

EDITORIAL: What's New for 1997

Bioconjugate Chemistry publishes high-quality research in all areas of conjugation chemistry. The Editors would like to expand the journal's coverage of topics relevant to combinatorial chemistry such as the reagents and methodology of attaching libraries to reporters, surfaces, or tags that add useful functionality. We will continue to offer authors of accepted **Review** articles the opportunity to submit an illustration for possible use on the cover of the issue where their article appears.

The 1997 Instructions to Authors for *Bioconjugate Chemistry*, which may be downloaded from the worldwide web address <http://pubs.acs.org/journals/bcches/index.html>, informs authors about practical aspects of electronic manuscript submission and the preparation of illustrations.

On an experimental basis, graphics files such as ChemDraw structures may be submitted on disk for highest-quality reproduction of some illustrations. Authors are requested to provide a copy of all illustrations reduced to single-column width (8.25 cm, 3.5 in.) to check legibility. Lettering and numbering should be no smaller than 2 mm in height upon reduction. Multiple-part figures should be combined on a single page.

Thanks to Our Reviewers

It is a pleasure to acknowledge the contributions of the reviewers of manuscripts submitted in 1996 for publication in *Bioconjugate Chemistry*. Their unselfish service has been essential in the shaping of the seventh volume of the journal. The scientific community is fortunate that its members are willing to share their time and specialized knowledge in this way. The list of reviewers is on the following page.

Claude F. Meares
Editor-in-Chief

List of Reviewers

Ralph Abraham
Maciej Adamczyk
Sudhir Agrawal
Eva Åkerblom
Terry Allen
Vernon L. Alvarez
Carolyn J. Anderson
Leslie D. Anderson
Yasushi Arano
Don Axworthy
Robert W. Baldwin
Marcel B. Bally
Rolf F. Barth
Jacqueline K. Barton
James K. Bashkin
Hagan Bayley
Jean-Paul Behr
Donald E. Bergstrom
G. V. Betageri
Purshotam Bhan
Gary Bignami
James Blake
David Blakey
Alexei A. Bogdanov
Philip N. Borer
Martin W. Brechbiel
Michael Brinkley
Art D. Broom
Tom Brown
Robert G. Bryant
David R. Bundle
Cynthia J. Burrows
Karin D. Caldwell
Jacek Capala
Paul Carter
C. Allen Chang
Chien-Hsing Ken Chang
Ravi V. J. Chari
Jik Chin
P. Dan Cook
Daniel J. Coughlin
Clark H. Cummins
David Curiel
Massad Damha
Gary S. David
Jean F. Desreux
Robert Dodge
Ruth Duncan
Richard H. Ebright
Fritz Eckstein
Bernard F. Erlanger
Arnold Falick
Gary Felsenfeld
BC9701813

Raymond A. Firestone
Harvey F. Fisher
Catherine Foulon
Keith R. Fox
Joseph Francisco
Alan R. Fritzberg
Jean Gariépy
Kieran F. Geoghegan
William F. Goeckler
Wayne Gombotz
David A. Goodwin
Marc Greenberg
Douglas Greiner
Gary L. Griffiths
Boyd E. Haley
Takeshi Hara
Jon Hangeland
Jim Haralambidis
Troy O. Harasym
Ronald Harvey
Richard Haugland
Robert E. Hearst
Sidney M. Hecht
Ned D. Heindel
F. Hillenkamp
Thomas Horn
Leaf Huang
James S. Huston
Jean-Louis Imbach
Thomas L. James
Donald M. Jerina
Brian H. Johnson
David K. Johnson
P. L. Jones
Roger Jones
George Just
Alexander V. Kabanov
Lou-Sing Kan
John A. Katzenellenbogen
John F. W. Keana
David E. Kerr
Ban An Khaw
Dalton King
Burma Kinsey
Hiromi Kitano
Eric T. Kool
Jindrich Kopecek
Robert Kroll
Ulrich Jorg Krull
Robert R. Kuntz
Mark J. Kurth
John M. Lambert
Robert Langer

Richard G. Lawton
Bernard Lebleu
J. S. Lee
Robert L. Letsinger
James Lewis
David Loakes
Thomas J. Lobl
Lawrence A. Loeb
Harri Lönnberg
Joseph Loo
Philip S. Low
Helmut R. Mäcke
L. James Maher
Sam A. Margolis
Luigi G. Marzilli
Pradip K. Mascharak
Phillip G. Mattingly
James A. McCloskey
Thomas Meehan
Damon L. Meyer
Karen L. Meyer
Rich B. Meyer
C. Russell Middaugh
Patrick Midoux
Michel Monsigny
Barbara M. Mueller
Akira Murakami
T. L. Nagabhushan
Sean O'Malley
Leslie E. Orgel
Giovanni Paganelli
William M. Pardridge
David Parker
Premal Patel
Dean Pettit
Vladimir N. Potaman
Glenn D. Prestwich
Tariq M. Rana
M. P. Reddy
Ralph Reisfeld
Mark A. Reynolds
Stacia M. Rink
Jean E. Rivier
Steven E. Rokita
Keith Rose
Peter G. Schultz
Petra Schwillie
William H. Scouten
Alec H. Sehon
Hartmut Seliger
Peter Senter
Jonathan L. Sessler
L. W. Seymour

Ben Shen
Clay Siegal
Nathan Siemers
David S. Sigman
Rajeeva Singh
Lloyd M. Smith
E. M. Southern
Caroline J. Springer
Suresh Srivastava
James J. Starling
Jacek Stawinski
Cy A. Stein
Stanley Stein
Michael P. Stone
Joanne Stubbe
Brian D. Sykes
Francis C. Szoka, Jr.
James P. Tam
T. J. Thomas
David H. Thompson
H. Holden Thorp
Nguyen T. Thuong
Louis X. Tiefenauer
Marcus A. Tius
Glen L. Tolman
Maria Tomasz
Vladimir P. Torchilin
Eishun Tsuchida
Thomas D. Tullius
Naoki Umamoto
Ganesan Vaidyanathan
Francesco M. Veronese
Wynn A. Volkert
Murthy Vrudhula
Ernst Wagner
E. Sally Ward
Michael J. Waring
Kyoichi A. Watanabe
David S. Watt
G. Wegner
Theodore G. Wensel
Ronald Wetzel
D. Scott Wilbur
Meir Wilchek
George S. Wilson
W. David Wilson
Martin L. Yarmush
Dale Yelton
Samuel Zalipsky
Michael Zalutsky
Jiri Zemlicka

COMMUNICATIONS

Comb-Type Polycations Effectively Stabilize DNA Triplex

Atsushi Maruyama,* Maiko Katoh, Tsutomu Ishihara, and Toshihiro Akaike

Department of Biomolecular Engineering, Tokyo Institute of Technology, 4259 Nagatsuta, Midori, Yokohama 226, Japan. Received May 6, 1996[®]

DNA triplex formation has been studied as a potential strategy for regulation of gene expression. The triplex is, however, unstable under physiological conditions, so that an effective stabilizer for the triplex formation is needed. Here is shown a novel strategy to stabilize the triplex based on the molecular design of a comb-type polycation. Linear polycations, such as poly(L-lysine) and poly(L-arginine), thermally stabilize DNA duplexes (and triplexes). The complexes between DNA and the polycation are irreversible and are liable to precipitate out of aqueous media. The irreversibility and phase separating properties of the complex impede association of single-stranded (ss) DNAs in the complex to form duplexes and triplexes. A comb-type polycation consisting of a poly(L-lysine) backbone and grafted chains of hydrophilic polymers was prepared. The comb-type copolymers increased solubility of their complex with DNA and suppressed conformational changes of DNA. Thermal melting curve analyses revealed that the comb-type copolymer markedly stabilized DNA triplexes and did not disturb ssDNAs in forming duplexes and triplexes. Reversible and one-step melting/reassociation transitions of poly(dA)·2poly(dT) triplex were shown in the presence of the copolymers. The stabilizing effect of the copolymer was larger than that of spermine, a polyamine considered effective in stabilizing triplexes. These results indicated that molecular design of polycations with a comb-type structure is a novel strategy to create efficient triplex stabilizers. Such comb-type copolymer consisting of various types of polycation backbones and hydrophilic graft chains may have many applications in which specific and precise interactions of polynucleotides are involved.

Deactivation of a target gene with oligonucleotides which form triplexes with that gene has been proven to be a potential strategy for regulation of gene translation (1, 2). Triplex formation is, however, unstable in physiological conditions, which limits the utility of the triplex strategy. To extend the usefulness of the triplex strategy, several compounds that stabilize triplexes have been investigated (3–7).

Polyamines, such as spermine, spermidine, and putrescine, stabilized duplexes and triplexes (8–10). The stabilizing effect of polyamines was largely due to neutralization of electrostatic repulsion among phosphate anions in DNA molecules associating in the triplex and duplex. Their effect was, however, reduced considerably under physiological conditions, because interaction of polyamines with DNA was hampered by coexisting cations (9–11).

For neutralizing the electrostatic repulsion among DNA strands associated in triplexes or duplexes, macromolecular polycations, such as poly(L-lysine) (PLL) and poly(L-arginine), are more effective than oligomeric cations, leading to a considerable rise in the melting temperature (T_m) of the duplex (12, 13). Polycations, however, interact strongly with polyanions to form irreversible polyion complexes (or inter-polyelectrolyte complexes) (13, 14). Polycations severely compacted the DNA conformation (15, 16). Coacervation or precipitation

of the complex occurred (12, 14). Single-stranded (ss) DNAs rarely form duplexes and triplexes in the presence of polycations, resulting in irreversibility of duplex and triplex transitions (melting and reassociation).

The reversible transition of DNA might be, therefore, attainable by increasing the solubility of the complex and reducing the conformational changes of DNA. For this approach, the interactions of polycations with DNA have to be regulated. The interactions of polycations with DNA could be regulated by modifying polycations with DNA-immiscible chains such as electrostatically neutral polymer chains that interfere with these interactions. Modification of polycations with hydrophilic chains like polysaccharides may improve the solubility of a DNA/polycation complex, leading to prevention of phase separation of the complex from aqueous medium. On the basis of the hypothesis mentioned above, we prepared comb-type copolymers of poly(L-lysine) with polysaccharide side chains and evaluated their ability to stabilize DNA triplexes.

The comb-type copolymers, PLL-graft-dextran, were prepared by a reductive amination reaction of PLL·HBr (100 mg, $M_w = 4.5 \times 10^4$ from Peptide Institute, Inc., Osaka, Japan) with dextran (Dex, 600 mg, $M_n = 5900$, Dextran T-10 from Pharmacia Biotech, Uppsala, Sweden) using sodium cyanoborohydride (30 mg, from Wako Pure Chemical Industries, Ltd., Osaka, Japan) as a reductant in dimethyl sulfoxide. After the mixture was incubated for 48 h at 40 °C, the copolymers were isolated by dialysis against water for 7 days using Spectra/Por membrane (MWCO = 12 000–14 000, Spectrum, Los Angeles, CA). Isolation of the resulting copolymers from unreacted Dex

* Author to whom correspondence should be addressed (telephone +81-45-924-5809; fax +81-45-924-5815; e-mail amaryam@bio.titech.ac.jp).

[®] Abstract published in *Advance ACS Abstracts*, December 15, 1996.

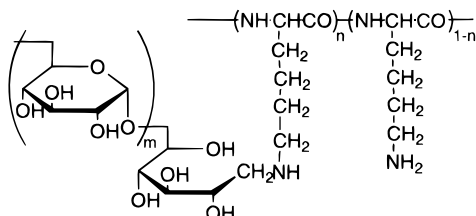


Figure 1. Structural formula of PLL-*graft*-Dex comb-type copolymer. The copolymer with $m = 36.5$ (calculated from the number-average MW of Dextran T-10) and $n = 0.2$ (determined by $^1\text{H-NMR}$ spectrum) was used in this study.

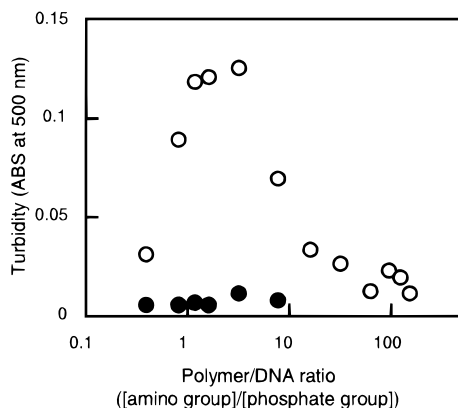


Figure 2. Turbidity of DNA solution to which the indicated amounts of PLL (○) or PLL-*graft*-Dex comb-type copolymer (●) were added. To 1 mL of 100 $\mu\text{g/mL}$ calf thymus DNA in Dulbecco's PBS was added the appropriate amount of polymers from 10 mg/mL stock solution at room temperature. The mixtures were diluted to 2.5 mL, followed by optical density measurement at 500 nm.

was confirmed by gel permeation chromatography on Waters Ultrahydrogel 250 and 500 columns connected with a multiangle light scattering detector and a differential refractive index detector. The molecular weight of the resulting copolymers was determined to be $M_n = 2.5 \times 10^5$ (as free salt). Composition of the copolymer was determined by $^1\text{H-NMR}$ spectrum in D_2O to be 90 wt % Dex and 10 wt % PLL, which meant that Dex chains were grafted onto an average of one of every five lysine units. Further, it was estimated that the coupling efficacy of Dex to PLL was $>90\%$. The structural formula of the copolymer is given in Figure 1.

The Dex-grafted chains on PLL increased the solubility of the complex with DNA. Figure 2 shows the turbidity change of calf thymus DNA in phosphate-buffered saline (PBS) by an addition of either PLL homopolymer or the comb-type graft copolymer. While significant turbidity appeared in PLL/DNA mixture, no turbidity was seen for corresponding comb-type copolymer mixtures. Thus, PLL-*graft*-Dex comb-type copolymer seems to form a soluble complex with DNA.

We then examined the comb-type copolymer for induced structural changes of DNA. Structural change of DNA is detectable by circular dichroism (CD). Figure 3 shows CD spectra of calf thymus DNA mixed with PLL homopolymer or the comb-type copolymer in 1/100 diluted PBS, where both mixtures are transparent. CD signals due to DNA base groups were considerably altered by the addition of PLL homopolymer. Complex formation between DNA and PLL is known to show cooperative association and irreversibility (13, 14). PLL condenses DNA into rod and toroid-like structures (15, 16), which accompanies a change in CD signals (14). In contrast to the PLL homopolymer, addition of the comb-type copolymers only shows a slight change. The CD signals did

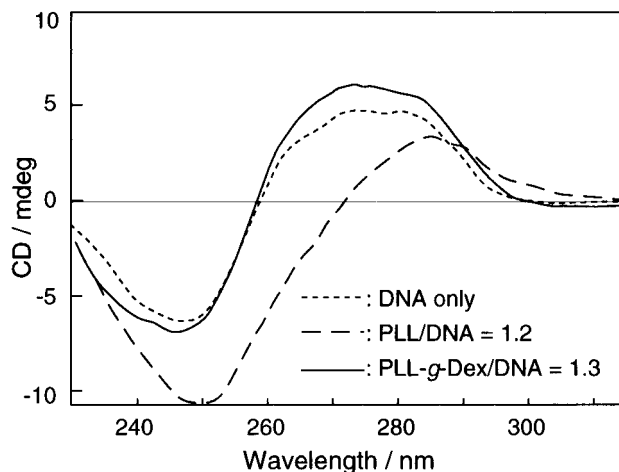


Figure 3. CD of calf thymus DNA mixed with PLL or PLL-*graft*-Dex comb-type copolymer in 1/100 diluted PBS at room temperature (ca. 20 $^\circ\text{C}$). The samples were created using the same procedure described in Figure 2, except PBS concentration. The DNA/comb-type copolymer mixture in PBS showed almost the same CD signal as that in this figure, while CD of the DNA/PLL mixture was not obtained because of turbidity and precipitation of the mixture.

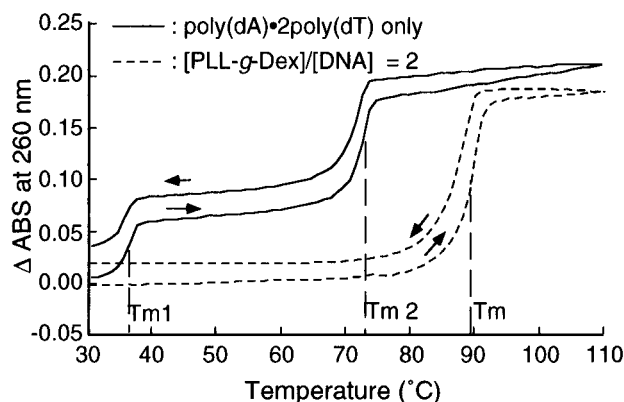


Figure 4. UV- T_m profile of poly(dA)•2poly(dT) triplex in the presence or absence of PLL-*graft*-Dex comb-type copolymer. Poly(dA) and poly(dT) were dissolved in 150 mM NaCl containing 10 mM sodium phosphate (pH 7.2) and 0.1 mM EDTA. Concentrations of the solutions were calculated using molar extinction coefficients of 8900 at 257 nm for poly(dA) and 9000 at 265 nm for poly(dT) (10). To a 1:2 mixture of poly(dA) and poly(dT) was added the comb-type copolymer at a polymer/DNA ([amino group]_{polymer}/[phosphate group]_{DNA}) ratio = 2. After dilution to a final DNA concentration of 14.5 (bp) $\mu\text{mol/L}$ with the same buffer, the mixtures were heated at 90 $^\circ\text{C}$ for 30 min, cooled to room temperature, and allowed to stand for 16 h. The UV- T_m curves were recorded at 0.2 K/min with a DU-640 spectrometer (Beckman) equipped with a micro- T_m apparatus.

not vary even when electrostatically excessive amounts of the copolymer were added (data not shown). Further, CD spectra of a comb-type copolymer/DNA mixture in PBS showed almost the same signals as that shown in Figure 3, while that of a PLL/DNA mixture was not obtained because of turbidity and precipitation of the mixture. Thus, the Dex graft was effective in preventing serious structural changes to DNA.

It was predictable from the results described above that the DNAs associated with the comb-type copolymer preserve an ability to form duplexes or triplexes. The stabilizing effect of the comb-type copolymers on DNA triplexes was then examined by recording thermal melting profiles with a UV spectrometer. Figure 4 shows UV- T_m curves of a poly(dA)•2poly(dT) triplex in PBS. At physiological ionic strength, the triplex showed two-step melting. The first transition at lower temperature (37

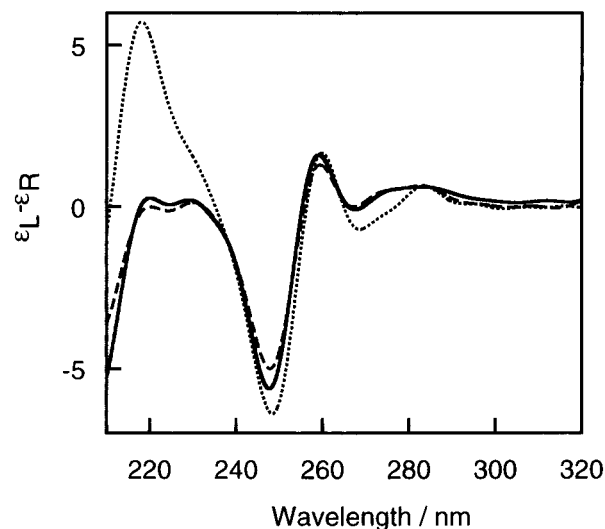


Figure 5. CDs of poly(dA)·poly(dT) duplex (dotted line), poly(dA)·2poly(dT) triplex (broken line), and the 2:1 mixture (solid line) of the comb-type copolymer and the triplex. The samples were prepared according to the same procedure as that described in Figure 4, except a 1:1 molar ratio of poly(dA)/poly(dT) was used for the duplex. CD measurements were done after T_m measurements. The spectra were recorded on a Jasco J-600 using a 0.5 cm length quartz cell at 20 nm/min as a scanning speed, 0.1 nm/point as a wavelength step, and 1 s/point as a time step. Each spectrum shown was the average of three scans and has been smoothed by a computer. The CD signal attributed to the comb-type copolymer was negligible under the condition.

°C) was the melting of the triplex to a duplex and a ssDNA, and the second transition at higher temperature (72 °C) was that of the duplex. In the presence of excess comb-type copolymers over DNAs, only one transition was observed at higher temperature (89 °C). As the magnitude in UV absorbance change (ΔABS) at T_m in the presence of the copolymer was equal to the sum of those at T_{m1} and T_{m2} in the absence of the copolymer, the transition is indicated to be a direct melting of the triplex to its constituting ssDNAs. The direct melting of the triplex was further indicated by ΔABS measurement with changing poly(dT)/poly(dA) molar ratio [while the concentration of poly(dA) was kept constant]. The ΔABS values reached a plateau at the changing poly(dT)/poly(dA) molar ratio over 2 (data not shown). It should be noted that the UV- T_m profile in the cooling process demonstrated reversibility of the transition even in the presence of the comb-type copolymer. It was indicated that the comb-type copolymer thermally stabilized the triplex but did not disturb triplex formation from its constituting ssDNAs. Formation of the poly(dA)·2poly(dT) triplex was further evaluated by CD measurements. As shown in Figure 5, whereas the CD spectrum of the poly(dA)·poly(dT) duplex has a strong positive band near 220 nm, the poly(dA)·2poly(dT) triplex has no positive band near this wavelength (17). The mixture of poly(dA)·2poly(dT) and the comb-type copolymers showed almost the same signals as the triplex alone even after T_m measurement. We conclude that the comb-type copolymers do not disturb inter-polynucleotide associations of ssDNAs to form the triplex.

The efficacy of the comb-type copolymer for stabilizing the triplex was then compared to that of spermine, a polyamine effective in triplex stabilization (10). Figure 6 shows the effects of comb-type copolymer and spermine on melting temperatures of the triplex at various stabilizer/DNA ratios. An electrostatically equivalent amount ($[\text{amino group}]_{\text{polymer}}/[\text{phosphate group}]_{\text{DNA}}$) of the comb-type copolymer increased the melting temperature of the

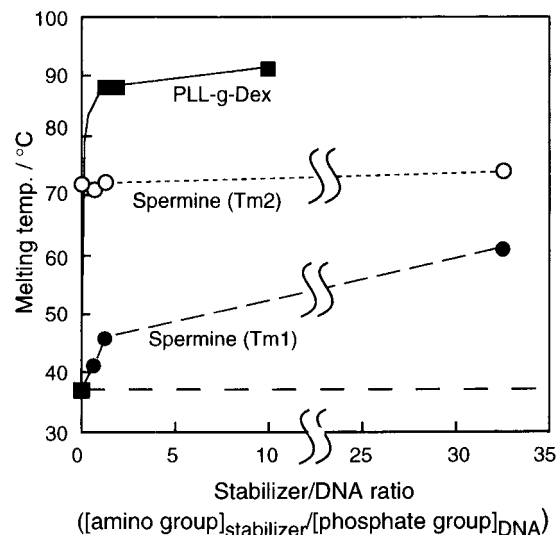


Figure 6. Stabilizing effect of spermine and the comb-type copolymer. All experiments were conducted under the conditions described in Figure 4. T_m was determined by generating the first derivative, dA/dT (where A and T are absorbance and temperature, respectively), of the UV- T_m curves.

triplex by 50 °C, while a large excess of spermine increased it by 20 °C. Moreover, one-step melting of the triplex was observed in the presence of the comb-type copolymer at a stabilizer/DNA ratio over 1, whereas two-step melting was still seen even in the presence of a large excess of spermine. Poly(dA)·2poly(dT) triplex stabilized with 7.5 μM spermine was reported to melt in a one-step manner in low ionic strength medium (10). The stabilizing effect was, however, significantly reduced in the presence of 0.15 M NaCl, resulting in the two-step melting of the triplex. Spermine is believed to be competitively displaced with Na cations. In contrast to spermine, the comb-type copolymer considerably stabilized the triplex of poly(dA)·2poly(dT). The one-step melting and considerable rise in T_m observed with an electrostatically equivalent amount of the comb-type copolymer implied its stable association with DNA.

The strong and stable stabilizing effect of the comb-type copolymer was considered to be directed by its high multivalency of cations. The copolymer, however, allows ssDNAs to form duplexes and triplexes. The Dex graft chains on the copolymer interfere with interaction between the PLL backbones and DNAs. Those graft chains might inhibit the close contact of DNAs to the PLL backbones and thereby dehydration and compaction, which are presumably involved in the irreversible complex formation between DNAs and homopolycations. Regardless of the weakened interaction, the comb-type copolymer could suppress the repulsive forces among DNA strands enough to stabilize the triplex.

In addition to the shielding effect upon the repulsive forces, Dex chains may play a role in stabilizing hydrogen bonding between base pairs. As the comb-type copolymer consists of 90 wt % Dex and 10 wt % PLL, the PLL backbone in the copolymer is likely surrounded by a phase concentrated with Dex segments. The DNAs that are attracted to the PLL backbone by electrostatic interactions are forced to merge with the Dex-enriched phases, which are low in dielectric constant. Such low dielectric environments might enhance hydrogen bonding between base pairs, leading to DNA triplex stabilization. It was reported that the triplex in a medium containing spermine was further stabilized by moderate concentrations of organic solvents (18). If the electrostatic repulsion was neutralized by polyamines or polycations,

medium with a low dielectric constant may further stabilize triplexes. Furthermore, specific interaction between Dex chains and DNA may affect the stabilization behavior (19).

These results indicate that the molecular design of polycations with a comb-type structure is a successful approach to create efficient triplex stabilizers. Comb-type copolymers consisting of various types of polycation backbones and hydrophilic graft chains may have many applications in which specific and precise interactions of polynucleotides are involved. Conjugation of triplex-forming oligonucleotides (TFOs) with the comb-type copolymer may allow specific and stable triplex formation at target genes. Modification of the comb-type copolymers with a cellular specific ligand and other functional groups will provide novel types of delivery systems for TFOs, which is not available with low molecular weight stabilizers.

ACKNOWLEDGMENT

We are grateful to Professor Mizuo Maeda of Kyushu University for helpful discussion.

LITERATURE CITED

- (1) Felsenfeld, G., Davies, D. R., and Rich, A. (1957) Formation of a three-stranded polynucleotide molecule. *J. Am. Chem. Soc.* **79**, 223–224.
- (2) For review: Hélène, C., and Toulme, J. J. (1990) Specific regulation of gene expression by antisense, sense and anti-gene nucleic acids. *Biochim. Biophys. Acta* **1049**, 99–125.
- (3) Le Doan, T., Perrouault, L., Praseuth, D., Habhouh, N., Decout, J. L., Thuong, N. T., Lhomme, J., and Hélène, C. (1987) Sequence-specific recognition, photocrosslinking and cleavage of the DNA double helix by an oligo-[α]-thymidylate covalently linked to an azidoproflavine derivative. *Nucleic Acids Res.* **15**, 7749–7760.
- (4) Tung, C-H., Breslauer, J. B., and Stein, S. (1993) Polyamine-linked oligonucleotides for DNA triplex formation. *Nucleic Acids Res.* **23**, 5489–5494.
- (5) Nara, H., Ono, A., and Matsuda, A. (1995) Nucleosides and nucleotides. 135. DNA duplex and triplex formation and resistance to nucleolytic degradation of oligodeoxynucleotides containing *syn*-norspermidine at the 5-position of 2'-deoxyuridine. *Bioconjugate Chem.* **6**, 54–61.
- (6) Mergny, J. L., Duval-Valentin, G., Nguyen, C. H., Perrouault, L., Faucon, B., Rougée, M., Montenay-Garestier, T., Bisagni, E., and Hélène, C. (1992) Triple helix-specific ligands. *Science* **256**, 1681–1684.
- (7) Potaman, V. N., and Sinden, R. R. (1995) Stabilization of triple-helical nucleic acids by basic oligopeptides. *Biochemistry* **34**, 14885–14892.
- (8) Hample, K. J., Crosson, P., and Lee, J. S. (1991) Polyamines favor DNA triplex formation at neutral pH. *Biochemistry* **30**, 4455–4459.
- (9) Hanvey, J. C., Williams, E. M., and Besterman, J. M. (1991) DNA triple-helix formation at physiologic pH and temperature. *Antisense Res. Dev.* **1**, 307–317.
- (10) Thomas, T., and Thomas, T. J. (1993) Selectivity of polyamines in triplex DNA stabilization. *Biochemistry* **32**, 14068–14074.
- (11) Murray, N. L., and Morgan, A. R. (1973) Enzymic and physical studies on the triplex dTn·dAn·rUn. *Can. J. Biochem.* **51**, 436–449.
- (12) Olins, D. E., Olins, A. L., and von Hippel, P. H. (1967) Model nucleoprotein complexes: Studies on the interaction of cationic homopolypeptides with DNA. *J. Mol. Biol.* **24**, 157–176.
- (13) Tsuboi, M. (1967) Helical complexes of poly-L-lysine and nucleic acids. In *Conformation of Biopolymers* (G. N. Ramachandran, Ed.) Vol. II, pp 689–702, Academic Press, New York.
- (14) von Hippel, P. H., and McGhee, J. D. (1972) DNA-protein interactions. *Annu. Rev. Biochem.* **41**, 231–300.
- (15) Haynes, M., Garrett, R. A., and Gratzner, W. B. (1970) Structure of nucleic acid-poly base complexes. *Biochemistry* **9**, 4410–4416.
- (16) Wagner, E., Cotten, M., Foisner, R., and Birnstiel, M. L. (1991) Transferrin-polycation-DNA complexes: The effect of polycations of the structure of the complex and DNA delivery to cells. *Proc. Natl. Acad. Sci. U.S.A.* **88**, 4255–4259.
- (17) Howard, F. B., Miles, H. T., Liu, K., Frazier, J., Raghunathan, G., and Sasisekharan, V. (1992) Structure of d(T)·d(A)·d(T): The DNA triple helix has B-form geometry with C2'-endo sugar pucker. *Biochemistry* **31**, 10671–10677.
- (18) Moser, H. E., and Dervan, P. B. (1987) Sequence-specific cleavage of double helical DNA by triple helix formation. *Science* **238**, 645–650.
- (19) Tajmir-Riahi, T. A., Naoui, M., and Diamantoglou, S. (1994) DNA-carbohydrate interaction. The effects of mono- and disaccharides on the solution structure of calf-thymus DNA. *J. Biomol. Struct. Dyn.* **12**, 217–234.

BC960071G

ARTICLES

Synthesis of a Novel [125 I]Neonicotinoid Photoaffinity Probe for the *Drosophila* Nicotinic Acetylcholine Receptor

Bachir Latli, Motohiro Tomizawa, and John E. Casida*

Environmental Chemistry and Toxicology Laboratory, Department of Environmental Science, Policy, and Management, University of California, Berkeley, California 94720-3112. Received August 12, 1996[®]

The insect nicotinic acetylcholine receptor (nAChR) is the target for the major insecticide imidacloprid (IMI) and for the first candidate photoaffinity probe described here. Addition to 1-[(6-chloro-3-pyridinyl)methyl]-4,5-dihydro-2-nitromethylene-1*H*-imidazolidine (the nitromethylene analog of the nitroimine IMI) of formaldehyde and any one of several primary amines is known to give hexahydro-8-nitroimidazo[1,2-*c*]pyrimidine derivatives. These imidazopyrimidines with a wide range of N-substituents were found to inhibit [3 H]IMI binding to the *Drosophila* or *Musca* nAChR by 50% (IC₅₀) at 0.7–38 nM. Esterification of the *N*-(2-hydroxyethyl) derivative with 2-azido-5-(trimethylstannyl)-benzoic acid and then iododestannylation using Na 125 I and chloramine-T provide the candidate photoaffinity probe 6-[2-(2-azido-5-[125 I]iodobenzoyl)ethyl]-1-[(6-chloro-3-pyridinyl)methyl]-1,2,3,5,6,7-hexahydro-8-nitroimidazo[1,2-*c*]pyrimidine. This compound (unlabeled) has an IC₅₀ of 8 nM for [3 H]-IMI binding in *Drosophila* head membranes, and the 125 I-labeled photoaffinity probe labels only a 66 kDa protein(s) at a specific site inhibited by (–)-nicotine, consistent with the insecticide-binding subunit of the nAChR.

INTRODUCTION

The nicotinic acetylcholine receptor (nAChR¹) is the target in insects for 1-[(6-chloro-3-pyridinyl)methyl]-4,5-dihydro-2-nitroimino-1*H*-imidazolidine (imidacloprid or IMI) and many analogs usually with (6-chloro-3-pyridinyl)methylamino and nitro substituents (1–3). This new class of insecticides is referred to as chloronicotinyls (4) or neonicotinoids (2). [3 H]IMI is the principal radioligand for characterizing and quantitating the insecticide binding site of the nAChR of *Drosophila melanogaster* (fruit fly) and *Musca domestica* (house fly) (5, 6) (Figure 1). The nitromethylene analog of IMI (CH-IMI) (2, 7–9) and an acyclic nitromethylene compound (nitenpyram) (6, 10, 11) (Figure 1) are of interest not only as potent insecticides but also as probes for exploring the structure of *Drosophila* and *Musca* nAChRs.

The insect nAChR is best understood for *Drosophila*, for which the structural features are deduced from molecular biology approaches (12) and the same three subunits of 69, 66, and 61 kDa have been isolated by chromatography on affinity columns based on α -bunga-

rotoxin (α -BGT) (a toxin from the elapidae snake *Bungarus multicinctus*, which is the classical competitive antagonist of the nAChR) and demethylnitenpyram (6). α -BGT cross-links with a protein(s) in *Drosophila* head membranes calculated to have a molecular mass of 42 kDa (13) and, as an azidosalicylate derivative, it photoaffinity labels a 66 kDa polypeptide in isolated *Drosophila* and *Musca* nAChRs (6). Although the neonicotinoids and α -BGT share the same binding site(s) in insects, on the basis of competition studies (1, 14), the site of insecticide binding is only partially defined with α -BGT since the molecular size is different, i.e. masses of 256 for IMI versus 8000 for α -BGT (3, 15). The photoaffinity probes used in characterizing the vertebrate (*Torpedo* electric organ) nAChR (16, 17) are not suitable for insects because of relatively low affinity or binding to a site not directly relevant for insecticidal activity (1, 11). The alternative is to specifically design a photoaffinity probe based on an IMI analog as in the case of our recent development of a nitenpyram analog as an affinity column for isolation of *Drosophila* and *Musca* nAChRs (6).

The design and development of the neonicotinoid photoaffinity probe involved the following steps: first, establish a site in the neonicotinoid for substitution allowing retention of moderate to high receptor potency in *Drosophila* brain membrane preparation; second, optimize the probe with candidate photoreactive substituents; and finally, prepare the radiolabeled photoaffinity ligand and test for light-dependent and protectable labeling of one or more nicotinic acetylcholine receptor subunits. The overall chemistry utilized is shown in Figure 1. Nitenpyram analogs were examined because of their successful use in preparing an affinity column (6). More extensive studies were made on nitromethylene imidazolidines such as CH-IMI since they are converted to insecticidal hexahydroimidazopyrimidines on ad-

* Author to whom correspondence should be addressed at the Environmental Chemistry and Toxicology Laboratory, Department of Environmental Science, Policy and Management, 114 Wellman Hall, University of California, Berkeley, CA 94720-3112 [telephone (510) 642-5424; fax (510) 642-6497; e-mail ectl@nature.berkeley.edu].

[®] Abstract published in *Advance ACS Abstracts*, December 1, 1996.

¹ Abbreviations: α -BGT, α -bungarotoxin; CH-IMI, nitromethylene analog of IMI; DCC, 1,3-dicyclohexylcarbodiimide; DMAP, 4-(dimethylamino)pyridine; EI, electron impact; EtOAc, ethyl acetate; FAB-HRMS, fast atom bombardment high-resolution MS; FAB-LRMS, fast atom bombardment low-resolution MS; Hex, hexane; IC₅₀, concentration of test compound for 50% inhibition of specific radioligand binding; IMI, imidacloprid; nAChR, nicotinic acetylcholine receptor.

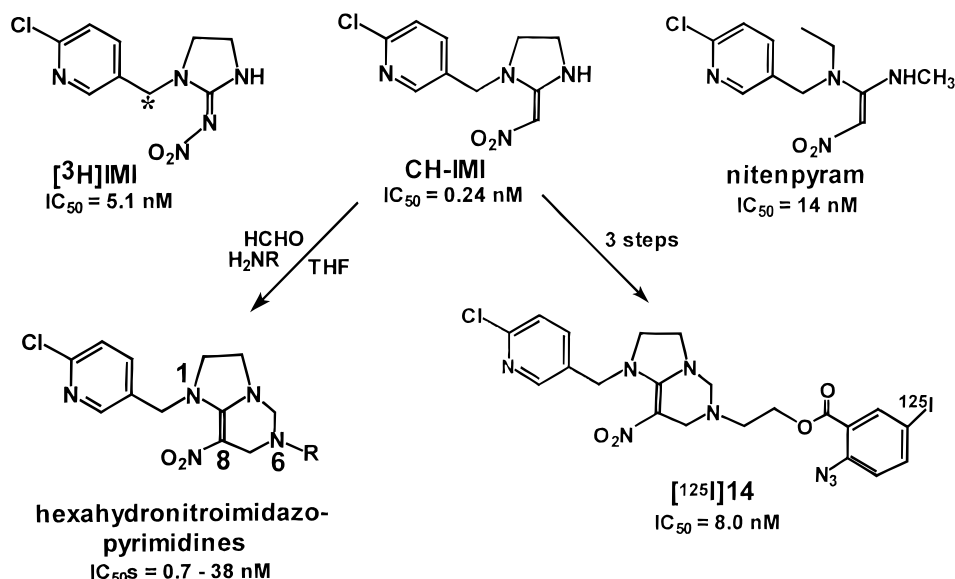


Figure 1. Structures of neonicotinoids including the radioligand ($[^3\text{H}]\text{IMI}$), analogs (CH-IMI and nitenpyram), derivatives, and the photoaffinity probe ($[^{125}\text{I}]\text{-14}$). Receptor potencies are indicated as concentrations for 50% inhibition (IC_{50}) of the displacement of $[^3\text{H}]\text{IMI}$ binding from *Drosophila* head membranes (data from this paper and ref 6).

dition of formaldehyde and a primary amine (18, 19). We find that fortunately the imidazopyrimidines derived from CH-IMI retain much of the affinity at the receptor of the parent compound and therefore allow the introduction of a variety of substituents in optimizing a candidate photoaffinity probe. Optimization studies ultimately led to synthesis of 6-[2-(2-azido-5- $[^{125}\text{I}]\text{-iodobenzoyl}$)ethyl]-1-[(6-chloro-3-pyridinyl)methyl]-1,2,3,5,6,7-hexahydro-8-nitroimidazo[1,2-c]pyrimidine ($[^{125}\text{I}]\text{-14}$) (Figure 1) as a candidate photoaffinity probe for the *Drosophila* nAChR.

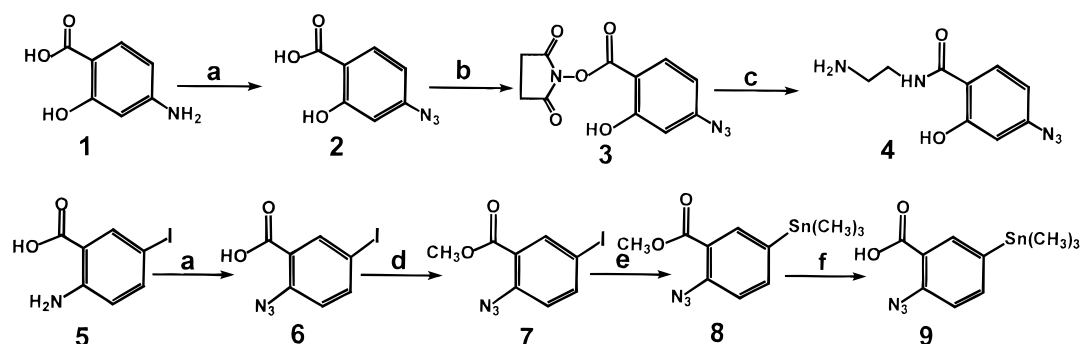
EXPERIMENTAL PROCEDURES

Materials. Silica gel TLC for analysis was performed with precoated plastic sheets ($4 \times 8 \text{ cm}$, 0.25 mm gel layer) with fluorescent indicator (Polygram R SILG/UV254, Macherey-Nagel, Germany) and for preparative purposes with precoated silica gel GF plates ($20 \times 20 \text{ cm}$, Analtech). NMR spectra were recorded for CDCl_3 solutions with a Bruker AM-300 or AM-400 spectrometer. Chemical shifts (δ in parts per million) are reported for ^1H at 300 Hz or 400 MHz and for ^{13}C at 75 MHz relative to internal tetramethylsilane and CDCl_3 , respectively. Mass spectra were acquired by GC/MS with a Hewlett-Packard 5971A or 5985B instrument in the electron impact (EI) mode (70 eV, 200 °C). Fast atom bombardment (FAB)-MS (both low and high resolution) was conducted with the Fisons ZAB2-EQ spectrometer. UV absorbances were measured on a Hewlett-Packard 8452A diode array spectrophotometer. Photoreactivity of the candidate photoaffinity probe was determined for a solution in absolute ethanol in a 1 cm quartz cell positioned 3 cm from four 350 nm lamps in a Rayonet photochemical reactor (The Southern New England Ultraviolet Co., Hamden, CT). Melting points are uncorrected and were recorded on a Fisher-Johns melting point apparatus. All reagents were obtained from Aldrich Chemical Co. (Milwaukee, WI) except EDTA, (–)-nicotine, ethylene glycol bis(β -aminoethyl ether)-*N,N,N,N*-tetraacetic acid, lithium dodecyl sulfate, and phenylmethanesulfonyl fluoride, which were obtained from Sigma Chemical Co. (St. Louis, MO). All solvents used were of reagent or HPLC grade. THF was distilled from sodium benzophenone under nitrogen in a recirculating still, with a deep blue color maintained in the distillation pot. Dioxane was dried by storage over molecular sieves.

Literature procedures were used to prepare 1-[(6-chloro-3-pyridinyl)methyl]-1-(ethylamino)-1-(methylthio)-2-nitroethene (6) and CH-IMI (7, 8). $[^3\text{H}]\text{IMI}$ at 25 Ci/mmol was prepared in this laboratory (5). L-[*N*-methyl- ^3H]-Nicotine ($[^3\text{H}]\text{nicotine}$) at 78 Ci/mmol and Na^{125}I at 584 MBq $^{125}\text{I}/\mu\text{g}$ of iodine ($\sim 2000 \text{ Ci/mmol}$) in dilute NaOH solution were purchased from DuPont NEN Research Products (Boston, MA) and Amersham Life Science Inc. (Arlington Heights, IL), respectively. Molecular mass markers were obtained from Bio-Rad (Richmond, CA). Liquid scintillation counting was performed with a Beckman LS 6000IC, using High Flash Point Cocktail, Safety-Solve, Research Products International Corp. (Mount Prospect, IL). Each intermediate and candidate probe was $>98\%$ pure on the basis of TLC and ^1H and ^{13}C NMR integrations. Compounds with photosensitive substituents were used in subdued light.

Synthesis of Azidohydroxybenzoyl (1–4), Azidoiodobenzoyl (5–7), and Azidotrimethylstannylbenzoyl (8, 9) Intermediates (Scheme 1). 4-Azido-2-hydroxybenzoic Acid (2). To a solution of 4-amino-2-hydroxybenzoic acid (1) (4.6 g, 30 mmol) in concentrated HCl (70 mL, 12 N) was added dropwise and with care at 0 °C a solution of sodium nitrite (6.21 g, 90 mmol) in cold water (30 mL). The mixture was stirred for 30 min before a solution of sodium azide (10 g, 155 mmol) in cold water (50 mL) was added slowly and dropwise. The resulting suspension was stirred at 0 °C for 3 h and then filtered, washed with cold water, and dried under vacuum to give 4.6 g of 2 as a brownish solid in 86% yield: mp = 165–167 °C; ^1H NMR (CDCl_3) δ 7.88 (d, $J = 8.03 \text{ Hz}$, 1H), 6.62 (d, $J = 8.03 \text{ Hz}$, 1H), 6.60 (s, 1H); ^{13}C NMR (CDCl_3) δ 172.82, 164.47, 148.47, 133.26, 111.17, 110.83, 107.74.

N-Hydroxysuccinimidyl-4-azido-2-hydroxybenzoate (3). To a stirred solution of 2 (2.33 g, 13 mmol) in dry THF (30 mL) was added *N*-hydroxysuccinimide (2.07 g, 18 mmol) at 0 °C followed by a solution of DCC (3.71 g, 18 mmol) in THF (2.0 mL), and the resulting mixture was stirred under nitrogen atmosphere for 6 h. It was then filtered and concentrated *in vacuo* to give 5.2 g of crude material. Purification by silica gel flash chromatography using CHCl_3 as eluent gave 3.6 g of product as a white solid in 100% yield: mp = 140–142 °C; $R_f = 0.73$ in MeOH/ CHCl_3 , 10:90; ^1H NMR (CDCl_3) δ 9.97 (d, $J = 8.64 \text{ Hz}$, 1H), 9.68 (s, 1H, OH), 6.68 (d, $J = 2.10 \text{ Hz}$, 1H), 6.62

Scheme 1. Preparation of Azidohydroxybenzoyl, Azidoiodobenzoyl, and Azidotrimethylstannylbenzoyl Intermediates^a

^a (a) HCl, NaNO₂, NaN₃, 86–90%; (b) NHS, DCC, THF, 100%; (c) H₂N(CH₂)₂NH₂, CH₃CN, THF, 91%; (d) MeOH, H₂SO₄, 100%; (e) Pd(PPh₃)₄, Me₃Sn–SnMe₃, dioxane, 67%; (f) LiOH, THF, 51%.

(dd, $J = 2.10, 8.64$ Hz, 1H), 2.93 (brs, 4H); ¹³C NMR (CDCl₃) δ 169.22, 163.83, 162.81, 149.32, 131.60, 111.11, 107.10, 104.62, 25.30.

N-(4-Azido-2-hydroxybenzoyl)ethylenediamine (4). A solution of **3** (1.1 g, 4.0 mmol) in dry THF (10 mL) was stirred at 0 °C under nitrogen atmosphere. Ethylenediamine (0.4 mL, 6.0 mmol) was added in acetonitrile (5.0 mL), and the resulting mixture was stirred overnight in the dark. The mixture was concentrated *in vacuo* and purified by preparative TLC (2.0 mm thickness plate) to give 0.8 g of **4** as a yellowish oil in 91% yield: $R_f = 0.1$ in MeOH/CHCl₃, 10:90; ¹H NMR (CDCl₃) δ 7.73 (d, $J = 8.61$ Hz, 1H), 6.54 (d, $J = 2.25$ Hz, 1H), 6.48 (dd, $J = 2.25, 8.61$ Hz, 1H), 3.49 (t, $J = 5.88$ Hz, 2H), 2.91 (t, $J = 5.88$ Hz, 2H), 2.74 (brs, NH₂, NH); ¹³C NMR (CDCl₃) δ 169.53, 165.1, 144.51, 129.61, 113.63, 108.51, 107.48, 41.26, 39.20; FAB-LRMS MH⁺ (10%), M⁺ (75%), 192 (100%); FAB-HRMS C₉H₁₁N₅O₂H⁺, calcd 222.0991, found 222.0941.

2-Azido-5-iodobenzoic Acid (6). To a solution of 2-amino-5-iodobenzoic acid (**5**) (5.26 g, 20 mmol) in concentrated HCl (60 mL, 12 N), stirred at 0 °C, was added a solution of NaNO₂ (4.14 g, 60 mmol) in water (25 mL). The resulting mixture was stirred for 30 min before NaN₃ (6.5 g, 100 mmol) in cold water (30 mL) was added dropwise, and the mixture was stirred overnight. It was then poured into ice and the solid was filtered and dried *in vacuo* to give 5.2 g of **6** as a cream colored solid in 90% yield: mp = 118–120 °C; $R_f = 0.75$ in MeOH/CHCl₃, 10:90; ¹H NMR (CDCl₃) δ 8.22 (d, $J = 2.21$ Hz, 1H), 7.75 (dd, $J = 2.21, 8.61$ Hz, 1H), 6.95 (d, $J = 8.61$ Hz, 1H); ¹³C NMR (CDCl₃) δ 169.31, 142.12, 141.12, 139.98, 123.72, 121.55, 87.50.

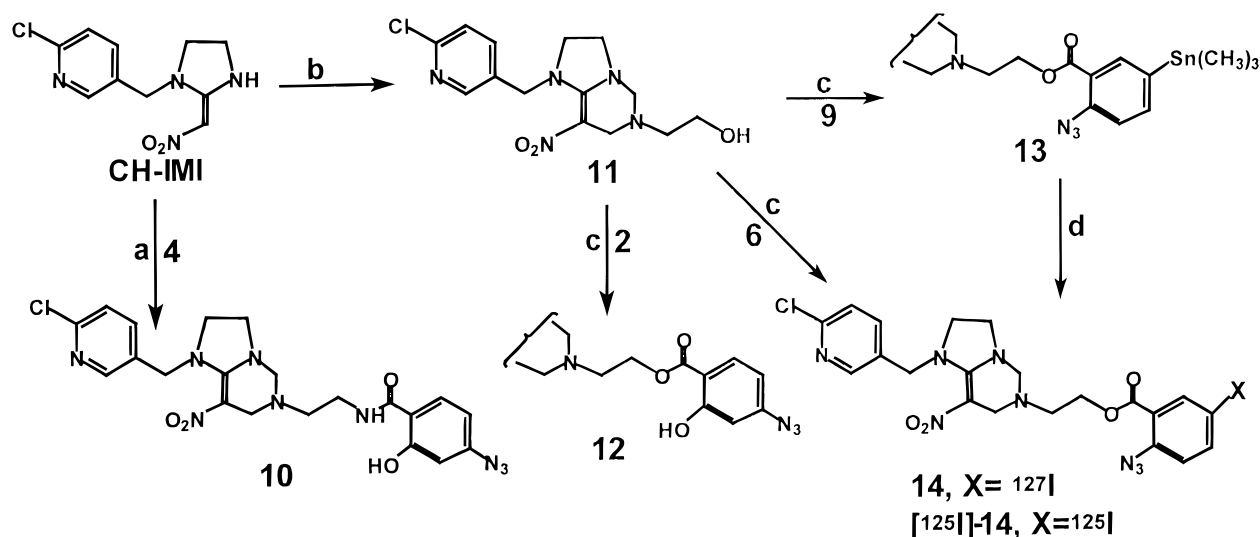
Methyl 2-Azido-5-iodobenzoate (7). To a solution of **6** (1.0 g, 3.46 mmol) in MeOH (50 mL) was added a few drops of concentrated H₂SO₄ (95–98%), and the mixture was stirred under reflux overnight. After the mixture cooled to room temperature, the solvent was evaporated and the residue was diluted in EtOAc. Aqueous workup with NaHCO₃ (5% solution), drying (MgSO₄), filtration, and concentration *in vacuo* followed by purification by silica gel flash chromatography using CHCl₃ as eluent gave 1.04 g (100% yield) of a solid as white needles: mp = 68–69 °C; $R_f = 0.68$ in EtOAc/Hex, 20:80; ¹H NMR (CDCl₃) δ 8.15 (d, $J = 2.12$ Hz, 1H), 7.80 (dd, $J = 2.12, 8.62$ Hz, 1H), 6.98 (d, $J = 8.62$ Hz, 1H), 3.90 (s, 3H); ¹³C NMR (CDCl₃) δ 163.83, 141.50, 140.08, 139.62, 123.86, 121.50, 87.15, 52.32.

Methyl 2-Azido-5-(trimethylstannyl)benzoate (8). A mixture of **7** (130 mg, 0.43 mmol) and tetrakis(triphenylphosphine)palladium(0) (10 mg, 8.65 μ mol) in anhydrous dioxane (5.0 mL) was made anaerobic by freezing, vacuum degassing, and introducing argon at-

mosphere three times at 0 °C. Then hexamethylditin (0.51 mL) was added, and the resulting mixture was stirred at 50 °C for 2 h. After the mixture cooled to room temperature, a saturated solution of NH₄Cl was added and the organic layer was extracted with EtOAc, dried (MgSO₄), filtered, and concentrated *in vacuo*. The pure product was isolated as a yellowish oil by silica gel flash chromatography using EtOAc in Hex (0–10%) as eluent to give 100 mg in 67% yield: $R_f = 0.78$ in EtOAc/Hex, 20:80; ¹H NMR (CDCl₃) δ 7.87 (d, $J = 1.16$ Hz, 1H), 7.58 (dd, $J = 1.16, 7.77$ Hz, 1H), 7.17 (d, $J = 7.77$ Hz, 1H), 3.87 (s, 3H), 0.27 (s, 9H); ¹³C NMR (CDCl₃) δ 166.30, 140.35, 139.84, 138.61, 138.50, 122.17, 120.40, 52.30, –9.23; EI-MS max mass for C₁₁H₁₅SnN₃O₂ as ¹²⁰Sn isotope, 341 (100%); EI-HRMS calcd 341.0276, found 341.0193 (M⁺ for tin and carbon isotopes pattern observed was similar to the one calculated).

2-Azido-5-(trimethylstannyl)benzoic Acid (9). To a solution of **8** (57 mg, 0.17 mmol) in THF (0.5 mL) was added a solution of LiOH (1 N solution, 0.34 mL). The mixture was stirred at 50 °C overnight and then cooled to room temperature and brought to pH ~7.0 by adding dropwise a potassium biphthalate buffer (0.05 M, pH 4). The aqueous fraction was extracted with CHCl₃, dried (MgSO₄), filtered, and concentrated *in vacuo*. Purification by silica gel flash chromatography using 3:1 Hex/EtOAc containing 2% acetic acid gave 28 mg of the desired acid as a yellowish solid: mp = 126–128 °C; $R_f = 0.16$ in EtOAc/Hex, 20:80; ¹H NMR (CDCl₃) δ 8.15 (d, $J = 2.1$ Hz, 1H), 7.72 (dd, $J = 2.1, 7.73$ Hz, 1H), 7.21 (d, $J = 7.73$ Hz, 1H), 0.32 (s, 9H); ¹³C NMR (CDCl₃) δ 169.21, 140.08, 139.95, 138.32, 132.98, 124.68, 119.03, –9.13.

Synthesis of Azidohydroxybenzoyl and Azidoiodobenzoyl Candidate Hexahydranitroimidazopyrimidine Photoaffinity Probes (10–14) (Scheme 2). **6-[2-(4-Azido-2-hydroxybenzamidy)ethyl]-1-[(6-chloro-3-pyridinyl)methyl]-1,2,3,5,6,7-hexahydro-8-nitroimidazo[1,2-c]pyrimidine (10).** To a solution of CH-IMI (127 mg, 0.50 mmol) and formaldehyde (85 μ L, 37% solution in water) in THF (5.0 mL) was added the diamine derivative (**4**) (110 mg, 0.50 mmol) in THF (5.0 mL), and the resulting mixture was stirred at room temperature overnight. Concentration *in vacuo* followed by purification by preparative TLC (2.0 mm thickness plate) gave 73 mg of the desired product as a yellowish solid in 29% yield: mp = 172–174 °C; $R_f = 0.63$ in MeOH/CHCl₃, 10:90; ¹H NMR (CDCl₃) δ 8.33 (d, $J = 2.4$ Hz, 1H), 7.82 (dd, $J = 2.4, 8.2$ Hz, 1H), 7.74 (d, $J = 8.2$ Hz, 1H), 7.33 (d, $J = 8.61$ Hz, 1H), 6.54 (d, $J = 2.25$ Hz, 1H), 6.44 (dd, $J = 2.25, 8.61$ Hz, 1H), 4.80 (s, 2H), 4.13 (s, 2H), 3.85 (s, 2H), 3.40–3.74 (m, 6H), 2.75 (t, $J = 5.88$ Hz, 2H); ¹³C NMR (CDCl₃) δ 169.94, 163.71, 158.41, 151.23, 149.37, 145.00, 139.93,

Scheme 2. Preparation of Azidohydroxybenzoyl and Azidoiodobenzoyl Candidate Hexahydroimidazopyrimidine Photoaffinity Probes^a

^a Structures of intermediates are given in Scheme 1. (a) HCHO, THF, 29%; (b) HCHO, H₂N(CH₂)₂OH, THF, 96%; (c) DCC, DMAP, CH₂Cl₂, 60–94%; (d) Na¹²⁵I, chloramine-T, MeOH, 20%.

131.54, 130.68, 125.02, 109.68, 107.44, 107.22, 103.66, 65.89, 50.88, 47.62, 37.86, 52.54, 52.18, 51.90; FAB-LRMS MH⁺ (60%), 154 (100%); FAB-HRMS C₂₁H₂₂ClN₉O₄H⁺, calcd 500.1561, found 500.1551; UV λ_{270} ϵ = 20 290, λ_{348} ϵ = 19 380.

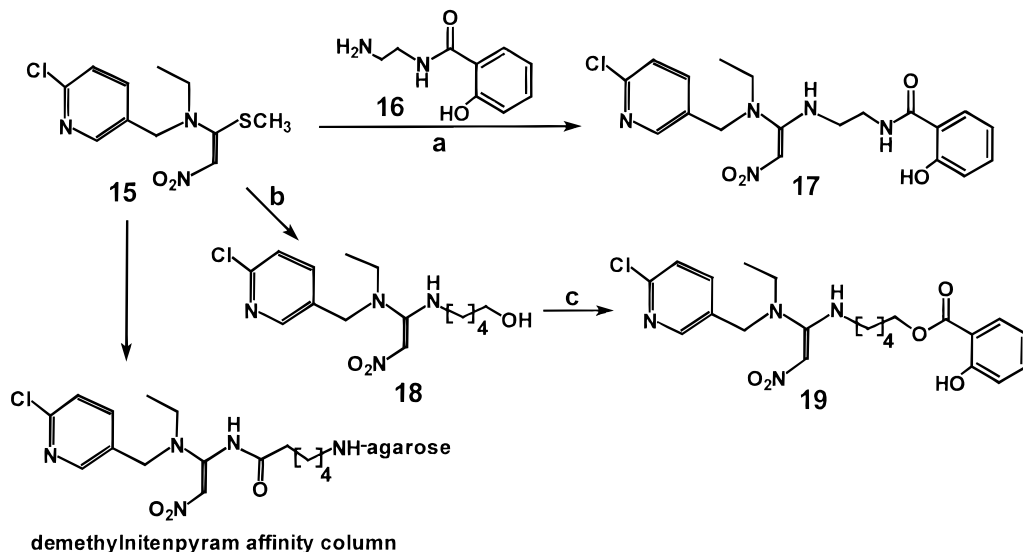
1-[6-(6-Chloro-3-pyridinyl)methyl]-1,2,3,5,6,7-hexahydro-6-(2-hydroxyethyl)-8-nitroimidazo[1,2-c]pyrimidine (11). To a solution of CH-IMI (254 mg, 1.0 mmol) in THF (20 mL) was added a solution of formaldehyde (0.153 mL, 37% solution in water) and ethanolamine (0.06 mL, 1.0 mmol). The resulting mixture was stirred overnight, concentrated *in vacuo*, and purified by preparative TLC (2.0 mm thickness plate) to give 312 mg of the desired product as a white solid in 96% yield: mp = 146–148 °C; R_f = 0.26 in MeOH/CHCl₃, 10:90; ¹H NMR (CDCl₃) δ 8.34 (d, J = 2.45 Hz, 1H), 7.86 (dd, J = 2.45, 8.26 Hz, 1H), 7.34 (d, J = 8.26 Hz, 1H), 4.84 (s, 2H), 4.11 (s, 2H), 3.88 (s, 2H), 3.73 (t, J = 5.16 Hz, 2H), 3.62 (m, 4H), 2.73 (t, J = 5.16 Hz, 2H); ¹³C NMR (CDCl₃) δ 157.45, 151.01, 149.07, 139.18, 130.76, 124.41, 102.97, 65.92, 59.63, 55.04, 52.17, 51.03, 49.29, 46.69; FAB-LRMS MH⁺ (26%), MLi⁺ (346, 12%); FAB-HRMS C₁₄H₁₈ClN₅O₃H⁺, calcd 340.1176, found 340.1169.

6-[2-(4-Azido-2-hydroxybenzoyl)ethyl]-1-[6-(6-chloro-3-pyridinyl)methyl]-1,2,3,5,6,7-hexahydro-8-nitroimidazo[1,2-c]pyrimidine (12). To a solution of 11 (68 mg, 0.20 mmol) in dry CH₂Cl₂ (12 mL) was added acid 2 (44 mg, 0.25 mmol), DMAP (30 mg, 0.25 mmol), and then DCC (66 mg, 0.32 mmol) in CH₂Cl₂ (2.0 mL). The resulting mixture was stirred overnight, concentrated *in vacuo*, and purified using preparative TLC (2.0 mm thickness plate) to give 94 mg of the product in 94% yield as a yellowish solid: mp = 142–144 °C; R_f = 0.7 in MeOH/CHCl₃, 10:90; ¹H NMR (CDCl₃) δ 8.34 (d, J = 2.40 Hz, 1H), 7.83 (m, 2H), 7.32 (d, J = 8.2 Hz, 1H), 6.62 (d, J = 2.10 Hz, 1H), 6.56 (dd, J = 2.10, 8.59 Hz, 1H), 4.83 (s, 2H), 4.49 (t, J = 5.55 Hz, 2H), 4.16 (s, 2H), 3.95 (s, 2H), 3.61 (m, 4H), 2.96 (t, J = 5.55 Hz, 2H); ¹³C NMR (CDCl₃) δ 169.21, 163.35, 157.28, 150.01, 149.06, 147.66, 139.24, 131.55, 130.58, 124.53, 110.66, 107.54, 107.24, 102.97, 65.97, 57.02, 52.21, 51.93, 50.83, 49.26, 46.51; FAB-LRMS MH⁺ (66%), 154 (100%); FAB-HRMS C₂₁H₂₁ClN₈O₅H⁺, calcd 501.1402, found 501.1393; UV λ_{272} ϵ = 24 020, λ_{352} ϵ = 13 790.

6-[2-(2-Azido-5-trimethylstannylbenzoyl)ethyl]-1-[6-(6-chloro-3-pyridinyl)methyl]-1,2,3,5,6,7-hexahydro-8-nitroim-

idazo[1,2-c]pyrimidine (13). Acid 9 (17 mg, 0.052 mmol), alcohol 11 (17 mg, 0.050 mmol), and DMAP (8 mg, 0.065 mmol) in dry CH₂Cl₂ (3.0 mL) were stirred at room temperature under nitrogen atmosphere. Then DCC (16 mg, 0.077 mmol) was added in CH₂Cl₂ (0.50 mL), the mixture was stirred overnight and concentrated *in vacuo*, and the residue was purified by preparative TLC (1.0 mm thickness plate) using MeOH/CHCl₃, 10:90, as eluent to give 10 mg of pure product as a yellowish solid in 31% yield: mp = decomposition at 130 °C; R_f = 0.73 in MeOH/CHCl₃, 10:90; ¹H NMR (CDCl₃) δ 8.34 (d, J = 2.35 Hz, 1H), 7.91 (d, J = 1.25 Hz, 1H), 7.86 (dd, J = 2.46, 8.24 Hz, 1H), 7.64 (dd, J = 1.25, 7.86 Hz, 1H), 7.31 (d, J = 8.24 Hz, 1H), 7.23 (d, J = 7.86 Hz, 1H), 4.83 (s, 2H), 4.47 (t, J = 5.75 Hz, 2H), 4.12 (s, 2H), 3.96 (s, 2H), 3.62 (m, 4H), 2.97 (t, J = 5.75 Hz, 2H), 0.32 (s, 9H); ¹³C NMR (CDCl₃) δ 165.84, 159.28, 151.03, 149.13, 140.71, 139.84, 139.34, 138.85, 138.71, 130.67, 124.59, 121.47, 119.27, 103.18, 65.53, 63.10, 52.24, 52.05, 51.93, 49.22, 46.54, -9.34; FAB-LRMS C₂₄H₂₉ClN₈O₄SnH⁺ (649, 70%), 267 (100%); FAB-HRMS max MH⁺ peak for ¹²⁰Sn isotope calcd 649.1101, found 649.1104.

6-[2-(2-Azido-5-iodobenzoyl)ethyl]-1-[6-(6-chloro-3-pyridinyl)methyl]-1,2,3,5,6,7-hexahydro-8-nitroimidazo[1,2-c]pyrimidine (14) from 11. A solution of alcohol 11 (68 mg, 0.20 mmol) in dry CH₂Cl₂ (12 mL) was stirred at room temperature under nitrogen atmosphere. Then acid 6 (58 mg, 0.20 mmol) and DMAP (30 mg, 0.25 mmol) were added followed by DCC (66 mg, 0.32 mmol) in dry CH₂Cl₂ (2.0 mL). The resulting mixture was stirred overnight and then concentrated *in vacuo*. The solid residue was purified by preparative TLC to give 110 mg of a yellowish solid in 91% yield (decomposed at 160 °C): R_f = 0.57 in MeOH/CHCl₃, 10:90; ¹H NMR (CDCl₃) δ 8.20 (d, J = 2.17 Hz, 1H), 8.14 (d, J = 2.11 Hz, 1H), 7.88 (dd, J = 2.11, 8.23 Hz, 1H), 7.82 (dd, J = 2.17, 8.49 Hz, 1H), 7.33 (d, J = 8.23 Hz, 1H), 7.00 (d, J = 8.49 Hz, 1H), 4.84 (s, 2H), 4.46 (t, J = 5.77 Hz, 2H), 4.09 (s, 2H), 3.96 (s, 2H), 3.61 (m, 4H), 2.94 (t, J = 5.77 Hz, 2H); ¹³C NMR (CDCl₃) δ 169.78, 163.68, 157.43, 151.22, 149.10, 142.03, 140.42, 140.32, 139.25, 130.65, 124.51, 121.76, 103.00, 87.40, 65.57, 63.24, 52.20, 51.74, 50.94, 49.21, 46.51; FAB-LRMS MH⁺ (58%), 225 (100%), 154 (30%); FAB-HRMS C₂₁H₂₀ClIN₈O₄H⁺, calcd 611.0419, found 611.0414; UV λ_{268} ϵ = 18 600; λ_{352} ϵ = 14 300.

Scheme 3. Preparation of Nitenpyram Analogs Including an Agarose Derivative as an Affinity Column^a

^a (a) EtOH, reflux, 29%; (b) H₂N(CH₂)₅OH, EtOH, reflux, 30%; (c) 2-hydroxybenzoic acid, DCC, DMAP, CH₂Cl₂, 44%.

Synthesis of **14 from **13**.** The method was validated by preparing unlabeled **14**. Thus, to a solution of **13** (1.3 mg, 2 μ mol of 1.0 mg/mL solution in MeOH) were added NaI (0.3 mg, 2 μ mol, 3 mg/mL solution in MeOH) and then chloramine-T (0.5 mg, 2 μ mol, 0.1 mL of a solution of 5 mg/mL in 200 mM phosphate buffer, pH 7.5). The resulting mixture was stirred for 10 min, the solvent evaporated under nitrogen, and the product taken up in CHCl₃. ¹H NMR data were identical to those of **14**, prepared via intermediates **11** and **6**, and comigrated with it on TLC.

Radiosynthesis of [¹²⁵I]-14** from **13**.** The above procedure was then used in the preparation of [¹²⁵I]-**14**. Thus, to a solution of Na¹²⁵I (5.6 mCi, 11 μ L) in dilute NaOH solution (pH 9.0) was injected the organotin precursor (**13**) (15 μ L, 0.1 mg/mL MeOH solution), followed by chloramine-T (6.0 μ L, 0.1 mg/mL 200 mM phosphate buffer solution, pH 7.5). The resulting mixture was shaken occasionally for 10 min before transfer to a vial for evaporation of the solvents under nitrogen. The residue was then dissolved in CHCl₃ and transferred to another vial, leaving insoluble materials behind. The ¹²⁵I-labeled product (1.0 mCi) cochromatographed with unlabeled **14** on TLC with the MeOH/CHCl₃ system above as observed by UV light and PhosphorImager (Molecular Dynamics, Sunnyvale, CA) detection.

Synthesis of Nitenpyram Analogs (15**–**19**) (Scheme 3).** 1-[(6-Chloro-3-pyridinyl)methyl]-1-(ethylamino)-1-[2-(2-hydroxybenzamidyl)ethyl]amino-2-nitroethene (**17**) via 1-[(6-Chloro-3-pyridinyl)methyl]-1-(ethylamino)-1-(methylthio)-2-nitroethene (**15**) and N-(2-Hydroxybenzoyl)ethylenediamine (**16**). A solution of **15** (100 mg, 0.35 mmol) and **16** (60 mg, 0.33 mmol, prepared similarly to intermediate **4** in Scheme 1) in EtOH (5.0 mL) was refluxed for 2 h and then concentrated *in vacuo* and purified by preparative TLC (1.0 mm layer thickness) to give 20 mg of product as a white solid (decomposed at 160 °C) in 29% yield: *R*_f = 0.5 in MeOH/CHCl₃, 10:90; ¹H NMR (CDCl₃) δ 8.23 (d, *J* = 2.52 Hz, 1H), 7.72 (dd, *J* = 1.75, 7.92 Hz, 1H), 7.52 (dd, *J* = 2.52, 8.25 Hz, 1H), 7.35 (s, OH), 7.30 (dt, *J* = 1.75, 8.29 Hz, 1H), 7.23 (d, *J* = 8.25 Hz, 1H), 6.83 (d, *J* = 8.29 Hz, 1H), 6.72 (t, *J* = 7.92 Hz, 1H), 6.49 (s, 1H), 4.48 (s, 2H), 3.76 (brs, 4H), 3.61 (m, 4H), 3.27 (q, *J* = 7.13 Hz, 2H), 1.16 (t, *J* = 7.13 Hz, 3H); ¹³C NMR (CDCl₃) δ 170.75, 163.59, 160.39, 150.66, 148.02, 137.98, 133.37, 130.11, 128.34, 128.13, 124.51, 119.16, 116.34,

101.01, 49.87, 46.47, 44.86, 38.84, 12.0; FAB-LRMS MH⁺ (420, 20%), 164 (100%); FAB-HRMS C₁₉H₂₂ClN₅O₄H⁺, calcd 420.1439, found 420.1448.

1-[(6-Chloro-3-pyridinyl)methyl]-1-(ethylamino)-1-(5-hydroxypentyl)amino-2-nitroethene (**18**). The above methylthio derivative (**15**) (144 mg, 0.50 mmol) was refluxed in EtOH (5.0 mL) with 5-amino-1-pentanol (53 mg, 0.51 mmol) for 2 h and then concentrated *in vacuo*. Purification by preparative TLC (1.0 mm thickness plate) gave 51 mg of a white solid in 30% yield: *R*_f = 0.67 in MeOH/CHCl₃, 20:80; ¹H NMR (CDCl₃) δ 9.69 (s, 1H, NH), 8.30 (d, *J* = 2.40 Hz, 1H), 7.53 (dd, *J* = 2.40, 8.22 Hz, 1H), 7.36 (d, *J* = 8.22 Hz, 1H), 6.51 (s, 1H), 4.33 (s, 2H), 3.64 (t, *J* = 7.73 Hz, 2H), 3.37 (m, 2H), 3.13 (q, *J* = 7.04 Hz, 2H), 1.45–1.82 (m, 8H), 1.19 (t, *J* = 7.04 Hz, 3H); ¹³C NMR (CDCl₃) δ 150.23, 148.77, 143.32, 137.97, 130.25, 124.65, 104.28, 62.18, 50.00, 45.90, 44.88, 31.98, 29.91, 23.00, 12.18.

1-[(6-Chloro-3-pyridinyl)methyl]-1-(ethylamino)-1-[5-(2-hydroxybenzoyl)pentyl]amino-2-nitroethene (**19**). To the above alcohol (**18**) (17 mg, 0.050 mmol) in dry DMF (0.50 mL) was added 2-hydroxybenzoic acid (7 mg, 0.053 mmol), DMAP (6.1 mg, 0.050 mmol), and DCC (10.3 mg, 0.050 mmol) in DMF (0.50 mL). The mixture was stirred overnight and then concentrated *in vacuo* and purified by preparative TLC to give 13 mg of **19** as a white solid in 44% yield: mp = 190–192 °C; *R*_f = 0.67 in MeOH/CHCl₃, 10:90; ¹H NMR (CDCl₃) δ 9.68 (s, 1H), 8.28 (d, *J* = 2.32 Hz, 1H), 7.83 (d, *J* = 7.97 Hz, 1H), 7.46 (m, 2H), 7.34 (d, *J* = 8.15 Hz, 1H), 6.97 (d, *J* = 7.97 Hz, 1H), 6.90 (t, *J* = 8.15 Hz, 1H), 6.51 (s, 1H), 4.34 (t, *J* = 6.12 Hz, 2H), 4.32 (s, 2H), 3.34 (t, *J* = 6.12 Hz, 2H), 3.10 (q, *J* = 7.03 Hz, 2H), 1.42–1.82 (m, 8H), 1.17 (t, *J* = 7.03 Hz, 3H); ¹³C NMR (CDCl₃) δ 170.35, 162.32, 160.81, 156.38, 151.72, 148.52, 137.98, 135.61, 130.25, 129.73, 124.60, 119.10, 117.38, 103.82, 64.69, 49.11, 45.81, 44.71, 29.64, 28.05, 23.14, 12.13; FAB-LRMS MH⁺ (80%), 225 (100%); FAB-HRMS C₂₂H₂₇ClN₄O₅H⁺, calcd 463.1748, found 463.1752.

Receptor Assays. Binding studies with *Drosophila* and *Musca* head membranes (θ) involved ~300 μ g of protein incubated with 2.5 nM [³H]IMI (25 Ci/mmol) for 60 min at 25 °C in a total volume of 250 μ L of 10 mM sodium phosphate buffer, pH 7.4, containing 100 mM NaCl, 5 mM EDTA, 3 mM ethylene glycol bis(β -aminoethyl ether)-*N,N,N,N*-tetraacetic acid, 0.1 mM phenyl-

methanesulfonyl fluoride, and 0.02% NaN_3 . Alternatively, rat whole brain membranes (20) ($\sim 800 \mu\text{g}$ of protein) were incubated for 10 min at 25°C with 5 nM [^3H]nicotine (78 Ci/mmol) in 250 μL of 20 mM Tris buffer, pH 7.4, containing 118 mM NaCl, 4.8 mM KCl, 2.5 mM CaCl_2 , 1.2 mM MgSO_4 , and 1 mM EDTA. The incubated mixtures were rapidly filtered on Whatman GF/B filters presoaked in 0.1% polyethylenimine. The filter was rinsed twice (for rat) or three times (for insects) with 2.5 mL of ice-cold 0.9% NaCl. Radioactivity remaining on the filter was determined by liquid scintillation counting. Specific binding was defined as the difference in radioactivity in the absence or presence of 25 μM unlabeled IMI (for [^3H]IMI binding) or 10 μM unlabeled (–)-nicotine (for [^3H]nicotine binding). IC_{50} values were calculated by iterative nonlinear least-squares regression.

Photoaffinity Labeling. The procedure was similar to that we used before with the azidosalicylate derivative of [^{125}I]- α -BGT and irradiation at 350 nm (6). *Drosophila* head membranes photoaffinity labeled with ~ 4 nM [^{125}I]-**14** (~ 2000 Ci/mmol) in the absence or presence of 10 mM (–)-nicotine were separated by lithium dodecyl sulfate–polyacrylamide gel electrophoresis. The radioactive band(s) was detected by PhosphorImager analysis and compared with molecular mass markers on the same gel.

RESULTS

Synthesis of Hexahydronitroimidazopyrimidines (Figure 1; Schemes 1 and 2). Reaction of an enamine, possessing an NH substituent, with suitable biselectrophiles leads to heterocyclization by bond formations at both nucleophilic sites (21). The desired product in the present study is obtained by stirring CH-IMI with a primary amine and formaldehyde in THF. The benzoyl derivatives **10** and **12** were initially examined because of extensive background on their use in the preparation of [^{125}I]-labeled ligands (22, 23). Synthesis included the preparation, on a multigram scale, of *N*-hydroxysuccinimidyl-4-azidosalicylic acid (**3**) (available commercially from Pierce) (22). Compound **3** on treatment with ethylenediamine gave amino analog **4**, which upon coupling with CH-IMI in the presence of formaldehyde gave the penultimate intermediate (**10**). This step, however, was very sluggish; the yields were improved greatly by using the benzoyl rather than the benzamidyl series. Ethanolamine is preferred over ethylenediamine in coupling with CH-IMI because the diamine can react with formaldehyde and give many cyclic products (24). Thus, ethanolamine and formaldehyde were reacted directly with CH-IMI to give the alcohol (**11**) in 96% yield (19) and then coupled to 4-azidosalicylic acid (**2**) using DCC in 94% yield. Iodination of **12** failed to give a clean reaction, and HPLC would be needed to isolate the product from the monoiodo and diiodo compounds and the starting material to determine the specific activity (25).

Synthesis of [^{125}I]Azidobenzoyl Photoaffinity Probe (Schemes 1 and 2). Iodine-125 can be easily introduced by destannylation of compound **13** in the presence of chloramine-T in methanol (26). Thus, 2-azido-5-iodobenzoic acid (**5**) was prepared in 90% yield from the amino precursor (**6**) and then coupled to the alcohol derivative (**11**) with DCC in 91% yield to give **14**. This compound has suitable photoreactivity with a half-life of <10 min at 0.071 mM in absolute ethanol under UV (350 nm) light (Figure 2). To synthesize the organotin derivative (**13**), 2-azido-5-iodobenzoic acid (**6**) was esterified to the methyl ester (**7**), and then stannylation was carried out to give **8** in anaerobic conditions using tetrakis(triphenylphosphine)palladium(0) in anhydrous

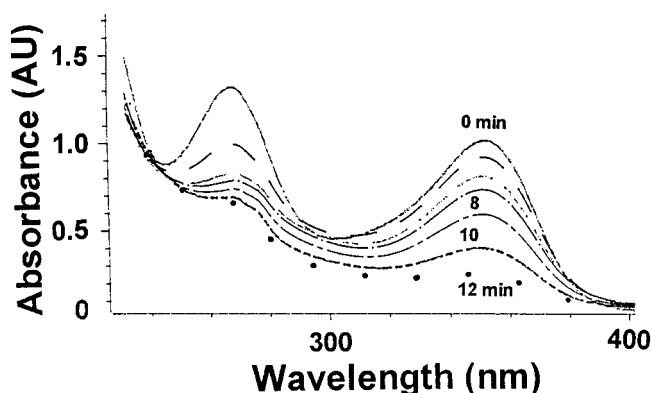


Figure 2. UV absorbance and photodecomposition of compound **14** in EtOH. The times are given for exposure to 350 nm light.

dioxane. Direct stannylation of the acid (**6**) failed to produce the desired product (26–28). Hydrolysis with 2 equiv of 1 N LiOH in THF (27) gave the free acid (**9**) which was coupled with the alcohol (**11**) as before. To prepare the [^{125}I]-labeled analog, a solution of the organotin derivative in MeOH was added to a dilute NaOH solution of Na [^{125}I] followed by a solution of chloramine-T in pH 7.5 phosphate buffer. This reaction was carried out in a well-ventilated hood behind lead shielding. The product was easily purified from the tin precursor by flash chromatography using silica gel packed in a Pasteur pipet and 1% MeOH in CHCl_3 as eluent.

Synthesis of Substituted Demethylnitenpyram Derivatives (Scheme 3). Model compounds were designed in which 2-hydroxybenzoic acid is coupled via a spacer to form demethylnitenpyram derivatives. The synthesis of compounds **17** and **19** included the preparation of a hydroxybenzoyl ethylenediamine derivative **16** by reacting *N*-hydroxysuccinimidyl-2-hydroxybenzoate with ethylenediamine as described above. This derivative was refluxed with the methylthionitroethene (**15**) to give **17** in 29% overall yield. To prepare **19**, compound **15** was reacted with 5-amino-1-pentanol to give the alcohol **18** in 30% yield. Coupling with 2-hydroxybenzoic acid gave **19** in 44% yield.

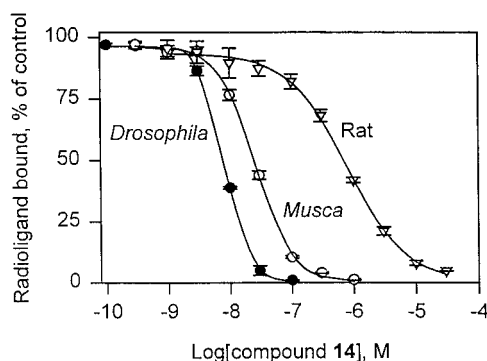
Potency of Nitenpyram Analogs and Hexahydronitroimidazopyrimidines as Inhibitors of [^3H]IMI Binding in *Drosophila* or *Musca* Head Membranes and of [^3H]Nicotine Binding in Rat Brain Membranes. The successful use of a demethylnitenpyram–agarose affinity column in isolation of the nAChRs of *Drosophila* and *Musca* prompted the synthesis of analogs as photoaffinity candidates (Scheme 3). Thus, nitenpyram analogs with amino and methylamino substituents have IC_{50} values for the *Drosophila* site of 2.2 and 14 nM, respectively (6). However, 2-hydroxybenzoyl analogs proved to be disappointing, with IC_{50} values for the *Drosophila* receptor of $22\,800 \pm 1050$ nM for compound **17** and 1310 ± 87 nM for analog **19**.

Hexahydronitroimidazopyrimidines with a variety of 6-substituents (Figure 1) maintain high potency as inhibitors of [^3H]IMI binding (Table 1). This includes alkyl and aralkyl moieties and various esters and amides with azidohydroxybenzoate and azidoiodobenzoate substituents. Two compounds in the series are of particular interest: the benzophenone as a candidate photoaffinity probe (29) and the azidoiodobenzoate (**14**). The latter compound was selected for radiosynthesis because of suitable potency (IC_{50} 8 nM for *Drosophila* and 25 nM for *Musca* nAChRs; Figure 3; Table 1) and the high specific activity and ease of radiosynthesis with iodine-125. Two analogs were also tested with rat brain

Table 1. Potency of Hexahydronitroimidazopyrimidines as Inhibitors of [³H]Imidacloprid Binding in *Drosophila* or *Musca* Head Membranes and [³H]Nicotine Binding in Rat Brain Membranes

6-substituent (compd no.) ^a	IC ₅₀ (nM ± SD) ^b
<i>Musca</i> (M) or <i>Drosophila</i> (D), [³ H]IMI	
–CH ₃	0.73 ± 0.37 (M)
–CH ₂ C ₆ H ₅	4.8 ± 1.4 (M)
–CH ₂ C ₆ H ₄ -4-Cl	3.3 ± 0.9 (M)
–CH ₂ -3-(6-Cl-pyridinyl)	6.4 ± 1.6 (M)
–(CH ₂) ₂ C ₆ H ₅	2.0 ± 0.6 (M)
–CH(C ₆ H ₅) ₂	21 ± 6 (M)
–C ₂ H ₄ NHC(O)C ₆ H ₃ -2-OH,4-N ₃ (10)	1.7 ± 0.0 (D)
–C ₂ H ₄ OC(O)CH ₃	4.6 ± 0.7 (M)
–C ₂ H ₄ OC(O)C ₆ H ₃ -2-OH,4-N ₃ (12)	6.1 ± 0.4 (D)
–C ₂ H ₄ OC(O)C ₆ H ₃ -2-N ₃ ,5-I (14)	8.0 ± 0.1 (D), 25 ± 1.5 (M)
–C ₂ H ₄ OC(O)C ₆ H ₃ -2-N ₃ ,5-Sn(CH ₃) ₃ (13)	38 ± 2 (D)
–C ₂ H ₄ OC(O)C ₆ H ₄ -4-C(O)C ₆ H ₅	2.3 ± 0.6 (M)
Rat, [³ H]Nicotine	
–C ₂ H ₄ NHC(O)C ₆ H ₃ -2-OH,4-N ₃ (10)	120 ± 10
–C ₂ H ₄ OC(O)C ₆ H ₃ -2-N ₃ ,5-I (14)	740 ± 73

^a R substituent at 6-position of hexahydronitroimidazopyrimidines (Figure 1). Numbers refer to candidate probes but not intermediates described in the text. Although not detailed here, other 6-substituents with similar potency at the *Musca* receptor are C₂H₅, *n*-C₃H₇, CH(CH₃)₂, *n*-C₄H₉, CH(CH₃)C₂H₅, CH₂CH(CH₃)₂, C(CH₃)₃, *n*-C₅H₁₁, C(CH₃)₂C₂H₅, C₂H₄CH(CH₃)₂, C(CH₃)₂C≡CH, cyclopropyl, cyclopentyl, cyclohexyl, pyridinyl-3-CH₂, CH(CH₃)C₆H₅, and adamantyl. ^b M = *Musca* and D = *Drosophila*, n = 3.

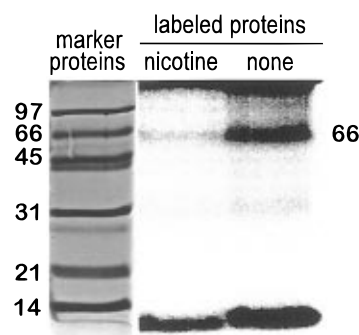
**Figure 3.** Displacement curves for compound **14** (unlabeled) on the [³H]IMI binding site in *Drosophila* and *Musca* head membranes and on the [³H]nicotine binding site in rat whole brain membranes.

membranes and [³H]nicotine binding revealing potencies of 71- and 93-fold less than with the *Drosophila* site (Table 1; Figure 3), indicating that with further optimization a photoaffinity probe might be achieved for the mammalian binding site.

Photoaffinity Labeling of 66 kDa Protein of *Drosophila* Head Membranes by [¹²⁵I]-14**.** A single protein band of 66 kDa is photoaffinity labeled by [¹²⁵I]-**14** and totally protected in the presence of 10 mM (–)-nicotine (Figure 4).

DISCUSSION

The discovery that optimized compounds with chloropyridinylmethylamino and nitromethylene substituents have outstanding insecticidal activity and very high affinity for a specific binding site in the insect nAChR provided the basis for preparing an affinity column reported recently (6) and candidate photoaffinity probes described here. The demethylnitenpyram series gave poorly active hydroxybenzoyl analogs as models for [¹²⁵I]-azido derivatives. Attention was then focused on the hexahydronitroimidazopyrimidine series, which is stable at neutral pH, by introducing a variety of substituents

**Figure 4.** Photoaffinity labeling of 66 kDa protein of *Drosophila* head membranes by [¹²⁵I]-**14**. Protein labeling was carried with or without nicotine, designated nicotine and none, respectively. Proteins are separated by lithium dodecyl sulfate–polyacrylamide gel electrophoresis and compared with protein standards (kDa and name): 14, lysozyme; 21, trypsin inhibitor; 31, carbonic anhydrase; 45, ovalbumin; 66, serum albumin; 97, phosphorylase *b*.

in the 6-position including alkyl, aralkyl, benzophenone, azidoxybenzamidyl (**10**), and azidoxybenzoyl derivatives (**12**). Clearly there is considerable structure latitude in groups' acceptability at this site. Iodination of the azidoxyaryls compounds was not complete even when using excess of iodinating reagents, giving a mixture of monoiodo and diiodo derivatives and unreacted starting material. Other analogs considered were the benzophenone or the acetate [as a model for the diazoacetate (**30**)], but introduction of iodine-125 in these candidates is not straightforward.

The preferred photoaffinity probe [¹²⁵I]-**14** is easily prepared from Na¹²⁵I by [¹²⁵I]iododestannylation with the highest specific activity obtainable, and the product is readily separated from starting material. The organotin derivative (**13**) is the precursor of choice for efficient introduction of iodine-125 into a ligand of this type. The precursor can be stored in MeOH solutions for prolonged time without significant decomposition. Compound **14** has suitable photoreactivity, and a preliminary study indicates that [¹²⁵I]-**14** covalently bound to *Drosophila* head membranes gives a derivatized protein at 66 kDa which appears to be associated with the ligand-binding subunit of the nAChR based on protection with (–)-nicotine.

In conclusion, this study describes the synthesis of a novel [¹²⁵I]neonicotinoid photoaffinity ligand by iododestannylation of a tin precursor with maximum ease of carrying out the labeling and separation of unreacted starting material. Further, the novel probe described appears to be suitable for photoaffinity labeling the insecticide-binding site of a putative nAChR subunit.

ACKNOWLEDGMENT

The study described was supported by Grant P01 ES00049 from the National Institute of Environmental Health Sciences, NIH. We received advice and assistance from our laboratory colleagues Gary B. Quistad and Pauline Yu. Donna Hackett and Gerald Rubin of the Department of Molecular and Cell Biology on this campus provided the *Drosophila*. Hélène Perrier (Merck Frosst Centre for Therapeutic Research, Quebec, Canada) made helpful suggestions on the synthesis of 2-azido-5-(trimethylstannyl)benzoic acid.

LITERATURE CITED

- (1) Liu, M.-Y., and Casida, J. E. (1993) High affinity binding of [³H]imidacloprid in the insect acetylcholine receptor. *Pestic. Biochem. Physiol.* 46, 40–46.

- (2) Tomizawa, M., and Yamamoto, I. (1993) Structure-activity relationships of nicotinoids and imidacloprid analogs. *J. Pestic. Sci.* **18**, 91–98.
- (3) Moriya, K., Shibuya, K., Hattori, Y., Tsuboi, S., Shiokawa, K., and Kagabu, S. (1992) 1-(6-Chloronicotiny)-2-nitroimino-imidazolidines and related compounds as potential new insecticides. *Biosci., Biotechnol., Biochem.* **56**, 364–365.
- (4) Leicht, W. (1996) Imidacloprid—a chloronicotiny insecticide. Biological activity and agricultural significance. *Pflanzenschutz-Nachr. Bayer* **49**, 71–84.
- (5) Latli, B., and Casida, J. E. (1992) [³H]Imidacloprid: synthesis of a candidate radioligand for the nicotinic acetylcholine receptor. *J. Labelled Compd. Radiopharm.* **31**, 609–613.
- (6) Tomizawa, M., Latli, B., and Casida, J. E. (1996) Novel neonicotinoid-agarose affinity column for *Drosophila* and *Musca* nicotinic acetylcholine receptors. *J. Neurochem.* **67**, 1669–1676.
- (7) Kagabu, S., Moriya, K., Shibuya, K., Hattori, Y., Tsuboi, S., and Shiokawa, K. (1992) 1-(6-Halonicotiny)-2-nitromethylene-imidazolidines as potential new insecticides. *Biosci., Biotechnol., Biochem.* **56**, 362–363.
- (8) Latli, B., Than, C., Morimoto, H., Williams, P. G., and Casida, J. E. (1996) [6-chloro-3-pyridylmethyl-³H]Neonicotinoids as high-affinity radioligands for the nicotinic acetylcholine receptor: preparation using NaB³H₄ and LiB³H₄. *J. Labelled Compd. Radiopharm.* **38**, 971–978.
- (9) Liu, M.-Y., Lanford, J., and Casida, J. E. (1993) Relevance of [³H]imidacloprid binding site in house fly head acetylcholine receptor to insecticidal activity of 2-nitromethylene- and 2-nitroimino-imidazolidines. *Pestic. Biochem. Physiol.* **46**, 200–206.
- (10) Minamida, I., Iwanaga, K., Tabuchi, T., Aoki, I., Fusaka, T., Ishizuka, H., and Okauchi, T. (1993) Synthesis and insecticidal activity of acyclic nitroethene compounds containing a heteroaryl methylamino group. *J. Pestic. Sci.* **18**, 41–48.
- (11) Tomizawa, M., Otsuka, H., Miyamoto, T., Eldefrawi, M. E., and Yamamoto, I. (1995) Pharmacological characteristics of insect nicotinic acetylcholine receptor with its ion channel and the comparison of the effect of nicotinoids and neonicotinoids. *J. Pestic. Sci.* **20**, 57–64.
- (12) Gundelfinger, E. D., and Hess, N. (1992) Nicotinic acetylcholine receptors of the central nervous system of *Drosophila*. *Biochim. Biophys. Acta* **1137**, 299–308.
- (13) Schloss, P., Mayser, W., Gundelfinger, E. D., and Betz, H. (1992) Cross-linking of ¹²⁵I- α -bungarotoxin to *Drosophila* head membranes identifies a 42 kDa toxin binding polypeptide. *Neurosci. Lett.* **145**, 63–66.
- (14) Tomizawa, M., and Yamamoto, I. (1992) Binding of nicotinoids and the related compounds to the insect nicotinic acetylcholine receptor. *J. Pestic. Sci.* **17**, 231–236.
- (15) Mebs, D., Narita, K., Iwanaga, S., Samejima, Y., and Lee, C. Y. (1971) Amino acid sequence of α -bungarotoxin from the venom of *Bungarus multicinctus*. *Biochem. Biophys. Res. Commun.* **44**, 711–716.
- (16) Galzi, J.-L., Revah, F., Bessis, A., and Changeux, J.-P. (1991) Functional architecture of the nicotinic acetylcholine receptor: from electric organ to brain. *Annu. Rev. Pharmacol.* **31**, 37–72.
- (17) Kotzyba-Hibert, F., Kapfer, I., and Goeldner, M. (1995) Recent trends in photoaffinity labeling. *Angew. Chem., Int. Ed. Engl.* **34**, 1296–1312.
- (18) Kishida, H., Sakamoto, N., Umeda, K., and Fujimoto, H. (1992) Preparation of nitropyrimidine derivatives as insecticides. *Jpn. Kokai Tokkyo Koho JP 04,173,788; Chem. Abstr.* **118**, 22251q.
- (19) Krüger, B.-W., Uhr, H., Kanellakopulos, J., Gesing, E. R. F., Wolf, H., Turberg, A., Mencke, N., Erdelen, C., Wachen-dorff-Neumann, U., and Hartwig, J. (1995) Substituierte 1,2,3,4-tetrahydro-5-nitro-pyrimidines. *Ger. Offen. DE 44 01 635 Al.*
- (20) Yamamoto, I., Yabuta, G., Tomizawa, M., Saito, T., Miyamoto, T., and Kagabu, S. (1995) Molecular mechanism for selective toxicity of nicotinoids and neonicotinoids. *J. Pestic. Sci.* **20**, 33–40.
- (21) Rajappa, S. (1981) Nitroenamines. Preparation, structure and synthetic potential. *Tetrahedron* **37**, 1453–1480.
- (22) Ji, T. H., and Ji, I. (1982) Macromolecular photoaffinity labeling with radioactive photoactivatable heterobifunctional reagents. *Anal. Biochem.* **121**, 286–289.
- (23) Ji, I., Shin, J., and Ji, T. H. (1985) Radioiodination of a photoactivatable heterobifunctional reagent. *Anal. Biochem.* **151**, 348–349.
- (24) Okawara, T., Ehara, S., Eto, M., Harano, K., and Furukawa, M. (1993) 7,15-Dioxo-4,8,12,16-tetraaza- and 4,7,8,12,15,16-hexaazaperhydropyrenes from glyoxal and polyfunctionalized compounds. *Tetrahedron Lett.* **34**, 4231–4232.
- (25) Beale, M. H., Hooley, R., Lewis, M. J., Smith, S. J., and Ward, J. L. (1995) Radio-iodinated gibberellin photoaffinity probes. *J. Chem. Soc., Perkin Trans. 1*, 657–663.
- (26) Perrier, H., Prasit, P., and Wang, Z. (1994) Synthesis of a radioactive photoaffinity arachidonic acid analog. *Tetrahedron Lett.* **35**, 1501–1502.
- (27) Mais, D. E., Bowling, N. L., True, T. A., Naka, M., Morinelli, T. A., Oatis, Jr., J. E., Hamanaka, N., and Halushka, P. V. (1991) Novel synthesis and biochemical properties of an [¹²⁵I]-labeled photoaffinity probe for thromboxane A₂/prostaglandin H₂ receptors. *J. Med. Chem.* **34**, 1511–1514.
- (28) Ali, H., and van Lier, J. E. (1996) Synthesis of radiopharmaceuticals via organotin intermediates. *Synthesis* **4**, 423–445.
- (29) Dormán, G., and Prestwich, G. D. (1994) Benzophenone photophores in biochemistry. *Biochemistry* **33**, 5661–5673.
- (30) Latli, B., and Prestwich, G. D. (1991) Synthesis of labeled (10R)-juvenile hormone III bisepoxide, and its photoaffinity analog, [12-³H]-(10R)-6,7,10,11-bisepoxyfarnesyl diazoacetate (BEFDA). *J. Labelled Compd. Radiopharm.* **29**, 1167–1173.

BC960066C

Conjugates of Oligonucleotides with Triplex-Specific Intercalating Agents. Stabilization of Triple-Helical DNA in the Promoter Region of the Gene for the α -Subunit of Interleukin 2 (IL-2R α)

Gail C. Silver,[†] Chi Hung Nguyen,[‡] Alexandre S. Boutorine,[†] Emile Bisagni,[‡] Thérèse Garestier,[†] and Claude Hélène^{*,†}

Laboratoire de Biophysique, Muséum National d'Histoire Naturelle, INSERM U201–CNRS URA 481, 43 rue Cuvier, 75231 Paris Cedex 05, France, and Laboratoire de Synthèse Organique, Institut Curie-Biologie, CNRS URA 1387, Bâtiment 110, 91405 Orsay, France. Received August 9, 1996[®]

The stabilization of triple-helical DNA under physiological conditions is an important goal for the control of gene expression using the antigene strategy, an approach whereby an oligonucleotide binds to the major groove of double-helical DNA to form a triple helix. To this end, triplex-specific intercalators, namely benzopyridoindole (BPI) and benzopyridoquinoxaline (BPQ) derivatives, have been conjugated to the 5' end or to an internucleotide position of a 15-mer oligonucleotide. These conjugates were then tested, using thermal denaturation experiments, for their ability to form and stabilize a triple-helical structure involving a 42-mer duplex target. All of the conjugates were found to do so. The B[h]PQ derivatives stabilized particularly well when attached to the 5' end with a ΔT_m of 15 °C and $-\Delta\Delta G_{37}^\circ$ of 3.4 kcal mol⁻¹ (pH 6.9, 140 mM KCl, 15 mM sodium cacodylate, 2 mM MgCl₂, 0.8 mM spermine). Though most of the derivatives when attached to the internucleotide position were not able to stabilize triple-helical DNA as well as when attached to the 5' end, one B[f]PQ derivative with an internucleotide attachment did so, with a ΔT_m of 13 °C and $-\Delta\Delta G_{37}^\circ$ of 2.8 kcal mol⁻¹. To a lesser degree, these conjugates were also able to stabilize duplex structures with single-stranded targets. Results were compared to the stabilization obtained with acridine conjugates as well as to a similar study performed with a different sequence.

INTRODUCTION

Oligonucleotides can recognize in a sequence-selective manner both single-stranded DNA (ssDNA¹) and double-stranded DNA (dsDNA). This feature has been exploited as a potential strategy for regulating gene expression with the purpose of treating genetic-based diseases (Hélène and Toulmé, 1990; Uhlmann and Peyman, 1990; Murray and Crockett, 1992; Crooke and Lebleu, 1993; Demesmaeker et al., 1995; Maher, 1996). By specifically recognizing and binding to m-RNA through Watson–Crick hydrogen bonds, an oligonucleotide may halt translation (antisense approach) (Stein and Cheng, 1993; Hélène, 1994; Pierga and Magdelenat, 1994). An oligonucleotide may also impede transcription by binding to the major groove of dsDNA (antigene approach) (Thuong and Hélène, 1993; Radhakrishnan and Patel, 1994a; Frank-Kamenetskii and Mirkin, 1995). In this latter approach, a (T,C)-containing third strand (pyrimidine motif) will bind parallel to the duplex purine strand with the formation of TA×T and CG×C⁺ base triplets using Hoogsteen bonds (Le Doan et al., 1987; Moser and Dervan, 1987; de los Santos et al., 1989; Rajagopal and Feigon, 1989). A (G,A)-containing third strand will run antiparallel and be bound through reverse Hoogsteen hydrogen bonds, forming CG×G and TA×A triplets (purine motif) (Beal and Dervan, 1991; Pilch et al., 1991). (G,T)-containing oligonucleotides can also form triple

helices (Durland et al., 1991) with an orientation that depends on sequence (Sun et al., 1991b; de Bizemont et al., 1996).

We have been interested in regulating gene expression via triple helix formation. One of the targets on which we have concentrated is a 15 bp oligopurine–oligopyrimidine sequence present in the promoter region of the gene coding for the α chain of the interleukin 2 receptor (IL-2R α), overlapping the binding sites for transcription factors NF κ B and SRF (Grigoriev et al., 1992) (Table 1). IL-2R α is a cellular receptor expressed in activated T-cells. The T-cell immune response is mediated by the binding of interleukin 2 to its high-affinity receptor (the α chain associated with the β and/or γ chains).

There are several limitations to the antigene strategy as a method for regulating gene expression. With a few exceptions (Svinarchuk et al., 1995), the stability of triple helices is limited under physiological conditions, due, in part, to the electrostatic repulsion between the third strand and the duplex, as well as the need for the cytosines on the third strand to be protonated in the pyrimidine motif. One strategy to improve triplex stability is to covalently attach DNA intercalators to the third strand (Hélène, 1989; Sun et al., 1989, 1991a; Giovannangeli et al., 1992; Thuong and Hélène, 1993). This approach has been used for the IL-2R α system using acridine-linked (Grigoriev et al., 1992, 1993a) and psoralen-linked (Grigoriev et al., 1993b) oligonucleotides. In both cases, specific inhibition of the transcription of reporter constructs containing the IL-2R α promoter in live cells was demonstrated.

In an attempt to look at more efficient chemical modifications of the third strand for the purpose of modulating *endogenous* gene expression, we have studied other intercalator–oligonucleotide conjugates. Benzopy-

* Author to whom correspondence should be addressed (e-mail am835@freenet.carleton.ca).

[†] Muséum National d'Histoire Naturelle.

[‡] Institut Curie-Biologie.

[®] Abstract published in *Advance ACS Abstracts*, December 15, 1996.

¹ Abbreviations: Ap, apurinic site; bp, base pair; BPI, benzopyridoindole; BPQ, benzopyridoquinoxaline; ds, double-stranded; Nb, nebularine; nt, nucleotide(s); ss, single-stranded.

Table 1. Thermal Melting Data of Triplex to Duplex Transitions for the BPI and BPQ Conjugates with the 42-mer Duplex Target at pH 6.9

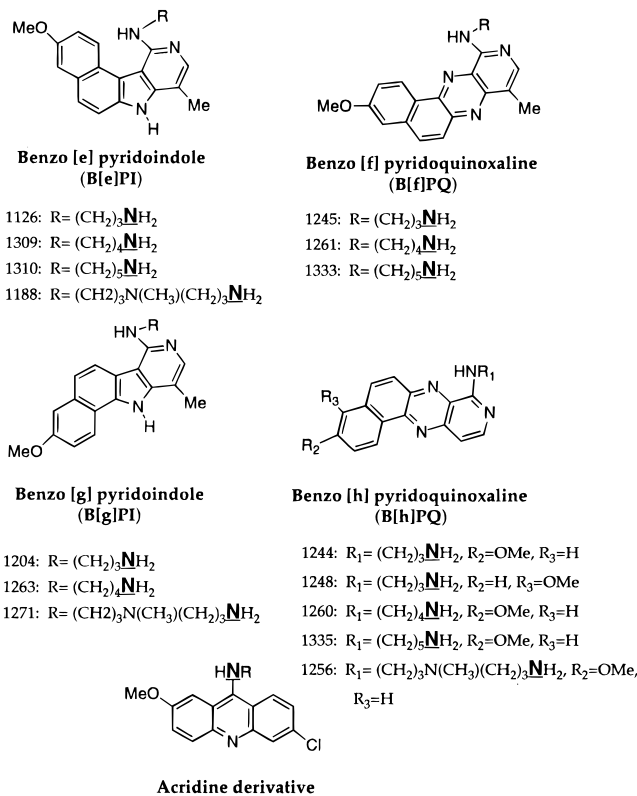
target duplex				
3'GATGCGGGTATTTTCCTCTCCCTCTAAGGGGACGGCAACTTC5'				
5'CTACGCCCATAAAGGAGAGGGGAGATTCCCTGCCGTTGAAG3'				
third strand				
X-TTTCCTCTCCCTCT3'				
Y				
third strand	linker arm	T _m (°C)	ΔT _m	
X = Y = no modification				
1	oligonucleotide 15IL2 (unmodified)	16	0	
Y = no modification; X =				
2	B[e]PI 1126 $-(CH_2)_3-$	22	6	
3	B[e]PI 1309 $-(CH_2)_4-$	27	11	
4	B[e]PI 1310 $-(CH_2)_5-$	28	12	
5	B[e]PI 1188 $-(CH_2)_3NMe(CH_2)_3-$	29	13	
6	B[g]PI 1204 $-(CH_2)_3-$	26	10	
7	B[g]PI 1263 $-(CH_2)_4-$	29	13	
8	B[g]PI 1271 $-(CH_2)_3NMe(CH_2)_3-$	28	12	
9	B[f]PQ 1245 $-(CH_2)_3-$	25	9	
10	B[f]PQ 1261 $-(CH_2)_4-$	26	10	
11	B[f]PQ 1333 $-(CH_2)_5-$	28	12	
12	B[h]PQ 1244 $-(CH_2)_3-$	26	10	
13	B[h]PQ 1248 $-(CH_2)_3-$	27	11	
14	B[h]PQ 1260 $-(CH_2)_4-$	31	15	
15	B[h]PQ 1335 $-(CH_2)_5-$	30	14	
16	B[h]PQ 1256 $-(CH_2)_3NMe(CH_2)_3-$	29	13	
17	acridine	29	13	
X = no modification; Y =				
18	B[e]PI 1126 $-(CH_2)_3-$	20	4	
19	B[e]PI 1188 $-(CH_2)_3NMe(CH_2)_3-$	20	4	
20	B[g]PI 1263 $-(CH_2)_4-$	20	4	
21	B[f]PQ 1261 $-(CH_2)_4-$	29	13	
22	B[h]PQ 1260 $-(CH_2)_4-$	21	5	
23	B[h]PQ 1256 $-(CH_2)_3NMe(CH_2)_3-$	23	7	
24	acridine	19	3	
5'TTNbTTTCCTCTCCCTCT3' (15IL2+Nb)				
5'TTApTTTCCTCTCCCTCT3' (15IL2+Ap)				
		8	-8	
		8	-8	

ridoindoles (BPI) (Nguyen et al., 1990) and benzopyridoquinoxalines (BPQ) (Nguyen et al., 1995) are classes of tetracyclic aromatic compounds (Figure 1) having antineoplastic activity. They have been shown to stabilize pyrimidine motif DNA triple helices in solution (Mergny et al., 1992; Escudé et al., 1995; Marchand et al., 1996) and can intercalate into both duplexes and triplexes but bind preferentially to triplexes (Mergny et al., 1992; Pilch et al., 1993).

In this study, we have covalently linked several BPI and BPQ intercalators to the 5' end or at an internucleotide position of a 15-mer third strand probe with the IL-2Rα sequence (Table 1). We have examined the ability of this series of oligonucleotide conjugates to stabilize triple helices *in vitro* under physiological conditions. The stability of triplexes formed from unmodified and acridine-modified oligonucleotide counterparts was also investigated. The results are compared to a similar study performed with a different triplex sequence (Silver et al., 1997).

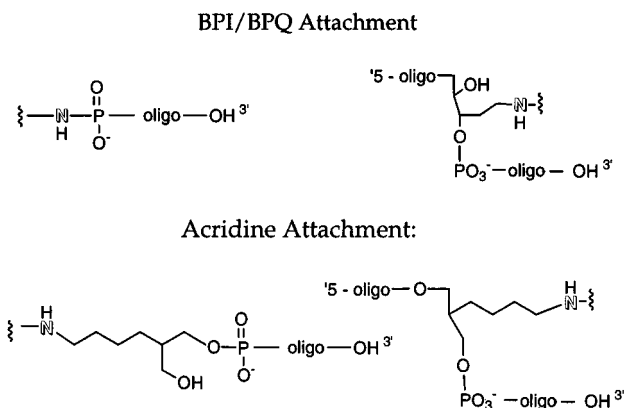
EXPERIMENTAL PROCEDURES

Oligonucleotides. Unmodified and acridine-modified (using 2-methoxy-6-chloro-9-aminoacridine) oligonucleotides were purchased from Eurogentec (Seraing, Belgium) or Genosys (Cambridge, England). The BPI- and BPQ-modified oligonucleotides were synthesized as described below. The linkage structures of the BPI, BPQ, and acridine-modified oligonucleotides are shown in Figure 2 for both the 5' and internal modifications. The

**Figure 1.** BPI (B[e]PI, B[g]PI), BPQ (B[f]PQ, B[h]PQ), and acridine derivatives. Oligonucleotides were attached to the terminal nitrogens on each of the side chains of the BPI and BPQ derivatives and to the nitrogen at position 9 of the acridine (indicated by boldface and underscoring).

Attachment through 5' end:

Attachment through internucleotide linkage:

**Figure 2.** Linkage structure of BPIs, BPQs, and acridine to oligonucleotides. Outlined characters indicate position of attachment to intercalator. Note that for BPI and BPQ derivatives, the NH group is that of the substituent R indicated in Figure 1, while for the acridine derivative the NH group is found in position 9 of the aromatic ring.

concentration of unmodified oligonucleotides was calculated using molar extinction coefficients at 260 nm derived using a nearest-neighbor model (Cantor et al., 1970; Rougée et al., 1992). The acridine-modified oligonucleotide concentration was calculated using $\epsilon_{424} = 8845 \text{ M}^{-1} \text{ cm}^{-1}$ (Asseline et al., 1984). The extinction coefficients for the BPI and BPQ conjugates were approximated by adding the experimentally derived extinction coefficient at 260 nm of the unconjugated BPI or BPQs in H₂O to the extinction coefficient for oligonucle-

Table 2. Thermodynamic Parameters for Triplex Formation^a

oligonucleotide– intercalator conjugate	ΔH° (kcal mol ⁻¹)	ΔS° [cal (mol K) ⁻¹]	ΔG°_{37} (kcal mol ⁻¹)
1 oligonucleotide 15IL2 (unmodified)	-68 ± 3	-208 ± 8	-3.5 ± 0.2
14 B[h]PQ 1260 (5' attachment)	-74 ± 3	-218 ± 10	-6.9 ± 0.1
17 acridine (5' attachment)	-73 ± 2	-217 ± 8	-6.2 ± 0.1
21 B[f]PQ 1261 (interior attachment)	-83 ± 4	-249 ± 13	-6.3 ± 0.1

^a The reported values correspond to the average of four experiments taking into account both the heating and cooling curves.

otide 15IL2 ($\epsilon_{260} = 116\,000\text{ M}^{-1}\text{ cm}^{-1}$). All concentrations are given on a per strand basis.

Syntheses. To covalently link the BPQ and BPI derivatives to the 5' end of the oligomers (Godovikova et al., 1986; Mergny et al., 1994), the hexadecyl trimethyl ammonium salt of 150 μg of 5'-phosphorylated 15IL2 (5'-TTTTCCTCTCCCTCT-3') was incubated with 6.6 mg of dipyrindyl disulfide, 7.9 mg of triphenylphosphine, and 5 μL of *N*-methylimidazole in 100 μL of dry DMSO for 15 min at room temperature. Five microliters of triethylamine was added followed by a solution of the BPQ or BPI derivative (20 μL , 30 mM in DMSO). After 20 min, the oligonucleotide was precipitated with 3% LiClO₄ in acetone, reprecipitated from water with EtOH, and purified by reversed phase HPLC. Average yield = 21%. The oligonucleotide–intercalator conjugates were characterized by UV–visible spectroscopy.

To attach the BPQ and BPI derivatives to the interior of the oligonucleotide (Vasseur et al., 1991), 100 μg of oligo 15IL2+A (5'-TTATTCCTCTCCCTCT-3') or 15IL2+Nb (5'-TTNbTTCCTCTCCCTCT-3') was depurinated in a 100 μL solution of 30 mM HCl/1 mM EDTA for 22 h at 37 °C [Bailly and Verly, 1987; to form oligo 15IL2+Ap (5'-TTApTTCCTCTCCCTCT-3')]. Following EtOH precipitation, the oligonucleotide was reacted with the BPQ or BPI derivative (2.5 mM), NaOAc (pH 5.2, 200 mM), and NaBH₃CN (50 mM) in a total volume of 100 μL for 2 h. The oligonucleotide was recovered by reversed phase HPLC. Average yield = 53%. The oligonucleotide–intercalator conjugates were characterized by UV–visible spectroscopy.

Thermal Denaturation Studies. Experiments were carried out in 140 mM KCl, 15 mM sodium cacodylate, 1.5 mM MgCl₂, and 0.8 mM spermine, pH 6.9. Cacodylate buffer was chosen due to the limited dependence of pH on temperature. Absorbance versus temperature curves were obtained using a Uvikon 940 spectrophotometer interfaced to an IBM computer. The temperature of the two six-cell holders was regulated by a Haake P2 circulating H₂O/glycerol (4:1) bath. The temperature was varied at a rate of 6 °C/h by a Haake PG20 thermoprogrammer. To monitor triplex-to-duplex transitions, the temperature was varied from 62 °C (equilibrated for 70 min) to 0 °C (maintained for 70 min) and returned to 62 °C. To monitor duplex-to-single-strand transitions, the temperature was varied from 90 °C (equilibrated for 70 min) to 40 °C (maintained for 70 min) and returned to 90 °C. Oligonucleotide concentrations were 1 μM of duplex and 1.5 μM of third strand. When intercalator was added free in solution, it was added at 1.5 μM . When the target was single-stranded and not double-stranded, the probe strand was added at 1.0 μM (Table 3). The absorbance at 260 and at 600 nm was recorded every 8.3 min. Corrections for spectrophotometric instability were made by subtracting the absor-

Table 3. T_m Values of Duplex to Single-Strand Transitions

target strand 3'GCCCATAAAAGGAGAGGGAGATTCC5'		
third strand X-TTTTCCTCTCCCTCT3' Y		
third strand	linker arm	T_m (°C)
X = Y = no modification		
1 unmodified 15IL2		54
Y = no modification; X =		
10 B[f]PQ 1261	-(CH ₂) ₄ -	58
13 B[h]PQ 1248	-(CH ₂) ₃ -	60
17 acridine		60
X = no modification; Y =		
21 B[f]PQ 1261	-(CH ₂) ₄ -	57
22 B[h]PQ 1260	-(CH ₂) ₄ -	58
23 B[h]PQ 1256	-(CH ₂) ₃ NMe(CH ₂) ₃ -	58
24 acridine		59

bance at 600 nm from that at 260 nm. There is some hysteresis in the heating and cooling curves, due to slow kinetics of formation and dissociation of the triple-helical complexes (Rougée et al., 1992). The difference between the cooling and heating curves varied between 0.5 and 2 °C at the T_m value depending on the identity of the third strand. T_m values were approximated as the maxima in dA/dT vs T plots of the heating curves. The uncertainty in T_m values reported is estimated at ± 1 °C on the basis of repetition of experiments. Values reported are an average of three to six experiments.

Thermodynamic Calculations. As the hysteresis was minimal for many of the melting curves, we could estimate thermodynamic parameters from some of these curves. The heating and cooling curves were analyzed separately, and it was found that the differences between the two values were insignificant.

The transition to the triplex, T, from the duplex, D, and the monomeric oligonucleotide, M, is given by



Thermodynamic parameters were derived from the melting curves using a two-state model which assumes that the species with incomplete base pairing are not significantly populated (Cantor and Schimmel, 1980; Rougée et al., 1992). A linear absorbance vs temperature relationship was assumed for the calculation of A_D and A_T , the absorbances of the double- and triple-stranded species, respectively. Equilibrium constants at different temperatures were then calculated, and the plot of $\ln K_{eq}$ vs T^{-1} was used to determine ΔH° , ΔS° , and ΔG° (37 °C) as previously described (Breslauer et al., 1975; Albergo et al., 1981; Petersheim and Turner, 1983; Rougée et al., 1992; Wang and Kool, 1995). Errors are reported as the standard deviation.

RESULTS

To study the ability of BPI and BPQ conjugates to form stable triple helices, UV thermal melting studies were performed with each conjugate (15 nt) in the presence of a 42 bp target duplex (see top of Table 1). Hyperchromicity at 260 nm accompanies the dissociation of the third strand from the duplex. The midpoint of this transition (T_m) indicates the relative stability of the triple helix. Comparisons were made with the unmodified third strand (15IL2) and with the acridine conjugates. The results of these studies are shown in Table 1. Examples of the profiles of the fraction of triplex formed as a function of temperature are shown in Figure 3. These

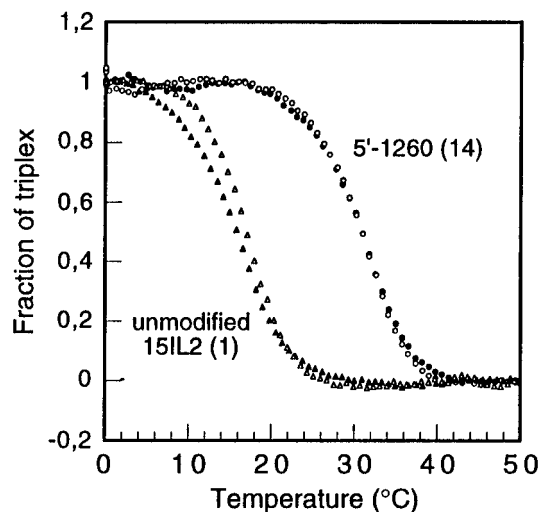


Figure 3. Fraction of triplex formed calculated from the graphs of absorbance vs temperature [$\chi_T = (A - A_D)/(A_T - A_D)$]. One example each is shown of the triplex formed with the unmodified third strand (triangles) or with oligonucleotide **14** (circles) in the presence of duplex (42R/Y). The calculations were performed separately on the heating (solid circles/triangles) and cooling (open circles/triangles) curves. Conditions are those described under Experimental Procedures.

curves allowed the calculation of several thermodynamic parameters (ΔG_{37}° , ΔH° , and ΔS°), which are given in Table 2.

These results show that all of the triple helices formed with the oligonucleotide conjugates are more stable than those formed with the unmodified probe (15IL2), yet there are significant variations depending on the point of attachment to the oligonucleotide and the specific intercalator used. The most stable triplex is formed with conjugate **14**, where a B[h]PQ with a butyl linker arm is attached to the 5' end. The triplex formed melts at 31 °C compared with 16 °C for the triplex formed with the free oligonucleotide (**1**) and 29 °C for the 5' acridine conjugate (**17**). The B[f]PQ derivative, 1261, attached to the interior of the 15-mer (**21**) melts at 29 °C. In terms of standard free energy, this corresponds to a stabilization of the triplex by 3.4 kcal mol⁻¹ at 37 °C for B[h]PQ 1260 attached to the 5' end of the 15-mer (**14**) as compared to 2.7 kcal mol⁻¹ for the acridine derivative (Table 2). The B[f]PQ derivative, 1261, attached to the interior of the 15-mer (**21**) stabilizes the triplex by 2.8 kcal mol⁻¹.

For the 5' attachments, comparing the four intercalators, for the $-(CH_2)_3-$ linker arm B[h]PQ = B[g]PI \geq B[f]PQ > B[e]PI, for the $-(CH_2)_4-$ linker arm B[h]PQ > B[g]PI > B[e]PI \geq B[f]PQ, for the $-(CH_2)_5-$ linker arm B[h]PQ > B[e]PI = B[f]PQ, and for the $-(CH_2)_3$ NMe- $(CH_3)_2-$ linker arm B[h]PQ = B[e]PI \geq B[g]PI. In summary, B[h]PQ seems to be the best ligand for stabilizing the triple helix. Also, a chain length of four carbons is optimal for B[f]PQ, but a slightly higher stabilization is obtained with a chain of 5 carbons for B[e]PI and B[h]PQ. A linker arm of three carbons gave consistently less stabilization. Different linker lengths were not tested for the acridine complexes. However, the one tested [$-(CH_2)_5-$] stabilizes well in comparison to most of the BPI and BPQ derivatives, except for B[h]PQ derivatives 1260 and 1335.

Attached to the interior position, the most stabilizing is the B[f]PQ with a linker arm of $-(CH_2)_4-$ (**21**), which has a T_m of 29 °C. This particular intercalator shows a remarkable stabilization compared with all of the other intercalators tested including acridine at this position.

As is to be expected, the oligonucleotide precursors for these conjugates, namely 15IL2+Nb or 15IL2+A, and the oligonucleotide with an apurinic site (15IL2+Ap) (see Experimental Procedures) are much less stable than the unmodified third strand. As fewer conjugates were tested for the interior modifications, it is more difficult to generalize. However, it appears that the B[f]PQ derivatives are much more stable than any of the other intercalator conjugates, whereas in the 5' position it was one of the worst.

The results with the intercalator-oligonucleotide conjugates were compared to the stabilization gained by triplexes with the intercalators free in solution. The plain third strand, 15IL2 (1.5 μ M), was mixed with the duplex solution (1 μ M) in the same buffer as that used for the conjugate studies. Significant triplex stabilization has been seen for solutions where a 10-fold higher concentration of intercalator was used (vs the triplex concentration) at pH 6.2 (Escudé et al., 1995). In the current study, a 1.5-fold concentration (1.5 μ M) of the BPI or BPQ derivatives and a pH of 6.9 were used. All tested BPI and BPQ derivatives led to ΔT_m values of 2 °C except B[h]PQ 1256 and B[g]PI 1271, which gave ΔT_m values of 6 and 3 °C, respectively. This is likely due to the extra positive charge localized on the tertiary nitrogen found in the longer linker arms of these two derivatives providing greater affinity for the negatively charged nucleic acids. That the first of these derivatives stabilizes more than the second has been confirmed by previous studies (Escudé et al., 1995; C. Escudé, personal communication). The addition of acridine to a triplex solution under these conditions did not stabilize the triplex.

BPIs and BPQs are known to preferentially stabilize triple-helical DNA structures over double-helical DNA when in solution (Mergny et al., 1992; Escudé et al., 1995; Marchand et al., 1996). Nevertheless, they do intercalate into duplex structures (Mergny et al., 1992). Therefore, it was of interest to measure the stability of double-helical complexes formed upon binding of the 15-mer-intercalator conjugates to a single-stranded target. A single-stranded sequence complementary to the oligonucleotide-BPI/BPQ conjugates was mixed in equimolar quantity (1 μ M) with different conjugates and the T_m of the duplex-to-single-strand transition was determined. The results are shown in Table 3. The stabilization seen varies between 3 and 6 °C depending on the conjugate.

To attach the intercalators to the interior of the probe strand, we chose to *add* an extra nucleotide to the probe strand, which was then depurinated so that the intercalator could be attached at this position. The reason we chose to do so was based on molecular modeling studies which had indicated that adding, rather than replacing, an existing nucleotide would provide the most energetically favorable possibility (unpublished calculations). The duplex "spreads apart" upon binding of an intercalator (Wilson, 1992; Zhou et al., 1995). Thus, the alignment of the bases in the duplex with the third strand is thought to be better through the addition rather than the replacement of a base. To test this, we performed some melting studies with a target sequence in which an extra base pair was added opposite to the position of depurination on the probe strand. The results are given in Table 4. When the probe strand also contained an extra nucleotide complementary to the base pair added to the target, the T_m remained at 16 °C. However, the T_m values observed with the oligonucleotide conjugates (**20**, **21**, and **23**) dropped (2–8 °C), indicating that these conjugates could not form a more stable conformation with the 43-mer duplexes as compared to the 42-mer duplex. It is interesting to note that the T_m of the 15IL2 oligonucle-

Table 4. Thermal Melting Data of Triplex to Duplex Transitions with Extra Base Pair (in bold) in Target Sequence

target duplex 3' GATGCGGGTAT TTZ TCCTCTCCCTCTAAGGGGACGGCAACTTC5' 5' CTACGCCCAT AAWA AGGAGAGGGAGATTCCTCTGCCGTGAAG3' third strand TTTTCCTCTCCCTCT3' Y				
		T _m (°C)		
third strand	linker arm	Z, W =		no extra bp (42-mer target)
		A, T	T, A	
5'-TTTTCCTCTCCCTCT-3' (15IL2)		7	14	16
5'-TTATTCCTCTCCCTCT-3'		7	7	not tested
5'-TTTTTCCTCTCCTCT-3'		not tested	16	not tested
Y =				
20	B[g]PI 1263 -(CH ₂) ₄ -	19	18	20
21	B[f]PQ 1261 -(CH ₂) ₄ -	21	23	29
23	B[h]PQ 1256 -(CH ₂) ₃ NMe(CH ₂) ₃ -	20	19	23
24	acridine	20	17	19

Table 5. T_m Values of Triplex to Duplex Transitions with a Blunt End Target Duplex^a

<div>target duplex</div> <div>3' <u>TTTTCCTCTCCCTCTAAGGGGACGGCAACTTC</u>5'</div> <div>5' <u>AAAAGGAGAGGGAGA</u>TTCCCTGCCGTTGAAG3'</div> <div>third strand</div> <div>X- TTTTCCTCTCCCTCT3'</div> <div>Y</div>					
		blunt end target ^a		standard target ^b	
third strand	linker arm	T _m	Δ T _m	T _m ^a	Δ T _m ^a
X = Y = no modification					
1	oligonucleotide 15IL2 (unmodified)	18	0	16	0
Y = no modification; X =					
10	B[f]PQ 1261 −(CH ₂) ₄ −	24	6	26	10
14	B[h]PQ 1260 −(CH ₂) ₄ −	28	10	31	15
16	B[h]PQ 1256 −(CH ₂) ₃ NMe(CH ₂) ₃ −	26	8	29	13
17	acridine	26	8	29	13
X = no modification; Y =					
21	B[f]PQ 1261 −(CH ₂) ₄ −	28	10	29	13
22	B[h]PQ 1260 −(CH ₂) ₄ −	22	4	21	5
23	B[h]PQ 1256 −(CH ₂) ₃ NMe(CH ₂) ₃ −	23	5	23	7
24	acridine	18	0	19	3

^a Shown above. ^b From Table 1.

otide also drops slightly with the 43-mer duplex (**Z**, **B** = T, A), even though it should also form a perfect triplex with the modified target. This phenomenon has previously been observed (J.-L. Mergny, personal communication). It is likely due to the distortion induced at the triplex–duplex junction which destabilizes the triple helix more for a py–py than for a pu–py step at the junction.

When the third strand hybridizes to the duplex, two sites are possible for intercalation of the BPI or BPQ derivatives: the duplex–triplex junction and within the triplex. To investigate the relative importance of intercalation at these two sites with the two types of conjugates synthesized, we performed melting temperature studies in the presence of a duplex where the overhanging 5' end (with respect to the purine strand) was removed (Table 5). As would be expected for intercalation within the triplex, the ΔT_m values for those conjugates where the intercalator is attached to the interior are almost the same as the ΔT_m values of these same conjugates with the standard (42R/Y) target. In the case where the intercalator was joined at the 5' end one sees a greater decrease in ΔT_m (i.e. 4–5 °C) when the overhanging duplex sequence is removed. Though not conclusive, these experiments suggest that when attached to the interior, the BPI/BPQ derivative intercalates within the triplex. However, when attached to the

5' end, a large part of the stabilization comes from intercalation into the junction. The T_m of the triplex formed with the unmodified third strand is somewhat higher with the blunt end target than with the target with the overhanging end (42R/Y). This is because the binding of a third strand induces a distortion of the triplex–duplex junction (Collier and Hélène, 1991), and the corresponding free energy has to be provided upon third strand binding leading to a destabilization of the complex.

A similar set of syntheses and melting experiments have previously been performed with a different sequence, called 14C3, shown in Table 6. These results are being reported elsewhere (Silver et al., 1996). However, a small selection of these 14C3 results is shown in Table 6 for the purpose of comparison. The 14C3 triplex is inherently more stable under the conditions used (the same as the present paper), as it contains only 21% cytosines vs 47% for the IL2Ra sequence. The pK_a of cytosines has been estimated at 4.7 in oligonucleotides (Manzini et al., 1990), and protonation is required for triplex formation. It is thus understandable that all of the T_m values obtained with the 14C3 sequence were higher than their 15IL2 counterparts.

However, it is interesting to note that the ΔT_m values for the 14C3 system were greater as well. The most significant Δ(ΔT_m) values [i.e. ΔT_m (14C3 system) – ΔT_m

Table 6. Selection of T_m Values for Triplex to Duplex Transitions in the 14C3 System^a

14C3 duplex + third strand		15IL2 duplex + third strand			
3' GCTCAATTCCTCTCTTTTCTTAAC TCG 5' 3' ...GGTATTTTCCTCTCCCTCTAAGG... 5'					
5' CGAGTTAAGAAGAAAAAGATTGAGC 3' 5' ...CCATAAAAGGAGAGGGGAGATTCC... 3'					
$\begin{array}{c} \text{X} - \text{TTCTCTCTCTTTTCT}^3' \\ \quad \quad \quad \text{Y} \end{array}$		$\begin{array}{c} \text{X} - \text{TTTCTCTCTCCCTCT}^3' \\ \quad \quad \quad \text{Y} \end{array}$			
third strand	linker arm	14C3		15IL2	
		T_m (°C)	ΔT_m	T_m (°C)	ΔT_m
X = Y = no modification					
unmodified (15IL2)		28	0	16	0
Y = no modification; X =					
B[f]PQ 1261	-(CH ₂) ₄ -	43	15	26	10
B[h]PQ 1260	-(CH ₂) ₄ -	51	23	31	15
acridine		45	17	29	13
X = no modification; Y =					
B[f]PQ 1261	-(CH ₂) ₄ -	45	17	29	13
B[h]PQ 1260	-(CH ₂) ₄ -	39	11	21	5
acridine		35	7	19	3

^a Buffer is the same as for the IL2 system.

(IL2 system)] were seen for 5' B[h]PQ attachments and for internally attached B[e]PIs. Thinking that the sequence around the site of the duplex–triplex junction could be influencing the amount of stability gained for the 5' attachments, we changed the duplex target sequence for the 14C3 system. In the IL2 system, at the junction the sequence is TATT in the pyrimidine strand, and for the 14C3 system it is AATT (see Table 6). So we changed the duplex target sequence for the 14C3 system to 3' GCTCTATTCTTCTTTTCTTAAC TCG 5' (outlined base indicates the one changed). The stability of the 14C3 triplexes formed with this target and a probe–intercalator conjugate was not lowered and in fact showed a 1–2 °C increase in T_m (data not shown), indicating that the conformation of the duplex–triplex junction is perhaps not responsible for the differences seen in ΔT_m values.

DISCUSSION

Certain DNA ligands have been shown to bind to DNA triple helices (Mergny et al., 1991; Scaria and Shafer, 1991; Durand et al., 1992; Park and Breslauer, 1992; Escudé et al., 1995). However, only a few compounds have been studied that *efficiently* and *selectively* bind to triple helices (Mergny et al., 1992; Lee et al., 1993; Wilson et al., 1993; Escudé et al., 1995; Fox et al., 1995; Latimer et al., 1995). Previous studies in our laboratory have concentrated on ligands of this latter type, namely benzopyridoindoles and benzopyridoquinoxalines. They stabilize the triple helix by intercalating between TA×T base triplets. Binding of these cationic derivatives to CG×C⁺ triplets is not favored due to the positive charge of this triplet. In this paper and another (Silver et al., 1996), we attached the BPI and BPQ derivatives to a run of thymines within the probe strand and examined the stability of triplexes formed with these conjugates.

The results of the current study indicate that all of the conjugates synthesized are able to stabilize the formation of DNA triple helices. However, certain conjugates did so to a greater extent. Differences were seen among the different derivatives and depended on which of the intercalators was attached, the length of the hydrocarbon linker chain, and the position of attachment to the probe strand. In general, better stabilization was seen with 5' attachments when arm lengths of at least four methyl- enes were used. The B[h]PQ derivatives worked par-

ticularly well here. That the B[f]PQ 1261 derivative (**21**) attached to the interior showed significant stabilization compared to both of the other intercalators attached at this position as well as to the same derivative attached to the 5' end suggests that this conjugate has a conformation allowing particularly favorable ligand–base stacking interactions within the triple-helical region. The mechanism by which these conjugates stabilize triple helices is likely the intercalation of the derivatives within the triplex (internal attachment) or at the duplex/triplex junction (5'-end attachment). When the BPI or BPQ is covalently attached to the oligonucleotide third strand, intramolecular interactions of the BPI or BPQ moiety with the bases of the third strand might also play a role in determining the thermodynamic parameters of the interactions of the conjugate with its target double helix.

It should be noted that the linker used to tether the BPI and BPQ derivatives to the oligonucleotide occupies a different position in the grooves of the triplex than when they are bound as *free* ligand. In the latter case, the linker is expected to be in the Watson–Crick groove for B[g]PI and B[h]PQ derivatives but has been shown to prefer the Watson–Hoogsteen groove for B[e]PI and B[f]PQ derivatives on the basis of molecular modeling (Escudé et al., 1995). [The nomenclature of the grooves has been previously described (Radhakrishnan and Patel, 1994b). The oligopyrimidine and oligopurine strand of the Watson–Crick duplex are *Watson* and *Crick*, respectively, and the third strand is *Hoogsteen*. Each groove of the triple helix is referred to by the names of the adjacent strands.] However, when attached to the third strand, the intercalating moiety is always introduced from the major groove side of the double helix. Therefore, B[g]PI and B[h]PQ should be in a less favorable position than B[e]PI and B[f]PQ. This seems to hold when the intercalator is attached to the interior of the third strand oligonucleotide but not when attached to the 5' end (Table 6). This might reflect the difference in the intercalation mode: within the triple-helical structure in the first case, at the duplex–triplex junction in the second case. On the other hand, the chemistry of dye attachment to the oligonucleotide is also different for an interior site and the 5' end (see Figure 2). A positive charge is still present on the linker when attachment occurs at an interior site as is the case for the free derivatives. This positive charge was taken into account for the modeling studies mentioned above. In contrast, the phosphoramidate linkage at the 5' end carries no positive charge, which may also explain the deviation from the results with the free ligands (Escudé et al., 1995).

It is informative to compare the current study with one performed with the 14C3 sequence (Table 6) (Silver et al., 1996). Both the T_m values and the ΔT_m values are significantly greater for the 14C3 system. The reason for the larger ΔT_m values is not obvious. Previous studies using the 14C3 sequence have suggested that the stretch of six TA×T base triplets is the major binding site for free BPI ligands (Mergny et al., 1992). When two thymines were replaced by two cytosines in the 14C3 sequence, leaving only four contiguous TA×T base triplets, a strong decrease in triple-helix stabilization was seen (Mergny et al., 1992). This probably occurs because the six contiguous TA×T base triplets provide a greater number of binding sites for the BPI ligands within the triplex. The IL2 sequence contains only a stretch of four TA×T base triplets, which might be one reason for the lower stabilization as compared to the 14C3 sequence. In addition, the four TA×T triplets of the IL2 sequence are located at the 5' end of the oligopurine target sequence, whereas the six TA×T triplets are located

toward the center of the 14C3 sequence. Finally, in the case of oligonucleotides with internal attachment of the ligands, the position of intercalation is only two base triplets away from the 5' end of the triplex structure in the case of the IL2 sequence. The last two thymines between the 5' end and the intercalator attachment site of the third-strand oligonucleotide might not be fully hydrogen-bonded to the two T·A base pairs of the target.

Despite the differences in sequence between the IL2 and 14C3, the same trends were seen with both systems in terms of which derivatives stabilized the most. To summarize, the B[h]PQs generally work particularly well and the B[f]PQs particularly poorly at stabilizing DNA triple helices when attached to the 5' end of the probe strand. As well, in both systems, for this site of attachment, the short linker arm, $-(CH_2)_3-$, does not work well. At the interior position, the results were somewhat more mixed, likely a result of several differences in the positioning of the intercalator. However, in both cases the B[f]PQ derivative 1261 shows great stabilization. For the 14C3 system the B[e]PIs also work well.

CONCLUSION

Benzopyridoindoles and benzopyridoquinoxalines have been shown to stabilize the formation of DNA triple helices when they are conjugated at both the 5' end and to an internucleotide position of the third-strand oligonucleotide. The particular derivative, the length of the linker arm, the point of attachment, and the sequence of base triplets around the ligand attachment site all play important roles in determining the stability of the triplexes formed. These results will be useful for studies using these conjugates to inhibit transcription in cellular systems as well as in the design of new oligonucleotide conjugates.

ACKNOWLEDGMENT

G.C.S. acknowledges the Ministère des Affaires Étrangères du Gouvernement Français for a Chateaubriand Fellowship as well as the support of the National Science Foundation (Grant INT 9403368).

LITERATURE CITED

- Albergo, D., Marky, L., Breslauer, K., and Turner, D. (1981) Thermodynamics of $(dG-dC)_3$ double-helix formation in water and deuterium oxide. *Biochemistry* 20, 1409–1413.
- Asseline, U., Delarue, M., Lancelot, G., Toulmé, F., Thuong, N. T., Montenay-Garestier, T., and Hélène, C. (1984) Nucleic acid-binding molecules with high affinity and base sequence specificity: intercalating agents covalently linked to oligodeoxynucleotides. *Proc. Natl. Acad. Sci. U.S.A.* 81, 3297–3301.
- Bailly, V., and Verly, W. G. (1987) *Escherichia coli* endonuclease III is not an endonuclease but a beta-elimination catalyst. *Biochem. J.* 242, 565–572.
- Beal, P. A., and Dervan, P. B. (1991) Second structural motif for recognition of DNA by oligonucleotide-directed triple-helix formation. *Science* 251, 1360–1363.
- Breslauer, K., Sturtevant, J., and Tinoco, I. J. (1975) Calorimetric and spectroscopic investigation of the helix-to-coil transition of a ribo-oligonucleotide. *J. Mol. Biol.* 99, 549–65.
- Cantor, C., and Schimmel, P. (1980) *Biophysical Chemistry*, Chapter 22, W. H. Freeman, San Francisco.
- Cantor, C. R., Warshaw, M. M., and Shapiro, H. (1970) Oligonucleotides interactions. III. Circular dichroism studies of the conformation of deoxyligonucleotides. *Biopolymers* 9, 1059–1077.
- Collier, D. A., and Hélène, C. (1991) Site-specific intercalation at the triplex-duplex junction induces a conformational change which is detectable by hypersensitivity of diethylpyrocarbonate. *Nucleic Acids Res.* 11, 4219–4224.
- Crooke, S. T., and Lebleu, B. (1993) *Antisense Research and Applications*, CRC Press, London.
- de Bizemont, T., Duval-Valentin, G., Sun, J.-S., Bisagni, E., Garestier, T., and Hélène, C. (1996) Alternate strand recognition of double-helical DNA by (T,G)-containing oligonucleotides in the presence of a triple helix-specific ligand. *Nucleic Acids Res.* 24, 1136–1143.
- de los Santos, C., Rosen, M., and Patel, D. (1989) NMR Studies of DNA (R+)-N(Y-)-N(Y+)-N triple helices in solution—imino and amino proton markers of TAT and CGC+ base-triple formation. *Biochemistry* 28, 7282–7289.
- Demesmaeker, A., Haner, R., Martin, P., and Moser, H. E. (1995) Antisense oligonucleotides. *Acc. Chem. Res.* 28, 366–374.
- Durand, M., Thuong, N. T., and Maurizot, J. C. (1992) Binding of netropsin to a DNA triple helix. *J. Biol. Chem.* 267, 24394–24399.
- Durland, R. H., Kessler, D. J., Gunnel, S., Duvic, M., Petit, B. M., and Hogan, M. E. (1991) Binding of triple helix forming oligonucleotides to sites in gene promoters. *Biochemistry* 30, 9246–9255.
- Escudé, C., Nguyen, C. H., Mergny, J.-L., Sun, J.-S., Bisagni, E., Garestier, T., and Hélène, C. (1995) Stabilization of triple helices by benzopyridoindole derivatives. *J. Am. Chem. Soc.* 117, 10212–10219.
- Fox, K. R., Polucci, P., Jenkins, T. C., and Neidle, S. (1995) A molecular anchor for stabilizing triple-helical DNA. *Proc. Natl. Acad. Sci. U.S.A.* 92, 7887–7891.
- Frank-Kamenetskii, M. D., and Mirkin, S. M. (1995) Triplex DNA structures. *Annu. Rev. Biochem.* 64, 65–95.
- Giovannangeli, C., Rougée, M., Montenay-Garestier, T., Thuong, N. T., and Hélène, C. (1992) Triple-helix formation by oligonucleotides containing the three bases thymine, cytosine, and guanine. *Proc. Natl. Acad. Sci. U.S.A.* 89, 8631–8635.
- Godovikova, T. S., Zarytova, V. F., and Khalimskaya, L. M. (1986) Synthesis of phosphoramidate derivatives of oligonucleotides. *Bioorgan. Khim.* 12, 475–481.
- Grigoriev, M., Praseuth, D., Robin, P., Hemar, A., Saison-Behmoaras, T., Dautry-Varsat, A., Thuong, N. T., Hélène, C., and Harel-Bellan, A. (1992) A triple helix-forming oligonucleotide-intercalator conjugate acts as a transcriptional repressor via inhibition of NF kappa B binding to interleukin-2 receptor alpha-regulatory sequence. *J. Biol. Chem.* 267, 3389–3395.
- Grigoriev, M., Praseuth, D., Guieysse, A.-L., Robin, P., Thuong, N. T., Hélène, C., and Harel-Bellan, A. (1993a) Inhibition of interleukin-2 receptor alpha-subunit gene expression by oligonucleotide-directed triple helix formation. *C. R. Acad. Sci. Paris, Ser. III* 316, 492–495.
- Grigoriev, M., Praseuth, D., Guieysse, A. L., Robin, P., Thuong, N. T., Hélène, C., and Harel-Bellan, A. (1993b) Inhibition of gene expression by triple helix-directed DNA cross-linking at specific sites. *Proc. Natl. Acad. Sci. U.S.A.* 90, 3501–3505.
- Hélène, C. (1989) Artificial control of gene expression by oligodeoxynucleotides covalently linked to intercalating agents. *Br. J. Cancer* 60, 157–160.
- Hélène, C. (1994) Control of oncogene expression by antisense nucleic acids. *Eur. J. Cancer* 30A, 1721–1726.
- Hélène, C., and Toulmé, J.-J. (1990) Specific regulation of gene expression by antisense, sense and antigene nucleic acids. *Biochim. Biophys. Acta* 1049, 99–125.
- Latimer, L. J. P., Payton, N., Forsyth, G., and Lee, J. S. (1995) The binding of analogues of coralyne and related heterocyclics to DNA triplexes. *Biochem. Cell Biol.* 73, 11–18.
- Le Doan, T., Perrouault, L., Praseuth, D., Habhou, N., Decout, J. L., Thuong, N. T., Lhomme, J., and Hélène, C. (1987) Sequence-specific recognition, photocrosslinking and cleavage of the DNA double helix by an oligo-[alpha]-thymidylate covalently linked to an azidoproflavine derivative. *Nucleic Acids Res.* 15, 7749–60.
- Lee, J. S., Latimer, L. J. P., and Hampel, K. J. (1993) Coralyne binds tightly to both T·A·T-containing and C·G·C+·containing DNA triplexes. *Biochemistry* 32, 5591–5597.
- Maher, L. (1996) Prospects for the therapeutic use of antigene oligonucleotides. *Cancer Invest.* 14, 66–82.
- Manzini, G., Xodo, L. E., Gasparotto, D., Quadrioglio, F., van der Marel, G. A., and van Boom, J. H. (1990) Triple helix formation by oligopurine-oligopyrimidine DNA fragments.

- Electrophoretic and thermodynamic behavior. *J. Mol. Biol.* **213**, 833–843.
- Marchand, C., Bailly, C., Nguyen, C. H., Bisagni, E., Garestier, T., Hélène, C., and Waring, M. J. (1996) Stabilization of triple helical DNA by a benzopyridoquinoxaline intercalator. *Biochemistry* **35**, 5022–5032.
- Mergny, J. L., Collier, D., Rougée, M., Montenay-Garestier, T., and Hélène, C. (1991) Intercalation of ethidium bromide into a triple-stranded oligonucleotide. *Nucleic Acids Res.* **19**, 1521–1526.
- Mergny, J. L., Duval-Valentin, G., Nguyen, C. H., Perrouault, L., Faucon, B., Rougée, M., Montenay-Garestier, T., Bisagni, E., and Hélène, C. (1992) Triple helix-specific ligands. *Science* **256**, 1681–1684.
- Mergny, J. L., Bourtoune, A. S., Garestier, T., Belloc, F., Rougée, M., Bulychev, N. V., Koshkin, A. A., Bourson, J., Lebedev, A. V., Valeur, B., Thuong, N. T., and Hélène, C. (1994) Fluorescence energy transfer as a probe for nucleic acid structures and sequences. *Nucleic Acids Res.* **22**, 920–928.
- Moser, H. E., and Dervan, P. B. (1987) Sequence-specific cleavage of double helical DNA by triple helix formation. *Science* **238**, 645–650.
- Murray, J. A. H., and Crockett, N. (1992) Antisense techniques: an overview. In *Antisense RNA and DNA* (J. A. H. Murray, Ed.) pp 1–48, Wiley, New York.
- Nguyen, C. H., Lhoste, J.-M., Lavelle, F., Bissery, M.-C., and Bisagni, E. (1990) Synthesis and antitumor activity of 1-[(di-alkylamino)alkyl]amino]-4-methyl-5H-pyrido[4,3-b]benzo[e]- and -benzo[g]indoles. A new class of antineoplastic agents. *J. Med. Chem.* **33**, 1519–1528.
- Nguyen, C. H., Fan, E., Riou, J.-F., Bissery, M.-C., Vrignaud, P., Lavelle, F., and Bisagni, E. (1995) Synthesis and biological evaluation of amino-substituted benzo[*a*]pyrido[4,3-*b*] and pyrido[3,4-*b*]quinoxalines: a new class of antineoplastic agents. *Anti-Cancer Drug Des.* **10**, 277–297.
- Park, Y. W., and Breslauer, K. J. (1992) Drug binding to higher ordered DNA structures—netropsin complexation with a nucleic acid triple helix. *Proc. Natl. Acad. Sci. U.S.A.* **89**, 6653–6657.
- Petersheim, M., and Turner, D. H. (1983) Base-stacking and base-pairing contributions to helix stability: thermodynamics of double-helix formation with CCGG, CCGGp, CCGGAp, ACCGGp, CCGGUp, and ACCGGUp. *Biochemistry* **22**, 256–263.
- Pierga, J., and Magdelenat, H. (1994) Applications of antisense oligonucleotides in oncology. *Cell. Mol. Biol.* **40**, 237–261.
- Pilch, D. S., Levenson, C., and Shafer, R. H. (1991) Structure, stability, and thermodynamics of a short intermolecular purine-purine-pyrimidine triple helix. *Biochemistry* **30**, 6081–6088.
- Pilch, D. S., Waring, M. J., Sun, J.-S., Rougée, M., Nguyen, C.-H., Bisagni, E., Garestier, T., and Hélène, C. (1993) Characterization of a triple helix-specific ligand. BePI {3-methoxy-7H-8-methyl-11-[(3'-amino)propylamino]-benzo[*e*]pyrido[4,3-*b*]indole} intercalates into both double-helical and triple-helical DNA. *J. Mol. Biol.* **232**, 926–946.
- Radhakrishnan, I., and Patel, D. J. (1994a) DNA triplexes: solution structures, hydration sites, energetics, interactions, and function. *Biochemistry* **33**, 11405–11416.
- Radhakrishnan, I., and Patel, D. J. (1994b) Solution structure and hydration patterns of a pyrimidine-purine-pyrimidine DNA triplex containing a novel T·CG base-triple. *J. Mol. Biol.* **241**, 600–619.
- Rajagopal, P., and Feigon, J. (1989) Triple-strand formation in the homopurine homopyrimidine DNA oligonucleotide-d(GA)₄ and oligonucleotide-d(TC)₄. *Nature* **339**, 637–640.
- Rougée, M., Faucon, B., Mergny, J. L., Barcelo, F., Giovannangeli, C., Garestier, T., and Hélène, C. (1992) Kinetics and thermodynamics of triple-helix formation: effects of ionic strength and mismatches. *Biochemistry* **31**, 9269–9278.
- Scaria, P. V., and Shafer, R. H. (1991) Binding of ethidium bromide to a DNA triple helix—evidence for intercalation. *J. Biol. Chem.* **266**, 5417–5423.
- Silver, G. C., Sun, J.-S., Nguyen, C. H., Bourtoune, A. S., Bisagni, E., and Hélène, C. (1997) Stable triple helical DNA complexes formed by benzopyridoindole- and benzopyridoquinoxaline-oligonucleotide conjugates. *J. Am. Chem. Soc.* **119**, 263–268.
- Stein, C. A., and Cheng, Y. (1993) Antisense oligonucleotides as therapeutic agents—is the bullet really magic? *Science* **261**, 1004–1012.
- Sun, J. S., François, J. C., Montenay-Garestier, T., Saison-Behmoaras, T., Roig, V., Chassignol, M., Thuong, N. T., and Hélène, C. (1989) Sequence-specific intercalating agents. Intercalation at specific sequences on duplex DNA via major-groove recognition by oligonucleotide intercalator conjugates. *Proc. Natl. Acad. Sci. U.S.A.* **86**, 9198–9202.
- Sun, J., Giovannangeli, C., François, J.-C., Kurfurst, R., Montenay-Garestier, T., Asseline, U., Saison-Behmoaras, T., Thuong, N. T., and Hélène, C. (1991a) Triple-helix formation by alpha-oligodeoxynucleotides and alpha-oligodeoxynucleotide intercalator conjugates. *Proc. Natl. Acad. Sci. U.S.A.* **88**, 6023–6027.
- Sun, J. S., de Bizemont, T., Duval-Valentin, G., Montenay-Garestier, T., and Hélène, C. (1991b) Extension of the range of recognition sequences for triple helix formation by oligonucleotides containing guanines and thymines. *C. R. Acad. Sci. Paris, Ser. III* **313**, 585–590.
- Svinarchuk, F., Paoletti, J., and Malvy, C. (1995) An unusually stable purine(purine-pyrimidine) short triplex—the third strand stabilizes double-stranded DNA. *J. Biol. Chem.* **270**, 14068–14071.
- Thuong, N. T., and Hélène, C. (1993) Sequence-specific recognition and modification of double-helical DNA by oligonucleotides. *Angew. Chem., Int. Ed. Engl.* **32**, 666–690.
- Uhlmann, E., and Peyman, A. (1990) Antisense oligonucleotides: a new therapeutic principle. *Chem. Rev.* **90**, 543–584.
- Vasseur, J.-J., Peoc'h, D., Rayner, B., and Imbach, J.-L. (1991) Derivatization of oligonucleotides through abasic site formation. *Nucleosides Nucleotides* **10**, 107–117.
- Wang, S., and Kool, E. T. (1995) Origins of the large differences in stability of DNA and RNA helices: C-5 methyl and 2'-hydroxyl effects. *Biochemistry* **34**, 4125–4132.
- Wilson, W. D. (1992) Reversible interactions of nucleic acids with small molecules. In *Nucleic Acids in Chemistry and Biology* (G. M. Blackburn and M. J. Gait, Eds.) 311 pp, Oxford University Press, Oxford, U.K.
- Wilson, W. D., Tanious, F. A., Mizan, S., Yao, S. J., Kiselyov, A. S., Zon, G., and Strekowski, L. (1993) DNA triple-helix specific intercalators as antigene enhancers—unfused aromatic cations. *Biochemistry* **32**, 10614–10621.
- Zhou, B. W., Puga, E., Sun, J. S., Garestier, T., and Hélène, C. (1995) Stable triple helices formed by acridine-containing oligonucleotides with oligopurine tracts of DNA interrupted by one or two pyrimidines. *J. Am. Chem. Soc.* **117**, 10425–10428.

BC9600675

Surface Modification of Hemoglobin Vesicles with Poly(ethylene glycol) and Effects on Aggregation, Viscosity, and Blood Flow during 90% Exchange Transfusion in Anesthetized Rats

Hiromi Sakai,[†] Shinji Takeoka,[†] Sung Ick Park,[†] Takehiro Kose,[†] Hiroyuki Nishide,[†] Yotaro Izumi,[‡] Akira Yoshizu,[‡] Koichi Kobayashi,[‡] and Eishun Tsuchida^{*,†}

Department of Polymer Chemistry, Advanced Research Institute for Science and Engineering, Waseda University, Tokyo 169, Japan, and Department of Surgery, School of Medicine, Keio University, Tokyo 160, Japan. Received May 16, 1996[⊗]

Poly(ethylene glycol) (PEG₅₀₀₀)-conjugated phosphatidylethanolamine was introduced onto the surface of hemoglobin vesicles (HbV); phospholipid vesicles encapsulating concentrated Hb ($d = 0.257 \pm 0.087 \mu\text{m}$; $P_{50} = 32 \text{ Torr}$). The obtained PEG-modified HbV (HbV-PEG) was studied for use as a red cell substitute from the viewpoint of rheology, surface properties, and hemodynamics. The viscosity of the unmodified HbV suspended in saline ($[\text{Hb}] = 10 \text{ g/dL}$) was 2.6 cP (shear rate = 358 s^{-1} , 37°C), less than that of human blood (4 cP). However, when suspended in a 5 g/dL albumin solution (HbV/albumin), it increased to 8 cP due to the molecular interaction between albumin and vesicles, and the viscosity increased with decreasing shear rate, *e.g.*, 37 cP at 0.58 s^{-1} . As for the HbV-PEG/albumin, on the other hand, the viscosity was 3.5 cP at 358 s^{-1} and was comparable with that of human blood. Optical microscopy showed formless flocculated aggregates of the unmodified HbV, while no aggregates were confirmed for the HbV-PEG. The steric hindrance of PEG chains seemed to be effective in preventing intervesicular access and the resulting aggregation. To estimate the flow profiles in the capillaries, the suspensions were allowed to penetrate through isopore membrane filters (pore size = $0.4\text{--}8 \mu\text{m}$, *cf.* capillary diameter = $4\text{--}10 \mu\text{m}$). The penetration rate of the HbV-PEG/albumin was higher than that of the unmodified HbV/albumin due to the suppression of aggregation, whereas both of them were significantly higher than that of human blood due to the smaller size of vesicles than RBC. Ninety percent exchange transfusion was performed with the HbV-PEG/albumin or HbV/albumin in anesthetized Wistar rats ($n = 6$). The blood flow in the abdominal aorta increased 1.5 times, and the total peripheral resistance decreased in the HbV-PEG/albumin-administered group in comparison with the HbV/albumin group. As for the blood gas parameters, the base excess and pH remained at higher levels in the HbV-PEG/albumin group, and the O_2 tension in mixed venous blood for the HbV-PEG/albumin group tended to be maintained at a higher level than that for the HbV/albumin group. Thus, the PEG modification of HbV reduced the viscosity by the suppression of aggregation and resulted in prompt blood circulation *in vivo*.

INTRODUCTION

To date, various efforts have been made to develop red cell substitutes, especially those utilizing Hb, to overcome the problems associated with blood transfusions such as the necessity for blood typing and cross-matching, blood-borne infections, and difficulties in storage (Chang, 1991; Winslow, 1995; Tsuchida, 1995). Hemoglobin vesicles (HbV)¹ or liposome-encapsulated hemoglobin (LEH) are candidates for red cell substitutes that have the cellular structure of phospholipid vesicles containing concentrated Hb (Djordjevic and Miller, 1980; Hunt *et al.*, 1985; Rudolph, 1995; Tsuchida and Takeoka, 1995). On the other hand, in the field of acellular Hb solutions such as chemically modified Hb and recombinant Hb, clinical trials are now underway (Winslow, 1995). However, vasoconstriction induced by acellular Hb solutions is reported. This is due to the trapping of endothelial-derived relaxation factor [EDRF; nitric oxide (NO)] by Hb with an intrinsic high affinity for NO (Vandegriff and Winslow, 1995; Tsai *et al.*, 1995). NO trapping also induces platelet activation (Olsen *et al.*, 1996). Com-

plexation of acellular Hb with endotoxin synergistically enhances the endotoxin biological activities, and it would be dangerous to use acellular Hb in septic shock (Kaca *et al.*, 1995). These problems seem to be related to the lack of physiological significance of the cellular structure of red blood cells (RBC), and it is expected that they will be solved by the encapsulation of Hb.

In previous papers, we have succeeded in preparing HbV with excellent physicochemical properties in terms of Hb encapsulation, Hb concentration, diameter control, oxygen affinity, *etc.* (Sakai *et al.*, 1996; Takeoka *et al.*, 1996). Moreover, in a 40% exchange transfusion with

* Author to whom correspondence should be addressed (fax +813-3209-5522; telephone +813-3209-8895).

[†]Waseda University.

[‡]Keio University.

[⊗] Abstract published in *Advance ACS Abstracts*, December 15, 1996.

¹ Abbreviations: Hb, hemoglobin; HbV, hemoglobin vesicles; RBC, red blood cell; PEG, poly(ethylene glycol); DDS, drug delivery system; HbV-PEG, poly(ethylene glycol)-modified hemoglobin vesicles; DPPC, 1,2-dipalmitoyl-*sn*-glycero-3-phosphatidylcholine; DPPG, 1,2-dipalmitoyl-*sn*-glycero-3-phosphatidylglycerol; PEG-DPPE, 1,2-dipalmitoyl-*sn*-glycero-3-phosphatidylethanolamine-*N*-[poly(ethylene glycol)]; HbV-PEG/albumin, HbV-PEG suspended in albumin; HbV/albumin, HbV suspended in albumin; PBS, phosphate-buffered saline; P_{50} , oxygen affinity; PLP, pyridoxal 5'-phosphate; MAP, mean arterial pressure; HR, heart rate; TPRI, total peripheral resistance index; PaO_2 , arterial blood oxygen tension; PaCO_2 , arterial blood carbon dioxide tension; PvO_2 , mixed venous blood oxygen tension; rPtO_2 , renal cortical tissue oxygen tension; sPtO_2 , skeletal muscle tissue oxygen tension; τ , shear stress; γ , shear rate.

the HbV suspended in saline, a high oxygen transporting capability of the HbV similar to that of the washed rat RBC was confirmed (Izumi *et al.*, 1996). Ninety percent exchange transfusion with the HbV was also successful in the presence of albumin as a plasma expander using rats (Izumi *et al.*, 1997).

Because the red cell substitutes are literally to be used as substitutes for a large amount of lost red blood cells, the rheological properties of HbV itself and the mixture with blood are important in relation to hemodynamics. Surface modification of phospholipid vesicles with some natural or synthetic glycolipids (Wu *et al.*, 1981; Allen *et al.*, 1987; Gabizon and Papahadjopoulos, 1988; Takeoka *et al.*, 1992) or poly(ethylene glycol) (PEG)-conjugated lipids (Kilbanov *et al.*, 1990; Woodle and Lasic, 1992; Woodle *et al.*, 1994; Harasym *et al.*, 1995; Zalipsky *et al.*, 1995) is known to improve the dispersion state of the vesicles and prolong the circulation time *in vivo* for drug delivery systems (DDS). For HbV, the surface was also modified to improve the dispersion state of the vesicles in the presence of water-soluble polymers or blood components (Yoshioka, 1991; Tsuchida and Takeoka, 1995). The PEG-modified HbV has been studied, and its oxygen transporting ability has been evaluated (Usuba *et al.*, 1993; Zheng *et al.*, 1993). PEG has thus been widely used for vesicular materials including DDS and HbV. However, little attention has been paid to the effect of the PEG modification on the low solution viscosity in the field of DDS because of the significantly low lipid concentration and small dosage. Also, these effects of PEG-modified HbV have not been clearly demonstrated in comparison with the unmodified HbV.

Using our HbV with high Hb encapsulation efficiency and high Hb concentration (Sakai *et al.*, 1996), we aimed to modify the surface with PEG chains by a simple method. The PEG-conjugated lipids with various molecular weights of PEG are currently commercially available, among which 2000 and 5000 seem to be most commonly used (Vertut-Do *et al.*, 1996). The effects of PEG, *e.g.*, longevity of circulation time and prevention of aggregation, increase with increasing chain length at the same molar composition. Our method enables PEG incorporation only on the outer surface of the vesicles; therefore, we thought that a smaller molar composition would be better not to disturb the lipid bilayer by the transbilayer asymmetry, and we selected a larger molecular weight of 5000. We tried to evaluate the HbV-PEG in comparison with the unmodified HbV, in terms of the dispersion state, rheological properties in a mixture with blood and the resulting oxygen transporting capabilities *in vivo* by observing the physiological responses to 90% exchange transfusion in anesthetized rats.

EXPERIMENTAL PROCEDURES

Preparation of HbV and Surface Modification with PEG-Phosphatidylethanolamine. HbV was prepared in the same manner as previously reported in the literature (Sakai *et al.*, 1993, 1995). The encapsulated carbonylhemoglobin (*ca.* 38 g/dL) contained pyridoxal 5'-phosphate (18 mM, Merck Co.) as an allosteric effector and DL-homocysteine (5 mM, Aldrich Chemical Co.) as a metHb reductant. The lipid bilayer was composed of Presome PPG-1 [a mixture of 1,2-dipalmitoyl-*sn*-glycero-3-phosphatidylcholine, (DPPC), cholesterol, and 1,2-dipalmitoyl-*sn*-glycero-3-phosphatidylglycerol (DPPG), Nippon Fine Chemicals Co.] and α -tocopherol (Merck Co.) at a molar composition of 5/5/1/0.1. After sizing by an extrusion method and removal of unencapsulated Hb using ultracentrifugation (50000g, 40 min), the surface modification of HbV with PEG was performed

by simply mixing the HbV suspension (lipid: 2.2 g/dL, 833 mL) with a saline solution of 1,2-dipalmitoyl-*sn*-glycero-3-phosphatidylethanolamine-*N*[poly(ethylene glycol)] (PEG-DPPE, Avanti Co., 0.1 g/dL, 231 mL) at 37 °C under a CO atmosphere and stirring for 30 min. The resulting HbV-PEG was diluted with saline to an Hb concentration of 0.5 g/dL, and carbonylhemoglobin was converted to oxyhemoglobin by illumination with visible light under an O₂ atmosphere (Chung *et al.*, 1995). After the ultracentrifugation and redispersion of the HbV-PEG in 5 g/dL of albumin solution (albumin 5% cutter, Bayer Co.) were repeated, the suspension was filtered through sterilizable filters (Dismic, Toyo Roshi Co.; pore size = 0.45 μ m). The free PEG-DPPE, which was not incorporated into the HbV, was removed during the process of ultracentrifugation (50000g, 40 min) and redispersion. Finally, the Hb concentration was regulated to 10 g/dL using the albumin solution to obtain HbV-PEG/albumin. The unmodified HbV suspended in the albumin solution (HbV/albumin) was prepared in the same manner.

Quantitative Analyses of PEG-DPPE. The freeze-dried powder of HbV-PEG was dispersed in CDCl₃, and the filtrate (filter paper, Toyo Roshi, 5B) was analyzed using ¹H-NMR spectroscopy (JEOL, EX-270). The PEG content was estimated from the intensity ratio of the PEG methylene proton peak (δ 3.63) to that of the choline methyl protons in DPPC (δ 3.39) (Yoshioka, 1991; Hamada *et al.*, 1995).

Viscosity and Optical Microscopy of HbV-PEG/Albumin Mixed with Human Blood. Human venous blood was drawn into EDTA (1 mg/mL blood)-containing tubes. The hematocrit of the blood was 55%. The HbV-PEG or HbV in albumin was mixed with the human blood at volume compositions of 0, 15, 30, 60, 90, and 100%. The rheological properties and density at 37 °C were measured with a capillary viscosimeter [Oscillatory Capillary Rheometer and Density Meter (OCR-D, Anton Parr)], where the sample in the measuring capillary (0.9948 mm in diameter, 100.2 mm in length) was set into sinusoidal oscillations at a given frequency of 2 Hz to mimic the pulsatile flow *in vivo* (Schneiditz *et al.*, 1985). The shear rate ranged from 0.58 to 358 s⁻¹. The whole measurement was performed within 6 h after blood collection. The dispersion states of the vesicles and RBC were observed with optical microscopy (Olympus BH-2) at a magnification of 750.

Permeability through Isopore Membranes. To mimic the blood flow in narrow capillaries, the permeabilities of human blood and the HbV-PEG/albumin and the HbV/albumin through filters were observed. Each isopore membrane filter (Nuclepore, Coaster Co.; pore size = 0.4, 0.6, 1.0, 2.0, 3.0, 5.0, 8.0 μ m; diameter = 25 mm) was attached to a high-pressure resistant chamber (Extruder, Lipex Biomembrane, Inc., Canada). The filtration area was regulated to 1 cm². After the suspension was prefiltered through disposable filters (Dismic, Toyo Roshi Co.; pore size = 0.45 μ m), 5 mL of the suspension was injected and 5 min later the initial filtration rate of the outlet volume was measured at a pressure of 0.3, 0.4, or 4 kg/cm² at 37 °C.

Protein Adsorption onto the Vesicular Surface. The unmodified and PEG-modified vesicles, which did not encapsulate Hb, were prepared with the same lipid composition in the same manner except that phosphate-buffered saline (PBS, pH 7.4, 37 °C) was used in place of a concentrated Hb solution for lipid hydration. After regulation of the lipid concentration to 3.4 g/dL, the vesicles were suspended in a 5% albumin solution and incubated for 3 and 12 h at 37 °C. The vesicles were separated by gel permeation chromatography (Sephacrose

CL-4B, Pharmacia; column size: height = 12 cm, diameter = 3 cm) with PBS as an eluent. It took about 5 min to obtain the fractions of HbV and HbV-PEG. The concentrations of total lipids in the fractions were calculated from the cholesterol concentration measured with a cholesterol oxidase-*p*-chlorophenol method (Cholesterol test II Wako, Wako Pure Chemicals Co.). The amount of adsorbed albumin was measured by *o*-phthalaldehyde (OPA) fluorescence assay (Peterson, 1983), in which the fluorescence ($\lambda_{\text{ex}} = 340$ nm, $\lambda_{\text{em}} = 440$ –455 nm) induced by the reaction of thiol groups on albumin with OPA was measured with a fluorometer (Jasco FP-550).

Ninety Percent Exchange Transfusion Protocol. The procedure was almost the same as that previously reported (Izumi *et al.*, 1996). Twelve Wistar rats (weight 348 ± 11 g, mean \pm SD) were anesthetized with an intraperitoneal injection of sodium pentobarbital (50 mg/kg). Two catheters (PE-20 tubing, o.d. = 0.8 mm, i.d. = 0.5 mm), one of which was introduced into the right jugular vein for sample infusion and the other into the right common carotid artery, were used for blood withdrawal. The catheter in the common carotid artery was then connected to a pressure transducer (Polygraph System, Nihon Koden, Tokyo) for continuous monitoring of the mean arterial pressure (MAP) and the heart rate (HR). Next, a median abdominal incision was made and a miniaturized 20-MHz pulsed doppler probe (HDP 20 20R, 2 mm in diameter, Crystal Biotech, Holliston, MA) was implanted on the abdominal aorta to measure the blood flow. The probe was connected to a pulsed doppler flow module (Model PD-20, Crystal Biotech) (Gardiner *et al.*, 1990; Haywood *et al.*, 1981). Needle-type polarographic oxygen electrodes (Intermedical Co.) were placed in the cortex of the kidney and the cervical muscle for continuous renal cortical and skeletal muscle tissue oxygen tension measurements (Nelmarkka *et al.*, 1982). Approximately 10 min was allowed for the parameters to stabilize. From the MAP, blood flow (Q), and body weight, the total peripheral resistance index (TPRI), which indicates the resistance to blood flow, was calculated using the following equation:

$$\text{TPRI} = (\text{MAP}/Q)/(\text{body weight}) \quad (1)$$

Ninety percent of the estimated total blood volume of the rat (50 mL/kg) was exchanged with the HbV-PEG/albumin (HbV-PEG group, $n = 6$) or the HbV/albumin (HbV group, $n = 6$) at 2 mL of withdrawal (via the common carotid artery)/infusion (via the jugular vein) cycles at a rate of 1 mL/min. Blood samples for hematocrit measurements and arterial and venous blood gas analyses (Corning 170 pH/blood gas analyzer, Corning Medical, Medfield, MA) were taken with a heparinized 2 mL syringe on the first withdrawal as basal values at exchange rates of around 10, 40, 60, 70, 80, and 90%, and 30 min after the completion of the exchange transfusion. All animal studies were approved by the Animal Care and Use Committee of Keio University. The care and handling of the rats were in accordance with the National Institutes of Health guidelines.

Data Analysis. Data are expressed as the mean \pm SD for the indicated number of animals. Data were evaluated using analysis of variance (ANOVA) followed by Fisher's protected least significant difference (PLSD) test. The level of confidence was placed at 95% for all experiments.

RESULTS AND DISCUSSION

1. Characteristics of HbV-PEG/Albumin as a Red Cell Substitute.

The characteristics of the HbV-PEG/

Table 1. Characteristics of HbV-PEG/Albumin in Comparison with Human Blood (RBC)

parameter	HbV-PEG/albumin	human blood
diameter (μm)	0.25 ± 0.08	ca. 8
P_{50} (Torr)	34	28
[Hb] (g/dL)	10	12–17
[lipid] (g/dL)	5.71	1.8–2.5 ^a
[Hb]/[lipid] (g/g)	1.75	ca. 31 ^b
O ₂ release (mL/dL)	6.1	5.5–7.7
metHb (%)	<3	<0.5
HbCO (%)	<2	<5
viscosity (cP at 230 s ⁻¹)	3.7	4–5
osmolarity (mOsm)	300	ca. 300
oncotic pressure (Torr)	20	ca. 25
pH	7.4	7.2–7.4
density (g/cm ³)	1.0336	1.05
hematocrit (%)	36 ^c	40–54

^a Total cell membrane components. ^b Weight ratio of Hb to total cell membrane components. ^c Volume percentage of HbV particles.

albumin are summarized in Table 1. The diameter was controlled to 0.25 ± 0.08 μm . By increasing the weight ratio of Hb to lipid to 1.74, the lipid concentration was reduced to 5.74 g/dL. This is the highest encapsulation efficiency ever reported, due to the control of intermolecular interactions during the assembling and sizing procedure of HbV (Takeoka *et al.*, 1996). The surface modifier, PEG-DPPE, was easily introduced onto the surface of HbV by the addition of the PEG-DPPE solution. Diameter changes were observed within experimental error. After the free PEG-DPPE was removed by repeating the centrifugation and redispersion, the content of PEG-DPPE was measured by ¹H NMR and the composition of the lipids was clarified to be DPPC/cholesterol/DPPG/ α -tocopherol/PEG-DPPE = 5/5/1/0.1/0.014 by molar ratio (PEG-DPPE = 0.13 mol %). More than 90% of the added PEG-DPPE was incorporated onto the outer surface of the HbV. The oxygen affinity, P_{50} (oxygen partial pressure required for the half-saturation of Hb with oxygen), was regulated to 32 Torr by coencapsulating PLP (18.6 mM). The amount of oxygen release was calculated to be 6.2 mL/100 mL, which was close to the 7.0 mL/100 mL of human blood due to the increased oxygen transporting efficiency (the difference in O₂ saturation between 40 and 110 Torr PO₂) of the HbV-PEG, 37%, compared to that of human red cells, 28%. No leakage of Hb was observed during and after the introduction of PEG-DPPE. The oxygen affinity of HbV-PEG was almost the same within experimental error, indicating that pH change in the inner aqueous phase and leakage of coencapsulated small molecules such as PLP, Na⁺, and Cl⁻, were negligibly small. The densities of the HbV-PEG/albumin and unmodified HbV/albumin suspensions were almost the same (1.0336 and 1.0335 g/cm³, respectively), and they were smaller than that of human blood (1.0525 g/cm³), mainly due to the fact that the concentration of albumin solution used is 5 g/dL, which is lower than the plasma protein concentration, ca. 7.5 g/dL. The concentration of albumin of the suspension is expressed as 3.2 g/dL due to 36% of the total volume being HbV particles.

2. Effect of PEG Conjugation on the Aggregation of HbV in Albumin Solution and Blood Mixture.

2.1. Optical Microscopic Observation of Dispersion States of HbV-PEG/Albumin. The dispersion states of the HbV-PEG/albumin and HbV/albumin when mixed with human blood were observed by optical microscopy (Figure 1). In the case of HbV-PEG/albumin, only RBCs were confirmed because of the small diameter of HbV-PEG (0.25 ± 0.08 μm), and no aggregate of HbV-PEG was confirmed in the photograph. In the case of HbV/albumin, on the other

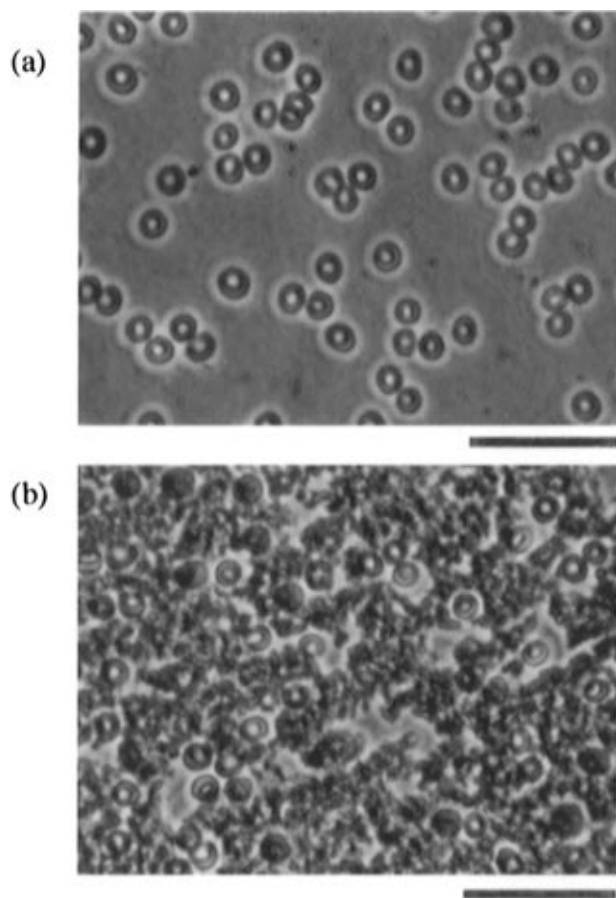


Figure 1. Optical microscopic observation of (a) HbV-PEG/albumin (30%) + blood (70%) and (b) HbV/albumin (30%) + blood (70%). The bars indicate 40 μm . Only the RBCs can be seen in (a), while the aggregates of HbV are seen between RBCs in (b).

hand, flocculated aggregates of the HbV were actually confirmed among the RBCs. The RBCs were neither aggregated nor deformed, indicating that both HbV and HbV-PEG did not interact with RBCs. The aggregates of HbV were actually observed before mixing with blood. It is quite obvious that PEG chains suppress the HbV aggregation.

2.2. Viscosities of HbV-PEG/Albumin and Mixtures with Blood. When the unmodified HbV was dispersed in PBS, the viscosity of the vesicular suspension became 2.6 cP (shear rate = 230 s^{-1}), which is lower than that of blood (Sakai *et al.*, 1996). However, when dispersed in a 5 g/dL albumin solution to adjust the colloidal osmotic pressure, the HbV/albumin showed 8 cP viscosity (shear rate = 358 s^{-1}), which was substantially higher than that of blood (3.7 cP). In Figure 2, the HbV/albumin shows a non-Newtonian flow typical for particle suspensions and higher viscosities, especially at lower shear rates. In the case of the HbV-PEG/albumin, on the other hand, the viscosity was significantly reduced in comparison with that of the unmodified HbV/albumin and was almost the same as that of human blood at any shear rates (*e.g.*, 3.5 cP at 358 s^{-1}). These results indicate that the unmodified HbV aggregates due to the molecular interaction of albumin with the vesicular surface and increases the viscosity, while the surface modification of the HbV with PEG chains suppresses HbV aggregation and provides a low viscosity almost the same as that of human blood.

The effect of compositions of PEG-DPPE on viscosity was previously studied at 0.063, 0.13, and 0.25 mol %, for which the viscosities at 10.2 s^{-1} were 5.8, 5.2, and 7.2 cP, respectively. All of the compositions showed a

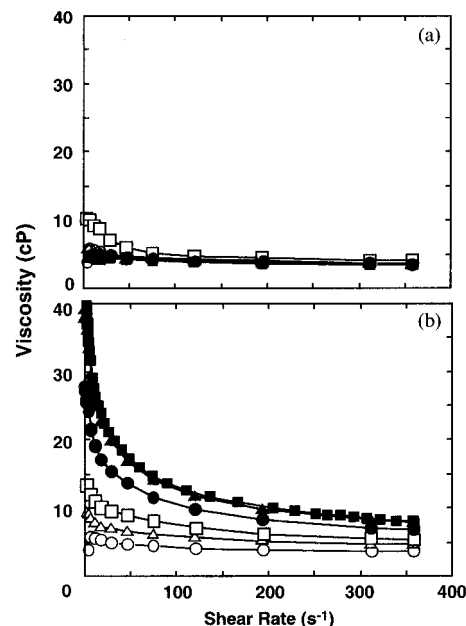


Figure 2. Shear rate dependence of the viscosity of (a) HbV-PEG/albumin and (b) HbV/albumin in the mixture with human blood measured with a capillary rheometer at 37 $^{\circ}\text{C}$. Blood volume (%): 0 (■), 10 (▲), 40 (●), 70 (□), 85 (△), 100 (○).

significant decrease in viscosity (*cf.* 22.5 cP without PEG-DPPE); however, the viscosity began to increase at 0.31 mol %. We therefore selected the composition at around 0.13 mol %.

When human blood was mixed with the HbV/albumin, the viscosity proportionally increased with increasing volume ratio of HbV/albumin. This indicates that the unmodified HbV already aggregates in the albumin solution, and there is no detectable additional interaction between the HbV/albumin and blood components from the rheological point of view. In the case of HbV-PEG/albumin, the viscosity was not changed at any shear rate and any mixing ratio, except at 30% HbV-PEG/albumin, at which there was a slight increase in viscosity; however, it is negligible in comparison with the high viscosity of the unmodified HbV/albumin.

Figure 3 shows the Casson plots for the mixtures of HbV/albumin or HbV-PEG/albumin with human blood, $\sqrt{\gamma}$ versus $\sqrt{\tau}$ (γ , shear rate; τ , shear stress). In the case of the HbV-PEG/albumin, all of the mixtures with blood coincided well with that of blood. A linear relationship indicates that the rheological property of the HbV-PEG agrees well with the Casson equation for a non-Newtonian fluid ($\sqrt{\tau} = k_0 + k_1\sqrt{\gamma}$) (Oka, 1984), with constants, $k_0 = 0.19 \pm 0.07$ (mean \pm SD) (dyn/cm^2) $^{1/2}$ and $k_1 = 0.18 \pm 0.002\text{ s}^{1/2}$. The stress yield (k_0^2), which indicates the change point from a solid to a fluid phase, seems to be similar to that of human blood. This linear relationship at all compositions indicates the absence of additional interaction with blood components. On the contrary, HbV/albumin showed a drastic increase in $\sqrt{\tau}$ at lower $\sqrt{\gamma}$ with increasing $\sqrt{\gamma}$ and then a linear relationship. The curves seem to fit the generalized Casson equation reported by Oka (1971). This equation is valid with the assumptions that the stress acts to break bonds between particles and that the shear rate acts independently in tending to prevent their reforming. Therefore, it can be easily surmised that the aggregates dissociate at the higher shear rates and that the sizes of HbV aggregates are different at each shear rate. The small stress yield for unmodified HbV/albumin may indicate that the aggregation is induced by the weak interaction between the albumin and vesicles.

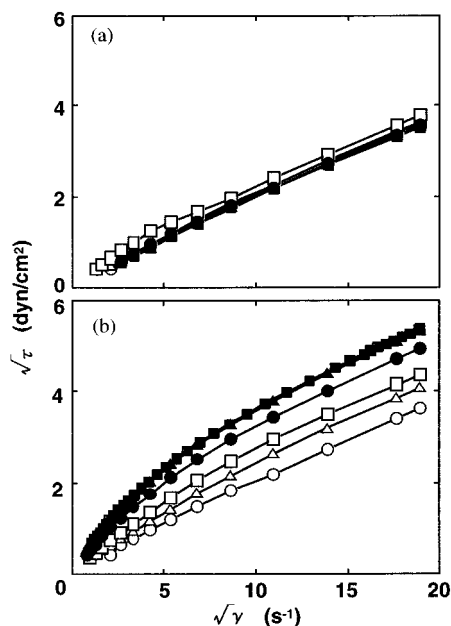


Figure 3. Casson plots for the (a) HbV-PEG/albumin and (b) HbV/albumin of the mixture with human blood. Casson equation: $\sqrt{\tau} = k_0 + k_1\sqrt{\gamma}$ (τ , shear stress; γ , shear rate; k_0 , k_1 , constants. Blood volume (%): 0 (■), 10 (▲), 40 (●), 70 (□), 85 (△), 100 (○).

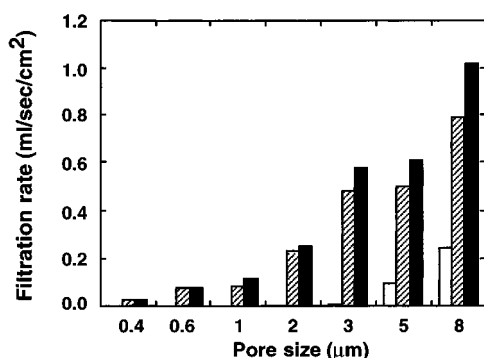


Figure 4. Comparison of the rates of penetration of the HbV/albumin (slashed bar), HbV-PEG/albumin (black bar), and human blood (white bar) through the Nuclepore isopore membrane filters at the applied pressure of 0.3 kg/cm² at 37 °C. For the membrane of 0.4 μ m pore size, the applied pressure was 0.5 kg/cm².

2.3. Permeability of HbV-PEG/Albumin through Isopores. In Figure 4, the permeabilities of the HbV-PEG/albumin, HbV/albumin, and human blood through isopore membranes are shown as a model of the blood flow through capillaries. This method is conventionally used for the RBC deformability measurement (Kukuchi and Koyama, 1984). The capillary and precapillary diameter is usually 3–15 μ m, and some narrow during circulatory failure such as hemorrhagic shock. A biconcave-shaped RBC with a diameter of 8 μ m deforms to a parachute-like configuration and permeates through the narrow capillaries. However, with decreasing pore size of the membranes from 5 to 2 μ m, the flow rate decreased for all suspensions, especially for human blood even though the applied pressure (0.3 kg/cm² \approx 220 Torr) is about twice that of normal blood pressure. When the pore diameter is 3 μ m, blood could hardly permeate, whereas both the unmodified HbV/albumin and HbV-PEG/albumin showed high permeability. The permeation through capillaries is very much influenced not only by viscosity but also by the capillary diameter. It was reported that the narrower the capillary is, the lower the viscosity of the blood is when the diameter of the artificial capillaries

decreased from 500 to 50 μ m with increased shear rate (Fahraeus and Lindqvist, 1931). However, when the diameter of the capillaries decreases to <4 μ m, the viscosity increases and finally there should be a limitation for the RBC penetration (Pries *et al.*, 1992). Due to the small size of HbV ($0.25 \pm 0.08 \mu$ m), both the HbV-PEG/albumin and HbV/albumin suspensions promptly permeate through the membrane filters with pores of sizes down to 0.4 μ m without changes in vesicular size or Hb leakage. Especially the HbV-PEG/albumin permeates more rapidly than the unmodified HbV/albumin because HbV-PEG did not aggregate. Even though the HbV/albumin showed aggregation in the optical microscopy, the aggregates dissociated at higher shear rates and permeated more promptly than expected. The difference in the permeation rate between the two suspensions becomes smaller, which should be related to the smaller difference in viscosity at higher shear rates in Figure 2. Both the HbV and HbV-PEG can penetrate through sterilizable filters of 0.45 μ m in pore size for preparation. No Hb leakage was confirmed, supporting the belief that the aggregation is reversible and that there is no deformation of the bilayer membrane. After the permeation, the suspension was ultracentrifuged, and the amount of PEG-DPPE in the supernatant was analyzed. However, no PEG-DPPE was detected. Therefore, PEG-DPPE was not removed during permeation through the pores of the membranes used in this experiment.

In spite of the fact that the viscometric properties of the HbV-PEG/albumin and blood are almost the same by viscometric analysis (Figures 2 and 3), the flow patterns in the capillaries *in vivo* would be influenced not only by the viscosity but also by the relationship between the diameters of the particles and capillaries.

3. Quantitative Analysis of Adsorbed Albumin onto the Vesicular Surface. The amounts of adsorbed albumin onto the vesicles after 3 and 12 h of incubation at 37 °C were quantitatively analyzed under the assumption that adsorbed albumin on the surface would induce vesicular aggregation. After 3 h, the amounts of albumin were 7 and 10 μ g/mg lipid for the unmodified and PEG-modified model vesicles, respectively. After 12 h, the amounts became 9 and 11 μ g/mg, respectively. At 11 μ g/mg, the surface of one vesicle (*ca.* 2.0×10^5 nm²) was calculated to be covered with *ca.* 100 albumin molecules (size: 3.8×15 nm); *ca.* 3% of the surface was covered with albumin. Some of the adsorbed albumin would be removed from the surface during gel permeation chromatography as Chonn *et al.* (1991) reported. However, the time required to obtain the HbV or HbV-PEG fraction was only 5 min and the desorption must be minimal. Contrary to the assumption, there was no significant difference between the modified and unmodified vesicles. PEG chains should prevent intervesicular access and aggregation rather than albumin adsorption. The repulsive interaction between PEG-modified surfaces has been clarified by the distance between the membranes using X-ray diffraction (Needham *et al.*, 1992) and the steric hindrance calculated using computer analysis (Torchilin *et al.*, 1994; Hristova and Needham, 1995). Because PEG chains do not completely cover the surface of the vesicles at the molar composition employed, albumin would penetrate through the PEG chain layers to the vesicular surface to be adsorbed. Even so, the repulsion between the PEG-modified vesicles, which are much larger than albumin, would be effective and the adsorbed albumin on the surface could not induce vesicular aggregation. This hypothesis is also supported by the results of Harasym *et al.* (1995), who found that the coupling of proteins onto PEG-modified phospholipid vesicles was not

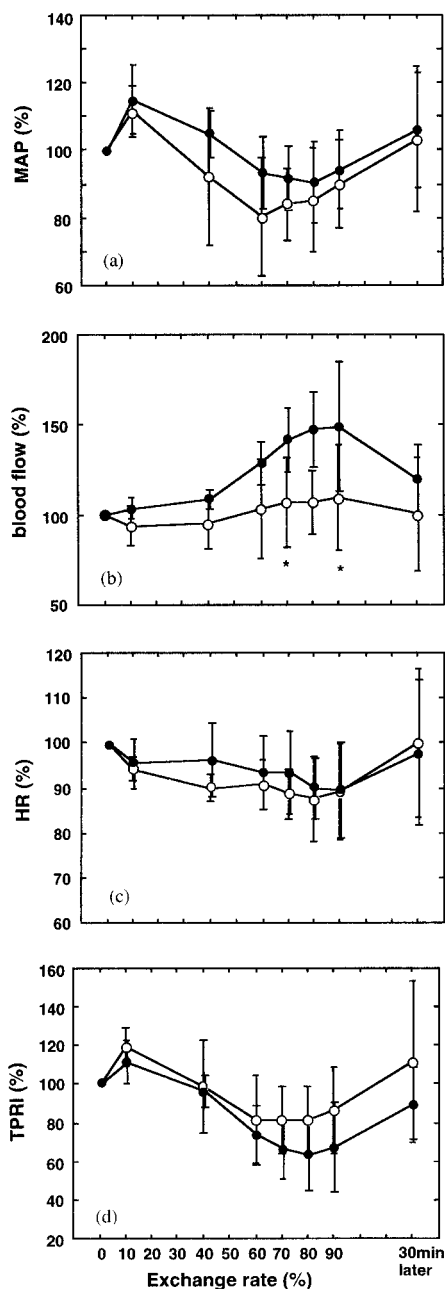


Figure 5. Changes in hemodynamic parameters during the 90% exchange transfusion with HbV/albumin (○, $n = 6$) and HbV-PEG/albumin (●, $n = 6$) and 30 min post-transfusion, shown as percentages of the basal values: (a) MAP, mean arterial pressure; (b) blood flow in abdominal aorta, significant differences at 70% ($p < 0.05$) and 90% ($p < 0.05$); (c) HR, heart rate; (d) TPRI, total peripheral resistance index.

retarded but that the aggregation during the coupling was suppressed by PEG chains.

4. Ninety Percent Exchange Transfusion. During the exchange transfusion, the hematocrit of both the HbV and HbV-PEG groups decreased from about 50 to 5%, indicating that almost 90% exchange transfusion was theoretically and actually performed. In the glass capillaries for hematocrit measurements, the HbV precipitated on the RBC layer, while the HbV-PEG did not, and it was still dispersed in the supernatant after centrifugation (12000g), indicating that the HbV-PEG is well dispersed even in the presence of blood components.

Figure 5 summarizes the changes in hemodynamic parameters, which are shown as percentages of the basal values. The HR remained normal in both groups. The MAP showed a slight transient increase for both groups

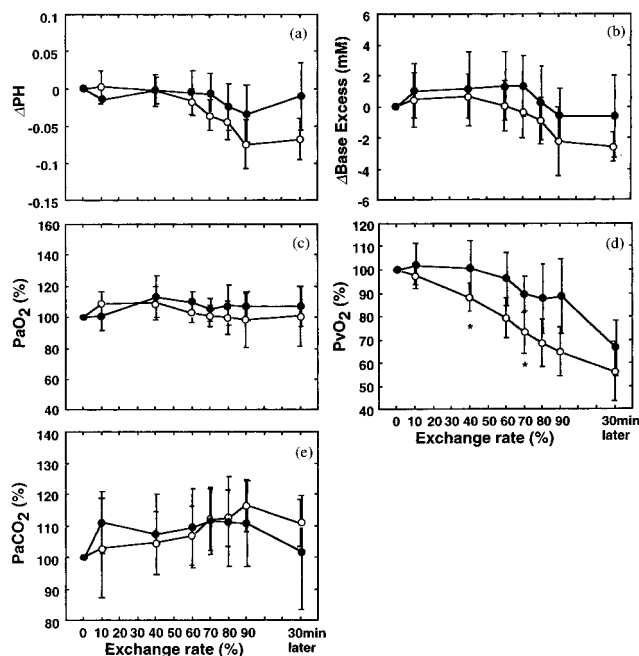


Figure 6. Changes in pH and blood gas parameters during the 90% exchange transfusion with HbV/albumin (○, $n = 6$) and HbV-PEG/albumin (●, $n = 6$) and 30 min post-transfusion: (a) pH, significant differences at 30 min post transfusion ($p < 0.05$); (b) base excess; (c) PaO₂, arterial blood partial oxygen tension; (d) PvO₂, mixed venous blood oxygen tension, significant differences at 40% ($p < 0.05$) and 70% ($p < 0.05$); (e) PaCO₂, arterial blood partial carbon dioxide tension. pH is shown as a difference from the basal value. Blood gas parameters are shown as percentages of the basal values.

and then decreased to 80–90% of the initial values. The transient increase at the first stage is maybe due to some form of immunological reaction accompanying the phospholipid vesicle injection as discussed later. The HbV-PEG group showed a significantly (*ca.* 50%) higher blood flow rate in the abdominal aorta with *ca.* 20% lower TPRI than the HbV group. This would be the result of the lower viscosity of the HbV-PEG/albumin, which promotes blood flow in the capillaries. The previous report of the 90% exchange transfusion with washed ratRBC/albumin (Hb = 10 g/dL) showed about a 30% increase in blood flow (Izumi *et al.*, 1997), less than that of HbV-PEG group, even though the HbV-PEG showed almost the same viscometric characteristics as mentioned above. This indicates that the rheological properties in narrow capillaries are not the same as those measured with the viscosimeter and that HbV-PEG would show prompt flow in the capillaries *in vivo* in just the same way as in the filter permeability measurements in Figure 4, because HbV-PEG is not aggregated and is smaller than RBC.

Parts a–d of Figure 6 show the differences in pH and the changes in blood gas parameters from the basal values. The pH began to decrease at an exchange ratio of around 60% for the HbV group. In spite of the fact that these levels of decreases are still small in comparison with the administration of albumin alone, as reported in the previous paper (Izumi *et al.*, 1997), the HbV-PEG group remained at a significantly higher level than the HbV group. The base excess values showed the same profiles. As for the arterial partial pressure of oxygen (PaO₂) and carbon dioxide (PaCO₂), both groups showed slight increases but remained in the normal range. The mixed venous partial oxygen pressure (PvO₂) of the HbV-PEG group was significantly higher than that of the HbV group. PvO₂ is a parameter for O₂ supply (Kobayashi *et al.*, 1995). Low PvO₂ indicates low oxygen saturation of

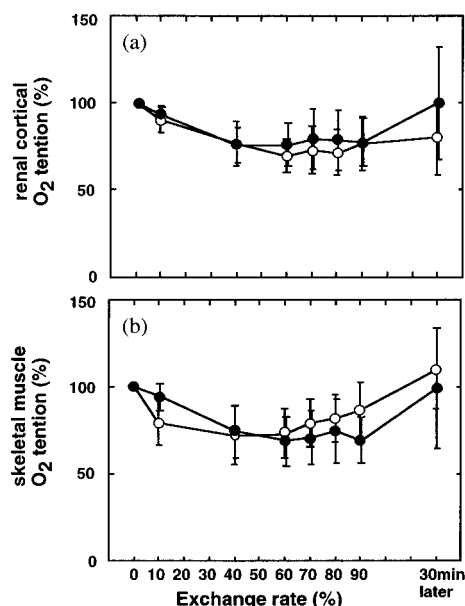


Figure 7. Changes in renal cortical (a) and skeletal muscle (b) tissue oxygen tensions measured by needle-type poplographic oxygen electrodes during the 90% exchange transfusion with HbV/albumin (○, $n = 6$) and HbV-PEG/albumin (●, $n = 6$) and 30 min post-transfusion. Both are shown as percentages of the basal values.

Hb, and a fall in PvO_2 implies decreased O_2 transport (Kandel and Aberman, 1983). The graph indicates that the HbV group is slightly hypoxic and the HbV-PEG shows better O_2 supply.

In spite of the fact that the PvO_2 was improved by the surface modification with PEG, the oxygen tensions at the renal cortex ($rPtO_2$) and skeletal muscle ($sPtO_2$) for both groups decreased to *ca.* 70% of the initial values at 90% exchange and were significantly low (Figure 7) in comparison with the RBC group ($rPtO_2 = 99\%$; $sPtO_2 = 99\%$ at 90% exchange; Izumi *et al.*, 1997), though they are significantly high in comparison with those who received only albumin ($rPtO_2 = 22\%$; $sPtO_2 = 35\%$ at 90% exchange; Izumi *et al.*, 1997). We presume that both the HbV and HbV-PEG somewhat influence the vasomotion, *e.g.*, indirect induction of vasoconstriction, which results in the decreased density of the capillaries and oxygen diffusion from capillaries to tissues. There is no difference in the high affinity of Hb for the endothelial-derived relaxation factor (nitric oxide) between HbV-PEG and HbV. One reason seems to be related to the shear stress in the capillaries. Some endothelial relaxation factor is reported to be generated in response to the shear stress in the capillaries (Malek and Izumo, 1995). The prompt flow of small HbV results in a shear stress decrease and vasoconstriction. The high fluidity in the vessels would adversely influence the vasomotion, and it would not always be convenient for blood flow (Tsai *et al.*, 1996). The other reason seems to be related to the immunological reaction accompanied by transient hypertension (Figure 5a) and thrombocytopenia, in which complements such as C3a would be generated and they would activate platelets and increase the thromboxane A_2 , which induces the vasoconstriction (Miyamoto *et al.*, 1988; Watanabe *et al.*, 1988; Loughley *et al.*, 1990; Rudolph, 1995). Anyway, both of the two groups recovered from the transient reaction and low tissue oxygen tensions at 30 min post exchange transfusion. All of the rats that received HbV/albumin or HbV-PEG/albumin survived for about 20 h, in spite of the fact that those which received only albumin died within 20 min post exchange transfusion.

In conclusion, the effects of the PEG modification of the HbV were observed as the suppression of inter-vesicular aggregation and prompt flow in vessels. This affects the hemodynamics, the increased blood flow, and the resulting stable blood gas parameters, indicating that HbV-PEG has the potential for efficient oxygen supply.

ACKNOWLEDGMENT

This work has been supported in part by Grants-in-Aid from the Ministry of Education, Science, and Culture, Japan (065159, 06771037, 07508005), the Ogasawara Foundation for the Promotion of Science and Engineering, and the Iwaki research fund. We are greatly indebted to Mr. Kenichi Hamada for skillful experimental works.

LITERATURE CITED

- Allen, T. M., and Cohn A. (1987) Large Unilamellar Liposomes with Low Uptake into the Reticuloendothelial System. *FEBS Lett.* 223, 42–46.
- Chang, T. M. S. (1991) Blood Substitutes Based on Modified Hemoglobin Prepared by Encapsulation or Crosslinking: An Overview. *Biomater. Artif. Cell Immobilization Biotechnol.* 20, 159–182.
- Chonn, A., Semple, S. C., and Cullis, P. R. (1991) Separation of Large Unilamellar Liposomes from Blood Components by a Spin Column Procedure: towards Identifying Plasma Proteins which Mediate Liposome Clearance in Vivo. *Biochim. Biophys. Acta* 1070, 215–222.
- Chung, J. E., Hamada, K., Sakai, H., Takeoka, S., and Tsuchida, E. (1995) Ligand Exchange Reaction of Carboxylhemoglobin to Oxyhemoglobin in a Hemoglobin Liquid Membrane. *Nihon Kagaku Kaishi* 2, 123–127.
- Djordjevic, L., and Miller, I. F. (1980) Synthetic Erythrocytes from Lipid Encapsulated Hemoglobin. *Exp. Hematol.* 8, 584–592.
- Fåhræus, R., and Lindqvist, T. (1931) The Viscosity of Blood in Narrow Capillary Tubes. *Am. J. Physiol.* 96, 562–568.
- Gabizon, A., and Papahadjopoulos, D. (1988) Liposome Formulations with Prolonged Circulation Time in Blood and Enhanced Uptake by Tumors. *Proc. Natl. Acad. Sci. U.S.A.* 85, 6949–6953.
- Gardiner, S. M., Compton, A. M., Bennett, T., and Hartley, C. J. (1990) Can Pulsed Doppler Technique Measure Changes in Aortic Blood Flow in Conscious Rats? *Am. J. Physiol.* 259, H448–H456.
- Hamada, K., Kose, T., Ohgushi, T., Sakai, H., Takeoka, S., Nishide, H., and Tsuchida, E. (1995) Assay Systems for the Components of Red Cell Substitutes (NRC). *Artif. Blood* 3, 96–101.
- Harasym, T. O., Tardi, P., Longman, S. A., Ansell, S. M., Bally, M. B., Cullis, P. R., and Choi, L. S. (1995) Poly(ethylene glycol)-modified Phospholipid Prevent Aggregation during Covalent Conjugation of Proteins to Liposomes. *Bioconjugate Chem.* 6, 1043–1802.
- Haywood, J. R., Shaffer, R. A., Fastenow, C., Fink, G. D., and Brody, M. J. (1981) Regional Blood Flow Measurement with Pulsed Doppler Flowmeter in Conscious Rat. *Am. J. Physiol.* 24, H273–H278.
- Hristova, K., and Needham, D. (1995) Phase Behavior of a Lipid/Polymer-Mixture in Aqueous Medium. *Macromolecules* 28, 991–1002.
- Hunt, C. A., Burnette, R. R., MacGregor, R. D., Strubbe, A. E., Lau, D. T., Taylor N., and Kawada, H. (1985) Synthesis and Evaluation of a Prototypal Artificial Red Cell. *Science* 30, 1165–1168.
- Izumi, Y., Sakai, H., Hamada, K., Takeoka, S., Yamahata, K., Katoh, H., Nishide, H., Tsuchida, E., and Kobayashi, K. (1996) Physiological Responses to Exchange Transfusion with Hemoglobin Vesicles as an Artificial Oxygen Carrier in Anesthetized Rats: Changes in Mean Arterial Pressure and Renal Cortical Tissue Oxygen Tension. *Crit. Care Med.* 24, 1869–1873.

- Izumi, Y., Sakai, H., Takeoka, S., Kose, T., Hamada, K., Yoshizu, A., Nishide, H., Tsuchida, E., and Kobayashi, K. (1997) Evaluation of the Capabilities of Hemoglobin Vesicles as an Artificial Oxygen Carriers in a Rat Exchange Transfusion Model. *ASAIO J.* (in press).
- Kaca, W., Roth, R. I., Vandegriff, K. D., Chen, G. C., Kuypers, F. A., Winslow, R. M., and Levin, J. (1995) Effects of Bacterial Endotoxin on Human Cross-Linked and Native Hemoglobins. *Biochemistry* 34, 11186–11185.
- Kandel, G., and Aberman, A. (1983) Mixed Venous Oxygen Saturation. Its Role in the Assessment of the Critically Ill Patient. *Arch. Intern. Med.* 143, 1400–1402.
- Kikuchi, Y., and Koyama, T. (1984) Red Blood Cell Deformability and Protein Adsorption on Red Blood Cell Surface. *Am. J. Physiol.* 247, H739–H747.
- Kilbanov, A., Maruyama, K., Torchilin V. P., and Huang L. (1990) Amphipatic Polyoxyethylenes Effectively Prolong the Circulation Time of Liposomes. *FEBS Lett.* 268, 235–237.
- King, R. G., and Copley, A. L. (1975) Some New Accessories to the Weissenberg Rheoginometer: An Exhibit. *Biorheology* 16, 355–360.
- Kobayashi, K., Tsuchida, E., and Nishide, H. (1995) Totally Synthetic Hemes: Their Characteristics and Oxygen-carrying Capacity in Dogs. *Artificial Red Cells* (E. Tsuchida, Ed.) pp 35–64, Wiley, New York.
- Loughley, H. C., Bally, M. B., Reihish, L. W., and Cullis, P. R. (1990) The Binding of Phosphatidylglycerol Liposomes to Rat Platelets is Mediated by Complement. *Thromb. Haemostasis* 64, 172–176.
- Malek, A. M., and Izumo, S. (1995) Control of Endothelial Cell Gene Expression by Flow. *J. Biomech.* 28, 1515–1528.
- Miyamoto, K., Schultz, E., Heath, T., Mitchell, M. D., Albertine, K. H., and Staub, N. C. (1988) Pulmonary Intravascular Macrophages and Hemodynamic Effects of Liposomes in Sheep. *J. Appl. Physiol.* 64, 1143–1152.
- Needham, D., McIntosh, T. J., and Lasic, D. D. (1992) Repulsive Interactions and Mechanical Stability of Polymer-grafted Lipid Membranes. *Biochim Biophys. Acta* 1108, 40–48.
- Nelimarkka, O., Halkola, L., and Niinikoski, J. (1982) Distribution of Renal Cortical and Medullary Tissue Oxygenation in Hemorrhagic Shock. *Acta Chir Scand.* 148, 213–219.
- Oka, S. (1971) An Approach to a Unified Theory of the Flow Behavior of Time-Independent Non-Newtonian Suspensions. *Jpn. J. Appl. Phys.* 10, 287–291.
- Oka, S. (1984) *Biorheology*, Shokabo Publisher, Tokyo.
- Olsen, S. B., Tang, D. B., Jackson, M. R., Gomez, E. R., Ayala, B., and Alving, B. M. (1996) Enhancement of Platelet Deposition by Cross-linked Hemoglobin in a Rat Carotid Endarterectomy Model. *Circulation* 93, 327–332.
- Peterson, G. L. (1983) Determination of total protein. *Methods Enzymol.* 91, 95–119.
- Pries, A. R., Neuhaus, D., and Gaehtgens, P. (1992) Blood Viscosity in Tube Flow: Dependence on Diameter and Hematocrit. *Am. J. Physiol.* 263, H1770–H1778.
- Prime, K. L., and Whitesides, G. M. (1993) Adsorption of Proteins onto the Surface Containing End-attached Oligo(ethylene Oxide): A Model System Using Self-Assembled Monolayers. *J. Am. Chem. Soc.* 115, 10714–10721.
- Rudolph, A. S. (1995) Encapsulation of Hemoglobin in Liposomes. *Blood Substitutes: Physiological Basis of Efficacy* (R. M. Winslow, K. D. Vandegriff, and M. Intaglietta, Eds.) pp 90–104, Birkhauser, Boston.
- Sakai, H., Takeoka, S., Yokohama, H., Seino, Y., Nishide, H., and Tsuchida, E. (1993) Purification of Concentrated Hemoglobin Using Organic Solvent and Heat Treatment. *Protein Expression Purif.* 4, 563–569.
- Sakai, H., Hamada, K., Takeoka, S., Nishide, H., and Tsuchida, E. (1996) Physical Characteristics of Hemoglobin Vesicles as Red Cell Substitutes. *Biotechnol. Prog.* 12, 119–125.
- Schneditz, D., Ribitsch V., and Kenner, T. (1985) Rheological Discrimination between Native, Rigid, and Aggregated Red Blood Cells in Oscillatory Flow. *Biorheology* 22, 209–219.
- Takeoka, S., Sakai, H., Takisada, M., and Tsuchida, E. (1992) Inhibition of Intervesicular Aggregation of Phospholipid Vesicles by Incorporation of Dialkyl Oligosaccharide Glycerol. *Chem. Lett.*, 1877–1880.
- Takeoka, S., Ohgushi, T., Ohmori, T., Terasa, K., Nishide, H., and Tsuchida, E. (1996) Layer Controlled Hemoglobin Vesicles by Interaction of Hemoglobin with Phospholipid Assembly. *Langmuir* 12, 1755–1759.
- Torchilin, V. P., Omelyaneko, V. G., Papisov, M. I., Bogdanov, Jr., A. A., Trubetskoy, V. S., Herron, J. N., and Gentry, C. A. (1994) Poly(ethylene glycol) on the Liposome Surface: on the Mechanism of Polymer-coated Liposome Longevity. *Biochim. Biophys. Acta* 1195, 11–20.
- Tsai, A. G., Kerger, H., and Intaglietta, M. (1995) Microcirculatory Consequences of Blood Substitution with $\alpha\alpha$ -Hemoglobin. *Blood Substitutes: Physiological Basis of Efficacy* (R. M. Winslow, K. D. Vandegriff, and M. Intaglietta, Eds.) pp 155–174, Birkhauser, Boston.
- Tsai, A. G., Kerger, H., and Intaglietta, M. (1996) Microvascular Oxygen Distribution: Effects due to Free Hemoglobin in Plasma. *Blood Substitutes: New Challenges* (R. M. Winslow, K. D. Vandegriff, and M. Intaglietta, Eds.) pp 124–131, Birkhauser, Boston.
- Tsuchida, E. (1995) Introduction: Overview and Perspective. *Artificial Red Cells* (E. Tsuchida, Ed.) pp 1–20, Wiley, New York.
- Tsuchida, E., and Takeoka, S. (1995) Stabilized Hemoglobin Vesicles. *Artificial Red Cells* (E. Tsuchida, Ed.) pp 35–64, Wiley, New York.
- Usuba, A., Miyazawa M., Motoki, R., Sakaguchi, K., Suzuki, K., Kamitani, T., and Takahashi, A. (1993) Oxygen Transport Capacity and Hemodynamic Effect of Newly Developed Artificial Blood "Neo Red Cells (NRC)". *Int. J. Artif. Organs* 16, 551–556.
- Vandegriff, K. D., and Winslow, R. M. (1995) The Theoretical Analysis of Oxygen Transport: A New Strategy for the Design of Hemoglobin-based Red Cell Substitutes. *Blood Substitutes: Physiological Basis of Efficacy* (R. M. Winslow, K. D. Vandegriff, and M. Intaglietta, Eds.) pp 143–154, Birkhauser, Boston.
- Vertut-Do, A., Ishiwata, H., and Miyajima, K. (1996) Binding and Uptake of Liposomes Containing a Poly(ethyleneglycol) Derivative of Cholesterol (Stealth Liposomes) by the Macrophage Cell Line J774: Influence of PEG Content and its Molecular Weight. *Biochim. Biophys. Acta* 1278, 19–28.
- Watanabe, M., Ohyanagi, H., and Saitoh, Y. (1988) Experimental Study on Anaphylactic Effects by Fluosol DA as an Oxygen Carrier. *Jpn J. Artif. Organs* 17, 1513–1522.
- Winslow, R. M. (1995) Blood Substitutes: A Moving Target. *Nature Med.* 1, 1212–1215.
- Woodle, M. C., and Lasic, D. D. (1992) Sterically Stabilized Liposomes. *Biochim. Biophys. Acta* 1113, 171–199.
- Woodle, M. C., Engbers, C. M., and Zalipsky, S. (1994) New Amphiphatic Polymer-Lipid Conjugates Forming Long Circulating Reticuloendothelial System-Evading Liposomes. *Bioconjugate Chem.* 5, 493–496.
- Wu, P.-S., Tin, G. W., Baldeschwieler, J. D., Shen, T. Y., and Ponpipom, M. M. (1981) Effect of Surface Modification on Aggregation of Phospholipid Vesicles. *Proc. Natl. Acad. Sci. U.S.A.* 78, 6211–6215.
- Yoshioka, H. (1991) Surface Modification of Haemoglobin-containing Liposomes with Polyethylene Glycol Prevents Liposome Aggregation in Blood Plasma. *Biomaterials* 12, 861–864.
- Zalipsky, S., Puntambeker, B., Boulikas, P., Engbers, P. B., and Woodle, M. C. (1995) Peptide Attachment to Extremities of Liposomal Surface Grafted PEG Chains: Preparation of the Long-Circulating Form of Laminin Pentapeptide, YIGSR. *Bioconjugate Chem.* 6, 705–708.
- Zheng, S., Beissinger, R., Sherwood, R. L., McCormick, D. L., Lasic D. D., and Martin, F. J. (1993) Liposome-encapsulated Hemoglobin: A Red Blood Cell Substitute. *J. Liposome Res.* 3, 575–588.

Electrochemistry of Methylene Blue Bound to a DNA-Modified Electrode

Shana O. Kelley and Jacqueline K. Barton*

Beckman Institute, Division of Chemistry and Chemical Engineering, California Institute of Technology, Pasadena, California 91125

Nicole M. Jackson and Michael G. Hill*

Department of Chemistry, Occidental College, Los Angeles, California 90041. Received August 1, 1996*

Gold surfaces have been derivatized with 15-base-pair double-stranded DNA oligonucleotides containing a pendant 5' hexanethiol linker. The electrochemistry of intercalated methylene blue has been investigated at these modified electrodes. Chronocoulometry, cyclic voltammetry, ellipsometry, and quantitation via ^{32}P labeling are all consistent with a surface coverage of $\geq 75\%$ with the DNA helices stacked at an angle from the electrode surface. Cyclic voltammetry at low methylene blue/duplex stoichiometries yields well-behaved surface waves with $E^\circ = -0.25\text{ V}$ (vs SCE), a value 0.03 V negative of that in aqueous solution. A binding isotherm for methylene blue at an electrode derivatized with the double-stranded sequence 5' SH-(CH₂)₆-p-AGTACAGTCATCGCG 3' was obtained from coulometric titrations and gave an affinity constant equal to $3.8(5) \times 10^6\text{ M}^{-1}$ with a saturation value of 1.4(2) methylene blue intercalators per DNA duplex. Taken together, these experiments support a model for the surface morphology in which DNA duplexes are densely packed; methylene blue therefore reversibly binds to sites in the DNA that are close to the bulk solution. Electrochemistry at DNA-derivatized electrodes provides a valuable methodology to examine DNA-bound redox reactions and may offer new insight into DNA-mediated electron transfers.

The π -stack of aromatic heterocycles contained within the DNA helix presents a unique medium in which to explore electron-transfer reactions (1). As the hydrophobic interior of DNA differs substantially from aqueous solution, the redox properties of molecules intercalatively bound (and of the nucleic acid bases themselves) may vary significantly from those in solution. Redox reactions in the π -stack are particularly important for understanding charge delocalization in DNA and its effect on base damage (2–4). However, the irreversible electrochemistry of the nucleic acid bases has made it difficult to monitor directly the redox behavior of bases in either their monomeric or extended π -stacked forms where electronic interactions perturb the π -systems of adjoining base steps (5–6). Both organic molecules and transition-metal complexes have been employed as indirect probes of the electronic properties of DNA (1, 7–15).

Photophysical studies on DNA have shown that the π -stack mediates ultrafast electron transfer ($k_{\text{ET}} \sim 10^{10}\text{ s}^{-1}$) (1). Although various systems are being explored (9–12), fast photoinduced electron-transfer kinetics are only observed when both donor and acceptor are intercalated into DNA (13–15); under such conditions, efficient luminescence quenching has been observed over 40 Å (13). Moreover, recent photochemical studies suggest that the extended DNA π -stack facilitates long-range oxidative base damage (4). These results all point to the base stack of DNA as an effective pathway for electron transfer.

Electrochemical studies of small molecule/DNA complexes have focused primarily on solution-phase phenomena, in which DNA-induced changes in redox potentials and/or diffusion constants of organic and inorganic spe-

cies have been analyzed to yield association constants (16, 17). In addition, rates of guanine oxidation catalyzed by electrochemically oxidized transition-metal complexes have been used to evaluate the solvent accessibility of bases for the detection of mismatches (18). Electrochemical signals triggered by the association of small molecules with DNA have also been applied in the design of other novel biosensors. Toward this end, oligonucleotides have been immobilized on electrode surfaces by a variety of linkages [e.g., thiols on gold (19, 20), carbodiimide coupling of guanine residues on glassy carbon (21), and alkanebisphosphonate films on Al³⁺-treated gold (22)] for use in hybridization assays. Both direct changes in mass (measured at a quartz crystal microbalance) (20) and changes in current (19, 21) or electrogenerated chemiluminescence (22) due to duplex-binding molecules have been used as reporters for double-stranded DNA. Gold surfaces modified with thiolated polynucleotides have also been used for the detection of metal ions and DNA-binding drugs (23).

To investigate the redox chemistry of molecules within the DNA environment, we have employed gold surfaces modified with double-stranded, thiol-terminated DNA (24). The covalent attachment of DNA directly to an electrode surface provides a controlled environment in which kinetic and thermodynamic parameters of DNA-bound species can be evaluated. To probe DNA on these modified surfaces, we have examined the electrochemistry of methylene blue (MB) (25), an aromatic heterocycle that binds strongly to DNA via intercalation (26). Here we report the electrochemistry, binding affinity, and electron-transfer dynamics of intercalated MB at a gold electrode modified with 15-base-pair oligonucleotide duplexes, singly derivatized with a 5'-hexylthiol tether.

* Authors to whom correspondence should be addressed.

© Abstract published in *Advance ACS Abstracts*, December 15, 1996.

EXPERIMENTAL SECTION

Materials. Phosphoramidite reagents (including the C₆ S–S thiol modifier) were obtained from Glen Research. Methylene blue (Sigma Chemical Co.), ferrocene carboxaldehyde, and octadecyl mercaptan (Aldrich) were used as received. Potassium ferrocyanide (Fisher) was recrystallized from aqueous solution prior to use. [γ -³²P]dATP was obtained from NEN-DuPont.

Synthesis of Derivatized Duplexes. 5' Mercapto-hexyloligonucleotides and underivatized complements were synthesized according to automated solid-phase techniques (27), using a disulfide protected linker (C₆ S–S thiol modifier). Sequences were purified by reversed phase HPLC, deprotected using dithiothreitol, and re-purified before hybridization to unmodified complements. Single-stranded oligonucleotides were characterized by matrix-assisted laser desorption/ionization time-of-flight mass spectrometry and HPLC retention times. Sequences prepared according to this method include 5' SH-(CH₂)₆-p-AGTGCGAA GCTGCGT 3', 5' SH-(CH₂)₆-p-AGTACAGTCATCGCG 3', and 5' SH-(CH₂)₆-p-AGTACAGTCATCAGT 3'. Duplexes were hybridized in deoxygenated 5 mM phosphate/50 mM NaCl (pH 7) by heating to 90 °C followed by slow cooling to room temperature. Unprotected duplexes were stored frozen under argon to prevent oxidation of the thiol.

Derivatization of Gold Electrodes. Bulk gold electrodes were polished successively with 0.3- and 0.05- μ m alumina (Buhler), sonicated for 30 min, and etched in 1.0 M sulfuric acid. Au(111) surfaces (28) were prepared by vapor deposition onto mica or glass. Electrodes were then modified by incubation in 0.1 mM solutions of derivatized DNA duplexes in 5 mM phosphate/50 mM NaCl (pH 7) for 12–48 h at ambient temperature. Modified electrodes were rinsed in buffer prior to use. For the investigation of DNA-modified electrodes at high MB loadings, deposition of the thiol-terminated DNA was performed in the presence of 0.6 mM MB; these electrodes were rinsed in 10 μ M MB/buffer solutions. CH₃(CH₂)₁₇-SH-modified electrodes were prepared by incubation in ethanol solutions for 48 h.

Electrochemistry. All electrochemical experiments were performed with a Bioanalytical Systems (BAS) Model CV-50W electrochemical analyzer. Cyclic voltammetry (CV) and chronocoulometry (CC) were carried out at 20 \pm 2 °C with a normal three-electrode configuration consisting of either a modified gold-disk or a hanging drop mercury working electrode and a saturated calomel reference electrode (SCE, Fisher Scientific). The working compartment of the electrochemical cell was separated from the reference compartment by a modified Luggin capillary. Potentials are reported versus SCE. Chronocoulometric measurements were corrected for double-layer charge as determined in buffer solutions. Heterogeneous electron-transfer rates were determined by cyclic voltammetry and analyzed as described previously (29). The electron-transfer kinetics of several previously reported systems (including benzo[*c*]cinnoline on gold and methylene blue on Hg) (30) were investigated using this method with our instrumentation, and in each case, excellent agreement with the literature values was observed.

Ellipsometry. Optical ellipsometry (λ = 632.8 nm) was carried out on dried samples at 25 °C using a Gaertner Model L116C ellipsometer.

³²P Labeling and Quantitation. A 15-base-pair oligonucleotide (5' CGCGATGACTGTACT 3') was 5' labeled with [γ -³²P]ATP and hybridized to a thiol-modified complement. Samples of Au(111) on mica (diameter

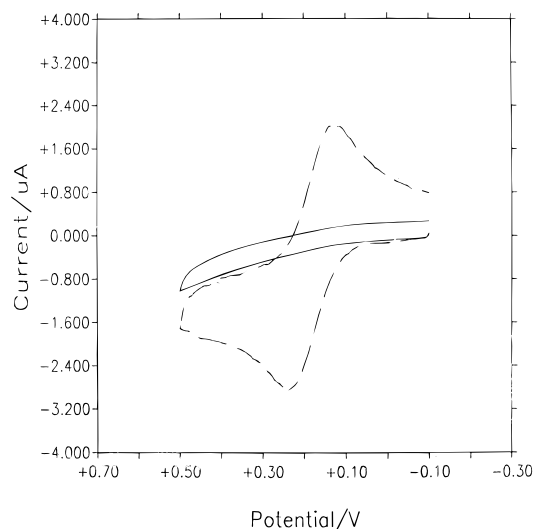


Figure 1. Cyclic voltammograms for 0.1 mM K₄[Fe(CN)₆] in 5 mM phosphate/50 mM NaCl (pH 7) at a DNA-modified (—) [5' SH-(CH₂)₆-p-AGTACAGTCATCGCG 3' + complement] and bare gold electrode (---). Scan rate = 100 mV/s; electrode area (*A*) = 0.02 cm².

= 0.41 cm) were treated with this duplex in the manner described above. After thorough rinsing in buffer solutions, dried samples were counted on a Beckman LS60001C scintillation counter, adjusted for attenuation by the presence of the mica, and compared to calibration standards that were prepared from known quantities of labeled oligonucleotide. The values obtained by scintillation counting and the surface areas of the modified mica were confirmed by analysis of the radioactivity of each sample by phosphorimager (Molecular Dynamics).

RESULTS

Surface Analysis. Modification of gold surfaces with 5'-thiol-terminated DNA duplexes was established by cyclic voltammetry, ellipsometry, and the direct quantitation of ³²P-labeled oligonucleotides on Au(111). The electrochemical window of 50 mM NaCl (pH 7) at DNA-modified gold extends from 0.70 to –0.70 V (versus SCE). The cyclic voltammograms of Fe(CN)₆^{4–} at bare and DNA-modified electrodes are shown in Figure 1. As ferrocyanide does not bind to the DNA polyanion, the lack of signal at the modified electrode implies essentially complete coverage by the thiol-terminated DNA. To ensure that Fe(CN)₆^{4–} was not merely electrostatically repelled from holes in the monolayer, a neutral probe, ferrocene carboxaldehyde, was investigated and gave a similar result.

Gold surface waves (generated by the formation and stripping of gold oxide) at bare and derivatized electrodes were also compared by cyclic voltammetry as a qualitative measure of the surface coverage (31, 32). These results suggest a very high loading (>85%). However, thiol–gold linkages are known to undergo oxidative desorption at high potentials (33), so an alternative method was used to quantitate the coverage.

DNA adsorbed on Au(111) was directly quantitated in a radioactive tagging (³²P) experiment. This assay yielded an average of 5.7(3) \times 10^{–12} mol of duplex DNA on a 0.14-cm² surface after 24 h of modification. From this value and the cross-sectional area of DNA (3.14 \times 10^{–12} cm²), the surface coverage was calculated as Γ = 4.1(2) \times 10^{–11} mol/cm², which corresponds to a close-packed fractional coverage of 0.75(3).

Ellipsometry of a 15-base-pair thiol-derivatized duplex on Au(111) was carried out and yielded an estimate for

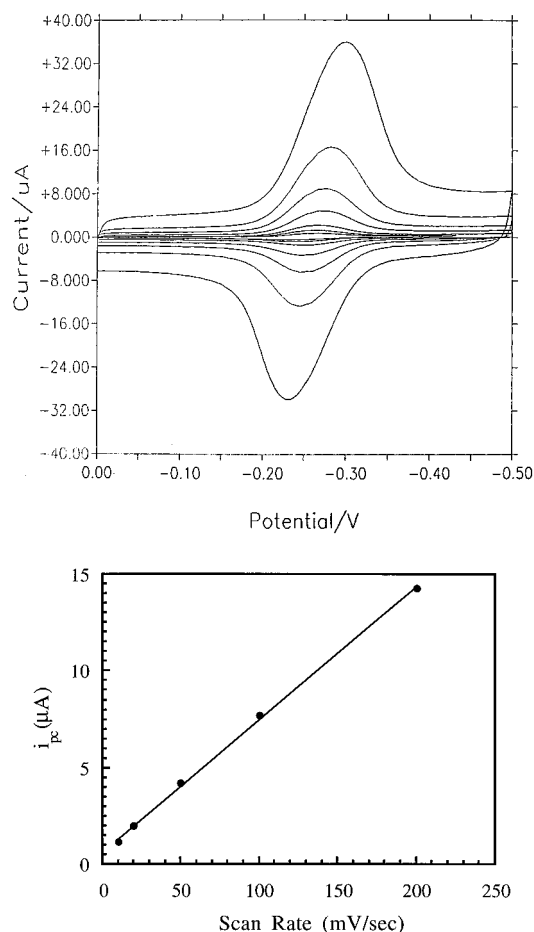


Figure 2. (A, top) Cyclic voltammetry of 1.0 μM methylene blue in 50 mM phosphate (pH 7) at a DNA-modified [5' SH-(CH₂)₆-p-AGTGCGAAGCTGCGT 3' + complement] electrode ($A = 0.7 \text{ cm}^2$; scan rate = 5, 10, 20, 50, 100, 200, and 500 mV/s). (B, bottom) Plot of i_{pc} vs scan rate.

the average monolayer thickness of 35 Å. As this measurement corresponds to an average thickness on the gold surface, it could reflect anywhere from 100% surface coverage with derivatized DNA duplexes stacked at an angle of 32° from the gold surface, to DNA helices oriented perpendicular to the surface with only 55% coverage, given a cylindrical DNA 15-mer duplex of 66-Å height (including the fully extended linker) and 20-Å diameter (34).

Cyclic Voltammetry of Methylene Blue. The cyclic voltammetry of 1.0 μM MB at a DNA-modified electrode is shown in Figure 2. The pronounced electrochemical response at such a low concentration is strong evidence that MB binds tightly and is electronically well coupled to the modified electrode surface. The reduction potential of MB at the DNA-modified electrode is -0.25 V (vs SCE), compared to -0.22 V at bare gold. A plot of cathodic peak current (i_{pc}) vs scan rate (ν) is linear (Figure 2B), establishing that MB is strongly adsorbed to the DNA-modified surface (35).

Qualitatively, ΔE_{p} increases as a function of scan rate (Figure 3), indicating slow electron-transfer kinetics on the CV time scale (29). For comparison, the peak separations are much less pronounced for MB adsorbed to a mercury surface, where the rate constant is reported as 1500 s^{-1} (25); at bare gold we observed essentially no peak splitting up to our fastest scan rates (50 V/s). Importantly, these measurements were all made at very low loadings of MB; thus, artifacts due to lateral charge migration or ohmic (iR) drop were minimized (at the largest currents used, iR was $<5 \text{ mV}$). These data

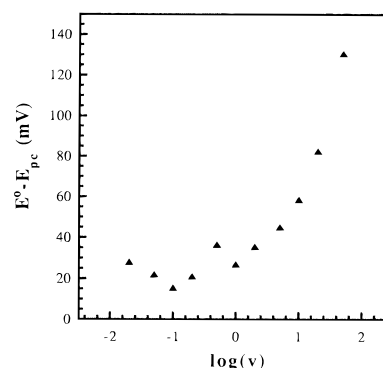


Figure 3. Plot of $E - E_{\text{pc}}$ vs $\log(\nu)$ for 0.1 μM methylene blue at a gold electrode derivatized with 5' SH-(CH₂)₆-p-AGTACAGT-CATCGCG 3' hybridized to its complement in 25 mM phosphate/75 mM NaCl (pH 7).

indicate that the electron-transfer rate is attenuated by the intercalation of MB into the DNA monolayer and that the rate is significantly faster at bare gold than at the derivatized surface. It is noteworthy that no appreciable differences in the CV responses were observed for the three oligonucleotide sequences examined.

Control experiments were also carried out to distinguish the binding characteristics of MB on different electrode surfaces. Coulometric experiments (36) on bare gold electrodes showed no evidence of adsorption of MB at sub-micromolar concentrations (Figure 4). In addition, electrodes treated with oligonucleotides lacking a thiol linker under the same conditions as those used for surface modification with the linker did not facilitate the subsequent adsorption of MB, and instead yielded irreproducible voltammetric responses that ranged from reversible to highly irreversible. Lastly, we contrast the behavior of MB at a DNA-modified electrode with that at a gold electrode modified with octadecanethiol (see Supporting Information). At the alkylthiol surface, cyclic voltammetry of MB reveals preferential binding to the surface in the reduced form, and a plot of i_{pc} vs $\nu^{1/2}$ is linear, consistent with diffusion of MB.

Determination of Methylene Blue Affinities. MB reversibly binds to DNA-modified electrodes, as established by transfer experiments in which the electrochemical response of a derivatized electrode was monitored during sequential and repetitive immersions in MB and MB-free solutions. The affinity of MB for the DNA-derivatized surface was determined using chronocoulometry (36). Figure 4 shows binding isotherms for MB at both DNA-modified [sequence = 5' SH-(CH₂)₆-p-AGTACAGT-CATCGCG 3'] and bare gold electrodes. The data obtained at the DNA-modified electrode were fit according to Langmuir's model (37), giving $K = 3.8(5) \times 10^6 \text{ M}^{-1}$ and $\Gamma_{\text{max}} = 1.2(1) \times 10^{-12} \text{ mol}$, where K is the association constant per site and Γ_{max} is the maximum number of MB binding sites (Figure 5). The good fit obtained with this model confirms independent, non-cooperative binding sites for MB on the 15-base-pair duplexes. Comparable values for K and Γ_{max} were obtained for the sequence 5' SH-(CH₂)₆-p-AGTACAGT-CATCAGT 3'. It is noteworthy that the affinity of MB to a bare gold electrode is significantly lower (Figure 4).

The value of Γ_{max} corresponds to a stoichiometry of 1.4(2) MB per 15-base-pair DNA duplex based upon 75% coverage of this surface. Yet maximum stoichiometries of MB bound to DNA in solution are expected to approach 7 MB per 15-base-pair oligonucleotide duplex (38). To test whether attachment of DNA to the electrode surface restricts access of MB, the electrochemistry of surfaces modified with duplexes presaturated with methylene blue

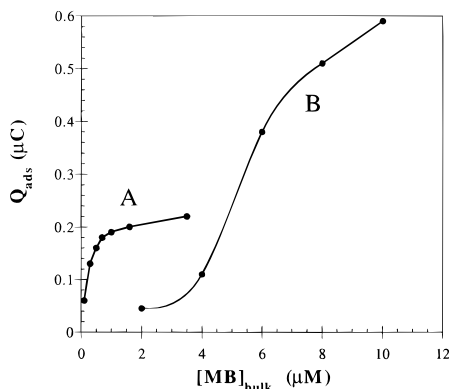


Figure 4. Adsorption isotherms for methylene blue (25 mM phosphate/75 mM NaCl, pH 7) at a gold electrode modified with 5' SH-(CH₂)₆-p-AGTACAGTCATCGCG 3' hybridized to its underivatized complement (A) and at a bare gold electrode (B). Surface concentrations were determined from the intercepts of Q vs $t^{1/2}$ curves obtained by chronocoulometry; $A = 0.02$ cm².

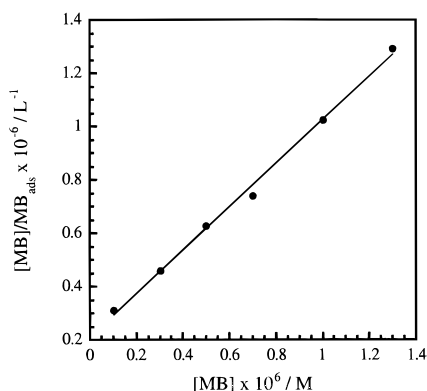


Figure 5. Plot of $[MB]/MB_{ads}$ vs $[MB]$ for the MB/DNA isotherm shown in Figure 4A. Data were analyzed as follows (37): $[MB]/MB_{ads} = (1/\Gamma_{max})[MB] + (1/K\Gamma_{max})$, where $[MB]$ is the bulk concentration of methylene blue, MB_{ads} is the number of moles of methylene blue adsorbed on the surface, and Γ_{max} is the number of methylene blue binding sites at saturation.

was investigated. Figure 6 shows the cyclic voltammogram of 10 μ M MB at an electrode derivatized with a 0.1 mM duplex solution that contained 0.6 mM MB (these conditions ensure that the DNA is almost entirely saturated, with a negligible concentration of MB free in solution). The very broad and cathodically shifted response is characteristic of interacting redox-active species (39). When this electrode was immersed in MB-free electrolyte, the response slowly decayed. Once the dissociation process was complete, the bulk concentration of MB was brought back to 10 μ M, but a much smaller response was observed. Importantly, the signal with 10 μ M MB was now identical to that observed for DNA-modified electrodes prepared in the absence of MB (i.e. not presaturated with MB). Integration of the currents shown in Figure 6 yields a 5:1 ratio, which is close to the ratio of saturation values expected for MB in solution versus that measured at the DNA-modified electrodes.

DISCUSSION

Gold Electrodes Derivatized with DNA. 5'-Thiol-terminated DNA duplexes covalently modify gold surfaces. Importantly, duplexes that lacked the thiol linker showed little and irreproducible adsorption to gold under identical conditions. Very high surface coverages of gold by thiol-terminated DNA were confirmed by evaluating the accessibility of the modified electrode to diffusing

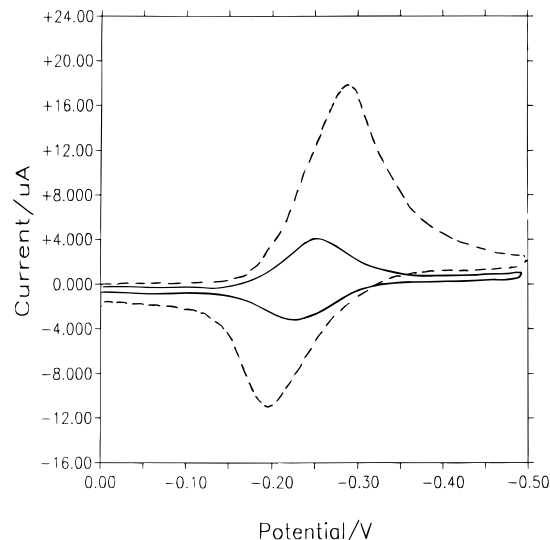


Figure 6. Cyclic voltammograms of 10 μ M methylene blue in 50 mM phosphate (pH 7) at an electrode ($A \sim 0.07$ cm²) modified with a solution containing 0.1 mM DNA [5' SH-(CH₂)₆-p-AGTGGGAAGCTGCGT 3' + complement] and 0.6 mM MB (dotted line) and the same electrode after buffer equilibration and subsequent restoration of the bulk concentration to 10 μ M MB (solid line).

species in solution, integrating the gold surface waves, and quantitating the radioactivity of ³²P-labeled DNA electrodes.

Although packing of the DNA on the surface is high, the DNA helices do not appear to lie flat on the electrode surface. Since quantitation of the DNA duplexes on the surface shows at least 75% coverage, such high loading of covalently bound duplexes can only be accommodated with the majority of DNA duplexes at a substantial angle from the surface. Moreover, since the duplexes are relatively short (representing 1.5 helical turns), they can also be considered quite rigid across the duplex. Ellipsometric measurements (albeit on dried samples) combined with electrochemical data also suggest that the helices are stacked at an angle with respect to the surface. Hence, the morphology of the DNA-modified surface appears to involve a densely packed array of duplexes. However, it is important to note that no direct information regarding the degree of order of DNA duplexes on the electrode has been obtained.

Electrochemistry of Intercalated MB. Micromolar solutions of MB yield well-defined voltammetric responses at electrodes modified with thiol-derivatized DNA (Figure 2). The reduction potential for intercalated MB is cathodically shifted (~ 30 mV) from the value in aqueous solution. For comparison, the reduction potentials for MB in dimethylformamide, acetonitrile, and acetone are, respectively, -0.50 , -0.52 , and -0.48 V vs SCE (corrected for the junction potential, using ferrocene/ferrocene as an internal standard). Wider variations in reduction potentials are observed in aqueous solution as a function of pH since the reduction is coupled to proton transfer. At low concentrations of MB (<0.1 μ M), the cyclic voltammograms exhibit full-widths at half-heights of ~ 55 mV. This value is slightly larger than the predicted 45 mV for a 2e⁻ Nernstian system. Starting at low loadings of MB, the voltammograms broaden until saturation in binding of MB to DNA is reached; the broadest cyclic voltammograms are observed at electrodes presaturated with MB. In each case, the cathodic and anodic peak splitting approaches zero at slow scan rates. The broadening (which depends directly upon loading of MB) therefore indicates a distribution of binding environ-

ments with slightly different reduction potentials. A systematic examination of these parameters as a function of sequence for this and other DNA-binding molecules will be instructive.

Importantly, the binding affinity of MB for the DNA-modified electrode [5' SH-(CH₂)₆-p-AGTACAGTCATCGCG 3'; $K = 3.8 \times 10^6 \text{ M}^{-1}$] is comparable to that found for DNA in solution ($K = 10^6 \text{ M}^{-1}$ in 50 mM NaCl) (26). A preference for GC-rich DNA has been noted in some studies; we do not observe a significant change in binding affinity with an electrode modified with the sequence 5' SH-(CH₂)₆-p-AGTACAGTCATCAGT 3', which does not contain adjacent GC base pairs near its 3' terminus.

While the equilibrium binding constants of MB to our DNA-modified electrodes are similar to those found for DNA in solution, the saturation values are not. Our observed Γ_{max} corresponds to roughly 1 MB per 15-base-pair duplex. This stoichiometry is significantly less than that of the MB/base-pair stoichiometry found in solution (26), where MB may occupy many (>5) neighbor excluded (38) sites on a 15-mer duplex. Indeed, if the oligonucleotides are presaturated with MB before attachment to the electrode surface, loadings of MB closer to that predicted by neighbor exclusion are detected electrochemically. However, once this presaturating MB dissociates from the surface (after the electrode is immersed in pure buffer), subsequent binding of MB to the electrode is again restricted. These observations fully support the notion that the DNA helices on the gold surface are tightly packed, necessitating that MB binds at sites close to the DNA/solvent interface. Owing to dense DNA packing and to the high affinity of MB for DNA, diffusion down into the DNA monolayer may be severely inhibited.

Although available data suggest that MB binds to DNA that is densely packed at an angle from the electrode surface, we also considered the possibility that the DNA is lying flat on the electrode. If this were the case, we might expect the CV response to more closely resemble that of MB adsorbed directly onto gold; the significant difference in ΔE_p as a function of scan rate strongly argues against this possibility. Moreover, if a flat orientation were more favorable, we would expect to see similar behavior when the surfaces were modified with DNA lacking the linker. Instead, in experiments with DNA noncovalently associated with the electrode, we observe only very weak and irreproducible signals for MB.

One might also consider that the DNA merely facilitates delivery of MB to the gold surface. However, our adsorption isotherms clearly indicate that MB binds more strongly to DNA-modified electrodes than to bare gold. Therefore, appreciable dissociation of MB from DNA to the gold surface is highly unlikely. In this light, it is interesting that the ratio of the maximum surface coverages for MB and thiol-modified DNA on gold (18×10^{-11} and $6 \times 10^{-11} \text{ mol/cm}^2$, respectively) corresponds roughly to the ratio of cross-sectional surface areas for methylene blue (1 nm^2) (25) and double-stranded DNA (3 nm^2) (34). Additionally, the electrochemistry of MB at an electrode modified with octadecanethiol provides further evidence against a channeling mechanism. At the alkylthiol surface, MB exhibits diffusional behavior and appears to bind more strongly in the reduced form. This is in stark contrast to the electrochemical response of MB at a DNA-modified electrode. The strength of the interaction between DNA and methylene blue afforded by intercalation makes it much more energetically favorable for the intercalator to remain bound rather than to diffuse to the electrode.

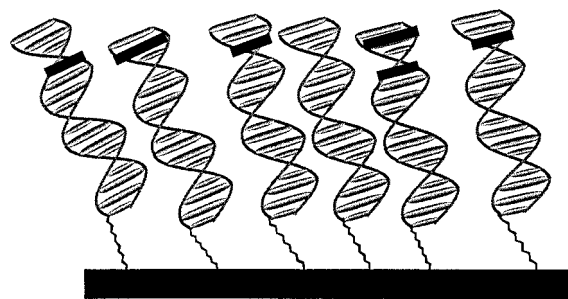


Figure 7. Schematic illustration depicting MB (dark rectangles) bound to 15-base-pair oligonucleotides attached to a gold surface. The lengths of the DNA helices and alkylthiol chains are shown to relative scale. Helices are shown at an average angle of 40° from the normal with a surface coverage of 80%; surfaces are realistically more heterogeneous than depicted.

These data may therefore be taken together in developing a model that describes the binding of MB to the DNA-derivatized surface. In this model (Figure 7), closely packed DNA helices are tethered to the gold surface via thiol linkages. Solution-borne MB binds reversibly to accessible duplex sites on the derivatized electrode, with an affinity comparable to that for duplex DNA in solution. Since the duplexes are tightly packed on the surface, however, access appears to be restricted primarily to those sites near the bulk solution. MB is therefore separated from the electrode by both the σ -system of the aliphatic linker ($\sim 15 \text{ \AA}$) and the π -stacked base pairs ($\sim 50 \text{ \AA}$), which lead to the intercalation site. As a result, electrochemical reduction of MB at the derivatized surface occurs over long distance through the DNA duplexes.

If this model is correct, our results lead to the suggestion that electron transfer through the double helix is remarkably efficient. For example, applying a decay constant (β) characteristic of σ -only arrays (0.95 \AA^{-1}) (41), we would expect the electron-transfer rate to drop by more than 22 orders of magnitude through the π -stack alone. The almost reversible response observed at scan rates up to 500 mV/s for MB at DNA-modified gold rules out a rate constant of this small magnitude.

We stress, however, that if MB intercalates into sites evenly dispersed throughout the modified surface, the observed electrochemical response may not uniquely support long-range electron transfer through DNA. Specifically, if the decay rate of electron transfer through DNA were steep enough, in principle only MB bound at the first base steps from the aliphatic linker would give an electrochemical response. In this scenario, the observed rate of electron transfer would be attenuated essentially only by tunneling through the hexylthiol tether, as the rates of electron transfer to MBs intercalated further out would be too slow to measure. Although we cannot completely rule out this possibility, the electrochemical response of MB at presaturated DNA-modified electrodes (Figure 6) seems to indicate that intercalators bound throughout the double helix can contribute to the observed currents. Moreover, given a relatively large β , if the intercalators were distributed throughout binding sites along the entire helices, we would predict much less reversible voltammograms, as a wide range of rate constants would contribute to the overall currents.

Therefore, from the data now available, it appears that as long as the MB is intercalated into the DNA-modified electrodes (be it near the solvent-exposed terminus of the adsorbed DNA or dispersed throughout the double helix) electron transfer over long distance through the DNA is exceptionally efficient. Studies employing well-defined systems in which the location of the intercalator is

precisely determined will be required to assess quantitatively the electronic coupling mediated by the π -stack of DNA.

CONCLUSIONS

DNA-derivatized electrodes offer a valuable tool to examine the redox behavior of species within the DNA environment. Electrochemistry on DNA-modified surfaces provides a convenient method to determine equilibrium binding parameters of redox-active species and may represent an alternative means to investigate the dynamics of DNA-mediated electron-transfer processes.

ACKNOWLEDGMENT

We are grateful to the NIH (GM49216 to J.K.B.), the Research Corporation (M.G.H.), the Camille and Henry Dreyfus Foundation (M.G.H.), and the NSF (DUE-9551647 to M.G.H.) for their financial support. In addition, we thank Ashish Bansal for assistance with the ellipsometry experiments and Professor F. C. Anson for helpful discussions.

Supporting Information Available: Kinetics fit for 0.1 μ M MB at a DNA-derivatized electrode; cyclic voltammogram of MB at an alkanethiol-modified gold electrode (5 pages). This material is contained in many libraries on microfiche, immediately follows this article in the microfilm version of the journal, can be ordered from the ACS, and can be downloaded from the Internet; see any current masthead page for ordering information and Internet access instructions.

LITERATURE CITED

- (1) Stemp, E. D. A., and Barton, J. K. (1996) Electron transfer between metal complexes bound to DNA: Is DNA a molecular wire? *Met. Ions Biol. Syst.* **33**, 325.
- (2) (a) Szent-Györgyi, A., Isenberg, I., and Baird, S. L. (1960) On the electron donating properties of carcinogens. *Proc. Natl. Acad. Sci. U.S.A.* **46**, 1444. (b) Snart, R. S. (1968) Photoelectric effects of deoxyribonucleic acid. *Biopolymers* **6**, 293. (c) Dee, D., and Baur, M. E. (1974) Charge and excitation migration in DNA chains. *J. Chem. Phys.* **60**, 541.
- (3) (a) Magan, J. D., Blau, W., Croke, D. T., McConnell, D. J., and Kelly, J. M. (1987) One-dimensional photoconductivity in DNA. *Chem. Phys. Lett.* **141**, 489. (b) Cullis, P. M., McClymont, J. D., and Symons, M. C. R. (1990) Electron conduction and trapping in DNA: an electron spin resonance study. *J. Chem. Soc., Faraday Trans. 86*, 591. (c) Houee-Levin, C., Gardes-Albert, M., Rouscilles, A., Ferradini, C., and Hickel, B. (1991) Intramolecular semiquinone disproportionation in DNA. Pulse radiolysis study of the one-electron reduction of daunorubicin intercalated in DNA. *Biochemistry* **30**, 8216. (d) Anderson, R. F., Patel, K. B., and Wilson, W. R. (1991) Determination of the one-electron reduction potential of electron-affinic compounds intercalated into DNA. *J. Chem. Soc., Faraday Trans. 87*, 3739.
- (4) Hall, D. B., Holmlin, R. E., and Barton, J. K. (1996) Oxidative DNA damage through long range electron transfer. *Nature* **382**, 731.
- (5) (a) Palecek, E., Kolar, V., Jelen, F., and Heinemann, U. (1990) Electrochemical analysis of the self-complementary B-DNA decamer d(CCAGGGCTGG). *Bioelectrochem. Bioenerg.* **23**, 285. (b) Brett, C. M. A., Brett, A. M. O., and Serrano, S. H. P. (1994) On the adsorption and electrochemical oxidation of DNA at glassy carbon electrodes. *J. Electroanal. Chem.* **366**, 225.
- (6) (a) Jovanovic, S. V., and Simic, M. G. (1986) One-electron redox potentials of purines and pyrimidines. *J. Phys. Chem.* **90**, 974. (b) Colson, A.-O., Besler, B., Close, D. M., and Sevilla, M. D. (1992) Ab initio molecular-orbital calculations of DNA bases and their radical ions in various protonation states: evidence for proton-transfer in GC base pair radical anions. *J. Phys. Chem.* **96**, 661.
- (7) Armitage, B., Yu, C., Devadoss, C., and Schuster, G. B. (1994) Cationic anthraquinone derivatives as catalytic DNA photonicases: mechanisms for DNA-damage and quinone recycling. *J. Am. Chem. Soc.* **116**, 9847.
- (8) (a) Johnston, D. H., Cheng, C. C., Campbell, K. J., and Thorp, H. H. (1994) Trans-dioxorhenium(V)-mediated electrocatalytic oxidation of DNA at indium tin oxide electrodes: voltammetric detection of DNA cleavage in solution. *Inorg. Chem.* **33**, 6388. (b) Cheng, C. C., Goll, J. G., Neyhart, G. A., Welch, T. W., Singh, P., and Thorp, H. H. (1995) Relative rates and potentials of competing redox processes during DNA cleavage: oxidation mechanisms and sequence-specific catalysis of the self-inactivation of oxometal oxidants by DNA. *J. Am. Chem. Soc.* **117**, 2970.
- (9) (a) Baguley, B. C., and LeBret, M. (1984) Quenching of DNA-ethidium fluorescence by amsacrine and other antitumor agents: a possible electron transfer effect. *Biochemistry* **23**, 937. (b) Fromhertz, P., and Rieger, B. (1986) Photoinduced electron transfer in DNA matrix from intercalated ethidium to condensed methylviologen. *J. Am. Chem. Soc.* **108**, 5361.
- (10) (a) Brun, A. M., and Harriman, A. (1992) Dynamics of electron transfer between intercalated polycyclic molecules: effect of interspersed bases. *J. Am. Chem. Soc.* **114**, 3656. (b) Brun, A. M., and Harriman, A. (1994) Energy-transfer and electron-transfer processes involving palladium porphyrins bound to DNA. *J. Am. Chem. Soc.* **116**, 10383.
- (11) Meade, T. J., and Kayyem, J. F. (1995) Electron-transfer through DNA: site-specific modification of duplex DNA with ruthenium donors and acceptors. *Angew. Chem., Int. Ed. Engl.* **34**, 352.
- (12) (a) Barton, J. K., Kumar, C. V., and Turro, N. J. (1986) DNA-mediated photoelectron transfer reactions. *J. Am. Chem. Soc.* **108**, 6391. (b) Purugganan, D., Kumar, C. V., Turro, N. J., and Barton, J. K. (1988) Accelerated electron-transfer between metal complexes mediated by DNA. *Science* **241**, 1645.
- (13) Murphy, C. J., Arkin, M. A., Ghatlia, N. D., Bossman, S., Turro, N. J., and Barton, J. K. (1993) Long-range photoinduced electron transfer through a DNA helix. *Science* **262**, 1025.
- (14) Murphy, C. J., Arkin, M. A., Ghatlia, N. D., Bossman, S., Turro, N. J., and Barton, J. K. (1994) Fast photoinduced electron transfer through DNA intercalation. *Proc. Natl. Acad. Sci. U.S.A.* **91**, 5315.
- (15) (a) Stemp, E. D. A., Arkin, M. R., and Barton, J. K. (1995) Electron-transfer between metallointercalators bound to DNA: spectral identification of the transient intermediate. *J. Am. Chem. Soc.* **117**, 2375. (b) Arkin, M. R., Stemp, E. D. A., Turro, C., Turro, N., and Barton, J. K. (1996) Luminescence quenching in supramolecular systems: a comparison of DNA-mediated and SDS micelle-mediated photoinduced electron transfer between metal complexes. *J. Am. Chem. Soc.* **118**, 2267. (c) Arkin, M. R., Stemp, E. D. A., Holmlin, R. E., Barton, J. K., Hörmann, A., Olson, E. J. C., and Barbara, P. A. (1996) Rates of DNA-mediated electron transfer between metallointercalators. *Science* **273**, 475. (d) Holmlin, R. E., Stemp, E. D. A., and Barton, J. K. (1996) Os(phen)₂dpz²⁺ in photoinduced DNA-mediated electron transfer reactions. *J. Am. Chem. Soc.* **118**, 5236.
- (16) (a) Carter, M. T., Rodriguez, M., and Bard, A. J. (1989) Voltammetric Studies of the interaction of metal chelates with DNA. 2. Tris-chelated complexes of cobalt(III) and iron(II) with 1,10-phenanthroline and 2,2'-bipyridine. *J. Am. Chem. Soc.* **111**, 8901. (b) Carter, M. T., and Bard, A. J. (1990) Electrochemical investigations of the interaction of metal chelates with DNA. 3. Electrogenated chemiluminescent investigation of the interaction of tris(1,10-phenanthroline)-ruthenium(II) with DNA. *Bioconjugate Chem.* **1**, 257. (c) Rodriguez, M., and Bard, A. J. (1990) Electrochemical studies of the interaction of metal chelates with DNA. 4. Voltammetric and electrogenerated chemiluminescent studies of the interaction of tris(2,2'-bipyridine)osmium(II) with DNA. *Anal. Chem.* **62**, 2658–2662.
- (17) (a) Welch, T. W., Corbett, A. H., and Thorp, H. H. (1995) Electrochemical determination of nucleic acid diffusion coefficients through noncovalent association of a redox-active probe. *J. Phys. Chem.* **99**, 11757. (b) Kelly, J. M., Lyons, M.

- E. G., and Van Der Putten, W. J. M. (1986) In *Electrochemistry, Sensors and Analysis* (M. R. Smyth and J. G. Vos, Eds.) pp 205–213, Elsevier, Amsterdam. (c) Molinier-Jumel, C., Malfroy, B., Raymond, J., Reynaud, J. A., and Aubel-Sadron, G. (1978) Electrochemical study of DNA-anthracyclines interaction. *Biochem. Biophys. Res. Commun.* **84**, 441. (d) Berg, H., Horn, G., Luthardt, U., and Ihn, W. (1981) Interaction of anthracycline antibiotics with biopolymers. Part V. Polarographic behavior and complexes with DNA. *Bioelectrochem. Bioenerg.* **8**, 537. (e) Plambeck, J., and Lown, J. W. (1984) Electrochemical studies of antitumor antibiotics. 5. An electrochemical method of measurement of the binding of doxorubicin and daunorubicin derivatives to DNA. *J. Electrochem. Soc.* **131**, 2556.
- (18) Johnston, D. H., Glasgow, K. C., and Thorp, H. H. (1995) Electrochemical measurement of the solvent accessibility of nucleobases using electron transfer between DNA and metal complexes. *J. Am. Chem. Soc.* **117**, 8933.
- (19) (a) Hashimoto, K., Ito, K., and Ishimori, Y. (1994) Sequence-specific gene detection with a gold electrode modified with DNA probes and an electrochemically active dye. *Anal. Chem.* **66**, 3830. (b) Hashimoto, K., Ito, K., and Ishimori, Y. (1994) Novel DNA sensor for electrochemical gene detection. *Anal. Chim. Acta* **286**, 219.
- (20) Okahata, Y., Matsunobu, Y., Ijio, K., Mukae, M., Murakami, A., and Makino, K. (1992) Hybridization of nucleic acids immobilized on a quartz crystal microbalance. *J. Am. Chem. Soc.* **114**, 8300.
- (21) Millan, K. M., and Mikkelsen, S. R. (1993) Sequence-selective biosensor for DNA based on electroactive hybridization indicators. *Anal. Chem.* **65**, 2317–2323.
- (22) (a) Xu, X.-H., Yang, H. C., Mallouk, T. E., and Bard, A. J. (1994) Immobilization of DNA on an aluminum(III) alkanebisphosphonate thin film with electrogenerated chemiluminescent detection. *J. Am. Chem. Soc.* **116**, 8386. (b) Xu, X.-H., and Bard, A. J. (1995) Immobilization and hybridization of DNA on an aluminum(III) alkanebisphosphonate thin film with electrogenerated chemiluminescent detection. *J. Am. Chem. Soc.* **117**, 2627.
- (23) (a) Maeda, M., Mitsuhashi, Y., Nakano, K., and Takagi, M. (1992) DNA-immobilized gold electrode for DNA-binding sensor. *Anal. Sci.* **8**, 83. (b) Maeda, M., Nakano, K., Uchida, S., and Takagi, M. (1994) Mg^{2+} -selective electrode comprising double-helical DNA as receptive entity. *Chem. Lett.* **1805**.
- (24) Ulman, A. (1991) *An Introduction to Ultrathin Organic Films: from Langmuir–Blodgett to Self-Assembly*, Academic Press, Boston.
- (25) (a) Zutic, V., Svetlicic, V., Lovric, M., Ruzic, I., and Chevalet, J. (1984) Electron-transfer kinetics of an adsorbed redox couple by double potential-step chronocoulometry: methylene blue leucomethylene blue. *J. Electroanal. Chem.* **177**, 253. (b) Svetlicic, V., Clavilier, J., Zutic, V., and Chevalet, J. (1991) Electrochemical evidence of 2-dimensional surface compounds of heterocyclic molecules at sulfur-covered gold and platinum. 1. Methylene blue. *J. Electroanal. Chem.* **312**, 205. (c) Ju, H., Zhou, J., Cai, C., and Chen, H. (1995) The electrochemical behavior of methylene blue at a microcylinder carbon-fiber electrode. *Electroanalysis* **7**, 1165.
- (26) (a) Bradley, D. F., Stellwagen, N. C., O'Konski, C. T., and Paulson, C. M. (1972) Electric birefringence and dichroism of acridine orange and methylene blue complexes with polynucleotides. *Biopolymers* **11**, 645. (b) Nordén, B., and Tjerneld, F. (1982) Structure of methylene blue-DNA complexes studied by linear and circular dichroism spectroscopy. *Biopolymers* **21**, 1713. (c) Tuite, E., and Nordén, B. (1994) Sequence-specific interactions of methylene blue with polynucleotides and DNA: a spectroscopic study. *J. Am. Chem. Soc.* **116**, 7548. (d) Tuite, E., and Kelly, J. M. (1995) The interaction of methylene blue, azure B, and thionine with DNA: formation of complexes with polynucleotides and mononucleotides as model systems. *Biopolymers* **35**, 419.
- (27) Beaucage, S. L., and Caruthers, M. H. (1981) Deoxynucleoside phosphoramidites: a new class of key intermediates for deoxypolynucleotide synthesis. *Tetrahedron Lett.* **22**, 1859.
- (28) (a) Widrig, C. A., Alves, C. A., and Porter, M. D. (1991) Scanning tunneling microscopy of ethanethiolate and normal-octadecanethiolate monolayers spontaneously adsorbed at gold surfaces. *J. Am. Chem. Soc.* **113**, 2805. (b) Zei, M. S., Nakai, Y., Lehmpfuhl, G., and Kolb, D. M. (1983) The structure of gold and silver films evaporated on glass: a LEED and RHEED study. *J. Electroanal. Chem.* **150**, 201.
- (29) (a) Nahir, T. M., Clark, R. A., and Bowden, E. F. (1994) Linear-sweep voltammetry of irreversible electron transfer in surface-confined species using Marcus theory. *Anal. Chem.* **66**, 2595. (b) Weber, K., and Creager, S. E. (1994) Voltammetry of redox-active groups irreversibly adsorbed onto electrodes: treatment using the Marcus relation between rate and overpotential. *Anal. Chem.* **66**, 3164. (c) Tender, L., Carter, M. T., and Murray, R. W. (1994) Cyclic voltammetric analysis of ferrocene alkanethiol monolayer electrode kinetics based on Marcus theory. *Anal. Chem.* **66**, 3173.
- (30) Laviron, E. (1975) A critical study of the factors causing the appearance of Brdicka's adsorption currents. Influence of the interactions between adsorbed molecules. *J. Electroanal. Chem.* **63**, 254.
- (31) Sabatini, E., Rubinstein, I., Maoz, R., and Sagiv, J. (1987) Organized self-assembling monolayers on electrodes. 1. Octadecyl derivatives on gold. *J. Electroanal. Chem.* **219**, 365.
- (32) Finklea, H. O., Snider, D. A., and Fedyk, J. (1990) Passivation of pinholes in octadecanethiol monolayers on gold electrodes by electrochemical polymerization of phenol. *Langmuir* **6**, 371.
- (33) Widrig, C. A., Chung, C., and Porter, M. D. (1991) The electrochemical desorption of n-alkanethiol monolayers from polycrystalline Au and Ag electrodes. *J. Electroanal. Chem.* **310**, 335.
- (34) Matthews, C. K., and Van Holde, K. E. (1990) *Biochemistry*, Benjamin Cummings, Redwood City, CA.
- (35) Bard, A. J., and Faulkner, L. R. (1980) *Electrochemical Methods*, Wiley and Sons, New York.
- (36) Christie, J. H., Anson, F. C., Lauer, G., and Osteryoung, R. A. (1963) Determination of charge passed following application of potential step in study of electrode processes. *Anal. Chem.* **35**, 1979.
- (37) Connors, K. A. (1987) *Binding Constants: The Measurement of Molecular Complex Stability*, Wiley-Interscience, New York.
- (38) Crothers, D. M. (1968) Calculation of binding isotherms for heterogeneous polymers. *Biopolymers* **6**, 575.
- (39) Chidsey, C. E. D., Bertozzi, C. R., Putvinski, T. M., and Majsce, A. M. (1990) Coadsorption of ferrocene-terminated and unsubstituted alkanethiols on gold: electroactive self-assembled monolayers. *J. Am. Chem. Soc.* **112**, 4301.
- (40) (a) Smalley, J. F., Feldberg, S. W., Chidsey, C. E. D., Linford, M. R., Newton, M. D., and Liu, Y. (1995) The kinetics of electron transfer through ferrocene-terminated alkanethiol monolayers on gold. *J. Phys. Chem.* **99**, 13141. (b) Finklea, H. O., and Hanshew, D. D. (1992) Electron-transfer kinetics in organized thiol monolayers with attached pentaamine-(pyridine)ruthenium redox centers. *J. Am. Chem. Soc.* **114**, 3173.
- (41) Marcus, R. A., Sutin, N. (1985) Electron transfers in chemistry and biology. *Biochim. Biophys. Acta* **811**, 265.

BC9600700

Influence of Endosome-Destabilizing Peptides on Efficacy of Anti-HIV Immunotoxins

Vladimir V. Tolstikov, Robert Cole, Hua Fang, and Seth H. Pincus*

Laboratory of Microbial Structure and Function, Rocky Mountain Laboratories, National Institute of Allergy and Infectious Diseases, National Institutes of Health, Hamilton, Montana 59840. Received June 13, 1996[®]

The effects on immunotoxin efficacy of fusogenic peptides derived from influenza virus hemagglutinin have been studied. These peptides have an amphipathic nature and change conformation from random at pH 7 to helical at pH 5. Fusogenic peptides are reported to destabilize endosomal membranes, resulting in the release of contents into the cytoplasm. The use of two related fusogenic peptides to enhance the efficacy of anti-HIV immunotoxins is described. The direct toxicity of the peptides was tested on HIV-infected H9/NL4-3 cells. Peptide HA24 was considerably more toxic than HA23. The peptides were mixed with two different immunotoxins. Immunotoxin action was enhanced by both peptides, with HA24 providing greater enhancement than HA23. Immunotoxins were then constructed by coupling HA23 or HA24 to the targeting antibody with disulfide-containing linkers. Peptide HA23 enhanced the activity of the immunotoxin 4–5-fold. Surprisingly, HA24 significantly inhibited immunotoxin activity. Coupling the peptides to the immunotoxin had no effect on antigen binding characteristics or the activity of the toxic moiety. Bafilomycin A₁, an agent that inhibits vacuolar acidification, markedly potentiated the effects of all immunotoxins. These results demonstrate that amphipathic peptides can influence the efficacy of immunotoxins, but in sometimes unpredictable ways.

Immunotoxins are bifunctional molecules containing a targeting portion, usually either an antibody or a ligand of a cell-surface receptor, and a toxic moiety. Immunotoxins bind to target cells and are internalized, and the toxic moiety is translocated to its site of action. The toxic moiety of a number of immunotoxins are polypeptides displaying enzymatic activity. Ricin A chain (RAC¹) depurinates an adenine residue in 28 S rRNA. Diphtheria toxin and pseudomonas exotoxin A (PE) exhibit ADP-ribosylating activity. These enzymatic activities, requiring translocation to the cytoplasm, arrest protein synthesis and cause cell death. Although the toxins are extremely potent, cytotoxic activity is limited by lysosomal degradation of the vast majority of internalized molecules (1, 2). Potentiation of immunotoxin action can be achieved by coadministration of drugs that inhibit lysosomal function, including monensin, chloroquine, and ammonium chloride (1, 3).

The use of amphipathic peptides that interact with the membrane bilayer and are able to destabilize membranes under acidic conditions can enhance the efficiency of gene transfer (4, 5) and cytoplasmic delivery of antisense oligonucleotides (6). The peptides have a random configuration at neutral pH but assume an amphipathic helix at acid pH. Peptides containing the N-terminal amino acid sequence of influenza virus hemagglutinin

have been demonstrated to lyse liposomes and erythrocytes at pH 5, but not at pH 7 (5). Such peptides were used to prepare covalent (4, 6) and noncovalent (5) plasmid or oligonucleotide conjugates/complexes. It is believed that once in the endosome, the fusogenic peptides self-assemble and form a transmembrane channel, thereby disrupting the vacuolar membrane and preventing lysosomal degradation of the transferred nucleic acids.

In the present paper, we study the use of such peptides to enhance the action of immunotoxins. As a model system, we have used anti-HIV immunotoxins targeted to the HIV envelope protein gp120, expressed on the surface of persistently infected cells (7–10). Peptides were either mixed with or conjugated to the immunotoxin. The results indicate that this approach can enhance the cytotoxicity of immunotoxins, but some unexpected phenomenon were observed.

EXPERIMENTAL PROCEDURES

Immunotoxin Synthesis. HA23 peptide, corresponding to the NH₂-terminal 20 amino acids (AA) of hemagglutinin extended with a 3 AA COOH-terminal tail (GLFEAIAAGFIENGWEGMIDGGGC), and the acidic mutant HA24 peptide, corresponding to the NH₂-terminal 23 amino acids with A7 replaced with E and having a COOH-terminal C (GLFEAIEGFIENGWEGMIDGWYGC), were synthesized on an automated peptide synthesizer using standard methods (Applied Biosystems Inc., Foster City, CA; Model 431A). The peptides were cleaved from the resin with trifluoroacetic acid/water/phenol/thioanisole/ethanedithiol (10:0.5:0.5:0.66). Crude peptides were dissolved in 20 mM ammonium bicarbonate with 300 μ L of 25% ammonia/L, reduced with dithiothreitol (DTT) and *N*-methylmercaptoacetamide (Fluka Chemika-BioChemika, Buchs, Switzerland), and purified by high-performance liquid chromatography (HPLC, preparative Nova-Pak HR C₁₈, Waters/Millipore, Milford, MA) on a 40–95% methanol gradient. The purity of the peptides was determined by analytical

* Address correspondence to this author at the Department of Microbiology, Montana State University, Bozeman MT 59717 [telephone (406) 994-6486; fax (406) 994-4926; e-mail umbbsp@gemini.oscs.montana.edu]. Address reprint requests c/o Susan Smaus, Rocky Mountain Laboratories, Hamilton, MT 59840.

[®] Abstract published in *Advance ACS Abstracts*, December 15, 1996.

¹ Abbreviations: DTT, dithiothreitol; ELISA, enzyme-linked immunosorbent assay; HPLC, high-performance liquid chromatography; LC-SPDP, sulfosuccinimidyl 6-[3'-(2-pyridylthio)propionamido]hexanoate; PAGE, polyacrylamide gel electrophoresis; PDP, pyridyldithiopropionyl; PE, pseudomonas exotoxin A; RAC, ricin A chain; SEM, standard error of the mean; SPDP, succinimidyl 3-(2-pyridylthio)propionate.

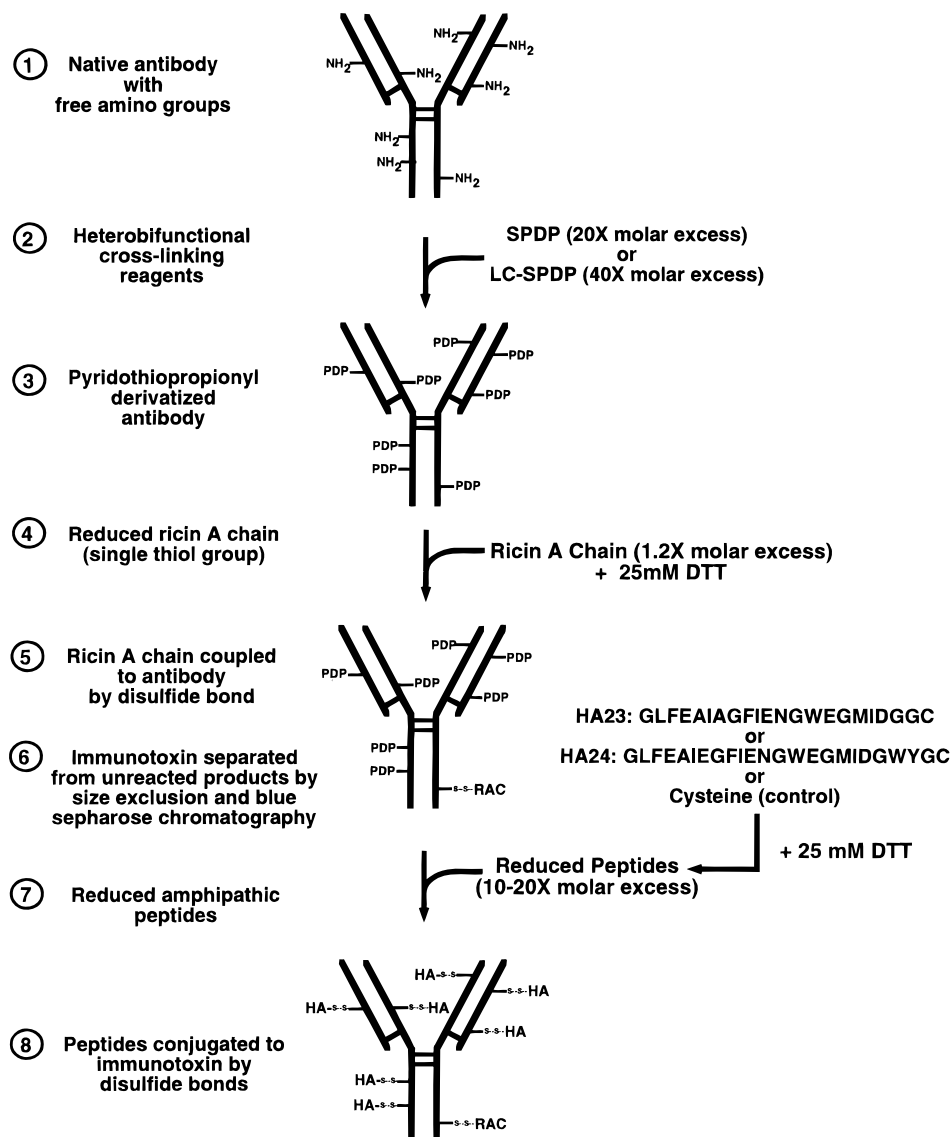


Figure 1. Construction of peptide-containing immunotoxins.

reversed phase HPLC. The amino acid sequence of both peptides was confirmed by sequence analysis (Applied Biosystems Inc., Model 470A protein sequencer equipped with a Model 120A PTH-amino acid analyzer).

A diagram of the conjugation scheme for the construction of the peptide-derivatized immunotoxins is shown in Figure 1. Monoclonal antibody 924 binds to the V3-loop of HIV gp120, strain IIIB (7). T7 is an irrelevant isotype matched antibody (11). Both were grown as hybridoma supernatants, purified on protein G-Sepharose (Pharmacia, Piscataway, NJ) and then by size exclusion HPLC (TSK-GEL G3000SW, TosoHaas, Japan). The antibody was treated with a 20-fold excess of sulfosuccinimidyl 6-[3'-(2-pyridylthio)propionamido]hexanoate (LC-SPDP; Pierce, Rockford, IL) or a 40-fold excess of succinimidyl 3-(2-pyridylthio)propionate (SPDP; Pierce) as previously described (12, 13). Modified antibodies were separated from an excess of reagent by size exclusion HPLC. The number of introduced pyridylthiopropionyl (PDP) groups was measured by reduction with 25 mM DTT and UV spectroscopy at 343 nm as described (14).

Deglycosylated ricin A chain (RAC; Inland Laboratories, DeSoto, TX) was reduced in the presence of 25 mM DTT and purified from DTT on Sephadex G-25M (Pharmacia) under nitrogen. A 1.2-fold molar excess of reduced

RAC was mixed with modified mAb, concentrated under nitrogen to 1 mg/mL of protein, and gently stirred for 48 h. Immunotoxins were separated from unreacted RAC by size exclusion HPLC. Unreacted mAb was separated by affinity chromatography on Blue Sepharose CL-6B (Pharmacia) as described (15). Purified immunotoxins were mixed with a 10–20-fold molar excess (relative to the amount of introduced PDP groups) of reduced HA23 or HA24 peptides or, as a control, cysteine, and gently stirred for 24 h. Modified immunotoxins were separated from unreacted peptides by size exclusion HPLC. The absence of the unreacted PDP groups was confirmed by measuring OD at 343 nm after reduction of purified immunoconjugates. There was no evidence of substitution of RAC by the peptides. The constitution of the immunotoxins was confirmed using SDS–polyacrylamide gel electrophoresis (PAGE) under both reducing and nonreducing conditions.

The immunotoxin CD4-PE40 is a chimeric fusion protein consisting of the two amino-terminal domains of CD4 coupled to the toxic domains of *Pseudomonas* exotoxin A (10, 16). It was the kind gift of Upjohn Laboratories (Kalamazoo, MI). Immunotoxins used in this study are summarized in the Table 1.

Immunoassay. Antigen binding and constitution of the immunotoxins were characterized by enzyme-linked

Table 1. Immunotoxins Used in This Study

immunotoxin	linker	specificity
T7-RAC	SPDP	synthetic polypeptide (Y,E)-A--K (irrelevant antigen)
CD4-PE40	fusion protein	CD4 binding site of HIV gp120
924-Ic-RAC	LC-SPDP	AA 309-318 (V3-loop) of gp120
924-Ic-RAC-HA23	LC-SPDP	AA 309-318 (V3-loop) of gp120
924-RAC	SPDP	AA 309-318 (V3-loop) of gp120
924-RAC-HA23	SPDP	AA 309-318 (V3-loop) of gp120
924-RAC-HA24	SPDP	AA 309-318 (V3-loop) of gp120

immunoassay (ELISA). Ninety-six-well U-bottom plates (Immulon-2, Dynatech, Chantilly, VA) were coated with a peptide corresponding to the V3-loop of gp120 (TRP-NNNTRKSIRIQRGPGRAFTVIGKIGNMRQAH) at 5 $\mu\text{g}/\text{mL}$ (17) and blocked with 3% BSA/0.1% Tween 20 in PBS. Plates were incubated with immunotoxins overnight at 4 °C. They were then washed and incubated with either guinea pig anti-RAC or rabbit anti-HA23 overnight at 4 °C. After washing, the plates were incubated with alkaline phosphatase-conjugated anti-guinea pig or rabbit Ig (Zymed Laboratories, South San Francisco, CA) for 2 h and washed again. As shown under Results, these anti-Ig do not cross-react with the mouse Ig component of the immunotoxin. Substrate (*p*-nitrophenyl phosphate; Sigma Chemical Co., St. Louis, MO) was added at 0.5 mg/mL, and OD₄₀₅ was determined 30–90 min later by using an automated ELISA reader (Bio-Rad Model 2550; Richmond, CA). Data are means and standard error of the mean (SEM) of triplicate samples.

Cell-Free Protein Synthesis. Untreated reticulocyte lysate *in vitro* translation kit was purchased from Ambion, Inc. (Austin, TX). Immunotoxin was added to a cell-free extract of rabbit reticulocyte lysate in the presence of [³⁵S]Met and incubated for 120 min at 37 °C. Protein was precipitated with trichloroacetic acid and the amount of label incorporated determined by liquid scintillation counting.

Assay of Immunotoxin Efficacy. The cytotoxic effect of the immunotoxins was tested on H9 cells persistently infected with the molecularly cloned strain of HIV-1 designated NL4-3 (7, 18, 19) by assaying [³⁵S]-Met incorporation into cellular proteins. Details of all techniques have previously been published (7). The results shown are means and SEM of triplicate samples.

RESULTS

Toxicity of Free Peptides on H9/NL4-3 Cells. Peptides HA23 and HA24 were tested for toxicity on persistently HIV-infected H9/NL4-3 cells at concentrations up to 1 mg/mL. HA23 peptide did not show any significant cytotoxicity, while a dose-dependent effect was obtained with HA24 peptide at concentrations as low as 125 $\mu\text{g}/\text{mL}$ (Figure 2). Thus, HA24 had greater direct toxicity upon HIV-infected cells. Similar results were obtained when both peptides were tested on uninfected H9 cells (data not shown). These results are consistent with previous studies showing greater membrane lysis by HA24 (5).

Effects of Mixing Peptides with Anti-HIV Immunotoxins. H9/NL4-3 cells were treated with suboptimal concentrations of immunotoxins (0.3 $\mu\text{g}/\text{mL}$) in the absence or presence of HA23 or HA24 (Figure 3). Peptides were tested at two concentrations within the nontoxic range for each peptide (the concentration of HA24 tested was lower than that of HA23). A small, dose-dependent enhancement of cytotoxicity was seen with each peptide. The effect was greater on CD4-PE40 than on 924-RAC. A marginal increase in toxicity of the irrelevant control immunotoxin was also observed.

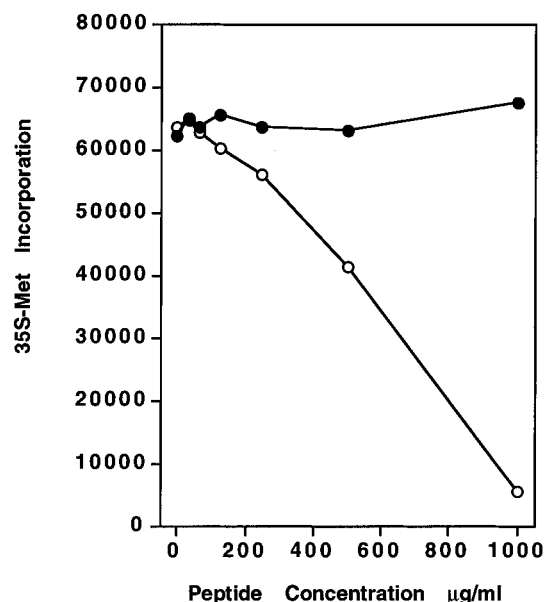


Figure 2. Inhibitory effect of peptides on H9/NL4-3 cells. 4×10^4 HIV-infected H9/NL4-3 cells were incubated with various concentrations of the HA23 (\bullet) or HA24 (\circ) peptide for 48 h in 200 μL per well. Cells were pulsed with [³⁵S]Met (0.5 $\mu\text{Ci}/\text{well}$) and incubated for an additional 24 h; the cellular proteins were harvested onto filter paper and counted in a scintillation counter. Results are counts per minute, means of triplicate values.

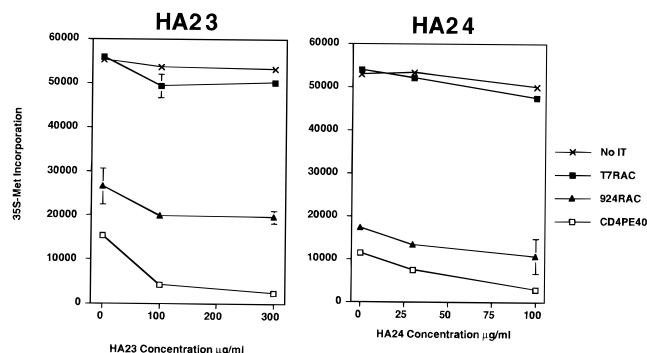


Figure 3. Effect of HA23 and HA24 peptides on cytotoxicity of anti-HIV immunotoxins. H9/NL4-3 cells were incubated with the indicated immunotoxin and various concentrations of free HA23 or HA24 peptides. Because of the differences in the direct toxicities of the two peptides, they were tested at different concentrations so that the direct effect of the peptides was comparable. Immunotoxins were used at a suboptimal concentration (0.3 $\mu\text{g}/\text{mL}$). Protein synthesis was assayed as in Figure 2. Results are means and SEM of triplicate values.

Synthesis and Characterization of Immunotoxins Conjugated to HA-Peptides. Immunotoxins were constructed by conjugating antibody 924 with an excess of disulfide-containing linkers (either SPDP, 6.8 Å length, or LC-SPDP, 15.6 Å length). RAC was next coupled to the antibody at an approximate ratio of 1:1. The 924-RAC conjugates were divided into aliquots and then coupled to HA23, HA24, or cysteine. Table 1 summarizes the different constructions that were made, and Figure 4 shows the results of nonreduced gradient SDS-PAGE performed on the immunotoxin preparations. Immunotoxins incorporating peptides had an increased molecular weight compared to those modified with cysteine. Those modified with SPDP incorporate more peptide, consistent with the greater degree of PDP modification obtained with this linker. The presence of approximately equimolar concentrations of antibody and RAC was confirmed by SDS-PAGE under reducing conditions and western blots (data not shown).

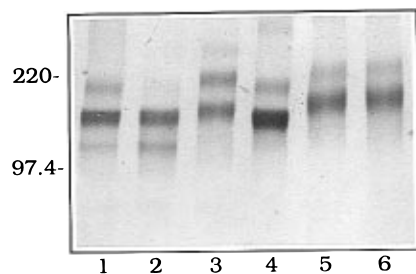


Figure 4. PAGE of immunotoxin preparations. Immunotoxins were run on polyacrylamide gradient (5–10%) gels under nonreducing conditions. Gels were stained with Coomassie blue. (Lane 1) T7-RAC; (lane 2) 924-lc-RAC; (lane 3) 924-lc-RAC-HA23; (lane 4) 924-RAC; (lane 5) 924-RAC-HA23; (lane 6) 924-RAC-HA24. Lanes 1 and 2 demonstrate the presence of breakdown products. Lanes 3–6 contain higher order multimers. The band containing monomeric immunotoxin is the most intense band in each lane.

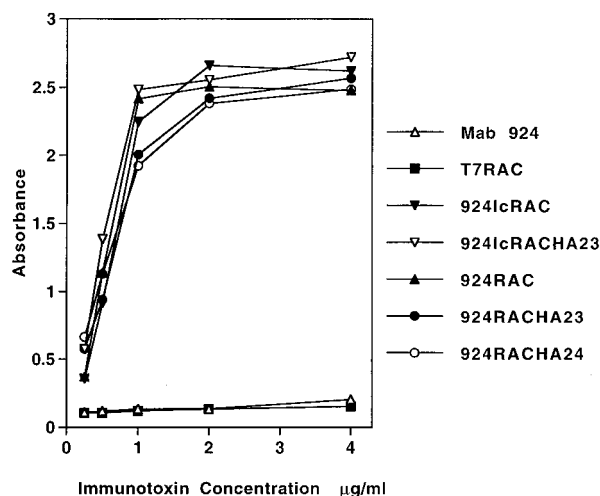


Figure 5. Identification of RAC in immunotoxins by ELISA. Microtiter wells were coated with a peptide representing the V3-loop of HIV gp120. Different immunotoxins over a range of concentrations were incubated in the wells, followed successively by guinea pig anti-ricin antibodies, alkaline phosphatase-conjugated anti-guinea pig Ig, and the addition of a chromogenic substrate. An important negative control is the use of unconjugated mab 924, which demonstrates that there is no cross-reaction between anti-guinea pig Ig and the mouse mab. Results are means of triplicate values.

The ability of immunotoxins to bind antigen was evaluated by ELISA. Using alkaline phosphatase-conjugated anti-mouse Ig, it was demonstrated that immunotoxins and unmodified antibody bound equivalently to antigen (not shown). The presence and amount of RAC in antigen-binding immunotoxins was measured using guinea pig anti-RAC antibody and an alkaline phosphatase-conjugated anti-guinea pig Ig to detect antigen-bound immunotoxin (Figure 5). The results show that all immunotoxin preparations contained equal amounts of RAC. The absence of binding to unconjugated antibody 924 demonstrates that the alkaline phosphatase-conjugated anti-guinea pig Ig did not cross-react with mouse Ig. We have defined the incorporation of peptides into immunotoxins in a similar fashion, using rabbit anti-HA23 antisera. Although this antiserum also reacted with HA24, reactivity was reduced by approximately half as measured by competitive ELISA (not shown). The presence of peptides in the appropriate immunotoxins is clearly shown in Figure 6, with 924-RAC-HA23 incorporating more peptide than 924-lc-RAC-HA23 as expected from the molecular weight of the conjugates (Figure 4).

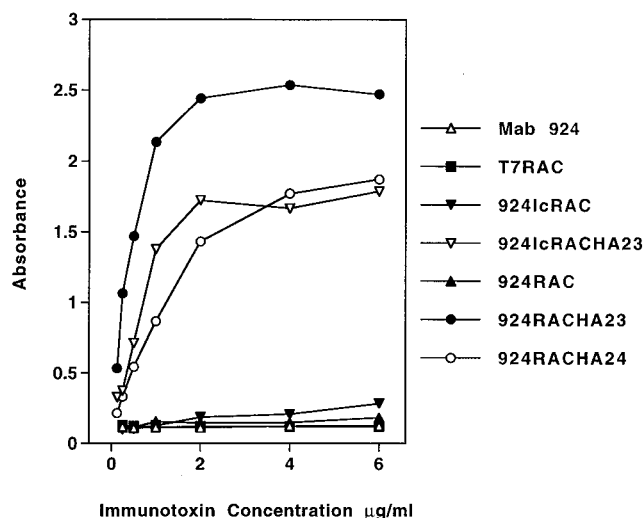


Figure 6. Identification of HA23 and HA24 in immunotoxins by ELISA. ELISA was performed as in Figure 5 but using rabbit anti-HA23 antiserum and an alkaline phosphatase-conjugated anti-rabbit Ig.

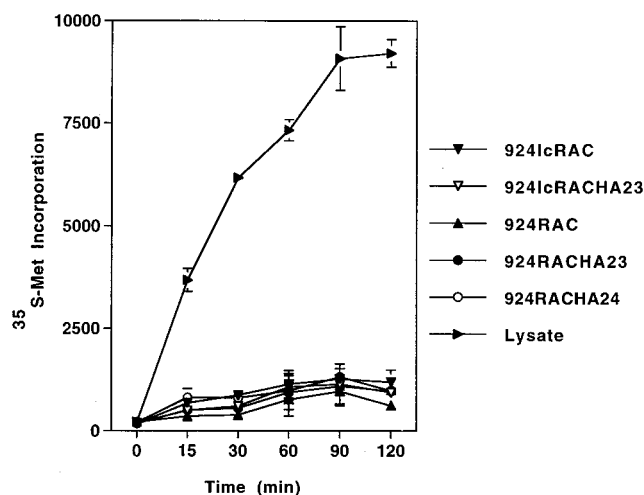


Figure 7. RAC enzymatic activity in immunotoxins. Inhibition of cell-free protein synthesis by immunotoxins was measured using rabbit reticulocyte lysate. The lysate is an assay mixture containing [35 S]Met and was incubated at 37 °C for 120 min with immunotoxins. [35 S]Met incorporated into protein was measured as counts per minute. Data labeled lysate indicates protein synthesis in the absence of any immunotoxin. Results are means and SEM of triplicate values.

To determine whether the incorporation of peptides into immunotoxins hindered the enzymatic function of RAC, we measured the ability of the immunotoxins to inhibit cell-free protein synthesis from a rabbit reticulocyte lysate. Protein synthesis was measured as the incorporation of [35 S]Met. All immunotoxins inhibited cell-free translation to an equivalent degree (Figure 7).

Cytotoxicity of Immunotoxin–Peptide Conjugates. The cytotoxic efficacy of immunotoxin–peptide conjugates was determined by measuring cellular protein synthesis in H9/NL4-3 cells. Conjugation of immunotoxins to HA23 enhanced cell killing 2–4-fold compared to the equivalent cysteine-containing immunotoxin (Figures 8 and 9). This was seen with two completely different immunotoxin preparations, indicating that this is not a fortuitous result from an exceptionally efficient immunotoxin conjugation. Surprisingly, incorporation of the more toxic HA24 peptide resulted in a 10-fold diminution in immunotoxin activity (Figure 9). None of the immunotoxins had any effect on uninfected H9 cells (not shown).

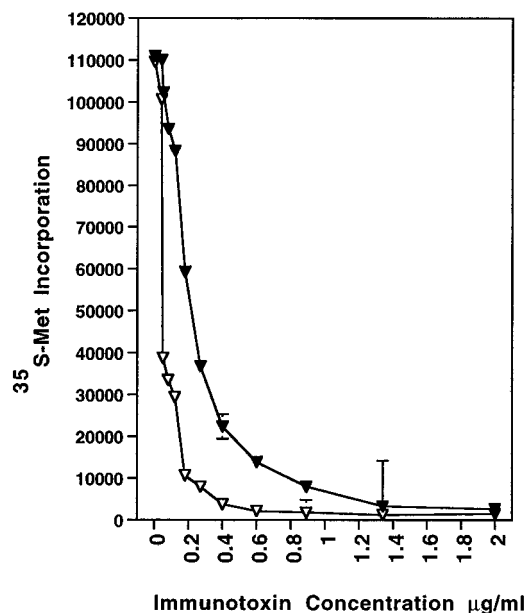


Figure 8. Enhancement of immunotoxin efficacy by incorporation of HA23 peptide. The comparative efficacy of two immunotoxins, differing only in the attachment of HA23 (∇) or cysteine (▼), was tested in H9/NL4-3 cells. Protein synthesis in target cells was measured during a 3-day culture period. Results are means and SEM of triplicate values.

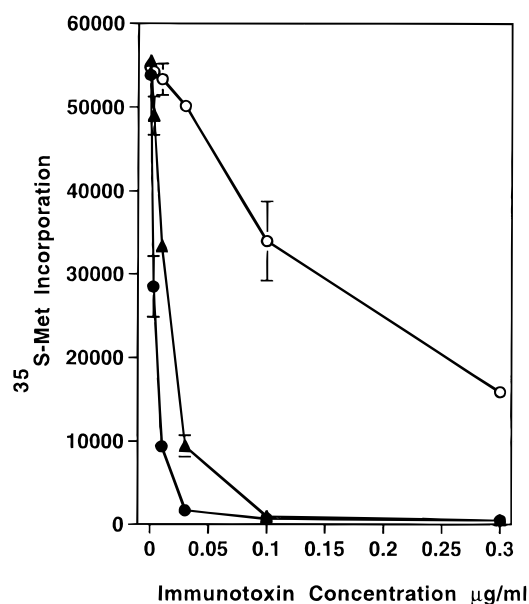


Figure 9. Contrasting effects of HA23 and HA24 on immunotoxin efficacy. Immunotoxins incorporating HA23 (●), HA24 (○), or cysteine (▲) were compared for cytotoxicity on H9/NL4-3 cells. Results are means and SEM of triplicate values.

Because vacuolar acidification is reportedly required for the action of the HA peptides (5), we have tested the effect of bafilomycin A₁, an inhibitor of the vacuolar H⁺ pump, on the immunotoxin-peptide constructs (Figure 10). Bafilomycin A₁ had an enhancing effect on all of the immunotoxins. However, even in the presence of bafilomycin A₁, the cytotoxic activity of 924-RAC-HA23 was greater and 924-RAC-HA24 was diminished in comparison to 924-RAC.

DISCUSSION

Inhibition of lysosomal function can potentiate the cytotoxic effects of immunotoxins because the majority of internalized immunotoxin molecules are degraded,

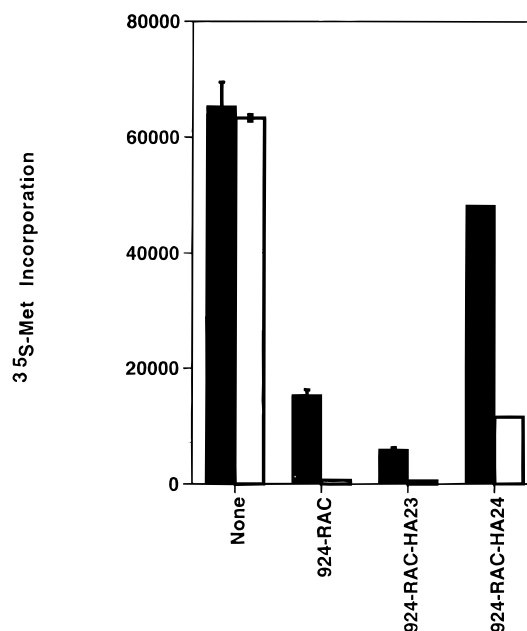


Figure 10. Effect of bafilomycin A₁ on immunotoxin action. Protein synthesis was assayed in H9/NL4-3 cells exposed to immunotoxin in the presence (□) or absence (■) of 3 nM bafilomycin A₁. Immunotoxins were used at 0.01 μg/mL. Results are means and SEM of triplicate values.

primarily in lysosomes, before they can reach their site of toxic action. In this paper we have explored the use of amphipathic peptides derived from the fusion region of the influenza hemagglutinin to enhance the activity of anti-HIV immunotoxins. Under appropriate conditions, the fusogenic peptides enhanced the activity of anti-HIV immunotoxins to the same degree as other inhibitors of lysosomal function, including monensin, chloroquine, and ammonium chloride (3).

The idea to use fusogenic peptides as enhancers of immunotoxin efficacy is based on the ability of these peptides to disrupt membranes at acidic pH (4, 5). The peptides have a random conformation at neutral pH but assume an amphipathic helix under acidic conditions. It is believed that once the endosome is acidified, the fusogenic peptides self-assemble and form a transmembrane channel, thereby disrupting the vacuolar membrane. This approach has been applied to the functional transfer of nucleic acids into target cells. Increased effects were seen with mixtures and with conjugates of nucleic acids with the fusogenic peptides (4, 5). A similar approach, using a genetic fusion of the N terminus of protein G of the vesicular stomatitis virus to ricin A chain, has demonstrated enhanced immunotoxin efficacy (20).

Peptides HA23 and HA24 were both tested in membrane lysis and gene transfer systems. Each was active in disrupting membranes and in increasing efficiency of gene transfer, with HA24 having greater activity than HA23 (5). Our studies of the toxicity of free peptides (Figure 2) and of the additive effect of peptides mixed with anti-HIV immunotoxins (Figure 3) confirm that HA24 is more toxic than HA23. Paradoxically, when the peptides were conjugated to the immunotoxin, HA23 enhanced cytotoxicity while HA24 markedly diminished the toxic effect of the immunotoxin.

The mechanism whereby the HA24 peptide inhibits, rather than enhances, the action of the immunotoxin conjugate is unclear. It does not prevent antigen binding or hinder the enzymatic activity of RAC. We do not believe that the differences are due to the amount of

peptide incorporated into the immunotoxin for the following reasons: 1. There is not simply a lack of enhancement but rather a marked inhibition of immunotoxin activity, suggesting that HA24 is actively interfering. 2. In preliminary studies (data not shown), immunotoxins conjugated with lower amounts of HA23 showed a lack of enhancement but no inhibition. One possibility to explain the inhibition of immunotoxin action by HA24 is that because it is so active in lysing membranes, the endocytic vacuole is lysed before reduction is complete and free RAC is not fully liberated from the immunotoxin complex.

We have demonstrated that the use of bafilomycin A₁ can markedly enhance the potency of immunotoxins. Bafilomycin A₁ is a specific poison of the vacuolar ATP-dependent proton pump. The most likely mechanism of potentiation of immunotoxin action is by inhibiting lysosomal degradation and allowing more RAC to reach the ribosomes, although other alterations of the intracellular routing of the immunotoxin cannot be ruled out. Bafilomycin A₁ has no effect on the processing or cell-surface display of the HIV envelope (data not shown).

Interestingly, the enhancing effect of HA23 and the inhibitory effect of HA24 were still active in the presence of bafilomycin A₁. This was unexpected because these peptides demonstrate greatest lytic activity under acid conditions. It is possible that the concentration of bafilomycin A₁ used did not fully prevent acidification of vacuoles, although we have also seen effects of these peptides in the presence of the lysosomal alkalinizing agent ammonium chloride (data not shown). Thus, these fusogenic peptides may also function under nonacidic conditions. While the ability of these peptides to lyse biological membranes is greatest at pH ≤ 5, some lytic activity has been reported at pH 7 (5).

The use of immunotoxins has been proposed for the treatment of cancer, autoimmune conditions, transplantation, and infectious diseases. Although significant problems are associated with the clinical use of immunotoxins, these therapies have shown some promise in early clinical trials. Methods that may potentiate the specific cytotoxic action of immunotoxins and not exacerbate the problems may prove useful. In this paper, we have demonstrated two novel approaches: the use of amphipathic peptides, either mixed with or conjugated to the immunotoxin, and bafilomycin A₁. Both most likely function through inhibition of lysosomal degradation of immunotoxins, and an additive effect of the two is seen (Figure 10). Although these effects were demonstrated using anti-HIV immunotoxins on HIV-infected cells, they should be generalizable to other targets of immunotoxin therapy.

ACKNOWLEDGMENT

This work was supported by NIAID intramural research funds and by the NIH Targeted AIDS Antiviral Program. We thank Carole Smaus and Susan Smaus for word-processing assistance, Robert Evans and Gary Hettrick for artwork, and John Swanson and Tom Duenning for helpful comments.

LITERATURE CITED

- (1) van Oosterhout, Y. V., Preijers, F. W., Wessels, H. M., and de Witte, T. (1992) Cytotoxicity of CD3-ricin A chain immunotoxins in relation to cellular uptake and degradation kinetics. *Cancer Res.* 52, 5921–5925.
- (2) Goldenberg, D. M. (1993) Monoclonal antibodies in cancer detection and therapy. *Am. J. Med.* 94, 297–312.
- (3) Pincus, S. H., McClure, J., and Fang, H. (1994) Use of anti-HIV immunotoxins as probes of the biology of HIV-infected cells. *Can. J. Infect. Dis.* 5 (Suppl. A), 23A–27A.
- (4) Wagner, E., Plank, C., Zatloukal, K., Cotten, M., and Birnstiel, M. L. (1992) Influenza virus hemagglutinin HA-2 N-terminal fusogenic peptides augment gene transfer by transferrin-polylysine-DNA complexes: toward a synthetic virus-like gene-transfer vehicle. *Proc. Natl. Acad. Sci. U.S.A.* 89, 7934–7938.
- (5) Plank, C., Oberhauser, B., Mechtler, K., Koch, C., and Wagner, E. (1994) The influence of endosome-disruptive peptides on gene transfer using synthetic virus-like gene transfer systems. *J. Biol. Chem.* 269, 12918–12924.
- (6) Bongartz, J.-P., Aubertin, A.-M., Milhaud, P. G., and Lebleu, B. (1994) Improved biological activity of antisense oligonucleotides conjugated to a fusogenic peptide. *Nucleic Acids Res.* 22, 4681–4688.
- (7) Pincus, S. H., Cole, R. L., Hersh, E. M., Lake, D., Masuho, Y., Durda, P. J., and McClure, J. (1991) In vitro efficacy of anti-HIV immunotoxins targeted by various antibodies to the envelope protein. *J. Immunol.* 146, 4315–4324.
- (8) Pincus, S. H., and McClure, J. (1993) Soluble CD4 enhances the efficacy of immunotoxins directed against gp41 of the human immunodeficiency virus. *Proc. Natl. Acad. Sci. U.S.A.* 90, 332–336.
- (9) Pincus, S. H., and Tolstikov, V. V. (1995) Anti-human immunodeficiency virus immunoconjugates. *Adv. Pharmacol.* 32, 205–242.
- (10) Berger, E. A., Clouse, K. A., Chaudhary, V. K., Chakrabarti, S., FitzGerald, D. J., Pastan, I., and Moss, B. (1989) CD4–*Pseudomonas* exotoxin hybrid protein blocks the spread of human immunodeficiency virus infection in vitro and is active against cells expressing the envelope glycoproteins from primate immunodeficiency retroviruses. *Proc. Natl. Acad. Sci. U.S.A.* 86, 9539–9543.
- (11) Pincus, S. H., Stocks, Jr., C. J., and Ewing, L. P. (1982) Monoclonal anti-(T,G)-A-L antibodies: characterization of fine specificity and idiotype expression. *Mol. Immunol.* 19, 1551–1559.
- (12) Fulton, R. J., Uhr, J. W., and Vitetta, E. S. (1986) The effect of antibody valency and lysosomotropic amines on the synergy between ricin A chain- and ricin B chain-containing immunotoxins. *J. Immunol.* 136, 3103–3109.
- (13) Pincus, S. H., Wehrly, K., and Chesebro, B. (1989) Treatment of HIV tissue culture infection with monoclonal antibody-ricin A chain conjugates. *J. Immunol.* 142, 3070–3075.
- (14) Carlsson, J., Drevin, H., and Axen, R. (1978) Protein thiolation and reversible protein-protein conjugation. *Biochem. J.* 173, 723–737.
- (15) Knowles, P. P., and Thorpe, P. E. (1987) Purification of immunotoxins containing ricin A-chain and abrin A-chain using blue sepharose CL-6B. *Anal. Biochem.* 160, 440–443.
- (16) Chaudhary, V. K., Mizukami, T., Fuerst, T. R., FitzGerald, D. J., Moss, B., Pastan, I., and Berger, E. A. (1988) Selective killing of HIV-infected cells by recombinant human CD4–*Pseudomonas* exotoxin hybrid protein. *Nature* 335, 369–372.
- (17) Pincus, S. H., Messer, K. G., Schwartz, D. H., Lewis, G. K., Graham, B. S., Blattner, W. A., and Fisher, G. (1993) Differences in the antibody response to human immunodeficiency virus-1 envelope glycoprotein (gp160) in infected laboratory workers and vaccinees. *J. Clin. Invest.* 91, 1987–1996.
- (18) Adachi, A., Gendelman, H. E., Koenig, S., Folks, T., Willey, R., Rabson, A., and Martin, M. A. (1986) Production of acquired immunodeficiency syndrome-associated retrovirus in human and nonhuman cells transfected with an infectious molecular clone. *J. Virol.* 59, 284–291.
- (19) Pincus, S. H., and Wehrly, K. (1990) AZT demonstrates anti-HIV-1 activity in persistently infected cell lines: implications for combination chemotherapy and immunotherapy. *J. Infect. Dis.* 162, 1233–1238.
- (20) Chignola, R., Anselmi, C., Dalla Serra, M., Franceschi, A., Fracasso, G., Pasti, M., Chiesa, E., Lord, J. M., Tridente, G., and Colombatti, M. (1995) Self-potentiation of ligand-toxin conjugates containing ricin A chain fused with viral structures. *J. Biol. Chem.* 270, 23345–23351.

Synthesis of the Protein Cutting Reagent Iron (S)-1-(*p*-Bromoacetamidobenzyl)ethylenediaminetetraacetate and Conjugation to Cysteine Side Chains

Douglas P. Greiner,^{†,‡} Reiko Miyake,[†] Justin K. Moran,^{†,§} A. Daniel Jones,^{||} Tomofumi Negishi,[⊥] Akira Ishihama,[⊥] and Claude F. Meares^{*,†}

Department of Chemistry, University of California, Davis, California 95616, Facility for Advanced Instrumentation, University of California, Davis, California 95616, and Department of Molecular Genetics, National Institute of Genetics, Mishima, Shizuoka 411, Japan. Received October 9, 1996[®]

Convenient methodology for preparation and conjugation of the protein-cutting iron chelate iron (S)-1-(*p*-bromoacetamidobenzyl)ethylenediaminetetraacetate (Fe-BABE) is given. This formulation of the reagent can be handled in a manner analogous to many other protein-labeling reagents, such as fluorescent probes or cross-linkers. By taking advantage of the recently discovered peptide hydrolysis reaction, the chelate may be tethered to a single site (e.g., a cysteine side chain) and used to map its proximity to individual peptide bonds by automated Edman sequencing of the protein fragments produced. The method is illustrated by conjugation of Fe-BABE to the carboxy terminal domain (amino acid residues 234–329) of the *Escherichia coli* RNA polymerase alpha subunit. The molecular mass of the protein conjugate was confirmed by electrospray ionization mass spectrometry.

Recently, we and others (1–3) have developed reagents based on small metal chelates that cleave polypeptide chains at sites determined by proximity to the chelate, apparently independent of the amino acid residues involved. By taking advantage of the recently discovered peptide hydrolysis reaction, the chelate may be tethered to a single site (e.g., a cysteine side chain) and used to map its proximity to individual peptide bonds (1). This methodology has rapidly developed to the point where it can be applied to complex biological systems such as membrane proteins (4).

Bifunctional chelating agents possess both a strong metal-binding moiety and a group that binds to a biological molecule (5). Since its original synthesis (6), the bifunctional chelating agent BABE¹ has been employed in a variety of ways to couple metal ions to biological molecules, including both radiopharmaceutical synthesis and targeted protein hydrolysis. Modified approaches to this and other related reagents have been developed in other laboratories (7, and references cited therein). Here we describe the preparation of a conve-

nient formulation of the protein cutting reagent Fe-BABE. This avoids the need to add iron after conjugation and can be handled in a manner analogous to many other protein-labeling reagents, such as fluorescent probes or cross-linkers.

To illustrate the conjugation method, the carboxy terminal domain (amino acid residues 234–329) of *Escherichia coli* RNA polymerase alpha subunit (alpha-CTD), which weighs 11 kDa and contains only one cysteine residue, was conjugated with Fe-BABE and the product isolated and characterized.

MATERIALS AND METHODS

One molar BH₃·THF, 10% palladium on carbon, bromoacetic acid, and bromoacetyl bromide were purchased from Aldrich Chemical Co. L-Phenylalanine was obtained from Sigma. The fluorescent dye CPM was purchased from Molecular Probes Inc. All other reagents were obtained from commercial sources and used without further purification. Pure water (18 MΩ cm⁻¹) was used throughout. All labware was either purchased as metal-free or acid-washed (8).

Thin Layer Chromatography. Plastic-backed silica gel TLC plates (Kieselgel 60 F₂₅₄, EM Science, Alltech) were developed in 95% EtOH/6.5 M NH₄OH (4:1 v/v). ⁵⁷Co metal binding assays and thiol plate TLC were performed according to the procedures of Moran *et al.* (9).

High-Performance Liquid Chromatography. HPLC was carried out on a Rainin three-pump HPXL system with titanium piston washing pump heads. UV absorbance was monitored at 254 nm. Analytical reversed-phase HPLC was performed at room temperature with a Dynamax 10 × 250 mm semipreparative C₁₈ column, flow rate 3 mL/min, to monitor the progress of reactions. Preparative reversed-phase HPLC, 12.5 mL/min, using a Dynamax 21.4 × 250 mm C₁₈ column was used for purification. The HPLC gradients used were as follows. (1) Solvent A, 0.1 M ammonium acetate, pH 6.0;

* Author to whom correspondence should be addressed [telephone (916) 752-0936; fax (916) 752-8938; e-mail cfmeares@ucdavis.edu].

[†] Department of Chemistry.

[‡] Present address: Genentech, Inc., Department of Process Science, 460 Pt. San Bruno Blvd., South San Francisco, CA 94080.

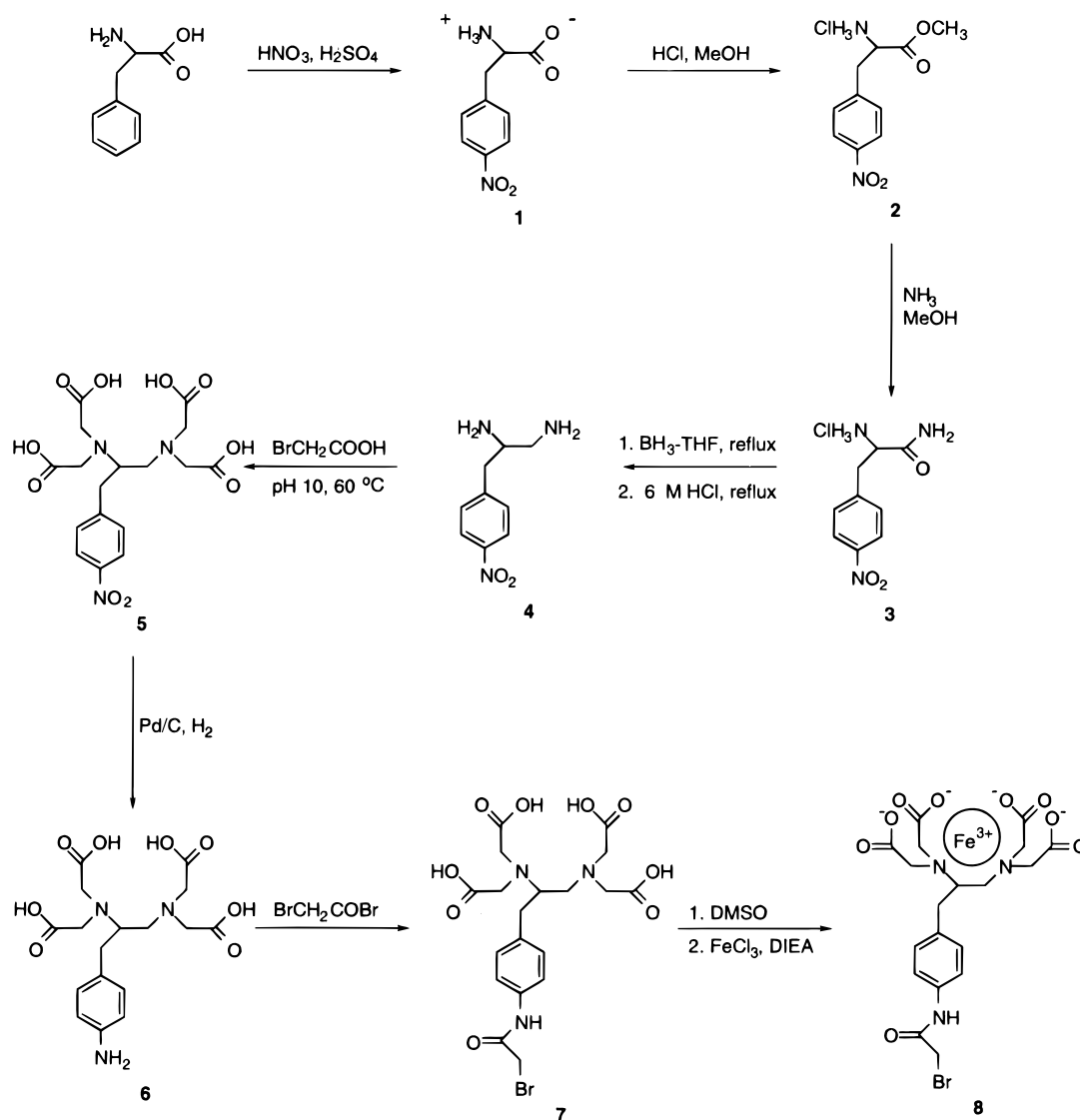
[§] Present address: Albert Einstein College of Medicine, Department of Nuclear Medicine, Montefiore Medical Park, 1695A Eastchester Rd., Bronx, NY 10461.

^{||} Facility for Advanced Instrumentation.

[⊥] Department of Molecular Genetics.

[®] Abstract published in *Advance ACS Abstracts*, December 15, 1996.

¹ BABE, (S)-1-(*p*-bromoacetamidobenzyl)ethylenediaminetetraacetic acid; BCA, bifunctional chelating agent; CPM, *N*-[4-[7-(diethylamino)-4-methylcoumarin-3-yl]phenyl]maleimide; DIEA, diisopropylethylamine; ESI, electrospray ionization mass spectrometry; HEPES, *N*-2-hydroxypiperazine-*N*-2-ethanesulfonic acid; MOPS, 3-morpholinopropanesulfonic acid.

Scheme 1. Synthesis of Fe-BABE

solvent B, methanol: 0–15% B, 0–30 min; 15–100% B, 30–35 min; 100% B, 35–40 min; 100–0% B, 40–45 min; 0% B, 45–55 min. (2) Solvent A, 0.1 M ammonium acetate, pH 6.0; solvent B, methanol: 15–30% B, 0–20 min; 30–100% B, 20–25 min; 100% B, 25–30 min; 100–15% B, 30–35 min; 15% B, 35–45 min. (3) Solvent A, 0.1 M sodium acetate, pH 6.0; solvent B, methanol: 15–30% B, 0–20 min; 30–100% B, 20–25 min; 100% B, 25–30 min; 100–15% B, 30–35 min; 15% B, 35–45 min.

Microbore HPLC. Protein conjugates were prepared for mass spectrometry by passage through a C_8 reversed phase column (Applied Biosystems, Aquapore RP-300, 7 μm , 250 \times 1.0 mm) at 80 $\mu\text{L}/\text{min}$ at room temperature on an Applied Biosystems Model 172 system. UV absorbance was monitored at 214 nm. Protein solvent A, H_2O + 0.06% CF_3COOH ; solvent B, CH_3CN + 0.06% CF_3COOH : 5–35% B, 0–60 min; 35% B, 60–660 min; 35–75% B, 660–700 min; 75–100% B, 700–710 min; 100% B, 710–720 min; 100–50% B, 720–721 min; 50% B, 721–731 min; 50–5% B, 731–733 min; 5% B, 733–748 min. Fe-BABE microbore analysis was performed with UV absorbance set to 260 nm. The Fe-BABE solvent gradient used was as follows. Solvent A, 0.1 M Et_3NH^+ acetate, pH 6.5, 5% CH_3CN ; solvent B, 0.1 M Et_3NH^+ acetate, pH 6.5, 75% CH_3CN : 0–80% B, 0–60 min; 80–100% B, 60–65 min.

NMR Spectroscopy. ^1H NMR spectra were obtained at 300 MHz on a GE QE-300 spectrometer. Chemical shifts are reported relative to HDO (4.80 ppm).

Mass Spectrometry. FAB mass spectra of small molecules were obtained on a ZAB-HS-2F mass spectrometer. Mass spectra of the protein and its conjugate were obtained using a Quattro-BQ mass spectrometer (VG Biotech, Altrincham, U.K.). Samples were introduced by loop injection at a flow rate of 3 $\mu\text{L}/\text{min}$, and positive ion electrospray mass spectra were obtained using a capillary voltage of 3.5 kV, a counter electrode voltage of 500 V, and a cone voltage of 50 V. The mass spectrometer was scanned over the range of m/z 200–2000 at a rate of 20 s/scan, and the spectra were summed. Calibration of the mass scale was performed using horse heart myoglobin as calibration standard. Molecular weights of peptides were determined by mathematical transformation of the electrospray spectra to a true mass scale spectrum using the maximum entropy transformation algorithm MaxEnt.

(S)-1-(p-Bromoacetamidobenzyl)ethylenediaminetetraacetic Acid (7). As described in the Supporting Information, L-phenylalanine was converted into p-aminobenzyl-EDTA (6) according to the procedure shown in Scheme 1. The pH of 16 mL of a 37.5 mM

aqueous solution of **6** (0.60 mmol) was adjusted to 7–8 (according to pH strips) using DIEA. This solution was added dropwise to a stirring solution of 300 μ L of bromoacetyl bromide in 16 mL of CHCl_3 . The aqueous phase was adjusted to pH 7.0 with 100 mL additions of DIEA and stirred vigorously. After 5 min of stirring, a small aliquot was analyzed on HPLC to check for completion by the disappearance of the starting material peak (retention time 4.5 min) and the appearance of the product peak (retention time 10 min). The layers were separated, and the aqueous phase was extracted with CHCl_3 . The pH of the aqueous phase was adjusted to 7–8 with DIEA and extracted again with CHCl_3 . The pH of the aqueous phase was adjusted to 2 with 3 M HCl and extracted five times with equal volumes of Et_2O . The pH was readjusted to 2 with 3 M HCl and the aqueous phase extracted five times with Et_2O . This was continued until the pH remained constant. Residual ether was removed from the aqueous solution under house vacuum. The pH of the solution was adjusted to 5 with DIEA, and the solution was divided into aliquots, frozen in $\text{N}_2(\text{l})$, and stored at -70°C . The concentration of the solution was determined by cobalt metal binding assay: purified yield, 0.43 mmol (72%); microbore HPLC (using the Fe-BABE gradient above), product peak, 10 min; FAB-MS, m/z 516, 518 ($\text{M} - \text{H}^-$); high-resolution MS, m/z 516.0628 measured, m/z 516.0618 calculated for $\text{C}_{19}\text{H}_{23}\text{O}_9\text{N}_3^{79}\text{Br}$.

Fe(III) [(S)-1-(p-Bromoacetamidobenzyl)ethylene-diaminetetraacetic acid] (8**)**. In a 5 mL pear-shaped flask, 1 mL of 20.6 mM BABE (**7**) was combined with 1 mL of DMSO. To remove the water, the volume of the solution was reduced to 0.7 mL via gentle evaporation at room temperature. Occasionally, a fine white precipitate of NaCl forms in the orange solution. The salt is removed by passing the solution through a 0.2 mm nylon syringe filter (Rainin). The chelator concentration (28.6 mM) was determined by ^{57}Co metal binding assay, and the alkylating capacity (86%) was determined by a thiol TLC assay (*9*). Then 286 μ L of 50 mM $\text{FeCl}_3 \cdot 6\text{H}_2\text{O}$ in DMSO was added to 500 μ L of BABE in DMSO. After vortex mixing, 20 μ L of DIEA (0.114 mmol) was added, and the yellow solution was mixed and allowed to stand at room temperature for 1 h. To measure the degree of saturation of the chelate with iron, a ^{57}Co competition experiment was performed by mixing the Fe(III)–BABE complex (**8**) with a 2-fold excess of ^{57}Co (*9*). Result: 97% saturation. The Fe(III)–BABE was divided into aliquots, frozen in liquid nitrogen, and stored at -70°C : yield, 0.012 mmol (83%); reversed-phase microbore HPLC (using Fe-BABE gradient above) product peak, 15 min.

Conjugation of **8 to Cys-269 in the C-Terminal Domain of *E. coli* RNA Polymerase α Subunit.** Alpha-CTD (*10*) in a TGE-50 mM NaCl buffer (10 mM Tris-HCl, pH 7.6, 5% glycerol, 0.1 mM EDTA, 50 mM NaCl) was exchanged into a conjugation buffer (10 mM MOPS, pH 8, 0.1 mM EDTA, 50 mM NaCl) by dialysis at 4°C . The 20 μ M protein was incubated with 400 μ M Fe-BABE at 37°C for 1 h. The reaction was quenched by the addition of an equal volume of 1 M Tris-HCl, pH 8, and dialyzed against a TGE-50 mM NaCl buffer at 4°C . The protein was purified by microbore HPLC as described above, completely dried under reduced pressure, and redissolved in water/acetonitrile (1:1) for mass spectrometry.

Assay of Free Sulfhydryl Groups. The concentration of free cysteine side chains was determined with the fluorescent reagent CPM on both unconjugated and conjugated proteins. The method of Parvari *et al.* (*11*) was slightly modified as follows: β -Mercaptoethanol standard solutions were prepared in MOPS buffer (10

mM MOPS, pH 7.9, 120 mM NaCl, 10 mM MgCl_2 , and 1.0 mM EDTA) at concentrations of 30, 20, 10, 5, 3, 1, 0.3, and 0.1 μ M. The protein sample in a TGE-50 mM NaCl buffer was exchanged into MOPS buffer by dialysis at 4°C , and the protein concentration was determined by micro-Bradford assay. A 15 μ L aliquot of 0.4 mM CPM in DMF was added to 15 μ L of each standard and each protein sample. After 1 h of incubation at room temperature, 3 mL of 1% Triton X-100 was added to each reaction. The intensity of fluorescence emission was measured on 2.9 mL samples, using a Perkin-Elmer LS 50B luminescence spectrometer. The excitation wavelength was 390 nm, and the emission wavelength was 473 nm.

RESULTS AND DISCUSSION

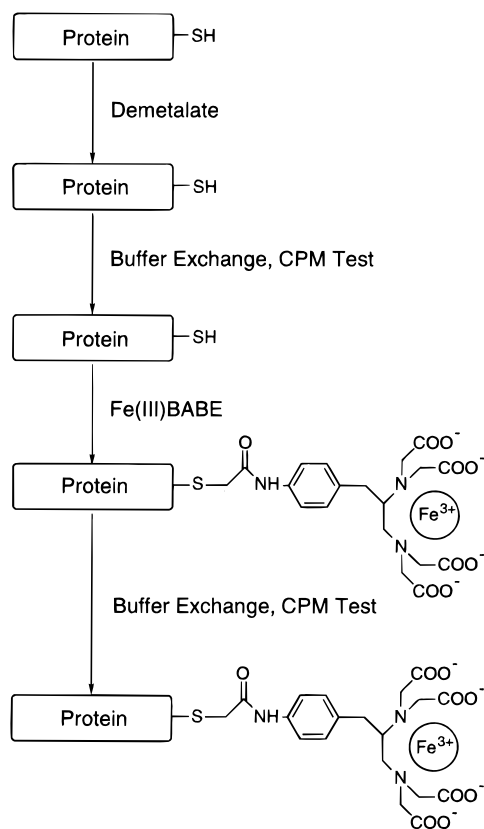
There are a number of different approaches to the use of metal complexes to map proteins. A recent example uses untethered chelates to map the overall surface and depends on changes in cutting sites to reveal binding interactions (*12, 13*). Another approach, employing a tethered reagent such as Fe-BABE, is similar in design to a cross-linking experiment (*3, 4*). Here it is essential that protein cutting is only due to the tethered reagent and not to unchelated metal coordinated directly to sites on the protein. In view of the results in ref *13*, we chose to prepare the iron chelate before conjugation to the protein, to avoid artifactual cutting by unchelated iron.

As reported by Moran *et al.* (*9*), the bromoacetylation reaction is quantitative as observed by HPLC. However, the reduced yield is due to sample loss during the necessarily extensive extraction workup of the product. The transfer of **7** into DMSO allows the reaction with ferric chloride to form **8** under mild nonhydrolyzing conditions. Furthermore, the difficulties associated with aqueous complexation of Fe(III), i.e. low pH, are avoided.

The preloaded bifunctional chelate (**8**) is used as a macromolecule modification reagent requiring only a single reaction to derivatize the target with Fe-EDTA. The general protocol for the derivatization is illustrated in Scheme 2. As shown, unless the macromolecule is stored in an EDTA buffer, the procedure begins by first demetalating the protein by incubation in a 0.1 M phosphate, pH 7.0, 20 mM EDTA buffer. Following the demetalation, the macromolecule is buffer exchanged (via size exclusion spin columns or dialysis) into a conjugation buffer composed of either 10–50 mM HEPES or MOPS, pH 8.0, and 0.1 mM EDTA. The presence of ≥ 0.1 mM EDTA is necessary to scavenge any unbound metal. Also, the conjugation buffer may contain simple salts (i.e. NaCl, KCl, MgCl_2 , NaOAc, etc.) and glycerol for macromolecular stability. The buffer must not contain free thiols.

Just prior to reaction, a sample of the macromolecule with the free cysteine is tested with CPM to quantify and confirm that it is available for conjugation. The amount of Fe-BABE added should be in 2–20-fold excess relative to the free thiol present. Since the reagent is in DMSO, to prevent possible denaturation the volume of chelate added should not exceed 5%. After the addition of Fe-BABE, the pH should be kept to $\text{pH } 8 \pm 0.5$ (adjust if necessary with DIEA). The conjugation reaction is performed at room temperature or 37°C for 0.5–1 h. The reaction is stopped by quenching with 1 M Tris buffer, pH 8, and/or buffer exchanging the macromolecule.

To demonstrate the conjugation procedure alpha-CTD was conjugated with Fe-BABE and analyzed by HPLC and mass spectrometry. The transformed ESI mass spectrum of unconjugated alpha-CTD shows only one

Scheme 2. Fe-BABE Conjugation to a Cysteine Side Chain

peak at mass 11 077, as expected for α residues 234–329 (Figure 1a). The mass spectrum of the Fe-BABE conjugated protein shows two peaks (Figure 1b); a peak at mass 11 076 for alpha-CTD and a peak at mass 11 566 corresponding to the conjugate of alpha-CTD with Fe-BABE (ΔMW 490, the mass of the iron chelate moiety). The conjugation yield determined by the CPM test was 40%, in good agreement with the yield determined from mass spectral peak ratios. Since mass spectrometry shows the fraction of protein conjugated and the species added, and the CPM test shows the loss of sulfhydryl groups, the combined results demonstrate that the Fe-BABE conjugation occurred at the cysteine side chain and not at other nucleophilic sites, such as histidine or lysine side chains.

As found by Ghaim *et al.* (4), cysteine residues on proteins fall into three categories. Some cysteines are unreactive toward alkylating reagents such as BABE or Fe-BABE (e.g., position 157 on subunit I of *E. coli* cytochrome *bd*); some are alkylated but produce no cleavage products upon treatment with ascorbate and peroxide (e.g., position 509 on subunit I of *E. coli* cytochrome *bd*); and some produce cleavage products (e.g., position 276 on subunit I of *E. coli* cytochrome *bd*). Cys-269 in the C-terminal domain of the *E. coli* RNA polymerase α subunit belongs to the second category; treatment with ascorbate and peroxide led to very little cleavage of the polypeptide backbone.

ACKNOWLEDGMENT

We thank Dr. Karin Hughes and Jeffrey Owens for helpful discussions and assistance with the CPM test. This work was supported by Research Grants GM25909 and CA16861 to C.F.M. from the National Institutes of Health and Grants NIEHS ES-04699 and ES-05707 for the purchase of the Quattro-BQ mass spectrometer.

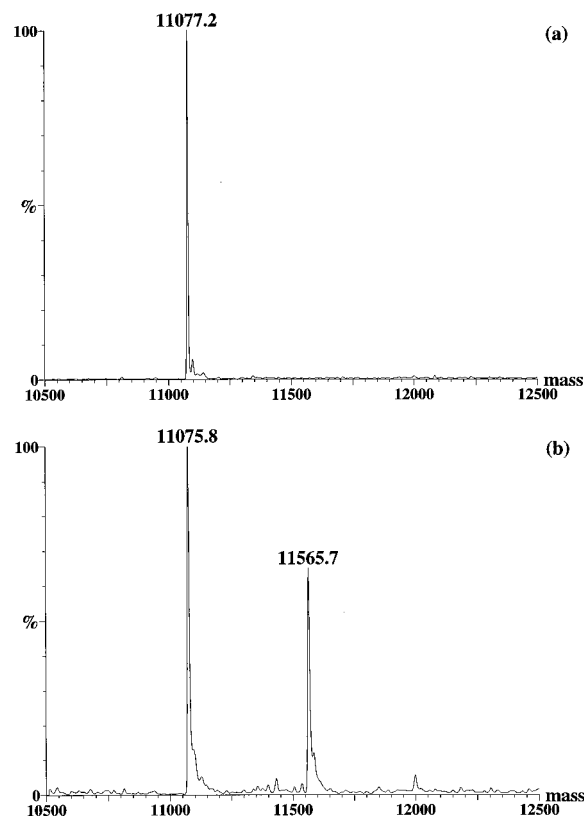


Figure 1. (a) Transformed ESI mass spectrum of the alpha-CTD subunit (11077 Da) before Fe-BABE conjugation. (b) Transformed ESI mass spectrum of the alpha-CTD subunit after the conjugation reaction, showing two peaks corresponding to unconjugated alpha-CTD subunit and Fe-BABE-conjugated alpha-CTD subunit.

Supporting Information Available: Descriptions of current methods for the syntheses of compounds **1–6**, available only via the Internet. See any current masthead page for ordering information.

LITERATURE CITED

- (1) Rana, T. M., and Meares, C. F. (1990) Specific Cleavage of a Protein by an Attached Iron Chelate. *J. Am. Chem. Soc.* 112, 2457–2458.
- (2) Rana, T. M., and Meares, C. F. (1991) Transfer of Oxygen from an Artificial Protease to Peptide Carbon During Proteolysis. *Proc. Natl. Acad. Sci. U.S.A.* 88, 10578–10582.
- (3) Ermacora, M. R., Ledman, D. W., and Fox, R. O. (1996) Mapping the Structure of a Non-Native State of Staphylococcal Nuclease. *Nat. Struct. Biol.* 3, 59–66.
- (4) Ghaim, J. B., Greiner, D. P., Meares, C. F., and Gennis, R. B. (1995) Proximity Mapping the Surface of a Membrane Protein Using an Artificial Protease: Demonstration That the Quinone-Binding Domain of Subunit I Is near the N-Terminal Region of Subunit II of Cytochrome *bd*. *Biochemistry* 34, 11311–11315.
- (5) Sundberg, M. W., Meares, C. F., Goodwin, D. A., and Diamanti, C. I. (1974) Chelating Agents for the Binding of Metal Ions to Macromolecules. *Nature (London)* 250, 587–588.
- (6) DeRiemer, L. H., Meares, C. F., Goodwin, D. A., and Diamanti, C. I. (1981) BLEDTA II: Synthesis of a New Tumor-Visualizing Derivative of Co(III)-Bleomycin. *J. Labelled Compd. Radiopharm.* 18, 1517–1534.
- (7) Hayward, M. M., Adrian, J. C., Jr., and Schepartz, A. (1995) Convenient Synthesis of Bifunctional Metal Chelates. *J. Org. Chem.* 60, 3924–3927.
- (8) Thiers, R. C. (1957) Contamination in Trace Element Analysis and Its Control. *Methods Biochem. Anal.* 5, 273–335.

- (9) Moran, J. K., Greiner, D. P., and Meares, C. F. (1995) Improved Synthesis of 6-[*p*-(Bromoacetamido)benzyl]-1,4,8,11-tetraazacyclotetradecane-*N,N',N'',N'''*-tetraacetic Acid and Development of a Thin-Layer Assay for Thiol-Reactive Bifunctional Chelating Agents. *Bioconjugate Chem.* 6, 296–301.
- (10) Jeon, Y. H., Negishi, T., Shirakawa, M., Yamazaki, T., Fujita, N., Ishihama, A., and Kyogoku, Y. (1995) Solution Structure of the Activator Contact Domain of the RNA Polymerase Alpha Subunit. *Science (Washington, D.C.)* 270, 1495–1497.
- (11) Parvari, R., Pecht, I., and Soreq, H. (1983) A Microfluorometric Assay for Cholinesterases, Suitable for Multiple Kinetic Determinations of Picomoles of Released Thiocoline. *Anal. Biochem.* 133, 450–456.
- (12) Heyduk, E., and Heyduk, T. (1994) Mapping Protein Domains Involved in Macromolecular Interactions: A Novel Protein Footprinting Approach. *Biochemistry* 33, 9643–9650.
- (13) Greiner, D. P., Hughes, K. A., Gunasekera, A. H., and Meares, C. F. (1996) Binding of the σ^{70} Protein to the Core Subunits of *Escherichia coli* RNA Polymerase, Studied by Iron-EDTA Protein Footprinting. *Proc. Natl. Acad. Sci. U.S.A.* 93, 71–75.

BC9600731

Site-Specific Photomodification of DNA by Porphyrin–Oligonucleotide Conjugates Synthesized via a Solid Phase H-Phosphonate Approach

Handong Li,[†] Olga S. Fedorova,^{†,‡} William R. Trumble,[§] T. Rick Fletcher,[†] and Leszek Czuchajowski*,[†]

Department of Chemistry and Department of Microbiology, Molecular Biology, and Biochemistry, University of Idaho, Moscow, Idaho 83844. Received July 31, 1996[®]

meso-Tris(4-pyridyl)[(ω-hydroxyhexamethylene)carbamoyl]phenyl]porphyrin was converted to its H-phosphonate derivative and conjugated using solid phase synthesis with the 5'-hydroxyl group of deoxyribonucleotides d(TCTTCCCA) and d(T)₁₂. These conjugates were transformed into their (*N*-methylpyridiniumyl)porphyrin analogs in the reaction with methyl iodide. A 532 nm laser beam was utilized to photoactivate both types of the conjugates in the presence of the target 22-mer and 16-mer oligonucleotides. Photoactivation of porphyrin–oligonucleotide conjugates resulted in site-specific DNA modification characterized by a main reaction site size of ~5 bases.

INTRODUCTION

Antisense oligonucleotides recognize a selected sequence on the target nucleic acid and can inhibit gene expression (1–3). Introduction of DNA-cleaving functional groups into an antisense oligonucleotide has been shown to generate site-directed damage on the target nucleic acids through chemical or photochemical reactions (4–6). A variety of chemical molecules have been covalently linked to oligonucleotides which were hybridized to cellular DNA to affect processes such as cellular uptake (2), nuclease resistance (3), and binding affinity (6).

Examples of those reactive molecules are alkylating agents such as aromatic (2-chloroethyl)amino derivatives (4–6), intercalating agents such as acridinium (3), ethidium, and phenazinium (6) derivatives, photoactivable cross-linkers such as psoralens (7–10), azides (11–13), or porphyrins (14–16), and artificial endonucleases such as EDTA–Fe(II) (17–19), Cu(I)–1,10-phenanthroline (20–21), bleomycin (22–23) or metalloporphyrins (24–32). The porphyrin–oligonucleotide conjugates and porphyrinyl–nucleoside derivatives (33–36) are of special interest to us due to their potential ability to modify nucleic acids either under dark conditions or under irradiation (37–39).

Sequence-specific modification of nucleic acids by porphyrin–oligonucleotide derivatives was reported using an excitation light wavelength around the porphyrin's Soret band (400–430 nm) (14–15) or in the case of porphyrin with an expanded structure such as lutetium(III) texatexaphyrin at an excitation wavelength of 732 nm (16). Porphyrins are used as anticancer agents in photodynamic therapy (PDT) (40). Their application as reactive groups of oligonucleotide derivatives in an antisense approach can result in selective inhibition of both oncogenes and proliferation of tumor cells (6).

Hitherto, only a few solution phase synthetic ap-

proaches have been reported for the preparation of the porphyrin–oligonucleotide conjugates. Amino derivatives of oligonucleotides were first made and then coupled with activated esters (15, 24–27, 29, 31, 32) or bromoalkyl derivatives (28) of porphyrin. Another method was based on the reaction between the activated 5'-phosphate group on an oligonucleotide and the amino group on a porphyrin (14, 28). Porphyrin with a hydroxyl group was also used as a monomer in triester solution phase synthesis of oligonucleotide derivatives (27).

Since porphyrin derivatives of oligonucleotides activated by light or active in dark conditions can be used as the selective anticancer drugs, simple and efficient synthetic methods for porphyrin–oligonucleotide conjugates are required to increase the availability. It appears that only the use of the porphyrin residue as the monomer in the synthesis of oligonucleotides leads to a high yield of conjugated product (27). Therefore, we developed a simple approach for producing porphyrin–oligonucleotide conjugates, based on the commercially available, fully protected resin-bound deoxyribooligonucleotides, synthesized by the phosphoramidite method. The porphyrin monomer was used in the form of the H-phosphonate derivative. The methodology of H-phosphonate coupling (41, 42) was modified to accomplish the porphyrin–oligonucleotide conjugation.

We chose two antisense oligonucleotides for application of this solid phase conjugation approach: a 12-mer of deoxyribothymidylate [d(T)₁₂], the complementary sequence to a riboadenylate track of single-stranded (+)-RNA in a wide variety of viruses such as potato virus Y and swine vesicular exanthema, and an 8-mer d(TCTTCCCA), the complementary fragment to the selected sequence of RNA of tick born encephalitis virus.

A green laser beam at 532 nm was applied to study the photoactivated modification of target nucleic acids in the presence of porphyrin–oligonucleotide conjugates. We found that photoactivation at porphyrin's Q band region (500–650 nm) was highly effective for modification of DNA. It is possible to suggest that porphyrin–oligonucleotide derivatives can be used as specific drugs in photodynamic therapy because the light source with this longer wavelength is more penetrating through tissue.

* To whom correspondence should be sent.

[†] Department of Chemistry.

[‡] Permanent address: Institute of Bioorganic Chemistry, Siberian Division of Russian Academy of Sciences, 630090 Novosibirsk, Russia.

[§] Department of Microbiology, Molecular Biology, and Biochemistry.

[®] Abstract published in *Advance ACS Abstracts*, January 1, 1997.

EXPERIMENTAL PROCEDURES

Materials. Fully protected resin-bound oligonucleotides synthesized by the phosphoramidite method were purchased from Bio-synthesis (Lewisville, TX). The target DNA sequences of d[(A₁₂)GTGT] (16-mer) and d(TGAATGGGAAGAGGGTCAGGT) (22-mer) were obtained from GIBCO BRL (Grand Island, NY). Oxidizers (I₂/pyridine/H₂O and H₂O/THF/Et₃N), adamantanecarbonyl chloride, pyridine, and acetonitrile were obtained from Glen Research Co. (Sterling, VA). All other chemicals were purchased from Aldrich Chemical Co. (Milwaukee, WI). ³²P labeling of the 16-mer and the 22-mer at their 5'-ends was accomplished using T4-polynucleotide kinase obtained from United States Biochemical (Cleveland, OH) and [γ -³²P]ATP purchased from New England Nuclear/Dupont (Boston, MA). Labeled oligomers were separated from the nonlabeled oligomers by electrophoresis in denaturing 20% polyacrylamide gels containing 7 M urea and subsequently electroeluted from the gel.

Synthesis of *meso*-Tris(4-*N*-pyridyl)[(methylcarboxy)phenyl]porphyrin 1. 4-Pyridaldehyde (16.1 g, 0.15 mol) and methyl 4-formylbenzoate (7.4 g, 0.05 mol) were dissolved in 600 mL of propionic acid and 10 mL of acetic anhydride in a 2000 mL flask. The solution was heated to 100 °C. Pyrrole (13.4 g, 0.2 mol) in 50 mL of propionic acid was added dropwise to the hot solution over 0.5 h. The solution became darker and was stirred and refluxed for an additional 1 h. At this point, about 600 mL of propionic acid was removed under vacuum. The residue was poured slowly into ice-cold 5% aqueous sodium bicarbonate with stirring. The black precipitate was washed with 5% aqueous sodium bicarbonate and then water until neutral and air-dried. The black solid was dissolved in chloroform, applied to a silica gel column, and eluted with chloroform and chloroform/methanol (50:1). The fifth fraction was collected and identified as compound **1**. The yield was 8%.

¹H NMR (CDCl₃, ppm): 9.03 (d, 6H, Py), 8.84 (m, 8H, β -pyrrole), 8.44 (d, 2H, phenyl), 8.27 (d, 2H, phenyl), 8.14 (d, 6H, Py), 4.10 (s, 3H, OCH₃), -2.93 (s, 2H, NH). MS (FAB): *m/z* 678 (M + 2). UV (CHCl₃, nm): 418 (Soret), 514, 548, 588, 644. MS (FAB): *m/z* 678 (M + 2), 647 (M + 2 - OCH₃).

Synthesis of *meso*-Tris(4-pyridyl)[[(ω -hydroxyhexamethylene)carbamoyl]phenyl]porphyrin 2. **1** (67.6 mg, 100 μ mol) and 6-aminoheptanol (2.0 g, excess) were introduced into a flask. The mixture was stirred at 65–70 °C under nitrogen for 48 h. The sublimated 6-aminoheptanol was melted down to the flask with a heating gun during the reaction. Aminoheptanol (1.5 g) was recovered by sublimation of the reaction mixture. The residue was introduced into ice/water and stirred for 10 min. The precipitate was collected and washed with ice/water until neutral and then air-dried. The dried purple solid was chromatographed on a silica gel (60–230 mesh) using 100:1 and 10:1 chloroform/methanol as eluent. Fraction 1 contained the starting material. Fraction 2 was identified as **2** with a yield of 80%.

¹H NMR (CDCl₃, ppm): 9.03 (d, 6H, Py), 8.82 (m, 8H, β -pyrrole), 8.30 (d, 2H, phenyl), 8.22 (d, 2H, phenyl), 8.15 (d, 6H, Py), 6.60 (t, 1H, NHCO), 3.76 (t, 2H, CH₂O), 3.68 (t, 2H, NCH₂), 1.81 (quint, 4H, CH₂CH₂), 1.74 (quint, 4H, CH₂CH₂), -2.91 (s, 2H, NH). MS (FAB): *m/z* 763 (M + 2), 663 [M + 3 - (CH₂)₆OH], 617 [M - CONH(CH₂)₆OH]. UV (CHCl₃, nm): 414 (Soret), 514, 548, 588, 644.

Synthesis of the H-Phosphonate Derivative of *meso*-Tris(4-pyridyl)[[(ω -hydroxyhexamethylene)carbamoyl]phenyl]porphyrin 3. **2** (15 mg, 20 μ mol) was dried under vacuum and dissolved in 10 mL of CH₂-

Table 1. UV–Vis Data of Porphyrins, Oligonucleotides, and Porphyrin–Oligonucleotide Conjugates

compound	UV	visible
	λ_{max} (nm), ϵ (M ⁻¹ cm ⁻¹)	λ_{max} (nm), ϵ (M ⁻¹ cm ⁻¹)
2	260, 4×10^4	406, 2.8×10^5
2-Me	260, 1.2×10^4	422, 2.2×10^5
4	260, 6.78×10^4	
5	260, 6.36×10^4	
6	266	416
7	268	416
8	268	430
9	266	430

Cl₂. A catalytic amount of triethylamine and 12 mg (21 μ mol) of tris(1,1,1,3,3,3-hexafluoro-2-propyl) phosphite were added. The reaction was completed in 10 min. A mixture of 1 M triethylamine bicarbonate (TEAB) and triethylamine (50:1 v:v) was added to the reaction mixture. After 30 min, the product was extracted with chloroform, washed with 1 M TEAB, and dried over anhydrous sodium sulfate. The chloroform layer was evaporated, and the residue was chromatographed on silica gel using chloroform/methanol/triethylamine (from 100:2:0 to 100:10:2). The second fraction was collected and washed with 1 M TEAB and dried with sodium sulfate. The porphyrin H-phosphonate **3** was obtained after evaporation of the chloroform with a 82% yield.

¹H NMR (DMSO-*d*₆, ppm): 9.05 (m, 6H, Py), 8.90 (m, 8H, β -pyrrole), 8.29 (m, 4H, phenyl), 8.26 (m, 6H, Py), 7.56 (s, 1H, NHCO), 5.67 (s, 1H, HP), 3.68 (m, 2H, CH₂O), 3.42 (m, 2H, CH₂NCO), 3.04 (quart, 2H, CH₂N), 1.68 (m, 4H, CH₂CH₂), 1.44 (m, 4H, CH₂CH₂), 1.15 (t, 3H, CH₃), -3.02 (s, 2H, NH). ³¹P NMR (DMSO-*d*₆, ppm): 1.76 (PH). MS (negative FAB): *m/z* 824 (M⁻). UV (CHCl₃/CH₃OH, 1:1, nm): 418 (Soret), 512, 548, 592, 638.

Synthesis of Conjugates of *meso*-Tris(4-pyridyl)-[(ω -hydroxyhexamethylene)carbamoyl]phenyl]porphyrin with Oligonucleotides d(TCTTCCCA) and d(T)₁₂ (6** and **7**, Respectively).** Fully protected resin-bound oligonucleotide (1 mmol) was packaged in a 1 mL syringe column which was connected to a vacuum line by a switch valve. All reaction agents and vessels were in a dry nitrogen glovebox. A procedure, closely approximating the reactions for automated DNA synthesis, was utilized as follows: (1) Detritylation was done with 2% Cl₂CHCOOH for 2 min. (2) Washing was done with CH₃CN and CH₃CN/pyridine for 2 min. (3) **3** (38 mg, 40 μ mol) dissolved in 1 mL of CH₃CN/pyridine and 20 mg (100 μ mol) of adamantanecarbonyl chloride was added immediately and applied to the column for 4 min. (4) Washing was done with CH₃CN/pyridine and CH₃CN for 2 min. (5) Oxidation was done with I₂/pyridine/H₂O and Et₃N/THF/H₂O for 5 min. (6) Washing was done with CH₃CN/pyridine and CH₃CN for 2 min. (7) Deprotection was done with concentrated NH₃·H₂O at room temperature for 12 h. The product was then lyophilized and redissolved in Tris-acetate/EDTA (TAE) buffer (pH 7.5) and purified on a Hewlett-Packard series 1050 HPLC apparatus with a variable wavelength UV detector set at 260 nm, using a Lichrospher 100 reverse phase C18 column (5 μ m). The solvent ramp followed a linear gradient from 9% CH₃CN and 91% 0.05 M TEAc (pH 7.5) at the beginning of each run to 81% CH₃CN and 19% 0.05 M TEAc (pH 7.5) at the end, 25 min later. The flow rate was 1.0 mL/min. HPLC profiles (shown in Figure 1) were recorded on a Hewlett-Packard 3396A integrator. The yields of **6** or **7** were about 60–70%. UV data are shown in Table 1.

Conjugates **6** and **7** were also analyzed by dynamic sieving capillary electrophoresis on a Biofocus 3000

Capillary Electrophoresis System (BioRad) using a coated column (length of 24 cm, diameter of 75 μm) in a buffer of 25 mM Tris-borate and 2 mM EDTA at pH 8.3. The absorption profiles (shown in Figure 2) were monitored at 260 nm for oligonucleotide moieties and at 416 nm for porphyrin units of the conjugates.

Concentrations of conjugates were estimated using absorption at 260 nm. The molar absorption coefficient at 260 nm was calculated as the sum of absorption for oligonucleotide and porphyrin moieties. The molar absorption coefficients of oligonucleotides at 260 nm were found using a procedure described in ref 43 to be $6.78 \times 10^4 \text{ M}^{-1} \text{ cm}^{-1}$ for d(TCTTCCCA) and $6.36 \times 10^4 \text{ M}^{-1} \text{ cm}^{-1}$ for d(T)₁₂. The molar absorption coefficient of porphyrin **2** was measured and is shown in Table 1.

Synthesis of *meso*-Tris(4-*N*-methylpyridiniumyl)-[(ω -hydroxyhexamethylene)carbamoyl]phenyl-porphyrin (2-Me**) and Its Conjugates with Oligonucleotides d(TCTTCCCA) and d(T)₁₂ (**8** and **9**, Respectively).** Compound **6**, **7**, or **2** was dissolved in DMF. Excess CH₃I was added, and the mixture was kept at room temperature for 3 h. *N*-Methylation of **2** was chosen as a model reaction for which completeness was monitored by TLC. The product **2-Me** was obtained by removing the excess CH₃I and DMF under vacuum with no need of further purification. The yield was 100%.

¹H NMR of **2-Me** (DMSO-*d*₆, ppm): 9.62 (d, 6H, 3, 5-Py), 9.18 (d, 6H, 2, 6-Py), 8.98 (m, 8H, β -pyrrole), 8.32 (m, 4H, phenyl), 4.72 (s, 9H, NCH₃), 3.48 (m, 4H, CH₂-CO and CH₂O), 1.67 (m, 4H, CH₂CH₂), 1.44 (m, 4H, CH₂-CH₂), -3.02 (s, 2H, porphyrin-NH).

UV [H₂O, λ_{max} (nm)]: 422, 520, 560, 592, 652. The molar absorption coefficient of porphyrin **2-Me** is presented in Table 1.

Compounds **8** and **9** were made in the same way as **2-Me**. Their UV-vis data are shown in Table 1. The red shifts of porphyrin Soret bands after conjugation with oligonucleotides are characteristic and consistent with our previous data (33).

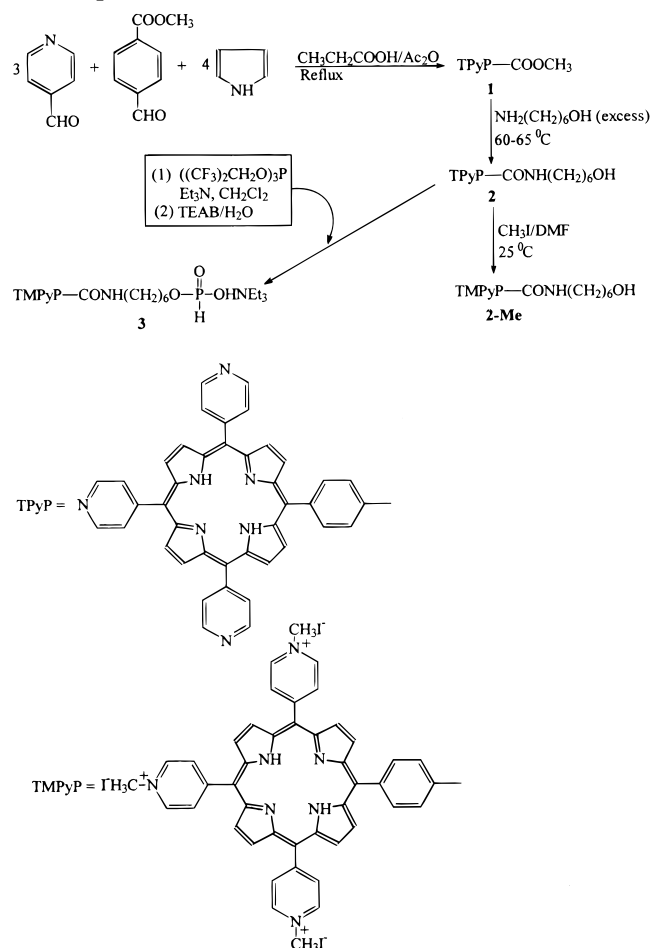
Photomodification of Target DNA. Photomodification reactions were carried out in a 20 μL buffer solution containing 10 nM [³²P]16-mer (or 22-mer), 0.2 M NaCl, 10 mM Tris-HCl, 1 mM EDTA (pH 7.5), and porphyrinyl derivatives of the 12-mer (or 8-mer) at 25 °C in a polypropylene Eppendorff tube. Tubes were placed in a horizontal position with caps opened in the path of a laser beam and irradiated for 10 min. The laser was a Nd:YAG laser at 532 nm with 25 mJ/pulse and 10 pulses/s.

After irradiation, the oligomers were precipitated by the addition of 100 μL of 2% LiClO₄/acetone solution. The precipitate was washed three times with 100 μL of acetone and dried under vacuum. If required, the oligomer pellets were suspended in 10 μL of 10% piperidine at 95 °C for 30 min. The solutions were cooled and subjected to a second LiClO₄/acetone precipitation. The precipitates were dissolved in 4 μL of water and 3 μL of 95% formamide containing 0.025% bromophenol blue and 0.025% xylene cyanol and loaded onto a 20% denaturing polyacrylamide sequencing gel (19:1 cross-linked, 20 cm \times 20 cm \times 0.4 mm). The gels were run at 50 W/cm and exposed on Kodak X-ray film. The autoradiograms of the gels were quantitized using an UltrosanXL densitometer (LKB, Sweden). The autoradiograms are shown in Figures 3 and 4. The densitometry data were plotted as shown in Figures 5–7.

RESULTS AND DISCUSSION

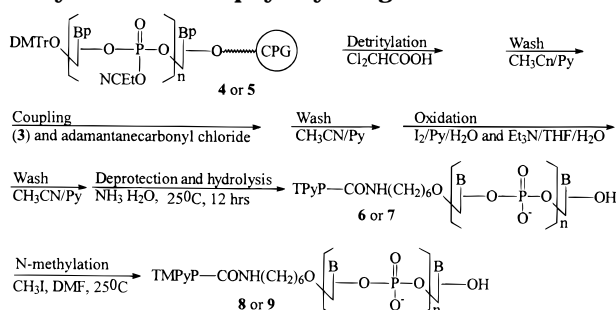
Synthesis of Porphyrin–Oligonucleotide Conjugates. Porphyrin–oligonucleotide conjugates were syn-

Scheme 1. Synthesis of the Porphyrin H-Phosphonates



thesized by coupling of the H-phosphonate derivative of oligonucleotide with fully protected oligonucleotides. For this purpose, a porphyrin ester **1** was synthesized by the Rothmund–Longo method (44). An ω -hydroxyhexamethylene group was introduced through an ester–amide exchange reaction which gave a new porphyrin **2** with a hydroxyl group in a high yield (Scheme 1). A small amount of acetic anhydride was added to the solvent of propionic acid to prevent the hydrolysis of the ester group. An ester–amide exchange reaction was found to be very efficient for derivatizing the porphyrin ester into new porphyrins with different functional groups, such as hydroxyl and amine. This is an easy way to make pure porphyrin derivatives compared with reactions previously reported in the literature that employed activation of porphyrin carboxylic acid in DMSO or DMF and produced a low yield (28). The *meso*-trispyridylporphyrin H-phosphonate **3**, as the coupling active compound, was synthesized using an efficient fluorinated agent (45). Compound **3** has good solubility in pyridine/acetonitrile solution, which is necessary for the coupling reaction. The H-phosphonate derivative was activated by adamantane-carbonyl chloride and coupled with the 5'-hydroxyl group of deoxyribonucleotides d(TCTTCCCA) **4** or d(T)₁₂ **5** bound on the resin (Scheme 2). The H-phosphonate group was oxidized by I₂ to phosphate. Hydrolysis, removing the conjugates from the resin, and deprotection were carried out in one step at room temperature. Conjugates **6** and **7** were purified by HPLC and converted to cationic porphyrin–oligonucleotides **8** and **9** by methyl iodide.

The coupling was allowed to proceed for less than 3 min to avoid the hydrolysis of the previously formed

Scheme 2. Solid Phase H-Phosphonate Approach to the Synthesis of Porphyrinyl Oligonucleotides^a

^a CPG = controlled pore glass. Bp = (phenylacetyl)deoxyadenosine, deoxythymidine, and (phenoxyacetyl)deoxycytosine. B = T, A, or C. **6** and **8** have an oligonucleotide sequence of TCTCCCA. **7** and **9** have an oligonucleotide sequence of (T)₁₂.

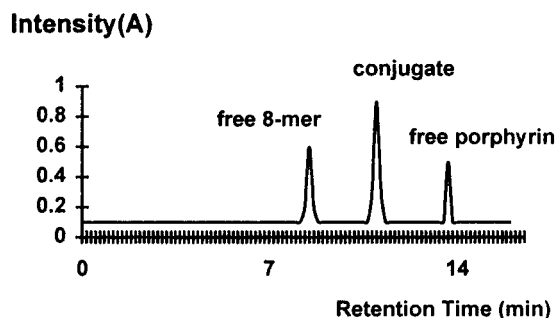


Figure 1. HPLC profile of coupling reaction products from porphyrin **3** and 8-mer **4**.

H-phosphonate diester. Adamantanecarbonyl chloride was chosen instead of pivaloyl chloride to minimize the capping of the oligonucleotide. The aliphatic amide bond on the porphyrin is stable under both room-temperature hydrolysis conditions and deprotection conditions in concentrated ammonium hydroxide.

HPLC and Capillary Electrophoresis. As may be seen in the HPLC elution profiles of conjugates (Figure 1), the free oligonucleotide was eluted first, the conjugate second, and the free porphyrin last. The free porphyrin is neutral and least polar, compared to the free anionic oligonucleotide or the conjugate. The retention time and the polarity are very well correlated on the reverse phase column. Each fraction was confirmed by the UV-vis spectrum.

As compared with acrylamide gel electrophoresis, capillary electrophoresis should provide more precise information. It is very easy to identify the porphyrin-oligonucleotide conjugate by applying two different detector wavelengths: 260 nm for oligonucleotides and 416 nm for porphyrin units. Only free oligonucleotides and porphyrin-oligonucleotide can be detected at 260 nm, while only free porphyrin and porphyrin-oligonucleotide can be detected at 416 nm. The capillary electrophoresis profiles are shown in Figure 2.

UV-Vis Spectra. Soret bands of pyridylporphyrin-oligonucleotide and of pyridiniumylporphyrin-oligonucleotide exhibited a red shift up to 10 nm compared to the free pyridylporphyrin and N-methylated pyridiniumylporphyrin.

Selective Photomodification of Target DNA. Synthesized porphyrin-oligonucleotide conjugates were tested for their abilities to modify the complementary nucleic acid strands under irradiation by visible light in the spectral region of the porphyrin Q-bands at 532 nm. Photomodification reactions were carried out with 5'-³²P-labeled targets, d(TGAATGGGAAGAGGGTCAGGTT) (22-

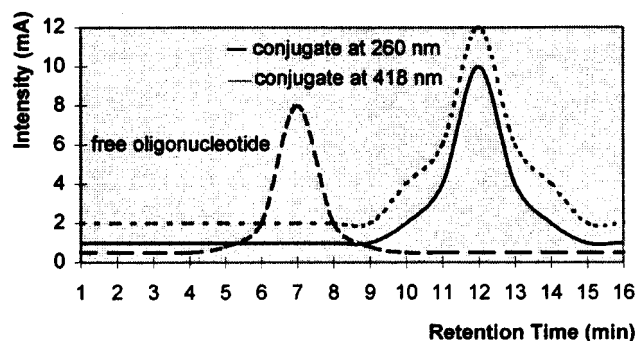


Figure 2. Capillary electrophoresis profile of purified conjugate **6** and pure oligonucleotide **4**.

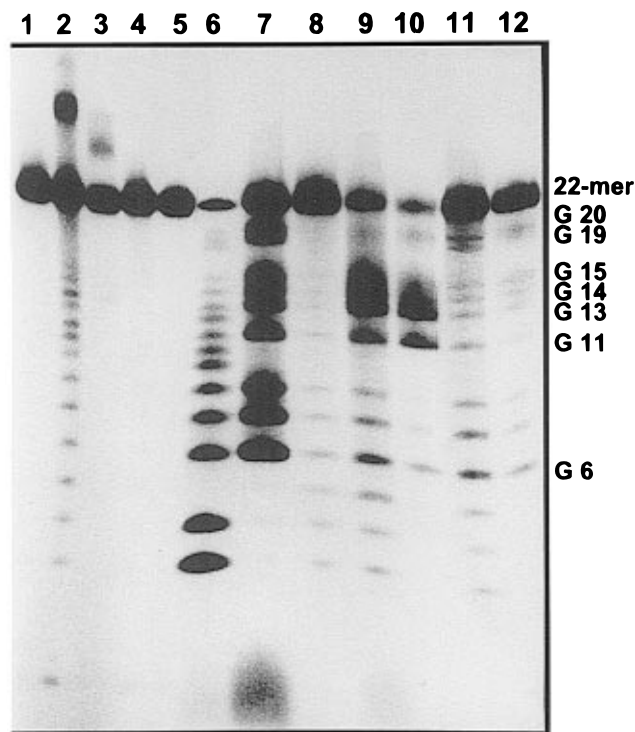
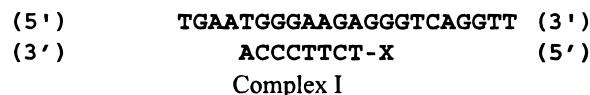
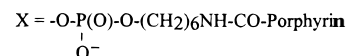


Figure 3. Autoradiogram of a 20% denaturing polyacrylamide gel showing photomodification products produced by irradiation of the 22-mer for 10 min: controls without porphyrinyl conjugates (lanes 1 and 8), in the presence of 4×10^{-6} M conjugates **6** (lanes 2 and 9), **7** (lanes 4 and 11), **8** (lanes 3 and 10), **9** (lanes 5 and 12), A + G (lane 6), and G (lane 7). Samples in lanes 9–12 were treated with piperidine.

mer) and d[(A)₁₂(GT)₂] (16-mer), at a concentration of $\sim 10^{-8}$ M. Concentrations of the porphyrin-oligonucleotide conjugates were equal to 4 μ M. In these equilibrium conditions, all targets must be in the form of a complex with the conjugate. The complementary complexes have the following structures:



where



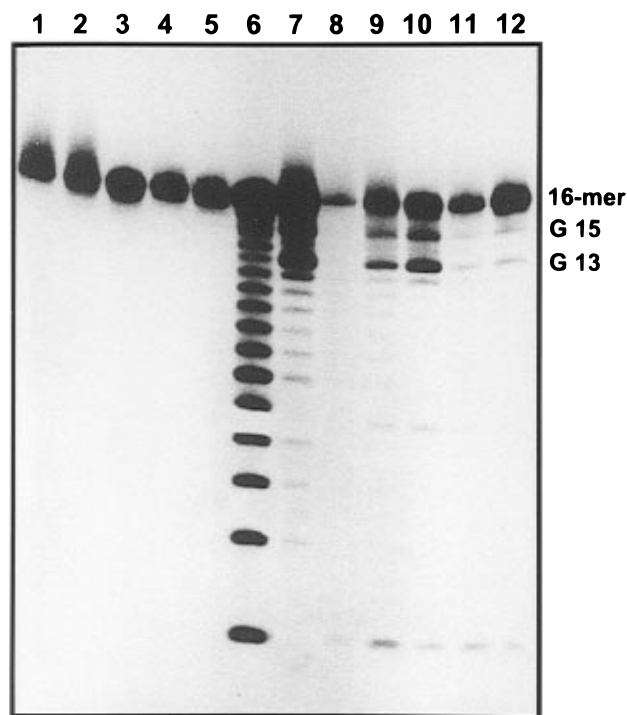


Figure 4. Autoradiogram of a 20% denaturing polyacrylamide gel showing photomodification products produced by irradiation of the 16-mer for 10 min: controls without porphyrinyl conjugates (lanes 1 and 8), in the presence of 4×10^{-6} M conjugates **6** (lanes 4 and 11), **7** (lanes 2 and 9), **8** (lanes 5 and 12), **9** (lanes 3 and 10), A + G (lane 6), and G (lane 7). Samples in lanes 9–12 were treated with piperidine.

The products were separated by 20% polyacrylamide gel electrophoresis under denaturing conditions, in the presence of 7 M urea. Results of control experiments and sequence-specific photomodification of the 22-mer and 16-mer are shown in Figures 3 and 4, respectively. The

modification sites were identified after piperidine cleavage from comigrating Maxam–Gilbert sequencing ladders (46), namely A + G and G. No photomodification of the targets was seen in the absence of the porphyrin conjugates (lanes 1 and 8). Slow-migrating bands (corresponding to cross-linked products) appeared above the bands corresponding to the starting materials when the 22-mer was irradiated in the presence of **6** and **8** (Figure 3, lanes 2 and 3, respectively). When these targets were irradiated in the presence of conjugates **7** and **9** which are not complementary to the targets, the cross-linked products were absent (see Figure 3, lanes 4 and 5). In the case where the 16-mer was irradiated in the presence of **7** and **9**, the bands of cross-linked products were absent (Figure 4, lanes 2 and 3, respectively). The photomodification sites were assigned after piperidine treatment of the reaction mixture and were observed primarily at G11, G13, G14, and G15 for the 22-mer (Figure 3, lanes 9 and 10). For the case of the 16-mer, specific modification products were observed only after the treatment by piperidine at G13 and G15 (Figure 4, lanes 9 and 10). This suggests that alkaline-labile photomodification occurred.

Densitograms are presented in Figures 5 and 6 for the photomodification of the 22-mer by reagents **6** and **8**, respectively, and in Figure 7 for the modification of the 16-mer by **7** and **9**. Figures 5–7 also show the absolute cleavage yields for each site after piperidine treatment and illustrate the data for both complementary and noncomplementary oligonucleotide conjugates. No specific photomodifications of the target 22-mer and 16-mer were observed in the presence of conjugates which could not hybridize with the target DNA. Modification by conjugates containing an uncharged porphyrinyl group **6** and **7** or a positively charged porphyrinyl group **8** and **9** showed slightly different efficiency and site selectivity (Figures 5–7).

For the 22-mer, the total yield, of cleavage ($\sim 77\%$ for

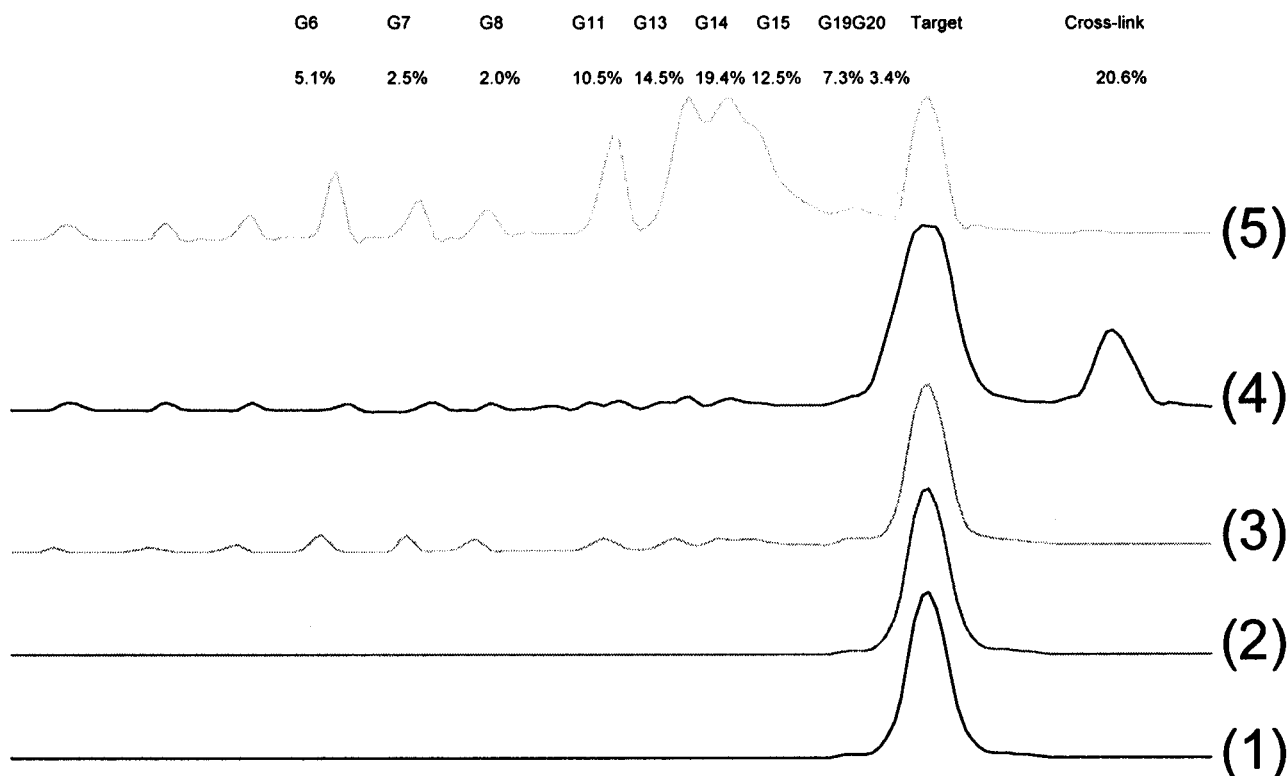


Figure 5. Densitograms of the gel electrophoretic separation of the reaction mixture, containing 22-mer target modified by conjugate **6**; the data for noncomplementary conjugate **7** are presented as the control (line 1, without conjugates; lines 2 and 3, $4 \mu\text{M}$ **7**, with **6** absent; and lines 4 and 5, $4 \mu\text{M}$ **6** with **7** absent). Samples for lines 1, 3, and 5 were treated with piperidine.

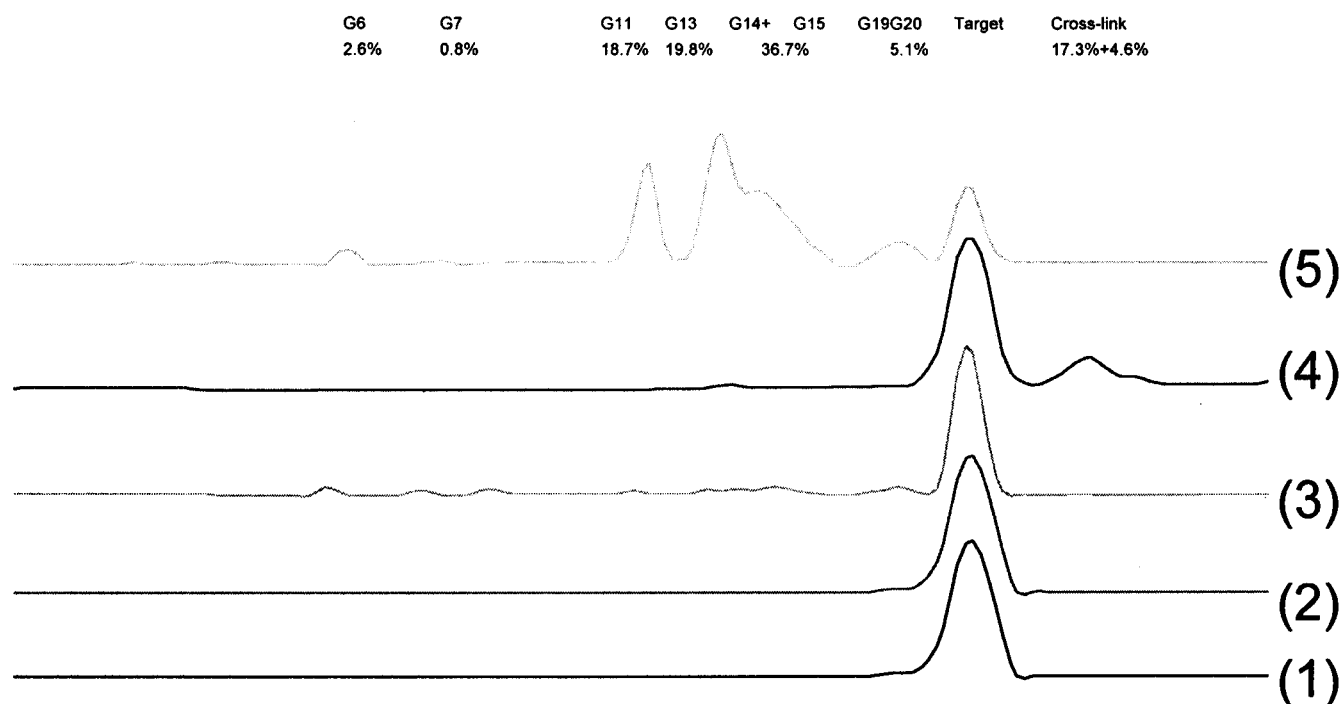


Figure 6. Densitograms of the gel electrophoretic separation of the reaction mixture, containing 22-mer target modified by conjugate **8**; the data for noncomplementary conjugate **9** are presented as the control (line 1, without conjugates; lines 2 and 3, 4 μ M **9** and with **8** absent; and lines 4 and 5, 4 μ M **8** with **9** absent). Samples for lines 1, 3, and 5 were treated with piperidine.

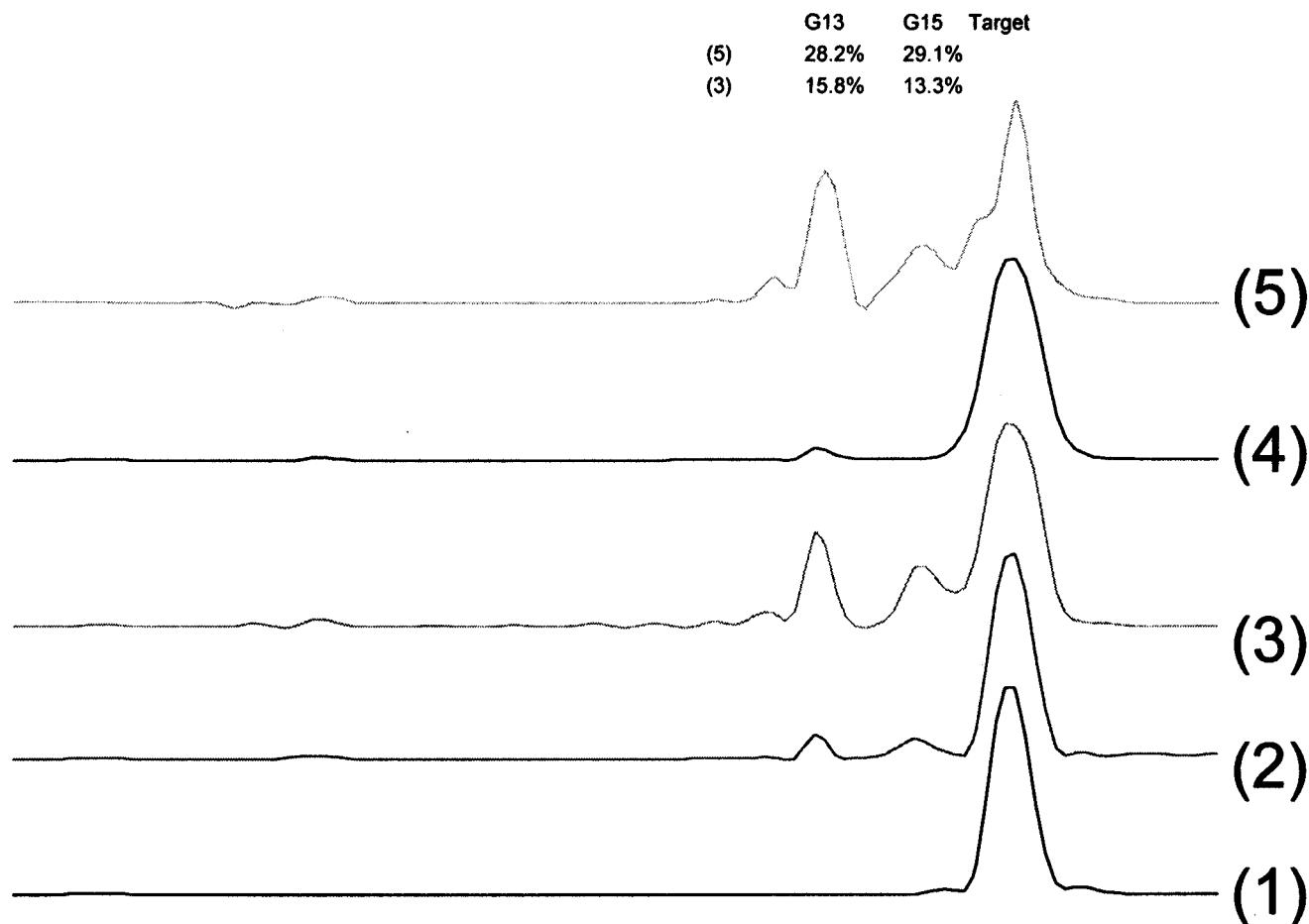


Figure 7. Densitograms of the gel electrophoretic separation of the reaction mixture, containing 16-mer target modified by conjugate **7** or **9**; the data for noncomplementary conjugates **6** and **8** are presented as the control (line 1, without conjugates; line 2, 4 μ M **6**; line 3, 4 μ M **7**; line 4, 4 μ M **8**; and line 5, 4 μ M **9**). Samples for lines 1–5 were treated with piperidine.

6 and ~84% for **8**) are higher than the yields of cross-linked products (~20%). Therefore, the alkaline-labile

modification of the 22-mer occurred also as in the case of the 16-mer.

The most intensively utilized modification site consisted of about five nucleotides. Two factors may account for this result. First, the dimension of the photoactive center porphyrin molecule is 18 Å (47), equivalent to one-half of a DNA helix turn. Second, a singlet molecular oxygen (1O_2)-modifying agent is presumed to form after sensitization by the porphyrin. The lifetime of this species is equal to 1–20 μ s in solution (48). Therefore, this molecule can migrate a large distance along the polynucleotide chain.

The results of this study demonstrate that the porphyrinyl groups of oligonucleotide conjugates can be activated by a green laser beam with a wavelength in the spectral region of the porphyrin's Q-bands. The photomodification efficiency is high with a total yield around 80% for a specific modification site of five nucleotides. This efficient site-directed photomodification of DNA suggests that porphyrinyl agents may be developed as anticancer or antiviral drugs for use in photodynamic therapy.

Our procedure provide an efficient method for producing porphyrin-oligonucleotide conjugates in sufficient quantity and with sufficient purity to make these compounds readily available for medical and chemical applications.

ACKNOWLEDGMENT

The authors thank V. V. Koval for the preparation of densitometric pictures and to the Idaho EPSCoR and SBOE in Boise, ID, for financial support.

LITERATURE CITED

- (1) Cohen, J. S., Ed. (1989) *Oligonucleotides: antisense inhibitors of gene expression*, MacMillan Press, London.
- (2) Wickstrom, E., Ed. (1991) *Prospects for antisense nucleic acid therapy of cancer and AIDS*, Wiley-Liss, Inc., New York.
- (3) Crooke, S. T., and Lebleu, B., Eds. (1993) *Antisense research and applications*, CRC Press, Boca Raton, FL.
- (4) Belikova, A. M., Zarytova, V. F., and Grineva, N. I. (1967) Synthesis of ribonucleotides and diribonucleotides phosphates containing 2-chloroethylamine and nitrogen mustard residues. *Tetrahedron Lett.*, 3557–3567.
- (5) Knorre, D. G., and Vlassov, V. V. (1989) *Affinity Modification of Biopolymers*, CRC Press, Boca Raton, FL.
- (6) Knorre, D. G., Vlassov, V. V., Zarytova, V. F., Lebedev, A. V., and Fedorova, O. S. (1994) *Design and targeted reaction of oligonucleotide derivatives*, CRC Press, Boca Raton, FL.
- (7) Sastry, S. S., Spielman, P., Dwyer, T. J., Wemmer, D. E., and Hearst, J. E. (1992) Recent advances in the synthesis and structure determination of site specifically psoralen-modified oligonucleotides. *J. Photochem. Photobiol. B*, 65–79.
- (8) Lee, B. L., Murakami, A., Blake, K. R., Lin, S.-B., and Miller, P. S. (1988) Interaction of psoralen-derivatized oligodeoxyribonucleoside methylphosphonates with single-stranded DNA. *Biochemistry* 27, 3197–3203.
- (9) Pieses, U., and English, U. (1989) Psoralen covalently linked to oligonucleotides: synthesis, sequence specific recognition of DNA and photo-cross-linking to pyrimidine residues of DNA. *Nucleic Acids Res.* 17, 285–299.
- (10) Woo, J., and Hopkins, P. B. (1991) Template-directed modification of single-stranded DNA by psoralen-tethered oligonucleotides: sites of photoadduct formation analyzed by sequence-specific and sequence-random cleavage. *J. Am. Chem. Soc.* 113, 5457–5459.
- (11) Decout, J.-L., Thuong, N. T., Lhomme, J., and Helene, C. (1987) Sequence-specific recognition, photocrosslinking and cleavage of the DNA double helix by an oligo-[α]-thymidylate covalently linked to an azidoproflavine derivative. *Nucleic Acids Res.* 15, 7749–7760.
- (12) Levina, A. S., Tabatadze, D. R., Khalimskaya, L. M., Prikhodko, T. A., Shishkin, G. V., Alexandrova, L. A., and Zarytova, V. F. (1993) Oligonucleotide derivatives bearing reactive and stabilizing groups attached to C5 of deoxyuridine. *Bioconjugate Chem.* 4, 319–325.
- (13) Koshkin, A. A., Kropachev, K. Yu., Mamaev, S. V., Bulychev, N. V., Lokhov, S. G., Vlassov, V. V., and Lebedev, A. V. (1994) Ethidium and azidoethidium oligonucleotide derivatives: synthesis, complementary complex formation and sequence-specific photomodification of the single-stranded and double-stranded target oligo- and polynucleotides. *J. Mol. Recognit.* 7, 177–178.
- (14) Fedorova, O. S., Savitskii, A. P., Shoikhet, K. G., and Ponomarev, G. V. (1990) Palladium(II)-coproporphyrin I as a photoactivable group in sequence-specific modification of nucleic acids by oligonucleotide derivatives. *FEBS Lett.* 259, 335–337.
- (15) Mastruzzo, L., Woisard, A., Ma, D. D. F., Rizzarelli, E., Favre, A., and Le Doan, T. (1994) Targeted photochemical modification of HIV-derived oligoribonucleotides by antisense oligodeoxynucleotides linked to porphyrins. *Photochem. Photobiol.* 60, 316–322.
- (16) Magda, D., Wright, M., Miller, R. A., Sessler, J. L., and Sanson, P. I. (1995) Sequence-specific photocleavage of DNA by an expanded porphyrin with irradiation above 700 nm. *J. Am. Chem. Soc.* 117, 3629–3630.
- (17) Boutorin, A. S., Vlassov, V. V., Kazakov, S. A., Kutiaev, I. V., and Podyminogin, M. A. (1984) Complementary addressed reagents carrying EDTA-Fe(II) groups for directed cleavage of single-stranded nucleic acids. *FEBS Lett.* 172, 43–46.
- (18) Chu, B. C. F., and Orgel, L. E. (1985) Nonenzymatic sequence-specific cleavage of single-stranded DNA. *Proc. Natl. Acad. Sci. U.S.A.* 82, 963–967.
- (19) Dreyer, G., and Dervan, P. B. (1985) Sequence-specific cleavage of single-stranded DNA. *Proc. Natl. Acad. Sci. U.S.A.* 82, 968–972.
- (20) Chen, C. B., and Sigman, D. S. (1986) Nuclease activity of 1,10-phenanthroline-copper: sequence-specific targeting. *Proc. Natl. Acad. Sci. U.S.A.* 63, 7147–7151.
- (21) Francois, J.-C., Saison-Behmoaras, T., Chassignol, M., Thuong, N. T., and Helene, C. (1989) Sequence-targeted cleavage of single- and double-stranded DNA by oligothymidylates covalently linked to 1,10-phenanthroline. *J. Biol. Chem.* 264, 5891–5898.
- (22) Sergeyev, D. S., Godovikova, T. S., and Zarytova, V. F. (1991) Direct cleavage of a DNA fragment by a bleomycin-oligonucleotide derivative. *FEBS Lett.* 280, 271–273.
- (23) Zarytova, V. F., Sergeev, D. S., and Godovikova, T. S. (1993) Synthesis of Bleomycin A5 Oligonucleotide Derivatives and Site-Specific Cleavage of the DNA Target. *Bioconjugate Chem.* 4, 189–193.
- (24) Le Doan, T., Perrouault, L., Helene, C., Chassignol, M., and Thuong, N. T. (1986) Targeted Cleavage of Polynucleotides by Complementary Oligonucleotide Covalently Linked to Iron-Porphyrins. *Biochemistry* 25, 6736–6739.
- (25) Le Doan, T., Perrouault, L., Chassignol, M., Thuong, N. T., and Helene, C. (1987) Sequence-targeted chemical modifications of nucleic acids by complementary oligonucleotides linked to porphyrins. *Nucleic Acids Res.* 15, 8643–8659.
- (26) Ivanova, E. M., Mamaev, S. V., Fedorova, O. S., and Frolova, E. I. (1988) Complementary addressed modification of single-stranded DNA fragment by ferrous-porphyrin derivative of oligonucleotide. *Bioorg. Khim.* 14, 551–554.
- (27) Frolova, E. I., Ivanova, E. M., Zarytova, V. F., Abramova, T. V., and Vlassov, V. V. (1990) Porphyrin-linked oligonucleotides. Synthesis and sequence-specific modification of ss-DNA. *FEBS Lett.* 269, 101–104.
- (28) Boutorin, A. S., Le Doan, T., Battioni, J. P., Mansuy, D., Dupre, D., and Helene, C. (1990) Rapid routes of synthesis of chemically reactive and highly radioactively labeled α - and β -oligonucleotide derivatives for *in vivo* studies. *Bioconjugate Chem.* 1, 350–356.
- (29) Casas, C., Lasey, C. J., and Meunier, B. (1993) Preparation of hybrid "DNA cleaver-oligonucleotide" molecules based on metallotris(methyl-pyridinium)porphyrin motif. *Bioconjugate Chem.* 4, 366–371.
- (30) Frolova, E. I., Fedorova, O. S., and Knorre, D. G. (1993) Kinetic study of the addressed modification by hemin derivatives of oligonucleotides. *Biochimie* 75, 5–12.

- (31) Mestre, B., Pratviel, G., and Meunier, B. (1995) Preparation and nuclease activity of hybrid "metallotris(methylpyridinium)porphyrin oligonucleotide" molecules having a 3'-loop for protection against 3'-exonucleases. *Bioconjugate Chem.* **6**, 466–472.
- (32) Magda, D., Miller, R. A., Sessler, J. L., and Iverson, B. L. (1994) Site-specific hydrolysis of RNA by europium(III) texaphyrin conjugated to synthetic oligodeoxyribonucleotide. *J. Am. Chem. Soc.* **116**, 7439–7440.
- (33) Li, H., and Czuchajowski, L. (1994) Ribofuranosides N-substituted with meso-porphyrin as nucleoside-like compounds. *Tetrahedron Lett.* **35** (11), 1629–1630.
- (34) Czuchajowski, L., Palka, A., Morra, M., and Wandrekar, V. (1993) Porphyrinyl nucleosides containing fluorinated nucleobases. *Tetrahedron Lett.* **34**, 5409–5412.
- (35) Czuchajowski, L., Habdas, J., Niedbala, H., and Wandrekar, V. (1992) Synthesis of Porphyrin-Nucleosides. *J. Heterocycl. Chem.* **29**, 479–484.
- (36) Li, H., Trumble, W. R., and Czuchajowski, L. (1997) Compounds Based on meso-Tris-(4-pyridyl)-p-acrylamidophenylporphyrin able to intercalate with DNA. *J. Heterocycl. Chem.* (in press).
- (37) Kochevar, I., Dunn, D. A. (1990) Photosensitized reactions of DNA: cleavage and addition. In *Bioorganic Photochemistry* (H. Morrison, Ed.) pp 273–315, John Wiley & Sons, New York.
- (38) Meunier, B. (1992) Metalloporphyrins as versatile catalysts for oxidation reactions and oxidative DNA cleavage. *Chem. Rev.* **92**, 1411–1456.
- (39) Knorre, D. G., Fedorova, O. S., and Frolova, E. I. (1993) Oxidative degradation of nucleic acids. *Russ. Chem. Rev. (Engl. Transl.)* **62**, 65–86.
- (40) Dolphin, D. (1994) Photomedicine and photodynamic therapy. *Can. J. Chem.* **72**, 1005–1013.
- (41) Froehler, B. C., and Matteucci, M. D. (1986) Nucleoside H-phosphonate: valuable intermediates in the synthesis of deoxynucleotides. *Tetrahedron Lett.* **27**, 469–472.
- (42) Gaffney, B. L., and Jones, R. A. (1988) Large-scale oligonucleotide synthesis by H-phosphonate method. *Tetrahedron Lett.* **29**, 2619–2622.
- (43) Fasman, G., Ed. (1975) *Handbook of Biochemistry and Molecular Biology. Nucleic Acids*, 3rd ed., p 175, CRC Press, Boca Raton, FL.
- (44) Adler, A. D., Longo, F. R., Finarell, J. D., Goldmacher, J., Assour, J., and Korsakoff, L. (1967) A simplified synthesis for meso-tetraporphyrins. *J. Org. Chem.* **32**, 476.
- (45) Sakatsume, O., Yamane, H., Takaku, H., and Yamamoto, N. (1990) Use of new phosphorylating and coupling agents in the synthesis of oligodeoxyribonucleotides via H-phosphonate approach. *Nucleic Acids Res.* **18**, 3327–3331.
- (46) Maxam, A. M., and Gilbert, W. (1980) Sequencing end-labelled DNA with base-specific chemical cleavages. *Methods Enzymol.* **65**, 499–560.
- (47) Ford, K. G., Pearl, L. H., and Neidle, S. (1987) Molecular modelling of the interactions of tetra-(4-methylpyridyl) porphyrin with TA and CG sites on DNA. *Nucleic Acids Res.* **16**, 6553–6562.
- (48) Kearns, D. R. (1971) Physical and chemical properties of singlet molecular oxygen. *Chem. Rev.* **71**, 395–427.

BC960074T

Dioleoylmelittin as a Novel Serum-Insensitive Reagent for Efficient Transfection of Mammalian Cells

J. Y. Legendre,* A. Trzeciak, B. Bohrmann, U. Deuschle, E. Kitas, and A. Supersaxo

Preclinical Research and Development, F. Hoffmann-La Roche AG, CH-4070 Basel, Switzerland.

Received August 29, 1996[®]

Amphipathic peptides can be useful effectors to enhance gene delivery. However, peptide/DNA complexes usually require additional effectors, such as fusogenic lipids, to mediate efficient transfection. Due to weak and/or multiple interactions between the various components of the system, the transfecting complexes are often heterogeneous and unstable in biological fluids. Accordingly, a hybrid molecule resulting from the covalent coupling of an amphipathic, membrane-disturbing peptide to a lipid moiety might create a stable and efficient peptide-based gene transfer system. The present work describes such a novel hybrid molecule, dioleoylmelittin, resulting from the conjugation of dioleoylphosphatidylethanolamine-*N*-[3-(2-pyridyldithio)propionate] with [Cys¹]melittin. Dioleoylmelittin had a lower hemolytic and membrane-disturbing activity than melittin. Size and zeta potential measurements, DNA gel electrophoresis, and electron microscopy showed that dioleoylmelittin, unlike melittin, was able to complex plasmid DNA to form spherical particles with a net positive charge and a diameter between 50 and 250 nm. These particles, prepared at an optimal 10/1 dioleoylmelittin/DNA ratio (w/w), mediated efficient transient transfection of reporter genes in cultured mammalian cells including primary cells. The luciferase activity induced by the dioleoylmelittin/DNA complex was 5–500-fold higher than that induced by a cationic lipid/DNA complex, depending on the cationic lipid and the cell-line. Surprisingly, the presence of 10–50% fetal calf serum during dioleoylmelittin-mediated transfection enhanced 1.5–3-fold gene expression. Dioleoylmelittin represents a new class of efficient peptide-based transfection reagents, especially suited for serum-sensitive cells.

INTRODUCTION

Gene delivery is recognized as a key issue in the future development of gene therapy. Indeed, several recent gene therapy clinical trials in humans have shown the limitations of viruses to deliver genes (1). Nonviral gene delivery systems could therefore provide an easier and safer alternative to viruses (2). However, the transfection efficiency of synthetic carriers is still lower than that of viral vectors.

Cationic lipids are the most widely used nonviral transfection reagents both in cell culture and in animals (3, 4). These transfection competent molecules are composed of a cationic moiety, which binds DNA by charge interactions, and a lipophilic tail. Therefore, cationic lipids have the dual ability of condensing DNA and fusing or destabilizing cell membranes (3, 4). Another emerging gene transfer strategy is the use of amphipathic peptides (5–11). These peptides are either fusogenic or permeabilize cell membranes and, hence, improve gene transfer. For example, the cyclic peptide gramicidin S can facilitate DNA delivery into cells in culture (8–10). However, efficient transfection with this peptide requires the addition of co-lipids such as dioleoylphosphatidylethanolamine (DOPE) or short-chain phospholipids; both interact with the hydrophobic face of the gramicidin S (8, 9). This binding usually occurs via weak interactions, and as a result, the transfecting particles are rather heterogeneous and unstable in biological fluids. Accordingly, hybrid molecules resulting from the covalent binding of a lipid moiety onto an amphipathic peptide might provide single, stable transfection compe-

tent reagents. The present work describes the synthesis of such a novel hybrid molecule, dioleoylmelittin. Melittin, a 26 amino acid peptide, is a well-characterized membrane-disturbing molecule (12). When complexed with plasmid DNA, its lipophilic derivative, dioleoylmelittin, forms homogeneous and small particles that mediate highly efficient transfection of cells in culture, even in the presence of serum.

MATERIALS AND METHODS

Synthesis of the Dioleoylmelittin. Continuous-flow solid-phase peptide synthesis was performed on a Milligen 9050 synthesizer, starting from a Tentagel S resin (0.22 mmol/g, Rapp Polymere, Tübingen, Germany), as described (13). All chiral amino acids were of the L-configuration. The base-labile 9-fluorenylmethoxycarbonyl (Fmoc) group was used for α -amino protection. Side chains were protected with the following protecting groups: 2,2,5,7,8-pentamethylchroman-6-sulfonyl (Pmc) for arginine, triphenylmethane (Trt) for cysteine and glutamine, *tert*-butoxycarbonyl (Boc) for lysine and tryptophan, and *tert*-butyl (But) for serine and threonine. Fmoc-amino acids (2.5 equivalent) were activated with an equivalent amount of 1,1,3,3-tetramethyl-2-(2-oxo)-1(2*H*)-pyridyluronium tetrafluoroborate (14) and diisopropylethylamine. Fmoc deprotection was achieved with 20% (v/v) piperidine in dimethylformamide. The resin-bound peptide was treated with a mixture of 86% trifluoroacetic acid, 10% ethanedithiol, and 4% water for 3 h. The reaction mixture was concentrated and poured into diethyl ether, and the precipitate was collected by filtration and lyophilized from water. The crude peptide was purified by preparative HPLC. The fractions of the main peak were collected, concentrated under reduced pressure, and lyophilized, yielding 94.5 mg of compound **I** (CIGAVLKVLTTGLPALISWIKRKRQQ). The homogeneity of compound **I** was confirmed by analytical reversed

* Address correspondence to this author at UPSA Laboratoires, 128 rue Danton, 92506 Rueil-Malmaison, France [telephone (33) 1.47.16.86.00; fax (33) 1.47.16.89.97].

[®] Abstract published in *Advance ACS Abstracts*, December 15, 1996.

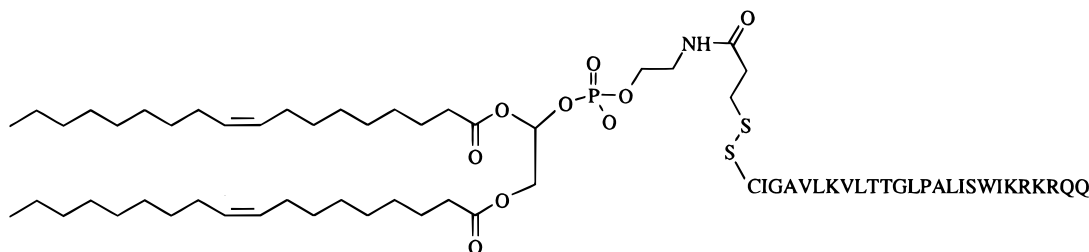


Figure 1. Structure of dioleoylmelittin.

phase HPLC, and the molecular weight was determined by ionization spray positive mode mass spectrometry: $M = 2892.6$ ($M + H$)⁺ (calculated 2892.6 for $C_{132}H_{231}N_{39}O_{35}$). Ten micromoles of compound **I** was dissolved in a mixture of 1 mL of 100 mM phosphate buffer (pH 6.5) and 1 mL of acetonitrile (15). Eleven micromoles of 1,2-dioleoyl-*sn*-glycero-3-phosphoethanolamine-*N*-[3-(2-pyridyldithio)propionate] (N-PDP-PE, Avanti Polar Lipids Inc., Birmingham, AL) in 2.8 mL of chloroform was then added. The mixture was left at room temperature for 1 h, and the organic solvent was removed by evaporation under nitrogen. The remaining solution was diluted with distilled water to a volume of 2.5 mL and passed through a Sephadex G-25 M column. The resulting lipopeptide, dioleoylmelittin (Figure 1), was eluted with distilled water and lyophilized, yielding 28.9 mg of a white solid. The molecular weight was determined by ionization spray positive mode mass spectrometry: $M = 3722$ (calculated 3722.7 for $C_{176}H_{311}N_{40}O_{40}PS_2$).

A control peptide resulting from the coupling of NPDP-PE with CKKKKK (dioleoyl- K_5) was prepared as above, yielding 60 mg of purified lyophilisate ($M = 1633.0$, calculated 1633.25 for $C_{79}H_{150}N_{13}O_{16}S_2$).

Hemolysis Test. Blood from beagle dogs was collected on lithium heparinate and centrifuged for 20 min at 1000*g*. Plasma and buffy coat were discarded, and red blood cells (RBC) were washed with isotonic saline and finally diluted to a concentration of about 6×10^8 cells/mL. Melittin (Sigma, St. Louis, MO; sequencing grade) or dioleoylmelittin, complexed or not with plasmid DNA at a 2/1 \pm charge ratio (assuming a charge of +5 for each peptide), was sequentially diluted with isotonic saline from 40 to 0.05 μ M in a 96-well plate. One hundred microliters of the RBC suspension was added per well, and the plate was incubated for 30 min at 37 °C. After centrifugation (15 min, 1000*g*), 80 μ L of each supernatant was transferred to a new 96-well plate and hemoglobin concentration was measured using a hemoglobin diagnostic kit (Roche diagnostic). Two hundred microliters of a 0.77 mM potassium cyanide solution was added per well, and after 10 min, absorbance was read at 560 nm using an ELISA plate reader. One hundred percent hemolysis was obtained by incubating the RBC with 1% Triton X-100. Background was measured after the RBC had been incubated in isotonic saline and was subtracted from each value.

Destabilization of Liposomes. Egg phosphatidylcholine liposomes (Lipoid, Ludwigshafen, Germany) were prepared by drying the lipids from a chloroform solution under vacuum and by rehydrating the lipid film with isotonic saline. Liposomes were then sonicated and extruded through polycarbonate filters with decreasing pore size (1, 0.4, 0.2 μ m) to generate liposomes with an apparent diameter of 203 ± 4 nm (16). Liposomes, at a final concentration of 1 mM in isotonic saline, were then incubated with increasing concentrations (from 5 to 140 μ M) of melittin or dioleoylmelittin. Five minutes after addition of the peptide to the liposomes, the modification

of the apparent diameter and the polydispersity of the liposomes was determined by dynamic light scattering (Zetasizer 4, Malvern Instruments, Southborough, MA).

Expression Vectors. The pGL3-CMV plasmid encoding for luciferase was constructed as follows: in a first step the *KpnI*–*BglII* TK promoter fragment from pT109luc (17) was introduced between the *KpnI* and *BglII* sites of pGL3basic (Promega, Madison, WI), respectively. From this construct the *XhoI*–*BglII* TK promoter was replaced by the CMV promoter excised as a 788 bp *XhoI*–*BamHI* fragment from pUHD10-1 (18), generating pGL3-CMV. The pCMV- β gal plasmid encoding for β -galactosidase was purchased from Clontech (Palo Alto, CA). Both plasmids were grown using standard methods and purified by column chromatography (Qiagen, Hilden, Germany).

Preparation of the Transfecting Complex. Dioleoylmelittin was dissolved in trifluoroethanol at a concentration of 1 mg/mL. One milliliter of the solution was dried under argon and then under high vacuum. The film was dissolved with 1 mL of 10 mM Tris maleate buffer (pH 6), and the solution was vortexed. Typical complex was prepared by diluting 10 μ g of plasmid DNA in a final volume of 200 μ L of sterile water in a polystyrene tube. Then, an appropriate amount (typically 100 μ L) of dioleoylmelittin was added dropwise and quickly mixed. The complex was allowed to stand at room temperature for 2–5 min before transfection. In some experiments, dioleoylmelittin was mixed with a 5-fold molar excess of DOPE (Avanti Polar Lipids) and subsequently added to plasmid DNA. The transfection efficiency of dioleoylmelittin was also compared to that of 1,2-bis(oleoyloxy)-3-(trimethylammonio)propane (DOTAP; Avanti Polar Lipids) and 1,3-dioleoyloxy-2-(6-carboxyspermyl)propylamide (DOSPER; Boehringer-Mannheim, Mannheim, Germany). DOTAP/DNA or DOSPER/DNA complexes were prepared according to the manufacturer's instructions and were used at a cationic liposome/DNA ratio of 5/1 (w/w). This corresponds to a 2/1 and 5/1 \pm cationic liposome/DNA charge ratio for DOTAP and DOSPER, respectively. The mean diameter of DOTAP/DNA and DOSPER/DNA complexes was 190 ± 10 nm, as determined by dynamic light scattering.

Transfection Experiments. CV-1 (monkey kidney fibroblasts) cells were plated at a density of about 2×10^4 cells per well in a 96-well plate (about 70–80% confluency) and grown for 24 h in 10% fetal calf serum (FCS, Gibco BRL, Grand Island, NY) containing medium. Transfection took place in 100 μ L of FCS-free Dulbecco's modified Eagle medium (DMEM), and 5 h later medium was removed and replaced by 10% FCS-containing medium. To each well was applied 0.2 μ g of plasmid DNA. In some experiments, transfection took place in 10% or 50% FCS-containing medium. Forty-eight hours later, β -galactosidase activity was measured. After medium removal, 50 μ L of 250 mM Tris Cl buffer (pH 8) containing 0.5% of Triton X-100 was added per well. Cells were frozen at -70 °C and then thawed at 37 °C, and 50 μ L of phosphate buffer saline (150 mM, pH 6, PBS) was added

per well. Finally, 150 μL of a 2 mg/mL solution of *o*-nitrophenyl galactopyranoside (Sigma) in 60 mM Na_2HPO_4 , 1 mM MgSO_4 , 10 mM KCl, and 50 mM β -mercaptoethanol was added per well. Optical density at 405 nm was measured after the plate was incubated for anywhere between 20 min and 1 h at 37 $^\circ\text{C}$, depending on the β -galactosidase activity. Values were computed from a β -galactosidase (Fluka) standard curve. Day-to-day β -galactosidase activity values usually varied by about 2-fold depending upon cell density and condition of the cells. Sensitivity of the assay was 50 μunits of β -galactosidase per well of CV-1 cells.

β -Galactosidase activity was also detected by cytochemical stain to evaluate the percentage of transfected cells (19). In this case, CV-1 cells and primary rabbit aorta smooth muscle cells (20) were grown in 60 mm dishes in 2 mL of appropriate medium. Two micrograms of pCMV β gal plasmid complexed with 20 μg of dioleoylmelittin was incubated with the cells during 5 h in 2 mL of serum-free medium. Forty-eight hours after transfection, cells were rinsed with PBS, fixed for 5 min with 4% formaldehyde in PBS, and then stained with X-Gal (5-bromo-4-chloro-3-indolyl- β -D-galactoside, Promega). The blue β -galactosidase-expressing cells were visualized under the microscope 2 h after staining and counted as the percentage of the total cell population.

The dioleoylmelittin transfection efficiency was also compared to that of cationic liposomes (DOTAP or DOSPER), and in this case a luciferase expression vector, pGL3-CMV, was used. Cell-lines CV-1, CHO-K1 (Chinese hamster ovary cells), and 293 (human kidney embryonic cells) were plated in six-well plates and grown for 24 h. Two micrograms of DNA complexed with either cationic liposomes or dioleoylmelittin was added per dish in 2 mL of 10% FCS-containing medium. Five hours later medium was removed and replaced by fresh 10% FCS-containing medium. Luciferase activity was measured 48 h later as previously described (21), and results were normalized to cell protein content (BCA protein assay reagent, Pierce, Rockford, IL).

Physicochemical Characterization. Size and zeta potential of the dioleoylmelittin/DNA complex were determined using a Zetasizer 4 (Malvern Instruments) after appropriate dilution in pure water. To estimate the interaction between plasmid DNA and dioleoylmelittin, plasmid DNA (0.5 μg) was mixed with increasing amounts of dioleoylmelittin (0–4 μg) and electrophoresed on a 0.8% agarose gel in the presence of ethidium bromide. Dioleoylmelittin/DNA complex was also imaged by electron microscopy (EM). For negative staining, a 5 μL aliquot of sample was adsorbed to a carbon-coated 200-mesh copper grid. Staining was done by adding directly 10 μL of 2% uranyl acetate to the adsorbed sample droplet, and the preparation was air-dried after removal of the excess of liquid with filter paper. Specimens were examined in a JEOL-1210 electron microscope operated at 100 kV. For cryoelectron microscopy of frozen-hydrated specimens, 5 μL of samples was applied to 700-mesh hexagonal copper grids. After the excess of solution was removed by blotting with filter paper, the grid was rapidly quench-frozen in a home-made guillotine-like device using liquid ethane as coolant. The frozen grids were mounted under liquid nitrogen in a side entry specimen holder (Model 626, Gatan, Pleasanton, CA) and examined at -172°C in a JEOL-1210 electron microscope equipped with an anticontaminator (Model TAC100, Oxford Instruments, Oxon, U.K.) and operated at 100 kV. Low-dose images were recorded 1.5–2.0 μ underfocus with an electron irradiation of approximately $10\text{ e}/\text{\AA}^2$ at a nominal magnification of 10 000–20 000. Digitized

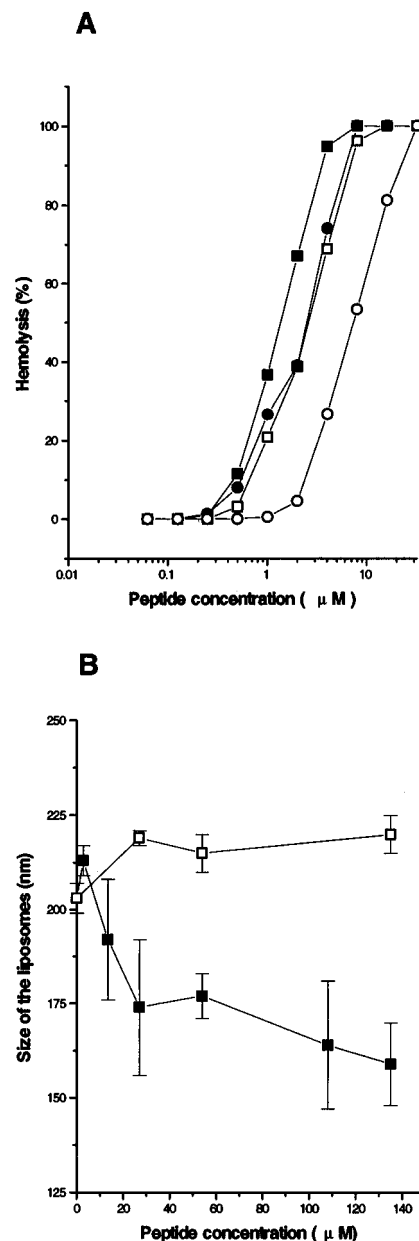


Figure 2. Hemolytic activity (A) and liposome-destabilizing activity (B) of melittin (■), melittin/DNA complex (●), dioleoylmelittin (□), and dioleoylmelittin/DNA complex (○). Complexes between peptides and DNA were prepared at a 2/1 (+/–) charge ratio, assuming 5 positive charges for each peptide.

micrographs were recorded with a slow scan CCD camera (Model 679, Gatan). Magnification calibration was done using negatively stained catalase crystals.

RESULTS

Membrane-Disturbing Activity of Melittin and Dioleoylmelittin Complexed or Not with Plasmid DNA. Two tests were used to evaluate the membrane-disturbing activity of dioleoylmelittin, as compared to melittin: the hemolytic activity and the solubilization of liposomes. When free melittin was incubated with erythrocytes at 37 $^\circ\text{C}$, 50% hemolysis could be detected at a peptide concentration of about 1.2 μM (Figure 2A). This concentration doubled when melittin was complexed with plasmid DNA. Dioleoylmelittin had a lower hemolytic activity than the original peptide, and 50% hemolysis was attained at a peptide concentration of 2.5 μM . After complexation with DNA, the dioleoylmelittin concentration that induced 50% hemolysis was 7 μM . At a

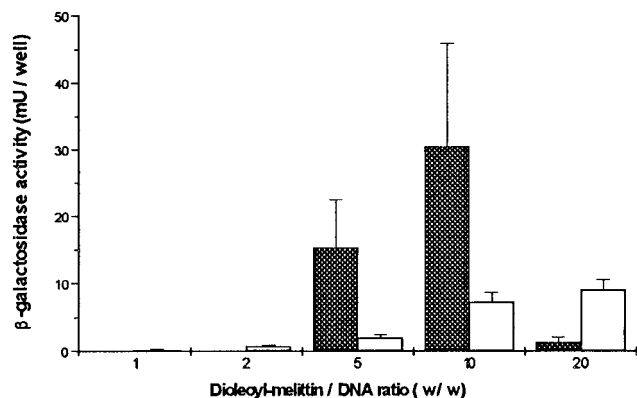


Figure 3. Effect of dioleoylmelittin/DNA ratio (w/w) on transfection efficiency of CV-1 cells in the presence (open bar) or absence (black bar) of DOPE in the complex. Results are the mean \pm SD of six wells in two separate experiments.

concentration of 5 μ M, melittin slightly increased the size of egg PC liposomes, but at concentrations above 10 μ M, it markedly decreased their size and increased their polydispersity (Figure 2B). This effect was attributed to the fusion of liposomes at low peptide/lipid ratios followed by the solubilization of the liposomes and the formation of discoidal structures at higher melittin concentrations (22). Conversely, dioleoylmelittin only slightly increased the size of the liposomes and did not modify their polydispersity in the range of concentration studied.

In Vitro Transfection with the Dioleoylmelittin/DNA Complex. The optimal dioleoylmelittin/DNA ratio for transfection of CV-1 cells was first determined (Figure 3). At a 1/1 or 2/1 dioleoylmelittin/DNA ratio (w/w), no transfection was detected. However, when the dioleoylmelittin/DNA ratio was at least 5/1 (w/w), β -galactosidase activity could be detected in CV-1 cells 48 h after transfection and the optimal dioleoylmelittin/DNA ratio was 10/1 (w/w). Above this ratio some toxicity appeared and transfection was reduced. When DOPE was added to the transfecting particles in a 5-fold molar excess to dioleoylmelittin, β -galactosidase activity was induced at dioleoylmelittin/DNA ratios at which DOPE-free formulations hardly mediated transfection. However, at the optimal ratio with DNA, the efficiency of the DOPE-containing formulations was reduced 5–10-fold as compared to the dioleoylmelittin alone. Furthermore, the control peptide dioleoyl-K₅ did not mediate any transfection of CV-1 cells at all lipopeptide/DNA ratios studied (data not shown).

Evaluation of the percentage of cells expressing β -galactosidase activity by cytochemical staining indicated that about 60–70% and 10–20% of the cells were transfected for CV-1 cells and primary rabbit aorta smooth muscle cells, respectively (data not shown).

The transfection efficiency of dioleoylmelittin was also compared to that of two commercially available cationic lipid transfection reagents, DOTAP and DOSPER, in various cell lines (Table 1). In the three cell lines studied, dioleoylmelittin mediated 3–40 and 25–500 times greater luciferase activity than DOSPER and DOTAP, respectively.

Effect of Serum and Lysomotropic Agents on Transfection Efficiency. Surprisingly, the presence of FCS in the medium had a favorable effect on the transfection efficiency of dioleoylmelittin in CV-1 cells (Figure 4). Ten percent FCS in the transfection medium slightly enhanced transfection, but 50% FCS enhanced β -galactosidase activity more than 2-fold. This effect was not cell line dependent since an improvement of transfection in the presence of serum was also observed for

Table 1. Transfection of Various Mammalian Cell Lines with Dioleoylmelittin Complex or Cationic Lipids

	luciferase activity		
	DOTAP	DOSPER	dioleoylmelittin
CHO-K1	2.69×10^6	2.50×10^7	5.19×10^8
CV-1	1.14×10^5	1.31×10^6	5.54×10^7
293	7.31×10^6	5.70×10^7	1.71×10^8

^a Results are expressed as light units per milligram of cell protein and are the mean of two experiments. Background (130 LU) was subtracted from each measurement.

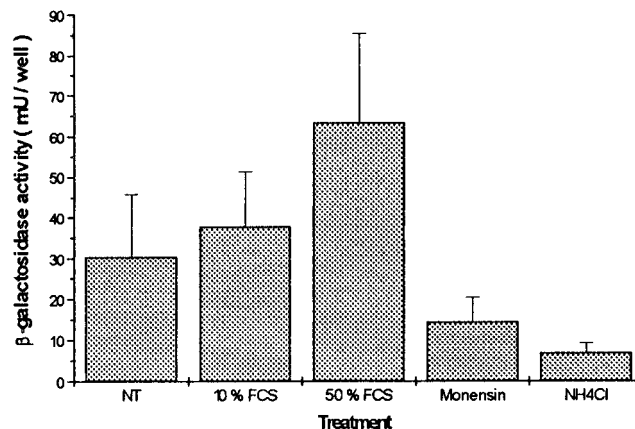


Figure 4. Effect of various agents on dioleoylmelittin-mediated transfection. NT, no treatment. Results are the mean \pm SD of at least 10 wells in three separate experiments.

293 or COS-1 cells (data not shown). Furthermore, cell viability was at least 96% in the absence or the presence of serum, suggesting that FCS did not improve transfection by protecting the cells from a possible toxic effect of the dioleoylmelittin.

To gain some insight into the mechanism whereby dioleoylmelittin brings about transfection, cells were also treated with various agents during the transfection procedure (Figure 4). Addition of lysomotropic agents, monensin (10 μ M) and ammonium chloride (20 mM), at the beginning of the 5 h incubation time reduced 2–3 times the transfection level mediated by the dioleoylmelittin. These compounds have been shown to enhance cationic lipid-mediated transfection in CV-1 cells (23).

Characterization of the Dioleoylmelittin/DNA Complex. Rehydration of the dioleoylmelittin film resulted in a clear solution. Under negative-stain EM this solution appeared as aggregates or micellar-like structures with a size between 5 and 10 nm (Figure 5a).

Dynamic light scattering indicated that homogeneous particles with an apparent diameter of about 170 nm were formed when dioleoylmelittin was added to DNA at a weight ratio between 2 and 4 (Figure 6). When increasing amounts of dioleoylmelittin were added, the mean size of the complex slightly increased to 250 nm. Addition of DOPE to the dioleoylmelittin/DNA complex led to less homogeneous particles of a size larger than 400 nm (data not shown). Zeta potential measurements showed that when dioleoylmelittin was added to the DNA solution, particles became more and more positive. Charge neutralization (zeta potential between -1 and $+1$ mV) was obtained at a dioleoylmelittin/DNA ratio between 4/1 and 8/1 (w/w) (Figure 6). Similarly, gel electrophoresis showed that plasmid DNA was completely retained in the agarose gel when mixed at a dioleoylmelittin/DNA weight ratio above 4/1 (data not shown). This finding was in good agreement with zeta potential measurements.

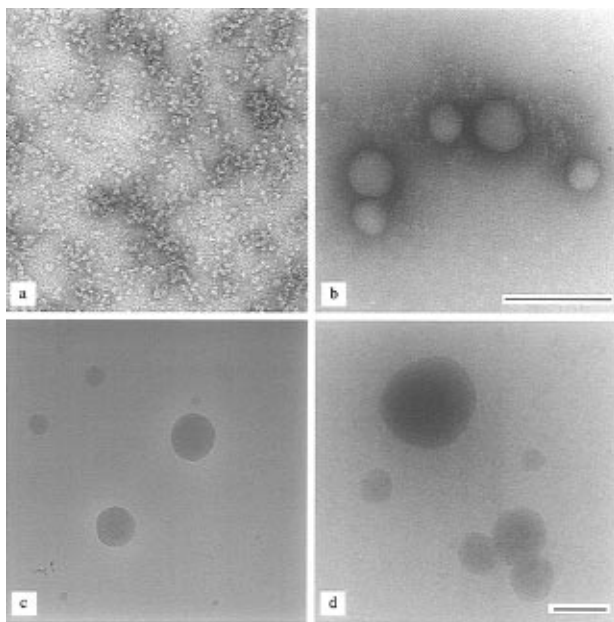


Figure 5. Electron micrographs of negative-stained (a, b) or frozen-hydrated (c, d) samples: dioleoylmelittin (a), dioleoylmelittin/DNA 10/1 (w/w) complex (b, d), and dioleoylmelittin/DNA 2/1 (w/w) complex (c). Bars represent 200 nm and are the same for (a) and (b) and for (c) and (d).

The dioleoylmelittin/DNA complex was also imaged by negative-stain EM and cryo-EM (Figure 5). At a 2/1 dioleoylmelittin/DNA weight ratio, spherical, filled particles with diameters between 50 and 150 nm were visualized under cryo-EM (Figure 5c). No aggregates or large structures were seen in any sample. Similar structures were observed for the 10/1 dioleoylmelittin/DNA complex (w/w), although particles larger than 200 nm were sometimes visualized in the sample (Figure 5d). Negative-stain EM revealed similar structures as for cryo-EM, albeit aggregated particles were seen more frequently (Figure 5b). These results confirmed the data obtained by laser light scattering.

DISCUSSION

Conjugation of 1,2-dioleoylphosphatidylethanolamine-*N*-[3-(2-pyridyldithio)propionate] with [Cys¹]melittin resulted in a hybrid molecule, the dioleoylmelittin, with properties different from those of the native peptide melittin. Indeed, although melittin binds DNA by charge interactions, the melittin/DNA complex does not mediate transfection and, due to the fast partitioning of melittin into cell membranes, induces high toxicity (8). In contrast, dioleoylmelittin was able to complex plasmid DNA to form homogeneous and small particles. The resulting dioleoylmelittin/DNA complex mediated efficient transfection of various cell types *in vitro*, including primary cells.

Dioleoylmelittin in aqueous solution forms aggregates that resemble micellar structures rather than liposomes. This characteristic distinguishes dioleoylmelittin from cationic lipids which spontaneously form liposomes in aqueous solution (24, 25). Unlike dioleoylmelittin/DNA complexes, cationic lipid/DNA complexes often appear as heterogeneous structures in EM (25–27). Recently, it has been shown that complexation of DNA with cationic lipids in a micellar state followed by dialysis of the preparation to remove the surfactant allowed the formation of small and stable particles (28). Therefore, due to a higher molecular motion, cationic amphiphiles in a micellar-like state could interact more favorably with plasmid DNA than in a liposomal state (29).

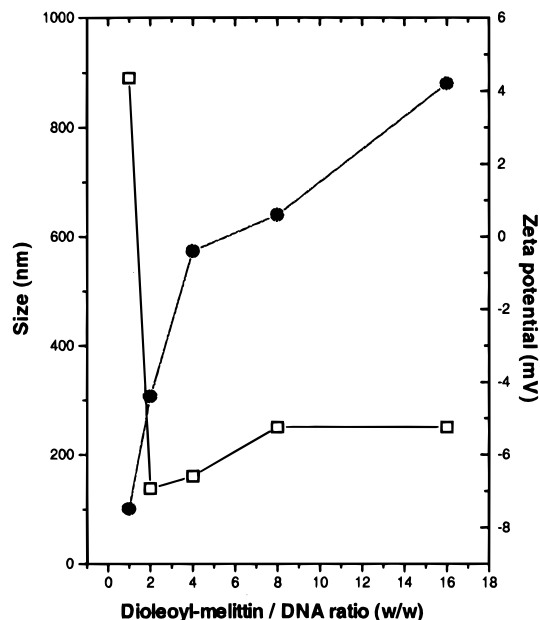


Figure 6. Evolution of the mean size (□) and the mean zeta potential (●) of the particles as a function of the dioleoylmelittin/DNA ratio (w/w).

The highest transfection of CV-1 cells was obtained for a 10/1 dioleoylmelittin/DNA ratio (w/w), which corresponds to a theoretical 5/1 \pm charge ratio, assuming 5 positive charges for dioleoylmelittin. The particles formed at this ratio had a net positive charge (zeta potential of 1.2 mV) and, as indicated by DNA gel electrophoresis, plasmid DNA was totally complexed by dioleoylmelittin. The absence of other structure in negative-stain EM or cryo-EM indicates that these particles are likely to be responsible for transfection.

Unlike other amphipathic molecule-based transfection systems, dioleoylmelittin did not require DOPE to mediate transfection (3, 4, 8). In contrast, at the optimal dioleoylmelittin/DNA ratio, addition of DOPE increased particle size and transfection efficiency decreased. Another interesting feature of the dioleoylmelittin system is its ability to mediate high transfection in the presence of serum. This is also in contrast to other transfection reagents such as cationic liposomes or the gramicidin S/DNA/DOPE complex for which 50% FCS in the transfection medium dramatically reduces transfection efficiency (8). This property should make dioleoylmelittin an attractive transfection reagent for serum-sensitive cell lines. Nevertheless, the reason FCS increases transfection is still unknown. The formation of small, compacted structures is undoubtedly an important feature to mediate high transfection in the presence of serum, as shown for cationic lipid- or polylysine-based systems (28, 30). However, other factors such as complement activation may be involved in the enhancement of dioleoylmelittin transfection efficiency by serum (31). We are currently investigating this possibility.

The cationic nature of the melittin moiety was necessary but not sufficient to mediate high levels of transfection. Indeed, replacement of the melittin by an oligolysine of five residues completely abolished transfection. Although high molecular weight polylysine covalently coupled with phosphatidylethanolamine can mediate transfection of cells in culture, scraping of the cells or addition of a helper lipid is required for efficient gene transfer with this reagent (32, 33). This indicates that the entry of DNA into cells and/or lysosomal escape using lipopolylysine is poor, which is due to the fact that

polylysine has no or limited membrane-disturbing activity. In contrast, both melittin and dioleoylmelittin can destabilize membranes, as shown by their ability in lysing red blood cells. However, melittin and dioleoylmelittin have somewhat different behaviors regarding their action on membranes. Dioleoylmelittin did not solubilize liposomes at concentrations below 140 μM , and the concentration that induced hemolysis was about 2–3-fold higher than that of melittin. This could explain why dioleoylmelittin, in contrast to melittin, did not induce cell toxicity at the concentrations used for transfection ($\leq 5 \mu\text{M}$).

Treatment of the cells with lysomotrophic agents during the transfection procedure decreased 2–3-fold the level of β -galactosidase expression. This observation suggests that DNA delivery using dioleoylmelittin may involve an endosomal/lysosomal pathway (23). Cationic lipid/DNA complexes also enter the cell by endocytosis (23, 34). Xu and Szoka have recently proposed that after endocytosis of the cationic lipid/DNA complex, destabilization of the early endosome occurs followed by a flip-flop of the anionic phospholipids of the endosomal membrane (35). Then, these anionic lipids diffuse into the complex to form ion pairs with cationic lipids, leading to the displacement of plasmid DNA from the transfecting complex. In the case of dioleoylmelittin, such a mechanism may also be possible since melittin can induce a rapid and extensive lipid flip-flop in membranes (36). Furthermore, the affinity of melittin for membrane-containing anionic lipids is 100-fold greater than for zwitterionic lipids (12). However, in contrast to cationic lipids for which lysomotrophic agents usually increase gene transfer efficiency (23), dioleoylmelittin transfection efficiency was decreased when monensin or ammonium chloride were present during transfection. Nevertheless, the exact mechanism whereby dioleoylmelittin is mediating transfection is still unresolved. In particular, it is unclear whether dioleoylmelittin is the actual transfecting agent or if it acts as a prodrug that releases the more active melittin after reduction of the disulfide bridge.

The use of dioleoylmelittin for *in vivo* gene transfer, especially in humans, may be precluded by the immunogenic potential of the melittin (37). However, similar hybrid molecules based on membrane-disturbing, non-immunogenic peptides could perhaps be engineered to deliver genes *in vivo*. In conclusion, dioleoylmelittin represents a new class of efficient, *in vitro* transfecting reagent, especially suited for serum-sensitive cells.

ACKNOWLEDGMENT

We are grateful to Dr. J. Fingerle (F. Hoffmann-La Roche) for providing rabbit aorta smooth muscle cells. We greatly appreciate the expertise of Mrs. B. Hennequin in the dioleoylmelittin purification.

LITERATURE CITED

- (1) Knowles, M. R., Hohneker, K. W., Zhou, Z., Olsen, J. C., Noah, T. L., Hu, P. C., Leigh, M. W., Engelhardt, J. F., Edwards, L. J., Jones, K. R., Grossman, M., Wilson, J. M., Johnson, L. G., and Boucher, R. C. (1995) A controlled study of adenoviral-vector-mediated gene transfer in the nasal epithelium of patients with cystic fibrosis. *N. Engl. J. Med.* 333, 823–831.
- (2) Ledley, F. D. (1995) Nonviral gene therapy: the promise of genes as pharmaceutical products. *Hum. Gene Ther.* 6, 1129–1144.
- (3) Behr, J. P. (1994) Gene transfer with synthetic cationic amphiphiles: prospects for gene therapy. *Bioconjugate Chem.* 5, 382–389.
- (4) Gao, X., and Huang, L. (1995) Cationic liposome-mediated gene transfer. *Gene Ther.* 2, 710–722.
- (5) Wagner, E., Plank, C., Zatloukal, K., Cotten, M., and Birnstiel, M. (1992) Influenza virus hemagglutinin HA-2 N-terminal fusogenic peptides augment gene transfer by transferrin-polylysine-DNA complexes: toward a synthetic virus-like gene transfer vehicle. *Proc. Natl. Acad. Sci. U.S.A.* 89, 7934–7938.
- (6) Haensler, J., and Szoka, F. C. (1993) Polyamidoamine cascade polymers mediate efficient transfection of cells in culture. *Bioconjugate Chem.* 4, 372–379.
- (7) Plank, C., Oberhauser, B., Mechtler, K., Koch, C., and Wagner, E. (1994) The influence of endosome-disruptive peptides on gene transfer using synthetic virus-like gene transfer systems. *J. Biol. Chem.* 269, 12918–12924.
- (8) Legendre, J. Y., and Szoka, F. C. (1993) Cyclic amphipathic peptide-DNA complexes mediate high efficiency transfection of adherent mammalian cells. *Proc. Natl. Acad. Sci. U.S.A.* 90, 893–897.
- (9) Legendre, J. Y., and Supersaxo, A. (1995) Short-chain phospholipids enhance amphipathic peptide-mediated gene transfer. *Biochem. Biophys. Res. Commun.* 217, 179–185.
- (10) Hara, T., Kuwasawa, H., Aramaki, Y., Takada, S., Koike, K., Ishidate, K., Kato, H., and Tsuchiya, S. (1996) Effects of fusogenic and DNA-binding amphiphilic compounds on the receptor-mediated gene transfer into hepatic cells by asialoglutin-labeled liposomes. *Biochim. Biophys. Acta* 1278, 51–58.
- (11) Kamata, H., Yagisawa, H., Takahashi, S., and Hirata, H. (1994) Amphiphilic peptides enhance the efficiency of liposome-mediated DNA transfection. *Nucleic Acids Res.* 22, 536–537.
- (12) Dempsey, C. E. (1990) The actions of melittin on membranes. *Biochim. Biophys. Acta* 1031, 143–161.
- (13) Atherton, E., and Sheppard, R. C. (1989) In *Solid Phase Peptide Synthesis: A Practical Approach* (D. Rickwoods and B. D. Hames, Eds.) IRL Press, Oxford, U.K.
- (14) Knorr, R., Trzeciak, A., Bannwarth, W., and Gillesen, D. (1989) New coupling reagents in peptide chemistry. *Tetrahedron Lett.* 30, 1927–1930.
- (15) Zuckermann, R., Corey, D., and Schultz, P. (1987) Efficient methods for attachment of thiol specific probes to the 3'-ends of synthetic oligodeoxyribonucleotides. *Nucleic Acids Res.* 15, 15305–15321.
- (16) Olson, F., Hunt, T., Szoka, F. C., Vail, W. J., and Papahadjopoulos, D. (1979) Preparation of liposomes of defined size distribution by extrusion through polycarbonate membranes. *Biochim. Biophys. Acta* 557, 9–23.
- (17) Nordeen, S. K. (1988) Luciferase reporter gene vectors for analysis of promoters and enhancers. *BioTechniques* 6, 454–458.
- (18) Deuschle, U., Pepperkok, R., Wang, F. B., Giordano, T. J., McAllister, W. T., Ansorge, W., and Bujard, H. (1989) Regulated expression of foreign genes in mammalian cells under the control of coliphage T3 RNA polymerase and lac repressor. *Proc. Natl. Acad. Sci. U.S.A.* 86, 5400–5404.
- (19) McGregor, G. R., Mogg, A. E., Burke, J. F., and Caskey, C. T. (1987) Histochemical staining of clonal mammalian cell lines expressing *E. coli* β galactosidase indicates heterogeneous expression of the bacterial gene. *Somat. Cell. Mol. Genet.* 13, 253–265.
- (20) Owens, G. K., and Thompson, L. G. (1986) Expression of smooth muscle specific isoactin in cultured smooth muscle cells: relationship between growth and cytodifferentiation. *J. Cell Biol.* 102, 343–352.
- (21) Brasier, A. R., Tate, J. E., and Habener, J. F. (1989) Optimized use of the firefly luciferase assay as a reporter gene in mammalian cell lines. *BioTechniques* 7, 1116–1122.
- (22) Dufourcq, J., Faucon, J. F., Fourche, G., Dasseux, J. L., Le Maire, M., and Gulik-Krzywicki, T. (1986) Morphological changes of phosphatidylcholine bilayers induced by melittin: vesicularization, fusion, discoidal particles. *Biochim. Biophys. Acta* 859, 33–48.
- (23) Legendre, J. Y., and Szoka, F. C. (1992) Delivery of plasmid DNA into mammalian cells using pH-sensitive liposomes: comparison with cationic liposomes. *Pharm. Res.* 9, 1235–1242.

- (24) Felgner, P. L., Gadek, T. R., Holm, M., Roman, R., Chan, H. W., Wenz, M., Northrop, J. P., Ringold, G. M., and Danielsen, M. (1987) Lipofection: a highly efficient, lipid-mediated DNA transfection procedure. *Proc. Natl. Acad. Sci. U.S.A.* 84, 7413–7417.
- (25) Gershon, H., Ghirlando, R., Guttman, S. B., and Minsky, A. (1993) Mode of formation and structural features of DNA-cationic liposome complexes used for transfection. *Biochemistry* 32, 7143–7151.
- (26) Sternberg, B., Sorgi, F. L., and Huang, L. (1994) New structures in complex formation between DNA and cationic liposomes visualized by freeze-fracture electron microscopy. *FEBS Lett.* 356, 361–366.
- (27) Gustafsson, J., Arvidson, G., Karlsson, G., and Almgren, M. (1995) Complexes between cationic liposomes and DNA visualized by cryo-TEM. *Biochim. Biophys. Acta* 1235, 305–312.
- (28) Hofland, H. E. J., Shephard, L., and Sullivan, S. M. (1996) Formation of stable cationic lipid/DNA complexes for gene transfer. *Proc. Natl. Acad. Sci. U.S.A.* 93, 7305–7309.
- (29) Behr, J. P. (1986) DNA strongly binds to micelles and vesicles containing lipopolyamines or lipointercalants. *Tetrahedron Lett.* 27, 5861–5864.
- (30) Vitiello, L., Chonn, A., Wasserman, J. D., Duff, C., and Worton, R. G. (1996) Condensation of plasmid DNA with polylysine improves liposome-mediated gene transfer into established and primary muscle cells. *Gene Ther.* 3, 396–404.
- (31) Plank, C., Mechtler, K., Szoka, F. C., and Wagner, E. (1996) Activation of the complement system by synthetic DNA complexes: a potential barrier for intravenous gene delivery. *Hum. Gene Ther.* 7, 1437–1446.
- (32) Zhou, X., Klibanov, A. L., and Huang, L. (1991) Lipophilic polylysines mediate efficient DNA transfection in mammalian cells. *Biochim. Biophys. Acta* 1065, 8–14.
- (33) Zhou, X., and Huang, L. (1994) DNA transfection mediated by cationic liposomes containing lipopolylysine: characterization and mechanism of action. *Biochim. Biophys. Acta* 1189, 195–203.
- (34) Zabner, J., Fasbender, A. J., Moninger, T., Poellinger, K. A., and Welsh, M. J. (1995) Cellular and molecular barriers to gene transfer by a cationic lipid. *J. Biol. Chem.* 270, 18997–19007.
- (35) Xu, Y., and Szoka, F. C. (1996) Mechanism of DNA release from cationic liposome/DNA complexes used in cell transfection. *Biochemistry* 35, 5616–5623.
- (36) Fattal, E., Nir, S., Parente, R. A., and Szoka, F. C. (1994) Pore-forming peptides induce rapid phospholipid flip-flop in membranes. *Biochemistry* 33, 6721–6730.
- (37) Kemeny, D. M., McKenzie-Mills, M., Harries, M. G., Youten, L. J. F., and Lessof, M. H. (1983) Antibodies to purified bee venom proteins and peptides. *J. Allergy Clin. Immunol.* 72, 376–385.

BC960076D

Optimization of Conditions for Formation and Analysis of Anti-CD19 FVS191 Single-Chain Fv Homodimer (scFv)₂

Duo Wang,[†] Erica Berven,[†] Quanzhi Li,[†] Fatih Uckun,[‡] and John H. Kersey^{*,†,§,||,⊥}

University of Minnesota Cancer Center, Biotherapy Institute, and Departments of Laboratory Medicine/Pathology and Pediatrics and Therapeutic Radiology, University of Minnesota, Minneapolis, Minnesota 55455. Received August 29, 1996[⊗]

In this report, we present the production of a dimeric form of anti-CD19 scFv, the FVS191cys (scFv)₂. Anti-CD19 scFv FVS191cys was constructed by engineering a cysteine residue at the C terminus of the V_L domain of scFv FVS191. FVS191cys (scFv)₂ was formed through a disulfide bond between two FVS191cys molecules. To optimize the yield of FVS191cys (scFv)₂, the effects of oxidation time, buffer pH, and temperature on the formation of dimeric scFv were analyzed. Our study indicates that the formation of FVS191cys (scFv)₂ is oxidation time- and buffer pH-dependent; a high pH buffer facilitates the formation of disulfide-linked (scFv)₂. The maximum yield of FVS191cys (scFv)₂ can be achieved when FVS191cys is air-oxidized at 4 °C, in buffer with a pH of 8.5–9. The biological activity of FVS191cys (scFv)₂ was analyzed by ELISA and an internalization assay. FVS191cys (scFv)₂ has a CD19 binding ability similar to that of its parental mAb B43 and is internalized by CD19 positive Nalm 6 cells. This study indicates that FVS191cys (scFv)₂ is a potential candidate for tumor diagnosis or therapy.

INTRODUCTION

Monoclonal antibodies (mAbs)¹ have been useful for antigen-specific targeting of tumor cells; however, the application of mAbs has demonstrated limited diffusion of mAbs from the vasculature into the tumor. The limited diffusion of intact antibodies is due to the large size of mAbs and the host effect elements of their Fc domains (1, 2). A recombinant single-chain Fv (scFv) composed of the minimal antigen binding domains, variable heavy chain (V_H) and variable light chain (V_L), is one-sixth of the size of a mAb (28 kDa). ScFvs have exhibited improved tumor penetration with higher tumor to normal tissue ratios than corresponding IgG or Fab and faster plasma clearance rates (3–5). However, scFvs have only one antigen binding arm which may decrease antigen binding affinity (4). Previous studies have demonstrated that homodimers of scFv [(scFv)₂], such as an anti-c-erb2 (scFv)₂, have exhibited divalent binding and increased retention in tumors as compared with the corresponding scFv monomers (6). Also, radiolabeled (scFv)₂ was found to have improved tumor imaging compared to Fab, monomeric scFv, and intact antibody (7). These studies suggest that dimers of scFvs may be useful candidates for tumor diagnoses and therapy.

Covalently linked (scFv)₂ have been generated by several different approaches: (i) forming a disulfide bond between carboxyl-terminal cysteine residues (6, 8), (ii) cross-linking with chemical linkers (6, 9), and (iii) forming covalent bundle helices or leucine zippers at the C terminus (10). The first method is carried out by introducing one cysteine at the 3' end of the scFv and forming a C-terminal disulfide bond through air oxidation. Chemical linking uses BMH or peptide-bridged MCA to link two scFvs (6). This method is complicated by the multiple steps involved in the chemical modification. Finally, engineering small peptides at the C terminus of scFv for formation of helix bundles or leucine zippers may be useful, but it may increase the immunogenicity of the molecules.

In this report, we studied the formation of dimeric forms of FVS191cys. FVS191 is an anti-CD19 scFv produced in our laboratory from the B43 hybridoma (11). FVS191cys was constructed by engineering a cysteine residue at the C terminus of FVS191. We focused on the production of a disulfide-linked (scFv)₂ because this species was relatively easy to generate and was stable in solution as chemically linked (scFv)₂ (6). It was observed that FVS191cys (scFv)₂ could be formed by air oxidation in basic buffers without any chemical modifications or manipulations. To optimize the conditions for formation of disulfide-linked (scFv)₂, we used FVS191cys as a model molecule to study the effects of oxidation time, buffer pH, and temperature on formation of FVS191cys (scFv)₂. In addition, the CD19 binding ability of FVS191cys (scFv)₂ was evaluated by ELISA. The internalization of FVS191cys (scFv)₂ by CD19 positive cells was also investigated.

MATERIALS AND METHODS

Construction of the Plasmid for the Expression of FVS191cys. The expression plasmid of FVS191cys was derived from pFVS191 (11). To insert an additional cysteine residue at the 3' end of the V_L gene, the pFVS191 plasmid was restricted with *Bgl*II and *Eco*RI and ligated with the annealed, complementary oligonucleotides of HLCys1 and HLCys2. The correct insertion of the oligonucleotides HLCys1/HLCys2 was verified by nu-

* To whom requests for reprints should be addressed at Box 86 UMHC, 420 Delaware St. SE, Minneapolis, MN 55455. Telephone: 612-625-4659. Fax: 612-624-8965. E-mail: kerse001@maroon.tc.umn.edu.

[†] University of Minnesota Cancer Center.

[‡] Biotherapy Institute.

[§] J.H.K. is a recipient of an Outstanding Investigator Grant Award (CA 49721) from the National Cancer Institute.

^{||} Department of Laboratory Medicine/Pathology.

[⊥] Department of Pediatrics and Therapeutic Radiology.

[⊗] Abstract published in *Advance ACS Abstracts*, January 1, 1997.

¹ Abbreviations: mAb, monoclonal antibody; scFv, single-chain Fv; scFv', single-chain Fv with C-terminal cysteine; (scFv)₂, dimeric single-chain Fv; BMH, 1,6-bis(maleimido)-hexane; MCA, *N,N*-bismaleimidocaproyl amino acid; SDS-PAGE, sodium dodecyl sulfate–polyacrylamide gel electrophoresis.

cleotide sequencing. The construction of pFVS191cys is shown in Figure 1.

Expression and Purification of FVS191cys. The pFVS191cys plasmid was transformed into *Escherichia coli* BL21(DE3) (Novagen, Madison, WI). The transformed bacterial cells were grown in 1 L of SOB medium (20 g of tryptone, 5 g of yeast extract, 0.5 g of NaCl, and 5 g of $\text{MgSO}_4 \cdot 7\text{H}_2\text{O}$ per liter) at 37 °C. When the absorbance of A_{600} of the bacterial culture reached 0.65, recombinant protein production was induced with 1 mM isopropyl β -D-thiogalactopyranoside (IPTG) for 1.5 h at 37 °C.

The inclusion bodies of FVS191cys were isolated using the following procedures. The harvested cell pellets were mixed with 50 mL of inclusion body separation (IBS) buffer (0.1 M KCl, 0.02 M Tris-HCl, 5 mM EDTA, and 0.1% Nonidet P-40 at pH 8.0) and sonicated. Lysozyme was added to the sonicated cell mixture to a final concentration of 0.2 mg/mL. After incubation at room temperature for 1 h, the cell lysate was frozen at -80 °C. Cell lysates were then thawed at room temperature, sonicated, and centrifuged at 17000g for 30 min at 4 °C. The supernatant was discarded, and the pellet was suspended in 50 mL of IBS buffer. Sodium deoxycholate (10%, w/v) was added to the suspensions for a final concentration of 2%. The mixture was stirred at room temperature for 1 h and centrifuged at 17000g for 30 min at 4 °C. The inclusion body pellet was washed by suspending in IBS buffer and centrifuging at 17000g for 30 min. The wash was repeated once with water, and the inclusion bodies were stored at -80 °C.

Refolding of FVS191cys. FVS191cys was denatured and refolded according to Buchner's method (12) with some modifications. The inclusion bodies of FVS191cys were dissolved in a denaturing buffer [0.1 M Tris, 6 M guanidine hydrochloride, 0.3 M dithioerythritol (DTE), and 0.002 M EDTA at pH 8] at room temperature for 2 h. Insoluble materials were removed by centrifugation at 30000g for 30 min. The soluble protein concentration was determined using Coomassie Plus Protein Assay Reagent (Pierce) and bovine serum albumin (BSA) as standards. The final concentration of protein in denaturing solution was adjusted with denaturing buffer up to 20 mg/mL. Renaturation of FVS191cys was carried out by a rapid 100-fold dilution of the denatured protein into refolding buffer [100 mM Tris-HCl, 500 mM L-arginine, 8 mM oxidized glutathione (GSSG), and 2 mM EDTA at pH 8] at 10 °C and incubation for 48 h.

Purification of Refolded FVS191cys. After renaturation, the FVS191cys was concentrated and dialyzed against phosphate-buffered saline (PBS) buffer using an Amicon RA2000 concentrator with a YM10 cartridge (Amicon, Beverly, MA). FVS191cys proteins were purified by FPLC using a Superdex 75 (16 \times 60 mm) gel filtration column (Pharmacia). Purified FVS191cys monomers were concentrated by ultrafiltration through a YM10 membrane (Amicon).

Formation of the FVS191cys Dimer. FVS191cys (scFv)₂ was formed by air oxidation of FVS191cys at 4 °C. To study the oxidation time and pH effects on FVS191cys (scFv)₂ formation, 500 μ L of 400 μ g/mL purified FVS191cys was injected into Slide-A-Lyzer 10K Dialysis Cassettes (Pierce) and dialyzed against Tris/EDTA/NaCl (TEN) buffer (10 mM Tris-HCl, 2 mM EDTA, and 100 mM NaCl at pH 6.5–12). After dialysis, the proteins were transferred into FALCON 2059 tubes and air-oxidized for 1, 5, 12, 16, 20, and 29 days at 4 °C. To examine the formation of FVS191cys (scFv)₂, 50 μ L of the protein sample was run on a 12% nonreducing SDS-PAGE (Bio-Rad, Hercules, CA) and visualized with

Coomassie Brilliant Blue R-250. The relative amounts of monomers and dimers of FVS191cys were quantified using a GS-700 imaging densitometer with the program of Molecular Analyst (Bio-Rad). The proportion of dimeric FVS191cys (% d) was calculated as % d = dimer/(monomer + dimer) \times 100%. This quantification method was tested with BSA standards, and the result indicated that this method could be used to compare the amounts of proteins.

To study the effect of dithiothreitol (DTT) reduction on the formation of dimeric FVS191cys, FVS191cys was reduced with DTT before air oxidation. Purified FVS191cys in PBS buffer was added by $1/100$ volume of 200 mM DTT and incubated at room temperature for 1 h. After reduction, DTT was removed by a PD10 column (Pharmacia). Reduced FVS191cys was dialyzed against TEN buffers with the pH at 7, 7.5, 8, 8.5, 9, and 10. The formation of dimeric FVS191cys was examined by 12% nonreducing SDS-PAGE after air oxidation for 1, 5, 12, 16, 20, and 29 days. The visualization and quantification of monomers and dimers of FVS191cys were performed as described above.

The effect of temperature on the formation of dimeric FVS191cys was evaluated as follows. FVS191cys in TEN buffer at pH 8 was incubated at 4 °C, room temperature, and 37 °C. After air oxidation for 4 h or longer, the formation of FVS191cys (scFv)₂ was examined by SDS-PAGE.

Purification of FVS191cys (scFv)₂. FVS191cys (scFv)₂ was purified by FPLC using a Superdex 75 column (HiLoad 16/60) (Pharmacia). PBS buffer was used as an elution buffer; the column was run at a flow rate of 1 mL/min. The fractions containing FVS191cys (scFv)₂ were collected and concentrated by ultrafiltration using a YM10 membrane (Amicon).

¹²⁵I Labeling of FVS191cys. Purified FVS191cys (scFv)₂ was labeled with radioiodine using the IODO-BEADS method of Pierce (Pierce, Rockford, IL). FVS191cys (scFv)₂ (100 μ g) in 100 μ L of PBS was incubated with 100 μ L of ¹²⁵I solution containing 1 mCi sodium iodine (NEN, Boston, MA) in a 1 mL Reacti-Vial. The reaction proceeded for 10 min at room temperature. The free iodine was separated from the labeled dimers with a Sephadex G-25 gel filtration column (Pharmacia). The specific activity of labeled FVS191cys (scFv)₂ was approximately 2 μ Ci/ μ g.

CD19 Antigen Binding Assay. The specific CD19 binding ability of FVS191cys (scFv)₂ was assessed by ¹²⁵I-labeled proteins. CD19 positive (Nalm 6) and CD19 negative (Molt 13 and Peer) cell lines were grown in RPMI 1640 tissue culture medium supplemented with 10% fetal bovine serum (FBS). The log phase cells were harvested by low-speed centrifugation, washed once with fresh medium, and adjusted to a final concentration of 2×10^8 cells/mL. The ¹²⁵I-labeled FVS191cys (scFv)₂ was diluted in fresh tissue culture medium to a final concentration of 200 ng/mL. Pellets of 0.1 mL of cell suspension from each cell line in duplicate were incubated with 400 μ L of labeled antibody solution at 4 °C for 1 h. After incubation, the cells were washed three times with 1 mL of fresh tissue culture medium. The radioactivity associated with pellets of each cell line was determined in a γ counter (Beckman).

The CD19 binding ability of FVS191cys (scFv)₂ was further assessed by a competitive ELISA. The ELISA method was performed as follows. Purified B43 mAb was conjugated to alkaline phosphatase (B43-AP) using a commercial conjugation kit (Pierce). The conjugates were used directly without further purification. A series of experiments were carried out to determine the optimal

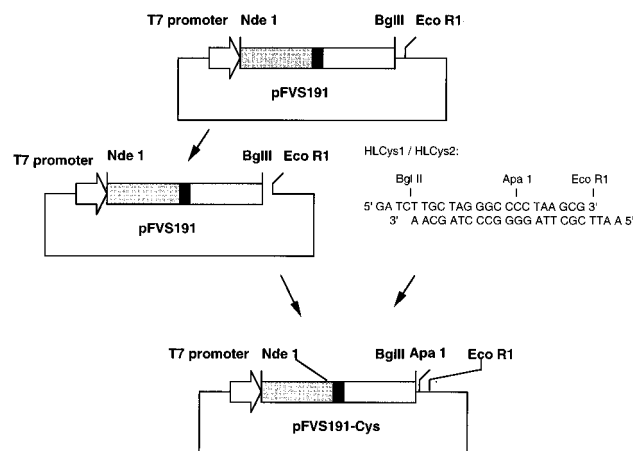


Figure 1. Cloning strategy used in the construction of FVS191cys. pFVS191 plasmid was restricted with enzyme *Bgl*III and *Eco*RI and inserted with annealed oligonucleotides HLCys1/HLCys2.

concentration of coating antigen and B43-AP for the ELISA. The CD19 antigens used in the ELISA were isolated from CD19 positive Daudi cells using the methods of Siegall et al. (13). ELISA plates (Immuron 4, Dynatech Laboratories Inc., Chantilly, VA) were coated with 50 μ L of isolated membrane proteins at a concentration of 80 μ g/mL. The plates were dried in a vacuum desiccator at 4 °C overnight and washed three times with PBS before use. Varying amounts of competing FVS191cys (scFv)₂ and a fixed amount of B43-AP (total volume of 100 μ L) were added to the wells and incubated at room temperature for 1 h. The final dilution of B43-AP was 1:2000. The plates were washed four times with PBS and incubated with 100 μ L of substrate solution at 4 °C overnight. The optical density of the wells was determined by an ELISA reader at 405 nm.

Internalization Assay. CD19 positive Nalm 6 cells were grown in RPMI 1640 medium supplemented with 10% FBS. The cells were harvested by centrifugation. ¹²⁵I-labeled FVS191cys (scFv)₂ (10 mg) was incubated with 1 \times 10⁸ cells in a volume of 5 mL and incubated on ice for 1 h. B43 mAb-blocked Nalm 6 cells were used as a control to assess nonspecific binding. After incubation, the cells were washed four times with cold RPMI 1640 without serum. Aliquots of 5 \times 10⁶ cells were transferred to 1 mL test tubes and incubated at 37 °C in a tissue culture incubator for various time intervals. Percentages of cell surface-bound, dissociated, internalized, and degraded FVS191cys (scFv)₂, based on the total cell-associated radioactivity at time 0, were determined according to the methods of Press et al. (14). Supernatants were separated from cell pellets by centrifugation. Precipitation of the supernatants by TCA further defined two portions of the labeled FVS191cys (scFv)₂: degraded FVS191cys (scFv)₂ (TCA nonperceptible) and dissociated FVS191cys (scFv)₂ (TCA perceptible). Cell pellets were treated with acid-papain; the radioactivity released by acid-papain treatment was regarded as cell surface-bound FVS191cys (scFv)₂, and the radioactivity associated with cell pellets after the treatment was seen as the internalized FVS191cys (scFv)₂.

RESULTS

FVS191cys Expression and Purification. A cysteine residue was introduced into the anti-CD19 scFv, FVS191, fragment by genetically engineering an additional codon at the 3' end of the gene encoding the V_L domain (Figure 1). The sulfhydryl group introduced to

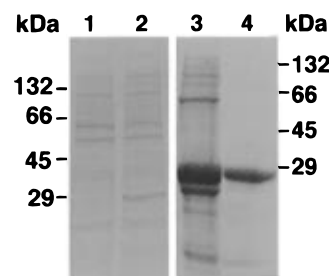


Figure 2. Expression and purification of FVS191cys. Electrophoretic analysis of samples on a 12% reducing SDS-PAGE: lane 1, total bacterial lysate of uninduced BL21(DE3) carrying pFVS191cys; lane 2, total cell lysate of IPTG-induced BL21(DE3) carrying pFVS191cys; lane 3, inclusion bodies of FVS191cys; and lane 4, refolded FVS191cys purified by FPLC. The sizes of molecular mass markers are indicated at each side of the gel.

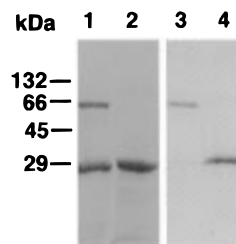


Figure 3. Formation and separation of FVS191cys (scFv)₂. Protein samples were analyzed by electrophoresis: lane 1, air-oxidized FVS191cys on a 12% nonreducing SDS-PAGE; lane 2, air-oxidized FVS191cys on a 12% reducing SDS-PAGE; lane 3, FVS191cys (scFv)₂ (peak II of FPLC) on a 12% nonreducing SDS-PAGE; and lane 4, FVS191cys monomers (peak III of FPLC) on a 12% nonreducing SDS-PAGE. The sizes of molecular mass markers are indicated on the left side of the gels.

the 3' end of FVS191 served as a specific site for the formation of disulfide-bonded dimeric FVS191cys. FVS191cys was produced as insoluble inclusion bodies by pFVS191cys-transformed BL21(DE3) *E. coli* cells. Figure 2 shows the expression and purification of FVS191cys on a SDS-PAGE. An average of 40 mg of FVS191cys inclusion bodies was isolated from 1 L of bacterial cell culture. The isolated FVS191cys was refolded in DTE-GSSG redox buffer. The final concentration of FVS191cys in refolding buffer influenced the refolding of FVS191cys. If the concentration of FVS191cys in refolding buffer were more than 20 mg/L, the amount of protein aggregates would increase. The refolded FVS191cys was purified by FPLC using a Superdex 75 column (Figure 2, lane 4).

Formation of the Disulfide-Bonded Dimer. FVS191cys scFv formed disulfide-linked homodimers through air oxidation. This was demonstrated by the formation of 56 kDa proteins when 28 kDa FVS191cys monomers were incubated at 4 °C (Figure 3, lane 1). The 56 kDa protein was reduced to a 28 kDa species in the presence of DTT (Figure 3, lane 2). After removal of DTT, the 28 kDa FVS191cys reformed the 56 kDa proteins (data not shown). This indicates that the 56 kDa protein is a disulfide-linked homodimer of FVS191cys.

FVS191cys (scFv)₂ was separated from monomers of FVS191cys by gel filtration chromatography. Figure 4 shows that FVS191cys (scFv)₂ was eluted from the Superdex 75 column in the second peak and FVS191cys monomers in the third peak. Fractions in the first peak contained high-molecular mass aggregates. The separated dimers and monomers of FVS191cys were examined by a nonreducing SDS-PAGE (Figure 3, lanes 3 and 4).

Time and pH Dependence of Dimer Formation. The formation of FVS191cys (scFv)₂ by air oxidation

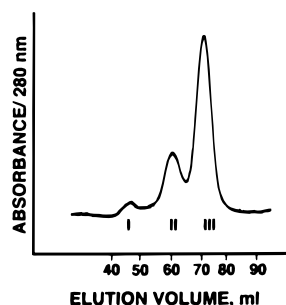


Figure 4. FPLC separation of monomeric (peak III), dimeric (peak II), and aggregates of FVS191cys (peak I) using a Superdex 75 column. Conditions for separation are described in Materials and Methods.

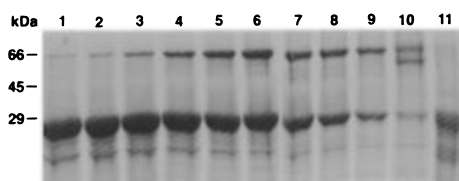


Figure 5. Formation of FVS191cys (scFv)₂ with various pHs. After air oxidation for 12 days at 4 °C, 50 μ L of protein samples in TEN buffer (pH 6–12) were electrophoresed on a 12% nonreducing SDS–PAGE. Lanes 1–11 are proteins with pH 6, 6.5, 7, 7.5, 8, 8.5, 9, 9.5, 10, 11, and 12, respectively. The sizes of molecular mass markers are indicated on the left side of the gel.

depends on the length of air oxidation time and the pH of the buffer. The amount of FVS191cys (scFv)₂ increased with oxidation time and buffer pH. Figure 5 shows the formation of FVS191cys (scFv)₂ with varied pH after air oxidation for 12 days at 4 °C. From pH 6 to 9, increasing amounts of dimeric FVS191cys were found with the increments of pH (Figure 5, lanes 1–9). These data indicate that pH affects the formation of (scFv)₂ and basic buffer conditions favor dimer formation. When the pH was over 9, some of the FVS191cys degraded and some formed high-molecular mass aggregates. Therefore, the total amounts of dimers and monomers of FVS191cys with a pH of >9 were reduced (Figure 5, lanes 8–11).

The formation of FVS191cys (scFv)₂ was studied by using both DTT-nonreduced FVS191cys and DTT-reduced FVS191cys. Various reaction times and buffer pHs were investigated for the formation of FVS191cys (scFv)₂. The percentages of FVS191cys dimers under the above conditions were tabulated in Table 1.

Temperature Effect on Dimer Formation. FVS191cys (scFv)₂ can be formed at 4 °C, room temperature, and 37 °C as shown in Figure 6. At room temperature and 37 °C, high-molecular mass aggregates of FVS191cys were found (Figure 6, lanes 2 and 3). No aggregation of FVS191cys was visible at 4 °C (Figure 6, lane 1). A greater proportion of dimers was formed at room temperature than at 4 °C; however, at room temperature, FVS191cys formed aggregates that reduced the population of reactive FVS191cys. Therefore, 4 °C is the best condition for formation of (scFv)₂.

Specific CD19 Binding by FVS191cys (scFv)₂. A specific antigen binding assay was carried out with ¹²⁵I-labeled FVS191cys (scFv)₂. When the radioactivity associated with cell pellets of CD19 positive cells (Nalm 6) was arbitrarily expressed as 100%, the radioactivity associated with Molt 13 and Peer (CD19 negative cells) were determined to be only 6.2 and 7.9%, respectively. These results demonstrate that the FVS191cys (scFv)₂ is highly specific for CD19 antigen positive cells.

An ELISA assay was used to compare the CD19 binding ability of FVS191cys (scFv)₂ with that of mAb B43 or FVS191cys. Figure 7 indicates that the IC₅₀ of FVS191cys (scFv)₂ is 1.45×10^{-9} , the IC₅₀ of mAb B43 is 1.32×10^{-9} , and the IC₅₀ of monomeric FVS191cys is 1.05×10^{-9} . Therefore, the three different forms of B43-derived proteins have similar CD19 binding abilities.

Internalization by CD19⁺ Cells. FVS191cys (scFv)₂ was internalized by CD19⁺ Nalm 6 cells, as shown in Figure 8. The amount of internalized FVS191cys (scFv)₂ increased with time, and the amount of cell surface-bound FVS191cys (scFv)₂ decreased correspondingly. The amount of degraded and dissociated FVS191cys (scFv)₂ remained relatively constant.

DISCUSSION

In this report, we have described the production of FVS191cys, an anti-CD19 scFv engineered with a C-terminal cysteine, and demonstrated that FVS191cys forms a disulfide-linked homodimer.

In this study, the effects of air oxidation time, buffer pH, and temperature on the formation of dimeric FVS191cys were investigated for the purpose of defining the optimal conditions for dimer formation. Our results indicate that formation of disulfide-linked (scFv)₂ is dependent on oxidation time and pH. Specially, the yield of (scFv)₂ increases with time and pH.

The time dependence of (scFv)₂ formation is related to the size and tertiary structure of the scFv' protein. The solubility of thiols affects the reaction rate of the disulfide bond formation between two molecules; the longer the peptides, the harder it is for oxidation to occur (15). The scFv' has a mass of 28 kDa, which is large for a peptide, and is, therefore, slow to form (scFv)₂. If the C-terminal cysteine of scFv' is sterically hindered, it would be more difficult to form a disulfide bond.

The pH dependence of dimer formation is due to the oxidation process. There are two steps involved in the air oxidation of thiols: the formation of a thiolate anion and the formation of a thiyl radical by electron transfer between the thiolate anion and oxygen (15). Therefore, oxidation is promoted under basic conditions. In our case, the maximum yield of FVS191cys (scFv)₂ was achieved at pH 8.5 or 9. Above pH 9, although the ratio of dimer to monomer of FVS191cys was high, the dimer yield is low because the total amount of FVS191cys was decreased. The reduction of FVS191cys was due to the high pH in which FVS191cys was unstable and was degraded.

FVS191cys aggregates at temperatures above 4 °C. Different scFv's may have different intrinsic tendencies to form multimers or aggregates (16). Those tendencies may be related to the tertiary structures of the scFv' and the distribution of charged or uncharged amino acids on the surfaces of the scFv' molecules. At higher temperatures, the disulfide bond of scFv' was less stable; FVS191cys was more likely to form covalently linked multimers. Therefore, 4 °C was the best condition for formation of (scFv)₂.

FVS191cys (scFv)₂ can be formed from DTT-nonreduced FVS191cys; this indicates that DTT reduction is not necessary for dimer formation. However, McCartney et al. (16, 17) suggested that DTT reduction was a necessary step for forming (scFv)₂. Their different conclusion may have resulted from the different method that they used to refold scFv'. They used urea–glutathione redox buffer to refold 741F8 scFv'; the final concentration of oxidized glutathione in the refolding buffer was 100 mM. Their refolding method converted reduced thiol groups of scFv' to mixed disulfides with

Table 1. Summary of the Percentage of Dimeric FVS191cys (% d) under Different Times and pHs^a

DTT-nonreduced FVS191cys							DTT-reduced FVS191cys						
pH	day 1	day 5	day 12	day 16	day 20	day 29	pH	day 1	day 5	day 12	day 16	day 20	day 29
6	1.4	13.0	3.3	6.1	5.1	7.4							
6.5	1.6	13.7	4.4	8.3	8.2	13.7							
7	2.0	14.7	9.0	14.7	16.2	22.4	7	5.5	5.9	11.0	24.8	19.9	42.4
7.5	2.8	14.7	17.0	25.8	27.4	35.0	7.5	7.7	3.5	14.9	28.7	25.5	36.1
8	4.6	24.0	26.4	35.2	36.1		8	8.5	4.7	16.0	29.8	28.7	32.6
8.5	7.5	21.0	32.7	39.0	33.1	38.4	8.5	9.8	5.5	17.8	28.9	29.5	33.4
9	11.5	29.4	34.0	43.1	43.3	44.7	9	12.7	7.9	18.3	30.6	29.9	35.6
9.5	14.4	35.0	38.9	46.8	47.8	51.2							
10	14.7	44.9	46.6	56.2	50.0		10	24.8	13.9	21.2	34.0	30.2	37.2

^a The calculation of % d for dimers from DTT-nonreduced and DTT-reduced FVS191cys is described in Materials and Methods.

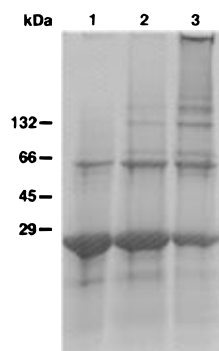


Figure 6. Formation of FVS191cys (scFv)₂ at 4 °C, room temperature, and 37 °C for 4 h. Proteins (50 μL) incubated at the above temperatures were electrophoresed on a 12% non-reducing SDS-PAGE: lane 1, proteins incubated at 4 °C; lane 2, proteins incubated at room temperature; and lane 3, proteins incubated at 37 °C. The sizes of molecular mass markers are indicated on the left side of the gel.

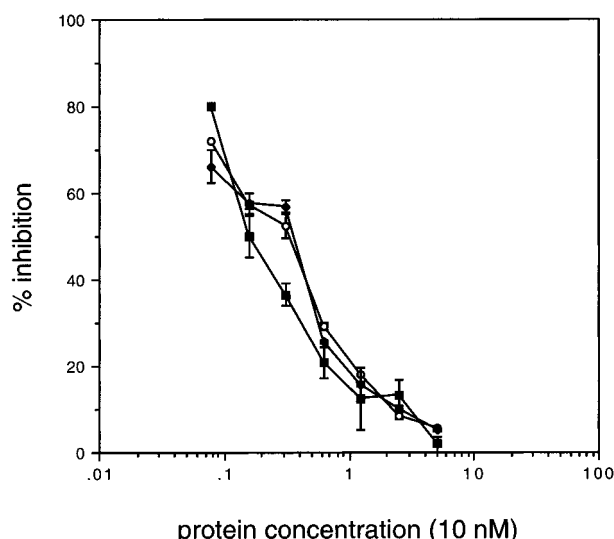


Figure 7. Affinity assay by competitive ELISA. Various amounts of FVS191cys (■), FVS191cys (scFv)₂ (●), and mAb B43 (○) were mixed up with a constant amount of B43-AP. The means of percentage inhibition of B43-AP binding were plotted against log molar concentrations of inhibition proteins. The bars represent a standard deviation.

glutathione; no thiol was available for forming a disulfide bond. Thus, DTT had to be used to eliminate the blocking group of C-terminal cysteines (16), and then the 741F8 (scFv)₂ was formed. In our study, however, we used DTE-GSSG redox buffer to refold FVS191cys; the final concentration of oxidized glutathione was 8 mM. Most FVS191cys compounds produced by our refolding method were not blocked by glutathione (data not shown). Therefore, DTT reduction was not necessary for formation of the FVS191cys (scFv)₂. DTT reduction is probably

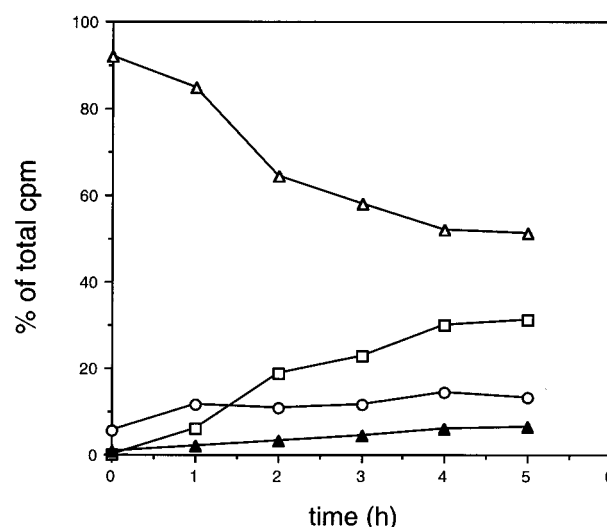


Figure 8. Internalization of ¹²⁵I-labeled FVS191cys (scFv)₂ by Nalm 6 cells. The percentage of radioactivity calculated as the percentage of total CPM was plotted against each time point. At each time point, cell pellets were separated from supernatants by low-speed centrifugation: (Δ) acid-papain released, cell surface-bound FVS191cys (scFv)₂; (□) internalized FVS191cys (scFv)₂ which could not be released by acid-papain treatment; (○) dissociated FVS191cys (scFv)₂ which was precipitated by TCA from supernatant; and (▲) degraded FVS191cys (scFv)₂ which could not be precipitated by TCA from supernatants.

only necessary when the refolded scFv's are blocked by glutathione. Among the two dimer formation methods, our method has the advantages of fewer experimental steps and lower cost since GSSG is an expensive chemical.

It was also observed that the yields of FVS191cys (scFv)₂ from different preparations were variable. This phenomenon may be due to the differences in the protein concentration. The relationship between the concentration of scFv and the formation of (scFv)₂ was studied by Desplancq et al. (18). They reported that the proportion of associated dimer to monomer was a function of concentration, with an increased concentration of monomer leading to an increased proportion of dimers. Their study indicates that formation of (scFv)₂ can be improved by increasing the concentration of scFv. We found that there was an upper limit for the concentration of FVS191cys monomers. If the concentration of FVS191cys is over 1.5 mg/mL, it will aggregate. The optimal concentration of scFv' for dimer formation has to be studied individually since different scFv's have different tendencies to aggregate.

The CD19 binding assay with ¹²⁵I-labeled FVS191cys (scFv)₂ revealed the specific antigen binding ability of FVS191cys (scFv)₂. The ELISA assay indicated that the antigen binding ability of FVS191cys (scFv)₂ was similar to that of parental mAb B43 and monomeric FVS191cys.

Thus, dimers formed through C-terminal cysteines maintained the original antigen binding capability. This result is consistent with other reports (8, 9, 19). The ELISA assay with a (scFv)₂ derived from mAb215 showed that the binding constant was quite close to that of the parental mAb and 4-fold higher than those of the scFv' monomers (8). Dimeric ScAb, a bivalent single-chain antibody fragment against *Pseudomonas aeruginosa*, had an antigen binding profile similar to that of the parental antibody (19). These results indicate that dimeric scFv' has the same antigen binding characters as the intact antibody from which it was derived.

To our knowledge, FVS191cys (scFv)₂ is the first dimeric scFv' to be analyzed in an internalization assay. FVS191cys (scFv)₂ can be internalized by CD19⁺ cells in a manner similar to that of its parental mAb B43 (unpublished data). This result indicates that FVS191cys (scFv)₂ can potentially replace intact mAb as tumor targeting agents on the basis of their antigen binding and internalization ability.

ScFvs containing C-terminal cysteines have proved to be very useful molecules. So far, several homodimers of scFvs have been formed through the C-terminal cysteines (6, 8, 17). The other studies have shown that the free sulfhydryl groups of scFvcys can be used to form heterodimers (7) or immunoconjugates with other chemical agents (8). In our laboratory, FVS191cys has been used to form a single-chain immunotoxin containing ricin A chain (unpublished data). Utilization of engineered cysteine to form disulfide-bonded molecules has also been employed to generate bivalent (9, 20) and bispecific (21) recombinant antibodies.

An alternative method for producing bivalent scFv is expression of protein in an *E. coli* system in which the proteins are secreted periplasmically. In periplasmic space, the proteins are refolded and assembled into the dimeric form (22). This method is more attractive when the proteins of interest can be produced in a large amount. In our studies, scFv FVS191 was expressed in such a system, but the yield was low.

In conclusion, we have demonstrated a simple and efficient method for producing disulfide-linked dimeric scFv' through C-terminal cysteines. In this method, scFv' is refolded in DTE-GSSG buffer and dimeric scFv' is formed by air oxidation in high-pH buffer. The formation of FVS191cys (scFv)₂ through air oxidation is time- and buffer pH-dependent. We found the optimal conditions for forming dimeric FVS191cys by air oxidation to be 4 °C and a pH between 8.5 to 9. The FVS191cys (scFv)₂ has a CD19 binding ability similar to that of its parental mAb B43 and is internalized by CD19 positive cells. Therefore, FVS191cys (scFv)₂ may be a good candidate for immunotargeting while being one-sixth of the size of the intact mAb.

ACKNOWLEDGMENTS

We gratefully thank Ms. Cedith Copenhaver for her help in reviewing and proofreading the manuscript.

LITERATURE CITED

- Jain, R. K. (1987) Transport of molecules in the tumor interstitium: a review. *Cancer Res.* 47, 3039–3051.
- Foon, K. A. (1989) Biological response modifiers: the new immunotherapy. *Cancer Res.* 49, 1621–1639.
- Yokota, T., Milenic, D. E., Whitlow, M., and Schlom, J. (1992) Rapid tumor penetration of a single-chain Fv and comparison with other immunoglobulin forms. *Cancer Res.* 52, 3402–3408.
- Milenic, D. E., Yokota, T., Filpula, D. R., Finkelman, M. A. J., Dodd, S. W., Wood, J. F., Whitlow, M., Snoy, P., and Schlom, J. (1991) Construction, binding properties, metabolism, and tumor targeting of a single-chain Fv derived from the pancarcinoma monoclonal antibody CC49. *Cancer Res.* 51, 6363–6371.
- Colcher, D., Bird, R., Roselli, M., Hardman, K., Johnson, D., Pope, S., Dodd, S. W., Pantoliano, M. W., Milenic, D. E., and Schlom, J. (1990) In vivo tumor targeting of a recombinant single-chain Fv antigen-binding protein. *J. Natl. Cancer Inst.* 82, 1191–1197.
- Adams, G. P., McCartney, J. E., Tai, M., Oppermann, H., Huston, J. S., Stafford, W. F., III, Bookman, M. A., Fand, I., Houston, L. L., and Weiner, L. M. (1993) Highly specific in vivo tumor targeting by monovalent and divalent forms of 741F8 anti-c-erbB2-2 single-chain Fv. *Cancer Res.* 53, 4026–4034.
- Tai, M.-S., McCartney, J. E., Adams, G. P., Jin, D., Hudziak, R. M., Oppermann, H., Laminet, A. A., Bookman, M. A., Wolf, E. J., Liu, S., Stafford, W. F., III, Fand, I., Houston, L. L., Weiner, L. M., and Huston, J. S. (1995) Targeting c-erbB2 expression tumors using single-chain Fv monomers and dimers. *Cancer Res.* 55, 5983–5989.
- Kipriyanov, S. M., Dubel, S., Breitling, F., Kontermann, R. D., and Little, M. (1994) Recombinant single-chain Fv fragments carrying C-terminal cysteine residues: production of bivalent and biotinylated miniantibodies. *Mol. Immunol.* 31 (14), 1047–1058.
- Cumber, A. J., Ward, E. S., Winter, G., Parnell, G. D., and Wawrzynczak, E. J. (1992) Comparative stabilities in vitro and in vivo of a recombinant mouse antibody FvCys fragment and a bisFvCys conjugate. *J. Immunol.* 149 (1), 120–126.
- Pack, P., and Pluckthun, A. (1992) Miniantibodies: use of amphipathic helices to produce functional, flexibly linked dimeric Fv fragments with high avidity in *Escherichia coli*. *Biochem. J.* 31 (6), 1579–1584.
- Bejeck, B., Wang, D., Berven, E., Pennell, C. A., Peiper, S. C., Poppema, S., Uckun, F., and Kersey, J. H. (1995) Development and characterization of three recombinant single chain antibody fragments (scFv) directed against the CD19 antigen. *Cancer Res.* 55, 2346–2351.
- Buchner, J., Pastan, I., and Brinkmann, U. (1992) A method for increasing the yield of properly folded recombinant fusion proteins: single-chain immunotoxins from renaturation of bacterial inclusion bodies. *Anal. Biochem.* 205, 263–270.
- Siegall, C. B., Chace, D., Mixan, B., Garrigues, U., Wan, H., Paul, L., Wolff, E., Hellstrom, I., and Hellstrom, K. E. (1994) In vitro and in vivo characterization of BR96 scFv-PE40. *J. Immunol.* 152 (2), 2376–2484.
- Press, O. W., Farr, A. G., Borroz, K. I., Anderson, K. A., and Martin, P. J. (1989) Endocytosis and degradation of monoclonal antibodies targeting human B-cell malignancies. *Cancer Res.* 49, 4906–4914.
- Ohno, A., and Oae, S. (1977) in *Organic Chemistry of Sulfur* (S. Oae, Ed.) pp 155–156, Plenum Press, New York.
- McCartney, J. E., Tai, M.-S., Hudziak, R. M., Adams, G. P., Weiner, L. M., Jin, D., Stafford, W. F., III, Liu, S., Bookman, M. A., Laminet, A. A., Fand, I., Houston, L. L., Oppermann, H., and Huston, J. S. (1994) Engineering disulfide-linked single-chain Fv dimers [(sFv)₂] with improved solution and targeting properties: anti-digoxin 26-10 (sFv) and anti-c-erbB-2 741F8 (sFv) made by protein folding and bonded through C-terminal cysteinyl peptides. *Protein Eng.* 8 (3), 301–314.
- McCartney, J. E., Tai, M. S., Oppermann, H., Jin, D., Warren, F. D., Weiner, L. M., Bookman, M. A., Stafford, W. F., III, Houston, L. L., and Huston, J. S. (1993) Refolding of single-chain Fv with C-terminal cysteine (sFv): formation of disulfide-bonded homodimers of anti-c-erbB-2 and anti-digoxin sFv. *Miami Short Rep.* 3, 91.
- Desplancq, D., King, D. J., Lawson, A. D. G., and Mountain, A. (1994) Multimerization behavior of single chain Fv variants for the tumor-binding antibody B72.3. *Protein Eng.* 7, 1027–1033.
- McGregor, D. P., Molloy, P. E., Cunningham, C., and Harris, W. J. (1994) Spontaneous assembly of bivalent single

- chain antibody fragments in *Escherichia coli*. *Mol. Immunol.* **31**, 219–226.
- (20) Carter, P., Kelley, R. F., Rodrigues, M. L., Snedecor, B., Covarrubias, M., Velligan, M., Wong, W. L. T., Rowland, A. M., Kotts, C. E., Carver, M. E., Yang, M., Bourell, J. H., Shepard, H. M., and Henner, D. (1992) High level *Escherichia coli* expression and production of a bivalent humanized antibody fragment. *Bio/Technology* **10**, 163–167.
- (21) Shalaby, M. R., Shepard, H. M., Presta, L., Rodrigues, M. L., Beverley, P. C. L., Feldmann, M., and Carter, P. (1992) Development of humanized bispecific antibodies reactive with cytotoxic lymphocytes and tumor cells overexpressing the HER2 protooncogene. *J. Exp. Med.* **175**, 2217–225.
- (22) Zhu, Z., Zapata, G., Shalaby, R., Snedecor, B., Chen, H., and Carter, P. (1996) High level secretion of a humanized bispecific diabody from *Escherichia coli*. *Bio/Technology* **14**, 192–196.

BC9600776

Influence of Coupling Method on the Luminescence Properties, Coupling Efficiency, and Binding Affinity of Antibodies Labeled with Europium(III) Chelates

Huriye Karşilayan,[†] Ilkka Hemmilä,^{*,‡} Harri Takalo,[‡] Airi Toivonen,[‡] Kim Pettersson,[§] Timo Lövgren,[§] and Veli-Matti Mukkala^{‡,||}

Yıldız Technical University, 80270 Şişli-Istanbul, Turkey, Wallac Oy, P.O. Box 10, FIN-20101 Turku, Finland, Department of Biotechnology, University of Turku, FIN-20520 Turku, Finland, and Department of Chemistry, University of Turku, FIN-20500 Turku, Finland. Received August 5, 1996*

A series of chelating 4-(phenylethynyl)pyridines having various 1,3,5-triazin-2-ylamino groups at the *para* position of the phenyl ring was synthesized. Their europium chelates were coupled to antibodies and the properties of antibody conjugates analyzed by fluorometry and in time-resolved fluorometric immunoassay. The substituents in the triazine ring were observed to have various effects on the chelate luminescence, the labeling properties of the chelates, and the immunoreactivity of labeled antibodies. The series of substituted triazinyl derivatives serves as a model of bioreactive groups that can be applied when certain properties are searched for, such as improved chelate solubilities, minimized internal quenching, different effects on the ligand triplet state, and stipulated coupling reactivities.

INTRODUCTION

Due to their unique luminescence properties, such as high quantum yield, large Stokes shift, narrow-banded emission lines, and, in particular, the very long lifetime of the excited state, lanthanide chelates have found wide label applications in bioaffinity-based fluorometric assays (1, 2). The use of lanthanide chelates as probes in time-resolved fluorometry enables the reduction of background level and so markedly improves the assay sensitivities (3).

A dissociative fluorescence enhancement system, commercialized under the trade name of DELFIA by Wallac, is today the most widely used chelate label technology. It is based on binding reagents (e.g. antibodies) labeled with a stable but nonluminescent chelate and a dissociative fluorescence development performed after completion of immunoreactions and washings. The technology is widely applied in clinical diagnostics, *in vitro* DNA hybridizations, cytotoxicity assays, and receptor–ligand binding assays (2, 4–6). Another chelate label system applies a fluorogenic chelator as the label and after-assay cationic saturation (7, 8). The actual label in that system consists of a derivative of *o*-phenanthroline-2,9-dicarboxylic acid. The used tetradentate ligand does not, however, provide the stability and protection needed when the chelate is used as a directly luminescent label.

A large number of multidentate, highly luminescent, and stable lanthanide chelates have been synthesized to be used as labels in time-resolved fluorometry (9–13). Such a chelate omits the separate development step and opens up new time-resolved fluorometric applications, such as simplified assays, homogeneous assays, and microimaging (2, 8). In the majority of the chelates

reported so far, an aromatic isothiocyanato group is employed in coupling of the chelate to proteins. The isothiocyanato group offers a mild and efficient coupling well suited for antibody labelings (5, 9, 10). However, quite frequently there is a need for alternative coupling reagents, e.g. to find more reactive intermediates, more hydrophilic substituents (12), or substituents having less adverse effect on the ligand triplet state and causing less internal quenching (13–16). A cyanuric acid condensation product, the 4,6-dichloro-1,3,5-triazin-2-ylamino group (DTA), provides an alternative, more reactive, more hydrophilic, and less quenching reactive group (12–14, 16). Because of its reactivity, it can be used for labeling of other amino acid residues besides cysteine and lysine and even labeling of sugars. The high reactivity can also be a disadvantage. We have found that a number of monoclonal antibodies lose easily their affinity when conjugated with DTA-activated chelate (unpublished data).

The present study was conducted to evaluate various less reactive DTA derivatives and their effects on chelate luminescence and antibody functionality by replacing one of the chlorine atoms in the triazine ring with a suitable substituent. {[4-(4-Aminophenylethynyl)pyridine-2,6-diyl]bis(methylenenitrilo)}tetrakis(acetic acid) (13) was used as the fluorogenic ligand modified with different 6-substituted 2,4-dichloro-1,3,5-triazines and isothiocyanate and iodoacetyl groups for comparison (1–3; Figure 1) (13). We used a solid-phase immunometric assay of prostate-specific antigen (PSA) as a model.

EXPERIMENTAL PROCEDURES

Reagents. The anti-PSA antibody (clone H 50), anti-PSA (clone H 117) coated microtitration plates, PSA standards, assay buffer, wash solution, and DELFIA Enhancement solution were obtained from Wallac Oy, Turku, Finland. In immunoassays and in determinations of affinity constants for labeled antibodies, an alternative measurement solution, LANFIA, was used. LANFIA solution contains, per liter, 50 mmol of glycine, 1.75 mol of NaSCN, 2.0 mmol of Na₂CO₃, 5.0% glycerol, 0.0005% Tween 40, 4.5 μmol of DTPA, and 20% 1-propanol with

* Author to whom correspondence should be addressed (telephone 358-2-2678111; fax 358-2-2678380).

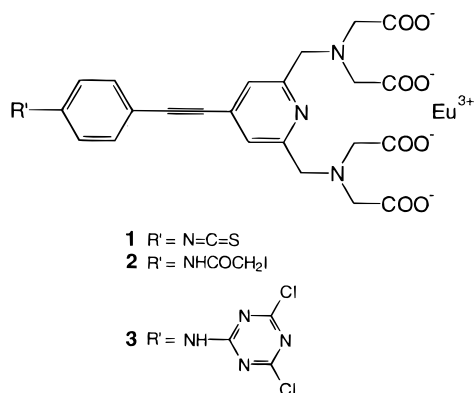
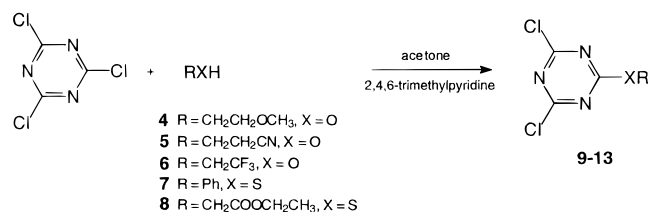
[†] Yıldız Technical University.

[‡] Wallac Oy.

[§] Department of Biotechnology.

^{||} Department of Chemistry.

© Abstract published in *Advance ACS Abstracts*, December 15, 1996.

**Figure 1.** Structure of chelates **1–3**.**Scheme 1. Synthesis of 6-Substituted 2,4-Dichloro-1,3,5-triazines (9–13)**

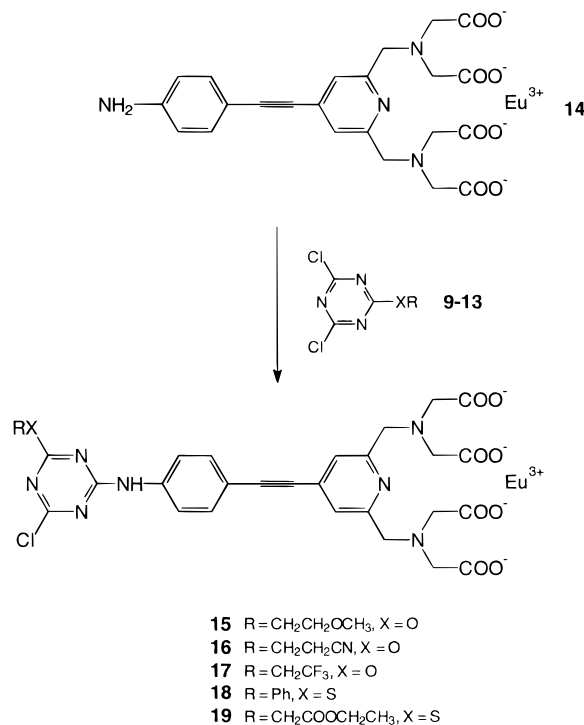
the final pH 10.0 (17). It dissociates immunocomplexes and creates optimized conditions for luminescence of that particular type of chelate. The assay buffers, other measuring buffers, and eluting buffers were based on TSA buffer consisting of 50 mM Tris-HCl, pH 7.75, 0.9% NaCl, and 0.05% NaN₃.

Equipment. Absorption spectra of the chelates were recorded with a Shimadzu UV-2100 spectrophotometer, emission spectra, luminescence yields, and decay times with a Perkin-Elmer LS5 luminescence spectrometer, and time-resolved fluorometric determinations of europium after the coupling reactions with a 1230 Arcus (Wallac Oy). Measurements of europium-labeled antibodies in immunoassays on microtitration plates were performed with a 1234 DELFIA Research fluorometer (Wallac Oy). A JEOL-JMN-GX400 spectrometer was used to record ¹H-NMR spectra at 400 MHz and a Perkin-Elmer 1600 FTIR spectrophotometer for IR spectra.

Synthesis of Activated Europium Chelates. General Synthesis of 6-Substituted 2,4-Dichloro-1,3,5-triazine (9–13, Scheme 1). A solution of alcohol (**4–6**) or thiol (**7, 8**) (12.0 mmol), acetone (5.0 mL), and 2,4,6-trimethylpyridine (1.45 g, 12.0 mmol) was slowly dropped into a cold solution of 2,4,6-trichloro-1,3,5-triazine (2.21 g, 12.0 mmol) in acetone (15.0 mL). The mixture was stirred for 0.5 h in an ice bath and for 3.0 h at room temperature and filtered. The filtrate was either evaporated to dryness or slowly poured into ice water, extracted with ethyl acetate, dried with Na₂SO₄, and evaporated to dryness. The product was purified by flash chromatography (FC).

2,4-Dichloro-6-(2-methoxyethoxy)-1,3,5-triazine (9): FC, silica gel, petroleum ether (40–60 °C)/ethyl acetate (5:2); yield, 80%; IR (film) 1544 ν(C=N), 1509 ν(C=N), 1347, 1303, 1254, 1055 cm⁻¹ ν(ether); UV (EtOH) 241 nm; ¹H NMR δ (CDCl₃) 3.42 (3 H, s), 3.75–3.77 (2 H, m), 4.64–4.66 (2 H, m).

2,4-Dichloro-6-(2-cyanoethoxy)-1,3,5-triazine (10): FC, silica gel, petroleum ether (40–60 °C)/ethyl acetate (5:1); yield, 43%; IR (film) 2257 ν(C≡N), 1544 ν(C=N), 1516 ν(C=N), 1360, 1307, 1257, 1058 cm⁻¹; UV (EtOH) 239 nm; ¹H NMR δ (CDCl₃) 2.91 (2 H, t, *J* = 6.5 Hz), 4.72 (2 H, t, *J* = 6.5 Hz).

Scheme 2. Synthesis of Europium(III) Chelates of 6-Substituted {2,2',2'',2'''}-[4-[4-[(4-Chloro-1,3,5-triazin-2-yl)amino]phenylethynyl]pyridine-2,6-diyl]-bis(methylenenitrilo)]tetrakis(acetic acid)} (15–19)

2,4-Dichloro-6-(2,2,2-trifluoroethoxy)-1,3,5-triazine (11): FC, silica gel, hexane/ethyl acetate (5:1); yield, 98%; IR (film) 1538 ν(C=N), 1303, 1259, 1172, 1085 cm⁻¹; UV (EtOH) 238 nm; ¹H NMR δ (CDCl₃) 4.90 (2 H, q, *J* = 7.9 Hz).

2,4-Dichloro-6-(thiophenoxy)-1,3,5-triazine (12): FC, silica gel, petroleum ether (40–60 °C)/ethyl acetate (10:1); yield, 28%; IR (film) 1505 ν(C=N), 1472 ν(C=N), 1260, 1244, 843 cm⁻¹; UV (EtOH) 263 nm; ¹H NMR δ (CDCl₃) 7.46–7.53 (3 H, m), 7.55–7.58 (2 H, m).

2,4-Dichloro-6-(ethoxycarbonylthiomethoxy)-1,3,5-triazine (13): FC, silica gel, petroleum ether (40–60 °C)/ethyl acetate (10:1); yield, 55%; IR (film) 1742 ν(C=O), 1515 ν(C=N), 1477 ν(C=N), 1304, 1266, 1244, 844 cm⁻¹; UV (EtOH) 260 nm; ¹H NMR δ (CDCl₃) 1.51 (3 H, t, *J* = 7.1 Hz), 4.17 (2 H, s), 4.47 (2 H, q, *J* = 7.1 Hz).

General Synthesis of Europium(III) Chelate of 6-Substituted {2,2',2'',2'''}-[4-[4-[(4-Chloro-1,3,5-triazin-2-yl)amino]phenylethynyl]pyridine-2,6-diyl]-bis(methylenenitrilo)]tetrakis(acetic acid)} (15–19, Scheme 2). A mixture of 6-substituted 2,4-dichloro-1,3,5-triazine (**9–13**) (0.10 mmol), acetone (1.0 mL), and water (1.0 mL) was added to a solution of compound **14** (**13**) (0.10 mmol) and 0.1 M NaOAc (1.5 mL, pH 4.9). After stirring for 30 min, the reaction mixture was treated with acetone, and the precipitate was centrifuged and washed with acetone. The purity of the chelates was tested with TLC plates. They were pure from any starting material. Before labeling, the chelates were dissolved in water and their europium concentrations were determined by using the DELFIA system.

Europium(III) Chelate of {2,2',2'',2'''}-[4-[4-[(4-Chloro-6-(2-methoxyethoxy)-1,3,5-triazin-2-yl)amino]phenylethynyl]pyridine-2,6-diyl]bis(methylenenitrilo)]tetrakis(acetic acid)} (15**):** IR (KBr) 2207 ν(C≡C), 1605, 1411 cm⁻¹ ν(C=O and C–O); UV (H₂O) 326, 298 (sh), 262 nm.

Europium(III) Chelate of {2,2',2'',2'''}-[4-[4-[(4-Chloro-6-(2-cyanoethoxy)-1,3,5-triazin-2-yl)amino]phenylethynyl]pyridine-2,6-diyl]bis(methylenenitrilo)]tetrakis(acetic acid)} (16**):** IR (KBr) 2207 ν(C≡C), 1605, 1411 cm⁻¹ ν(C=O and C–O); UV (H₂O) 326, 298 (sh), 262 nm.

Table 1. Labeling Properties of Europium(III) Chelates 1–3 and 15–19, Labeling Yields, Aggregation Percentages, and Affinities of the Chelate-Labeled Anti-PSA Antibodies^a

chelate, R' or R	labeling efficiency, %		labeling yield Eu/IgG		aggregation, %		affinity	
	pH 8.0	pH 9.5	pH 8.0	pH 9.5	pH 8.0	pH 9.5	pH 8.0	pH 9.5
S=C=N– (1)	2.3	10.0	4.7	3.0	2	0	1.1×10^9	1.6×10^9
I–CH ₂ COHN– (2)	0.4	4.8	2.0	2.4			3.0×10^8	1.5×10^9
DTA– (3)	4.0	26.5	8.0	5.3	10	0	8.6×10^7	2.1×10^8
CH ₃ OCH ₂ CH ₂ –O– (15)	0.7	6.2	2.6	3.1	24	0	1.4×10^7	5.7×10^8
NC–CH ₂ CH ₂ –O– (16)	1.2	7.2	4.7	3.6	15	0	7.7×10^7	1.5×10^9
CF ₃ CH ₂ –O– (17)		8.8		4.4		2		5.1×10^8
phenyl–S– (18)	1.6	25.0	5.0	7.5	14	0	1.7×10^8	4.6×10^8
CH ₃ CH ₂ O–OCCH ₂ –S– (19)	0.6	8.6	1.8	2.6	5	3	3.5×10^8	6.7×10^8

^aLabelings in borate buffer with molar excesses of 200- (chelates 1 and 3), 300- (chelates 18 and 19), and 500-fold (chelate 2) and in carbonate buffer (pH 9.5) with excess ratios of 20 (chelate 3), 30 (chelate 1, 18, and 19), and 50 (chelates 2, 15, and 17).

(16): IR (KBr) 2259 ν (C≡N), 2207 ν (C≡C), 1602, 1412 cm^{-1} ν (C=O and C–O); UV (H₂O) 327, 298 (sh), 262 nm.

Europium(III) Chelate of {2,2',2'',2'''-[4-[4-[4-Chloro-6-(2,2,2-trifluoroethoxy)-1,3,5-triazin-2-yl]amino]phenylethynyl]pyridine-2,6-diyl]bis(methylenenitrilo)]tetrakis(acetic acid)} (17): IR (KBr) 2205 ν (C≡C), 1603, 1406 cm^{-1} ν (C=O and C–O); UV (H₂O) 328, 300 (sh), 260 nm.

Europium(III) Chelate of {2,2',2'',2'''-[4-[4-[4-Chloro-6-(thiophenoxy)-1,3,5-triazin-2-yl]amino]phenylethynyl]pyridine-2,6-diyl]bis(methylenenitrilo)]tetrakis(acetic acid)} (18): IR (KBr) 2206 ν (C≡C), 1604, 1398 cm^{-1} ν (C=O and C–O); UV (H₂O) 329, 260 nm.

Europium(III) Chelate of {2,2',2'',2'''-[4-[4-[4-Chloro-6-(ethoxycarbonylthiomethoxy)-1,3,5-triazin-2-yl]amino]phenylethynyl]pyridine-2,6-diyl]bis(methylenenitrilo)]tetrakis(acetic acid)} (19): IR (KBr) 2208 ν (C≡C), 1603, 1398 cm^{-1} ν (C=O and C–O); UV (H₂O) 330, 255 nm.

Labeling of Antibodies. The anti-PSA antibodies were labeled in 0.5 mg batches with different amounts of the chelates, either in carbonate buffer, pH 9.5, or borate buffer, pH 8.0. The conjugation was allowed to proceed at room temperature overnight. The effects of stoichiometric labeling ratio (Eu/IgG) and labeling pH (carbonate buffer at pH 10, 10.5, and 11) were further studied with the chelate 18. The labeling ratio was determined by measuring the europium concentrations of reagent solutions by the dissociative enhancement system (DELFA) (6). After the appropriate volume of stock solution was added, the labeling volume was adjusted to 1 mL. Labeled IgG fractions were purified by gel filtration on a column containing Sephadex G-50 (1.5 × 10 cm) and Sepharose 6B (1.5 × 30 cm) by eluting with TSA buffer. The labeling ratios were analyzed by recording UV absorbance at 280 and 330 nm (12) and by measuring the total europium concentrations (6).

Luminescence Properties of Chelate-Labeled Antibodies. Antibody-coupled chelates were characterized by absorption and by luminescence in various buffers. Europium (0.1 μM) in DELFIA Enhancement solution was used as a standard in spectrofluorimetry (luminescence yield, $\epsilon \times \Phi$, 26 300) (12). The measurement time was adjusted from 10 μs to 5 ms to integrate all emissions of each chelate regardless of decay time. The buffers were TSA buffer containing 0.5% bovine albumin and the LANFIA solution. The emission intensities of the most intense emission line ca. 613 nm are recorded.

Determination of Antibody Affinities, Specific Binding, and Nonspecific Binding. The affinities of the antibody conjugates were measured as previously described (18). Microtitration plate coated with anti-PSA antibody were first incubated with 1 ng of PSA in 25 μL of TSA buffer containing 7.5% bovine serum albumin. Thereafter, six different concentrations of labeled antibodies (from 6.25 to 200 ng in 100 μL of DELFIA assay buffer) were added and incubated at room temperature

for 2 h with slow shaking. After washings, the bound europium was measured with the DELFIA system (6). After the portion of nonspecific binding was subtracted from each value, the affinity was calculated according to the method of Scatchard (19). A sandwich assay of PSA was used to analyze the specific binding of labeled antibodies using 100 ng/mL PSA standard and nonspecific binding using zero calibrator.

RESULTS AND DISCUSSION

The reaction between 2,4,6-trichloro-1,3,5-triazine and suitable alcohols (4–6) or thiols (7, 8) in acetone and 2,4,6-trimethylpyridine gave only 6-substituted 2,4-dichloro-1,3,5-triazines (9–13, Scheme 1) without any formation of di- or trisubstituted byproducts. The syntheses of activated chelates (15–19) were performed by coupling triazines (9–13) to the europium(III) chelate having an aromatic amino group (14) (Scheme 2) (13).

The labeling properties of the chelates 1–3 and 15–19 were studied by labeling anti-PSA antibodies both in a borate buffer, pH 8.0 and in a carbonate buffer, pH 9.5. Chelate concentrations were adjusted (from 200- to 500-fold molar excess in pH 8.0 and from 20- to 50-fold in pH 9.5) to obtain similar degrees of labeling. The labeling efficiencies (given as percentage binding from the amount added), obtained ratios (Eu/IgG), aggregations (the percentage of protein aggregation), and affinities are given in Table 1. The DTA group (3) clearly had the highest labeling efficiency (4% at pH 8.0 and 26.5% at pH 9.5). Substitution of one chlorine atom in the triazine ring (15–19) decreased the reactivity to varying degrees. In all substituents, the labeling efficiency was greatly improved when pH was increased from 8 to 9.5, due to increased deprotonation of amino groups. In contrast to isothiocyanate coupling, which according to our experience tends to cause aggregations, losses of affinity, and increased nonspecific binding backgrounds when the labeling is done at high pH values (20), labeling with DTA and DTA derivatives resulted in higher affinities and less aggregations when done at pH 9.5 as compared to 8.0 (Table 1). The somewhat negative effect of DTA coupling to anti-PSA antibody was partly eliminated by chlorine substitutions (chelates 18 and 19).

The luminescence properties of the chelate-labeled antibodies are given in Table 2. In TSA buffer with albumin, the luminescence yields ($\epsilon \times \Phi$) are relatively analogous regardless of the activation method with the exception of isothiocyanate, which has clearly lower luminescence in TSA buffer. The decay times of these heptadentate chelates ($\approx 390 \mu\text{s}$) confirm that the remaining two coordination sites of the europium ion are occupied by two water molecules (20). In LANFIA solution the decay time is increased from 380–400 to over 800 μs (Table 2), as a result of either optimized environ-

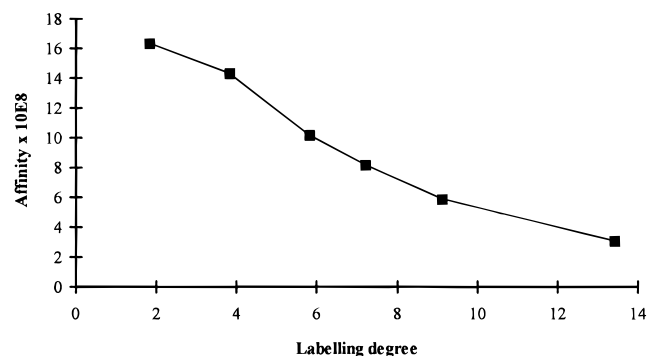
Table 2. Luminescence Yields ($\epsilon \times \Phi$) and Decay Times of Europium(III) Chelate (1–3 and 15–19) Labeled Antibodies in TSA Buffer and in LANFIA Solution

chelate R' or R	$\epsilon \times \Phi$		decay time, μ s	
	TSA–albumin	LANFIA solution	TSA–albumin	LANFIA solution
S=C=N– (1)	550	3400	380	770
I–CH ₂ COHN– (2)	1200	2600	400	920
DTA– (3)	1100	3700	400	830
CH ₃ OCH ₂ CH ₂ –O– (15)	1400	6600	390	840
NC–CH ₂ CH ₂ –O– (16)	1100	3700	400	830
CF ₃ CH ₂ –O– (17)	1600	5000	380	850
phenyl–S– (18)	920	3400	380	840
CH ₃ CH ₂ O–OCCH ₂ –S– (19)	1200	4500	380	880

Table 3. Effect of Labeling pH on Anti-PSA Antibody Affinity, Specific Binding, and Background^a

labeling pH	Eu/IgG	affinity 10E8	specific signal/Eu	background/Eu	signal/background
8.0	5.0	1.7	3500	130	27
9.5	7.5	4.6	30000	270	110
10.0	4.7	7.6	26000	290	89
10.5	5.8	10.1	41000	390	110
11.0	4.5	9.5	39000	570	68

^a Labeling with the chelate **18** in pH from 8.0 to 11.

**Figure 2.** Effect of labeling degree on the affinity of anti-PSA antibody. Labelings were done at pH 10.5 with increasing amounts of chelate **18**.

ment and decreased quenching or the replacement of the coordinated water molecules.

The effect of labeling pH was further evaluated with thiophenoxy derivative (**18**) by labeling anti-PSA antibodies in a series of increasing pH values (from 8.0 to 11.0). The analyzed affinities, specific signals, and backgrounds (normalized by dividing with labeling yield) are given in Table 3. The results confirm the data given in Table 1. The increase of pH up to pH 10.5 resulted in less decrease in affinity. On the other hand, there was a slight but clear increase in nonspecific binding beyond pH 9.5. These data are not, however, sufficient to accurately determine the optimum conjugation pH for that combination.

The effect of increasing labeling yields on the antibody affinity was studied by labeling anti-PSA antibody at pH 10.5 with increasing amounts of the thiophenoxy derivative (**18**). Increase in Eu/IgG steadily decreased the affinity from 16.4×10^8 with 1.8 Eu/IgG to 3.3×10^8 with 13.4 Eu/IgG (Figure 2). As shown earlier (13), the total luminescence of chelate-labeled antibody correlates directly with the labeling level, because the long Stokes shift eliminates inner filter quenching. In an immunoassay, the 5 time difference in affinity was compensated by a 7.4-fold increase in signal, and without extensive further studies, the data does not give definite answer to eventual optimal labeling level.

The performance of the labeled antibodies was briefly validated with the model assay of PSA. The correlation between the actual signal and antibody affinity, however, was poor. The signal correlated slightly better with relative luminescence intensities (data not shown). The poor correlation may relate to imprecisions in measured values or unknown factors related to immunoassays. Similarly, the nonspecific binding (highest with conjugates of chelate **18** and lowest of chelates **15** and **16**) did not exactly correlate with observed aggregation percentages (highest with **15**, **16**, and **18**).

As a conclusion, our study showed that the modifications of the reactive groups on the luminescent chelate both changed the luminescence properties of the chelate and had an impact on the immunoreactivity of labeled antibodies. The triazinyl derivatives provide a wide range of alternatives with various reactivities, hydrophilic properties, and various effects on antibody affinity and nonspecific binding properties. Despite the fact that the chosen model chelate did not clearly reveal the differences between the different substitutions (due to its high hydrophilicity and less critical triplet state energy), the DTA coupling and its modifications serve as valuable tools, particularly for larger, more hydrophobic chelates, in labelings where DTA may be too aggressive and with terbium chelates with ligands having a triplet state at a critical energy level.

ACKNOWLEDGMENT

We thank Ms. Teija Ristelä for revising the language.

LITERATURE CITED

- (1) Hemmilä, I. (1990) *Application of Fluorescence in Immunoassays*, Wiley, New York.
- (2) Hemmilä, I., Ståhlberg, T., and Mottram, P. (Eds.) (1994) *Bioanalytical Applications of Labeling Technologies*, Wallac, Turku.
- (3) Soini, E., and Hemmilä, I. (1979) Fluoroimmunoassay: present status and key problems. *Clin. Chem.* 25, 353–361.
- (4) Hemmilä, I. (1988) Lanthanides as probes for time-resolved fluorometric immunoassays. *Scand. J. Clin. Lab. Invest.* 4, 389–400.
- (5) Mikkala, V.-M., Mikola, H., and Hemmilä, I. (1989) The synthesis and use of activated N-benzyl derivatives of diethylenetriaminetetraacetic acids: alternative reagents for labeling of antibodies with metal ions. *Anal. Biochem.* 176, 319–325.
- (6) Hemmilä, I., Dakubu, S., Mikkala, V.-M., Siitari, H., and Lövgren, T. (1984) Europium as a label in time-resolved immunofluorometric assays. *Anal. Biochem.* 137, 335–343.
- (7) Evangelista, R. A., Pollak, A., Allore, B., Templeton, E. F., Morton, R. C., and Diamandis, E. P. (1988) A new europium chelate for protein labeling and time-resolved fluorescence applications. *Clin. Biochem.* 21, 173–178.
- (8) Gudgin Dickson, E. F., Pollak, A., and Diamandis, E. P. (1995) Time-resolved detection of lanthanide luminescence for ultrasensitive bioanalytical assays. *J. Photochem. Photobiol. B: Biol.* 27, 3–19.
- (9) Mikkala, V.-M., Sund, C., Kwiatkowski, M., Pasanen, P., Högberg, M., Kankare, J., and Takalo, H. (1992) New heteroaromatic complexing agents and luminescence of their europium(III) and terbium(III) chelates. *Helv. Chim. Acta* 75, 1621–1632.
- (10) Takalo, H., Hänninen, E., and Kankare, J. (1993) Luminescence of Eu(III) chelates of substituted 4-phenylethynylpyridines as ligands. *Helv. Chim. Acta* 76, 877–883.
- (11) Mikola, H., Takalo, H., and Hemmilä, I. (1995) Syntheses and properties of luminescent chelate labels and labeled haptenic antigens for homogenic immunoassays. *Bioconjugate Chem.* 6, 235–241.
- (12) Mikkala, V.-M., Helenius, M., Hemmilä, I., Kankare, J., and Takalo, H. (1993) Development of luminescent europium-

- (III) and terbium(III) chelates of 2,2':6',2''-terpyridine derivatives for protein labeling. *Helv. Chim. Acta* 76, 1–18.
- (13) Takalo, H., Mikkala, V.-M., Mikola, H., Liitti, P., and Hemmilä, I. (1994) Synthesis of europium(III) chelates suitable for labeling of bioactive molecules. *Bioconjugate Chem.* 5, 278–282.
- (14) Hemmilä, I., Mikkala, V.-M., and Takalo, H. (1996) Development of lanthanide chelate labels for diagnostic assays. *J. Alloys Compd.* (in press).
- (15) Latva, M., Takalo, H., Mikkala, V.-M., Matachescu, C., Rodriguez-Ubis, J. C., and Kankare, J. (1996) Correlation between luminescence efficiencies of europium(III) and terbium(III) chelates and triplet state energy levels. *J. Lumin.* (submitted for publication).
- (16) Takalo, H., Mikkala, V.-M., Meriö, L., Rodriguez-Ubis, J. C., Sedano, R., Juanes, O., and Brunet, E. (1996) Development of luminescent terbium(III) chelates for protein labeling—effect of triplet state energy level. *Helv. Chim. Acta* (submitted for publication).
- (17) Mitrinen, K., Pettersson K., Piironen, T., Björk, T., Lilja, H., and Lövgren, T. (1995) A novel dual-label one-step immunoassay for simultaneous measurement of free and total PSA concentrations and ratios in serum. *Clin. Chem.* 41, 1115–1120.
- (18) Pettersson, K. S. I., and Söderholm, J. M. (1991) Individual differences in lutropin immunoreactivity revealed by monoclonal antibodies. *Clin. Chem.* 37, 333–340.
- (19) Scatchard, G. (1949) The attractions of proteins for small molecules and ions. *Ann. N. Y. Acad. Sci.* 51, 660–672.
- (20) Pettersson, K. (1990) Immunofluoromeric assays of LH with special reference to sensitivity and specificity. Ph.D. Thesis, Åbo Akademi, Turku, Finland.
- (21) De W. Horrocks, W., Jr., and Sudnick, D. S. (1981) Lanthanide ion luminescence probes of the structure of biological macromolecules. *Acc. Chem. Res.* 14, 384–392.

BC960075L

Chromogenic Lactate–Leukocyte Esterase Substrates

Gary M. Johnson* and Robert Schaeper

Diagnostics Division, Bayer Corporation, Elkhart, Indiana 46515. Received June 24, 1996[®]

The first successful reported use of lactate-based chromogenic, colorimetric substrates for a serine protease-based enzyme is described. A series of hydroxy-protected 5-phenyl-3-hydroxypyrrolyl L-lactate substrates of the general formula RO-Lac-OPP were prepared and formulated into reagents for the determination of leukocytes in dry phase formats.

INTRODUCTION

The presence of leukocytes in urine is indicative of inflammation or infection. Human leukocyte elastase (HLE) is a serine protease contained within leukocytes, which is associated with physiological processes (1, 2) such as rheumatoid arthritis, adult respiratory distress syndrome, glomerulonephritis, pulmonary emphysema, and phagocytosis. Over the past 20 years, many types of substrates (3–9) have been developed to study the reactivity and specificity of HLE. One substrate (10) has been used to detect HLE in biological fluids as a diagnostic reagent strip in a urinary leukocyte assay (10, 11) known as LEUKOSTIX.

The assay operates by the general principle outlined in Scheme 1 using a test strip containing the reagents 3-[(*N*-tosylalaninyl)oxy]-5-phenylpyrrole (PPTA) and 4-sulfo-1,2-naphthoquinone 1-diazide (DNSA). When a urine sample containing HLE is applied to the strip, the enzyme catalyzes the hydrolysis of PPTA. This releases 3-hydroxy-5-phenylpyrrole (HOPP), which reacts with the diazide to produce a colored azo dye. The concentration of leukocytes in the sample is estimated by comparing the intensity of the final color to a standard color chart or by measuring the reflectance with a clinical reflectance meter such as CLINITEK-10.

We were interested in identifying new classes of HLE substrates that yield similar or greater sensitivity toward HLE. We report herein the synthesis and evaluation of a new class of chromogenic, colorimetric esterase substrates, hydroxy-protected 5-phenyl-3-hydroxypyrrolyl L-lactates (12) of the general formula RO-Lac-OPP. These substrates have reactivity and stability comparable to that of the corresponding isostere substrate 5-phenyl-3-hydroxypyrrolyl tosyl-L-alaninate (10), Ts-Ala-OPP.

CHEMISTRY

The synthesis of 3-(*O*-tosyl-L-lactoyl)-5-phenylpyrrole (TsO-Lac-OPP, **4a**) depicted in Scheme 2 is typical of the sequence used to prepare the lactic acid substrates (12) (RO-Lac-OPP, **4a–e**). Tosyl chloride is added to L-lactic acid ethyl ester in the presence of TEA to provide the intermediate *O*-tosyl ester (**1a**), in a 91% yield. This intermediate is then hydrolyzed with ethanolic NaOH at 0 °C, which after acidic workup provides the intermediate *O*-tosyl acid (**2a**) in a 76% yield. The acid (**2a**) is then quantitatively converted into the corresponding acid chloride (**3a**) with neat thionyl chloride. **3a** was then added to a chilled solution of 3-hydroxy-5-phenylpyrrole (HOPP) in the presence of pyridine at 0 °C to provide TsO-Lac-OPP (**4a**) in a 71% yield before purification.

Table 1 summarizes the synthesized chromogenic lactic acid substrates (**4a–e**), prepared similarly in like yields.

RESULTS AND DISCUSSION

It is well established (13) that hydrolysis of synthetic substrates by the serine protease HLE requires a small alkyl amino acid such as alanine or valine at the P₁ site as demonstrated by the substrate 5-phenyl-3-hydroxypyrrolyl tosyl-L-alaninate, Ts-Ala-OPP [the nomenclature of Schechter and Berger (14) is used to designate the individual amino acid residue (P₁, P₂, P_{1'}, or P_{2'}) of a peptide substrate]. Likewise, diagnostic test strips that detect the presence of HLE contain an alanine substrate along with a diazonium salt that acts as the color-generating system (Scheme 1).

The reactivity of these types of dry reagent strips toward an analyte is generally quantified by monitoring the intensity of reflected light at specific wavelengths (i.e. 557 nm for the LEUKOSTIX reagent) and applying the standard Kubelka–Munk equation (28): $K/S = (1 - R)^2 / (2R)$, where K = the absorption coefficient, S = the scattering coefficient, and R = the intensity of reflected light. Use of the equation permits color development to be proportional to analyte concentration. In addition, for the LEUKOSTIX reagent, linear kinetics are also observed over 2 min when the equation is applied.

In an average urine specimen, diagnostic reagent strips that contain an alanine substrate detect in 2 min at least 19 ng/mL HLE, which is the trace response with the LEUKOSTIX reagent strip. Lactic acid, is the non-amino acid, oxygen isostere of alanine, and it is well established that changes made to the substrate can dramatically affect the hydrolysis kinetics (15). Published work (15–22) on lactate derivatives with orientations at P₁ has previously shown that lactates act as inhibitors. Table 2 shows that the direct substitution of the phenylpyrrole ester of alanine with the phenylpyrrole ester of lactic acid produces a highly reactive substrate. As with its alanine parent, an assay incorporating this lactate derivative readily detects 19 ng/mL HLE. Similarly, Table 3 shows that substitutions made to the N terminus also produce reactive substrates. In each case, the assays using the lactate substrates readily detect 19 ng/mL HLE.

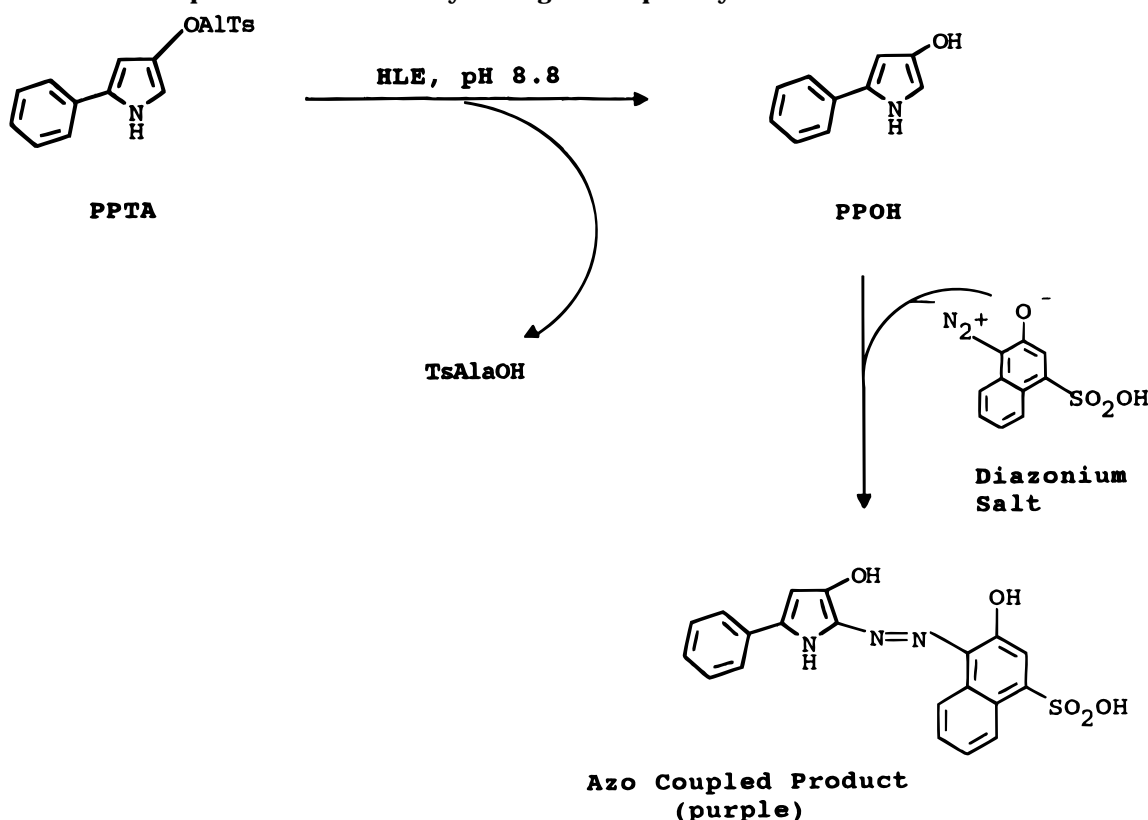
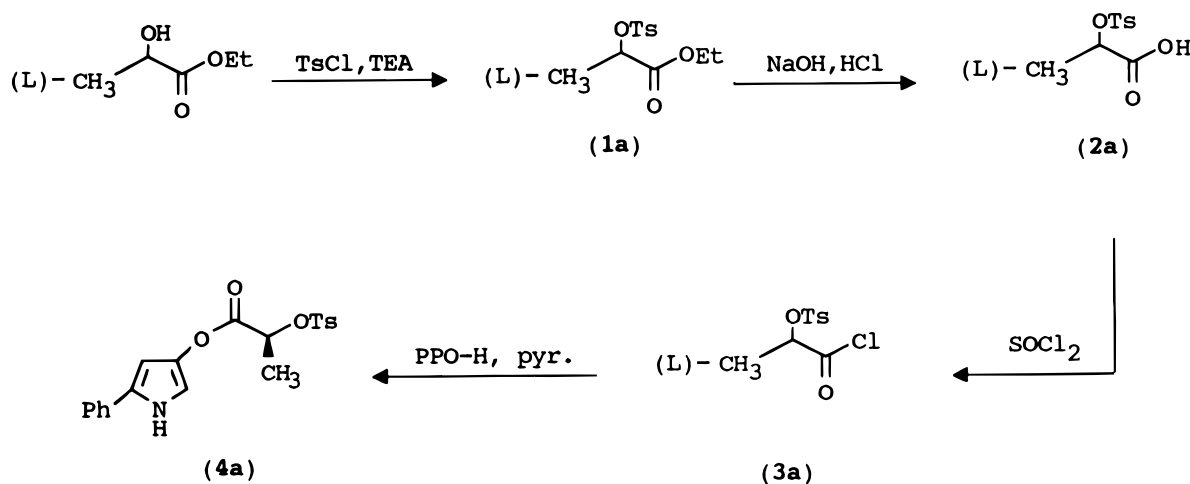
The substrates listed in Tables 2 and 3 contain an *N*-tosyl CH₃-phenyl-SO₂ terminal group, while conventional HLE substrates (13) generally contain amide linkages. Jackson et al. (23) recently confirmed that the N-terminal group dramatically influences reaction kinetics. Substituting a sulfonyl group for the amide group is shown to enhance the hydrolysis kinetics (23). Thus, Table 4 shows a dramatic decrease in hydrolysis when the sulfonyl group is changed to a C=O group. It is known (23, 24) for both the *N*-tosyl alaninate ester and

[®] Abstract published in *Advance ACS Abstracts*, January 1, 1997.

Table 1

	lactic acid ethyl ester analogs ^a		(5-phenyl-3-hydroxypyrrolyl)lactate products ^a
1a	L-Ts-OCH(CH ₃)CO ₂ Et	4a	Ts-Lac-OPP
1b	L-nPr-SO ₂ -OCH(CH ₃)CO ₂ Et	4b	nPr-SO ₂ -Lac-OPP
1c	L-PhCO-OCH(CH ₃)CO ₂ Et	4c	PhCO-Lac-OPP
1d	L-MeSucc-SO ₂ -OCH(CH ₃)CO ₂ Et	4d	MeOSucc-SO ₂ -Lac-OPP
1e	L-thiophene-SO ₂ -OCH(CH ₃)CO ₂ Et	4e	thiophene-SO ₂ -Lac-OPP

^a Where OPP = 5-phenyl-3-hydroxypyrrolyl, Lac = lactate, Ts = tosyl, PhCO = benzoyl, nPr = *n*-propyl, MeSucc = methoxysuccinyl, and SO₂ = sulfonyl.

Scheme 1. Reaction Sequence for the Leukocyte Reagent Strip Assay**Scheme 2. Synthetic Sequence for Ts-Lac-OPP (4a)**

the *N*-carbobenzoxy alaninate ester substrates that the rate-limiting step is the deacylation of the enzyme–acyl intermediate. The dramatic change observed in the hydrolysis rates when the *N*-terminal C=O group is incorporated suggests that the acyl enzyme deacylates faster with sulfonyl groups.

The performance of lactate substrates with different types of *N*-sulfonyl groups shown in Table 3 is similar to

and at times superior to that of the natural alanine amino acid substrates. Thus, a wide variety of blocking groups can be used, ranging from simple alkyl through aromatic groups. Many functional groups can be envisioned, and this work would anticipate that such substrates would be highly reactive, providing that a sulfonyl group exists between the functional group and the O terminus of the lactate.

Table 2

compound	HLE ^a (ng/mL)	response at 120 s			
		R = alanine		R = lactate (4a)	
		K/S	change	K/S	change
tosyl-R-OPP	0	0.048	—	0.046	—
	19	0.316	0.268	0.348	0.302

^a Results are obtained after immersing the reagent strips in solutions and observing the response at 557 nm after 2 min.

Table 3

compound	HLE ^a (ng/mL)	response at 120 s			
		R = alanine		R = lactate (4a,b,d,e)	
		K/S	change	K/S	change
tosyl-R-OPP	0	0.034	—	—	—
	19	0.343	0.309	—	—
	48	0.822	0.788	—	—
nPr-SO ₂ -R-OPP	0	0.050	—	0.100	—
	19	0.363	0.313	0.498	0.398
	48	0.881	0.831	1.049	0.949
CH ₃ O-CO(CH ₂) ₂ - SO ₂ -R-OPP	0	0.074	—	0.177	—
	19	0.435	0.361	0.514	0.337
	48	0.976	0.902	0.916	0.739
thiophene-SO ₂ -R-OPP	0	0.050	—	0.050	—
	19	0.224	0.174	0.385	0.335

^a In an average urine, 48 ng/mL HLE produces a small result with the LEUKOSTIX reagent strip. Results are obtained after immersing the reagent strips in solutions and observing the response at 557 nm after 2 min.

Table 4

compound	HLE ^a (ng/mL)	response at 120 s			
		R = alanine		R = lactate (4c)	
		K/S	change	K/S	change
PhCO-R-OPP	0	0.038	—	0.041	—
	19	0.039	0.001	0.106	0.065

^a Results are obtained after immersing the reagent strips in solutions and observing the response at 557 nm after 2 min.

In this paper, we have demonstrated that lactate esters can act as substrates for HLE. Other groups (15–22) utilizing different enzymes and different substrates indicate that lactate esters either directly or indirectly affect enzymatic reactivity. Much of the previous work focused on designing inhibitors of HLE and other enzymes. In the chymotrypsin work of Ingles (25), he reported a 10-fold decrease in the enzymatic rate and a decrease in stereospecificity when phenyl lactate was substituted for phenylalanine. It was suggested that an important hydrogen-bonding interaction has been eliminated. An additional explanation for the apparent change in reactivity was found during the course of our experiments. We observed that, in the presence of 0.25 M NaCl, the reactivity of the lactate derivatives decreases by 33%. Consequently, experimental conditions such as ionic strength can influence the observed reactivity.

SUMMARY

In summary, it is well established that simple amino acid compounds can function as colorimetric, chromogenic HLE enzyme substrates. In this manuscript, we have demonstrated that lactate esters of varying length and functional composition act as highly reactive substrates for human leukocyte elastase.

MATERIALS AND METHODS

HLE was obtained from Athens Research Technology (Athens, GA). Buffer salts were analytical grade from

Fisher or Aldrich. DMSO and acetone were obtained from J. T. Baker, Inc. (Phillipsburg, NJ), and decanol was from Sigma Chemical Co. (St. Louis, MO). Polyvinylpyrrolidone (PVP) was obtained from Polysciences Inc. (Warrington, PA). Diazonium salts were prepared as previously described (26).

IR spectra were recorded on a Perkin-Elmer 710B spectrophotometer. NMR spectra were recorded on a GE 300NB-MHz spectrometer. Mass spectra were determined on a HP5985A instrument by fast atom bombardment (FAB) with direct introduction. Thin layer chromatography was carried out on Merck GF 254 silica plates. Optical rotations were determined on a PE141 polarimeter. C/H/N analyses were done by Galbraith Labs (Knoxville, TN).

HLE was dissolved in 50 mM sodium acetate (pH 4.5) buffer, and the concentration of HLE was determined spectrophotometrically according to the method of Baugh and Travis (29). Reagent papers were prepared by impregnating Whatman 3M filter paper with 0.8 M borate/NaOH (pH 8.8) buffer containing 1% PVP K60 and dried in an air foil dryer. The dried paper was subsequently immersed in a solution containing 1.1 mM substrate, 0.7 mM 6-nitro-1,2-naphthoquinone diazide, 1.5% decanol, and 3% DMSO and then dried as above. The reagent paper was made into reagent test strips that consisted of 0.2 in. squares of the final impregnated paper, which was adhered via double-stick adhesive to a polystyrene carrier. The reagent strip was quickly immersed in the testing solution [100 mM NaOAc (pH 5.6), 4 mM benzoic acid, 0.0025% yellow #7, and 0.00002% red #40] that contained 0 or 19 ng/mL HLE. After 2 min, the color intensity was measured with a clinical reflectance meter, the CLINITEK-10. The intensity of the reflected light was quantified by applying the standard Kubulka–Monk equation (28).

EXPERIMENTAL PROCEDURES

Step 1. To L-lactic acid ethyl ester (5.00 g, 4.81 mL, 42.3 mmol) in CH₂Cl₂ (50 mL) at 0 °C (ice bath), under argon, was added tosyl chloride (8.1 g, 42.3 mmol) in one portion with stirring. Triethylamine (5.57 g, 7.67 mL, 55 mmol) was added dropwise via syringe, and the reaction mixture was stirred for 7 h at 0 °C. The reaction mixture was then poured over a solution of 1 M aqueous HCl (75 mL) and ice (75 g). After separation, the organic layers were dried over MgSO₄, filtered, and concentrated *in vacuo* to give 10.5 g (91%) of crude product (1a).

Step 2. The crude L-tosyl lactate ethyl ester (10.5 g, 38.6 mmol, 1a) in absolute ethanol (12 mL) was added dropwise via addition funnel (1/4 h) to a chilled (0 °C, ice bath) solution of NaOH (1.8 g, 46 mmol) in distilled water (20 mL). After the mixture was stirred for 5 h under argon at 0 °C, the reaction was carefully quenched via dropwise addition of concentrated HCl to pH 2. Solid NaCl was added to saturation, and the aqueous layer was extracted with CH₂Cl₂ (4 × 50 mL). The organic phase was then dried over MgSO₄, filtered, and concentrated *in vacuo* to give 7.17 g (76%) of crude product (2a).

Step 3. The crude L-O-tosyllactic acid (1.50 g, 6.15 mmol, 2a) was placed in a 25 mL round bottom flask under argon equipped with a reflux condenser. Thionyl chloride (10.12 g, 6.2 mL, 85 mmol) was added in one portion and the reaction mixture placed into an oil bath, preheated to 50 °C, and stirred for 2 h. The reaction mixture was then cooled and placed in an ice bath, and ice cold hexane (25 mL) was added. When no solid product was observed, the solution was concentrated *in vacuo* to give 1.6 g (quantitative) of crude yellow oil (3a).

Step 4. To a chilled solution (0 °C, ice bath) of 5-phenyl-3-hydroxypyrrole (986 mg, 6.20 mmol) in CH₂-Cl₂ (30 mL) under argon was added pyridine (1.5 mL, 18.6 mmol) dropwise via syringe, followed immediately by rapid dropwise addition of a solution of L-*O*-tosyllactic acid chloride (1.60 g, 6.11 mmol, **3a**) in CH₂Cl₂ (5.0 mL). The residual contents were then added dropwise with an additional 5.0 mL of CH₂Cl₂. The reaction mixture was stirred for 1 h at 0 °C, allowed to come to room temperature over approximately 1 h further, and then stirred overnight at room temperature (16 h).

The reaction mixture was then extracted with aqueous 1 M HCl (2 × 25 mL), and the combined aqueous phases were back-extracted with CH₂Cl₂ (25 mL). The combined organic layers were then extracted with saturated aqueous bicarbonate (2 × 25 mL). After back-extraction of the basic aqueous phase, the combined organic layers were treated with norite carbon and MgSO₄, filtered, and concentrated *in vacuo*. The resulting oil was dissolved in hexane/EtOAc (1:1, 25 mL), treated with norite carbon once more, filtered, and concentrated *in vacuo* to give 1.7 g (71%) of solid crude product (**4a**).

This material was triturated with warm hexane (10 mL) followed by hexane/EtOAc (4:1, 2 × 8 mL), and decanted, and the resultant solid was dried under vacuum to provide 1.04 g of a pink solid. This material was dissolved in hexane/EtOAc (1:1), treated with norite carbon, filtered, and concentrated *in vacuo* at room temperature to give 932 mg (unoptimized yield) of creme product (**4a**).

Product 4a: ¹H NMR (300 MHz, CDCl₃, ppm) 1.65 (d, 3H), 2.42 (s, 3H), 5.12 (qu, 1H), 6.26 (dd, 1H), 6.84 (dd, 1H), 7.18–7.5 (m, 7H), 7.84 (d, 2H), 8.15 (brs, 1H); ¹³C NMR (75 MHz, CDCl₃, ppm) 18.51 (methyl), 21.66 (methyl), 73.96 (CH, lactate), 93.39 (CH, pyrrole), 107.89 (CH, pyrrole), 123.84 (CH, aromatic), 126.85 (CH, aromatic), 128.12 (CH, aromatic), 128.97 (CH, aromatic), 129.87 (CH, aromatic), 166.68 (C=O); EI/MS (18 EV, DIP) 385 (M⁺, 21.8), 227 (2.3), 199 (22.4), 158 (67.5), 155 (BASE), 91 (41.7); IR: (CDCl₃, cm⁻¹) 3450, 3022, 1770, 1600, 1570, 1550, 1514, 1450, 1370, 1260, 1240; optical rotation (λ = 578 nm) 10 mg sample, 1 mL of MeOH, room temperature, 1 cm cell, -64.8°. Anal. Calcd: C, 62.39; H, 4.97; N, 3.63; S, 8.33. Found: C, 62.44; H, 5.03; N, 3.57; S, 8.65.

Product 4b: ¹H NMR (300 MHz, CDCl₃, ppm) 1.10 (t, 3H), 1.75 (d, 3H), 2.20 (m, 2H), 3.30 (m, 2H), 5.35 (qu, 1H), 6.41 (dd, 1H), 6.95 (dd, 1H), 7.20–7.60 (m, 5H), 8.30 (brs, 1H); ¹³C NMR (75 MHz, CDCl₃, ppm) 12.87 (methyl), 17.23 (methylene), 18.59 (methyl), 53.64 (methylene), 73.49 (CH, lactate), 98.32 (CH, pyrrole), 107.94 (CH, pyrrole), 123.86 (CH, aromatic), 126.90 (CH, aromatic), 128.96 (CH, aromatic), 166.5 (C=O); FAB/MS 337.2 (M⁺, 55), 159 (BASE); IR: (CDCl₃, cm⁻¹) 3400, 3010, 2980, 1768, 1573, 1512, 1454, 1400, 1360, 1254, 1169; optical rotation (λ = 578 nm) 13 mg sample, 1 mL of MeOH, room temperature, 1 cm cell, -48.5°. Anal. Calcd: C, 56.97; H, 5.64; N, 4.15; S, 9.49. Found: C, 57.06; H, 5.75; N, 3.87; S, 9.91.

Product 4c: ¹H NMR (300 MHz, CDCl₃, ppm) 1.75 (d, 3H), 5.55 (qu, 1H), 6.40 (dd, 1H), 6.95 (dd, 1H), 7.15–7.7 (m, 8H), 8.1 (d, 2H), 8.2 (brs, 1H); ¹³C NMR (75 MHz, CDCl₃, ppm) 17.13 (methyl), 69.08 (CH, lactate), 98.57 (CH, pyrrole), 108.03 (CH, pyrrole), 123.82 (CH, aromatic), 126.68 (CH, aromatic), 128.41 (CH, aromatic), 128.89 (CH, aromatic), 129.91 (CH, aromatic), 133.33 (CH, aromatic), 165.98 (C=O), 166.48 (C=O); EI/MS (18 EV, DIP) 335 (M⁺, 3.1), 177 (42.8), 149 (22.2), 105 (BASE), 77 (0.7); IR: (CDCl₃, cm⁻¹) 3400, 3000, 1763, 1723, 1606, 1585, 1573, 1512, 1452, 1318, 1177; optical

rotation (λ = 578 nm) 12 mg sample, 1 mL of MeOH, room temperature, 1 cm cell, +13.3°. Anal. Calcd: C, 71.64; H, 5.07; N, 4.18. Found: C, 71.92; H, 5.22; N, 4.28.

Product 4d: ¹H NMR (300 MHz, CDCl₃, ppm) 1.78 (d, 3H), 1.98 (t, 2H), 2.62 (t, 2H), 2.75 (s, 3H), 5.37 (qu, 1H), 6.42 (brs, 1H), 6.98 (brs, 1H), 7.2–7.55 (m, 5H), 8.2 (brs, 1H); ¹³C NMR (75 MHz, CDCl₃, ppm) 18.52 (methyl), 28.42 (methylene), 47.29 (methylene), 52.4 (methyl), 74.14 (CH, lactate), 98.37 (CH, pyrrole), 107.93 (CH, pyrrole), 123.89 (CH, aromatic), 126.94 (CH, aromatic), 128.98 (CH, aromatic); FAB/MS 381 (M⁺, 63), 186 (8.5), 159 (BASE), 91 (12), 55 (24.5); IR: (CDCl₃, cm⁻¹) 3450, 3000, 1751, 1741, 1572, 1513, 1453, 1439, 1359, 1319, 1255; optical rotation (λ = 578 nm) 7 mg sample, 1 mL of MeOH, room temperature, 1 cm cell, -27.1°. Anal. Calcd: C, 53.54; H, 4.99; N, 3.67; S, 8.39. Found: C, 53.05; H, 5.07; N, 3.41; S, 7.75.

Product 4e: ¹H NMR (300 MHz, CDCl₃, ppm) 1.70 (d, 3H), 5.19 (qu, 1H), 6.32 (dd, 1H), 6.85 (dd, 1H), 7.12 (t, 1H), 7.20–7.50 (m, 5H), 7.70 (dd, 1H), 7.79 (dd, 1H), 8.19 (brs, 1H); ¹³C NMR (75 MHz, CDCl₃, ppm) 18.44 (methyl), 74.91 (CH, lactate), 98.34 (CH, pyrrole), 107.90 (CH, pyrrole), 123.85 (CH, aromatic), 126.85 (CH, aromatic), 127.54 (CH, thiophene), 128.95 (CH, aromatic), 134.09 (CH, thiophene), 134.71 (CH, thiophene); EI/MS (18 EV, DIP) 377 (M⁺, 63.1), 236 (4.4), 191 (13.8), 164 (4.9), 159 (BASE), 147 (66.1), 99 (8.2), 83 (1.1); IR (CDCl₃, cm⁻¹) 3450, 3050, 2940, 1760, 1573, 1509, 1453, 1404, 1378; optical rotation (λ = 578 nm) 12 mg sample, 1 mL of MeOH, room temperature, 1 cm cell, -34.3°. Anal. Calcd: C, 54.1; H, 3.98; N, 3.71; S, 16.98. Found: C, 53.4; H, 4.16; N, 3.69; S, 16.81.

LITERATURE CITED

- (1) Powers, J. C., Kam, C. M., Hou, H., Oleksyszyn, J., and Meyer, E. F. (1992) in *Biochemistry of Pulmonary Emphysema* (C. Grassi, J. Travis, L. Casali, and M. Luisetti, Eds.) pp 123–141, Springer-Verlag, London.
- (2) Bieth, J. G. (1989) *Human Neutrophil Elastase*. In *Elastin and Elastases*, Vol. II, pp 23–31, CRC Press, Inc., Boca Raton, FL.
- (3) Ashe, B. M., and Zimmerman, M. (1980) Fluorogenic substrates for human leukocyte and porcine pancreatic elastase. *J. Appl. Biochem.*, 445–447.
- (4) Powers, J. C., Harper, J. W., Cook, R. R., Roberts, C. J., and McLaughlin, B. J. (1984) Active Site Mapping of Serine Proteases Using Tripeptide Thiobenzyl Ester Substrates. *Biochemistry* 23, 2995–3002.
- (5) Nakajima, K., Powers, J. C., Ashe, B. M., and Zimmerman, M. (1979) Mapping the Extended Substrate Binding Site of Cathepsin G and Human Leukocyte Elastase. Studies with Peptide Substrates related to the alpha-1-Proteinase Inhibitor. *J. Biol. Chem.* 254, 4027–4032.
- (6) Castillo, M. J., Nakajima, X., Zimmerman, M., and Powers, J. C. (1979) Sensitive substrates for human leukocyte and porcine pancreatic elastase: a study of the merits of various chromophoric and fluorogenic leaving groups in assays for serine proteases. *Anal. Biochem.* 99, 53–64.
- (7) Stein, R. L., Viscarello, B. R., and Wildonger, R. A. (1984) Catalysis by human leukocyte elastase. Rate limiting deacylation for specific *p*-nitroanilides and amides. *J. Am. Chem. Soc.* 106, 796–798.
- (8) Stein, R. L., Strimpler, A. M., Hori, H., and Powers, J. C. (1987) Catalysis by Human Leukocyte Elastase: Mechanistic Insights into Specificity Requirement. *Biochemistry* 26, 1301–1305.
- (9) Stein, R. L., Strimpler, A. M., Hori, H., and Powers, J. C. (1987) Catalysis by Human Leukocyte Elastase: Proton Inventory as a Mechanistic Probe. *Biochemistry* 26, 1305–1314.
- (10) Corey, P. F., Skjold, A. L., Pendergrass, J. H., and Stover, L. (1987) Composition and Test Device for Determining the

- Presence of Leukocytes, Esterase and Protease in a Test Sample, U.S. Patent 4,657,855.
- (11) Skjold, A. C., and Hugel, H. (1987) Composition and Test Device for Determining the Presence of Leukocytes Containing a Zwitterion Coupling Reagent, U.S. Patent 4,637,979.
- (12) Johnson, G. M., and Schaeper, R. J. (1995 and 1996) Test Device for Determining the Presence of Leukocyte Cells, Esterase or Protease in a Test Sample, U.S. Patent 5,464,739; U.S. Patent 5,512,450.
- (13) Bieth, J. G. (1989) Mechanism of Action of Elastases. In *Elastin and Elastases*, Vol. II, pp 23–31, CRC Press, Inc., Boca Raton, FL.
- (14) Schechter, I., and Berger, A. (1967) On the size of the active site of proteases. I. Papain. *Biochem. Biophys. Res. Commun.* 27, 157–162.
- (15) Dorn, C. P., and Yang, S. S. (1977) Peptide Carbazates, U.S. Patent 4,064,236.
- (16) Dorn, C. P., Zimmerman, M., Yang, S. S., Yurewicz, E. C., Ashe, B. M., Frankshun, R., and Jones, H. (1977) Proteinase Inhibitors 1. Inhibitors of Elastase. *J. Med. Chem.* 20, 1464–1468.
- (17) Digenis, G., Agha, B. J., Tsuji, K., Kato, M., and Shinogi, M. (1986) Peptidyl Carbamates Incorporating Amino Acid Isosteres as Novel Elastase Inhibitors. *J. Med. Chem.* 29, 1468–1476.
- (18) Krantz, A., Spencer, R. W., Tam, T. F., Liak, T. J., Copp, L. J., Thomas, E. M., and Rafferty, S. P. (1990) Design and Synthesis of 4H-3,1-Benzoxazin-4-ones as Potent Alternate Substrate Inhibitors of HLE. *J. Med. Chem.* 33, 464–479.
- (19) Umezawa, H., Takeuchi, T., Aoyagi, T., Morishima, H., and Takamatsu, A. (1977) N-Lactoyl Peptides, JP 52,057,121.
- (20) Kellog, R. M., and Moorlag, H. (1990) Pig Liver Esterase Catalyzed Hydrolyses of Racemic Alpha-substituted Alpha-hydroxy Esters. *J. Org. Chem.* 55, 5878–5881.
- (21) Kellog, R. M., and Moorlag, H. (1991) Pig Liver Esterase Catalyzed Hydrolyses of Alpha-substituted Alpha-hydroxy Esters: The Influence of Substituents. *Tetrahedron: Asymmetry* 2, 705–720.
- (22) Kraicsovits, F., and Otvos, L. Effect of the Alcohol Moiety upon Reactivity and Stereospecificity in Alpha-Chymotrypsin-catalyzed Ester Hydrolysis. *Symp. Pap.—IUPAC Int. Symp. Chem. Nat. Prod.*, 11th, 37–40.
- (23) Jackson, D. S., Brown, A. D., Schaeper, R. J., and Powers, J. C. (1995) A Kinetic Study of the Hydrolysis of the N-Tosylalanine Ester of 3-Hydroxy-5-phenylpyrrole and Related Compounds by Human Leukocyte Elastase. *Arch. Biochem. Biophys.* 323, 108–114.
- (24) Stein, R. L. (1983) Catalysis by human Leukocyte Elastase: Substrate Structural Dependence of Rate-Limiting Protolytic Catalysis and Operation of the Charge Relay System. *J. Am. Chem. Soc.* 105, 5111–5116.
- (25) Ingles, D. W., and Knowles, J. R. (1968) The Stereospecificity of Alpha-Chymotrypsin. *Biochem. J.* 108, 561–569.
- (26) Putter, R. (1965) In *Methoden der Organischen Chemie* (E. Muller, Ed.) pp 89–92, George Thieme Verlag, Stuttgart.
- (27) Baugh, R. J., and Travis, J. (1976) Human Leukocyte Granule Elastase: Rapid Isolation and Characterization. *Biochemistry* 15, 836–841.
- (28) Kortum, G. (1976) *Reflectance Spectroscopy: Principles, Methods, & Applications*, Springer-Verlag, New York.

BC960081H

Peptide-Mediated Gene Delivery: Influence of Peptide Structure on Gene Expression

Manpreet S. Wadhwa,[†] Wendy T. Collard, Roger C. Adami, Donald L. McKenzie, and Kevin G. Rice*

Divisions of Medicinal Chemistry and Pharmaceutics, College of Pharmacy, University of Michigan, 428 Church Street, Ann Arbor, Michigan 48109. Received September 13, 1996[®]

Cationic peptides possessing a single cysteine, tryptophan, and lysine repeat were synthesized to define the minimal peptide length needed to mediate transient gene expression in mammalian cells. The N-terminal cysteine in each peptide was either alkylated or oxidatively dimerized to produce peptides possessing lysine chains of 3, 6, 8, 13, 16, 18, 26, and 36 residues. Each synthetic peptide was studied for its ability to condense plasmid DNA and compared to polylysine₁₉ and cationic lipids to establish relative *in vitro* gene transfer efficiency in HepG2 and COS 7 cells. Peptides with lysine repeats of 13 or more bound DNA tightly and produced condensates that decreased in mean diameter from 231 to 53 nm as lysine chain length increased. In contrast, peptides possessing 8 or fewer lysine residues were similar to polylysine₁₉, which bound DNA weakly and produced large (0.7–3 μ m) DNA condensates. The luciferase expression was elevated 1000-fold after HepG2 cells were transfected with DNA condensates prepared with alkylated Cys-Trp-Lys₁₈ (AlkCWK₁₈) versus polylysine₁₉. The gene transfer efficiencies of AlkCWK₁₈ and cationic lipids were equivalent in HepG2 cells but different by 10-fold in COS 7 cells. A 40-fold reduction in particle size and a 1000-fold amplification in transfection efficiency for AlkCWK₁₈ DNA condensates relative to polylysine₁₉ DNA condensates suggest a contribution from tryptophan that leads to enhanced gene transfer properties for AlkCWK₁₈. Tryptophan-containing cationic peptides result in the formation of small DNA condensates that mediate efficient nonspecific gene transfer in mammalian cells. Due to their low toxicity, these peptides may find utility as carriers for nonspecific gene delivery or may be developed further as low molecular weight DNA condensing agents used in targeted gene delivery systems.

Nonviral gene delivery systems are being developed to transfect mammalian host cells with foreign genes (1–3). Plasmids encoding transgenes are complexed with carriers that facilitate the transfer of the DNA across the cell membrane for delivery to the nucleus. The efficiency of gene transfer into cells directly influences the resultant gene expression levels. Thereby, optimizing transfer efficiency is often necessary to achieve therapeutically relevant gene expression levels in a variety of host cells (4, 5).

Nonviral gene delivery systems rely on carrier molecules to bind and condense DNA into small particles that facilitate DNA entry into cells through endocytosis or pinocytosis (1). In addition, the carrier molecules act as scaffolding to which ligands may be attached to achieve site specific targeting of DNA (6–15).

The most commonly used DNA condensing agent for the development of nonviral gene delivery systems is polylysine in the size range of dp 90–450 (6–15). Its amino groups have been derivatized with asialoorosomucoid, transferrin, carbohydrates, folate, lectins, antibodies, or other proteins to provide specificity in cell recognition, without compromising its binding affinity for DNA (6–15). However, the high molecular weight and polydispersity of polylysine also contribute to a lack of chemical control in coupling macromolecular ligands, which leads to heterogeneity in polylysine-based carrier molecules. This can complicate the formulation of DNA

carrier complexes and limits the ability to systematically optimize carrier design to achieve maximal efficiency (16, 17).

To refine targeted gene delivery carriers aimed at transfecting hepatocytes via the asialoglycoprotein receptor, we previously developed a low molecular weight carrier (4500) by attaching a single complex carbohydrate ligand to low molecular weight polylysine (dp 19) (18). This glycopeptide bound to DNA and efficiently transfected HepG2 cells *in vitro* via the asialoglycoprotein receptor, establishing that low molecular weight glycopeptide carriers can function as efficiently as a macromolecular glycoconjugate carriers. However, despite the low molecular weight of this glycopeptide, the polydispersity of polylysine₁₉ and the lack of control of the carbohydrate coupling site both contributed to heterogeneity, limiting further opportunity for optimization.

In the present study we have taken the next step toward developing homogeneous glycopeptide carriers by attempting to define the minimal polylysine chain length that leads to DNA condensation. Earlier studies examined the influence of polylysine chain length for transferrin–polylysine-mediated gene delivery and found that the transfection efficiency decreased below dp 300 (12, 19). Another study examined the particle size of DNA condensates produced with polylysine varying in size from dp 30 to 1500 and found that low molecular weight polylysine condensed DNA into small particles (20–30 nm) and was also less toxic to cells in culture (20). Still others have quantitatively examined the binding of lysine-rich peptides (dp 3–10) to single- and double-stranded oligonucleotides and noted an enhancement in the binding affinity when increasing polylysine chain length up to dp 10 (21–23). Notably, the peptides utilized in these studies contained a tryptophan residue that allowed monitoring of DNA binding via fluorescence.

* Author to whom correspondence should be addressed [telephone (313) 763-1032; fax (313) 763-2022; e-mail krice@umich.edu].

[†] Present address: GeneMedicine, Inc., 8301 New Trails Drive, The Woodlands, TX 77381-4248.

[®] Abstract published in *Advance ACS Abstracts*, December 15, 1996.

A recent paper also highlighted the utility of a low molecular weight peptide (dp 13) possessing a lysine repeat of 8 as a DNA condensing for enhancing gene transfer (24). When coformulated with a fusogenic peptide and a plasmid encoding luciferase, this peptide mediated gene transfer in several cell lines, including hepatocytes, with efficiency comparable to that of cationic lipid mediated gene delivery.

The synthetic peptides used in the present study also possess a lysine repeat, which was varied from 3 to 36 residues and incorporated one or more tryptophan and cysteine residues. The results establish that a peptide of 13–18 lysine residues possessing a single tryptophan residue enhances gene transfer to cells in culture by up to 3 orders of magnitude relative to comparable polylysine peptides lacking a tryptophan. The mechanism of peptide-mediated gene transfer is related to the efficiency of condensing DNA into small particles. It is proposed that tryptophan plays a specific role in organizing the DNA binding of cationic peptides to produce small condensates that exhibit enhanced gene transfer efficiency. Therefore, tryptophan-containing peptides represent a new class of low molecular weight condensing agents that may be modified with ligands to produce low molecular weight carriers for site specific gene delivery.

MATERIALS AND METHODS

N-terminal Fmoc protected amino acids, and all other reagents for peptide synthesis, were obtained from Advanced ChemTech, Lexington, KY. Minimum essential media (MEM¹), Sephadex G-25, dithiothreitol, iodoacetamide, iodoacetic acid, and polylysine₁₉ (MW 1000–4000) were purchased from Sigma Chemical Co., St. Louis, MO. Ethanedithiol (EDT) was purchased from Aldrich Chemical Co., Milwaukee, WI. Trifluoroacetic acid (TFA) was purchased from Fisher Scientific, Pittsburgh, PA. LB media, LB agar, D-luciferin, and luciferase from *Photinus pyralis* (EC 1.13.12.7) were obtained from Boehringer Mannheim, Indianapolis, IN. HepG2 and COS 7 cells were from the American Type Culture Collection, Rockville, MD. Dulbecco's modified Eagle medium (DMEM), media supplements, and heat inactivated "qualified" fetal bovine serum (FBS) were from Gibco BRL, Grand Island, NY. Bradford reagent was purchased from Bio-Rad, Hercules, CA, and thiazole orange was a gift from Beckton Dickinson Immunocytometry Systems, San Jose, CA. The 5.6 kb plasmid pCMVL encoding the reporter gene luciferase under the control of the cytomegalovirus promoter was a gift from Dr. M. A. Hickman at the University of California, Davis. Peptide purification was performed using a semipreparative (10 μ m) C₁₈ RP-HPLC column from Vydac, Hesperia, CA. HPLC was performed using a computer-interfaced HPLC and fraction collector from ISCO, Lincoln, NE.

DNA Purification and Peptide Synthesis. Plasmid DNA was prepared by the alkaline lysis method and purified on cesium chloride gradient (25). Peptides were prepared by solid phase peptide synthesis on Fmoc-L-Boc-lysine-Wang resin (*p*-benzyloxybenzyl alcohol resin, 1% divinyl benzene cross-linked, 100–200 mesh) at a 136 μ mol scale (0.68 mmol/g resin). The synthesis was

accomplished using a computer-interfaced Model 90 synthesizer from Advanced Chemtech. Lysine and tryptophan side chains were Boc protected, and the sulfhydryl side chain of cysteine was protected with a trityl group. A 6 molar excess of N-terminal Fmoc-protected amino acid was activated *in situ* in the reaction vessel by adding equimolar diisopropylcarbodiimide and *N*-hydroxybenzotriazole in a total reaction volume of 18 mL. Coupling was carried out for 1 h and was followed with a capping cycle for 30 min with 10% acetic anhydride in 1% diisopropylethylamine. Fmoc deblocking was performed with 25% piperidine for 12 min. All reagents were dissolved in dimethylformamide.

At completion, the resin-conjugated peptide was washed with dichloromethane, dried, and weighed. Cleavage was performed in a solution of TFA/EDT/water (95:2.5:2.5 v/v) for 30 min at room temperature, which simultaneously deprotected the amino acid side chains. The peptide solution was extracted with diethyl ether, concentrated by rotary evaporation, and freeze-dried. Lyophilized crude peptides were dissolved in degassed and nitrogen-purged 0.1% TFA. Peptides (3 μ mol per injection) were purified on a semipreparative (2 \times 25 cm) C₁₈ RP-HPLC column eluted at 10 mL/min with 0.1% TFA and acetonitrile (5–20% over 40 min) while absorbance was monitored at 280 nm, 1.0 AUFS. Purified peptides were concentrated by rotary evaporation, lyophilized, and stored dry at –20 °C.

Lyophilized peptides (1 μ mol) were dissolved in 1 mL of nitrogen-purged 50 mM Tris HCl (pH 7.5) and reduced by the addition of 250 μ L of 100 mM dithiothreitol prepared in the same buffer by reacting at room temperature for 30 min. Alkylation was carried out by adding 25 mg of solid iodoacetamide or iodoacetic acid followed by reaction for 1 h at room temperature. The alkylated peptides were acidified to pH 2.0 with TFA and purified by RP-HPLC as described above. The yield of each purified peptide (approximately 25%) was determined from the absorbance of tryptophan ($\epsilon_{280\text{nm}} = 5600 \text{ M}^{-1} \text{ cm}^{-1}$). The TFA salt of polylysine₁₉ was prepared by chromatographing the hydrobromide salt on RP-HPLC eluted with 0.1% TFA and acetonitrile while detecting 214 nm as described above. The concentration of polylysine₁₉ was established by fluorescamine analysis (26) using a calibrated standard of AlkCWK₁₈ as a reference.

Dimeric peptides were prepared by dissolving 1 μ mol of each purified CWK_{*n*} (*n* = 3, 8, 13, or 18) peptide in Tris HCl (pH 7.5) followed by reaction at 37 °C for 24 h. Each dimeric peptide was purified using RP-HPLC as described above and quantified by Abs_{280nm} ($\epsilon = 11\,200 \text{ M}^{-1} \text{ cm}^{-1}$).

Peptides were characterized using MALDI-TOF-MS. The peptide (1 nmol) was reconstituted in 100 μ L of 0.1% acetic acid, and 1 μ L was applied to the target and analyzed using a Vestec-2000 Laser Tec Research laser desorption linear time of flight mass spectrometer using insulin as the internal standard. The instrument was operated with 23 kV ion accelerating voltage and 3 kV multiplier voltage using a 337 nm VSL-SS& ND nitrogen laser with a 3 ns pulse width.

Formulation of Peptide DNA Condensates. Peptide DNA condensates were prepared at a final DNA concentration of 20 μ g/mL and at a peptide/DNA stoichiometry varying from 0.1 to 1.5 nmol of peptide/ μ g of DNA. The condensates were formed by adding peptide (2–30 nmol) prepared in 500 μ L of isotonic Hepes-buffered mannitol (HBM, 0.27 M mannitol, 5 mM sodium Hepes, pH 7.5) to 20 μ g of DNA in 500 μ L of HBM while vortexing, followed by equilibration at room temperature for 30 min.

¹ Abbreviations: RP-HPLC, reversed phase high-performance liquid chromatography; CWK, cysteine–tryptophan–lysine; TFA, trifluoroacetic acid; EDT, ethanedithiol; MALDI-TOF-MS, matrix-assisted time of flight mass spectrometry; RLU, relative light units; DTT, dithiothreitol; FBS, fetal bovine serum; MEM, minimal essential media; DMEM, Dulbecco's modified Eagle media; HBM, Hepes-buffered mannitol; QELS, quasi-elastic light scattering.

Sedimentation of DNA condensates was evaluated by measuring the concentration of DNA in solution before and after centrifugation. After peptide DNA condensates were formed as described above, a 50 μ L aliquot (1 μ g of DNA) was diluted in 1 mL of water and the $Abs_{260\text{ nm}}$ was determined on a Beckman DU640 spectrophotometer. Following centrifugation at 13000*g* for 4 min at room temperature, an identical aliquot was diluted with 1 mL of water and the concentration of DNA remaining in solution was determined. The ratio of absorbances subtracted from unity and multiplied by 100 was defined as the percent sedimentation.

Peptide binding to DNA was monitored by a fluorescence titration assay (18). A 1 μ g aliquot of the peptide DNA condensate prepared as described above was diluted to 1 mL in HBM containing 0.1 μ M thiazole orange. The fluorescence of the intercalated dye was measured on an LS50B fluorometer (Perkin-Elmer, U.K.) in a microcuvette by exciting at 500 nm while monitoring emission at 530 nm, with the slits set at 15 and 20 nm and photomultiplier gain set to 700 V. DNA condensation was monitored by measuring total scattered light at 90° by setting both monochromators to 500 nm and decreasing slit widths to 2.5 nm. Fluorescence and scattered light intensity blanks were subtracted from all values before data analysis.

Transmission electron microscopy was performed by immobilizing condensed DNA on carbon-coated copper grids (3 mm diameter, 400 mesh; Electron Microscopy Sciences, Fort Washington, PA). Grids were glow discharged, and 3 μ L of peptide DNA condensate (20 μ g/mL), prepared as described above, was placed on the grid for 5 min. The grids were blotted dry and then stained by floating for 1.5 min on each of three 100 μ L drops of uranyl acetate (1%, in 95% ethanol) followed by rinsing with 0.4% detergent solution (PhotoFlo, Kodak) and drying. Electron microscopy was performed using a Philips EM-100 transmission electron microscope.

Particle size analysis was measured for peptide DNA condensates prepared at a DNA concentration of 20 μ g/mL in HBM and at a stoichiometry of 0.8 or 1.0 (DiCWK₃) nmol of peptide/ μ g of DNA. Samples were analyzed using a Nicomp 370 Autodilute submicrometer particle sizer in the solid particle mode, and acquisition was continued until the fit error was <10. The mean diameter and population distribution were computed from the diffusion coefficient using functions supplied by the instrument.

In Vitro Gene Transfection. HepG2 cells (2×10^6 cells) were plated on 6 \times 35 mm wells and grown to 40–70% confluency in MEM supplemented with 10% FBS, penicillin, and streptomycin (10 000 units/mL), sodium pyruvate (100 mM), and L-glutamine (200 mM). Transfections were performed in MEM (2 mL/35 mm well) with 2% FBS, with or without 80 μ M chloroquine. Peptide DNA condensates (10 μ g of DNA in 0.5 mL of HBM) were added dropwise to triplicate wells. After 5 h of incubation at 37 °C, the medium was replaced with MEM supplemented with 10% FBS.

Luciferase expression was determined at 24 h with some modification of a published method (27). Cells were washed twice with ice-cold phosphate-buffered saline (calcium and magnesium free) and then treated with 0.5 mL of ice-cold lysis buffer (25 mM Tris chloride, pH 7.8, 1 mM EDTA, 8 mM magnesium chloride, 1% Triton X-100, 1 mM DTT) for 10 min. The cell lysate mixture was scraped, transferred to 1.5 mL microcentrifuge tubes, and centrifuged for 7 min at 13000*g* at 4 °C to pellet debris.

Lysis buffer (300 μ L), sodium ATP (4 μ L of a 180 mM solution, pH 7, 4 °C), and cell lysate (100 μ L, 4 °C) were combined in a test tube, briefly mixed, and immediately placed in the luminometer. Luciferase relative light units (RLU) were recorded on a Lumat LB 9501 (Berthold Systems, Germany) with 10 s integration after automatic injection of 100 μ L of 0.5 mM D-luciferin (prepared fresh in lysis buffer without DTT). The RLU were converted into femtomoles using a standard curve generated each day using luciferase dissolved in Tris acetate, pH 7.5, and stored at –20 °C. The standard curve was constructed by adding a known amount of the enzyme (0.01–100 fmol with specific activity of 2.5 nanounits/fmol) to 35 mm wells containing 40–70% confluent HepG2 or COS 7 cells. The cells were processed as described above, resulting in a standard curve with an average slope of 130 000 RLU/fmol of enzyme.

Protein concentrations were measured by Bradford assay using bovine serum albumin as a standard (28). The amount of luciferase recovered in each sample was normalized to milligrams of protein, and the mean and standard deviation obtained from each triplicate are reported.

COS 7 cells were plated at 72 000 cells per well and grown to 50% confluency in DMEM (Gibco BRL) supplemented with penicillin (10 000 units/mL), L-glutamine (200 mM), and 10% FBS for 24 h. The cells were transfected as described for HepG2 cells.

Lipofectace (Gibco BRL, 1:2.5 w/w dimethyl dioctadecylammonium bromide and dioleoylphosphatidylethanolamine) was used to mediate nonspecific gene transfection according to the manufacturer's instructions. The ratio of DNA to Lipofectace was optimized for both COS 7 and HepG2 cells. An optimal DNA/Lipofectace ratio was achieved by dissolving 10 μ g of DNA in 100 μ L of serum free media (SFM) followed by adding 60 μ L of Lipofectace prepared in 140 μ L of SFM. The Lipofectace DNA complex was then diluted with 1.7 mL of SFM and used to transfect HepG2 or COS 7 cells for 5 h followed by replacement of the transfecting media with supplemented 10% FBS. The cells were incubated for a total of 24 h, then harvested, and analyzed for luciferase as described above.

Dose response curves were prepared by varying the dose from 1 to 50 μ g of DNA while keeping the peptide/DNA stoichiometry fixed at 0.6 nmol/ μ g of DNA and normalizing the volume to 0.5 mL. Alternatively, a dose response curve for Lipofectace was prepared by varying the DNA dose from 1 to 20 μ g while keeping the stoichiometry of Lipofectace to DNA constant and normalizing the total volume of each dose to 2 mL with SFM.

RESULTS

Design of Peptides for Gene Delivery. Cationic peptides were designed to probe the minimal size needed to mediate efficient gene transfer in mammalian cells. The synthetic strategy involved comparison of four peptides with various lysine chain lengths in the range of 3–18 residues. During peptide synthesis, truncated peptides were capped by N-acetylation and a tryptophan residue was placed near the N terminus to provide a chromophore for identification of full-length sequences during purification. This residue allows quantitation of peptide concentration and is also intended for use in monitoring fluorescence to evaluate peptide binding to DNA as previously described (21). In addition, each peptide possessed an N-terminal cysteine residue as a potential ligand attachment site.

The four peptides were alkylated with iodoacetamide to provide AlkCWK_{*n*} (where *n* = 3, 8, 13, or 18 residues)

Table 1. Peptides for Gene Delivery

name	sequence	mass (obsd/calcd ^a)
AlkCWK ₃	Alk-S-Cys-Trp-(Lys) ₃	750.2/750.0
AlkCWK ₈	Alk-S-Cys-Trp-(Lys) ₈	1391.1/1390.9
AlkCWK ₁₃	Alk-S-Cys-Trp-(Lys) ₁₃	2031.1/2031.8
AlkCWK ₁₈	Alk-S-Cys-Trp-(Lys) ₁₈	2672.7/2672.5
DiCWK ₃	(Lys) ₃ -Trp-Cys-S-S-Cys-Trp-(Lys) ₃	1382.5/1382.8
DiCWK ₈	(Lys) ₈ -Trp-Cys-S-S-Cys-Trp-(Lys) ₈	2664.5/2665.2
DiCWK ₁₃	(Lys) ₁₃ -Trp-Cys-S-S-Cys-Trp-(Lys) ₁₃	3946.2/3945.9
DiCWK ₁₈	(Lys) ₁₈ -Trp-Cys-S-S-Cys-Trp-(Lys) ₁₈	5227.8/5227.9
polylysine ₁₉	(Lys) ₁₉	nd ^b /2435.8

^a Masses are calculated as the average $M + 1$ of the free base.

^b The mass of polylysine₁₉ was not determined due to polydispersity.

(Table 1). A further extension of this peptide series was accomplished by allowing the cysteine of each monomeric peptide to oxidize, resulting in a panel of homodimeric peptides each possessing two tryptophans and a discontinuous lysine repeat of either 6, 16, 26, or 36 residues in length (Table 1). Each alkylated peptide and dimeric peptide was characterized using MALDI-TOF-MS, which produced a dominant ion corresponding to the anticipated molecular weight of each peptide (Table 1).

Purified AlkCWK₃, AlkCWK₈, AlkCWK₁₃, and AlkCWK₁₈ each demonstrated a minor (10%) peak eluting later than the major product on RP-HPLC. On storage in an acid solution, the minor peak increased proportionally to the loss of the major product. The new product was isolated and analyzed by MALDI-TOF-MS, which verified a loss of 17 amu. A byproduct of identical mass loss was formed for each of AlkCWK₃, AlkCWK₈, AlkCWK₁₃, and AlkCWK₁₈. We speculate that the new product represents a cyclization of N-terminal amine with the acetamido group attached to cysteine leading to the loss of ammonia. The proposed cyclic byproduct of AlkCWK₁₈ was isolated and found to be functionally equivalent to the parent structure in transfection assays. Substitution of iodoacetic acid for iodoacetamide in the alkylation step led to an AlkCWK₁₈ peptide that was acid stable and functionally equivalent in formulation and biological assays.

Peptide Binding to Plasmid DNA. Peptides were studied for DNA binding using a dye exclusion assay that has been described previously (18). Peptide binding to DNA leads to exclusion of thiazole orange intercalation and a decrease in fluorescence. Titration of AlkCWK₃, AlkCWK₈, AlkCWK₁₃, or AlkCWK₁₈ with DNA in the range of 0.1–1.5 nmol of peptide/ μ g of DNA led to a reduction in fluorescence except for the smallest peptide (AlkCWK₃), which failed to exclude the intercalator within the titration range (Figure 1A). An asymptote in the fluorescence decline was observed at a stoichiometry of 0.6, 0.4, or 0.2 nmol of peptide/ μ g of DNA for AlkCWK₈, AlkCWK₁₃, or AlkCWK₁₈, respectively (Figure 1A). The relative fluorescence intensity at peptide/DNA stoichiometries above the asymptote established that AlkCWK₁₃ and AlkCWK₁₈ were able to exclude thiazole orange intercalation more efficiently than AlkCWK₈.

Dimeric peptides (DiCWK_{*n*}, *n* = 8, 13, 18) also possessed high affinity for DNA as evidenced by the stoichiometry of the fluorescence asymptote and the reduction in residual fluorescence, both of which correlated with the number of lysine residues (Figure 1B). Of this series, DiCWK₃ possessed weak affinity for DNA and thereby produced an asymptote at a stoichiometry of 1 nmol of peptide/ μ g of DNA.

In contrast to these results, polylysine₁₉ demonstrated a markedly different fluorescence titration curve compared to the alkylated or dimeric peptides of comparable

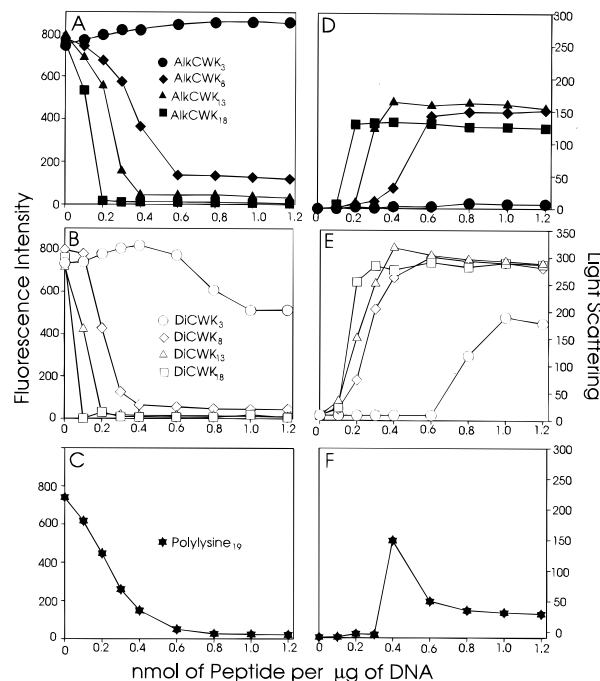


Figure 1. Fluorescence and light scattering titration of peptides with DNA. (A) Thiazole orange fluorescence was determined after titrating AlkCWK₃, AlkCWK₈, AlkCWK₁₃, or AlkCWK₁₈ with DNA as described under Materials and Methods. (D) Total light scattering measured simultaneously for each peptide DNA condensate. (B, E) Results of the fluorescence and light scattering titration using DiCWK₃, DiCWK₈, DiCWK₁₃, or DiCWK₁₈, respectively. (C, F) Fluorescence and light scattering titration of DNA with polylysine₁₉, respectively. Each titration represents the average of three determinations with average standard deviations of 7.4% for the fluorescence titration and 6.2% for the light scattering assay (error bars not shown).

length (Figure 1C). Even though polylysine₁₉ has a similar number of lysine residues as AlkCWK₁₈, its fluorescence asymptote occurs at a stoichiometry of approximately 0.6 nmol of peptide/ μ g of DNA. This result suggests that polylysine₁₉ binding to DNA is weak relative to AlkCWK₁₈.

Condensation of DNA with Peptides. Total light scattering at 90° was used to detect the peptide stoichiometry at which condensed DNA particles were formed (18, 29). Titration of AlkCWK₈, AlkCWK₁₃, or AlkCWK₁₈ with DNA produced a maximal total light scattering at stoichiometries that corresponded to the asymptote observed in the fluorescence exclusion assay (Figure 1D). A plateau in the light scattering profile observed at stoichiometries of 0.6, 0.4, and 0.2 for AlkCWK₈, AlkCWK₁₃, and AlkCWK₁₈, respectively, established the complete condensation of DNA at or above this peptide/DNA ratio. In contrast, titration of DNA with AlkCWK₃ failed to produce an increase in the light scattering, supporting earlier observations that indicate AlkCWK₃ fails to bind to DNA.

Titration of the dimeric peptides with DNA each produced condensates detected by light scattering (Figure 1E). Although the plateau light scattering levels for each dimeric peptide DNA condensate were nearly indistinguishable, the stoichiometry at which the plateau was achieved occurred at 0.6, 0.4, and 0.2 nmol of peptide/ μ g of DNA for DiCWK₈, DiCWK₁₃, and DiCWK₁₈, respectively. A weaker binding affinity for DiCWK₃ was evident from the plateau in light scattering which occurred at a stoichiometry of 1 nmol/ μ g of DNA (Figure 1E).

The light scattering profile for polylysine₁₉ was very distinct from that obtained for alkylated and dimeric

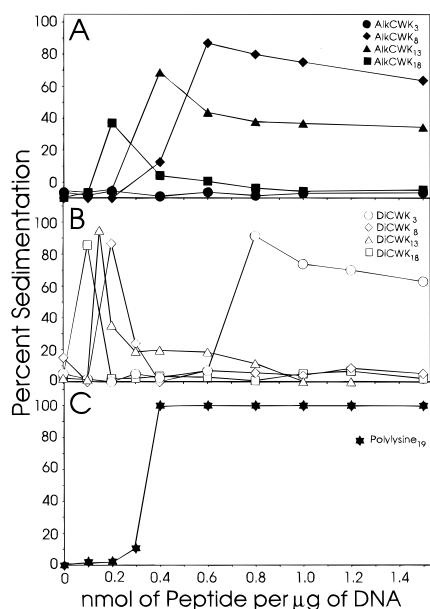


Figure 2. Sedimentation of peptide DNA condensates. The percent of DNA sedimented following centrifugation of peptide-induced DNA condensates is shown. The peptide/DNA stoichiometry was varied from 0.1 to 1.5 nmol of peptide/ μ g of DNA in HBM at a total DNA concentration of 20 μ g/mL. (A) Results for AlkCWK₃, AlkCWK₈, AlkCWK₁₃, and AlkCWK₁₈; (B) results for DiCWK₃, DiCWK₈, DiCWK₁₃, and DiCWK₁₈; (C) results for polylysine₁₉. The average standard deviation for the assay was 8.6% (error bars not shown).

peptides. A sharp increase occurred at a stoichiometry of 0.4 nmol/ μ g of DNA, which declined to approximately 50 light scattering units at higher peptide/DNA stoichiometries (Figure 1F). This light scattering titration profile distinguished the condensation properties of polylysine₁₉ from CWK_n peptides, suggesting differences in the particle size for polylysine₁₉ DNA condensates.

Sedimentation of DNA Condensates. To evaluate the relative particle size of DNA condensates prepared at stoichiometries ranging from 0.1 to 1.5 nmol of peptide/ μ g of DNA, a sedimentation assay was utilized to measure the DNA remaining in suspension following centrifugation at 13000*g* for 4 min (18) (Figure 2). Titration of DNA with AlkCWK₃ resulted in the complete recovery of the DNA following centrifugation, supporting earlier findings that indicate AlkCWK₃ fails to bind and condense DNA into particles. Alternatively, AlkCWK₈, AlkCWK₁₃, and AlkCWK₁₈ each produced maximal sedimentation at a stoichiometry that roughly correlates with the stoichiometry calculated for a charge neutral complex (Figure 2A). At stoichiometries greater than charge neutral, AlkCWK₈ condensates sedimented to a greater extent than AlkCWK₁₃ or AlkCWK₁₈ condensates, indicating their larger size.

A similar trend was observed when dimeric peptide DNA condensates were sedimented. The maximal sedimentation was observed at a stoichiometry of 0.8, 0.2, 0.15, and 0.1 nmol of peptide/ μ g of DNA for DiCWK₃, DiCWK₈, DiCWK₁₃, and DiCWK₁₈, respectively (Figure 2B). At stoichiometries above the calculated charge neutral point DiCWK₈, DiCWK₁₃, and DiCWK₁₈ DNA condensates failed to sediment, suggesting they are smaller in size (Figure 2B). It is also evident that DiCWK₃ DNA condensates were large due to the observed sedimentation (70–80%) at stoichiometries above the charge neutralization point (Figure 2B).

In contrast, polylysine₁₉ DNA condensates sedimented completely at 0.2 nmol of peptide/ μ g of DNA and failed to recover at higher stoichiometries. These data estab-

Table 2. QELS Particle Size Distribution

peptide DNA condensate ^a	particle size population	
	diameter ^b (nm)	σ^c (nm)
polylysine ₁₉	3102	297
AlkCWK ₃		
AlkCWK ₈	2412	354
AlkCWK ₁₃	231	107
AlkCWK ₁₈	78	30
DiCWK ₃	724	154
DiCWK ₈	53	24
DiCWK ₁₃	56	29
DiCWK ₁₈	64	27

^a Peptide DNA condensates were prepared at a concentration of 20 μ g/mL of DNA and at stoichiometry of 0.8 or 1.0 nmol (DiCWK₃) of peptide/ μ g of DNA in HBM. ^b Represents the mean diameter of particles. ^c Standard deviation of the population.

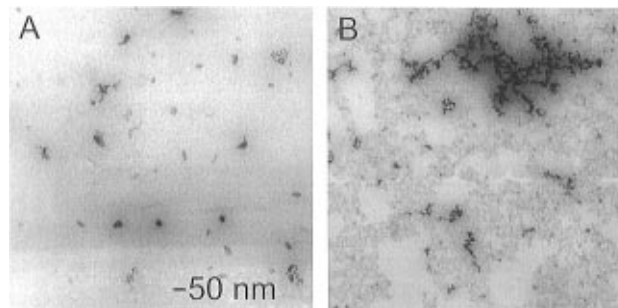


Figure 3. Electron microscopy of DNA condensates. The electron micrographs are shown for DNA condensates prepared at 0.5 nmol of peptide/ μ g of DNA for AlkCWK₁₈ (A) and at 0.8 nmol of peptide/ μ g of DNA for polylysine₁₉ (B). The calibration bar shown is 50 nm in length.

lished that once polylysine₁₉ DNA condensates are formed, they remained large throughout the titration range (Figure 2C).

Particle Size and Distribution. DNA condensates were prepared with alkylated peptides, dimeric peptides, and polylysine₁₉ at a stoichiometry of 0.8 nmol of peptide/ μ g of DNA, and particle sizes were compared using quasi-elastic light scattering (QELS). A population of particles with average diameters of 0.7–3.1 μ m was determined for polylysine₁₉, AlkCWK₈, and DiCWK₃ DNA condensates, whereas no particles were detected for AlkCWK₃ DNA condensates (Table 2), consistent with the results of sedimentation analysis.

Each alkylated or dimeric peptide possessing 13 lysine residues or more produced a population of particles with mean diameters of 53–231 nm (Table 2). It should be noted that particle populations were most often bimodal, possessing a major (>90%) smaller diameter population and a minor larger diameter population which contributed to the large standard deviation of the average particle size (Table 2).

Particle sizes determined by QELS were substantiated by analyzing DNA condensates using electron microscopy. Figure 3 compares the particle size and morphology for AlkCWK₁₈ and polylysine₁₉ DNA condensates. The images demonstrate that condensates produced with AlkCWK₁₈ are relatively uniform particles with diameters of approximately 50–100 nm, whereas polylysine₁₉-induced condensates were large flocculated particles, consistent with the result of particle size analysis by QELS (Figure 3).

In Vitro Gene Expression of Peptide DNA Condensates. Luciferase reporter gene expression was analyzed following transfection of HepG2 or COS 7 cells with peptide DNA condensates prepared at stoichiometries ranging from 0.1 to 1.5 nmol of peptide/ μ g of DNA.

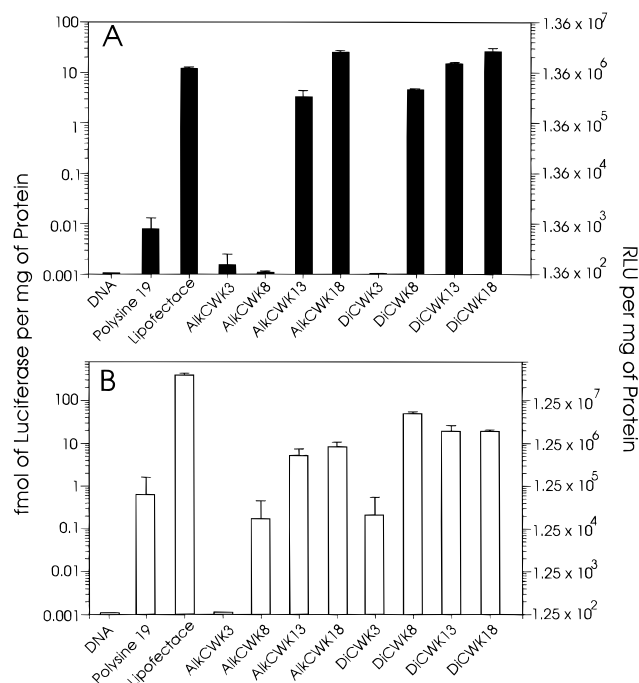


Figure 4. In vitro gene expression in HepG2 and COS 7 cells. Luciferase reporter gene expression is shown for DNA condensates prepared using alkylated peptides, dimeric peptides, polylysine₁₉, and Lipofectace. Chloroquine (80 μ M) was included in the transfecting media for peptides and polylysine₁₉. (A) Gene expression determined in HepG2 cells; (B) gene expression in COS 7 cells. Each bar represents the mean and standard deviation of three determinations.

A 10-fold enhancement in the gene expression level was achieved when chloroquine was included in the transfecting media. For each peptide-condensing agent, the maximal reporter gene expression occurred at a peptide/DNA stoichiometry that corresponds to the fully condensed DNA as determined by the asymptote in the light scattering assay (Figure 1D,E,F) (18). At stoichiometries greater than that required to achieve condensation, the gene expression remained constant. Thereby, the relative gene expression levels were compared for each peptide DNA condensate at a fixed stoichiometry of 0.8 or 1.0 nmol (DiCWK₃) of peptide/ μ g of DNA, which was sufficient for each peptide to fully condense DNA.

Transfection of HepG2 with 10 μ g of either uncomplexed plasmid DNA, AlkCWK₃ or AlkCWK₈, DiCWK₃, or polylysine₁₉ DNA condensates failed to produce significant reporter gene expression (Figure 4A). This result supported formulation experiments that predicted these peptides either fail to condense DNA (AlkCWK₃) or produce condensates that are large (0.7–3.1 μ m). Alternatively, AlkCWK₁₃, AlkCWK₁₈, DiCWK₈, DiCWK₁₃, and DiCWK₁₈ DNA condensates each demonstrated significant gene transfer efficiency that was 2–3 orders of magnitude greater than that of polylysine₁₉. Lipofectace-mediated gene expression levels were also found to be identical to peptide-mediated expression levels in HepG2 cells (Figure 4A).

To verify that peptide-mediated gene delivery was not dependent on the existence of cell type specific receptors, the reporter gene expression in HepG2 cells was compared to that in COS 7 cells (Figure 4B). Significant differences were observed for the transfection of COS 7 versus HepG2 cells such that only uncomplexed DNA and AlkCWK₃ DNA condensates failed to produce measurable gene expression levels. AlkCWK₈, DiCWK₃, and polylysine₁₉ DNA condensates each mediated a significant gene expression in COS 7 cells despite their inactivity

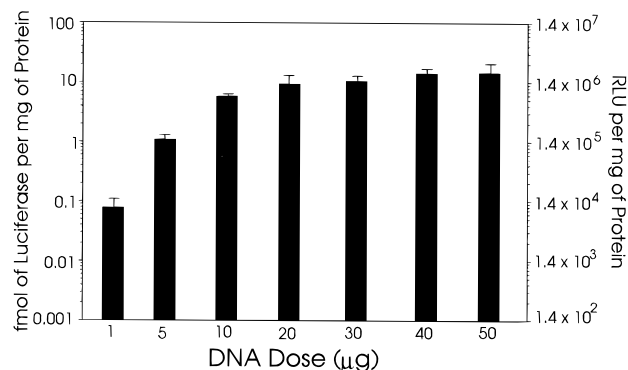


Figure 5. Dose response for peptide-mediated gene delivery. Luciferase gene expression levels in HepG2 are compared using an escalating dose of AlkCWK₁₈ DNA condensate prepared at a stoichiometry of 0.6 nmol/ μ g of DNA.

in transfecting HepG2 cells. However, the gene expression level mediated by these peptides was still 1–2 orders of magnitude below that afforded by AlkCWK₁₃, AlkCWK₁₈, DiCWK₈, DiCWK₁₃, and DiCWK₁₈ (Figure 4B). Also, Lipofectace-mediated gene expression in COS 7 cells was 1 order of magnitude greater than peptide-mediated gene delivery. These results suggest that the size restriction of peptide DNA condensates is less stringent in COS 7 cells compared to HepG2 cells.

To establish the effect of dose response using peptide DNA condensates, HepG2 cells were treated with escalating doses of AlkCWK₁₈ DNA condensates and Lipofectace DNA formulations. As demonstrated in Figure 5, a dose response curve for the AlkCWK₁₈ DNA condensate plateaus at 20 μ g of DNA and remains constant at higher doses, whereas the toxicity of Lipofectace above 10 μ g of DNA (data not shown) leads to reduced expression levels at higher doses.

DISCUSSION

The efficiency of carrier-mediated gene delivery depends on the reversible association of condensing molecules with plasmid DNA (1–3). The carriers that have been used most often are composed of polymers or lipids that bind to anionic sites on DNA. In the case of cationic peptides, this leads to condensation of plasmid DNA into small particles that gain entry into the target cell via nonspecific fluid phase pinocytosis (1). Attachment of ligands adds specificity to the delivery system and likewise alters the mode of DNA transfer across cell membranes such that DNA and ligand cotransfer via receptor-mediated endocytosis (5–15).

Previously we demonstrated that a low molecular weight glycopeptide mediated gene transfer to hepatocytes via the asialoglycoprotein receptor (18). Since this glycopeptide was prepared from low molecular weight polydisperse polylysine (dp 19), we sought to systematically optimize the peptide portion of the glycopeptide as a first step to improve its efficiency as a carrier for nonviral gene delivery.

The results establish that low molecular weight peptides possessing six or more lysine residues bind with sufficient affinity to condense DNA at stoichiometries above the charge neutral point (Figure 1). However, condensation of DNA is not sufficient to ensure significant transfection levels since AlkCWK₈, DiCWK₃, and polylysine₁₉ each produced DNA condensates but failed to mediate significant gene transfer in HepG2 cells (Figure 4A). The success or failure of individual peptide DNA condensates to mediate gene expression appears to be related to particle size such that larger condensates

are less efficiently pinocytosed (2). For HepG2 cells an apparent size restriction exists that excludes large DNA condensates. This is demonstrated by comparison of the transfection efficiency for AlkCWK₈ DNA condensates of 2.4 μm size relative to AlkCWK₁₃ DNA condensates, which possess an average diameter of 231 nm (Figure 4A). The addition of five lysine residues decreases particle size 10-fold, which leads to a 1000-fold amplification in gene transfer efficiency. Further reductions in the DNA particle diameters in the range of 231–53 nm only led to an additional 10-fold increase in transfection levels (Figure 4A). The size requirements described above for transfecting HepG2 cells are less stringent for COS 7 cells. Large (0.7–3.1 μm) peptide DNA condensates are moderately efficient at mediating transfection in COS 7 cells but are still 10–100-fold less efficient than smaller DNA condensates (Figure 4B).

The equivalent transfer efficiency of peptide DNA condensates into either HepG2 or COS 7 cells suggests a nonspecific mechanism related to the cationic nature of the condensates (1, 2). We have also transfected 293T cells with peptide DNA condensates (data not shown), which resulted in a similar high level of gene expression. Comparable gene expression levels were obtained using peptide or Lipofectace to mediate DNA transfer in HepG2 cells, whereas Lipofectace-mediated gene delivery was found to be more efficient than peptide-mediated gene delivery in COS 7 cells (Figure 4). These results reflect cell type specific differences that must be considered in the development of gene delivery systems (1, 2).

The discovery of a class of low molecular weight peptides that efficiently condense DNA into small particles is a major finding of this study. Apparently, some structural feature of AlkCWK_n peptides allows more efficient condensation of DNA relative to polylysine. This is demonstrated most clearly by AlkCWK₁₈, which condenses DNA into particles that are 40-fold smaller (78 nm) than those produced by polylysine₁₉ (3.1 μm). Given that the lysine chain lengths of these two peptides are nearly equivalent, the N-terminal cysteine or tryptophan is presumably responsible for the enhanced condensing activity. To investigate the structural requirements of an efficient DNA condensing peptide, we synthesized an isomer of AlkCWK₁₈ also possessing 18 lysine residues but in which cysteine is relocated to the C terminus and tryptophan is the N terminus (WK₁₈C). The alkylated and dimeric form of this peptide each mediated gene transfer as efficiently as AlkCWK₁₈ (data not shown), suggesting that the location of cysteine may not be key to the reported activity. On the basis of this and other observations discussed below, we hypothesize that tryptophan may be primarily responsible for the enhanced condensation activity of AlkCWK₁₈ compared to polylysine₁₉.

A tryptophan residue may increase the binding affinity between cationic peptides and DNA. Evidence supporting this hypothesis comes from the stoichiometry of AlkCWK₁₈ (0.2 nmol of peptide/ μg of DNA) needed to exclude intercalator binding to DNA versus that for polylysine₁₉ (0.6 nmol of peptide/ μg of DNA) (Figure 1A,C). Lohman and co-workers also identified a function for tryptophan in altering cationic peptide binding to DNA and RNA (22, 23). Curiously, they determined an enhancement in the entropy of peptide binding to DNA when substituting tryptophan for lysine (22, 23). However, this was offset by a decrease in the enthalpy of binding, leading to a net zero change in the association constant (22, 23). These studies also established that the location of tryptophan is not important and that multiple tryptophan residues do not influence the magnitude of

the association constant despite changes in the enthalpic and entropic contributions (22, 23). Recently, a low molecular weight cationic peptide possessing alanine, tyrosine, 10 lysines, and tryptophan has been co-complexed with a fusogenic peptide and DNA to achieve a 5 order of magnitude amplification in gene expression in HepG2 cells relative to uncomplexed DNA (24). The efficient DNA condensing activity of this low molecular weight peptide may also be linked the tryptophan residue, which flanks the polylysine sequence.

The precise mechanism of how tryptophan functions to increase binding affinity and decrease particle size is uncertain; however, it may relate to its ability to intercalate into DNA leading to an observed fluorescence quench (21–23). Tryptophan's hydrophobic interaction with DNA may organize the peptide binding on DNA, facilitating the formation of intermolecular ion pairs between multiple lysine residues and the DNA phosphate backbone.

Preparation of small DNA condensates has also recently been reported using polylysine dp 30 at a stoichiometric excess of 1.2 nmol/ μg of DNA (20). The present study establishes that simple amino acid substitutions allow polylysine peptides as small as dp 13 to acquire the necessary affinity to condense DNA into small particles at low stoichiometric excess.

The development of homogeneous peptides that actively condense DNA into small particles is an important advance toward the development of low molecular weight carriers for targeted gene delivery. Attachment of a receptor ligand such as a carbohydrate or peptide to a single cysteine residue should endow specificity to the gene delivery system and allow further systematic optimization of low molecular weight carriers for receptor-mediated gene delivery.

ACKNOWLEDGMENT

We acknowledge financial support for this work from NIH GM48049. The DNA used for these studies was prepared by Anna Calcagno. We also acknowledge technical assistance in performing mass spectroscopy by Bao-Jen Shyong at the Carbohydrate and Protein core facility, University of Michigan. Electron microscopy studies were performed with technical assistance from Bruce Donohoe and Chris Edwards in the Department of Cell Biology and Anatomy, University of Michigan. The QELS particle size analysis was performed with assistance from Ramachandran Chandrasekharan at the College of Pharmacy, University of Michigan.

LITERATURE CITED

- (1) Behr, J. P. (1994) Gene Transfer with Synthetic Cationic Amphiphiles: Prospects for Gene Therapy. *Bioconjugate Chem.* 5, 382–389.
- (2) Ledley, F. D. (1995) Nonviral Gene Therapy: The Promise of Genes as Pharmaceuticals. *Hum. Gene Ther.* 6, 1129–1144.
- (3) Christiano, R. J., and Roth, J. A. (1995) Molecular Conjugates: a Targeted Gene Delivery Vector For Molecular Medicine. *J. Mol. Med.* 73, 479–486.
- (4) Ledley, T. S., and Ledley, F. D. (1994) Multicompartment, Numerical Model of Cellular Events in the Pharmacokinetics of Gene Therapies. *Hum. Gene Ther.* 5, 679–691.
- (5) Michael, S. I., and Curiel, D. T. (1994) Strategies to Achieve Targeted Gene Delivery Via the Receptor-Mediated Endocytosis Pathway. *Gene Ther.* 1, 223–232.
- (6) Wu, G. Y., and Wu, C. H. (1988) Evidence for Targeted Gene Delivery to HepG2 Hepatoma Cells in Vitro. *Biochemistry* 27, 887–892.
- (7) Wu, G. Y., and Wu, C. Y. (1988) Receptor-Mediated Gene Delivery and Expression in Vivo. *J. Biol. Chem.* 263, 14621–14624.

- (8) Hockett, B., Ariatti, M., and Hawtrey, A. O. (1990) Evidence for Targeted Gene Transfer by Receptor-Mediated Endocytosis. Stable Expression Following Insulin-Directed Entry of Neo Into HepG2 Cells. *Biochem. Pharmacol.* **40**, 253–263.
- (9) Thurnher, M., Wagner, E., Clausen, H., Mechtler, K., Rusconi, S., Dinter, A., Birnstiel, M. L., Berger, E. G., and Cotten, M. (1994) Carbohydrate Receptor-Mediated Gene Transfer to Human T-Leukaemic Cells. *Glycobiology* **4**, 429–435.
- (10) Rojanasakul, Y., Wang, L. Y., Malanga, C. J., Ma, J. K. H., and Liaw J. (1994) Targeted Gene Delivery to Alveolar Macrophages via Fc Receptor-Mediated Endocytosis. *Pharm. Res.* **11**, 1731–1736.
- (11) Midoux, P., Mendes, C., Legrand, A., Raimond, J., Mayer, R., Monsigny, M., and Roche, C. (1993) Specific Gene Transfer Mediated by Lactosylated Poly(L-Lysine) into Hepatoma Cells. *Nucleic Acid Res.* **21**, 871–878.
- (12) Wagner, E., Zenke, M., Cotten, M., Beug, H., and Birnstiel, M. L. (1990) Transferrin-Polycation conjugates as Carriers for DNA Uptake into Cells. *Proc. Natl. Acad. Sci. U.S.A.* **87**, 3410–3414.
- (13) Merwin, J. R., Noell, G. S., Thomas, W. L., Chiou, H. C., DeRome, M. E., McKee, T. D., Spitalny, G. L., and Findeis, M. A. (1994) Targeted Delivery of DNA using YEE (GalNAcAH)3, a Synthetic Glycopeptide Ligand for the Asialoglycoprotein Receptor. *Bioconjugate Chem.* **5**, 612–620.
- (14) Yin, W., and Cheng, P. W. (1994) Lectin Conjugate-Directed Gene Transfer to Airway Epithelial Cells. *Biochem. Biophys. Res. Commun.* **205**, 826–833.
- (15) Gottschalk, S., Cristiano, R. J., Smith, L. C., and Woo, S. L. C. (1994) Folate Receptor Mediated DNA Delivery into Tumor Cells: Potosomal Disruption Results in Enhanced Gene Expression. *Gene Ther.* **1**, 185–191.
- (16) McKee, T. D., DeRome, M. E., Wu, G. Y., and Findeis, M. A. (1994) Preparation of Asialoorosomucoid-Polylysine Conjugates. *Bioconjugate Chem.* **5**, 306–311.
- (17) Erbacher, P., Roche, A. C., Monsigny, M., and Midoux, P. (1995) Glycosylated Polylysine/DNA Complexes: Gene Transfer Efficiency in Relation with the Size and Sugar Substitution Level of Glycosylated Polylysines and with the Plasmid Size. *Bioconjugate Chem.* **6**, 401–410.
- (18) Wadhwa, M., Knoell, D. L., Young, A. P., and Rice, K. G. (1995) Targeted Gene Delivery with A Low Molecular Weight Glycopeptide. *Bioconjugate Chem.* **6**, 283–291.
- (19) Taxman, D. J., Lee, E. S., and Wojchowski, D. M. (1993) Receptor-Targeted Transfection Using Stable Maleimido Transferrin/Thio-Polyl(L-Lysine) Conjugates. *Anal. Biochem.* **213**, 97–103.
- (20) Wolfert, M. A., and Seymour, L. W. (1996) Atomic Force Microscopic Analysis of the Influence of the Molecular Weight of Poly(L-Lysine) on the Size of Polyelectrolyte Complexes Formed with DNA. *Gene Ther.* **3**, 269–273.
- (21) Bujalowski, W., and Lohman, T. M. (1987) A General Method of Analysis of Ligand-Macromolecule Equilibria Using a Spectroscopic Signal from the Ligand To Monitor Binding. Application to *Escherichia coli* Single-Strand Binding Protein-Nucleic Acid Interactions. *Biochemistry* **26**, 3099–3106.
- (22) Mascotti, D. P., and Lohman, T. M. (1992) Cooperative Binding of Polyamines Induces the *Escherichia coli* Single-Strand Binding Protein-DNA Binding Mode Transitions. *Biochemistry* **31**, 8932–8946.
- (23) Mascotti, D. P., and Lohman, T. M. (1993) Thermodynamics of Single-Stranded RNA and DNA Interactions with Oligolysines Containing Tryptophan. Effects of Base Composition. *Biochemistry* **32**, 10568–10579.
- (24) Gottschalk, S., Sparrow, J. T., Hauer, J., Mims, M. P., Leland, F. E., Woo, S. L. C., and Smith, L. C. (1996) A Novel DNA-Peptide Complex for Efficient Gene Transfer and Expression in Mammalian Cells. *Gene Ther.* **3**, 448–457.
- (25) Sambrook, J., Fritsch, E. F., and Maniatis, T. (1989) *Molecular Cloning: A Laboratory Manual*, Cold Spring Harbor Laboratory Press, Plainview, NY.
- (26) Naoi, M., and Lee, Y. C. (1974) A Fluorometric Measurement of Ligands Incorporated into BrCn-Activated Polysaccharides. *Anal. Biochem.* **57**, 640–644.
- (27) Brasier, A. R., Tate, J. E., and Harener, J. F. (1989) Optimized Use of the Firefly Luciferase Assay as a Reporter Gene in Mammalian Cell Lines. *BioTechniques* **7**, 1116–1122.
- (28) Bradford, M. M. (1976) A Rapid and Sensitive Method for the Quantitation of Microgram Quantities of Protein Utilizing the Principle of Protein-Dye Binding. *Anal. Biochem.* **72**, 248–254.
- (29) Wilson, R. W., and Bloomfield, V. A. (1979) Counterion-induced Condensation of Deoxyribonucleic Acid. A Light Scattering Study. *Biochemistry* **18**, 2192–2196.

BC960079Q

TECHNICAL NOTES

Characterization of Oligodeoxyribonucleotide–Polyethylene Glycol Conjugates by Electrospray Mass Spectrometry

Theodore M. Tarasow,* David Tinnermeier, and Carina Zyzniewski

NeXstar Pharmaceuticals Inc., 2860 Wilderness Place, Boulder, Colorado 80301. Received September 26, 1996[®]

Electrospray mass spectrometry (ESMS) was used to characterize a number of differently functionalized polyethylene glycol–oligodeoxyribonucleotide conjugates. Sample preparation was found to be crucial to obtaining quality data. The resolution and precision of ESMS allowed for the identification of individual conjugates differing in MW by a single ethylene glycol unit with an accuracy of ≤ 1 (0.02% of the molecular weight). In addition, ESMS was shown to be valuable in identifying chromatographically unresolvable components of a derivatized polyethylene glycol–oligonucleotide conjugate mixture.

INTRODUCTION

Interest in oligonucleotides as research tools, diagnostic reagents, and therapeutics has increased dramatically. As scientific probes, oligonucleotides and oligonucleotide conjugates have been used in both macromolecular structural research and reaction mechanism investigations. From a commercial perspective, these molecules have shown promise as therapeutic and diagnostic agents (1). Potential oligonucleotide therapeutics include anti-sense molecules (2, 3), ribozymes (4), and oligonucleotides obtained from the systematic evolution of ligands by exponential enrichment (SELEX) (1, 5, 6). In particular, the SELEX-derived compounds are of intense pharmaceutical interest because of the high affinity and exquisite selectivity demonstrated for a broad range of targets. However, oligonucleotides as drugs suffer from two drawbacks, the first being their susceptibility to hydrolytic and enzymatic degradation and the second being their lack of bioavailability. A general strategy for overcoming these shortcomings has been chemical modification of oligonucleotides such that their inherent stability and bioavailability are increased (3, 7). In addition, oligonucleotides have been modified to facilitate their incorporation into stabilizers and delivery vehicles such as liposomes (8).

Oligonucleotide modifications have included conjugation of cholesterol (9, 10), fatty acids (12, 13), polycations (8, 11), proteins (14), and polymers (15, 16) to name a few. Characterization of these molecules is crucial to gaining knowledge about their mode of action and to qualify them as drug candidates. Unfortunately, the process of chemically modifying oligonucleotides often results in multiple reaction products, especially when polymers are involved, making characterization difficult. Most product characterizations have included some change in physical property such as a band shift in gel electrophoresis or a peak shift in high-performance liquid chromatography (HPLC). Although these techniques suggest a modification has taken place, they do not directly allude to the identity of the reaction product or

products. Furthermore, when multiple products are produced, these techniques are often unable to resolve the resulting mixture and identify the individual components. Analytical hurdles such as these were encountered early on in our efforts to produce 5' polyethylene glycol (PEG)-modified oligonucleotides using standard automated synthetic techniques. Somewhat similar conjugates had been prepared in the past (16); however, our oligonucleotide conjugate targets were designed with longer PEG units than previously described. As a result, new methods were required to prepare these compounds, and improved analytical analysis proved to be key in developing these procedures.

Mass spectrometry (MS) offers a characterization technique superior to those discussed above by providing a direct measurement of the molecular weight of the molecule or molecules of interest (17). In addition, one of the many valuable uses of MS has been mixture analysis, making the technique potentially useful for analyzing reaction product mixtures produced by the chemical modification of oligonucleotides. Indeed, two accounts revealed matrix-assisted laser desorption/ionization mass spectrometry (MALDI MS) to be a useful tool for the characterization of oligonucleotide–PEG conjugates (16, 18). However, the resolution and accuracy of MALDI are limited and decrease significantly with increasing molecular weight (MW). These limitations are especially evident in the MALDI analyses of the PEG–oligonucleotide conjugates where the polydispersity of the PEG polymer results in multiple species with similar molecular weights. These species became less resolved as the length of the oligonucleotide and/or the polymer was increased. Another MS technique which offers superior resolution and accuracy is electrospray mass spectrometry (ESMS). ESMS generates and detects multiple charge states of the sample, which upon reconstruction yields the molecular weights of the species present (19). Because of the mild ionization process and the increased measurable molecular weight range, ESMS has been particularly useful for characterizing large biomolecules (17), such as proteins (20), protein conjugates (21), protein–ligand complexes (22) and oligonucleotides (23, 24). Herein, we report the characterization of a variety of functionalized oligodeoxyribonucleotide–PEG conjugates by electrospray mass spec-

* Author to whom correspondence should be addressed. Telephone: (303) 546-7702. Fax: (303) 444-0672.

[®] Abstract published in *Advance ACS Abstracts*, January 1, 1997.

trometry. Further, we demonstrate the utility of ESMS in analyzing multiple reaction products as a result of the chemical modification of oligonucleotide-PEG conjugates. We also describe good yielding methods for the incorporation of PEG molecules with average molecular weights up to 2000 in oligonucleotide conjugates by automated synthesis using standard phosphoramidite chemistry.

EXPERIMENTAL PROCEDURES

General. Monoamino-PEG-2000 (average M_n of ≈ 2000) and monomethoxy-PEG-2000 were purchased from Shearwater Polymers Inc. (Huntsville, AL) and used as received. All other chemicals were purchased from Aldrich Chemical Co. and used as received unless otherwise specified. HPLC was performed on a Rainin Dynamax HPLC instrument equipped with a Rainin UV D-II dual-wavelength detector. Vydac C4 reverse phase HPLC columns were used with triethylammonium acetate (TEAA) at pH 7.0 and acetonitrile (MeCN) as eluents. NMR spectra were obtained on a Bruker AMX 300 instrument.

Functionalized PEG. The functionalized PEG molecules used to produce compounds **2–4** were prepared by acylation of monoamino-PEG-2000 with either the *N*-hydroxysuccinimide (NHS)-activated ester or the *p*-nitrophenyl-activated carbonate of the corresponding functional modification. The derivatized PEG compounds were purified by flash silica gel chromatography and precipitation from tetrahydrofuran (THF) with diethyl ether. The identities of the PEG molecules were confirmed by ^1H NMR.

The (*N*-acetylamino)cyclohexadienyl-PEG molecule used to synthesize compound **5** was prepared by addition of amino-PEG to the boron tetrafluoride salt of cyclohexadienylumiron(0) tricarbonyl with subsequent oxidative elimination of the iron tricarbonyl using ceric ammonium nitrate (T. Dewey, C. Zyzniewski, and B. Eaton, unpublished results). The derivatized PEG molecule was purified and characterized in a manner similar to that described above.

PEG Phosphoramidite Synthesis. All steps were carried out under an argon atmosphere using inert atmosphere techniques. THF was freshly distilled from potassium/benzophenone prior to use. The primary amine on the PEG used to prepare compound **1** was protected as the 9-fluorenylmethyl carbamate (fmoc) prior to phosphoramidite synthesis. The derivatized PEG (150 mg, 0.07 mmol) was dissolved in THF (1.5 mL) and added to a solution of 18.2 mg (0.077 mmol) of (2-cyanoethyl)-*N,N*-diisopropylchlorophosphoramidite and 14.7 mg (0.114 mmol) of diisopropylethylamine in THF (0.5 mL). The reagents were allowed to react at room temperature for 30 min, after which ^{31}P NMR indicated that the reaction was complete. Excess phosphoryl chloride as detected by ^{31}P NMR was quenched by the addition of methanol (20 μL). The mixture was then filtered through glass wool and the solvent removed under reduced pressure. The PEG phosphoramidite was used immediately in the automated oligonucleotide conjugation described below.

Oligonucleotide-PEG Conjugate Synthesis. All oligonucleotide-PEG conjugates were synthesized on an ABI 392 DNA synthesizer using standard cycles and conditions except for coupling of the PEG phosphoramidite. Reagents, including phosphoramidites, were obtained from Glen Research. All syntheses were performed at the 1 μmol scale using a Pharmacia polystyrene support. The PEG phosphoramidite was dissolved in anhydrous acetonitrile to a final concentration of 50 mM. Coupling of PEG phosphoramidite was achieved using a

modified ABI 1 μmol CE coupling cycle. The coupling time was increased to 45 min, and an additional coupling cycle was inserted prior to capping. Oligonucleotide cleavage from the polystyrene support and deprotection were carried out in concentrated NH_4OH at 55 $^\circ\text{C}$ for 12–16 h. The oligonucleotide-PEG conjugates were purified by HPLC using a 15 to 40% acetonitrile gradient over 20 min. Retention times of the oligonucleotide conjugates varied depending on what functionality was present at the end of the PEG. Due to the degree of polymerization and polydisperse nature of the PEG, conjugates typically eluted as an envelope of moderately resolved peaks. Oligonucleotide-PEG conjugates were collected, concentrated to dryness, dissolved in water, and quantitated by UV spectroscopy ($\epsilon_{260} \approx 91\,600$). Yields were typically 40–60%. These samples were used directly in the MS experiments described below.

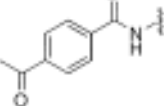
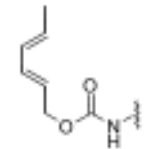
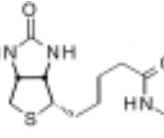
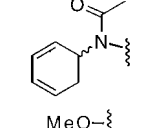
The alternative route to functionalized oligonucleotide-PEG conjugates **2** and **4** involved reaction of the amino-PEG-oligonucleotide (**1**) with the NHS ester of either 4-acetobenzoic acid or biotin, respectively. The resulting reaction mixture was HPLC purified as above and subjected to ESMS analysis. In both cases, HPLC was ineffective at separating the desired compounds, **2** and **4**, from undesired side products.

MS Analysis of Oligonucleotide-PEG Conjugates. Electrospray mass spectrometry was performed on a Fisons Quattro II (Beverly, MA) triple-quadrupole mass spectrometer using the negative ion mode. The first detector was used for mass detection. Nitrogen was used as the nebulizer gas at 20 L/h and the drying gas at 300 L/h. The cone voltage was -30 V , the capillary 2.65 kV, and the HV lens 0.33 kV. The source temperature was maintained at 80 $^\circ\text{C}$. Samples (10 μL) were injected via flow injection using a Rheodyne 7125 (Cotati, CA) manual injector with a 20 μL stainless steel loop. A Harvard apparatus model 22 (South Natick, MA) syringe pump was used to deliver 1:1 methanol/ H_2O (v/v) containing 0.1% triethylamine at 10 $\mu\text{L}/\text{min}$ to the mass spectrometer. All solvents used were HPLC grade and were obtained from Fisher Scientific (Fair Lawn, NJ). Data were acquired at 5 ms dwell, 0.1 step size between m/z 350 and 2000. The spectra were averaged across the entire sample plug, and background was subtracted. The instrument was calibrated using a 2 $\mu\text{g}/\mu\text{L}$ NaI solution. At least three charge states were used to determine the reported weights. The deviation reported is the error associated with the molecular weight calculation using several charge states. Transformation of the raw data was accomplished using MaxEnt, included in the MassLynx software from Fisons.

RESULTS AND DISCUSSION

Synthesis of Oligonucleotide Conjugates. A variety of oligonucleotide-PEG conjugates have been prepared in good yields using automated synthesis. The more efficient approach involved preparing the desired monohydroxy-PEG compound, converting it to the phosphoramidite, and coupling it to the oligonucleotide using a modified automated synthesis reaction cycle. This strategy resulted in good yields of HPLC-purified PEG-2000 (average M_n of ≈ 2000)-oligonucleotide conjugates as determined by UV quantitation. Crucial to obtaining reasonable yields were the support, coupling times, and repetitive coupling procedure. Yields were found to be lower with CPG supports than with polystyrene resins. In addition, CPG yields were highly dependent on pore size, with 2000 \AA supports giving the best yields. Increasing the coupling time to 45 min and including an

Table 1. Functionalized Polyethylene Glycol–Oligodeoxyribonucleotide Conjugates Studied, Their Calculated Molecular Weights, and Their Measured Molecular Weights as Determined by ESMS

$\text{R}-\text{CH}_2-\text{CH}_2-(\text{O}-\text{CH}_2-\text{CH}_2)_n-\text{OH}$				
compound	R	n	calculated MW	measured MW
1	$\text{H}_2\text{N}-$	50	5323.4	5324.2 ± 0.3
2	$\text{H}_2\text{N}-$	50	5469.4	5468.3 ± 0.3
3		43	5139.2	5140.2 ± 0.9
4		43	5241.2	5240.5 ± 0.5
5		43	5135.2	5135.7 ± 0.2
6		42	4986.1	4986.4 ± 0.9

additional coupling step were also found to dramatically increase the yield of the conjugate.

An alternative, less efficient approach to differently functionalized PEG–oligonucleotide molecules was chemical modification of the PEG after conjugation to the 10-mer oligonucleotide. For example, the amino-PEG-2000–10-mer **1** was modified with various acylating reagents and the resulting functionalized oligonucleotide–PEG conjugate HPLC purified. Modification of the amino group generally resulted in a significant shift in the retention time, thus allowing for facile purification. However, some modifications resulted in unresolvable mixtures, in which case the MS proved invaluable to analysis of the product mixture (*vide infra*). In all cases, this approach resulted in significantly lower yields compared to yields obtained by modifying the PEG prior to automated oligonucleotide conjugation.

ESMS Analysis of Oligonucleotide Conjugates. Representative ESMS spectra for the conjugates listed in Table 1 are shown in Figure 1. The peaks fall into charge state envelopes in which each envelope consists of molecules of like charge and is spread over a range of m/z ratios due to the polydisperse nature of the PEG. The resolution of ESMS is demonstrated by the near baseline separation of peaks within an envelope, where the difference between two peaks represents one ethylene glycol unit. The smaller peaks observed within an envelope correspond to salt adducts of the parent molecule. Sample preparation is crucial to obtaining quality ESMS data. Conjugates should be purified using volatile buffers such as triethylammonium acetate or triethylammonium bicarbonate and should always be dissolved in deionized water. Contaminating cations, particularly sodium and potassium ions, can render a spectrum impossible to assign if present in high enough amounts. Undesired counterions can be exchanged using triethyl-

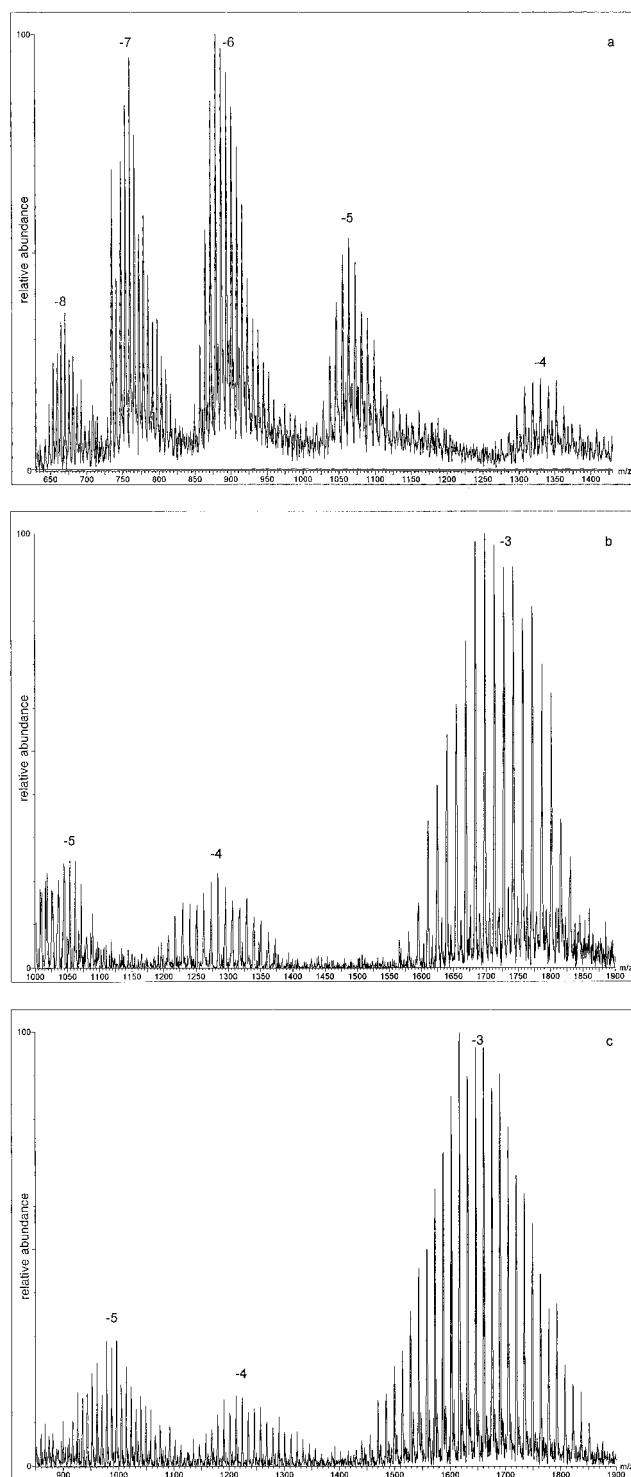


Figure 1. Representative ESMS spectra of selected oligoconjugates listed in Table 1. All data were obtained under conditions described in Experimental Procedures. Mass envelope charge states have been labeled: (a) compound **1**, (b) compound **3**, and (c) compound **5**.

ammonium buffers in either ion exchange HPLC, reverse phase HPLC, size exclusion chromatography, or dialysis.

Reconstruction of Figure 1a yielded the spectrum shown in Figure 2. Like the primary spectrum, the reconstructed spectrum shows the polydisperse nature of the PEG–oligonucleotide conjugate, but it also illustrates the accuracy of the ESMS technique. The molecular weight values listed in Table 1 agree well with the calculated molecular weights. Typically, a difference of less than 0.02% was obtained. Accuracy does not

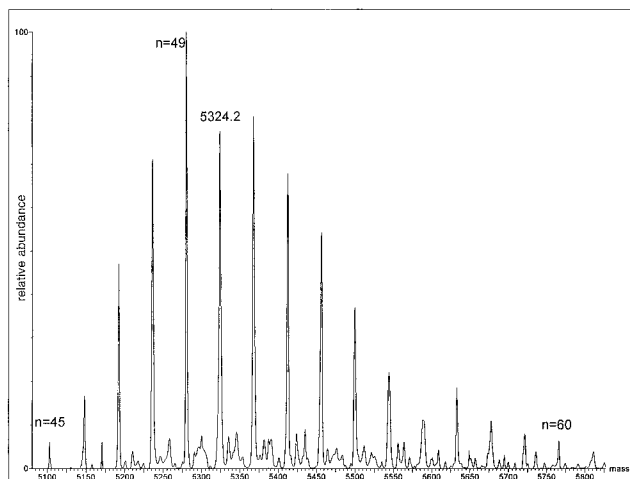


Figure 2. Reconstructed spectrum of Figure 1a. The value of n is indicated for the maximum and minimum number of polyethylene glycol units, as well as for the most abundant species. The peak corresponding to the measured molecular weight reported in Table 1 is also labeled.

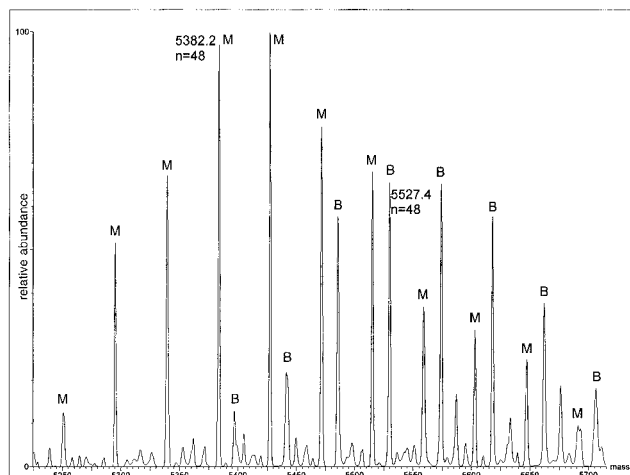


Figure 3. Reconstruction of mixture analysis data showing the mono (M) and bis (B) adduct mass envelopes. The two differently modified conjugates were the result of the derivatization of compound **1** with the NHS ester of 4-acetylbenzoic acid. The measured molecular weights for the $n = 48$, mono, and bis adducts have been labeled.

appear to be sequence dependent because ESMS analyses of oligonucleotide-PEG conjugates similar to those reported here, differing only in sequence, have generated equally accurate results (T. M. Tarasow, D. Tinnermeier, and C. Zyzanski, unpublished results). Furthermore, the resolution of ESMS provides data for the determination of oligonucleotide-PEG physical characteristics such as the range and distribution of PEG chain lengths. For example, using the reconstructed spectrum shown in Figure 2, the number of polyethylene glycol units ranges from 45 to 60 with a maximum around 49 units. These values can be easily determined for each batch of oligonucleotide conjugate to assure consistency in product and to help correlate physical differences between lots.

Figure 3 demonstrates the ability of ESMS to deconvolute chromatographically unresolvable mixtures. Modification of the amino-PEG-10-mer (**1**) with the NHS ester of 4-acetylbenzoic acid generated mono and bis addition products which were not resolvable by HPLC. Although the mass envelopes for the two products overlap, the ESMS-reconstructed spectrum was baseline resolved (Figure 3). The identity of the two components in the mixture could be assigned as the mono ($M_{r\text{-meas}} =$

5382.2 ± 0.4 , $M_{r\text{-calc}} = 5381.4$, $n = 48$) and bis ($M_{r\text{-meas}} = 5527.4 \pm 0.2$, $M_{r\text{-calc}} = 5527.4$, $n = 48$) acetophenone adducts. The synthetic modification of oligonucleotides quite often results in multiple products such as these, and while ESMS does not identify the regiochemistry of modification, it does provide data to more accurately characterize the reaction products.

Conjugation of PEG to oligonucleotides has been used to increase hydrolytic stability (16), to provide a flexible linker between oligonucleotides and other molecules (14, 25), and to purify oligonucleotides (26). While the utility of oligonucleotide-PEG conjugation is obvious, the characterization of the reaction products has been incomplete. The polymeric nature of PEG introduces additional analytical hurdles. Mass spectrometry techniques such as MALDI are less than ideal for the analysis of oligonucleotide-PEG conjugates with high degrees of polymerization ($n > 30$) due to poor resolution between MS peaks (16, 18). We have shown ES-quadrupole MS to be a valuable tool for the accurate and resolute analysis of a variety of highly polymerized, functionalized oligonucleotide-PEG conjugates. We anticipate that this technique will be widely applicable to the analysis of other polymer-modified oligonucleotides as well. In the future, the concept may even be extended to collision-induced dissociation ESMS/MS experiments (23) in which more detailed structural data of synthetically modified oligonucleotides may be obtained.

ACKNOWLEDGMENT

The authors thank Pamela Crain, James McCloskey, Bruce Eaton, and Russ Lehrman for thoughtful discussions and suggestions.

LITERATURE CITED

- (1) Gold, L. (1995) Oligonucleotides as Research, Diagnostic, and Therapeutic Agents. *J. Biol. Chem.* 270, 13581–13584.
- (2) Stein, C. A., and Cheng, Y.-C. (1993) Antisense Oligonucleotides as Therapeutic Agents-Is the Bullet Really Magical? *Science* 261, 1004–1012.
- (3) Uhlmann, E., and Peyman, A. (1990) Antisense Oligonucleotides: A New Therapeutic Principle. *Chem. Rev.* 90, 543–583.
- (4) Ohkawa, J., Koguma, T., Kohda, T., and Taira, K. (1995) Ribozymes: From Mechanistic Studies to Applications *In Vivo*. *J. Biochem.* 118, 251–258.
- (5) Gold, L., Polisky, B., Uhlenbeck, O., and Yarus, M. (1995) Diversity of Oligonucleotide Functions. *Annu. Rev. Biochem.* 64, 763–797.
- (6) Klug, S. J., and Famulok, M. (1994) All you wanted to know about SELEX. *Mol. Biol. Rep.* 20, 97–107.
- (7) Goodchild, J. (1990) Conjugates of Oligonucleotides and Modified Oligonucleotides: A Review of Their Synthesis and Properties. *Bioconjugate Chem.* 1, 165–187.
- (8) Wang, S., Lee, R. J., Cauchon, G., Gorenstein, D. G., and Low, P. S. (1995) Delivery of antisense oligodeoxynucleotides against the human epidermal growth factor receptor into cultured KB cells with liposomes conjugated to folate via polyethylene glycol. *Proc. Natl. Acad. Sci. U.S.A.* 92, 3318–3322.
- (9) Manoharan, M., Tivel, K. L., Andrade, L. K., Mohan, V., Condon, T. P., Bennett, C. F., and Cook, P. D. (1995) Oligonucleotide conjugates: alteration of the pharmacokinetic properties of antisense agents. *Nucleosides Nucleotides* 14, 969–973.
- (10) Reed, M. W., Adams, A. D., Nelson, J. S., and Meyer, R. B., Jr. (1991) Acridine- and cholesterol-derivatized solid supports for improved synthesis of 3'-modified oligonucleotides. *Bioconjugate Chem.* 2, 217–225.
- (11) Shea, R. G., Marsters, J. C., and Bischoffberger, N. (1990) Synthesis, hybridization properties and antiviral activity of lipid-oligodeoxynucleotide conjugates. *Nucleic Acids Res.* 18, 3777–3783.

- (12) Vinogradov, S. V., Suzdaltseva, Y. G., and Kabanov, A. V. (1996) Block Polycationic Oligonucleotide Derivative: Synthesis and Inhibition of Herpes Virus Reproduction. *Bioconjugate Chem.* 7, 3–6.
- (13) Lemaitre, M., Bayard, B., and Lebleu, B. (1987) Specific antiviral activity of a poly(L-lysine)-conjugated oligodeoxyribonucleotide sequence complementary to vesicular stomatitis virus N protein mRNA initiation site. *Proc. Natl. Acad. Sci. U.S.A.* 84, 648–652.
- (14) Jones, D. S., Hachmann, J. P., Osgood, S. A., Hayag, M. S., Barstad, P. A., Iverson, G. M., and Coutts, S. M. (1994) Conjugates of Double-Stranded Oligonucleotides with Poly(ethylene glycol) and Keyhole Limpet Hemocyanin: A Model for Treating Systemic Lupus Erythematosus. *Bioconjugate Chem.* 5, 390–399.
- (15) Jaschke, A., Furste, J. P., Cech, D., and Erdmann, V. A. (1993) Automated Incorporation of Polyethylene Glycol into Synthetic Oligonucleotides. *Tetrahedron Lett.* 34, 301–304.
- (16) Jaschke, A., Furste, J. P., Nordhoff, E., Hillenkamp, F., Cech, D., and Erdmann, V. A. (1994) Synthesis and properties of oligodeoxyribonucleotide-polyethylene glycol conjugates. *Nucleic Acids Res.* 22, 4810–4817.
- (17) Burlingame, A. L., Boyd, R. K., and Gaskell, S. J. (1996) Mass Spectrometry. *Anal. Chem.* 68, 599–651.
- (18) Jaschke, A., Bald, R., Nordhoff, E., Hillenkamp, F., Cech, D., Erdmann, V. A., and Furste, J. P. (1996) Synthesis and Analytical Characterization of RNA-Polyethylene Glycol Conjugates. *Nucleosides Nucleotides* 15, 1519–1529.
- (19) Fenn, J. B., Mann, M., Meng, C. K., Wong, S. F., and Whitehouse, C. M. (1989) Electrospray Ionization for Mass Spectrometry of Large Biomolecules. *Science* 246, 64–71.
- (20) Smith, R. D., Loo, J. A., Edmonds, C. G., Barinaga, C. J., and Udseth, H. R. (1990) New Developments in Biochemical Mass Spectrometry: Electrospray Ionization. *Anal. Chem.* 62, 882–899.
- (21) Bennet, K. L.; Smith, S. V., Lambrecht, R. M., Truscott, R. J. W., and Sheil, M. M. (1996) Rapid Characterization of Chemically-Modified Proteins by Electrospray Mass Spectrometry. *Bioconjugate Chem.* 7, 16–22.
- (22) Przybylski, M., and Glocker, M. O. (1996) Electrospray mass spectrometry of biomacromolecular complexes with noncovalent interactions—new analytical perspectives for supramolecular chemistry and molecular recognition processes. *Angew. Chem., Int. Ed. Engl.* 35, 806–826.
- (23) Ni, J., Pomerantz, S. C., Rozenski, J., Zhang, Y., and McCloskey, J. A. (1996) Interpretation of Oligonucleotide Mass Spectra for Determination of Sequence Using Electrospray Ionization and Tandem Mass Spectrometry. *Anal. Chem.* 68, 1989–1999.
- (24) Little, D. P., and McLafferty, F. W. (1995) Sequencing 50-mer DNAs Using Electrospray Tandem Mass Spectroscopy and Complementary Fragmentation Methods. *J. Am. Chem. Soc.* 117, 6783–6784.
- (25) Durand, M., Chevrier, K., Chassignol, M., Thuong, N. T., and Maurizot, J. C. (1990) Circular dichroism studies of an oligodeoxyribonucleotide containing a hairpin loop made of a hexaethylene glycol chain: conformation and stability. *Nucleic Acids Res.* 18, 6353–6359.
- (26) Jaschke, A., Furste, J. P., Erdmann, V. A., and Cech, D. (1994) Hybridization-based affinity partitioning of nucleic acids using PEG-coupled oligonucleotides. *Nucleic Acids Res.* 22, 1880–1884.

BC960082+

Determination of the Extent of Protein Biotinylation by Fluorescence Binding Assay

Srivatsa V. Rao,[†] Kimberly W. Anderson,^{*,†} and Leonidas G. Bachas^{*,‡}

Department of Chemical and Materials Engineering and Department of Chemistry, University of Kentucky, Lexington, Kentucky 40506. Received June 30, 1996[⊗]

A method was developed to determine the total amount of biotin present in biotinylated protein conjugates. Conjugates of bovine serum albumin, alkaline phosphatase, and horseradish peroxidase were used in this case study. The extent of biotinylation was determined by complete acid hydrolysis or by enzymatic digestion using proteinase K to release biotin from the biotinylated proteins, followed by sensitive detection of biotin using a coupled HPLC–binding assay system. This detection system is based on the enhancement of the fluorescence of streptavidin-FITC by biotin. The extent of biotinylation determined by this method was compared with the values obtained by a conventional colorimetric method that is based on the displacement of the dye 4-hydroxyazobenzene-2-carboxylic acid (HABA) from the binding sites of avidin. It was found that, because the described method determines the amount of liberated biotin after hydrolysis, it does not suffer from steric hindrance problems associated with the ability of biotin on a protein surface to displace HABA from avidin. Therefore, this method can provide a more accurate determination of the extent of biotinylation. It was also determined that the acid hydrolysis of the biotinylated protein was more effective in releasing the conjugated biotin compared to enzymatic digestion by proteinase K.

INTRODUCTION

Biotin has an extraordinarily high affinity for (strept-)avidin with reported dissociation constants of $\sim 10^{-15}$ and $\sim 10^{-14}$ M for avidin and streptavidin, respectively (Green, 1990). Each (strept)avidin molecule has four binding sites that can bind biotin and biotinylated compounds. Further, a variety of biotinylating reagents are commercially available that can be used to attach biotin to proteins, nucleic acids, carbohydrates, and other biomolecules with relative ease (Wilchek and Bayer, 1990). This has led to an explosive growth in the use of biotin–(strept)avidin systems in various biotechnological, analytical, and therapeutical applications (Diamandis and Christopoulos, 1991; Wilchek and Bayer, 1988).

Biotinylation of proteins is generally achieved by an amidation reaction in which the free amino groups on lysine residues and the N terminus of proteins are reacted with an activated biotin derivative that is typically an *N*-hydroxysuccinimide (NHS) ester (Bayer and Wilchek, 1990). Sometimes, derivatives that introduce a spacer between the biotin and the protein surface are used to increase the accessibility of biotin toward (strept-)avidin (Barbarakis et al., 1993a). Knowledge of the degree of biotinylation is of importance in the characterization of biotinylated proteins for use in optimized binding assays, bioreactors, and biosensors.

Currently known methods for determining the extent of biotinylation of proteins can be broadly grouped into two categories: those that measure the accessible biotin on the protein, and those that measure the total biotinylation. 4-Hydroxyazobenzene-2-carboxylic acid (HABA) titration is one of the most commonly used methods to determine the extent of biotinylation (Bayer and Wilchek, 1990). In this case, HABA binds to avidin to give an absorption maximum at 500 nm. When biotin or biotin-

ylated proteins are added, biotin displaces HABA from avidin and the absorbance at 500 nm is reduced. The decrease in absorbance is then used to determine the extent of biotinylation. Because this method is based on an absorbance measurement, HABA titration suffers from low sensitivity. As a result, amounts typically in the order of several nanomoles of protein are required for the determination of the degree of biotinylation. More sensitive methods for biotin determination should reduce the amount of biotinylated protein sacrificed for this purpose.

Der-Bailian et al. (1990) developed a method to determine the degree of biotinylation that is based on quenching of the natural fluorescence of avidin by biotin moieties on the biotinylated protein. This method, though simple, sensitive, and reproducible, suffers from steric hindrance effects (i.e., not all biotin on a protein can simultaneously bind to avidin) and thus underestimates the extent of biotinylation. Shah et al. (1994) have developed a different method that is based on the competition between fluorescein-labeled biotin and the biotinylated protein toward an anti-biotin monoclonal antibody. The fluorescence polarization of the fluorescein-labeled biotin was measured and correlated to the extent of biotinylation. This method also suffers from steric hindrance effects that lead to underestimation of the extent of biotinylation. However, the two techniques mentioned above may be useful in determining the amount of functional (i.e., available for binding) biotins on proteins, although there still may be some questions raised about the proper calibration of the methods; that is, biotin cannot be used as a standard in these assays because it may induce a different fluorescence signal than the biotinylated protein (Mei et al., 1994). Smith et al. (1991) have reported a different method for the determination of the degree of protein biotinylation. This requires biotinylation with an ϵ -aminohexanoic acid derivative of biotin. After acid hydrolysis, amino acid analysis yields the number of aminohexanoic acids per protein, which is equal to the degree of biotinylation of the protein. This method has picomolar sensitivity, but can be used only if the bio-

* Authors to whom correspondence should be addressed.

[†] Department of Chemical and Materials Engineering.

[‡] Department of Chemistry.

[⊗] Abstract published in *Advance ACS Abstracts*, December 15, 1996.

tinylated residue has incorporated an ϵ -aminohexanoic acid spacer arm. Consequently, despite the extensive use of biotinylated proteins in a variety of applications, the literature on their characterization is sparse (Kurosky et al., 1993; Miles and Garcia, 1995; Miller et al., 1994; Yem et al., 1989), especially in terms of a general method that determines the total number of biotin moieties attached per protein molecule. Therefore, it is desirable to develop a new method that allows the accurate determination of the degree of biotinylation.

In this paper, we describe a method developed in our laboratory for the determination of the amount of biotin present in biotinylated proteins. This method is based on the complete acid hydrolysis of the biotinylated protein, followed by separation of the released biotin by HPLC, and determination of the amount of biotin present using a highly sensitive postcolumn reaction detection system that is based on a fluorescence binding assay. This method was also compared to an alternative hydrolysis approach that involved enzymatic digestion of the biotinylated protein using proteinase K.

EXPERIMENTAL PROCEDURES

Reagents. Biotin, horseradish peroxidase (HRP) type VIA, biotinylated bovine serum albumin (b-BSA), biotinamidocaproyl-labeled bovine serum albumin (bcap-BSA), biotinylated alkaline phosphatase (b-AP), avidin, *N*-hydroxysuccinimidobiotin (BNHS), sodium dodecyl sulfate (SDS), and proteinase K were all purchased from Sigma (St. Louis, MO). HABA and *N,N*-dimethylformamide (DMF) (ACS reagent grade), were obtained from Aldrich (Milwaukee, WI). Tris[hydroxymethyl]aminomethane (Tris) was from Research Organics (Cleveland, OH) and ethylenediaminetetraacetic acid (EDTA) from Mallinckrodt (St. Louis, MO). Streptavidin-FITC was purchased from Vector Laboratories (Burlingame, CA). Protein concentrations were determined according to the BCA protein assay (Pierce, Rockford, IL). Deionized water (Milli Q water purification system; Millipore, Bedford, MA) was used in the preparation of all solutions.

HPLC with Postcolumn Reaction Detection. The experimental setup used in this work consisted of a Rainin (Woburn, MA) HPLC system, which was interfaced with a Macintosh computer (Apple Computer, Cupertino, CA). The system included a Rainin Rabbit solvent-delivery system and a Rheodyne (Berkeley, CA) Model 7125 injector with a 20- μ L sample loop. The samples were separated using a reversed-phase 5 μ m Microsorb C₁₈ column (250 \times 4.6 mm i.d.) (Rainin). An 80:20 (v/v) mixture of phosphate buffer, pH 7.0, and methanol was used as the mobile phase at a flow rate of 0.4 mL/min.

The effluent stream from the HPLC column was mixed with the reagent stream containing 2 mg/L streptavidin labeled with fluorescein isothiocyanate (streptavidin-FITC) prepared by diluting a stock solution (purchased as 1 mg/mL solution) with 100 mM phosphate buffer, pH 8.4. The reagent solution was pumped by an ISCO (Lincoln, NE) Model LC-2600 syringe pump at a flow rate of 1 mL/min and was merged with the column effluent through a tee-connector followed by a 10.0-m knitted open-tubular (KOT) reactor made from PTFE tubing (0.5 mm i. d., 14-mm helix diameter) (Przyjazny et al., 1993). The binding of biotin to streptavidin-FITC resulted in an enhancement of fluorescence intensity (Hentz and Bachas, 1995). Detection of the change in fluorescence was carried out by using a Fluorolog-2 spectrofluorometer (SPEX Industries, Edison, NJ) with a μ -fluorescence flow cell (20- μ L cell volume; NSG Precision Cells, Farmingdale, NY). The excitation was set at 495 nm, and the

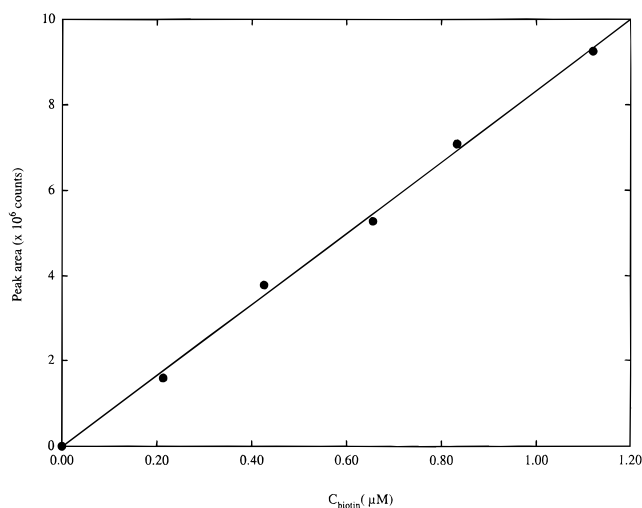


Figure 1. Calibration plot for biotin using the streptavidin-FITC-based postcolumn reaction detection system.

emission was monitored at 518 nm. The excitation and emission slit widths were each set at 2 nm. The SPEX spectrofluorometer was operated in the photon-counting mode. A calibration plot for biotin was prepared daily using biotin standards, and the corresponding peak areas were employed to estimate the amount of biotin present in each of the samples. A typical calibration plot is given in Figure 1.

Biotinylation of HRP. For the preparation of biotinylated HRP (b-HRP), HRP was dissolved in 100 mM sodium hydrogen carbonate solution, adjusted to pH 8, to obtain a 10 mg/mL solution. Sufficient volume of a BNHS solution (100 mM BNHS in DMF) was added to 100 μ L of an HRP solution to achieve an initial molar ratio of BNHS to HRP of 100. The biotinylation reaction was carried out in Reactivials (Pierce) for 3 h at room temperature. The reaction mixture was then dialyzed against phosphate buffer saline to remove unreacted BNHS.

Acid Hydrolysis of Biotinylated Proteins. The biotinylated proteins were hydrolyzed with 6 M HCl in an evacuated vacuole at 110 °C for 18–24 h and dried in a vacuum centrifuge (Savant Instruments, Hickville, NY). The samples were then dissolved in a known amount of deionized water and analyzed for the amount of biotin present.

Enzymatic Digestion of Biotinylated Proteins. The biotinylated proteins were digested with proteinase K and dissolved in 100 mM Tris-HCl buffer, pH 7.8, containing 5 mM EDTA and 0.5% (v/v) SDS. The molar ratio of proteinase K to biotinylated protein was 1:25 or 1:50. The digestion was carried out for 3 or 24 h at 37 °C. In all cases, the corresponding nonbiotinylated proteins were also processed under similar conditions and used as control samples. The digestion reaction was terminated by boiling the reaction mixture for 15 min. The samples were then used for biotin determination.

RESULTS AND DISCUSSION

The HABA titration method provides an estimate of the accessible biotin but not the true extent of biotinylation of a protein, because some of the biotin moieties on the protein may not be accessible for binding to avidin as shown in Figure 2. In scenario A, where both the biotins are accessible to avidin, the HABA titration gives an accurate value of the extent of biotinylation. However, erroneous results may be obtained with highly biotinylated proteins because of possible cross-linking between

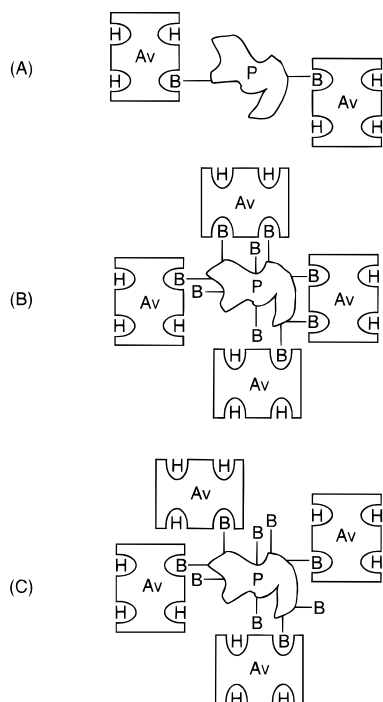


Figure 2. Depending on the nature of biotinylated protein, the HABA titration may give erroneous results: (A) degree of biotinylation is 2 as determined by HABA titration; (B) degree of biotinylation is determined to be 6; (C) degree of biotinylation is determined to be 4 for the same conjugate as in (B). Av, B, P, and H represent avidin, biotin, protein, and HABA, respectively.

avidin and biotinylated protein molecules (as a result of the availability of four binding sites on avidin) and/or steric hindrance effects, all of which may prohibit some of the biotin moieties on the surface of the protein from binding to avidin. The effect of steric hindrance is illustrated in Figure 2 (parts B and C), where for the same conjugate the accessible biotin in scenario B is 6 and in C is 4. This is also true for other assays that are based on the interaction between the biotinylated protein and avidin, streptavidin, or anti-biotin antibodies (Der-Bailian et al., 1990; Shah et al., 1994). Therefore, the HABA titration and the other methods that use intact biotinylated protein typically underestimate the extent of biotinylation and may not even be accurate at calculating the functional biotins on the protein molecule because of steric/cross-linking effects. Further, as mentioned earlier, additional questions may be raised about the ability of some of these methods to determine the degree of functional biotin on proteins, because free biotin and biotinylated protein have a different effect on the intrinsic fluorescence of avidin (Mei et al., 1994).

Bayer and Wilchek (1990) have reported that one of the ways to circumvent the problems described above is to digest the biotinylated protein with proteinase K and determine the amount of free biotin released. This should give the true degree of biotinylation. As demonstrated in the present study (*vide infra*) and depending on the protein, the enzymatic digestion may lead to incomplete hydrolysis of the biotinylated protein and thus inaccurate results.

To determine the total number of biotin moieties attached per protein molecule, a highly sensitive method was developed in our laboratory, which is based on complete hydrolysis of the biotinylated protein followed by a fluorescence binding assay that monitors the enhancement of fluorescence of streptavidin-FITC by biotin. Complete hydrolysis of the protein is necessary because biotin and biotinylated peptides could induce different

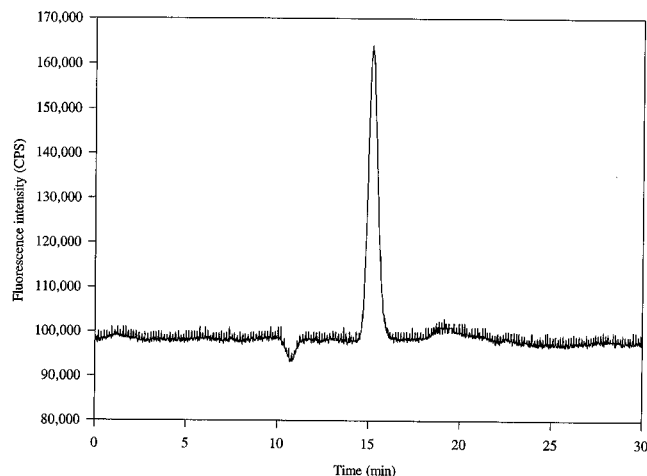


Figure 3. Separation and detection of free biotin released by a 24-h proteinase K digestion from b-HRP (moles of b-HRP/mole of proteinase K = 25).

fluorescence enhancement to streptavidin-FITC (Barbarakis et al., 1993b), which may give erroneous results for the degree of biotinylation. By coupling a postcolumn reaction detection system based on this fluorescence binding assay to a HPLC separation, it is possible to verify the complete hydrolysis of the protein. It should be noted that the method has no interferences from amino acids that are not biotinylated, because these compounds do not induce a change in the fluorescence of streptavidin-FITC. The coupled HPLC-binding assay system also has good detection limits (4×10^{-13} mol of biotin), which reduces the amount of biotinylated protein needed for the assay.

Proteinase K digestion and acid hydrolysis were investigated as methods for the release of biotin from the biotinylated proteins. It was reported earlier that, in about 3 h, proteinase K digests protein completely (Bayer and Wilchek, 1990; Ebeling et al., 1974). It was found, however, that 3 h was not enough to completely digest b-HRP, and therefore longer digestion times were used for this purpose. The chromatogram of the digest after a 24-h hydrolysis with proteinase K is shown in Figure 3, where biotin elutes out at 15.2 min (the hold-up time is 10.8 min). These data, in conjunction with a calibration plot for biotin (see Experimental Procedures), were used to calculate the extent of biotinylation, which was found to be 1.8 biotins per HRP molecule. Given that biotinylation was performed with a 100-fold excess of BNHS, this value of the degree of biotinylation is consistent with previous observations reporting that only 2 of the 7 amino groups of HRP (6 lysines and the N terminus) are accessible for modification by NHS esters (Paek et al., 1993; Zaitsev et al., 1992). The small peak at ~19 min is most probably due to a biotinylated peptide and suggests incomplete hydrolysis of b-HRP even after a 24-h digestion with proteinase K. As anticipated, the chromatograms corresponding to the hydrolysis product of the nonbiotinylated proteins had no peaks, which indicates the selective nature of the postcolumn reaction detection system used toward the biotin moiety.

As shown in Figure 3, prolonged digestion of b-HRP with proteinase K does not always give complete hydrolysis. This is more pronounced in Figure 4, which shows the chromatogram obtained when b-BSA was digested for 3 h with proteinase K in amounts that were 25-fold less than b-BSA on a mole-to-mole basis. The additional peaks at retention times longer than that of biotin (biotin elutes at ~15 min) indicate that the hydrolysis of the protein was incomplete. It should be mentioned that the

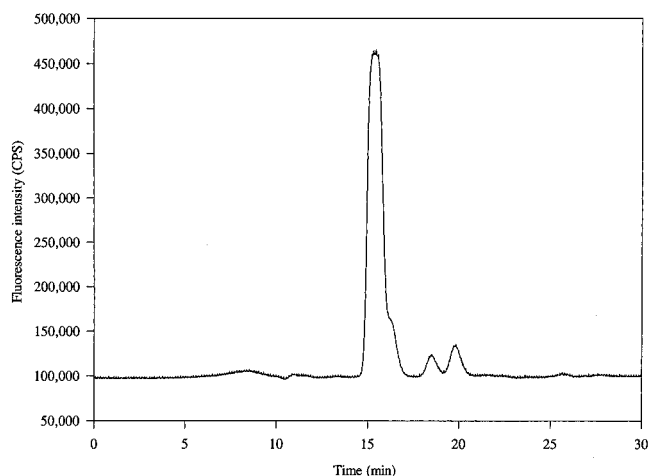


Figure 4. Separation and detection of free biotin released by a 3-h proteinase K digestion from b-BSA (moles of b-BSA/mole of proteinase K = 25).

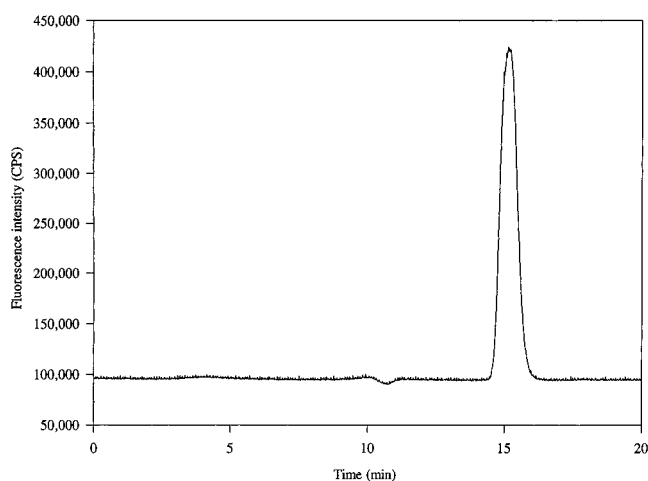


Figure 5. Separation and detection of acid-hydrolyzed b-BSA.

postcolumn reaction detection system used is highly selective and only detects biotin or biotinylated compounds. Thus, the additional peaks at 18.4 and 19.8 min are most probably due to biotinylated peptides. It was also found that the amount of proteinase K plays a role in the extent of hydrolysis and that an increase in the amount of proteinase K used causes an increase in the amount of biotin released. However, it was not possible to eliminate the additional chromatographic peaks by altering the amount of proteinase K used and/or the digestion time. The additional peaks were persistent even after 24 h of digestion with proteinase K. Therefore, proteinase K is not the ideal reagent to cause complete release of biotin, and this was verified as shown in Figure 4 by using the coupled HPLC–fluorescence system.

Hydrolysis of proteins with concentrated HCl is commonly used to achieve complete digestion of proteins prior to amino acid analysis. Given the shortcomings of the proteinase K digestion, acid hydrolysis in evacuated vacuoles was performed on b-BSA, b-HRP, and b-AP. When b-BSA, b-HRP, and b-AP were analyzed for biotin, the chromatograms showed a single peak due to biotin. Figure 5 depicts a typical chromatogram of an acid-hydrolyzed biotinylated protein. The values of the degree of biotinylation obtained by this method are higher than those determined by HABA titration (Table 1). The HABA titration gave degrees of biotinylation of 8.6 for b-BSA and 1.9 for b-HRP, while it was found by the method described above using acid hydrolysis combined with fluorescence binding assay that the ratios of (moles

Table 1. Comparison of Different Methods Used To Estimate the Extent of Biotinylation of b-HRP and b-BSA

method of determination	b-HRP	b-BSA
HABA titration	1.9	8.6
after enzymatic digestion with proteinase K, 3 h	0.8	10.1
after enzymatic digestion with proteinase K, 24 h	1.8	10.4
after acid hydrolysis	1.9	11.8

of biotin)/(mole of b-BSA) were 11.8 and 1.9, respectively. In the case of biotinylated alkaline phosphatase the chromatogram of the acid-hydrolyzed product also showed a single peak that corresponds to biotin. From these data the degree of biotinylation was estimated to be 6.2, while the enzymatically digested sample of the same conjugate gave a degree of biotinylation of 4.5.

Because it is based on the determination of the amount of free biotin released from a biotinylated conjugate, the proposed method does not suffer from the bane of steric hindrance. Biotin and biotinylated analogs when reacted with streptavidin-FITC enhance the fluorescence intensity by different amounts (Barbarakis et al., 1993b). Therefore, complete hydrolysis, as reflected in a single peak for free biotin when using the HPLC–fluorescence detection method, is important for the accurate determination of biotin present and, thus, the degree of biotinylation. In the case of enzymatic digestion, the digest contains a few biotinylated peptides along with the released free biotin (e.g., see Figure 4). Therefore, enzymatic digestion does not provide accurate results.

Biotinylating reagents that incorporate a spacer arm between biotin and the protein have also been used to reduce steric hindrance in the interaction with strept(avidin) (Barbarakis et al., 1992; Wilchek and Bayer, 1990). In that regard, a conjugate of BSA with a long-chain biotin derivative (bcap-BSA) was studied to compare the proposed method with the HABA titration. The HABA titration gave a degree of biotinylation of 10.9, while the acid hydrolysis followed by the HPLC–fluorescence detection gave a degree of biotinylation of 12.2. Thus, the HABA titration underestimates the degree of biotinylation of b-BSA (data discussed above) and bcap-BSA by 27% and 9.9%, respectively. The HABA titration has less relative error with bcap-BSA than with b-BSA, which is not surprising given the presence of the spacer arm between biotin and BSA. This allows for better accessibility of the attached biotin to avidin. However, even in bcap-BSA there are still on average 1.3 biotins per BSA molecule that are sterically hindered from binding to avidin. Complete acid hydrolysis of bcap-BSA, on the other hand, provides the total amount of biotin conjugated to the protein.

In conclusion, the method described in this paper is able to give an accurate estimation of the degree of biotinylation. The method has an excellent detection limit of 2×10^{-8} M for biotin. The acid hydrolysis to release biotin is superior to enzymatic digestion as it leads to complete hydrolysis of the protein. The enzymatic digestion is dependent on the amount of proteinase K used and the time of digestion. The currently described method should pose no problems when the degree of biotinylation of proteins prepared by using BNHS or longer chain esters of NHS is determined.

ACKNOWLEDGMENT

This work was supported by grants from the National Science Foundation and the Department of Energy. We thank Michael Russ, from the Macromolecular Structure Analysis Facility, for acid hydrolysis of proteins.

LITERATURE CITED

- Barbarakis, M. S., Daunert, S., and Bachas, L. G. (1992) Effect of Different Binding Proteins on the Detection Limits and Sensitivity of Assays Based on Biotinylated Adenosine Deaminase. *Bioconjugate Chem.* 3, 225–229.
- Barbarakis, M. S., Qaisi, W. G., Daunert, S., and Bachas, L. G. (1993a) Observation of "Hook Effects" in the Inhibition and Dose-Response Curves of Biotin Assays Based on the Interaction of Biotinylated Glucose Oxidase with Strept(avidin). *Anal. Chem.* 65, 457–460.
- Barbarakis, M. S., Smith-Palmer, T., Bachas, L. G., Chen, S., and Van Der Meer, W. (1993b) Enhancement of the Emission Intensity of Fluorescence-Labeled Avidin by Biotin and Biotin Derivatives. Evaluation of Different Fluorophores for Improved Sensitivity. *Talanta* 40, 1139–1145.
- Bayer, E. A., and Wilchek, M. (1990) Protein Biotinylation. *Methods Enzymol.* 184, 138–160.
- Der-Bailian, G. P., Gomez, B., Masino, R. S., and Parce, J. W. (1990) A Fluorometric Method for Determining the Degree of Biotinylation of Proteins. *J. Immunol. Methods* 126, 281–285.
- Diamandis, E. P., and Christopoulos, T. K. (1991) The Biotin-(Strept)avidin System, Principles and Applications in Biotechnology. *Clin. Chem.* 37, 625–636.
- Ebeling, W., Hennrich, N., Klockow, M., Metz, H., Orth, H. D., and Lang, H. (1974) Proteinase K from *Tritirachium album* Limber. *Eur. J. Biochem.* 47, 91–97.
- Green, N. M. (1990) Avidin and Streptavidin. *Methods Enzymol.* 184, 51–67.
- Hentz, N. G., and Bachas, L. G. (1995) Class-Selective Detection System for Liquid Chromatography Based on the Streptavidin-Biotin Interaction. *Anal. Chem.* 67, 1014–1018.
- Kurosky, A., Miller, B. T., and Knock, S. L. (1993) Kinetic Analysis of Biotinylation of Specific Residues of Peptides by High-Performance Chromatography. *J. Chromatogr.* 631, 281–287.
- Mei, G., Pugliese, L., Rostao, N., Toma, L., Bolognesi, M., and Finazzi-Agró, A. (1994) Biotin and Biotin Analogues Specifically Modify the Fluorescence Decay of Avidin. *J. Mol. Biol.* 242, 539–565.
- Miles, D., and Garcia, A. (1995) Separation of Biotin Labeled Proteins from Their Unlabeled Counterparts Using Immobilized Platinum Affinity Chromatography. *J. Chromatogr.* 702, 173–189.
- Miller, B. T., Rogers, E. M., Smith, J. S., and Kurosky, A. (1994) Identification and Characterization of O-Biotinylated Hydroxy Amino Acid Residues in Peptides. *Anal. Biochem.* 219, 240–248.
- Paek, S., Bachas, L. G., and Schramm, W. (1993) Defined Analyte-Enzyme Conjugates as Signal Generators in Immunoassays. *Anal. Biochem.* 210, 145–154.
- Przyjazny, A., Hentz, N. G., and Bachas, L. G. (1993) Sensitive and Selective Liquid Chromatographic Postcolumn Reaction Detection System for Biotin and Biocytin Using a Homogeneous Fluorescence-Linked Assay. *J. Chromatogr.* 654, 79–86.
- Shah, D., Salbilla, V., Richerson, R., and Brown III, W. (1994) Determination of Biotin in Biotin-Conjugated Protein by Measuring Fluorescence Polarization. *Clin. Chem.* 40, 2112–2113.
- Smith, J. S., Miller, B. T., Knock, S. L., and Kurosky, A. (1991) Biotinylated Peptides/Proteins. *Anal. Biochem.* 197, 247–253.
- Wilchek, M., and Bayer, E. A. (1988) The Avidin-Biotin Complex in Bioanalytical Applications. *Anal. Biochem.* 171, 1–32.
- Wilchek, M., and Bayer, E. A. (1990) Biotin-Containing Reagents. *Methods Enzymol.* 184, 123–138.
- Yem, A. W., Zurcher-Neely, H. A., Richard, K. A., Staite, N. D., Heinrichson, R. L., and Deibel, M. R. (1989) Biotinylation of Reactive Amino Groups in Native Recombinant Human Interleukin-1 β . *J. Biol. Chem.* 264, 17691–17697.
- Zaitzu K, Ohnishi, M., Nanami M., and Ohkura, Y. (1992) Evaluation of the Numbers of Functional Groups Introduced into Horseradish Peroxidase in Reactions with Four Heterobifunctional Reagents. *Chem. Pharm. Bull.* 40, 2205–2207.

BC960080P

COMMUNICATIONS

Synthesis of Oligonucleotides Containing 3'-Alkylcarboxylic Acids Using a Palladium Labile Oligonucleotide Solid Phase Synthesis Support

Tracy J. Matray, Dong Jin Yoo, Dustin L. McMin, and Marc M. Greenberg*

Department of Chemistry, Colorado State University, Fort Collins, Colorado 80523. Received October 31, 1996[®]

Oligonucleotides containing a 3'-alkylcarboxylic acid are isolated using a Pd(0)-catalyzed cleavage reaction, in yields that are in most cases within experimental error of those isolated using standard oligonucleotide cleavage conditions (concentrated NH_4OH). In contrast to results obtained with photolabile solid phase synthesis supports, no reduction in isolated yields of the oligonucleotides is observed when their length is increased from 20 to 40 nucleotides. The oligonucleotides are characterized by anion exchange HPLC, electrospray mass spectrometry, and enzymatic digestion. When methyl phosphoramidites are employed in the synthesis of the biopolymers, **3** serves as an orthogonal solid phase oligonucleotide synthesis support.

Solid phase oligonucleotide synthesis has advanced to a very efficient state. Scientists working with nucleic acids now have a wide variety of methodologies available for preparing native oligonucleotides, as well as biopolymers containing modified backbones, nucleobases, and sugars (1). These recent advances in solid phase synthesis have led to strategies for the synthesis of oligonucleotide conjugates (2–5). Both naturally occurring and synthetic oligonucleotide conjugates show promise as therapeutic agents and diagnostic probes. For example, it has been shown that oligonucleotide bioconjugates can facilitate the transport of potential antisense agents through cell membranes (6–8). The methodology for synthesizing bioconjugates, particularly those in which the covalent linkage is at the 3'-terminus of the oligonucleotide, has lagged behind the aforementioned aspects of nucleic acid synthesis (9). One approach to bioconjugate formation involves utilizing fully depro-

tected oligonucleotides as substrates. The poor solubility of such substrates in many organic solvents limits the scope of reactions that can be utilized to effect conjugation. Another difficulty associated with this method of oligonucleotide conjugate formation is attributable to side reactions occurring with the exocyclic amines located throughout the biopolymer (10, 11).

To ameliorate these limitations, we, and others, have suggested utilizing protected oligonucleotides (retaining their nucleobase and phosphate protecting groups) that contain a single exposed functional group as substrates for nucleic acid conjugation reactions (12–16). Before such a bioconjugation strategy is pursued, it is necessary to develop methodology for cleaving protected oligonucleotides containing a single functional group at their 3'-termini from their solid phase supports. We have previously reported on several orthogonal solid phase supports that utilize the *o*-nitrobenzyl photoredox reaction (12–14). Oligonucleotides containing 3'-hydroxy- and 3'-alkylcarboxylic acids and 3'-alkylamines have been

* Abstract published in *Advance ACS Abstracts*, February 15, 1997.

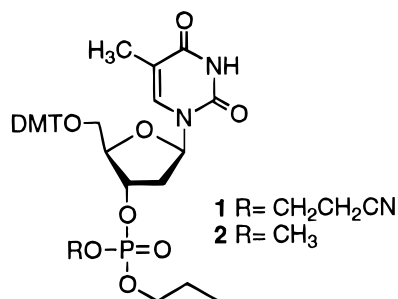
Table 1. Isolated Yields of Fully Deprotected Oligonucleotides Obtained via Pd(0)-Mediated Cleavage^a

oligo-nucleotide	phosphate protecting group	reaction time (h)	isolated yield ^b (%)
8	β -cyanoethyl	7	102 \pm 7
8	methyl	7	93 \pm 7
8	methyl	5	93 \pm 8
9	methyl	5	91 \pm 13
10	methyl	5	77 \pm 7
11	β -cyanoethyl	5	105 \pm 10

^a Pd(0) cleavage reactions were carried out as described in footnote 2. ^b Determined as described in footnote 1.

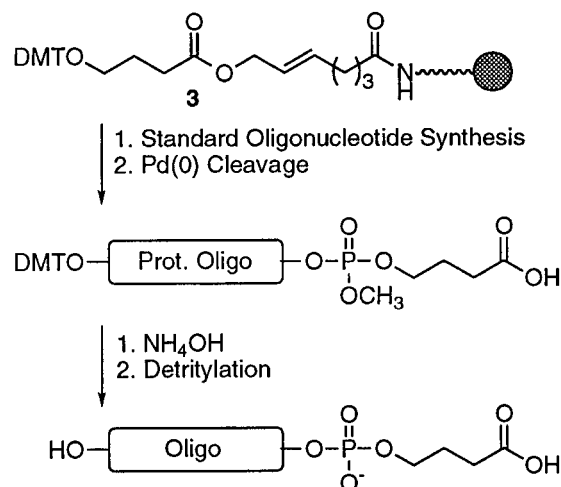
obtained using these supports. These supports are compatible with commercially available reagents and automated oligonucleotide synthesis protocols. Isolated yields as high as 98% of oligonucleotides containing photodamage below detectable limits have been obtained using commonly available irradiation sources (12, 13).¹ A shortcoming of these photolabile synthesis supports was revealed during the synthesis of longer oligonucleotides. A decrease in yield was observed as the length of the biopolymer was increased from 20 to 40 nucleotides (12). This decrease in yield was attributed to greater competition for light by the protected biopolymer with the *o*-nitrobenzyl chromophore. While yields can be increased by extending the irradiation period, this also increases the amount of photodamage. This observation prompted us to investigate an alternative reaction for the cleavage of protected oligonucleotides from solid phase supports.

In designing a new generation of orthogonal oligonucleotide synthesis supports for which the cleavage reaction would not be dependent upon biopolymer length, we chose to utilize the proven Pd(0)-catalyzed allyl transfer reaction (17–21). This reaction has been used successfully for deprotecting the exocyclic amines of nucleobases and the phosphate diesters during oligonucleotide synthesis, as well as an orthogonal linker for peptide synthesis. Prior to commencing the synthesis of an appropriate solid support, we sought to ensure that the conditions employed to cleave the allyloxy linker were orthogonal with respect to the oligonucleotide protecting groups used in commercially available reagents. The stability of amide protecting groups for the exocyclic amines was not a concern. In addition, the 5'-*O*-dimethoxytrityl group of **1** was stable to Pd₂(dba)₃·CHCl₃



and PPh₃ in *n*-BuNH₂/HCO₂H (1.2 M) between 25 and 55 °C for up to 7 h. However, contrary to assumptions in a recent paper, the β -cyanoethyl group was cleaved completely within 1 h at 55 °C under these conditions

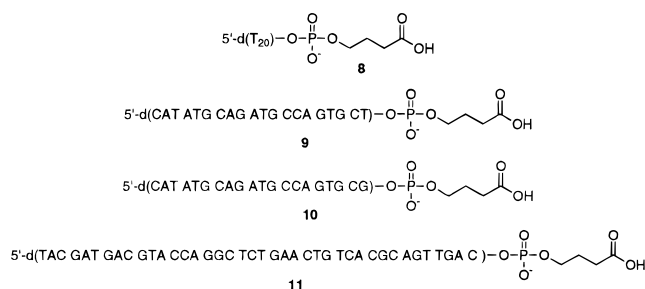
¹ Yields of oligonucleotides obtained from orthogonal solid phase supports are determined via comparison of the isolated yield of oligonucleotide obtained via Pd(0) cleavage and subsequent NH₄OH treatment versus that obtained via direct NH₄OH treatment of resin-bound oligonucleotide from the same oligonucleotide synthesis.

Scheme 1

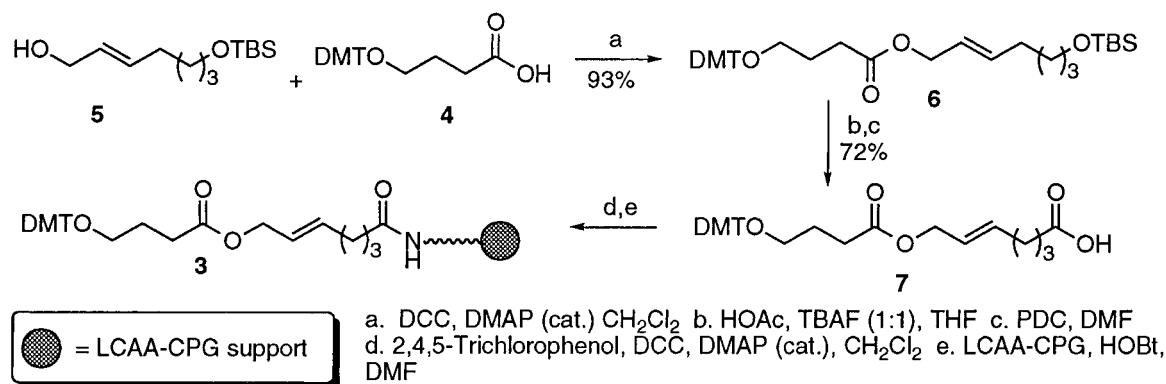
(16). This problem was alleviated using monomer **2**. The *O*-methyl phosphate triester was shown to undergo only minor (\approx 10%) decomposition over the course of 7 h at 55 °C in the presence of these reagents.

Having established the suitability of the Pd(0)-catalyzed allyl transfer reaction as the basis for an orthogonal solid phase support, **3** was designed to function as a universal solid phase synthesis support for the preparation of oligonucleotides containing 3'-alkylcarboxylic acids (Scheme 1) (14). Support **3** was rapidly assembled in a convergent manner via the coupling of previously reported **4** and **5** (Scheme 2) (14, 22). The long-chain alkylamine controlled pore glass support (LCAA-CPG) was loaded (45 μ mol/g) using the trichlorophenyl ester of **7**. Oligonucleotides were synthesized on **3** using standard oligonucleotide synthesis cycles, in which (while not necessary) the 5'-*O*-dimethoxytrityl group was removed prior to cleavage of the oligonucleotide from the support. With the exception of the substitution of *t*-BuOOH in CH₂Cl₂ for I₂ in pyridine/H₂O (to guard against iodination of the double bond), all oligonucleotide synthesis reagents used were commercially available (17).

Conditions for the cleavage of oligonucleotides from **3** were optimized utilizing the isolation of an eicosameric polythymidylate (**8**). The yields were determined for fully deprotected, gel-purified oligonucleotides.¹ Consequently, cleavage reactions could be carried out on oligonucleotides prepared using β -cyanoethyl or methyl protected phosphoramidites. Initial Pd(0)-catalyzed cleavage reactions were carried out under the conditions prescribed for the removal of phosphate and nucleobase amine protecting groups (17). To obtain tractable material, it was necessary to remove the *n*-butylamine/formic acid buffer and phosphine reagent prior to treating the cleaved oligonucleotide with NH₄OH. However, removal of the large excess of PPh₃ via trituration of the residue with hexanes proved difficult. The amorphous organic material obtained was difficult to handle, resulting in erratic yields of isolated **8**. Utilization of bis(diphen-



Scheme 2



ylphosphino)ethane (DIPHOS) in place of PPh_3 enabled us to employ only 5 equiv of phosphine ligand relative to $\text{Pd}_2(\text{dba})_3 \cdot \text{CHCl}_3$.² Subsequent workup of the protected oligonucleotide yielded a more tractable material. Yields of eicosameric polythymidylate within experimental error of those obtained via direct ammonolysis were achieved from *O*- β -cyanoethyl phosphate protected oligonucleotides after 7 h at 55 °C (Table 1).¹ Eicosameric polythymidylates containing phosphate protecting groups (*O*-methyl) that are orthogonal with regard to the Pd(0)-mediated cleavage were also isolated in quantitative yields (Table 1). Further optimization of the reaction conditions proved that 5 h was sufficient to effect complete cleavage of the oligonucleotide from the solid support.

Electrospray mass spectrometry (ESMS) proved that the alkylcarboxy group remained intact during the various deprotection and purification procedures. Only a small amount of dealkylated material was formed. We believe that the dealkylated material results from formation of the dianion during NH_4OH deprotection, followed by intramolecular displacement of the phosphate-terminated oligonucleotide. ESMS could not distinguish between the polythymidylates cleaved directly from **3** with NH_4OH and those cleaved with Pd(0), as they differ by only 1 mass unit. However, the two products are separable on anion exchange HPLC, where **8** eluted more than 1 min later than the respective amide obtained from NH_4OH treatment of resin-bound oligonucleotide.

² Typical procedure for palladium(0)-mediated cleavage of CPG-bound oligonucleotides: In a typical procedure, $\text{Pd}_2(\text{dba})_3 \cdot \text{CHCl}_3$ (0.5 mg, 0.5 μmol) was added to a mixture of the appropriate oligonucleotide that was synthesized on **3** (1 mg, $\approx 0.05 \mu\text{mol}$) and 1,2-bis(diphenylphosphino)ethane (1 mg, 2.5 μmol) in THF (170 μL , sparged with N_2 for 30 min). After addition of *n*-butylamine (18 mg, 240 μmol , sparged with N_2 for 30 min) and formic acid (11 mg, 240 μmol , sparged with N_2 for 30 min), the mixture was vortexed well and heated at 55 °C. The reaction vessel was vortexed approximately every 15–30 min. After the appropriate reaction time, the solution was transferred to a vial and concentrated *in vacuo* to give a black residue. The residue was dissolved in a 1:1 mixture (by volume) of THF/ H_2O (1 mL) and evaporated to dryness. This process was repeated a second time. The residue was then triturated with hexanes (2 \times 2 mL), dissolved in CH_3CN (1 mL), and filtered through a nylon filter (0.45 μm). The filter was washed well with CH_3CN (3 mL) and then H_2O (3 mL). All of the washings were combined and evaporated to dryness *in vacuo*. The residue was suspended in concentrated NH_4OH and heated for 10 h at 55 °C. After the NH_4OH was removed *in vacuo*, the residue was suspended in formamide loading buffer (70 μL) containing sodium *N,N*-diethyldithiocarbamic acid (30 mM) and purified by denaturing polyacrylamide gel electrophoresis (20% polyacrylamide). The oligonucleotide was extracted from the gel slice with NaCl (0.2 M) and EDTA (1 mM) and desalted using a reversed phase purification cartridge.

Using the optimized conditions for cleaving methyl phosphate protected polythymidylates, we examined the suitability of the methodology for obtaining oligonucleotides containing all four native nucleotides. We determined that the yields of oligonucleotides prepared on **3** and cleaved via Pd(0) were not strongly dependent upon sequence or length (Table 1).¹ Furthermore, enzymatic digestion of heteropolymers prepared on **3** using β -cyanoethyl phosphoramidites that were cleaved with Pd(0) reveals that no extraneous nucleosides are formed, demonstrating that the Pd(0) cleavage process does not damage the biopolymer.

In summary, we have utilized Pd(0)-catalyzed cleavage of allyl groups to cleave oligonucleotides, conjugated to alkylcarboxylic acids at their 3'-termini, from their solid phase synthesis supports in very high yield.¹ The cleavage reaction is orthogonal to commercially available *O*-methyl phosphoramidite protecting groups. This methodology should prove to be highly useful for the preparation of more elaborate oligonucleotide conjugates.

ACKNOWLEDGMENT

This research was supported by the National Science Foundation (CHE-9424040). M.M.G. is a fellow of the Alfred P. Sloan Foundation. We are grateful to Dr. Laurent Bellon (Ribozyne Pharmaceuticals Inc.) for stimulating discussion.

Supporting Information Available: Enzymatic digest of an eicosameric oligonucleotide and an electrospray mass spectrum of **8** (4 pages). Ordering information is given on any current masthead page.

LITERATURE CITED

- (1) Beaucage, S. L., and Iyer, R. P. (1993) The Synthesis of Modified Oligonucleotides by the Phosphoramidite Approach and Their Applications. *Tetrahedron* 49, 6123–6194.
- (2) Truffert, J.-C., Lorthioir, O., Asseline, U., Thuong, N. T., and Brack, A. (1994) On-Line Solid Phase Synthesis of Oligonucleotide-Peptide Hybrids Using Silica Supports. *Tetrahedron Lett.* 35, 2353–2356.
- (3) de la Torre, B. G., Aviñó, A., Tarrason, G., Piulats, J., Albericio, F., and Eritja, R. (1994) Stepwise Solid-Phase Synthesis of Oligonucleotide-Peptide Hybrids. *Tetrahedron Lett.* 35, 2733–2736.
- (4) MacKellar, C., Graham, D., Will, D. W., Burgess, S., and Brown, T. (1992) Synthesis and Physical Properties of Anti-HIV Antisense Oligonucleotides Bearing Terminal Lipophilic Groups. *Nucleic Acids Res.* 20, 3411–3417.
- (5) Haralambidis, J., Angus, K., Pownall, S., Duncan, L., Chai, M., and Tregear, G. W. (1990) The Preparation of Polyamide Oligonucleotide Probes Containing Multiple Non-Radioactive Labels. *Nucleic Acids Res.* 18, 501–505.

- (6) Jones, D. S., Hachmann, J. P., Osgood, S. A., Hayag, M. S., Barstad, P. A., Iverson, G. M., and Coutts, S. M. (1994) Conjugates of Double-Stranded Oligonucleotides With Poly-(ethylene glycol) and Keyhole Limpet Hemocyanin: A Model for Treating Systemic Lupus Erythematosus. *Bioconjugate Chem.* **5**, 390–399.
- (7) Leonetti, J-P., Degols, G., and Lebleu, B. (1990) Biological Activity of Oligonucleotide-Poly(L-lysine) Conjugates: Mechanism of Cell Uptake. *Bioconjugate Chem.* **1**, 149–153.
- (8) Letsinger, R. L., Zhang, G., Sun, D. K., Ikeuchi, T., and Sarin, P. S. (1989) Cholesteryl-Conjugated Oligonucleotides: Synthesis, Properties, and Activity as Inhibitors of Replication of Human Immunodeficiency Virus in Cell Culture. *Proc. Natl. Acad. Sci. U.S.A.* **86**, 6553–6556.
- (9) Goodchild, J. (1990) Conjugates of Oligonucleotides and Modified Oligonucleotides: A Review of Their Synthesis and Properties. *Bioconjugate Chem.* **1**, 165–187.
- (10) Ghosh, S. S., and Musso, G. F. (1987) Covalent Attachment of Oligonucleotides to Solid Supports. *Nucleic Acids Res.* **15**, 5353–5372.
- (11) Bischoff, R., Coull, J. M., and Regnier, F. E. (1987) Introduction of 5'-Terminal Functional Groups Into Synthetic Oligonucleotides For Selective Immobilization. *Anal. Biochem.* **164**, 336–344.
- (12) McMinn, D. L., and Greenberg, M. M. (1996) Novel Solid Phase Synthesis Supports For The Preparation of Oligonucleotides Containing 3'-Alkyl Amines. *Tetrahedron* **52**, 3827–3840.
- (13) Venkatesan, H., and Greenberg, M. M. (1996) Improved Utility of Photolabile Solid Phase Synthesis Supports For The Synthesis of Oligonucleotides Containing 3'-Hydroxyl Termini. *J. Org. Chem.* **61**, 525–529.
- (14) Yoo, D. J., and Greenberg, M. M. (1995) Synthesis of Oligonucleotides Containing 3'-Alkyl Carboxylic Acids Using Universal Photolabile Solid Phase Synthesis Supports. *J. Org. Chem.* **60**, 3358–3364.
- (15) Matray, T. J., Yoo, D. J., and Greenberg, M. M. (1996) Palladium Labile Oligonucleotide Synthesis Supports. *Abstracts of Papers*, 211th National Meeting of the American Chemical Society, New Orleans, LA, Division of Organic Chemistry Abstract 119, American Chemical Society, Washington, DC.
- (16) Zhang, X., and Jones, R. A. (1996) Solid-Phase Synthesis of Peptide Aminoalkylamides Using An Allyl Linker. *Tetrahedron Lett.* **37**, 3789–3790.
- (17) Hayakawa, Y., Wakabayashi, S., Kato, H., and Noyori, R. (1990) The Allylic Protection Method in Solid-Phase Oligonucleotide Synthesis. An Efficient Preparation of Solid-Anchored DNA Oligomers. *J. Am. Chem. Soc.* **112**, 1691–1696.
- (18) Seitz, O., and Kunz, H. (1995) A Novel Allylic Anchor for Solid-Phase Synthesis-Synthesis of Protected and Unprotected O-Glycosylated Mucin-Type Glycopeptides. *Angew. Chem., Int. Ed. Engl.* **34**, 803–805.
- (19) Kunz, H., and Dombo, B. (1988) Solid Phase Synthesis of Peptides and Glycopeptides on Polymeric Supports With Allylic Anchor Groups. *Angew. Chem., Int. Ed. Engl.* **27**, 711–713.
- (20) L-Williams, P., Merzouk, A., Guibé, F., Albericio, F., and Giralt, E. (1994) Solid-Phase Synthesis of Peptides Using Allylic Anchoring Groups 2. Palladium-Catalysed Cleavage of Fmoc-Protected Peptides. *Tetrahedron Lett.* **35**, 4437–4440.
- (21) Kaljuste, K., and Undén, A. (1996) Solid-Phase Synthesis of Peptide Aminoalkylamides Using an Allyl Linker. *Tetrahedron Lett.* **37**, 3031–3034.
- (22) Nicolaou, K. C., Prasad, C. V. C., Somers, P. K., and Hwang, C-K. (1989) Activation of 6-Endo Over 5-Exo Hydroxyl Epoxide Opening. Stereoselective and Ring Selective Synthesis of Tetrahydrofuran and Tetrahydropyran Systems. *J. Am. Chem. Soc.* **111**, 5330–5334.

BC970013A

Supporting Information for: Synthesis of Oligonucleotides Containing 3'-Alkyl Carboxylic Acids Using a Palladium Labile Solid Phase Synthesis Support.

Tracy J. Matray, Dong Jin Yoo, Dustin L. McMinn and Marc M. Greenberg*
Department of Chemistry, Colorado State University
Fort Collins, CO 80523

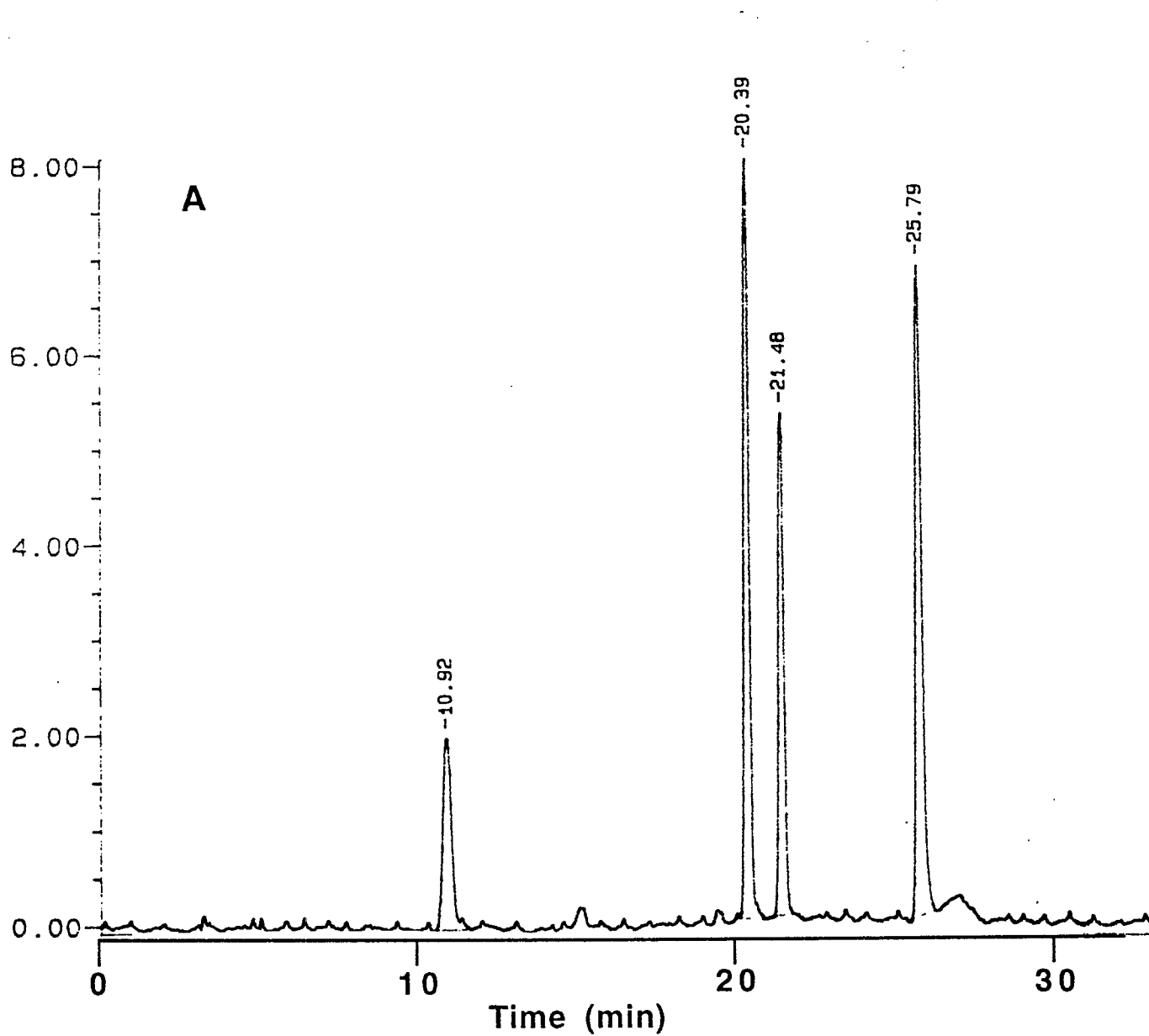
Enclosed herein is additional primary data concerning the characterization of oligonucleotides obtained from the Pd(0) cleavage methodology presented. This data includes:

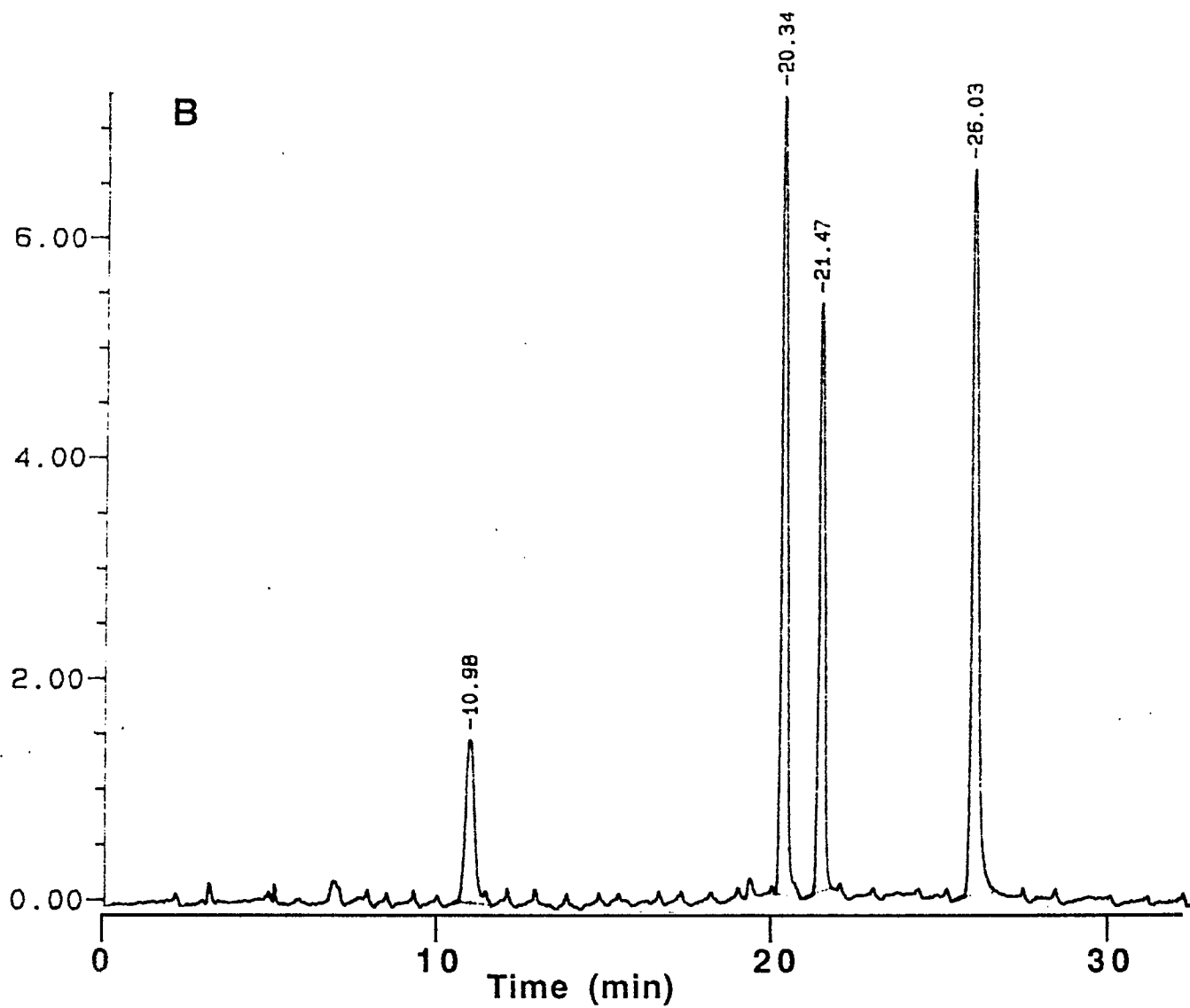
1. Enzymatic digests of eicosameric oligonucleotides of identical sequence obtained via direct ammonolysis (Labelled: A) of the biopolymer, and that isolated via ammonolysis following Pd(0) cleavage (Labelled: B) of the oligonucleotide. The oligonucleotide was synthesized using β -cyanoethyl phosphoramidites. The enzymatic digestion was carried out via standard procedures using snake venom phosphodiesterase, followed by dephosphorylation using calf intestine alkaline phosphatase. For an example of the description of such a procedure, see: Greenberg, M. M. and Gilmore, J. L. *J. Org. Chem.* **1994**, *59*, 746. The oligonucleotide digested is that shown below.

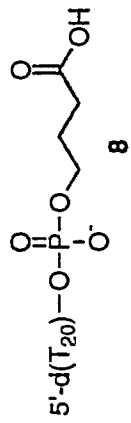
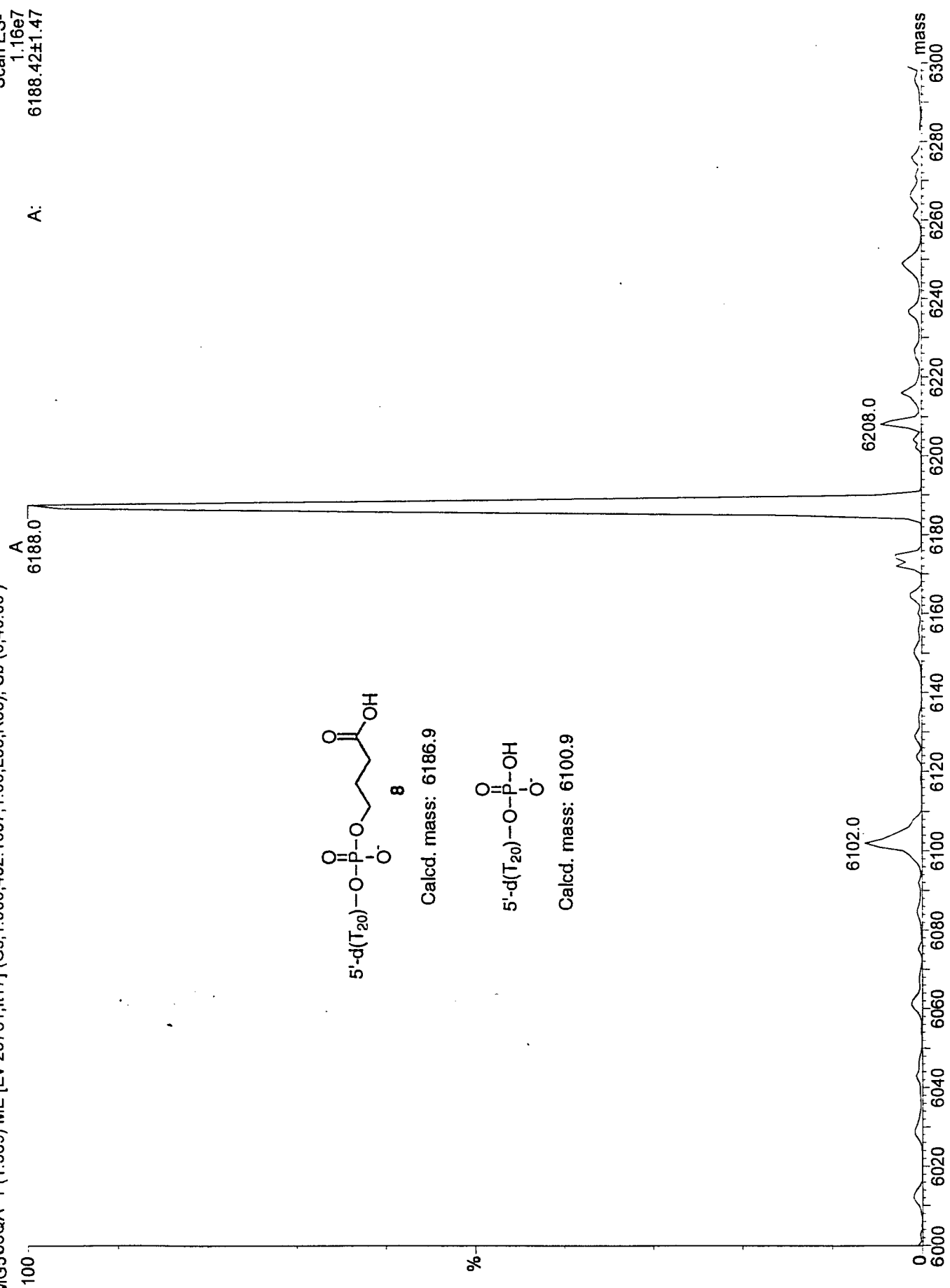


2. Electrospray mass spectrum of an eicosameric polythymidylate isolated via the Pd(0) cleavage procedure described in the manuscript. The observed ions are within one atomic mass unit of the calculated masses for **8** and the dealkylated product.

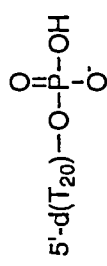
BC970013A







Calcd. mass: 6186.9



Calcd. mass: 6100.9

Presentation of Ligands on Hydroxylapatite

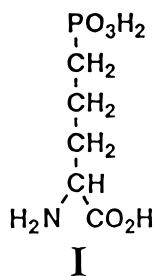
Barbara C. F. Chu and Leslie E. Orgel*

The Salk Institute for Biological Studies, P.O. Box 85800, San Diego, California 92186-5800.
Received December 17, 1996[®]

Conjugates of biotin with the decamer of glutamic acid (glu₁₀) and the trimer of D,L-2-amino-5-phosphonovaleric acid (**I**) have been synthesized, and it has been shown that they mediate the binding of avidin to hydroxylapatite. In a similar way a conjugate of methotrexate with glu₁₀ mediates the binding of dihydrofolate reductase to the mineral. The presentation of ligands on the hydroxylapatite component of bone may find applications in clinical medicine.

Peptides containing several aspartic and glutamic acid residues, oligonucleotides, and other polyanions bind strongly but reversibly to hydroxylapatite; this is the basis of hydroxylapatite chromatography (1, 2). We have recently found that oligomers of glutamic acid as short as the hexamer bind quantitatively to hydroxylapatite and are not removed by washing with water or a 0.1 M NaCl solution (3). This suggests that negatively charged polypeptides might be used as linkers to bind ligands to the mineral component of bone with controllable affinity and retention time. In this paper we show that conjugates of biotin and methotrexate with negatively charged peptides may be used to mediate the binding of avidin and dihydrofolate reductase, respectively, to hydroxylapatite.

Glu₁₀ was synthesized by the Peptide Biology Laboratory at The Salk Institute. D,L-2-Amino-5-phosphonovaleric acid (**I**), methotrexate (MTX), chicken liver dihy-



drofolate reductase (DHFR), and *N*-hydroxysuccinimide (N-OH-succ) were obtained from Sigma; 1,1-carbonyldiimidazole (CDI) and dicyclohexylcarbodiimide (DCC) were from Aldrich. Succinimidyl-6-(biotinamido) hexanoate (NHS-LC-Biotin II) was obtained from Pierce, streptavidin from Boehringer, ¹²⁵I-labeled streptavidin from Amersham, and hydroxylapatite (HA) from Bio-Rad.

The biotin derivative of glu₁₀ was synthesized by reacting 25 nmol of the oligomer with 190 nmol of NHS-LC-Biotin II in 20 μ L of 0.1 M NaHCO₃ buffer at pH 8.4 for 45 min. The product was purified on a C₁₈ column using a 0.1% TFA/acetonitrile gradient and its identity confirmed by LDMS (calculated for C₆₆H₉₇N₁₃O₃₄S + Na⁺ 1670.6; found 1670.7).

The MTX derivative of glu₁₀ was synthesized via an *N*-hydroxysuccinimide intermediate (4). A solution (40 μ L) containing 0.05 M MTX, 0.05 M N-OH-succ, and 0.05 M DCC in DMF was allowed to stand at room temperature for 1 h and then at 2–4 °C overnight. Ten microliters of the resulting solution was added to 5–25 nmol of glu₁₀ in 30 μ L of 0.02 M NaHCO₃ at pH 8.2. The reaction mixture was shaken in the dark for 4 h and then diluted with 70 μ L of water. Unreacted MTX and salts were removed by shaking the reaction mixture with 10 mg of HA overnight, removing the supernatant, and washing the HA with water. Glu₁₀ and its MTX conjugate were eluted by shaking the HA with 2 \times 50 μ L of 0.02 M pyrophosphate for 30 min. The conjugate was purified by HPLC on a C₁₈ column. Its identity was confirmed by LDMS (calculated for C₇₀H₉₂N₁₈O₃₅ + H⁺ 1745.6; found 1745.0).

Oligomers of D,L-2-amino-5-phosphonovaleric acid (pvl) were synthesized from the monomer (**I**) using carbonyldiimidazole (CDI) as a condensing agent (5). A solution of the monomer at pH 8 (0.05–0.1 M) was added to a 3-fold excess of solid CDI, and the resulting solution was allowed to stand for 6 h (or overnight). Products ranging from the dimer to the pentamer were identified by paper chromatography (*n*-PrOH/NH₃/H₂O 7:1:2), and samples of the oligomers were eluted from the paper. HPLC of the reaction mixture on an RPC-5 column gave a series of peaks that were assigned to oligomers of known length by cochromatography with the material eluted from paper.

To determine the shortest oligomer that binds to HA, 2–3 μ g of the dimer, trimer, tetramer, or pentamer was separately shaken with 10 mg of HA, and any oligomer retained by the HA was eluted with K₄P₂O₇ as described above. HPLC analysis of the supernatant and K₄P₂O₇ eluate showed that trimers and longer oligomers of pvl were found only in the eluate and therefore had been bound by the HA. Dimers were not bound to HA and were found in the supernatant fraction.

To obtain the biotin derivative of (pvl)₃, 6 μ g of the tripeptide isolated from RPC-5 was first adsorbed to 10 mg of HA. The solid was separated by centrifugation and washed with H₂O to remove Tris and other components of the HPLC buffer. (Pvl)₃ was then eluted with pyrophosphate as described above. (Pvl)₃ (5–10 μ g) in 20 μ L of buffer containing 0.2 M pyrophosphate and 0.2 M NaHCO₃ (pH 8.4) was added to 0.1 mg of solid NHS-LC-Biotin II. The reaction mixture was then allowed to stand for 1 h at room temperature. The biotinyl derivative of the tripeptide was purified and isolated using an

* Author to whom correspondence should be addressed [telephone (619) 453-4100, ext 1321; fax (619) 558-7359; e-mail orgel@sc2.salk.com].

[®] Abstract published in *Advance ACS Abstracts*, February 15, 1997.

Table 1. Biotin-Mediated Binding of Streptavidin to Hydroxylapatite

	% [125 I]streptavidin in supernatant	% [125 I]streptavidin on hydroxylapatite
glu ₁₀	97	3
pvl ₃	97	3
biotin-glu ₁₀	25	75
biotin-pvl ₃	32	68

RPC-5 column. Its identity was confirmed by ESMS (calculated for C₃₁H₅₇N₆O₁₆P₃S - H 893.2; found 893).

To recruit streptavidin to HA, 1 nmol of biotin-glu₁₀ or biotin-(pvl)₃ was first shaken with 1 mg of HA in 20 μ L of 0.01 M Tris-ClO₄ for 6 h (or overnight) at room temperature. The supernatant was removed by centrifugation, and the HA was washed with 100 μ L of water. A solution of 0.1 nmol of [125 I]-labeled streptavidin (25 000–50 000 cpm) in 100 μ L of buffer containing 1 M KCl and 0.01 M phosphate at pH 6.5 was added to the HA and shaken for 45 min. The supernatant was removed by centrifugation and the HA washed several times with 200 μ L of H₂O. The amounts of radioactivity found in the supernatant, wash, and HA fractions were then measured (see Table 1). In control experiments, biotin-glu₁₀ was replaced by glu₁₀ and biotin-(pvl)₃ was replaced by (pvl)₃. When a peptide bound to the HA was ligated to biotin about 70% of the streptavidin was recruited to the HA and 25–30% remained in the supernatant (Table 1). In the control experiments no more than 5% of the streptavidin was bound to the HA. Clearly the preadsorption of biotin conjugates of negatively charged polypeptides greatly enhances the adsorption of avidin to HA.

To recruit dihydrofolate reductase to HA, 1 nmol of MTX-glu₁₀ was adsorbed to HA as described above for biotin-glu₁₀. DHFR (0.52 nmol) in 200 μ L of buffer containing 0.1 M ammonium sulfate, 0.01 M potassium phosphate, at pH 6.4, and 5% glycerol was added to the HA and shaken for 45 min. The HA was separated from the supernatant, washed with 100 μ L of water, and then eluted twice with 20 μ L of 0.02 M K₄P₂O₇. In control experiments the MTX-glu₁₀ was replaced by glu₁₀. The supernatant, the washes, and the pyrophosphate eluate were analyzed on a 6% acrylamide SDS gel using Coomassie Blue to visualize DHFR. Figure 1 shows that in the control experiments with glu₁₀ more than 75% of the DHFR was found in the supernatant (Figure 1, lane 1) and only a small amount in the pyrophosphate eluate (Figure 1, lane 3). In experiments involving MTX-glu₁₀ more than 75% of the DHFR was found in the pyrophosphate eluate (Figure 1, lane 6) and very little in the supernatant (Figure 1, lane 4). Preadsorption of MTX-glu₁₀, therefore, greatly increases the amount of DHFR that binds to HA.

The above results show that conjugates of various ligands with anionic polypeptides adsorbed noncovalently on hydroxylapatite could be used as supports for affinity chromatography. More importantly, HA presents special opportunities in a related context, because it is the main mineral component of bone. The surface of bone is freely accessible to molecules in the extracellular fluid even if they are as large as proteins (6). The bisphosphonates, small molecules carrying four negative charges, have been used extensively to attach technetium to hydroxylapatite for bone scintigraphy (7). One example of the recruitment of an anticancer drug, methotrexate, to bone using a bisphosphonate has been reported (8). We believe that anionic polypeptides may prove particularly convenient as carriers of ligands to bone and may sometimes have advantages over the bisphosphonates.

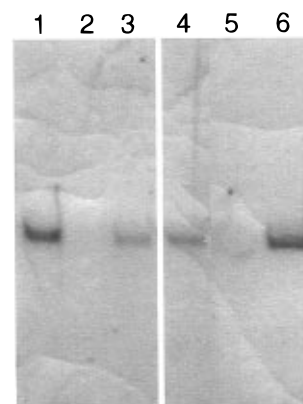


Figure 1. Coomassie Blue stained SDS gel showing DHFR in the supernatant (lanes 1 and 4), the wash (lanes 2 and 5), or the pyrophosphate eluate (lanes 3 and 6) after shaking a solution of the enzyme with glu₁₀-bound hydroxylapatite (HA) (lanes 1–3) or with MTX-glu₁₀-bound HA (lanes 4–6). One nanomole of glu₁₀ or MTX-glu₁₀ was shaken with 1 mg of HA for 6 h. Excess peptide was removed by washing. The glu₁₀- or MTX-glu₁₀-bound HA was then shaken with 0.52 nmol of DHFR for 45 min. The supernatant was removed by centrifugation and the HA washed with 100 μ L of water. The glu₁₀ and MTX-glu₁₀ together with any bound DHFR were eluted from the HA by shaking with 2 \times 50 μ L of pyrophosphate solution for 30 min.

The mechanism of action of bisphosphonates on bone resorption is not fully understood, but it seems clear that it is not entirely a matter of adsorption to hydroxylapatite. The properties of osteoblasts are profoundly affected by submicromolar concentrations of bisphosphonates, suggesting that they attach to receptors, possibly pyrophosphate receptors, on the cell surface (9). The structures of polypeptides are completely unrelated to that of inorganic pyrophosphate, so by using them as carriers it should be possible to dissociate the direct effects of adsorption to HA from the indirect effects due to interaction with extracellular receptors on osteoblasts (or osteoclasts).

Polypeptides are uniquely convenient as carriers, because effective automated methods are already available for their synthesis, and the use of combinatorial peptide libraries is well-established. The strength of adsorption of the carriers could easily be controlled via their length, while more or less degradable carriers could be obtained by varying the ratio of D- to L-residues. In the special case of a peptide ligand, the ligand and the anionic carrier could be assembled in a single solid-phase peptide synthesis. Presentation of ligands on HA that interact directly with receptors on osteoblasts or osteoclasts, or which recruit proteins to bone, may find applications in medicine.

ACKNOWLEDGMENT

This work was supported by Grant GM33023 from the National Institute for Allergy and Infectious Diseases and Grant NAWG-1660 from the National Aeronautics and Space Administration. We are grateful to Prof. A. Michael Parfitt (University of Arkansas for Medical Sciences) for much helpful advice. We thank Aubrey R. Hill, Jr., for technical assistance and Sylvia Bailey for manuscript preparation.

LITERATURE CITED

- (1) Bernardi, G. (1971) Chromatography of Proteins on Hydroxylapatite. In *Methods in Enzymology*. Vol. XXII. Enzyme purification and related techniques (W. B. Jakoby, Ed.) pp 325–339, Academic Press, New York.

- (2) Bernardi, G. (1973) Chromatography of Proteins on Hydroxyapatite. In *Methods in Enzymology. Vol. XXVII. Enzyme Structure, Part D* (C. H. W. Hirs and S. N. Timasheff, Eds.) pp 471–479, Academic Press, New York.
- (3) Chu, B. C. F., Hill, A. R., Jr., and Orgel, L. E. (1996) Unpublished results.
- (4) Kulkarni, P. N., Huntley Blair, A., and Chose, T. I. (1981) Covalent binding of methotrexate to immunoglobulins and the effect of antibody-linked drug on tumor growth *in vivo*. *Cancer Res.* 41, 2700–2706.
- (5) Ehler, K. W., and Orgel, L. E. (1976) *N,N*-carbonyldiimidazole-induced peptide formation in aqueous solution. *Biochim. Biophys. Acta* 434, 233–243.
- (6) Doty, S. B., Robinson, R. A., and Schofield, B. (1976) Morphology of Bone and Histochemical Staining Characteristics of Bone Cells. In *Handbook of Physiology. Section 7: Endocrinology* (G. D. Aurbach, Ed.) pp 3–23, American Physiological Society, Washington, DC.
- (7) Fogelman, I., Maisey, M. N., and Clarke, S. E. M. (1994) *An Atlas of Clinical Nuclear Medicine*, pp 1–110, Mosby, St. Louis, MO.
- (8) Hosain, F., Spencer, R. P., Couthon, H. M., and Stuirtz, G. L. (1994) Targeted delivery of antineoplastic agent to bone: biodistribution studies of technetium-99m-labeled gem-bisphosphonate conjugate of methotrexate. *J. Nuclear Med.* 37, 105–107.
- (9) Fleisch, H. (1995) *Bisphosphonates in Bone Disease*, pp 47–54, Parthenon, New York.

BC970015V

ARTICLES

Mitogenic Activities of Water-Soluble and -Insoluble Insulin Conjugates

Guoping Chen, Yoshihiro Ito,* and Yukio Imanishi

Department of Material Chemistry, Faculty of Engineering, Kyoto University, Kyoto 606-01, Japan. Received May 3, 1996[®]

Insulin was covalently bound to water-soluble polymers such as poly(oxyethylene) and poly(acrylic acid). The former and the latter product are water-soluble monovalent and multivalent conjugates, respectively. Insulin was also bound to a poly(acrylic acid)-grafted polystyrene film, to form a water-insoluble multivalent conjugate. The matrix polymer was prepared by graft polymerization of acrylic acid initiated by glow-discharged polystyrene film. Insulin coupled with poly(oxyethylene) reduced the mitogenic activity, but the poly(acrylic acid)–insulin conjugate stimulated cell growth more than native insulin. A concentration of immobilized insulin much lower than that of native insulin and the water-soluble insulin conjugates accelerated cell growth. The maximal mitogenic effect of the immobilized insulin was greater than that of native insulin or the water-soluble insulin conjugates. The findings suggest that the mitogenic effect of the water-insoluble, multivalent insulin conjugate lasts longer than that of the water-soluble conjugates, owing to the absence of internalization into the cell.

INTRODUCTION

Developments in molecular biology have revealed the importance of biosignaling polypeptides, including growth factors and cytokines. The covalent binding of biosignal molecules to a soluble or insoluble matrix has a wide range of applications, ranging from the elucidation of biosignaling mechanisms and receptor isolation to clinical therapeutics such as drug delivery and tissue regeneration systems (1–4). The binding of biosignal molecules to their specific receptors may lead to specific complexes which are assembled and internalized into the cytoplasm with a portion of the receptors returning to the cell surface (down-regulation). However, whether all of these processes are necessary has not been clarified. If the internalization of biosignal–receptor complexes is not indispensable for signal transduction, biosignal molecules covalently linked to water-insoluble matrix should be active.

We showed that insulin immobilized on various water-insoluble matrices enhances the growth of anchorage-dependent cells more than native insulin (5, 6). We considered that this effect was due to long-lasting signal transduction due to inhibited down-regulation (7). However, the growth-acceleration effect of immobilized insulin might involve effects arising from chemical modifications of the insulin and the generation of a multivalent ligand system. These effects of immobilized insulin have not been thoroughly investigated.

In the present study, to clarify the effect of chemical modification and the generation of a multivalent ligand system, we synthesized insulin–poly(oxyethylene) or insulin–poly(acrylic acid) conjugates and compared their effects with those of insulin immobilized to a poly(acrylic acid)-grafted polystyrene film.

MATERIALS AND METHODS

Materials. Insulin (Ins) (bovine origin, no. I-5500) and tresylated ω -methoxypoly(oxyethylene) (POE, MW = 5000) were purchased from Sigma Chemical Co. (St. Louis). [¹²⁵I]Insulin was purchased from Daiichi Chemical Ltd. (Tokyo). Poly(acrylic acid) (PAA, MW = 15 000), acrylic acid, and Clear-sol I were purchased from Nacalai Tesque, Inc. (Kyoto, Japan). Polystyrene (PSt) was purchased from Wako Pure Chemical Ltd. (Osaka, Japan) and purified by precipitation in methanol before use.

Poly(oxyethylene) Conjugates. The synthetic scheme is shown in Figure 1a (8). A phosphate-buffered solution (pH 7.0, 0.5 mL) containing tresylated POE (100 μ g) and the same solution (0.5 mL) containing insulin (1 mg) with or without [¹²⁵I]insulin were mixed and stirred for 24 h at 4 °C. The product was purified by ultrafiltration (Millipore Molecut II, filtration off below 10 kDa) and referred to as Ins–POE. The formation of the insulin conjugate was confirmed by high-performance liquid chromatography (HPLC) using a column packed with Cosmosil 5Diol-120, purchased from Nacalai Tesque, Inc. [eluent, 0.02 M phosphate buffer (pH 7.0) and 0.2 M NaCl; elution rate, 1.0 mL/min at room temperature; detection, absorbance at 280 nm].

Poly(acrylic acid) Conjugates. The synthetic scheme is shown in Figure 1b. A phosphate-buffered solution (pH 7.0, 0.5 mL) containing PAA (100 μ g) was mixed with the same solution (0.5 mL) containing 1-ethyl-3-[3-(dimethylamino)propyl]carbodiimide hydrochloride (water-soluble carbodiimide, WSC, 1 mg), and the mixture was stirred for 24 h at 4 °C. The solution containing activated PAA was quickly ultrafiltrated (Millipore Molecut II, filtration off below 10 kDa), mixed with a phosphate-buffered solution (pH 7.0, 1 mL) containing insulin (1 mg) with or without [¹²⁵I]insulin, and then stirred at 4 °C for 24 h. Thereafter, a phosphate-buffered solution containing glycine (10 mg, 1 mL) was added to the reaction mixture and left at 4 °C for a further 6 h to block any

[®] Abstract published in *Advance ACS Abstracts*, December 15, 1996.

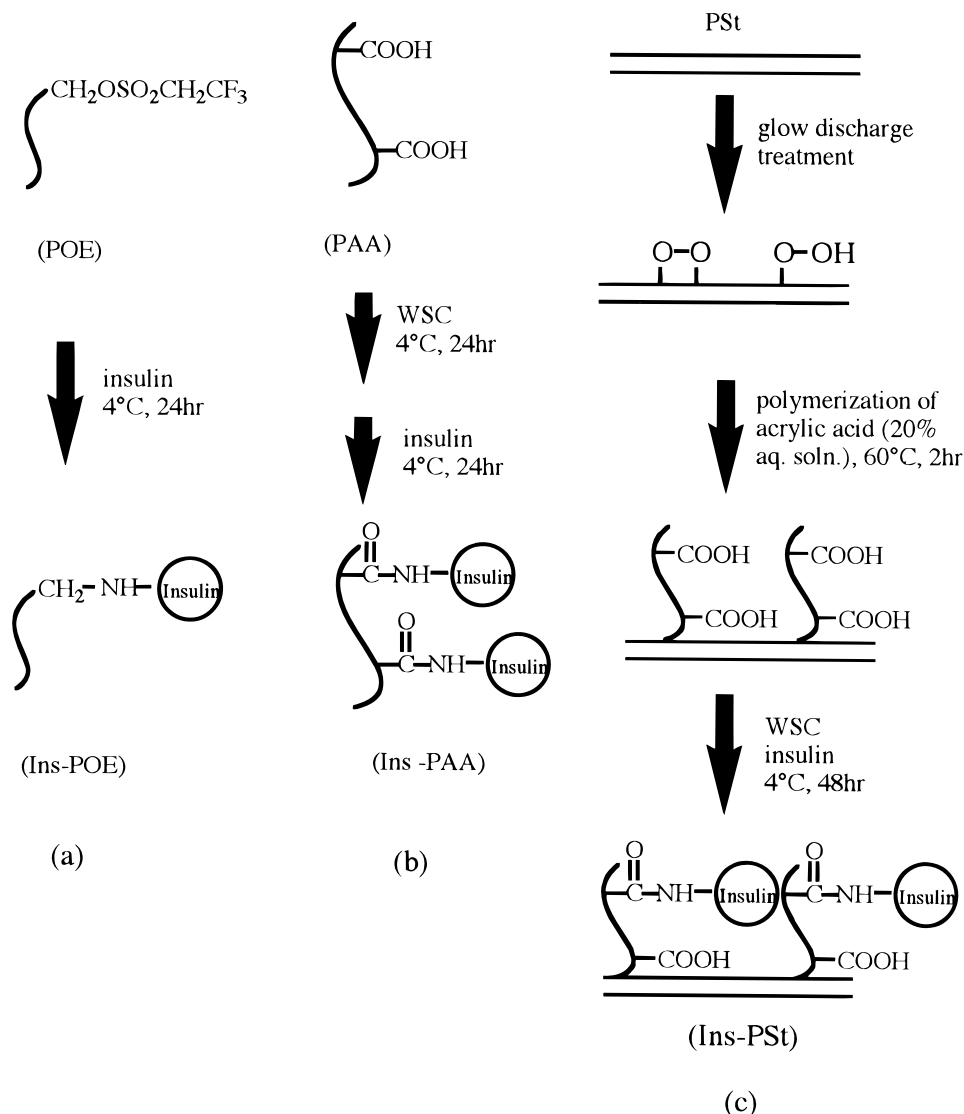


Figure 1. Synthetic schemes of insulin conjugates with (a) poly(oxyethylene) (POE), (b) poly(acrylic acid) (PAA), and (c) poly(acrylic acid)-grafted polystyrene (PSt) film. WSC is water-soluble carbodiimide.

activated carboxylic groups of PAA that remained unreacted. The product was purified by ultrafiltration and is referred to as Ins-PAA. The formation of Ins-PAA was confirmed by HPLC as described above for Ins-POE.

Immobilization of Insulin onto a Poly(acrylic acid)-Grafted Polystyrene Film. The synthetic scheme is shown in Figure 1c. A PSt film was cast from a toluene solution (15 wt %) on a circular glass plate (diameter, 15 mm). The film was glow-discharged (200 W) with a high-frequency wave generator (Nihon Koshuha Co., Yokohama, Japan) for 20 s under a pressure of 5.65 Pa. The film was exposed to air and incubated in a solution of acrylic acid (20 wt %) for 24 h at 60°C . The PAA-grafted PSt film was washed with distilled water until the absence of unreacted monomer and unbound PAA in the wash was confirmed by a pH monitor.

The PAA-grafted PSt film was immersed in a phosphate-buffered solution (pH 7.0) containing WSC (1 mg/mL) and ^{125}I insulin of various concentrations at 4°C for 48 h. After immobilization, the film was repeatedly washed with phosphate-buffered saline [PBS (pH 7.4), NaCl (8.0 g), KCl (0.2 g), KH_2PO_4 (0.2 g), NaH_2PO_4 (1.15 g), MgCl_2 (0.1 g), and CaCl_2 (0.1 g in 1 L of distilled water)] until the absence of ^{125}I insulin in the wash was confirmed. Non-radiolabeled insulin was immobilized under the same conditions. The immobilized insulin is

referred to as Ins-PSt. An insulin-adsorbed PSt film was prepared in a similar manner without using WSC. These films were disinfected with 70% ethanol and washed with sterilized PBS for biological experiments.

Measurement of Contact Angle, Electron Spectroscopy for Chemical Analysis (ESCA), Surface Concentration of Carboxylic Acid, and Composition of Conjugates. The contact angle of an air bubble placed on polystyrene film was measured to assess the surface wettability. Prior to the measurement, the PSt film was incubated at 37°C for 24 h. Surface modifications of polystyrene film were analyzed by ESCA using a Perkin-Elmer 5500 series multi-technique apparatus on freeze-dried samples. The surface amount of carboxylic acid was measured using rhodamine 6G as reported (5).

The composition of insulin in the conjugates was determined by measuring ^{125}I and fluorescence. The labeled conjugates were prepared by the same methods as the nonlabeled conjugates. The fluorescence was measured at 345 nm by excitation at 280 nm. The insulin contents were calculated by comparing the radioactivity and fluorescence intensity of insulin conjugates with that of insulin per unit weight.

Cell Culture and Growth Assay. Mouse fibroblast STO cells were subcultured in Dulbecco's modified Ea-

gle's minimum essential medium (DMEM) supplemented with 10% fetal bovine serum (FBS), purchased from Nissui Pharmaceutical Co. Ltd. (Tokyo).

The STO cells were harvested using PBS without magnesium or calcium ions [PBS(-)], containing 0.15% (w/v) trypsin (2000 units/g) and 0.02% (w/v) ethylenediaminetetraacetic acid (EDTA). The cells were washed once with DMEM containing FBS and once with DMEM, then suspended in DMEM (2×10^4 cells/well), and incubated in 24-well plates containing insulin conjugates in DMEM (1 mL/well) under a 5% CO₂ atmosphere at 37 °C. The cell growth was determined by measuring the uptake of [³H]thymidine (9). After cell culture for 45 h, the cells were incubated with [³H]thymidine for a further 3 h. Subsequently, the cells were washed once with PBS and three times with ice-cooled TCA (10 wt %) and then solubilized with 0.5 N NaOH. The lysate was neutralized with 5 N HCl and then mixed with Clear-sol I, and the radioactivity was measured.

Insulin Association with Cells. To determine the internalization into cells and specific or nonspecific complexation with the cell surface of the insulin conjugates (insulin association), STO cells were cultured in the presence of ¹²⁵I-labeled insulin conjugates for 3, 24, and 48 h. After three washes with PBS(-), the cells were detached from culture plates using PBS(-) containing 0.02 wt % EDTA until cells adhering to the plates became undetectable by optical microscopy. The cells were collected by centrifugation, and the radioactivity was measured in a γ counter.

RESULTS

Synthesis of Water-Soluble Insulin Conjugates.

Figure 2 shows the HPLC elution profile of the native insulin and the insulin conjugates with POE and PAA. Ins-POE eluted faster than the native insulin or POE. The Ins-PAA conjugate eluted faster than native insulin or PAA. Measuring the ¹²⁵I-labeled insulin showed that the insulin contents in Ins-POE and Ins-PAA were 0.95 ± 0.09 and 4.06 ± 0.22 mol/mol, respectively (\pm standard deviation, $n = 5$). Fluorescence measurements indicated that the contents in Ins-POE and Ins-PAA were 0.98 ± 0.11 and 3.90 ± 0.15 mol/mol, respectively (\pm standard deviation, $n = 3$). These results demonstrated that Ins-POE was composed of about one insulin molecule and one poly(oxyethylene) chain and that Ins-PAA contained about four insulin molecules in one poly(acrylic acid) chain.

Graft Copolymerization and Insulin Immobilization. The surface composition of polystyrene film after various manipulations was analyzed by ESCA, and the results are shown in Table 1. After glow discharge, the content of oxygen in the film surface increased, showing the formation of peroxides, alcohols, and other oxidation products. After graft polymerization of acrylic acid, the oxygen content increased, indicating the presence of PAA (O, 40%). The concentration of COOH groups on the PAA-grafted PSt film as determined with rhodamine 6G was $(4.3 \pm 0.2) \times 10^{-8}$ mol/cm². The content of oxygen decreased, and that of nitrogen became detectable by insulin immobilization (N, 15.4%; O, 18.4%). The surface wettability of the polystyrene film after various manipulations was estimated in terms of the contact angle of air bubbles in water, and the results are shown in Table 1. Glow discharge and graft polymerization of acrylic acid increased the wettability. Insulin immobilization slightly decreased the wettability of PAA-grafted PSt film.

PAA-grafted Pst film was immersed in an aqueous solution of insulin in the presence or absence of water-

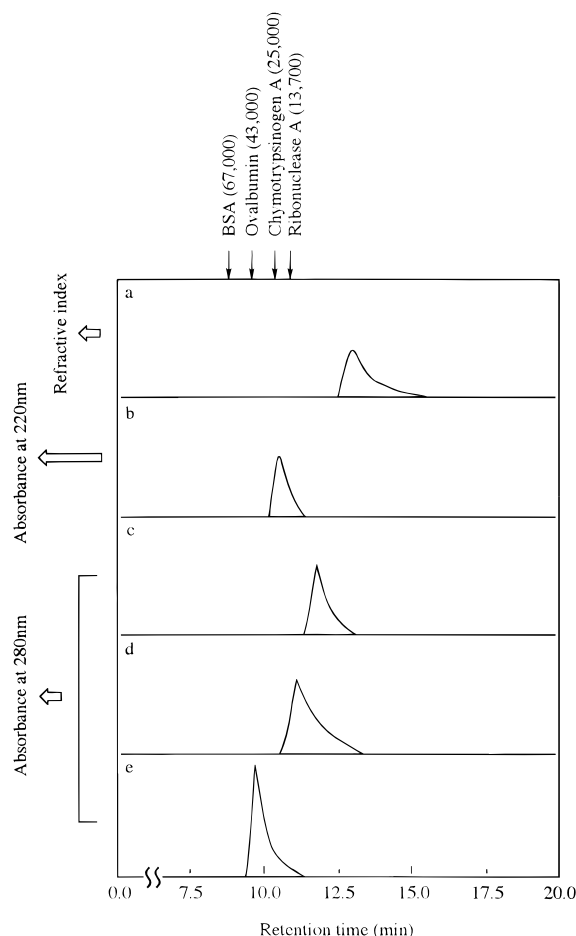


Figure 2. HPLC elution profiles of (a) POE, (b) PAA, (c) native insulin, (d) Ins-POE, and (e) Ins-PAA. BSA is bovine serum albumin. The number indicates the molecular weight.

Table 1. Surface Properties of Polystyrene Film as Investigated by ESCA and Contact Angle Measurement

sample	element composition (%)			contact angle of air in water
	C	O	N	
PSt	97.8	2.2	0.0	$88 \pm 3^\circ$
glow-discharged PSt	88.7	11.3	0.0	$42 \pm 3^\circ$
PAA-grafted PSt	78.1	21.9	0.0	$35 \pm 3^\circ$
Ins-PSt ^a	73.3	15.7	11.0	$38 \pm 2^\circ$

^a PAA-grafted PSt immobilized with insulin ($0.684 \mu\text{g}/\text{cm}^2$).

soluble carbodiimide. The film was then repeatedly washed with PBS until insulin release from the film was undetectable. Complete removal of insulin, which was weakly adsorbed on the film, required over 20 washes. The amount of insulin immobilized or adsorbed on the PAA-grafted PSt film was measured using radiolabeled insulin, and the results are shown in Figure 3. With increasing feed concentrations, the amount of immobilized insulin increased. The maximal surface concentration of immobilized insulin corresponded to complete coverage of the film surface with insulin. A small amount of noncovalently (physically) adsorbed insulin was found on the film surface after repeated washing with PBS.

Table 2 shows that the covalently immobilized insulin was not released under any conditions investigated, while the adsorbed insulin was released into the culture medium or taken up by cells under some conditions.

The association of insulin conjugates with cells during culture is shown in Figure 4. Insulin internalization was slightly suppressed by binding to POE but enhanced by that to PAA. On the other hand, Ins-PSt was completely free from insulin internalization, while insulin nonco-

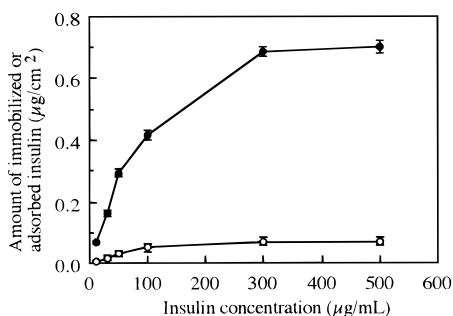


Figure 3. Amount of insulin adsorbed (○) or immobilized (●) on PAA-PSt film. Bars represent the standard deviation. $n = 6$.

Table 2. Percentage of Insulin Released during a 48 h Incubation under Various Conditions

culture condition	state of insulin on polystyrene film	
	immobilization	adsorption
serum-free medium with cells		
in medium	0.0	3.3 ± 2.0
in cells	0.0	26.6 ± 6.0
serum-free medium without cells	0.0	1.3 ± 0.6
serum-containing medium	0.0	10.0 ± 1.3
PBS	0.0	0.0

valently adsorbed on PAA-grafted PSt film was very slowly taken up by the cells.

Mitogenic Activities of Insulin Conjugates. Figure 5 shows the rate of DNA synthesis in mouse fibroblast STO cells cultured in the presence of various insulin conjugates. The mitogenic effect of Ins-POE was lower than that of native insulin. The effect of Ins-PAA was a little higher than that of the native insulin. Small amounts of Ins-PSt (0.1–0.05-fold the amount of native insulin) stimulated DNA synthesis in STO cells. The maximal mitogenic effect of Ins-PSt was much greater than that of the water-soluble insulin conjugates investigated.

DISCUSSION

Soluble Insulin Conjugates. Insulin has two chains, A and B, and three amino groups, A1-glycine, B1-phenylalanine, and B29-lysine. The reactivity is $A1 > B29 > B1$. The N terminus of the A chain is the most reactive and is considered to be in the neighborhood of the receptor binding site (10). Markussen et al. (11) coupled insulin selectively through the B1 amino group to divinyl sulfone-activated agarose using insulin that was protected in positions A1 and B29, to construct a high-capacity affinity chromatography system for insulin receptors. On the other hand, Schoelson et al. (12) incorporated benzoylphenylalanine, a photoactivable amino acid, into position 25 of the B chain by chemical synthesis and enzymatic semisynthesis to investigate the interaction between insulin and the receptor. They concluded that the efficiency of cross-linking was unusually high, ranging from 60 to 100%, and the cross-linking resulted in receptor and kinase activation. Weiland et al. (13) synthesized a covalently dimerized insulin derivative B29,B29'-suberoylinsulin and indicated that the derivative competitively inhibited insulin-stimulated DNA synthesis in 3T3-L1 fatty fibroblasts. However, it had no effect on mature rat adipocytes. These results demonstrate that it is difficult to estimate the activity of modified insulin.

In this study, the mitogenic effect of insulin was reduced by coupling to poly(oxyethylene). We considered the fact that the POE molecule hindered access of the

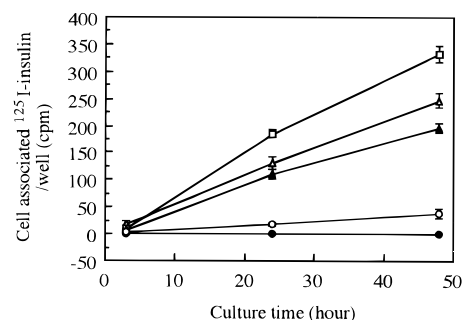


Figure 4. Time-dependent association with mouse fibroblast STO cells during culture in the presence of (Δ) native insulin, (▲) Ins-POE, (□) Ins-PAA, (●) Ins-PSt, and (○) insulin adsorbed on PAA-PSt. Bars represent the standard deviation. $n = 6$.

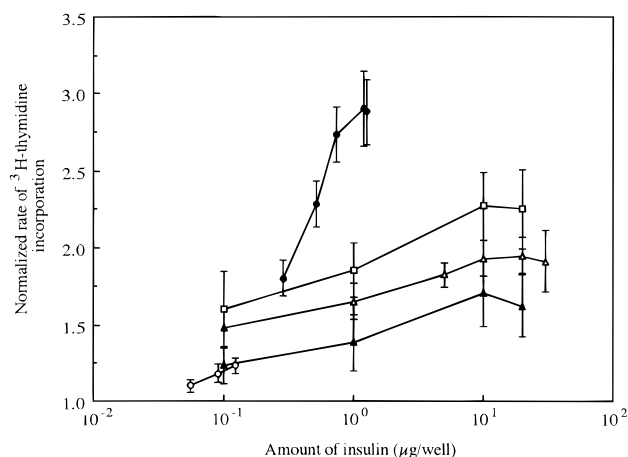


Figure 5. Growth rate of mouse fibroblast STO cells in the presence of (Δ) native insulin, (▲) Ins-POE, (□) Ins-PAA, (●) Ins-PSt, and (○) insulin adsorbed on PAA-PSt. Bars represent the standard deviation. $n = 6$.

insulin to the receptor because insulin is linked to POE mainly through the chemically reactive and biologically active sites, A1 and B29. However, the Ins-PAA conjugate apparently possessed higher mitogenic activity than the Ins-POE conjugate, although we also considered the fact that insulin is linked to PAA through A1 and B29. This should be due to the multivalency of Ins-PAA. The Ins-PAA conjugate can be active by enhancing receptor dimerization, as well as the aggregation and internalization of insulin conjugate-receptor complex.

Insoluble Insulin Conjugates. Covalent immobilization by insulin onto the polymer matrix was first reported by Cuatrecasas in 1969, who found that the immobilized insulin stimulates isolated fat cells (14). However, Oka and Topper found that some material with insulin-like activity was released from insulin-Sepharose (15). This substance had greater activity than native insulin and was referred to as superactive insulin. Wilchek and co-workers (16) considered the fact that the biological effects attributed to the insulin-Sepharose conjugate may be best explained in terms of insulin/serum protein-substituted guanidine released from the Sepharose matrix during cell culture.

The present study showed that immobilized insulin, Ins-PSt, was more mitogenic than Ins-PAA. In addition to multivalency, some other mechanisms must be operating in the action of Ins-PSt. We reported that insulin immobilized on surface-hydrolyzed poly(methyl methacrylate) film activated insulin receptors longer than soluble insulin, due to inhibited down-regulation (7). Ins-PSt should also activate the cellular signal-transduction

system over a long period without internalization. Membrane-anchored growth factors or cytokines regulate cells as "juxtacrine stimulators" (17). Immobilized insulin is considered to be "an artificial juxtacrine stimulator". The high activity of the artificial system will extend the concept of juxtacrine stimulation.

Proteins physically adsorb onto solid materials, and it is impossible to completely remove them by washing (18, 19). Therefore, some noncovalently adsorbed insulin remained on poly(acrylic acid)-grafted polystyrene film even after repeated washing. However, the amount was very small; it was slowly released from the surface, and the mitogenic effect was negligible. In Ins-PSt, insulin was covalently bound and none was released during cell culture. There should be no space where insulin could physically adsorb on the activated PAA-grafted PSt film surface.

Another problem concerning the insulin-Sepharose gel conjugate is the porosity or the rough surface of the matrix, which hinders access of cells to immobilized insulin. Horwitz and co-workers (4) pointed out the importance of a smooth surface in the activity of immobilized biosignal proteins and reported that interleukin-2 immobilized to plasma-treated polystyrene film maintained the viability of an interleukin-2-dependent cell line.

In the present investigation, the effectiveness of insulin immobilization on insoluble matrix was demonstrated by comparing Ins-PSt with Ins-PAA or Ins-POE conjugates. The effectiveness probably arose from inhibited internalization. A comparison of two types of immobilization matrices, polystyrene film and Sepharose gel, indicated that the smooth film surface induced efficient interaction of immobilized insulin with adsorbed cells. We quantified the contribution of the lack of internalization to the activity of immobilized biosignal proteins for the first time, using smooth polystyrene film.

ACKNOWLEDGMENT

We acknowledge Prof. K. Saito of the Radioisotope Center of Kyoto University for his supervision on the radioisotope experiments. This work was partially supported by a grant-in-aid for scientific research from the Ministry of Education, Science, Culture, and Sports of Japan and partially supported by the Nissan Science Foundation.

LITERATURE CITED

- (1) Venter, J. C. (1982) Immobilized and insolubilized drugs, hormones, and neurotransmitters: properties, mechanisms of action and applications. *Pharm. Rev.* 34, 153–187.
- (2) Goodson, R. J., and Katre, N. V. (1990) Site-directed polyglycation of recombinant interleukin-2 at its glycosylation site. *BioTechnology* 8, 343–346.
- (3) Capala, J., Barth, R. F., Bendayan, M., Lauzon, M., Adams, D. M., Soloway, A. H., Fenstermaker, R. A., and Carlsson, J. (1996) Borated epidermal growth factor as a potential targeting agent of boron neutron capture therapy of brain tumors. *Bioconjugate Chem.* 7, 1–15.
- (4) Horwitz, J. I., Toner, M., Tompkins, R. G., and Yarmush, M. L. (1993) Immobilized IL-2 preserves the viability of an IL-2 dependent cell line. *Mol. Immunol.* 30, 1041–1048.
- (5) Ito, Y., Liu, S. Q., and Imanishi, Y. (1991) Enhancement of cell growth on growth-factor-immobilized polymer film. *Bio-materials* 12, 449–453.
- (6) Zheng, J., It, Y., and Imanishi, Y. (1995) Growth enhancement of anchorage-dependent and anchorage-independent cells by coimmobilization of insulin with polyallylamine and gelatin. *Biotechnol. Prog.* 11, 677–681.
- (7) Ito, Y., Zheng, J., Imanishi, Y., Yonezawa, K., and Kasuga, M. (1996) Protein-free cell culture on an artificial substrate with covalently immobilized insulin. *Proc. Natl. Acad. Sci. U.S.A.* 93, 3598–3601.
- (8) Delgado, C., Patel, J. N., Francis, G. E., and Fisher, D. (1990) Coupling of poly(ethylene glycol) to albumin under very mild conditions by activation with tresyl chloride: characterization of the conjugate by partitioning in aqueous two-phase systems. *Biotechnol. Appl. Biochem.* 12, 119–128.
- (9) Nishi, N., Matuo, Y., Muguruma, Y., Yoshitake, Y., Nishikawa, K., and Wasa, F. (1985) A human prostatic growth factor (hPGF): partial purification and characterization. *Biochem. Biophys. Res. Commun.* 132, 1103–1109.
- (10) Schuettler, A., and Brandenburg, D. (1982) Preparation and properties of covalently linked insulin dimers. *Hoppe-Seyler's Z. Physiol. Chem.* 363, 317–330.
- (11) Markussen, J., Halstroem, J., Wiberg, F., and Schaeffer, L. (1991) Immobilized insulin for high capacity affinity chromatography of insulin receptors. *J. Biol. Chem.* 266, 18814–18818.
- (12) Schoelson, S. E., Lee, J., Lynch, C. S., Backer, J. M., and Pilch, P. F. (1993) Bpa^{B25} insulins, photoactivatable analogues that quantitatively cross-link, radiolabel, and activate the insulin receptor. *J. Biol. Chem.* 268, 4085–4091.
- (13) Weiland, M., Brandenburg, C., Brandenburg, D., and Joost, H. G. (1990) Antagonistic effects of a covalently dimerized insulin derivative on insulin receptors in 3T3-L1 adipocytes. *Proc. Natl. Acad. Sci. U.S.A.* 87, 1154–1158.
- (14) Cuatrecasas, P. (1969) Interaction of insulin with the cell membrane: primary action of insulin. *Proc. Natl. Acad. Sci. U.S.A.* 63, 450–457.
- (15) Oka, T., and Topper, Y. J. (1974) A soluble super-active form of insulin. *Proc. Natl. Acad. Sci. U.S.A.* 71, 1630–1633.
- (16) Wilchek, M., Oka, T., and Topper, Y. J. (1975) Structure of a soluble super-active insulin is revealed by the nature of the complex between cyanogen bromide-activated Sepharose and amines. *Proc. Natl. Acad. Sci. U.S.A.* 72, 1055–1058.
- (17) Massague, J., and Pandiella, A. (1993) Membrane-anchored growth factors. *Annu. Rev. Biochem.* 62, 515–541.
- (18) Brynda, E., Houska, M., Kalal, J., and Cepalova, N. A. (1980) Adsorption of human fibrinogen and human serum albumin onto polyethylene. *Am. Biomed. Eng.* 8, 245–252.
- (19) Van Straaten, J., and Peppas, N. A. (1991) Modelling of protein adsorption on polymeric surfaces. *J. Biomater. Sci., Polym. Ed.* 2, 91–111.

BC960068X

Poly(ethylene glycol)-Grafted Liposomes with Oligopeptide or Oligosaccharide Ligands Appended to the Termini of the Polymer Chains

Samuel Zalipsky,^{*,†} Nasreen Mullah,[†] Jennifer A. Harding,[†] Joshua Gittelman,[†] Luke Guo,[†] and Shawn A. DeFrees[‡]

SEQUUS Pharmaceuticals, Inc., 960 Hamilton Court, Menlo Park, California 94025, and Cytel Corporation, 3525 John Hopkins Court, San Diego, California 92121. Received August 31, 1996[®]

Novel conjugates tailor-made for inclusion in liposomal formulations, containing distearoylphosphatidylethanolamine (DSPE) as a lipid anchor, heterobifunctional polyethylene glycol (PEG) with a molecular weight of 2000 as a linking moiety, and a biological cell adhesive ligand [YIGSR peptide or Sialyl Lewis^x oligosaccharide (SLX)], were synthesized. They were characterized by NMR, chromatography, and matrix-assisted laser desorption ionization–time of flight mass spectrometry (MALDI–TOFMS). Inclusion of either of the ligand–PEG–lipid conjugates (2 mol %) in a lecithin/cholesterol/methoxy-PEG₂₀₀₀-DSPE (55:40:3 mole ratio) lipid mixture followed by preparation of unilamellar vesicles (100 nm) resulted in positioning of 55% of the YIGSR and 63% of the SLX ligands on the periphery of the outer surface-grafted polymeric “brush”, as determined by a combination of specific enzymatic alterations of each ligand and HPLC. Similar densities of ligand-bearing PEG chains were incorporated into liposomes by simply incubating (37 °C, 5 h) either one of the ligand–PEG–lipid conjugates with preformed lipid vesicles. This conjugate insertion process was aggregation free. Using enzymatic derivatization–HPLC, it was demonstrated that all the ligands incorporated into lipid membranes by this new approach were positioned exclusively on the outer leaflet of the liposomal bilayers. Since liposomes of this type are intended for *in vivo* use as long-circulating, ligand-presenting platforms, the insertion approach is preferable because of the more efficient utilization of ligand–PEG–lipid conjugates.

INTRODUCTION

Liposomes, spherical self-enclosed vesicles composed of amphiphilic lipids, constitute one of the most important and extensively studied classes of supramolecular constructs. They play an important role in a variety of subdisciplines ranging from studies of biological recognition to catalysis and chemical separations (1). Unilamellar liposomes of natural phospholipids loaded in their aqueous compartment with biologically active substances were long considered promising vehicles for improvement of *in vivo* properties of drugs. However, this promise was largely unfulfilled due to the tendency of liposomes to interact with plasma components, a process resulting in their rapid clearance from systemic circulation with concomitant accumulation by organs of the mononuclear phagocyte system (primarily liver and spleen). It has been discovered that grafting of flexible water soluble polymers on the surface of liposomes circumvents this problem to a large extent [see reviews (2–6)]. The optimal formulations of polymer-grafted liposomes (approximately 100 nm in diameter) have been obtained by including in the total lipid mixture 3–7 mol % of methoxypoly(ethylene glycol) with a molecular weight of 2000 in the form of distearoylphosphatidylethanolamine (mPEG-DSPE¹) conjugate, in addition to phosphatidylcholine (PC) and cholesterol. Although some other amphipatic polymers, most notably poly(2-methyl-2-oxazolines) (7, 8), were also able to convey comparable beneficial properties to liposomes, PEG remains the principal

polymer used for modification of liposomal surfaces. Such formulations possess extraordinarily long *in vivo* plasma circulation times (terminal $T_{1/2}$ = 45 h in humans, with most of the dose cleared under the longer half-life) (9). This property offers new opportunities for utilization of such polymer-grafted liposomes as long-circulating platforms presenting biologically relevant ligands. This type of system is useful for ligand-mediated targeting or as a means of increasing systemic exposure of small biologically active substance ligands, which, in their free form, are cleared from blood circulation very rapidly. Potentially useful ligands could be vitamins (10, 11), peptides (12), oligosaccharides (13), as well as macromolecules like immunoglobulins (14–17), other proteins (18), and polysaccharides (3). Since the surface of PEG liposome is covered by mobile, highly water-solvated polymer chains, it is logical to form covalent attachments with the biological ligands of interest through the end groups of these chains (19, 20). This allows for maximal exposure of the ligands on the periphery of the liposomes. The more conventional methods of binding ligands to polar head group residues of liposomal lipid components resulted in interference by the surface-grafted PEG chains in both the conjugation reactions and the interaction of the bound ligand with the intended target (15, 16). Several end group-functionalized PEG–lipid conjugates were recently introduced to facilitate the development of liposomes with ligands linked to the termini of the grafted PEG chains (17, 19–21). There are two principal approaches to preparation of such systems. One involves preparation of lipid vesicles containing the

* Address correspondence to Dr. Samuel Zalipsky, SEQUUS Pharmaceuticals, Inc., 960 Hamilton Court, Menlo Park, CA 94025. Telephone: 415-323-9011. Fax: 415-617-3080. E-mail: SamuelZ@SEQUUS.com.

[†] SEQUUS Pharmaceuticals, Inc.

[‡] Cytel Corp.

[®] Abstract published in *Advance ACS Abstracts*, January 1, 1997.

¹ Abbreviations: PEG, poly(ethylene glycol); mPEG-DSPE, methoxy-PEG–distearoylphosphatidylethanolamine; YIGSR, Tyr-Ile-Gly-Ser-Arg; SLX, Sialyl Lewis^x; PHPC, partially hydrogenated soy phosphatidylcholine; PDP, 3-(2-pyridyldithio)propionyl; MALDI–TOFMS, matrix-assisted laser desorption ionization–time of flight mass spectrometry.

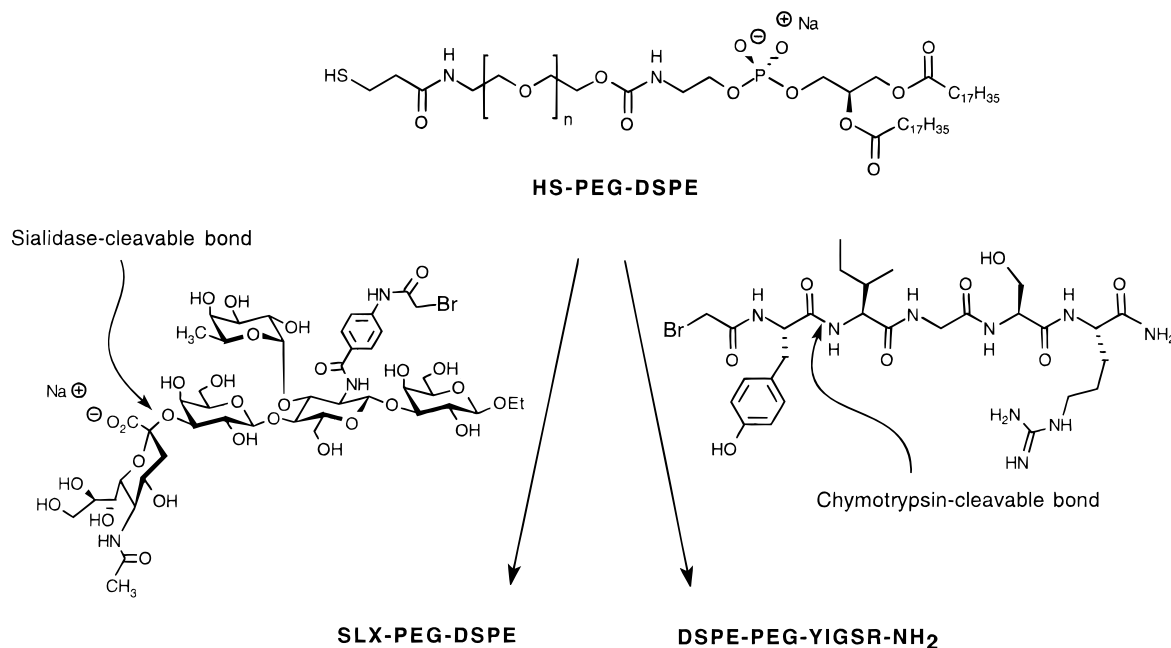


Figure 1. Schematic depiction of the conjugation reactions.

appropriate amounts of X-PEG-lipid, where X is a reactive functionality, which is then used for covalent fixation of the appropriate ligands (12, 17, 18). An alternative methodology involves the initial preparation of a three-component conjugate of the general structure ligand-PEG-lipid, followed by formulation of the liposomes (10, 13). Since in the first approach the conjugation reaction is done after liposome formation, it unavoidably leaves some reactive functional groups on the inner leaflet of the lipid bilayer and often some on the outer leaflet as well. On the other hand, if the liposomes are formulated with the preformed three-component conjugates, some of the valuable ligands inevitably are facing the enclosed aqueous compartment and thus become unavailable for their intended interaction with their biological targets.

In this manuscript, we present the results of synthesis and formulation of two new PEG-phospholipid conjugates of biological-cell adhesive ligands (Figure 1): the peptide, Tyr-Ile-Gly-Ser-Arg (YIGSR), and the oligosaccharide, Sial α 2,3Gal β 1,4(Fuc α 1,3)GlcNAc (Sialyl LewisX, SLX), each representing a major group of potentially useful substances. The pentapeptide sequence is the shortest fragment of basement membrane glycoprotein, laminin, retaining the binding activity to laminin cell surface receptors. This binding was implicated in metastasis and angiogenesis processes (22, 23). SLX is recognized *in vivo* by E-, P-, and L-selectin, which play an important role in inflammation-related tissue injury (24). The conjugates were designed to fit in liposomal membranes of mPEG-grafted lecithin/cholesterol vesicles so that the biologically active ligands would be positioned on the periphery of the grafted polymer chains. Our results show that formulations obtained by mixing either of the conjugates with the appropriate lipid components and forming 100 nm unilamellar liposomes had approximately 60% of the ligands expressed on the exterior. After careful characterization of this type of lipid vesicle, we devised an improved method for formulation of ligand-bearing polymer-grafted liposomes which contain ligand-polymer components exclusively on the outer leaflet of the lipid bilayer. Thus, the new method overcomes the limitations of both of the above-mentioned approaches to ligand-bearing PEG liposomes. This is the first

description of this methodology, which holds great promise in development of long-circulating liposomes carrying biologically active ligands on their exterior.

RESULTS AND DISCUSSION

Synthesis of Conjugates. Our synthesis strategy, schematically depicted in Figure 1, relied on the nucleophilic displacement reaction between bromoacetylated oligosaccharide or oligopeptide ligands and thiol-terminated PEG-DSPE. The use of a DSPE-based lipid anchor was warranted to maximize the lipid bilayer affinity (25) and to minimize the ability of the produced conjugates to dissociate from liposomal bilayers (26). The bromoacetyl-thiol coupling reaction was previously used for preparation of various protein and peptide adducts (27–30). The thiol component was generated by a facile reduction of 3-(2-pyridyldithio)propionate residue of PDP-PEG-DSPE, derived from PEG₂₀₀₀ (17), with tributylphosphine (28). The peptide derivative, N^ε-(bromoacetyl)-YIGSR-NH₂, was prepared by standard solid-phase peptide synthesis (30). The reactive derivative of SLX containing bromoacetylated *p*-aminobenzoyl, appended onto the amino group of the glucosamine residue of the pentasaccharide, was assembled through a series of chemical and enzymatic steps as described elsewhere (13). The conjugation reaction between the thiol and bromoacetyl components proceeded only moderately under conventional conditions often employed in protein chemistry, e.g. aqueous buffer and close to neutral pH (30). After some optimization of reaction conditions, the best results were obtained by carrying out the coupling in DMF/aqueous bicarbonate (9:1, v/v) in the presence of potassium iodide. Under these conditions, we were able to obtain approximately 70% yields of reverse-phase silica-purified YIGSR or SLX conjugates of DSPE-PEG. Both conjugates were characterized by NMR, chromatography, and mass spectrometry. Figure 2 depicts the spectra obtained by MALDI-TOFMS analysis of the conjugates. Both produced a series of 44 Da-spaced lines centered around 3540 and 4056 Da for the pentapeptide and pentasaccharide conjugates, respectively, i.e. within 44 Da, the molecular mass of one ethylene oxide unit, of the theoretical values (3496 and 4012 Da). These results represent one of the first uses of MALDI-TOFMS for char-

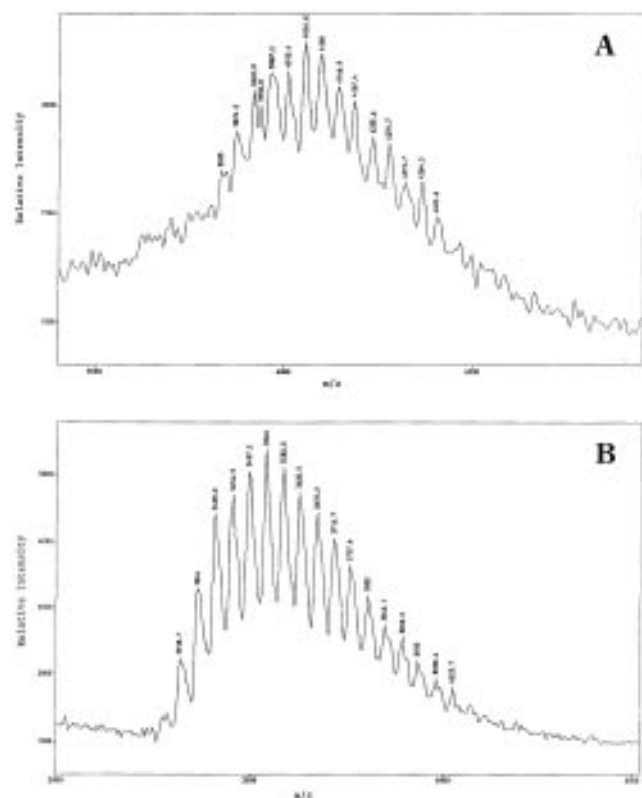


Figure 2. MALDI-TOFMS spectra of SLX-PEG-DSPE (A) and DSPE-PEG-YIGSR-NH₂ (B).

acterization of conjugates of three different components assembled in a well-defined manner (31). Both of the three-component conjugates formed clear aqueous solutions thought to be micellar in analogy to previously described solutions of mPEG-DSPE (32, 33).

Liposome Formulation and Quantitation of External Ligands. Standard methodology of lipid film hydration followed by extrusion was utilized to form liposomes containing 2 mol % of one of the ligand-PEG-lipid conjugates. On the basis of our previous experience with optimal formulations of mPEG-grafted liposomes, the total content of PEG-lipid (sum of mPEG-DSPE and ligand-PEG-DSPE) was kept at 5 mole %, while the remainder of the components was PHPC and cholesterol (55:40 mole ratio) (2, 12, 13, 17). As demonstrated by cryoelectron microscopy (Figure 3), liposomes obtained by this methodology were predominantly unilamellar. The total content of each ligand-PEG-lipid was determined by HPLC. In the case of the YIGSR ligand, we also confirmed the content of the pentapeptide by amino acid analysis. Since potential applications of these systems involve interaction of the ligand residues with the corresponding target receptors, it is the outer leaflet-bound ligand that is of primary importance. In essence, the ligand moieties facing the interior aqueous compartment are going to be wasted. In order to determine the amounts of external surface-bound ligands, we devised a strategy involving an enzymatic alteration of each of the ligands followed by HPLC determination of the amounts of starting materials and products.

There are three primary reasons for choosing this strategy. (A) Enzymes are large proteins, and thus, they are not able to diffuse through lipid bilayers. (B) Enzymatic reactions take place under conditions mild enough that they do not cause liposomal bilayer mixing and reformation. (C) Finally, enzymatic reactions are clean; i.e. they produce only one product and will proceed until the supply of accessible substrate is completely

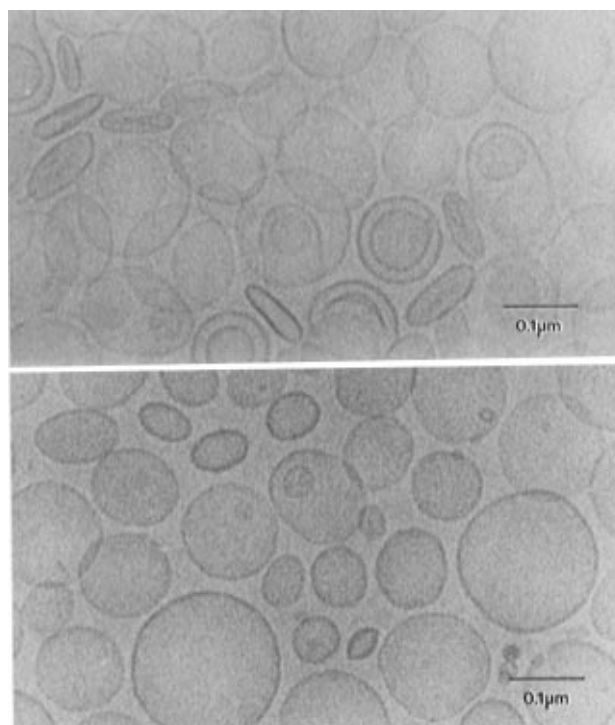


Figure 3. Cryoelectron micrographs of control (top, PHPC/cholesterol/mPEG-DSPE, 55:40:5 mole ratio, ≈ 100 nm diameter) and SLX-containing liposomes (bottom, PHPC/cholesterol/mPEG-DSPE/SLX-PEG-DSPE, 55:40:3:2 mole ratio, ≈ 100 nm diameter). Courtesy of Dr. Peter M. Frederik.

depleted. For this purpose, we chose two enzymatic cleavage reactions using readily available enzymes: sialidase and chymotrypsin. The sites of cleavage on each of the ligand residues are shown with arrows in Figure 1. Thus, enzymatic reactions performed on ligand-containing liposomes resulted in the appropriate alterations of enzyme-accessible ligand residues. Both enzymatic reactions (sialidase with SLX and chymotrypsin with YIGSR) were monitored by HPLC, which showed distinct peaks of the appropriate ligand-PEG-lipid conjugates and their enzymatically modified products. The micellar samples of both ligand-PEG-DSPE's subjected to such treatment proceeded cleanly to completion, yielding one-peak products on HPLC. Figure 4 illustrates the chromatogram of SLX-PEG-DSPE before, during, and after completion of the sialidase-mediated cleavage of the oligosaccharide. Similar chromatograms were observed in the course of DSPE-PEG-YIGSR-NH₂ digestion with chymotrypsin (data not shown). Integration of starting material and product peaks in the process of each of the enzymatic reactions provided information about the accessibility of each ligand. As can be seen from Figure 5, chymotryptic digestion of YIGSR-containing liposomes proceeded readily up to a point of approximately 55% conversion to the product, DSPE-PEG-Y. The product: starting material ratio did not change even after extended incubation with the enzyme. Since we established that all the accessible, micellar substrate is cleaved by the enzyme, this observation is consistent with 55% of the conjugate being anchored in the outer leaflet of the liposomal bilayer. Similar experiments performed with SLX liposomes showed that sialidase converted approximately 63% of liposomal SLX-PEG-DSPE into a single-peak product, LX-PEG-DSPE. Both enzymatic reactions were controlled for their activity in the presence of ligand-free liposomes.

These experiments established that slightly more than half of the total ligand-PEG-lipid conjugates (55 and

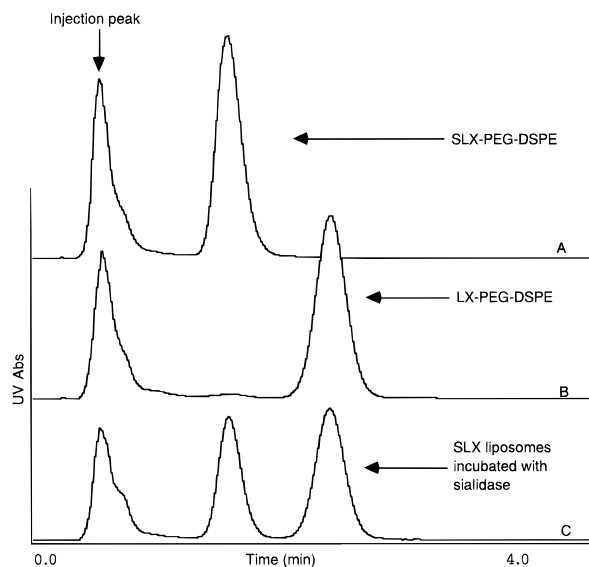


Figure 4. HPLC chromatograms of SLX-PEG-DSPE before (A) and after completion of sialidase-mediated cleavage of micellar or liposome-inserted conjugate (B). The bottom chromatogram (C), showing 63% LX-PEG-DSPE and 37% SLX-PEG-DSPE, was obtained after extensive sialidase-mediated cleavage of SLX liposomes made by premixing of all the lipid components. An identical peak profile was observed during partial cleavage of the micellar conjugate.

63%, respectively, for YIGSR and SLX liposomes) were accessible to enzymatic cleavage and thus were positioned on the external leaflets of the liposomal bilayers. These measurements of the external ligands are in accord with a simple picture of spherical unilamellar liposome geometry. Assuming a 100 nm diameter ($R = 50$ nm) and a 4 nm bilayer thickness (internal radius $r = 46$ nm), the percent of the ligand on the external leaflet should be $4\pi R^2 / (4\pi R^2 + 4\pi r^2)$, which equals 54%. Bulkier head groups of lipids, as well as deviations from the strictly spherical shape of vesicles (see Figure 3), should cause further preference for the outer surface (*1*). In comparison to YIGSR, SLX is a larger ligand. It is also a more rigid residue, and the attachment site was positioned on the second sugar moiety, further enhancing the requirements for steric accommodation. Thus, we think it is reasonable that, under otherwise identical formulation conditions, a somewhat larger percentage of SLX than YIGSR is positioned on the external surface of the liposomal bilayer.

Liposomes Bearing Ligands Exclusively on the Outer Surface. Since liposomes of this type are intended for *in vivo* applications as ligand-presenting long-circulating platforms, only the ligand residues on the external leaflet are potentially capable of interaction with their intended biological targets. Thus, it is apparent that maximal expression of the ligands on the external surface is desirable, and the inner leaflet-bound ligands are in essence wasted. Furthermore, preparation of three-component conjugates of the type described here, containing expensive biologically active ligands, is considered to be a formidable challenge. In light of these considerations, a formulation containing similar densities of ligand-PEG-lipid conjugates anchored exclusively on the external surface of the liposomal bilayer is preferable to more conventional preparations, which inevitably result in a substantial fraction of the valuable three-component conjugates being on the inner leaflet.

It has been known that incubation of some lipids with liposomes or biological cells can result in their incorporation into the lipid bilayer (*34*). Recently, Uster *et al.*

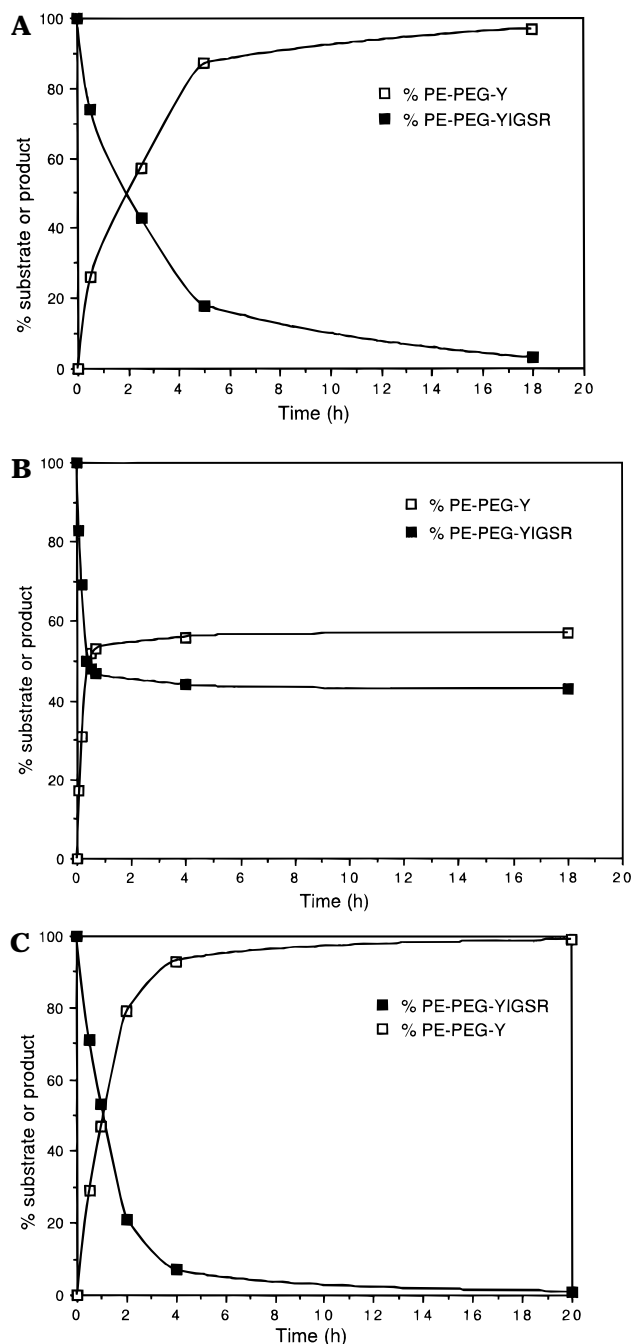


Figure 5. Results of HPLC followup of chymotryptic cleavage of DSPE-PEG-YIGSR-NH₂ (1–2 units per micromole of peptide) in a micellar form (A), liposomal formulation (PHPC/cholesterol/mPEG-DSPE/DSPE-PEG-YIGSR-NH₂, 55:40:3:2 mole ratio) obtained by the lipid film hydration–extrusion method (B), and liposomal formulation prepared by insertion of the three-component conjugate (1.2 mol %) into preformed liposomes (PHPC/cholesterol/mPEG-DSPE, 55:40:3 mole ratio) (C).

demonstrated that mPEG-DSPE can be inserted into lipid vesicles composed of lecithin/cholesterol, resulting in external surface PEG-grafted liposomes with physical and biological characteristics similar to those of liposomes obtained by hydration–extrusion of the mixture of all the lipids (*33*). Building on these precedents, we devised a method for preparation of ligand-bearing polymer-grafted liposomes containing ligand residues only on the external surface. In a few biological experiments, it was demonstrated that inclusion of 2 mol % of SLX-PEG-DSPE in mixed lipid film hydration–extrusion formulations resulted in good biological activity (*13, 35*). Therefore, our aim was to achieve the same external surface ligand

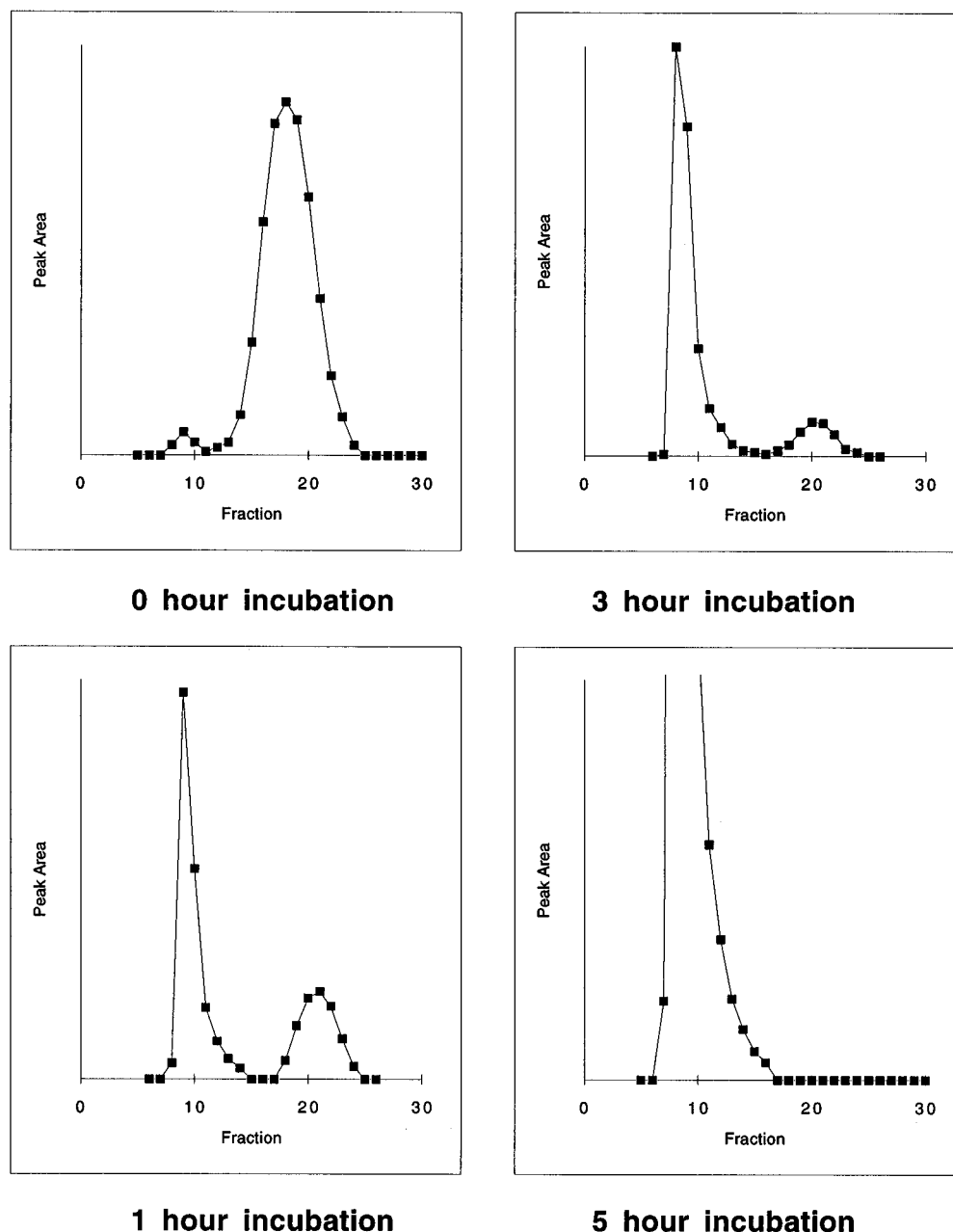


Figure 6. Separation of liposomes (peak centered around fraction 10) and micelles (peak centered around fraction 20) by size exclusion chromatography on a Biogel A50M column. Samples were taken at different time intervals after incubating SLX-PEG-DSPE (1.2 mol %) at 37 °C with preformed liposomes (PHPC/cholesterol/mPEG-DSPE, 55:40:3 mole ratio, ≈ 100 nm diameter).

density of ligand-PEG-lipid conjugates while keeping the amount of the mPEG component unchanged. According to the enzymatic cleavage experiments, approximately 60% of the ligand conjugates were on the external surface, which corresponds to 1.2 mol % of total lipid. Therefore, ligand-PEG-lipid conjugates corresponding to this amount were incubated with preformed PHPC/cholesterol liposomes containing 3 mol % of mPEG-DSPE. Thus, in contrast to previously published lipid insertion experiments (33), the starting liposomes contained mPEG-DSPE on both sides of the lipid bilayers. In exploratory experiments at various time intervals, aliquots of the liposomes incubated with SLX-PEG-DSPE at 37 °C were withdrawn and the liposomal peak was separated from the micellar conjugate by size exclusion chromatography (Figure 6). HPLC was used to determine the amounts of the ligand-containing conjugate in each of the fractions. As shown in Figure 7, insertion of the SLX-PEG-DSPE conjugate into the preformed liposomes proceeded readily at 37 °C and

noticeably more slowly at ambient temperature. Essentially, the same time course of the insertion process (data not shown) was observed upon incubation of DSPE-PEG-YIGSR-NH₂ with PHPC/cholesterol/mPEG-DSPE (55:40:3 mole ratio) liposomes. On the basis of these results, preparative batches of liposomes were obtained by 5 h of incubation at 37 °C of the appropriate amounts of either one of the three-component conjugates with the preformed liposomes. As summarized in Table 1, the average particle size determined by dynamic light scattering was only slightly increased during this process. The completeness of the incorporation of the ligand-PEG-DSPE conjugates was monitored by size exclusion chromatography. If all the inserted conjugate indeed becomes part of the external leaflet, then all the ligand in such a formulation should be available for the corresponding enzymatic cleavage. As shown in Figure 5C, and in contrast to results depicted in Figure 5B, all the liposome-inserted DSPE-PEG-YIGSR-NH₂ was completely consumed by chymotrypsin digestion. Incubation

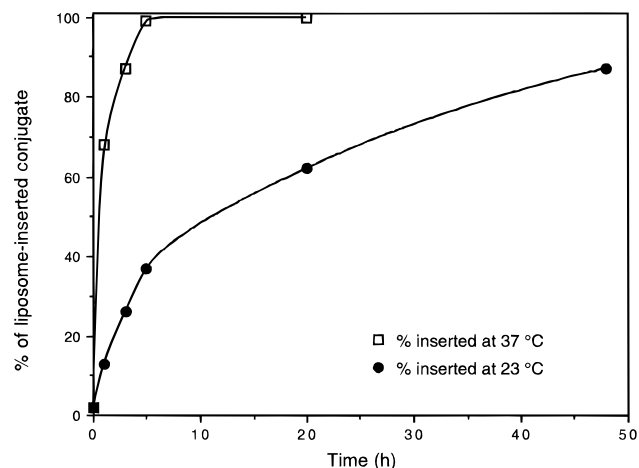


Figure 7. Time course of SLX-PEG-DSPE (1.2 mol %) insertion into the preformed liposomes (same composition and size as in Figure 6).

Table 1. Summary of Particle Sizes of YIGSR and SLX Liposomes before and after Insertion of the Corresponding Three-Component Conjugates into the External Leaflet of Preformed Unilamellar Vesicles^a

liposomal sample type		particle size (nm)	
		90° angle	30° angle
YIGSR	before insertion	100	177
	after insertion	105	233
SLX	before insertion	98	126
	after insertion	99	137

^a Unilamellar vesicles (PHPC/cholesterol/mPEG-DSPE, 55:40:3 mole ratio) prepared by film hydration–extrusion as described in Experimental Procedures were incubated for 20 h at 37 °C with either DSPE-PEG–SLX or –YIGSR conjugates (1.2 mol %). This amount of the three-component conjugate ($2\% \times 0.6 = 1.2\%$) when completely inserted results in the same amount of external leaflet-bound ligands as formulations obtained by hydration–extrusion of PHPC/cholesterol/mPEG DSPE/ligand–PEG-DSPE in a molar ratio of 55:40:3:2. Note that larger particles scatter light much more intensely at the 30° angle than smaller particles, which biases the measurement taken at the 30° angle toward the larger particles. Thus, the apparent particle size taken at the 30° angle increases much more than those taken at the 90° angle.

of SLX-bearing liposomes prepared via the insertion process with sialidase also resulted in consumption of the entire three-component conjugate and its conversion into a single HPLC identifiable product, LX-PEG-DSPE (Figure 4B). These observations confirm that the inserted three-component conjugates are positioned exclusively on the external surface of the liposomes.

Summary and Conclusions. We demonstrated the synthesis of two conjugates composed of three components: DSPE, heterobifunctional PEG acting as a linking moiety, and an oligopeptide or an oligosaccharide cell adhesive ligand. The composition and purity of the three-part constructs, confirmed by NMR and chromatography, were further corroborated by MALDI–TOFMS. The conjugates were designed for incorporation into mPEG-grafted liposomes so that the biological ligand in such formulations would be positioned right at the periphery of the polymeric brush. Using a novel combination of enzymatic cleavage and HPLC analysis, we demonstrated that 100 nm liposomes containing such three-component conjugates prepared by the traditional lipid film hydration–extrusion process express only slightly more than half (55–63%) of the total ligands on their external surface, while the rest of the ligand moieties face the internal aqueous compartment and thus are unavailable for interactions with potential biological targets. To assure more efficient utilization of ligand–PEG–lipid

conjugates, we prepared liposomal formulations via a new approach utilizing bilayer insertion of the three-component conjugates. By this method, ligand-bearing PEG-grafted liposomes with the same ligand and mPEG external surface densities as in previously biologically tested traditional formulations were readily attainable.

EXPERIMENTAL PROCEDURES

Materials and Methods. mPEG-DSPE (21), PDP-PEG-DSPE (17), and the bromoacetylated derivative of Sialyl-Lewis^x (13) were prepared as described elsewhere. N^B-(Bromoacetyl)-YIGSR-NH₂ was purchased from AnaSpec, Inc. (San Jose, CA). The enzymes, sialidase from *Vibrio cholerae* and chymotrypsin, were purchased from Oxford GlycoSystems (Rosedale, NY) and Sigma (St. Louis, MO), respectively. Partially hydrogenated soybean phosphatidylcholine (PHPC, iodine value of 35) and cholesterol were obtained from Lipoid (Ludwigshafen, Germany) and Croda (Fullerton, CA), respectively. Thin layer chromatography (TLC) on silica gel GF plates (Analtech, Newark, DE) was visualized with iodine vapor, Dragendorff- (36) and phenol-sulfuric acid spray reagents, and UV light for detection of lipid, PEG, saccharide, and UV-absorbing ligands. NMR spectra was recorded on a 360 MHz Nicolet instrument at Acorn NMR (Fremont, Ca). Matrix-assisted laser desorption/ionization-time of flight mass spectrometry (MALDI–TOFMS) was carried out at M-Scan, Inc. (West Chester, PA) on a VG ToFSpec mass spectrometer utilizing a UV nitrogen laser at 337 nm and a VAX 4000 data station. Spectra of DSPE-PEG–oligopeptide or –oligosaccharide were acquired from 0.1 mg/mL solutions of the conjugates in 50 mM NaCl, containing *trans*-3-indoleacrylic acid (matrix material) and insulin (internal standard). The liposome particle size was determined by dynamic light scattering (Coulter N4MD, Hialeah, FL). Shimadzu and Rainin HPLC systems were used interchangeably. Amino acid analysis was performed on hydrolyzed aliquots of peptide liposomes at the Protein Structure Laboratory of the University of California, Davis.

Preparation of HS-PEG-DSPE. Tributylphosphine (80 μ L, 0.32 mmol) was added under N₂ to a clear solution of PDP-PEG-DSPE (200 mg, 0.064 mmol) in isopropanol/water (1:4, 6 mL) containing EDTA (10 mM). After 2 h, TLC (CHCl₃:CH₃OH:H₂O = 90:18:2) revealed that the reaction was complete. The starting material ($R_f = 0.56$) absorbed UV and was positive to Dragendorff spray. The product, HS-PEG-DSPE ($R_f = 0.58$), did not absorb UV but was positive to Dragendorff spray. The byproduct, 2-thiopyridone, was observed under UV light ($R_f = 0.65$). The reaction mixture was lyophilized. The yellowish solid residue was triturated with ether (3 \times 3 mL). The residual white solid (196 mg, 99% yield) was dried under a water aspirator pressure and then *in vacuo* over P₂O₅. It was used directly in the next step.

Preparation of SLX-PEG-DSPE. The bromoacetylated derivative of SLX (98 mg, 0.08 mmol) was added to a DMF (2.8 mL) solution of HS-PEG-DSPE (197 mg, 0.07 mmol) followed by potassium iodide (14.3 mg, 0.086 mmol). After \approx 5 min, a NaHCO₃ (0.4 M)/Na₂EDTA (10 mM) solution (pH 8.0, 328 μ L, 0.13 mmol of bicarbonate) was added. The reaction mixture was stirred at room temperature overnight. After 21 h, TLC (CHCl₃:CH₃OH:H₂O = 75:36:6) showed the SLX-PEG-DSPE product ($R_f = 0.37$, visualized by UV, Dragendorff and phenol/H₂SO₄ sprays) and weak spots of the starting materials: SLX derivative ($R_f = 0.0$) and HS-PEG-DSPE ($R_f = 0.85$). Water (12 mL) was added to the reaction mixture, and it was loaded onto a C8 silica column (8 g, 1 \times 40 cm, LC-8 Supelclean, Supelco). The column was eluted with

a stepwise gradient of methanol (0 to 70% v/v) in water (10% increments every 20 mL) and then 15:80:5 water/methanol/chloroform (60 mL). The product-containing fractions were pooled and evaporated at ambient temperature, producing colorless thick liquid. It was dissolved in *tert*-butanol (5 mL), lyophilized, and further dried *in vacuo* over P_2O_5 to yield a white fluffy solid (203 mg, 74%). 1H -NMR (CD_3OD): δ 0.88 (t, CH_3 -lipid, 6H), 1.15 (d, H-6 Fuc, 3H), 1.19 (t, OCH_2CH_3 , 3H), 1.29 (bs, $(CH_2)_n$, 56H), 1.61 (bm, $CH_2CH_2C=O$, 4H), 1.73 (t, H-3_{ax}-Sial, 1H), 2.01 (s, NHAc, 3H), 2.32 (2 \times t, CH_2CO , 4H), 2.58 (t, SCH_2CH_2CONH , 2H), 2.87 (dd, H-3_{eq}-Sial, 1H), 2.93 (t, SCH_2CH_2CONH , 2H), 3.35 (m, $NHCH_2$, 4H), 3.64 (s, PEG, \approx 180H), 3.7–4 (m, overlapping sugar peaks and $CH_2PO_4CH_2$, 8H), 4–4.31 (m, overlapping, 5H), 4.43 (dd, $CHCH_2CO$, 1H), 4.54 (d, H-1 Gal, 1H), 4.83 (m, H-5 Fuc, 1H), 4.90 (d, H-1 GlcN, 1H), 5.06 (d, H-1 Fuc, 1H), 5.2 (m, $POCH_2CHCH_2$, 1H), 7.70 and 7.84 (2 \times d, phenyl, 4H). MALDI-TOFMS (Figure 2A) produced a bell-shaped distribution of ions spaced at equal 44 ± 1 Da intervals and centered at 4056 Da (theory, 4012 Da).

Preparation of DSPE-PEG-YIGSR-NH₂. HS-PEG-DSPE (196 mg, 0.07 mmol) and *N*^ε-(bromoacetyl)-YIGSR-NH₂ (54.2 mg, 0.07 mmol, 1.2 equiv) were dissolved in DMF (2 mL) and treated with potassium iodide (14.1 mg, 0.09 mmol, 1.3 equiv), followed by a $NaHCO_3$ (0.4 M)/ Na_2EDTA (10 mmol) solution (pH 8.0, 326 μ L). After 21 h of stirring, TLC ($CHCl_3:CH_3OH:H_2O = 75:36:6$) confirmed the presence of expected product ($R_f = 0.55$) along with small amounts of the starting thiol and peptide derivatives. The reaction mixture was diluted with 5 mL of water and loaded onto a C8 silica column (8 g, 1 \times 40 cm, LC-8 Supelclean, Supelco), which was eluted with another 12 mL of water followed by a methanol gradient (0 to 70% v/v) in water (10% increments every 25 mL) and then 10:80:10 water/methanol/chloroform (60 mL). The product-containing fractions were pooled and evaporated at ambient temperature, producing colorless thick liquid. It was dissolved in *tert*-butanol (5 mL), lyophilized, and further dried *in vacuo* over P_2O_5 to yield a white fluffy solid (174 mg, 69% yield). 1H -NMR (CD_3OD): δ 0.9 (3 \times t, CH_3 of Ile and lipid, 12H), 1.2 (m, 1H), 1.26 (s, CH_2 , 56H), 1.58 (bm, $CH_2CH_2C=O$, 4H), 1.7 (m, 1H), 2.31 (2 \times t, $CH_2C=O$, 4H), 2.45 (t, SCH_2CH_2CONH), 2.7 (t, SCH_2CH_2CONH), 2.9 and 3.1 (dd, peptide, 2H), 3.2 (m, 2H), 3.35 (m, $NHCH_2$, 4H), 3.45 (t, 2H), 3.64 (s, PEG, \approx 180H), 3.7 (m, 4H), 3.9 (m, CH_2PO_4 , 4H), 4.0 (m, 3H), 4.15–4.2 (overlapping peaks, 4H), 4.3–4.45 (overlapping peaks, 3H), 4.6 (m, 2H), 5.2 (m, PO_4CH_2CH , 1H), 6.7 and 7.1 (2 \times d, phenyl of Tyr, 4H). MALDI-TOFMS (Figure 2B) produced a bell-shaped distribution of ions spaced at equal 44 ± 1 Da intervals and centered at 3540 Da (theory, 3496 Da).

Liposome Preparation. The ligand-containing liposomes were composed of PHPC, cholesterol, mPEG-DSPE, and ligand-PEG-lipid at a molar ratio of 55:40:3:2. All liposomes were prepared by mixing chloroform and/or methanol solutions of different lipids in a round bottom flask. The solvents were removed by rotary evaporation, and the dried lipid film produced was hydrated with either sodium phosphate buffer (10 mM, 140 mM NaCl, pH 7) or HEPES buffer (25 mM, 150 mM NaCl, pH 7) to produce large multilamellar vesicles. The resulting vesicles were passed repeatedly under pressure through 0.2, 0.1, and 0.05 μ m pore size polycarbonate membranes (37), until the average size distribution for the diameter (monitored by dynamic light scattering) was approximately 100 nm. The mean particle diameter measured from 12 different batches ranged from 92 to 111 nm with an average of 98 nm. The content of the

SLX-PEG-DSPE or DSPE-PEG-YIGSR-NH₂ in liposomes was determined by HPLC at 272 nm using reverse-phase HPLC. Quantitation of SLX-PEG-DSPE (Symmetry C8 column, 1 mL, Waters Associates, Milford, MA, mobile phase of 92% aqueous methanol containing 20 mM ammonium phosphate at pH 7.0) in the liposome preparations was greater than 97% of the amounts used in the corresponding formulations. A Prodigy C8 column (Phenomenex, Torrance, CA) with 92% aqueous methanol, containing 0.1% TFA, was used for detection and quantitation of DSPE-PEG-YIGSR-NH₂ and its digestion product. The amino acid composition of YIGSR liposomes determined by amino acids analysis was as follows: Tyr, 0.97; Ile, 1.00; Gly, 0.98; Ser, 0.96; and Arg, 1.08. The peptide content in 2 mol % formulations calculated from phosphate and amino acid analysis was in the range of 28–32 mmol per mole of phospholipid, which was in accord with the ligand contents determined by HPLC.

Cryoelectron microscopy photographs were obtained by previously published method of Dr. P. M. Frederik (38).

Quantitation of Outer Leaflet-Bound Ligands.

Liposomes containing SLX-PEG-DSPE (2 mol %, 12.5 μ mol/mL) were incubated for 16 h with sialidase (1 unit/mL) at 37 °C in the digestion buffer (50 mM histidine, 4 mM $CaCl_2$, and 150 mg/mL BSA at pH 6.5). Samples were diluted 10 fold with methanol and analyzed by HPLC. These experiments showed consistently that 62–64% of the initial oligosaccharide-containing conjugate was converted into the product, while 36–38% of the starting conjugate remained unchanged. Under the same conditions, micellar samples of SLX-PEG-DSPE (elution time of 1.5 min) were completely converted into a single-peak product (2.4 min), LX-PEG-DSPE. Liposomes containing DSPE-PEG-YIGSR-NH₂ (2 mol %) were digested with chymotrypsin (1–2 units per micromole of peptide) in HEPES buffer (25 mM, pH 7.2, 37 °C). At different time intervals, aliquots were taken, diluted with methanol, and analyzed by HPLC. The starting peptide conjugate eluted at 4.2 min, while the single-peak product, DSPE-PEG-Y, eluted at 7.6 min. Liposomal samples of peptide conjugates were cleaved with chymotrypsin to the extent of 52–59%. The remaining 41–48% of the starting conjugate, presumably localized in the inner leaflets of the liposomal bilayers, was not altered by the enzymatic reaction (Figure 5B).

Insertion of Ligand-PEG-DSPE Conjugates into Preformed Liposomes.

Liposomes were prepared as before with 3 mol % of mPEG-DSPE and no ligand conjugates. They were then incubated at ambient temperature or 37 °C for up to 48 h with amounts corresponding to 1.2 mol % of SLX-PEG-DSPE or DSPE-PEG-YIGSR-NH₂ (equal to 60% of 2 mol % in the original formulations). At various time points, free ligand conjugates (micelles) were separated from inserted ligands (liposomes) by size exclusion chromatography (SEC). For SLX liposomes, a Biogel A50M column equilibrated with 10 mM sodium phosphate, 140 mM sodium chloride, and 0.02% NaN_3 at pH 6.5 was used. For YIGSR-containing liposomes, a Sepharose 4B column was used with 10% sucrose and 10 mM HEPES at pH 7.0 as eluent. Fractions (1 mL) were collected, diluted 1:10 in methanol, and analyzed for ligand content by HPLC (see Figure 6).

ACKNOWLEDGMENT

We thank Dr. Paul Uster of SEQUUS Pharmaceuticals, Inc., for useful discussions about the lipid insertion phenomena and Dr. Peter M. Frederik of the University of Maastricht for preparation of cryoelectron micrographs of liposomes.

LITERATURE CITED

- (1) Lasic, D. D. (1993) *Liposomes: From Physics to applications*, Elsevier, Amsterdam.
- (2) Woodle, M. C., and Lasic, D. D. (1992) Sterically stabilized liposomes. *Biochim. Biophys. Acta* 1113, 171–199.
- (3) Sato, T., and Sunamoto, J. (1992) Recent aspects in the use of liposomes in biotechnology and medicine. *Prog. Lipid Res.* 31, 345–372.
- (4) Allen, T. M. (1994) The use of glycolipids and hydrophilic polymers in avoiding rapid uptake of liposomes by the mononuclear phagocyte system. *Adv. Drug Delivery Rev.* 13, 285–309.
- (5) Lasic, D. D., and Needham, D. (1995) The "Stealth" liposome: A prototypical biomaterial. *Chem. Rev.* 95, 2601–2628.
- (6) Lasic, D., and Martin, F., Eds. (1995) *Stealth Liposomes*, CRC Press, Boca Raton, FL.
- (7) Woodle, M. C., Engbers, C. M., and Zalipsky, S. (1994) New amphipatic polymer-lipid conjugates forming long-circulating reticuloendothelial system-evading liposomes. *Bioconjugate Chem.* 5, 493–496.
- (8) Zalipsky, S., Hansen, C. B., Oaks, J. M., and Allen, T. M. (1996) Evaluation of blood clearance rates and biodistribution of poly(2-oxazoline)-grafted liposomes. *J. Pharm. Sci.* 85, 133–137.
- (9) Gabizon, A., Catane, R., Uziely, B., Kaufman, B., Safra, T., Cohen, R., Martin, F., Huang, A., and Barenholz, Y. (1994) Prolonged circulation time and enhanced accumulation in malignant exudates of doxorubicin encapsulated in polyethylene glycol coated liposomes. *Cancer Res.* 54, 987–992.
- (10) Lee, R. J., and Low, P. S. (1994) Delivery of liposomes into cultured KB cells via folate receptor-mediated endocytosis. *J. Biol. Chem.* 269, 3198–3204.
- (11) Vogel, K., Wang, S., Lee, R. J., Chmielewski, J., and Low, P. S. (1996) Peptide-mediated release of folate-targeted liposome contents from endosomal compartments. *J. Am. Chem. Soc.* 118, 1581–1586.
- (12) Zalipsky, S., Puntambekar, B., Bolikas, P., Engbers, C. M., and Woodle, M. C. (1995) Peptide attachment to extremities of liposomal surface grafted PEG chains: Preparation of the long-circulating form of laminin pentapeptide, YIGSR. *Bioconjugate Chem.* 6, 705–708.
- (13) DeFrees, S. A., Phillips, L., Guo, L., and Zalipsky, S. (1996) Sialyl Lewis^x liposomes as a multivalent ligand and inhibitor of E-Selectin mediated cellular adhesion. *J. Am. Chem. Soc.* 118, 6101–6104.
- (14) Zalipsky, S., Hansen, C. B., Lopes de Menezes, D. E., and Allen, T. M. (1996) Long-circulating, polyethylene glycol-grafted immunoliposomes. *J. Controlled Release* 39, 153–161.
- (15) Klibanov, A. L., Maruyama, K., Beckerleg, A. M., Torchilin, V. P., and Huang, L. (1991) Activity of amphipatic poly(ethylene glycol) 5000 to prolong the circulation time of liposomes depends on the liposome size and is unfavorable for immunoliposome binding to target. *Biochim. Biophys. Acta* 1062, 142–148.
- (16) Hansen, C. B., Kao, G. Y., Moase, E. H., Zalipsky, S., and Allen, T. M. (1995) Attachment of Antibodies to Sterically Stabilized Liposomes: Evaluation, Comparison and Optimization of Coupling Procedures. *Biochim. Biophys. Acta* 1239, 133–144.
- (17) Allen, T. M., Brandeis, E., Hansen, C. B., Kao, G. Y., and Zalipsky, S. (1995) A new strategy for attachment of antibodies to sterically stabilized liposomes resulting in efficient targeting to cancer cells. *Biochim. Biophys. Acta* 1237, 99–108.
- (18) Blume, G., Cevc, G., Crommelin, M. D. J. A., Bakker-Woudenberg, I. A. J. M., Kluft, C., and Storm, G. (1993) Specific targeting with poly(ethylene glycol)-modified liposomes: coupling of homing devices to the ends of the polymeric chains combines effective target binding with long circulation times. *Biochim. Biophys. Acta* 1149, 180–184.
- (19) Zalipsky, S. (1995) Polyethylene glycol-lipid conjugates. In *Stealth Liposomes* (D. Lasic and F. Martin, Eds.) pp 93–102, CRC Press, Boca Raton, FL.
- (20) Zalipsky, S. (1995) Chemistry of polyethylene glycol conjugates with biologically active molecules. *Adv. Drug Delivery Rev.* 16, 157–182.
- (21) Zalipsky, S. (1993) Synthesis of an end-group functionalized polyethylene glycol-lipid conjugate for preparation of polymer-grafted liposomes. *Bioconjugate Chem.* 4, 296–299.
- (22) Iwamoto, Y., Robey, F. A., Graf, J., Sasaki, M., Kleinman, H. K., Yamada, Y., and Martin, G. R. (1987) YIGSR, a synthetic laminin pentapeptide, inhibits experimental metastasis formation. *Science* 238, 1132–1134.
- (23) Sakamoto, N., Iwahana, M., Tanaka, N. G., and Osada, Y. (1991) Inhibition of angiogenesis and tumor growth by a synthetic laminine peptide, CDPGYIGSR-NH₂. *Cancer Res.* 51, 903–906.
- (24) Phillips, M. L., Nudelman, E., Gaeta, F. C. A., Perez, M., Singhal, A. K., Hakomori, S., and Paulson, J. C. (1990) ELAM-1 mediates cell adhesion by recognition of a carbohydrate ligand, sialyl-Le^x. *Science* 250, 1130–1132.
- (25) Parr, M. J., Ansell, S. M., Choi, L. S., and Cullis, P. R. (1994) Factors influencing the retention and chemical stability of poly(ethylene glycol)-lipid conjugates incorporated into large unilamellar vesicles. *Biochim. Biophys. Acta* 1195, 21–30.
- (26) Silvius, J. R., and Zuckerman, M. J. (1993) Interbilayer transfer of phospholipid-anchored macromolecules via monomer diffusion. *Biochemistry* 32, 3153–3161.
- (27) Bernatowicz, M. S., and Matsueda, G. R. (1986) Preparation of peptide-protein immunogens using N-succinimidyl bromoacetate as a heterobifunctional crosslinking reagent. *Anal. Biochem.* 155, 95–102.
- (28) Kolodny, N., and Robey, F. A. (1990) Conjugation of synthetic peptides to proteins: Quantitation from S-carboxymethylcysteine released upon acid hydrolysis. *Anal. Biochem.* 187, 136–140.
- (29) Dawson, P. E., and Kent, S. B. H. (1993) Convenient total synthesis of a 4-helix TASP molecule by chemoselective ligation. *J. Am. Chem. Soc.* 115, 7263–7266.
- (30) Robey, F. A. (1994) Bromoacetylated synthetic peptides. *Methods Mol. Biol.* 35, 73–90.
- (31) Lee, S., Winnik, M. A., Whittall, R. M., and Li, L. (1996) Synthesis of symmetric fluorescently labeled poly(ethylene glycols) using phosphoramidites of pyrenebutanol and their characterization by MALDI mass spectrometry. *Macromolecules* 29, 3060–3072.
- (32) Hristova, K., Kenworthy, A., and McIntosh, T. J. (1995) Effect of bilayer composition on the phase behavior of liposomal suspensions containing poly(ethylene glycol)-lipids. *Macromolecules* 28, 7693–7699.
- (33) Uster, P. S., Allen, T. M., Daniels, B. E., Mendez, C. J., Newman, M. S., and Zhu, G. Z. (1996) Insertion of poly(ethylene glycol) derivatized phospholipid into pre-formed liposomes results in prolonged in vivo circulation time. *FEBS Lett.* 386, 243–246.
- (34) Kanda, S., Inoue, K., Nojima, S., Utsumi, H., and Wiegandt, H. (1982) Incorporation of ganglioside and spin-labeled ganglioside analogue into cell and liposomal membranes. *J. Biochem.* 91, 2095–2098.
- (35) Murohara, T., Margiotta, J., Phillips, L. M., Paulson, J. C., DeFrees, S., Zalipsky, S., Guo, L., and Lefer, A. M. (1995) Cardioprotection by liposome-conjugates sialyl Lewis^x-oligosaccharide in myocardial ischemia and reperfusion injury. *Cardiovasc. Res.* 30, 965–974.
- (36) Bürger, K. (1963) Spurennachweis und Quantitative Bestimmung von grenzflächenaktiven Polyäthylenoxidverbindungen und von Polyäthylenglycolen. *Z. Anal. Chem.* 196, 251–259.
- (37) Olson, F., Hunt, C. A., Szoka, F. C., Vail, W. J., and Papahadjopoulos, D. (1979) Preparation of liposomes of defined size distribution by extrusion through polycarbonate membranes. *Biochim. Biophys. Acta* 557, 9–23.
- (38) Frederik, P. M., Stuart, M. C. A., Bomans, P. H. H., Busing, W. M., Burger, K. N. H., and Verkleij, A. J. (1991) Perspective and limitations of cryo-electron microscopy: From model systems to biological specimens. *J. Microsc. (Oxford)* 161, 253–262.

Oligonucleotides Tethering Hoechst 33258 Derivatives: Effect of the Conjugation Site on Duplex Stabilization and Fluorescence Properties

Kristin Wiederholt, Sharanabasava B. Rajur, and Larry W. McLaughlin*

Department of Chemistry, Merkert Chemistry Center, Boston College, Chestnut Hill, Massachusetts 02167.
Received September 26, 1996[®]

A series of DNA conjugates have been prepared in which two different derivatives of Hoechst 33258 have been tethered to a sequence containing a 5'-GAATTC-3' target site. The two derivatives differ only in the length of the tether between the DNA and the Hoechst fluorophore. By using a DNA backbone labeling protocol, one in which the Hoechst dye is tethered to an internucleotide phosphoramidate residue, it was possible to easily vary the site of attachment with respect to the A-T rich binding site. When tethered outside the GAATTC sequence, little if any helix stabilization results upon hybridization of the conjugate to its complementary sequence. As the site of conjugation is moved to one end of the target sequence and finally within the AATT sequence, more effective helix stabilization results. When tethered between the two A residues, or between the A and T residue, a ΔT_m of at least +20 °C is observed. Upon hybridization and formation of the B-form DNA, binding by the tethered Hoechst dye results, and the bound dye becomes brightly fluorescent. Upon a simple titration of the single-stranded conjugate with the complementary target sequence the quantum yield enhancement for hybridization only appears to be 5–7-fold at best. These fluorescence effects, generally less dramatic than those observed with other sequences, result from an increase in quantum yield for the single-stranded conjugate relative to the free Hoechst 33258. Heating the single-stranded conjugate reduces the inherent fluorescence of the single-stranded conjugate to a level comparable with that of the free Hoechst dye. In experiments monitoring absorbance vs temperature, a cooperative transition is observed for the single-stranded conjugate. Both the high quantum yield observed for the single-stranded conjugate and the observed thermally induced transition suggest that the single-stranded conjugate can dimerize (at the GAATTC site), mediated by the groove-binding fluorophore.

INTRODUCTION

The Hoechst dyes are a class of extended heterocycles based upon the bisbenzimidazole ring system that are capable of binding in the minor groove of B-form DNA at A-T-rich sequences. The flexible nature of this extended heterocyclic ring system permits the dye to adopt a conformation that is isohelical with the minor groove and thus optimize binding to double-stranded DNA (1). Crystallographic analyses (2–5) have confirmed the minor groove nature of these dye–DNA complexes and suggested that the preference for binding in A-T-rich sequences is the ability of the benzimidazole rings to penetrate deeply within the groove structure, where they can make hydrogen bonding contacts with specific thymine *O*-carbonyls and adenine *N*³-nitrogens (2–5). Electrostatic effects (6) and van der Waals contacts (7) also play an important role in complex formation. The presence of G residues in the DNA duplex results in one or more *N*²-amino groups protruding into the minor groove, and the presence of this functional group prevents penetration by the dye into the groove structure (8, 9). The sequence preferences for complex formation by Hoechst 33258 require a minimum of four contiguous A-T (T-A) base pairs (8, 10–14) with the double-stranded sequences AAAA·TTTT and AATT·AATT being the preferred binding sites. However, the exact nature of the binding may differ depending upon the target sequence; different sets of crystallographic analyses have indicated

that the position of the Hoechst 33258 fluorophore in the target sequence (GAATTC)₂ can be across the ATTC sequence (2) or across the AATT sequence (3, 5), and similar differences are observed for the target (CAAATTTG)₂ (15, 16).

In addition to their groove-binding characteristics, the Hoechst dyes have fluorescent properties with a relatively large Stokes shift (17). Although only moderately fluorescent in aqueous solution, upon binding to double-stranded DNA they exhibit a dramatically enhanced quantum yield (18). These effects appear to be related to the tight binding within the minor groove, where the excited state is protected from the aqueous solution and from processes involving nonradiative decay of the excited state (17). The fluorescence characteristics of bisbenzimidazoles have been used to automate DNA content assays (19–21), to determine cell numbers (22, 23), and to sort chromosomes (24). The quantum yield effects for these dyes are sensitive enough to permit the detection of one target cell per million in mixed cell populations using appropriate instrumentation (25).

The development of DNA conjugates that rely upon the well-characterized Watson–Crick hydrogen bonding interactions for sequence targeting, and also tether a ligand capable of reporting upon the hybridization event, should be important in the development of DNA-based diagnostics, such as *in situ* hybridization probes. In the current work, the ligand is a groove-binding agent that requires formation of the B-form DNA minor groove to initiate binding. In this respect, hybridization by the conjugate is required to trigger the binding event by the tethered ligand. The resultant fluorescent signal reports on the success of this event. We have previously described (26)

* Author to whom correspondence should be addressed [telephone (617) 552-3622; fax (617) 552-2705; e-mail larry.mclaughlin@bc.edu].

[®] Abstract published in *Advance ACS Abstracts*, February 1, 1997.

the synthesis of two Hoechst 33258 analogues used to prepare the DNA–Hoechst conjugates. In the present paper we examine a specific binding site (GAATTC)₂ containing four A-T (T-A) base pairs and determine how placement of the tethered Hoechst analogues affects both helix stability and the fluorescence properties of the conjugate/target hybridization complex.

EXPERIMENTAL PROCEDURES

Materials. Oligodeoxynucleotides were synthesized using 2'-deoxynucleoside phosphoramidites on an Applied Biosystems 381A DNA synthesizer. The four common 2'-deoxynucleoside phosphoramidites containing aryl- or isobutyrylamides were purchased from BioGenex (San Ramon, CA). H-phosphonate derivatives were obtained from Glen Research (Sterling, VA). The controlled pore glass support containing the 3'-terminal nucleoside was a product of CPG Inc. (Fairfield, NJ). Cystamine dihydrochloride, adamantanecarbonyl chloride, anhydrous solvents, and ammonium hydroxide were all obtained from the Aldrich Chemical Co. (Milwaukee, WI).

Nuclease P1 and snake venom phosphodiesterase were products of Boehringer Mannheim (Indianapolis, IN). Acrylamide and bis(acrylamide) were obtained from ICN Biomedicals (Cleveland, OH). Thin layer chromatography was performed on aluminum-backed precoated silica gel 60 F254 plates purchased from EM Science (Gibbstown, NJ). UV measurements for thermal denaturation studies employed an AVIV 14DS spectrophotometer equipped with digital temperature control. Fluorescence emission spectra were collected on a Shimadzu RF5000U fluorescence spectrophotometer containing a Shimadzu DR-15 microprocessor and graphics display terminal.

Methods. *Syntheses.* The synthesis of the two Hoechst derivatives **3** and **4** has been described elsewhere (26), and the DNA–Hoechst conjugates were prepared using a thiol-containing linker attached to the DNA backbone (27). The site of the cystamine-based linker was determined by the position at which the nucleoside H-phosphonate derivative was incorporated. For conjugation sites i and ii, the H-phosphonate of dG was employed, and for conjugation sites iii and iv the H-phosphonate derivative of dA was used.

Oligonucleotide Conjugation. To 1 A₂₆₀ unit of a single diastereomer of the desired dodecamer in 100 mM Tris·HCl, pH 8, was added DTT to a concentration of 10 mM, and the mixture was incubated at 50 °C for 1 h. HPLC analysis [50 mM triethylammonium acetate, pH 7.0, with a linear gradient of acetonitrile (7–28% over 30 min)] after this time period indicated the complete absence of the triphenylmethylacetyl-protected sequence (retention time ~ 28 min) and the presence of a new peak (retention time ~ 9 min). The bromoacetylated Hoechst derivative (**3** or **4**) in DMF was added to this reaction mixture to a concentration of 15 mM (40% DMF). The reaction mixture was shaken at ambient temperature for 48 h (a precipitate appeared during this period). An equal amount of formamide was added to the reaction mixtures; they were heated to 90 °C (to dissolve aggregates) and loaded directly onto the gel for isolation by electrophoresis.

The conjugated product was purified on a 20% denaturing (7 M urea) polyacrylamide gel. A fluorescent band (365 nm excitation) was present at a position that was retarded slightly from that of the oligomer containing the cystamine-based linker. This band was excised from the gel, crushed, and soaked in 0.3 M sodium acetate, pH 6. The gel was removed and the product desalted using a C₁₈ Sep-Pak column and a water/methanol gradient. The conjugated oligomer was eluted with

approximately 80% methanol in water. Yields varied, typically 0.3–0.5 A₂₆₀ units. The product exhibited a UV–vis spectrum having characteristics of both DNA (λ_{max} = 260 nm) and the Hoechst fluorophore (λ_{max} = 342 nm).

T_m Values. T_m values were obtained for complexes containing a 1:1 mixture of the conjugate and its complementary sequence in 21 mM HEPES, pH 7.5, containing 100 mM NaCl and 20 mM MgCl₂ at duplex concentrations in the low micromolar range (1–2 μ M). Solutions were heated to 90 °C and then cooled slowly to 0 °C prior to analysis. The samples were then heated in 0.5 or 1.0 °C steps, and absorbance readings were taken after a period of temperature stabilization. Absorbance and temperature readings were plotted using Igor software. T_m values were determined from first- and second-order derivatives, as well as graphically from the absorbance vs temperature plots.

Fluorescence Measurements. Fluorescence measurements were made in solutions typically containing ~1 μ M of the DNA–Hoechst conjugate in 21 mM HEPES, pH 7.5, containing 100 mM NaCl and 20 mM MgCl₂. All emission measurements were made with the following list of parameters: slit width, Ex/Em = 10 nm/10 nm, low sensitivity, medium speed. Samples were introduced into a 1.25 mL cell thermally isolated with a water jacket. Temperature was controlled with a recirculating water bath typically at 20 or 90 °C. Fluorescence emissions were measured at 470 nm with an excitation wavelength of 342 nm. The fluorescence enhancement (ΔF) values were ratios obtained at 450 nm. This emission wavelength represented the emission maximum for the duplex conjugates and was slightly off the emission maximum for the single-stranded conjugates.

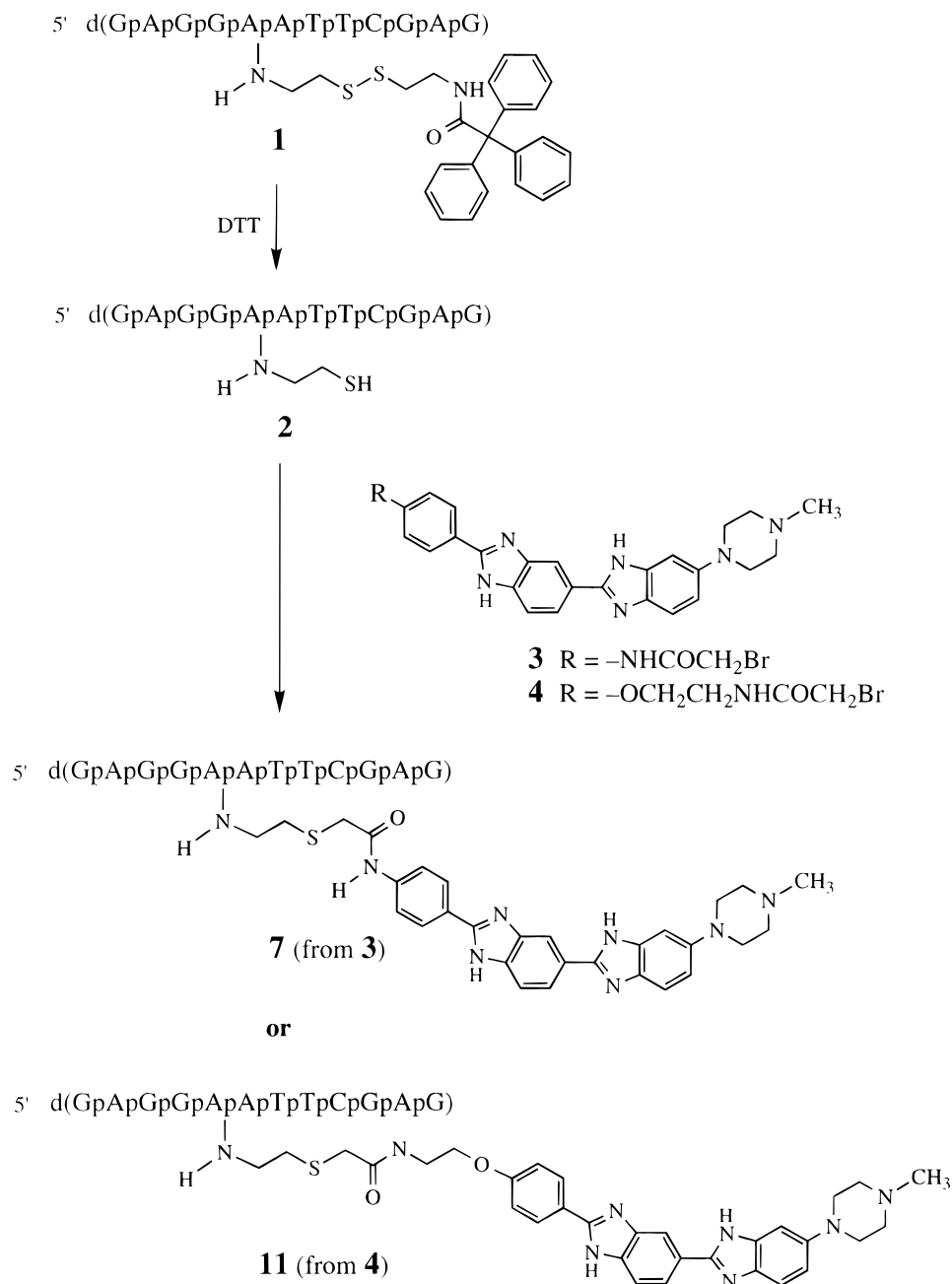
RESULTS AND DISCUSSION

We have previously described the preparation of a series of DNA–Hoechst conjugates and characterized their thermal denaturation and fluorescence properties for a sequence target containing six contiguous A-T¹ base pairs (26). In the present work we examine complex formation between the conjugate and a target sequence containing only a four base-pair binding site for the Hoechst derivative and then determine how the site of conjugation impacts both helix stabilization and the fluorescence properties of the conjugated complexes. A four base-pair target site is required for binding by Hoechst 33258, and both AAAA·TTTT and (AATT)₂ have been shown to be the preferred four base-pair binding sites (8, 10–14). For this study we chose the binding site (GAATTC)₂ in which the palindromic four base-pair A-T-rich target site is flanked by two G-C base pairs. This target site has been used previously in crystal structure analyses (2, 3, 5) and identified by DNA footprinting studies using Hoechst 33258 (8, 10–14).

Synthesis of the Oligonucleotide Conjugates. The parent Hoechst 33258 cannot be covalently tethered to the oligonucleotides of interest without the introduction of appropriate functionality. We have described the synthesis of two Hoechst analogues (**3** and **4**, Scheme 1) (26) in which a bromoacetamide tether is incorporated into the terminal phenyl moiety of the parent fluorophore. The two analogues differ only in the nature of the tether. Hoechst derivative **4** contains an additional three atoms (–OCH₂CH₂–) to lengthen the tether slightly with respect to **3**. Both derivatives can be conjugated to an alkyl thiol in aqueous solutions at pH 8.

¹ All letter abbreviations refer to the 2'-deoxynucleosides.

Scheme 1



The two Hoechst analogues were conjugated to the DNA sequences using a postsynthetic approach. To vary the site of conjugation within the DNA sequence, we have employed a backbone labeling procedure (27, 28) in which the dye is tethered to a short thiol linker incorporated into the DNA sequence as a phosphoramidate internucleotide linkage. The internucleotide phosphoramidate is prepared by oxidation of an H-phosphonate linkage, immediately after its introduction to the DNA sequence, using pyridine/CCl₄ and the *N*-(triphenylmethylacetamyl)-cystamine (27). Oxidation of the H-phosphonate generates two isomeric phosphoramidate conjugates, the *Rp* and *Sp* diastereomers, tethering the *N*-triphenylacetamide derivative of cystamine (**1**, Scheme 1). Placement of the bulky triphenylacetamide on the linker attached to the stereochemical center of the phosphoramidates facilitated the separation of the *Rp* and *Sp* isomers during isolation by HPLC in most cases. A typical chromatogram is illustrated in Figure 1. After elution of the failed sequences, both those representing failed couplings and those representing failed oxidation of the

intermediate H-phosphonate, the two phosphoramidate diastereomers (a and b) tethering the triphenylacetamide-protected linker are eluted. The early eluting isomer "a" has been tentatively assigned as the *Rp* diastereomer (26), while the later eluting isomer "b" has been tentatively assigned as the *Sp* diastereomer. The yield of dodecamers tethering the cystamine-based linker is roughly half that expected for the native sequence. We believe this loss in yield results from hydrolysis of the putative phosphorochloridate (29, 30), the expected intermediate in the oxidation reaction. Owing to the reactivity of this intermediate with water, effective oxidation in the presence of the cystamine-based linker occurs only under strictly anhydrous conditions, and trace amounts of water will drastically reduce expected yields—and generally result in increased amounts of failed sequences (note the early eluting peaks in Figure 1). Equal amounts of both diastereomers were obtained in all cases, and only in one case were the diastereomeric sequences unresolvable. When the cystamine-based tether was placed at the internucleotide linkage between

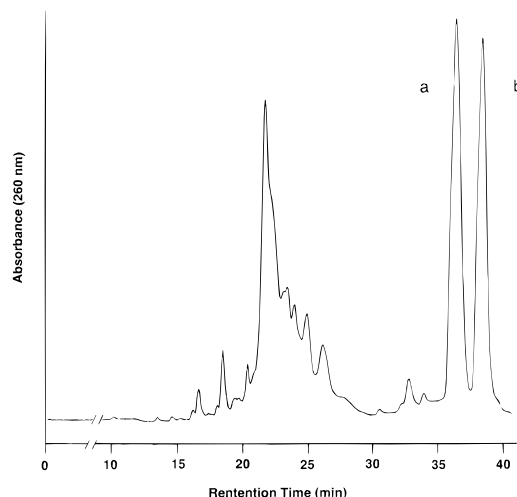


Figure 1. HPLC isolation of the two phosphoramidate diastereomers (a and b) for the dodecameric sequence 5'-d[GpApGpGpAp(NHCH₂CH₂S-SCH₂CH₂NHCOPh₃)-ApTpTpCpGpApG]. HPLC conditions are described under Experimental Procedures.

Table 1. DNA-Hoechst Conjugates: Helix Stabilization and Fluorescence Characteristics

		Conjugation Site:				
		i	ii	iii	iv	
		↓	↓	↓	↓	
		(5') -d(GpApGpGpApApTpTpCpGpApG)				
		(3') d(CpTpCpCpTpTpApApGpCpTpC)				
conjugate	Hoechst deriv	site of conjgn	isomer ^a	T _m ^b (°C)	ΔF ^c	ΔF* ^d
native duplex				51		
native duplex	33258			60	2.5 ^e	
5	3	i	(Rp)	53	1.3	16
5	3	i	(Sp)	60	1.1	12
6	3	ii	(Rp) + (Sp)	63	2.1	9
7	3	iii	(Rp)	75	2.6	15
7	3	iii	(Sp)	61	3.8	13
8	3	iv	(Rp)	73	4.1	16
8	3	iv	(Sp)	56	2.7	14
9	4	i	(Rp)	57	1.1	18
9	4	i	(Sp)	65	1.4	19
10	4	ii	(Rp) + (Sp)	57	2.7	20
11	4	iii	(Rp)	73	2.0	27
11	4	iii	(Sp)	67	1.8	30
12	4	iv	(Rp)	72	6.7	35
12	4	iv	(Sp)	67	4.7	37

^a Assignment of specific diastereomers is based upon arguments made elsewhere (26). The use of parentheses is to indicate that the assignments are tentative and are not yet corroborated by structural data. ^b T_m values are the average of at least two determinations and have an estimated error range of ±1 °C. ^c ΔF represents the ratio of the emission at 450 nm for the double-stranded conjugate relative to the single-stranded conjugate after titration by the complementary target. ^d ΔF* represents the ratio of the emission at 470 nm for the double-stranded conjugate relative to the single-stranded conjugate at 90 °C, after titration by the complementary target. ^e This value was obtained by comparing a solution of 1 μM Hoechst 33258 and 1 μM single-stranded GAATTC-containing sequence and then titrating this solution with the complementary target single-stranded DNA. The alternate experiment, comparing the fluorescence of 1 μM Hoechst 33258 and then titrating with excess DNA duplex, results in a ΔF = 26 (see text).

the G and A residues (site ii, Table 1), the diastereomeric sequences coeluted. For the conjugates **6** and **10** (Table 1), we could only prepare the requisite DNA sequence tethering the cystamine-based linker as a diastereomeric mixture.

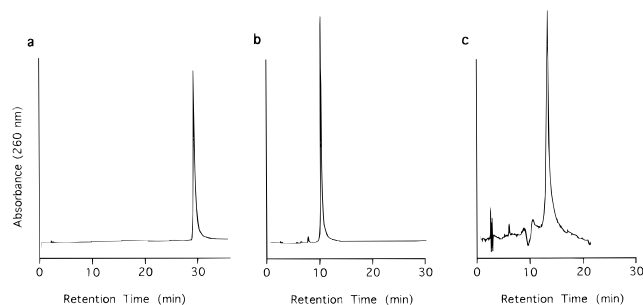


Figure 2. HPLC analyses of dodecameric sequences tethering (a) the triphenylacetamide derivative of cystamine (**1**), (b) the unmasked thiol (**2**), and (c) a Hoechst 33258 conjugate (**11**) (see Scheme 1). A peak with the same retention time as that in (c) was also present when the detector was set at 345 nm and a sample of **11** analyzed under the same HPLC conditions. HPLC conditions: 50 mM triethylammonium acetate, pH 7.0, with a linear gradient of acetonitrile (7–28% over 30 min). Retention times for the various dodecameric conjugates did not vary significantly with sequence or with the Hoechst derivative.

The conjugates were formed by cleavage of the disulfide bond to unmask the reactive thiol linker (**2**) and then treatment with either of the Hoechst analogues **3** or **4** (Scheme 1). After isolation by polyacrylamide gel electrophoresis, conjugates of the type **7** or **11** were obtained as both the *Rp* and the *Sp* diastereomers (as noted above, **6** and **10** were obtained as isomeric mixtures). We were unable to isolate the conjugated oligonucleotides by HPLC, largely due to the problems of aggregation of the excess fluorophore in the reaction mixture. The Hoechst derivatives are known to aggregate in aqueous solutions at concentrations above 30 μM, and the conjugations reactions, while performed in aqueous/DMF mixtures, required dye concentrations of roughly 15 mM. However, after completion of the reaction, the aggregates could be dissolved by the addition of excess DMF and then the product isolated by loading the entire reaction mixture onto a denaturing polyacrylamide gel. After electrophoresis, and excision and isolation of the fluorescent band from the gel, the conjugates (stored at concentrations of ~10 μM) could be analyzed by HPLC. HPLC analysis indicated that the initially prepared triphenylacetamide-protected sequence (Figure 2a), the unmasked thiol (Figure 2b), and the Hoechst conjugate (Figure 2c) could all be effectively resolved. Each conjugate exhibited a UV-vis absorbance spectrum characteristic of the absorption maximum for DNA (260 nm) as well as that for the Hoechst derivative (345 nm) (Figure 3).

T_m Characteristics of the Oligonucleotide Conjugates. The native dodecameric duplex exhibited a T_m value of 51 °C (Table 1). In the presence of 1 equiv of Hoechst 33258, the T_m was raised by 9 °C. We cannot determine from this assay whether a single complex is present since the fluorophore is known to bind to DNA by more than one mode. Nevertheless, the increased T_m suggests some minor groove binding, presumably at the A-T-rich site, with attendant helix stabilization. We then examined a series of conjugates prepared from the Hoechst derivative **3**. With the fluorophore tethered between the two G residues (**5**), but outside the (AATT)₂ binding site (conjugation site i), moderate helix stabilization was present for one isomer (ΔT_m = +9 °C), but the second diastereomer was less effective than the free fluorophore in stabilizing the dodecameric duplex. Contrary to previous observations, it is the *Sp* diastereomer that affords the more effective helix stabilizing characteristics. When tethered between the G and A residues at the end of the A-T binding site (conjugate ii), only the diastereomeric mixture was available, but this mixture

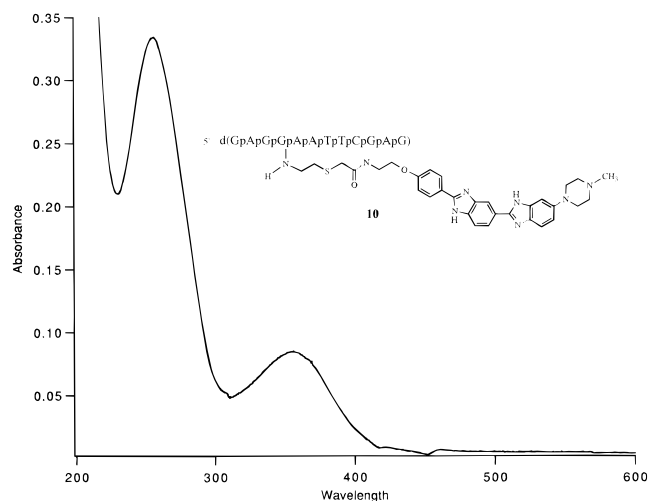


Figure 3. (a) Structure and UV-vis spectrum of the DNA-Hoechst conjugate (**9**) formed by the reaction of **4** with the dodecamer 5'-d(GpApGpGp(NHCH₂CH₂SH)ApApTpTpCpTpApG) tethering an unmasked thiol.

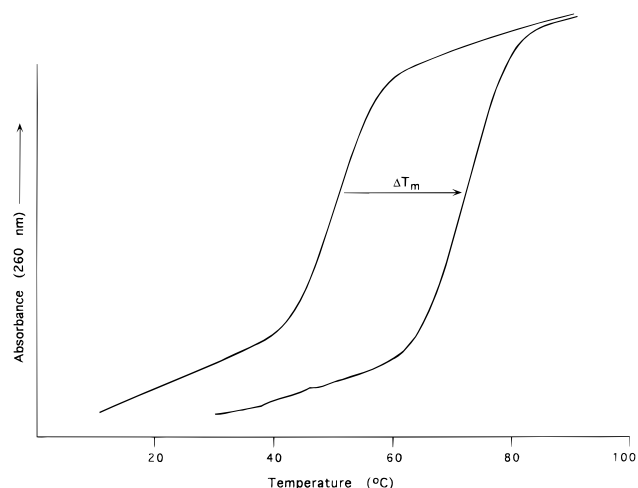


Figure 4. Absorbance vs temperature plots for the native dodecamer (left-side transition) and the conjugate **12** (*Rp* diastereomer) complexed to its complementary sequence (right-hand transition). The arrow indicates the approximate change in T_m value between the two samples (ΔT_m).

provided a 12 °C enhancement in T_m —likely an average value between the *Rp* and *Sp* diastereomers. In a previous study (26) the *Rp* diastereomers were always more effective than the *Sp* isomers in stabilizing the DNA duplex. This observation suggests that the purified *Rp*, if available, might exhibit a more significant T_m effect. In fact, this expectation was met with both conjugates **7** and **8**. In both of these latter examples, the *Rp* isomers resulted in T_m values that were 22–24 °C higher than that of the native duplex (Table 1). An example of two typical absorbance vs temperature transitions for a conjugate that effectively stabilizes the DNA duplex is illustrated in Figure 4. Both *Sp* diastereomers of **7** and **8** were also reasonably effective in stabilizing the DNA dodecamer (ΔT_m values of +10 and +5 °C, respectively). We have attributed the differences in helix stabilizing effects for the *Rp* and the *Sp* isomers to orientation effects related to the diastereomeric character of the linker. The *Rp* diastereomer orients the linker more toward the minor groove side of the DNA duplex, while the *Sp* diastereomer presents the linker more toward the major groove. The more effective helix stabilization by the *Rp* isomers of conjugates **7** and **8** is again consistent with

this relative orientation of the ligands tethered to the DNA backbone (26).

The *Rp* diastereomer **5** was not capable of providing very effective helix stabilization, but this result is more likely to reflect the position of the linker rather than any diastereomeric consequences. It remains unclear why the *Sp* diastereomer appeared more effective with this sequence, but even these effects are relatively moderate. With the tether placed outside the A-T-rich binding site, it is likely that the linker restricts access by the Hoechst derivative to the A-T-rich binding site. With the tether incorporated into the terminal phenyl ring of the Hoechst fluorophore, one might expect that positioning the linker near the end of the binding site would be most effective. With such a positioning, the Hoechst derivative would be directed along the binding site, ostensibly in its preferred binding mode. In this respect, conjugate **6** would appear to provide the optimal positioning for the linker. However, both sites that place the linker more toward the center of the binding target (iii and iv, Table 1) appear to provide nearly identical, and the most impressive, T_m effects. This result could reflect that there is sufficient linker flexibility to permit similar binding from either tethered position or that more than one binding mode within the (AATT)₂ minor groove is possible. Crystal structure analyses indicate that two modes of binding by Hoechst 33258 are possible within the (GAATTC)₂ binding site, differing in position by one base pair (2, 3, 5).

The DNA conjugates formed from the Hoechst derivative **4** differ from those described above in that the tether consists of an additional three atoms (–CH₂CH₂O–), which could provide additional flexibility in binding to the target A-T site. Tethering **4** outside the A-T-rich binding site between the two G residues (conjugation site i, Table 1) resulted in slightly more effective helix stabilization that correlated with the results for **3**. For the diastereomeric mixture of conjugate **10**, which tethered between the G and the A residues (conjugate ii, Table 1), only moderate stabilization was observed. However, for the remaining two conjugation sites (iii and iv, Table 1), both *Rp* diastereomers (**11** and **12**) provided in excess of a 20 °C enhancement in T_m values (see Figure 4). The corresponding *Sp* diastereomers were again not as effective but stabilized the helix somewhat more effectively than did the corresponding conjugates prepared from **3**.

Although it not clear why, conjugation at site ii with the derivative prepared from **3** resulted in a sequence that was more effective at helix stabilization than the corresponding derivative prepared from **4**. This suggests the role of the tether in some complexes is not fully elucidated, particularly with the minimum four base-pair binding site. Nevertheless, the most helix stabilizing conjugates were those that resulted from placing the linker within the targeted binding site. At both sites iii and iv the *Rp* diastereomers were most effective at helix stabilization, and this observation is also consistent with those regarding the conjugates prepared from **3**, as well as those prepared previously for a binding site composed of six contiguous A-T base pairs (26).

Fluorescence Properties. The four base-pair sequence (AATT)₂ should provide an effective binding site for the fluorophore, but the sequences outside the binding site may impact the nature of the groove, particularly its width, and result in less than optimal protection of the excited state from collisional decay processes involving water (17). At a concentration of 1 μM Hoechst 33258, in the presence of 1 μM single-stranded oligonucleotide, 5'-d(GpApGpGpApApTpTpCpGpApG), titra-

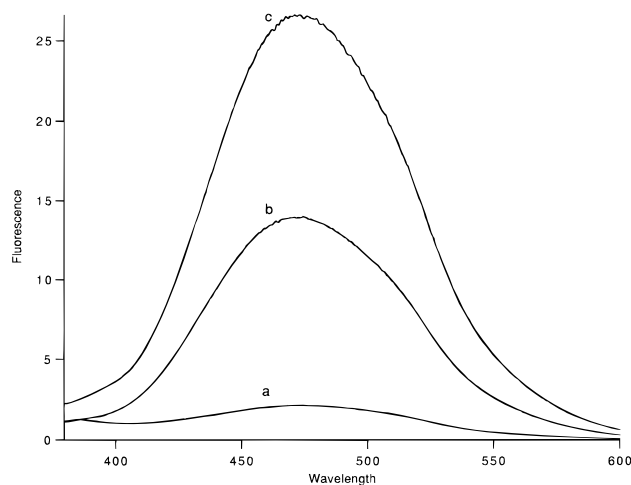


Figure 5. Fluorescence emission spectra ($\lambda_{\text{ex}} = 342$) for the single-stranded conjugate 5'-d(GpApGpGpAp(NHCH₂CH₂S-Hoechst)ApTpTpCpTpApG) (Rp **11**) (a) at 90 °C, (b) at 20 °C, and (c) in the presence of the complementary target at 20 °C after heating and cooling.

tion with the complementary sequence, 5'-d(CpTpCp-GpApApTpTpCpCpTpC) resulted in a moderate 2.5-fold enhancement in quantum yield. However, the alternate experiment, titration of free Hoechst 33258 by the *double-stranded* sequence, resulted in a 26-fold enhancement in quantum yield, very similar to what has been observed in other studies (18, 26). The solution containing free Hoechst 33258, and that containing the free fluorophore with one of the single strands of the GAATTC-containing sequence, differed in quantum yield by 10-fold. These differences in quantum yield enhancement suggest that the GAATTC-containing sequence, although not a complete palindrome, is capable of adopting a secondary structure in solution, perhaps mediated by the Hoechst 33258 groove binder, that results in significant enhancement in the emission quantum yield.

Tethering the minor groove-binding fluorophore to the oligonucleotide probe results in similar moderate increases in quantum yield upon hybridization. The process can be envisioned to occur in two steps, one a recognition event between the probe and the target sequence. Hybridization creates the minor groove-binding site and triggers the second step, that of ligand binding. Since each sequence tethers but a single ligand, the fluorescence properties of each complex should reflect the presence of a single ligand. For each sequence, the fluorescence of the single-stranded conjugate was measured, and then the sequence was titrated with the complementary target sequence. After the addition of each aliquot, the fluorescence spectrum was again measured, and the result obtained with 1 equiv of the complementary strand is illustrated in Figure 5c. The ratio of the emissions at 470 nm for the initial single-stranded conjugate and the final double-stranded conjugate was used to determine the fluorescence enhancement (ΔF) values (Table 1). The most significant fluorescence enhancement occurred with conjugate **12**, in which the dye is tethered essentially in the center of the target sequence. One diastereomer results in nearly a 7-fold increase in quantum yield, while the second diastereomer has a value nearly 5-fold larger than that measured for the single-stranded conjugate. These two complexes also exhibit some of the highest T_m values (72 and 67 °C, respectively) observed in this study; both properties suggest that the tethered ligand is most effectively bound to the DNA duplex, and the A-T-rich target site, when tethered in the center of the sequence.

Although the diastereomers of sequence **11** also exhibit relatively high T_m values, the fluorescence properties are more moderate. These observations suggest that the fluorescence characteristics of such complexes may be more sensitive to the nature of the binding event, and in some cases the ligand may not effectively penetrate the groove structure sufficiently well to avoid some relaxation effects by nonradiative (e.g., collisional) processes.

However, it is possible that the single-stranded conjugates can result in the formation of some secondary structure as noted above for the unconjugated sequences in the presence of Hoechst 33258. For example, they can undergo a self-complementary partial duplex assembly using the central palindromic (GAATTC)₂ sequence, with additional stabilization by one of the tethered groove-binding agents. Such a complex could also exhibit a significant enhanced fluorescence emission signal such as that observed for the free Hoechst dye in the presence of the unconjugated sequences. Dissociation of this palindromic partial duplex, followed by association with the complementary target sequence during the titration experiments, would result in only moderate apparent quantum yield enhancement effects—exactly what has been observed. Since we could not physically separate the tethered ligand and DNA sequence, instead we heated the single-stranded conjugates in an attempt to destabilize such structures and release the bound fluorophore. Under these conditions we observed a cooperative transition similar to that expected for a helix-to-coil transition. A decrease in the quantum yield of the emission spectrum for the single-stranded conjugate was also observed during heating over the temperature range 10–90 °C. The fluorescence observed for the single-stranded conjugate at 20 °C (Figure 5b) was reduced (Figure 5a) to a level comparable with that of free Hoechst 33258.

We then compared the fluorescence enhancement values for the complexes prepared by two procedures: (i) the single-stranded conjugate was titrated with the complementary target at 20 °C, and (ii) after formation of the 1:1 conjugated duplex, the complex was heated and cooled prior to fluorescence measurements. Regardless of the procedure used, the quantum yields observed in the fluorescence emission spectra were essentially the same, suggesting that simple titration by the complementary target sequence disrupts the putative GAATTC dimer and results in the formation of the conjugate–target duplex (in some cases the emission for the heated/cooled sample was very slightly reduced, reflecting perhaps minor amounts of degradation). With the presence of the dimerized single-stranded conjugate, and the inherent fluorescence enhancement from this complex, the ΔF values observed for the double-stranded conjugate–target complex seem, at best, only moderate (Table 1, compare parts b and c of Figure 5). We obtained a second set of fluorescence enhancement values (ΔF^* , Table 1) in which we compared the fluorescence emission spectra of the double-stranded conjugates (at 20 °C) with the single-stranded conjugates at 90 °C (compare parts a and c of Figure 5). Heating the single-stranded conjugate disrupts the putative dimer and permits a comparison of the fluorescence for the unbound (but tethered) ligand with that of the corresponding conjugated duplex containing the bound ligand. The quantum yield for the single-stranded conjugate typically decreases by roughly an order of magnitude with heating. At higher temperature, nonradiative collisional effects may be slightly increased, thus improving the apparent quantum yield enhancement. For example, when free Hoechst 33258 is titrated with the native, nominally single-stranded

GAATTC sequence, the quantum yield increases roughly 35-fold—consistent with expectations for the (GAATTC)₂ binding site. However, when this complex is heated at 90 °C, the quantum yield decreases an apparent 46-fold—presumably because of the enhanced collisional effects at higher temperatures. Thus, a comparison of the observed emission values for the single-stranded (90 °C) and double-stranded (at 20 °C) conjugates must be done cautiously. Nevertheless, the quantum yield enhancements were now found to be as high as 37-fold, similar to, or greater than, that observed for the free Hoechst 33258 (Table 1). In general, duplexes containing the Hoechst derivative **4** (with the longer linker) tethered near or at the center of the AATT sequence resulted in the highest enhancement values when compared with the heat denatured single-stranded conjugate (27–37-fold). These differences are likely to reflect the greater flexibility afforded the ligand by the longer linker, but even the shorter linker present in complexes prepared from **3** results in quantum yield enhancements from 9- to 16-fold.

Conclusions. We have shown that the tethered derivative of Hoechst 33258 can be used to target the four base-pair sequence (AATT)₂ and provide significant helix stabilization. The most effective position for the linker, employed to tether the fluorophore, is at the center of the targeted binding site. Both types of DNA conjugates, those prepared from either **3** or **4**, enhance the *T_m* values of the duplex by more than 20 °C when present as the tentatively assigned *Rp* diastereomer. The fluorescence properties after titration of the single-stranded conjugates with the target sequence are less defining and appear at best only moderate. However, fluorescence vs temperature, and absorbance vs temperature, plots indicate that the single-stranded conjugates adopt some secondary structure, most likely dimerization about the palindromic GAATTC core sequence. Heating the single-stranded conjugates reduced their fluorescence properties, consistent with a dimerized complex about the tethered Hoechst dye. Although titration by the complementary target sequence disrupts the secondary structure present in the single-stranded conjugate and permits complex formation, the results of this study suggest that probe sequences containing palindromic sequences rich in A-T base pairs may suffer from dimerization effects mediated by such groove-binding agents.

ACKNOWLEDGMENT

This work was supported by a grant from the NIH (GM37065).

LITERATURE CITED

- (1) Goodsell, D., and Dickerson, R. E. (1986) Isohelical analysis of DNA groove-binding drugs. *J. Med. Chem.* 29, 727–733.
- (2) Pjura, P. E., Grzeskowiak, K., and Dickerson, R. E. (1987) Binding of Hoechst 33258 to the minor groove of B-DNA. *J. Mol. Biol.* 197, 257–271.
- (3) Teng, M.-K., Usman, N., Frederick, C. A., and Wang, A. H.-J. (1988) The molecular structure of the complex of Hoechst 33258 and the DNA dodecamer d(CGCGAATTCGCG). *Nucleic Acids Res.* 16, 2671–2675.
- (4) de C. T. Carrondo, M. A. F., Coll, M., Aymami, J., Wang, A. H.-J., van der Marel, G. A., van Boom, J. H., and Rich, A. (1989) Binding of a Hoechst dye to d(CGCGATATCGCG) and its influence on the conformation of the DNA fragment. *Biochemistry* 28, 7849–7859.
- (5) Quintana, J. R., Lipanov, A. A., and Dickerson, R. E. (1991) Low-temperature crystallographic analyses of the binding of Hoechst 33258 to the double-helical DNA dodecamer C-G-C-G-A-A-T-T-C-G-C-G. *Biochemistry* 30, 10294–10306.
- (6) Kissinger, K. L., Drowicki, K., Dabrowiak, J. C., and Lown, J. W. (1987) Molecular recognition between oligopeptides and nucleic acids. Monocationic imidazole lexitropsin that display enhanced GC sequence dependent DNA binding. *Biochemistry* 26, 5590–5595.
- (7) Lee, M., Drowicki, K., Hartley, J. A., Pon, R. T., and Lown, J. W. (1988) Molecular recognition between oligopeptides and nucleic acids: Influence of van der Waals contacts in determining the 3'-terminus of DNA sequences read by monocationic lexitropsins. *J. Am. Chem. Soc.* 110, 3641–3649.
- (8) Harshman, K. D., and Dervan, P. B. (1985) Molecular recognition of B-DNA by Hoechst 33258. *Nucleic Acids Res.* 13, 4825–4835.
- (9) Martin, R. F., and Holmes, N. (1983) Use of an ¹²⁵I-labeled DNA ligand to probe DNA structure. *Nature* 302, 452–454.
- (10) Fox, K. R., and Waring, M. J. (1984) DNA structural variations produced by actinomycin and distamycin as revealed by DNAase I footprinting. *Nucleic Acids Res.* 12, 9271–9285.
- (11) Portugal, J., and Waring, M. J. (1987) Comparison of binding sites in DNA for Berenil, Netropsin and Distamycin as revealed by DNAase I footprinting. *Eur. J. Biochem.* 167, 281–289.
- (12) Portugal, J., and Waring, M. J. (1988) Assignment of DNA binding sites for 4',6'-diamidine-2-phenyl indole and bis-benzimidazole (Hoechst 33258). A comparative footprinting study. *Biochim. Biophys. Acta* 949, 158–168.
- (13) van Dyke, M. W., Hertzberg, R. P., and Dervan, P. B. (1982) Map of Distamycin, Netropsin and Actinomycin binding sites on heterogeneous DNA: DNA cleavage-inhibition patterns with methidium propyl-EDTA-Fe(II). *Proc. Natl. Acad. Sci. U.S.A.* 79, 5470–5474.
- (14) Abu-Daya, A., Brown, P. M., and Fox, K. R. (1995) DNA sequence preferences of several AT-selective minor groove binding ligands. *Nucleic Acids Res.* 17, 3385–3392.
- (15) Spink, N., Brown, D. G., Skelly, J. V., and Neidle, S. (1994) Sequence-dependent effects in drug-DNA interactions: The crystal structure of Hoechst 33258 bound to the d(CGCAAATTTGCG)₂ duplex. *Nucleic Acids Res.* 22, 1607–1612.
- (16) Vega, M. C., Garci Saez, I., Aymami, J., Eritja, R., van der Marel, G. A., van Boom, J. H., Rich, A., and Coll, M. (1994) Three dimensional crystal structure of the A-T tract DNA dodecamer d(CGCAAATTTGCG)₂ complexed with the minor groove binding drug Hoechst 33258. *Eur. J. Biochem.* 222, 721–726.
- (17) Zimmer, C., and Wahnert, U. (1986) Nonintercalating DNA binding ligands: Specificity of the interaction and their use as tools in biophysical, biochemical and biological investigations of genetic material. *Prog. Biophys. Mol. Biol.* 47, 31–112.
- (18) Looitens, F. G., Regenfuss, P., Zechel, A., Dumortier, L., and Clegg, R. M. (1990) Binding characteristics of Hoechst 33258 with calf thymus DNA, poly [d(A-T)] and d(CCGGAATTCGCG): Multiple stoichiometries and determination of tight binding with a wide spectrum of site affinities. *Biochemistry* 29, 9029–9039.
- (19) Sterzel, W., Bedford, P., and Eisenbrand, G. (1985) Automated determination of DNA using the fluorochrome Hoechst 33258. *Anal. Biochem.* 147, 462–470.
- (20) Araki, T., Yamamoto, A., and Yamada, M. (1987) *Histochemistry* 87, 331–338.
- (21) Karawajew, L., Rudchenko, S., Wlasik, T., and Trakht, I. (1990) Flow sorting of hybrid hybridomas using the DNA stain Hoechst 33258. *J. Immunol. Methods* 129, 277–282.
- (22) Downs, T. R., and Wilfinger, W. W. (1983) Fluorometric quantification of DNA in cells and tissue. *Anal. Biochem.* 131, 538–547.
- (23) Adams, C. J., and Storrie, B. (1981) A simple DNA-dependent fluorescence enhancement assay for cell number. *Histochem. Cytochem.* 29, 326–334.
- (24) Arndt-Jovin, D. J., and Jovin, T. M. (1990) Fluorescence labeling and microscopy of DNA. *Cytometry* 11, 80–89.

- (25) Lee, B. R., Haseman, D. B., and Reynolds, C. P. (1989) A digital image microscopy system for rare-event detection using fluorescent probes. *Cytometry* 10, 256–266.
- (26) Wiederholt, K., Rajur, S. B., Giuliano, J. J., O'Donnell, M. J., and McLaughlin, L. W. (1996) DNA-tethered Hoechst groove-binding agents: Duplex stabilization and fluorescence properties. *J. Am. Chem. Soc.* 118, 7055–7062.
- (27) O'Donnell, M. J., Hebert, N., and McLaughlin, L. W. (1994) The stereospecific introduction of reporter groups to oligodeoxynucleotides by the labeling of individual phosphorus diastereomers. *Bioorg. Med. Chem. Lett.* 4, 1001–1004.
- (28) Fidanza, J., and McLaughlin, L. W. (1992) The use of a thiol tether for the sequence-specific attachment of reporter groups to DNA. *J. Org. Chem.* 57, 2340–2346.
- (29) Blackburn, G. M., Cohen, J. S., and Todd, A. R. (1966) Synthesis of dialkyl phosphates from monoalkyl phosphonates. Direct oxidative esterification. *J. Chem. Soc.*, 239–245.
- (30) Atherton, F. R., Openshaw, H. T., and Todd, A. R. (1945) Dibenzyl chlorophosphonate as a phosphorylating agent. *J. Chem. Soc.*, 660–663.

BC960086E

Amine-Reactive Forms of a Luminescent Diethylenetriaminepentaacetic Acid Chelate of Terbium and Europium: Attachment to DNA and Energy Transfer Measurements

Min Li[†] and Paul R. Selvin*

Department of Chemistry, University of California, Berkeley, California 94720, and Life Sciences Division, Lawrence Berkeley National Laboratory, Berkeley, California. Received July 24, 1996[®]

An isothiocyanate form of a lanthanide chelate which is highly luminescent when bound to terbium or europium has been synthesized. The chelate consists of diethylenetriaminepentaacetic acid (DTPA) covalently joined to a chromophore, 7-amino-4-methyl-2(1*H*)-quinolinone (cs124), and to *L*-*p*-aminophenylalanine, in which the aromatic amine was further converted to an isothiocyanate group. Ethylenediamine was also used in place of aminophenylalanine, but the isothiocyanate formed from the aliphatic amine was significantly less reactive. Site-specific attachments to triglycine and to the 5' ends of amine-modified DNA oligomers have been made. In addition, as an alternative method of coupling to macromolecules, DTPA anhydride–cs124 can be used to react specifically with a 5' amine group on base-deprotected synthetic DNA oligomers. Synthesis and purification is relatively straightforward in both cases, and luminescent properties are favorable for several applications, including as nonisotopic labels, as long-lifetime alternatives to fluorophores in imaging and diagnostics and particularly as donors in luminescence resonance energy transfer. Energy transfer measurements are consistent with previously reported measurements using different attachment mechanisms.

INTRODUCTION

Luminescent lanthanide chelates have highly unusual spectral characteristics that make them useful nonisotopic alternatives to radioactive probes (1–5), as alternatives to organic fluorophores, particularly where there are problems of background autofluorescence (6–9), and as donors in luminescence resonance energy transfer (10–16). These characteristics include millisecond lifetime, sharply spiked emission spectrum (<10 nm fwhm), large Stokes shifts (>150 nm), no self-quenching (17, 18), high quantum yield for lanthanide luminescence (~1), and excellent solubility.

A commonly used luminescent lanthanide chelate is diethylenetriaminepentaacetic acid (DTPA),¹ covalently attached to an organic chromophore, the latter acting as an antenna or sensitizer to absorb the excitation light and overcome the weak absorbance of the lanthanides (11, 19–22). We have previously shown that carbostyryl 124 bound to DTPA (11, 12) or to other polyamino-carboxylate chelates (23) can sensitize both europium and terbium, and the complex is an excellent donor in resonance energy transfer experiments.

Conjugation of DTPA–chromophore moieties is most often done through the dianhydride form of DTPA (24), where one anhydride reacts with an amine-containing chromophore and the other with amine-containing biomolecules (11, 17, 19, 21, 22). For conjugation, however,

the dianhydride has several disadvantages: (1) The anhydride is nonspecific in which nucleophilic acyl substitution reactions occur readily. When reacting with DNA, this concern led us to use base-protected DNA in our previous work (11, 12). However, base deprotection required strongly alkaline conditions, which we found cause significant cleavage of the DTPA–cs124 amide bond, particularly on longer DNAs, and more mild conditions led to questions of incomplete deprotection (12). (2) The anhydride is water-labile. (3) The dianhydride can lead to a number of products, including DTPA disubstituted with chromophore, DTPA attached to the macromolecule with no sensitizer, and macromolecules cross-linked by DTPA. (4) The length of the linker arm between DTPA and the macromolecule is fixed.

A number of groups have made isothiocyanate forms attached to the backbone of DTPA (without a sensitizer), in part to overcome these problems (25–28). The synthesis, however, involves many steps and is time-consuming, and its extension to DTPA-modified with a sensitizer is not necessarily straightforward. We have synthesized an isothiocyanate form of DTPA–cs124 by utilizing one of the carboxyl groups: caDTPA is reacted with cs124, followed by addition of diamino-compound, and one of the amines is then converted to an isothiocyanate group (29, 30). The synthesis is straightforward, and the isothiocyanate group formed from an aromatic amine is highly reactive and does not interfere with lanthanide luminescence. Furthermore, the amide-bond formed from one of the carboxyl groups is able to maintain coordination to the lanthanide (31) and the binding constant is sufficiently high for most practical purposes. We have also revisited the reaction of DTPA–cs124 anhydride with DNA (11, 12) and have found conditions in which base-deprotected DNA can be conjugated without side reactions.

EXPERIMENTAL METHODS

Chemicals. The following chemicals were purchased from Aldrich: diethylenetriaminepentaacetic acid dian-

* Address correspondence to this author at Calvin Laboratory, University of California, Berkeley, Berkeley CA 94720 [telephone (510) 486-6786; fax (510) 486-6059; e-mail prselvin@lbl.gov].

[†] Present address: Union Carbide Corp. Technical Center, 3200/3300 Kanawha Turnpike, S. Charleston, WV 25303.

[®] Abstract published in *Advance ACS Abstracts*, February 1, 1997.

¹ Abbreviations: DTPA, diethylenetriaminepentaacetic acid; caDTPA, dianhydride of DTPA; cs124 or carbostyryl 124, 7-amino-4-methyl-2(1*H*)-quinolinone; DMSO, dimethyl sulfoxide; DMF, dimethylformamide; EDA, ethylenediamine; HPLC, high-performance liquid chromatography.

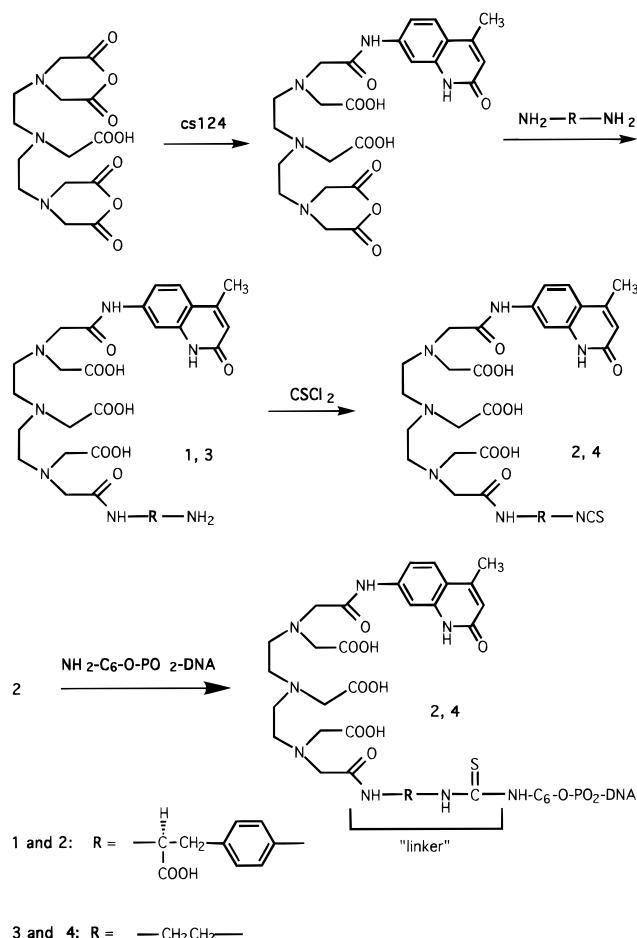


Figure 1. Synthesis of isothiocyanate formed from DTPA-cs124 attached to ethylenediamine (**4**) or L-*p*-aminophenylalanine (**2**) and conjugation with amino-modified DNA. When using the anhydride-based conjugation (see text) with an amine-containing compound, the indicated "linker" is absent.

hydride; 7-amino-4-methyl-2(1*H*)-quinolinone; anhydrous *N,N*-dimethylformamide; anhydrous dimethyl sulfoxide; triethylamine; ethylenediamine; thiophosgene; europium chloride hexahydrate (99.99%); terbium chloride hexahydrate (99.999%). L-*p*-Aminophenylalanine was purchased from Sigma. Distilled and deionized water (18 MΩ cm⁻¹) was used throughout. All glassware was washed with a mixed acid solution and thoroughly rinsed with deionized, distilled water (32). All plastic (metal-free) labware was purchased from Bio-Rad. All chemicals were of the purest grade available.

Purification. High-performance liquid chromatography was performed at room temperature on either a Beckman Model 100 system or a Waters 600E with a Dynamax C₁₈ column (Rainin) for reversed-phase purification and a GenPak Fax (Waters) 4.6 × 100 mm column for anion exchange purification. The UV-absorbing fractions were detected at 328 nm for cs-124 compounds and at 260 nm for DNA oligos.

Synthesis (Figure 1). DTPA-cs124-L-*p*-Aminophenylalanine (**1**). To a solution of caDTPA (200 mg, 560 μmol) in 5 mL of DMF and 300 μL of triethylamine was added dropwise cs124 (115.5 mg, 1.2 × 560 μmol) in 2 mL of DMF. After 45 min, the reaction mixture was added dropwise to a solution of L-*p*-aminophenylalanine (121 mg, 1.2 × 560 μmol) in 5 mL of DMSO and 100 μL of triethylamine. After 3 h of stirring, the solvent was evaporated to dryness under reduced pressure and the residue was redissolved in 5 mL of 1 M triethylammonium acetate, pH 6.5. The product was purified by

reversed-phase HPLC using a 21.4 × 250 mm C₁₈ column (Dynamax 60 Å) with a flow rate of 12.5 mL/min. A 15-min linear gradient, from 10% to 15% solvent B (solvent A, 0.1 M triethylammonium acetate, pH 6.5; solvent B, CH₃CN), was used. The peak at retention time 14.5 min was collected and dried to give **1** as a light yellow solid: yield, 115 mg, 29%; ¹H NMR δ (D₂O, pD = 6.5) 2.16 (3H, s), 2.7–3.4 (16H, m), 3.50 (2H, s), 3.60 (2H, s), 4.23 (1H, m), 6.13 (1H, s), 6.88 (2H, d), 6.95 (2H, d), 7.08 (1H, d), 7.33 (1H, d), 7.35 (1H, s); FAB-MS, *m/e* 712 (M + H⁺).

DTPA-cs124-L-(*p*-Isothiocyanato)phenylalanine (**2**). Compound **1** (50 mg, 70 μmol) in 40 mL of 0.5 M HCl was added to 30 mL of CCl₄ (85% in CCl₄) at room temperature. The reaction was stirred vigorously for 1 h. The aqueous phase was washed with chloroform (5 × 5 mL) to remove excess CCl₄ and then purified by reversed-phase HPLC using a 21.4 × 250 mm C₁₈ column (Dynamax 60 Å) with a flow rate of 12.5 mL/min. A 25-min linear gradient, from 10% to 50% solvent B (solvent A, 0.1% CF₃COOH in H₂O; solvent B, CH₃CN), was used. The major peak at retention time 24 min was collected and dried to give **2** as a white solid: yield, 16 mg, 30%; ¹H NMR δ (CD₃OD) 2.42 (3H, s), 3.06 (2H, t), 3.15 (2H, t), 3.38 (8H, m), 3.51 (2H, s), 3.61 (2H, s), 3.92 (2H, s), 4.56 (1H, m), 6.35 (1H, s), 6.02 (2H, d), 7.09 (2H, d), 7.35 (1H, d), 7.65 (1H, d), 7.90 (1H, s); FAB-MS, *m/e* 754 (M + H⁺).

DTPA-cs124-EDA (**3**). To a solution of caDTPA (500 mg, 1.4 mmol) in 30 mL of DMF and 1 mL of triethylamine was added dropwise cs124 (240 mg, 1.4 mmol) in 4 mL of DMF and stirred. After 30 min, 5 mL (75 mmol) of ethylenediamine (EDA) was added, forming a white precipitate. The reaction was stirred for 2 h at room temperature and then stored in a refrigerator overnight, forming a brown precipitate. The precipitate turned white after several washes with 2-propanol and was finally washed with ether and dried overnight under vacuum. To remove excess EDA, the solid was redissolved in H₂O, loaded on a C₁₈ Sep-Pak (Waters), washed with 12 mL of 0.4 M NaOAc, pH 6, and 6 mL of H₂O, and eluted with 50% MeOH/H₂O. HPLC analysis [30-min linear gradient from 15% to 60% solvent B (solvent A, 0.1% CF₃COOH in H₂O; solvent B, CH₃CN), 3 mL/min with 10 × 250 mm C₁₈ Dynamax 60 Å column] showed two well-resolved peaks. The first peak at 16 min was confirmed to be DTPA-cs124-EDA: FAB-MS, *m/e* 592 (M + H⁺). The second peak at retention time 19 min was DTPA-(cs124)₂.

DTPA-cs124-EDA-Isothiocyanate (**4**). Approximately 10 mg of the precipitate containing **3** was dissolved in 3 mL of H₂O. Three milliliters of CCl₄/CCl₄ (85%) was added [precipitation of DTPA-(cs124)₂ was observed], followed by addition of solid CaCO₃. After 30 min of vigorous stirring, HPLC analysis of the supernatant showed that the DTPA-cs124-EDA peak at retention time 16 min (see **3**) was quantitatively converted to a peak with retention time 22 min, later shown to be **4**. The solution was extracted with CHCl₃, and the precipitate containing DTPA-(cs124)₂ was removed by centrifugation. The material in the water phase was purified by HPLC using a 15-min linear gradient, from 15% to 40% solvent B (solvent A, 0.1% CF₃COOH in H₂O; solvent B, CH₃CN) with a 21.4 × 250 mm C₁₈ Dynamax 60 Å column at a flow rate of 12.5 mL/min: FAB-MS, *m/e* 634 (M + H⁺).

Conjugation of **2 to DNA Oligo.** Thirty microliters of 0.1 M NaHCO₃, pH 7, was added to dried synthetic DNA oligo [10-mer with C6-amino linker at 5' end, 50 nmol; sequence: NH₂-CCT-AGA-GTG-G (12)]. The solution was mixed with compound **2** (20 × 50 nmol, dried by

SpeedVac prior to use). The pH of solution was adjusted to 9–10 using Et_3N aqueous solution. The mixture was incubated at 37 °C overnight and then passed through a P-6 column. The fraction was further purified on a reversed-phase HPLC using a $10 \times 250 \text{ C}_{18}$ column (Dynamax, 300 Å) with a flow rate of 3 mL/min. A 60-min linear gradient, from 10% to 25% solvent B (solvent A, 0.1 M triethylammonium acetate, pH 6.5; solvent B, CH_3CN) was used. Peak at 37 min was collected to give the conjugate. Unconjugated DNA eluted at 18 min. Yield: 40–80% based on HPLC profiles. Mass (by time-of-flight MALDI): 4006 (calcd 4008). A second peak, not fully resolved, eluted less than 1 min later and was found to contain an approximately equal mixture of product and a compound of 56 extra mass units. Further purification by anion exchange [120-min gradient from 20% to 55% B with a flow rate of 0.5 mL/min (solvent A, 25 mM Tris HCl, pH 8.0, in 10% CH_3CN ; solvent B, 25 mM Tris HCl, pH 8.0, and 1 M NaCl in 10% CH_3CN)] yielded two well-resolved peaks at 48 and 50 min, with the first peak containing twice the area and corresponding to the expected mass and the second peak corresponding to the species of 56 extra mass units. Conjugation with a 14-mer with C6-amino linker at 5' end, $\text{NH}_2\text{-CCT-AGC-AGC-AGT-GG}$, was over 90% on the basis of HPLC profiles. Conjugation of **2** with the same DNA lacking a 5' amine showed no reaction.

Conjugation of caDTPA–cs124 to DNA Oligo. To a solution of ca-DTPA (7.1 mg, 20 μmol) in 100 μL of DMSO and 11 μL Et_3N was added dropwise cs124 (5.1 mg, 1.5 $\times 20 \mu\text{mol}$) in 60 μL of DMSO at room temperature. After a 0.5 h, 43 μL of reaction solution was mixed with synthetic DNA oligos (e.g., 14-mer or 20-mer with C6-amino linker at 5' end, 10 nmol, reversed-phase HPLC purified) in 60 μL of DMSO and 26 μL of 0.1 M Et_3NOAc , pH 8. The mixture was incubated at room temperature overnight and then passed through a P-6 column. The fraction was further purified on a reversed-phase HPLC using a $10 \times 250 \text{ C}_{18}$ column (Dynamax, 300 Å) with a flow rate of 3 mL/min. A 60-min linear gradient, from 5% to 25% solvent B (solvent A, 0.1 M triethylammonium acetate, pH 6.5; solvent B, CH_3CN) was used. The peak at 44 min was collected and dried to give the conjugate: yield, 30–80% based on HPLC profiles; mass, 5011 (14-mer, calcd 5010), 6906 (20-mer, calcd 6906). Further anion exchange purification (see above) displayed a major single peak, with a second small (<10%) peak of 56 extra mass units. Conjugation of caDTPA–cs124 with the same DNA lacking a 5' amine showed no reaction.

Hybridization Conditions. DNA oligomers were hybridized to their complement in 10 mM Tris, pH 8.0, 10 mM MgCl_2 , and 150 mM NaCl by heating to 65–70 °C and cooling over a period of 15–60 min to either room temperature or 5 °C. The solvent was either H_2O or D_2O (99.9%; Aldrich). For energy transfer measurement, and an increasing amount of acceptor-labeled strand [tetramethylrhodamine (TMR) is the acceptor for terbium; Cy5 is the acceptor for europium] was added to lanthanide-labeled DNA at approximately 0.25 μM . Complementary DNA (labeled or unlabeled) was synthesized and purified as previously described (11, 12).

Spectroscopy. Absorption measurements were made on a Hewlett-Packard 8452A spectrometer. Time-resolved and gated luminescence measurements were made on a laboratory-built spectrometer used previously (11, 12, 23) utilizing 337-nm pulsed excitation (5 ns, 40 Hz) and photon-counting detection (GaAs PMT and multichannel scalar with 2- μs resolution). Terbium emission was monitored at 546 nm and europium emis-

sion at 617 nm. Data were curve-fit to one or two exponentials using TableCurve software (Jandel Scientific).

Metal Binding. All of the chelate-conjugated compounds were added in 1:1 molar ratio with a solution of TbCl_3 or EuCl_3 in triethylammonium acetate, pH 5. The solutions were incubated at room temperature for 30 min and diluted in the appropriate spectroscopy buffer.

RESULTS AND DISCUSSION

Proof of Structure. Figure 1 shows the synthesis pathways of two isothiocyanate forms of DTPA–cs124, **2** and **4**. Several lines of evidence confirm the synthesis and purity of the compounds. Single well-resolved HPLC peaks were found for the products, with starting materials running at different retention rates—conversion of the amine to an isothiocyanate resulted in significantly extended retention; mass spectroscopy confirmed the expected mass; NMR showed the expected peaks with no significant impurity components; both isothiocyanate forms reacted quantitatively with an excess of triglycine as determined by a shift in retention time in HPLC and by mass spectroscopy analysis; products were highly luminescent with terbium and europium, whereas starting materials mixed with lanthanides showed no significant lanthanide luminescence; absorption spectra showed characteristic spectra of carbostyryl as a 7-amide (maximum at 328 nm with secondary maximum at 342 nm (23)).

Reactivity Testing of –NCS Group. Compounds **2** and **4** were each mixed with ~50-fold excess of triglycine in a solution of 0.1 M triethylammonium acetate, pH 9, for 0.5 h at room temperature. HPLC analysis [30-min linear gradient 15–60% solvent B (solvent A, 0.1% CF_3COOH in H_2O ; solvent B, CH_3CN ; 3 mL/min with $10 \times 250 \text{ mm C}_{18}$ Dynamax 60 Å column] of the reaction mixtures showed a peak corresponding to **2** at retention time 23 min converted quantitatively to a peak at 13 min (FAB-MS, m/e 943 [$\text{M} + \text{H}^+$]) and a peak of **4** at retention time 16 min was quantitatively converted to a peak at 11 min, respectively. Under conditions appropriate for labeling amine-modified DNA (up to a 50-fold excess of **4** over DNA; see above), we found that **2** but not **4** was sufficiently reactive. This is in agreement with the results of Mujumdar et al., who found that an isothiocyanate of cyanine dyes formed from an aromatic—but not aliphatic—amine was sufficiently reactive with amine-containing biomolecules (33).

Proof of Conjugation to DNA. **2** and caDTPA–cs124 were each reacted with base-deprotected and HPLC-purified synthetic DNA oligomers containing a 5' amine. After both reversed-phase and anion exchange HPLC, well-resolved peaks of the expected product mass were isolated. Control reactions with DNA lacking a 5' amine showed no reaction of either **2** or caDTPA–cs124 with the amines of the (deprotected) DNA bases. For similar reaction conditions, no significant reaction of **4** with DNA was observed. With **2** there was a minor but significant second peak of 56 extra mass units which was not well resolved by reversed-phase HPLC alone but was resolved after additional anion exchange. The source of this extra mass is unknown, though it is possible that the chelate bound some trace heavy metals. The two peaks displayed identical luminescent properties after lanthanides were added, and both hybridized approximately equally well to complementary DNA. Nevertheless, we routinely purified the conjugated DNA by both reversed-phase and anion exchange HPLC to isolate the product of proper molecular weight and found that this gave the best hybridization results.

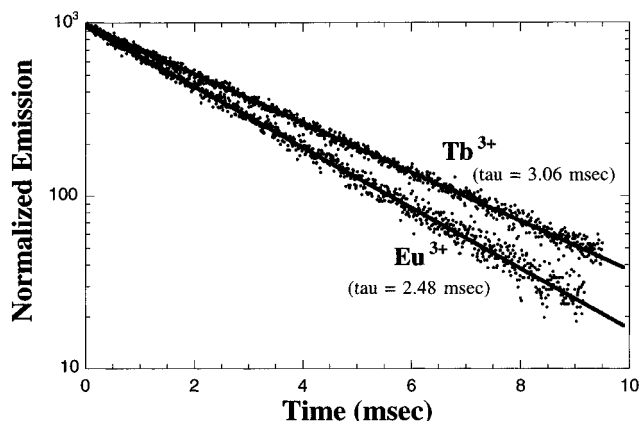


Figure 2. Lifetime of Tb^{3+} and Eu^{3+} bound to **2** attached to the 5' amine group of synthetic DNA. The Tb data are for DNA hybridized to an unlabeled complement. Solution conditions are the same as in Table 1. Data were acquired every 2 μs , digitally binned every 10 μs , and curve fit to a single exponential which showed no residual structure and $r^2 > 0.99$.

Table 1. Lanthanide Excited State Lifetime Attached to DNA^a

sample	H ₂ O; RT (ms)	D ₂ O; RT (ms)	D ₂ O; 5 °C (ms)
Tb-anhydride	1.5 (1.25)	2.38 (2.0)	2.98 (2.1–2.5)
Tb-ITC	1.43 (1.35)	2.50 (2.19)	3.06
Eu-anhydride	0.63 (0.63)	(2.38)	2.41 (2.46)
Eu-ITC	(0.60)	2.39	2.45

^a The table shows the excited state lifetime of terbium or europium attached to DNA either via **2** or via the anhydride reaction. The numbers in parentheses correspond to unhybridized DNA, those not in parentheses to lanthanide-labeled DNA hybridized to an unlabeled complement. Data were taken at 10 mM Tris, pH 8.0, 10 mM MgCl_2 , 150 mM NaCl. In some cases, particularly the single-stranded DNA, there was a minor component (<10%) with a highly quenched lifetime (a few hundred microseconds), likely caused by interaction of the chelate with the DNA bases. The relatively large spread in the data for the Tb-anhydride unhybridized data is due to variability in the temperature regulation of the cuvette.

Luminescence Measurements. *Triglycine Complexes.* Terbium and europium luminescence of both **2** and **4** conjugated to triglycine had lifetimes and intensities unchanged from the unmodified DTPA-cs124. This indicates that modification of the chelate complex with these isothiocyanate groups does not alter the luminescence properties of the bound lanthanide.

DNA Complexes. Figure 2 shows luminescence of **2** bound to Eu^{3+} or Tb^{3+} , conjugated to DNA, and hybridized to its DNA complement in a D_2O -based buffer. Table 1 summarizes the lifetime of both **2** and the anhydride DTPA-cs124 conjugated to DNA under a variety of solvent, temperature, and hybridization conditions. The Eu lifetime is relatively insensitive to environmental conditions, except for the well-known quenching effect of H_2O when ligated in the primary coordination sphere (34–36). The Eu lifetime of 2.48 ms shown in Figure 2 is very similar to that of the unconjugated, unmodified Eu-DTPA-cs124 [2.42 ms (23)] and to that of the Eu-DTPA-cs124 complexed to DNA via the anhydride reaction [2.48 ms, this work; 2.5 ms (11)]. As reported previously for the anhydride form (11), the Eu lifetime for both the isothiocyanate and the anhydride reactions changes <5% between single- and double-stranded DNA.

The terbium excited state lifetime when the chelate is bound to DNA is more sensitive to environmental conditions—temperature, salt, and hybridization conditions—than europium under similar conditions. The terbium lifetime in DTPA-cs124 not attached to a

macromolecule is insensitive to these conditions (23). It is likely that the origin of this greater sensitivity is due to strong interaction between the chelate and the DNA bases, and this interaction affects the excited state lifetime of Tb^{3+} more than Eu^{3+} (likely because of the greater energy of the terbium excited state). The 3.063 ms terbium lifetime in Figure 2 is somewhat longer than that of the unmodified Tb-DTPA-cs124 [2.63 ms (23)] and very similar to the lifetime of Tb-DTPA-cs124 complexed to DNA via the anhydride reaction and hybridized [2.98 ms, this work; 2.81 ms (12)]. (The small difference appears to be due to slightly lower temperature used in the current work, although both are reported as “5 °C”.) As we found previously for the anhydride reaction (12), the lifetime of the terbium when bound to DNA via the isothiocyanate increases upon hybridization (2.19 ms for single-stranded, 2.50 ms for double-stranded; both at room temperature and in D_2O buffer) and decreases with temperature (2.50 ms in D_2O at room temperature; 3.06 ms in D_2O buffer at 5 °C for the double-stranded, isothiocyanate-form) and increases slightly with salt. The emission intensity of the lanthanide complexes also decreases upon attachment to DNA (roughly 5–10-fold). In contrast, the terbium lifetime in the unreacted form is temperature and salt independent (23). These observations imply that the chelate interacts strongly with the DNA, and this interaction is modulated by hybridization, temperature, and salt. More specifically, hybridization increases the terbium lifetime, which is consistent with the symmetry in the crystal field surrounding the terbium increasing upon hybridization. In addition, particularly in the single-stranded form, the cs124 may be able to interact with bases, forming a new energy level which can lead to nonradiative deexcitation. We find, for example, that in the single-stranded case, terbium (but not europium) can have a small (typically $\leq 10\%$ amplitude) component of a few hundred microseconds, indicating a species which is quenched. The amplitude of this component generally decreases with increasing salt and with hybridization.

Energy Transfer Measurements: ITC-Based Reactions. We have performed energy transfer measurements by hybridizing the chelate-labeled DNA to a complementary DNA containing an acceptor dye attached to the 5' end, in analogy to our previous work (11–13). For Eu, we used Cy5 as the acceptor, and for Tb, we used tetramethylrhodamine (TMR) as the acceptor. Addition of 0.25 Cy5-labeled DNA per Eu-DTPA-cs124-ITC-14-mer-DNA yielded a biexponential donor lifetime at 617 nm of 22% $\exp(-t/786 \mu\text{s}) + 78\% \exp(-t/2405 \mu\text{s})$, indicating 67% energy transfer ($1-786 \mu\text{s}/2.41 \text{ ms}$) and a distance of 62.2 Å ($R_0 = 70 \text{ Å}$) for the hybridized species in D_2O buffer. As expected, addition of further amounts of Cy5 increased the amplitude of the short-time component, without changing its lifetime (see also below). For Eu bound via the anhydride, we found 70% energy transfer (60.8 Å) for the hybridized species (see below). These distances are in excellent agreement with the 61.2 Å found previously using the Tb-anhydride chelate attached to the same 14-mer (12).

Energy transfer from terbium bound to a 10-mer DNA via the isothiocyanate also yielded results consistent with previous (and current) anhydride-based reactions. In D_2O buffer, at room temperature, for example, an intermediate point in the titration with a TMR-labeled strand yielded a donor lifetime at 546 nm of 43% $\exp(-t/355 \mu\text{s}) + 67\% \exp(-t/2187 \mu\text{s})$. Previously, we found 329 and 2101 μs , respectively (12).

Energy Transfer Using Anhydride Reaction: Comparison to Previous Work. We repeated our previ-

ously published energy transfer measurements (11, 12) on the 10-mer DNA, which was based on a base-protected anhydride-coupling reaction, using our new anhydride-coupling procedure. The repeatability was excellent: In the current work, the terbium lifetime of terbium-labeled DNA hybridized to a TMR-labeled complement is 328–343 μ s, corresponding to 88% energy transfer (previous value 328 μ s, 88% energy transfer), and the terbium lifetime of the unhybridized donor strand is 2.19 ms (previous value 2.10 ms), although this latter value is fairly temperature-sensitive, increasing to as much as 2.50 ms if the temperature is not carefully controlled. The sensitized emission of the TMR is 333–356 μ s (326 μ s, previous value), in excellent agreement with the donor lifetime of the hybridized species.

Similar agreement is found with the Eu-anhydride–10-mer DNA hybridized to Cy5 complement (11). In this work, the unhybridized donor lifetime is 2.41 ms (previous value 2.40–2.52 ms) and the hybridized lifetime is 0.19 ms, corresponding to 92% energy transfer (previous values 0.22 ms, 91% energy transfer). The sensitized emission lifetime of Cy5 at 668 nm is 0.24 ms (previous value 0.25 ms).

Energy Transfer: Hybridization Conditions. Although no effort was made to achieve optimal hybridization conditions in this work, we generally found that our simple (but commonly used) hybridization procedure did not yield 100% hybridized donor strand, even with a 1.25-fold excess of acceptor strand and at 5 °C, which was well below the melting temperature of the DNAs. The amount of unhybridized donor strand varied from 10% to 50% (typically 10–20%). We generally found that DNA chelate purified by both reversed-phase and anion exchange yielded higher percentage of hybridization than those purified only by reversed phase, although this result is not rigorous and the reason for it is unclear. Since each strand was shown to be pure, we do not believe the unhybridized donor strand is due to some fraction of donor strand that cannot hybridize. Complete hybridization was achieved after gel purification to isolate the double-stranded complex under nondenaturing conditions (37): luminescence measurements on the DNA in gel fragments yielding a single exponential and quenched donor lifetime. Presumably kinetically trapped single-stranded DNA complexes were formed in solution in our simple hybridization procedures. We note that lanthanide-based energy transfer, with the capability to accurately measure multiexponential donor lifetimes, has the ability to detect even a relatively small percentage of unhybridized strands. Standard fluorescence resonance energy transfer does not have this ability. We believe, therefore, that caution should be exercised in assuming complete hybridization in FRET experiments and that gel purification of the double-stranded complex may be necessary, as others have found (37).

Conclusion. We have synthesized, purified, and spectrally characterized new isothiocyanate derivatives of DTPA–cs124 bound to small molecules and to DNA oligomers. We have also optimized conditions for the anhydride-based reaction of DTPA–cs124 with base-protected DNA and shown that specific reaction at a 5' amine can be achieved without side reaction at the DNA bases. Finally, we have used these new products in luminescence resonance energy transfer measurements and have shown that the results are consistent with previously published measurements. The facile attachment to biomolecules of luminescent lanthanide chelates should increase the utility of these compounds.

ACKNOWLEDGMENT

We acknowledge financial support from NIH Grants AR44420 and GM41911 and from the Office of Energy Research, Office of Health and Environmental Research of the Department of Energy, under Contract DE AC03-76SF00098. M.L. was supported by Postdoctoral Training Grant NIH 2-T32 ES07075. We also acknowledge the excellent technical assistance of the UCSF Mass Spectrometry Facility (A. L. Burlingame, Director), Biomedical Research Program of National Center Research Resources, NIH NCRR BRTP 01614, and the excellent mass spectroscopy assistance of Lynn Myers of the Midland Certified Reagent Co.

LITERATURE CITED

- (1) Yu, H., and Diamandis, E. P. (1993) *Clin. Chem.* 39, 2108.
- (2) Oser, A., Collasius, M., and Valet, G. (1990) *Anal. Biochem.* 191, 295.
- (3) Saha, A. K., Kross, K., Kloszewski, E. D., Upson, D. A., Toner, J. L., Snow, R. A., Black, C. D. V., and Desai, V. C. (1993) *J. Am. Chem. Soc.* 115, 11032.
- (4) Soini, E., and Lovgren, T. (1987) *CRC Crit. Rev. Anal. Chem.* 18, 104.
- (5) Hemmälä, I., Dakubu, S., Mikkala, V.-M., Siitari, H., and Lovgren, T. (1984) *Anal. Biochem.* 137, 335.
- (6) Seveus, L., Vaisala, M., Syrjanen, S., Sandberg, M., Kuusisto, A., Harju, R., Salo, J., Hemmälä, I., Kojola, H., and Soini, E. (1992) *Cytometry* 13, 329.
- (7) Seveus, L., Vaisala, M., Hemmälä, I., Kojola, H., Roomans, G. M., and Soini, E. (1994) *Microsc. Res. Techn.* 28, 149.
- (8) Marriott, G., Clegg, R. M., Arndt-Jovin, D. J., and Jovin, T. M. (1991) *Biophys. J.* 60, 1374.
- (9) Marriott, G., Heidecker, M., Diamandis, E. P., and Yan-Marriott, Y. (1994) *Biophys. J.* 67, 957.
- (10) Stryer, L., Thomas, D. D., and Meares, C. F. Diffusion-Enhanced Fluorescence Energy Transfer. In *Annual Review of Biophysics and Bioengineering* (L. J. Mullins, Ed.) Vol. 11, 203 pp, Annual Reviews, Palo Alto, CA, 1982.
- (11) Selvin, P. R., Rana, T. M., and Hearst, J. E. (1994) *J. Am. Chem. Soc.* 116, 6029.
- (12) Selvin, P. R., and Hearst, J. E. (1994) *Proc. Natl. Acad. Sci. U.S.A.* 91, 10024.
- (13) Selvin, P. R. Fluorescence Resonance Energy Transfer. In *Methods in Enzymology* (K. Sauer, Ed.) Vol. 246, 300 pp, Academic Press, Orlando, FL, 1995.
- (14) Mathis, G. (1993) *Clin. Chem.* 39, 1953.
- (15) Mathis, G. (1995) *Clin. Chem.* 41, 1391.
- (16) Selvin, P. R. (1997) *IEEE J. Sel. Top. Quantum Electron.* (in press).
- (17) Canfi, A., Bailey, M. P., and Rocks, B. F. (1989) *Analyst* 114, 1908.
- (18) Takalo, H., Mikkala, V.-M., Mikola, H., Liitti, P., and Hemmälä, I. (1994) *Bioconjugate Chem.* 5, 278.
- (19) Bailey, M. P., Rocks, B. F., and Riley, C. (1984) *Analyst* 109, 1449.
- (20) Canfi, A., Bailey, M. P., and Rocks, B. F. (1989) *Analyst* 114, 1405.
- (21) Ando, T., Yamamoto, T., Kobayashi, N., and Munekata, E. (1992) *Biochim. Biophys. Acta* 1102, 186.
- (22) Saavedra, S. S., and Picozza, E. G. (1989) *Analyst* 114, 835.
- (23) Li, M., and Selvin, P. R. (1995) *J. Am. Chem. Soc.* 117, 8132.
- (24) Hnatowich, D. J., Layne, W. W., Childs, R. L., Lanteigne, D., Davis, M. A., Griffin, T. W., and Doherty, P. W. (1983) *Science* 220, 613.
- (25) Keana, J. F., and Mann, J. S. (1990) *J. Org. Chem.* 55, 2868.
- (26) Westerberg, D. A., Carney, P. L., Rogers, P. E., Kline, S. J., and Johnson, D. K. (1989) *J. Med. Chem.* 32, 236.
- (27) Brechbiel, M. W., Gansow, O. A., Atcher, R. W., Schlom, J., Esteban, J., Simpson, D. E., and Colcher, D. (1986) *Inorg. Chem.* 25, 2772.

- (28) Mikkala, V.-M., Mikola, H., and Hemmila, I. (1989) *Anal. Biochem.* 176, 319.
- (29) Meares, C. F., McCall, M. J., Reardan, D. T., Goodwin, D. A., Diamanti, C. I., and McTigue, M. (1984) *Anal. Biochem.* 142, 68.
- (30) Drobnica, L., Kristian, P., and Augustin, J. In *The Chemistry of Cyanates and their Thio Derivatives* (S. Patai, Ed.) 1003 pp. Wiley, New York, 1977.
- (31) Selvin, P. R., Jancarik, J., Li, M., and Hung, L.-W. (1996) *Inorg. Chem.* 35, 700.
- (32) Thiers, R. C. (1957) *Methods Biochem. Anal.* 5, 273.
- (33) Mujumdar, R. B., Ernst, L. A., Mujumdar, S. R., Lewis, C. J., and Waggoner, A. S. (1989) *Cytometry* 10, 11.
- (34) Horrocks, W. D., Jr., Schmidt, G. F., Sudnick, D. R., Kittrell, C., and Bernheim, R. A. (1977) *J. Am. Chem. Soc.* 99, 2378.
- (35) Horrocks, W. D., Jr., and Sudnick, D. R. (1979) *J. Am. Chem. Soc.* 101, 334.
- (36) Bunzli, J.-C. G. Luminescent Probes. In *Lanthanide Probes in Life, Chemical and Earth Sciences, Theory and Practice* (B. J.-C. G. Choppin and G. R. Choppin, Eds.) 219 pp, Elsevier, New York, 1989.
- (37) Clegg, R. M., Murchie, A. I., Zechel, A., and Lilley, D. M. (1993) *Proc. Natl. Acad. Sci. U.S.A.* 90, 2994.

BC960085M

Immunoassay Reagents for Thyroid Testing. 2. Binding Properties and Energetic Parameters of a T₄ Monoclonal Antibody and Its Fab Fragment with a Library of Thyroxine Analog Biosensors Using Surface Plasmon Resonance

Maciej Adamczyk,* John C. Gebler, Angelo H. Gunasekera, Phillip G. Mattingly, and You Pan

Diagnostics Division, Division Organic Chemistry (9-NM), Abbott Laboratories, Building AP 20, 100 Abbott Park Road, Abbott Park, Illinois 60064. Received November 6, 1996[®]

A library of 16 thyroxine analog biosensors were prepared for use on the BIAcore surface plasmon resonance instrument. An anti-thyroxine monoclonal antibody and its Fab fragment were tested with each biosensor to generate the association and dissociation rate constants, equilibrium association constants, and Gibbs free energy values for characterizing the binding event.

INTRODUCTION

The literature has stressed the need for well-characterized immunoreagents used in immunoassays (1–9). While haptens, tracers, immunoconjugates, and antibodies are routinely characterized to determine their identity and purity, their kinetic and thermodynamic properties are seldom acquired. However, these parameters are useful at all stages of immunoassay development from selection of the antibody through determining the structural features important in the design of the tracer. Characterizing the avidity of the antibody for a particular ligand should be at least as critical as determining its subtype, molecular weight, or purity. Determination of these binding parameters can be a laborious endeavor (10). However, the use of the automated BIAcore (Pharmacia) technology greatly simplifies this task, thus creating a convenient reference method. The BIAcore instrument allows biomolecular interaction analysis (BIA) in real time based on the surface plasmon resonance (SPR) phenomenon (11). Briefly, one member of the hapten–antibody pair is conjugated to the hydrophilic dextran matrix supported on the gold layer of the SPR chip to form a biosensor. A solution of the other binding member is introduced at a constant rate to the surface of the biosensor. Binding causes a change in the refractive index measured at the surface, generating an instrument response which is directly related to the change in the mass concentration in the surface layer. The resulting response is transformed by the instrument software to a sensorgram that depicts response units (RU) versus time (*t*). Nonlinear or linear regression analysis of the sensorgram curves provides the value for the rates of association (k_a) and dissociation (k_d) and, thus, the equilibrium association constant (K_A) and the change of free energy (ΔG) for the binding event.

Our continuing interest in immunoreagents for thyroid testing led us to compare the binding interaction of a structurally diverse library of thyroxine analog biosensors with a previously described anti-thyroxine monoclonal antibody (5) and its Fab fragment using the BIAcore surface plasmon resonance instrument. Our aim was to characterize both of these binding proteins in terms of

their association and dissociation rate constants, equilibrium association constants, and Gibbs free energy values in their reaction with potential ligand structures and to further elucidate those structural features which are important for the binding interaction.

MATERIALS AND METHODS

Sodium D-thyroxine pentahydrate, sodium L-3,3',5-triiodothyronine, L-3,5-diiodothyronine, 3,3',5-triiodothyropropionic acid, 3,3',5,5'-tetraiodothyropropionic acid, and 3,3',5-triiodothyroacetic acid were obtained from Sigma Chemical Co. (St. Louis, MO). D-3,3',5-Triiodothyronine was obtained from ICN Biochemicals (Cleveland, OH). Sodium L-thyroxine pentahydrate and all other synthetic reagents were obtained from Aldrich Chemical Co. (Milwaukee, WI) unless otherwise noted. Synthesized compounds were purified by HPLC [Waters (Millford, MA) system consisting of a model 590 pump, a Lambda-Max 481 UV detector, a model 745B data module, and a 40 × 100 mm μ Bondapak C18 column; flow rate, 45 mL/min]. Analytical HPLC was performed on a Beckman Gold system with UV detection using a Waters 8 × 100 mm μ Bondapak C18 column. ¹H NMR spectra were recorded at 300 MHz on a Varian Gemini spectrometer (Palo Alto, CA). Chemical shifts are reported in parts per million (δ) using tetramethylsilane (TMS) as the internal reference; coupling constants (*J*) are in hertz. Elemental analyses were performed by Robertson Microлит Laboratories, Inc. (Madison, NJ). Melting points were performed on an Electrothermal model 9100 digital melting point apparatus (Gillette, NJ) and are uncorrected. Electrospray ionization mass spectrometry (ESI/MS) was carried out on a Perkin-Elmer (Norwalk, CT) Sciex API 100 Benchtop system employing the Turbo IonSpray ion source. LC/ESI/MS was performed on the API 100 apparatus interfaced with a binary microbore HPLC system (Ultra Plus, Microtech Scientific, Sunnyvale, CA) equipped with a PLRP-S column (2.1 × 50 mm, Polymer Laboratories, Amherst, MA). Dialysis was carried out using SpectaPor 12–14 kDa molecular weight cutoff dialysis tubing (Scientific Products, McGaw, IL). SDS–PAGE was performed on a BioRad (Hercules, CA) Minigel system utilizing 12.5% polyacrylamide gels (7 cm × 10 cm × 1 mm), followed by staining with Coomassie Blue. Gel permeation chromatography was carried out on a Pharmacia P-50 system with UV detection at 280 nm. Surface plasmon resonance (SPR) measurements

* Author to whom correspondence should be addressed. Telephone: (847) 937-0225. Fax: (847) 938-8927. E-mail: adamczyk@apmac.abbott.com.

[®] Abstract published in *Advance ACS Abstracts*, February 15, 1997.

were carried out on a Pharmacia BIAcore automated system using CM-5 four-channel sensor chips. Reagents for the BIAcore instrument consisted of HBS buffer [10 mM Hepes (pH 7.4), 150 mM NaCl, 3.4 mM EDTA, and 0.05% surfactant P-20], a coupling kit containing *N*-hydroxysuccinimide (NHS), *N*-ethyl-*N*-(3-(diethylamino)-propyl)carbodiimide (EDAC), and 1 M ethanolamine hydrochloride (pH 8.5), all from Pharmacia. Anti-thyroxine mAb (5) and anti-theophylline mAb were obtained from the Abbott cell culture facility (Abbott Laboratories, Abbott Park, IL).

3'-Bromo-3,5,5-triiodo-L-thyronine (4). To a solution of **5** (240 mg, 0.397 mmol) in NaHCO₃ (50 mg, 0.596 mmol)/H₂O (15 mL) with 50 μ L of methylamine (40% aqueous) was added I₂ (101 mg, 0.397 mmol), followed by stirring for 1 h. After removal of the solvent in vacuo, the residue was dissolved in DMF (6 mL) and purified by HPLC (40:60:0.05 CH₃CN/H₂O/TFA; retention time, 6.7 min) to give the product **4** (295 mg, 37%). ¹H NMR (CD₃OD): 7.84 (2 H, s), 7.12 (1 H, d, *J* = 3), 6.92 (1 H, d, *J* = 3), 4.15 (1 H, m), 3.19 (1 H, dd, *J* = 14, 5), 2.94 (1 H, dd, *J* = 14, 6). ESI/MS (negative ion mode) *m/z*: 729 (M - H)⁻. Mp: 214–216 °C dec (lit. 236–238 °C) (12).

3'-Bromo-3,5-diiodo-L-thyronine (5). Bromine (49 μ L, 0.95 mmol) was added to a solution of 3,5-diiodo-L-thyronine (**3**, L-T₂, 500 mg, 0.95 mmol) in AcOH (10 mL) containing 2 drops of concentrated HCl and stirred. After 40 min, the solvent was evaporated and the residue was dissolved in EtOH (6 mL). The solution was purified by HPLC (33:67:0.05 CH₃CN/H₂O/TFA; retention time, 5.6 min) to give the product **4** (415 mg, 69%). ¹H NMR (DMSO-*d*₆): 7.83 (2 H, s), 6.94 (1 H, d, *J* = 6.6), 6.81 (1 H, s), 6.65 (1 H, m), 4.06 (1 H, m), 3.14 (1 H, m), 2.99 (1 H, m). ESI/MS *m/z*: 604, 606 (M)⁺. Mp: 240–242 °C dec (lit. 246–248 °C) (12).

3',5'-Dibromo-3,5-triiodo-L-thyronine (6). Bromine (123 μ L, 2.38 mmol) was added to a solution of 3,5-diiodo-L-thyronine (**3**, L-T₂, 500 mg, 0.97 mmol) in AcOH (4 mL) containing 2 drops of concentrated HCl and stirred. After 2 h, another portion of Br₂ (50 μ L, 0.38 mmol) and AcOH (4 mL) were added. The resulting solution was stirred for 30 min. After evaporation of the solvent, the residue was dissolved in EtOH (6 mL) and purified by HPLC (37:63:0.05 CH₃CN/H₂O/TFA; retention time, 6.9 min) to give the product **6** (493 mg, 76%). ¹H NMR (DMSO-*d*₆): 7.83 (2 H, s), 6.95 (2 H, s), 3.61 (1 H, m), 3.18 (1 H, m), 2.86 (1 H, m). ESI/MS *m/z*: 682, 684, 686 (M)⁺. Mp: 259–261 °C dec (lit. 262–264 °C) (12).

L-Thyroxine Dimethylamide TFA Salt (7). (A) L-Thyroxine sodium salt pentahydrate (**1**, L-T₄, 7.75 g, 8.72 mmol) was dissolved in THF (50 mL) and water (50 mL, pH was adjusted to 10 with 1 N NaOH). Di-*tert*-butyl dicarbonate (1.75 g, 10 mmol) was added and the solution stirred. After 2 h, THF was evaporated in vacuo. The aqueous layer was diluted with water (30 mL) and acidified with HCl to pH 2. The white precipitate was collected and dried over P₂O₅ to give *N-tert*-Boc-L-thyroxine (7.6 g, 99%). ¹H NMR (DMSO-*d*₆): 7.78 (2 H, s), 7.19 (1 H, b), 7.03 (2 H, s), 4.14 (1 H, m), 3.05 (1 H, m), 2.73 (1 H, m), 1.30 (9 H, s). ESI/MS (negative ion mode) *m/z*: 876 (M - H)⁻. Mp: 206–208 °C (D isomer, lit. 211–213 °C) (13). Analytical HPLC (70:30:0.05 CH₃CN/H₂O/TFA; retention time, 4.76 min, 98% purity). (B) *N-tert*-Boc-L-thyroxine (424 mg, 0.48 mmol), EDAC (186 mg, 0.97 mmol), and NHS (111 mg, 0.97 mmol) in DMF (8 mL) were stirred for 1.5 h. Dimethylamine (40% aqueous, 2 mL, 18 mmol) was added to this solution and stirred. After 1 h, the solution was acidified with TFA. The reaction mixture was purified by HPLC (70:30:0.05 CH₃CN/H₂O/TFA; retention time, 5.94 min) to give *N-*

tert-Boc-L-thyroxine dimethylamide (312 mg, 71%). ¹H NMR (CD₃OD): 7.82 (2 H, s), 7.08 (2 H, s), 4.85 (1 H, m), 3.01 (3 H, s), 2.93–2.85 (3 H, s; 2 H, m), 1.42 (9 H, s). ESI/MS (negative ion mode) *m/z*: 903 (M - H)⁻. (C) *N-tert*-Boc-L-thyroxine dimethylamide (107 mg, 0.19 mmol) was stirred in TFA (2 mL) for 30 min and then evaporated in vacuo to give L-thyroxine dimethylamide TFA salt (**7**) which was used in subsequent reactions without further purification.

3,3',5-Triiodo-L-thyronine dimethylamide TFA salt (8) was prepared from 3,3',5-triiodo-L-thyronine sodium salt (**2**, L-T₃) following the procedure for **7**, above. (A) Compound **2** (2.58 g, 3.96 mmol) gave *N-tert*-Boc-3,3',5-triiodo-L-thyronine (2.85 g, 97%). ¹H NMR (DMSO-*d*₆): 10.01 (1 H, b), 7.80 (2 H, s), 7.19 (1 H, d, *J* = 9), 6.95 (1 H, s), 6.81 (1 H, d, *J* = 9), 6.54 (1 H, b), 4.14 (1 H, m), 3.06 (1 H, m), 2.74 (1 H, m), 1.32 (9 H, s). (B) *N-tert*-Boc-3,3',5'-triiodo-L-thyronine (416 mg, 0.554 mmol) gave *N-tert*-Boc-3,3',5'-triiodo-L-thyronine dimethylamide (314 mg, 73%). HPLC (63:37:0.05 CH₃CN/H₂O/TFA; retention time, 6.19 min). ¹H NMR (CD₃OD): 7.81 (2 H, s), 6.97 (1 H, d, *J* = 3), 6.75 (1 H, d, *J* = 9), 6.62 (1 H, dd, *J* = 3, 9), 4.73 (1 H, m), 3.02 (3 H, s), 2.93 (3 H, s), 2.85 (2 H, m), 1.42 (9 H, s). ESI/MS *m/z*: 779 (M + NH₄)⁺. (C) *N-tert*-Boc-3,3',5-triiodo-L-thyronine dimethylamide (106 mg, 0.14 mmol) gave compound **8** which was used as the crude salt in subsequent reactions without further purification.

O-Methyl-L-thyroxine TFA Salt (9) (14). (A) To a solution of *N-tert*-Boc-L-thyroxine (550 mg, 0.63 mmol) in DMF (7 mL) were added K₂CO₃ (433 mg, 3.14 mmol) and CH₃I (300 μ L, 4.82 mmol). After being stirred for 1 h, the reaction mixture was directly purified by column chromatography (SiO₂, 30% EtOAc in hexane) to give *O*-methyl-*N-tert*-Boc-L-thyroxine methyl ester (490 mg, 90%). ¹H NMR (CDCl₃): 7.73 (2 H, s), 7.26 (1 H, d, *J* = 3), 6.74 (2 H, m), 5.13 (1 H, b), 4.56 (1 H, m), 3.84 (3 H, s), 3.76 (3 H, s), 3.09 (1 H, m), 2.97 (1 H, m), 1.45 (9 H, s). ESI/MS *m/z*: 797 (M + NH₄)⁺. (B) A solution of *O*-methyl-*N-tert*-Boc-L-thyroxine methyl ester (432 mg, 0.48 mmol) and LiOH·H₂O (100 mg, 2.39 mmol) in THF (7 mL) and H₂O (7 mL) were stirred for 1 h. The reaction mixture was acidified with 1 N HCl to pH 2 and extracted with EtOAc (4 × 20 mL). The extract was dried over anhydrous sodium sulfate, filtered, and evaporated in vacuo to give *N-tert*-Boc-*O*-methyl-L-thyroxine (393 mg, 92%). ¹H NMR (CD₃OD): 7.80 (2 H, s), 7.15 (1 H, s), 6.84 (1 H, d, *J* = 9), 6.66 (1 H, d, *J* = 9), 4.34 (1 H, m), 3.79 (3 H, s), 3.14 (1 H, dd, *J* = 5, 9), 2.85 (1 H, dd, *J* = 9, 4), 1.41 (9 H, s). ESI/MS *m/z*: 783 (M + NH₄)⁺. (C) Treatment of *N-tert*-Boc-*O*-methyl-L-thyroxine (370 mg, 0.42 mmol) with TFA (4 mL) gave compound **9** in quantitative yield which was used in subsequent reactions without further purification.

O-Methyl-3,3',5-triiodo-L-thyronine TFA salt (10) (15) was prepared following the procedure given above for compound **9**. (A) *N-tert*-Boc-3,3',5'-triiodo-L-thyronine (487 mg, 0.65 mmol) gave *O*-methyl-*N-tert*-Boc-3,3',5'-triiodo-L-thyronine methyl ester (451 mg, 87%). ¹H NMR (CDCl₃): 7.64 (2 H, s), 7.15 (2 H, s), 5.15 (1 H, b), 4.56 (1 H, m), 3.83 (3 H, s), 3.76 (3 H, s), 3.07 (1 H, m), 2.96 (1 H, m), 1.45 (9 H, s). ESI/MS (negative ion mode) *m/z*: 904 (M - H)⁻. (B) *O*-Methyl-*N-tert*-Boc-3,3',5'-triiodo-L-thyronine methyl ester (410 mg, 0.53 mmol) gave *N-tert*-Boc-*O*-methyl-3,3',5'-triiodo-L-thyronine (386 mg, 96%). ¹H NMR (CD₃OD): 7.78 (2 H, s), 7.13 (2 H, s), 4.37 (1 H, m), 3.78 (3 H, s), 3.16 (1 H, m), 2.89 (1 H, m), 1.41 (9 H, s). ESI/MS (negative ion mode) *m/z*: 890 (M - H)⁻. (C) *N-tert*-Boc-*O*-methyl-3,3',5'-triiodo-L-thyronine (366 mg,

0.528 mmol) gave compound **10** in quantitative yield and was used in subsequent reactions without further purification.

General Procedure for Conjugation of Linker to Amino-Substituted Analogs. (A) A solution of *N*-tert-Boc-6-aminocaproic acid (9.4 g, 40.6 mmol), EDAC (19.4 g, 101 mmol), and *N*-hydroxysuccinimide (11.6 g, 101 mmol) in DMF (100 mL) was stirred for 20 h. The solvent was removed in vacuo. The residue was dissolved in ether (50 mL) and washed with buffer (200 mL, 50 mM phosphate, pH 6). The extract was dried over anhydrous sodium sulfate, filtered, and evaporated in vacuo to give *N*-tert-Boc-6-aminocaproic acid succinimidyl active ester (12.1 g, 91%). ¹H NMR (CDCl₃): 4.60 (1 H, b), 3.12 (2 H, m), 2.85 (4 H, s), 2.62 (2 H, m), 1.5–1.35 (13 H, m, s). ESI/MS *m/z*: 329 (M + H)⁺. (B) To a stirred solution of the amine (or TFA ammonium salt) (0.4 mmol) and *N*-tert-Boc-6-aminocaproic acid succinimidyl active ester (0.6 mmol) in DMF (6 mL) was added diisopropylethylamine (0.2 mL, 1.15 mmol). After analytical HPLC showed complete reaction (1 h), the reaction mixture was purified by preparative HPLC.

Compound 15L was obtained from compound **1L** (66%). HPLC (58:42:0.05 CH₃CN/H₂O/TFA; retention time, 7.6 min). ¹H NMR (CD₃OD): 7.80 (2 H, s), 7.07 (2 H, s), 4.67 (1 H, m), 3.29 (1 H, m), 3.00 (2 H, m), 2.93 (1 H, m), 2.20 (2 H, m), 1.56 (2 H, m), 1.42 (11 H, s, m), 1.28 (2 H, m). ESI/MS *m/z*: 991 (M + H)⁺. Anal. Calcd for C₂₆H₃₀I₄N₂O₇·CF₃CO₂H: C, 30.43; H, 2.80; N, 2.53. Found: C, 30.48; H, 2.69; N, 2.62.

Compound 15D was obtained from compound **1D** (83%). HPLC (60:40:0.05 CH₃CN/H₂O/TFA; retention time, 6.4 min). ¹H NMR (DMSO-*d*₆): 9.27 (1 H, b), 8.15 (1 H, d, *J* = 8.7), 7.78 (2 H, s), 7.03 (2 H, s), 6.70 (1 H, b), 4.43 (1 H, m), 3.04 (1 H, dd, *J* = 3, 8.6), 2.85 (2 H, m), 2.76 (1 H, m), 2.02 (2 H, m), 1.34 (13 H, s, m), 1.14 (2 H, m). ESI/MS *m/z*: 990 (M)⁺. Anal. Calcd for C₂₆H₃₀I₄N₂O₇·CF₃CO₂H: C, 30.43; H, 2.80; N, 2.53. Found: C, 30.49; H, 2.5; N, 2.64.

Compound 16L was obtained from compound **2L** (68%). HPLC (55:45:0.05 CH₃CN/H₂O/TFA; flow rate, 45 mL/min; retention time, 8.4 min). ¹H NMR (CD₃OD): 7.77 (2 H, s), 7.01 (1 H, s), 6.72 (1 H, d, *J* = 9), 6.57 (1 H, d, *J* = 9), 4.65 (1 H, m), 3.20 (1 H, dd, *J* = 4.6, 13.6), 3.00 (2 H, m), 2.89 (1 H, m), 2.19 (2 H, m), 1.55 (2 H, m), 1.34 (13 H, s, m), 1.27 (2 H, m). ESI/MS *m/z*: 865 (M + H)⁺. Anal. Calcd for C₂₆H₃₁I₃N₂O₇·CF₃CO₂H: C, 34.34; H, 3.27; N, 2.86. Found: C, 34.49; H, 3.22; N, 2.95.

Compound 16D was obtained from compound **2L** (85%). HPLC (55:45:0.05 CH₃CN/H₂O/TFA; retention time, 6.06 min). ¹H NMR (DMSO-*d*₆): 8.13 (1 H, d, *J* = 8.4), 7.76 (2 H, s), 6.93 (1 H, d, *J* = 3), 6.79 (1 H, d, *J* = 8.7), 6.69 (1 H, m), 6.55 (1 H, dd, *J* = 3, 8.6), 4.42 (1 H, m), 3.06 (1 H, dd, *J* = 4.6, 13.6), 2.85 (2 H, m), 2.83 (1 H, m), 2.05 (2 H, m), 1.34 (13 H, s, m), 1.13 (2 H, m). ESI/MS *m/z*: 865 (M + H)⁺. Anal. Calcd for C₂₆H₃₁I₃N₂O₇·CF₃CO₂H: C, 34.34; H, 3.27; N, 2.86. Found: C, 34.65; H, 3.26; N, 3.10.

Compound 17 was obtained from compound **3** (82%). HPLC (50:50:0.05 CH₃CN/H₂O/TFA; retention time, 6.4 min). ¹H NMR (DMSO-*d*₆): 8.15 (1 H, d, *J* = 8.1), 7.75 (2 H, s), 6.69 (1 H, m), 6.68 (2 H, d, *J* = 6.3), 6.48 (2 H, d, *J* = 6.2), 4.41 (1 H, m), 3.01 (1 H, dd, *J* = 3, 7.5), 2.88–2.72 (5 H, m), 2.05 (2 H, m), 1.34 (11 H, s, m), 1.29 (2 H, m). ESI/MS *m/z*: 739 (M + H)⁺. Anal. Calcd for C₂₆H₃₂I₂N₂O₇: C, 42.25; H, 4.33; I, 34.40; N, 3.79. Found: C, 41.92; H, 4.1; I, 34.11; N, 3.72.

Compound 18 was obtained from compound **4** (92%). HPLC (60:40:0.05 CH₃CN/H₂O/TFA; retention time, 6.05 min). ¹H NMR (DMSO-*d*₆): 7.80 (2 H, s), 7.06 (1 H, d, *J*

= 3), 6.85 (1 H, d, *J* = 3), 4.69 (1 H, dd, *J* = 10, 5), 3.22 (1 H, dd, *J* = 13, 4), 3.00 (2 H, t, *J* = 7), 2.89 (1 H, dd, *J* = 14, 10), 2.19 (2 H, t, *J* = 8), 1.55 (2 H, t, *J* = 7), 1.41 (11 H, s, m). ESI/MS (negative ion mode) *m/z*: 943 (M)[−]. Anal. Calcd for C₂₆H₃₀BrI₃N₂O₇: C, 33.08; H, 3.18; N, 2.97. Found: C, 32.78; H, 2.92; N, 2.90.

Compound 19 was obtained from compound **5** (83%). HPLC (58:42:0.05 CH₃CN/H₂O/TFA; retention time, 5.7 min). ¹H NMR (DMSO-*d*₆): 7.79 (2 H, s), 6.83 (1 H, d, *J* = 6.6), 6.80 (1 H, s), 6.53 (1 H, d, *J* = 6.6), 4.68 (1 H, m), 3.20 (1 H, m), 3.00 (2 H), 2.89 (1 H, m), 2.22 (2 H, m), 1.55 (2 H, m), 1.42 (11 H, s, m), 1.29 (2 H, m). ESI/MS *m/z*: 819 (M + H)⁺.

Compound 20 was obtained from compound **6** (93%). HPLC (60:40:0.05 CH₃CN/H₂O/TFA; retention time, 5.4 min). ¹H NMR (DMSO-*d*₆): 7.80 (2 H, s), 6.85 (2 H, d, s), 4.68 (1 H, m), 3.25 (1 H, m), 3.00 (2 H), 2.90 (1 H, m), 2.20 (2 H, m), 1.55 (2 H, m), 1.42 (11 H, s, m), 1.27 (2 H, m). ESI/MS *m/z*: 897 (M + H)⁺.

Compound 21 was obtained from compound **7** (68%). HPLC (65:35:0.05 CH₃CN/H₂O/TFA; retention time, 6.5 min). ¹H NMR (CD₃OD): 7.83 (2 H, s), 7.07 (2 H, s), 5.06 (1 H, m), 3.03–2.93 (3 H, s; 2 H, m), 2.93–2.83 (3 H, s; 2 H, m), 2.19 (2 H, m), 1.55 (2 H, m), 1.42 (10 H, s, m), 1.23 (3 H, m). ESI/MS *m/z*: 1018 (M + H)⁺.

Compound 22 was obtained from compound **8** (78%). HPLC (63:37:0.05 CH₃CN/H₂O/TFA; retention time, 5.5 min). ¹H NMR (CD₃OD): 7.81 (2 H, s), 6.95 (1 H, d, *J* = 3), 6.74 (1 H, d, *J* = 9), 6.62 (1 H, dd, *J* = 3, 9), 5.48 (1 H, m), 3.02–2.95 (3 H, s; 2 H, m), 2.93 (3 H, s), 2.85 (2 H, m), 2.19 (2 H, m), 1.55 (2 H, m), 1.42 (10 H, s, m), 1.23 (3 H, m). ESI/MS *m/z*: 892 (M + H)⁺.

Compound 23 was obtained from compound **9** (94%). SiO₂ column (10–20% MeOH in CHCl₃). ¹H NMR (DMSO-*d*₆): 7.75 (2 H, s), 7.15 (2 H, s), 4.27 (1 H, m), 3.73 (3 H, s), 3.18 (1 H, m), 2.98 (2 H, m), 2.80 (1 H, m), 2.02 (2 H, m), 1.37 (13 H, s, m), 1.14 (2 H, m). ESI/MS *m/z*: 1005 (M + H)⁺. Anal. Calcd for C₂₇H₃₂I₄N₂O₇·CF₃CO₂H: C, 31.12; H, 2.95; N, 2.50. Found: C, 31.19; H, 2.88; N, 2.60.

Compound 24 was obtained from compound **10** (70%). SiO₂ column (10–25% MeOH in CHCl₃). ¹H NMR (CD₃OD): 7.80 (2 H, s), 7.14 (1 H, d, *J* = 3), 6.76 (1 H), 6.64 (1 H), 4.52 (1 H, m), 3.77 (3 H, s), 3.27 (1 H, m), 3.01 (2 H, m), 2.85 (1 H, m), 2.22 (2 H, m), 1.56 (2 H, m), 1.40 (11 H, s, m), 1.27 (2 H, m). ESI/MS *m/z*: 896 (M + NH₄)⁺.

Compound 28 was obtained from compound **14** (83%). HPLC (47:53:0.05 CH₃CN/H₂O/TFA; retention time, 6.3 min). ¹H NMR (DMSO-*d*₆): 9.35 (1 H, b), 8.08 (1 H, d, *J* = 8.1), 7.65 (2 H, s), 6.71 (1 H, b), 4.29 (1 H, m), 2.88–2.81 (4 H, m), 2.71 (2 H, m), 2.05 (2 H, m), 1.34 (11 H, s, m), 1.14 (2 H, m). ESI/MS *m/z*: 647 (M + H)⁺. Anal. Calcd for C₂₀H₂₈I₂N₂O₆: C, 37.14; H, 4.33; I, 39.30; N, 4.33. Found: C, 37.21; H, 4.39; I, 38.93; N, 4.52.

General Procedure for Conjugation of Linker to Carboxy-Substituted Analogs (25–27). A solution of the acid (**11–13**, 0.07 mmol), EDAC (0.141 mmol), NHS (0.14 mmol), and *N*-tert-Boc-hexamethylenediamine (0.14 mmol) in DMF (3 mL) was stirred for 30 h. The reaction mixture was purified by HPLC.

Compound 25 was obtained from compound **11** (35%). HPLC (70:30:0.05 CH₃CN/H₂O/TFA; retention time, 6.9 min). ¹H NMR (DMSO): 9.30 (1 H, s), 8.05 (1 H, b), 7.79 (2 H, s), 7.05 (2 H, s), 6.74 (1 H, b), 3.38 (2 H), 3.01 (2 H, m), 2.87 (2 H, m), 1.34 (13 H, s, m), 1.20 (4 H, m). ESI/MS *m/z*: 947 (M)⁺, 847 [M – CO₂C(CH₃)₃]⁺. Anal. Calcd for C₂₅H₃₀I₄N₂O₅: C, 31.70; H, 3.17; I, 53.69; N, 2.96. Found: C, 31.94; H, 3.09; I, 53.62; N, 2.89.

Compound 26 was obtained from compound **12** (33%). HPLC (63:37:0.05 CH₃CN/H₂O/TFA; retention time, 6.8

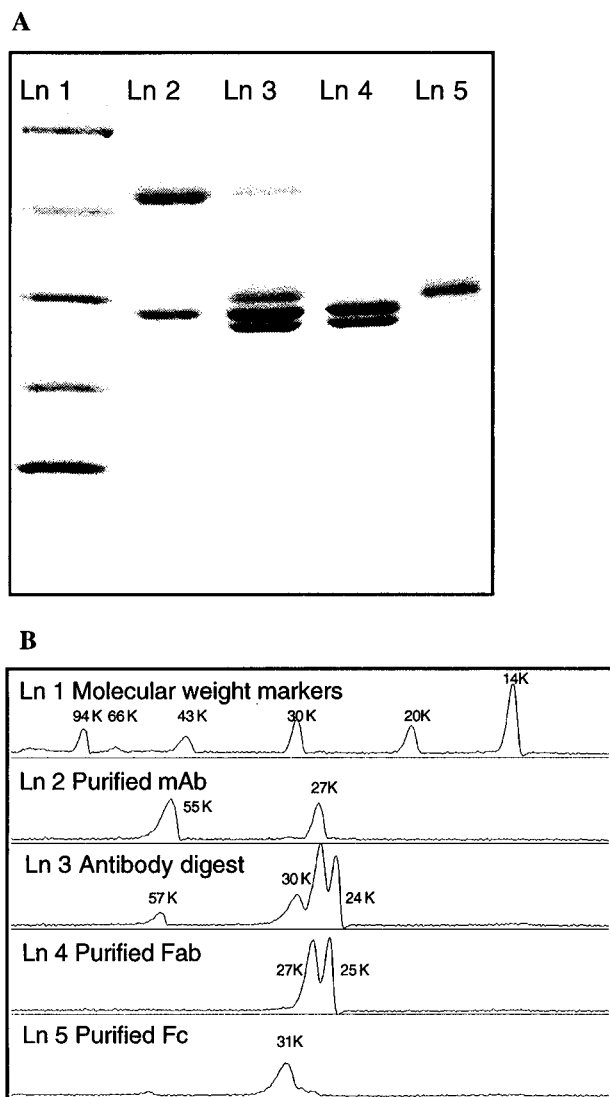


Figure 1. Gel electrophoresis. (A) SDS-PAGE of anti-T₄ monoclonal antibody and anti-T₄ Fab. (B) NIH Image digital plot of lane 1, molecular mass standards [phosphorylase b (94 kDa), BSA 966 kDa, ovalbumin (43 kDa), carbonic anhydrase (30 kDa), trypsin inhibitor (20 kDa), and lysozyme (14.5 kDa)]; lane 2, purified mAb; lane 3, antibody digest; lane 4, purified Fab fragment; and lane 5, purified Fc fragment.

min). ¹H NMR (DMSO-*d*₆): 10.01 (1 H, s), 8.05 (1 H, m), 7.78 (2 H, s), 6.96 (1 H, d, *J* = 3), 6.80 (1 H, d, *J* = 8.7), 6.74 (1 H, m), 6.57 (1 H, d, *J* = 8.7), 3.36 (4 H, m), 3.03 (2 H, m), 2.87 (2 H, m), 1.34 (13 H, s, m), 1.21 (2 H, m). ESI/MS *m/z*: 821 (M + H)⁺. Anal. Calcd for C₂₅H₃₁I₃N₂O₅: C, 36.57; H, 3.78; I, 46.45; N, 3.41. Found: C, 36.44; H, 3.66; I, 45.98; N, 3.24.

Compound 27 was obtained from compound **12** (34%). HPLC (65:35:0.05 CH₃CN/H₂O/TFA; retention time, 6.4 min). ¹H NMR (DMSO-*d*₆): 10.01 (1 H, s), 7.79 (1 H, m), 7.73 (2 H, s), 6.93 (1 H, d, *J* = 3), 6.80 (1 H, d, *J* = 9), 6.77 (1 H, m), 6.58 (1 H, dd, *J* = 3, 9), 2.98 (2 H, m), 2.86 (2 H, m), 2.75 (2 H, m), 3.36 (2 H, m), 1.34 (9 H, s; 2 H, m), 1.18 (2 H, m). ESI/MS *m/z*: 835 (M + H)⁺.

Anti-Thyroxine Monoclonal Antibody Preparation. The anti-thyroxine-mAb (**5**) derived from cell line ATCC HB1125 (American Type Culture Collection, Rockville, MD) which was raised against T₄ conjugate **59** (**3**) was purified using a Pharmacia FPLC system as follows. The tissue culture media containing anti-T₄ mAb (150 mL) was centrifuged at 3500*g* and filtered through a 0.2 μm filter to remove hybridoma cells. The super-

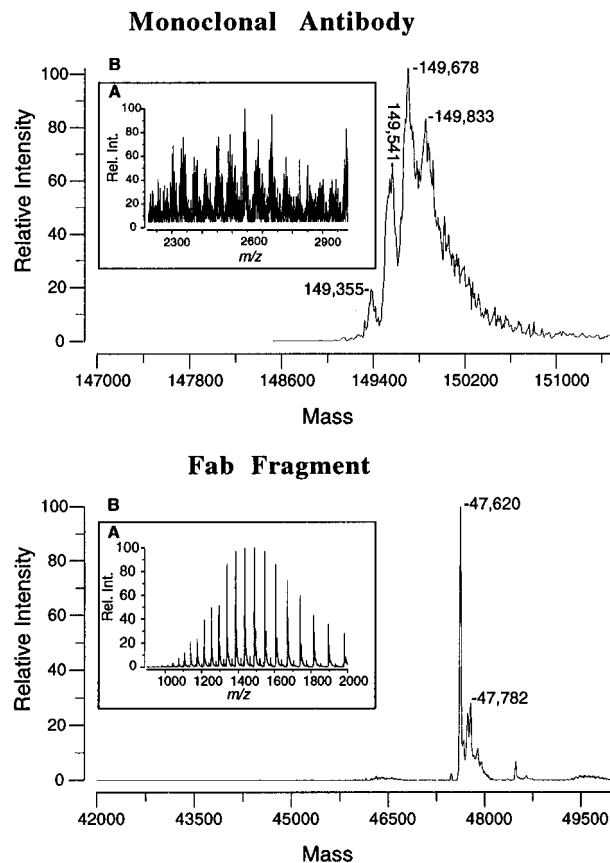


Figure 2. ESI/MS of anti-T₄ mAb and its Fab fragment. (A) Raw mass spectrum. (B) Deconvoluted mass spectrum.

natant was applied at a rate of 10 mL/min to a protein-A column (26 mm × 20 cm, 75 mL, Pharmacia) which had been equilibrated with IgG binding buffer (500 mL, Pierce). The protein-A column with bound monoclonal antibodies was further washed with IgG binding buffer (500 mL), and anti-T₄ mAb was eluted with IgG elution buffer (500 mL, Pierce), monitoring at 280 nm. Fractions (4 × 30 mL) containing the desired component were collected, combined, and dialyzed against PBS buffer (4 × 4 L, 2 days, 4 °C). The antibody concentration was 4.86 mg/mL as determined by UV spectroscopy at 280 nm using an absorption coefficient of 1.4 (16) and verified by the micro-BCA protein assay (17) reagent kit (Pierce) using mouse IgG as a standard protein. Purified anti-T₄ mAb was characterized for purity by SDS-PAGE (Figure 1), and its molecular weight was determined by LC/ESI mass spectrometry (Figure 2) according to the methods reported below. The total recovery of the purified anti-T₄ mAb was 194 mg.

Anti-Thyroxine Fab Preparation. The digestion of anti-T₄ mAb was carried out with the ImmunoPure Fab Preparation Kit (Pierce) according to the manufacturer's protocol. Thus, purified anti-T₄ mAb (40 mg) in digestion buffer (2 mL; 20 mM NaH₂PO₄, 10 mM EDTA, and 20 mM cysteine at pH 7.0) was incubated for 5 h in a 37 °C incubator-shaker with immobilized papain (2 mL). Papain-digested anti-T₄ mAb was passed through an immobilized protein-A column (2 mL) supplied with the kit to remove undigested mAb and the Fc fragments. The protein-A column was washed again with an additional ImmunoPure binding buffer (15 mL). Column flow-through and column washes were pooled and concentrated to 4 mL using a Centrprep-30 concentrator (Amicon, Beverly, MA). Concentrated anti-T₄ Fab was dialyzed against PBS (4 × 4 L, 2 days, 4 °C). The

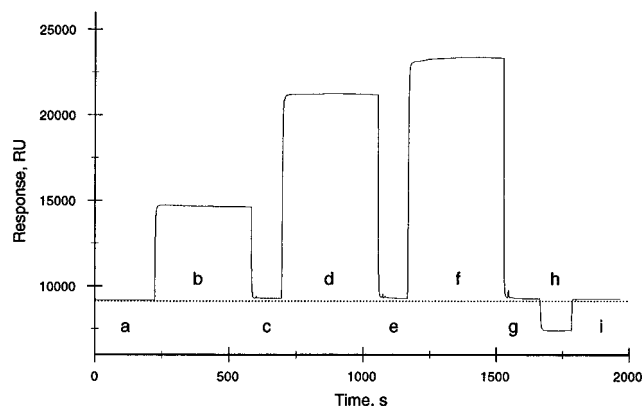


Figure 3. Sensorgram for activation and conjugation to a sensor chip: (a) buffer baseline, (b) EDAC/NHS activation, (c) buffer wash, (d) thyroxine analog conjugation, (e) buffer wash, (f) ethanolamine quench, (g) buffer wash, (h) HCl wash, (i) buffer wash, and (---) reference line for ΔRU .

concentration of anti-T₄ Fab was 11.8 mg/mL as determined by the micro-BCA method using mouse IgG as a standard protein. Purified anti-T₄ Fab was characterized for purity by SDS-PAGE (Figure 1), and its molecular weight was determined by LC/ESI mass spectrometry (Figure 2) according to the methods reported below. The total recovery of the purified anti-T₄ FAB was 9 mg (~65% yield).

Analysis by Gel Electrophoresis. The antibody samples were dissolved in SDS-PAGE sample buffer (10 mM TRIS/HCl, 1 mM EDTA, 2.5% SDS, and 5.0% β -mercaptoethanol at pH 8.0) and heated to 100 °C for 5

min. Gels were loaded with 15 μ L of sample and run under denaturing conditions using the manufacturer's protocol. Upon completion, the gels were stained with Coomassie Blue using a standard developing routine from the manufacturer. The resulting gels were evaluated first by scanning (Apple OneScanner, Apple Computers, Cupertino, CA) and then analyzing the image with the gel plotting macros of NIH Image (version 1.58, public domain image processing and analysis program for the Apple Macintosh PowerPC from the NIH, Bethesda, MD, downloaded from zippy.nimh.nih.gov).

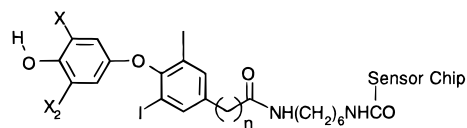
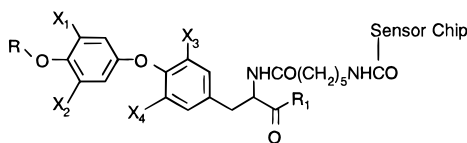
Mass Spectrometry Analysis. Monoclonal Antibody.

A solution of anti-T₄ mAb (1 mg/mL, 0.1% formic acid) was injected into the LC/ESI/MS apparatus and eluted with a linear gradient of 90:10 TFA (0.1% aqueous)/acetonitrile to 100% acetonitrile over 40 min at a flow rate of 75 μ L/min. The column output was directly interfaced to the mass spectrometer ion source. ESI/MS operating parameters were as follows: interface auxiliary air flow of 5 L/min at 400 °C and nebulizer air flow of 1.5 L/min, ion spray voltage (IS) of 4.8 kV, and orifice voltage (OR) of 80 V. The instrument scanned a mass range of 2200–3000 m/z in 0.1 amu steps for a total scan time of 8 s. The resulting spectra were reconstructed using the manufacturer's software (BioMultiview version 1.2) (Figure 2).

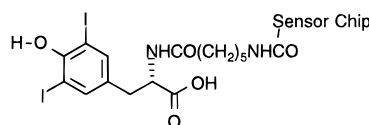
Fab Fragment. A solution of anti-T₄ Fab (1 mg/mL, 0.1% formic acid) was injected into the LC/ESI/MS apparatus and eluted with a linear gradient of 90:10 TFA (0.1% aqueous)/acetonitrile to 100% acetonitrile over 20 min at a flow rate of 100 μ L/min. The column output was directly interfaced to the mass spectrometer ion

Table 1. Biosensors Prepared and Their Binding Properties with Anti-Thyroxine Monoclonal Antibody^a

no.	R	X ₁	X ₂	X ₃	X ₄	R ₁	k_a (M ⁻¹ s ⁻¹) × 10 ⁶	k_d (s ⁻¹) × 10 ⁻⁵	K_A (M ⁻¹) × 10 ⁸	ΔG (kcal/mol)	$\Delta\Delta G$ (kcal/mol)
43L	H	I	I	I	I	OH	3 ± 0.34	6 ± 0.95	525 ± 97.4	-14.5	0
43D	H	I	I	I	I	OH	2 ± 0.47	4 ± 0.18	647 ± 120	-14.7	-0.2
44L	H	H	I	I	I	OH	2 ± 0.75	77 ± 19	29 ± 11.7	-12.9	1.6
44D	H	H	I	I	I	OH	3 ± 0.30	84 ± 9	32 ± 5.23	-12.9	1.6
45	H	H	H	I	I	OH	— ^b	—	—	—	—
46	H	I	Br	I	I	OH	2 ± 0.37	11 ± 2.6	187 ± 54.6	-14.2	0.3
47	H	H	Br	I	I	OH	5 ± 0.60	317 ± 49	15 ± 3.09	-12.4	2.1
48	H	Br	Br	I	I	OH	3 ± 0.45	18 ± 4.8	152 ± 51.0	-13.8	0.7
49	H	I	I	I	I	N(CH ₃) ₂	1 ± 0.07	1 ± 0.03	1140 ± 76.2	-15.0	-0.5
50	H	H	I	I	I	N(CH ₃) ₂	5 ± 0.25	592 ± 93	9 ± 1.39	-12.2	2.3
51	CH ₃	I	I	I	I	OH	—	—	—	—	—
52	CH ₃	H	I	I	I	OH	—	—	—	—	—



no.	n	X ₁	X ₂
53	1	I	I
54	1	H	I
55	2	H	I



56

^a All data are from nonlinear regression analysis of sensorgram curves. ^b — indicates that no binding was observed at the concentrations tested.

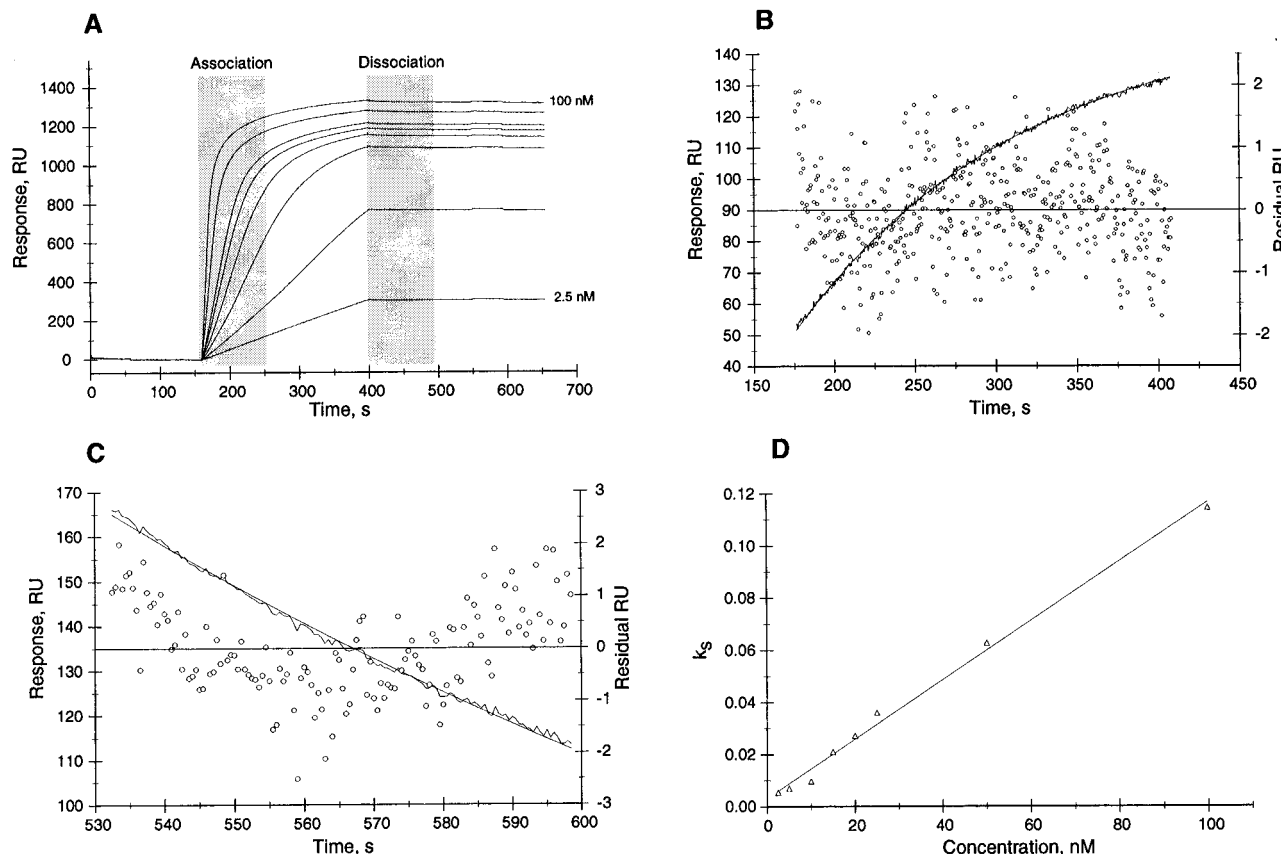


Figure 4. SPR analysis with sensor 43L and T₄ monoclonal antibody. (A) Sensorgrams generated with 2.5, 5, 10, 15, 20, 25, 50, and 100 nM mAb. (B) Nonlinear regression plot of the association phase. (C) Nonlinear regression plot of the dissociation phase. (D) Linear regression plot.

source. ESI/MS operating parameters were as follows: interface auxiliary air flow of 4 L/min at 350 °C and nebulizer air flow of 1.5 L/min, ion spray voltage (IS) of 4.8 kV, and orifice voltage (OR) of 20 V. The instrument scanned a mass range of 700–2000 *m/z* in 0.25 amu steps for a total scan time of 5.2 s. The resulting spectra were reconstructed using the manufacturer's software (Bio-Multiview version 1.2) (Figure 2).

Conjugation of Thyroxine Analogs to Sensor Chips. (A) *Removing the tert-Boc Protecting Group.* A solution of the *tert*-Boc-protected analog (**15–28**) (5.2 mmol) in TFA (0.2 mL) was stirred for 30 min. After removal of the solvent in vacuo, the resulting TFA salt (**29–42**) was used for conjugation to the sensor chip without further purification.

(B) *Activation and Coupling to the Sensor Chip for Direct Kinetic Analysis* (18) (Figure 3). The CM-5 sensor chip was placed in the automated BIAcore instrument, and the HBS buffer flow was started (5 μ L/min), giving an instrument response as shown in region a. After about 4 min, the activation solution (5 μ L/min, 0.2 M EDAC and 0.05 M NHS) was injected (region b). After 6 min, HBS buffer was introduced (5 μ L/min, 90 s) (region c), before the thyroxine analog solution (**29–42**, 5 μ g/mL in 10% EtOH, 50 mM NaHCO₃, and 500 mM NaCl at pH 8.5) was added (region d). After 6 min, HBS buffer was again introduced (5 μ L/min, 2 min, region e), before the unreacted active ester groups remaining on the biosensor chip were blocked with ethanolamine (5 μ L/min, 1 M, 6 min, region f). Finally, the sensor surface was washed with HBS buffer (5 μ L/min, 2 min, region g), aqueous HCl (5 μ L/min, 100 mM, 2 min, region h), and HBS buffer (5 μ L/min, 4 min, region i) to remove any residual noncovalently attached thyroxine analog. All immobilization steps were performed automatically by

the BIAcore instrument to produce the biosensors **43–56** (Table 1).

Kinetic Analysis. Eight concentrations (0.5–100 nM in HBS buffer) of the binding protein (anti-T₄ mAb or anti-T₄ Fab) were each injected over the surface of each thyroxine analog biosensor (**43–56**) for 360 s at a rate of 5 μ L/min. Afterward, the binding protein solution was replaced with HBS buffer alone and the dissociation of the protein from the biosensor surface was monitored for 200 s. Any remaining bound proteins were dissociated by washing with formic acid (10 s, 1 M) in order to regenerate the biosensor. The association and dissociation rates were calculated by selecting regions from the binding and dissociation phases of the sensorgrams that corresponded to a 1:1 binding interaction (19) (Figure 4). Equilibrium affinity constants were derived from the ratio of association and dissociation constants. All experiments were performed at 25 °C. Data were collected at 2 Hz intervals and analyzed using least-squares statistics built into BIAevaluation 1.1.1 software (Pharmacia) on a NEC personal computer.

Analysis for Nonspecific Binding. (A) A control sensor chip lacking any ligand was prepared following the general procedure for conjugation presented above but substituting buffer for the ligand solution. Anti-T₄ mAb and anti-T₄ Fab were used in the direct kinetic analysis following the above procedure. The resulting sensorgrams are shown in panels A and B of Figure 5, respectively. (B) The binding of anti-theophylline mAb to each of the thyroxine analog biosensors (**43–56**) was evaluated under the same conditions as those used for anti-T₄ mAb and anti-T₄ Fab in the direct kinetic analysis, above. Six concentrations (0.5–100 nM) of anti-theophylline mAb were injected over the biosensor surfaces and the sensorgrams recorded (Figure 5C).

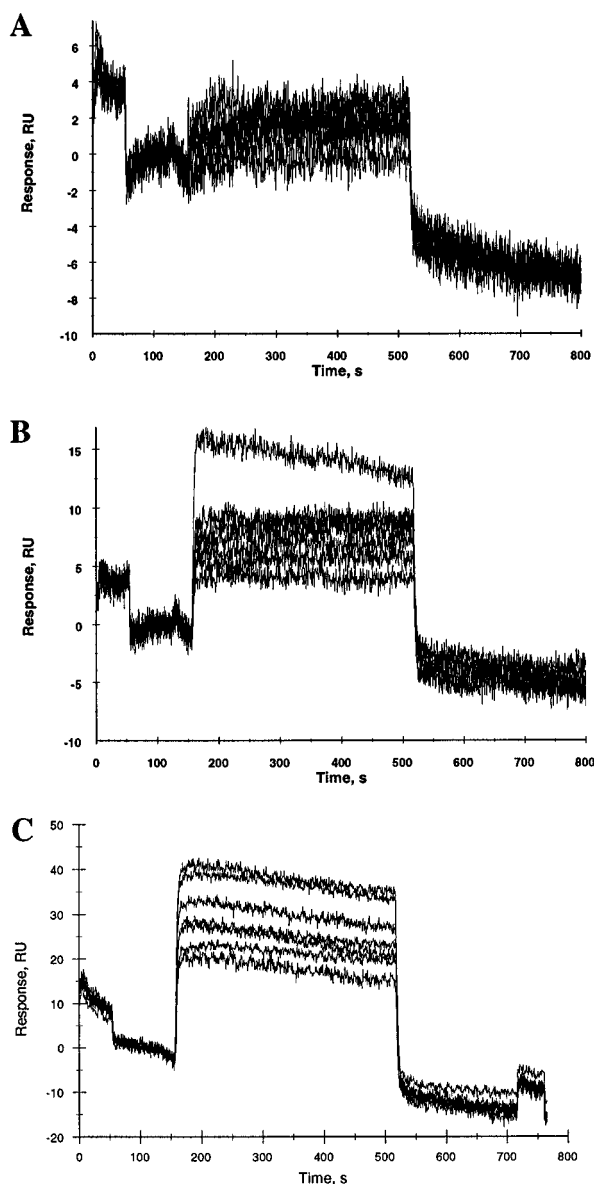


Figure 5. Sensorgrams showing the absence of nonspecific binding. (A) Sensorgrams generated with 2.5, 5, 10, 15, 20, 25, 50, and 100 nM mAb with no ligand on the sensor chip. (B) Sensorgrams generated with 2.5, 5, 10, 15, 20, 25, 50, and 100 nM Fab with no ligand on the sensor chip. (C) Sensorgrams generated with 2.5, 5, 10, 15, 20, 25, 50, and 100 nM theophylline mAb and sensor 43L.

RESULTS

Preparation of Thyroxine Biosensors. Derivatization of the carboxylated surface of the sensor chip first required the preparation of the chosen thyroxine analogs bearing aminoalkyl linkers. As detailed in Scheme 1, commercially available T_4 (**1**, L and D enantiomers), T_3 (**2**, L and D enantiomers), and T_2 (**3**) were employed directly in the reaction scheme without further modification. The bromo analogs **4–6** were prepared according to literature procedures (12, 20). Thus, **5** and **6** were obtained directly by bromination of T_2 (**3**), while **4** was prepared by the iodination of BrT_2 (**5**). Attempted bromination of T_3 (**2L**) led only to Br_2T_2 (**6**). Dimethylamide compounds **7** and **8** were prepared through the carbodiimide-mediated coupling of the corresponding *N*-*tert*-Boc-protected derivatives of T_4 (**1L**) and T_3 (**2L**) with excess aqueous dimethylamine and subsequent deprotection with TFA. The known *O*-methyl-substituted T_4 (**14**) and T_3 (**15**) compounds were likewise issued as

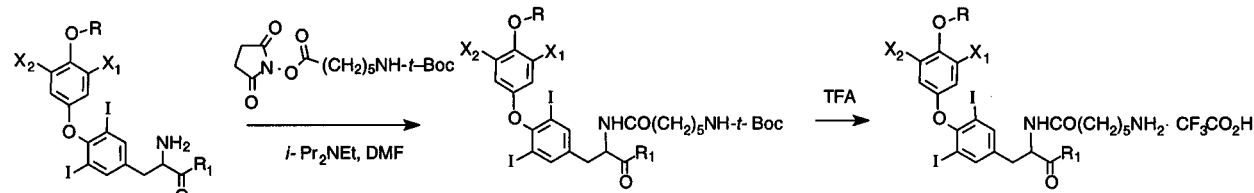
the TFA salts **9** and **10** in 83% overall yield, from the *N*-*tert*-Boc-protected derivatives after methylation with methyl iodide in the presence of potassium carbonate and deprotection with TFA. Analogs **1–10** were coupled with the NHS ester of *N*-*tert*-Boc-6-aminocaproic acid to give compounds **15–24** in 66–94% yield after preparative HPLC. Deprotection with TFA gave the aminoalkyl-substituted thyroxine analogs. Thyroalkanoic acids **11–13** (Scheme 2) were coupled to mono-*N*-*tert*-Boc-hexanediamine (**21**), giving compounds **25** and **26** (33–35% yield), and subsequently deprotected to give the requisite aminoalkyl derivatives **39–41**. The aminoalkyl-substituted 3,5-diiodothyrosine derivative **42** was prepared as shown in Scheme 3.

Conjugation of low-molecular weight ligands as typified by the L - T_4 analog **29** to the BIAcore sensor chips allowed the generation of the sensorgram illustrated in Figure 3. Buffer alone (region a) gave a baseline response of 9174 RU. Activation of the carboxylated surface of the chip with EDAC and NHS to give the NHS active esters produced a change of 6000 RU (region b). Washing returned the sensorgram to near baseline (9290 RU, region c). Introduction of the ligand-bearing reactive amino groups (region d) led to covalent attachment via newly formed amide bonds with a change of 12 000 RU. After washing, the instrument response fell to 9326 RU (region e). Final blocking of unreacted active esters on the solid surface with ethanolamine (region f) caused a rise in RU of 15 000. Washing with buffer, aqueous HCl, and buffer again gave the final biosensor chip. As expected for low-molecular weight ligands, the 36 Δ RU (region e – region i) after conjugation was too small to be a reliable indicator of ligand density. Successful conjugation was confirmed, however, on equilibration of the sensors with anti- T_4 mAb (Figure 4) where the Δ RU was dramatically larger. For our experiments, conjugation using the optimum concentration of the aminoalkyl thyroxine analogs (**29–42**) (5 μ g/mL) gave rise to a maximum Δ RU of about 1000 at saturation levels of anti- T_4 mAb for the resulting biosensors (**43–56**). These biosensors were suitable for use in the direct kinetic analysis, below.

To show that the interaction of anti- T_4 mAb was specific for the analyte on the biosensor and not to the dextran surface, three experiments were performed. First, a blank sensor was treated under the normal conjugation protocol except that buffer was substituted for the thyroxine analog ligand. Anti-thyroxine mAb and Fab were tested at eight concentrations with the sensor. The resulting sensorgrams are depicted in panels A and B of Figure 5, respectively. Finally, thyroxine sensor **43L** was equilibrated with anti-theophylline monoclonal antibody (Figure 5C). The sensorgram in all three experiments showed a very small Δ RU response within the noise level of the instrument. Additionally, the recorded response appeared to be random. It did not correspond to the incremental changes in the antibody concentration, thus indicating no binding.

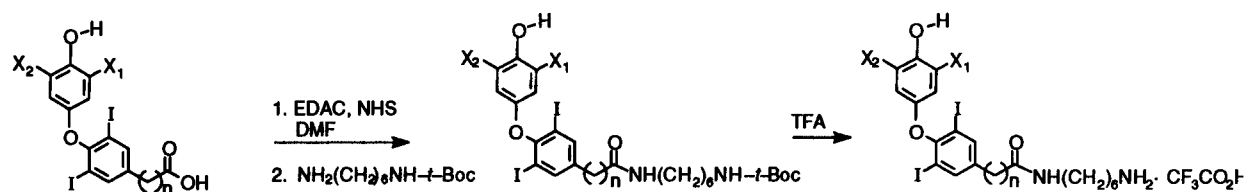
Preparation of T_4 mAb and Fab. For this study, the desired monoclonal antibody to T_4 was obtained from tissue culture media after filtration, centrifugation, and protein-A column chromatography. After dialysis, the concentration of the antibody was found to be 4.86 mg/mL by UV spectroscopy. Assay by the micro-BCA method found the concentration to be 4.99 mg/mL, which was in close agreement with the UV value. Analysis by SDS-PAGE showed two bands (Figure 1). The upper band corresponded to the heavy chain of the antibody, with an apparent molecular weight of 55 kDa, while the light chain appeared as a sharp band at 27 kDa. LC/ESI/MS

Scheme 1



	R	X ₁	X ₂	R ₁		
1 (L)	H	I	I	ONa·5H ₂ O	15 (L)	29 (L)
1 (D)	H	I	I	ONa·5H ₂ O	15 (D)	29 (D)
2 (L)	H	H	I	ONa	16 (L)	30 (L)
2 (D)	H	H	I	OH	16 (D)	30 (D)
3	H	H	H	OH	17	31
4	H	I	Br	OH	18	32
5	H	H	Br	OH	19	33
6	H	Br	Br	OH	20	34
7 ¹	H	I	I	N(CH ₃) ₂	21	35
8 ¹	H	H	I	N(CH ₃) ₂	22	36
9 ¹	CH ₃	I	I	OH	23	37
10 ¹	CH ₃	H	I	OH	24	38

Scheme 2



	n	X ₁	X ₂		
11	1	I	I	25	39
12	1	H	I	26	40
13	2	H	I	27	41

Scheme 3

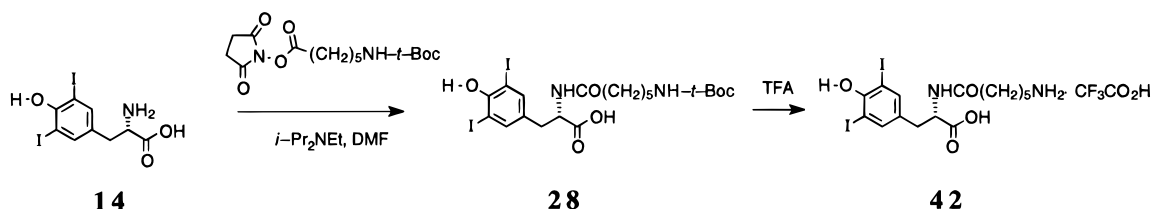


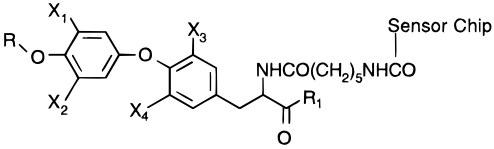
(Figure 2) of the antibody gave a series of multicharged ions centered at m/z 2600 (inset A). Deconvolution showed four species (inset B) with molecular weights of 149 355 (20%), 149 541 (65%), 149 678 (100%), and 149 833 Da (85%), consistent with the expected mass of an intact monoclonal antibody (22, 23).

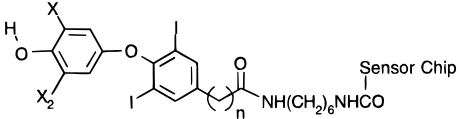
Digestion of the monoclonal antibody with papain produced a mixture containing the unreacted mAb, and the Fc and Fab fragments. Chromatography (protein-A) gave the Fab fragment in the void volume in 65% yield after dialysis. The final concentration of anti-T₄ Fab was 11.8 mg/mL (micro-BCA). SDS-PAGE (Figure 1) showed two bands (27 and 25 kDa) and no detectable mAb or Fc fragment. LC/ESI/MS (Figure 2) showed a series of multicharged species centered at m/z 1500 (inset A). On

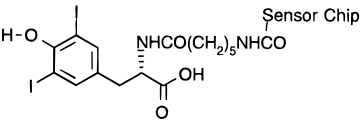
deconvolution (inset B), a single narrow peak was predominant at m/z 47 620 (100%), accompanied by a broad peak centered at m/z 47 782 (30%).

Direct Kinetic Analysis. Monoclonal Antibody to T₄. Each thyroxine analog biosensor (43–56) was tested with the purified anti-T₄ mAb at eight concentrations ranging from 0.5 to 100 nM on the BIAcore instrument to produce a series of sensorgrams. Typical results are illustrated in Figure 4A using biosensor 43L. The concentration-dependent binding kinetics of anti-T₄ mAb to biosensor 43L displayed in the sensorgrams were consistent with a two-component interaction model, i.e., $A + B \rightleftharpoons AB$, during the first 100 s of the association and dissociation phases. In panels B and C of Figure 4, the solid curves (with the left y-axis) represent the fitted data for these

Table 2. Binding Properties of Anti-Thyroxine Monoclonal Antibody Fab Fragment^a

											
no.	R	X ₁	X ₂	X ₃	X ₄	R ₁	k_a (M ⁻¹ s ⁻¹) × 10 ⁶	k_d (s ⁻¹) × 10 ⁻⁵	K_A (M ⁻¹) × 10 ⁸	ΔG (kcal/mol)	$\Delta\Delta G$ (kcal/mol)
43L	H	I	I	I	I	OH	2 ± 0.22	15 ± 1.2	128 ± 18.1	-13.7	0
43D	H	I	I	I	I	OH	2 ± 0.23	45 ± 6.5	49 ± 8.21	-13.2	0.5
44L	H	H	I	I	I	OH	6 ± 0.84	491 ± 92	13 ± 2.86	-12.4	1.3
44D	H	H	I	I	I	OH	7 ± 0.42	920 ± 102	8 ± 0.96	-12.0	1.7
45	H	H	H	I	I	OH	— ^b	—	—	—	—
46	H	I	Br	I	I	OH	2 ± 0.12	45 ± 2.1	51 ± 3.38	-13.2	1.0
47	H	H	Br	I	I	OH	3 ± 0.90	267 ± 33	11 ± 3.65	-12.3	1.4
48	H	Br	Br	I	I	OH	3 ± 0.38	101 ± 7.1	28 ± 4.30	-12.8	0.9
49	H	I	I	I	I	N(CH ₃) ₂	1 ± 0.32	6 ± 0.22	114 ± 81.1	-13.6	0.1
50	H	H	I	I	I	N(CH ₃) ₂	1 ± 0.16	704 ± 36	1 ± 0.24	-10.9	2.8
51	CH ₃	I	I	I	I	OH	—	—	—	—	—
52	CH ₃	H	I	I	I	OH	—	—	—	—	—

											
no.	n	X ₁	X ₂								
53	1	I	I				—	—	—	—	—
54	1	H	I				—	—	—	—	—
55	2	H	I				10 ± 0.17	1640 ± 39	6 ± 0.18	-11.9	1.8

											
56							—	—	—	—	—

^a All data are from nonlinear regression analysis of sensorgram curves. ^b — indicates that no binding was observed at the concentration tested.

regions of the association and dissociation phases, respectively. The coplotted residuals (right *y*-axis and the *x*-axis) show the difference between the fitted data and the experimental data for each point. The uniform distribution of points in the residual plots is typical for the proposed 1:1 binding model and indicates a good fit of the data (24). The plots were used to determine k_a and k_d (Table 1). Figure 4D shows the result of the linear regression analysis of the sensorgrams shown in Figure 4A, as a plot of k_s versus concentration, where k_s is the slope of dRU/dt versus RU_f . The slope of this plot is k_a , and the *y*-intercept is k_d . The resulting values were in close agreement with those in Table 1.

The T₂ analog (45), the *O*-methyl derivatives (51 and 52), the thyroacetic acids (53 and 54), and the tyrosine compound (56) showed no binding at the concentrations tested. Of the ligands that bound, all but 49 appeared to bind according to the proposed 1:1 binding model. The residual plots of the association and dissociation phases of the sensorgram for sensor 49 (not shown) were decidedly skewed, indicating a deviation from the model. Nonetheless, the association rate constant (k_a) values for all of the binding structures were similar, ranging from 1 to 7 × 10⁶ M⁻¹ s⁻¹. However, the recorded dissociation rate constants for the same structures exhibited a much wider range of values (1–592 × 10⁻⁵ s⁻¹). The equilibrium association constants, K_A , were derived from the equation

$$K_A = k_a/k_d$$

Of the analog biosensor surfaces that bound the T₄ mAb,

values of K_A ranged from 9 to 1140 × 10⁸ M⁻¹. The analogs fell into four groups. T₄ mAb had the highest affinity for the enantiomeric thyroxine analog sensors (43L,D) and the thyroxine dimethylamide sensor (49), all of which were linked through the α-amino group. The next group consisted of the mono- (46) and dibromo-substituted (48) analogs of thyroxine. T₃ derivatives (44L,D), like the thyroxine sensors, showed no preference for the stereochemistry of the α-amino group. The group with the lowest affinity included the monobromo T₃ analog (47), T₃ dimethylamide (50), and the T₃ derivative lacking the α-amino group (55). The values for the change in free energy on binding of the analog surfaces with T₄ mAb were obtained from the equation

$$\Delta G = -RT \ln(K_A)$$

and ranged from -12.2 to -15.0 kcal/mol. Using the ΔG value for sensor 43L as a point of reference, $\Delta\Delta G$ was determined from the equation

$$\Delta\Delta G = \Delta G_{\text{obs}} - \Delta G_{43L}$$

A difference of up to 2.8 kcal/mol was seen with the sensors that exhibited binding to the antibody.

Monoclonal Antibody Fab to T₄. Following the same evaluation and data reduction protocols used for the intact T₄ mAb, the binding kinetics of purified Fab to the biosensors (43–56) were recorded (Table 2). Those surfaces that bound T₄ mAb also bound the Fab fragment. All the binding events appeared to follow the proposed 1:1 interaction of the model based on the residual plots

and the low χ^2 values obtained from analysis of the sensorgrams. The association rate constants (k_a) were similar to those recorded for the whole antibody, $1\text{--}10 \times 10^6 \text{ M}^{-1} \text{ s}^{-1}$, while the dissociation rates were from 1- to 11-fold higher. Equilibrium association constants ranged from 1 to $128 \times 10^8 \text{ M}^{-1}$. Again, the sensors could be separated into four groups with similar K_A values. The thyroxine sensor (**44L**) and the thyroxine dimethylamide (**49**) had the highest affinity constants, followed by the D enantiomer of the thyroxine sensor (**43D**). Unlike the intact antibody, the Fab fragment had a slight preference for the naturally occurring L stereochemistry. The mono- (**46**) and dibromothyroxine sensors (**48**) were next in the affinity ranking. T₃ (**44L,D**), T₃ dimethylamide (**50**), and thyropropionic acid (**55**) had the lowest affinity for the Fab fragment of those derivatives that bound. Values for ΔG spanned the range from -13.7 to -10.9 kcal/mol , giving $\Delta\Delta G$ values of $0\text{--}2.8 \text{ kcal/mol}$.

DISCUSSION

T₄ (3,5,3',5'-tetraiodothyronine or thyroxine) is a powerful hormone with far-reaching and diverse physiological effects. As the predominant hormone secreted from the thyroid gland, T₄ is essential for normal metabolic and neural activity. Only 0.05% of T₄ freely circulates in the blood, while the rest is bound to proteins such as thyroid binding globulin (TBG), thyroid binding pre-albumins, and albumins. The concentration of T₄ in serum is an important diagnostic indicator of thyroid function (25). The most common method of measuring serum levels of T₄ in the United States and Japan has been homogeneous fluorescence polarization immunoassay (FPIA) (26). An earlier report has dealt with the design and synthesis of T₄ FPIA immunoreagents (3). The increasing need for higher sample throughput, ease of automation, and economy in today's cost-conscious health care environment has brought about a renewed interest in heterogeneous immunoassays for T₄. The immunoreagents that have optimal performance in a homogeneous assay need not display similar performance in a heterogeneous format. Traditionally, the choice of reagents has been arrived at empirically by matching an antibody with a tracer in a particular assay format. This labor intensive approach has been successful but could have been greatly simplified if the basic kinetic and thermodynamic binding parameters of the immunoreagents had been known *a priori*. Such biospecific interactions are dynamic events which are reflected in the rates of association (k_a) and dissociation (k_d) of the binding molecules. From these values, equilibrium binding constants (K_A) can be determined. Additionally, the change of the K_A -derived Gibbs free energy (ΔG) during the binding event offers a convenient means of relating changes in hapten structure to changes in binding to protein. These critical immunocomponent properties can be determined by surface plasmon resonance on the automated BIAcore system.

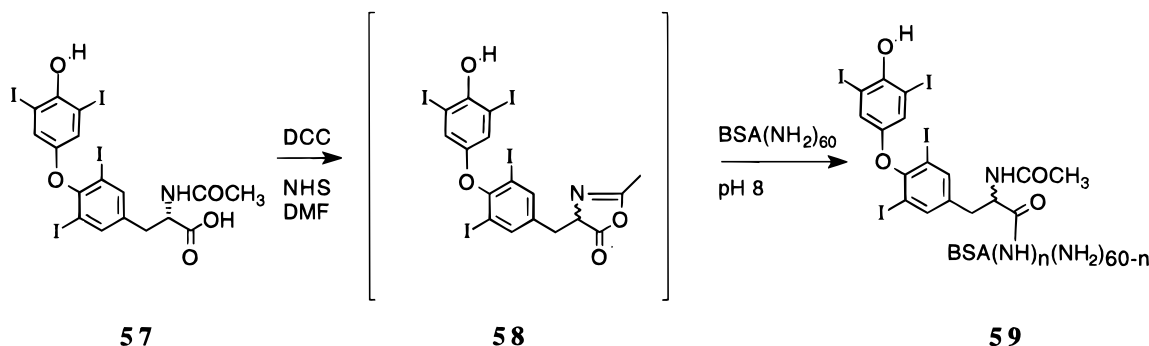
In the approach presented here, one member of a binding pair is conjugated to the surface of a sensor chip while the other is injected in solution over the surface at a constant rate. The instrument response is directly related to the change in mass on the surface of the biosensor. When both the binding components are macromolecules, the choice of which component to conjugate to the sensor is largely arbitrary. Conjugation of either component to the sensor will generate a substantial initial rise in RU, and subsequent association with the other component will generate a large ΔRU . The kinetics of the interaction may not be the same for both approaches simply because the process of conjugation can

change the conformation and reactivity of the species involved (27).

Relatively few studies on the BIAcore system have been reported in which a low-molecular weight ligand (like T₄) interacts with a large binding protein (like an antibody). In this case, the choice of which component to conjugate to the sensor surface is critical due to instrument constraints. Conjugation of the antibody to the sensor surface induces a large shift in RU in accordance with the large mass of the protein, but the subsequent interaction with the ligand produces a small shift that cannot be measured reliably. Although, advances in the BIAcore instrument and the accompanying increase in the sensitivity of the detector have been reported to mitigate this limitation (28). As in the case of the bimacromolecular interaction cited above, it is difficult to assess what effect immobilization of the binding protein on the sensor chip has on its binding properties. Three approaches to conjugation of low-molecular weight ligands to the sensor chip have been reported. One approach has been to conjugate the ligand to a carrier protein, which can then be coupled to the sensor surface (29–34). A concern with this protocol is that the intermediate bioconjugate is a heterogeneous species requiring an additional conjugation step and characterization to produce reliable biosensors. Low-molecular mass ligands have also been attached to the sensor surface indirectly by use of the streptavidin–biotin interaction. A sensor covalently linked to streptavidin captures the biotinylated ligand which subsequently interacts with the binding protein to form a sandwich (35). Sensors of this type have a limited lifetime and tend to “leak”. Sensors made by the direct conjugation of the ligand to the biosensor surface are more rugged (35, 36) and well-defined. However, when the small ligand is bound to the surface, there is only a small shift in RU (Figure 3) so loading cannot be quantitated directly. Only on binding with the antibody can a large and easily quantitated ΔRU be obtained. This latter conjugation procedure was chosen for the present study. This method of evaluating the kinetic and thermodynamic properties of these immunocomponents mimics the characteristics of heterogeneous assays and avoids concerns about altering the binding site conformation of the antibody but requires the construction of a different biosensor for each ligand tested. Alternative methods (37) that would mimic homogeneous assay conditions are of interest but were not the subject of this study.

The T₄ mAb that is the principle subject of this investigation was obtained from immunization with the *N*-acetyl-T₄–bovine serum albumin (BSA) conjugate prepared as shown in Scheme 4. While the L enantiomer of *N*-acetyl-T₄ was used as the starting material, we expected from our own model studies (38) that the conjugated hapten would be racemized as a result of azalactone (39) formation during the activation. Racemization of *N*-acyl amino acids under carbodiimide coupling conditions is well-known (40). It was critical to probe whether the monoclonal antibody that resulted from this immunogen recognized the chiral center of the analyte. Thus, biosensors **43L**, **43D**, **44L**, and **44D** were prepared with care to avoid racemization of the chiral haptens. In particular, the dimethyl amides (**7** and **8**, Scheme 1) were prepared from L-T₄ and L-T₃ by activation of the *N*-tert-Boc amino acids under conditions that avoid racemization. Each of the other thyroxine analogs included in the library of biosensors was chosen to probe other structural requirements of the antibody. Sensors **43–48** were prepared to test how the degree and type of halogenation in the terminal aryl ring affected binding, while sensor

Scheme 4



56 tested whether that aryl group was necessary at all. Sensors **49** and **50** were prepared to address the necessity of the ionizable carboxyl group, while **51** and **52** reflected the absence of the ionizable phenol. Thyroalkanoic acid sensors **53–55** were employed to test the need for the α -amino group.

On the basis of the structure of the immunogen which was used to generate the monoclonal antibody, we expected that the diphenyl ether ring system would be a major antigenic determinant. Moreover, the molecular architecture of the hapten close to the site of conjugation to the carrier protein is known to render the resulting antibody relatively indifferent to changes surrounding the site of attachment (3). The data obtained from the surface plasmon resonance analysis on the BIAcore system (Table 1) supported our suppositions. The free energy of binding (ΔG) of the thyroxine analog sensors to the antibody became less favorable with the loss of each halogen from the terminal aryl ring (**43L** > **46** \approx **48** > **44L** > **47** \gg **45**). The initial iodo–bromo exchange on going from **43L** to **46** resulted in a 0.3 kcal/mol increase in ΔG . Removal of one iodo group (**43L** versus **44L**) resulted in a further increase in ΔG of 1.6 kcal/mol. The trend continued until the T_2 derivative (**45**) showed no binding at the concentrations studied. Likewise, the tyrosine derivative (**56**) which lacked the B-ring of the diphenyl ether entirely showed no binding. Eliminating the phenolic HO group by conversion to the corresponding methyl ether, as in sensors **51** and **52**, also prevented antibody binding. It seemed then that the binding of the mAb was indeed sensitive to changes in the diphenyl ether moiety.

Both the degree of halogenation and the presence of a free phenol were important determinants for binding. These observations may be directly related to the acidity of the phenolic HO group. It would be expected that changing a substituent from iodo to bromo would result in a decrease in pK_a of 0.1 [based on the literature (41) pK_a values for *o*-iodophenol and *o*-bromophenol of 8.5 and 8.4, respectively]. Replacing the iodo group with hydrogen would cause a much larger decrease of 1.5–2 pK_a units (based on the following pK_a data: 6.79, T_4 ; 8.86, T_3 ; and 10.28, T_2) (12). A change of 1 pK_a unit equals 1.32 kcal/mol. The $\Delta\Delta G$ of the antibody binding reaction between sensors **43L** and **44L** (ΔpK_a of 2.1) amounted to only 1.6 kcal/mol, about half of the expected value based on the change in pK_a of the analogs. A similar trend in antibody–thyroxine analog binding was seen by Rokos et al. (12). They reported cross reactivity data in an RIA format of several thyroxine analogs with an antibody directed toward an α -amino-linked L- T_4 ethyl ester immunogen. In their study, T_4 , Br T_3 , and Br T_2 (similar in structure to sensors **43L**, **46**, and **48**, respectively) displayed cross reactivity of 100, 85.6, and 47.6%,

respectively, while 3'-isopropyl- T_3 cross reacted only 8.9%. In their study, as well as ours, as the halogenation decreased, so did binding to the antibody. We conclude that, while the interaction of the phenolic HO group with this antibody is important, it need not be the only contributing factor. The higher polarizability of the iodo versus the bromo substituent may also contribute to the results noted here.

The SPR-derived binding data indicated that our mAb recognized both enantiomers of the thyroxine biosensors (**43L,D**) and the triiodothyronine biosensors (**44L,D**) to an equal degree, supporting the expectation that the antibody would not be sensitive to changes surrounding the chiral center. The dimethylamide-substituted sensors (**49** and **50**) showed affinity for the antibody nearly equivalent to that for the corresponding carboxy-substituted analogs (**43L** and **44L**). The triiodothyropropionic acid-derived sensor (**55**) which was linked via the carboxylic acid, thus lacking the chiral center, α -amino, and free carboxyl groups, had similar binding to the corresponding T_3 dimethylamide sensor (**50**). In light of the insensitivity of this mAb to changes in the structure surrounding the chiral center, α -amino, and carboxyl groups, it was surprising that neither the tetraiodo- nor the triiodothyroacetic acid analogs (**53** and **54**, respectively), which differed by a single methylene unit from sensor **55**, showed any binding to the antibody.

With only minor variations, the kinetic and thermodynamic values obtained from the SPR analysis of the Fab fragment with the same series of biosensors (Table 2) followed the same trend as seen with the whole antibody. In absolute terms, the values for ΔG for the Fab fragment were on average 0.8 kcal/mol less favorable than those seen with the mAb. The Fab fragment had very slight bias for the L enantiomer of thyroxine sensor (**43L**) and the triiodothyronine sensor (**44L**), unlike the intact antibody.

The kinetic binding data obtained for the Fab with the thyroxine analog sensors followed a true 1:1 binding event model which was represented by the dissociation and the association phases of the sensorgrams; i.e., dissociation rates were independent of the concentration of Fab (42). In contrast, this was true only for about the first 100 s of the dissociation phases in the mAb–thyroxine analog sensors binding sensorgrams. Thus, the rate constants obtained with the Fab fragment would appear to be absolute kinetic parameters, while in the case of the mAb, the numbers would represent apparent binding constants.

CONCLUSION

A library of ligand analogs were designed to probe the structural requirements for the binding interaction be-

tween hapten and antibody. The binding properties of the antibody were conveniently obtained using surface plasmon resonance on the automated BIAcore instrument. Conjugation of the ligand analogs to the SPR chip obviated concern about altering the conformation of the antibody while still mimicking a heterogeneous assay format but required the preparation of a separate biosensor for each ligand.

The data from the SPR analysis for the interaction of anti-T₄ mAb and its Fab fragment with a structurally diverse library of thyroxine analog biosensors pointed to the important contribution of the diphenyl ether ring system and the ionizable phenolic hydroxyl group to the interaction. Affinities recorded for the bivalent mAb and the monovalent Fab differed by a factor of 2–13. Additionally, the intact antibody was blind to the chirality of the hapten, whereas the monovalent Fab had a slight preference for the L enantiomers of the analogs of T₄ and T₃.

LITERATURE CITED

- (1) Henry, C. (1996) FDA, reform and the well-characterized biologic. *Anal. Chem.* 68, 674A–677A.
- (2) Adamczyk, M., Gebler, J. C., and Mattingly, P. G. (1996) Characterization of protein-hapten conjugates. 2. Electro-spray mass spectrometry of bovine serum albumin-hapten conjugates. *Bioconjugate Chem.* 7, 475–481.
- (3) Adamczyk, M., Fino, L., Fishpaugh, J. R., Johnson, D. D., and Mattingly, P. G. (1994) Immunoassay reagents for thyroid testing. 1. Synthesis of thyroxine conjugates. *Bioconjugate Chem.* 5, 459–462.
- (4) Adamczyk, M., Buko, A., Chen, Y.-Y., Fishpaugh, J. R., Gebler, J. C., and Johnson, D. D. (1994) Characterization of protein-hapten conjugates. 1. Matrix-assisted laser desorption ionization mass spectrometry of immuno BSA-hapten conjugates and comparison with other characterization methods. *Bioconjugate Chem.* 5, 631–635.
- (5) Adamczyk, M., Johnson, D. D., Mattingly, P. G., Clarisse, D. E., Tyner, J. D., and Perkowitz, M. M. (1994) Reagents and methods for the detection and quantification of thyroxine in fluid samples. U.S. Patent 5,359,093; *Chem. Abs.* 122, 24579.
- (6) Adamczyk, M., Fishpaugh, J., Harrington, C., Johnson, D., and Vanderbilt, A. (1993) Immunoassay reagents for psychoactive drugs. II. The method for the development of antibodies specific to imipramine and desipramine. *J. Immunol. Methods* 163, 187–197.
- (7) Adamczyk, M., Chen, Y. Y., and Fishpaugh, J. (1993) Lipase mediated diastereoselective hydrolysis of steroidal 3-(O-carboxymethyl) oxime methyl esters. *Tetrahedron: Asymmetry* 4, 1467–1468.
- (8) Adamczyk, M., Chen, Y.-Y., and Fishpaugh, J. (1993) Preparation and high-performance liquid chromatographic analysis of syn and anti isomers of steroidal 3-(O-carboxymethyl) oximes. *J. Chromatogr.* 657, 345–348.
- (9) Adamczyk, M., Fishpaugh, J., Harrington, C., Hartter, D., Johnson, D., and Vanderbilt, A. (1993) Immunoassay reagents for psychoactive drugs. I. The method for the development of antibodies specific to amitriptyline and nortriptyline. *J. Immunol. Methods* 162, 47–58.
- (10) van Regenmortel, M. H. V., and Azimzadeh, A. (1994) Determination of antibody affinity. In *Immunochemistry* (C. J. van Oss and M. H. V. van Regenmortel, Eds.) pp 805–828, Marcel Dekker, Inc., New York.
- (11) Karlsson, R., and Fägerstam, L. G. (1994) Biosensor techniques. In *Immunochemistry* (C. J. van Oss and M. H. V. van Regenmortel, Eds.) pp 949–970, Marcel Dekker, Inc., New York.
- (12) Rokos, H., and Steinmaus, H. (1981) Synthesis and investigation of substituted iodothyronines with the aim of obtaining radiochemically stable ¹²⁵I-tracers of high specific activity. *J. Clin. Chem. Clin. Biochem.* 19, 191–194.
- (13) Ércegyi, J., Seprődi, J., Vadasz, Z., Nikolics, K., Teplán, I., Mező, I., Kanyickska, B., and Kovács, M. (1988) Synthesis and biological activity of novel hydrophobic D-amino acid-6 analogues of the gonadotropin-releasing hormone. *Acta Chim. Hung.* 125, 821–830.
- (14) Myers, C. S. (1932) Some derivatives of diiodotyrosine and thyroxine. The action of acetic anhydride on diiodotyrosine. *J. Am. Chem. Soc.* 54, 3718–3725.
- (15) Blank, B., Greenberg, C. M., and Kerwin, J. F. (1964) Thyromimetics. III. The synthesis and relative thyromimetic activities of some 4'-ethers of iodinated thyronines and thyroalkanoic acids. *J. Med. Chem.* 7, 53–56.
- (16) Hudson, L., and Hay, F. C. (1989) *Practical Immunology*, 3rd ed., Blackwell Scientific Publications, Oxford, England.
- (17) Redinbaugh, M. G., and Turley, R. B. (1986) Adaptation of bicinchoninic acid protein assay for use with microtiter plated and sucrose gradient fractions. *Anal. Biochem.* 153, 267–271.
- (18) Löfås, S., and Johnsson, B. (1990) A novel hydrogel matrix on gold surface plasmon resonance sensors for fast and efficient covalent immobilization of ligands. *J. Chem. Soc., Chem. Commun.* 21, 1526–1528.
- (19) Karlsson, R., Michalesson, A., and Mattsson, L. (1991) Kinetic analysis of monoclonal antibody-antigen interactions with a new biosensor based analytical system. *J. Immunol. Methods* 145, 229–240.
- (20) Dibbo, A., Sly, J. C. P., Stephenson, L., Walker, T., Warburton, W. K., and Whiting, K. D. E. (1961) The synthesis of thyroxine and related compounds. Part XVII. The preparation of some additional compounds related to thyroxine. *J. Chem. Soc.*, 2890–2902.
- (21) Krapcho, A. P., and Kuell, C. S. (1990) Mono-protected diamines. N-tert-butoxycarbonyl- α - ω -alkanediamines from α - ω -alkanediamines. *Synth. Commun.* 20, 2559–2564.
- (22) Ashton, D. S., Beddell, C. R., Cooper, D. J., Craig, S. J., Lines, A. C., Oliver, R. W. A., and Smith, M. A. (1995) Mass spectrometry of the humanized monoclonal antibody CAM-PATH 1H. *Anal. Chem.* 67, 835–842.
- (23) Bennett, K. L., Hick, L. A., Truscott, R. J. W., Sheil, M. M., and Smith, S. M. (1995) Optimum conditions for electro-spray mass spectrometry of a monoclonal antibody. *J. Mass Spectrom.* 30, 769–771.
- (24) BIAevaluation software handbook (1995) pp 4–8, Pharmacia, Uppsala, Sweden.
- (25) Alexander, N. M. (1984) Thyroid function tests. *Clin. Chem.* 30, 827–828.
- (26) Wild, D. (1994) Thyroid. In *The Immunoassay handbook* (D. Wild, Ed.) p 331, Stockton Press, New York.
- (27) Karlsson, R., Mo, J. A., and Holmdahl, R. (1995) Binding of autoreactive mouse anti-type II collagen antibodies derived from the primary and the secondary immune-response investigated with the biosensor technique. *J. Immunol. Methods* 188, 63–71.
- (28) Karlsson, R., and Stahlberg, R. (1995) Surface plasmon resonance interactions involving low-molecular-weight analytes and for determination of low affinities. *Anal. Biochem.* 228, 274–280.
- (29) Pak, R. H., Primus, F. J., Rickard-Dickson, K. J., Ng, L. L., Kane, R. R., and Hawthorne, M. F. (1995) Preparation and properties of nido-carborane-specific monoclonal antibodies for potential use in boron neutron capture therapy for cancer. *Proc. Natl. Acad. Sci. U.S.A.* 92, 6986–6990.
- (30) Zeder-Lutz, G., van Regenmortel, M. H., Wenger, R., and Altschuh, D. (1994) Interaction of cyclosporin A and two cyclosporin analogs with cyclophilin: relationship between structure and binding. *J. Chromatogr. Biomed. Appl.* 662, 301–306.
- (31) Laukkanen, M. L., Alfthan, K., and Keinänen, K. (1994) Functional immunoliposomes harboring a biosynthetically lipid-tagged single-chain antibody. *Biochemistry* 33, 11664–11670.
- (32) Zeder-Lutz, G., Altschuh, D., Geysen, H. M., Trifileff, E., Sommermeyer, G., and van Regenmortel, M. H. (1993) Monoclonal antipeptide antibodies: affinity and kinetic rate constants measured for the peptide and the cognate protein using a biosensor technology. *Mol. Immunol.* 30, 145–155.
- (33) Zeder-Lutz, G., Wenger, R., van Regenmortel, M. H. V., and Altschuh, D. (1993) Interaction of cyclosporin A with Fab fragment or cyclophilin. Affinity measurements and time-dependent changes in binding. *FEBS Lett.* 326, 153–157.

- (34) Zeder-Lutz, G., Altschuh, D., Denery-Papini, S., Briand, J. P., Tribbick, G., and van Regenmortel, M. H. (1993) Epitope analysis using kinetic measurements of antibody binding to synthetic peptides presenting single amino acid substitutions. *J. Mol. Recognit.* 6, 71–79.
- (35) Khilko, S. N., Corr, M., Boyd, L. F., Lees, A., Inman, J. K., and Margulies, D. H. (1993) Direct detection of major histocompatibility complex class I binding to antigenic peptides using surface plasmon resonance. *J. Biol. Chem.* 268, 15425–15434.
- (36) Sternesjö, A., Mellgren, C., and Björck, L. (1995) Determination of sulfamethazine residues in milk by a surface plasmon resonance-based biosensor assay. *Anal. Biochem.* 226, 175–181.
- (37) Karlsson, R. (1994) Real-time competitive kinetic analysis of interactions between low-molecular-weight ligands in solution and surface-immobilized receptors. *Anal. Biochem.* 221, 142–151.
- (38) Adamczyk, M., Johnson, D. J., Mattingly, P. G., and Pan, Y., Unpublished observations.
- (39) Greenstein, J. P., and Winitz, M. (1984) Chemical procedures for the synthesis of peptides. In *Chemistry of the amino acids*, pp 832–838, Robert E. Krieger Publishing Co., Inc., Malabar, FL.
- (40) Bodanszky, M. (1984) Side reactions in peptide synthesis. In *Principles of peptide synthesis*, pp 158–162, Springer-Verlag, New York.
- (41) Albert, A., and Serjeant, E. P. (1984) *The Determination of Ionization constants: A Laboratory manual*, 3rd ed., p 150, Methuen, Inc., New York.
- (42) Nice, E. C., McInerney, T. L., and Jackson, D. C. (1996) Analysis of the interaction between a synthetic peptide of influenza virus hemagglutinin and monoclonal antibodies using an optical biosensor. *Mol. Immunol.* 33, 659–670.

BC960088Z

New and Versatile Ternary Ligand System for Technetium Radiopharmaceuticals: Water Soluble Phosphines and Tricine as Coligands in Labeling a Hydrazinonicotinamide-Modified Cyclic Glycoprotein IIb/IIIa Receptor Antagonist with ^{99m}Tc

D. Scott Edwards,* Shuang Liu,* John A. Barrett, Anthony R. Harris, Richard J. Looby, Marisa C. Ziegler, Stuart J. Heminway, and Timothy R. Carroll

The DuPont Merck Pharmaceutical Company, Radiopharmaceuticals Division, 331 Treble Cove Road, North Billerica, Massachusetts 01862. Received October 28, 1996*

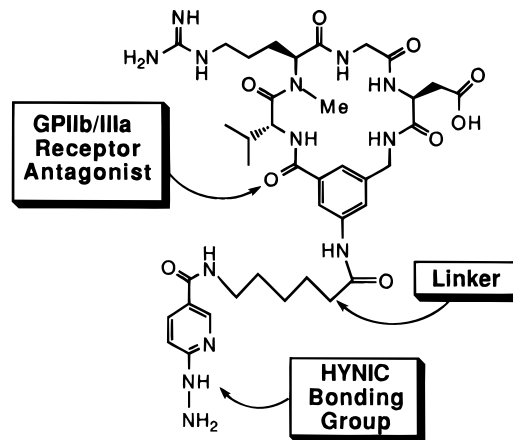
A hydrazinonicotinamide-functionalized cyclic platelet glycoprotein IIb/IIIa (GPIIb/IIIa) receptor antagonist [cyclo(D-Val-NMeArg-Gly-Asp-Mamb(5-(6-(6-hydrazinonicotinamido)hexanamido)) (HYNICTide)] was labeled with ^{99m}Tc using tricine and a water soluble phosphine (TPPTS, trisodium triphenylphosphine-3,3',3''-trisulfonate; TPPDS, disodium triphenylphosphine-3,3'-disulfonate; or TPPMS, sodium triphenylphosphine-3-monosulfonate) as coligands. The synthesis of technetium complexes, $^{99m}\text{Tc}(\text{HYNICTide})(\text{L})(\text{tricine})$ (**1**, **L** = TPPTS; **2**, **L** = TPPDS; **3**, **L** = TPPMS), can be performed in one or two steps in high yield and with high specific activity ($\geq 20\,000\text{ Ci/mmol}$). For example, the reaction of the HYNICTide, ^{99m}Tc pertechnetate, stannous chloride, and tricine at pH 4–5 and room temperature results in the complex $^{99m}\text{Tc}(\text{HYNICTide})(\text{tricine})_2$, which reacts with TPPTS (50 °C for 30 min) to give complex **1** in $\geq 90\%$ yield as determined by radio-HPLC. Complexes **1–3** are formed as equal mixtures of two isomeric forms and are stable for $\geq 6\text{ h}$ in the reaction mixture and in dilute solution. Both isomeric forms of complex **1** were found by a platelet-binding assay to contain the ^{99m}Tc -labeled HYNICTide and possess biological activity. The composition of these complexes was determined to be 1:1:1:1 for Tc:HYNICTide:L:tricine through a series of mixed ligand experiments on the tracer (^{99m}Tc) level. Surprisingly, this composition is maintained over a wide range of relative ligand ratios. The relative bonding capability of the three phosphine coligands to the Tc was determined by spiking various amounts of TPPDS or TPPMS into TPPTS and falls in the order TPPMS > TPPDS > TPPTS. The lipophilicity of the ^{99m}Tc HYNICTide complexes can be systematically varied by the choice of the phosphine and aminocarboxylate coligands. Using the combination of tricine and a phosphine ligand, HYNIC-derivatized peptides or other small molecules can be labeled with ^{99m}Tc in high specific activity and with high stability for potential use as radiopharmaceuticals.

INTRODUCTION

We have been actively pursuing a research program to develop a thrombus imaging agent by labeling a platelet glycoprotein IIb/IIIa (GPIIb/IIIa) receptor antagonist with ^{99m}Tc (1–6). Recently, we reported the ^{99m}Tc labeling of a hydrazinonicotinamide-conjugated GPIIb/IIIa antagonist (HYNICTide in Chart 1). We found that the HYNICTide can be labeled using tricine as the coligand and forms the complex $^{99m}\text{Tc}(\text{HYNICTide})(\text{tricine})_2$ with specific activity $\geq 20\,000\text{ Ci/mmol}$. However, $^{99m}\text{Tc}(\text{HYNICTide})(\text{tricine})_2$ is not stable in solution and exists in many isomeric forms, which we attribute to coordination isomerism from the hydrazine moiety of the HYNICTide and the tricine coligand (5). Although the biological data from animal studies in a canine arteriovenous (AV) shunt and a deep venous thrombosis (DVT) model show that the complex $^{99m}\text{Tc}(\text{HYNICTide})(\text{tricine})_2$ is able to image both arterial and venous thrombus (3), it would still be difficult to develop for clinical use because of the solution instability and the presence of the many isomeric forms.

To prepare ^{99m}Tc HYNICTide complexes with higher solution stability and less isomerism, we used ethylene-

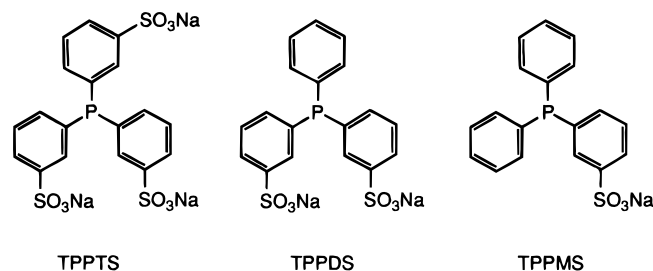
Chart 1. Cyclic HYNICTide



diamine-*N,N'*-diacetic acid (EDDA), which is more symmetrical and potentially tetradentate, as the coligand to label the HYNICTide. We found that EDDA forms the complex $^{99m}\text{Tc}(\text{HYNICTide})(\text{EDDA})$, with much higher solution stability and less isomerism (5). However, the HPLC data showed that the complex $^{99m}\text{Tc}(\text{HYNICTide})(\text{EDDA})$ exists in at least three isomeric forms. The use of *N*-substituted EDDA analogs produces ^{99m}Tc HYNICTide complexes with different lipophilicity but offers no improvement with respect to minimizing the number of coordination isomers. Thus, EDDA and its *N*-substituted

* Authors to whom correspondence should be addressed [telephone (508) 671-8311 (D.S.E.) and (508) 671-8696 (S.L.); fax (508) 436-7500].

© Abstract published in *Advance ACS Abstracts*, February 15, 1997.

Chart 2. Structures of Three Water Soluble Phosphines

analogs are not ideal coligands for the ^{99m}Tc -labeling of the HYNICTide.

In this paper, we describe an alternative approach, in which a water soluble phosphine [Chart 2; trisodium triphenylphosphine-3,3',3''-trisulfonate (TPPTS); disodium triphenylphosphine-3,3'-disulfonate (TPPDS); sodium triphenylphosphine-3-monosulfonate (TPPMS)] is used as the second coligand to form a ternary ligand system. To our surprise, these monodentate water soluble phosphines react readily with $^{99m}\text{Tc}(\text{HYNICTide})\text{-(tricine)}_2$, replace one of its two tricine coligands, and form the technetium complexes $^{99m}\text{Tc}(\text{HYNICTide})(\text{tricine})(\text{L})$ (**1**, **L** = TPPTS; **2**, TPPDS; **3**, TPPMS) in high yield and high specific activity ($\geq 20\,000\text{ Ci/mmol}$). Complexes **1–3** are very stable in both the kit matrix and dilute solutions. By two reversed phase HPLC methods, we found that these complexes are formed as equal mixtures of two species. Through a series of mixed ligand experiments, we determined the composition of these complexes to be 1:1:1:1 for Tc:HYNICTide:L:tricine (**L** = TPPTS, TPPDS, and TPPMS). This composition is maintained over a wide range of relative ligand ratios. We also evaluated these three complexes in the canine AV shunt and DVT models for their potential use as thrombus imaging agents. The results of the biological evaluation will be described in a companion report (7).

EXPERIMENTAL PROCEDURES

Materials. TPPTS and tetrabutylammonium dihydrogen phosphate (TBAP) were purchased from Aldrich Chemical Co. TPPTS was purified according to the literature method (8) before use for radiolabeling. TPPDS was prepared and purified according to the procedure described in the literature (9). TPPMS was purchased from TCI America, Portland, OR, and was used as received. *N*-(6-Hydrazinonicotinyl)-D-phenylalanine methyl ester hydrochloride was received as a gift from Michael J. Abrams and J. D. Higgins III, Johnson-Matthey Pharmaceutical, Wester Chester, PA. $\text{Na}^{99m}\text{TcO}_4$ was obtained from a Technelite $^{99}\text{Mo}/^{99m}\text{Tc}$ generator, DuPont Merck Pharmaceutical Co., North Billerica, MA. Deionized water was obtained from a Millipore MilliQ Water System and was of $>18\text{ M}\Omega$ quality. The synthesis and biological properties of the cyclic GPIIb/IIIa HYNICTide will be reported elsewhere (10, 11).

Instruments and Methods. The high-performance liquid chromatography (HPLC) methods used a Hewlett-Packard Model 1050 or Model 1090 instrument with radiometric detector. The instant thin layer chromatography (ITLC) method used Gelman Sciences silica gel strips and a 1:1 mixture of acetone and saline as eluant.

HPLC Method 1 used a Zorbax Rx C_{18} column (4.6 mm \times 250 mm, 80 Å pore size) at a flow rate of 1.0 mL/min with a gradient mobile phase from 100% A [95:5 (0.025 M, pH 3.7, phosphate buffer/0.005 M TBAP):acetonitrile] to 90% A and 10% B [20:80 (0.025 M, pH 3.7, phosphate

Table 1. Radio-HPLC Data for Complexes 1–3

L	complex	yield (%)	retention time ^a (min)
TPPTS	1	≥ 90	11.0/11.4
TPPDS	2	≥ 90	14.5/15.0
TPPMS	3	≥ 90	17.4/17.8

^a Using HPLC method 2.

buffer/0.005 M TBAP):acetonitrile] at 20 min, 40% B at 30 min, and 100% B at 33 min.

HPLC Method 2 used a Vydac C_{18} column (4.6 mm \times 250 mm, 300 Å pore size) at a flow rate of 1 mL/min with a gradient mobile phase starting from 100% A (10 mM phosphate buffer, pH 6) to 30% B (acetonitrile) at 15 min and 75% B at 25 min.

HPLC Method 3 used a heated (50 °C) Zorbax C_{18} column (4.6 mm \times 250 mm, 80 Å pore size) at a flow rate of 1 mL/min with a gradient mobile phase starting from 95% A (0.01 M phosphate buffer, pH 6) and 5% B (acetonitrile) to 13% B at 15 min and 75% B at 20 min.

HPLC Method 4 used a heated (50 °C) Zorbax C_{18} column (4.6 mm \times 250 mm, 80 Å pore size) at a flow rate of 1 mL/min. The mobile phase is isocratic from 0 to 12 min using 100% A [90:10 (0.025 M phosphate buffer, pH 8):acetonitrile] and from 13 to 45 min using 100% B [87:13 (0.025 M phosphate buffer, pH 8):acetonitrile].

Synthesis of Complexes 1–3. Two-Step Synthesis. To a 10 mL vial were added 0.2 mL of the HYNICTide solution (50 $\mu\text{g/mL}$ in H_2O), 0.2–0.4 mL of tricine solution (100 mg/mL in H_2O), 0.5 mL of $^{99m}\text{TcO}_4^-$ solution (100 mCi/mL in saline), and 25 μL of $\text{SnCl}_2\cdot 2\text{H}_2\text{O}$ solution (1.0 mg/mL in 0.1 N HCl). The reaction mixture was allowed to stand at room temperature for 30 min. The HPLC showed radiochemical purity (RCP) of $\geq 95\%$ for the resulting complex $^{99m}\text{Tc}(\text{HYNICTide})(\text{tricine})_2$. To the solution was added 0.1 mL of phosphine solution (10 mg/mL in H_2O). The reaction mixture was heated at 50 °C for 30 min and analyzed by HPLC and ITLC.

One-Step Synthesis. To a 10 mL vial were added 0.2–0.4 mL of tricine solution (100 mg/mL in H_2O), 0.2 mL of HYNICTide solution (50 $\mu\text{g/mL}$ in H_2O), 0.1 mL of phosphine solution (10 mg/mL in H_2O), 0.5 mL of $^{99m}\text{TcO}_4^-$ solution (100 mCi/mL in saline), and 25 μL of $\text{SnCl}_2\cdot 2\text{H}_2\text{O}$ solution (1.0 mg/mL in 0.1 N HCl). The pH was adjusted to 4–5. The reaction mixture was heated at 50 °C for 30 min and analyzed by HPLC and ITLC. The ^{99m}Tc HYNICTide complexes prepared according to this approach were shown by HPLC to be identical to those prepared according to the two-step synthesis. The radiolabeling yields for complexes **1–3** along with their HPLC (method 2) data are summarized in Table 1.

Composition Studies on ^{99m}Tc -HYNICTide Complexes. Determination of the Number of HYNICTide Ligands. To a 10 mL vial was added 0.4 mL of tricine solution (100 mg/mL in H_2O), followed by 0.2 mL of HYNICTide solution (50 $\mu\text{g/mL}$ in H_2O), 0.2 mL of *N*-(6-hydrazinonicotinyl)-D-phenylalanine methyl ester hydrochloride solution (50 $\mu\text{g/mL}$ in H_2O), 0.5 mL of $^{99m}\text{TcO}_4^-$ solution (100 mCi/mL in saline), and 10 μL of $\text{SnCl}_2\cdot 2\text{H}_2\text{O}$ solution (10 mg/mL in 1.0 N HCl). The reaction mixture was heated at 50 °C for about 20 min. To the solution was added 0.1 mL of TPPTS solution (10 mg/mL in H_2O). The mixture was heated at 50 °C for another 30 min and was then analyzed by HPLC (method 3).

Determination of the Number of Phosphine Ligands. To a 10 mL vial were added 0.2 mL of HYNICTide solution (50 $\mu\text{g/mL}$ in H_2O), 0.4 mL of tricine (100 mg/mL in H_2O), 0.2 mL of TPPTS solution (20 mg/mL in

H₂O), 0.2 mL of TPPDS solution (10 mg/mL in H₂O), 0.5 mL of ^{99m}TcO₄⁻ solution (100 mCi/mL in saline), and 25 μ L of SnCl₂·2H₂O solution (1.0 mg/mL in 0.1 N HCl). The reaction mixture was heated at 50 °C for 30 min and was then analyzed by HPLC (method 4).

Determination of the Number of Tricine Ligands. To a 10 mL vial was added 0.1 mL of TPPTS solution (10 mg/mL in H₂O), followed by 0.2 mL of HYNICTide solution (50 μ g/mL in H₂O), 0.1 mL of tricine solution (200 mg/mL in H₂O), 0.5 mL of glycine solution (200 mg/mL in H₂O), 0.5 mL of ^{99m}TcO₄⁻ solution (100 mCi/mL in saline), and 25 μ L of SnCl₂·2H₂O solution (1 mg/mL in 0.1 N HCl). The mixture was heated at 50 °C for 30 min and then analyzed by HPLC (method 3).

Solution Stability Studies. *Solution Stability of Complex 1 in Kit Matrix.* Complex **1** in the kit matrix was analyzed by HPLC (method 3) without dilution. Aliquots of the reaction mixture were placed in eight autosampler vials and analyzed sequentially over 6 h.

Solution Stability of Complex 1 in Solution with 10-Fold Dilution. Aliquots (0.3 mL) of complex **1** were diluted with either 0.9% saline (2.7 mL) or 2 wt % tricine in saline (2.7 mL); the diluted solutions were analyzed by HPLC as described above.

Solution Stability of Complex 1 in Solution with 100-Fold Dilution. Aliquots (0.1 mL) of complex **1** were diluted with either saline (9.9 mL) or 2 wt % tricine in saline (9.9 mL); the diluted solutions were analyzed by HPLC as described above.

Solution Stability of Isolated Peaks. The two peaks of complex **1** were collected separately using HPLC method 3. The collected fractions were each divided into two separate 10 mL vials. The pH was adjusted to 4.0 in one vial and to 8.0 in the other. These solutions were monitored for ~24 h by HPLC.

TPPDS and TPPMS Spiking Studies. To each of four 10 mL vials was added 0.2 mL of HYNICTide solution (50 μ g/mL in H₂O), followed by 0.4 mL of tricine solution (100 mg/mL in H₂O), 0.1 mL of TPPTS solution (10 mg/mL in H₂O), 0.1 mL of H₂O containing various amounts of TPPDS (0, 50, 100, or 500 μ g) or TPPMS (0, 50, 100, or 200 μ g), 0.2 mL of ^{99m}TcO₄⁻ solution (200 mCi/mL in saline), and 25 μ L of SnCl₂·2H₂O solution (1.0 mg/mL in 0.1 N HCl). The pH was adjusted to 4–5. The reaction mixture was heated at 80 °C for 30 min and analyzed by HPLC (method 2).

Platelet-Binding Assay. The platelet-binding assay was performed according to the literature method (12) with some modification. Canine venous whole blood was collected into citrate-containing syringes (sodium citrate final concentration 0.38 wt %, Ricca Chemical Co., Arlington, TX). To form platelet-rich plasma, the whole blood was centrifuged at 900 rpm for 10 min (Sorvall Model RT6000B Rotor H1000B, DuPont Medical Products, Newtown, CT) and the supernatant retained. The platelets were rendered quiescent via the addition of aspirin (Sigma Chemical Co., St. Louis, MO) to obtain a final concentration of 50 μ M, prior to their incubation at 37 °C for 20 min. At the end of the 20 min incubation period, prostaglandin E₁ (final concentration 0.9 μ M, Sigma) was added and the pH was adjusted to 6.5–7 using 3.8 wt % sodium citrate (pH 5.5). The preparation was centrifuged at 2300 rpm for 10 min and the supernatant discarded. Approximately 3 mL of Tyrodes buffer was added, and the preparation was placed on a gel filtration column containing Sepharose CL-4B (Pharmacia Biotech, Uppsala, Sweden). The platelet fraction was collected and the platelets were counted on a cell analyzer (Simex K-1000, Baxter, Chicago, IL). The aliquot was

adjusted to achieve a final concentration of 1.8×10^7 platelets/well.

This assay was performed in a 96 well microtiter plate, and the reagents (expressed as final concentration) were added in the following order: Tyrodes buffer, calcium chloride (2 mM, BioData Corp., Horsham, PA), thrombin (0.1 unit/mL, Sigma), and platelets (1.8×10^7 platelets/well). After 2 min of incubation at room temperature, hirudin (0.5 unit/mL, Sigma) and the test agent (HPLC-purified complex **1** or one of its two isolated radiometric peaks) were added. The microtiter plate was incubated at room temperature for an additional 15 min, followed by centrifugation at 3000 rpm for 10 min. The pellet and supernatant were separated, and incorporation of complex **1** and its two isolated radiometric peaks was determined via gamma scintillation counting.

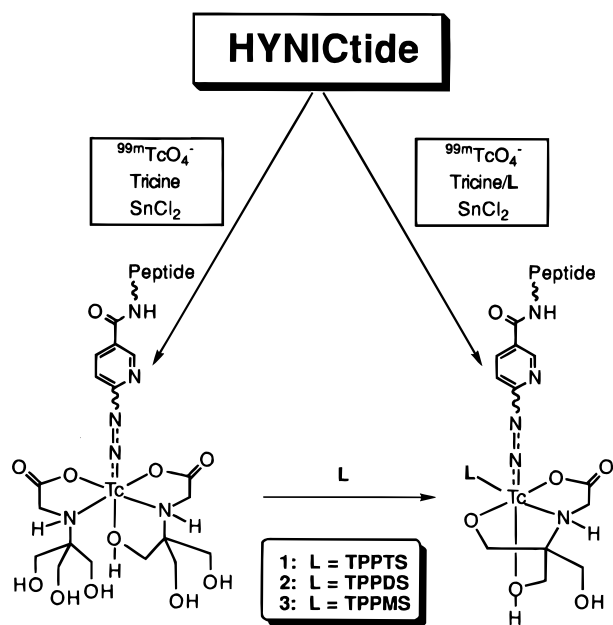
RESULTS AND DISCUSSION

Recently, Abrams and co-workers reported the use of HYNIC technology in labeling polyclonal IgG with ^{99m}Tc for imaging focal sites of infection (13–17). This technology has also been used for the ^{99m}Tc-labeling of chemotactic peptides (18–20) and antisense and DNA oligonucleotides (21–23). Since the HYNIC group can only occupy one or two sites in the technetium coordination sphere, a coligand such as glucoheptonate or tricine is required. It has been shown that the specific activity of the ^{99m}Tc-labeled polyclonal IgG using tricine as a coligand is much higher than that obtained using glucoheptonate (15–17).

We have labeled the HYNICTide (Chart 1) using tricine as the coligand to form the complex [^{99m}Tc(HYNICTide)(tricine)₂] (**5**). We found that the complex [^{99m}Tc(HYNICTide)(tricine)₂] is not stable in solution, particularly under dilute conditions, and exists in many isomeric forms, which we attribute to coordination isomerism from the hydrazine moiety of the HYNICTide and the two tricine coligands. To reduce the number of coordination isomers, we have used other more symmetrical polydentate aminocarboxylates (such as EDDA) as coligands for the radiolabeling. Although the complex [^{99m}Tc(HYNICTide)(EDDA)] has higher solution stability and less coordination isomerism, the radio-HPLC data show that it exists in at least three isomeric forms, which interconvert in solution (**5**). Therefore, EDDA and its N-substituted analogs are not ideal coligands for the ^{99m}Tc-labeling of the HYNICTide.

An alternative approach to reduce the coordination isomerism is to introduce an additional coligand (**L**), which may replace one of the two unsymmetrical, multidentate tricine coligands in [^{99m}Tc(HYNICTide)(tricine)₂] to form a complex [^{99m}Tc(HYNICTide)(tricine)(**L**)] with a ternary ligand system. The use of an appropriate additional coligand (**L**) may impart constraints on the possible coordination modes of the tricine and hydrazine ligands, thereby minimizing the number of possible coordination isomers. These constraints may arise from either a steric or electronic preference for the coordination of **L**. For this purpose, we have chosen three bulky monodentate water soluble phosphines (Chart 2) as the additional coligand for the ^{99m}Tc-labeling of the HYNICTide.

Triphenylphosphine itself is known to form complexes with Tc in various oxidation states (24). A number of Tc-hydrazido and Tc-diazenido complexes with monodentate and bidentate phosphine ligands have been reported (25–31), with well-defined coordination geometries, including complexes formed on the tracer level (^{99m}Tc) in aqueous solution (27). The sulfonate groups are expected to be deprotonated under physiological conditions, resulting in increased hydrophilicity and

Chart 3. Synthesis of Complexes 1–3

potentially improved target to background ratios for the technetium complexes (7).

Synthesis of Complexes 1–3. Synthesis (Chart 3) of complexes 1–3 can be achieved either in two steps, in which the complex $^{99m}\text{Tc}(\text{HYNICTide})(\text{tricine})_2$ is formed first and then reacts with TPPTS, TPPDS, and TPPMS, respectively, or in one step by direct reduction of ^{99m}Tc -pertechnetate with stannous chloride in the presence of the HYNICTide, tricine, and a phosphine coligand. The reaction is carried out by heating the reaction mixture at 50 °C for 30 min. The relative amounts of the three ligands can cover a wide range. The tricine concentration can be from 10 to 100 mg/mL. Using lower tricine concentration (<10 mg/mL) results in the formation of a significant amount of ^{99m}Tc colloid. The phosphine concentration can be from 1.0 to 5.0 mg/mL. Low phosphine coligand concentration results in either incomplete conversion of $^{99m}\text{Tc}(\text{HYNICTide})(\text{tricine})_2$ to complexes 1, 2, or 3 in the two-step synthesis or the formation of $^{99m}\text{Tc}(\text{HYNICTide})(\text{tricine})_2$ as a radioimpurity in the one-step synthesis.

The concentration of the HYNICTide can range from 1 to 100 $\mu\text{g/mL}$. The radiolabeling yields (Table 1) for complexes 1–3 are usually $\geq 90\%$ using 5 μg of HYNICTide (4.69×10^{-9} mol, FW = 1066 for HYNICTide-2TFA) and 100 mCi of ^{99m}Tc pertechnetate ($\sim 7 \times 10^{-10}$ mol of ^{99m}Tc and ^{99}Tc for 24 h generator). The HYNICTide/Tc ratio is about 7:1 under these conditions. Very high specific activity ($\sim 20\,000$ mCi/ μmol) can be achieved for complexes 1–3 without postlabeling purification. The radiolabeling efficiency of this new ternary ligand system is comparable to that obtained using tricine coligand only (5). Since the ^{99m}Tc HYNICTide complexes require no postlabeling purification, this procedure is amenable for clinical application.

HPLC Characterization. In our previous contribution (5), we found that the radio-HPLC (method 1) chromatogram of $^{99m}\text{Tc}(\text{HYNICTide})(\text{tricine})_2$ (Figure 1) showed at least 10 partially resolved peaks with retention times ranging from 20 to 28 min. To our surprise, the reaction of $^{99m}\text{Tc}(\text{HYNICTide})(\text{tricine})_2$ with TPPTS produces complex 1, which shows only one peak at 33.2 min (Figure 2) using the same method. However, by a gradient reversed phase method (method 2), we found two partially resolved peaks (Figure 3) for complex 1.

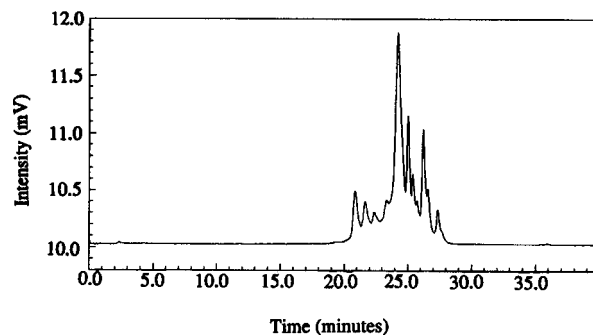


Figure 1. Radio-HPLC chromatogram for complex $^{99m}\text{Tc}(\text{HYNICTide})(\text{tricine})_2$.

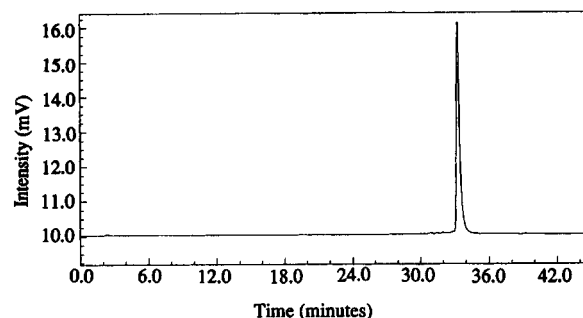


Figure 2. Radio-HPLC chromatogram (method 1) for complex 1.

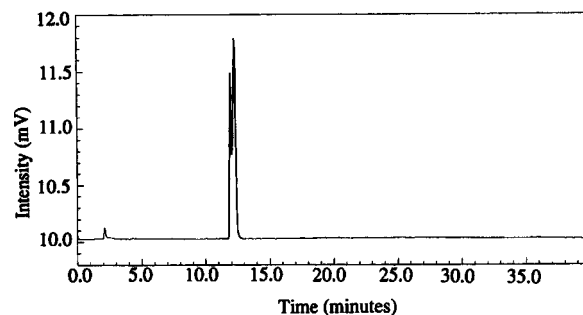


Figure 3. Radio-HPLC chromatogram (method 2) for complex 1.

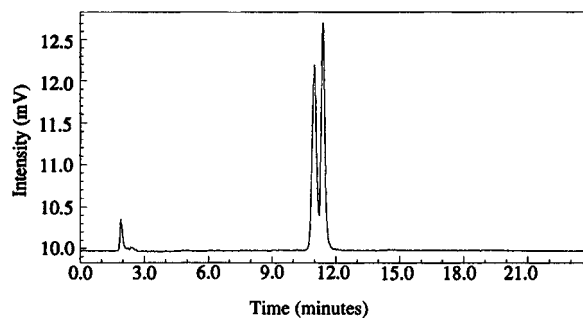


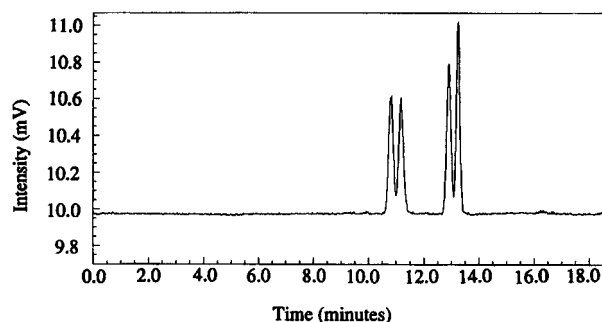
Figure 4. Radio-HPLC chromatogram (method 3) for complex 1.

Using a different gradient HPLC method (method 3) or an isocratic reversed phase method (method 4), we were able to resolve the two peaks (Figures 3 and 4), with the area ratio being approximately 1:1. We also found that the complex prepared according to the two-step synthesis is exactly the same as that prepared according to the one-step synthesis. It is remarkable that the use of a simple monodentate phosphine ligand forms a new ternary ligand system and reduces the number of isomeric forms from >10 for $^{99m}\text{Tc}(\text{HYNICTide})(\text{tricine})_2$ to only 2 for complex 1.

Table 2. Results for Platelet-Binding Assay

compound	percentage ^a activity bonded to canine platelet GPIIb/IIIa receptor
complex 1 (combined)	99
peak 1	98
peak 2	98

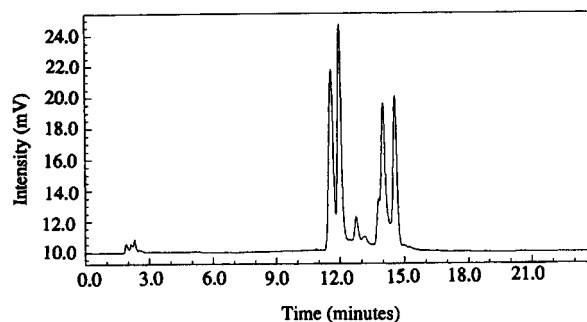
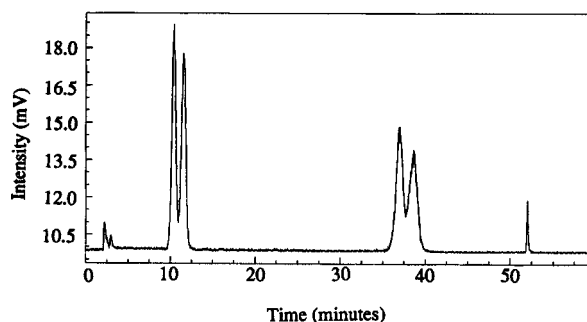
^a The mean value of a single determination performed in triplicate.

**Figure 5.** Radio-HPLC chromatogram (method 2) for complex **1** and [^{99m}Tc(HYNIC-D-Phe-OMe)(TPPTS)(tricine)].

Platelet-Binding Assay. A platelet-binding assay (12) was used to determine if the two peaks assigned as complex **1** do, in fact, represent species comprised of the ^{99m}Tc-labeled HYNICTide and are competent to bind to platelets. In this assay, there is marked excess of receptor to eliminate competition for the GPIIb/IIIa receptor sites. The assay was based on the following data. There are approximately 74 000 copies of the GPIIb/IIIa receptor per platelet; and $1 \times 10^7 - 2 \times 10^7$ platelets/well. In addition, we assumed that competition from fibrinogen released from platelet alpha granules does not effectively compete with our test agent. Thus, the receptor saturation should occur at approximately 12 nM of test agent.

We separated the two peaks using radio-HPLC method 3. The collected fractions were evaporated to dryness, redissolved in 0.9% saline, and diluted to the required concentration for the platelet-binding assay. As a control, we also collected both peaks as one fraction (combined peaks 1 and 2). The HPLC purified complex **1** (combined) and the two radiometric peaks were assessed at a fixed concentration of 10 pM. It was found that the HPLC-purified complex **1** (combined) and its two radiometric peaks bind to the gel-filtered canine platelets to the same extent (Table 2), demonstrating clearly that both isolated peaks contain the ^{99m}Tc-labeled HYNICTide and possess biological activity.

Composition Studies of [^{99m}Tc]HYNICTide Complexes. A mixed ligand experiment was performed to determine the number of HYNICTides bonded to the Tc. In this experiment, the HYNICTide and a model compound, *N*-(6-hydrazinonicotinyl)-D-phenylalanine methyl ester (HYNIC-D-Phe-OMe), were used in the same reaction mixture. After the radiolabeling, the reaction mixture was analyzed by radio-HPLC (method 3). If only one HYNICTide is bonded to the Tc, the chromatogram is expected to show two sets of peaks, one set from complex **1** and the other from the complex [^{99m}Tc(HYNIC-D-Phe-OMe)(tricine)(TPPTS)]. If there were two HYNIC-containing ligands in each complex, a third set of peaks from the mixed ligand complex, [^{99m}Tc(HYNICTide)-(HYNIC-D-Phe-OMe)(tricine)(TPPTS)], is expected. The presence of only two sets of peaks in the radio-HPLC chromatogram (Figure 5) demonstrates clearly that there is only one HYNICTide bonded to the Tc in complex **1**, and by inference to complexes **2** and **3**.

**Figure 6.** Radio-HPLC chromatogram (method 2) for complex **1** and [^{99m}Tc(HYNICTide)(TPPTS)(glycine)₂].**Figure 7.** Radio-HPLC chromatogram (method 3) for complexes **1** and **2**.

The number of tricine coligands in complex **1** was determined similarly using tricine and glycine as competing coligands. We used a 12:1 molar ratio of glycine to tricine since the bidentate glycine is not as strong a ligand as tricine. Figure 6 shows the radio-HPLC chromatogram (method 3) of the resulting reaction mixture. Two sets of peaks from complex **1** and [^{99m}Tc(HYNICTide)-(TPPTS)(Gly)₂] are seen at 12 and 14 min, respectively, suggesting that there is only one tricine coligand in complex **1**, and by inference in complexes **2** and **3**. The small peaks between these two sets of peaks are evident in the chromatogram obtained using glycine only.

The number of TPPTS coligands in complex **1** was determined similarly to that for the HYNICTide using TPPTS and TPPDS as competing coligands. The presence of two sets of distinctive peaks at 12 and 36 min in the radio-HPLC chromatogram (Figure 7) for complexes **1** and **2**, respectively, indicates clearly that there is only one phosphine coligand bonded to the Tc in these complexes.

On the basis of these data, we conclude that these technetium complexes contain one HYNICTide, one tricine, and one phosphine coligand (TPPTS, TPPDS, and TPPMS). It has been reported that on the carrier-added (⁹⁹Tc) level the reaction of [⁹⁹Tc]tricine complex with 2 equiv of HYNIC-D-Phe-OMe results in formation of two technetium complexes: [⁹⁹Tc(HYNIC-D-Phe-OMe)(tricine)]⁻ and [⁹⁹Tc(HYNIC-D-Phe-OMe)₂(tricine)₂]⁻ (16). On the tracer level (^{99m}Tc), however, the reaction of [^{99m}Tc]tricine complex with excess HYNICTide results in complex **1** as the only detectable product. No bis(HYNICTide) technetium complex was observed even at a HYNICTide concentration of ~100 μg/mL. We also carried out the synthesis of complex **1** changing the level of each component. Surprisingly, the 1:1:1 composition for Tc: HYNICTide:tricine:TPPTS was retained over a wide range of relative ligand ratios (HYNICTide, 1–100 μg; tricine, 10–100 mg; TPPTS, 1–5 mg).

Solution Stability Studies. Another advantage using this new ternary ligand system is the high solution stability of complexes **1–3**. We examined the solution

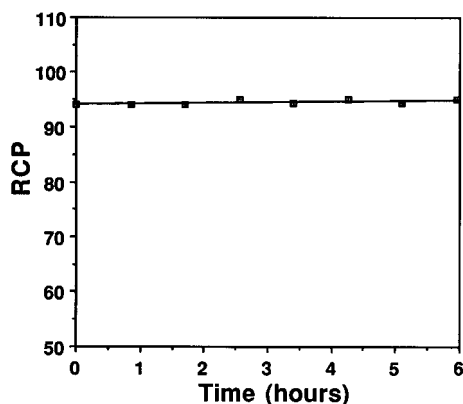


Figure 8. Plot of RCP vs time for complex **1** in the kit matrix.

stability of complex **1** both in the kit matrix and in solutions with 10- and 100-fold dilutions. For complex **1** in the kit matrix, the stability was assessed by radio-HPLC (method 3) by performing eight injections over ~6 h. For complex **1** in the dilute solutions, the reaction mixture was first diluted with either 2 wt % tricine solution or 0.9% saline, and the diluted solutions were monitored in a similar fashion. Figure 8 shows the plot of RCP (radiochemical purity) vs time for complex **1** in the kit matrix. Plots of RCP vs time for complex **1** in solutions with 10- and 100-fold dilutions are shown in Figures SI and SII, respectively. It is clear that complex **1** is stable for ≥ 6 h in solution and the peak ratio remains relatively constant.

We also examined the stability of the two isolated peaks of complex **1** in solutions at different pH values. The collected solution of each peak was divided into two fractions, and the pH was adjusted to 4 in one fraction and to 8 in the other. These fractions were monitored by radio-HPLC (method 3). It was found that both peaks are stable for at least 6 h in solution between pH 4 and 8 (Figures SIII and SIV). No interconversion was observed for the two isolated peaks under conditions used in this study.

Apparently, the use of this new ternary ligand system offers several major advantages. First, bonding of the phosphine coligand to the Tc dramatically reduces the number of isomeric forms of the [^{99m}Tc]HYNICTide complexes. Second, the solution stability of [^{99m}Tc]HYNICTide complexes is dramatically improved. Finally, the hydrophilicity of [^{99m}Tc]HYNICTide complexes with the new ternary ligand system can be tuned by either altering the number of sulfonate groups or using water soluble phosphines with other polar functionality. The tricine coligand can also be substituted by other potentially tetradentate aminocarboxylates, such as dicine [*N*-bis(hydroxymethyl)methylglycine] and bicine [*N,N*-bis(hydroxymethyl)glycine]. However, the specific activity of [^{99m}Tc]HYNICTide complexes using dicine and bicine as coligands is not as high as that of the corresponding tricine complexes. This is consistent with the literature results reported by Abrams and co-workers, who found that the [^{99m}Tc]tricine precursor complex has the highest reactivity with hydrazines (15).

In the past decade, the ligand design for technetium radiopharmaceuticals has been focused on preparing polydentate chelators [e.g., N_3S triamidethiols (32–34), N_2S_2 diamidedithiols (34–38), N_2S_2 diaminedithiols (39–50), N_2S_2 monoamide monoaminodithiols (51–54), *N*-4-oxopentan-2-ylidene-*N*-pyrrol-2-ylmethylethane-1,2-diamine ($\text{H}_3\text{MRP-20}$) (55, 56), and propylene amine oxime (PnAO) (57, 58)], which are able to form stable complexes with a 1:1 Tc:ligand ratio. Some of these chelators have

been successfully used to label proteins (37, 38), and peptides (34, 48) with ^{99m}Tc for the development of target specific radiopharmaceuticals. A binary ligand system containing a tetradentate N_2O_2 and two monodentate ether-substituted phosphine ligands was reported to form cationic Tc(III) complexes such as $^{99m}\text{Tc-Q3}$ (59, 60), which is used as a heart imaging agent. Very few binary ligand systems are used for the ^{99m}Tc -labeling of proteins and peptides.

Recently, tridentate ligands containing the SNS donor set were used in the synthesis of brain imaging agents (61, 62). The combination of a dianionic tridentate SNS ligand with a monodentate thiolate produces a binary ligand system that can bind to the Tc=O core and form neutral square-pyramidal technetium complexes. This “3 + 1” concept has been used for ^{99m}Tc -labeling of dopamine transporters (63, 64). The ternary ligand system described in this study contains three different ligands: a bifunctional coupling group (HYNIC), a monodentate phosphine, and the tetradentate tricine coligand. It is remarkable that these three different ligands react in one step with [^{99m}Tc]pertechnetate in the presence of stannous chloride and form a technetium complex with only two isomeric forms. This represents the first example of a ternary ligand system used for the ^{99m}Tc -labeling of peptides, proteins, or other biologically active molecules.

Traditionally, the development of a new class of ^{99m}Tc radiopharmaceuticals involves synthesis and characterization of new technetium complexes using macroscopic amounts of ^{99}Tc , followed by the translation of the macroscopic ^{99}Tc chemistry to the tracer level (^{99m}Tc) chemistry. The composition and structure of ^{99m}Tc complexes are determined by various spectroscopic (IR, NMR, and FAB-MS) and X-ray crystallographic studies on the corresponding ^{99}Tc analogs. In this study, we used a simple mixed ligand experiment to determine the composition of ^{99m}Tc complexes. The composition of complex **1** determined with this method is completely consistent with that of the corresponding ^{99}Tc analog, [^{99}Tc](HYNICTide)(TPPTS)(tricine), determined with ^1H NMR methods (65). This methodology also applies to the composition determination for ^{99m}Tc complexes with other binary or ternary ligand systems.

On the basis of the mixed ligand experiments, it is quite clear that complex **1** contains one HYNICTide, one tricine, and one TPPTS. However, the technetium oxidation state and the exact nature of bonding between these ligands (HYNIC, tricine, and phosphine) and the Tc metal center are not yet clear. It has been proposed that the technetium oxidation state in the [^{99m}Tc]tricine complex is +5 (15–17). However, the oxidation state might change when the HYNIC group and phosphine coligand are bonded to the Tc center. Furthermore, the technetium oxidation state largely depends on how the HYNIC group binds to the Tc and how one counts the charge on the HYNIC ligand.

When the HYNICTide binds to the Tc, it likely occupies one site of the Tc coordination sphere by forming either a Tc-hydrazido or Tc-diazenido bond. Complexes containing Tc-hydrazido and Tc-diazenido bonds have been previously reported and characterized by X-ray crystallography (25–31). If one assumes that the coordination geometry around the Tc is distorted octahedral, the tricine coligand is expected to be tetradentate. Several possible explanations can be envisaged for the existence of two isomeric forms of these complexes, including the resolution of diastereomers resulting from the chiral center on the coordinated tricine and different geometric orientations of the diazenido ligand due to restricted

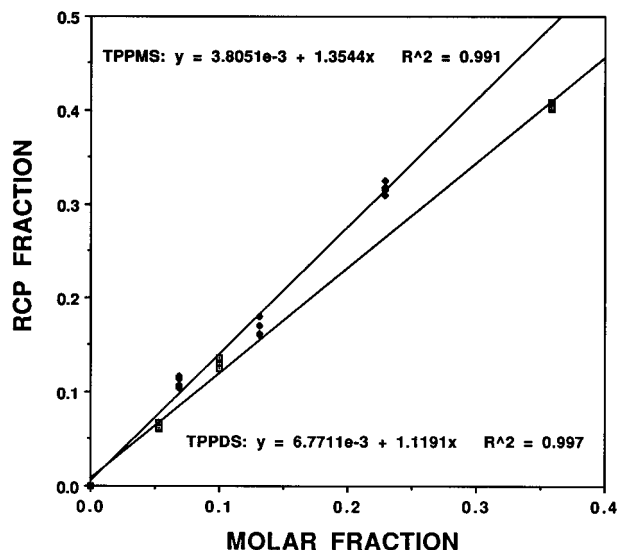


Figure 9. Plot of RCP fraction versus molar fraction.

rotation around the Tc=N and N=N bonds. Efforts are continuing to better understand the complex coordination chemistry of this unique ternary ligand system.

The electron-withdrawing sulfonato groups have profound impact on the donating capability of the phosphine coligands. To study their relative donating capability, we performed mixed ligand experiments by spiking a range of amounts of either TPPDS or TPPMS, respectively, into the TPPTS solution. Plotting (Figure 9) the ratio of the yield of the ternary complex of the added phosphine to the total yield of the two ternary complexes $[RCP2/(RCP1 + RCP2)]$ versus the mole fraction TPPDS/(TPPDS + TPPTS) should give a measure of their relative bonding affinity. For TPPDS, a slope of 1.12 indicates that TPPDS is 1.12 times more powerful than TPPTS in coordinating to the Tc. For TPPMS, plotting RCP3/(RCP1 + RCP3) versus TPPMS/(TPPMS + TPPTS) also gives a straight line with slope of 1.35, suggesting that TPPMS is 1.35 times more powerful than TPPTS. It is clear that as the number of electron-withdrawing sulfonato groups on the benzene rings decreases, the electron density on the phosphine donor atom increases; therefore, the σ -donating capability increases. The relative donating capability for three water soluble phosphine coligands falls in the order TPPMS > TPPDS > TPPTS, as expected.

CONCLUSION

A hydrazinonicotinamide-functionalized cyclic GPIIb/IIIa receptor antagonist [HYNICTide: cyclo(D-Val-NMe-Arg-Gly-Asp-Mamb(5-(6-(6-hydrazinonicotinamido)hexanamide)))] was labeled with ^{99m}Tc using tricine and a water soluble phosphine (TPPTS, TPPDS, or TPPMS) as coligand. The combination of HYNICTide, tricine, and phosphine produces a new ternary ligand system which forms technetium complexes, $[^{99m}\text{Tc}(\text{HYNICTide})(\text{L})(\text{tricine})]$ (**1**, L = TPPTS; **2**, L = TPPDS; **3**, L = TPPMS), with high specific activity ($\geq 20\,000$ Ci/mmol) and high stability. Using two reversed phase radio-HPLC methods, we found that complexes **1–3** exist as equal mixtures of two isomeric forms, both of which contain the radio-labeled HYNICTide and have the capability to bind to platelets as demonstrated in a platelet-binding assay (for complex **1**). The composition of these complexes was determined to be 1:1:1:1 (Tc:HYNICTide:L:tricine) through a series of mixed ligand experiments and is maintained over a wide range of relative ligand ratios. Using the mixed ligand experiment, we also demonstrated that the

binding capability of the aryl phosphine ligand, L, to the Tc increases as the number of sulfonato groups decreases. The lipophilicity of these technetium complexes can be systematically varied by the choice of the phosphine coligand. The tricine coligand can also be replaced by other potentially tetradentate aminocarboxylates such as bicine, dicine (15), and EDDA. However, tricine remains the best with respect to the labeling efficiency. Using the combination of an aminocarboxylate and a phosphine as coligands, HYNIC-derivatized peptides or other biologically active small molecules can be labeled with ^{99m}Tc in high specific activity and high stability for potential use as radiopharmaceuticals.

ACKNOWLEDGMENT

Acknowledgement is made to Dr. J. L. Glajch and M. J. Poirier for the use of their radio-HPLC method (method 1), to Dr. M. J. Abrams and Dr. J. D. Higgins III for the synthesis of *N*-(6-hydrazinonicotinyl)-D-phenylalanine methyl ester hydrochloride, to P. R. Damphousse for the synthesis of TPPDS, and to Dr. T. D. Harris, Dr. M. Rajopadhye, Dr. D. Glowacka, J. P. Bourque, P. R. Damphousse, and K. Yu for the synthesis of the cyclic GPIIb/IIIa HYNICTide, cyclo[D-Val-NMeArg-Gly-Asp-Mamb(5-(6-(6-hydrazinonicotinamido)hexanamide))].

Supporting Information Available: Two diagrams showing the solution stability of complex **1** in solution with 10-fold (Figure SI) and 100-fold (Figure SII) dilution, and HPLC chromatograms (Figures SIII and SVI) for the two isolated peaks at $t = 30$ min and 6 h (4 pages). Ordering information is given on any current masthead page.

LITERATURE CITED

- Barrett, J. A., Heminway, S. J., Damphousse, D. J., Thomas, J. R., Looby, R. J., Edwards, D. S., Harris, T. D., Rajopadhye, M., Liu, S., and Carroll, T. R. (1994) Platelet GP IIB/IIIa antagonists in the canine arteriovenous shunt: potential thrombus imaging agents. *J. Nucl. Med.* **35**, 52P (Abstract 202).
- Harris, T. D., Barrett, J. A., Bourque, J. P., Carroll, T. R., Damphousse, P. R., Edwards, D. S., Glowacka, D., Liu, S., Looby, R. J., Poirier, M. J., Rajopadhye, M., and Yu, K. (1994) Design and synthesis of radiolabeled GPIIb/IIIa receptor antagonists as potential thrombus imaging agents. *J. Nucl. Med.* **35**, 245P (Abstract 1005).
- Barrett, J. A., Bresnick, M. R., Crocker, A. C., Damphousse, D. J., Hampson, J. R., Heminway, S. J., Mazaika, T. J., Kagan, M., Lazewatsky, J. L., Edwards, D. S., Liu, S., Harris, T. D., Rajopadhye, M., and Carroll, T. R. (1995) RP-431: a potential thrombus imaging agent. *J. Nucl. Med.* **36**, 16P (Abstract 55).
- Liu, S., Edwards, D. S., Looby, R. J., Harris, A. R., Poirier, M. J., Barrett, J. A., Heminway, S. J., and Carroll, T. R. (1996) Labeling a hydrazino nicotinamide-modified cyclic IIB/IIIa receptor antagonist with ^{99m}Tc using aminocarboxylates as coligands. *Bioconjugate Chem.* **7**, 63–71.
- Liu, S., Edwards, D. S., Looby, R. J., Harris, A. R., Poirier, M. J., Rajopadhye, M., and Bourque, J. P. (1996) Labeling cyclic IIB/IIIa receptor antagonists with ^{99m}Tc by the pre-formed chelate approach. *Bioconjugate Chem.* **7**, 196–203.
- Barrett, J. A., Damphousse, D. J., Heminway, S. J., Liu, S., Edwards, D. S., Looby, R. J., and Carroll, T. R. (1996) Biological evaluation of ^{99m}Tc -labeled cyclic GPIIb/IIIa receptor antagonists in the canine arteriovenous shunt and deep vein thrombosis models: effects of chelators on biological properties of ^{99m}Tc -chelator-peptide conjugates. *Bioconjugate Chem.* **7**, 203–208.
- Barrett, J. A., Crocker, A. C., Damphousse, D. J., Heminway, S. J., Liu, S., Edwards, D. S., Harris, A. R., Looby, R. J., and Carroll, T. R. (1997) Biological evaluation of thrombus imaging agents utilizing water soluble phosphines and tricine

- as coligands when used to label a hydrazino nicotinamide-modified cyclic glycoprotein IIb/IIIa receptor antagonist with ^{99m}Tc . *Bioconjugate Chem.* 8, 155–160.
- (8) Bartik, T., Bartik, B., Hanson, B. E., Glass, T., and Bebout, W. E. (1992) Comments on the synthesis of trisulfonated triphenylphosphine: reaction monitoring by NMR spectroscopy. *Inorg. Chem.* 31, 2667–2670.
- (9) Kuntz, E. (1981) Catalytic hydroformylation of olefins. U.S. Pat. 4,248,802.
- (10) Harris, T. D., Rajopadhye, M., Damphousse, P. R., Glowacka, D., Yu, K., Bourque, J. P., Barrett, J. A., Damphousse, D. J., Heminway, S. J., Lazewatsky, Mazaika, T., and Carroll, T. R. (1996) Tc-99m-labeled fibrinogen receptor antagonists: design and synthesis of cyclic RGD peptides for the detection of thrombi. *Bioorg. Med. Chem. Lett.* 6, 1741–1746.
- (11) Rajopadhye, M., Harris, T. D., Yu, K., Glowacka, D., Damphousse, P. R., Barrett, J. A., Heminway, S. J., Edwards, D. S., and Carroll, T. R. (1996) Synthesis, evaluation and Tc-99m complexation of a hydrazinonicotinyl conjugate of a GP IIb/IIIa antagonist cyclic peptide for the detection of deep vein thrombosis. *Bioorg. Med. Chem. Lett.* (submitted for publication).
- (12) Plow, E. F., Marguerie, G., and Ginsberg, M. (1987) Fibrinogen, fibrinogen receptors and the peptides that inhibit these interactions. *Biochem. Pharmacol.* 36, 4035–4041.
- (13) Schwartz, D. A., Abrams, M. J., Hauser, M. M., Gaul, F. E., Larsen, S. K., Rauh, D., and Zubieta, J. A. (1991) Preparation of hydrazino-modified proteins and their use for the synthesis of ^{99m}Tc -protein conjugates. *Bioconjugate Chem.* 2, 334–336.
- (14) Abrams, M. J., Juweid, M., tenKate, C. I., Schwartz, D. A., Hauser, M. M., Gaul, F. E., Fuccello, A. J., Rubin, R. H., Strauss, H. W., and Fischman, A. J. (1990) Technetium-99m-human polyclonal IgG radiolabeled via the hydrazino nicotinamide derivative for imaging focal sites of infection in rats. *J. Nucl. Med.* 31, 2022–2028.
- (15) Larson, S. K., Abrams, M. J., Higgins III, J. D., Solomon, H. F., Babich, J. W., and Fischman, A. J. (1994) Technetium complexes of tricine: useful precursor for the ^{99m}Tc labeling of hydrazino nicotinamide modified human polyclonal IgG. *J. Nucl. Med.* 35, 105P (Abstract 418).
- (16) Larson, S. K., Caldwell, G., Higgins III, J. D., Abrams, M. J., and Solomon, H. F. (1994) Technetium complex of tricine: useful precursor for the ^{99m}Tc labeling of hydrazino nicotinamide modified proteins. *J. Labelled Compd. Radiopharm.* 35, 1–2.
- (17) Larson, S. K., Solomon, H. F., Caldwell, G., and Abrams, M. J. (1995) ^{99m}Tc /Tricine: a useful precursor complex for the radiolabeling of hydrazinonicotinate protein conjugates. *Bioconjugate Chem.* 6, 635–638.
- (18) Babich, J. W., Solomon, H., Pike, M. C., Kroon, D., Graham, W., Abrams, M. J., Tompkins, R. G., Rubin, R. H., and Fischman, A. J. (1993) Technetium-99m-labeled hydrazino nicotinamide derivatized chemotactic peptide analogs for imaging focal sites of bacterial infection. *J. Nucl. Med.* 34, 1967–1974.
- (19) Babich, J. W., and Fischman, A. J. (1995) Effect of “coligand” on the biodistribution of ^{99m}Tc -labeled hydrazino nicotinic acid derivatized chemotactic peptides. *Nucl. Med. Biol.* 22, 25–30.
- (20) Fischman, A. J., Babich, J. W., and Rubin, R. H. (1994) Infection imaging with technetium-99m-labeled chemotactic peptide analogs. *Semin. Nucl. Med.* 24, 154–168.
- (21) Dewanjee, M. K., Ghalfouripour, A. K., Subramanian, M., Hanna, M., Kapadvanjwala, M., Serafini, A. N., Ezuddin, S., Lopez, D., and Sfakianakis, G. N. (1994) Labeling antisense deoxyoligonucleotide with Tc-99m and hybridization with c-myc oncogene mRNA in P388 leukemic cells. *J. Labelled Compd. Radiopharm.* 35, 40–42.
- (22) Dewanjee, M. K., Abrams, M. J., Wu, S. M., Kapadvanjwala, M., Serafini, A. N., and Sfakianakis, G. N. (1995) Technetium-99m labeled single-strand DNA probe for imaging thrombin in viscera formed during cardiopulmonary bypass. *J. Nucl. Med.* 36, 16P (Abstract 54).
- (23) Hnatowich, D. J., Winnard Jr., P., Virzi, F., Fogarski, M., Sano, T., Smith, C. L., Cantor, C. L., and Rusckowski, M. (1995) Technetium-99m labeling of DNA oligonucleotides. *J. Nucl. Med.* 36, 2306–2314.
- (24) Deutsch, E., Libson, K., Jurrison, S., and Lindoy, L. F. (1983) Technetium chemistry and technetium radiopharmaceuticals. *Prog. Inorg. Chem.* 30, 75–139.
- (25) Nicholson, T., de Vries, N., Davison, A., and Jones, A. G. (1989) Synthesis and characterization of aryldiazenido technetium complexes and their protonation reactions. The X-ray structure of $[\text{TcCl}(\text{PPh}_3)_2(\text{NNC}_6\text{H}_4\text{Br})_2]$. *Technetium and Rhenium in Chemistry and Nuclear Medicine* (M. Nicolini, G. Bandoli, and U. Mazzi, Eds.) Vol. 3, pp 95–108, Cortina International, Verona.
- (26) Abrams, M. J., Larsen, S. K., Shaikh, S. N., and Zubieta, J. (1991) Investigation of technetium-organohydrazine coordination chemistry. The crystal and molecular structures of $[\text{TcCl}_2(\text{C}_8\text{H}_5\text{N}_4)(\text{PPh}_3)_2] \cdot 0.75\text{C}_7\text{H}_8$ and $[\text{TcNCl}_2(\text{PPh}_3)_2] \cdot 0.25\text{CH}_2\text{Cl}_2$. *Inorg. Chim. Acta* 185, 7–15.
- (27) Archer, C. M., Dilworth, J. R., Jobanputra, P., Thompson, R. M., McPartlin, M., Povey, D. C., Smith, G. W., and Kelly, J. D. (1990) Development of new technetium cores containing technetium-nitrogen multiple bonds. Synthesis and characterization of some diazenido-, hydrazido- and imido- complexes of technetium. *Polyhedron* 9, 1497–1502.
- (28) Dilworth, J. R., Jobanputra, P., Thompson, R. M., Archer, C. M., Povey, D. C., Kelly, J. D., and Hiller, W. (1992) Crystal structure of a diazenido-dithiocarbamate complex of technetium, $[\text{Tc}(\text{NNC}_6\text{H}_4\text{Cl})((\text{CH}_3)_2\text{NCS})_2(\text{PPh}_3)]$. *Z. Naturforsch.* 46, 449–452.
- (29) Archer, C. M., Dilworth, J. R., Jobanputra, P., Thompson, R. M., McPartin, M., and Hiller, W. (1993) Technetium diazenido complexes. Part 1. Synthesis and structures of $[\text{TcCl}(\text{NNC}_6\text{H}_4\text{Cl-4})_2(\text{PPh}_3)_2]$ and $[\text{TcCl}(\text{NNPh})(\text{Ph}_2\text{PCH}_2\text{CH}_2\text{PPh}_2)_2][\text{PF}_6] \cdot \text{H}_2\text{O}$. *J. Chem. Soc., Dalton Trans.*, 897–904.
- (30) Dilworth, J. R., Jobanputra, P., Thompson, R. M., Povey, D. C., Archer, C. M., and Kelly, J. D. (1994) Technetium diazenido complexes. Part 2. Substitution chemistry of $[\text{TcCl}(\text{NNC}_6\text{H}_4\text{Cl-4})_2(\text{PPh}_3)_2]$ and the synthesis of technetium diazenido-complexes directly from $[\text{NH}_4][\text{TcO}_4]$. *J. Chem. Soc., Dalton Trans.*, 1251–1256.
- (31) Cook, J., Davison, A., Jones, A. J., and Davis, W. M. (1990) The reaction chemistry of $\text{HTc}(\text{CO})_3(\text{PPh}_3)_2$. *Technetium and Rhenium in Chemistry and Nuclear Medicine* (M. Nicolini, G. Bandoli, and U. Mazzi, Eds.) Vol. 3, pp 65–68, Cortina International, Verona.
- (32) Bormans, G., Cleynehen, B., Adriaens, P., De Roo, M., and Verbruggen, A. (1993) Synthesis and labeling characteristics of ^{99m}Tc -mercaptoacetyltri-peptides. *J. Labelled Compd. Radiopharm.* 33, 1065–1078.
- (33) Grummon, G., Rajagopalan, R., Palenik, G. J., Koziol, A. E., and Nosco, D. L. (1995) Synthesis, characterization and crystal structures of technetium(V)-oxo complexes useful in nuclear medicine. 1. Complexes of mercaptoacetylglutylglycylglycine (MAG_3) and its methyl ester derivative ($\text{MAG}_3\text{-OMe}$). *Inorg. Chem.* 34, 1764–1772.
- (34) Liu, S., and Edwards, D. S. (1995) New N_2S_2 diamidedithiol and N_3S triamidedithiols as bifunctional chelating agents for labeling small peptides with technetium-99m. *Technetium and Rhenium in Chemistry and Nuclear Medicine* (M. Nicolini, G. Banoli, and U. Mazzi, Eds.) Vol. 4, pp 383–393, SGEEditoriali, Padova.
- (35) Davison, A., Jones, A. G., Orvig, C., and Sohn, M. (1981) A new class of oxotechnetium(5+) chelate complexes containing a TcON_2S_2 core. *Inorg. Chem.* 20, 1629–1632.
- (36) Rao, T. N., Adhikesavalu, D., Camerman, A., and Fritzberg, A. R. (1990) Technetium(V) and rhenium(V) complexes of 2,3-bis(mercaptoacetamido)-propanoate. Chelate ring stereochemistry and influence on chemical and biological properties. *J. Am. Chem. Soc.* 112, 5798–5804.
- (37) Fritzberg, A. R., Abrams, P. G., Beaumier, P. L., Kasina, S., Morgan, A. C., Rao, T. N., Reno, J. M., Sanderson, J. A., Srinivasan, A., and Wilbur, D. S. (1988) Specific and stable labeling of antibodies with technetium-99m with a diamide dithiolate chelating agent. *Proc. Natl. Acad. Sci. U.S.A.* 85, 4025–4029.
- (38) Kasina, S., Rao, T. N., Srinivasan, A., Sanderson, J. A., Fitzner, J. N., Reno, J. M., Beaumier, P. L., and Fritzberg, A. R. (1991) Development and biological evaluation of a kit

- for preformed chelate technetium-99m radiolabeling of an antibody Fab fragment using a diamide dimercaptide chelating agent. *J. Nucl. Med.* **32**, 1445–1451.
- (39) Edwards, D. S., Cheesman, E. H., Watson, M. W., Maheu, L. J., Nguyen, S. A., Dimitre, L., Nason, T., Watson, A. D., and Walovitch, R. (1990) Synthesis and characterization of technetium and rhenium complexes of *N,N*-1,2-ethylenediybis-L-cysteine. Neurolite® and its metabolites. *Technetium and Rhenium in Chemistry and Nuclear Medicine* (M. Nicolini, G. Banoli, and U. Mazzi, Eds.) Vol. 3, pp 431–444, Cortina International, Verona.
- (40) Kung, H. F., Molnar, M., Billings, J., and Blau, M. (1984) Synthesis and biodistribution of neutral lipid-soluble Tc-99m complexes that cross the blood-brain barrier. *J. Nucl. Med.* **25**, 326–332.
- (41) Kung, H. F., Guo, Y. Z., Yu, C. C., Billings, J., Subramanyam, V., and Calabrese, J. C. (1989) New brain perfusion imaging agents based on ^{99m}Tc-bis(aminoethanethiol) complexes: Stereoisomers and biodistribution. *J. Med. Chem.* **32**, 433–437.
- (42) Mach, R. H., Kung, H. F., Jungwiwattanaporn, P., and Guo, Y. Z. (1991) Synthesis and biodistribution of a new class of ^{99m}Tc-labeled fatty acid analogs for myocardial imaging. *Nucl. Med. Biol.* **18**, 215–226.
- (43) Mach, R. H., Kung, H. F., Guo, Y. Z., Yu, C. C., Subramanyam, V., and Calabrese, J. C. (1989) Synthesis, characterization and biodistribution of neutral and lipid-soluble ^{99m}Tc-PAT-HM and ^{99m}Tc-TMR for brain imaging. *Nucl. Med. Biol.* **16**, 829–837.
- (44) Oya, S., Kung, M. P., Frederick, D., and Kung, H. F. (1995) New bisaminoethanethiol (BAT) ligands which form two interconvertible Tc-99m complexes. *Nucl. Med. Biol.* **22**, 749–757.
- (45) Francesconi, L. C., Graczyk, G., Wehrli, S., Shaikh, S. N., McClinton, D., Liu, S., Zubietta, J., and Kung, H. F. (1993) Synthesis and characterization of neutral MVO (M = Tc, Re) Amine-thiol complexes containing a pendant phenylpiperidine group. *Inorg. Chem.* **32**, 3114–3124.
- (46) Lever, S. Z., Sun, S.-Y., Scheffel, U. A., Kaltovich, F. A., Baidoo, K. E., Goldfarb, H., and Wagner, Jr., H. N. (1994) Pulmonary accumulation of neutral diamine dithiol complexes of technetium-99m. *J. Pharm. Sci.* **84**, 802–809.
- (47) Baidoo, K. E., and Lever, S. Z. (1990) Synthesis of a diaminedithiol bifunctional chelating agent for incorporation of technetium-99m into biomolecules. *Bioconjugate Chem.* **1**, 132–137.
- (48) Baidoo, K. E., Scheffel, U., Finley, P., Lever, S. Z., and Wagner, Jr. H. N. (1994) No carrier added (NCA) Tc-99m-diaminedithiolate derivatives of chemotactic peptides for imaging inflammation. *J. Nucl. Med.* **35**, 19P (Abstract 67).
- (49) Eisenhut, M., Missfeldt, M., Lehmann, W. D., and Karas, M. (1991) Synthesis of a bis(aminoethanethiol) ligand with an activated ester group for protein conjugation and ^{99m}Tc-labeling. *J. Labelled Compd. Radiopharm.* **29**, 1283–1291.
- (50) Eisenhut, M., Lehmann, W. D., Becker, W., Elser, H., Strittmatter, W., Baum, R. P., Valerius, T., Repp, R., and Deo, Y. (1996) Bifunctional NHS-BAT ester for antibody conjugation and stable technetium-99m labeling: conjugation chemistry, immunoreactivity and kit formulation. *J. Nucl. Med.* **37**, 362–370.
- (51) O'Neil, J. P., Wilson, S. R., and Katzenellenbogen, J. A. (1994) Preparation and structural characterization of monoamine-monoamide bis(thiol) oxo complexes of technetium(V) and rhenium(V). *Inorg. Chem.* **33**, 319–323.
- (52) Gustavson, L. M., Rao, T. N., Jones, D. S., and Fritzberg, A. R. (1991) Synthesis of a new class of Tc chelating agents: N₂S₂ monoaminemonoamide (MAMA) ligands. *Tetrahedron Lett.* **32**, 5485–5488.
- (53) Mahmood, A., Wolff, J. A., Davison, A., and Jones, A. J. (1995) Technetium and rhenium complexes of amine amide dithiol ligands: ligand synthesis and metal complexes. *Technetium and Rhenium in Chemistry and Nuclear Medicine* (M. Nicolini, G. Banoli, and U. Mazzi, Eds.) Vol. 4, pp 211–215, SGEEditorali, Padova.
- (54) Kung, H. F., Bradshaw, J. E., Chumpradit, S., Zhang, Z. P., Kung, M. P., Mu, M., and Frederick, D. (1995) New TcO(III) and ReO(III) N₂S₂ complexes as potential CNS 5-HT_{1A} receptor imaging agents. *Technetium and Rhenium in Chemistry and Nuclear Medicine* (M. Nicolini, G. Banoli, and U. Mazzi, Eds.) Vol. 4, pp 293–298, SGEEditorali, Padova.
- (55) Morgan, G. F., Deblaton, M., Hussein, W., Thornback, J. R., Evrard, G., Durant, F., Stach, J., Abram, U., and Abram, S. (1991) Rhenium(V) and technetium(V) complexes with *N*-[2(1H-pyrolomethyl)]-*N*-(4-pentene-3-one-2)ethane-1,2-diamine (C₁₂H₁₆N₃O, MRP 20). X-ray crystal structures of H₃-MRP 20 and TcO(MRP 20). *Inorg. Chim. Acta* **190**, 257–264.
- (56) Bossuyt, A., Morgan, G. F., Deblaton, M., Pirotte, R., Chirico, A., Clements, P., Vandenbroeck, P., and Thornback, J. R. (1991) Technetium-99m-MRP20, a potential brain perfusion agent: in vivo biodistribution and SPECT studies in normal male volunteers. *J. Nucl. Med.* **32**, 399–403.
- (57) Troutner, D. E., Volkert, W. A., Hoffman, T. J., and Holmes, R. A. (1984) A neutral lipophilic complex of ^{99m}Tc with a multidentate amine oxime. *Int. J. Appl. Radiat. Isot.* **35**, 467–470.
- (58) Jurisson, S., Aston, K., Fair, C. K., Schlemper, E. O., Sharp, P. R., and Troutner, D. E. (1987) Effect of ring size on properties of technetium amine oxime complexes. X-ray structures of TcO₂Pent(AO)₂, which contains an unusual eight-membered chelate ring, and of TcOEn(AO)₂. *Inorg. Chem.* **26**, 3576–3582.
- (59) Libson, K., Messa, C., Kwiatkowski, M., Zito, F., Best, T., Colombo, F., Mattarrese, M., Wang, X., Fragasso, G., Fazio, F., and Deutsch, E. (1990) Development of new ^{99m}Tc myocardial perfusion imaging agents. *Technetium and Rhenium in Chemistry and Nuclear Medicine* (M. Nicolini, G. Banoli, and U. Mazzi, Eds.) Vol. 3, pp 365–368, Cortina International, Verona.
- (60) Biniakiewicz, D. S., Washburn, L. C., McGoron, A. J., and Gerson, M. C. (1995) Synthesis and biodistribution of new Tc-99m Q-series complexes with ester functionality. *J. Nucl. Med.* **36**, 17P (Abstract 59).
- (61) Spyriounis, D. M., Pelecanou, M., Stassinopoulou, C. I., Raptopoulou, C. P., Terzis, A., and Chiotellis, E. (1995) Synthesis and characterization of oxotechnetium(V) complexes with aza-substituted 2,6-dimethyl-4-azaheptane-2,6-dithiol ligands and benzyl mercaptan as coligand. *Inorg. Chem.* **34**, 1077–1082.
- (62) Mastrostamatis, S. G., Papadopoulos, M. S., Pirmettis, I. C., Paschali, E., Varvarigou, A. D., Stassinopoulou, C. I., Raptopoulou, C. P., Terzis, A., and Chiotellis, E. (1994) Tridentate ligands containing the SNS donor atom set as a novel backbone for the development of technetium brain-imaging agents. *J. Med. Chem.* **37**, 1077–1082.
- (63) Meegalla, S., Plössl, K., Kung, M.-P., Stevenson, D. A., Liable-Sand, L. M., Rheingold, A. L., and Kung, H. F. (1995) First example of a ^{99m}Tc complex as a dopamine transporter imaging agent. *J. Am. Chem. Soc.* **117**, 11037–11038.
- (64) Meegalla, S., Plössl, K., Kung, M.-P., Chumpradit, S., Stevenson, D. A., Frederick, D., and Kung, H. F. (1996) Tc-99m-labeled tropanes as dopamine transporter imaging agents. *Bioconjugate Chem.* **7**, 421–429.
- (65) Liu, S., and Edwards, D. S. Unpublished results.

BC970002H

Volume 8, Number 2, March/April 1997.

D. Scott Edwards,* Shuang Liu,* John A. Barrett,
Anthony R. Harris, Richard J. Looby, Marisa C.
Ziegler, Stuart J. Heminway, and Timothy R.
Carroll

NEW AND VERSATILE TERNARY LIGAND
SYSTEM FOR TECHNETIUM RADIOPHARMA-
CEUTICALS: WATER SOLUBLE PHOSPHINES
AND TRICINE AS COLIGANDS IN LABELING A
HYDRAZINONICOTINAMIDE-MODIFIED CYCLIC
GLYCOPROTEIN IIb/IIIa RECEPTOR ANTAGO-
NIST WITH ^{99m}Tc

Page 150. The caption for Figure 6 should read as follows. Radio-HPLC chromatogram (method 3) for complex **1** and [$^{99m}\text{Tc}(\text{HYNICtide})(\text{TPPTS})(\text{glycine})_2$]. The caption for Figure 7 should read as follows. Radio-HPLC chromatogram (method 4) for complexes **1** and **2**.

BC980199T

S1043-1802(98)00199-2

Published on Web 08/27/1998

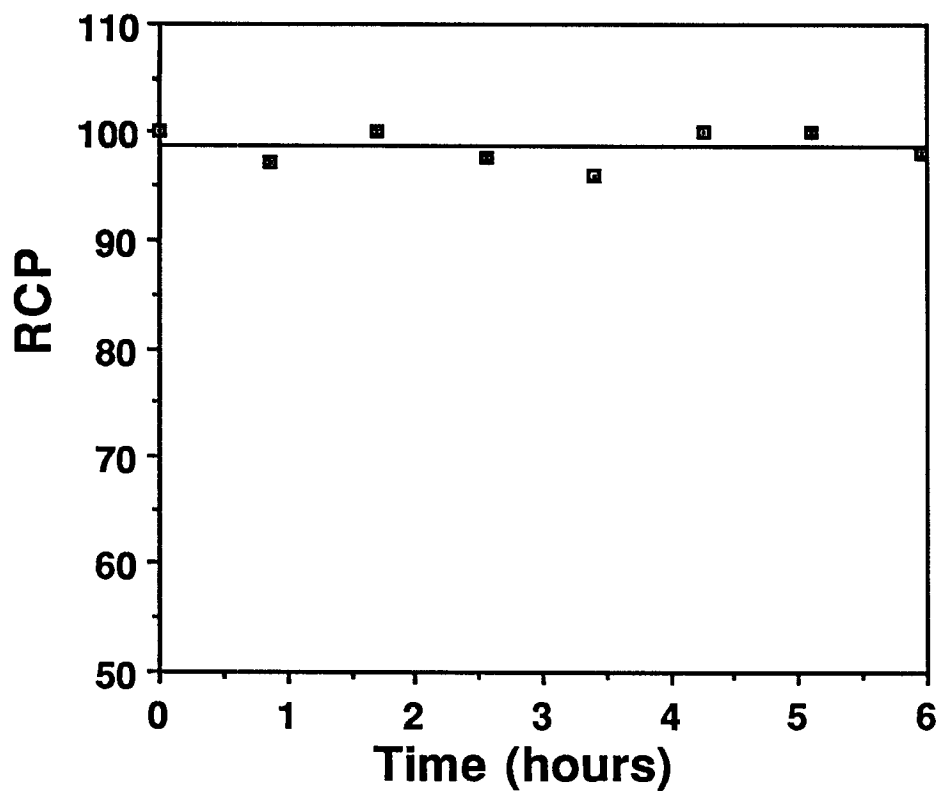


Figure SI. RCP versus time for complex **1** in solution with 10-fold dilution.

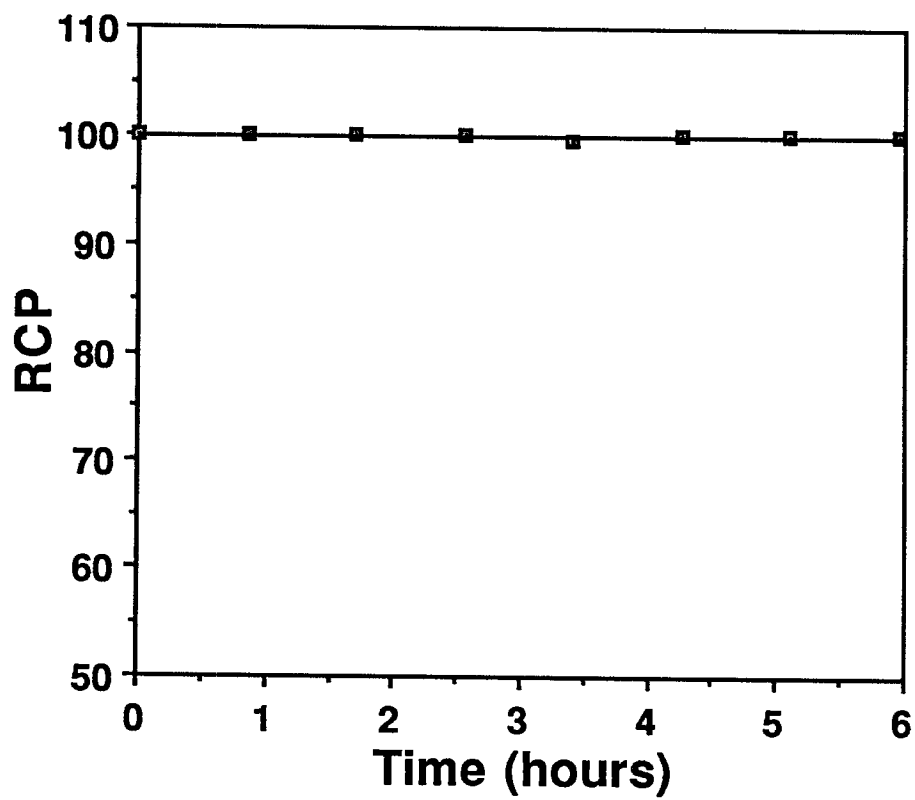


Figure SII. RCP1 versus time for complex **1** in solution with 100-fold dilution.

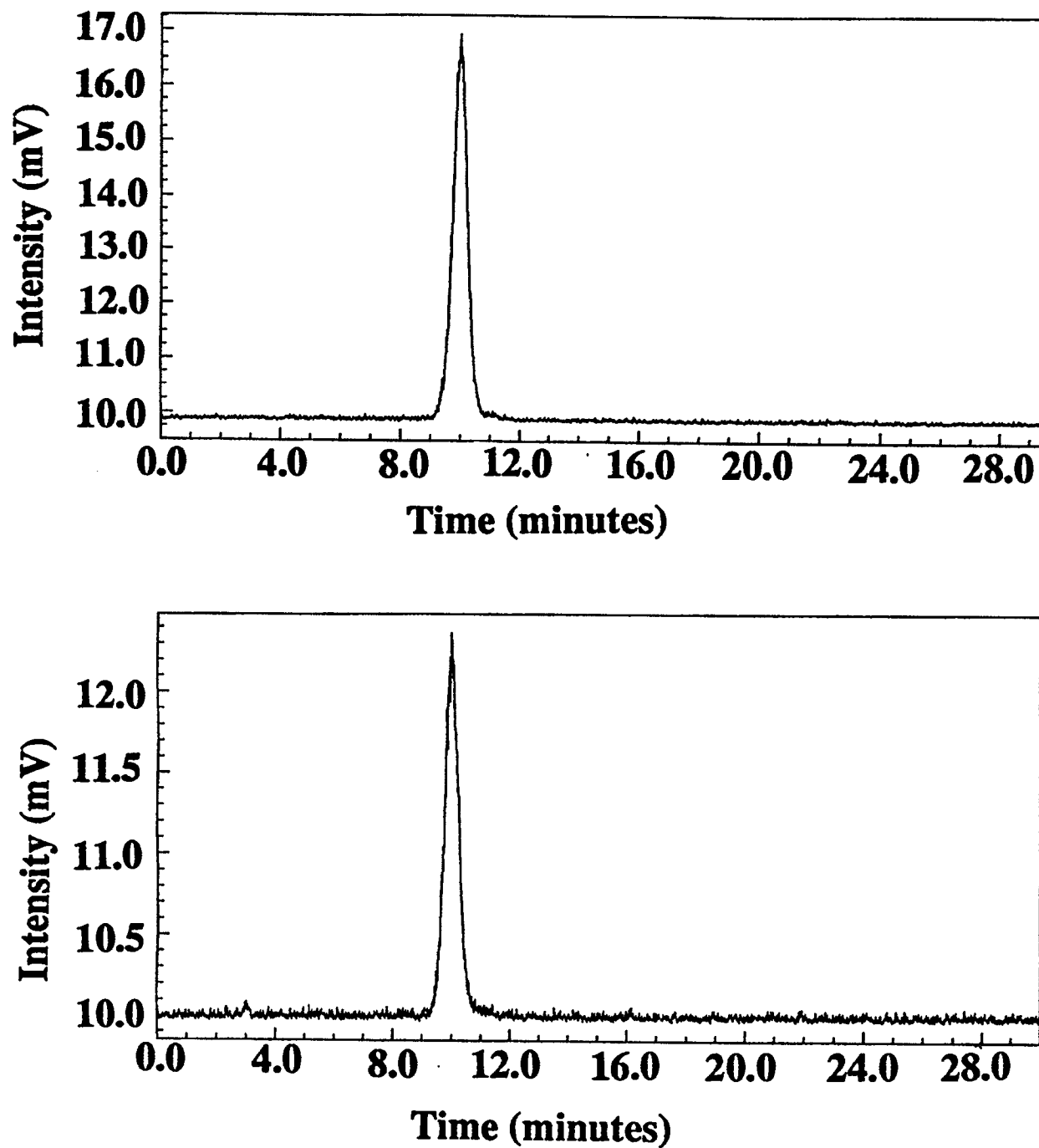


Figure SIII. Radio-HPLC chromatogram (method 4) for the peak 1 ($R_t = 10$ min) at 30 min (top) and 6 h (bottom).

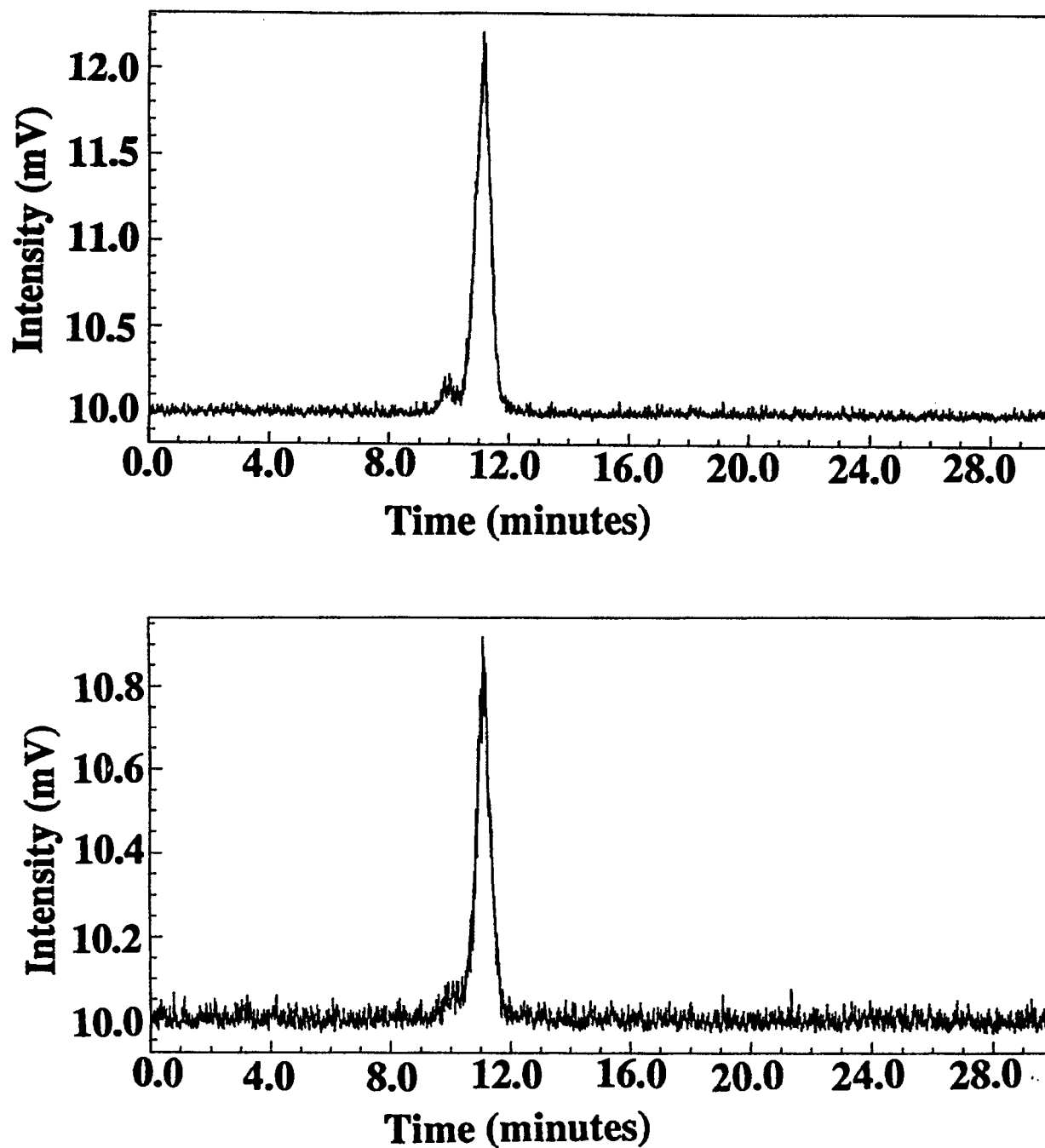


Figure SIV. Radio-HPLC chromatogram (method 4) for the peak 2 ($R_t = 11$ min) at 30 min (top) and 6 h (bottom).

Biological Evaluation of Thrombus Imaging Agents Utilizing Water Soluble Phosphines and Tricine as Coligands When Used To Label a Hydrazinonicotinamide-Modified Cyclic Glycoprotein IIb/IIIa Receptor Antagonist with ^{99m}Tc

John A. Barrett,* Andrew C. Crocker, David J. Damphousse, Stuart J. Heminway, Shuang Liu,*
D. Scott Edwards, Joel L. Lazewatsky, Mikhail Kagan, Theresa J. Mazaika, and Timothy R. Carroll

The DuPont Merck Pharmaceutical Company, Radiopharmaceuticals Division, 331 Treble Cove Road,
North Billerica, Massachusetts 01862. Received October 28, 1996[®]

A hydrazinonicotinamide-functionalized cyclic glycoprotein IIb/IIIa (GPIIb/IIIa) receptor antagonist [cyclo(D-Val-NMeArg-Gly-Asp-Mamb(5-(6-(6-hydrazinonicotinamido)hexanamide))) (HYNICTide)] was labeled with ^{99m}Tc using tricine and a water soluble phosphine [trisodium triphenylphosphine-3,3',3''-trisulfonate (TPPTS); disodium triphenylphosphine-3,3'-disulfonate (TPPDS); or sodium triphenylphosphine-3-monosulfonate (TPPMS)] as coligands. Three complexes, [^{99m}Tc (HYNICTide)(L)(tricine)] (**1**, **L** = TPPTS; **2**, **L** = TPPDS; **3**, **L** = TPPMS), were evaluated in the canine arteriovenous shunt (AV shunt) model and canine deep vein thrombosis imaging (DVT) model. All three agents were adequately incorporated into the arterial and venous portions of the growing thrombus (7.8–9.9 and 0.2–3.7% ID/g, respectively) in the canine AV shunt model. In the canine DVT model all three complexes had thrombus uptake that far exceeded the negative control, [^{99m}Tc]albumin. The findings indicate similar incorporation into a venous thrombus (% ID/g = 2.86 ± 0.4 , 3.4 ± 0.9 , and 3.38 ± 1.1 for complexes **1**, **2**, and **3**, respectively) and similar blood clearance with a $t_{1/2}$ of approximately 90 min. Gamma camera scintigraphy allowed visualization of deep vein thrombosis in as little as 15 min with the thrombus/muscle ratios being 3.8 ± 0.8 , 2.8 ± 0.4 , and 3.0 ± 0.8 for complexes **1**, **2**, and **3**, respectively. The visualization of the thrombus improved over time, and the thrombus/muscle ratios were 9.7 ± 1.9 , 13.8 ± 3.6 , and 9.4 ± 2 for complexes **1**, **2**, and **3**, respectively, at 120 min postinjection. The administration of complexes **1–3** did not alter platelet function, hemodynamics, or the coagulation cascade. Furthermore, complexes **1–3** did not significantly differ in their uptake into the growing thrombus, blood clearance, and target to background ratios. Therefore, all three complexes have the capability to detect rapidly growing venous and arterial thrombi.

INTRODUCTION

Our thrombus research program has focused on development of a thrombus imaging agent by labeling a platelet glycoprotein IIb/IIIa (GPIIb/IIIa) receptor antagonist with ^{99m}Tc (*1–7*). In our previous paper (*1*), we described the ^{99m}Tc -labeling of a platelet GPIIb/IIIa receptor antagonist [[cyclo(D-Val-NMeArg-Gly-Asp-Mamb(5-(6-(6-hydrazinonicotinamido)hexanamide))) (HYNICTide)] using tricine and water soluble phosphines [trisodium triphenylphosphine-3,3',3''-trisulfonate (TPPTS); disodium triphenylphosphine-3,3'-disulfonate (TPPDS); sodium triphenylphosphine-3-monosulfonate (TPPMS)] as coligands. The combination of HYNICTide with tricine and phosphine produces a new and versatile ternary ligand system, which forms technetium complexes, [^{99m}Tc (HYNICTide)(L)(tricine)] (Figure 1, **1**, **L** = TPPTS; **2**, **L** = TPPDS; **3**, **L** = TPPMS), in high yield and high specific activity ($\geq 20\,000$ Ci/mmol). It was found that these complexes are formed as equal mixtures of two isomeric forms and are stable for ≥ 6 h in both the reaction mixture and dilute solutions. As a continuation of that study, we now present the biological evaluation of complexes **1–3** in the canine arteriovenous (AV) shunt and deep vein thrombosis (DVT) models.

Deep vein thrombus is the result of a hypercoagulable state coupled with a period of stasis occurring in a low-shear environment. The end result is the formation of a fibrin-rich thrombus which also contains some platelets and erythrocytes. In contrast, an arterial thrombus is the result of the rupture of an atherosclerotic plaque occurring under high-shear conditions, resulting in the formation of a platelet-rich thrombus (*8*). The GPIIb/IIIa complex is expressed on the membrane surface of activated platelets and plays an integral role in platelet aggregation and thrombus formation (*9*). Initial events in thrombus formation frequently entail the activation of platelets by thrombogenic conditions and their subsequent aggregation (*10*). Since the GPIIb/IIIa complex is expressed only on the membrane surface of activated platelets, the GPIIb/IIIa receptor makes an excellent target for the development of a thrombus imaging agent. Existing diagnostic modalities are inadequate to diagnose and determine the morphology of the evolving thrombus (*11*). Thus, the development of agents that will not only detect the location but, in addition, determine the age of the thrombi is a critical unmet need in nuclear diagnostic medicine.

EXPERIMENTAL PROCEDURES

Materials. TPPTS was purchased from Aldrich Chemical Co. TPPDS was prepared and purified according to the procedure described in the literature (*6*). TPPMS was purchased from TCI America, Portland, OR, and was used as received. $\text{Na}^{99m}\text{TcO}_4$ was obtained from a com-

* Authors to whom correspondence should be addressed [telephone (508) 671-8696 (S.L.) or (508) 671-8341 (J.A.B.); fax (508) 436-7500].

[®] Abstract published in *Advance ACS Abstracts*, February 15, 1997.

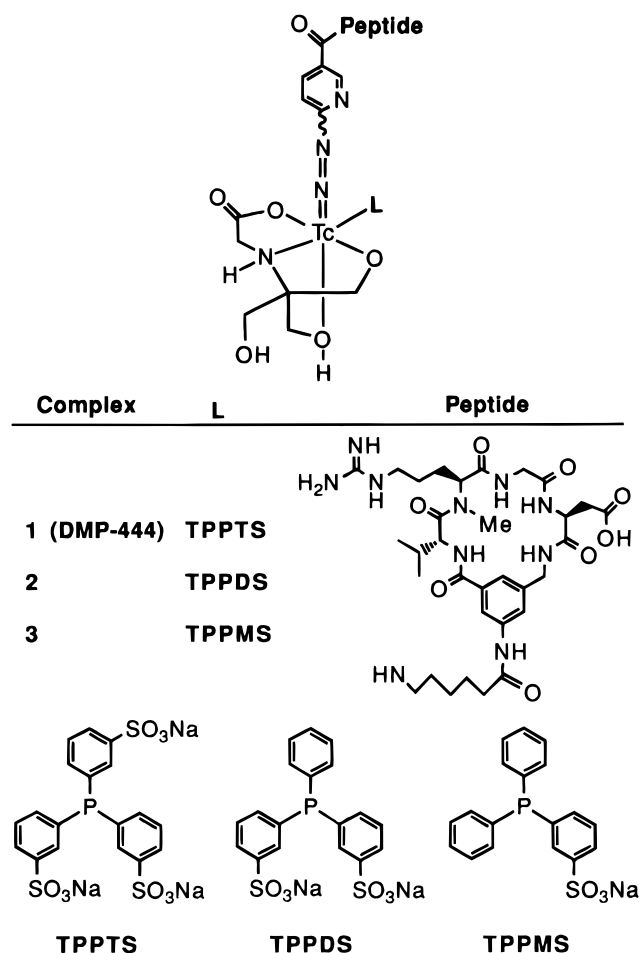


Figure 1. HYNICTide complexes and three water soluble phosphine coligands.

mercial DuPont Merck $^{99}\text{Mo}/^{99\text{m}}\text{Tc}$ generator, N. Billerica, MA. $^{99\text{m}}\text{Tc}$ [albumin, canine ^{125}I]fibrinogen, and ^{111}In -oxine kits were purchased from Medi-Physics Inc., Arlington Heights, IL, and were used as directed. Deionized water was obtained from a Millipore MilliQ Water System and was of $>18\text{ M}\Omega$ quality.

Methods. The radio-HPLC method used a Hewlett-Packard Model 1050 instrument, a reversed phase Vydac C_{18} column ($4.6\text{ mm} \times 250\text{ mm}$, 300 \AA pore size) at a flow rate of 1 mL/min with the mobile phase starting from 100% A (0.01 M phosphate buffer, pH 6) to 30% B (acetonitrile) at 15 min and 75% B at 25 min . The ITLC method used Gelman Sciences silica gel strips and a $1:1$ mixture of acetone and saline as eluant.

The $^{99\text{m}}\text{Tc}$ labeling of the cyclic GPIIb/IIIa HYNICTide was achieved following the previously described procedure (1) with some modification. To a clean 10 mL vial were added 0.5 mL of tricine solution (80 mg/mL in H_2O , pH 5), the HYNICTide solution ($50\text{ }\mu\text{g/mL}$ in H_2O ; 0.1 mL for DVT model and 0.2 mL for AV shunt model), 0.2 mL of phosphine coligand solution (5 mg/mL in H_2O), 19 mCi of pertechnetate in 0.5 mL of saline, and $25\text{ }\mu\text{L}$ of $\text{SnCl}_2 \cdot 2\text{H}_2\text{O}$ solution (1 mg/mL in 0.1 N HCl). The pH was adjusted to $4-5$. The reaction mixture was heated in a water bath at $80\text{ }^\circ\text{C}$ for 30 min and was then analyzed by radio-HPLC and ITLC. The radiochemical purity (RCP) for complexes **1-3** was $\geq 90\%$ with no detectable $^{99\text{m}}\text{Tc}$ colloid. Doses for biological evaluation were prepared by dilution with 2.0% tricine solution in saline to the required concentration: 0.3 mCi/mL for the AV shunt model and 1.5 mCi/mL for the DVT. The diluted solutions were reanalyzed by radio-HPLC before the animal study.

Canine Arteriovenous Shunt Methodology. Adult beagle dogs of either sex ($9-13\text{ kg}$) were anesthetized with pentobarbital sodium (35 mg/kg iv) and ventilated with room air via an endotracheal tube (12 strokes/min , 25 mL/kg). For arterial pressure determination, the left carotid artery was cannulated with a saline-filled polyethylene catheter (PE-240) and connected to a Statham pressure transducer (Model P23ID, Gould Co., Oxnard, CA). Mean arterial blood pressure was determined via damping the pulsatile pressure signal. Heart rate was monitored using a cardiometer (Grass Instrument Inc., Quincy, MA) triggered from a lead II electrocardiogram generated by limb leads. A jugular vein was cannulated (PE-240) for drug administration. Both femoral arteries and femoral veins were cannulated with silicon-treated (Sigmacote, Sigma Chemical Co., St. Louis, MO), saline-filled polyethylene tubing (PE-200) and connected with a 5 cm section of silicon-treated tubing (PE-240) to form extra corporeal arteriovenous (AV) shunts. Shunt patency was monitored using a Doppler flow system (Model VF-1, Crystal Biotech Inc., Hopkinton, MA) and flow probe ($2-3.5\text{ mm}$, Crystal Biotech) placed proximal to the locus of the shunt. All parameters were monitored continuously on a Model 7D polygraph recorder (Grass Instrument Inc., Quincy, MA) at a paper speed of 10 mm/min or 10 mm/s .

On completion of a 15 min postsurgical stabilization period, an occlusive thrombus was formed by the introduction of a thrombogenic surface ($4-0$ braided silk thread, 5 cm in length, Ethicon Inc., Somerville, NJ) into one shunt with the other serving as a control. A 1 h shunt period was employed with the test agent ($\sim 3.0\text{ mCi}$ in 10 mL) administered as an infusion over 5 min , beginning 5 min before insertion of the first thrombogenic surface. The thrombus formed was comprised of a platelet-rich component on the thrombogenic surface and a fibrin-rich tail. At the end of the 1 h shunt period, the silk was carefully removed, the portions separated and weighed. The percent incorporation was determined via well counting (LKB Model 1282, Wallac Inc., Gaithersburg, MD). Thrombus weight was calculated by subtracting the weight of the silk prior to placement from the total weight of the silk on removal from the shunt. Arterial blood was withdrawn prior to infusion and every 30 min thereafter for determination of blood clearance, whole blood collagen-induced platelet aggregation, prothrombin time (PT), activated partial thromboplastin time (APTT), and platelet count. Template bleeding time was also performed prior to infusion and every 30 min thereafter.

^{111}In Platelets Preparation. The isolation and ^{111}In -labeling of platelets were performed according to the literature method (12) with some modification. Canine arterial blood (40 mL) was withdrawn in 2.5% ACD solution (2.5 g of trisodium citrate, 1.4 g of citric acid, and 2.0 g of dextrose in 100 mL of H_2O , pH 4.5). An additional 20 mL of blood was drawn in 3.8% sodium citrate solution, which serves as control. The samples were centrifuged at 1400 rpm for 15 min to form platelet-rich plasma (PRP) and platelet-poor plasma (PPP). The ACD-PRP was pelleted (2800 rpm for 15 min) and washed twice with ACD. The platelet pellet was resuspended in ACD (2 mL), and $60-100\text{ }\mu\text{Ci}$ of ^{111}In -oxine was added. The suspension was incubated at $37\text{ }^\circ\text{C}$ for 5 min , followed by the addition of PPP (5 mL). The suspension was centrifuged at 2800 rpm for 10 min . The supernatant and platelet pellet were counted to assess labeling efficiency ($>80\%$ in all cases). The platelet pellet was resuspended in PPP (5 mL) and platelet viability determined by comparing collagen-induced platelet ag-

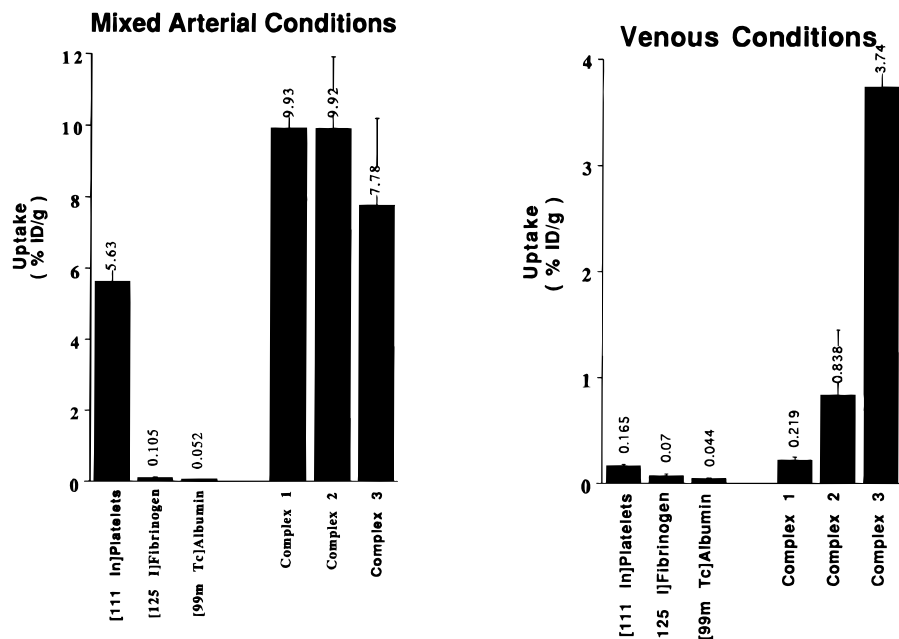


Figure 2. Thrombus uptakes for [¹²⁵I]fibrinogen, [¹¹¹In]platelets, [^{99m}Tc]albumin, and complexes 1–3 under both venous and arterial conditions in the canine AV shunt model. All values are expressed as the mean \pm SEM; $N = 10$ for [¹¹¹In]platelets and [¹²⁵I]fibrinogen (except for venous conditions, where $N = 5$), $N = 4$ for albumin, $N = 6$ for complex 1, $N = 3$ for complex 2, and $N = 2$ for complex 3.

gregation using nonlabeled and ¹¹¹In-labeled platelets. Only those [¹¹¹In]platelet preparations that were within 25% of control were injected into the animal.

Canine Deep Vein Thrombosis Methodology. This model incorporates the triad of events (hypercoagulable state, period of stasis, low-shear environment) essential for the formation of a venous fibrin-rich actively growing thrombus. Adult beagle dogs of either sex (9–13 kg) were anesthetized with pentobarbital sodium (35 mg/kg iv) and ventilated with room air via an endotracheal tube (12 strokes/min, 25 mL/kg). For arterial pressure determination, the right femoral artery was cannulated with a saline-filled polyethylene catheter connected to a pressure transducer (Model P231D, Gould Co.). Heart rate was monitored using a cardiometer (Grass Instrument Inc.) triggered from a lead II electrocardiogram generated by limb leads. The right femoral vein was cannulated for drug administration. For the induction of a venous thrombus, a 5 cm segment of both jugular veins was isolated and circumscribed with silk suture. A balloon catheter (3–4 F, Baxter Co., McGraw Park, IL) was advanced from the facial vein into the jugular vein. A microthermister probe (Physitemp Co., Clifton, NJ) was placed on the vessel, which serves as an indirect measure of venous flow. A period of stasis and hypercoagulability was induced by inflating the balloon and the local administration of 5 units of thrombin (American Diagnostica, Greenwich, CT) into the occluded segment. Fifteen minutes later, the balloon was deflated and flow reestablished as verified by the microthermister probe.

The test agent was administered over 5 min beginning at reflux. Serial images were acquired using a gamma camera (Digital Dyna Camera, Picker International, Cleveland, OH) every 5 min for 2 h and region of interest and target to background ratios calculated. Arterial blood was withdrawn prior to administration and every 30 min thereafter for determination of blood clearance, hematology, platelet function, and coagulation status. At the end of the protocol the animal was euthanized with an overdose of pentobarbital and the vessel excised. The thrombus was removed and weighed, and the amount of

incorporation was determined via a gamma well counter (LKB 1282, Wallac Inc., Gaithersburg, MD).

Hematologic Studies. Platelet, WBC, and RBC counts and hematocrit determinations were performed on whole blood collected in 2 mg/mL disodium EDTA using a Sysmex K1000 (TEA Medical Electronics Co., Los Alamitos, CA). Template bleeding time was assessed via an incision in the lower lip (Surgicutt, Baxter Co.) and the time to formation of a clot monitored. Whole blood platelet aggregation was measured using a lumiaggregometer (Chrono-Log Co., Havertown, PA) by recording the change in impedance (platelet aggregation). Blood samples were collected in 10 mM sodium citrate and diluted 50% with saline supplemented with 0.5 mM Ca. Aggregation was induced with collagen (5 μ g/mL, Chrono-Log Co.), and the changes in impedance were recorded over 6 min. APTT and PT were monitored using a microsample coagulation analyzer (MCA-210, BIO/DATA Co., Horsham, PA).

Data Analysis. All values are expressed as the mean \pm SEM. In the DVT studies the target (thrombus) uptake was calculated by drawing a 4 \times 4 pixel area in the region of interest and determining the average intensity. Background values were determined in a similar manner. Blood background was calculated using the jugular vein just distal to the locus of the thrombus. Statistical analysis consisted of a one-way analysis of variance and, when appropriate, Student's paired *t*-test, two-tailed probability for assessing differences within treatment and a Newman-Keuls test for assessing differences between means of treatment groups. Differences were considered significant at $P \leq 0.05$.

RESULTS AND DISCUSSION

In this study, we used a canine AV shunt model and a canine DVT imaging model to evaluate three platelet GPIIb/IIIa antagonists, [^{99m}Tc(HYNICtide)(L)(tricine)] (1, L = TPPTS; 2, L = TPPDS; 3, L = TPPMS), for their potential use in the detection of rapidly growing arterial and venous thrombi. The thrombus formed in the AV shunt model was comprised of a platelet-rich head

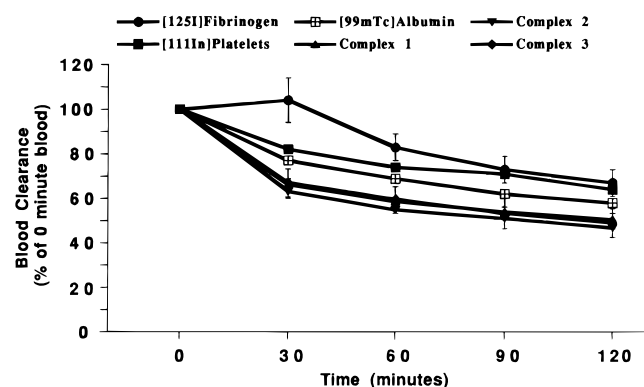


Figure 3. Blood clearance of $[^{125}\text{I}]$ fibrinogen, $[^{111}\text{In}]$ platelets, $[^{99\text{m}}\text{Tc}]$ albumin, and complexes 1–3, expressed as a percentage of the end of infusion value in the canine AV shunt model. All values are expressed as the mean \pm SEM; $N = 10$ for $[^{111}\text{In}]$ platelets and $[^{125}\text{I}]$ fibrinogen (except for venous conditions, where $N = 5$), $N = 4$ for $[^{99\text{m}}\text{Tc}]$ albumin, $N = 6$ for complex 1, $N = 3$ for complex 2, and $N = 2$ for complex 3.

(arterial conditions) and a fibrin-rich tail (venous conditions), which allowed the rapid assessment of an agent under both arterial and venous conditions. To validate this model, the amount of incorporation of $[^{111}\text{In}]$ platelets (58 μCi), $[^{125}\text{I}]$ fibrinogen (106 μCi), and $[^{99\text{m}}\text{Tc}]$ albumin (153 μCi) was assessed via well counting. $[^{111}\text{In}]$ platelets and $[^{125}\text{I}]$ fibrinogen were adequately incorporated into the growing thrombus with $[^{111}\text{In}]$ platelets favoring the platelet-rich head ($5.63 \pm 0.6\%$ ID/g) with lesser amounts of incorporation observed in the fibrin-rich tail ($0.17 \pm 0.02\%$ ID/g). Similar amounts of $[^{125}\text{I}]$ fibrinogen were incorporated under both the arterial and venous conditions (0.11 ± 0.02 vs $0.07 \pm 0.02\%$ ID/g, respectively), while little incorporation was observed with $[^{99\text{m}}\text{Tc}]$ albumin (arterial, $0.05 \pm 0.01\%$ ID/g; venous, $0.04 \pm 0.001\%$ ID/g) (Figure 2). The administration of $[^{111}\text{In}]$ platelets, $[^{125}\text{I}]$ fibrinogen, and $[^{99\text{m}}\text{Tc}]$ albumin did not alter any of the parameters studied (Table 1). Thus, the deposition on the thrombogenic surface mimics that of arterial conditions, i.e. high-shear, platelet-rich thrombus, and the platelet-poor tail mimics that of a venous thrombus, i.e. platelet-poor, low-shear environment.

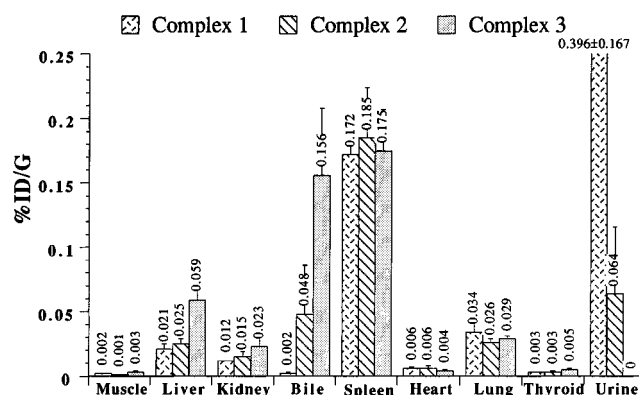


Figure 4. Biodistribution of complexes 1–3. All values are expressed as the mean \pm SEM; $N = 6$ for complex 1, $N = 3$ for complex 2, and $N = 2$ for complex 3.

Complexes 1–3 were assessed in the canine AV shunt model, and all show incorporation into a growing thrombus in both the platelet-rich arterial portion and the venous platelet-poor tail (Figure 2). The greatest uptake of complexes 1–3 was observed under arterial conditions, which reflects the platelet-rich environment. Similar uptakes between complexes 1, 2, and 3 were seen under arterial conditions (arterial range, 7.78–9.93% ID/g), and all have significantly greater uptake than $[^{125}\text{I}]$ fibrinogen and $[^{99\text{m}}\text{Tc}]$ albumin. Complex 1 also exhibited significantly greater uptake under arterial conditions than $[^{111}\text{In}]$ platelets ($P \leq 0.05$). Venous conditions, as expected, demonstrated less uptake in the platelet-poor tail, with all three complexes having greater uptake than $[^{125}\text{I}]$ fibrinogen and $[^{99\text{m}}\text{Tc}]$ albumin ($P \leq 0.05$). Complex 3 appeared to have greater uptake; however, this apparent difference was not statistically significant due to interanimal variability. The uptake of complex 3 ranged from 1.2 to 6.2% ID/g. Complexes 1–3 share similar blood clearance with a half-life of about 90 min (Figure 3). The biodistribution data demonstrated that complexes 1 and 2 are preferentially renally excreted, while complex 3 was preferentially excreted via the hepatobiliary route (Figure 4). $[^{99\text{m}}\text{Tc}]$ albumin was renally cleared, while $[^{125}\text{I}]$ fibrinogen demonstrated a mixed hepatobil-

Table 1. Summary of the Hematological and Hemodynamic Effects of $[^{99\text{m}}\text{Tc}]$ Albumin and Complexes 1–3 at 1 mCi/kg iv in the Canine DVT Model and $[^{111}\text{In}]$ Platelets/ $[^{125}\text{I}]$ Fibrinogen at 150 $\mu\text{Ci/kg}$ iv in the Canine AV Shunt Model

treatment	parameter ^a				
	heart rate (bpm)	mean arterial pressure (mmHg)	APTT (s)	platelet count ($\times 10^3$)	aggregation (ohms)
$[^{111}\text{In}]$ platelets/ $[^{125}\text{I}]$ fibrinogen					
control	135 \pm 5	113 \pm 8	17 \pm 1	272 \pm 17	27 \pm 3
EOI	128 \pm 5	113 \pm 7	21 \pm 2	264 \pm 17	29 \pm 2
1 h postinfusion	124 \pm 5	112 \pm 7	17 \pm 1	264 \pm 19	29 \pm 2
$[^{99\text{m}}\text{Tc}]$ albumin					
control	150 \pm 6	124 \pm 8	15 \pm 0	281 \pm 8	24 \pm 1
EOI	150 \pm 5	124 \pm 8	15 \pm 1	289 \pm 11	27 \pm 3
1 h postinfusion	147 \pm 7	124 \pm 10	15 \pm 1	284 \pm 17	23 \pm 2
complex 1					
control	139 \pm 5	118 \pm 7	16 \pm 1	278 \pm 12	21 \pm 2
EOI	139 \pm 4	111 \pm 6	16 \pm 2	291 \pm 9	22 \pm 1
1 h postinfusion	138 \pm 6	109 \pm 1	15 \pm 3	287 \pm 4	23 \pm 2
complex 2					
control	121 \pm 8	88 \pm 15	16 \pm 1	267 \pm 20	22 \pm 2
EOI	109 \pm 1	78 \pm 13	14 \pm 1	225 \pm 13	20 \pm 4
1 h postinfusion	113 \pm 6	84 \pm 10	14 \pm 1	264 \pm 21	26 \pm 1
complex 3					
control	164 \pm 7	94 \pm 8	16 \pm 1	281 \pm 37	22 \pm 3
EOI	163 \pm 7	97 \pm 11	16 \pm 1	279 \pm 37	19 \pm 2
1 h postinfusion	166 \pm 11	103 \pm 8	15 \pm 1	281 \pm 45	22 \pm 3

^a All values are expressed as the mean \pm SEM; $N = 10$ for $[^{111}\text{In}]$ platelets and $[^{125}\text{I}]$ fibrinogen, $N = 4$ for $[^{99\text{m}}\text{Tc}]$ albumin and complex 1, $N = 3$ for complex 2, and $N = 2$ for complex 3.

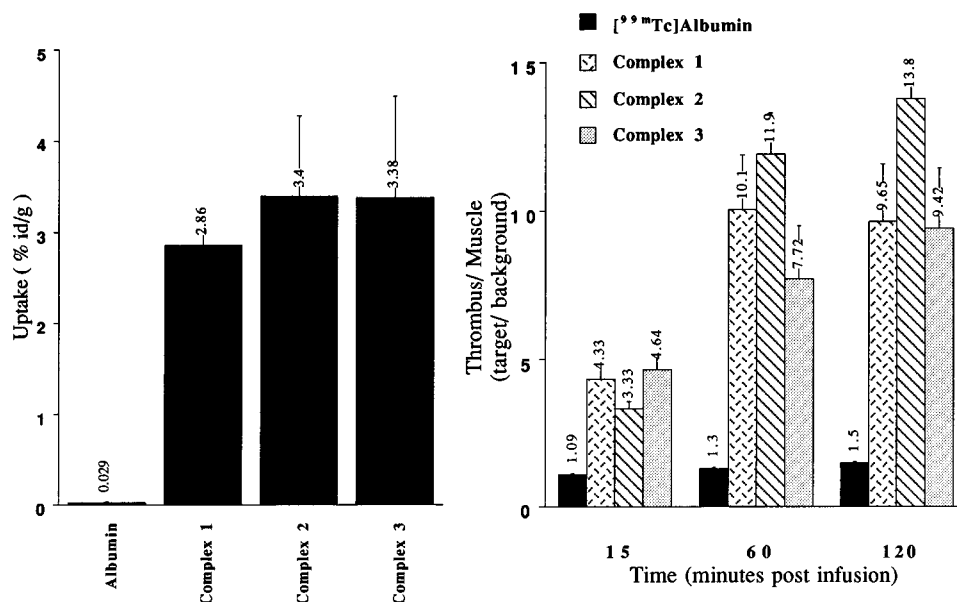


Figure 5. Canine DVT thrombus uptake at 120 min (left) and thrombus/blood ratio (right) for [¹²⁵I]fibrinogen, [¹¹¹In]platelets, [^{99m}Tc]albumin, and complexes 1–3 under both venous and arterial conditions. The thrombus uptake and target/background ratios for all three complexes were significantly greater ($P < 0.05$) than for [^{99m}Tc]albumin. There were no significant differences between complexes 1, 2, and 3 ($P < 0.5$). Target to background ratios were calculated on the basis of an average 4×4 pixel area in the region of interest. All values are expressed as the mean \pm SEM; $N = 6$ for [^{99m}Tc]albumin, $N = 5$ for complex 1, $N = 4$ for complex 2, and $N = 4$ for complex 3.

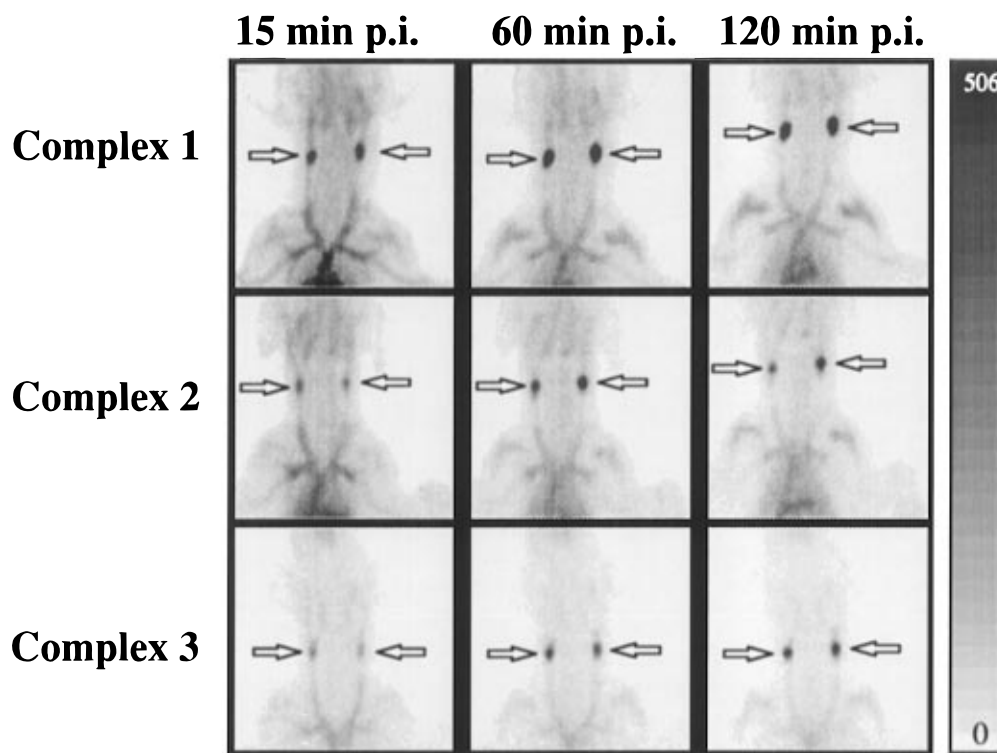


Figure 6. Representative DVT images of complexes 1–3 at 15, 60, and 120 min postinfusion. The bar to the right of the images indicates the scale from 0 (white) to 506 (greatest/black). The images have not been filtered. Arrows indicate presence of thrombus in jugular veins.

lary/renal excretion pattern. In contrast, [¹¹¹In]platelets were sequestered in the spleen.

Complexes 1–3 and [^{99m}Tc]albumin have been evaluated in the canine deep vein thrombosis imaging model (DVT). The sample data from the LKB gamma well counter show no significant difference between the three complexes in respect to % ID/g, although all three are significantly greater than [^{99m}Tc]albumin ($P \leq 0.05$, Figure 5). All three complexes demonstrated similar rates of clearance from the circulating blood.

Representative unfiltered images of the three complexes in the DVT imaging model at 15, 60, and 120 min postinfusion are shown in Figure 6. The scale to the right of the images represents a fixed scale that increases to the hottest or most dense pixel represented by 506 (black). The region of interest (ROI) data acquired from the images are shown in Figure 6 as target to background ratios. Complexes 1, 2, and 3 were rapidly incorporated into the growing thrombus, which can be easily visualized by 15 min with the thrombus/muscle ratios of 3.8 ± 0.8 ,

2.8 ± 0.4 , and 3.0 ± 0.8 , respectively. Increased uptake over time was also observed with exceptional imaging at 60 min. All three complexes are significantly greater than [^{99m}Tc]albumin with respect to ROI data ($P \leq 0.05$). Hematologic and hemodynamic data were unaffected by the administration of the complexes and remained in normal range throughout the DVT study (Table 1). The present study is in agreement with the work of Oster et al. (14), who demonstrated that the 7E3 antibody, directed against the platelet GPIIb/IIIa receptor, was capable of detecting both arterial and venous thrombi. More recently, a series of disintegrins derived from snake venom demonstrated limited utility in detecting venous thrombi (15). In addition, a ^{99m}Tc -labeled peptide (P280) that targets the platelet GPIIb/IIIa site has been shown to detect growing venous thrombi in man (16). Thus, on the basis of these data the targeting of the platelet GPIIb/IIIa receptor is a viable approach for detecting thromboembolic events throughout the body.

In summary, complexes 1–3 show remarkably similar incorporation into a growing thrombus and blood clearance with a $t_{1/2}$ of 90 min. None of the compounds affected hemodynamics or hematological values, which was consistent with the subtherapeutic levels administered. In addition, complexes 1–3 exhibit similar abilities to detect a growing thrombus within 15 min postinjection. Further, complexes 1–3 did not significantly differ in their uptake into the growing thrombus, blood clearance, and target to background ratio. Therefore, it is concluded that all three agents are able to detect rapidly growing venous and arterial thrombi.

ACKNOWLEDGMENT

Acknowledgment is made to P. R. Damphousse for the synthesis of TPPDS and to Dr. T. D. Harris, Dr. M. Rajopadhye, Dr. D. Glowacka, J. P. Bourque, P. R. Damphousse, and K. Yu for the synthesis of the cyclic GPIIb/IIIa HYNICTide, cyclo[d-Val-NMeArg-Gly-Asp-Mamb(5-(6-(6-hydrazinonicotinamido)hexanamide))].

LITERATURE CITED

- Edwards, D. S., Liu, S., Barrett, J. A., Harris, A. R., Looby, R. J., Ziegler, M. C., Heminway, S. J., and Carroll, T. R. (1997) A new and versatile ternary ligand system for technetium radiopharmaceuticals: water soluble phosphines and tricine as coligands in labeling a hydrazino nicotinamide-modified cyclic glycoprotein IIb/IIIa receptor antagonist with ^{99m}Tc . *Bioconjugate Chem.* 8, 146–154.
- Barrett, J. A., Heminway, S. J., Damphousse, D. J., Thomas, J. R., Looby, R. J., Edwards, D. S., Harris, T. D., Rajopadhye, M., Liu, S., and Carroll, T. R. (1994) Platelet GP IIb/IIIa antagonists in the canine arteriovenous shunt: potential thrombus imaging agents. *J. Nucl. Med.* 35, 52P (Abstract 202).
- Harris, T. D., Rajopadhye, M., Damphousse, P. R., Glowacka, D., Yu, K., Bourque, J., Barrett, J. A., Damphousse, D. J., Heminway, S. J., Lazewatsky, J., Mazaika, T., and Carroll, T. R. (1996) Tc-99m-labeled fibrinogen receptor antagonists: Design and synthesis of cyclic RGD peptides for the detection of thrombi. *Bioorg. Med. Chem. Lett.* 6, 1741–1746.
- Barrett, J. A., Bresnick, M., Crocker, A., Damphousse, D. J., Hampson, J. R., Heminway, S. J., Mazaika, T. J., Kagan, M., Lazewatsky, J., Edwards, D. S., Liu, S., Harris, T. D., Rajopadhye, M., and Carroll, T. R. (1995) RP-431: a potential thrombus imaging agent. *J. Nucl. Med.* 36, 16P (Abstract 55).
- Liu, S., Edwards, D. S., Looby, R. J., Harris, A. R., Poirier, M. J., Barrett, J. A., and Heminway, S. J. (1996) Labeling a hydrazino nicotinamide-modified cyclic IIb/IIIa receptor antagonist with ^{99m}Tc using aminocarboxylates as coligands. *Bioconjugate Chem.* 7, 63–71.
- Liu, S., Edwards, D. S., Looby, R. J., Harris, A. R., Poirier, M. J., Rajopadhye, M., and Bourque, J. P. (1996) Labeling cyclic IIb/IIIa receptor antagonists with ^{99m}Tc by the preformed chelate approach. *Bioconjugate Chem.* 7, 196–202.
- Barrett, J. A., Damphousse, D. J., Heminway, S. J., Liu, S., Edwards, D. S., Looby, R. J., and Carroll, T. R. (1996) Biological evaluation of ^{99m}Tc -labeled cyclic GPIIb/IIIa receptor antagonists in the canine arteriovenous shunt and deep vein thrombosis models: effects of chelators on biological properties of ^{99m}Tc -chelator-peptide conjugates. *Bioconjugate Chem.* 7, 203–208.
- Knight, L. C. (1990) Radiopharmaceuticals for thrombus detection. *Semin. Nucl. Med.* 20, 52–67.
- Fuster, V., Stein, B., Badimon, L., and Chesebro, J. (1988) Antithrombotic therapy after myocardial reperfusion in acute myocardial infarction. *J. Am. Col. Cardiol.* 12, 78A–84A.
- Plow, E. F., Marguerie, G., and Ginsberg, M. (1987) Fibrinogen, fibrinogen receptors and the peptides that inhibit these interactions. *Biochem. Pharmacol.* 36, 4035–4041.
- Shattil, S. J., Hoxie, J. A., Cunningham, M., and Brass, L. F. (1985) Changes in the platelet membrane glycoprotein IIb/IIIa complex during platelet activation. *J. Biol. Chem.* 260, 11107–11110.
- Thakur, M. L., Welch, M. J., Joist, J. H., and Coleman, R. E. (1976) In-111 labeled platelets: studies on preparation and evaluation of in vitro and in vivo function. *Thrombus Res.* 9, 345–357.
- Haskel, E., Adams, S., Feigen, L., Saffitz, J., Gorczynski, R., Sobel, D., and Abendschein, D. (1989) Prevention of reoccluding platelet-rich thrombi in canine femoral arteries with a novel peptide antagonist of platelet glycoprotein IIb/IIIa receptors. *Circulation* 80, 1775–1782.
- Oster, Z., Srivastava, S., Som, P., Meinken, G., Scudder, L., Yamamoto, K., Atkins, H., Brill, A., and Collier, B. (1985) Thrombus radioimmunoscintigraphy: An approach using monoclonal antiplatelet antibody. *Proc. Natl. Acad. Sci. U.S.A.* 82, 3465–3468.
- Knight, L., Maurer, A., and Romano, J. (1996) Comparison of iodine-123-disintegrins for imaging thrombi and emboli in a canine model. *J. Nucl. Med.* 37, 476–482.
- Muto, P., Lastoria, S., Varrella, P., Vergara, E., Salvatore, M., Morgano, G., Lister-James, J., Bernardy, J., Dean, R., Wencker, D., and Borer, J. (1995) Detecting deep venous thrombosis with technetium-99m-labeled synthetic peptide P280. *J. Nucl. Med.* 36, 1384–1391.

BC970001P

Synthesis of Cobalamin Dimers Using Isophthalate Cross-Linking of Corrin Ring Carboxylates and Evaluation of Their Binding to Transcobalamin II

Pradip M. Pathare,[†] D. Scott Wilbur,^{*,†} Donald K. Hamlin,[†] Shannon Heusser,[†] Edward V. Quadros,[‡] Patricia McLoughlin,[‡] and A. Charles Morgan^{†,§}

Department of Radiation Oncology, University of Washington, Seattle, Washington 98195, VA Medical Center—SUNY Health Science Center, Brooklyn, New York 11209, and Receptagen Corporation, Edmonds, Washington 98020. Received August 21, 1996[®]

Several cobalamin (Cbl) dimers have been prepared for evaluation as potential antiproliferative agents in the treatment of AIDS-related lymphoma. The Cbl dimers were synthesized by cross-linking Cbl carboxylates, produced by acid hydrolysis of the *b*-, *d*-, and *e*-propionamide side chains of cyanocobalamin (CN-Cbl), through an isophthalate molecule. Linking molecules were used between the Cbl carboxylates and the isophthalate moiety. The linkers were incorporated to provide a distance between the two Cbl molecules such that the dimeric Cbls might bind two molecules of transcobalamin II (TCII), the Cbl transport protein in plasma. Initially, the linking moiety used was 1,12-diaminododecane, but the resulting dimers had low aqueous solubility. To improve the solubility of the dimers, 4,7,10-trioxa-1,13-tridecanediamine was employed as the linking moiety. This improved the water solubility of the dimers considerably, while retaining the distance between the Cbl molecules at 41–42 Å (fully extended). To introduce additional substitution on Cbl dimers, 5-aminoisophthalic acid was used as the cross-linking reagent. *p*-Iodobenzoyl and *p*-(tri-*n*-butylstannyl)benzoyl conjugates of 5-aminoisophthalate were synthesized and used to prepare Cbl dimers. The stannylbenzoyl-conjugated Cbl dimers were prepared as precursors to be used in radioiodination reactions, and the iodobenzoyl-conjugated Cbl dimers were prepared as HPLC standards for the radioiodinated product. Attempts to iodinate/radioiodinate the stannylbenzoyl Cbl dimers were unsuccessful. Although an explanation for this is not readily apparent, the failure to react may be due to the lipophilicity of the linker used and the steric environment of the two Cbl moieties. A biotinylated derivative of 5-aminoisophthalate was also synthesized and used to prepare biotinylated-Cbl dimers. In a competitive rhTCII binding assay with [⁵⁷Co]CN-Cbl, Cbl dimers containing the lipophilic diaminododecane linking moiety had decreased binding avidities compared to those of Cbl monomers substituted at the same corrin ring carboxylate. However, Cbl dimers containing the water-solubilizing trioxadecanamine linker appeared to have avidities similar to those of the Cbl monomers.

INTRODUCTION

Cobalamins (Cbls¹) are cofactors in enzymatic pathways associated with DNA and protein synthesis in cells (1, 2). Actively dividing cells, such as hematopoietic cells in bone marrow, avidly take up Cbls. Importantly, it has been noted that Cbls play a significant metabolic role in human leukemia cells (3, 4). These facts have led us to investigate the application of Cbl depletion to the therapy of rapidly dividing and proliferating cells found in

leukemias and lymphomas. Evidence for such an antiproliferative therapeutic approach is not without precedent as previous investigations have shown that therapeutic responses could be obtained in patients when they were isolated in an atmosphere containing the anesthetic agent nitrous oxide (N₂O) (5, 6). N₂O administration causes an oxidative inactivation of Cbl, depleting cells in the body of metabolically active forms of Cbl. The use of N₂O, while effective for inactivation of Cbl, presents several problems for its general application to the therapy of leukemias or lymphomas. One major problem is that patients are required to stay in an atmosphere of N₂O for extended periods of time, which results in extended hospitalization and the need for constant patient monitoring. Additionally, serious neurological side effects have been observed in some patients undergoing this treatment. Further, the nonspecific nature of the oxidation of Cbl with N₂O can have effects on many different biological systems and may lead to a number of toxicities. Thus, an alternative approach for depletion of cellular Cbl was conceived.

We have begun to investigate a novel approach to depletion of cellular Cbl which is directed at developing a pharmaceutical capable of blocking entry of endogenous Cbls into cells. Since the entry of Cbls into cells at physiological concentrations appears to be completely dependent on a receptor-mediated process (7), we are investigating synthetic Cbl derivatives designed to in-

* Address correspondence to this author at the Department of Radiation Oncology, University of Washington, 2121 N. 35th St., Seattle, WA 98103-9103 [telephone (206) 685-3085; fax (206) 685-9630; e-mail dswilbur@u.washington.edu].

[†] University of Washington.

[‡] VA Medical Center—SUNY Health Science Center.

[§] Receptagen Corp.

[®] Abstract published in *Advance ACS Abstracts*, February 15, 1997.

¹ Abbreviations: Cbl(s), cobalamin(s); CN-Cbl, cyanocobalamin; DCC, dicyclohexylcarbodiimide; DMF, dimethylformamide; DMSO, dimethyl sulfoxide; EDC, 1-[3-(dimethylamino)propyl]-3-ethylcarbodiimide; 2HEDS, 2-hydroxyethyl sulfide; HSA, human serum albumin; LC, liquid chromatography; 3NBA, 3-nitrobenzyl alcohol; NCS, *N*-chlorosuccinimide; NHS, *N*-hydroxysuccinimide; PBS, phosphate-buffered saline; rt, room temperature; TCII, transcobalamin II; rhTCII, recombinant human transcobalamin II; TFP, tetrafluorophenyl; TFP-OH, tetrafluorophenol; TFP-OTFA, tetrafluorophenyl trifluoroacetate.

terfere with the receptor-mediated cellular uptake of endogenous Cbls. It is known that cellular uptake of Cbls is a complex and highly regulated process which involves (1) transport of Cbl in plasma via a high-affinity serum Cbl binding protein, transcobalamin II (TCII) (8); (2) cell surface binding of the Cbl/TCII complex with a glycoprotein receptor (9); (3) internalization of the Cbl/TCII/receptor complex; and (4) release of the Cbl to the cytoplasm. Importantly, it has been shown in leukemia cells (e.g. L1210 and K562 cell lines) that the Cbl/TCII cell surface receptor density, which is directly related to Cbl uptake, is up-regulated during proliferation and down-regulated during quiescence (10). Although the process of receptor-mediated uptake and delivery of Cbls to cytoplasm is not fully understood, it has been shown that the lysosomotropic agent chloroquine and the monocarboxylate proton ionophore monensin can drastically decrease the Cbl/TCII surface receptor concentration in K562 leukemia cells (10). The lack of information available on the effect of alterations in the Cbl molecule on receptor trafficking and release of Cbl to cytoplasm makes it impossible to have a rational design of Cbl derivatives. Therefore, our initial investigations have involved synthesizing a number of Cbl derivatives containing a variety of appended groups for evaluation in cellular proliferation assays. To focus our synthetic efforts somewhat, we reasoned that Cbl derivatives containing appended highly lipophilic groups (e.g. fatty acids), highly ionic groups (e.g. alkyl sulfonates), or lysosomotropic agents (e.g. polyamines) (11) might result in retention of the Cbl, and possibly the retention of TCII/cell surface receptor, in endosomes and/or lysosomes.

When considering possible Cbl derivatives for synthesis, we became intrigued by derivatives that contain two or more Cbl moieties on the same molecule. Of the many derivatives that might be prepared, it appeared that binding with more than one TCII molecule had a higher potential for altering the receptor recycling process. Following this logic, we became interested in dimeric Cbl derivatives as they presented less of a synthetic challenge than molecules with multiple Cbl moieties. Since our approach was to utilize the Cbl/TCII receptor-mediated cell internalization process, it was apparent that any synthetic Cbl derivative prepared must bind with the plasma protein TCII as effectively as endogenous Cbl. Previous studies by this group (12, 13) and several other groups (14–17) have shown that conjugation of chemical moieties on the corrin ring side chains provides a stable attachment to the Cbl moiety which, depending on the location of attachment, has a varying effect on the binding with TCII. That variability of binding has been found to range from 3 orders of magnitude decreased binding relative to cyanocobalamin (CN-Cbl), **1**, for conjugates at the *c*-acetamide side chain, to nearly equivalent binding to TCII for the *e*-propionamide side chain conjugates (12). Thus, cobalamin dimers that were linked through corrin ring attachments were targeted. As with other Cbl derivatives, we felt that the cobalamin dimers should be designed such that it was possible to append functional groups that could change the physical nature (e.g. lipophilicity and ionic nature), or add lysosomotropic properties, to the dimers, so a trifunctional cross-linking moiety was included in the design. Further, it seemed important to design the Cbl dimers in a manner that separated the Cbl moieties by a significant distance such that binding with two TCII molecules might be achieved.

Reported herein are the synthesis and preliminary binding studies of 14 Cbl dimers. The dimers prepared employ isophthalic acid or aminoisophthalic acid moi-

eties to cross-link corrin ring Cbl-carboxylates (*b*-, *d*-, or *e*-isomers). Cross-linking was accomplished by incorporating linker molecules, containing two terminal amino groups, between the Cbl carboxylates and the carboxylates of isophthalic acid. As part of the investigation, Cbl dimers containing arylstannanes were prepared such that radioiodine might be incorporated through an iododestannylation reaction (18, 19). Biotinylated Cbl dimers were also prepared in the investigation. Binding of 11 Cbl dimers with recombinant human TCII (rhTCII), relative to [⁵⁷Co]CN-Cbl, was measured in a competitive binding assay.

EXPERIMENTAL PROCEDURES

General. All chemicals purchased from commercial sources were of analytical grade or better and were used without further purification. Cyanocobalamin (CN-Cbl; vitamin B₁₂) was obtained from Sigma Chemical Co. (St. Louis, MO). *N*-Hydroxysuccinimide and isophthaloyl dichloride were purchased from Lancaster Synthesis Inc. (Windham, NH). All other reagents were obtained from Aldrich Chemical Co. (Milwaukee, WI). Solvents for HPLC analysis were obtained as HPLC grade and were filtered (0.2 μm) prior to use. Ion exchange chromatography was conducted with 200–400 mesh strongly basic anion, 2% cross-linked Dowex 1 chloride (Aldrich). Amberlite XAD-2 nonionic polymeric adsorbent and octadecyl functionalized silica gel for column chromatography were also obtained from Aldrich. Bio-Sil NH₂ (aminopropyl bonded silica) (40–63 μm) for column packing was purchased from Bio-Rad Laboratories (Hercules, CA). Phosphate-buffered saline (PBS) was prepared as a solution containing 8.1 mM Na₂PO₄, 1.2 mM KH₂PO₄, and 138 mM NaCl, pH 7.4. Human serum albumin (HSA) was obtained from Miles, Inc. (Elkhart, IN).

Molecular modeling of Cbl dimers was conducted to estimate the distance between the Cbl moieties. The modeling was conducted with ChemDraw Plus/Chem3D Pro software (CambridgeSoft Corp., Burlington, MA) on a Macintosh 8100/80 computer. Structures of the Cbl cross-linking reagents were drawn (fully extended) and minimized for structural error and energy, and interatomic distances were obtained directly from the computer program.

Spectroscopic Data. ¹H NMR spectra were obtained on either a Bruker AC-300 (300 MHz) or a Bruker AC-500 (500 MHz) instrument. The chemical shifts are expressed as parts per million using tetramethylsilane as an internal standard (δ = 0.0 ppm). IR data were obtained on a Perkin-Elmer 1420 infrared spectrophotometer. UV data were obtained on a Perkin-Elmer Lambda 2 UV–vis spectrophotometer or a Shimadzu UV 160U spectrophotometer. UV absorbances were obtained as previously described (12). Mass spectral data were obtained on a VG 70SEQ mass spectrometer with 11250J data system. Fast atom bombardment (FAB⁺) mass spectral data were obtained at 8 kV using a matrix of 3-nitrobenzyl alcohol (3NBA) or a matrix of 90% thioglycerol, 9% DMSO, and 1% TFA (DMIX). We were unable to find conditions for obtaining mass spectral data with the stannylbenzoyl-Cbl dimers **27–29**.

Identity of the Cbl derivatives was established by mass spectral and NMR data (see Supporting Information). Elemental analyses were not obtained for the Cbl dimers due to the difficulties encountered previously with monomeric Cbls (12, 13). Purity of the Cbl derivatives was established by HPLC analysis (see Supporting Information).

Analytical Chromatography. HPLC separations of compounds were obtained on a Hewlett-Packard quater-

nary 1050 gradient pumping system with a variable wavelength UV detector (360 nm). Analysis of the HPLC data was conducted on Hewlett-Packard HPLC Chemstation software. All reactions were monitored by HPLC.

Separations of the CN-Cbl, **1**, and Cbl derivatives **2–10** were conducted on an aminopropyl-silica column at a flow rate of 1 mL/min. The HPLC separations of the precursor compounds **1–7** were conducted on a 5 μ m, 4.6 mm \times 250 mm aminopropyl column (Rainin microsorb-MV amino column) eluting with 58 mM pyridine acetate, pH 4.4, in H₂O/THF (96:4) solution (9). Retention times for the Cbls evaluated with this system were as follows: **1** = 2.7 min; **2** = 3.8 min; **3** = 4.4 min; **4** = 5.1 min; **5** = 2.2 min; **6** = 2.2 min; **7** = 2.2 min; **8** = 2.3 min; and **10** = 2.3 min.

HPLC separations for benzoylaminoisophthalate **11–14** were conducted on a Hewlett-Packard LiChrospher 100 RP-18 (5 μ m; 4.6 mm \times 125 mm) C₁₈ column using a gradient solvent system. Solvent A in the gradient was MeOH. Solvent B was H₂O. Starting from 70% A, the initial solvent mixture was held for 2 min, then the gradient was increased to 100% A over the next 10 min, and 100% A was held for 5 min. The gradient was decreased in percentage of A to 70% over the next 5 min. Retention times under these conditions were as follows: **11** = 3 min (solvent front); **12** = 6.6 min; **13** = 14.8 min; and **14** = 21.9 min.

HPLC separations for aminocaproate–biotin derivatives **15–20** and for dimers **21–31** were conducted on a C₁₈ reversed phase column employing a gradient. Solvent A in the gradient was methanol. Solvent B was aqueous 1% acetic acid. The gradient was begun at 40% A and was held at that composition for 2 min, and then the percentage of A was linearly increased to 100% over the next 10 min. The gradient was held at 100% A for 20 min. Retention times under these conditions for dimers were as follows: **15** = 6.1 min; **16** = 12.9 min; **17** = 7.2 min; **18** = 12.7 min; **19** = 8.4 min; **20** = 14.8 min; **21** = 12.6 min; **22** = 12.3 min; **23** = 13.0 min; **24** = 13.5 min; **25** = 13.8 min; **26** = 13.9 min; **27** = 8.6 min; **28** = 8.7 min; **29** = 9.0 min; **30** = 12.8 min; and **31** = 12.8 min.

For HPLC chromatography of dimers **32–34**, reversed phase chromatography was conducted at a flow rate of 1 mL/min. Solvent A in the gradient was methanol. Solvent B was H₂O. The gradient was held at the starting mixture of 70% A for 2 min, and then the percentage of A was linearly increased to 100% over the next 10 min. Retention times for the compounds examined under these conditions were as follows: **32** = 10.4 min; **33** = 10.8 min; and **34** = 10.8 min.

Preparative LC. A preparative LC system containing a Rainin Rabbit-plus peristaltic pump and a Dynamax Model FC-1 fraction collector was used to obtain pure samples of Cbl derivatives. Compounds were separated on either an aminopropyl silica column (1000 mm \times 25 mm; 40–63 μ m; Alltech) or a C₁₈ reversed phase column (25 mm \times 500 mm; octadecyl; Aldrich). Isolation of purified products was aided by evaluation of collected fractions from the preparative LC on an analytical HPLC column.

Preparation of Cyanocobalamin Monocarboxylic Acids **2, 3, or 4.** The *b*-, *d*-, and *e*-Cbl monocarboxylates (**2, 3, and 4**, respectively) were prepared as previously reported (12). Briefly, CN-Cbl was hydrolyzed in 0.1 N HCl over 10 days at room temperature. Following the hydrolysis reaction, the isomeric monocarboxylates were separated from starting CN-Cbl and from di- and triacids by ion exchange chromatography. Separation of the individual carboxylate isomers was accomplished by

preparative liquid chromatography on an aminopropyl-silica column (25 mm \times 1000 mm) at a flow rate of 0.15 mL/min.

General Procedure for Conjugation of **2, 3, or 4 with **1,12-Diaminododecane**; **Synthesis of **5, 6, and 7****.** The conjugation of the Cbl-monocarboxylates with diaminododecane was accomplished as previously described (12). Briefly, reaction of **2, 3, or 4** with diaminododecane, EDC, or NHS and in a 1:1 mixture of DMF and H₂O for 4 days yielded the desired compounds after purification by ion exchange chromatography.

Conjugation of Cyanocobalamin Monocarboxylic Acid with **4,7,10-Trioxa-1,13-Tridecanediamine; **Synthesis of **8 and 10****.** A 2.0 g (1.47 mmol) quantity of a CN-Cbl monocarboxylic acid, **2 or 4**, and 0.68 g (5.9 mmol) of NHS were dissolved in 100 mL of water. To that mixture was added 1.46 g (29 mmol) of NaCN, then 16 g (36 mmol) of 4,7,10-trioxa-1,13-tridecanediamine was added, and the pH was adjusted to 6 with 1 N HCl. To that solution was added 1.14 g (5.9 mmol) of EDC, and the pH of the solution was readjusted to 5.5. The reaction mixture was then stirred overnight in the dark at rt. In five intervals of 6–14 h, 0.68 g of NHS and 1.14 g of EDC were added to the solution, with the pH value readjusted to 5.5 each time. After a total reaction time of 4 days, the solution was evaporated to dryness. The residue was washed with 100 mL of acetone, and the solvent was decanted. The remaining solid was dissolved in 50 mL of H₂O and applied to an Amberlite XAD-2 (200 g; 4 cm \times 60 cm) column. The column was eluted with 1 L of water, and then the desired product was eluted with 500 mL of methanol. The methanol fractions were evaporated to dryness, and the residue was dissolved in 25 mL of water and was applied to a ion exchange column (100 g; 2.5 cm \times 60 cm; acetate form; 200–400 mesh). The final product was eluted using 250 mL of water, thereby leaving nonconverted Cbl-acid bound to the column, which was later eluted with 0.04 mol/L sodium acetate buffer, pH 4.7. The fractions containing the final product were evaporated to dryness and then washed with acetone and filtered. The solid obtained was recrystallized from aqueous acetone.

b-Isomer (**8**): yield, 2.0 g (87%); mp, 213–217 °C with decomposition; ¹H NMR (MeOH-*d*₄) δ 0.44 (s, 3H), 1.17 (d, 5H), 1.25 (d, 4H), 1.36 (d, 7H), 1.45 (s, 4H), 1.74 (m, 10H), 1.88 (s, 11H), 2.27 (d, 8H), 2.34 (m, 11H), 2.56 (m, 11H), 3.17 (t, 3H), 3.2 (m, 9H), 3.3 (m, 6H), 3.4 (m, 4H), 3.5 (s, 7H), 3.58 (s, 8H), 3.6 (m, 11H), 3.7 (m, 1H), 3.88 (m, 1H), 4.07 (m, 1H), 4.1 (m, 1H), 4.17 (m, 1H), 4.3 (m, 1H), 4.5 (m, 1H), 4.6 (m, 1H), 6.04 (d, 1H), 6.27 (s, 1H), 6.52 (s, 1H), 7.13 (d, 1H), 7.25 (s, 1H); MS (FAB⁺) mass calcd for C₇₃H₁₀₉N₁₅O₁₈CoP 1557, found 1558 (M + H)⁺; IR (KBr, cm⁻¹) 3400, 3200, 2950, 2060, 1660, 1570, 1490, 1060; UV (H₂O) λ_{361} (ϵ = 17 500).

e-Isomer (**10**): yield, 1.5 g (65%); mp, 112–116 °C with decomposition; ¹H NMR (MeOH-*d*₄) δ 0.44 (s, 3H), 1.18 (s, 3H), 1.25 (d, 5H), 1.37 (d, 8H), 1.45 (s, 4H), 1.74 (m, 10H), 1.88 (s, 11H), 2.28 (d, 7H), 2.3 (m, 15H), 2.56 (d, 11H), 3.17 (t, 3H), 3.2 (t, 4H), 3.3 (m, 11H), 3.4 (m, 4H), 3.5 (s, 7H), 3.58 (d, 3H), 3.6 (m, 5H), 3.7 (m, 1H), 4.0 (m, 1H), 4.1 (d, 1H), 4.19 (m, 1H), 4.3 (m, 1H), 4.5 (d, 1H), 4.6 (m, 1H), 6.05 (d, 1H), 6.27 (s, 1H), 6.57 (s, 1H), 7.1 (d, 1H), 7.25 (s, 1H); MS (FAB⁺) mass calcd for C₇₃H₁₀₉N₁₅O₁₈CoP 1557, found 1558 (M + H)⁺; IR (KBr, cm⁻¹) 3400, 3200, 2950, 2060, 1660, 1570, 1490, 1060; UV (H₂O) λ_{361} (ϵ = 12 800).

p-Iodobenzoyl-5-aminoisophthalic Acid, **12.** A 5.0 g (28 mmol) quantity of 5-amino-isophthalic acid, **11**, was dissolved in 30 mL of 1 N NaOH and placed in an ice/water bath. To the cold solution was added 7.5 g (28

mmol) of 4-iodobenzoyl chloride in 60 mL of acetonitrile, dropwise. The thick white precipitate was stirred for 10 min before the ice/water bath was removed, and the mixture was allowed to stir for an additional 10 min. The reaction mixture was adjusted to pH 4 with acetic acid and the resulting solid collected. This solid was dissolved in 30 mL of 1 N NaOH and washed with 2×50 mL of ether. The resulting aqueous solution was filtered and acidified to pH 4 with acetic acid. The white precipitate was collected and dried under high vacuum to yield 11.6 g (99+%) of **12**: mp >300 °C; ^1H NMR (DMSO- d_6) δ 7.84 (d, 2H, $J = 4.1$ Hz), 7.94 (d, 2H, $J = 4.2$ Hz), 8.27 (s, 1H), 8.51 (d, 2H, $J = 0.7$ Hz); IR (Nujol, cm^{-1}) 3570, 3300, 1645, 1580, 1525, 760; HRMS (FAB $^+$; DMIX) ($M + \text{H}$) $^+$ mass calcd for $\text{C}_{15}\text{H}_{11}\text{INO}_5$ 411.9682, found 411.9696.

p-Iodobenzoyl-5-aminoisophthalate DiTFP Ester, 13. A 5.0 g (12.2 mmol) quantity of **12** was suspended in 100 mL of anhydrous ethyl acetate. To this suspension was added 12.5 g (73 mmol) of 2,3,5,6-tetrafluorophenol (TFP-OH) followed by 5.0 g (24.2 mmol) of 1,3-dicyclohexylcarbodiimide (DCC). This suspension was stirred at rt for 3 days before filtering off the solid and washing with an additional 20 mL of ethyl acetate. The filtrate was evaporated to dryness. The resulting sticky white solid was suspended in 50 mL of acetonitrile, stirred for 30 min, and filtered to yield 3.75 g of **13** as a white solid (43%): mp 250–251 °C; ^1H NMR (DMSO- d_6) δ 7.81 (d, 2H, $J = 4.3$ Hz), 7.94 (d, 2H, $J = 4.2$ Hz), 8.04 (m, 2H), 8.57 (t, 1H, $J = 1.4$ Hz), 9.06 (d, 2H, $J = 0.7$ Hz); IR (Nujol, cm^{-1}) 3220, 3060, 1750, 1655, 1520, 1485, 1330, 1195, 1110, 1085, 955, 945; HRMS (FAB $^+$; 3NBA) ($M + \text{H}$) $^+$ mass calcd for $\text{C}_{27}\text{H}_{11}\text{F}_8\text{INO}_5$ 707.9554, found 707.9552.

p-(Tri-*n*-butylstannyl)benzoyl-5-aminoisophthalate DiTFP Ester, 14. A 2.0 g (2.8 mmol) quantity of **13** was dissolved in 20 mL of dry toluene under argon. To this solution was added 2.8 mL (5.5 mmol) of bis-(tributyltin), followed by 40 mg (0.04 mmol) of tetrakis-(triphenylphosphine)palladium(0). The mixture was stirred at rt for 15 min before heating to 80 °C for 2 h. After 2 h, an additional 40 mg of palladium catalyst was added. Within 1 h the mixture had turned black. After cooling to rt, the toluene was removed by rotary evaporation. The resulting black oil was taken into 20 mL of ethyl acetate and dried onto 10 g of silica gel while on a rotary evaporator. The oil-coated silica was added to the top of a 250 g (40×3.5 cm) silica gel column. The column was initially eluted with hexanes containing 5% acetic acid, but after eluting with 600 mL, the solvent was changed to 90:10 hexanes/ethyl acetate (containing 5% acetic acid). Fractions 14–16 were combined and dried to yield 1.5 g of **14** as a white solid (62%): mp 120–123 °C; ^1H NMR (CDCl_3) δ 0.89 (t, 9H, $J = 7.3$ Hz), 1.11 (m, 6H), 1.36 (m, 15H), 1.55 (m, 6H), 7.07 (m, 2H), 7.62 (d, 2H, $J = 4.1$ Hz), 7.84 (d, 2H, $J = 4.1$ Hz), 8.38 (s, 1H), 8.76 (t, 1H, $J = 1.6$ Hz), 8.87 (d, 2H, $J = 0.7$ Hz); IR (Nujol, cm^{-1}) 1750, 1645, 1520, 1480, 1185, 1100, 1085; MS (FAB $^+$) mass calcd (isotopic abundance) 868 (38%), 869 (37%), 870 (75%), 871 (53%), 872 (100%), 873 (41%), 874 (21%); mass found 868 (47%), 869 (42%), 870 (82%), 871 (55%), 872 (100%), 873 (42%), 874 (26%).

Biotin TFP Ester, 16. A 3.0 g (12.3 mmol) quantity of biotin, **15**, was dissolved in 60 mL of warm (70 °C) DMF under argon atmosphere. The solution was cooled to ambient temperature, and 2.79 g (13.5 mmol) of DCC was added, followed by 40.8 g (24.6 mmol) of TFP-OH. The reaction mixture was cooled to 0 °C and stirred at that temperature for 0.5 h. It was brought back to ambient temperature and stirred for another 4–5 h. The mixture was filtered and the filtrate evaporated to

dryness. The resultant solid was washed with 50 mL of acetonitrile and dried to yield 5.0 g (98%) of **16** as a white solid: mp 185–187 °C (20); ^1H NMR (DMSO- d_6) δ 1.4 (m, 2H), 1.7 (m, 2H), 2.5 (t, 2H), 2.8 (t, 2H), 3.1 (m, 1H), 4.1 (m, 1H), 4.3 (m, 1H), 6.4 (d, 2H), 7.9 (m, 1H); IR (KBr, cm^{-1}) 3250, 2915, 1790, 1710, 1520, 1480, 1090.

Biotin–Aminocaproate TFP Ester, 18. A 0.99 g quantity (7.5 mmol) of 6-aminocaproic acid was dissolved in 75 mL of H_2O . To this mixture was added 0.5 mL of triethylamine, followed by a solution of 1.96 g (5 mmol) of **16** in warm acetonitrile (300 mL). The reaction was stirred overnight at rt. It was filtered, washed with 50 mL of H_2O , and dried under high vacuum to yield 0.870 g (47%) of **17**. Additional material was obtained by evaporating the filtrate to dryness, dissolving the residue in 75 mL of CH_3CN , and allowing the CH_3CN solution to cool to rt. The resultant solid was filtered, washed with warm acetonitrile, and dried under high vacuum to give an additional 0.6 g. Total yield of **17** was 1.47 g (79%): mp 225–227 °C; ^1H NMR (DMSO- d_6) δ 1.2–1.6 (m, 8H), 2.0 (t, 2H), 2.2 (t, 2H), 2.5 (dd, 2H), 2.8 (dd, 2H), 3.1 (m, 3H), 4.1 (m, 1H), 4.3 (m, 1H), 6.4 (d, 2H), 7.7 (m, 1H); IR (KBr, cm^{-1}) 3280, 2915, 1710, 1630, 1540, 1260, 1030.

A 1.0 g quantity (2.68 mmol) of **17** was dissolved in 50 mL of DMSO. To that solution was added 0.4 mL of triethylamine, followed by 1.05 g (4.02 mmol) of TFP-OTFA (21). The reaction mixture was stirred at rt for 15–20 min and then evaporated to dryness. The residue was washed with ether and dichloromethane. The resulting solid was dried under vacuum to yield 1.24 g (89%) of **18**: mp 139–141 °C; ^1H NMR (DMSO- d_6) δ 1.2 (t, 2H), 1.3–1.7 (m, 5H), 2.1 (t, 2H), 2.6 (dd, 2H), 2.8 (m, 4H), 3.1 (m, 4H), 4.2 (m, 1H), 4.4 (m, 1H), 6.4 (d, 2H), 7.8 (t, 1H), 8.0 (m, 1H); IR (KBr, cm^{-1}) 3300, 2940, 1785, 1690, 1640, 1520, 950; HRMS (FAB $^+$, 3NBA) ($M + \text{H}$) $^+$ mass calcd for $\text{C}_{22}\text{H}_{28}\text{F}_4\text{N}_3\text{O}_4\text{S}$ 506.1737, found 506.1732.

Biotin–Aminocaproate 5-Aminoisophthalic Acid DiTFP Ester, 20. A 0.35 g (0.67 mmol) quantity of **18** was dissolved in 40 mL of DMF. To that solution was added 80 μL of triethylamine, followed by 0.182 g (1.01 mmol) of 5-aminoisophthalic acid. The reaction was stirred at rt for 8 days, with triethylamine (80 μL) added every 24 h. It was then evaporated to dryness, and the residue was applied to a silica column. The column was initially eluted with 450 mL of acetonitrile, followed by 40 mL of methanol, and then DMF, collecting 20 mL fractions. The fractions containing the final product (HPLC monitored) were evaporated to dryness to yield 230 mg (65%) of **19**: mp 193–195 °C; ^1H NMR (DMSO- d_6) δ 1.3–1.7 (m, 8H), 2.1 (t, 2H), 2.3 (t, 2H), 2.6 (m, 2H), 2.8 (m, 2H), 3.1 (m, 3H), 4.1 (m, 1H), 4.3 (m, 1H), 6.4 (d, 2H), 7.8 (t, 1H), 8.1 (m, 1H), 8.46 (s, 2H); IR (KBr, cm^{-1}) 3280, 2920, 1710, 1690, 1640, 1240, 1100, 900; HRMS (FAB $^+$, 3NBA) ($M + \text{H}$) $^+$ mass calcd for $\text{C}_{24}\text{H}_{33}\text{N}_4\text{O}_7\text{S}$ 521.2070, found 521.2070.

A 200 mg (0.376 mmol) quantity of **19** was dissolved in 30 mL of DMF under argon atmosphere. To this solution was added 241 mg (0.94 mmol) of TFP-OTFA by a transfer using a double-ended needle. That addition was followed by addition of 112 μL of triethylamine. The reaction mixture was stirred at rt for 24 h (HPLC monitored) and then evaporated to dryness. The light brown oil was triturated with ether, and the solution was filtered and washed with 50 mL of additional ether to yield 250 mg (86%) of **20**: mp 135–137 °C; ^1H NMR (DMSO- d_6) δ 1.3–1.7 (m, 8H), 2.1 (t, 2H), 2.3 (t, 2H), 2.6 (m, 2H), 2.8 (m, 2H), 3.1 (m, 3H), 4.2 (m, 1H), 4.4 (m, 1H), 6.4 (d, 2H), 7.8 (t, 1H), 8.1 (m, 2H), 8.57 (s, 1H), 8.9 (s, 2H); IR (KBr, cm^{-1}) 3280, 2920, 1260, 1200, 1690,

1520, 1185, 950; HRMS ($M + H$)⁺ mass calcd for $C_{36}H_{32}F_8N_4O_7S$ 817.1942, found 817.1920.

Conjugation of Cyanocobalamin Monocarboxylic Acid Diaminododecane with Isophthaloyl Dichloride; Synthesis of 21–23. To a solution of 0.300 g (0.192 mmol) of **5**, **6**, or **7** in 30 mL of DMF was added 18 μ L of triethylamine. To that solution was added 0.195 g (0.096 mmol) of isophthaloyl dichloride over a period of 10–15 min. The reaction mixture was stirred at 55–60 °C for 48 h. It was then evaporated to dryness. The solid residue was dissolved in 20 mL of methanol/H₂O (7:3) and eluted on a preparative reversed phase column (500 mm \times 25 mm) with the same solvent. The fractions containing the product were evaporated to dryness.

b-Acid Dimer (21): yield, 121 mg (38%); mp 220–222 °C with decomposition; ¹H NMR (D₂O) δ 0.43 (s, 6H, C-20 CH₃), 1.17 (s, 8H), 1.22 (d, 13H), 1.29 (s, 45H), 1.36 (d, 22H), 1.44 (s, 10H), 1.6 (m, 8H), 1.87 (s, 8H), 2.04 (m, 10H), 2.25 (s, 12H), 2.36 (m, 8H), 2.55 (d, 20H), 2.8 (m, 8H), 3.15 (m, 8H), 3.29 (s, 10H), 3.36 (m, 14H), 3.6 (m, 4H), 3.73 (m, 2H), 3.9 (d, 2H), 4.07 (m, 2H), 4.12 (m, 2H), 4.16 (m, 2H), 4.3 (m, 2H), 4.5 (m, 2H), 4.6 (s, 2H), 4.66 (m, 2H), 6.0 (s, 2H), 6.26 (d, 2H), 6.6 (s, 2H), 7.1 (s, 2H), 7.25 (s, 2H), 7.54 (t, 1H), 7.93 (d, 2H), 8.25 (s, 1H); MS (FAB⁺) mass calcd for $C_{158}H_{228}N_{30}O_{30}Co_2P_2$ 3208,² found 3208 (M)⁺; IR (KBr, cm⁻¹) 3400, 3200, 2950, 2060, 1660, 1570, 1490, 1060; UV (MeOH) λ_{360} (ϵ = 33 900).

d-Acid Dimer (22): yield, 96 mg (30%); mp 217–220 °C with decomposition; ¹H NMR (D₂O) δ 0.43 (s, 6H, C-20 CH₃), 1.18 (s, 8H), 1.3 (m, 36H), 1.37 (m, 12H), 1.46 (s, 10H), 1.6 (m, 8H), 1.9 (d, 12H), 2.05 (m, 10H), 2.2 (d, 16H), 2.35 (m, 8H), 2.6 (d, 18H), 2.8–3.0 (m, 16H), 3.15 (m, 6H), 3.3 (s, 8H), 3.37 (m, 14H), 3.6 (m, 4H), 3.76 (m, 2H), 3.9 (d, 2H), 4.07 (m, 2H), 4.12 (m, 2H), 4.18 (m, 2H), 4.3 (m, 2H), 4.5 (m, 2H), 4.6 (s, 2H), 4.68 (m, 2H), 6.0 (s, 2H), 6.26 (d, 2H), 6.6 (s, 2H), 7.1 (s, 2H), 7.25 (s, 2H), 7.54 (t, 1H), 7.95 (d, 2H), 8.25 (s, 1H); MS (FAB⁺) mass calcd for $C_{158}H_{228}N_{30}O_{30}Co_2P_2$ 3208, found 3208 (M)⁺; IR (KBr, cm⁻¹) 3400, 3200, 2950, 2060, 1660, 1570, 1490, 1060; UV (MeOH) λ_{360} (ϵ = 42 400).

e-Acid Dimer (23): yield, 96 mg (30%); mp 225–228 °C with decomposition; ¹H NMR (D₂O) δ 0.43 (s, 6H), 1.16 (s, 8H), 1.29 (m, 36H), 1.35 (d, 12H), 1.44 (s, 10H), 1.53 (m, 6H), 1.6 (m, 8H), 1.85 (s, 12H), 2.03 (m, 8H), 2.25 (d, 12H), 2.33 (m, 8H), 2.54 (d, 20H), 2.8 (m, 8H), 3.13 (m, 8H), 3.28 (s, 12H), 3.35 (m, 12H), 3.6 (m, 4H), 3.73 (m, 2H), 3.9 (d, 2H), 4.07 (m, 2H), 4.12 (m, 2H), 4.16 (m, 2H), 4.3 (m, 2H), 4.5 (m, 2H), 4.64 (m, 2H), 4.7 (s, 2H), 6.0 (s, 2H), 6.26 (d, 2H), 6.6 (s, 2H), 7.1 (s, 2H), 7.25 (s, 2H), 7.54 (t, 1H), 7.93 (d, 2H), 8.25 (s, 1H); MS (FAB⁺) mass calcd for $C_{158}H_{228}N_{30}O_{30}Co_2P_2$ 3208, found 3209 (M + H)⁺; IR (KBr, cm⁻¹) 3400, 3200, 2950, 2060, 1660, 1570, 1490, 1060; UV (MeOH) λ_{360} (ϵ = 31 700).

Conjugation of Cyanocobalamin Monocarboxylic Acid Diaminododecane with p-Iodobenzoyl Aminoisophthalate; Synthesis of 24–26. To a solution containing 0.30 g (0.192 mmol) of **5**, **6**, or **7** in 40 mL of a 3:1 mixture of DMF/H₂O was added 18 μ L of triethylamine. To that solution was added 68 mg (0.096 mmol) of **13** over a 5–10 min period. The reaction mixture was stirred at rt for 4–5 h and then evaporated to dryness. The solid residue was dissolved in 20 mL of a 4:1 MeOH/H₂O mixture and applied to a preparative reversed phase column (500 mm \times 25 mm), which was eluted with the

same solvent. The fractions containing the product were evaporated to dryness.

b-Acid Dimer (24): yield, 258 mg (70%); mp 285–290 °C with decomposition; ¹H NMR (D₂O) δ 0.43 (s, 6H), 1.17 (s, 8H), 1.22 (d, 13H), 1.29 (s, 45H), 1.36 (d, 22H), 1.44 (s, 10H), 1.6 (m, 8H), 1.86 (s, 12H), 2.04 (m, 10H), 2.25 (s, 12H), 2.36 (m, 8H), 2.55 (d, 20H), 2.83 (m, 8H), 3.15 (m, 8H), 3.29 (s, 10H), 3.36 (m, 8H), 3.58 (m, 2H), 3.65 (m, 2H), 3.75 (m, 2H), 3.9 (d, 2H), 4.06 (m, 2H), 4.12 (m, 2H), 4.16 (m, 2H), 4.3 (m, 2H), 4.5 (m, 2H), 4.57 (s, 2H), 4.65 (m, 2H), 6.0 (s, 2H), 6.26 (d, 2H), 6.5 (s, 2H), 7.1 (s, 2H), 7.25 (s, 2H), 7.7 (d, 2H), 7.89 (d, 2H), 7.98 (s, 1H), 8.26 (s, 2H); MS (FAB⁺) mass calcd for $C_{165}H_{232}O_{31}N_{31}Co_2P_2I$ 3453, found 3453 (M)⁺; IR (KBr, cm⁻¹) 3400, 3200, 2950, 2060, 1660, 1570, 1490, 1060; UV (MeOH) λ_{360} (ϵ = 41 500).

d-Acid Dimer (25): yield, 280 mg (76%); mp 230–233 °C with decomposition; ¹H NMR (D₂O) δ 0.43 (s, 6H), 1.19 (s, 8H), 1.3 (m, 36H), 1.37 (d, 12H), 1.46 (s, 10H), 1.63 (m, 8H), 1.87 (s, 12H), 2.05 (m, 10H), 2.27 (d, 16H), 2.35 (m, 8H), 2.6 (d, 18H), 2.8 (s, 8H), 3.0 (s, 10H), 3.15 (m, 8H), 3.3 (d, 8H), 3.37 (m, 14H), 3.6 (m, 2H), 3.68 (d, 2H), 3.76 (m, 2H), 3.9 (d, 2H), 4.07 (m, 2H), 4.12 (m, 2H), 4.18 (m, 2H), 4.3 (m, 2H), 4.5 (m, 2H), 4.64 (m, 4H), 6.0 (s, 2H), 6.26 (d, 2H), 6.6 (s, 2H), 7.1 (s, 2H), 7.25 (s, 2H), 7.7 (d, 2H), 7.9 (d, 2H), 7.99 (d, 1H), 8.28 (s, 2H); MS (FAB⁺) mass calcd for $C_{165}H_{232}O_{31}N_{31}Co_2P_2I$ 3453, found 3453 (M)⁺; IR (KBr, cm⁻¹) 3400, 3200, 2950, 2060, 1660, 1570, 1490, 1060; UV (MeOH) λ_{360} (ϵ = 48 900).

e-Acid Dimer (26): yield, 265 mg (72%); mp 253–255 °C with decomposition; ¹H NMR (D₂O) δ 0.43 (s, 6H), 1.16 (s, 8H), 1.22 (d, 12H), 1.33 (m, 36H), 1.43 (s, 10H), 1.53 (m, 6H), 1.6 (m, 8H), 1.86 (s, 12H), 2.03 (m, 8H), 2.25 (d, 12H), 2.33 (m, 8H), 2.54 (d, 20H), 2.8 (s, 4H), 3.0 (s, 4H), 3.28 (s, 10H), 3.35 (m, 8H), 3.58 (m, 2H), 3.65 (m, 2H), 3.73 (m, 2H), 3.88 (d, 2H), 4.05 (m, 2H), 4.1 (m, 2H), 4.17 (m, 2H), 4.3 (m, 2H), 4.5 (m, 2H), 4.57 (s, 2H), 4.63 (m, 2H), 6.0 (s, 2H), 6.26 (d, 2H), 6.5 (s, 2H), 7.1 (s, 2H), 7.25 (s, 2H), 7.7 (d, 2H), 7.89 (d, 2H), 7.98 (s, 1H), 8.26 (s, 2H); MS (FAB⁺) mass calcd for $C_{165}H_{232}O_{31}N_{31}Co_2P_2I$ 3453, found 3452 (M)²; IR (KBr, cm⁻¹) 3400, 3200, 2950, 2060, 1660, 1570, 1490, 1060; UV (MeOH) λ_{360} (ϵ = 48 200).

Conjugation of Cyanocobalamin Monocarboxylic Acid Diaminododecane with p-(Tri-n-butylstannyl)-benzoyl Aminoisophthalate; Synthesis of 27–29. To a solution containing 0.10 g (0.065 mmol) of **5**, **6**, or **7** in 40 mL of a 3:1 mixture of DMF/H₂O was added 6 μ L of triethylamine. To that solution was added 28 mg (0.033 mmol) of **14** over a 5–10 min period. The reaction mixture was stirred at rt for 12–14 h and then evaporated to dryness. The residue was washed with 100 mL of acetone, and the solvent was decanted.

b-Acid Dimer (27): yield, 93 mg (72%); mp >300 °C; ¹H NMR (D₂O) δ 0.43 (s, 6H, C-20 CH₃), 0.88 (t, 9H), 1.12 (t, 12H), 1.17 (d, 8H), 1.22 (d, 13H), 1.29 (s, 45H), 1.36 (d, 22H), 1.44 (s, 10H), 1.6 (m, 8H), 1.87 (d, 12H), 2.04 (m, 10H), 2.25 (s, 12H), 2.36 (m, 8H), 2.55 (d, 20H), 2.8 (m, 8H), 3.15 (m, 8H), 3.29 (s, 10H), 3.36 (m, 14H), 3.6 (m, 4H), 3.73 (m, 2H), 3.9 (d, 2H), 4.07 (m, 2H), 4.12 (m, 2H), 4.16 (m, 2H), 4.3 (m, 2H), 4.5 (m, 2H), 4.66 (m, 2H), 6.0 (s, 2H), 6.26 (d, 2H), 6.6 (s, 2H), 7.1 (s, 2H), 7.25 (s, 2H), 7.6 (d, 2H), 7.9 (d, 2H), 7.98 (br s, 1H), 8.28 (br s, 2H); IR (KBr, cm⁻¹) 3400, 3200, 2950, 2060, 1660, 1570, 1490, 1060; UV (MeOH) λ_{360} (ϵ = 59 300).

d-Acid Dimer (28): yield, 90 mg (70%); mp 208–212 °C with decomposition; ¹H NMR (D₂O) δ 0.43 (s, 6H), 0.88 (t, 9H), 1.15 (t, 12H), 1.19 (s, 8H), 1.3 (m, 36H), 1.37 (d, 12H), 1.46 (s, 10H), 1.6 (m, 8H), 1.9 (s, 12H), 2.05 (m, 10H), 2.28 (d, 16H), 2.35 (m, 8H), 2.6 (d, 18H), 2.8–2.9

² Obtaining exact mass values for molecules of >3000 amu is difficult. It is believed that the difference of 1 mass unit obtained is a reflection of the difficulty in assigning mass units to the spectrometer data, not an indication that the mass is different from that calculated for the desired compound.

(m, 16H), 3.15 (m, 8H), 3.3 (s, 8H), 3.37 (m, 14H), 3.6 (m, 4H), 3.76 (m, 2H), 3.9 (d, 2H), 4.07 (m, 2H), 4.12 (m, 2H), 4.18 (m, 2H), 4.3 (m, 2H), 4.5 (m, 2H), 4.68 (m, 2H), 6.0 (s, 2H), 6.26 (d, 2H), 6.6 (s, 2H), 7.1 (s, 2H), 7.25 (d, 2H), 7.6 (d, 2H), 7.9 (d, 2H), 7.99 (br s, 1H), 8.28 (br s, 2H); IR (KBr, cm^{-1}) 3400, 3200, 2950, 2060, 1660, 1570, 1490, 1060; UV (MeOH) λ_{360} ($\epsilon = 47\,700$).

e-Acid Dimer (29): yield, 100 mg (78%); mp 202–205 °C with decomposition; ^1H NMR (D_2O) δ 0.43 (s, 6H), 0.88 (t, 9H), 1.12 (t, 12H), 1.15 (s, 8H), 1.29 (m, 36H), 1.35 (d, 12H), 1.44 (s, 10H), 1.53 (m, 6H), 1.6 (m, 8H), 1.86 (d, 12H), 2.03 (m, 8H), 2.25 (d, 12H), 2.33 (m, 8H), 2.54 (d, 20H), 2.8 (m, 8H), 3.13 (m, 8H), 3.28 (s, 10H), 3.35 (m, 10H), 3.6 (m, 4H), 3.73 (m, 2H), 3.9 (d, 2H), 4.05 (m, 2H), 4.1 (m, 2H), 4.17 (m, 2H), 4.3 (m, 2H), 4.5 (m, 2H), 4.6 (m, 2H), 6.0 (s, 2H), 6.26 (d, 2H), 6.6 (s, 2H), 7.1 (s, 2H), 7.25 (s, 2H), 7.6 (d, 2H), 7.9 (d, 2H), 7.98 (br s, 1H), 8.28 (br s, 2H); IR (KBr, cm^{-1}) 3400, 3200, 2950, 2060, 1660, 1570, 1490, 1060; UV (MeOH) λ_{360} ($\epsilon = 41\,900$).

Conjugation of Cyanocobalamin Monocarboxylic Acid Diaminododecane with Biotin–Aminocaproate Aminoisophthalate; Synthesis of 30 and 31. To a solution of containing 0.20 g (0.13 mmol) of **5**, **6**, or **7** in 40 mL of a 3:1 mixture of DMF/ H_2O was added 12 μL of triethylamine. To that solution was added 50 mg (0.065 mmol) of **20** over a 5–10 min period. The reaction mixture was stirred at rt for 3 h and then was evaporated to dryness. The residue was washed with 100 mL of acetone, and the solvent was decanted.

b-Acid Dimer (30): yield, 124 mg (62%); mp 195–198 °C with decomposition; ^1H NMR ($\text{MeOH}-d_4$) δ 0.43 (s, 6H), 1.17 (s, 8H), 1.3 (m, 20H), 1.35 (m, 22H), 1.46 (s, 10H), 1.6 (m, 8H), 1.8 (m, 6H), 1.87 (m, 10H), 2.0 (m, 4H), 2.17 (s, 10H), 2.25 (s, 12H), 2.57 (d, 16H), 3.16 (m, 9H), 3.29 (s, 8H), 3.37 (m, 6H), 3.6 (m, 4H), 3.76 (m, 2H), 3.9 (d, 2H), 4.07 (m, 4H), 4.16 (m, 2H), 4.28 (m, 4H), 4.5 (m, 4H), 4.7 (m, 2H), 6.04 (s, 2H), 6.26 (d, 2H), 6.5 (s, 2H), 7.1 (s, 2H), 7.2 (s, 2H), 7.9 (d, 1H), 8.1 (s, 2H); MS (FAB^+) mass calcd for $\text{C}_{174}\text{H}_{254}\text{N}_{34}\text{O}_{33}\text{Co}_2\text{P}_2\text{S}$ 3562, found 3561 (M^+); IR (KBr, cm^{-1}) 3400, 3200, 2950, 2060, 1660, 1570, 1490, 1060; UV (MeOH) λ_{360} ($\epsilon = 38\,700$).

e-Acid Dimer (31): yield, 100 mg (50%); mp > 300 °C; ^1H NMR ($\text{MeOH}-d_4$) δ 0.43 (s, 6H), 1.17 (s, 8H), 1.3 (m, 20H), 1.35 (m, 22H), 1.43 (s, 10H), 1.53 (m, 8H), 1.7 (m, 6H), 1.87 (m, 6H), 2.0 (m, 4H), 2.13 (s, 10H), 2.25 (d, 10H), 2.52 (d, 16H), 3.16 (m, 6H), 3.29 (s, 10H), 3.37 (m, 6H), 3.6 (m, 4H), 3.73 (m, 2H), 3.9 (d, 2H), 4.07 (m, 4H), 4.16 (m, 2H), 4.26 (m, 4H), 4.5 (m, 4H), 4.64 (m, 2H), 6.04 (s, 2H), 6.26 (d, 2H), 6.6 (s, 2H), 7.1 (s, 2H), 7.23 (s, 2H), 7.9 (d, 1H), 8.1 (s, 2H); MS (FAB^+) mass calcd for $\text{C}_{174}\text{H}_{254}\text{N}_{34}\text{O}_{33}\text{Co}_2\text{P}_2\text{S}$ 3562, found 3562 (M^+); IR (KBr, cm^{-1}) 3400, 3200, 2950, 2060, 1660, 1570, 1490, 1060; UV (MeOH) λ_{360} ($\epsilon = 40\,000$).

Conjugation of Cyanocobalamin Monocarboxylic Acid–Trioxadiazine with Isophthaloyl Dichloride; Synthesis of 32. To a solution containing 300 mg (0.193 mmol) of **8** in 20 mL of DMF was added 30 μL of triethylamine. To that solution was added 19.5 mg (0.096 mmol) of isophthaloyl dichloride over a 10–15 min period. The reaction mixture was stirred at rt for 4–5 days, and 30 μL of triethylamine was added after each 24 h period. After evaporating to dryness, the solid was dissolved in 20 mL of a 1:1 methanol/ H_2O mixture and was applied to a preparative reversed phase column (25 mm \times 500 mm), which was eluted with the same solvent. The fractions containing the final product were evaporated to dryness.

b-Acid Dimer (32): yield, 100 mg (32%); mp 195–198 °C with decomposition; ^1H NMR ($\text{MeOH}-d_4$) δ 0.44 (s, 6H), 1.18 (s, 6H), 1.25 (d, 7H), 1.31 (t, 20H), 1.36 (s, 14H),

1.45 (s, 8H), 1.74 (m, 20H), 1.88 (d, 15H), 2.27 (s, 11H), 2.37 (m, 22H), 2.56 (d, 20H), 2.85 (s, 5H), 2.99 (s, 2H), 3.2 (m, 18H), 3.3 (m, 12H), 3.4 (m, 10H), 3.5 (s, 14H), 3.58 (s, 18H), 3.6 (s, 30H), 3.9 (d, 4H), 4.0 (d, 2H), 4.1 (d, 2H), 4.18 (d, 2H), 4.3 (m, 2H), 4.5 (m, 2H), 4.7 (m, 2H), 6.0 (s, 2H), 6.28 (s, 2H), 6.56 (s, 2H), 7.1 (s, 2H), 7.25 (s, 2H), 7.56 (m, 1H), 7.8 (d, 2H), 8.3 (s, 1H); MS (FAB^+) mass calcd for $\text{C}_{154}\text{H}_{220}\text{N}_{30}\text{O}_{36}\text{Co}_2\text{P}_2$ 3245, found 3245 (M^+); IR (KBr, cm^{-1}) 3400, 3200, 2950, 2060, 1660, 1570, 1490, 1060; UV (H_2O) λ_{361} ($\epsilon = 33\,900$).

Conjugation of Cyanocobalamin Monocarboxylic Acid–Trioxadiazine with DiTFP Ester of Biotin–Aminocaproate Aminoisophthalate; Synthesis of 33 and 34. To a solution containing 300 mg (0.193 mmol) **8** or **10** in 15 mL of DMF was added 30 μL of triethylamine. To that solution was added 79 mg (97 mmol) of **20** over a 5–10 min period. The reaction mixture was stirred at rt for 3–4 days (HPLC monitored), adding 30 μL of triethylamine after each 24 h period. The reaction mixture was then evaporated to dryness. The solid residue was dissolved in 20 mL of a 1:1 methanol/ H_2O mixture and applied to a preparative reversed phase column (25 mm \times 500 mm), which was eluted with the same solvent. The fractions containing the product were evaporated to dryness.

b-Acid Dimer (33): yield, 160 mg (53%); mp 192–195 °C with decomposition; ^1H NMR ($\text{MeOH}-d_4$) δ 0.43 (s, 6H), 1.17 (s, 6H), 1.24 (d, 8H), 1.36 (d, 16H), 1.44 (s, 6H), 1.73 (m, 20H), 1.87 (m, 12H), 2.26 (s, 10H), 2.4 (m, 14H), 2.55 (m, 18H), 3.17–3.3 (m, 30H), 3.6 (m, 40H), 3.73 (m, 2H), 3.9 (m, 2H), 4.06 (m, 2H), 4.1 (m, 2H), 4.17 (d, 2H), 4.3 (m, 4H), 4.47 (m, 4H), 4.6 (m, 2H), 4.66 (m, 2H), 6.03 (s, 2H), 6.27 (s, 2H), 6.55 (s, 2H), 7.12 (s, 2H), 7.25 (s, 2H), 7.9 (s, 1H), 8.16 (s, 2H); MS (FAB^+) mass calcd for $\text{C}_{170}\text{H}_{246}\text{N}_{34}\text{O}_{39}\text{Co}_2\text{P}_2\text{S}$ 3602, found 3602 (M^+); IR (KBr, cm^{-1}) 3400, 3200, 2950, 2060, 1660, 1570, 1490, 1060; UV (H_2O) λ_{360} ($\epsilon = 35\,300$).

e-Acid Dimer (34): yield, 120 mg (40%); mp 235–239 °C with decomposition; ^1H NMR ($\text{MeOH}-d_4$) δ 0.43 (s, 6H), 1.17 (d, 6H), 1.24 (d, 8H), 1.36 (d, 16H), 1.43 (s, 6H), 1.73 (m, 20H), 1.87 (m, 12H), 2.26 (d, 10H), 2.35 (m, 14H), 2.55 (m, 18H), 3.17–3.3 (m, 30H), 3.6 (m, 40H), 3.73 (m, 2H), 3.88 (m, 2H), 4.07 (m, 2H), 4.1 (m, 2H), 4.18 (d, 2H), 4.3 (m, 4H), 4.47 (m, 4H), 4.57 (m, 2H), 4.65 (m, 2H), 6.03 (s, 2H), 6.27 (s, 2H), 6.56 (s, 2H), 7.11 (s, 2H), 7.25 (s, 2H), 7.9 (s, 1H), 8.16 (s, 2H); MS (FAB^+) mass calcd for $\text{C}_{170}\text{H}_{246}\text{N}_{34}\text{O}_{39}\text{Co}_2\text{P}_2\text{S}$ 3602, found 3603 ($\text{M} + \text{H}^+$); IR (KBr, cm^{-1}) 3400, 3200, 2950, 2060, 1660, 1570, 1490, 1060; UV (H_2O) λ_{360} ($\epsilon = 31\,400$).

Binding of Cobalamin Derivatives with rhTCII. Recombinant human transcobalamin II (rhTCII) was prepared as previously reported (22). Stock solutions of Cbl derivatives were prepared by dissolving 2 mg in 100–200 μL of DMSO, followed by dilution to 1.0 mL with H_2O . Quantification of the Cbl derivatives was accomplished by UV, based on the measured extinction coefficients at 360 nm (data provided with individual compounds). Thus, a 20 μL aliquot of the stock Cbl solution was diluted to 1 mL with H_2O , and the absorbance at 360 nm was measured. An aliquot of the original solution was diluted to obtain a 1 μM solution, which was further diluted to 0.1 μM for use in the assay.

rhTCII was partially purified on a cation exchange column as previously described (23). The rhTCII was diluted in PBS containing 0.025% HSA to bind approximately 10 pmol of CN-Cbl (**1**)/mL. Aliquots of 100 μL of the rhTCII solution were added to tubes containing 0.01 pmol of [^{57}Co]-**1** and 0.1–30 pmol of unmodified **1** or Cbl derivatives **2–18**. The solution volume in each tube was adjusted to 1.0 mL with PBS, and the samples

Table 1. Binding of Cbl Dimers with rhTCII Relative to CN-Cbl, 1

cobalamin (compound no.)	50% binding inhibition for [⁵⁷ Co]CN-Cbl ^a	% relative rhTCII binding
1	1	100
21	111	0.9
22	284	0.35
23	5	20
24	52	1.9
25	6	16
26	1.8	56
30	26	3.8
31	4.5	22
32	23	4.3
33	23	4.3
34	1.8	56

^a The binding inhibition quantity is that amount (pmol) of Cbl derivative required to inhibit by 50% the binding of 0.01 pmol of [⁵⁷Co]CN-Cbl and was obtained by dividing 100 by the 50% binding inhibition quantity.

were incubated at rt for 1 h. The protein-bound [⁵⁷Co]-**1** was then separated from free [⁵⁷Co]-**1** by adsorption to hemoglobin-coated charcoal (24). The amount of radioactivity in each fraction was determined in a gamma counter. The decrease in binding of [⁵⁷Co]-**1** in the presence of various amounts of a Cbl derivative was calculated and graphed (Figure 2). The quantities of each derivative required to inhibit the binding of [⁵⁷Co]CN-Cbl to rhTCII by 50% was determined, and the apparent affinities of the compounds relative to CN-Cbl were calculated (Table 1).

RESULTS AND DISCUSSION

There are only a few reported examples of the preparation of Cbl dimers. In one example, it is proposed that Co–S–S–Co Cbl dimers are prepared from reaction with hydrosulfide ion (25). More recently, cobalt oligomethylene bridged dimers [Co–(CH₂)_{*n*}–Co, where *n* = 4–6] have been prepared as potential “latent alkanediyl diradicals” (26). Since our ultimate goal is to obtain Cbl derivatives that could be used as therapeutic pharmaceuticals, the light sensitivity and instability of previously described cobalt-linked dimers made them unsuitable. Therefore, we directed our efforts to the synthesis of novel new Cbl dimers that are designed to be stable to degradation. The synthetic approach chosen for preparation of stable Cbl dimers was to employ a di- or trifunctional cross-linking reagent that could couple two Cbl corrin ring carboxylates through linking moieties, as depicted in Figure 1. While bioactive Cbl dimers may be obtained with a difunctional cross-linking reagent, the desire to incorporate other functionalities into the dimers led us to consider a trifunctional reagent. This cross-linking arrangement allows for attachment of other chemical moieties with specific biological properties without having to make a second attachment on the Cbl moiety. Since we were interested in the possibility of binding two TCII molecules to the same Cbl dimer, the distance between the two Cbl moieties was considered to be critical for formation of such a complex. The linker molecules employed have 14–15 atoms in the chain, and linking of two of these with the isophthalic acid cross-linking moiety provides a 41–42 Å (fully extended) distance between the Cbls. This distance was thought to be adequate to bind two TCII molecules.

Synthesis of Cobalamin Dimers and Precursor Molecules. Our approach to preparing the Cbl dimers was to synthesize the diamino-linker adduct of Cbl carboxylates first and then couple the two adducts with the cross-linking reagent. This approach was chosen

because the Cbl diamino-linker adducts had been previously prepared for related studies (12, 13). The initial dimeric Cbls synthesized (Chart 2) incorporated diaminododecane adducts **5–7** (Chart 1) with isophthalate cross-linking moieties. The alkylamino derivatives **5**, **6**, and **7** were prepared by conjugation of the Cbl-carboxylates **2**, **3**, or **4** with diaminododecane using the water soluble carbodiimide, EDC,³ in DMF. The carboxylates were prepared from mild acid hydrolysis of CN-Cbl, **1**, followed by careful separation of the isomers on a preparative LC system employing an aminopropyl-silica column (12). Synthesis of the isomeric Cbl dimers **21–23** was accomplished by reacting one of the diaminododecane adducts, **5**, **6**, or **7**, with isophthaloyl dichloride. All three isomeric derivatives (e.g. *b*, *d*, and *e*) were prepared to compare the TCII binding of dimeric molecules with their monomeric counterparts.

Radioiodination of Cbl dimers was initiated to evaluate the biological properties of these compounds. We have previously shown that, while direct radioiodination of Cbl does not yield the desired product, radioiodination of Cbls could be accomplished by conjugation with arylstannane moieties (13). In general, incorporation of high specific activity radioiodine into a benzoyl moiety is readily achieved from the corresponding trialkylstannyl benzoate intermediates (18). One approach to obtaining radioiodinated dimers was to prepare them from stannylbenzoyl adducts of aminoisophthalate cross-linked Cbls. Thus, *p*-(tri-*n*-butylstannyl)benzoyl-containing isophthaloyl dimers **27–29** were prepared to be used for incorporation of radioiodine into the dimers, and *p*-iodobenzoyl-containing isophthaloyl dimers **24–26** were prepared as HPLC standards for radioiodinated Cbl derivatives.

Prior to the synthesis of the Cbl dimers **24–29**, the requisite activated isophthaloyl derivatives had to be prepared. The synthesis of ditetrafluorophenyl (TFP) esters of the iodobenzoyl and stannylbenzoyl adducts of 5-aminoisophthalic acid, **13** and **14**, is shown in Scheme 1. Conjugation of *p*-iodobenzoyl chloride with 5-aminoisophthalic acid gave a nearly quantitative yield of the crude adduct, **12**. Preparation of the di-TFP ester **13** was accomplished in 43% yield by reacting **12** with DCC and TFP-OH in ethyl acetate. Conversion of the aryl iodide, **13**, into the aryl stannane, **14**, was accomplished in 62% yield using bis(tributyltin) and palladium catalyst.

Biotinylated Cbl dimers were of interest as reagents for analytical studies. Therefore, Cbl dimers **30** and **31** were prepared. Rather than preparing all three isomeric biotinylated derivatives, only the Cbls containing *b*- and *e*-propionic acid side chains (**2** and **4**) were employed for cross-linking reactions. Indeed, we were primarily interested in the *e*-isomer of the biotinylated dimer as it was expected to have the highest binding with TCII, but since the Cbl *e*-carboxylate was available in small quantities, initial development of cross-linking reaction conditions was conducted with the more abundant *b*-carboxylate, **2**. Prior to cross-linking the aminoalkyl-Cbls **5** or **7**, a carboxylate activated–biotinylated aminoisophthalic acid derivative, **20**, had to be prepared. Although *N*-hydroxysuccinimido ester of biotin–aminocaproate was commercially available,⁴ the high cost of this reagent led us to synthesize the corresponding TFP ester, **18** (Scheme 2). Reaction of **18** with 5-aminoisophthalic acid provided

³ EDC is also referred to as EDAC (Sigma Chemical Co., St. Louis, MO); 1-ethyl-3-(3-(dimethylamino)propyl)carbodiimide.

⁴ For example: sulfosuccinimido-6-(biotinamido)hexanoate is available from Pierce (Rockford, IL) as NHS-LC-Biotin, and biotinamidocaproate *N*-hydroxysuccinimido ester is available from Sigma Chemical Co. (St. Louis, MO).

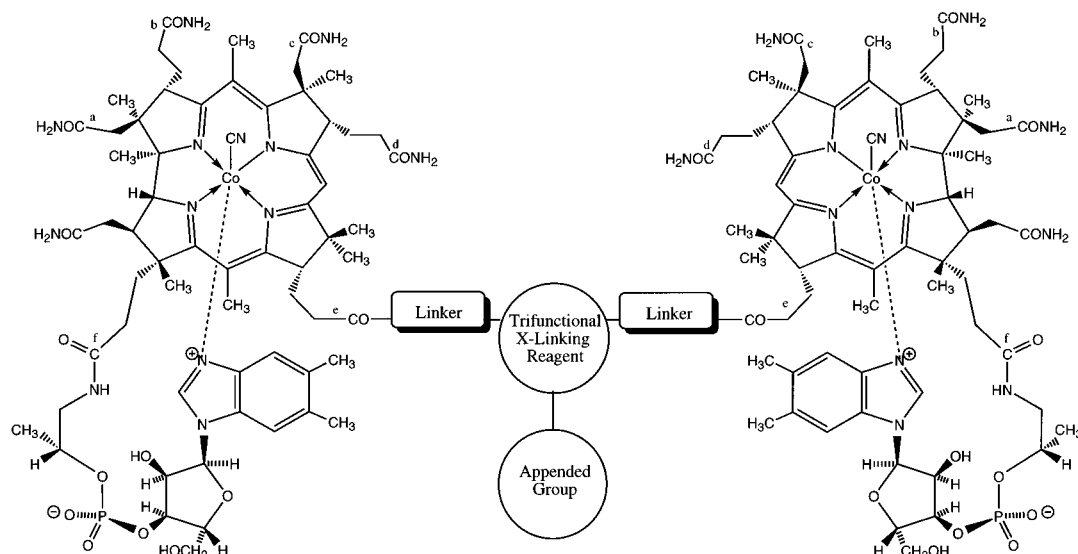
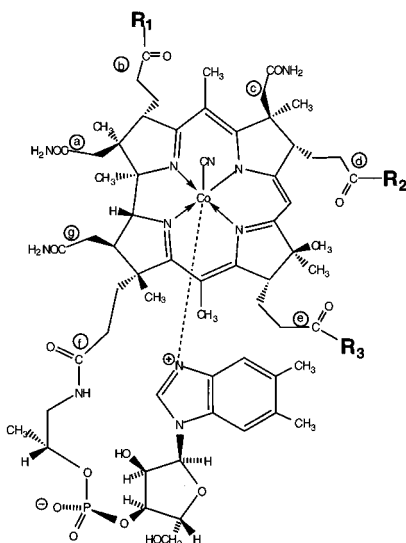


Figure 1. General schematic representation of CN-Cbl dimers. The dimers contain two Cbl moieties, two linking moieties, a cross-linking moiety, and, where desired, an appended group. This example depicts corrin ring *e*-propionamide attachment.

Chart 1. Structures of Cyanocobalamin Diamino Spacer Adducts

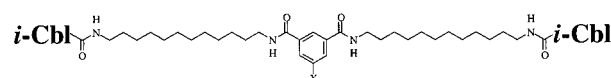


- 1 $R_1 = \text{NH}_2$; $R_2 = \text{NH}_2$; $R_3 = \text{NH}_2$
- 2 $R_1 = \text{OH}$; $R_2 = \text{NH}_2$; $R_3 = \text{NH}_2$
- 3 $R_1 = \text{NH}_2$; $R_2 = \text{OH}$; $R_3 = \text{NH}_2$
- 4 $R_1 = \text{NH}_2$; $R_2 = \text{NH}_2$; $R_3 = \text{OH}$
- 5 $R_1 = \text{HN}(\text{CH}_2)_{12}\text{NH}_2$; $R_2 = \text{NH}_2$; $R_3 = \text{NH}_2$
- 6 $R_1 = \text{NH}_2$; $R_2 = \text{HN}(\text{CH}_2)_{12}\text{NH}_2$; $R_3 = \text{NH}_2$
- 7 $R_1 = \text{NH}_2$; $R_2 = \text{NH}_2$; $R_3 = \text{HN}(\text{CH}_2)_{12}\text{NH}_2$
- 8 $R_1 = \text{HN}(\text{CH}_2)_3(\text{OCH}_2\text{CH}_2)_2\text{O}(\text{CH}_2)_3\text{NH}_2$; $R_2 = \text{NH}_2$; $R_3 = \text{NH}_2$
- 9 $R_1 = \text{NH}_2$; $R_2 = \text{HN}(\text{CH}_2)_3(\text{OCH}_2\text{CH}_2)_2\text{O}(\text{CH}_2)_3\text{NH}_2$; $R_3 = \text{NH}_2$
- 10 $R_1 = \text{NH}_2$; $R_2 = \text{NH}_2$; $R_3 = \text{HN}(\text{CH}_2)_3(\text{OCH}_2\text{CH}_2)_2\text{O}(\text{CH}_2)_3\text{NH}_2$

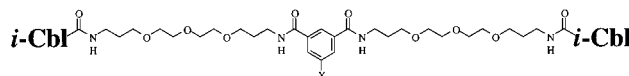
19 in 65% yield, and further conversion to **20** using the transesterification reagent tetrafluorophenyl trifluoroacetate (TFP-OCOCF₃) (**21**) was accomplished in 86% yield.

It became apparent after the synthesis of Cbl dimers **21–31** that they had limited water solubility. Fortunately, very low concentrations of Cbls are required to obtain biological data with these compounds, permitting *in vitro* evaluations to be conducted. However, the increased lipophilicity of the compounds was considered to be a potential problem with nonspecific binding and

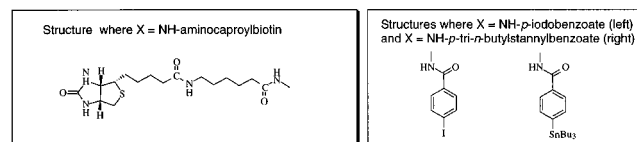
Chart 2. Cyanocobalamin Dimers Synthesized^a



- 21 $i = b$; $X = \text{H}$
- 22 $i = d$; $X = \text{H}$
- 23 $i = e$; $X = \text{H}$
- 24 $i = b$; $X = \text{NH-}p\text{-iodobenzoate}$
- 25 $i = d$; $X = \text{NH-}p\text{-iodobenzoate}$
- 26 $i = e$; $X = \text{NH-}p\text{-iodobenzoate}$
- 27 $i = b$; $X = \text{NH-}p\text{-tri-}n\text{-butylstannylbenzoate}$
- 28 $i = d$; $X = \text{NH-}p\text{-tri-}n\text{-butylstannylbenzoate}$
- 29 $i = e$; $X = \text{NH-}p\text{-tri-}n\text{-butylstannylbenzoate}$
- 30 $i = b$; $X = \text{NH-aminocaproylbiotin}$
- 31 $i = e$; $X = \text{NH-aminocaproylbiotin}$

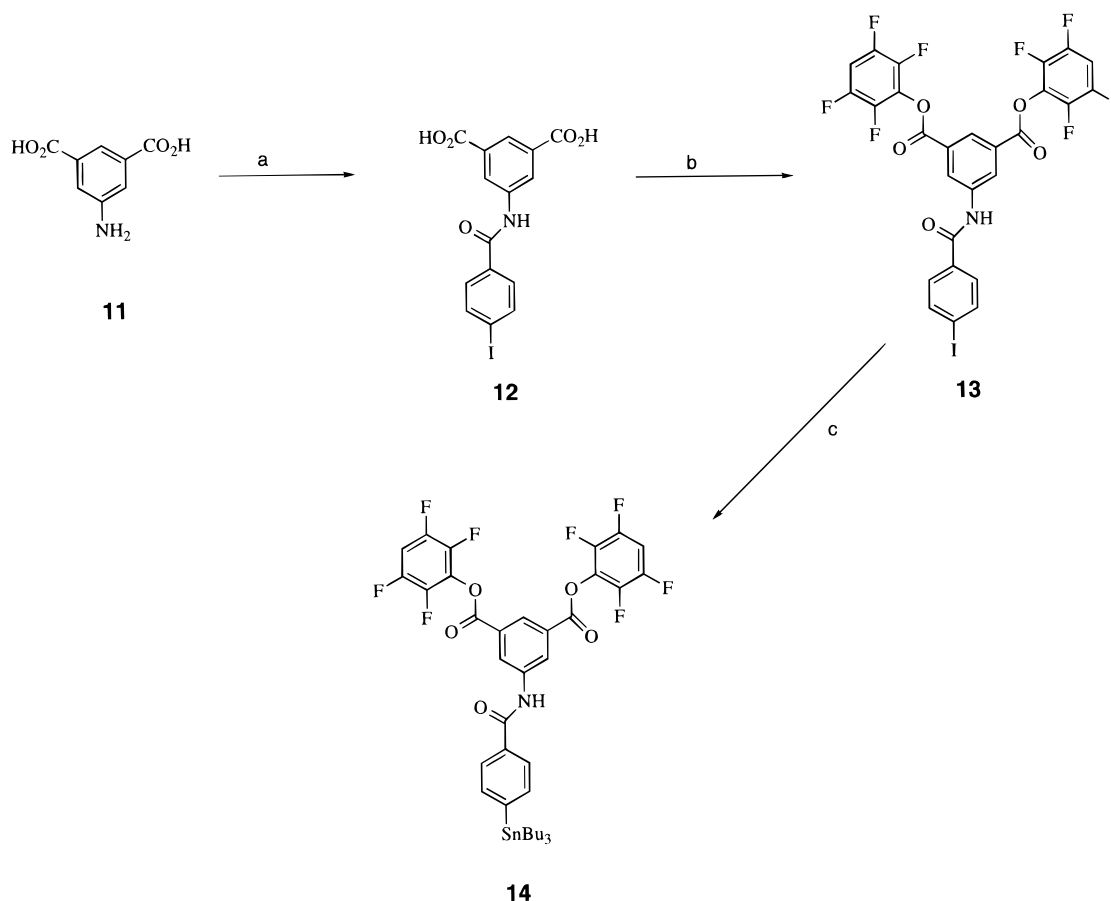


- 32 $i = b$; $X = \text{H}$
- 33 $i = b$; $X = \text{NH-aminocaproylbiotin}$
- 34 $i = e$; $X = \text{NH-aminocaproylbiotin}$



^a *i*-Cbl are isomers of Cbl carboxylates **2** (*b*), **3** (*d*), or **4** (*e*).

could ultimately make formulation of a pharmaceutical more difficult. Therefore, a method of water solubilization for the dimers was sought. The favored approach to solving this problem was to incorporate a more water soluble linking moiety. Thus, commercially available 4,7,10-trioxa-1,13-tridecanediamine was conjugated with two isomeric Cbl carboxylates, **2** and **4**, to yield Cbl adducts **8** and **10**. This linking arm is nearly the same length as the diaminododecane linker, resulting in distances between Cbl carboxylates of 41.6 Å for **23** (and related compounds) and 42.6 Å for **32** (and related compounds). The reason for preparing only the *b*- and *e*-isomers was based on availability of carboxylates as described previously. Conjugation of **8** with isophthaloyl dichloride provided Cbl dimer, **32**. Importantly, that compound was more soluble in water than its diaminododecane counterpart. Due to the anticipated increased water solubility of the simple isophthalate cross-linked molecules, the biotin dimers **33** and **34** were synthesized. The biotinylated Cbl dimers **33** and **34** were synthesized in 40–53% yield from the reaction of **8** or **10** with the

Scheme 1. Synthesis of Isophthalate DiTFP Ester Containing Iodobenzoate or Stannylbenzoate

^a 1 N NaOH/iodobenzoyl chloride/0 °C. ^b TFP-OH/DCC/3 days. ^c Bu₃Sn₂/(Ph₃P)₄Pd(O)/toluene/80 °C.

aminoisophthalate di-TFP ester **20**. Again, the resulting Cbl dimers were found to be more soluble in aqueous medium than their diaminododecane counterparts, **30** and **31**.

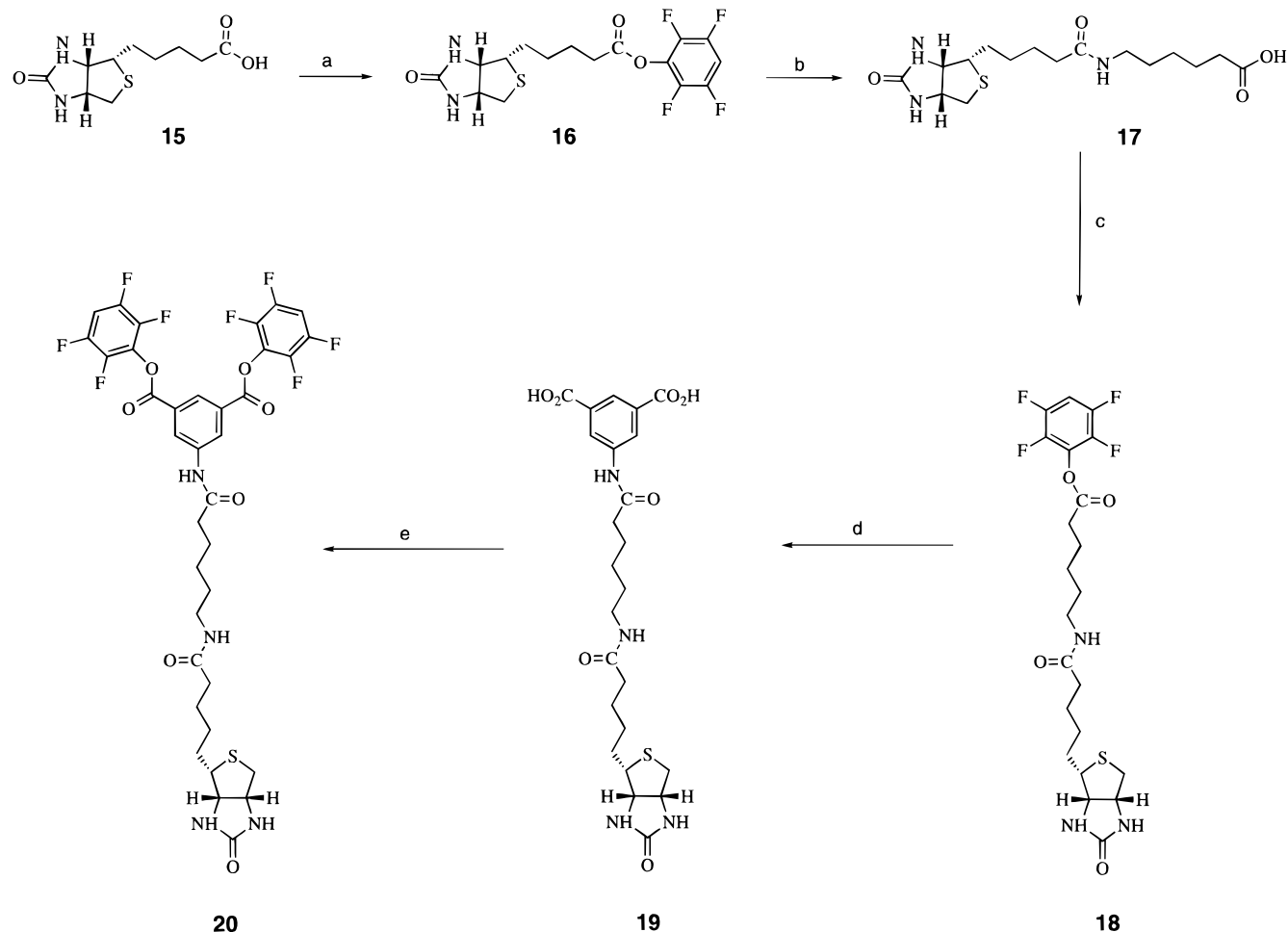
Iodination Reactions. Iodination and radioiodination of Cbl derivatives containing arylstannanes must be conducted under (near) neutral conditions or a side reaction for the formation of *c*-lactone can predominate (13). Attempts at iodination of HPLC purified stannyl derivatives **27–29** in MeOH using NaI and *N*-chlorosuccinimide (NCS)⁵ over a 30 min period resulted in no change in the starting material. Attempts at iodination using NaI/NCS in 5% HOAc/MeOH also did not alter the starting material. Because there was a concern that the iodide ion was somehow being inactivated toward oxidation with NCS (e.g. being bonded to the Co in the corrin ring), ICl was investigated as the iodination reagent. Attempts to iodinate **29** with ICl in MeOH over a 30 min period also failed to change the starting material; however, reaction of ICl in 5% HOAc/MeOH resulted in conversion to another compound. Unfortunately, the new compound was not the desired iodinated product as its HPLC retention time was not the same as that of **26**. Although the data obtained were insufficient to determine the nature of the new compound, it seems likely that it is the *c*-lactone derivative of **26**. An evaluation of the radioiodination of **29** also did not provide the desired compound.

The lack of conversion of the arylstannanes (**27–29**) to aryl iodides (**24–26**) was surprising. Under the reac-

tion conditions employed, no previous iodinations of arylstannyl-derivatized compounds have failed to affect rapid (generally <1 min) and nearly quantitative substitution of the stannyl group. This failure to react with electrophilic iodine could be due to unique nature of the Cbls synthesized. The mass spectral data and chemical shifts of butyl and aryl protons in the NMR spectra indicated that the arylstannane is present in the dimer. However, the HPLC retention time of the arylstannane derivatives **27–29** was not as expected. Generally on reversed phase HPLC, aryltri-*n*-butylstannyl derivatives are retained much longer than the corresponding aryl iodide derivatives. This was not the case with compounds **27–29**, as they had shorter retention times (8.6–9.0 min) than the corresponding aryl iodides **24–26** (14.1–14.2 min). Since the spectral data suggest that the compounds are as depicted in Table 2, it is very difficult to understand how this increased polarity is obtained in the arylstannyl Cbl dimers. We can only hypothesize that the lipophilic linker arms and the lipophilic arylstannane are somehow compressed between the more hydrophilic Cbl moieties, perhaps causing a shift in the benzimidazole rings or other portion of the molecule, making it more hydrophilic. It is anticipated that we will be able to obtain more information on the structures through a crystal structure determination of the aryl iodide derivative **26**. An attempt to obtain the crystal structure of **26** is underway.

Competitive Binding with TCII. Cbl dimers were evaluated for their binding to rhTCII in a competitive assay that measures the binding relative to CN-Cbl (**12**). The assay employed partially purified rhTCII as the binding protein, and high specific activity (e.g. 200 μCi/

⁵ These reagents were used because the conditions mimic the radioiodination reaction conditions where NCS oxidizes Na[*I] to an electrophilic species *in situ*.

Scheme 2. Synthesis of Isophthalate DiTFP Ester Containing Aminocaproylbiotin Substituent

^a DCC/DMF/TFP/0 °C. ^b Aminocaproic acid/Et₃N. ^c DMSO/Et₃N/TFP-OTFA. ^d DMF/Et₃N/5-aminoisophthalic acid/8 days. ^e DMF/Et₃N/TFP-OTFA.

μg) [⁵⁷Co]CN-Cbl as the tracer. The assay measures the decrease in the binding of [⁵⁷Co]CN-Cbl in the presence of increasing concentrations of a Cbl dimer. The competitive binding curves for Cbl dimers are shown in Figure 2. The binding curves for the four isophthalate cross-linked dimers, **21**–**23** and **32**, relative to CN-Cbl, **1**, are shown in Figure 2A. The data show that the *e*-isomer, **23**, binds more avidly than the *b*-isomer, **21**, or the *d*-isomer, **22**. It is interesting to note that the compounds of **21**–**23** appear to bind less avidly than the corresponding monomeric Cbls **5**–**7**, previously tested (12). The differences observed could be due to the decreased water solubility of the dimers compared to the monomers. Indeed, water solubility appears to affect Cbl binding as the more water soluble trioxadiazine-linked Cbl-*b*-dimer, **32**, bound more avidly than the diaminododecane Cbl-*b*-dimer, **21**.

Evaluation of iodobenzoyl-containing Cbl dimers, **24**–**26**, provided similar results to those observed for the other diaminododecane-containing dimers **21**–**23** (Figure 2B). Again, only the *e*-isomer, **26**, bound competitively with [⁵⁷Co]-**1**, and its binding appeared to be reduced from that of the monomeric counterpart **7**. Binding assays were not conducted on the stannylbenzoate-containing dimers **27**–**29** as these compounds were only to be used as intermediates to prepare (radio)iodinated derivatives **24**–**26**.

The results obtained for the biotinylated derivatives **30**, **31**, **33**, and **34** are shown in Figure 2C. Binding of the water-solubilized *b*- and *e*-isomers, **33** and **34**, to

rhTCII is similar to the isomeric monomers **5** and **7**. The *e*-isomer, **31**, which contains the less water soluble diaminododecane linking moiety, does not bind as competitively as the corresponding more water soluble *e*-isomer, **34**. Again, this difference may be due to the lower water solubility of **31**. Relative binding data for the Cbl dimers are provided in Table 1. From the data, the decrease in binding (from 100%) and the effect of various modifications in the Cbl dimers on binding can be readily assessed. It is interesting to note that substitution on the isophthalate moiety appears to have little effect on TCII binding, whereas there is a significant improvement in binding with the addition of the trioxadiazine linker.

One of the questions we attempted to address in this investigation was whether a Cbl dimer could bind two TCII protein molecules. On the basis of the data obtained from the competitive binding assay, it appears that under the assay conditions (e.g. excess Cbl), only one Cbl moiety in the dimers bound with rhTCII. However, unless large quantities (e.g. micrograms–milligrams) of a dimer were injected in patients, the amount of TCII should be in excess even when considering endogenous Cbls (8, 29). The results obtained in the competitive binding assay are not surprising as it seems likely that binding of a Cbl dimer with the one TCII molecule could occur at a rate similar to a monomer but that the second TCII molecule would have to combine with a Cbl that was highly sterically hindered from the side that had bound TCII. This would suggest that binding with a second TCII

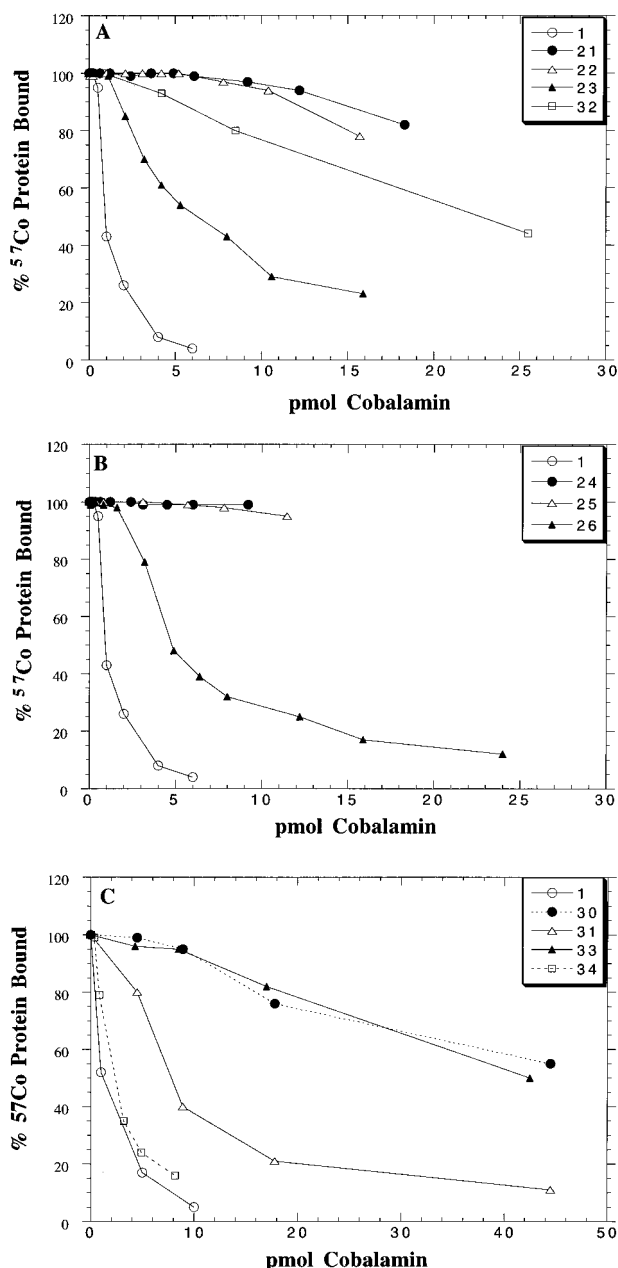


Figure 2. Competitive binding curves for $[^{57}\text{Co}]\text{CN-Cbl}$, **1**, and Cbl dimers **21–26** and **30–34** with rhTCII. To obtain the data, a quantity of rhTCII that would bind approximately 1 pmol of CN-Cbl was mixed with 0.01 pmol of $[^{57}\text{Co}]\text{-1}$ and 0.01–30 pmol of unmodified **1** or Cbl dimer. The mixture was diluted with PBS/HSA and incubated at rt for 1 h. Free Cbl was adsorbed onto hemoglobin-coated charcoal, and the protein-bound radioactivity in the supernatant fraction was measured. The amount of protein-bound ^{57}Co versus the amount of Cbl derivative present is plotted in panels A–C. Panel A (top) compares the competitive binding of the isophthalate cross-linked Cbl dimers that employed diaminododecane linker (**21**, **22**, **23**) and trioxadecanamine linker (**32**) with CN-Cbl (**1**). Panel B (middle) compares the competitive binding of *p*-iodobenzoyl-5-aminoisophthalate cross-linked Cbl dimers (**24**, **25**, **26**) with **1**. Panel C (bottom) compares the competitive binding of biotin containing Cbl dimers that employed the diaminododecane linker (**30**, **31**) and the trioxadecanamine linker (**33**, **34**) with **1**.

molecule might occur at a much slower rate. Determination of whether the dimers described herein bind with two rhTCII molecules when the TCII is in excess has proven to be difficult with *partially purified* rhTCII. Thus, future studies will be directed at obtaining radioiodinated Cbl dimers to improve sensitivity of detecting

Cbl/TCII complexes by electrophoresis and size exclusion HPLC.

SUMMARY

Fourteen isophthalate cross-linked Cbl dimers have been synthesized. To our knowledge, the reported compounds represent the first preparation of Cbl dimers that are coupled at a position other than at the Co atom. The Cbl dimers were prepared by cross-linking with carboxylate-activated derivatives of isophthalic acid or derivatized aminoisophthalic acid. To provide a distance between the Cbl moieties such that two TCII proteins might bind a Cbl dimer, linking molecules were incorporated between the Cbl moieties and the isophthalic acid moieties. The linker first evaluated, 1,12-diaminododecane, was found to decrease the water solubility of the Cbls considerably; therefore, a more water soluble linker, 4,7,10-trioxo-1,13-tridecanediamine, was also evaluated. The trioxatridecanediamine improved the water solubility significantly. In the investigation, Cbl dimers were evaluated for their binding with rhTCII. Analysis of the binding data shows that most of the Cbl dimers bound less avidly to rhTCII than CN-Cbl. As expected, the Cbl *ε*-carboxylate derived dimers bound most avidly of the three isomeric carboxylates studied. The more water soluble dimers bound rhTCII more avidly than their aliphatic counterparts, resulting in binding that was nearly equivalent to that of CN-Cbl for the *ε*-carboxylate isomer.

In this initial investigation, the Cbl dimers synthesized have provided basic information about their chemistry and binding to TCII. Studies are planned to prepare additional water soluble Cbl dimers and to obtain radioiodinated Cbl dimers. Once a radioiodinated Cbl dimer is obtained, the question of whether it can bind two TCII molecules will be assessed. It is anticipated that more highly derivatized Cbl dimers will be needed to be effective in Cbl/TCII cell surface receptor depletion, but all Cbl derivatives synthesized will be evaluated for potency as antiproliferative agents in *in vitro* assays. The data obtained from *in vitro* analyses will be reported elsewhere.

ACKNOWLEDGMENT

We thank Dr. Ross Lawrence (Medicinal Chemistry Department, University of Washington) for his efforts in obtaining mass spectral data on the Cbl derivatives. We are grateful for the financial support provided by Receptagen Corp. to conduct these studies.

Supporting Information Available: HPLC chromatograms and ^1H NMR spectra of trioxadecanamine Cbl derivatives **8–10**, Cbl dimers **21–34**, iodobenzoyl and stannylbenzoyl aminoisophthalates **13** and **14**, and biotinylated derivatives **18**, **19**, and **20** (39 pages). Ordering information is given on any current masthead page.

LITERATURE CITED

- Banerjee, R. V., and Matthews, R. G. (1990) Cobalamin-Dependent Methionine Synthase. *FASEB J.* **4**, 1450–1459.
- Weissbach, H., and Taylor R. T. (1968) Metabolic Role of Vitamin B₁₂. *Vitamins and Hormones* (R. S. Harris, I. G. Wool, and J. A. Loraine, Eds.) Vol. 26, pp 395–412, Academic Press, New York.
- Myasishcheva, N. V. (1990) Cobalamin metabolism in acute lymphoblastic leukaemia in children. *Biomedicine and Physiology of Vitamin B₁₂* (J. C. Linnell and H. R. Bhatt, Eds.) pp 193–198, Children's Medical Charity, London.
- Faludy, J. E., and Linnell, J. C. (1990) Cobalamin metabolism in human leukæmia cell lines: a pilot study. *Biomedicine*

- and Physiology of Vitamin B₁₂ (J. C. Linnell and H. R. Bhatt, Eds.) pp 199–205, Children's Medical Charity, London.
- (5) Lassen, H. C. A., and Kristensen, H. S. (1959) Remission in chronic myeloid leukaemia following prolonged nitrous oxide inhalation. *Danish Med. Bull.* 6, 252–254.
 - (6) Eastwood, D. W., Green, C. D., Lambdin, M. A., and Gardner, R. (1963) Effect of nitrous oxide on the white-cell count in leukemia. *New Engl. J. Med.* 268, 297–299.
 - (7) Hall, A. C. (1990) The role of Transcobalamin II in the cellular uptake of cobalamin. *Biomedicine and Physiology of Vitamin B₁₂* (J. C. Linnell and H. R. Bhatt, Eds.) pp 239–253, Children's Medical Charity, London.
 - (8) Seetharam, B. (1994) Gastrointestinal Absorption and Transport of Cobalamin (Vitamin B₁₂). *Physiology of the Gastrointestinal Tract* (L. R. Johnson, Ed.) pp 1997–2026, Raven Press, New York.
 - (9) Quadros, E. V., Sai, P., and Rothenberg, S. P. (1994) Characterization of the Human Placental Membrane Receptor for Transcobalamin II–Cobalamin. *Arch. Biochem. Biophys.* 308, 192–199.
 - (10) Jacobsen, D. W., Amagasaki, T., and Green, R. (1990) Synthesis and recycling of the Transcobalamin II receptor. *Biomedicine and Physiology of Vitamin B₁₂* (J. C. Linnell and H. R. Bhatt, Eds.) pp 293–306, Children's Medical Charity, London.
 - (11) De Duve, C., de Barsy, T., Poole, B., Trouet, A., Tulkens, P., and Van Hoof, F. (1974) Lysosomotropic Agents. *Biochem. Biopharmacol.* 23, 2495–2531.
 - (12) Pathare, P. M., Wilbur, D. S., Heusser, S., Quadros, E. V., McLoughlin, P., and Morgan, A. C. (1996) Synthesis of Cobalamin-Biotin Conjugates Which Vary in Position of Coupling. An Evaluation of the Location of Conjugated Groups on Transcobalamin II Binding. *Bioconjugate Chem.* 7, 217–232.
 - (13) Wilbur, D. S., Hamlin, D. K., Pathare, P. M., Heusser, S., Vessella, R. L., Buhler, K. R., Stray, J. E., Daniel, J., Quadros, E. V., McLoughlin, P., and Morgan, A. C. (1995) Synthesis and *nca*-Radioiodination of Arylstannylcobalamin Conjugates. Evaluation of Aryliodocobalamin Conjugate Binding to Transcobalamin II and Biodistribution in Mice. *Bioconjugate Chem.* 7, 461–474.
 - (14) Bonnett, R. (1982) Reactions of the Corrin Macrocyclic. *B₁₂: Vol. I—Chemistry* (D. Dolphin, Ed.) pp 201–243, Wiley, New York.
 - (15) Morley, C. G. D., Blakley, R. L., and Hogenkamp, H. P. C. (1968) Analogs of Deoxyadenosylcobalamin with Alterations in a Side Chain of the Corrin Ring. *Biochemistry* 7, 1231–1239.
 - (16) Kenley, J. S., Leighton, M., and Bradbeer, C. (1978) Transport of Vitamin B₁₂ in *Escherichia coli*. Corrinoid Specificity of the Outer Membrane Receptor. *J. Biol. Chem.* 253, 1341–1346.
 - (17) Toraya, T., Krodel, E., Mildvan, A. S., and Abeles, R. H. (1979) Role of Peripheral Side Chains of Vitamin B₁₂ Coenzymes in the Reaction Catalyzed by Dioldehydrase. *Biochemistry* 18, 417–426.
 - (18) Wilbur, D. S. (1992) Radiohalogenation of Proteins: An Overview of Radionuclides, Labeling Methods, and Reagents for Conjugate Labeling. *Bioconjugate Chem.* 3, 433–470.
 - (19) Kabalka, G. W., and Varma, R. S. (1989) The Synthesis of Radiolabeled Compounds Via Organometallic Intermediates. *Tetrahedron* 45, 6601–6621.
 - (20) Wilbur, D. S., Hamlin, D. K., Vessella, R. L., Stray, J. E., Buhler, K. R., Stayton, P. S., Klumb, L. H., Pathare, P. M., and Weerawarna, S. A. (1996) Antibody Fragments in Tumor Pretargeting. Evaluation of Biotinylated Fab' Co-Localization with Recombinant Streptavidin and Avidin. *Bioconjugate Chem.* 7, 689–702.
 - (21) Gamper, H. B., Reed, M. W., Cox, T., Viroso, J. S., Adams, A. D., Gall, A. A., Scholler, J. K., and Meyer, R. B. (1993) Facile preparation of nuclease resistant 3' modified oligodeoxynucleotides. *Nucleic Acids Res.* 21, 145–150.
 - (22) Quadros, E. V., Sai, P., and Rothenberg, S. P. (1993) Functional human transcobalamin II isoproteins are secreted by insect cells using the Baculovirus expression system. *Blood* 81, 1239–1245.
 - (23) Quadros, E. V., Rothenberg, S. P., Pan, Y. Ch. E., and Stein, S. (1986) Purification and molecular characterization of human transcobalamin II. *J. Biol. Chem.* 261, 15455–15460.
 - (24) Lau, K. S., Gottlieb, C., Wasserman, L. R., and Herbert, V. (1965) Measurement of serum vitamin B₁₂ level using radioisotope dilution and coated charcoal. *Blood* 26, 202–214.
 - (25) Toohey, J. I. (1993) Hydrosulfide Derivatives of Cobalamins. *J. Inorg. Biochem.* 49, 189–199.
 - (26) Krautler, B., Derer, T., Liu, T., Muhlecker, W., Puchberger, M., Gruber, K., and Kratky, C. (1995) Oligomethylene-Bridged Vitamin B₁₂ Dimers. *Angew. Chem., Int. Ed. Engl.* 34, 84–86.
 - (27) Linnell, J. C. (1975) The fate of Cobalamins *in vivo*. In *Cobalamin. Biochemistry and Pathophysiology* (B. M. Babior, Ed.) Chapter 6, pp 287–333, Wiley, New York.

BC970003+

SUPPORTING INFORMATION

BC 970003†

for manuscript entitled:

SYNTHESIS OF COBALAMIN DIMERS USING ISOPHTHALATE CROSS-LINKING OF CORRIN RING CARBOXYLATES AND EVALUATION OF THEIR BINDING TO TRANSCOBALAMIN II.

Pradip M. Pathare[†], D. Scott Wilbur^{*†}, Donald K. Hamlin[†], Shannon Heusser[†], Edward V. Quadros[‡],
Patricia McLoughlin[‡], and A. Charles Morgan^{§,†}

[†]Department of Radiation Oncology, University of Washington, Seattle, WA 98195,

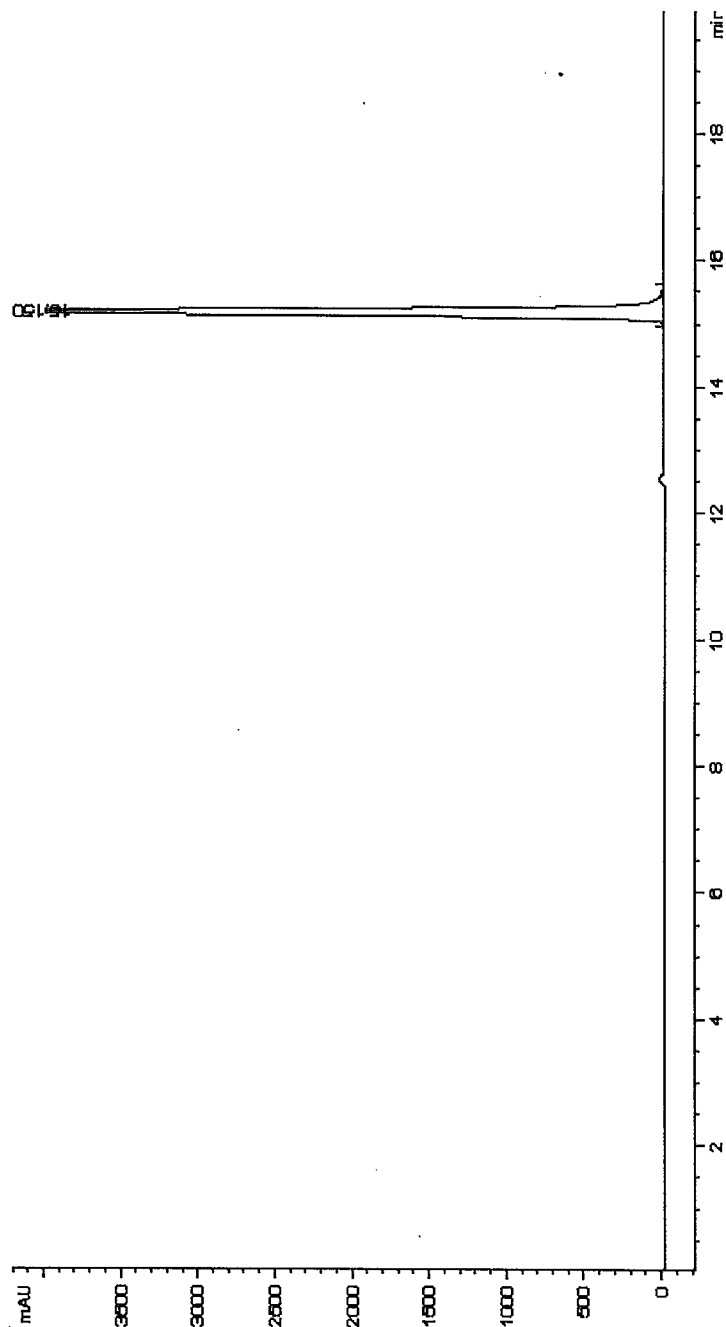
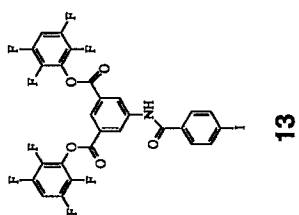
[‡]VA Medical Center-SUNY Health Science Center, Brooklyn, NY 11209,

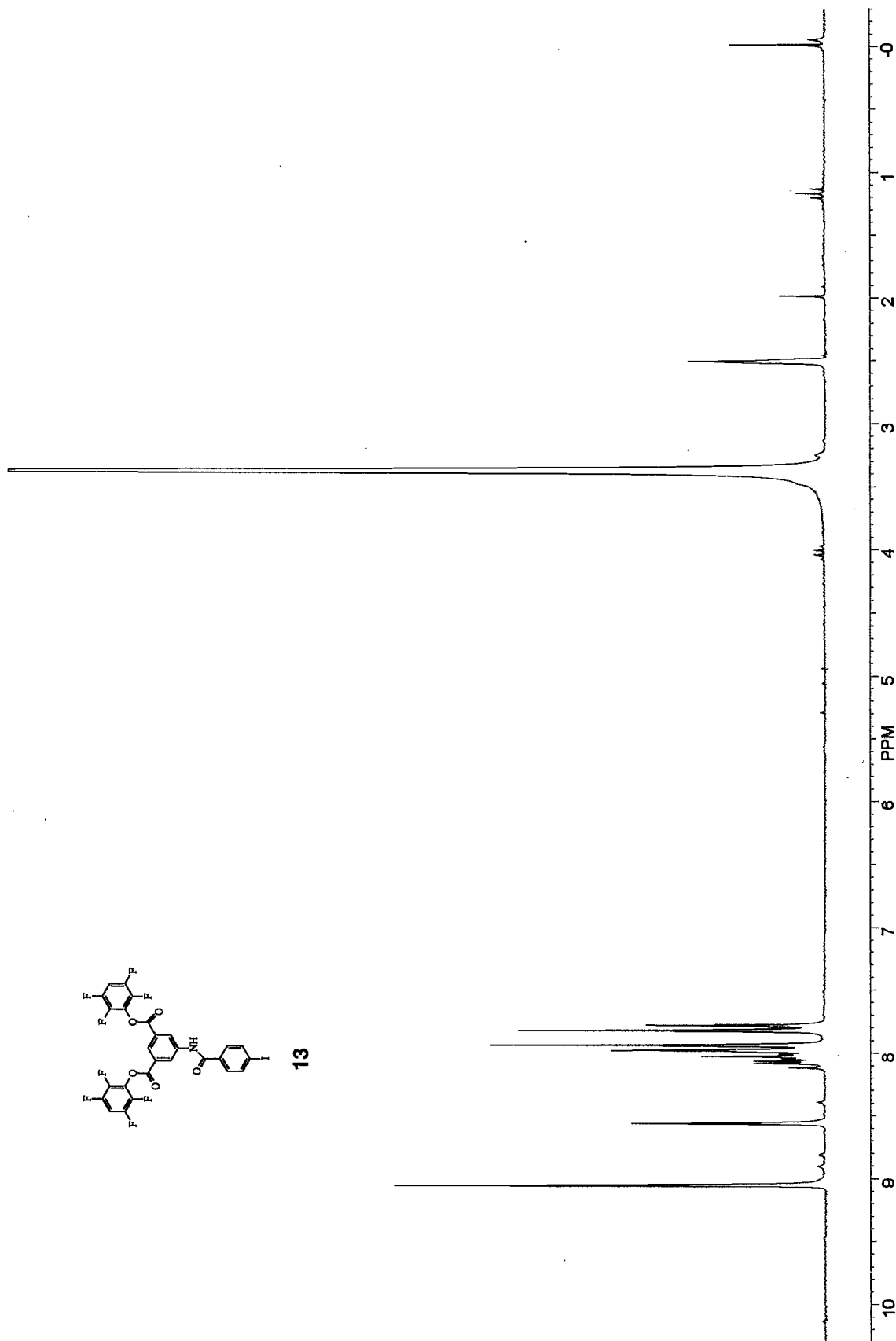
and [§]Receptagen Corporation, Edmonds, WA 98020

Comments on Spectra and Chromatograms:

Note that the HPLC chromatograms of cobalamins were obtained from compounds purified by reversed-phase HPLC for analytical purposes. In most examples, the NMR spectra was obtained from purified material, but not necessarily as highly purified as the analytical HPLC samples. The stannylbenzoyl cobalamin derivatives **27**, **28**, **29** were not purified as they were not found to be useful in the iodination / radioiodination reactions. Thus, the HPLC and NMR data for these compounds reflect the crude reaction products. Compound **28** (*d*-isomer) was purified by HPLC to show that the iodination / radioiodination reactions were not affected by purity.

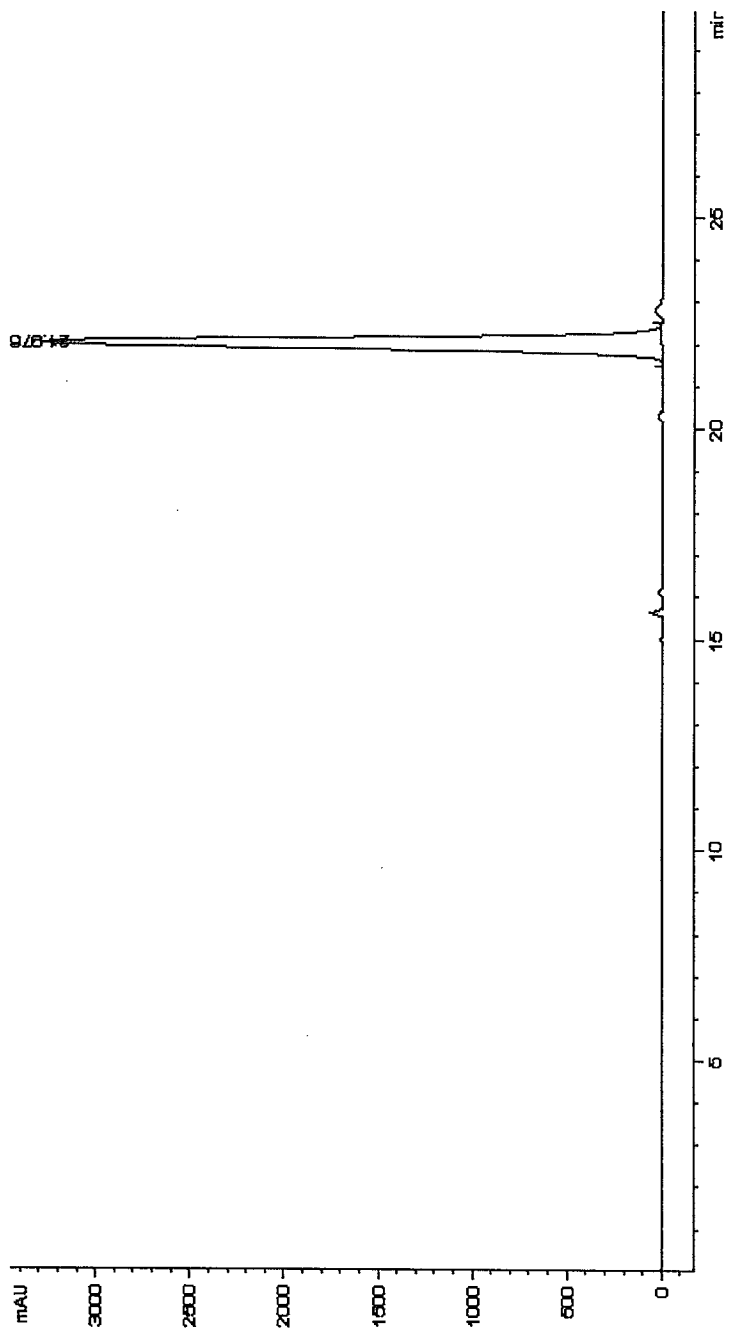
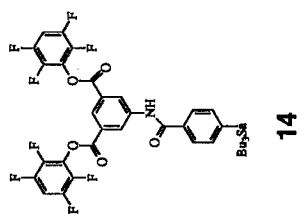
**CONFIDENTIAL
COMMUNICATION**

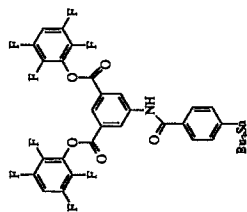




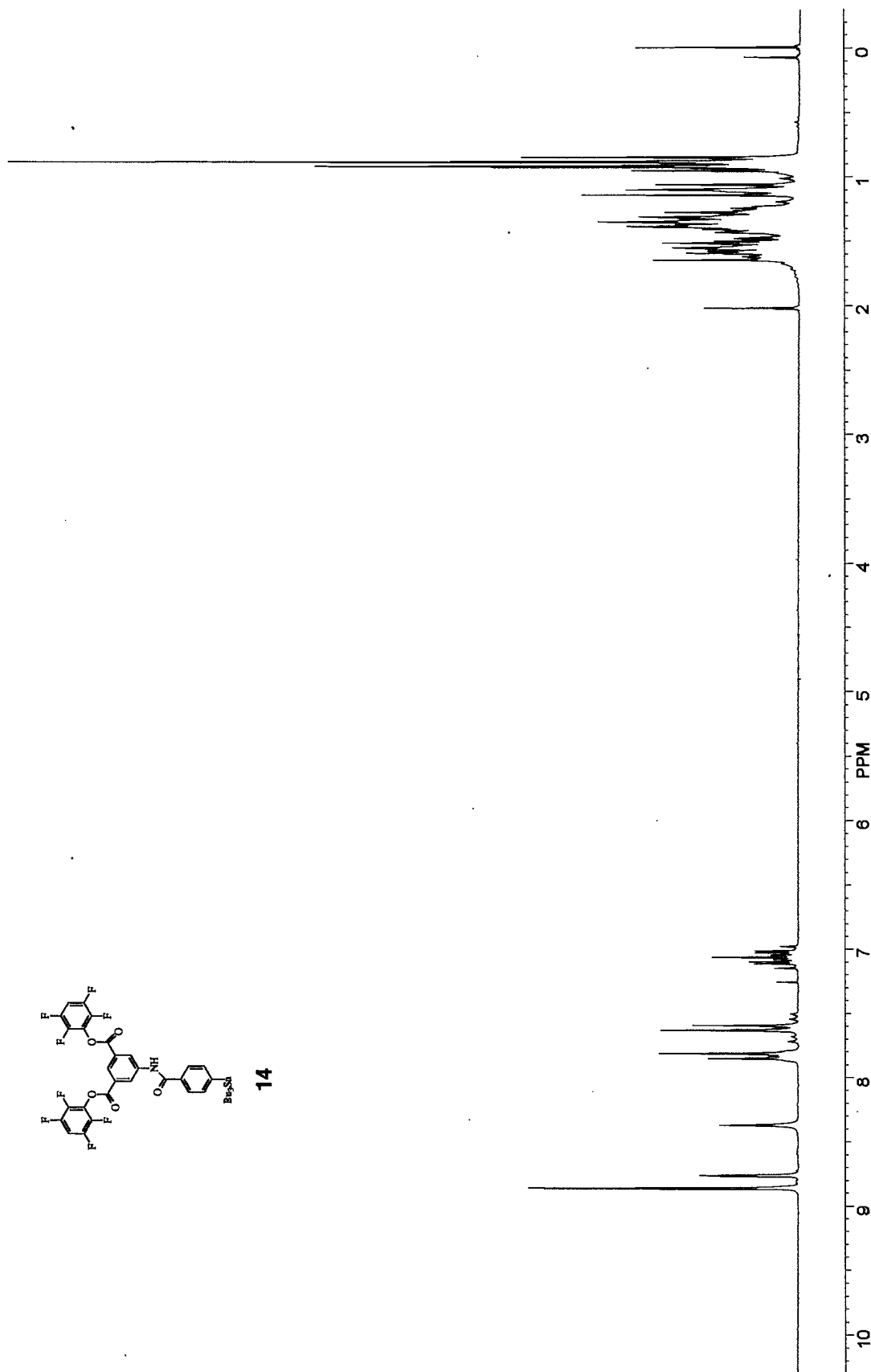
200 MHz; DMSO-d₆

4



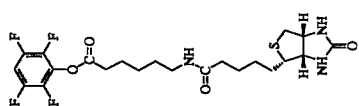


14

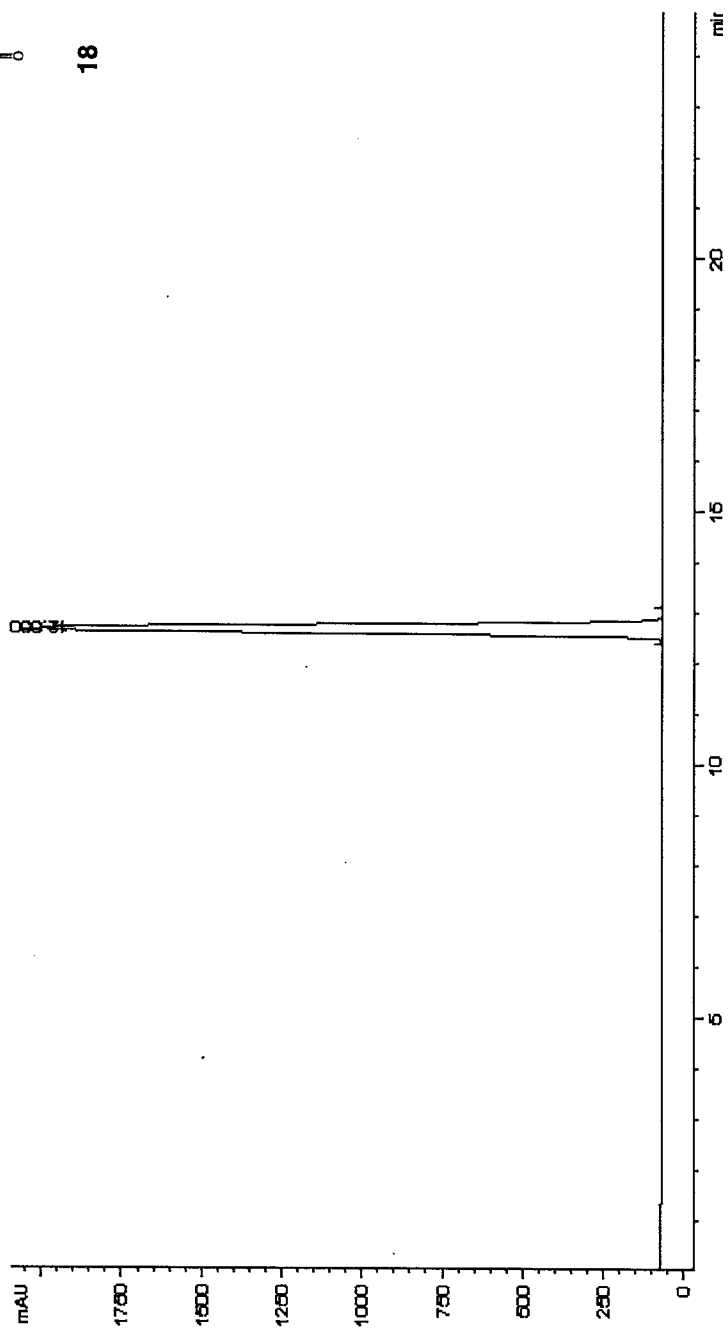


200 MHz; CDCl₃

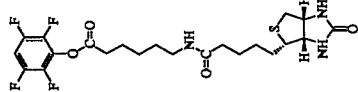
6



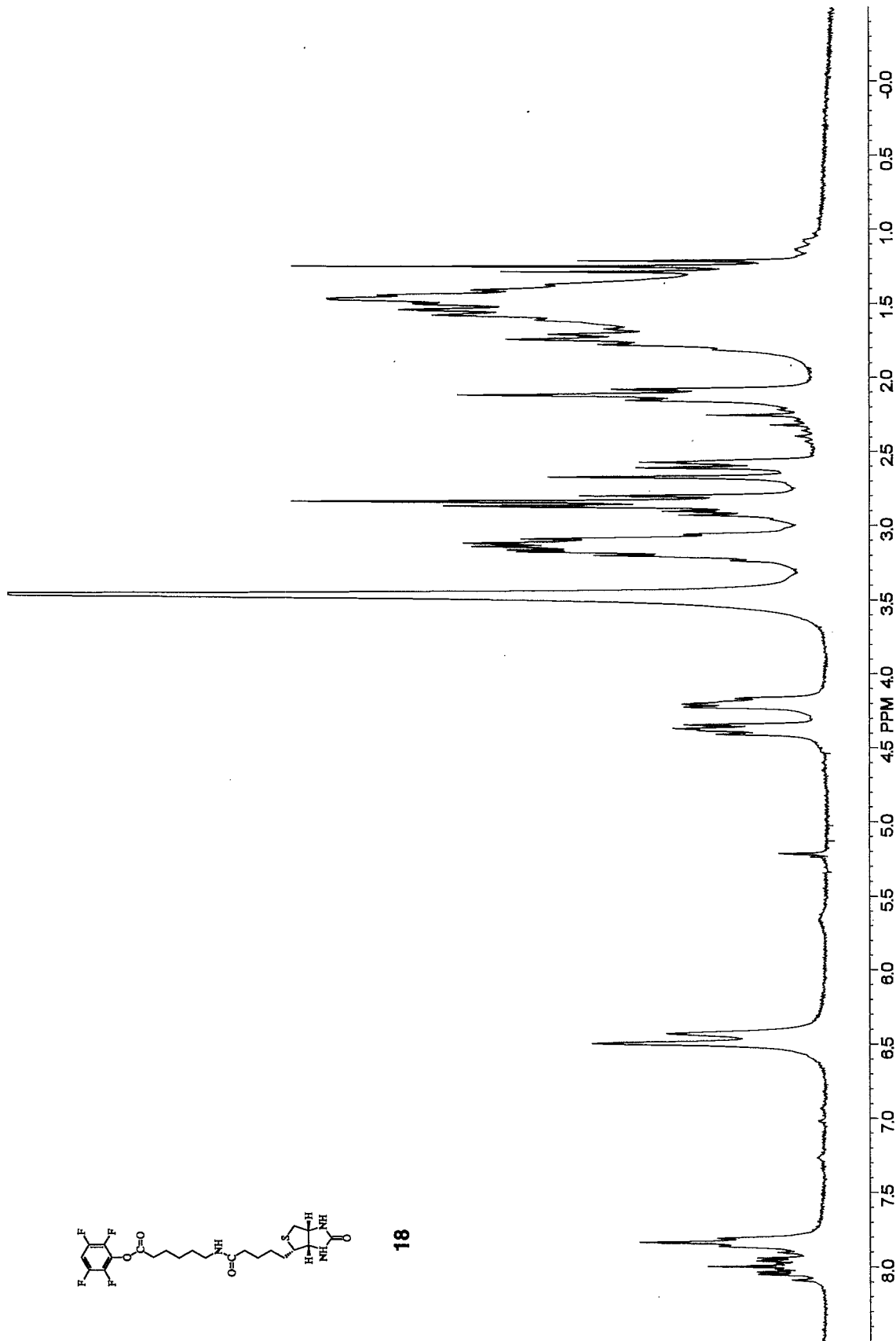
18



7

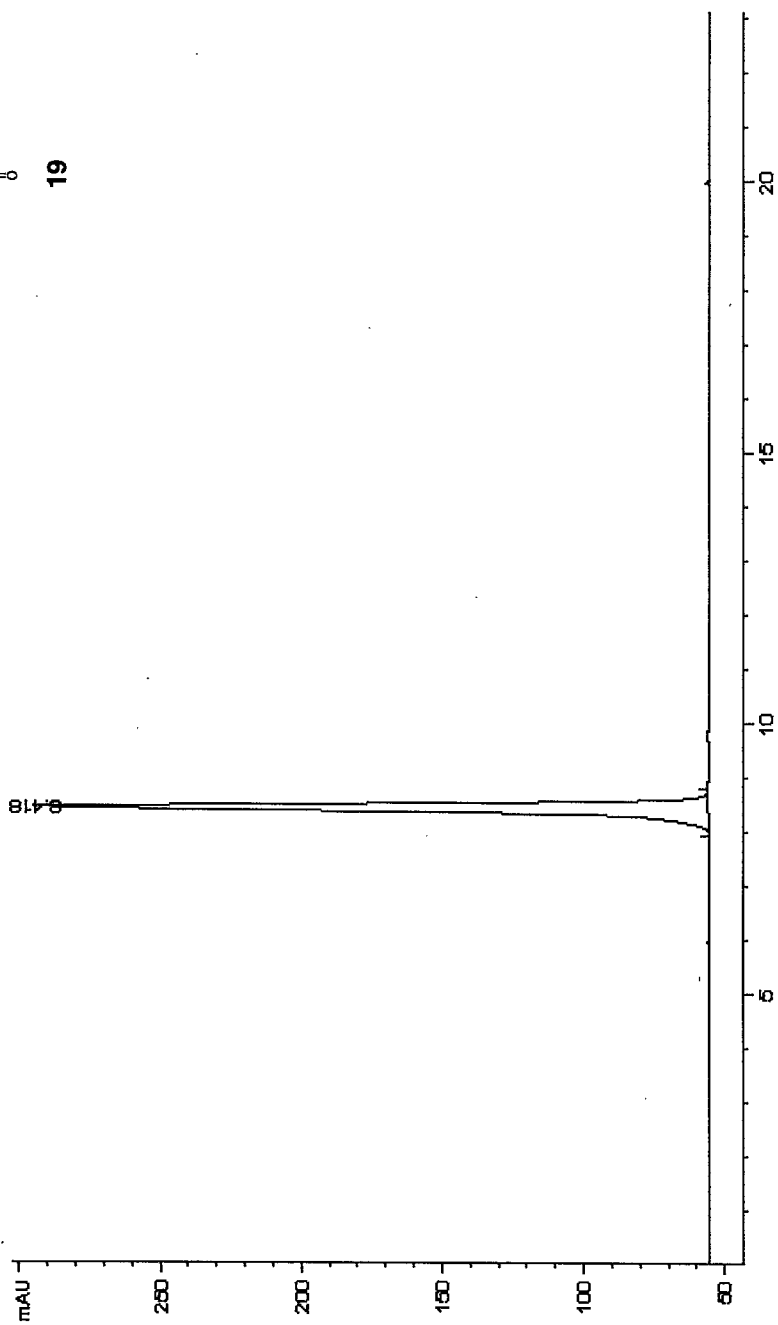
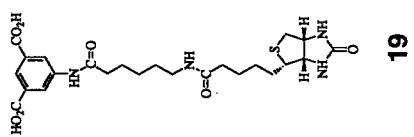


18

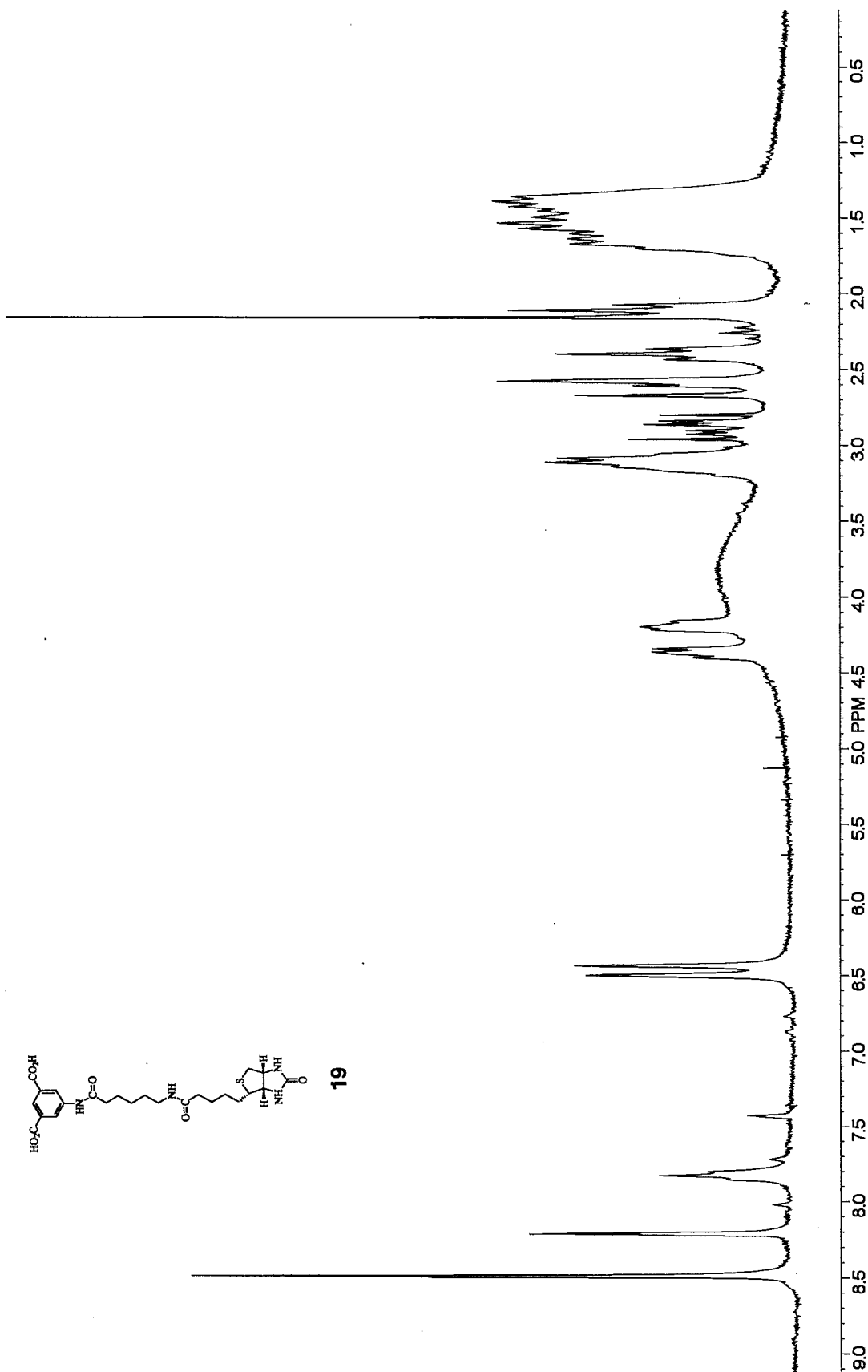


200 MHz; DMSO-d₆

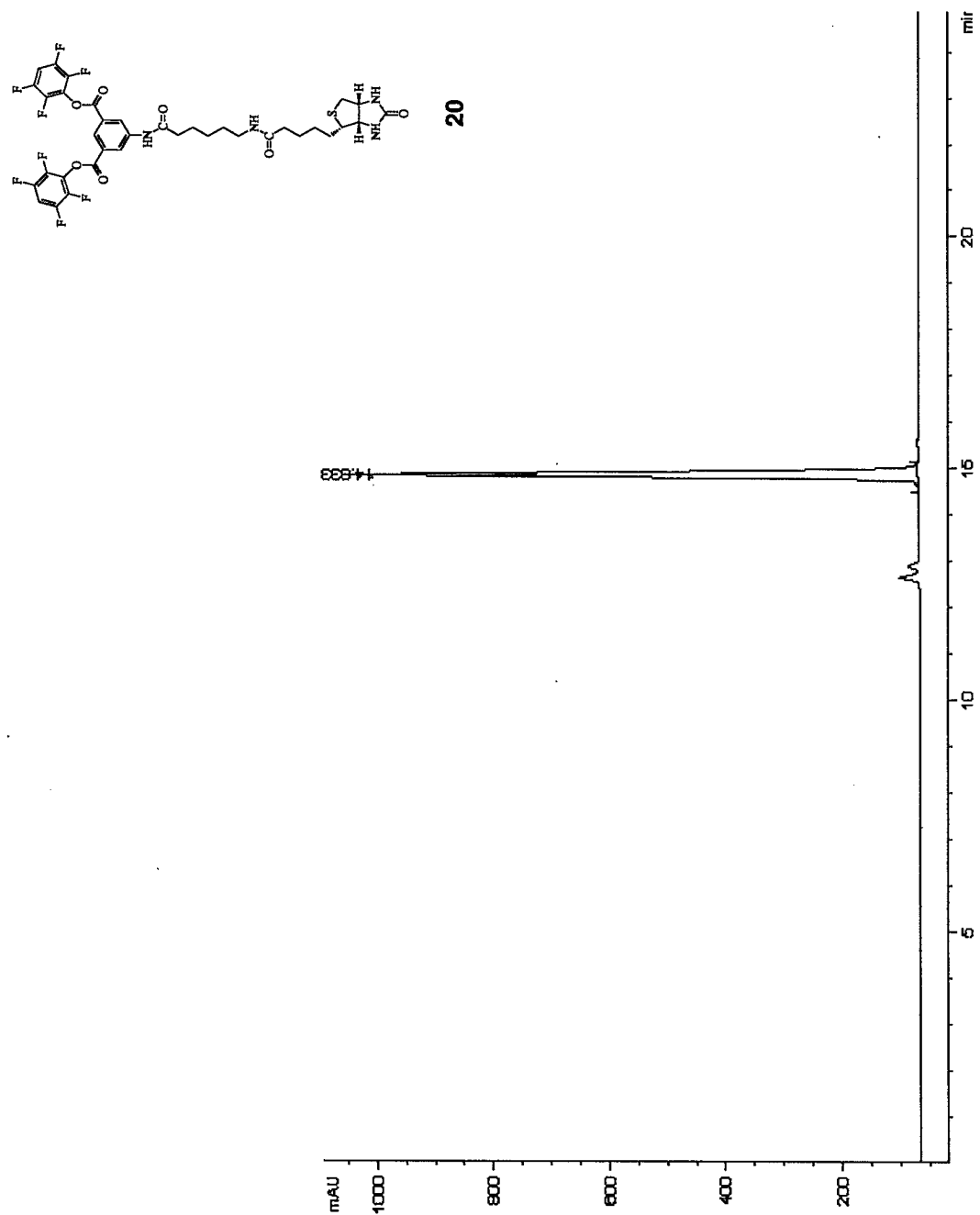
8

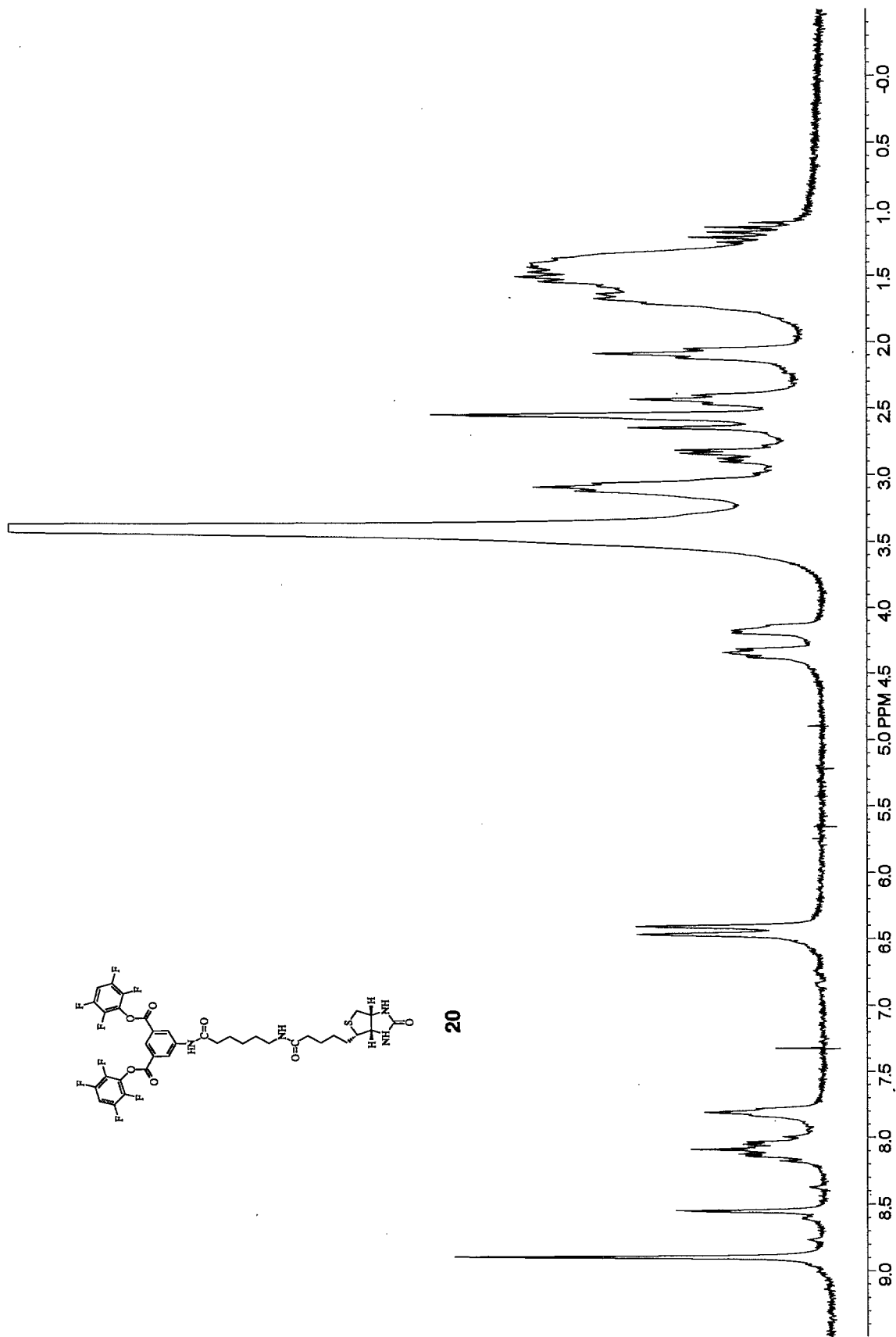


9

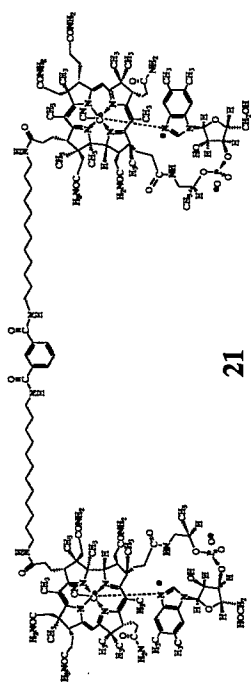


200 MHz; DMSO-d₆

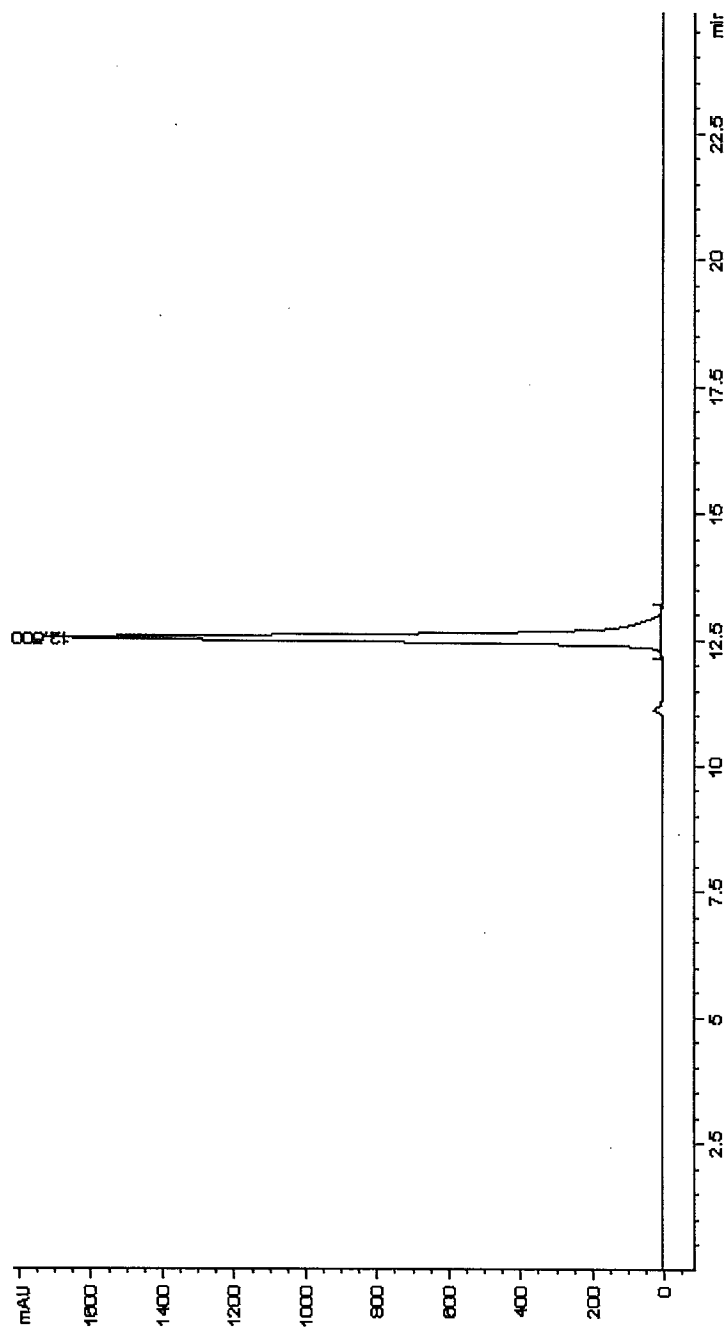




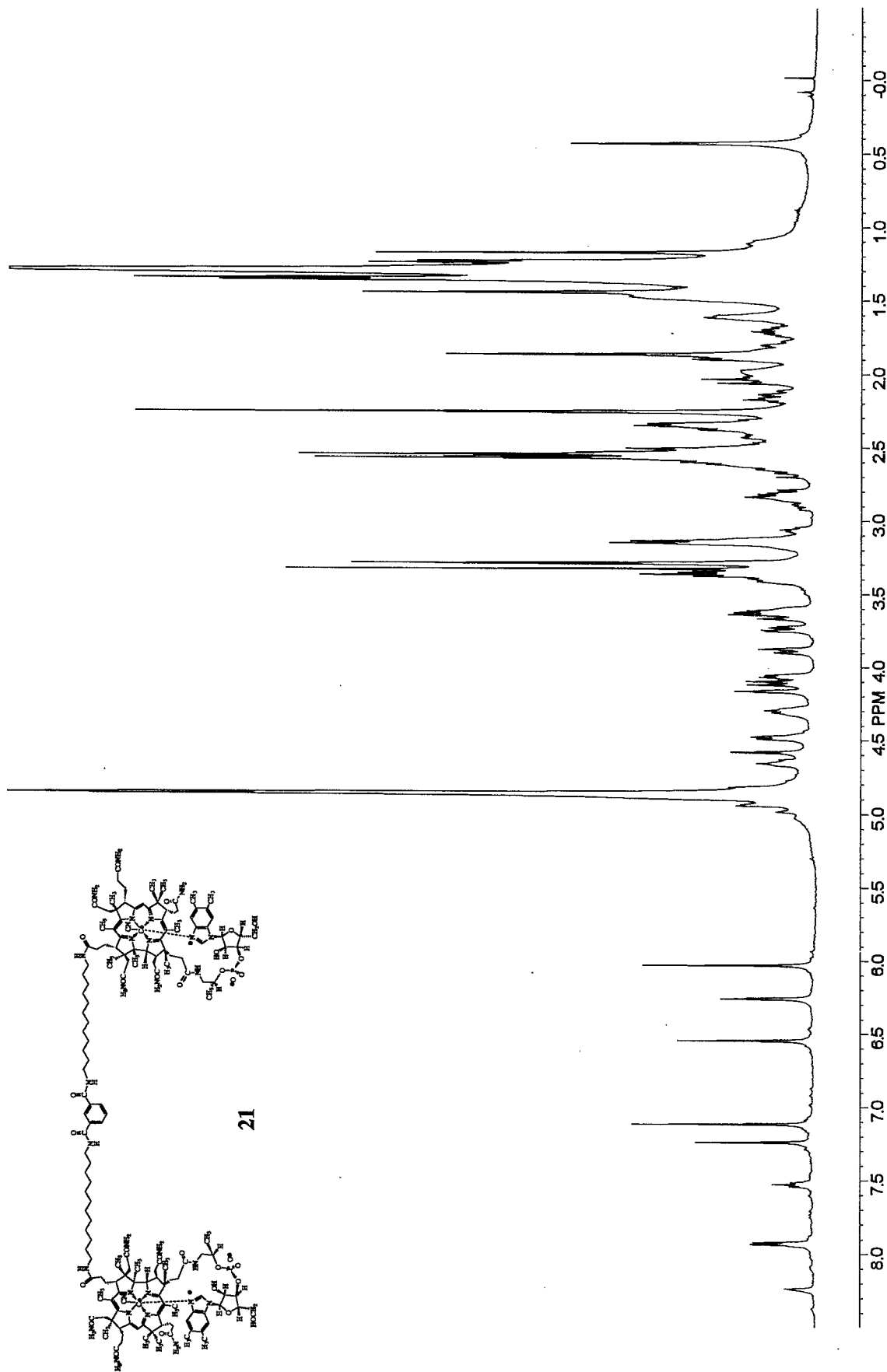
200 MHz; DMSO-d₆



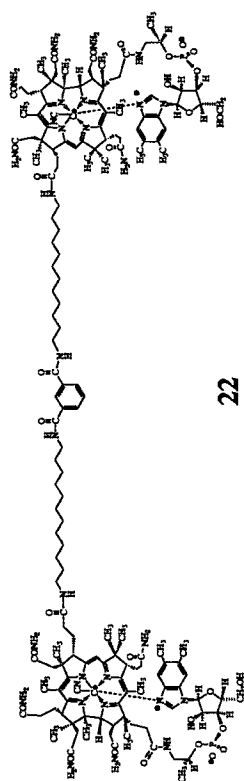
21



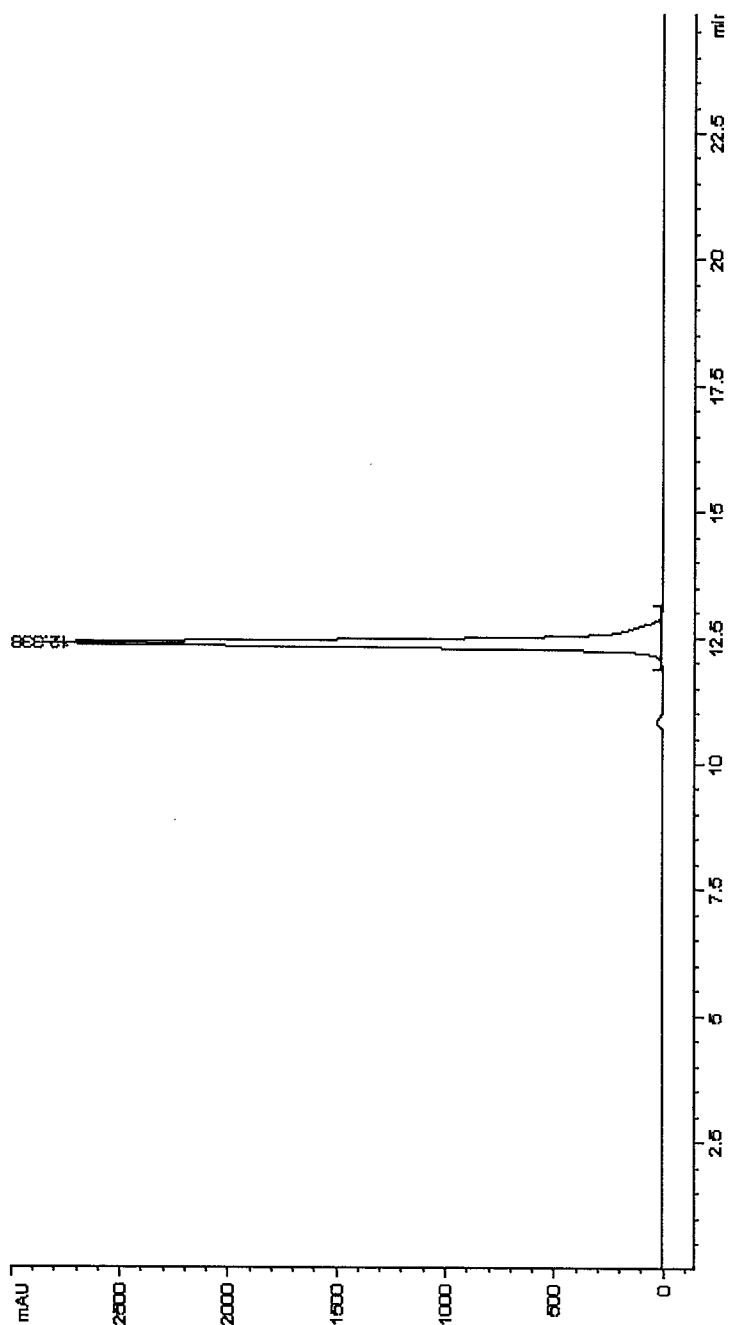
13



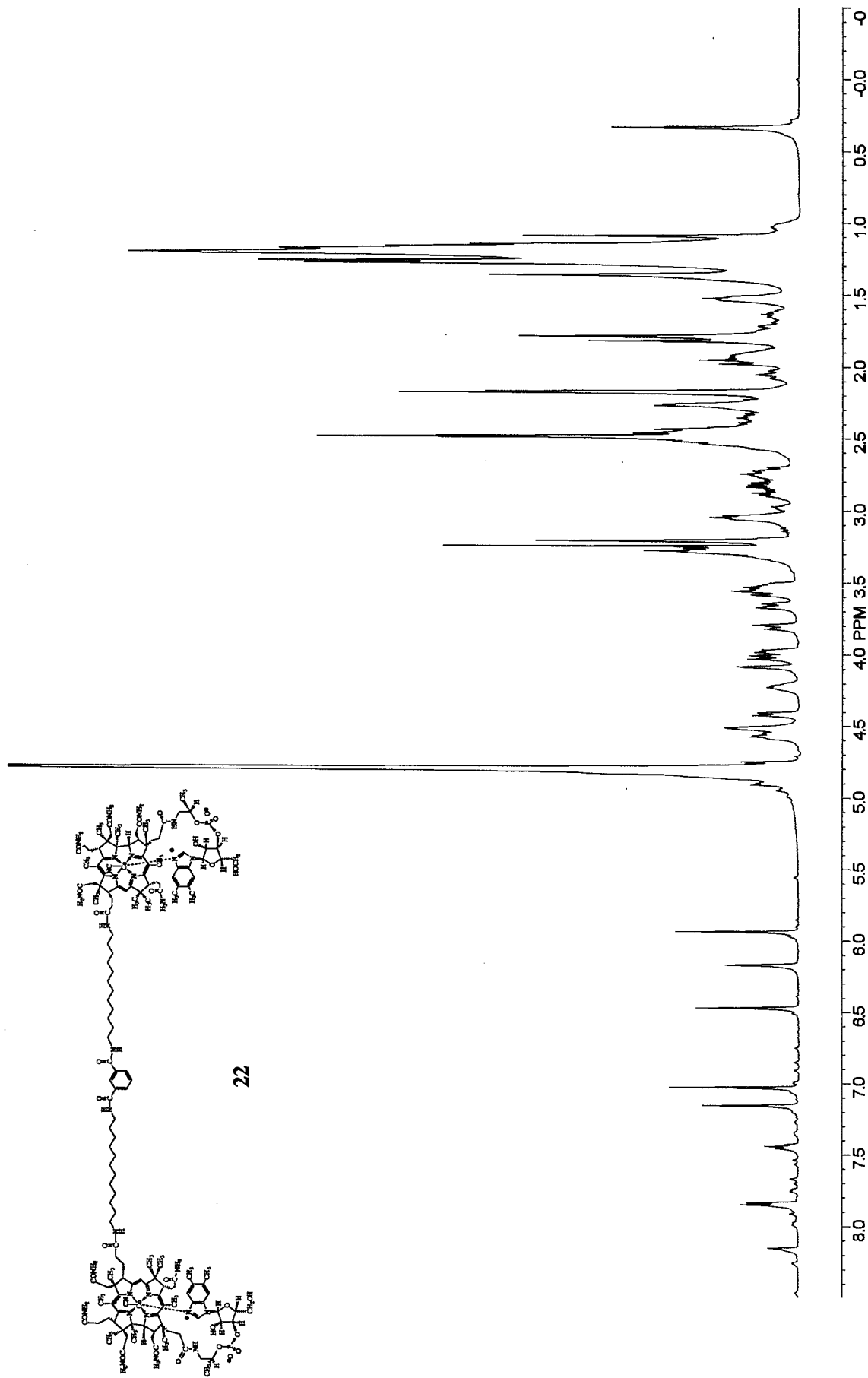
500 MHz; MeOH-d₄



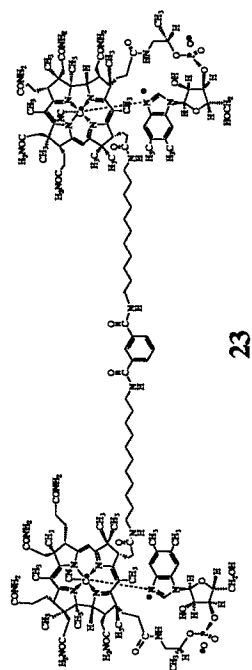
22



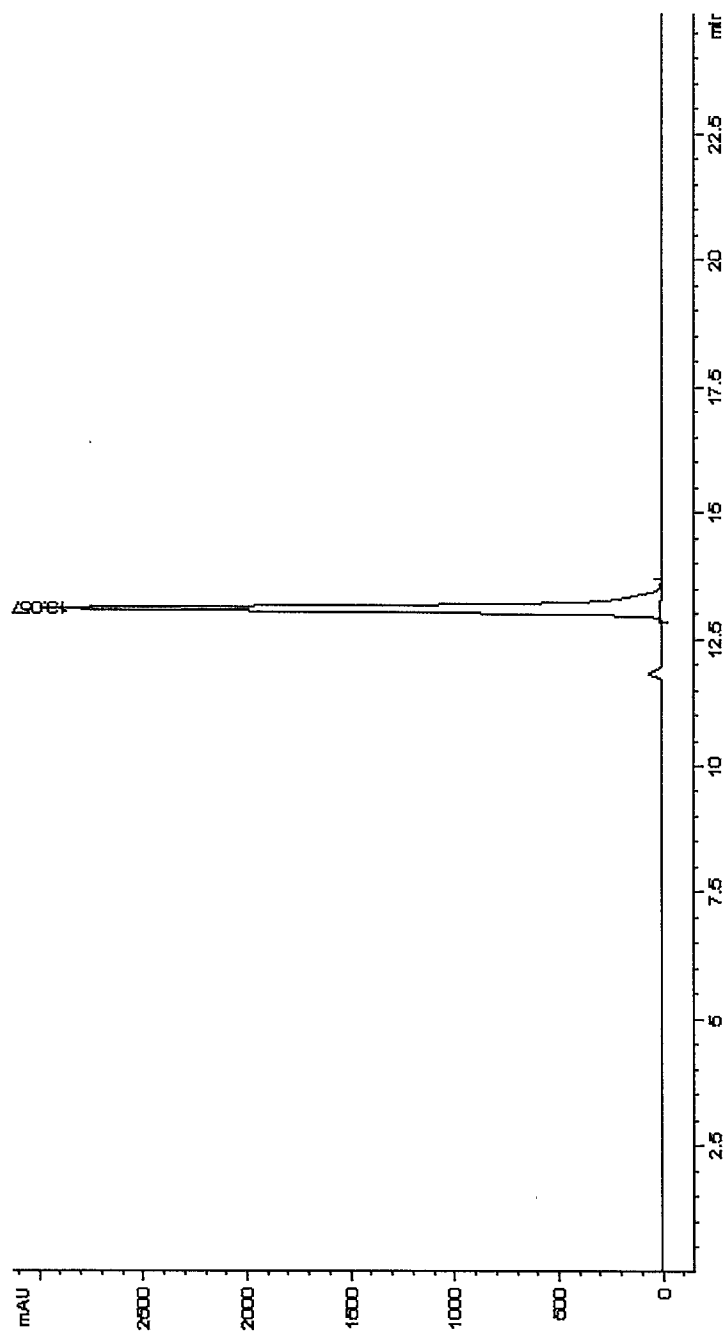
15

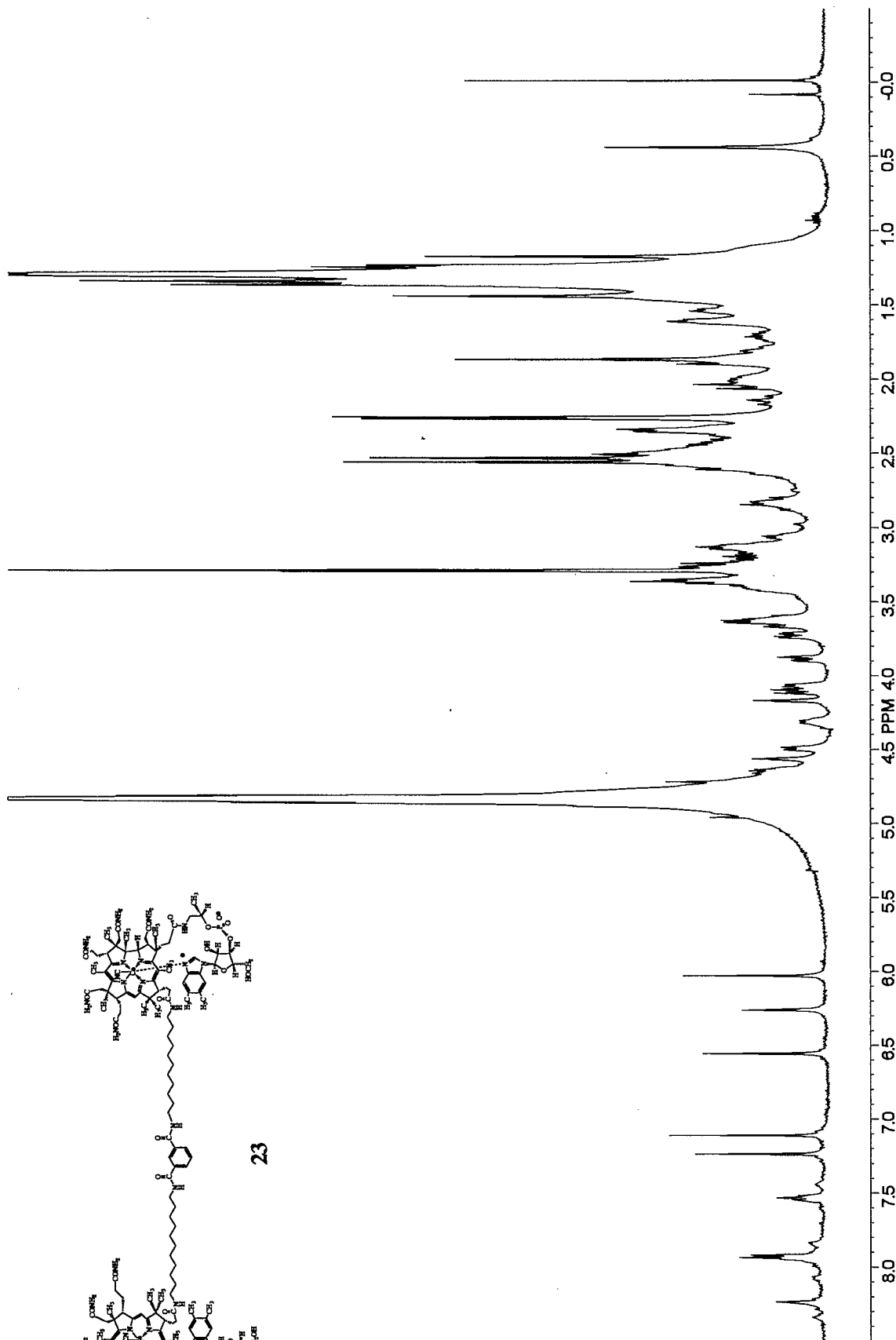


500 MHz; MeOH-d₄



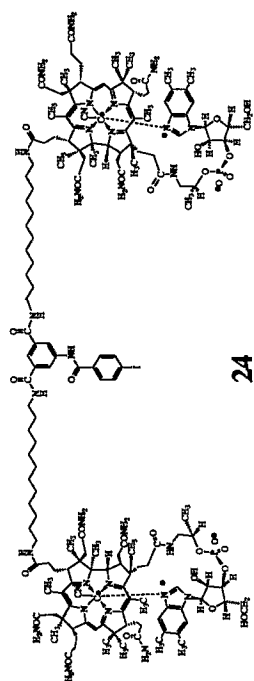
23



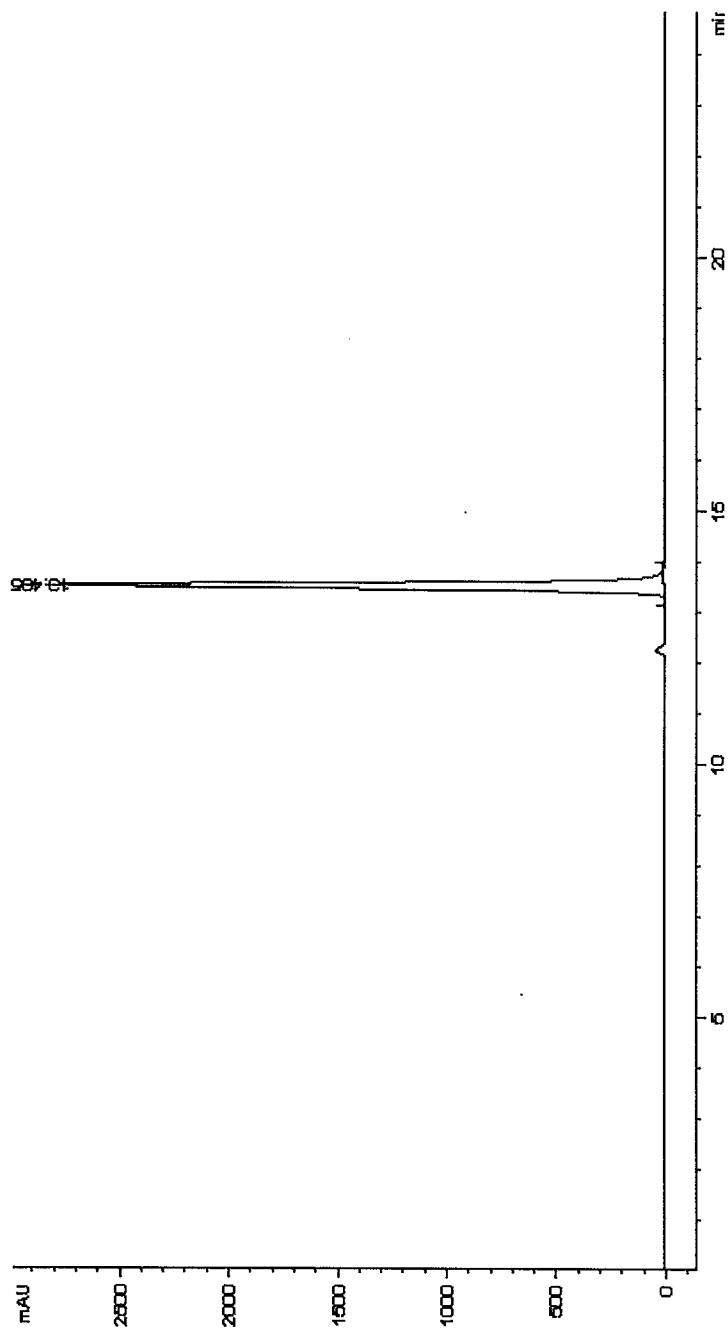


500 MHz; MeOH-d₄

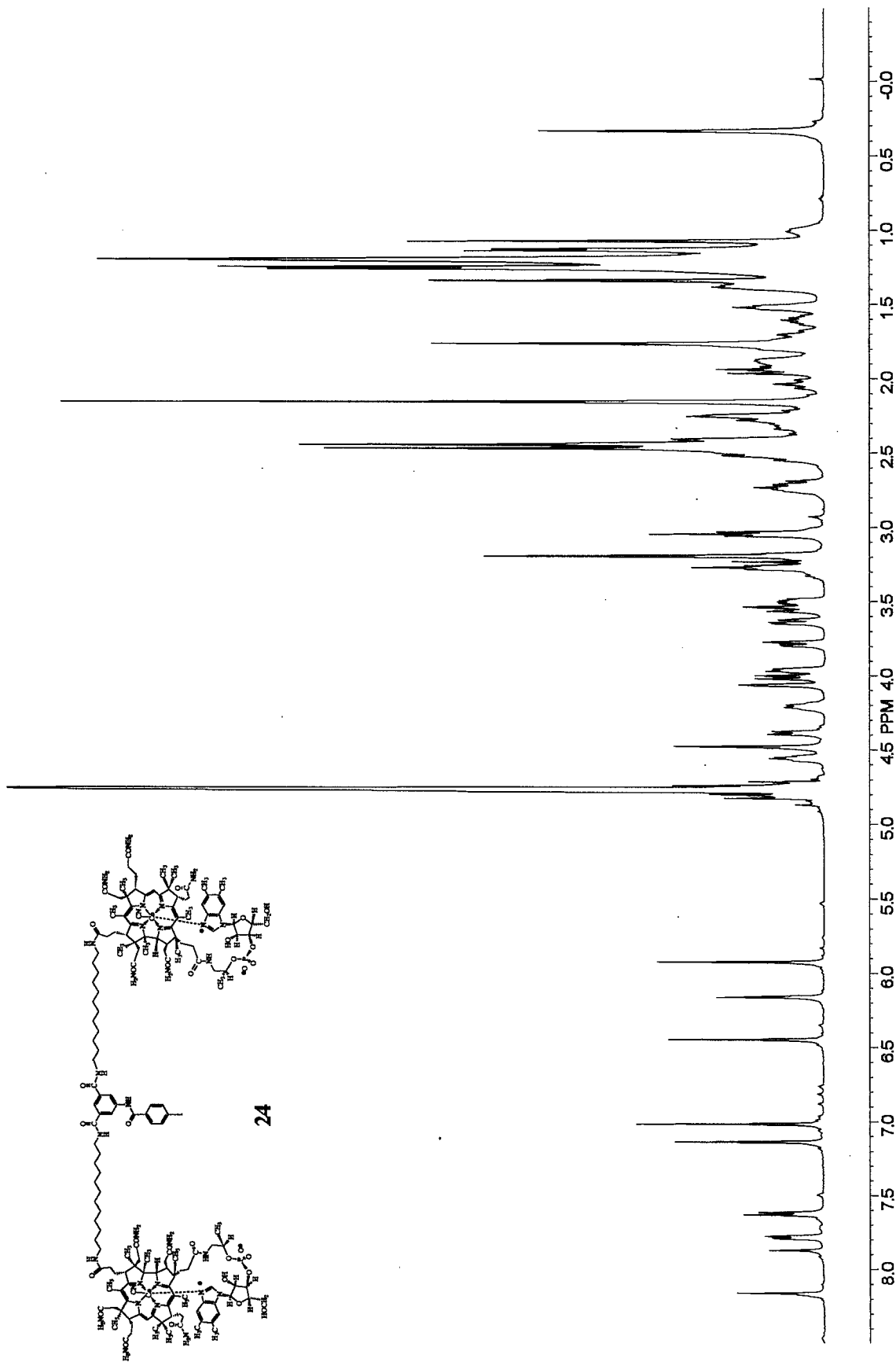
16



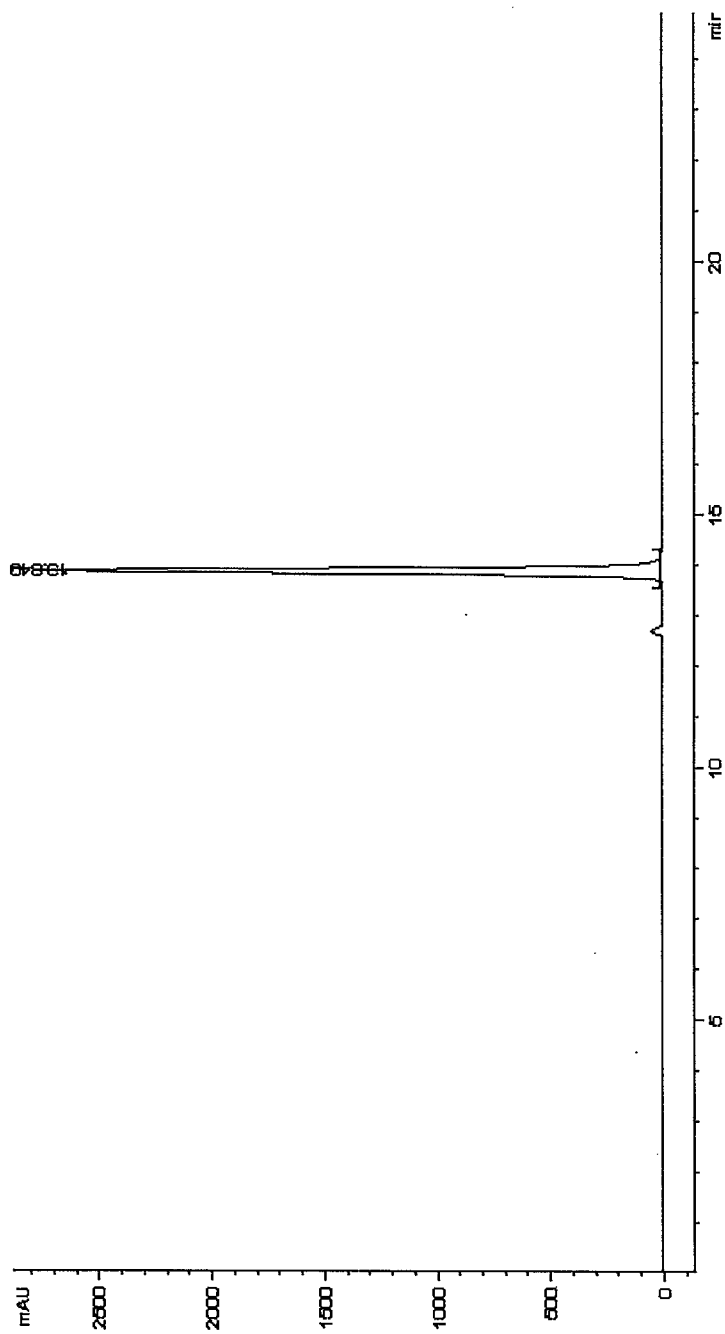
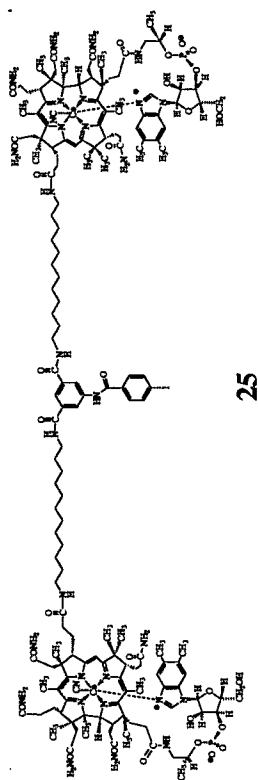
24

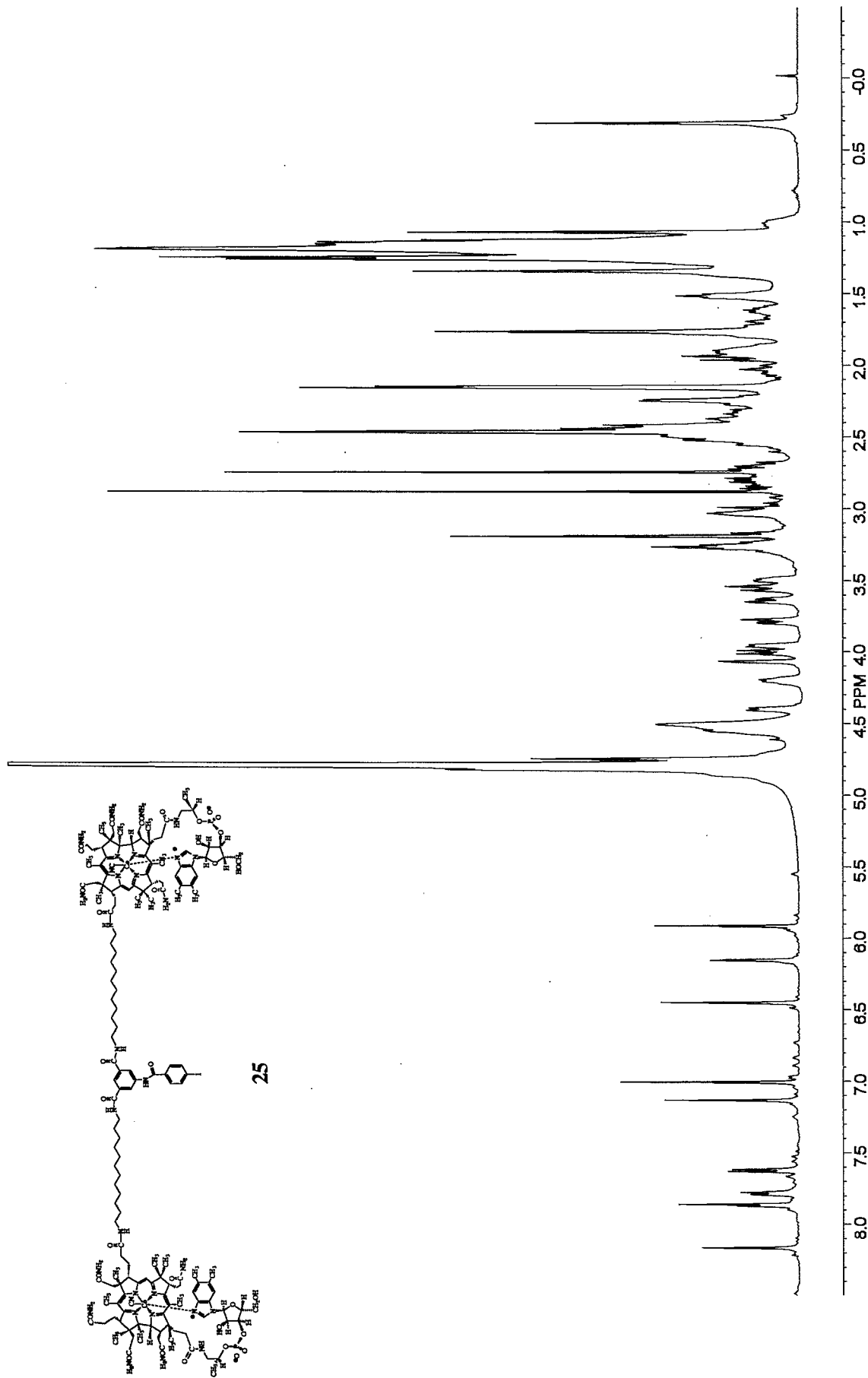


1-7

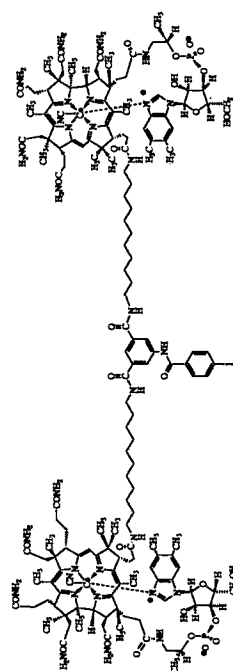


500 MHz; MeOH-d₄

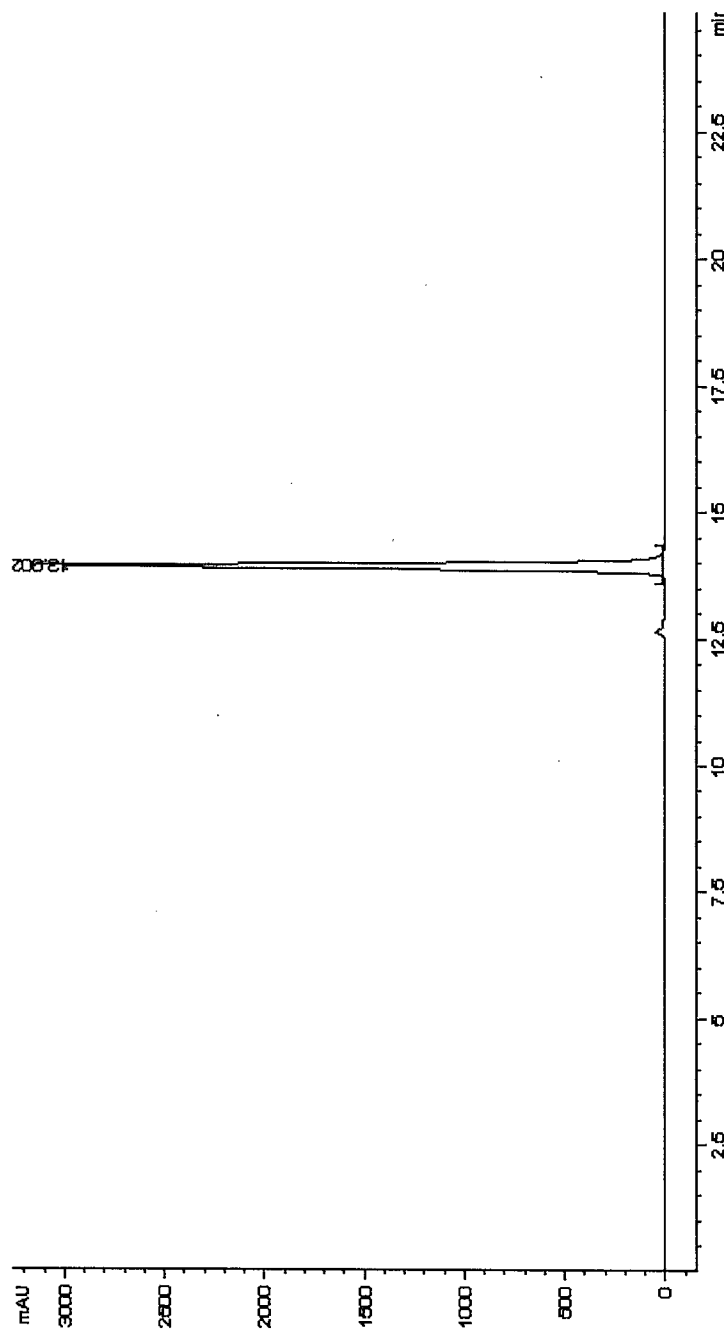




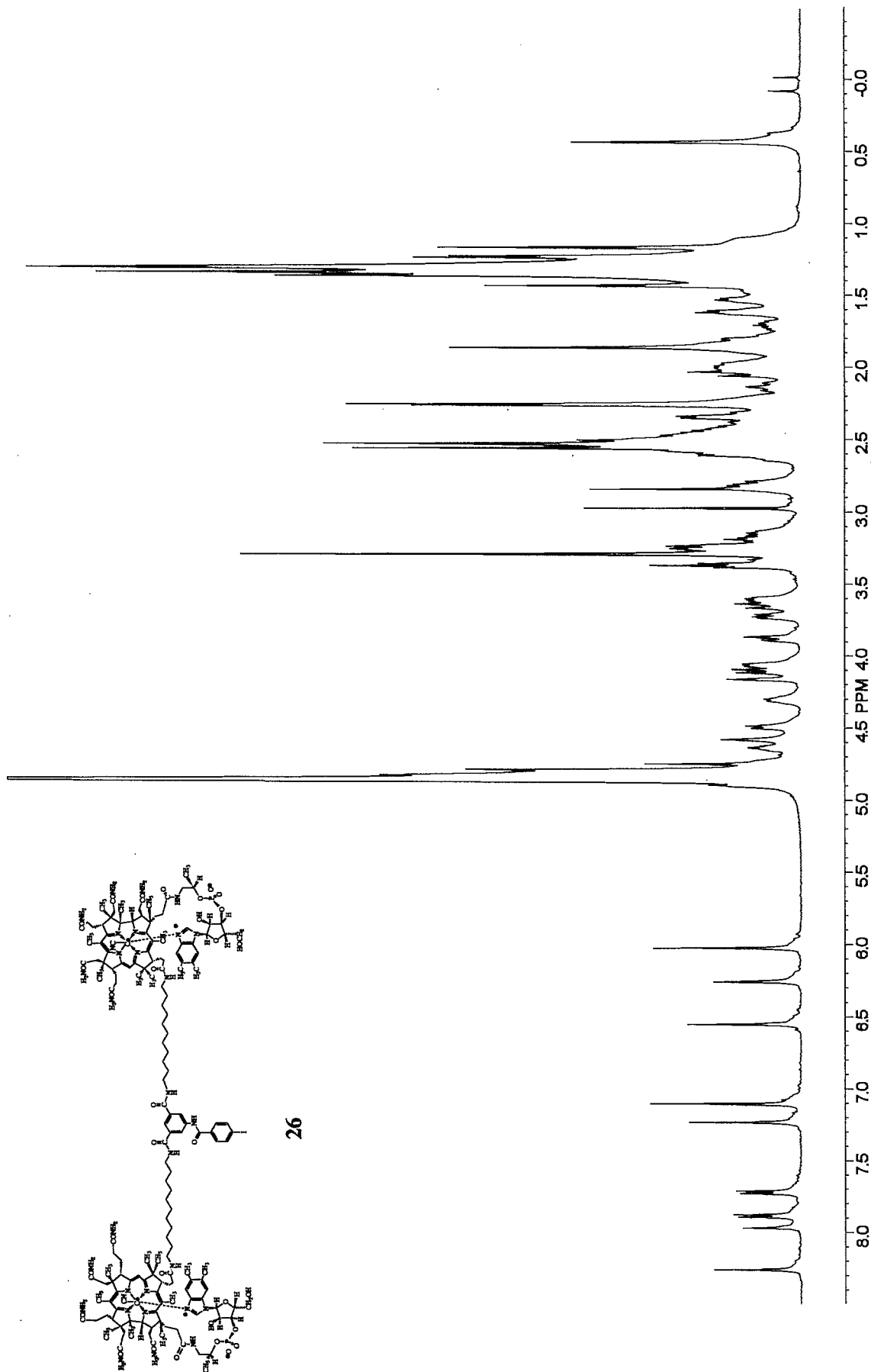
500 MHz; MeOH-d₄



26



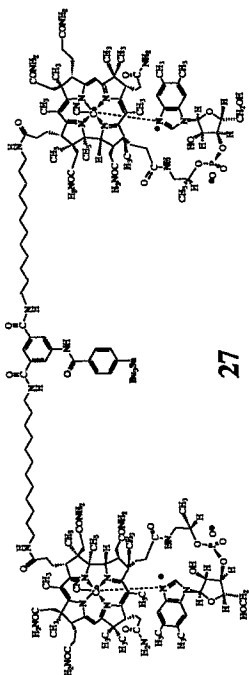
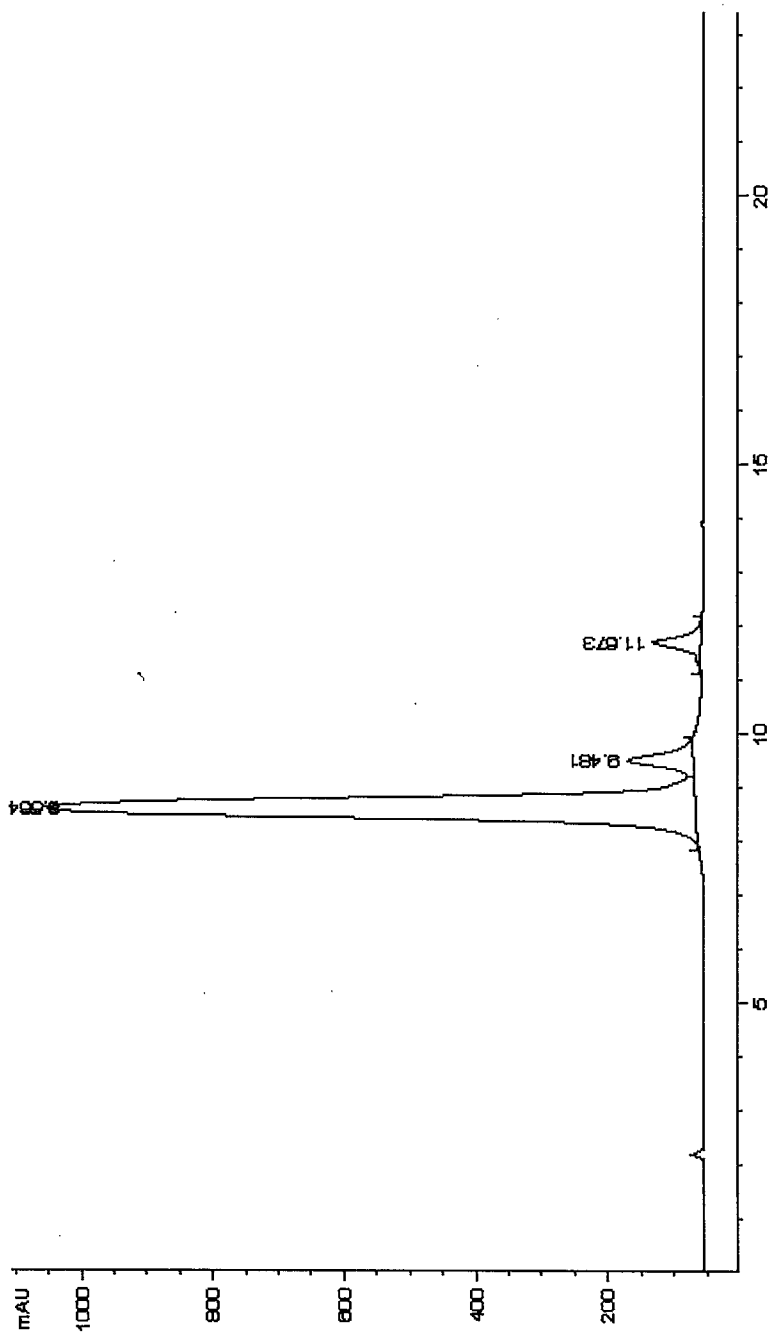
23



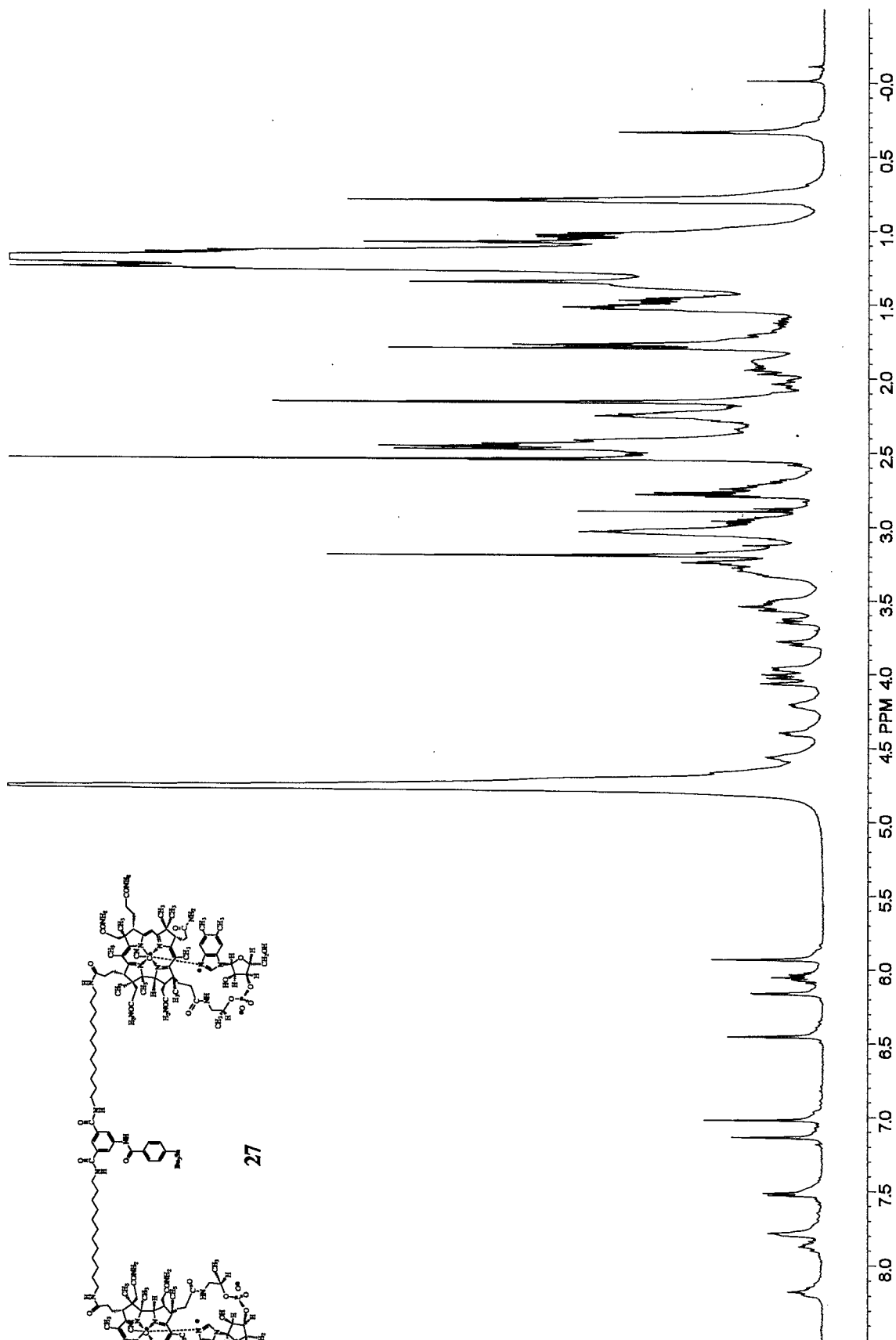
500 MHz; MeOH-d₄

26

24

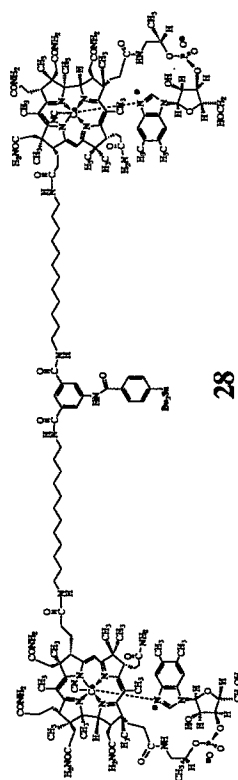


27

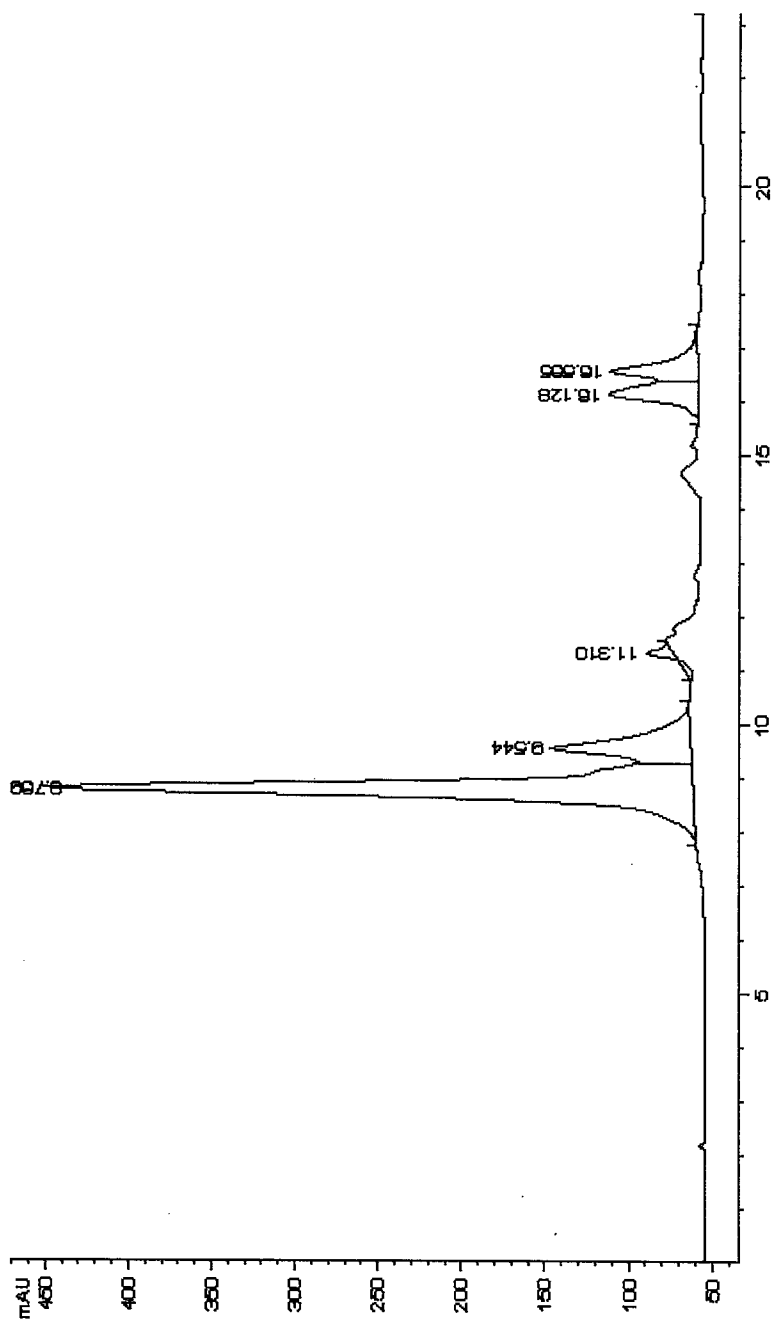


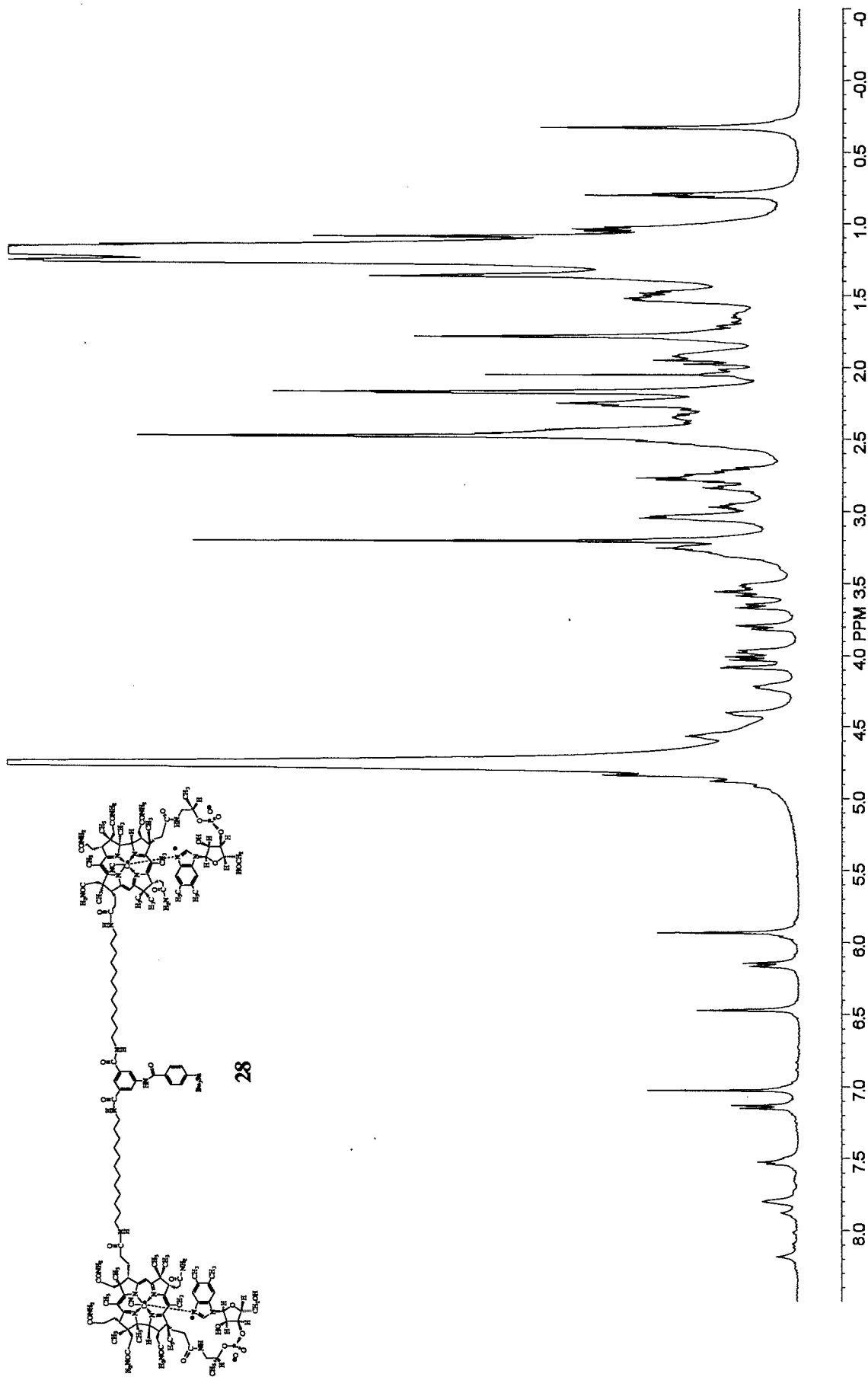
500 MHz; MeOH-d₄

26



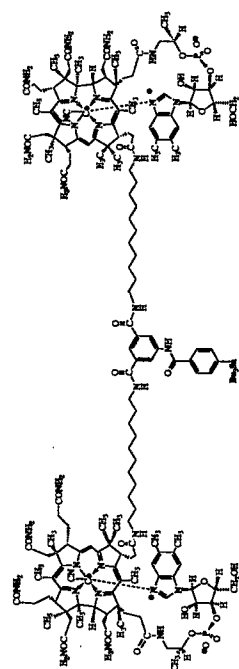
28



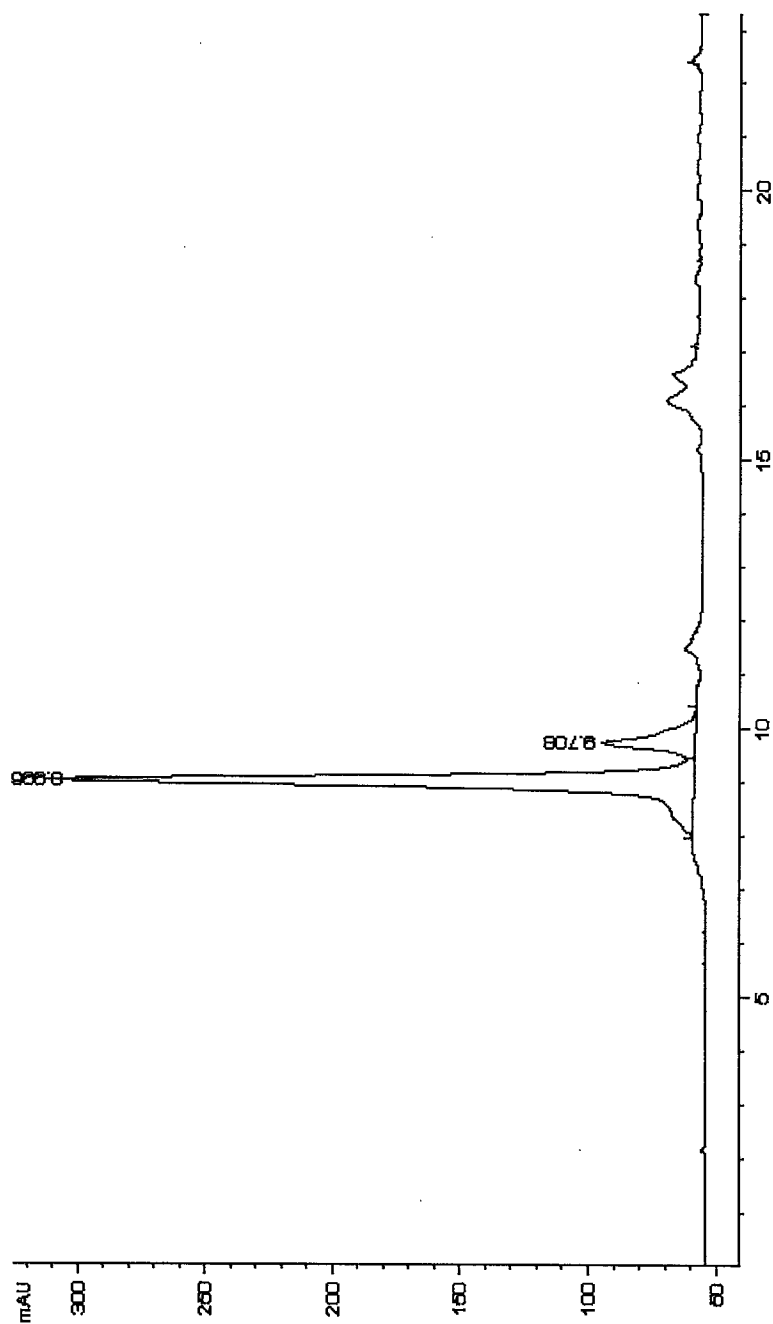


500 MHz; MeOH-d₄

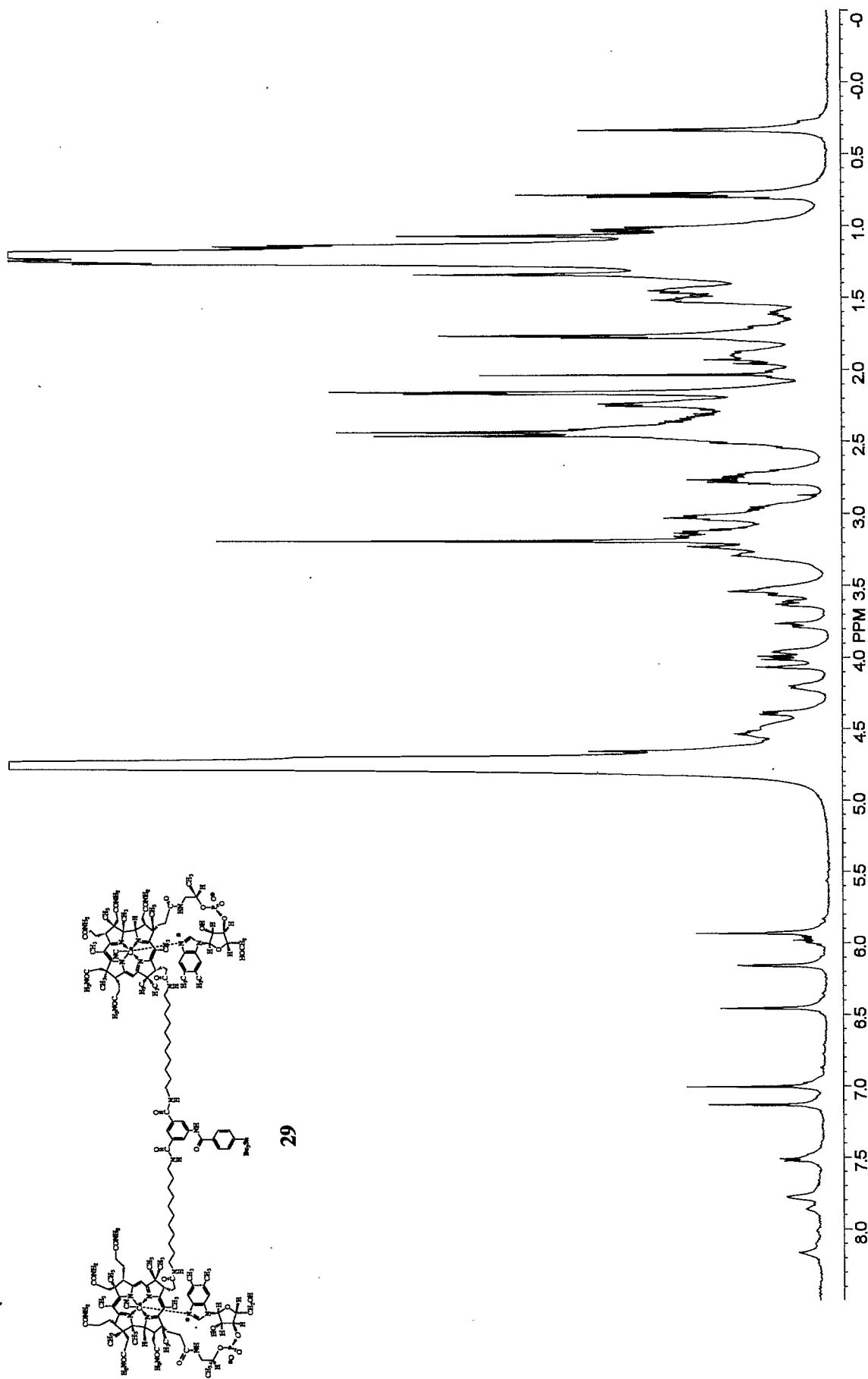
4



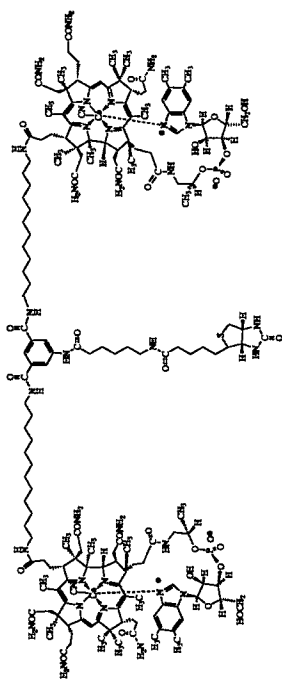
29



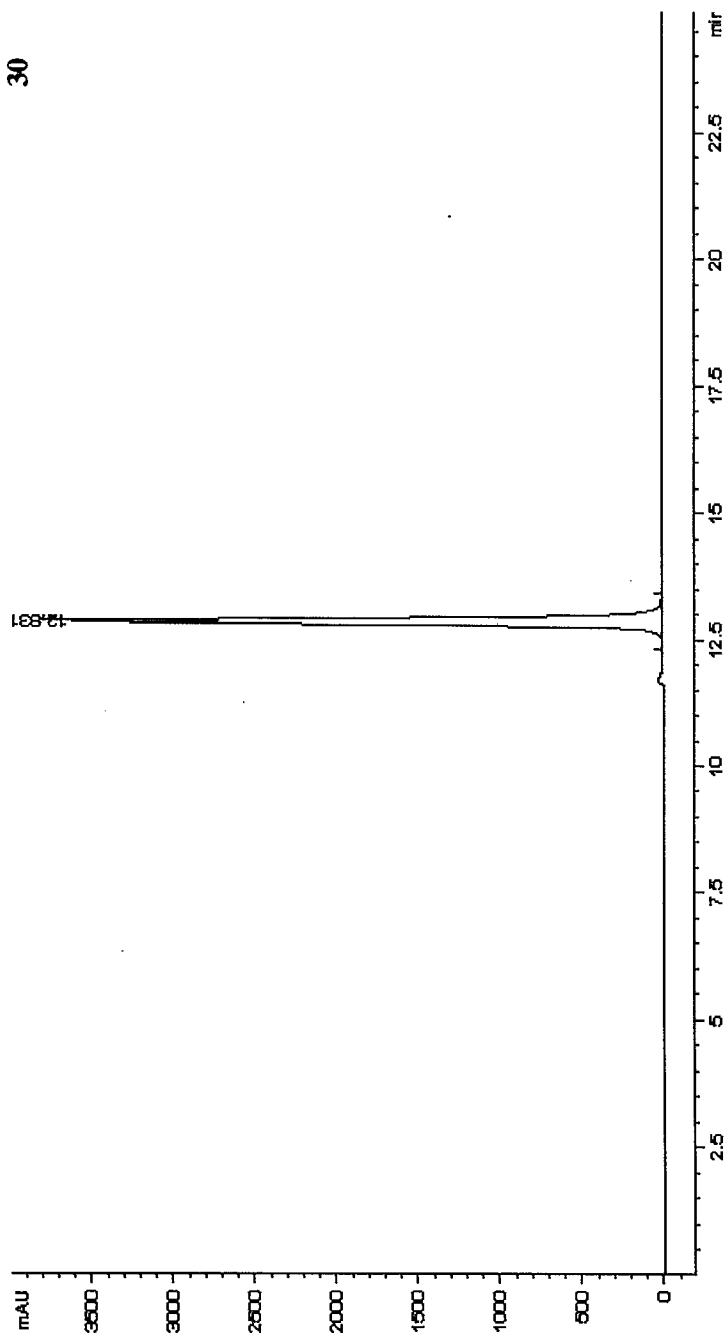
29

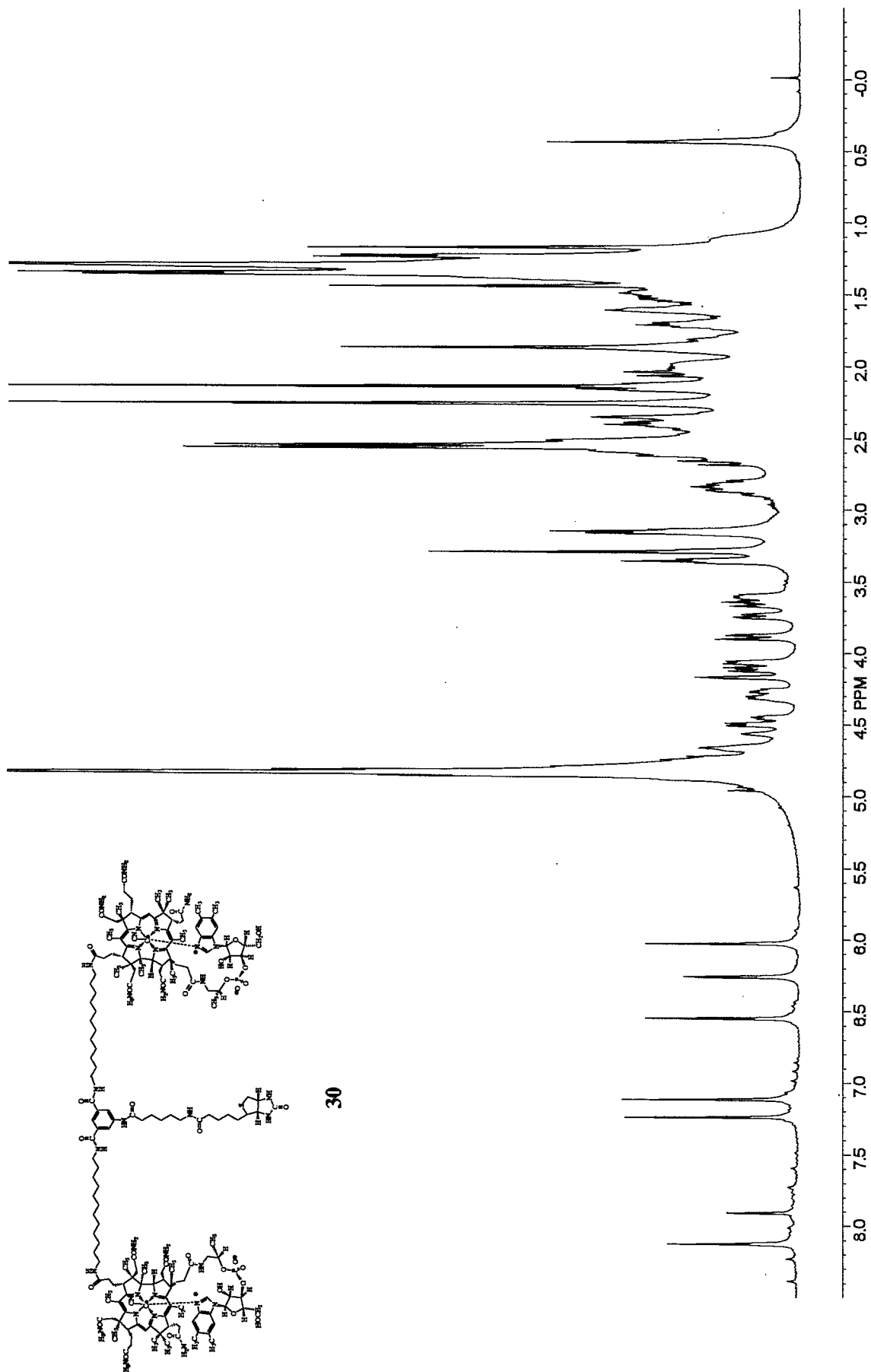


500 MHz; MeOH-d₄



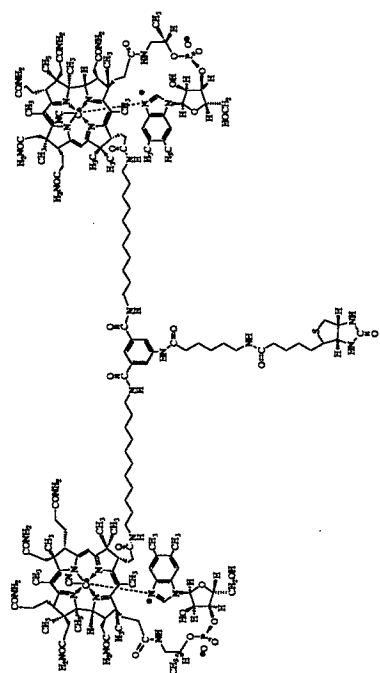
30



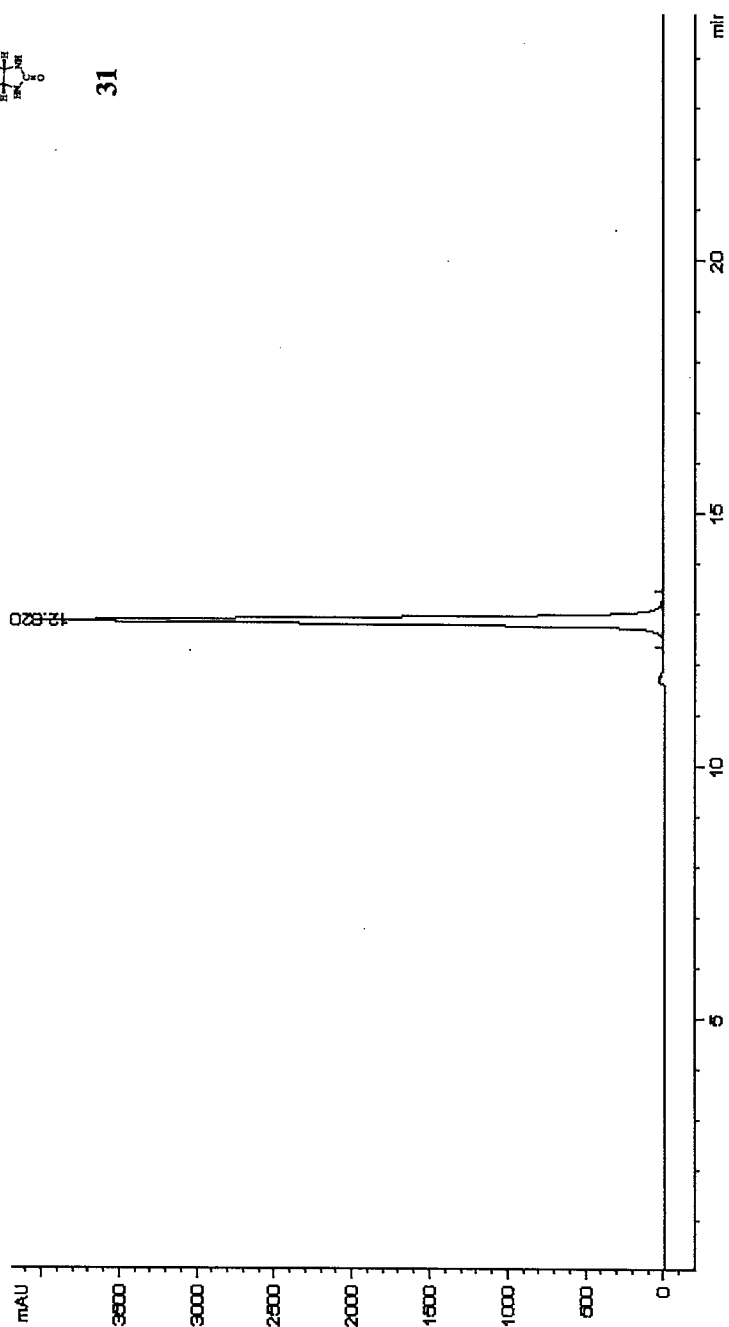


500 MHz; MeOH-d₄

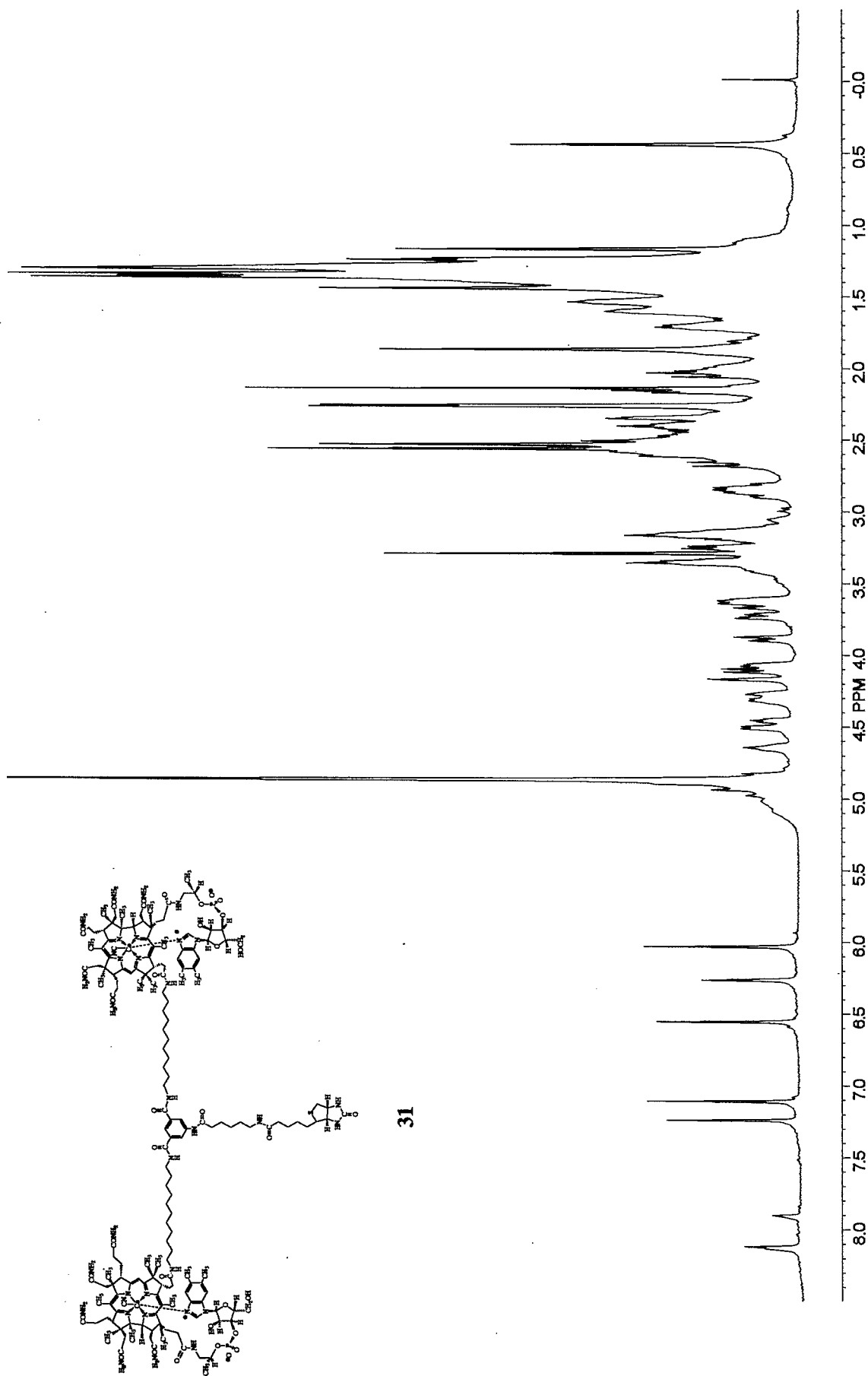
22



31

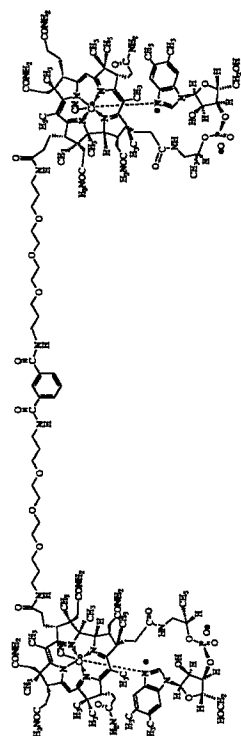


33

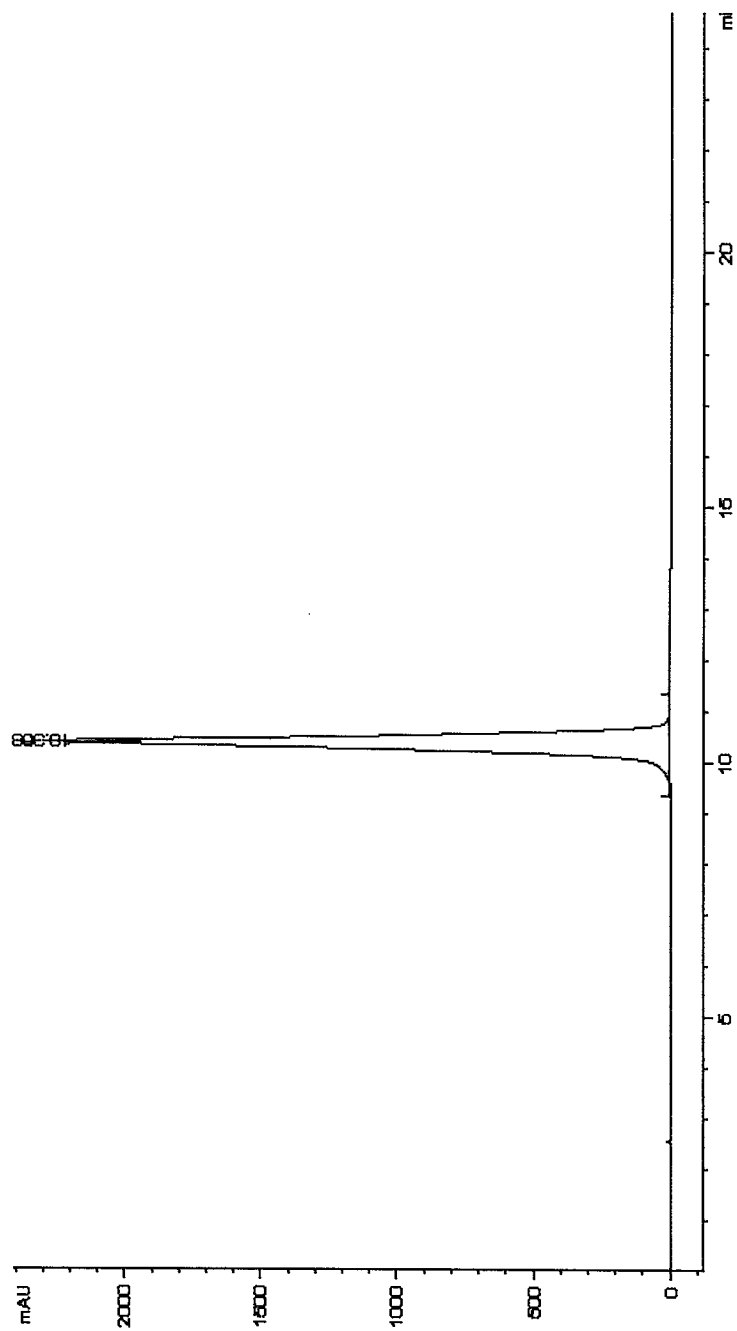


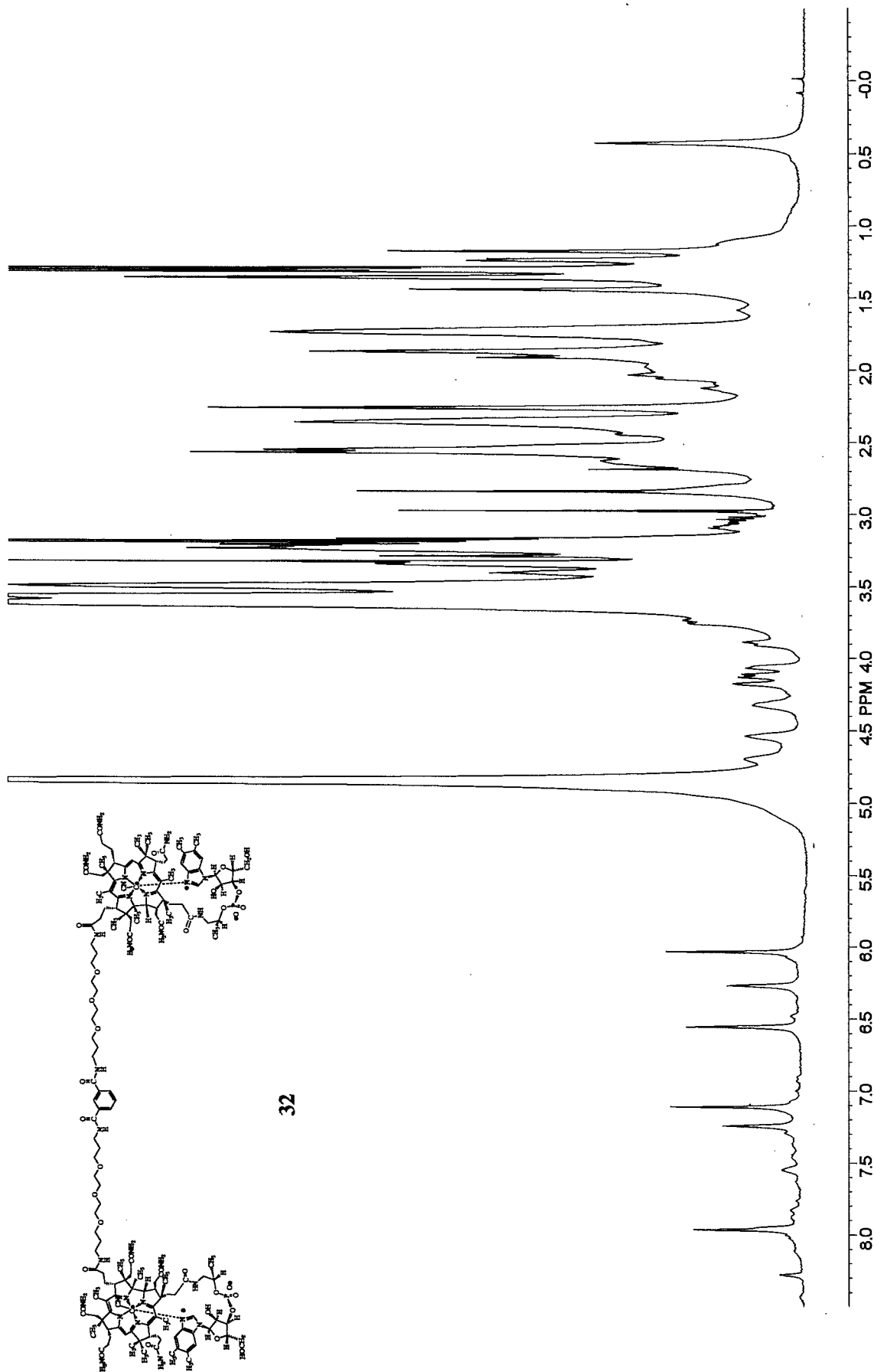
500 MHz; MeOH-d₄

34



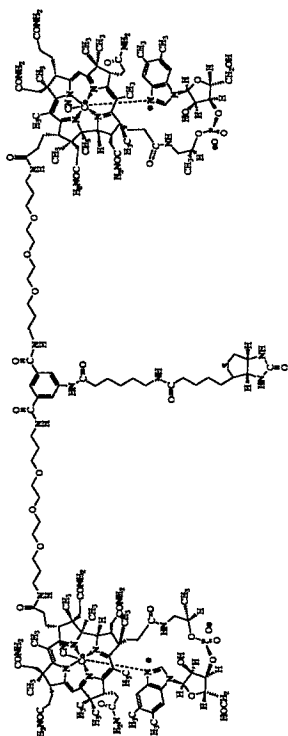
32



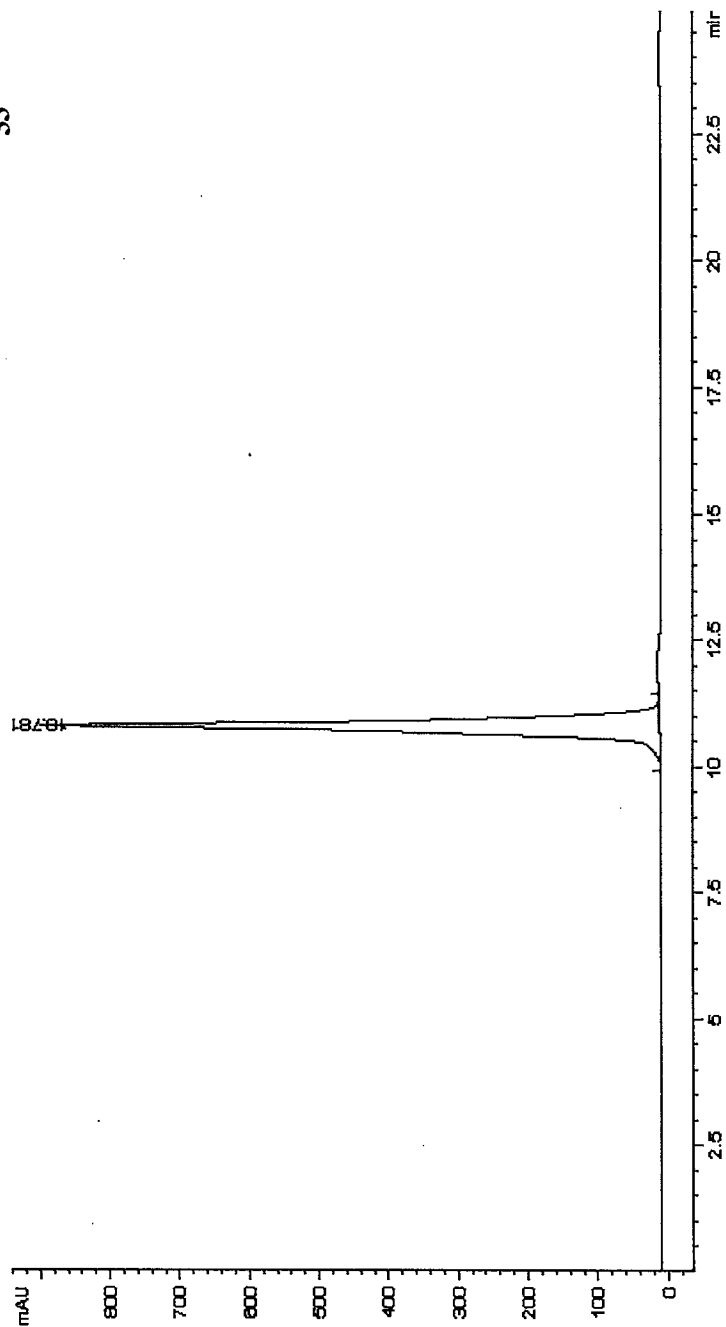


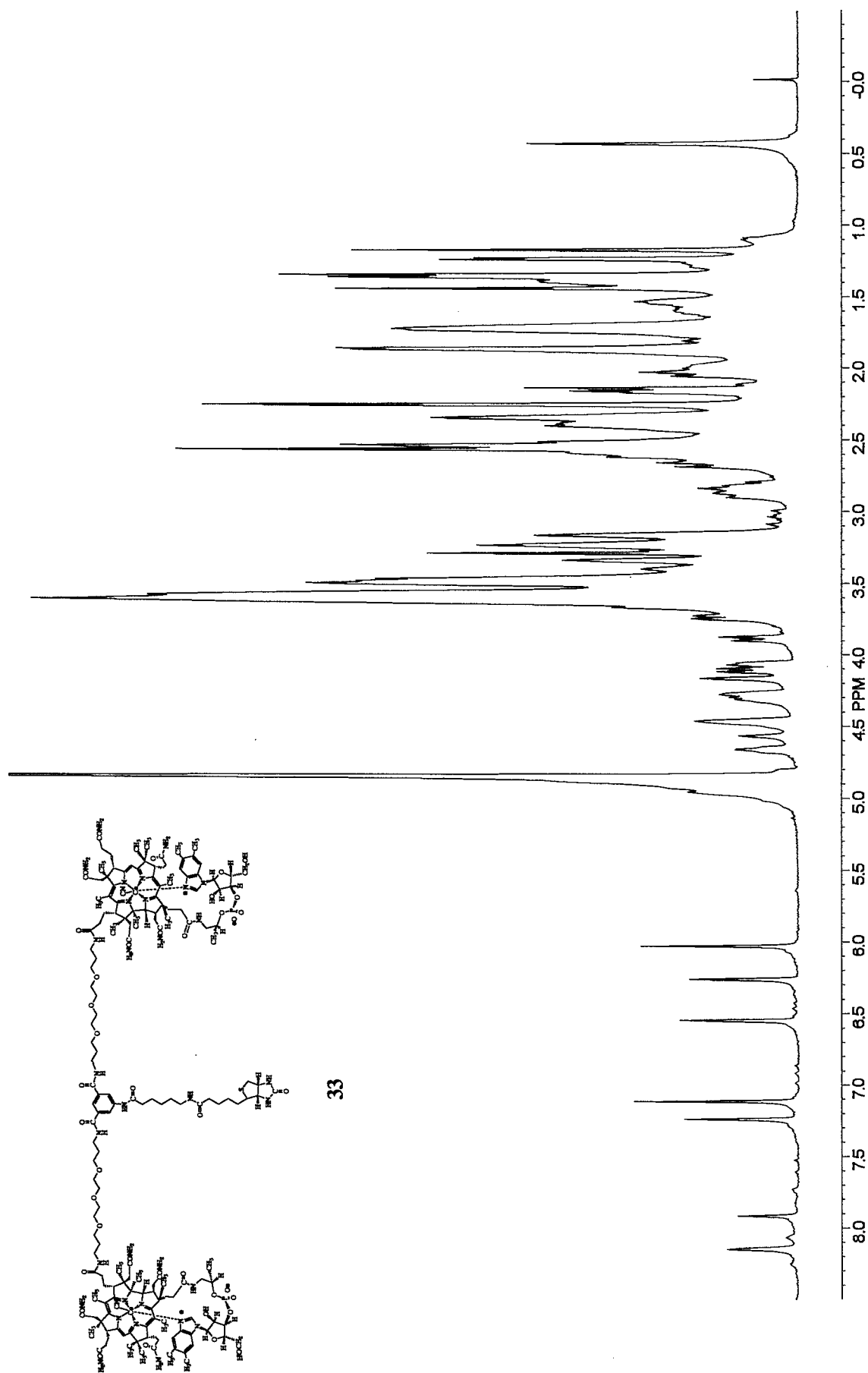
500 MHz; MeOH-d₄

36



33

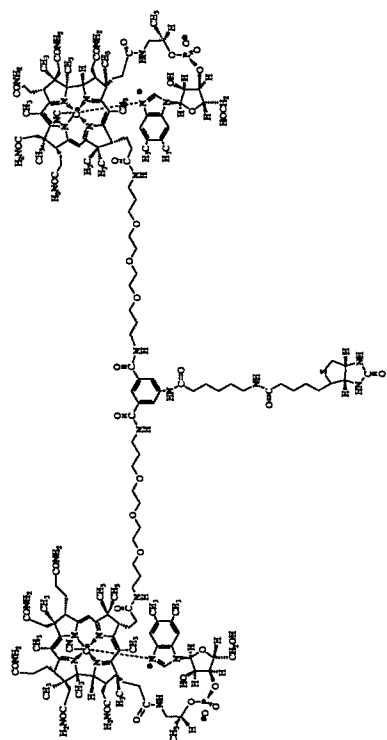




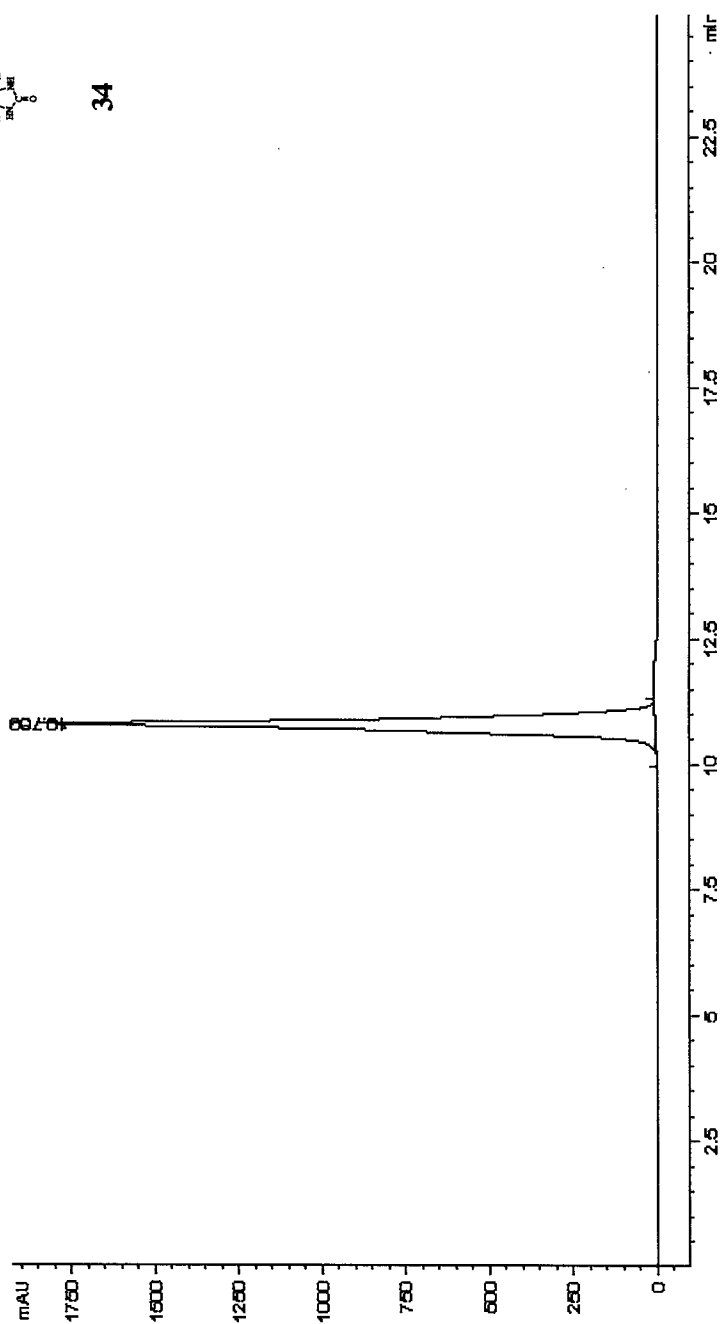
500 MHz; MeOH-d₄

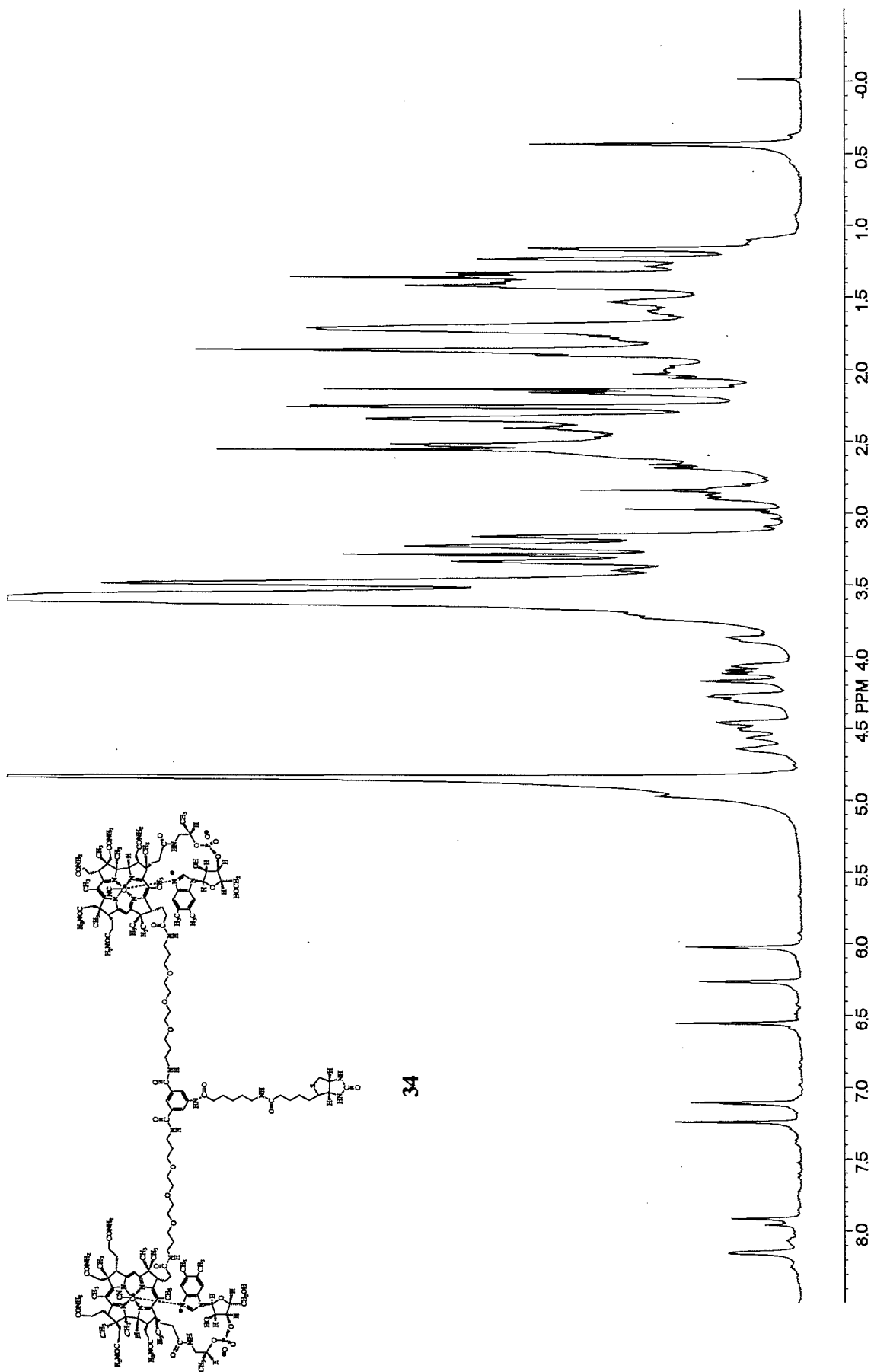
37

08



34





500 MHz; MeOH-d₄

Radiation-Induced Formation of 3,4-Dihydroxyphenylalanine in Tyrosine-Containing Peptides and Proteins as a Function of X-Irradiation Dose

Rama Jain, Harold G. Freund, Edwin Budzinsky, and Minoti Sharma*

Department of Biophysics, Roswell Park Cancer Institute, Buffalo, New York 14263 . Received October 7, 1996[⊗]

Radiation-induced formation of 3,4-dihydroxyphenylalanine (DOPA) in Tyr and Tyr-containing peptides and proteins was investigated as a function of X-irradiation dose. Irradiated Tyr (0–30 Gy) and the acid hydrolysates of irradiated peptide and protein (0–240 Gy) were conjugated with dansyl chloride. The dansylated amino acids were analyzed by reversed-phase HPLC using fluorescence detection. Formation of DOPA, determined by integrated peak area, increased with dose. Analysis of the major product from irradiated tripeptide Tyr-Gly-Gly detected Gly and DOPA (2:1). Extension of the model study to irradiated BSA and RNase A showed correlation of DOPA formation with Tyr modification up to 120 Gy. Higher dose induced further transformation of DOPA. The fluorescence signal of dansylated DOPA was linear from 1.5 nmol to 0.5 pmol (correlation coefficient of 0.999, $n = 3$). The detection limit allows the detection of 1 molecule of DOPA/300 molecules of BSA in 5 μ g of dansylated hydrolysate. Most standard amino acid analysis techniques are limited to detect normal residues of protein. Protein-bound DOPA has been suggested to have a role in the replenishment of reduced transition metal ion involved free-radical-generating system *in vivo*. Sensitive analysis of protein-bound DOPA will be useful to study amplification of the radical-damaging event.

INTRODUCTION

There is increasing evidence that the oxidative modification of proteins may be physiologically important, serving as a "marking" step for initiation of protein degradation (1, 2). Oxygen radicals are formed ubiquitously in biological systems by both enzymatic and metal-ion-catalyzed oxidation (MCO) (3). Recent advances in the understanding of the chemistry of oxygen free radical and its role in modification of biological molecules have led to the recognition that oxygen free radicals are involved in physiological processes of aging as well as in the pathogenesis of age-related disease (4, 5). The findings that some amino acid residues are oxidized to carbonyl derivatives by active oxygen species produced during ionizing radiation, MCO, and ozone led to the development of sensitive assays for their detection and quantitation (6, 7). However, carbonyl compounds are highly reactive toward nucleophiles in biological systems. As a result, although useful as indicators of steady-state oxidation to proteins, carbonyl compounds may not be good candidate for assaying cumulative damage to long-lived proteins by oxidative reactions (8). The nucleic acids in crude tissue extracts and the unwashed free reagents used are two major problems often encountered in this assay (9). Besides, the introduction of carbonyl groups into amino acid residues does not indicate the involvement of a specific amino acid.

All aliphatic amino acids are potential targets of modification by radiolysis (10), but aromatic amino acid residues of proteins are particularly sensitive to oxidation by ozone, singlet-oxygen, radiolysis, and MCO. The formation of formylkynurenine from Trp, 3,4-dihydroxyphenylalanine (DOPA) from Tyr, and *o*-Tyr from Phe as major oxidation products was recognized several decades ago (11–14). Histidine residues are converted

to asparagine, aspartic acid, and 2-oxohistidine (5, 15, 16). Under anaerobic conditions, radiolytically generated radicals promote considerable protein–protein cross-linkage through \cdot OH-facilitated $-S-S$ and Tyr-Tyr (DT) bonding (17). Several oxidation products of Trp including *N*-formylkynurenine have been identified in the mature human lens (18, 19).

Fluorescence spectroscopy is used generally to measure the formation of DT and oxidation products of Trp. Upon irradiation at 325 nm, DT exhibits strong fluorescence at 410–420 nm. However, evidence based on spectrophotometric measurement of fluorescent emission at 410 nm for formation of DT has been cautioned due to the contribution of similar fluorescence at 400–450 nm by Trp oxidation and other protein modification when excited at 325 nm (7, 18). In a more specific procedure for DT and *o*-Tyr (20), deuterium-labeled DT and *o*-Tyr were added as internal standards to protein hydrolysates. Then, following enrichment, the amino acids were converted to their *N*-pentafluoropropyl *O*-isopropyl esters and analyzed by selected ion monitoring GC/MS. This technique requires the synthesis of deuterated amino acids for internal standards as well as derivatization of all the functional groups. For preparation of isopropyl esters the samples require heating at 110 $^{\circ}$ C. All modified amino acids may not survive such a drastic condition. Due to intrinsic sensitivity, 2-oxohistidine could be identified by HPLC analysis using electrochemical detection (21). A recent report on stabilization of this amino acid during derivatization has allowed the detection of 2-oxohistidine by fluorescence labeling (22).

The direct evidence that tyrosine residues in protein are converted to DOPA is rare (4). Protein-bound DOPA (PB-DOPA) may well be a more widespread component of protein and peptide than is generally accepted. The main reason for this suggestion is that DOPA derivatives are eclipsed by other amino acids in the standard analytical procedures. The same may be true with other chemical indicators of protein oxidation. The routine method for dealing with chromatographically ambiguous

* To whom all correspondence should be addressed. Phone: (716) 845-8296. FAX: (716) 845-8899.

[⊗] Abstract published in *Advance ACS Abstracts*, February 15, 1997.

PTH (phenylthiohydantoin) derivatives involved back hydrolysis of the PTH-amino acid in hydroiodic acid vapor (23). This procedure is frequently inconclusive due to the oxidative degradation of PTH-amino acids. Resolution of DOPA as its PTH derivative requires use of temperature jumps and solvent gradation (24).

The current high interest in oxidation-linked mechanism of disease (25) dictates that improved assay for oxidative stress be thoroughly explored. A systematic approach to develop a sensitive assay for routine analysis of oxidized amino acids discussed earlier is still lacking. Our laboratory is currently engaged in developing a technique to assay the chemical indicators of protein oxidation without relying on their intrinsic sensitivity. This report describes the analysis of induction of DOPA in peptides and proteins as a function of ionizing-radiation dose.

MATERIALS AND METHODS

Materials. Dns-Cl (5-dimethylaminonaphthalene-1-sulfonyl chloride), Dns-amino acids, L-DOPA, peptide TyrGlyGly, BSA (bovine serum albumin), and RNase A (ribonuclease A) were obtained from Sigma (St. Louis, MO). The standard amino acids and constant boiling 6 N HCl ampules were purchased from Pierce (Rockford, IL).

Eluents. HPLC grade solvents and analytical reagents (Baker analyzed) were used to prepare buffers for the various solvent systems used in the analysis (see figure legends). The working buffer (30 mM sodium phosphate, pH 6.5) was prepared daily from 0.3 M stock by dilution with double distilled, deionized water. All solvents were filtered through a Rainin nylon-66 filter (0.2 μ m) and degassed prior to use. A high-pressure inline filter (SSL, 0.5 μ m) was used as a further safeguard between the pump and the injector valve.

Apparatus. For most HPLC analysis, a microsorb C18 column (5 μ m, 4.6 mm i.d., 25 cm) and a HPXL pump from Rainin Instrument Co., Inc., to deliver the solvent (1 mL/min) were used with a Shimadzu fluorescence detector RF-530 to monitor the dansylated amino acids. For highly sensitive fluorescence detection, a fully programmable pump system from Rainin with a FL-750 B McPherson detector equipped with a high-sensitive accessory unit was used. In the McPherson detector the dansylated amino acids were irradiated at 365 nm with a xenon-mercury lamp. A typical spectrum of xenon-mercury shows 30% more output at 365 nm than at 340 nm, used commonly to excite dansylated derivatives. The dansylated amino acids, when scanned at stop flow mode, showed maximum emission at 520 nm. A Radial-Pak 8MBC18 cartridge (10 μ m, 8 mm i.d., 10 cm) from Waters and a variable-wavelength detector with an Altex spectrophotometer flow cell were used for isolation of a peak of interest from one 100 μ g sample per run.

A GE Maxitron 250 X-ray, operated at 240 KV, was used to irradiate the samples in distilled deionized water (0.33 mg/mL). Oxygen was bubbled through the solution for 20 min prior to and during the entire process of irradiation. When multidosages are needed from a sample to study the irradiation effect as a function of irradiation dose (1 Gy = 100 rad), aliquots were withdrawn during the irradiation so that the first withdrawn aliquot has zero dosage and the remaining aliquots have the sum of dosages up to the time each aliquot is withdrawn.

Hydrolysis of Peptide and Protein. Peptides and proteins were hydrolyzed with 6 N hydrochloric acid at 110° C in Millipore-Water's Pico Tag Work station following manufacturer's standard protocol. Typically

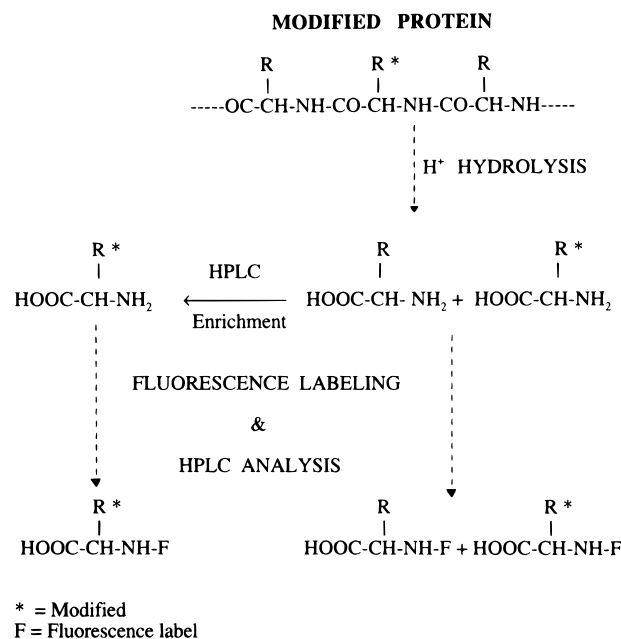


Figure 1. Schematic representation for assaying protein modification by fluorescence labeling.

5–10 μ g samples and 200 μ L of hydrochloric acid containing 1% (w/v) double distilled phenol were placed in the Pyrex sample vial (6 \times 50 mm, corning) and the reaction vial (pico tag), respectively. After 20 h the sample vials were placed in a clean reaction vial and left for 30 min under vacuum to dry the samples. We observed that the same procedure could be scaled up to 50 μ g per vial.

Dansylation of Amino Acids. The conditions for dansylation of amino acids were similar to those used by Tapuhi et al. (26) and Oray et al. (27). A Dns-Cl solution (4.5 mg/mL) was freshly prepared weekly with HPLC grade acetonitrile. The aqueous solutions of the amino acid mixture (1–10 nmol) and hydrolysates of peptides and proteins (0.1–1 nmol), after transferring from the hydrolysis vial to 1.5 mL Eppendorf tubes with 50 μ L of distilled deionized water, were lyophilized in a vacuum centrifuge. The residues were dissolved in 50 mM sodium borate buffer, pH 9.5. The ratio of Dns-Cl to buffer was 1:2, and the volume used varied according to the total concentration of Dns-susceptible amino groups present in the sample. The optimal conditions for the dansylation reaction were found to be at ratios of Dns-Cl to amino acids of 5:1 to 10:1 as reported (26). The reaction was carried at room temperature in the dark for 60 min. The reaction mixture was filtered on an ultrafree microcentrifuge unit (0.22 μ m) to remove any particulate material seen during dansylation. The filtrate was then subjected to HPLC analysis or stored at –22 °C until analyzed. The dansylated samples, as monitored by HPLC analysis, were found to be quite stable under these conditions.

RESULTS

Figure 1 outlines the scheme used for assaying DOPA in X-irradiated proteins. Briefly, modified protein is subjected to acid hydrolysis to release both normal and modified amino acids. The hydrolysate is labeled with Dns-Cl. Optimum elution conditions are devised to resolve the modified amino acid from the normal amino acids by HPLC using fluorescence detection. Alternately, the modified amino acid is enriched by HPLC, prior to dansylation, from the normal amino acids. The enriched

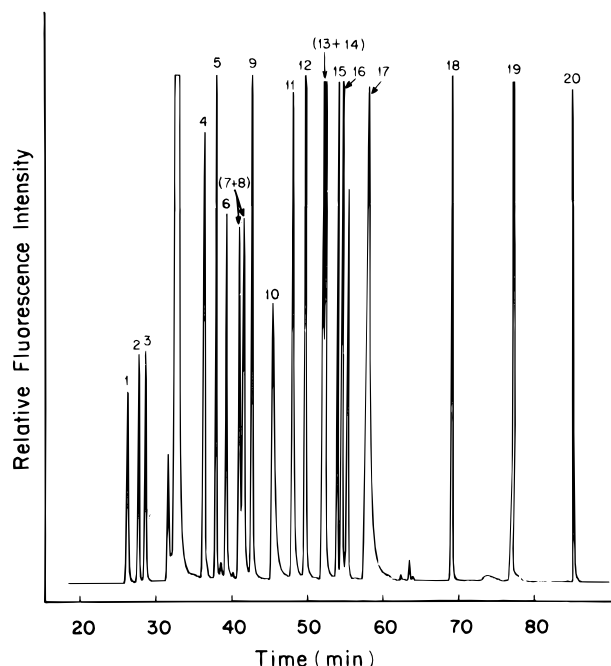


Figure 2. HPLC resolution of dansylated amino acids on a reversed phase C18 column (5 μ m, 4.6 mm i.d., 25 cm) using a 90 min linear gradient of 8–90% acetonitrile in 30 mM sodium phosphate, pH 6.5. Detection: excitation 340 nm, emission 520 nm. The peaks 1–20 correspond to Asp, Glu, Asn, Gln, Ser, Leu, Gly + Thr, Arg, Pro, Val, Met, Ile + Leu, Trp, Phe, Cys, Lys, Tyr, and DOPA, respectively.

amino acid is then labeled with Dns-Cl and analyzed by HPLC using fluorescence detection.

Figure 2 shows HPLC analysis of a mixture of dansylated amino acids. Except for Gly and Thr and Ile and Leu pairs, a 90 min linear gradient of 8–60% acetonitrile in 30 mM sodium phosphate buffer, pH 6.5, resolved all other amino acids including DOPA. Extension of the gradient from 90 to 120 min resolves the Gly and Thr pair (not shown). The reproducibility of the system was evaluated by injecting the mixture on different days. The average deviation of the retention times and areas were within 1% and 5%, respectively, $n = 5$.

Figure 3 shows the formation of DOPA from Tyr (top) and a modified peptide from the tripeptide Tyr-Gly-Gly (bottom) as a function of irradiation dose. The irradiated samples were labeled with Dns-Cl and analyzed by reversed-phase HPLC. A 50% solution of acetonitrile in 30 mM sodium phosphate, pH 6.5, under isocratic condition, and a 20 min linear gradient of 40–60% acetonitrile in the same buffer followed by a 20 min isocratic run with 60% acetonitrile were used to analyze the irradiation products formed from Tyr and Tyr-containing peptide, respectively. The percent modification of the peptide was calculated on the basis of the integrated peak area of the major modified peak shown in Figure 4 b. As described in the Materials and Methods, the samples (0.33 μ g/mL) were irradiated in aqueous solution in the presence of oxygen. The results shown in Figure 3 are an average of three separate runs from each dose used in the study.

Figure 4a shows the HPLC profile of the peptide (Gly-Gly-Tyr) prior to irradiation. The major modified peak shown in the profile from the irradiated peptide (see Figure 4b) was isolated by HPLC. Profiles c and d in Figure 4 show HPLC analysis of the precolumn derivatized acid hydrolysates from unmodified and modified peptides, respectively. The use of a 50 min linear gradient from 22 to 60% acetonitrile in phosphate buffer detected Gly, Tyr, and its modified amino acid in the

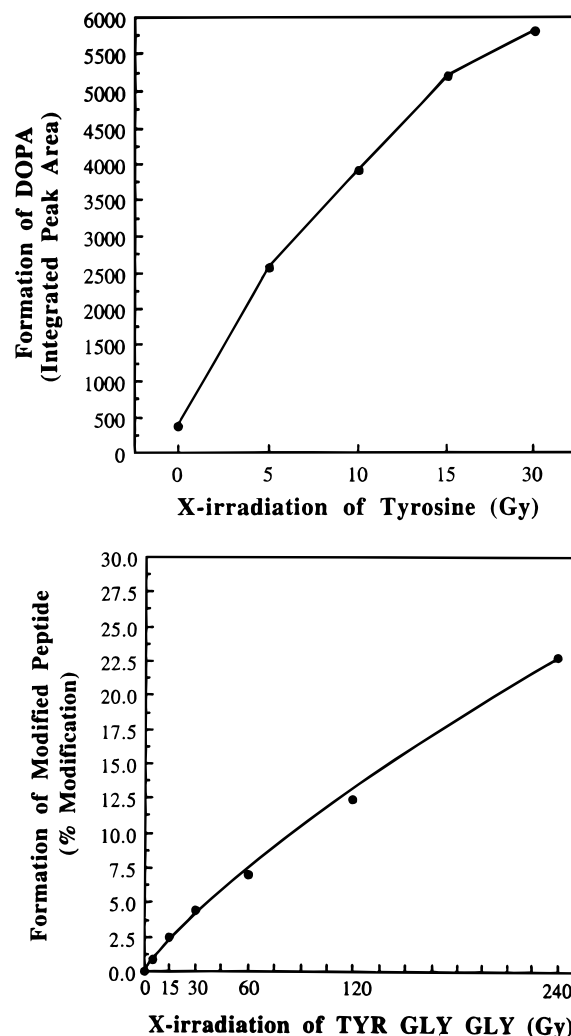


Figure 3. Formation of DOPA from Tyr (top) and a modified peptide from Tyr-Gly-Gly (bottom) as a function of irradiation dose (Gy).

dansylated hydrolysates. The identity of the peak at 36 min in the Figure 4d was confirmed as DOPA by cochromatography with authentic marker (results not shown). The amino acid composition of the peptides as Gly:Tyr (2:1) and Gly:DOPA (2:1) in profiles c and d showed that the major modified peptide in profile b resulted from conversion of the Tyr residue to DOPA during the irradiation. These results also support the stability of DOPA under the experimental conditions. The high level of recovery (>98%) of DOPA was also determined by adding a known amount of DOPA to the unmodified peptide prior to hydrolysis and HPLC analysis of the dansylated hydrolysate.

Figure 5 shows the HPLC profiles for assaying DOPA in (a) BSA as a control, (b) irradiated BSA, and (c) irradiated RNase A. The identities of peaks 1 and 2 in the profiles were confirmed as Tyr and DOPA by cochromatography of the postlabeled hydrolysate from irradiated RNase A with authentic Tyr and DOPA (see Figure 5d). The use of a 50% solution of acetonitrile in phosphate buffer as an eluent allowed the detection of Tyr and DOPA from the hydrolysate under isocratic conditions. Figure 6 shows analysis of Tyr modification to DOPA in RNase A (left) and BSA (right) as a function of irradiation dose. The percent formation of DOPA correlates with the percent modification of Tyr up to 120 Gy for both of the proteins. At higher doses (240 Gy), the yield of DOPA represents approximately 50% of Tyrosine modification. The recovery of most other amino

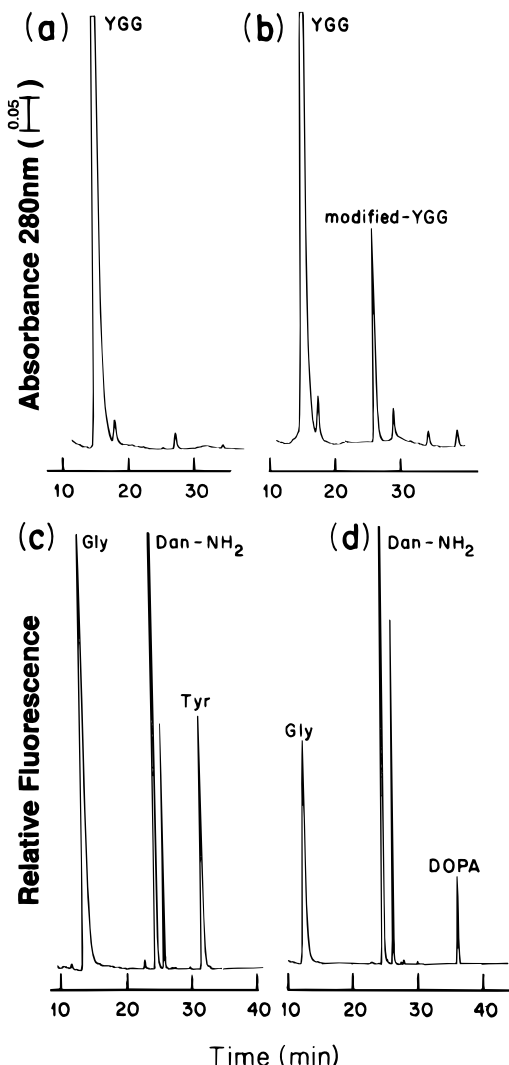


Figure 4. HPLC analysis of Tyr-Gly-Gly (a) and X-irradiated Tyr-Gly-Gly (b) on a Radial-Pak C18 cartridge using a 30 min linear gradient of 0–60% acetonitrile in 0.05% TFA; fluorescence labeling assay of Tyr-Gly-Gly (c) and modified-Tyr-Gly-Gly using a 50 min linear gradient of 22–60% acetonitrile in 30 mM phosphate buffer, pH 6.5.

acids also were affected 25–30% with respect to the control. For each dose, the same amount of dansylated hydrolysate (1.66 μ g) was analyzed under the conditions described in Figure 2. In agreement with the reported study (8) there was no change in valine content of the irradiated samples compared to the control. To correct for variation in protein content, tyrosine was normalized to valine content of an aliquot of original hydrolysate. The effect of each dose on Tyr content and subsequently on DOPA formation was determined from three separate experiments. The coefficient of variation was found to be 3% for DOPA and 5% for Tyr, respectively.

DISCUSSION

The scheme outlined in Figure 1 for protein modification assay involves the preparation and characterization of a modified amino acid of interest as an authentic marker. Determination of the effects of acid hydrolysis and labeling conditions on the stability of the marker and the quantitative labeling are some other considerations that require systematic investigation prior to application of the technique to study protein modification. In the present study, DOPA is available commercially and as discussed earlier was found to be quite stable to acid

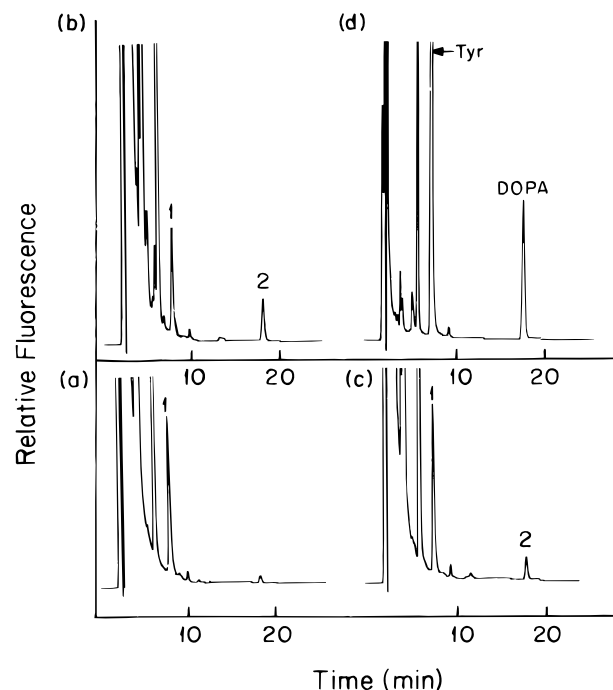


Figure 5. Fluorescence labeling assay of (a) BSA, (b) X-irradiated BSA, (c) X-irradiated RNase A, and (d) cochromatography of c with authentic Tyr (peak 1) plus DOPA (peak 2) by reversed-phase HPLC using 50% acetonitrile solution in 30 mM phosphate buffer, pH 6.5.

hydrolysis conditions. Fluorescence labeling of DOPA with Dns-Cl was monitored by HPLC analysis of the labeling reaction mixture. Comparison of the integrated peak area with respect to a standard dansylated amino acid, showed quantitative labeling yield under the conditions used routinely for derivatization of standard amino acid. Successful application of the assay also depends on devising appropriate HPLC conditions to resolve the modified amino acids of interest from the standard amino acids. The chromatographic characteristic of the modified amino acid generated by subjecting a specific amino acid to a specific modification condition usually serves to identify the same lesion in protein exposed to the same condition. The identity of the peak of interest is confirmed further by cochromatography with authentic marker. Figure 2 shows the resolution of dansylated DOPA from the standard dansylated amino acids by reversed-phase HPLC. For those modified amino acids that do not resolve well from the standard amino acids, resolution could be improved by HPLC enrichment of the modified amino acids prior to labeling as outlined in the schematic representation of the assay (Figure 1). In this alternative procedure a fraction corresponding to the retention time of the authentic marker is collected during the HPLC analysis of the hydrolysate. The profile is monitored by UV absorption, usually at 280 nm. The collected fraction is lyophilized and labeled with Dns-Cl for sensitive detection of the peak of interest by fluorescence detector. Since most of the standard amino acids are eliminated during this procedure, HPLC analysis of the labeled amino acid can be carried out either isocratically or under a gradient system of short duration depending on the nature of modification of the amino acid. This approach will reduce background interference and improve detection limit substantially (28).

HPLC analysis of precolumn derivatized amino acids appears to be a valid alternative to classical ion-exchange chromatography with the subsequent postcolumn ninhydrin derivative (29). Precolumn derivatization of amino acid is performed using PTH, *o*-phthalaldehyde

(OPA), and Dns-Cl. The dansyl derivatives were selected for the present study because the quantitative preparation of the amino acid derivatives is easy and they are stable (26). The use of dansylated derivatives also avoids the loss of cysteine and proline which cannot be detected by the standard amino acid detection derivatives with OPA. Dansyl label has high quantum efficiency. Previously we reported sub-femtomole detection of dansylated nucleic acid by HPLC using laser-induced fluorescence detection (30). Separation of dansylated amino acid by HPLC has been reported earlier (27, 29, 31, 32). So far, all of the reported studies have dealt with the separation of standard amino acids. In a reported HPLC analysis using 30 mM phosphate buffer, pH 6.5, and acetonitrile, a complex three-step gradient was used for the separation of the standard dansylated amino acids (27). Using the same solvents Figure 2 shows resolution of 20 standard amino acids including one modified amino acid (DOPA) in a linear 90 min gradient. To our knowledge, this is the first report of analysis of a dansylated derivative of a modified amino acid.

Analysis of the major modified peak isolated from irradiated tripeptide Tyr-Gly-Gly validated the technique for DOPA analysis (Figure 4). The formation of DOPA could also be detected in the dansylated hydrolysate of the peptide before isolating the major modified peak from the hydrolysate. However, the peak was isolated to determine the amino acid composition which confirmed that the conversion of Tyr to DOPA was the major modification induced by ionizing radiation. The hydrophobicity and, as a result, the retention times of dansylated Gly differed considerably from those of dansylated Tyr and DOPA in reversed-phase HPLC analysis (see Figure 2). However, appropriate HPLC conditions were devised which allowed the determination of integrated peak ratios of Gly and Tyr in the unmodified and Gly and DOPA in the modified under the same conditions (Figure 4c,d).

Having validated the technique for assaying modified amino acid in the tripeptide, the model study was extended to detect the formation of DOPA in X-irradiated BSA and RNase A (Figure 5). BSA which contains several Tyr and two Trp residues is a representative protein model for oxidative modification (17). Ribonuclease A which lacks Trp has been subject of a number of radiobiological investigation due to its low molecular weight and known structure (33). The isocratic conditions chosen for the HPLC analysis shown in Figure 5 were convenient for rapid detection of tyrosine modification in the protein hydrolysates. However, for quantitative purposes, the samples were analyzed under the HPLC conditions described in Figure 2. The identities of peaks 1 and 2 in the profiles shown in Figure 5 were confirmed as Tyr and DOPA by cochromatography with authentic markers (Figure 5d). Figure 6 shows the formation of DOPA in RNase A (left) and BSA (right) as a function of irradiation dose. The results were obtained from analysis of 1.66 μ g of dansylated hydrolysates. The formula weight of RNase A is approximately five times less than that of BSA. In the same quantity of hydrolysate from each protein, the Tyr content was higher in RNase A than in BSA. In each case, as discussed earlier, the content of Tyr was normalized with respect to valine to determine the % modification.

Using a conventional fluorescence detector, we observed that the relationship of fluorescence signal and concentration of dansylated DOPA was linear from 1.5 nmol to 0.5 pmol with a correlation coefficient of 0.999, $n = 3$. This detection limit of fluorescence postlabeling assay of dansylated DOPA allows the detection of 1

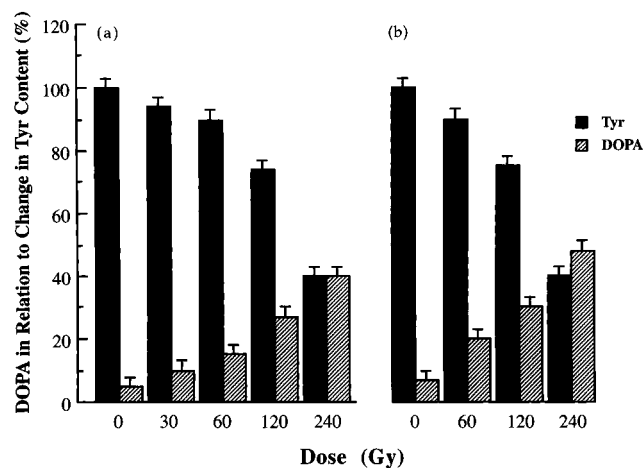


Figure 6. Formation of DOPA in relation to Tyrosine content of X-irradiated RNase A (left) and BSA (right) as a function of irradiation dose (Gy).

molecule of DOPA/300 molecules of BSA in a 5 μ g protein sample. Dose-related appearance of protein-bound DOPA in BSA was reported by fluorometric detection (excitation, 280 nm; emission, 320 nm) using 10 times more sample and a dose range 230–920 Gy in the presence of oxygen (34). However, the present study shows that at doses higher than 120 Gy the percent of formation of DOPA does not correlate with the percent of modification of Tyr. When samples were irradiated with a dose range 200–600 Gy, a broad peak with a retention time longer than that of DOPA appeared, the intensity of which increased with dose at the expense of the DOPA peak (results not shown). Although the peak was not identified, such an observation combined with the generation of brownish yellow color seen in the irradiated samples suggests further transformation of DOPA with higher dose, leading perhaps to the formation of some polymeric material. Besides, the percent recoveries of most other amino acids in both the proteins were also affected 30% or more at 240 Gy.

Free DOPA and other reactive quinones have been implicated in a number of disease states (35). Protein-bound DOPA may have a role in the replenishment of reduced transition metal ion involved in a free-radical-generating system *in vivo* (36). This would result in amplification of the radical-damaging event that originally generated protein-bound DOPA. Since most standard amino acid analysis techniques are limited to detect normal residues of protein, sensitive assay of low-level oxidized amino acids implicated in protein oxidation will be useful for monitoring oxidative stress-related physiological and pathological processes.

ACKNOWLEDGMENT

Supported in part by National Cancer Institute Grant CA46896. Authors thank H. C. Box for the use of the X-ray source.

LITERATURE CITED

- (1) Stadtman, E. R. (1992) Protein oxidation and aging. *Science* 257, 1220–1224.
- (2) Davies, K. J. A. (1993) Protein modification by oxidants and the role of proteolytic enzyme. *Biochem. Soc. Trans.* 21, 346–353.
- (3) Cross, C. E., Halliwell, B., Borish, E. T., Pryor, W. A., Ames, B. N., Saul, R. L., McCord, J. M., and Harman, D. (1987) Oxygen radicals and human disease. *Ann. Int. Med.* 107, 526–545.

- (4) Stadtman, E. R. (1993) Oxidation of free amino acids and amino acid residues in proteins by radiolysis and by metal-catalyzed reactions. *Annu. Rev. Biochem.* **62**, 797–821.
- (5) Stadtman, E. R. (1995) Role of oxidized amino acids in protein breakdown and stability. *Methods Enzymol.* **258**, 379–393.
- (6) Levine, R. L., Garland, D., Oliver, C. N., Amici, A., Climent, I., Lenz, A.-G., Ahn, B.-W., Shaltiel, S., and Stadtman, E. R. (1990) Determination of carbonyl content in oxidatively modified proteins. *Methods Enzymol.* **186**, 464–478.
- (7) Levine, R. L., Williams, J. A., Stadtman, E. R., and Shacter, E. (1994) Carbonyl assays for determination of oxidatively modified proteins. *Methods Enzymol.* **233**, 346–357.
- (8) Huggins, T. G., Wells-Knecht, M. C., Detorie, N. A., Baynes, J. W., and Thorpe, S. R. (1993) Formation of o-tyrosine and dityrosine in proteins during radiolytic and metal-catalyzed oxidation. *J. Biol. Chem.* **268**, 12341–12347.
- (9) Cao, G., and Culter, R. G. (1995) Difficulties in measuring reactive protein carbonyls in tissues using 2,4-dinitrophenylhydrazines. *Arch. Biochem. Biophys.* **320**, 106–114.
- (10) Garrison, W. M. (1987) Reaction mechanisms in the radiolysis of peptides, polypeptides, and proteins. *Chem. Rev.* **87**, 381–398.
- (11) Alexander, P., Rosen, D. (1961) A comparison of the effects of X-rays and alpha rays on some proteins and amino acids in dilute aqueous solution. *Radiation Res.* **15**, 475–488.
- (12) Fletcher, G. L., and Okada, S. (1961) Radiation-induced formation of dihydroxyphenylalanine from tyrosine and tyrosine-containing peptides in aqueous solution. *Radiat. Res.* **15**, 349–354.
- (13) Rowbottom, J. (1955) The radiolysis of aqueous solutions of tyrosine. *J. Biol. Chem.* **212**, 877–885.
- (14) Vermeil, C., and Lefort, M. (1955) Production de tyrosine par action des rayons γ sur les solutions aqueuses de phenylalanine. *C. R. Acad. Sci. Paris* **244**, 889–891.
- (15) Farber, J. M., and Levine, R. L. (1986) Sequence of a peptide susceptible to mixed-function oxidation. *J. Biol. Chem.* **261**, 4574–4578.
- (16) Uchida, K., and Kawakishi, S. (1989) Ascorbate-mediated specific oxidation of the imidazole ring in a histidine derivative. *Bioorg. Chem.* **17**, 330–343.
- (17) Davies, K. J. A., Delsignore, M. E., and Lin, S. W. (1987) Protein damage and degradation by oxygen radicals. *J. Biol. Chem.* **262**, 9902–9907.
- (18) Guptasarma, P., and Balasubramanian, D. (1992) Hydroxyl radical mediated damage to proteins, with special reference to the crystallins. *Biochemistry* **31**, 4296–4303.
- (19) Sen, A. C., Ueno, N., and Chakrabarti, B. (1992) Studies on human lens: origin and development of fluorescent pigments. *Photochem. Photobiol.* **55**, 753–764.
- (20) Wells-Knecht, M. C., Huggins, T. G., Dyer, D. G., Thorpe, S. R., and Baynes, J. W. (1993) Oxidized amino acids in lens protein with age. *J. Biol. Chem.* **268**, 12348–12352.
- (21) Uchida, K., and Kawakishi, S. (1994) Identification of oxidized histidine generated at the active site of Cu/Zn-superoxide dismutase exposed to H_2O_2 . *J. Biol. Chem.* **269**, 2405–2410.
- (22) Lewis, S. A., and Levine, R. L. (1995) Determination of 2-oxohistidine by amino acid analysis. *Anal. Biochem.* **231**, 440–446.
- (23) Ozols, J., Gerard, C., and Nobrega, F. G. (1976) Proteolytic cleavage of horse liver cytochrome b₅. *J. Biol. Chem.* **251**, 6767–6774.
- (24) Waite, J. H. (1991) *Anal. Biochem.* **192**, 429–433.
- (25) Davies, K. J. A., Ed. (1991) *Detection of peptidyl-3,4-dihydroxyphenylalanine by amino acid analysis and microsequencing techniques. Oxidative damage and repair: chemical, biological and medical aspects*, Pergamon Press, Oxford, U.K.
- (26) Tapuhi, Y., Schmidt, D. E., Linder, W., and Krager, B. L. (1981) Dansylation of amino acids for high-performance liquid chromatography analysis. *Anal. Biochem.* **115**, 123–129.
- (27) Oray, B., Lu, H. S., and Gracy, R. W. (1983) High-performance liquid chromatographic separation of Dns-amino acid derivatives and applications to peptide and protein structural studies. *J. Chromatogr.* **270**, 253–266.
- (28) Randerath, K., Randerath, E., Danna, T. F., Van Golen, K. L. and Putnam, K. L. (1989) A new sensitive ^{32}P -postlabeling assay based on the specific enzymatic conversion of bulky DNA lesions to radiolabeled dinucleotides and nucleoside monophosphates. *Carcinogenesis* **10**, 1231–1239.
- (29) Marquez, F. J., Quesada, A. R., Sanchez-Jimenez, F., and Nimez De Castro, I. (1986) Determination of 27 dansyl amino acid derivatives in biological fluids by reversed-phase high-performance liquid chromatography. *J. Chromatogr.* **380**, 275–283.
- (30) Sharma, M., and Freund, H. G. (1991) Development of laser-induced fluorescence detection to assay DNA damage. In *Optical Methods for Ultrasensitive Detection and Analysis: Techniques and Applications* (B. L. Fearey, Ed.) Proceedings of SPIE 1435, pp 280–291, SPIE, Bellingham, WA.
- (31) Tapuhi, Y., Miller, N., and Krager, B. L. (1981) Practical considerations in the chiral separation of Dns-amino acids by reversed-phase liquid chromatography using metal chelate additives. *J. Chromatogr.* **205**, 325–337.
- (32) Reitsma, B. H., and Yeung, E. S. (1987) Optical activity and ultraviolet absorbance detection of dansyl L-amino acids separated by gradient liquid chromatography. *Anal. Chem.* **59**, 1059–1061.
- (33) Boguta, G., and Dancewicz, A. M. (1983) Radiolytic and enzymatic dimerization of tyrosyl residues in insulin, ribonuclease, papain and collagen. *Int. J. Radiat. Biol.* **43**, 249–265.
- (34) Gieseg, S. P., Simpson, J. A., Charlton, T. S., Duncan, M. W., and Dean, R. T. (1993) Protein-bound 3,4-dihydroxyphenylalanine is a major reductant formed during hydroxyl radical damage to protein. *Biochemistry* **32**, 4780–4786.
- (35) O'Brien, P. J. (1991) Molecular mechanism of quinone cytotoxicity. *Chem.-Biol. Interact.* **80**, 1–41.
- (36) Dean, R. T., Gebicki, J., Gieseg, S. P., Grant, A. J., and Simpson, J. A. (1992) Hypothesis: a damaging role in aging for reactive protein oxidation products? *Mutat. Res.* **275**, 387–393.

BC9700042

Synthesis and Preliminary Biological Evaluation of (3-Iodobenzoyl)norbiotinamide and ((5-Iodo-3-pyridinyl)carbonyl)norbiotinamide: Two Radioiodinated Biotin Conjugates with Improved Stability

Catherine F. Foulon,* Kevin L. Alston, and Michael R. Zalutsky

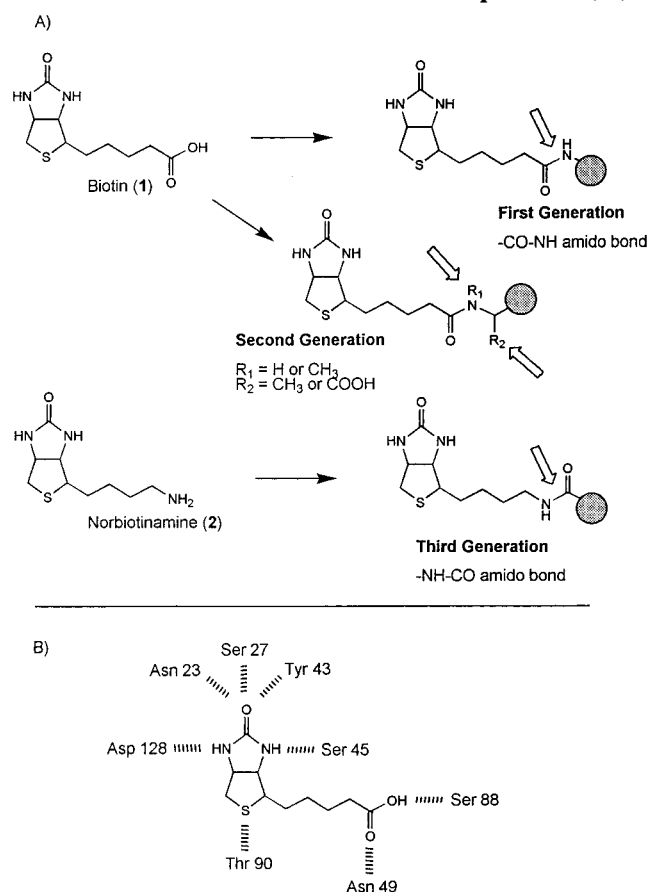
Department of Radiology, Duke University Medical Center, Durham, North Carolina 27710. Received November 20, 1996[®]

A new class of radioiodinated biotin conjugates is described in which the amido bond between biotin and the labeled prosthetic group is reversed. One conjugate, (3-[¹²⁵I]iodobenzoyl)norbiotinamide (**4c**, [¹²⁵I]IBB) was labeled with Na¹²⁵I in one step from (3-(tributylstannyl)benzoyl)norbiotinamide (**4b**, TBB) via a demetalation reaction. However, the analogous reaction with ((5-(tributylstannyl)-3-pyridinyl)carbonyl)norbiotinamide (**6b**, TPB) failed to yield ((5-[¹³¹I]iodo-3-pyridinyl)carbonyl)norbiotinamide (**6c**, [¹³¹I]IPB), necessitating a two-step approach for synthesizing [¹³¹I]IPB. The binding of [¹²⁵I]IBB and [¹³¹I]IPB to streptavidin in vitro was identical to that of biotinyl-3-[¹²⁵I]iodoanilide, a conjugate with an amido bond with normal configuration. Both [¹²⁵I]IBB and [¹³¹I]IPB were stable in serum while the first-generation compound was rapidly degraded. The biodistribution patterns of [¹²⁵I]IBB and [¹³¹I]IPB in mice are consistent with limited degradation of these conjugates by biotinidase and deiodinases.

INTRODUCTION

The utilization of radiolabeled antibodies (MAbs)¹ for the localization and therapy of tumors has been impaired by the inability to achieve high tumor-to-normal tissue ratios in a time frame compatible with those of many radionuclides of potential clinical interest (1). Among the approaches being explored to circumvent this problem is pre-targeting, which involves separate administration of the MAb and the radionuclide. This strategy most frequently attempts to exploit the high affinity of biotin (1), a 244D vitamin found in low concentration in blood and tissues, for the 65 kD proteins avidin (2) or streptavidin (3). The feasibility of targeting radiolabeled biotin derivatives to (strept)avidin-conjugated MAbs previously localized on tumors was first demonstrated nearly a decade ago (4). The structural elements of biotin involved in binding to (strept)avidin are the urea moiety and the nonoxidized thioether (5), thus leaving the carboxylic group available for modification. For this reason, radio-labeled biotin derivatives generally have been prepared by direct functionalization of the carboxyl group of the vitamin, resulting in a CO–NH amido bond (Scheme 1).

Scheme 1. (A) Different Generations of Radiolabeled Biotin Derivatives and (B) Interaction between Biotin and Amino Acid Residues of Streptavidin (29)



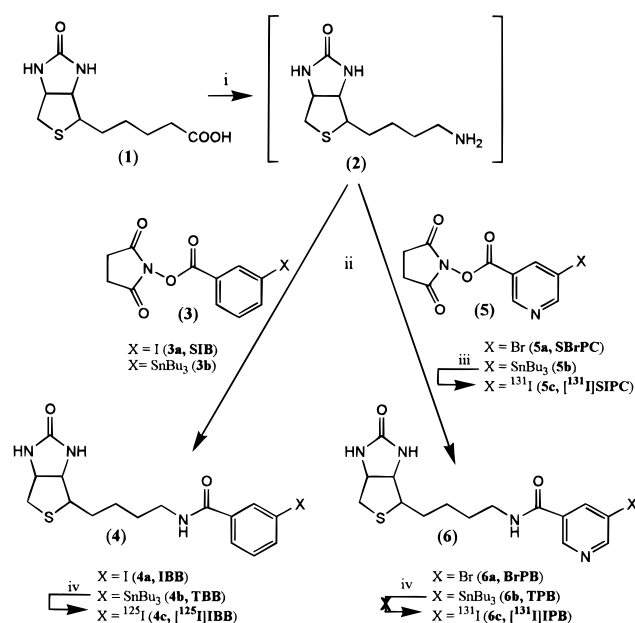
* Corresponding author: Catherine F. Foulon, Ph.D., Department of Radiology, Box 3808, Duke University Medical Center, Durham, NC 27710 (telephone, 919-684-7705; FAX, 919-684-7122; e-mail, cfoulon@acpub.duke.edu).

[®] Abstract published in *Advance ACS Abstracts*, February 15, 1997.

¹ Abbreviations used: MAbs, monoclonal antibodies; SIB, *N*-succinimidyl 3-iodobenzoate; SIPC, *N*-succinimidyl 5-iodo-3-pyridinecarboxylate; SBrPC, *N*-succinimidyl 5-bromo-3-pyridinecarboxylate; IBB, (3-iodobenzoyl)norbiotinamide; [¹²⁵I]IBB, (3-[¹²⁵I]iodobenzoyl)norbiotinamide; TBB, (3-(tributylstannyl)benzoyl)norbiotinamide; BrPB, ((5-bromo-3-pyridinyl)carbonyl)norbiotinamide; [¹³¹I]IPB, ((5-[¹³¹I]iodo-3-pyridinyl)carbonyl)norbiotinamide; TPB, ((5-(tributylstannyl)-3-pyridinyl)carbonyl)norbiotinamide; IBA, biotinyl-3-iodoanilide; [¹²⁵I]IBA, biotinyl-3-[¹²⁵I]iodoanilide; [²¹¹At]AtBA, biotinyl-3-[²¹¹At]atatoanilide; CSF, cerebrospinal fluid; ITLC, instant thin layer chromatography; Asn, asparagine; Asp, aspartic acid; Ser, serine; Tyr, tyrosine.

This tactic, designated as First Generation, has been utilized to prepare biotin conjugates labeled with a wide variety of radionuclides including ^{123/125/131}I (6–9), ¹⁸F (10), ²¹¹At (11), ⁹⁰Y (12), ¹¹¹In (13, 14), ⁶⁷Ga (15), and ^{99m}Tc (16). Although most of these derivatives maintain a high

Scheme 2. Preparation of Third-Generation Biotin Derivatives^a



^a (i) *t*BuOH, TEA, diphenylphosphoryl azide. (ii) DMF, water, TEA. (iii) Na¹³¹I, NCS, CHCl₃, AcOH, 65 °C, 10 min. (iv) Na^{125/131}I, NCS, MeOH, Na₂S₂O₅, room temperature, 20 s.

affinity for (strept)avidin and have good stability in vitro, direct and indirect evidence suggests that these radiolabeled biotin conjugates are rapidly metabolized in vivo. The catabolic pathways involved include oxidation of the sulfur, cleavage of the valeryl chain, loss of the radiolabel, and cleavage of the radiolabeled prosthetic group by the action of biotinamide amino hydrolase (EC 3.5.1.12, biotinidase) (17). Avoiding biotinidase degradation has been attempted previously by introducing steric hindrance at the level of the amido bond, depicted in Scheme 1 as Second Generation (18, 19).

In this study, we have evaluated two radioiodinated biotin conjugates which have been designed to be resistant to degradation by both biotinidase and deiodinases. We attempted to impair recognition by biotinidase through the use of a reversed amido bond (i.e., NH–CO bond) between the valeryl chain of biotin and the prosthetic group, depicted in Scheme 1 as Third Generation. The templates used for radioiodination were selected on the basis of our previous experience with *N*-succinimidyl 3-iodobenzoate (**3a**, SIB) and *N*-succinimidyl 5-iodo-3-pyridinecarboxylate (**5c**, SIPC) as depicted on Scheme 2 (20–22). MAbs labeled via these reagents exhibited very low levels of deiodination in vivo and yielded labeled catabolites which were rapidly excreted via the urine, two properties of interest for improved radioiodinated biotin conjugates. (3-[¹²⁵I]Iodobenzoyl)norbiotinamide (**4c**, [¹²⁵I]-IBB) was prepared in one step from (3-(tributylstannyl)-benzoyl)norbiotinamide (**4b**, TBB) via a demetalation reaction. However, the analogous reaction of ((5-(tributylstannyl)-3-pyridinyl)carbonyl)norbiotinamide (**6b**, TPB) failed to yield ((5-[¹³¹I]iodo-3-pyridinyl)carbonyl)norbiotinamide (**6c**, [¹³¹I]IPB) necessitating a two-step approach for synthesizing [¹³¹I]IPB. We chose to radiolabel each of these compounds with a different isotope of iodine in order to evaluate their in vitro and in vivo biological properties simultaneously, by paired-label experiments. Both [¹²⁵I]IBB and [¹³¹I]IPB exhibited good stability and streptavidin binding, in vitro, and tissue distribution profiles in mice consistent with limited degradation by biotinidase and deiodinases.

EXPERIMENTAL PROCEDURES

Materials. Streptavidin was purchased from Sigma Chemical Co. St. Louis, MO, and all other chemicals were obtained from Aldrich, Milwaukee, WI. Norbiotinamine hydrochloride (**2**) was purchased from Molecular Probes, Eugene, OR, for preparing the radiohalogenated conjugates, whereas crude **2**, prepared as reported by Szalecki (23), was utilized for the synthesis of standards. *N*-Succinimidyl 3-iodobenzoate (SIB, **3a**), *N*-succinimidyl 3-(tributylstannyl)benzoate (**3b**), *N*-succinimidyl 5-bromo-3-pyridinecarboxylate (SBrPC, **5a**) and *N*-succinimidyl 5-(tributylstannyl)-3-pyridinecarboxylate (**5b**) were prepared as described in previous publications (21, 24). Biotinyl-3-[^{125/127}I]iodoanilide ([^{125/127}I]IBA) was prepared according to a previously reported procedure (25). Sodium [¹²⁵I]iodide and sodium [¹³¹I]iodide in 0.1 N NaOH were obtained from Dupont New England Nuclear, Billerica, MA. tC18 cartridges were purchased from Waters, Milford, MA.

HPLC purifications were conducted on a Beckman system (Model 126 pump, Model 168 UV detector, Model 170 radioactivity detector) connected to a Model 406 analog interface module. Chromatography was performed using either a reverse-phase column (Adsorbosphere C18, 10 μm, 250 × 4.6 mm, eluted with methanol: water, 55:45 at 1 mL/min) or a normal-phase column (Adsorbosphere Silica, 10 μm, 250 × 4.6 mm, eluted with hexane:ethyl acetate:acetic acid, 65:34.3:0.7 at 1 mL/min), both obtained from Alltech, Deerfield, IL. TLC was performed on silica gel IB2-F Baker-Flex sheets (J.T. Baker, Phillipsburg, NJ). Silica gel impregnated glass fiber ITLC plates were purchased from Gelman Science, Ann Arbor, MI, and cut in 1.5- × 8-cm strips. Radioactivity was quantified using a LKB 1282 Compugamma dual-channel, automated γ counter. Higher levels of activity were measured using a Capintec CRC-7R radioisotope calibrator. Elemental analyses were performed by Atlantic Microlab, Norcross, GA. ¹H NMR spectra were recorded on a General Electric Midfield 300 MHz spectrometer.

Norbiotinamine (2). This product was prepared as described by Szalecki (23). Briefly, to a flask (predried at 110 °C for 48 h) containing biotin (**1** (0.49 g, 2.01 mmol) dissolved in 20 mL of *tert*-butyl alcohol were added diphenylphosphoryl azide (475 μL, 2.21 mmol) and triethylamine (308 μL, 2.21 mmol). The reaction mixture was refluxed for 18 h under argon atmosphere, the solvent removed by rotative evaporation, and the oily residue dissolved in a 50% methanolic solution of 6 N HCl (20 mL) and stirred overnight. Solvents were removed using a vacuum pump, affording an oil (1.84 g) which was not purified further before reaction with the *N*-succinimidyl ester **3a**, **3b**, **5a**, or **5b**.

Preparation of IBB (4a), TBB (4b), BrPB (6a), and TPB (6b): General Procedure. The crude oil **2** was dissolved in DMF:water (4:1), and the pH was made basic using triethylamine. The *N*-succinimidyl ester derivative **3a**, **3b**, **5a**, or **5b** (1.2 equiv) in DMF was added to the above mixture and stirred at room temperature for at least 3 h. The reaction was monitored by TLC (chloroform:methanol, 6:1). The solvent was removed by rotative evaporation and the product subjected to column chromatography (silica gel, chloroform:methanol, 6:1). The desired fractions were pooled, evaporated to dryness, and recrystallized in DMF:H₂O (1:1). The white crystals thus obtained were filtered off and further dried under vacuum. The products were stored under argon at 4 °C.

(3-Iodobenzoyl)norbiotinamide (IBB, 4a). IBB was obtained as white crystals, in 18.3% yield. *R_f* (TLC)

= 0.53. Anal. Calcd for $C_{16}H_{20}N_3O_2SI$: C, 43.15; H, 4.52; N, 9.44. Found: C, 43.21; H, 4.56; N, 9.35. 1H NMR (DMSO- d_6), δ (ppm): 8.52 (t, 1H, NHCO), 8.16 (s, 1H, ArH2), 7.87 (d, 1H, ArH6), 7.83 (d, 1H, ArH4), 7.26 (t, 1H, ArH5), 6.45 (s, 1H, NHCO), 6.35 (s, 1H, NHCO), 4.29 (q, 1H, CHN), 4.13 (t, 1H, CHN), 3.22 (m, 2H, CH_2N), 3.11 (q, 1H, SCH), 2.81 (m, 2H, SCH_2), 1.62–1.36 (m, 6H, $(CH_2)_3$). M_p = 185–190 °C.

(3-(Tributylstannyl)benzoyl)norbiotinamide (TBB, 4b). TBB was isolated as white crystals, in 22% yield. R_f (TLC) = 0.67. Anal. Calcd for $C_{28}H_{47}N_3O_2SSn$: C, 55.27; H, 7.79; N, 6.91. Found: C, 55.07; H, 7.59; N, 6.83. 1H NMR ($CDCl_3$) δ (ppm): 8.41 (m, 1H, NHCO), 7.86 (s, 1H, ArH2), 7.72 (d, 1H, ArH6), 7.54 (d, 1H, ArH4), 7.39 (t, 1H, ArH5), 6.45 (s, 1H, NHCO), 6.35 (s, 1H, NHCO), 4.29 (m, 1H, CHN), 4.14 (m, 1H, CHN), 3.24 (m, 2H, CH_2N), 3.11 (m, 1H, SCH), 2.80 (m, 2H, SCH_2), 1.50–0.83 (m, 33H, 3 nBu + $(CH_2)_3$). M_p = 154–155 °C.

((5-Bromo-3-pyridinyl)carbonyl)norbiotinamide (BrPB, 6a). BrPB was afforded as white crystals, in 14.5% yield. R_f (TLC) = 0.39. Anal. Calcd for $C_{15}H_{19}N_4O_2SBr$: C, 45.12; H, 4.80; N, 14.03. Found: C, 45.19; H, 4.80; N, 13.95. 1H NMR (DMSO- d_6) δ (ppm): 8.85 (s, 1H, ArH2), 8.74 (d, 1H, ArH6), 8.61 (t, 1H, NHCO), 8.29 (s, 1H, ArH4), 6.36 (s, 1H, NHCO), 6.27 (s, 1H, NHCO), 4.20 (q, 1H, CHN), 4.05 (t, 1H, CHN), 3.15 (d, 2H, CH_2N), 3.00 (m, 1H, SCH), 2.71 (m, 2H, SCH_2), 1.42–1.28 (m, 6H, $(CH_2)_3$). M_p = 227–228 °C.

((5-(Tributylstannyl)-3-pyridinyl)carbonyl)norbiotinamide (TPB, 6b). TPB was obtained as white crystals, in 24% yield. R_f (TLC) = 0.55. Anal. Calcd for $C_{27}H_{46}N_4O_2SSn$: C, 53.21; H, 7.61; N, 9.19. Found: C, 53.11; H, 7.56; N, 9.10. 1H NMR (DMSO- d_6) δ (ppm): 8.83 (s, 1H, ArH2), 8.61 (s, 1H, ArH6), 8.56 (m, 1H, NHCO), 8.14 (s, 1H, ArH4), 6.39 (s, 1H, NHCO), 6.29 (s, 1H, NHCO), 4.24 (m, 1H, CHN), 4.07 (m, 1H, CHN), 3.15 (m, 2H, CH_2N), 3.05 (m, 1H, SCH), 2.78 (m, 2H, SCH_2), 1.46–0.80 (m, 33H, 3 nBu + $(CH_2)_3$). M_p = 134–138 °C.

***N*-Succinimidyl 5-[^{131}I]Iodo-3-pyridinecarboxylate ([^{131}I]SIPC, 5c).** To a vial containing $Na^{131}I$ (1 mCi) were added acetic acid:chloroform [5:95 (10 μ L)], *N*-chlorosuccinimide (10 μ L, 13.3 mg/mL of chloroform), and **5b** (10 μ L, 5 mg/100 μ L of chloroform). The vial was vortexed, and the reaction was allowed to proceed at 65 °C for 10 min. The product **5c** was isolated by HPLC (normal-phase column eluted with hexane:ethyl acetate:acetic acid, 65:34.3:0.7, at 1 mL/min). The product eluting at 14 min was concentrated under a stream of nitrogen and used directly for the next reaction.

Preparation of [^{131}I]IPB (6c). A solution of commercial **2**-HCl in pH 8.5 borate buffer (200 μ L, 2 mg/mL) was added to a vial containing 500 μ Ci of [^{131}I]SIPC **5c**. The reaction was performed at room temperature for 20 min, and the sample was purified on HPLC (C18 column, 55% methanol, 1 mL/min). The desired product was collected at 6.4 min and concentrated by elution through a tC18 cartridge; [^{131}I]IPB was isolated in 0.5 mL of methanol. The solvent was evaporated under a stream of nitrogen, and **6c** was reconstituted in water for use in the in vitro and in vivo studies. Radiolabeling yields ranged between 75 and 82%.

Preparation of [^{125}I]IBB (4c). $Na^{125}I$ (500 μ Ci) was added to a vial containing TBB (**4b**) (100 μ g in 100 μ L of methanol) along with *N*-chlorosuccinimide (20 μ L, 2 mg/mL of methanol). The vial was vortexed for a maximum of 20 s, and a saturated aqueous solution of sodium metabisulfite was added (2 \times 200 μ L). The product was purified on HPLC (C18 column, 1 mL/min, 55% MeOH), and **4c** was collected at 8.9 min. After evaporation, **4c**

was dissolved in 10 mL of water and concentrated on a tC18 cartridge; [^{125}I]IBB was collected in 0.5 mL of methanol, which was evaporated under a stream of nitrogen. The radiolabeling yields averaged 62%. The product was stored in methanol at 4 °C and was stable for up to 1 week.

In Vitro Binding to Streptavidin. The in vitro binding of the radioiodinated biotin derivatives to streptavidin was assessed. A constant activity (4 μ Ci in 100 μ L of distilled water) of [^{125}I]IBB, [^{131}I]IPB, or [^{125}I]IBA was mixed with increasing amounts of streptavidin (0–50 μ g, 100 μ L of distilled water) in a 1.5-mL polypropylene conical vial. The vials were placed on an orbital shaker and incubated at 37 °C for 5 h, and a 5- μ L aliquot was removed for analysis by silica gel ITLC. The plates were eluted with distilled water:ethanol (1:1). The radioiodinated biotin–streptavidin complex stayed at the origin whereas the free biotinylated compound moved with the solvent front. Each plate was cut horizontally, 1.5 cm above the origin, and the activity levels in the two parts were quantified. The percentage of radioiodine activity associated with the biotin–streptavidin complex was calculated as follows: the activity at the baseline multiplied by 100, divided the activity at the baseline and on the upper part of the plate.

In Vitro Stability in Serum, Cerebrospinal Fluid (CSF), and Distilled Water. A mixture of [^{125}I]IBB and [^{131}I]IPB (4 μ Ci each in a total volume of 20 μ L of distilled water) was incubated at 37 °C in 1.5-mL polypropylene centrifuge tubes with 200 μ L of either mouse serum, human serum, human CSF, or distilled water. An additional experiment was performed in single-label format to measure the stability of [^{125}I]IBA (4 μ Ci per tube). All measurements were performed in triplicate. The stability of [^{125}I]IBB and [^{131}I]IPB was monitored over 24 h by silica gel TLC eluted with chloroform:methanol (90:10). Plates were covered with tape to prevent the loss of volatile species. At each time point, an aliquot (4 μ L) from each tube was co-spotted on TLC with the appropriate cold standard; IBB, BrPB, and IBA had R_f values of 0.55, 0.48, and 0.51, respectively, under these conditions. The plates were cut into three sections: part A, below the spot of the cold standard, where the sulfoxide byproducts (R_f = 0.30) migrate, part B, with an R_f corresponding to the cold standard, and part C, with R_f greater than the cold standard, where iodide (R_f = 0.95), iodobenzoic acid, bromonicotinic acid (both R_f = 0.80), and 3-iodoaniline (R_f = 0.81) are found. The TLC sections were counted for radioactivity in the γ counter using a dual- or single-channel program as appropriate. The percentage of intact radioiodinated biotin conjugate was calculated from the following ratio: (activity in part B)/(activities in parts A + B + C) multiplied by 100.

Tissue Distribution. A paired-label experiment was performed to compare the tissue distribution of [^{125}I]IBB and [^{131}I]IPB. Normal BALB/c mice weighting 20–25 g were injected intravenously with [^{125}I]IBB (5 μ Ci, 100 μ L of saline) and [^{131}I]IPB (5 μ Ci, 100 μ L of saline). Groups of five animals were euthanized by halothane overdose at 5, 30, and 60 min as well as 6, 12, and 18 h. The organs were weighted and the ^{125}I and ^{131}I activity levels counted in the γ counter using a dual-channel program. The percentage of injected dose localized per organ was calculated; blood, muscle, and bone were assumed to account for 6%, 40%, and 10% of body weight, respectively. Statistical analysis of the differences between ^{125}I and ^{131}I tissue levels was performed using a paired *t*-test with P < 0.05 considered to be significant.

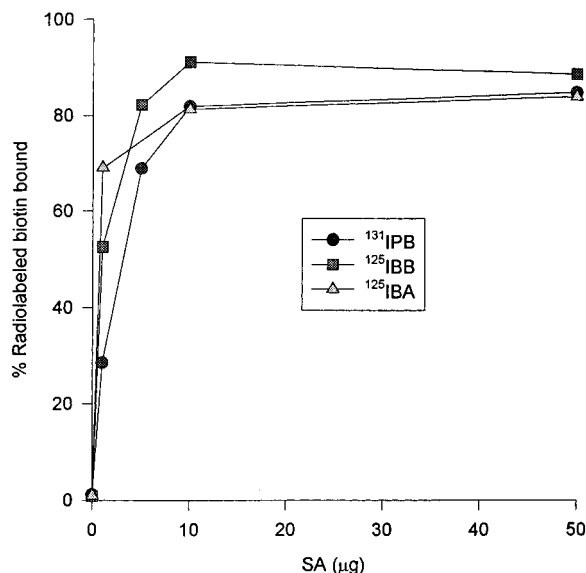


Figure 1. In vitro binding of [^{125}I]IBB, [^{131}I]IPB, and [^{125}I]IBA to streptavidin as a function of streptavidin concentration.

RESULTS

Radiochemical Synthesis. The preparation of [^{125}I]IBB was readily accomplished by destannylation of TBB using Na^{125}I and *N*-chlorosuccinimide as the oxidant. The total time required for synthesis and purification was 40 min with an average yield of 62%. The sulfoxide byproduct also was produced in 2–10% yield but was removed by HPLC. [^{125}I]IBB was identified by coelution with an authentic IBB standard at 8.9 min. No peak corresponding to IBB was observed by the UV detector during HPLC purification, consistent with the preparation of [^{125}I]IBB at the no-carrier-added level. Attempts to prepare [^{131}I]IPB in a one-step fashion from TPB using the same conditions were not successful. Modifying the reaction conditions through the use of other oxidants (iodogen, hydrogen peroxide), acid (acetic acid, hydrochloric acid), and elevated temperature (65 °C) were fruitless. Hence, a two-step procedure was utilized for the synthesis of [^{131}I]IPB. First, [^{131}I]SIPC was prepared from **5b** and isolated by HPLC in an average yield of 60%. This intermediate then was reacted in alkaline medium with commercial norbiotamine hydrochloride, and the reaction mixture was subjected to HPLC. The yield for this step was 80%. The identity of [^{131}I]IPB was established by coelution with a BrPB standard (6.4 min). With these reaction conditions, the sulfoxide byproduct was not produced. The lack of cold peak on the UV trace corresponding to IPB during HPLC purification is consistent with preparation of [^{131}I]IPB at the no-carrier-added level. Both [^{131}I]IPB and [^{125}I]IBB were stable for at least 1 week when stored in methanol at 4 °C.

Binding to Streptavidin In Vitro. The binding of [^{125}I]IBB and [^{131}I]IPB to streptavidin was evaluated in vitro in order to determine whether inversion of the amido bond impaired the affinity of these conjugates for streptavidin. Instant thin layer chromatography (ITLC) was used to separate bound and unbound radioligand, and [^{125}I]IBA was tested under identical conditions as a control. As shown in Figure 1, binding saturation curves for the three biotin derivatives were nearly identical. For example, in the presence of 50 μg of streptavidin, the percentage of radioligand bound was $88.5 \pm 1.0\%$ for [^{125}I]IBB, $84.7 \pm 0.1\%$ for [^{131}I]IPB, and $83.8 \pm 6.3\%$ for [^{125}I]IBA, indicating that inversion of the amido bond did not interfere with binding to streptavidin.

In Vitro Stability. The in vitro stability of the three radioiodinated biotin conjugates was compared following incubation with mouse serum, human serum, human CSF, and distilled water at 37 °C. Essentially all of the radioiodine activity remaining associated with intact [^{125}I]IBB, [^{131}I]IPB, and [^{125}I]IBA in distilled water (Figure 2A), CSF (Figure 2B) and human serum (Figure 2C). The stability of [^{125}I]IBB and [^{131}I]IPB was evaluated for 6 days, and in these three media, 90% or more of the radioactivity remained associated with the conjugate for 4 days. With time, an increasing fraction of radioiodine activity was found in the lower part of the TLC plate, consistent with the R_f of the sulfoxide byproducts. The activity at the top of the TLC plate reflects either the cleavage of the prosthetic group or deiodination. With the exception of the value measured for [^{125}I]IBB in human serum at 3 days ($3.4 \pm 2.6\%$), less than 2% of the activity eluted in the top part of the TLC plate. More striking differences were observed in murine serum (Figure 2D). The first-generation compound, [^{125}I]IBA, was degraded rapidly, with only $38.4 \pm 1.5\%$ and $14.2 \pm 1.6\%$ remaining after 30 min and 6 h, respectively. Most of the radioactivity ($61.1 \pm 1.4\%$, 30 min; $83.7 \pm 1.2\%$, 6 h) was found at the top of the TLC plate. In contrast, the percentage of radioiodine activity remaining as [^{125}I]IBB and [^{131}I]IPB in mouse serum at 6 h was $99.2 \pm 0.5\%$ and $97.9 \pm 0.4\%$, respectively. By 4 days, these values had decreased to $86.0 \pm 2.0\%$ and $88.2 \pm 2.5\%$. The percentage of activity moving to the top of the TLC plate was significantly higher from day 1 to 6 for [^{125}I]IBB (1.5 to 3.3%) than for [^{131}I]IPB (0.05 to 0.6%).

Tissue Distribution. The tissue distribution in normal mice of [^{125}I]IBB and [^{131}I]IPB was investigated in a paired-label experiment, and the results are presented in Table 1. Both compounds were cleared rapidly from the blood, with less than 1% of the injected dose remaining at 1 h. Although total recovery of urine was not performed, the level of activity in the urine sample obtained at necropsy was 22–26% at 1 h, suggesting rapid excretion of both tracers. Thyroid levels of ^{125}I and ^{131}I were less than 0.25% at all time points, consistent with a low degree of deiodination for both conjugates. Both [^{125}I]IBB and [^{131}I]IPB cleared rapidly from most normal tissues; however, retention of ^{131}I was significantly lower ($P < 0.05$, paired *t*-test) than that of ^{125}I in liver, spleen, lungs, heart, kidneys, and blood at most time points. High levels of both biotin conjugates were observed in the intestines during the first hour after injection; however, by 18 h, less than 1% of the injected dose remained in the intestines. The %ID in the intestines for [^{131}I]IPB was higher than that for [^{125}I]IBB with these differences being significant at all time points.

DISCUSSION

Antibody-mediated pre-targeting is an attractive strategy for the selective delivery of radionuclides to tumors because it attempts to exploit the specificity of the Mab without the disadvantages associated with its macromolecular size, namely slow blood clearance and poor diffusion. Multistep approaches have evolved which utilize the biotin–(strept)avidin system, with or without clearing agent, to improve target-to-normal tissue ratios. Encouraging results have been obtained in both diagnostic and therapeutic trials in patients (16, 26, 27) and animal models (1, 13). Efforts are underway to improve pre-targeting through the optimization of each component of this strategy, including the nature of the MAb–streptavidin conjugate, the clearing agent and the radiolabeled biotin derivative (12, 28).

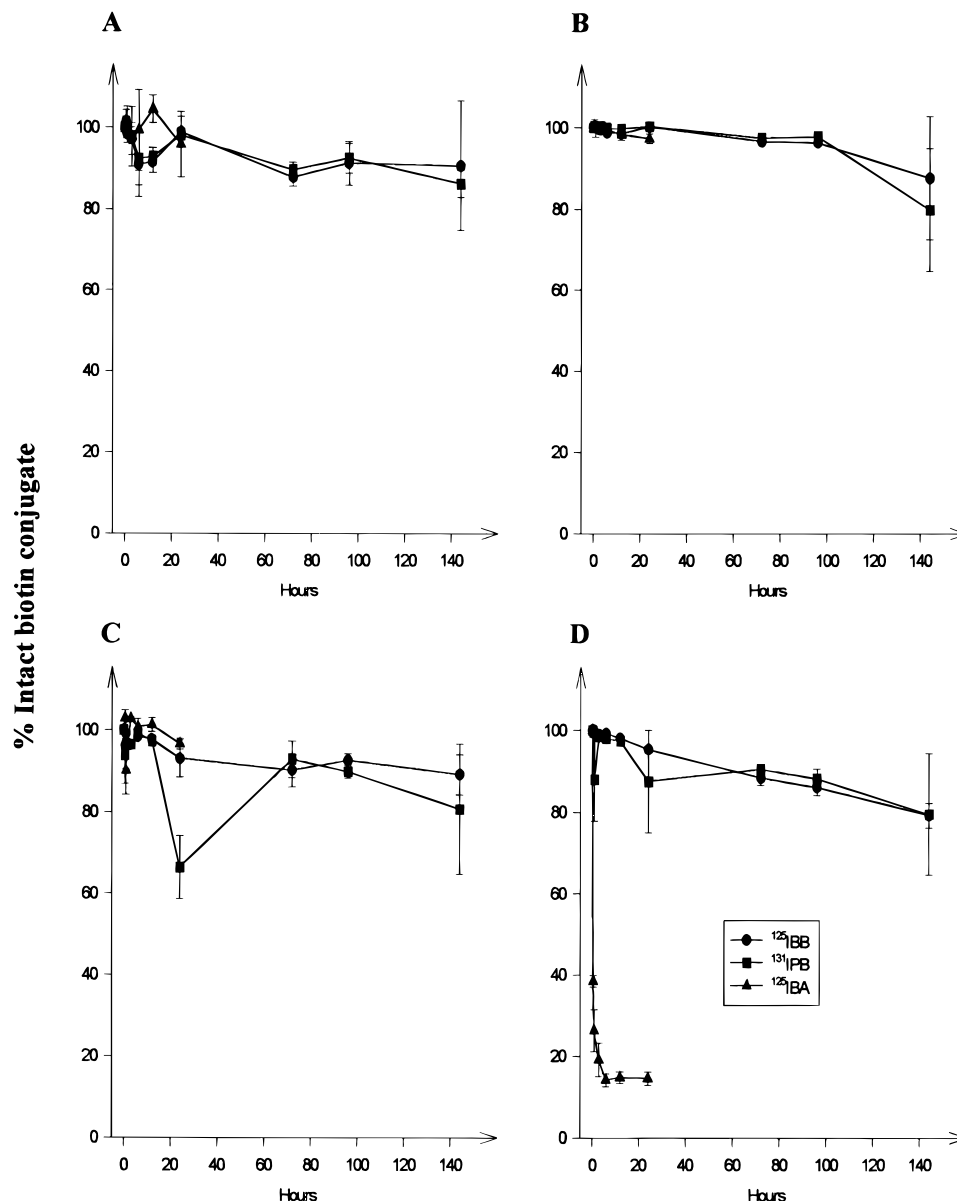


Figure 2. Profiles of metabolites of $[^{125}\text{I}]\text{IBB}$, $[^{131}\text{I}]\text{IPB}$, and $[^{125}\text{I}]\text{IBA}$ after incubation in distilled water (A), human CSF (B), human serum (C), and murine serum (D).

The goal of the current study was to develop a better radioiodinated biotin conjugate for use in pre-targeting. Two conjugates have been evaluated with regard to the following criteria: (a) ease of radiosynthesis, (b) retention of binding to streptavidin, (c) stability toward dehalogenation and degradation by biotinidase, and (d) clearance of activity from normal tissues.

The design of radiolabeled biotin conjugates is facilitated by the considerable amount of information available concerning the structural elements of biotin which are involved in binding to (strept)avidin as well as processing by biotinidase. Binding of the vitamin to (strept)avidin occurs via the interaction of its ureido moiety with five amino acids on these proteins (Asp 128, Asn 23, Ser 27, Tyr 43, and Ser 45) and its nonoxidized sulfur to Thr 90 (29) (Scheme 1). Thus, the carboxylic group is available to react with a wide variety of compounds, including radiolabeled prosthetic groups. However, since hydrogen bonds are established between the sp^2 oxygen and the hydroxyl group of biotin and Asn 49 and Ser 88, respectively (29), radiolabeled biotin conjugates in which these functionalities are modified can lose their potency for binding to (strept)avidin (10, 30).

A wide variety of first-generation radiolabeled biotin conjugates have been synthesized via an amino residue on the prosthetic group, resulting in the formation of a CO-NH amido bond (Scheme 1). Alkyl chain or aromatic group spacers have been used to bridge the vitamin and metal-labeled chelate conjugates (15, 16, 28, 30) or halogen-labeled prosthetic groups (6–11). Most of these biotin derivatives exhibit a good affinity for streptavidin; however, it does not appear that these conjugates remain intact after exposure to biological fluids in vitro or administration in vivo. For example, the biotinyl-3-halogenoanilides $[^{125}\text{I}]\text{IBA}$ and $[^{211}\text{At}]\text{AtBA}$ are rapidly converted to their corresponding haloanilines in murine serum in vitro (11), suggesting that cleavage of the CO-NH amido bond had occurred.

The rapid degradation of biotin conjugates such as $[^{125}\text{I}]\text{IBA}$ most likely reflects the actions of biotinamide amino hydrolase (EC 3.5.1.12, biotinidase). This enzyme specifically cleaves the CO-NH amido bond between the vitamin and the amino group of ϵ -lysyl residues of four classes of biotin-dependent carboxylases or nutritive proteins (31). Previous efforts to design more stable radiolabeled biotin derivatives by impairing the action

Table 1. Tissue Distribution of Radioactivity after Injection of [¹²⁵I]IBB and [¹³¹I]IPB in Mice^a

tissue	% injected dose					
	5 min	30 min	1 h	6 h	12 h	18 h
[¹²⁵I]IBB						
liver	26.35 ± 1.80	17.11 ± 2.35	8.56 ± 1.47	0.09 ± 0.03	0.07 ± 0.04	0.03 ± 0.02
spleen	0.15 ± 0.02	0.09 ± 0.01	0.06 ± 0.02	0.00 ± 0.00	0.00 ± 0.00	0.00 ± 0.01
lungs	1.10 ± 0.20	0.58 ± 0.10	0.33 ± 0.06	0.01 ± 0.00	0.01 ± 0.00	0.00 ± 0.00
heart	0.73 ± 0.03	0.31 ± 0.02	0.14 ± 0.02	0.00 ± 0.00	0.00 ± 0.00	0.00 ± 0.00
kidneys	8.50 ± 1.30	4.11 ± 0.24	1.85 ± 0.19	0.03 ± 0.01	0.02 ± 0.01	0.01 ± 0.00
bladder	0.11 ± 0.11	0.58 ± 0.53	0.30 ± 0.26	0.07 ± 0.15	0.00 ± 0.00	0.00 ± 0.00
stomach	1.35 ± 0.45	1.84 ± 0.61	1.33 ± 0.98	0.04 ± 0.05	0.37 ± 0.35	0.03 ± 0.02
sm. int.	11.28 ± 0.17	17.01 ± 2.22	21.54 ± 3.17	0.39 ± 0.20	1.15 ± 0.91	0.07 ± 0.05
lar. int.	2.21 ± 0.20	4.55 ± 1.31	7.06 ± 2.15	6.86 ± 4.64	1.72 ± 0.26	0.29 ± 0.23
thyroid	0.18 ± 0.06	0.07 ± 0.02	0.08 ± 0.03	0.04 ± 0.01	0.05 ± 0.01	0.08 ± 0.01
muscle	16.27 ± 0.79	10.73 ± 0.52	7.27 ± 1.28	0.50 ± 0.13	0.09 ± 0.04	0.03 ± 0.00
bone	2.02 ± 0.26	1.12 ± 0.31	0.75 ± 0.26	0.19 ± 0.10	0.02 ± 0.02	0.00 ± 0.00
urine	2.19 ± 2.57	10.98 ± 6.69	22.22 ± 3.69	4.38 ± 7.45	0.40 ± 0.67	0.01 ± 0.01
blood	3.08 ± 0.13	1.79 ± 0.19	0.91 ± 0.10	0.07 ± 0.01	0.03 ± 0.01	0.03 ± 0.01
brain	0.05 ± 0.01	0.05 ± 0.02	0.06 ± 0.07	0.01 ± 0.02	0.00 ± 0.00	0.00 ± 0.00
[¹³¹I]IPB						
liver	22.84 ± 2.08	7.87 ± 1.36	3.50 ± 1.48	0.03 ± 0.01	0.04 ± 0.02	0.01 ± 0.00
spleen	0.11 ± 0.02	0.04 ± 0.01	0.04 ± 0.04	0.00 ± 0.00	0.00 ± 0.00	0.00 ± 0.00
lungs	0.83 ± 0.21	0.25 ± 0.07	0.11 ± 0.05	0.00 ± 0.00	0.00 ± 0.00	0.00 ± 0.00
heart	0.46 ± 0.02	0.11 ± 0.02	0.04 ± 0.01	0.00 ± 0.00	0.00 ± 0.00	0.00 ± 0.00
kidneys	6.16 ± 1.47	1.17 ± 0.19	0.30 ± 0.06	0.01 ± 0.00	0.01 ± 0.01	0.00 ± 0.00
bladder	0.22 ± 0.29	0.80 ± 0.76	0.34 ± 0.27	0.05 ± 0.11	0.00 ± 0.00	0.00 ± 0.00
stomach	1.64 ± 0.68	2.50 ± 0.83	1.30 ± 0.92	0.05 ± 0.05	0.44 ± 0.47	0.04 ± 0.03
sm. int.	16.50 ± 2.77	30.86 ± 3.33	35.71 ± 4.42	0.28 ± 0.15	1.69 ± 1.42	0.10 ± 0.07
lar. int.	2.57 ± 0.19	5.45 ± 1.73	7.80 ± 2.78	10.91 ± 6.61	2.84 ± 2.31	0.39 ± 0.31
thyroid	0.11 ± 0.03	0.09 ± 0.02	0.14 ± 0.05	0.10 ± 0.02	0.13 ± 0.04	0.22 ± 0.06
muscle	13.55 ± 1.42	5.27 ± 0.37	3.46 ± 1.03	0.45 ± 0.06	0.08 ± 0.06	0.02 ± 0.01
bone	2.01 ± 0.36	0.84 ± 0.49	0.54 ± 0.21	0.31 ± 0.23	0.03 ± 0.01	0.02 ± 0.01
urine	6.66 ± 7.56	16.77 ± 10.21	26.27 ± 5.59	3.55 ± 6.12	0.46 ± 0.60	0.03 ± 0.04
blood	2.98 ± 0.21	0.95 ± 0.19	0.36 ± 0.06	0.03 ± 0.01	0.02 ± 0.01	0.01 ± 0.01
brain	0.03 ± 0.01	0.02 ± 0.00	0.03 ± 0.04	0.02 ± 0.03	0.00 ± 0.00	0.00 ± 0.00

^a IV injection, mean ± standard deviation of five animals (sm. int., small intestine; lar. int., large intestine).

of biotinidase have focused on generating steric hindrance at the level of the amido bond (Scheme 1), either by substitution on the carbon in the vicinal position of the nitrogen (15, 19) or by methylation of the nitrogen itself (19).

Herein, we describe an alternate approach for the preparation of a more stable radiohalogenated biotin conjugate in which the amido bond between the vitamin and the prosthetic group is reversed (i.e., NH–CO bond, Scheme 1). To accomplish this, it was necessary to modify the vitamin such that a primary amino group be present. The extension of the alkyl chain via reaction with a diamino spacer was not suitable since this would lead to a first-generation compound. Therefore, we decided to transform the terminal carboxylic group of biotin into a primary amine. Although this compound, norbiotamine **2**, is now commercially available, we followed a recently published procedure (23) to prepare **2** from biotin. Isolation of the amino derivative from the starting material was problematic since both display the same polarity and lack UV absorbance. We proceeded directly to the coupling of **2** to the active esters (Scheme 2). Once the biotin moiety was coupled to the benzoyl or pyridyl group, the resulting product became UV absorbing, facilitating its purification using column chromatography. We were then able to prepare the two halogenated cold standards, IBB and BrPB, in adequate yield. The brominated analogue of SIPC, previously established as a valid substitute for the iodinated derivative (21), was used for convenience.

The sensitivity of biotin to oxidizing agents has been documented previously and has long prevented the direct radioiodination of biotin conjugates due to concerns about the production of non-avidin-binding sulfoxide byproducts (32). However, we have shown recently that the kinetics of iododestannylation occur faster than those of oxidation

and that the formation of the sulfoxide byproducts can be minimized by using a 20 s reaction time (25). Under these conditions, [¹²⁵I]IBB could be synthesized in about 60% yield in a single step from TBB along with 0–10% of the sulfoxide byproducts (which can be removed by HPLC). Synthesis of [¹³¹I]IPB from TPB in a single step could not be accomplished. This is not surprising since, unlike SIB, radioiododestannylation of SIPC requires elevated temperatures (21). Nonetheless, synthesis of [¹³¹I]IPB was readily achieved in two steps. An advantage of this procedure is that it avoids direct exposure of biotin to the oxidant *N*-chlorosuccinimide, and as a result, only negligible amounts of sulfoxide byproducts were produced. Disadvantages include the longer preparation time and the need for different columns and solvents for the two HPLC purification steps that are required.

The binding of [¹²⁵I]IBB and [¹³¹I]IPB to streptavidin was measured in vitro to determine whether inversion of the amido bond altered this interaction. This was a potential concern because the side chain of the biotin molecule is involved in streptavidin binding (29) and modifications of this side chain have been shown to influence the affinity of the biotin–avidin interaction (7). Our results indicate that [¹²⁵I]IBB and [¹³¹I]IPB binding to streptavidin was saturable and virtually identical with that of [¹²⁵I]IBA, a biotin analogue which we previously have shown to have the same affinity for streptavidin as biotin itself (25).

The in vitro stability of [¹²⁵I]IBB and [¹³¹I]IPB was compared to that of the first-generation biotin conjugate, [¹²⁵I]IBA, in the presence of distilled water, murine and human serum, and human CSF. Biotinidase levels in CSF are about 0.5% of those encountered in serum (33), and this medium was studied because of the potential for utilizing radiohalogenated biotin conjugates in the treatment of neoplastic meningitis (34). All three radio-

iodinated biotin conjugates were stable in distilled water and CSF with minor degradation seen in human serum. In murine serum, degradation of [^{125}I]IBA was rapid while both [^{125}I]IBB and [^{131}I]IPB remained intact. Even after 4 days incubation in murine serum at 37 °C, more than 85% of the radioiodine activity was still associated with [^{125}I]IBB and [^{131}I]IPB. Furthermore, nearly all of the remainder of the activity was present as the sulfoxide byproduct. These results suggest that inversion of the amido bond markedly increased the stability of [^{125}I]IBB and [^{131}I]IPB in murine serum, presumably by minimizing recognition of these conjugates by biotinidase.

The tissue distribution of radioiodine activity after injection of [^{125}I]IBB and [^{131}I]IPB was measured in normal mice. Thyroid uptake of both conjugates was low and at comparable levels to those observed previously with analogously labeled MAb conjugates (20–22, 35). The percentage of the injected dose of [^{125}I]IBB and [^{131}I]IPB found in the thyroid was about 5 times lower ($P = 0.0012$) than that reported for [^{125}I]IBA (11). Both [^{125}I]IBB and [^{131}I]IPB cleared rapidly from the blood pool and normal tissues as would be anticipated for these low-molecular-weight compounds. The retention of [^{131}I]IPB in normal tissues generally was lower than that of [^{125}I]IBB. This behavior is consistent with the lower lipophilicity and more rapid tissue clearance of 5-iodonicotinic acid compared with 3-iodobenzoic acid (21, 35).

In contrast to levels seen in other normal tissues, a high percentage of the injected dose of [^{125}I]IBB and [^{131}I]IPB was observed in the intestines at early time points. These levels were two to three times higher ($P = 0.0001$) than those seen previously with [^{125}I]IBA. Only limited information is available concerning the intestinal uptake of other radiolabeled biotin conjugates since published studies have not included data for intestines (10, 30). The accumulation of radioactivity in intestines with [^{125}I]IBB and [^{131}I]IPB could reflect the behavior of a labeled catabolite of these conjugates; however, neither 3-iodobenzoic acid nor 5-iodonicotinic acid (nor their MAB conjugates) exhibit significant accumulation in the intestines (20–22, 35). A more likely explanation is that this tissue distribution pattern reflects the behavior of radioiodinated biotin itself, since this new generation of derivatives is not subjected to cleavage by serum biotinidase. This possibility is consistent with the known biosynthetic pathways of vitamins, including biotin (36), and the demonstration of biotin uptake and biotinidase activity in the intestines (37, 38).

In conclusion, we have described the synthesis and biological characterization of a new class of biotin conjugates in which the labeled prosthetic group is linked to biotin via a reversed amido bond. The two radioiodinated conjugates [^{125}I]IBB and [^{131}I]IPB exhibited a high affinity for streptavidin and were found stable in vitro. The distribution of these compounds in normal mice was consistent with that anticipated for biotin conjugates which were resistant to both deiodination and the action of biotinidase. Taken together, these results suggest that this class of biotin conjugates may offer significant advantages for pre-targeting strategies.

ACKNOWLEDGMENT

The excellent technical assistance of Susan Slade is gratefully acknowledged. This work was supported by National Institutes of Health Grants CA42324, NS20023, and CA14236 and Grants 95ER62021 and 96ER62148 from the Department of Energy.

LITERATURE CITED

- Reilly, R. M., Sandhy, J., Alvarez-Diez, T. M., Gallinger, S., Kirsh, J., and Stern, H. (1995) Problems of delivery of monoclonal antibodies: Pharmaceuticals and pharmacokinetic solutions. *Clin. Pharmacokinet.* 28, 126–142.
- Green, N. M. (1975) Avidin. *Adv. Protein Chem.* 29, 85–133.
- Chalet, L., and Wolf, F. J. (1964) The properties of streptavidin, a biotin-binding protein produced by *streptomyces*. *Arch. Biochem. Biophys.* 106, 1–5.
- Hnatowich, D. J., Virzi, F., and Rusckowski, M. (1987) Investigation of avidin and biotin for imaging applications. *J. Nucl. Med.* 28, 1294–1302.
- Liu, F.-T., and Leonard, N. J. (1979) Avidin–Biotin Interaction. Synthesis, Oxidation, and Spectroscopic Properties of Linked Models. *J. Am. Chem. Soc.* 101, 996–1005.
- Livianou, E., Evangelitos, G. P., and Ithakissios, D. S. (1987) Radioiodinated biotin derivative for *in vitro* radioassays. *J. Nucl. Med.* 28, 1430–1434.
- Garlick, R. K., and Giese, R. W. (1988) Avidin binding of radiolabeled biotin derivatives. *J. Biol. Chem.* 263, 210–215.
- Khawli, L. A., and Kassiss, A. I. (1992) Novel synthesis of radioiodinated biotin derivatives. *Nucl. Med. Biol.* 19, 297–30.
- Kortylewicz, Z. P., Baranowska-Kortylewicz, J., Adelstein, S. J., Carmel, A. D., and Kassiss, A. I. (1994) Radiolabeled biotin amides from triazenylo precursors: synthesis, binding and *in vivo* properties. *J. Labelled Compd. Radiopharm.* 34, 1129–1146.
- Shoup, T. M., Fischman, A. J., Jaywood, S., Babich, J. W., Strauss, H. W., and Elmaleh, D. R. (1994) Synthesis of fluorine-18-labeled biotin derivatives: biodistribution and infection localization. *J. Nucl. Med.* 35, 1685–1690.
- Foulon, C. F., Schoultz, B. W., and Zalutsky, M. R. (1997) Preparation and biological evaluation of an astatine-211 labeled biotin conjugate: biotinyl-3-[^{211}At]astatoanilide. *Nucl. Med. Biol.* (in press).
- Beaumont, P. L., Axworthy, D. B., Fritzberg, A. R., Hylarides, M. D., Mallett, R. W., Gustavson, L. M., Su, F.-M., and Reno, J. M. (1995) The pharmacology of pretargeting components: optimizing therapeutic targeting. *Q. J. Nucl. Med.* 39, 20–52.
- Alvarez-Diez, T. M., Polihronis, J., and Reilly, R. M. (1996) Pretargeted tumour imaging with streptavidin immunoconjugates of monoclonal antibody CC49 and ^{111}In -DTPA-biotin. *Nucl. Med. Biol.* 23, 459–466.
- Samuel, A., Paganelli, G., Chiesa, R., Sudati, F., Calvito, M., Melissano, G., Grossi, A., and Fazio, F. (1996) Detection of prosthetic vascular graft infection using avidin/ ^{111}In -biotin scintigraphy. *J. Nucl. Med.* 37, 55–61.
- Hashmi, M., and Rosebrough, S. F. (1995) Synthesis, pharmacokinetics, and biodistribution of ^{67}Ga deferoxamine-acetyl-cysteinylbiotin. *Drug Met. Disp.* 23, 1362–1367.
- Paganelli, G., Magnani, P., Zito, F., Lucignani, G., Sudati, F., Truci, G., Motti, E., Terreni, M., Pollo, B., Giovanelli, M., Canal, N., Scotti, G., Comi, G., Koch, P., Maecke, H. R., and Fazio, F. (1994) Pre-targeted immunodetection in glioma patients: tumour localization and single-photon emission tomography imaging of [$^{99\text{m}}\text{Tc}$]PnAO-biotin. *Eur. J. Nucl. Med.* 21, 314–321.
- Wang, K.-S., Patel, A., and Mock, D. M. (1996) The metabolite profile of radioisotope-labeled biotin in rats indicates that rat biotin metabolism is similar to that in humans. *J. Nutr.* 126, 1852–1857.
- Rosebrough, S. F. (1993) Plasma stability and pharmacokinetics of radiolabeled deferoxamine-biotin derivatives. *J. Pharmacol. Exp. Ther.* 265, 408–415.
- Wilbur, D. S., Hamlin, D. K., Pathare, P. M., Weerawarna, W. A., Vessella, R. L., Stray, J. E., Stayton, P. S., and Klumb, L. A. (1996) Synthesis and radiolabeling of water soluble, biotinidase resistant radioiodinated derivatives. *Tumor Targeting* 2, 185–186 (abstract).
- Zalutsky, M. R., Noska, M. A., Colapinto, E. V., Garg, P. K., and Bigner, D. D. (1989) Enhanced tumor localization and *in vivo* stability of a monoclonal antibody radioiodinated using *N*-succinimidyl-3-(tri-*n*-butylstannyl)benzoate (ATE). *Cancer Res.* 49, 5543–5549.
- Garg, S., Garg, P. K., and Zalutsky, M. R. (1991) *N*-Succinimidyl-5-(trialkylstannyl)-3-pyridinecarboxylate: A New Class of Reagents for Proteins Radioiodination. *Bioconjugate Chem.* 2, 50–56.

- (22) Garg, P. K., Alston, K. L., and Zalutsky, M. R. (1995) Catabolism of Radioiodinated Murine Monoclonal Antibody F(ab')₂ Fragment Labeled using N-Succinimidyl-3-iodobenzoate and Iodogen Methods. *Bioconjugate Chem.* 6, 493–501.
- (23) Szalecki, W. (1996) Synthesis of Norbiotinamine and Its Derivatives. *Bioconjugate Chem.* 7, 271–273.
- (24) Zalutsky, M. R., and Narula, A. S. (1987) A method for the radiohalogenation of proteins resulting in decreased thyroid uptake of radioiodine. *Appl. Radiat. Isot.* 38, 1051–1055.
- (25) Foulon, C. F., Adelstein, S. J., and Kassis, A. I. (1996) One-step synthesis of radioiodinated biotin derivatives. *Bioorg. Med. Chem. Lett.* 6, 779–784.
- (26) Paganelli, G., Grana, C., Chinol, M., De Cicco, C., Florenza, M., Cremonesi, M., Tarditi, L., Franceschini, R., Zoboli, S., De Braud, F., and Siccaldi, A. G. (1996) Therapy trial in malignant glioma patients with Y-90-biotin in a three step pretargeting approach. *J. Nucl. Med.* 37(Suppl.), 169P–170P (abstract).
- (27) Paganelli, A. S. G., Chiesa, R., Sudati, F., Calvitto, M., Melissano, G., Grossi, A., and Fazio, F. (1996) Detection of prosthetic vascular graft infection using avidin/indium-111-biotin scintigraphy. *J. Nucl. Med.* 37, 55–61.
- (28) Axworthy, D. B., Fritzberg, A. R., Hylarides, M. D., Mallett, R. W., Theodore, L. J., Gustavson, L. M., Su, F.-M., Beaumier, P. L., and Reno, J. M. (1995) Preclinical evaluation of an anti-tumor monoclonal antibody/streptavidin conjugate for pre-targeted ⁹⁰Y radioimmunotherapy in a mouse xenograft model. *J. Immunother.* 16, 138 (abstract).
- (29) Weber, P. C., Pantoliano, M. W., and Salemme, F. R. (1995) Crystallographic and thermodynamic comparison of structurally diverse molecules binding to streptavidin. *Acta Crystallogr. D* 51, 590–596.
- (30) Virzi, F., Fritz, B., Ruscowski, M., Gionet, M., Misra, H., and Hnatowich, D. J. (1991) New indium-111 labeled biotin derivatives for improved immunotargeting. *Nucl. Med. Biol.* 18, 719–726.
- (31) Chauhan, J., and Dakshinamurti, K. (1986) Purification and characterization of human serum biotinidase. *J. Biol. Chem.* 261, 4268–4275.
- (32) Windholz, M., Budavari, S., Blumetti, R. F., and Otterbein, E. S., Eds. (1983) *Merck Index*, 10th ed., p 174, Merck, Rahway, NJ.
- (33) DeFelice, C., Hayakawa, K., Nikei, K., Higushi, S., Tanaka, T., Watanabe, T., and Hihi, I. (1994) Changes in cerebrospinal fluid biotinidase activity in *Staphylococcus aureus* meningitis. *Brain Dev.* 1, 156–8.
- (34) Bigner, D. D., Brown, M., Coleman, R. E., Friedman, A. H., Friedman, H. S., McLendon, R. E., Bigner, S. H., Zhao, X.-G., Wickstrand, C. J., Pegram, C. N., Kerby, T., and Zalutsky, M. R. (1995) Phase I studies of treatment of malignant gliomas and neoplastic meningitis with ¹³¹I- radiolabeled monoclonal antibodies anti-tenascin 81C6 and anti-chondroitin proteoglycan sulfate Me1-14 F(ab')₂—a preliminary report. *J. Neuro-Oncol.* 24, 109–122.
- (35) Garg, S., Garg, P. K., Zhao, X.-G., Friedman, H. S., Bigner, D. D., and Zalutsky, M. R. (1993) Radioiodination of a monoclonal antibody using N-succinimidyl 5-iodo-3-pyridine carboxylate. *Nucl. Med. Biol.* 20, 835–842.
- (36) Suormala, T., Wick, H., Bonjour, J.-P., and Baumgartner, E. R. (1985) Intestinal absorption and renal excretion of biotin in patients with biotinidase deficiency. *Eur. J. Pediatr.* 144, 21–26.
- (37) Leon-del-Rio, A., Velasquez, A., Vizcaino, G., Robles-Diaz, G., and Gonzalez-Noriega, A. (1990) Association of pancreatic biotinidase activity and intestinal uptake of biotin and biocytin in Hamster and rat. *Ann. Nutr. Metab.* 34, 266–272.
- (38) Dakshinamurti, K., Chauhan, J., and Ebrahim, H. (1987) Intestinal absorption of biotin and biocytin in the rat. *Biosci. Rep.* 7, 667–673.

BC970006M

Chemoenzymatic Synthesis and Lectin Binding Properties of Dendritic *N*-Acetyllactosamine

Diana Zanini and René Roy*

Department of Chemistry, University of Ottawa, Ottawa, Ontario, Canada K1N 6N5.

Received September 5, 1996[©]

Proof that multivalency amplifies individual carbohydrate–protein interactions is growing. *N*-Acetylglucosamine (GlcNAc)-based dendrimers with valencies of two (**9**), four (**10**), and eight (**11**) were prepared in fair to excellent yields (65–99%) on the basis of the rational scaffolding of L-lysine on solid phase using established Fmoc and HOBt chemistry. These GlcNAc dendrimers were then further transformed enzymatically (79–90% yields) into dendritic *N*-acetyllactosamine (LacNAc) derivatives [di- (**12**), tetra- (**13**), and octavalent (**14**)] using UDPglucose, UDP-glucose 4'-epimerase, and GlcNAc β -1,4-galactosyltransferase. GlcNAc and LacNAc dendrimers were used to inhibit lectin–porcine stomach mucin interactions. Wheat germ agglutinin and *Erythrina cristagalli* lectin were used for GlcNAc and LacNAc dendrimers, respectively. Di-, tetra-, and octavalent GlcNAc dendrimers exhibited IC₅₀s of 3100, 509, and 88 μ M (6200, 2040, and 703 μ M, with respect to monomeric GlcNAc content). IC₅₀s for the LacNAc series were 341, 143, and 86 μ M (682, 574, and 692 μ M, as compared with monomeric LacNAc content). These data represent more than 20-fold increases in inhibitory potential for dendritic GlcNAc as compared to that for monomeric GlcNAc. Studies with *E. cristagalli* do not reveal significant increased inhibitory potential with multivalency.

INTRODUCTION

Carbohydrates are involved in numerous biological functions, including cellular recognition, adhesion, cell growth regulation, cancer cell metastasis, and inflammation (*1*). However, it is known that individual carbohydrate–protein interactions are generally of low affinity (*2*). It is therefore important to investigate how such weak carbohydrate–protein interactions can be amplified in successful recognition processes. In fact, amplified interactions can be observed on the basis of the glycoside cluster effect (*3*). That is, the multivalent nature of cell surface carbohydrates may act cooperatively to increase the overall binding avidity of these interactions. Evidence for the requirement of multivalency for tight binding is growing. Glycopolymers (*4*) and, more recently, glycodendrimers (*5*) have been used to show that inhibitory potencies of glycosides are increased when carbohydrates are properly presented in multivalent form. This multivalency or cluster effect has been well characterized for asialoglycoprotein hepatic receptors (*6*) and for the inhibition of influenza virus attachment to host sialylated receptors (*4, 5*).

N-Acetyllactosamine [*O*-(β -D-galactopyranosyl)-(1–4)-2-acetamido-2-deoxy-D-glucopyranose; Gal β (1–4)GlcNAc, LacNAc] is well known as a biologically important disaccharide core structure of lactosaminoglycans, tumor-associated antigenic carbohydrates, and many carbohydrate receptors in glycoproteins and glycolipids (*7, 8*). Specifically, LacNAc-containing compounds have been implicated in mouse colon cancers (*9*), some thyroid disorders (*10*), the sexual transmission of the *H. ducreyi* pathogen (*11*), and corneal epithelial cell migration (*12*). To date, only a few hypervalent LacNAc clusters have been prepared for use in studies aimed at understanding these interactions. These LacNAc-based glycopeptides and glycopolymers have ill-defined chemical structures (*13*). They vary in size and carbohydrate density and,

as such, may not constitute ideal candidates for precise quantitative measurements.

Alternatively, dendrimers with covalently attached glycoside residues represent novel and chemically well-defined biopolymers with controlled densities (*14*). In addition, bidirectional dendrimers can be used advantageously as models for cell surface multiantennary glycoproteins as they share similar structural characteristics (*15*). It therefore seems natural to turn our attention to the synthesis of dendritic LacNAc conjugates as probes for the study of *N*-acetyllactosamine–protein interactions.

Purely chemical strategies for the synthesis of such compounds is not an easy task, and owing to the stereo- and regioselectivity in the formation of glycoside linkages, chemoenzymatic methodologies have been regarded as important tools for the preparation of structurally complex oligosaccharides (*16*).

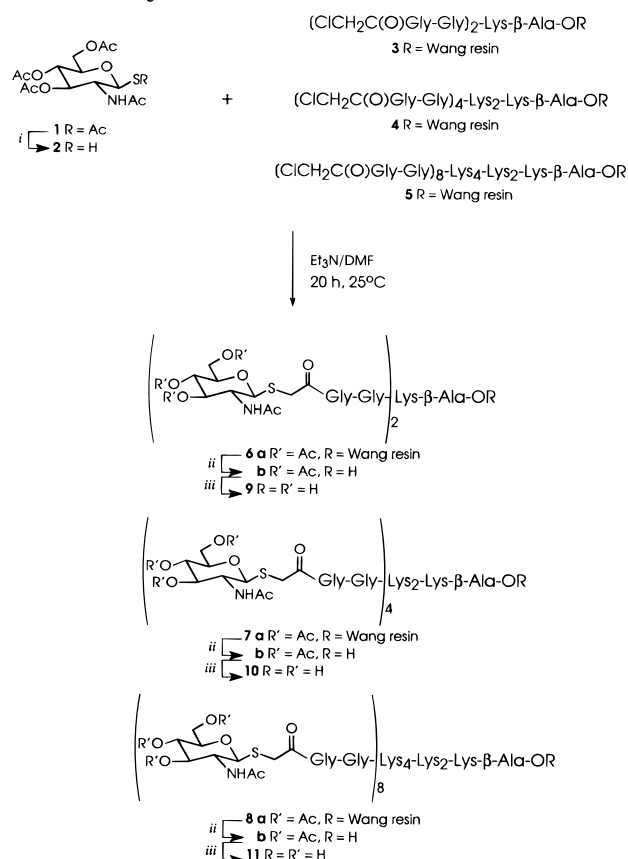
Herein, we present the efficient chemoenzymatic syntheses of *N*-acetyllactosamine dendrimers. Also, the specific binding properties of families of *N*-acetylglucosamine and LacNAc dendrimers with wheat germ agglutinin (WGA) and *Erythrina cristagalli* lectin (ECA) will be discussed.

MATERIALS AND METHODS

UDPglucose, bovine serum albumin, UDP-glucose 4'-epimerase (EC 5.1.3.2), calf intestinal alkaline phosphatase (EC 3.1.3.1), GlcNAc β -1,4-galactosyltransferase (EC 2.4.1.22), lectin from *Triticum vulgaris* (wheat germ agglutinin, WGA) peroxidase labeled, and porcine stomach mucin type III was purchased from Sigma. The lectin from *E. cristagalli* (ECA) peroxidase labeled was obtained from E-Y Laboratories (San Mateo, CA). Thiolated *N*-acetylglucosamine derivative **2** (2-acetamido-3,4,6-tri-*O*-acetyl-2-deoxy-1-thio- β -D-glucopyranose, GlcNAc) (*17*) and *N*-chloroacetylated dendrimers were prepared as previously described (*5*).

The ¹H and ¹³C NMR spectra were recorded on a Bruker 500 MHz AMX NMR spectrometer. Proton

* Abstract published in *Advance ACS Abstracts*, February 15, 1997.

Scheme 1. Synthesis of GlcNAc Dendrimers 9–11^a

^a (i) H₂NNH₂·HOAc, DMF, N₂, 25 °C, 15 min; (ii) 95% aqueous TFA, 1.5 h; (iii) NaOMe/MeOH, 1.5 h, then H⁺ resin.

chemical shifts (δ) are given relative to internal dimethyl sulfoxide (2.49 ppm) for DMSO-*d*₆ solutions and to internal HOD (4.76 ppm) for D₂O solutions. Carbon chemical shifts are given relative to DMSO-*d*₆ (39.4 ppm). Assignments were based on COSY, HMQC, and/or DEPT experiments. Mass spectra were obtained on a Kratos Concept ITH spectrometer (FAB-MS, glycerol matrix). Gel permeation chromatography (GPC) was performed using Biogel P-2 and Sephadex G-50 columns using water as eluent. Optical densities (ODs) for the ELLA tests were measured on a Dynatech MR600 microplate reader.

Peracetylated Glucosamine Dendrimers (6a–8a). *N*-Chloroacetylated dendrimer backbones 3–5 (Scheme 1) were synthesized as previously described (5, 17). Coupling of 1-thio-*N*-acetylglucosamine derivative 2 (17) with dendrimers 3–5 was done on solid phase. Polymer-supported (Wang resin, 0.58 mmol/g substitution) dendrimers 3–5 were placed in a 1% Et₃N/DMF solution containing compound 2 (1.2 equiv per *N*-chloroacetyl functionality; 0.45, 0.34, and 0.24 mmol/g substitution for dendrimers 3–5, respectively). Agitation of the mixture was maintained for 16 h by bubbling nitrogen through the solution. Before the bulk of the dendrimers was released from the polymeric support, aliquots were withdrawn and hydrolyzed (95% aqueous TFA, 1.5 h). The completeness of the reaction was monitored by ¹H NMR spectra of the dendritic GlcNAc which showed characteristic signals for any residual *N*-chloroacetyl group at 4.12 ppm (DMSO-*d*₆). Where required, couplings were repeated.

Polymer-bound glycodendrimers 6a–8a were released from the polymeric support (95% TFA, 1.5 h) and obtained in 65–99% yields after dissolution in a minimum amount of neat TFA and precipitation in ether.

Compound 6b: ¹H NMR (DMSO-*d*₆) δ 1.16 (m, 2H, lysyl γ-CH₂), 1.33 (m, 2H, lysyl δ-CH₂), 1.46 and 1.61 (2m, 2H, lysyl β-CH₂, nonequivalent), 1.75 (s, 6H, NAc), 1.90, 1.95, 2.00 (3s, 18H, OAc), 2.36 (t, 2H, *J* = 7 Hz, β-alanyl α-CH₂), 3.00 (m, 2H, lysyl ε-CH₂), 3.20 (m, 2H, β-alanyl β-CH₂), 3.30 and 3.38 (2d, 2 × 2H, *J* = 14.1 Hz, SCH₂S), 3.66 (d, 2H, *J* = 5.8 Hz, glycylic CH₂), 3.73 (m, 6H, glycylic CH₂S), 3.81 (m, 2H, H-5), 3.89 (dd, 2H, *J*_{2,3} = 9.89 Hz), 4.00 (d, 2H, *J*_{5,6} = 10.3 Hz, H-6), 4.14 (m, 3H, lysyl α-CH, H-6'), 4.77 (d, 2H, *J*_{1,2} = 10.3 Hz, H-1), 4.86 (dd, 2H, *J*_{3,4} = 9.74 Hz, *J*_{4,5} = 9.74 Hz, H-4), 5.05 (dd, 2H, H-3), 7.73 (m, 1H, lysyl ε-NH), 7.90 (m, 2H, β-alanyl NH, lysyl α-NH), 7.98 (d, 2H, *J* = 9.26 Hz, NHAc), 8.12 and 8.20 (2m, 2 × 2H, glycylic NHs); ¹³C NMR δ 20.3, 20.4, 20.5 (OAc), 22.6 (NHAc), 22.7 (lysyl α-C), 28.7 (lysyl δ-C), 31.7 (lysyl β-C), 32.6 (SCH₂S), 33.7 (β-alanyl α-C), 34.8 (β-alanyl β-C), 38.4 (lysyl ε-C), 42.0 and 42.4 (glycylic Cs), 52.0 (C-2), 52.5 (lysyl α-C), 61.9 (C-6), 68.4 (C-4), 73.6 (C-3), 74.7 (C-5), 82.8 (C-1), 168.4 to 172.8 (C=Os); FAB-MS (positive) calcd for C₄₉H₇₃N₉O₂₅S₂ 1252.3, found 1253.2 (*M* + 1, 19.8%).

Compound 7b: ¹H NMR (DMSO-*d*₆) δ 2.35 (t, 2H, *J* = 6.8 Hz, β-alanyl α-CH₂), 3.00 (m, 6H, lysyl ε-CH₂), 4.77 (d, 4H, *J*_{1,2} = 10.3 Hz, H-1); ¹³C NMR δ 22.6 (NHAc), 32.6 (SCH₂S), 82.8 (C-1); FAB-MS (pos.) calcd for C₁₀₁H₁₅₁N₁₉O₄₉S₄ 2543.6, found 2544.3 (*M* + 1, 0.5%).

Compound 8b: ¹H NMR (DMSO-*d*₆) δ 2.35 (t, 2H, *J* = 6.7 Hz, β-alanyl α-CH₂), 3.00 (m, ¹⁴H, lysyl ε-CH₂), 4.77 (d, 8H, *J*_{1,2} = 10.4 Hz, H-1); ¹³C NMR δ 22.6 (NHAc), 32.5 (SCH₂S), 82.7 (C-1).

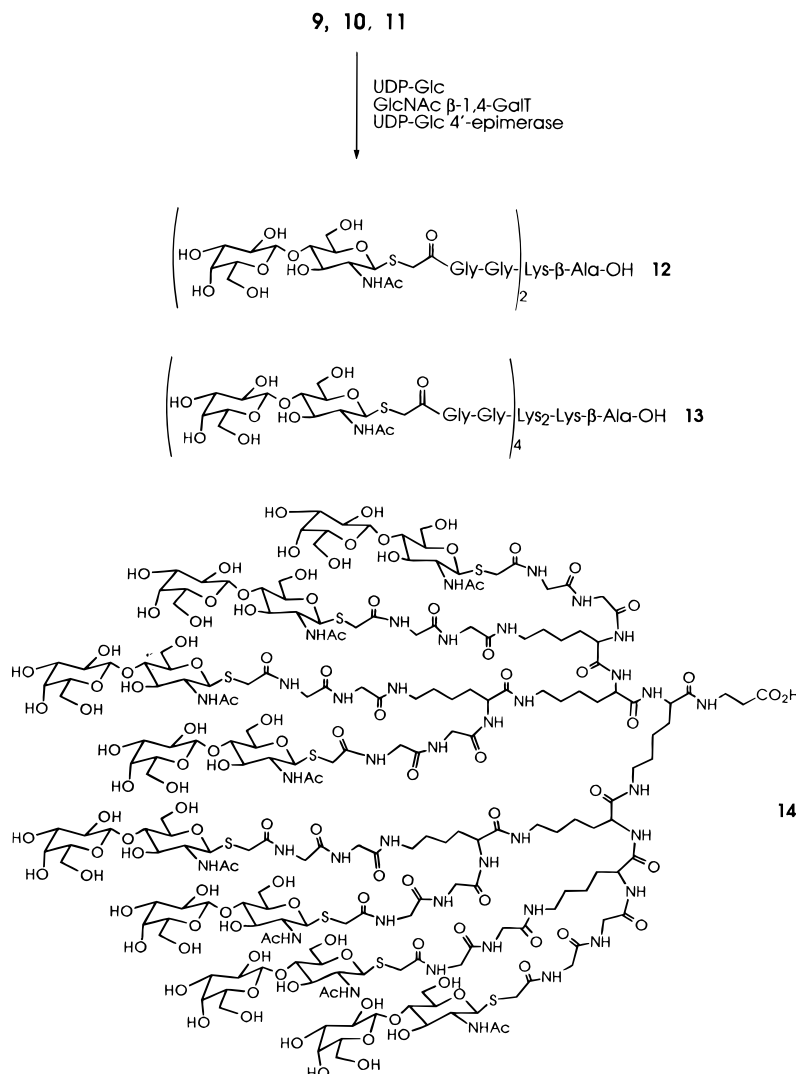
De-O-acetylated *N*-Acetylglucosamine Dendrimers (9–11). Each of the polymer free glycodendrimers (6b–8b) was de-O-acetylated with NaOMe/MeOH (25 °C, 1.5 h) followed by H⁺ resin treatment to give dendrimers 9–11 in quantitative yields.

Compound 9: ¹H NMR (D₂O) δ 1.40 (m, 2H, lysyl γ-CH₂), 1.57 (m, 2H, lysyl δ-CH₂), 1.77 and 1.83 (2m, 2H, lysyl β-CH₂, nonequivalent), 2.09 (s, 6H, NAc), 2.66 (t, 2H, *J* = 6.5 Hz, β-alanyl α-CH₂), 3.26 (t, 2H, *J* = 6.9 Hz, lysyl ε-CH₂), 3.46 to 3.97 (m, 26H, β-alanyl β-CH₂, glycylic CH₂S, SCH₂S, H-2, H-3, H-4, H-5, H-6, H-6'), 4.27 (m, 1H, lysyl α-CH), 4.74 (dd, 2H, H-1); ¹³C NMR δ 21.7 (NHAc), 21.8 (lysyl α-C), 27.3 (lysyl δ-C), 30.1 (lysyl β-C), 32.9 (SCH₂S), 33.0 (β-alanyl α-C), 34.7 (β-alanyl β-C), 38.5 (lysyl ε-C), 53.5 (lysyl α-C), 83.5 (C-1), 41.8, 42.0, 42.4, 54.0, 60.4, 69.2, 74.5, 79.4, and 81.3 (glycylic Cs, C-2, C-3, C-4, C-5, C-6), 170.6–175.6 (C=Os); FAB-MS (pos.) calcd for C₃₇H₆₁N₉O₁₉S₂ 999.4, found 1000.6 (*M* + 1, <1%).

Compound 10: ¹H NMR (D₂O) δ 2.09 (s, 12H, NAc), 2.66 (t, 2H, *J* = 6.5 Hz, β-alanyl α-CH₂), 3.26 (m, 6H, lysyl ε-CH₂), 4.74 (dd, 4H, H-1); ¹³C NMR δ 21.7 (NHAc), 83.5 (C-1).

Compound 11: ¹H NMR (D₂O) δ 2.11 (s, 24H, NAc), 2.68 (t, 2H, *J* = 6.1 Hz, β-alanyl α-CH₂), 3.28 (m, ¹⁴H, lysyl ε-CH₂), 4.75 (dd, 8H, H-1); ¹³C NMR δ 21.7 (NHAc), 83.5 (C-1).

***N*-Acetyllactosamine Dendrimers (12–14).** Enzymatic reactions were performed according to established procedures (18). Five milligram portions of GlcNAc dendrimers 9–11 were dissolved in 50 mM sodium cacodylate (pH 7.4, 565 μL) containing bovine serum albumin (0.5 mg), 1.1 μmol of MnCl₂, 3.4 μmol of NaN₃, 28.3 μmol of UDPglucose, 200 milliunits of GlcNAc β-1,4-galactosyltransferase (EC 2.4.1.22), 1 unit of UDP-glucose 4'-epimerase (EC 5.1.3.2), and 4 units of calf intestinal phosphatase (EC 3.1.3.1). The reaction mixture was incubated at 37 °C for 5 days while the pH was maintained at 7.4 by periodic addition of 0.1 M NaOH (Scheme 2).

Scheme 2. Chemoenzymatic Synthesis of LacNAc Dendrimers 12–14

LacNAc dendrimers were isolated by gel permeation chromatography on both a Biogel P-2 column (2.3 × 90 cm) and a Sephadex G-50 column (2.3 × 75 cm) using H₂O as eluent. Isolated yields were 79–90%. NMR data (D₂O, Figure 1) showed complete galactosyl incorporation as measured by the H-1 galactose signal at 4.55 ppm relative to the H-1 GlcNAc, the NAc GlcNAc, and β-alanyl α-CH₂ signals at 4.78, 2.11, and 2.57 ppm, respectively.

Compound 12: ¹H NMR (D₂O) δ 1.40 (m, 2H, lysyl γ-CH₂), 1.59 (m, 2H, lysyl δ-CH₂), 1.79 and 1.87 (2m, 2H, lysyl β-CH₂, nonequivalent), 2.11 (2s, 6H, NAc), 2.57 (t, 2H, *J* = 6.7 Hz, β-alanyl α-CH₂), 3.28 (t, 2H, *J* = 6.9 Hz, lysyl ε-CH₂), 3.42 to 4.11 (m, 38H, β-alanyl β-CH₂, glycylic CH₂s, SCH₂s, H-2, H-3, H-4, H-5, H-6, H-6' of GlcNAc and H-2, H-3, H-4, H-5, H-6, H-6' of Gal), 4.30 (dd, 1H, *J*_{lysylα,lysylβ} = 8.7 Hz, *J*_{lysylα,lysylβ'} = 3.2 Hz, lysyl α-CH), 4.55 (d, 2H, *J*_{1,2} = 7.8 Hz, H-1 Gal), 4.77 and 4.79 (dd, 2H, H-1 GlcNAc, nonequivalent); ¹³C NMR δ 21.7 (NHAc), 21.8 (lysyl α-C), 27.3 (lysyl δ-C), 30.1 (lysyl β-C), 32.9 (SCH₂s), 33.0 (β-alanyl α-C), 34.7 (β-alanyl β-C), 38.5 (lysyl ε-C), 83.5 (C-1 GlcNAc), 102.5 (C-1 Gal); FAB-MS (pos.) calcd for C₄₉H₈₁N₉O₂₉S₂ 1323.4, found 1324.3 (*M* + 1, 1.8%).

Compound 13: ¹H NMR (D₂O) δ 2.11 (s, 12H, NAc), 2.60 (m, 2H, β-alanyl α-CH₂), 3.28 (m, 6H, lysyl ε-CH₂), 4.55 (d, 4H, *J*_{1,2} = 8.1 Hz, H-1 Gal), 4.77 (dd, 4H, H-1 GlcNAc, nonequivalent); ¹³C NMR δ 21.7 (NHAc), 83.5 (C-1 GlcNAc), 102.5 (C-1 Gal).

Compound 14: ¹H NMR (D₂O) δ 2.11 (s, 24H, NAc), 2.47 (m, 2H, β-alanyl α-CH₂), 3.27 (m, 14H, lysyl ε-CH₂), 4.55 (d, 8H, *J*_{1,2} = 7.8 Hz, H-1 Gal), 4.77 and 4.79 (dd, 8H, H-1 GlcNAc, nonequivalent); ¹³C NMR δ 21.7 (NHAc), 83.5 (C-1 GlcNAc), 102.5 (C-1 Gal).

Enzyme-Linked Lectin Assays (ELLAs). Linbro (Titertek) microtitration plates were coated with porcine stomach mucin type III at 100 μL/well with a 5 μg/mL stock solution in 0.01 M phosphate buffer (pH 7.3). The wells were then washed three times with 300 μL/well with 0.01 M phosphate buffer (pH 7.3) containing 0.05% (v/v) Tween 20 (PBST). Washing with PBST was repeated after each incubation period. Wells were then blocked with 150 μL/well with 1% BSA/PBS for 1 h at 37 °C. After washing, wells were filled with 100 μL/well of inhibitor solutions and incubated again at 37 °C for 1 h. Inhibitors used include allyl 2-acetamido-2-deoxy-α-D-glucopyranoside (monomeric GlcNAc **15**) (**19**) and *O*-(β-D-galactopyranosyl)-(1-4)-2-acetamido-2-deoxy-β-D-glucopyranosyl azide (monomeric LacNAc **16**) (**20**) as reference monovalent compounds (Figure 4), di- (**9**), tetra- (**10**), and octavalent (**11**) GlcNAc dendrimers, and di- (**12**), tetra- (**13**), and octavalent (**14**) LacNAc dendrimers. Each inhibitor was added in serial 2-fold dilutions (60 μL/well) in PBS with the appropriate lectin–enzyme conjugate concentration (1000-fold dilution of a 1 mg/mL stock WGA solution in PBS for GlcNAc-based compounds and a 100-fold dilution of a 1 mg/mL stock solution of *E*.

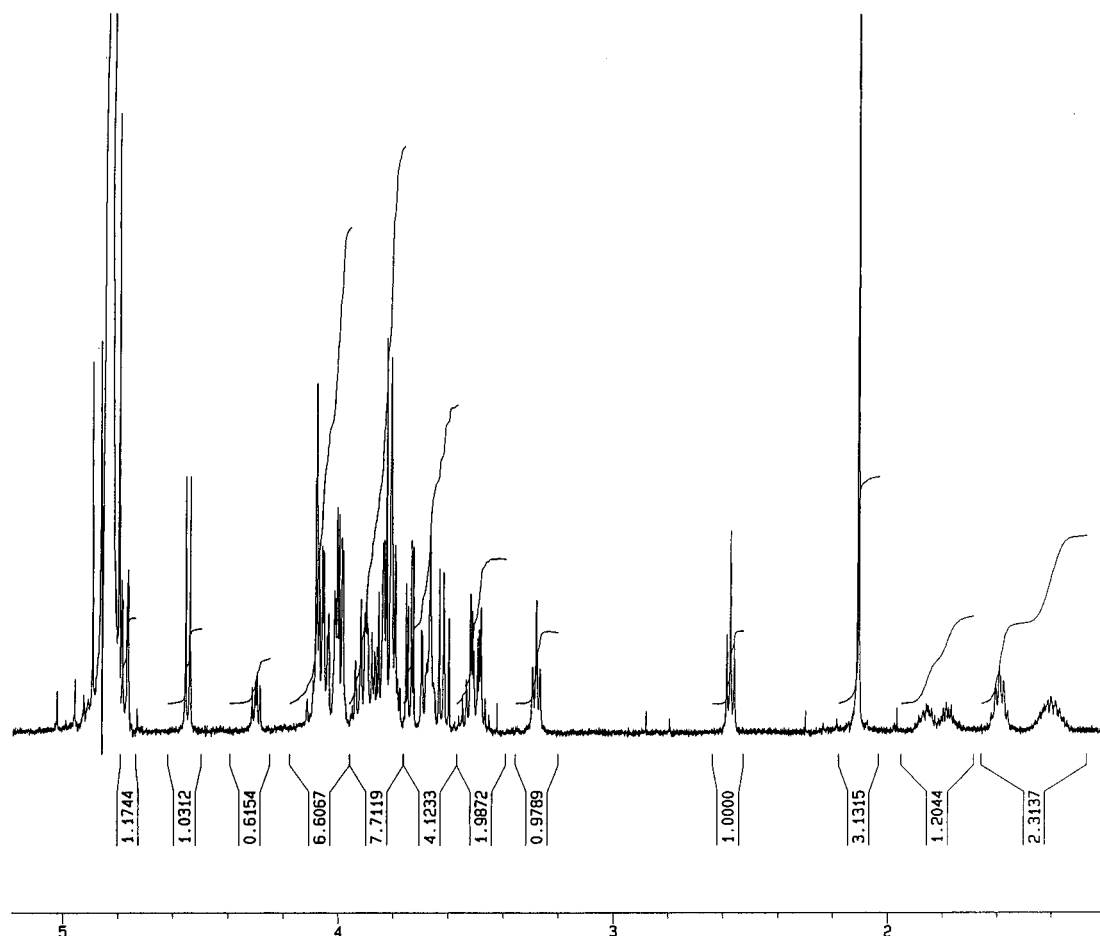


Figure 1. ^1H NMR (D_2O , 500 MHz) spectrum of divalent *N*-acetylglucosamine dendrimer **12**.

crisagalli lectin in PBS for dendritic LacNAc) on Nunclon (Delta) microtiter plates and incubated at 37 °C for 1 h. These inhibitor solutions (100 μL) were transferred to the antigen-coated plates and incubated for a second hour. The plates were washed, and 50 μL /well 2,2'-azinobis(3-ethylbenzothiazoline-6-sulfonic acid) diammonium salt (ABTS) (1 mg per 4 mL) in citrate phosphate buffer (0.2 M, pH 4.0 with 0.015% H_2O_2) was added. The reaction was stopped after 20 min by adding 50 μL /well of 1 M H_2SO_4 , and the optical density was measured at 410 nm relative to 570 nm. Percent inhibition was calculated as follows:

$$\% \text{ inhibition} = \frac{[A_{(\text{no inhibitor})} - A_{(\text{with inhibitor})}]/A_{(\text{no inhibitor})} \times 100}$$

IC_{50} s were reported as the concentration required for 50% inhibition of the coating antigen. All tests were performed in triplicate.

RESULTS AND DISCUSSION

GlcNAc-ending dendrimers with valencies of two (**9**), four (**10**), and eight (**11**) were synthesized in fair to excellent yields (65–99%) using chemical synthesis based on the rational scaffolding of L-lysine core structures on solid phase. The convergent strategy (Scheme 1) involved the solid-phase synthesis of *N*-chloroacetylated glycylglycine-capped multibranched L-lysine as previously described (5). Each *N*-chloroacetyl group was then substituted with the peracetylated 1-thio GlcNAc derivative **2**. Hydrolysis from the resin (95% TFA) and protecting group removal (NaOMe, MeOH) afforded **9–11**.

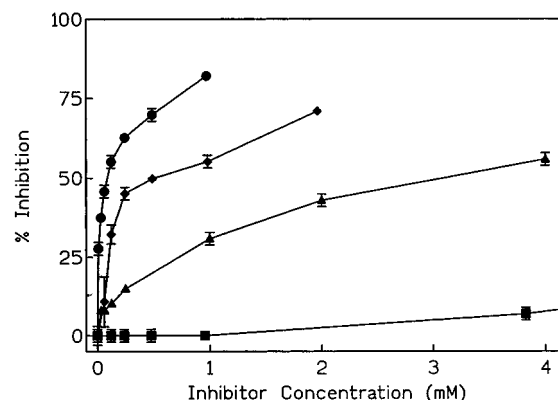


Figure 2. Inhibition curves for the binding of WGA to porcine stomach mucin type III: allyl 2-acetamido-2-deoxy- α -D-glucopyranoside (\blacksquare) and GlcNAc dendrimers **9** (\blacktriangle), **10** (\blacklozenge), and **11** (\bullet).

These GlcNAc-based dendrimers were then enzymatically transformed into di- (**12**), tetra- (**13**), and octavalent (**14**) LacNAc dendrimers (Scheme 2). Isolated yields were excellent (79–90%) and were indicative of the efficiency of this chemoenzymatic strategy. These results also indicate that even the shorter arms of the dendritic lysine core were sufficiently long and free of steric hindrance to be amenable to enzymatic transformations. While the enzymatic galactosylation of *N*-acetylglucosamine is known, this is the first reported achievement of the enzymatic conversion of GlcNAc to LacNAc on a synthetic dendrimer.

Porcine stomach mucin was used as a model coating antigen for carbohydrate–glycoprotein interactions as it is readily available and contains both *N*-acetylglucos-

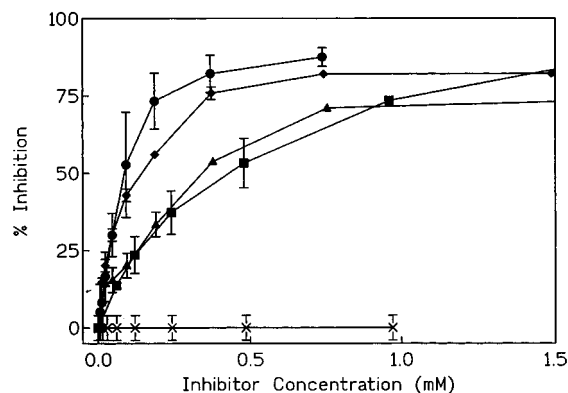


Figure 3. Inhibition curves for the binding of *E. cristagalli* to porcine stomach mucin type III: *O*-(β -D-galactopyranosyl)-(1-4)-2-acetamido-2-deoxy- β -D-glucopyranosyl azide (monomeric LacNAc) (■), LacNAc dendrimers **12** (▲), **13** (◆), and **14** (●), and octameric GlcNAc **11** (×).

Table 1. Results for the Inhibition of Binding of HRPO-Labeled WGA or ECA to Porcine Stomach Mucin by *N*-Acetylglucosamine Dendrimers 9–11 and by *N*-Acetylglucosamine Dendrimers 12–14

compound	IC ₅₀ (mM) ^a	relative potency
allyl α -D-GlcNAc 15	>15 ^b	—
9 (dimer)	3.1 (6.2)	>4.8
10 (tetramer)	0.51 (2.0)	>25.4
11 (octamer)	0.088 (0.7)	>170
azido- β -LacNAc 16	0.43	1
12 (dimer)	0.34 (0.68)	1.3
13 (tetramer)	0.14 (0.57)	3.0
14 (octamer)	0.086 (0.69)	5.0

^a Values in parentheses refer to IC₅₀s expressed relative to monomeric GlcNAc or LacNAc content. ^b At a concentration of 15.3 mM, **15** showed 15.1% inhibition.

amine and *N*-acetylglucosamine in high concentrations to allow for effective microtiter plate enzyme-linked inhibition assays (ELLAs) (21). WGA is a tetravalent lectin that binds GlcNAc moieties (22). Thus, it was used for inhibition testing using GlcNAc dendrimers **9–11**. To test *N*-acetylglucosamine dendrimers **12–14**, it was necessary to use a lectin specific to LacNAc and one that would not bind GlcNAc. For this reason, inhibition of carbohydrate–porcine stomach mucin interactions with dendrimers **12–14** was performed with *E. cristagalli* lectin (ECA). ECA is a divalent lectin, and binding studies have revealed that *N*-acetylglucosamine exhibits the highest affinity for ECA, where most of the binding energy is contributed by the nonreducing terminal galactose residue (23, 24). ECA–protein interactions are therefore not inhibited by GlcNAc residues. Thus, inhibition of binding of ECA to porcine stomach mucin by newly synthesized glycodendrimers **12–14** would unequivocally demonstrate galactose incorporation and inhibitory potency.

GlcNAc dendrimers having valencies of two (**9**), four (**10**), and eight (**11**) exhibited IC₅₀s of 3100, 509, and 88 μ M, respectively, in the inhibition of WGA–porcine stomach mucin type III binding. This represents IC₅₀ values of more than 6200, 2040, and 703 μ M, respectively, as compared to that of monomeric GlcNAc **15** (at concentrations of >15 mM, allyl 2-acetamido-2-deoxy- α -D-glucopyranoside exhibited 15% inhibition, Table 1). When IC₅₀s are plotted relative to monomer as a function of dendrimer valency, the curve generated for this set of data clearly indicates that multivalency enhances inhibitory potencies for the WGA–porcine stomach mucin type III interaction (Figure 5). The inhibitory potential of

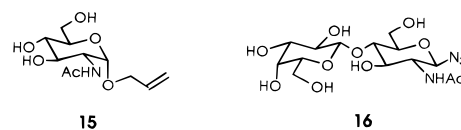


Figure 4.

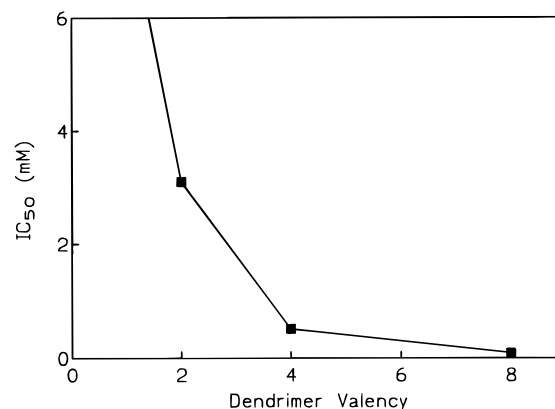


Figure 5. IC₅₀s as a function of dendrimer valency for GlcNAc dendrimers **9–11** (■).

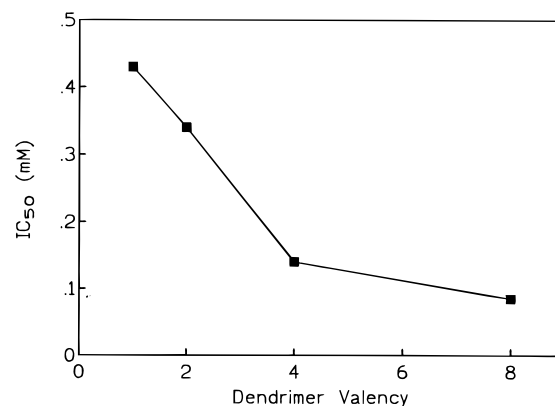


Figure 6. IC₅₀s as a function of dendrimer valency for LacNAc dendrimers **12–14** (■).

dendrimer **11** represents more than a 20-fold increase over that of the analogous monomer **15**.

Thus, ELLA inhibition of binding of lectin to porcine stomach mucin by dendrimers **9–11** (Figures 2 and 3) showed a steady increase in the inhibitory potency as a function of GlcNAc content.

Di- (**12**), tetra- (**13**), and octavalent (**14**) LacNAc dendrimers, when used in the inhibition of binding of *E. cristagalli* lectin to porcine stomach mucin type III by ELLA, showed IC₅₀ values of 341, 143, and 86 μ M, respectively [682, 574, and 692 μ M, respectively, as compared to that of *O*-(β -D-galactopyranosyl)-(1-4)-2-acetamido-2-deoxy- β -D-glucopyranosyl azide (azido- β -LacNAc) **16**, Table 1]. As a control, octameric GlcNAc **11** did not inhibit the lectin–mucin interaction. When expressed on a per hapten basis, the average binding potency of **12–14** indicates that LacNAc residues in these dendrimers were not strong ligands toward ECA. In this case, no cluster effect was observed. One explanation may be that the presentation of the carbohydrate residues plays an important role in this particular carbohydrate–lectin interaction and perhaps the LacNAc residues in the form presented here are not properly scaffolded to confer steady increases as a function of multivalency. Indeed, this phenomenon has been previously observed for LacNAc clusters (24). These data do not negate the overall importance of the multivalency or glycosidic cluster effect in carbohydrate–protein interactions.

Rather, they stress the need for well-designed glycoforms. Of importance though is the fact that these results nicely confirm the enzymatic incorporation of galactose residues in the LacNAc dendrimers. No inhibition would have been observed without proper galactosylation of GlcNAc dendrimers since octavalent GlcNAc dendrimer **11** did not inhibit the binding at all.

The above results indicate that, indeed, multivalency can amplify carbohydrate–protein interactions. However, this effect is variable for each individual interaction, and to what extent multivalency plays a role in such interactions is still under active investigation.

ACKNOWLEDGMENT

We are grateful to the National Sciences and Engineering Research Council of Canada (NSERC) for financial assistance and a postgraduate scholarship to D.Z.

Supporting Information Available: ^1H and ^{13}C NMR spectra of compounds **6b–8b** and **9–14** (18 pages). Ordering information is given on any current masthead page.

LITERATURE CITED

- Varki, A. (1993) Biological roles of oligosaccharides: all of the theories are correct. *Glycobiology* 3, 97.
- Toone, E. J. (1994) Structure and energetics of protein-carbohydrate complexes. *Curr. Opin. Struct. Biol.* 4, 719.
- Lee, Y. C. (1992). Biochemistry of carbohydrate-protein interaction. *FASEB J.* 6, 3193.
- (a) Roy, R., and Laferrière, C. A. (1988) Synthesis of antigenic copolymers of N-acetylneuraminic acid binding to wheat germ agglutinin and antibodies. *Carbohydr. Res.* 177, C1. (b) Gamian, A., Chomik, M., Laferrière, C. A., and Roy, R. (1991) Inhibition of Influenza A virus hemagglutinin and induction of interferon by synthetic sialylated glycoconjugates. *Can. J. Microbiol.* 37, 233. (c) Roy, R., Andersson, F. O., Harms, G., Kelm, S., and Schauer, R. (1992) Synthesis of esterase-resistant 9-O-acetylated polysialosides as inhibitors of Influenza C virus hemagglutinin. *Angew. Chem., Int. Ed. Engl.* 31, 1478. (d) Byramova, N. E., Mochalova, L. V., Belyanchikov, I. M., Matrosovich, M. N., and Bovin, N. V. (1991) Synthesis of sialic acid pseudopolysaccharides by coupling of spacer connected Neu5Ac with activated polymer. *J. Carbohydr. Chem.* 10, 691. (e) Sigal, G. B., Mammen, M., Dahmann, G., and Whitesides, G. M. (1996) Polyacrylamides bearing pendant alpha-sialoside groups strongly inhibit agglutination of erythrocytes by Influenza virus—the strong inhibition reflects enhanced binding through cooperative polyvalent interactions. *J. Am. Chem. Soc.* 118, 3789 and references cited therein.
- (a) Roy, R., Zanini, D., Meunier, S., and Romanowska, A. (1993) Solid-phase synthesis of dendritic sialoside inhibitors of Influenza A virus haemagglutinin. *J. Chem. Soc., Chem. Commun.*, 1869. (b) Roy, R., Zanini, D., Meunier, S., and Romanowska, A. (1994) Synthesis and antigenic properties of sialic acid based dendrimers. *ACS Symp. Ser.* 560, 104.
- Lee, R. T., and Lee, Y. C. (1994) in *Neoglycoconjugates: Preparations and Applications* (Y. C. Lee and R. T. Lee, Eds.) p 23, Academic Press, San Diego.
- Ando, K., Kikugawa, K., and Beppu, M. (1994) Involvement of sialylated poly-N-acetyllactosaminyl sugar chains of band 3 glycoprotein on senescent erythrocytes in anti-band 3 autoantibody binding. *J. Biol. Chem.* 269, 19394.
- Eggins, I., Fenderson, B. A., Toyokuni, T., Dean, B., Stroud, M. R., and Hakomori, S. -I. (1989) Specific interaction between Le^x and Le^x determinants. *J. Biol. Chem.* 264, 9476.
- Kawakami, H., Ito, M., Miura, Y., and Hirano, H. (1994) Involvement of N-acetyllactosamine containing sugar structures in the liver metastasis of mouse colon carcinoma (colon 26) cells. *J. Gastroenterol. Hepatol.* 9, 567.
- Fenouillet, E., Thibault, V., and Miquelis, R. (1995) On the relationship between completion of N-acetyllactosamine oligosaccharide units and iodine content of thyroglobulin: a reinvestigation. *Endocrinology* 136, 4204.
- Melaugh, W., Phillips, N. J., Campagnari, A. A., Tullius, M. V., and Gibson, B. W. (1994) Structure of the major oligosaccharide from the liposaccharide of *Hemophilus ducreyi* strain 35000 and evidence for additional glycoforms. *Biochemistry* 33, 13070.
- Panjwani, N., Zhao, Z., Ahmad, S., Yang, Z. T., Jungalwala, F., and Baum, J. (1995) Neolacto-glycosphingolipids, potential mediators of corneal epithelial cell migration. *J. Biol. Chem.* 270, 14015.
- (a) Schuster, M., Wang, P., Paulson, J. C., and Wong, C.-H. (1994) Solid-phase chemical-enzymatic synthesis of glycopeptides and oligosaccharides. *J. Am. Chem. Soc.* 116, 1135. (b) Unverzagt, C., Kelm, S., and Paulson, J. C. (1994) Chemical and enzymatic synthesis of multivalent sialoglycopeptides. *Carbohydr. Res.* 251, 285. (c) Nishimura, S.-I., Matsuoka, K., and Lee, Y. C. (1994) Chemoenzymatic oligosaccharide synthesis on a soluble polymeric carrier. *Tetrahedron Lett.* 31, 5657 and references cited therein.
- (a) Roy, R. (1996) Glycodendrimers: a new class of biopolymers. *Polym. News* 21, 226. (b) Roy, R. (1996) Syntheses and some applications of chemically defined multivalent glycoconjugates. *Curr. Opin. Struct. Biol.* 6, 692.
- (a) Ardoin, N., and Astruc, D. (1995) Molecular trees—from syntheses towards applications. *Bull. Soc. Chim. Fr.*, 875. (b) Issberner, J., Moors, R., and Vögtle, F. (1994) Dendrimers: from generations and functional groups to functions. *Angew. Chem., Int. Ed. Engl.* 33, 2413. (c) Fréchet, J. M. J. (1994) Functional polymers and dendrimers: reactivity, molecular architecture, and interfacial energy. *Science* 263, 1710 and references cited therein.
- (a) Wong, C.-H., Halcomb, R. L., Ichikawa, Y., and Kajimoto, T. (1995) Enzymes in organic synthesis: application to the problems of carbohydrate recognition (part 1). *Angew. Chem., Int. Ed. Engl.* 34, 412. (b) Wong, C.-H., Halcomb, R. L., Ichikawa, Y., and Kajimoto, T. (1995) Enzymes in organic synthesis: application to the problems of carbohydrate recognition (part 2). *Angew. Chem., Int. Ed. Engl.* 34, 521.
- Zanini, D., Park, W. K. C., and Roy, R. (1995) Synthesis of novel dendritic glycosides. *Tetrahedron Lett.* 36, 7383.
- Unverzagt, C., Kunz, H., and Paulson, J. C. (1990) High efficiency synthesis of sialyloligosaccharides and sialoglycopeptides. *J. Am. Chem. Soc.* 112, 9308.
- Lee, Y. C., and Lee, R. T. (1974) Synthesis of 3-(2-aminoethylthio)propyl glycosides. *Carbohydr. Res.* 37, 193.
- Park, W. K. C. (1995) Design and synthesis of GM3- and lactose-containing multivalent conjugates. Ph.D. Thesis, University of Ottawa, Ottawa, ON.
- Gottschalk, A., and Bhargava, A. S. (1972) in *Glycoproteins: Their Composition, Structure and Function* (A. Gottschalk, Ed.) pp 821–829, Elsevier Publishing Co., New York.
- Goldstein, I. J., and Poretz, R. D. (1986) Isolation, Physicochemical Characterization, and Carbohydrate-Binding Specificity of Lectins. In *The Lectins Properties, Functions, and Applications in Biology and Medicine* (I. E. Liener, N. Sharon, and I. J. Goldstein, Eds.) pp 103–115, Academic Press, Inc., Orlando.
- Goldstein, I. J. and Poretz, R. D. (1986) Isolation, Physicochemical Characterization, and Carbohydrate-Binding Specificity of Lectins. In *The Lectins Properties, Functions, and Applications in Biology and Medicine* (I. E. Liener, N. Sharon, and I. J. Goldstein, Eds.) pp 160–163, Academic Press, Inc., Orlando.
- Bhattacharyya, L., Haraldsson, M., Sharon, N., Lis, H., and Brewer F. (1989) Binding and precipitating activities of Erythrina lectins with complex type carbohydrates and synthetic cluster glycosides. A comparative study of the lectins from *E. Corallodendron*, *E. Cristagalli*, *E. Flabelliformis*, and *E. Indica*. *Glycoconjugate J.* 6, 141.

Current Data Parameters
NAME diana_dz589c
EXPNO 1
PROCNO 1

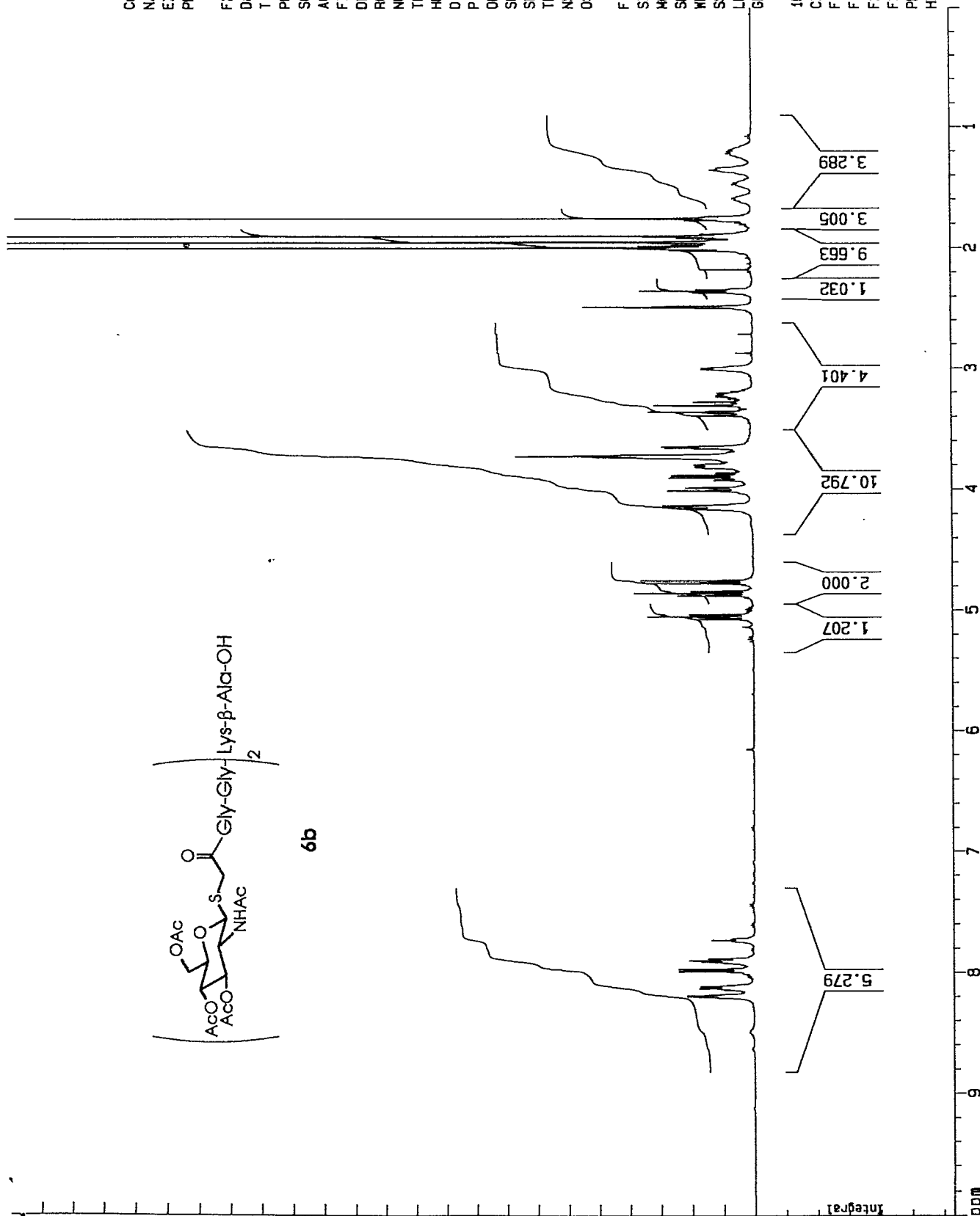
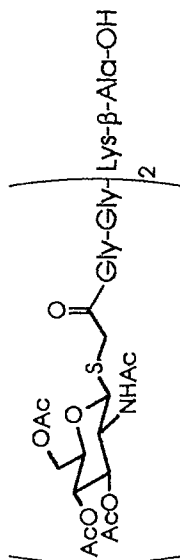
F2 - Acquisition Parameters

Date 950425
Time 12.50
PULPROG zg
SOLVENT dms0
AQ 4.6530762
FIDRES 0.107456
OW 71.0
RG 512
NUCLEUS 1H
TE 300.0
HL1 0
D1 0.0100000
P1 3.0
DE 88.8
SF01 500.1405972
SWH 7042.25
TD 65536
NS 8
DS 0

F1 - Processing parameters

SI 32768
MC2 GF
SF 500.1377944
WDW EM
SSB 0
LB 0.30
GB 0

1D NMR plot parameters
CX 22.00
FIP 10.000
F1 5001.38
F2 0.000
F2 0.00
PPMCM 0.45455
HZCM 227.33536



Current Data Parameters
 NAME diana_gz589c
 EXPNO 4
 PROCNO 1

F2 - Acquisition Paramet

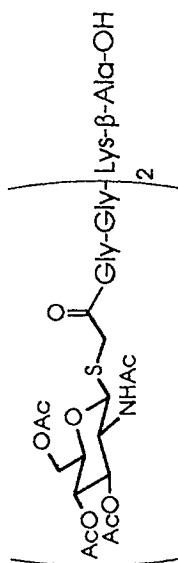
Date 950425
 Time 14.20
 PULPROG zgdc
 SOLVENT CDC13
 AQ 1.0485960
 FIDRES 0.476937
 DW 16.0
 RG 32768
 NUCLEUS 13C
 TE 300.0
 D1 0.0300000
 P31 70.0
 S2 22
 HL1 22
 D1 1.0000000
 P1 5.0
 DE 20.0
 SF01 125.7724464
 SMH 31250.00
 TD 65536
 NS 1385
 DS 0

F1 - Processing paramete

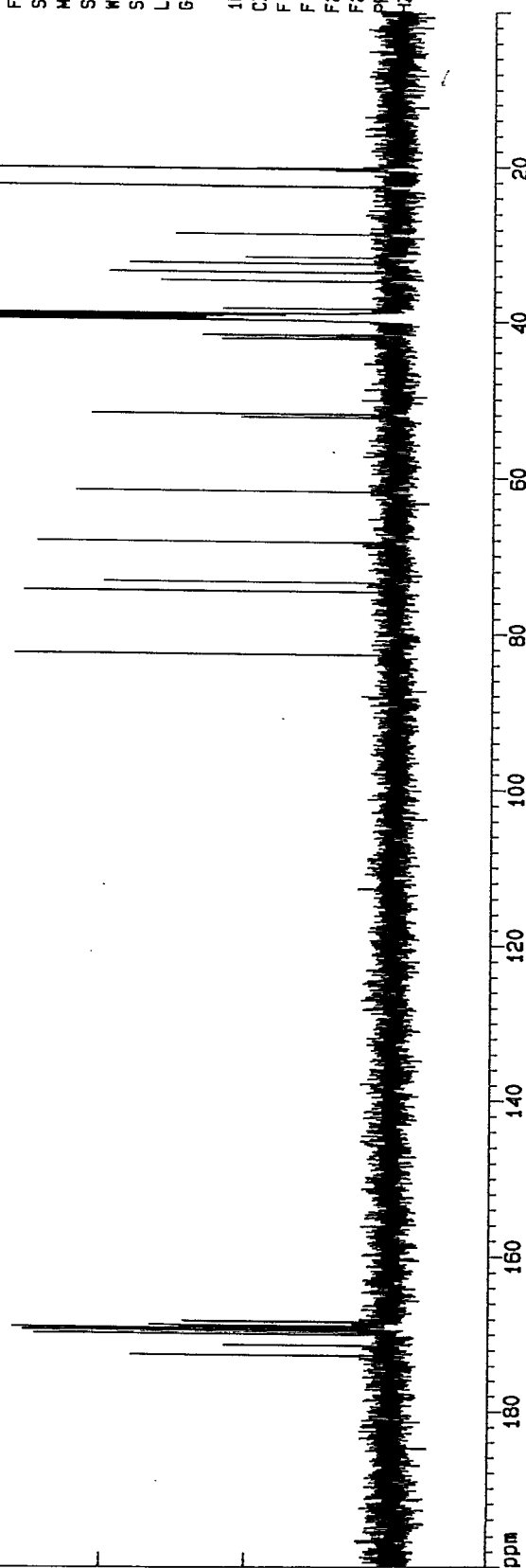
SI 32768
 MC2 GF
 SF 125.7598047
 WDW EM
 SSB 0
 LB 1.00
 GB 0

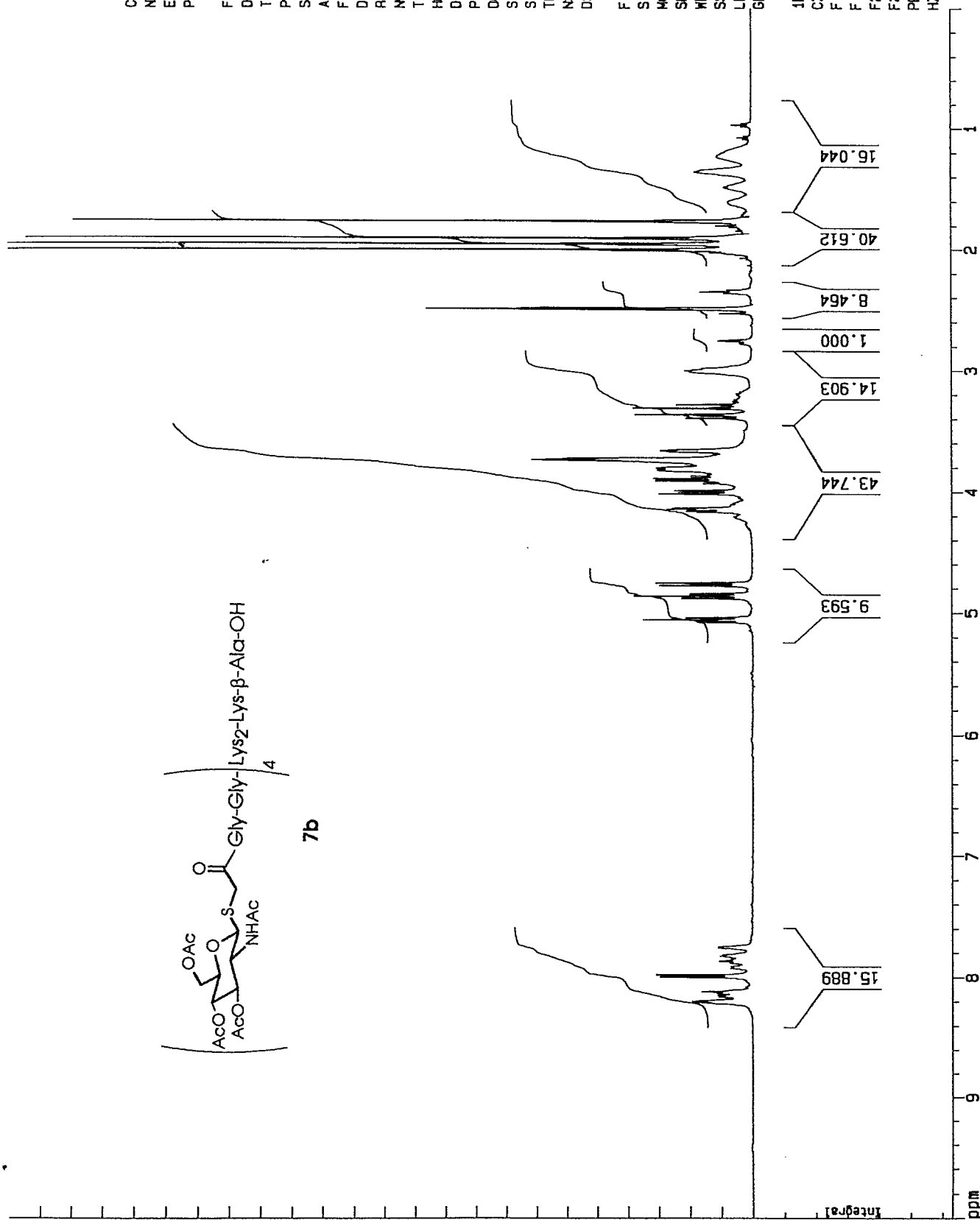
1D NMR plot parameters

CX 22.00
 F1P 200.000
 F1 25151.96
 F2P 0.000
 F2 0.00
 PPCHM 9.09091
 HZCH 1143.27100



6b





Current Data Parameters
NAME diana_02509c

EXPNO	1
PROCNO	1

F2 - Acquisition Param.
Date 950511

Time	13.17
END PROG	70

entry	solvent	yield (%)
1	DMF	65
2	DMF	65
3	DMF	65
4	DMF	65
5	DMF	65
6	DMF	65
7	DMF	65
8	DMF	65
9	DMF	65
10	DMF	65
11	DMF	65
12	DMF	65
13	DMF	65
14	DMF	65
15	DMF	65
16	DMF	65
17	DMF	65
18	DMF	65
19	DMF	65
20	DMF	65
21	DMF	65
22	DMF	65
23	DMF	65
24	DMF	65
25	DMF	65
26	DMF	65
27	DMF	65
28	DMF	65
29	DMF	65
30	DMF	65
31	DMF	65
32	DMF	65
33	DMF	65
34	DMF	65
35	DMF	65
36	DMF	65
37	DMF	65
38	DMF	65
39	DMF	65
40	DMF	65
41	DMF	65
42	DMF	65
43	DMF	65
44	DMF	65
45	DMF	65
46	DMF	65
47	DMF	65
48	DMF	65
49	DMF	65
50	DMF	65
51	DMF	65
52	DMF	65
53	DMF	65
54	DMF	65
55	DMF	65
56	DMF	65
57	DMF	65
58	DMF	65
59	DMF	65
60	DMF	65
61	DMF	65
62	DMF	65
63	DMF	65
64	DMF	65
65	DMF	65
66	DMF	65
67	DMF	65
68	DMF	65
69	DMF	65
70	DMF	65
71	DMF	65
72	DMF	65
73	DMF	65
74	DMF	65
75	DMF	65
76	DMF	65
77	DMF	65
78	DMF	65
79	DMF	65
80	DMF	65
81	DMF	65
82	DMF	65
83	DMF	65
84	DMF	65
85	DMF	65
86	DMF	65
87	DMF	65
88	DMF	65
89	DMF	65
90	DMF	65
91	DMF	65
92	DMF	65
93	DMF	65
94	DMF	65
95	DMF	65
96	DMF	65
97	DMF	65
98	DMF	65
99	DMF	65
100	DMF	65

AG	4.6530/62
FIDRES	0.107455

DW	71.0
AG	1024

NUCLEUS
TE
300.0
1H

HL1	0
D1	0.0100000

P1	3.0
DE	88.8

SF01 500.1405972
SWH 7042.25

TD	65536
NS	8

050

F1 - Processing parameter	32768
SI	

MC2 OF
SF 500 1377944

0
ME
ME

0	
0.30	
0	

083

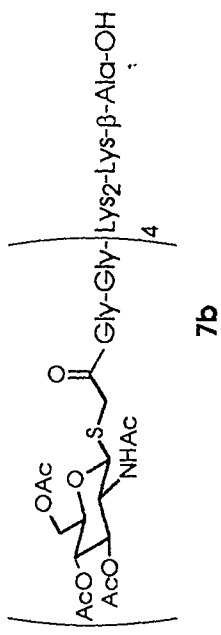
1D NMR plot parameters	
CX	22.00

F1P	5.370
F1	2685.70

F2p	2.196
F2	1098.15

0.14428	ppmCM
72.16134	H7CM

ESTAT: 37 4021

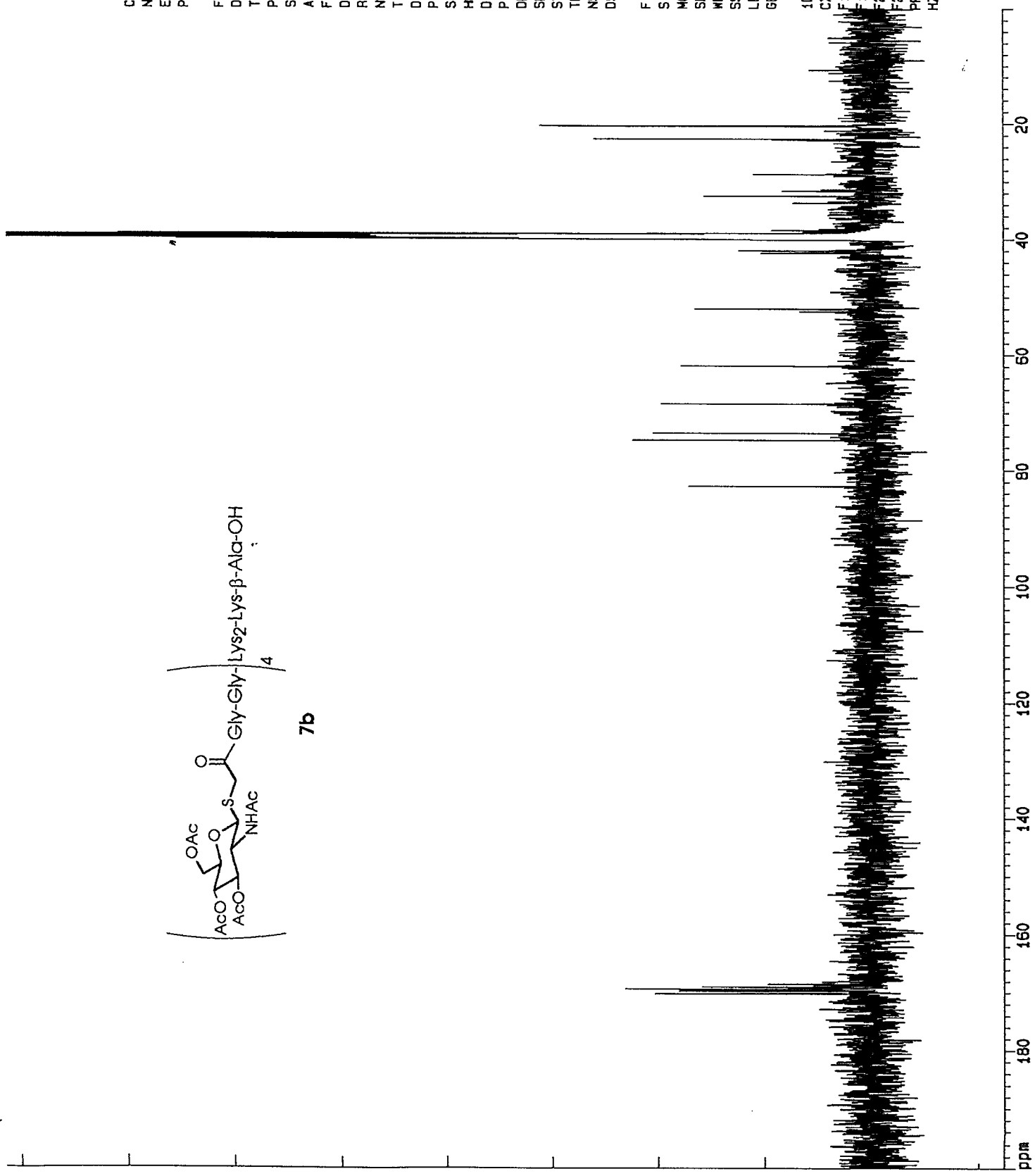


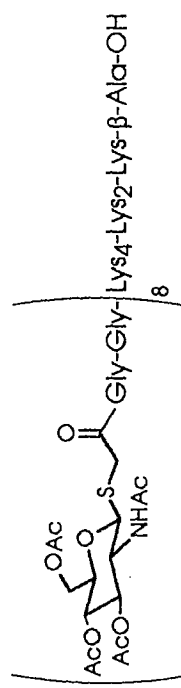
Current Data Parameters
 NAME diana_dz589c
 EXPNO 4
 PROCNO 1

F2 - Acquisition Parameters
 Date 950511
 Time 14.03
 PULPROG zgpg
 SOLVENT CDC13
 AQ 1.0485960
 FIDRES 0.476837
 DQ 16.0
 RG 32768
 NUCLEUS 13C
 TE 300.0
 D11 0.0300000
 P31 70.0
 S2 22
 HL1 22
 D1 1.0000000
 P1 5.0
 DE 20.0
 SFO1 125.7724464
 SWH 31250.00
 TD 65536
 NS 534
 DS 0

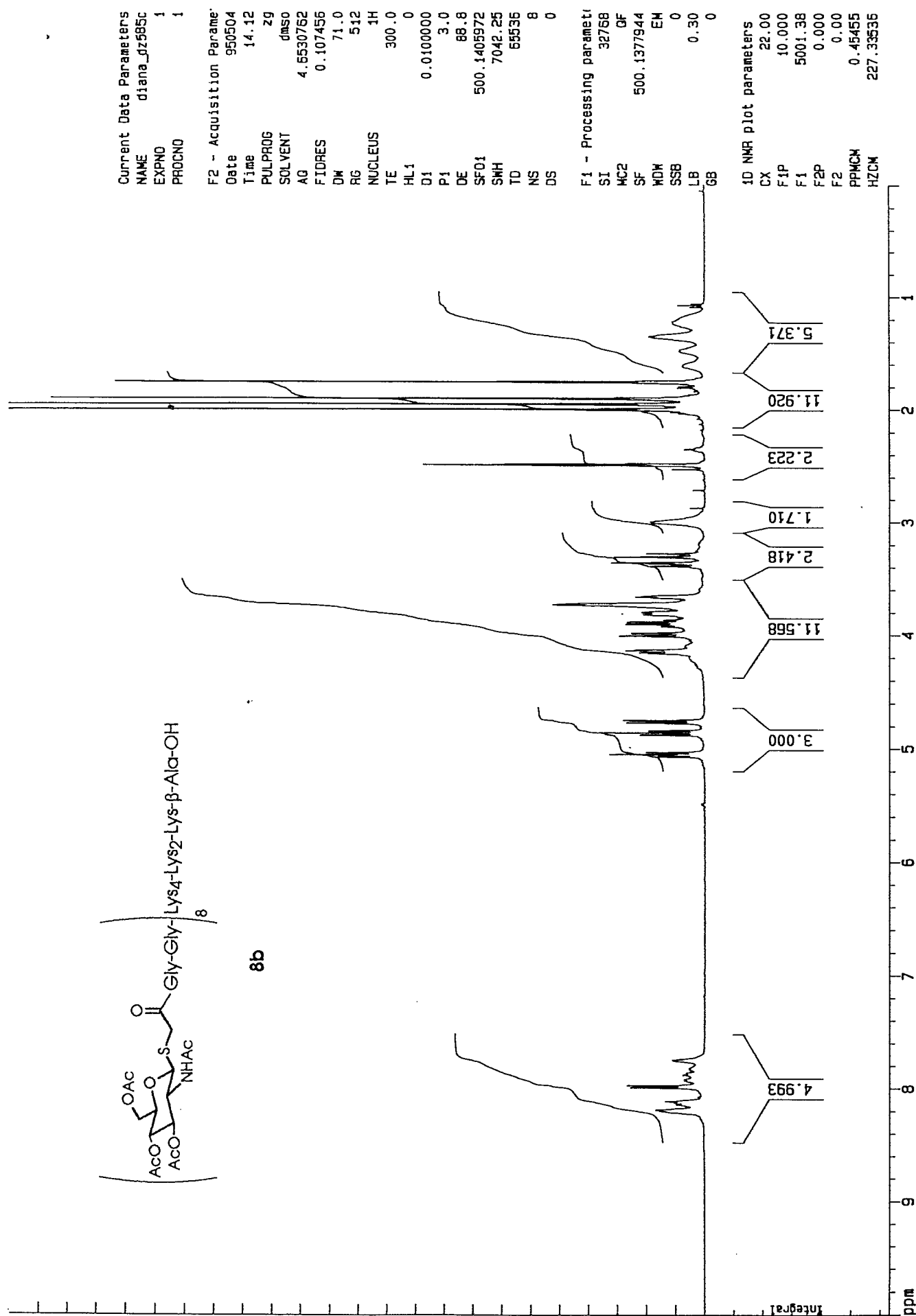
F1 - Processing parameters
 SI 32768
 MC2 GF
 SF 125.7598047
 WDW EM
 SSB 0
 LB 2.00
 GB 0

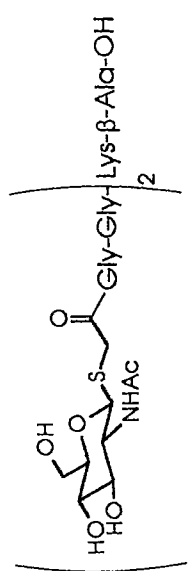
1D NMR plot parameters
 CX 22.00
 F1P 200.000
 E1 25151.96
 F2P 0.000
 F2 0.00
 PPMCH 9.09091
 HZCH 1143.27100



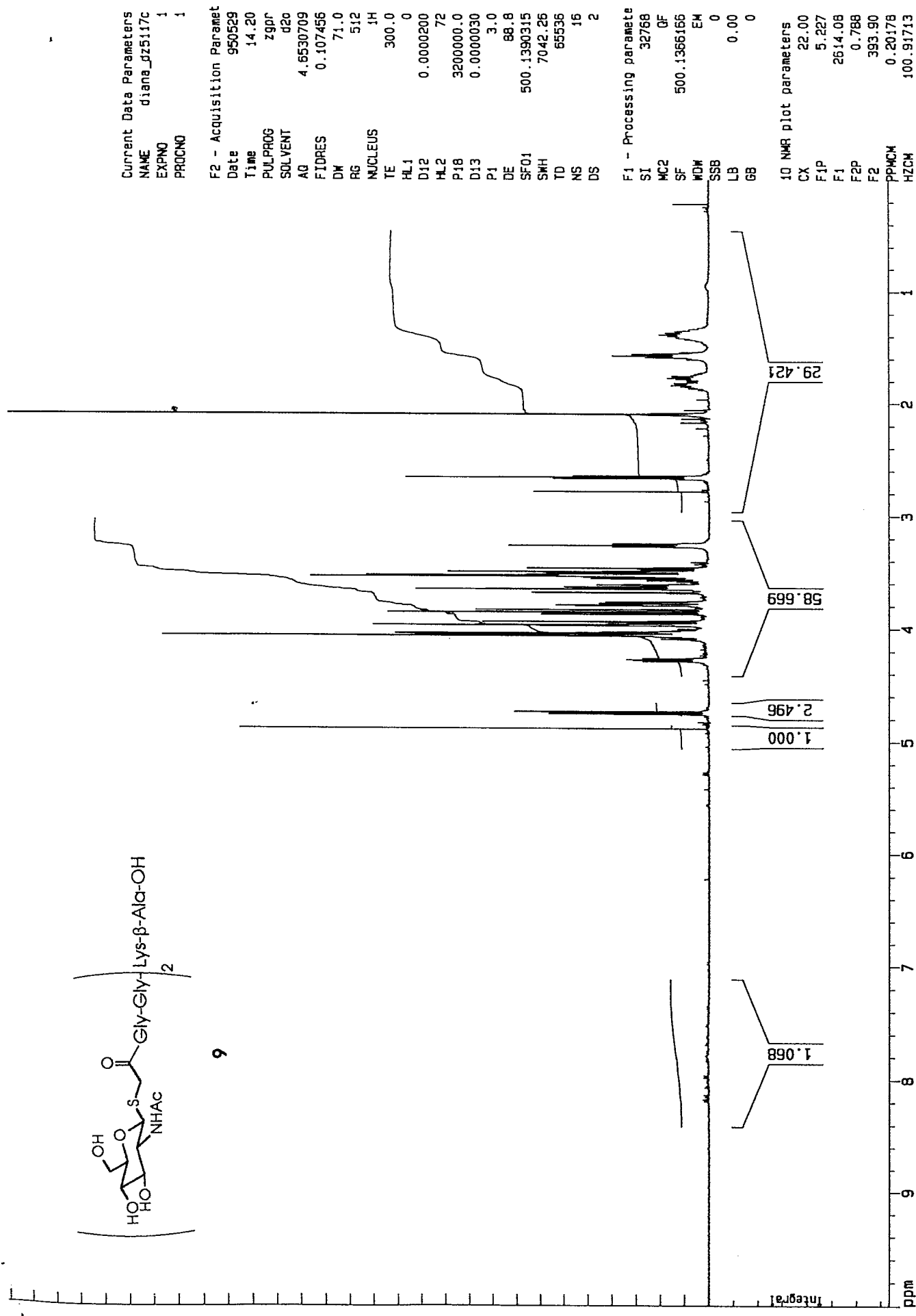


8b





9



Current Data Parameters
 NAME diana_gz517c
 EXPNO 1
 PROCNO 1

F2 - Acquisition Parameters
 Date 950529
 Time 14.20
 PULPROG zgpg
 SOLVENT d2o
 AQ 4.6530709
 FIDRES 0.107456
 DW 71.0
 RG 512
 NUCLEUS 1H
 TE 300.0
 HL1 0
 D12 0.0000200
 HL2 72
 P18 3200000.0
 D13 0.0000030
 P1 3.0
 DE 88.8
 SF01 500.1390315
 SWH 7042.26
 TD 65536
 NS 16
 DS 2

F1 - Processing parameters
 SI 32768
 MC2 GF
 SF 500.1366166
 WDW EM
 SSB 0
 LB 0.00
 GB 0

10 NMR plot parameters
 CX 22.00
 F1P 5.227
 F1 2614.08
 F2P 0.788
 F2 393.90
 PPMCM 0.20178
 HZCM 100.91713

Current Data Parameters
NAME diana_dz5117c
EXPNO 4
PROCNO 1

F2 - Acquisition Parameters

Date 950529
Time 15.02

PULPROG zgpg
SOLVENT d2o

AQ 1.0485960
FIDRES 0.476837

DW 16.0
RG 32768

NUCLEUS 13C
TE 300.0

D11 0.0300000
P31 70.0

S2 22
HL1 22

D1 1.0000000
P1 5.0

DE 20.0
SF01 125.7724464

SWH 31250.00
TD 65536

NS 2048
DS 0

F1 - Processing parameters

SI 32768
MC2 OF

SF 125.7595330
WDW EM

SSB 0
LB 1.00

GB 0

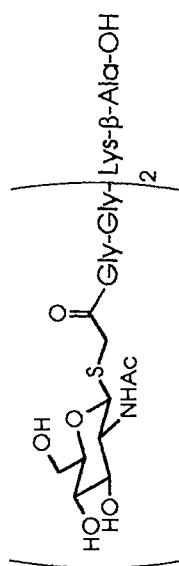
1D NMR plot parameters

CX 22.00
FIP 200.000

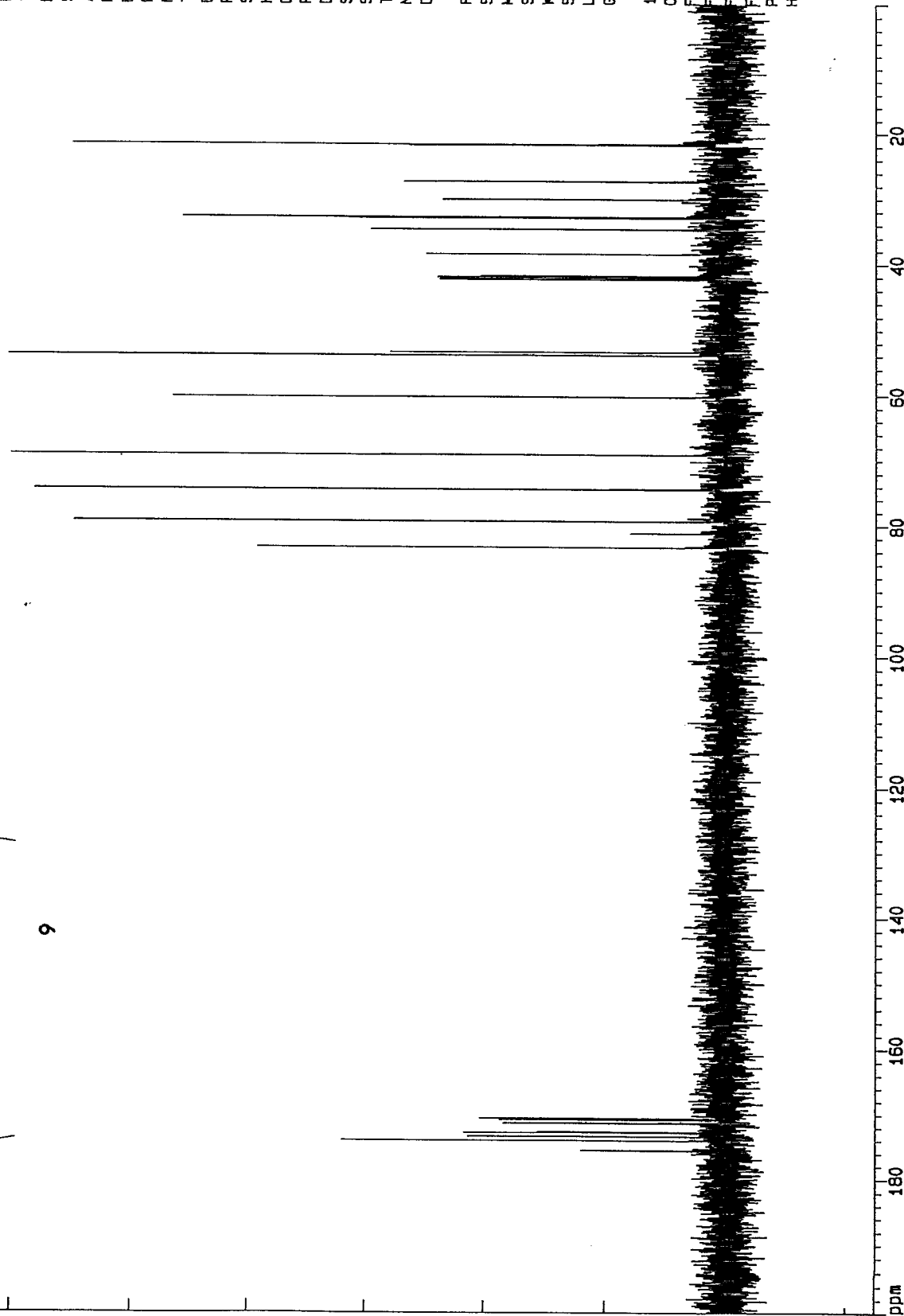
F1 25151.91
F2 0.000

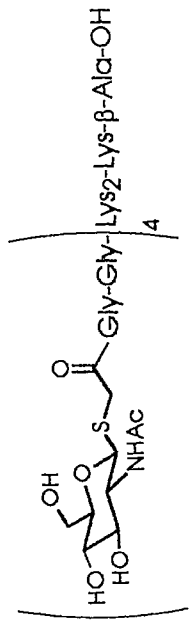
F2 0.00
PPMCH 9.09031

HZCM 1143.26855

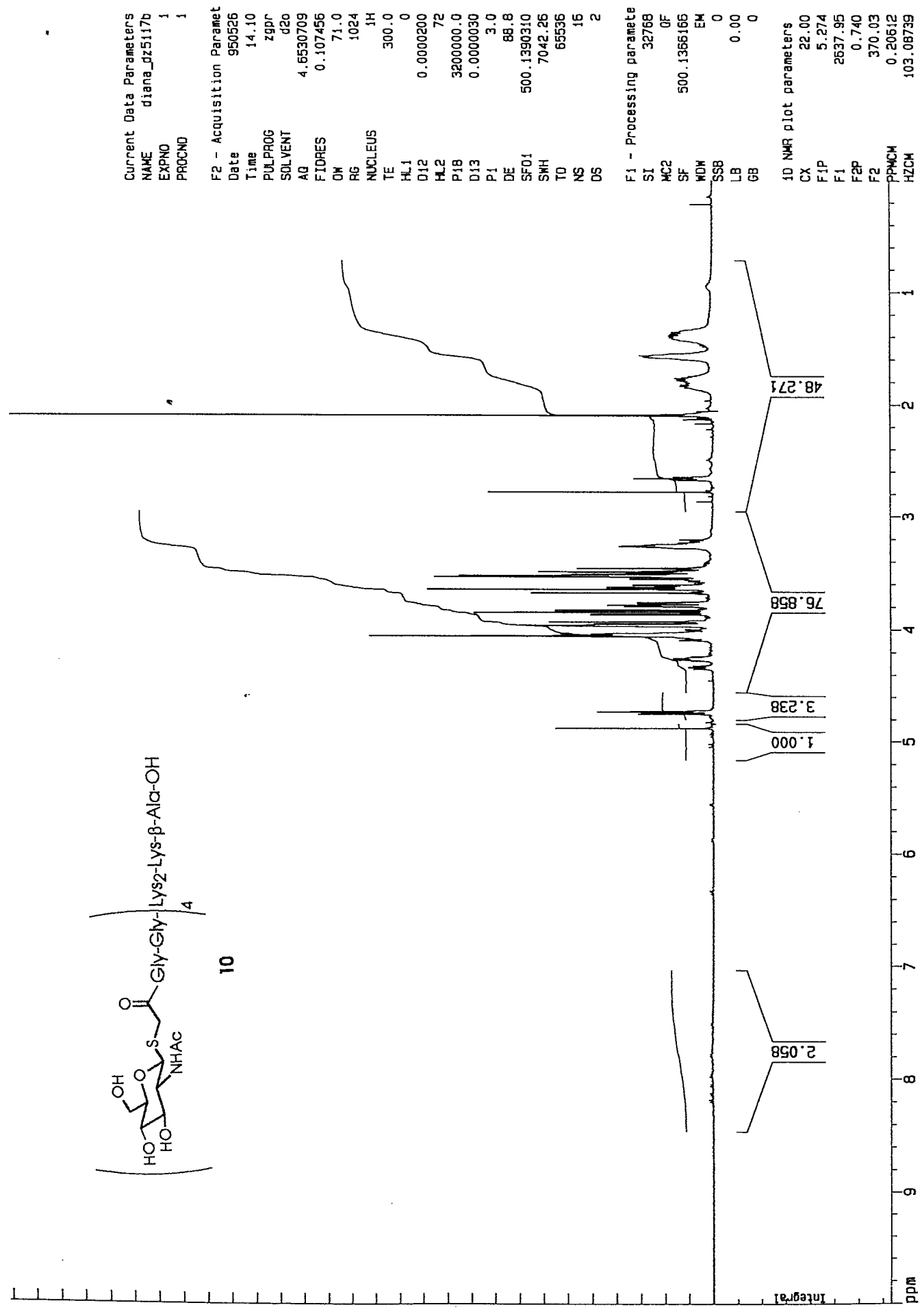


9





10



Current Data Parameters
NAME diana_dz5117b
EXPNO 4
PROCNO 1

F2 - Acquisition Paramet

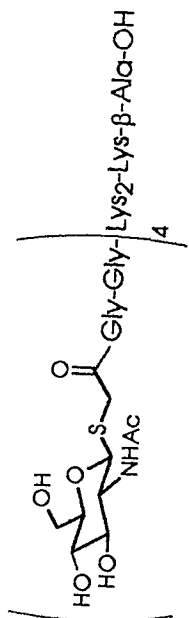
Date 950526
Time 16.35
PULPROG zgdc
SOLVENT CDC13
AQ 1.0485960
FIDRES 0.476837
DQ 16.0
RG 32768
NUCLEUS 13C
TE 300.0
D11 0.0300000
P31 70.0
S2 22
HL1 22
D1 1.0000000
P1 5.0
DE 20.0
SF01 125.772464
SWH 31250.00
TD 65536
NS 15384
DS 0

F1 - Processing paramete

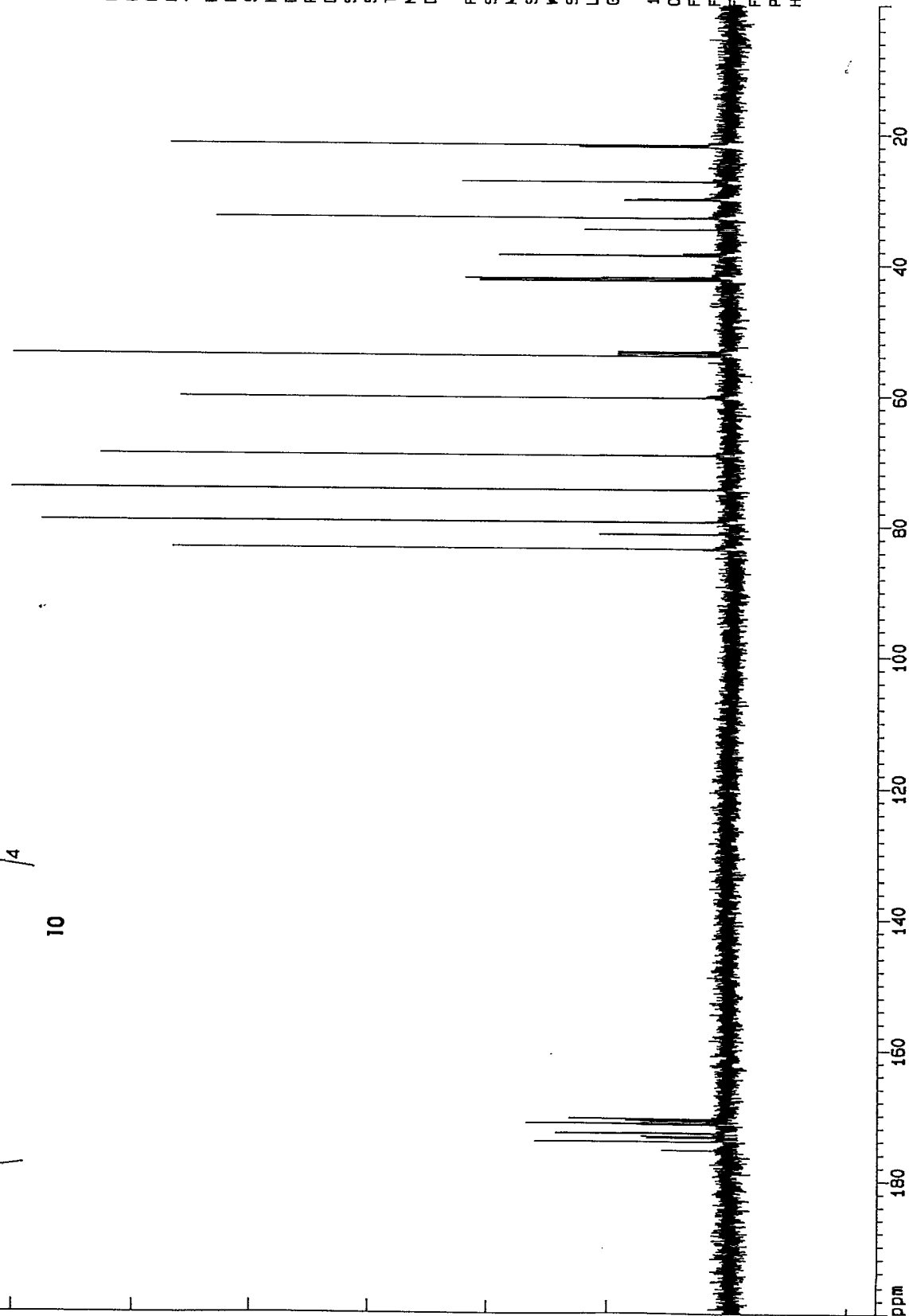
SI 32768
MC2 GF
SF 125.7595330
WDW EM
SSB 0
LB 1.00
GB 0

ID NMR plot parameters

CX 22.00
F1P 200.000
F1 25151.91
F2P 0.000
F2 0.00
PPMCH 9.09091
HZCM 1143.26855



10

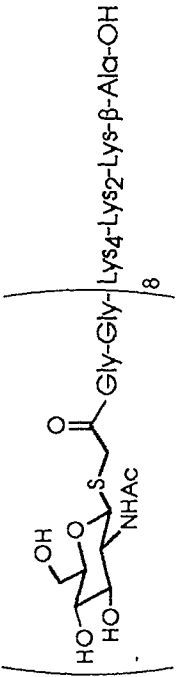
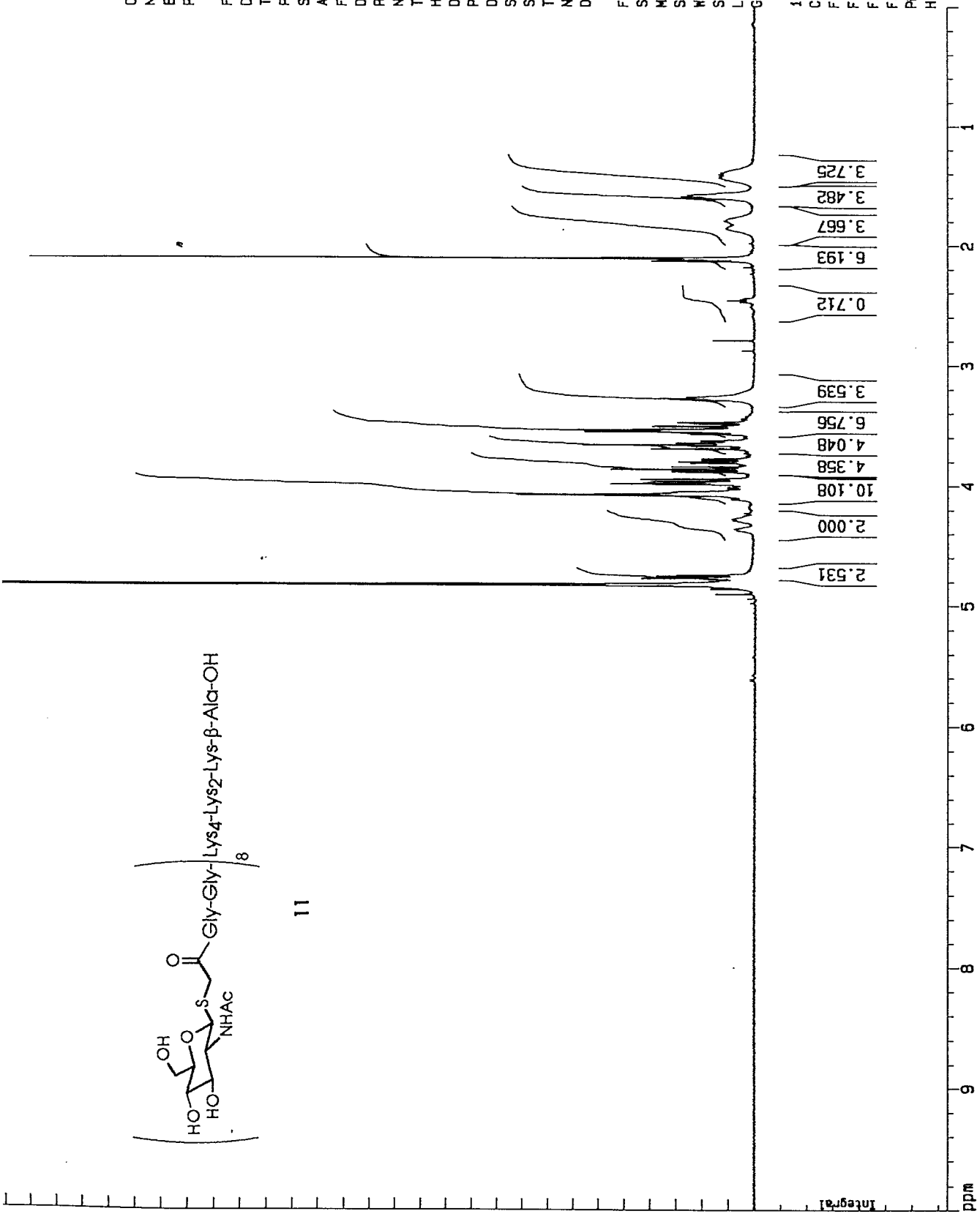


Current Data Parameters
NAME diana_pz86
EXPNO 1
PROCNO 1

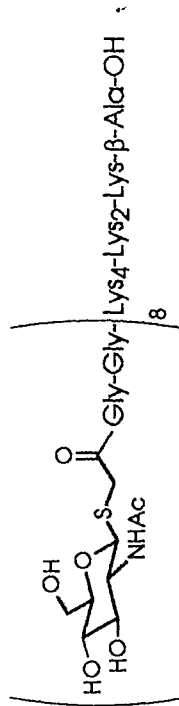
F2 - Acquisition Parameters
Date 960226
Time 17.09
PULPROG zg
SOLVENT d2o
AQ 4.6530671
FIDRES 0.107456
DM 71.0
RG 2048
NUCLEUS 1H
TE 300.0
HL1 0
D1 0.0100000
P1 3.0
DE 88.8
SF01 500.1394550
SHH 7042.27
TD 65536
NS 32
DS 0

F1 - Processing parameters
SI 32768
MC2 GF
SF 500.1366166
WDW EM
SSB 0
LB 0.00
GB 0

1D NMR plot parameters
CX 22.00
F1P 10.000
F1 5001.37
F2P 0.000
F2 0.00
PPMCM 0.45455
HZCM 227.33482

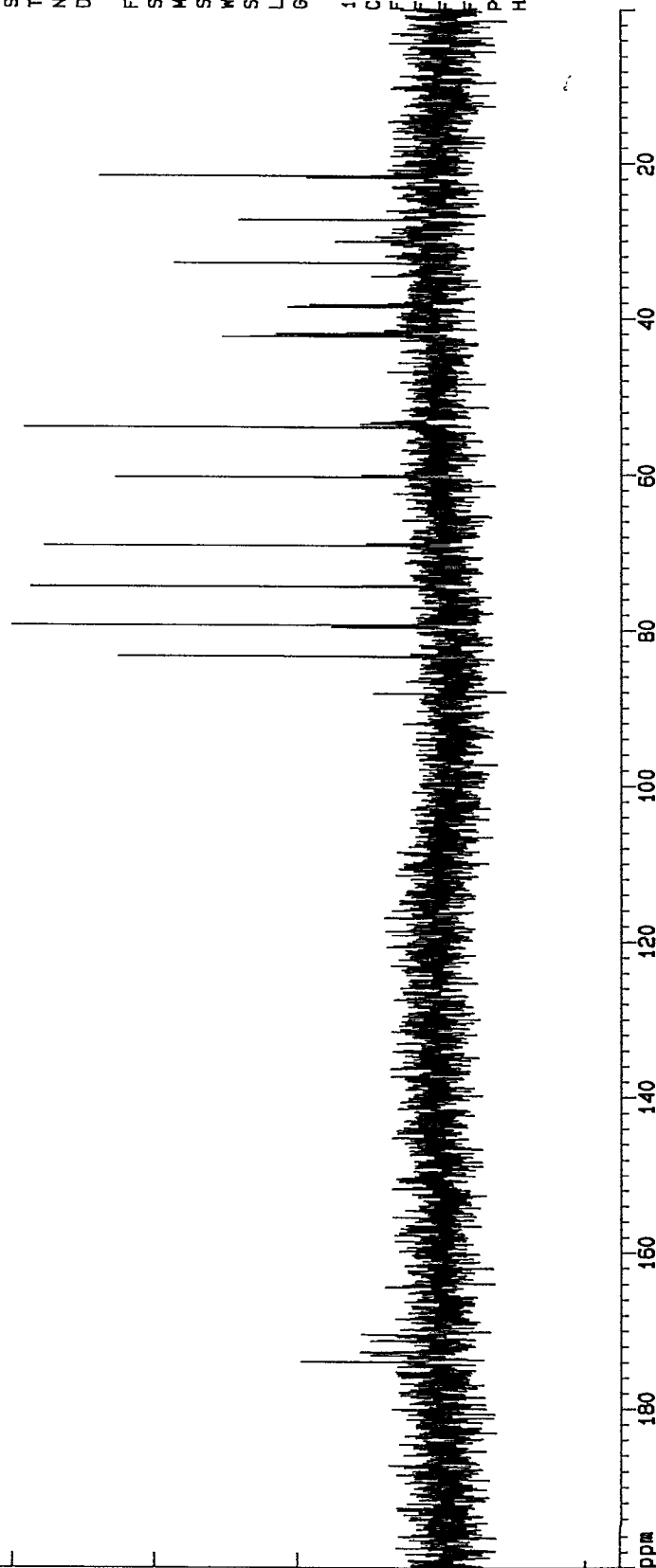


11



11

Current Data Parameters
NAME diana_dz3134b
EXPNO 4
PROCNO 1
F2 - Acquisition Paramet
Date 950307
Time 20.59
PULPROG zgdc
SOLVENT CDC13
AQ 1.0485960
FIDRES 0.475837
DQ 16.0
RG 32768
NUCLEUS 13C
TE 300.0
D11 0.0300000
P31 70.0
S2 22
HL1 22
D1 1.0000000
P1 5.0
DE 20.0
SF01 125.7724464
SWH 31250.00
TQ 65536
NS 16384
DS 0
F1 - Processing paramete
SI 32768
MC2 GF
SF 125.7595330
WDW EM
SSB 0
LB 2.00
GB 0
1D NMR plot parameters
CX 22.00
FIP 200.000
F1 25151.91
F2 0.000
F2 0.00
PPMCH 9.09091
HZCM 1143.26855



12

Current Data Parameters
NAME diana_d7519b
EXPNO 1
PROCNO 1

F2 - Acquisition Parameters

Date 960307
Time 17.05

PULPROG zg

SOLVENT d2o

AQ 4.6530571

FIDRES 0.107456

DM 71.0

RG 2048

NUCLEUS 1H

TE 300.0

HL1 0

D1 0.0100000

P1 3.0

DE 88.8

SF01 500.1394650

SWH 7042.27

TD 65536

NS 16

DS 0

F1 - Processing parameters

SF 32768

HC2 OF

SF 500.1366166

WDW EM

SSB 0

LB 0.00

GB 0

1D NMR plot parameters

CX 22.00

FJP 10.000

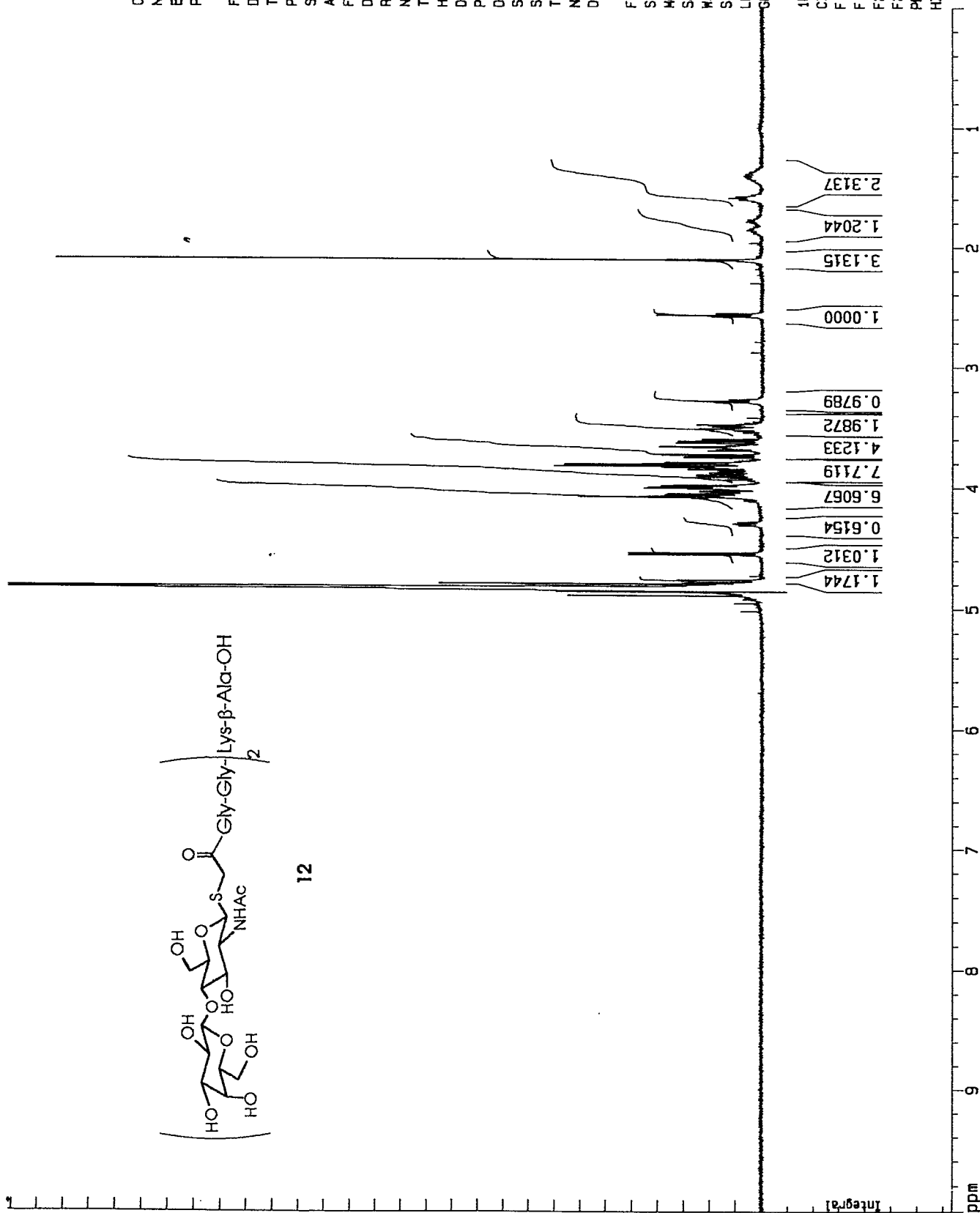
F1 5001.37

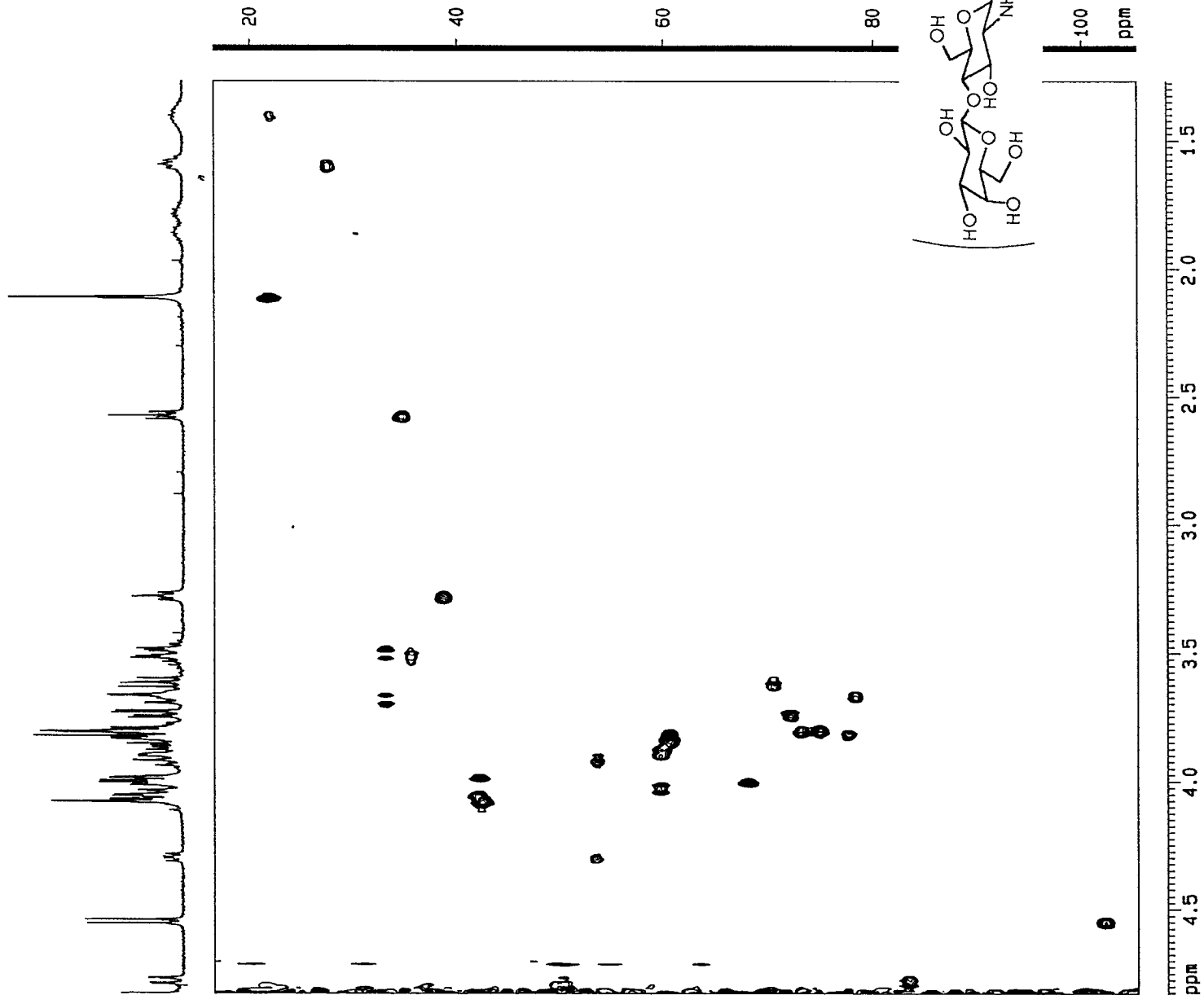
F2 0.000

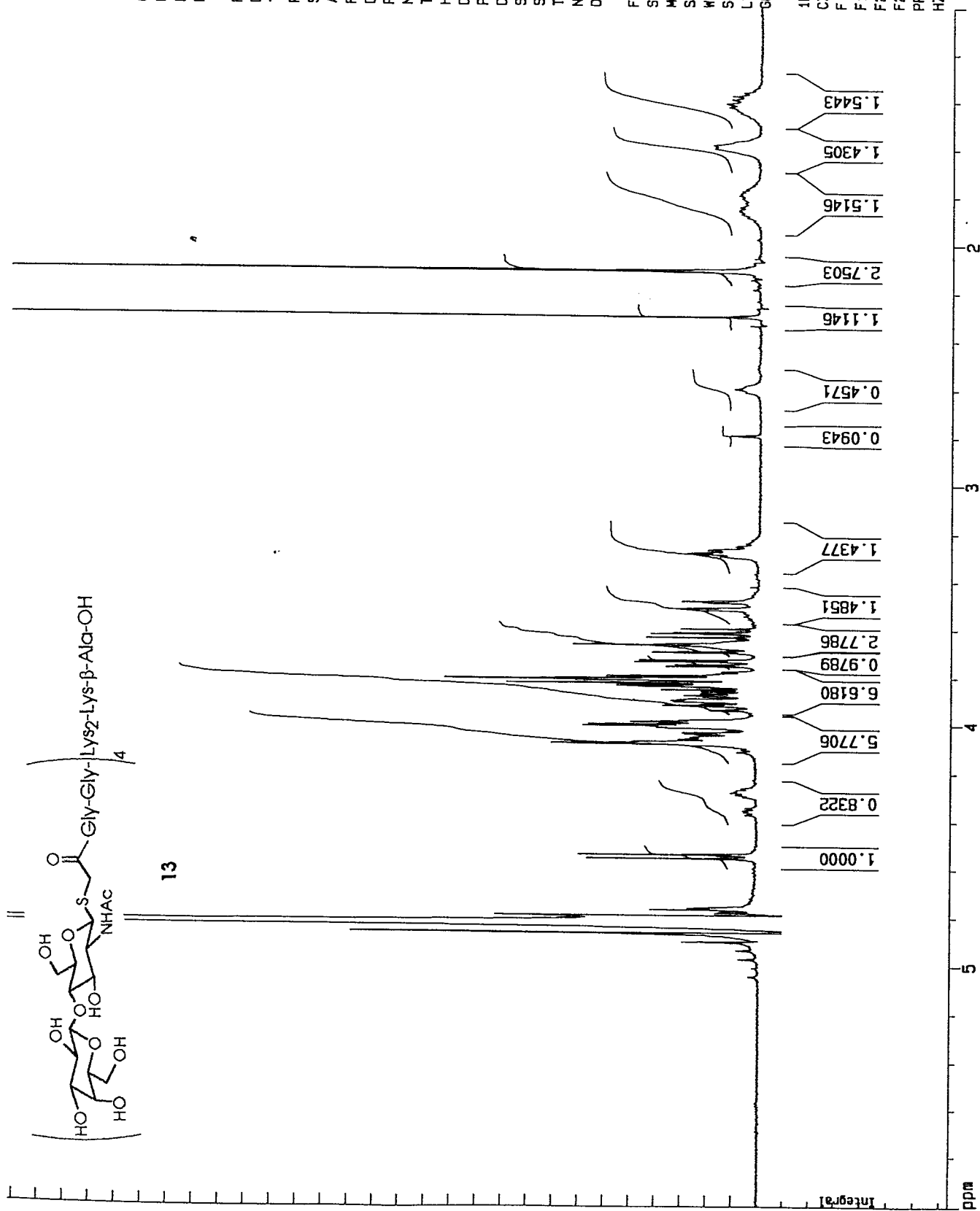
F2 0.00

PPMCM 0.45455

HZCM 227.33482





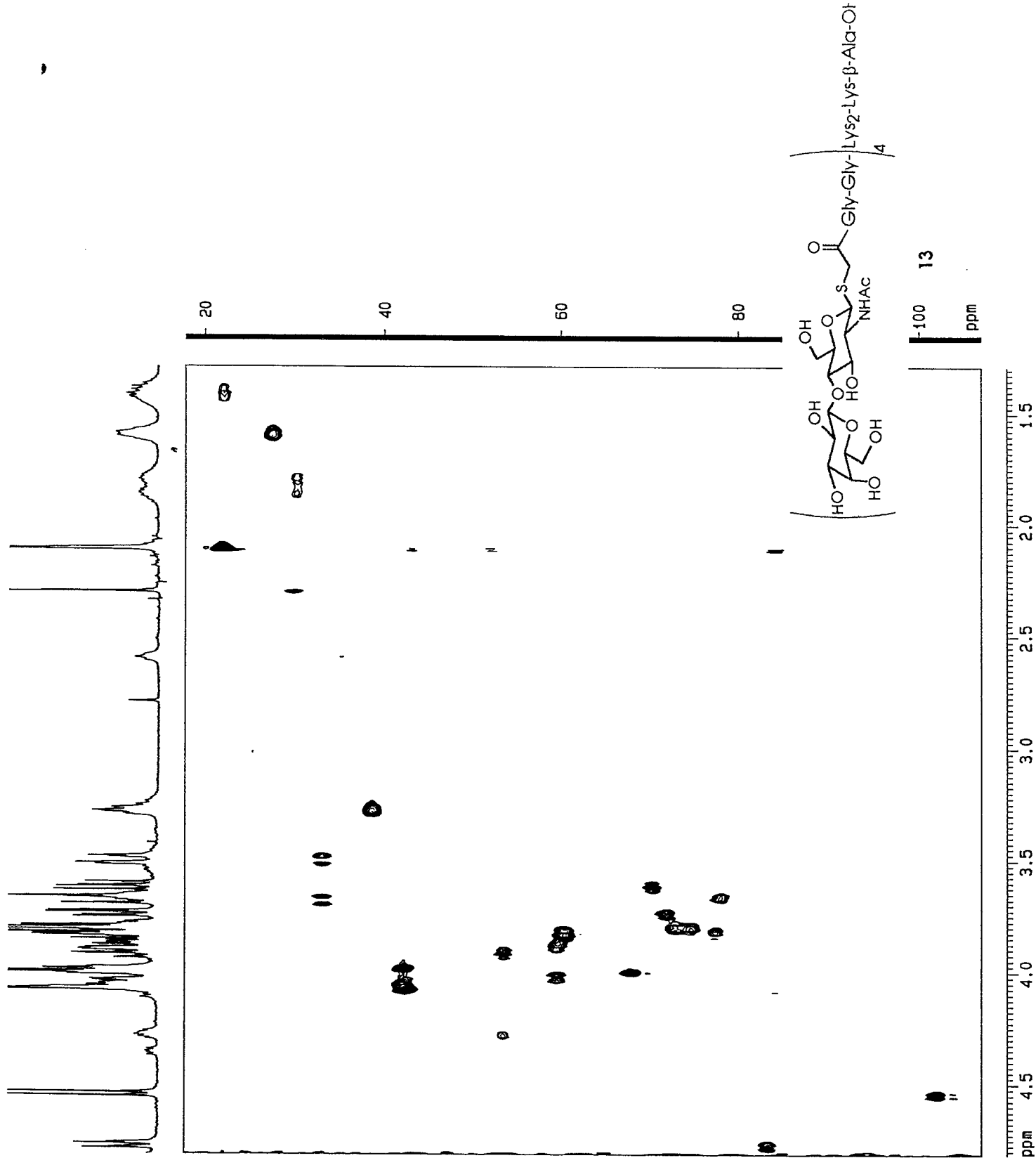


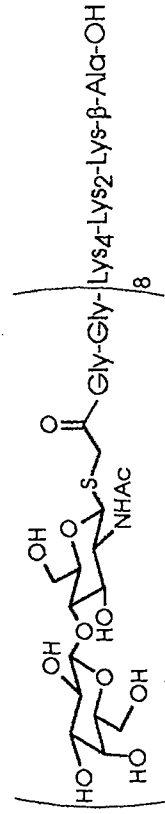
Current Data Parameters
NAME diana_gz617b
EXPNO 1
PROCNO 1

F2 - Acquisition Parameters
Date 960313
Time 16.55
PULPROG zg
SOLVENT d2o
AQ 4.6530571
FIDRES 0.107456
DQ 71.0
RG 1024
NUCLEUS 1H
TE 300.0
HL1 0
D1 0.0100000
P1 3.0
DE 88.8
SF01 500.1394650
SWH 7042.27
TD 65536
NS 32
DS 0

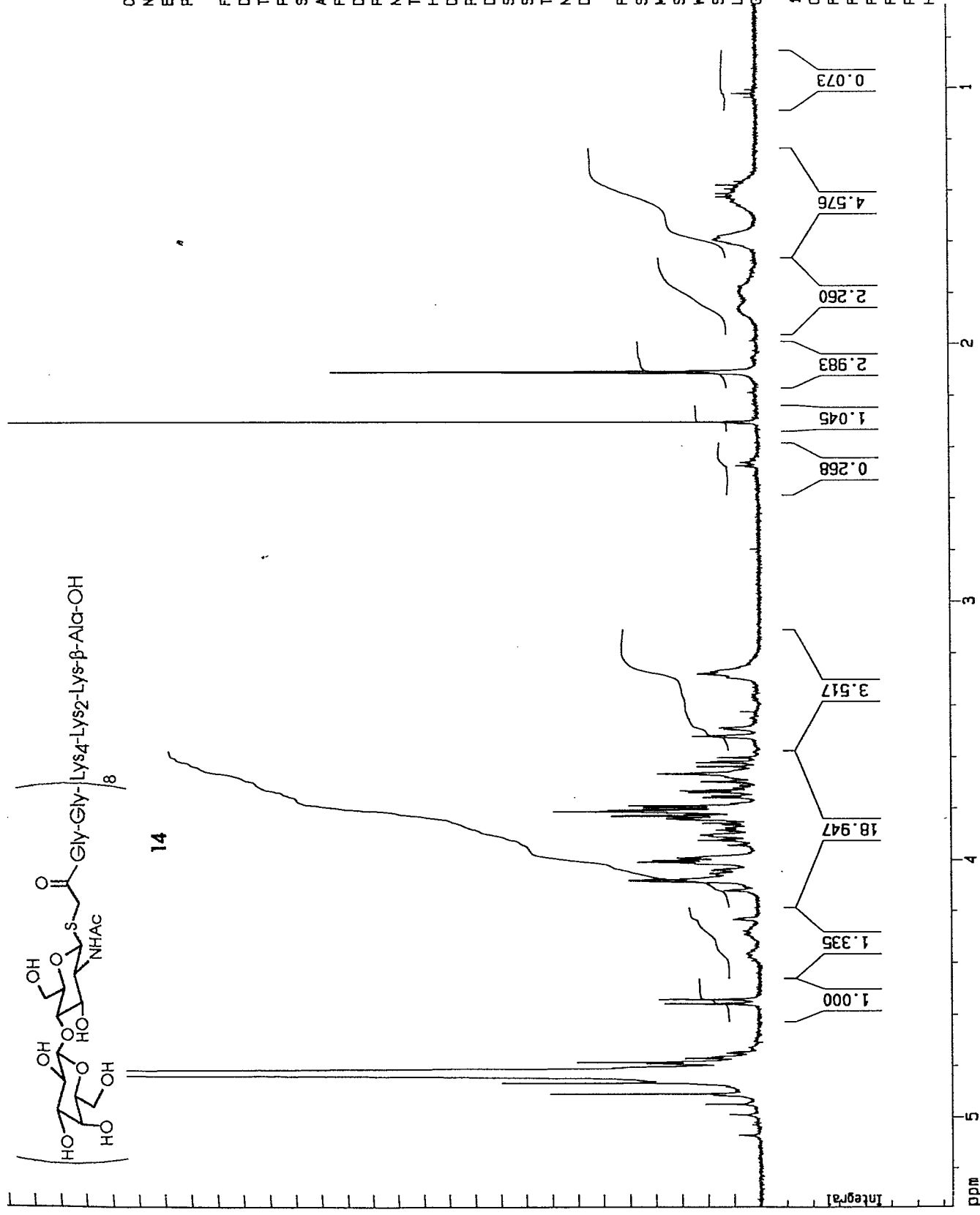
F1 - Processing parameters
SI 32768
MC2 GF
SF 500.1366165
WDW EM
SSB 0
LB 0.00
GB 0

1D NMR plot parameters
CX 22.00
F1P 4.687
F1 2344.32
F2P 2.480
F2 1240.20
PPMCM 0.10035
HZCM 50.18729





14

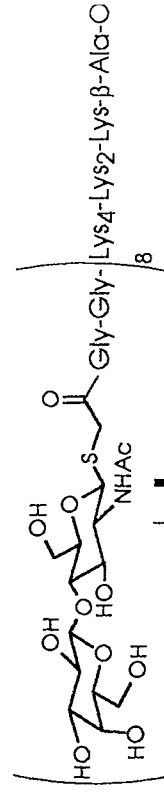
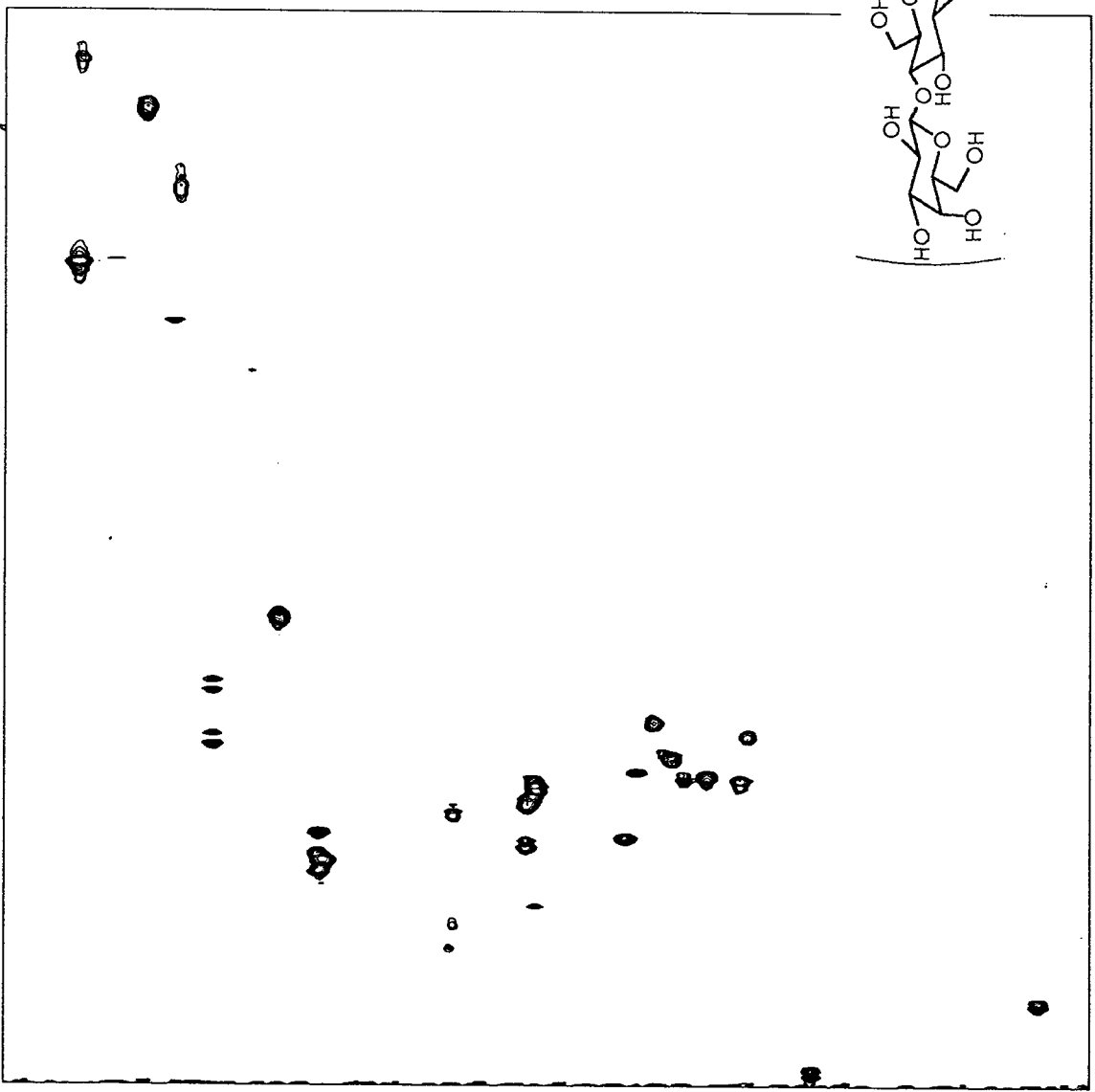


Current Data Parameters
 NAME diana_dz57b
 EXPNO 1
 PROCNO 1

F2 - Acquisition Parameters
 Date 960313
 Time 14.56
 PULPROG zg
 SOLVENT d2o
 AQ 4.6530671
 FIDRES 0.107456
 DW 71.0
 RG 2048
 NUCLEUS 1H
 TE 300.0
 HL1 0
 D1 0.0100000
 P1 3.0
 DE 88.8
 SF01 500.1394650
 SMH 7042.27
 TD 65536
 NS 32
 DS 0

F1 - Processing parameters
 SI 32768
 MC2 GF
 SF 500.1366166
 WDW EM
 SSB 0
 LB 0.00
 GB 0

1D NMR plot parameters
 CX 22.00
 F1P 5.346
 F1 2673.76
 F2P 0.658
 F2 334.22
 PPMCM 0.21263
 HZCM 106.34278



Versatile Linker Chemistry for Synthesis of 3'-Modified DNA

Matthew H. Lyttle,* Howard Adams, Derek Hudson, and Ronald M. Cook

Biosearch Technologies Inc., 40 Mark Drive, San Rafael, California 94903. Received November 14, 1996*

A general method is described for the solid phase supported synthesis of DNA containing 3'-terminal phosphodiester modified with linkers bearing either amino, thiol, or hydroxyl groups. These products are all made from a common intermediate, obtained by the reaction of trimellitic anhydride chloride with aminopropyl CPG. The anhydride-derivatized support was then reacted with three appropriate bifunctional spacers, giving DMT-protected hydroxyl solid supports bearing the masked functionality as an ester, amide, or thioester. DNA synthesis was then performed, followed by ammonia cleavage and deprotection, giving the hydroxyl-, amino-, or thiol-functionalized DNA 3'-phosphate diesters, respectively. Test mononucleotides synthesized with each of the new supports were identical with control mononucleotides made with 5'-immobilized nucleosides and alkylhydroxyl, alkylamino, and alkylthio phosphoramidites. The new supports were then used to prepare several 3'-modified oligonucleotides, which were characterized by gel electrophoresis, HPLC, and MALDI mass spectroscopy. The amino- and thiol-functionalized DNAs were conjugated with chromophores, and purification of these products was facilitated by use of reversed phase cartridges.

INTRODUCTION

The preparation of DNA containing unnatural 3'-terminal groups has become increasingly important in antisense applications (1) and for the attachment of reporter groups (2, 3). A variety of synthetic methods have been developed to meet these needs (4–8). We present a simple and yet general way to obtain such important materials.

Our work is based on an earlier contribution by Petrie et al. (9) in which a phthalimide-based linker, prepared and immobilized on controlled pore glass (CPG) in four steps, was used to prepare 3'-aminoalkyl phosphate functionalized oligonucleotides. A functionally analogous structure 4 may be prepared in two steps by treating aminopropyl CPG with trimellitic anhydride chloride 1, followed by reaction with 6-amino-1-hexanol (Figure 1). Automated DNA synthesis, followed by basic workup, gave the desired 3'-(6-amino)hexanol 1-phosphorylated oligonucleotides. Furthermore, the immobilized anhydride support 2 could be reacted with other nucleophiles. 1,3-Propanediol or 6-(4,4'-dimethoxytrityl)oxy-1-thiohexane gave the immobilized ester 3 and the thioester 5, respectively, which were then used in automated DNA synthesis to give 3'-hydroxyl or thioalkyl phosphate functionalized oligonucleotides.

MATERIALS AND METHODS

Aqueous ammonia, mercaptoethanol, Tris free base, and silver nitrate were of reagent grade from J. T. Baker; dichloromethane (DCM), pyridine, dimethylformamide (DMF), and acetonitrile were of Omnisolve grade from VWR. *N*-Methylimidazole, 6-amino-1-hexanol, 1,3-propanediol, triethylamine (TEA), dithiothreitol, Tris-HCl, and trimellitic anhydride chloride were from Aldrich. 4,4'-Dimethoxytrityl chloride was obtained from Chem Impex and fluorescein-5-maleimide from Pierce. Aminopropyl- and nucleoside-derivatized 1000 Å CPG and 5,6-carboxy-fluorescein succinimide ester were from Biosearch Technologies, Inc. MALDI mass spectroscopy was performed

by the University of Michigan Protein and Carbohydrate Structure Facility.

Synthesis of the Supports. 3-*N*-(1,3,4-Trimellityl-3,4-anhydride) Aminopropylsilane, 2. Aminopropyl CPG (5 g) was placed in a 125 mL Erlenmeyer flask with stopper. A solution of trimellitic anhydride chloride 1 (1 g) in a mixture of pyridine (10 mL) and methylene chloride (40 mL) was added, and the mixture was swirled every 10 min for 1 h. The CPG was poured into a sintered glass funnel and washed with methylene chloride (3 × 50 mL) and acetonitrile (3 × 50 mL). The support was dried *in vacuo* and tested for the presence of amino groups with a Kaiser test (10) and found to be negative.

1-DMT-*O*-dihydroxypropyl-3-*O*-(4' or 5'-trimellityl)-1'-*N*-trimellityl)aminopropylsilane, 3. Support 2 (2 g) was treated with a solution of 1,3-propanediol (1 mL) and *N*-methylimidazole (0.5 mL) in DMF (10 mL) for 3 h. The support was washed and dried as above and then slurried in dry pyridine (100 mL); DMT chloride (1 g) was then added. The mixture was shaken periodically, then allowed to sit overnight, and was washed and dried as previously (loading: 36 μmol/g by colorimetric DMT loading assay).

1-DMT-*O*-aminohydroxyhexan-6-*N*-(4' or 5'-trimellityl)-1'-*N*-trimellityl)aminopropylsilane, 4. Support 2 (2 g) was treated with a solution of 6-amino-1-hexanol (2 g) in DMF (10 mL) for 3 h. The support was washed and dried as previously. The material was reacted with DMT chloride as described above for 3, giving a loading of 76 μmol/g.

6-DMT-*O*-thiohydroxyhexan-1-*S*-(4' or 5'-trimellityl)-1'-*N*-trimellityl)aminopropylsilane, 5. Support 2 (2 g) was treated with a solution of 6-mercapto-1-*O*-DMT-hexane (1 g, ref 11) with 1 mL of TEA in DMF (10 mL) for 3 h. The support was washed as for 3 and dried to give a loading of 31 μmol/g.

Mononucleotide Synthesis. Automated DNA synthesis was performed on a Biosearch 8750 DNA synthesizer, with Beckman (Fullerton) amidites. A 0.4 M solution of 5-(ethylthio)-1*H*-tetrazole (AIC Corp, Strathmore) in acetonitrile was used as the amidite activator, with all other reagents the same as those previously described (12). 6-(4-Methoxytrityl)amino-1-*O*-(diisopropylaminocynoethyl)hexyl phosphoramidite was prepared according to the procedure of Sinha and Cook (13);

* Author to whom correspondence should be addressed [telephone (415) 479-8710; fax (415) 479-1606; e-mail BTIDNA@aol.com].

© Abstract published in *Advance ACS Abstracts*, February 15, 1997.

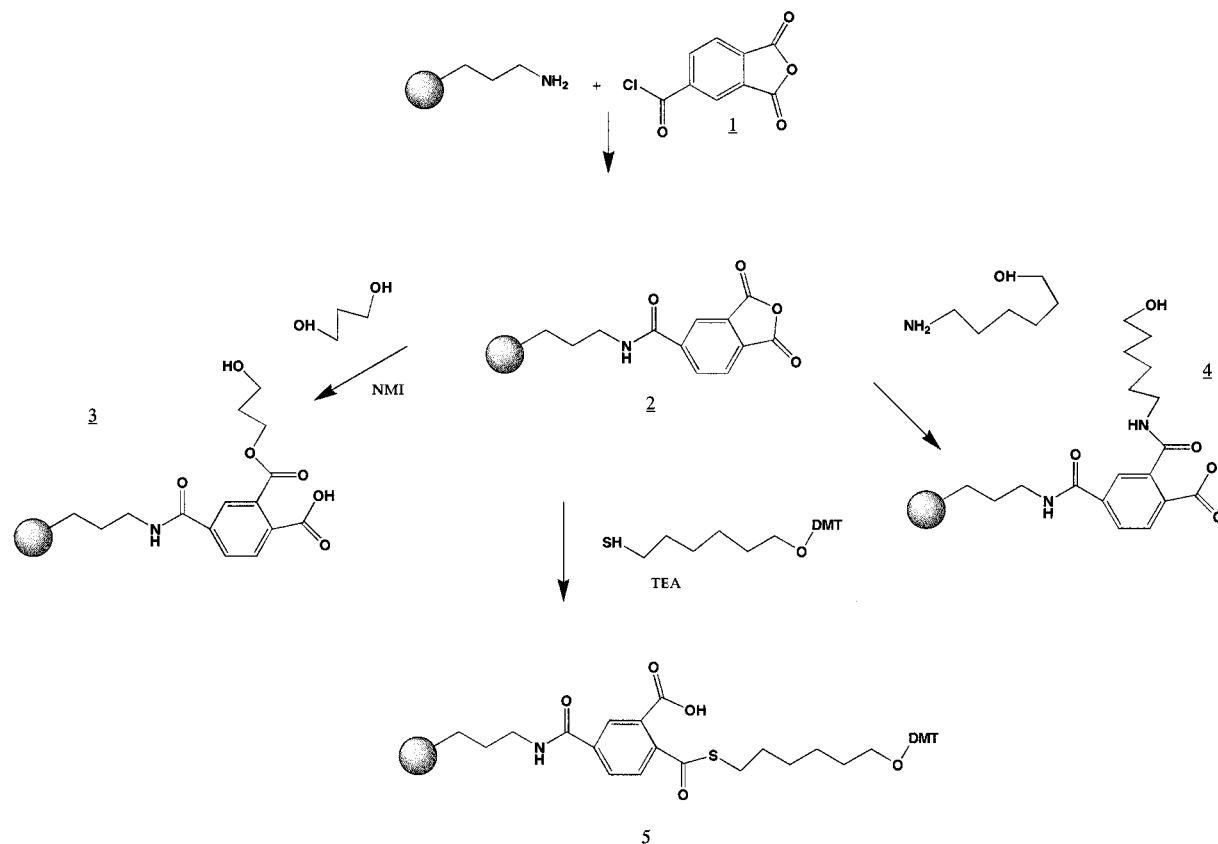


Figure 1. Synthesis of 3–5 from 2.

6-(trityl)thio-1-*O*-(diisopropylaminocyanoethyl)hexyl phosphoramidite was made according to the procedure of Connolly and Rider (14), and 3-*O*-(4,4'-dimethoxytrityl)-1-*O*-(diisopropylaminocyanoethyl)propyl phosphoramidite was synthesized with protocols described in Jaschke et al. (15). 5'-Succinoylnucleoside CPG (ILO CPG, inverse linkage CPG) was prepared as in Ortiago et al. (16). Control mononucleotide synthesis by conjugation of reporter group amidites onto ILO CPG was accomplished by semimanual methods as follows: The column containing the support was detritylated on the DNA synthesizer and thoroughly rinsed with dry CH_3CN . The liquid was removed from the column by an argon drying instrument step. The column was removed from the instrument. For a 200 nmol synthesis, the reporter group amidite solution (200 μL of a 100 mg/mL, dissolved under argon) was taken up in a 1 mL tuberculin syringe (luer slip-tip) and 200 μL of 0.31 M 5-(ethylthio)-1*H*-tetrazole in CH_3CN in a second syringe. One syringe was inserted into each end of the column, and the syringe containing the amidite was discharged into the column. Excess volume was allowed to enter the syringe containing the 5-(ethylthio)-1*H*-tetrazole solution. Next, the other syringe was discharged, while the first syringe was allowed to fill with the mixed fluid. The process was repeated (three times), and the column was allowed to stand for 2 min. The syringes were removed, the column was placed back on the instrument, and oxidation and washing steps were performed. For the DMT and MMT group containing products, deprotection was accomplished on the instrument with 3% dichloroacetic acid in DCM. The column was then rinsed with CH_3CN on the instrument, the support was removed from the column and then treated with concentrated ammonia in a sealed tube for 24 h at 55 $^\circ\text{C}$. The tube was cooled and the ammonia solution evaporated for further analysis. For the thiotrityl sample, 1 M AgNO_3 (500 μL) was pushed slowly through the

column over 10 min and then washed by water (3 mL). Next, 5% (v:v) aqueous mercaptoethanol (500 μL) was applied for a duration of 10 min, followed by washing with water (3 mL). The thiol mononucleotide was then ammonia cleaved as above. For the test mononucleotides, 200 nmol DNA synthesis columns packed with either 3, 4, or 5 were coupled with T amidite with standard automated DNA synthesis protocols and reagents as mentioned above. The DMT group was removed, and the CPG was treated with ammonia and heat for 18–24 h. For the thiohexyl test mononucleotide, DTT (2–3 mg) was added to the ammonia solution before the onset of heating. The samples were then dried under vacuum and redissolved in 20% acetonitrile in water for subsequent analysis.

3'-Modified Oligonucleotide Synthesis. DNA synthesis columns were packed with either 3, 4, or 5, and the DNA fragments (see Table 1) were synthesized with standard protocols and reagents. The 5'-DMT groups were left attached, and for the 3'-aminoethyl- or 3'-hydroxypropyl-derivatized fragments 18–24 h of 55 $^\circ\text{C}$ heating in concentrated aqueous ammonia (1 mL) was used to cleave the DNA from the support. For the 3'-thiohexyl DNA, 2–3 mg of DTT was added to the ammonia solution before the onset of heating. The samples were cooled, and the DNA was isolated with a reversed phase cartridge and protocols (17). The DNA was evaporated for analysis or conjugation.

Reversed Phase HPLC Conditions. The dried sample was dissolved in 20% acetonitrile in water, and 2–20 μL of this solution, depending on the concentration, was injected onto a C_{18} 3.3 cm cartridge (PE-ABI, 0258-0164) with detection at 260 nm, eluted at 1 mL/min with a gradient of 100% A (0.1 N ammonium acetate) for 2 min, 100% A to 90% A (B was 100% acetonitrile) over 10 min, then 90% A to 50% A over 10 min, and then back to 100% A over 1 min.

Table 1. Yields and Purity of 3'-Fluorescein Conjugates

sequence ^a	synthesis scale (nM)	yield ^b (ODs)	% conv ^c	ODs isolated ^d	HPLC purity ^e (%)
14-merNH ₂	200	18.7	75	3.0	95
14-merNH ₂	1000	43.9	>99	22.0	85 ^f
16-merNH ₂	1000	47.5	95	16.0	86
19-merNH ₂	1000	68.0	>99	16.6	84 ^f
20-merNH ₂	1000	64.3	93	22.5	94
14-merSH	1000	30.0	39		
16-merSH	1000	25.5	19	8.2	49
19-merSH	1000	34.0	49		
20-merSH	1000	24.0	24	16.9	34

^a 14-mer sequence = 5'-dCCGAGTACTAATCA-3'; 16-mer = 5'-dATACTTATCATGAGCC-3'; 19-mer = T₁₉; 20-mer = 5'-dTCCAGTCATCGAGGTCATA-3'. ^b Yield of unconjugated DNA obtained after first Micropure Cartridge purification. ^c HPLC examination of size exclusion isolated material, after fluorescein conjugation. ^d Yield of fluorescein conjugate purified by Micropure Cartridge. ^e Purity of isolated probe, by HPLC. ^f Modified final purification: loaded onto the reversed phase cartridge in 3% aqueous ammonia, product eluted with 28% aqueous ammonia.

Anion Exchange HPLC. The dried sample was dissolved in 20% acetonitrile in water, and 2–20 μ L of this solution, depending on the concentration, was injected onto a 16 \times 40 mm Shodex DEAE 420-N 4 cM column (Phenomenex) eluted with a gradient to 100% B over 20 min. Buffer A was 0.025 M Tris-HCl, 0.01 M Tris; buffer B was A plus 1.0 M NaCl.

Fluorescein Conjugation Studies. For the 3'-amino-hexyl-modified DNA, 5,6-carboxyfluorescein succinimide ester (1 mg/10 ODs of DNA) was dissolved in DMSO (100 μ L) and added to a 2 mL screw cap polyethylene tube containing the purified DNA, followed by an aqueous solution 1 M in Na₂CO₃ and 1 M in NaHCO₃ (500 μ L). The tube was sealed and allowed to stand for 18–24 h at room temperature in the dark. The liquid was evaporated under vacuum, and the residue was dissolved in 2 mL of 0.05 M NH₄OAc in HPLC grade water. The solution was applied to a 1 \times 20 cm Sephadex G-25 column (Sigma catalog no. G-25-80) packed and eluted with 0.05 M NH₄OAc in HPLC grade water. The tagged DNA eluted rapidly as a green solution after 5–10 mL of liquid had eluted, and this fraction was collected and reduced to a solid under vacuum. The solid was dissolved in 15% aqueous ammonia (1 mL) and applied to a reversed phase cartridge (17), which had been pre-equilibrated with acetonitrile (4 mL) followed by 1 M triethylamine acetate (4 mL). The solution of the conjugate was reloaded twice and washed with 3% aqueous ammonia (4 mL) followed by water (4 mL). Some faint green color was sometimes observed to elute during the aqueous ammonia washes. Next, the column was washed with 20% acetonitrile in water (3 mL), and the strongly green liquid that emerged was collected and evaporated under vacuum to a solid for further analysis.

For the 3'-thiohexyl-modified DNA, 2 mg of fluorescein-5-maleimide (2 mg/10 ODs of DNA to be conjugated) was dissolved in DMF (100 μ L) and added to a 2 mL screw cap polyethylene tube containing the purified thiohexyl DNA isolated as above. Next, 50 mM sodium phosphate/150 mM sodium chloride, pH 7.2, buffer (500 μ L) was added. The tube was sealed, mixed, and allowed to stand for 18–24 h at room temperature in the dark. The liquid was evaporated under vacuum, and the residue was processed further as above.

RESULTS AND DISCUSSION

The three new supports (3–5) were synthesized from common intermediate **2**, obtained by the reaction of trimellitic anhydride chloride and aminopropyl CPG.

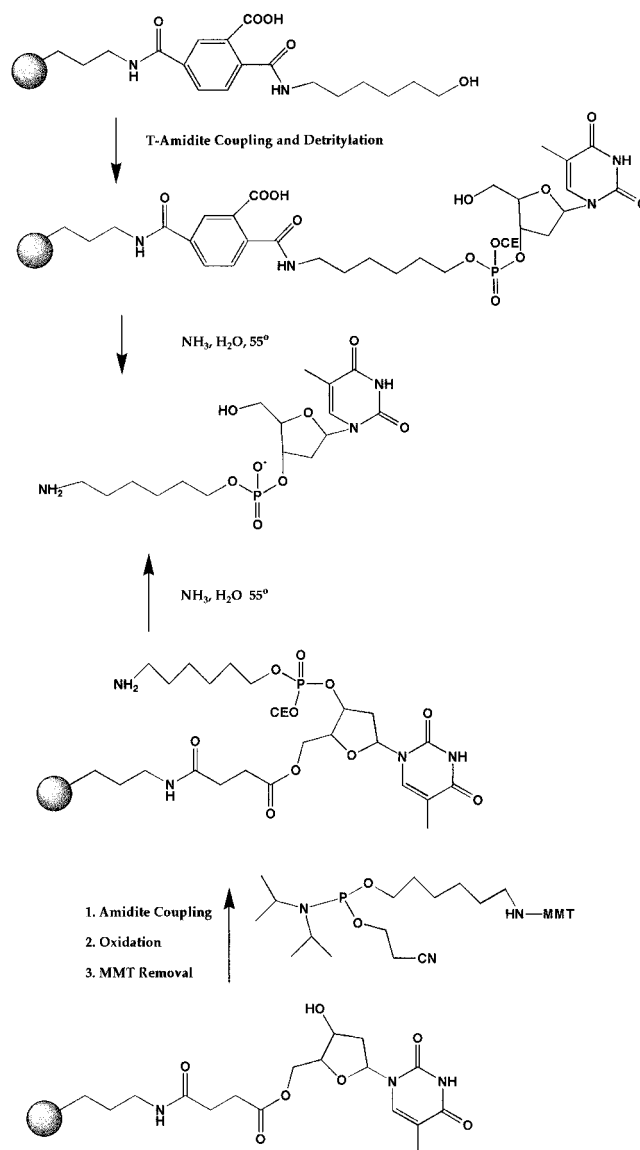


Figure 2. Synthesis of 3'-amino-hexyl phosphate functionalized T from two different solid supports.

Solutions of bifunctional linkers were added, and subsequent washing gave the hydroxyl-functionalized supports (Figure 1). In the case of the propanediol- and amino-hexanol-functionalized materials, the supports could be synthesized without protection of the additional hydroxyl group. A DMT group was added to these to gauge the loading during automated DNA synthesis. It was found necessary to protect the hydroxy groups of heterobifunctional spacers containing additional thiol functionality; otherwise, heterogeneous products were obtained after DNA synthesis. Insufficient differential reactivity between the OH and SH groups toward the immobilized anhydride most likely produces a mixture of both ester and thioester linked supports, the former giving rise to an undesired product.

To confirm the identity of the 3'-terminal functionality obtained from the use of 3–5, control mononucleotides were prepared by adding amidites containing amino-hexyl (13), thiohexyl (14), and hydroxypropyl (15) functional groups to a 3'-hydroxyl nucleoside immobilized through its 5'-hydroxyl group. These were then compared to the analogous structures prepared by coupling a single phosphoramidite nucleotide to 3–5. The experiment is shown schematically for the amino-hexyl case in Figure 2. After aqueous ammonia workup, the control mono-

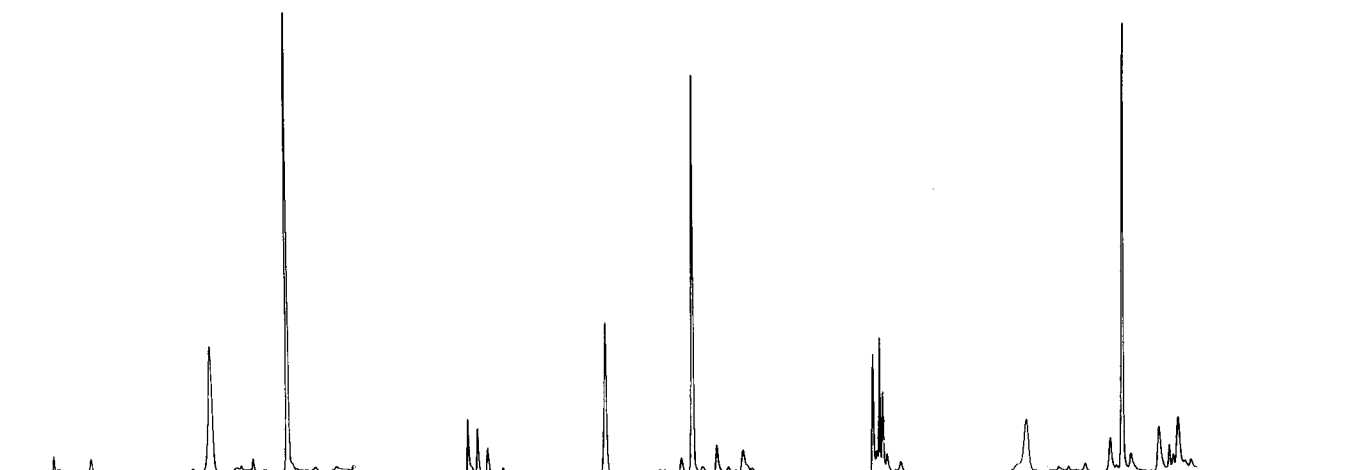
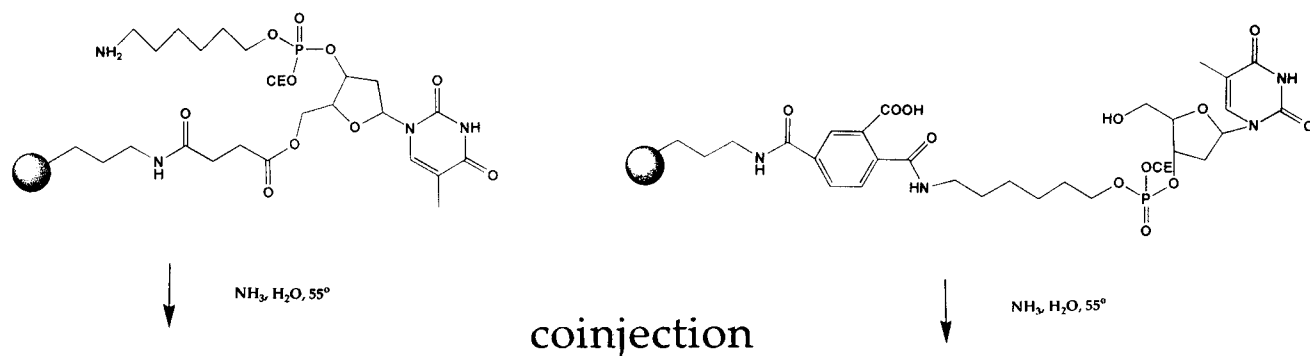


Figure 3. Reversed phase HPLC analysis of products made in Figure 2. The peak at about 5 min is T nucleoside; the other minor peaks were not identified.

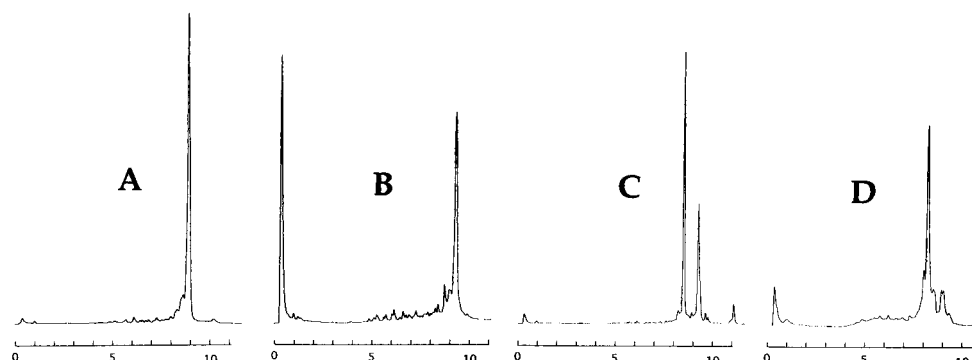


Figure 4. Anion exchange HPLC of 14-mers with 3' modification, after reversed phase cartridge purification: (A) 14-mer with 3'-hydroxypropyl phosphate; (B) 14-mer with 3'-thiohexyl phosphate; (C) 14-mer with 3'-aminoethyl phosphate and 24 h of ammoniolysis; (D) same as (C) with 8 days additional heating in concentrated ammonia.

nucleotides were found to be identical to those produced from **3–5**, according to coelution of the major products on reversed phase HPLC (Figure 3 shows the result with the aminoethyl example). DTT was added to the thiol-functionalized product to curtail oxidative dimerization.

Several longer DNA fragments were then synthesized on the new supports (Table 1). A 14-mer 5'-dCCGAG-TACTATTCA-3' was synthesized on **3**, **4**, and **5**, as well as with conventional dA-derivatized CPG. Overall coupling yields were similar in the four cases, and no evidence was observed for instability of the linkages during synthesis or problems arising from the pendant unblocked carboxyl groups. The DNA was cleaved from the CPG with aqueous ammonia and heating and purified on a reversed phase cartridge (17). Yields of purified DNA compared favorably with the amount normally obtained for cartridge purification at these two synthesis scales (see Table 1). MALDI mass spectroscopy (Table 2) showed the correct increase in mass for the 3'-modified 14-mers when compared to the spectrum of the unmodi-

Table 2. Observed MALDI Masses of Unmodified and 3'-Modified DNA^a

3' terminus	mass	calcd diff	found diff
unmodified	4217.2		
hydroxypropyl	4357.3	138.1	140.1
aminoethyl	4400.0	179.2	182.8
thiohexyl	4524.9 ^b	195.3	193.7

^a Experimental error is ± 4.2 amu. ^b M/e-TFA.

fied 14-mer. Anion exchange HPLC of the three analogs (Figure 4) showed that good quality products were obtained in the case of the 3'-thiohexyl and 3'-propanol examples. For the 3'-aminoethyl-derivatized 14-mer, a substantial later eluting contaminant (20–30%) was present (Figure 4C). This could be somewhat diminished by prolonged heating with ammonia (Figure 4D shows the ammonia/DNA solution after 8 days of additional heating, after CPG removal), suggesting that this contaminant is unhydrolyzed amide with the mellitic acid linker. A recent paper (18) describes difficulty in removal

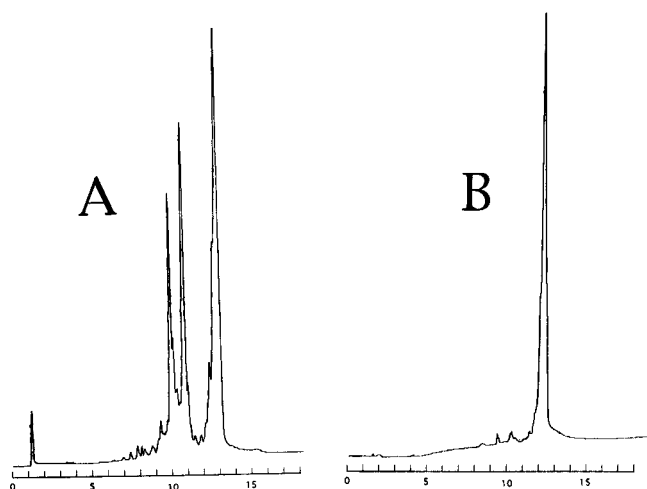


Figure 5. (A) Anion exchange HPLC of crude 3'-aminoethyl 14-mer conjugate with 5,6-carboxyfluorescein ONSu active ester. (B) purified compound isolated using reversed phase cartridge. A Gen-Pak Fax anion exchange HPLC column (Waters) was used instead of the Shodex column.

of phthaloyl groups from alkylamines by basic hydrolysis, in accord with this observation. However, the loss of material due to this side reaction was compensated by the yield of DNA obtained because of the high loading of the support. The later eluting contaminant did not interfere in subsequent reactions involving conjugation of the 3'-aminoethyl-functionalized material and was separated from the desired fluorescein conjugate with a reversed phase cartridge procedure (see below).

Our findings contrast with an earlier study implying that final products free of contaminants were obtained when a similar structure was used for DNA synthesis followed by hydrolysis with aqueous ammonia and heating (9). The later eluting impurity generated when 3'-amino-linked DNA was synthesized on **4** could be suppressed somewhat by using 1:1 methylamine/concentrated ammonia for 24 h at 60 °C as the basic workup step (data not shown). The use of methylamine as a component in the hydrolysis step necessitates the use of *N*⁴-acetyl dC phosphoramidite (in lieu of *N*⁴-benzoyl dC) during synthesis, because of a side reaction (19). Since the product still contains the unhydrolyzed impurity, this modification will not be worthwhile for most applications.

Another possibility is that the later eluting contaminant may result from reverse addition of the 6-amino-1-hexanol to the anhydride CPG **2**. DNA synthesized on this species would have a terminal hydroxyl instead of an amine and, hence, an additional net negative charge, eluting later in anion exchange HPLC. This was ruled out by the synthesis of **4** using 6-amino-1-*O*-DMT hexanol (20) and subsequent DNA synthesis followed by basic hydrolysis. The products obtained from **4** synthesized in this way had the same amount of the later eluting contaminant (data not shown).

The importance of hydroxylalkyl-functionalized DNA in antisense work is discussed in ref 15. The use of 3'-amino- and thiol-functionalized DNA in fluorescent dye conjugation was accomplished using variations on published protocols (21, 22). For the above 3'-amino-linked 14-mer DNA fragment made at a 200 nmol scale, about 75% conversion was obtained with 50 equiv of a mixture of fluorescein 5- and 6-carboxyhydroxysuccinimide active esters (see Figure 5A; Figure 4C shows the unreacted amino-functionalized oligonucleotide). This product could be purified to ca. 95% purity by a simple reversed phase cartridge method (see Figure 5B). Better amine conjugation efficiency (>90%) was obtained at larger synthesis

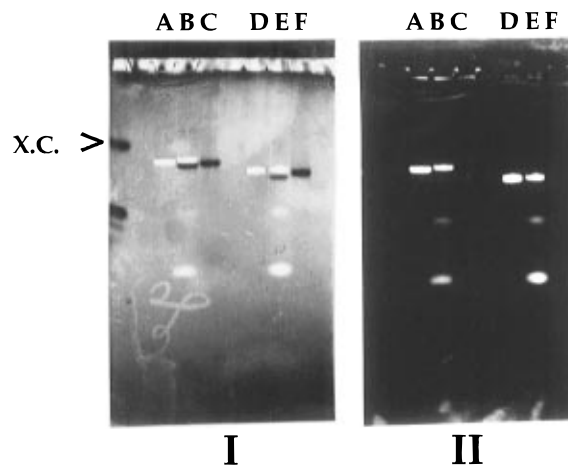


Figure 6. 20% PAGE of purified dye conjugated DNA and unconjugated fragments: (I) illumination with 254 nm UV and fluorescent backing; (II) illumination with 312 nm UV and black backing; X.C., xylene cyanol; (lane A) fluorescein-conjugated 3'-aminoethyl 20-mer; (lane B) fluorescein-conjugated 3'-thiohexyl 20-mer; (lane C) 3'-aminoethyl 20-mer; (lane D) fluorescein-conjugated 3'-aminoethyl 16-mer; (lane E) fluorescein-conjugated 3'-thiohexyl 16-mer; (lane F) 3'-aminoethyl 16-mer.

scales, perhaps because of concentration effects. Table 1 shows results with 16-mer and 20-mer examples at the 1 μ mol scale. The corresponding 3'-thiol-modified DNA gave lower efficiencies when conjugated with 100 equiv of fluorescein-5-maleimide (Table 1, 19–49% vs 75–>99%). Since very little dimerization of the thiol-containing DNA was observed during the reactions, the cause of these lower yields remains unclear. They may be due to solubility problems or the quality of the commercial fluorescein-5-maleimide used. Cartridge purification of the thiol-linked conjugates was also less effective, perhaps due to the lower polarity of the thiohexyl 3' moiety compared to the corresponding aminoethyl, leading to stronger binding of the starting material, the thiohexyl DNA, to the stationary phase and hence less effective purification. A 20% cross-linked PAGE gel of 3'-conjugated DNA fragments, made with both 3'-terminal modifications, showed strongly fluorescent products with about the same mobility on the gel as the underivatized DNA (Figure 6). The gel lanes of the thiol-linked conjugates contain some underivatized material, in accord with HPLC analysis.

CONCLUSION

An immobilized anhydride intermediate has been used in the synthesis of solid supports that provide 3'-modified DNA containing 3'-alkyl OH, SH, and NH₂ end groups. The structural integrity and utility of the 3'-modifications have been demonstrated. The thioester linkage of **5** has been shown to survive the conditions of automated DNA synthesis and may be useful in other systems where a terminal thiol group is desired after aqueous basic workup. Simple methods for isolating 3'-fluorescein conjugates with the SH- and NH₂-modified DNA have been developed.

In principle, the method is compatible with other homo- or heterobifunctional linkages, provided transient protection is used or the functional groups have sufficient differential reactivity. Also, only a single support is required for the generation of any single class of 3'-modified nucleotide. This new method is, therefore, more versatile and more easily implemented than many of the 3' derivatization methods previously presented. Our new linker methods may also be useful in other areas of solid

phase supported chemistry, such as peptide or combinatorial library synthesis.

LITERATURE CITED

- (1) Zerial, A., Thuong, N. T., and Helene, C. (1987) Selective Inhibition of the Cytopathic Effect of Type A Influenza Viruses by Oligonucleotides Linked to an Intercalating Agent. *Nucleic Acids Res.* **15**, 9909–9919.
- (2) Goodchild, J. (1990) Conjugates of Oligonucleotides and Modified Oligonucleotides: A Review of their Synthesis and Properties. *Bioconjugate Chem.* **1**, 165–187.
- (3) Tyagi, S., and Kramer, F. R. (1996) Molecular Beacons: Probes that Fluoresce upon Hybridization. *Nat. Biotechnol.* **14**, 303–308.
- (4) Nelson, P., Frye, R. A., and Lieu, E. (1989) Bifunctional oligonucleotide probes synthesized using a novel CPG support are able to detect single base pair mutations. *Nucleic Acids Res.* **17**, 7187–7194.
- (5) Asseline, U., and Thuong, N. T. (1990) New Solid Phase for Automated Synthesis of Oligonucleotides containing an aminoalkyl linker at their 3'-end. *Tetrahedron Lett.* **31**, 81–84.
- (6) Zuckermann, R., Corey, C., and Shultz, P. (1987) Efficient methods for attachment of thiol specific probes to the 3'-ends of synthetic oligodeoxyribonucleotides. *Nucleic Acids Res.* **15**, 5305–5321.
- (7) Hovinen, J., Guzaev, A., Azhayav, A., and Lonnberg, H. (1993) Synthesis of 3'-Functionalized Oligonucleotides on a Single Solid Support. *Tetrahedron Lett.* **34**, 8169–8172.
- (8) Gupta, K. C., Sharma, P., Sathyanarayana, S. and Kumar, P. (1990) A Universal Solid Support for the Synthesis of 3'-Thiol Group Containing Oligonucleotides. *Tetrahedron Lett.* **31**, 2471–2474.
- (9) Petrie, C. R., Reed, M. W., Adams, D., and Meyer, R. B. (1992) An Improved CPG Support for the Synthesis of 3'-Amine-Tailed Oligonucleotides. *Bioconjugate Chem.* **3**, 85–87.
- (10) Stewart, J. M., and Young, J. D. (1984) In *Solid Phase Peptide Synthesis*, p 105, Pierce Chemical Co., Rockford, IL.
- (11) Gupta, K. C., Sharma, P., Kumar, P., and Sathyanarayana, S. (1991) A general method for the synthesis of 3'-sulfhydryl and phosphate group containing oligonucleotides. *Nucleic Acids Res.* **19**, 3019–3025.
- (12) Wang, Y. Y., Lyttle, M. H., and Borer, P. N. (1990) Enzymatic and NMR analysis of oligoribonucleotides synthesized with 2'-*tert*-butyldimethylsilyl protected cyanoethylphosphoramidite monomers. *Nucleic Acids Res.* **18**, 3347–3352.
- (13) Sinha, N. D., and Cook, R. M. (1988) The preparation and application of functionalised synthetic oligonucleotides: III. Use of H-phosphonate derivatives of protected amino-hexanol and mercapto-propanol or -hexanol. *Nucleic Acids Res.* **16**, 2659–2669.
- (14) Connolly, B. A., and Rider, P. (1985) Chemical synthesis of oligonucleotides containing a free sulphhydryl group and subsequent attachment of thiol specific probes. *Nucleic Acids Res.* **13**, 4485–4502.
- (15) Jaschke, A., Furste, J. P., Cech, D., and Erdmann, V. A. (1993) Automated Incorporation of Polyethylene Glycol into Synthetic Oligonucleotides. *Tetrahedron Lett.* **34**, 301–304.
- (16) Ortiago, J., Rosch, H., Selter, H., Fröhlich, A., Lorenz, A., Montenarh, M., and Seliger, H. (1992) Antisense Effect of Oligonucleotides with Inverted Terminal Internucleotidic Linkages: A Minimal Modification Protecting against Nucleolytic Degradation. *Antisense Res. Dev.* **2**, 129–146.
- (17) Biosearch Technologies, Inc., reversed phase DNA purification cartridge and protocols.
- (18) Kahn, M. N. (1996) Suggested Improvement in the Ing-Manske Procedure and Gabriel Synthesis of Primary Amines: Kinetic Study on Alkylamine Hydrolysis of *N*-Phthaloylglycine and Acid Hydrolysis of *N*-(α -Carboxybenzoyl)glycine in Aqueous Organic Solvents. *J. Org. Chem.* **61**, 8063–8068.
- (19) Reddy, M. P., Hanna, N. D., and Farouqi, F. (1994) Fast Cleavage and deprotection of oligonucleotides. *Tetrahedron Lett.* **35**, 4311–4314.
- (20) 6-*N*-Fmoc-1-*O*-DMT hexanol was prepared with methods similar to those in: Vu, H., Joyce, N., Reiger, M., Walker, D., Goldknopf, I., Hill, T. S., Jayaraman, K., and Mulvey, D. (1995) Use of Phthaloyl Protecting Group for the Automated Synthesis of 3'-[(hydroxypropyl)amino] and 3'-[(hydroxypropyl)triglycyl] oligonucleotide Conjugates. *Bioconjugate Chem.* **6**, 599–608. The Fmoc group was removed with ammonia before addition of the resulting 6-amino-1-*O*-DMT hexanol to **2**.
- (21) Khanna, P. L., and Ullman, E. F. (1980) 4',5'-Dimethoxy-6-carboxyfluorescein: A Novel Dipole-Dipole coupled fluorescence energy transfer acceptor useful for fluorescence immunoassays. *Anal. Biochem.* **108**, 156.
- (22) Curtis, S. K., and Cowden, R. R. (1980) Demonstration of sulfhydryl and disulfide groups by a fluorescent maleimide procedure. *Histochemistry* **68**, 23–28.

BC970010Y

Efficient Functionalization of 2',5'-Oligoadenyates with Sulfur

Krystyna Lesiak[†] and Paul F. Torrence*

Section on Biomedical Chemistry, Laboratory of Medicinal Chemistry,
National Institute of Diabetes and Digestive and Kidney Diseases, National Institutes of Health,
Bethesda, Maryland 20892. Received November 18, 1996[©]

To derivatize the 2'-terminus of 2',5'-oligoadenyates with a thiol group, the reaction of periodate-oxidized nucleotide and 2',5'-oligonucleotide with aminothiols was explored. Two separate synthetic approaches were employed, both of which relied upon the use of S-protected thiols. In one approach, 5'AMP was oxidized with sodium periodate to dialdehyde, which was reacted with cystamine hydrochloride. Sodium cyanoborohydride reduction of the unisolated intermediate ainal gave compound **4**. The second approach involved reaction of *S*-(2-tetrahydropyranyl)cysteamine with the dialdehyde obtained by periodate oxidation of 5'AMP to yield, after reduction with Na(CN)BH₃, the S-protected adduct **3**. Intermediate **3** could be oxidized with aqueous iodine to give disulfide **4**. Disulfide **4**, obtained by either of the above routes, was reduced with dithiothreitol (DTT) to the thiol **5**. This same reaction sequence was applied to 2–5A tetramer monophosphate, p5'A2'[p5'A2']₂p5'A (**6a**), to give via **6b** the 2'-terminal-modified derivative **6c**. Aqueous iodine oxidation of **6c** provided the disulfide **7**, which reacted with DTT to give quantitative conversion to product, the free thiol **8**. Both the disulfide **7** and the *S*-tetrahydropyranyl-protected derivative (**6c**) were bound effectively to the 2–5A-dependent RNase L of mouse L cells with IC₅₀ values of 1×10^{-9} M for **7** and 8×10^{-10} M for **6c**, not significantly different from the corresponding value for the parent unmodified 2–5A (**6a**) itself.

INTRODUCTION

Conjugates of 2',5'-oligoadenyates (2–5A's) (**1**, **2**) with small molecules and macromolecules, including carbohydrates, proteins, and nucleic acids, are of growing importance for affinity purification (**3**), affinity labeling (**4**), and targeted degradation of specific RNAs (**5–8**). Thiol-modified oligonucleotides present several conjugate construction advantages including sulfur's enhanced nucleophilicity, ease of disulfide-based conjugation, and the ready reversibility of the latter. Approaches that generally have been used for derivatizations with thiols have included direct synthesis from mononucleotidic precursors (**9–12**), including introduction of the modification into the starting nucleotide affixed to the solid support matrix (**13**). Since these latter procedures are not applicable to preformed nucleic acids, Chu and Orgel (**14**) exploited 5'-derivatization via 5'-phosphoramidate formation with cysteamine or cystamine. Such 5'-derivatization is not possible in the case of 2–5A since the 5'-terminus must bear a free phosphate or polyphosphate for maximum interaction with a key enzyme of the 2–5A system, the RNase L (**1**, **2**). Soukup and associates (**15**) employed phosphoramidite methodology to synthesize an oligonucleotide bearing a 3'-terminal primary amino group which was subsequently reacted with sulfosuccinimidyl-2-(biotinamidoethyl)-1,3-dithiopropionate. This conjugation product bore a disulfide bond in the linker moiety between the oligo and the biotin. Reduction provided a means of cleaving the biotin group from the oligonucleotide domain. Again, however, this approach would not be compatible with the need to derivatize a preformed oligonucleotide.

A valuable route to oligoribonucleotide 3'-modification involves periodate oxidization of the 3'-ribonucleotide to a dialdehyde, which is reacted with an amine or amino acid to yield a Schiff base, reduction of which by borohydride gives a product in which the 3'-terminal ribose is transformed to an N-substituted morpholine (**16–21**). We have explored this theme to functionalize 2',5'-oligoadenyate with a 2'-terminal thiol or a disulfide moiety.

EXPERIMENTAL PROCEDURES

Chemicals. Adenosine 5'-monophosphate, cysteamine (2-aminoethanethiol) hydrochloride, and cystamine [2,2'-dithiobis(ethylamine)] hydrochloride were from Aldrich (Milwaukee, WI). Fluka was the source for 3,4-dihydro-2H-pyran, while sodium periodate was from Sigma (St. Louis, MO), and 1,4-dithiothreitol was from Schwarz-Mann (Orangeburg, NY). 2',5'-Oligoadenyate trimer 5'-monophosphate was synthesized according to the procedure of Sawai (**22**) and purified by reversed-phase HPLC (Zorbax ODS).

HPLC. Analytical HPLC was carried out on a Zorbax ODS column (9.4 mm × 25 cm) using a linear gradient of 0–100% solvent B in buffer A, where A was 0.05 M ammonium phosphate of pH 7.0 and B was MeOH/H₂O (1:1) and the flow rate was 2 mL/min. Detection was by UV.

Physical Measurements. Proton NMR spectra were recorded on a Varian 220 MHz or 300 MHz spectrometer. ¹³C NMR spectra were recorded with the latter instrument operating at 75.5 MHz. Ultraviolet spectra were obtained on a Hewlett-Packard 8450 UV–vis spectrophotometer. Chemical ionization mass spectra were obtained on a Finnegan Extrel 1015 with NH₃ as carrier gas. Obtaining the mass spectrum of compound **3** required its conversion first to the free acid (with Dowex 50[H⁺]) and then (after lypophilization) silylation by reaction with bis(triethylsilyl)acetamide in DMF.

Enzymatic Procedures. Digestions with bacteria alkaline phosphatase (*Escherichia coli*) and snake venom

* Address correspondence to this author at Bldg 8, Rm B2A02 [e-mail torrence@helix.nih.gov; telephone (301) 496-2653; fax (301) 402-0589].

[†] Present address: Codon Pharmaceuticals, Inc., 200 Perry Parkway, Gaithersburg, MD 20877.

[©] Abstract published in *Advance ACS Abstracts*, February 15, 1997.

phosphodiesterase (*Crotalus adamanteus*, Worthington) were performed as described previously (23). The preparation of mouse L cell extracts and the procedures and reagents for the radiobinding assay to RNase L were also as described in the literature (4–6, 21).

Synthesis of *S*-(2-Tetrahydropyranyl)cysteamine Hydrochloride. Cysteamine hydrochloride (2.0 g, 17.6 mmol) was made anhydrous by addition and evaporation with ethanol/toluene (2:1, 3 × 50 mL). The resulting solid was suspended in 3,4-dihydropyran (50 mL), and this mixture was refluxed for 1 h. After evaporation of dihydropyran, the residue was recrystallized twice from EtOAc/EtOH (5:1) to give 1.86 g (9.54 mmol, 53.4%) of *S*-(2-tetrahydropyranyl)cysteamine hydrochloride, mp 142–145 °C; mass spectrum, m/z 162 [(M + H)⁺]; ¹H NMR (CD₃OD) δ 1.6 and 1.9 (br m, 6, C-3, C-4, and C-5 of THP), 2.8–3.1 (m, 2, cysteamine CH₂–N), 3.1–3.3 (m, 2H, cysteamine CH₂–S), 3.6 and 4.0 (br m, 1 each, THP C-6 H's), 5.9 (m, 1, C-2 H). Anal. Calcd for C₇H₁₆NOSCl: C, 42.52; H, 8.17; N, 7.08; Cl, 17.93; S, 16.22. Found: C, 42.34; H, 8.18; N, 7.14; Cl, 18.04; S, 16.52.

Preparation of 6'-Monophosphoryl-[3'-aza-3'-(β-*S*-tetrahydropyranylthioethylene)-1',2,3,4-tetradexopyranosyl]-adenine (3). Sodium periodate (0.5 mL of 0.1 M in H₂O, 0.05 mmol) was added in one portion to a pH 6.0 solution of 5'AMP (Na salt, 0.5 mL of 0.1 M in H₂O, 0.05 mmol), and the resulting mixture was kept in the dark at 0 °C for 30 min. To destroy unreacted periodate, ethylene glycol (200 mL of 1 M aqueous solution, 0.2 mmol) then was added, and the resultant solution maintained at 0 °C for an additional 10 min. *S*-(2-Tetrahydropyranyl)cysteamine hydrochloride (0.5 mL of 0.5 M solution in H₂O, 0.25 mmol) was added, and the pH of the reaction mixture was adjusted to 8.5–9.0 with 1 M NaOH. The resulting mixture was maintained at 0 °C for 30 min, and then sodium cyanoborohydride (total of 0.1 mmol, 0.5 mL of 0.5 M in water) was added. This reaction mixture was kept at 0 °C for 1 h, during which time the pH was maintained at 7.0 by the addition of 10% HOAc. The excess of cyanoborohydride was removed by treatment with acetone at pH 5 for 1 h. (All procedures using cyanoborohydride were conducted in a chemical fume hood.) Finally, the reaction mixture was diluted 10-fold with water, and the diluted solution was applied to a DEAE-Sephadex A-25 column (HCO₃[−] form, 1 × 15 cm). Elution was accomplished with a linear gradient of 0.05–0.5 M triethylammonium bicarbonate (TEAB) (pH 7.0, total of 500 mL). Fractions (4 mL) were collected. The desired product was found in fractions 42–52 (buffer concentration approximately 0.2 M). TEAB was removed by repeated additions and evaporations of water. Product 3 was isolated as a sodium salt by precipitation from a solution of 1% sodium iodide in acetone. Compound 3 had an HPLC retention time of 44.5 min in the above specified system. The final yield was 610 A₂₅₉ units (0.04 mmol, 80% yield): mass spectrum, m/z 691 [(M + H)⁺, trisilylated 3] and 763 [(M + H)⁺, tetrasilylated 3]; ¹H NMR (D₂O) δ 1.51, 1.72, and 1.82 (br m, 3, 4, and 5 methylenes of THP group), 2.35 (t, 1, ²J_{H4'–H4''} = ³J_{H4'–H5'} = 11.4 Hz, H4'), 2.80 (br m, 5H, H2' and exocyclic CH₂–N and CH₂–S), 2.87 (d, 1 H, ²J_{H4'–H4''} = 11.2 Hz, H4''), 3.21 (d, 1, ²J_{H2'–H2''} = 10.3 Hz, H2'), 3.52 (m, 1, CH₂–O of THP), 3.89 (m, 2, H6' and H6''), 3.96 (m, 1, CH₂–O of THP), 4.16 (m, 1, H5'), 4.84 (m, 1, S–CH–O), 5.85 (dd, 1, ³J_{H1'–H2'} = 10.4 Hz, ³J_{H1'–H2''} < 2 Hz), 8.11 (s, 1, purine 2H), 8.24 (s, 1, purine 8H); ¹³C NMR (D₂O) δ 21.69 (C4 of THP), 24.92 (C-5 of THP), 26.12 (CH₂–S), 31.28 (C3 of THP), 52.35 (C-4'), 54.41 (C2'), 57.40 (CH₂–N of cysteamine), 64.80 (C6'), 66.19 (C6 of THP), 75.37 (C5', ³J = 8.0 Hz), 79.41 (C1'), 82.85

(C2, THP), 118.46 (adenine C5), 140.2 (adenine C8), 148.32 (adenine C4), 152.86 (adenine C2), 155.61 (adenine C6).

Bis[6'-monophosphoryl-3'-aza-1'-(9-adenyl)-1',2,3,4-tetradexopyranosyl-3'-β-ethylene] Disulfide (4). Compound 4 was obtained in the same way as compound 3 from 0.2 mmol of AMP 2',3'-dialdehyde (prepared as above) and 1 mmol of cystamine hydrochloride (2 mL, 0.5 M, adjusted to pH 9.0 with NaOH). The product was purified by means of DEAE-Sephadex A-25 (HCO₃[−] form, 1.6 × 25 cm column) chromatography employing a linear gradient of 0.05–0.6 M TEAB, pH 7.5. Fractions of 4 mL were collected with the product being eluted in fractions 94–114 (buffer concentration approximately 0.5 M). TEAB was removed by repeated addition and evaporation of water, and the sodium salt of 4 was isolated by precipitation from 1% NaI in acetone. The final yield was 630 A₂₅₉ units (0.042 mmol, 23%). Compound 4 had an HPLC retention time of 39.0 min: ¹H NMR (D₂O) δ 2.33 (t, 1, ²J_{H4'–H4''} = ³J_{H4'–H5'} = 11.4 Hz, H4'), 2.74 (t, 1, ²J_{H2'–H2''} = ³J_{H2'–H1'} = 10.7 Hz, H2'), 2.94 (m, 4, S–CH₂–CH₂–N), 3.01 (d, 1, ²J_{H4'–H4''} = 11.7 Hz, H4'), 3.20 (d, 1, ²J_{H2'–H2''} = 10.7 Hz, H2''), 3.85 (m, 2, H6' and H6''), 4.13 (m, 1, H5'), 5.72 (dd, 1, ³J_{H1'–H2'} = 8.3, ³J_{H1'–H2''} < 2 Hz, H1'), 8.02 (s, 1, adenine H2), 8.18 (s, 1, adenine H8); ¹³C NMR (D₂O) δ 34.20 (CH₂–S), 52.57 (C4'), 54.36 (C2'), 56.50 (CH₂–N), 64.57 (C6'), 75.46 (d, ³J = 8.0 Hz, C5'), 79.44 (C1'), 118.28 (adenine C5), 140.02 (adenine C8), 148.03 (adenine C4), 152.71 (adenine C2), 155.40 (adenine C6).

Oxidation of Compound 3 with Aqueous Iodine. The sodium salt of compound 3 (950 A₂₅₉ units, 0.6 mmol) was dissolved in H₂O (750 mL), and iodine (0.05 M in 0.05 M NaI) was added in 10 mL portions at 0 °C. The addition of iodine solution was continued until a light brown color persisted for 1–2 min. At this point, TLC revealed that the reaction was completed as judged by the disappearance of starting material.

The excess iodine was removed by evaporation *in vacuo* at 10–20 °C (until the light brown color disappeared). The remaining solution was diluted 10-fold with water and applied to a DEAE-Sephadex A-25 (HCO₃[−]) column (1 × 15 cm), and the column was eluted with a linear gradient of 0.05–0.45 M, pH 7.5, TEAB. Fractions of 4 mL were collected, and the desired product was found in fractions 81–102 (approximately 0.4 M TEAB). The yield of oxidized product was 510 A₂₅₉ units (0.31 mmol, 52%). The product was identical by both TLC and HPLC with the product of the reaction of oxidized AMP (2) with cysteamine, i.e., compound 4.

Reaction of Compound 4 with Dithiothreitol. An aqueous solution of dithiothreitol (DTT, 1 mL of 1 M, 1 mmol) was added to a solution of compound 4 (500 A₂₅₉ units, 0.32 mmol) in H₂O. After 10 min at 0 °C, HPLC analysis revealed the presence of two major compounds with retention times of 31.6 min (82%) and 33.7 min (13%), respectively. This mixture was applied to a DEAE-Sephadex A-25 column (1 × 15 cm, HCO₃[−] form) which was eluted with a linear gradient of 0.05–0.3 M TEAB, pH 7.5. The total elution volume was 500 mL, and 4 mL fractions were collected. Fractions 40–62 contained two compounds, both of which were eluted at significantly lower salt concentration than was required to elute the starting material, compound 4. One compound had a retention time of 32.1 min (68%) and was identical with the major product in the original DTT reaction mixture. It was assigned the structure of 5. The second compound, which had a retention time of 39.3 min (26%), was identified as the starting disulfide 4. Free thiol 5 was very sensitive to air oxidation; for instance, when a

solution of **4** was reduced with β -mercaptoethanol, HPLC showed quantitative conversion to **5**. However, lyophilization of the solution resulted in complete conversion back to disulfide **4**.

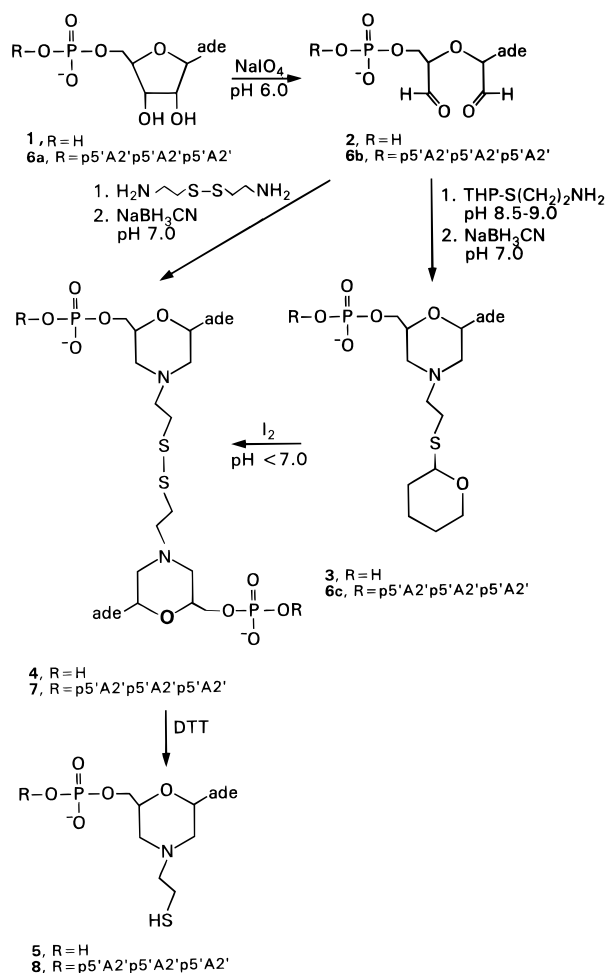
Reaction of 5'-Monophosphoryladenyl(2'→5')adenyl(2'→5')adenyl(2'→5')adenosine with S-(2-Tetrahydropyranyl)cysteamine. **Preparation of 6c.** A procedure was employed that was similar to the synthesis of compound **3**. Specifically, the oligonucleotide p5'A2'p5'A2'p5'A2'p5'A (240 A_{259} units, 5 mmol) in 200 mL of H₂O was oxidized with NaIO₄ (60 mL of a 1 M aqueous solution, 6 mmol) at 0 °C. Excess periodate was destroyed with ethylene glycol (30 mL of 1 M aqueous solution), and then S-(2-tetrahydropyranyl)cysteamine (50 mL of 0.5 M, 25 mmol) was added in one portion. The pH of the reaction mixture was adjusted to 8.5–9.0. After 40 min of reaction at 0 °C, a solution of sodium cyanoborohydride (25 mmol in 50 mL of H₂O) was added, and the pH again adjusted, this time to approximately 7.0. The pH was maintained at about 7 by addition of 10% HOAc. After 1 h at 0 °C, the excess sodium cyanoborohydride was destroyed with acetone at pH 5. The resulting mixture was diluted 10-fold with H₂O and applied to a DEAE-Sephadex A-25 column (HCO₃⁻ form, 1 × 10 cm). The column was eluted with a linear gradient (0.05–0.6 M, total of 500 mL) of TEAB, pH 7.5. Fractions of 4 mL were collected. Product **6c** was eluted in fractions 63–71. After removal of TEAB by repeated addition and evaporation of H₂O, compound **6c** was converted to the sodium salt by treatment with NaI/acetone as before. The final yield was 133 A_{258} units (2.77 mmol, 55.4%). Compound **6c** had a retention time of 37.1 min. Bacterial alkaline phosphatase treatment of **6c** gave only one product which had a higher retention time of 41.39 min, as expected for the production of the less polar 5'-unphosphorylated core. Snake venom phosphodiesterase digestion of **6** resulted in the generation of 5'AMP and compound **3** in the required 3:1 ratio. However, in addition to the expected products, an additional product with a slightly greater retention time than 5'AMP (13.54 min compared to 13.03 for AMP) was formed in 13% yield.

Reaction of Compound 6c with Iodine. **Preparation of Compound 7.** Compound **6c** (70 A_{258} units, 1.46 mmol), in 300 mL of H₂O, was oxidized according to the identical procedure used for the oxidation of compound **3**. After completion of the reaction, the entire mixture was applied to a DEAE-Sephadex A-25 column (Cl⁻ form, 1 × 10 cm). Elution was accomplished with a linear gradient of 0.05–0.6 M LiCl (total of 500 mL). Fractions of 4 mL were collected. The product (**7**) was eluted in fractions 93–110 (LiCl concentration of approximately 0.55 M). These fractions were reduced to dryness *in vacuo*, and the residue was dried by two azeotropic evaporations with ethanol/benzene (1:2, 2 × 100 mL). Acetone (50 mL) was added to the residue. After the resultant mixture was stirred for 5–10 min, the insoluble component was centrifuged down, washed with acetone (2 × 5 mL), and then dried *in vacuo*. The final yield was 55 A_{258} units (1.15 mmol, 79%). Compound **7** had an HPLC retention time of 30.4 min.

RESULTS AND DISCUSSION

The reaction of periodate-oxidized ribonucleotides or oligoribonucleotides with amines or amino acids followed by reduction with borohydride gives products in which the ribose (or terminal ribose in the case of oligoribonucleotides) has been transformed to the corresponding morpholine derivatives (17, 18, 21). However, when we attempted to extend this reaction to conjugation of the simple aminothiols, 2-aminoethanethiol (cysteamine), we

Scheme 1



noted the formation of three major products and at least five minor products, none of which were identified (results not shown). We surmise that this result may be due to the reactivity of thiols with the aldehyde groups generated in the oxidation step (24, 25).

Guided by the above hypothesis, we explored protection of the reactive thiol functionality during the dialdehyde–amine conjugation reaction. Two separate but convergent approaches were employed.

The first approach (Scheme 1) used the natural disulfide of cysteamine, namely, cystamine. Thus, 5'AMP was oxidized with sodium periodate to the dialdehyde, which was reacted with cystamine hydrochloride followed by sodium cyanoborohydride reduction to give compound **4**.

The second synthetic approach used the tetrahydropyranyl group for S-protection. Thus, S-(2-tetrahydropyranyl)cysteamine was obtained in good yield by refluxing a suspension of cysteamine hydrochloride with 3,4-dihydropyran. This method was similar to that reported for protection of cysteine (26); however, in this case, no solvent was used. In turn, S-(2-tetrahydropyranyl)-cysteamine was reacted with periodate-oxidized 5'AMP to yield, after reduction with Na(CN)BH₃, the S-protected adduct **3**. It was particularly important to destroy all of the excess periodate before addition of protected thiol due to its high oxidation susceptibility (27, 28). Compound **3** could be deprotected with aqueous iodine (29) to give, after purification, a 52% yield of product identical in all respects to disulfide **4** above, obtained from the reaction of oxidized AMP with cystamine. Pilot reactions under various pH conditions demonstrated that the pH of the reaction mixture should not be higher than 6 to avoid overoxidation.

Disulfide **4**, obtained by either of the above routes, was reduced with DTT to the thiol **5** (Scheme 1). HPLC showed an 82% conversion to compound **5** during the DTT reaction. Although the thiol **5** was formed in high yield according to direct HPLC analysis of the reaction mixture, we were unable to isolate the pure free thiol (**5**) itself since it was contaminated by the disulfide **4**, apparently formed during workup by the facile air oxidation of compound **5**. Such ready oxidation of oligonucleotides bearing 3'-terminal thiols has been observed previously (13).

This successful reaction sequence was applied to 2-5A tetramer monophosphate, p5'A2'[p5'A2']₂p5'A. Synthetic conditions used to prepare **3** readily converted p5'A2'-[p5'A2']₂p5'A (**6a**) to the 2'-terminal-modified derivative **6c** in moderate yield. Characterization of compound **6c** was through snake venom phosphodiesterase digestion, which produced both 5'AMP and **3** in the requisite 3:1 ratio. A small amount of an additional compound was generated under these latter digestion conditions. We speculate that this arises from the partial decomposition of **3**, but this reaction product has not been characterized further.

Aqueous iodine oxidation of compound **6c** provided disulfide **7** in high yield. Characteristically, disulfide **7** could be 5'-dephosphorylated by bacterial alkaline phosphatase. Snake venom phosphodiesterase digestion gave, as expected, 5'AMP and the disulfide **4** in a 3:1 ratio. Limited digestion with a mixture of both bacterial alkaline phosphatase and snake venom phosphodiesterase further characterized the essential structural elements of the molecule by production of adenosine, 5'AMP, A2'p5'A, A2'p5'A2'p5'A, and compound **4**. The disulfide **7** reacted cleanly with DTT to give quantitative conversion to a product that was not isolated but was presumed to be the free thiol (**8**), in analogy to the reduction of **4** to **5**.

Both disulfide **7** and the *S*-tetrahydropyranyl-protected derivative were evaluated for their ability to bind to the 2-5A-dependent RNase L of mouse L cells. The concentrations (IC₅₀ values) of these derivatives required for replacement of 50% of the radiolabeled probe, p5'A2'p5'A2'p5'A2'p5'A3'[^32P]p5'C3'p, from the enzyme were 1 × 10⁻⁹ M for **7** and 8 × 10⁻¹⁰ M for **6c**, not significantly different from the corresponding value for 2-5A tetramer 5'-monophosphate itself. Assay conditions normally include an excess of β-mercaptoethanol, so that the disulfide would be reduced to the free thiol, and the IC₅₀ for **7** would be for the reduced oligonucleotide, not compound **7**.

CONCLUSIONS

The reaction of *S*-protected aminothiols with periodate-oxidized 3'-ribonucleotide-terminated oligonucleotides provides a viable synthetic approach to the introduction of thiols into preformed oligonucleotides. Specifically, we have demonstrated the key steps in this method using 5'AMP as a model and by applying it to the 2',5'-linked oligonucleotide, p5'A2'p5'A2'p5'A2'p5'A. However, in principle this chemistry should be applicable to any nucleic acid bearing a 3' (or 2')-terminal ribose, so long as no modified nucleotides are present which would be incompatible with the specific reactions involved in this derivatization.

As a practical matter, which preparative methodology would be preferable: (a) direct conjugation to cystamine or (b) reaction with *S*-(2-tetrahydropyranyl)cystamine and subsequent oxidation? A decision would depend upon the specific substrate under consideration. The faster approach would be cystamine conjugation, but this

would be limited by the relatively low yield of product and the increased difficulty of product purification. Thus, the latter method would be restricted to the simplest substrates, such as the mononucleotide AMP. For the more complex oligonucleotide substrates, the two-step sequence of conjugation with *S*-(2-tetrahydropyranyl)-cystamine followed by iodine oxidation would be preferable since the higher yields of the individual steps would allow more facile product purification.

LITERATURE CITED

- (1) Johnston, M. I., and Torrence, P. F. (1984) The role of interferon-induced proteins, double-stranded RNA, and 2',5'-oligoadenylate on the interferon-mediated inhibition of viral translation. In *Interferon: Mechanisms of Production and Action* (R. Friedman, Ed.) Vol. 3, pp 189-298, Elsevier Science, Amsterdam.
- (2) Torrence, P. F., Xiao, W., Li, G., and Khamnei, S. (1994) Development of 2',5'-oligonucleotides as potential therapeutic agents. *Curr. Med. Chem.* 1, 176-191.
- (3) Silverman, R. H., Jung, D. D., Nolan-Sorden, N. L., Diefenbach, C. W., Kedar, V. P., and SenGupta, D. N. (1988) Purification and analysis of murine 2-5A-dependent RNase. *J. Biol. Chem.* 263, 7336-7341.
- (4) Nolan-Sorden, N., Lesiak, K., Bayard, K., Torrence, P. F., and Silverman, R. H. (1990) Photochemical crosslinking in oligonucleotide-protein complexes between a bromine-substituted 2-5A-analog and 2-5A-dependent RNase by ultraviolet lamp or laser. *Anal. Biochem.* 184, 298-304.
- (5) Torrence, P. F., Maitra, R. K., Lesiak, K., Khamnei, S., Zhou, A., and Silverman, R. H. (1993) Targeting RNA for degradation with a (2',5')-oligoadenylate-antisense chimera. *Proc. Natl. Acad. Sci. U.S.A.* 90, 1300-1304.
- (6) Lesiak, K., Khamnei, S., and Torrence, P. F. (1993) 2',5'-Oligoadenylate-antisense chimeras: synthesis and properties. *Bioconjugate Chem.* 4, 467-472.
- (7) Maran, A., Maitra, R. K., Kumar, A., Dong, B., Xiao, W., Li, G., Williams, B. R., Torrence, P. F., and Silverman, R. H. (1994) Blockage of NK-kB signaling by selective ablation of an mRNA target by 2-5A-antisense chimeras. *Science* 265, 789-792.
- (8) Maitra, R. K., Li, G., Xiao, W., Dong, B., Torrence, P. F., and Silverman, R. H. (1995) Catalytic cleavage of an RNA target by 2-5A-antisense and RNase L. *J. Biol. Chem.* 270, 15071-15075.
- (9) Connolly, B. A. (1991) Oligonucleotides containing modified bases. In *Oligonucleotides and Analogues: A Practical Approach* (F. Eckstein, Ed.) pp 155-183, IRL Press, New York.
- (10) Sinha, N. D., and Striepeke, S. (1991) Oligonucleotides with reporter groups attached to the 5'-terminus. In *Oligonucleotides and Analogues: A Practical Approach* (F. Eckstein, Ed.) pp 185-210, IRL Press, New York.
- (11) Blanks, R., and McLaughlin, L. W. (1991) Oligonucleotides for affinity chromatography. In *Oligonucleotides and Analogues: A Practical Approach* (F. Eckstein, Ed.) pp 241-254, IRL Press, New York.
- (12) Beaucage, S. L., and Iyer, R. P. (1993) The synthesis of modified oligonucleotides by the phosphoramidite approach and their applications. *Tetrahedron* 49, 6123-6194.
- (13) Zuckerman, R., Corey, D., and Schultz, P. (1987) Efficient methods for attachment of thiol-specific probes to the 3'-ends of synthetic oligoribonucleotides. *Nucleic Acids Res.* 15, 5305-5321.
- (14) Chu, B. C. F., and Orgel, L. E. (1988) Ligation of oligonucleotides to nucleic acids or proteins via disulfide bonds. *Nucleic Acids Res.* 16, 3671-3690.
- (15) Soukup, G. A., Cerny, R. L., and Maher, L. J., III (1995) Preparation of oligonucleotide-biotin conjugates with cleavable linkers. *Bioconjugate Chem.* 6, 135-138.
- (16) Brown, D. M., and Read, A. P. (1965) Nucleotides. Part XLIX. The reduction of the adduct of periodate-oxidized adenosine 5'-phosphate and methylamine. *J. Chem. Soc.*, 5072-5074.

- (17) Khym, J. X. (1963) The reaction of methylamine with periodate-oxidized adenosine 5'-phosphate. *Biochemistry* 2, 344-350.
- (18) Jones, A. S., Markham, A. F., and Walker, R. T. (1976) A simple method for the preparation of "ribonucleoside dialdehydes" and some comments on their structure. *J. Chem. Soc., Perkin Trans. 1*, 1567-1570.
- (19) RajBhandary, U. L. (1968) Studies on polynucleotides. LXXVII. The labeling of end groups in polynucleotides chains: the selective modification of diol end groups in ribonucleic acids. *J. Biol. Chem.* 243, 556-564.
- (20) Hansske, F., and Cramer, F. (1979) Modification of the 3'-terminus of tRNA by periodate oxidation and subsequent reaction with hydrazides. *Methods Enzymol.* 59, 172-181.
- (21) Imai, J., Johnston, M. I., and Torrence, P. F. (1982) Chemical modification potentiates the biological activities of 2-5A and its congeners. *J. Biol. Chem.* 257, 12739-12745.
- (22) Sawai, H., Shibata, T., and Ohno, M. (1981) Preparation of oligoadenylates with 2',5' linkage using Pb^{+2} ion catalyst. *Tetrahedron* 37, 481-485.
- (23) Lesiak, K., Imai, J., Floyd-Smith, G., and Torrence, P. F. (1983) Biological activities of phosphodiester linkage isomers of 2-5A. *J. Biol. Chem.* 258, 13082-13088.
- (24) Lienhard, G. E., and Jencks, W. P. (1966) Thiol addition to the carbonyl group. Equilibria and kinetics. *J. Am. Chem. Soc.* 88, 3982-3995.
- (25) Fitzpatrick, P. F., and Massey, V. (1982) Thiazolodine-2-carboxylic acid, an adduct of cysteamine and glyoxylate, as a substrate for D-amino acid oxidase. *J. Biol. Chem.* 257, 1166-1171.
- (26) Holland, G. F., and Cohen, L. A. (1958) Studies on the synthesis of insulin peptides. *J. Am. Chem. Soc.* 80, 3765-3769.
- (27) Capozzi, G., and Modena, G. (1974) Oxidation of thiols. In *The Chemistry of the Thiol Group* (S. Patai, Ed.) pp 785-840, Wiley, New York.
- (28) Doi, J. T., and Musker, W. K. (1985) A general mechanism for the oxidative cleavage of amine disulfides and cystine in aqueous iodine. Isolation of cyclic sulfenamides. *J. Org. Chem.* 50, 1-4.
- (29) Hiskey, R. G., and Tucker, W. K. (1985) Chemistry of aliphatic disulfides. IV. Studies on the synthesis of open-chain unsymmetrical cystine derivatives. *J. Am. Chem. Soc.* 107, 4789-4797.

BC970012I

Post-synthetically Ligated Ribozymes: An Alternative Approach to Iterative Solid-Phase Synthesis

Laurent Bellon,^{*,†} Christopher T. Workman,[†] Thale C. Jarvis,[‡] and Francine E. Wincott[†]

Departments of Oligonucleotide Chemistry and Cell Biology, Ribozyme Pharmaceuticals, Inc., 2950 Wilderness Place, Boulder, Colorado 80301. Received November 25, 1996[⊗]

To improve the overall yield of ribozyme synthesis, a convergent approach, based on the post-synthetic formation of an amino linker between two half-ribozymes was investigated. Borane-pyridine-mediated reductive amination of 3'-phosphoglycaldehyde-5'-half-ribozymes with 5'-aminoethyl-3'-half-ribozymes generated the corresponding amino-linked ribozymes in yields >77% on different scales. The investigation of a variety of reducing agents is discussed together with a kinetic analysis of the selected coupling reaction. These post-synthetically ligated ribozymes exhibited slightly reduced *in vitro* catalytic activity and cell efficacy.

INTRODUCTION

Ribozymes are RNA enzymes (Cech, 1993; Symons, 1994) that can be designed to cleave other RNA molecules. *trans*-Cleaving hammerhead ribozymes show great promise as therapeutic agents due to their inherent catalytic activity combined with highly specific binding to a chosen target RNA (Christoffersen and Marr, 1995). Improvements in the chemical synthesis of RNA (Wincott et al., 1995; Scaringe et al., 1990) have led to the site-specific introduction of various chemical modifications into hammerhead ribozymes providing nuclease resistance (Usman and Cedergren, 1992; Yang et al., 1992) and enhanced catalytic activity (Beigelman et al., 1995; Burgin et al., 1996). Because of the iterative nature of solid-phase oligoribonucleotide synthesis, only modest chemical yields of a 37-mer ribozyme can be achieved. Moreover, the necessary reversed-phase and anion-exchange purification steps further diminish this yield due to the inherent difficulty in separating the full-length ribozyme from the failures. As part of an ongoing effort to overcome these limitations, our group has designed an alternative approach (Bellon et al., 1996) in which two half-ribozymes are synthesized using known solid-phase methodologies. These halves contain complementary chemical functionalities that allow post-synthetic chemical ligation through a covalent linkage. Due to their lengths and the iterative synthesis process, the half-ribozymes are obtained in greater yield as compared to a full-length ribozyme. Therefore, this half-ribozyme approach has a theoretical advantage over the purely solid-phase procedure, with respect to yields, provided that the post-synthetic chemical ligation proceeds efficiently.

We describe herein the design, synthesis, and reductive amination coupling of half-ribozymes, on a pilot scale, together with a kinetic analysis of the conjugation reaction. The optimized conditions were then applied to a larger scale synthesis (50 μ mol), allowing a direct comparison between the half-ribozyme strategy and classical recurrent ribozyme synthesis. Catalytic activity and cell culture efficacy of the amino-linked ribozymes are also discussed.

MATERIALS AND METHODS

General Methods. Glyceryl-CPG and aminoethyl linker phosphoramidite were purchased from GlenResearch, Sterling, VA. Sodium cyanoborohydride, sodium borohydride, sodium triacetoxymethylborohydride, borane-pyridine, borane dimethylamine, and amberlyst A-26 borohydride were obtained from Aldrich Chemical Co., Milwaukee, WI. Sep-Pak Plus (C₁₈) purification cartridges were obtained from Waters Corp., Milford, MA.

Oxidative Cleavage of the 3'-Phosphoglyceryl-5'-half-ribozyme. A typical procedure is represented with half-ribozyme **4**. Half-ribozyme **4** (100 μ L, 50 nmol) was oxidized over 30 min with 10 equiv of aqueous NaIO₄ (1 μ L, 500 mM).

Small-Scale Desalting of the Ribozymes after Periodate Oxidation or Anion-Exchange HPLC. A typical procedure is represented with half-ribozyme **8**. The crude oxidized 3'-phosphoglycaldehyde-5'-half-ribozyme **8** was applied to a Waters Sep-Pak Plus (C₁₈) cartridge conditioned with CH₃CN/MeOH/H₂O (1:1:1, 10 mL) and SuperQ H₂O (20 mL). Following sample application, the cartridge was washed with SuperQ H₂O (10 mL) to remove formaldehyde and excess sodium periodate or excess sodium chloride in the case of anion-exchange-purified samples. Product was then eluted from the column with CH₃CN/MeOH/H₂O (1:1:1, 10 mL) and dried under reduced pressure.

Reductive Amination Ligation of 5'- and 3'-Half-Ribozymes. A typical procedure is represented by the synthesis of the amino-linked ribozyme **9**. 3'-Phosphoglycaldehyde-5'-half-ribozyme **8** (10 μ L, 500 μ M) and 5'-aminoethyl-3'-half-ribozyme **5** (10 μ L, 500 μ M) were mixed in a 1.5 mL Eppendorf tube. Sodium *N*₂-acetamido-2-iminodiacetate (ADA) (20 μ L of 200 mM, pH 6.2) was then added (125 μ M half-ribozyme final concentration). Reductive amination coupling was initiated with borane-pyridine in EtOH (1 μ L, 160 mM, 30 equiv). Reaction was sampled (0.5 μ L, 60 pmol) every few hours and diluted in water (200 μ L, 180 μ L injected) for HPLC analysis.

Analytical Anion-Exchange HPLC. All analyticals were run on a Hewlett-Packard 1090 HPLC using a Dionex NucleoPac PA-100 column, 4 \times 250 mm. Perchlorate buffers (buffer A = 10 mM NaClO₄/1 mM Tris-HCl; buffer B = 300 mM NaClO₄/1 mM Tris-HCl, both pH 9.3) and column heating to 50 $^{\circ}$ C were standard conditions. Analyticals were run with 30–60 pmol of ribozyme injected in a volume of 180 μ L. Half-ribozymes

* Author to whom correspondence should be addressed (e-mail lbellon@rpi.com).

[†] Department of Oligonucleotide Chemistry.

[‡] Department of Cell Biology.

[⊗] Abstract published in *Advance ACS Abstracts*, February 15, 1997.

were analyzed on a 30–60% B gradient over 12 min. Oxidized 3'-phosphoglycaldehyde-5'-half-ribozymes were run at 80 °C on a 45–75% B gradient over 12 min. Reductive amination reactions were analyzed on a 40–70% B gradient over 12 min.

Small-Scale Purification of the Amino-Linked Ribozymes. Crude samples (5 mL) were injected onto a Dionex NucleoPac PA-100, 22 × 250 mm (90 mL), column equilibrated with buffer A (buffer A = 20 mM NaCl/10% EtOH/1 mM Tris·HCl; buffer B = 1 M NaCl/10% EtOH/1 mM Tris·HCl, both pH 9.3). The linked ribozymes were purified at elevated temperatures since heat was necessary to melt the hybrid formed between the unreacted halves. A 55–70% B gradient was applied over 60 min. A 10 mL/min flow rate was used, and fractions were collected every minute. Fractions containing full-length product >80% by peak area were pooled and desalted using the method described for **8**.

Large-Scale Reversed-Phase HPLC Purification of the 5'-Half-Ribozyme **4 and Full-Length Control RPI.3718.** The crude material from a large-scale tritylation (50 μ mol) synthesis was applied to a Pharmacia Source 15RP 16/10 column equilibrated in 100% buffer A (buffer A = 1 M NaCl/5 mM Tris·HCl, pH 9.0; buffer B = 60% EtOH/5 mM Tris·HCl, pH 9.0) on a FPLC system (Pharmacia Biotech). A gradient from 0 to 40% B in 4 column volumes (CVs), from 40 to 42% B in 5 CVs, and then from 42 to 100% B in 3 CVs was applied at a flow rate of 10 mL/min (300 cm/h). Fractions containing over 60% full-length material by HPLC were pooled and subjected to manual detritylation with HCl. The solution was acidified to pH 2 (20–40 mM HCl) with 1 M HCl for 15 min. The pH of the solution was then adjusted to pH 7 with Tris base (1 M Tris base, pH 11–12). This material was analyzed by HPLC at >70% full-length by area.

Large-Scale Anion-Exchange HPLC Purification of the Half-Ribozymes **4 and **5**, Full-Length Control RPI.3718, and Amino-Linked Ribozyme **9**.** The reversed-phase purified, detritylated material was applied to a Pharmacia Source 15Q 26/10 (50 mL) anion-exchange column on a Pharmacia FPLC system. A NaCl gradient (buffer A = 20 mM NaCl/5 mM Tris·HCl, pH 9; buffer B = 1 M NaCl/5 mM Tris·HCl, pH 9) was applied at a flow rate of 10 mL/min. The half-ribozymes were purified using a 30–50% B gradient in 40 CVs. For the full-length control, RPI.3718, a gradient from 40 to 60% B in 40 CVs was used. The linked ribozyme **9** was purified at 55 °C with a gradient from 60 to 80% B in 20 CVs. The fractions containing over 80% full-length material were pooled. This material was analyzed by HPLC at >85% full-length by area.

Large-Scale Desalting of the 3'-Phosphoglycaldehyde-5'-half-ribozyme **8 and of the Anion-Exchange-Purified Ribozymes.** The ribozyme solutions were applied to a 1.6 × 10 cm (20 mL) bed of Bondapak C₁₈ 125 Å (37–55 μ M) packed in a Pharmacia HR 16/10 column pre-equilibrated in water. Application and desalting were run at a flow rate of 10 mL/min. Ribozyme was cleared from the column with a step gradient to 30% EtOH in water. All UV-absorbing fractions were pooled and dried under reduced pressure.

Electrospray Mass Spectrometry. Desalting was performed using a modified ammonium acetate precipitation procedure (Stults and Marsters, 1991). Ribozyme (10 nmol) was suspended in SuperQ water (30 μ L). NH₄-OAc (50 μ L, 5 M, pH 5.6) was added and the solution vortexed. After 10 min, absolute EtOH (600 μ L) was added and the ribozyme solution vortexed and placed in the –70 °C freezer overnight. Samples were centrifuged

(14 000 rpm, 30 min), and supernatant was carefully removed. The pellets were treated twice more with this procedure to ensure efficient ammonium exchange. ES-MS was performed on a Fison Instruments VG Quattro-SG quadrupole mass spectrometer. Desalted and ammonium-exchanged samples were suspended in deionized water (1 nmol/ μ L). The ribozyme solution (1 μ L) was added to an acetonitrile (ACN) solution [17 μ L, 80% ACN/2.5 mM 1,2 diaminocyclohexane-*N,N,N,N*-tetraacetic acid (CDTA)/0.1%TEA]. The ribozyme/ACN solution was injected through a fused silica loop (10 μ L) at 4 μ L/min. The instrument was run in ES(–) mode (cone voltage = 42 V) on a mass range of 400–1500.

Ribozyme Catalytic Activity Assay. RPI.3718, amino-linked ribozyme **9**, its inactive version, and 5'-³²P-end-labeled substrate **3** were heated separately in reaction buffer (50 mM Tris·HCl, pH 8.0; 40 mM MgCl₂) to 95 °C for 2 min, quenched on ice, and equilibrated to the final reaction temperature (37 °C) prior to the start of the reactions. Reactions were carried out in enzyme excess and were started by mixing ~1 nM substrate with 500 nM ribozyme in a final volume of 50 μ L. Aliquots of 5 μ L were removed at 0.5, 1, 2.5, 5, 10, 15, 20, 30, and 60 min, quenched in formamide loading buffer, and loaded onto 15% polyacrylamide/7 M urea gels. The fraction of substrate and product present at each time point was determined by quantitation of scanned images from a Molecular Dynamics PhosphorImager. Ribozyme cleavage rates were calculated from plots of the fraction of substrate remaining vs time using a double-exponential curve fit (Kaleidagraph, Synergy Software) (Burgin et al., 1996). For RPI.3718, the fast portion of the curve represented 54% of the total reaction; therefore, the observed cleavage rate (k_{obs}) was taken from fits of the first exponential. For amino-linked ribozyme **9**, the slow portion of the curve represented 93% of the total reaction; therefore, the observed cleavage rate (k_{obs}) was taken from fits of the second exponential.

Smooth Muscle Cell Proliferation Assay. Rat aortic smooth muscle cells (RASMC) were isolated and propagated as described (Jarvis et al., 1996a). Cell proliferation assays were performed according to a modification of the method of Jarvis et al. (1996a). Briefly, cells were set at a density of 5000 cells per well in a 24-well tissue culture plate and cultured in Dulbecco's Modified Eagle's Medium (DMEM) containing 10% FBS for 24 h at 37 °C in a 5% CO₂ atmosphere. Cells were then washed twice in Dulbecco's phosphate-buffered saline (DPBS) and serum starved in DMEM containing 0.5% fetal bovine serum (FBS) for 48 h to induce a quiescent state. Cells were then washed twice with DPBS and treated with 0.5 mL per well of 100 nM ribozyme complexed with 7.2 μ g/mL LipofectAMINE (GIBCO-BRL) for 1.5 h at 37 °C. Ribozyme/lipid complexes were then removed, and the cells were washed twice with DPBS and incubated in DMEM containing 0.25% FBS for an additional 6 h. Cells were then stimulated to proliferate by addition of 10% FBS. Cell proliferation was measured by incorporation of BrdU as described (Jarvis et al., 1996a).

RESULTS AND DISCUSSION

Synthetic Strategy. A realistic averaged stepwise chemical yield (ASWY) of 96.5% can be routinely obtained for ribozyme synthesis as determined by the ratio (μ mol of FLR/ μ mol scale)^{1/n} × 100, where μ mol of FLR is the amount of full-length ribozyme in the crude mixture, μ mol scale is the scale of synthesis and *n* is the number of synthesis cycles. This half-ribozyme approach has a theoretical advantage over the iterative procedure with

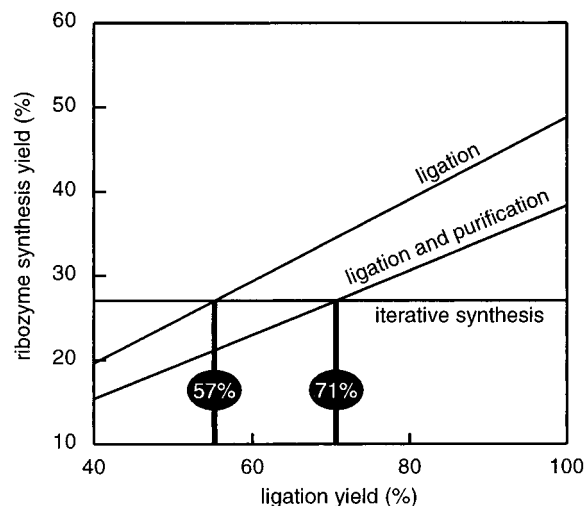


Figure 1. Theoretical chemical yield comparison between half-ribozyme approach and iterative ribozyme synthesis. Ligated ribozyme synthesis yields are calculated as follows: (49% \times ligation yield), where 49% is the 21-mer half-ribozyme synthesis yield as determined from a 96.5% ASWY; or (49% \times ligation yield) \times 80%, where 80% is the recovery yield of the additional purification step for the convergent route. The selected break-even point for the two strategies corresponds to 71%.

respect to yields. A 96.5% ASWY correlates in 28% theoretical yield for a 37-mer ribozyme, 49% theoretical yield for a 21-mer half-ribozyme, and 56% theoretical yield for a 17-mer half-ribozyme. A critical requirement is the chemical ligation yield of the two halves to form the full-length ribozyme (Figure 1). We have determined that a minimum coupling yield of 57% is theoretically sufficient to compete with iterative synthesis (49% \times 57% = 28%). However, the convergent route requires an additional purification step to separate the chemically ligated full-length ribozyme from the unreacted halves. Therefore, we have set the threshold that ensures the advantage of this segmented approach over iterative synthesis at 71% half-ribozyme coupling yield (Figure 1). It is clear from Figure 1 that any improvement in the ligation efficiency that raises it above 71% will provide a greater amount of full-length ribozyme. Ideally, quantitative ligation efficiency would lead to 39% FLR, to be compared with 28% for the iterative approach (Figure 1).

Design of Half-Ribozymes. An important requirement for this strategy to be successful is that the site of chemical ligation must not interfere with the ribozyme core to ensure that full catalytic activity is retained. It has been previously shown that the stem II or loop II of the hammerhead ribozyme is not essential for catalytic activity (Bellon et al., 1996; Tuschl et al., 1993; Benseler et al., 1993; Beigelman et al., 1994; Hendry et al., 1994). Similarly to our previous work (Bellon et al., 1996), the standard GAAA tetraloop II and the stem II region of the generic, nuclease stable ribozyme motif (Beigelman et al., 1995; Burgin et al., 1996), as represented by RPI.3718 (Jarvis et al., 1996a) **1** (Figure 2), were modified to accommodate post-synthetic chemical coupling (Figure 3). Chemical ligation or conjugation of oligonucleotides can be greatly enhanced by the presence of a template (Gryaznov and Letsinger, 1993; Herrlein et al., 1995). Therefore, we assumed that successful coupling reaction

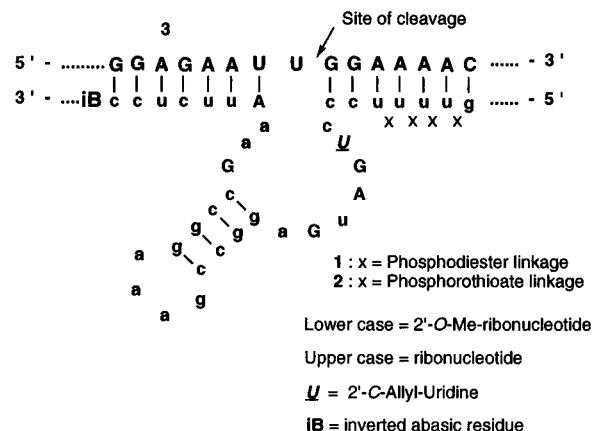


Figure 2. Structures of RPI.3718 **1**, RPI.3718S **2**, and the RNA substrate **3**.

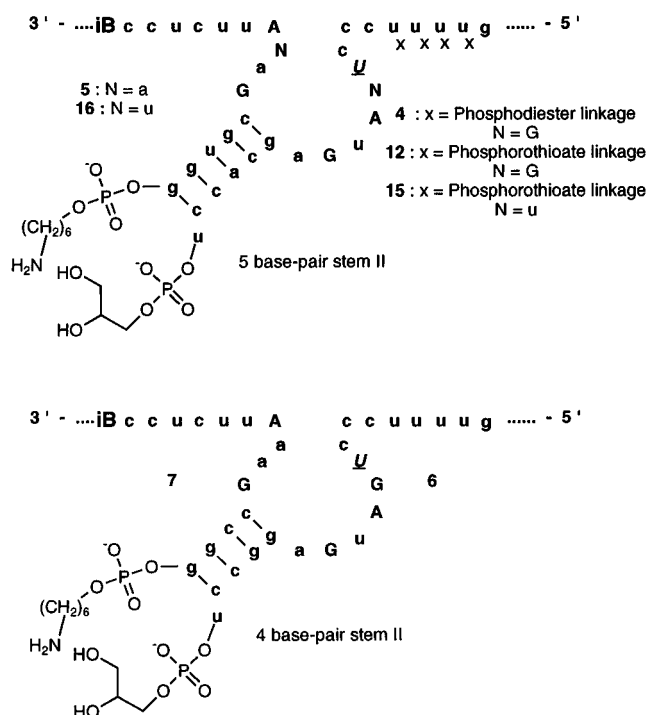


Figure 3. Structures of the 5 base-pair and 4 base-pair stem II half-ribozymes **4**, **5**, **12**, **15**, and **16** and **6** and **7**, respectively.

of the two half-ribozymes relied upon formation of the stem II bringing the two chemical moieties within close proximity to one another. Free energies predicting duplex stability of the suitable 5'-3' (**4.5** or **6.7**) and undesired 5'-5' (**4.4** or **6.6**) or 3'-3' (**5.5** or **7.7**) duplexes were calculated (Freier et al., 1986) with the standard self-complementarity ggcc stem II (as represented in **6** and **7**, Figure 3) or with a modified gcacc five base-pair stem II (as represented in **4** and **5**, Figure 3) (Table 1). The ΔG° values were clearly in favor of the 5 base pair stem II ensuring the formation of the correct duplex **4.5** by -3.3 kcal mol $^{-1}$ over the other possible duplexes **4.4** or **5.5**.

Furthermore, a uridyl residue was introduced between the 3'-phosphoglyceryl moiety and the stem II in the 5'-half-ribozyme **4** (Figure 3) to allow spatial bridging between the primary amine of **5** and the carbonyl

Table 1. Free Energies ΔG° Calculation Based on Nearest-Neighbor Model, 37 °C, 1 M NaCl or 10 mM Mg $^{2+}$

stem II	5 bp (gcacc)			4 bp (ggcc)		
duplex	4.5 (5'-3')	4.4 (5'-5')	5.5 (3'-3')	6.7 (5'-3')	6.6 (5'-5')	7.7 (3'-3')
ΔG° (kcal mol $^{-1}$)	-11.7	-8.4	-8.4	-10.4	-10.4	-10.4

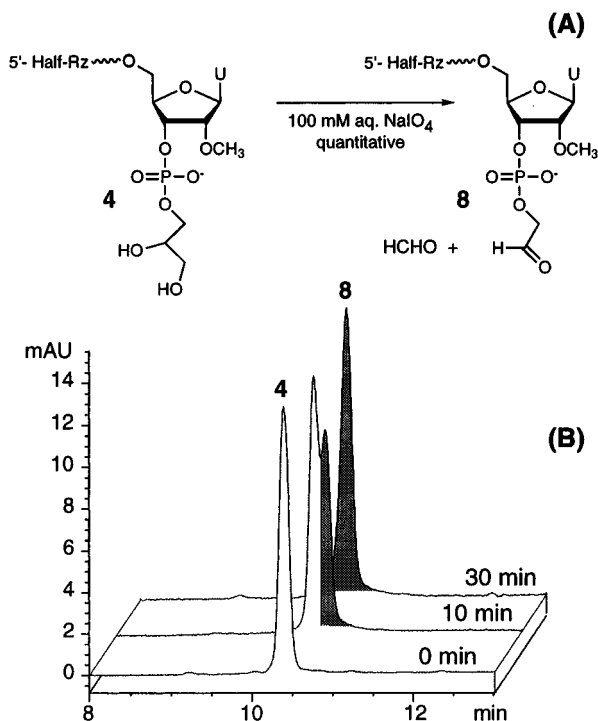


Figure 4. (A) NaIO₄-mediated oxidative cleavage of the 3'-phosphoglyceryl-5'-half-ribozyme **4** to the 3'-phosphoglycaldehyde **8**. (B) Anion-exchange HPLC analysis of the oxidative cleavage reaction after 0, 10, and 30 min.

functionality of the oxidized **4**. Indeed, preliminary work on morpholino-linked ribozymes (Bellon et al., 1996) indicated that a single atom difference between an aminoethyl linker and an aminoethylene glycol linker had a tremendous influence on the extent of product formation (data not shown).

Reductive Amination Coupling of Half-Ribozymes.

We selected a linear amino linkage to covalently bridge the 5'- and 3'-half-ribozyme since reductive amination chemistry has been applied effectively to a wide range of oligonucleotide substrates under aqueous conditions (Goodchild, 1990; Morvan et al., 1996; Deschamp and Sonveaux, 1995; Harambilis et al., 1994; Lemaitre et al., 1987). The previously studied morpholino linkage (Bellon et al., 1996) was not chosen here because of long reaction time together with the formation of two linked products.

Half-ribozymes **4** and **5**, derived from RPI.3718, were synthesized on a 2.5 μ mol scale on glyceryl-controlled pore glass (Urata and Akagi, 1993) and on an inverted abasic polystyrene (Jarvis et al., 1996b), respectively, and then purified according to standard methods (Wincott et al., 1995). The 3'-phosphoglyceryl-5'-half-ribozyme **4** (125 μ M aqueous solution) was subjected to oxidative cleavage with 10 molar equiv of a 100 mM aqueous solution of sodium periodate (Figure 4A). Complete conversion of **4** to the 3'-phosphoglycaldehyde-5'-half-ribozyme **8** could be observed within 30 min (Figure 4B). Since the periodate-mediated oxidation of the 3'-phosphoglyceryl **4** generates 1 molar equiv of highly reactive formaldehyde, **8** was eluted from the reaction mixture on a Sep-Pak C₁₈ cartridge (Waters Corp.). Half-ribozymes **8** (125 μ M) and **5** (500 μ M) were then reacted with 30 molar equiv of aqueous NaBH₃CN (Borch et al., 1971) (500 mM) in ADA buffer (100 mM), pH 6.0 (Figure 5A). Unlike the morpholino ribozyme (Bellon et al., 1996), after 7 days of reaction, a substantial amount of unreacted 3'-phosphoglycaldehyde **8** could be observed (Figure 5B). After HPLC purification, **9** was identified as the desired amino-

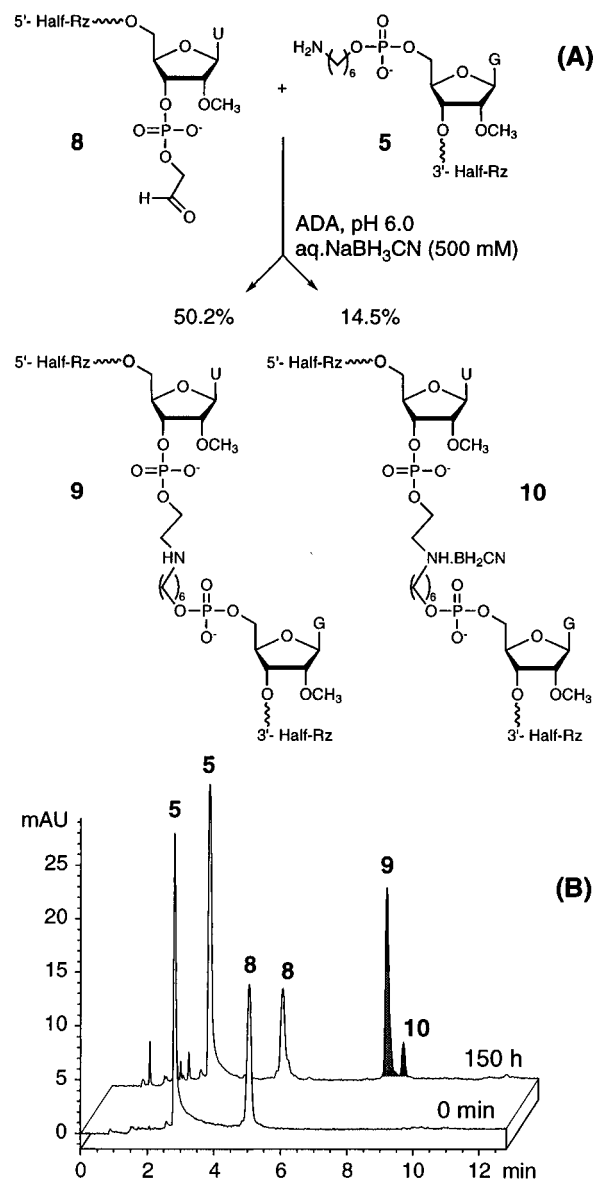


Figure 5. (A) NaBH₃CN-mediated coupling of the amino-linked ribozymes **9** and **10**. (B) Anion-exchange HPLC analysis of the reductive amination of **8** with **5** after 0 and 150 h.

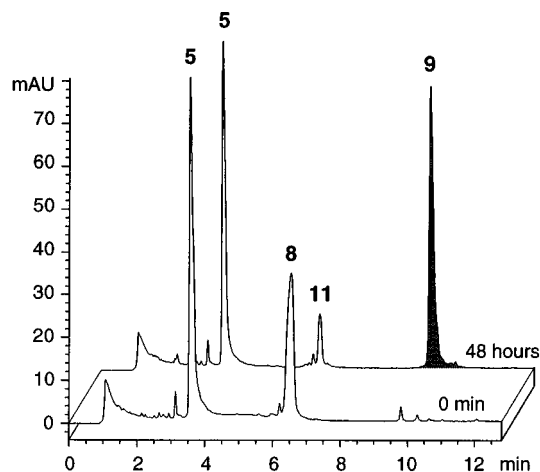
linked ribozyme on the basis of ES-MS analysis (calcd 11928.6, found 11929.0). Product **10** was assigned as a cyanoborane adduct in accordance with our previous data (Bellon et al., 1996). As a result of the incomplete reaction of the half-ribozymes, in addition to the undesired formation of the adduct **10**, the amino-linked ribozyme, **9**, was obtained in only 50.2% yield (Table 2). Since the necessary 71% coupling efficiency (Figure 1) was not obtained, we investigated other reducing agents to suppress the formation of the adduct as in **10** yet allow faster and higher yielding synthesis of **9**.

We assumed that the borane adduct formation could be prevented with the use of borane reducing reagents already complexed with an amine (Pelter et al., 1988). Such amine-borane complexes have reducing properties similar to those of hydroborates (Pelter et al., 1988), which are known to be rather selective for Schiff base reduction. We investigated the use of borane-pyridine (Pelter et al., 1984; Bomann et al., 1995; Moorman, 1993) and borane-dimethylamine (Billman and McDowell, 1961) complexes together with other types of hydroborates such as sodium borohydride (Abdel-Magid et al., 1994), sodium triacetoxyborohydride (Abdel-Magid et al., 1990; Hart

Table 2. Reductive Amination of **8 (125 μ M) with **5** (500 μ M) in ADA (100 mM, pH 6.0) with 30 Molar Equiv of Reducing Agent for 48 h at Room Temperature^a**

	reducing agent					
	NaBH ₃ CN ^b	NaBH(OAc) ₃ ^c	BH ₄ ·Amberlyst A-26 ^d	NaBH ₄ ^c	BH ₃ ·Pyr ^e	BH ₃ ·HNMe ₂ ^c
9 (%)	50.2	NR ^f	NR	NR	81.2	4.4
10 (%)	14.5	NR	NR	NR	NR	NR

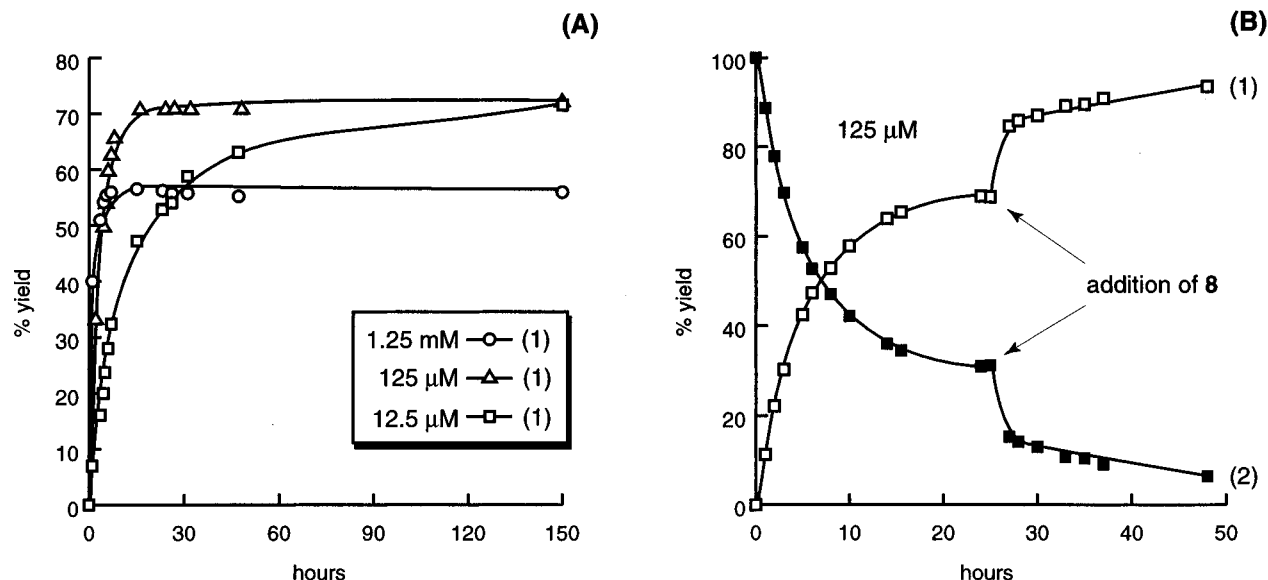
^a Yields are expressed as μ mol ratio \times 100 based on the disappearance of the limiting reagent **8**. ^b 500 mM in H₂O, 7 days of reaction. ^c 100 mM in H₂O. ^d 2.5 mmol equiv of BH₄⁻ g⁻¹ of resin. ^e 80 mM in EtOH. ^f NR, no significant reaction after 48 h.

**Figure 6.** Anion-exchange HPLC analysis of the borane-pyridine-mediated coupling of the amino-linked ribozyme **9** after 0 and 48 h of reaction.

and Leroy, 1995), or borohydride exchange resins (Yoon et al., 1993; Gibson and Bailey, 1977). Half-ribozymes **8** (125 μ M) and **5** (500 μ M) were reacted in ADA buffer (100 mM), pH 6.0, in the presence of 30 molar equiv of the reducing agent for 48 h (Table 2). As seen from Table 2, borane-pyridine complex produced a very high yield of the amino-linked ribozyme **9** without the concomitant formation of a second ligated product. A small amount of unreacted 5'-half-ribozyme was still observed after 48 h of reaction (Figure 6). Following anion-exchange purification, this material was subjected to ES-MS to determine whether **8** could have been reduced (Andrews and Crawford, 1980) into the corresponding 3'-phosphoglycol, **11** (Urata and Akagi, 1993), thereby competing

with the reductive amination. The mass analysis (calcd 6652.2, found 6653.0) was in agreement with the molecular weight of alcohol **11**, although **8** (calcd 6650.2) and **11** (calcd 6652.2) only differ by 2 atomic mass units. The fact that **11** did not react with the 5'-aminoheptyl-3'-half-ribozyme **5** when subjected to the same reductive amination conditions (data not shown) provided supportive evidence regarding the 3'-phosphoglycol nature of **11**. Reducing the molar equivalent of borane-pyridine to 5 equiv lengthened considerably the reaction time (over 5 days) without preventing the formation of **11**. Adding the 30 molar equiv in two portions at a 12 h interval did not change the scope of the reaction (data not shown).

Kinetic Analysis of the Borane-Pyridine-Mediated Half-Ribozyme Coupling. To prepare for the large-scale (50 μ mol) comparison of the half-ribozyme approach vs recurrent synthesis, we felt it was important to fine-tune reaction conditions giving rise to the amino-linked ribozyme **9**. In particular, optimal reaction time and concentration of the halves were investigated. Coupling reactions were set in ADA buffer (100 mM), pH 6.0, in the presence of 30 molar equiv of BH₃·Pyr (800 mM in ethanol) with 1.25 mM, 125 μ M, or 12.5 μ M of the 3'-phosphoglycaldehyde-5'-half-ribozyme **8** and the 5'-aminoheptyl-3'-half-ribozyme **5** (1:1 stoichiometry). Anion-exchange HPLC monitoring of the coupling reaction allowed us to plot the formation of the amino-linked ribozyme, **9** (expressed in percent yield), vs time (Figure 7A). The 125 and 12.5 μ M reactions reached the same 72% coupling yield after 24 and 150 h, respectively, whereas a final 56% coupling efficiency could be obtained after only 5 h with the high 1.25 mM concentration (Figure 7A). Extending the reaction time up to 150 h for the three concentrations did not have any significant impact on the amount of product formed. One possible

**Figure 7.** (A) Kinetic plots of the formation of **9** over time using 1.25 mM, 125 μ M, or 12.5 μ M stoichiometric amounts of half-ribozymes **5** and **8**. (B) Kinetic plot of the rescue reaction using 125 μ M **5** and $2 \times$ 125 μ M **8**: (1) formation of **9**; (2) consumption of **5**.

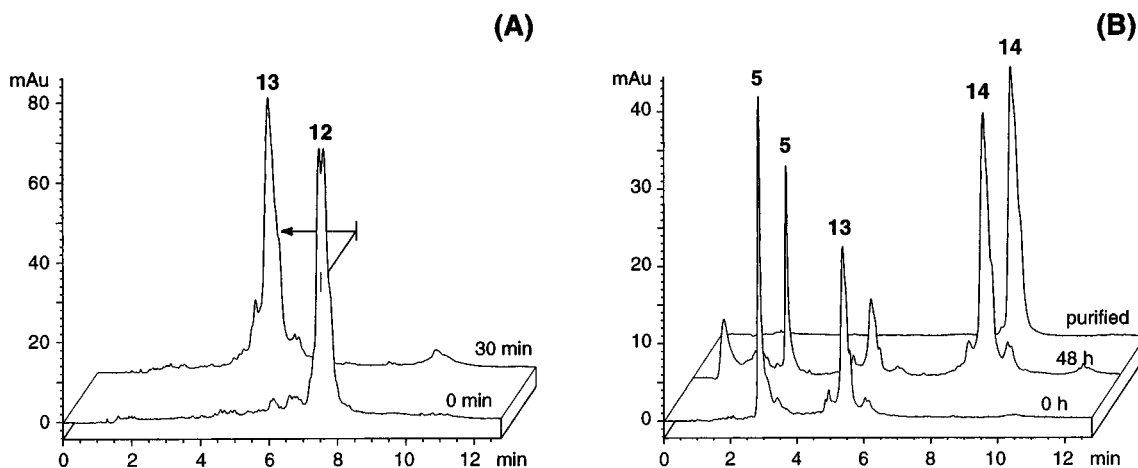


Figure 8. (A) Anion-exchange HPLC analysis of the NaIO_4 -mediated oxidative cleavage of the thiolated 3'-phosphoglyceryl-half-ribozyme **12** to the 3'-phosphoglycaldehyde **13**, after 0 and 30 min reaction times. (B) Anion-exchange HPLC analysis of the borane-pyridine-mediated coupling of the amino-linked ribozyme, **14**, after 0 and 48 h of reaction and after purification.

Table 3. Initial Velocities of the Reductive Amination Cross-Coupling Reaction

	half-ribozyme 5 and 8 concentration		
	1.25 mM	125 μM	12.5 μM
k_{obs} (h^{-1})	0.611	0.290	0.086

explanation for this "plateau" effect is that the 3'-phosphoglycaldehyde-5'-half-ribozyme **8** was competitively reduced into the corresponding alcohol (Andrews and Crawford, 1980) during the reductive amination with **5**. To further validate this hypothesis, we designed a "rescue" experiment in which another equivalent of half-ribozyme **8** was added to the 125 μM reaction after 24 h. As predicted, this procedure increased the final coupling yield to 93.6% after 48 h (Figure 7B). Another "rescue" experiment in which a molar equivalent of **5** was added to the 125 μM reaction after 24 h did not have any effect on the formation of the product **9** (data not shown), corroborating the fact that **8** was consumed in a side reaction. Since these "rescue" experiments did not use the desired 1:1 stoichiometry, the single mixing of an equimolar amount of half-ribozymes (125 μM) together with a 24 h reaction time was selected for the 50 μmol large-scale comparison. The experimental time points (Figure 7A) were treated (Burgin et al., 1996) using a double-exponential curve algorithm (KaleidaGraph). Kinetic analyses of the initial velocities of the reactions revealed a direct relationship between half-ribozyme concentration and the initial rate constant (Table 3). The lower yield (72%) obtained in these kinetic experiments was attributed to the 1:1 stoichiometry since it is known that reductive amination works optimally in the presence of a 5-fold excess of the amine residue (Borch et al., 1971).

Catalytic Activity of the Amino-Linked Ribozyme **9 and Its "Inactive" Counterpart.** Once the amino-linked ribozyme **9** was synthesized and characterized, it was critical to ascertain the effect of this chemical linkage on the ribozyme activity. "Active" amino-linked ribozyme **9**, its "inactive" counterpart containing two mutations in the catalytic core that abolish cleavage activity (Beigelman et al., 1995; Jarvis et al., 1996) (see **4** and **5**, Figure 3), and the control RPI.3718 were assayed under single-turnover conditions for their cleavage rate on short substrate **3** (Figure 2). The amino-linked ribozyme **9** was approximately 10 times slower than RPI.3718 (Table 4), confirming that one can extensively modify the stem II/loop II region without dramatically affecting cleavage activity. As expected, the inactive amino-linked ribozyme completely lacked detectable catalytic activity.

Table 4. Cleavage Rate of the Substrate **3** by the "Active" Ribozyme **9**, Its "Inactive" Analog, and RPI.3718^a

	ribozyme		
	"active" 9	"inactive" 9	RPI.3718
k_{obs} (min^{-1})	0.012	<0.0001	0.144

^a Over 82%, 55%, and 0% of the substrate **3** was cleaved over 1 h with ribozymes RPI.3718, **9**, and inactive **9**, respectively. ^b [Rz] = 500 nM, [**3**] ~ 1 nM, 50 mM Tris-HCl, pH 8.0, 37 °C, 40 mM Mg^{2+} .

Cell Efficacy of Phosphorothioate-Containing Amino-Linked Ribozyme **14 and Its "Inactive" Counterpart **17**.** Equally important was to assess the cell culture efficacy (Jarvis et al., 1996a,b) of these amino-linked ribozymes as compared to the control RPI.3718 **2**. It has been shown that one to four phosphorothioates linkages are required at the 5'-end of the ribozyme to optimize cell efficacy of the ribozyme (Jarvis et al., 1996b). Therefore, the 3'-phosphoglyceryl-5'-half-ribozyme **12**, containing four phosphorothioate linkages at the 5'-end (Figure 3), was synthesized and periodate-oxidized under the same conditions as described for its all-phosphodiester analog **4**. Interestingly, a negative shift in the retention time was observed for the 3'-phosphoglycaldehyde **13** (Figure 8A), suggesting that in addition to the desired oxidative cleavage of the 3'-*cis*-diol, nonspecific oxidation of the phosphorothioate linkages to their phosphodiester analogs may have occurred. After Sep-Pak desalting, **13** (177 μM in ADA, 100 mM, pH 6.0) was reductively aminated with the aminohexyl-half-ribozyme **5** under the borane-pyridine conditions (Figure 8B). The expected partially thiolated amino-linked ribozyme **14** was formed and subsequently purified on anion-exchange HPLC. After ammonium acetate precipitation, this material was subjected to ES-MS analysis to assess its phosphorothioate content. As seen from the electrospray mass spectrum (Figure 9), two peaks corresponding to **14** with one remaining phosphorothioate linkage (calcd 11944.7, found 11944.0) or two remaining phosphorothioates (calcd 11960.7, found 11961.0) could be identified. This clearly confirmed that oxidation of at least two phosphorothioate linkages to their oxygenated homologs had occurred during the periodate-mediated oxidative cleavage. Surprisingly, no material corresponding to the all-phosphodiester amino-linked ribozyme **9** was observed, indicating that at least one of the thiolated positions seems to be particularly resistant toward oxidation. Desulfurization of phospho-

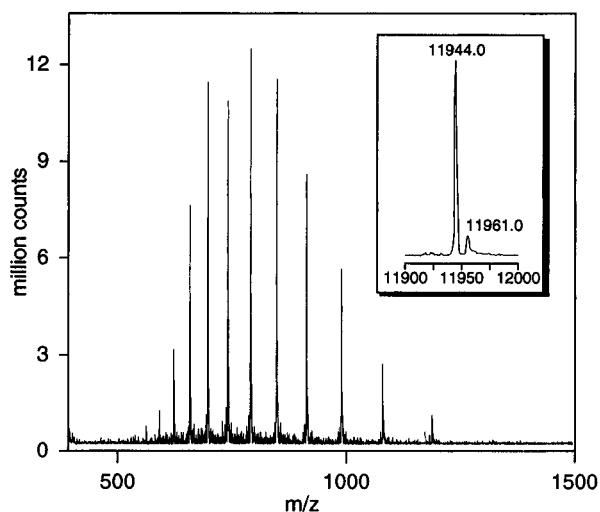


Figure 9. ES-MS for **14** (4.5 μ M) in 80% $\text{CH}_3\text{CN}/\text{H}_2\text{O}$, 0.1% TEA with CDTA, charge states 11– to 19–. The computer-deconvoluted masses are represented in the inset.

rothioate linkages using diverse oxidizing reagents is a commonly used method for base composition analysis of thiolated oligonucleotides (Connolly et al., 1984; Schuette et al., 1994; Wyrzykiewicz and Cole, 1994). To the best of our knowledge, a single study (Agrawal et al., 1990) describes the use of sodium periodate as the oxidizing agent. Base composition on phosphorothioate-containing ribozymes performed in our hands necessitated the use of 250 equiv of sodium periodate per phosphorothioate linkage at 37 $^\circ\text{C}$ over 2 h to complete full oxidation (D. Sweedler, unpublished data). Therefore, we were not expecting such an overwhelming side reaction under the relatively mild conditions used (a maximum of 2.5 equiv of NaIO_4 per phosphorothioate linkage, 30 min at room temperature). The exact position(s) of the(se) remaining phosphorothioate linkage(s) on the ribozyme is (are) under investigation using a modification of the iodethanol method developed by Gish and Eckstein (1988). The “inactive” version **17** of the amino-linked ribozyme **14** was synthesized similarly from half-ribozymes **15** and **16** (Figure 3). The same phosphorothioate/phosphodiester distribution could be observed as determined by ES-MS (**17** with one $\text{P}=\text{S}$, calcd 11896.6, found 11896.0; **17** with two $\text{P}=\text{S}$, calcd 11912.7, found 11912.0).

RPI.3718S **2** is a chemically stabilized 37-mer ribozyme targeted against site 575 of the proto-oncogene *c-myc* mRNA; it contains four phosphorothioate linkages at the 5'-end. RPI.3718S has been shown to inhibit vascular smooth muscle cell proliferation with an IC_{50} of approximately 75 nM (Jarvis et al., 1996a). “Active” and “inactive” amino-linked ribozymes **14** and **17**, respectively, together with the “active” control RPI.3718S and its inactive version RPI.3704 (Jarvis et al., 1996a) were delivered to quiescent RASCs using LipofectAMINE as a cationic lipid vehicle. The cells were stimulated with 10% fetal bovine serum, and cell proliferation was measured by a bromodeoxyuridine incorporation assay (Jarvis et al., 1996a). As seen in Figure 10, treatment of the cells with the catalytically active ribozymes **14** and RPI.3718S resulted in a significant inhibition of proliferation, whereas the “inactive” version (**17** or RPI.3704) failed to inhibit. It is apparent that a significant window of inhibition of cell proliferation exists between “active” and “inactive” ribozymes, confirming the mode of action of the ribozymes. Furthermore, the extent of this inhibition by the amino-linked ribozyme **14** is similar to that obtained with the control RPI.3718S. This clearly demonstrates that post-synthetically ligated ribozymes are as

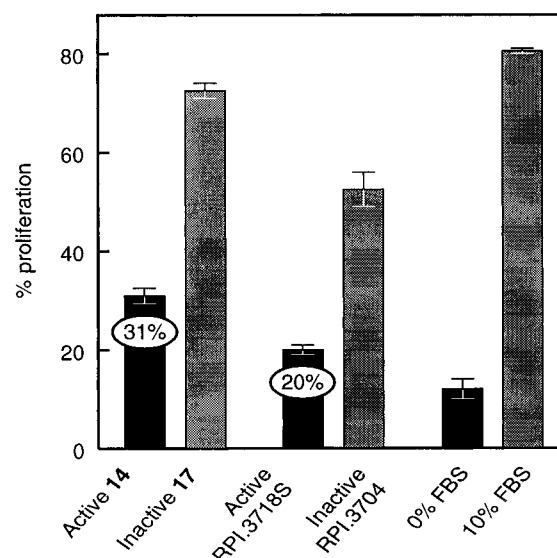


Figure 10. RASCs were treated with ribozymes complexed with cationic lipid as described under Materials and Methods. Cell proliferation is displayed as the percentage of cells that undergo DNA replication in response to serum stimulation. The 0% and 10% FBS controls show the proliferative response of untreated cells in the absence of or presence of serum.

potent as their traditionally synthesized analogs in inhibiting *c-myc* mRNA-induced cell proliferation. In agreement with previous work (Jarvis et al., 1996a), the slightly diminished inhibition of cell proliferation can be attributed to the presence of only one and two thiolated linkages in the amino-linked ribozyme, **14**, whereas RPI.3718S contains four phosphorothioate linkages.

50 μ mol Large-Scale Comparison between Half-Ribozyme Approach and Iterative Synthesis. Cleavage activity and cell culture efficacy of these amino-linked ribozymes having been demonstrated, it was imperative to study the scale-up of this post-synthetic coupling to validate the theoretical advantage of the half-ribozyme approach in terms of yields (Figure 1). Therefore, the 5'-half-ribozyme-3'-phosphoglyceryl **4**, 3'-half-ribozyme-5'-aminoethyl **5**, and RPI.3718 (Figures 2 and 3) were synthesized on a 50 μ mol scale on a 390Z ABI synthesizer using known methodologies (Wincott et al., 1995). RPI.3718 and **4** were then purified using the routine two-step (trityl-on reversed-phase and trityl-off anion-exchange) purification, whereas **5** was submitted to a single anion-exchange procedure since it did not contain a trityl group at the 5'-end. As predicted from a 96.5% ASWY, RPI.3718 was obtained in 26.1% chemical yield at the crude reaction mixture stage. This yield was further diminished to 17.7% after purification (3102 $\text{AU}_{260\text{ nm}}$, 8.88 μ mol, Figure 11A) with a 96.3% HPLC spectrophotometric purity at 260 nm. The 5'-aminoethyl-3'-half-ribozyme, **5**, was obtained in 52.7% yield at the crude level, corrected to 34.9% after purification (2667 $\text{AU}_{260\text{ nm}}$, 18.45 μ mol, 97.9% HPLC purity, Figure 11A). More surprising was the much lower chemical yield obtained for the 3'-phosphoglyceryl-half-ribozyme, **4** (18.5%, 1750 $\text{AU}_{260\text{ nm}}$ before purification, Figure 11A), synthesized on glyceryl-CPG (63 μ mol g^{-1} , Glen Research). Analysis of the trityl release data indicated a sharp drop of the trityl cation-induced conductivity after the first coupling of the 2'-*O*-methyluridyl residue onto the glyceryl-CPG, while the conductivity remained constant thereafter. This suggested that the first coupling on the solid support was not optimal. Highly loaded ($>40\ \mu\text{mol g}^{-1}$) CPG solid supports are known (Wright et al., 1993) to lose the mechanical and fluidic properties suitable for large-scale

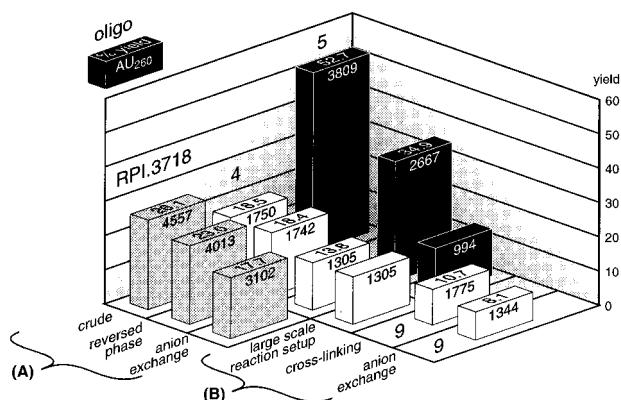


Figure 11. (A) Chemical yields of RPI.3718, half-ribozymes **4** and **5** after synthesis, reversed-phase and anion-exchange purification. (B) Chemical yield of the amino-linked ribozyme **9** after coupling and anion-exchange purification.

synthesis. Therefore, we functionalized highly cross-linked aminomethyl polystyrene solid support (McCollum and Andrus, 1991) with 1-*O*-dimethoxytritylglycerol according to a known procedure (Urata and Akagi, 1993). Under these conditions, glyceryl polystyrene solid support was obtained with a $11.6 \mu\text{mol g}^{-1}$ loading yield. Unfortunately, **4** synthesized from this resin was not obtained in any better yield as compared to CPG. This led us to believe that the electron-withdrawing acetoxy group (Urata and Akagi, 1993) adjacent to the dimethoxytrityl residue diminished the reactivity of the primary hydroxyl group generated after detritylation.

It was obvious that since **4** was obtained with a lower chemical yield ($6.88 \mu\text{mol}$) than the full-length control RPI.3718 ($8.88 \mu\text{mol}$, Figure 11), the coupling of the two halves could not generate more material than the iterative synthesis. However, the coupling study was completed to evaluate the scale-up of the pilot reactions (Figure 11B). 3'-Phosphoglyceryl-half-ribozyme **4** ($1305 \text{ AU}_{260 \text{ nm}}$, $6.88 \mu\text{mol}$) was oxidized as above into the 3'-phosphoglycaldehyde **8**, which was desalted on reversed-phase HPLC to remove excess NaIO_4 and formaldehyde. The aldehyde **8** was coupled in ADA buffer (100 mM, pH 6.0) with a stoichiometric amount of 5'-aminohexyl-half-ribozyme **5** ($994 \text{ AU}_{260 \text{ nm}}$, $6.88 \mu\text{mol}$, Figure 11B, final half-ribozymes concentration = $116 \mu\text{M}$) in the presence of 30 molar equiv of $\text{BH}_3 \cdot \text{Pyr}$ (80 mM in ethanol) for 24 h. As expected, the amino-linked ribozyme **9** was obtained cleanly in 77.6% coupling yield, well above the 71% threshold (Figure 1). After a final anion-exchange HPLC purification step to remove the unreacted 5'- and 3'-halves, $1344 \text{ AU}_{260 \text{ nm}}$ ($4.04 \mu\text{mol}$) of **9** exhibiting a 97.4% HPLC spectrophotometric purity at 260 nm was isolated (Figure 11B). This corresponds to a 58.7% coupling yield after purification. However, due to the low yield of its precursor **4**, the chemically ligated ribozyme **9** was only obtained with a 8.1% overall yield to be compared with the 17.7% overall yield for RPI.3718 (Figure 11).

CONCLUSION

Post-synthetically amino-linked ribozymes have been shown to possess the necessary cleavage activity and cell efficacy required to be considered as alternatives to solid-phase synthesized ribozymes. Furthermore, it has been demonstrated, on both small- and large-scale, that the post-synthetic assembling of half-ribozymes through a reductive amination coupling reaction meets the theoretical yield requirement to be competitive with iterative synthesis. However, this yield advantage is counterbal-

anced by the necessity of using a 3'-phosphoglyceryl-5'-half-ribozyme that cannot be synthesized in satisfactory yields.

ACKNOWLEDGMENT

We thank Susan Grimm, Victor Mokler, and Lara Maloney for the synthesis and purification of the different oligoribonucleotides, James McSwiggen for free energy calculations, Carolyn Gonzalez for catalytic activity assay, Alex Burgin for fruitful kinetic discussions, and Nassim Usman for continuous support.

LITERATURE CITED

- Abdel-Magid, A. H., Harris, B. D., and Maryanoff, C. A. (1994) A Reductive Amination/Lactamization Procedure Using Borohydride Reagents. *Synlett*, 81–83.
- Abdel-Magid, A. H., Maryanoff, C. A., and Carson, K. G. (1990) Reductive Amination of Aldehydes and Ketones by Using Sodium Triacetoxyborohydride. *Tetrahedron Lett.* 31, 5595–5598.
- Agrawal, S., Tang, J. Y., and Brown, D. M. (1990) Analytical Study of Phosphorothioate Analogues of Oligodeoxynucleotides Using High-Performance Liquid Chromatography. *J. Chromatogr.* 509, 396–399.
- Andrews, G. C., and Crawford, T. C. (1980) The Synthetic Utility of Amine Borane Reagents in the Reduction of Aldehydes and Ketones. *Tetrahedron Lett.* 21, 693–696.
- Beigelman, L., McSwiggen, J., Draper, K., Gonzalez, C., Jensen, K., Karpeisky, A., Modak, A., Matulic-Adamic, J., DiRenzo, A., Haeblerli, P., Sweedler, D., Tracz, D., Grimm, S., Wincott, F., and Usman, N. (1995) Chemical Modifications of Hammerhead Ribozymes. *J. Biol. Chem.* 270, 25702–25708.
- Beigelman, L., Karpeisky, A., and Usman, N. (1994) Synthesis of 1-Deoxy-D-Ribofuranose Phosphoramidite and the Incorporation of Abasic Nucleotides in Stem-loop II of a Hammerhead Ribozyme. *Bioorg. Med. Chem. Lett.* 4, 1715–1720.
- Bellon, L., Workman, C., Sherrer, J., Usman, N., and Wincott, F. (1996) Morpholino-Linked Ribozymes: A Convergent Synthetic Approach. *J. Am. Chem. Soc.* 118, 3771–3772.
- Benseler, F., Fu, D. J., Ludwig, J., and McLaughlin, L. W. (1993) Hammerhead-like Molecules Containing Non-Nucleoside Linkers Are Active RNA Catalysts. *J. Am. Chem. Soc.* 115, 8483–8484.
- Billman, J. H., and McDowell, J. W. (1961) Reduction of Schiff Bases. III. Reduction with Dimethylamine Borane. *J. Org. Chem.* 26, 1437–1440.
- Bomann, M. D., Guch, I. C., and DiMare, M. (1995) A Mild, Pyridine-Borane-Based Reductive Amination Protocol. *J. Org. Chem.* 60, 5995–5996.
- Borch, R. F., Bernstein, M. D., and Durst, H. D. (1971) The Cyanohydrinborate Anion as a Selective Reducing Agent. *J. Am. Chem. Soc.* 93, 2897–2904.
- Burgin, A. B., Gonzalez, C., Matulic-Adamic, J., Karpeisky, A. M., Usman, N., McSwiggen, J., and Beigelman, L. (1996) Chemically Modified Hammerhead Ribozymes with Improved Catalytic Rates. *Biochemistry* 35, 14090–14097.
- Cech, T. R. (1992) Ribozyme Engineering. *Curr. Opin. Struct. Biol.* 2, 605–609.
- Christoffersen, R. E., and Marr, J. J. (1995) Ribozymes as Human Therapeutic Agents. *J. Med. Chem.* 38, 2023–2037.
- Connolly, B. A., Potter, B. V. L., Eckstein, F., Pingoud, A., and Grotjham, L. (1984) Synthesis and Characterization of an Octanucleotide Containing the EcoRI recognition Sequence with a Phosphorothioate Group at the Cleavage Site. *Biochemistry* 23, 3443–3453.
- Deschamps, M., and Sonveaux, E. (1995) Aldehyde Functions in Synthetic Oligonucleotides. *Nucleosides Nucleotides* 14, 867–870.
- Freier, S. M., Kierzek, R., Jaeger, J. A., Sugimoto, N., Caruthers, M. H., Neilson, T., and Turner, D. H. (1986) Improved Free Energy Parameters for Predictions of RNA Duplex Stability. *Proc. Natl. Acad. Sci. U.S.A.* 83, 9373–9377.
- Gibson, H. W., and Bailey, F. C. (1977) Chemical Modification of Polymers. Borohydride reducing Agents Derived from Anion Exchange Resins. *J. Chem. Soc., Chem. Commun.*, 815.

- Gish, G., and Eckstein, F. (1988) DNA and RNA Sequence Determination Based on Phosphorothioate Chemistry. *Science* 240, 1520–1522.
- Goodchild, J. (1990) Conjugates of Oligonucleotides and Modified Oligonucleotides: A Review of Their Synthesis and Properties. *Bioconjugate Chem.* 1, 165–187.
- Gryaznov, S. M., and Letsinger, R. L. (1993) Chemical Ligation of Oligonucleotides in the Presence and Absence of a Template. *J. Am. Chem. Soc.* 115, 3808–3809.
- Harambilis, J., Lagniton, L., and Tregear, G. W. (1994) The Preparation of Enzyme-Labelled Oligonucleotides by Reductive Amination. *Bioorg. Med. Chem. Lett.* 4, 1005–1010.
- Hart, D. J., and Leroy, V. (1995) Some Observations Regarding the Stereochemical Course of Iminium Ion Reductions: An Example of the Size Difference Between Sodium Cyanoborohydride and Sodium Triacetoxyborohydride. *Tetrahedron* 51, 5757–5770.
- Hendry, P., Moghaddam, M. J., McCall, M. J., Jennings, P. A., Ebel, S., and Brown, T. (1994) Using Linkers to Investigate the Spatial Separation of the Conserved Nucleotides A9 and G12 in the Hammerhead Ribozyme. *Biochim. Biophys. Acta* 1219, 405–412.
- Herrlein, M. K., Nelson, J. S., and Letsinger, R. L. (1995) A Covalent Lock for Self-Assembled Oligonucleotide Conjugates. *J. Am. Chem. Soc.* 117, 10151–10152.
- Jarvis, T. C., Alby, L. J., Beaudry, A. A., Wincott, F. E., Beigelman, L., McSwiggen, J. A., Usman, N., and Stinchcomb, D. T. (1996a) Inhibition of Vascular Smooth Muscle Cell Proliferation by Ribozymes that Cleave c-myc mRNA. *RNA* 2, 419–428.
- Jarvis, T. C., Wincott, F. E., Alby, L. J., McSwiggen, J. A., Beigelman, L., Gustofson, J., DiRenzo, A., Levy, K., Arthur, M., Matulic-Adamic, J., Karpeisky, A., Gonzalez, C., Woolf, T. M., Usman, N., and Stinchcomb, D. T. (1996b) Optimizing the Cell Efficacy of Synthetic Ribozymes: Site Selection and Chemical Modifications of Ribozymes Targeting the Proto-oncogen c-myc. *J. Biol. Chem.* 271, 29107–29112.
- Lemaitre, M., Bayard, B., and Lebleu, B. (1987) Specific Antiviral Activity of a Poly(L-lysine)-Conjugated Oligodeoxyribonucleotide Sequence Complementary to Vesicular Stomatitis Virus N Protein mRNA Initiation Site. *Proc. Natl. Acad. Sci. U.S.A.* 84, 648–652.
- McCullum, C., and Andrus, A. (1991) An Optimized Polystyrene Support for Rapid Efficient Oligonucleotide Synthesis. *Tetrahedron Lett.* 32, 4069–4072.
- Moorman, A. E. (1993) Reductive Amination of Piperidines with Aldehydes Using Borane-Pyridine. *Synth. Commun.* 23, 789–795.
- Morvan, F., Sanghvi, Y. S., Perbost, M., Vasseur, J. J., and Bellon, L. (1996) Oligonucleotides Mimics for Antisense Therapeutics: Solution-Phase Synthesis and Automated Solid-Support Synthesis of MMI-Linked Oligomers. *J. Am. Chem. Soc.* 118, 255–256.
- Pelter, A., Smith, K., and Brown, H. C. (1988) *Borane Reagents, Best Synthetic Methods Series*, pp 45–47, 131, Academic Press, San Diego.
- Pelter, A., Rosser, R. M., and Mills, S. (1984) Reductive Aminations of Ketones and Aldehydes Using Borane-Pyridine. *J. Chem. Soc., Perkin Trans. 1*, 717–720.
- Scaringe, S. A., Francklyn, C., and Usman, N. (1990) Chemical Synthesis of Biologically Active Oligoribonucleotides Using β -Cyanoethyl Protected Ribonucleoside Phosphoramidites. *Nucleic Acids Res.* 18, 5433–5441.
- Schuette, J. M., Cole, D. L., and Srivatz, G. S. (1994) Development and Validation of a Method for Routine Base Composition Analysis of Phosphorothioate Oligonucleotides. *J. Pharm. Biomed. Anal.* 12, 1345–1353.
- Stults, J. T., and Marsters, J. C. (1991) Improved Electrospray Ionization of Synthetic Oligodeoxynucleotides. *Rapid Commun. Mass Spectrom.* 5, 359–363.
- Symons, R. H. (1994) Ribozymes. *Curr. Opin. Struct. Biol.* 4, 322–330.
- Tsou, D., Hampel, A., Andrus, A., and Vinayak, R. (1995) Large Scale Synthesis of Oligoribonucleotides on High-loaded Polystyrene (HLP) Support. *Nucleosides Nucleotides* 14, 1481–1492.
- Tuschl, T., and Eckstein, F. (1993) Hammerhead Ribozymes: Importance of Stem-loop II for Activity. *Proc. Natl. Acad. Sci. U.S.A.* 90, 6991–6994.
- Urata, H., and Akagi, M. (1993) A Convenient Synthesis of Oligonucleotides with a 3'-Phosphoglycolate and 3'-Phosphoglycaldehyde Terminus. *Tetrahedron Lett.* 34, 4015–4018.
- Usman, N., and Cedergren, R. J. (1992) Exploiting the Chemical Synthesis of RNA. *Trends Biochem. Sci.* 17, 334–339.
- Wincott, F., DiRenzo, A., Shaffer, C., Grimm, S., Tracz, D., Workman, C., Sweedler, D., Gonzalez, C., Scaringe, S., and Usman, N. (1995) Synthesis, Deprotection, Analysis and Purification of RNA and Ribozymes. *Nucleic Acids Res.* 23, 2677–2684.
- Wright, P., Lloyd, D., Rapp, W., and Andrus, A. (1993) Large Scale Synthesis of Oligonucleotides via Phosphoramidite Nucleosides and a High-loaded Polystyrene Support. *Tetrahedron Lett.* 34, 3373–3376.
- Wyrzykiewicz, T. K., and Cole, D. L. (1994) Sequencing of Oligonucleotide Phosphorothioates Based on Solid-Supported Desulfurization. *Nucleic Acids Res.* 22, 2667–2669.
- Yang, J.-H., Usman, N., Chartrand, P., and Cedergren, R. J. (1992) Minimum Ribonucleotide Requirement for Catalysis by the RNA Hammerhead Domain. *Biochemistry* 31, 5005–5009.
- Yoon, N. M., Kim, E. G., Son, H. S., and Coi, J. (1993) Borohydride Exchange Resin, A New Reducing Agent for Reductive Amination. *Synth. Commun.* 23, 1595–1599.

BC970011Q

Influence of Membrane-Active Peptides on Lipospermine/DNA Complex Mediated Gene Transfer

Antoine Kichler,^{†,‡} Karl Mechtler,[§] Jean-Paul Behr,^{||} and Ernst Wagner^{*,†,⊥}

Institute of Biochemistry, University of Vienna, Dr. Bohrgasse 9/3, A-1030 Vienna, Research Institute of Molecular Pathology, A-1030 Vienna, Austria, Université Louis Pasteur, URA 1386 du CNRS, F-67400 Strasbourg-Illkirch, France, and Boehringer Ingelheim Research and Development Vienna, Dr. Boehringerergasse 5-11, A-1121 Vienna, Austria. Received October 24, 1996[⊗]

To explore whether endosomal release presents a major barrier to lipospermine-mediated gene delivery, acidic membrane-active peptides derived from influenza virus or artificial sequences were incorporated into DNA/dioctadecylamidoglycylspermine (=Transfectam) complexes. Depending on the cell line used, gene expression levels are approximately 3–30-fold higher than those obtained by applying DNA complexed to optimal amounts of Transfectam alone. In addition, gene transfer efficiency of DNA complexes with lower amounts of Transfectam (1.5–2 charge equiv) is increased by a factor of up to 1000 by peptides INF6 (influenza virus derived sequence) and INF10 (artificial sequence). The helper lipids 1,2-dioleoylphosphatidylethanolamine, egg phosphatidylethanolamine, and 1,2-dioleoyl-*rac*-glycerol also can enhance the gene transfer. Thus, endosomal escape seems to be only a moderate barrier for optimized, positively charged DNA/Transfectam complexes, but a substantial bottleneck for less positively charged complexes.

INTRODUCTION

Gene therapy relies on strategies that allow efficient and safe introduction of genetic information into human cells. Although most gene therapy protocols use recombinant viral vectors, the limitations of those biological vectors have prompted the design of a great variety of new synthetic systems, among which mono- and polycationic amphipathic molecules, able to complex DNA, have proven to be very attractive (Felgner et al., 1987, 1994; Behr et al., 1989; Leventis and Silviu, 1990; Gao and Huang, 1991; Rose et al., 1991; Hawley-Nelson et al., 1993; Solodin et al., 1995). This class of vectors has been shown to be applicable for *in vivo* administration in experimental animals (Brigham et al., 1989; Alton et al., 1993; Zhu et al., 1993; Canonico et al., 1994; Liu et al., 1995; Schwartz et al., 1995; Thierry et al., 1995) and in clinical trials (Nabel et al., 1993; Caplen et al., 1995). Despite the advances, the efficiency of these vectors, based on number of administered genes, remains orders of magnitude behind that of viral vectors. Efforts to further improve lipid-based gene transfer have been primarily focused on the direct modification of the cationic lipid (acyl chains, spacer arm, hydrophilic part; Felgner et al., 1994; Remy et al., 1994); the mechanism and the limiting steps of gene delivery remain unclear. Packaging of DNA into compact particles, uptake into the cell, release from internal vesicles, release of the DNA from the cationic lipid, and transfer into the nucleus are considered important steps of DNA delivery. Complexation of cationic lipids and DNA results in the formation of nucleolipidic particles (Behr, 1994; Sternberg et al.,

1994; Gao and Huang, 1996), which bind to the cell membrane surface by charge interaction, and endocytosis seems to be an efficient and the major delivery pathway (Legendre and Szoka, 1992; Behr, 1993; Zhou and Huang, 1994; Wrobel and Collins, 1995; Zabner et al., 1995) in many cell types. However, subsequent steps, i.e. the transport of DNA from the endosome to the cytoplasm and thence to the nucleus (Zabner et al., 1995) and the release of DNA from the cationic lipid (Zabner et al., 1995; Xu and Szoka, 1996), are considered to represent bottlenecks in successful gene transfer. Release of DNA from endosomes is suggested to proceed by destabilization of the endosomal membrane triggered by mixing the cationic lipids with the cellular anionic lipids (Leventis and Silviu, 1990; Xu and Szoka, 1996); it is, however, unclear how efficiently this mechanism proceeds.

The goal of this work was to evaluate whether gene expression mediated by the lipospermine Transfectam (dioctadecylamidoglycylspermine, DOGS¹) (Behr et al., 1989) can be further enhanced by adding compounds that should facilitate the transfer across the endosomal membrane. As membrane-destabilizing agents we used amphipathic peptides (Plank et al., 1994; Mechtler and Wagner, 1997) as well as helper lipids (Duzgunes et al., 1989; Leventis and Silviu, 1990; Felgner et al., 1994; Zhou and Huang, 1994; Remy et al., 1995) added to Transfectam/DNA. Amphipathic peptides were previously found to strongly (up to ≥ 1000 -fold) enhance polycation-based gene transfer (Plank et al., 1994; Gottschalk, 1996; Mechtler and Wagner, 1997; Zauner, 1995). As reported in this paper, we found that incorporation of peptides into Transfectam/DNA complexes results in (only) 3–30-fold higher gene expression as

* Author to whom correspondence should be addressed [telephone (+43) 1-80105-783; fax (+43) 1-80105-782; e-mail WagnerE@Bender.co.at].

[†] University of Vienna.

[‡] Present address: Centre de Biophysique Moléculaire, Glycobiologie, Rue Charles-Sadron, 45000 Orléans, France.

[§] Research Institute of Molecular Biology.

^{||} Université Louis Pasteur.

[⊥] Boehringer Ingelheim.

[⊗] Abstract published in *Advance ACS Abstracts*, February 15, 1997.

¹ Abbreviations: DOG, 1,2-dioleoyl-*rac*-glycerol; DOGS, dioctadecylamidoglycylspermine = Transfectam; DOPE, 1,2-dioleoyl-*sn*-glycero-3-phosphoethanolamine; EPC, egg phosphatidylcholine; EPE, egg phosphatidylethanolamine; FCS, fetal calf serum; Fmoc, *N*-(9-fluorenyl)methoxycarbonyl; HBS, Hepes-buffered saline (150 mM NaCl, 20 mM Hepes, pH 7.3); HBTU, [O-(1*H*-benzotriazol-1-yl)-*N,N,N,N*-tetramethyluronium hexafluorophosphate]; MOG, 1-monooleoyl-*rac*-glycerol; SM, sphingomyelin.

Table 1. Sequences and Origins of the Different Membrane-Active Peptides

peptide	origin	specificity for low pH	sequence (N → C terminus)	ref
melittin	peptide from bee venom	no	GIGAV LKVL TGLPA LISWI KRKRQQ	<i>a</i>
INF6	influenza HA-2 (see <i>b</i>)	no	GLF GAI AGFI ENGW EGMI DGWYG	<i>b</i>
INF5	dimeric HA-2 acidic mutant	yes	GLF EAI EGFI ENGW EGNI DG _{JK} GLF EAI EGFI ENGW EGNI DG	<i>b</i>
INFA	influenza HA-2 alanine mutant	no	GLF EAI EAFI ENAW EAMI DAWYG	<i>c</i>
EGLA-I	artificial sequence	yes	GLFL GLA [EGLA] ₄ EGL ECLA GGSC	<i>c</i>
INF10	influenza HA-2 ECLA hybride	yes	GLF ELA ECLA ELGW ECLA EGWYGC	<i>c</i>

^a Benachir and Lafleur (1995). ^b N-terminal sequences of influenza virus hemagglutinin subunit HA-2 [see Plank et al. (1994)]; n, norleucine; K, carboxyl-terminal lysine modified at *N*^α and *N*^ε. ^c Mechtler and Wagner (1997).

compared to optimized, positively charged Transfectam/DNA complexes. This suggests that for Transfectam/DNA complexes the escape of DNA from endocytic vesicles is an existing, but minor, bottleneck. However, transfection of more electroneutral formulations is strongly increased by peptides and helper lipids by up to 1000-fold, indicating that for these particles endosomal escape is a limiting step.

MATERIALS AND METHODS

Materials. The plasmid pCMVL, coding for the *Photinus pyralis* luciferase gene under control of the cytomegalovirus enhancer/promoter, has been described (Plank et al., 1992). Endotoxin content was measured by the *Limulus amoebocyte* lysate assay (BioWhittaker, Walkersville, MD). Lipopolysaccharide content of pCMVL used in transfection experiments was 0.2 endotoxin unit/ μ g of DNA. Transfectam was synthesized as described (Behr et al., 1989) and is available from Promega (Madison, WI). Chloroquine, bafilomycin A₁, DOPE, MOG, DOG, EPE, EPC, cholesterol, and melittin (from bee venom) were obtained from Sigma (St. Louis, MO).

Peptide Synthesis. Peptides described in Table 1 were assembled on an Applied Biosystems 433 synthesizer with feedback monitoring by using fluorenylmethoxycarbonyl (Fmoc)-protected amino acids. Amino acids were coupled by the HBTU activation method (Fastmoc^U; 0.25 mmol scale; Knorr et al., 1989). The following side chain protecting groups were used: (Boc)Lys, (t-Bu)Glu, (t-Bu)Asp, and (Trt)Asn.

The synthesis and purification of the INF5 and INF6 peptides are described in Plank et al. (1994). The peptides INFA, INF10, and ECLA-I were synthesized according to the method of Mechtler and Wagner (1997). In brief, for ECLA-I, an HMP-resin (TentaGel R PHB; 0.22 mmol/g, Rapp Polymere) was chosen, using a mixture of 70% *N*-methylpyrrolidone/30% dimethylformamide (DMF) as solvent. Peptides INFA and INF10 were synthesized on a Cys(Trt) preloaded aminomethylated polystyrene resin with a *p*-carboxytrityl chloride linker (0.52 mmol/g; PepChem, Tübingen, Germany) using DMF as solvent.

The peptides were cleaved from the resin, and side chain protecting groups were removed with a mixture of trifluoroacetic acid/water/phenol/thioanisole/ethanedithiol (10:0.5:0.75:0.5:0.25) for 1.5 h at room temperature. Crude peptides were precipitated by dropwise addition of diethyl ether and were collected by centrifugation. Peptides were washed three times with ether and subsequently dried under a stream of argon followed by high vacuum. Crude peptides, dissolved in 1 M triethylammonium bicarbonate (pH 9), were subjected to gel filtration (Sephadex G-10; 20 mM triethylammonium acetate, pH 7.3). The purified peptide fractions were freeze-dried in a Speedvac (Savant) and stored as a powder at -80 °C.

The purity of the peptides was determined by analytical reversed phase HPLC, and peptide identities were confirmed by time-of-flight mass spectroscopy performed with a Finnigan MAT Lasermat instrument. Purified peptides were stored at -80 °C as lyophilized powder or in a 75:25 (v/v) HBS/glycerol mixture. Peptide INF6 lost its biological activity when stored in solution, most likely by structural changes involving aggregation (changes in HPLC profile). The membrane disruption activity of the peptides was tested in liposome and erythrocyte lysis assays (Plank et al., 1994; Mechtler and Wagner, 1997).

Liposome Leakage Assay. The ability of peptides INF6 and INF10, in free form or associated with Transfectam, to disrupt liposomes was assayed by the release of calcein from liposomes loaded with a self-quenching concentration of calcein. Liposomes (lipid compositions in molar ratio: EPC/EPE/cholesterol/SM, 10:3:5:2) were prepared as described (Mechtler and Wagner, 1997) by reversed phase evaporation with an aqueous phase of 100 mM calcein (dissolved by addition of 3.75 equiv of sodium hydroxide) and 50 mM NaCl and extruded through a 100 nm polycarbonate filter to obtain a uniform size distribution. The liposomes were separated from unincorporated material by gel filtration on Sepharose 4B with an iso-osmotic buffer (200 mM NaCl, 25 mM HEPES, pH 7.3). For the leakage assay in 96 well microtiter plates, the liposome stock solution was diluted (10 μ L/mL) in assay buffer (200 mM sodium chloride containing 20 mM citrate, pH 5.5, or 20 mM HEPES, pH 7.3). Fivefold serial dilutions of the test samples (stock solutions in 100 μ L of buffer: 5 μ g of peptide INF6 or 7.5 μ g of INF10, either in free form or associated with 7.5 μ g of Transfectam) were prepared in a 96 well microtiter plate (rows B–G). Row H was left as blank. Eighty microliters of the serial dilution of the test samples was added to 100 μ L of the liposome solution in another 96 well microtiter plate (final lipid concentration: 15 μ M) and, after 20 min of incubation at room temperature, assayed for calcein fluorescence at 515 nm (excitation 495 nm) on a microtiter plate fluorescence photometer (Perkin-Elmer). The value for 100% leakage was obtained by addition of 1 μ L of a 10% Triton X-100 solution to row A; row H (liposomes without peptide) was defined as 0% leakage.

Preparation of the Cationic Lipid/DNA Complexes with/without Membrane-Active Peptides or Helper Lipids. Complexes of DNA and Transfectam were prepared as described (Barthel et al., 1993). Briefly, plasmid DNA (3 μ g) and the desired amount of Transfectam were each diluted into 75 μ L of 150 mM NaCl and gently mixed. After 10–20 min, the two solutions were mixed. After an additional 10 min, the mixture was diluted with serum-free medium to a final volume of 2 mL; 1 mL of the transfection mixture was put on each well of the duplicate.

We use the term "charge equivalent" to indicate the amount of lipid used for a transfection; 1 charge equiv corresponds to the amount required to neutralize all of

the negative charges carried by the phosphate groups of the plasmid. For example, 3 μg of DNA corresponds to 9 nmol of negative charges; the charge ratio is calculated by taking into account the fact that 1 mol of Transfectam carries three positive charges, as three ammonium groups are protonated at physiological pH; according to this calculation, 3 μg of nucleic acid is neutralized by 3 nmol (3.8 μg) of Transfectam.

Membrane-active peptides (0.5 or 1 mg/mL solutions in HBS/glycerol, 3:1) were added to the preformed Transfectam/DNA complexes; after a 10–20 min period, the transfection volume was adjusted to 2 mL with culture medium, and 1 mL of this transfection mixture per well was pipetted onto the cells.

Helper lipids (DOPE, DOG, EPC, EPE, MOG) and cholesterol were diluted in ethanol containing a trace of methylene chloride (10 μL in 1 mL ethanol). The Transfectam/DNA/helper lipid complexes were formed by mixing the desired amounts of Transfectam/helper lipid (the amounts of helper lipids used are given in equivalents (mole/mole) to Transfectam) prior to dilution with the DNA solution.

Chromatography of Peptide/Transfectam/DNA Complexes. To demonstrate that the negatively charged peptides (at physiological pH) are bound via electrostatic interactions to the Transfectam 2 equiv/DNA complex, we subjected purified INF5 (90 μg) or Transfectam 2 equiv/60 μg of DNA with/without 90 μg of INF5 to gel filtration (Superose 12 HR10-30, Pharmacia, 10 \times 300 mm, HBS, flow rate 0.5 mL/min). Free peptide was detected by spectrophotometry measuring at 280 and 230 nm.

Cell Culture. Media, horse serum, and fetal calf serum (FCS) were from Gibco-BRL (Gaithersburg, MD). Culture media were supplemented with 2 mM L-glutamine and antibiotics. Human melanoma cells (H225) were kindly provided by S. Schreiber and G. Stingl (University of Vienna, Austria). BNL CL.2 (mouse embryonic liver cells), A549 (human lung carcinoma cells), and M-3 (Cloudman S91 melanoma cells; clone M-3) were obtained from ATCC (Rockville, MD). H225 cells were cultured in Roswell Park Memorial Institute (RPMI) medium 1640/10% FCS/1 mM sodium pyruvate, A549 cells in Dulbecco's Modified Eagle Medium (DMEM)/10% FCS, BNL CL.2 cells in high-glucose DMEM/10% FCS, and M-3 cells in Ham's-F10 medium/15% horse serum/5% FCS.

Transfection of Cells. Fifty thousand to seventy-five thousand cells per well for 24 well plates (Nunc, Roskilde, Denmark) and 150 000 cells per well for 6 well plates were plated the day before transfection. For all experiments, the final transfection volume was 1 mL per well. After 3–4 h, transfection medium was replaced with fresh medium containing 10% FCS. Luciferase activity was assayed 24 h after transfection. Each experiment was carried out several times; within a series, experiments were done in duplicate.

Luciferase Activity. Cells were harvested after 24 h in 150–200 μL of 250 mM Tris (pH 7.3)/0.5% Triton X-100. The cell lysate was then transferred to 1.5 mL Eppendorf tubes and centrifuged for 5 min at 10000g to pellet debris. Luciferase light units were recorded (using a Clinilumat LB9502 instrument from Berthold, Bad Wildbad, Germany) from an aliquot of the supernatant (20 μL) with 10 s integration after automatic injection of freshly prepared luciferin solution (Cotten et al., 1991). Luciferase background (150–250 light units) was subtracted from each value, and the transfection efficiencies were expressed as total light units per well and are the

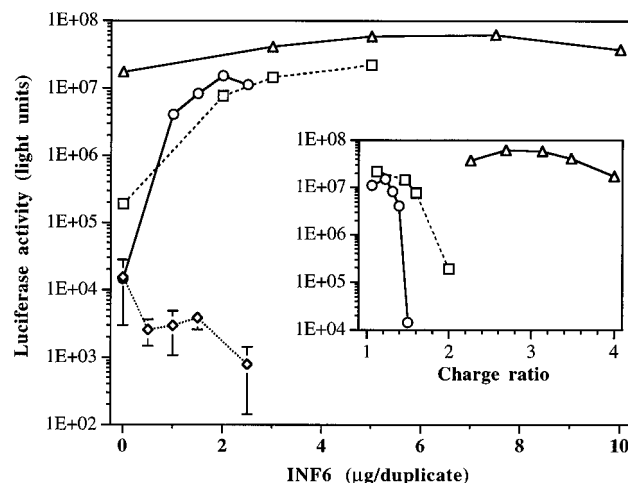


Figure 1. Transfection efficiency of Transfectam/DNA/INF6 complexes. Complexes of 1 (\diamond), 1.5 (\circ), 2 (\square), and 4 (\triangle) charge equivalents of Transfectam/3 μg of pCMV in the presence of increasing amounts of the membrane-active peptide INF6 were used. DNA complexes were mixed with RPMI 1640 culture medium and added to the human melanoma cells H225 (75 000 cells per well in 24 well plates). After 4 h, the transfection medium was replaced by fresh RPMI containing 10% FCS. The cells were harvested 24 h after transfection and assayed for luciferase activity. Total luciferase activity of the cells is shown and is the mean of duplicates (\pm SD). (Insert) Representation of the luciferase activity versus the calculated charge ratio (Transfectam/DNA + INF6; \pm) of the different complexes. As the negatively charged peptide INF6 (four negative charges per molecule at neutral pH) associates with the positively charged lipospermine/DNA complex, the charge ratio \pm is modified.

means of duplicates. The Bradford dye-binding assay (Bio-Rad, Hercules, CA) was used to quantify the protein content.

Flow Cytometry. Plasmid DNA was incubated with the fluorescent intercalator dye YOYO-1 (Molecular Probes, Eugene, OR; ca. 1 dye molecule/300 bp), after which complexes were mixed as described above. The complexes were added to 300 000 H225 cells per well (6 well plates) at either 4 $^{\circ}\text{C}$ (cell surface association) or 37 $^{\circ}\text{C}$ (cell surface association and cellular uptake) for 4 h. The cells were washed twice with cold PBS and harvested with 1 mM EDTA in PBS. Cells were then analyzed on a FACScan (Becton Dickinson, San Jose, CA).

RESULTS

Increased Efficiency of Lipospermine/DNA Complexes through Membrane-Active Peptides. Complexes of plasmid pCMV (encoding a luciferase reporter gene) and 1, 1.5, 2, or 4 charge equiv of Transfectam in combination with various amounts of the membrane-active peptide INF6 (see Table 1) were prepared. As the influenza-derived peptide INF6 has four negative charges at pH 7, it will associate, via electrostatic interactions, with the cationic lipid/DNA particles. Almost all of the peptide was found to bind to the transfecting particles (as determined by chromatography, see Materials and Methods). Transfection efficiencies were determined by using human H225 melanoma cells (Figure 1) and several other cell lines (Figure 2). As shown in Figure 1, a 100–1000-fold increase could be observed upon addition of INF6 when 2 and 1.5 equiv, respectively, of lipid were used. In optimal conditions (4 equiv) only a slight enhancement (up to 5-fold) could be obtained in H225 cells. No enhancement was observed when neutral particles (1 charge equiv) were used, presumably because only few peptides can bind to these complexes. In fact, interactions with the cell membrane might be reduced

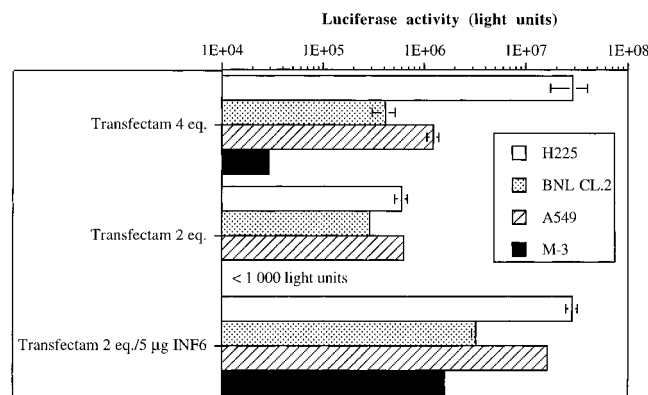


Figure 2. Peptide effect can be observed on several cell lines. The efficiency of Transfectam 2 equiv/pCMVL/5 µg of INF6 complexes was tested on H225, BNL CL.2, and A549 cells (100 000–150 000 cells plated per well in 6 well plates) and on M-3 cells (60 000 cells per well plated in a 24 well plate coated with 0.1% gelatin). Total luciferase activity of the cells is shown and is the mean of duplicates (\pm SD).

because residual positive charges on the complex required for cell interaction have been masked by the peptide association. The insert of Figure 1 presents the transfection efficiency of Transfectam/DNA/INF6 complexes versus the theoretical charge ratio (\pm) of the complexes. High luciferase expression can be achieved with almost electroneutral lipid-based vectors.

We tested several other cell lines to determine whether the effects of the membrane-active peptide on lipospermine-mediated gene transfer is specific for H225 melanoma cells or not (see Figure 2). The results obtained on mouse embryonic liver cells (BNL CL.2), human lung carcinoma cells (A549), and murine melanoma cells (M-3) demonstrate that the enhancement of transfection efficiency through addition of INF6 to DNA/2 equiv of Transfectam is a more general phenomenon. The extent of increase in gene expression mediated by the peptide is cell type dependent; while in H225 cells with DNA/2equiv of Transfectam/INF6 similar results were obtained as with DNA/4equiv of Transfectam (see also Figure 1), in the other tested cell lines approximately 10–50-fold higher expression levels were obtained.

To determine whether the peptide might influence the association of the DNA complexes with the cell, flow cytometry studies of various transfection complexes were performed on H225 cells. For this purpose the plasmid DNA was labeled with the intercalator YOYO-1 (Rye et al., 1992; Hirons et al., 1994) before formation of the lipid/DNA complex. As shown in Figure 3, the association of the Transfectam/DNA complexes with the cell surface varies with the charge ratio: with 2 equiv, a heterogeneous cell population is found, while at 4 equiv a classical Gauss curve is obtained. Addition of membrane-active peptides to 2 equiv (or 4 equiv, not shown) of Transfectam does not significantly modify the association with the cell (compare parts B and C of Figure 3), at either 37 or 4 °C (not shown). These experiments suggest that the peptide acts as expected; that is, it improves the release of the complexes from the endosomes.

Enhancement Is Peptide Sequence Dependent. Previous work with ligand/polylysine DNA complexes in association with membrane-destabilizing peptides showed that peptides with specificity for low pH were the most useful (Plank et al., 1994; Mechtler and Wagner, 1997). Our preliminary results (described above) led us to test a series of membrane-active peptides (Table 1) in association with 2 charge equiv of Transfectam.

The peptides INF6, INF4, and melittin, which possess a good membrane disruption activity but no specificity

for low pH (Plank et al., 1994; Mechtler and Wagner, 1997), displayed different behaviors: INF4 and INF6 (negatively charged) increased the transfection efficiency of 2 charge equiv of Transfectam 10- and ~200-fold respectively, while melittin (positively charged) only slightly increased the luciferase expression (Figure 4). Moreover, melittin was highly toxic at 2.5 µg/mL. The peptides INF5 and INF10, which can efficiently disrupt membranes at pH 5.0 (Plank et al., 1994; Mechtler and Wagner, 1997), gave better results than the INF4 peptide but were less efficient than the INF6 derivative. The artificial pH-specific peptide EGLA-I, in which one of the alanine residues in the repeat of GALA (Parente et al., 1988a,b) has been replaced by glycine (Mechtler and Wagner, 1997), gave results comparable to those of the INF5 peptide but had less activity than INF6.

Thus, the most efficient peptide in combination with Transfectam appeared to be peptide INF6 whose membrane-destabilizing activity is pH independent. To confirm that the peptides are still active when ionically bound to the cationic lipid/DNA complex, we measured leakage activity of the two most efficient peptides, INF10 (Figure 5A) and INF6 (Figure 5B), either in free form or associated with Transfectam, using calcein-loaded liposomes of natural lipid composition (EPC/EPE/cholesterol/SM) at neutral or acidic pH. As can be seen, the peptides efficiently release calcein also in combination with Transfectam, although the activity is diminished in quantity. In quality, the characteristics of the peptides are retained: INF10 shows specificity for acidic pH, whereas INF6 is effective at both pH levels.

To check whether the peptides may act at the level of acidic endocytic vesicles, we measured the level of reporter gene expression obtained with Transfectam 2 equiv/DNA + peptide in the presence or absence of the specific inhibitor of the vacuolar proton pump bafilomycin A₁ (Bowman et al., 1988; Yoshimori et al., 1991). As expected, the INF10 formulation (with specificity for low pH) was more sensitive to bafilomycin (5-fold decreased gene expression) than the INF6 formulation (see Figure 6). Note that transferrin-polylysine/acidic-peptide mediated gene transfer was shown to be also inhibited approximately 5-fold by bafilomycin (Plank et al., 1994; Zauner et al., 1995). Bafilomycin did not decrease the efficiency of 4 charge equiv of Transfectam. This latter observation is consistent with the buffering properties of the spermine headgroup (Behr, 1994).

Combination with Neutral Lipids (Helper Lipids) Affects the Transfection Efficiency. The efficiency of Transfectam/DNA complexes near electroneutrality is strongly increased when 1.5–2 equiv of the helper lipid DOPE (moles per mole to Transfectam) is added (Remy et al., 1995). We tried to find other lipids able to increase the efficiency of Transfectam when such suboptimal amounts were used. The combination of 2 charge equiv of Transfectam with 1–3 equiv (mol/mol) of DOPE, EPE, or DOG resulted in 10–20-fold higher gene expression levels (Figure 7). MOG enhanced expression approximately 4-fold, whereas EPC and cholesterol could not improve the transfection efficiency on H225 cells. An additional increase—up to 7-fold—of the Transfectam/DOPE formulation could be obtained by mixing DOG (1 mol % to DOPE) with these two lipids (data not shown). The effect of DOPE and DOG relies presumably on their ability to induce fusion and to stabilize H_{II} phases (Duzgunes et al., 1989; Siegel et al., 1989). The addition of DOPE to 2 charge equiv of Transfectam completely changes the FACScan profile (compare parts B and D of Figure 3): the cell population is more homogeneous and

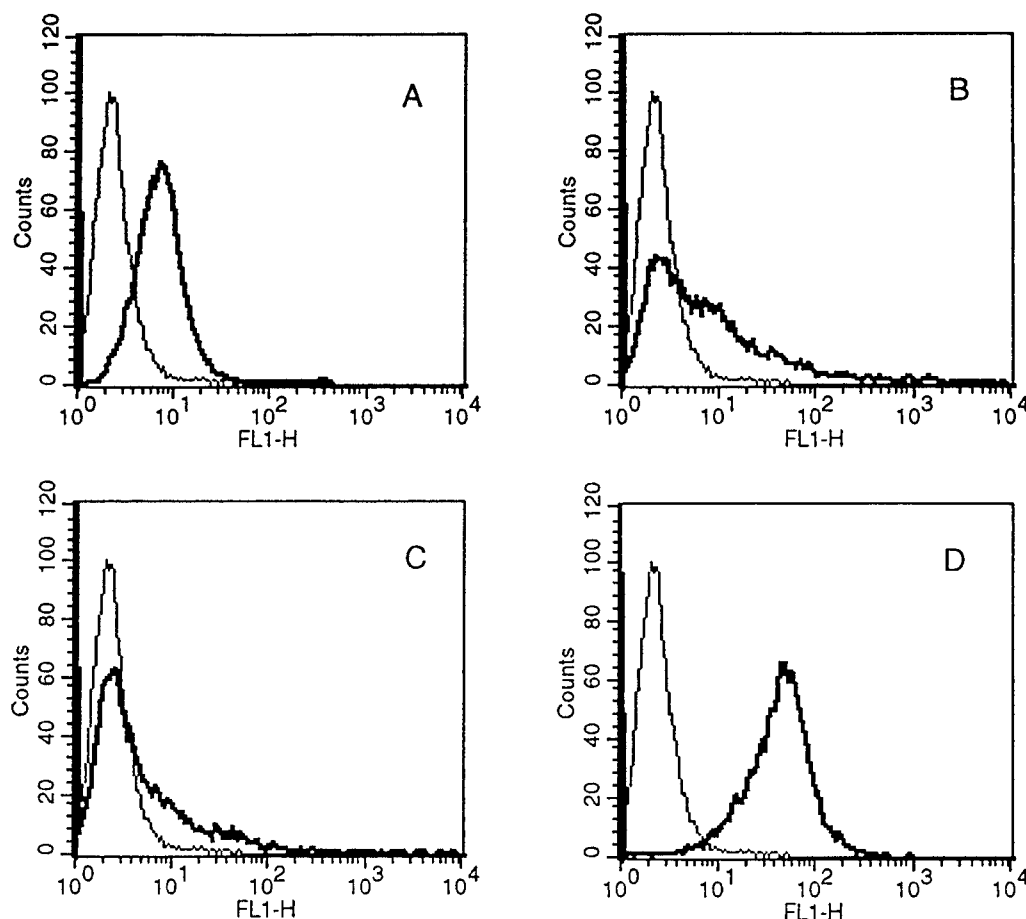


Figure 3. FACS analysis. Three hundred thousand H225 cells were incubated in the presence of transfection complexes containing 1.5 μ g of YOYO-1-labeled pCMVL and either Transfectam 4 (A) or 2 equiv (B), Transfectam 2 equiv/1.5 μ g of INF5 (C), or Transfectam 2 equiv/1.5 equiv of DOPE (D). After 4 h, the cells were washed twice with PBS, harvested with 1 mM EDTA/PBS, and analyzed by FACS (thick lines). Cells incubated with YOYO-1-labeled DNA alone were indistinguishable from unstained control cells and are shown as negative control (thin lines).

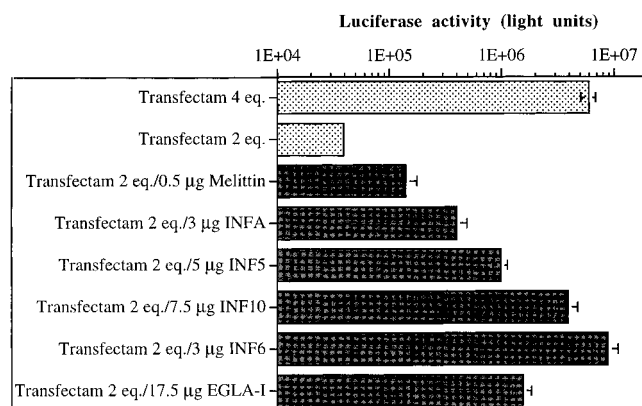


Figure 4. Several peptides are able to increase the efficiency of Transfectam 2 equiv. Increasing amounts of peptide were added to Transfectam 2 equiv/3 μ g of DNA complexes (as described under Materials and Methods and Figure 1). The best formulation for each peptide is compared to Transfectam 4 and 2 charge equivalents. Total luciferase activity of the cells is shown and is the mean of duplicates (\pm SD).

the cell association and uptake are higher with than without helper lipid.

DISCUSSION

The efficiency of DNA transfer mediated by cationic lipids or polycations is dependent on many factors, including size and structure of complexes, immunogenicity, stability in serum and against intracellular enzymes, binding and uptake into the cell, release into the

cytoplasm and transfer into the nucleus, or the release of the DNA from the cationic carrier.

Transfection based on receptor-mediated endocytosis of polylysine conjugate/DNA particles is thought to be particularly limited in efficiency by the accumulation of DNA complexes in intracellular vesicles. Methods to destabilize the endosomal membrane, such as addition of replication-defective adenoviruses (Curiel et al., 1991), membrane-active peptides derived from influenza virus (Wagner et al., 1992; Plank et al., 1994) or from rhinovirus (Zauner et al., 1995), and—in some cell types—the use of lysosomotropic agents (Wagner et al., 1994) or glycerol (Zauner et al., 1996), have been shown to strongly enhance the level of gene expression.

There is mounting evidence that DNA delivery seems to take place by endocytosis also in cationic lipid-based gene transfer (Felgner et al., 1987, 1994; Behr et al., 1989; Leventis and Silvius, 1990; Gao and Huang, 1991; Rose et al., 1991; Hawley-Nelson et al., 1993; Solodin et al., 1995; Legendre and Szoka, 1992; Behr, 1993; Zhou and Huang, 1994; Wrobel and Collins, 1995; Zabner et al., 1995). Cationic lipid-based gene transfer has been found to be efficient in a great variety of cells; in contrast to polylysine-based gene transfer, it has been less clear whether the release of the DNA from endosomal compartments is limiting this method of gene transfer (Leventis and Silvius, 1990; Zabner et al., 1995; Xu and Szoka, 1996). This also may depend on the nature of the particular applied cationic lipid or lipid mixture.

Using the lipospermine Transfectam, it was found in previous studies that transfection efficiency was optimal

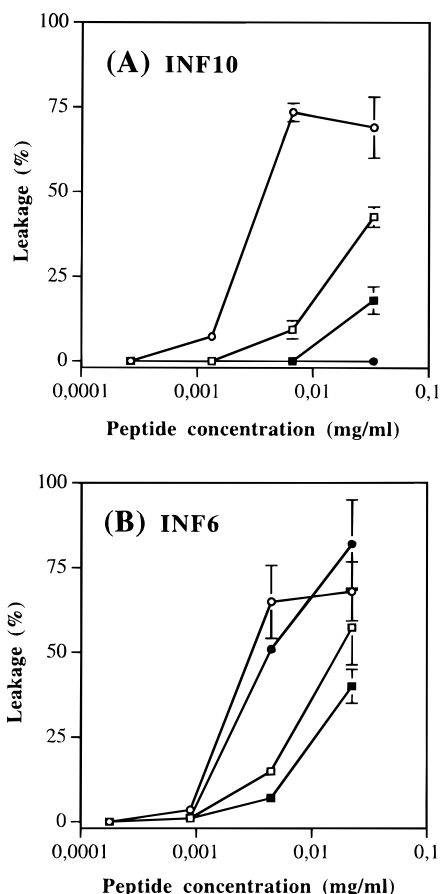


Figure 5. Liposome leakage assay. The leakage activity of peptides INF10 (A) and INF6 (B), in free form (circles) or associated with Transfectam (squares), was determined at pH 7.3 (solid symbols) and 5.5 (open symbols) on EPC/EPE/cholesterol/SM (10:3:5:2) liposomes loaded with 100 mM calcein.

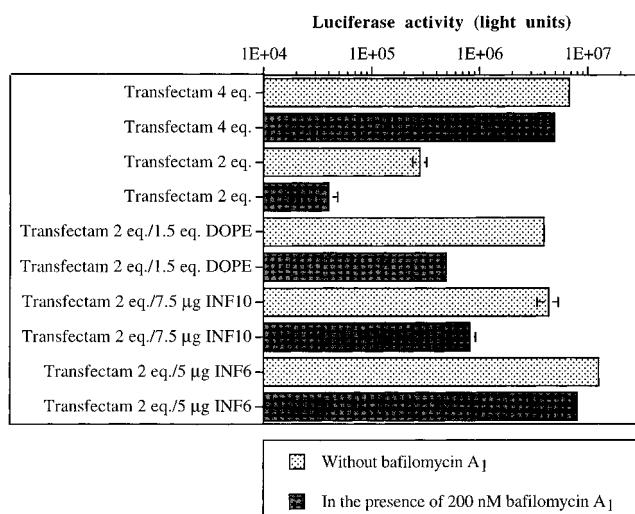


Figure 6. Effects of bafilomycin A₁ on the transfection efficiencies of Transfectam/DNA/peptide or DOPE complexes. Transfection of H225 cells was performed in the absence (light bars) or presence (dark bars) of bafilomycin A₁ (final concentration 200 nM). After 4 h of incubation, the medium was replaced by a fresh one containing 10% FCS. Total luciferase activity of the cells is shown and is the mean of duplicates (±SD).

when the charge ratio of cationic lipid to DNA was highly positive (i.e. about 3–6; Barthel et al., 1993). The positive charges promote binding and uptake of the complex into cells. In addition, Transfectam has endosome buffering capacity (pK_a of the least basic secondary amine ca. 5.4), thus protecting DNA from enzymatic

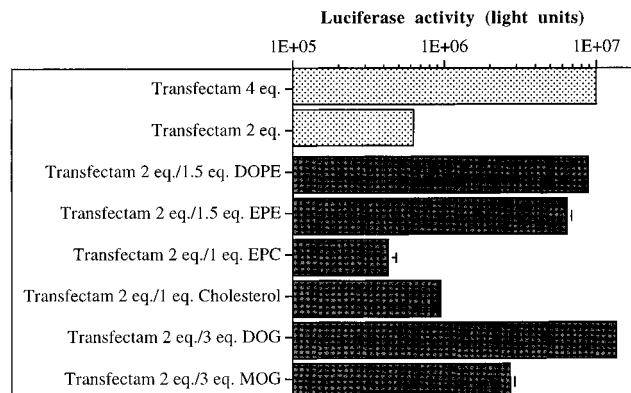


Figure 7. Helper lipids are able to increase the efficiency of 2 charge equiv of Transfectam. Transfection complexes were prepared as described under Materials and Methods. Total luciferase activity of the cells is shown and is the mean of duplicates (±SD).

degradation and potentially causing also some osmotic destabilization of buffered endosomes (Behr, 1994).

We were interested whether the efficiency of Transfectam-mediated plasmid delivery can be enhanced by incorporating influenza-derived peptides. This series of peptides has been previously shown to be able to disrupt liposomes, erythrocytes, or endosomes of cultured cells, enhancing receptor-mediated gene transfer up to approximately 1000-fold (Plank et al., 1994; Mechtler and Wagner, 1997). When optimal amounts of Transfectam are used in association with membrane-destabilizing peptides, a significant, but only moderate (3–30-fold), enhancement of the gene expression was obtained (Figures 1 and 2). Thus, in this context, escape from endocytotic vesicles seems not to be a major bottleneck of gene transfer. Related findings were reported by Kamata et al. (1994), who showed that two influenza-derived peptides can increase the level of gene expression of the commercially available formulation Lipofectin by up to a factor of 5.

However, when we used less positively charged complexes, the addition of membrane-active peptides resulted in up to a 1000-fold increase in expression (1.5 charge equiv of Transfectam in the presence of 2 μg of INF6), reaching or surpassing the level obtained with the optimized amounts of cationic lipid (Figures 1 and 2). The peptide did not change binding of DNA to the cell (Figure 3). Consistent with the working hypothesis that the peptides act on an endosomal level, the effect mediated by the pH-specific peptide INF10 was sensitive to endosomal neutralization by bafilomycin A₁ (Figure 6). Among the peptides tested, only the acidic (negatively charged) ones gave good results in combination with Transfectam. This is in agreement with the hypothesis that for improved endosomal escape of DNA the peptides have to be in the same endocytotic vesicles as the lipid/DNA complexes, which is the case when (negatively charged) peptides are ionically bound to the positively charged Transfectam/DNA particles. The order of efficiency of peptides, when associated with 2 charge equiv of Transfectam, was found to be as follows: INF6 > INF10 > EGLA-I, INF5 > INFA > melittin (Figure 4). These results are different from those obtained with the ligand/polylysine-based system. While INF5 was found to be the best peptide in association with transferrin/polylysine, and approximately 50-fold more effective than INF6 (Plank et al., 1994; Mechtler and Wagner, 1997), in Transfectam-based gene transfer INF5 is 10 times less efficient than INF6. Peptide INF5 has membrane disruption activity only at acidic pH, whereas INF6 is also

active at neutral pH. In lipid-free polylysine-based gene transfer such an activity at neutral pH results in toxic side effects, which were not observed in cells transfected with peptide INF6 in the liposomal system. An additional possible explanation for the higher efficiency of peptide INF6 (compared to INF5 or INF10) is a reduced acidification of endosomes resulting from the buffer capacity of Transfectam (Behr, 1994).

It has recently been shown that highly efficient DNA complexes with low charge (2 equiv of Transfectam) can also be generated by the inclusion of the helper lipid DOPE (Remy et al., 1995). We compared this type of complex with the peptide-containing complexes. The enhancement by DOPE is thought to rely on its capacity for transition from the bilayer ($L\alpha$) phase to the inverted hexagonal (H_{II}) phase. The endosomal protonation promotes this transition, resulting in membrane-active activity (Allen et al., 1990; Litzinger and Huang, 1992; Farhood et al., 1995). Our FACS data suggest an additional, potentially important effect of the helper lipid: the cell association of the transfection complexes is far more pronounced when 1.5 equiv of DOPE is added to 2 charge equiv of Transfectam (Figure 3D) than when the lipospermine is used alone. This suggests that DOPE not only improves the escape of DNA from the endosomes but also increases cell association (and uptake) of the complexes. The existence of this second effect of DOPE is also supported by the fact that the Transfectam/DOPE efficiency is only partially abolished by the presence of the vacuolar proton pump inhibitor bafilomycin A_1 (Figure 6).

Besides DOPE, we used several other lipids in combination with Transfectam to compare their helper capacity with the activity of the membrane-active peptides. EPE and DOG, but not EPC or cholesterol, could enhance the gene expression in H225 cells (Figure 7) to an extent similar to that shown by peptides INF6 and INF10. The lipids that enhance are diacylglycerols, i.e. lipids which do not form stable lamellar structure due to a small headgroup surface. This reinforces the conclusion that the helper lipid has to possess a membrane destabilization activity.

These results show that the modes of action of Transfectam and polylysine after endocytosis of DNA complexes are different. In contrast to polylysine-mediated gene transfer, gene transfer mediated by optimized positively charged Transfectam/DNA complexes cannot be greatly enhanced by the addition of membrane-active peptides, DOPE, glycerol (Zauner et al., 1996), or replication defective adenoviruses [when added to Transfectam/DNA at up to 30 000 particles per cell, data not shown; see also Zabner et al. (1995)]. This finding is not unexpected and is in agreement with the hypothesis that a surplus of positively charged lipids in the DNA complex can directly destabilize the endosomal membrane by lipid mixing (Leventis and Silvius, 1990; Xu and Szoka, 1996) and/or osmotic stress resulting from endosomal protonation of the surplus of Transfectam. In keeping with these hypotheses, the transfection efficiency of DNA complexed with lower, suboptimum amounts of lipids (i.e. 1.5–2 charge equiv) can be increased up to 1000-fold by a membrane-active peptide (without influencing cell association). This confirms that for these particles endosomal escape is a limiting step, similar to what has been observed for polylysine-based gene delivery.

Efficient lipid/DNA transfection complexes that possess a charge ratio near neutrality may be useful for *in vivo* gene transfer. They might be prerequisite for selective, targeted liposomal gene transfer by specific receptor ligands (Remy et al., 1995; Compagnon et al., 1996). This

is also supported by recently published findings of Lee and Huang (1996), who demonstrated that folate-targeted liposome/DNA complexes carrying a net positive charge lose their specificity. In addition, as has also been shown for the polylysine-based system (Plank et al., 1996), positively charged lipid/DNA complexes interact with serum complement; only electroneutral particles do not activate the complement system. This correlates well with the *in vivo* results obtained by Schwartz et al. (1995): they observed highest reporter gene expression when low positively charged Transfectam/DNA complexes (i.e. 0.8 or 1.8 equiv) were used in combination with the lipid DOPE. Thus, for *in vivo* applications, the charge ratio between the carrier and nucleic acids seems to be a key parameter, meaning that Transfectam/DNA/membrane-active peptides might be an alternative to other cationic lipid formulations.

ACKNOWLEDGMENT

We thank Helen Kirlappos for excellent technical support. We are grateful to Ciaran Morrison and Wolfgang Zauner for helpful discussions and to Matt Cotten and Tim Skern for critical review of the manuscript. This work was done with the financial support of the Austrian Science Foundation (FWF).

LITERATURE CITED

- Allen, T. M., Hong, K., and Papahadjopoulos, D. (1990) Membrane contact, fusion, and hexagonal (H_{II}) transitions in phosphatidylethanolamine liposomes. *Biochemistry* 29, 2976–2985.
- Alton, E. W., Middleton, P. G., Caplen, N. J., Smith, S. N., Steel, D. M., Munkonge, F. M., Jeffery, P. K., Geddes, D. M., Hart, S. L., Williamson, R., Fasold, K. I., Miller, A. D., Dickinson, P., Stevenson, B. J., McLachlan, G., Dorin, J. R., and Porteous, D. J. (1993) Non-invasive liposome-mediated gene delivery can correct the ion transport defect in cystic fibrosis mutant mice. *Nat. Genet.* 5, 135–142.
- Barthel, F., Remy, J.-S., Loeffler, J.-P., and Behr, J.-P. (1993) Gene transfer optimization with lipospermine-coated DNA. *DNA Cell Biol.* 12, 553–560.
- Behr, J.-P. (1993) Synthetic gene transfer vectors. *Acc. Chem. Res.* 26, 274–278.
- Behr, J.-P. (1994) Gene transfer with synthetic cationic amphiphiles: prospects for gene therapy. *Bioconjugate Chem.* 5, 382–389.
- Behr, J.-P., Demeneix, B., Loeffler, J.-P., and Perez-Mutul, J. (1989) Efficient gene transfer into mammalian primary endocrine cells with lipopolyamine-coated DNA. *Proc. Natl. Acad. Sci. U.S.A.* 86, 6982–6986.
- Benachir, T., and Lafleur, M. (1995) Study of vesicle leakage induced by melittin. *Biochim. Biophys. Acta* 1235, 452–460.
- Bowman, E. J., Siebers, A., and Altendorf, K. (1988) Bafilomycins: a class of inhibitors of membrane ATPases from microorganisms, animal cells, and plant cells. *Proc. Natl. Acad. Sci. U.S.A.* 85, 7972–7976.
- Brigham, K. L., Meyrick, B., Christman, B., Magnuson, M., King, G., and Berry, L. C. (1989) *In vivo* transfection of murine lungs with a functioning prokaryotic gene using a liposome vehicle. *Am. J. Med. Sci.* 298, 278–281.
- Canonica, A. E., Plitman, J. D., Conary, J. T., Meyrick, B. O., and Brigham, K. L. (1994) No lung toxicity after repeated aerosol or intravenous delivery of plasmid-cationic liposome complexes. *J. Appl. Physiol.* 77, 415–419.
- Caplen, N. J., Alton, E. W. F. W., Middleton, P. G., Dorin, J. R., Stevenson, B. J., Gao, X., Durham, S. R., Jeffery, P. K., Hodson, M. E., Coutelle, C., Huang, L., Porteous, D. J., Williamson, R., and Geddes, D. M. (1995) Liposome-mediated CFTR gene transfer to the nasal epithelium of patients with cystic fibrosis. *Nat. Med.* 1, 39–46.
- Compagnon, B., Moradpour, D., Alford, D. R., Larsen, C. E., Stevenson, M. J., Wands, J. R., and Nicolau, C. (1997) Enhanced gene delivery and expression in human hepato-

- cellular carcinoma cells by cationic immunoliposomes. *J. Liposome Res.* 7, 127–141.
- Cotten, M., Wagner, E., and Birnstiel, M. L. (1991) Receptor-mediated transport of DNA into eukaryotic cells. *Methods Enzymol.* 217, 618–644.
- Curiel, D. T., Agarwal, S., Wagner, E., and Cotten, M. (1991) Adenovirus enhancement of transferrin-polylysine-mediated gene delivery. *Proc. Natl. Acad. Sci. U.S.A.* 88, 8850–8854.
- Duzgunes, N., Goldstein, J. A., Friend, D. S., and Felgner, P. L. (1989) Fusion of liposomes containing a novel cationic lipid, N-[2,3-(dioleoyloxy)propyl]-N,N,N-trimethylammonium: induction by multivalent anions and asymmetric fusion with acidic phospholipid vesicles. *Biochemistry* 28, 9179–9184.
- Farhood, H., Serbina, N., and Huang, L. (1995) The role of dioleoyl phosphatidylethanolamine in cationic liposome mediated gene transfer. *Biochim. Biophys. Acta* 1235, 289–295.
- Felgner, P. L., Gadek, T. R., Holm, M., Roman, R., Chan, H. W., Wenz, M., Northrop, J. P., Ringold, G. M., and Danielsen, M. (1987) Lipofection: a highly efficient, lipid-mediated DNA-transfection procedure. *Proc. Natl. Acad. Sci. U.S.A.* 84, 7413–7417.
- Felgner, J. H., Kumar, R., Sridhar, C. N., Wheeler, C. J., Tsai, Y. J., Border, R., Ramsey, P., Martin, M., and Felgner, P. L. (1994) Enhanced gene delivery and mechanism studies with a novel series of cationic lipid formulations. *J. Biol. Chem.* 269, 2550–2561.
- Gao, X., and Huang, L. (1991) A novel cationic liposome reagent for efficient transfection of mammalian cells. *Biochem. Biophys. Res. Commun.* 179, 280–285.
- Gao, X., and Huang, L. (1996) Potentiation of cationic liposome-mediated gene delivery by polycations. *Biochemistry* 35, 1027–1036.
- Gottschalk, S., Sparrow, J. T., Hauer, J., Mims, M. P., Leland, F. E., Woo, S. L. C., and Smith, L. C. (1996) A novel DNA-peptide complex for efficient gene transfer and expression in mammalian cells. *Gene Ther.* 3, 448–457.
- Hawley-Nelson, P., Ciccarone, V., Gebeyehu, G., Jessee, J., and Felgner, P. L. (1993) Lipofectamine reagent: a new, higher efficiency polycationic liposome transfection reagent. *Focus* 15, 73–79.
- Hirons, G. T., Fawcett, J. J., and Crissman, H. A. (1994) TOTO and YOYO: new very bright fluorochromes for DNA content analyses by flow cytometry. *Cytometry* 15, 129–140.
- Kamata, H., Yagisawa, H., Takahashi, S., and Hirata, H. (1994) Amphiphilic peptides enhance the efficiency of liposome-mediated DNA transfection. *Nucleic Acids Res.* 22, 536–537.
- Knorr, R., Trzeciak, A., Bannwarth, W., and Gillesse, D. (1989) New coupling reagents in peptide chemistry. *Tetrahedron Lett.* 30, 1927–1930.
- Lee, R. J., and Huang, L. (1996) Folate-targeted, anionic liposome-entrapped polylysine-condensed DNA for tumor cell-specific gene transfer. *J. Biol. Chem.* 271, 8481–8487.
- Legendre, J. Y., and Szoka, F. C. (1992) Delivery of plasmid DNA into mammalian cell lines using pH-sensitive liposomes: comparison with cationic liposomes. *Pharm. Res.* 9, 1235–1242.
- Leventis, R., and Silvius, J. R. (1990) Interactions of mammalian cells with lipid dispersions containing novel metabolizable cationic amphiphiles. *Biochim. Biophys. Acta* 1023, 124–132.
- Litzinger, D. C., and Huang, L. (1992) Phosphatidylethanolamine liposomes: drug delivery, gene transfer and immunodiagnostic applications. *Biochim. Biophys. Acta* 1113, 201–227.
- Liu, Y., Liggit, D., Zhong, W., Tu, G. H., Gaensler, K., and Debs, R. (1995) Cationic liposome-mediated intravenous gene delivery. *J. Biol. Chem.* 270, 24864–24870.
- Mechtler, K., and Wagner, E. (1997) Influenza peptide enhanced gene transfer: the role of peptide sequences. *New J. Chem.* 21 (1), 105–111.
- Nabel, G. J., Nabel, E. G., Yang, Z.-Y., Fox, B. A., Plautz, G. E., Gao, X., Huang, L., Shu, S., Gordon, D., and Chang, A. E. (1993) Direct gene transfer with DNA-liposome complexes in melanoma: expression, biologic activity, and lack of toxicity in humans. *Proc. Natl. Acad. Sci. U.S.A.* 90, 11307–11311.
- Parente, R. A., Nir, S., and Szoka, F. C. (1988a) pH-dependent fusion of phosphatidylcholine small vesicles. Induction by a synthetic amphipathic peptide. *J. Biol. Chem.* 263, 4724–473.
- Parente, R. A., Nir, S., and Szoka, F. C. (1988b) Association of a pH-sensitive peptide with membrane vesicles: role of amino acid sequence. *Biochemistry* 27, 8720–8727.
- Plank, C., Zatloukal, K., Cotten, M., Mechtler, K., and Wagner, E. (1992) Gene transfer into hepatocytes using asialoglycoprotein receptor mediated endocytosis of DNA complexed with an artificial tetra-antennary galactose ligand. *Bioconjugate Chem.* 3, 533–539.
- Plank, C., Oberhauser, B., Mechtler, K., Koch, C., and Wagner, E. (1994) The influence of endosome-disruptive peptides on gene transfer using synthetic virus-like gene transfer systems. *J. Biol. Chem.* 269, 12918–12924.
- Plank, C., Mechtler, K., Szoka, F., and Wagner, E. (1996) Activation of the complement system by synthetic DNA complexes: a potential barrier for intravenous gene delivery. *Hum. Gene Ther.* 7, 1437–1446.
- Remy, J.-S., Sirlin, C., Vierling, P., and Behr, J.-P. (1994) Gene transfer with a series of lipophilic DNA-binding molecules. *Bioconjugate Chem.* 5, 647–654.
- Remy, J.-S., Kichler, A., Mordvinov, V., Schuber, F., and Behr, J.-P. (1995) Targeted gene transfer into hepatoma cells with lipopolyamine-condensed DNA particles bearing multi-antennary galactosyl ligands: a stage towards artificial viruses. *Proc. Natl. Acad. Sci. U.S.A.* 92, 1744–1748.
- Rose, J. K., Buonocore, L., and Whitt, M. A. (1991) A new cationic liposome reagent mediating nearly quantitative transfection of animal cells. *BioTechniques* 10, 520–525.
- Rye, H. S., Yue, S., Wemmer, D. E., Quesada, M. A., Haugland, R. P., Mathies, R. A., and Glazer, A. N. (1992) Stable fluorescent complexes of double-stranded DNA with bis-intercalating asymmetric cyanine dyes: properties and applications. *Nucleic Acids Res.* 20, 2803–2812.
- Schwartz, B., Benoist, C., Abdallah, B., Scherman, D., Behr, J.-P., and Demeneix, B. A. (1995) Lipospermine-based gene transfer into newborn mouse brain is optimized by a low lipospermine/DNA charge ratio. *Hum. Gene Ther.* 6, 1515–1524.
- Siegel, D. P., Banschbach, J., Alford, D., Ellens, H., Lis, L. J., Quinn, P. J., Yeagle, P. L., and Bentz, J. (1989) Physiological levels of diacylglycerols in phospholipid membranes induce membrane fusion and destabilize inverted phases. *Biochemistry* 28, 3703–3709.
- Solodin, I., Brown, C. S., Bruno, C. Y., Jang, E. H., Debs, R. J., and Heath, T. D. (1995) A novel series of amphiphilic imidazolium compounds for in vitro and in vivo gene delivery. *Biochemistry* 34, 13537–13544.
- Sternberg, B., Sorgi, F. L., and Huang, L. (1994) New structures in complex formation between DNA and cationic liposomes visualized by freeze-fracture electron microscopy. *FEBS Lett.* 356, 361–366.
- Thierry, A. R., Lunardi-Iskandar, Y., Bryant, J. L., Rabinovich, P., Gallo, R. C., and Mahan, L. C. (1995) Systemic gene therapy: biodistribution and long-term expression of a transgene in mice. *Proc. Natl. Acad. Sci. U.S.A.* 92, 9742–9746.
- Wagner, E., Plank, C., Zatloukal, K., Cotten, M., and Birnstiel, M. L. (1992) Influenza virus hemagglutinin HA-2 N-terminal fusogenic peptides augment gene transfer by transferrin-polylysine-DNA complexes: toward a synthetic virus-like gene-transfer vehicle. *Proc. Natl. Acad. Sci. U.S.A.* 89, 7934–7938.
- Wagner, E., Curiel, D. T., and Cotten, M. (1994) Delivery of drugs, proteins and genes into cells using transferrin as a ligand for receptor-mediated endocytosis. *Adv. Drug Delivery Rev.* 14, 113–135.
- Wrobel, I., and Collins, D. (1995) Fusion of cationic liposomes with mammalian cells occurs after endocytosis. *Biochim. Biophys. Acta* 1235, 296–304.
- Xu, Y., and Szoka, F. C. (1996) Mechanism of DNA release from cationic liposome/DNA complexes used in cell transfection. *Biochemistry* 35, 5616–5623.

- Yoshimori, T., Yamamoto, A., Moriyama, Y., Futai, M., and Tashiro, Y. (1991) Bafilomycin A₁, a specific inhibitor of vacuolar-type H⁺-ATPase, inhibits acidification and protein degradation in lysosomes of cultured cells. *J. Biol. Chem.* **266**, 17707–17712.
- Zabner, J., Fasbender, A. J., Moninger, T., Poellinger, K. A., and Welsh, M. J. (1995) Cellular and molecular barriers to gene transfer by a cationic lipid. *J. Biol. Chem.* **270**, 18997–19007.
- Zauner, W., Blaas, D., Kuchler, E., and Wagner, E. (1995) Rhinovirus mediated endosomal release of transfection complexes. *J. Virol.* **69**, 1085–1092.
- Zauner, W., Kichler, A., Schmidt, W., Sinski, A., and Wagner, E. (1996) Glycerol enhancement of ligand-polylysine/DNA transfection. *BioTechniques* **20**, 905–913.
- Zhou, X., and Huang, L. (1994) DNA transfection mediated by cationic liposomes containing lipopolylysine: characterization and mechanism of action. *Biochim. Biophys. Acta* **1189**, 195–203.
- Zhu, N., Liggitt, D., Liu, Y., and Debs, R. (1993) Systemic gene expression after intravenous DNA delivery into adult mice. *Science* **261**, 209–211.

BC970009Z

Nuclease Activity and Binding Characteristics of a Cationic “Manganese Porphyrin–Bis(benzimidazole) Dye (Hoechst 33258)” Conjugate

Silvana Frau, Jean Bernadou,* and Bernard Meunier*

Laboratoire de Chimie de Coordination du CNRS, 205, route de Narbonne, 31077 Toulouse cedex, France.
Received July 22, 1996*

To increase the binding affinity and/or the sequence selectivity of the chemical nuclease manganese(III) tetrakis(4-*N*-methylpyridiniumyl)porphyrin, we synthesized a conjugate molecule by associating a tris(4-*N*-methylpyridiniumyl)metalloporphyrin motif to Hoechst 33258 (H33258), a DNA minor groove binding dye known for its selective affinity for A·T tracts. Selected double-stranded (ds) 35-mer oligodeoxyribonucleotides have been used to probe DNA chain breakages induced by the manganese derivative of the conjugate after activation by potassium monopersulfate. Gel electrophoresis analyses show that DNA cuts were generated by the metalloporphyrin moiety of the hybrid molecule, with the H33258 entity interacting in two different possible orientations, upstream or downstream, with its preferred affinity site inside the minor groove. Also studied was the cleavage of a ds 29-mer oligodeoxyribonucleotide containing two stretches of A·T basepair (bp) which clearly showed that the hybrid can occupy the binding region at least in four preferred ways. These cleavage experiments support the strong and selective interaction of the metalloporphyrin–dye hybrid with DNA and allow the estimate of 10 bp as an average size for the affinity site of an isolated conjugate molecule. Further studies by UV–visible spectroscopy, DNA melting temperature determinations, and DNase I footprinting showed, for higher concentrations of H33258 conjugate, a preferential interaction of only the H33258 moiety with DNA (estimated binding site size 6–7 bp) with the porphyrin entity pushed out of the groove and, for the highest concentrations, self-aggregation of the H33258 conjugate all along the DNA strand in a nonselective mode.

INTRODUCTION

Inhibition of gene expression by creating specific irreversible damage on DNA might be a potentially useful strategy. Such achievement is based on the preparation of molecules able to damage selected sequences on the targeted DNA. Based on bleomycin, an antitumor antibiotic agent combining both DNA binding properties and ability to cleave DNA (1, 2), a variety of DNA binders linked to cleaving reagents have been prepared: distamycin–EDTA iron (3), bis(1,10-phenanthroline)–copper (I) (4), and Hoechst 33258–1,10-phenanthroline–copper (I) (5).

The metalloporphyrin [*meso*-tetrakis(4-*N*-methylpyridiniumyl)porphyrinato]manganese(III) activated with an oxygen atom donor such as KHSO₅ is able to cleave double-stranded (ds) DNA at nanomolar concentration (6). The active form generated in situ with KHSO₅ is a Mn^V–oxo complex reminiscent of the activated form of cytochrome P-450 (7). The mechanism of DNA cleavage

involves the oxidative activation of C₁–H or C₅–H bonds of deoxyriboses in a ratio depending on the presence of triplets of adenine–thymine basepairs (bp's) (8, 9). To increase the binding affinity and/or to modulate the cleavage specificity of this chemical nuclease (which is itself sequence specific, cutting at three adjacent A·T residues), a [tris(4-*N*-methylpyridiniumyl)porphyrinato]manganese(III) moiety has been previously coupled with intercalating agents (10–12), oligonucleotides (13–15), and peptide nucleic acids (16). DNA minor groove binders have also been extensively studied for their capacity to bind to defined sequences of DNA. Netropsin, one of them, has been recently covalently attached to a cationic porphyrin (17). Here, we focused our interest on another minor groove binder, the bis(benzimidazole) dye Hoechst 33258 (H33258 for short, 2'-(4-hydroxyphenyl)-5-(4-methyl-1-piperazinyl)-2,5'-bis(1*H*-benzimidazole)) that was attached to a cationic manganese porphyrin. Interactions between H33258 and nucleic acids have been studied in detail by X-ray diffraction (18–22), NMR spectroscopy (23–26), fluorescence spectroscopy (27–29), electric linear dichroism (30), and a range of other biophysical methods (31–33). From all of these data, it appears that the high-affinity site of H33258 is a quadruplet of adenine–thymine bp's. Concerning this quadruplet, the exact nature of the sequence as also the nature of the flanking bases may modulate the interaction of H33258 (32).

So, association of a cationic metalloporphyrin and H33258 could lead to an efficient nuclease with an improved affinity for DNA and an increased selectivity for A·T rich regions (H33258 should enhance the affinity and direct the specificity of the hybrid). Here, we remind that binding of the general transcription factor TATA box binding protein (TBP, i.e. a protein with high affinity for

* Abbreviations: (A·T)₃, triplets of adenine–thymine base pairs; bp, base pair; CT-DNA, calf thymus DNA; DMF, dimethylformamide; ds, double-stranded; FAB, fast atom bombardment; Hepes, *N*-(2-hydroxyethyl)piperazine-*N*-2-ethanesulfonic acid; H33258, Hoechst 33258; MnTMPyP, pentaacetate of manganese(III) *meso*-tetrakis(4-*N*-methylpyridiniumyl)porphyrin; MnTrisMPyP, tetraacetate of manganese(III) 5-[4-[4-(carboxy)-1-butoxy]phenyl]-10,15,20-tris(4-*N*-methylpyridiniumyl)porphyrin; ODN, oligodeoxynucleotide; P/D, [DNA polymer in base pairs]/[dye] ratio; poly(dA)·(dT), polydeoxyadenylic acid–polythymidylic acid; poly[d(A-T)·d(A-T)], poly(deoxyadenylic acid–thymidylic acid); poly(dG)·(dC), polydeoxyguanylic acid–polydeoxycytidylic acid; poly[d(G-C)·d(G-C)], poly(deoxyguanylic acid–deoxycytidylic acid); TBP, TATA box binding protein; *T*_m, melting temperature; Tris, tris(hydroxymethyl)aminomethane.

* Abstract published in *Advance ACS Abstracts*, February 15, 1997.

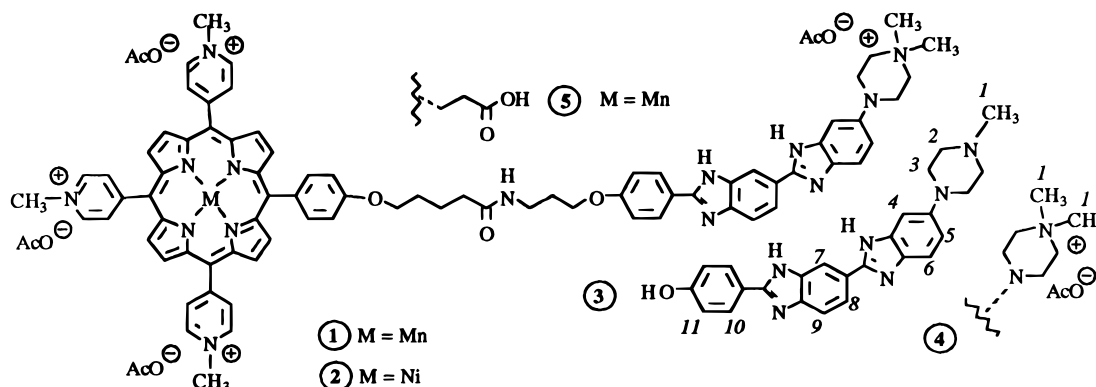


Figure 1. Structures of the conjugate molecules **1** ($M = \text{Mn}$) and **2** ($M = \text{Ni}$), H33258 **3** and its methylated analogue **4**, and the porphyrin precursor **5** ($M = \text{Mn}$).

A·T rich sequences) to a promotor located upstream from the transcription start site is essential for the accurate and efficient initiation of transcription (34). Causing damage on DNA on such regions could inhibit transcription. On the other hand, it has been recently demonstrated that some minor groove binders (like H33258) are effective inhibitors of the formation of a DNA/TBP complex (35) or topoisomerases (36, 37). Adding a reactive entity such as a metalloporphyrin endowed with oxidative properties should improve the efficiency of this class of inhibitors.

We report here, in a first part, cleavage experiments performed with the conjugate molecule "manganese porphyrin–H33258" **1** (Figure 1) on a series of synthetic oligonucleotides. These ODNs were built to contain or not (i) one well-characterized affinity site of H33258 [5'-CAAATTTG-3'] (32) and (ii) one or two affinity sites of MnTMPyP [(A·T)₃] (8).

The other part of this article concerns additional physicochemical data to discuss the behavior in solution and the mode of interaction of conjugate **1** with DNA models. On the basis of melting temperature determinations, DNase I footprinting experiments in the presence of the conjugate, and UV–vis spectroscopy studies in the presence of varying concentrations of poly(dA)·(dT), poly[d(A·T)·d(A·T)], and poly(dG)·(dC), we can propose a model of the interaction of conjugate **1** with DNA.

EXPERIMENTAL PROCEDURES

Spectrometry. UV–visible spectral measurements were carried out on a diode array HP8452 spectrometer using a 1 cm quartz cuvette. NMR spectra were recorded on a Bruker AM250. FAB mass spectroscopy was performed on a Nermag R1010.

Preparation of Compounds 1, 2, and 5 (Figure 1). The porphyrin precursor **5** and the hybrid molecules **1** and **2** were synthesized according to previously reported methods (13 (5); 38, 39 (1 and 2)).

Preparation of the H33258 Analogue 4 (Figure 1). The hydrochloride salt (94 mg, 0.15 mmol) of H33258 (3HCl, 5H₂O, from Aldrich) was dissolved in 30 mL of water. The free base **3** was precipitated by addition of 30 mL of aqueous 5% NaHCO₃, extracted with a large excess of ethyl acetate, and crystallized in this solvent (59 mg, 95% yield). NMR data were in agreement with the literature (40). Methylation of **3** to give **4** was obtained as follows: 11 mg (0.026 mmol) of **3** and 15 μL (0.26 mmol) of CH₃I were mixed in 2.3 mL of DMF for 1.5 h at room temperature. The evolution of the reaction was followed by TLC (R_f values on silica gel were 0.32 for **3** and 0.0 for **4** with CH₂Cl₂/MeOH (50/50) as the eluent). The crude product was precipitated with a

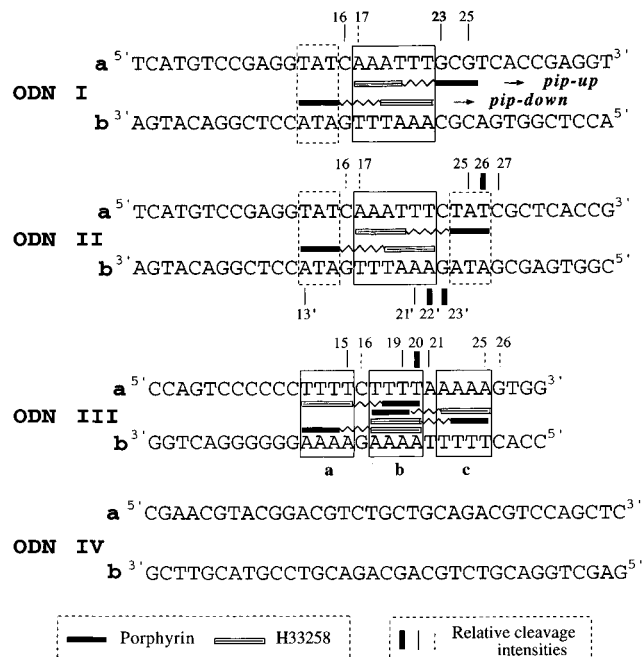


Figure 2. Bases sequences of ODNs and schematic representation of conjugate **1** in its site. Solid boxes show the possible ways the conjugate **1** (and more precisely the H33258 moiety) can occupy the binding region. Dashed boxes (ODNs I and II) indicate the position of the metalloporphyrin in its preferred (A·T)₃ site. Bars indicate the cleavage positions induced by **1** in the presence of KHSO₅.

mixture of MeOH and Et₂O (14 mg, 0.025 mmol, 95% yield). MS (FAB in DMF): m/z 439.5 (M^+). ¹H NMR (CD₃COOD), δ ppm: 8.34 (1H, s, H₇), 8.12 (1H, d, $J = 9$ Hz, H₈), 7.97 (2H, d, $J = 9$ Hz, H₁₀), 7.87 (1H, d, $J = 9$ Hz, H₉), 7.65 (1H, d, $J = 9$ Hz, H₆), 7.29 (1H, d, $J = 9$ Hz, H₅), 7.17 (1H, s, H₄), 6.98 (2H, d, $J = 9$ Hz, H₁₁), 3.71 (8H, m, H₂, H₃), 3.40 (6H, s, H₁). UV–vis (6 μM in MeOH), λ nm ($\epsilon_M \times 10^{-3}$, M⁻¹ cm⁻¹): 262 (20), 340 (40).

Oligonucleotides: Syntheses and Labeling. The eight oligonucleotides used in this study (ODN Ia,b, ODN IIa,b, ODN IIIa,b, and ODN IVa,b; Figure 2) were synthesized by a standard solid-phase (β -cyanoethyl)-phosphoramidite chemistry on a Cyclone Plus DNA synthesizer from Milligen Biosearch. Concentrations of single-stranded oligonucleotides were determined by UV titration at 260 nm: $\epsilon_M \times 10^{-3}$, M⁻¹ cm⁻¹ = 337 (ODN Ia), 342 (Ib), 329 (ODN IIa), 355 (IIb), 263 (ODN IIIa), 285 (IIIb), 326 (ODN IVa), 322 (IVb). They were labeled at the 5'-end by reaction with γ -[³²P]ATP and T4 polynucleotide kinase using a standard procedure.

Cleavage and Footprinting Experiments. Double-stranded ODNs I–IV were formed as follows: to a

solution (8 μ L) containing 100 nM (final concentration) 5'-labeled single strand in 100 mM NaCl and 40 mM Tris buffer (pH 8) was added a solution of the complementary strand in the same solvent (4 μ L, final concentration 100 nM). After 5 min of heating at 90 °C, the hybridization of the duplex was achieved by slowly cooling the solution to 25 °C. Conjugate **1** (4 μ L, final concentration varying from 20 nM to 10 μ M) was preincubated with the duplex for 1.5 h at 37 °C. For cleavage experiments, 4 μ L of 5 mM KHSO₅ solution (final concentration 1 mM) was added and the reaction was allowed to proceed for 1 h at 37 °C. The reaction was stopped by addition of 1 μ L of 1 M Hepes buffer (pH 8). For alkaline treatment (in order to reveal lesions on G bases of the target duplex), the reaction solution was heated at 90 °C for 30 min in the presence of a 1 M piperidine solution. In DNase I footprinting experiments, the enzyme (from Gibco BRL, 4 μ L, 1 unit) was added to 16 μ L of a solution containing the duplex (5'-³²P-labeled on one strand) preincubated with **1** and was allowed to react for 5 min at 4 °C. In both cases (footprinting and cleavage experiments), the samples were diluted after reaction with 1 μ L of yeast tRNA (10 mg/mL) and 100 μ L of 0.3 M sodium acetate (pH 5.2) and then precipitated with 300 μ L of cold ethanol. The pellet was finally rinsed with 70% aqueous ethanol and lyophilized. Fragments of DNA were analyzed by denaturing (7 M urea) 20% polyacrylamide gel (4 h at 2000 V). Establishment of sequences involved guanine and guanine-adenine specific cleavage of DNA (Maxam and Gilbert protocols) and for ODN **I**, reference to the cleavage pattern of the 5'- and 3'-labeled polymer in the presence of DNase I.

DNA Models. Poly(dA)·(dT), poly[d(A-T)·d(A-T)], poly(dG)·(dC), and poly[d(G-C)·d(G-C)] (purchased from Sigma) were used without purification. Concentrations (always calculated in base pairs) were determined by UV titration using the following molar extinction coefficients. ϵ_{M} , M⁻¹ cm⁻¹ bp⁻¹: poly(dA)·(dT), 12 000 (260 nm); poly(dG)·(dC), 14 800 (253 nm); poly[d(G-C)·d(G-C)], 16 800 (254 nm) (41); poly[d(A-T)·d(A-T)], 13 200 (262 nm) (42).

Influence of H33258 and Related Compounds on the Melting Temperature of Poly[d(A-T)·d(A-T)]. Duplex dissociation was followed by UV spectroscopy at 260 nm. Melting curves were obtained with a diode array HP 8452 spectrophotometer equipped with a Peltier temperature controller; heating increments were of 2 °C from 36 to 58 °C (with 3 min of stabilization after each increment) and then of 1 °C (with 3 min stabilization) to go to 90 °C. One centimeter path length cuvettes were used for data collection. The duplex absorbance was measured by using a solution containing 75 μ M bp target duplex poly(dA)·(dT) dissolved in 1.2 mL of 40 mM Tris (pH 8) and 100 mM NaCl. For T_m experiments the concentration ratio of DNA bp over ligand was P/D = 5. The melting temperatures of the DNA target–minor groove binder (**1**, **4**, or **5**) complexes were determined after subtraction of solvent absorbance.

UV–Vis Absorption Studies for Mixtures of Conjugate **1 and Poly[d(A-T)·d(A-T)], Poly(dA)·(dT), Poly(dG)·(dC), and Poly[d(G-C)·d(G-C)].** UV–vis absorption spectra were recorded for mixtures of **1** and various DNA polymers in 40 mM Tris (pH 8) and 100 mM NaCl, at room temperature. The molarity of **1** was 2, 5, or 10 μ M, and the molarity of the DNA polymers varies in the range 0–200 μ M bp. The complex was allowed to equilibrate for 1.5 h at 37 °C before measurements. Variations of absorbance maxima for H33258 chromophore and at the Soret band (intense absorption band of porphyrins in the visible spectrum) were followed

according to increasing concentrations of DNA polymers in the range P/D = 0–20 (Figure 5).

RESULTS

Cleavage Experiments on ODNs I–IV with the Conjugate **1/KHSO₅ System.** For all of the following experiments performed on synthetic ODNs, the concentration of ds target duplex was 100 nM. Nuclease activity of conjugate **1** (see Figure 1 for structures of the manganese derivative **1**; conjugate **2** is the nickel analogue which was used as a control with no nuclease activity) was studied on two ODNs containing both sites of high affinity for H33258 and manganese porphyrin (ODN I and ODN II), on one ODN with two A·T tracts (ODN III), and on another one (ODN IV) containing no more than two consecutive A·T bp (see Figure 2 for sequences). In conjugate **1**, due to the constraints of the synthesis, the H33258 moiety was methylated on the nitrogen of the methylpiperazine to give an additional cationic center. Incidence of this point will be discussed further.

Footprinting and Cleavage Experiments on ODN Ia. The affinity of **1** for DNA is, in part, due to the four positive charges present in its structure (three *N*-methylpyridiniumyl groups on Mn porphyrin and one ammonium on H33258 moiety). To make sure that neither the supplementary methyl group on H33258 nor the presence of the metalloporphyrin moiety changed the intrinsic affinity of H33258 for DNA, we performed a DNase I footprinting study on ODN **I** in the presence of compounds **1**, **3**, and **4**. They all reacted in the same way: the three ligands protected the (A·T)₆ site at low concentration and complete protection was reached for concentrations up to 100–200 nM (Figure 3). This is clearly shown in lanes 8 (**1**), 19 (**3**), and 24 (**4**) where the bands corresponding to the hydrolysis of the phosphodiester bonds A19–A20 (very weak band), T20–T21 (weak), T21–T22, and G23–C24 completely disappeared. Even if the steric hindrance of the piperazine ring is more important in **4** compared to **3**, it did not seem to have any influence on the recognition of the affinity site. The same conclusions are also valid concerning the presence of the metalloporphyrin substituent attached to the H33258 part in **1**. Footprinting with **1** exhibited selective protection of the (A·T)₆ site at low concentration (half-protection with 20 nM, lane 6; complete protection with 100 nM, lane 8; Figure 3). Additionally, for concentrations higher than 2 or 3 μ M (lanes 10–14), the bound drug was found to prevent DNase I from cleaving all along the ODN strand. Controls with the porphyrin precursor **5** or with the parent dye H33258 **3** or its methylated derivative **4** did not show any particular protection of the duplex at such high concentrations (see lanes 17, 22, and 27 for experiments performed in the presence of 10 μ M of **5**, **3**, and **4**, respectively). This point will be discussed at the same time as the spectroscopic behavior of conjugate **1** in the presence of varying amounts of DNA polymers.

We can also notice that footprinting experiments with the porphyrin precursor **5** did not exhibit any particular protection except at high concentration (10 μ M, lane 17) where some decrease in intensity of the enzymatic digestion bands T15–C16 and C16–A17 was observed and might correspond to a lower affinity of the metalloporphyrin motif (compared to H33258) for its own preferred binding site, the TAT triplet located at T13A14T15.

Figure 4 shows the results of cleavage experiments performed on ODN **I** with compound **1** activated by potassium monopersulfate. Degradation of labeled ODN **Ia** occurred on both sides of the sequence (A·T)₆: on the

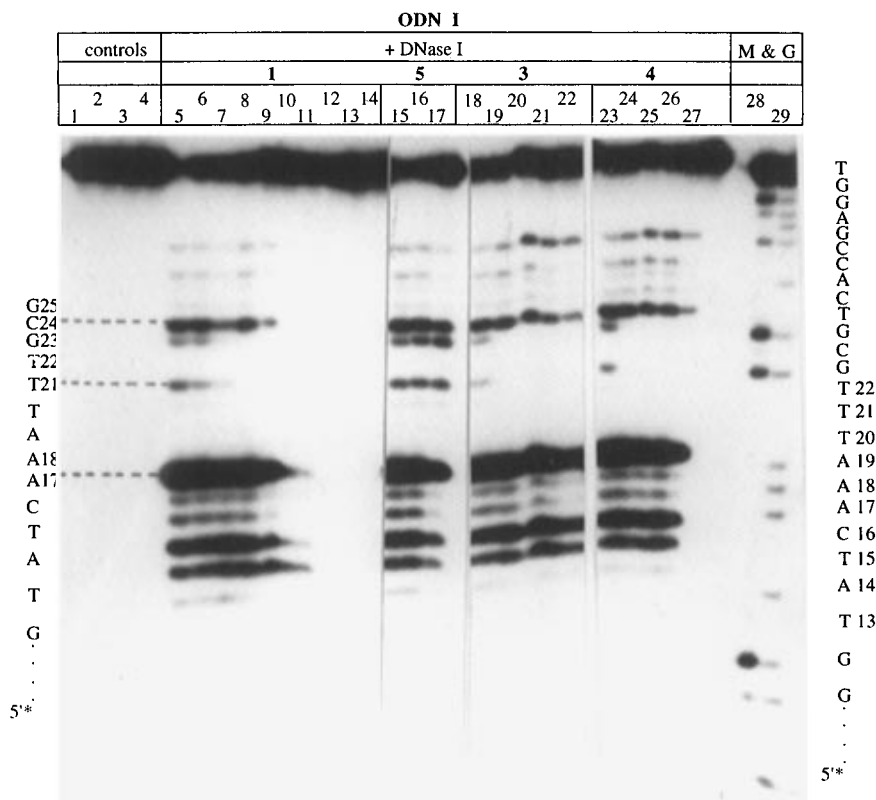


Figure 3. Footprinting on ODN **I** (**Ia** was 5'-³²P-labeled). Target was 100 nM in Tris-HCl (40 mM, pH 8) and NaCl (100 mM). Digestion by DNase I was performed for 5 min at 4 °C. Duplex alone: lane 1. Duplex in the presence of **1**, **3**, and **4**: lanes 2–4. DNase I cleavage in the absence of ligand: lane 5. DNase I cleavage in the presence of various concentrations of **1** (0.02, 0.05, 0.1, 1, 2, 3.5, 5, 7.5, and 10 μ M): lanes 6–14. DNase I cleavage in the presence of the porphyrin precursor **5** (0.1, 1 and 10 μ M): lanes 15–17. DNase I cleavage in the presence of H33258 **3** (0.02, 0.2, 2, 5, and 10 μ M): lanes 18–22. DNase I cleavage in the presence of the H33258 analogue **4** (0.02, 0.2, 2, 5, and 10 μ M): lanes 23–27. Lanes 28 and 29 are sequencing Maxam and Gilbert, G and GA. On the left is indicated the sequence established for DNase I cleavage.

5'-side, where one (A·T)₃ triplet was present, two main individual bands appeared at C16 and A17 (lanes 2–4); on the 3'-side, where no (A·T)₃ triplet was present, the pattern of cleavage consisted of a smear stretching from approximately C24 to A28 (lanes 2–4). After heating at 90 °C during 1 h in the presence of 1 M piperidine, the two discrete bands at C16 and A17 observed by direct cleavage resisted piperidine treatment when the smear from C24 to A28 was transformed to discrete cleavage bands corresponding mainly to G23 and G25 (lanes 5–7). This pattern with cleavage bands of rather similar intensities on both sides of the H33258 affinity site suggests that conjugate **1** can adopt two different possible orientations in this site. In a control experiment we checked that the redox inactive nickel derivative **2** was not able to induce any damage on this DNA target (not shown).

Cleavage pattern with MnTMPyP showed the main cleavage sites at T15/C16/A17, on the 3'-side of the TAT triplet, and also at T20/T21/T22, on the 3'-side of the three overlapping triplets located from positions A17 to T21, which confirmed A·T triplets as preferred sites of DNA interaction of the "free" metalloporphyrin (positions of cleavage are indicated by arrows on the left of Figure 4) (8, 43, 44). A secondary site of cleavage was also observed at A28 when relatively drastic cleavage occurred; 43).

Cleavage on ODN II. To confirm the two possible orientations of conjugate **1** within the minor groove, we used ODN **II** which possesses two (A·T)₃ triplets on both sides of the high-affinity site of H33258. If the Mn porphyrin moiety can point toward the 3'-end as well as 5'-end of strand **a** or **b** of the duplex, then two distinct

oxidation sites must be observed. Effectively, the pattern of cleavage products supported the existence of two cleaving sites presenting well-defined breaks at C16, A17 and A25, T26, C27 on strand **a** and C12', A13' and A21', A22', G23' on strand **b** (lanes 8–13; Figure 4). The position of the cleavage bands on strand **b** corresponded to a shift of three or four bases toward the 3'-end as compared with breaks on strand **a**, meaning that the Mn porphyrin moiety was located and reacted inside the minor groove of the target duplex. Cleavage intensity increased when the concentration of conjugate **1** was increased (lanes 8–10), but for P/D = 3.5 (10 equiv of conjugate per duplex molecule, lane 11), the intensity slightly decreased. These facts will be correlated in the Discussion with UV–vis spectroscopy results supporting nonspecific interactions of the conjugate all along the double-stranded DNA when the duplex is overloaded with conjugate molecules. We must also note the more intense cleavage on the 3'-side of the (A·T)₃ triplet at positions 24–26 compared to that one at positions 13–15.

When we compared the nuclease activity of MnTMPyP and conjugate **1** on this target, we saw that positions of cleaving sites observed with conjugate **1** were clearly different than with MnTMPyP (see arrows on the sequence of ODN **IIa** for MnTMPyP cleavage sites, Figure 4).

Cleavage on ODN III. The main sites of cleavage were observed at T15, T19, T20 (the most intense), and A21 and to a minor extent at A25 and G26, while MnTMPyP induced cleavage on the 3'-side of all (A·T)₃ triplets of the duplex: T15 and C16, T20, A21, A22, A23, A24, A25, and G26. Conjugate **1** seemed to be able to select a particular high-affinity site in the A·T track of this

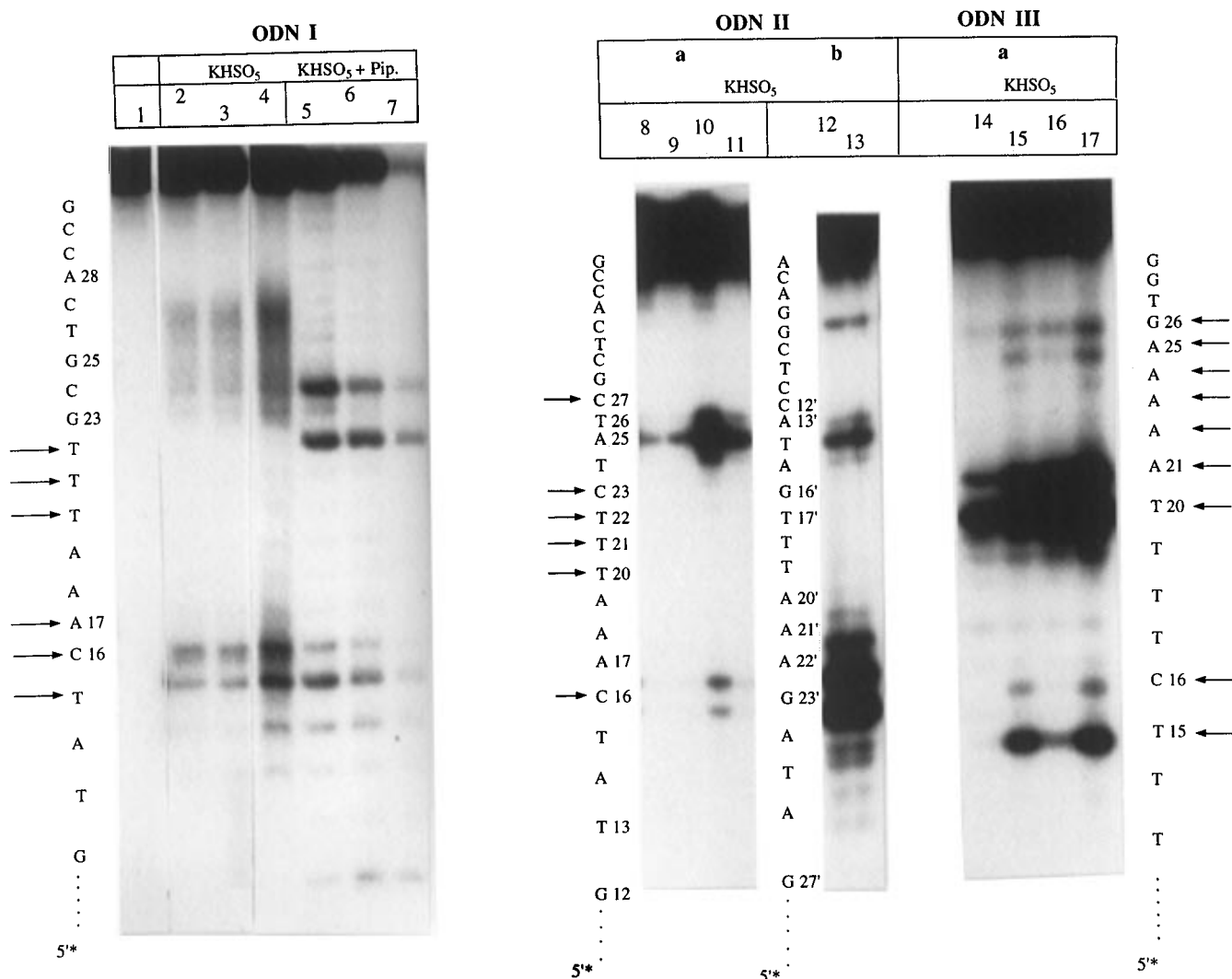


Figure 4. Cleavage on ODN I (**Ia** 5'-³²P-labeled), ODN II (either ODN **IIa** or ODN **IIb** was 5'-³²P-labeled), and ODN III (**IIIa** was 5'-³²P-labeled). Target was 100 nM in Tris-HCl (40 mM, pH 8) and NaCl (100 mM). ODN I: cleavage was performed in the presence of 1 mM KHSO₅ for varying concentration of conjugate **1** (0.1, 0.5, and 1 μ M) without (lanes 2–4) or with alkali treatment (lanes 5–7). Alkali treatment control on the duplex alone: lane 1. ODN II cleavage was performed in the presence of 1 mM KHSO₅ for varying concentration of conjugate **1**: 0.05, 0.1, 0.5, and 1 μ M (lanes 8–11) for study of ODN **IIa** and 0.5 and 1 μ M (lanes 12 and 13) for study of ODN **IIb**. ODN III: cleavage was performed in the presence of KHSO₅ (500 μ M, lanes 14 and 15; 1 mM, lanes 16 and 17) for two concentrations of conjugate **1** (0.5 μ M, lanes 14 and 16; 1 μ M, lanes 15 and 17). Arrows indicate the cleavage positions induced by MnTMPyP in the presence of KHSO₅.

duplex, with for the lower concentrations a selective cleavage at T20 (see lane 14 in Figure 4).

Cleavage on ODN IV (Data Not Shown). Duplex ODN IV was designed as a control. In the absence of A·T triplets, MnTMPyP was unable to find a strong high-affinity site but can cause some weak (unspecific) oxidations on C5, G6, C9, G10, G18, G21, and G27 on strand **a**, or G14, G23, and G35 on strand **b**. At similar concentrations, conjugate **1** did not seem to interact at all with this duplex: no cleavage bands were observed.

Cleavage with the Ni Derivative 2. The same cleavage experiments as described above were performed on ODNs **I**, **II**, **III**, and **IV** with the Ni conjugate **2** as a control. In all cases, no nuclease activity was detected.

Interaction of Conjugate 1 with DNA Models. *Stabilization of Duplex Structure Due to the Presence of MnTMPyP, 1, or Related Precursor 4.* Thermal melting experiments were carried out with poly[d(A-T)·d(A-T)] and the ligands MnTMPyP, **1**, or **4** in a ratio P/D = 5. In these conditions we could observe that the methylated H33258 derivative **4** and MnTMPyP as well as the conjugate **1** gave a noticeable increase of the overall stability of the duplex (T_m values were increased of about

30 °C) similar to that described for H33258 itself ($\Delta T_m > 25$ °C, 45). With poly(dG)·(dC), no significant change in T_m values ($\Delta T_m \leq 4$ °C) was observed.

Absorption Behavior of 1 in the Presence of Synthetic DNA Polymers. The absorption spectrum of **1** (final concentration 2 μ M, Figure 5) in buffer pH 8 showed two main maxima at 470 nm (0.064 OD unit, Soret band of manganese porphyrin) and 340 nm (0.048 OD unit, H33258 chromophore). The progressive addition of poly-(dA)·(dT) or poly[d(A-T)·d(A-T)] produced at low [DNA bp]/[dye] mole ratios (P/D = 0.5) a decrease in absorbance of the Soret band (lower value = 0.040 OD unit) and a decrease (lower value = 0.029 OD unit) and a bathochromic shift of the maximum of H33258 chromophore (Figure 5). Then, there was a progressive increase in absorbance when increasing P/D and the maximal hyperchromicity was observed at P/D = 10 (DNA concentration about 20 μ M) with maxima values raising 0.113 OD unit (Soret band) and 0.064 OD unit (with a shift to 350 nm of the H33258 chromophore). When the starting concentration of **1** was increased to 5 or 10 μ M, the minimal DNA concentration sufficient to induce maximal hyperchromicity increased to 40–50 μ M bp or 100 μ M

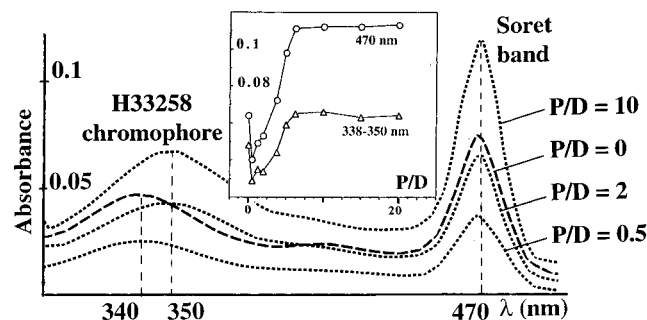


Figure 5. UV-visible absorption spectra for poly[d(A-T)·d(A-T)]/conjugate **1** mixtures in varying ratios in buffer (pH 8). Molarity of **1** was 2 μ M. Inset: dependence of absorbance maxima at 338–350 nm (H33258 chromophore) and 470 nm (Soret band) for increasing concentrations of poly[d(A-T)·d(A-T)] ($P/D = 0$ –20).

Table 1. Determination, at Two Wavelengths, of DNA bp Concentrations (μ M) Which Gave Half-Hyperchromic Effects When the Conjugate **1** Interacted with Poly[d(A-T)·d(A-T)] in Varying Concentrations^a

	2 μ M 1	5 μ M 1	10 μ M 1
at 470 nm	8.5	26	42.5
at 340–350 nm	7.5	28.5	52.5

^a Linear correlations between $y = [\text{bp}]$ and $x = [\text{1}]$: at 470 nm, $y = 2.13 + 4.15x$, $R = 0.97$; at 340–350 nm, $y = -1.90 + 5.54x$, $R = 0.99$.

bp, respectively. Implications of this dependence on conjugate **1** concentration will be discussed later. Using poly(dG)·(dC) or poly[d(G-C)·d(G-C)], no significant change in absorption characteristics could be observed.

Half hyperchromic effects estimated between the lowest absorption value observed after initial addition of A·T polymers ($P/D = 0.5$ –2) and the highest value of absorption reached for high DNA concentration ($P/D \geq 10$) were observed for DNA concentrations depending on the concentration of conjugate **1** as indicated with data collected at both 470 (Soret band) and 340–350 nm (H33258 chromophore) in Table 1 and Figure 5. The linear correlations presented in caption of Table 1 allowed us to exclude the association/dissociation equilibrium for formation of the conjugate **1**:DNA complex as the explanation of this phenomenon (see Discussion).

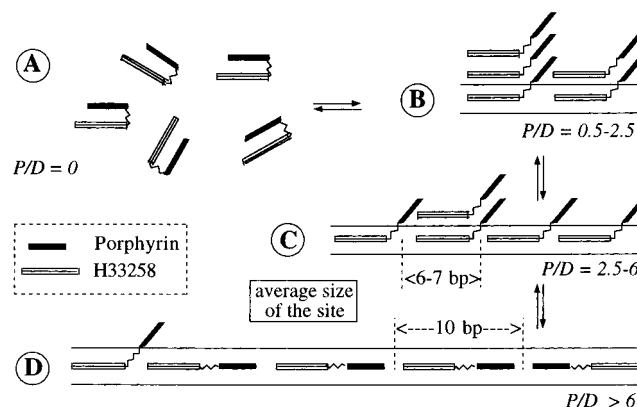
DISCUSSION

Cationic metalloporphyrins are well-established efficient chemical nucleases (9, 46). We coupled such a reactive entity to H33258, a B-DNA minor groove binder, to take advantage of its capacity to bind to (A·T)₄ sequences of DNA. Interaction of this conjugate with ds DNA was investigated through studies on nuclease activity, footprinting experiments, and UV-vis behavior in the presence of DNA models (hypochromic/hyperchromic effects and increase in stabilization of the duplex).

We used in this study synthetic DNA polymers and also four synthetic ds oligonucleotides (Figure 2): ODN **I** and ODN **II** possessed high-affinity sites for both H33258 and porphyrin moieties ([A·T]₄ and [A·T]₃, respectively); ODN **III** contained two tracts of A·T bp's. The last oligonucleotide (ODN **IV**), devoid of any A·T triplets, was a control for which **1** should have a very weak affinity.

During the multistep synthesis of conjugate **1**, the H33258 moiety was methylated on the piperazine ring (38) in the same time as the tripyridylporphyrin was converted into the tris(methylpyridinium)porphyrin. A first question was, does this additional methyl group on piperazine as well as the presence of the bulky Mn

Scheme 1. Ways of Binding of Conjugate **1** in the Minor Groove of DNA Models Depending on the DNA bp/Dye Ratio (P/D)^a



^a Conjugate **1** molecules may exist (A) free in solution as self stacked entities, (B) aggregated outside (or possibly inside) the minor groove of DNA, (C) either aggregated or unstacked in the minor groove (in the situation around half-hyperchromicity conditions), or (D) interacting with the DNA sites without any stacking with other conjugate molecules (the porphyrin moiety is probably located in the DNA minor groove for the highest values of P/D).

porphyrin attached to the H33258 modify the dye affinity for A·T rich sequences of DNA? The pattern of the enzymatic digestion with DNase I in footprinting experiments (Figure 3) gave a negative answer to this question. These studies were performed on ODN **I** interacting with conjugate **1**, H33258 **3**, or its methylated derivative **4** and showed that these three compounds protected the same sequence at similar concentrations and with the same efficiency. These data allowed us to conclude that neither the methylation of piperazine ring on H33258 moiety nor the presence of linked Mn porphyrin in conjugate **1** did affect the selectivity and the strength of interaction of the dye moiety with its usual recognition site. However, at high concentrations of ligand (above 1 μ M, $P/D \leq 3.5$, less than 3.5 bp for one ligand molecule), we could observe that the behavior of conjugate **1** differed from those of compounds **3** and **4**. In these conditions, only the first one gave a nonspecific protection all along the duplex (complete protection was observed at concentrations above 3.5 μ M, $P/D \leq 1$). This fact may be interpreted as self-aggregation of conjugate **1** along the minor groove as indicated in Scheme 1 (form B; more than two stacked molecules is a likely situation for the lowest values of P/D): the first conjugate molecule interacts with its specific site in the minor groove, then the second and the following ones aggregate, probably outside of the groove in a nonspecific way reminiscent of the nonspecific (charge- or dye-mediated) binding previously observed for H33258 by Loontjens et al. (28). Additional support for this schematic representation is given by the UV-vis study discussed further.

We have also compared T_m values of poly(dA·dT) and poly(dG·dC) in the absence and in the presence of MnTMPyP, **1**, or **4**. The observed increase of the T_m value for interaction of **1** with poly(dA·dT) conformed with literature data for H33258 (27, 45). The fact that ΔT_m was almost the same for conjugate **1** and precursor molecules allowed us to suggest that a strong interaction in the minor groove correspond to a high stabilization of the duplex form of DNA. Conjugate **1** did not interact strongly with poly(dG·dC).

The nuclease activity of conjugate **1** was then studied in order to have a best knowledge of the nature of its

interaction (sequence specificity, orientation of the ligand) with synthetic oligonucleotides.

ODN **I** and ODN **II** were built to contain a sextuplet AAATTT, which is a favorite site for H33258 (22), and also, in its close vicinity, one or two (A·T)₃ triplets which are high-affinity sites for the cationic Mn^{III} porphyrin, MnTMPyP (8). Two distinct cleavage sites were pointed out on each strand, indicating that conjugate **1** can interact with its affinity site with two different orientations, as it is shown in Figure 2 and in agreement with the so-called "piperazine-up" (pip-up) and "piperazine-down" (pip-down) orientation; for example, "pip-up" means that the piperazine end of H33258 is oriented toward the 5'-end of the upper strand in the usual representation of ODNs (21).

Another noteworthy fact was the dissymmetry on the intensity of cleavage at the two sites for ODNs **IIa,b**. The pip-up orientation was predominant and gave the most efficient cleavages. Although the H33258 site is a self-complementary one, the two possible polarities for conjugate **1** in its site were not equivalent underlining the role of the flanking bases (C or G on the 5'-side of the H33258 site AAAT for ODN **IIa** or **IIb**, respectively; T on the 3'-side in both cases) in directing the nature of the interaction. For ODN **I** where the flanking bases were identical whatever was the orientation of the conjugate in its site (C on the 5'-side and T on the 3'-side of the H33258 site AAAT), the cleavage extent was rather similar on the two strands. In addition, this result indicates that the presence of a porphyrin affinity site on one side did not help to discriminate between the two orientations.

These results obtained in solution confirmed the crystallographic data on H33258/dodecanucleotide (CG-CAAATTTGCG)₂, which gives the 5'-AAAT sequence as the main site of interaction. However, neither from these cleavage results (Figure 4) nor from footprinting studies (Figure 3) can it be completely excluded that **1** interacts with the central quadruplet AATT which has been recently shown to be a high-affinity site for H33258 (32). When an (A·T)₃ sequence was adjacent to the AAATTT site, on one side (ODN **I**) or on both sides (ODN **II**), well-defined cleavage was directly observed on the 3'-side of the A·T triplet. When such a sequence was absent, as it is the case on one side of the AAATTT site of ODN **I**, then the site of cleavage appeared like a "smear" which gave, after alkaline treatment, well-defined bands located at G positions. This particular behavior was recently attributed to oxidative damage on G bases present at or near the cleavage site (47), indicating a cutting pattern strongly dependent on the oxidizability of the bases present at this site.

When cleavage experiments were carried out with the ODN **II** duplex which contains one (A·T)₃ sequence on each side of the H33258 high-affinity site, two breaks illustrating the two polarities were detected on each strand and showed a shift (of four bp) of the cleavage position in the 3' direction, on one strand compared to the complementary one. This was typical for an interaction of the cleaving reagent in the minor groove (48). Additionally, the four-bp shift and the fact that fragments comigrated like Maxam–Gilbert cleavage products strongly support at this site an oxidative C5' chemistry as initial damage on the deoxyribose (8, 9). An oxidative C1' chemistry, the other mode of DNA cleavage previously described for cationic metalloporphyrins (9), might be discarded since we never observed on electrophoresis gels ODN fragments carrying the characteristic α,β -unsaturated lactone at their 3' end which are known to

migrate ahead of the corresponding 3'-phosphate-ending fragments (9, 49, 50).

Experiments performed with ODN **III** showed three distinct cleavage sites with different relative intensities. On the basis of cleavage data obtained with ODN **I** and ODN **II** and the two possible orientations of conjugate **1** within the different (A·T)₄ sequences on ODN **III**, we can propose four potential ways of interaction which depend on the preference of the H33258 moiety for some particular sequences of bases in the (A·T)₄ site, boxes **a** (pip-up), **b** (pip-up and pip-down), and **c** (pip-down), to explain the observed cleavage patterns (Figure 2). The combination of these four possibilities gave distinct cleavage intensities on the different sites, e.g. T20 was the most intense cleavage band and may result from the conjunction of two positions of conjugate **1**, in box **a** (pip-up) and in box **c** (pip-down).

For all ODNs (**I**, **II**, or **III**), the observed pattern of binding/damage supports the preference of the conjugate for A·T tetranucleotide site and underlines the role of base sequence in this site as also the nature of flanking bases, probably in relation with variation of DNA conformations (31, 51). The cleavage patterns with conjugate **1** appeared substantially different from those observed for MnTMPyP, in which classical cuts are located on the nucleotide adjacent on the 3'-side of each (A·T)₃ triplet, i.e. for ODN **II**, for example, on C16, T20, T21, T22, C23 (weak), and C27 (ODN **IIa**) and C12', G16', T17', T18', T19', G23', and A24' (ODN **IIb**). The presence of the H33258 vector attached to the Mn porphyrin precursor clearly changed and directed the metalloporphyrin selectivity toward targets close to the H33258 binding site. This probably results of the 100-fold higher DNA affinity of H33258 compared to that of MnTMPyP ($K_{\text{aff}} = 10^8 \text{ M}^{-1}$ (28) and $K_{\text{aff}} = 10^6 \text{ M}^{-1}$ (12), respectively).

When no quadruplet of A·T bp was present, like in ODN **IV**, and only at high concentrations of the conjugate ($>2 \mu\text{M}$), a nonspecific and very weak cleavage activity was detected and appeared as a "smear". This nonspecific interaction, also observed in footprinting experiments for ODN **I** at similar concentrations, might correspond to charge- or dye-mediated nonspecific binding of conjugate **1**. It might explain the low efficiency of cleavage because the aggregation of conjugate **1** molecules should favor self-bleaching of the Mn porphyrin entities rather than oxidative cleavage on DNA. Such a phenomenon could also explain the low intensity of cleavage observed for high conjugate **1** concentrations in ODN **II** cleavage experiments (Figure 4, lane 11).

Indeed, this proposal was confirmed with results obtained by UV–vis spectroscopy in concentration conditions far beyond the DNA concentrations giving an association/dissociation equilibrium. If we looked at variation of absorption of **1** in the presence of various concentrations of DNA (Figure 5), the first hypochromicity step (for P/D < 2.5) should result from complete aggregation of **1**, initiated by a tightly bound conjugate molecule in the minor groove of the DNA polymer, which led to polymeric stacking interactions outside (or inside) the minor groove (Scheme 1, form B; for a discussion on the different possible polymeric associations, see ref 28). Around the half-hyperchromic concentration conditions (P/D = 2.5–6), both aggregated and unstacked molecules can exist (form C). On the other hand, when DNA concentration was sufficient (P/D > 6 , form D; for the upper values of P/D, the most likely mode of interaction involves both porphyrin and H33258 moieties lying in the minor groove), then conjugate molecules interacted with the minor groove without self-stacking and, thus,

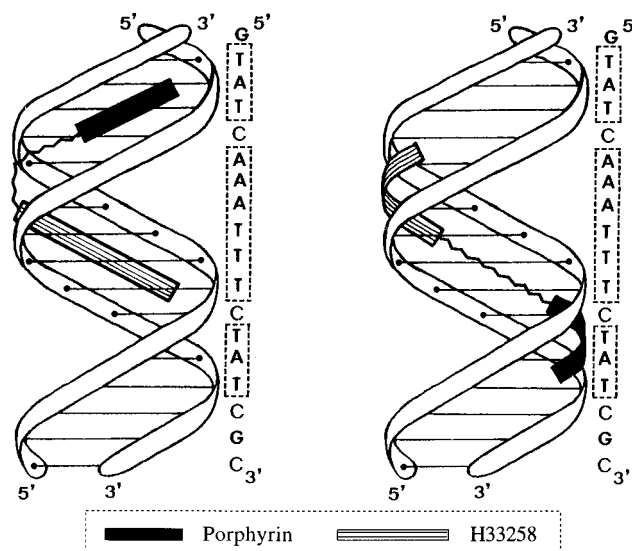
the absorption of both Mn porphyrin and H33258 chromophores was exalted (relatively to forms A or B) and reached a maximum for $P/D > 6$. The same behavior was observed whatever was the initial concentration of conjugate molecule (2, 5, or 10 μM). A ratio $P/D \geq 6$ was always necessary to dissociate aggregated molecules present along the DNA strand and to give complete interaction of isolated molecules with DNA sites. In the absence of DNA, the self-stacked structure A (Scheme 1) is the most likely for **1**, since this conjugate strictly obeyed the Beer–Lambert's law in neutral solution in the range 0–10 μM (data not shown), when the parent dye H33258 in similar conditions (28) presents a concentration-dependent decrease of ϵ values at 338 nm indicating formation of dye aggregates.

The variation of spectroscopic data has been already described for H33258 in the presence of CT-DNA (52) as also the formation of DNA-stacked H33258 complexes (28). Thus, if we suppose that interaction of conjugate **1** with DNA is similar to that of H33258, it is logical that this aggregation occurred when an excess of conjugate vs DNA bp was present. Moreover, we must note the crucial role of the porphyrin moiety which greatly enhanced the propensity of H33258 dye to aggregate: indeed, in footprinting experiments, the conjugate **1** completely protected the DNA duplex against hydrolytic cleavage by DNase I in conditions (2–10 μM) where H33258 itself was inefficient (lanes 10–14 to be compared with lanes 20–22, Figure 3). Extension of the overall number of aromatic rings involved in the stacking process (form B, Scheme 1) could explain this increase of stability.

In addition, we observed that the bp concentration necessary to reach half of the hyperchromic effect (see Results and Table 1) was linearly correlated with concentration of conjugate **1** (see footnote of Table 1). This fact excludes the possibility of an association/dissociation equilibrium (in this case, the DNA bp concentration needed to give half-bound ligand should be independent of the initial concentration of ligand) and supports the hypothesis of a redistribution between the nonspecific interaction of stacked conjugate molecules and a specific interaction with isolated conjugate molecules bound to their preferred affinity site inside the minor groove (Scheme 1, redistribution from B to C and D). In these conditions, about five bp per conjugate **1** molecule (deduced from the linear correlations presented in caption of Table 1 ($y/x \approx 4.2\text{--}5.5$) was the mean value necessary to observe the half-hyperchromic effect. If we consider dimers/monomers in similar proportion as the most likely distribution at this point, then the average size of the interaction site for **1** should be $4 \times 5/3 \approx 6.5$ bp (number of conjugate molecules \times size of binding site/number of occupied binding sites). This last value, probably slightly overestimated due to arrangements which were not strictly from end to end and which included also upstream and downstream orientations of the conjugate, is in agreement with the previously reported size of the affinity site of H33258 and indicates that, in this range of DNA bp/conjugate concentrations, only the H33258 part interacts with the minor groove, the porphyrin moiety being pushed outside of DNA (Scheme 1, form C).

All of these observations were only available for poly(dA)·(dT) and poly[d(A-T)·d(A-T)]. With poly(dG)·(dC) or poly[d(G-C)·d(G-C)], variations of characteristic absorption bands of **1** were not significant supporting a very low affinity of **1** for G-C rich polymers. These spectroscopic results are in agreement with the low level of DNA cleavage observed on ODN **IV** with conjugate **1**.

Chart 1. Schematic Representation of the Two Possible Orientations of Conjugate **1 in Its Site of Interaction with ODN **II****



CONCLUSION

In conclusion, we synthesized a conjugate molecule Mn porphyrin–H33258 by associating an efficient chemical nuclease to a highly selective (A·T)₄ binding agent. We could check that chemical modifications introduced on the H33258 entity, especially the covalent linkage of the bulky metalloporphyrin, did not modify its intrinsic binding properties: the H33258 entity was still directing the sequence specificity of the conjugate, not the metalloporphyrin moiety.

Analyses of DNA breaks induced after chemical activation of conjugate **1** at low concentration allowed us to localize its site of interaction and to estimate its size at about 10 bp's. At this site, the conjugate may interact with the piperazine residue oriented either in the 5'- or 3'-direction, giving two possibilities of breaks on each strand. These breaks, when an A·T triplet was adjacent to the H33258 site, resulted from the usual 5'-deoxyribose oxidative chemistry; in the absence of such a triplet, damage probably affected the guanine base(s) present at or near the site of cleavage. At high concentrations of conjugate (with respect to the concentration of DNA target), nonspecific interactions of stacked conjugate molecules all along the DNA double strand were observed.

One example of the two possible interactions of conjugate **1** with its target is presented in Chart 1.

Without question, as it was shown on several ds oligonucleotides, the attachment of the cleaver motif [tris-(4-*N*-methylpyridiniumyl)porphyrinato]manganese(III) to the minor groove binder H33258 as a vector allowed specific recognition and cleavage of the DNA target. These data provided additional support for further investigations on such DNA damaging drugs in the field of molecular biology or pharmacology.

ACKNOWLEDGMENT

This work was supported by the Centre National de la Recherche Scientifique (CNRS) and the Région Midi-Pyrénées.

LITERATURE CITED

- (1) Hecht, S. M. (1986) The chemistry of activated bleomycin. *Acc. Chem. Res.* 19, 383–391.

- (2) Stubbe, J., and Kozarich, J. W. (1987) Mechanisms of bleomycin-induced DNA degradation. *Chem. Rev.* **87**, 1107–1136.
- (3) Dervan, P. B. (1986) Design of sequence-specific DNA binding molecules. *Science* **232**, 464–471.
- (4) Sigman, D. S. (1986) Nuclease activity of 1,10-Phenanthroline-Copper ion. *Acc. Chem. Res.* **19**, 180–186.
- (5) Chen, C. H. B., Mazumder, A., Constant, J. F., and Sigman, D. S. (1993) Nuclease activity of 1,10-Phenanthroline-copper. New conjugates with low molecular weight targeting ligands. *Bioconjugate Chem.* **4**, 69–77.
- (6) Bernadou, J., Pratviel, G., Bennis, F., Girardet, M., and Meunier, B. (1989) Potassium monopersulfate and a water-soluble manganese porphyrin complex [Mn(TMPyP)](OAc)₅ as an efficient reagent for the oxidative cleavage of DNA. *Biochemistry* **28**, 7268–7275.
- (7) Pitié, M., Bernadou, J., and Meunier, B. (1995) Oxidation at carbon-1' of DNA deoxyriboses by the MnTMPyP/KHSO₅ system results from a cytochrome P-450 type hydroxylation reaction. *J. Am. Chem. Soc.* **117**, 2935–2936.
- (8) Pitié, M., Pratviel, G., Bernadou, J., and Meunier, B. (1992) Preferential hydroxylation by chemical nuclease *meso*-tetakis-(4-*N*-methylpyridiniumyl) porphyrinato-manganese (III) pentaacetate/KHSO₅ at the 5' carbon of deoxyriboses on both 3' sites of three contiguous A-T base pairs in short double-stranded oligonucleotides. *Proc. Natl. Acad. Sci. U.S.A.* **89**, 3967–3971.
- (9) Pratviel, G., Bernadou, J., and Meunier, B. (1995) Carbon-Hydrogen bonds of DNA sugar units as targets for chemical nucleases and drugs. *Angew. Chem., Int. Ed. Engl.* **34**, 746–769.
- (10) Ding, L., Etemad-Moghadam, G., and Meunier, B. (1990) Oxidative cleavage of DNA mediated by hybrid "metalloporphyrin-ellipticine" molecules and functionalized metalloporphyrin precursors. *Biochemistry* **29**, 7868–7875.
- (11) Ding, L., Etemad-Moghadam, G., Cros, S., Auclair, C., and Meunier, B. (1991) Water-soluble cytotoxic hybrid molecules "cationic metalloporphyrin-ellipticine" having a high affinity for DNA. *J. Med. Chem.* **34**, 900–906.
- (12) Ding, L., Bernadou, J., and Meunier, B. (1991) Oxidative degradation of cationic metalloporphyrins in the presence of nucleic acids: a way to binding constants? *Bioconjugate Chem.* **2**, 201–206.
- (13) Casas, C., Lacey, C. J., and Meunier, B. (1993) Preparation of hybrid "DNA cleaver-oligonucleotides" molecules based on a metaltris(methylpyridiniumyl)porphyrin motif. *Bioconjugate Chem.* **4**, 366–371.
- (14) Pitié, M., Casas, C., Lacey, C. J., Pratviel, G., Bernadou, J., and Meunier, B. (1993) Efficient cleavage of a 35-mer single-stranded DNA containing the initiation codon of the TAT gene of HIV-1 by a targeted cationic manganese porphyrin. *Angew. Chem., Int. Ed. Engl.* **32**, 557–559.
- (15) Bigey, P., Pratviel, G., and Meunier, B. (1995) Cleavage of double-stranded DNA by "metalloporphyrin-linker-oligonucleotide" molecules: influence of the linker. *Nucleic Acids. Res.* **23**, 3894–3900.
- (16) Bigey, P., Sönnischsen, S. H., Nielsen, P. E., and Meunier, B. (1996) Manuscript in preparation.
- (17) Anneheim-Herbelin, G., Perrée-Fauvet, M., Gaudemer, A., Helissay, P., and Giorgi-Renault, S. (1993) Porphyrin-Netropsin: a potential ligand of DNA. *Tetrahedron Lett.* **34**, 7263–7266.
- (18) Pjura, P. E., Grzeskowiak, K., and Dickerson, R. E. (1987) Binding of Hoechst 33258 to the minor groove of B-DNA. *J. Mol. Biol.* **197**, 257–271.
- (19) Teng, M. K., Usman, N., Frederick, C. A., and Wang, A. H. J. (1988) The molecular structure of the complex of Hoechst 33258 and the DNA dodecamer d(CGCGAATTCGCG). *Nucleic Acids Res.* **16**, 2671–2690.
- (20) Carrondo, M. A. A. F. de C. T., Coll, M., Aymami, J., Wang, A. H. J., van der Mard, G. A., van Bom, J. H., and Rich, A. (1989) Binding of a Hoechst dye to d(CGCGATATCGCG) and its influence on the conformation of the DNA fragment. *Biochemistry* **28**, 7849–7859.
- (21) Quintana, J. R., Lipanov, A. A., and Dickerson, R. E. (1991) Low-temperature crystallographic analyses of the binding of Hoechst 33258 to the double-helical DNA dodecamer CGCGAATTCGCG. *Biochemistry* **30**, 10294–10306.
- (22) Spink, N., Brown, D. G., Skelly, J. V., and Neidle, S. (1994) Sequence-dependent effects in drug-DNA interaction: the crystal structure of Hoechst 33258 bound to d(CGCAAA-TTTGCG)₂ duplex. *Nucleic Acids Res.* **22**, 1607–1612.
- (23) Parkinson, J. A., Barber, J., Douglas, K. T., Rosamund, J., and Sharpless, D. (1990) Minor-groove recognition of the self-complementary duplex d(CGCGAATTCGCG)₂ by Hoechst 33258: a high-field NMR study. *Biochemistry* **29**, 10181–10190.
- (24) Parkinson, J. A., Ebrahimi, S. E., Mc Kie, J. H., and Douglas, K. T. (1994) Molecular design of DNA-directed ligands with specific interactions: solution NMR studies of the interaction of a *m*-Hydroxy Analogue of Hoechst 33258 with d(CGCGAATTCGCG)₂. *Biochemistry* **33**, 8442–8452.
- (25) Embrey, K. J., Searle, M. S., and Craik, D. J. (1991) Probing the interaction of Hoechst 33258 with an A-T rich oligonucleotide duplex using ¹H NMR spectroscopy. *J. Chem. Soc., Chem. Commun.* 1770–1771.
- (26) Parkinson, J. A., Barber, J., Buckingham, B. A., Douglas, K. T., and Morris, G. A. (1992) Hoechst 33258 and its complex with the oligonucleotide d(CGCGAATTCGCG)₂: ¹H NMR assignments and dynamics. *Magn. Reson. Chem.* **30**, 1064–1069.
- (27) Comings, D. E. (1975) Mechanisms of chromosome binding. VIII Hoechst 33258-DNA interaction. *Chromosoma* **52**, 229–243.
- (28) Loontjens, F. G., Regenfus, P., Zechel, A., Dumortier, L., and Clegg, R. M. (1990) Binding characteristics of Hoechst 33258 with calf thymus DNA, Poly[d(A-T)], and d(CCGG-AATTCGG): Multiple stoichiometries and determination of tight binding with a wide spectrum of site affinities. *Biochemistry* **29**, 9029–9039.
- (29) Kalnins, K. K., Pestov, D. V., and Roshchina, Y. K. (1994) Absorption and fluorescence spectra of the probe Hoechst 33258. *J. Photochem. Photobiol. A: Chem.* **83**, 39–47.
- (30) Bailly, C., Colson, P., Henichart, J. P., and Houssier, C. (1993) The different binding modes of Hoechst 33258 to DNA studied by electric linear dichroism. *Nucleic Acids. Res.* **21**, 3705–3709.
- (31) Martin, R. F., and Holmes, N. (1983) Use of an ¹²⁵I-labelled DNA ligand to probe DNA structure. *Nature* **302**, 452–454.
- (32) Abu-Daya, A., Brown, P. M., and Fox, K. R. (1995) DNA sequence preferences of several AT-selective minor groove binding ligands. *Nucleic Acids Res.* **23**, 3385–3392.
- (33) Bathini, Y., Rao, K. E., Shea, R. G., and Lown, J. W. (1990) Molecular recognition between ligands and nucleic acids: Novel pyridine- and benzoxazole-containing agents related to Hoechst 33258 that exhibit altered DNA sequence specificity deduced from footprinting analysis and spectroscopic studies. *Chem. Res. Toxicol.* **3**, 268–280.
- (34) Drapkin, R., Merino, A., and Reinberg, D. (1993) Regulation of RNA polymerase II transcription. *Curr. Opin. Cell Biol.* **5**, 469–476.
- (35) Chiang, S. Y., Welch, J., Rauscher, F. J., and Beerman, T. A. (1994) Effects of minor groove binding drugs on the interaction of TATA box binding protein and TFIIA with DNA. *Biochemistry* **33**, 7033–7040.
- (36) Woyanowski, J. M., Mchugh, M., Sigmund, R. D., and Beerman, T. A. (1989) Modulation of Topoisomerase II catalytic activity by DNA minor groove binding agents distamycin, Hoechst 33258 and 4',6-Diamidine-2-phenylindole. *Mol. Pharmacol.* **35**, 177–182.
- (37) Chen, A. Y., Yu, C., Gatto, B., and Liu, L. F. (1993) DNA minor groove-binding ligands: a different class of mammalian DNA topoisomerase I inhibitors. *Proc. Natl. Acad. Sci. U.S.A.* **90**, 8131–8135.
- (38) Frau, S., Bernadou, J., Meunier, B., Delaunay, J. C., and Vercauteren, J. (1995) Synthesis and characterization of a cationic "manganese porphyrin-bisbenzimidazole dye (Hoechst 33258)" conjugate as a potential sequence-selective DNA cleaver. *New J. Chem.* **19**, 873–876.
- (39) Bigey, P., Frau, S., Loup, C., Claparols, C., Bernadou, J., and Meunier, B. (1996) Preparation and characterization by electrospray mass spectrometry of cationic metalloporphyrin DNA cleavers. *Bull. Soc. Chim. Fr.* **133**, 679–689.

- (40) Martin, R. F., Pardee, M., Kelly, D. P., and Mack, P. (1986) Synthesis and characterisation of 2-iodo-4-[5''-(4'''-methylpiperazin-1'''-yl)-2'',5'-bi-1*H*-benzimidazol-2'-yl]phenol (iodoHoechst 33258) and 2,5-disubstituted benzimidazole model compounds. *Aust. J. Chem.* **39**, 373–381.
- (41) Wells, R. D., Larson, J. E., Grant, R. C., Shortle, B. E., and Cantor, C. R. (1970) Physicochemical studies on polydeoxyribonucleotides containing defined repeating nucleotide sequences. *J. Mol. Biol.* **54**, 465–497.
- (42) Imman, R. B., and Baldwin, R. L. (1962) Helix-random coil transition in synthetic DNAs of alternating sequence. *J. Mol. Biol.* **5**, 172–184.
- (43) Pratviel, G., Duarte, V., Bernadou, J., and Meunier, B. (1993) Nonenzymatic cleavage and ligation of DNA at a three AT base pair site. A two-step "pseudohydrolysis" of DNA. *J. Am. Chem. Soc.* **115**, 7939–7943.
- (44) Pitié, M., Pratviel, G., Bernadou, J., and Meunier, B. (1993) Characterization of PAGE bands from 3'-labeled short DNA fragments resulting from oxidative cleavage by "MnTMPyP/KHSO₅". Drastic modifications of band migrations by 5'-end sugar residues. *The Activation of Dioxygen and Homogeneous Catalytic Oxidation* (D. H. R. Barton, E. A. E. Martell, and D. T. Sawyer, Eds.), pp 333–346, Plenum Publishing Corp., New York.
- (45) Wilson, W. D., Ratmeyer, L., Zhao, M., Strekowski, L., and Boykin, D. (1993) The search for structure-specific nucleic acid-interactive drugs: effects of compound structure on RNA versus DNA interaction strength. *Biochemistry* **32**, 4098–4104.
- (46) Pratviel, G., Bernadou, J., and Meunier, B. (1996) Selective DNA cleavage by metalloporphyrin derivatives. *Met. Ions Biol. Syst.* **33**, 399–426.
- (47) Mestre, B., Jakobs, A., Pratviel, G., and Meunier, B. (1996) Structure/nuclease activity relationship of DNA cleavers based on cationic metalloporphyrin-oligonucleotide conjugate. *Biochemistry* **35**, 9140–9149.
- (48) Sluka, J. P., Griffin, J. H., Mack, D. P., and Dervan, P. B. (1990) Reagents and methods for the solid-phase synthesis of protein-EDTA for use in affinity cleaving. *J. Am. Chem. Soc.* **112**, 6369–6374.
- (49) Kuwabara, M., Yoon, C., Goyne, T., Thederahn, T., and Sigman, D. S. (1986) Nuclease activity of 1,10-phenanthroline-copper ion: reaction with CGCGAATTCGCG and its complexes with netropsin and *EcoRI*. *Biochemistry* **25**, 7401–7408.
- (50) Kappen, L. S., Goldberg, I. H., Wu, S. H., Stubbe, J., Worth, L., and Kozarich, J. W. (1990) Isotope effects on the sequence specific cleavage of dC in d(AGC) sequences by neocarzinostatin: elucidation of chemistry of minor lesions. *J. Am. Chem. Soc.* **112**, 2797–2798.
- (51) Frau, S., Bernadou, J., and Meunier, B. (1996) Hoechst 33258, a specific DNA minor groove binder. *Bull. Soc. Chim. Fr.* **133**, 1053–1070.
- (52) Steiner, R. F., and Sternberg, H. (1979) The interaction of Hoechst 33258 with natural and biosynthetic nucleic acids. *Arch. Biochem. Biophys.* **197**, 580–588.

BC970007E

Time-Resolved Fluorescence Detection of Oligonucleotide Hybridization on a Single Microparticle: Covalent Immobilization of Oligonucleotides and Quantitation of a Model System

Harri Hakala and Harri Lönnberg*

Department of Chemistry, University of Turku, FIN-20014 Turku, Finland. Received October 15, 1996®

Several alternative methods have been described for the immobilization of oligodeoxyribonucleotides to uniformly sized glycidyl methacrylate/ethylene dimethacrylate particles. Hybridization of complementary oligodeoxyribonucleotides labeled with photoluminescent europium(III) chelates to these particle-bound oligonucleotide probes was followed by subjecting a single microparticle to a time-resolved fluorescence measurement. The hybridization was further quantified by releasing the europium ion to a fluorescence enhancement solution and determining its concentration against europium(III) chloride standards. Both the efficiency and kinetics of the hybridization were observed to depend markedly on the linker employed to tether the oligonucleotide probes to the particles. These effects and those of the experimental conditions, such as oligonucleotide concentration in solution, oligonucleotide density on particles, and number of particles in a given volume of assay solution, are discussed.

INTRODUCTION

Detection of gene mutations by assays based on oligonucleotide hybridization has gained increasing popularity in clinical diagnostics since the introduction of efficient amplification techniques, such as polymerase chain reaction (PCR) (1). Since a reliable diagnosis of a given genetic disease often requires detection of multiple DNA mutations, simultaneous analysis of several potentially mutated sequences from a single biological sample appears highly desirable. Covalent immobilization of arrays of allele-specific oligonucleotides to a glass plate has recently been shown to offer a feasible basis for the development of such multiparameter analysis (2–4). The fluorescent labeled PCR products are hybridized to a support-bound oligonucleotide array, and the identity of the hybridized sequences is then determined by the location of fluorescent spots on the support. Alternatively, microscopic particles, each bearing a given allele-specific oligonucleotide and a reporter group defining the particle category, may be used for the same purpose (5). A mixture of particles is used as the solid support in the hybridization assay, and subsequently each particle is separately subjected to measurement to identify the particle category and to quantitate the possible hybridization with a complementary fluorescent labeled oligonucleotide in the PCR sample. We have previously (6) demonstrated that a highly sensitive miniaturized assay format may be developed by using uniformly sized (50 μm) glycidyl methacrylate/ethylene dimethacrylate particles (7) for covalent immobilization of the oligonucleotide probes and a photoluminescent europium(III) chelate (8) for oligonucleotide labeling instead of conventional organic fluorophores. Accordingly, time-resolved fluorescence detection may be used, enabling efficient elimination of background fluorescence. We now report on covalent immobilization of the oligonucleotide probes to microparticles and quantitation of the hybridization by

time-resolved fluorescence. The factors affecting the kinetics and efficiency of hybridization are discussed.

EXPERIMENTAL PROCEDURES

Materials. Uniformly sized (50 μm) porous glycidyl methacrylate/ethylene dimethacrylate particles (1) prepared by SINTEF Applied Chemistry (Norway) (7) were used for immobilization of the oligonucleotide probes. The particles were obtained by copolymerization of glycidyl methacrylate (40%) with ethylene dimethylacrylate (60%) (37% matrix) and derivatized with bis(3-aminopropyl)-amine reacted with the particle-bound epoxy functions. The density of the primary amino functions was of the order of 1 mmol g^{-1} , the surface area 137 $\text{m}^2 \text{g}^{-1}$, and the total pore volume 0.822 mL g^{-1} . The pore size ranged from <5 to 500 nm, the average size being of the order of 30 nm.

Preparation of SH-Derivatized Particles 3 and 5. Particles bearing *N*-(mercaptoacetyl) functional groups (3) were prepared as follows. The amino functions of particles 1 were partly acylated with the pyridinium salt of dithiodiglycolic acid, as described previously (9) for long-chain alkylamine controlled pore glass support. Accordingly, the particles (0.1 g) were treated with a mixture of dithiodiglycolic acid (0.01 mmol), *N,N*-diisopropylcarbodiimide (0.02 mmol) and *N*-hydroxysuccinimide (0.01 mmol) in pyridine (4 mL). After 0.5 h, the particles were washed with pyridine, and the unreacted amino functions were acetylated by treating the particles four times for 15 min with a mixture of acetic anhydride, pyridine, and 1-methylimidazole (1:5:1 v/v; 7 mL). The capped particles 2 were washed with pyridine and ether and then dried for 30 min under reduced pressure. The particle-bound disulfide bonds were finally cleaved with methanolic 1,4-dithio-D,L-threitol (1 mL of 0.5 M solution) in the presence of triethylamine (3 μM) to give the SH-derivatized particles 3. The loading of the mercapto functions of these particles, determined by the 2-thiopyridone response (10), was 80 $\mu\text{mol g}^{-1}$.

Particles bearing *N*-(ω -mercaptoundecanoyl) functional groups (5) were prepared via acylation of particles 1 with 10-undecenoic acid to 4, followed by radical addition of thioacetic acid to the terminal double bond of the *N*-(10-

* Author to whom correspondence should be addressed (telephone 358-2-333 6770; fax 358-2-333 6770; e-mail harri.lonnberg@utu.fi).

® Abstract published in *Advance ACS Abstracts*, February 15, 1997.

undecenoyl) group and ammonolysis of the resulting thioester. The experimental details have been published elsewhere (11). According to the 2-thiopyridone response, the loading of the mercapto groups was $22 \mu\text{mol g}^{-1}$.

Preparation of NH_2 -Derivatized Particles 7. The amino functions of particles 1 were partly acylated with *N*-Fmoc-protected β -alanine. For this purpose, the particles (0.1 g) were treated with a mixture of *N*-Fmoc- β -alanine (0.1 mmol), *N,N*-diisopropylcarbodiimide (0.2 mmol) and *N*-hydroxysuccinimide (0.1 mmol) in pyridine (4 mL). After 1 h, the particles were washed with pyridine, and the unreacted amino functions were repeatedly acetylated as described above for particles 2. The Fmoc loading of the capped particles (6) was determined by detecting fluorometrically the amount of dibenzofulvene released upon treatment of part of the particles with a 1:4 mixture of 40% aqueous methylamine and pyridine. The loading was observed to be $20 \mu\text{mol g}^{-1}$. Finally, the Fmoc protection was removed with morpholine in pyridine (20%; 0.5 h), and the particles (7) were washed with pyridine and ether and dried under reduced pressure.

Immobilization of Oligonucleotides to the SH-Derivatized Particles 3 and 5. A 3'-[*N*-(6-amino-3,4-dithiahexyl)carboxamidomethyl] phosphate conjugate 8 of the 16-meric oligodeoxyribonucleotide 5'-d(CCTATGATGAATATAG)-3' was prepared by phosphoramidite chemistry as described previously (12) and converted to the *S*-(2-pyridyl) disulfide conjugate 9 via reduction with 1,4-dithio-D,L-threitol (25 mM; 4 h) in aqueous solution and subsequent reoxidation of the chromatographically isolated oligomer with bis(2-pyridyl) disulfide (3 mM; 17 h) in ethanol. The activated oligonucleotide conjugate 9 was finally purified by RP HPLC (Nucleosil 300 C₁₈, 4×250 mm, 5 μm ; buffer A, 0.05 M aqueous NH_4OAc ; buffer B, 0.05 M NH_4OAc in 65% aqueous MeCN; flow rate 1 mL min⁻¹; linear gradient from 0 to 30% B in A in 30 min) and desalted. When the SH-derivatized particles 3 (1.4 mg) or 5 (1.7 mg) were treated with the desired amount of 9 (from 0.25 to 3 OD) in aqueous solution (500 μL) for 24 h, the oligonucleotide was quantitatively attached to the particles giving 10 and 11, respectively, as indicated by complete disappearance of the nucleobase absorption at 260 nm and concomitant appearance of the 2-thiopyridone absorption at 343 nm. In this manner oligonucleotide loadings ranging from 1 to 8 $\mu\text{mol g}^{-1}$ were obtained. Finally, the unreacted mercapto functions were capped with maleimide in a 1:1 mixture of pyridine and ethanol (1 mL of 0.5 M solution). The particles were washed with pyridine and ether and dried under reduced pressure.

Alternatively, a 3'-[*N*-(2-aminoethyl)carboxamidomethyl] phosphate conjugate 12 of the same 16-meric oligodeoxyribonucleotide probe (0.25 OD, 1.5 nmol) was prepared, as described previously (12). The primary amino function of 12 was allowed to react with 30-fold excess of 2,4,6-trichlorotriazine in aqueous solution (96 μL) in the presence of *N,N*-diisopropylethylamine (135 nmol). After 5 min, the SH-derivatized particles 3 (2.0 mg) were added, and the reaction was allowed to proceed for 20 h. According to time-dependent UV absorption spectra of the solution, the oligonucleotide was quantitatively attached to the particles, giving an oligonucleotide loading of $0.7 \mu\text{mol g}^{-1}$. The particles were washed with water, and the unreacted mercapto functions were capped with maleimide, as described above for 10 and 11. The capped particles 13 were finally washed with pyridine and ether and dried under reduced pressure.

Immobilization of Oligonucleotides to the NH_2 -Derivatized Particles 7. The 3'-[*N*-(2-aminoethyl)carboxamidomethyl] phosphate conjugate 12 (0.30 OD,

1.8 nmol) was activated with 15-fold excess of 2,4,6-trichlorotriazine. After 5 min, particles 7 (2.3 mg) were added, and the reaction was allowed to proceed for 20 h. Quantitative attachment of 12 to the particles resulted in an oligonucleotide loading $0.8 \mu\text{mol g}^{-1}$. The particles obtained (14) were washed with pyridine and ether and dried under reduced pressure.

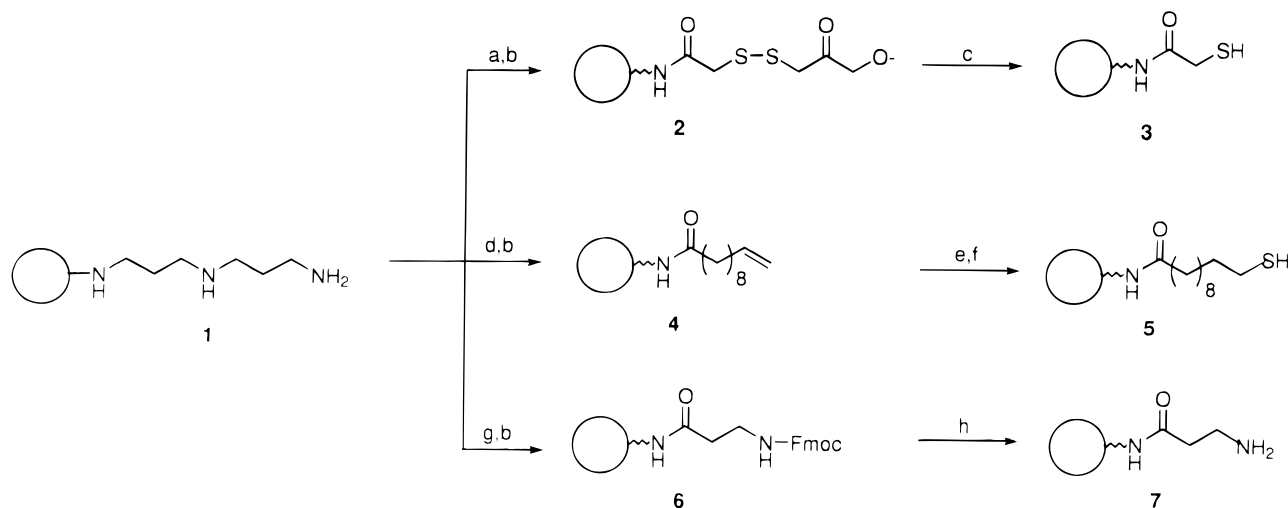
Fluorescent Oligonucleotide Conjugates. The fluorescent oligonucleotide conjugates used in hybridization assays were obtained by assembling sequences 5'-d(CTATATTCATCATAGGAAACACCAAAGATGATA-TTX₅C)-3' [X = *N*⁴-aminohexyl-2'-deoxycytidine; 15], as described previously (13), and labeling (14) them with a photoluminescent Eu(III) chelate, {2,2',2'',2'''-[4'-{4'''-[(4,6-dichloro-1,3,5-triazin-2-yl)aminophenyl]-2,2':6,2''-terpyridine-6,6''-diyl}bis(methylenenitrilo)}tetrakis-(acetato)}europium(III) (8). The extent of labeling was determined by releasing Eu(III) ion in solution with a fluorescence enhancement solution and measuring the fluorescence intensity on a time-resolved fluorometer against a europium(III) chloride standard solution (15). 15 was observed to be fully labeled, bearing thus 5 Eu(III) chelates. A similarly labeled 32-mer, 5'-d(X₂₀-ATCATCTTTGGT)-3' (16), was prepared to determine the unspecific binding of oligonucleotides to particles 10, 11, 13, and 14. The extent of labeling was determined to be 17 chelates per oligomer.

Hybridization Assays. The hybridization assays were carried out in a Tris buffer (50 mM, pH 7.5, 0.01% Tween 20, 0.5 M NaCl). Usually 50 particles were incubated in 10 μL of the buffer containing a known amount of the fluorescently labeled oligonucleotide (15 or 16). However, for examining the kinetics of hybridization, the total volume was 100 μL and aliquots of 10 μL were withdrawn. Hybridization reactions were typically allowed to proceed for 24 h. The particles were usually washed twice with 200 μL of glycine buffer (50 mM, pH 10), containing 20% propanol, and then transferred into a quartz capillary tube for measurement. However, when the kinetics of hybridization was followed, only one wash with 300 μL of buffer was carried out. The fluorescence emission of each particle was determined separately on a time-resolved microfluorometer based on a Nikon TDM inverted microscope, as previously described in detail (6). Typically 10 individual particles were measured, the standard deviation ranging from 2 to 8%. To convert the intensity of the fluorescence signal to number of europium(III) ions, and hence to number of oligonucleotides hybridized, the europium(III) ion was in some cases released in solution with a fluorescence enhancement solution, and the fluorescence emission was measured on a time-resolved fluorometer against a europium(III) chloride standard solution (15).

RESULTS AND DISCUSSION

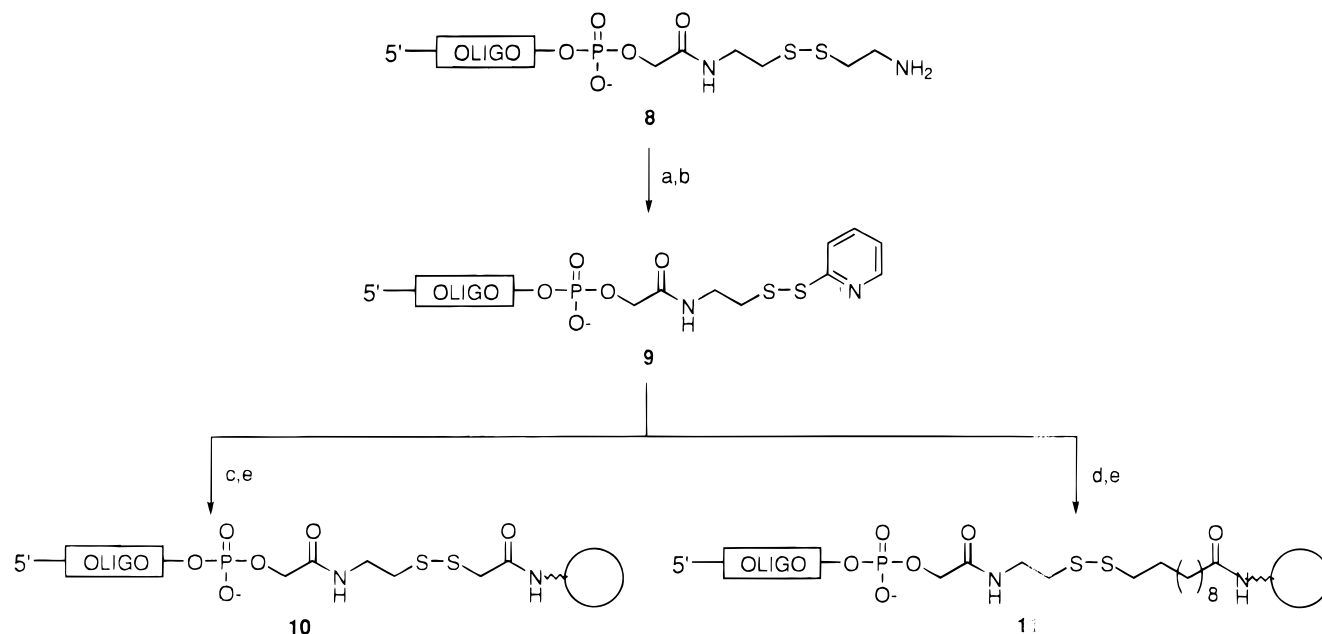
Covalent Immobilization of Oligonucleotides to Microparticles. Uniformly sized (50 μm) porous microparticles (1) prepared by copolymerization of glycidyl methacrylate (40%) with ethylene dimethylacrylate (60%) and functionalized with primary amino groups (7) were used for the immobilization of a 16-mer oligodeoxyribonucleotide, 5'-d(CCTATGATGAATATAG)-3'. For this purpose, the particles were further derivatized in one of the three alternative manners depicted in Scheme 1. Accordingly, a desired proportion of the amino functions of particles 1 was first acylated with either dithiodiglycolic acid to give 2, 10-undecenoic acid to give 4, or *N*-Fmoc- β -alanine to give 6, and the rest of the amino groups were acetylated. Reductive cleavage of the disulfide bond of particles 2 with 1,4-dithio-D,L-threitol gave

Scheme 1



^a HOOCCH₂SSCH₂COOH/HO-Su/DIPC/Py. ^b Ac₂O/MI/Py. ^c DTT/Et₃N/MeOH. ^d H₂C=CH(CH₂)₈COOH/HO-Su/DIPC/Py. ^e AcSH, (PhCOO)₂. ^f *n*-BuNH₂/MeOH. ^g *N*-Fmoc-β-Ala/HO-Su/DIPC/Py. ^h Morpholine/Py. HO-Su, *N*-hydroxysuccinimide; DIPC, *N,N*-diisopropylcarbodiimide; Py, pyridine; MI, 1-methylimidazole; DTT, 1,4-dithio-D,L-threitol.

Scheme 2



^a DTT, aq. ^b PySSPy/EtOH. ^c **3**/aq. ^d **5**/aq. ^e Maleimide/pyridine/EtOH. DTT, 1,4-dithio-D,L-threitol; PySSPy, bis(2-pyridyl) disulfide; OLIGO, 5'-d(CCTATGATGAATATAG-3').

N-mercaptoacetylated particles **3**, radical addition of thioacetic acid to the terminal double bond of particles **4** and subsequent ammonolysis gave *N*-(ω-mercapto-undecanoyl) functionalized particles **5** (11), and removal of the *N*-Fmoc protection from particles **6** gave particles **7**. A 3'-[*N*-(6-amino-3,4-dithiahexyl)carboxamidomethyl] phosphate conjugate **8** of the 16-meric oligodeoxynucleotide was then prepared (12), converted to the *S*-(2-pyridyl) disulfide conjugate **9**, and reacted with SH-derivatized particles **3** and **5** to result in covalent immobilization via a disulfide linkage (**10** and **11** in Scheme 2). Immobilization to particles **3** was also achieved by activating the 3'-[*N*-(2-aminoethyl)carboxamidomethyl] phosphate oligonucleotide **12** (12) with 2,4,6-trichlorotriazine (**13** in Scheme 3). In the same manner, the oligonucleotide conjugate **12** was attached to the NH₂-derivatized particles **7** (**14** in Scheme 3). The oligonucleotide loading of the particles ranged from 0.7 to 8 μmol g⁻¹.

Kinetics of Hybridization to Particle-Bound Oligonucleotides. The hybridization of the fluorescent oligonucleotide conjugate **15** to the particle-bound oligonucleotides was followed by shaking 500 microparticles (**10**, **11**, **13**, **14**) in 100 μL of Tris buffer (50 mM, pH 7.5, containing 0.5 M NaCl and 0.01% Tween) containing **15** at nanomolar concentrations. Aliquots of 10 μL (50 particles) were withdrawn at appropriate intervals. The particles were washed with 300 μL of glycine buffer, and the fluorescence emission of a single particle was measured by time-resolved fluorometry. The results obtained at 25 °C are presented in Figure 1. With each particle, unspecific binding of the noncomplementary oligonucleotide **16** was negligible; <1% of **16** was bound to the particles. Even with particles exhibiting the poorest hybridization properties, the sequence specific signal represented >10% of the total amount of the labeled oligomer. Accordingly, the background signal referring to unspecific binding of **16** remained always <10% of the

Scheme 3

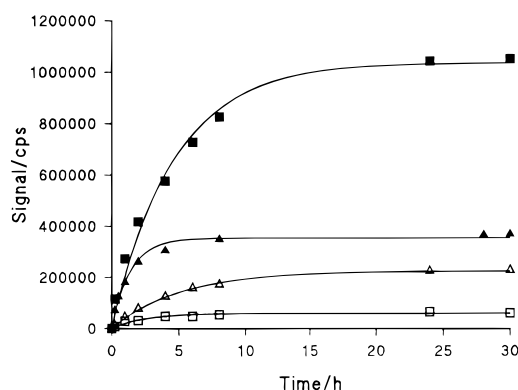
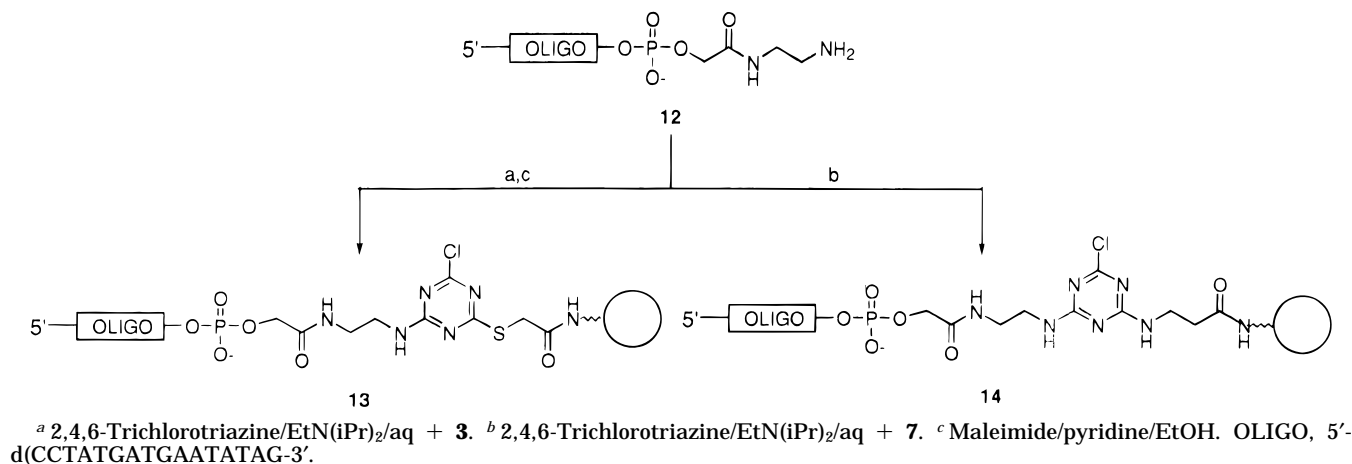


Figure 1. Kinetics of hybridization of fluorescent labeled oligonucleotide **15** with a complementary sequence covalently immobilized via various linkers to glycidyl methacrylate/ethylene dimethacrylate particles: (\blacktriangle) **10**, (\blacksquare) **11**, (\triangle) **13**, (\square) **14**.

specific one resulting from binding of **15**, usually only a couple of percent. The low level of unspecific binding was further verified by replacing the base triplet T7C8A9 of **15** with a triplet G7T8G9. This three-base mismatch was sufficient to result in complete disappearance of sequence specific signal of **15**.

As seen, the kinetics of hybridization depend considerably on the structure of the linker employed to tether the oligonucleotide to the particle. The half-saturation took place in 1.2, 4, 4, and 3 h with **10**, **11**, **13**, and **14**, respectively. All of these half-lives were practically independent of the initial concentration of **15**, as long as the amount of **15** was small compared to that of the covalently immobilized oligonucleotides. Under these conditions, i.e. when the immobilized sequences are present in large excess, the hybridization obeys rather well the kinetics of two reversible first-order reactions, the rates of the opposite reactions being proportional to the amount of **15** in solution and hybridized to the particle, respectively. The curves indicated in Figure 1 represent the best least-squares fit obtained on the basis of this simple model. As seen, no systematic deviation from the assumed kinetics occurs.

Somewhat unexpectedly, the density of immobilized oligonucleotides on the particle had practically no effect on the hybridization kinetics. For example, particles **11** having oligonucleotide loadings of 1 and 6 $\mu\text{mol g}^{-1}$ both underwent half-saturation in 4 h (data not shown). Increasing the number of particles in a given volume of the hybridization mixture, in turn, markedly reduced the time needed to reach the equilibrium. In fact, the half-life of hybridization was observed to be approximately inversely proportional to the number of particles. In

summary, when the amount of particle-bound oligonucleotide probes is much higher than that of the complementary oligonucleotide (**15**) in solution, the hybridization can be accelerated by increasing the area of the solid support in contact with the solution, but not by increasing the oligonucleotide density, keeping the surface area constant.

Calibration of the Fluorescence Measurement from a Single Microparticle. The efficiency of hybridization, i.e. the proportion of the fluorescent oligonucleotide conjugate **15** hybridized to particles **10**, **11**, **13**, and **14**, was quantified as follows. Two sets of hybridization assays on particles **10** were carried out, changing the initial concentration of **15** from 1.7 pM to 1.7 μM , i.e. from 10^9 to 10^{12} molecules of **15** per reaction (50 particles in 10 μL). After the hybridization equilibrium had settled, one set of particles was subjected to microfluorometry measurements by the single-particle techniques used above. From the other set of washed particles, europium(III) ion was released to solution and determined according to the DELFIA protocol (15). Similarly, the amount of **15** in the solution phase before and after the hybridization assay was determined by releasing the europium(III) ion from **15** and determining its amount by DELFIA. The sum of the amount of europium(III) ion released from the solution and solid phase after hybridization was always equal to the amount of europium(III) ion released from the solution phase before hybridization. Plotting of the microfluorometry signals determined from single particles against the amount of europium(III) ion released from the particles and quantified by DELFIA gave the calibration line depicted in Figure 2. Approximately 50 particles were used in each europium release assay. The possible contribution of unspecific binding was always estimated with the aid of the labeled noncomplementary oligonucleotide, **16**. In all cases this contribution was negligible. As seen from Figure 2, the microfluorometry signal is linearly related to the number of europium(III) ions on particle over a range of 3 orders of magnitude, in striking contrast to the behavior of conventional fluorophores. This calibration line was exploited to convert the microfluorometry signals to the amount of europium(III) ion on the particle and further to the amount of **15** hybridized to the particle. Comparison of the total amount of **15** on all particles to the total amount of **15** initially added to the system then enabled estimation of the hybridization efficiency.

Efficiency of Hybridization. All of the particles studied (**10**, **11**, **13**, **14**) exhibited selective hybridization with the complementary oligonucleotide (**15**) in solution. Binding of a noncomplementary oligonucleotide conjugate

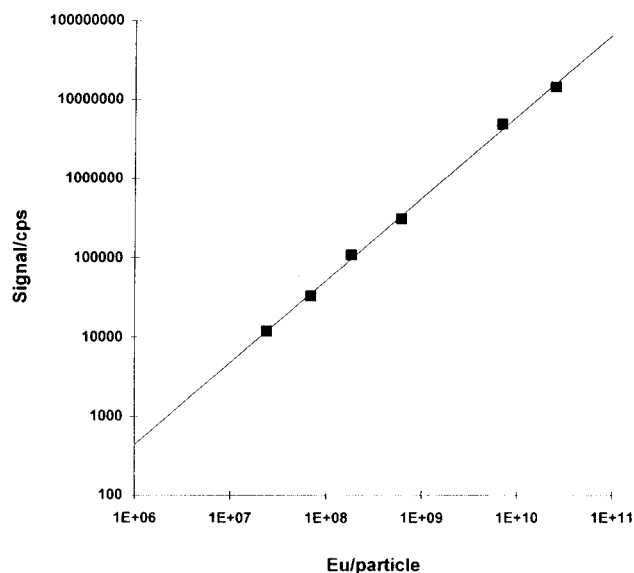


Figure 2. Intensity of the microfluorometer signal of a single particle plotted against the number of europium(III) ions on the particle.

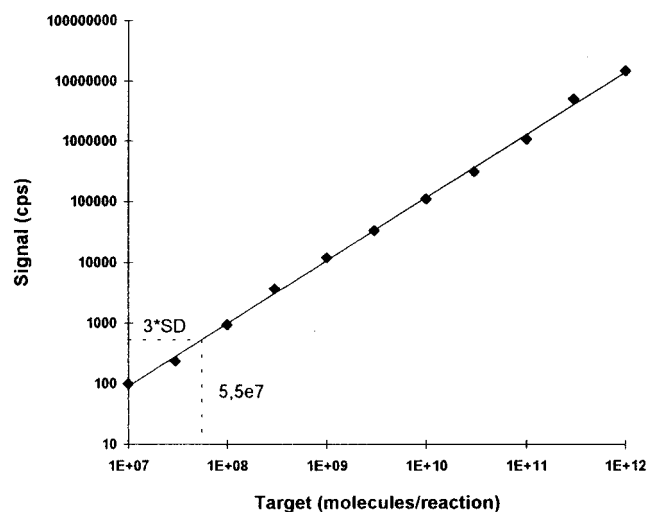


Figure 3. Intensity of the microfluorometer signal of a single particle plotted against the number of labeled oligonucleotide molecules used in the hybridization assay.

(16) was always negligible. As mentioned above, the structure of the linker used to tether the oligonucleotide probe to the particle markedly affects the kinetics of hybridization. Unfortunately, the kinetics and efficiency of hybridization do not correlate; as seen from Figure 1, faster hybridization does not necessarily mean more efficient hybridization. Application of the calibration curve in Figure 2 to the data in Figure 1 (and several similar measurements) gave average hybridization efficiencies of 25, 80, 20, and 10% for particles **10**, **11**, **13**, and **14**, respectively. Accordingly, tethering of oligonucleotide probes to particles via a long hydrocarbon chain, as with particles **11**, appears preferable, in spite of the fact that the kinetics of hybridization is slower than with some other alternatives studied.

With all of the particles studied, the efficiency of hybridization was observed to be, analogously to the kinetics of hybridization, independent of the concentration of the complementary oligonucleotide (**15**) over a wide range. As an example, the data obtained with particles **10** are given in Figure 3. Experiments with the same particles (**10**) also showed that the density of the covalently immobilized oligonucleotide probes exerts only

a minor effect on the efficiency of hybridization, as long as the particle-bound oligonucleotide probes are present in large excess. Increasing the oligonucleotide loading from 1 to 8 $\mu\text{mol g}^{-1}$ increased the hybridization efficiency from 25 to 40%. Interestingly, tethering 4 $\mu\text{mol g}^{-1}$ of a pentameric T₅ sequence to these particles, keeping the loading of the recognizing oligonucleotide probe at 1 $\mu\text{mol g}^{-1}$, also increased the hybridization efficiency of **15** from 25 to 40%, while the unspecific oligonucleotide binding remained at low level. The physicochemical basis of the enhanced binding is obscure, but the observation suggests that truncated oligonucleotide sequences on the particles are not necessarily detrimental to the binding properties. Possibly, the desired oligonucleotide probes could be assembled directly on the microparticles without a marked loss of efficiency and selectivity of hybridization.

From the point of view of potential applications, the relatively slow kinetics of hybridization form the major hurdle to overcome. As discussed in the foregoing, increasing the number of particles, i.e. increasing the surface area and keeping the density of immobilized probes constant, reduces the time needed to reach equilibrium. At the same time the efficiency of hybridization appeared to remain almost unaltered. Accordingly, high particle density would enable short assay times. Unfortunately, the fluorescence intensity when determined from a single particle is inversely proportional to the number of particles, and hence what one wins in time is lost in sensitivity. The attempts to accelerate the hybridization by increasing the temperature led to a similar result. Increasing the temperature from 25 to 40 °C reduced the apparent half-life of hybridization to approximately half of the original value, but simultaneously the hybridization efficiency was decreased by almost 50%.

ACKNOWLEDGMENT

We thank Dr. Ruth Schmid, SINTEF (Norway), for the generous gift of the particles employed and Prof. Timo Lövgren, Dr. Antti Iitiä, and Ms. Pia Heinonen for helpful discussions. We gratefully acknowledge financial support from the Academy of Finland, the Research Council for Natural Sciences and Technology.

LITERATURE CITED

- (1) Saiki, R., Gelfand, D. H., Stoffel, S., Scharf, S. J., Higuchi, R., Horn, G. T., Mullis, K. B., and Erlich, H. A. (1988) Primer-directed enzymatic amplification of DNA with a thermostable DNA polymerase. *Science* **239**, 487–491.
- (2) Southern, E. M., Maskos, U., and Elder, J. K. (1992) Analyzing and comparing nucleic acid sequences by hybridization to arrays of oligonucleotides: Evaluation using experimental models. *Genomics* **13**, 1008–1017.
- (3) Southern, E. M., Case-Green, S. C., Elder, J. K., Johnson, M., Mir, K. U., Wang, L., and Williams, J. C. (1994) Arrays of complementary oligonucleotides for analysing the hybridization behaviour of nucleic acids. *Nucleic Acids Res.* **22**, 1368–1373.
- (4) Guo, Z., Guilfoyle, R. A., Thiel, A. J., Wang, R., and Smith, L. M. (1994) Direct fluorescence analysis of genetic polymorphisms by hybridization with oligonucleotide arrays on glass supports. *Nucleic Acids Res.* **22**, 5456–5465.
- (5) Soini, E. (1991) Biospecific multianalyte assay method. U.S. Pat. 5,028,545.
- (6) Lövgren, T., Heinonen, P., Lehtinen, P., Hakala, H., Heinola, J., Harju, R., Takalo, H., Mukkala, V.-M., Schmid, R., Lönnberg, H., Pettersson, K., and Iitiä, A. (1996) Sensitive bioaffinity assays on individual microparticles using time-resolved fluorometry. *Clin. Chem.* (submitted for publication).
- (7) Ugelstad, J., Berge, A., Ellingsen, T., Schmid, R., Nilsen, T.-N., Mørk, P. C., Stenstad, P., Hornes, E., and Olsvik, Ø. (1992)

- Preparation and application of new monosized polymer particles. *Prog. Polym. Sci.* 17, 87–161.
- (8) Mikkala, V.-M., Helenius, M., Hemmälä, I., Kankare, J., and Takalo, H. (1993) Development of luminescent europium(III) and terbium(III) chelates of 2,2':6',2''-terpyridine derivatives for protein labelling. *Helv. Chim. Acta* 76, 1361–1378.
- (9) Hovinen, J., Guzaev, A., Azhayeve, E., Azhayeve, A., and Lönnberg, H. (1995) Imidazole tethered oligodeoxyribonucleotides: synthesis and RNA cleaving activity. *J. Org. Chem.* 60, 2205–2209.
- (10) Brocklehurst, K., and Little, G. (1973) Reactions of papain and of low-molecular-weight thiols with some aromatic disulphides. *Biochem. J.* 133, 67–80.
- (11) Salo, H., Guzaev, A., Azhayeve, A., and Lönnberg, H. (1996) Disulfide tethered solid supports for oligonucleotide synthesis and a comparative study on their resistance to ammonolysis. *Collect. Czech. Chem. Commun.* 61 (special issue), S110–111.
- (12) Hovinen, J., Guzaev, A., Azhayeve, A., and Lönnberg, H. (1994) Novel solid supports for the preparation of 3'-derivatized oligonucleotides: introduction of 3'-alkylphosphate tether groups bearing amino, carboxy, carboxamido, and mercapto functionalities. *Tetrahedron* 50, 7203–7218.
- (13) Sund, C., Ylikoski, J., Hurskainen, P., and Kwiatkowski, M. (1988) Construction of europium (Eu³⁺)-labeled oligo DNA hybridization probes. *Nucleosides Nucleotides* 7, 655–659.
- (14) Lövgren, T., Iitiä, A., Hurskainen, P., and Dahlen, P. (1995) Detection of lanthanide chelates by time-resolved fluorescence. In *Blotting and Sequencing* (L. Kricka, Ed.) pp 350–358, Academic Press, San Diego, CA.
- (15) Hemmälä, I., Dakubu, S., Mikkala, V.-M., Siitari, H., and Lövgren, T. (1984) Europium as a label in time-resolved immunofluorometric assays. *Anal. Biochem.* 137, 335–343.

BC9700143

Synthesis of ^{125}I -Labeled Oligonucleotides from Tributylstannylbenzamide Conjugates

Michael W. Reed,^{*,†} Igor G. Panyutin,[‡] Don Hamlin,[§] Deborah D. Lucas,[†] and D. Scott Wilbur[§]

Epoch Pharmaceuticals Inc., 1725 220th Street S.E. No. 104, Bothell, Washington 98021, Department of Nuclear Medicine, Clinical Center, National Institutes of Health, Bethesda, Maryland 20892, and Department of Radiation Oncology, University of Washington, Seattle, Washington 98195. Received October 16, 1996[®]

A rapid and efficient method for the synthesis of ^{125}I -labeled oligodeoxynucleotides (^{125}I ODNs) is described. The key intermediates are tributylstannylbenzamide-modified ODNs (Sn-ODNs). Reaction conditions are described for the preparation of 5'-modified Sn-ODNs. Treatment with NaI and chloramine T gave conversion to the desired I-ODN, which was easily isolated by reversed phase chromatography. Thermal denaturation (T_m) studies showed that hybridization properties were not disturbed by the 4-iodobenzamide modification. An ^{125}I ODN was prepared and characterized by hybridization to ^{32}P -labeled DNA targets. Sequence specific cleavage of the target DNA strand by ^{125}I was measured.

INTRODUCTION

^{125}I -labeled oligodeoxynucleotides (^{125}I ODNs)¹ have been used for years as probes to detect complementary nucleic acids. Appropriately labeled ^{125}I ODNs can also act as efficient, sequence specific, DNA cleavage agents (1). The nuclear decay process of ^{125}I (electron capture and internal conversion) generates ~ 22 low-energy electrons that dissipate their energy within a few nanometers of the decay site (2). If this decay process (Auger emission) occurs in close proximity to duplex DNA, double-strand breaks can occur with $\sim 100\%$ efficiency/decay event. The short DNA cleavage range of the Auger emitting isotopes makes them promising agents for sequence specific targeting by oligonucleotides. For example, when ^{125}I -labeled deoxycytidine (^{125}I dC) was enzymatically incorporated into a single position in an ODN and hybridized to a complementary ssDNA target, more than 70% of the cleavage products were found within 15–20 Å of the site of ^{125}I decay (1). Recently it has been shown that an ^{125}I -dC labeled triplex forming ODN can specifically cleave a homopurine sequence in a plasmid DNA target containing the *nef* gene of HIV. Each ^{125}I decay gave approximately 0.8 dsDNA breaks (3).

As a result of its efficient DNA cleavage properties, ^{125}I is extremely cytotoxic when incorporated into the DNA of dividing cells as ^{125}I dU (4). Therapeutic (anticancer) implications of Auger emitting radionuclides have been reviewed (5). Although ^{125}I is an efficient DNA cleavage agent, its 60 day half-life is an obvious disadvantage for *in vivo* applications. The shorter half-life, Auger emitting isotope ^{123}I (13.2 h half-life) has also been shown to be cytotoxic when incorporated into DNA using ^{123}I dU (6)

or targeted to DNA using ^{123}I -labeled estrogens (7). The DNA cleavage efficiency of ^{123}I dU incorporated into cellular DNA has been determined (8). Each decay of ^{123}I gave 0.45–0.74 dsDNA breaks if DNA repair is accounted for. Radiolabeling of ODNs with ^{123}I has not been reported.

This paper describes a rapid and convenient radiolabeling method for making I-ODNs from tributylstannylbenzamide-modified ODN intermediates (Sn-ODNs). Aryl tin intermediates have been valuable for radiolabeling small molecular weight compounds via halodestannylation reactions (9). A 15-mer ODN bearing a 5'-terminal hexylamine linker was used to develop the conjugation chemistry. The effect of the 4-iodobenzamide linker system on hybridization properties of nontadioactive (^{127}I) labeled ODNs was studied spectrophotometrically. The terminally modified ^{125}I ODN was then prepared and hybridized to a ^{32}P -labeled ssDNA target. Analysis of the ^{32}P fragments after 15 days showed sequence specific DNA cleavage at the site of the attached ^{125}I . Our ultimate goal is to prepare ^{123}I -labeled ODNs and to determine how the position of attachment of ^{125}I and ^{123}I affects DNA cleavage efficiency of I-ODNs.

EXPERIMENTAL PROCEDURES

General Chemical Procedures. Reversed phase HPLC analysis of nonradioactive compounds used a Rainin pump system. Pump control and data processing used a Rainin Dynamax chromatographic software package (Macintosh). Aqueous solutions were dried at <1 Torr on a Speed Vac centrifugal evaporator (Savant Instruments, Farmingdale, NY). T_m studies were performed on a Perkin-Elmer Lambda 2S UV-vis spectrophotometer equipped with a PTP6 thermal programmer. Radio-HPLC was done on a Beckman pump system with an in-line γ detector (Beckman Model 170). Alternatively, radio-HPLC was done on a Hewlett-Packard pump system with an IN/US γ -RAM detector. To account for variations in HPLC systems, retention times of the ^{125}I ODNs were always verified by injection of nonradioactive standards. Isolated radiochemical yields were determined using a Capintec dose calibrator.

Synthesis of Oligodeoxynucleotides. ODNs were prepared on an Applied Biosystems Model 384 synthesizer using the 1 μmol protocols supplied by the manufacturer. Protected β -cyanoethyl phosphoramidites, CPG

* Author to whom correspondence should be addressed [telephone (206) 485-8566; fax 206/486-8336; e-mail mreed@epochpharm.com].

[†] Epoch Pharmaceuticals.

[‡] National Institutes of Health.

[§] University of Washington.

[®] Abstract published in *Advance ACS Abstracts*, March 1, 1997.

¹ Abbreviations: ODN, oligodeoxynucleotide; I-ODN, iodinated ODN; Sn-ODN, tributyltin-modified ODN; ssDNA, single-stranded DNA; dsDNA, double-stranded DNA; ChT, chloramine T (sodium salt of *N*-chloro-*p*-toluenesulfonamide); TEAA, triethylammonium acetate; PAGE, polyacrylamide gel electrophoresis; PBS, phosphate-buffered saline.

supports, deblocking solutions, cap reagents, oxidizing solutions, and tetrazole solutions were purchased from Glen Research (Sterling, VA). The structure and sequence of the amine-modified ODN (**1**) used in this study are shown in Figure 1. The sequence of the 42-mer target (ODN **4**) is shown below. The underlined region is complementary to modified ODN **1**.

5'-CCAGCAGCCTCCCGCGACGATGCCCTCAACGTTAGCTTCAC

The 3'-hexanol modification was introduced into ODN **1** through use of a hexanol-modified CPG support (10). The 5'-aminoethyl modification was introduced into **1** using an N-MMT-hexanolamine phosphoramidite linker (Glen Research). HPLC purification, detritylation, and butanol precipitation of the synthetic ODNs were carried out as previously described (11).

Characterization of Modified ODNs. The concentrations of all ODNs were determined from the UV absorbance at 260 nm in PBS (pH 7.2). An extinction coefficient for each ODN was determined using a nearest-neighbor model (12), correcting for the molecular weight (but not ϵ) of appended modifications. The value for ϵ was used to calculate a theoretical ratio of A_{260} to concentration in micrograms per milliliter as listed in Table 1. All modified ODNs were analyzed by HPLC using the method described in Figure 2. Retention times are listed in Table 1. ODN purity was further confirmed by polyacrylamide gel electrophoresis. PAGE was carried out under denaturing conditions (7 M urea) using cross-linked 20% gels [bis(acrylamide)/acrylamide, 1:19; $0.4 \times 170 \times 390$ mm] at 45 W for 40 min. TBE (pH 8.3; 100 mM Tris base, 100 mM boric acid, 1 mM EDTA) was used as a running buffer. Bromophenol blue was used as a marker. The nucleotidic bands were visualized by silver staining. Unless otherwise noted, all modified ODNs were >95% pure by HPLC and one major band by PAGE.

5'-Modified Sn-ODN (2). To 0.13 mL of a 0.77 mM solution of ODN **1** ($0.10 \mu\text{mol}$) were added 0.1 mL of 1 M sodium borate buffer (pH 8.3) and 0.3 mL of 0.1 M sodium borate buffer (pH 8.3) in a 1.7 mL Eppendorf tube. A solution of 5 mg ($10 \mu\text{mol}$) of *N*-hydroxysuccinimidyl 4-*tri*-(*n*-butyl)stannylbenzoate (13) in 0.5 mL of THF was added, and the milky emulsion was shaken for 16 h. The mixture was concentrated to a volume of ~ 0.1 mL on a Speed Vac to remove THF. The cloudy solution was dissolved in 0.4 mL of 0.1 M TEAA (pH 7.5) and filtered through a $0.45 \mu\text{m}$ syringe filter. The filter was rinsed with an additional 0.2 mL of buffer, and the combined filtrate was purified by HPLC using the conditions described in Figure 2. The desired product (31 min peak) was collected, and 0.1 mL of 1 M borate buffer (pH 8.3) was added before taking to dryness on a Speed Vac. The white solid product was reconstituted with 0.5 mL of water, and the concentration was determined by A_{260} measurement. Recovery of **2** was 0.23 mg (42% yield).

5'-Modified [¹²⁵I]ODN (3). *Method A.* To 12 μL of an 83 μM solution of Sn-ODN **2** (1 nmol) were added 7.5 μL (5 nmol) of a 0.1 mg/mL solution of sodium iodide and 6.9 μL of 0.1 M borate buffer (pH 8.3). Reaction was initiated by adding 4.56 μL (20 nmol) of a 1 mg/mL solution of chloramine T hydrate (ChT) in water. After 5 min, the reaction was quenched with 5 μL of a 10 mg/mL solution of sodium bisulfite. The reaction was analyzed by HPLC and showed complete conversion of **2** (31 min) to the desired product **3** (16 min) as shown in Figure 2.

Method B. To 0.127 mL of a 0.79 mM solution of ODN **1** ($0.10 \mu\text{mol}$) were added 0.1 mL of 1 M sodium borate buffer (pH 8.3) and 0.3 mL of 0.1 M sodium borate buffer

(pH 8.3) in a 1.7 mL Eppendorf tube. A solution of 4-iodobenzoyl chloride (2.5 mg, $9.4 \mu\text{mol}$) in 0.5 mL of THF was added, and the solution was kept at room temperature for 16 h. HPLC showed complete reaction of **1** (8.7 min). The reaction mixture was diluted to 2 mL and purified by centrifugal ultrafiltration through a 1000 MW cutoff concentrator (Filtron). This process removed excess hydrolyzed acid chloride and gave the desired product **3** in 97% purity as evidenced by HPLC. The retentate was diluted to 0.5 mL with water, and concentration was determined by A_{260} measurement. Recovery of **3** was 0.41 mg (77% yield). This product coeluted with **3** prepared according to method A and was used for thermal denaturation experiments.

Thermal Denaturation Studies. The hybridization properties of all modified ODNs were examined by forming duplexes with complementary ODN **4** and determining the melting temperatures (T_m). Each ODN was present at 2 μM in pH 7.2 PBS (9.2 mM disodium phosphate, 0.8 mM monosodium phosphate, 0.131 M sodium chloride). UV absorbance was measured as the samples were heated from 10 to 90 °C with a temperature increase of 0.5 °C/min. Thermal dissociation curves were obtained from A_{260} vs temperature. The T_m was determined from the derivative maximum. Data from one representative run are given in Table 1.

Radiolabeling Procedures. The volatile nature of ¹²⁵I dictates certain handling precautions. Radiohalogenation of ODNs was carried out in a Plexiglas "iodination box", which had its own exhaust fan and charcoal filter (Radiation Physics, Beltsville, MD) and which was placed within a fume hood. ¹²⁵I was handled using standard syringe techniques. Labeling reactions were conducted in a reaction vessel that was vented to the inside of the iodination box through a 10 mL syringe filled with charcoal. Double gloves were routinely used to prevent the volatile halogens from penetrating the first glove layer. Commercially available "sleeve protectors" were used to decrease contamination of lab coats. Monitoring with a Geiger counter was conducted continually throughout an experiment. Between 24 and 72 h postlabeling, investigators should have a thyroid bioassay conducted.

Conversion of 2 to [¹²⁵I]ODN (3). To a solution of 11 μg (2 nmol) of Sn-ODN **2** in 22 μL of 0.1 M borate buffer (pH 8.3) were added 1.41 mCi (~ 0.64 nmol, 2200 Ci/mmol) of Na¹²⁵I in 3 μL of 0.1 M NaOH (New England Nuclear) and 20 μg (88 nmol) of ChT in 20 μL of water. After 15 min, the reaction was quenched with 10 μL of sodium bisulfite (10 mg/mL). A 5 μL aliquot of the crude reaction mixture was analyzed by radio-HPLC. The γ -detector indicated 69% conversion of ¹²⁵I to the desired I-ODN **3** (22 min peak) as shown in Figure 3. The remaining [¹²⁵I]ODN reaction mixture was loaded on a Poly-Pak reversed phase syringe cartridge (Glen Research) and eluted first with 2 mL of TEAA and then with 2 mL of 20% acetonitrile in TEAA. Fractions of ~ 0.5 mL were collected, and each was measured in the dose calibrator. The most concentrated fraction (no. 5) contained 0.384 mCi (27% radiochemical yield) of [¹²⁵I]ODN **3**. Radio-HPLC analysis of this sample showed 96% purity. Earlier radioactive fractions were not analyzed for purity.

Alternatively, the [¹²⁵I]ODN product was isolated from the reaction mixture by reversed phase HPLC. In a separate labeling run, 50 pmol of **2** in 20 μL of 50 mM borate buffer (pH 8.5) was treated with 350 μCi (~ 160 pmol) of Na¹²⁵I and 20 μg of ChT. After 10 min, the reaction was quenched with 10 μL of sodium bisulfite (10 mg/mL). The mixture was passed through a Sephadex G-50 microspin column (Pharmacia). The product (**3**) was

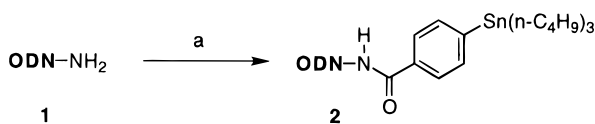
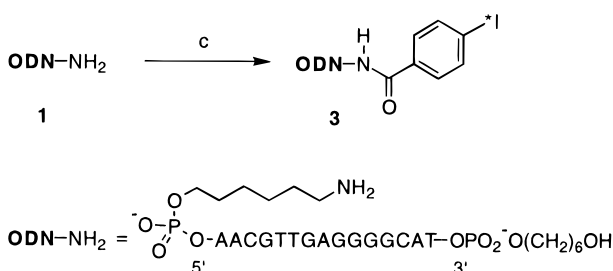
Method A (^{125}I , ^{127}I):**Method B** (^{127}I):

Figure 1. Synthesis of I-ODN conjugates. Reagents: (a) 4-(tributylstannyl)-benzoate, NHS ester; (b) Na⁺I⁻, chloramine T; (c) 4-iodobenzoyl chloride.

recovered in 50 μL of TES buffer buffer (50 mM Tris, pH 8, 50 mM NaCl, 1 mM EDTA) and contained 25 μCi of ^{125}I while 320 μCi was retained by the column. HPLC purification used a 150 \times 4.6 mm C₁₈ column (Supelcosil LC-18-T) and the gradient specified in Figure 2. The radioactive peak corresponding to product (11–16 min) was collected in 0.5 mL fractions. Fractions 3–5 (3.8 μCi , 1.73 pmol) were combined and taken to dryness on the Speed Vac. The residue was dissolved in 10 μL of TES buffer. [^{125}I]ODN **3** appeared as a single band by both denaturing and nondenaturing PAGE.

Duplex Preparation with [^{125}I]ODN (3). The 42-mer target (ODN **4**) complementary to ODN **3** was purified by gel electrophoresis prior to 5'- ^{32}P labeling with [^{32}P]- γ -ATP using T4 polynucleotide kinase. The product was purified on a Pharmacia Microspin G50 gel filtration column according to the manufacturer's protocol, and its final concentration was estimated to be 0.25 pmol/ μL on the basis of quantitative recovery of ODN. HPLC-purified [^{125}I]ODN **3a** (0.4 pmol, 2.5 μL) and ODN **4** (0.25 pmol, 1 μL) were annealed at 40 $^{\circ}\text{C}$ for 10 min in 1 \times TES buffer. Two different duplex solutions were prepared with final volumes of either 25 μL (sample D1) or 10 μL (sample D2). The products of annealing were analyzed in 20% native PAGE as shown in Figure 4. Extent of duplex formation was quantitated using a FUJI BioImager BAS1500 and MacBAS software.

DNA Strand Break Analysis. After 15 days at -70°C , the duplex samples D1 and D2 described above were analyzed for fragmentation of the ssDNA target by 10% denaturing PAGE as shown in Figure 5 (panel A). The bands corresponding to fragmentation of each duplex were quantitated on the FUJI BioImager, and the distribution of breaks in [^{32}P]ODN **4** for sample D2 are presented in Figure 5 (panel B). A control sample containing [^{32}P]ODN **4** but no [^{125}I]ODN **3a** showed trace bands that were subtracted as background.

RESULTS

The conjugation and iodination chemistry were developed using the nonradioactive isotope of iodine (^{127}I). As shown in Figure 1, two methods were used to prepare iodinated ODNs, but only method A was used to prepare ^{125}I -labeled ODNs. An amine-modified ODN (**1**) was treated with *N*-hydroxysuccinimidyl *p*-tributylstannyl-

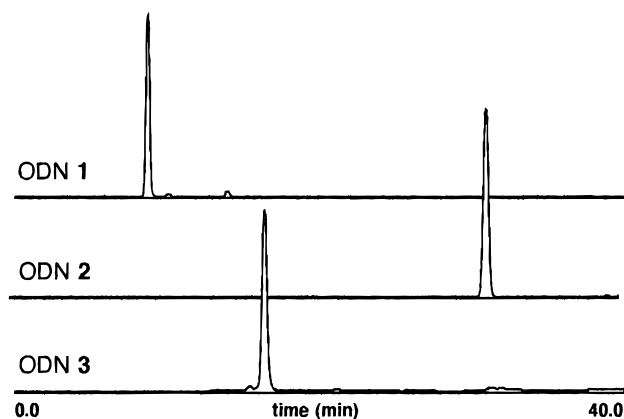


Figure 2. HPLC chromatograms describing synthesis of I-ODN **3** from Sn-ODN **2**, as shown in Figure 1 (method A). The HPLC system used a 250 \times 4.6 mm C₁₈ column (Rainin Dynamax 300 Å) and a gradient of 5–85% solvent B over 40 min (flow rate = 1 mL/min), where solvent A = 0.1 M triethylammonium acetate (pH 7.5), solvent B = acetonitrile; detection was by UV absorbance at 260 nm. Chromatogram for ODN **3** shows the reaction mixture 5 min after treatment of ODN **2** with NaI and chloramine T.

benzoate to give the key Sn-ODN precursor (**2**). Conversion to the desired I-ODN (**3**) was accomplished by treatment with excess NaI and ChT. To confirm the structure of the I-ODN prepared from Sn-ODN intermediate, I-ODN (**3**) was also prepared directly from **1** by reaction with 4-iodobenzoyl chloride (method B).

The structure and sequence of the starting amine-modified ODN (**1**) are shown in Figure 1. The ODN sequence is a 15-mer that is complementary to the initiation codon region of the *c-myc* oncogene. The 3'-hexanol modification was introduced into the ODN to improve serum stability (10). The 5'-hexylamine linker group was readily introduced into **1** on the DNA synthesizer using a commercially available phosphoramidite.

Preparation of the Sn-ODN was complicated by poor water solubility of the lipophilic tributyltin NHS ester. Suitable reaction conditions for synthesis of **2** used an excess of the NHS ester in an emulsion of THF and borate buffer (pH 8.3). Reversed phase HPLC analysis showed complete conversion of **1** to **2** after several hours. As shown in Figure 2, the lipophilic Sn-ODN (31 min retention time) was isolated by HPLC in high purity. Only 42% yield was obtained, presumably due to losses in the prior filtration step. The organometallic product destannylates under acidic conditions, so the Sn-ODN solutions were stored at pH 8 or above. These solutions had good stability (<5% degradation after 6 months at 0–5 $^{\circ}\text{C}$).

Treatment of **2** with 20 equiv of NaI and ChT gave complete conversion of the Sn-ODN to the I-ODN (**3**). After 5 min, HPLC analysis showed no remaining **2** and a new peak at 16 min. To prove that this peak was indeed the desired product, the same I-ODN product (**3**) was prepared using method B. Treatment of **1** with 4-iodobenzoyl chloride in borate buffer/THF gave 77% yield of a product (**3**) that coeluted with the I-ODN product from method A. Method B was more convenient for the larger scale preparations of I-ODN needed for T_m studies.

HPLC retention times and other physical properties of the modified 15-mer ODNs are listed in Table 1. Hybridization properties were determined by measuring the melting temperature (T_m) of DNA duplexes formed with a complementary 42-mer ODN target (**4**). The T_m data show that the 4-iodobenzamide modification has little effect on the ability of **3** to form stable duplexes. In

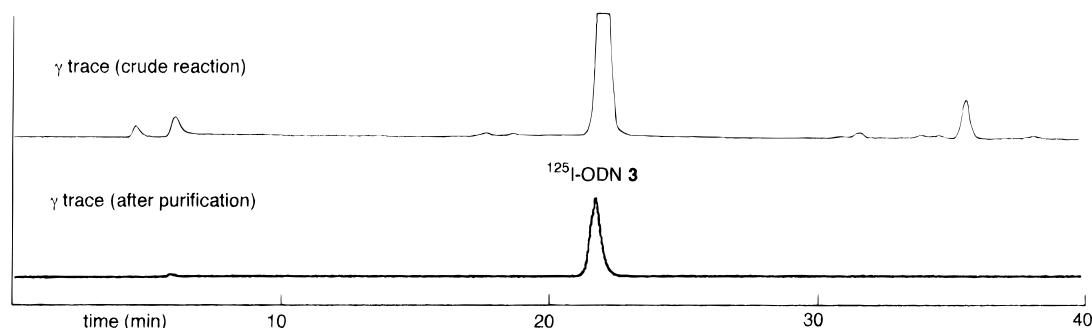


Figure 3. Radio-HPLC analysis of crude and purified [¹²⁵I]ODN **3**. The HPLC system is described in Figure 2. Upper trace is reaction mixture 10 min after addition of ChT. Lower trace is [¹²⁵I]ODN **3** after reversed phase (syringe column) purification.

Table 1. Properties of Modified ODNs^a

ODN	MW	A ₂₆₀ = 1 ^b (μg/mL)	HPLC ^c (min)	T _m ^d (°C)
1	5016	33.1	8.7	58.8
2	5409	35.7	31	57.4
3	5246	34.6	16	59.6

^a Sequences and structures of modified ODNs are shown in Figure 1. ^b Calculated concentration of ODN that gives 1.00 absorbance unit at 260 nm. ^c Elution time; C₁₈ HPLC conditions described in Figure 2. ^d Determined for 2 μM solutions of modified ODN and complementary 42-mer ODN **4** as described under Experimental Procedures.

fact, a slight increase in *T_m* (0.8 °C) was observed. The bulky tributylstannylbenzamide group in **2** gave a slight drop in *T_m* (1.4 °C), but even this ODN formed stable duplex structures as evidenced by the normally shaped melting curve.

After the hybridization properties were evaluated with the nonradioactive [¹²⁷I]ODN, the [¹²⁵I]-labeled ODN was prepared from the Sn-ODN intermediate. Radioiodination of Sn-ODN **2** with 1.41 mCi of [¹²⁵I] gave facile conversion to [¹²⁵I]ODN **3**. The reaction conditions were similar to that described for [¹²⁷I], except that 3.6-fold excess of the Sn-ODN was used to drive incorporation of the more valuable radionuclide. After 5 min, the reaction mix was quenched with sodium bisulfite (to reduce volatile iodine byproducts) and analyzed by reversed phase HPLC. As shown in Figure 3, the Na¹²⁵I (4–6 min retention time) was efficiently converted to a product with the same retention time (22 min) as the [¹²⁷I]ODN standard (**3**). Although the product peak was off scale on the chart recorder, the γ-detector indicated 69% conversion of [¹²⁵I] to the desired I-ODN **3**. A late eluting side product (35 min) was also present in the labeling mixture. The UV trace (not shown) was noisy due to the small injection volume but showed unreacted Sn-ODN (34 min).

[¹²⁵I]ODN **3** was purified by passing the reaction mixture through a disposable reversed phase syringe cartridge. These columns are routinely used for "tritylon" purification of synthetic ODNs. We used the protocol supplied by the manufacturer to isolate the desired product (0.38 mCi) in ~0.5 mL of 20% acetonitrile/TEAA. HPLC analysis of this material showed 96% purity by γ detection, and no detectable Sn-ODN by UV. The radioactive forerun was not analyzed for purity but presumably contained the remaining [¹²⁵I]ODN **3** and unreacted radioiodine. The excess of unreacted Sn-ODN was easily separated from the I-ODN product.

In a separate radiolabeling reaction, 3.2 equiv of [¹²⁵I] was used in relation to Sn-ODN **2**. After removal of unreacted [¹²⁵I] by gel filtration chromatography, analytical HPLC showed no unreacted Sn-ODN and some residual [¹²⁵I]. Further purification was accomplished by HPLC. Although the in-line radiometric detector gave

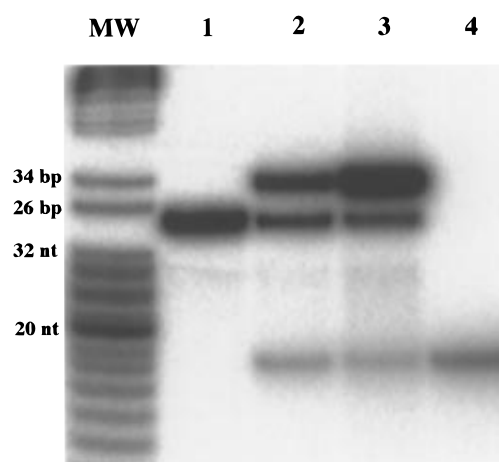


Figure 4. Nondenaturing PAGE showing duplexes formed from [¹²⁵I]ODN **3** and ³²P-labeled ODN **4**. Molecular weight (MW) markers: mixture of ³²P-labeled pBR322 Msp 1 digest and 8–32 oligo dT. Lanes: (1) [³²P]ODN **4**; (2) duplex D1; (3) duplex D2; (4) [¹²⁵I]ODN **3**.

better control over the purification process, radiochemical yield was low (3.5%) due to nonspecific adsorption to the C₁₈ packing. The fraction containing [¹²⁵I]ODN **3** was dried *in vacuo* and reconstituted in the desired buffer for the DNA cleavage assay. Nondenaturing PAGE analysis of this fraction showed one radioactive band (Figure 4, lane 4).

To study hybridization properties of [¹²⁵I]ODN **3**, a 5'-³²P-labeled 42-mer (ODN **4**) was prepared. A solution of 0.4 pmol (1.6 equiv) of I-ODN was annealed with an estimated 0.25 pmol of **4**. We assumed complete recovery of ³²P-labeled **4** from a gel filtration spin column on the basis of the manufacturer's claims of >90% recovery and our prior experience with these columns. Two different duplex solutions were prepared with different ODN **3** concentrations. These preparations were assayed for duplex formation by nondenaturing PAGE as shown in Figure 4. The less concentrated sample (D1) showed 65% of the slower moving duplex band, whereas sample D2 showed 89% duplex formation. As expected, both samples showed unhybridized I-ODN. The samples were frozen in liquid nitrogen and kept at -70 °C for strand break analysis of ODN **4**.

After 15 days of storage, the [¹²⁵I]ODN **3a**/[³²P]ODN **4** duplexes were analyzed for fragmentation by denaturing PAGE as shown in Figure 5A. The length of the 5'-³²P-labeled fragments in lanes 1 and 2 provides evidence for sequence specific cleavage by [¹²⁵I] decay. The position of the breaks relative to the sequence of ODN **4** was determined by counting the bands from the top of the gel. Breaks at a given position are due to complete removal of the corresponding base and result in a fragment *n* - 1 nucleotides long, where *n* is the position

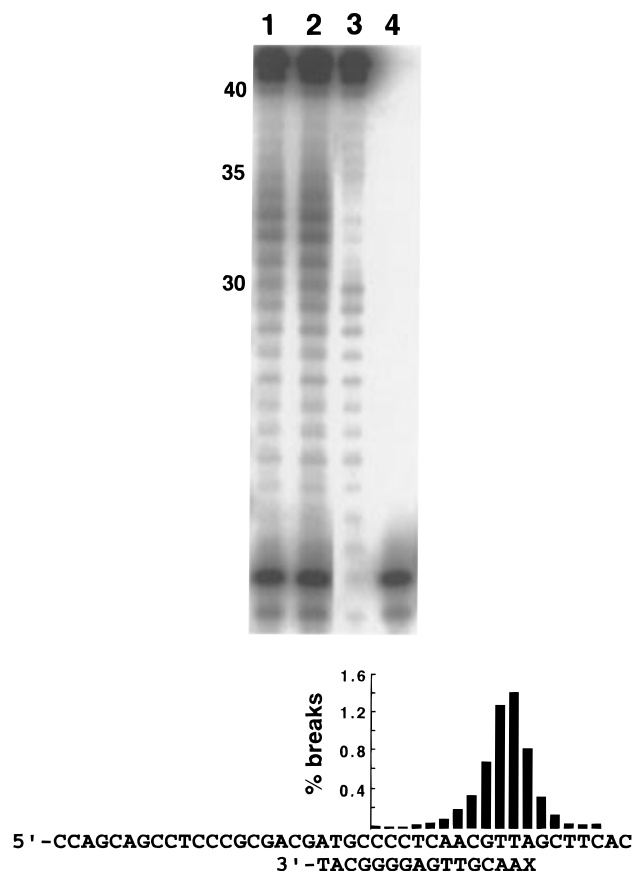


Figure 5. (A, top) 10% denaturing PAGE showing fragmentation of ODN **4** after 15 days of decay. Lanes: (1) duplex D1; (2) duplex D2; (3) [^{32}P]ODN **4**; (4) [^{125}I]ODN **3**. (B, bottom) Bar graph showing distribution and relative intensity of breaks at individual bases of ODN **4** for duplex D2. X indicates position of attachment of iodobenzamide conjugate group. Total yield of strand breaks was 4.6% for D1 and 6.6% for D2.

of the nucleotide from the 5'-end. For example, a break at T34 (maximum in Figure 5B) corresponds to the 33 nucleotide long fragment in the gel. The bar graph in Figure 5B shows the relative intensity of these cleavage bands for the more concentrated duplex sample (D2) and how their position corresponds to the sequence of ODN **4**. The pattern of breaks for sample D1 was identical, but the intensity of each band was slightly lower. The value of each bar represents percent intensity of the band compared to the sum of the intensities of all bands including the top band (unbroken ODN **4**). The total yields of the strand breaks were calculated to be 4.6% for sample D1 and 6.6% for sample D2.

DISCUSSION

Before the advent of automated ODN synthesis, ^{125}I -labeled DNA probes were obtained by direct treatment with thallium chloride and sodium iodide at elevated temperature (14). The oxidized form of ^{125}I (I^+) reacts with random cytosine bases in the DNA to give 5,6-saturated pyrimidine residues. The harsh reaction conditions degraded the DNA and gave mixtures of iodinated products. Direct iodination of the cytosine residues is undesirable since the modified bases compromise hybridization properties of shorter probes.

Automated synthesis of 3'-labeled [^{125}I]ODNs from a [^{125}I]dU-modified solid support has been reported (15). The I-ODN products were used as PCR primers for preparation of internally modified [^{125}I]ODNs. This method is unsuitable for labeling with shorter half-life radiohalogens. More direct methods for radioiodination

of ODNs use conjugate groups that can be selectively iodinated. For example, 5'-hexylamine-modified ODNs have been chemically conjugated to 4-hydroxyphenyl (16) or 4-methoxyphenyl groups (17). Recently, a phosphoramidite reagent has been developed that allows direct incorporation of 4-hydroxyphenyl groups into 5-methyl dC nucleotides using a DNA synthesizer (18). To ensure that no cytosine residues react (and to speed the reaction), the modified ODN is generally present in large excess with respect to the small quantities of radioiodine that are used. Unreacted (carrier) ODN must be separated from the I-ODN since it competes for complementary nucleic acid target sites. This separation is difficult for the conjugates studied to date.

The radioiodination method reported here uses a tributylstannylbenzamide precursor (Sn-ODN **2**). The major advantage of this new radiolabeling procedure is that unreacted Sn-ODN and free iodine are easily separated from the desired I-ODN product. The lipophilic organometallic precursor was soluble and stable in aqueous buffer (pH 8.3). The hexylamine linker arm in ODN **1** reacted cleanly with tributylstannylbenzoic acid NHS ester to give **2**. This active ester has been used for labeling monoclonal antibodies with a number of radiohalogens (19). The strong UV absorbance of ODNs allowed the iodination chemistry to be developed using ^{127}I and reversed phase HPLC methods. Conversion of the Sn-ODN to I-ODN **3** proceeded quantitatively when excess NaI was used. The identity of **3** was confirmed by preparation via a more direct route (Figure 1, method B). T_m studies showed that the addition of the 4-iodobenzamide conjugate group did not adversely affect hybridization.

Radioiodination of ODN **2** with ^{125}I gave 69% conversion to [^{125}I]ODN **3**. The large shift in retention time allowed easy isolation and identification of the I-ODN product. Reversed phase chromatography using a disposable syringe cartridge gave 27% isolated yield of no carrier added [^{125}I]ODN **3** in 96% purity. A large excess of Sn-ODN was not required to drive the reaction, but a slight excess ensured complete reaction of the relatively expensive radioisotope. Although a C_{18} stationary phase was useful for analytical HPLC, recovery was poor in a preparative mode. We are experimenting with other reversed phase packings and HPLC methods to improve radiochemical yields.

The hybridization and DNA cleavage properties of [^{125}I]ODN **3** were studied using gel electrophoresis assays. We were especially interested in the effect of the relatively long 5'-linker in **3** on DNA cleavage efficiency. The reported 15–20 Å cleavage range (1) of [^{125}I]dC or [^{125}I]dU-modified ODNs hybridized to ssDNA targets may be an ideal situation. Substitution of ^{125}I at the 5-position of the pyrimidine ring essentially "locks" it into the major groove, approximately 5 Å from the axis of the B-form DNA helix. We suspected that the hexylaminebenzamide linker arm used to attach ^{125}I to the 5'-terminus might be too long (~16 Å) and flexible to allow efficient DNA cleavage.

Nondenaturing PAGE analysis of the duplex formed between [^{125}I]ODN **3** and 42-mer ODN **4** showed that extent of duplex formation was concentration dependent. Duplex sample D1 (10 nM in **4**) showed 65% dsDNA, whereas sample D2 (25 nM in **4**) showed 89% dsDNA. After 15 days (16% ^{125}I decay), the duplex samples were assayed for strand breaks using denaturing PAGE (Figure 5). Samples showed a Gaussian distribution of DNA fragments typical for strand breaks caused by ^{125}I . Taking into account that only 65% and 89% of ODN **4** formed duplexes, we recalculated the effective yield of

breaks as 7.1% and 7.4% for D1 and D2, correspondingly. Therefore, the yields in terms of breaks per decay were 0.44 and 0.46.

It is interesting that the DNA fragment of maximum intensity corresponds to the position of attachment of the 5'-terminal [¹²⁵I]benzamide containing linker. If this linker were stretched out in either the 5'- or 3'-direction, then the pattern of bands would be expected to shift (up to five nucleotides). The high cleavage efficiency (0.45 break per decay) indicates that the ¹²⁵I atom is constrained close to the sugar-phosphate backbone of the target DNA strand, much like the geometry obtained from labeling at the 5-position of the pyrimidine ring. It is not clear how the DNA cleavage efficiency of these different linker systems compares since no values have been reported for cleavage of ssDNA targets with ¹²⁵I-labeled dC or dU. Results showed 0.8 ds break per decay from ¹²⁵I-dC-labeled triplex forming ODNs that lie in the major groove of target dsDNA (3). Further investigations are planned to explore the effect of different linker systems on the DNA cleavage properties of ¹²⁵I. For example, 5-(aminoalkyl)uridine linkers can be used to prepare internally modified ODNs that constrain the iodobenzamide group in the major groove of duplex DNA. The rapid radioiodination method reported here should also allow the DNA cleavage properties of ¹²³I to be explored.

LITERATURE CITED

- (1) Martin, R. F., and Haseltine, W. A. (1981) Range of radiochemical damage to DNA with decay of iodine-125. *Science* 213, 896.
- (2) Charlton, D. E., and Booz, J. (1981) A Monte Carlo treatment of the decay of ¹²⁵I. *Radiat. Res.* 87, 10.
- (3) Panyutin, I. G., and Neumann, R. D. (1994) Sequence-specific DNA double-strand breaks induced by triplex forming ¹²⁵I labeled oligonucleotides. *Nucleic Acids Res.* 22, 4979.
- (4) Bloomer, W. D., and Adelstein, S. J. (1977) 5-¹²⁵I-iododeoxyuridine as prototype for radionuclide therapy with Auger emitters. *Nature* 265, 620.
- (5) Kassis, A. I., Adelstein, J., and Bloomer, W. D. (1987) *Therapeutic Implications of Auger-Emitting Radionuclides. Radionuclides in Therapy* (R. P. Spencer et al., Eds.) pp 120-134, CRC Press, Boca Raton, FL.
- (6) Makrigiorgos, G. M., Kassis, A. I., Baranowska-Kortylewicz, J., McElvany, K. D., Welch, M. J., Sastry, K. S. R., and Adelstein, S. J. (1989) Radiotoxicity of 5-[¹²³I]iodo-2'-deoxyuridine in V79 cells: a comparison with 5-[¹²⁵I]iodo-2'-deoxyuridine. *Radiat. Res.* 118, 532.
- (7) DeSombre, E. R., Shafii, B., Hanson, R. N., Kuivanen, P. C., and Hughes, A. (1992) Estrogen receptor-directed radiotoxicity with Auger electrons: specificity and mean lethal dose. *Cancer Res.* 52, 5752.
- (8) Makrigiorgos, G. M., Berman, R. M., Baranowska-Kortylewicz, J., Bump, E., Humm, J. L., Adelstein, S. J., and Kassis, A. I. (1992) DNA damage produced in V79 cells by DNA-incorporated Iodine-123: a comparison with iodine-125. *Radiat. Res.* 129, 309.
- (9) Coenen, H. H., Moerlein, S. M., and Stocklin, G. (1983) No-carrier-added radiohalogenation methods with heavy halogens. *Radiochim. Acta* 34, 47.
- (10) Gamper, H. B., Reed, M. W., Cox, T., Virosco, J. S., Adams, A. D., Gall, A. A., Scholler, J. K., and Meyer, R. B. (1993) Facile preparation of nuclease resistant 3'-modified oligodeoxynucleotides. *Nucleic Acids Res.* 21, 145.
- (11) Reed, M. W., Adams, A. D., Nelson, J. S., and Meyer, R. B., Jr. (1991) Acridine and cholesterol derivatized solid supports for improved synthesis of 3'-modified oligonucleotides. *Bioconjugate Chem.* 2, 217.
- (12) Cantor, C. R., Warshaw, M. M., and Shapiro, H. (1970) Oligonucleotide interactions. III. Circular dichroism studies of the conformation of deoxypolynucleotides. *Biopolymers* 9, 1059.
- (13) Wilbur, D. S., Hadley, S. W., Hylarides, M. D., Abrams, P. G., Beaumier, P. L., Morgan, A. C., Reno, J., and Fritzberg, A. R. (1989) Development of a stable radioiodinating reagent to label monoclonal antibodies for radiotherapy of cancer. *J. Nucl. Med.* 30, 216.
- (14) Commerford, S. L. (1971) Iodination of nucleic acids in vitro. *Biochemistry* 10, 1993.
- (15) Scherberg, N., Bloch, I., and Gardner, P. (1992) Site-specific incorporation of [¹²⁵I]iododeoxyuridine into DNA. *Appl. Radiat. Isot.* 43, 923.
- (16) Dattagupta, N., and Knowles, W. EP 0198207.
- (17) Dewanjee, M. K., Ghafouripour, A. K., Werner, R. K., Serafini, A. N., and Sfakianakis, G. N. (1991) Development of sensitive radioiodinated anti-sense oligonucleotide probes by conjugation technique. *Bioconjugate Chem.* 2, 195.
- (18) Fontanel, M. L., Bazin, H., Roget, A., and Téoule, R. (1993) Synthesis and use of 4-hydroxyphenyl derivatized phosphoramidites in the selective radioiodination of oligonucleotide probes. *J. Labelled Compd. Radiopharm.* 33, 717.
- (19) Wilbur, D. S. (1992) Radiohalogenation of proteins: an overview of radionuclides, labeling methods, and reagents for conjugate labeling. *Bioconjugate Chem.* 3, 433.

BC970016N

TECHNICAL NOTES

Effect of Cast Solvent on the Electron Transfer Reaction for Poly(ethylene oxide)-Modified Myoglobin on the Electrode in Poly(ethylene oxide) Oligomers

Natsue Y. Kawahara, Waki Ohkubo, and Hiroyuki Ohno*

Department of Biotechnology, Tokyo University of Agriculture & Technology, Koganei, Tokyo 184, Japan.
Received July 14, 1996[®]

Myoglobin from horse skeletal muscle was modified with poly(ethylene oxide) (PEO) with an average molecular weight of 2000 or 5000. Myoglobin was soluble after this modification in several organic solvents and PEO oligomers. The electron transfer reactions of PEO-modified myoglobin cast on the indium tin oxide (ITO) glass electrode were investigated by cyclic voltammetry. The PEO-modified myoglobin, cast on the electrode from water or a methanol solution, showed quasi-reversible redox reactions in PEO (average MW of 400). On the other hand, no redox response was seen in PEO-modified myoglobin cast on it using chloroform or benzene as a casting solvent. A clear redox response of the PEO-modified myoglobin was observed after methanol treatment of these layers cast from chloroform or a benzene solution. This suggests that the conformational change of the adsorbed PEO-modified myoglobin layer on the ITO electrode cast from chloroform or a benzene solution was not irreversible. The cast condition of PEO-modified myoglobin on the ITO glass electrode was revealed to affect the electron transfer reaction for protein considerably in PEO oligomers.

INTRODUCTION

Poly(ethylene oxide) (PEO)–protein hybrid was the most popular material in bioconjugate chemistry (1, 2). There are many papers on the enzymatic activity (3–6) and structure (7, 8) of PEO-modified proteins. Further, various methods for PEO modification of proteins were also reported (9–12). PEO modification of proteins is known to provide a nonimmunogenic response, and it also supports the improved solubility of these proteins in nonaqueous media keeping their functions. PEO is not only a polymer for protein modification but also a typical base material for preparing an ion conductive polymer matrix (13–15). Since PEO has a unit structure ($\text{CH}_2\text{-OCH}_2$) quite similar to that of water, we are studying the electrochemistry of a variety of water-soluble molecules in PEO (16–18).

On the other hand, there are extensive studies on the electrochemical characteristics of heme proteins such as cytochrome *c* (19–24), myoglobin (25–28), and so on in buffer solution. These redox reactions of heme proteins have been analyzed in only aqueous solutions. We mentioned PEO as a nonaqueous medium for electrochemical reaction of PEO-modified heme proteins. By using PEO as a solvent for electrochemistry of PEO-modified heme proteins, a novel electrochemical redox response is expected. Myoglobin is one of the water-soluble proteins, and it showed a direct electron transfer reaction at the electrode in a buffer solution without any mediator (25–28). PEO-modified myoglobin was then expected to be soluble in PEO oligomers, and it shows redox behavior similar to that in an aqueous medium.

As expected, PEO-modified myoglobin was also soluble in PEO oligomers and showed quasi-reversible electron transfer reactions at an indium tin oxide (ITO) glass electrode without any mediator in PEO oligomers (29–31). The electron transfer reaction of that was quite slow in PEO oligomers. PEO-modified myoglobin was cast on the electrode to eliminate the effect of the diffusion of proteins (30). However, there was no detailed knowledge on the redox response of PEO-modified myoglobin cast on the ITO electrode. The study of the relationship between the electrode response and the casting state of proteins on the electrode was an important subject in the field of electrochemistry for PEO-modified heme proteins in nonaqueous media.

Here we wish to show the effect of casting solvents on the direct electron transfer reaction of PEO-modified myoglobin on the electrode in salt-containing PEO oligomers.

EXPERIMENTAL SECTION

Materials. Myoglobin from horse skeletal muscle (Mb) (Sigma M-0630) was used without further purification. PEO₄₀₀ (average MW of 400) containing no additive such as an antioxidant was purchased from NOF Co. Ltd. PEO₄₀₀ containing 0.20 mol dm⁻³ KCl was used as a solvent after drying *in vacuo* at 60 °C for 3 days. PEO monomethyl ethers with molecular weights of 750, 2000, and 5000 were purchased from Aldrich Co. Ltd. All other reagents, not noted here, were purchased as analytical grade from Kanto Chemical Co. Ltd.

An indium tin oxide (ITO) glass electrode (ITO layer thickness of 1300 Å, surface resistance of 30.9 Ω/square) was purchased from Oji Tobi Co. Ltd. These were used as working and counter electrodes for cyclic voltammetry measurements after washing with acetone and then with chloroform. Silver wire (ϕ of 0.5 mm) was purchased as an electrode from Tokuriki Honten Co. Ltd.

* To whom correspondence should be addressed. Phone: +81-423-88-7024. Fax: +81-423-88-7012. E-mail: ohnoh@cc.tuat.ac.jp.

[®] Abstract published in *Advance ACS Abstracts*, February 15, 1997.

Table 1. Effect of the Molecular Weight of PEO for the Modification of Myoglobin on the Solubility in Organic Solvent^a

MW ^b	no. ^c	MeOH ^d	EtOH ^e	chloroform	benzene	acetone	CCl ₄ ^f	EtAc ^g
750	15	—	—	—	—	—	—	—
2000	18	+	±	+	+	±	—	—
5000	18	+	+	+	+	+	±	+

^a +, soluble; ±, sparingly soluble; and —, insoluble. ^b Average molecular weight of modified PEO on protein. ^c Number of PEO chains per Mb. ^d Methyl alcohol. ^e Ethyl alcohol. ^f Carbon tetrachloride. ^g Ethyl acetate.

Synthesis of PEO-Modified Mb. The activated PEO (A-PEO) was synthesized according to the conventional method (29). First, PEO succinate was prepared by reacting PEO monomethyl ether and succinic anhydride. Then, A-PEO was prepared by reacting PEO succinate and *N*-hydroxysuccinimide. Mb was stirred with A-PEO for 1 h at 30 °C in a 0.05 mol dm⁻³ borate buffer solution at pH 9.0. A-PEO is known to react with amino groups of Mb in an aqueous medium. Mb was modified with A-PEO with average molecular weights of 750, 2000, or 5000. The unbound A-PEO was removed by ultrafiltration (Millipore, PTGC10K) using distilled water. PEO-modified Mb (PEO-Mb) in the dry state was prepared by the lyophilization (Tokyo Rika, FDU-540) of this solution.

Determination of the Degree of PEO Modification. The average number of PEO chains on one Mb was estimated from the titration results of amino groups of Mb by 2,4,6-trinitrobenzenesulfonic acid (32–34). The average number of PEO molecules with an average MW of 750, 2000, and 5000 attached onto one molecule of Mb was estimated to be 15 ± 1, 18 ± 1, and 18 ± 1, respectively.

UV-Vis Spectroscopy. Mb, having 18 PEO₅₀₀₀ chains, was dissolved in several organic solvents to a final concentration of 1.0 × 10⁻⁵ mol dm⁻³. The PEO-Mb solution was introduced into a quartz cuvette with a light path length of 10.0 mm. The UV-vis absorption spectrum was recorded with a Shimadzu UV-2200A spectrophotometer at room temperature.

Cyclic Voltammetry Measurement. Mb, modified with 18 chains of PEO₂₀₀₀ on average, was individually dissolved in casting solvents (water, methanol, chloroform, or benzene) to a concentration of 7.0 × 10⁻⁵ mol dm⁻³. Distilled casting solvent was used for all experiments. The PEO-Mb solution was cast onto the ITO glass electrode with a casting density of 10 μL cm⁻². After drying, the ITO glass electrode as a working electrode was faced with another ITO glass electrode as a counter one. They were fixed as a thin layer cell with silicone resin and dried *in vacuo* for 1 h. The thickness of the thin layer cell was 100 μm. Then polished silver wire (0.5 mm φ) was further introduced as a reference electrode. After complete drying, the cell system was soaked with PEO₄₀₀ (average MW of 400) containing 0.20 mol dm⁻³ KCl, and the solution was then raised in the cell by the capillary action. The electron transfer reaction of PEO-Mb cast on the ITO electrode in PEO₄₀₀ was investigated with cyclic voltammetry (Fuso Seisakusho HECS 972, 321B) at room temperature under a nitrogen atmosphere.

RESULTS AND DISCUSSION

Property of PEO-Mb in Organic Solvents. The solubility of synthesized poly(ethylene oxide)-modified myoglobin (PEO-Mb) in organic solvents is shown in Table 1. Since Mb, modified with PEO₇₅₀ (average MW of 750), was not soluble in those organic solvents, this hybrid was not used for further experiments. Longer PEO chains (≥2000) onto the proteins were preferable for making Mb soluble in organic solvents. Newly

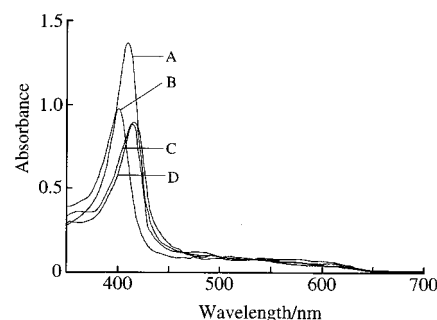


Figure 1. UV-vis spectra of PEO-Mb in various solvents at room temperature. PEO₅₀₀₀-Mb was dissolved in phosphate buffer at pH 7.4 (A), methanol (B), chloroform (C), and benzene (D).

prepared PEO-Mb, having 18 chains of PEO₂₀₀₀, was soluble in water, methanol, chloroform, and benzene. When Mb was modified with PEO₅₀₀₀, PEO₅₀₀₀-Mb became more soluble in various organic solvents. This suggested that PEO₂₀₀₀ and PEO₅₀₀₀ were preferred material for the modification of myoglobin to dissolve it in organic solvents. This result is in agreement with that reported by Inada et al. (3–7).

The conformation of newly prepared PEO-Mb was analyzed in several organic solvents. UV-vis spectrophotometry revealed that PEO-Mb showed spectra in organic solvents and an aqueous solution as shown in Figure 1. The difference of both the absorbance and wavelength at the absorption maximum was observed in the different solvents. The UV-vis spectrum of PEO-Mb was affected by the solvent species, suggesting a small conformational change. The PEO-Mb in buffer solution (Figure 1A) exhibited an absorption maximum at the Soret band that is the same as that of unmodified Mb (oxidized form) in an aqueous solution (29). The absorption maximum at the Soret band, arising from π - π^* transitions of the heme active site, was not influenced by the PEO modification. Little shifts of Soret bands (400.0–414.7 nm) for PEO-Mb (Fe³⁺) were found in different solvents which means a little structural change around heme in PEO-Mb. Even after PEO modification, the solvent species was revealed to affect the chemical environment of heme in PEO-Mb. Furthermore, a strong conformational change of PEO-Mb in organic solvents was not found by absorption at 200–250 nm with CD spectrometry (data not shown).

Electrochemistry of PEO-Mb Cast on the ITO Electrode in a PEO Oligomer. Figure 2 shows cyclic voltammograms of PEO-Mb in PEO₄₀₀, where the PEO-Mb was cast onto the ITO electrode with various casting solvents. The PEO-Mb, cast from aqueous and methanol solutions, showed clear redox peaks in PEO₄₀₀. On the other hand, no response was seen for those cast from chloroform and benzene solutions. The conformation of PEO-Mb was suggested not to be strongly changed even in chloroform and benzene by UV-vis and CD spectrometry as mentioned above; however, the nature of the PEO-Mb film on the ITO glass electrode after casting seemed to be changed by casting solvent species. The dimensional characteristics of adsorbed PEO-Mb at the

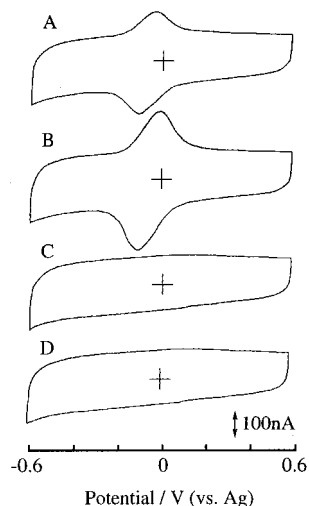


Figure 2. Cyclic voltammograms of PEO-Mb on the ITO electrode cast from water (A), methanol (B), chloroform (C), and benzene (D). The voltammograms were taken in PEO₄₀₀ containing 0.5 mol dm⁻³ KCl, recorded with a sweep rate of 33 mV s⁻¹ at room temperature.

molecular level on the electrode should not be suitable for electron transfer when it was cast from a chloroform or benzene solution. A distinct difference in solubility of PEO-Mb in organic solvents, such as methanol, chloroform, or benzene, was not observed as seen in Table 1. However, spread-out forms of PEO chains onto Mb may be affected by solvent species. Macroscopically, the PEO-Mb cast ITO glass electrodes, prepared from water or a methanol solution, was transparent. Against these, those films cast from chloroform or benzene were obscure opaque. The PEO-Mb cast from chloroform or benzene might be assembled as massive particles on the electrode during the drying process. This flocculation might inhibit the electron transfer with the ITO glass electrode. It was also observed that the different morphology of PEO cast on the glass plate was formed by the casting solvent. It was quite similar to that for PEO-Mb cast on ITO glass electrode. The nature of PEO-Mb cast on the electrode from organic solvents should depend on the conformation and/or aggregated state of the modified PEO chains. When chloroform or benzene was used as a casting solvent, modified PEO chains of PEO-Mb were adsorbed on the electrode and inhibited the electron transfer between the protein and the ITO electrode. A very small conformational change affected by the redox processes has been detected by FTIR spectroscopy (35). This result supported the fact that the conformation of PEO-Mb adsorbed on the ITO electrode was an important factor in keeping the electrochemical activity of proteins.

Since PEO-Mb showed no response when it was cast from chloroform and benzene, a small amount of methanol was added dropwise onto these modified electrodes, and the redox response was analyzed in PEO₄₀₀ as shown in Figure 3. As a result, a clear redox response of the PEO-Mb was found after methanol treatment. This clearly supports the fact that both chloroform- and benzene-cast PEO-Mb films, i.e., redox inactive ones, were shifted to be redox active. The conformational change of the adsorbed PEO-Mb layer on the electrode cast from chloroform or benzene was not irreversible. Niki and his co-workers reported that three conformations of adsorbed cytochrome *c*₃ on the surface of mercury. These conformational changes are reported to be irreversible and depend on the applied potential (36). In our study, the electrochemical activity of adsorbed proteins on the electrode was changed and it depended on

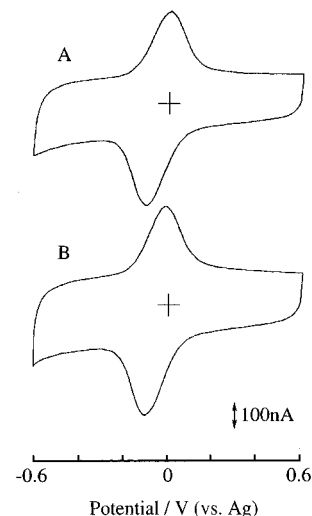


Figure 3. Cyclic voltammograms of PEO-Mb on the ITO electrode with methanol post-treatment after casting from chloroform (A) or benzene (B) in PEO₄₀₀ containing KCl. The sweep rate was 33 mV s⁻¹ at room temperature.

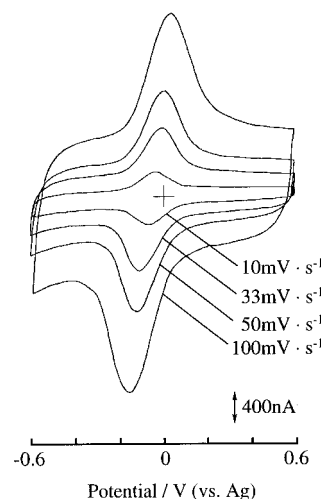


Figure 4. Cyclic voltammograms of PEO-Mb on the ITO electrode with methanol post-treatment after casting from benzene solution in PEO₄₀₀ containing KCl. The sweep rates were 10, 33, 50, and 100 mV s⁻¹ at room temperature.

the casting solvent. The property of the adsorbate was influenced by the species of electrode, protein, solvent, and method. This is also consistent with the reported result, which described the nature of the electrode surface as a decisive factor for the electron transfer between protein and electrode. On the other hand, the important role of hydration for the indium oxide electrode surface in the electrode transfer reaction of proteins has already been reported by several researchers (19, 27). The electroactivity for PEO-Mb cast on the ITO electrode from the organic solvent may be influenced by the surface hydrophilicity of the electrode.

The PEO-Mb was post-treated with methanol after casting on the ITO glass electrode from benzene solution, and its cyclic voltammograms were recorded at various sweep rates in PEO₄₀₀ (Figure 4). The electrochemical response for PEO-Mb on the ITO glass electrode was stable with continuous cycling for at least 24 h. The formal potential of PEO-Mb, estimated from the anodic and cathodic peak potentials, is -57 mV vs Ag, and the ratio of the anodic to cathodic peak currents is 0.89 ± 0.05 in the sweep rate range from 5 to 100 mV s⁻¹. The formal redox potential of cast PEO-Mb on the electrode in PEO₄₀₀, obtained in our study, shifted to a positive side

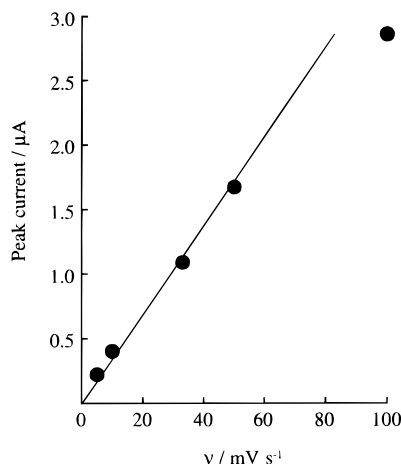


Figure 5. Sweep rate dependence of the cathodic peak current for PEO-Mb on the ITO electrode with methanol post-treatment after casting from benzene solution in PEO₄₀₀ containing KCl at room temperature.

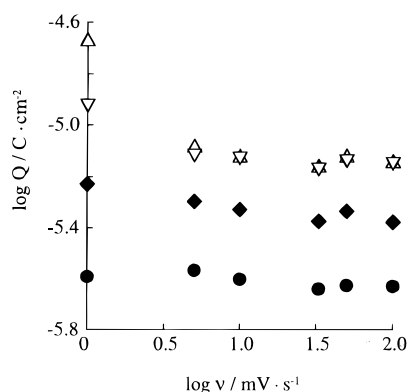


Figure 6. Effect of the sweep rate (ν) on the quantity of electricity (Q) for the reduction of cast PEO-Mb on the ITO electrode in PEO₄₀₀ containing KCl. The casting solvents were as follows: water (●), methanol (◆), chloroform and then methanol (post-treatment) (▽), and benzene and then methanol (post-treatment) (△).

compared with that of purified myoglobin in buffer solution (26). However, it is in fairly good agreement with that of PEO-Mb dissolved in PEO₂₀₀ (−55 mV vs Ag). A shift of the formal redox potential of PEO-Mb in PEO₄₀₀ is considered to be due to the PEO being a solvent. The peak separation of PEO-Mb cast onto the ITO glass electrode slightly increased with increasing sweep rates. Both the anodic and cathodic peak currents of the PEO-Mb cast on the ITO glass electrode depended on the sweep rate in PEO₄₀₀ as shown in Figure 5. It increased linearly in the sweep rate range up to 50 mV s^{−1}, suggesting that an electron transfer process should be the rate-determining step.

There is a small sweep rate dependence on the quantity of electricity (Q) in a wide sweep rate range from 1.0 to 100 mV s^{−1} as shown in Figure 6. Since the Q value was affected by the casting solvent species, the casting solvent was strongly suggested to affect the molecular packing of PEO-Mb on the ITO glass electrode. For example, it was 4.0×10^{-6} C for those cast from methanol and 2.3×10^{-6} C from water regardless of the sweep rate between 5.0 and 100 mV s^{−1}. Sweep rate-independent Q values were consistent with the result of the direct electron transfer between the ITO glass electrode and PEO-Mb at the interface of the electrode. This Q value was reasonable when the molecular cross section of PEO-Mb was estimated to be about 2000 Å²/molecule and taking surface roughness of the ITO electrode into

consideration. The calculated Q value was 4.0×10^{-6} C when the mean surface area of the ITO electrode was estimated to be 5 times larger than the apparent one. This is in good agreement with that obtained in this experiment as mentioned above. It is apparent that a rapid electron transfer occurred between the ITO glass electrode and only PEO-Mbs which were in direct contact with the electrode. A larger Q value was detected by decreasing the sweep rate to less than 1.0 mV s^{−1} only when organic solvent was used as a casting solvent. This increased Q value was constant during repeated scanning with the sweep rate of 1.0 mV s^{−1}. This suggests the possibility of intermolecular electron transfer perpendicular to the electrode between adjacent PEO-Mbs in the cast layer.

CONCLUSIONS

PEO-modified myoglobin, having 18 chains of PEO with an average molecular weight of 2000 or 5000, was soluble in organic solvents such as methanol, chloroform, and benzene. Water and methanol provided excellent casting conditions for such PEO-Mbs, and quasi-reversible electron transfer reaction was observed between PEO-Mb and the ITO glass electrode. Against this, the PEO-Mb, cast from a chloroform or benzene solution, showed no redox response in PEO oligomers. This electroinactive PEO-Hb layer was not irreversible and became electroactive after treatment with methanol. For the cast system, the casting condition of protein on the electrode was a very important factor for an electron transfer reaction of PEO-Mb in PEO oligomers.

ACKNOWLEDGMENT

The present study was supported by a Grant-in-Aid for Scientific Research from the Ministry of Education, Science, Sports and Culture, Japan (08246101).

LITERATURE CITED

- (1) Inada, Y., Matsushima, A., Hiroto, M., Nishimura, H., and Kodera, Y. (1994) Modification of Proteins with Polyethylene Glycol Derivatives: Neoglycoconjugates. *Methods Enzymol.* 242, 65–93.
- (2) Harris, J. M. (1990) Introduction to Biotechnical and Biomedical Applications of Poly(Ethylene Glycol). In *Poly(Ethylene Glycol) Chemistry: Biotechnical and Biomedical Applications* (Harris, J. M., Ed.) pp 1–14, Plenum Press, New York.
- (3) Takahashi, K., Yoshimoto, T., Ajima, A., Tamaura, Y., and Inada, I. (1984) Modified Lipase Catalyzes Ester Synthesis in Benzene, Substrate Specificity. *Enzyme* 32, 235–240.
- (4) Matsushima, A., Okada, M., and Inada, Y. (1984) Chymotrypsin Modified with Polyethylene Glycol Catalyzes Peptide Synthesis Reaction in Benzene. *FEBS Lett.* 178, 275–277.
- (5) Inada, Y., Matsushima, A., Kodera, Y., and Nishimura, H. (1990) Polyethylene Glycol (PEG)-Protein Conjugates: Application to Biomedical and Biotechnological Processes. *J. Bioact. Compat. Polym.* 5, 343–364.
- (6) Gaertner, H., and Puigserver, A. (1989) Kinetics and Specificity of Serine Proteases in Peptide Synthesis Catalyzed in Organic Solvents. *Eur. J. Biochem.* 181, 207–213.
- (7) Mabrouk, P. A. (1995) The Use of Nonaqueous Media to Probe Biochemically Significant Enzyme Intermediates: The Generation and Stabilization of Horseradish Peroxidase Compound II in Neat Benzene Solution at Room Temperature. *J. Am. Chem. Soc.* 117, 2141–2146.
- (8) Mabrouk, P. A. (1994) Effect of Pegylation on the Structure and Function of Horse Cytochrome c. *Bioconjugate Chem.* 5, 236–241.
- (9) Kodera, Y., Sekine, T., Yasukohchi, T., Kiri, Y., Hiroto, M., Matsushima, A., and Inada, Y. (1994) Stabilization of L-Asparaginase Modified with Comb-Shaped Poly(ethylene

- glycol) Derivatives, in vivo and in vitro. *Bioconjugate Chem.* 5, 283–286.
- (10) Zalipsky, S. (1995) Functionalized Poly(ethylene glycol) for Preparation of Biologically Relevant Conjugates. *Bioconjugate Chem.* 6, 150–165.
- (11) Gaertner, H. F., and Offord, R. E. (1996) Site-Specific Attachment of Functionalized Poly(ethylene glycol) to the Amino Terminus of Proteins. *Bioconjugate Chem.* 7, 38–44.
- (12) Monfardini, C., Schiavon, O., Caliceti, P., Morpurgo, M., Harris, J. M., and Veronese, F. M. (1995) A Branched Monomethoxypoly(ethylene glycol) for Protein Modification. *Bioconjugate Chem.* 6, 62–69.
- (13) MacCallum, J. R., and Vincent, C. A., Eds. (1987) *Polymer Electrolyte Reviews-I*, Elsevier Applied Science, London.
- (14) MacCallum J. R., and Vincent, C. A., Eds. (1989) *Polymer Electrolyte Reviews-II*, Elsevier Applied Science, London.
- (15) Gray, F. M. (1991) *Solid Polymer Electrolytes*, VCH Publishers, New York, and references therein.
- (16) Shi, G., and Ohno, H. (1991) Electrochemical Behavior of Hemin and PEO-Hemin in Ion-Conductive Polymer Matrixes. *J. Electroanal. Chem.* 314, 59–69.
- (17) Ohno, H., and Ishikura, K. (1992) Effect of Supporting Electrolytes on the Redox Response of Poly(xylyl viologen) and its Polymer Complex with Poly(styrene sulfonate) in Poly(ethylene oxide) Oligomers. *Polym. Adv. Technol.* 4, 114–118.
- (18) Ohno, H., and Satoh, H. (1993) Solubility, Diffusion Coefficient and Ionic Conductivity of Alkyl Viologens in Poly(ethylene oxide) and its Derivatives. *J. Electroanal. Chem.* 360, 27–37.
- (19) Yeh, P., and Kuwana, T. (1977) Reversible Electrode Reaction of Cytochrome *c*. *Chem. Lett.*, 1145.
- (20) Bowden, E. F., Hawkrige, F. M., Chlebowski, J. F., Bancroft, E. E., Thorpe, C., and Blount, H. N. (1982) Cyclic Voltammetry and Derivative Cyclic Voltabsorptometry of Purified Horse Heart Cytochrome *c* at Tin-doped Indium Oxide Optically Transparent Electrodes. *J. Am. Chem. Soc.* 104, 7641–7644.
- (21) Taniguchi, I., Toyosawa, K., Yamaguchi, H., and Yasukouchi, K. (1982) Voltammetric Response of Horse Cytochrome *c* at a Gold Electrode in the Presence of Sulfur-Bridged Bipyridines. *J. Electroanal. Chem.* 140, 187–193.
- (22) Song, S., Clark, R. A., Bowden, E. F., and Tarlov, M. J. (1993) Characterization of Cytochrome *c*/Alkanethiolate Structures Prepared by Self-Assembly on Gold. *J. Phys. Chem.* 97, 6564–6572.
- (23) Feng, Z. Q., Imabayashi, S., Kakiuchi, T., and Niki, K. (1995) Electroreflectance Spectroscopic Study of the Electron Transfer Rate of Cytochrome *c* Electrostatically Immobilized on the ω -Carboxyl Alkanethiol Monolayer modified Gold Electrode. *J. Electroanal. Chem.* 394, 149–154.
- (24) Bowden, E. D., Hawkrige, F. M., Blount, H. N., Srinivasan, S., Chiamadzhev, Y. A., Bockris, J. O., Conway, B. E., and Yeager, E., Eds. (1985) *Comprehensive Treatise of Electrochemistry*, Vol. 10, Plenum Press, New York.
- (25) King, B. C., Hawkrige, F. M., and Hoffman, B. M. (1992) Electrochemical Studies of Cyanometmyoglobin and Metmyoglobin: Implications for Long-Range Electron Transfer in Proteins. *J. Am. Chem. Soc.* 114, 10603–10608.
- (26) Taniguchi, I., Watanabe, K., Tominaga, M., and Hawkrige, F. M. (1992) Direct Electron Transfer of Horse Heart Myoglobin at an Indium Oxide Electrode. *J. Electroanal. Chem.* 333, 331–338.
- (27) Tominaga, M., Kumagai, T., Takita, S., and Taniguchi, I. (1993) Effect of Surface Hydrophilicity of an Indium Oxide Electrode on Direct Electron Transfer of Myoglobins. *Chem. Lett.*, 1771–1774.
- (28) Niu, J., Guo, Y., and Dong, S. (1995) The Direct Electrochemistry of Cryo-Hydrogel Immobilized Myoglobin at a Glassy Carbon Electrode. *J. Electroanal. Chem.* 399, 41–46.
- (29) Ohno, H., and Tsukuda, T. (1992) Electron-Transfer Reaction of Polyethylene Oxide-modified Myoglobin in Polyethylene oxide oligomers. *J. Electroanal. Chem.* 341, 137–149.
- (30) Ohno, H., and Tsukuda, T. (1994) Electron Transfer Reaction of Poly(ethylene oxide)-modified Myoglobin coated on an ITO Electrode in Poly(ethylene oxide) Oligomers. *J. Electroanal. Chem.* 367, 189–194.
- (31) Ohno, H., Ohkubo, W., and Yamaguchi, N. (1994) Conformation and Electrochemical Reduction of Myoglobin in PEO Oligomers. *Polym. Adv. Technol.* 5, 411–415.
- (32) Okuyama, T., and Satake, K. (1960) On the Preparation and Properties of 2,4,6-Trinitrophenyl-Amino Acid and -Peptides. *J. Biochem.* 47, 454–466.
- (33) Satake, K., Okuyama, T., Ohashi, M., and Shinoda, T. (1960) The Spectrophotometric Determination of Amine, Amino Acid and Peptide with 2,4,6-Trinitrobenzene 1-Sulfonic Acid. *J. Biochem.* 47, 654–660.
- (34) Haynes, R., Osuga, D. T., and Feeney, R. E. (1967) Modification of Amino Groups in Inhibitors of Proteolytic Enzymes. *Biochemistry* 6, 541–547.
- (35) Schlereth, D. D., Fernandez, V. M., and Mantele, W. (1993) Protein Conformational Changes in Tetraheme Cytochromes Detected by FTIR Spectroelectrochemistry: *Desulfovibrio desulfuricans* Norway 4 and *Desulfovibrio gigas* Cytochromes *c*₃. *Biochemistry* 32, 9199–9208.
- (36) Zhang, D., Wilson, G. S., and Niki, K. (1994) Electrochemistry of Adsorbed Cytochrome *c*₃ on Mercury, Glassy Carbon, and Gold Electrodes. *Anal. Chem.* 66, 3873–3811.

BC960089R

Synthesis of an Amino Acid Analogue To Incorporate *p*-Aminobenzyl-EDTA in Peptides

Anne In. Song[†] and Tariq M. Rana*

Department of Pharmacology, Robert Wood Johnson Medical School, University of Medicine and Dentistry of New Jersey, 675 Hoes Lane, Piscataway, New Jersey 08854. Received July 24, 1996[®]

A convenient and straightforward synthesis of an amino acid analog, [*p*-(*N*- α -Fmoc-L-aspartic acid- β -amido)benzyl]-EDTA tetra-*tert*-butyl ester, compatible with Fmoc solid phase peptide synthesis strategy is described. This reagent was used to incorporate *p*-aminobenzyl-EDTA at an internal sequence position in an HIV-1 Tat protein fragment. After cleavage from the resin and standard deprotection, the peptide was purified by high-performance liquid chromatography and characterized by mass spectrometry. Through this methodology, flexible linkers of different lengths and containing various structures can be placed between the α -carbon backbone of peptides and metal chelates. These peptides will provide a new class of affinity cleaving reagents that can be directed against protein and nucleic acid targets.

Interaction of transition metal complexes with nucleic acids and proteins makes them a useful tool in molecular biology. Metal complexes can be synthesized for specific recognition and cleavage of nucleic acids, or they can be used as nonspecific nucleases (for an excellent review, see ref 1). Shape-selective metal complexes have been designed to target specific DNA and RNA structures (2–4). An iron–EDTA complex cleaves DNA nonspecifically and can be applied to determine the helical periodicity of DNA and structural details of bent DNA (5, 6). Cleavage of DNA and RNA by metal chelates is an important new approach to characterize specific structural features of nucleic acids and their complexes in solutions (7–11). The metal chelate attachment converts sequence-specific DNA-binding protein or oligonucleotide to sequence-specific DNA-cleaving molecules that function under physiological pH, temperature, and salt conditions (9, 10, 12–16).

As with nucleic acids, methods for specific and non-specific cleavage of proteins have been developed. Site-specific cleavage of proteins is achieved by introducing a metal-binding site at one position in a polypeptide chain or attaching it to protein binding ligands (17–26). Recently, an Fe-EDTA-catalyzed protein cleavage method has been applied to complex biological systems such as membrane proteins (27). Nonspecific protein cleavage by an untethered Fe-EDTA has been recently applied to map protein domains involved in macromolecular interactions such as the surface of a DNA-binding protein (28) and interactions between subunits of the multisubunit RNA polymerase (29). Artificial proteolytic reagents would be extremely useful to characterize important structural features of proteins and their complexes under physiological conditions.

To accurately probe structure–function relationships in nucleic acids, proteins, and nucleic acid–protein complexes by affinity cleaving methods, the development of both general and specific methods for single-site

modification of the peptide sidechain is required. Reagents potentially useful for such experiments are the “bifunctional chelating agents,” so called because they incorporate a strong metal-chelating group and a chemically reactive functional group. Bifunctional chelating agents have been synthesized and used to provide biological molecules with the nuclear, physical, and chemical properties of chelated metal ions (30–32).

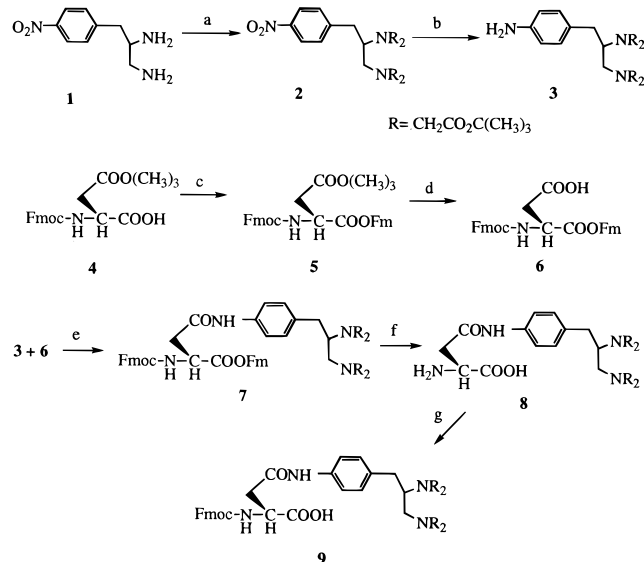
To prepare peptides labeled with metal chelates, protected derivatives of EDTA analogs compatible with Merrifield solid phase protein synthesis using *N*-*tert*-butyloxycarbonyl (Boc)-protected amino acids were developed (13, 33–35). There are two major concerns about this synthetic strategy: (a) repetitive TFA acidolysis in Boc-group deprotection could lead to acid-catalyzed side reactions and (b) cleavage and deprotection of peptides requires HF and specific laboratory setup which is not available to many researchers. Due to these concerns 9-fluorenylmethyl carbamate (Fmoc) solid phase peptide synthesis was developed which employs *N*- α -Fmoc amino acids (36). In this strategy, the Fmoc group is deprotected with piperidine and TFA is required only for the final cleavage and deprotection step. In this paper, we have synthesized an amino acid analog, [*p*-(*N*- α -Fmoc-L-aspartic acid- β -amido)benzyl]-EDTA tetra-*tert*-butyl ester (**9**). We report here a new selective protection scheme for the preparation of amino acid analog **9** which is designed to be compatible with the Fmoc solid phase peptide synthesis strategy. The synthetic route for this synthesis is outlined in Scheme 1. EDTA analog **3** was synthesized with modifications of the method published by Studer and Meares (37).

To test the use of reagent **9** to incorporate *p*-aminobenzyl-EDTA in internal sequence of a peptide, we synthesized a fragment of HIV-1 Tat protein (amino acids 56–72) on an automated peptide synthesizer. We used standard HOBt/DCC peptide synthesis protocols to incorporate reagent **9** in the peptide sequence. The amino acid sequence of the Tat peptide contained Arg-X-Pro-Pro-Gln-Gly-Ser-Gln-Thr-His-Gln-Val-Ser-Leu-Ser-Lys-Gln, where X was the modified amino acid **9**. After standard TFA deprotection, the peptide was purified and characterized by mass spectrometry, which confirmed the incorporation of EDTA in the peptide sequence. Tat protein is a potent transactivator of transcription from the viral long terminal repeat and acts by binding to a stem-loop RNA

* Author to whom correspondence should be addressed [telephone (908) 235-4082; fax (908) 235-4073; e-mail rana@umdnj.edu].

[†] Present address: Department of Chemistry, Hartwick College, Oneonta, NY 13820.

[®] Abstract published in *Advance ACS Abstracts*, February 1, 1997.

Scheme 1

a. $\text{BrCH}_2\text{CO}_2\text{C}(\text{CH}_3)_3$, $\text{KI}/\text{K}_2\text{CO}_3$ b. Pd/C , K_2CO_3 , H_2 c. DCC/DMAP , FmOH d. TFA
e. DCC , HOBT f. 20% Piperidine g. $\text{Fmoc-OSu}/\text{DME}$.

structure called TAR RNA (38). Tat peptides modified with metal chelates at various sequence positions would provide a class of affinity cleaving reagents that can be directed against TAR RNA, and these studies are in progress.

EXPERIMENTAL SECTION

Anhydrous DMF, *N,N*-diisopropylethylamine, fluorene-methanol, TFA, piperidine, DMAP, and 10% Pd on charcoal were purchased from Aldrich. DCC and HOBT were obtained from Sigma. *N*- α -Fmoc- β -*tert*-butyl ester L-aspartic acid was purchased from Bachem. All chemicals were of reagent grade unless otherwise specified. NMR spectra were recorded at 200 MHz on a Gemini 200 spectrometer (Varian). The FAB MS spectrum was recorded using *m*-nitrobenzoic acid/NaI as matrix. IR spectra were obtained on a Perkin-Elmer FT 1600 as thin film. TLC was performed with precoated 0.2 mm silica gel 60 F-254 TLC plates (EM Reagents, Darmstadt, Germany).

(*p*-Nitrobenzyl)-EDTA Tetra-*tert*-butyl Ester (2). To a 100 mL round-bottom flask were added 0.92 g (3.4 mmol) of (*p*-nitrobenzyl)ethylenediamine dihydrochloride and 50 mL of dry acetonitrile. The flask was flushed with nitrogen for 10 min, and to the stirring mixture were added 2.46 g (17.7 mmol) of K_2CO_3 and 0.64 g (3.8 mmol) of KI. Finally, *tert*-butyl bromoacetate (2.9 mL, 17.9 mmol) was added to the mixture slowly. The mixture was refluxed at 105 °C for 120 h in the dark and then cooled to room temperature. Evaporation of solvent gave brown oil containing powdery deposit. The crude mixture was dissolved in methylene chloride and filtered through a glass frit, and the solid was washed with more methylene chloride until the powder on top of the frit turned white. The filtrate was collected and evaporated to give a yellow oil, which was silica gel column purified with 10% ethyl acetate in methylene chloride. The ^1H NMR showed several kinds of para-disubstituted phenyl groups, seemingly a mixture of mono-, di-, tri-, and tetraprotected EDTA moieties. Another silica gel column with 5% ethyl acetate in CH_2Cl_2 gave the final product (1.53 g, 2.4 mmol, 70.6% yield): IR 1731 cm^{-1} ($\text{C}=\text{O}$, br s); ^1H NMR (CDCl_3) δ 8.03 (2H, d, 8.76 Hz), 7.42 (2H, d, 8.42 Hz),

3.37 (4H, s), 3.34 (4H, s), 3.30 (2H, m), 2.95 (2H, m), 2.34 (1H, m), 1.36 (36H, s); ^{13}C NMR δ 171.42, 171.09, 149.41, 146.66, 130.69, 123.64, 63.52, 56.89, 56.08, 53.81, 37.54, 28.54, 28.49.

(*p*-Aminobenzyl)-EDTA Tetra-*tert*-butyl Ester (3). To dried compound 2 (1.5 g, 2.3 mmol) in 100 mL of THF were added 415 mg (3.0 mmol) of K_2CO_3 and 400 mg of 10% Pd/C under nitrogen flow at room temperature. After addition, hydrogen inlet was used instead of nitrogen, and with vigorous stirring and strong hydrogen flow, the mixture was allowed to react overnight at room temperature under H_2 atmosphere. The reaction mixture was filtered through a glass frit, and the solid was washed with more THF. The collected solution was evaporated to give a yellow oil. Silica gel column separation with ethyl acetate and another column with methylene chloride gave yellow oil, which was identified as pure product by ^1H and ^{13}C NMR spectra (0.78 mg, 1.3 mmol, 56.5% yield): IR 1731 cm^{-1} ($\text{C}=\text{O}$, br s); ^1H NMR in CDCl_3 δ 6.98 (2H, d, 8.18 Hz), 6.57 (2H, d, 8.22 Hz), 5.29 (2H, s), 3.48 (4H, s), 3.43 (4H, s), 3.03 (1H, m), 2.81 (2H, m), 2.55 (2H, m), 1.43 (18H, s), 1.40 (18H, s); ^{13}C NMR δ 172.05, 171.58, 145.11, 130.23, 115.62, 63.54, 56.69, 55.35, 53.92, 35.69, 20.50.

***N*- α -Fmoc- β -*tert*-butyl Ester L-Aspartic Acid 9-Fluorenylmethyl Ester (5).** To a 25 mL round-bottom flask was added compound 4 (0.411 g, 1 mmol) dissolved in 5 mL of methylene chloride. At 0 °C, 206 mg (1 mmol) of DCC and 2 mg of DMAP were added to the mixture and stirred for 1 h at the same temperature. Prepared solution of 9-fluorenylmethanol (216 mg, 1.1 mmol) in 2 mL of CH_2Cl_2 was added, and the mixture was stirred overnight at room temperature. Filtration to remove white salt (DCU) and evaporation of the filtrate gave a light yellowish oil. Silica gel column with 30% ethyl acetate in petroleum ether gave 0.5 g of colorless oil and 0.1 g of white solid. NMR confirmed the oily compound as the product (0.5 g, 0.85 mmol, 85% yield): ^1H NMR (CDCl_3) δ 7.50 (16H, m), 6.00 (1H, d, 8.5 Hz, NH), 4.76 (1H, dt), 4.48 (4H, 2d), 4.29 (2H, 2t), 2.94 (2H, dd, 4.48 Hz, 15.10 Hz), 1.48 (9H, s); ^{13}C NMR δ 171.49, 170.54, 156.55, 144.41, 144.27, 144.03, 141.81, 128.42, 128.27, 127.74, 127.62, 125.59, 125.56, 120.60, 120.54, 68.33, 67.84, 51.24, 47.66, 47.23, 38.27, 28.57.

***N*- α -Fmoc- α -9-fluorenylmethyl Ester L-Aspartic Acid (6).** At 0 °C, 1.5 mL of trifluoroacetic acid was added to 0.309 g (0.52 mmol) of 5 in 4 mL of methylene chloride. The mixture was stirred for 2 h at 0 °C, and the solvent was evaporated under vacuum. Complete dryness gave 0.25 g (0.47 mmol, 90.4% yield) of white powder, which was confirmed to be 6 by mass spectrum: ^1H NMR (CD_3OD) δ 7.80–7.27 (16H, m), 4.70–4.20 (7H, m), 2.80 (2H, m).

[*p*-(*N*- α -Fmoc L-aspartic acid 9-fluorenylmethyl ester β -amido)benzyl]-EDTA Tetra-*tert*-butyl Ester (7). To a 25 mL round-bottom flask containing 126 mg of 6 (0.24 mmol) was added 50 mg (0.37 mmol) of HOBT in 5 mL of 1:1 mixture of THF and DMF. DCC (100 mg, 0.48 mmol) in 3 mL of methylene chloride and 0.5 mL of IPEA were added to keep the pH about 8. The reaction mixture was stirred for 30 min at 0 °C and for 2 h at room temperature. Without filtration, compound 3 (0.14 g, 0.225 mmol) in 3 mL of THF was added to the mixture and left for stirring overnight. TLC in 15% petroleum ether/ethyl acetate showed two spots, one corresponding to the mixture of Fmoc derivatives and another to the coupled product. Spin chromatotron separation with 80% petroleum ether in ethyl acetate gave 150 mg of pure product (0.13 mmol) as yellow oil, which was identified by NMR and high-resolution mass spectra to be com-

pound **7** (MS = 1137.581, theor = 1137.580; 58% yield): IR 1731 cm^{-1} (C=O, br s); ^1H NMR (CDCl_3) δ 7.50 (20H, m), 6.25 (1H, d), 4.50 (7H, m), 3.49 (4H, s), 3.44 (4H, s), 2.85 (8H, m), 1.44 (18H, s), 1.41 (18H, s); ^{13}C NMR δ 171.83, 171.41, 168.40, 156.80, 144.30, 144.16, 144.09, 144.00, 141.74, 137.31, 135.78, 130.29, 128.28, 128.20, 127.69, 127.60, 125.65, 125.51, 120.47, 120.28, 68.18, 67.88, 63.81, 60.92, 56.81, 55.94, 54.06, 51.31, 47.55, 47.15, 39.03, 36.83, 28.63, 21.58, 14.70.

[p-(L-Aspartic acid β -amido)benzyl]-EDTA Tetra-*tert*-butyl Ester (8**).** To 150 mg of **7** (0.13 mmol) was added 5 mL of 20% piperidine in methylene chloride, and the mixture was stirred for 2.5 h. The solvent was evaporated completely. The obtained yellow solid was washed with a minimal amount of ether and filtered through a micropipet with cotton. White solid, which was not ether soluble, was washed again with 2 mL of ether. The filtrate, which contains the product and Fmoc derivatives, was concentrated. The resulting yellow oil was fractionally crystallized in petroleum ether (72.4% yield; M + Na = 759.3065, theor = 759.3061): IR 1731 cm^{-1} (C=O, br s); ^1H NMR (CDCl_3) δ 7.55 (2H, d), 7.10 (2H, d), 3.42 (8H, 2br s), 3.20–2.50 (8H, m), 1.42 (18H, s), 1.40 (18H, s).

[p-(N- α -Fmoc-L-aspartic acid β -amido)benzyl]-EDTA Tetra-*tert*-butyl Ester (9**).** To a round-bottom flask was transferred compound **8** (405 mg, 0.55 mmol), and 10 mL of 10% Na_2CO_3 was added. A solution of 270 mg of Fmoc-OSu (0.8 mmol) in 20 mL of DME was also added to the mixture. The reaction mixture was stirred for 5 h at room temperature. After the solvent was evaporated, 10 mL of H_2O was added to the crude mixture and the pH was adjusted to 7 with 1 N HCl. The mixture was extracted with ethyl acetate and washed with H_2O and brine. Spin chromatotron purification with 50% ethyl acetate in methanol gave 200 mg (0.21 mmol) of yellow oil as the product (38% yield; M + Na = 959.503, theor = 959.502): IR 1731 cm^{-1} (C=O, br s); ^1H NMR (CDCl_3) δ 7.7–7.0 (12H, m), 3.32 (8H, m), 3.20–2.20 (14H, m), 1.53 (18H, s), 1.47 (18H, s).

PEPTIDE SYNTHESIS

All Fmoc-amino acids, piperidine, 4-(dimethylamino)-pyridine, dichloromethane, *N,N*-dimethylformamide, 1-hydroxybenzotriazole (HOBt), 2-(1*H*-benzotriazo-1-yl)-1,1,3,3-tetramethyluronium hexafluorophosphate (HBTU), diisopropylethylamine, and HMP-linked polystyrene resin were obtained from Applied Biosystems Division, Perkin-Elmer. Trifluoroacetic acid, 1,2-ethanedithiol, phenol, and thioanisole were from Sigma. Tat-derived peptide (from amino acids 56–72) was synthesized on an Applied Biosystems 431A peptide synthesizer using standard FastMoc protocols. Reagent **9** was incorporated in the peptide sequence by HOBt/DCC peptide coupling procedures. Cleavage and deprotection of the peptide was carried out in 2 mL of reagent K for 6 h at room temperature. Reagent K contained 1.75 mL of TFA, 100 μL of thioanisole, 100 μL of water, and 50 μL of ethanedithiol (**39**). After cleavage from the resin, peptide was purified by HPLC on a Zorbax 300 SB-C₈ column. The mass of fully deprotected and purified peptides was confirmed by FAB mass spectrometry: calculated mass for Tat (56–72 containing Asp-aminobenzyl-EDTA at position 57) = 2494.6, found 2495.6 (M + H).

ACKNOWLEDGMENT

We thank Xilu Wang for critical reading of the manuscript. This research was supported by Research Grant AI 34785-01 from the National Institutes of Health.

LITERATURE CITED

- (1) Tullius, T. D. (1989) In *Metal-DNA Chemistry* (T. D. Tullius, Ed.) pp 1–23, American Chemical Society, Washington, DC.
- (2) Pyle, A. M., Long, E. C., and Barton, J. K. (1989) Shape-selective targeting of DNA by (phenanthroquinone diimine) rhodium (III) photocleaving agents. *J. Am. Chem. Soc.* **111**, 4520–4522.
- (3) Chow, C. S., and Barton, J. K. (1990) Shape-selective cleavage of tRNA^{phe} by transition-metal complexes. *J. Am. Chem. Soc.* **112**, 2839–2841.
- (4) Chow, C. S., Behlen, L. S., Uhlenbeck, O. C., and Barton, J. K. (1992) Recognition of tertiary structure in tRNAs by Rh-(phen)₂ph³⁺, a new reagent for RNA structure-function mapping. *Biochemistry* **31**, 972–982.
- (5) Tullius, T. D., and Dombroski, B. A. (1985) Iron(II) EDTA used to measure the helical twist along any DNA molecule. *Science* **230**, 679–681.
- (6) Price, M. A., and Tullius, T. D. (1992) Using hydroxyl radical to probe DNA structure. *Methods Enzymol.* **212**, 194–219.
- (7) Latham, J. A., and Cech, T. R. (1989) Defining the Inside and Outside of a Catalytic RNA Molecule. *Science* **245**, 276–282.
- (8) Celander, D. W., and Cech, T. R. (1991) Visualizing the higher order folding of a catalytic RNA molecule. *Science* **251**, 401–407.
- (9) Dreyer, G. B., and Dervan, P. B. (1985) Sequence-specific Cleavage of Single-stranded DNA: Oligodeoxynucleotide-EDTA-Fe(II). *Proc. Natl. Acad. Sci. U.S.A.* **82**, 968–972.
- (10) Moser, H. E., and Dervan, P. B. (1987) Sequence-Specific Cleavage of Double Helical DNA by Triple Helix Formation. *Science* **238**, 645–650.
- (11) Han, H., Schepartz, A., Pellegrini, M., and Dervan, P. B. (1994) Mapping RNA regions in eukaryotic ribosomes that are accessible to methidiumpropyl-EDTA-Fe(II) and EDTA-Fe(II). *Biochemistry* **33**, 9831–9844.
- (12) Chen, C.-H. B., and Sigman, D. S. (1987) Chemical conversion of a DNA-binding protein into a site-specific nuclease. *Science* **237**, 1197–1201.
- (13) Sluka, J. P., Horvath, S. J., Bruist, M. F., Simon, M. I., and Dervan, P. B. (1987) Synthesis of a sequence-specific DNA-cleaving Peptide. *Science* **238**, 1129–1132.
- (14) François, J.-C., et al. (1989) Sequence-Specific recognition and Cleavage of Duplex DNA via Triple-Helix Formation by Oligonucleotides Covalently Linked to a Phenanthroline-copper Chelate. *Proc. Natl. Acad. Sci. U.S.A.* **86**, 9702–9706.
- (15) Ebright, R. H., Ebright, Y. W., Pendergrast, P. S., and Gunasekera, A. (1990) Conversion of a helix-turn-helix motif sequence-specific DNA binding protein into a site-specific DNA cleavage agent. *Proc. Natl. Acad. Sci. U.S.A.* **87**, 2882–2886.
- (16) Ebright, Y. W., Chen, Y., Ludescher, R. D., and Ebright, R. H. (1993) N-(iodoacetyl)-p-phenylenediamine-EDTA: a reagent for high-efficiency incorporation of an EDTA-metal complex at a rationally selected site within a protein. *Bioconjugate Chem.* **4**, 219–225.
- (17) Rana, T. M., and Meares, C. F. (1990) Specific Cleavage of a Protein by an Attached Iron Chelate. *J. Am. Chem. Soc.* **112**, 2457–2458.
- (18) Schepartz, A., and Cuenoud, B. (1990) Site-specific cleavage of the protein calmodulin using a trifluoperazine-based affinity reagent. *J. Am. Chem. Soc.* **112**, 3247–3249.
- (19) Hoyer, D., Cho, H., and Schultz, P. G. (1990) A new strategy for selective protein cleavage. *J. Am. Chem. Soc.* **112**, 3249–3250.
- (20) Rana, T. M., and Meares, C. F. (1991) Iron Chelate-Mediated Proteolysis: Protein Structure Dependence. *J. Am. Chem. Soc.* **113**, 1859–1861.
- (21) Rana, T. M., and Meares, C. F. (1991) Transfer of Oxygen from an Artificial Protease to Peptide Carbon During Proteolysis. *Proc. Natl. Acad. Sci. U.S.A.* **88**, 10578–10582.
- (22) Cuenoud, B., Tarasow, T. M., and Schepartz, A. (1992) A new strategy for directed protein cleavage. *Tetrahedron Lett.* **33**, 895–898.
- (23) Ermacora, M. R., Delfino, J. M., Cuenoud, B., Schepartz, A., and Fox, R. O. (1992) Conformation-dependent cleavage of staphylococcal nuclease with a disulfide-linked iron chelate. *Proc. Natl. Acad. Sci. U.S.A.* **89**, 6383–6387.

- (24) Ermacora, M. R., Ledman, D. W., Hellinga, H. W., Hsu, G. W., and Fox, R. O. (1994) Mapping staphylococcal nuclease conformation using an EDTA-Fe derivative attached to genetically engineered cysteine residue. *Biochemistry* 33, 13625–13641.
- (25) Wu, J., Perrin, D. M., Sigman, D. S., and Kaback, H. R. (1995) Helix packing of lactose permease in *Escherichia coli* studies by site-directed chemical cleavage. *Proc. Natl. Acad. Sci. U.S.A.* 92, 9186–9190.
- (26) Parac, T. N., and Kostić, N. M. (1996) Effects of linkage isomerism and of acid-base equilibria on reactivity and catalytic turnover in hydrolytic cleavage of histidyl peptides coordinated to palladium(II). Identification of the active complex between Palladium(II) and histidyl residue. *J. Am. Chem. Soc.* 118, 5946–5951.
- (27) Ghaim, J. B., Greiner, D. P., Meares, C. F., and Gennis, R. B. (1995) Proximity mapping the surface of a membrane protein using an artificial protease: demonstration that the quinone-binding domain of subunit I is near the N-terminal region of subunit II of cytochrome *bd*. *Biochemistry* 34, 11311–11315.
- (28) Heyduk, E., and Heyduk, T. (1994) Mapping protein domains involved in macromolecular interactions: a novel protein footprinting approach. *Biochemistry* 33, 9643–9650.
- (29) Greiner, D. P., Hughes, K. A., Gunasekera, A. H., and Meares, C. F. (1996) Binding of σ^{70} protein to the core subunits of *Escherichia coli* RNA polymerase, studies by iron-EDTA protein footprinting. *Proc. Natl. Acad. Sci. U.S.A.* 93, 71–75.
- (30) Sundberg, M. W., Meares, C. F., Goodwin, D. A., and Diamanti, C. I. (1974) Selective binding of metal ions to macromolecules using bifunctional analogs of EDTA. *J. Med. Chem.* 17, 1304–1307.
- (31) Meares, C. F., and Wensel, T. G. (1984) Metal Chelates as Probes for Biological Systems. *Acc. Chem. Res.* 17, 202–209.
- (32) Meares, C. F., and Goodwin, D. A. (1984) Linking Radiometals to Proteins with Bifunctional Chelating Agents. *J. Protein Chem.* 3, 215–227.
- (33) Sluka, J. P., Griffin, J. H., Mack, D. P., and Dervan, P. B. (1990) Reagents and methods for the solid-phase synthesis of Protein-EDTA for use in affinity cleaving. *J. Am. Chem. Soc.* 112, 6369–6374.
- (34) Cuenoud, B., and Schepartz, A. (1991) Synthesis of N- α -Boc-N- ϵ -tribenzyl EDTA-L-lysine. An amino acid analogue suitable for solid phase peptide synthesis. *Tetrahedron* 47, 2535–2542.
- (35) Arya, R., and Gariépy, J. (1991) Rapid synthesis and introduction of a protected EDTA-like group during the solid-phase assembly of peptides. *Bioconjugate Chem.* 2, 323–326.
- (36) Fields, G. B., and Noble, R. L. (1990) *Int. J. Pept. Protein Res.* 35, 161–214.
- (37) Studer, M., and Meares, C. F. (1992) A convenient and flexible approach for introducing linkers on bifunctional chelating agents. *Bioconjugate Chem.* 3, 420–423.
- (38) Jones, K. A., and Peterlin, B. M. (1994) Control of RNA Initiation and Elongation at The HIV-1 Promoter. *Annu. Rev. Biochem.* 63, 717–743.
- (39) King, D. S., Fields, C. G., and Fields, G. B. (1990) A cleavage method which minimizes side reactions following Fmoc solid phase peptide synthesis. *Int. J. Pept. Protein Res.* 36, 255–266.

BC960084U

Preparation of Succinimidyl and Pentafluorophenyl Active Esters of 5- and 6- Carboxyfluorescein

Maciej Adamczyk,* Jeffrey R. Fishpauqh, and Kevin J. Heuser

Diagnostic Division, Division Organic Chemistry (D-9NM), Building AP-20, Abbott Laboratories, 100 Abbott Park Road, Abbott Park, IL 60064-3500. Received November 8, 1996[®]

A mixture of 5- and 6-carboxyfluorescein was activated with 1-[3-(dimethylamino)propyl]-3-ethylcarbodiimide hydrochloride in the presence of either *N*-hydroxysuccinimide or pentafluorophenol to give the corresponding succinimidyl and pentafluorophenyl esters. The regioisomeric mixtures were separated to give the 5- and 6- succinimidyl and pentafluorophenyl active esters in >98% purity.

INTRODUCTION

Fluorescein derivatives have been widely used as fluorescent markers in bioanalytical chemistry (1–5) and have found exceptional utility as the fluorophores of choice in fluorescent polarization immunoassays (FPIA) used for monitoring the level of drugs and hormones in human fluids (6, 7). Active esters of 5- and 6-carboxyfluorescein¹ are used for production of labels and conjugates (1, 4, 8–10). The 5- and 6-carboxyfluorescein mixture (61:39 isomer ratio) is commercially available (11). The pure isomers are also available, but at a high cost, while the pure succinimidyl active esters can be purchased at a cost of \$7600/g (12). From the literature (13, 14) only limited information is available for the preparation, purification, and analysis of the fluorescein succinimidyl active esters, while the corresponding pentafluorophenyl active esters, which usually possess higher hydrolytic stability (15), have not been previously reported. Thus, there is a need for an efficient and cost effective method for the preparation of these active esters. We now report a method for the preparation of 5- and 6-carboxyfluorescein succinimidyl (**2a** and **2b**, respectively) and new pentafluorophenyl (**2c** and **2d**) active esters from the inexpensive, commercially available mixture of 5(6)-carboxyfluorescein (**1**) as shown in Scheme 1.

MATERIALS AND METHODS

All reagents were purchased from Aldrich Chemical Co. (Milwaukee, WI) except for 5(6)-carboxyfluorescein (**1**), which was purchased from Kodak (Rochester, NY), and these chemicals were used without further purification. Solvents were of HPLC grade and used without further purification. Silica gel 60 (230–400 mesh) was purchased from EM Science (Gibbstown, NJ). Biotage FLASH 75 purification system and KP-SIL silica cartridges (32–63 μ m, 60A, 7.5 \times 30 cm) were purchased from Biotage, Inc. (Charlottesville, VA). ¹H NMR spectra were recorded at 300 MHz, on a Varian Gemini 300 spectrometer. Electrospray ionization mass spectra were recorded on a Perkin-Elmer Sciex API 100 instrument. Elemental analyses were performed by Robertson-Microlit Laboratories, Inc. (Madison, NJ). Analytical HPLC

was performed using a Waters (Milford, MA) 8 \times 100 mm μ Bondapak radial compression C₁₈ column with a flow rate of 2 mL/min and UV detection at 225 nm. Preparative HPLC was performed using a Waters 40 \times 100 mm μ Bondapak radial compression C₁₈ column with a flow rate of 45 mL/min and UV detection at 225 nm.

5- and 6- Carboxyfluorescein Succinimidyl Active Esters (2a, 2b). To a solution of 5(6)-carboxyfluorescein (5.0 g, 13.3 mmol) in anhydrous *N,N*-dimethylformamide (DMF; 50 mL) was added 1-[3-(dimethylamino)propyl]-3-ethylcarbodiimide hydrochloride (EDAC; 3.1 g, 16.0 mmol) followed by *N*-hydroxysuccinimide (HOSu; 1.9 g, 16.0 mmol). The reaction was covered with foil, stirred under nitrogen, and monitored by analytical HPLC (22% CH₃CN/22% MeOH/56% aqueous 0.1% formic acid). After 4.5 h, additional EDAC (510 mg, 0.2 equiv) was added, and the reaction was stirred for an additional 18.5 h. The reaction mixture was rinsed into a separatory funnel with DMF (10 mL) and diluted with acetone (200 mL). Buffer (0.05 M, pH 6 phosphate buffer, 250 mL) was added, and the mixture was extracted with diethyl ether (Et₂O)/ethyl acetate (EtOAc) (2:1, 300 mL). The organic layer was separated, and the aqueous layer was extracted two times with Et₂O/EtOAc (2:1, 250 mL). The combined organic extracts were washed with water (3 \times 200 mL) and brine (1 \times 250 mL), dried over Na₂SO₄, and filtered, and the solvents were removed *in vacuo* to afford 4.7 g of crude 5(6)-carboxyfluorescein succinimidyl active esters. Separation of the isomers on the Biotage system was performed as follows: (a) the Biotage column was equilibrated with 2 L of eluent (15% acetone/85% toluene containing 0.05% acetic acid); (b) crude active ester mixture, adsorbed onto silica gel (50 g), was loaded into the SIM (16); and (c) the isomers were eluted at a main system pressure of 100 psi and solvent pressure of 55–60 psi, to afford 1.7 g of **2a** (<2% of **2b** present) and 1.2 g of **2b** (<3% of **2a** present). For further purification, each lot was adsorbed onto silica gel (10–15 g), loaded into the SIM, and purified using the previous conditions to afford 795 mg of **2a** (21% yield, >99% pure with <0.1% of **2b** present) and 780 mg of **2b** (32% yield, >99% pure with <0.1% of **2a** present). Complete spectral and analytical data are shown in Tables 1 and 2.

Flash Chromatography. The crude reaction mixture (4.7 g) adsorbed onto silica (50 g) was loaded onto an equilibrated flash column (14 \times 30 cm bed of silica) and separated (17) to afford 1.2 g of **2a** (<0.1% of **2b** present) and 1.5 g of **2b** (24% of **2a** present).

Preparative HPLC. A crude mixture (50 mg) was separated by reversed phase preparative HPLC (25% CH₃CN/75% aqueous 0.1% formic acid) to afford **2a** (27

* Author to whom correspondence should be addressed [telephone (847) 937-0225; fax (847) 938-8927; e-mail adamczyk@apmac.abbott.com].

[®] Abstract published in *Advance ACS Abstracts*, February 1, 1997.

¹5(6)-Carboxyfluorescein is also known as 4(5)-carboxyfluorescein.

Scheme 1

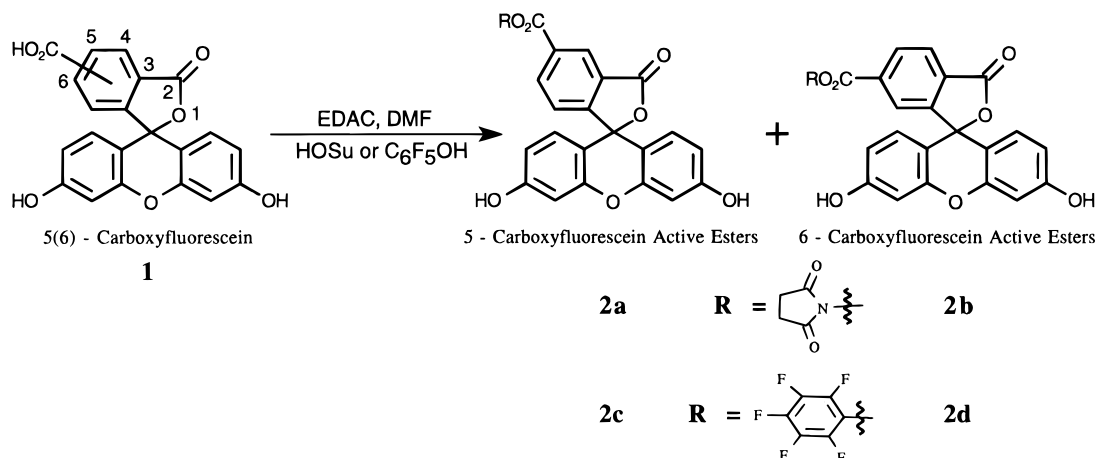


Table 1. Preparation of Fluorescein Active Esters 2a–d

compd	yield (%)	HPLC ^{a,b}		molecular formula	ESI-MS (M + H) ⁺	elemental analysis (found)			
		retention time (min)	purity (%)			C	H	N	F
2a	21	11.69	99	C ₂₅ H ₁₅ NO ₉	474.0	63.43 (63.74)	3.19 (3.43)	2.96 (3.04)	
2b	32	9.68	99	C ₂₅ H ₁₅ NO ₉	474.0	63.43 (63.16)	3.19 (3.36)	2.96 (2.86)	
2c	25	7.20	99	C ₂₇ H ₁₁ F ₅ O ₇	543.2	59.79 (60.17)	2.04 (1.96)		17.51 (17.61)
2d	13	6.14	98	C ₂₇ H ₁₁ F ₅ O ₇	543.2	59.79 (59.81)	2.04 (1.79)		17.51 (17.36)

^a Solvent system for **2a**, **2b** = 43% (1:1 CH₃CN/MeOH)/57% aqueous 0.1% formic acid. ^b Solvent system for **2c**, **2d** = 70% (1:1 CH₃CN/MeOH)/30% aqueous 0.1% formic acid.

Table 2. NMR Data for Fluorescein Active Esters 2a–d

compd	¹ H NMR (DMSO- <i>d</i> ₆) (δ, ppm; <i>J</i> , Hz)									
2a	10.18 (s, 2H), 8.54 (s, 1H), 8.43 (d, 1H, <i>J</i> = 8.07), 7.56 (d, 1H, <i>J</i> = 8.14), 6.75–6.66 (m, 4H), 6.60–6.50 (m, 2H), 2.93 (s, 4H)									
2b	10.17 (s, 2H), 8.39 (d, 1H, <i>J</i> = 8.07), 8.25 (d, 1H, <i>J</i> = 8.04), 7.92 (s, 1H), 6.75–6.61 (m, 4H), 6.60–6.50 (m, 2H), 2.88 (s, 4H)									
2c	10.18 (s, 2H), 8.64 (s, 1H), 8.50 (d, 1H, <i>J</i> = 8.10), 7.55 (d, 1H, <i>J</i> = 8.10), 6.75–6.65 (m, 4H), 6.60–6.50 (m, 2H)									
2d	10.18 (s, 2H), 8.45 (d, 1H, <i>J</i> = 8.10), 8.24 (d, 1H, <i>J</i> = 7.96), 7.98 (s, 1H), 6.72–6.63 (m, 4H), 6.61–6.50 (m, 2H)									

mg, 5% hydrolysis observed) and **2b** (18 mg, 12% hydrolysis observed).

5- and 6-Carboxyfluorescein Pentafluorophenyl Active Esters (2c, 2d). To a solution of 5(6)-carboxyfluorescein (5.0 g, 13.3 mmol) in anhydrous DMF (40 mL) was added EDAC (3.1 g, 16.0 mmol) followed by a solution of pentafluorophenol (3.0 g, 16.0 mmol) in DMF (10 mL). The reaction flask was covered with foil, and the reaction was monitored by analytical HPLC (35% CH₃CN/35% MeOH/30% aqueous 0.1% formic acid). After stirring under nitrogen for 22 h, the reaction was worked up as described above to afford 6.3 g of crude 5(6)-carboxyfluorescein pentafluorophenyl active esters. Partial separation on the Biotage system using the method and eluents described above for **2a** and **2b** gave 3.2 g of the active ester mixture **2c** and **2d** with no observed separation between the 5 and 6 regioisomers. Separation by flash chromatography was achieved by adsorbing the mixture onto silica (25 g), loading it onto an equilibrated flash column (70% ethyl acetate/30% toluene, 7.5 × 23 cm bed of silica), and eluting (18) to afford 1.1 g of **2c** (25% yield, >99% with <0.5% of **2d** present), 814 mg of a mixture, and 555 mg of **2d** (>91% with 6% of **2c** present). Partially separated **2d** was adsorbed onto silica (5 g), loaded onto an equilibrated flash column (20% acetone/80% toluene containing 0.1% acetic acid, 3 × 20 cm bed of silica), and further purified using the above solvent system to afford 350 mg of **2d** (13% yield, >98% with <1.8% of **2c** present). Complete spectral and analytical data are shown in Tables 1 and 2.

Preparative HPLC. A crude mixture (65 mg) was separated by reversed phase preparative HPLC (55% CH₃CN/45% aqueous 0.1% formic acid) to afford **2c** (21

mg) and **2d** (17 mg); however, only small amounts of material could be loaded onto the 40 × 100 column per run (30 min, ~95 runs needed to separate the total 6.3 g of mixture).

RESULTS AND DISCUSSION

The mixture of **1** was reacted with EDAC and HOSu in anhydrous DMF to convert each acid to its respective succinimidyl active ester (**2a** and **2b**). Workup conditions consisted of pouring the crude reaction mixture into a separatory funnel, adding pH 6 buffer solution, and extracting with a mixture of ether/ethyl acetate (2:1). The selection of solvent combination was necessary to fully maximize extraction of the desired active esters and minimize the presence of HOSu, while the choice of pH 6 phosphate buffer prevented undesired hydrolysis. This workup gave active esters **2a** and **2b** with <0.5% of the starting acids. Separation of the active esters was attempted according to three different methods: flash chromatography, preparative reversed phase HPLC with a 40 × 100 mm radial compression column, and the Biotage FLASH 75 system.

Separation by flash chromatography was inefficient since it did not afford good resolution between the two fluorescein succinimidyl ester regioisomers. Preparative reversed phase HPLC separation was attempted using a 50 mg mixture of **2a** and **2b** and resulted in complete separation of the two isomers, but with partial hydrolysis (5–12%) of the active esters. A third method was sought that would combine the ease of use of flash chromatography with the separation capabilities of HPLC. The Biotage FLASH 75 system, introduced in 1994, was attractive because it is designed for milligram to kilogram

scale separations and provides solutions to critical operational problems typically found with glass columns: speed, safety, and performance (19). For gram scale separations, Biotage cartridges operate at higher pressures (85–120 psi) with higher flow rates (100–300 mL/min) than flash chromatography, which results in shorter run times (19). This self-contained system reduces the concern of using glass columns under pressure, while its radial compression technology eliminates voids and channels that often occur in conventional flash chromatography (19).

Separation of the crude mixture of fluorescein succinimidyl esters using the Biotage FLASH 75 system afforded good separation of **2a** from **2b** (both >97% by analytical HPLC). Further purification afforded **2a** and **2b** with purity >99%, see Table 1. A disadvantage for any silica gel based chromatographic separation of active esters is hydrolysis of the active ester while on the column, which frequently leads to diminished product yields. Mass recoveries using the Biotage system were in general <80%. This method of separation was found to be the most effective for the production of fluorescein succinimidyl active esters **2a** and **2b**.

Pentafluorophenyl active esters were prepared in a similar manner as the succinimidyl esters using EDAC/pentafluorophenol (C₆F₅OH), and separation was also attempted according to the three methods described for **2a** and **2b**. Preparative reversed phase HPLC separated **2c** and **2d** (<0.5% hydrolysis); however, this is a time-consuming process by which only a relatively small amount of material (65 mg) could be separated in a 30 min run using a 40 × 100 mm radial compression cartridge. The Biotage system was ineffective in separating **2c** and **2d**; however, rapid separation of the active esters from other components present after aqueous workup was achieved. Further purification of the active ester mixture by flash chromatography afforded **2c** and **2d** in low to moderate yields and high purity (>98%, see Table 1). In this case, the combination of Biotage and flash chromatography was found to be the most effective for obtaining the desired pentafluorophenyl active esters **2c** and **2d**.

In summary, our method transforms the inexpensive, commercially available 5(6)-carboxyfluorescein (**1**) to the highly useful 5- and 6-carboxyfluorescein succinimidyl active esters (**2a** and **2b**) and pentafluorophenyl active esters (**2c** and **2d**). Separation on the Biotage system gave very pure (>99%) succinimidyl active esters, and the combination of Biotage and flash chromatography afforded very pure (>98%) pentafluorophenyl active esters. These procedures allow for the rapid and cost effective production of these carboxyfluorescein active

esters, and the Biotage FLASH 75 system offers the advantages of safety, reproducibility, and speed over other techniques for the separation of larger amounts of material.

LITERATURE CITED

- (1) Haughland, R. P. (1991) *Biosensors with Fiberoptics* (D. L. Wise and D. Wingard, Eds.) p 85–109, Humana Press, Clifton, NJ.
- (2) Bright, F. V. (1988) Bioanalytical Applications of Fluorescence Spectroscopy. *Anal. Chem.* 60, 1031A–1039A.
- (3) Owens, M. A., and Loken, M. R. (1995) *Flow Cytometry: Principles for Clinical Laboratory Practice*, pp 28–29, Wiley-Liss, New York.
- (4) Haughland, R. P. (1992) *Handbook of Fluorescent Probes and Research Chemicals*, Molecular Probes, Eugene, OR.
- (5) Miki, M. (1987) The Recovery of the Polymerizability of Lys-61-Labelled Actin by the Addition of Phalloidin. *Eur. J. Biochem.* 164, 229–235.
- (6) Lu-Steffes, M., et al. (1982) Fluorescence Polarization Immunoassay IV. Determination of Phenytoin and Phenobarbital in Human Serum and Plasma. *Clin. Chem.* 28, 2278–2282.
- (7) Adamczyk, M., Harrington, C., and Johnson, D. (1994) Reagents and Methods for the Quantification of Imipramine and Desipramine in Biological Fluids. U.S. Pat. 5,340,750.
- (8) Bodanszky, M. (1979) *The Peptides*, Vol. 1, pp 106–175, Academic Press, New York.
- (9) Bodanszky, M. (1984) *Principles of Peptide Synthesis*, pp 28–49, Springer-Verlag, New York.
- (10) Reference 4, p 26.
- (11) The mixture is available from Fluka (Ronkonkoma, NY) and Kodak. Analytical HPLC revealed a 61:39 ratio using the Waters system described under Materials and Methods and eluting with 20% CH₃CN/20% MeOH/60% aqueous 0.1% formic acid.
- (12) Molecular Probes, Eugene, OR. 1996 price \$380 per 50 mg, 20 × \$380/50 mg = \$7600/g.
- (13) Yoshida, R. A. (1980) Support Ligand Analog Fluorescer Conjugate and Serum Assay Method Involving Such Conjugate. Eur. Pat. Appl. 0015695.
- (14) Vanderbilt, A. S., Osikowicz, E. W., Fino, J. R., and Shipchandler, M. T. (1986) Total Estriol Fluorescence Polarization Immunoassay. Eur. Pat. Appl. 0200960.
- (15) Imming, P., and Jung, M.-H. (1995) Pentafluorophenyl Esters of Dicarboxylic Acids. *Arch. Pharm.* 328, 87–91.
- (16) Stainless steel sample injection module (SIM) which delivers sample onto the cartridge.
- (17) Eluted with 15% acetone/85% toluene containing 0.05% acetic acid.
- (18) Eluted with 70% ethyl acetate/30% toluene (6000 mL), then 90% ethyl acetate/10% toluene (4000 mL), then 100% acetone containing 0.1% acetic acid (2000 mL).
- (19) Biotage FLASH 75 system user's manual, version 2.0 (1995).

BC9600877

CORRECTIONS

Volume 7, Number 6, November/December 1996.

Richard B. Greenwald,* Annapurna Pendri,
Anthony Martinez, Carl Gilbert, and Patricia
Bradley

PEG THIAZOLIDINE-2-THIONE, A NOVEL REA-
GENT FOR FACILE PROTEIN MODIFICATION:
CONJUGATION OF BOVINE HEMOGLOBIN

Page 638. The entry in the fourth column and second
row of Table 1 should be 36.

Page 640. In the legend for Figure 1, **9** should appear
in place of **8**, in both cases.

BC960196L

ARTICLES

Syntheses of Haptens Containing Dioxaphosphorinan Methoxyacetic Acid Linker Arms for the Production of Antibodies to Organophosphate Pesticides

Wolter ten Hoeve,[†] Hans Wynberg,[†] William T. Jones,^{*,‡} Dawn Harvey,[‡] Gordon B. Ryan,[‡] and Paul H. S. Reynolds[‡]

Syncom, University of Groningen, Groningen, The Netherlands, and Plant Improvement Division, The Horticulture and Food Research Institute of New Zealand, Private Bag 11 030, Palmerston North, New Zealand. Received October 16, 1996[®]

Four generic heterobifunctional reagents, namely 2-(2-chloro-5-methyl-1,3,2-dioxaphosphorinan-5-yl)methoxyacetic acid methyl ester, *p*-sulfide, 2-(2-chloro-5-methyl-1,3,2-dioxaphosphorinan-5-yl)-methoxyacetic acid methyl ester, *p*-oxide, 2-(2-mercapto-5-methyl-1,3,2-dioxaphosphorinan-5-yl)-methoxyacetic acid bispotassium salt, *p*-sulfide-, and (2-methoxy-5-methyl-1,3,2-dioxaphosphorinan-5-yl)methoxyacetic acid, methyl ester, have been synthesized and used to prepare organophosphate, thiophosphate, and dithiophosphate haptens containing a functional carboxyl group which can be used to conjugate the haptens to proteins. These hapten-protein conjugates have been used as antigens for preparing polyclonal sera against all classes of organophosphate pesticides. The eight examples used protein-hapten conjugates of chlorpyrifos, parathion, diazinon, paraoxon, azinphos, dimethoate, demeton, and dichlorvos. These were all immunogenic and resulted in sera containing antibodies that recognized the corresponding parent pesticide with high specificity.

INTRODUCTION

Residues of pesticides used for protection of horticultural crops against insect infestations need to be monitored from a human health as well as an economic perspective. Legal maximum residue limits are stipulated by both national and international regulatory agencies for many of these compounds in most food crops

and products. Increasingly, levels of such residues are being monitored by the international and domestic agencies.

Accordingly, there is a need for internationally acceptable, rapid, reliable, sensitive, and cost-effective assay systems for determining the presence of these compounds. Suitably designed immunoassay-based tests can fulfill all these requirements. Modern immunoassays are based on two important phenomena: (i) the extraordinary discriminatory power of antibodies and (ii) detection systems that allow the reaction of the antibody with its hapten to be quantified at low concentrations of the reactants (antibody and hapten).

The use of enzyme immunoassays (EIAs) and solid phase technology has brought about widespread use of these techniques. An excellent review of enzyme immu-

* Address correspondence to Dr. W. T. Jones, The Horticulture and Food Research Institute of New Zealand, Batchelar Research Centre, Private Bag 11 030, Palmerston North, New Zealand. Telephone: +64-6-356-8080. Fax: +64-6-351-7031.

[†] University of Groningen.

[‡] The Horticulture and Food Research Institute of New Zealand.

[®] Abstract published in *Advance ACS Abstracts*, April 1, 1997.

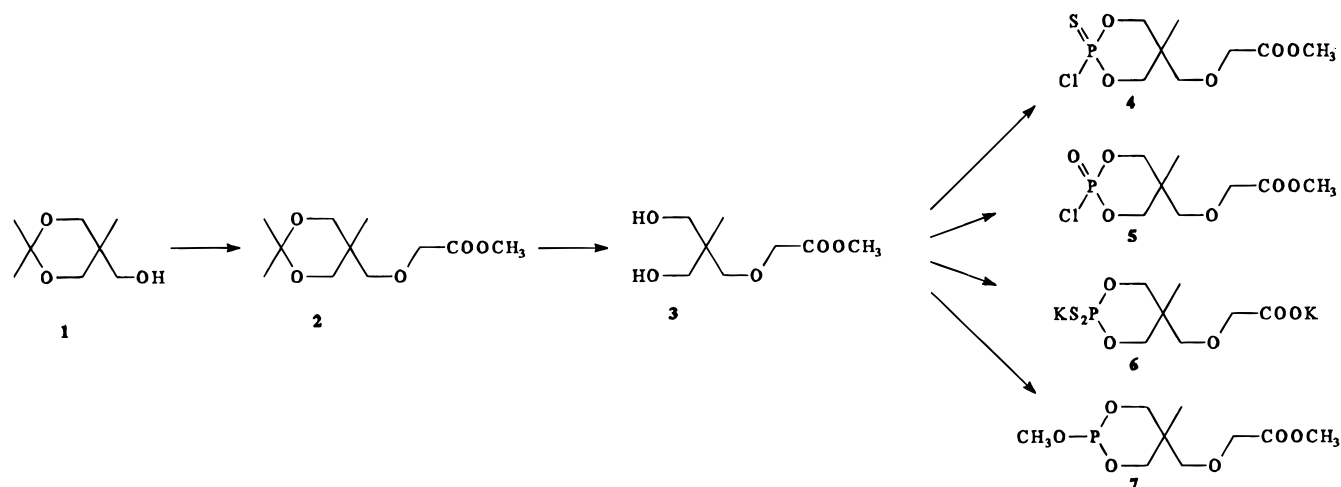


Figure 1. Synthetic scheme for the production of generic intermediates for synthesis of organophosphate, organothiophosphates, and organodithiophosphate haptens.

noassay is provided by Tijssen (1990). A large number of assays have been developed for aflatoxins (Chu *et al.*, 1991) and herbicides and insecticides (Aston *et al.*, 1992).

Residues are small molecules ($M_r < 1000$) and are usually unable to invoke an immune response when injected into animals. These molecules therefore have to be conjugated to larger immunogenic carrier molecules to produce the desired response. The organophosphate group of pesticides, being small molecules, are not immunogenic, nor can the majority of them be readily conjugated to a suitable carrier protein to render them antigenic. Until recently, antibodies have been raised only to those organophosphates that could easily be modified to allow coupling of the modified pesticide to the carrier protein (parathion, Ercegovich *et al.*, 1981; paraoxon, Brimfield *et al.*, 1985; Heldman *et al.*, 1985).

Heldman *et al.* (1985) produced antibodies to paraoxon by conjugation via a β -alanine linker attached through the phosphate atom. McAdam *et al.* (1992) described the production of haptens for preparing antibodies to fenitrothion. This entailed coupling the hapten through the phosphate group to the carrier protein and produced haptens resembling those of Heldman *et al.* (1985). This method of coupling through the phosphate group produced the best antibodies (Hill *et al.*, 1992). McAdam and Skerritt (1993) described the use of *tert*-butyl-3-[[chloro(methoxy)phosphorothioyl]amino]propanoate as a generic intermediate in preparing haptens of the organothiophosphate pesticides and successfully raised antibodies to fenitrothion, chlorpyrifos-methyl, and pyrimphos-methyl.

This work describes the synthesis of new generic heterobifunctional intermediates containing a dioxaphosphorinane ring which can be used to synthesize organophosphate, thiophosphate, and dithiophosphate haptens containing a functional carboxyl group to conjugate to proteins. These hapten-protein conjugates can be used as antigens for preparing antibodies for use in the development of specific immunoassays for the detection of specific pesticides.

RESULTS

Synthesis of Haptens and Conjugates. Access to haptens of some common organophosphate pesticides was investigated in the first instance through replacement of the methoxy or ethoxy group in these pesticides by another alkoxy group which would contain an amino or carboxylic acid function. The difficulties encountered in attaining such unsymmetrical compounds in a pure state

led to the investigation of an approach in which both methoxy and ethoxy groups were replaced by a group that would lead to a more symmetrical compound. Such a compound would presumably be easier to purify. On this basis, a 1,3-propanediol was chosen which contained a group at position 2 with a protected carboxylic acid function. 2-(Hydroxymethyl)-1,3-propanediol is commercially available and can be converted easily to 5-(hydroxymethyl)-2-methyl-1,3-dioxane (Gash, 1972). We reasoned that functionalization of the free hydroxy group leading to a group containing a carboxylic ester function, followed by coupling of the deprotected diol part to the phosphorus atom of pesticides, and finally selective hydrolysis of the carboxylic ester should lead to the desired haptens.

In practice, this approach (shown in Figure 1) appeared to be useful for the preparation of a series of haptens. Treatment of 5-(hydroxymethyl)-2-methyl-1,3-dioxane **1** with 2 equiv of sodium hydride in DMF followed by the addition of bromoacetic acid gave the sodium salt of the coupled product. This was directly reacted with dimethyl sulfate to furnish the methyl ester **2**. In order to gain access to the desired haptens, it was necessary to transform the acetal moiety into a diol, while maintaining the ester moiety intact. Common acidic cleavage methods led to the loss of the ester group, but under mild conditions, using pyridinium *p*-toluenesulfonate, the acetal was preferentially cleaved. The resulting crude diol **3** was used in the following transformations to prepare a set of generic intermediates useful for syntheses of organophosphate, organothiophosphate, and organodithiophosphate haptens.

(1) Treatment with thiophosphoryl dichloride and triethylamine in toluene gave a mixture of two isomeric (chlorine atom *cis* or *trans*, respectively) thionodioxaphosphorinanes **4**, the major isomer of which could be isolated as a crystalline compound. (2) Treatment with phosphoryl chloride and triethylamine in toluene gave a mixture of two isomeric dioxaphosphorinanes **5** which, in our hands, were inseparable. (3) Heating with phosphorus pentasulfide in toluene followed by treatment with potassium hydroxide resulted in the precipitation of the bispotassium salt **6**. (4) Stirring with trimethylphosphite and trimethylamine (Edmundson *et al.*, 1985) gave the distillable cyclic phosphite **7**.

The precursors **4–7** were then used for the preparation of the following haptens (Figure 2).

(a) *Chlorpyrifos*. The sodium salt of trichloropyridinol (obtained from the pyridinol with sodium hydride in DMF) was reacted with the crystalline isomer of chloride **4** in DMF at room temperature (RT). The resulting crystalline ester **8** could be hydrolyzed, under very mild basic conditions, viz., potassium carbonate in water, methanol, and THF, to the hapten, crystalline acid **9**.

(b) *Parathion*. 4-Nitrophenol was coupled to chloride **4** as described for chlorpyrifos to yield crystalline ester **10**. The ester was hydrolyzed with lithium hydroxide, resulting in crystalline acid **11**.

(c) *Diazinon*. The sodium salt of isopropylmethylpyrimidinol was reacted with chloride **4** to furnish crystalline ester **12**. Hydrolysis with potassium carbonate gave crystalline acid **13**.

(d) *Paraoxon*. 4-Nitrophenol was reacted with the mixture of isomeric chlorides **5**, resulting in two isomeric esters **14**, which could be separated by recrystallization. The paraoxon hapten **15** was prepared by potassium carbonate hydrolysis of the methyl ester. The use of lithium hydroxide, as for parathion, led to hydrolysis of the phosphate ester.

(e) *Azinphos*. The bispotassium salt **6** was treated with 1 equiv of hydrochloric acid to protonate the weaker carboxylic acid function and reacted with 3-(chloromethyl)-1,2,3-benzotriazin-4(3*H*)-one in acetone to give hapten **16** which was purified through acid-base separation and by crystallization.

(f) *Dimethoate*. This was prepared as for azinphos. *N*-Methylchloroacetamide was reacted with bispotassium salt **6** to give crystalline acid **17**.

(g) *Demeton*. Access to hapten **19** was possible by making use of the known O-S rearrangement (Sasse, 1964). Ethylthioethanol was reacted with butyllithium followed by addition of chloride **4**. The resulting ester **18** slowly underwent O-S rearrangement. However, the product could not be hydrolyzed to acid **19** without completely destroying the molecule. Therefore, ester **18** was hydrolyzed before rearrangement took place. The resulting crude acid slowly underwent O-S rearrangement, and hapten **19** was obtained in low yield as a crystalline solid.

(h) *Dichlorvos*. Phosphite **7** was reacted with anhydrous chloral by the Perkow reaction (Gallenkamp, 1982) to yield crude ester **20** which was hydrolyzed with potassium carbonate to the crystalline acid **21** together with an unknown acid. The desired hapten **21** was purified from the unknown acid by washing with ether and recrystallization from water/methanol.

None of the haptens inhibited cholinesterase activity at 200 ppm when tested with a commercial kit (Enzytec Inc.). This contrasts with the parent pesticides which gave 100% cholinesterase inhibition at concentrations ranging from 0.3 to 2.0 ppm. No deterioration has been observed when haptens were stored dry at 4 °C for 2 years.

Production of Antibodies to Haptens. The carboxyl function on haptens **9**, **11**, **13**, **15–17**, **19**, and **21** was activated to a succinimidyl ester (Langone and Vanakis, 1975) and coupled to free amines on ovalbumin (OVA) or mouse serum albumin (MSA) to produce antigens with which to immunize mice or to use as plating antigens for enzyme-linked immunoassays (ELISAs), respectively.

Using this procedure, conjugates were prepared with the degree of coupling between being 8 and 20 mol of hapten per mole of OVA and 12–30 mol of hapten per mole of MSA. OVA immunoconjugates of haptens were injected into mice, and the resulting antisera were assessed in an ELISA format as described in Materials

and Methods. In all cases, immunization resulted in the production of antisera recognizing haptens conjugated to MSA. No reaction was observed when preimmune sera were reacted with MSA-haptens or when sera from immunized mice were tested against MSA. Thus, a specific reaction to the hapten was apparent.

Optimal plating concentrations of MSA-hapten and sera dilution of individual mice to give an absorbance at 492 nm of 0.8–1.2 were established for each antigen by checkerboard titration. Competition, defined as the inhibition of binding of antibody to microwell plates as a result of incubation with organophosphate pesticide or hapten, was observed in all experiments for the pesticide resembling the hapten (i.e., chlorpyrifos for the chlorpyrifos hapten) used to immunize mice. Within a particular assay, variation was observed between mice in the I_{50} and in the useful range (I_{20} – I_{80}) for measuring of organophosphate, with specific results as follows.

(a) *Chlorpyrifos Immunoconjugate*. The optimal dilutions of MSA-hapten were 25, 90, 50, and 25 ng/mL and of sera 1/32000, 1/64000, 1/32000, and 1/32000 for mouse **1–4**, respectively. I_{50} , I_{20} , and I_{80} for chlorpyrifos using mouse **1** and **2** sera were 300 ng/mL, 60 ng/mL, and 1.5 μ g/mL and mouse **3** and **4** sera 150, 25, and 860 ng/mL, respectively. Competition was not measurable at concentrations of paraoxon, parathion, and azinphos-methyl up to 200 μ g/mL. The chlorpyrifos hapten had an I_{50} of 20 ng/mL; I_{20} = 1 ng/mL and I_{80} = 100 ng/mL for all mice.

(b) *Parathion Immunoconjugate*. The optimal dilutions of MSA-hapten were 25, 25, 50, and 50 ng/mL and of sera 1/32000, 1/64000, 1/32000, and 1/64000 for mouse **1–4**, respectively. I_{50} , I_{20} , and I_{80} for parathion using mouse **1** serum were 1.2 μ g/mL, 80 ng/mL, and 16 μ g/mL, using mouse **2** serum were 800 ng/mL, 60 ng/mL, and 11 μ g/mL, using mouse **3** serum were 4 μ g/mL, 300 ng/mL, and 31 μ g/mL, and using mouse **4** serum were 2.1 μ g/mL, 350 ng/mL, and 33 μ g/mL, respectively. For all mouse sera, no competition was observed with chlorpyrifos and azinphos. Paraoxon showed cross reactivities of 0.6 and 0.4% for mouse **1** and **2**, respectively, and no cross reaction for mouse **3** and **4** sera. Competition with parathion hapten gave an I_{50} of 20–25 ng/mL, an I_{20} of 1–2 ng/mL, and an I_{80} of 80–100 ng/mL.

(c) *Paraoxon Immunoconjugate*. The optimal dilutions of MSA-hapten were 200, 150, 25, and 25 ng/mL and of sera 1/16000, 1/32000, 1/8000, and 1/16000 for mouse **1–4**, respectively. I_{50} , I_{20} , and I_{80} for paraoxon using mouse **1** serum were 8.1, 1.2, and 46 μ g/mL, using mouse **2** serum were 2.2 μ g/mL, 710 ng/mL, and 105 μ g/mL, using mouse **3** serum were 8, 1.2, and 43 μ g/mL, and using mouse **4** serum were 2 μ g/mL, 200 ng/mL, and 23 μ g/mL, respectively. No cross reaction was observed for any sera from mice injected with paraoxon-hapten immunoconjugates, with parathion, chlorpyrifos, or azinphos-methyl or -ethyl. The paraoxon hapten gave an I_{50} of 20 ng/mL, an I_{20} of 2 ng/mL and an I_{80} of 100 ng/mL.

(d) *Azinphos Immunoconjugate*. The optimal dilutions of MSA-hapten were 25, 12.5, 25, and 25 ng/mL and of sera 1/64000 for mouse **1–4**, respectively. I_{50} , I_{20} , and I_{80} for azinphos-methyl using mouse **1** and **3** sera were 4 μ g/mL, 400 ng/mL, and 30 μ g/mL, using mouse **2** serum were 20 μ g/mL, 800 ng/mL, and 120 μ g/mL, and using mouse **4** serum were 800 ng/mL, 20 ng/mL, and 34 μ g/mL. Chlorpyrifos and paraoxon showed no cross reaction. Parathion showed cross reaction at 1–2% azinphos-methyl. Azinphos-ethyl was slightly more competitive than azinphos-methyl. For the azinphos hapten, I_{50} ranged from 6 to 10 ng/mL, I_{20} from 1 to 2 ng/mL, and I_{80} from 60 to 100 ng/mL.

(e) *Demeton Immunoconjugate*. The optimal dilutions

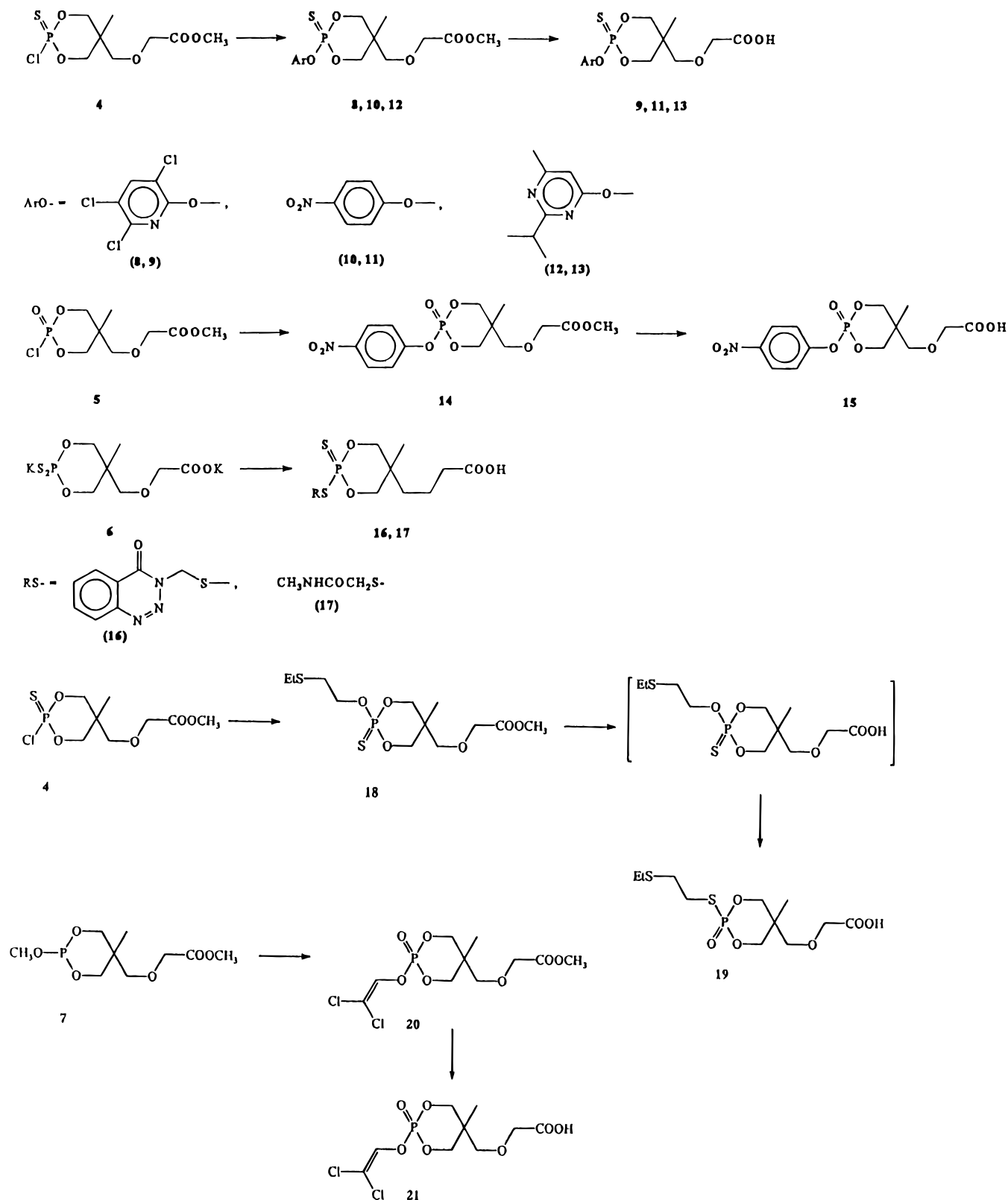


Figure 2. Overall synthetic scheme for organophosphate haptens.

of MSA-hapten were 25, 200, 50, and 50 ng/mL and of sera dilution of 1/32000, 1/64000, 1/128000, and 1/32000 for mouse 1–4, respectively. I_{50} , I_{20} , and I_{80} for demeton using mouse 1 and mouse 4 sera were 20 μ g/mL, 800 ng/mL, and 120 μ g/mL, using mouse 3 serum were 66, 7, and >200 μ g/mL, and using mouse 2 serum were 20.0, 1.8, and 80.0 μ g/mL, respectively. For the demeton hapten, I_{50} ranged from 10 to 20 ng/mL, I_{20} from 2 to 6 ng/mL, and I_{80} from 80 to 150 ng/mL.

(f) *Dimethoate Immunoconjugate.* The optimal dilutions of MSA-hapten were 500, 250, 500, and 500 ng/mL and of sera dilution 1/32000, 1/10000, 1/64000, and 1/64000 for mouse 1–4, respectively. I_{50} , I_{20} , and I_{80} for dimethoate using mouse 1–3 sera were 45, 6, and 180 μ g/mL and using mouse 4 serum were 66, 7, and >200 μ g/mL, respectively. For the dimethoate hapten, I_{50} ranged from 20 to 30 ng/mL, I_{20} from 4 to 10 ng/mL, and I_{80} from 90 to 150 ng/mL.

(g) *Dichlorvos Immunoconjugate*. The optimal dilutions of MSA-hapten were 90, 250, 500, and 500 ng/mL and of sera 1/32000 for mouse 1–4, respectively. I_{50} , I_{20} , and I_{80} for dichlorvos using mouse 1, 2, and 4 sera were 80, 12, and >200 μ g/mL and using mouse 3 serum were 200, 35, and >200 μ g/mL, respectively. For the dichlorvos hapten, I_{50} ranged from 20 to 40 ng/mL, I_{20} from 5 to 15 ng/mL, and I_{80} from 90 to 180 ng/mL.

(h) *Diazinon Immunoconjugate*. The optimal dilutions of MSA-hapten were 250, 500, 250, and 250 ng/mL and of sera 1/25000, 1/12800, 1/25000, and 1/25000 for mouse 1–4, respectively. I_{50} , I_{20} , and I_{80} for diazinon using mouse 1 serum were 2.1 μ g/mL, 250 ng/mL, and 15 μ g/mL, using mouse 2 serum were 1.4 μ g/mL, <45 ng/mL, and 10.2 μ g/mL, using mouse 3 serum were 750 ng/mL, 70 ng/mL, and 9 μ g/mL, and using mouse 4 serum were 750 ng/mL, 130 ng/mL, and 8 μ g/mL, respectively.

DISCUSSION

Development of an immunoassay for a small hapten requires covalent attachment of the hapten to an immunogenic carrier protein to generate reagent antibodies. The small molecule may already have a functional group that can be conjugated to the carrier, but frequently, a derivative of the hapten must be synthesized for conjugation to occur (Van Emon *et al.*, 1985). The nature of the linker arm and its position on the organophosphate hapten molecule will affect the specificity of the antibody and the ability of the free hapten to react with the antibody, although invariably, the hapten–protein immunoconjugate does react with the antibody.

Antibodies generated to hapten–protein immunoconjugates must therefore be tested to show that they react with the free hapten, with the parent organophosphate, as well as with the immunoconjugate. Antibodies must also be tested for their specificity; i.e., do they cross react with other small molecules having some of the common structural features found in the hapten used for immunization. Generally, the specificity of the antibody is highest for that part of the molecule most distal to the site of conjugation (Nugent, 1992).

We have described the syntheses of four novel generic intermediates that can be used to prepare organophosphate haptens of the phosphate, phosphorothioate, and phosphorodithioate groups. The generic intermediates are based on the dioxaphosphorinane ring and contain a protected carboxylic function which, after synthesis of the protected hapten, can be deprotected under mild conditions to yield stable haptens. Since the carboxyl group, which is used to couple the hapten to the carrier protein, is located distal to the unique functions of the hapten, we have synthesized hapten conjugates that should favor the production of antibodies that possess a high degree of specificity for individual organophosphate pesticides.

Mice immunized with the OVA-hapten conjugates elicited a strong immune response, resulting in antibodies of high titer to the corresponding MSA-hapten immunoconjugates. Furthermore, results indicated that a proportion of the antibody mixture recognized the parent organophosphate pesticide as well as the conjugated and unconjugated haptens. In all cases, under the conditions used, the unconjugated hapten was more effective in competing than was the parent pesticide, indicating that the dioxane ring of the linker arm plays a role in the structure of the epitope recognized by the major species of antibody present in polyclonal sera. It was further noticeable that haptens containing aromatic or heterocyclic structures produced polyclonal sera that were inhibited by lower concentrations of the corresponding pesticide than sera prepared from haptens containing

smaller aliphatic chains. Presumably, in these cases, the dioxane ring may play a more important role in filling the paratope of the major species of immunoglobulin present in the polyclonal sera.

The aim of the research reported in this paper was to show the applicability of our synthetic schemes, based on “generic” intermediates, in preparing haptens suitable for preparing antibodies to all classes of organophosphate pesticides. We have therefore given eight examples from the diverse groups of phosphates, thiophosphates, and dithiophosphates containing aliphatic, aromatic, and heterocyclic esters and shown that in each case the hapten conjugates are immunogenic and mice produce sera containing antibodies that recognize the parent pesticide. Although the concentrations of pesticide required to inhibit 50% binding of sera to MSA-hapten conjugates were in the nanogram to microgram per milliliter range and possibly of too low a sensitivity to be of use for developing polyclonal sera-based immunoassays for detection of organophosphates, we have recently been able to prepare hybridoma cell lines from the mice described in this paper, which secrete monoclonal antibodies (MAbs) to chlorpyrifos, parathion, diazinon (W. T. Jones and G. B. Ryan, unpublished results), and azinphos (Jones *et al.*, 1995) that can be used to develop sensitive assays. In our experience, 10–20% of hybridomas secreting antibodies to the hapten conjugate also recognize the parent pesticide in a competitive ELISA and it has been possible to select high-affinity antibodies with minimal cross reactivity to other organophosphates. For example, we recently described (Jones *et al.*, 1995) the production of monoclonals to azinphos, which only showed cross reactivity between azinphos-methyl and -ethyl and were able to develop an ELISA with a limit of detection of 80 pg/mL. We have also prepared monoclonal antibodies to the parathion hapten and easily been able to select high-affinity antibodies, some of which recognize also paraoxon while others show no cross reactivity to paraoxon, to chlorpyrifos which showed 0.4% cross reactivity to fenitrothion but no detectable cross reactivities to other pesticides and to diazinon, which gave 0.1 and 0.25% cross reactivity with etrimfos- and pyrimifos-methyl, respectively, but no detectable reactions to other pesticides (W. T. Jones and G. B. Ryan, unpublished results). Thus, in all cases, we have been able to select MAbs that when used in ELISAs resulted in greater sensitivity (limit of detection in the picogram per milliliter range) and higher specificity for the organophosphate pesticide than the corresponding polyclonal sera.

We have therefore described the synthesis of four generic heterobifunctional intermediates that can be used to prepare suitable haptens for preparing antibodies for the development of sensitive and highly specific immunoassays for individual organophosphates of phosphate, monothioate, and dithioate classes. Furthermore, the stability and undetectable level of cholinesterase inhibition are important features of the hapten and the protein conjugates in considering their usage in the development of immunoassay kits (Nugent, 1992).

MATERIALS AND METHODS

Bovine serum albumin (BSA), ovalbumin (OVA), Tween-20, horseradish peroxidase (HRP), peroxidase-labeled sheep anti-mouse IgG (γ chain specific), α -phenylenediamine (OPD), and succinimidylpyridyldithiopropionic acid (SPDP) were obtained from Sigma Chemical Co. (St. Louis, MO). *N*-Hydroxysuccinimide (NHS) and *N*-ethyl-*N*-[3'-(dimethylamino)propyl]carbodiimide hydrochloride (EDC) were from Pierce Ltd. (Rockford, IL). MicroELISA flat bottom F16 modules (Maxisorb) were obtained from

Nunc (Roskilde, Denmark). Pesticides were purchased from Chem Services (West Chester, PA). All other reagents and solvents used in the synthesis of haptens were reagent grade, and all other solvents used in other procedures were of analytical grade or better. NMR spectra were recorded on a 60 or 200 MHz spectrophotometer.

Synthesis of Haptens. *5-(Hydroxymethyl)-2,2,5-trimethyl-1,3-dioxane.* A mixture of 2-(hydroxymethyl)-2-methyl-1,3-propanediol (240 g, 2 mol), acetone (120 g, 2 mol), a few crystals of *p*-toluenesulfonic acid, and benzene (800 mL) was heated under reflux for 24 h with azeotropic removal of water. The reaction mixture was concentrated by rotary evaporation, and the residue purified by bulb-to-bulb distillation, to yield 288.8 g (1.805 mol, 90%) of the desired alcohol **1**, with a bp of 80 °C (0.2 mmHg). ¹H-NMR (CDCl₃): δ 0.8 (s, 3H), 1.35 (s, 3H), 1.40 (s, 3H), 3.5–3.7 (m, 6H).

2-(2,2,5-Trimethyl-1,3-dioxan-5-yl)methoxyacetic Acid, Methyl Ester. Alcohol (**2**, 285 g, 1.78 mol) dissolved in 200 mL of DMF was added to sodium hydride (157 g, 55–65% in mineral oil, washed twice with 300 mL of hexane) in 800 mL of DMF. The reaction mix was cooled in ice/water to maintain the temperature of 10–25 °C and stirred for 3 h at RT. Bromoacetic acid (249 g, 1.79 mol) in DMF (500 mL) was added over a 2 h period with ice cooling and mechanical stirring to maintain the temperature at 16–22 °C. The reaction mixture solidified, and DMF (1 L) was added and the suspension stirred overnight at RT.

The mixture was warmed to 30 °C and stirred for a further 2 h at 37 °C. Dimethyl sulfate (210 mL, 2.22 mol) was added and the mixture maintained at 30–35 °C for 2 h, cooling where necessary, in ice. The suspension was stirred for 5 h at RT and rotary evaporated to remove most of the DMF.

Water (1 L) and toluene (1 L) were added to the residue; the mixture was shaken, and the layers were allowed to separate. The aqueous layer was extracted with 750 mL of toluene, and the combined toluene layers were washed with 2 × 1 L of water. The toluene layer was dried and evaporated. The residue was purified by bulb-to-bulb distillation to yield 240.2 g (1.035 mol, 58%) of the desired product **2**. ¹H-NMR (CDCl₃): δ 0.85 (s, 3H), 1.35 (s, 3H), 1.40 (s, 3H), 3.5–3.7 (AB, *J* = 12 Hz, 4H), 3.5 (s, 2H), 3.7 (s, 3H), 4.1 (s, 2H). ¹³C-NMR (CDCl₃): δ 17.9, 20.7, 26.6, 34.3, 51.6, 66.2, 68.7, 74.5, 97.8, 170.9.

2-[3-Hydroxy-2-(hydroxymethyl)-2-methylpropoxy]acetic Acid, Methyl Ester. Pyridinium *p*-toluenesulfonate (6.9 g, 27.5 mmol) was added to a solution of the acetal ester **2** obtained above (96.0 g, 0.414 mol) in 450 mL of methanol, followed by 120 mL of water. The solution was stirred for 4 h, during which time a total of 400 mL water was added in 100 mL portions. The resulting solution was rotary evaporated, and 100 mL of toluene was added to the residue. This solution was rotary evaporated, and a further 100 mL of toluene was added. Rotary evaporation of this solution yielded 90 g of the desired product **3**. ¹H-NMR (CDCl₃): δ 0.8 (s, 3H), 3.4 (s, 2H), 3.5 (s, 4H), 3.6 (s, 2H), 3.7 (s, 3H), 4.1 (s, 2H).

*2-(2-Chloro-5-methyl-1,3,2-dioxaphosphorinan-5-yl)methoxyacetic Acid, Methyl Ester, *p*-Sulfide.* The crude diol **3** obtained above (27.3 g, containing 3.1 g of pyridinium *p*-toluenesulfonate) was dissolved in 100 mL of toluene, and to this was added pyridine (25 mL, 0.316 mol). The mixture was cooled to 10–15 °C, and thiophosphoryl chloride (distilled, 26 g, 0.153 mol) was then added over a 3 min period (the temperature of the mixture was allowed to rise to 25–30 °C). The suspen-

sion was stirred overnight at RT. Water (250 mL) and toluene (100 mL) were then added; the resultant mixture was shaken, and the layers were separated. The organic layer was then washed with 250 mL of water, and the aqueous layers were extracted with 100 mL of toluene. The combined toluene layers were then dried over sodium sulfate and rotary evaporated. The resultant residue was dissolved in a small amount of toluene and filtered over a column of aluminum oxide (5 × 3 cm), and the product eluted from this column with toluene. The filtrate was evaporated and the residue stirred overnight with a mixture of 30 mL of ether and 30 mL of ligroin (bp of 40–60 °C). After cooling to –10 °C for 2 h, the suspension was filtered with suction and the solid phase then washed with a 2/3 mixture of ether and ligroin. This procedure yielded 12.95 g of the product **4** which, by NMR, appeared to be principally comprised of one isomer. The crystallization filtrate was then evaporated, leaving a residue of 12.72 g which, by NMR, appeared to be a 1/2 mixture of the crystalline and liquid isomers **4**. The total yield was 25.67 g (88.0 mmol, 71% yield based on acetal ester **2**). The crystalline isomer had singlets at δ 0.9, 3.7, and 4.1 ppm. Both isomers had multiplets in the δ 3.8–4.8 ppm region.

*2-(2-Chloro-5-methyl-1,3,2-dioxaphosphorinan-5-yl)methoxyacetic Acid, Methyl Ester, *p*-Oxide.* The oxygen analogue **5** was prepared in a manner identical to the preparation of **4**, using phosphoryl chloride in place of thiophosphoryl chloride. After filtration of the crude product over aluminum oxide, and evaporation of the toluene eluate, the product (21.8 g, 80 mmol, 63% yield based on the acetal ester **2**) was obtained as an oily mixture of two isomers **5**. Attempted purification through vacuum distillation resulted in almost complete decomposition. ¹H-NMR (CDCl₃): δ 1.0 (s), 1.3 (s) (ratio of about 2/1), 3.3–4.7 (m) with singlets at 3.4, 3.7, and 4.1.

*2-(2-Mercapto-5-methyl-1,3,2-dioxaphosphorinan-5-yl)methoxyacetic Acid, Bispotassium Salt, *p*-Sulfide.* Diol **3** (35.4 g, 0.184 mol) (see above) was dissolved in 300 mL of toluene. Phosphorus pentasulfide (35.4 g, 0.144 mol) was then added and the suspension stirred first for 1 h at 60–70 °C, then overnight at RT, and finally at 80–90 °C for 3 h (most of the phosphorus pentasulfide dissolved during the heating process). The mixture was then vacuum filtered, and the solids were washed with toluene. The filtrate was evaporated, and 200 mL of methanol was added to the residue, followed by the addition of 30 g of potassium hydroxide in 100 mL of methanol over a 15 min period (with cooling, the temperature was allowed to rise to approximately 35 °C). The resultant suspension was filtered under vacuum and the solid phase washed with methanol. The yield was 31.9 g (91.7 mmol, 56% based on the acetal ester **2**) of the colorless bispotassium salt **6**. This product was then recrystallized from a mixture of ethanol and water. ¹H-NMR (D₂O): δ 1.0 (s, 3H), 3.5 (s, 2H), 3.9, 4.0 (s, 4H), 4.25 (s, 2H).

(2-Methoxy-5-methyl-1,3,2-dioxaphosphorinan-5-yl)methoxyacetic Acid, Methyl Ester. The acetal ester **2** (42 g, 0.181 mol) was converted to diol **3** in the usual way using 200 mL of methanol, 2.1 g of pyridinium *p*-toluenesulfonate, and 240 mL of water. The resultant diol was stirred with 400 mL of toluene, 33 g of trimethyl phosphite (0.266 mol), and 16 drops of triethylamine for 3 days [see Edmundson *et al.* (1985) for a similar procedure]. After rotary evaporation at 300 mmHg and 40 °C, the residue was washed with 2 × 100 mL of water, dried, and evaporated. The residue was then purified by bulb-to-bulb distillation at 0.1 mmHg to give 28.21 g of the pure product **7** (0.112 mol, 62%). ¹H-NMR (CCl₄):

δ 0.75 s and 1.2 s (ratio of 2/1), 3.1–4.7 (m) with singlets at 3.3, 3.5, 3.6, and 4.0.

2-[5-Methyl-2-(3,5,6-trichloropyridin-2-oxy)-1,3,2-dioxaphosphorinan-5-yl]methoxyacetic Acid, *p*-Sulfide (*Chlorpyrifos Hapten*). DMF (50 mL) was first added to sodium hydride in mineral oil (50–55%, 1.94 g, 44.4 mmol, washed twice with 40 mL of ligroin), after which trichloropyridinol (9.2 g, 46.3 mmol) was added in portions over 10 min. After the mixture was stirred for 30 min, the crystalline isomer **4**, obtained above, was added (10.15 g, 35.18 mmol), followed by an additional 10 mL of DMF. After being stirred for 3 days at RT, the mixture was poured into 500 mL of water (containing 10 g of sodium bicarbonate). The product was then extracted with 500 mL and then 250 mL of chloroform, and the combined organic layers were first washed with 500 mL of water, dried, and evaporated. The residue, which solidified on standing, could be purified by stirring with a 1/1 mixture of ether and ligroin to yield a single isomeric product. ¹H-NMR (CDCl₃): δ 1.0 (s, 3H), 3.8 (s, 5H), 4.2 (s, 2H), 4.2–4.4 (m, 4H), 7.9 (s, 1H). ¹³C-NMR (CDCl₃): δ 16.1, 36.2, 51.7, 68.5, 71.8, 74.0, 121.0, 127.4, 141.1, 144.2, 150.2, 170.4. Similarly, from the oily mixture of chlorides **4**, a mixture of esters **8** was obtained. The more soluble isomer had singlets at δ 1.3, 3.3, 3.7, 3.9, and 7.9 ppm and a multiplet at δ 3.7–4.8 ppm.

THF (75 mL), followed by 75 mL of methanol, was added to the methyl ester **8** (15.0 g) obtained above. A solution of potassium carbonate (5.28 g, 38.3 mmol in 35 mL of water) was added over a period of 10 min, followed by the addition of 50 mL of water over a 15 min period. After the mixture was stirred for 2 h, 500 mL of water was added and the mixture then extracted first with 400 mL of a 3/1 mixture of toluene and ethanol and then with 300 mL of toluene, to remove the unreacted ester **8**. The combined aqueous layers were acidified by the addition of 10 mL of concentrated hydrochloric acid and then extracted with 4 \times 250 mL of toluene. The combined toluene layers were then dried and rotary evaporated to yield a residue which was dissolved in 100 mL of warm methanol. Water (about 60 mL) was added, followed by some seed crystals. After the mixture was stirred at RT for some time, the precipitate was collected by vacuum filtration. The precipitate **9** so obtained weighed 6.50 g and, on the basis of NMR, appeared to consist of a single isomer. Using the same procedure, a further 1.78 g of **9** was obtained from the filtrate. NMR revealed this product to consist of a 3/2 mixture of the more soluble and less soluble isomers. The total yield was 8.28 g (18.97 mmol, 54% yield based on chloride **4**). Similarly, from the oily mixture of chlorides **4** obtained above, the acid **9** was obtained (after the methanol/water purification) as a 5/2 mixture of the more soluble and less soluble isomers. ¹H-NMR (CDCl₃) for the less soluble isomer: singlets at δ 1.0 (3H), 3.7 (2H), 4.8 (2H), 7.8 (1H), 8.9 (1H, broad), multiplet at δ 3.8–4.9. ¹H-NMR (CDCl₃) for the more soluble isomer: singlets at δ 1.3, 3.4 (broad), 7.8, multiplet at δ 3.7–4.9.

2-[5-Methyl-2-(4-nitrophenoxy)-1,3,2-dioxaphosphorinan-5-yl]methoxyacetic Acid, *p*-Sulfide (*Parathion Hapten*). 4-Nitrophenol (3.00 g, 20 mmol) was added in 0.5 g portions to a mixture of sodium hydride (1.10 g, 50–55%, 22.9 mmol, washed twice with 30 mL of ligroin) and DMF (30 mL). After the mixture was stirred for 1 h, 5.15 g (20 mmol) of crystalline chloride **4** was added and the mixture stirred for 3 days at RT. The reaction mixture was then poured into 250 mL of a 4% sodium bicarbonate solution and the product extracted with 250 mL of toluene. Washing with 2 \times 250 mL of water followed by drying and evaporation gave the crude product as a 3/2

mixture of isomers (by NMR). Addition of 50 mL of ether yielded a solid which, after filtration and washing with ether, gave 2.07 g of methyl ester **10** (one isomer by NMR, major isomer in the crude product). Similarly, from 5.15 g of the oily mixture of chlorides **4** was obtained 1.59 g of a single isomer. The ether filtrates of both products were combined, evaporated, treated with 50 mL of ether and a small amount of ligroin, and then stored at –15 °C to give 3.45 g of product **10** (3/2 mixture of the more soluble and less soluble isomers). The total yield was 7.31 g (18.7 mmol, 47% yield). ¹H-NMR (CDCl₃) of the less soluble isomer: δ 1.0 (s, 3H), 3.7 (s, 5H), 4.1 (s, 4H), 4.1–4.35 (AB, *J* = 12 Hz, 2H), 7.1–8.2 (AB, *J* = 9 Hz, 4H). The more soluble isomer had a singlet at 1.3 ppm, and a complicated pattern in the 3.4–4.9 ppm range with singlets at 3.4, 3.7, and 4.0 ppm.

Sufficient THF (about 20 mL) was added to 3.66 g (9.36 mmol) of the single isomer ester **10** in methanol (70 mL) to completely solubilize the mixture. Lithium hydroxide (232 mg, 9.65 mmol) in 20 mL of 1/3 water/methanol was added with stirring over 30 min. This mixture was further stirred for 1 h and then poured into 500 mL of water. This solution was extracted with 250 mL of toluene, which was washed with 50 mL of water. The combined aqueous layers were acidified by the addition of 1.5 mL of concentrated hydrochloric acid and then extracted with 2 \times 250 mL of toluene. The combined toluene layers were dried and evaporated to give a solid residue, which was then stirred with ether. Subsequent filtration and washing with ether yielded 1.26 g of the free acid of the less soluble isomer **11**.

Similarly, 1.01 g of the more soluble isomer (isomer ratio of 2/1) was obtained from 3.45 g of the mixture of esters **10** (see above) after this mixture had been treated with ether. From the combined filtrates of both reactions, a further 0.79 g of an almost 1/1 mixture of isomers was obtained following treatment with ether. The total yield was 3.06 g (8.12 mmol, 43%). ¹H-NMR (CDCl₃) of the less soluble isomer: δ 1.0 (s, 3H), 3.6–4.6 (m), 3.8 (s), 4.2 (s, 8H), 7.5–8.6 (AB, *J* = 9 Hz, 4H). The more soluble isomer had singlets at δ 1.3, 3.45, and 4.1 ppm.

2-[5-Methyl-2-(2-isopropyl-6-methylpyrimidin-4-oxy)-1,3,2-dioxaphosphorinan-5-yl]methoxyacetic Acid, *p*-Sulfide (*Diazinon Hapten*). DMF (30 mL), followed by 2-isopropyl-6-methyl-4-pyrimidinol (4.7 g, 30.9 mmol) added in portions over 5 min, was added to sodium hydride in mineral oil (50–55%, 1.13 g, 25.9 mmol, washed twice with pentane). After the mixture was stirred for 4 h, crystalline isomer **4** (6.8 g, 23.6 mmol) was added and the mixture stirred for a further 2 days at RT. The resultant mixture was then added to 300 mL of sodium carbonate and 500 mL of toluene and the solution mixed. The layers were separated, and the toluene phase was back washed with 300 mL of water, dried, and evaporated. The oily residue, ester **12**, was dissolved in 150 mL of 1/1 THF/MeOH.

Aqueous sodium carbonate (5.5 g in 50 mL of water) was added with stirring for 30 min. Water (50 mL) was added and the mixture stirred for a further 4 h followed by the addition of another 300 mL of water. The mixture was extracted with 2 \times 300 mL of toluene, and the toluene layer was back washed with 250 mL of water. The combined aqueous layers were acidified by the addition of concentrated hydrochloric acid (10 mL) and then extracted with 3 \times 250 mL of toluene. The toluene was dried and evaporated and the residue stirred overnight with ether (50 mL). The residue was then filtered and washed with ether to yield the desired product **13** (4.31 mmol, 18% yield based on chloride **4**). ¹H-NMR (CDCl₃): δ 1.0 (s, 3H), 1.35 (s, 3H), 1.4 (s, 3H), 2.6 (s,

3H), 3.2 (m, 1H), 3.8 (s, 2H), 4.2–4.5 (m, 6H), 4.25 (s, 6H), 6.9 (s, 1H).

2-[5-Methyl-2-(4-nitrophenoxy)-1,3,2-dioxaphosphorinan-5-yl]methoxyacetic Acid, p-Oxide (Paraoxon Hapten). 4-Nitrophenol (10.2 g, 73.4 mmol) was added over a 10 min period to a mixture of sodium hydride (3.14 g, 50–55%, 72 mmol, washed twice with 40 mL of ligroin) and 75 mL of DMF. After the mixture was stirred for an additional 30 min, chloride **5** (16.9 g, 62.0 mmol) in 20 mL of DMF was added. This mixture was stirred for 3 days at RT and then poured into 500 mL of 2% sodium bicarbonate solution. The product was extracted with 500 mL of toluene and the toluene layer washed with 2 × 500 mL of water, dried, and evaporated. Ether (100 mL) was then added to the residue (which consisted of two methyl ester isomers in a 3/2 ratio) and the mixture stirred for 2 h. The solid was then filtered off and washed with ether to give 12.6 g of material principally comprised of the less soluble major isomer **14**. Evaporation of the filtrate left 7.94 g of material, the major constituent of which was the other isomer. The total yield was 20.54 g of methyl ester **14** (54.8 mmol, 88%). ¹H-NMR (CDCl₃) of the less soluble isomer: δ 1.0 (s, 3H), 3.7 (s, 5H), 3.9–4.8 (m, 6H), 4.15 (s, 6H), 7.2–8.3 (AB, *J* = 9 Hz, 4H). ¹H-NMR (CDCl₃) of the more soluble isomer: δ 1.3 (s, 3H), 3.4 (s, 2H), 3.7 (s, 3H), 3.9–4.9 (m, 6H), 4.0 (s, 6H), 7.2–8.3 (AB, *J* = 9 Hz, 4H).

Methanol (100 mL) was added to a solution of ester **14** (10.1 g, 26.9 mmol, less soluble isomer) in 160 mL of THF. This was followed by the dropwise addition of a solution of potassium carbonate (4.20 g, 30.4 mmol) in 50 mL of water over a 15 min period. A further 100 mL of water was subsequently added over a 5 min period. After being stirred at RT for 90 min, the reaction mixture was poured into 750 mL of water. Extraction with 2 × 300 mL of toluene, followed by washing of the combined toluene layers with 150 mL of water, removed unreacted ester **14**. The combined aqueous layers were acidified by the addition of about 6 mL of concentrated hydrochloric acid and then extracted with 3 × 300 mL of toluene. Drying and rotary evaporation of these toluene layers yielded a solid residue which was then stirred with a small amount of ether. Subsequent filtration and washing with ether gave 4.70 g of the acid **15** (13.0 mmol, 48% yield). ¹H-NMR (CDCl₃/DMSO-*d*₆): δ 0.95 (s, 3H), 3.7 (s, 2H), 3.9–4.6 (m, 6H), 4.05 (s, 6H), 7.2–8.2 (AB, *J* = 9 Hz, 4H).

2-[5-Methyl-2-[[4-oxo-1,2,3-benzotriazin-3(4H)-yl]thio]-1,3,2-dioxaphosphorinan-5-yl]methoxyacetic Acid, p-Sulfide (Azinphos Hapten). Concentrated hydrochloric acid (3.3 g, 1.172 mmol) was added to a suspension of the bispotassium salt **6** (11.0 g, 31.6 mmol) in 100 mL of methanol followed by 30 mL of water. The resulting clear solution was evaporated completely, and the residue was dissolved in absolute ethanol (100 mL) by warming the stirred suspension. Toluene (100 mL) was added and the mixture evaporated to dryness. Toluene (100 mL) was added to the residue and the mixture rotary evaporated again. The solid residue was dissolved in acetone (100 mL), and 3-(chloromethyl)-1,2,3-benzotriazin-4(3*H*)-one [6.13 g, 31.36 mmol, prepared according to Lorenz (1957)] was added. The mixture was stirred for 64 h at RT and evaporated. The residue was stirred with a mixture of potassium carbonate (6.0 g, 43.5 mmol), water (150 mL), and toluene (150 mL). The aqueous layer was extracted with toluene (250 mL), and the toluene layers were extracted with water (150 mL). The combined aqueous layers were acidified with concentrated hydrochloric acid (10 mL) and extracted with toluene (2 × 250 mL), washed with water (150 mL), dried, and evaporated to a viscous

oil which solidified on standing. The solid was stirred in ether, filtered, and washed with ether to give 6.08 g of the desired product **16** (45% yield based on **6**) as a 1/1 mixture of isomers. These isomers are probably the result of attack on either the axial sulfur or the equatorial sulfur atom in the dipotassium salt **6**. ¹H-NMR (CDCl₃) of **16** (a 1/1 mixture of isomers): δ 0.9 (s, 3H), 1.25 (s, 3H), 3.5 (s, 2H), 3.7 (s, 2H), 3.8–4.6 (m, 6H), 5.7 (s, 2H), 6.0 (s, 2H), 7.5–8.5 (m, 4H).

2-[5-Methyl-2-[[2-(methylamino)-2-oxoethyl]thio]-1,3,2-dioxaphosphorinan-5-yl]methoxyacetic Acid, p-Sulfide (Dimethoate Hapten). Hydrochloric acid (4.21 g, 40.5 mmol), followed by 30 mL water, was added to a suspension of the bispotassium salt **6** (14.67 g, 42.16 mmol). The resultant solution was evaporated to dryness, the residue resuspended in absolute ethanol (100 mL), and the suspension warmed and then re-evaporated to dryness. Toluene (100 mL) was added to the residue, and the suspension was again evaporated. This procedure was repeated one more time. Acetone (100 mL), followed by *N*-methylchloroacetamide (5.05 g, 46.98 mmol), was then added to the residue; the mixture was stirred for 3 days at RT and then evaporated. Potassium carbonate (8.80 g) in water (250 mL), followed by 250 mL of toluene, was added to the residue. After the mixture was stirred for 15 min, the layers were separated, the aqueous layer was extracted with 250 mL of toluene, and the combined organic layers were washed with 100 mL of water. To the combined aqueous layers was added 17 mL of concentrated hydrochloric acid, and the resulting mixture was extracted with 3 × 200 mL of chloroform. The chloroform layers were dried and evaporated to leave 8.2 g of residue. Concentrated ammonia (5 mL) was added to the residue and the solution evaporated to dryness. Acetone was added to the residue; the mixture was stirred, and the resulting solid (the ammonium salt of **17**) was filtered off and washed with acetone. This gave 2.77 g of product (single isomer by NMR, apparently only one of the two possible isomers is formed or one of the two possible isomers is much less soluble than the other isomer), which was then dissolved in 100 mL of water. Concentrated hydrochloric acid (2 mL) was added and the mixture extracted with 3 × 100 mL of chloroform. Drying and evaporation left a residue from which, on stirring with ether, the pure acid **17** was precipitated. Subsequent filtration and washing yielded 1.765 g (5.15 mmol, 12% based on **6**). ¹H-NMR (CDCl₃): δ 1.0 (s, 3H), 2.8 (s, 3H), 2.9 (s, 3H), 3.4 (s, 2H), 3.7 (s, 2H), 3.6 (s, 2H), 3.8–4.6 (m, 6H), 4.1 (s, 6H), 6.5 (broad s, 1H), 9.3 (s, 1H).

2-[2-[[2-(Ethylthio)ethyl]thio]-5-methyl-1,3,2-dioxaphosphorinan-5-yl]methoxyacetic Acid 17, p-Oxide (Demeton Hapten). *n*-Butyllithium (18 mL, ca. 2.25 M in hexanes, 40.5 mmol) was added over 5 min to an ice-cooled solution of ethylthioethanol (4.26 g, 40 mmol) in 50 mL of THF. The suspension was stirred for 1 h at RT and cooled with ice, and the acid chloride **4** (mixture of isomers, 11.60 g, 40.2 mmol), dissolved in 15 mL of THF, was then added over 10 min. This mixture was stirred overnight at RT and poured into 250 mL of water, and the product was extracted with 2 × 200 mL of toluene. The combined toluene layers were washed with 3 × 100 mL of water, dried, and evaporated. The residue, **18**, was then dissolved in a mixture of 100 mL of methanol and 100 mL of THF. A solution of 5.50 g of potassium carbonate (39.9 mmol) in 50 mL of water was added over 10 min, followed by the addition of 100 mL of water over 30 min. This solution was then stirred for 3 h at RT, poured into 500 mL of water, and extracted with 2 × 250 mL of chloroform (some sodium chloride being added). The combined chloroform layers were washed with 2 × 100 mL of water

(some ethanol being added). The combined aqueous layers were acidified by the addition of 10 mL of concentrated hydrochloric acid and then extracted with 3 × 250 mL of chloroform. After drying and evaporation, a residue was obtained which was then stirred in 50 mL of toluene at RT for 10 days (this allowed slow isomerization from the sulfide to the oxide). The solution was evaporated and the residue stirred for a further 2 days at RT with ether to precipitate the desired **19** (one isomer precipitates). Filtration and washing with ether afforded a final yield of 350 mg of **19** (1.02 mmol, 2.5% based on acid chloride **4**). ¹H-NMR (CDCl₃): δ 1.0 (s, 3H), 1.3 (t, *J* = 7 Hz, 3H), 2.3–3.4 (m, 6H), 3.7 (s, 2H), 3.9–4.6 (m, 6H), 4.0 and 4.1 (s, 6H), 9.6 (1H).

2-[2-[(2,2-Dichloroethenyl)oxy]-5-methyl-1,3,2-dioxaphosphorinan-5-yl]methoxyacetic Acid, p-Oxide (Dichlorvos Hapten). The phosphite **7** obtained above was dissolved in 150 mL of toluene and 20.0 g of chloral (0.136 mol) in 25 mL of toluene added over a 15 min period with ice cooling. The solution was first stirred for 1 h at 0–10 °C and then for 3 h at RT, after which time it was evaporated to dryness, leaving as a residue the crude methyl ester **20**. ¹H-NMR (CCl₄): δ 1.0 and 1.3 (s, 3H, ratio of 1/2), 3.2–4.7 (m) and singlets at 3.3, 3.7, 4.0, and 4.1 (11H), 7.0 (d, *J* = 6 Hz, 1H). The crude ester was dissolved in a mixture of 100 mL of THF and 150 mL of methanol, and a solution of 15.0 g of potassium carbonate (0.109 mol) in 100 mL of water was then added in 10 min. A further 100 mL of water was added over 15 min and the mixture then stirred at RT for 3 h. Water (500 mL) was added and the mixture extracted with 2 × 250 mL of chloroform. The organic layers were washed with 250 mL of water. The chloroform layers contained impurities and starting ester. Chloroform (250 mL) was added to the combined aqueous layers, followed (with stirring) by 25 mL of concentrated hydrochloric acid. The layers were separated, and the aqueous layer was extracted with 2 × 250 mL of chloroform. Drying and evaporation yielded 11.6 g of crude product which was then stirred with 100 mL of ether to give a colorless solid. Filtration and washing with ether afforded 5.17 g of a mixture of **21** and an unknown acid which did not contain (NMR) a vinyl proton. Evaporation of the filtrate yielded crude **21** which was dissolved in 25 mL of methanol. Water (40 mL) was added dropwise with stirring, upon which pure **21** crystallized (the unknown acid proved to be much more soluble in water/methanol than **21**). Filtration and washing with water/methanol (3/1) yielded 2.10 g (6.27 mmol, 6% based on the phosphite **7**, mainly one isomer) of pure **21**. Repetition of the latter procedure gave one isomer of **21**. ¹H-NMR (CDCl₃): δ 1.3 (s, 3H), 3.4 (s, 2H), 3.8–4.8 (m, 8H), 4.0 (s, 8H), 7.0 (d, *J* = 5 Hz, 1H), 9.5 (broad s, 1H).

Synthesis of Hapten–Protein Conjugates. The haptens were conjugated to carrier proteins MSA and OVA using the active ester procedure (Langone and Van Vunakis, 1975). Briefly, the hapten (0.2 mM) was dissolved in 1 mL of dimethylformamide (DMF), and to this were added 30 mg of NHS and 40 mg of EDC; the mixture was stirred for 2 h at RT to convert the carboxyl group into the succinimidyl ester function. MSA (60 mg) or OVA (40 mg) was dissolved in 1.8 mL of distilled water, cooled in ice and DMF (1.2 mL) slowly added to the dissolved protein in stirred reactivials (Pierce Chemicals). The hapten–NHS esters (50 μL) were added to the protein solutions and incubated overnight at 4 °C. The reaction mixture was dialyzed exhaustively against distilled water and stored at –70 °C in aliquots. The number of moles of hapten per mole of protein was determined using protein estimation (Bradford, 1976)

and phosphorus (atomic absorption spectroscopy) to determine the moles of conjugated hapten.

Anti-Cholinesterase Activity of Haptens and Organophosphate Pesticides. Organophosphate pesticides and their haptens were tested for their ability to inhibit cholinesterase activity using a pesticide biosensor detector kit (Enzytec Inc., Kansas City, MO). The lowest concentration to inhibit a positive reaction was determined for each test molecule using the manufacturer's protocol.

Immunization of Mice. Female mice (Balb/c PN X DBA, four mice) 6–8 weeks old were immunized at intraperitoneal (IP) and subcutaneous (SC) sites with 100 μg of OVA–hapten conjugates in complete Freund's adjuvant (CFA).

The mice received a further three immunizations at 28 day intervals of 50 μg of conjugate in incomplete Freund's adjuvant (IFA). Blood was taken from each mouse, prior to the first immunization (preimmune) and 10 days following the fourth immunization, and tested for antibodies against the hapten–MSA conjugates and the parent pesticide.

Micro-ELISA Procedures. Microtiter wells were coated with hapten–MSA conjugates for 3 h at 37 °C in phosphate-buffered saline (100 μL per well). BSA (2%) in phosphate-buffered saline (PBS) was used to block the remaining protein-binding sites on the microwell surface.

Stock solutions of pesticides and synthetic intermediates were prepared by dissolving the appropriate compound in methanol (10 mg/mL). Standard solutions (20 × working concentration) were prepared by dilution of the stock solution into methanol. Working standards (2 × final concentration; 3 ng/mL to 200 μg/mL) were prepared by diluting 1 mL of the standard solutions with 9 mL of dilution buffer [PBST (PBS and 0.1% Tween-20) containing 2% BSA].

Optimal conditions for ELISA (Jones *et al.*, 1992) were determined by varying the incubation time and reagent concentrations. Between additions of reagents, the plates were washed six times with PBST. Substrate (OPD, 40 mg of 100 mL citrate/phosphate buffer at pH 5.0 containing 40 μL of 30% H₂O₂; 200 μL/well) was added, and the plates were incubated at RT for 30 min. The peroxidase reaction was stopped by addition of 4 M sulfuric acid (50 μL/well), and the absorbance was measured at 492 nm (*A*₄₉₂) in a Dynatech MR 5000 plate reader with Biolinx 1.0 software (Dynatech Laboratories, Inc., Chantilly, VA).

Serum in dilution buffer (100 μL/well) was added to wells for 2 h at 37 °C. Antibodies to hapten conjugates were detected after incubation with peroxidase-labeled anti-mouse IgG (1/2000 in dilution buffer, 1 h, 37 °C) and addition of peroxidase substrate. Sera reacting with conjugate were further tested using a competitive ELISA for reactivity with pesticides. Plates were coated with hapten conjugates at minimal dilution to achieve an *A*₄₉₂ of <0.050 when incubated with peroxidase-labeled anti-mouse IgG (1/2000). Sera were diluted to determine the concentration which gives an absorbance of approximately 1.0 (*C*_{1.0}) when detected as described above.

Equal volumes of sera diluted to 2*C*_{1.0} and serial dilutions of pesticide, prepared as described above, were mixed and incubated at 37 °C for 1 h. These solutions (100 μL) were added to the microwells, coated with hapten conjugate, and incubated for 3 h at 37 °C. The wells were washed and incubated with peroxidase-labeled anti-mouse IgG (Sigma Chemicals Fc specific antibody at 1/2000 dilution, 100 μL/well) for 1 h at 37 °C. Wells were washed and developed with substrate as described above. Standard curves were generated, and the concentrations of pesticide inhibiting binding of sera to

microwell plate by 20% (I_{20}), 50% (I_{50}), and 80% (I_{80}) were determined. The percent cross reactivity was determined as the ratio of I_{50} for the parent pesticide divided by I_{50} for test compound $\times 100$.

LITERATURE CITED

- Aston, J. P., Britton, D. W., Wraith, M. J., and Wright, A. S. (1992) Enzyme-linked competitive immunoassay. In *Emerging Strategies for Pesticide Analysis* (T. Cairns and J. Sherma, Eds.) pp 309–329, CRC Press, London.
- Bradford, M. M. (1976) A rapid and sensitive method for the determination of microgram quantities of protein using the principle of protein-dye binding. *Anal. Biochem.* **72**, 248–254.
- Brimfield, A. A., Lentz, D. E., Graham, C., and Hunter, W. (1985) Mouse monoclonal antibodies against paraoxon: Potential reagents for immunoassays with constant immunochemical characteristics. *J. Agric. Food Chem.* **33**, 1237–1242.
- Centro, E. R., Johnson, W. J., and Sehon, A. H. (1970) Antibodies to two common pesticides, DDT and malathion. *Int. Arch. Allergy Appl. Immunol.* **37**, 1–13.
- Chu, F. S. (1991) Current immunochemical methods for mycotoxin analysis. *Am. Chem. Soc. Symp. Ser.* **451**, 140–157.
- Edmundson, R. D., Johnson, O., Jones, E. W., and King, T. J. (1985) Cyclic organophosphorus compounds. Part 21. Crystallographic and spectroscopic assignments of configuration at phosphorus in 2-Chloro-4-isopropyl-5,5-dimethyl-1,3,2 λ^5 -dioxaphosphorinan-2-ones and in 2-Methoxy-4-isopropyl-5,5-dimethyl-1,3,2-dioxaphosphorinanes. *J. Chem. Soc., Perkin Trans. 2*, 69.
- Ercogovich, C. D., Vallejo, R. P., Gettig, R. R., Woods, L., Bogus, E. R., and Mumma, R. O. (1981) Development of a radioimmunoassay for parathion. *J. Agric. Food Chem.* **29**, 559–563.
- Gallenkamp, B., Hofer, W., Kruger, B.-W., Maurer, F., and Pfister, T. (1982) Phosphorsäure-Derivate. In *Houben-Weyl, Methoden der Organischen Chemie* (M. Regitz, Ed.) Vol. 2, pp 590–591, Georg Thieme Verlag, Stuttgart and New York.
- Gash, V. W. (1972) Dineoalkyl ethers. A general synthesis of the symmetrical ethers. *J. Org. Chem.* **37**, 2197.
- Haas, J. H., and Guardia, E. J. (1968) Production of antibodies against insecticide-protein conjugates. *Proc. Soc. Exp. Biol. Med.* **129**, 546–551.
- Heldman, E., Balan, A., Horowitz, O., Ben-Zion, S., and Torton, M. (1985) A novel immunoassay with direct relevance to protection against organophosphate poisoning. *FEBS Lett.* **180**, 243–248.
- Hill, A. S., Beasley, H. P., McAdam, D. P., and Skerritt, J. H. (1992) Mono- and polyclonal antibodies to the organophosphate fenitrothion 2. Antibody specificity and assay performance. *J. Agric. Food Chem.* **40**, 1471–1474.
- Jones, W. T., Jones, S. D., Liddane, C. P., and Reynolds, P. H. S. (1992) Measurement of aspartate aminotransferase-P₂ in developing lupin nodules using a two site ELISA employing monoclonal antibodies. *Aust. J. Plant Physiol.* **19**, 147–153.
- Jones, W. T., Wynberg, H., and Ten Hoeve, W. (1993) Immunological detection of organophosphates. PCT WO 93/17030.
- Jones, W. T., Harvey, D., Jones, S. D., Wynberg, H., Ten Hoeve, W., and Reynolds, P. H. S. (1995) Monoclonal antibodies specific for the organophosphate pesticide Azinphos-methyl. *Food Agric. Immunol.* **7**, 9–19.
- Langone, J. J., and Van Vunakis, H. (1975) Radioimmunoassay for dieldrin and aldrin. *Res. Commun. Chem. Pathol. Pharmacol.* **10**, 163–171.
- Lorenz, W. (1957) Derivatives of thiophosphoric acid. *Chem. Abstr.* **51**, 2888i.
- McAdam, D. A., Hill, A. S., Beasley, H. L., and Skerritt, J. H. (1992) Mono- and polyclonal antibodies to the organophosphate fenitrothion. 1. Approaches to hapten-protein conjugates. *J. Agric. Food Chem.* **40**, 1466–1470.
- McAdam, D. P., and Skerritt, J. H. (1993) Synthesis of organothiophosphate antigens for the development of specific immunoassays. *Aust. J. Chem.* **46**, 959–967.
- Nugent, P. A. (1992) Enzyme-linked competitive immunoassay. In *Emerging Strategies for Pesticide Analysis* (T. Cairns and J. Sherma, Eds.) pp 247–258, CRC Press, London.
- Sasse, K. (1964) Organische Derivate der Phosphorsäure. In *Houben-Weyl, Methoden der Organischen Chemie* (E. Müller, Ed.) Vol. 12/2, pp 348–366, Georg Thieme Verlag, Stuttgart.
- Tijssen, P. (1990) Practice and theory of enzyme immunoassay. In *Laboratory Techniques in Biochemistry and Molecular Biology* (R. H. Burden and P. H. Knippenburg, Eds.) pp 221–278, Elsevier, New York, Amsterdam, Oxford.
- Van Emon, J. M., Seiber, J. N., and Hammock, B. D. (1985) in *Bioregulators for Pest Control* (P. A. Hedin, Ed.) American Chemical Society Symposium Series 276, American Chemical Society, Washington, DC.

BC970022J

DNA Binding and Cleavage by a Cationic Manganese Porphyrin–Peptide Nucleic Acid Conjugate

Pascal Bigey,[†] Søren Holst Sønnichsen,[‡] Bernard Meunier,[†] and Peter E. Nielsen^{*,‡}

Laboratoire de Chimie de Coordination du CNRS, 205 route de Narbonne, F-31077 Toulouse Cedex, France, and Center for Biomolecular Recognition, Department of Biochemistry B, The Panum Institute, Blegdamsvej 3c, DK-2200 N Copenhagen, Denmark. Received November 11, 1996[⊗]

A cationic manganese porphyrin–peptide nucleic acid (PNA) conjugate has been prepared and used to cleave a double-stranded DNA target. Cleavage experiments were performed with a 247-base pair restriction DNA fragment containing a 10-base pair homopurine binding target for the PNA. Oxidative activation by this Mn porphyrin–PNA conjugate leads to sequence specific, 3'-staggered cleavage of both DNA strands near the strand displacement junction. Furthermore, the Mn porphyrin–PNA porphyrin conjugates bind over 100-fold better to double-stranded DNA compared to the native PNA.

INTRODUCTION

The sequence specific recognition of double-stranded DNA is an essential biological process performed by DNA-binding proteins and involved in the regulation of transcription, replication, recombination, and DNA repair. The design of synthetic molecules that bind sequence specifically to unique sites on human DNA, thereby to some extent mimicking the action of the natural proteins, may have major implications for the treatment of genetic, oncogenic, and viral diseases. Oligonucleotide (via triple-helix binding), oligopeptide, or protein fragments have been used during the past decade (1–3). More recently, homopyrimidine peptide nucleic acids (PNAs) were shown to form stable triplexes with single-stranded DNA and to invade double-stranded DNA, thereby providing a novel approach to sequence specific DNA recognition (4–6).

Encouraged by the work on oxidative DNA cleavage by tetrakis(4-*N*-methylpyridiniumyl)porphyrinatomanganese(III) activated by potassium monopersulfate (KH₂SO₅) (7–9) and the attachment of trimethylpyridiniumylporphyrinatomanganese(III) motif (Mn-TrisMPyP-COOH) to oligonucleotides (10–12), we found it of interest to prepare a metalloporphyrin–PNA conjugate using the same porphyrin precursor to utilize the DNA targeting properties of the PNA. Here we report the preparation of such a "cationic manganese porphyrin–PNA" molecule (see Figure 1 for structure) and its ability to cleave a double-stranded DNA target.

EXPERIMENTAL PROCEDURES

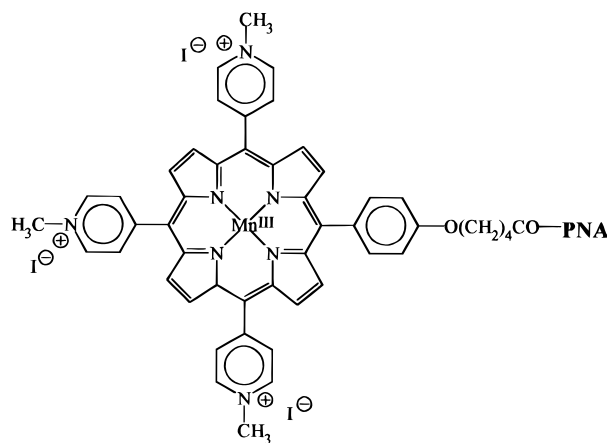
Preparation of Mn-TrisMPyP–PNA Conjugate 1 (See Chart 1 and Figure 1 for Structure). The metallated cationic porphyrin precursor MnTrisMPyP-COOH was prepared according to the procedure given in ref 13 and activated by 1,1'-carbonyldiimidazole (CDI) and 1-hydroxybenzotriazole (HOBt) according to the procedure given in ref 10. MnTrisMPyP-COOH (1 mg, 62.5 nmol) was dissolved in 110 μ L of dry dimethylformamide (DMF), and CDI (1.5 mg, 9.2 μ mol) was added. The mixture was allowed to react for 1 h at room temperature before addition of a solution of HOBt (1.7 mg, 12 mmol in 40 μ L of dry DMF). After an extra 1 h

Chart 1. Sequences of DNA Duplex Target (in Bold) and of PNA-*n* or Conjugate *n*^a

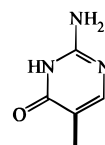
5'-----TCGACCTGCAGT**TTTCTTCTT**CTGCAGGCATGCAAGC-----
3'-----AGCTGGACGTC**AAAAGAAGA**AGACGCTCCGTACGTTTCG-----

X-TTJTJTJT-TT-(ado)_{*n*}-TTTTCTTCTT-NH₂ (PNA or PNA-conjugate 1)

^a X = H-(ado)_{*n*} for PNA-*n* (*n* = 1, 2, 3) and MnTrisMPyP-(ado)_{*n*} for conjugate *n* [ado = 8-amino-3,6-dioxaoctanoyl [–HN(CH₂CH₂O)₂CH₂CO–]; J = pseudoisocytosine].



Mn-TrisMPyP-PNA conjugate



J = Pseudoisocytosine

Figure 1. Structure of the metalloporphyrin part of the PNA conjugates and of the J-base: pseudoisocytosine.

at room temperature, the excess of CDI was eliminated by addition of 30 μ L of 20 mM sodium 4-morpholinopropanesulfonate (MOPS) buffer, pH 7.5, and 5 μ L of pyridine was added. The activated ester solution was added to 9 OD units of PNA-1 (57 nmol) dissolved in 30 μ L of 20 mM MOPS buffer, pH 7.5. The reaction was allowed to proceed for 45 min at room temperature. One

* Author to whom correspondence should be addressed.

[†] Laboratoire de Chimie de Coordination du CNRS.

[‡] The Panum Institute.

⊗ Abstract published in *Advance ACS Abstracts*, April 1, 1997.

milliliter of cold ethanol was then added, and the mixture was allowed to precipitate overnight at -20°C . After centrifugation, the supernatant was discarded. The precipitate was dissolved in water, and conjugate **1** was purified on a C₁₈ Sep-Pak cartridge from Millipore. The yield of the conjugate was 80–90% (based on starting PNA) after purification. Conjugate **1** (and **2** and **3**) was characterized by laser desorption mass spectrometry (MALDI-TOF) on a Kratos MALDI-II instrument. The main peak was detected at 6671 (and 6809 and 6962) and corresponds to the molecular weight of conjugate **1** (and **2** and **3**). [Calcd $M = 6670$ (6815 and 6960) without axial ligand on the metal and with all of the counterions of the 4-*N*-methylpyridiniumyl residues of the metalloporphyrin moiety being removed. This should give a trication, the metalloporphyrin having three 4-*N*-methylpyridiniumyl residues. As only a monocation was observed, this probably implies the loss of two protons.]

The PNA was synthesized according to the procedures given in refs 14, 15, and 16. Concentrations of PNA were determined at 260 nm (assuming that base extinction coefficients are identical in oligonucleotides and PNAs).

DNA Cleavage Experiments. The ³²P-labeled *Eco*RI–*Pvu*II restriction fragment of plasmid pA8G2 (see ref 6 for details) was mixed with conjugate **1** (for concentrations, see caption of Figure 3) in a 20 μL volume of TE buffer (10 mM Tris-HCl, pH 7.4, 1 mM EDTA). The mixture was incubated for 2 h at 37°C , and then 0.6 μL of a 2 M NaCl solution or 2 μL of salmon DNA was added as desired. The resulting mixture was allowed to equilibrate at room temperature for 1 h.

For cleaving experiments, 2 μL of a 5 mM KHSO₅ solution was added at room temperature to the hybridization mixture and the reaction was allowed to proceed for 15 min. The reaction was stopped by the addition of 1 μL of 100 mM Hepes buffer (pH 8). Samples were then diluted with 1 μL of yeast tRNA (10 mg/mL) and 100 μL of 0.3 M sodium acetate (pH 5.2), precipitated with 350 μL of absolute ethanol, and finally rinsed with 70% aqueous ethanol and lyophilized. The DNA was analyzed on a 10% denaturing polyacrylamide gel, and radioactive fragments were visualized by autoradiography. Autoradiograms were scanned using a Molecular Dynamics laser densitometry scanner.

RESULTS AND DISCUSSION

The manganese porphyrin moiety was linked to the amino end of the PNA molecule, and the hybrid molecule was characterized by mass spectrometry. The DNA target and PNA shown in Chart 1 were used in the present study.

We used a bis-PNA that is able to invade double-stranded DNA by strand displacement (4–6, 16, 17) in a bimolecular process. To optimize triplex formation (16), we used cytosines in the antiparallel (Watson–Crick recognizing) strand, while pseudoisocytosines (termed J; see Figure 1 for structure)—that allow Hoogsteen hydrogen bond formation independent of pH (16)—were used in the parallel (Hoogsteen recognizing) strand.

Binding of conjugates **1**, **2**, and **3** to a 247-base pair duplex DNA restriction fragment containing a 10-base binding site for the PNA (Chart 1) was studied using electrophoretic mobility shift assay (Figure 2), and the pseudo affinity constant K_d^{ps} for all three conjugates was 25 nM. This pseudo affinity constant, which more accurately reflects the binding rate constant (18), was over 100-fold higher for the manganese porphyrin–PNA conjugates than for the free PNAs ($K_d^{\text{ps}} \approx 10$ mM). We ascribe this dramatically improved binding efficiency of the conjugate to the high affinity of the metalloporphyrin

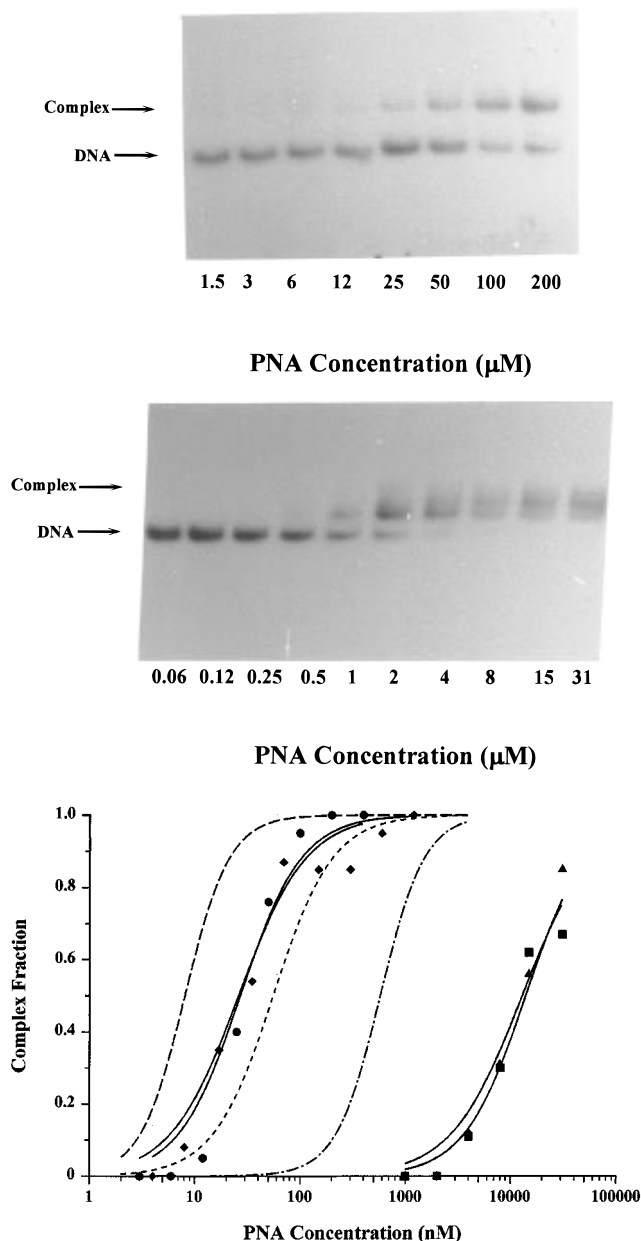


Figure 2. (a, b) Gel shift analysis of the DNA binding of PNA **1** (a) and metalloporphyrin–PNA conjugate **1** (b). (At present we do not know if the appearance of multiple bands at higher concentrations (>4 mM) is due to complexes of different conformation or structure, but it is unlikely that they represent different binding sites since no other obvious targets are present in the DNA fragment.) (c) Binding isotherms of the DNA binding of PNA **1** (■) and **2** (▲) and metalloporphyrin–PNA conjugates **1** (●) and **2** (◆). For comparison, the binding isotherms of three other bis-PNAs with total charges of +2 (in the form of one lysine and the terminal amino group) (– · –), +4 (3 lysines) (– – –), or +5 (4 lysines) (– – –) are also shown.

moiety for the minor groove of double-stranded DNA, which will effectively increase the local concentration of the PNA moiety close to the DNA helix and thus increase the probability of duplex invasion. Additional charges *per se* have been shown to increase binding efficiency [Nielsen and Demidov (in preparation), 19, 20], but the manganese porphyrin–PNA conjugates that have three positive charges bind even better than an analogous PNA with four positive charges but without the manganese porphyrin moiety (Figure 2).

Oxidation activation of the targeted manganese porphyrin with potassium monopersulfate (see ref 9 for the formation and the reactivity of manganese–oxo porphy-

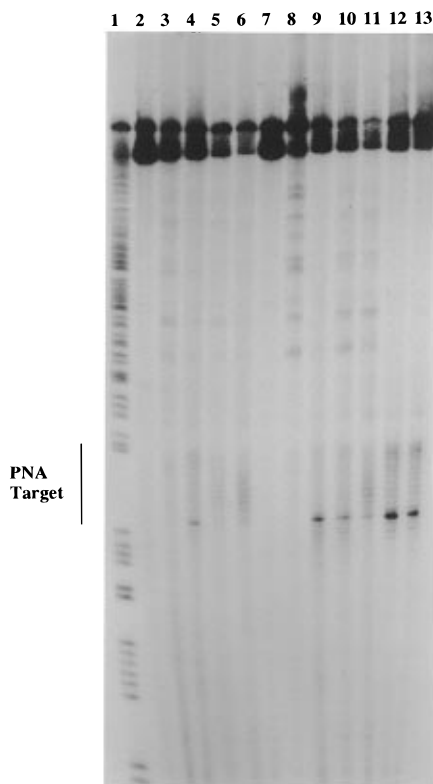


Figure 3. Sequence selective oxidative cleavage of a double-stranded DNA target by the metalloporphyrin-PNA conjugate **1**. (Lane 1) A/G sequence reaction; (lane 2) control with KHSO_5 and free PNA **1**; (lane 3) control with metalloporphyrin precursor ($1 \mu\text{M}$) and KHSO_5 and free PNA **1**; (lanes 4–6) cleavage with porphyrin-PNA conjugate **1** (0.1 , 0.3 , and $1 \mu\text{M}$, respectively) and KHSO_5 ; (lane 7) as lane 3 except for the presence of 50 mM NaCl ; (lane 8) as lane 7 except for the presence of $1 \mu\text{M}$ control PNA (without conjugated porphyrin); (lanes 9–11) as lanes 4–6 except for the presence of 50 mM NaCl ; (lanes 12 and 13) as lanes 5 and 6 except for the presence of salmon sperm DNA ($1 \mu\text{g/mL}$).

rin complexes in water solutions) led to sequence specific cleavage of this long DNA fragment proximal to the PNA target. The main cleavage occurred at the duplex-to-triplex junction as a discrete band (Figure 3, lanes 4, 9, and 12; Figure 4a), whereas control experiments with the free metalloporphyrin in the presence of free PNA-**1** led to very little cleavage at the PNA target (Figure 3, lane 3; Figure 4). Cleavage with conjugate **1** on the purine-rich strand under the same conditions occurred primarily at the triplex-to-duplex junction (Figure 4c,d), whereas hardly any cleavage was observed inside the binding site. Some cleavage also took place at the 5'-end of the purine target (Figure 4a,d). This cleavage could be due to the formation of a kinetically trapped complex in which the PNA binds eight bases in the opposite direction (Figure 4f). (Conjugates **1–3** gave virtually identical cleavage results.) It is noteworthy that the cleavage occurs at a 3'-staggered fashion across the two DNA target strands, thereby indicating that the cleavage takes place from the minor groove in full accordance with the expected binding mode of the porphyrin, although it should be considered that the DNA helix is most probably significantly distorted proximal to the strand displacement loop. It is also interesting that conjugates **2** and **3**, in which the linker between the PNA and the porphyrin is increased, cleave the DNA at virtually the same positions as conjugate **1**. These results indicate that the precise site of cleavage to a significant extent is determined by the altered/distorted DNA structure proximal to the PNA binding loop. Finally, we notice that increased concen-

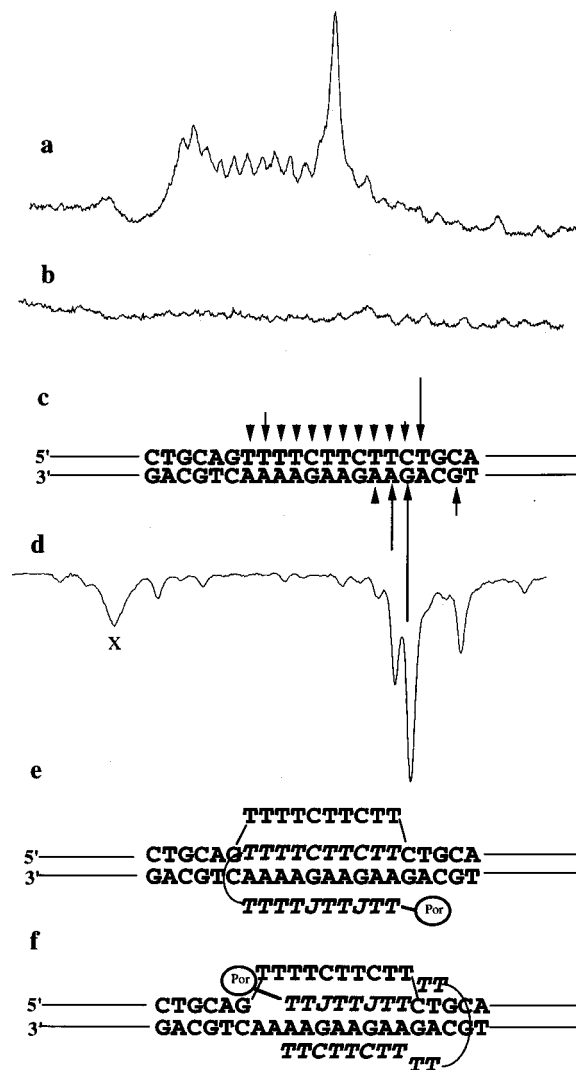


Figure 4. Densitometric scanning and schematic representations of the cleavage results: (a) cleavage of the pyrimidine strand by the metalloporphyrin-PNA conjugate **1** (corresponding to lane 4 of the autoradiogram presented in Figure 3); (b) control (corresponding to lane 3); (c) cleavage positions on the double-stranded DNA target; (d) cleavage of the purine strand by the metalloporphyrin-PNA conjugate **1** (analogous to the experiment of lane 4 in Figure 3, but performed on a DNA fragment with the ^{32}P -label at the 5'-end of the *Eco*RI site; X denotes a background band also present in the control samples); (e) schematic structure of the PNA DNA strand displacement complex showing the position of the metalloporphyrin group (por); (f) alternative complex (minor) that may account for the slight cleavage at the 5'-end of the pyrimidine strand of the target.

trations of the porphyrin-PNA conjugate decrease the site specific cleavage (Figure 3, lanes 5 and 6) and that addition of carrier DNA both restores this cleavage and suppresses unspecific cleavage at other sites of the DNA fragment (Figure 3, lanes 12 and 13), as would be expected since lower affinity sites are titrated out by the carrier DNA without affecting the high-affinity target.

No efforts to optimize the cleavage reaction with the metalloporphyrin-PNA conjugates have been undertaken. Thus, it is likely that the relatively low yields (estimated as 5–10%) observed in the experiments presented here can be improved once the mechanism of the cleavage reaction and the DNA binding of these metalloporphyrin-PNA conjugates are better understood. Furthermore, the properties and efficiencies of the present DNA cleavers should be directly compared with

other analogous PNA conjugates based on Fe (20) or Ni (21) redox chemistry.

In conclusion, conjugation to the cationic porphyrin dramatically enhances the duplex invasion potency of the PNA. Furthermore, the oxidative activation of a manganese porphyrin–PNA hybrid molecule allows the cationic metalloporphyrin to efficiently create irreversible damages on the double-stranded DNA target at the expected sites. Thus, further studies of such metalloporphyrin–PNA hybrid molecules are of interest in the development of sequence specific gene targeting and cleaving reagents.

ACKNOWLEDGMENT

P.B. is indebted to CNRS and Région Midi-Pyrénées for a fellowship. This work was supported by the French Agency for AIDS Research (ANRS), Région Midi-Pyrénées, and CNRS (B.M.) and by The Danish National Research Foundation (P.E.N.).

LITERATURE CITED

- (1) Nielsen, P. E. (1991) Sequence Selective DNA Recognition by Synthetic Ligands. *Bioconjugate Chem.* 2, 1–12.
- (2) Moser, H., and Dervan, P. B. (1987) Sequence specific cleavage of double helical DNA by triplex formation. *Science* 238, 645–650.
- (3) Thuong, N. T., and Hélène, C. (1993) Sequence specific recognition and modification of double-helical DNA by oligonucleotides. *Angew. Chem., Int. Ed. Engl.* 32, 666.
- (4) Nielsen, P. E., Egholm, M., Berg, R. H., and Buchardt, O. (1991) Sequence selective recognition of DNA by strand displacement with a thymine-substituted polyamide. *Science* 254, 1497–1500.
- (5) Cherny, D. Y., Belotserkovskii, B. P., Frank-Kamenetskii, M. D., Egholm, M., Buchardt, O., Berg, R. H., and Nielsen, P. E. (1993) DNA unwinding upon strand displacement of binding of PNA to double stranded DNA. *Proc. Natl. Acad. Sci. U.S.A.* 90, 667–1670.
- (6) Nielsen, P. E., Egholm, M., and Buchardt, O. (1994) Evidence for (PNA)₂/DNA triplex structure upon binding of PNA to dsDNA by strand displacement. *J. Mol. Recognit.* 7, 165–70.
- (7) Pitié, M., Pratviel, G., Bernadou, J., and Meunier, B. (1992) *Proc. Natl. Acad. Sci. U.S.A.* 89, 3967.
- (8) Pratviel, G., Duarte, V., Bernadou, J., and Meunier, B. (1993) Nonenzymatic Cleavage and Ligation of DNA at a Three A·T Base Pair Site. A Two-Step "Pseudohydrolysis" of DNA. *J. Am. Chem. Soc.* 115, 7939.
- (9) Pitié, M., Bernadou, J., and Meunier, B. (1995) Oxidation at Carbon-1' of DNA Deoxyribose by the Mn-TMPyP/KHSO₅ System Results from a Cytochrome P-450-Type Hydroxylation Reaction. *J. Am. Chem. Soc.* 117, 2935.
- (10) Pitié, M., Casas, C., Lacey, C. J., Pratviel, G., Bernadou, J., and Meunier, B. (1993) Selective Cleavage of a 35-mer Single-stranded DNA Containing the Initiation Codon of the TAT Gene of HIV-1 by a Tailored Cationic Manganese Porphyrin. *Angew. Chem., Int. Ed. Engl.* 32, 557–559.
- (11) Casas, C., Lacey, C. J., and Meunier, B. (1993) Preparation of Hybrid "DNA Cleaver-Oligonucleotide" Molecules based on a Metallotriss(methylpyridiniumyl)porphyrin Motif. *Bioconjugate Chem.* 4, 366–271.
- (12) Bigey, P., Pratviel, G., Meunier, B. (1995) DNA cleavage by a metalloporphyrin-spermidine-oligonucleotide" molecule. *J. Chem. Soc., Chem Commun.*, 181–182.
- (13) Casas, C., Saint-Jalmes, B., Loup, C., Lacey, C. J., and Meunier, B. (1993) Synthesis of Cationic Metalloporphyrin Precursors Related to the Design of DNA Cleavers. *J. Org. Chem.* 58, 2913.
- (14) Dueholm, K. L., Egholm, M., Behrens, C., Christensen, L., Hansen, H. F., Vulpius, T., Petersen, K., Berg, R. H., Nielsen, P. E., and Buchardt, O. (1994) Synthesis of peptide nucleic acid monomers containing the four natural nucleobases: thymine, cytosine, adenine and guanine, and their oligomerization. *J. Org. Chem.* 59, 5767–5773.
- (15) Christensen, L., Fitzpatrick, R., Gildea, B., Petersen, K. H., Hansen, H. F., Koch, T., Egholm, M., Buchardt, O., Nielsen, P. E., Coull, J., and Berg, R. H. (1995) Solid-phase synthesis of peptide nucleic acids (PNA). *J. Peptide Sci.* 3, 175–183.
- (16) Egholm, M., Christensen, L., Dueholm, K., Buchardt, O., Coull, J., and Nielsen, P. E. (1995) Efficient pH independent sequence specific DNA binding by pseudoisocytosine-containing bis-PNA. *Nucleic Acids Res.* 23, 217–222.
- (17) Griffith, M. C., Risen, L. M., Greig, M. J., Lesnik, E. A., Sprangle, K. G., Griffey, R. H., Kiely, J. S., and Freier, S. M. (1995) Single and Bis Peptide Nucleic Acids as Triplexing Agents: Binding and Stoichiometry. *J. Am. Chem. Soc.* 117, 831–832.
- (18) Demidov, V. V., Yavnilovich, M. V., Belotserkovskii, B. P., Frank-Kamenetskii, M. D., and Nielsen, P. E. (1995) Kinetics and mechanism of PNA binding to duplex DNA. *Proc. Natl. Acad. Sci. U.S.A.* 92, 2637–2641.
- (19) Veselkov, A. G., Demidov, V. V., Nielsen, P. E., and Frank-Kamenetskii, M. (1996) A new class of genome rare cutters. *Nucleic Acids Res.* 24, 2483–2487.
- (20) Lohse, J., Hui, C., Sönnichsen, S. H., and Nielsen, P. E. (1996) Sequence selective DNA cleavage by PNA-NTA conjugates. In *DNA and RNA Cleavers and Chemotherapy of Cancer and Viral Diseases*, NATO ASI Series (Meunier, B., Ed.) pp 133–141.
- (21) Footer, M., Egholm, M., Kron, S., Coull, J. M., and Matsudera, P. (1996) Biochemical evidence that a D-loop is part of a four-stranded PNA–DNA bundle. Nickel-mediated cleavage of duplex DNA by a Gly-Gly-His bis-PNA. *Biochemistry* 35, 10673–10679.

BC9700190

Nucleosides and Nucleotides. 160. Synthesis of Oligodeoxyribonucleotides Containing 5-(*N*-Aminoalkyl)carbamoyl-2'-deoxyuridines by a New Postsynthetic Modification Method and Their Thermal Stability and Nuclease-Resistance Properties[†]

Noriyasu Haginoya, Akira Ono,[‡] Yukari Nomura, Yoshihito Ueno, and Akira Matsuda*

Faculty of Pharmaceutical Sciences, Hokkaido University, Kita-12, Nishi-6, Kita-ku, Sapporo 060, Japan.
Received August 29, 1996[⊗]

Heptadecadeoxynucleotides containing 5-(*N*-aminoethyl- or *N*-aminohexyl)carbamoyl-2'-deoxyuridines (**E** or **H**) were synthesized using a newly developed postsynthetic modification method. As a convertible nucleoside unit, 5-methoxycarbonyl-2'-deoxyuridine (**1**) was initially incorporated into oligodeoxynucleotides (ODNs) according to the phosphoramidite method at various positions using a DNA synthesizer. Fully protected ODNs attached to a solid support were treated with alkyldiamines such as ethylenediamine and 1,6-hexanediamine to give the above modified ODNs. The thermal stability, resistance toward nuclease digestion, and stability in fetal calf serum of the modified ODNs were studied. An increase in the number of 5-(*N*-aminoethyl)carbamoyl-2'-deoxyuridines (**E**) in the ODNs was found to effectively stabilize duplex formation with both the corresponding complementary DNA and RNA and protect against nucleolytic hydrolysis by snake venom phosphodiesterase. In particular, the half-life of ODN **19**, which contained four **E** residues, was about 162 h in the presence of the nuclease. Furthermore, **19** was also stable in medium containing 10% fetal calf serum with a $t_{1/2}$ of about 48 h, while $t_{1/2}$ for the corresponding unmodified ODN was 13 min.

INTRODUCTION

Various oligodeoxyribonucleotide (ODN¹) analogues containing modified backbones or linker groups have been synthesized and used for biological and biophysical studies, such as antisense studies (1–7). For antisense studies, phosphorothioate and methylphosphonate analogues have been extensively used due to their nuclease-resistance properties, since a natural phosphodiester linkage in DNA is a good substrate for ubiquitous nucleases (7). However, these backbone-modified analogues have several drawbacks for use in antisense studies: (1) Phosphorothioate ODNs have lower binding affinity for their complementary strands than phosphodiester ODNs, possibly due to their diastereomer formation (8–11). (2) Although the role of RNase H cleavage in the antisense strategy is not clearly understood, it has been reported that the RNA is not a substrate for the enzyme when the methylphosphonate ODN is the complementary strand (12, 13). (3) Nonspecific binding of phosphorothioate ODNs to certain proteins was more frequent than that of the corresponding phosphodiester

ODNs, perhaps due to an inherited characteristic of the P=S bond (14, 15). Several attempts have been made to overcome these problems. One of the most promising methods is to use natural phosphodiester ODNs if they are resistant to nucleolytic digestion.

Recently, we reported the synthesis of ODNs with normal phosphodiester linkages containing a 2'-deoxyuridine analogue that carries an aminoalkyl tether at the 1'-position. We found that these were more resistant to nuclease P1 and venom phosphodiesterase than unmodified ODNs (16, 17). We also synthesized ODNs containing a novel 2'-deoxyuridine analogue with *syn*-norspermidine at the 5-position, which not only stabilized both duplex and triplex formation but also protected against hydrolysis by nuclease P1 and snake venom phosphodiesterase (18). Increased stability of *N*²-imidazolylpropylguanine- and *N*²-imidazolyl-2-aminoadenine-modified ODNs toward nucleases and thermal denaturation has also been reported (19). It is also well-known that bacteriophage ϕ W-14 DNA contains up to 50% α -putrescinyllthymine in place of thymine and is more resistant to nucleolytic enzymes such as DNase I and venom phosphodiesterase than unmodified DNAs (20–24). In addition, this modification results in a higher melting temperature (T_m) than that expected for unmodified DNA on the basis of the GC content (23, 24). However, short synthetic ODNs containing α -putrescinyllthymine were found to reduce thermal stability compared with their parent ODNs in our laboratory (25). On the basis of the result of this study, we thought that the length of the amino linkers and the distal position of the amino group would be important factors in protecting against nuclease degradation and stabilizing duplex and triplex formation.

A classical method for the synthesis of ODNs with such amino linkers is to first prepare such nucleoside phosphoramidite units separately and then to incorporate

* Author to whom correspondence should be addressed [telephone (011) 706-3228; fax (011) 706-4980; e-mail matuda@pharm.hokudai.ac.jp].

[†] For Part 159 in this series, see: Nishizono, N., Koike, N., Yamagata, Y., Fujii, S., Matsuda, A. (1996) Synthesis of thietane nucleosides via the Pummerer reaction as a key step. *Tetrahedron Lett.* 37, 7569–7572.

[‡] Present address: Department of Chemistry, Faculty of Science, Tokyo Metropolitan University, Minamiosawa, Hachioji, Tokyo 192-03, Japan.

[⊗] Abstract published in *Advance ACS Abstracts*, April 1, 1997.

¹ Abbreviations: ODN, oligodeoxyribonucleotide; DMAP, 4-(dimethylamino)pyridine; DMTr, dimethoxytrityl; EDTA, ethylenediaminetetraacetic acid; TEAA, triethylammonium acetate; TEAB, triethylammonium bicarbonate; FCS, fetal calf serum; HPLC, high-performance liquid chromatography; T_m , melting temperature; PAGE, polyacrylamide gel electrophoresis.

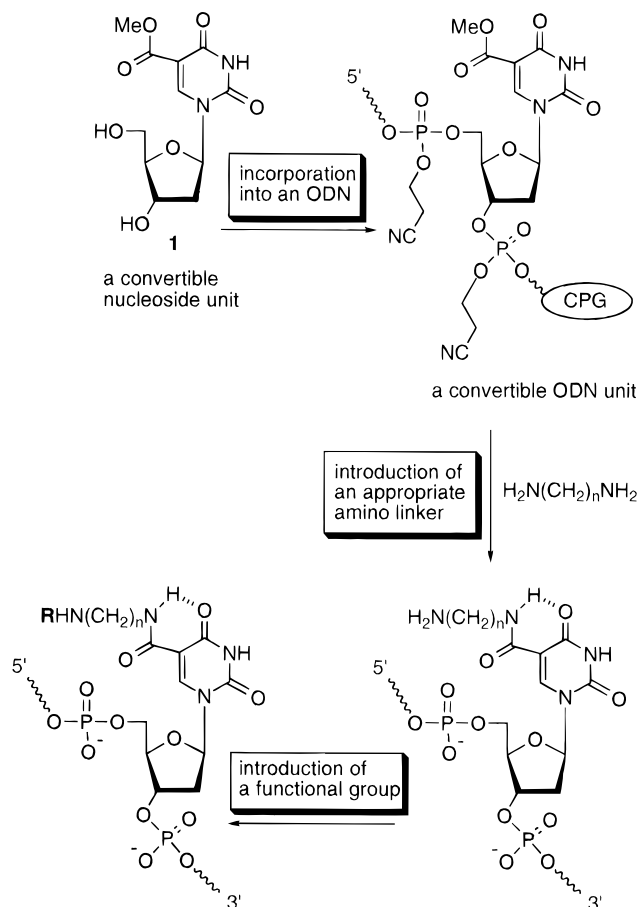


Figure 1. Postsynthetic modification method.

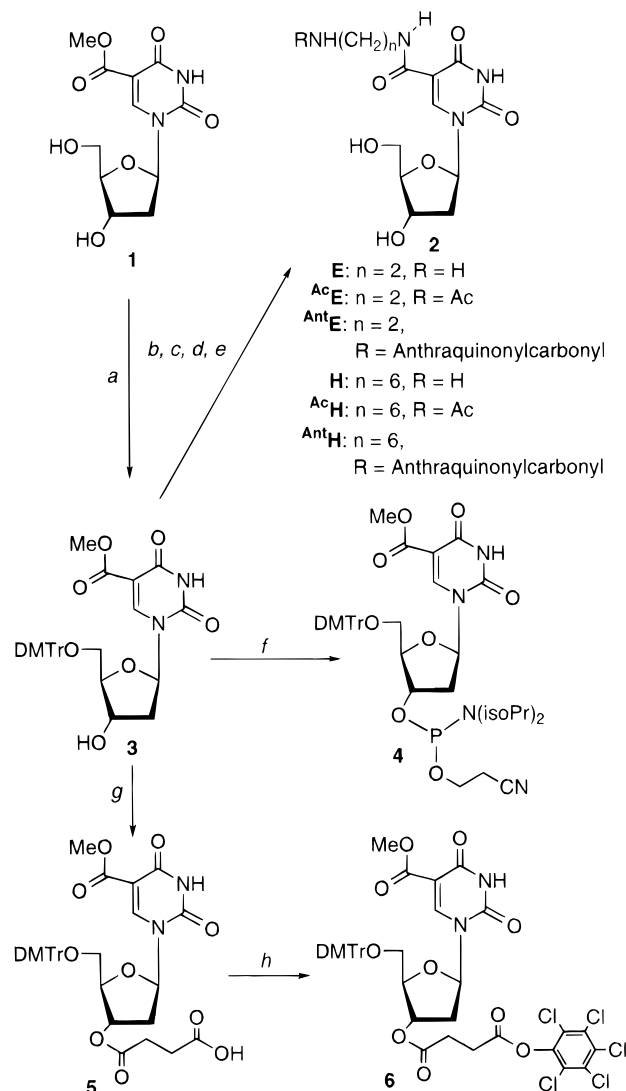
them into ODNs by an automated DNA synthesizer (26). However, this method sometimes involves tedious protection-deprotection processes and solubility problems in the synthesis of the mononucleotide units. In particular, when the optimum length of the linker group for a desired function is not known, several nucleoside phosphoramidite units with linkers of various lengths have to be constructed separately, and these mononucleotide units have to be incorporated independently. To avoid such time-consuming processes, postsynthetic modifications have been developed (27–32). In these methods, a nucleoside unit with a leaving group within a molecule (a convertible nucleoside unit), which should be stable under the conditions of DNA synthetic cycles, is initially introduced into an ODN (a convertible ODN unit) and then appropriately modified linkers and/or further functionalized linkers are introduced into the ODNs. Thus, postsynthetic modification would be suitable for identifying the proper length of the linkers.

We previously developed a new convertible nucleoside, 5-methoxycarbonyl-2'-deoxyuridine (**1**), which reacts smoothly with alkyldiamines in MeOH under mild conditions, and developed a new postsynthetic modification method using **1** as a convertible nucleoside unit as shown in Figure 1 (33). In this paper, we describe the synthesis of ODNs containing 5-(*N*-aminoethyl- or *N*-aminohexyl)-carbamoyl-2'-deoxyuridines (**E** or **H**) using this new postsynthetic modification, their thermal stabilization properties, their protective effects against nucleolytic enzymes, and their stability in FCS.

RESULTS AND DISCUSSION

Synthesis. As a convertible nucleoside unit, 5-(methoxycarbonyl)-2'-deoxyuridine (**1**) was synthesized via pal-

Scheme 1^a



^a (a) DMTrCl, pyridine, room temperature; (b) (1) $\text{NH}_2(\text{CH}_2)_n\text{NH}_2$ ($n = 2$ or 6), MeOH, room temperature, (2) aqueous 80% AcOH, room temperature; (c) (1) Ac_2O , DMAP, pyridine, room temperature, (2) NH_3/MeOH , room temperature; (d) (1) b, (2) anthraquinone-2-carboxylic acid, 1-ethyl-3-[3-(dimethylamino)propyl]carbodiimide hydrochloride, pyridine and DMF, room temperature; (e) aqueous 80% AcOH, room temperature; (f) 2-cyanoethyl *N,N*-diisopropylphosphoramidochloride, *N,N*-diisopropylethylamine, CH_2Cl_2 , room temperature; (g) succinic anhydride, pyridine, 70 °C; (h) pentachlorophenol, 1-ethyl-3-[3-(dimethylamino)propyl]carbodiimide hydrochloride, DMF.

ladium-catalyzed carbonylation of a commercially available 5-iodo-2'-deoxyuridine with carbon monoxide in MeOH (33). Compound **1** was converted to 5'-*O*-dimethoxytrityl (DMTr) derivative **3** and then phosphoramidite unit **4** according to a standard protocol without modifications. To incorporate **1** into the 3'-end of the ODNs, **3** was further derivatized to its 3'-*O*-succinate **5**, which was then coupled with pentachlorophenol to give **6**. Reaction of **6** with a controlled pore glass (CPG) gave a solid support containing **1** (21.9 $\mu\text{mol/g}$) (Scheme 1).

For the synthesis of reference nucleosides, **3** was treated with ethylenediamine or 1,6-hexanediamine in MeOH at room temperature to give the corresponding 5-(*N*-aminoalkyl)carbamoyl-2'-deoxyuridines (**2**; **E** and **H**) after detritylation. *N*-Acetamidoethyl- (**AcE**), *N*-acetamidoethyl- (**AcH**), *N*-(2-anthraquinonylcarbonyl)aminoethyl- (**AntE**), and *N*-(2-anthraquinonylcarbonyl)amino-

Table 1. Thermal Denaturation and PAGE Relative Mobility of Duplexes and Triplexes^a

	ODNs ^b	DNA-DNA ^c			DNA-RNA ^d	triplex ^e	relative mobility (%)
		0.01 M NaCl <i>T_m</i> (°C)	0.1 M NaCl <i>T_m</i> (°C)	ΔT_m (°C)	0.1 M NaCl <i>T_m</i> (°C)	0.5 M NaCl <i>T_m</i> (°C)	
7	5'-d[T(MT) ₈]-3' (control)	49	63	14	69	36	100
8	5'-d[(TM) ₄ E(MT) ₄]-3'	53	64	11	68	34	ND
9	5'-d[E(TM) ₈]-3'	54	ND	ND	68	36	ND
10	5'-d[E(MT) ₃ ME(MT) ₃ ME]-3'	55	66	11	71	31	ND
11	5'-d[E(MT) ₂ MEMTME(MT) ₂ ME]-3'	57	67	10	71	26	ND
12	5'-d[(TM) ₄ AntE(MT) ₄]-3'	55	66	11	68	33	ND
13	5'-d[AntE(TM) ₈]-3'	56	ND	ND	67	39	ND
14	5'-d[AntE(MT) ₃ MAntE(MT) ₃ MAntE]-3'	51	66	15	67	ND	ND
15	5'-d[AntE(MT) ₂ MAntEMTMAntE(MT) ₂ MAntE]-3'	56	69	13	68	ND	ND
16	5'-d[(TM) ₄ H(MT) ₄]-3'	53	ND	ND	70	37	96
17	5'-d[H(TM) ₈]-3'	55	ND	ND	69	34	ND
18	5'-d[H(MT) ₃ MH(MT) ₃ MH]-3'	57	66	9	72	32	86
19	5'-d[H(MT) ₂ MHMTMH(MT) ₂ MH]-3'	61	70	9	75	25	82
20	5'-d[(TM) ₄ AntH(MT) ₄]-3'	57	67	10	69	34	ND
21	5'-d[AntH(TM) ₈]-3'	58	ND	ND	69	41	ND
22	5'-d[AntH(MT) ₃ MAntH(MT) ₃ MAntH]-3'	61	72	11	71	ND	ND
23	5'-d[AntH(MT) ₂ MAntHMTMAntH(MT) ₂ MAntH]-3'	63	72	9	70	ND	ND
24	5'-d[(TM) ₄ AcH(MT) ₄]-3'	51	ND	ND	ND	32	98
25	5'-d[AcH(TM) ₈]-3'	51	ND	ND	ND	ND	ND
26	5'-d[AcH(MT) ₃ MAcH(MT) ₃ MAcH]-3'	49	63	14	ND	26	91
27	5'-d[AcH(MT) ₂ MAcHMTMAcH(MT) ₂ MAcH]-3'	50	62	12	ND	17	89

^a Experimental conditions are described under Experimental Procedures. ^b M = 2'-deoxy-5-methylcytidine. E, AcE, AntE, H, AcH, and AntH, see Scheme 1. ^c The complementary ODN: 5'-d[TG(GA)₉GGT]-3' (**28**). ^d The complementary RNA: 5'-r[(AG)₈A]-3' (**30**). ^e The target sequence: 5'-d[AG(TC)₉C(T)₅AG(GA)₉CT]-3' (**29**). ^f ND, not determined.

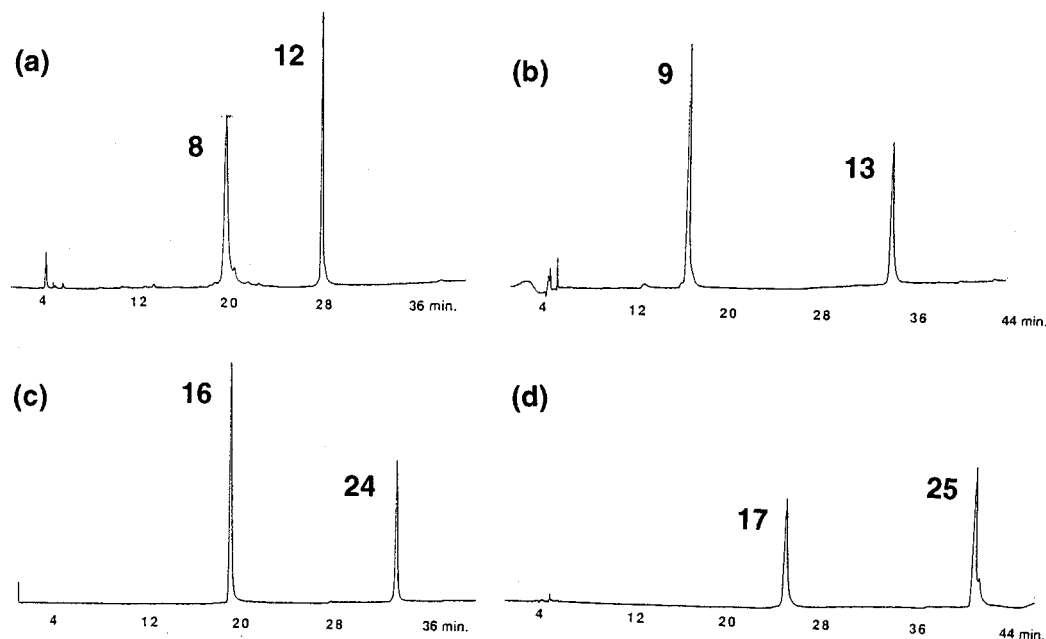


Figure 2. Examples of HPLC profiles of the ODNs with a C₁₈ column: (a) co-injection of **8** and **12**; (b) co-injection of **9** and **13**; (c) co-injection of **16** and **24**; (d) co-injection of **17** and **25**. We used a linear gradient of CH₃CN from 10 to 15% (20 min) and then from 15 to 30% (20 min) in 0.1 M TEAA buffer (pH 6.8).

hexyl- (AntH) carbamoyl derivatives were also synthesized from **3** or the corresponding amino derivatives.

Heptadecamers containing various numbers of **1** at various positions were synthesized on a DNA synthesizer using **4** and/or the solid support bearing **1**. The average coupling yield of **4** was 97% using a 0.1–0.12 M solution of **4** in CH₃CN and a coupling time of 360 s. Each fully protected ODN linked to the solid support was treated with a large excess of ethylenediamine or 1,6-hexanediamine in MeOH at room temperature or at 45 °C for 12–14 h. This treatment produced simultaneous conversion of the methoxycarbonyl group into the (*N*-aminoalkyl)-carbamoyl group, deprotection, and detachment from the solid support. Subsequent purification by C₁₈ column chromatography and following detritylation gave the corresponding heptadecamers **8–11** and **16–19** (Table

1), which were further purified by ion-exchange column chromatography followed by C₁₈ HPLC. It was necessary to remove excess 1,6-hexanediamine using Sephadex G-25 column chromatography prior to further purification. Starting from 1 μmol of nucleoside residues attached to the CPG, 8.5–23 OD units (at 254 nm) of ODNs were obtained. Reactions of these ODNs with Ac₂O or *N*-[(anthraquinone-2-carbonyl)oxyl]succinimide (**17**) at room temperature gave the desired functionalized ODNs **12–15** and **20–27** (Table 1) in good yields, which showed single peaks by HPLC analyses with C₁₈ HPLC (some examples are shown in Figure 2).

To confirm the presence of modified nucleosides in the heptadecamers, each ODN was completely hydrolyzed to the corresponding nucleosides by a mixture of snake venom phosphodiesterase and alkaline phosphatase, and

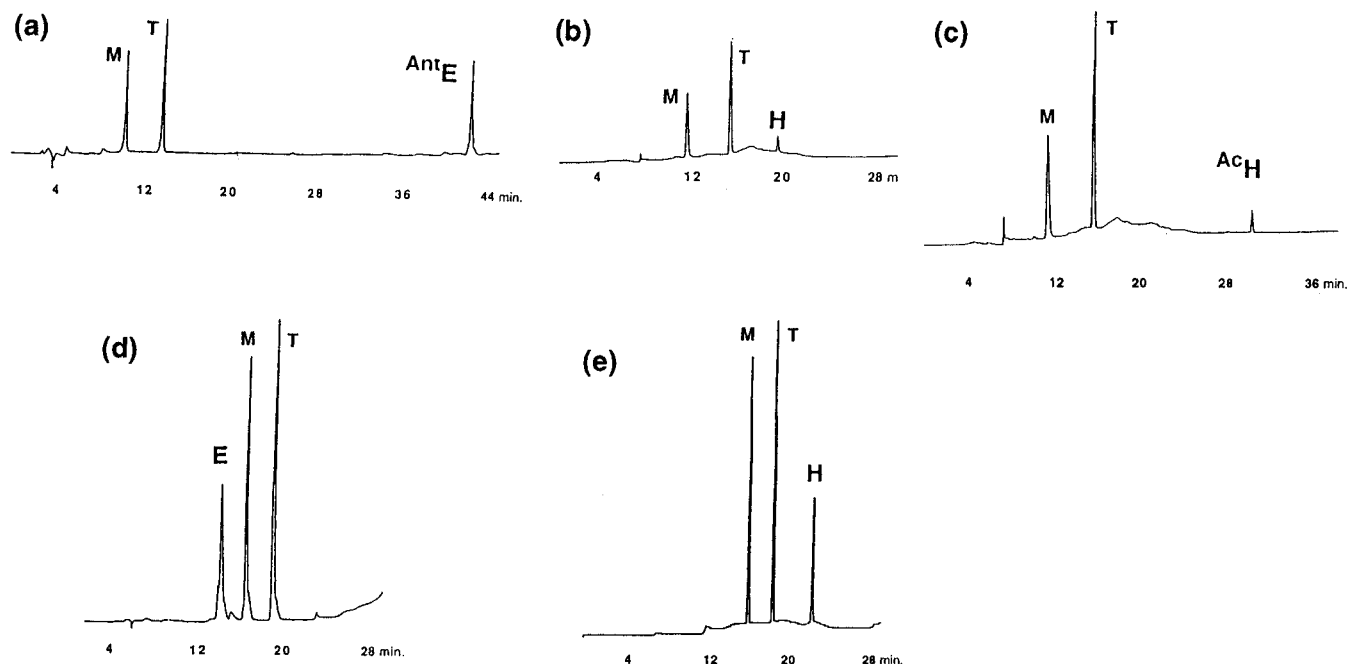


Figure 3. Examples of a profiles of HPLC analysis of a nucleoside mixture obtained by complete hydrolysis of ODNs by an enzyme mixture with a C₁₈ column: (a) **13**; (b) **17**; (c) **25**; (d) **10**; (e) **18**. For the nucleoside mixture containing **E** or **H**, HPLC was performed with a linear gradient of CH₃CN from 0 to 25% (20 min) and then from 25 to 60% (5 min) in 0.1 M TEAA buffer (pH 6.8). For the nucleoside mixture containing **AntE** or **AcH**, HPLC was performed with a linear gradient of CH₃CN from 0 to 25% (20 min) and then from 25 to 80% (25 min) in 0.1 M TEAA buffer (pH 6.8).

the nucleoside composition was analyzed by HPLC (several examples are shown in Figure 3). Peaks corresponding to the modified nucleosides, confirmed by coelution with authentic samples, were observed, and the composition of the nucleosides calculated from the areas of the peaks was close to the theoretical value. Thus, this postsynthetic modification, in which we reacted ethylenediamine and 1,6-hexanediamine with a solid support containing the convertible nucleoside **1**, worked well without problems.

Duplex and Triplex Formation by Heptadecamers. Duplex formation of the heptadecamers **8–27** with the complementary ODN, 5'-d[TG(GA)₉GGT]-3' (**28**), was studied by thermal denaturation in 0.01 M NaCl. One transition was observed in the melting profile of each duplex. *T_m* values are shown in Table 1. All of the ODNs bearing the terminal amino groups and the intercalator stabilized the duplex formation. The thermal stabilities of the duplexes formed by **28** and ODNs **9** or **17**, which bore one molecule of **E** or **H** at the 5'-end, were almost the same, and therefore, at the 5'-end, the effect did not depend on the length of the linker, although the *T_m* values are higher than that of the control (5 and 6 °C, respectively). The ODNs **13** and **21**, which bore the anthraquinone group at the terminal amino group (**AntE** and **AntH**), showed even higher *T_m* values (7 and 9 °C, respectively), while the acetamidohexyl derivative **25** had a decreased *T_m*, which was still higher than that of the control duplex. Incorporation of one modified nucleoside at the center of ODNs such as **8**, **12**, **16**, **20**, and **24** had less of a stabilizing effect on duplex formation. However, with an increase in the number of **E** or **H** in heptadecamers such as **10**, **11**, **18**, and **19**, duplex stability increased somewhat proportionally and the increase in the *T_m* values was greater for ODNs containing **H** (**18** and **19**) than for those containing **E** (**10** and **11**). Since a stabilizing effect was not observed for ODNs containing **AcH** (**26** and **27**), the enhanced thermal stability of the duplexes is likely due to the effect of the terminal ammonium ion, which may be close to the phosphate

anion of the complementary strand or the self-strand. Introduction of the anthraquinone group to the terminal amino group, although it counteracts the stabilizing effect of the ammonium ion, gave higher *T_m* values than the control duplex, while an increase in the number of **AntE** or **AntH** did not produce a cumulative effect on the *T_m* values.

The importance of the ammonium ion in stabilizing duplexes was further examined in two ways. First, *T_m* values were compared under conditions of a higher (0.1 M NaCl) ionic strength (Table 1). $\Delta T_m [T_m (0.1 \text{ M NaCl}) - T_m (0.01 \text{ M NaCl})]$ for the control duplex (14 °C) was greater than those of duplexes **28** and **8** (11 °C), **10** (11 °C), **11** (10 °C), **18** (9 °C), and **19** (9 °C), whereas ΔT_m values (14 and 12 °C, respectively) for duplexes with ODNs containing **AcH** (**26** and **27**) were similar to or slightly lower than that of the control duplex. Thus, the effect of salt concentration on duplex stability indicates that the terminal ammonium ion stabilized duplex formation by neutralizing phosphate anions, which is consistent with a recent paper by Hashimoto *et al.* (34). For duplexes containing the intercalator group, the effects of intercalation on the stabilization of duplex formation should also be taken into account. Second, the polyacrylamide gel electrophoretic mobility (PAGE mobility) of **7** was compared with those of ODNs containing **H** and **AcH** using 5'-³²P-labeled ODNs. Relative PAGE mobility is calculated in Table 1. An increase in the number of **H** clearly decreased the relative mobility from 96 to 82%, although with an increase in size, changes with **AcH** were less than those with **H**. Therefore, it is clear that the ammonium ion at the terminal position of the linker can contribute to the stabilization of duplex formation.

Stable duplex formation with mRNA is one of the most important factors in antisense research. Therefore, duplex formation by heptadecamers with the complementary RNA strand, 5'-r[(AG)₈A]-3' (**30**), was next studied by thermal denaturation in a buffer of 0.01 M sodium cacodylate (pH 7) containing 0.1 M NaCl. As

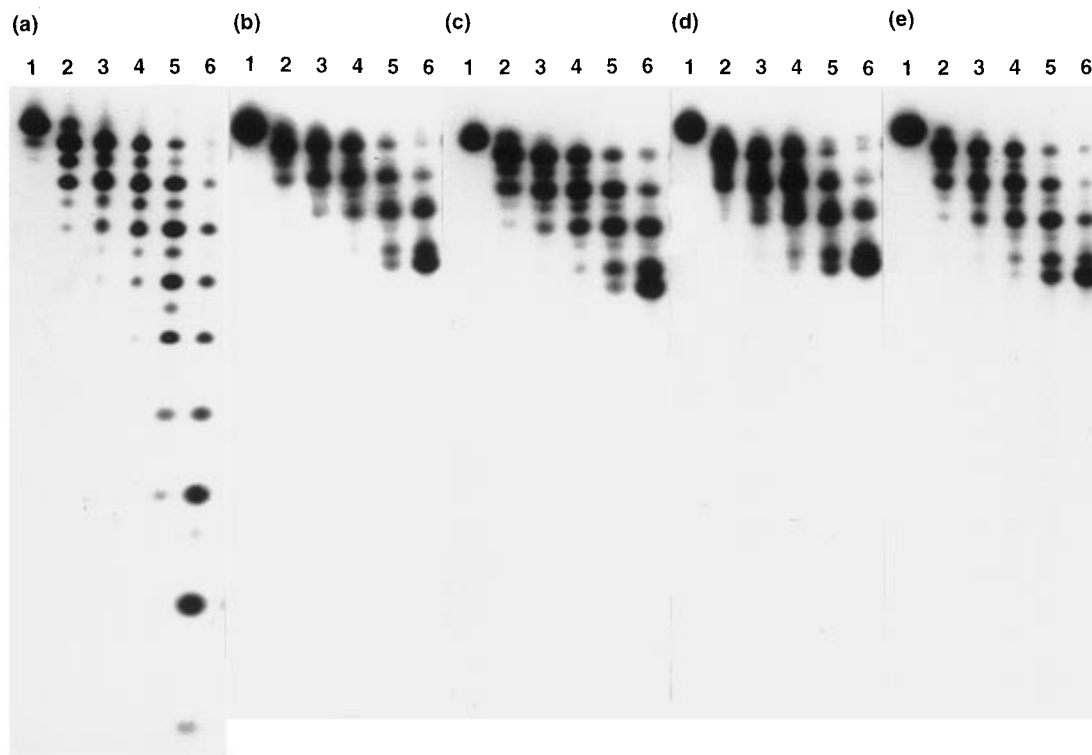


Figure 4. PAGE of 5'-³²P-labeled ODNs hydrolyzed by snake venom phosphodiesterase: (a) **7**; (b) **8**; (c) **16**; (d) **12**; (e) **20**. ODNs were incubated with venom phosphodiesterase for 0 min (lane 1), 10 min (lane 2), 20 min (lane 3), 30 min (lane 4), 1 h (lane 5), and 2 h (lane 6). Experimental conditions are described under Experimental Procedures.

shown in Table 1, T_m values gradually increased when the number of modified nucleosides **E** or **H** increased in the ODNs. The increase in T_m values in ODNs containing **H** was greater than in ODNs containing **E** and a 6 °C increase was observed in **19**, which contains four **H**s in the ODN. On the other hand, attachment of the intercalator to the amino terminus did not produce a cumulative increase in T_m values. This tendency was different from that in duplexes with **28**. The data indicated structural differences between the DNA–DNA duplexes and the DNA–RNA duplexes, and the bulky intercalator may not be well-accommodated in the narrow major groove formed by the DNA–RNA duplexes.

Triplex formation by heptadecamers with the target duplex, d[AG(TC)₉C(T)₅AG(GA)₉CT]-3' (**29**), was also studied by thermal denaturation in a buffer containing 0.5 M NaCl (pH 7.0). Two transitions were observed in a melting profile of each triplex. Transitions at higher T_m values due to the melting of the target duplex **29** (88 °C) and transitions at lower T_m values due to dissociation of the third strands from the triplexes were observed (Table 1). While heptadecamers containing one molecule of **E** at both the 5'-end and at the center, as well as those with **H** at the 5'-end, did not stabilize triplex formation, the ODN containing one molecule of **H** at the center showed slight stabilization. When the terminal amino group was modified by the anthraquinone group, T_m values increased to 3 °C for **13** and to 5 °C for **21**, compared with that of the control triplex (36 °C), while ODNs **12** and **20** destabilized triplex formation. However, when the number of **E** or **H** together with **A^cH** per molecule increased, the T_m values tended to decrease. Therefore, further experiments are needed to identify the proper length for stabilizing triplex formation.

A postsynthetic modification method is a convenient approach to constructing ODNs with functional groups. Our newly developed method would be superior to the previously reported nucleobase-modified methods (27–

32) with regard to the thermal stability of both DNA–DNA and DNA–RNA duplexes. Substitutions of *O*⁴-(2,4,6-trimethylphenyl)uracil (**27**) and *O*⁶-phenylpurine (**28**) in ODNs by various amino nucleophiles to give ODNs with *N*⁴-aminoalkylcytosines and *N*⁶-aminoalkyladenines, respectively, have been reported. However, the introduction of linkers at the exocyclic amino groups reduced the T_m values of duplexes with unmodified complementary ODNs, due to a decrease in the acidity of exocyclic NH groups, which would be unfavorable for hydrogen bonding to the complementary nucleobases. The replacements of thymine by α-putrescinythymine (**25**) and 5-ω-amino-hexyluracil (**34**) also reduced the thermal stability of the duplexes. The pK_a value of the N3-H in **E** was measured by titration to be 8.1 (33), which is 1.7 units lower than that of thymidine and 1.2 units lower than that of 2'-deoxyuridine (35). Since incorporation of 5-propynyl-uracil (**36**, **37**) and 5-heteroaryluracils (**38**) into ODNs gives increased T_m values compared with unmodified duplexes, the introduction of such electron-withdrawing groups at the 5-position of uracil is important to obtain the thermal stability of duplexes.

In addition, a variety of amino nucleophiles can be conveniently incorporated into ODNs using our method, and the most suitable length of linkers for desired functions can be easily identified. Thus, the 1,6-diaminohexane linker was found to stabilize duplex formation with either DNA or RNA as a complementary strand, but not triplex formation. The importance of the ammonium ion was estimated by the effect of the salt concentration on T_m and by changes in mobility on PAGE. This is also supported by the fact that an increase in the number of ammonium ions in an ODN results in greater duplex stability. The terminal ammonium ion in **H** may effectively neutralize the phosphate negative charge, although whether its distal position is close to the phosphate anion in the complementary strand or that in the self-strand remains to be clarified. Moreover, an in-

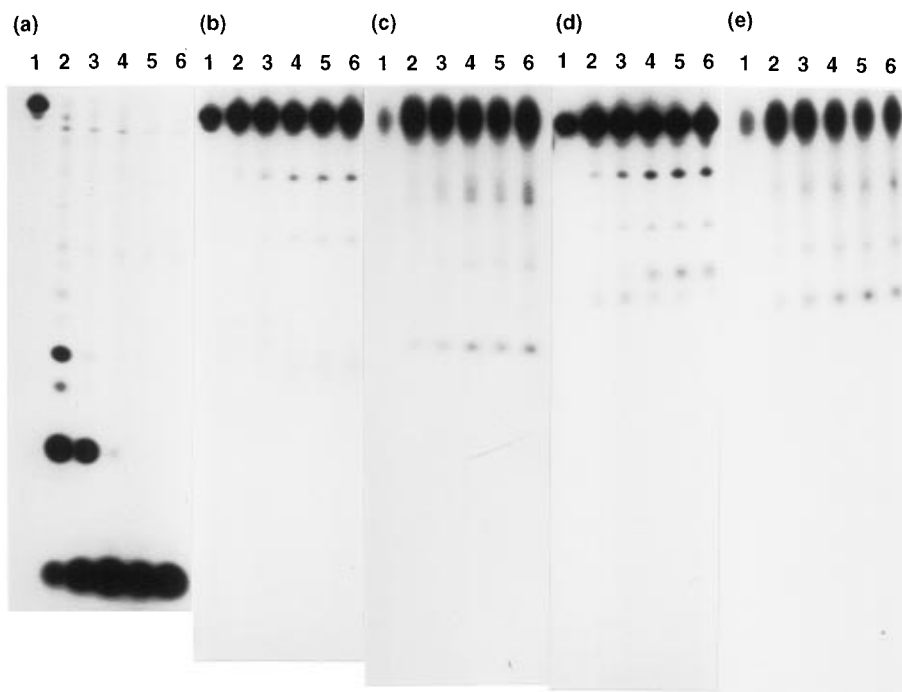


Figure 5. PAGE of 5'- ^{32}P -labeled ODNs hydrolyzed by snake venom phosphodiesterase: (a) **7**; (b) **11**; (c) **19**; (d) **15**; (e) **23**. ODNs were incubated with venom phosphodiesterase for 0 h (lane 1), 3 h (lane 2), 6 h (lane 3), 12 h (lane 4), 24 h (lane 5), and 48 h (lane 6). Experimental conditions are described under Experimental Procedures.

tramolecular hydrogen bond between the O^4 atom and one of the carbamoyl protons was observed in the crystal structure of 5-carbamoyl-2'-deoxyuridine (**33**). Although it is not clear whether this conformational fixation contributes to stabilization of the duplexes, the enhanced hydrogen-donor ability at N3-H and the neutralizing effect of the terminal ammonium ion should work in cooperation to give duplex stabilization. Therefore, ODNs containing **H** can be useful for antisense studies if they have nuclease-resistance properties.

Nuclease Resistance of Modified ODNs. Resistance of the heptadecamers to nucleolytic digestion was examined next. The heptadecamers **8**, **12**, **16**, and **20**, which carried modified nucleosides in their centers, were labeled at the 5'-end with ^{32}P and incubated with snake venom phosphodiesterase, a 3'-exonuclease. The reactions were then analyzed by 20% PAGE under denaturing conditions (Figure 4). Due to a difference in the rate of hydrolysis between 5'-TpM-3' linkages and 5'-MpT-3' linkages, spots for the newly generated ODNs containing an M residue at the 3'-end were faint, while spots for ODNs containing a T residue at the 3'-end were bold. Although the control **7** was hydrolyzed randomly within 2 h, all of the modified ODNs were hydrolyzed only at the 3'-side of the modified nucleosides. The phosphodiester linkages at the 5'-side of the modified nucleosides were completely resistant to the nuclease for 2 h.

On the other hand, the ^{32}P -labeled ODNs **11**, **15**, **19**, and **23**, which contained four modified nucleoside residues, were completely resistant to the nuclease for 2 h under the same conditions (data not shown). After 3 h, they began to be gradually hydrolyzed, and the half-lives of these ODNs were about 105, 126, 162, and 48 h, respectively (Figure 5). The control ODN **7** was completely hydrolyzed randomly within 3 h under the same conditions. Thus, ODNs containing 5-(*N*-aminoalkyl)-carbamoyluracils and with an anthraquinone group at the terminal amino group were fairly stable against the nuclease, although other nucleases with different substrate specificity remain to be elucidated.

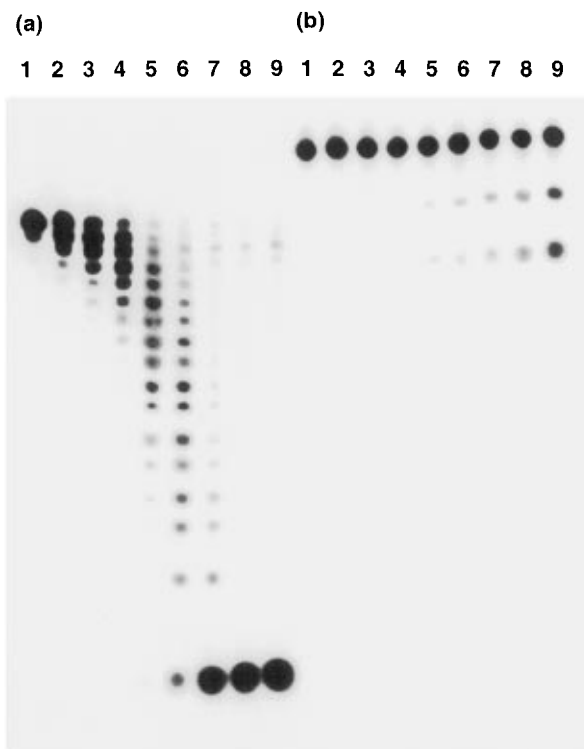


Figure 6. PAGE of 5'- ^{32}P -labeled ODNs incubated in the medium containing 10% FCS: (a) **7**; (b) **19**. ODNs were incubated for 0 min (lane 1), 15 min (lane 2), 30 min (lane 3), 1 h (lane 4), 3 h (lane 5), 5 h (lane 6), 10 h (lane 7), 24 h (lane 8), and 48 h (lane 9). Experimental conditions are described under Experimental Procedures.

Next, we compared the stabilities of **7** and **19** in a medium containing 10% FCS. A mixture of ^{32}P -labeled **7** or **19** (at the 5'-ends) with their unlabeled ODN (25 μM) was incubated separately in FCS, which was partially heat-denatured for 30 min at 56 $^{\circ}\text{C}$ prior to use, and analyzed by 20% PAGE under denaturing conditions (Figure 6). The half-lives of these ODNs were 13 min

and 48 h, respectively. This experiment clearly shows that **19** is fairly stable in the presence of 10% fetal calf serum (FCS). Thus, due to both the thermal stabilization and nuclease resistance conferred by the 5-(*N*-amino-hexyl)carbamoyl substituent, ODNs containing **H** should be suitable for use as antisense ODNs.

CONCLUSION

A new postsynthetic modification method was developed using 5-(methoxycarbonyl)-2'-deoxyuridine (**1**) as a convertible nucleoside unit. After incorporation of **1** into ODNs attached to a solid support, treatment of the resin with alkyldiamines proceeded concomitantly with several processes, such as incorporation of the alkyldiamines into the ODN, deprotection, and detachment from the solid support to give the desired modified ODNs in which modified uracils were incorporated in appropriate numbers and positions. Furthermore, the modified heptadecamers were fairly stable to nuclease degradation using a 3'-exonuclease and to FCS. These properties make the ODNs potentially useful as antisense ODNs. Related studies are currently underway in our laboratory.

EXPERIMENTAL PROCEDURES

General Experimental Data. TLC was done on Merck Kieselgel F254 precoated plates (Merck). The silica gel, the neutralized silica gel, or the silanized silica gel used for column chromatography was YMC gel 60A (70–230 mesh) (YMC Co., Ltd.), ICN silica 60A (ICN Biochemicals), or preparative C₁₈ (Waters, 125Å). Melting points were measured on a Yanagimoto MP-3 micro melting point apparatus (Yanagimoto) and are uncorrected. Fast atom bombardment mass spectrometry (FAB-MS) was measured on a JEOL JMS-HX110 (JEOL) at an ionizing voltage of 70 eV. The ¹H NMR spectra were recorded on a JEOL JNM-GX 270 (270 MHz) or JEOL EX 400 (400 MHz) spectrometer (JEOL) with tetramethylsilane as an internal standard. Chemical shifts are reported in parts per million (δ), and signals are expressed as s (singlet), d (doublet), t (triplet), m (multiplet), or br (broad). All exchangeable protons were detected by disappearance on the addition of D₂O. UV absorption spectra were recorded with a Shimadzu UV-240 spectrophotometer (Shimadzu Co.).

5-(Methoxycarbonyl)-5'-*O*-(dimethoxytrityl)-2'-deoxyuridine (3**).** Dimethoxytrityl chloride (12.4 g, 36.7 mmol) was added to a solution of **1** (33) (10.0 g, 34.9 mmol) in anhydrous pyridine (100 mL), and the mixture was stirred overnight at room temperature. EtOH (10 mL) was added to the mixture, and the whole was stirred for 10 min. The mixture was concentrated *in vacuo* and was taken in CHCl₃, which was washed with saturated aqueous NaHCO₃ (two times) and brine. The separated organic phase was dried (Na₂SO₄) and concentrated to dryness. The residue was purified on a silica gel column (6 × 35 cm) with 0–8% MeOH in CHCl₃ containing 0.2% pyridine to give **3** (18.3 g, 87%, as a white foam): FAB-MS, *m/z* 590 (M⁺ + 1); NMR (CDCl₃) δ 8.69 (1 H, s, H-6), 8.23 (1 H, br s, 3-NH), 6.81–7.45 (13 H, m, Ph), 6.26 (1 H, t, H-1', *J*_{1',2'} = 6.7 Hz), 4.40–4.47 (1 H, m, H-3'), 4.03–4.09 (1 H, m, H-4'), 3.80 (6 H, s, OMe), 3.54 (1 H, dd, H-5'a, *J*_{5'a,4'} = 4.0, *J*_{gem} = 10.5 Hz), 3.33 (1 H, dd, H-5'b, *J*_{5'b,4'} = 3.4, *J*_{gem} = 10.5 Hz), 3.30 (3 H, s, CO₂Me), 2.52 (1 H, ddd, H-2'a, *J*_{2'a,1'} = 6.7, *J*_{2'a,3'} = 4.0, *J*_{gem} = 12.3 Hz), 2.29 (1 H, dd, H-2'b, *J*_{2'b,1'} = 6.7, *J*_{gem} = 12.3 Hz), 2.01–1.92 (1 H, m, 3'-OH).

5-[(*N*-Aminoethyl)carbamoyl]-2'-deoxyuridine (E**).** Ethylenediamine (2.0 mL, 23 mmol) was added to a solution of **3** (400 mg, 0.68 mmol) in MeOH (4 mL), and

the mixture was stirred for 2 days at room temperature. The volatiles were removed *in vacuo*, and the residue was taken in CHCl₃, which was washed with saturated aqueous KH₂PO₄ (two times) and brine. The separated organic phase was dried (Na₂SO₄) and concentrated. The residue was dissolved in aqueous 80% AcOH (10 mL), and the mixture was stirred for 5.5 h at room temperature. The solvent was removed *in vacuo*, and the residue was coevaporated several times with H₂O. The residue was partitioned between H₂O and Et₂O (two times). The H₂O phase was concentrated, and the residue was crystallized from Et₂O with saturated H₂O to give **E** (157 mg, 73%): mp 218 °C (dec); FAB-MS, *m/z* 315 (M⁺ + 1); UV λ_{max} (H₂O) 277 nm (ε 15 100), λ_{max} (0.1 N HCl) 276 nm (ε 17 000), λ_{max} (0.1 N NaOH) 276 nm (ε 14 000); NMR (D₂O) δ 8.63 (1 H, s, H-6), 6.29 (1 H, t, H-1', *J*_{1',2'} = 6.5 Hz), 4.41–4.51 (1 H, m, H-3'), 4.05–4.12 (1 H, m, H-4'), 3.85 (1 H, dd, H-5'a, *J*_{5'a,4'} = 4.2, *J*_{gem} = 11.0 Hz), 3.77 (1 H, dd, H-5'b, *J*_{5'b,4'} = 3.5, *J*_{gem} = 11.0 Hz), 3.65 (2 H, t, CONDCHa₂CHb₂, *J*_{a,b} = 5.5 Hz), 3.16 (2 H, t, CONDCHa₂CHb₂, *J*_{b,a} = 5.5 Hz), 2.18–2.43 (2 H, m, H-2'a,b). Anal. (C₁₂H₁₈N₄O₆·1/2H₂O): C, 44.58; H, 5.92; N, 17.33. Found: C, 44.52; H, 5.76; N, 17.36.

5-[(*N*-Acetamidoethyl)carbamoyl]-2'-deoxyuridine (^{Ac}E**).** Acetic anhydride (0.13 mL, 1.44 mmol) was added to a solution of **E** (100 mg, 0.32 mmol) in pyridine (4 mL) containing DMAP (10 mg), and the reaction mixture was stirred for 2 days at room temperature. H₂O (1 mL) was added to the mixture, and the whole was further stirred for 10 min. The solvent was removed *in vacuo*, and the residue was coevaporated several times with H₂O. The residue was treated with NH₃/MeOH (saturated at 0 °C, 4 mL) overnight at room temperature, and the solvent was removed *in vacuo*. The residue was purified on a silica gel column (1.9 × 5 cm) with 0–20% MeOH in CHCl₃ to give **^{Ac}E** (37 mg, 31% as a white crystal): mp 203–205 °C; FAB-MS, *m/z* 357 (M⁺ + 1); UV λ_{max} (H₂O) 277 nm (ε 12 900), λ_{max} (0.1 N HCl) 276 nm (ε 14 300), λ_{max} (0.1 N NaOH) 277 nm (ε 13 800); NMR (DMSO-*d*₆) δ 11.86 (1 H, br s, 3-NH), 8.75 (1 H, t, 5-CONH, *J* = 5.5 Hz), 8.69 (1 H, s, H-6), 7.92–7.94 (1 H, m, AcNH), 6.12 (1 H, dd, H-1', *J*_{1',2'a} = 7.1, *J*_{1',2'b} = 6.1 Hz), 5.26 (1 H, d, 3'-OH, *J* = 3.9 Hz), 4.98–5.01 (1 H, m, 5'-OH), 4.21–4.24 (1 H, m, H-3'), 3.83–3.87 (1 H, m, H-4'), 3.55–3.57 (2 H, m, H-5'a,b), 3.25–3.38 (2 H, m, 5-CONHCHa₂CHb₂), 3.15 (2 H, dt, 5-CONHCHa₂CHb₂, *J*_{b,a} = 6.0, *J*_{b,NH} = 5.5 Hz), 2.12–2.18 (2 H, m, H-2'a,b), 1.78 (3 H, s, Ac). Anal. Calcd for C₁₄H₂₀N₄O₇: C, 47.19; H, 5.66; N, 15.72. Found: C, 47.06; H, 5.78; N, 15.51.

5-[[*N*-(2-Anthraquinonylcarbonyl)amino]ethyl]-carbamoyl]-2'-deoxyuridine (^{Ant}E**).** Ethylenediamine (0.50 mL, 5.75 mmol) was added to a solution of **3** (59 mg, 0.10 mmol) in MeOH (2 mL), and the mixture was stirred for 2 days at room temperature. The solvent was removed *in vacuo* and the residue was taken in CHCl₃, which was washed with saturated aqueous KH₂PO₄ (two times) and brine. The separated organic phase was dried (Na₂SO₄) and concentrated. Anthraquinone-2-carboxylic acid (76 mg, 0.30 mmol) and 1-ethyl-3-[3-(dimethylamino)propyl]carbodiimide hydrochloride (57 mg, 0.30 mmol) were added to a solution of the residue in a mixture of pyridine and DMF (1:1, 2 mL). The reaction mixture was stirred overnight at room temperature and was diluted with CHCl₃. The solution was washed successively with H₂O (two times), saturated aqueous NaHCO₃ (two times), and brine. The separated organic phase was dried (Na₂SO₄) and was concentrated to dryness. The residue was treated with NH₃/MeOH (saturated at 0 °C, 5 mL) overnight at room temperature, and the solvent was removed. The residue was further treated with aqueous

80% AcOH (5 mL) for 2 h at room temperature. The solvent was removed, and the residue was coevaporated with H₂O. The residue was purified on a silica gel column (1.1 × 14 cm) with 0–8% MeOH in CHCl₃ to give **AntE** (18 mg, 31% as an oil). A part of the sample was crystallized from EtOH: mp 187–189 °C; FAB-MS, *m/z* 549 (*M*⁺ + 1); NMR (DMSO-*d*₆) δ 11.86 (1 H, br s, 3-NH), 9.06–9.08 (1 H, m, anthraquinone-CONH), 8.87–8.89 (1 H, m, 5-CONH), 8.71 (1 H, s, H-6), 7.95–8.65 (7 H, m, anthraquinone), 6.12 (1 H, t, H-1', *J*_{1',2'} = 6.6 Hz), 5.28 (1 H, d, 3'-OH), 5.01 (1 H, t, 5'-OH), 4.21–4.24 (1 H, m, H-3'), 3.84–3.85 (1 H, m, H-4'), 3.53–3.57 (2 H, m, H-5'a,b), 3.43–3.50 (4 H, m, NCH₂CH₂N), 2.13–2.20 (2 H, m, H-2'a,b). Anal. Calcd for C₂₇H₂₄N₄O₉: C, 59.12; H, 4.41; N, 10.21. Found: C, 58.93; H, 4.60; N, 10.08.

5-[(N-Aminohexyl)carbamoyl]-2'-deoxyuridine (H). To a solution of **3** (2.0 g, 3.39 mmol) in MeOH (30 mL) was added 1,6-diaminohexane (11.8 g, 101 mmol), and the mixture was stirred overnight at room temperature. Workup and the detritiation were done as described for the synthesis of **E** to give **H** (704 mg, 56%, crystallized from MeOH): mp 213 °C; FAB-MS, *m/z* 371 (*M*⁺ + 1); UV λ_{max} (H₂O) 276 nm (ε 12 300), λ_{max} (0.1 N HCl) 277 nm (ε 14 200), λ_{max} (0.1 N NaOH) 276 nm (ε 12 100); NMR (DMSO-*d*₆ + D₂O) δ 8.67 (1 H, s, H-6), 6.12 (1 H, t, H-1', *J*_{1',2'} = 6.5 Hz), 4.24–4.22 (1 H, m, H-3'), 3.88–3.84 (1 H, m, H-4'), 3.57–3.55 (2 H, m, H-5'a,b), 3.32–3.24 (4 H, m, 5-CONHCH₂CH₂), 2.21–2.12 (2 H, m, H-2'a,b), 1.54–1.24 [8 H, m, -(CH₂)₄]. Anal. Calcd for C₁₆H₂₆N₄O₆·1/2 H₂O: C, 50.65; H, 7.17; N, 14.77. Found: C, 50.73; H, 7.08; N, 14.52.

5-[(N-Acetamidohexyl)carbamoyl]-2'-deoxyuridine (AcH). To a solution of **3** (200 mg, 0.34 mmol) in MeOH (4 mL) was added 1,6-diaminohexane (788 mg, 6.80 mmol). The mixture was stirred for 3 days at room temperature. The volatile was removed *in vacuo*, and pyridine (6 mL) was added to the residue. The resulting precipitates were removed by filtration, and Ac₂O (0.60 mL, 15.3 mmol) and DMAP (41 mg, 0.34 mmol) were added to the filtrate. The mixture was stirred overnight at room temperature. H₂O (1 mL) was added to the mixture, the solvent was concentrated, and the residue was coevaporated several times with H₂O. The residue was taken in CHCl₃, which was washed with saturated aqueous NaHCO₃ (two times) and brine. The separated organic phase was dried (Na₂SO₄) and concentrated. The residue was treated with aqueous 80% AcOH (10 mL) overnight at room temperature. The solvent was removed *in vacuo* and coevaporated several times with H₂O. The residue was kept in NH₃/MeOH (saturated at 0 °C, 4 mL) overnight at room temperature, and the solvent was concentrated *in vacuo*. The residue was purified on a silica gel column (2.5 × 13 cm) with 0–15% MeOH in CHCl₃ to give **AcH** (98 mg, 70%, as a white solid): mp 162–163 °C; FAB-MS, *m/z* 413 (*M*⁺ + 1); UV λ_{max} (H₂O) 277 nm (ε 13 700), λ_{max} (0.1 N HCl) 276 nm (ε 14 700), λ_{max} (0.1 N NaOH) 276 nm (ε 14 300); NMR (DMSO-*d*₆) δ 11.86 (1 H, br s, 3-NH), 8.70 (1 H, t, 5-CONH, *J* = 6.3 Hz), 8.67 (1 H, s, H-6), 7.76 (1 H, br s, AcNH), 6.12 (1 H, t, H-1', *J*_{1',2'} = 6.5 Hz), 5.28 (1 H, d, 3'-OH, *J* = 3.9 Hz), 4.98–5.00 (1 H, m, 5'-OH), 4.23–4.24 (1 H, m, H-3'), 3.85–3.86 (1 H, m, H-4'), 3.54–3.56 (2 H, m, H-5'a,b), 3.24 (2 H, q, 5-CONHCH₂CH₂, *J*_{a,b} = *J*_{a,NH} = 6.6 Hz), 2.99 (2 H, q, CONHCH₂CH₂, *J*_{b,a} = *J*_{b,NH} = 6.3 Hz), 2.12–2.20 (2 H, m, H-2'a,b), 1.77 (3 H, s, Ac), 1.24–1.48 [8 H, m, -(CH₂)₄]. Anal. Calcd for C₁₈H₂₈N₄O₇·1/2 H₂O: C, 51.30; H, 6.94; N, 13.29. Found: C, 51.46; H, 6.87; N, 13.26.

5-[(N-Anthraquinonylcarbamoyl)amino]hexyl]-carbamoyl]-2'-deoxyuridine (AntH). A mixture of **3**

(400 mg, 0.609 mmol) and 1,6-diaminohexane (2.12 g, 18.3 mmol) in MeOH (10 mL) was heated for 2 days at 50 °C. Workup and condensation with anthraquinone-2-carboxylic acid (231 mg, 0.914 mmol) and 1-ethyl-3-[3-(dimethylamino)propyl]carbodiimide hydrochloride (174 mg, 0.914 mmol) were done as described for the synthesis of **AntE** to give **AntH** (42 mg, 11% as a yellow solid): mp 200–201 °C; FAB-MS, *m/z* 605 (*M*⁺); UV λ_{max} (MeOH) 257 nm (ε 30 900), 309 nm (ε 3 000), 319 nm (ε 3 200), 323 nm (ε 3 300), λ_{max} (0.1 N HCl) 258 nm (ε 35 000), 271 nm (ε 18 800), 278 nm (ε 19 100), 327 nm (ε 3 900), λ_{max} (0.1 N NaOH) 258 nm (ε 35 700), 278 nm (ε 20 000), 328 nm (ε 4 900); NMR (DMSO-*d*₆) δ 11.86 (1 H, br s, 3-NH), 8.94 (1 H, t, 5-CONH, *J* = 5.5 Hz), 8.73 (1 H, t, CH₂-NHCO), 8.69 (1 H, s, H-6), 8.66 (1 H, s, ant-H), 8.33 (2 H, d, ant-H, *J* = 6.3 Hz), 8.27 (1 H, d, ant-H, *J* = 4.8 Hz), 8.24 (2 H, d, ant-H, *J* = 4.8 Hz), 7.99–7.96 (2 H, m, ant-H), 6.13 (1 H, t, H-1', *J*_{1',2'} = 6.5 Hz), 5.28 (1 H, d, 3'-OH, *J* = 4.2 Hz), 5.00 (1 H, m, 5'-OH, *J* = 4.8 Hz), 4.26–4.23 (1 H, m, H-3'), 3.86 (1 H, dt, H-4', *J*_{4',5'a} = *J*_{4',3'} = 3.5 Hz), 3.58–3.55 (2 H, m, H-5'a,b), 3.27 (2 H, q, 5-CONHCH₂CH₂, *J*_{a,b} = *J*_{a,NH} = 6.5 Hz), 2.21–2.14 (2 H, q, CONHCH₂CH₂, *J*_{b,a} = 6.5 Hz), 2.21–2.14 (2 H, m, H-2'a,b), 1.59–1.36 [8 H, m, -(CH₂)₄]. Anal. Calcd for C₃₁H₃₂N₄O₉·MeOH: C, 60.37; H, 5.70; N, 8.80. Found: C, 60.09; H, 5.66; N, 8.59.

β-Cyanoethyl [5-(Methoxycarbonyl)-5'-O-(dimethoxytrityl)-2'-deoxyuridin-3'-O-yl]-N,N-diisopropylphosphoramidite (4). After successive coevaporation with pyridine, **3** (0.50 g, 0.85 mmol) was dissolved in anhydrous CH₂Cl₂ (10 mL) containing *N,N*-diisopropylethylamine (0.29 mL, 1.7 mmol). 2-Cyanoethyl *N,N*-diisopropylphosphoramidochloride (0.22 mL, 1.28 mmol) was added to the solution, and the reaction mixture was stirred for 50 min at room temperature. The mixture was diluted with CHCl₃ and washed with saturated aqueous NaHCO₃ (two times) and brine. The separated organic phase was dried (Na₂SO₄) and concentrated. The residue was purified on a neutral silica gel column (2.2 × 10 cm) with EtOAc to give **4** (0.57 g, 85% as white foam): FAB-MS, *m/z* 789 (*M*⁺); ³¹P NMR (CDCl₃) 144.59 and 144.08.

5-(Methoxycarbonyl)-5'-O-(dimethoxytrityl)-3'-O-[(pentachlorophenyl)succinyl]-2'-deoxyuridine (6). Succinic anhydride (51 mg, 0.51 mmol) was added to a solution of **3** (200 mg, 0.34 mmol) in anhydrous pyridine (3 mL). The mixture was stirred at 70 °C overnight. H₂O (10 mL) was added to the mixture, and the whole was further stirred for 10 min. The solvent was removed *in vacuo*, and the residue was purified over a silica gel column (1.9 × 15 cm) with 0–10% MeOH in CHCl₃ to give **5** (198 mg, 85% as a pale brown foam): FAB-MS, *m/z* 688 (*M*⁺ + 1). Pentachlorophenol (88 mg, 0.34 mmol) and 1-ethyl-3-[3-(dimethylamino)propyl]carbodiimide hydrochloride (81 mg, 0.42 mmol) were added to a solution of **5** (198 mg, 0.29 mmol) in DMF (2 mL). The mixture was stirred for 4 h at room temperature and then diluted with EtOAc. The solution was washed successively with H₂O (two times), saturated aqueous NaHCO₃ (two times), and brine. The separated organic phase was dried (Na₂SO₄) and concentrated. The residue was purified over a neutral silica gel column (2.2 × 21 cm) with EtOAc/hexane (1:1) to give **6** (121 mg, 46% as a white foam): FAB-MS, *m/z* 936 (*M*⁺); NMR (CDCl₃) δ 8.71 (1 H, s, H-6), 8.03 (1 H, br s, 3-NH), 6.81–7.42 (13 H, m, Ph), 6.26 (1 H, dd, H-1', *J*_{1',2'a} = 5.2, *J*_{1',2'b} = 8.8 Hz), 5.31–5.34 (1 H, m, H-3'), 4.15–4.18 (1 H, m, H-4'), 3.79 (6 H, s, OMe), 3.56 (1 H, dd, H-5'a, *J*_{5'a,4'} = 3.3, *J*_{gem} = 10.7 Hz), 3.33 (1 H, dd, H-5'b, *J*_{5'b,4'} = 2.8, *J*_{gem} = 10.7 Hz), 3.24 (3 H, s, CO₂Me), 3.02 (2 H, t, 3'-OCOCH₂CH₂, *J*_{3',2'} = 6.6 Hz).

$J_{a,b} = 6.5$ Hz), 2.77 (2 H, t, 3'-OCOCH₂CHb₂, $J_{b,a} = 6.5$ Hz), 2.05–2.58 (2 H, m, H-2'a,b).

Synthesis of the CPG Support Containing 5-(Methoxycarbonyl)-5'-*O*-(dimethoxytrityl)-2'-deoxyuridine. Aminopropyl CPG (376 mg, 32.3 μ mol, 85.7 μ mol/g, CPG Inc., NJ) was added to a solution of **6** (121 mg, 129 mmol) in anhydrous DMF (1 mL), and the mixture was kept for 22 h at room temperature. After the resin was washed with anhydrous pyridine, 1 mL of a capping solution (0.1 M DMAP in pyridine/Ac₂O = 9:1) was added, and the whole was kept for 2 h at room temperature. The resin was washed with EtOH and acetone and was dried under vacuum. The amount of loaded nucleoside to the solid support is 21.9 μ mol/g from the calculation of released dimethoxytrityl cation by 0.1 M *p*-toluene-sulfonic acid in CH₃CN.

Synthesis of ODNs. ODNs were synthesized on a DNA synthesizer (Applied Biosystem Model 381A, CA) according to the phosphoramidite method using 1 μ mol of nucleoside residue attached to the resin (39). For the incorporation of 5-methylcytidine, β -cyanoethyl [*N*-(dimethylamino)methylene]-5'-*O*-(dimethoxytrityl)-2'-deoxy-5-methylcytidin-3'-*O*-yl]-*N,N*-diisopropylphosphoramidite was used (0.1 M in CH₃CN solution). Then, fully protected ODNs bearing the solid support were treated with ethylenediamine (1 mL) or 1,6-hexanediamine (400 mg) in MeOH (1 mL) at room temperature or at 45 °C for 12–14 h. After filtration of the resin, which was washed well with MeOH, the filtrate was concentrated *in vacuo*. The residue obtained from the reaction with ethylenediamine was purified by C₁₈ silica gel column chromatography (1.0 \times 7 cm) with a linear gradient of CH₃CN from 0 to 30% in 0.1 M TEAA buffer (pH 7.2). The residue obtained from the reaction with 1,6-hexanediamine was chromatographed on Sephadex G-25 (1.7 \times 27 cm) with 0.1 M TEAA buffer (pH 7.2) before purification on the C₁₈ column. Fractions were concentrated, and the residue was treated with 80% AcOH at room temperature for 20 min; then the solution was concentrated, and the residue was coevaporated with water. The residue was dissolved in water, and the solution was washed with Et₂O; then the H₂O layer was concentrated to give a deprotected ODN. The sample was purified on a DEAE cellulose column (1 \times 9 cm) with a linear gradient from 0.1 to 1.0 M TEAB buffer (pH 8) and then further purified by HPLC with a C₁₈ silica gel column (Inertsil ODS-2, GL Science Inc.) using a gradient of solution A (5% CH₃CN in 0.1 N TEAA buffer, pH 7.0) and solution B (50% CH₃CN in 0.1 N TEAA buffer) to give **8** (23.0), **9** (12.6), **10** (8.5), **11** (11.7), **16** (20.4), **17** (12.4), **18** (16.6), and **19** (14.5). The yields are indicated in parentheses as OD units at 260 nm starting from 1 μ mol scale.

Acetylation of ODNs. A solution containing each ODN (1.0 OD unit at 254 nm) and acetic anhydride (2 μ L) in 0.2 M HEPES buffer (200 μ L, pH 7.2) was kept for 1 h at room temperature. Concentrated NH₄OH (400 μ L) was added to the mixture, and the whole was kept overnight at 4 °C. The solvent was removed *in vacuo*, and the residue was purified by HPLC with the C₁₈ column. Average yields for **24**–**27** were >70%.

Reaction of ODNs with *N*-(Anthraquinone-2-carbonyl)oxy)succinimide. A solution containing each ODN (0.5–3.0 OD units at 254 nm) and *N*-(anthraquinone-2-carbonyl)oxy)succinimide (**17**) (50 μ L, 20 mg/mL in DMF) in 0.05 M NaHCO₃/Na₂CO₃ (50 μ L, pH 10.3) was kept overnight at room temperature. The solvent was removed *in vacuo*, and the residue was taken in H₂O (300 μ L). The solution was acidified by adding 1 N HCl (10–20 μ L) to pH 3–4 and was washed with EtOAc (eight

times). The aqueous phase was neutralized by adding saturated aqueous NaHCO₃, and each ODN was purified by HPLC with the C₁₈ column. Average yields for **12**–**15** and **20**–**23** were more than 70%.

Complete Hydrolysis of ODNs. A solution containing alkaline phosphatase (0.4 unit, Takara Shuzo Co., Ltd.) in 0.1 M Tris-HCl (pH 7.7) and 2 mM MgCl₂ (total 130 μ L) was heated on boiling water for 10 min to inactivate adenosine deaminase activity contaminated in the enzyme solution. The solution and snake venom phosphodiesterase (10 μ g, Boehringer Mannheim) were added to each ODN (0.2 OD unit), and the whole was incubated at 37 °C for 24 h. After heating on boiling water for 5 min, cold EtOH (320 μ L) was added to the reaction mixture, and the whole was kept at –20 °C for 1 h. The cold solution was centrifuged for 20 min (12 000 rpm), and then a supernatant was separated and concentrated. The residue was analyzed by HPLC with the C₁₈ column.

Thermal Denaturation. Each solution contains each ODN (3 μ M) and the complementary strand **28** (3 μ M) and **30** (3 μ M) or the target duplex **29** (3 μ M) in an appropriate buffer. The solution containing each ODN was heated 70 °C for 20 min, then cooled gradually to an appropriate temperature, and used for the thermal denaturation studies. Thermally induced transition of each mixture was monitored at 260 nm on a Gilford Response II. Sample temperature was increased 1 °C/min. Each T_m is given as an average of three measurements.

Partial Hydrolysis of ODN with Venom Phosphodiesterase. Each ODN labeled with ³²P at the 5' end (0.01 OD unit) (**40**) was incubated with venom phosphodiesterase (0.4 mg) in the presence of Torula RNA (0.3 OD unit at 260 nm) in a buffer containing 37.5 mM Tris-HCl (pH 8.0) and 7.5 mM MgCl₂ (total 20 μ L) at 37 °C. Aliquots of the reaction mixture were separated and added to a solution of EDTA (5 mM, 10 μ L) at appropriate periods, and then the mixtures were heated at 100 °C for 3 min. The solutions were analyzed by electrophoresis on 20% polyacrylamide gel containing 8 M urea (**40**). Densities of radioactivity of the gel were visualized by a Bio-imaging Analyzer (Bas 2000, Fuji, Co. Ltd.).

Stability of **19 in the Medium Containing FCS.** The ODN **7** or **19** labeled with ³²P at the 5' end (10 pmol) was mixed with the corresponding unlabeled ODN (each 1 nmol). The mixture was incubated in RPMI 1640 medium (40 μ L) containing 10% FCS (heat-denatured at 56 °C for 30 min prior to use) at 37 °C. Aliquots (4 μ L) of the reaction mixture were separated and added to a solution of EDTA (5 mM, 10 μ L) at appropriate periods, and then the mixtures were heated at 100 °C for 5 min. The solutions were analyzed by electrophoresis on 20% polyacrylamide gel containing 8 M urea. The gels were analyzed as described above.

ACKNOWLEDGMENT

This work was supported in part by a Grant-in-Aid for Scientific Research from the Ministry of Education, Science, Sports, and Culture, Japan.

LITERATURE CITED

- (1) Cohen, J. S., Ed. (1989) *Oligodeoxynucleotides: Antisense Inhibitors of Gene Expression*, The Macmillan Press Ltd., London.
- (2) Uhlmann, E., and Peyman, A. (1990) Antisense oligonucleotides: a new therapeutic principle. *Chem. Rev.* 90, 544–584.
- (3) Beaucage, S. L., and Iyer, R. P. (1992) The synthesis of oligonucleotides via the phosphoramidite approach: advances and applications. *Tetrahedron* 48, 2223–2311.

- (4) Crooke, S. T. (1992) Therapeutic applications of oligonucleotides. *Annu. Rev. Pharmacol. Toxicol.* **32**, 329–376.
- (5) Beaucage, S. L., and Iyer, R. P. (1993) The functionalization of oligonucleotides via phosphoramidite derivatives. *Tetrahedron* **49**, 1925–1963.
- (6) Beaucage, S. L., and Iyer, R. P. (1993) The synthesis of modified oligonucleotides by the phosphoramidite approach and their application. *Tetrahedron* **49**, 6123–6194.
- (7) Crooke, S. T., and Lebleu, B., Eds. (1993) *Antisense Research and Applications*, CRC Press, Boca Raton, FL.
- (8) Cosstick, R., and Eckstein, E. (1985) Synthesis of d(GC) and d(CG) octamers containing alternating phosphorothioate linkages: effect of the phosphorothioate group on the B-Z transition. *Biochemistry* **24**, 3630–3638.
- (9) LaPlanche, L. A., James, T. L., Powell, C., Wilson, W. D., Uznanski, B., Stec, W. J., Summers, M. F., and Zon, G. (1986) Phosphorothioate-modified oligonucleotides. III. NMR and UV spectroscopic studies of the Rp-Rp, Sp-Sp, and Rp-Sp duplexes, [d(CGsAATTCC)]₂, derived from diastereomeric O-ethyl phosphorothioates. *Nucleic Acids Res.* **14**, 9081–9093.
- (10) Latimer, L. J. P., Hampel, K., and Lee, J. S. (1989) Synthetic repeating sequence DNAs containing phosphorothioates: nuclease sensitivity and triplex formation. *Nucleic Acids Res.* **17**, 1549–1561.
- (11) Hacia, J. G., Wold, B. J., and Dervan, P. B. (1994) Phosphorothioate oligonucleotide-directed triple helix formation. *Biochemistry* **33**, 5367–5369.
- (12) Tidd, S. M., Hawley, P., Warenus, H. M., and Gibson, I. (1988) Evaluation of N-ras oncogene antisense, sense, and nonsense sequence methylphosphonate oligonucleotide analogues. *Anti-Cancer Drug Des.* **3**, 117–127.
- (13) Walder, R. Y., and Walder, J. A. (1988) Role of RNase H in hybrid-arrested translation by antisense oligonucleotides. *Proc. Natl. Acad. Sci. U.S.A.* **85**, 5011–5015.
- (14) Stein, C. A. (1995) Phosphorothioate oligodeoxynucleotides: Antisense or anti-protein? *Antisense Res. Dev.* **5**, 241 and references cited therein.
- (15) Agrawal, S. (1996) Antisense oligonucleotides: towards clinical trials. *Trends Biotechnol.* **14**, 376–387.
- (16) Ono, A., Dan, A., and Matsuda, A. (1993) Synthesis of oligonucleotides containing a novel 2'-deoxyuridine analogue that carries an aminoalkyl tether at 1'-position; stabilization of duplex formation by an intercalating group accommodated in the minor groove. *Biomed. Chem. Lett.* **3**, 615–618.
- (17) Ono, A., Dan, A., and Matsuda, A. (1993) Synthesis of oligonucleotides carrying linker groups at the 1'-position of sugar residues. *Bioconjugate Chem.* **4**, 499–508.
- (18) Nara, H., Ono, A., and Matsuda, A. (1995) DNA duplex and triplex formation and resistance to nucleolytic degradation of oligodeoxynucleotides containing *syn*-norspermidine at the 5-position of 2'-deoxyuridine. *Bioconjugate Chem.* **6**, 54–61.
- (19) Ramasamy, K. S., Zounes, M., Gonzalez, C., Freier, S. M., Lesnik, E. A., Cummins, L. L., Griffey, R. H., Monia, B. P., and Cook, P. D. (1994) Remarkable enhancement of binding affinity of heterocycle-modified DNA to DNA and RNA. Synthesis, characterization and biophysical evaluation of N²-imidazolylpropylguanine and N²-imidazolyl-2-aminoadenine modified oligonucleotides. *Tetrahedron Lett.* **35**, 215–218.
- (20) Warren, R. A. J. (1980) Modified bases in bacteriophage DNAs. *Annu. Rev. Microbiol.* **34**, 137–158.
- (21) Wiberg, J. S. (1967) Amber mutants of bacteriophage T4 defective in deoxycytidine diphosphatase and deoxycytidine triphosphatase. Role of 5-hydroxymethylcytosine in bacteriophage deoxyribonucleic acid. *J. Biol. Chem.* **242**, 5824–5829.
- (22) Kropinski, A. M. B., Bose, R. J., and Warren, R. A. J. (1973) 5-(4-Aminobutylaminomethyl)uracil, an unusual pyrimidine from the deoxyribonucleic acid of bacteriophage ΦW-14. *Biochemistry* **12**, 151–157.
- (23) Cohen, S. S., and McComic, F. P. (1979) Polyamines and virus multiplication. *Adv. Virus Res.* **24**, 331–387.
- (24) Neuhaud, J., Maltman, K. L., and Warren, R. A. J. (1980) Bacteriophage ΦW-14-infected pseudomonas acidovorans synthesizes hydroxymethyldeoxyuridine triphosphate. *J. Virol.* **34**, 347–353.
- (25) Takeda, T., Ikeda, K., Mizuno, Y., and Ueda, T. (1987) Synthesis and properties of deoxyligonucleotides containing putrescinylythymine. *Chem. Pharm. Bull.* **35**, 3558–3567.
- (26) Manoharan, M. (1993) Designer antisense oligonucleotides: conjugation chemistry and functionality placement. In *Antisense Research and Applications* (S. T. Crooke and B. Lebleu, Eds.) pp 303–349, CRC Press, .
- (27) MacMillan, A. M., and Verdine, G. L. (1990) Synthesis of functionally tethered oligonucleotides by the convertible nucleoside approach. *J. Org. Chem.* **55**, 5931–5933.
- (28) MacMillan, A. M., and Verdine, G. L. (1991) Engineering tethered DNA molecules by the convertible nucleoside approach. *Tetrahedron* **47**, 2603–2616.
- (29) Coleman, R. S., and Kesicki, E. A. (1994) Synthesis and postsynthetic modification of oligonucleotides containing 4-thio-2'-deoxyuridine. *J. Am. Chem. Soc.* **116**, 11636–11642.
- (30) Xu, Y.-Z., Zheng, Q., and Swann, P. (1992) Synthesis and duplex stability of oligodeoxynucleotides containing 6-mercaptopurine. *Tetrahedron* **48**, 1729–1740.
- (31) Gao, H., Fathi, R., Gaffney, B. L., Goswami, B., Kung, P.-P., Rhee, Y., Jin, R., and Jones, R. A. (1992) 6-O-(Pentafluorophenyl)-2'-deoxyguanosine: a versatile synthon for nucleoside and oligonucleotide synthesis. *J. Org. Chem.* **57**, 6954–6959.
- (32) Kim, S. J., Stone, M. P., Harris, C. M., and Harris, T. M. (1992) A postoligomerization synthesis of oligodeoxynucleotides containing polycyclic aromatic hydrocarbon adducts at the N⁶ position of deoxyadenosine. *J. Am. Chem. Soc.* **114**, 5480–5481.
- (33) Ono, A., Haginoya, N., Kiyokawa, M., Minakawa, N., and Matsuda, A. (1993) A novel and convenient post-synthetic modification method for the synthesis of oligodeoxyribonucleotides carrying amino linkers at the 5-position of 2'-deoxyuridine. *Biomed. Chem. Lett.* **4**, 361–366.
- (34) Hashimoto, H., Nelson, M. G., and Switzer, C. (1993) Zwitterionic DNA. *J. Am. Chem. Soc.* **115**, 7128–7134.
- (35) Shabarova, Z., and Bogdanov, A. (1994) *Advanced Organic Chemistry of Nucleic Acids*, VCH Publishers, New York.
- (36) Froehler, B. C., Wadwani, S., Terhorst, T. J., and Gerrard, S. R. (1992) Oligodeoxynucleotides containing C-5 propyne analogs of 2'-deoxyuridine and 2'-deoxycytidine. *Tetrahedron Lett.* **33**, 5307–5310.
- (37) Moulds, C., Lewis, J. G., Froehler, B. C., Grant, D., Huang, T., Milligan, J. F., Matteucci, M. D., and Wagner, R. W. (1995) Site and mechanism of antisense inhibition by C-5 propyne oligonucleotides. *Biochemistry* **34**, 5044–5053.
- (38) Gutierrez, A. J., Terhorst, T. J., Matteucci, M. D., and Froehler, B. C. (1994) 5-Heteroaryl-2'-deoxyuridine analogs. Synthesis and incorporation into high-affinity oligonucleotides. *J. Am. Chem. Soc.* **116**, 5540–5544.
- (39) Atrinson, A., and Smith, M. (1984) *Oligonucleotide Synthesis: A Practical Approach* (M. J. Gait, Ed.) IRL Press, Oxford, U.K.
- (40) Maniatis, T., Fritsch, E. F., and Sambrook, J. (1982) *Molecular Cloning*, Cold Spring Harbor Laboratory, Cold Spring Harbor, NY.

Synthesis of Conjugates for a Barbiturate Screening Assay

Maciej Adamczyk,* Jonathan Grote, Jeanine Douglas, Robert Dubler, and Charles Harrington

Department of Chemistry (D9NM), Abbott Diagnostics Division, Abbott Laboratories, 100 Abbott Park Road, Abbott Park, Illinois 60064-3500. Received November 29, 1996*

Novel derivatives of barbiturates functionalized with free carboxylic acids were designed and synthesized. Coupling of 5-cyclopentyl-5-carboxycrotylbarbituric acid via its active ester to an aminofluorescein derivative produced a fluorescent tracer. Conjugation of the 5-cyclopentenyl-5-carboxyethylbarbituric acid via its mixed anhydride to thyroglobulin allowed for subsequent development of a polyclonal antibody which was evaluated for binding in a fluorescence polarization immunoassay format with various barbiturates. The binding studies showed good cross-reactivity of a variety of barbiturates containing both aromatic and aliphatic 5-substituents with the tested antisera. The relationship between the immunogen architecture, the chemical structure of the binding analytes, and the characteristics of the antisera is also presented.

INTRODUCTION

Barbiturates are central nervous system depressants that are frequently administered on a therapeutic basis as sedatives, hypnotics, and anticonvulsants. These drugs have been known for several decades, having been introduced into therapeutic use by Fisher and von Mering in the early 1900s (1). A large number of different barbiturates have since been synthesized, several of which are still in use (2).

Disubstitution at the 5-position is required for pharmacological activity, as unsubstituted or 5-monosubstituted barbituric acids demonstrate no CNS activity. Small structural variations in these 5-substituents cause substantial changes in the drug's physiological effects and duration (2). Because of the rapid onset of their CNS activity, the most frequently abused barbiturates (including secobarbital, pentobarbital, and amobarbital) have alone or in combination with other drugs been frequently used to commit suicide (3, 4). Therefore, rapid determination of the presence or absence of barbiturates in a comatose patient prior to emergency medical treatment can be the difference between life and death (4).

Structurally, barbiturates can be divided into two classes: those containing aliphatic 5-substituents (such as secobarbital, Figure 1) and those containing an aromatic 5-substituent (such as phenobarbital, Figure 1).

The ideal screening assay for barbiturates would allow for rapid determination of the presence or absence of a variety of structures with subtle structural differences. Competitive binding immunoassay techniques are advantageous over chromatographic techniques such as high-performance liquid chromatography (HPLC) and gas chromatography (GC) for this purpose, since chromatographic techniques need initial sample extraction and have lengthy assay time requirements (5). However, immunoassay techniques such as enzyme immunoassay (EIA) and substrate-linked fluorescence immunoassay (SLFIA) both contain enzymes that are sensitive to enzyme inhibitors or other reactive enzymes contained in the sample (6), while radioimmunoassay (RIA) has other severe shortcomings, including short shelf life

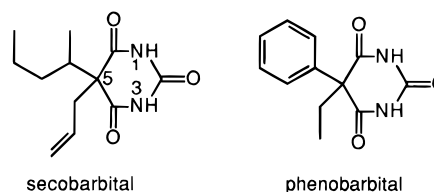
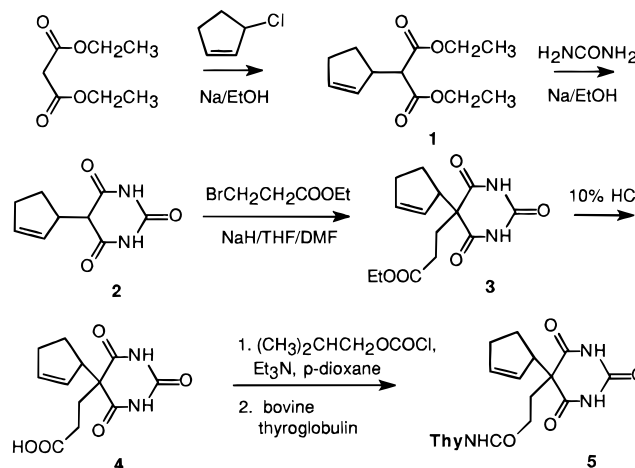


Figure 1. Structures of secobarbital and phenobarbital.

Scheme 1. Synthesis of the Barbiturate Immunogen

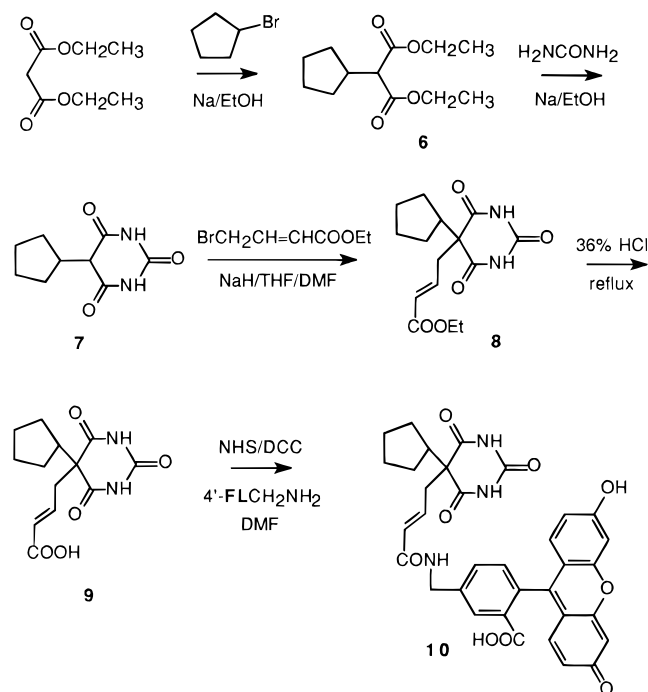


reagents and the hazards of working with, storage of, and disposal of radioactive materials (7). Alternatively, fluorescence polarization immunoassay (FPIA) is ideally suited for automation and employs fluorescent tracers and antibodies, thus avoiding the disadvantages associated with enzyme sensitivity and the hazards of radio-labeled tracers (8).

The quality of a screening immunoassay greatly depends on the availability of antibodies that are specific for the target class of analytes. In this work, we present the design and synthesis of a hapten that shows the structural properties of both the aliphatic and aromatic classes of barbiturates (Scheme 1). This hapten was conjugated to prepare an immunogen useful for eliciting antibodies in sheep. A complementary fluorescent tracer was also synthesized (Scheme 2). The binding characteristics of the obtained antibodies were assessed with various barbiturates in competition with the fluorescent tracer.

* Author to whom correspondence should be addressed [telephone (847) 937-0225; fax (847) 938-8927; e-mail adamczyk@apmac.abbott.com].

© Abstract published in *Advance ACS Abstracts*, April 15, 1997.

Scheme 2. Synthesis of the Barbiturate Tracer**MATERIALS AND METHODS**

All reagents were purchased from Aldrich Chemical Co., Inc., Milwaukee, WI, and were used without further purification, except where noted. Solvents (HPLC grade) and silica gel were obtained from E. Merck Science, Darmstadt, Germany, and were used without further purification. ^1H NMR and ^{13}C NMR were recorded at 300 and 75 MHz, respectively, on a Varian Gemini 300 spectrometer with tetramethylsilane (TMS) as internal standard. Electrospray mass spectrometry (ESMS) was performed on a Perkin-Elmer Siex API III. HPLC was performed on a Waters RCM C_{18} (8 \times 100 mm) reversed phase μ Bondapak column at 2 mL/min (detection at 220 nm) with the solvent indicated.

Preparation of the Barbiturate Immunogen (5). Dicyclopentadiene (50 mL) was depolymerized (9), providing 31.22 g of cyclopentadiene. To the cyclopentadiene cooled to -78°C was added gaseous HCl (9) in portions until the weight had increased to 46.4 g. The resulting crude 3-chlorocyclopentene was added in portions to a preformed solution of sodium diethylmalonate, prepared by adding diethyl malonate (73 mL, 0.48 mol) to a solution of sodium (11.0 g, 0.48 mol) in ethanol (200 mL). Each addition of the 3-chlorocyclopentene produced a noticeably exothermic reaction. After the addition was complete, the resulting yellow suspension was refluxed for 14 h. Most of the ethanol was removed by rotary evaporation from the cooled solution, and the residue was diluted with 300 mL of water. The solution was extracted with ether (3 \times 100 mL), and the combined ether extracts were washed with water (2 \times 50 mL), dried over MgSO_4 , and concentrated to a red oil. Distillation provided 45.194 g (42%) of diethyl cyclopentenylmalonate (**1**) as a colorless oil: bp $99\text{--}103^\circ\text{C}$ (0.8 mm); ^1H NMR (CDCl_3) δ 5.81 (ddd, olef H, 1H, $J = 5.7, 4.5$, and 2.3 Hz), 5.66 (ddd, olef H, 1H, $J = 5.7, 4.3$, and 2.1 Hz), 4.18 (q, ethyl CH_2 , 4H, $J = 7.1$ Hz), 3.34 (m, allyl CH, 1H), 3.22 (d, 1H, malonate CH, $J = 9.6$ Hz), 2.34 (m, allyl CH_2 , 2H), 2.13 (m, aliph CH, 1H), 1.60 (m, aliph CH, 1H), 1.25 (t, ethyl CH_3 , 6H, $J = 7.2$ Hz); ^{13}C NMR (CDCl_3) δ 168.9, 168.8, 132.9, 131.6, 61.1, 57.0, 45.2, 31.6, 27.7, 14.0; ESMS, m/z 227 ($\text{M} + \text{H}$) $^+$, 244 ($\text{M} + \text{NH}_4$) $^+$.

To a solution of sodium (3.51 g, 153 mmol) in ethanol (50 mL) was added urea (3.05 g, 51 mmol) and diethyl cyclopentenylmalonate (**1**, 10.00 g, 44.2 mmol). After 14 h of refluxing, the white suspension was dissolved in water and acidified to pH ~ 2 . The off-white solid collected by filtration was crystallized from ~ 200 mL of 30% ethanol/water, to provide 5.656 g (66%) of cyclopentenylbarbituric acid (**2**) as tan plates, mp $192\text{--}193^\circ\text{C}$. An additional 1.314 g of light brown powdery crystals (17%) with mp $186\text{--}188^\circ\text{C}$ was obtained by concentration to 80 mL and crystallization over 14 h. Both materials showed the following: ^1H NMR ($\text{DMSO}-d_6$) δ 11.17 (s, barb. NH, 1H), 11.13 (s, barb. NH, 1H), 5.80 (m, olef CH, 1H), 5.59 (m, olef CH, 1H), 3.30 (br s, allyl CH + barb. CH, 2H), 2.22–2.08 (m, allyl CH_2 , 2H), 2.01–1.78 (m, aliph. CH_2 , 2H); ^{13}C NMR ($\text{DMSO}-d_6$) δ 170.4, 170.2, 151.3, 133.2, 130.4, 52.2, 48.5, 31.7, 26.2; ESMS, m/z 195 ($\text{M} - \text{H}$) $^-$.

Sodium hydride (95%, 135 mg, 5.36 mmol) was suspended in 2 mL of tetrahydrofuran (THF), and a solution of 5-cyclopentenylbarbituric acid (**2**, 1.00 g, 5.10 mmol) in 18 mL of dimethylformamide (DMF) was added. After 4 h of stirring, ethyl 3-bromopropionate (0.72 mL, 5.61 mmol) and potassium iodide (169 mg, 1.02 mmol) were added, and the reaction was refluxed for 24 h. The reaction mixture was poured into 100 mL of water and extracted with ethyl acetate (3 \times 50 mL). The combined extracts were washed with water (2 \times 50 mL), dried over MgSO_4 , and concentrated. Chromatography on a 2 \times 18 cm column of silica gel, eluting with 100 mL each of 30, 40, and 50% EtOAc/hexanes, provided 1.159 g (77%) of the disubstituted barbituric acid ester (**3**) as a white solid: mp $93\text{--}94^\circ\text{C}$; ^1H NMR (CDCl_3) δ 8.77 (s, barb. NH, 1H), 8.67 (s, barb. NH, 1H), 5.93 (m, olef CH, 1H), 5.64 (m, olef CH, 1H), 4.08 (q, ethyl CH_2 , 2H, $J = 7.5$ Hz), 3.29 (m, allyl CH, 1H), 2.42–2.25 (m, allyl CH_2 + propionate CH_2CH_2 , 6H), 2.05–1.97 (m, aliph cyclopentenyl CH_2 , 2H), 1.21 (t, ethyl CH_3 , 3H, $J = 7.2$ Hz); ^{13}C NMR (CDCl_3) δ 172.6, 171.3, 170.9, 149.2, 136.0, 60.8, 57.9, 56.6, 31.9, 29.7, 27.5, 24.5, 14.0; ESMS, m/z 293 ($\text{M} - \text{H}$) $^-$.

The barbiturate ester (**3**, 200 mg, 0.68 mmol) was suspended in a solution of 1.0 mL of 10% HCl in 1.0 mL of dioxane and stirred for 24 days at ambient temperature. HPLC showed that $>90\%$ of a single product had been formed. The resulting solution was purified by preparative reversed phase HPLC on a C_{18} μ Bondapak 40 mm \times 100 mm PrepPak column, eluting at 40 mL/min with 35% acetonitrile/65% 0.05% CF_3COOH in water, to produce 167 mg (92%) of the acid **4** as a white solid: ^1H NMR ($\text{DMSO}-d_6$) δ 12.10 (br s, COOH, 1H), 11.43 (s, barb. NH, 1H), 11.37 (s, barb. NH, 1H), 5.88 (m, olef CH, 1H), 5.54 (m, olef CH, 1H), 3.11 (s, allyl CH, 1H), 2.19–2.12 (allyl CH_2 , 2H), 2.05–1.80 (m, aliph CH_2 s, 6H); ^{13}C NMR (CDCl_3) δ 173.7, 172.0, 171.8, 150.3, 134.6, 56.7, 55.5, 31.6, 29.5, 27.2, 24.1; ESMS, m/z 265 ($\text{M} - \text{H}$) $^-$.

To a solution of the acid (**4**, 20.7 mg, 77 μmol) in *p*-dioxane (1.6 mL) were added isobutyl chloroformate (17 μL , 134 μmol) and triethylamine (17 μL , 125 μmol). After 2 h of stirring at ambient temperature, the dioxane mixture solution was added to a rapidly stirred solution of 318 mg of bovine thyroglobulin in 17 mL of 0.05 M, pH 9.5, borate buffer. After 2 h of stirring at ambient temperature, the solution was dialyzed against 0.05 M, pH 7.5, phosphate (five changes, at least 8 h between changes), to produce the immunogen **5**. TNBS titration (**10**) indicated that 70% of the available amino groups had been modified.

Preparation of the Barbiturate Tracer (10). Sodium (9.2 g, 0.40 mol) was carefully dissolved in ethanol (150 mL), and diethyl malonate (60 mL, 0.40 mol) was added. After a brief period of stirring, cyclopentyl bromide (44 mL, 0.40 mol) was added, and the reaction mixture was refluxed for 14 h. The suspension was poured into 100 mL of water and extracted with ethyl acetate (3×100 mL). The combined extracts were dried over MgSO_4 and concentrated. Distillation afforded 66.535 g (73%) of diethyl cyclopentylmalonate (**6**) as a clear colorless oil: bp $104\text{--}106^\circ\text{C}$ (3 mm Hg); ^1H NMR (CDCl_3) δ 4.16 (q, ethyl CH_2 , 4H, $J = 7.1$ Hz), 3.15 (d, malonate CH, 1H, $J = 10.3$ Hz), 2.45 (m, cyclopent CH, 1H), 1.85–1.51 (m, cyclopent CH_2 , 8H), 1.24 (t, ethyl CH_3 , 6H, $J = 7.2$ Hz); ^{13}C NMR (CDCl_3) δ 169.2, 61.0, 57.3, 39.4, 30.6, 24.8, 13.9; ESMS, m/z 229 ($\text{M} + \text{H}$) $^+$, 246 ($\text{M} + \text{NH}_4$) $^+$.

Sodium (11.3 g, 490 mmol) was carefully dissolved in 150 mL of ethanol, and urea (9.80 g, 163 mmol) was added, followed by diethyl cyclopentylmalonate (32.409 g, 142 mmol). After 14 h of refluxing, the suspension was poured into water, and the mixture was acidified to pH ~ 2 . The white crystals collected by filtration were recrystallized from ~ 200 mL of 30% ethanol/water, to provided 21.243 g (80%) of cyclopentylbarbituric acid (**7**) as white plates: mp $222\text{--}223^\circ\text{C}$; ^1H NMR ($\text{DMSO}-d_6$) δ 9.56 (br s, barb. NH, 2H) 3.37 (d, 1H, barb. CH, $J = 10.8$ Hz), 2.42 (m, cyclopent CH, 1H), 1.71–1.44 (m, cyclopent CH_2 , 8H); ^{13}C NMR ($\text{DMSO}-d_6$) δ 170.8, 151.4, 51.7, 42.4, 29.0, 24.3; ESMS, m/z 195 ($\text{M} - \text{H}$) $^-$.

Sodium hydride (95%, 271 mg, 10.7 mmol) was suspended in DMF, and a solution of 5-cyclopentylbarbituric acid (2.00 g, 10.2 mmol) in 40 mL of 85% DMF/THF was added. After 3 h of stirring, ethyl 4-bromocrotonate (1.54 mL, 11.2 mmol) and potassium iodide (423 mg, 2.55 mmol) were added, and the reaction was refluxed for 14 h. The reaction was poured into 100 mL of water and extracted with ethyl acetate (2×100 mL). The combined extracts were washed with water (3×50 mL), dried over MgSO_4 , and concentrated. Chromatography on a 3×30 cm column of silica gel, eluting with 100 mL each of 20, 30, 40, 50, and 70% EtOAc/hexanes, provided 1.917 g of a clear pale yellow oil. Crystallization of this material from EtOAc/hexanes provided 1.602 g (51%) of disubstituted barbiturate ester (**8**) as a white solid: mp $141\text{--}142^\circ\text{C}$; ^1H NMR (CDCl_3) δ 7.98 (br s, barb. NH, 2H), 6.65 (dt, 1H, β -olef CH, $J = 14.3$ and 7.5 Hz), 5.90 (d, α -olef CH, 1H, $J = 14.3$ Hz), 4.15 (q, ethyl CH_2 , 2H, $J = 7.2$ Hz), 2.92 (dd, allyl CH_2 , 2H, $J = 7.7$ and 1.1 Hz), 2.43 (m, cyclopent CH, 1H), 1.78–1.49 (m, cyclopent CH_2 , 8H), 1.26 (t, ethyl CH_3 , 3H, $J = 7.1$ Hz); ^{13}C NMR (CDCl_3) δ 171.0, 166.2, 149.3, 126.3, 60.6, 57.7, 50.0, 36.2, 27.1, 24.1, 21.1, 14.0; ESMS, m/z 307 ($\text{M} - \text{H}$) $^-$.

The barbiturate ester (**8**, 200 mg, 0.65 mmol) was suspended in 12 mL of concentrated HCl and refluxed for 45 min. Concentration furnished a white solid, which was crystallized from water to yield 173 mg (95%) of the disubstituted barbiturate acid (**9**) as white needles: mp $217\text{--}218^\circ\text{C}$; ^1H NMR ($\text{DMSO}-d_6$) δ 11.55 (br s, NH and COOH, 3H), 6.48 (dt, β -olef CH, 1H, $J = 15.5$ and 7.7 Hz), 5.72 (d, α -olef CH, 1H, $J = 15.5$ Hz), 2.76 (d, allyl CH_2 , 1H, $J = 7.0$), 2.26 (m, cyclopent CH, 1H), 1.72–1.34 (m, cyclopent CH_2 , 8H); ^{13}C NMR (CDCl_3) δ 181.8, 176.7, 160.0, 152.1, 135.7, 66.3, 58.8, 45.5, 36.8, 34.0; ESMS, m/z 279 ($\text{M} - \text{H}$) $^-$.

To a solution of the acid **9** (20 mg, 71 μmol) in DMF (100 μL) were added *N*-hydroxysuccinimide (11 mg, 93 μmol) and dicyclohexylcarbodiimide (16 mg, 78 μmol). After 8 h of stirring, 4'-aminomethylfluorescein hydrochloride (28 mg, 71 μmol) and triethylamine (10 μL , 71

μmol) were added, and the suspension was stirred for 96 h. Concentration furnished an orange solid, which was dissolved in methanol and purified by preparative reversed phase HPLC on a C_{18} $\mu\text{Bondapak}$ 40 mm \times 100 mm PrepPak column, eluting at 40 mL/min with 38% $\text{CH}_3\text{CN}/62\%$ 0.05% CF_3COOH in water (220 nm), to produce 26 mg (59%) of the fluorescent tracer **10** as a bright yellow solid: $R_T = 5.68$ min (45% $\text{CH}_3\text{CN}/55\%$ 0.05% CF_3COOH in water); ESMS, m/z 622 ($\text{M} - \text{H}$) $^-$.

Immunization of Animals and Preparation of Antisera. Eight sheep were initially immunized with 1 mg of immunogen in 1.0 mL of complete Freund's adjuvant. The sheep were subsequently bled 7–10 days after immunization and then boosted monthly with 0.5 mg of the immunogen in 0.5 mL of incomplete Freund's adjuvant until the response was mature, after which time the animals were boosted with 0.5 mg of the immunogen monthly. From the blood obtained from each animal every 2 weeks, the serum was separated and stored at -20°C . Antisera titers rose slowly and demonstrated consistent titer after about 6 months. Production bleeds (~ 200 mL) collected for 16 weeks were combined to give the antisera pool, which is characterized below.

Evaluation of the Pooled Antisera. The antisera pool was evaluated by fluorescence polarization immunoassay on an Abbott TDx analyzer equipped with Revision 15 software and operated as described in the TDx system operation manual (8) and Popelka et al. (11) using TDx dilution buffer (0.1 M phosphate buffer, pH 7.4, with 0.1% bovine γ -globulin and 0.1% sodium azide). Except where noted, antisera and tracer were added to the internal 3-POT serum vial (S) and tracer vial (T) containers, respectively. Analyte was added to the sample well of the disposable sample cartridge. Polarization measurements were recorded in millipolarization units (mP).

To measure antisera activity, serial dilutions of antibody were added directly to the cuvette, and polarization measurements were made with and without analyte. In these experiments, the serum vial was filled with TDx dilution buffer. Displacement (ΔmP) was calculated by taking the difference between the polarizations of tracer binding without analyte minus tracer binding with analyte. The working titer was selected from the dilution having the maximum displacement. The antisera were further evaluated by comparing the zero calibrator and the A–F span. Once consistent pool-to-pool titer and performance were obtained, the antisera pools were evaluated on the AxSYM analyzer.

Standards were prepared by the addition of analytically pure secobarbital to normal human urine diluent (confirmed to be negative for barbiturates) at concentrations of 0, 200, 400, 700, 1200, and 2000 ng/mL. Using a four-parameter weighted curve fit (duplicate determinations), a calibration curve was constructed (Figure 2). Mean responses to these standards were established using multiple instruments and stored in barcode form for each antisera pool. The two-point Master Calibration Curve thus derived is specific for each pool and refits the standard six-point calibration curve based on the response of an individual instrument to the two-point curve.

Sensitivity of the assay was determined by identifying the lowest measurable concentration of drug in human urine that could be distinguished from a sample known to contain 0 ng/mL of the drug with a 95% confidence limit ($n = 20$). Replicates of a human urine sample known to be negative for barbiturates and the 0 ng/mL standard were both analyzed. The standard deviation of the replicates was then calculated, and twice this

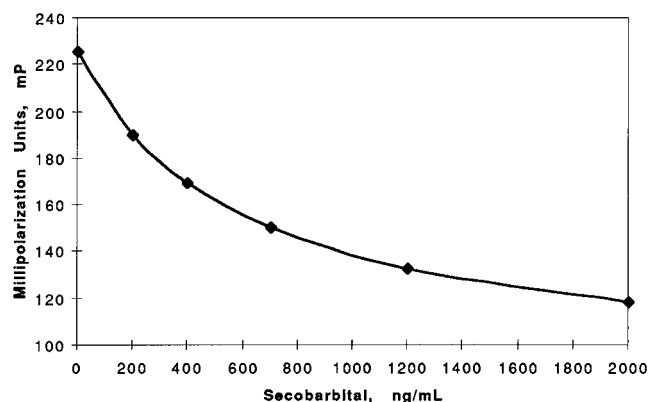


Figure 2. Standard curve with secobarbital as calibrator.

number was subtracted from the average of the replicates in each case.

The antisera was tested for binding with several different barbiturates. Percent cross-reactivity was calculated as $100 \times$ the measured concentration of drug divided by the concentration of analyte added.

RESULTS

Immunogen and Tracer Synthesis. The first step toward development of an immunoassay is to prepare a carefully designed immunogen. This was accomplished by selective conjugation of the unsaturated acid (**4**, Scheme 1) linked at its 5-position to bovine thyroglobulin. This acid was derived from ester (**3**) via hydrolysis at ambient temperature. Attempted hydrolysis at higher temperatures resulted in lower yields of difficultly purified products. Formation of cyclopentenylbarbituric acid (**2**) was derived ultimately from dicyclopentadiene, via cracking to cyclopentadiene (**9**), low-temperature addition of HCl gas (**9**), and addition of the resulting allylic chloride to a preformed solution of sodium diethylmalonate. Formation of the monosubstituted barbituric acid was performed prior to propionate alkylation instead of attempting to form the barbituric acid ring with a bisalkylated malonate, since the presence of the third propionate ester could result in side reactions and lower yields in the formation of the barbiturate ring.

The isobutyl mixed anhydride was formed by reaction with isobutyl chloroformate and triethylamine in *p*-dioxane, and reaction with bovine thyroglobulin produced the desired immunogen (**5**). Analysis by TNBS (**10**) showed that 70% of the available amino groups of the thyroglobulin had been modified.

The multistep synthesis of the tracer proceeded along a similar path (Scheme 2). Cyclopentylmalonate (**6**) was synthesized by alkylation with commercially available cyclopentyl bromide. The second alkylation was again performed after barbiturate formation for the same reasons noted above. Thus, the crotonate side chain was introduced by alkylation of barbituric acid **7** with sodium hydride in the presence of potassium iodide. Carboxylic acid **9** produced via acid hydrolysis of ester **8** was activated as described above and reacted with 4'-aminomethylfluorescein to produce the fluorescent tracer **10**.

Antisera Characterization. All animals responded by producing consistently titered antiserum after about 6 months. The maximum displacement identified for the mature pool of antisera was obtained at 1/76000 dilution, which gave a dynamic range of 107 mP (Figure 2) when tested against secobarbital. Using a two-point calibration curve, negative urine yielded a sensitivity of 34 ng/mL, and the 0 ng/mL standard a sensitivity of 37 ng/mL. With a standard six-point calibration curve, values of 24 and

Table 1. Cross-Reactivities of Barbiturates in Barbiturate Screening Assay

compd	concn added (ng/mL)	concn obsd (ng/mL)	% cross-reactivity
cyclopentobarbital	200	898.9	449.45
butabarbital	200	420.2	210.10
talbutal	200	361.7	180.85
alphenal	200	312.9	156.45
butalbital	200	226.9	113.45
secobarbital	200	200.0	100.00
brallobarbital	200	133.3	66.65
aprobital	200	128.0	64.00
pentobarbital	200	107.5	53.75
phenobarbital	200	105.6	52.83
butobarbital	400	199.2	49.80
allobarbital	400	90.9	22.73
amobarbital	700	183.6	26.23
thiopental	2000	140.3	7.02
veronal	2000	94.9	4.75
5-ethyl-5-(4-hydroxyphenyl)-barbituric acid	2000	70.6	3.53
hexobarbital	100000	291.6	0.292
metharbital	1000000	438.3	0.044
methohexital	1000000	344.3	0.034

Table 2. Cross-Reactivities of Structurally Similar Compounds

compd	concn added (ng/mL)	concn obsd (ng/mL)	% cross-reactivity
glutethimide	10000	451	4.510
primidone	100000	248.7	0.250
aminoglutethimide	100000	203.9	0.204
5-(<i>p</i> -hydroxyphenyl)-5-phenylhydantoin (HPPH)	500000	243.6	0.049

27 ng/mL were obtained. These values are statistically indistinguishable. The assay was thus able to detect concentrations of secobarbital at <40 ng/mL.

Good cross-reactivity was obtained in the screening assay with a number of different barbiturates, including those containing both aliphatic and aromatic 5-substituents, at clinically observed concentrations. Of the 18 barbiturates tested, 13 demonstrated cross-reactivities of >22% (Table 1, upper two groups). Other barbiturates showed lower cross-reactivity: veronal, thiopental, and 5-ethyl-5-(4-hydroxyphenyl)barbituric acid (4-hydroxyphenobarbital, a phenobarbital metabolite) showed limited (3–7%) cross-reactivity at 2000 ng/mL, while hexobarbital, metharbital, and methohexital showed (<1%) cross-reactivity that was observable only at extremely high concentrations.

Additionally, cross-reactivity was evaluated with structurally similar compounds (Table 2). These compounds generally showed low (<1%) cross-reactivities observable only at extremely high concentrations. Glutethimide showed limited cross-reactivity (4.5%) at 10000 ng/mL.

DISCUSSION

An ideal screening assay for barbiturates would allow for rapid, automated determination of the presence of frequently abused barbiturates with equivalent recognition at similar concentrations. In the design of an immunogen, taking structural information into account can be critical in generating a response that will lead to the desired reactivity profiles. Our previous work has stressed the important relationship between the architecture of the immunoconjugate used for the inoculation of the animals and the characteristics of the antibodies obtained (12–15).

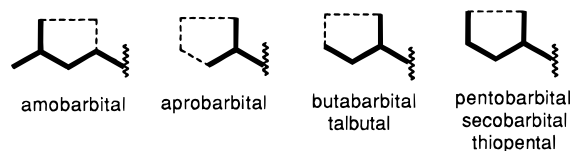


Figure 3. Larger 5-substituent structure of several barbiturates.

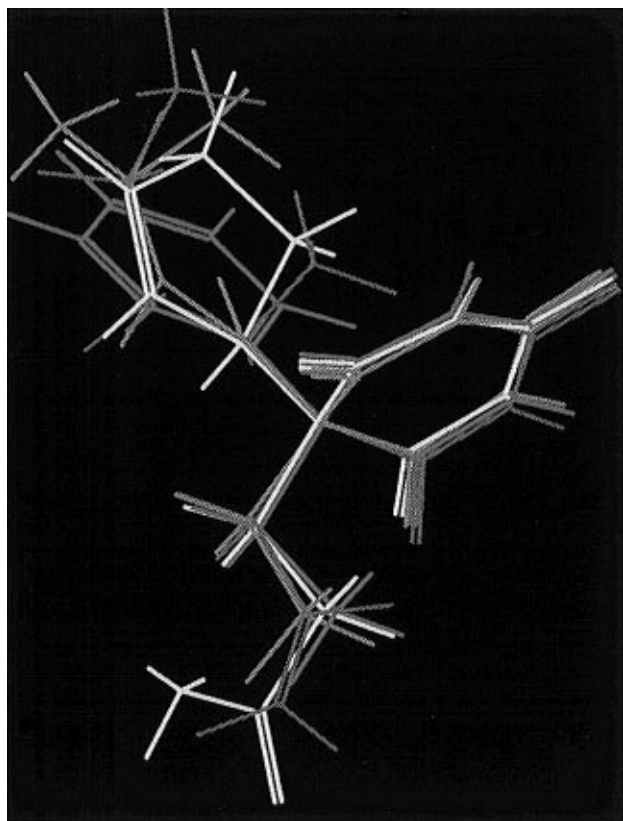


Figure 4. Overlay of the energy-minimized structures of hapten **4** (yellow), secobarbital (green), amobarbital (blue), and phenobarbital (red).

For a screening assay, one needs antibodies with a broad recognition of the class of molecules of interest. For barbiturates, three structural elements are important to closely mimic: the pyrimidinetrione ring, the larger 5-substituent, and the smaller 5-substituent. The imide hydrogens on the pyrimidinetrione ring are particularly important, as they take an active role in hydrogen bonding within the active site, a key interactive force in antibody binding (16).

While the smaller 5-substituent shows little variability (generally ethyl or allyl), considerable variation is observed in the larger 5-substituent (Figures 3 and 5). Thus, linking the barbiturate hapten via the smaller unbranched 5-substituent would appear to be the best strategy, in order to leave the remaining more important determinants fully exposed for optimal antibody recognition. An aliphatic carboxyethyl linker was thus chosen.

Further consideration of the structures of most of the aliphatic barbiturates leads one to observe that the larger of the two 5-substituents, while not always cyclic, can be considered as a fragment of a cyclopentyl ring structure (Figure 3). While conformational studies have shown that unsubstituted noncyclic aliphatic structures are not planar (unsubstituted cyclohexyl rings, for example, exist in the well-known chairlike conformation), phenyl rings are flat, due to the densities of shared π electron structure above and below the plane of the six-membered carbon ring. Electron densities are important

antigenic determinants, since the mechanism of antibody binding relies on the three-dimensional orientation of electron densities rather than on the recognition of chemical structure as such (16). Alternatively, the static conformation of a cyclopentyl ring is much like an envelope, with four atoms in a single plane and the remaining atom above the plane (like the flap of the envelope). In the time-averaged picture, rapid transformation occurs, resulting in each atom temporarily assuming the flap position. The choice of a cyclopentenyl ring as our larger 5-substituent thus offered both the three-dimensional and the π electron character we required for developing an antibody that would detect both aliphatic and aromatic types of 5-substituents of barbiturates. Therefore, hapten **4** became our target.

Tracer design also requires careful consideration of structural information. While a good starting point is frequently the same hapten used in the assay, some discreet modifications in structure are frequently needed to make the tracer bind less strongly, so that in a competitive format it can be effectively displaced by analytes whose structures may not be as well recognized by the antibody. Since several barbiturates contain an allyl group as a 5-substituent, a natural, but slightly different, choice for the linking arm of the tracer was a crotyl substituent. Cyclopentyl was chosen as the another 5-substituent slightly different from the cyclopentenyl group of the hapten, and the crotyl-functionalized cyclopentyl barbiturate **9** became the desired precursor for the tracer.

To better illustrate the previously described structural requirements of barbiturates, molecular modeling was performed (17). Shown in Figure 4 is an overlay of the energy-minimized structures of secobarbital (green) and amobarbital (blue), two frequently abused barbiturates, phenobarbital (cyan), the most frequently prescribed barbiturate containing an aromatic 5-substituent, and the cyclopentenyl barbiturate haptan 4 (yellow). Clearly observable is the structural homology between the barbituric acid ring and the smaller of the two 5-substituents. Even though the larger of the 5-substituents does not display the same spacial homology, rotational changes are possible about the 5-position bonds, as are conformational changes with all of the 5-substituents except the phenyl ring. Such changes would be expected during a normal multistep binding event with an antibody binding site capable of considerable flexibility (16).

As indicated by the cross-reactivity listed in Table 1, desirable recognition was obtained with a variety of different barbiturates at clinically observed concentrations. In all, 13 barbiturates were effectively recognized in the assay at clinically observed concentrations. Secobarbital was selected as the calibrator for the assay and thus shows 100% cross-reactivity. Cyclopentobarbital showed the highest recognition, since it has the greatest structural homology with the hapten. The relatively higher recognition demonstrated by secobarbital and alphenal, which contain a 5-allyl group, as compared to pentobarbital and phenobarbital, which are structurally identical except for their 5-ethyl group (Figure 5), indicates that barbiturates containing a 5-allyl group demonstrate better competitive binding against the fluorescent tracer, which contains an olefinic linker. Talbutal contains a branched 5-isobutyl group, which is structurally more similar to hapten **4** than the smaller 5-isopropyl group of aprobarbital, the 5-bromoallyl group of brallobarbital, or the unbranched 5-allyl group of allobarbital, and thus displays better recognition. Size and branching of the larger 5-substituent are thus observed to be important factors in recognition. Even butalbital, which

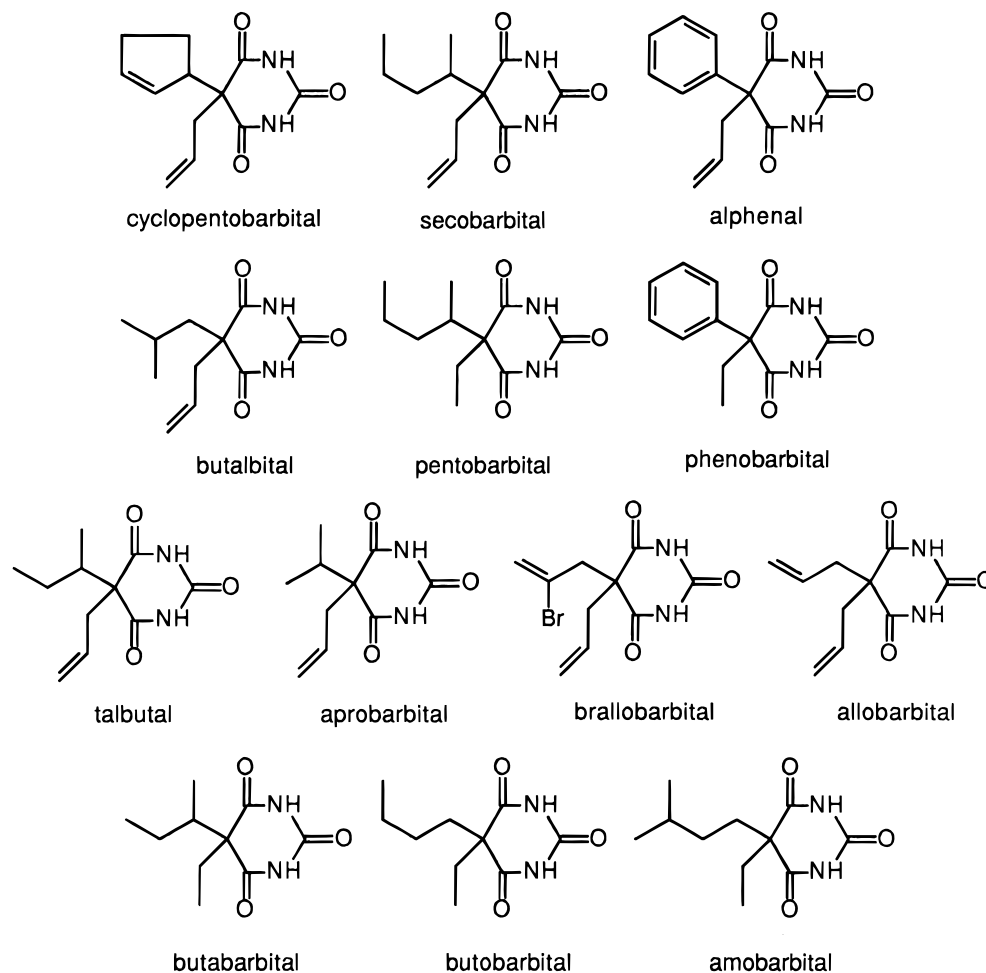


Figure 5. Structural comparisons of barbiturates.

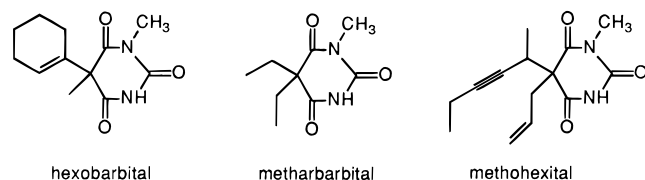


Figure 6. Structures of barbiturates with extremely low recognition.

contains an isobutyl group that would appear to be a poor fit with antisera raised to a hapten containing a cyclic 5-substituent, shows excellent recognition. Barbiturates containing a 5-ethyl substituent generally showed lower recognition. Butabarbital, which contains a branched 5-substituent, would be expected to show higher cross-reactivity than its structural isomer butobarbital, which contains an unbranched 5-butyl group, due to a greater homology with the cyclic group of the hapten. Amobarbital shows lower recognition as compared to other 5-ethyl barbiturates, since its isopentyl group contains a methyl group, which is a poor fit with this antisera (see also Figures 3 and 4, blue structure).

Metharbitol, methohexital, and hexobarbital all showed very low recognition (observable only at extremely high concentrations). This is not surprising, in view of the fact that these barbiturates each have an *N*-methyl group present on the barbiturate ring in place of one of the pyrimidinetrione hydrogens, as shown in Figure 6. For example, veronal is structurally identical to metharbitol, except it lacks the *N*-methyl substituent and, as indicated in Table 1, shows significantly better recognition than metharbitol. The considerably larger size of the *N*-

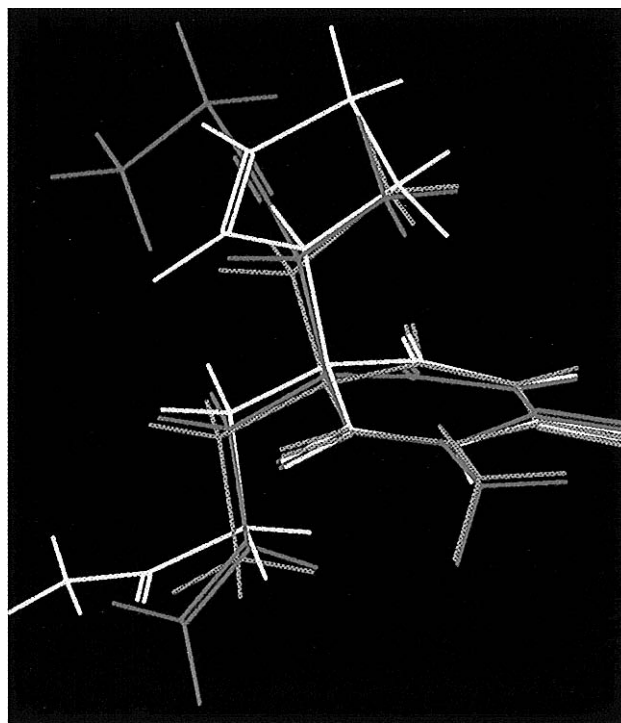


Figure 7. Overlay of the energy-minimized structures of hapten 4 (yellow), metharbitol (blue), and methohexital (red).

methyl group (in place of hydrogen), as well as substitution with a group which can no longer serve as a hydrogen bond donor, demonstrates that influencing both

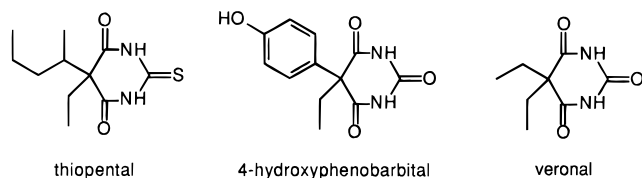


Figure 8. Structures of barbiturates with limited recognition.

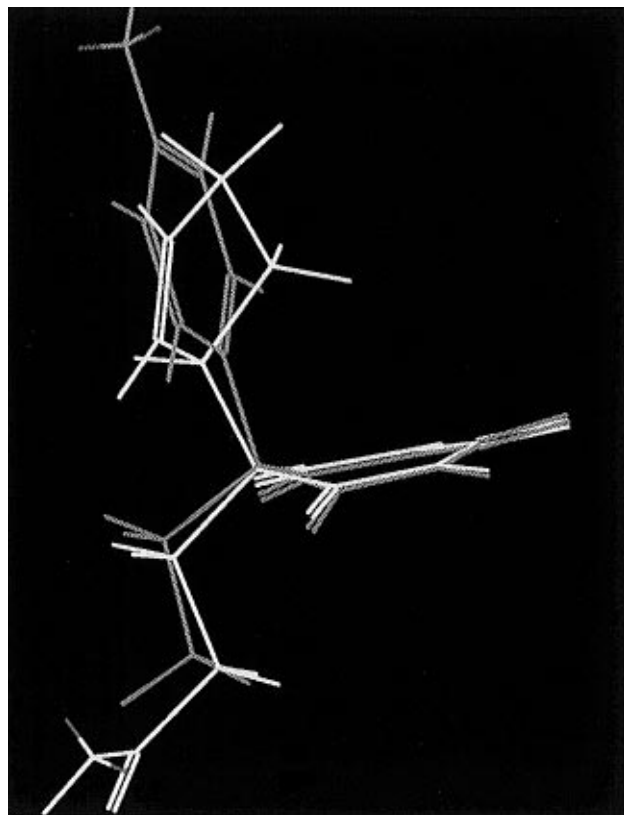


Figure 9. Overlay of the energy-minimized structures of hapten 4 (yellow) and 4-hydroxyphenobarbital (blue).

the van der Waals (hydrophobic) and electrostatic components of binding forces can have a profound effect on antibody recognition. Methohexital also has a pentynyl group which orients four carbons in a sterically inflexible linear arrangement. An overlay of the energy-minimized structures of hapten 4 with metharbital and methohexital (Figure 7) further illustrates the difference the pyrimidinetrione methyl substituent introduces. These molecular features render these barbiturates significantly less susceptible to recognition by the antibody developed here, and thus, these compounds demonstrated measurable cross-reactivity only when tested at very high concentrations.

The specificity of the antibody was further illustrated by the limited recognition observed for 4-hydroxyphenobarbital, thiopental, and veronal at 2000 ng/mL. As seen in Figure 8, thiopental is structurally identical to secobarbital, except that thiopental has a sulfur atom in place of the 3-position pyrimidinetrione oxygen. This contrast between secobarbital and thiopental is analogous to Kollman's study of the recognition of biotin and thiobiotin by streptavidin (18, 19). Kollman expresses binding free energy as a function of the interactions of the analyte with both the solvent and binding protein. Thiobiotin binds much more weakly to streptavidin than biotin, because binding free energy is reduced much more by the O \rightarrow S substitution than the solvent interactions, since three hydrogen bonds of the uriedo oxygen to

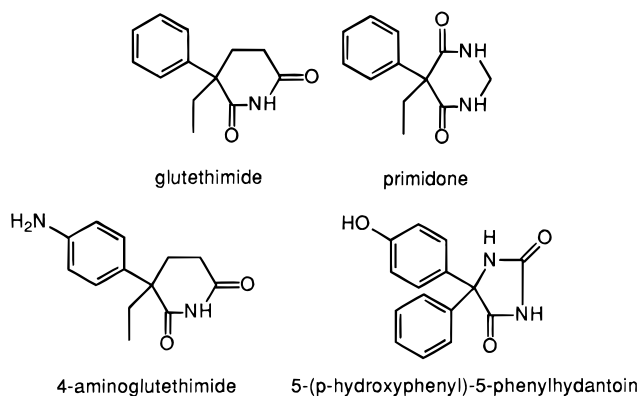


Figure 10. Structurally similar compounds.

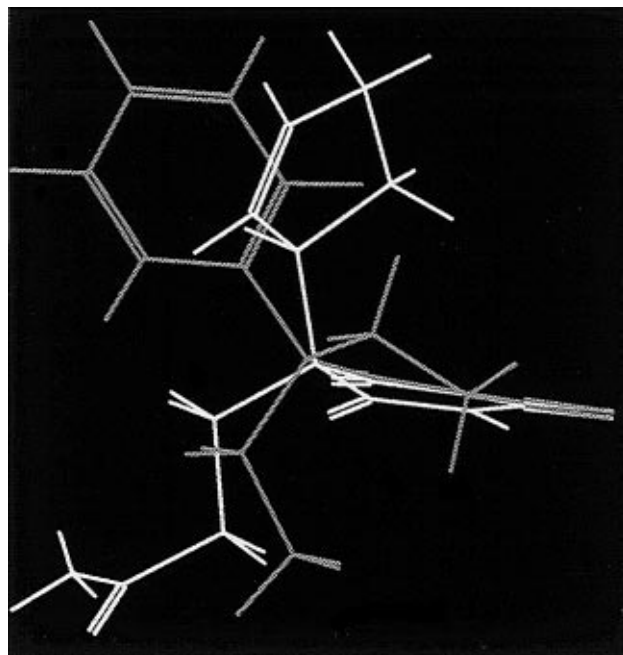


Figure 11. Overlay of the energy-minimized structures of hapten 4 (yellow) and glutethimide (blue).

protein are affected. Presumably, similar effects, resulting in lower recognition, are operating in this case.

On the other hand, 4-hydroxyphenobarbital has a phenolic hydroxy group on the larger of the 5-substituents. The hydroxyl group is sterically larger than the corresponding hydrogen atom in phenobarbital and, due to the polarity of the group, would not be well accommodated by an antibody designed to accommodate hydrophobic 5-substituents. An overlay of hapten 4 with 4-hydroxyphenobarbital (blue structure, Figure 9) further illustrates this point. The attenuated recognition thus observed in comparison to phenobarbital (Table 1) would be expected. Veronal contains two 5-ethyl groups, which would offer poorer van der Waals interactions with the antibody than the saturated butyl groups of analogous 5-ethyl barbiturates butabarbital or butobarbital. Veronal thus displays a lower cross-reactivity in this assay.

Additionally, cross-reactivity was tested with structurally similar compounds that are not barbiturates and was found to be extremely low. Glutethimide (Figure 10), an addictive, rarely prescribed sedative-hypnotic, had to be tested at 10 000 ng/mL to detect any cross-reactivity. While glutethimide is structurally similar to phenobarbital, it possesses two methylene groups in place of the 3- and 4-position imide functionality and thus lacks the hydrogen bonding potential of phenobarbital at these positions. The two methylenes also render its hetero-

cyclic ring less planar than a barbiturate ring and thus affect the antibody van der Waals interactions as well. Figure 11 further illustrates these differences. Primidone also resembles phenobarbital, but has a methylene in place of the 2-position carbonyl. In addition to the differences in heterocyclic structure, both aminoglutethimide and 5-(4-hydroxyphenyl)-5-phenylhydantoin also have polar or charged groups on the phenyl ring which are larger than the analogous hydrogen and would not be well recognized by an antibody designed to accommodate hydrophobic 5-substituents. All of these structures are thus poorly recognized in this assay.

In conclusion, we have provided methods for the development of antisera suitable for a barbiturate screen assay by rational design of immunocomponents. We have demonstrated that a carefully designed immunogen is responsible for the characteristics of the antisera generated. In fact, the antisera generated here demonstrate the desired recognition of a series of clinically important barbiturates. The reactivities observed are attributable to the relationship between the architecture of the immunogen, the characteristics of the resulting antisera, the structure of the fluorescent tracer, and the structures of the barbiturates being tested.

LITERATURE CITED

- (1) Volwiler, E. H. (1925) Alkyl-allyl barbituric acids. *J. Am. Chem. Soc.* 47, 2236–2240.
- (2) Rall, T. W. (1975) Hypnotics and Sedatives; Ethanol. *The Pharmacological Basis of Therapeutics* (A. G. Gilman, T. W. Rall, A. S. Nies, and P. Taylor, Eds.) pp 102–123, Pergamon Press, New York.
- (3) Stead, A. H., et al. (1981) Drug Misuse—The Barbiturate Problem. *J. Forensic Sci. Soc.* 21, 41–53.
- (4) Wesson, D. R., and Smith, D. E. (1977) *Barbiturates: Their Use, Misuse, and Abuse*, pp 18–89, Human Sciences Press, New York.
- (5) Adamczyk, M., Dubler, R. E., Grote, J., Jonas, P. J., and Nelson, J. A. (1991) Barbiturate assay, tracers, immunogens, antibodies, and kit. Eur. Pat. Appl. 0 457 213 A2.
- (6) Pesce, A. J., and Michael, J. G. (1992) Artifacts and limitations of enzyme immunoassay. *J. Immunol. Methods* 150, 111–119.
- (7) Mehta, A. C. (1992) A critical appraisal of chromatographic and immunoassay techniques for clinical drug analysis. *J. Clin. Pharm. Ther.* 17, 325–331.
- (8) TDx System Operation Manual (9520-22), Abbott Laboratories, Abbott Park, IL 60064.
- (9) Moffett, R. B. (1962) Cyclopentadiene and 3-Chlorocyclopentene. *Organic Syntheses*, Collect. Vol. IV, p 238, Wiley, New York.
- (10) Shinoda, T., and Tsuzukida, Y. (1974) Identification of rapidly trinitrophenylating amino groups of human Bence-Jones proteins. *J. Biochem.* 75, 23.
- (11) Popelka, S. R., Miller, D. M., Holen, J. T., and Kelso, D. M. (1981) Fluorescence polarization II. Analyzer for the rapid and precise measurement of fluorescence polarization using disposable cuvettes. *Clin. Chem.* 27, 1198–1201.
- (12) Adamczyk, M., Fishpaugh, J., Harrington, C., Hartter, D., Johnson, D., and Vanderbilt, A. (1993) Immunoassay reagents for psychoactive drugs. I. The method for the development of antibodies specific to amitriptyline and nortriptyline. *J. Immunol. Methods* 162, 47–58.
- (13) Adamczyk, M., Fishpaugh, J., Harrington, C., Johnson, D., and Vanderbilt, A. (1993) Immunoassay reagents for psychoactive drugs. II. The method for the development of antibodies specific to imipramine and desipramine. *J. Immunol. Methods* 162, 187–197.
- (14) Adamczyk, M., Fino, L., Fishpaugh, J., Johnson, D., and Mattingly, P. G. (1994) Immunoassay Reagents for Thyroid Testing. I. Synthesis of Thyroxine Conjugates. *Bioconjugate Chem.* 5, 459–462.
- (15) Adamczyk, M., Johnson, D. D., Mattingly, P. G., Clarisse, D. E., Tyner, J. D., and Perkowitz, M. M. (1994) Reagents and methods for the detection and quantification of thyroxine in fluid samples. U.S. Pat. 5,359,093; *Chem. Abstr.* 122, 24579.
- (16) Davies, C. (1994) Immunoassay Design. *The Immunoassay Handbook* (D. Wild, Ed.) pp 15–44, Stockton Press, New York.
- (17) Energy minimizations and overlays were performed using Chem 3D Plus software available from Cambridge Scientific Computing, Suite 61, 875 Massachusetts Ave., Cambridge, MA, 02139. While energy-minimized structures are not necessarily representative of the molecular conformations that bind to antibodies, we chose energy minimization to provide a common denominator by which various barbiturates could be equitably compared.
- (18) Kollman, P. A. (1996) Advances and Continuing Challenges in Achieving Realistic and Predictive Simulations of the Properties of Organic and Biological Molecules. *Acc. Chem. Res.* 29, 461–469.
- (19) Miyamoto, S., and Kollman, P. A. (1993) Absolute and Relative Binding Free Energy Calculations of the Interaction of Biotin and Its Analogs with Streptavidin Using Molecular Dynamics/Free Energy Perturbation Approaches. *Proteins* 16, 223–245.

BC9700345

Radiolabeling of Epidermal Growth Factor with ^{99m}Tc and *in Vivo* Localization following Intracerebral Injection into Normal and Glioma-Bearing Rats

Jacek Capala,^{*,†} Rolf F. Barth,[†] Michael Q. Bailey,^{‡,§} Robert A. Fenstermaker,^{||} Michael J. Marek,[⊥] and Buck A. Rhodes[⊥]

Departments of Pathology and Veterinary Clinical Sciences, The Ohio State University, Columbus, Ohio 43210, Department of Neurosurgery, Roswell Park Cancer Institute, Buffalo, New York 14273, and RhoMed Inc., Albuquerque, New Mexico 87109. Received October 28, 1996[®]

High grade gliomas may have amplified expression of the epidermal growth factor receptor (EGFR) gene *c-erb-B*, which often is associated with increased expression of transmembrane EGFR. The purpose of the present study was to develop a method for labeling EGF with ^{99m}Tc and to determine whether the resulting radioligand would localize, following intracerebral injection, in rats bearing EGFR-positive gliomas. EGF has a relatively low molecular mass (~6 kDa) compared to monoclonal antibodies, and this has allowed smaller bioconjugates, which should diffuse more rapidly within the brain and more effectively target disseminated glioma cells, to be constructed. In the present study, EGF has been labeled with either ^{131}I or ^{99m}Tc , and *in vitro* uptake of the resulting radioligand has been investigated using C6_{EGFR} rat glioma cells, which had been transfected with the EGFR gene. Cellular uptake of ^{131}I radioactivity peaked after ~30 min of incubation with [^{131}I]EGF, following which time it declined, while ^{99m}Tc radioactivity continued to increase over a 6 h incubation with [^{99m}Tc]EGF. To determine if radiolabeled EGF had *in vivo* tumor-localizing properties, C6_{EGFR} glioma cells were implanted stereotactically into the brains of Fischer rats. Four weeks later, either ^{99m}Tc - or ^{131}I -labeled EGF was injected intracerebrally into normal or glioma-bearing animals using the same stereotactic coordinates. External gamma scintigraphy revealed that ^{131}I radioactivity disappeared rapidly from the brain regions of tumor-bearing animals compared to ^{99m}Tc , ~50% of which remained in the tumor for up to 12 h. In contrast, only ~20% remained in the brains of non-tumor-bearing animals after 6 h. These studies are the first to describe a method for radiolabeling EGF with ^{99m}Tc and to detect it by external scintigraphy in the brains of tumor-bearing animals.

INTRODUCTION

Epidermal growth factor (EGF)¹ is a ~6 kDa, single-chain, 53 amino acid containing polypeptide (Carpenter and Cohen, 1979), which usually is promptly internalized and transferred to lysosomes, where both EGF and its receptor (EGFR) are degraded (Carpenter, 1987; Todderund and Carpenter, 1989). The relatively low molecular mass of EGF has permitted construction of relatively small bioconjugates, which have high affinity for EGFR on tumor cells (Capala et al., 1993, 1996) and possibly could be used to target receptor-positive tumors, especially those in the brain, for either diagnosis or therapy (Harris, 1990; Carlsson et al., 1994).

The majority of high grade gliomas have amplified expression of the EGFR gene, *c-erb-B*, which often is associated with an increase in cell surface receptor expression (Torp et al., 1991; Mondjtahedi and Dean, 1994). As reported by Bigner et al. (1990), 45% of 33 human glioma biopsies showed amplification of the EGFR gene. Subsequently, this was confirmed by Ekstrand et al. (1991) and Tuzi et al. (1991). Gene amplification often results in significantly increased expression of EGFR on the surface membrane of tumor cells (Bigner et al., 1990; Torp et al., 1991). Due to the cellular heterogeneity of high grade gliomas, the distribution of EGFR in each individual tumor is not uniform, but, in 25 of 42 human gliomas studied by Torp et al., more than 50% of the tumor cells bound biotinylated EGF. Because the number of EGFR on tumor cells may be 100 times greater than that on normal, untransformed cells, EGFR has been considered as a potential target for the specific delivery of tumoricidal agents using mAbs against the EGFR or their fragments (Mendelsohn, 1988; Sato and Sato 1989; Modjtahedi and Dean, 1991; Lofts and Gullick, 1994). Preliminary clinical trials have been carried out using anti-EGFR mAbs as a delivery agents of ^{131}I for radioimmunotherapy of brain tumors (Epenetos et al., 1985; Kalofonos et al., 1989; Brady et al., 1991; Snelling et al., 1995), and although no definitive conclusion can yet be made about therapeutic efficacy, no significant toxicity was observed and there was some evidence of a clinical response. One major problem, however, is that only a very small amount of systemically administered anti-EGFR monoclonal antibody (mAb) localizes within the brain tumor. In a recently reported phase I clinical

* Address correspondence to this author at the Medical Department, Brookhaven National Laboratory, Upton, NY 11973 [telephone (516) 344-2693; fax (516) 344-5311; e-mail capala@bnl.gov].

[†] Department of Pathology, The Ohio State University.

[‡] Veterinary Clinical Sciences, The Ohio State University.

[§] Present address: Midwest Veterinary Diagnostic Imaging, Inc., 5678 Moorgate Dr., Columbus, OH 43235.

^{||} Roswell Park Cancer Institute.

[⊥] RhoMed Inc.

[®] Abstract published in *Advance ACS Abstracts*, April 15, 1997.

¹ Abbreviations: BBB, blood–brain barrier; BNCT, boron neutron capture therapy; DMEM, Dulbecco's Modified Eagle's Medium; EDTA, ethylenediaminetetraacetic acid; EGF, epidermal growth factor; EGFR, epidermal growth factor receptor; ip, intraperitoneal; iv, intravenous; mAb, monoclonal antibody; PBS, phosphate-buffered saline; PET, positron emission tomography; SPECT, single photon emission computer tomography; TLC, thin layer chromatography.

study (Faillot et al., 1996) on the possible use of anti-EGFR mAb for the treatment of malignant gliomas, the fraction of antibody recovered per gram of tumor 48 h following continuous intravenous (iv) infusion was in the range of 0.00001–0.0001% of the injected dose per gram. Targeting the EGFR by means of EGF is another approach for delivering potentially tumoricidal agents to malignant gliomas expressing increased amounts of EGFR. The preparation of ^{131}I -labeled EGF for targeted radiotherapy (Capala et al., 1990, 1991; Andersson et al., 1992; Carlsson et al., 1994) and of ^{10}B -labeled EGF as a potential delivery agent for boron neutron capture therapy (BNCT; Capala et al., 1996) previously has been reported.

The purpose of the present study was to extend our previous work to develop a method for radiolabeling EGF with $^{99\text{m}}\text{Tc}$, a gamma-emitting radionuclide whose short half-life (6.8 h) and favorable energy spectrum allow optimal imaging with minimal biological damage. Such a radioligand may be used to identify those tumors with increased amounts of EGFR for better, receptor specific, therapeutic targeting. In this paper we describe a simple method for radiolabeling EGF with $^{99\text{m}}\text{Tc}$ and compare the *in vitro* and *in vivo* properties of [$^{99\text{m}}\text{Tc}$]EGF with those of [^{131}I]EGF.

EXPERIMENTAL PROCEDURES

EGF. Human recombinant EGF, which previously has been shown to bind with high affinity to the EGFR on human glioma U-343MG (Capala et al., 1993) and rat C6_{EGFR} glioma cells (Fenstermaker et al., 1995), was purchased from Upstate Biotechnology, Inc., Lake Placid, NY.

Cells. All cell lines were grown in Dulbecco's Modified Eagle's Medium (DMEM; Gibco, Grand Island, NY) supplemented with 10% fetal bovine serum (Sigma, St. Louis, MO), L-glutamine (2 mM), solution I (1 mM oxaloacetic acid, 0.2 IU/mL crystalline insulin, 0.5 mM sodium pyruvate), streptomycin (100 mg/mL), and penicillin (100 IU/mL) in a humidified atmosphere at 37 °C. The parental C6 rat glioma cells (American Type Culture Collection, Rockville, MD) were transfected with the gene encoding EGFR (Fenstermaker et al., 1995) to yield stable transfectants, designated C6_{EGFR}. As determined by a radioligand binding assay and Scatchard analysis, parental C6 cells did not express EGFR, while transfected cells expressed 3×10^6 receptor sites/cell (Fenstermaker et al., 1995).

Intracerebral Rat Tumor Model. Male CD Fischer rats, weighing 236 ± 16 g (mean \pm SD), were purchased from Harlan Sprague Dawley, Indianapolis, IN, and were maintained on standard rat chow and water *ad libitum*. Intracerebral implantation of C6_{EGFR} tumor cells was carried out according to the method of Clendenon et al. (1990). Animals were anesthetized by intraperitoneal (ip) injection of a 1.6/1.0 mixture of ketamine (100 mg/mL)/xylazine (20 mg/mL) at a dose of 1.3 mL/kg and placed in a stereotactic frame (David Kopf Instruments, Tujunga, CA). The surface of the skull was exposed by a midline incision, and a small burr hole was drilled at a location 7 mm anterior to the interaural line and 3.5 mm to the right of the midline. Then, a precision-milled plastic screw equipped with an injection port was screwed into the hole. Tumor cells (10^5), mixed with serum-free DMEM (10 mL) containing 1.25% low melting point agarose (gelling temperature < 30 °C), were injected into the right caudate nucleus over 10 s. At the end of the procedure the viability of the remaining cells was determined by means of the trypan blue exclusion method. To allow for the implanted glioma cells to produce a tumor of adequate size, *in vivo* studies were carried out 4 weeks

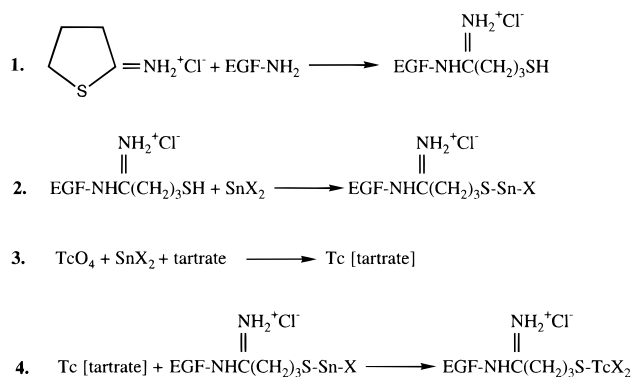


Figure 1. Chemical scheme for radiolabeling EGF with $^{99\text{m}}\text{Tc}$ pertechnetate as modified from the original postulated by Rhodes (1991).

following tumor cells implantation. On the basis of previous studies with this tumor model (San-Galli et al., 1989), as well as our own with the C6 (Fenstermaker et al., 1995) and F98 gliomas (Clendenon et al., 1990; Barth et al., 1997), animals injected intracerebrally die as a result of the expanding brain tumor, which at the time of death is ~ 5 –6 mm in diameter.

Radiolabeling of EGF with ^{131}I . As previously described (Capala et al., 1990), EGF was radioiodinated by means of the chloramine-T method. Briefly, 10 μg of lyophilized EGF was dissolved in 100 μL of 0.25 M potassium phosphate buffer, pH 7.5, and incubated for 1 min with 1 mCi of sodium [^{131}I]iodide and 20 μL of freshly prepared chloramine-T solution (2 mg/mL in 0.5 M phosphate buffer, pH 7.5). The reaction was quenched by adding 50 μL of freshly prepared sodium metabisulfite solution (2 mg/mL in 0.5 M phosphate buffer, pH 7.5). Unbound ^{131}I was separated from [^{131}I]EGF using a desalting, Sephadex G-25 column (PD-10, Pharmacia Biotech, Piscataway, NJ) and eluted with phosphate-buffered saline (PBS), pH 7.2.

Radiolabeling of EGF with $^{99\text{m}}\text{Tc}$. The chemical procedure employed to radiolabel EGF with $^{99\text{m}}\text{Tc}$ pertechnetate is shown in Figure 1. To introduce a thiol group into the terminal amino group of EGF, 400 mg of EGF first was reacted at ambient temperature with 2-iminothiolane (Pierce, Rockford, IL; $50\times$ molar excess) in 600 mL of 7 mM potassium phosphate, 0.1 M NaCl, 1 mM EDTA, and 60 mM triethanolamine under a nitrogen atmosphere for 1 h. Excess, unreacted 2-iminothiolane was separated from EGF using a PD-10 column (Pharmacia Biotech) eluted with protein elution buffer (0.15 M NaCl, 40 mM potassium monohydrate phthalate, 10 mM potassium sodium tartrate, 4 mg/mL inositol, 4 mg/mL glycine, pH 5.6). One milliliter fractions were collected, and protein concentrations were determined spectrophotometrically by measuring absorbance at 280 nm using a Beckman DU-6 spectrophotometer (Beckman Instruments Inc., Irvine, CA). Aliquots of each fraction were mixed with Ellman's reagent [5,5-dithiobis(2-nitrobenzoic acid)] in 0.1 M sodium phosphate buffer, and absorbance at 412 nm was measured spectrophotometrically to determine the presence of sulfhydryl groups. Fractions containing EGF-SH were concentrated by means of Centricon 3 microconcentrators (Amicon, Danvers, MA), and then, the direct labeling method of Rhodes (1991) was used to attach $^{99\text{m}}\text{Tc}$ to thiolated EGF. Modified EGF-SH in protein elution buffer was mixed 1:1 with a nitrogen-purged reducing solution (20 mM potassium monohydrophthalate, 10 mM potassium–sodium tartrate, 1.5 mM stannous tartrate, pH 5.6) and reacted with $^{99\text{m}}\text{Tc}$ sodium pertechnetate (10 mCi) at

ambient temperature for 1–10 min. The reaction mixture was applied to a PD-10 column, eluted with PBS, pH 7.2, and the overall recovery of ^{99m}Tc was determined by collecting the total column effluent and comparing the radioactivity present in it with the radioactivity added to the column. To determine the labeling efficiency, the yield was multiplied by the percentage of ^{99m}Tc associated with the peptide peak. The amount of free pertechnetate and unbound ^{99m}Tc was estimated by thin layer chromatography (TLC) on TLC-SG strips (Gelman Sciences, Ann Arbor, MI) using 85% ethanol as a mobile phase, which separated the soluble, unbound, migrating with the solvent, free ^{99m}Tc pertechnetate from the nonmigrating [^{99m}Tc]EGF. The ratio of bound ^{99m}Tc was expressed as radioactivity detected in the first (origin) half of the strip divided by the total radioactivity, with all measurements corrected for background. Radiocolloid was determined using serum albumin-coated silica gel strips. In this case the ethanol–ammonia–water (2:1:5) mixture was the mobile phase and colloid-bound ^{99m}Tc remained at the origin, while free ^{99m}Tc pertechnetate and radiolabeled EGF migrated with the solvent. The stability of [^{99m}Tc]EGF was determined at various times up to 24 h following labeling.

In Vitro Cellular Uptake and Retention of EGF-Delivered ^{99m}Tc and ^{131}I Radioactivity. Cellular uptake of ^{99m}Tc was determined as follows. C6_{EGFR} glioma cells ($\sim 2 \times 10^5$ per well), grown in 24-well plates (Corning, Corning, NY), were incubated at 4 °C for 90 min in cell culture medium containing various concentrations of [^{99m}Tc]EGF in the range 0.00165–165 nM. At the end of each experiment, the cells were washed with cold PBS and the cell-associated radioactivity was determined by gamma scintillation counting (Tm Analytic, Model 1185, Elk Grove Village, IL). Wild type C6 cells, which did not express EGF receptors, were used as controls to assess background, nonspecific binding, and this was subtracted from the total counts obtained for each sample. Repeated attempts to determine the affinity constant (K_A) of [^{99m}Tc]EGF by a direct binding assay were unsuccessful due to high levels of nonspecific binding (data not shown). Cellular retention of the EGF-delivered radioactivity was determined in the next series of experiments. C6_{EGFR} cells, grown in 24-well plates ($\sim 10^5$ cells/well), were incubated at 37 °C with medium containing 165 nM [^{99m}Tc]– or [^{131}I]EGF for periods of time ranging from 5 min to 6 or 3 h, respectively. In another experiment, the cells were exposed to 165 nM radiolabeled EGF at 37 °C for 30 min, and then the cells were washed and incubated in supplemented DMEM for periods of time ranging from 5 min to 2.5 or 5.5 h. Cell-associated radioactivity and that in the medium were measured by gamma scintillation counting. Again, wild type C6 cells were used as controls and background counts due to nonspecific binding were subtracted from the total counts obtained for each test sample.

Scintigraphic Studies. Four weeks after intracerebral implantation of tumor cells, non-tumor- and tumor-bearing rats were injected either intracerebrally or intratumorally with 1.7–2.3 μg (34–43 μCi) of [^{99m}Tc]EGF or with 1–5 μg (60–200 μCi) of [^{131}I]EGF. The distribution of radioactivity was monitored by means of external scintigraphy using a Sigma 410 gamma camera with a low-energy collimator optimized for ^{99m}Tc detection. The gamma camera was interfaced with a Technicare 560 computer (Ohio-Nuclear, Inc., Solon, OH) for the imaging data collection and processing. Three to five animals were used in each study. The quantity of ^{131}I or ^{99m}Tc radioactivity retained in the brains of non-tumor- and tumor-bearing animals was determined as a function

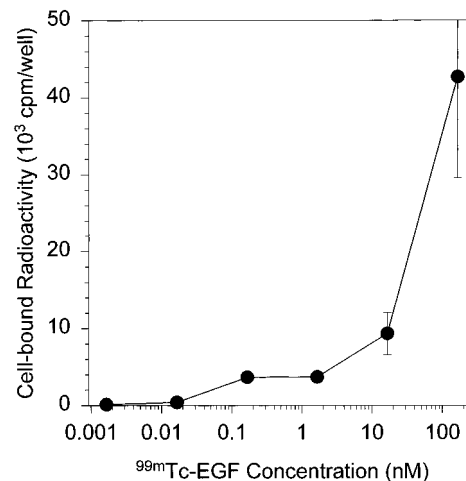


Figure 2. Cell-associated ^{99m}Tc radioactivity following incubation of C6_{EGFR} cells with [^{99m}Tc]EGF. The cells ($\sim 2 \times 10^5$ cells/well) were incubated with increasing concentrations (0.00165–165 nM) of [^{99m}Tc]EGF at 4 °C for 90 min and then washed, and cell-associated radioactivity was determined by gamma scintillation counting. Background values resulting from non-specific binding, obtained from control parental C6 cells, which do not express EGFR, were subtracted at each [^{99m}Tc]EGF concentration. The mean value and the maximum variation of results from two or three samples are shown for each point.

of time, using intrinsic features of the computers' software, which permitted calculation of the average number of counts per pixel in each outlined region of interest.

RESULTS

Radiolabeling of EGF with ^{99m}Tc . The labeling efficiency of EGF-SH with ^{99m}Tc sodium pertechnetate increased from 77% after a reaction time of 1 min to 87% after 10 min, and the estimated specific activities of radiolabeled EGF ranged from 18 to 21 mCi/mg. Since the differences in the efficiency were insignificant, a 1 min reaction time was used to minimize possible damage to the EGF molecule as a result of the reducing conditions of the reaction. As determined by TLC on silica gel strips using 85% ethanol as the solvent phase, and on serum albumin-coated silica gel strips using ethanol–ammonia–water mixture as the solvent phase, $\sim 97\%$ of the ^{99m}Tc radioactivity in the protein peak remained bound to EGF at ambient temperature for up to 24 h.

In Vitro Cellular Uptake and Retention of EGF-Delivered ^{99m}Tc and ^{131}I Radioactivity. [^{99m}Tc]EGF binding as a function of its concentration and ^{99m}Tc uptake as a function of time of incubation with [^{99m}Tc]EGF were studied *in vitro* using C6_{EGFR} cells. Direct binding of [^{99m}Tc]EGF to C6_{EGFR} cells was assessed by measuring cell-associated radioactivity following incubation with increasing concentrations (0.00165–165 nM) of [^{99m}Tc]EGF. As shown in Figure 2, there was a stepwise rather than linear increase of the cell-bound radioactivity with increasing concentrations of the bioconjugate. Similar experiments carried out with wild type C6 cells, which do not express EGFR, showed an order of magnitude lower binding at each concentration, and background due to this nonspecific binding has been subtracted. Cell-bound radioactivity as a function of time following incubation with [^{131}I]EGF or [^{99m}Tc]EGF is shown in Figure 3. Continuous incubation with [^{99m}Tc]EGF resulted in an increase of cell-associated radioactivity proportional to the time of incubation, while incubation with [^{131}I]EGF produced a peak value of cell associated radioactivity at ~ 30 min followed by a 30% decrease over the next 2 h due to release of ^{131}I from the cells after EGF

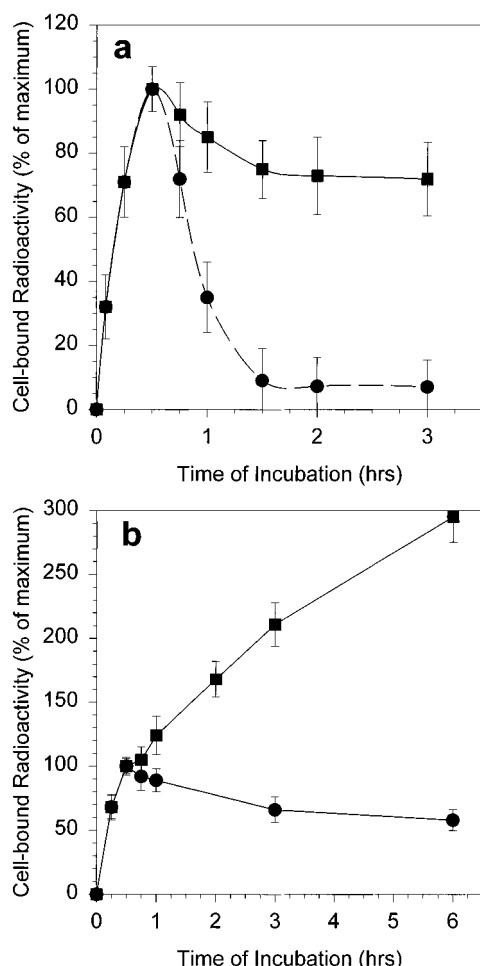


Figure 3. Cell-bound radioactivity as a function of time following incubation with 165 nM $[^{131}\text{I}]\text{EGF}$ (a) or $[^{99\text{m}}\text{Tc}]\text{EGF}$ (b): (■) continuous incubation with radiolabeled EGF; (●) incubation in medium devoid of radiolabeled EGF. The cells were seeded into 24 well plates (~ 105 cells/well) and then, following 30 min of incubation with radiolabeled EGF, incubated further with or without 165 nM radiolabeled EGF. Background values resulting from nonspecific binding, obtained from control parental C6 cells, which do not express EGFR, were subtracted at each EGF concentration. The mean values and standard deviations obtained from triplicate samples are shown.

had been catabolized. When a 30 min incubation of cells with $[^{131}\text{I}]\text{-}$ or $[^{99\text{m}}\text{Tc}]\text{EGF}$ was followed by incubation in medium devoid of radiolabeled EGF, ^{131}I radioactivity was released from the cells after EGF had been catabolized, while approximately 60% of the $^{99\text{m}}\text{Tc}$ radioactivity was retained within the cells for at least 6 h. At this time, the reason for the continued cellular retention of either $^{99\text{m}}\text{Tc}$ -labeled EGF or free $^{99\text{m}}\text{Tc}$ is unknown, but it is possible either that radiolabeling may have altered the catabolism of EGF or that $^{99\text{m}}\text{Tc}$ was retained within cells after EGF had been degraded.

Scintigraphic Studies. Scans were carried out after injection of radiolabeled EGF into 4-week-old tumors or into the corresponding sites of non-tumor-bearing animals. Figures 4 and 5 show images obtained 6 h following injection of $[^{131}\text{I}]\text{-}$ or $[^{99\text{m}}\text{Tc}]\text{EGF}$, respectively. ^{131}I radioactivity disappeared more rapidly from the brain regions of tumor-bearing animals compared to non-tumor-bearing animals. This probably was due to the release of iodine following rapid internalization and degradation of $[^{131}\text{I}]\text{EGF}$ by brain tumor cells. The scans of animals injected with $^{99\text{m}}\text{Tc}$ -labeled EGF, on the other hand, showed that radioactivity persisted in the brain regions of the tumor-bearing animals, but was dispersed

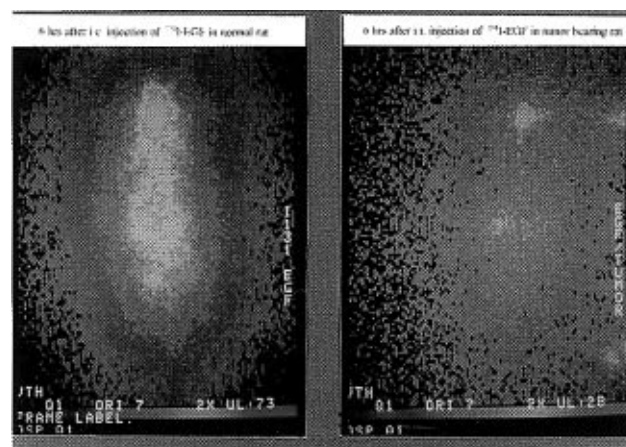


Figure 4. Scans of ^{131}I distribution following ic injection of ~ 5 μg of $[^{131}\text{I}]\text{EGF}$ (200 μCi) in normal rats (left panel) or intratumoral injection of ~ 1 μg of $[^{131}\text{I}]\text{EGF}$ (60 μCi) in tumor-bearing rats (right panel). The tumors were grown for 4 weeks to reach an estimated size of 5 mm in diameter.

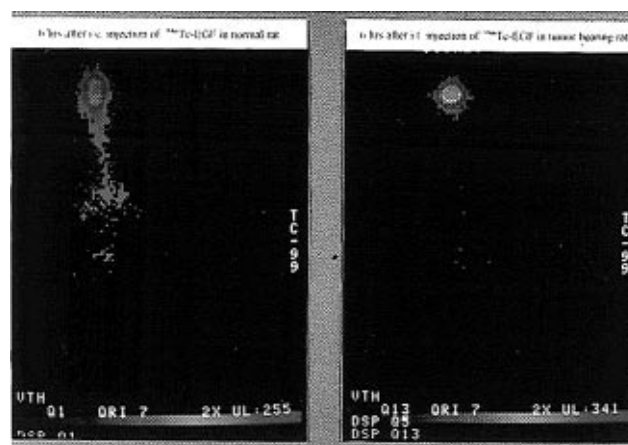


Figure 5. Scans of $^{99\text{m}}\text{Tc}$ distribution following ic injection of ~ 2.3 μg of $[^{99\text{m}}\text{Tc}]\text{EGF}$ (43 μCi) in non-tumor-bearing control rats (left panel) or intratumoral injection of ~ 1.7 μg of $[^{99\text{m}}\text{Tc}]\text{EGF}$ (34 μCi) in glioma-bearing rats (right panel). The tumors were grown for 4 weeks to reach an estimated size of 5 mm in diameter.

in non-tumor-bearing animals (Figure 5). Relative quantitative changes of radioactivity retained in the brain regions of tumor-bearing versus normal rats following injection of ^{131}I - or $^{99\text{m}}\text{Tc}$ -labeled EGF were determined by comparing counts per pixel recorded by the gamma camera. The changes of ^{131}I radioactivity detected in the brain regions were faster in tumor-bearing and slower in non-tumor-bearing control rats (Figure 6a). A different localization pattern was observed for $^{99\text{m}}\text{Tc}$, where $\sim 50\%$ of the radioactivity persisted in the brain regions of tumor-bearing animals for up to 12 h, while only $\sim 20\%$ remained in the brain region of non-tumor-bearing rats after 6 h (Figure 6b). Because it was impossible to precisely define the regions of interest corresponding to other organs on each image, changes of radioactivity in organs such as liver, kidneys, and thyroid could be assessed only qualitatively rather than quantitatively. Comparison of the images obtained with $[^{131}\text{I}]\text{EGF}$ indicated that less activity was present in the liver and it accumulated more quickly in the thyroid of tumor-bearing animals compared to non-tumor-bearing controls.

DISCUSSION

In the present study, we have described a method for radiolabeling EGF with $^{99\text{m}}\text{Tc}$ pertechnetate using a

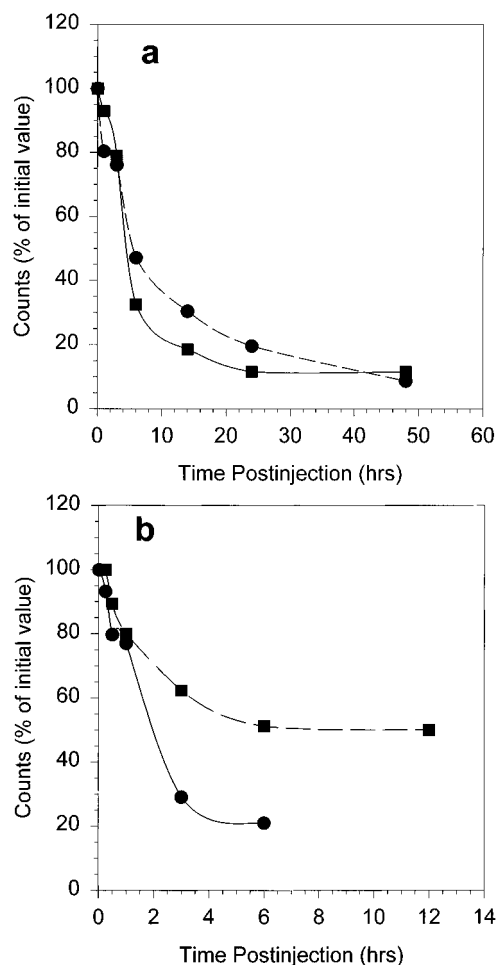


Figure 6. Quantitative evaluation of ^{131}I (a) or ^{99m}Tc (b) radioactivity retained in the brain of control (●) or tumor-bearing animals (■) following ic injection of radiolabeled EGF.

procedure originally described by Rhodes et al. (1991) for the direct labeling of proteins. However, before radiolabeling of EGF could be carried out, it was necessary to introduce a thiol group into the amino-terminal end of the EGF molecule. Although the heterobifunctional reagent *N*-succinimidyl 3-(2-pyridyldithio)propionate could have been used to derivatize EGF, this probably would have broken internal cysteine bonds, thereby changing the tertiary structure of the molecule. To minimize these changes and to preserve EGF's ability to bind to its receptors, thiolation was carried out under mild conditions with 2-iminothiolane.

Using rats bearing intracerebral implants of C6_{EGFR} glioma that express EGFR, we studied the *in vivo* localization of radiolabeled EGF following intratumoral or intracerebral injection. As determined by external scintigraphy, ^{131}I radioactivity disappeared more rapidly from the brain regions of tumor-bearing compared to control animals. This may have been due to the release of iodine following rapid internalization and degradation of [^{131}I]EGF in tumor cells, which would correlate with our *in vitro* observation that cell-associated ^{131}I activity rapidly disappeared after [^{131}I]EGF-containing medium had been replaced with EGF-free medium. This phenomenon also has been observed in human fibroblasts (Carpenter and Cohen, 1976) and in human glioblastoma cells (Capala et al., 1993). As determined by gel filtration of the incubation medium, in both cases the radioactivity released from the cells was in a low molecular mass form. Following intratumoral injection, EGF most likely was catabolized by tumor cells, as suggested by the rapid loss

of ^{131}I radioactivity from the brain, lower levels of radioactivity in the liver, and faster accumulation of iodine in the thyroid. On the other hand, following injection of ^{99m}Tc -labeled EGF into tumor-bearing rats, ~50% of ^{99m}Tc remained in the brain regions for up to 12 h, compared to only ~20% remaining after 6 h in non-tumor-bearing animals. These findings also correlated with our *in vitro* data, which showed that 60% of ^{99m}Tc remained cell-associated for at least 6 h following 30 min of incubation with [^{99m}Tc]EGF. It is possible that the covalent sulfur–technetium bond, which is produced during the labeling procedure described above, was stronger than the carbon–iodine bond produced by the chloramine-T iodination method. Furthermore, there are specific dehalogenating enzymes that could cause the release of iodine from proteins (Wilbur, 1992; Carrasquillo, 1993) and, thereby, decrease stability of the iodinated EGF. On the other hand, since technetium is not a naturally occurring element, there are no specific enzymes that degrade Tc-labeled proteins, which could explain the differences in *in vitro* and *in vivo* pharmacokinetics of ^{131}I - and ^{99m}Tc -labeled EGF. Increased stability of ^{99m}Tc -, ^{186}Re -, and ^{188}Re -labeled mAbs and peptide-based ligands has been reported previously (Zamora et al., 1993, 1996; Rhodes et al., 1995). However, tumor retention and biodistribution profiles of the ^{131}I -labeled somastatin analogue, RC-160, were similar to those of [^{188}Re]RC-160 (Zamora et al., 1996). At this time we do not know whether the ^{99m}Tc pertechnetate inhibited the degradation of EGF or whether the radionuclide was retained following intracellular degradation of EGF.

Zamora et al. (1996) have successfully used [^{188}Re]RC-160, a directly radiolabeled somastatin analogue, to treat xenografts of a somastatin-receptor-positive human prostate adenocarcinoma grown in nude mice. Since the chemistry of ^{186}Re or ^{188}Re perrhenate is similar to that of ^{99m}Tc pertechnetate, EGF might be useful as a tumor-targeting agent for these radionuclides (Griffiths et al., 1994). Rémy et al. (1995) have produced a human EGF-(1–51) construct that included a branched peptide with four metal-chelating sites, which could be radiolabeled with ^{111}In . The resulting bioconjugate retained the receptor-binding properties of the native EGF *in vitro*. Scott Robson et al. (1991) have described a method for radiolabeling EGF with positron-emitting ^{76}Br and have compared [^{76}Br]EGF to [^{125}I]EGF *in vitro* and *in vivo*. [^{125}I]EGF and [^{76}Br]EGF bound equally well to EGF-positive glioma cells *in vitro*. The *in vivo* studies showed that the biodistributions of both radioconjugates were similar following intravenous injection into normal rats, although the biological half-life of ^{76}Br was greater than that of ^{125}I in some organs.

As recently reviewed by Carlsson et al. (1994), EGF also might be used as a targeting agent for boron neutron capture therapy, the success of which depends upon the delivery of a large number of boron atoms to tumor cells (Barth et al., 1996). Carlsson et al. have produced an EGF–dextran containing ~1000 boron atoms per conjugate unit and have shown that the ^{131}I radioactivity delivered to the tumor cells by EGF–dextran–tyrosine- ^{131}I remained cell-associated for at least 20–24 h. Recently, we have described a method for boronating EGF by linking EGF to a boron-containing starburst dendrimer (Capala et al., 1996). The resulting bioconjugates contained ~960 boron atoms per molecule of EGF, specifically bound to the EGFR on tumor cells, and were internalized and localized in lysosomes, where they persisted for up to 3 h.

The blood–brain barrier (BBB), which effectively limits the diffusion of both low and high molecular mass

substances from the vascular compartment to both normal brain and tumor within it (Brightman, 1989), is an obstacle to the delivery of EGF radioconjugates to brain tumor following systemic injection. Nevertheless, there are a number of strategies that could be used to circumvent this problem. Radiolabeled EGF could be injected either into the tumor, as we did in the present study, or into the site from which the tumor had been surgically resected (Liebert et al., 1990; Riva et al., 1994). Alternatively, radiolabeled EGF might be delivered directly into the brain, using polymers (Brem et al., 1991) or implantable pumps (Kroin and Penn, 1989; Madrit et al., 1991) that would release it over a longer period of time. The intracarotid infusion of a hyperosmotic solution (1.373 mOsmol/mL) of mannitol can disrupt the BBB (Neuwelt et al., 1986), and this approach significantly increased the tumor uptake of both intact mAbs (Neuwelt et al., 1994) and their F(ab) and F(ab')₂ fragments in brain-tumor-bearing rodents (Neuwelt et al., 1988), as well as low molecular mass boron compounds in glioma-bearing rats (Barth et al., 1997; Yang et al., 1996, 1997a,b). Studies currently are in progress in our laboratory to further evaluate intratumoral versus intracarotid injection, with or without BBB disruption, of ^{99m}Tc-labeled and boronated EGF. These studies should provide relevant information concerning the optimal route for the administration of EGF to brain-tumor-bearing rodents, and if these are sufficiently promising, then studies in larger animals such as canines would be warranted to assess the feasibility of using EGF as a targeting agent for either diagnosis or therapy of human brain tumors. EGF-based bioconjugates also might be used to target other kinds of tumors, such as sarcomas and squamous carcinomas, whose cells have been shown to express increased amounts of EGF (Carpenter, 1987; Helseth et al., 1990). [^{99m}Tc]EGF radioconjugates might be useful for evaluating *in vivo* EGFR expression, as well as optimizing the route of delivery of other EGF bioconjugates such as [⁷⁶Br]EGF for positron emission tomography, boronated EGF for BNCT, or [¹⁸⁶Re]- or [¹⁸⁸Re]EGF for targeted radiotherapy of EGFR positive tumors. Further studies will determine whether any of these approaches are successful.

ACKNOWLEDGMENT

This work has been supported by U.S. Department of Energy Grant DE-AC02-76CH000016.

LITERATURE CITED

- Andersson, A., Capala, J., and Carlsson, J. (1992) Effects of EGF-dextran-tyrosine-¹³¹I Conjugates on the Clonogenic Survival of Cultured Glioma Cells. *J. Neuro-Oncol.* **14**, 213–223.
- Barth, R. F., Soloway, A. H., and Brugger, R. M. (1996) Boron Neutron Capture Therapy of Brain Tumors: Past History, Current Status, and Future Potential. *Cancer Invest.* **14**, 534–550.
- Barth, R. F., Yang, W., Rotaru, J. H., Moeschberger, M. L., Joel, D. D., Nawrocky, M. M., Goodman, J. H., and Soloway, A. H. (1997) Boron Neutron Capture Therapy of Brain Tumors: Enhanced Survival Following Intracarotid Injection of either Sodium Borocaptate or Borophenylalanine with or without Blood-Brain Barrier Disruption. *Cancer Res.* **57**, 1129–1136.
- Bigner, S. H., Humphrey, P. A., Wong, A. J., Vogelstein, B., Mark, J., Friedman, H. S., and Bigner, D. D. (1990) Characterization of the Epidermal Growth Factor Receptor in Human Glioma Cell Lines and Xenografts. *Cancer Res.* **50**, 8017–8022.
- Brady L. W., Miyamoto, C., Woo, D., Rachover, M., Emrich, J., Bender, H., Dadparvar, S., Steplewski, Z., Koprowski, H., Black, P., Lazzaro, B., Nair, S., McCormack, T., Nieves, J., Morabito, M., and Eshleman, J. (1991) Malignant Astrocytomas Treated with Iodine-125 Labelled Monoclonal Antibody 425 Against Epidermal Growth Factor Receptors: A Phase II Trial. *Int. J. Radiat. Oncol. Biol. Phys.* **22**, 225–230.
- Brem, H., Mahaley, Jr., M. S., Vick, N. A., Black, K. L., Schold, Jr., S. C., Burger, P. C., Friedman, A. H., Ciric, I. S., Eller, T. W., Cozzenes, J. W., and Kenealy, J. N. (1991) Interstitial Chemotherapy with Drug Polymer Implants for the Treatment of Recurrent Gliomas. *J. Neurosurg.* **74**, 441–446.
- Brightman, M. W. (1989) The Anatomic Basis of the Blood-Brain Barrier. *Implications of the Blood-Brain Barrier and Its Manipulation* (E. A. Neuwelt, Ed.) Vol. 1, pp 53–83, Plenum Publishing, New York.
- Capala, J., and Carlsson, J. (1991) Influence of Chloroquine and Lidocaine on the Therapeutic Effects of ¹³¹I-EGF. Studies on Cultured Glioma Cells. *Int. J. Radiat. Biol.* **60**, 497–510.
- Capala, J., Prähle, M., Scott Robson, S., Pontén, J., Westermarck, B., and Carlsson, J. (1990) Effects of ¹³¹I-EGF on Cultured Human Glioma Cells. *J. Neuro-Oncol.* **9**, 201–210.
- Capala, J., Barth, R. F., Adams, D. M., Soloway, A. H., and Carlsson, J. (1993) Epidermal Growth Factor as a Potential Targeting Agent for Delivery of ¹⁰B to Malignant Gliomas. *Advances of Neutron Capture Therapy* (A. H. Soloway, R. F. Barth, and D. E. Carpenter, Eds.) pp 371–375, Plenum Press, New York.
- Capala, J., Barth, R. F., Bendayan, M., Lauzon, M., Adams, D. M., Soloway, A. H., Fenstermaker, R. A., and Carlsson, J. (1996) Boronated Epidermal Growth Factor as a Potential Targeting Agent for Boron Neutron Capture Therapy of Brain Tumors. *Bioconjugate Chem.* **7**, 7–15.
- Carlsson, J., Gedda, L., Grönvik, C., Hartman, T., Lindström, A., Lindström, P., Lundqvist, H., Löfvist, A., Malmqvist, J., Olsson, P., Essand, M., Pontén, J., Sjöberg, S., and Westermarck, B. (1994) Strategy for Boron Neutron Capture Therapy Against Tumor Cells with Over-Expression of the Epidermal Growth Factor-Receptor. *Int. J. Radiat. Oncol. Biol. Phys.* **30**, 105–115.
- Carpenter, G. (1987) Receptors for Epidermal Growth Factor and Other Polypeptide Mitogens. *Annu. Rev. Biochem.* **56**, 881–914.
- Carpenter, G., and Cohen, S. (1976) ¹²⁵I-Labeled Epidermal Growth Factor. Binding, Internalization, and Degradation in Human Fibroblasts. *J. Cell Biol.* **71**, 159–171.
- Carpenter, G., and Cohen, S. (1979) Epidermal Growth Factor. *Annu. Rev. Biochem.* **48**, 193–216.
- Carrasquillo, J. (1993) Imaging and dosimetry determinations using radiolabeled antibodies. *Cancer Treat. Res.* **68**, 65–97.
- Clendenon, N. R., Barth, R. F., Gordon, W. A., Goodman, J. H., Alam, F., Staubus, A. E., Boesel, C. P., Yates, A. J., Moeschberger, M. L., Fairchild, R. G., and Kalef-Ezra, J. A. (1990) Boron Neutron Capture Therapy of a Rat Glioma. *Neurosurgery* **26**, 47–55.
- Ekstrand, A. J., James, C. D., Cavenee, W. K., Selinger, B., Petterson, R. E., and Collins, V. P. (1991) Genes for Epidermal Growth Factor Receptor, Transforming Growth Factor α , and Epidermal Growth Factor and Their Expression in Human Gliomas *in Vivo*. *Cancer Res.* **51**, 521–527.
- Epenetos, A. A., Courtney-Luck N., Pickering, D., Hooker, G., Durbin, H., Lavender, J. P., and McKenzie, C. G. (1985) Antibody Guided Irradiation of Brain Glioma by Arterial Infusion of Radioactive Monoclonal Antibody against Epidermal Growth Factor Receptor and Blood Group A Antigen. *Br. Med. J.* **290**, 1463–1466.
- Faillot, T., Magdelénat, H., Mady, E., Stasiecki, P., Fohanno, D., Gropp, P., Poisson, M., and Delattre, J.-Y. (1996) A Phase I Study of Anti-epidermal Growth Factor Receptor Monoclonal Antibody for the Treatment of Malignant Gliomas. *Neurosurgery* **39**, 478–483.
- Fenstermaker, R. A., Capala, J., Barth, R. F., Hujer, A., Kung, H.-J., and Kaetzer, Jr., D. M. (1995) The Effect of Epidermal Growth Factor Receptors (EGFR) Expression on *in Vivo* Growth of Rat C6 Glioma Cells. *Leukemia* **9** (Suppl. 1), S106–S112.
- Griffiths, G. L., Goldenberg, D. M., Diril, H., and Hansen, H. J. (1994) Technetium-99m, Rhenium-186, and Rhenium-188 Direct-Labeled Antibodies. *Cancer* **73**, 761–768.

- Harris, A. L. (1990) The Epidermal Growth Factor Receptor as a Target for Therapy. *Cancer Cells* 2, 321–323.
- Helseth, E., Brogger, A., Dalen, A., Fure, H., Johansen, S. G., Lier, M. E., Skandsen, T., Unsrard, G., and Vik, R. (1990) Polysomy of Chromosome 7 is Associated with Amplification and Overexpression of the EGF-Receptor Gene in a Human Carcinoma Cell Line Delivered from a Brain Metastasis. *Acta Pathol., Microbiol. Immunol. Scand.* 98, 996–1004.
- Kalofonos, H. P., Pawlikowska, T. R., Hemingway, A., Courtenay-Luck, N., Dhokia, B., Snook, D., Sivolapenko, G. B., Hooker, G. R., McKenzie, C. G., Lavender, P. J., Thomas, D. G. T., and Epenetos, A. A. (1989) Antibody Guided Diagnosis and Therapy of Brain Gliomas Using Radiolabeled Monoclonal Antibodies Against Epidermal Growth Factor Receptor and Placental Alkaline Phosphatase. *J. Nucl. Med.* 30, 1636–1645.
- Kroin, J. F., and Penn, R. D. (1989) Implantable Pumps to Deliver Drugs Directly into CNS. *Implications of The Blood Brain Barrier and Its Manipulation* (E. A. Neuwelt, Ed.) Vol. 2, pp 601–615, Plenum Medical Book, New York.
- Liebert, M., Wahl, R. L., Lawless, G., McKeever, P. E., Taren, J. A., Beierwalters, W. H., and Brasswell, R. (1990) Direct Stereotactic Intracerebral Injection of Monoclonal Antibodies and Their Fragments: A Potential Approach to Brain Tumor Immunotherapy. *Am. J. Physiol. Imaging* 5, 55–59.
- Lofts, F. J., and Gullick, W. J. (1994) Growth Factor Receptors as Targets. *New Molecular Targets for Cancer Chemotherapy* (D. J. Kerr and P. Workman, Eds.) pp 45–66, CRC Press, Boca Raton.
- Madrit, Y., Feigenbaum Langer, L., Brem, H., and Langer, R. (1991) New Directions for the Delivery of Drugs and Other Substances to the Central Nervous System. *Semin. Pharmacol.* 22, 299–324.
- Mendelsohn, J. (1988) Growth Factor Receptors as Targets for Antitumor Therapy with Monoclonal Antibodies. *Prog. Allergy* 45, 147–160.
- Modjtahedi, H., and Dean, C. (1991) The Receptor for EGF and Its Ligands: Expression, Prognostic Value and Target for Therapy in Cancer (Review). *Int. J. Oncol.* 4, 227–296.
- Neuwelt, E. A., Howieson, J., Frenkel, E. P., Specht, H. D., Weigel, R., Buchman, C. G., and Hill, S. A. (1986) Therapeutic Efficacy of Multiagent Chemotherapy with Drug Delivery Enhancement by Blood-Brain Barrier Modification in Glioblastoma. *Neurosurgery* 19, 573–582.
- Neuwelt, E. A., Barnett, P. A., Hellström, I., Hellström, K. E., Beaumier, P., McCormick, C. I., and Weigel, R. M. (1988) Delivery of Melanoma-associated Immunoglobulin Monoclonal Antibody and Fab Fragments to Normal Brain Utilizing Osmotic Blood-Brain Barrier Disruption. *Cancer Res.* 48, 4725–4729.
- Neuwelt, E. A., Barnett, P. A., Hellström, K. E., Hellström, I., McCormick, C. I., and Ramsey, F. L. (1994) Effect of Blood-Brain Barrier Disruption on Intact and Fragmented Monoclonal Antibody Localization in Intracerebral Human Lung Carcinoma Xenografts. *J. Nucl. Med.* 35, 1831–1841.
- Rémy, S., Reilly, M. R., Sheldon, K., and Gariépy, J. (1995) A New Radioligand for the Epidermal Growth Factor Receptor: ^{111}In Labeled Human Epidermal Growth Factor Derivatized with a Bifunctional Metal-Chelating Peptide. *Bioconjugate Chem.* 6, 683–690.
- Rhodes, B. A. (1991) Direct Labeling of Proteins with ^{99m}Tc (Review). *Nucl. Med. Biol.* 18, 667–676.
- Rhodes, B. A., Zamora, P. O., Marek, M. J., Sharma, S. D., and Wall, F. J. (1995) Direct ^{99m}Tc Labeling of Peptides: Factors that Alter Radiochemical Yields and *in vivo* Stability. *Technetium and Rhenium in Chemistry and Nuclear Medicine* 4 (M. Nicolini, G. Bandolini, and U. Mazzi, Eds.) pp 319–325, SG Editoriale, Padova, Italy.
- Riva, P., Arista, A., Tison, V., Sturiale, C., Franceschi, G., Spinelli, A., Riva, N., Casi, M., Moscatelli, G., and Frattarelli, M. (1994) Intralesional Radioimmunotherapy of Malignant Gliomas. An Effective Treatment in Recurrent Tumors. *Cancer* 73 (Suppl. 3), 1076–1082.
- San-Galli, F., Vrignaud, P., Riert, J., Coindre, J. M., and Cohadon, F. (1989) Assessment of the Experimental Model of Transplanted Glioblastoma in Wistar Rats. *J. Neuro-Oncol.* 7, 299–304.
- Sato, G. H., and Sato, J. D. (1989) Growth Factor Receptor Monoclonal Antibodies and Cancer Immunotherapy. *J. Int. Cancer Inst.* 81, 1600–1601.
- Scott Robson, S., Capala, J., Carlsson, J., Malmberg, P., and Lundqvist, H. (1991) Distribution and Stability in the Rat of a $^{76}\text{Br}/^{125}\text{I}$ -labeled Polypeptide, Epidermal Growth Factor. *Nucl. Med. Biol.* 18, 241–246.
- Snelling, L., Miyamoto, C. T., Bender, H., Brady, L. W., Steplewski, Z., Class, R., Emrich, J., and Rackover, M. A. (1995) Epidermal Growth Factor Receptor 425 Monoclonal Antibodies Radiolabeled with Iodine-125 in the Adjuvant Treatment of High-Grade Astrocytomas. *Hybridoma* 14, 111–114.
- Todderud, G., and Carpenter, G. (1989) Epidermal Growth Factor: the Receptors and Its Function. *BioFactors* 2, 11–15.
- Torp, S. H., Helseth, E., Dalen, A., and Unsgaard, G. (1991) Epidermal Growth Factor Receptor Expression in Human Gliomas. *Cancer Immunol. Immunother.* 33, 61–64.
- Tuzi, N. L., Venter, D. J., Kumar, S., Staddon, S. L., Lemoine, N. R., and Gullick, W. J. (1991) Expression of Growth Factor Receptors in Human Brain Tumors. *Br. J. Cancer* 63, 227–233.
- Wilbur, D. S. (1992) Radiohalogenation of Proteins: An Overview of Radionuclides, Labeling Methods, and Reagents for Conjugate Labeling. *Bioconjugate Chem.* 3, 333–370.
- Yang, W., Barth, R. F., Carpenter, D. E., and Goodman, J. H. (1996) Enhanced Delivery of Boronophenylalanine to Brain Tumors for Neutron Capture Therapy by Means of Carotid Injection and Blood-Brain Barrier Disruption. *Neurosurgery* 38, 985–992.
- Yang, W., Barth, R. F., Rotaru, J. H., Moenschberger, M. L., Carpenter D. E., Joel, D. D., Nawrocki, M. M., and Goodman, J. (1997a) Enhanced Survival of Glioma Bearing Rats Following Boron Neutron Capture Therapy with Blood Brain Barrier Disruption and Intracarotid Injection of Boronphenylalanine. *J. Neuro-Oncol.* 33, 59–70.
- Yang, W., Barth, R. F., Rotaru, J. H., Moenschberger, M. L., Joel, D. D., Nawrocki, M. M., Goodman, J., and Soloway A. F. (1997b) Boron Neutron Capture Therapy of Brain Tumors: Enhanced Survival Following Intracarotid Injection of Sodium Borocaptate with or without Blood-Brain Barrier Disruption. *Int. J. Radiat. Oncol. Biol. Phys.* 37, 663–672.
- Zamora, P. O., Eshima, D., Shattuck, L. A., Marek, M. J., and Rhodes, B. A. (1993) Can Blood Retention of ^{99m}Tc and ^{188}Re Labeled Antibodies be Predicted *in vitro* by Challenge with Cysteine? *J. Nucl. Med.* 34, 246P.
- Zamora, P. O., Gulhke, S., Bender, H., Diekmann, D., Rhodes, B. A., Biersack, H.-J., and Knapp, Jr., F. F. (1996) Experimental Radiotherapy of Receptor-Positive Human Prostate Adenocarcinoma with ^{188}Re -RC-160, a Directly-Radiolabeled Somastatin Analogue. *Int. J. Cancer.* 65, 214–220.

BC970031S

Synthesis of a New Photoreactive Derivative of Dipyridamole and Its Use in the Manufacture of Artificial Surfaces with Low Thrombogenicity

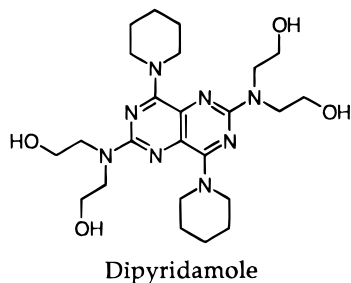
Yvette B. J. Aldenhoff,[†] A. Paul Pijpers,[‡] and Leo H. Koole^{*,†}

Centre for Biomaterials Research, Maastricht University, P.O. Box 616, 6200 MD Maastricht, The Netherlands, and DSM Research, Geleen, The Netherlands. Received November 15, 1996[®]

Photoimmobilization of dipyridamole (Persantin) was accomplished through the use of a new synthetic conjugate molecule, **1**. Persantin is a powerful inhibitor of platelet activation and aggregation and is widely used as a vasodilator. Conjugate **1** consists of triply protected dipyridamole [three of the four hydroxyl groups carry a *tert*-butyldimethylsilyl (TBDMS) protective group] and the photoreactive 4-azidobenzoyl group. A short hydrophilic spacer chain, derived from triethylene glycol, separates the protected dipyridamole system and the photoreactive group. Compound **1** was immobilized on polyurethane sheets (Pellethane D-55) through irradiation with ultraviolet (UV) light, and the protective groups were removed afterward. The resulting modified polyurethane surfaces were characterized by different physicochemical techniques: UV extinction, contact angle measurements (captive bubble technique), and X-ray photoelectron spectroscopy (XPS). The UV extinction measurements showed the presence of 13 ± 1 nmol of immobilized dipyridamole/cm². The contact angle measurements revealed that the modified surface was markedly more hydrophilic than the control (i.e. unmodified polyurethane). XPS measurements clearly established the presence of immobilized dipyridamole in the outermost layers of the modified surface. This was especially clear from the XPS spectra recorded at a low take-off angle ($\sim 6^\circ$). Furthermore, the XPS spectra showed that the TBDMS protective groups had been quantitatively removed during the deprotection/washing treatment. The *in vitro* blood compatibility of the modified surface was studied with the thrombin generation assay as developed in our group, as well as with scanning electron microscopy. The thrombin generation test produced a lag time of 1275 s for the modified surface, as opposed to 569 s for the control. Scanning electron microscopy showed that far fewer platelets adhere to the modified surface (approximately $7 \times 10^3/\text{mm}^2$) as compared to the control (approximately $6 \times 10^2/\text{mm}^2$). Taken together, the experimental data reveal that the modified surface has excellent blood compatibility *in vitro*. It is discussed that the use of conjugate **1** leads to simultaneous exposure of dipyridamole at the modified surface and to a marked increase of the surface hydrophilicity, which is likely to hamper adsorption of plasma proteins. The combination of these effects is uniquely related to the molecular buildup of **1**. Conjugate **1** will be used in future work that is aimed at preparing small-caliber polyurethane vascular grafts with a blood compatible luminal surface.

INTRODUCTION

Dipyridamole is a nontoxic drug that acts as an inhibitor of the activation and aggregation of blood platelets (1, 2). The drug is also a powerful vasodilator, i.e. a substance which induces widening of the blood vessels after its systemic injection (1, 2). Dipyridamole,



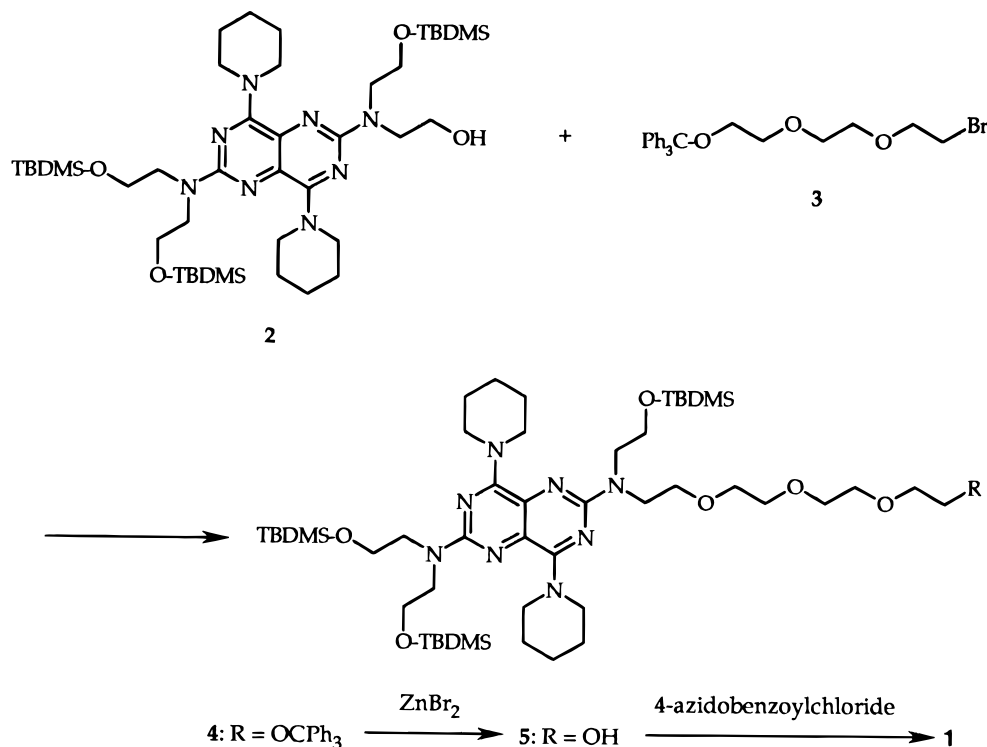
which is marketed as Persantin, is commonly administered to patients before and after percutaneous transluminal coronary angioplasty ("Dottering"), mostly in com-

bination with aspirin. We became interested in dipyridamole in the course of our work, which is aimed at the manufacture of new materials with improved blood compatibility. We concentrate both on the preparation and on the testing (*in vitro* and *in vivo*) of such materials (3–7). Blood clotting as a result of the contact between blood and an artificial surface remains perhaps the most important problem in the development of improved cardiovascular devices. We know, particularly from the pioneering work of Vroman et al. (8–10), that contact between blood and an artificial surface immediately leads to adsorption of plasma proteins. Adsorbed proteins may be displaced by others, and these processes probably occur within several minutes. Proteins in the adsorbed state adopt a different molecular conformation as compared to the circulating state, and platelets and leukocytes may adhere via receptor sites that match structural patterns of an adsorbate. It has become clear that immunoglobulins, fibronectin, and fibrinogen have specific significance as adsorbates (11). When a platelet is activated through this mechanism, it may in turn trigger other platelets and induce generation of thrombin, leading to deposition of fibrin. These events will result in the formation of a thrombus. Recent work by Bamford

[†] Maastricht University.

[‡] DSM Research.

[®] Abstract published in *Advance ACS Abstracts*, April 1, 1997.

Scheme 1. Preparation of Conjugate Molecule 1

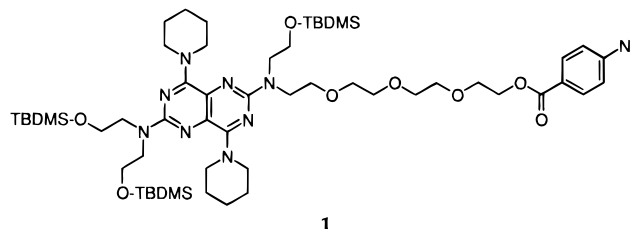
et al. implied that dipyridamole could play a role in the development of new blood-compatible materials (12, 13). Bamford et al. chemically coupled dipyridamole to a series of water-soluble macromolecules and subsequently showed that the drug retained its platelet-inhibitory activity. In some cases, the drug was even slightly potentiated. As the macromolecular vehicles containing dipyridamole cannot cross the platelet's membrane, these experiments revealed—although in an indirect manner—that dipyridamole can exert its function via a putative receptor site on the exterior of the platelet.

Later, we could also show that coupling of dipyridamole onto water-insoluble polymers (e.g., the polyurethane Pellethane D-55) markedly contributes to the blood compatibility of the surface, at least *in vitro* (3). Evidence in support of an inhibitory action of immobilized dipyridamole on contacting platelets has accumulated. Our data, taken together, suggest that the platelet inhibition by immobilized dipyridamole counteracts or overrules platelet activation by adsorbed plasma proteins (e.g., fibronectin or fibrinogen).

Immobilization of dipyridamole onto the surface of water-insoluble polymers was accomplished through a novel photoimmobilization technique (3–5, 14). To this end, we synthesized a series of novel molecules, which consist of a triply *tert*-butyldimethylsilyl (TBDMS)-protected (15) dipyridamole connected to a 4-azidobenzoyl group. It could be demonstrated that such conjugate molecules can be covalently coupled to a polyurethane surface via irradiation with ultraviolet (UV) light (14). The 4-azidobenzoyl group loses molecular nitrogen (N_2) upon UV irradiation, and this photoreaction generates a highly reactive (electrophilic) didehydroazepine structure (16–18). Then, reaction with a nucleophilic site at the polymer surface (e.g., a urethane NH group) generates a new covalent bond between the conjugate and the polymer surface.

We report here a comprehensive study on a new conjugate molecule, **1**, which has the characteristic

feature that the (protected) dipyridamole unit is linked to 4-azidobenzoyl via a *short hydrophilic* spacer chain.



We decided to prepare and test such a system since we anticipated that a hydrophilic spacer chain could facilitate exposure of the deprotected dipyridamole in the aqueous boundary layer at the polymer's surface. We report consecutively (i) synthesis of **1**, (ii) photoimmobilization of **1** on polyurethane sheets, (iii) deprotection and purification, (iv) physicochemical characterization of the modified surfaces (contact angles, XPS), and (v) *in vitro* tests of the blood compatibility of modified and unmodified surfaces. Moreover, it is described how compound **1** can be immobilized on the luminal surface of a short polyurethane vascular graft, which will be used in followup *in vivo* investigations.

MATERIALS AND METHODS

Preparation of Conjugate 1. The synthesis route to **1** is outlined in Scheme 1. The preparation started out with tris[*tert*-butyldimethylsilyl]dipyridamole (**2**), which was prepared from dipyridamole as described earlier (14). Compound **2** was reacted with 1-(2'-*O*-tritylethoxy)-2-(2'-bromoethoxy)ethane (**3**) in the presence of sodium hydride (19). This reaction afforded compound **4**, which was subsequently treated with zinc bromide to cleave the trityl group (20). The resulting alcohol, **5**, was esterified through reaction with 4-azidobenzoyl chloride. This reaction afforded the desired conjugate structure **1**, in 18% overall yield based on **2**. Purity and identity of conjugate **1** and all synthetic intermediates were estab-

lished unequivocally. Different analytical techniques, including chromatography (thin layer), high-field nuclear magnetic resonance (NMR, 400 MHz for ^1H), and fast atom bombardment mass spectrometry, were used.

All solvents and starting materials were of the highest available purity or were purified as specified. Pyridine and dichloromethane were distilled from calcium hydride and stored over Linde 3Å molecular sieves. Triethylamine was distilled from calcium hydride and stored over potassium hydroxide pellets. Tetrahydrofuran was passed through an alumina column, distilled from calcium hydride, and stored over Linde 3Å molecular sieves. Methanol was predried with iodine and magnesium turnings, distilled, and stored over Linde 3Å molecular sieves. Thin layer chromatography was performed on glass plates (3 × 10 cm) with a fluorescent indicator. Silica gel 60 (particle size 0.063–0.200 mm) was used for column chromatography. Mass spectra were run on a Kratos MS 80 RF instrument. ^1H NMR and ^{13}C NMR were recorded at 399.9 and 100.6 MHz, respectively, on a Varian Unity-Plus spectrometer, using deuterated chloroform or deuterated methyl sulfoxide as the solvent. Tetramethylsilane was used as the internal reference (δ = 0.00 ppm).

Preparation of 1-(2'-*O*-Triphenylmethylethoxy)-2-(2'-bromoethoxy)ethane (3). To a stirred solution of triethylene glycol (75.09 g, 500.00 mmol) and 4-(dimethylamino)pyridine (0.38 g, 3.13 mmol) in 125 mL of anhydrous pyridine was added triphenylmethyl chloride (17.42 g, 63.50 mmol) in 10 portions during 3 h. The solution was stirred for 16 h under exclusion of moisture. Then, pyridine was removed (last traces were removed by coevaporation with toluene). The residue was taken up in dichloromethane and washed with saturated aqueous bicarbonate (three times) and water (three times). The organic layer was dried on magnesium sulfate, filtered, and concentrated to dryness under reduced pressure. The crude product was applied to a silica gel column. Elution with 1:1 petroleum ether/ethyl acetate afforded pure 1-(2'-*O*-triphenylmethylethoxy)-2-(2'-hydroxyethoxy)ethane (i.e. monotritylated triethylene glycol) as a viscous oil: R_f (petroleum ether/ethyl acetate 1:1) = 0.38; yield, 20.56 g (84%); ^1H NMR (CDCl_3) δ 7.50–7.15 (15H, m, CPh_3), 3.66 (8H, m, $\text{OCH}_2\text{CH}_2\text{O}$), 3.59 (2H, t, CH_2OH), 3.24 (2H, t, CH_2OCPh_3), 2.95 (1H, br s, OH); ^{13}C NMR (CDCl_3) δ 144.09, 128.70, 127.80, 126.98, 86.59, 72.60, 70.68, 63.29, 61.69.

A solution of bromine (12.27 g, 76.81 mmol) in anhydrous dichloromethane (60 mL) was added dropwise to a solution of triphenylphosphine (18.60 g, 70.90 mmol) in anhydrous dichloromethane (125 mL). The addition was stopped as the yellow-brown color of free bromine persisted. Subsequently, anhydrous triethylamine (10.76 g, 106.35 mmol) and a solution of 1-(2'-*O*-triphenylmethylethoxy)-2-(2'-hydroxyethoxy)ethane (20.19 g, 59.08 mmol) in 75 mL of anhydrous dichloromethane were added dropwise. The resulting mixture was stirred for 1 h under exclusion of moisture. Then, all volatiles were removed under reduced pressure. The residue was taken up in diethyl ether and washed with water. The organic layer was dried on magnesium sulfate, filtered, and concentrated to dryness under reduced pressure. The crude product was applied to a silica gel column. Elution with dichloromethane afforded **3** as a white solid: R_f (dichloromethane) = 0.43; yield, 23.85 g (89%); ^1H NMR (CDCl_3) δ 7.50–7.18 (15H, m, CPh_3), 3.85 (2H, t, $\text{CH}_2\text{-Br}$), 3.70 (6H, m, $\text{OCH}_2\text{CH}_2\text{O}$), 3.44 (2H, t, CH_2O), 3.21 (2H, t, CH_2CPh_3); ^{13}C NMR (CDCl_3) δ 144.08, 128.69, 127.74, 126.91, 86.6, 71.28, 70.79, 70.75, 70.66, 63.31, 30.34; mp, 57.8 °C.

Preparation of Compound 5. Sodium hydride (60%, 0.906 g, 22.65 mmol) was added to a solution of **2** (3.84 g, 4.53 mmol) (**19**) in 50 mL of anhydrous tetrahydrofuran. The mixture was sonicated under argon for 15 min. Then, compound **3** (2.27 g, 4.98 mmol) was added and the reaction mixture was magnetically stirred for 16 h. The reaction mixture was poured into saturated aqueous ammonium chloride (150 mL), which was extracted with ethyl acetate. The combined organic layers were dried on magnesium sulfate, filtered, and concentrated to dryness under reduced pressure. The residue (crude **4**) was taken up in 10 mL of anhydrous dichloromethane and treated with 2 mL of anhydrous methanol and anhydrous zinc bromide (10.00 g, 45.00 mmol). This reaction mixture was magnetically stirred for 2 h. The solvents were evaporated under reduced pressure, and the residue was taken up in ethyl acetate and washed consecutively with a 0.1 M citric acid, saturated bicarbonate, and brine. The organic layer was dried on magnesium sulfate, filtered, and concentrated to dryness under reduced pressure. Crude **5** was applied to a silica gel column. Elution with 1:1 petroleum ether/ethyl acetate afforded pure **5** as a yellow viscous oil: yield, 1.10 g (25%); ^1H NMR (CDCl_3) δ 4.70–3.80 (34H, m, $\text{CH}_2\text{-N}$ and $\text{CH}_2\text{-O}$), 1.68–1.62 (12H, br s, CH_2 of piperidine rings), 0.84 (27H, s, *t*-Bu), 0.02 (18H, s, $\text{CH}_3\text{-Si}$).

Preparation of 4-Azidobenzoyl Chloride. A solution of 4-azidobenzoic acid (7.50 g, 45.98 mmol) (**21**) and thionyl chloride (16.29 g, 138.04 mmol) in 250 mL of anhydrous tetrahydrofuran was refluxed for 30 min. All volatiles were removed under reduced pressure (in the hood, stench). The solid residue was recrystallized from hexane to give pure 4-azidobenzoyl chloride as a yellowish solid: yield, 6.76 g (81%); ^1H NMR (CDCl_3) δ 8.05 (2H, d, aromatic H), 7.05 (2H, d, aromatic H); ^{13}C NMR ($\text{DMSO}-d_6$) δ 166.39, 143.87, 131.15, 127.20, 119.34, 119.05.

Preparation of Compound 1. Compound **5** (1.35 g, 1.39 mmol) and 4-azidobenzoyl chloride (0.28 g, 1.52 mmol) were dissolved in 50 mL of anhydrous pyridine, and the solution was magnetically stirred for 3 h. Then, pyridine was evaporated (last traces were removed by coevaporation with toluene). The residue was taken up in ethyl acetate and washed with 0.1 M citric acid, saturated bicarbonate, and brine. The organic layer was dried on magnesium sulfate, filtered, and concentrated to dryness under reduced pressure. The crude product was applied to a silica gel column. Elution with 4:1 petroleum ether/ethyl acetate afforded pure **1** as a yellow-brown oil: R_f (petroleum ether/ethyl acetate 1:1) = 0.68; yield, 1.12 g (72%); ^1H NMR (CDCl_3) δ 8.02 (2H, d, aromatic H), 7.02 (2H, d, aromatic H), 4.43 [2H, t, $\text{CH}_2\text{-C(O)}$], 4.05–3.48 (32H, m, $\text{CH}_2\text{-N}$ and $\text{CH}_2\text{-O}$), 1.65 (12H, br s, CH_2 of piperidine rings), 0.95 (27H, s, *t*-Bu), 0.02 (18H, s, $\text{CH}_3\text{-Si}$); ^{13}C NMR (CDCl_3) δ 160.34, 160.28, 153.69, 132.54, 131.51, 118.76, 70.36, 70.49, 69.76, 69.21, 64.18, 61.48, 51.50, 51.28, 48.82, 48.63, 26.24, 25.94, 25.12, 18.29, -5.32; FABMS, calcd for $\text{C}_{55}\text{H}_{97}\text{N}_{11}\text{O}_8\text{Si}_3$ m/z = 1224, obsd m/z = 1225 ($\text{M} + \text{H}$) $^+$.

Preparation of Modified Polyurethane Surfaces. Throughout our experiments, we used a medical grade polyurethane foil (Pellethane D-55). The foil had a smooth surface (as could be verified with scanning electron microscopy) and was transparent; its thickness was 0.4 mm. Compound **1** was dissolved in 2-propanol (concentration 1 mM), and this solution was sprayed onto several specimens of the polyurethane foil (dimensions 50 × 50 mm). A compressed-air sprayer was used (tube-type, Aldrich Z12,629-2). During spraying, the polymer surface was placed horizontally and consecutively wetted,

dried (air föhn), and turned by 90°. The procedure of wetting, drying, and turning was repeated 20 times. Then, each foil was irradiated for 15 min with a Philips HPA 1000 high-power UV lamp (Philips Lighting, Eindhoven, The Netherlands). The distance between the lamp and the foil surface was 30 cm. Technical details on the lamp are as follows: nominal power, 930 W; radiation output (mW/cm², measured at 1.00 m distance), UV-A 2500, UV-B 900, UV-C 230. After irradiation, each foil was thoroughly washed with 2-propanol and immersed for 24 h in a stirred solution of tetrabutylammonium fluoride in nitromethane (22). This reagent is known to effectively cleave the TBDMS groups. Each foil was then thoroughly washed with 2-propanol and water and stored in dry form.

Physicochemical Characterization of the Modified Surfaces. The UV extinction of dipyrindamole provided a convenient means to obtain an estimate of the surface concentration. The UV absorption spectrum of dipyrindamole shows a maximum at $\lambda = 408$ nm. The molar extinction coefficient at this wavelength is 4397 L mol⁻¹ cm⁻¹. A piece of the unmodified polyurethane (138.79 mm²) was dissolved in tetrahydrofuran (4.50 mL). The UV extinction spectrum was measured and stored in the digital memory of the spectrometer. Then, a similar piece of the modified polyurethane (139.67 mm²) was dissolved in 4.53 mL of tetrahydrofuran (same concentration as the blank). The UV extinction was measured at 408 nm, and the density of immobilized dipyrindamole coupled to the polyurethane was calculated (3).

Contact angle measurements were performed according to the captive bubble method (23). The contact angle apparatus consists of a traveling microscope with a 40× eyepiece with fine right-angle crosshairs and a long-distance objective, a variable intensity light source, and a micrometer-adjustable X-Y stage vertically mounted on an optical bench. The stage contains a plexiglass box. The polyurethane sheets were held on the underside of a polycarbonate plate with the modified surface exposed. The box was then filled with doubly distilled water, and the plate containing the polyurethane sheet was lowered in the box until the polyurethane sheet was completely immersed. A bubble of air with a volume of ~0.1 mL was positioned under the surface and the contact angle was measured.

For the X-ray photoelectron spectroscopy (XPS) experiments, polyurethane sheets were mounted on a standard sample holder and inserted via a separately pumped load lock into a Leybold MAX200 XPS instrument. Sample areas of 4 × 7 mm² were analyzed. Mg K α (1253.6 eV) radiation of a Mg/Al double-anode X-ray tube (13 kV, 20 mA) was used. The spectrometer was calibrated using Ag, Cu, and Au (24). At the used pass energy of 48 eV, the full width at half-maximum for Ag 3d_{5/2} was 0.95 eV. The base pressure in the analysis chamber was well below 1 × 10⁻⁹ mbar. The instrument was controlled by a HP A400 computer, and a Leybold DS100 data system was used for data acquisition and analysis. For the quantitative analysis the spectra were corrected for the analyzer transmission function, and a linear background was subtracted (25). Sensitivity factors were calculated, using the approach of Nöller et al. (26) and the Scofield cross sections (27). For energy referencing a C 1s binding energy of 285.0 eV for aliphatic carbon was used (28). The samples were measured with different take-off angles. Besides the usual angle (90°), the sample holder was rotated in such a way that a take-off angle of ~6° was obtained. Derivatization of the hydroxyls of the dipyrindamole by trifluoroacetic anhydride was achieved

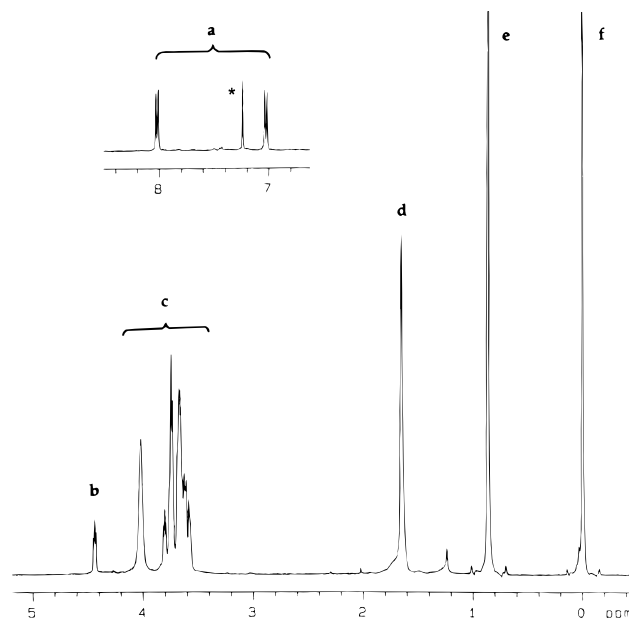


Figure 1. 400 MHz ¹H NMR spectrum of **1**, dissolved in CDCl₃. Spectral parameters: spectral width, 6000 Hz; number of transients, 8; time domain, 32K; size, 64K; Fourier transformation without application of a spectral window. Assignments: (a) aromatic protons from the azidobenzoyl group; (b) CH₂C(O); (c) CH₂-N and CH₂-O; (d) CH₂ of piperidine rings; (e) *tert*-butyl; (f) CH₃-Si; (*) solvent signal (CHCl₃).

by exposing the polyurethane surface to trifluoroacetic anhydride vapor for 5 min in a sealed vessel (29). The polyurethane surface was then removed and dried.

Biochemical Characterization. The unmodified and modified surfaces were subjected to the *in vitro* thrombin generation assay developed by Lindhout et al. (30) and described extensively in our previous work (3, 7, 31). Two reference materials were included in the assay: polyethylene (PE), which has a high surface thrombogenicity, and poly(vinyl chloride) (PVC), which is a relatively passive material. Note that the blood was taken from a healthy donor; the blood plasma was anticoagulated with citrate prior to the assay, and the addition of calcium chloride marks the actual start of the experiment.

Following incubation with platelet-rich plasma, the unmodified and modified surfaces were subjected to scanning electron microscopy (SEM) to study the morphology of adhered platelets. The platelets attached to the polyurethane surfaces were fixed with glutaraldehyde. The specimens were then dehydrated with ethanol, subjected to critical point drying, and sputter-coated with gold.

RESULTS

Physicochemical Characterization. The chemical synthesis of conjugate compound **1** proceeded smoothly. Figure 1 shows the 400 MHz proton NMR spectrum of **1**, dissolved in deuterated chloroform. The spectrum clearly reveals the identity and purity of the product. Fast atom bombardment mass spectrometry provided further evidence for the identity of **1** (*vide supra*).

Measurements of the surface density of immobilized dipyrindamole were performed through UV spectrophotometry. The modified surfaces (dimensions approximately 50 × 50 mm) showed uniform density of immobilized dipyrindamole. This was concluded after comparison of different pieces (dimensions 10 × 15 mm), cut out of the foil. All physicochemical and biochemical experi-

Table 1. Contact Angles Measured with the Captive Bubble Method for the Unmodified and Modified Surfaces

unmodified surface		modified surface	
49.5	51.2	19.1	22.3
50.6	49.8	25.3	21.5
47.3		20.8	

ments reported here correspond with a surface density of 13 ± 1 nmol/cm² of immobilized dipyridamole.

Table 1 compiles the results of the water contact angle measurements on both the unmodified and modified surfaces. The contact angles were measured with the captive-bubble method. Under each surface, five air bubbles (~ 0.1 mL) were placed, and height (h) and diameter (d) of the bubbles were measured. The contact angle α was then calculated from the formula (23)

$$\alpha = \cos^{-1}[-1 + 2h/d]$$

The data in Table 1 clearly show that the modified surface is more hydrophilic than the unmodified surface.

Furthermore, both surfaces were studied with XPS. As expected, oxygen, nitrogen, and carbon were detected. No contaminations were found on either surface. The observed binding energies for the oxygen, nitrogen, and carbon species are in good agreement with those of Beamson and Briggs (28). The spectra were analyzed by applying curve deconvolution, using a Gaussian line shape. The N 1s narrow-scan subspectrum was used to get more detailed information on the nature of the surface. The increase of the N 1s signal was not significant, and this inspired us to measure the modified surface also under another take-off angle. This enables one to look more at the outermost layer of the modified surface. The sample holder was rotated in such a way that a take-off angle of $\sim 6^\circ$ was obtained. This experiment clearly showed a change in surface chemistry, which could be derived from changes in the peak shape of the narrow-scan spectra. Figure 2 shows the expansion of the N 1s narrow-scan spectrum measured at a take-off angle of 90° . Figure 3 shows the expansion of the N 1s narrow-scan spectrum measured at a take-off angle of $\sim 6^\circ$. The N 1s line is less intense, but broadened, consistent with the presence of another nitrogen functionality in the outermost surface layer (aromatic nitrogen from the dipyridamole). Table 2 gives the atomic percent C, N, and O and the elemental ratios C/O and C/N for the unmodified and modified surfaces. Another important conclusion that can be drawn from the XPS spectra of the modified surface is that the Si protective groups were completely removed in the deprotection/washing steps following the irradiation with ultraviolet light. The XPS spectra do not show the very characteristic Si signals at approximately 102 (Si 2p) and 153 (Si 2s) eV. For this reason, we expected the presence of free hydroxyl groups (three OH groups for each immobilized dipyridamole) for the modified surface. This expectation could be verified by exposure of the modified surface to a vapor of tetrafluoroacetic anhydride in a sealed vessel. The anhydride then reacts with free hydroxyl groups to form the trifluoroacetic ester. This vapor-phase labeling of hydroxyl groups has been shown to be very successful (29). The CF₃ tag is easily detected since two extra peaks appear in the XPS spectrum: (i) the F 1s line at approximately 690 eV and (ii) the F Auger line at approximately 600 eV (Mg K α radiation; see ref 28, p 236, and ref 29). Figure 4 shows the overall XPS scan of the modified surface (take-off angle of $\sim 6^\circ$). Figure 5 shows the XPS scan of the modified surface after

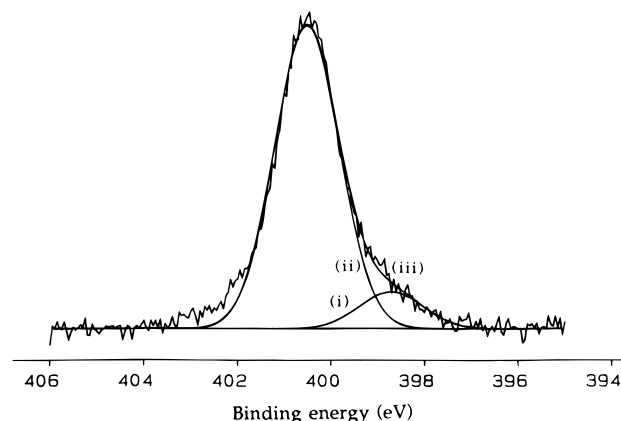


Figure 2. N 1s narrow-scan XPS spectrum of the modified surface measured at a take-off angle of 90° . The experimental spectrum can be simulated by adding the simulated spectra i and ii. Note that (iii), which equals (i) + (ii), fits the experimental spectrum; (i) corresponds with the aromatic N of the dipyridamole ring system, and (ii) corresponds with the N atoms of the polymer urethane groups, and the nonaromatic Ns of dipyridamole.

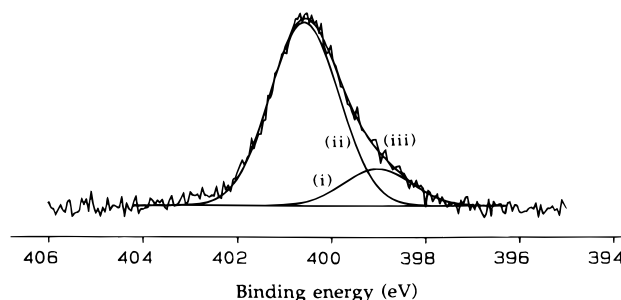


Figure 3. N 1s narrow-scan XPS spectrum of the modified surface measured at a take-off angle of $\sim 6^\circ$. Spectral simulation was accomplished as described in the legend to Figure 2.

Table 2. Elemental Atomic Percentages and Elemental Ratios Measured by XPS for the Unmodified and Modified Surfaces

atom	unmodified surface	modified surface	
	take-off angle 90°	take-off angle 90°	take-off angle $\sim 6^\circ$
% C	80	79	82
% N	3.1	4.3	2.8
% O	17	17	15
C/O	4.7	4.6	5.5
C/N	25.8	18.4	29.3

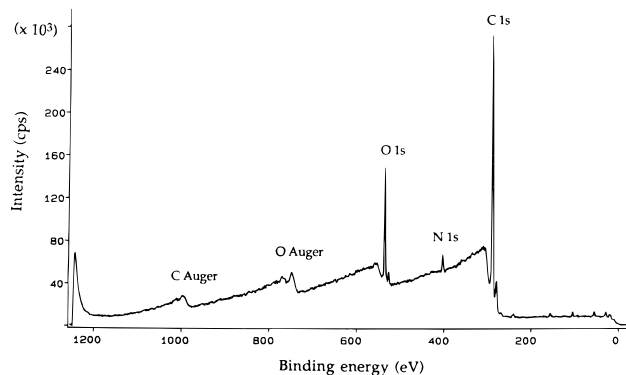


Figure 4. Overall XPS spectrum of the modified surface measured at a take-off angle of $\sim 6^\circ$.

its exposure to tetrafluoroacetic anhydride vapor (take-off angle of $\sim 6^\circ$). This labeling clearly revealed the presence of free hydroxyl groups on the modified surface, which is consistent with the presence of immobilized and fully deprotected dipyridamole.

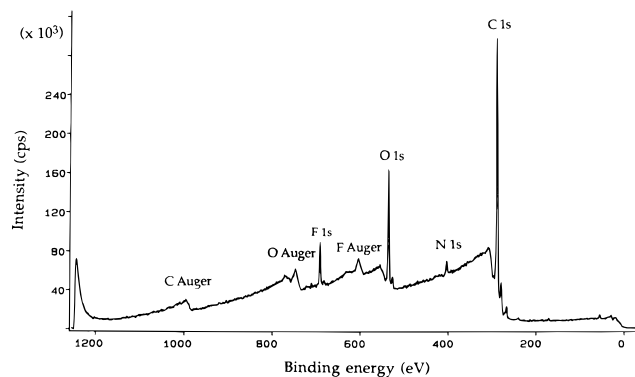


Figure 5. Overall XPS spectrum of the modified surface exposed to trifluoroacetic anhydride vapor measured at a take-off angle of $\sim 6^\circ$.

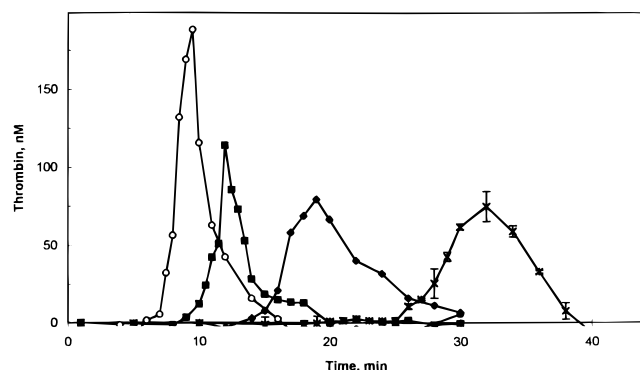


Figure 6. Thrombin generation curves measured for four different surfaces. The thrombin generation curves were corrected for the amidolytic activity of the α_2 m-thrombin complex (32). Assignments: (○) PE; (■) polyurethane; (◆) PVC; (×) modified polyurethane.

Table 3. Results of the Thrombin Generation Test

material	lag time (s)	[thrombin] _{max} (nM)
PE	395	169
PVC	859	79
polyurethane	569	85
modified polyurethane	1267; 1282	68; 75

Biochemical Characterization. The unmodified and modified surfaces were subjected to the *in vitro* thrombogenicity test developed by Lindhout et al. (30). PE, a highly thrombogenic material, PVC, a relatively passive material, and unmodified polyurethane were used as reference materials. The assay produces a thrombin generation curve for each surface tested. The experiments on the modified surface were performed in duplicate. Figure 6 shows the thrombin generation curves for both the unmodified and modified surfaces, exposed to human platelet-rich blood plasma. Each thrombin generation curve yields two parameters, which are directly related to the thrombogenicity of the material. The first parameter is the lag time, i.e. the time elapsing between the moment of recalcification and the moment at which the free thrombin concentration starts to increase. The second parameter is the maximal concentration of free thrombin reached during the experiment. The results of these experiments with all surfaces are compiled in Table 3. It should be noted that the maximum thrombin concentrations were obtained after correction of the experimental thrombin generation curves for the residual amidolytic activity of the thrombin- α_2 -macroglobulin complex according to the method of Hemker et al. (32). The thrombogenicity of the different surfaces decreases in the following order: PE > polyurethane > PVC > modified polyurethane. The

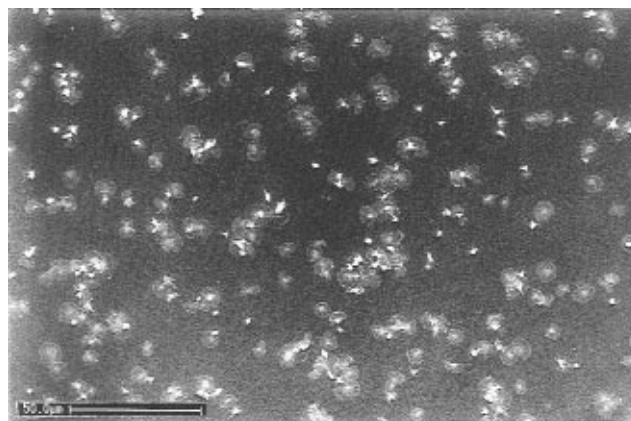


Figure 7. Overview scanning electron micrograph of the unmodified surface after incubation with platelet-rich plasma.

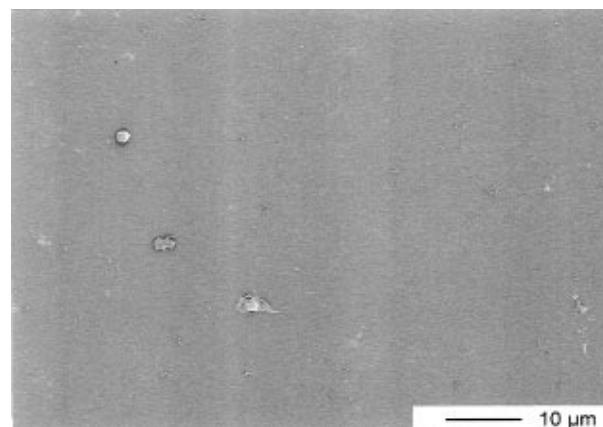


Figure 8. Overview scanning electron micrograph of the modified surface after incubation with platelet-rich plasma.

surface immobilization of compound **1** leads to a decrease of the thrombogenicity of the polyurethane; the lag time increases from 569 s for the unmodified polyurethane to 1267 and 1282 s (duplicate) for the modified surface. The maximum free thrombin concentration decreases from 85 nM for the unmodified polyurethane to 68 and 75 nM (duplicate) for the modified surface.

The unmodified and modified surfaces were further studied with SEM to look at the adherence and activation of platelets on the surfaces. The unmodified surface was covered to a large extent by activated/spreaded platelets, as is shown in Figure 7. From the scanning electron micrographs, a surface density of approximately 7×10^3 platelets/mm² could be estimated. The modified surface showed far less adhered platelets (Figure 8); the scanning electron micrograph indicated a surface density of approximately 6×10^2 platelets/mm². This implies that the surface modification results in a decrease of platelet adhesion by, roughly, 1 order of magnitude. This finding is in good agreement with our previous work (3, 5). Figure 9 shows a detail scanning electron micrograph of an individual platelet, adhered to the modified surface. While this particular platelet merely shows the formation of small pseudopodia, and no spreading, it should be noted that spread platelets could also be found on the modified surface.

DISCUSSION AND CONCLUDING REMARKS

The present results clearly demonstrate that dipyrindamole can be immobilized onto polyurethane surfaces through use of conjugate **1**. A combination of different physical analytical techniques reveals the presence of fully deprotected dipyrindamole in the outermost layer of

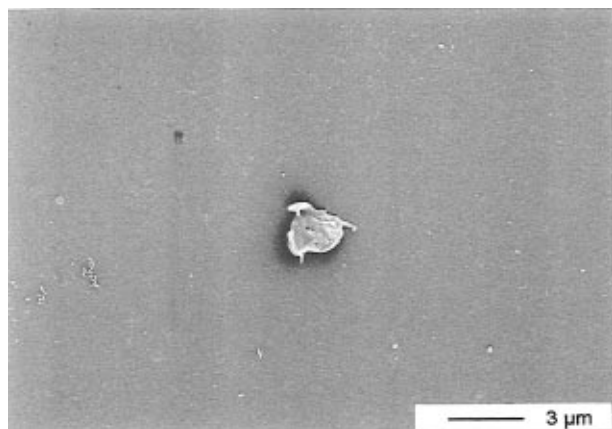


Figure 9. Detailed scanning electron micrograph showing the morphology of a platelet adhered to the modified surface. Formation of small pseudopodia is noted.

the modified surface. Furthermore, the modified surface features a markedly increased hydrophilicity, as compared to the control (i.e. unmodified polyurethane). This can be attributed to the short polyethylene glycol spacer chain that bridges dipyridamole to the polymer surface.

To the best of our knowledge, the present results show for the first time that it is possible to couple a pharmacologically active drug to a polymer surface via a chain of covalent bonds and to simultaneously achieve a substantial increase of the surface hydrophilicity. We believe that this combination of effects holds promise with respect to passivation of artificial surfaces. From the classic work of Vroman and others (*vide supra*), it is known that contact between blood and an artificial surface first leads to adsorption of plasma proteins and then to activation of platelets or leukocytes, which recognize one or more specific structural patterns of the proteinaceous adsorbates. A modified surface as studied in our present work interferes with this mechanism at two different stages: (i) the hydrophilic nature of the surface leads to substantial hydration and hence to a diminished affinity for proteins; (ii) the exposure of a platelet inhibitory agent (dipyridamole in our case) suppresses activation of contacting blood platelets.

We did not perform a quantitative comparison of the modified surfaces based on **1** and those to which dipyridamole was coupled either directly or via a short hydrophobic spacer chain. Nevertheless, our thrombin generation assay suggests that photoimmobilization of **1** leads to the best results (15). This idea is reinforced by a comparison of the scanning electron micrographs. Figure 8 (this work) shows that the modified polyurethane surface, prepared with conjugate **1**, adsorbs far fewer platelets after exposure to human platelet-rich plasma (approximately $7 \times 10^3/\text{mm}^2$) as compared to the control (approximately $6 \times 10^2/\text{mm}^2$). Upon use of a short hydrophobic spacer chain $[-\text{C}(\text{O})\text{CH}_2\text{CH}_2\text{CH}_2\text{O}-]$, we previously found that platelet adhesion was also markedly suppressed (in comparison with the control) (3). However, the platelets present on the latter surface showed substantial spreading and formation of pseudopodia.

On the basis of our experience with photoimmobilization of dipyridamole to polyurethane surfaces, we are currently working on photoimmobilization of conjugate **1** on the luminal surface of a polyurethane vascular graft. This graft has an inner diameter of 5 mm and a flexible, compliant, and porous wall structure. Our results with this new vascular graft (*in vitro* and *in vivo*) will be published later.

LITERATURE CITED

- (1) Oates, J. A., Wood, A. J. J., and Fitzgerald, G. A. (1987) Medical intelligence drug therapy dipyridamole. *N. Engl. J. Med.* **316**, 1247–1257.
- (2) Singh, J. P., Rothfuss, K. J., Wiernicki, T. R., Lacefield, W. B., Kurtz, W. L., Brown, R. F., Brune, K. A., Bailey, D., and Dubé, G. P. (1994) Dipyridamole directly inhibits vascular smooth muscle cell proliferation *in vitro* and *in vivo*: implications in the treatment of restenosis after angioplasty. *J. Am. Coll. Cardiol.* **23**, 665–671.
- (3) Aldenhoff, Y. B. J., and Koole, L. H. (1995) Studies on a new strategy for surface modification of polymeric biomaterials. *J. Biomed. Mater. Res.* **29**, 917–928.
- (4) Kuijpers, J. M. H., Kardaun, G. A., Blezer, R., Pijpers, A. P., and Koole, L. H. (1995) Immobilization of theophylline on medical-grade polyurethane inhibits surface-induced activation of bloodplatelets. *J. Am. Chem. Soc.* **117**, 8691–8697.
- (5) Aldenhoff, Y. B. J., Blezer, R., Lindhout, T., and Koole, L. H. (1997) Photo-immobilization of dipyridamole (Persantin) at the surface of polyurethane biomaterials: reduction of *in vitro* thrombogenicity. *Biomaterials* **18**, 167–172.
- (6) Kruff, M. A. B., Benzina, A., Blezer, R., and Koole, L. H. (1996) Studies on radio-opaque polymeric biomaterials with potential applications to endovascular prostheses. *Biomaterials* **17**, 1803–1812.
- (7) Kruff, M. A. B., Benzina, A., Bär, F., van der Veen, F. H., Bastiaansen, C. W. M., Blezer, R., Lindhout, T., and Koole, L. H. (1994) Studies on two new radiopaque polymeric biomaterials. *J. Biomed. Mater. Res.* **28**, 1259–1266.
- (8) Vroman, L., and Adams, A. L. (1969) Findings with the recording ellipsometer suggesting rapid exchange of specific plasma proteins at liquid-solid interfaces. *Surf. Sci.* **16**, 438–446.
- (9) Brash, J. L. (1987) The fate of fibrinogen following adsorption at the blood-biomaterial interface. *Ann. N. Y. Acad. Sci.* **516**, 206–222.
- (10) Vroman, L. (1988) The life of an artificial device in contact with blood: Initial events and their effect on its final state. *Bull. N. Y. Acad. Med.* **64**, 352–357.
- (11) Grinnell, F. (1987) Fibronectin adsorption on material surfaces. *Ann. N. Y. Acad. Sci.* **516**, 280–290.
- (12) Bamford, C. H., and Al-Lamee, K. G. (1992) Chemical methods for improving haemocompatibility of synthetic polymers. *Clin. Mater.* **10**, 243–250.
- (13) Bamford, C. H., Al-Lamee, K. G., Middleton, I., and Can, R. (1990) Chemical modification of polymers to increase blood compatibility. *Bull. Soc. Chim. Belg.* **99**, 919–925.
- (14) van der Heiden, A. P., and Koole, L. H. (1996) Photochemical coupling of aryl azides to poly(etherurethane) surfaces: studies with a fluorescent model compound. *Macromolecules* **29**, 7012–7015.
- (15) Witkowski, S., Koteswar, R., Ramiya, H. P., Haluska, P. V., and Fried, J. (1992) Total synthesis of (+)-10,10-difluorothromboxane A_2 and its 9, 11 and 15 stereoisomers. *J. Am. Chem. Soc.* **114**, 8464–8472.
- (16) Leyva, E. L., Platz, M. S., Persy, G., and Wirtz, J. J. (1986) Photochemistry of phenyl azide: the role of singlet and triplet phenylnitrene as transient intermediates. *J. Am. Chem. Soc.* **108**, 3783–3790.
- (17) Li, Y.-Z., Kirby, J. P., George, M. W., Poliakoff, M., and Schuster, G. B. (1988) 1,2-Didehydroazepines from the photolysis of substituted aryl azides: analysis of their chemical and physical properties by time-resolved spectroscopic methods. *J. Am. Chem. Soc.* **110**, 8092–8098.
- (18) Smith, P. A. S. (1984) *Azides and Nitrenes; Reactivity and Utility* (E. F. V. Scriven, Ed.) Academic Press, Orlando, FL.
- (19) Wu, J. C., Xi, Z., Gioeli, C., and Chattopadhyaya, J. (1991) Intramolecular cyclization-trapping of carbon radicals by olefins as means to functionalize 2'- and 3'-carbons in β -D-nucleosides. *Tetrahedron* **47**, 2237–2254.
- (20) Kohli, V., Blöcker, H., and Köster, H. (1980) The triphenylmethyl (trityl) group and its use in nucleotide chemistry. *Tetrahedron Lett.* **21**, 2683–2686.
- (21) Bretschneider, H., and Rager, H. (1950) Darstellung aromatischer azidverbindungen nach der Dutt-Wormallschen reaktion. *Monatsh. Chem.* **81**, 970–980.

- (22) Corey, E. J., and Venkateswarly, A. (1972) Protection of hydroxyl groups as *tert*-butyldimethylsilyl derivatives. *J. Am. Chem. Soc.* **94**, 6190–6191.
- (23) King, R. N., Andrade, J. D., Ma, S. M., Gregonis, D. E., and Brostrom, L. R. (1995) Interfacial tensions at acrylic hydrogel-water interfaces. *J. Colloid Interface Sci.* **103**, 62–75.
- (24) Seah, M. P. (1989) Post-1989 calibration energies for X-ray photoelectron spectrometers and the 1990 Josephson constant. *Surf. Interface Anal.* **14**, 488.
- (25) Berresheim, K., Mattern-Klosson, M., and Wilmers, M. (1991) A standard form spectra for quantitative ESCA-analysis. *Fresenius' J. Anal. Chem.* **341**, 121–124.
- (26) Nöller, H. G., Polaschegg, H. D., and Schillalies, H. (1974) A step towards quantitative electron spectroscopy measurements by improved electron optics. *J. Electron Spectrosc. Relat. Phenom.* **5**, 705–723.
- (27) Scofield, J. H. (1976) Hartree-slater subshell photoionization cross-sections at 1254 and 1487 eV. *J. Electron Spectrosc. Relat. Phenom.* **8**, 129–137.
- (28) Beamson, G., and Briggs, D. (1992) *High Resolution XPS of Organic Polymers*, Wiley, Chichester, U.K.
- (29) Ameen, A. P., Ward, R. J., Short, R. D., Beamson, G., and Briggs, D. (1993) A high-resolution X-ray photoelectron spectroscopy study of trifluoroacetic anhydride labelling of hydroxyl groups: demonstration of the β shift due to $-\text{OC}(\text{O})\text{CF}_3$. *Polym. Prepr. (Am. Chem. Soc. Div. Poly. Chem.)* **34**, 1795–1799.
- (30) Lindhout, T., Baruch, D., Schoen, P., Franssen, J., and Hemker, H. C. (1986) Thrombin generation and inactivation in the presence of antithrombin III and heparin. *Biochemistry* **25**, 5962–5970.
- (31) Lindhout, T., Blezer, R., Maassen, C., Heijnen, V., and Reutelingsperger, C. P. M. (1995) Platelet procoagulant surface as an essential parameter for the *in vitro* evaluation of the blood compatibility of polymers. *J. Mater. Sci.: Mater. Med.* **6**, 367–372.
- (32) Hemker, H. C., Willems, G., and Béguin, S. (1986) A computer assisted method to obtain the prothrombin activation velocity in whole plasma independent of thrombin decay processes. *Thromb. Haemostasis* **56**, 9–17.

BC970020Z

^{99m}Tc -Labeled σ -Receptor-Binding Complex: Synthesis, Characterization, and Specific Binding to Human Ductal Breast Carcinoma (T47D) Cells

Christy S. John,^{*,†} Benjamin B. Lim,[†] Brian C. Geyer,[†] Bertold J. Vilner,[‡] and Wayne D. Bowen[‡]

Radiopharmaceutical Chemistry Section, Department of Radiology, George Washington University Medical Center, Washington, D.C. 20037, and Unit on Receptor Biochemistry and Pharmacology, Laboratory of Medicinal Chemistry, NIDDK, National Institutes of Health, Bethesda, Maryland 20892. Received September 20, 1996[⊗]

σ -Receptors have recently been shown to be expressed in a variety of human tumor cells. In an attempt to prepare ^{99m}Tc chelates that would bind to σ -receptors and be useful for imaging σ -receptor-positive tumors, we have synthesized and characterized a bisaminothiol (BAT) chelate appended with a σ -receptor pharmacophore. The synthesis of target ligand **VII** was accomplished in three steps starting from bicyclic imidazolidino[1,2-*d*]dithiazapine. The labeling of the BAT ligand with ^{99m}Tc was carried out in high yields (>80%) using stannous tartarate as a reducing agent, resulting in the target σ -receptor-binding chelate [^{99m}Tc]BAT-EN6, **III**. Similarly, ^{99g}Tc chelate with ligand **VII** was prepared from ammonium pertechnetate by reduction with stannous tartarate. ^{99m}Tc -radiolabeled chelate was purified by reversed phase HPLC, and cell binding with human breast ductal carcinoma (T47D) was performed. A high degree of specific binding (90–97%) was obtained when σ -receptor ligands such as halogenated phenylethylenediamines were used to determine nonspecific binding. A modest affinity dose-dependent inhibition of binding was found with BD1008, **I**, and 4-IPEMP, **II** ($\text{IC}_{50} = 47 \pm 2$ and 59 ± 5 nM, respectively), known σ -ligands. No specific binding was found with [^{99m}Tc]BAT, **VIII** [without appended σ -pharmacophore (*N*-alkyl-substituted ethylenediamine)], showing that biological activity resulted from the pendent pharmacophore. ^{99g}Tc complex was found to be a potent inhibitor ($K_i = 42.7 \pm 8.5$ nM) of [^3H]DTG binding in guinea pig brain membranes. Scatchard analysis of [^{99m}Tc]BAT-EN6 (spiked with [^{99g}Tc]BAT-EN6) binding in T47D breast cancer cells showed a saturable binding, with a K_d of 43.5 ± 14.7 nM and a B_{max} of 3121 ± 130 fmol/(mg of protein). A biodistribution study of [^{99m}Tc]BAT-EN6 chelates in Sprague Dawley rats showed hepatic clearance, as expected. A blocking study at 4 h postinjection using 2 μmol of BD1008 with [^{99m}Tc]BAT-EN6 showed a significant decrease of radiopharmaceutical in liver (15.32 vs 22.31% ID/organ) and kidney (1.01 vs 2.21% ID/organ), organs known to possess high concentrations of σ -receptors. These results imply that [^{99m}Tc]BAT-EN6 binds with high affinity to σ -receptors expressed in human breast tumor cells, and it may be useful for imaging breast cancer.

INTRODUCTION

Recently, we have been interested in the development of molecular probes for imaging σ -receptor sites on tumors. σ -Receptors exist in at least two distinct subtypes termed σ -1 and σ -2 (*1*). Tritiated σ -ligand probes such as (+)-pentazocine (a σ -1 selective ligand) (*2*) and tritiated 1,3- σ -ditolylguanidine (DTG, a σ non-subtype selective ligand) (*3*) were recently used to characterize the expression of σ -receptors on various human tumor cell lines and to establish the pharmacological profiles for various drugs. A very high density of both σ -1 and σ -2 receptor subtypes was expressed on many human and rodent tumor cell lines [$B_{\text{max}} = 1000$ – 4000 fmol/(mg of protein)] (*4*). High levels of σ -receptors have also been reported in the membrane preparations from surgically removed solid human tumor tissue using [^3H]DTG (*5*). Furthermore, σ -receptors expressed in human melanoma cells (*6*), breast cancer cells (*7*, *8*), non-

small cell lung carcinoma (*9*), and human prostate tumor (*10*) cells have been characterized using different radioiodinated σ -ligands. Scatchard analysis of [^{125}I]-4-(*N*-benzylpiperidin-4-yl)-4-iodobenzamide binding in human breast adenocarcinoma (MCF-7) cells revealed that breast cancer cells possess approximately 1 million receptors per cell (*4*). σ -Receptors are therefore very attractive targets for the development of diagnostic probes. Hence, we embarked on a study of ^{99m}Tc -radiolabeled chelates that would bind to the σ sites because of the excellent physical characteristics of this radionuclide.

^{99m}Tc is one of the most widely used radionuclides in clinical nuclear medicine due to its instant availability from the $^{99}\text{Mo}/^{99m}\text{Tc}$ generator, ideal physical properties ($t_{1/2} = 6.02$ h; γ -energy = 140 keV), an absence of β -emissions, a low radiation burden to patients, and its low cost. One of the major challenges in the development of receptor-based ^{99m}Tc radiopharmaceuticals for diagnostic imaging is the design and synthesis of high-affinity ^{99m}Tc chelates for specific receptor sites. In order to provide in vivo stability to the radiolabel, ^{99m}Tc has to be complexed to a chelate. Thus, a molecule suitable for imaging a particular receptor site would possess a chelating moiety and a pharmacological entity appended to the chelate. This generally results in an increase in steric bulk of the molecule, and the affinity for the receptors is often compromised. In recent years, some progress has been made for imaging steroid receptors (*11*), muscarinic

* Address correspondence to Christy S. John, Ph.D., Radiopharmaceutical Chemistry Section, Department of Radiology, The George Washington University Medical Center, 661 Ross Hall, 2300 I St. NW, Washington, D.C. 20037. Telephone: (202) 994-5031. Fax: (202) 994-0417. E-mail: Johncs@gwis2.circ.gwu.edu.

[†] George Washington University Medical Center.

[‡] National Institutes of Health.

[⊗] Abstract published in *Advance ACS Abstracts*, March 1, 1997.

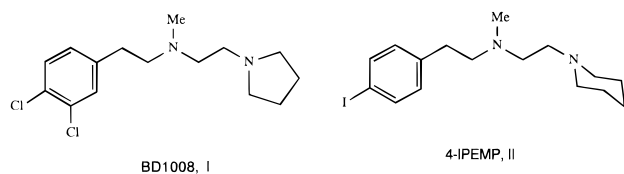
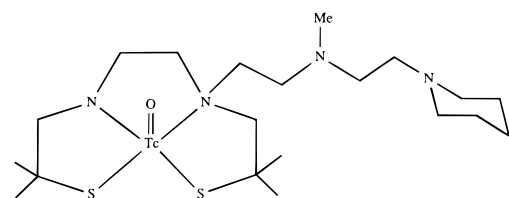
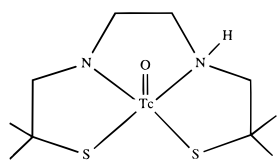


Figure 1. Structures of σ -receptor-binding substituted ethylenediamine ligands.



[Tc-99m]BAT-EN6, III, Chelate-Pharmacophore Complex



[Tc-99m]BAT, VIII, Parent Chelate

Figure 2. Structures of [^{99m}Tc]BAT chelates.

receptors (12), and vesamicol receptors (13) using bisaminothiol-based ^{99m}Tc chelates.

Halogen-substituted arylenediamines have been studied extensively for their σ -affinities (14, 15). BD1008 [*N*-2-[(3,4-dichlorophenyl)ethyl]-*N*-methyl-2-pyrrolidinylethylamine], **I**, is one of the most potent halogenated arylenediamine derivatives. One congener of this series, *N*-[2-(4-iodophenyl)ethyl]-*N*-methyl-2-(1-piperidinylethylamine) (4-IPEMP, **II**), has recently been well-studied (Figure 1) (16). Compound **II** showed very high specific binding to human breast and melanoma tumor cells. The inhibition binding isotherms for 4-[^{125}I]PEMP in guinea pig brain also were consistent with σ -receptor pharmacology. On the basis of the structure-activity relationship of de Costa et al. (14), we reasoned that the substituted ethylenediamine portion of **II** is the molecular recognition fragment that imparts high affinity for σ -receptor, with the halogen-substituted aromatic ring occupying the lipophilic pocket of the receptor. Therefore, we decided to append the *N*-methyl-2-piperidinylethylamine pharmacophore into a basic bisaminoethanethiol ligand **VIII** (Figure 2) (that is known to form highly stable, neutral, and lipophilic complexes with ^{99m}Tc) to test the hypothesis that this molecular recognition fragment would impart specificity for the σ -receptors to the resulting ^{99m}Tc -labeled complex. In this article, we report preliminary results of the synthesis of our target ligand **VII**, its complexation with ^{99m}Tc and ^{99}Tc , and the preliminary pharmacological characterization and in vivo distribution of the resulting complexes.

EXPERIMENTAL PROCEDURES

General. All chemicals and reagents not otherwise noted were purchased from Aldrich Chemical Co. Melting points were determined with a Fisher-Johns apparatus and are reported uncorrected. ^1H NMR spectra were recorded on a Bruker 300 AM spectrometer. The thin-layer chromatography (TLC) system consisted of Analtech uniplat silica gel GF plates (250 μm , 10 \times 20

cm). Mass spectra (chemical ionization or electron impact) were recorded on a Finnigan 1015 mass spectrometer. For ^{99}Tc complex, electrospray ionization (ESI) mass spectra was obtained using the Finnigan TSQ700 triple-quadrupole mass spectrometer. $\text{Na}^{99m}\text{TcO}_4$ was eluted with the $^{99}\text{Mo}/^{99m}\text{Tc}$ generator obtained from DuPont Merck (Billerica, MA). Elemental analysis was performed by Quantitative Technologies, Inc. (Whitehouse, NJ). Imidazolidino[1,2-*d*]dithiazepine (**IV**) was prepared according to a published method (17).

Chemical Synthesis. *Reaction of Imidazolidino[1,2-*d*]dithiazepine (IV) with Chloroacetyl Chloride.* To a solution of imidazolidino[1,2-*d*]dithiazepine (8.6 g, 37 mmol) in CHCl_3 (50 mL) was added 10% NaOH (50 mL), and the mixture was cooled with an ice/water bath. To this was added chloroacetyl chloride (4.2 mL, 53.3 mmol), and the mixture was stirred for 1 h. The bath was removed, and the mixture was stirred for an additional 0.5 h. The organic layer was separated, dried over anhydrous sodium sulfate, and evaporated to a thick oil. This oil was dissolved in ethyl acetate/hexanes (1:5) to give white solid **V** (5.2 g, 45%): ^1H NMR (CDCl_3) δ 1.23 (s, 3H), 1.24 (s, 3H), 1.27 (s, 3H), 1.34 (s, 3H), 2.58 (d, J = 15 Hz, 1H), 2.83–2.87 (m, 1H), 3.24 (m, 1H), 3.32 (d, J = 15 Hz, 1H), 3.45–3.55 (m, 1H), 3.70–3.76 (m, 1H), 4.04 (s, 2H), 4.71 (s, 1H). Anal. Calcd for $\text{C}_{12}\text{H}_{21}\text{N}_2\text{OS}_2\text{Cl}$: C, 46.66; H, 6.85; N, 9.07. Found: C, 46.75; H, 6.68; N, 9.03.

Reaction of V with N-Methyl-2-(1-piperidinyl)ethylamine. To a solution of **V** (6.0 g, 20 mmol) in dry DMF (50 mL) was added powdered potassium carbonate (3.3 g, 23.9 mmol). To this was added *N*-methyl-2-(1-piperidinyl)ethylamine (4.26 g, 29.9 mmol), and the mixture was stirred overnight at room temperature. This was evaporated to dryness under vacuum and washed with water (2 \times 50 mL). This was redissolved in chloroform, washed with water, and dried over anhydrous sodium sulfate. The organic layer was evaporated to dryness. This oil was converted to hydrochloride salt and recrystallized from 20% ethanol in acetonitrile to give quantitative yields of **VI**: ^1H NMR (CDCl_3) δ 1.17–1.26 (m, 12H), 1.33–1.49 (m, 6H), 2.21 (s, 3H), 2.3–2.5 (m, 9H), 2.5–2.7 (m, 1H), 2.9–3.1 (m, 2H), 3.2–3.3 (m, 3H), 3.9–4.0 (m, 1H), 4.65 (s, 1H). Anal. Calcd for $\text{C}_{20}\text{H}_{38}\text{N}_4\text{OS}_2$: C, 57.93; H, 9.24; N, 13.51. Found: C, 58.05; H, 9.12; N, 13.39.

Reduction of VI with LAH. To the suspension of LAH (2.2 g) in THF (100 mL) was added a solution of amide (4.0 g), and the mixture was heated at reflux for 19 h. The reaction was quenched with saturated aqueous NH_4Cl , and ether (50 mL) was added and filtered through a pad of Celite. The solid was washed with ether (3 \times 50 mL), and to the combined ether layer was added ethanol saturated with HCl to give a sticky white solid **VII**. To this more was added ethanol to give a powdery white solid (2.0 g, 38%): MS (m/e) 403 [M + 1] $^+$.

Radiochemical Synthesis. *Preparation of [^{99m}Tc]BAT-EN6 Complex.* An aqueous solution of ligand **VII** (1.0 mg/mL) was prepared. To a 0.2 mL solution of the ligand was added 2.0 mCi of $\text{Na}^{99m}\text{TcO}_4$. A freshly prepared solution from a saturated aqueous stannous tartarate (0.2 mL) was added to the mixture and the mixture incubated at room temperature for 10 min. A saturated solution of sodium bicarbonate (0.2 mL) was added to the mixture, and [^{99m}Tc]EN6 was vortexed and extracted in 1.0 mL of chloroform. The organic layer was separated from the aqueous layer, evaporated under a stream of air, dissolved in methanol, and purified by HPLC. The desired fractions were collected and solvents

removed in vacuo and dissolved in normal saline for cell binding studies.

Preparation of [^{99g}Tc]BAT-EN6 Complex. To a 20 mL scintillation vial were added ammonium pertechnetate (104 mg, 0.57 mmol), hydrochloride salt of ligand **VII** (273 mg, 0.59 mmol), and 50% aqueous ethanol (10 mL). The mixture was stirred at room temperature, and solid stannous tartarate (154 mg) was added. The contents were stirred at room temperature overnight, whereby the color of the solvent turned light brown. The complex was extracted from the solvent by addition of (2×1 mL) chloroform. The organic layers were combined and evaporated overnight in a hood, and [^{99g}Tc]BAT-EN6 complex was purified by passing through a silica gel column eluting with 90:10 $\text{CHCl}_3/\text{MeOH}$: MS (m/z) 517 (MH^+).

BIOLOGICAL PROCEDURES

Cell Culture. Human ductal breast carcinoma cells (T47D) were purchased from ATCC, (Rockville, MD) and cultured in serum-supplemented 1640 RPMI containing 10% heat-inactivated fetal bovine serum (GIBCO) at 37 °C. The cells were adherent and split weekly in a 1:20 ratio using trypsin/EDTA (GIBCO).

In Vitro σ -Receptor Binding Assays. The binding assays were carried out essentially as previously described using guinea pig brain membranes with some modifications (8a,b). Guinea pig brain membranes (500 μg of proteins) were incubated with 5 nM [^3H]DTG (39.4 Ci/mmol) and various concentrations of competing ligand in 0.5 mL of Tris-HCl (pH 8.0) for 120 min at 25 °C. Nonspecific binding was determined in the presence of 10 μM haloperidol. [^{99g}Tc]BAT-EN6 was used in 12 concentrations ranging from 0.05 to 10 000 nM. Assays were determined by dilution with 5 mL of ice-cold 10 mM Tris-HCl (pH 8.0) and filtration through glass fiber filters using a Brandel cell harvester (Brandel, Gaithersburg, MD). Filters were then washed twice with ice-cold buffer. Filters were soaked in 0.5% poly(ethyleneimine) for at least 30 min at 25 °C prior to use. The filters were then counted in CytoScint (ICN, Costa Mesa, CA) after an overnight extraction of counts. In order to control for possible interference with tritium β counting from ^{99g}Tc β emission, parallel curves were run under exactly the same conditions using membranes and 0.05–10 000 nM [^{99g}Tc]BAT-EN6, except with the omission of [^3H]DTG. No radioactivity above background could be detected in the tritium channel at [^{99g}Tc]BAT-EN6 concentrations up to 1000 nM; thus, no correction was necessary. IC_{50} values were determined using the computerized iterative curve-fitting program GraphPAD Inplot4 (GraphPAD Software, San Diego, CA).

Competition Binding Studies in T47D Cells. The cells were scraped using a cell scraper from T75 culture flasks and centrifuged in a Sorvall 6000B centrifuge at a speed of 4000 rpm. The growth medium was removed, and the cell pellet was resuspended in RPMI 1600 serum free media. The affinity of compounds for sites labeled by [^{99m}Tc]BAT-EN6 in human breast cancer cells was determined by heterologous in vitro competitive binding assays in whole cells. The following method was used. A small aliquot of the cell suspension (100 μL) was incubated with [^{99m}Tc]BAT-EN6 and varying concentrations (10^{-4} – 10^{-12} M) of aryethylenediamines, keeping a total volume of 1.0 mL constant. The cells were incubated at 37 °C for 1 h and subsequently filtered through a Brandel cell harvester (Brandel) and washed with deionized cold water. The radioactivity associated with the cells on filters was counted on a Beckman (DP 5500) γ counter. The optimum pH for the binding was found

to be between 7 and 8. Each data point represents an average of three values. The K_i values are average of two experiments. The data were analyzed with the iterative nonlinear least-squares curve-fitting program GraphPAD Inplot (GraphPAD Software). The Cheng–Prusoff equation was then used to convert IC_{50} values to apparent K_i values.

Saturation Binding and Scatchard Analysis. Saturation binding and Scatchard analysis of [^{99m}Tc]BAT-EN6 were carried out in membranes from T47D human ductal breast cells, which were prepared as described previously (4). A methanol/sodium phosphate buffer (pH 8.0) solution of carrier free [^{99m}Tc]BAT-EN6 in trace concentration was mixed in equal proportion with a 10 μM solution of [^{99g}Tc]BAT-EN6 to approximately 0.35 Ci/mmol. This solution was diluted into glass or polypropylene assay tubes to final concentrations ranging from 1 to 1000 nM. Incubations were carried out in a final volume of 0.25 mL of 50 mM Tris-HCl containing 250 μg of membrane protein for 120 min at 37 °C. Nonspecific binding was determined at each radioligand concentration in the presence of 10 μM BD1008, a ligand with high affinity for both σ -1 and σ -2 receptors. Assays were terminated by addition of 0.5 mL of ice-cold 10 mM Tris-HCl (pH 8.0) and filtration through glass fiber filters. Filters were then washed twice with 0.5 mL of ice-cold buffer and counted in a γ counter. Filters were soaked in 0.5% poly(ethyleneimine) for at least 30 min prior to use in order to reduce nonspecific binding of radioligand to filters. Each experiment was carried out in duplicate. Data were analyzed using the iterative curve-fitting program BDATA (Baltimore, MD).

Animal Biodistribution and Blocking Studies in Rats. Sprague–Dawley rats (200–250 g) were anesthetized with ketamine/xylazine and injected intravenously with [^{99m}Tc]BAT-EN6 (10–20 μCi) in 0.2 mL of saline containing up to 20% ethanol solution. At 0.5, 1, and 4 h postinjection, blood samples were drawn by cardiac puncture, and the rats were sacrificed thereafter by cardiectomy while under ketamine/xylazine anesthesia. The organs of interest were then excised, blotted with tissue paper, and weighed, and the radioactivity was counted. The percent injected dose/organ was determined by comparison of the tissue radioactivity with suitably diluted, known quantity aliquots of the injected dose. For in vivo blocking studies, 2.16 μmol of BD1008 was premixed with [^{99m}Tc]BAT-EN6 and then injected through the tail vein. The animals were sacrificed at 4 h postinjection, and the organs of interest were removed and handled as above.

RESULTS AND DISCUSSION

The synthesis of the tetradentate N_2S_2 ligand was achieved (Scheme 1) through the sodium borohydride-initiated transannular cyclization of 1,2-dithia-5,8-diazacyclodeca-4,8-dienes (17). The resulting bicyclic imidazolidino[1,2-*d*]dithiazapine **IV** was acylated with chloroacetyl chloride in a mixture of chloroform and 10% aqueous sodium hydroxide. The acylated imidazolidino[1,2-*d*]dithiazapine **V** was then alkylated with *N*-(methylethyl)piperidine to produce amide **VI**. Reduction of this amide using lithium aluminum hydride in THF gave the desired ligand **VII** possessing free bisaminothiol groups for chelating ^{99m}Tc along with the pendent recognition elements for σ -receptor affinity. The labeling of **VII** with ^{99m}Tc was carried out in high yields (80–95%) by incubating an aqueous solution of ligand with generator-eluted sodium [^{99m}Tc]pertechnetate (carrier free) in the presence of freshly prepared stannous tartarate which was the reducing agent. The lipid soluble ^{99m}Tc complex

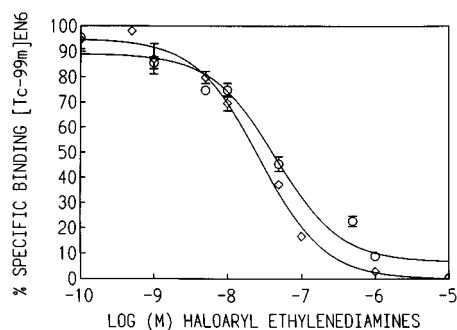
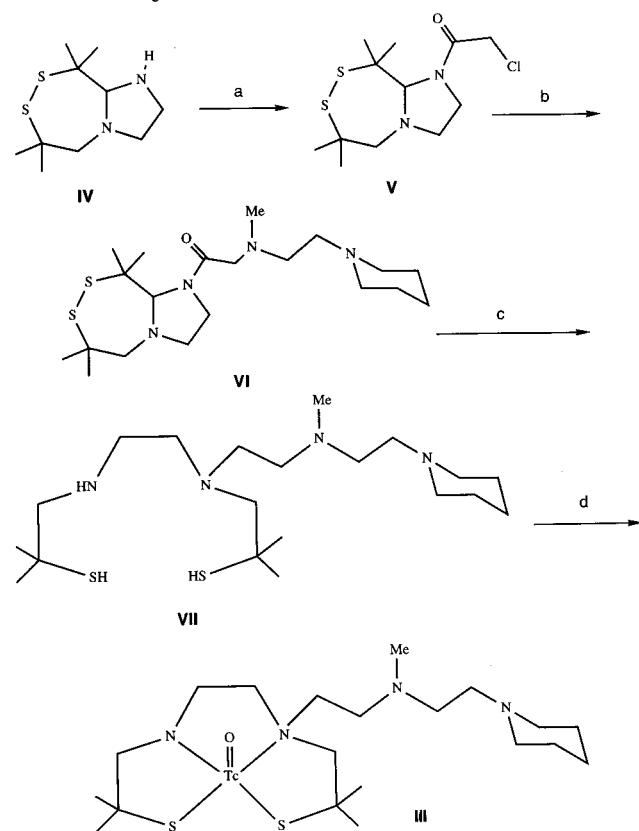


Figure 3. Inhibition binding isotherms of [^{99m}Tc]BAT-EN6 with substituted haloarylethylenediamines in human ductal carcinoma (T47D) cells. Diamonds represent BD1008, and circles represent IPEMP.

Scheme 1. Synthesis of [^{99m}Tc]N₂S₂-Conjugated Substituted Ethylenediamine^a



III [^{99m}Tc]BAT-EN6 was extracted from the aqueous solution using chloroform and purified by using C-18 reversed phase HPLC column [retention time = 15 min, 90:10 methanol/trishydrochloride (10 mM, pH 4.5) buffer]. It is well-known for BAT ligands that they form a square pyramidal technetium(V)-oxo core with the oxo group occupying the apical position. The complexation of *N*-monoalkylated BAT ligands with technetium results in the formation of syn and anti diastereomeric isomers each as a pair of enantiomers. The stereochemistry reflects the orientation of the *N*-alkyl group, syn or anti, with respect to apical oxygen (18). An HPLC trace of ^{99m}Tc complex indicated two peaks related to syn and anti isomers in an approximate ratio of 55:45. A ground state (^{99g}Tc) complex of the ligand was prepared by reaction with ammonium pertechnetate using stannous tartarate as a reducing agent. As expected, a neutral, lipophilic, Tc^{VO} complex was obtained that was characterized by electrospray ionization mass spectroscopy ($\text{MH}^+ = 517$). The mass spectral fragmentation [a loss of $[\text{SC}(\text{CH}_3)_2-$

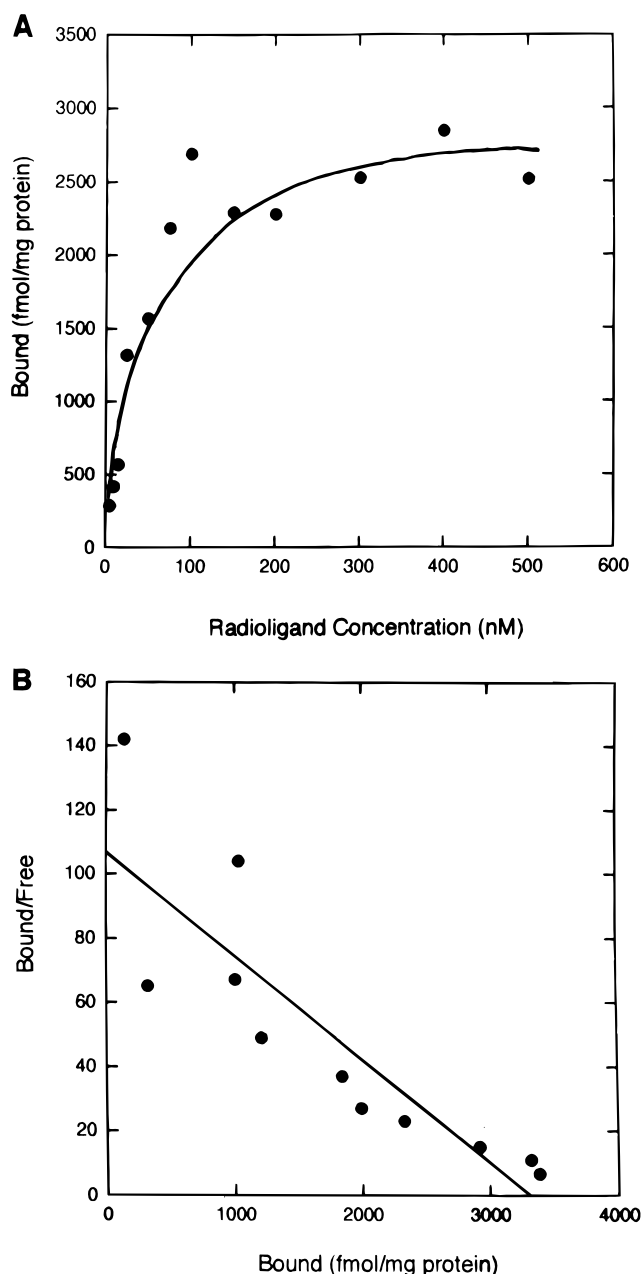


Figure 4. Saturation analysis of [^{99m}Tc]BAT-EN6 binding in T47D breast cancer cell membranes. Panel A shows the saturation plot, and panel B shows the Scatchard plot.

$\text{CH}_2]$ ($m/z = 429$) was also consistent with the chemical structure. The HPLC retention times for both ^{99m}Tc and ^{99g}Tc were identical under identical conditions, indicating the formation of the same species with carrier free and the ground state radionuclide.

The receptor binding specificity of ^{99m}Tc complex **III** was determined by its binding to human ductal breast cancer (T47D) cells. We have shown previously that T47D cells possess a high density of both σ -1 and σ -2 sites (4). A high degree of specific binding (90–97%) of ^{99m}Tc complex **III** was obtained when σ -receptor ligands such as halogenated phenylethylenediamines (BD1008 and IPEMP) were used to determine nonspecific binding. In order to determine that this binding was related to σ -receptors in T47D cells, two high-affinity σ -ligands BD1008 and IPEMP [$K_i = 2.1 \pm 0.8$ and 0.82 ± 0.13 nM, respectively, for σ -1 sites in guinea pig brain against [^3H](+)-pentazocine and $K_i = 8.1 \pm 2.2$ and 15.2 ± 2.35 nM, respectively, for σ -2 sites in rat liver membrane preparation against [^3H]DTG in the presence of dextrallorphan]

Table 1. Tissue Distribution of [^{99m}Tc]BAT-EN6 in Sprague-Dawley Rats^a

tissue	0.5 h	1.0 h	4.0 h	4.0 h with 2.10 μmol of BD1008
blood	5.13 \pm 1.03	4.45 \pm 0.74	2.33 \pm 0.18	0.82 \pm 0.02
heart	0.27 \pm 0.01	0.20 \pm 0.03	0.14 \pm 0.01	0.06 \pm 0.01
liver	14.42 \pm 2.01	16.85 \pm 2.05	22.31 \pm 2.37	15.32 \pm 1.21
lung	2.21 \pm 0.33	2.07 \pm 0.95	1.32 \pm 0.20	0.62 \pm 0.10
kidney	3.48 \pm 0.30	3.02 \pm 0.45	2.21 \pm 0.19	1.01 \pm 0.10
spleen	0.77 \pm 0.08	0.66 \pm 0.06	0.50 \pm 0.05	0.23 \pm 0.07
stomach	3.32 \pm 0.85	1.38 \pm 0.19	1.13 \pm 0.60	1.36 \pm 0.55
small intestine	5.29 \pm 2.70	11.63 \pm 3.97	14.52 \pm 2.86	13.65 \pm 2.90
large intestine	0.24 \pm 0.12	0.36 \pm 0.21	0.52 \pm 0.19	0.42 \pm 0.11
muscle	11.32 \pm 1.66	10.01 \pm 0.81	9.45 \pm 1.22	5.77 \pm 1.65
brain	0.04 \pm 0.01	0.03 \pm 0.01	0.03 \pm 0.01	0.02 \pm 0.00

^a % ID/organ \pm SD; $n = 6$.

were used in competition experiments. A dose-dependent inhibition of binding of ^{99m}Tc complex **III** was observed using BD1008 and IPEMP ligands ($\text{IC}_{50} = 47 \pm 2$ and 59 ± 5 nM, respectively), indicating that it is labeling σ -receptors (Figure 3). In order to determine the binding affinity of the ^{99m}Tc chelate, the binding studies of ^{99g}Tc complex were studied in guinea pig brain membranes against [^3H]DTG (a known σ -ligand). A high-affinity dose-dependent inhibition of binding of [^3H]DTG was found in the presence of ^{99g}Tc complex, indicating the binding at σ sites. The K_i value for ^{99g}Tc complex was found to be 42.7 ± 8.57 nM. This represents a combined binding affinity for σ -1 and σ -2 subtypes as [^3H]DTG is a σ nonsubtype selective ligand. An exact affinity of ^{99g}Tc chelate at the individual σ subtypes is currently being investigated. The affinity of the two isomers (syn and anti) for the receptor sites also remains to be studied. It should be noted, however, that there was no specific binding of the parent ^{99m}Tc complex **VIII** (Figure 2) without the pendent pharmacophore, confirming that binding activity resulted from the pendent ethylenediamine moiety and indicating that the binding was to σ sites.

The saturation binding of [^{99m}Tc]BAT-EN6 in membrane preparations of T47D cells was studied using Scatchard analysis. The incubation of an increasing concentration of HPLC-purified [^{99m}Tc]BAT-EN6 chelate [spiked with a known concentration of [^{99g}Tc]BAT-EN6] showed a saturable binding, with a K_d of 43.5 ± 14.7 nM and a B_{max} of 3121 ± 130 fmol/(mg of protein). The data from a representative experiment are shown in Figure 4 (panel A shows the saturation plot and panel B shows the Scatchard plot). The binding saturates with increasing concentration of the tracer, and a high B_{max} was found. This result is consistent with our earlier findings, where we had shown that a high density of σ -receptors [$3000\text{--}3500$ fmol/(mg of protein)] was expressed in T47D cells on the basis of [^3H]DTG binding in T47D cell membranes. The biodistribution of [^{99m}Tc]BAT-EN6 in Sprague-Dawley rats (Table 1) showed a hepatobiliary excretion, as expected. The tracer cleared quickly from the blood pool and was extracted in high amounts by liver (14.42% ID/organ at 30 min and 22.31% ID/organ at 4 h postinjection). A good uptake of the tracer was also found in lungs and kidneys. The evidence for in vivo receptor binding was established by in vivo blocking of specific binding with BD1008. The uptake of the radiopharmaceutical at 4 h post-iv injection was 2.21% ID/organ in the kidney, whereas uptake in the presence of 2 μmol of BD1008 was 1.01% ID/organ (Table 1). Thus, a co-injection of ^{99m}Tc complex along with 2 μmol of BD1008 in male Sprague-Dawley rats resulted in an inhibition of binding of about 55% at 4 h post-iv injection in the kidneys, an organ that is known to possess high densities of both σ -1 and σ -2 receptors (19). Similarly, a significant

reduction of radioactivity was also found in liver (32%) and lungs (50%) at 4 h postinjection.

CONCLUSION

In summary, the results presented here indicated that the bisaminothiol ligand system possessing the pendent σ -receptor pharmacophore complexed with ^{99m}Tc in very high yields. This complex displayed a very high specific binding in T47D breast cancer cells and a dose-dependent inhibition of binding with known σ -ligands. No specific binding was found with ^{99m}Tc chelate without substituted ethylenediamine pharmacophore. Furthermore, the in vivo blocking study revealed a significant reduction of the uptake of the ^{99m}Tc complex in kidneys. This is the first ^{99m}Tc chelate shown to bind σ -receptor sites in human breast cancer cells. Derivatives of this chelating ligand system or another chelating ligand (to alter in vivo distribution) possessing the σ -pharmacophore may be useful for diagnostic receptor scintigraphy of σ -receptor-positive tumors.

ACKNOWLEDGMENT

We acknowledge Dr. C. E. Costello (Boston University School of Medicine) and Mr. Noel Whittaker (NIDDK, NIH) for mass spectroscopic studies. Financial support of this work by the Department of Radiology, George Washington University Medical Center, is gratefully acknowledged. We are grateful to Prof. John Katzenellenbogen for helpful suggestions and comments on the manuscript.

LITERATURE CITED

- (1) (a) Hellewell, S. B., and Bowen, W. D. (1990) A σ -like binding site in rat pheochromocytoma (PC12) cells: Decreased affinity for (+)-benzomorphans and lower molecular weight suggest a different σ -receptor form from that in guinea pig brain. *Brain Res.* 527, 244–253. (b) Quirion, R., Bowen, W. D., Itzhak, Y., Junien, J. L., Musacchio, J. M., Rothman, R. B., Su, T. P., Tam, S. W., and Taylor, D. P. (1992) A proposal for the classification of σ binding sites. *Trends Pharmacol. Sci.* 13, 85–86.
- (2) (a) Bowen, W. D., de Costa, B. R., Hellewell, S. B., Walker, J. M., and Rice, K. C. (1993) [^3H](+)-Pentazocine: A potent and highly selective benzomorphan-based probe for σ -1 receptors. *Mol. Neuropharmacol.* 3, 117–126. (b) de Costa, B. R., Bowen, W. D., Hellewell, S. B., Walker, J. M., Thurkauf, A., Jacobson, A. E., and Rice, K. C. (1989) Synthesis and evaluation of optically pure [^3H](+)-pentazocine, a highly potent and selective radioligand for σ receptors. *FEBS Lett.* 251, 53–58.
- (3) Weber, E., Sonders, M., Quarum, M., McLean, S., Pou, S., and Keana, J. F. W. (1986) 1,3-Di(2-[5- ^3H]tolyl)guanidine: a selective ligand that labels σ type receptors for psychotomimetic opiates and antipsychotic drugs. *Proc. Natl. Acad. Sci. U.S.A.* 83, 8784–8788.

- (4) Vilner, B. J., John, C. S., and Bowen, W. D. (1995) σ -1 and σ -2 receptors are expressed in a wide variety of human and rodent tumor cell lines. *Cancer Res.* 55, 408–413.
- (5) (a) Thomas, G. E., Szucs, M., Mamone, J. Y., Bem, W. T., Rush, M. D., Johnson, F. E., and Coscia, C. J. (1990) σ and opioid receptors in human brain tumors. *Life Sci.* 46, 1279–1286. (b) Bem, W. T., Thomas, G. E., Mamone, J. Y., Homan, S. M., Levy, B. K., Johnson, F. E., and Coscia, C. J. (1991) Overexpression of σ -receptors in nonneural human tumors. *Cancer Res.* 51, 6558–6562. (c) John, C. S., Vilner, B. J., Schwartz, A. M., and Bowen, W. D. (1996) Characterization of σ -receptor binding sites in human biopsied solid breast tumors. *J. Nucl. Med.* 37, 267P (abstract).
- (6) John, C. S., Bowen, W. D., Saga, T., Kinuya, S., Vilner, B. J., Baumgold, J., Paik, C. H., Reba R. C., Neumann, R. D., Varma, V. M., and McAfee, J. G. (1993) A malignant melanoma imaging agent: synthesis, characterization, in vitro binding and biodistribution of iodine-125-(2-piperidinyl-aminoethyl)-4-iodobenzamide. *J. Nucl. Med.* 34, 2169–2175.
- (7) John, C. S., Vilner, B. J., and Bowen, W. D. (1994) Synthesis and characterization of [¹²⁵I]-N-(N-benzylpiperidin-4-yl)-4-iodobenzamide, a new σ -receptor radiopharmaceutical: high affinity binding to MCF-7 breast tumor cells. *J. Med. Chem.* 37, 1737–1739.
- (8) John, C. S., Vilner, B. J., Gulden, M. E., Efange, S. M. N., Langason, R. B., Moody, T. W., and Bowen, W. D. (1995) Synthesis and pharmacological characterization of 4-[¹²⁵I]-N-(N-benzylpiperidin-4-yl)-4-iodobenzamide: a high affinity σ -receptor ligand for potential imaging of breast cancer. *Cancer Res.* 55, 3022–3027.
- (9) John, C. S., Bowen, W. D., Varma, V. M., McAfee, J. G., and Moody, T. W. (1995) σ -Receptors are expressed in human non-small cell lung carcinoma. *Life Sci.* 56, 2385–2392.
- (10) (a) John, C. S., Venugopal, R., Li, J., Bowen, W. D., Varma, V. M., and Thakur, M. L. (1996) Characterization and targeting of σ -receptor binding sites in human prostate tumor cells. *J. Nucl. Med.* 37, 205P (abstract). (b) John, C. S., Gulden, M. E., Li, J., McAfee, J. G., Bowen, W. D., and Thakur, M. L. (1997) Synthesis, in-vitro binding and pharmacokinetics of radioiodinated (N-benzylpiperidin-4-yl)-2-iodobenzamide: σ -receptor marker for human prostate tumors. (Manuscript submitted for publication.)
- (11) (a) DiZio, J. P., Anderson, C. J., Davison, A., Ehrhardt, G. J., Carlson, K. E., Welch, M. J., and Katzenellenbogen, J. A. (1992) Technetium- and rhenium-labeled progestins: synthesis, receptor binding and in-vivo distribution of an 111-substituted progestin labeled with technetium-99 and rhenium-186. *J. Nucl. Med.* 33, 558–569. (b) O'Neil, J. P., Carlson, K. E., Anderson, C. J., Welch, M. J., and Katzenellenbogen, J. A. (1994) Progestin radiopharmaceuticals labeled with technetium and rhenium: synthesis, binding affinity, and in-vivo distribution of a new progestin N₂S₂-metal conjugate. *Bioconjugate Chem.* 5, 182–193.
- (12) Lever, S. Z., Baidoo, K. E., Mahmood, A., Matsumura, K., Scheffel, U., and Wagner, H. N. (1994) Novel technetium ligands with affinity for the muscarinic cholinergic receptors. *Nucl. Med. Biol.* 21, 157–164.
- (13) Del Rosario, R. B., Jung, Y.-W., Baidoo, K. E., Lever, S. Z., and Wieland, D. M. (1994) Synthesis and in vivo evaluation of a ^{99m}Tc-DADT-benzovesamicol: a potential marker for cholinergic neurons. *Nucl. Med. Biol.* 21, 197–203.
- (14) de Costa, B. R., Radesca, L., Di Paolo, L., and Bowen, W. D. (1992) Synthesis, characterization and biological evaluation of a novel class of N-(arylethyl)-N-alkyl-2-(1-pyrrolidinyl)ethylamines: structural requirements and binding affinity at the σ -receptors. *J. Med. Chem.* 35, 38–47.
- (15) de Costa, B. R., Radesca, L., Dominguez, C., Di Paolo, L., and Bowen, W. D. (1992) Synthesis and receptor binding properties of fluoro- and iodo-substituted high affinity σ -receptor ligands: Identification of potential PET and SPECT σ -receptor imaging agents. *J. Med. Chem.* 35, 2221–2230.
- (16) (a) John, C. S., Vilner, B. J., and Bowen, W. D. (1995) Synthesis, binding characteristics and in-vivo clearance of 4-[I-125]PEMP: a σ -receptor ligand for imaging tumors. *J. Nucl. Med.* 36, 6P (abstract). (b) John, C. S., Gulden, M. E., Vilner, B. J., and Bowen, W. D. (1996) Synthesis, in vitro validation and in vivo pharmacokinetics of [¹²⁵I]N-[2-(4-iodophenyl)ethyl]-N-methyl-2-(1-piperidinyl)ethylamine: a high affinity ligand for imaging σ -receptor-positive tumors. *Nucl. Med. Biol.* 23, 761–766.
- (17) Joshua, A. V., Scott, J. R., Sondhi, S. M., Ball, R. G., and Lown, J. W. (1987) Transannular cyclizations of 1,2-dithia-5,8-diazacyclodeca-4,8-dienes during borohydride reduction. *J. Org. Chem.* 52, 2447–2451.
- (18) (a) DiZio, J. P., Fiaschi, R., Davison, A., Jones, A. G., and Katzenellenbogen, J. A. (1991) Progestin-rhenium complexes: metal-labeled steroids with high receptor binding affinity, potential receptor-directed agents for diagnostic imaging or therapy. *Bioconjugate Chem.* 2, 353–366. (b) Mahmood, A., Baidoo, K. E., and Lever, S. Z. (1990) Stereoisomers of neutral oxotechnetium(V) and oxorhenium(V) complexes. In *Technetium in Chemistry and Nuclear Medicine* (M. Nicolini, G. Bandoli, and U. Mazzi, Eds.) Vol. 3, pp 119–124, Cortina International, Verona.
- (19) Hellewell, S. B., Bruce, A., Feinstein, G., Orringer, J., Williams, W., and Bowen, W. D. (1994) Rat liver and kidney contain high densities of σ -1 and σ -2 receptors: characterization by ligand binding and photoaffinity labeling. *Eur. J. Pharmacol., Mol. Pharmacol. Sect.* 268, 9–18.

BC9700087

Critical Parameters for Adduct Formation of the Carcinogen (+)-*anti*-Benzo[*a*]pyrene-7,8-dihydrodiol 9,10-Epoxy with Oligonucleotides

Mario Funk,[†] Ingrid Pontén,[†] Albrecht Seidel,[‡] and Bengt Jernström^{*,†}

Institute of Environmental Medicine, Division of Biochemical Toxicology, Karolinska Institutet, S-17177 Stockholm, Sweden, and Department of Toxicology, University of Mainz, D-55131 Mainz, Germany. Received May 15, 1996[®]

Various parameters relevant for the formation of dG adducts produced in the reaction of individual benzo[*a*]pyrene diol epoxide (BPDE) stereoisomers with oligonucleotides have been studied. Reaction time, temperature, pH, molar ratio of diol epoxide and oligonucleotide, base sequence, and buffer system were shown to affect the amount of (+)-*anti*-BPDE dG adducts formed. Optimum experimental conditions for dG adduct formation were different depending on the base sequence context of the oligonucleotide employed [5'-d(CCTATAGATATCC) or 5'-d(CCTATTGCTATCC)]. In general, low temperature to allow a longer reaction time, slightly alkaline Tris-HCl (pH 7.5–8.0) or alkaline phosphate buffer (pH 11), low concentration of organic solvent, and a molar excess of (+)-*anti*-BPDE promote dG adduct formation with an oligonucleotide. Low incubation temperature and Tris-HCl buffer also favor dG adduct formation of (–)-*anti*-BPDE and both enantiomers of *syn*-BPDE to both 5'-d(CCTATAGATATCC) and 5'-d(CCTATTGCTATCC).

INTRODUCTION

Since its detection as one of the principal carcinogens in coal tar (Cook *et al.*, 1933), benzo[*a*]pyrene has served as an important model substrate for investigating the mutagenic and carcinogenic properties of polycyclic aromatic hydrocarbons (PAH¹). Benzo[*a*]pyrene is not biologically active *per se*, but requires metabolic activation to elicit its hazardous properties. The most widely accepted metabolic activation pathway involves (i) arene oxide formation at the 7,8-position by action of CYP 1A1, (ii) epoxide hydrolase catalyzed ring opening of the intermediate arene oxide to produce the *trans*-7,8-dihydrodiol, and (iii) a second attack by CYP 1A1 in the bay region at the 9,10-position of the dihydrodiol. The latter reaction preferentially results in the formation of the 7(*R*),8(*S*)-dihydroxy-9(*S*),10(*R*)-epoxy-7,8,9,10-tetrahydrobenzo[*a*]pyrene [(+)-*anti*-BPDE; Figure 1] and, to a lesser extent, of the 7(*R*),8(*S*)-dihydroxy-9(*R*),10(*S*)-epoxy-7,8,9,10-tetrahydrobenzo[*a*]pyrene [(–)-*syn*-BPDE] (Thakker *et al.*, 1977; Yang *et al.*, 1977a; Jerina *et al.*, 1985).

Among the four possible stereoisomeric bay-region diol epoxides the (+)-*anti*-BPDE reveals the highest mutagenic and carcinogenic activity in most mammalian test systems (Thakker *et al.*, 1977; Stevens *et al.*, 1985; Wislocki and Lu, 1988). This biological activity appears to be causally linked to covalent binding of (+)-*anti*-BPDE to DNA, which occurs almost exclusively at the exocyclic

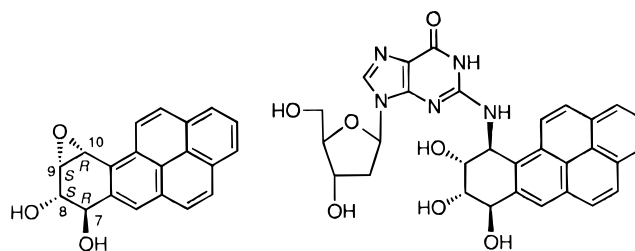


Figure 1. Absolute structures of (+)-*anti*-BPDE (left) and its *trans*-(+)-*anti*-BPDE-*N*²-dG adduct (right) predominantly formed on reaction with DNA.

amino group of deoxyguanosine (dG) (Jeffrey *et al.*, 1976). Stereochemically favored is the *trans* opening of the oxirane ring by nucleophilic attack of the amino group at the benzylic C-10 position (Cheng *et al.*, 1989); the structure of the adduct emerged from this reaction is shown in Figure 1. In contrast, the reaction of (–)-*anti*-BPDE and the two enantiomers of *syn*-BPDE with DNA is much less selective regarding dG *vs* dA binding and the stereochemical course of the oxirane ring opening. Thus, binding to dG *vs* dA residues depends on the absolute stereochemistry of the diol epoxide and results in different ratios of adducts with *cis* and *trans* stereochemistry (Cheng *et al.*, 1989; Sayer *et al.*, 1991).

To get insights into the underlying mechanisms of mutagenesis and carcinogenesis, it is of pivotal interest to investigate the structural and physicochemical properties of defined DNA adducts in specific oligonucleotide sequences by spectroscopic methods as well as to perform studies with adducted sequences in biological systems (Cosman *et al.*, 1990; Geacintov *et al.*, 1991; Margulis *et al.*, 1993; Jernström and Gräslund, 1994). However, experimental access to the required amounts of material for structure investigations by spectroscopic methods, in particular by 2D NMR, provides a strong limitation in this field of research.

The chemical synthesis of defined adducted oligonucleotides with the control about the *cis* and *trans* stereochemistry has been demonstrated (Lee *et al.*, 1990, 1995; Zajc *et al.*, 1992; Kim *et al.*, 1992; Lakshman *et al.*, 1992;

* Address correspondence to this author at the Institute of Environmental Medicine, Division of Biochemical Toxicology, Karolinska Institutet, Box 210, S-17177 Stockholm, Sweden (e-mail Bengt.Jernstrom@imm.ki.se).

[†] Karolinska Institutet.

[‡] University of Mainz.

[®] Abstract published in *Advance ACS Abstracts*, April 1, 1997.

¹ PAH, polycyclic aromatic hydrocarbons; BPDE, benzo[*a*]pyrene diol epoxide; (+)-*anti*-BPDE, 7(*R*),8(*S*)-dihydroxy-9(*S*),10(*R*)-epoxy-7,8,9,10-tetrahydrobenzo[*a*]pyrene; (–)-*anti*-BPDE, 7(*S*),8(*R*)-dihydroxy-9(*R*),10(*S*)-epoxy-7,8,9,10-tetrahydrobenzo[*a*]pyrene; (+)-*syn*-BPDE, 7(*S*),8(*R*)-dihydroxy-9(*S*),10(*R*)-epoxy-7,8,9,10-tetrahydrobenzo[*a*]pyrene; (–)-*syn*-BPDE, 7(*R*),8(*S*)-dihydroxy-9(*R*),10(*S*)-epoxy-7,8,9,10-tetrahydrobenzo[*a*]pyrene; DMSO, dimethyl sulfoxide; THF, tetrahydrofuran; DMF, dimethylformamide; TEA, triethylamine.

Steinbrecher *et al.*, 1993), but it includes quite material-intensive and laborious working steps to obtain larger quantities, and the methodology seems to be more successful for the preparation of oligonucleotides with dA adducts of diol epoxides. A much faster approach is provided by the direct synthesis, which includes incubation of the diol epoxide with the oligonucleotide and subsequent separation of the sequences bearing individual adducts. However, it is necessary to perform this reaction repeatedly to produce required amounts since the yields in specific modified oligonucleotides obtained by this method are usually relatively low. Therefore, upscaling of the direct synthesis of dG-specific modified oligonucleotides by incubation of diol epoxides with oligonucleotides has been considered to be an attractive goal. The direct method for the synthesis of modified oligonucleotides containing defined diol epoxide adducts of BPDE by reaction of racemates or individual configurational isomers of BPDE with a single-stranded oligonucleotide of short length followed by HPLC separation of the resulting modified sequences and adduct characterization was initially developed by Geacintov and co-workers (Cosman *et al.*, 1990). The availability of oligonucleotides containing a single or more structurally defined adducts derived from BPDE binding at the exocyclic amino group of dG has proven to be of great importance in elucidating structural features of this type of adduct and their relationship to effects in biological and biochemical systems. For instance, the conformation of structurally defined BPDE–dG adducts site-specifically positioned in double-stranded oligonucleotide has been successfully elucidated by high-resolution NMR [Cosman *et al.*, 1992, 1993; de los Santos *et al.*, 1992; Fountain and Krugh, 1995 (reviewed in Geacintov *et al.* (1997))], the effect of individual BPDE–dG adducts on DNA replication, transcription, or transcription-associated activities and repair have been studied in *in vitro* systems (Hruszkewycz *et al.*, 1991; Shibutani *et al.*, 1993; Zou *et al.*, 1995; Persson *et al.*, 1996), and attempts to elucidate the mechanisms underlying BPDE–dG adduct-induced mutations have been carried out in bacterial systems (Jelinsky *et al.*, 1995).

To elucidate and to rationalize the experimental conditions being most important in promoting the formation of dG adducts by reacting the individual (+)-*anti*-BPDE stereoisomer directly with an oligonucleotide, the influence of temperature, pH, solvent polarity, the molar ratio of diol epoxide/oligonucleotide, reaction time, buffer system, and the oligonucleotide sequence context was investigated. Adduct yields using different sequence context in the oligonucleotide have been compared for all four BPDE stereoisomers under standard reaction conditions.

EXPERIMENTAL SECTION

Caution: Benzo[a]pyrene diol epoxides are carcinogens, and thus experimental handling must be carried out under special safety conditions, e.g. those outlined in the NCI guidelines.

Materials. The optically active stereoisomers of BPDE were synthesized as described previously (Pontén *et al.*, 1996 and references cited therein). Oligonucleotides were obtained from Kebo, Stockholm, Sweden. Their purity was checked by HPLC (see below). Other chemicals and solvents used were purchased from different commercial sources and were of analytical or HPLC grade.

Reaction of BPDE with Oligonucleotides. As a standard system the reaction of the oligonucleotide 5'-(CCTATAGATATCC) with (+)-*anti*-BPDE was selected. In the system used here the oligonucleotide was dissolved

in 50 mM Tris-HCl/0.5 mM EDTA at pH 7.5 (measured at 20 °C) to a final concentration of 50–70 μ M together with a 5-fold molar excess of BPDE, added as a single portion dissolved in dimethyl sulfoxide (DMSO; final concentration of DMSO was 8.5%). The addition of sodium chloride has been avoided since high concentrations of chloride ions have been shown to favor *cis* adduct formation (Wolfe *et al.*, 1994). The mixture was kept at 0 °C in the dark for 5 h followed by storage at 4 °C for at least overnight to allow the reaction to be completed before HPLC analysis. The rates of (+)-*anti*-BPDE hydrolysis leading to tetraols and of the adduct formation were determined after the excess of BPDE was trapped with alkaline 2-mercaptoethanol [*cf.* Michaud *et al.* (1983) and Dock *et al.* (1987)] at different time points and subsequent HPLC analysis of the products.

The effect of temperature on the adduct formation was studied using the standard conditions (see above) and with the reaction temperature varied between 0 and 40 °C. It should be noted that increased temperature is associated with a reduction in pH; the pH of the standard buffer at 20 °C (7.5) changes to 7.9 at 0 °C and to 7.2 at 40 °C. To see if the increased adduct formation observed for (+)-*anti*-BPDE at lower temperature can be considered as a more general phenomenon, the corresponding (–)-*anti*-BPDE as well as both enantiomers of *syn*-BPDE were reacted with 5'-d(CCTATAGATATCC) or 5'-d(CCTATTGCTATCC) at 0 and 20 °C. In another set of experiments with (+)-*anti*-BPDE, the standard Tris-HCl buffer, pH 7.5, was adjusted at 20 °C to a pH varying between 6.0 and 9.5.

The influence of selected organic solvents on the reaction yield was studied by addition of various amounts of DMSO, tetrahydrofuran (THF), and dimethylformamide (DMF). The final volume concentrations of these solvents were 2%, 10%, and 25%, respectively. All other reaction parameters were used according to the standard procedure.

To study the effect of base sequence context on adduct formation, the extent of binding of (+)-*anti*-BPDE to dG in the oligonucleotides 5'-d(CCTATAGATATCC) and 5'-d(CCTATTGCTATCC) was compared under standard conditions as described above and at 20 °C.

The influence of different buffer systems, near-neutral Tris-HCl buffer or phosphate buffer supplemented with 1.5% triethylamine (TEA) (Margulis *et al.*, 1993), and incubation time on the adduct yield was also investigated.

HPLC Analysis. The analysis of diol epoxide oligonucleotide adducts was in principal performed as described earlier (Pontén *et al.*, 1994, 1996). In brief, a Dynamax (Rainin Instrument Co., Woburn, MA) reversed phase column (C₁₈, 5 μ m, 300 Å, 4.6 \times 250 mm) equipped with a precolumn and thermostated at 37 °C was used as stationary phase. The mobile phase consisted of 0.1 M triethylammonium acetate, pH 7.0 (solvent A), and a 1:1 mixture of this solution with acetonitrile (solvent B) at a flow rate of 1.5 mL/min. The samples were eluted with a gradient from 10% to 25% solvent B in solvent A over 10 min, isocratically for 10 min with 25% solvent B in solvent A followed by a 10 min gradient from 25% to 30% solvent B in solvent A, and finally 30% to 60% solvent B in solvent A over 10 min.

Analysis of diol epoxide–mercaptoethanol conjugates was performed essentially as previously described (Dock *et al.*, 1987). Briefly, a Nova-Pak reversed phase column (C₁₈, 4 μ m, 3.9 \times 150 mm, Waters, Milford, MA) and a solvent system composed of 25 mM ammonium acetate, pH 4.0 (solvent A) and acetonitrile (solvent B) delivered at 1 mL/min were employed. The samples were eluted

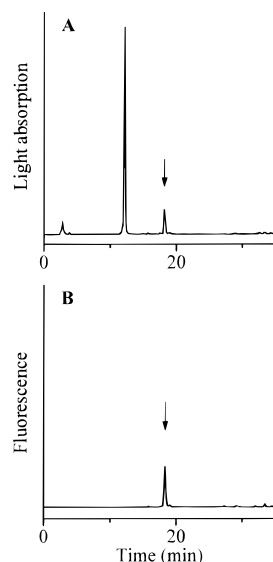


Figure 2. HPLC elution profiles of the reaction products of the (+)-*anti*-BPDE-modified oligonucleotide 5'-d(CCTATAGATATCC) monitored by light absorbance at 260 nm (A) and by fluorescence emission at 400 nm ($\lambda_{\text{excitation}} = 350$ nm) (B).

with a gradient ranging from 20% to 40% solvent B in solvent A during 20 min.

Adduct Identification. Studying single-stranded oligonucleotides containing a single dG in a number of different sequence contexts, Margulis *et al.* (1993) demonstrated that dG in 5'-AGA exhibited the lowest reactivity and dG in 5'-TGC the highest reactivity with (+)-*anti*-BPDE. In this study we have used the two oligonucleotides 5'-d(CCTATAGATATCC) and 5'-d(CCTATTGCTATCC), each containing one of the target sequences and, therefore, representing an experimental system with a broad range of reactivity. The overall yield of dG adducts and the individual adduct distribution (adducts with *cis* or *trans* stereochemistry) resulting from the reaction of the oligonucleotides with all four possible stereoisomers of BPDE have been estimated from HPLC analysis (Figure 2). The amount of N^2 -dG adducts was calculated from the sum of unmodified and dG-modified oligonucleotide peak areas. Identification and characterization of the dG adducts formed by the reaction of (+)-*anti*-BPDE within the triplet 5'-TGC or 5'-AGA have been described by Margulis *et al.* (1993), of *anti*- or *syn*-BPDE within 5'-AGA by Pontén *et al.* (1994 and 1996, respectively), and of (-)-*syn*-BPDE within 5'-TGC by Pontén *et al.* (1997). The stereochemistry of the major dG adduct formed from (-)-*anti*-BPDE (*trans* adduct) and (+)-*syn*-BPDE (*cis* adduct) within the sequence context 5'-TGC was determined by circular dichroism measurements (Pradhan *et al.*, 1997).

RESULTS AND DISCUSSION

Effect of Time, Temperature, and Buffer System on the Binding of BPDE to 5'-d(CCTATAGATATCC) and 5'-d(CCTATTGCTATCC). Figure 3 shows the extent of adduct formation of (+)-*anti*-BPDE (defined as the proportion of oligonucleotides reacted with BPDE) as a function of time and under different experimental conditions. In general, the 50 μ M oligonucleotide was incubated with 250 μ M diol epoxide. This concentration by far exceeds the solubility of BPDE in aqueous solutions, and thus the compound is expected to be partly present in aggregates or microcrystals. Parts A and B of Figure 3 demonstrate that both temperature and buffer

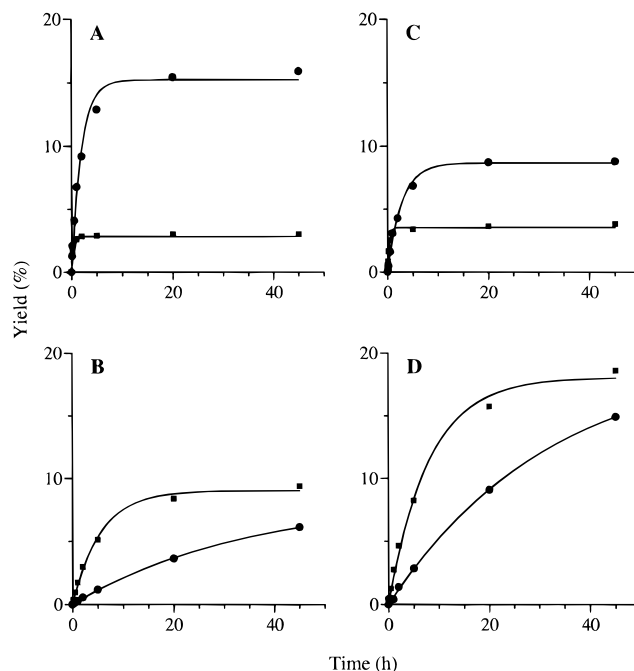


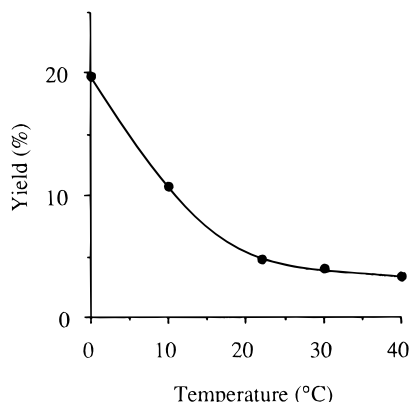
Figure 3. Time-dependent formation of the *trans* adducts of (+)-*anti*-BPDE with the oligonucleotide 5'-d(CCTATAGATATCC) at 0 and 20 °C in Tris-HCl (pH 7.5) (A) and at 0 and 20 °C in phosphate/TEA buffer (B) and of (+)-*anti*-BPDE with 5'-d(CCTATTGCTATCC) at 0 and 20 °C in Tris-HCl (pH 7.5) (C) and at 0 and 20 °C in phosphate/TEA buffer (D): incubation at 0 °C (●) and 20 °C (■). For further experimental details, see Experimental Section.

system greatly influence the rate of adduct formation. In Tris buffer the maximum binding of (+)-*anti*-BPDE to 5'-d(CCTATAGATATCC) was attained after approximately 1 h at 20 °C or after 5 h at 0 °C. The large influence of low temperature on adduct formation is remarkable (Figure 3A). Replacing the Tris buffer with phosphate supplemented with 1.5% TEA results in a markedly reduced rate of adduct formation. In this system the reaction at 20 °C with 5'-d(CCTATAGATATCC) seemed to approach completion after about 20 h of incubation. At 0 °C the reaction is far from complete even after 45 h of incubation. Parts C and D of Figure 3 show the extent of adduct formation to 5'-d(CCTATTGCTATCC) in Tris or alkaline phosphate buffer. It is obvious that the change in sequence context from 5'-AGA to 5'-TGC in conjunction with the buffer system used greatly influences adduct formation. In Tris buffer the initial rate of adduct formation and adduct yield are substantially lower with 5'-d(CCTATTGCTATCC) and the effect of temperature is less pronounced (Figure 3C). In contrast, in alkaline phosphate buffer a higher yield of adducts was obtained with 5'-d(CCTATTGCTATCC) at both 0 and 20 °C. The results in Figure 3D indicate that prolonged incubation ($\gg 45$ h) most probably results in a similar adduct yield. This is also clear from the data compiled in Table 1 obtained from a number of experiments in which the reaction of (+)-*anti*-BPDE with 5'-d(CCTATAGATATCC) or 5'-d(CCTATTGCTATCC) has been allowed to continue to completion or near completion. In fact, in the presence of phosphate buffer no statistically significant difference in adduct yields at 0 or 20 °C was observed. The preference of (+)-*anti*-BPDE to react with dG in 5'-TGC rather than with dG in 5'-AGA in alkaline phosphate buffer observed here is in full agreement with the results of Margulis *et al.* (1993). The influence of the base sequence context on adduct formation will be further discussed below.

Table 1. Yields of Trans Adducts Formed between (+)-*anti*-BPDE and 5'-d(CCTATAGATATCC) or 5'-d(CCTATTGCTATCC): Effect of Different Buffer Systems and Temperature Dependence

system	temp (°C)	5'-AGA	5'-TGC
Tris-HCl buffer, pH 7.9 ^a	0	16.7 ± 2.7 (16) ^b	7.5 ± 1.2 (7)
	20 ^c	3.4 ± 1.6 (5)	2.9 ± 0.8 (5)
PO ₄ /TEA buffer, pH 11 ^d	0	6.1 ± 2.3 (6)	11.4 ± 4.7 (8)
	20	7.7 ± 3.3 (8)	18.1 ± 8.4 (9)

^a Incubation time in Tris buffer, ≥20 h. ^b Number of experiments (*n*) is given in parentheses. ^c The pH at 20 °C in Tris buffer is 7.5. ^d Incubation time in phosphate buffer, ≥45 h.

**Figure 4.** Yield of trans adducts formed between (+)-*anti*-BPDE and 5'-d(CCTATAGATATCC) as a function of temperature.

The buffer- and temperature-dependent shift of preferred sequence context shown here has certain implications for the universal applicability of previous studies.

The difference in adduct yields in the presence of Tris or phosphate buffer cannot be due to a different pH values of the reaction medium, since higher pH results in lower binding efficiencies in Tris buffer (*vide infra*). Furthermore, addition of 1.5% TEA to the Tris-buffered system did not improve adduct yields (data not shown).

The experiments described above demonstrate that the temperature is an important factor when (+)-*anti*-BPDE is reacted with oligonucleotides in Tris buffer. To study this in more detail, the diol epoxide was incubated with 5'-d(CCTATAGATATCC) at temperatures ranging from 0 to 40 °C. As shown in Figure 4 an exponential decline of the reaction yield from about 20% at 0 °C to about 5% at 40 °C was observed (*cf.* Table 1). It should be noted that the increased temperature is associated with a reduced pH in Tris buffer (7.9 at 0 °C and 7.2 at 20 °C). However, it is unlikely that differences in pH had any significant effect on adduct formation (*vide infra*).

The most obvious explanation for the increased adduct formation at low temperature is the increased average lifetime of the diol epoxide molecules allowing an increased formation of hydrophobic BPDE-oligonucleotide complexes, a process that possibly precedes adduct formation. This interpretation is in agreement with previous observations (Geacintov *et al.*, 1988) as well as recent findings of Geacintov *et al.* (personal communication). The major chemical reaction pathways of BPDE in the experimental systems described here are hydrolysis to tetraols and adduct formation. The results demonstrate that the contribution of tetraol formation to the overall reaction, as exemplified by the experiments with (+)-*anti*-BPDE, is considerably smaller at low temperature (Figure 3).

To see if the increased adduct formation observed for (+)-*anti*-BPDE at lower temperature can be considered

as a more general phenomenon, the corresponding (–)-*anti*-enantiomer as well as the (+)- and (–)-*syn*-BPDE enantiomers were reacted with 5'-d(CCTATAGATATCC) or 5'-d(CCTATTGCTATCC) at 0 and 20 °C. The results are compiled in Table 2, including those obtained with (+)-*anti*-BPDE (*cf.* Table 1) for comparison. As can be seen, increasing the temperature from 0 to 20 °C reduced the relative yields of oligonucleotide adducts with all four BPDE stereoisomers. Interestingly, the temperature effect seems to be dependent on the flanking bases since the reduction in adduct formation with the 5'-AGA sequence is significantly more pronounced than with the 5'-TGC sequence. The absolute oligonucleotide modifications obtained within the 5'-AGA sequence at 0 °C were approximately 17%, 6%, 2.5%, and 3.5% for (+)-*anti*-BPDE, (–)-*anti*-BPDE, (+)-*syn*-BPDE, and (–)-*syn*-BPDE, respectively. With the exception of (+)-*anti*-BPDE (*cf.* Table 1), changing the sequence context from 5'-AGA to 5'-TGC had little or no effect on the amount of adducts formed from BPDE isomers at 0 °C with the oligonucleotides (Table 2, *cf.* Table 1). Despite the fact that the total yield was reduced, an increase in the reaction temperature significantly influenced the *cis* vs *trans* stereochemistry of the adducts formed, and the formation of adducts with *cis* stereochemistry was favored for each BPDE stereoisomer investigated (Table 2).

Effect of pH on the Adduct Formation. As evident from the results shown in Figure 5, the optimum pH for adduct formation in Tris buffer at 0 °C is between 7.5 and 8.0. Under these conditions about 20% modified oligonucleotide was obtained.

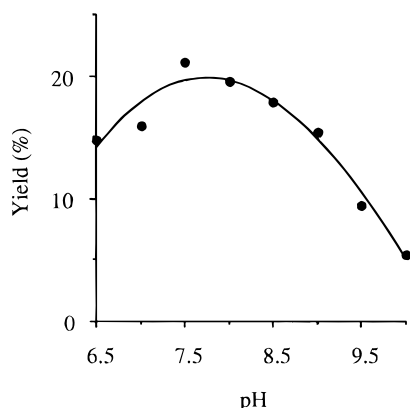
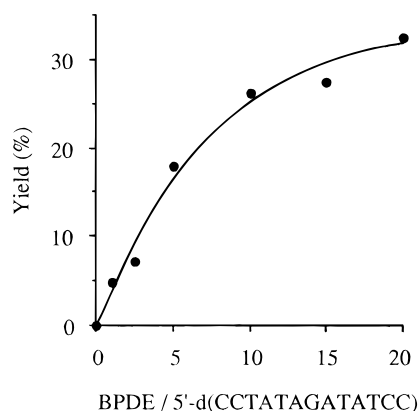
Effect of Solvent Polarity on the Adduct Formation. Addition of DMSO or THF up to 10% had no significant effect on adduct formation in Tris buffer at 0 °C. However, a further increase to 25% of DMSO or THF substantially reduced the extent of adduct formation (data not shown). The inhibitory effect of relatively high THF concentrations on adduct formation has also been observed by Geacintov *et al.* (personal communication). The presence of DMF strongly inhibited the reaction at all concentrations tested and almost abolished diol epoxide binding at 25% (data not shown). Differences in the ease of formation of intercalation complexes depending on the defined sequence context have recently been discussed to explain the nearest-neighbor effects on the ratio of *cis* vs *trans* adduct formation of diol epoxides with double-stranded oligonucleotides (Cheh *et al.*, 1994). The effects of organic solvents on adduct formation observed here suggest that the diol epoxide also in the single-stranded oligonucleotide has to be oriented in a well-defined manner relative to the exocyclic amino group of dG for efficient reaction. The marked decrease in reaction yields observed with the strong polar organic solvent DMF is probably due to a conformational change of the single-stranded oligonucleotide accompanied by a destruction of the catalytic environment. Lack of a specific oligonucleotide conformation results in very poor reaction yields, as has also been observed for direct reactions of BPDE and single nucleotides and/or nucleosides (M. Funk and B. Jernström, unpublished observations).

Effect of Molar Excess of BPDE and of Tetraols on Adduct Formation. As shown in Figure 6, increasing the molar ratios of (+)-*anti*-BPDE and the oligonucleotide (varied from 1:1 to 20:1) resulted in ratios of up to 5:1 in a nearly linear improvement of the reaction yield [*cf.* Margulis *et al.* (1993)]. At higher ratios the improvement in adduct yield was reduced, which might be due to an overproportional hydrolysis to tetraols favored at higher diol epoxide/oligonucleotide ratios. However, at

Table 2. Yields of Adducts Formed between Individual BPDE Stereoisomers and 5'-d(CCTATAGATATCC) or 5'-d(CCTATTGCTATCC) in Tris-HCl Buffer (pH 7.9) at 0 °C and at 20 °C (pH 7.5)

sequence	temp (°C)	(+)- <i>anti</i> -BPDE	(-)- <i>anti</i> -BPDE	(+)- <i>syn</i> -BPDE	(-)- <i>syn</i> -BPDE
5'-AGA ^a	0	1.00 ^{b,c} (97) ^d	1.00 ^{b,c} (89)	1.00 ^{b,c} (21)	1.00 ^{b,e} (1)
	20	0.24 ± 0.08 (76)	0.39 ± 0.05 (66)	0.39 ± 0.07 (7)	0.34 ± 0.05 (0)
5'-TGC ^f	0	1.00 ^{b,g} (83)	1.00 ^{b,g} (60)	1.00 ^{b,g} (10)	1.00 ^{b,g} (0)
	20	0.52 ± 0.09 (57)	0.69 ± 0.04 (35)	0.54 ± 0.16 (19)	0.64 ± 0.01 (0)

^a Data shown from four experiments. ^b Amount of adducts set to 1.00. ^c Percentage of adducts formed (see Table 1). ^d Percentage of trans adducts. ^e Total amount of adducts formed, 5.9 ± 0.8, 2.5 ± 0.5, and 3.5 ± 0.6 for (-)-*anti*-BPDE/, (+)-*syn*-BPDE/, and (-)-*syn*-BPDE/5'-AGA, respectively. ^f Data shown from two experiments. ^g Total amount of adducts formed, 5.5 ± 0.6, 3.1 ± 0, and 3.0 ± 0.4 for (-)-*anti*-BPDE/, (+)-*syn*-BPDE/, and (-)-*syn*-BPDE/5'-TGC, respectively.

**Figure 5.** Yield of trans adducts formed between (+)-*anti*-BPDE and 5'-d(CCTATAGATATCC) as a function of pH. The pH values given represent those at the incubation temperature of 0 °C.**Figure 6.** Yield of trans adducts formed between (+)-*anti*-BPDE and 5'-d(CCTATAGATATCC) as a function of increasing diol epoxide/oligonucleotide molar ratio.

ratios exceeding 20:1 an adduct yield of >30% can be accomplished. In terms of efficient use of BPDE in Tris buffer, a 5–10-fold molar excess of (+)-*anti*-BPDE seems to be optimal.

Incubations under standard conditions using (+)-*anti*-BPDE in the presence of the tetraol, which is formed by trans hydrolysis of *anti*-BPDE, at a concentration equimolar to that of (+)-*anti*-BPDE lead to a diminished reaction yield (about 12%; data not shown). This effect is most probably caused by the competition between the tetraol and the diol epoxide for potential noncovalent binding sites preceding adduct formation. The noncovalent interaction of tetraols to duplexed DNA (Ibanez *et al.*, 1980) and single-stranded oligonucleotides (Geacintov *et al.*, personal communication) has been demonstrated. The inhibitory effect of tetraols has to be taken into account when one is performing the reaction by stepwise addition of BPDE aliquots to the oligonucleotide-containing solution (Cosman *et al.*, 1990; Fountain and Krugh, 1995). Stepwise addition of (+)-*anti*-BPDE aliquots rather than

a single addition of the total amount had no effect on reaction yields in the Tris-buffered system (data not shown). This may be due to the presence of tetraols and, consequently, to a reduced ease of adduct formation [*cf.* Liu *et al.* (1996)].

Oligonucleotide-Catalyzed Hydrolysis of (+)-*anti*-BPDE. DNA catalyzes the hydrolysis of BPDE (Geacintov *et al.*, 1980, 1982; MacLeod and Selkirk, 1982; MacLeod and Zachary, 1985a). The increased rate of hydrolysis can probably be attributed to a general-acid catalysis due to protonation of the phosphate diester groups (Michaud *et al.*, 1983) and/or the nucleophilic properties of these groups resulting in the formation of unstable phosphotriesters (Gamper *et al.*, 1977; Di Raddo and Chan, 1983). Also, the exocyclic amino group of dG has been suggested to play a role in the catalysis (MacLeod and Zachary, 1985b). Considering that hydrolysis of BPDE constitutes the major competing reaction of adduct formation, it was of interest to study the catalytic properties of the parts of the oligonucleotide sequence flanking the dG position, which are not directly involved in adduct formation. The oligonucleotide 5'-d(CCTATAIATATCC), in which dG was replaced by deoxyinosine (dI), was incubated with (+)-*anti*-BPDE, and differences of the oligonucleotide in single- or double-stranded form to catalyze hydrolysis to tetraols were studied. A partial duplex was obtained by hybridization with 5'-d(ATATCTATA). For comparison, the diol epoxide was also allowed to undergo hydrolysis in standard buffer. The plot of the remaining diol epoxide (determined as the 2-mercaptoethanol conjugate) vs reaction time revealed an exponential decline of the diol epoxide concentration both in the absence and in the presence of DNA [Figure 7; *cf.* Michaud *et al.* (1983)]. The diol epoxide half-life ($t_{1/2}$) values were obtained from plots of the logarithm of residual (+)-*anti*-BPDE vs time (Michaud *et al.*, 1983; Dock *et al.*, 1987). The $t_{1/2}$ of (+)-*anti*-BPDE in Tris buffer at 0 °C was estimated to be 2.8 h. The presence of single-stranded oligonucleotide increased the rate of hydrolysis ($t_{1/2}$ = 1.6 h). A further increase in the rate of hydrolysis was observed in the presence of the partial oligonucleotide duplex ($t_{1/2}$ = 1.1 h; see Figure 7). We conclude from these experiments that the hydrolytic properties of double-stranded DNA compared to the single-stranded form do not seem to be of qualitative difference; the double-stranded oligonucleotide behaves in our system approximately as a double molar equivalent of the single-stranded form. Thus, a DNA duplex is *per se* not more efficient in catalyzing hydrolysis than a corresponding amount of single-stranded DNA. Furthermore, the base sequence seems to be of little importance in catalyzing hydrolysis since no difference in rates was observed in the presence of 5'-d(CCTATAGATATCC) or 5'-d(CCTATTGCTATCC).

Effect of Base Sequence Context on Adduct Formation. The oligonucleotides 5'-d(CCTATAGATATCC) and 5'-d(CCTATTGCTATCC) were employed,

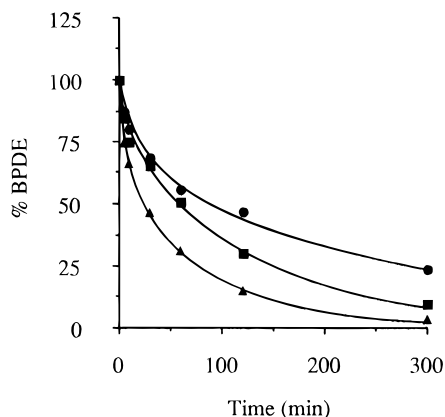


Figure 7. Hydrolysis of (+)-anti-BPDE ($c = 300 \mu\text{M}$) at 0°C in 50 mM Tris-HCl buffer (pH 7.9): (●) in the absence of oligonucleotide; (■) in the presence of $50 \mu\text{M}$ of the oligonucleotide 5'-d(CCTATAIATATCC); (▲) in the presence of $50 \mu\text{M}$ of the oligonucleotide 5'-d(CCTATAIATATCC) and $50 \mu\text{M}$ of the oligonucleotide 5'-d(ATATCTATA).

both with a central dG as the binding site but having different bases at the adjacent 5' and 3' sides, as well as buffer systems based on Tris-HCl or sodium phosphate. The extents of binding of (+)-anti-BPDE to dG in the two oligonucleotides were compared. As shown previously (Figure 3 and Table 1), the overall amount of dG adducts formed with the oligonucleotide containing 5'-AGA was about 2-fold higher relative to the one containing 5'-TGC under standard conditions (Tris buffer, pH 7.5 at 0°C). This was unexpected since previous results with (+)-anti-BPDE and the oligonucleotides 5'-d(CTATAGATATC) and 5'-d(CTATTGCTATC) demonstrated the opposite reactivity (Margulis *et al.*, 1993). In their study the diol epoxide was incubated with the oligomers overnight at room temperature in sodium phosphate supplemented with TEA and sodium chloride. The results showed that dG surrounded by pyrimidines in general yields higher amounts of adducts than dG surrounded by purines. It was suggested that purines flanking dG lower the reactivity by steric effects due to their bulkiness and/or noncovalent interactions with the diol epoxide. Either mechanism is expected to decrease the optimum conditions for the formation of bimolecular transition state complexes. Taken together, the results indicate that flanking purines seem to promote the formation of a bimolecular dG/BPDE transition state in Tris buffer but have the opposite effect in phosphate buffer. The reason for this discrepancy is presently not completely understood.

Earlier studies have been performed with both native DNA and oligomers in single- or double-stranded form to establish the influence of flanking bases on adduct formation of BPDE stereoisomers with dG (Reardon *et al.*, 1989; Kootstra *et al.*, 1989; Osborne, 1990; Schwartz *et al.*, 1994). Osborne (1990) studied the effect of sequence context on the binding of (+)-anti-BPDE to dG in a series of self-complementary oligonucleotides. The diol epoxide and oligonucleotide duplex were incubated at 0°C in slightly acidic sodium cacodylate buffer overnight, and the results showed lowest yields of adduct formation with dG flanked by dA and dT and highest yields with dG in mixed d(GC) sequences [*cf.* Kootstra *et al.* (1989)]. In a more recent study (Schwartz *et al.*, 1994), the base sequence selectivity in binding of (+)-anti-BPDE to self-complementary oligonucleotides was investigated. In this case the diol epoxide was incubated with the oligonucleotide duplex at 0°C in neutral Hepes/sodium chloride buffer overnight. Consistent with previ-

ous results (Osborne, 1990) the study showed that dG surrounded by dC reacted to the greatest extent, whereas dG surrounded by dA and dT gave the lowest yield of adducts. A preference of (+)-anti-BPDE for dG flanked by another dG on either the 5'- or 3'-side was also noted. These latter results are in contrast to those obtained by Margulis *et al.* (1993) and Mao *et al.* (1995) on single-stranded oligomers.

The strong influence of the buffer system on the preferred sequence context for (+)-anti-BPDE binding was most unexpected in the present study. The factors underlying the shift in the binding preference from pur-dG-pur in Tris buffer to pyr-dG-pyr in phosphate buffer (Table 1) seem to warrant further investigation. As mentioned before, the buffer- and temperature-dependent shift of preferred sequence context shown here has certain implications for the universal applicability of previous studies.

CONCLUSIONS

From the experiments reacting (+)-anti-BPDE with two different oligonucleotide sequences in Tris buffer we conclude that (i) low incubation temperature, slightly alkaline pH, and high diol epoxide/oligonucleotide ratios promote adduct formation; (ii) elevated temperature promotes the formation of adducts with *cis* stereochemistry; (iii) the reaction time required to complete the reaction is <10 h; (iv) the addition of tetraols, being hydrolysis products of BPDE, or high amounts of an organic solvent inhibits the reaction; and (v) a substantially higher yield of adducts with *trans* stereochemistry (17%) is obtained with flanking purines (5'-AGA) than with flanking pyrimidines (5'-TGC). The same set of experiments performed with (+)-anti-BPDE in the phosphate/TEA-buffered system revealed that (i) temperature is in general of less importance for adduct formation (see below), provided that the reaction is allowed to go to completion (incubation time >20 h depending on the temperature); and (ii) a similar high yield of *trans* adducts (18%) is obtained upon reaction with 5'-d(CTATTGCTATCC), whereas the yield with the 13-mer containing 5'-AGA was substantially lower.

Taking the results of the present study together, incubation time and temperature along with the varying lifetime of a given PAH diol epoxide in different buffer systems and, as a consequence, greatly varying rates of adduct formation may also be factors that have to be taken into account when one is interpreting the results from studies on the sequence selectivity of diol epoxide binding.

ACKNOWLEDGMENT

This study was supported by grants from the Swedish Cancer Society, the Swedish Work Environmental Fund, and the Deutsche Forschungsgemeinschaft (SFB 302). We thank Professor Nicholas E. Geacintov for valuable comments on this work.

LITERATURE CITED

- Cheh, A. M., Yagi, H., and Jerina, D. M. (1994) Effect of DNA base sequence on the configuration of deoxyadenosine adducts formed by the fjord region diol epoxide, (+)-(1R,2S,3R,4S)-3,4-dihydroxy-1,2-epoxy-1,2,3,4-tetrahydrobenzo[*c*]phenanthrene. *Biochemistry* 33, 12911–12919.
- Cheng, S. C., Hilton, B. D., Roman, J. M., and Dipple, A. (1989) DNA adducts from carcinogenic and noncarcinogenic enantiomers of benzo[*a*]pyrene dihydrodiol epoxide. *Chem. Res. Toxicol.* 2, 334–340.
- Cook, J. M., Hewett, C. L., and Hieger, I. (1933) The isolation of a cancer producing hydrocarbon from coal tar. Parts I, II and III. *J. Chem. Soc.*, 395–405.

- Cosman, M., Ibanez, V., Geacintov, N. E., and Harvey, R. G. (1990) Preparation and isolation of adducts in high yield derived from the binding of two benzo[a]pyrene-7,8-dihydroxy-9,10-oxide stereoisomers to the oligonucleotide d(ATAT-GTATA). *Carcinogenesis (London)* 11, 1667–1672.
- Cosman, M., de los Santos, C., Fiala, R., Hingerty, B. E., Singh, S. B., Ibanez, V., Margulis, L. A., Geacintov, N. E., Broyde, S., and Patel, D. J. (1992) Solution conformation of the major adduct between the carcinogen (+)-anti-benzo[a]pyrene diol epoxide and DNA. *Proc. Natl. Acad. Sci. U.S.A.* 89, 1914–1918.
- Cosman, M., de los Santos, C., Fiala, R., Hingerty, B. E., Ibanez, V., Luna, E., Harvey, R. G., Geacintov, N. E., Broyde, S., and Patel, D. J. (1993) Solution conformation of the (+)-cis-anti-[BP]GC adduct in a DNA duplex: intercalation of the covalently attached benzo[a]pyrenyl ring into the helix and displacement of the modified deoxyguanosine. *Biochemistry* 32, 4145–4154.
- de los Santos, C., Cosman, M., Hingerty, B. E., Ibanez, V., Margulis, L. A., Geacintov, N. E., Broyde, S., and Patel, D. J. (1992) Influence of benzo[a]pyrene diol epoxide chirality on solution conformations of DNA covalent adducts: the (–)-trans-anti-[BP]GC adduct structure and comparison with the (+)-trans-anti-[BP]GC enantiomer. *Biochemistry* 31, 5245–5252.
- Di Raddo, P., and Chan, T.-H. (1983) Reactions of phosphodiester with epoxides of polycyclic aromatic hydrocarbons. *J. Chem. Soc., Chem. Commun.*, 16–17.
- Dock, L., Martinez, M., and Jernström, B. (1987) Increased stability of 7 β , 8 α -dihydroxy-9 α ,10 α -epoxy-7,8,9,10-tetrahydrobenzo[a]pyrene through interaction with subcellular fractions of rat liver. *Chem.-Biol. Interact.* 61, 31–44.
- Fountain, M. A., and Krugh, T. R. (1995) Structural characterization of a (+)-trans-anti-benzo[a]pyrene-DNA adduct using NMR, restrained energy minimization, and molecular dynamics. *Biochemistry* 34, 3152–3161.
- Gamper, H. B., Tung, A. S., Straub, K., Bartholomew, J. C., and Calvin, M. (1977) DNA strand scission by benzo[a]pyrene diol epoxides. *Science* 197, 671–674.
- Geacintov, N. E., Ibanez, V., Gagliano, A. G., Yoshida, H., and Harvey, R. G. (1980) Kinetics of hydrolysis to tetraols and binding of benzo[a]pyrene 7,8-dihydrodiol 9,10-oxide and its tetraol derivatives to DNA. Conformation of adducts. *Biochem. Biophys. Res. Commun.* 92, 1335–1342.
- Geacintov, N. E., Yoshida, H., Ibanez, V., and Harvey, R. G. (1982) Noncovalent binding of 7 β ,8 α -dihydroxy-9 α ,10 α -epoxy tetrahydrobenzo[a]pyrene to deoxyribonucleic acid and its catalytic effect on the hydrolysis of the diol epoxide to tetraol. *Biochemistry* 21, 1864–1869.
- Geacintov, N. E., Shahbaz, M., Ibanez, V., Moussaoui, K., and Harvey, R. (1988) Base-sequence dependence of noncovalent complex formation and reactivity of benzo[a]pyrene diol epoxide with polynucleotides. *Biochemistry* 27, 8380–8387.
- Geacintov, N. E., Cosman, M., Mao, B., Alfano, A., Ibanez, V., and Harvey, R. G. (1991) Spectroscopic characteristics and site/siteII classification of cis and trans-benzo[a]pyrene diol epoxide enantiomer-guanosine adducts in oligonucleotides and polynucleotides. *Carcinogenesis (London)* 12, 2099–2108.
- Geacintov, N. E., Cosman, M., Hingerty, B. E., Amin, S., Broyde, S., and Patel, D. J. (1997) NMR solution structures of stereoisomeric polycyclic aromatic carcinogen-DNA adducts: principles, patterns and diversity. *Chem. Res. Toxicol.* 10, 111–146.
- Hruszkewycz, A. M., Canella, K. A., Peltonen, K., Kotrappa, L., and Dipple, A. (1992) DNA polymerase action on benzo[a]pyrene-DNA adducts. *Carcinogenesis (London)* 13, 2347–2352.
- Ibanez, V., Geacintov, N. E., Gagliano, A. G., Brandimarte, S., and Harvey, R. G. (1980) Physical binding of tetraols derived from 7,8-dihydroxy-9,10-epoxybenzo[a]pyrene to DNA. *J. Am. Chem. Soc.* 102, 5661–5666.
- Jeffrey, A. M., Jeanette, K. W., Blobstein, S. H., Weinstein, I. B., Beland, F. A., Harvey, R. G., Kasai, H., Miura, I., and Nakanishi, K. (1976) Benzo[a]pyrene-nucleic acid derivative found in vivo: structure of benzo[a]pyrenetetrahydrodiol epoxide-guanosine adduct. *J. Am. Chem. Soc.* 98, 5714–5715.
- Jelinsky, S. A., Liu, T., Geacintov, N. E., and Loechler, E. L. (1995) The major, N²-Gua adduct of the (+)-anti-benzo[a]pyrene diol epoxide is capable of inducing G \rightarrow A and G \rightarrow C, in addition to G \rightarrow T, mutations. *Biochemistry* 34, 13545–13553.
- Jerina, D. M., Sayer, J. M., Yagi, H., van Bladeren, P. J., Thakker, D. R., Levin, W., Chang, R. L., Wood, A. W., and Conney, A. H. (1985) Stereoselective metabolism of polycyclic aromatic hydrocarbons to carcinogenic metabolites. In *Microssomes and Drug Oxidations* (A. R. Boobis, J. Cadwell, F. De Matteis, and C. R. Elcombe, Eds.) pp 310–319, Taylor & Francis, London.
- Jernström, B., and Gräslund, A. (1994) Covalent binding of benzo[a]pyrene 7,8-dihydrodiol 9,10-epoxides to DNA: molecular structures, induced mutations and biological consequences. *Biophys. Chem.* 49, 185–199.
- Kim, S. J., Stone, M. P., Harris, C. M., and Harris, T. M. (1992) A postligomerization synthesis of oligodesoxynucleotides containing polycyclic aromatic hydrocarbon adducts at the N⁶ position of desoxyadenosine. *J. Am. Chem. Soc.* 114, 5480–5481.
- Kootstra, A., Lew, L. K., Nairn, R. S., and MacLeod, M. C. (1989) Preferential modification of GC boxes by benzo[a]pyrene-7,8-diol-9,10-epoxide. *Mol. Carcinogen.* 1, 239–244.
- Lakshman, M. K., Sayer, J. M., Yagi, H., and Jerina, D. M. (1992) Synthesis and duplex-forming properties of a nonanucleotide containing an N⁶-desoxyadenosine adduct of a bay-region diol epoxide. *J. Org. Chem.* 57, 4585–4590.
- Lee, H., Hinz, M., Stezowski, J. J., and Harvey, R. G. (1990) Synthesis of polycyclic aromatic hydrocarbon-nucleoside and oligonucleotide adducts specifically alkylated on the amino functions of deoxyguanosine and deoxyadenosine. *Tetrahedron Lett.* 31, 6773–6776.
- Lee, H. M., Luna, E., Hinz, M., Stezowski, J. J., Kiselyov, A. S., and Harvey, R. G. (1995) Synthesis of oligonucleotide adducts of the bay region diol epoxide metabolites of carcinogenic polycyclic aromatic hydrocarbons. *J. Org. Chem.* 60, 5604–5613.
- Liu, T., Xu, J., Tsao, H., Li, B., Xu, R., Yang, C., Amin, S., Moriya, M., and Geacintov, N. E. (1996) Base sequence-dependent bends in site-specific benzo[a]pyrene diol epoxide-modified oligonucleotide duplexes. *Chem. Res. Toxicol.* 9, 255–261.
- MacLeod, M. C., and Selkirk, J. K. (1982) Physical interactions of isomeric benzo[a]pyrene diol-epoxides with DNA. *Carcinogenesis (London)* 3, 287–292.
- MacLeod, M. C., and Zachary, K. L. (1985a) Catalysis of carcinogen detoxification by DNA: comparison of enantiomeric diol epoxides. *Chem.-Biol. Interact.* 54, 45–55.
- MacLeod, M. C., and Zachary, K. L. (1985b) Involvement of the exocyclic amino group of desoxyguanosine in DNA-catalysed carcinogen detoxification. *Carcinogenesis (London)* 6, 147–149.
- Mao, B., Xu, J., Li, B., Margulis, L. A., Smirnov, S., Ya, N.-Q., Courtney, S. H., and Geacintov, N. E. (1995) Synthesis and characterization of covalent adducts derived from the binding of benzo[a]pyrene diol epoxide to a -GGG- sequence in a deoxyoligonucleotide. *Carcinogenesis (London)* 16, 357–365.
- Margulis, L. A., Ibanez, V., and Geacintov, N. E. (1993) Base-sequence dependence of covalent binding of benzo[a]pyrene diol epoxide to guanine in oligodeoxyribonucleotides. *Chem. Res. Toxicol.* 6, 59–63.
- Michaud, D. P., Gupta, S. C., Whalen, D. L., Sayer, J. M., and Jerina, D. M. (1983) Effects of pH and salt concentration on the hydrolysis of a benzo[a]pyrene 7,8-diol-9,10-epoxide catalyzed by DNA and polyadenylic acid. *Chem.-Biol. Interact.* 44, 41–52.
- Osborne, M. E. (1990) Sequence specificity in the reaction of benzopyrene diol epoxide with DNA. *Chem.-Biol. Interact.* 75, 131–140.
- Persson, Å., Pontén, I., Cotgreave, I., and Jernström, B. (1996) Inhibitory effects on the DNA binding of AP-1 transcription factor to an AP-1 binding site modified by benzo[a]pyrene 7,8-dihydrodiol 9,10-epoxide diastereomers. *Carcinogenesis (London)* 17, 1963–1969.
- Pontén, I., Kim, S. K., Gräslund, A., Nordén, B., and Jernström, B. (1994) Spectroscopic studies of the trans-adducts derived

- from (+)- and (-)-*anti*-benzo[*a*]pyrene 7,8-dihydrodiol 9,10-epoxide and the oligonucleotide 5'-d(CCTATAGATATCC). *Carcinogenesis (London)* 15, 2207-2213.
- Pontén, I., Seidel, A., Gräslund, A., and Jernström, B. (1996) Synthesis and characterization of adducts derived from the *syn*-diastereomer of benzo[*a*]pyrene 7,8-dihydrodiol 9,10-epoxide and the 5'-d(CCTATAGATATCC) oligonucleotide. *Chem. Res. Toxicol.* 9, 188-196.
- Pontén, I., Ström, K., Seidel, A., Gräslund, A., and Jernström, B. (1997) Base sequence preference of (+)-*anti*- and (-)-*syn*-benzo[*a*]pyrene 7,8-dihydrodiol 9,10-epoxide stereoisomers in the covalent binding to guanine in single stranded oligonucleotides. (Manuscript in preparation.)
- Pradhan, P., Jernström, B., Seidel, A., and Gräslund, A. (1997) Induced circular dichroism of benzo[*a*]pyrene diol epoxide stereoisomers covalently bound to DNA. (Manuscript in preparation.)
- Reardon, D. B., Bigger, C. A. H., Strandberg, J., Yagi, H., Jerina, D. M., and Dipple, A. (1989) Sequence selectivity in the reaction of optically active hydrocarbon dihydrodiol epoxides with rat H-ras DNA. *Chem. Res. Toxicol.* 2, 12-14.
- Sayer, J. M., Chadha, A., Agarwal, S. K., Yeh, H. J. C., Yagi, H., and Jerina, D. M. (1991) Covalent nucleoside adducts of benzo[*a*]pyrene 7,8-diol 9,10-epoxides: structural reinvestigation and characterization of a novel adenosine adduct on the ribose moiety. *J. Org. Chem.* 56, 20-29.
- Schwartz, J. J., Lau, H. S., and Baird, W. M. (1994) Base sequence selectivity in the binding of 7(R),8(S)-dihydroxy-9(S),10(R)-epoxy-7,8,9,10-tetrahydrobenzo[*a*]pyrene to oligodeoxy-ribonucleotide duplexes. *Chem. Res. Toxicol.* 7, 29-40.
- Shibutani, S., Margulis, L. A., Geacintov, N. E., and Grollman, A. P. (1993) Translesional synthesis on a DNA template containing a single stereoisomer of dG-(+)- or dG-(-)-*anti*-BPDE (7,8-dihydroxy-*anti*-9,10-epoxy-7,8,9,10-tetrahydrobenzo[*a*]pyrene). *Biochemistry* 32, 7531-7541.
- Steinbrecher, T., Becker, A., Stezowski, J. J., Oesch, F., and Seidel, A. (1993) Synthesis of oligodeoxynucleotides containing diastereomeric dihydrodiol epoxide-*N*⁶-deoxyadenosine adducts of polycyclic aromatic hydrocarbons. *Tetrahedron Lett.* 34, 1773-1774.
- Stevens, C. W., Bouck, N., Burgess, J. A., and Fahl, W. E. (1985) Benzo[*a*]pyrene diol-epoxides: different mutagenic efficiency in human and bacterial cells. *Mutat. Res.* 152, 5-14.
- Thakker, D. R., Yagi, H., Levin, W., Lu, A. Y. H., Conney, A. H., and Jerina, D. M. (1977) Stereospecificity of microsomal and purified epoxide hydrolase from rat liver. *J. Biol. Chem.* 252, 6328-6334.
- Wislocki, P., and Lu, A. Y. H. (1988) Carcinogenicity and mutagenicity of proximate and ultimate carcinogens of polycyclic aromatic hydrocarbons. In *Polycyclic Aromatic Hydrocarbon Carcinogenesis: Structure-Activity Relationships* (S. K. Yang and B. D. Silverman, Eds.) pp 2-31, CRC Press, Boca Raton, FL.
- Wolfe, A. R., Yamamoto, J., and Meehan, T. (1994) Chloride ions catalyze the formation of cis adducts in the binding of *anti*-benzo[*a*]pyrene diol epoxide to nucleic acids. *Proc. Natl. Acad. Sci. U.S.A.* 91, 1371-1375.
- Yang, S. K., Roller, P. P., and Gelboin, H. V. (1977) Enzymatic mechanism of benzo[*a*]pyrene conversion to phenols and diols and an improved high-pressure liquid chromatographic separation of benzo[*a*]pyrene derivatives. *Biochemistry* 16, 3680-3686.
- Zajc, B., Lakshman, M. K., Sayer, J. M., and Jerina, D. M. (1992) Epoxide and diol epoxide adducts of polycyclic aromatic hydrocarbons at the exocyclic amino group of deoxyadenosine. *Tetrahedron Lett.* 33, 3409-3412.
- Zou, Y., Liu, T.-M., Geacintov, N. E., and Van Houten, B. (1995) Interaction of the UvrABC nuclease system with a DNA duplex containing a single stereoisomer of dG-(+)- or dG-(-)-*anti*-BPDE. *Biochemistry* 34, 13582-13593.

BC9700188

A 15-Base Acridine-Conjugated Oligodeoxynucleotide Forms Triplex DNA with Its IL-2R α Promoter Target with Greatly Improved Avidity

Jan Klysik,^{*,†,‡,§} Berma M. Kinsey,^{†,‡} Pascal Hua,^{†,||} G. Alexander Glass,[†] and Frank M. Orson^{†,‡,§}

Veterans Affairs Medical Center Research Center on AIDS and HIV Infections and Department of Internal Medicine, Department of Microbiology and Immunology, and Department of Otolaryngology, Baylor College of Medicine, Building 109, Room 226, VAMC, 2002 Holcombe Boulevard, Houston, Texas 77030. Received August 12, 1996[®]

Attachment of 6,9-diamino-2-methoxyacridine to the 5' end of a purine-rich oligodeoxynucleotide targeting a 15 bp oligopurine-oligopyrimidine stretch in the promoter region of the interleukin-2 receptor alpha chain (IL-2R α) gene results in an approximately 500-fold increase in its triplex forming avidity as determined by both band shift assay and DMS footprinting (K_d lowered from 2.5 μ M to 5 nM). This oligonucleotide participates in Mg²⁺-dependent three-stranded DNA formation in which it is oriented antiparallel relative to the purine strand of the target duplex as determined by acridine moiety sensitized photoreactivity with the target duplex DNA. The oligonucleotides used in these studies were synthesized with a 3-amino-2-hydroxypropyl group at the 3' end to protect against exonucleolytic degradation for future *in vivo* applications. The 3'-amino group underwent partial removal, probably during the NaOH deprotection step. Both the 3'-amino and the 3'-free forms of the oligo have the same binding avidity and specificity. The interaction of the third strand with its target is sequence specific and can be essentially abolished by a point G \rightarrow T transversion 4 bases away from the 3' end of the target oligopurine block or severely reduced by other mutations within the target duplex. Thus, the attachment of the acridine moiety to the 5' end of the oligonucleotide does not seem to substantially compromise the sequence specificity of binding. Additionally, the oligonucleotide composed of G and A nucleotides was found to be superior to the oligonucleotide containing G and T residues since the difference in avidity of binding to the same target site was 17-fold.

INTRODUCTION

Stretches of oligopurine-oligopyrimidine duplex DNA have the unique property of being able to associate with an internally (Hanvey et al., 1988; Htun and Dahlberg, 1988; Klysik, 1995; Klysik et al., 1991; Lyamichev et al., 1986) or externally (Cheng and Pettitt, 1992; Hélène, 1991; Hélène and Toulme, 1990) provided third strand to form triple-stranded helical DNA structures via Hoogsteen or reverse Hoogsteen hydrogen bond interactions. Triplexes are of considerable interest as they could be useful in the regulation of gene expression (Dervan, 1989; Hélène and Toulmé, 1989), the delivery of a desired mutagen to its specific nuclear target (Giovannangeli et al., 1992; Praseuth et al., 1988; Wang et al., 1996), the specific fragmentation of the genome at designated sites (Moser and Dervan, 1987; Orson et al., 1996b), or DNA purification by triplex affinity capture (Ito et al., 1992). Many potential oligopurine/oligopyrimidine genomic target sites do not exceed 15 base pairs in length. One way to enhance the binding of such short oligonucleotides is to attach an intercalating agent to one end of the chain (Grigoriev et al., 1992; Orson et al., 1994; Sun et al., 1989; Zhou et al., 1995). In the present studies we have chosen as an intercalating agent 6,9-diamino-2-methoxyacri-

dine (DAMA), which is similar to the well-known vital nuclear stain rivanol. It has a bright greenish-yellow fluorescence that can be detected by UV illumination.

In prior studies of DAMA-conjugated oligonucleotides, we established that the structure of the link between the acridine and the oligo has a great influence on triplex stability (Orson et al., 1994). For example, the best linker–DAMA combination was capable of reducing the effective K_d of T₁₀ to its ideal target sequence from >250 μ M to 1 μ M. In this paper we extend these studies to oligonucleotides targeting a 15 bp oligopurine sequence in the promoter region of the interleukin-2 receptor alpha (IL-2R α) gene (Leonard et al., 1985). IL-2 receptors are of substantial importance in the normal functioning of the immune system (Diamantstein and Osawa, 1986; Strom et al., 1992; Williams et al., 1988). An abnormal expression of IL-2R α is associated with many lymphoid malignancies including adult T-cell leukemia, hairy cell leukemia, acute and chronic granulocytic leukemia, cutaneous T-cell lymphoma, and Hodgkin's disease. An increased expression of the IL-2 receptor has been documented to take place in a long list of autoimmune diseases including rheumatoid arthritis, systemic lupus erythematosus, insulin-dependent diabetes mellitus, and many others. Also, elevated expression of the IL-2R α chain on the surface of T cells occurs in allograft rejection. Since the IL-2R α subunit is required for high-affinity IL-2 binding, selective regulation of IL-2 interaction with its cognate receptor may be achieved by regulation of IL-2R α gene expression. The promoter of the IL-2R α receptor gene offers a 15 bp long oligopurine stretch that can be targeted by an appropriate oligonucleotide (Grig-

* Address correspondence to this author at Building 109, Room 226, Veterans Affairs Medical Center, 2002 Holcombe Blvd., Houston, TX 77030.

[†] Veterans Affairs Medical Center Research Center on AIDS and HIV Infections.

[‡] Department of Internal Medicine.

[§] Department of Microbiology and Immunology.

^{||} Department of Otolaryngology.

[®] Abstract published in *Advance ACS Abstracts*, April 1, 1997.

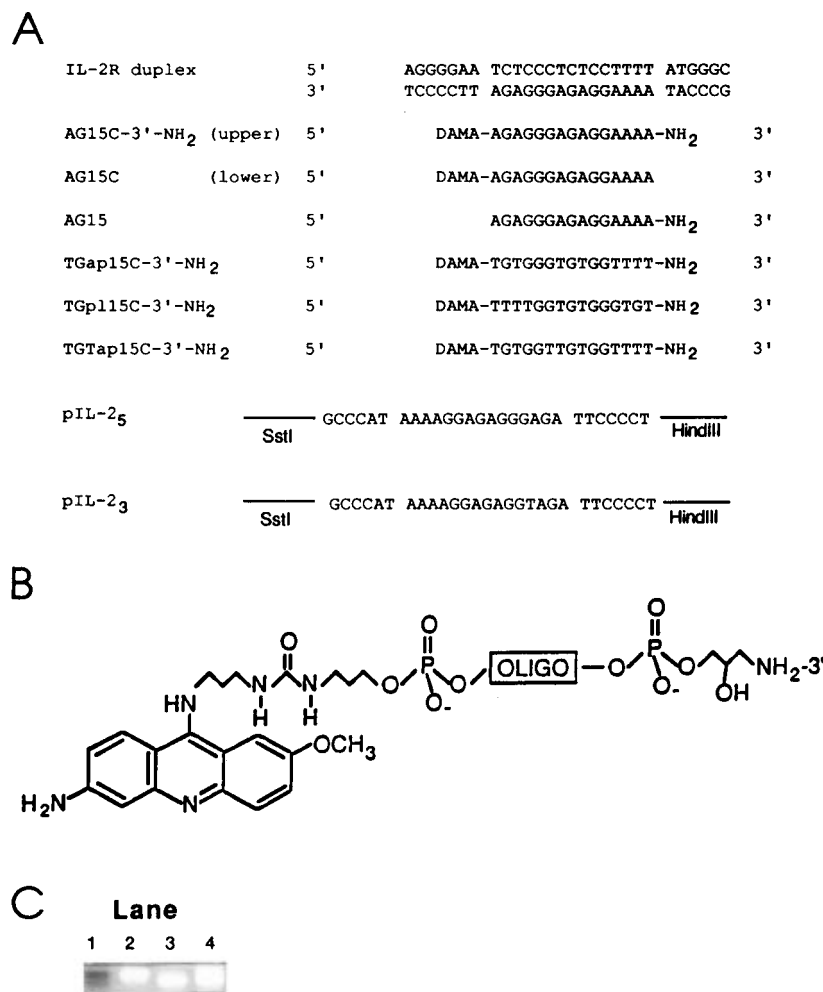


Figure 1. DNAs used in these studies. (A) List of synthetic oligonucleotides and plasmid inserts. AG15C-3'-NH₂ is the derivative as shown in panel B and migrates as the slower (upper) band when separated on an acrylamide gel (cf. panel C). AG15C refers to the 3'-unmodified derivative, which migrates more rapidly (lower band) in an acrylamide gel (cf. panel C). The identities of both AG15C-3'-NH₂ and AG15C were confirmed by MALDI-TOF mass spectrometry. AG15 (5'-DAMA-unconjugated) appears to be a mixture of 3'-modified and 3'-unmodified molecules. TGap15C-3'-NH₂ is a 3'-modified and 5'-acridine-conjugated oligonucleotide composed of G and T nucleotides and designed to bind the target duplex in an antiparallel orientation. TGap15C-3'-NH₂ is an oligonucleotide similar to TGap15C-3'-NH₂ except that it is designed to bind in the parallel orientation. TGTap15C-3'-NH₂ is an oligonucleotide identical to TGap15C-3'-NH₂ except for a single G → T transversion within the sequence. (B) Structural formula for the conjugated oligos containing a 3-amino-2-hydroxypropyl group at the 3' end. (C) Relative migration of individual species on an acrylamide gel: (lane 1) AG15; (lane 2) purified AG15C-3'-NH₂; (lane 3) purified AG15C (no 3-amino-2-hydroxypropyl phosphate); (lane 4) mixture obtained after synthesis and HPLC purification (referred to as AG15C mix elsewhere in the text). Note that the acridine derivatives produce bright fluorescent bands, whereas AG15-3'-NH₂ gives a dark band upon UV shadowing. One hundred picomoles of DNA is present in each lane.

oriev et al., 1992; Orson et al., 1991). In this paper we have characterized oligonucleotides conjugated to an acridine (DAMA) derivative by DMS footprinting. We found that acridine conjugation enhances binding of an oligonucleotide composed of G and A residues about 500-fold while maintaining a high degree of binding specificity. An acridine-conjugated oligonucleotide composed of G and T nucleotides, on the other hand, bound to the target sequence less efficiently.

EXPERIMENTAL PROCEDURES

Synthesis and Purification of Oligonucleotides.

Oligonucleotides listed in Figure 1 were synthesized and HPLC purified as described previously (Orson et al., 1996a). We further separated AG15C-3'-NH₂ (upper band migrating more slowly) from the more rapidly migrating AG15C (no 3-amino-2-hydroxypropyl phosphate) (Figure 1C) in a preparative denaturing acrylamide gel. Denaturing acrylamide gel separation was also used to purify TGap15C-3'-NH₂, TGpl15C-3'-NH₂, and TGTap15C-3'-NH₂. Target duplexes were made by

annealing equimolar amounts of complementary strands under conditions described before (Orson et al., 1996a). The duplexes were further purified by hydroxyapatite chromatography to separate any residual single-stranded oligonucleotide.

Mass Spectrometry. The matrix-assisted laser desorption/ionization time of flight mass spectrometry of the upper (AG15C-3'-NH₂) and lower (AG15C) bands were performed at The Midland Certified Reagent Co.

Plasmids. pIL-2₅ was obtained by cloning the IL duplex (Figure 1A) into a *Hinc*II site of the pUC19 vector. pIL-2₃ was the same as pIL-2₅ except for point transversion within the oligopurine tract (Figure 1A). Plasmids were purified by CsCl/ethidium bromide banding. The inserts were verified by Maxam and Gilbert sequencing (Maxam and Gilbert, 1980) and used for footprinting experiments.

Conditions for Triple-Helix Formation. Unless indicated otherwise, the specified amounts of third-strand and duplex DNA were mixed together in a volume of 10 mL containing 10 mM MgCl₂ and either 10 mM Tris

buffer, pH 7.4. or 80 mM Tris-borate buffer, pH 8.2. The third-strand bindings were equivalent in either buffer.

Band Shift Assay. Separation of triplex from duplex DNA and unbound oligonucleotide was performed on 12–16% acrylamide gels run in 100 mM TES/50 mM Tris buffer, pH 7.4, containing 10 mM MgCl₂ as described previously (Orson et al., 1994). K_d values were determined under conditions in which 50% of the oligonucleotide was bound to its target according to the equation $K_d = (OD)/T$, where O is the concentration of the oligo, D is the concentration of the duplex, and T is the concentration of the triplex.

DMS Footprinting. The *HindIII*–*SstI* restriction fragment from pIL-2₅ or pIL-2₃ containing the target sequence was labeled using [³²P]dATPαP and Klenow polymerase and then mixed with the third strand (concentration as indicated) in triplex binding buffer (80 mM Tris-borate, pH 8.2, 10 mM MgCl₂). Unless stated otherwise, samples were equilibrated overnight at room temperature and DMS was added to a final concentration of 0.5%. The reaction was stopped after 3.5 min at room temperature by adding 1 μL of 5 M 2-mercaptoethanol. The DNA was precipitated with 4 volumes of ethanol, treated with 1 M piperidine at 90 °C for 30 min, vacuum dried, dissolved in formamide, and loaded on the sequencing gel.

Photocleavage Reaction. The ³²P-labeled *HindIII*–*SstI* restriction fragment from pIL-2₅ (0.1 nM) containing the IL target sequence (Figure 1A) was mixed with AG15-3'-NH₂ (100 nM) or AG15C (100 nM) in triplex binding buffer and preincubated overnight at room temperature. Samples (10 μL) contained in 0.5 mL Eppendorf tubes were exposed to sunlight for the indicated period of time. The illuminated samples were either precipitated with ethanol, cleaved with hot piperidine, vacuum dried, dissolved in formamide, and loaded on a sequencing gel or denatured for 5 min at 90 °C, treated with 0.5% DMS for 3.5 min at room temperature, cleaved with piperidine, and subjected to sequencing gel electrophoresis.

Quantitation of the Gels. Autoradiograms were traced and quantitated using video densitometry [IMAGE for Macintosh (Wayne Rasband, NCI Bethesda, MD)]. In calculations of the K_d values derived from footprinting experiments, the individual lanes were standardized by dividing the intensities of the protected bands within the oligopurine tract over the intensities of three unprotected bands and plotted as a function of the concentration of the third strand.

RESULTS

Figure 1A lists the oligonucleotides and cloned fragments employed in these studies. AG15C-3'-NH₂ and AG15C are synthetic oligonucleotides designed to bind antiparallel relative to the purine strand of the IL-2Rα target duplex by forming G:G·A and A:A·T triads (Klysik et al., 1991; Kohwi and Kohwi-Shigematsu, 1988). AG15C-3'-NH₂ has a 3-amino-2-hydroxypropyl group attached at the 3'-phosphate terminus as a protection against cellular nucleases for future *in vivo* applications. The full formula is shown in Figure 1B. In the course of the NaOH deprotection of AG15C-3'-NH₂, some of the 3'-amino groups are eliminated (Vu et al., 1995), leading to the appearance of two electrophoretically distinct products (Figure 1C, lane 4). As determined by mass spectrometry, the upper band (referred to as AG15C-3'-NH₂, Figure 1A) is the expected 3'-amino derivative, whereas the lower band lacks the 3-amino-2-hydroxypropyl phosphate group. Since this 3'-amino-modifier product (Glen Research, Sterling, VA) is frequently used as a protecting group against cellular degradation of oligos

(McShan et al., 1992; Orson et al., 1991; Zendegeui et al., 1992), it was of interest to assess the binding properties of both forms of the oligonucleotide to the target IL-2Rα sequence relative to that of the unconjugated AG15-3'-NH₂ counterpart.

The Binding of AG15C-3'-NH₂ Oligonucleotide Is Enhanced 500-fold When the Acridine (DAMA) Is Attached to Its 5' End. Our prior band shift determinations performed using a nonseparated mixture of AG15C and AG15C-3'-NH₂ (AG15C-mix) resulted in a K_d of 5 nM (Orson et al., 1996a). Band shift analysis is an inexpensive, fast, and simple way to characterize the triplex binding properties of synthetic oligonucleotides, and for this reason it has been used routinely in such determinations. However, since the individual components of the mixture separate during gel electrophoresis, the results of this assay may not reflect the equilibrium state of the system. We therefore performed footprinting analyses using dimethyl sulfate (DMS) (Hanvey et al., 1988; Klysik, 1992, 1995). DMS, which alkylates the N-7 of G residues in B DNA, is a chemical widely used for assessing DNA structure. It is especially suitable for assaying triplex DNA because when the N-7 atom is involved in Hoogsteen hydrogen bond formation, the G of the duplex is relatively protected against this chemical.

Figure 2A shows the results of the footprinting analysis performed at 37 °C with AG15C-3'-NH₂ and with AG15-3'-NH₂, which does not carry the DAMA function at the 5' end. Almost 70% diminution in the intensities of the bands corresponding to the G residues of the target oligopurine segment can be detected at 10 nM concentration of AG15C-3'-NH₂. The protection of the oligopurine segment of the duplex increases further as the oligonucleotide concentration increases. Quantitation of the data presented in Figure 2A revealed that 50% protection of the oligopurine tract (K_d) occurs at a 5 nM concentration of AG15C-3'-NH₂ under the conditions applied in this experiment. However, for acridine-free AG15-3'-NH₂ oligonucleotide (Figure 2A) the K_d was found to be 500-fold higher (2.5 μM). Figure 2B compares the binding properties of AG15C-3'-NH₂ and AG15C as determined by footprinting analysis performed at 37 °C. No difference was found between the two forms of these DAMA-conjugated oligos.

In summary, the footprinting analysis presented above indicates that the attachment of the DAMA acridine to the 5' end of the AG15-3'-NH₂ (to produce AG15C-3'-NH₂) significantly enhances its binding to the target sequence by reducing its K_d value from 2.5 μM to 5 nM.

Acridine (DAMA) Attached to the 5' End of the Oligonucleotide Does Not Substantially Compromise Specificity of Binding. Intercalation of an acridine between the planar bases of the double helix is not sequence specific. Thus, it was of interest to determine whether attachment of DAMA to the 5' end of a triplex forming oligonucleotide would compromise the specificity of triplex formation. For the purpose of these investigations we synthesized and cloned an oligopurine target identical to that found in IL-2Rα promoter except that it contained a single point G → T transversion (see pIL-2₃ in Figure 1A). The *HindIII*–*SstI* restriction fragment containing this mutated sequence was used in footprinting experiments with AG15C-3'-NH₂ serving as a third strand. Figure 3B shows the effect of increasing concentrations of AG15C-3'-NH₂ on the DMS reactivity of G residues in the mutated target duplex. No protection could be detected even at the highest concentration of AG15C-3'-NH₂ employed (10 μM). Thus, a single transversion in the target duplex is capable of affecting substantially the specific binding of the third strand.

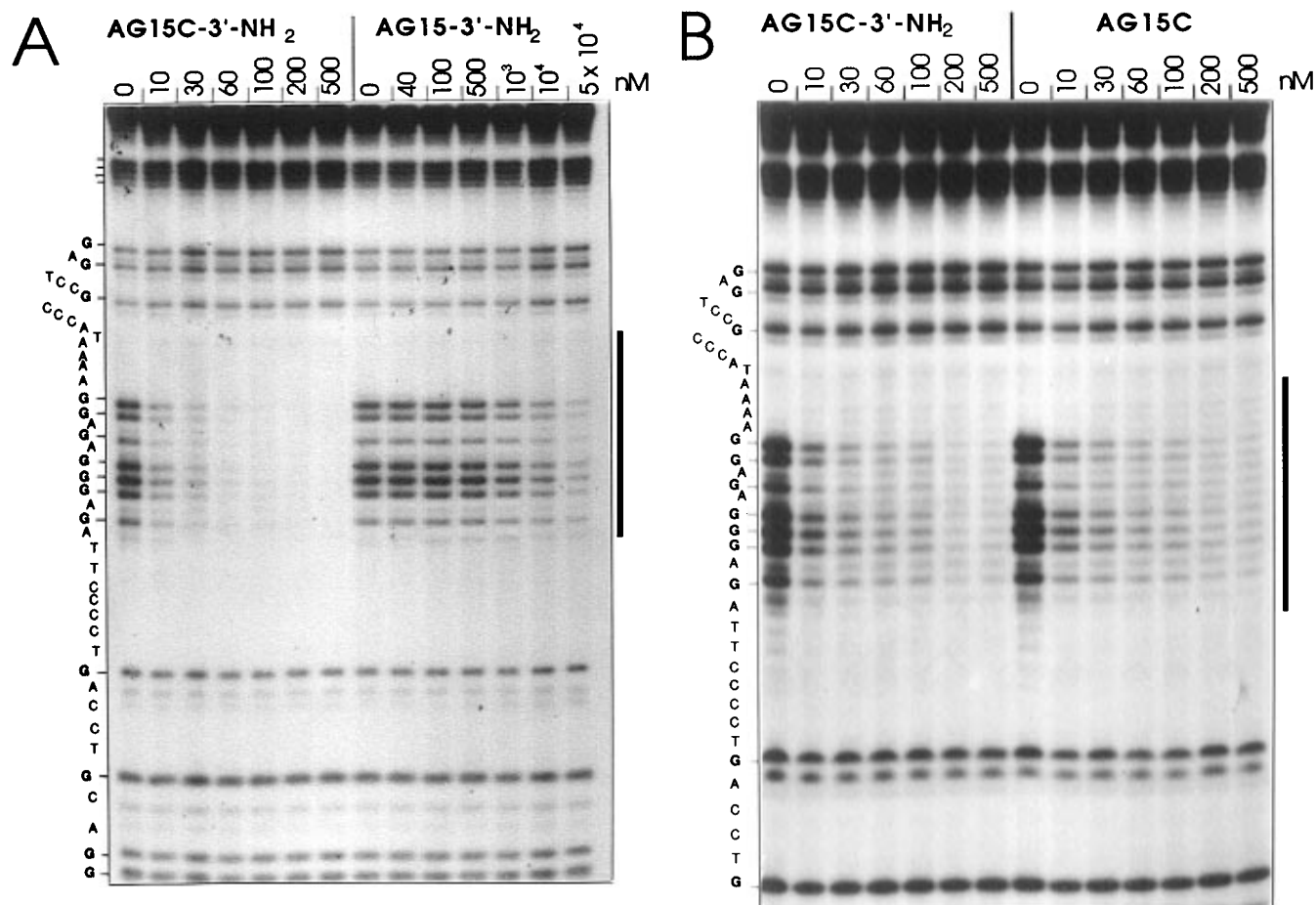


Figure 2. DMS footprinting. (A) DMS footprinting of the IL-2R α target duplex sequence cloned within the pIL-2₅ plasmid as a function of third strand concentration. The *Hind*III–*Sst*I restriction fragment from pIL-2₅ was labeled at the 3' end of the purine strand and used as a duplex target (<0.1 nM) to preform the triplex in a buffer containing 10 mM MgCl₂. Samples were equilibrated at 37 °C for 4 days. Treatment with DMS (see Experimental Procedures) was also done at 37 °C. The bar indicates the oligopurine target sequence. Concentration of the oligonucleotide is shown above each lane. Quantitation of the autoradiograms was as described under Experimental Procedures. (B) Footprinting of AG15C-3'-NH₂ and AG15C with DMS. Other details are as in panel A.

Some mutations in the target duplex seem to be more effective in preventing triplex formation than others. Using the band shift assay technique, we have determined K_d values for the mixture of AG15C-3'-NH₂ and AG15C and numerous duplexes carrying mutations in the targeted sequence (Table 1). The mutated duplexes fall into two categories: (i) those with mutations in the block of three G's located closer to the 3' end of the oligopurine strand of the duplex and 4–6 bp away from the intercalation site of the acridine attached to the third strand and (ii) those with mutations in the block of two G's located closer to the 5' end of the oligopurine strand and distal to the intercalation site of the acridine. In general, mutations within the block of three G residues were more effective in preventing triplex DNA formation. As expected, double mutations destabilized triplex DNA more profoundly than single-point mutations. Greater than 500-fold decreases in binding avidity have been observed in all cases except for the G \rightarrow T transversion (50-fold decrease) and G \rightarrow A transition (100-fold decrease) within the block of two G's (see Table 1, duplexes 2 and 4).

Taken all together, these results strongly indicate that the sequence-dependent recognition of the target sequence is not significantly compromised by the attachment of DAMA to the 5' end of the third-strand oligonucleotide.

Potassium Ions Have an Effect on the Binding of AG15C-3'-NH₂. Figure 3A shows the DMS footprinting experiment performed with AG15C-3'-NH₂ as a function of increasing concentration of KCl present in the stan-

dard triplex binding reaction. At a concentration of 10 mM and lower, KCl does not seem to have any significant effect on the binding properties of the DAMA-conjugated oligonucleotide. However, 55% inhibition of protection of the target duplex against DMS was observed at 100 mM KCl (Figure 3A, cf. lanes 1, 2, and 7). As the concentration of KCl increased to 200 mM, only 16% of the target duplex protection remained, compared to the sample containing no KCl (cf. lanes 1, 2, and 8). Thus, similar to unconjugated oligos composed of G and A residues, DAMA-conjugated oligonucleotide AG15C-3'-NH₂ is sensitive to physiological concentrations of potassium cations. However, the potassium-mediated inhibition seems to be less pronounced compared with similar studies in which nonconjugated oligonucleotides were used (Cheng and Van Dyke, 1993; Olivas and Maher, 1995).

DAMA-Sensitized Photooxidation Reaction Demonstrates Antiparallel Orientation of AG15C-3'-NH₂ Relative to the Oligopurine Strand of the Target Duplex. Upon light illumination, DNA can undergo a process of photooxidation in the presence of a sensitizing dye (Pooler and Valenzano, 1981). In general, double-substituted purines (i.e. G residues) are more sensitive than other bases, but any base can be dye-sensitized and photooxidized (Rahn and Patrick, 1976). DAMA attached to the 5' end of AG15-3'-NH₂ can be regarded as a sensitizing dye which may promote photoreactivity of the bases at the site of intercalation. Thus, when triplex DNA is preformed using AG15C-3'-NH₂ and exposed to

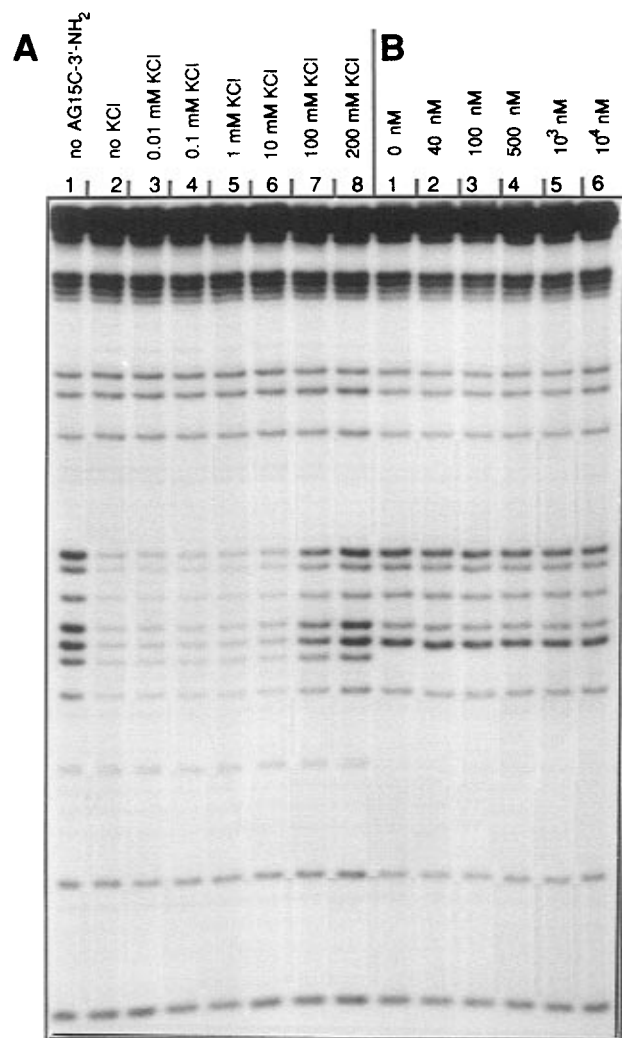


Figure 3. Effect of KCl concentration and of point mutation of the target duplex on binding of AG15C-3'-NH₂. (A) Labeled *Hind*III-*Sst*I restriction fragment (<0.1 nM) was mixed with AG15C-3'-NH₂ (100 nM) and equilibrated overnight in the triplex binding buffer (containing 10 mM Mg²⁺) supplemented with increasing concentration of KCl as indicated above each lane. DMS footprinting was performed as described under Experimental Procedures. (B) The *Hind*III-*Sst*I restriction fragment from pIL-2₃ was labeled at the 3' end of the purine strand and used for preforming the triplex DNA with AG15C-3'-NH₂ (concentrations as indicated). Conditions of the experiment and DMS treatment were as described in the legend to Figure 2.

light, specific degradation of the target duplex could be expected 3' to the oligopurine block of the oligopurine duplex strand, if the orientation of the third strand is antiparallel relative to the oligopurine strand of the target duplex.

Table 1. Band Shift Dissociation Constants of AG15C-3'-NH₂ and AG15C Mixture at 25 °C for Targets Containing Mutations

		binding strand of the target duplex																					K_d (nM)	
1	3'	—	—	—	A	G	A	G	G	G	A	G	A	G	G	A	A	A	A	—	—	—	5'	5
2	3'	—	—	—	A	G	A	G	G	G	A	G	A	G	T	A	A	A	A	—	—	—	5'	240
3	3'	—	—	—	A	G	A	G	G	G	A	G	A	G	C	A	A	A	A	—	—	—	5'	2500
4	3'	—	—	—	A	G	A	G	G	G	A	G	A	G	A	A	A	A	A	—	—	—	5'	500
5	3'	—	—	—	A	G	A	G	G	G	A	G	A	G	T	T	A	A	A	—	—	—	5'	10000
6	3'	—	—	—	A	G	A	G	G	G	A	G	A	G	C	C	A	A	A	—	—	—	5'	5000
7	3'	—	—	—	A	G	A	G	G	T	A	G	A	G	G	G	A	A	A	—	—	—	5'	3000
8	3'	—	—	—	A	G	A	G	G	C	A	G	A	G	G	G	A	A	A	—	—	—	5'	11000
9	3'	—	—	—	A	G	A	G	G	A	A	G	A	G	G	G	A	A	A	—	—	—	5'	18000
10	3'	—	—	—	A	G	A	G	G	T	T	G	A	G	G	G	A	A	A	—	—	—	5'	> 50000
11	3'	—	—	—	A	G	A	G	G	C	C	G	A	G	G	G	A	A	A	—	—	—	5'	> 50000
12	3'	—	—	—	A	G	A	T	G	G	A	G	A	G	G	G	A	A	A	—	—	—	5'	> 20000

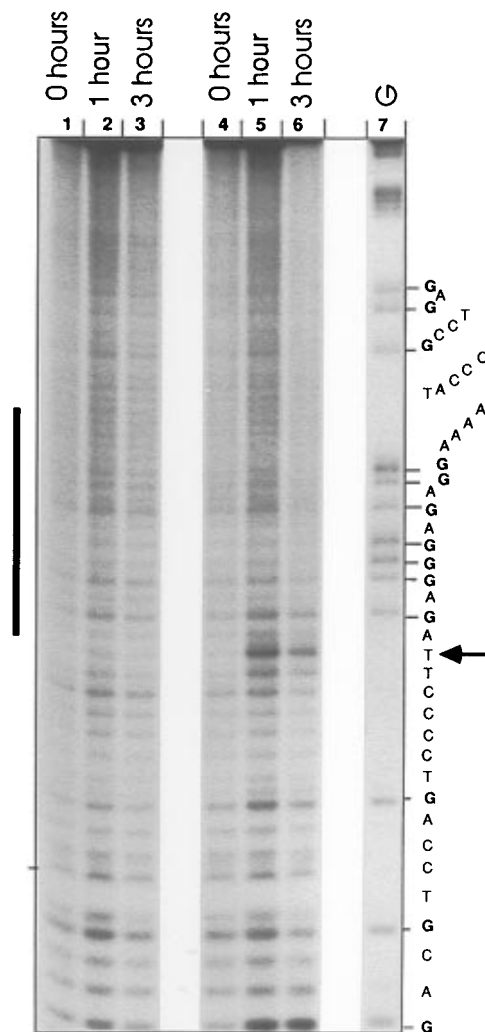


Figure 4. Acridine-sensitized triplex-mediated cleavage of the target duplex. The labeled *Hind*III-*Sst*I insert of pIL-2₅ (concentration < 0.1 nM) was mixed with 100 nM AG15C-3'-NH₂ (lanes 1-3) or 100 nM AG15C-3'-NH₂ (lanes 4-6) in triplex binding buffer. After overnight equilibration at room temperature, samples were exposed for the indicated period of time to sunlight in 0.5 mL Eppendorf tubes. The DNA was precipitated, treated with 1 M hot piperidine for 30 min, vacuum dried, dissolved in formamide, and resolved on a sequencing gel. G refers to the Maxam and Gilbert sequencing reaction (Maxam and Gilbert, 1980). An arrow indicates the DAMA-sensitized photocleavage band.

Figure 4 presents the results of such an analysis. When the mixture of AG15C-3'-NH₂ (no acridine) and the labeled restriction fragment containing the target oligopurine block was illuminated with sunlight for 0, 1, and 3 h (Figure 4A, lanes 1-3, respectively), followed by treatment with hot piperidine and resolution of the

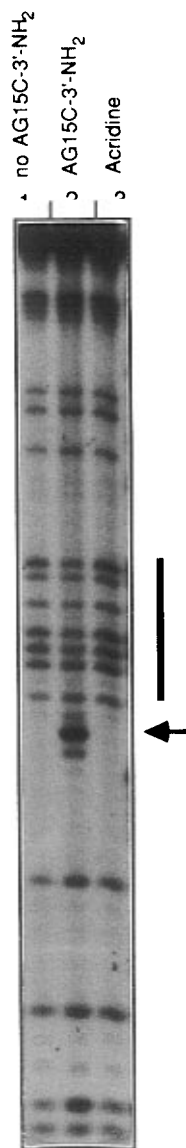


Figure 5. Acridine-sensitized triplex-mediated cleavage of the target duplex. The experiment was performed as described in the legend to Figure 4 except that the samples after illumination with the sunlight (45 min) were heated for 5 min at 90 °C, modified with 0.5% DMS for 3.5 min, and then subjected to piperidine cleavage. The sample shown in lane 1 contained no AG15C-3'-NH₂. The sample in lane 2 contained 100 nM AG15C-3'-NH₂, whereas the sample in lane 3 contained 100 nM unconjugated DAMA acridine.

products on the sequencing gel, a background degradation pattern developed. For the triplex preformed with AG15C-3'-NH₂ (lanes 4–6) a similar illumination-induced background degradation could be observed. However, a strongly enhanced band can be seen after 1 or 3 h of illumination (lanes 5 and 6) that is not present in the background pattern of the nonilluminated sample (lane 4) or in the samples containing AG15-3'-NH₂ (lanes 1–3).

An even more pronounced site specific DAMA-sensitized photocleavage effect was obtained when the illuminated DNA was denatured and treated with DMS prior to the piperidine cleavage step (Figure 5). The sample with AG15C-3'-NH₂ omitted (lane 1) resulted in the expected pattern of bands indicating degradation of the sequence at G residues. When the third strand was present (lane 2), a strong band corresponding to a T residue at the 3' flank of the oligopurine block becomes visible in addition to the regular pattern resulting from cleavages at methylated G residues. This band is triplex

specific since no selectively enhanced degradation can be obtained with intercalator alone (lane 3).

The appearance of this band (see arrows in Figures 4 and 5) indicates an acridine-induced and triplex-mediated site specific photoreactivity. The most reactive base is a T residue adjacent to the 3' end of the oligopurine sequence. Since the DAMA group is attached to the 5' end of the oligo, the AG15C-3'-NH₂ must be oriented antiparallel relative to the purine strand of the target duplex.

An Acridine-Conjugated Oligonucleotide Containing Exclusively T and G Nucleotides Binds 17 Times Less Efficiently than a Conjugated Oligonucleotide Composed of G and A Residues. When designing an oligonucleotide for binding to the specific oligopurine duplex target at neutral pH, it is widely accepted that a G residue in the third strand binds well to the GC Watson–Crick base pair of the target duplex, forming a G:GC triad (Dervan, 1989; Hélène, 1991; Kohwi and Kohwi-Shigematsu, 1988). However, for the AT base pair of the duplex, a stable triad can form by an interaction with either a T residue (T:AT) or an A residue (A:AT) (Beal and Dervan, 1991; Klysik et al., 1991; Orson et al., 1996a; Zendegui et al., 1992). Since third-strand oligonucleotides can be composed exclusively of G's and A's or G's and T's (Beal and Dervan, 1991; Jayasena and Johnston, 1992; Orson et al., 1996a; Young et al., 1991), it was of interest to compare the binding avidity of acridine-conjugated oligonucleotides based on these two motifs. We have synthesized and purified an oligonucleotide TGap15C-3'-NH₂ that is identical to AG15C-3'-NH₂ except that all A residues were replaced with T residues (see Figure 1). It should bind antiparallel to the purine strand of the Watson–Crick IL-2R α target duplex. Figure 6, lanes 1–7, shows an example of DMS footprinting performed as a function of increasing concentration of TGap15C-3'-NH₂ using the *Hind*III–*Sst*I restriction fragment of pIL-2₅. As the concentration of TGap15C-3'-NH₂ increased, the oligopurine block became increasingly protected against DMS modification. Quantitation of the data revealed that 50% inhibition of the DMS reactivity of G residues in the oligopurine block of the duplex (K_d) took place at 88 nM TGap15C-3'-NH₂ (an average of three independent experiments). Thus, the dissociation constant of TGap15C-3'-NH₂ was 17 times higher than that of the AG15C-3'-NH₂ (K_d = 5 nM).

Figure 6, lanes 8–14, shows the footprinting analysis of the TGap15C-3'-NH₂ composed of G and T nucleotides and designed to bind parallel to the IL-2R α target duplex. No binding could be detected within the concentration range tested. We also assessed the binding properties of TGTap15C-3'-NH₂, the sequence of which is identical to that of TGap15C-3'-NH₂ except for having one G \rightarrow T transversion (see Figure 1). The T:GC mismatch severely affected binding, and the DMS methylation reaction was not inhibited even at a concentration of 10 μ M (data not shown).

DISCUSSION

In this paper we have assessed the effect of acridine conjugation on the binding avidity and specificity of the 15 base oligonucleotide targeting the IL-2R α binding site. We found that attachment of DAMA to the 5' end of AG15-3'-NH₂ profoundly lowers the K_d . This has been determined by band shift assay (Orson et al., 1996a) and footprinting analysis, with the two methods providing comparable results. A 500-fold decrease in the K_d value is of particular significance since the targeted site is short, and concentrations in the low nanomolar range may be required for effective future applications *in vivo*.

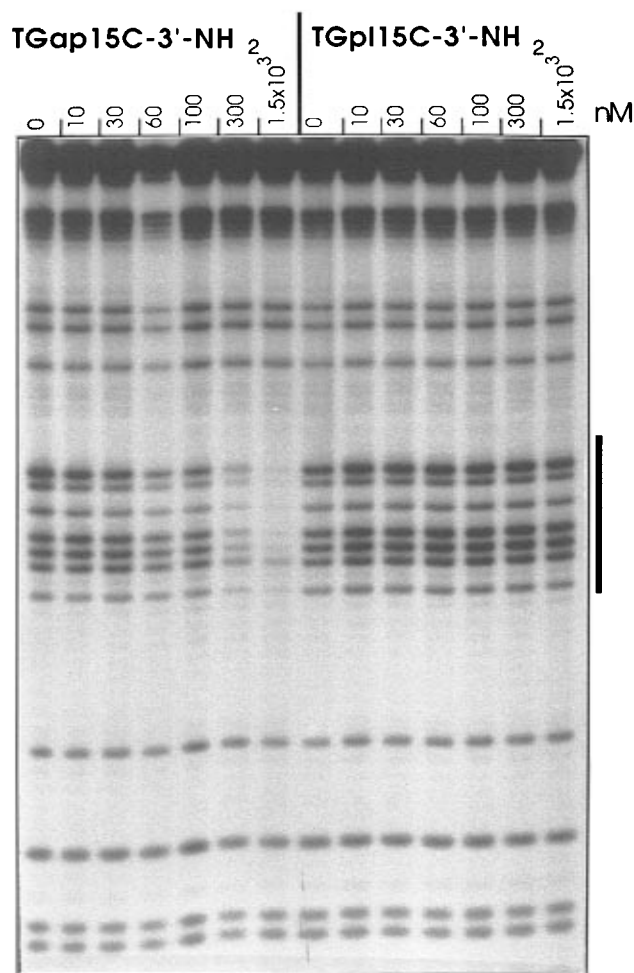


Figure 6. Example of DMS footprinting of the IL-2R α target duplex sequence cloned within the pIL-2 β plasmid as a function of TGap15C-3'-NH $_2$ or TGpl15C-3'-NH $_2$ concentration. The concentration of the oligonucleotide is shown above each lane. Quantitation of the autoradiograms was as described under Experimental Procedures. For other details see legend to Figure 2A.

An enhancement of binding achieved by the attachment of a different acridine to the 5' end of an oligo has been reported before (Grigoriev et al., 1992, 1993; Sun et al., 1989). However, our data provide a quantitative description of the equilibrium binding enhancement induced by acridine attachment to a third strand composed exclusively of purine bases. It is important to remember that the 500-fold lower K_d seen in the course of this work could be achieved only after prior optimization of the linker structure used to attach the DAMA portion to the synthetic oligonucleotide (Orson et al., 1994).

The 3'-amino group was included in the DAMA-conjugated oligonucleotides to protect them from exonucleolytic degradation in future *in vivo* experiments (McShan et al., 1992; Orson et al., 1991). However, preparation of the oligo resulted in a mixture of the 3'-amino protected and unprotected forms (Vu et al., 1995). The two species were separated on a gel (Figure 1C) and their identities confirmed by mass spectral analysis. They were then characterized with respect to their triplex forming capacity. We found that both AG15C-3'-NH $_2$ and AG15C had the same affinity toward the target duplex sequence (Figure 2B). Furthermore, the acridine-conjugated oligonucleotides composed of G's and A's (AG15C-3'-NH $_2$ and AG15C) appeared to have superior binding avidity compared to an oligonucleotide composed of G's and T's (TGap15C-3'-NH $_2$).

As expected, binding of the third strand was affected by mutations in the target duplex. The degree to which the triplex became destabilized depended on the nature of the mutation (Greenberg and Dervan, 1995) as well as on the location of the mutation (Cheng and van Dyke, 1994) within the targeted sequence (Table 1). The smallest effects were observed for the G \rightarrow T transversion and G \rightarrow A transition located in the block of two G's. This is consistent with prior work demonstrating a relatively lower triplex destabilization effect for G \cdot TA and G \cdot AT triads (Fossella et al., 1993; Yoon et al., 1992). Mutations in the block of three G residues affected binding capacity of the duplex more than the mutations in the block of two G's. Although the reason for this is not entirely clear, it is most likely related to (i) the local nucleotide composition surrounding the mutated site, (ii) the distance of the mutation from the acridine intercalation site, or (iii) a combination of these two factors.

It was unexpected to find that the DAMA-sensitized photoreactivity is primarily limited to the single base immediately adjacent to the oligopurine tract. This may reflect a precise and unique intercalation point stereochemically compatible with the triplex state and the linker structure. Alternatively, the structure of the triplex/B-DNA junction located immediately adjacent to the oligopurine block may offer a greatly preferred site for intercalation of this acridine as suggested by others (Collier et al., 1991).

The interaction of AG15C-3'-NH $_2$ or AG15C with the duplex target remained similar with respect to all of the basic properties characteristic of unfunctionalized oligos composed of purine bases: (i) Mg $^{2+}$ ions were required in the binding buffer (McShan et al., 1992) at a concentration of ≥ 5 mM; (ii) binding was affected, but not abolished, by KCl at concentrations of 100–200 mM; however, the KCl-mediated triplex inhibition was less pronounced than the inhibition reported for similar but nonconjugated oligonucleotides (Cheng and Van Dyke, 1993; Olivas and Maher, 1995); (iii) the specificity of binding of the acridine-derivatized oligo to the target sequence remained very high, such that specific mutations in the 15 bp long target sequence either essentially abolished binding (Figure 3B) or significantly reduced it (Table 1) depending on the position and nature of the mutation; (iv) the orientation of the acridine-conjugated oligo remained antiparallel relative to the oligopurine strand of the target duplex as determined by an acridine-sensitized photodynamic oxidation reaction (Birg et al., 1990) (Figure 4), even though in theory the sequence could allow parallel binding via the first 9 bases adjacent to the acridine (the methodology used herein may be of general applicability in cases of other dye-conjugated oligonucleotides); (v) the kinetics of triplex formation was slow (Maher et al., 1990), so that no binding of AG15C-3'-NH $_2$ to the oligopurine target could be detected after 1 h of preforming the triplex at 22 $^{\circ}$ C, but the reaction was virtually complete by 24 h (data not shown).

Potential applications of synthetic oligonucleotides in the regulation of gene expression are widely recognized (Dervan, 1990; Hélène and Toulme, 1990), and such oligos may be utilized both for basic science and for medicine. There are several examples where the regulation of gene expression achieved by oligonucleotide treatment of cells in culture is well established (McShan et al., 1992; Roy, 1993). The work presented herein encourages and justifies further studies of AG15C-3'-NH $_2$ type molecules as potential regulators of IL-2R α expression. In more general terms, conjugation of DAMA to synthetic oligonucleotides may be particularly advantageous in the case of many other genes where the target oligopurine

sequence is relatively short and binding enhancement needs to be introduced via oligonucleotide modification.

ACKNOWLEDGMENT

Supported by the Department of Veterans Affairs, NIH AI28071, and NIH NS32583. We are grateful to R. Griffey (ISIS Pharmaceutical), Xiaolian Gao (University of Houston), and Chau-Wen Chou (Arizona State University) for help in interpretation of mass spectrometry data.

LITERATURE CITED

- Beal, P. A., and Dervan, P. B. (1991) Second structural motif for recognition of DNA by oligonucleotide-directed triple helix formation. *Science* 251, 1360–1363.
- Birg, F., Praseuth, D., Zerial, A., Thuong, N. T., Asseline, U., Doan, T. L., and Hélène, C. (1990) Inhibition of simian virus 40 DNA replication in CV-1 cells by an oligodeoxynucleotide covalently linked to an intercalating agent. *Nucleic Acids Res.* 18, 2901–2908.
- Cheng, A.-J., and van Dyke, M. W. (1993) Monovalent cation effects on intermolecular purine-purine-pyrimidine triple-helix formation. *Nucleic Acids Res.* 21, 5630–5635.
- Cheng, A.-J., and van Dyke, M. W. (1994) Oligodeoxyribonucleotide length and sequence effects on intermolecular purine-purine-pyrimidine triple-helix formation. *Nucleic Acids Res.* 22, 4742–4747.
- Cheng, Y.-K., and Pettitt, B. M. (1992) Stabilities of double- and triple-stranded helical nucleic acids. *Prog. Biophys. Mol. Biol.* 58, 225–257.
- Collier, D. A., Mergny, J. L., Thuong, N. T., and Hélène, C. (1991) Site-specific intercalation at the triplex-duplex junction induces a conformational change which is detectable by hypersensitivity to diethylpyrocarbonate. *Nucleic Acids Res.* 19, 4219–4224.
- Dervan, P. B. (1989) Oligonucleotide recognition of double-helical DNA by triple-helix formation. In *Oligodeoxynucleotides: Antisense Inhibitors of Gene Expression* (J. S. Cohen, Ed.) pp 197–210, CRC Press, Boca Raton, FL.
- Dervan, P. B. (1990) Chemical methods for the site-specific cleavage of genome DNA. In *Structure and Methods, Vol. 1: Human Genome Initiative and DNA Recombination* (R. H. Sarma and M. H. Sarma, Eds.) Adenine Press, Schenectady, NY.
- Diamantstein, T., and Osawa, H. (1986) The interleukin-2 receptor, its physiology and a new approach to a selective immunosuppressive therapy by anti-interleukin-2 receptor. *Immunol. Rev.* 92, 5–27.
- Fossella, J. A., Kim, Y. J., Shih, H., Richards, E. G., and Fresco, J. R. (1993) Relative specificities in binding of Watson-Crick base pairs by third strand residues in a DNA pyrimidine triplex motif. *Nucleic Acids Res.* 21, 4511–4515.
- Giovannangeli, C., Thuong, N. T., and Hélène, C. (1992) Oligodeoxynucleotide-directed photo-induced cross-linking of HIV proviral DNA via triple-helix formation. *Nucleic Acids Res.* 20, 4275–4281.
- Greenberg, W. A., and Dervan, P. B. (1995) Energetics of formation of sixteen triple helical complexes which vary at a single position within a purine motif. *J. Am. Chem. Soc.* 117, 5016–5022.
- Grigoriev, M., Praseuth, D., Robin, P., Hemar, A., Saison-Behmoaras, T., Dautry-Varsat, A., Thuong, N. T., Hélène, C. T., and Harel-Bellan, A. (1992) A triple helix-forming oligonucleotide-intercalator conjugate acts as a transcriptional repressor via inhibition of NFkB binding to interleukin-2 receptor alpha-regulatory sequence. *J. Biol. Chem.* 267, 3389–3395.
- Grigoriev, M., Praseuth, D., Guieysse, A. L., Robin, P., Thuong, N. T., Hélène, C., and Harel-Bellan, A. (1993) Inhibition of gene expression by triple helix-directed DNA cross-linking at specific sites. *Proc. Natl. Acad. Sci. U.S.A.* 90, 3501–3505.
- Hanvey, J. C., Klysik, J., and Wells, R. D. (1988) Influence of DNA sequence on the formation of non-B right-handed helices in oligopurine-oligopyrimidine inserts in plasmids. *J. Biol. Chem.* 263, 7386–7396.
- Hélène, C. (1991) Rational design of sequence-specific oncogene inhibitors based on antisense and antigene oligonucleotides. *Eur. J. Cancer* 27, 1466–1471.
- Hélène, C., and Toulmé, J.-J. (1989) Control of gene expression by oligodeoxynucleotides covalently linked to intercalating agents and nucleic acid-cleaving reagents. In *Oligodeoxynucleotides: Antisense Inhibitors of Gene Expression* (J. S. Cohen, Ed.) pp 137–172, CRC Press, Boca Raton, FL.
- Hélène, C., and Toulmé, J.-J. (1990) Specific regulation of gene expression by antisense, sense and antigene nucleic acids. *Biochim. Biophys. Acta* 1049, 99–125.
- Htun, H., and Dahlberg, J. E. (1988) Single strands, triple strands, and kinks in H-DNA. *Science* 241, 1791–1796.
- Ito, T., Smith, C. L., and Cantor, C. R. (1992) Sequence-specific DNA purification by triplex affinity capture. *Proc. Natl. Acad. Sci. U.S.A.* 89, 495–498.
- Jayasena, S. D., and Johnston, B. H. (1992) Intramolecular triple-helix formation at (PuPy)·(Pu-Py) tracts: recognition of alternate Sstrands via Pu-PuPy and Py-PuPy base triplets. *Biochemistry* 31, 320–327.
- Klysik, J. (1992) Cruciform extrusion facilitates intramolecular triplex formation between distal oligopurine:oligopyrimidine tracts. Long range effects. *J. Biol. Chem.* 267, 17430–17437.
- Klysik, J. (1995) An intramolecular triplex structure from non-mirror repeated sequence containing both PyPuPy and Pu-PuPy triads. *J. Mol. Biol.* 245, 499–507.
- Klysik, J., Rippe, K., and Jovin, T. M. (1991) Parallel-stranded DNA under topological stress: rearrangement of (dA)₁₅·(dT)₁₅ to a d(A·A·T)_n triplex. *Nucleic Acids Res.* 19, 7145–7154.
- Kohwi, Y., and Kohwi-Shigematsu, T. (1988) Magnesium ion-dependent triple-helix structure formed by homopurine-homopyrimidine sequences in supercoiled plasmid DNA. *Proc. Natl. Acad. Sci. U.S.A.* 85, 3781–3785.
- Leonard, W. J., Depper, J. M., Kanehisa, M., Kronke, M., Pfeffer, N. J., Svetlik, P. B., Sullivan, M., and Greene, W. C. (1985) Structure of the human interleukin-2 receptor gene. *Science* 230, 633–639.
- Lyamichev, V. I., Mirkin, S. M., and Frank-Kamenetskii, M. D. (1986) Structures of homopurine-homopyrimidine tract in supercoiled DNA. *J. Biomol. Struct. Dyn.* 3, 667–669.
- Maier, L. J., Dervan, P. B., and Wold, B. J. (1990) Kinetic analysis of oligodeoxyribonucleotide-directed triple-helix formation on DNA. *Biochemistry* 29, 8820–8826.
- Maxam, A. M., and Gilbert, W. (1980) Sequencing end-labeled DNA with base-specific chemical cleavages. *Methods Enzymol.* 65, 499–560.
- McShan, W. M., Rossen, R. D., Laughter, A. H., Trial, J., Kessler, D. J., Zendegui, J. G., Hogan, M. E., and Orson, F. M. (1992) Inhibition of transcription of HIV-1 in infected human cells by oligodeoxynucleotides designed to form DNA triple helices. *J. Biol. Chem.* 267, 5712–5721.
- Moser, H. E., and Dervan, P. B. (1987) Sequence-specific cleavage of double helical DNA by triple helix formation. *Science* 238, 645–650.
- Olivas, W. M., and Maher III, L. J. (1995) Overcoming potassium-mediated triplex inhibition. *Nucleic Acids Res.* 23, 1936–1941.
- Orson, F. M., Thomas, D. W., McShan, W. M., Kessler, D. J., and Hogan, M. E. (1991) Oligonucleotide inhibition of IL2Ra mRNA transcription by promoter region collinear triplex formation in lymphocytes. *Nucleic Acids Res.* 19, 3435–3441.
- Orson, F., Kinsey, B., and McShan, W. (1994) Linkage structures strongly influence the binding cooperativity of DNA intercalators conjugated to triplex forming oligonucleotides. *Nucleic Acids Res.* 22, 479–484.
- Orson, F. M., Klysik, J., Glass, G. A., and Kinsey, B. M. (1996a) Comparison of triple helix formation by polypurine versus polypyrimidine oligodeoxynucleotides when conjugated to a DNA intercalator. *J. Exp. Ther. Oncol.* 1, 177–185.
- Orson, F. M., McShan, W. M., and Kinsey, B. M. (1996b) Sequence specific binding and cleavage of duplex DNA by a radioiodinated intercalator linked triplex forming oligonucleotide. *Nucl. Med. Biol.* 23, 519–524.
- Pooler, J. P., and Valenzano, D. P. (1981) Dye-sensitized photodynamic inactivation of cells. *Med. Phys.* 8, 614–628.
- Praseuth, D., Perrouault, L., Le, D. T., Chassignol, M., Thuong, N., and Hélène, C. (1988) Sequence-specific binding and

- photocrosslinking of alpha and beta oligodeoxynucleotides to the major groove of DNA via triple-helix formation. *Proc. Natl. Acad. Sci. U.S.A.* **85**, 1349–1353.
- Rahn, R. O., and Patrick, M. H. (1976) Photochemistry of DNA: secondary structure, photosensitization, base substitution, and exogenous molecules. In *Photochemistry and Photobiology of Nucleic Acids* (S. Y. Wang, Ed.) Vol. 2, pp 123–129, Academic Press, New York.
- Roy, C. (1993) Inhibition of gene transcription by purine rich triplex forming oligodeoxyribonucleotides. *Nucleic Acids Res.* **21**, 2845–2852.
- Strom, T. B., Kelley, V. R., Woodworth, T. G., and Murphy, J. R. (1992) Interleukin-2 receptor-directed immunosuppressive therapies: antibody- or cytokine-based targeting molecules. *Immunol. Rev.* **129**, 131–163.
- Sun, J.-S., Francois, J.-C., Montenay-Garestier, T., Saison-Behmoaras, T., Roig, V., Thuong, N. T., and Hélène, C. (1989) Sequence-specific intercalating agents: Intercalation at specific sequences on duplex DNA via major groove recognition by oligonucleotide-intercalator conjugates. *Proc. Natl. Acad. Sci. U.S.A.* **86**, 9198–9202.
- Vu, H., Joyce, N., Rieger, M., Walker, D., Goldknopf, I., Hill, T. S., Jayaraman, K., and Mulvey, D. (1995) Use of phthaloyl protecting group for automated synthesis of 3'-[(hydroxypropyl)amino] and 3'-[(hydroxypropyl)triglycyl] oligonucleotide conjugates. *Bioconjugate Chem.* **6**, 599–607.
- Wang, G., Seidman, M. M., and Glazer, P. M. (1996) Mutagenesis in mammalian cells induced by triple helix formation and transcription-coupled repair. *Science* **271**, 802–805.
- Williams, J. M., Kelley, V. E., Kirkman, R. L., Tilney, N. L., Shapiro, M. E., Murphy, J. R., and Strom, T. B. (1988) *Immunol. Invest.* **16**, 687–723.
- Yoon, K., Hobbs, C. A., Koch, J., Sardano, M., Kutny, R., and Weis, A. L. (1992) Elucidation of the sequence-specific third-strand recognition of four Watson-Crick base pairs in a pyrimidine triple helix motif: T·AT, C·GC, T·CG, and G·TA. *Proc. Natl. Acad. Sci. U.S.A.* **89**, 3840–3844.
- Young, S. L., Krawczyk, S. H., Matteucci, M. D., and Toole, J. J. (1991) Triple helix formation inhibits transcription elongation in vitro. *Proc. Natl. Acad. Sci. U.S.A.* **88**, 10023–10026.
- Zendegui, J. G., Vasquez, K. M., Tinsley, J. H., Kessler, D. J., and Hogan, M. E. (1992) In vivo stability and kinetics of absorption and disposition of 3' phosphopropyl amine oligonucleotides. *Nucleic Acids Res.* **20**, 307–314.
- Zhou, B.-W., Puga, E., Sun, J.-S., Garestier, T., and Hélène, C. (1995) Stable triple helices formed by acridine-containing oligonucleotides with oligopurine tracts of DNA interrupted by one or two pyrimidines. *J. Am. Chem. Soc.* **117**, 10425–10428.

BC970017F

New Coupling Reagents for the Preparation of Disulfide Cross-Linked Conjugates with Increased Stability

Silvia Arpicco, Franco Dosio, Paola Brusa, Paola Crosasso, and Luigi Cattel*

Dipartimento di Scienza e Tecnologia del Farmaco, V. P. Giuria 9,
10125 Torino, Italy. Received September 30, 1996[®]

To improve the *in vivo* stability of disulfide-linked immunotoxins (ITs), a series of sterically hindered cross-linking reagents were designed and synthesized. These ligands are characterized by a thioimide group linked to an *S*-acetyl thiol or a substituted arylthio group. To select the reagent of choice, several arylthiothioimides, substituted with a methyl or a phenyl group adjacent to the disulfide, were analyzed in thiol–disulfide exchange reactions. Also analyzed were the following: (i) the stability and solubility of the linkers in aqueous solution, (ii) the rate of protein derivatization, and (iii) the steric hindrance due to methyl or phenyl group substituents toward cleavage of the disulfide bond by glutathione. Ethyl *S*-acetyl 3-mercaptopropionthioimide (M-AMPT) was chosen as reagent to prepare two types of stable disulfide-containing AR-3–gelonin conjugates (IT2 and IT3). IT2 was prepared by a 3-(4-carboxamidophenylthio)propionthioimide (CDPT)-derivatized antibody coupled to the M-AMPT-derivatized gelonin to afford a conjugate characterized by the presence of a methyl group adjacent to the sulfide bond. In the IT3 conjugate, an M-AMPT-derivatized toxin was coupled to the antibody thiolated with M-AMPT and then activated with Ellman's reagent (DNTB). The *in vitro* and *in vivo* stabilities of the three immunoconjugates were assayed, respectively, (i) by adding an excess of glutathione and monitoring protein release and (ii) by studying their pharmacokinetic behaviors. The specificity and cytotoxicity of all ITs were analyzed on target and unrelated cell lines, and no significant differences in activity were observed. IT3, consisting of a symmetrical dimethyl-substituted disulfide bond, was substantially more stable *in vivo* ($t_{1/2\beta} = 88.3$ h) than the corresponding IT2, characterized by a disulfide-protected monomethyl substituent bond ($t_{1/2\beta} = 60.2$ h) compared to the unhindered conjugate IT1 ($t_{1/2\beta} = 27.9$ h). This family of cross-linking reagents therefore offers advantages, such as minimal perturbation of the protein structure and controlled reactivity due to the thioimide moiety, as well as the capacity to yield immunotoxins possessing substantial stability *in vivo*.

INTRODUCTION

Immunotoxins (ITs¹) are a class of therapeutic agents composed of antibodies linked to a proteic toxin, constructed as both chemical conjugates and fusion proteins (1–3).

Chemical conjugation of the antibody and the toxin is generally accomplished by means of cross-linking agents such as *N*-succinimidyl 3-(2-pyridyldithio)propionate (SPDP) or 2-iminothiolane (2-IT) to introduce a disulfide bond between the proteins (4–7). The presence of a reducible disulfide bond is a prerequisite for cytotoxicity of ITs constituted by RIP-1 (ribosome inactivating protein) linked to a monoclonal antibody (mAb) directed to

a tumor-associated antigen (1, 8, 9). In particular, the A-chain type ITs containing a nonreducible thioether bond are much less cytotoxic than those containing a labile disulfide bond. On the other hand, such conjugates are unstable *in vivo*, because cleavage of the disulfide bond regenerates free antibody and toxin (10–12). Premature cleavage reduces the amount of conjugate that can bind to target cells; in addition, released antibody remains in circulation longer than the conjugate and can compete with intact conjugate for target cell binding. Thus, in multiple-dose therapeutic treatment, IT potency may decrease because tumor antigens are masked by the previously released antibody. Ideally, an immunotoxin should be labile enough to facilitate intracellular cytotoxicity but sufficiently stable to survive administration and delivery *in vivo*. Attempts to minimize this problem have focused on the synthesis of hindered cross-linking reagents in which bulky side chains proximal to the disulfide bond afford protection from nucleophilic attack (13–17). These “second generation” ITs are stable and long-lived and are highly toxic to target cells. One of these, consisting of mAb covalently bound to the deglycosylated ricin A chain by hindered disulfide linkers, has been successfully used in clinical trials for the treatment of non-Hodgkin's (B-cell) lymphoma (18).

In preceding papers, we have reported the preparation of two new acyclic thioimide cross-linking reagents, 3-(4-carboxamidophenylthio)propionthioimide (CDPT) and ethyl *S*-acetylpropionthioimide (AMPT) (19, 20). We used these reagents to prepare immunotoxins made from the RIP-1 gelonin (21) and the AR-3 mAb that recognizes the CAR-3 antigen widely expressed among

* Author to whom correspondence should be addressed (telephone ++39.11.6707697; fax ++39.11.6707695; e-mail cattel@ch.unito.it).

[®] Abstract published in *Advance ACS Abstracts*, April 1, 1997.

¹ Abbreviations: ITs, immunotoxins; M-AMPT, ethyl *S*-acetyl-3-mercaptopropionthioimide; CDPT, 3-(4-carboxamidophenylthio)propionthioimide; DNTB, Ellman's reagent; SPDP, *N*-succinimidyl 3-(2-pyridyldithio)propionate; 2-IT, 2-iminothiolane; RIP-1, ribosome inactivating protein; mAb, monoclonal antibody; AMPT, ethyl *S*-acetylpropionthioimide; THF, tetrahydrofuran; Ph-AMPT, ethyl *S*-acetyl-3-mercaptopropionthioimide; M-CDPT, ethyl 3-(4-carboxamidophenylthio)butyrylthioimide; Ph-CDPT, carboxymethyl 3-phenyl-3-(4-carboxamidophenylthio)propionthioimide; PBS, phosphate-buffered saline; DMF, dimethylformamide; TNB, 5-mercapto-2-nitrobenzoic acid; DTT, dithiothreitol; GSH, reduced glutathione; SDS–PAGE, sodium dodecyl sulfate–polyacrylamide gel electrophoresis; SMPT, 4-[(succinimidyl)oxy]carbonyl- α -methyl- α -(2-pyridyldithio)toluene.

human adenocarcinomas of the stomach, colon, pancreas, ovary, and uterus (22). These ITs were found to be more effective than the corresponding conjugates made by *N*-succinimidyl ester linkers, taking advantage of the ability to amidinate proteins, thus preserving a positive charge on the molecule. These reagents also offer an additional advantage over 2-IT to introduce thiol groups into proteins because during the coupling procedure the sulfhydryl group remains protected from air oxidation, and the acetyl group can be subsequently cleaved in mild conditions by hydroxylamine to give the thiol group.

In this study, in an effort to improve the *in vivo* stability of our thioimide cross-linking reagents, we synthesized a series of thioimide-based sterically hindered reagents provided either with a thioacetyl or with a substituted arylthio group. These reagents were then used to prepare immunotoxins that have improved *in vitro* and *in vivo* stability. The conjugates made by these new cross-linkers have *in vitro* cytotoxic activity similar to that of the corresponding unhindered derivatives.

EXPERIMENTAL PROCEDURES

Materials. Thiolacetic acid and cinnamionitrile were obtained from Merck (Milan, Italy). Crotononitrile, ethanethiol, mercaptoacetic acid, dichloromethane anhydrous, and Ellman's reagent (DTNB) were from Aldrich (Milwaukee, WI).

Diethyl ether was distilled from lithium aluminum hydride, and dry tetrahydrofuran (THF) was obtained by distillation from sodium.

General Procedures. Melting points were determined with a Reichert Kofler apparatus and are uncorrected.

¹H NMR spectra were recorded on a JEOL PMX-60 spectrometer, operating at 60 MHz, with tetramethylsilane as internal standard. IR spectra were obtained as KBr disks on a Shimadzu FT-IR 8101 M spectrophotometer; wavelengths are given in inverse centimeters. Mass spectra were obtained with a Finnigan-MAT TSQ-700 or with a VG Analytical 70-70 EQ-HF spectrometer. Ultraviolet spectra were recorded on a Beckman DU-70 spectrophotometer.

The reactions were checked on F₂₅₄ silica gel precoated sheets (Merck). Purification was done by column flash chromatography on silica gel 60 (Merck, 230–400 mesh) or by distillation under reduced pressure with Kugelrohr apparatus.

3-(Acetylthio)butyronitrile (1). Thiolacetic acid (20.7 mL, 0.29 mol) was added dropwise to crotononitrile (18.81 mL, 0.232 mol) under an argon atmosphere, and the reaction mixture was stirred for 24 h at room temperature and then refluxed for 1 h. The unreacted products were eliminated under reduced pressure (15 mmHg, 50 °C); distillation of the product (3 mmHg, 100 °C) then gave a yellow oil, which slowly crystallized at room temperature (16.6 g, 50%): ¹H NMR (CDCl₃) δ 3.8 (m, 1H, CH), 3.0 (d, 2H, CH₂), 2.4 (s, 3H, SAc), 1.5 (d, 3H, CH₃).

3-(Acetylthio)-3-phenylpropionitrile (2). Thiolacetic acid (12 mL, 0.169 mol) was added slowly to cinnamionitrile (20 mL, 0.159 mol) under an argon atmosphere, and the reaction mixture was refluxed for 3 h to give a pale yellow precipitate that was washed several times with ethanol to remove unreacted products (26 g, 80%): ¹H NMR (CDCl₃) δ 7.6 (m, 5H, Ar-H), 5.1 (t, 1H, CH), 3.2 (d, 2H, CH₂), 2.3 (s, 3H, SAc).

5-(3-Cyano-2-propyldithio)-2-nitrobenzoic Acid (4). To 3-(acetylthio)butyronitrile (22.9 g, 0.16 mol) was added an excess of 12% aqueous sodium hydroxide, and the mixture was stirred at 25 °C for 12 h. After extraction

with diethyl ether under Ar, the aqueous layer was acidified with 6 N H₂SO₄ and reextracted with ether. Evaporation of the dried ether extracts of this aqueous layer yielded 3-mercaptoputyronitrile (**3**) as a dark yellow oil, which was purified by distillation under reduced pressure (70 °C, 3 mmHg) (6 g, 38%): ¹H NMR (CDCl₃) δ 3.3 (m, 1H, CH), 2.7 (d, 2H, CH₂), 1.9 (d, 1H, SH), 1.5 (d, 3H, CH₃). 3-Mercaptoputyronitrile (0.5 g, 0.005 mol) in methanol was added to a solution of DTNB (3.96 g, 0.01 mol) in 250 mL of sodium phosphate buffer, pH 7.4, deaerated and saturated with Ar. After stirring for 4 h at 25 °C, the solution was acidified with 1 N HCl and extracted with ethyl acetate; the organic layers were pooled, dried, and concentrated *in vacuo* to give a crude product, which was purified by flash chromatography with elution in dichloromethane/methanol/acetic acid (99/0.5/0.5, v/v). The pure product **4** was obtained as a pale yellow oil (0.82 g, 55%): ¹H NMR (CDCl₃) δ 9.2 (s, 1H, COOH), 8.2 (m, 3H, Ar-H), 3.3 (t, 1H, CH), 2.8 (d, 2H, CH₂), 1.7 (d, 3H, CH₃).

5-(2-Cyano-1-phenylethylthio)-2-nitrobenzoic Acid (6). 3-(Acetylthio)-3-phenylpropionitrile (24.2 g, 0.118 mol) was hydrolyzed for 12 h at room temperature with an excess of aqueous sodium hydroxide; the mixture was then extracted with ether, as described below, and evaporated to give a yellow oil, which was purified by flash chromatography with elution in petroleum ether/dichloromethane (90/10, v/v) to give 7.7 g of 3-mercaptop-3-phenylpropionitrile (**5**) (40%): ¹H NMR (CDCl₃) δ 7.5 (m, 5H, Ar-H), 4.4 (q, 1H, CH), 3.1 (d, 2H, CH₂), 2.2 (s, 1H, SH). Compound **6** was prepared in a manner analogous to that of **4** and was purified by flash chromatography (dichloromethane/methanol/acetic acid 97.5/2/0.5) to give an orange oil (0.467 g, 54%): ¹H NMR (CDCl₃) δ 9.8 (s, 1H, COOH), 7.5 (m, 3H, Ar-H), 7.1 (m, 5H, Ar-H) 4.25 (m, 1H, CH), 3.1 (d, 2H, CH₂).

4-(3-Cyano-2-propyldithio)benzamide (7). To 4-carbamoylbenzenesulfenyl chloride (3.62 g, 0.0193 mol) dissolved in 100 mL of hot glacial acetic acid was added 3-mercaptoputyronitrile (1.95 g, 0.0193 mol) in 1.5 mL of glacial acetic acid. The reaction mixture was stirred at 90 °C for 45 min and, after the mixture had cooled to room temperature, 300 mL of water was added and the mixture was left for 12 h at 4 °C. The resulting precipitate was filtrated and the solution was extracted with ethyl acetate; the organic extracts were dried and evaporated under reduced pressure. The residue and the precipitate previously obtained were pooled and purified by flash chromatography using diethyl ether as eluent to give **7** as white crystals (2.43 g, 50%): mp 140 °C; ¹H NMR (CD₃COCD₃) δ 8.2 (d, 2H, Ar-H), 7.8 (d, 2H, Ar-H), 3.5 (m, 1H, CH), 2.9 (d, 2H, CH₂), 1.5 (d, 3H, CH₃).

4-[(2-Cyano-1-phenylethyl)dithio]benzamide (8). The procedure used to prepare **7** was followed. The crude product was purified by flash chromatography (diethyl ether/ethyl acetate, 99.5/0.5) to give a yellow solid (3.1 g, 50%): mp 115–117 °C; ¹H NMR (CDCl₃) δ 7.8 (q, 4H, Ar-H), 7.5 (m, 5H, Ar-H), 6.5 (s, 2H, NH₂), 4.3 (m, 1H, CH), 3.1 (d, 2H, CH₂).

General Procedure for Preparation of Thioimide Ester Hydrochlorides (9–15). Hydrogen chloride gas, dried by passing through concentrated sulfuric acid in two washing bottles, was bubbled through ice-cold ethanethiol (3.25 mL, 0.0435 mol) or mercaptoacetic acid (3.5 mL, 0.0435 mol) for the derivative **14**, for 1 h. The purified nitriles (0.00435 mol) diluted in anhydrous diethyl ether (**1** and **4**), dry THF (**2** and **7**), and anhydrous dichloromethane (**6** and **8**) were quickly added to the cold solution under stirring, and the reaction was left overnight at 0 °C. Anhydrous cold diethyl ether was then

added to the reaction mixture, which was left at -20°C until a crystalline solid was formed. The supernatant was decanted, and the precipitate was washed with anhydrous diethyl ether under argon and dried under reduced pressure at room temperature.

Ethyl S-Acetyl-3-mercaptopropionthioimide Ester Hydrochloride (M-AMPT, 9): yield 0.79 g (75%); mp 112°C ; ^1H NMR (CDCl_3) δ 3.4–3.2 (m, 5H, $-\text{SCH}_2\text{CH}_3$, CH and CH_2), 2.43 (s, 3H, SAc), 1.6 (d, 3H, CH_3), 1.43 (t, 3H, $-\text{SCH}_2\text{CH}_3$); IR (KBr) cm^{-1} 3300–2400 (NH), 1690 (C=O), 1620 (C=N), 1360 (SAc); MS-EI, m/z (relative intensity) 206 (M^+ , 7), 162 (100), 145 (53), 130 (20), 102 (65), 89 (20), 75 (33), 61 (52), 43 (100).

Ethyl S-Acetyl-3-mercaptopropionthioimide ester hydrochloride (Ph-AMPT, 10): yield 1.1 g (84%); mp 85°C ; ^1H NMR (CDCl_3) δ 7.6 (m, 5H, Ar-H), 4.9 (t, 1H, CH), 3.9–3.3 (m, 4H, $-\text{SCH}_2\text{CH}_3$, and CH_2), 2.5 (s, 3H, SAc), 1.6 (t, 3H, $-\text{SCH}_2\text{CH}_3$); IR (KBr) cm^{-1} 3300–2400 (NH), 1730 (C=O), 1610 (C=N), 1360 (SAc); MS-EI, m/z (relative intensity) 268 (M^+ , 8), 130 (100), 103 (40), 77 (35), 43 (38).

Ethyl 3-[(3-Carboxy-4-nitrophenyl)dithio]butyrythioimide Ester Hydrochloride (11): yield 1.3 g (78%); mp 112°C ; ^1H NMR (CD_3OD) δ 8.2 (m, 3H, Ar-H), 3.8–3.2 (m, 5H, $-\text{SCH}_2\text{CH}_3$, CH and CH_2), 1.5 (q, 3H, CH_3), 1.25 (t, 3H, $-\text{SCH}_2\text{CH}_3$); IR (KBr) cm^{-1} 3300–2500 (NH and OH), 1610 (C=N), 1570, 1530 (NO_2), 1370 (NO_2).

Ethyl 3-Phenyl-[(3-carboxy-4-nitrophenyl)dithio]propionthioimide Ester Hydrochloride (12): yield 1.6 g (80%); mp 120°C ; ^1H NMR (CD_3OD) δ 7.4 (m, 3H, Ar-H), 7 (m, 5H, Ar-H), 3.8–3.2 (m, 5H, $-\text{SCH}_2\text{CH}_3$, CH and CH_2), 1.25 (t, 3H, $-\text{SCH}_2\text{CH}_3$); IR (KBr) cm^{-1} 3300–2500 (NH and OH), 1610 (C=N), 1570, 1530 (NO_2), 1370 (NO_2).

Ethyl 3-[(4-Carboxamidophenyl)dithio]butyrythioimide Ester Hydrochloride (M-CDPT, 13): yield 1.17 g (77%); mp 118°C ; ^1H NMR ($\text{DMSO}-d_6$) δ 8.2 (d, 2H, Ar-H), 7.8 (d, 2H, Ar-H), 4.1 (m, 1H, CH), 3.4–3.2 (m, 4H, $-\text{SCH}_2\text{CH}_3$ and CH_2), 1.5 (d, 3H, CH_3), 1.25 (t, 3H, $-\text{SCH}_2\text{CH}_3$); IR (KBr) cm^{-1} 3300–2200 (NH_2 and NH_2^+), 1650 (C=O), 1620 (C=N); MS-EI, m/z (relative intensity) 315 (M^+ , 38), 254 (8), 226 (18), 212 (100), 195 (20), 163 (100), 153 (18), 89 (18), 44 (10).

Carboxymethyl 3-Phenyl-3-[(4-carboxamidophenyl)dithio]propionthioimide Ester Hydrochloride (Ph-CDCT, 14): yield 1.5 g (78%); mp 115°C ; ^1H NMR ($\text{DMSO}-d_6$) δ 7.8 (q, 4H, Ar-H), 7.4 (m, 5H, Ar-H), 4.5 (t, 1H, CH), 3.6 (s, 2H, $-\text{SCH}_2\text{COOH}$), 2.85 (d, 2H, CH_2); IR (KBr) cm^{-1} 3300–2200 (NH_2 and NH_2^+), 1650 (C=O), 1620 (C=N); MS (FAB^+) 407 (M^+ + 1).

Ethyl 3-Phenyl-3-[(4-carboxamidophenyl)dithio]propionthioimide Ester Hydrochloride (Ph-CDPT, 15): yield 1.36 g (78%); mp 120°C ; ^1H NMR ($\text{DMSO}-d_6$) δ 7.8 (q, 4H, Ar-H), 7.3 (m, 5H, Ar-H), 4.2 (t, 1H, CH), 3.4–3.2 (m, 4H, $-\text{SCH}_2\text{CH}_3$ and CH_2), 1.3 (t, 3H, $-\text{SCH}_2\text{CH}_3$); IR (KBr) cm^{-1} 3300–2200 (NH_2 and NH_2^+), 1650 (C=O), 1620 (C=N); MS (FAB^+) 377 (M^+ + 1).

Determination of Aryldithio Group Reactivity. Stock solutions (0.25 mM) of disulfides **4**, **6**, **7**, and **8** were prepared in ethanol (95%) and diluted to 0.028 mM with sodium phosphate buffer (0.0056 M Na_2HPO_4 , 0.014 M $\text{NaH}_2\text{PO}_4 \cdot \text{H}_2\text{O}$, 0.2 M NaCl, 0.003 M EDTA disodium salt, pH 6.5), deaerated and flushed with Ar. To 900 μL of each disulfide solution in a photometer cell was quickly added 100 μL of different concentrations of freshly prepared solutions of cysteine hydrochloride monohydrate (0.5 and 1 mM) in the same buffer. The thiol–disulfide exchange reaction was then monitored by recording the absorbance–time curve relative to the displacement of the substituted thiophenol (which is

balanced with its ionized form) in the presence of double and quadruple molar excesses of cysteine.

The kinetic constants were calculated (19) using the second-order equation

$$dx/dt = k(a - x)(b - x); \quad k = \frac{1}{t(a - b)} \ln \frac{(b - x)a}{(a - x)b}$$

where a is initial aryldithio derivative molar concentration, b is initial cysteine molar concentration, and x is thiophenol molar concentration at time t (s). The value of x is calculated by the equation

$$dx/dt = k(A - A_0/A_{\text{inf}} - A_0)a$$

where A is the absorbance at time t (s), A_0 is the initial absorbance of the aryl disulfide, and A_{inf} is the final absorbance at 100% of reaction with cysteine.

For each couple A/t relative to the registered kinetic curves, the value of x and the kinetic constant k ($\text{L} \cdot \text{mol}^{-1} \cdot \text{s}^{-1}$) were calculated.

Reaction of Thioimide with AR-3 mAb and Determination of Degree of Derivatization. The mouse IgG1 monoclonal antibody AR-3 was purified from ascitic fluid with affinity chromatography on Sepharose Cl–protein A. A solution of AR-3 (60 μM , 1 mL) in PBS–EDTA (100 mM sodium phosphate, 100 mM NaCl, 1 mM EDTA, pH 7.4), deaerated and flushed with Ar, was mixed at 25°C with different molar excesses (10-, 20-, 30-fold) of the linkers **9**, **10**, **13**, and **14** previously dissolved in absolute ethanol (**9**, **10**) or anhydrous dimethylformamide (DMF) (**13** and **14**) (40 μL). The degree of derivatization was evaluated at different time intervals after purification from the excess of ligands by gel filtration on a 15×55 mm Bio-Gel P6-DG column (Bio-Rad, Hercules, CA) pre-equilibrated in PBS–EDTA at 20°C .

The number of thioacetylated groups linked to the protein was calculated spectrophotometrically by reaction of the sample with the deacetylating reagent hydroxylamine hydrochloride (0.5 M, 12.5 mM EDTA, pH 7.4) followed by thiol–disulfide exchange with DTNB as described by Duncan (23). Determination of the aryldithio groups linked to AR-3 was evaluated following the release of thiolated anion at 313 nm, after incubation of the protein sample (1 mL) in the presence of 2-mercaptoethanol in PBS–EDTA (11 mM sodium phosphate, 50 μL) and NaOH (1 M, 40 μL) to a final pH of 8.8–9.4. The molar absorptivity value for the 4-carboxamidophenylthiolate anion under these conditions at 313 nm was $15\,200 \pm 300$.

Disulfide Bond Stability in Modified AR-3. The protein (33.3 μM , 1 mL) was reacted with the ligands M-AMPT, Ph-AMPT, M-CDPT, and Ph-CDCT and with the analogous unhindered thioimides AMPT and CDPT, previously prepared in our laboratory (19), so as to incorporate an average of 1–1.2 mol of linkers/mol of protein.

Before purification in the derivatization mixture, the thioacetylated groups were replaced with TNB by deacetylation with hydroxylamine solution and successive exchange with DTNB 800 μM for 1 h at 25°C .

The samples were purified by gel centrifugation as described below.

The linker/protein ratio was spectrophotometrically determined by quantifying the release of TNB at 412 nm after the addition of a solution of dithiothreitol (DTT, 50 mM); the release of 4-carboxamidophenylthiolate anion was followed at 313 nm as described below.

To test the stability of the disulfide bond introduced into proteins, the samples were incubated with reduced glutathione (GSH) (2 and 4 molar excess with respect to thiol groups linked), and the release of thiophenol was spectrophotometrically followed at 412 or 313 nm.

Preparation and Purification of Immunoconjugates. Gelonin solution (Inland Laboratories, Inc., Austin, TX) (187 μ M, 1 mL) was stirred with ethanolic solutions of AMPT (64.2 mM, 30 μ L) or M-AMPT (51 mM, 30 μ L) for 30 min at 25 °C so as to incorporate an average of 1–1.1 linkers/mol of gelonin. The mixture was purified by gel centrifugation. The purified antibody dissolved in PBS–EDTA was separately reacted with two different cross-linkers, CDPT and M-AMPT.

The method used to derivatize AR-3 with CDPT is described in ref 20; briefly, the cross-linker (16 μ M, 43 μ L) in dry DMF was reacted for 30 min at 25 °C with AR-3 (47 μ M, 890 μ L) to obtain a molar ratio of 1:1.2 (AR-3/CDPT).

The reaction of AR-3 with M-AMPT proceeded as follows: M-AMPT in absolute ethanol (11 mM, 40 μ L) was added to the solution of the mAb (44.6 μ M, 1 mL), and the mixture was stirred for 30 min at 25 °C; then solutions of hydroxylamine (0.5 M, 100 μ L) and DTNB (40 mM, 30 μ L) were added and the reaction was stirred for 1 h. The AR-3/M-AMPT molar ratio was 1:1.1. In both cases the mixture was purified by gel centrifugation.

The derivatized mAb and RIP were mixed in the presence of a solution of hydroxylamine (1:10, v/v). The conjugation reactions proceeded for 5 h at 25 °C followed by 18 h at 4 °C; at the end of the reaction a solution of *N*-ethylmaleimide (20 mM, 20 μ L) was added to block free thiol groups.

Immunoconjugates were purified as follows: the reaction mixtures were centrifuged and the supernatants applied to an HPLC gel filtration column (TSK G 3000 SW, 7.5 \times 600 mm) in several steps and eluted in sodium phosphate buffer, pH 6.8 (50 mM phosphate, 0.15 M NaCl). The fractions containing unreacted mAb and conjugate were pooled, concentrated, dialyzed against 50 mM phosphate buffer/10 mM NaCl, pH 7.4, and loaded onto an Affi-Gel Blue column (7 \times 50 mm) preequilibrated in the same buffer. Unconjugated AR-3 did not bind to the solid phase under these conditions of ionic strength and was eluted. The conjugates were then eluted with the same buffer containing 1 M NaCl. The fractions containing immunoconjugates were dialyzed and concentrated.

Purity of the immunotoxins was monitored by sodium dodecyl sulfate–polyacrylamide gel electrophoresis (SDS–PAGE) using 4–15% precast gels (Bio-Rad) under non-reducing conditions and Coomassie blue staining.

In Vitro Study of Disulfide Bond Stability. The *in vitro* stability of the bond in the various conjugates was evaluated in two different ways. In the first method the samples (1 mg/mL, 3 μ L) were incubated for 1 h at 37 °C with solutions of GSH (3 μ L) in increasing excess (from 3- to 10000-fold), and the reaction was stopped by addition of excess of iodoacetamide. The samples were then tested by densitometric analysis of SDS–PAGE 4–15% precast gels stained by Coomassie blue to calculate the amount of mAb released (2202 ULTROSCAN Laser Densitometer, LKB, Bromma, Sweden). The other experiment was similar to the procedure of Carroll (16): immunotoxins (5.5 μ M, 10 μ L) were incubated for 1 h at 37 °C with different concentrations of GSH (from 30- to 3000-fold), and iodoacetamide was then added; the samples were dialyzed by a microdialyzer System 500 (Pierce, Rockford, IL) to remove the low molecular weight products and then chromatographed on a Zorbax Bio

Series GF 250 column (DuPont, Newtown, CT) equilibrated in 0.2 M Na₂HPO₄, pH 7.5. The elution was monitored at 280 nm, and the amount of gelonin released was quantified by area integration (CBS-10A Communications Bus Module, Shimadzu, Duisburg, Germany).

Cytotoxicity Assay. The cell lines used were HT-29, a human colon adenocarcinoma expressing the CAR-3 antigen, as target cell line, and the MeWo human melanoma as control. These cell lines were tested in the presence of serial dilutions of three immunotoxins, according to the method of Cattel et al. (24). The results were expressed as percentage of [³H]leucine incorporation with respect to control (background values subtracted).

Pharmacokinetic Evaluation. The immunoconjugates were labeled with ¹²⁵I according to the iodogen method (25) to specific activity of approximately of 7 mCi/mg. Pharmacokinetic studies were performed as previously described (26) using female Balb/c mice (1 month old, 18–20 g; Charles River Italia, Milan, Italy); care and handling of animals were in accordance with the provisions of the European Economic Community Council Directive 86/209 recognized and adopted by the Italian Government (approval decree no. 230/95 B). The mice drank water plus 0.2% (v/v) Lugol solution 3 days before and during the experiment to block thyroid iodine uptake. The animals were treated with 4.5 μ Ci (135–180 μ g/kg) of conjugate. The samples were diluted in a carrier solution of PBS, pH 7.4, containing 0.1% bovine serum albumin to a volume of 100 μ L. The solutions were injected intravenously (iv) into the tail vein (groups of three animals each). Blood samples were taken from the retroorbital plexus at various times (0, 0.5, 1, 2, 4, 6, 24, 48, 72, and 144 h); both the Pasteur capillary and the Eppendorf vials used for the sample collections were washed in a heparin solution 1 day before use. Because blood was taken from each animal no more than four times, the different groups were overlapped to cover the chosen time range. The experiments were repeated three or four times.

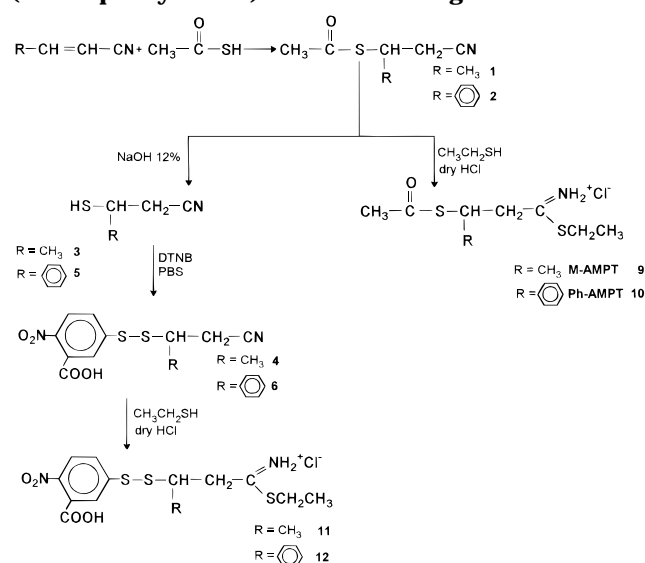
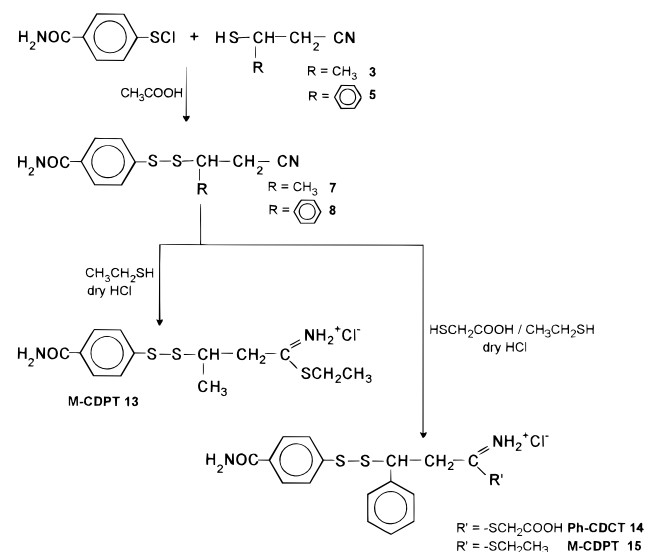
The treatment of blood samples was quite similar to that described by Scott (27): samples were diluted to the same volume of 54 mM aqueous iodoacetamide to prevent oxidation of free thiol groups possibly formed; proteins were rapidly precipitated with 1 mL of cold trichloroacetic acid (12.5%, w/v). The samples were directly counted in a gamma counter (L'ACN, Milan, Italy) and then centrifuged; the resultant pellets were counted separately from the supernatants and used to determine the pharmacokinetic parameter.

The plasma samples from each time point were also analyzed by 7.5% SDS–PAGE gels using volumes containing 350–3000 cpm. Autoradiographs of the dried gels were obtained and analyzed with a Phosphor Imaging GS-250 (Bio-Rad); then the immunotoxin and antibody areas were calculated with Molecular Analyst software version 1.2 (Bio-Rad).

Pharmacokinetic parameters were determined from a two-compartment analysis using the program PCNONLIN (Statistical Consultants, Inc., Lexington, KY).

RESULTS

Chemistry. The S-acetylated thioimide ester hydrochlorides M-AMPT **9** and Ph-AMPT **10** were prepared as shown in Scheme 1. The precursor nitriles **1** and **2** were prepared by the addition of thiolacetic acid to the unsaturated nitriles according to the method of Holmberg and Schjamberg (28). Transformation to the corresponding thioimide followed the Pinner synthesis (29) by the

Scheme 1. Synthesis of S-Acetylated and 3-Carboxy-(4-nitrophenyldithio)thioimide Reagents**Scheme 2. Synthesis of (4-Carboxamidophenylthio)thioimides**

addition of the nitrile to a solution of ethanethiol previously saturated with dry hydrogen chloride.

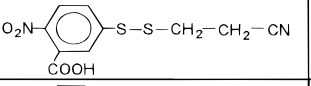
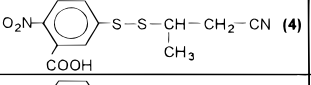
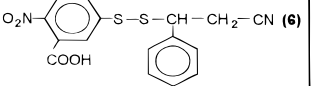
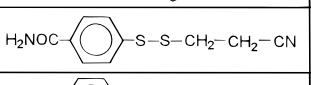
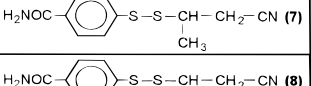
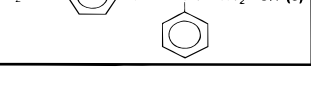
The (3-carboxy-4-nitrophenyldithio)thioimides **11** and **12** were synthesized from the corresponding nitriles **4** and **6** (Scheme 1) prepared by a reaction of thiol-disulfide exchange between DTNB and 3-mercaptoputyrionitrile (**3**) or 3-mercapto-3-phenylpropionitrile (**5**) previously obtained by hydrolysis of respective thioacetylated derivatives (**1** and **2**).

The carboxamidoaryldithio derivatives M-CDPT **13**, Ph-CDCT **14**, and Ph-CDPT **15** were prepared from the corresponding nitriles **7** and **8** (Scheme 2) obtained by the reaction of 4-carbamoylbenzenesulfenyl chloride (**30**) with the mercaptans **3** and **5**. For preparation of the ligand **14**, the classical Pinner reaction was modified using mercaptoacetic acid instead of ethanethiol. In this way it was possible to increase the hydrophilicity of the poorly water soluble phenyl-substituted linker by replacing the *S*-ethyl function by an *S*-carboxymethyl group.

The compounds were characterized by 1H NMR, IR, and MS.

The thioimides required storage under very anhydrous conditions and were kept in tightly stoppered flasks at $-20^\circ C$ under Ar.

Table 1. Aryldithio Group Reactivity

COMPOUND	k (Lmol ⁻¹ s ⁻¹)
	330±10
	21.2±2
	19.6±2
	51.2±2
	4.5±0.5
	7.6±1

Kinetic Studies. To verify the relationship between steric hindrance and stability of the disulfide bond in the (aryldithio)thioimide linker series, we studied the reactivity toward thiol-disulfide exchange in the precursor nitrile derivatives **4**, **6**, **7**, and **8** using cysteine as thiol reagent (**19**).

The progress of disulfide reductive scission was followed at 412 or 313 nm (for TNB or carboxamidophenylthiolate anion, respectively), and the relative rate constants k (L·mol⁻¹·s⁻¹) were calculated. The rate constants obtained using 2-fold molar excess of cysteine are shown in Table 1 and compared to the value obtained for the unhindered derivatives 5-[(2-cyanoethyl)dithio]-2-nitrobenzoic acid and 4-[(2-cyanoethyl)dithio]benzamide. As shown in Table 1, the lower value of the rate constant in the hindered compounds **4**, **6**, **7**, and **8** relative to that found for the unhindered derivatives indicates a reduction in the reactivity of cysteine toward thiol-disulfide exchange, and the comparable k values suggest that the methyl and phenyl groups conferred similar stability to the disulfide bond.

Among the compounds tested, the 3-carboxy-4-nitrophenyldithio series showed higher reactivity than the carboxamidophenyldithio derivatives. Derivatives **4** and **6** were in turn transformed by synthesis to the corresponding thioimide derivatives **11** and **12**, which did not show sufficient stability in aqueous media to allow their use as cross-linkage reagents, while compound **15** was excluded from further experiments because of its very low water solubility. Instead, the thioimide derivatives **13** and **14**, obtained from the less reactive nitrile precursors **7** and **8**, were much more stable in aqueous solution. Consequently, we chose the hindered derivatives M-CDPT **13** and Ph-CDCT **14** as linkers for further testing of protein derivatization.

Reaction of Thioimide with Protein. The reactivity of linkers **9**, **10**, **13**, and **14** toward the lysyl ϵ -amino groups of AR-3 was evaluated. Degrees of derivatization versus time using a fixed molar excess of linker (pH 7.4, 20 $^\circ C$) are shown in Figure 1.

For these reagents, prolonging the reaction time increased the degree of substitution on the protein in proportion to the molar excess of ligand; after 2 h of reaction, no increase appeared. As shown in Figure 1, the hindered derivatives, being more lipophilic and hence less soluble in the aqueous buffer, were generally less

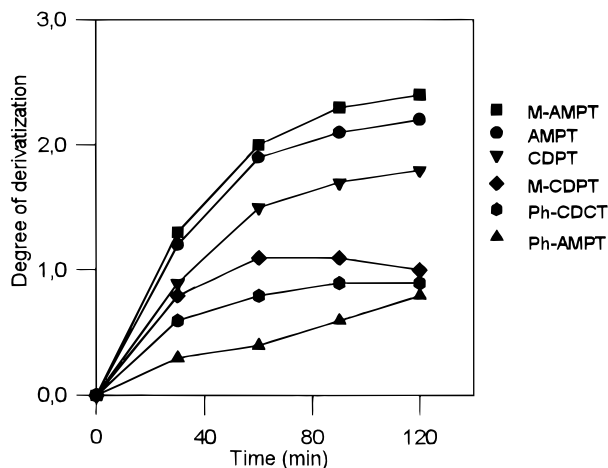


Figure 1. AR-3 derivatization degree with various thioimide esters. The mAb (60 μ M) was reacted with a fixed molar excess of ligand ($\times 10$); the derivatization efficacy was evaluated at different time intervals after purification from the excess of ligand as described under Experimental Procedures. The points represent the arithmetic means of three determinations. SDs (not reported) were $<10\%$ of the means.

reactive toward protein, the exception being M-AMPT, which showed roughly the same reactivity as the parent AMPT.

Stability of Model Disulfides in Derivatized AR-3. The relative stability of the disulfide bond introduced into AR-3 by derivatization with ligands M-AMPT **9**, Ph-AMPT **10**, M-CDPT **13**, and Ph-CDCT **14** was analyzed by comparison with the parent unhindered linkers AMPT and CDPT (**19**) using GSH as reducing agent.

To study the stability of the S-acetylated thioimide linkers (AMPT, M-AMPT, and Ph-AMPT) after derivatization with the protein, the thioacetylated groups were replaced by TNB by deacetylation with hydroxylamine followed by exchange with DTNB. In this way it was possible to measure the strength of the disulfide bond introduced in the protein by following spectrophotometrically the release of TNB at 412 nm after the addition of GSH (Figure 2A).

Instead, to analyze the stability of the dithio group introduced in the AR-3 protein after derivatization with the series of the (carboxamidophenylthio)thioimide linkers (CDPT, M-CDPT, and Ph-CDCT), it was sufficient to measure spectrophotometrically the release of the carboxamidophenylthiolate anion at 313 nm after addition of GSH (Figure 2B). Figure 2 indicates that there is an increase in stability of the disulfide bond after introduction of a methyl or phenyl group in an adjacent position. As it was found for the kinetic constant values of the nitrile precursors (Table 1), M-CDPT is the most stable compound among the carboxamido derivatives, while among the TNB derivatives, the most stable toward thiol–disulfide exchange was that derived by the Ph-AMPT linker.

Parts A and B of Figure 2 also show a different value for the release of thiophenol due to higher thiol–disulfide exchange reactivity in TNB-modified derivatives.

Preparation of Immunotoxins. Gelonin, a 30 kDa cytotoxic single-chain glycoprotein obtained from the seeds of *Gelonium multiflorum* (**31**, **32**), was selected as toxin to generate ITs after chemical conjugation with the monoclonal antibody AR-3. According to the preceding results, three different coupling procedures were followed to compare the relative stability of the immunotoxins.

IT1 (Scheme 3). The CDPT ligand was first reacted with the mAb to introduce 1.2 arylthio groups/protein

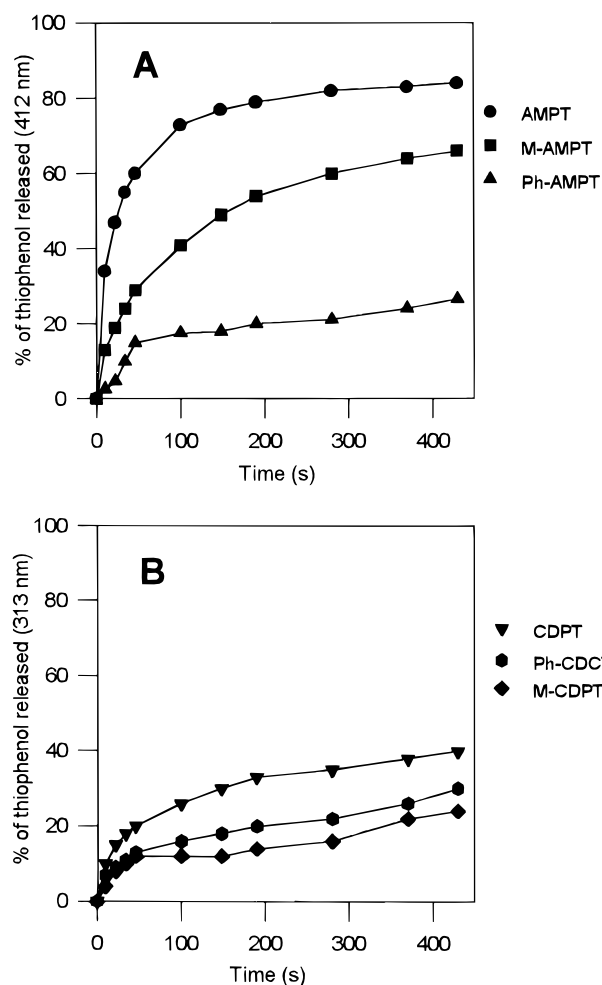


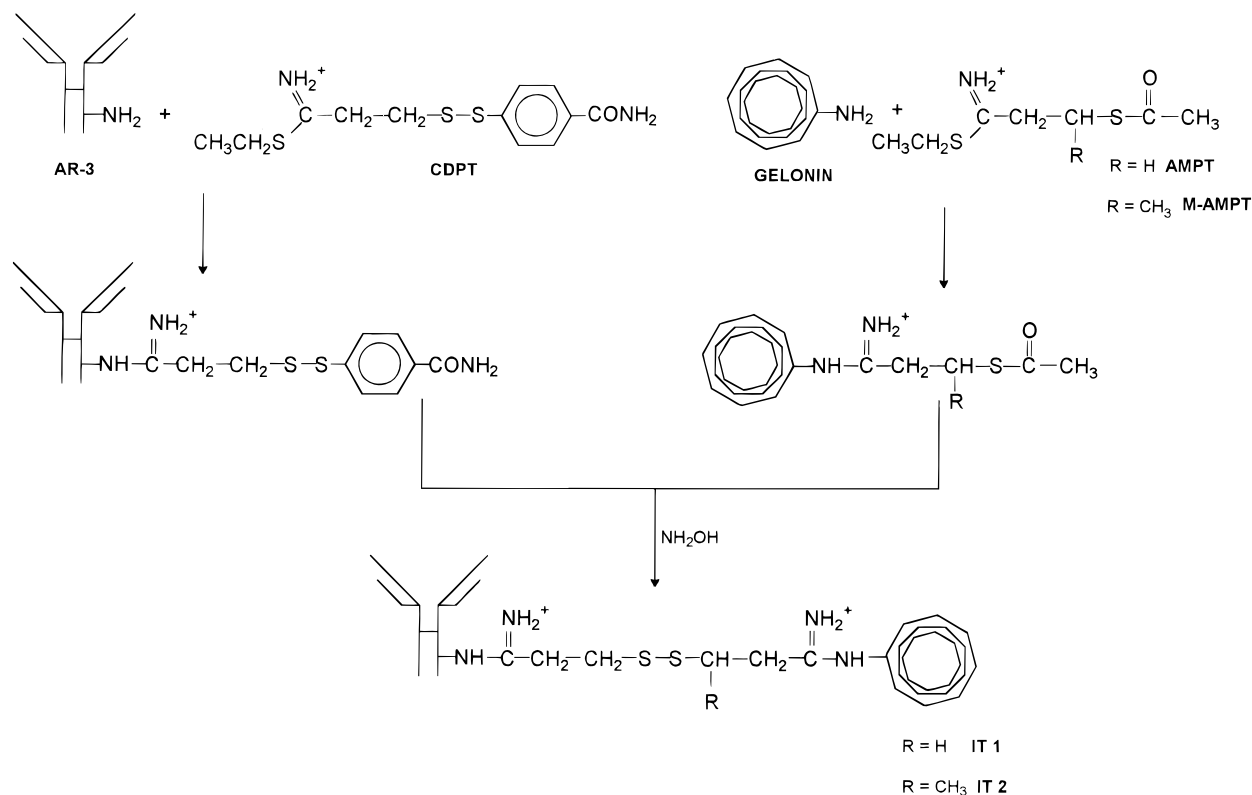
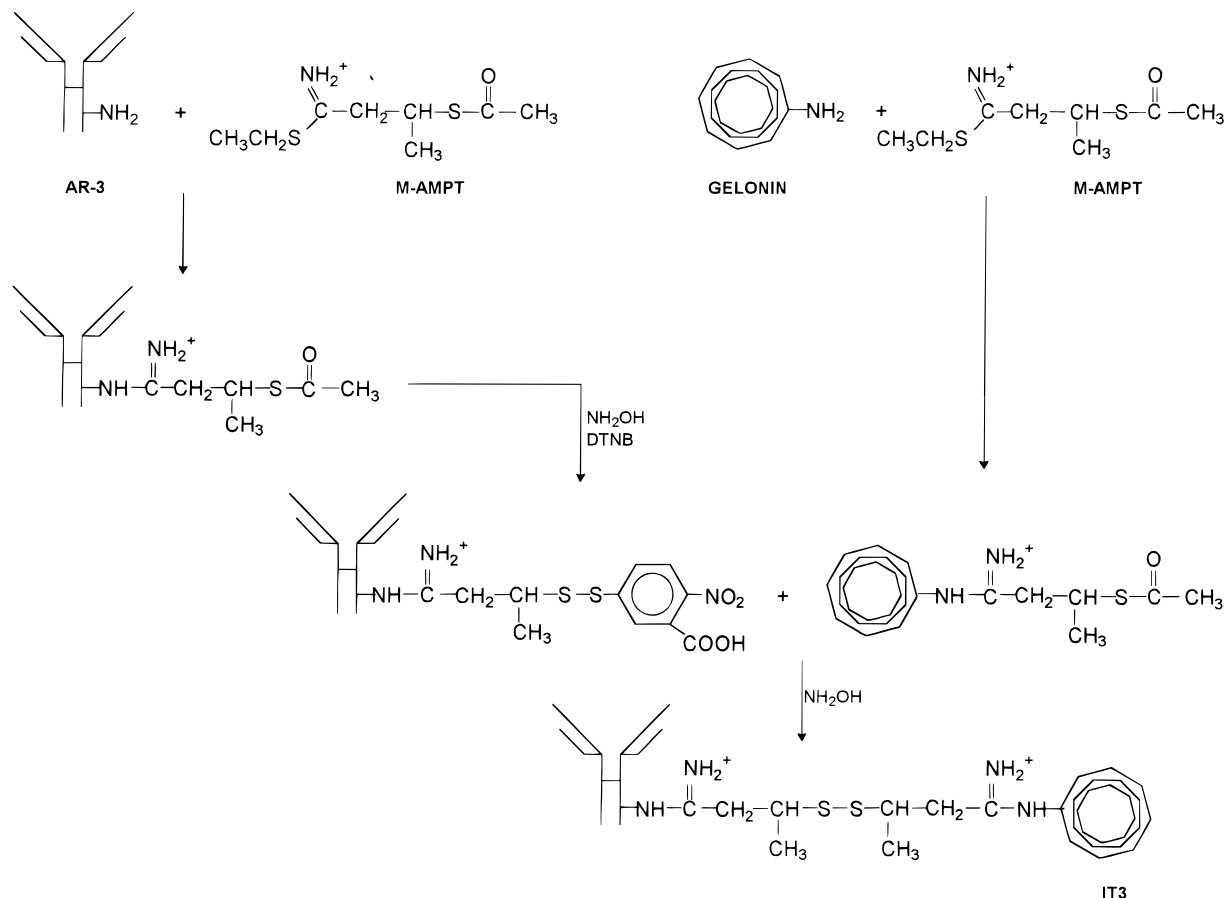
Figure 2. Stability of disulfide bond introduced into AR-3 by derivatization with different linkers so as to incorporate an average of 1–1.2 mol of linkers/mol of antibody. The release of thiophenol was monitored spectrophotometrically after the addition of GSH. In (A) the release was followed at 412 nm after the substitution of S-acetylthio group with TNB, while in (B) the release was followed at 313 nm. Results were normalized by dividing the absorbance at any time point by that obtained with an excess of DTT and multiplying the product by 100. The points represent the arithmetic means of three determinations. SDs (not reported) were $<8\%$ of the means.

molecule, whereas 1–1.1 acetylthio residues were introduced into gelonin with AMPT; the derivatized proteins were coupled in the presence of hydroxylamine to deprotect the acetylthio groups to obtain the corresponding IT.

IT2 (Scheme 3). The CDPT-modified AR-3 was reacted with the gelonin previously thioacetylated with the hindered linker M-AMPT (0.9–1.1 groups).

IT3 (Scheme 4). Both proteins were derivatized with M-AMPT by introducing 0.9–1.1 acetylthio groups; the modified mAb was then deacetylated with hydroxylamine and reacted with DTNB and further directly coupled to the S-acetyl-containing gelonin in the presence of hydroxylamine by a thiol–disulfide exchange reaction. In this way the disulfide group was protected by the introduction of two symmetric methyl groups in the protein–protein linkage.

All of the coupling reactions proceeded for 5 h at 25 $^{\circ}$ C and for 18 h at 4 $^{\circ}$ C, and then aliquots were analyzed by SDS–PAGE (Figure 3). The ITs (IT1 and IT2) prepared using CDPT as ligand gave pure conjugate with a molar ratio 1:1 mAb/gelonin at 85%; in fact, the carboxamidophenylthiolate leaving group, being less

Scheme 3. Preparation of IT1 and IT2**Scheme 4. Preparation of IT3**

reactive, produced the monoconjugate species in higher yield compared with the TNB leaving group.

The results showed an inverse correlation between disulfide bond stability and efficiency of conjugation in

this order: $\text{IT1} \geq \text{IT2} > \text{IT3}$; conjugation yields were approximately 10% for IT1 and IT2 and 3–4% for IT3.

The disulfide-linked immunotoxins were purified by HPLC gel filtration to remove the aggregates and the

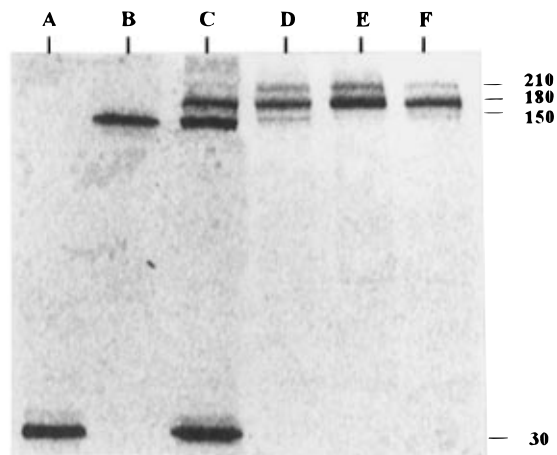


Figure 3. SDS-PAGE analysis of AR-3, gelonin, and ITs. Samples were run on a 4–15% polyacrylamide gel under nonreducing conditions and Coomassie blue staining: (lane A) gelonin; (lane B) AR-3; (lane C) crude IT; (lane D) IT3; (lane E) IT2; (lane F) IT1.

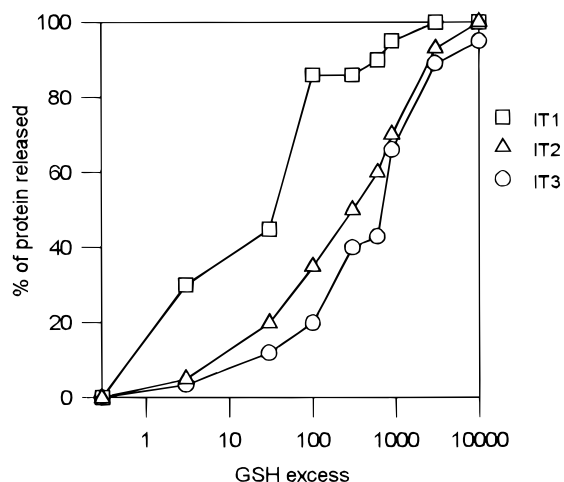


Figure 4. Release of mAb from the immunoconjugates. The conjugates were incubated with different concentrations of GSH for 1 h at 37 °C. The amounts released were measured by densitometric analysis of SDS-PAGE. Results are the average of three independent experiments (SDs were <10%).

unreacted toxin; then to completely remove the free mAb from the conjugate, the mixtures were subjected to Affi-Gel Blue affinity chromatography.

Disulfide Bond Stability of Conjugates *in Vitro*. To test the *in vitro* stability of the immunotoxins, two types of experiments were done using GSH as reagent. First, the samples, after incubation with different excesses of GSH, were tested by densitometric analysis of SDS-PAGE; the results showed less release of mAb from conjugates IT2 and IT3 containing a steric hindrance (Figure 4). In the second experiment the release of toxin after reaction with GSH was monitored by HPLC and quantified by area integration (data not shown).

The results obtained with the two methods were comparable. However, using an excess of GSH >7000, the cleavage of the mAb disulfide bond was measurable only by the SDS procedure.

Evaluation of the Specific Cytotoxicity of Immunoconjugates. The cytotoxicity of each immunoconjugate was evaluated on target (HT-29) and control (MeWo) cell lines. The three conjugates showed the same activity in inhibition of protein synthesis since the IC_{50} values were around 0.2–0.3 nM. All of the immunotoxins were less effective on the nontarget MeWo cells (Figure 5).

Pharmacokinetics. To check the *in vivo* stability of

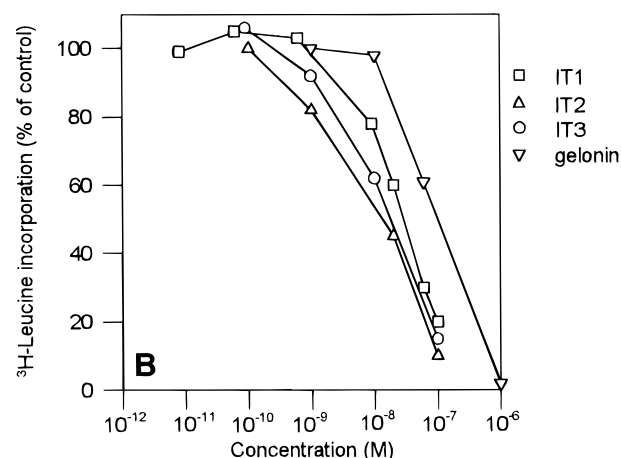
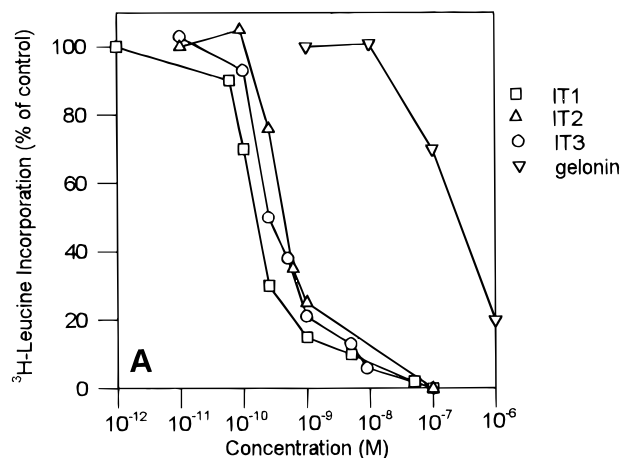


Figure 5. Inhibition of [3H]leucine incorporation in HT-29 (target cell) (A) and MeWo (control cell) (B). The points represent the arithmetic means of three determinations. SDs values (not reported) were <10% of the means.

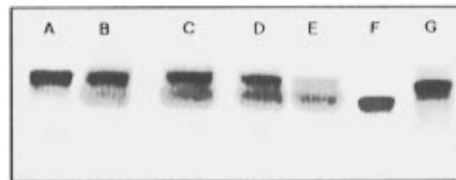


Figure 6. Autoradiograph of 7.5% SDS-PAGE gels of plasma samples taken at various time intervals from mice that had been given iv injections of IT2: (lanes A–E) plasma samples taken at 0, 6, 24, 48, and 144 h after injection, respectively; (lane F) AR-3; (lane G) IT2.

the hindered and unhindered disulfide bond, pharmacokinetic behavior after iv bolus administration in Balb/c mice was evaluated. Each immunotoxin was radio-labeled with ^{125}I and injected iv in groups of mice. Blood samples were collected at interval times, and radioactivity was determined. The plasma samples were analyzed by SDS-PAGE autoradiography and densitometry (Figure 6). The rate at which the unhindered conjugate IT1 broke down to release the free antibody *in vivo* was faster than that of IT2 and IT3. For these, the plasma samples contained approximately equal amounts of intact immunotoxin and released mAb 42–48 h after injection. As was found *in vitro*, IT1 appeared to uncouple more quickly *in vivo*; in fact, the conjugate band decreased to 50% after about 6–8 h.

Plasma concentrations of immunotoxin at each time point were used to construct pharmacokinetic curves for each conjugate (Figure 7). Computerized analysis of the

Table 2. Pharmacokinetic Parameters^a

	A ($\mu\text{g/mL}$)	B ($\mu\text{g/mL}$)	$T_{1/2\alpha}$ (h)	$T_{1/2\beta}$ (h)	AUC ($\mu\text{g}\cdot\text{h}\cdot\text{mL}^{-1}$)	Cl (mL/h)	V_{SS} (mL)	MRT (h)
IT1	0.63 ± 0.06	0.094 ± 0.006	1.8 ± 0.22	27.9 ± 1.39	5.4 ± 0.21	0.49 ± 0.02	14.2 ± 0.77	28.8 ± 1.61
IT2	0.65 ± 0.05	0.10 ± 0.005	1.9 ± 0.21	60.2 ± 1.81	10 ± 0.38	0.34 ± 0.011	20 ± 1.20	56 ± 3.58
IT3	0.76 ± 0.06	0.098 ± 0.005	2.2 ± 0.22	88.3 ± 4.42	15 ± 0.51	0.25 ± 0.0092	27 ± 1.52	107 ± 7.28
AR-3	1.5 ± 0.13	0.72 ± 0.039	2.23 ± 0.25	138.6 ± 5.54	148 ± 5.18	0.014 ± 0.0006	4.1 ± 0.22	215 ± 13.5

^a The values were obtained by adopting a two-compartment open pharmacokinetic model.

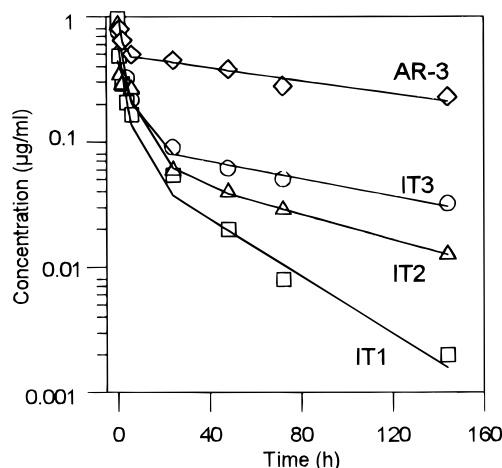


Figure 7. Blood clearance. Mice were given iv injections of radioiodinated immunotoxins, and blood samples were removed at various time intervals later. The percentage of the injected dose that corresponded to intact immunotoxin was determined with plasma samples both by γ counting and by scanning autoradiographs of SDS gels. The points represent the arithmetic means of three determinations. SDs (not reported) were <9% of the means.

clearance data using an open two-compartment pharmacokinetic model gave the parameters shown in Table 2.

The elimination curves were biphasic, having an initial rapid α phase followed by a slower β phase. The immunoconjugates most stable *in vitro* (IT2 and IT3) were eliminated more slowly, while IT1 was cleared rapidly, as shown by progressive increase of the respective β -phase half-lives (from 27.9 h for the unhindered IT1 to 60.2 and 88.3 h for the hindered IT2 and IT3, respectively). In contrast, the enhanced stability of the linker did not effect the α phase half-life, which mainly influences the distribution.

DISCUSSION

In an attempt to evaluate factors affecting immunoconjugate preparation and potency, we developed a series of heterobifunctional cross-linking reagents (19). In this study we synthesized linkers that should be useful to prepare immunotoxins containing disulfide bonds with improved stability *in vivo*. Two different types of bifunctional linkers were synthesized: (1) a set of differently substituted (aryldithio)thioimide derivatives based on an amine-reactive thioimide function and a dithiophenyl group able to perform thiol–disulfide exchange reactions; (2) a series of thioimide derivatives containing a protected *S*-acetyl thiol group. These types of linker share in common reactivity toward lysyl ϵ -amino groups, generating an amidinated linkage and thereby preserving the positive charge of the protein. Some authors have reported that modification of gelonin with reagents that forms positively charged amidines preserves its activity, while it is inactivated by derivatization with *N*-hydroxy-succinimide esters (33). These linkers were designed to generate a protected disulfide linkage after protein–protein conjugation in which a methyl or phenyl group is bound to the carbon atom adjacent to the dithio bond.

To assess the ability of the cross-linking reagents to produce immunoconjugates highly stable *in vivo* but reducible intracellularly, we developed different test procedures.

In the aryldithio series we first tested the reactivity of the precursor nitrile derivatives (hindered versus unhindered) in a thiol–disulfide exchange type using cysteine as thiolating reagent. By considering the kinetic constant values of the thiol–disulfide exchange reaction of the two parent unhindered compounds, 4-[(2-cyanoethyl)dithio]benzamide and 5-[(2-cyanoethyl)dithio]-2-nitrobenzoic acid, we found the major factor in determining the reactivity toward cysteine to be the presence of strong electron-withdrawing groups in the aromatic ring (19). In both cases stability of the linker was strongly enhanced when a methyl or a phenyl group was bound to the carbon near the disulfide bond. For practical purposes we selected the carboxamidothioimide derivatives **13** and **14** to further test the reactivity of this set of linkers toward the protein, since the more reactive **11** and **12** were not sufficiently stable in aqueous buffer.

The next step was to evaluate the ability of the linkers to derivatize the AR-3 mAb and to check the stability of the disulfide group introduced. Reactivity toward the protein strongly decreased when a phenyl group was bound to the carbon atom adjacent to the disulfide bond. In contrast, with a different series of 5-substituted 2-iminothiolanes, reactivity with protein amino groups was unaffected by ring substituents (34). Probably in our series some factors limited the overall reaction kinetics as the aqueous solubility became predominant.

To choose the best hindered cross-linking for preparation of stable disulfide-linked immunotoxins, different features were evaluated, such as (a) stability and solubility of the linker in aqueous solution, (b) reactivity of the linker toward the model protein, and (c) the protective effect of the methyl or phenyl groups toward disulfide bond cleavage. Taking these factors together, M-AMPT appeared to be the best balanced coupling reagent. We therefore applied two coupling procedures taking M-AMPT as reference linker in constructing stable dithio bond-containing immunotoxins: (1) a CDPT-derivatized antibody coupled to M-AMPT-thiolated gelonin to introduce one methyl group adjacent to the disulfide bond (IT2); (2) an M-AMPT-derivatized gelonin coupled to the antibody first derivatized with M-AMPT followed by activation of the thiol group by DTNB (IT3). In this case we introduced symmetrical methyl groups at each end of the dithio linkage. As reference we synthesized an unhindered IT by using CDPT and AMPT to derivatize the antibody and the gelonin respectively (IT1).

Conjugates IT1, IT2, and IT3 showed almost the same cytotoxic activity toward the target HT-29 cell line, whereas they were nearly ineffective on the nontarget MeWo cell line.

In vivo the stability of the hindered versus the unhindered immunotoxins was verified by studying the pharmacokinetic behavior after iv bolus administration in Balb/c mice.

All three ITs had similar α phase half-lives, suggesting

that reducibility of the linkage is not a limiting factor during the α phase.

Instead, in the β phase the sterically hindered conjugate IT2 had a significantly longer half-life (60.2 h) compared with that of the unmodified disulfide IT1 (27.9 h), while the symmetrical dimethyl disulfide-linked IT3 (88.3 h) had the longest β phase half-life. To our knowledge, this is the longest β phase half-life so far reported for an immunotoxin in rodents. Potentially increased *in vivo* therapeutical efficacy of the hindered immunoconjugates was also suggested by the increases in the AUC and MRT values.

Thorpe, both in preclinical and clinical studies (14, 17, 18), showed that IT with a methyl-hindered linker had greater antitumor activity, when given in equimolar dose, than IT with unhindered linkers. Excellent *in vivo* stability as well as favorable pharmacokinetics were also shown in a colorectal tumor-directed immunotoxin (35). Other authors disagreed; studying the *in vivo* therapeutic efficacy of two anti CD7-saporin ITs constructed with either hindered (SMPT) or unhindered (SPDP) linkers, they were unable to show any significant difference (36). It is possible that in some cases the tertiary structure of the coupled protein surrounding the linkage may inhibit the ability of GSH to cleave the disulfide bond in the IT (37). Indeed, it was shown that Abrin A chain IT was less susceptible to cleavage *in vitro* and *in vivo* than other ITs made with ricin A chain, gelonin, or momordin (38).

In conclusion, all of our data are in agreement with previous findings that the introduction of a hindered disulfide linkage into ITs has little or no effect on pharmacological potency (14–16), suggesting that disulfide cleavage is not the rate-limiting step in intoxication of cell by AR-3–gelonin conjugates. Moreover, resistance to cleavage of dithio bond *in vitro* or *in vivo* is directly related to the degree of steric hindrance afforded by the group adjacent to the disulfide bond.

We noted that ITs such as IT3 made with a symmetrical dimethyl-substituted disulfide bond showed a substantially greater *in vivo* stability than the monomethyl-substituted IT2. When two geminal methyl groups are linked to the α -carbon adjacent to the dithio bond, comparable stability and plasma elimination profiles have been observed in comparison to the monomethyl-substituted IT (16).

It will be possible to extend the approach described to design protein–protein or drug–protein conjugates in which controlled time-dependent release of the drug, following systemic delivery, is desirable.

ACKNOWLEDGMENT

We appreciate the excellent technical assistance of Mr. D. Zonari. We thank V. Rossi for the gift of AR-3 monoclonal antibody and Dr. A. Pecorale for the protein radiolabeling, both from Sorin Biomedica, Saluggia, and Prof. G. Bussolati, Dipartimento di Scienze Biomediche ed Oncologia Umana of Turin, for using the Phosphor Imaging. This work was supported by MURST (40–60%), by Associazione Italiana per la Ricerca sul Cancro, by Azienda Ospedaliera San Giovanni Battista, and by CNR grants.

LITERATURE CITED

- Vitetta, E. S., Thorpe, P. E., and Uhr, J. W. (1993) Immunotoxins: magic bullets or misguided missiles? *Immunol. Today* 14, 252–259.
- Wawrzynczak, E. J. (1992) Rational design of immunotoxins: current progress and future prospects. *Anti-Cancer Drug Des.* 7, 427–441.
- Brinkmann, U., and Pastan, I. (1994) Immunotoxins against cancer. *Biochim. Biophys. Acta* 1198, 27–45.
- Carlsson, J., Drevin, H., and Axen, R. (1978) Protein thiolation and reversible protein-protein conjugation. *Biochem. J.* 173, 723–737.
- Gros, O., Jansen, F. K., and Vidal, H. J. (1985) Biochemical aspects of immunotoxin preparation. *J. Immunol. Methods* 81, 283–297.
- King, T. P., Li, Y., and Kochoomian, L. (1978) Preparation of protein conjugates via intermolecular disulfide bond formation. *Biochemistry* 17, 1499–1506.
- Thorpe, P. E., Blakey, D. C., Brown, A. N. F., Knowles, P. P., Knyba, R. E., Wallace, P. M., Watson, G. J., and Wawrzynczak, E. J. (1987) Comparison of two anti-Thy 1.1-abrin A-chain immunotoxins prepared with different cross-linking agents: antitumor effects, *in vivo* fate, and tumor cell mutants. *J. Natl. Cancer Inst.* 79, 1101–1111.
- Masuh, Y., Kishida, K., Saito, M., Umemoto, N., and Hara, T. (1982) Importance of the antigen-binding valency and the nature of the cross-linking bond in ricin A-chain conjugates with antibody. *J. Biochem.* 91, 1583–1591.
- Wawrzynczak, E. J., and Thorpe, P. E. (1988) Effect of chemical linkage upon the stability and cytotoxic activity of A chain immunotoxins. In *Immunotoxins* (A. E. Frankel, Ed.) pp 239–251, Kluwer, Boston.
- Worrell, N. R., Cumber, A. J., Parnell, G. D., Ross, W. C., and Forrester, J. A. (1986) Fate of an antibody-ricin A chain conjugate administered to normal rats. *Biochem. Pharmacol.* 35, 417–423.
- Blakey, D. C., Watson, G. J., Knowles, P. P., and Thorpe, P. E. (1987) Effect of chemical deglycosylation of ricin A chain on the *in vivo* fate and cytotoxic activity of an immunotoxin composed of ricin A chain and anti-Thy1.1 antibody. *Cancer Res.* 47, 947–952.
- Letvin, N. L., Goldmacher, V. S., Ritz, J., Yetz, J. M., Schlossman, S. F., and Lambert, J. M. (1986) *In vivo* administration of lymphocyte-specific monoclonal antibodies in nonhuman primates. *In vivo* stability of disulfide-linked immunotoxin conjugates. *J. Clin. Invest.* 77, 977–984.
- Worrell, N. R., Cumber, A. J., Parnell, G. D., Mirza, A., Forrester, J. A., and Ross, W. C. J. (1986) Effect of linkage variation on pharmacokinetics of ricin A chain-antibody conjugates in normal rats. *Anti-Cancer Drug Des.* 1, 179–188.
- Thorpe, P. E., Wallace, P. M., Knowles, P. P., Relf, M. G., Brown, A. N. F., Watson, G. J., Knyba, R. E., Wawrzynczak, E. J., and Blakey, D. C. (1987) New coupling agents for the synthesis of immunotoxins containing a hindered disulfide bond with improved stability *in vivo*. *Cancer Res.* 47, 5924–5931.
- Greenfield, L., Bloch, W., and Moreland, M. (1990) Thiol-containing cross-linking agent with enhanced steric hindrance. *Bioconjugate Chem.* 1, 400–410.
- Carroll, S. F., Bernhard, S. L., Goff, D. A., Bauer, R. J., Leach, W., and Kung, A. H. C. (1994) Enhanced stability *in vitro* and *in vivo* of immunoconjugate prepared with 5-methyl-2-iminothiolane. *Bioconjugate Chem.* 5, 248–256.
- Ghetie, V., Thorpe, P., Ghetie, M. A., Knowles, P., Uhr, J. W., and Vitetta, E. S. (1991) The GLP large scale preparation of immunotoxins containing deglycosylated ricin A chain and a hindered disulfide bond. *J. Immunol. Methods* 142, 223–230.
- Amlot, P. L., Stone, M. J., Cunningham, D., Fay, J., Newman, J., Collins, R., May, R., McCarthy, M., Richardson, J., Ghetie, V., Ramilo, O., Thorpe, P. E., Uhr, J. W., and Vitetta, E. S. (1993) A phase I study of an anti-CD22-deglycosylated ricin A chain immunotoxin in the treatment of B-cell lymphomas resistant to conventional therapy. *Blood* 82, 2624–2633.
- Delprino, L., Giacomotti, M., Dosio, F., Brusa, P., Ceruti, M., Grosa, G., and Cattel, L. (1993) Toxin-targeted design for anticancer therapy. I: synthesis and biological evaluation of new thioimide heterobifunctional reagents. *J. Pharm. Sci.* 82, 506–512.
- Delprino, L., Giacomotti, M., Dosio, F., Brusa, P., Ceruti, M., Grosa, G., and Cattel, L. (1993) Toxin-targeted design for anticancer therapy. II: preparation and biological comparison

- of different chemically linked gelonin-antibody conjugates. *J. Pharm. Sci.* **82**, 699–704.
- (21) Thorpe, P. E., Brown, A. N. F., Ross, W. C. J., Cumber, A. J., Detre, S. I., Edwards, D. C., Davies, A. J. S., and Stirpe, F. (1981) Cytotoxicity acquired by conjugation of an anti-Thy_{1.1} monoclonal antibody and the ribosome inactivating protein, gelonin. *Eur. J. Biochem.* **116**, 447–454.
- (22) Prat, M., Morra, I., Bussolati, G., and Comoglio, P. M. (1985) CAR-3, a monoclonal antibody-defined antigen expressed on human carcinomas. *Cancer Res.* **45**, 5799–5807.
- (23) Duncan, R. J. S., Weston, P. D., and Wrigglesworth, R. (1983) A new reagent which may be used to introduce sulfhydryl groups into proteins, and its use in the preparation of conjugates for immunoassay. *Anal. Biochem.* **132**, 68–73.
- (24) Cattel, L., Delprino, L., Brusa, P., Dosio, F., Comoglio, P. M., and Prat, M. (1988) Comparison of blocked and non-blocked ricin-antibody immunotoxins against human gastric carcinoma and colorectal adenocarcinoma cell lines. *Cancer Immunol. Immunother.* **27**, 233–240.
- (25) Fraker, P. J., and Speck, J. D. (1978) Protein and cell membrane iodinations with a sparingly soluble chloroamide, 1,2,4,6-tetrachloro-3a,6a-diphenylglycouril. *Biochem. Biophys. Res. Commun.* **80**, 849–857.
- (26) Dosio, F., Brusa, P., Delprino, L., Grosa, G., Ceruti, M., and Cattel, L. (1994) A new approach in the synthesis of immunotoxins: ribosome inactivating protein noncovalently bound to monoclonal antibody. *J. Pharm. Sci.* **83**, 206–211.
- (27) Scott, C. F. Jr., Goldmacher, V. S., Lamber, J. M., Jackson J. V., and McIntyre, G. D. (1987) An immunotoxin composed of a monoclonal antitransferrin receptor antibody linked by a disulfide bond to the ribosome-inactivating protein gelonin: potent in vitro and in vivo effects against human tumor. *J. Natl. Cancer Inst.* **79**, 1163–1172.
- (28) Holmberg, B., and Schjamberg, E. (1940) Omattade syror och tioattiksyra. *Ark. Kemi, Mineral. Geol.* **40A** (7), 1–10.
- (29) Roger, R., and Neilson, D. G. (1961) The chemistry of imidates. *Chem. Rev.* **61**, 179–211.
- (30) Behforouz, M., and Kerwood, J. E. (1969) Alkyl and arylkyl sulfenimides. *J. Org. Chem.* **34**, 51–55.
- (31) Stirpe, F., Olsnes, S., and Pihl, A. (1980) Gelonin a new inhibitor of protein synthesis, non toxic to intact cells. *J. Biol. Chem.* **255**, 6947–6953.
- (32) Rosenblum, M. G., Kohr, W. A., Beattie, K. L., Beattie, W. G., Marks, W., Toman, P. D., and Cheung, L. (1995) Amino acid sequence analysis, gene construction, cloning, and expression of gelonin, a toxin derived from *Gelonium multiflorum*. *J. Interferon Cytokine Res.* **15**, 547–555.
- (33) Lambert, J. M., Senter, P. D., Yau-Young, A., Blatter, W. A., and Goldmacher, V. S. (1985) Purified immunotoxins that are reactive with human lymphoid cells. *J. Biol. Chem.* **260**, 12035–12041.
- (34) Goff, D. A., and Carroll, S. F. (1990) Substituted 2-iminothiolanes: reagents for the preparation of disulfide cross-linked conjugates with increased stability. *Bioconjugate Chem.* **1**, 381–386.
- (35) Calvete, J. A., Newell, D. R., Charlton, C. J., and Wright, A. F. (1993) Pharmacokinetic studies in mice with ICI D0490, a novel recombinant ricin A-chain immunotoxin. *Br. J. Cancer* **67**, 1310–1315.
- (36) Flavell, D. J., Boehm, D. A., Okayama, K., Kohler, J. A., and Flavell, S. U. (1994) Therapy of human T-cell acute lymphoblastic leukaemia in severe combined immunodeficient mice with two different anti-CD7-saporin immunotoxins containing hindered or non-hindered disulphide cross-linkers. *Int. J. Cancer* **58**, 407–414.
- (37) Cumber, A. J., Westwood, J. H., Henry, R. V., Parnell, G. D., Coles, B. F., and Wawrzynczak, E. J. (1992) Structural features of the antibody-A chain linkage that influence the activity and stability of ricin A chain immunotoxins. *Bioconjugate Chem.* **3**, 397–401.
- (38) Wawrzynczak, E. J., Cumber, A. J., Henry, R. V., May, J., Newell, D. R., Parnell, G. D., Worrell, N. R., and Forrester, J. A. (1990) Pharmacokinetics in the rat of a panel of immunotoxins made with abrin A chain, ricin A chain, gelonin, and momordin. *Cancer Res.* **50**, 7519–7526.

BC970025W

Single-Chain Fv/Folate Conjugates Mediate Efficient Lysis of Folate-Receptor-Positive Tumor Cells

Bryan K. Cho,[†] Edward J. Roy,^{‡§} Todd A. Patrick,[§] and David M. Kranz^{*,†}

Department of Biochemistry, Department of Psychology, and Neuroscience Program, University of Illinois, 600 South Matthews Avenue, Urbana, Illinois 61801-3792. Received October 11, 1996[®]

Bispecific antibodies that bind to a tumor antigen and the T cell receptor (TCR) redirect cytotoxic T lymphocytes (CTL) to lyse tumor cells which have escaped normal immune recognition mechanisms. One well-characterized tumor antigen, the folate receptor (FR), is expressed on most ovarian carcinomas and some types of brain cancer. Recently, it was shown that conjugates of folate and anti-TCR antibodies are extremely potent bispecific agents that target tumor cells expressing the high-affinity folate receptor, but not normal cells expressing only the reduced folate carrier protein. In this paper, it is shown that the size of these conjugates can be reduced to the smallest bispecific agent yet described (30 kDa) by attaching folate to a single-chain antibody, scFv, of the anti-TCR antibody KJ16. The scFv/folate conjugates are as effective as IgG/folate conjugates in mediating lysis of FR⁺ tumor cells by CTL. The optimal folate density was in the range of 5–15 folate molecules per scFv or IgG molecule, which yielded half-maximal lysis values (EC₅₀) of approximately 40 pM (1.2 ng/mL for scFv). Finally, the scFv/folate conjugates could efficiently target tumor cells even in the presence of free folic acid at concentrations that are normally found in serum. Compared to conventional bispecific antibodies, the small size of scFv/folate conjugates may prove advantageous in the ability to penetrate tumors and in reduced immunogenicity.

INTRODUCTION

It has been known for over 50 years that the immune system is capable of attacking and eliminating very large tumor burdens but sometimes fails to do so (1). Although the basis of this "escape" is incompletely understood (2), one mechanism involves the failure of tumor cells to express antigens in a context that is essential for recognition by the immune system [reviewed by Pardoll (3)]. Another mechanism might be the loss of costimulatory ligands and adhesion molecules that aid in the recognition and activation of T cells (4).

One potential way to direct T cells or other immune effector cells against tumor cells is with bispecific antibodies [reviewed by Fanger (5)]. Bispecific antibodies can be constructed to recognize two separate antigens, one on the tumor surface and the other on the surface of a cytotoxic T cell (e.g. TCR¹). Many tumor cells have potential target antigens that are tumor-specific or quantitatively more abundant on tumor cells than normal

cells (tumor-associated). By bringing together the tumor cell and an activated T cell, bispecific antibodies can redirect the cytotoxicity of T cells against tumors. Previous work has demonstrated the effectiveness of bispecific antibodies against tumors *in vitro* and *in vivo* and some clinical trials have been initiated (e.g. see refs 6–12). It has generally been agreed that optimizing the properties of bispecific antibodies should improve their clinical effectiveness.

Among the tumor antigens targeted with bispecific antibodies has been the high-affinity folate receptor (FR), also called the folate binding protein. The FR is now known to be expressed at elevated levels on many human tumors, including ovarian carcinomas [e.g. one study showed that 98% of ovarian tumors express the FR (13)], choroid plexus carcinomas, and ependymomas (14, 15). These cancers affect a significant segment of the population: ovarian cancer is the fourth leading cause of cancer death among women (16) and at least 30% of early childhood tumors are diagnosed as ependymoma or choroid plexus tumors (17, 18).

The presence of high levels of FR on human tumor cells has made it an attractive candidate for tumor-specific therapeutics. Monoclonal antibodies to the human FR have been generated and shown to be effective at targeting FR⁺ tumors *in vitro* (19–21). Clinical trials with radiolabeled antibodies and anti-FR/anti-CD3 bispecific antibodies have recently been initiated (9, 10, 12). Another approach has been to use the endocytic properties of the FR to deliver toxins or antisense nucleotides to the interior of malignant cells (22, 23). Although relatively low levels of FR mRNA have been detected in most normal human tissues (14), several studies have shown that normal choroid plexus, kidney, thyroid, colon, and placenta may have elevated levels [14, 24, 25; reviewed by Antony (26)]. Despite the presence of FR on normal human tissue, clinical trials using the anti-FR/anti-CD3 bispecific antibody have not demonstrated any toxicity associated with cytolysis of normal FR expressing tissue (9, 10).

* Author to whom correspondence should be addressed [telephone (217) 244-2821; fax (217) 244-5858; e-mail d-kranz@uiuc.edu].

[†] Department of Biochemistry.

[‡] Department of Psychology.

[§] Neuroscience Program.

[®] Abstract published in *Advance ACS Abstracts*, April 1, 1997.

¹ Abbreviations: CTL, cytotoxic T lymphocyte; FR, folate receptor; TCR, T cell receptor; scFv, single-chain antibody binding domain; MHC, major histocompatibility complex; K_D, dissociation constant; SV40, simian virus 40; EC₅₀, concentration of antibody/folate conjugate required for half-maximal CTL mediated cytotoxicity; fol, folate; EDC, 1-ethyl-3-[3-(dimethylamino)propyl]carbodiimide hydrochloride; FITC, 5-aminofluorescein isothiocyanate; Ga, gallium; Fab, antigen binding fragment derived from papain digestion of Ig molecule; V regions, variable regions of IgG heavy and light chains; ϵ , extinction coefficient; SDS, sodium dodecyl sulfate; PAGE, polyacrylamide gel electrophoresis; PBS, 10 mM phosphate buffer, 150 mM NaCl, pH 7.3; PBS-BSA, PBS containing 0.1% bovine serum albumin; MTX, methotrexate.

The high intrinsic affinity of folate for FR ($K_d \sim 1$ nM) suggested to us that attachment of folate directly to an anti-TCR antibody might efficiently target FR⁺ tumor cells for lysis by T cells. We recently reported that such conjugates have very potent targeting activity without adversely affecting normal cells that express only the reduced folate carrier protein [$K_d \sim 1.5 \times 10^{-6}$ (27)], which is responsible for normal dietary uptake of folate and the transport of folate-based dihydrofolate reductase inhibitors such as methotrexate. It is reasonable to predict that the most effective agents for targeting solid tumors will have reduced sizes that allow greater tumor penetration. For instance, comparative biodistribution studies with ¹²⁵I-labeled IgG, F(ab)₂, Fab fragments, and scFv in human colon carcinoma xenografts in athymic mice demonstrated that scFv molecules penetrated tumor more rapidly, to a greater depth, and more uniformly than other forms of the antibody (28).

In this paper, a 29-kDa scFv of the anti-V β 8 antibody KJ16 (29) was conjugated with folate and its targeting potential was evaluated *in vitro*. Cytotoxicity assays with these preparations showed that lysis of mouse FR⁺ tumor cells was highly specific and correlated directly with FR density ($r = 0.93$). Comparison between folate-labeled-IgG and scFv demonstrated that both conjugates have nearly identical targeting efficiencies ($EC_{50} = 40$ pM), and lysis with scFv/folate could be detected at concentrations as low as 1 pM. Direct competition experiments with free folate demonstrated that the scFv/folate conjugate could effectively target FR⁺ tumor cells even at folate concentrations above normal serum levels. The reduced size of the scFv/folate compared to other bispecific reagents as well as its high potency suggests that it has potential for *in vivo* therapy. In addition, the conjugate may serve as a model for the development of future novel bispecific agents that contain small ligands specific for tumor cell surface antigens.

EXPERIMENTAL PROCEDURES

Cell Lines and Antibodies. The following DBA/2-derived tumor cell lines were maintained in RPMI 1640 containing 5 mM HEPES, 10% fetal calf serum, 1.3 mM L-glutamine, 100 units of penicillin/mL, 100 μ g/mL streptomycin, and 50 μ M 2-mercaptoethanol: Mel, murine erythroleukemia cell (30); La, a subline of Mel selected on low folate (31); L1210, a murine leukemia cell line (32); and F2-MTX^rA, a MTX-resistant subline of L1210 selected for increased expression of FR- β by growth on low folic acid (33). La expresses primarily the α isoform of folate receptor (FR), F2-MTX^rA expresses only the FR- β isoform, and L1210 expresses both α and β isoforms. CTL clone 2C, a V β 8⁺ alloreactive cell line specific for L^d (34), was maintained in the same RPMI medium supplemented with 10% (v/v) supernatant from concanavalin A-stimulated rat spleen cells, 5% methyl α -mannoside, and mitomycin C treated BALB/c mouse spleen cells as stimulators. KJ16 is a rat IgG antibody specific for the V β 8.1–2 domains of the TCR (35) and was provided by Drs. Kappler and Marrack. KJ16 monoclonal antibody was prepared from tissue culture supernatant generated in a Vita-Fiber miniflow path bioreactor (Amicon) and concentrated by precipitating twice in 50% ammonium sulfate. KJ16 Fab fragments, FITC-labeled Fab fragments, and KJ16 scFv were generated and purified as described previously (29). Briefly, scFv was refolded from inclusion bodies, and monomeric scFv was purified by G-200 HPLC purification. Monoclonal antibody 30.5.7 is specific for the major histocompatibility complex (MHC) class I product L^d (36) and was prepared as ascites

fluid and used without further purification in some cytotoxicity assays.

Preparation of Antibody/Folate Conjugates. Folate was coupled through its carboxyl groups to antibody amine groups using a carbodiimide procedure described previously (27, 37). Unless indicated, a 5-fold molar excess of 1-ethyl-3-[3-(dimethylamino)propyl]carbodiimide hydrochloride (EDC, Pierce Chemical Co.) was added to folate (Sigma) dissolved in dimethyl sulfoxide. After 30 min at room temperature in the dark, a 20–700-fold molar excess of the EDC-activated folate was added to 0.1–0.5 mg of antibody in 0.1 M MOPS, pH 7.5. After 1 h at room temperature, the sample was either applied to a Sephadex G-25 column pre-equilibrated in 0.1 M MOPS or immediately dialyzed into phosphate-buffered saline (PBS; 10 mM sodium phosphate, 150 mM sodium chloride, pH 7.3). If passed over a G-25 column, the excluded-peak fractions were pooled and dialyzed against PBS. After dialysis, protein concentrations were determined using the bicinchoninic assay (Pierce) using a protein A purified intact mouse antibody as the standard. Antibody conjugates were also analyzed spectrophotometrically at 363 nm, and the density of the folate per antibody was calculated by dividing the molar concentration of folate on the conjugate (A_{363}/ϵ_M ; $\epsilon_M = 6197$ M⁻¹) by the antibody concentration. Folate densities obtained ranged from ~ 1 to ~ 120 folates/antibody. Conjugates were stored at 4 °C in the dark.

Mass Spectrometry. Mass spectra were obtained on a ToFSpec using electrospray ionization. Samples were dialyzed against 1 mM potassium phosphate buffer, pH 8.0, and concentrated to 10–25 pmol/mL. Analysis was performed by the Mass Spectrometry Laboratory, School of Chemical Science, University of Illinois.

Folate Binding Assays. Binding assays were conducted by using ¹²⁵I-labeled folate (NEN; specific activity = 2200 Ci/mmol; 1 Ci = 37 GBq). Cells were washed with PBS containing 0.1% bovine serum albumin, pH 7.3 (PBS-BSA), to remove excess free folate present in the cell culture medium. Cells, labeled folate, and competitors were incubated in triplicate in 50 μ L of PBS-BSA for 1 h at 37 °C. Incubation at 37 °C has previously been shown to produce levels of binding similar to that obtained with acid pretreatment (27). Samples were loaded into tubes containing 300 μ L of oil [80% (v/v) dibutyl phthalate/20% (v/v) olive oil], and bound and free ligand were separated by a 3 s centrifugation at 12000g. Tubes were frozen and cut to allow the radioactivity in the cell pellet and supernatants to be quantitated separately.

T Cell Receptor Binding Assays. The relative affinity of the scFv/folate conjugates for the TCR was determined by a competition assay with 5-aminofluorescein isothiocyanate (FITC)-labeled KJ16 Fab fragments as previously described (29). In brief, various concentrations of antibody were added to triplicate sets of 6×10^5 2C cells in the presence of a constant amount of FITC-labeled Fab fragments. After a 30 min incubation on ice, the entire mixture (antibody + FITC-labeled Fab fragments + 2C cells) was passed through a flow cytometer without washing. Inhibition by various KJ16 preparations was measured by quantitating the decrease in bound fluorescence by flow cytometry (performed with a Coulter Electronics EPICS 752 at the University of Illinois Biotechnology Center). The concentrations of unlabeled antibody giving 50% inhibition (IC_{50}) were determined relative to the maximum fluorescence (in the absence of inhibitor) and the background fluorescence (in the presence of a large excess of intact antibody).

Cytotoxicity Assays. Tumor cells were labeled with

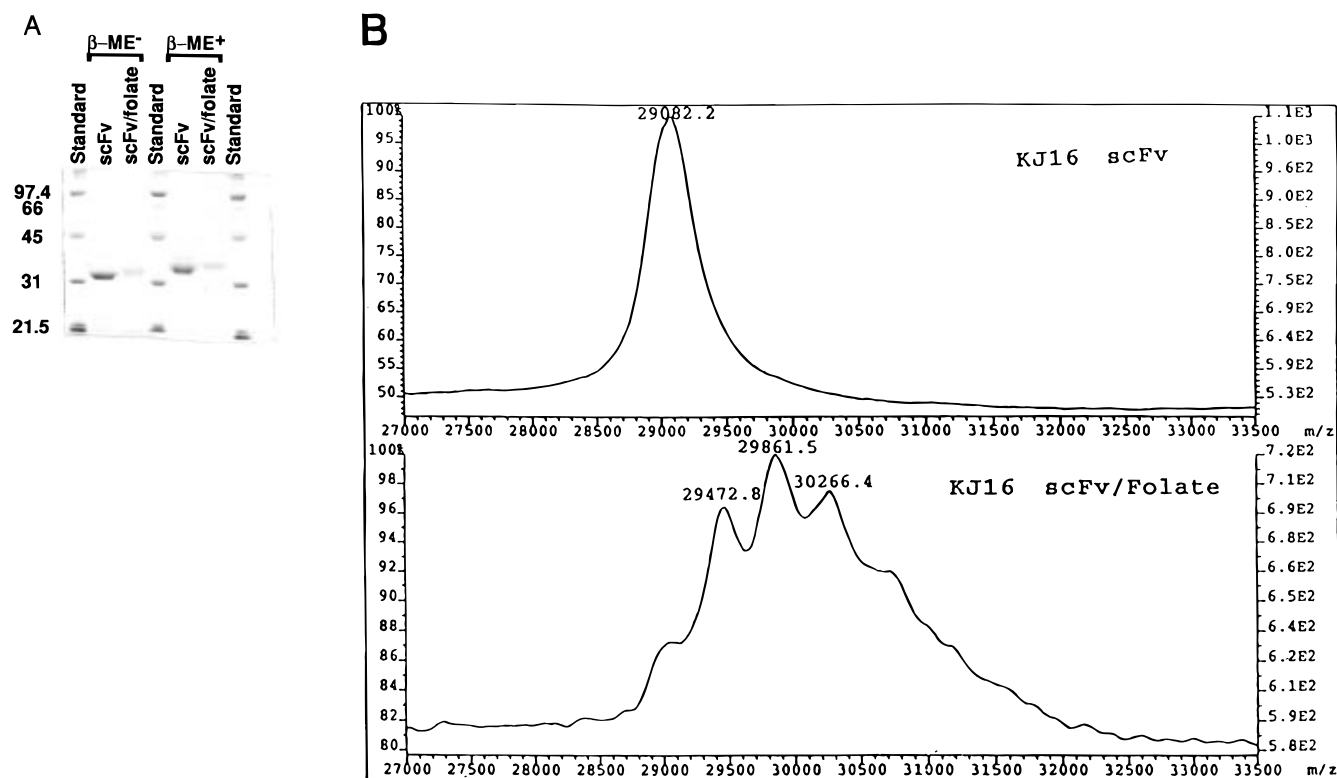


Figure 1. SDS-PAGE analysis and mass spectra of purified preparations of scFv KJ16 and scFv/folate conjugate: (A) samples were electrophoresed through a 10% polyacrylamide gel under reducing and nonreducing conditions, and proteins were visualized by staining with Coomassie Blue; (B) samples were concentrated, dialyzed against 1 mM potassium phosphate buffer, pH 8.0, and mass spectra were obtained on a ToFSpec using electrospray ionization. Purified scFv existed as a single species with a molecular mass of 29 082 Da. In contrast, folate-labeled scFv existed as a collection of antibody populations, each differing by the molecular mass of a folate molecule (~400 Da), detectable up to 7 folates per antibody.

50–100 μ L of ^{51}Cr (2.5 mCi/mL) for 60 min at 37 $^{\circ}\text{C}$, washed twice with folate-free RPMI 1640 medium containing 5% (v/v) fetal calf serum (folate-free media), and used in 96-well plate cytotoxicity assays at 10^4 cells per well. Because each of these cell lines also expressed the alloantigen L^d, which is recognized by CTL 2C, assays were performed in the presence of anti-L^d antibody to minimize non-FR-mediated lysis. Ascites of anti-L^d antibody 30.5.7 was diluted 1:100 into folate-free media containing effector cells (2C). Effector cells were added to target cells at an effector-to-target cell ratio of 5:1. Antibodies and folate/antibody conjugates were diluted in folate-free media and added to triplicate wells at various concentrations. Plates were incubated at 37 $^{\circ}\text{C}$ for 4 h in 5% CO_2 , and supernatants were removed for γ counting. For the inhibition of scFv/folate by free folate, a nonsaturating concentration of scFv/folate (3 nM) that would generate maximal cytotoxicity was used together with various concentrations of free folate. Unless indicated otherwise, the specific release mediated by the folate conjugates was determined by subtracting the release in the absence of the conjugates [e.g. % specific release = (experimental counts – spontaneous counts)/(maximal counts – spontaneous counts) \times 100].

EC_{50} values (i.e. the concentration of antibody/folate conjugate required for half-maximal specific lysis) were determined by linear regression. Among independent experiments, EC_{50} values and maximum cytotoxicity could vary for the same conjugate preparation primarily due to differences in CTL activity. For example, noticeable reductions in CTL 2C activity can be observed after multiple passages *in vitro* (unpublished data, D.M.K.). Therefore, for comparison of EC_{50} values from different experiments (i.e. Figure 5B), assay results were normalized by dividing each calculated EC_{50} by the EC_{50} of the

most potent conjugate in a given experiment [e.g. $\text{EC}_{50}^{\text{normalized}} = (\text{EC}_{50}/\text{EC}_{50}^{\text{low}})$]. The inverse of this normalized value, $[(\text{EC}_{50}^{\text{normalized}})^{-1}]$, which we have called the targeting index] was plotted as a function of folate density on the antibody, where a targeting index = 1 specifies the most potent conjugate.

RESULTS

Characterization of scFv/Folate Conjugates. The scFv of KJ16, an anti-V β 8 antibody, was purified from *Escherichia coli* inclusion bodies after guanidine denaturation, refolding, and HPLC gel filtration. Purified scFv migrated as an apparent 35-kDa protein on SDS-PAGE gels (Figure 1A). Folate was coupled to the scFv using the carbodiimide (EDC) reaction, which links carboxyl groups of folate to primary amine groups on the protein. In the engineering of the scFv, the V_L and V_H domains were joined by the 26 residue linker, 205s, that contains 8 lysine residues (29, 38). We reasoned that the presence of multiple lysine residues in a highly accessible, solvent-exposed region may result in higher folate densities in the linker region as opposed to the antibody V regions. In initial studies, folate was coupled to the scFv at a 100:1 folate to antibody molar ratio. Under these conditions, scFv/folate preparations contained an average of 3–8 folates per antibody ($N = 3$), on the basis of spectrophotometric analysis. Consistent with this finding, migration of the scFv/folate conjugate on SDS-PAGE gels was slightly slower than that of scFv and the band was more diffuse (Figure 1A).

The folate density determined by photometry does not provide information about the heterogeneity of the conjugates. To determine the range of epitope densities within a single preparation, scFv/folate conjugates were

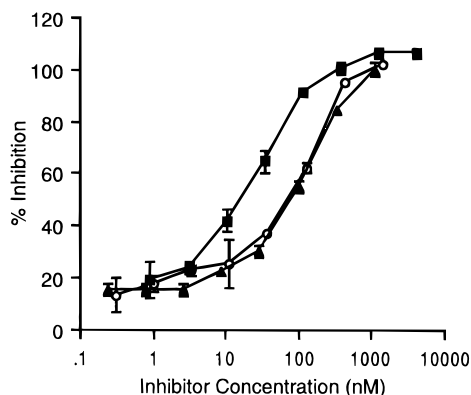


Figure 2. Binding of KJ16 scFv/folate to cell surface T cell receptor. The binding of FITC-labeled KJ16 Fab fragments to the V β 8-positive T cell clone 2C was inhibited by purified scFv/folate, scFv, or Fab fragments. A total of 6×10^5 2C cells was incubated for 30 min at 4 °C with FITC-labeled KJ16 Fab fragments ($\sim 7.0 \times 10^{-8}$ M) and various concentrations of folate-labeled scFv KJ16 (7.8 fol/scFv, \blacktriangle), unlabeled scFv (\blacksquare), and unlabeled Fab fragments (\circ). A relative affinity of the scFv/folate was determined by comparing the concentrations required to inhibit 50% of the FITC-labeled Fab fragments from binding the 2C TCR.

examined by electrospray ionization mass spectrometry (Figure 1B). Unlabeled scFv demonstrated a single peak with a molecular mass of 29 082 Da. In contrast, folate-labeled scFv existed as a collection of antibody populations, each differing by the molecular mass of a folate molecule (~ 400 Da), detectable up to 7 folates per antibody. Integration of mass spectra showed that $>85\%$ of the scFv molecules were labeled with one or more folate molecules. Folate densities estimated from mass spectra were generally 1.5–2-fold lower than densities estimated by spectrophotometry. This could in part be due to lower solubility of high-density conjugates under conditions required for mass spectrometry or to the dissociation of some folate molecules during ionization.

Binding of scFv/Folate Conjugates to the T Cell Receptor. To examine if folate conjugation affected the binding of scFv antibodies to the TCR, a scFv/folate conjugate was compared with unlabeled scFv. In a competitive flow cytometric assay, fluorescein-labeled KJ16 Fab fragments were inhibited from binding the V β 8-positive CTL clone 2C by unlabeled Fab fragments, scFv, or scFv/folate (Figure 2). As shown previously, scFv antibodies have an approximate 3-fold higher apparent affinity than Fab fragments, possibly because of the presence of noncovalently associated scFv dimers (29). Comparison of folate-labeled and unlabeled scFv showed that the folate conjugate had an apparent affinity ~ 3 -fold lower than scFv (i.e. approximately equal to KJ16 Fab fragments). This decreased binding, compared to unlabeled scFv, could be due either to chemical modification of active site residues with folate or to the interference of dimer formation by folate. The fact that folate conjugates bound the TCR as well as KJ16 Fab fragments, which have a K_D of ~ 130 nM (29, 39), indicated that the conjugates have potential to mediate lysis of target cells by CTLs.

Binding of scFv/Folate Conjugates to Folate Receptors on Tumor Cells. The ability of scFv/folate conjugates to bind folate receptors (FR) on the surface of tumor cells was examined by a competition binding assay using 125 I-labeled folate as the labeled ligand (Figure 3). The competition assay used the F2-MTX^A cell line that expresses the β isoform of the FR. Competitors included various concentrations of free folate, unlabeled scFv, and three different scFv/folate preparations. Examination of

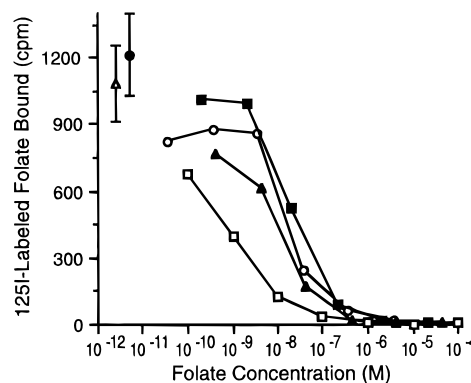


Figure 3. Binding of KJ16 scFv/folate to folate receptors. 125 I-labeled folate ($\sim 1.8 \times 10^{-10}$ M, 2000 Ci/mM) was incubated with F2-MTX^A cells in the presence or absence of competitors for 1 h at 37 °C. Concentrations refer to folate rather than antibody concentrations. Competitors included free folate (\square) and KJ16 scFv/folate conjugates with different folate densities: 2.8 fol/scFv (\circ), 9.2 fol/scFv (\blacksquare), and 20.4 fol/scFv (\blacktriangle). Inhibition was not observed in the absence of competitor (Δ) or in the presence of unconjugated scFv (\bullet) (error shown is \pm average SEM).

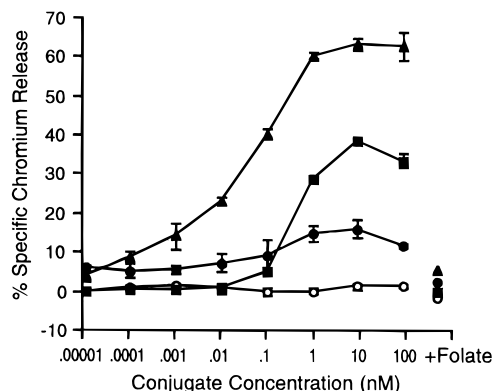


Figure 4. Cytotoxicity assay of various tumor cell lines with the scFv/folate conjugate and CTL clone 2C. Various concentrations of the scFv/folate conjugate were incubated with 51 Cr-labeled tumor cells and CTL 2C for 4 h at an effector-to-target ratio of 5:1. Experiments were performed in the presence of anti-L^d antibody to minimize lysis due to recognition of L^d, the nominal ligand for CTL 2C. Lysis correlated directly with the level of FR expressed by the cell line: F2-MTX^A (200 000 sites/cell, \blacktriangle); La (60 000 sites/cell, \blacksquare); L1210 (8 000 sites/cell, \bullet); Mel (not detectable FR, \circ). Assays with free folate at a final concentration of $1.5 \mu\text{M}$ were performed with the scFv/folate conjugate at a concentration of 0.09 nM (+ folate).

the binding curves showed that folate-conjugated antibody, but not unlabeled scFv, binds to the FR⁺ tumor cell line. However, on the basis of molar folate concentration, the folate conjugates had a relative affinity that was approximately 10–30-fold less than that of free folate. This decrease in apparent affinity was consistent with previous observations (27) and could be partly attributed to the carbodiimide labeling procedure. This procedure links folate through either the α or γ carboxyl group, but only linkage through the γ carboxyl retains binding (40). It is also possible that receptor-mediated internalization or decreased accessibility of the FR may also explain the lower apparent affinity of the folate conjugate. Included in the latter is the possibility that neighboring folates or amino acids sterically hinder interaction with the FR.

CTL-Mediated Lysis of FR⁺ Tumor Cells by scFv/Folate Conjugates. The specificity and efficiency of tumor targeting with scFv/folate conjugates were examined in a 51 Cr release assay with CTL clone 2C (Figure 4). Four different tumor cell lines that have a range of cell surface FR densities were used as target cells: F2-

MTX^rA (200 000 sites/cell); La (60 000 sites/cell); L1210 (8 000 sites/cell); Mel (no detectable FR). Each of the FR⁺ cell lines was lysed in the presence of the scFv/folate conjugate, and the extent of lysis was directly correlated with the expression level of the FR ($r = 0.93$). Lysis was completely inhibited by free folate, indicating that targeting of the tumor cells was specifically mediated by the folate receptor and not some other cell surface molecule. The lysis mediated by these conjugates was highly specific (e.g. the FR⁻ cell line Mel was not lysed by the conjugate even at concentrations over 10^5 times that required for detectable killing of the FR⁺ cell line F2-MTX^rA) and extremely potent (e.g. lysis was detectable at concentrations as low as 1 pM of scFv/folate). The slight reduction in observed lysis at the highest concentrations of conjugate occurs because excess bispecific antibody yields monospecific binding without cell-to-cell cross-linking (41). The presence of reduced folate carrier protein (as present in Mel and in all other normal cells) does not result in cell destruction. It is important to point out that the FR density reportedly on ovarian tumors is even higher (~1 million/cell) than those on these tumor cell lines (21).

Effects of Folate Density on Targeting. To examine the effects of folate density and labeling on the targeting efficiency of scFv/folate conjugates, the antibody was labeled with folate under various carbodiimide-mediated coupling conditions. The carbodiimide EDC couples folate through the free carboxyl groups, but when used in the presence of protein, it may also lead to protein modification and subsequent precipitation or inactivation. To evaluate the optimal levels of EDC for folate coupling, several different concentrations of EDC at a constant folate concentration were used during coupling. EDC used at either 13 or 65 mM generated conjugates with approximately equal targeting efficiency. EDC used at 260 mM yielded conjugates with reduced efficiency and frequently led to protein precipitation (data not shown).

To directly examine the effect of folate density, activated folate was prepared at a constant EDC/folate ratio (5:1) and conjugates were produced by adding different ratios of activated folate to the scFv protein. After dialysis to remove unreacted folate and excess EDC, conjugates were evaluated by spectrophotometry to determine folate densities and cytotoxicity assays to evaluate targeting efficiency. Folate densities ranged from approximately 1 to 20 folates per scFv. As shown in Figure 5A, each of the conjugates was capable of mediating lysis of the FR⁺ tumor cell line by CTL clone 2C. However, conjugates with either the lowest density (1.3 folates/scFv) or highest density (20.4 folates/scFv) were 5–10-fold less effective than conjugates with intermediate folate densities.

To better evaluate the effects of folate density, the above experiment was performed with several additional folate conjugate preparations. To directly compare the results of these assays, the EC₅₀ of each conjugate was determined by linear regression and divided by the EC₅₀ of the conjugate that yielded the highest targeting efficiency (i.e. the lowest EC₅₀; see Experimental Procedures). A plot of the normalized targeting values as a function of the folate density (Figure 5B) demonstrates that optimal folate density appears to be in the range of 5–15 folates/scFv. At higher folate densities, the targeting efficiency of the conjugates is generally lower and more variable than those of conjugates with an intermediate amount of folate. The reduction in targeting efficiency at higher folate densities is not due to the inability of these conjugates to bind to FR⁺ cells (Figure 3), but is likely a consequence of chemical modification

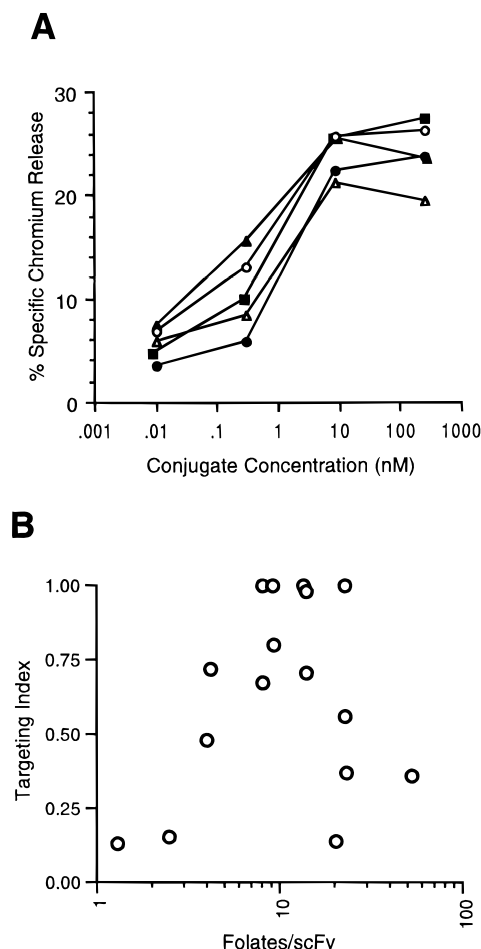


Figure 5. Effect of folate density on targeting with scFv/folate conjugates: (A) scFv/folate conjugates with different folate densities were prepared by labeling scFv protein with various amounts activated folate, using an EDC/folate ratio of 5:1 (EDC = 65 mM). Folate densities were 1.3 fol/scFv, ●; 4.0 fol/scFv, ■; 9.2 fol/scFv, ▲; 9.3 fol/scFv, ○; and 20.4 fol/scFv, △. Conjugates were tested in cytotoxicity assays using F2-MTX^rA and CTL 2C. (B) Relative targeting efficiency of various scFv/folate conjugates as a function of increasing folate density. Targeting index values were determined by normalizing EC₅₀ values of the various conjugates with the most effective conjugate (value = 1) (see Experimental Procedures for details). Each open circle (○) represents a single scFv/folate conjugate prepared using an EDC/folate ratio of 5:1 (EDC 33–65 mM) and tested in cytotoxicity assays using F2-MTX^rA and CTL 2C.

of amino acid residues important in TCR binding by the scFv or in scFv stability.

Comparison of Intact Antibody and scFv. To determine the relative effectiveness of intact KJ16 IgG versus scFv-KJ16, both forms were labeled with folate at a 100:1 molar ratio of activated folate to antibody and under identical EDC reaction conditions (33 mM EDC, 6.7 mM folate). These conditions yielded folate densities of 7 and 5 for the scFv and intact antibody, respectively. Cytotoxicity assays with these preparations showed nearly identical targeting efficiencies for the intact and scFv forms of KJ16 (Figure 6). The concentration required to obtain 50% of the maximal specific release (EC₅₀) was approximately 40 pM (1.2 ng/mL for scFv). Comparison of intact and scFv conjugates in an ¹²⁵I-labeled folate binding assay indicated no significant difference in their ability to bind FR (data not shown).

Intact KJ16 antibody was also labeled at various folate densities to determine if targeting efficiency could be optimized further. Conjugates were again evaluated by spectrophotometry to determine folate densities and cytotoxicity assays to evaluate targeting efficiency (Fig-

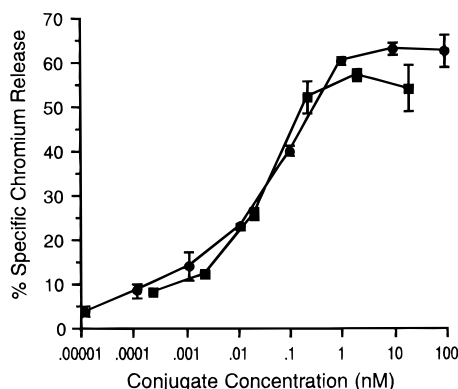


Figure 6. Comparison of scFv/folate and IgG/folate in CTL-mediated lysis of tumor cells. Folate was conjugated to KJ16 scFv and intact antibody under identical conditions (3.3 mM EDC, 100:1 molar ratio of folate/antibody), yielding conjugates with 7 fol/scFv (●) and 5 fol/IgG (■). Cytotoxicity assays were performed with these conjugates using ^{51}Cr -labeled F2-MTX^rA cells and CTL clone 2C.

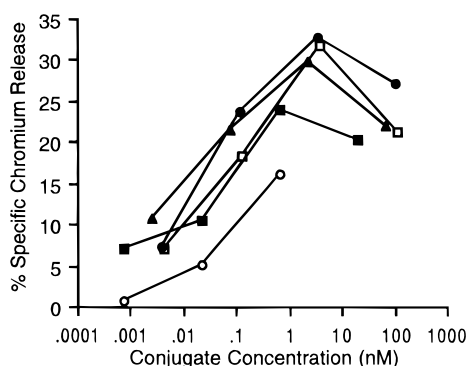


Figure 7. Effect of folate density on targeting with IgG/folate conjugates. Intact antibody was labeled at several folate concentrations to determine if, like scFv, a specific range of folate density would yield the optimal targeting effectiveness. Conjugates with the following densities were assayed with ^{51}Cr -labeled F2-MTX^rA cells and CTL clone 2C: 4.5 fol/IgG, □; 7.0 fol/IgG, ●; 13.6 fol/IgG, ▲; 56.7 fol/IgG, ■; and 126.2 fol/IgG, ○.

ure 7). Folate densities ranged from approximately 4–126 folates/antibody molecule. As shown with scFv preparations, high and low folate density resulted in decreased targeting effectiveness for the intact antibody. As with scFv preparations, the optimal densities appear to be in the range of 5–15 folates/antibody, as determined by spectrophotometry.

Inhibition of scFv/Folate Conjugate-Mediated Lysis by Free Folate. Normal serum folate may reduce the effectiveness of the scFv/folate conjugate by competing for the folate receptor *in vivo*. A ^{51}Cr release assay was used to evaluate the effectiveness of the scFv/folate conjugate-mediated lysis at biologically relevant concentrations of free folate (Figure 8). Free folate was diluted in folate-free media, and various concentrations were added to triplicate wells containing ^{51}Cr -labeled F2-MTX^rA cells, 2C effector cells, and a fixed, nonsaturating concentration of scFv/folate conjugate (3 nM) that would generate maximal specific release. The resulting titration curve demonstrated that at normal human serum folate levels [9–36 nM (42, 43)] the scFv/folate conjugate retained most of its activity. For instance, at 20 nM folate, the scFv/folate conjugate exhibited over 80% of its CTL-mediated targeting potential. Although murine serum folate levels are significantly higher than normal human serum values (124–700 nM) due to folate-rich chow (44, 45), even at these elevated folate concentra-

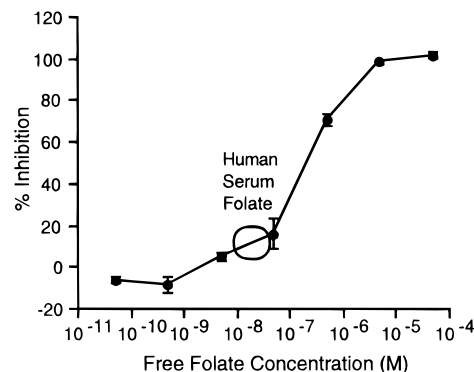


Figure 8. Inhibition of scFv/folate-mediated lysis by free folate. Various concentrations of free folate were added to triplicate wells containing ^{51}Cr -labeled F2-MTX^rA cells, 2C effector cells, and a fixed, nonsaturating concentration of scFv/folate conjugate (~8 fol/scFv) that would yield maximal specific release (3 nM). Inhibition was calculated as a function of the specific release in the absence of folate competitor. Normal human serum folate concentrations range from 9 to 36 nM (42, 43).

tions, the scFv/folate conjugate exhibited 30–60% of its targeting potential.

DISCUSSION

The most effective agents for targeting solid tumors will likely have reduced sizes that allow greater tumor penetration. This paper characterizes the smallest bispecific agent yet described for redirecting the activity of immune effector cells against tumors. Initial bispecific antibody studies to target ovarian tumors that express high-affinity FR have used intact heterobifunctional antibodies (~150 kDa) that bind to CD3 and the FR. These agents showed efficacy in animal models, and they have recently entered testing in clinical trials (9, 10, 12). Although not yet reported for anti-FR antibodies, several laboratories have shown that it is possible to engineer smaller bispecific antibodies of ~60 kDa by linking two scFv regions (41, 46, 47). Here we show that the size of a bispecific targeting agent can be reduced even further to ~30 kDa for the scFv/folate conjugates. Furthermore, the targeting efficiency of the engineered scFv/folate conjugate is comparable to that of the native intact antibody/folate conjugates.

For coupling of folate to the anti-V β 8 scFv KJ16, a carbodiimide reaction that links the carboxyl groups of folate to the amino groups of the antibody was used. KJ16 scFv binds to the cell surface TCR with an affinity that is similar to that of the intact KJ16 antibody (29). The V_L and V_H regions of the scFv are linked by a 26 amino acid region that contains 8 lysine residues. We reasoned that this charged linker would be accessible to folate, would be located distal to the binding site, and would contain multiple attachment sites for folate through the EDC reaction. Under coupling conditions where folate concentrations are nonsaturating, the scFv and intact antibody have comparable densities of folate attached per molecule (~5–15 folates/molecule), despite the 5-fold greater size of the intact antibody. Cytolytic assays demonstrated that these conjugates have very similar targeting efficiencies (Figure 6).

Although folate is probably attached to lysines present in the linker, the scFv/folate conjugates are actually heterogeneous populations as evidenced by mass spectra (Figure 1B). Within a scFv/folate preparation there are most likely conjugates with enhanced targeting properties and conjugates with diminished targeting properties. The former could include not only those with folate at an accessible location but perhaps those with multiple

folates that allow for multivalent interactions with FRs on tumor cells. Conjugates which have diminished bispecific properties would include those that have folate attached through amine groups in the scFv active site or in regions which destabilize the V_L – V_H interaction. These are analogous to those preparations derived with very high folate densities, where the targeting efficiency is significantly reduced (Figures 5 and 7).

Several considerations suggest that further optimization of the scFv/folate conjugates could yield even more potent agents. The anti-TCR antibody KJ16 has a relatively modest K_D of ~ 100 nM (29). Our laboratory is currently engineering higher affinity anti-TCR antibodies by antibody display methods; antibodies with $K_D \leq 1$ nM have been routinely generated using similar approaches (48). In addition, the affinity of the scFv/folate conjugate for the FR⁺ tumor cells was up to 30-fold less than the affinity of free folate for the FR (Figure 3). Coupling of folate through the γ carboxyl, plus homogeneous linkage perhaps through cysteine or multiple cysteines, should improve the affinity for the FR. Alternatively, other folate analogs with higher affinity than folate could be employed (49). The use of these strategies should allow the development of scFv conjugates that have EC_{50} values considerably less than those described in this paper.

It is of significant note that the scFv agent described here not only is the smallest agent but is at least as potent *in vitro* as bispecific antibodies described in the literature. For example, the EC_{50} of other bispecific agents range from 1 to 100 ng/mL (21, 50–52). Various other antibody or folate-based targeting agents have EC_{50} values that range from 0.1 to 200 ng/mL (e.g. refs 37, 40, 53–56). *In vitro* assays for these other agents typically involved 24 h incubation periods, while the cytotoxicity assays for CTL-mediated lysis, described here and elsewhere, are 4 h incubations. Thus, there is reason to believe that the scFv/folate conjugate has considerable promise *in vivo*. It has an EC_{50} of approximately 1 ng/mL, is smaller than the other agents, and remains effective at folate levels found in normal human serum. The scFv/folate targeting effect was inhibitable by free folate, but only at concentrations that were considerably higher (>1000-fold) than the folate conjugate concentration (Figure 8). Schodin *et al.* (57) have previously shown that <1% of the total number of TCRs per CTL need to be triggered for CTL-mediated cytotoxicity to occur. Thus, it is possible that >90% of the folate/antibody conjugates were inhibited from binding the target cell but sufficient conjugate remained bound to trigger maximal lysis.

The fact that the scFv/folate conjugate is in direct competition with serum folate also brings about the intriguing possibility of modulating the effectiveness of scFv/folate conjugate treatment by altering the levels of serum folate. For instance, recent studies with mice have shown that serum folate can be intentionally decreased up to 100-fold with special low-folate diets (44, 45). The decreased folate concentration greatly enhanced the ability of a ^{67}Ga -labeled deferoxamine/folate conjugate to image FR⁺ tumors *in vivo* (44). We envision that similar low-folate diets will likewise enhance the therapeutic effectiveness of the scFv/folate conjugate. Conversely, serum folate could be increased in situations where nonspecific T cell interactions lead to adverse side effects. Thus, the use of folate as the small molecule ligand specific for a tumor antigen may allow for additional levels of regulation normally not available with other immunotargeting agents.

In vivo tests to compare scFv and intact folate conjugates are currently underway in SV40 transgenic mice

that develop choroid plexus tumors exhibiting elevated levels of the high affinity folate receptor (58). Preliminary results indicate that T cells specifically infiltrate the tumor after treatment with the scFv/folate conjugate (B.K.C., T.A.P., D.M.K., and E.J.R., unpublished data). At this time, it is unclear whether conjugate-bound T cells extravasate into the tumor or if T cells first extravasate into the tumor and subsequently recognize the conjugate bound to cell surface FR. The latter mechanism would favor the enhanced tumor penetration characteristics of the smaller scFv molecule and would likely lead to increased therapeutic effectiveness.

ACKNOWLEDGMENT

We thank Drs. John Kappler and Philippa Marrack for providing the KJ16 hybridoma line, Carol Schlueter for providing the anti-L^d ascites fluid, and Drs. Brigle, Spinella, and Goldman for the DBA/2 tumor cell lines. This work was supported by grants from the University of Illinois Research Board (E.J.R.), the National Institutes of Health (AI35990, E.J.R. and D.M.K.), the Department of the Army (DAMD17-94-J-4347, D.M.K.), and the National Institutes of Mental Health (MH11189-01, T.A.P.). The ToFSpec mass spectrometer was purchased in part with Grant RR07141 from the Division of Research Resources, National Institutes of Health. Mass spectrometry was performed by Nelson Huang.

LITERATURE CITED

- (1) Gorer, P. A. (1937) The genetic and antigenic basis of tumor transplantation. *J. Pathol. Bacteriol.* 44, 691–697.
- (2) Boon, T. (1993) Teaching the immune system to fight cancer. *Sci. Am.* 268, 82–89.
- (3) Pardoll, D. M. (1994) A new look for the 1990s. *Nature* 369, 357–358.
- (4) Klein, G., and Boon, T. (1993) Tumor immunology: present perspectives. *Curr. Opin. Immunol.* 5, 687–692.
- (5) Fanger, M. W., Morganelli, P. M., and Guyre, P. M. (1992) Bispecific antibodies. *Crit. Rev. Immunol.* 12, 101–124.
- (6) Liu, M. A., Nussbaum, S. R., and Eisen, H. N. (1988) Hormone conjugated with antibody to CD3 mediates cytotoxic T cell lysis of human melanoma cells. *Science* 239, 395–398.
- (7) Nitta, T., Yagita, H., Sato, K., Okumura, K., and Ishii, S. (1990) Preliminary trials of specific targeting therapy against malignant glioma. *Lancet* 335, 368–371.
- (8) Chen, J., Zhou, J. H., Mokotoff, M., Fanger, M. W., and Ball, E. D. (1995) Lysis of small cell carcinoma of the lung (SCCL) cells by cytokine-activated monocytes and natural killer cells in the presence of bispecific immunoconjugates containing a gastrin-releasing peptide (GRP) analog or a GRP antagonist. *J. Hematother.* 4, 369–376.
- (9) Canevari, S., Miotti, S., Bottero, F., Valota, O., and Colnaghi, M. I. (1993) Ovarian carcinoma therapy with monoclonal antibodies. *Hybridoma* 12, 501–507.
- (10) Canevari, S., Stoter, G., Arienti, F., Bolis, G., Colnaghi, M. I., Di Re, E. M., Eggermont, A. M. M., Goey, S. H., Gratama, J. W., Lamers, C. H. J., Nooy, M. A., Parmiani, G., Raspagliesi, F., Ravagnani, F., Scarfone, G., Trimbos, J. B., Warnaar, S. O., and Bolhuis, R. L. H. (1995) Regression of advanced ovarian carcinoma by intraperitoneal treatment with autologous T lymphocytes retargeted by a bispecific monoclonal antibody. *J. Natl. Cancer Inst.* 87, 1463–1469.
- (11) Weiner, L. M., Clark, J. I., Davey, M., Li, W. S., Garcia de Palazzo, I., Ring, D. B., and Alpaugh, R. K. (1995) Phase I trial of 2B1, a bispecific monoclonal antibody targeting c-erbB-2 and Fc gamma RIII. *Cancer Res.* 55, 4586–4593.
- (12) Lamers, C. H., Gratama, J. W., Warnaar, S. O., Stoter, G., and Bolhuis, R. L. (1995) Inhibition of bispecific monoclonal antibody (bsAb)-targeted cytotoxicity by human anti-mouse antibodies in ovarian carcinoma patients treated with bsAb-targeted activated T-lymphocytes. *Int. J. Cancer.* 60, 450–457.

- (13) Buist, M. R., Molthoff, C. F. M., Kenemans, P., and Meijer, C. J. L. M. (1995) Distribution of OV-TL 3 and MOv18 in normal and malignant ovarian tissue. *J. Clin. Pathol.* **48**, 631–636.
- (14) Ross, J. F., Chaudhuri, P. K., and Ratnam, M. (1994) Differential regulation of folate receptor isoforms in normal and malignant tissues in vivo and in established cell lines. Physiologic and clinical implications. *Cancer* **73**, 2432–2443.
- (15) Weitman, S. D., Frazier, K. M., and Kamen, B. A. (1994) The folate receptor in central nervous system malignancies of childhood. *J. Neurooncol.* **21**, 107–112.
- (16) Knapp, R. C., and Berkowitz, R. S. (1993) *Gynecologic Oncology*, 250 pp, McGraw-Hill, New York.
- (17) Allen, J., Wisoff, J., Helson, L., Pearce, J., and Arenson, E. (1992) Choroid plexus carcinoma—responses to chemotherapy alone in newly diagnosed young children. *J. Neuro-Oncol.* **12**, 69–74.
- (18) Dohrmann, G. J., Farwell, J. R., and Flannery, J. T. (1976) Ependymomas and ependymoblastomas in children. *J. Neurosurg.* **45**, 273–283.
- (19) Coney, L. R., Tomassetti, A., Carayannopoulos, L., Frasca, V., Kamen, B. A., Colnaghi, M. I., and Zurawski, V. R., Jr. (1991) Cloning of a tumor-associated antigen: MOv18 and MOv19 antibodies recognize a folate-binding protein. *Cancer Res.* **51**, 6125–6132.
- (20) van Ravenswaay Claassen, H. H., van de Griend, R. J., Mezzananza, D., Bolhuis, R. L., Warnaar, S. O., and Fleuren, G. J. (1993) Analysis of production, purification, and cytolytic potential of bi-specific antibodies reactive with ovarian-carcinoma-associated antigens and the T-cell antigen CD3. *Int. J. Cancer* **55**, 128–136.
- (21) Coney, L. R., Mezzananza, D., Sanborn, D., Casalini, P., Colnaghi, M. I., and Zurawski, V. R. (1994) Chimeric murine human antibodies directed against folate binding receptor are efficient mediators of ovarian carcinoma cell killing. *Cancer Res.* **54**, 2448–2455.
- (22) Leamon, C. P., and Low, P. S. (1994) Selective targeting of malignant cells with cytotoxin-folate conjugates. *J. Drug Target.* **2**, 101–112.
- (23) Wang, S., Lee, R. J., Cauchon, G., Gorenstein, D. G., and Low, P. S. (1995) Delivery of antisense oligodeoxyribonucleotides against the human epidermal growth factor receptor into cultured KB cells with liposomes conjugated to folate via polyethylene glycol. *Proc. Natl. Acad. Sci. U.S.A.* **92**, 3318–3322.
- (24) Weitman, S. D., Lark, R. H., Coney, L. R., Fort, D. W., Frasca, V., Zurawski, V. R., Jr., and Kamen, B. A. (1992) Distribution of the folate receptor GP38 in normal and malignant cell lines and tissues. *Cancer Res.* **52**, 3396–3401.
- (25) Weitman, S. D., Weinberg, A. G., Coney, L. R., Zurawski, V. R., Jennings, D. S., and Kamen, B. A. (1992) Cellular localization of the folate receptor: potential role in drug toxicity and folate homeostasis. *Cancer Res.* **52**, 6708–6711.
- (26) Antony, A. C. (1996) Folate receptors. *Annu. Rev. Nutr.* **16**, 501–521.
- (27) Kranz, D. M., Patrick, T. A., Brigle, K. E., Spinella, M. J., and Roy, E. J. (1995) Conjugates of folate and anti-T cell receptor antibodies specifically target folate-receptor-positive tumor cells for lysis. *Proc. Natl. Acad. Sci. U.S.A.* **92**, 9057–9061.
- (28) Yokota, T., Milenic, D. E., Whitlow, M., and Schlom, J. (1992) Rapid tumor penetration of a single-chain Fv and comparison with other immunoglobulin forms. *Cancer Res.* **52**, 3402–3408.
- (29) Cho, B. K., Schodin, B. A., and Kranz, D. M. (1995) Characterization of a single-chain antibody to the β -chain of the T cell receptor. *J. Biol. Chem.* **270**, 25819–25826.
- (30) Friend, C., Patuleia, M. C., and De Harven, E. (1966) Erythrocytic maturation *in vitro* of murine (Friend) virus-induced leukemic cells. *NCI Monographs No. 22*, 505–522.
- (31) Brigle, K. E., Spinella, M. J., Westin, E. H., and Goldman, I. D. (1994) Increased expression and characterization of two distinct folate binding proteins in murine erythroleukemia cells. *Biochem. Pharmacol.* **47**, 337–345.
- (32) Law, L. W., B. D. T., Boyle, P. J., and Miller, J. H. (1949) Observations on the effect of a folic-acid antagonist on transplantable lymphoid leukemias in mice. *J. Natl. Cancer Inst.* **10**, 179–192.
- (33) Brigle, K. E., Seither, R. L., Westin, E. H., and Goldman, I. D. (1994) Increased expression and genomic organization of a folate-binding protein homologous to the human placental isoform in L1210 murine leukemia cell lines with a defective reduced folate carrier. *J. Biol. Chem.* **269**, 4267–4272.
- (34) Kranz, D. M., Sherman, D. H., Sitkovsky, M. V., Pasternack, M. S., and Eisen, H. N. (1984) Immunoprecipitation of cell surface structure of cloned cytotoxic T lymphocytes by clone-specific antisera. *Proc. Natl. Acad. Sci. U.S.A.* **81**, 573–577.
- (35) Haskins, K., Hannum, C., White, J., Rhoem, N., Kubo, R., Kappler, J., and Marrack, K. (1984) The antigen-specific major histocompatibility complex-restricted receptor on T cells. VI. An antibody to a receptor allotype. *J. Exp. Med.* **160**, 452–471.
- (36) Ozato, K., Hansen, T. H., and Sachs, D. H. (1980) Monoclonal antibodies to mouse MHC antigens. II. Antibodies to the H-2L^d antigen, the product of a third polymorphic locus of the mouse major histocompatibility complex. *J. Immunol.* **125**, 2473–2477.
- (37) Leamon, C. P., and Low, P. S. (1992) Cytotoxicity of momordin-folate conjugates in cultured human cells. *J. Biol. Chem.* **267**, 24966–24971.
- (38) Whitlow, M., and Filpula, D. (1991) Single-chain Fv proteins and their fusion proteins. *Methods: A Companion to Methods in Enzymology*, Vol. 2, pp 97–105, Academic, San Diego.
- (39) Rojo, J. M., and Janeway, C. A., Jr. (1988) The biologic activity of anti-T cell receptor V region monoclonal antibodies is determined by the epitope recognized. *J. Immunol.* **140**, 1081–1088.
- (40) Leamon, C. P., Pastan, I., and Low, P. S. (1993) Cytotoxicity of folate-*Pseudomonas* exotoxin conjugates toward tumor cells. Contribution of translocation domain. *J. Biol. Chem.* **268**, 24847–24854.
- (41) Gruber, M., Schodin, B., Wilson, E., and Kranz, D. M. (1994) Efficient tumor cell lysis mediated by a bispecific single-chain antibody expressed in *E. coli*. *J. Immunol.* **152**, 5368–5374.
- (42) Kutsy, R. J. (1981) *Handbook of Vitamins, Minerals, and Hormones*, 2nd ed., 492 pp, Van Nostrand Reinhold, New York.
- (43) Lentner, C. (1984) *Geigy Scientific Tables, 8th rev., Physical chemistry, composition of blood, hematology, somatometric data*, Vol. 3, 131 pp, Ciba-Geigy Limited, Basle, Switzerland.
- (44) Mathias, C. J., Wang, S., Lee, R. J., Waters, D. J., Low, P. S., and Green, M. A. (1996) Tumor-selective radiopharmaceutical targeting via receptor-mediate endocytosis of gallium-67-deferoxamine-folate. *J. Nucl. Med.* **37**, 1003–1008.
- (45) Gospe Jr., S. M., Gietzen, D. W., Summers, P. J., Lunetta, J. M., Miller, J. W., Selhub, J., Ellis, W. G., and Clifford, A. J. (1995) Behavioral and neurochemical changes in folate-deficient mice. *Physiol. Behav.* **58**, 935–941.
- (46) Hollinger, P., Prospero, T., and Winter, G. (1993) “Diabodies”: Small bivalent and bispecific antibody fragments. *Proc. Natl. Acad. Sci. U.S.A.* **90**, 6444–6448.
- (47) Kurucz, I., Titus, J. A., Jost, C. R., Jacobus, C. M., and Segal, D. M. (1995) Retargeting of CTL by an efficiently refolded bispecific single-chain Fv dimer produced in bacteria. *J. Immunol.* **154**, 4576–4582.
- (48) Winter, G., Griffiths, A. D., Hawkins, R. E., and Hoogenboom, H. R. (1994) Making antibodies by phage display technology. *Annu. Rev. Immunol.* **12**, 433–455.
- (49) Elwood, P. C., Kane, M. A., Portillo, R. M., and Kolhouse, J. F. (1986) The isolation, characterization, and comparison of the membrane-associated and soluble folate-binding proteins from human KB cells. *J. Biol. Chem.* **261**, 15416–15423.
- (50) Mack, M., Riethmuller, G., and Kufer, P. (1995) A small bispecific antibody construct expressed as a functional single-chain molecule with high tumor cell cytotoxicity. *Proc. Natl. Acad. Sci. U.S.A.* **92**, 7021–7025.
- (51) Zhu, Z., Zapata, G., Shalaby, R., Snedecor, B., Chen, H., and Carter, P. (1996) High level secretion of a humanized bispecific diabody from *Escherichia coli*. *Biotechnology* **14**, 192–196.

- (52) Sugiyama, Y., Aihara, M., Shibamori, M., Deguchi, K., Imagawa, K., Kikuchi, M., Momata, H., Azuma, T., Okada, H., Alper, Ö., Hitomi, J., and Yamaguchi, K. (1992) *In vitro* anti-tumor activity of anti-*c-erbB-2* x anti-CD3 ϵ bifunctional monoclonal antibody. *Jpn. J. Cancer Res.* 83, 563–267.
- (53) Chaudhary, V. K., Queen, C., Junghans, R. P., Waldmann, T. A., FitzGerald, D. J., and Pastan, I. (1989) A recombinant immunotoxin consisting of two antibody variable domains fused to *Pseudomonas* exotoxin. *Nature* 339, 394–397.
- (54) Chaudhary, V. K., Gallo, M. G., FitzGerald, D. J., and Pastan, I. (1990) A recombinant single-chain immunotoxin composed of anti-Tac variable regions and a truncated diphtheria toxin. *Proc. Natl. Acad. Sci. U.S.A.* 87, 9491–9494.
- (55) Burrows, F. J., and Thorpe, P. E. (1993) Eradication of large solid tumors in mice with an immunotoxin directed against tumor vasculature. *Proc. Natl. Acad. Sci. U.S.A.* 90, 8996–9000.
- (56) Wels, W., Harwerth, I. M., Mueller, M., Groner, B., and Hynes, N. E. (1992) Selective inhibition of tumor cell growth by a recombinant single-chain antibody-toxin specific for the *erbB-2* receptor. *Cancer Res.* 52, 6310–6317.
- (57) Schodin, B. A., Tsomides, T. J., and Kranz, D. M. (1996) Correlation between the number of T cell receptors required for T cell activation and TCR-ligand affinity. *Immunity* 5, 137–146.
- (58) Patrick, T. A., Kranz, D. M., Van Dyke, T. A., and Roy, E. J. (1997) Folate receptors as potential therapeutic targets in choroid plexus tumors of SV40 transgenic mice. *J. Neuro-Oncol.* (in press).

BC9700244

Synthesis and Characterization of Rhenium-Complexed α -Melanotropin Analogs

Michael F. Giblin,[†] Silvia S. Jurisson,[‡] and Thomas P. Quinn^{*,†}

Departments of Biochemistry and Chemistry, University of Missouri—Columbia, Columbia, Missouri 65211.
Received September 30, 1996[®]

Receptor binding peptides labeled with medically important radionuclides such as technetium and rhenium are an important tool for the imaging and treatment of many forms of cancer. This paper describes a method of labeling peptides with rhenium using a natural amino acid chelating moiety. The structural characteristics of this chelate moiety, *N*-acetyl-cysteine-glycine-cysteine-glycine (NAC-CGCG) complexed with nonradioactive rhenium, have been investigated. The stability of this peptide–metal complex has been evaluated on the tracer level using radioactive rhenium-186. The rhenium-bound peptide has been appended to the N termini of receptor binding α -melanocyte stimulating hormone (α -MSH, NAc-Ser-Tyr-Ser-Met-Glu-His-Phe-Arg-Trp-Gly-Lys-Pro-Val-NH₂) fragments via solid phase peptide synthesis. Bioassays and receptor binding studies of the resulting complexes demonstrate that the fragments retained biological activity and exhibited receptor binding constants ranging from 0.3 to 1.1 nM. This method could provide a general means of labeling bioactive peptide fragments that would simplify product purification and characterization.

INTRODUCTION

Biologically active molecules that selectively interact with specific cell types are attractive vehicles for radioisotope delivery. Peptides, which possess specific affinities for receptors upregulated in certain malignancies (1), are receiving increasing attention due to their *in vivo* targeting and pharmacokinetic properties. Small peptides such as somatostatin (1–3), vasoactive intestinal peptide (4, 5), chemotactic peptides (6–10), and the α -melanocyte stimulating hormone (α -MSH)¹ (11–14) have all shown promise as radioisotope delivery agents.

The group VIIA transition metals technetium (Tc) and rhenium (Re) are among the most commonly used radioisotopes in medicine due to the favorable emission energies and decay properties of the radioactive isotopes Tc-99m, Re-186, and Re-188 (15). As a result, increasing attention has been focused on developing methods of attaching these radionuclides to bioactive peptide sequences. Currently, the most common approaches to labeling peptide hormones have involved attachment of either In-111 or I-123 (2–4, 11–14). For the coordination of Tc and Re, many studies have shown that ligand

systems containing two nitrogen atoms and two thiol sulfur atoms (N₂S₂ systems) are effective (16–25). Often, these chelating systems are built via organic syntheses of varying complexity. In some cases, researchers have taken advantage of solid phase peptide synthesis to design peptide chelators that either lack sulfur or contain sulfur in the context of non-natural groups such as the mercaptoacetyl group (23, 24, 26, 27). More recent studies have demonstrated that amino acid sequences such as Cys-Gly-Cys, Cys-Thr-Cys, and Gly-Gly-Cys can be used to coordinate Tc-99m in peptides (1, 7–10, 28) and proteins (29).

In this paper, we have used conventional ¹H and ¹³C NMR methods to characterize the solution conformation of the peptide *N*-Acetyl-Cys-Gly-Cys-Gly (NAC-CGCG) complexed to a nonradioactive rhenium(V)–oxo core. The remarkable stability of this peptide–metal complex allowed us to synthesize, purify, and then append this complex to the N termini of α -melanocyte stimulating hormone (α -MSH, NAc-Ser-Tyr-Ser-Met-Glu-His-Phe-Arg-Trp-Gly-Lys-Pro-Val-NH₂) receptor binding fragments. The attachment of the metal-complexed peptide was carried out as the last step of a conventional solid phase peptide synthesis (SPPS). Attachment of the peptide–metal complex to the N termini of the α -MSH fragments resulted in readily purifiable products which were labeled with rhenium and retained receptor binding affinity. This coupling was also carried out on the tracer level with Re-186-labeled NAC-CGCG and resulted in a readily purifiable radiolabeled peptide product. These experiments show that SPPS can be used to attach preformed peptide–metal chelates to bioactive peptides. This method of labeling peptides could have general use as a means of obtaining high specific activity rhenium-labeled bioactive peptides.

EXPERIMENTAL PROCEDURES

Sodium [¹⁸⁶Re]perrhenate (530 Ci/mmol) was obtained from the Missouri University Research Reactor (MURR). [¹²⁵I]-labeled [Nle⁴,D-Phe⁷]- α -MSH (1700 Ci/mmol) was obtained from Advanced Chemtech in Louisville, KY. Fmoc amino acids and automated peptide synthesis reagents were obtained from Applied Biosystems (Foster City, CA). Dithiothreitol (DTT), methanol (MeOH), di-

* Address correspondence to this author at the Department of Biochemistry, 117 Schweitzer Hall, University of Missouri—Columbia, Columbia, MO 65211 [telephone (573) 882-6099; fax (573) 882-5635; e-mail bctquinn@muccmail.missouri.edu].

[†] Department of Biochemistry.

[‡] Department of Chemistry.

[®] Abstract published in *Advance ACS Abstracts*, April 1, 1997.

¹ Abbreviations: NAc, *N*-acetyl; CGCG, Cys-Gly-Cys-Gly; ReO, rhenium(V)–oxo; Nle, norleucine; α -MSH, NAc-Ser-Tyr-Ser-Met-Glu-His-Phe-Arg-Trp-Gly-Lys-Pro-Val-NH₂; [D-Phe⁷]- α -MSH_{5–10}-NH₂, Glu-His-D-Phe-Arg-Trp-Gly-NH₂; [Nle⁴,D-Phe⁷]- α -MSH, Ser-Tyr-Ser-Nle-Glu-His-D-Phe-Arg-Trp-Gly-Lys-Pro-Val-NH₂; SPPS, solid phase peptide synthesis; RP-HPLC, reversed phase high-performance liquid chromatography; Trt, trityl; COSY, correlated spectroscopy; NOESY, nuclear Overhauser effect and exchange spectroscopy; HMBC, heteronuclear multiple bond connectivity correlated spectroscopy; TPPI, time-proportional phase incrementation; FAB-MS, fast-atom bombardment mass spectroscopy; Fmoc, fluorenylmethoxycarbonyl; HBTU, 2-(1*H*-benzotriazol-1-yl)-1,1,3,3-tetramethyluronium hexafluorophosphate; HOBt, *N*-hydroxybenzotriazole; DIEA, *N,N*-diisopropylethylamine; HEPES, *N*-(2-hydroxyethyl)piperazine-*N*-2-ethanesulfonic acid; PBS, phosphate-buffered saline.

ethyl ether, *N*-methylpyrrolidinone (NMP), and dichloromethane (DCM) were obtained from Fisher Scientific (St. Louis, MO). Thioanisole, ethanedithiol, and dicyclohexylcarbodiimide (DCC) were obtained from Aldrich Chemical Co. (St. Louis, MO). Trifluoroacetic acid (TFA) was obtained from Sigma Chemical Co. (St. Louis, MO).

Preparation of NAc-CGCG. The peptide was synthesized by conventional SPPS techniques, using Fmoc/HBTU chemistry (30). The synthesis was carried out on a Synergy desktop peptide synthesizer from Applied Biosystems. The peptide was N-terminally acetylated by activation of excess glacial acetic acid after deprotection of the N-terminal Cys residue. Cleavage and deprotection were carried out by incubation in a 36:2:1:1 mix of TFA/thioanisole/ethanedithiol/water for 2 h. This solution was then filtered and the product precipitated with diethyl ether. The resulting precipitate was dried, dissolved in 1 mM DTT, and lyophilized.

Preparation of Nonradioactive ReO-NAc-CGCG. Labeling of compounds followed roughly the procedure of Hansen et al. (31). Fifteen milligrams of NAc-CGCG was dissolved in 1 mL of 62% MeOH, and the pH was adjusted to about 8 with 1 M NaOH. $\text{ReOCl}_3(\text{Me}_2\text{S})\text{-(OPPh}_3\text{)}$ (26 mg) (32, 33) was added as a solid, giving a green suspension. Heating at 60–70 °C for 60 min resulted in an orange-brown solution. The reaction mixture was filtered to remove an H_2O -insoluble gray precipitate and purified by RP-HPLC. Purification was carried out on a C_{18} semipreparative HPLC column (Vydac), utilizing a 30 min gradient of 3–12% acetonitrile/0.1% TFA in H_2O /0.1% TFA. Product elution was monitored by UV detection at 400 nm using an Isco V⁴ absorbance detector. The product peak (retention time = 24 min) was collected and lyophilized.

Preparation of $^{186}\text{ReO-NAc-CGCG}$. The radiolabeled peptide complex was prepared by substitution onto ^{186}Re -labeled citrate. Briefly, 0.235 mCi of $\text{Na}^{186}\text{ReO}_4$ was added to 0.8 mL of degassed, 1 M sodium citrate, pH 8.8, containing 250 mg of stannous tartrate. After 10 min at room temperature, 0.1 mg of reduced NAc-CGCG was added, and the solution was allowed to stir for 1 h at 65–70 °C. Isolation of the resulting complex proceeded as for the nonradioactive complex, with the exception that radioactivity was monitored using a Radiomatic Series A-200 radiochromotography detector.

Evaluation of Labeled Peptide Stability. The *in vitro* stability of the nonradioactive rhenium complex was evaluated by incubation at room temperature with the cleavage/deblocking mixture. Samples were taken at various times and analyzed by RP-HPLC. The stability of the radioactive complex was assessed by diluting the reaction mixture 1:2 into fresh solutions of 20 and 2 mM L-cysteine. Again, RP-HPLC was used to quantitate complex stability over time.

Structural Determination Using ^1H and ^{13}C NMR. A sample of 5–10 mg of purified complex was solubilized in 80% H_2O /20% D_2O . ^1H spectra were referenced to the H_2O peak at 4.75 ppm. ^{13}C spectra were externally referenced to dioxane at 67.4 ppm. All spectra were collected at 298 K on a Bruker AMX500 spectrometer. Scalar connectivities were obtained from COSY experiments; sequential assignments were made on the basis of NOESY experiments. The NOESY mixing time was 200 ms. All spectra were recorded using the time-proportional phase incrementation (TPPI) method. In most cases the spectral width was 6000 Hz. Typically, the data set size was $2048(t_2) \times 256(t_1)$ blocks with 16 scans/fid. H_2O suppression was carried out by presaturation (1.5 s) at the water frequency during the relaxation delay between scans (as well as during the mixing time

in NOESY expts). NMR spectra were processed with the NMR software within the SYBYL program (Tripos, Inc.) on an SGI Indigo R4000 workstation. Data sets were multiplied by a 0–90° shifted sinebell squared transformation function and zero-filled to 1024 K in t_1 prior to Fourier transformation. The assignment of indices 1 and 2 to methylene protons follows the convention that the lower index denotes the most downfield shifted resonance of the pair.

Attachment of the Nonradioactive Complex to Bioactive α -MSH Sequences. The peptides $[\text{D-Phe}^7]\text{-}\alpha\text{-MSH}_{5-10}\text{-NH}_2$ and $\text{NAC-}[\text{Nle}^4, \text{D-Phe}^7]\text{-}\alpha\text{-MSH}$ were synthesized by conventional SPPS techniques, as previously described (30). As a final step, the Fmoc group was removed from the N-terminal residue by piperidine deprotection, and ReO-NAc-CGCG was coupled to the growing chains via its free Gly_4 carboxylate. In each case, the final coupling step was repeated twice to ensure maximal incorporation of the rhenium-labeled fragment, since the molar amount of ReO-NAc-CGCG used was less than the theoretical 0.25 μmol needed for maximum yield. The rhenium-labeled α -MSH peptide analogs were cleaved from the resin and deprotected in a 36:2:1:1 mix of TFA/thioanisole/ethanedithiol/water. This solution was then filtered and the product precipitated in diethyl ether; the precipitate was dried, dissolved in H_2O , and lyophilized. The identity of rhenium-containing peptides was confirmed by fast-atom bombardment–mass spectroscopy (FAB-MS). For $\text{ReO-NAc-CGCG-}[\text{D-Phe}^7]\text{-}\alpha\text{-MSH}_{5-10}\text{-NH}_2$, the $(\text{M} + \text{H})^+$ peak was observed at m/z 1392.2 (calculated 1391.6). For $\text{ReO-NAc-CGCG-}[\text{Nle}^4, \text{D-Phe}^7]\text{-}\alpha\text{-MSH}$, the $(\text{M} + \text{H})^+$ peak was observed at m/z 2166.5 (calculated 2166.5).

Attachment of $^{186}\text{Re-NAc-CGCG}$ to a Bioactive α -MSH Sequence. Purified, lyophilized $^{186}\text{Re-NAc-CGCG}$ (1.4×10^{-11} mol) was solubilized in NMP and added to 8 mg of blocked peptide resin containing 1.6×10^{-6} mol of $[\text{D-Phe}^7]\text{-}\alpha\text{-MSH}_{5-10}\text{-NH}_2$. A mixture of 1.6×10^{-4} mol of HOBT/DIEA in NMP was added, followed by the addition of 1.6×10^{-4} mol of DCC on ice. The solution was allowed to stir on ice for 1 h and for an additional 3.5 h at room temperature. At that time the resin was thoroughly rinsed with NMP, 1:1 MeOH/DCM, and DCM and allowed to dry. After drying, the resin was deprotected by incubation in a 36:2:1:1 mix of TFA/thioanisole/ethanedithiol/water. After 2 h, the cleavage/deprotection mix was centrifuged, and the supernatant was applied directly to a C_{18} RP-HPLC column (Vydac).

Measurement of Melanin Production by B16 F1 Murine Melanoma Cells. Peptide bioactivity was determined by measuring melanin production in an *in vitro* assay using B16 F1 murine melanoma cells acquired from the American Type Tissue Culture collection. The assay followed the method developed by Siegrist and Eberle (34). Briefly, cells were seeded in 96 well tissue culture plates and allowed to attach to the plates overnight. At that time, cells were exposed to various concentrations of peptides to be tested. After 12–24 h, the peptide solutions were removed and fresh medium was added to each well. After an additional 3–5 days, the absorbance of each cell-containing well was measured at 405 nm in a Vmax kinetic microplate reader from Molecular Devices. Absorbance values were compared to a standard curve obtained using synthetic melanin from Sigma. The standard curve was linear over the experimental range of absorbance values.

Quantitation of Peptide Binding to B16 F1 Cells. Quantitative receptor binding assays were carried out following a method described previously (35, 36). Cells were seeded at a density of 5×10^5 cells per well in 24

Table 1. ^1H NMR Resonance Assignments for NAc-CGCG and ReO-NAc-CGCG^a

resonance	NAc-CGCG δ	ReO-NAc-CGCG δ	$\Delta\delta^b$
acetyl methyl	2.05	2.06	0.01
Cys1 α H	4.50	5.10	0.06
Cys1 β H1	2.93	2.79	-0.14
Cys1 β H2	2.93	3.46	0.53
Gly2 α H1	3.99	4.59	0.60
Gly2 α H2	3.99	4.59	0.60
Cys3 α H	4.59	5.07	0.48
Cys3 β H1	2.93	3.63	0.70
Cys3 β H2	2.93	4.19	1.26
Gly4 α H1	3.99	3.86	-0.13
Gly4 α H2	3.99	3.86	-0.13
Cys1NH	8.40	7.79	-0.61
Gly2NH	8.45		
Cys3NH	8.24		
Gly4NH	8.61	8.43	-0.18

^a Chemical shifts relative to H₂O at $\delta = 4.75$ ppm. ^b $\Delta\delta = (\delta_{\text{metal-bound}} - \delta_{\text{metal-free}})$.

well tissue culture plates and allowed to attach overnight. Cells were then exposed to various concentrations of peptides to be tested in 0.5 mL of binding media. The binding medium consisted of 25 mM HEPES/NaOH (pH 7.4), 0.2% BSA, and 0.3 mM 1,10-phenanthroline and contained approximately 100 000 cpm of [¹²⁵I]-[Nle⁴,D-Phe⁷]- α -MSH (37) per 0.5 mL. Cells were incubated in this mixture at 4 °C for 8 h, then rinsed with PBS, lysed with 1 M NaOH, and counted in a 1275 minigamma gamma counter from LKB Wallac.

RESULTS

Synthesis of Rhenium–Peptide Complexes. The nonradioactive ReO-NAc-CGCG complex was synthesized utilizing the ReOCl₃(Me₂S)(OPPH₃) exchange ligand (32, 33). The radioactive ¹⁸⁶ReO-NAc-CGCG complex was synthesized via a direct labeling reaction with citrate as the exchange ligand. Both metal complexes were found to coelute under the RP-HPLC conditions used to purify them, indicating the complexes differ only in isotopic composition. The purified nonradioactive complex was characterized by NMR.

Assignment of ^1H Resonances. Sequence specific ^1H resonance assignments of NAc-CGCG and ReO-NAc-CGCG were made using COSY and NOESY spectra (38). Assignments for both compounds are given in Table 1. Deprotonation of two amide nitrogens occurred during the metal complexation reaction. The assignment of the deprotonated amide nitrogens was determined by an intrasidue NOE between the *N*-acetyl methyl group and the Cys¹ amide proton. A Cys³ α H-Gly⁴NH sequential NOE is also present, showing that the amide nitrogens of Gly² and Cys³ are deprotonated and presumably involved in metal coordination. A minor species (<10%), assumed to be an isomer, was also present in the sample. After a period of 1 week, no increase in the intensity of these signals was observed, indicating that the minor species is not a degradation product. 1D spectra of NAc-CGCG and ReO-NAc-CGCG are shown in Figure 1.

Chemical Shift Changes upon Metal Coordination. ^1H chemical shift changes between metal-free and metal-bound forms of the peptide are given in Table 1. The α -protons of both Cys residues are found to shift downfield in the rhenium compound, as is to be expected upon thiol coordination of an electropositive transition metal (25). It is generally thought that metal coordination should have the effect of deshielding nearby protons in a ^1H spectrum due either to the electron withdrawing effect of the metal or to the magnetic anisotropy of the metal–oxo bond. It might be expected therefore that the

β proton resonances should be further shifted downfield. While this is the case for the Cys³ β protons, Cys¹ β H₁ is seen to resonate upfield in the metal-bound form, while Cys¹ β H₂ is slightly less deshielded than Cys¹ α H.

¹³C chemical shift assignments for ReO-NAc-CGCG are shown in Table 2. These assignments were made via an HMBC (39) spectrum of the complex acquired at 298 K. The ¹³C chemical shifts of the complex were compared to average ¹³C chemical shifts for nonterminal Cys and Gly residues in model peptides (40). The results of this comparison are also given in Table 2. Downfield shifts of the Cys¹ and Gly² carbonyl ¹³C resonances were expected due to metal coordination by the proximal amide nitrogens. The Cys³ and Gly⁴ carbonyl carbons, which both lie outside the torsionally constrained metal coordinating rings, are found to be only slightly deshielded. The α carbons of both Cys¹ and Cys³ are deshielded in the metal-bound peptide. However, Cys³ α resonates 11.4 ppm further downfield than Cys¹ α . Also, Cys¹ β is actually shielded relative to average Cys β carbons in non-terminal cysteines of metal-free peptides, while Cys³ β is deshielded 8.7 ppm.

Torsional Angles Derived from 3J -Coupling Data. The structure of ReO-NAc-CGCG derived from NMR data consists of three fused heterocycles (Figure 2). J -coupling information derived from resolution-enhanced 1D spectra and 2D ^1H –¹³C HMBC spectra suggests specific ranges for the torsional angles about Cys¹ ϕ , Gly³ ϕ , Cys¹ χ , and Cys³ χ (Table 3). Since the ring structures are essentially locked by coordination to the metal, the measured 3J values probably reflect a single preferred χ angle, rather than an interconverting rotamer population. Dihedrals external to the three-ring system, however, such as the ϕ angles of Cys¹ and Cys³, are more properly viewed as free to rotate in solution.

Measured $^3J_{\alpha\text{H}\beta\text{H}}$ values for Cys¹ β H₁ and Cys¹ β H₂ indicate that these protons are trans and gauche, respectively, with respect to Cys¹ α H. The $^3J_{\alpha\text{H}\beta\text{H}}$ coupling constants of Cys³ suggest that Cys³ β H₁ and Cys³ β H₂ are intermediate between gauche and trans positions with respect to Cys³ α H. The χ angle of Cys³ derived from the experimental J -coupling values results in an average conformation that is essentially midway between the high energy eclipsed and low energy staggered conformations.

The observation of intermediate $^3J_{\alpha\text{H}\beta\text{H}}$ values for Cys³ is consistent with the observed HMBC intensities. The HMBC signal relating C³ β H₁ and C³CO is more intense than that relating C³ β H₂ and C³CO, indicating a more trans Cys³ β H₁-Cys³ β C-Cys³ α C-Cys³CO torsion and a more gauche C³ β H₂-C³ β C-C³ α C-C³CO torsion.

Stability of ReO-NAc-CGCG. To determine whether the nonradioactive complex would be able to withstand the conditions involved in SPPS, the stability of the ReO-NAc-CGCG complex was tested by a 2 h incubation in the cleavage/deprotection mix. This mix contains an 800-fold excess of free thiol groups, so this provides a rigorous stability test of the peptide–rhenium complex. The stability of this complex, as assessed by RP-HPLC, was such that no degradation was observed after 2 h. The stability of the ¹⁸⁶ReO-NAc-CGCG complex was tested by competition against various concentrations of L-cysteine. The complex showed essentially no degradation after 5.5 h in 1 mM cysteine, and 80% of the complex remained after 12 h in 10 mM cysteine.

Attachment of ReO-NAc-CGCG to a Bioactive Peptide Sequence. Two α -MSH-derived peptide sequences, [D-Phe⁷]- α -MSH_{5–10}-NH₂ and [Nle⁴,D-Phe⁷]- α -MSH (37), were N-terminally labeled with the ReO-NAc-CGCG moiety. In the peptide synthesis reactions, the rhenium was used as a blocking group, preventing the

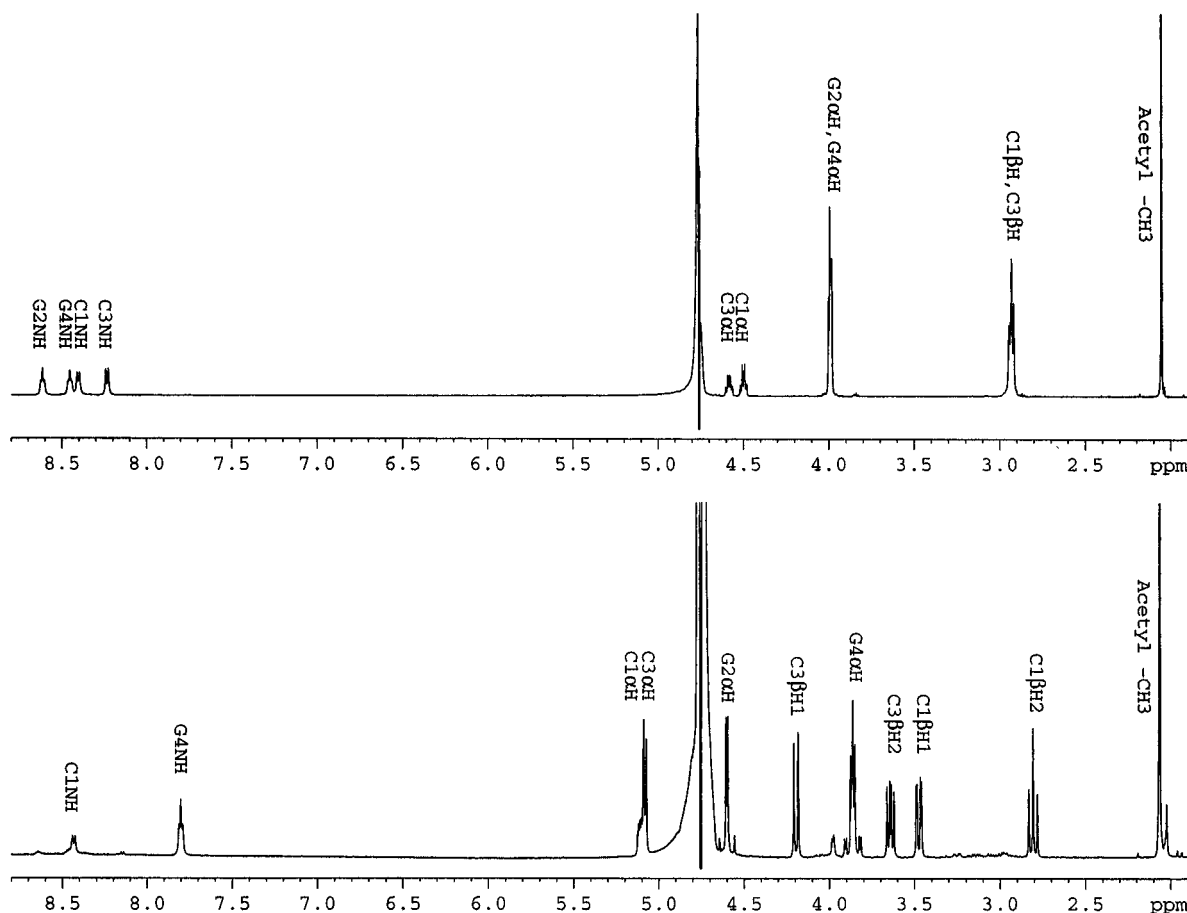


Figure 1. ^1H NMR spectra of NAc-CGCG (top) and ReO-NAc-CGCG (bottom). Both spectra were acquired in 90% $\text{H}_2\text{O}/10\%$ D_2O at 298 K.

Table 2. ^{13}C NMR Resonance Assignments for ReO-NAc-CGCG Compared with Average Values (δ_{av}) for Nonterminal Residues (37)

resonance	δ^a ReO-NAc-CGCG	δ_{av}^{37}	$\Delta\delta^b$
acetyl methyl	22.8		
acetyl C=O	174.3		
Cys1C α	58.6	53.5	5.1
Cys1C β	34.4	39.6	-5.2
Cys1C=O	180.2	173.5	6.7
Gly2C α	61.1	43.5	17.6
Gly2C=O	192.4	172.1	20.3
Cys3C α	70.0	53.5	16.5
Cys3C β	48.3	39.6	8.7
Cys3C=O	174.7	173.5	1.2
Gly4C α	41.9	43.5	-1.6
Gly4C=O	174.0	172.1	1.9

^a Chemical shifts relative to dioxane at $\delta = 67.4$ ppm. ^b $\Delta\delta = (\delta_{\text{metal-bound}} - \delta_{\text{av}})$.

cysteine thiols from participating in side reactions. After cleavage/deprotection (see Experimental Procedures), the peptide products were subjected to C_{18} RP-HPLC.

In each case, the reaction yielded one major rhenium-containing product. Some unconjugated α -MSH fragment was also present since the reactions were carried out with an excess of α -MSH fragment present. The rhenium-containing product was more hydrophobic than the attached α -MSH sequences alone, thus simplifying purification of the final labeled product.

[D-Phe⁷]- α -MSH₅₋₁₀-NH₂ was also labeled with ^{186}ReO -NAc-CGCG via peptide synthesis techniques (see Experimental Procedures). The result of this reaction was a highly pure radiolabeled product (Figure 3). This product was easily separable from nonradioactive [D-Phe⁷]- α -MSH₅₋₁₀-NH₂ due to the relatively large difference in

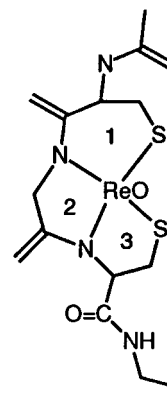


Figure 2. Structure of ReO-NAc-CGCG.

Table 3. Coupling Data for ReO-NAc-CGCG

residue	$^3J_{\text{aNH}}^a$ (Hz)	ϕ^b (deg)	$^3J_{\text{ab1}}^a$ (Hz)	χ'^b (deg)	$^3J_{\text{ab2}}^a$ (Hz)	χ''^b (deg)
Cys1	7.7	$\pm 137, \pm 29$	12.5	± 180	3.2	$\pm 110, \pm 62$
Cys3			8.0	$\pm 138, \pm 25$	<1.5	± 85
Gly4	5.5	+124, +43				

^a Observed coupling constants from NMR data. ^b Torsion angles calculated using the Karplus-type equation $^3J = 11.0 \cos^2 \phi - 1.4 \cos \phi + 1.6 \sin^2 \phi$.²¹

hydrophobicity between the two compounds. The purity of product resulting from this synthesis strategy compares quite favorably to the product resulting from a postconjugate chelation strategy. The use of ^{186}ReO -NAc-CGCG as a preformed chelate precludes nonspecific binding of ^{186}Re to other uncharacterized sites within peptides.

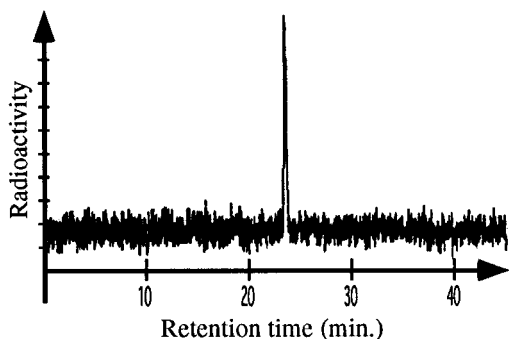


Figure 3. HPLC profile showing the radioactive product of the ^{186}Re -NAC-CGCG-[D-Phe⁷]- α -MSH₅₋₁₀-NH₂ conjugation reaction. The radioactive product was shown to coelute with the previously characterized nonradioactive standard.

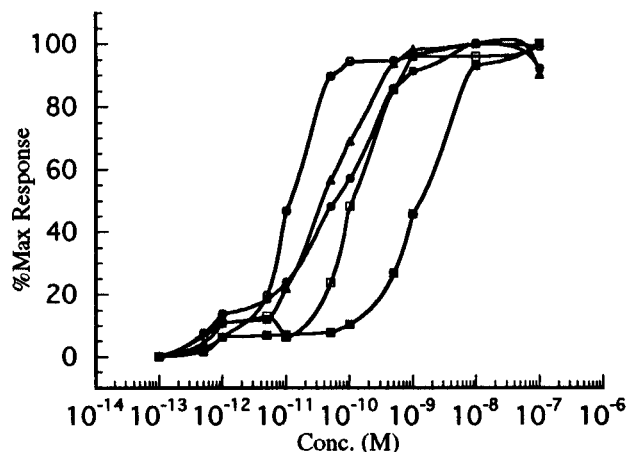


Figure 4. Sigmoidal dose-response curves indicating melanogenic response of B16 F1 murine melanoma cells to various concentrations of (▲) α -MSH, (□) [D-Phe⁷]- α -MSH₅₋₁₀-NH₂, (■) ReO-NAC-CGCG-[D-Phe⁷]- α -MSH₅₋₁₀-NH₂, (○) NAc-[Nle⁴,D-Phe⁷]- α -MSH, and (●) ReO-NAC-CGCG-[Nle⁴,D-Phe⁷]- α -MSH.

Table 4. EC₅₀ and K_i Values for Various α -MSH Analogs

compound	K _i (M)	EC ₅₀ (M)
α -MSH	8.8×10^{-10}	3.4×10^{-11}
[D-Phe ⁷]- α -MSH ₅₋₁₀ -NH ₂	4.6×10^{-8}	9.8×10^{-11}
ReO-NAC-CGCG-[D-Phe ⁷]- α -MSH ₅₋₁₀ -NH ₂	1.1×10^{-8}	1.1×10^{-9}
NAc-[Nle ⁴ ,D-Phe ⁷]- α -MSH	1.8×10^{-10}	1.1×10^{-11}
ReO-NAC-CGCG-[Nle ⁴ ,D-Phe ⁷]- α -MSH	3.0×10^{-10}	3.9×10^{-11}

Bioactivity and Receptor Binding Affinity. The bioactivity of these peptide-metal complexes was assayed by measuring stimulation of melanin production by B16 F1 murine melanoma cells (Figure 4). ReO-NAC-CGCG-conjugated [D-Phe⁷]- α -MSH₅₋₁₀-NH₂ and [Nle⁴,D-Phe⁷]- α -MSH peptides displayed a 4–10-fold reduction in melanin production compared to the uncomplexed parent peptides (Table 4). The EC₅₀ value for melanin production in response to [Nle⁴,D-Phe⁷]- α -MSH was found to be 1.1×10^{-11} M, a control value that is in good agreement with previously published values (36).

Receptor binding assays were performed on both ReO-NAC-CGCG-conjugated and unconjugated peptides (Figure 5). The ReO-NAC-CGCG-[Nle⁴,D-Phe⁷]- α -MSH and ReO-NAC-CGCG-[D-Phe⁷]- α -MSH₅₋₁₀-NH₂ conjugates exhibited a 1.5-fold decrease and a 4-fold increase in receptor binding affinity, respectively, compared to the parent uncomplexed peptide sequences (Table 4). Results from the melanin biosynthesis and receptor binding assays demonstrated that conjugation of ReO-NAC-CGCG to the N termini of the α -MSH analogs yielded minimal

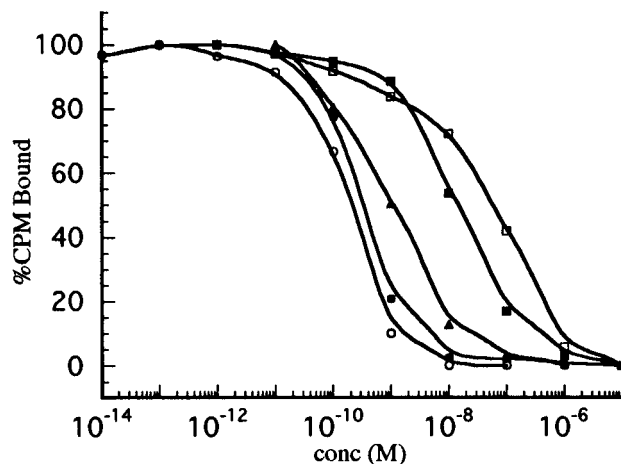


Figure 5. Sigmoidal dose-response curves showing inhibition of binding of ^{125}I -Nle⁴,D-Phe⁷- α -MSH to B16 F1 murine melanoma cells by (▲) α -MSH, (□) [D-Phe⁷]- α -MSH₅₋₁₀-NH₂, (■) ReO-NAC-CGCG-[D-Phe⁷]- α -MSH₅₋₁₀-NH₂, (○) NAc-[Nle⁴,D-Phe⁷]- α -MSH, and (●) ReO-NAC-CGCG-[Nle⁴,D-Phe⁷]- α -MSH.

effects on both their biological activities and receptor binding affinities.

DISCUSSION

Certain bioactive peptides, including α -MSH (41), permit relatively bulky substitutions at their amino terminus. The ability to append a metal-peptide pre-chelate to a bioactive peptide sequence via SPPS could be advantageous in several respects. For example, such a procedure could simplify subsequent purification of a radiolabeled bioactive complex, since the labeled compound has quite different chromatographic characteristics compared with the unlabeled compound. This results in a radiotracer that is not contaminated with unlabeled peptide.

The peptide NAC-CGCG was used as a metal-binding moiety to coordinate rhenium. The results of the conformational analysis of ReO-NAC-CGCG demonstrate that the metal is coordinated by two cysteine sulfurs and two intervening amide nitrogens. The structure as a whole can be considered as consisting of three fused heterocycles (Figure 2), with ring 1 including Cys¹S and Gly²N heteroatoms and rings 2 and 3 numbered anti-clockwise from ring 1. There is a strong analogy between the structure of this compound and the structure of rhenium-bound mercaptoacetyl triglycine (MAG3) (26, 31, 43). Three crystal structures of metal-bound analogs of MAG3 are available in the Cambridge Crystallographic Database. Rings 2 and 3 of ReO-NAC-CGCG are directly comparable to the MAG3 structures, while ring 1 departs significantly from MAG3 geometry.

Alignment of ReO-NAC-CGCG ring 2 with the analogous ring of MAG3 (43), using the fit algorithm within the SYBYL molecular modeling program, resulted in an almost perfect alignment. Slight differences in alignment between ring 3 and the C-terminal ring of MAG3 can be accounted for by the lack of a planar peptide bond in ring 3 and by the replacement of the nitrogen donor in MAG3 with sulfur in ReO-NAC-CGCG.

The additional carbon atom in ring 1 relative to MAG3 results in a deviation from the square pyramidal coordination of the ReO core. Placement of the sulfur of Cys¹ in the plane of the other three donor atoms would yield a distorted coordination geometry in which the Cys¹S–Cys³S distance is shorter than it would be in an ideal square plane. Alternatively, the NMR data suggest a different conformation for ring 1 in which both Cys¹S and

Cys1 β C lie slightly below the plane of the other three donor atoms. ^{13}C and ^1H chemical shift data indicate that the β carbon of Cys1 lies below the plane of the other three donor atoms. It has been found previously that in technetium- and rhenium-containing compounds, groups in an *anti* configuration relative to the metal-oxo group tend to resonate upfield relative to analogous groups in a *syn* configuration (25, 44). That the sulfur of Cys1 is also located beneath this plane is supported by $^3J_{\alpha\text{H}\beta\text{H}}$ coupling data, suggestive of a *gauche/trans* relationship between the two Cys1 β protons and Cys1 αH . Confirmation of our model, however, awaits a crystal structure of the complex.

The stability of the ReO-NAC-CGCG complex enabled us to append it directly to the N termini of biologically active peptides using standard SPPS chemistry. Conjugation of the ReO-NAC-CGCG moiety to the N termini of the α -MSH analogs had a minimal effect on bioactivity and receptor binding affinity. The binding affinity of NAc-[Nle 4 ,D-Phe 7]- α -MSH decreased <2-fold upon addition of ReO-NAC-CGCG, indicating that the addition of spacer atoms between the coordinating moiety and the bioactive peptide sequence is not required. The binding affinity of the [D-Phe 7]- α -MSH $_{5-10}$ -NH $_2$ analog was actually seen to increase upon addition of ReO-NAC-CGCG, an effect that might be explained by the known preference for a hydrophobic moiety at the α -MSH N terminus.

The reduction in EC $_{50}$ and K_i values for the conjugated and parent [D-Phe 7]- α -MSH $_{5-10}$ -NH $_2$ analogs compared to the NAc-[Nle 4 ,D-Phe 7]- α -MSH analogs is directly attributable to differences in amino acid sequence length. The truncated [D-Phe 7]- α -MSH $_{5-10}$ -NH $_2$ fragment lacks the C-terminal three amino acids as well as the N-terminal four amino acids that are present in the wild-type hormone. Each of these sequences has been implicated as being important for the binding of the wild-type hormone to the murine α -MSH receptor (36). Although the smaller fragment has a lower binding affinity to the α -MSH receptor *in vitro*, its smaller size and increased hydrophilicity may benefit its biodistribution *in vivo*. Experiments to test this hypothesis are currently in progress.

CONCLUSION

The labeling of truncated α -MSH fragments with the ReO-NAC-CGCG chelate demonstrates that the Cys-Gly-Cys peptide sequence when complexed with rhenium can be used in SPPS as a preformed ^{186}Re bifunctional chelate. The resulting labeled bioconjugates showed specific binding affinity for the α -MSH receptor and were demonstrated to retain bioactivity. The synthesis of these compounds serves to show that preformed peptide-metal coordination compounds can be successfully incorporated into bioactive peptide sequences by conventional SPPS techniques. Further, the labeled product can be obtained in a highly pure form, easily purified away from potentially contaminating unlabeled peptide species. Whether the peptidic nature of the chelating moiety has any effect on the *in vivo* metabolism of the radiotracer is currently being investigated.

This method could provide a general means of labeling bioactive peptides with preformed radiolabeled chelates that contain a free -COOH group. Amino acid based chelates such as MAG3 could be labeled with ^{186}Re and then coupled to biologically active peptide sequences during automated synthesis. Likewise, this technique could be used to append radiolabeled N $_2$ S $_2$ heterocyclic chelates to peptides. The only requirements are that the chelate complex contains an activatable carboxylate group and is stable in the deblocking/deprotection mix.

Additionally, the use of a natural amino acid chelate has other possible benefits that can be realized using a postconjugate chelation approach. Cysteine-containing amino acid sequences such as Cys-Gly-Cys or Gly-Gly-Cys (29) can be genetically engineered into larger biomolecules such as antibody fragments. Recombinant fragments can then be radiolabeled under mild conditions, with increased labeling efficiency.

The pure radiolabeled peptide-rhenium complexes produced by the preformed chelate approach described here have the metal incorporated into the peptide structure at a specific, known position. In contrast, any postlabeling scheme, even of relatively small peptides, is likely to result in a mixture of labeled peptides, of which many are not N $_2$ S $_2$ rhenium conjugates and therefore have lower intrinsic stability. In the future, this method could provide a means of producing medically useful peptide radiopharmaceuticals of high specific activity and purity.

ACKNOWLEDGMENT

This work was supported by DOE Grant DE FG02 93ER61661 and NSF NMR Instrumentation Grant 8908304.

LITERATURE CITED

- (1) Vallabhajosula, S., Moyer, B. R., Lister-James, J., McBride, B. J., Lipszyc, H., Lee, H., Bastidas, D., and Dean, R. T. (1996) Preclinical evaluation of technetium-99m-labeled somatostatin receptor-binding peptides. *J. Nucl. Med.* 37, 1016-1022.
- (2) Bakker, W. H., Albert, R., Bruns, C., Breeman, W. A. P., Hofland, L. J., Marbach, P., Pless, J., Pralet, D., Stoltz, B., Koper, J. W., Lamberts, S. W. J., Visser, T. J., and Krenning, E. P. (1991) [Indium-111-DPTA-D-Phe-1]-octreotide, a potential radiopharmaceutical for imaging somatostatin receptor positive tumors: synthesis, radiolabeling, and *in vitro* validation. *Life Sci.* 49, 1583-1591.
- (3) Krenning, E. P., Bakker, W. H., Kooij, P. P. M., Breeman, W. A. P., Oei, H. Y., deJong, M., Reubi, J. C., Visser, T. J., Bruns, C., Kwekkeboom, D. J., Reijs, A. E. M., van Hagen, P. M., Koper, J. W., and Lamberts, S. W. J. (1992) Somatostatin receptor scintigraphy with indium-111-DPTA-D-Phe-1-octreotide in man: metabolism, dosimetry, and comparison with iodine-123-Tyr-3-octreotide. *J. Nucl. Med.* 33, 652-658.
- (4) Virgolini, I., Kurtaran, A., Raderer, M., Leimer, M., Angelberger, P., Havlik, E., Li, S., Scheithauer, W., Niederle, B., Valent, P., and Eichler, H. (1995) Vasoactive intestinal peptide receptor scintigraphy. *J. Med. Chem.* 36, 1732-1739.
- (5) Reubi, J. C. (1995) In vitro identification of vasoactive intestinal peptide receptors in human tumors: implications for tumor imaging. *J. Med. Chem.* 36, 1846-1853.
- (6) Babich, J. W., Graham, W., Barrow, S. A., Dragotakes, S. C., Tompkins, R. G., Rubin, R. H., and Fischman, A. J. (1993) Technetium-99m-labeled chemotactic peptides: comparison with indium-111-labeled white blood cells for localizing acute bacterial infection in the rabbit. *J. Nucl. Med.* 34, 2176-2181.
- (7) Knight, L. C., Radcliffe, R., Maurer, A. H., Rodwell, J. D., and Alvarez, V. L. (1994) Thrombus imaging with technetium-99m synthetic peptides based upon the binding domain of a monoclonal antibody to activated platelets. *J. Nucl. Med.* 35, 282-288.
- (8) Muto, P., Lastoria, S., Varrella, P., Vergara, E., Salvatore, M., Morgano, G., Lister-James, J., Bernardy, J. D., Dean, R. T., Wencker, D., and Borer, J. S. (1995) Detecting deep venous thrombosis with technetium-99m-labeled synthetic peptide P280. *J. Nucl. Med.* 36, 1384-1391.
- (9) Lister-James, J., McBride, W. J., Buttram, S., Civitello, E. R., Martel, L. J., Pearson, D. A., Wilson, D. M., and Dean, R. T. (1995) Technetium-99m chelate-containing receptor-binding peptides. In *Technetium and Rhenium in Chemistry and Nuclear Medicine 4* (M. Nicolini, G. Bandoli, U. Mazzi, Eds.) pp 269-274, SGEEditoriali, Padova, Italy.
- (10) Barrett, J., Edwards, S., Harris, T., Rajopadhye, M., Lazewatsky, J., Liu, S., Damphousse, D., Heminway, S.,

- Mazaika, T., Thomas, J., Carroll, T., and Smith, J. (1995) The development of a technetium-99m agent for imaging deep vein thrombosis. In *Technetium and Rhenium in Chemistry and Nuclear Medicine 4* (M. Nicolini, G. Bandoli, U. Mazzi, Eds.) pp 275–280, SGEEditoriali, Padova, Italy.
- (11) Bard, D. R., Knight, C. G., and Page-Thomas, D. P. (1990) A chelating derivative of α -melanocyte stimulating hormone as a potential imaging agent for malignant melanoma. *Br. J. Cancer* 62, 919–922.
- (12) Bard, D. R., Knight, C. G., and Page-Thomas, D. P. (1990) Targeting of a chelating derivative of a short-chain analogue of α -melanocyte stimulating hormone to Cloudman S91 melanomas. *Biochem. Soc. Trans.* 18, 882–883.
- (13) Wraight, E. P., Bard, D. R., Maughan, T. S., Knight, C. G., and Page-Thomas, D. P. (1992) The use of a chelating derivative of α -melanocyte stimulating hormone for the clinical imaging of malignant melanoma. *Br. J. Radiol.* 65, 112–118.
- (14) Bagutti, C., Stolz, B., Albert, R., Bruns, C., Pless, J., and Eberle, A. N. (1994) [^{111}In]-DTPA-labeled analogues of α -melanocyte-stimulating hormone for melanoma targeting: receptor binding *in vitro* and *in vivo*. *Int. J. Cancer* 58, 749–755.
- (15) Deutsch, E., Libson, K., Vanderheyden, J., Ketrang, A. R., and Maxon, H. R. (1986) The chemistry of rhenium and technetium as related to the use of isotopes of these elements in therapeutic and diagnostic nuclear medicine. *Nucl. Med. Biol.* 13, 465–477.
- (16) Davison, A., Jones, A. G., Orvig, C., and Sohn, M. (1981) A new class of oxotechnetium(5+) chelate complexes containing a TcN_2S_2 core. *Inorg. Chem.* 20, 1629–1632.
- (17) Bryson, N., Dewan, J. C., Lister-James, J., Jones, A. G., and Davison, A. (1988) Neutral technetium(V) complexes with amide-thiol-thioether chelating ligands. *Inorg. Chem.* 27, 2154–2161.
- (18) Rao, T. N., Adhikesavalu, D., Camerman, A., and Fritzberg, A. R. (1990) Technetium(V) and rhenium(V) complexes of 2,3-bis(mercaptoacetamido)propanoate. Chelate ring stereochemistry and influence on chemical and biological properties. *J. Am. Chem. Soc.* 112, 5798–5804.
- (19) John, C. S., Francesconi, L. C., Kung, H. F., Wehrli, S., Graczyk, G., and Carroll, P. (1992) Synthesis and characterization of neutral oxotechnetium(V) bisaminoethanethiol complexes: potential brain imaging agents. *Polyhedron* 11, 1145–1155.
- (20) Coulais, Y., Cros, G., Darbieu, M. H., Gantet, P., Tafani, J. A. M., Vende, D., Pasqualini, R., and Guiraud, R. (1993) Synthesis, characterization, and biodistribution of new $^{99\text{m}}\text{Tc}$ oxo and nitrido complexes of unsaturated tetradentate (N_2S_2) ligands. *Nucl. Med. Biol.* 20, 263–268.
- (21) Volkert, W. A., Hoffman, T. J., Roth, C., Corlija, M., and Holmes, R. A. (1993) The design and properties of $^{99\text{m}}\text{Tc}$ chelates for brain perfusion imaging. *Radiochim. Acta* 63, 205–208.
- (22) Marzilli, L. G., Banaszczuk, M. G., Hansen, L., Kuklenyik, Z., Cini, R., and Taylor, A. (1994) Linking deprotonation and denticity of chelate ligands. Rhenium(V) oxo analogues of technetium-99m radiopharmaceuticals containing N_2S_2 chelate ligands. *Inorg. Chem.* 33, 4850–4860.
- (23) Chi, D. Y., Wilson, S. R., and Katzenellenbogen, J. A. (1995) Crystal structure of a bis(amido)bis(thiolato)oxorhenium(V) complex from silica gel. *Inorg. Chem.* 34, 1624–1625.
- (24) Fritzberg, A. R., Kasina, S., Eshima, D., and Johnson, D. L. (1986) Synthesis and biological evaluation of technetium-99m MAG_3 as a hippuran replacement. *J. Nucl. Med.* 27, 111–116.
- (25) O'Neil, J. P., Wilson, S. R., and Katzenellenbogen, J. A. (1994) Preparation and structural characterization of monoamine-monoamide bis(thiol) oxo complexes of technetium(V) and rhenium(V). *Inorg. Chem.* 33, 319–323.
- (26) Grummon, G., Rajagopalan, R., Palenik, G. J., Koziol, A. E., and Nosco, D. L. (1995) Synthesis, characterization, and crystal structures of technetium(V)-oxo complexes useful in nuclear medicine. 1. Complexes of mercaptoacetylglucylglycylglycine (MAG_3) and its methyl ester derivative ($\text{MAG}_3\text{-OMe}$). *Inorg. Chem.* 34, 1764–1772.
- (27) Cleynhens, B., Adriaens, P., Boonen, C., Vanbilloen, H., Van Nerom, C., and Verbruggen, A. M. (1994) Synthesis and biological evaluation of the four isomers of $^{99\text{m}}\text{Tc}$ -cysteinyltriglycine, an amino substituted derivative of $^{99\text{m}}\text{Tc}$ - MAG_3 . *J. Nucl. Biol. Med.* 38 (4 Suppl. 1), 69–74.
- (28) Mather, S. J., Ellison, D., and Bard, D. S. (1995) Technetium-99m labelled hybrid receptor-binding peptides. In *Technetium and Rhenium in Chemistry and Nuclear Medicine 4* (M. Nicolini, G. Bandoli, U. Mazzi, Eds.) pp 491–497, SGEEditoriali, Padova, Italy.
- (29) George, A. J. T., Jamar, F., Tai, M. S., Heelan, B. T., Adams, G. P., McCartney, J. E., Houston, L. L., Weiner, L. M., Oppermann, H., Peters, A. M., and Huston, J. S. (1995) Radiometal labeling of recombinant technetium-99m coordination by single-chain Fv antibody fusion proteins through a C-terminal cysteinyl peptide. *Proc. Natl. Acad. Sci. U.S.A.* 92, 8358–8362.
- (30) Bodanszky, M., and Bodanszky, A. (1994) *The Practice of Peptide Synthesis*, 2nd ed., Springer-Verlag, Berlin.
- (31) Hansen, L., Cini, R., Taylor, A., and Marzilli, L. G. (1992) Rhenium(V) oxo complexes relevant to technetium renal imaging agents derived from mercaptoacetylglucylglycylaminobenzoic acid isomers. Structural and molecular mechanics studies. *Inorg. Chem.* 31, 2801–2808.
- (32) Grove, D. E., and Wilkinson, G. (1966) Oxo-complexes of rhenium(V). *J. Chem. Soc. A*, 1224–1230.
- (33) Bryan, J. C., Stenkamp, R. E., Tulip, T. H., and Mayer, J. M. (1987) Oxygen atom transfer between rhenium, sulfur, and phosphorus. Characterization and reactivity of $\text{Re}(\text{O})\text{Cl}_3(\text{Me}_2\text{S})(\text{OPPh}_3)$ and $\text{Re}(\text{O})\text{Cl}_3(\text{CNCMe}_3)_2$. *Inorg. Chem.* 26, 2283–2288.
- (34) Siegrist, W., and Eberle, A. N. (1986) *In situ* melanin assay for MSH using mouse B16 melanoma cells in culture. *Anal. Biochem.* 159, 191–197.
- (35) Siegrist, W., Oestreicher, M., Stutz, S., Girard, J., and Eberle, A. N. (1988) Radioreceptor assay for α -MSH using mouse B16 melanoma cells. *J. Recept. Res.* 8, 323–343.
- (36) Sahm, U. G., Olivier, G. W. J., Branch, S. K., Moss, S. H., and Pouton, C. W. (1994) Influence of α -MSH terminal amino acids on binding affinity and biological activity in melanoma cells. *Peptides* 15, 441–446.
- (37) Sawyer, T. K., Sanfilippo, P. J., Hruby, V. J., Engel, M. H., Heward, C. B., Burnett, J. B., and Hadley, M. E. (1980) [$\text{Nle}^4, \text{D-Phe}^7$] α -melanocyte stimulating hormone: a highly potent α -melanotropin with ultralong biological activity. *Proc. Natl. Acad. Sci. U.S.A.* 77, 5754–5758.
- (38) Wüthrich, K. (1986) *NMR of Proteins and Nucleic Acids*, Wiley, New York.
- (39) Bax, A., and Summers, M. F. (1986) ^1H and ^{13}C assignments from sensitivity-enhanced detection of heteronuclear multiple-bond connectivity by 2D multiple quantum NMR. *J. Am. Chem. Soc.* 108, 2093–2094.
- (40) Jardetzky, O., and Roberts, G. C. G. (1981) *NMR in Molecular Biology*, Academic Press, New York.
- (41) Chaturvedi, D. N., Knittel, J. J., Hruby, V. J., Castrucci, A. M., and Hadley, M. E. (1984) Synthesis and biological actions of highly potent and prolonged acting biotin-labeled melanotropins. *J. Med. Chem.* 27, 1406–1410.
- (42) Sawyer, T. K., Hruby, V. J., Darman, P. S., and Hadley, M. E. (1982) [$\text{half-Cys}^4, \text{half-Cys}^{10}$]- α -melanocyte-stimulating hormone: a cyclic α -melanotropin exhibiting superagonist biological activity. *Proc. Natl. Acad. Sci. U.S.A.* 79, 1751–1755.
- (43) Rao, T. N., Adhikesavalu, D., Camerman, A., and Fritzberg, A. R. (1991) Synthesis and characterization of monooxorhenium(V) complexes of mercaptoacetylglucylglycylglycine. Crystal structure of tetrabutylammonium oxo(mercaptoacetylglucylglycylglycine)rhenate(V). *Inorg. Chim. Acta* 180, 63–67.
- (44) Lever, S. Z., Baidoo, K. E., and Mahmood, A. (1990) Structure proof of *syn/anti* isomerism in N-alkylated diaminedithiol (DADT) complexes of technetium. *Inorg. Chim. Acta* 176, 183–184.

Kinetic Analysis of Sequence-Specific Alkylation of DNA by Pyrimidine Oligodeoxyribonucleotide-Directed Triple-Helix Formation

Matthew J. Taylor and Peter B. Dervan*

Arnold and Mabel Beckman Laboratories of Chemical Synthesis, Division of Chemistry and Chemical Engineering, California Institute of Technology, Pasadena, California 91125. Received March 12, 1997*

Attachment of a nondiffusible bromoacetyl electrophile to the 5-position of a thymine at the 5'-end of a pyrimidine oligodeoxyribonucleotide affords sequence-specific alkylation of a guanine base in duplex DNA two base pairs to the 5'-side of a local triple-helical complex. Products resulting from reaction of 5'-³ETTTT^{Me}CTTTT^{Me}CTTTT^{Me}CTTTT-3' at 37 °C with a 29 base pair target duplex are determined by a gel mobility analysis to be oligonucleotides terminating in 5'- and 3'-phosphate functional groups, consistent with a mechanism involving alkylation, glycosidic bond cleavage, and base-promoted strand cleavage. The guanine-(linker)-oligonucleotide conjugate formed upon triple-helix-mediated alkylation at the N⁷ position of a guanine base in a 60 base pair duplex was identified by enzymatic phosphodiester hydrolysis of the alkylation products followed by reversed phase HPLC analysis. To determine the rate enhancement achieved by oligonucleotide-directed alkylation of duplex DNA, a comparison of rates of alkylation at N⁷ of guanine in double-stranded DNA by the *N*-bromoacetyloligonucleotide and 2-bromoacetamide was performed by a polyacrylamide gel assay. The reaction within the triple-helical complex on a restriction fragment was determined at 200 nM *N*-bromoacetyloligonucleotide to have a first-order rate constant k_1 of $(2.7 \pm 0.5) \times 10^{-5} \text{ s}^{-1}$ ($t_{1/2} = 7.2 \text{ h}$). The reaction of 2-bromoacetamide with a 39 base pair duplex of sequence corresponding to the restriction fragment targeted by triple-helix formation was determined to have a second-order rate constant k_2 of $(3.6 \pm 0.3) \times 10^{-5} \text{ M}^{-1} \text{ s}^{-1}$. A comparison of the first-order and second-order rate constants for the unimolecular and bimolecular alkylation reactions provides an effective molarity of 0.8 M for bromoacetyl within the triple-helical complex.

INTRODUCTION

The design of sequence-specific DNA-cleaving molecules requires the integration of recognition and cleavage in a single molecule. Three approaches to the bifunctional design of these molecules include attachment of functional groups to DNA-binding molecules that can achieve oxidation of the deoxyribose backbone (1), electrophilic modification of the bases (2), or hydrolysis of the phosphodiester bond. Of these classes, DNA-binding molecules that perform electrophilic modification of the bases can provide additional specificity due to the different nucleophilicity of positions on the bases in DNA (e.g. N⁷ of guanine or N³ of adenine).

Oligonucleotide-directed triple-helix formation is one of the most powerful methods for the sequence-specific recognition of single sites within megabase pair double-helical DNA (3, 4). Pyrimidine oligodeoxyribonucleotides bind purine tracts in the major groove of DNA parallel to the purine Watson–Crick strand, through formation of specific Hoogsteen hydrogen bonds to the purine Watson–Crick bases (Figure 1). Specificity is derived from thymine (T) recognition of adenine–thymine (AT) base pairs (TAT triplet) and N³-protonated cytosine (C⁺) recognition of guanine–cytosine (GC) base pairs (C⁺GC triplet).

Efforts have been successful in the use of oligonucleotides for directing electrophiles to react at the N⁷-position of guanine in the major groove via triple-helix formation (5). Early examples utilizing 5'-aromatic chloroethyl-

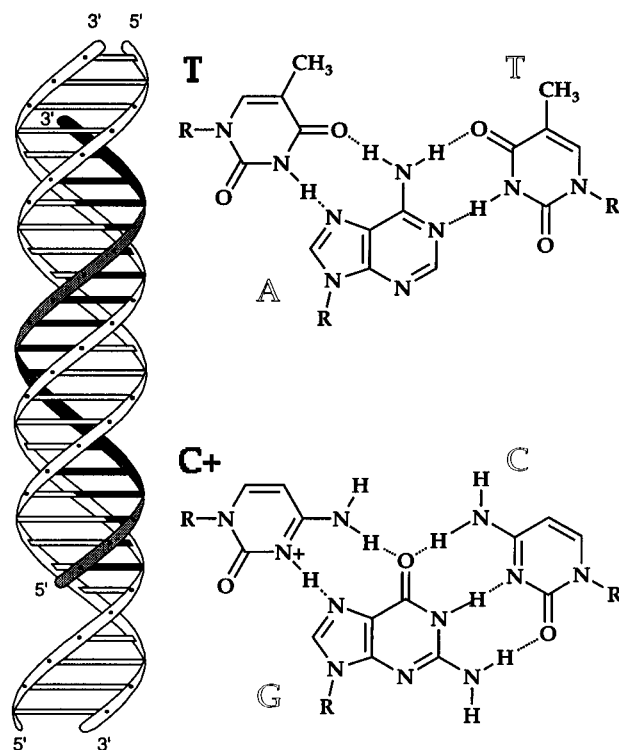


Figure 1. Model representing a pyrimidine-rich oligonucleotide bound in the major groove of double-stranded DNA and base triplets formed upon binding.

amine-modified pyrimidine oligonucleotides demonstrated alkylation at adjacent guanine bases with modest yield (5a,b). Ethano-5-methyl-2'-deoxycytidine residues at the 3'-end of oligonucleotides (5d,e) and oligonucle-

* Author to whom correspondence should be addressed [telephone (818) 395-6002; fax (818) 683-8753; e-mail dervan@cco.caltech.edu].

© Abstract published in *Advance ACS Abstracts*, April 15, 1997.

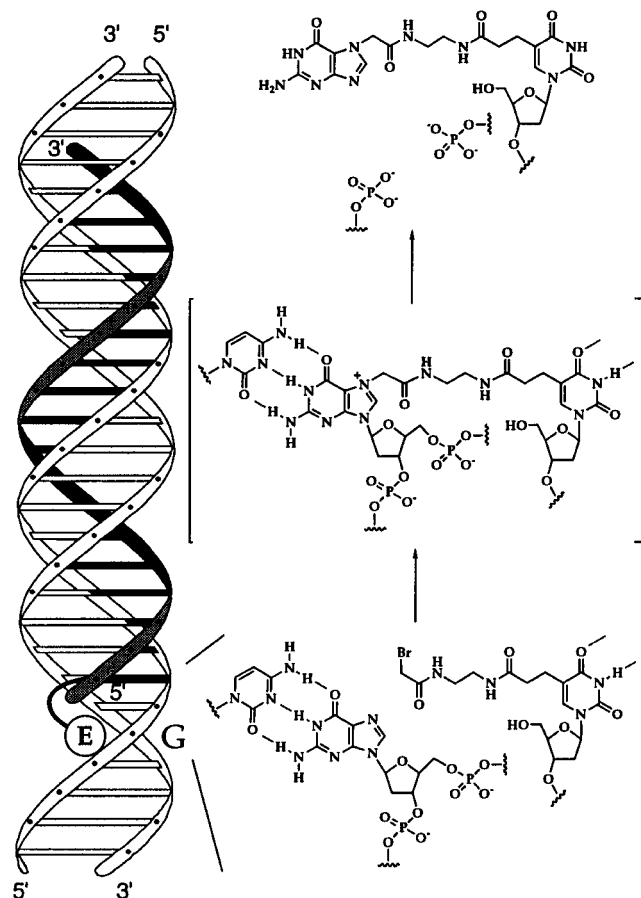


Figure 2. Bromoacetyl electrophile is localized in the major groove by triple-helix formation proximal to a GC base pair (G) in the Watson–Crick duplex target site. Alkylation at N7 of guanine followed by depurination results in cleavage of the deoxyribose backbone.

otides equipped with *N*-bromoacetyl at the 5'-end react with one strand of a duplex DNA target site in very high yield (5c). Pyrimidine oligodeoxyribonucleotides bound in the major groove and equipped with a bromoacetyl moiety at the 5'-end position the electrophile proximal to a guanine 2 base pairs to the 5'-side of the target sequence. Reaction of the electrophilic carbon of *N*-bromoacetyl with N⁷ of the guanine base adjacent to the local triple helix results in covalent attachment of the oligonucleotide to the target sequence. Upon warming in the presence of base, depurination at the position of alkylation occurs and cleavage of one strand of the DNA backbone is observed (5c) (Figure 2).

More recently, alkylation of both strands of double-helical DNA has been demonstrated (6). Pyrimidine oligonucleotides modified at both the 5'-end (for same-strand alkylation) and 3'-end (for opposite-strand alkylation) with aromatic chloroethylamines cross-link short double-helical DNA at guanine bases separated by 22–26 base pairs in 80% yield (6b). *N*-Bromoacetyl oligonucleotides bind adjacent inverted purine tracts on double-helical DNA by triple-helix formation and alkylate single guanine positions on opposite strands (6a). Double-strand cleavage at a single site within yeast chromosome III occurs in 85–90% yield, demonstrating the utility of this nonenzymatic approach for atom-specific reaction and cleavage of megabase pair double-helical DNA. Further design of these systems will undoubtedly benefit from an understanding in quantitative terms of what has been gained in reaction rate and specificity upon covalent attachment of electrophiles to oligonucleotides for alkylation of DNA.

We report here a product and kinetic analysis of pyrimidine oligonucleotide-directed bromoacetyl alkylation of double-stranded DNA. Products of N⁷ alkylation of guanine in the target duplex DNA and the pyrimidine-rich Hoogsteen strand of the bound triple-helical complex are characterized. Rate constants for the alkylation reaction at N⁷ of guanine within the triple-helical complex and the reaction of 2-bromoacetamide with N⁷ of guanine within duplex DNA are determined, allowing for an estimate of the effective molarity of bromoacetyl obtained upon attachment of the electrophile to the Hoogsteen strand of a local triple-helical complex.

EXPERIMENTAL PROCEDURES

¹H NMR and ¹³C NMR spectra were recorded at 300 MHz on a General Electric QE 300 Spectrometer. Chemical shifts were recorded in parts per million using the proteo NMR solvent as a reference. Biochemical manipulations were carried out according to standard procedures (7) unless otherwise noted. Adenine-specific (8) and guanine-specific (7) sequencing reactions were performed as previously described. Radioactive nucleotides were purchased from Amersham and ICN. T4 polynucleotide kinase, calf alkaline phosphatase, Klenow fragment, and glycogen were obtained from Boehringer Mannheim. *Hind*III was obtained from New England Biolabs. *Ssp*I was obtained from Gibco/BRL. Terminal transferase was obtained from USB. Dimethyl sulfate, piperidine, and 2-bromoacetamide were obtained from Aldrich. Purity of 2-bromoacetamide was verified by ¹H NMR. Acrylamide was purchased from Bio-Rad. Cobalt hexamine trichloride was obtained from Fluka. Snake venom phosphodiesterase (type VIII) was purchased from Sigma. NAP-5, NAP-25, and NICK columns were purchased from Pharmacia. All reagents were used without further purification unless otherwise noted. High-resolution FAB mass spectra were obtained at the California Institute of Technology Chemistry/Biology Mass Spectrometry Facility. Matrix-assisted laser desorption/ionization time of flight mass spectra were obtained at the Protein and Peptide Microanalytical Facility at the California Institute of Technology.

High-pressure liquid chromatography (HPLC) was performed on a Hewlett-Packard 1090 liquid chromatograph with a HPLC 3D Chemstation. Analytical reversed phase HPLC was performed on a Vydac 201HS reversed phase HPLC column. Oligonucleotide purification was accomplished on a Pharmacia LKB FPLC using a ProRPC HR 16/10 reversed phase column (160 mm × 10 mm). Ion retardation resin (AG 11A8) and cation exchange cellulose (Cellex-CM) were purchased from Bio-Rad. Reversed phase resin (LiChroprep RP-18) was purchased from EM Separations.

Synthesis and Purification of Oligonucleotides.

Oligonucleotides were synthesized on an Applied Biosystems Model 380B DNA synthesizer using standard phosphoramidite chemistry (9) and deprotected with concentrated NH₄OH at 55 °C for 24 h. Following lyophilization, purification of 5'-OH-oligonucleotide was achieved using denaturing polyacrylamide gel electrophoresis. Purification of the 5'-O-dimethoxytrityl oligonucleotide was achieved using reversed phase FPLC (solvent A, 100 mM ammonium acetate, pH 7.0; solvent B, 40% acetonitrile in solvent A). Following lyophilization of appropriate fractions and removal of the dimethoxytrityl protecting group (80% acetic acid for 20 min followed by lyophilization), purification of the deprotected oligonucleotide was achieved by reversed phase FPLC. Following purification, oligonucleotides were desalted on a Sep-Pak car-

tridge (Waters) and quantitated by UV-vis spectroscopy (extinction coefficients in $M^{-1} \text{ cm}^{-1}$: dT = 8 700, dG = 11 500, dA = 15 400, dC = 7 400).

Synthesis and Analysis of *N*-Bromoacetyloligonucleotides. Fmoc-protected aminonucleoside (5c) was incorporated at the 5'-end of the oligonucleotide 5'-TTT^{Me}-CTTTT^{Me}C^{Me}CTTT^{Me}CTTTT-3' as the 5'-O-DMT-3'-phosphoramidite with a modification of standard coupling protocols. The last coupling step in the oligonucleotide synthesis was performed with a 0.15 M solution of the β -cyanoethyl phosphoramidite in tetrahydrofuran (distilled from calcium hydride) on a 1 μmol scale. Following deprotection at 55 °C for 15 h, the 5'-O-DMT-oligonucleotide was purified by reversed phase FPLC, deprotected, and further purified by reversed phase FPLC. Acylation of the resulting oligonucleotide-amine was then performed. Ten nanomoles of oligonucleotide was dissolved in 10 μL of 200 mM borate buffer, pH 8.9. Ten microliters of a 30 mM solution of freshly prepared *N*-hydroxysuccinimide bromoacetate in *N,N*-dimethylformamide (stored over molecular sieves) was added, the resulting solution mixed well, and, after 30 s, diluted to 0.5 mL with water and passed through an NAP-5 column (Sephadex G-25, equilibrated with water). Following elution with 1.0 mL of water, the *N*-bromoacetyloligonucleotide was quantitated by UV-vis spectroscopy (extinction coefficient of 153 000 $M^{-1} \text{ cm}^{-1}$ determined from the sum of dT = 8 700, dT^E = 8 700, and 5-methyl-dC = 5 700) and stored at -20 °C. The reaction was judged quantitative by HPLC analysis of enzyme degradation products. To the oligonucleotide were added 18 μL of water, 2.5 μL of 10 \times dephosphorylation buffer (500 mM Tris-HCl, 1 mM EDTA, pH 8.5), 2.5 μL of 2 M MgCl_2 , and 2 μL of snake venom phosphodiesterase (2 units/0.7 mL of enzyme). Following incubation at 37 °C for 2 h, samples were filtered (0.2 μm Nylon-66 membrane, Rainin) and 23.5 μL was injected. HPLC conditions: Vydac C₁₈ 201HS reversed phase column preequilibrated to 50 °C; solvent A, 100 mM ammonium acetate, pH 6.0; solvent B, acetonitrile; gradient, 0–10 min at 0% B, 10–40 min to 5% B, 40–60 min at 5% B, 60–70 min to 10% B, 70–85 min at 10% B, 85–90 min to 0% B. Retention times and relative peak areas: 5-methyl-2'-deoxycytidine 5'-monophosphate, 10.3 min, 2.6; thymidine 5'-monophosphate, 15.0 min, 14.6; hydroxy-(linker)-thymidine, 35.2 min, 0.2; bromo-(linker)-thymidine, 52.6 min, 0.8. Mass spectrum of *N*-bromoacetyloligonucleotide (MALDI-TOF): calcd 5934.9, found 5935.7.

5'-³²P-End Labeling of the 29 Base Pair Duplex. Fifty picomoles of single-stranded oligonucleotide 5'-GCTAGTAAAGAAAAGGAAAGAAAAGTCG-3' was labeled with ³²P at the 5'-end by treatment with 45 units of T4-polynucleotide kinase and [γ -³²P]dATP γ P for 45 min at 37 °C. Following phenol/chloroform extraction, ethanol precipitation, and hybridization with 100 pmol of complementary single-stranded oligonucleotide, the 5'-³²P-end-labeled duplex was subjected to 14% nondenaturing polyacrylamide gel electrophoresis, visualized by autoradiography, excised from the gel, and eluted with 200 mM NaCl/1 mM EDTA at 37 °C overnight. The DNA was filtered (0.45 μm), ethanol precipitated, passed through a NICK column (Sephadex G-50, equilibrated with water), and stored at -20 °C.

3'-³²P-End Labeling of 29 Base Pair Duplex. Fifty picomoles of single-stranded oligonucleotide 5'-GCTAGTAAAGAAAAGGAAAGAAAAGTCG-3' was labeled with [α -³²P]ddA α P at the 3'-end by treatment with 85 units of terminal deoxynucleotidyl transferase and [α -³²P]ddATP α P for 45 min at 37 °C. Unincorporated nucleotide was removed by passage through a NICK column (Sephadex

G-50, equilibrated with water), then butanol was extracted, and the nucleotide was lyophilized to dryness. Radiolabeled single-stranded oligonucleotide was then subjected to 20% denaturing polyacrylamide gel electrophoresis, visualized by autoradiography, excised from the gel, and eluted with 200 mM NaCl/1 mM EDTA at 37 °C overnight. The DNA was filtered (0.45 μm) and ethanol precipitated. Following hybridization with 100 pmol of complementary single strand, the 3'-³²P-end-labeled duplex was purified by 14% nondenaturing polyacrylamide gel electrophoresis, visualized by autoradiography, excised from the gel, and eluted with 200 mM NaCl/1 mM EDTA at 37 °C overnight. The DNA was filtered (0.45 μm), ethanol precipitated, passed through a NICK column (Sephadex G-50, equilibrated with water), and stored at -20 °C.

Enzymatic Characterization of DNA Termini. End-labeled 29 base pair duplex (100 000 cpm) with and without *N*-bromoacetyloligonucleotide (2.5 μM) was incubated in 20 mM HEPES, pH 6.8, with 1 mM $\text{Co}(\text{NH}_3)_6\text{Cl}_3$ in a volume of 20 μL at 4 °C for 2 h and then at 37 °C for 24 h. Two microliters of glycogen in water (20 mg/mL), 2 μL of 3 M sodium acetate, pH 5, and 60 μL of absolute ethanol were then added. Following chilling at -70 °C for 20 min and centrifugation at 14 000 rpm for 40 min, the supernatant was discarded. Seventy percent ethanol/water was added, and following centrifugation at 14 000 rpm for 5 min, the supernatant was discarded. Fifty microliters of water was added and, after vigorous mixing, the reaction was dried *in vacuo*. To each tube was added 100 μL of 10% piperidine. Following incubation at 90 °C for 30 min, reactions were dried *in vacuo*. Samples were then lyophilized twice from 50 μL of water.

For the 3'-end analysis, a portion (10 000 cpm) of 5'-³²P-end-labeled product as well as products of dimethyl sulfate cleavage were dissolved in separate reactions in dephosphorylation buffer (20 mM Tris-HCl, pH 6.6, 20 mM MgCl_2 , 10 mM β -mercaptoethanol), and 10 units of T4 polynucleotide kinase was added. After 1 h at 37 °C, reactions were ethanol precipitated. For the 5'-end analysis, a portion (20 000 cpm) of the 3'-[α -³²P]ddA-end-labeled product as well as products of dimethyl sulfate cleavage were dissolved in separate reactions in calf alkaline phosphatase (CAP) buffer, and 2 units of CAP was added. After 45 min at 37 °C, reactions were ethanol precipitated. Reaction products, as well as control and G-reactions, were dissolved in formamide loading buffer and subjected to gel electrophoresis on 1:20 cross-linked 20% denaturing polyacrylamide gels. Following electrophoresis, gels were visualized by autoradiography.

***N*-Hydroxysuccinimide 2-Bromoacetate (10).** To a solution of *N*-hydroxysuccinimide (0.6 g, 5.4 mmol) and 2-bromoacetic acid (0.75 g, 5.4 mmol) in dioxane (30 mL) was added *N,N*-dicyclohexylcarbodiimide (1.3 g, 6.5 mmol). The resulting white suspension was stirred for 2 h and then filtered into 100 mL of petroleum ether. The resulting white precipitate was collected by filtration, washed with petroleum ether, and dried *in vacuo* to provide 0.5 g (38%) of *N*-hydroxysuccinimide 2-bromoacetate as a white, crystalline solid: ¹H NMR (DMSO-*d*₆) δ 2.82 (s, 4H), 4.62 (s, 2H); ¹³C NMR (DMSO-*d*₆) δ 23.1, 26.0, 164.7, 170.3; IR (KBr) 3060 (vw), 2990 (vw), 2943 (vw), 1812 (m), 1781 (m), 1736 (s), 1356 (m), 1211 (m), 1074 (m) cm^{-1} ; HRMS calcd for C₆H₆NO₄Br 234.9479, found 234.9469.

Amino-(Linker)-Thymidine (T-NH₂). To a flask containing 237 mg (0.75 mmol) of thymidine methyl ester **1** (11) was added 5 mL of ethylenediamine (freshly distilled from sodium hydroxide). The clear solution was stirred at 50 °C for 7 h and then at room temperature

for 16 h. The ethylenediamine was removed *in vacuo* to give a clear oil. Evaporation with methanol/toluene to remove trace ethylenediamine yielded a clear oil, and upon repeated evaporation with acetonitrile, 247 mg (96%) of **T-NH₂** was obtained as a white, hygroscopic, fluffy solid: ¹H NMR (CD₃OH) δ 2.08–2.15 (m, 2H), 2.29–2.33 (m, 2H), 2.47–2.52 (m, 2H), 2.56–2.61 (m, 2H), 3.11 (dd, *J* = 6.4 Hz, *J* = 2.3 Hz, 2H), 3.66 (dd, *J* = 21 Hz, *J* = 4 Hz, 2H), 3.79 (q, *J* = 3.4 Hz, 1H), 4.28 (m, 1H), 6.18 (t, *J* = 6.7 Hz, 1H), 7.70 (s, 1H); ¹³C NMR (CD₃OH) δ 24.3, 35.8, 41.2, 41.9, 42.8, 62.9, 72.1, 86.3, 88.8, 114.1, 138.8, 152.5, 166.1, 175.3; IR (KBr) 3362 (s), 3261 (m), 2937 (w), 2855 (w), 1702 (s), 1637 (s), 1560 (m), 1282 (m), 1104 (m), 926 (w) cm⁻¹; HRMS calcd for C₁₄H₂₂N₄O₆ 342.1534, found 342.1561.

Bromo-(Linker)-Thymidine (T-Br). To a solution of **T-NH₂** (19 mg, 55 μmol) in water (0.2 mL) was added *N*-hydroxysuccinimide 2-bromoacetate (25 mg, 106 μmol). The solution was vigorously mixed for 5 min and then loaded onto a 2 g Sep-Pak cartridge equilibrated with water. The column was washed first with water and then with 50% acetonitrile/water. Lyophilization afforded 6 mg (24%) of **T-Br** as a fluffy, white solid: ¹H NMR (D₂O) δ 2.29–2.38 (m, 2H), 2.40–2.45 (t, *J* = 7.1 Hz, 2H), 2.56–2.61 (t, *J* = 5.9 Hz, 2H), 3.30 (s, 4H), 3.71–3.81 (m, 2H), 3.86 (s, 2H), 3.87–3.89 (m, 1H), 3.98–4.02 (m, 1H), 4.41–4.46 (m, 1H), 6.23–6.28 (t, *J* = 6.7 Hz, 1H), 7.65 (s, 1H); ¹³C NMR (D₂O) δ 23.0, 28.1, 34.4, 38.4, 38.8, 39.3, 61.2, 70.5, 85.2, 86.6, 113.3, 138.3, 151.6, 165.6, 170.2, 175.5; IR (KBr) 3507 (m), 3365 (s), 3049 (m), 2931 (m), 2802 (w), 1686 (s), 1655 (s), 1625 (m), 1560 (m), 1424 (m), 1048 (m) cm⁻¹; HRMS calcd for C₁₆H₂₄N₄O₇Br 463.0823, found 463.0821.

Hydroxy-(Linker)-Thymidine (T-OH). To a solution of *N*-hydroxysuccinimide (1.5 g, 13.2 mmol) and glycolic acid (1 g, 13.2 mmol) in dioxane (16 mL) was added *N,N*-dicyclohexylcarbodiimide (3.3 g, 15.8 mmol). The resulting white suspension was stirred for 2 h and then filtered into 100 mL of petroleum ether. The resulting white precipitate was collected by filtration, washed with petroleum ether, and dried *in vacuo* to provide 1.2 g of a white solid, used without further purification. To a solution of **T-NH₂** (44 mg, 129 μmol) in water (0.44 mL) was added the NHS-ester of glycolic acid (34 mg). The solution was vigorously mixed for 5 min and then stirred for 4 h. The reaction mixture was dried *in vacuo* to a yellow oil. The oil was dissolved in 50% aqueous acetonitrile (300 μL) and then adsorbed onto silica gel. Column chromatography (0–7% water/acetonitrile), followed by adsorption and elution from reversed phase resin (LiChroprep RP-18) afforded 7 mg (14%) of **T-OH** as a white solid: ¹H NMR (DMSO-*d*₆) δ 2.03–2.07 (m, 2H), 2.20–2.26 (t, *J* = 7.4 Hz, 2H), 2.38–2.43 (t, *J* = 7.4 Hz, 2H), 3.08–3.14 (m, 4H), 3.53–3.58 (m, 2H), 3.73–3.75 (m, 1H), 3.77 (s, 2H), 4.21–4.23 (m, 1H), 5.01–5.05 (m, 1H), 5.22–5.24 (d, *J* = 4 Hz, 1H), 6.12–6.17 (t, *J* = 6.9 Hz, 1H), 7.63 (s, 1H), 7.81–7.84 (m, 1H), 7.85–7.90 (m, 1H), 11.28 (s, 1H); ¹³C NMR (D₂O) δ 23.0, 34.4, 38.4, 38.6, 38.8, 60.9, 61.2, 70.5, 85.2, 86.6, 113.3, 138.3, 151.5, 165.5, 175.2, 175.5; IR (KBr) 3448 (s), 3413 (s), 3072 (m), 2931 (m), 1690 (s), 1655 (s), 1561 (m), 1543 (m), 1273 (m), 1096 (m), 1032 (w) cm⁻¹; HRMS calcd for C₁₆H₂₄N₄O₈ 400.1588, found 400.1607.

***N*-Carboxymethylguanine (12).** To a flask containing guanosine (1.8 g, 6.6 mmol), iodoacetic acid (4.8 g, 26 mmol), and lithium hydroxide (0.31 g, 12.8 mmol) was added 12 mL of water. The resulting suspension was stirred at reflux for 70 min, during which time a clear, dark red solution was formed. The solution was cooled, and solid sodium thiosulfate was added until the red

solution turned to a light pink color. The solution was then adjusted to pH 5.5 with LiOH(s). After storage overnight at 4 °C, the pink precipitate was collected by filtration. Following recrystallization from 5% aqueous acetic acid 350 mg (26%) of *N*-carboxymethylguanine was obtained as a pale pink solid: ¹H NMR (NaOD/D₂O) δ 4.86 (s, 1H), 7.71 (s, 1H); ¹³C NMR (NaOD/D₂O/DMSO-*d*₆) δ 40.0 (DMSO-*d*₆), 50.8, 111.6, 144.0, 160.0, 162.2, 166.5, 176.5; IR (KBr) 3537 (s), 3316 (s), 3124 (s), 2694 (s), 1659 (s), 1502 (w), 1474 (m), 1232 (m), 1103 (w), 897 (w) cm⁻¹; HRMS calcd for C₇H₇N₅O₃ 209.0548, found 209.0545.

Guanine-(Linker)-Thymidine (T-G). To 1.5 mL of 50% aqueous pyridine, pH 8.5, was added *N*-carboxymethylguanine (20 mg, 96 μmol), 4-nitrophenol (133 mg, 960 μmol), and thymidine-amine **T-NH₂** (36 mg, 105 μmol). 1-[3-(Dimethylamino)propyl]-3-ethylcarbodiimide hydrochloride (EDCI) (total 576 μmol) was then added to the resulting yellow solution in portions of 1/5 equivalent. The solution was lyophilized, dissolved in 2 mL of 10 mM NH₄OAc, pH 4.5, and extracted with an equal amount of chloroform. Removal of residual pyridine was achieved by passage of the aqueous solution through cation exchange cellulose (CM-Sephadex). The reaction was then subjected to purification by reversed phase chromatography (LiChroprep C₁₈ resin), affording a further purified mixture of adduct **T-G** and *p*-nitrophenol, which was then lyophilized, dissolved in water, and passed through ion retardation resin (Bio-Rad AG 11A8) to remove *p*-nitrophenol. Lyophilization afforded the authentic standard **T-G** (2 mg) as a fluffy, white solid: ¹H NMR (DMSO-*d*₆) δ 2.04–2.08 (m, 2H), 2.21–2.26 (t, *J* = 7.4 Hz, 2H), 2.38–2.43 (t, *J* = 7.5 Hz, 2H), 3.31 (s, 4H), 3.53–3.57 (m, 2H), 3.73–3.77 (m, 1H), 4.21–4.23 (m, 1H), 4.85 (s, 2H), 5.01–5.04 (t, *J* = 5.1 Hz, 1H), 5.23–5.24 (d, *J* = 4.2 Hz, 1H), 6.10 (s, 2H), 6.13–6.17 (t, *J* = 6.9 Hz, 1H), 7.65 (s, 1H), 7.79–7.81 (s, 1H), 7.83 (s, 1H), 8.17 (s, 1H), 10.72 (s, 1H), 11.31 (s, 1H); ¹³C NMR (DMSO-*d*₆) δ 23.0, 34.5, 38.5, 38.9, 39.8, 48.6, 61.7, 70.7, 84.3, 87.6, 109.0, 113.1, 137.6, 144.5, 150.8, 153.2, 155.2, 160.1, 163.8, 167.4, 172.0; IR (KBr) 3358 (s), 2924 (m), 2848 (w), 1686 (s), 1560 (m), 1384 (m), 1273 (w), 1108 (w) cm⁻¹; HRMS calcd for C₂₁H₂₇N₉O₈ 533.1977, found 533.1989.

HPLC Analysis of Products of Oligonucleotide-Directed Alkylation. Twenty nanomoles of single-stranded oligonucleotide 5'-TCGGTACCCGGGATCT-AAAGTAAAGAAAAGAAAAGAAAAGCTTT-CTTCTTCCCTATC-3' (ε = 6.0 × 10⁵ M⁻¹ cm⁻¹) and complementary oligonucleotide (ε = 5.7 × 10⁵ M⁻¹ cm⁻¹) were hybridized as follows: Oligonucleotides were combined in 400 μL of water and passed through a NAP-5 column (Sephadex G-25, equilibrated with water). To the 1.0 mL of eluent in a 1.7 mL microfuge tube was added 100 μL of 200 mM HEPES, pH 7.0. The solution was heated to 90 °C for 9 min and then cooled to room temperature. After 15 h, the resulting solution was then combined in a 15 mL Falcon tube with 4.5 mL of water, 570 μL of 200 mM HEPES, pH 7.0, and a stirbar. After the solution was cooled to 4 °C with stirring, 20 nmol of *N*-bromoacetyl oligonucleotide in 1 mL of water was added, followed by 170 μL of 8 mM cobalt hexamine trichloride (to give a final concentration of 2.7 μM oligonucleotides). This solution was stirred at 4 °C for 1.5 h and then placed in an oil bath equilibrated to 37 °C. The cloudy solution was stirred, and after 10 min, the first aliquot (1.1 mL, 3 nmol) was removed for workup. The sample was pipetted into a 1.7 mL microfuge tube with 100 μL of 2 M sodium chloride (170 mM NaCl final concentration). The resulting clear

solution was heated to 90 °C for 15 min and then cooled to room temperature. The solution was diluted to 2.5 mL and passed through a NAP-25 column (Sephadex G-25, equilibrated with water), the 3.5 mL eluent was collected in two 2 mL microfuge tubes, and the solutions were dried *in vacuo*. Product was then transferred to a 0.7 mL microfuge tube with 100 μ L of water, followed by washes of three 100 μ L aliquots of water to ensure complete transfer of material. Samples were then dried *in vacuo* and stored at -20 °C. The above procedure was repeated at time points of 3, 7, 10.5, 19.2, 29, and 69.5 h (relative to the time of the first sample withdrawn from the reaction mixture).

Just prior to HPLC analysis, to each tube were added 18 μ L of water, 2.5 μ L of 10 \times dephosphorylation buffer (500 mM Tris-HCl/1 mM EDTA, pH 8.5), 2.5 μ L of 2 M MgCl₂, and 2 μ L of snake venom phosphodiesterase (2 units/0.7 mL of enzyme). Following incubation at 37 °C for 2 h, samples were filtered (0.2 μ m Nylon-66 membrane, Rainin) and 23.5 μ L was injected. A blank run with 23.5 μ L of water injected between each run was performed to prevent contamination of HPLC chromatograms from previous runs. HPLC conditions: Vydac C₁₈ 201HS reversed phase column preequilibrated to 50 °C; solvent A, 100 mM ammonium acetate, pH 6.0; solvent B, acetonitrile; gradient, 0–10 min at 0% B, 10–40 min to 5% B, 40–60 min at 5% B, 60–70 min to 10% B, 70–85 min at 10% B, 85–90 min to 0% B. Retention times: 2'-deoxycytidine 5'-monophosphate, 7.7 min; 5-methyl-2'-deoxycytidine 5'-monophosphate, 10.7 min; thymidine 5'-monophosphate, 14.5 min; 2'-deoxyadenosine 5'-monophosphate, 26.6 min; hydroxy-(linker)-thymidine nucleoside, 38.4 min; guanine-(linker)-thymidine nucleoside, 47.8 min; bromo-(linker)-thymidine nucleoside, 55.2 min; undigested oligodeoxyribonucleotides, 70–80 min; authentic standard T-G injected under identical solution conditions, 48.5 min; hydroxy-(linker)-thymidine, 39.0 min; bromo-(linker)-thymidine, 55.5 min.

Cloning of Plasmid pUCINET. The plasmid pUCINET was constructed by ligation of the duplex formed between oligonucleotides of sequence 5'-GATCATACACATACTAATACTAGTAAAAGAAAAGGAAAGAAAA-3' and 5'-TCGATTTTCTTTCTTTCTTTTACTAGTATTAGTATGTGTAT-3' with pUC19 previously digested with *Bam*HI and *Sal*I. Ligation products were used to transform Epicurian Coli XL 1 Blue competent cells. Colonies were selected for α -complementation on Luria-Bertani medium agar plates containing 50 μ g/mL ampicillin and XGAL and IPTG solution. Large scale plasmid purification was performed using Qiagen purification kits according to the manufacturer's protocol. Plasmid DNA concentration was determined from absorbance at 260 nm using the relation 1 OD unit = 50 μ g/mL duplex DNA. The sequence of the inserted region was verified by dideoxy sequencing of the resulting recombinant plasmid.

Kinetic Measurements: N-Bromoacetyloligonucleotide Alkylation of the 666 Base Pair Restriction Fragment. Plasmid pUCINET was linearized with the restriction enzyme *Hind*III. Eight micrograms of DNA was labeled at the 3'-end using Klenow to incorporate [α -³²P]dATP α P and [α -³²P]TTP α P. Following a chase fill-in with dATP, TTP, dCTP, and dGTP the reaction was extracted with phenol/chloroform, and the 3'-³²P-end-labeled DNA ethanol precipitated. The DNA was digested with *Ssp*I, producing fragments 2 and 0.7 kbp in size. Following ethanol precipitation, separation by 5% polyacrylamide gel electrophoresis, and visualization of the gel by autoradiography, the 666 base pair fragment containing the target site was excised from the gel and eluted with 200 mM NaCl/1 mM EDTA at 37 °C over-

night. The radiolabeled restriction fragment was filtered (0.45 μ m), ethanol precipitated, and passed through a NICK column (Sephadex G-50, equilibrated with water); ¹/₁₀ volume of 200 mM Bis-Tris acetate, pH 7.0, was added, and the mixture was stored at -20 °C.

A 2 \times stock solution was made containing 3'-³²P-end-labeled *Hind*III/*Ssp*I pUCINET restriction fragment (4 000 cpm/ μ L), 40 mM Bis-Tris acetate, pH 7.0, and 1.6 mM cobalt hexammine trichloride. The stock solutions were then aliquoted into microfuge tubes, and to each was added an equivalent volume of 2 \times aqueous N-bromoacetyloligonucleotide at 2, 0.4, and 0.2 μ M concentrations. The solutions were incubated overnight at 8 °C, and then each was split into seven tubes and put at 37 °C. After 30 min, the first tube (arbitrarily designated time equals zero) was quenched by the addition of 2 μ L of glycogen (20 mg/mL), 2 μ L of 3 M sodium acetate, and 60 μ L of ethanol. Samples were stored at -80 °C until completion of the experiment. Subsequent time points were treated as described. The samples were then centrifuged at 14 000 rpm for 30 min, the supernatants discarded, and reactions dried *in vacuo*. One hundred microliters of 10% aqueous piperidine was added, and reactions were heated to 90 °C for 30 min. Reactions were lyophilized, then lyophilized twice from 50 μ L of water, and dissolved in formamide loading buffer. Separation of products was performed by 1:20 cross-linked 8% denaturing polyacrylamide gel electrophoresis (5 000 cpm/lane). Dried polyacrylamide gels were analyzed by storage phosphor autoradiogram.

Band densities were determined by quantitative analysis of storage phosphor autoradiograms using a PhosphorImager (Model 400S) and Image Quant (Molecular Dynamics) software. Integrated volumes were determined for individual bands, and numerical values were transferred to Microsoft Excel. Bands were assigned as depicted in Figure 7 to determine values for [D]_i and [D]_o, and ln([D]_i/[D]_o) was plotted versus time using the program KaleidaGraph to determine from the slope the value for *k*₁. Kinetics were first-order in target DNA concentration over 2 half-lives and provided rate constants of (2.4 \pm 0.3) \times 10⁻⁵, (2.7 \pm 0.5) \times 10⁻⁵, and (1.6 \pm 0.4) \times 10⁻⁵ s⁻¹ for 1, 0.2, and 0.1 μ M concentrations of N-bromoacetyloligonucleotide, respectively.

Kinetic Measurements: 2-Bromoacetamide Alkylation of the 39 Base Pair Duplex. Fifty picomoles of single-stranded oligonucleotide 5'-ATACACATACATACTAGTAAAAGAAAAGGAAAGAAAA-3' was labeled with ³²P at the 5'-end by treatment with 45 units of T4 polynucleotide kinase and [γ -³²P]dATP γ P for 45 min at 37 °C. Following ethanol precipitation the DNA was resuspended in formamide loading buffer and purified by 20% denaturing polyacrylamide gel electrophoresis. Following elution, ethanol precipitation, and hybridization with excess complementary single-stranded oligonucleotide, the 5'-³²P-end-labeled duplex was then subjected to 12% nondenaturing polyacrylamide gel electrophoresis, visualized by autoradiography, excised from the gel, and eluted with 200 mM NaCl/1 mM EDTA at 37 °C overnight. The DNA was filtered (0.45 μ m), ethanol precipitated, and passed through a NICK column (Sephadex G-50, equilibrated with water); ¹/₁₀ volume of 200 mM Bis-Tris acetate, pH 7.0, was added, and the mixture was stored at -20 °C.

A 2 \times stock solution was made containing 5'-³²P-end-labeled 39 base pair duplex (8 000 cpm/ μ L), 40 mM Bis-Tris acetate, pH 7.0, and 1.6 mM cobalt hexammine trichloride. The stock solutions were then aliquoted into microfuge tubes, and to each was added an equivalent volume of 2 \times aqueous 2-bromoacetamide (made fresh,

volumetrically) at 20, 40, 60, 100, 120, 140, 160, and 180 mM concentrations. Reactions were each then aliquoted to six microfuge tubes and incubated at 37 °C for 25 min. The first tube (arbitrarily designated time equals zero) was quenched by brief exposure to liquid nitrogen, followed by the addition of 2 μ L of glycogen (20 mg/mL), 2 μ L of 3 M sodium acetate, and 60 μ L of ethanol. Samples were stored at -80 °C until completion of the experiment, and subsequent time points were treated as described. The samples were then centrifuged at 14 000 rpm for 30 min, the supernatants discarded, and reactions dried *in vacuo*. One hundred microliters of 10% aqueous piperidine was added, and reactions were heated to 90 °C for 30 min. Reactions were lyophilized, then lyophilized twice from 50 μ L of water, and dissolved in formamide loading buffer. Separation of products was performed by 1:20 cross-linked 15% denaturing polyacrylamide gel electrophoresis (10 000 cpm/lane). Dried polyacrylamide gels were analyzed by storage phosphor autoradiography.

Band densities were determined by quantitative analysis of storage phosphor autoradiography as described above. Bands were assigned as depicted in Figure 9 to determine values for $[D]_i$ and $[D]_t$, and $[D]_i/[D]_t$ was plotted versus time using the program Kaleidagraph to determine from the slope values for k_{obs} for two or three rate determinations at each concentration of 2-bromoacetamide. An analysis of the data indicated that disappearance of fully intact DNA at the highest concentration of 2-bromoacetamide (90 mM) over 3 half-lives followed pseudo-first-order kinetics. In subsequent determinations of observed rate constants, initial rates were used providing values of $(3.4 \pm 0.2) \times 10^{-7}$, $(6.4 \pm 0.8) \times 10^{-7}$, $(9.6 \pm 0.9) \times 10^{-7}$, $(1.7 \pm 0.2) \times 10^{-6}$, $(2.2 \pm 0.1) \times 10^{-6}$, $(2.4 \pm 0.01) \times 10^{-6}$, $(2.4 \pm 0.1) \times 10^{-6}$, and $(3.4 \pm 0.1) \times 10^{-6} \text{ s}^{-1}$ for 10, 20, 30, 50, 60, 70, 80, and 90 mM 2-bromoacetamide concentrations, respectively. Average k_{obs} values were then plotted against concentration of 2-bromoacetamide to determine, from the slope of the line, a rate constant k_2 of $(3.6 \pm 0.3) \times 10^{-5} \text{ M}^{-1} \text{ s}^{-1}$.

RESULTS AND DISCUSSION

Products of Reaction at Target Duplex. The production of phosphate termini is consistent with a mechanism involving base-promoted DNA cleavage at the abasic site within the target duplex resulting from alkylation at the N⁷ position of guanine and depurination. The 29 base pair duplex of sequence composition 5'-GCTAGTAAAAGAAAAGGAAAGAAAAGTTCG-3' possessing a GC base pair 2 base pairs to the 5'-side of the homopurine tract was synthesized and 5'- or 3'-³²P-end labeled for 3'- and 5'-terminal analysis, respectively. Radiolabeled duplexes were reacted with *N*-bromoacetyl oligonucleotide of sequence composition 5'-ETTTT^{Me}-CTTTT^{Me}C^{Me}CTTTT^{Me}CTTTT-3' at 2.5 μ M concentration (20 mM HEPES, pH 6.8, 1 mM cobalt hexammine trichloride) for 24 h at 37 °C, and following piperidine treatment (90 °C, 30 min), the reactions were analyzed by high-resolution polyacrylamide gel electrophoresis. Treatment of the radiolabeled duplex with dimethyl sulfate followed by piperidine affords authentic standards of the expected phosphate-terminal oligonucleotides (13). Alkylation by the *N*-bromoacetyl oligonucleotide occurs at the targeted guanine base proximal to the local triple helix, and oligonucleotide products comigrate by gel electrophoresis with products of dimethyl sulfate-treated DNA (Figure 3).

For further evidence of terminal phosphate functionality at the site of strand cleavage, oligonucleotide products were treated with the appropriate enzyme to achieve

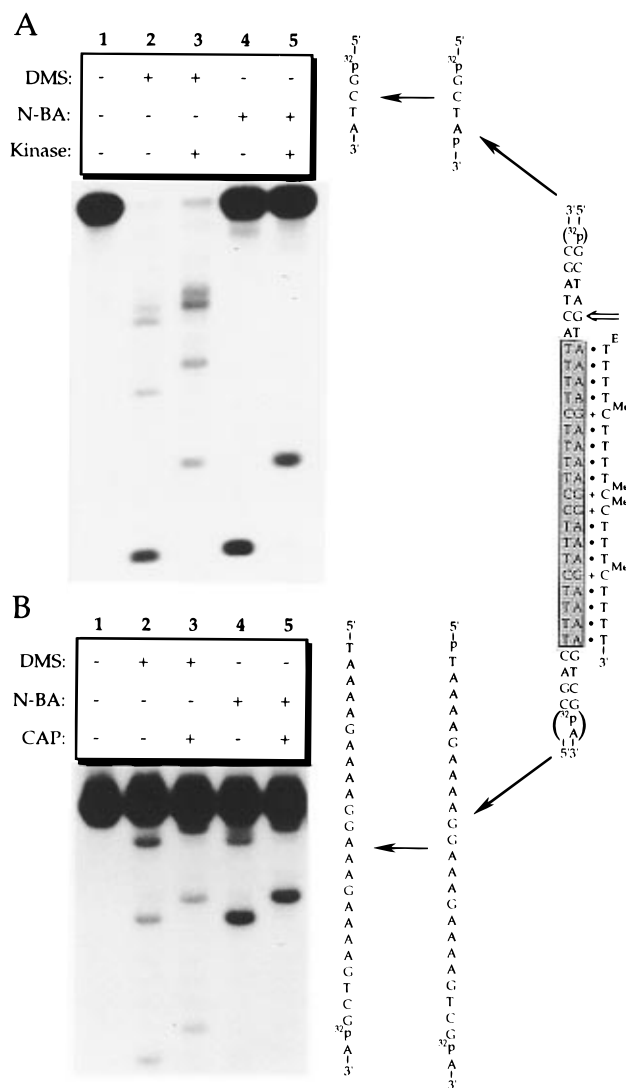


Figure 3. Autoradiograms of 20% denaturing polyacrylamide gels used for characterization of the DNA termini resulting from oligonucleotide-directed alkylation and base-promoted strand cleavage at the targeted guanine base: (A) 3'-end analysis using a 5'-end-labeled 29 base pair target duplex and T4 polynucleotide kinase; (B) 5'-end analysis using a 3'-end-labeled 29 base pair target duplex and calf alkaline phosphatase. (Lane 1) Controls, 24 h with no *N*-bromoacetyl oligonucleotide; (lane 2) duplex treated with dimethyl sulfate; (lane 3) enzymatically treated dimethyl sulfate products; (lane 4) duplex treated with 2.5 μ M *N*-bromoacetyl oligonucleotide for 24 h; (lane 5) enzymatically treated products of oligonucleotide-directed alkylation. TE is bromoacetyl attached to the 5-position of thymine, and MeC is 5-methyl-2'-deoxycytidine, previously shown to facilitate binding in oligonucleotide-directed triple-helix formation.

hydrolysis of the 5'- and 3'-phosphate groups. The 5'-end-labeled oligonucleotide fragment possessing the putative 3'-phosphate produced in the alkylation reaction was subjected to treatment with T4 polynucleotide kinase, an enzyme that can catalyze the hydrolysis of 3'-phosphate groups (14). Following this treatment, a retardation of gel mobility is observed (Figure 3A). The observed shift in gel mobility is identical to that observed for the products of dimethyl sulfate alkylation of DNA subjected to kinase treatment. The analysis was repeated for the 3'-³²P-end-labeled product possessing the putative 5'-phosphate using calf alkaline phosphatase, an enzyme that can catalyze the hydrolysis of 5'-phosphate groups. Again, a product of slower mobility is produced, and the observed shift in gel mobility for the phosphatase-treated products of dimethyl sulfate

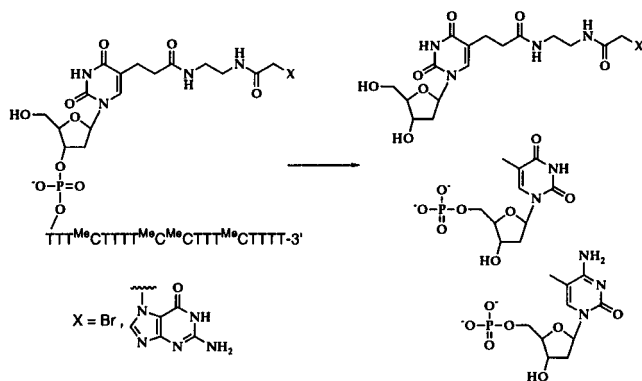


Figure 4. Enzymatic phosphodiester hydrolysis of the modified pyrimidine-rich Hoogsteen strand by the 3'-exonuclease snake venom phosphodiesterase produces thymidine nucleosides with linker arm modifications at the 5-position, thymidine 5'-monophosphate, and 5-methyl-2'-deoxycytidine 5'-monophosphate. These products can then be separated and identified by reversed-phase HPLC.

alkylation of DNA is equivalent (Figure 3B). These data are consistent with the formation of phosphate termini at the site of strand cleavage.

Identification of the Guanine-(Linker)-Oligonucleotide Conjugate Formed in the Alkylation Reaction. Alkylation at the N⁷ atom of guanine within the Watson-Crick duplex is achieved by the bromoacetyl electrophile appended to the 5'-end of the Hoogsteen strand bound in the local triple-helical complex. Identification of the guanine-(linker)-oligonucleotide conjugate formed after depurination would provide direct evidence for covalent bond formation. To address this issue, reversed phase HPLC analysis can be performed on the reaction products enzymatically digested by a 3'-exonuclease. Products of this hydrolysis reaction are nucleotides (resulting from internal and 3'-terminal residues) and nucleosides (resulting from 5'-terminal residues) (Figure 4) (15). Nucleosides resulting from modifications of the linker arm at the 5-position of the 5'-terminal thymidine in the pyrimidine-rich Hoogsteen strand can then be separated by standard reversed phase chromatographic techniques from a potentially large background of nucleotides.

N-Bromoacetyloligonucleotide (20 nmol, 2.7 μ M) of sequence composition 5'-ETTTT^{Me}CTTTT^{Me}C^{Me}CTTT^{Me}-CTTTT-3' was bound to the 60 base pair duplex (20 nmol, 2.7 μ M) of sequence composition 5'-TCGGTAC-CCGGGATCTAAAGTAAAGAAAGGAAAGAAAGCTTTCTTCTCCCTATC-3' and a time course performed (20 mM HEPES, pH 7.0, 0.2 mM cobalt hexammine trichloride, 37 °C). Three nanomole aliquots were removed over time and heated to 90 °C to depurinate N⁷-alkylated guanine bases (16). Cleavage products were then digested with snake venom phosphodiesterase and subjected to HPLC analysis. For comparison, standards of products expected from enzymatic digestion of unreacted *N*-bromoacetyloligonucleotide, as well as products of N⁷-alkylation of guanine and hydrolysis of starting material, were synthesized from the thymidine methyl ester **1** (11) (Figure 5).

The reversed phase HPLC analysis of the reaction products is shown in Figure 6. The authentic guanine-(linker)-thymidine standard (**T-G**) expected from the alkylation reaction elutes at 48.5 min under these HPLC conditions (Figure 6a). Featured in the time course (Figure 6b-d) is the presence of a compound with a retention time of 47.8 min (**T-G**, Figure 6). The relative amount of this product increases during the course of the reaction and comigrates upon coinjection with the au-

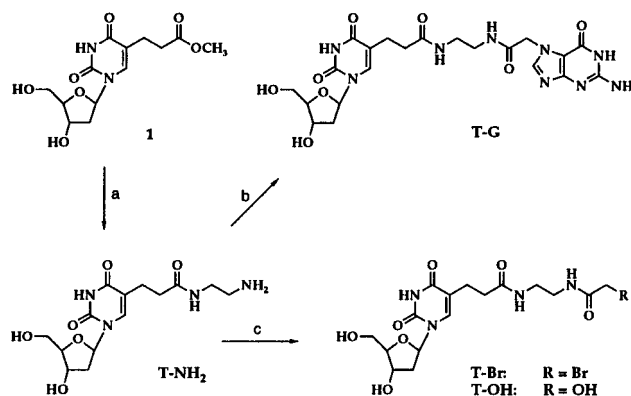


Figure 5. Scheme for the synthesis of authentic standards for HPLC analysis of products of oligonucleotide-directed alkylation of duplex DNA: (a) ethylenediamine (neat), 23 h; (b) *N*-carboxymethylguanine, 4-nitrophenol, pyridine/water, EDCI; (c) *N*-hydroxysuccinimidyl 2-bromoacetate, water (for **T-Br**) or *N*-hydroxysuccinimidyl 2-hydroxyacetate, water (for **T-OH**).

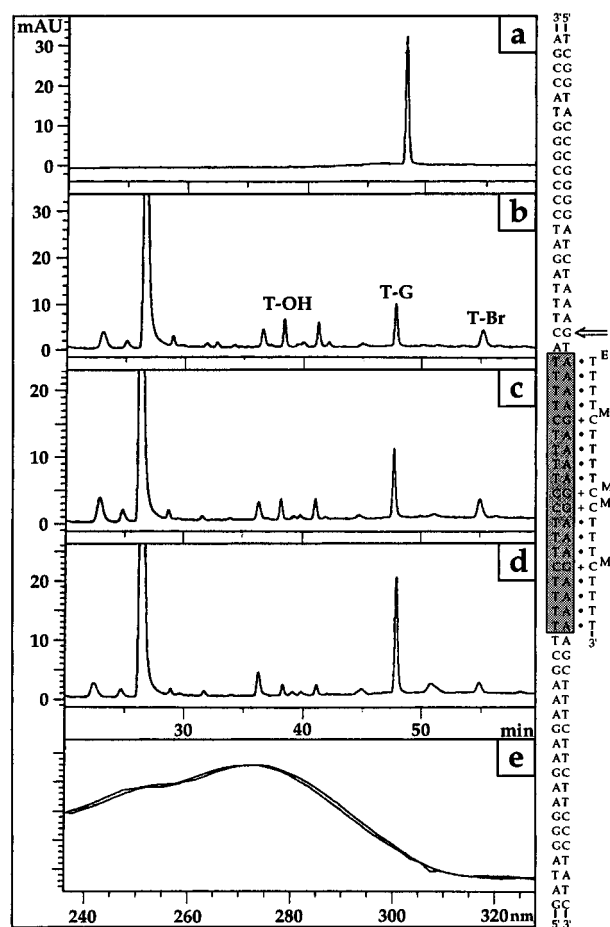


Figure 6. HPLC analysis of the enzymatically digested products of oligonucleotide-directed alkylation of double-stranded DNA. Peak heights for the time course are normalized according to peak area ratio with 5-methyl-2'-deoxycytidine 5'-monophosphate, and chromatograms were monitored at 260 nm: (a) HPLC trace of authentic guanine-(linker)-thymidine standard **T-G**; (b-d) HPLC traces of enzyme digests of oligonucleotides (3 nmol) from an alkylation reaction at times 3, 10.5, and 29 h; (e) UV spectrum of the peak at 47.8 min in (d) superimposed and normalized with the UV spectrum of authentic standard **T-G** in (a). Labels for peak assignments are as follows: **T-OH** for hydroxy-(linker)-thymidine, **T-G** for guanine-(linker)-thymidine, and **T-Br** for bromo-(linker)-thymidine nucleoside.

thentic standard **T-G** (data not shown). The amount of 5-methyl-2'-deoxycytidine 5'-monophosphate (retention

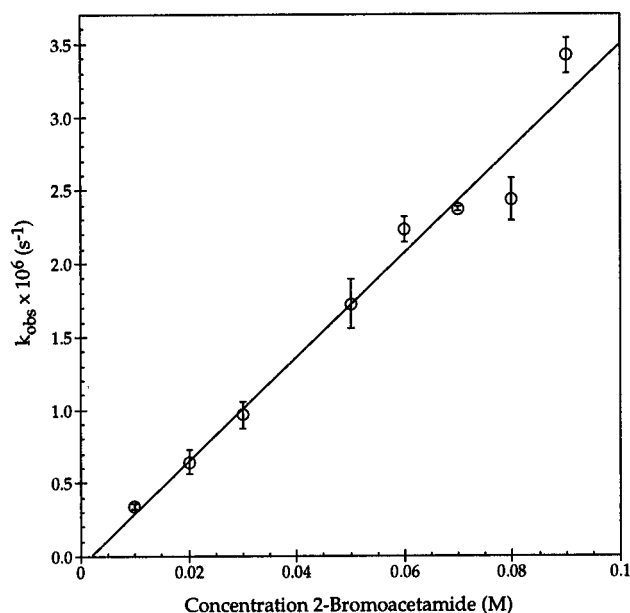


Figure 10. Determination of the rate constant k_2 for the intermolecular alkylation reaction of 2-bromoacetamide at the N⁷ position of guanine within duplex DNA. Shown is a plot of k_{obs} versus concentration of 2-bromoacetamide, which provides from the slope a rate constant k_2 of $(3.6 \pm 0.3) \times 10^{-5} \text{ M}^{-1} \text{ s}^{-1}$ for the alkylation reaction. Error bars represent standard deviation about the mean for two or three rate determinations at each concentration of 2-bromoacetamide.

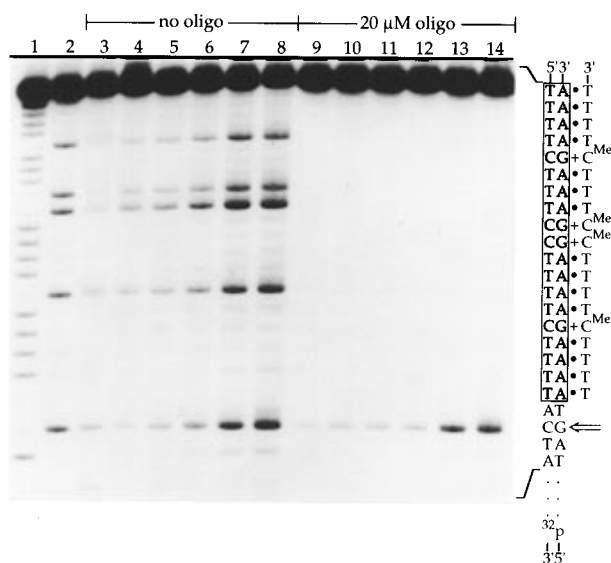


Figure 11. Autoradiogram of a 15% denaturing polyacrylamide gel used to determine the effect of local triple helix formation on the rate of alkylation at N⁷ of guanine in duplex DNA by 2-bromoacetamide: (lane 1) A-specific sequencing reaction; (lane 2) G-specific sequencing reaction; (lanes 3–8) reaction of 80 mM 2-bromoacetamide with duplex DNA at times 0, 0.5, 1.0, 2.0, 4.9, and 7.9 h; (lanes 9–14) reaction of 80 mM 2-bromoacetamide with triplex DNA at times 0, 0.5, 1.0, 2.0, 4.9, and 7.9 h.

philic functionality was synthesized and 2-bromoacetamide alkylation reactions were performed in the presence (20 μM) and absence of the Hoogsteen strand of the local triple-helical complex (Figure 11). Binding of the Hoogsteen strand in the major groove protects the N⁷ position of guanine from alkylation, resulting in a footprint at the binding site on the duplex. The data then provides observed rate constants at 80 mM 2-bromoacetamide concentration of $(2.4 \pm 0.1) \times 10^{-6}$ and $(1.2 \pm 0.1) \times 10^{-6} \text{ s}^{-1}$ for alkylation of the targeted guanine base in double-helical and triple-helical DNA, respectively.

This indicates an approximate 2-fold decrease in the rate of nucleophilic substitution upon local triple-helix formation.

The effective molarity of bromoacetyl at one position in the duplex upon localization of the alkylation reaction by oligonucleotide-directed triple-helix formation can be derived from the ratio of rate constants for the unimolecular and bimolecular reactions. This provides an effective local concentration of bromoacetyl at the targeted G-C base pair of 0.8 M in the bound complex. Though encouraging with regard to convenient reaction times in this system ($t_{1/2} = 7.2 \text{ h}$ at 200 nM concentration of oligonucleotide), this value does not nearly approach the effective molarities obtained by enzymes (19), revealing current limitations in the design of bifunctional molecules for recognition and reaction on DNA.

ACKNOWLEDGMENT

We are grateful for generous support from the National Institutes of Health (GM-35724).

LITERATURE CITED

- (1) (a) Hertzberg, R. P., and Dervan, P. B. (1982) Cleavage of Double-Helical DNA by (Methidiumpropyl-EDTA)iron(II). *J. Am. Chem. Soc.* 104, 313. (b) Hertzberg, R. P., and Dervan, P. B. (1984) Cleavage of DNA with Methidiumpropyl-EDTA-Iron(II): Reaction Conditions and Product Analyses. *Biochemistry* 23, 3934. (c) Schultz, P. G., Taylor, J. S., and Dervan, P. B. (1982) Design and Synthesis of a Sequence-Specific DNA Cleaving Molecule. (Distamycin-EDTA)iron(II). *J. Am. Chem. Soc.* 104, 6861. (d) Mack, D. P., Iverson, B. L., and Dervan, P. B. (1988) Design and Chemical Synthesis of a Sequence-Specific DNA-Cleaving Protein. *J. Am. Chem. Soc.* 110, 7572. (e) Mack, D. P., and Dervan, P. B. (1990) Nickel-Mediated Sequence-Specific Oxidative Cleavage of DNA by a Designed Metalloprotein. *J. Am. Chem. Soc.* 112, 4604. (f) Bruice, T. W., Wise, J. G., Rosser, D. S. E., and Sigman, D. S. (1991) Conversion of Lambda Phage Cro into an Operator-Specific Nuclease. *J. Am. Chem. Soc.* 113, 5446.
- (2) (a) Baker, B. F., and Dervan, P. B. (1985) Sequence-Specific Cleavage of Double-Helical DNA. *N-Bromoacetyldistamycin*. *J. Am. Chem. Soc.* 107, 8266. (b) Baker, B. F., and Dervan, P. B. (1989) Sequence-Specific Cleavage of DNA by *N*-Bromoacetyldistamycin—Product and Kinetic Analysis. *J. Am. Chem. Soc.* 111, 2700. (c) Boger, D. L., and Mesini, P. (1995) DNA Alkylation Properties of CC-1065 and Duocarmycin Analogs Incorporating the 2,3,10,10a-Tetrahydrocyclopropa[*d*]benzo[*h*]quinol-5-one Alkylation Subunit—Identification of Subtle Structural Features that Contribute to the Regioselectivity of the Adenine N3 Alkylation Reaction. *J. Am. Chem. Soc.* 117, 11647.
- (3) (a) Moser, H. E., and Dervan, P. B. (1987) Sequence-Specific Cleavage of Double Helical DNA by Triple Helix Formation. *Science* 238, 645. (b) Povsic, T. J., and Dervan, P. B. (1989) Triple Helix Formation by Oligonucleotides on DNA Extended to the Physiological pH Range. *J. Am. Chem. Soc.* 111, 3059. (c) Strobel, S. A., and Dervan, P. B. (1991) Single-Site Enzymatic Cleavage of Yeast Genomic DNA Mediated by Triple Helix Formation. *Nature* 350, 172.
- (4) (a) LeDoan, T., Perrouault, L., Praseuth, D., Habhou, N., Decout, J.-L., Thuong, N. T., Lhomme, J., and Helene, C. (1987) Sequence-Specific Recognition, Photocrosslinking, and Cleavage of the DNA Double Helix by an Oligo-[α]-Thymidylate Covalently Linked to an Azidoproflavine Derivative. *Nucleic Acids Res.* 15, 7749. (b) Perrouault, L., Asseline, U., Rivalle, C., Thuong, N. T., Bisagni, E., Giovannangeli, C., Le Doan, T., and Helene, C. (1990) Sequence-Specific Artificial Photoinduced Endonucleases Based on Triple Helix-Forming Oligonucleotides. *Nature* 344, 358. (c) Thuong, N. T., and Helene, C. (1993) Sequence-Specific Recognition and Modification of Double-Helical DNA by Oligonucleotides. *Angew. Chem., Int. Ed. Engl.* 32, 666.
- (5) (a) Fedorova, O. S., Knorre, D. G., Podust, L. M., and Zarytova, V. F. (1988) Complementary Addressed Modifica-

- tion of Double-Stranded DNA within a Ternary Complex. *FEBS Lett.* **228**, 273. (b) Vlassov, V. V., Gaidamakov, S. A., Zarytova, V. F., Knorre, D. G., Levina, A. S., Nikonova, A. A., Podust, L. M., and Fedorova, O. S. (1988) Sequence-Specific Chemical Modification of Double-Stranded DNA with Alkylating Oligodeoxyribonucleotide Derivatives. *Gene* **72**, 313. (c) Povsic, T. J., and Dervan, P. B. (1990) Sequence-Specific Alkylation of Double-Helical DNA by Oligonucleotide-Directed Triple-Helix Formation. *J. Am. Chem. Soc.* **112**, 9428. (d) Shaw, J.-P., Milligan, J. F., Krawczyk, S. H., and Matteucci, M. (1991) Specific, High Efficiency, Triple-Helix-Mediated Cross-Linking to Duplex DNA. *J. Am. Chem. Soc.* **113**, 7765. (e) Young, S. L., Krawczyk, S. H., Matteucci, M. D., and Toole, J. J. (1991) Triple Helix Formation Inhibits Transcription Elongation *In Vitro*. *Proc. Natl. Acad. Sci. U.S.A.* **88**, 10023.
- (6) (a) Povsic, T. J., Strobel, S. A., and Dervan, P. B. (1992) Sequence-Specific Double-Strand Alkylation and Cleavage of DNA Mediated by Triple-Helix Formation. *J. Am. Chem. Soc.* **114**, 5934. (b) Kutuyavin, I. V., Gamper, H. B., Gall, A. A., and Meyer, R. B. (1993) Efficient, Specific Interstrand Cross-Linking of Double-Stranded DNA by a Chlorambucil-Modified, Triplex-Forming Oligonucleotide. *J. Am. Chem. Soc.* **115**, 9303.
- (7) Sambrook, J., Fritsch, E. F., and Maniatis, T. (1989) *Molecular Cloning*, Cold Spring Harbor Laboratory, Cold Spring Harbor, NY.
- (8) Iverson, B. L., and Dervan, P. B. (1993) Adenine-Specific DNA Chemical Sequencing Reaction. *Methods Enzymol.* **218**, 222.
- (9) Gait, M. J. (1984) *Oligonucleotide Synthesis: A Practical Approach*, IRL Press, Oxford, U.K., and references cited therein.
- (10) (a) de Groot, N., Lapidot, Y., Panet, A., and Wolman, Y. (1966) The Synthesis of N-Acetylphenylalanyl-sRNA. *Biochem. Biophys. Res. Commun.* **25**, 17. (b) Pelligrini, M., Oen, H., and Cantor, C. R. (1972) Covalent Attachment of a Peptidyl-Transfer RNA Analog to the 50S Subunit of *Escherichia coli* Ribosomes. *Proc. Natl. Acad. Sci. U.S.A.* **69**, 837.
- (11) Dreyer, G. B., and Dervan, P. B. (1985) Sequence-Specific Cleavage of Single-Stranded DNA: Oligodeoxynucleotide-EDTA-Fe(II). *Proc. Natl. Acad. Sci. U.S.A.* **82**, 968.
- (12) Zurlo, J., Curphey, T. J., Hiley, R., and Longnecker, D. S. (1982) Identification of 7-Carboxymethylguanine in DNA from Pancreatic Acinar Cells Exposed to Azaserine. *Cancer Res.* **42**, 1286.
- (13) Maxam, A. M., and Gilbert, W. (1980) Sequencing End-Labeled DNA with Base-Specific Chemical Cleavages. *Methods Enzymol.* **65**, 499.
- (14) Cameron, V., and Uhlenbeck, O. C. (1977) 3'-Phosphatase Activity in T4 Polynucleotide Kinase. *Biochemistry* **16**, 5120.
- (15) Razzell, W. E., and Khorana, H. G. (1959) Studies on Polynucleotides: IV. Enzyme Degradation. The Stepwise Action of Venom Phosphodiesterase on Deoxyribo-Oligonucleotides. *J. Biol. Chem.* **234**, 2114.
- (16) Hemminki, K., Peltonen, K., and Vodicka, P. (1989) Depurination from DNA of 7-(2-Aminoethyl)-Guanine and Ring-Opened 7-Methylguanines. *Chem.-Biol. Interact.* **70**, 289.
- (17) Bevington, P. R., and Robinson, D. K. (1990) *Data Reduction and Error Analysis for the Physical Sciences*, 2nd ed., McGraw-Hill, New York.
- (18) Frost, A. A., and Pearson, R. G. (1961) *Kinetics and Mechanism*, 2nd ed., pp 40-46, Wiley, New York.
- (19) Page, M. I., and Jencks, W. P. (1971) Entropic Contributions to Rate Accelerations in Enzymic and Intramolecular Reactions and the Chelate Effect. *Proc. Natl. Acad. Sci. U.S.A.* **68**, 1678.

BC970035X

Biodistribution and Catabolism of Ga-67-Labeled Anti-Tac dsFv Fragment

Chuanchu Wu,[†] Elaine Jagoda,[‡] Martin Brechbiel,[†] Keith O. Webber,[§] Ira Pastan,[§] Otto Gansow,[†] and William C. Eckelman^{*,†}

Radiation Oncology Branch, National Cancer Institute, Laboratory of Molecular Biology, Division of Cancer Biology, National Cancer Institute, and Positron Emission Tomography Department, Clinical Center, National Institutes of Health, Bethesda, Maryland 20892. Received November 1, 1996[®]

The disulfide-linked fragment (dsFv) of the antibody to the α subunit of the IL2 receptor has been radiolabeled with a [Ga-67] Ga-2-(*p*-SCN-Bz)-NOTA derivative linked through an isothiocyanato group to either the ϵ -amino group of lysine or the α -amino group of the N-terminal amino acids. This low molecular weight protein (LMWP) has been proposed as a tumor diagnostic agent. However, >60% of the injected dose localized in the mouse kidney. The major catabolites (>95%) in the kidney were identified as the Ga-2-(*p*-SCN-Bz)-NOTA conjugate with either lysine or methionine, with no evidence of transchelation of Ga-67. Since different amino acids in the dsFv were radiolabeled according to this procedure, it was possible to study the relative residence times of the various catabolites. The methionine conjugate had a significantly shorter residence time than the lysine conjugate in the same kidney. Labeling the appropriate amino acid in a LMWP may lead to reduced residence times and increased diagnostic or therapeutic ratios.

INTRODUCTION

Many fragments of monoclonal antibodies have been radiolabeled with metallic radionuclides to take advantage of the variety of decay characteristics (1). In most cases, the conjugate containing the metallic radionuclide has a longer residence time in the kidney than the radioiodinated form of the fragment. For example, dsFv,¹ a high-affinity antibody fragment to the IL-2 receptor, has been labeled with I-125 using the Bolton–Hunter reagent and with In-111(2). The radioactivities in the kidney at 0.5, 6, and 24 h for the In-111-labeled dsFv were 142, 124, and 57% ID/g, whereas for the Bolton–Hunter iodinated dsFv the radioactivities in the kidney at 0.25, 6, and 24 h were 121, 2.5, and 0.21% ID/g. Likewise, Schott et al. compared I-125-labeled Fv fragment of CC49 with the Lu-177-labeled Fv fragment (3). The activities in the kidney of the former were 10.0, 2.1, and 0.1% ID/g at 1, 6, and 24 h, whereas the latter had kidney activities of 241, 219, and 198% ID/g at the same time points. Recently, Choi et al. have shown that directly radioiodinated dsFv is deiodinated in the kidney so that iodide is the predominant catabolite in the blood (4). However, the more rapid efflux of iodinated fragments begs the question of whether the retention of metallic radionuclides is due to the slow release of radiolabeled catabolites from the kidney back into the blood stream or to transchelation to metal binding sites in the kidney. To minimize transchelation in the kidney,

we have chosen Ga complexed by NOTA because of its known stability at low pH (1). The purpose of this study is to synthesize anti-TAC dsFv labeled with Ga-67 using Ga-67 2-(*p*-SCN-Bz)-NOTA and to identify and quantitate each chemical species of the Ga-67 in kidney tissue of tumor-bearing mice at various times postinjection.

MATERIALS AND METHODS

All of the HPLC separations were performed by using a Dionex system equipped with a Model GPM-2 gradient pump and a Gilson Model 112 UV monitor operating at 254 or 280 nm as well as an IN/US γ -RAM flow-through radioactivity detector.

The analytical size exclusion chromatography was performed with two columns, a TSK G2000SW_{XL} (30 cm \times 7.8 mm) and a TSK G3000SW (15 cm \times 7.8 mm) in series with PBS elution at 1.0 mL/min. The semipreparative size exclusion chromatography was performed with TSK G3000SW (60 cm \times 21.5 mm) with 0.15 M NH₄OAc, pH 7.0, at a flow rate of 2.5 mL/min. The analytical reversed-phase chromatography was carried out on a Beckman RP column (25 cm \times 4.6 mm) at 1 mL/min using a binary linear gradient of 0–100% B/25 min (solvent A = 0.05 M HOAc/0.05 M Et₃N, pH 7.0; solvent B = MeOH). The semipreparative reversed-phase chromatography was performed with an AltexUltrasphere ODS RP column (25 cm \times 10 mm, Alltech, Deerfield, IL) using a binary linear gradient of 0–100% B/50 min at a flow rate of 2.0 mL/min [solvent A = 0.1% trifluoroacetic acid (TFA) in H₂O, solvent B = 0.1% TFA in acetonitrile]. The solution was evaporated to \sim 1 mL at room temperature using a rotary evaporator and then lyophilized.

Ion-pair reversed-phase chromatography was performed using a Beckman IP column (25 cm \times 4.6 mm) using 0.02 M NaH₂PO₄/0.01 M (*n*-C₄H₉)₄NOH, pH 7.0, with the percent methanol increasing from 0 to 100% in a linear fashion over 34 min. Recovery of Ga-67 activity in HPLC analysis was >98% for all of the chromatographic procedures.

Radiolabeling Studies. The anti-Tac dsFv was prepared and characterized in the Laboratory of Molec-

* Address correspondence to this author at the PET Department, Clinical Center, Bldg. 10, Rm. 1C495, 10 Center Dr., MSC 1180, Bethesda, MD 20892-1180 [telephone (301) 496-6455; fax (301) 402-3521; e-mail Eckelman@nmdpet.cc.nih.gov].

[†] Radiation Oncology Branch.

[‡] Positron Emission Tomography Department.

[§] Laboratory of Molecular Biology.

[®] Abstract published in *Advance ACS Abstracts*, April 15, 1997.

¹ Abbreviations: 2-(*p*-SCN-Bz)-, 2-(*p*-isothiocyanatobenzyl)-1,4,7-triazacyclononane-1,4,7-triacetic acid; LMWP, low molecular weight protein; anti-Tac, antibody to the α subunit of the IL2 α receptor; dsFv, disulfide-linked Fv; Met, methionine; Lys, lysine.

Table 1. Biodistribution of Ga-67 NOTA-dsFv in Tumor-Bearing Nude Mice (% ID/g \pm SD; $n = 5$)

	15 min	45 min	90 min	6 h	24 h
blood	2.19 \pm 0.34	0.65 \pm 0.17	0.58 \pm 0.09	0.13 \pm 0.01	0.028 \pm 0.007
heart	1.74 \pm 0.42	0.40 \pm 0.07	0.38 \pm 0.09	0.10 \pm 0.01	0.038 \pm 0.015
lungs	2.99 \pm 0.51	1.53 \pm 0.31	1.09 \pm 0.14	0.54 \pm 0.20	0.320 \pm 0.24
liver	1.00 \pm 0.13	0.61 \pm 0.10	0.63 \pm 0.05	0.35 \pm 0.03	0.190 \pm 0.035
spleen	0.82 \pm 0.19	0.42 \pm 0.05	0.41 \pm 0.07	0.25 \pm 0.05	0.081 \pm 0.02
kidneys	204.7 \pm 33.1	197.7 \pm 41.8	203.4 \pm 35.1	137.4 \pm 11.6	70.95 \pm 21.5
A431	2.66 \pm 0.93	1.71 \pm 0.54	0.50 \pm 0.06	0.16 \pm 9.04	0.29 \pm 0.16
ATAC4	4.51 \pm 0.55	2.04 \pm 0.35	2.96 \pm 1.62	2.14 \pm 0.61	0.83 \pm 0.06
muscle	0.73 \pm 0.10	0.29 \pm 0.04	0.25 \pm 0.02	0.04 \pm 0.02	0.042 \pm 0.01

ular Biology, Division of Cancer Biology, National Cancer Institute (5).

The bifunctional chelating agent 2-(*p*-SCN-Bz)-NOTA labeled with ^{14}C at a specific activity of 1.04 mCi/mmol was prepared as described earlier (6). The anti-Tac dsFv was conjugated with 2-(*p*-SCN-Bz)-NOTA at an initial ligand-to-protein molar ratio of 2.5 and then purified by following the procedure reported previously (7). The final ligand-to-protein molar ratio was determined by measuring both the protein concentration by UV and the ligand concentration by liquid scintillation counting. The Ga-67 compound was prepared by adding to the solution of Ga-67 in HCl, 0.01 M acetylacetone to obtain a final concentration of 0.4 mM. After the pH of the solution was adjusted to 5–6 with 3 M ammonium acetate, the anti-Tac antibody, conjugated to the bifunctional chelating agent 2-(*p*-SCN-Bz)-NOTA, was then added, and the mixture was incubated for 30 min at room temperature. After incubation at room temperature for an additional 5 min with 5 μL of 0.1 M EDTA, the anti-Tac-2 conjugate of (*p*-SCN-Bz)-NOTA-Ga-67 conjugate was purified by size exclusion HPLC.

Preparation of Amino Acid Conjugated NOTA–Ga Complexes. The amino acid–NOTA conjugates were prepared by reaction of large excess of amino acid (lysine, methionine, *N*-acetyllysine, and glutamine from Aldrich Chemical Co., St. Louis, MO) with 2-(*p*-SCN-Bz)-NOTA (ca. 1 mg) in 0.1 M bicarbonate/carbonate buffer, pH 8.5, at room temperature overnight. The conjugate was then labeled with Ga-67 as described above and then purified using reversed-phase chromatography.

The conjugate was also complexed with stable Ga at pH 6.0–6.5 for mass spectra analysis. The product in this case was purified using the semipreparative reversed-phase chromatography. In addition to analysis by HPLC, FAB spectra were obtained on a JOEL SX102 mass spectrometer operated at an accelerating voltage of 10 kV. Samples were desorbed from a matrix using 6 keV xenon atoms. Mass measurements in FAB are performed at 10 000 resolution using electric field scans with the sample peak bracketed by two poly(ethylene glycol) reference ions. For the methionine conjugate of GaNOTA ($\text{C}_{25}\text{H}_{34}\text{GaN}_5\text{O}_8\text{S}_2$), MS *m/e* 666.42 (M^+), for the ϵ -aminolysine conjugate of GaNOTA ($\text{C}_{26}\text{H}_{37}\text{GaN}_6\text{O}_8\text{S}$) MS *m/e* 663.40 (M^+); for the α -aminolysine conjugate of GaNOTA ($\text{C}_{26}\text{H}_{37}\text{GaN}_6\text{O}_8\text{S}$), MS *m/e* 663.40 (M^+); for the α -*N*-acetyllysine conjugate of GaNOTA ($\text{C}_{28}\text{H}_{39}\text{GaN}_6\text{O}_9\text{S}$), MS *m/e* 705.43 (M^+); and for glutamine ($\text{C}_{25}\text{H}_{33}\text{GaN}_6\text{O}_9\text{S}$), MS *m/e* 663.35 (M^+).

Biodistribution Studies and Procedure for the Assay of Catabolites. Both A431 cells, a human epidermoid cancer cell line that has been shown to yield subcutaneous tumors with high efficiency in immunologically incompetent mice, and A431 cells transfected using molecular biology techniques to express the IL-2 α receptor (ATAC4) were implanted in nude mice on opposite flanks following the procedure of Choi et al. (4). Five sets of five mice each were injected with the Ga-67 2-(*p*-SCN-

Table 2. Extraction of Kidney Tissue from Normal (n) Mice or Tumor-Bearing (t) Mice Injected with Ga-67 NOTA-dsFv (Percent of Total Radioactivity)

	45 min (t)	45 min (t)	45 min (n)	6 h (t)	24 h (t)
(1) EtOH	41.9			49.4	50.4
(2) PBS	13.7			24.7	25.6
pellet	44.5			25.9	24.0
(1) PBS		19.6	20.5	49.6 ^a	
(2) EtOH		33.3	27.9	28.6 ^a	
pellet		47	51.5	21.8	

^a Extracted with 2 \times extractant (PBS or EtOH) to tissue (mL/g). The other samples were extracted at 1:1 ratios. Samples were extracted using either (1) EtOH followed by (2) PBS or (1) PBS followed by (2) EtOH.

Bz)-NOTA conjugate of dsFv at a specific activity of 12.5–15.7 mCi/mg ($n = 3$). Four mice received 10 μCi (for the biodistribution study) and one mouse received 120 μCi (for the metabolite study) in each set. Mice were sacrificed at 15, 45, 90, 360, and 1440 min after injection. The tissues of interest were excised from each animal and counted with a gamma counter. Urine was taken at the time of sacrifice and therefore represents the catabolites present at that time and not a quantitative analysis of excreted metabolites. Diluted injectates were also counted as standards (Table 1).

For the 45, 360, and 1440 min blood samples, serum was separated by centrifugation from red cells and mixed with an equal volume of PBS for size exclusion chromatography. Duplicate blood samples were taken, and serum was separated, extracted with an equal volume of EtOH, freeze-dried, dissolved in the initial HPLC eluent, and analyzed on a reversed HPLC column to separate catabolites. The kidneys were homogenized and extracted twice using an equal volume of cold EtOH, followed by two additional extractions using an equal volume of cold PBS, and kept on ice. For the 45 min time point, the kidneys of one mouse were divided in half, with half from this mouse extracted twice with EtOH followed by extraction twice with PBS and the other half extracted twice with PBS followed by extraction twice with EtOH. The activities in each extractants and the pellets were counted. For the 6 h study in which PBS was used before EtOH (Table 2), the volume of extractant to tissue was 2:1 (mL/g). The percent catabolites was determined using the analytical procedures described below (Table 3).

For the detailed extraction studies carried out at 6 h (Table 4), each tissue sample was homogenized after addition of the next extractant and larger volumes of extractant to tissue were used as indicated in Table 4. The EtOH extractants were mixed with an equal volume of water, freeze-dried, dissolved with HPLC initial eluent, filtered with 0.22 μm centrifuge filters, and analyzed on size exclusion, reversed-phase, and ion-pair reversed-phase columns, respectively. The PBS extractants were directly analyzed with size exclusion chromatography after filtration. For reversed-phase and ion-pair reversed-phase chromatography, the PBS extractants were puri-

Table 3. Percent Catabolites as Ga-67-NOTA Amino Acids in Extraction Fractions of Kidney from Normal (n) Mice or Tumor-Bearing (t) Mice Injected with Ga-67 NOTA-dsFv^a

time	extractant	dsFv	Lys	Met	no I.D.
(1) 45 min (t)	(1) EtOH	0	40.3	38.5	21.1
	(2) PBS	24.4	45.4	20.6	9.6
(2) 45 min (t)	(1) PBS	30.9	17.8	42.2	9.1
	(2) EtOH	0	42.1	36.5	21.4
(3) 45 min (n)	(1) PBS	31.5	18.3	45.8	4.4
	(2) EtOH	0	43.2	37.3	19.5
(4) 6 h (t)	(1) EtOH	0	>85	<3	<15
	(2) PBS	0	>85	<3	<15
(5) 24 h (t)	(1) EtOH	0	>90	0	<10
	(2) PBS	0	>90	0	<10

^a Percentage of total radioactivity recovered by extraction. See Table 2 for extraction efficiencies using either EtOH followed by PBS or PBS followed by EtOH. Lys, lysine; Met, methionine

fied using a semipreparative size exclusion chromatography column, and the fractions containing low molecular weight species were collected, freeze-dried, diluted with HPLC eluent, and then analyzed. The urine samples were analyzed after filtration. The retention times of Ga-67 compounds in mouse urine and the extracts of mouse kidney were analyzed by ion-pair reversed-phase chromatography (Figure 1) and compared to a mixture of standards of Ga-67 2-(*p*-SCN-Bz)-NOTA amino acid conjugates (Figure 2).

RESULTS

The overall radiochemical yield obtained after Ga-67 was added to the anti-Tac antibody conjugated to the bifunctional chelating agent 2-(*p*-SCN-Bz)-NOTA was 90% based on Ga-67. The resulting dsFv was analyzed according to the method described in Choi et al. (4) and had a immunoreactivity of >80%. In two experiments, the ratios of NOTA to dsFv in the dsFv-2-(*p*-SCN-Bz)-NOTA conjugates were 0.86 and 1.15, respectively. The specific activities of the dsFv conjugate of Ga-67-2-(*p*-SCN-Bz)-NOTA were between 12.8 and 15.7 mCi/mg.

The biodistribution in tumor-bearing mice showed high uptake in the kidney of 205% ID/g, which remained constant from 15 to 90 min and then fell to 140% ID/g at 6 h and 70% ID/g at 24 h. Specific tumor uptake was shown by retention of Ga-67 in ATAC4 tumor versus a control tumor (A431) in the same mouse (4). The specific-to-nonspecific tumor ratio reached 6 at 90 min and 13 at 6 h. The radioactivity cleared rapidly from the blood: 2.2% ID/g at 15 min to 0.1% ID/g at 6 h (Table 1).

In preliminary experiments to determine the catabolites, the kidney tissue of the mice sacrificed at 45 min was extracted using two procedures: the first involved extracting with EtOH followed by PBS, and the second consisted of extracting with PBS followed by EtOH. Both procedures resulted in 50–55% extraction of the Ga-67 activity in kidneys. For those mice sacrificed at 6 and 24 h, the kidney tissue was extracted with EtOH followed by PBS, and 75% of Ga-67 activity was extracted.

Three HPLC methods were used to identify the catabolites in serum, kidney, and urine. At 45 min the radioactivity in the serum was predominantly unchanged dsFv. At 6 and 24 h postinjection, the radioactivity in the serum was below detection limits. Size exclusion chromatography was used to measure the Ga-67 bound to dsFv. As expected, dsFv-bound Ga-67 was not found in any of the EtOH extracts of the kidneys because EtOH most likely denatured the dsFv. In both normal and tumor-bearing mice sacrificed at 45 min with PBS as the initial extractant of the kidneys, 31% dsFv was found, which is ~6% of total activity in the kidney (PBS

extracted ~20% Ga-67, see Table 2). With PBS as the second extractant, 24% dsFv was found, which is ~3% of total activity in the kidneys. At 6 and 24 h no dsFv was found in the PBS extract, and no dsFv was found in any of the urine samples.

The major catabolites in kidney were the ϵ -aminolysine conjugate and the α -aminomethionine conjugate of the Ga-67 2-(*p*-SCN-Bz)-NOTA derivative (Table 3; Figure 1). These catabolites were also found in the urine samples. Another catabolite was observed but could not be identified unequivocally. Both chains of dsFv have N-terminal methionine, although other amino acids may be introduced during the genetically engineered production of the light and heavy chain in *Escherichia coli*. When kidney homogenates were extracted from mice sacrificed at 45 min with PBS followed by EtOH, the concentration of Met > Lys in PBS, whereas in EtOH the two were equal. In the urine Met predominated (>95%). In the kidney at 6 h, both the PBS and the EtOH contained Lys (>95%). The urine samples taken at that time contained Lys. Met appears to be cleared more rapidly from the kidney (Figure 1).

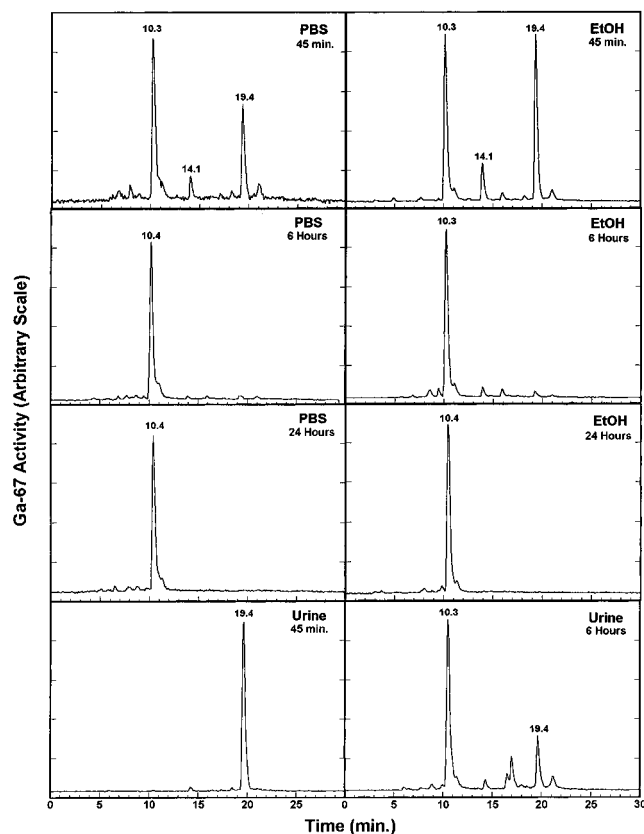
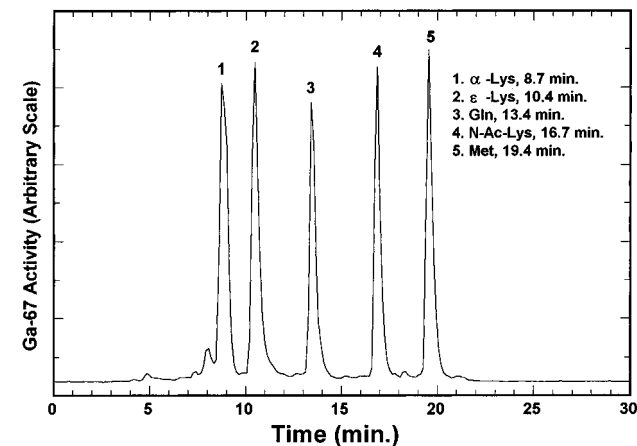
To better define the chemical form of the radioactivity that was not extracted from kidney tissue, we carried out additional experiments using various extraction procedures, larger extractant to tissue ratios, and more frequent homogenization between extractions (Table 4). The results show that using various extraction paradigms, the total amount of radioactivity extracted was always >90%. Chromatographic analysis of the extracted radioactivity for each paradigm gave >95% of the ϵ -aminolysine conjugate of the Ga-67 2-(*p*-SCN-Bz)-NOTA derivative. We found no radioactive peaks with the retention time of Ga-67 EDTA (13.1 min) in any of the extracts. If Ga-67 is weakly bound to protein, we would expect to see Ga-67 EDTA formed. Since we found >95% of the radioactivity in the kidney at 6 h to be in the form of the ϵ -aminolysine conjugate of the Ga-67 2-(*p*-SCN-Bz)-NOTA derivative, we believe that the Ga-67 NOTA complex is stable in vivo and that retention of radioactivity in the kidney can be attributed to slow kinetics of the catabolites rather than to retention of Ga-67 in the kidney as a transchelated product with kidney proteins.

DISCUSSION

Monoclonal antibodies have been used for both diagnosis and therapy. In an attempt to increase whole body clearance and the time to maximum target to nontarget ratio, many investigators have pursued LMWP. As the molecular weight or size decreases, the glomerular sieving coefficient increases. The primary mechanism of kidney uptake of LMWP is by endocytosis in the proximal tubules (8). No simple theory explains the difference between the uptake of various LMWP, although many experiments varying molecular size, isoelectric points, etc. have been carried out (9). However, the catabolites of various LMWP have been studied. Christensen and Maunsback have shown that I-125-labeled lysozyme was taken up by the proximal tubules and that monoiodotyrosine was the major catabolite (10). Johnson and Maack also reported that iodotyrosine was the major catabolite from human GH (11). Choi et al. have found that F-18 fluoromethylbenzoyl-labeled antiTac dsFv leads to both fluoromethylbenzoyllysine and fluoromethylbenzoyl- α -N-acetyllysine (4). The former was the major catabolite in the blood while the latter was the major catabolite in the urine, presumably because the N-acetyl derivative is not taken up in the proximal tubules as shown by direct injection of the radiolabeled catabolites in mice (4).

Table 4. Extraction of Kidney Tissue from Normal Mice at 6 h after Injection of Ga-67 NOTA-dsFv (Percent of Total Radioactivity)

	1st extr	2nd extr	3rd extr	4th extr	5th extr	pellet
1	4 × PBS, 25.2	4 × PBS, 19.2	4 × EtOH, 34.3	4 × EDTA, 14.0		7.3
2	8 × PBS, 40.8	8 × PBS, 19.2	8 × EtOH, 29.4	8 × EDTA, 6.6		4.0
3	8 × PBS, 22.6	8 × PBS, 13.0	8 × EtOH, 44.1	8 × EtOH, 1.6	8 × EDTA, 12.4	6.3
4	8 × PBS, 36.8	8 × PBS, 14.8	8 × EtOH, 35.6	8 × EtOH, 1.2	8 × EDTA, 6.9	4.6

**Figure 1.** Ion-pair reversed-phase chromatography after extraction of mouse urine and the extractants of mouse kidney using PBS and ethanol.**Figure 2.** Separation of a standard mixture of Ga-67 2-(p-SCN-Bz)-NOTA amino acid conjugates (α -Lys, α -amino-linked lysine; ϵ -Lys, ϵ -amino-linked lysine; Gln, α -amino-linked glutamine; N-Ac-Lys, ϵ -amino-linked N -acetyllysine; and Met, α -amino-linked methionine) by ion-pair reversed-phase chromatography.

Rogers et al. analyzed kidney catabolites after injection of In-111 DTPA-1a3-F(ab')₂ and found that the major catabolite was In-111-DTPA- ϵ -lysine (12). However, they did not report the retention time of the standard for the N -acetyl analog of In-111-DTPA- ϵ -lysine. Garg et al. found that in the 3 h kidney supernatant after injection

of the radiolabeled Me1-14 F(ab')₂, 92% of the low molecular weight catabolites were present as [¹²⁵I]iodobenzoic acid using N -succinimidyl 3-iodobenzoate, but with iodogen, iodide was the major catabolite (13, 14). Finally Rogers et al. have studied radiolabeled 1A3-F(ab')₂ using four bifunctional chelates for copper. The kidney metabolism of Cu-67 4-[(1,4,8,11-tetraazacyclotetradec-1-yl)methyl]benzoic acid F(ab')₂ conjugate showed at one day postinjection a small molecular weight catabolite that was either a lysine or N -terminal amino acid derivative of the bifunctional chelates (15).

There are two approaches to reducing the residence time and amount of uptake in the kidney. It has been shown by Morgenson and Solling that large doses of lysine will block renal uptake of albumin, free light chains, and β -2-microglobulin (16). Kobayashi et al. have taken that approach in recent studies with radiolabeled anti-Tac dsFv (17). The other approach is to decrease the residence time in the kidney. This approach usually involves the use of hydrolyzable linkers (18). We tested the hypothesis that transchelation will not occur if we use a chelate that is stable over a broad pH range. This appears to be the case for the Ga-67 NOTA complex employed in this study in that we found only the original dsFv and amino acid-containing catabolites in the analysis of the kidney, the blood, and the urine. In the process of radiolabeling the dsFv using the isothiocyanato linking group with the amino groups in dsFv, both the ϵ -amino group of lysine and the α -amino group of the terminal methionines were labeled. Rana and Meares have reported this possibility with a similar reagent (19). The genetically engineered heavy and light chains of anti-Tac dsFv contain 13 lysine groups and terminal methionine groups on each chain (2). Because these two amino acids were labeled, we were able to directly compare the transit times of the two Ga-67 NOTA-amino acid conjugates. It appears that the methionine conjugate has the shorter residence time in the kidney compared to the lysine conjugate. We did not detect the N -acetyllysine conjugate, although this was a major catabolite of F-18-labeled fluoromethylbenzoyl-dsFv (5).

To the best of our knowledge, this is the first example of the differential clearance of two amino acid conjugates from the kidney. There are only a few studies on the nature of the efflux transporter in the proximal renal cells (20), so further analysis of the pathways in the proximal renal tubular cells is warranted before this finding can be widely applied. However, this information can lead to the design of LMWP labeled using bifunctional chelates that have decreased residence time in the kidney. Key factors in the design appear to be using a chelating agent that binds radiometals at low pH and finding the appropriate combination of chelate and amino acid which is rapidly transported out of the renal cells.

ACKNOWLEDGMENT

We appreciate the assistance of the Structural Mass Spectra Group, NIDDK (Dr. L. Pannell), and Dr. Chang Paik for his helpful discussions on the extraction procedure.

LITERATURE CITED

- (1) Jankowski, K. J., and Parker, D. (1993) Diagnosis and therapy with antibody conjugates of metal radioisotopes. *Adv. Metals Med.* 1, 29–73.
- (2) Webber, K. O., Kreitman, R. J., and Pastan, I. (1995) Rapid and Specific Uptake of Anti-Tac Disulfide-stabilized Fv by Interleukin-2 Receptor-bearing Tumors. *Cancer Res.* 55, 318–323.
- (3) Schott, M. E., Milenic, D. E., Yokota, T., Whitlow, M., Wood, J. F., Fordyce, W. A., Cheng, R. C., and Schlom, J. (1992) Differential Metabolic Patterns of Iodinated versus Radio-metal Chelated Anticarcinoma Single-Chain Fv Molecules. *Cancer Res.* 52, 6413–6417.
- (4) Choi, C. W., Lang, L., Lee, J. T., Webber, K. O., Yoo, T. M., Chang, H. K., Le, N., Jagoda, E., Paik, C. H., Pastan, I., Eckelman, W. C., and Carrasquillo, J. A. (1995) Biodistribution of [¹⁸F]- and [¹²⁵I]-labeled anti-Tac disulfide stabilized Fv fragments in nude mice with IL-2 α receptor positive tumor xenografts. *Cancer Res.* 55, 5323–5329.
- (5) Webber, K. O., Reiter, Y., Brinkmann, U., Kreitman, R., and Pastan, I. (1995) Preparation and characterization of a disulfide-stabilized Fv fragment of the anti-Tac antibody: comparison with its single-chain analog. *Mol. Immunol.* 32, 249–258.
- (6) McMurphy, T. J., Brechbiel, M., Wu, C., and Gansow, O. A. (1993) Synthesis of 2-(p-thiocyanatobenzyl)-1,4,7-triazacyclononane-1,4,7-triacetic acid: application of the 4-methoxy-2,3,6-trimethylbenzenesulfonamide protecting group in the synthesis of macrocyclic polyamines. *Bioconjugate Chem.* 4, 236–245.
- (7) Mirzadeh, S., Brechbiel, M. W., Atcher, R. W., and Gansow, O. A. (1990) Radiometal labeling of immunoproteins: covalent linkage of 2-(4-isothiocyanatobenzyl)diethylenetriaminepentaacetic acid ligands to immunoglobulin. *Bioconjugate Chem.* 1, 59–65.
- (8) Maack, T., Johnson, V., Sen, T. K., Figueiredo, J., and Sigulem, D. (1979) Renal filtration, transport, and metabolism of low-molecular-weight proteins: a review. *Kidney Int.* 16, 251–270.
- (9) Maack, T., Park, C. H., and Camargo, M. J. F. (1992) Renal Filtration, Transport, and Metabolism of Proteins. In *The Kidney: Physiology and Pathophysiology*, 2nd ed. (D. W. Seldin and G. Giebisch, Eds.) pp 3005–3038, Raven Press, New York.
- (10) Christensen, E. I., and Maunsbach, A. B. (1974) Intralysosomal digestion of lysozyme in renal proximal tubule cells. *Kidney Int.* 6, 396–407.
- (11) Johnson, V., and Maack, T. (1977) Renal extraction, filtration, absorption, and catabolism of growth hormone. *Am. J. Physiol.* 233, F185–F196.
- (12) Rogers, B. E., Franano, F. N., Duncan, J. R., Edwards, W. B., Anderson, C. J., Connett, J. M., and Welch, M. J. (1995) Identification of metabolites of ¹¹¹In-diethylenetriaminepentaacetic monoclonal antibodies and antibody fragments in vivo. *Cancer Res. (Suppl.)* 55, 5714s–5720s.
- (13) Garg, P. K., Alston, K. L., and Zalutsky, M. R. (1996) Catabolism of label from an F(ab')₂ fragment radioiodinated using N-succinimidyl 3-iodobenzoate and iodogen methods. *J. Labelled Compd. Radiopharm.* 35, 539–541.
- (14) Garg, P. K., Alston, K. L., and Zalutsky, M. R. (1995) Catabolism of radioiodinated murine monoclonal antibody F(ab')₂ fragment labeled using N-succinimidyl 3-iodobenzoate and iodogen methods. *Bioconjugate Chem.* 6, 493–501.
- (15) Rogers, B. E., Anderson, C. J., Connett, J. M., Guo, L. W., Edwards, W. B., Sherman, E. L. C., Zinn, K. R., and Welch, M. J. (1996) Comparison of four bifunctional chelates for radiolabeling monoclonal antibodies with copper radioisotopes: biodistribution and metabolism. *Bioconjugate Chem.* 7, 511–522.
- (16) Solling, K., and Morgenson, C. E. (1977) Studies on the mechanism of renal tubular protein reabsorption. *Proc. Eur. Dial. Transplant Assoc.* 14, 543–549.
- (17) Kobayashi, H., Yoo, T. M., Kim, I. S., Kim, M.-K., Le, N., Webber, K. O., Pastan, I., Paik, C. H., Eckelman, W. C., and Carrasquillo, J. A. (1996) L-Lysine effectively blocks renal uptake of ¹²⁵I or ^{99m}Tc labeled anti-tac dsFv. *Cancer Res.* 56, 3788–3795.
- (18) Franssen, E. J. F., Koiter, J., Kuipers, C. A. M., Bruins, A. P., Moolenaar, F., de Zeeuw, D., Kruizinga, W. H., Kellogg, R. M., and Meijer, D. K. F. (1992) Low molecular weight proteins as carriers for renal drug targeting. Preparation of drug-protein conjugates and drug-spacer derivatives and their catabolism in renal cortex homogenates and lysosomal lysates. *J. Med. Chem.* 35, 1246–1259.
- (19) Rana, T. M., and Meares, C. F. (1990) N-terminal modification of immunoglobulin polypeptide chains tagged with isothiocyanato chelates. *Bioconjugate Chem.* 1, 357–362.
- (20) Christensen, J. N. (1989) Distinguishing amino acid transport systems of a given cell or tissue. *Methods Enzymol.* 173, 576–616.

BC970032K

Regiospecific Solid-Phase Synthesis of Branched Oligonucleotides. Effect of Vicinal 2',5'- (or 2',3'-) and 3',5'-Phosphodiester Linkages on the Formation of Hairpin DNA

Ravinderjit S. Braich and Masad J. Damha*

Department of Chemistry, Otto Maass Chemistry Building, McGill University, 801 Sherbrooke Street West, Montreal, Quebec, Canada H3A 2K6. Received January 13, 1997*

A general procedure for the solid-phase regiospecific synthesis of branched oligonucleotides (bNA) analogues using readily available phosphoramidite reagents has been developed. The key feature of this method is use of the solid-phase phosphoramidite procedure to assemble linear oligonucleotide sequences and sequential removal of the phosphate (β -cyanoethyl or methyl) and silyl protecting groups without detaching the nascent oligonucleotide from the solid support. Conversion of the phosphate backbone into the more stable phosphodiester linkages allows for removal of the 2'-*O*-*tert*-butyldimethylsilyl protecting group without cleavage or isomerization at the branch point. This method allows for the formation of branched oligonucleotides with sequences of arbitrary base composition, length, and orientation around the branch point junction, including a "Y"-shaped octadecamer d(TACTA)-rA[^{2',5'}d(GTATGT)]^{3',5'}d(CAAGTT). Studies to explore structural effects in the use of a branched adenosine as replacement for nucleotide loops in duplex and triplex DNA are also described. Branched oligonucleotides of the type rA[^{2',5'}dC_ndA_{10-5'}]^{3',5'}dC_ndT_{10-3'} and rA[^{2',5'}dC_n3',3'dA_{10-5'}]^{3',5'}dC_nT_{10-3'} form hairpin duplexes with thermal stability comparable to or better than that of one with a natural deoxynucleotide loop.

INTRODUCTION

Branched nucleic acids (bNAs) have been the subject of a number of scientific studies since the discovery of RNA "forks" and "lariats" (1–4) and multicopy single-stranded DNA (msDNA) in prokaryotic and eukaryotic cells (5, 6). msDNA is a chimera of DNA and RNA found in some prokaryotes having a branched or forked structure wherein the 5'-nucleotide of a single-stranded DNA chain is esterified to the 2'-hydroxyl of an internal residue of the RNA chain. The novelty of these structures has raised interest as to their possible role in regulating RNA splicing and debranching. In addition, there has been increasing recent interest in synthetic branched DNA and RNA for use in diagnostic applications (7), as "molecular anchors" for inducing the formation of novel triple-helical DNA (8–13), and as tools for studying branched RNA/RNA complexes (9) and the substrate specificity of debranching enzymes (14, 15).

We have been describing in detail a methodology for the solid-phase synthesis of open-chain forked or "Y" RNA and DNAs such as a branched 18-mer UACUAA(2'-GUAUGU)3'-GUAUGU, in which the branchpoint adenosine nucleotide (A) is linked to identical GUAUGU "tails" via vicinal 2',5'- and 3',5'-phosphodiester bonds (16). The branched "V" 21-mer rA(2'dT₁₀)3'dT₁₀ (10) and a "dendritic" 87-mer structure have also been synthesized from this laboratory (17, 18). Our synthetic "convergent" strategy is based on our discovery that nucleosides 2',3'-*O*-bisphosphoramidite synthons react with adjacent solid-support bound chains, yielding symmetric "V"-like molecules. Synthesis is then continued in the 3'-to-5' direction from the apex of the "V" to yield forked or "Y" structures. More recently, we developed a convergent method that

generates a mixture of bRNA's with 2'- and 3'-chains of different base composition, e.g., A(2'-GUAUGU)3'-CAAGUU (19). Although this is the easiest way to prepare an array of branched oligoribonucleotides having different 2'- and 3'-chain sequences (requiring commercially available building blocks), this method necessitates separation of very similar branched molecules. It is therefore only practical for "combinatorial" or biochemical investigations in which the amount of material needed is very small.

All other synthetic strategies reported so far for the regiospecific assembly of branched oligonucleotides mimicking the natural lariat structures are based upon solution-phase phosphotriester methods, except for the recent and elegant work by Sproat and co-workers, who use a "divergent" solid-phase phosphoramidite strategy (20). This strategy has permitted the synthesis of medium size branched oligoribonucleotides; however, it requires the use of elaborate phosphoramidites and branchpoint synthons, which limits the ease and speed of a potential synthesis. Given this limitation, and those of our current methods, we directed our attention toward alternative strategies for the regiospecific synthesis of branched oligonucleotides. As a starting point, we have chosen to regiospecifically synthesize branched ("Y"-shaped) oligonucleotides consisting of three DNA chains joined to the 2', 3', and 5'-positions of an adenosine branchpoint. The synthesis of branched oligonucleotides in which 2'-deoxyribose is substituted for ribose sugars would be useful for studying the substrate specificity of debranching enzymes and for evaluating the role of 2'-OH groups in enzyme–bRNA interactions. Furthermore, the conformational rigidity imparted to the DNA chains, by the branchpoint ribose, could be exploited to preorganize and induce the formation of duplex and triplex DNA.

Here we describe a facile method for the regiospecific synthesis of branched oligodeoxynucleotides. Some sequences were synthesized only on the basis of mimicking the structure of naturally occurring branched introns

* Author to whom correspondence should be addressed [telephone (514) 398-7552; fax (514) 398-3797; e-mail damha@omc.lan.mcgill.ca].

© Abstract published in *Advance ACS Abstracts*, April 15, 1997.

Table 1. Branched Sequences Synthesized for This Study

Sequence	Branched Oligonucleotide
1	$5\text{-HO}_d(\text{TAC TA}) \text{rA}^{2\text{'-}5\text{'}}_d(\text{GTA TGT})\text{-}3'$ $3\text{'-}5\text{'}_d(\text{CAA GTT})\text{-}3'$
2	$5\text{-HO}_d(\text{TAC TA}) \text{rA}^{2\text{'-}5\text{'}}_d(\text{I TA TGT})\text{-}3'$ $3\text{'-}5\text{'}_d(\text{CAA GTT})\text{-}3'$
3	$5\text{-HO}_{\text{rA}}^{2\text{'-}5\text{'}}_d(\text{TTT TTT TTT T})\text{-}3'$ $3\text{'-}5\text{'}_d(\text{TTT TTT TTT T})\text{-}3'$
4	$5\text{-HO}_{\text{rA}}^{2\text{'-}5\text{'}}_d(\text{T}^{3\text{'-}3'}\text{T}^{5\text{'-}3'}\text{T TTT TTT T})\text{-}5'$ $3\text{'-}5\text{'}_d(\text{TTT TTT TTT T})\text{-}3'$
5	$5\text{-HO}_{\text{rA}}^{2\text{'-}3'}_d(\text{T}^{5\text{'-}3'}\text{TT TTT TTT T})\text{-}5'$ $3\text{'-}5\text{'}_d(\text{TTT TTT TTT T})\text{-}3'$
6	$5\text{-HO}_{\text{rA}}^{2\text{'-}3'}_d(\text{A}^{5\text{'-}3'}\text{AA AAA AAA A})\text{-}5'$ $3\text{'-}5\text{'}_d(\text{TTT TTT TTT T})\text{-}3'$
7	$5\text{-HO}_{\text{rA}}^{2\text{'-}3'}_d(\text{C}^{5\text{'-}3'}\text{AA AAA AAA A})\text{-}5'$ $3\text{'-}5\text{'}_d(\text{CTT TTT TTT T})\text{-}3'$
8	$5\text{-HO}_{\text{rA}}^{2\text{'-}3'}_d(\text{C}^{5\text{'-}3'}\text{CA AAA AAA A})\text{-}5'$ $3\text{'-}5\text{'}_d(\text{CCT TTT TTT T})\text{-}3'$
9	$5\text{-HO}_{\text{rA}}^{2\text{'-}5\text{'}}_d(\text{CC}^{3\text{'-}3'}\text{A}^{5\text{'-}3'}\text{AA AAA AA})\text{-}5'$ $3\text{'-}5\text{'}_d(\text{CCT TTT TTT T})\text{-}3'$

(e.g., **1** and **2**, Table 1). Others were prepared to explore structural effects in the use of a branched adenosine as a replacement for nucleotide loops in a hairpin (duplex) DNA (**6**–**9**).

EXPERIMENTAL PROCEDURES

Reversed-phase C₁₈ Sep-Pak cartridges were obtained from Waters (Milford, MA). Polyacrylamide gel electrophoresis (PAGE) reagents were purchased from Bio-Rad (Toronto). Fused silica capillaries, for capillary electrophoresis (CE), were obtained from Polymicro Technologies (Phoenix, AZ). Long-chain alkylamine controlled pore glass (CPG) bearing deoxyribonucleosides were prepared using our protocols (21). Tetra-*n*-butylammonium fluoride (1 M) in tetrahydrofuran (THF; desilylating reagent) and (methacryloxypropyl)trimethoxysilane were purchased from Aldrich. Enzymes were purchased from Boehringer Mannheim (Quebec). Incubation buffers for enzyme digestions were prepared using sterilized deionized water, filtered through a sterile 0.2 μm -pore filter and stored at -20°C prior to use. Snake-venom phosphodiesterase (SVPDE)/alkaline phosphatase (AP) incubations were performed in 50 mM Tris-HCl/10 mM MgCl₂, pH 8, while Nuclease P1/AP incubations were performed in 0.1 M Tris-HCl/1 mM ZnCl₂, pH 7.2.

Synthesis of Branched Oligonucleotides. Branched oligomers, the structures of which are illustrated in Table 1, were synthesized on an Applied Biosystems DNA synthesizer (Model 381A) via phosphoramidite chemistry.

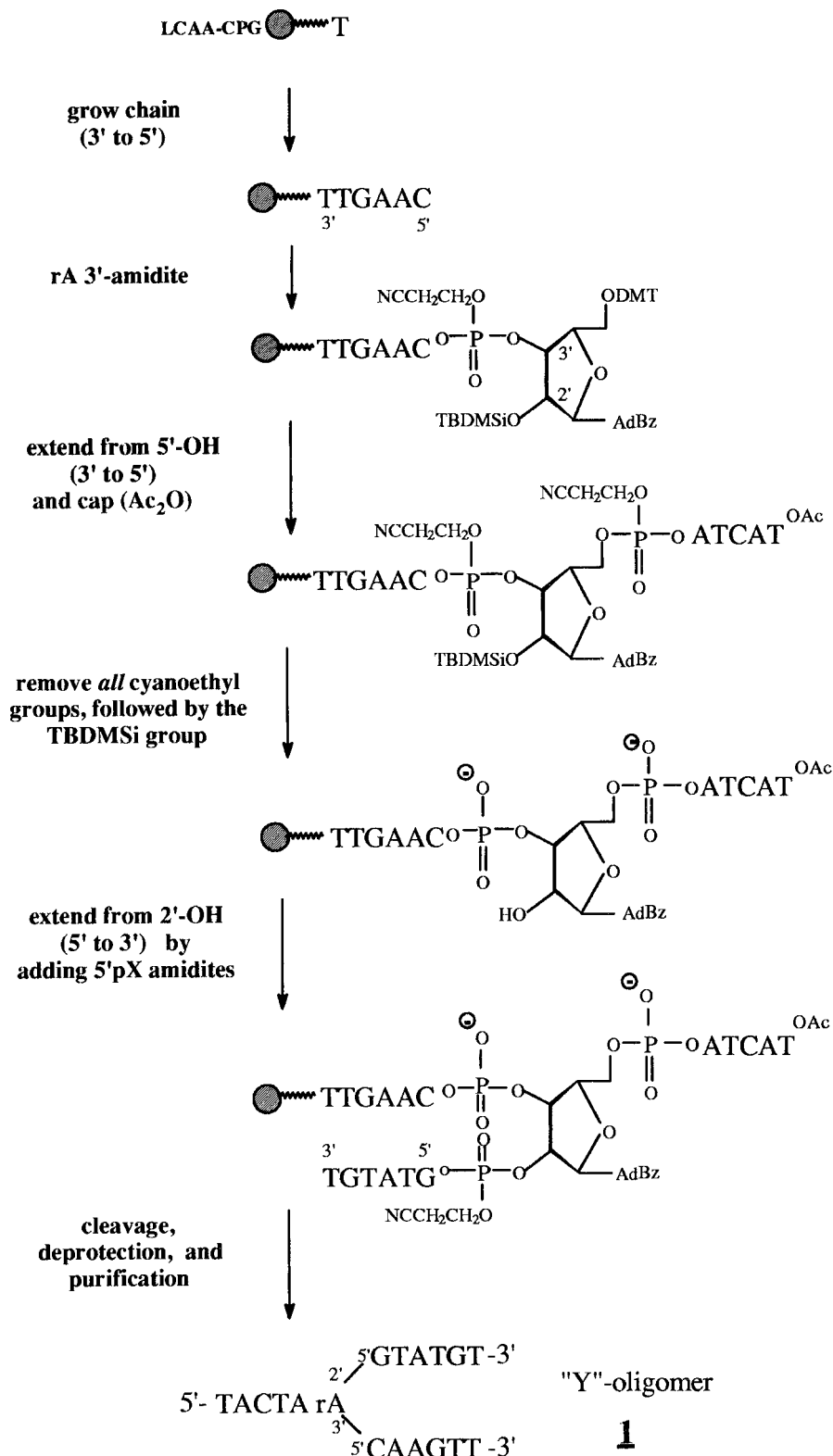
The procedure can be illustrated by describing the synthesis of **1**. The linear sequence 3',5'-linked 5'-HO-d(TACTA)-rA-d(CAAGTT)-3' was synthesized by the normal synthesis cycle (22), and the free 5'-hydroxyl group was capped by running the capping (Ac₂O) cycle. The synthesis column was removed from the synthesizer and the solid support dried by flushing argon through the column. All phosphate protecting groups were removed by treating the support with a solution of NEt₃/dioxane/thiophenol (10 mL, 2:2:1 v/v/v) (when rA methylamidite was used as branching synthon) or NEt₃/CH₃CN (10 mL, 4:6 v/v) (when rA β -cyanoethylamidite was used as branching synthon). This step is done via a syringe by pushing the deprotection solution through the column over a 90 min period (room temperature). The solid support was then washed extensively with EtOH (30 mL, for methyl protection only) and CH₃CN (30 mL), followed by THF (30 mL). Removal of the 2'-silyl protecting group was carried out by pushing a solution of 1 M TBAF/THF (1 mL) through the synthesis column over a period of 10 min. After the removal of silyl protecting group, the support was washed with THF (50 mL), followed by CH₃CN (50 mL). The column was then reinstalled on the synthesizer and synthesis continued by the normal cycle for the addition of 5'-phosphoramidites except that the first addition required the use of more concentrated phosphoramidite solution (0.3 M) and longer coupling times (30 min) (see Table 2). Average coupling yields (trityl assay method) for 5'-phosphoramidites couplings were in the range of 95–98%. CPG-bound oligomers were deprotected under standard conditions (concentrated NH₄OH/ethanol; 4:1, room temperature, 48 h). Following deprotection, the branched oligomers (**1**–**7**) were purified by polyacrylamide gel electrophoresis (PAGE) and desalted by reversed-phase chromatography on C₁₈ Sep-Pak cartridges (22). Alternatively, 5'-tritylated oligonucleotides can be purified by reversed-phase chromatography on OPC cartridges (as in the case of **8** and **9**) using supplier's specification (Dalton Chemical Co., Toronto).

Analysis and Characterization of Oligonucleotides. For enzymatic digestions, 0.5 A₂₆₀ unit of the purified lyophilized branched oligomer **1** was dissolved in the appropriate buffer (20 μL), and to this was added either SVPDE (1 μL , 0.002 U) and AP (1 μL , 9 U) or nuclease P1 (3 μL , 0.9 U) and AP (1 μL , 9 U). After incubation was complete (37 $^\circ\text{C}$, 24 h), the samples were lyophilized to dryness, redissolved in 15 μL of sterilized water, and analyzed by HPLC as described below.

HPLC analysis of enzymatic digests was carried out on a Waters Max 480 system (Millipore) equipped with dual 501 pumps, UK6 injector, and a 480 tunable UV detector, with the gradient being controlled by a 600E gradient controller and solvent delivery system. Analyses were conducted at 254 nm under the following conditions: reversed-phase Whatman Partisil ODS-2 column (10 μm , 4.6 \times 250 mm, Chromatographic Specialties); mobile phase solvent A, 20 mM KH₂PO₄ (pH 5.5); solvent B, methanol, gradient 0–50% solvent B in 25 min. Peak areas and the previously reported extinction coefficient values at 254 nm (23) were used to calculate relative concentrations of monomers.

Capillary electrophoresis analyses were carried out on a CE system constructed at McGill (24). Capillary, 75 μm i.d., contained 9% (w/v) acrylamide and had a total length of 55 cm and separation length of 35 cm. Samples were injected electrokinetically by applying a voltage of 9 kV for 30 s to 3 min depending on sample concentration.

Melting Experiments. Melting experiments were carried out in 50 mM magnesium chloride/10 mM Tris-

Scheme 1. Regiospecific, Divergent Synthesis of Branched Oligonucleotides

HCl, pH 7.3. The solution was loaded into a cuvette, and the absorbance versus temperature profile was recorded using a Cary 3E UV-vis spectrophotometer fitted with a thermostated cell block and temperature controller. The cell block was continuously purged with dry nitrogen to prevent moisture condensation at low temperatures. Solutions containing the hairpin duplexes (1.1–110 μ M range) or triplex **6**/dT₁₀ (2.2 μ M) were transferred to the cuvette and heated to 90 °C for 5 min and then cooled to 5.0 °C for 1–12 h. The solutions were heated at a rate

of 0.5 °C/min, and the absorbance at 260 nm was measured. The melting curve was then obtained as described above. T_m values were calculated from the first derivative of the melting curve. Precision in T_m values, determined from variance of repeated experiments, is no greater than ± 0.5 °C.

Molecular Modeling. These studies were performed in the AMBER force field developed for nucleic acids (Hypercube's HyperChem 3.0). The cutoff function (switched: inner = 10 Å and outer = 14 Å) and the RMS

Table 2. Conditions and Yields of Branched Oligonucleotide Synthesis

sequence	scale (μ mol)	% coupling yield ^a			crude ^b A_{260} U	purification (A_{260} U) ^c	
		rA ^d	2'5'pX	next		loaded	recovered
1	1.0	95	91	99	87	25	7.4
2^e	0.6	61 ^e	60 ^f	78	29	20	3.1
3	1.0	100	97	101	131	25	2.8
3	1.0	97 ^g	99	111	64	25	6.2
4	1.0	87	115	86	45	20	2.1
5	1.0	97	89	93	85	25	6.0
6	1.0	98	81	83	43	25	2.6
7	1.0	89	91	92	123	20	3.1
8	0.1	97	124	102	10	8	1.4
9	0.1	97	111	135	9	7	1.9

^a Coupling yield of the 2',5'-pX residue was calculated relative to coupling of branchpoint A. ^b Total oligomer recovered after cleavage and deprotection. ^c PAGE followed by desalting with C₁₈ Sep-Pak cartridges. Sequences **8** and **9** were purified by the "trityl-on" reversed-phase procedure (OPC purification matrix). ^d Unless otherwise indicated, rA^{Bz}-5'-O-DMT-2'-O-silyl-3'-O-cyanoethylphosphoramidite was used as the branching synthon. ^e rA^{Bz}-5'-O-DMT-3'-O-silyl-2'-O-cyanoethylphosphoramidite. ^f Lower coupling reflects the inadvertent use of lower concentration (0.1 M) of the phosphoramidite solution after the branchpoint. ^g rA^{Bz}-5'-O-DMT-2'-O-silyl-3'-O-methylphosphoramidite used.

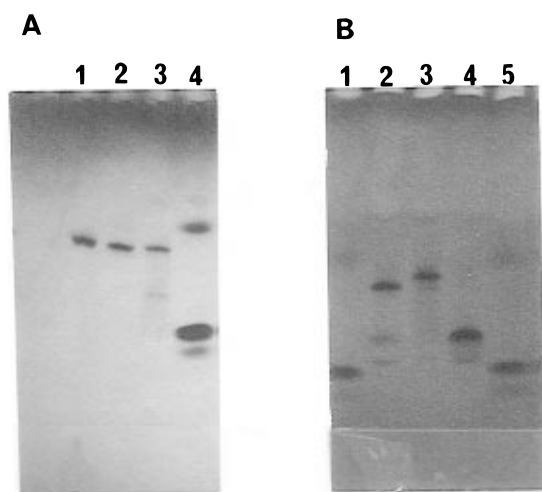


Figure 1. Electrophoresis of branched oligonucleotides on a 24% polyacrylamide/7 M urea gel: (A) lane 1, oligomer **3** prepared by the present divergent method; lane 2, authentic sample of oligomer **3** prepared by a convergent method (16); lane 3, crude sample of **3** prepared by the present divergent method; lane 4, marker dyes bromophenol blue (fast) and xylene cyanol (slow); (B) lanes 1 and 5, marker dyes; lane 2, branched 18-mer TACTAA(2'-GTATGT)3'-GTATGT (16); lane 3, branched 18-mer **1**; lane 4, linear 12-mer TACTArA2'5'GTATGT.

gradient were kept constant at 10^{-5} kcal/mol Å. The branched pentaloops for **6**, **8**, and **9** were first minimized individually. These were then capped to A/T duplexes built in the classical B-form. Three preliminary structures were minimized, and short simulations (10–70 ps) were performed in vacuum on unconstrained helices. A stereoview of the most energetically favored structure of **9** is shown in Figure 5.

RESULTS AND DISCUSSION

Synthesis of Branched Oligodeoxynucleotides. Our methodology is illustrated in Scheme 1 for the synthesis of branched 18-mer **1**. This oligonucleotide has all conserved nucleobases and mimics the naturally occurring sequence found in *Staphylococcus cerevisiae* lariat introns (Table 1). The commercially available *N*⁶-benzoyl-5'-dimethoxytrityl-2'-O-*tert*-butyldimethylsilyladenosine is the key building block in our strategy because

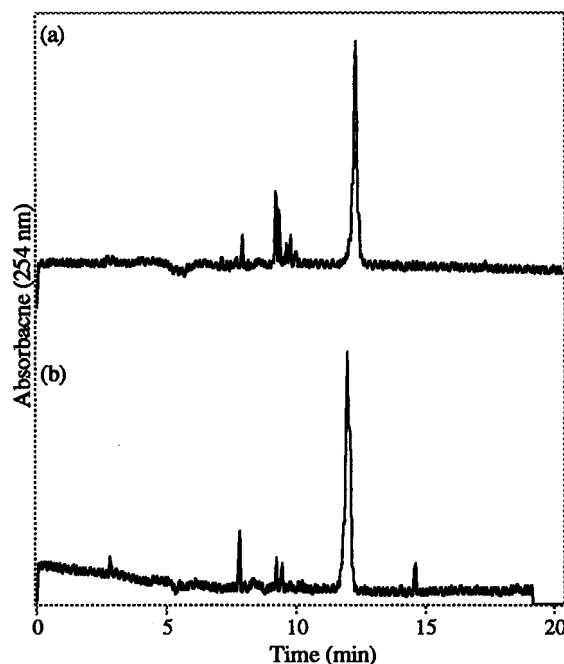


Figure 2. Capillary gel electrophoresis of branched oligomer **3**: (a) crude sample obtained from the convergent method (16); (b) crude sample obtained by the present divergent method. See Experimental Procedures for conditions.

it allows sequential extension of the chain from the branchpoint rA in all three directions. The other synthons required are 2'-deoxynucleoside-3'-O- or 5'-O-cyanoethylphosphoramidite monomers, which are also commercially available. Long-chain alkylamine CPG served as the solid support and was derivatized with the 3'-terminal nucleoside as previously described (21). The synthesis began by assembly of the linear tridecanucleotide 5'-d(TACTA)-rA-d(CAA GTT)-3' in the normal 3'-to-5' fashion. Following acetylation of the terminal 5'-hydroxyl group, the support was treated with triethylamine/acetonitrile solution (4:6 v/v, 1.5 h, room temperature) to affect the removal of all cyanoethyl phosphate protecting groups, thus providing an oligomer with an intrinsically more stable *phosphodiester* backbone (25). This is necessary because deblocking of a 2'-OH group vicinal to a 3',5'-*phosphotriester* linkage under neutral, acidic, or basic conditions has been shown to lead to phosphoryl migration and/or chain cleavage (26–29).

An important feature was the use of fluoride ions to effect the removal of the 2'-O-TBDMSi without "dissolving" the solid support (SiO₂) and/or detaching the oligomer from its surface. Thus, the silyl group was removed from riboadenosine by treatment of the support with 1 M tetra-*n*-butylammonium fluoride/THF (10 min, room temperature), followed by washing with THF and acetonitrile. Model experiments with DMT-dT-(LCAA-CPG) showed that extended treatment with fluoride (15, 30, and 60 min) leads to significant cleavage of the nucleoside from the solid support (10%, 25%, and >65%, respectively). At this point, the 2'-chain (5'-GTA TGT-3') was synthesized in the 5'-to-3' direction using commercially available 5'-phosphoramidite derivatives (30). To force branching at the sterically hindered 2'-hydroxyl group, both the concentration and the coupling time of the first 5'-amidite (dG) were tripled to 0.3 M and 30 min, respectively (12, 31). Under these conditions coupling proceeded with 91% efficiency. Lower amidite concentrations (0.10 M) resulted in significantly lower coupling yields (ca. 60%, e.g., **2**, Table 2). Synthesis under

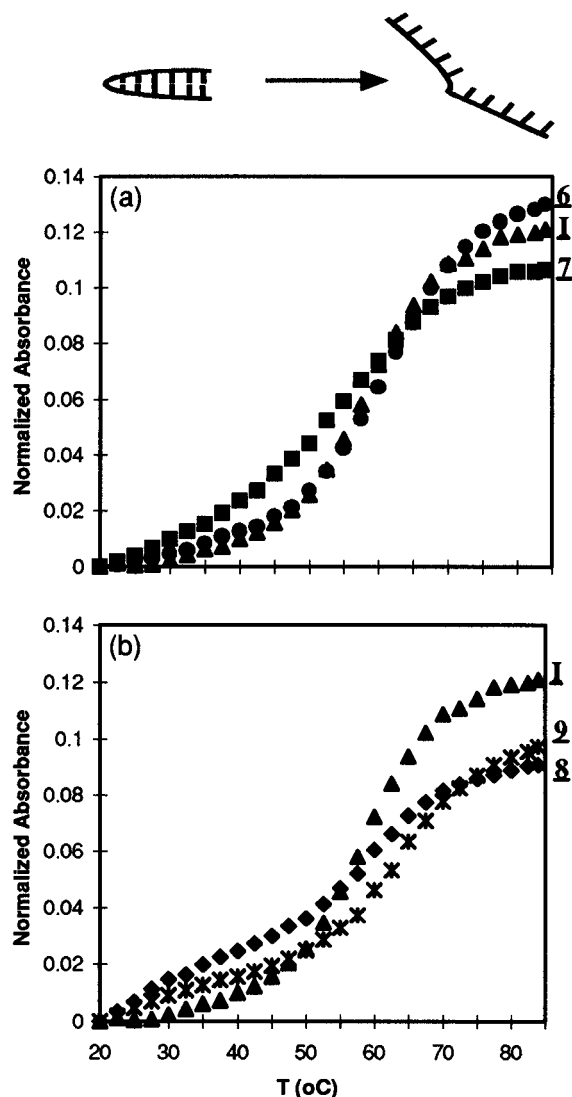


Figure 3. Melting curves of branched and linear hairpin structures in 50 mM MgCl_2 /10 mM Tris-HCl buffer, pH 7.3: (a) 6, 7, and I; (b) 8, 9, and I. Oligomer concentration was 1.1 μM .

standard conditions was then continued until the desired "Y"-mer 1 was assembled.

The successful completion of 1 was followed by the synthesis of eight other "V"- and "Y"-shaped oligonucleotides 2–9 (Table 1). Sequence 2 mimics a lariat structure in which the conserved 2'-guanine base has been replaced by hypoxanthine. Apart from the use of deoxyinosine as the 2'-residue, the other major difference in the preparation of 1 and that of 2 was the use of adenosine 2'-*O*-cyanoethylphosphoramidite instead of the regioisomeric 3'-*O*-cyanoethylphosphoramidite. Thus, 5'-d(TACTA)-rA^{2',5'}d(ITATGT)-3' was first assembled in the

conventional 3'-to-5' direction and capped (Ac_2O). This was followed by removal of the cyanoethyl and 3'-silyl groups and assembly of the 3'-branch, namely d(CAA GTT). All other aspects of branch assembly, deprotection procedures, and handling remained invariant. Under the conditions used (0.5 M tetrazole, room temperature, 30 min), the branch rA-3'-amidite isomer coupled (95%) with greater efficiency than the 2'-amidite isomer (61%). However, if 5-ethylthio-1H-tetrazole is used instead of tetrazole as the acid catalyst, both 2' and 3'-amidite couple with similar (97–99%) efficiency (Wasner and Damha, unpublished results). For the preparation of sequence 3, both rA-3'-*O*-methyl and cyanoethyl protected phosphoramidites were used as the branching synthon (Table 2). In the case of methyl protection, a thiophenoxide step was used to cleave the methyl phosphate protecting group at the branchpoint rA prior to 2'-desilylation and 2'-chain assembly. Presumably, the thiophenoxide step also removes the cyanoethyl groups attached to the deoxynucleotide residues. Coupling yields at various stages of these syntheses (as determined by the trityl assay method) as well as isolated yields of oligomers are given in Table 2.

The branched oligonucleotides were removed from the support and deblocked by treatment with 15 M aqueous ammonia/ethanol 4:1 v/v (room temperature, 48 h). Removal of the ammoniacal solution furnished the crude products. Initial characterization and purification of oligomers was accomplished by electrophoresis by comparison of mobilities to linear oligomers and to authentic samples of branched oligonucleotides. For example, a sample of 3 produced via the convergent approach (10, 16) was the same as a sample produced by the present method, as shown by PAGE and CE (Figures 1A and 2) and by thermal dissociation of antiparallel T/A:T triplexes formed with dA_{10} (10). Also, a sample of 1 (18-mer) exhibited similar electrophoretic mobility to a "Y"-18-mer prepared via the convergent approach (Figure 1B). The oligonucleotides were purified by either preparative gel electrophoresis or reversed-phase (trityl-on) chromatography. In the former case, the major band was cut out under UV shadow, extracted with water at 37 °C overnight, and desalted by reversed-phase chromatography (Sep-Pak cartridges). Isolated yields of crude and purified oligonucleotides are reported in Table 2.

As a further check on the branched structure and nucleotide composition, a small sample of 1 and 2 was subjected to enzymatic hydrolysis and the resulting products were identified by reversed-phase HPLC. Treatment with snake venom phosphodiesterase (*Crotalus durissus*) and alkaline phosphatase (AP) (from calf intestine) gave the expected nucleoside composition. Furthermore, treatment with nuclease P1 (*Penicillium citrinum*)/AP gave the branched core trinucleoside diphosphate A(2'dG)3'dC (32) and nucleosides in the expected ratios (data not shown).



Figure 4. Melting temperatures and structures of branched and linear hairpin DNA (50 mM MgCl_2 /10 mM Tris-HCl buffer, pH 7.3).

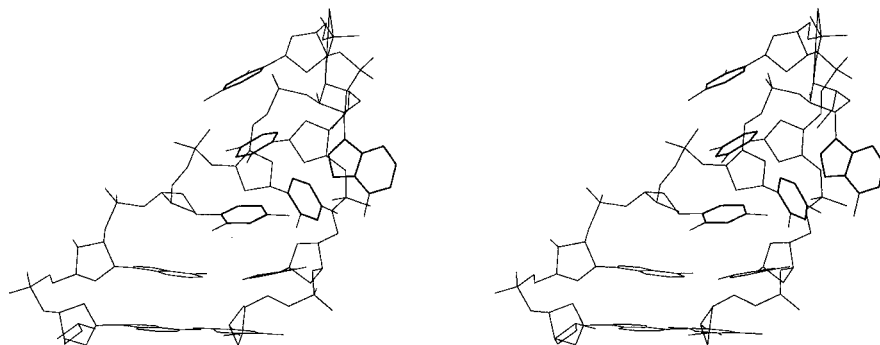


Figure 5. Stereoview of an energy-minimized structure of branched hairpin **9**. Bases in the pentaloop structure are shown in boldface; only two A:T base pairs (bottom) are shown for clarity.

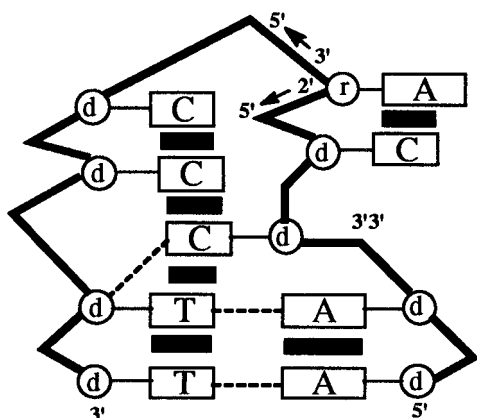


Figure 6. Schematic representation of the structural features of stacking interactions of the branched pentaloop structure of hairpin **9**. Symbols: ribose (r); deoxyribose (d); base stacking (■); hydrogen bonds (---).

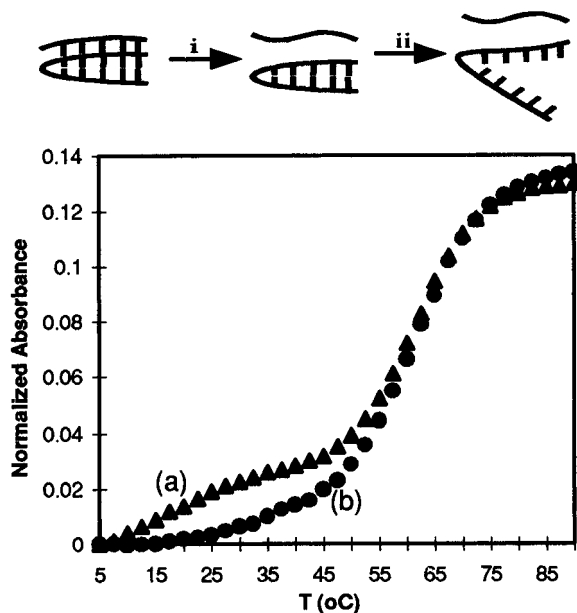


Figure 7. Melting curves of (a) **6**:dT₁₀ and (b) **6** in 50 mM MgCl₂/10 mM Tris-HCl buffer, pH 7.3.

Branched Nucleic Acid Hairpins. Compounds **6–9** were designed to test the effect of the branchpoint “linker” in systems potentially capable of folding into a hairpin duplex structure. Compounds **6–9** exhibit single cooperative melting transitions (T_m) that are independent of oligonucleotide concentrations over a 10–100-fold range (50 mM MgCl₂/10 mM Tris, pH 7.3) (Figure 3). In addition, their T_m values are >28 °C higher than for double-stranded complexes formed from two independent strands e.g., dA₁₀ + dT₁₀, T_m = 32 °C. These results

support the view that branched oligomers can form hydrogen-bonded, base-stacked structures reversibly in solution by folding intramolecularly to a hairpin conformation.

Molecular modeling performed on hairpins **6–8** suggests that their structure is energetically most favorable when the “loop” is composed of a heptanucleotide (5'...AXX-3',2'rA-3',5'YYT...3') and the “stem” has seven A/T base-paired residues. In agreement with the view that **6–8** have similar folded structures, the temperatures of dissociation of these complexes are comparable (58–61 °C, Figure 4). By contrast, the energetically optimized structure of compound **9** (the constitutional isomer of **8**) can accommodate an additional A/T base pair, leaving a loop that is only five unpaired bases (5'...CC-5',2'rA-3',5'CC...3') that is constrained sterically by the requirements of loop closing. It is noteworthy that the structural features of the dC-5',2'rA-3',5'dC residues in this loop are in excellent agreement with the NMR-derived structure of small branched RNA fragments (33, 34), the most significant being the extensive base–base stacking interactions between the central rA and the 2',5'-dC residue (... dC5'↔2'rA ...) (Figures 5 and 6). The remaining three dC residues in **9** also base–base stack in a way that is reminiscent of stable nucleic acid hairpins (35). Such stacking interactions are less important in the minimized structure of **8**, and this is due to the structural constraints of the vicinal 2',3'/3',5' linkages. Since, in fact, the T_m value is 6 °C greater for compound **9** than for **8**, or an unmodified hairpin with identical stem and loop sequences (**I**, Figure 4), we conclude that the pentaloop contributes significantly to the stabilization of **9**. The favorable stabilization derived from the branched pentaloop structure in **9** is also evident when its thermal dissociation (64.1 °C) is compared to that of a model hairpin with an identical stem but a four-unit (CCCC) loop (60.7 °C), the optimum loop length for DNA hairpins (35). We speculate that extensive base stacking interactions within the branched pentaloop provide, at least in part, the structural basis for the gain of thermal stability observed in **9** relative to **I** (35). Additional studies on various branched pentaloops containing various sequence combinations will be necessary to test this hypothesis.

Triplex Formation. Association of a Branched A:T Hairpin with dT₁₀. We have also conducted preliminary studies on the interaction of branched hairpins with single-stranded DNA, namely, dT₁₀ with hairpin **6**. dT₁₀ forms a stable complex with **6** in Tris buffer (pH 7.3, 50 mM MgCl₂) as indicated by the presence of two well-separated transitions (Figure 7). The lower temperature transition (21.5 °C) is nearly coincident with the first transition given by the classical dA₁₀:2dT₁₀ triplex (T_m = 19 °C) and corresponds to the process triplex

→ dT₁₀ + duplex (36). The lower temperature transition (21.5 °C) is therefore attributed to dissociation of dT₁₀ from the triplex dT₁₀:6, whereas the high-temperature transition (61.5 °C) corresponds to the helix-to-coil transition of duplex 6 (Figure 3). This result demonstrates that a unimolecular branched duplex (hairpin) can interact with a pyrimidine sequence to form a triplex structure. We note that the unique folded structure of branched single-stranded loops may confer desirable resistance against degradative nucleases (37). These characteristics combined may be significant in the development of antisense therapeutic agents that target single-stranded RNA via triple-helix formation (38–40).

In summary, an efficient and regiospecific synthesis of "V"- and "Y"-shaped oligonucleotides has been developed. We have also demonstrated that ribonucleoside branchpoints can be used as linkers to stabilize hybridization and to direct folding of oligonucleotide strands into duplex structures. In one example, insertion of a branchpoint ribonucleoside in the loop of a DNA hairpin has increased the stability of the hairpin duplex. A branched hairpin structure was found to bind single-stranded DNA via triplex formation. These properties combined make branched oligonucleotides appealing choices for use as novel probes for studying nucleic acid structure and as sequence selective oligonucleotides that can interact with single-stranded nucleic acids. Branched oligonucleotides of the type described here may also serve as probes for studying RNA processing in the cell.

ACKNOWLEDGMENT

We thank Dr. W. C. Purdy and Dr. T. Tadey for assistance in capillary electrophoresis analysis of oligonucleotides and Dr. D. N. Harpp for continued support. This research was supported by grants from NSERC (Collaborative Program) and FCAR (Quebec).

LITERATURE CITED

- (1) Wallace, J. C., and Edmonds, M. (1983) Polyadenylated nuclear RNA contains branches. *Proc. Natl. Acad. Sci. U.S.A.* **80**, 950–954.
- (2) Domedy, H., Apostol, B., Lin, R.-J., Newman, A., Brody, E., and Abelson, J. (1984) Lariat structures are in vivo intermediates in yeast pre-mRNA splicing. *Cell* **39**, 611–621.
- (3) Ruskin, B., Krainer, A. R., Maniatis, T., and Green, M. R. (1984) Excision of an intact intron as a novel lariat structure during pre-mRNA splicing in vitro. *Cell* **38**, 317–331.
- (4) Padgett, R. A., Konarska, M. M., Grabowski, P. J., Hardy, S. F., and Sharp, P. A. (1984) Lariat RNA's as intermediates and products in the splicing of messenger precursors. *Science* **225**, 898–903.
- (5) Inouye, S., Furuichi, T., Dhundle, A., and Inouye, M. (1987) *Molecular Biology of RNA: New Perspectives* (M. Inouye and B. S. Dudoek, Eds.) pp 271, Academic Press, San Diego, CA.
- (6) Yee, T., Furuichi, T., Inouye, S., and Inouye, M. (1984) Multicopy single-stranded DNA isolated from a Gram-negative bacterium, *Myxococcus xanthus*. *Cell* **38**, 203–209.
- (7) Urdea, M., Horn, T., Fultz, T., Anderson, M., Runnings, J., Hamren, S., Ahle, D., and Chang, C.-A. (1991) Branched DNA amplification multimers for the sensitive, direct detection of human hepatitis viruses. *Nucleic Acids Res. Symp. Ser.* **24**, 197–200.
- (8) Hudson, R. H. E., and Damha, M. J. (1993) Association of branched nucleic acids. *Nucleic Acids Res. Symp. Ser.* **29**, 97–99.
- (9) Hudson, R. H. E., Ganeshan, K., and Damha, M. J. (1994) Branched nucleic acids: synthesis and biological applications. *Carbohydrate Modifications in Antisense Research* (Y. S. Sanghvi and P. D. Cook, Eds.) ACS Symposium Series 580, pp 133–152, American Chemical Society, Washington, DC.
- (10) Hudson, R. H. E., Uddin, A. H., and Damha, M. J. (1995) Association of branched nucleic acids: structural and physicochemical analysis of antiparallel T:AT triple-helical DNA. *J. Am. Chem. Soc.* **117**, 12470–12477.
- (11) Azhayeva, E., Azhayev, A., Guzaev, A., Hovinen, J., and Lönnberg, H. (1995) Looped oligonucleotides form stable hybrid complexes with a single-stranded DNA. *Nucleic Acids Res.* **23**, 1170–1176.
- (12) Brandenburg, G., Petersen, G. V., Rasmussen, K., and Wengel, J. (1995) Branched oligodeoxynucleotides: a new synthetic strategy and formation of strong intra- and intermolecular triple helical complexes. *Bioorg. Med. Chem. Lett.* **5**, 791–794.
- (13) von Büren, M., Petersen, G. V., Rasmussen, K., Brandenburg, G., Wengel, J., and Kirpekar, F. (1995) Branched oligodeoxynucleotides: automated synthesis and triple helical hybridization studies. *Tetrahedron* **51**, 8491–8501.
- (14) Nam, K., Hudson, R. H. E., Chapman, K. B., Ganeshan, K., Damha, M. J., and Boeke, J. D. (1994) Yeast lariat debranching enzyme: substrate and sequence specificity. *J. Biol. Chem.* **269**, 20613–20621.
- (15) Sproat, B. S., Beijer, B., Grøtli, M., Ryder, U., Morand, K. L., and Lamond, A. I. (1994) Novel solid-phase synthesis of branched oligoribonucleotides, including a substrate for RNA debranching enzyme. *J. Chem. Soc., Perkin Trans. 1*, 419–430.
- (16) Damha, M. J., Ganeshan, K., Hudson, R. H. E., and Zabarylo, S. V. (1992) Solid-phase synthesis of branched oligoribonucleotides related to messenger RNA splicing intermediates. *Nucleic Acids Res.* **20**, 6565–6573.
- (17) Hudson, R. H. E., and Damha, M. J. (1993) Nucleic acid dendrimers: novel biopolymer structures. *J. Am. Chem. Soc.* **115**, 2119–2124.
- (18) Amato, I. (1993) How to drive nucleic acids up a tree. *Science* **260**, 491.
- (19) Ganeshan, K., Tadey, T., Nam, K., Braich, R., Purdy, W. C., Boeke, J. D., and Damha, M. J. (1995) Novel approaches to the synthesis and analysis of branched RNA. *Nucleosides Nucleotides* **14**, 1009–1013.
- (20) Grøtli, M., and Sproat, B. S. (1995) A universal solid-phase synthesis of branched oligoribonucleotides. *J. Chem. Soc., Chem Commun.*, 495–497.
- (21) Damha, M. J., Ginnaris, P. A., and Zabarylo, S. V. (1990) An improved procedure for derivatization of controlled-pore glass beads for solid-phase oligonucleotide synthesis. *Nucleic Acids Res.* **18**, 3813–3821.
- (22) Damha, M. J., and Ogilvie, K. K. (1993) Oligoribonucleotide synthesis. *Protocols for Oligonucleotide and Analogues: Synthesis and Properties, Methods in Molecular Biology* (S. Agrawal, Ed.) pp 81–114, Humana Press, Totowa, NJ.
- (23) Pon, R. T. (1984) Ph.D. Thesis, McGill University, Montreal, PQ, Canada.
- (24) Tanya, T., and Purdy, W. C. (1994) Capillary electrophoretic separation of nucleotide isomers via complexation with cyclodextrin and borate. *J. Chromatogr. B* **657**, 365–372.
- (25) Kierzek, R., Kopp, D. W., Edmons, M., and Caruthers, M. H. (1986) Chemical synthesis of branched RNA. *Nucleic Acids Res.* **14**, 4751–4764.
- (26) Brown, D. M., Magrath, D. I., and Todd, A. R. (1955) *J. Chem. Soc.*, 4496.
- (27) de Rooij, J. F. M., Willie-Hazeleger, G., Burgers, P. M. J., and van Boom, J. H. (1979) Neighbouring group participation in the unblocking of phosphotriesters of nucleic acids. *Nucleic Acids Res.* **6**, 2237–2259.
- (28) Damha, M. J., Pon, R. T., and Ogilvie, K. K. (1985) Chemical synthesis of branched RNA: novel trinucleotide diphosphates containing vicinal 2'-5' and 3'-5' phosphodiester linkages. *Tetrahedron Lett.* **26**, 4839–4842.
- (29) Reese, C. B., and Skone, P. A. (1985) Action of acid on oligoribonucleotide phosphotriester intermediates. Effect of released vicinal hydroxy functions. *Nucleic Acids Res.* **13**, 5215–5231.
- (30) van de Sande, J. H., Ramsing, N. B., Germann, M. W., Elhorst, W., Kalisch, B. W., Kitzing, E. V., Pon, R. T., Clegg, R. C., and Jovin, T. M. (1988) Parallel stranded DNA. *Science* **241**, 551–557.
- (31) Damha, M. J., Usman, N., and Ogilvie, K. K. (1989) Solution and solid phase chemical synthesis of arabinonucleotides. *Can. J. Chem.* **67**, 831–839.

- (32) Damha, M. J., and Ogilvie, K. K. (1988) Synthesis and spectroscopic analysis of branched RNA fragments: messenger RNA splicing intermediates. *J. Org. Chem.* **53**, 3710–3722.
- (33) Damha, M. J., and Ogilvie, K. K. (1988) Conformational properties of branched RNA fragments in aqueous solution. *Biochemistry* **27**, 9403–6416.
- (34) Sund, C., Agback, P., Koole, L. H., Sandström, A., and Chattopadhyaya, J. (1992) Assessment of competing 2'-5' versus 3'-5' stackings in solution structure of branched-RNA by ^1H - and ^{31}P -NMR spectroscopy. *Tetrahedron* **48**, 695–718.
- (35) Varani, G. (1995) Exceptionally stable nucleic acid hairpins. *Annu. Rev. Biophys. Biomol. Struct.* **24**, 379–404.
- (36) Pilch, D. S., Levenson, C., and Shafer, R. H. (1990) Structural analysis of the $(\text{dA})_{10}\cdot 2(\text{dT})_{10}$ triple helix. *Proc. Natl. Acad. Sci. U.S.A.* **87**, 1942–1946.
- (37) Tang, J. Y., Temsamani, J., and Agrawal, S. (1993) Self-stabilized antisense oligodeoxynucleotide phosphorothioates: properties and anti-HIV activity. *Nucleic Acids Res.* **21**, 2729–2735.
- (38) Giovannangeli, C., Monteray-Garestier, T., Rougée, M., Chassignol, M., Thuong, N. T., and Hélène, C. (1991) Single-stranded DNA as a target for triple-helix formation. *J. Am. Chem. Soc.* **113**, 7775–7777.
- (39) Salunkhe, M., Wu, T., and Letsinger, R. L. (1992) Control of folding and binding of oligonucleotides by use of a non-nucleotide linker. *J. Am. Chem. Soc.* **114**, 8768–8772.
- (40) Wang, S., and Kool, E. T. (1994) Recognition of single-stranded nucleic acids by triplex formation: the binding of pyrimidine-rich sequences. *J. Am. Chem. Soc.* **116**, 8857–8858.

BC9700300

Detection of Oligonucleotide Hybridization on a Single Microparticle by Time-Resolved Fluorometry: Hybridization Assays on Polymer Particles Obtained by Direct Solid Phase Assembly of the Oligonucleotide Probes

Harri Hakala,[†] Pia Heinonen,[‡] Antti Iitiä,[‡] and Harri Lönnberg^{*,†}

Departments of Chemistry and Biotechnology, University of Turku, FIN-20014 Turku, Finland. Received December 19, 1996[®]

Oligodeoxyribonucleotides were assembled by conventional phosphoramidite chemistry on uniformly sized (50 μm) porous glycidyl methacrylate/ethylene dimethacrylate (SINTEF) and compact polystyrene (Dynosphere) particles, the aminoalkyl side chains of which were further derivatized with DMTrO-acetyl groups. The linker was completely resistant toward ammonolytic deprotection of the base moieties. The quality of oligonucleotides was assessed by repeating the synthesis on the same particles derivatized with a cleavable ester linker. The ability of the oligonucleotide-coated particles to bind complementary sequences via hybridization was examined by following the attachment of oligonucleotides bearing a photoluminescent europium(III) chelate to the particles. The fluorescence emission was measured directly on a single particle. The effects of the following factors on the kinetics and efficiency of hybridization were studied: number of particles in a given volume of the assay solution, loading of oligonucleotide on the particle, concentration of the target oligonucleotide in solution, length of the hybridizing sequence, presence of noncomplementary sequences, and ionic strength. The fluorescence signal measured on a single particle after hybridization was observed to be proportional to the concentration of the target oligonucleotide in solution over a concentration range of 5 orders of magnitude.

INTRODUCTION

Solid supports bearing covalently immobilized synthetic oligodeoxyribonucleotides have recently received considerable interest owing to their possible applications in mixed phase hybridization assays (1–11). In particular, assays that enable simultaneous detection of several polynucleotides from a single biological sample have been developed on these bases: arrays of allele-specific oligonucleotides are attached to a glass plate, hybridization with a mixture of fluorescently tagged PCR amplified sequences is carried out, and the hybridized sequences are recognized by location of fluorescent spots on the support (8, 9). We have recently tried to evaluate the feasibility of an alternative approach based on the following principle (12). A mixture of microscopic particles, each of which bears a given allele-specific oligonucleotide and a reporter group defining the particle category, is used as the solid phase. After hybridization, individual particles are separately subjected to two parallel measurements: one identifies the particle category, and the other quantifies the hybridized oligonucleotide. As a first part of these studies, we have previously (11) described several methods for covalent immobilization of oligonucleotide probes to uniformly sized particles (50 μm) made of a glycidyl methacrylate/ethylene dimethacrylate copolymer particle. The hybridization of the particle-bound probes with oligonucleotides bearing a photoluminescent europium chelate was then detected by time-resolved fluorescence measurement of a single

particle. The best hybridization yields were observed to be 80% on using sequences forming 16 complementary base-pairs. We now demonstrate that the same polymer particles may be used, after appropriate derivatization, as a solid support in automated oligonucleotide synthesis by the phosphoramidite approach. The oligonucleotide-coated particles obtained in this manner exhibit, somewhat unexpectedly, hybridization properties as good as those of the best solid phases prepared by postsynthetic immobilization of appropriately derivatized purified oligonucleotides.

EXPERIMENTAL PROCEDURES

Materials. The porous and compact particles on which the oligonucleotide probes were assembled were products of SINTEF Applied Chemistry (Trondheim, Norway) and Dyno Particles AS (Trondheim, Norway), respectively. The porous particles (**1**) were copolymers of glycidyl methacrylate (40%) and ethylene dimethacrylate (60%) (37% matrix), derivatized with primary amino functions by reacting bis(3-aminopropyl)amine with the particle-bound epoxy groups (13). The density of the primary amino groups of these particles is of the order of 1 mmol g^{-1} , the surface area 137 $\text{m}^2 \text{g}^{-1}$, and the total pore volume 0.822 mL g^{-1} . The pore size ranges from <5 to 500 nm, the average size being 30 nm. The compact particles (**2**; Dynospheres Exp-SS-50-RACQ) were made of polystyrene, having a mean particle diameter of 56 μm (% CV 1.3). These particles are functionalized with ethylenediamine groups, the density of the primary amino functions being 1.3 $\mu\text{mol g}^{-1}$.

Derivatization of Microparticles for Oligonucleotide Synthesis. The porous particles (**1**) were acylated with pyridinium DMTrO-acetate and capped with acetic anhydride, as described previously (14) (Scheme 1). The *N*-(DMTrO-acetyl) loading of the particles (**3**), when determined by the DMTr-cation assay (15), ranged from

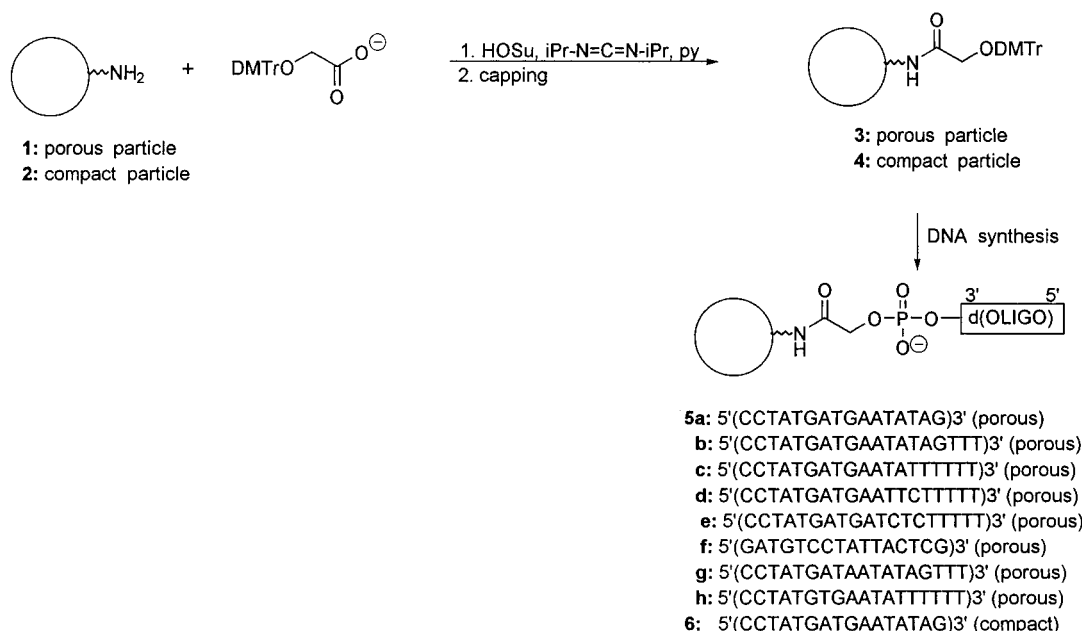
* Author to whom correspondence should be addressed (telephone +358-2-333 6770; fax +358-2-333 6770; e-mail harri.lonnberg@utu.fi).

[†] Department of Chemistry.

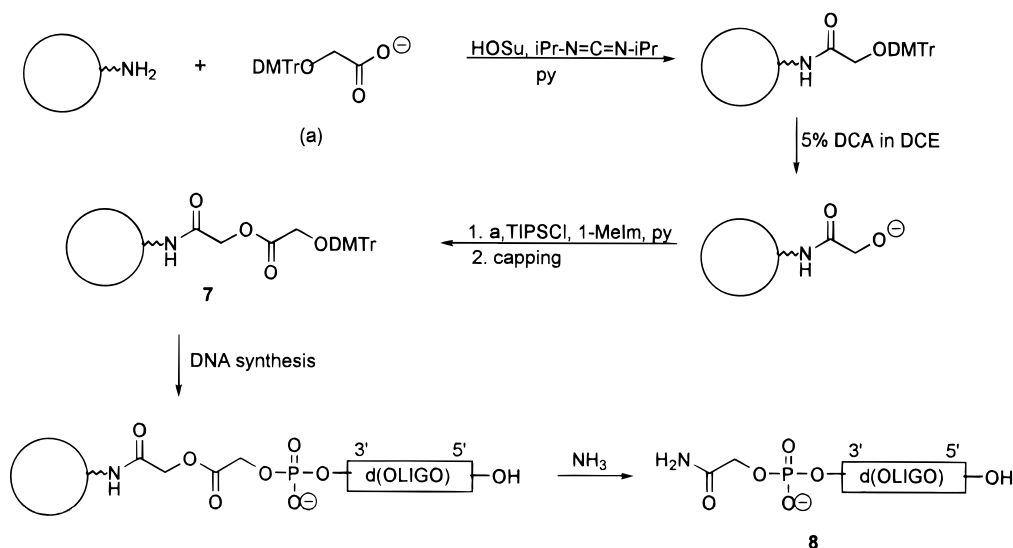
[‡] Department of Biotechnology.

[®] Abstract published in *Advance ACS Abstracts*, April 15, 1997.

Scheme 1



Scheme 2



1 to 160 $\mu\text{mol g}^{-1}$. The compact particles (2) were similarly converted to *N*-(DMTrO-acetylated) particles 4, exhibiting a DMTr-loading of 0.15 $\mu\text{mol g}^{-1}$.

Oligonucleotide Synthesis on Microparticles 3 and 4. An appropriate amount of particles 3 or 4 was loaded in the column of a DNA synthesizer (ABI 392), and the desired oligodeoxyribonucleotide was assembled in a 0.2 μmol scale using standard phosphoramidite chemistry. According to the DMTr-cation response, the stepwise coupling efficiency ranged from 90 to 98%, giving a total efficiency of 30–50%. The yield of the first two to three couplings was exceptionally low (90–93%), while the subsequent couplings exhibited a normal efficiency (97–98%). In all likelihood the low initial coupling yields result from the fact the solid support employed is not optimized for oligonucleotide synthesis. The amido linker of particles 3 and 4 was completely resistant toward conventional ammonolytic deprotection of the base moieties. After ammonolysis, the particles bearing the desired oligonucleotide sequence [porous particles: 5a 5'-d(CCTATGATGAATATAG)-3', 5b 5'-d(CCTATGATGAATATAGTTT)-3', 5c 5'-d(CCTATGATGAATATTTTTT)-3', 5d 5'-d(CCTATGATGAATTCTTTTT)-3',

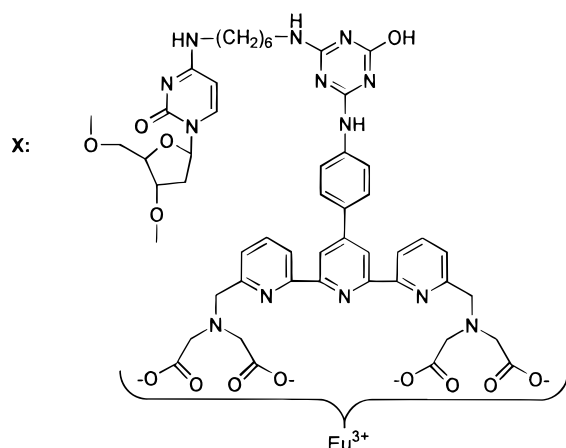
5e 5'-d(CCTATGATGATCTCTTTTT)-3', 5f 5'-d(GATGTCCTATTACTCG)-3', 5g 5'-d(CCTATGATAATATAGTTT)-3', 5h 5'-d(CCTATGTGAATATTTTTT)-3'; compact particles: 6 5'-d(CCTATGATGAATATAG)-3'] were dried under reduced pressure, removed from the column, and washed with the buffer used in the hybridization assays.

To evaluate the quality of oligonucleotide synthesis on particles 3, the 16-mer sequence 5'-d(CCTATGATGAATATAG)-3' was assembled on the same particles bearing a short cleavable linker (Scheme 2). For this purpose, particles 3, having a DMTr loading of 22 $\mu\text{mol g}^{-1}$, were detritylated with 5% dichloroacetic acid in 1,2-dichloroethane, and the released hydroxy functions were again acylated with pyridinium DMTrO-acetate and capped to give particles 7. The 16-mer sequence was assembled on these particles. Upon ammonolysis, the oligonucleotides were released as 3'-carboxamidomethyl phosphates (8) (14), and the composition of the product mixture was analyzed by ion-exchange HPLC on a Synchropak AX-300 column (4.6 \times 250 mm, 6.5 μm ; buffer A, 0.05 M KH_2PO_4 in 50% aqueous formamide, pH 5.6; buffer B, buffer A + 0.6 M $(\text{NH}_4)_2\text{SO}_4$; flow rate, 1 mL min^{-1} ; linear gradient from 0 to 60% buffer B in 60

Scheme 3

9 5'-d(CTATATTCATCATAGGAAACACCAAAGATGATATTX₅C)3'

10 5'-d(X₂₀ATCATCTTTGGT)3'



min). The area of the main signal at $t_R = 42$ min, referring to the desired 16-mer conjugate, was 42% of total signal area, all shorter sequences being evenly distributed.

Fluorescent Oligonucleotide Conjugates (9, 10).

The fluorescently tagged oligonucleotide used for the characterization of the hybridization properties of particles **5a–h** and **6** was a 41-mer (**9**), 5'-d(CTATATTCATCATAGGAAACACCAAAGATGATATTX₅C)-3', where X stands for *N*⁴-(aminohexyl)-2'-deoxycytidine tethered to a 2,4,6-trichloro-1,3,5-triazine-activated photoluminescent europium(III) chelate, {2,2',2'',2'''-{{4'-{4'''-[4,6-dichloro-1,3,5-triazin-2-yl]amino]phenyl}-2,2':6',2'':6'',2''':6'''-terpyridine-6,6''-diyl}bis(methylenenitrilo)}tetrakis(acetato)europium(III) (**16**). A similarly labeled 32-mer (**10**), 5'-d(X₂₀ATCATCTTTGGT)-3', was used to determine the extent of unspecific binding of oligonucleotides to particles **5a–h** and **6**. The preparation of these oligonucleotide conjugates has been described previously (**11**).

Hybridization Assays. The hybridization assays were carried out as described previously (**11**).

RESULTS

Solid Phase Assembly of Oligonucleotides on Polymer Particles.

Two different types of microparticles, both having a diameter of approximately 50 μm , were used as a solid support to assemble the oligonucleotide probes and to characterize the hybridization properties of the oligonucleotide-coated particles obtained. The porous particles (**1**) were made of a copolymer of glycidyl methacrylate (40%) and ethylene dimethylacrylate (60%). Their average pore size was of the order of 30 nm, and the density of primary amino groups was 1 mmol g^{-1} . The compact particles (**2**) were made of polystyrene, and they bore primary amino groups 1.3 $\mu\text{mol g}^{-1}$. Both particles were further derivatized by acylating a desired proportion of the amino functions with DMTrO-acetic acid and capping the rest of the amino groups by repeated acetylations (Scheme 1). The loading of the *N*-(DMTrO-acetyl) groups was determined by the DMTr-cation assay (**15**). These particles (**3**, **4**) were used as a solid support in automated oligonucleotide synthesis according to the conventional phosphoramidite strategy. The oligonucleotide chains thus became bonded to the support via an amide linkage, which was observed to be completely resistant toward deprotection of the base moieties by ammonolysis.

The sequences assembled on porous particles (**3**) were 5'-d(CCTATGATGAATATAG)-3' (**5a**), 5'-d(CCTATGATGAATATAGTTT)-3' (**5b**), 5'-d(CCTATGATGAATATTTT)-3' (**5c**), 5'-d(CCTATGATGAATCTTTTT)-3' (**5d**), 5'-d(CCTATGATGATCTCTTTTT)-3' (**5e**), 5'-d(GATGTCCTATTACTCG)-3' (**5f**), 5'-d(CCTATGATAATATAGTTT)-3' (**5g**), and 5'-d(CCTATGTGAATATTTTTT)-3' (**5h**) and that on compact particles (**4**) 5'-d(CCTATGATGAATATAG)-3' (**6**). On the basis of the DMTr-cation response of the consecutive couplings, about one-third of the growing chains reached the full length, the rest of the chains remaining truncated. To evaluate the homogeneity of the assembled oligonucleotides in more detail, the synthesis was repeated on particles **3** bearing a short cleavable linker. Accordingly, the particles **3** were detritylated and DMTrO-acetic acid was esterified with the free hydroxy functions (Scheme 2) (**14**). The unreacted hydroxy groups were capped, and the oligonucleotide was assembled on these particles (**7**). Upon ammonolytic deprotection of the base moieties, the oligonucleotide was released as a 3'-carboxamidomethyl phosphate (**8**) (**14**). Ion-exchange HPLC analysis of the crude oligonucleotide mixture revealed that about 40% of all nucleotidic units were present in completed 16-mer chains, while the rest were rather evenly distributed among shorter sequences.

Hybridization Properties of the Particle-Bound Oligonucleotides.

A fluorescently tagged 41-mer oligonucleotide (**9**), 5'-d(CTATATTCATCATAGGAAACACCAAAGATGATATTX₅C)-3', where X stands for *N*⁴-(aminohexyl)-2'-deoxycytidine tethered to a 2,4,6-trichloro-1,3,5-triazine-activated photoluminescent europium(III) chelate, {2,2',2'',2'''-{{4'-{4'''-[4,6-dichloro-1,3,5-triazin-2-yl]amino]phenyl}-2,2':6',2'':6'',2''':6'''-terpyridine-6,6''-diyl}bis(methylenenitrilo)}tetrakis(acetato)europium(III) (**16**), was used to elucidate the hybridization properties of particles **5a–h** and **6**. The sequence complementary to the particle-bound 16-mer is indicated by bold letters. The kinetics of hybridization was followed at 25 °C by shaking 500–5000 particles in 100 μL of Tris buffer (50 mM, pH 7.5, containing 0.5 M NaCl and 0.01% Tween) containing **9** at a concentration of 5 nM. Accordingly, the particle-bound oligonucleotides were always present in large excess compared to the fluorescently tagged oligomer **9** (5×10^{-13} mol vs $>3 \times 10^{-11}$ mol). Aliquots of 10 μL (50–500 particles) were withdrawn at appropriate intervals. The particles were washed, and a single particle was subjected to a time-resolved fluorescence measurement, as described previously (**10**, **11**). Typically 10 individual particles were measured, the standard deviation ranging from 2 to 8%. To estimate the contribution of unspecific adsorption of the labeled oligomer to the particles, a comparative study with a noncomplementary fluorescently tagged oligomer, 5'-d(X₂₀ATCATCTTTGGT)-3', was carried out. The unspecific binding was in all cases negligible, <1% of **10** being attached to the particles.

To transform the observed fluorescence emission of a single particle to the number of fluorescently tagged oligomers hybridized to the particle, two sets of particles **5a** were subjected to hybridization with the tagged oligomer **9**, the initial concentration of which was varied from 17 pM to 170 nM. After 20 h of incubation, one set of particles was measured by the single-particle technique, while from the other set europium(III) ion was released to solution and determined according to the DELFIA protocol (**17**). Additionally, the amount of **9** in solution before and after hybridization was determined by DELFIA. The fact that the difference between the amount of europium(III) in solution phase before and after hybridization always was equal to the amount

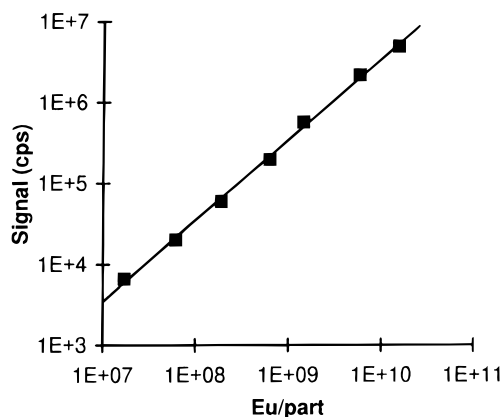


Figure 1. Intensity of the microfluorometer signal measured from a single oligonucleotide-coated polymer particle (**5a**) after hybridization as a function of the number of europium(III) ions released from the same particle when treated according to the DELFIA protocol (17).

released from the particles after hybridization lends considerable support to the reliability of the determination. Figure 1 shows the calibration line obtained and used throughout this work to transform the microfluorometry signals to the number of fluorescently tagged oligonucleotide molecules.

Figure 2 shows the hybridization kinetics observed with porous particles **5a**, the oligonucleotide loading of which was $1 \mu\text{mol g}^{-1}$. As previously discussed in more detail (11), the hybridization obeys the kinetics of two reversible first-order reactions under the experimental conditions, that is, when the immobilized oligomers are present in large excess (all curves indicated represent the best least-squares fit obtained on the basis of this model). The half-lives observed on using 5, 10, and 50 particles/ μL were 3.6 h, 1.3 h, and 22 min, respectively. In other words, the rate of hybridization appears to be proportional to the number of particles in a given volume of the hybridization solution. By contrast, the amount of oligonucleotide **9** hybridized to the particles is almost independent of the number of particles, and hence the intensity of the fluorescence emission measured from a single particle is inversely proportional to the number of particles used in the assay. This is clearly seen from Figure 3, in which the signal of a single particle after equilibration is plotted against the number of particles used in the assay. Accordingly, what one wins in time is lost in sensitivity of detection. The rate of hybridization is with compact particles **6** comparable to that with porous particles (data not shown).

While the rate of hybridization may be increased by increasing the number of particles in a given volume of the hybridization solution, increasing the density of oligonucleotides on particles does not have a similar effect. The data in Figure 4 clearly show that the oligonucleotide density has practically no effect on either the hybridization kinetics or the amount of oligonucleotide **9** hybridized, as long as the number of particles remains constant; oligonucleotide loadings of 1 and $9 \mu\text{mol g}^{-1}$ gave very similar results.

The concentration of oligonucleotide **9** in the hybridization solution had no effect on the kinetics of hybridization. The kinetics remained unaltered when the concentration of **9** was decreased from 5 to 0.17 nM (Figure 5). Similarly, the hybridization efficiency (the mole fraction of **9** hybridized to the particles) remained unchanged over a wide concentration range. In Figure 6 the intensity of the fluorescence emission from a single porous particle (**5a**) is plotted against the concentration of **9** in the assay.

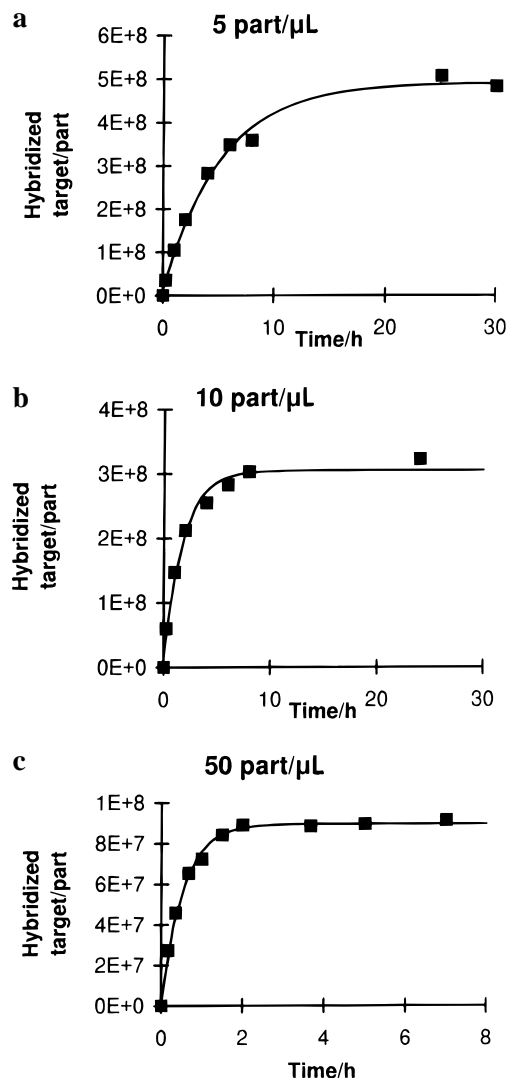


Figure 2. Kinetics of hybridization of a fluorescently tagged oligonucleotide (**9**) with the complementary 16-mer probes on a porous polymer particle (**5a**) at 25 °C: the effect of the number of particles in a given volume of the assay solution. The initial concentration of **9** was 5 nM, and the loading of the oligonucleotide probe on the particles was $1 \mu\text{mol g}^{-1}$.

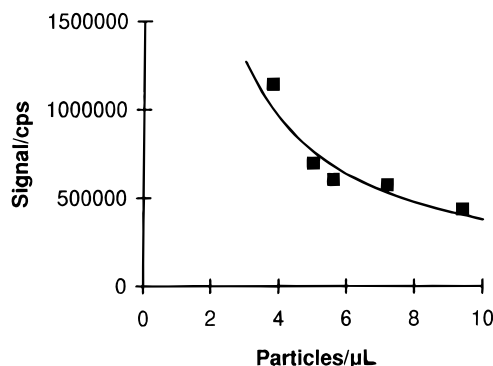


Figure 3. Intensity of the microfluorometer signal measured from a single polymer particle (**5a**) after hybridization plotted against the number of particles used in the assay.

As seen, the plot remains strictly linear over 5 orders of magnitude. With compact particles (**6**) the linear range is more narrow, owing to the fact that the particle becomes saturated with **9** at high concentrations (Figure 7). With porous particles, this kind of saturation could only be achieved by using a mixture of **9** (1%) and the corresponding unlabeled oligomer (99%). Otherwise, the

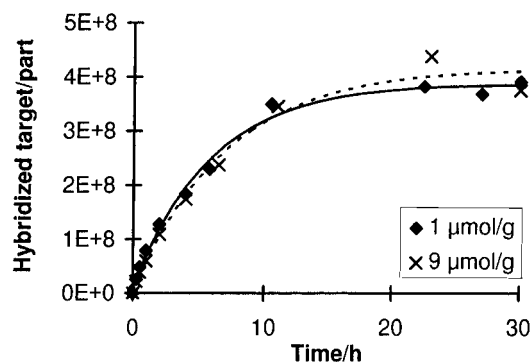


Figure 4. Kinetics of hybridization of a fluorescently tagged oligonucleotide (**9**) with the complementary 16-mer probes on a porous polymer particle (**5a**) at 25 °C: the effect of the oligonucleotide loading on the particle. The data refer to experiments with 5 particles/ μL of the assay solution. The initial concentration of **9** was 5 nM.

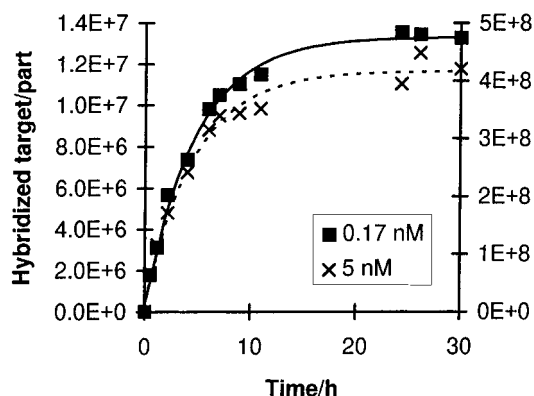


Figure 5. Kinetics of hybridization of a fluorescently tagged oligonucleotide (**9**) with the complementary 16-mer probes on a porous particle (**5a**) at 25 °C: the effect of the concentration of the fluorescently tagged oligomer. The data refer to experiments with 5 particles/ μL . The concentrations of **9** were 5 and 0.17 nM.

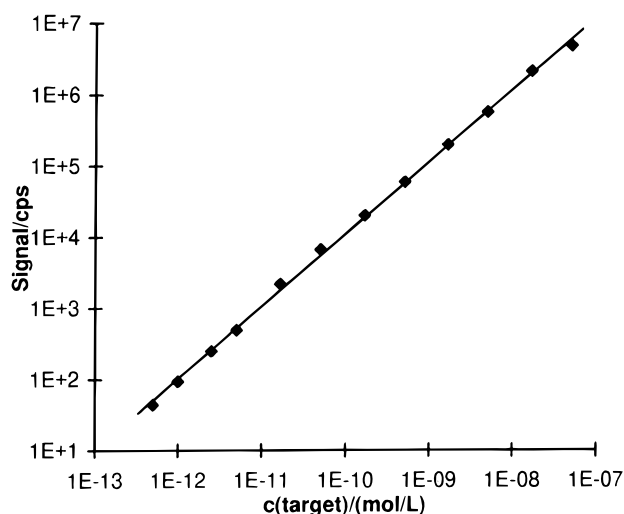


Figure 6. Hybridization of a fluorescently tagged oligonucleotide (**9**) with the complementary 16-mer probes on a porous polymer particle (**5a**) at 25 °C: the effect of the concentration of **9** in the assay solution. The data refer to experiments with 5 particles/ μL of the assay solution and oligonucleotide loading of 1 $\mu\text{mol g}^{-1}$ on particles.

signal became too intense to be measured. Interestingly, the saturation takes place in the same concentration range of **9** when the oligonucleotide loading on the particle is 1 $\mu\text{mol g}^{-1}$ and when it is 9 $\mu\text{mol g}^{-1}$ (Figure 8). In the former case (1 $\mu\text{mol g}^{-1}$) the saturation level

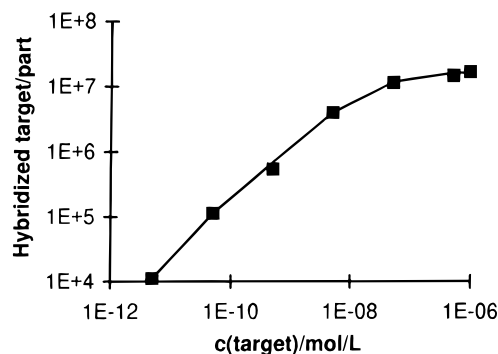


Figure 7. Saturation of compact oligonucleotide-coated particles (**6**) with a fluorescently tagged oligonucleotide (**9**) at 25 °C: the number of **9** hybridized to a single particle as a function of the concentration of **9** in the assay solution. The oligonucleotide loading of the particles was 0.1 $\mu\text{mol g}^{-1}$.

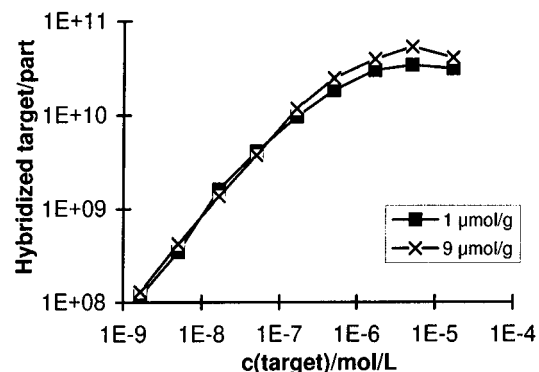


Figure 8. Saturation of porous oligonucleotide-coated particles (**5a**) with a fluorescently tagged oligonucleotide (**9**) at 25 °C: the number of **9** hybridized to a single particle as a function of the concentration of **9** in the assay solution. The oligonucleotide loading of the particles was either 1 or 9 $\mu\text{mol g}^{-1}$.

is reached only when practically all of the 16-mer sequences on the particles are engaged in hybridization, while in the latter case (9 $\mu\text{mol g}^{-1}$) saturation occurs when only 15% of the particle-bound sequences are hybridized. Noncomplementary oligonucleotides or hs-DNA could be present in 300-fold excess compared to **9** (on the basis of the number of nucleosidic units) without any significant influence on either the kinetics or efficiency of hybridization (data not shown).

The effect of ionic strength on the efficiency of hybridization was expected (18, 19). Addition of sodium chloride markedly enhanced hybridization up to the ionic strength of 0.2 M, but had minor effect thereafter (data not shown). Simultaneously, the unspecific binding was also increased, but under all conditions it remained almost negligible, <2% of the sequence-specific signal in spite of the fact that the complementary oligomer **9** bore only 5 photoluminescent chelates and the noncomplementary one (**10**) 17 chelates. When **9** was incubated with particles bearing a noncomplementary sequence (**5f**), the signal observed was <0.3% of that referring to the sequence-specific binding to **5a**.

To elucidate how strongly the hybridization efficiency depends on the length of the complementary sequences, comparative measurements with particles **5b–e** were carried out. All of these particles have immobilized a 19-mer sequence complementary to the fluorescently tagged oligomer (**9**) over 16 (**5b**), 14 (**5c**), 12 (**5d**), and 10 (**5e**) bases from the free 5' terminus of the particle-bound oligonucleotide. The hybridization efficiencies observed were 61, 49, 7, and 0.6%, respectively. The results remained unchanged when the concentration of **9** was

varied from 0.17 to 17 nM. Comparison of the hybridization efficiency of **5b** to **5a** further reveals that the hybridization is not markedly enhanced by adding extra nucleotides between the linker and the sequence engaged in hybridization.

To verify the specificity of hybridization, a one-base nonterminal deletion was made on particles **5b** and **5c**, bearing 16-mer and 14-mer complementary sequences to **9**, respectively. With the 16-mer sequence, that is, when **5b** is replaced with **5g**, the hybridization efficiency dropped from 61 to 3.0% due to this deletion, and with the 14-mer sequence (**5c** replaced with **5h**) the hybridization efficiency dropped from 49 to 2.5%. A three-base mutation in the fluorescently tagged oligonucleotide **9** (a triplet T7C8A9 replaced with G7T8G9) decreased the affinity to **5a** from 61 to 1%.

DISCUSSION

The results presented above clearly show that both porous and compact polymer particles bearing 3'-attached oligonucleotide probes (**5a–h**, **6**) may be conveniently prepared by direct solid phase assembly of oligonucleotides on particles (**3**, **4**), the aminoalkyl chains of which are derivatized with *N*-(DMTrO-acetyl) groups (and the unreacted amino functions capped by acetylation, Scheme 1). The amido linker obtained is completely stable toward conventional deprotection of the base moieties by ammonolysis. With porous particles, the oligonucleotide density on the particle may be easily varied from 1 to 40 $\mu\text{mol g}^{-1}$ by changing the *N*-(DMTrO-acetyl) loading on the particle, whereas with compact particles the maximal loading is 3 orders of magnitude lower. The efficiency of oligonucleotide synthesis on these polymer particles (**3**, **4**) is not as good as on CPG. On preparing 16-meric sequences, 40% of the nucleotide units were, according to ion-exchange HPLC of the released oligomer, present in the full-length sequence, the remaining 60% being rather evenly distributed among truncated sequences. In spite of this, the particles exhibited hybridization properties as good as those of particles prepared previously (11) by postsynthetic covalent immobilization of purified oligonucleotides to the same particles. Among the latter particles only one, bearing a disulfide linker [5'-oligo-*O*(3')-PO(*O*-)OCH₂CONHCH₂CH₂SS(CH₂)₁₀CONH particle], showed a somewhat higher hybridization efficiency (80 vs 60% on using complementarity of 16 base-pairs). However, even those particles exhibited higher unspecific binding (unspecific to specific = 1:200) than the particles of the present work (unspecific to specific = 1:600; determined by comparing the binding of **10** and **9**). In other words, the oligonucleotide-coated particles obtained by direct oligonucleotide assembly appear to be even more applicable to mixed-phase hybridization assays than those prepared by more laborious postsynthetic immobilization of purified oligonucleotides.

Complementarity over a sequence of 16 base-pairs is sufficient to ensure that >50% of the target oligonucleotide in solution is hybridized to the particles. With 12 base-pairs, the hybridization efficiency is already <10%. To achieve optimal binding, the ionic strength must be >0.1 M. Under such conditions, neither noncomplementary oligonucleotides nor DNA is able to interfere with the sequence-specific binding, even if present in large excess. In spite of the fact that the particles bear truncated sequences in addition to the desired full-length probe, the specificity of hybridization appears reasonable. For example, a one-base deletion in the middle of a 16- or 14-mer sequence resulted in a 20-fold decrease in the hybridization efficiency.

The hybridization efficiency of the oligonucleotide-coated porous particles (**5a**) described in the present work is comparable to that of other solid phases bearing covalently immobilized oligonucleotides (1, 4, 6, 20). Time-resolved fluorescence detection of oligonucleotides tagged with a photoluminescent europium(III) chelate, however, offers a major advantage: the emission measured from a single particle after hybridization is strictly proportional to the concentration of the target oligonucleotide in solution over a range of 5 orders of magnitude (Figure 6). In other words, the linear region in the assay is clearly wider than reported previously (9, 21). The major concern, in turn, is the prolonged incubation needed to reach the equilibrium between the solution and solid phase. On using 5 particles/ μL of the assay solution, this takes 20 h. Comparable reaction times have been reported for oligonucleotide-arrays on glass support (9), but by miniaturization of the system the reaction times have been reduced even to 5 min (21). With polymer particles, the reaction time may be shortened by increasing the number of particles in a given volume of the assay solution (Figure 2), but not by increasing the density of oligonucleotide probes on the particle (Figure 4). The potential of this approach has been well demonstrated in literature (1, 20, 22, 23). Unfortunately, the situation is no longer as simple when one wishes to measure the intensity of the fluorescence emission directly on a single polymer particle. If the number of particles is increased, the fluorescently tagged target oligonucleotide present in the assay solution will be evenly distributed among increasing number of particles (Figure 3), and hence the emission of a single particle is decreased. In other words, one has to make a compromise between the assay time and sensitivity. In spite of this limitation, polymer particles on which oligonucleotide probes may be directly assembled show potential as solid phases in hybridization assays that are based on measurement of the emission of photoluminescent lanthanide chelates directly from a single particle. In this manner, a high sensitivity and linear response of the signal to analyte concentration over an exceptionally wide concentration range are achieved.

ACKNOWLEDGMENT

The particles employed were a generous gift of Dr. Ruth Schmid, SINTEF (Norway). Financial support from the Academy of Finland, the Research Council for Natural Sciences and Technology, is gratefully acknowledged.

LITERATURE CITED

- (1) Gingeras, T. R., Kwok, D. Y., and Davis, G. R. (1987) Hybridization properties of immobilized nucleic acids. *Nucleic Acids Res.* 15, 5373–5390.
- (2) Van Ness, J., Kalbfleisch, S., Petrie, C. R., Reed, M. W., Tabone, J. C., and Vermeulen, N. M. J. (1991) A versatile solid support system for oligodeoxynucleotide probe-based hybridization assays. *Nucleic Acids Res.* 19, 3345–3350.
- (3) Maskos, U., and Southern, E. M. (1992) Parallel analysis of oligodeoxyribonucleotide (oligonucleotide) interactions. I. Analysis of factors influencing oligonucleotide duplex formation. *Nucleic Acids Res.* 20, 1675–1678.
- (4) Maskos, U., and Southern, E. M. (1992) Oligonucleotide hybridizations on glass supports: a novel linker for oligonucleotide synthesis and hybridization properties of oligonucleotides synthesized in situ. *Nucleic Acids Res.* 20, 1679–1684.
- (5) Southern, E. M., Maskos, U., and Elder, J. K. (1992) Analyzing and comparing nucleic acid sequences by hybridization to arrays of oligonucleotides: evaluation using experimental models. *Genomics* 13, 1008–1017.
- (6) Kumar, A. (1994) Development of suitable linkage for oligonucleotide synthesis and preliminary hybridization stud-

- ies on oligonucleotides synthesized in situ. *Nucleosides Nucleotides* 13, 2125–2134.
- (7) Williams, J. C., Case-Green, S. C., Mir, K. U., and Southern, E. M. (1994) Studies of oligonucleotide interactions by hybridization to arrays: the influence of dangling ends on duplex yield. *Nucleic Acids Res.* 22, 1365–1367.
- (8) Southern, E. M., Case-Green, S. C., Elder, J. K., Johnson, M., Mir, K. U., Wang, L., and Williams, J. C. (1994) Arrays of complementary oligonucleotides for analysing the hybridization behaviour of nucleic acids. *Nucleic Acids Res.* 22, 1368–1373.
- (9) Guo, Z., Guilfoyle, R. A., Thiel, A. J., Wang, R., and Smith, L. M. (1994) Direct fluorescence analysis of genetic polymorphisms by hybridization with oligonucleotide arrays on glass supports. *Nucleic Acids Res.* 22, 5456–5465.
- (10) Lövgren, T., Heinonen, P., Hakala, H., Heinola, J., Harju, R., Takalo, H., Mikkala, V.-M., Schmid, R., Lönnberg, H., Pettersson, K., and Iitiä, A. Sensitive bioaffinity assays on individual microparticles using time-resolved fluorometry. *Clin. Chem.* (submitted for publication).
- (11) Hakala, H., and Lönnberg, H. Time-resolved fluorescence detection of oligonucleotide hybridization on a single microparticle: covalent immobilization of oligonucleotides and quantitation of a model system. *Bioconjugate Chem.* (in press).
- (12) Soini, E. (1991) Biospecific multianalyte assay method. U.S. Pat. 5,028,545.
- (13) Ugelstad, J., Berge, A., Ellingsen, T., Schmid, R., Nilsen, T.-N., Mørk, P. C., Stenstad, P., Hornes, E., and Olsvik, Ø. (1992) Preparation and application of new monosized polymer particles. *Prog. Polym. Sci.* 17, 87–161.
- (14) Hovinen, J., Guzaev, A., Azhayev, A., and Lönnberg, H. (1994) Novel solid supports for the preparation of 3'-derivatized oligonucleotides: introduction of 3'-alkylphosphate tether groups bearing amino, carboxy, carboxamido, and mercapto functionalities. *Tetrahedron* 50, 7203–7218.
- (15) Atkinson, T., and Smith, M. (1984) In *Oligonucleotide Synthesis: A Practical Approach* (M. J. Gait, Ed.) p 48, IRL Press, Oxford, U.K.
- (16) Mikkala, V.-M., Helenius, M., Hemmilä, I., Kankare, J., and Takalo, H. (1993) Development of luminescent europium(III) and terbium(III) chelates of 2,2':6',2''-terpyridine derivatives for protein labelling. *Helv. Chim. Acta* 76, 1361–1378.
- (17) Hemmilä, I., Dakubu, S., Mikkala, V.-M., Siitari, H., and Lövgren, T. (1984) Europium as a label in time-resolved immunofluorometric assays. *Anal. Biochem.* 137, 335–343.
- (18) Breslauer, K. J., Frank, R., Blöcker, H., and Marky, L. A. (1986) Predicting DNA duplex stability from the base sequence. *Proc. Natl. Acad. Sci. U.S.A.* 83, 3746–3750.
- (19) Rychlik, W., and Rhoads, R. E. (1989) A computer program for choosing optimal oligonucleotides for filter hybridization, sequencing and *in vitro* amplification of DNA. *Nucleic Acids Res.* 17, 8543–8551.
- (20) Lund, V., Schmid, R., Rickwood, D., and Hornes, E. (1988) Assessment for covalent binding of nucleic acids to magnetic beads, Dynabeads™, and the characteristics of the bound nucleic acids in hybridization reactions. *Nucleic Acids Res.* 16, 10861–10880.
- (21) Stimpson, D. I., Hoijer, J. V., Hsieh, W., Jou, C., Gordon, J., Theriault, T., Gamble, R., and Baldeschwieler, J. D. (1995) Real-time detection of DNA hybridization and melting on oligonucleotide arrays by using optical wave guides. *Proc. Natl. Acad. Sci. U.S.A.* 92, 6379–6383.
- (22) Albretsen, C., Kalland, K.-H., Haukanes, B.-I., Hävarstein, L.-S., and Kleppe, K. (1990) Applications of magnetic beads with covalently attached oligonucleotides in hybridization: isolation and detection of specific measles virus mRNA from a crude cell lysate. *Anal. Biochem.* 189, 40–50.
- (23) Bush, C. E., Michele, L. J. D., Peterson, W. R., Sherman, D. G., and Godsey, J. H. (1992) Solid-phase time-resolved fluorescence detection of human immunodeficiency virus polymerase chain reaction amplification products. *Anal. Biochem.* 202, 146–151.

BC970033C

Synthesis of New *d*-Propoxyphene Derivatives and the Development of a Microparticle-Based Immunoassay for the Detection of Propoxyphene and Norpropoxyphene

Robert S. Wu,* A. J. McNally, Ian A. Pilcher, and Salvatore J. Salamone

Research and Development, Roche Diagnostic Systems, Inc., 1080 U.S. Highway 202, Somerville, New Jersey 08876-3771. Received May 6, 1996[®]

The synthesis of [*S*-(*R,S*)]-4-[[methyl[2-methyl-3-(1-oxopropoxy)-3,4-diphenylbutyl]amino]-1-oxobutoxy]-2,5-pyrrolidinedione (propoxyphene active ester, **2**) is described. This was used as an intermediate to prepare a propoxyphene immunogen, [*S*-(*R,S*)]-4-[[methyl[2-methyl-3-(1-oxopropoxy)-3,4-diphenylbutyl]amino]-1-oxobutyl-Bovine Thyroglobulin (**3**). This immunogen was then used to generate antibodies which demonstrate good cross-reactivity to *d*-propoxyphene, *d*-norpropoxyphene, and other propoxyphene metabolites. In addition, these antibodies were shown to have very low cross-reactivity to methadone, a structurally related compound. The introduction of an aminomethyl benzoate spacer into the propoxyphene active ester (**2**), followed by the activation of the carboxylic acid, provided for a more stable active ester (**5**). This stable active ester, together with the antibodies generated from the propoxyphene immunogen, has led to the development of an immunoassay based on the Kinetic Interaction of Microparticles in Solution (KIMS).

INTRODUCTION

d-Propoxyphene (PPX), (2*S*:3*R*)-4-dimethylamino-1,2-diphenyl-3-methyl-2-propionoxybutane, (known as Darvon) is a mild narcotic analgesic. The drug is widely prescribed, and overdose has been associated with a large number of fatalities (*1*). PPX by itself or in conjunction with other drugs, including alcohol, can be toxic. In addition to exerting respiratory depressant effects common to all μ agonist narcotics (*2*), PPX and norpropoxyphene (NPPX), its major metabolite, also act as local anesthetics for the treatment of mild to moderate pain disorders. Essentially all PPX abuse is due to oral ingestion, and peak plasma concentration occurs within 1–2 h after a single oral dose. The drug is metabolized primarily *via* double N-demethylation to NPPX and dinorpropoxyphene (DNPPX), both appearing as metabolites in urine. Urinary excretion (*3*) in a 20 h period following a 130 mg single oral dose of PPX, expressed as percent dose, was 1.1% PPX, 13.2% NPPX, and 0.7% DNPPX. The half-lives (*4*) of the metabolites are much longer than those of the parent compound, with a mean of 27 h. Common physical methods for analysis of PPX and its metabolites are GC/MS (*5, 6*) and LC (*7, 8*). A more convenient method of analysis is carried out by the use of commercial screening immunoassays, with several immunoassays being available. The assays include technologies that are enzyme-based (*9, 10*), fluorescence polarization (*11*), and radioimmunoassay (RIA). In this paper, we describe the synthesis of a new PPX hapten and the corresponding derivative for use as a label in a newly developed microparticle-based immunoassay (*12*). Like other OnLine immunoassays (*13*), this new assay utilizes the Kinetic Interaction of Microparticles in Solution (KIMS), as measured by changes in light transmission (*14, 15*). Because of the reported greater occurrence of NPPX in urine (*3, 4*), it is necessary to have an assay that detects both PPX and NPPX. Thus, the first two steps involved in this strategy for the development of this

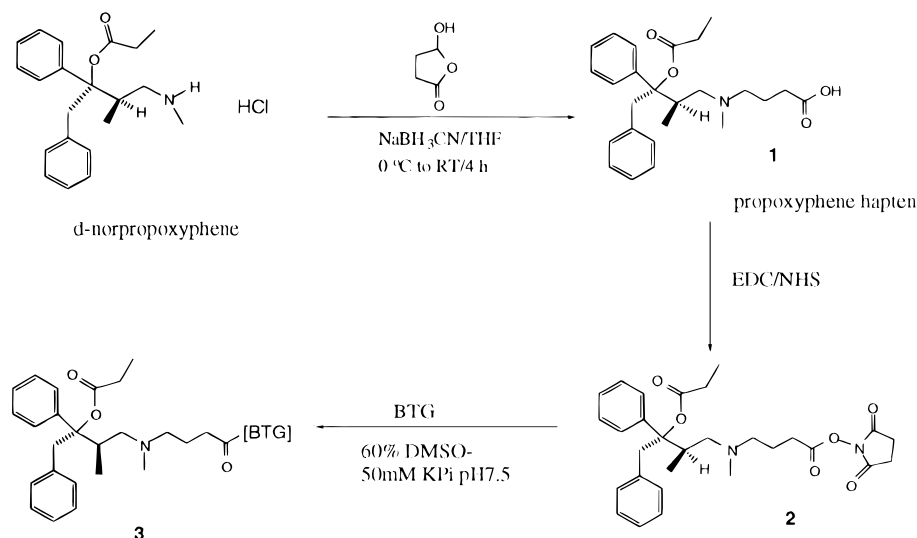
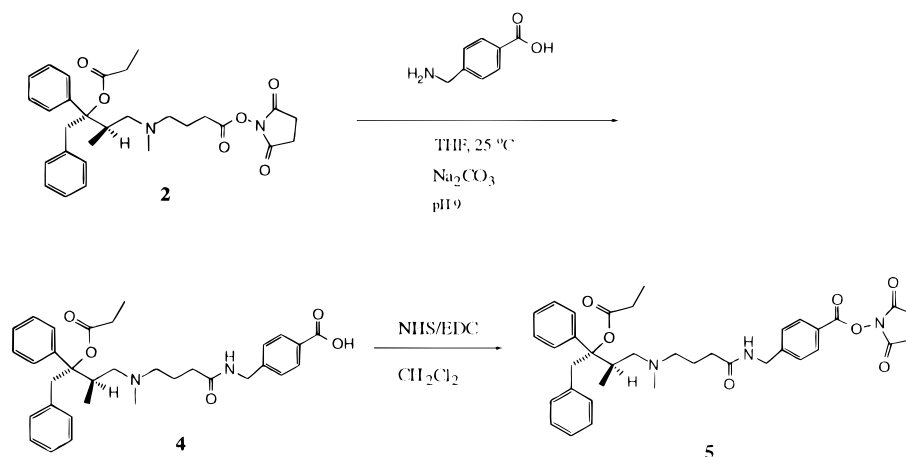
immunoassay are the preparation of antibodies and labels that allow for the recognition of both compounds. A PPX hapten immunogen (**3**) was synthesized as shown in Scheme 1 and used to develop antibodies capable of recognizing PPX and NPPX. In addition, a PPX *N*-hydroxysuccinimide ester bearing an aromatic spacer (**5**) was prepared as the label (Scheme 2). For the development of a microparticle-based assay, **5** was covalently coupled to a carrier protein, and this conjugate was then covalently linked to a microparticle. Thus, this newly developed microparticle–label conjugate allows for the competitive displacement of both PPX and NPPX in the immunoassay.

EXPERIMENTAL PROCEDURES

General. All solvents were obtained from Fisher Scientific unless stated otherwise. All flash-grade silica gel and silica gel preparative TLC plates were obtained from E.M. Science. 1-Ethyl-3-(dimethylaminopropyl)-carbodiimide hydrochloride (EDC), 1-*N*-hydroxybenzotriazole hydrate (NHB·H₂O), *d*-propoxyphene hydrochloride, *d*-norpropoxyphene hydrochloride, methadone hydrochloride, and goat IgG were obtained from Sigma. Dicyclohexyl carbodiimide (DCC), 4-bromo-ethylbutyrate, cesium carbonate, sodium cyanoborohydride (NaCNBH₃), *N*-hydroxysuccinimide, succinic semialdehyde (15% solution in water), and 1-cyclohexyl-3-(2-morpholinoethyl)-carbodiimide metho-*p*-toluene sulfonate (CMC) were obtained from Aldrich. Trinitrobenzenesulfonic acid (TNBS) was obtained from Pierce. Proton nuclear magnetic resonance (¹H-NMR) spectra were recorded at 200 MHz or at 400 MHz on either a Varian XL-200 or a Varian XL-400 spectrometer, respectively. Coupling constants are given in hertz (Hz). The abbreviations used are: s, singlet; d, doublet; t, triplet; m, multiplet. All aqueous buffers and proteins were obtained from Sigma, and carboxyl modified microparticles were obtained from Rhone-Poulenc. The Coomassie protein assay reagent was obtained from Bio-Rad. PPX immunoassay can be performed on many different instruments: Roche COBAS MIRA, Roche COBAS FARA, Hitachi 717/747, Olympus

* Author to whom correspondence should be addressed. Telephone: 908-253-7931.

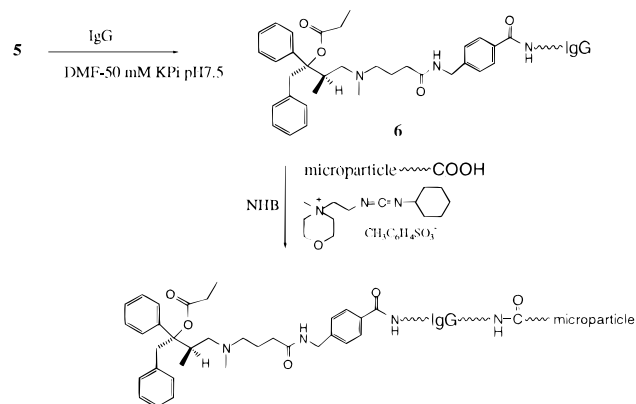
[®] Abstract published in *Advance ACS Abstracts*, May 1, 1997.

Scheme 1. Synthesis of the PPX Hapten 1**Scheme 2. Synthesis of the PPX Label 5**

AU 800, and Olympus AU 5200 series. Described in this publication, COBAS MIRA from Roche Diagnostic Systems was used for the immunoassay. All samples were analyzed using point-to-point curve-fitting model with PPX concentrations of 0, 150, 300, and 600 ng/mL as the calibrators.

Characterization of the Conjugate. The protein concentration is determined by the Coomassie protein assay and is also known as the Bradford method (16). Bovine serum albumin (BSA) was used as the reference. For immunogen, the degree of drug substitution on the protein conjugate was determined by the ability of remaining uncoupled lysine residues to react with TNBS (17, 18). Unmodified BTG at the same concentration as the conjugate was treated in the same manner with TNBS to provide a blank. This procedure produces a yellow complex with an absorbance maximum at 325 nm and was used to calculate the drug substitution expressed as percent modification. Typically, immunogens with a lysine modification of greater than 50% are used for animal immunization. The degree of drug substitution of the IgG conjugate was not determined. The resulting drug-protein conjugate was coupled to the microparticle as outlined in Scheme 3.

Animal Immunization. Three sheep were placed on an immunization program according to an adaptation of a reported procedure (19). Briefly, immunogen 3 was emulsified with Complete Freund's adjuvant, and each sheep received multiple site injections across the back using 1 mg of the immunogen. At the second week, the

Scheme 3. The Preparation of PPX-protein-microparticle Conjugate

animals received booster immunizations containing 1 mg of the immunogen emulsified in Incomplete Freund's adjuvant. This injection was repeated twice, followed by a monthly injection of 0.5 mg of the immunogen/Incomplete Freund's adjuvant mixture for a period of 6 months. Each animal was then bled and serum was separated from the clot by centrifugation to provide the antisera.

Preparation of [S-(R,S)]-4-[Methyl[2-methyl-3-(1-oxopropoxy)-3,4-diphenylbutyl]amino]butanoic Acid (1). To a 15% solution of succinic semialdehyde (4.24 mL, 0.69 g, 6.8 mmol) was added tetrahydrofuran (THF) (15

mL), NPPX (1.89 g, 5.23 mmol) and NaCNBH₃ (328 mg, 5.23 mmol) at 0–4 °C. The mixture was stirred for 2 h while allowing the reaction to reach room temperature (RT). Thin layer chromatography (TLC) revealed a complete disappearance of the starting material (Silica Gel, 85:15 CH₂Cl₂/MeOH). To this was added 1 N HCl (15 mL), and the reaction mixture was stirred for an additional 2 h. The reaction flask was then placed under reduced pressure to remove THF, and the remaining aqueous phase was adjusted to pH 6–7 with 1.0 N NaOH. The aqueous layer was extracted with CH₂Cl₂ (3 × 20 mL). The combined organic layer was washed with saturated NaHCO₃ (2 × 10 mL) and H₂O (2 × 10 mL), dried over anhydrous Na₂SO₄, and evaporated under reduced pressure to give 1.358 g (63%) of white solids with a good purity under TLC examination. *R_f* = 0.37 (85:15 CH₂Cl₂/MeOH).

IR (KBr): ν 1733 (ester), 1726 (COOH) cm⁻¹. MS-FAB: *m/z* 412 (M + 1). ¹H-NMR (400 MHz, CDCl₃): δ 7.40–7.01(m, 10H), 3.90 (d, *J* = 14, 1H), 3.76 (d, *J* = 14, 1H), 2.89–2.86(2 br s, 1H), 2.79 (m, 1H), 2.65 (m, 1H), 2.51 (m, 2H), 2.33 (s, 3H), 2.25 (q, *J* = 7, 2H), 2.00 (t, *J* = 10, 1H), 1.72 (br m, 2H), 1.16 (d, *J* = 7, 3H), 1.06 (t, *J* = 7, 3H). [α]_D = +73.5° (*c* = 0.695%, CHCl₃); *d*-propoxyphenes [α]_D = +54.5° (*c* = 1%, CHCl₃).

Preparation of [S(R,S)]-[4-[Methyl[2-methyl-3-(1-oxopropoxy)-3,4-diphenylbutyl]amino]-1-oxobutoxy]-2,5-pyrrolidinedione (2). To a solution of **1** (101 mg, 0.225 mmol) in dry CH₂Cl₂ (5 mL of freshly distilled over CaH₂) was added EDC (86 mg, 0.45 mmol) and *N*-hydroxysuccinimide (51.7 mg, 0.45 mmol). The reaction mixture was stirred for 18 h under argon, then washed with 0.2 N HCl (2 × 3 mL), saturated NaHCO₃ (2 × 5 mL), and H₂O (2 × 5 mL), and finally dried over anhydrous Na₂SO₄. The solvent was evaporated to dryness to afford 125 mg of white foam (92%). This active ester was found to degrade to the starting material upon a prolonged standing. An attempt to obtain an analytical grade sample by column chromatography using silica gel gave back the starting material **1**. The active ester (**2**) was generally prepared fresh and was used immediately in the following reactions.

IR (KBr): ν 3434 (broad OH), 1814 (NHS ester), 1738 (ester) cm⁻¹. LR (+) MS-FAB: *M*, 508; observed, 509 (M + H). ¹H-NMR (400 MHz, CDCl₃): δ 7.42–7.00 (m, 10H), 3.87 and 3.76 (2d, *J* = 14, 2H), 3.20–1.85 (m, 11H), 2.84 (s, 4H), 2.75–2.56 (2s, 3H, distereomeric salts), 2.69 (s, 3H), 1.22 (q, *J* = 7, 2H), 1.06 (t, *J* = 7, 3H).

Preparation of [S(R,S)]-1-[4-[4-[Methyl[2-methyl-3-(1-oxopropoxy)-3,4-diphenylbutyl]amino]oxobutoxy]amino methyl]benzoic acid (4). A solution of 2.0 g (0.0132 mol) of 4-(aminomethyl)benzoic acid in THF (135 mL) and H₂O (65 mL) was adjusted with 1 N NaOH (5 mL) to give a pH of about 9 or 10. To this was then added a solution of freshly prepared **2** (6.7 g, 0.0132 mol in 135 mL of THF). The reaction was driven to completion by the addition of 1 N NaOH over a period of 1 h (25 mL of 1 N NaOH total). The reaction was then neutralized to pH 6.5 with 6 N HCl, diluted with CH₂Cl₂ (500 mL) and washed with saturated brine solution (250 mL). The aqueous layer was then extracted with CH₂Cl₂ (250 mL). The organic layers were combined and washed with 50 mM K₂HPO₄, pH 8 (250 mL), dried over anhydrous Na₂SO₄ and concentrated under reduced pressure to yield 6.7 g (93.5%) of a white amorphous solid. NMR showed this to be approximately 85–90% pure. This compound may be used without further purification. The above solid was chromatographed on silica gel (350 g) using 9:1 methylene CH₂Cl₂/MeOH to remove front running impurities, followed by 75:25 CH₂Cl₂/MeOH to

elute the product. A yield of 5.02 g (70%) of a white amorphous solid was obtained.

IR (KBr): ν 1733 (ester), 1653 (amide), 705 (C₆H₅) cm⁻¹. LR (+) LSIMS: 545 (M + 1). ¹H-NMR (400 MHz, MeOH-*d*₄): δ 7.91 and 7.24 (d, *J* = 8.3 Hz, 4H), 7.37–7.01 (m, 10H), 4.36 (s, 2H), 3.84 (s, 2H), 2.72 (m, 1H), 2.53 (br d, 1H), 2.30 (m, 1H), 2.26 (q, *J* = 7.5 Hz, 2H), 2.18 (m, 3H), 2.07 (s, 3H), 1.67 (m, 2H), and 1.05–1.00 (m, 6H). [α]_D = +25.1° (*c* = 1%, EtOH).

Preparation of [S(R,S)]-1-[4-[4-[Methyl[2-methyl-3-(1-oxopropoxy)-3,4-diphenylbutyl]amino]-1-oxobutoxy]aminomethyl]phenyl]carbonyl]oxy]-2,5-pyrrolidinedione (5). A round-bottom flask was charged with 170 mg (0.31 mmol) of **4**, 119 mg (0.62 mmol) of EDC, 71.3 mg (0.62 mmol) of *N*-hydroxysuccinimide, and 6 mL of freshly distilled CH₂Cl₂. The reaction mixture was stirred overnight under an argon atmosphere. This was then washed with saturated NaHCO₃ (2 × 5 mL) and water (2 × 5 mL) and dried over anhydrous Na₂SO₄. Solvent was removed under reduced pressure to afford 169 mg (85%) of white foam. TLC *R_f* = 0.33 (85:15 CH₂Cl₂/MeOH). Eighty five milligrams of this material was purified over a silica gel column (1.5 cm i.d. × 18 cm length) and eluted with a mixture of solvents consisting of 85:15 CH₂Cl₂/absolute EtOH to yield 72 mg (85% recovery) of white foam.

IR (KBr): ν 1773 and 1742 (ester), 1668 (amide) cm⁻¹. ¹H-NMR (400 MHz, CDCl₃): δ 8.07 and 7.38 (d, *J* = 8 Hz, 4H), 7.34–6.94 (m, 10H), 7.08 (br t, 1H, NH), 4.46 (d, *J* = 4.8 Hz), 3.79 (dd, *J* = ~15 Hz, 2H), 2.91 (br s, 4H), 2.80 (br m, 1H), 2.42 (br d, 1H), 2.27–2.18 (m, 6H), 2.01 (s, 3H), 1.74–1.61 (m, 3H), 1.02 (t, *J* = 7.8 Hz, 3H), and 0.97 (d, *J* = 6.9 Hz, 3H). MS (+) FAB: 642 (M + 1). [α]_D = +29.1° (*c* = 1%, CHCl₃).

Preparation of PPX Immunogen, [S(R,S)]-4-[Methyl[2-methyl-3-(1-oxopropoxy)-3,4-diphenylbutyl]amino]-1-oxobutyl-BTG (3). A solution of Bovine Thyroglobulin (BTG) (650 mg, 9.7 × 10⁻⁴ mmol, 18 mL of 36.2 mg/mL in 50 mM potassium phosphate (KP_i) (pH = 7.5) was cooled in an ice bath (this was to keep the protein solution cool while adding DMSO), and DMSO (54 mL) was added dropwise. The resulting homogeneous solution was set aside while letting the temperature equilibrate to RT. A freshly prepared NHS ester **2** (99.8 mg) was dissolved in dry dimethyl sulfoxide (DMSO) (1 mL). The hapten solution was immediately added dropwise to the previously prepared BTG solution. The reaction mixture remained homogeneous. This was stirred for 18 h at RT and poured into a dialysis bag of a 50 kDa cut-off. The bag was dialyzed against 50 mM KP_i, pH 7.5, until an exchange of 1000000-fold was achieved. The resulting conjugate was then filtered through a 0.22 μ m sterile filter. The protein concentration (Coomassie protein assay kit) was determined to be 5.6 mg/mL, and the lysine modification (17, 18) was 93% with a total protein recovery of 88%.

Preparation of PPX-IgG Conjugate (6). Three milligrams of the NHS ester (**5**) was dissolved in 3 mL of dry DMSO (over molecular sieves) to make a 1 mg/mL hapten solution. This was set aside. A solution of goat IgG (200 mg, 1.25 μ mol) in 5 mL of 50 mM K₂HPO₄ (pH 7.5) was cooled with an ice bath. To this was added slowly 4.2 mL of DMSO. The temperature was allowed to equilibrate to 25 °C, and 0.8 mL of the previously prepared hapten solution (1.25 μ mol) was added dropwise with stirring. Stirring was continued for 18 h at RT. The resulting conjugate was placed in a dialysis bag of 10 kDa cut-off. The dialysis was carried out according to the protocols described above. At the end of dialysis, the conjugate was filtered through a 0.22 μ m sterile filter to

yield 13 mL of the propoxyphene conjugate. Protein concentration of the conjugate was determined to be 6.7 mg/mL by the Coomassie protein assay. The degree of drug substitution was not determined. This conjugate was serially diluted with nonconjugated IgG in 50 mM bicarbonate buffer (pH 7.5) to provide molar ratios of 1:2, 1:4, 1:8, and 1:16 of conjugated IgG to nonconjugated IgG. The resulting mixture at each dilution molar ratio was coupled to the microparticle described in the following procedure.

Coupling of PPX-IgG Conjugate to the Microparticle. Ten milliliters of carboxyl modified microparticle (10% solids of 0.21 μ m) was first washed, by centrifugation at 10000*g*, with a 0.1% Tween-20 solution. To each milliliter of the particle, 20 mL of 0.1% Tween-water was added, centrifuged (10000*g*), decanted, and resuspended. This process was repeated five times and the microparticle concentration was then adjusted to 3% w/v with a 0.1% Tween-20 solution. Two milliliters of 1-*N*-hydroxybenzotriazole hydrate (NHB, 25 mg/mL, 0.37 mmol), previously dissolved in DMSO, was added slowly to the 30 mL of microparticle suspension, under rapid stirring conditions. The suspension was then stirred for 10 min at 25 °C. To this suspension was added 2.9 mL of a freshly prepared CMC carbodiimide solution (50 mg/mL, 0.34 mmol), and the mixture was stirred slowly for 3 h at 25 °C. The material was then washed by the method of centrifugation described above. The washed, activated microparticle (50 mL) was immediately mixed with 162.5 mg of IgG-propoxyphene conjugate diluted in 50 mM sodium bicarbonate, pH 8.6, which contains 1 mol of drug (initial molar ratio) per mol of IgG. This mixture was allowed to stir for 15 h at 25 °C. The conjugate-coupled microparticle was then mixed with 37.5 mL of 50 mM sodium bicarbonate, pH 8.6, containing 13.5 mg/mL (3.0 mmol) total IgG in order to block the unreacted sites. After blocking, the material was again washed by the method of centrifugation described using a wash solution of 10 mM potassium phosphate, pH 7.5, containing 0.09% sodium azide and 0.1% Tween-20. The washed microparticle was then resuspended in this buffer at 1.0% w/v solids.

Development of the PPX Immunoassay. Four key components were needed for this assay. (1) The antibody reagent was made by placing the titrated antibody in a solution of 50 mM HEPES, pH 6.5, containing 0.1% BSA, 0.5% sodium chloride, 0.09% NaN₃, and 0.1% sheep IgG as the protein stabilizer. (2) A reaction buffer containing 50 mM PIPES, pH 7.0, with 2–3% polyethylene glycol (PEG, MW 15000–20000), 2% sodium chloride, and 0.09% sodium azide. (3) A microparticle reagent, diluted from a 1% stock solution to 0.2% solids in a buffer containing 10 mM potassium phosphate, pH 7.5, 0.09% sodium azide, and 0.1% Tween-20. (4) PPX calibrators at concentrations between 0 and 600 ng/mL in normal human urine containing 0.05% sodium azide. A dose response curve was generated by adjusting the antibody concentration to give maximum displacement in the appropriate concentration range.

RESULTS AND DISCUSSION

Synthesis of the PPX Immunogen. It is generally accepted that the antibodies formed on injection of an antigen to an animal recognize preferentially the part of the molecule that is furthest from the attachment site of the hapten to carrier protein (20). Since we wished to have an antibody that can recognize both PPX and NPPX, it was advantageous to design one hapten derivative displaying a structure common to both drugs. PPX

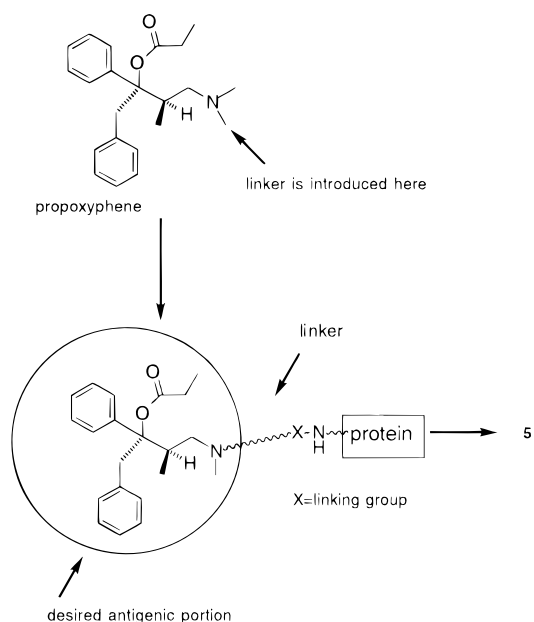


Figure 1. Design of the propoxyphene hapten used to prepare the immunogen.

differs from NPPX by having an additional methyl group on the amino group. In the design of the immunogen (see Figure 1), a drug linker arm was attached at the nitrogen center such that the exposed antigenic region would have the structure common to both the PPX and NPPX molecules. In addition, the linker arm must have a group to which the protein carrier can be covalently coupled. To accomplish this, NPPX appeared to be the ideal starting material, as the secondary amine group could be derivatized to allow the introduction of a tether.

The introduction of a butanoic tether to prepare the PPX hapten 1 was accomplished by a reductive amination procedure as outlined in Scheme 1. This method was more direct than a two-step procedure which has been generally carried out by *N*-alkylation (21) of NPPX with ethyl 4-bromobutyrate, followed by saponification of the ethyl ester to the acid 1. The reductive-amination approach was more viable in that it affords 1 in a high yield. Activation of the acid 1 to the NHS ester 2 is straightforward, and upon addition of BTG, the propoxyphene immunogen 3 was prepared.

Synthesis of the PPX Label Used in the Immunoassay. The aim was to synthesize an activated PPX derivative which could be linked to a water soluble protein carrier, and then this conjugate could be covalently coupled to a microparticle. This coupled microparticle could then act as a label. The coupled microparticle and selected PPX/NPPX antibodies were then used to generate an assay based on the KIMS technology. In the absence of free drug, the antibody binds the drug-microparticle conjugate causing the formation of particle aggregates. The formation of these aggregates causes increased light scattering and is monitored by the changes in light transmission (14). When a urine sample containing the drug in question is present, this drug competes with the microparticle-bound drug derivative for antibody binding. The antibody bound to the free drug in the sample is no longer available to promote particle aggregation, and subsequent particle cross-linking is inhibited. In principle, compound 2 could be utilized as a label since this molecule contained a 4-carbon spacer that was sufficiently flexible for antibody recognition. However, the NHS ester 2 (Scheme 1) is not sufficiently stable as it hydrolyzes back to the acid 1 upon storage. This observation is also consistent with the

finding in this laboratory where an aliphatic NHS ester bearing a tertiary amine in the molecule has a very short life (21). The hydrolysis is most likely caused by the presence of residual water in the sample. Hydrolysis proceeded through a base-catalyzed process induced by the basic tertiary nitrogen group on the molecule. This problem is especially troublesome because the compound is labile and thus causes inconvenience in a routine preparation of the protein conjugate. On the other hand, an NHS ester directly attached to an aryl group appears to be resistant to hydrolysis despite the presence of a tertiary amine in the same molecule. Therefore, we made the corresponding benzoate NHS ester **5** by Scheme 2. This active ester has been found to be more stable and was suitable for our studies.

Synthesis of PPX-Microparticle Conjugate. In producing the activated microparticle, drug conjugates with several different molar ratios of the drug to protein were evaluated to determine the optimal ratio that produced the best dose response curve. When working with microparticle technology, it is important that proper agglutination occurs in the absence of free antigen. Proper amounts of drug conjugate must be coupled to each microparticle so that an equivalence point can be reached allowing the crosslinking of microparticles by antibody. Excess antigen load or excess antibody in the system will prevent the formation of the large aggregates produced by crosslinking.

Each substituted microparticle was then titrated against the antibody to determine the performance of the drug conjugate. The dilution ratio of the conjugate to IgG that gave the most sensitive dose response, and the lowest nonspecific binding (agglutination rate in the absence of antibody) was selected. This was determined to be a dilution ratio of 1:4.

Generation of an Immunoassay for the Detection of PPX and its Assay Precision. Using the PPX conjugate coupled microparticle (0.21 μm) and the antibodies generated from the described immunogen, an immunoassay was developed for COBAS MIRA analyzer. This analyzer is an automated instrument that has the capacity of adding immunoassay reagents and samples into cuvettes to give test results at the rate of 50 tests per h. The MIRA instrument first pipettes 10 μL of urine along with 85 μL of antibody with one syringe and 100 μL of sample diluent with a second syringe into a cuvette. The instrument then mixes the pipetted reagents, and the sample syringe pipettes 24 μL of microparticle reagent to the cuvette along with 25 μL of water. It then again mixes the reagents and monitors the reaction kinetics at 500 nm in 25 s intervals for 12 read points (5 min). An end point analysis with a point-to-point curve fit model is used to plot the difference in absorbance between each calibrator, and a dose response curve is generated. Figure 2 illustrates a typical standard curve that can be obtained using PPX calibrators as standards. In addition, Table 1A shows that when the precision of the assay was assessed, the % coefficient variation (CV) was less than 7% for several points in a single run. When the interassay precision was assessed, the % CV was less than 8% for all points, taken from five runs over five days. Table 1B shows that, in all cases tested, the positive threshold controls (120% cut-off value; 360 ng/mL) yielded positive determination, while conversely, the negative threshold controls (80% the cutoff, 240 ng/mL) were uniformly negative.

Cross-Reactivity of Antibodies to PPX and NPPX-Like Compounds. Three sheep were placed on an immunization program, as described in the methods section using immunogen **3** shown in Scheme 1. At the

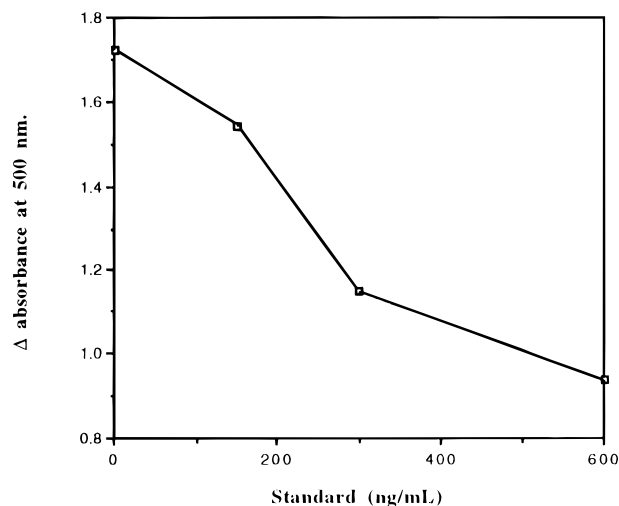


Figure 2.

Table 1

(A) intra-assay precision ($n = 20$)

mean		SD	CV%
ng/mL ^a	ng/mL ^b		
150	140	8.2	5.8
240	265	5.6	2.1
300	301	17.9	5.9
360	405	25.9	6.4

inter-assay precision (5 runs of $n = 20$)

150	144	11.6	8.1
240	262	7.8	3.0
300	307	17.3	5.6
360	406	25.9	6.3

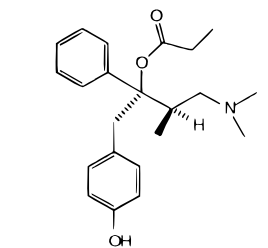
(B) qualitative precision

control ^c	number tested	positive results	negative results	predicted frequency
0.8×	200	0	200	100% negative reading
1.2×	200	200	0	100% positive reading

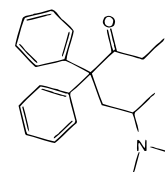
^a Concentration of propoxyphene in urine standard, theoretical spike value. ^b Concentration of propoxyphene measured experimentally by the assay. ^c 0.8× = urine control containing propoxyphene at 80% of the cutoff concentration, and 1.2× = urine control containing propoxyphene at 120% of the cutoff concentration.

Table 2

compound	approximate ng/mL equivalent to 300 ng/mL propoxyphene	approximate percent cross reactivity
<i>d</i> -norpropoxyphene	390	77
<i>d</i> - <i>p</i> -hydroxypropoxyphene	1 408	21
methadone	1 034 500	0.03



d-*p*-hydroxypropoxyphene



methadone

end of six months, the test sera were assayed for titer and cross reactivity to all of the structurally related cross-reactants shown in Table 2. The titer, which was defined as 50% of saturation, was determined using ELISA and KIMS. Two sheep were found to respond well in binding

Table 3

sample	theoretical recovery (ng/mL)	actual recovery (ng/mL)	spiked (ng/mL)
propoxyphene			
1	240	227	240
2	240	224	240
3	360	345	360
4	360	372	360
norpropoxyphene			
1	270 ^a	242	350
2	270 ^a	251	350
3	385 ^a	350	500
4	385 ^a	378	500

^a Calculated from spiked sample $x\%$ cross-reactivity.

Table 4

sample	propoxyphene GC/MS (ng/mL)	norpropoxyphene GC/MS (ng/mL)	OnLine (ng/mL)
13	71	3640	>600
15	76	229	>600
22	244	14 300	>600
23	202	9360	>600
28	34	11 900	>600
32	224	23 600	>600

to PPX with the antisera titer in the range 1:512 to 1:1024. A pool of the antisera of equal volume was made and used to develop the immunoassay. The ability of the polyclonal antibodies to bind PPX was demonstrated (Figure 2), and the cross-reactivity to NPPX, *p*-hydroxy-PPX(4-dimethylamino-1-(4-hydroxyphenyl)-2-phenyl-3-methyl-2-propionoxybutane), and methadone was evaluated as shown in Table 2. The cross-reactivity is expressed in two ways, the approximate percent cross-reactivity and the approximate nanogram per milliliter equivalence to give a positive result of 300 ng/mL. To further confirm that these antibodies detect both PPX and NPPX, urine samples were spiked with given amounts of PPX and NPPX, and values were determined by testing these samples in the immunoassay. These spike and recovery studies are reported in Table 3. This table shows the theoretical and actual value obtained based on 100% cross-reactivity to PPX and 77% cross-reactivity to NPPX.

Sixty-four positive clinical samples with known PPX and NPPX values determined by GC/MS were also tested. All of these clinical samples were positive in the immunoassay. Fifty-eight of these clinical samples had GC/MS PPX values of greater than 300 ng/mL. Six clinical samples showed levels of PPX less than 300 ng/mL and had high levels of NPPX by GC/MS analysis (Table 4). The positive response of these six samples by the immunoassay demonstrated the value of increased sensitivity for NPPX.

In summary, we have synthesized a new PPX immunogen that elicited cross-reactive polyclonal antibodies directed to PPX and NPPX. This was accomplished by designing an immunogen having a linker arm tethered to the tertiary amino group of the PPX molecule. This allowed for the principal binding of the antibodies to be directed toward the structural elements common to both PPX and NPPX. In addition, we have synthesized a new label that demonstrates good stability, providing ease of use in the preparation of PPX-protein conjugates and for routine use in the OnLine assay. This microparticle-based assay provided increased sensitivity for detecting both PPX and NPPX in human urine samples compared to assays employing antibodies specific to only PPX.

LITERATURE CITED

- (1) Soumerai, S., Avorn, J., Gortmaker, S., and Hawley, S. (1987). Effect of government and commercial warnings on reducing prescription misuse: The case of propoxyphene. *Am. J. Public Health* 77, 1518–1523.
- (2) Karch, S. B., Ed. (1993) *The Pathology of Drug Abuse*, Chapter 5, Narcotics, pp 269, CRC Press, Boca Raton, FL.
- (3) McMahon, R. E., Sullivan, H. R., Due, S. L., and Marshall, F. J. (1973) The Metabolite Pattern of d-Propoxyphene in Man. *Life Sci.* 12, 463–473.
- (4) Baselt, R. E., and Cravey, R. H., Eds. (1989) *Disposition of Toxic Drugs and Chemicals in Man*, 3rd ed. pp 724, Year Book Medical Publishers, Inc., Chicago.
- (5) Margot, P. A., Crouch, D. J., Finkle, B. S., Johnson, J. R., and Deyman, M. E. (1983) Capillary and Packed Column GC Determination of Propoxyphene and nor-propoxyphene in Biological Samples: Analytical Problems and Improvements. *J. Chromatogr. Sci.* 21, 201–204.
- (6) Millard, B. J., Sheinin, E. B., and Benson, W. R. (1980) Thermal Decomposition of Propoxyphene during GLC Analysis. *J. Pharm. Sci.* 69, 1177–1179.
- (7) Angelo, H. R., and Christensen, J. M. (1985) Gas Chromatographic Method for the determination of Dextropropoxyphene and Nor-dextropropoxyphene in human plasma, serum and urine. *J. Chromatogr.* 345, 413–418.
- (8) Kunka, R. L., Yong, C. L., Ladik, C. F., and Bates, T. R. (1985) Liquid Chromatography Determination of Propoxyphene and nor-propoxyphene in Plasma and Breast milk. *J. Pharm. Sci.* 74, 103–104.
- (9) Klinger, R. A. (1990) Direct Automated EMIT d.a.u. analysis of N, N-dimethylformamide-modified serum, plasma, and Postmortem Blood for Amphetamines, Barbiturates, Methadone, Methaqualone, Phencyclidine and Propoxyphene. *J. Anal. Toxicol.* 14, 288–291.
- (10) Marr, G., Weingarten, P., Le, M., Rouhani, R., Loor, R., and Khanna, P. (1994) *CEDIA Cannabinoids (THC) Assay for Urine Drug Testing*, Am. Assoc. Forensic Sci. Annual Meeting, Abstract No. K1, p 185.
- (11) Kintz, P., and Mangin, P. (1993) Abbott Propoxyphene Assay: Evaluation and Comparison of TDx and GC/MS Methods. *J. Anal. Toxicol.* 17, 222–224.
- (12) McNally, A. J., Pilcher, I. A., Wu, R., Salamone, S. J., Brewington, S., King, J. W., and Irving, J. (1996) Evaluation of the OnLine Immunoassay for Propoxyphene: Comparison to EMIT II and GC-MS. *J. Anal. Toxicol.* 20, 537–540.
- (13) Armbruster, D., Schwarzhoff, R., Pierce, B., and Hubster, E. (1993) Method Comparison of Emit II and OnLine with RIA for Drug Screening. *J. Forensic Sci.* 38 (6), 1326–1341.
- (14) Looney, C. E. (1984) High-sensitivity Light Scattering Immunoassays. *J. Clin. Immunoassay* 7, 90–95.
- (15) Adler, F. L., and Liu, C. T. (1971) Detection of Morphine by Hemaagglutination-inhibition. *J. Immunol.* 106 (6), 1684–1685.
- (16) Bradford, M. M. (1976) A Rapid and Sensitive Method for the Quantitative determination of Micrograms quantities of Protein Utilizing the Principal Protein-Dye Binding. *Anal. Biochem.* 72, 248–254.
- (17) Goldfarb, A. R. (1966) A Kinetic Study of the Reactions of Amino acids and Peptides with Trinitrobenzenesulfonic acid. *Biochem.* 5, 2570–2574.
- (18) Snyder, S. L., and Sobocinski, P. Z. (1975) An Improved 2,4,6-Trinitrobenzenesulfonic acid method for the Determination of Amines. *Anal. Biochem.* 64, 284–288.
- (19) Erlanger, B. F. (1980) The Preparation of Antigenic Hapten Carrier Conjugates: a Survey. *Methods Enzymol.* 70, 85–104.
- (20) Vaitukaitis, J. L. (1981) Production of Antisera with Small Dose of Immunogen. *Methods Enzymol.* 73B, 46–52.
- (21) Unpublished procedure.

CORRECTIONS

Volume 8, Number 3, May/June 1997.

Robert S. Wu,* A. J. McNally, Ian A. Pitcher, and
Salvatore J. Salamone

SYNTHESIS OF NEW *d*-PROPOXYPHENE
DERIVATIVES AND THE DEVELOPMENT OF A
MICROPARTICLE-BASED IMMUNOASSAY FOR
THE DETECTION OF PROPOXYPHENE AND
NORPROPOXYPHENE

The authors include as one of the authors on the paper
Shaker Rashid. The authors also gratefully acknowledge
Dr. Lili Arabshahi, Mr. Stephen Vitone, and Mr. Fauzi
Rashid for their technical assistance.

BC9702009

S1043-1802(97)00200-0

Published on Web 03/20/1998

Structural Determination of the Conjugate of Human Serum Albumin with a Mitomycin C Derivative, KW-2149, by Matrix-Assisted Laser Desorption/Ionization Mass Spectrometry

Tohru Yasuzawa and Kenneth B. Tomer*

Laboratory of Structural Biology, National Institute of Environmental Health Sciences, P.O. Box 12233, Research Triangle Park, North Carolina 27709. Received December 9, 1996[®]

A new mitomycin C derivative, KW-2149, is known to form a covalent conjugate with human serum albumin (HSA). This conjugate exhibits $1/20$ of the anticellular activity of unconjugated KW-2149. Structural studies of this conjugate were carried out using a combination of enzymatic digestion, high-performance liquid chromatography (HPLC), and matrix-assisted laser desorption/ionization (MALDI) mass spectrometry. The tryptic peptide T5 (residues 21–41) was the only peptide found to be modified by KW-2149 moieties, the [γ -L-glutamylamino]ethylthio group or the (2-aminoethyl)thio group, through a disulfide bond. Although the latter peptide lost its mitomycin C moiety in the course of tryptic digestion, these data strongly suggest that KW-2149 was bound to Cys-34, the only free cysteine on HSA.

INTRODUCTION

Drug–protein binding is one of the essential factors in analyzing pharmacokinetics because it can affect the distribution, metabolism, and excretion of a drug within the body. It is also known that one drug can compete with a second drug for the drug-binding site on serum proteins in man which is the case with clofibrate and warfarin (1). This drug substitution phenomenon can alter the drug concentration levels in blood, causing side effects in some cases. For this reason, identifying the drug-binding site on serum proteins of each drug is necessary for developing new drugs and using them safely.

A large number of small molecules, including many drugs, bind reversibly to serum proteins, which act as circulatory transporters (2). The most abundant protein in the human circulatory system is serum albumin (HSA). The protein (HSA, $M_r = 65K$) consists of a single, nonglycosylated, polypeptide containing 585 amino acids (Figure 1), one free thiol (Cys-34), and a total of 17 disulfide bridges (3, 4). The drug-binding sites of HSA have been well studied, and two major binding sites have been identified (5–9). It is known that some compounds, such as penicillin, acyl glucuronide, and glucose, bind covalently to HSA via transacylation or via the formation of a Schiff base at lysine or tyrosine residues (10–15). The cysteine residue is also a covalent binding site, to which biological thiols bind through a disulfide linkage (2).

Recently, a new mitomycin C derivative, KW-2149 (Figure 2), has been reported (16–20). This compound exhibits a broad spectrum antitumor activity in experimental tumor models, including mitomycin C-resistant tumors. It is also less hematotoxic than mitomycin C. The metabolic half-life of KW-2149 is very rapid with a $t_{1/2}$ of 9.7 min. One of the major metabolites of KW-2149 has been identified as the albumin conjugate (18). This conjugate still has $1/20$ of the anticellular activity of

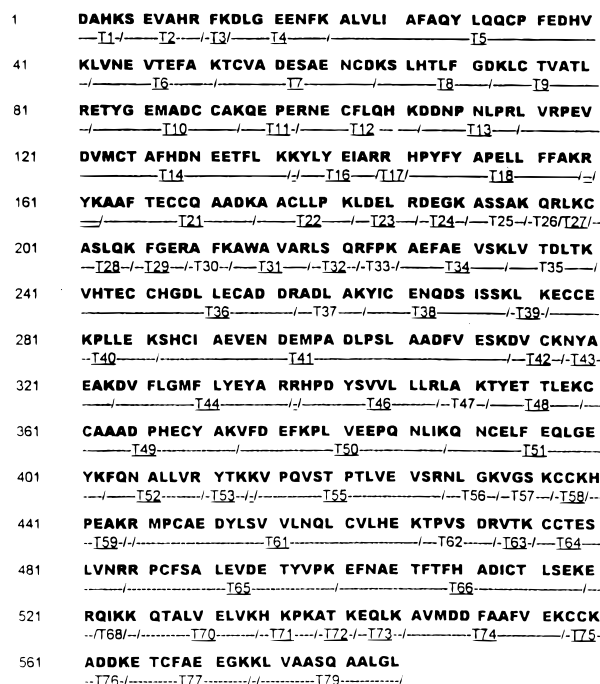


Figure 1. Amino acid sequence of HSA deduced from cDNA sequences by Putnam *et al.* (3). Underlined tryptic fragment labels indicate that the tryptic fragment was observed by MALDI-MS.

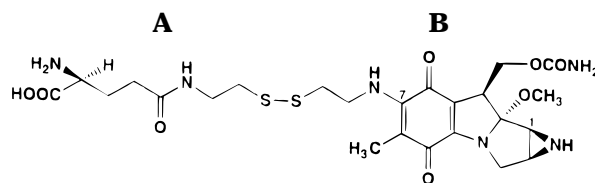


Figure 2. Chemical structure of KW-2149. This compound is composed of two sulfides, γ -L-glutamylcysteine and 7-N-(2-mercaptoethyl)mitomycin C. These two parts are described as left-half (A) and right-half (B) sulfides of KW-2149, respectively, in this paper.

unconjugated KW-2149. Because KW-2149 contains a disulfide bond, it is proposed that it binds to HSA at a

* Corresponding author. Phone: (919) 541-1966. Fax: (919) 541-7880. E-mail: tomer@niehs.nih.gov.

[®] Abstract published in *Advance ACS Abstracts*, May 1, 1997.

cysteine residue through formation of a disulfide linkage. There is a great interest in the structure of this conjugate in view of not only the drug-protein binding but also the activation mechanism of this mitomycin C-HSA disulfide. In the study of the activation mechanism of KW-2149, thiol molecules such as glutathione and cysteine were found to significantly enhance the cytotoxicity of this drug possibly through reduction of the disulfide moiety of KW-2149 to a sulfur ion which in turn activates the quinone ring to the corresponding semiquinone by an intramolecular reaction (21). The albumin conjugate of KW-2149 may be activated by the same mechanism. This proposed activation mechanism differs from that of mitomycin C which proceeds through reductive activation by DT-diaphorase and cytochrome P450 reductase (22, 23). The difference between the two activation mechanisms is thought to be the reason why KW-2149 is effective against mitomycin C-resistant tumors.

The formation of a conjugate with HSA which still has potent anticellular activity is one of the characteristic features of KW-2149. Understanding this phenomenon, and especially identifying the structure of the conjugate, are of great interest in the analysis of the pharmacokinetics of KW-2149, as well as in the study of the activation mechanisms of this drug. We have undertaken a study to determine the structure of the conjugate, including the position of attachment between KW-2149 and HSA, using a combination of enzymatic digestion, high-performance liquid chromatography (HPLC) separation, and matrix-assisted laser desorption/ionization mass spectrometry (MALDI-MS).

EXPERIMENTAL PROCEDURES

Chemicals and Materials. Human serum albumin (HSA), fraction V, fatty acid free, was purchased from Bayer Corp. (Kankakee, IL). Sequencing grade trypsin and carboxypeptidase P were purchased from Boehringer Mannheim GmbH (Indianapolis, IN). 7-*N*-[2-[[2-(γ -L-Glutamylamino)ethyl]dithio]ethyl]mitomycin C (KW-2149) was synthesized in the Pharmaceutical Research Laboratories, Kyowa Hakko Kogyo Co., Ltd. (Shizuoka, Japan). Acetonitrile, obtained from Fisher Scientific (Pittsburgh, PA), water, obtained from J. T. Baker (Phillipsburg, NJ), and trifluoroacetic acid (TFA), obtained from Pierce (Rockford, IL), were HPLC grade. Dithiothreitol (DTT) and α -cyano-4-hydroxycinnamic acid (CHCA) were purchased from Aldrich Chemical Co. (Milwaukee, WI). CHCA was recrystallized from methanol before using as a matrix. All other chemicals were of reagent grade. The Slide-A-Lyzer 10K dialysis cassettes (10 000 MW cutoff) were purchased from Pierce.

MALDI-TOF. MALDI mass spectra were obtained on a Voyager-RP time-of-flight mass spectrometer (PerSeptive Biosystems, Framingham, MA) in the linear mode with an accelerating voltage of 30 kV and a 1.3 m flight path. A saturated solution of α -cyano-4-hydroxycinnamic acid dissolved in EtOH/H₂O/HCO₂H (45:45:10, v/v/v) or water/acetonitrile (2:1, v/v) was used as a matrix. The instrument is equipped with a nitrogen laser operating at 337 nm. The spectra presented in this paper represent averages of 64 or 128 laser shots. To analyze the fragment ions that dissociate from the original ion in the flight tube, post-source decay (PSD) analysis was carried out using timed ion selection, which allows only ions of a selected mass of interest to pass to the detector, in the reflector mode (24). These PSD experiments are the reflectron time-of-flight equivalents of MS/MS experiments. The time-of-flight data were externally calibrated

using bovine serum albumin, horse heart cytochrome c, oxidized insulin B chain, angiotensin I, and CHCA as standards.

HPLC. Two model 6000A chromatographic pumps, a model 441 UV detector, and a model 660 solvent programmer (Waters, Milford, MA) were used for all HPLC analyses. Separations were carried out on a Protein C-4 (250 \times 4.6 mm inside diameter, 10 μ m particles) reverse phase column (Vydac, Hesperia, CA) using as solvents 0.1% TFA in water (A) and in acetonitrile (B) at a flow rate of 1 mL/min. The gradients used were 5 to 70% B over 20 min for the KW-2149-HSA conjugate and 0 to 65% B over 50 min for the tryptic digests of HSA and the KW-2149-HSA conjugate.

Preparation of the KW-2149-HSA Conjugate. HSA (240 mg, 3.61 mmol) and KW-2149 (10.8 mg, 18.1 μ mol) were dissolved in water (2.2 mL) and incubated at 37 $^{\circ}$ C for 24 h. After incubation, the protein was dialyzed against water at 4 $^{\circ}$ C for 12 h and then lyophilized.

Determination of the Binding Ratio of KW-2149 to HSA. The binding ratio of KW-2149 (mitomycin C moiety) to HSA was estimated by UV absorbance at 375 nm using KW-2149 as a calibration standard. The concentrations of the KW-2149 standard were 3, 6, 12, and 24 μ g/mL, and that of the KW-2149-HSA conjugate was 2 mg/mL.

Tryptic Digestion. To a solution of the KW-2149-HSA conjugate (2 mg) in 50 mM ammonium bicarbonate at pH 7.9 (0.5 mL) was added trypsin (14 μ g), and the solution was incubated at 37 $^{\circ}$ C for 24 h. The hydrolysis was stopped by lyophilization. The tryptic digestion of HSA was carried out in the same manner.

Carboxypeptidase P Digestion. To a solution of each conjugate between T5 and KW-2149 in 50 mM ammonium acetate at pH 4.7 (100 μ L) was added carboxypeptidase P (0.1 μ g), and the solution was incubated at room temperature. Aliquots of the solution (20 μ L) were taken at 5, 15, 30, and 60 min and 5 h and lyophilized. Each aliquot was redissolved in water (2 μ L) prior to analysis by MALDI-MS.

DTT Reduction of the Disulfide-Linked Peptides. To a solution of a disulfide-linked peptide in water (2 μ L) was added an excess amount of 50 mM DTT (2 μ L). Ambient air was displaced by nitrogen, and the sample, under nitrogen, was sealed, and allowed to stand overnight at room temperature. The reaction mixture (0.5 μ L) was mixed with the matrix solution (0.5 μ L) on the MALDI target and dried.

RESULTS AND DISCUSSION

Preparation of the Conjugate of KW-2149 with HSA. The conjugate of HSA with KW-2149 was prepared by incubating HSA with KW-2149 (molar ratio of 1:5 HSA:KW-2149) in water at 37 $^{\circ}$ C for 24 h. Figure 3A shows the HPLC chromatogram of the incubation mixture detected at 365 nm, characteristic of the mitomycin C chromophore. There is an absorption peak, peak b, just before 20 min, which corresponds to the retention time of HSA detected at 214 nm (data not shown). This peak did not disappear after dialysis with a 10K MW cutoff (Figure 3B). This evidence clearly shows the presence of covalent binding between HSA and a species containing the mitomycin C chromophore. Peak a is unchanged KW-2149, and the remaining peaks are removed by dialysis with a 10K MW cutoff, indicating they are low-molecular weight decomposition products. The ratio of the mitomycin C moiety to HSA, determined from a KW-2149 calibration curve, was in the range of 0.5–0.8, showing that the HPLC fraction is actually a

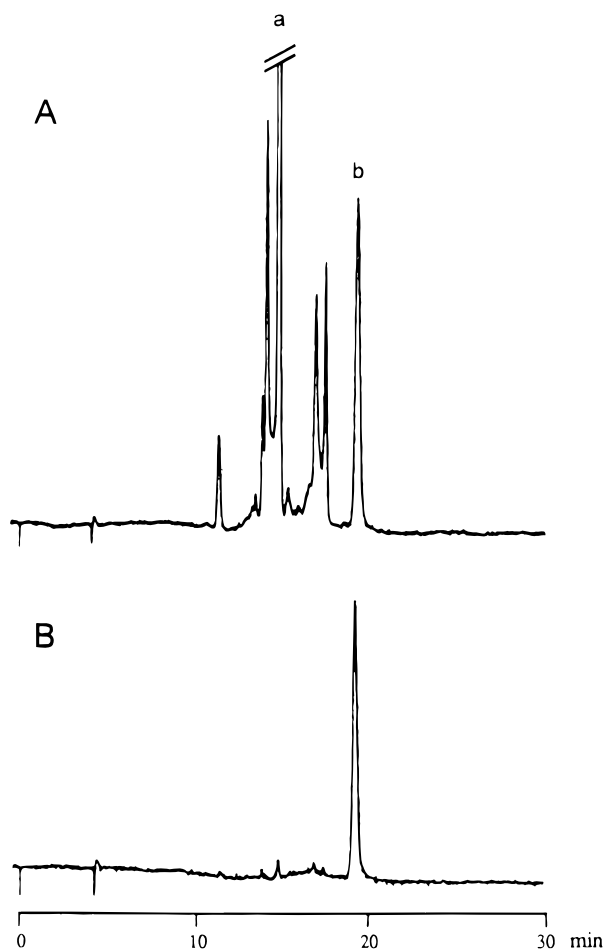


Figure 3. HPLC chromatogram of (A) the incubation mixture of HSA with KW-2149 and (B) that after dialysis detected at 365 nm. Peak a is unchanged KW-2149, peak b is the conjugate of HSA with KW-2149, and the other peaks are the decomposition products of KW-2149.

mixture of the KW-2149–HSA conjugate and intact HSA. The structural determination of the conjugate was performed without further purification. The obtained conjugate was analyzed by MALDI-MS using CHCA as a matrix. The observed molecular weight from the mean of five measurements of HSA was $66\,347.9 \pm 2.6$ (calcd, 66 438.2), and that of the reaction product (a mixture of conjugated and nonconjugated HSA) was $66\,513.9 \pm 8.6$. The shift in average mass also indicates that conjugation has occurred.

Peptide Mapping of HSA and the Conjugate Using MALDI Mass Spectra of an Unfractionated Tryptic Digest. As KW-2149 contains a disulfide bond, it was proposed that KW-2149 is linked to a cysteine residue(s) in HSA through a disulfide linkage which results from a disproportionation reaction between the two sulfides. To determine the position on HSA to which KW-2149 binds, tryptic digestions of intact and of KW-2149-linked HSA were performed, and peptide maps were obtained. These peptide maps, especially the disulfide-linked peptides, were compared.

HSA. Reduced HSA is predicted to give rise to 79 fragments by tryptic digestion (Figure 1). In nonreduced HSA, some of those peptides are linked through disulfide bonds (T9–T10–T12, T14–T21–T22, T28–T36, T38–T40–T41, T42–T49, T51–T58–T61–T64–T65, and T66–T75–T77). The tryptic peptides obtained by digestion of HSA were analyzed by MALDI (Figure 4A) using EtOH/H₂O/HCOOH as a solvent in target preparation. The peptides observed, including six of seven expected

disulfide-linked peptides, covered 396 amino acid residues in HSA. Using water/acetonitrile as a solvent for target preparation to obtain the peaks of small peptides, 34 more amino acids were determined (25). In total, 73% of the amino acid residues in HSA were identified by MALDI-MS of the unfractionated peptides, with 90% coverage obtained from a combination of analyses of fractionated and unfractionated peptides (Figure 1). T5, which contains the only free cysteine (Cys-34), and the largest disulfide-linked peptide, T51–T58–T61–T64–T65, were not observed. (T5 was, however, observed when the HSA tryptic digest was reduced with DTT prior to analysis). For the latter peptide, however, the smaller peptides corresponding to reductive cleavage of the disulfide linkage between T61 and T64 and between T58 and T61 (T51–T58–T61 and T61–T64–T65, respectively) as well as cleavage between each component peptide (T51, T61, T64, and T65) were observed. Such cleavages at disulfide linkage were also observed for the other disulfide-linked peptides.

As mentioned above, T5 was not observed in the MALDI spectrum of the tryptic digest of unmodified HSA. Because ions arising from T5 (including parts of KW-2149) and T51–T58–T61–T64–T65 were observed in the tryptic digest of the conjugate (see below), the nonobservation of T5 was not due to ionization/suppression effects in the peptide mixture or to the degradation of those molecular ions. It was therefore hypothesized that T5 existed in the tryptic digest of HSA as a set of mixed sulfides.

DTT reduction of the tryptic digest of HSA shifted the weights of almost all of the peptides previously observed above 3000 to lower weights (Figure 4C, T14, T36, T41, T65, and T66 and peaks around MW 2500 are enhanced), thus confirming that the original peaks resulted from disulfide-linked peptides.

In the tryptic digest of HSA (Figure 4A), there are several peaks between MW 3000 and 5000 (m/z 4772, 4446, 4307, 3454, and 3306) which can be assigned to disulfide-linked peptides which are not observed in the tryptic digest of the conjugate (Figure 4B). Some of these peaks correspond to disulfide-linked peptides of T5 with other cysteine–peptides. Also, the series of T51–T58–T61–T64–T65 ions observed in the conjugate digest (Figure 4B) were not observed in the spectrum of the HSA digest (Figure 4A). T5, which was also missing in the tryptic digest of HSA (Figure 4A), was clearly observed upon DTT reduction (Figure 4C), showing that this peptide existed as a disulfide-linked peptide prior to reduction. This evidence shows that, in the case of HSA, the disproportionation reaction between T5 and disulfide-linked peptides, especially T51–T58–T61–T64–T65 and related peptides, occurred during the course of the tryptic digestion, resulting in rather complex mixed disulfides.

These results are comparable to previous reports on the proteolytic mapping of HSA and of HSA adducts using mass spectral characterization by fast atom bombardment ionization (26–31) and by electrospray ionization (32, 33).

HSA-KW-2149 Conjugate. The MALDI mass spectrum of the tryptic digest of the HSA conjugate with KW-2149 differed from that of intact HSA, especially above MW 7000 (Figure 4B). Four new peaks were observed in that range (m/z 8113, 7793, 7542, and 7228) and were assigned to the disulfide-linked peptide T51–T58–T61–T64–T65 and to several peptides arising from incomplete cleavages. Furthermore, two peaks, m/z 2509 and 2637, were observed in the spectrum of the conjugate which were not observed in HSA itself. These two peaks could

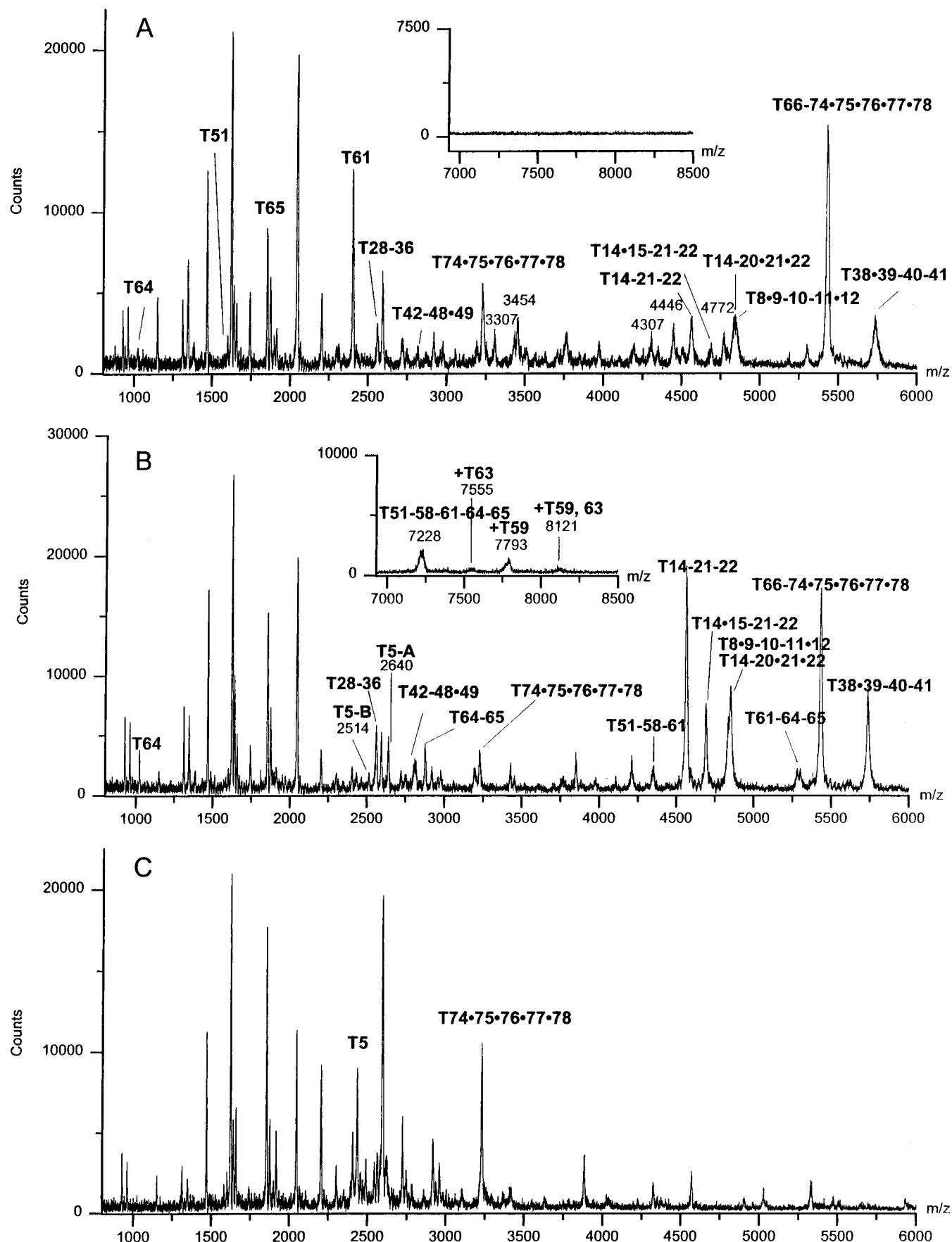


Figure 4. MALDI mass spectra of the tryptic digest of (A) HSA, (B) the KW-2149-HSA conjugate, and (C) that of HSA after DTT reduction. The dot and hyphen in the assignments indicate uncleaved peptides and disulfide bonds, respectively. The +T63, +T59, and +T59, 63 in the inset show the missed cleavages added to T51-T58-T61-T64-T65.

not be assigned to known tryptic fragments, but do correspond in weight to adducts of T5 with each sulfide

of KW-2149. Characterization of these two peaks by HPLC separation of the tryptic digest followed by MALDI-

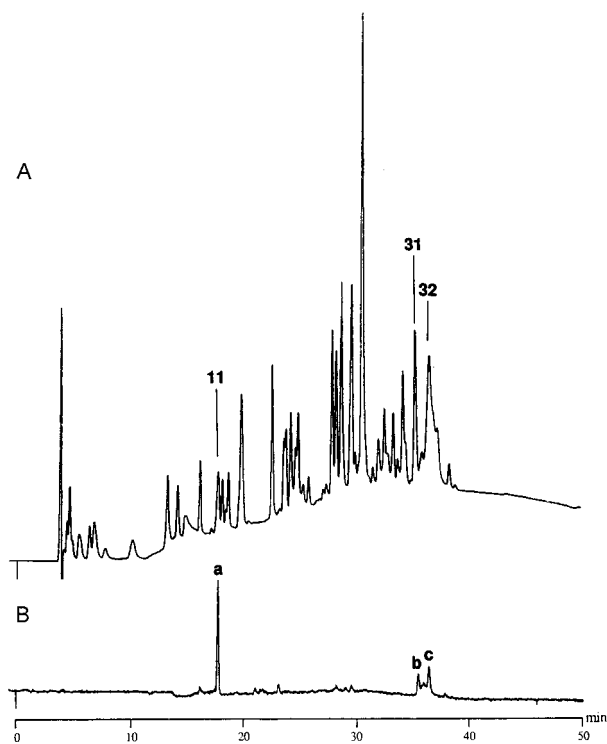


Figure 5. HPLC chromatogram of the tryptic digest of the KW-2149-HSA conjugate detected at (A) 214 nm and (B) 365 nm.

MS is detailed below. Eighty-two percent of the amino acid sequence of HSA was identified by the MALDI-MS of unfractionated tryptic peptides of the HSA conjugate.

Comparison of HPLC Fractionated Peptides from HSA and the Conjugate by MALDI-MS. To compare the tryptic peptides obtained from HSA with those obtained from the KW-2149-linked HSA in more detail, HPLC separations were carried out (Figure 5). Figure 5A shows the HPLC chromatogram of the tryptic digest of KW-2149-linked HSA detected at 214 nm. All peaks were collected, and the MALDI mass spectrum of each fraction was compared with that of the corresponding fraction from the tryptic digest of HSA (HPLC data not shown). The peaks which showed absorbance at 365 nm (Figure 5B) were also collected and analyzed by MALDI-MS. Although peak a is the major peak observed at 365 nm, no molecular ion corresponding to a possible KW-2149 conjugate was observed, but an ion corresponding to the protonated molecular ion of T71-72 was observed (peak a coeluted with peak 11 detected at 214 nm; see Figure 5). This peak also cochromatographed with that of the major degradation product of KW-2149 itself. The mass spectra of the other two peaks, peaks b and c, contained ions of m/z 44 019 and 67 039, respectively. The former corresponds to the peptide from residues 5-389, and the latter is unhydrolyzed KW-2149-HSA conjugate. Since there are no tryptic peptides found that absorb at 365 nm while the intact conjugate does, we postulate that the KW-2149-linked peptide was degraded to release the mitomycin C moiety during the course of tryptic digestion. The major difference in the chromatograms of HSA and of the conjugate detected at 214 nm is the presence of several peaks in the conjugate eluting between 30 and 34 min (Figure 5A), which were assigned to disulfide-linked peptides, including T51-T58-T61-T64-T65, by MALDI-MS. As for the MALDI-MS of the tryptic digest of HSA, no ion corresponding to the series of T51-T58-T61-T64-T65 peptides was observed in the MALDI mass spectra of any of the HPLC fractions.

These results are in agreement with those obtained from the unfractionated tryptic digest of HSA (Figure 4A).

The disulfide-linked peptides isolated by HPLC exhibited a characteristic pattern in MALDI-MS. Patterson and Katta reported that single disulfide-linked peptides gave molecular ions corresponding to their reduced-form peptides as well as ions corresponding to the intact peptides in MALDI-MS (34). The same phenomenon was observed in the multi-disulfide-linked peptides studied here as well. Figure 6A shows the MALDI mass spectrum of the tryptic peptide T51-T58-T61-T64-T65, in which five peptides are connected to each other through four disulfide linkages. All combinations of the reduced forms of the peptide except T58 were observed, proving unambiguously the structure of this peptide. T58 (M_r = 352) was not observed as is often the case with low-mass peptides (<500) under these MALDI conditions. The results obtained after DTT reduction confirm the components of this peptide (Figure 6B). By observation of the reduced-form ions, all disulfide-linked peptides present in the tryptic digests were identified.

The reduced-form ions could arise either from *in situ* reduction of the peptide or from fragmentation of the protonated molecular ion. To further investigate these possibilities, a post-source decay (24) spectrum of a peptide containing a single disulfide linkage, T28-T36, was obtained. Figure 7 shows the MALDI mass spectrum of T28-T36 and its post-source decay (PSD) spectrum. Two reduced-form ions attributable to T28 and to T36 are clearly observed in the MALDI mass spectrum. Neither of these ions is present in the PSD spectrum. Ions arising from amide bond cleavages from each C-terminal and C-S bond cleavages on each side of the disulfide group are observed. These data verify that the reduced-form ions did not arise through a gas phase process, in agreement with the result of Patterson and Katta (34).

Two additional disulfide-linked peptides, eluting between 35 and 37 min in Figure 5A, were observed in the HPLC chromatogram of the tryptic digest of KW-2149-linked HSA. The mass spectrum of fraction 31 showed a molecular ion at m/z 2637 and an accompanying reduced-form ion at m/z 2433. This could correspond to the conjugate of the tryptic peptide T5 with the left-half sulfide of KW-2149 (Figure 8, compound T5-A). DTT reduction eliminated the peak at m/z 2637 completely, but the peak at m/z 2433 still remained, confirming the structure as a disulfide-linked peptide. The second peptide was observed in fraction 32. The mass spectrum of this fraction showed a molecular ion at m/z 2509. This could correspond to the conjugate of T5 with 2-aminoethanethiol, the right-half sulfide of KW-2149 but without the mitomycin C group connected at its N-7 position (Figure 9, compound T5-B). The presence of m/z 2434 as well as the disappearance of m/z 2509 by DTT reduction supported the assignment of this disulfide-linked peptide. The presence of these two peptides indicates that a disproportionation reaction had occurred between HSA (Cys-34) and KW-2149 which formed two conjugates: HSA conjugated with γ -L-glutamylcysteamine and 7-N-(2-mercaptoethyl)mitomycin C. The latter conjugate then underwent bond cleavage at the N-7 position of mitomycin C during tryptic digestion. The mechanism of this bond cleavage is not clear. The presence, however, of the disulfide-linked peptide between T5 and cysteamine and the released mitomycin C chromophore detected at 365 nm in HPLC in the tryptic digest of the conjugate as well as the presence of 365 nm absorption in intact conjugate indicate that the whole

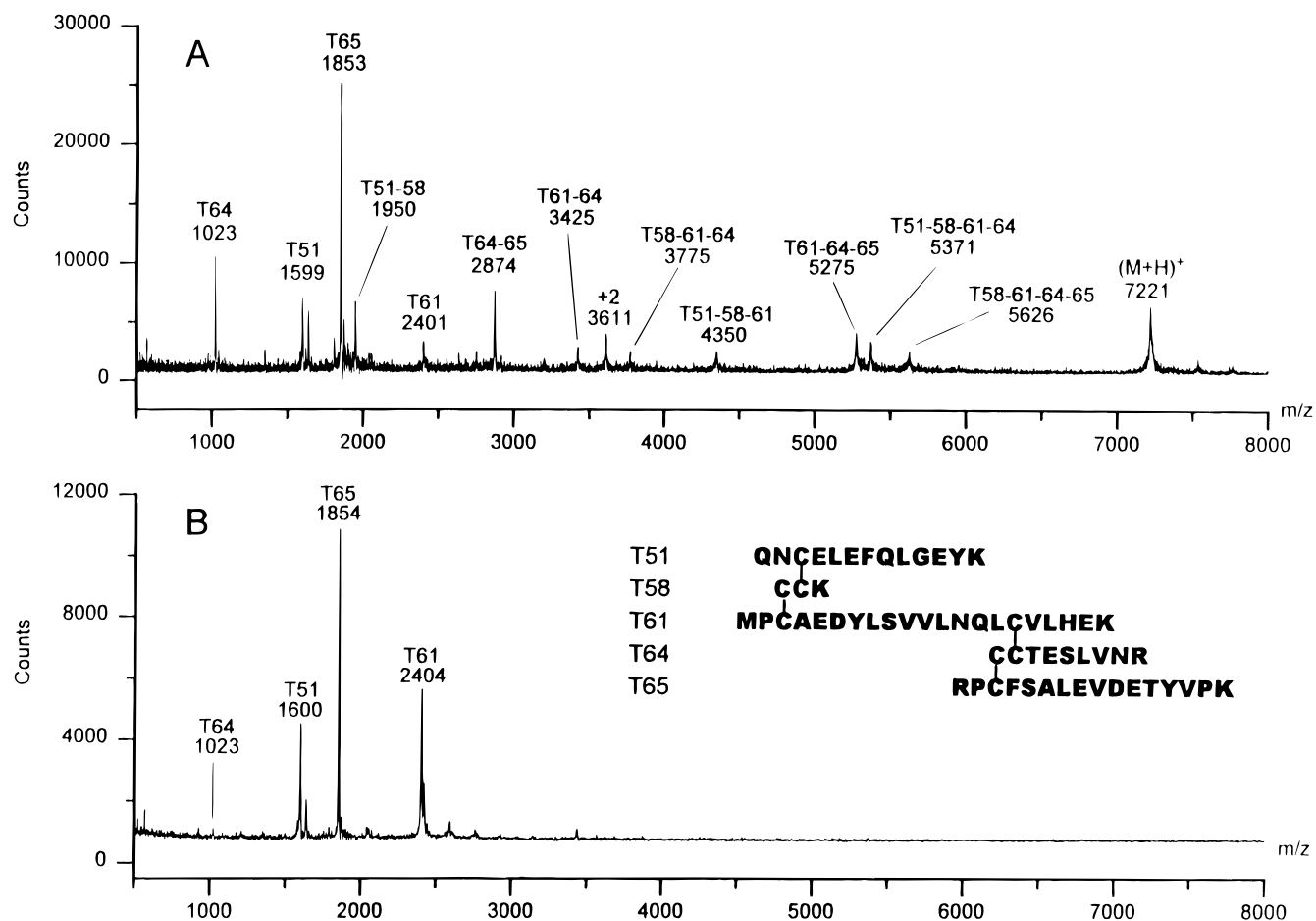


Figure 6. MALDI mass spectra of (A) HPLC peak 29 (T51–T58–T61–T64–T65) and (B) that after DTT reduction. The +2 indicates the doubly protonated molecular ion.

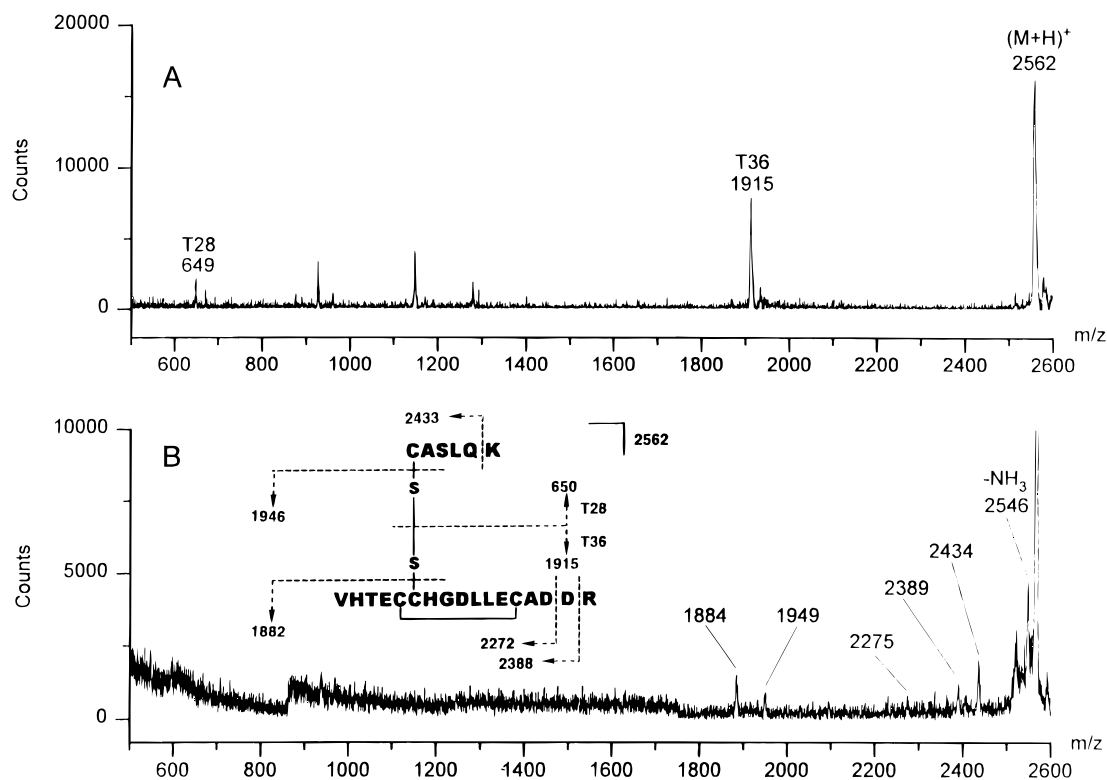


Figure 7. Comparison of (A) the spectrum of HPLC peak 17 (T28–T36) obtained in the linear mode and (B) the PSD spectrum of *m/z* 2562.

right-half sulfide of KW-2149 was originally linked to Cys-34 through a disulfide bond.

The structures of the two peptides proposed to be bound to the KW-2149 moieties were confirmed by

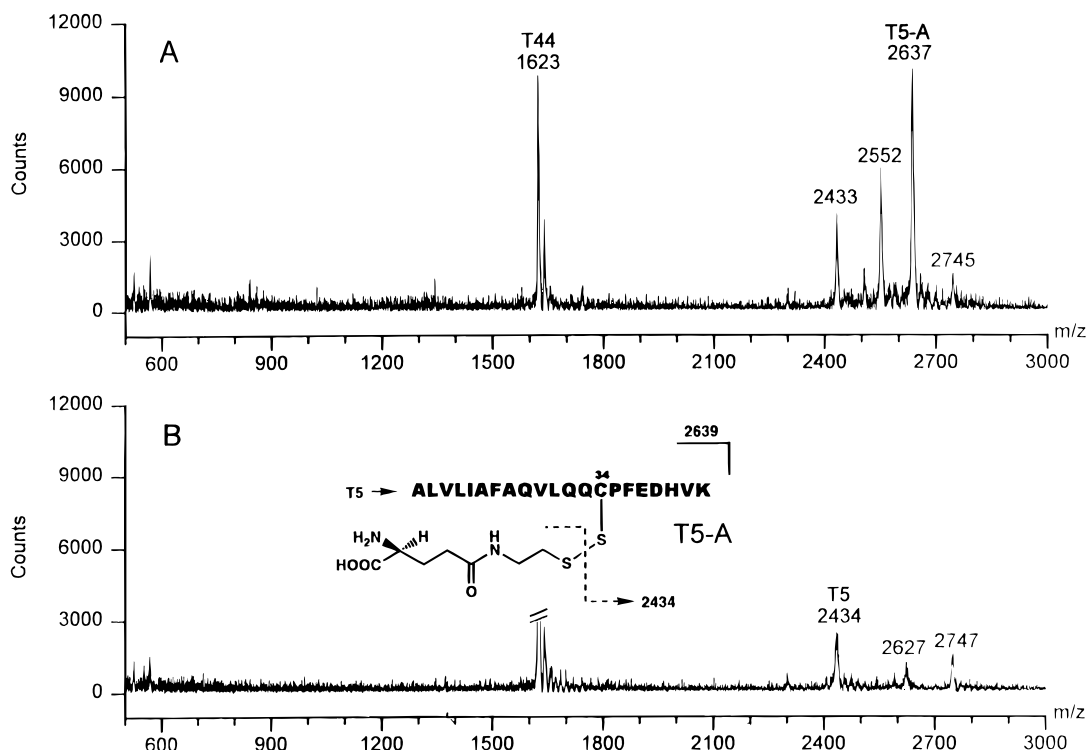


Figure 8. MALDI mass spectra of (A) HPLC peak 31 and (B) HPLC peak 31 after DTT reduction. This fraction contains several peptides as well as T5-A.

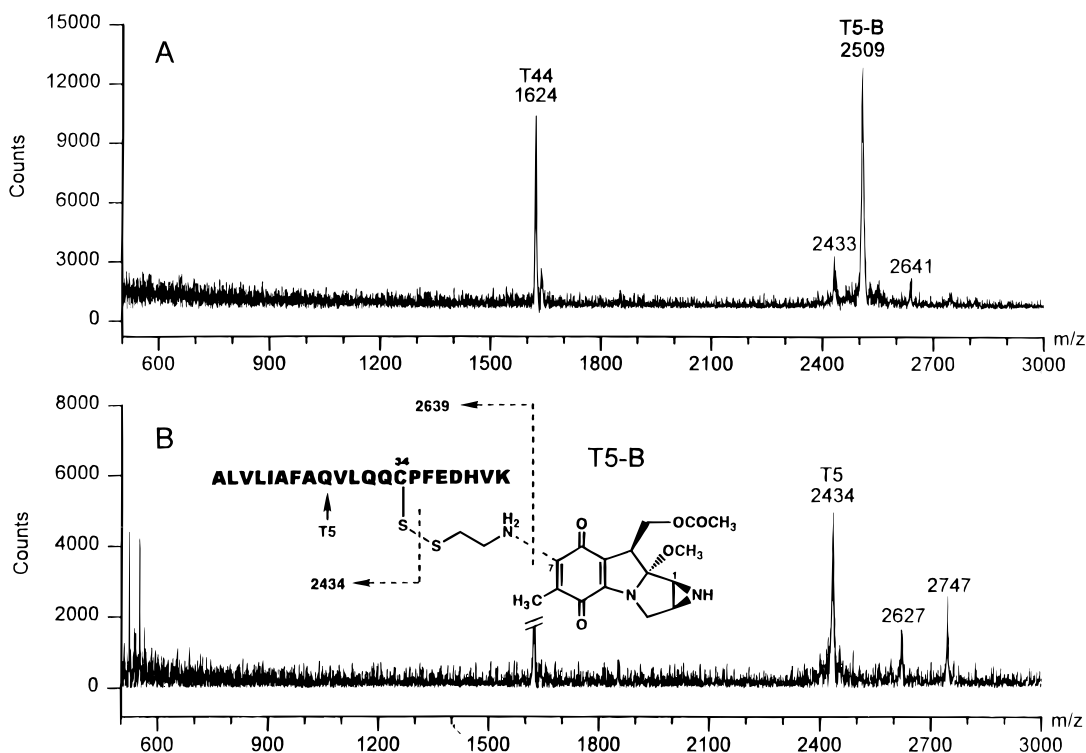


Figure 9. MALDI mass spectra of (A) HPLC peak 32 and (B) HPLC peak 32 after DTT reduction. This fraction contains several peptides as well as T5-B.

carboxypeptidase Y C-terminal sequencing which was followed by MALDI-MS. Losses of up to four residues (DHVK-COOH) in the T5- γ -L-glutamylcysteamine disulfide (T5-A) and up to five residues (EDHVK-COOH) in the T5-cysteamine disulfide (T5-B) were identified.

Because no other peptide containing the KW-2149 moiety was found, Cys-34 was determined to be the only site where KW-2149 was linked to HSA. It has been reported that Cys-34 in HSA has the most reactive sulfhydryl group (pK_{SH} of 5) among serum proteins and

is easily oxidized by biological thiols such as cysteine and glutathione (2, 35). From this point of view, it is reasonable to expect that the disulfide in KW-2149 can be a good oxidant for free sulfhydryl (Cys-34) in formation of the mixed KW-2149-HSA complex.

Summary. KW-2149 is a new mitomycin C derivative which shows a superior antitumor activity and less hematotoxicity, as well as a different activation mechanism compared with that of mitomycin C. In the study of the drug metabolism of KW-2149 in mice, three active

metabolites had been found. One of them, the albumin conjugate, was thought to be composed of disulfide linkage(s) between cysteine in HSA and the sulfide group in KW-2149, but there was no chemical evidence up to now for this structure. In the experiments described in this report, we determined that both halves of the disulfide in KW-2149 are linked to Cys-34 through new disulfide bonds. This structure clearly shows the possibility that the mitomycin C moiety in the conjugate, the active pharmacophore, can easily be released by biological thiols such as glutathione, cysteine, and other thiol molecules. This chemical evidence provides what appears to be useful information for further studies of the mechanism of action and/or pharmacokinetic studies of this drug.

LITERATURE CITED

- (1) Bjornsson, T. D., Meffin, P. J., Swezey, S., and Blaschke, T. F. (1979) Clofibrate Displaces Warfarin from Plasma Protein in Man: An Example of a Pure Displacement Interaction. *J. Pharmacol. Exp. Ther.* **20**, 316–321.
- (2) Carter, D. C., and Ho, J. X. (1994) Structure of Serum Albumin. *Adv. Protein Chem.* **45**, 153–203.
- (3) Takahashi, N., Takahashi, Y., Blumberg, B. S., and Putnam, F. W. (1987) Amino Acid Substitutions in Genetic Variants of Human Serum Albumin and in Sequences Inferred from Molecular Cloning. *Proc. Natl. Acad. Sci. U.S.A.* **84**, 4413–4417.
- (4) He, X. M., and Carter, D. C. (1992) Atomic Structure and Chemistry of Human Serum Albumin. *Nature* **358**, 209–215.
- (5) Sudlow, G., Birkett, D. J., and Wade, D. N. (1975) The Characterization of Two Specific Drug Binding Sites on Human Serum Albumin. *Mol. Pharmacol.* **11**, 824–832.
- (6) Sudlow, G., Birkett, D. J., and Wade, D. N. (1976) Further Characterization of Specific Drug Binding Sites on Human Serum Albumin. *Mol. Pharmacol.* **12**, 1052–1061.
- (7) Sjöholm, I., Ekman, B., Kober, A., Ljungstedt-Pahlman, I., Seiving, B., and Sjödin, T. (1979) Binding of Drugs to Human Serum Albumin: XI. The Specificity of Three Binding Sites as Studied with Albumin Immobilized in Microparticles. *Mol. Pharmacol.* **16**, 767–777.
- (8) Fehske, K. J., Schlafer, U., Wollert, U., and Muller, W. E. (1982) Characterization of an Important Drug Binding Area on Human Serum Albumin Including the High-Affinity Binding Sites of Warfarin and Azapropazone. *Mol. Pharmacol.* **21**, 387–393.
- (9) Yamasaki, K., Miyoshi, T., Maruyama, T., Takadate, A., and Otagiri, M. (1994) Characterization of Region Ic in Site I on Human Serum Albumin. Microenvironmental Analysis Using Fluorescence Spectroscopy. *Biol. Pharm. Bull.* **17**, 1656–1622.
- (10) Rocha, J., Bohner, J., and Kompf, J. (1995) Transient Bisalbuminemia: Separation by Isoelectric Focusing of Human Albumin Fractions Linked to Different Numbers of Benzylpenicilloyl Groups. *Electrophoresis* **16**, 1031–1033.
- (11) Dickinson, R. G., Baker, P. V., and King, A. R. (1994) Studies on The Reactivity of Acyl Glucuronides VII. Salicyl Acyl Glucuronide Reactivity In Vitro and Covalent Binding of Salicylic Acid to Plasma Protein of Humans Taking Aspirin. *Biochem. Pharmacol.* **47**, 469–476.
- (12) Grubb, N., Weil, A., and Caldwell, J. (1993) Studies on the In Vitro Reactivity of Clofibril and Fenofibril Glucuronides. Evidence for Protein Binding via a Schiff's Base Mechanism. *Biochem. Pharmacol.* **46**, 357–364.
- (13) Bohnet, J. P., Fonda, M. L., and Feldhoff, R. C. (1992) Identification of Lys190 as the Primary Binding Site for Pyridoxal 5'-Phosphate in Human Serum Albumin. *FEBS Lett.* **298**, 266–268.
- (14) Wells, D. S., Janssen, F. W., and Ruelius, H. W. (1987) Interactions Between Oxaprozin Glucuronide and Human Serum Albumin. *Xenobiotica* **17**, 1437–1449.
- (15) Tsuchiya, S., Sakurai, T., and Sekiguchi, S. (1984) Non-enzymatic Glucosylation of Human Serum Albumin and Its Influence on Binding Capacity of Sulfonyleureas. *Biochem. Pharmacol.* **33**, 2967–2971.
- (16) Kono, M., Saitoh, Y., Kasai, M., Sato, A., Shirahata, K., Morimoto, M., and Ashizawa, T. (1989) Synthesis and Antitumor Activity of a Novel Water Soluble Mitomycin Analog: 7-N-[2-[[2-(γ -L-glutamylamino)ethyl]dithio]ethyl]mitomycin C. *Chem. Pharm. Bull.* **37**, 1128–1130.
- (17) Morimoto, M., Ashizawa, T., Ohno, H., Azuma, M., Kobayashi, E., Okabe, M., Gomi, K., Kono, M., Saito, Y., Kanda, Y., Arai, H., Sato, A., Kasai, M., and Tsuruo, T. (1991) Antitumor Activity of 7-N-[2-[[2-(γ -L-glutamylamino)ethyl]dithio]ethyl]mitomycin C (KW-2149), Against Murine and Human Tumors and a Mitomycin C-resistant Tumor in Vitro and In Vivo. *Cancer Res.* **51**, 110–115.
- (18) Kobayashi, S., Ushiki, J., Takai, K., Okumura, S., Kono, M., Kasai, M., Gomi, K., Morimoto, M., Ueno, H., and Hirata, H. (1993) Disposition and Metabolism of KW-2149, a Novel Anticancer Agent. *Cancer Chemother. Pharmacol.* **32**, 143–150.
- (19) Ashizawa, T., Okabe, M., Gomi, K., and Hirata, T. (1993) Reduced Bone Marrow Toxicity of KW-2149, a Mitomycin C Derivative, in Mice. *Anticancer Drugs* **4**, 181–188.
- (20) Fujii, N., Arai, H., Saito, H., Kasai, M., and Nakano, H. (1993) Induction of Protein-DNA Complexes in HeLa S3 Cells by KW-2149, a New Derivative of Mitomycin C. *Cancer Res.* **53**, 4466–4468.
- (21) Lee, J. H., Naito, M., and Tsuruo, T. (1994) Nonenzymatic Reductive Activation of 7-N-[2-[[2-(γ -L-glutamylamino)ethyl]dithio]ethyl]mitomycin C by Thiol Molecules: a Novel Mitomycin C Derivative Effective on Mitomycin C-Resistant Tumor Cells. *Cancer Res.* **54**, 2398–2403.
- (22) Bligh, H. F., Bartozek, A., Robson, C. N., Hickson, I. D., Kasper, C. B., Beggs, J. D., and Wolf, C. R. (1990) Activation of Mitomycin C by NADPH: Cytochrome P-450 Reductase. *Cancer Res.* **50**, 7789–7792.
- (23) Siegel, D., Beall, H., Senekowitsch, C., Kasai, M., Arai, H., Gibson, N. W., and Ross, D. (1992) Bioreductive Activation of Mitomycin C by DT-Diaphorase. *Biochemistry* **31**, 7879–7885.
- (24) Kaufmann, R., Spengler, B., and Lutzenkirchen, F. (1993) Mass Spectrometric Sequencing of Linear Peptides by Product-ion Analysis in a Reflectron Time-of-flight Mass Spectrometer Using Matrix-assisted Laser Desorption Ionization. *Rapid Commun. Mass Spectrom.* **7**, 902–910.
- (25) Cohen, S. L., and Chait, B. T. (1996) Influence of Matrix Solution Conditions on the MALDI-MS Analysis of Peptides and Proteins. *Anal. Chem.* **68**, 31–37.
- (26) Ding, A., Ojingwa, J. C., McDonagh, A. F., Burlingame, A. L., and Benet, L. Z. (1993) Evidence for Covalent Binding of Acyl Glucuronides to Serum Albumin via an Imine Mechanism as Revealed by Tandem Mass Spectrometry. *Proc. Natl. Acad. Sci. U.S.A.* **90**, 3797–3801.
- (27) Finch, J. W., Crouch, R. K., Knapp, D. R., and Schey, K. L. (1993) Mass Spectrometric Identification of Modifications to Human Serum Albumin Treated with Hydrogen Peroxide. *Arch. Biochem. Biophys.* **305**, 595–599.
- (28) Campagnini, A., Fisichella, S., Foti, S., Saletti, R., and Sardo, L. (1994) Tryptic Peptide Mapping of Sequence 1–298 of Human Serum Albumin by High-Performance Liquid Chromatography and Fast-Atom Bombardment Mass Spectrometry. *Rapid Commun. Mass Spectrom.* **8**, 459–464.
- (29) Fisichella, S., Foti, S., Maccarrone, G., and Saletti, R. (1995) Tryptic Peptide Mapping of Sequence 299–585 of Human Serum Albumin by High-Performance Liquid Chromatography and Fast Atom Bombardment Mass Spectrometry. *J. Chromatogr. A* **693**, 33–44.
- (30) Ding, A., Zia-Amirhosseini, P., McDonagh, A. F., Burlingame, A. L., and Benet, L. Z. (1995) Reactivity of Tolmetin Glucuronide with Human Serum Albumin. Identification of Binding Sites and Mechanisms of Reaction by Tandem Mass Spectrometry. *Drug Metab. Dispos.* **23**, 369–376.
- (31) Zia-Amirhosseini, P., Ding, A., Burlingame, A. L., McDonagh, A. G., and Benet, L. Z. (1995) Synthesis and Mass-Spectrometric Characterization of Human Serum Albumins Modified by Covalent Binding of Two Non-steroidal Anti-inflammatory Drugs: Tolmetin and Zomepirac. *Biochem. J.* **311**, 431–435.

- (32) Day, B. W., Skipper, P. L., Zaia, J., Singh, K., and Tannenbaum, S. R. (1994) Enantiospecificity of Covalent Adduct Formation by Benzo[a]pyrene *anti*-Diol Epoxide with Human Serum Albumin. *Chem. Res. Toxicol.* 7, 829–835.
- (33) Clerc, F. F., Monegier, B., Faucher, D., Pourcet, C., Holt, J. C., Tang, S. Y., Van Dorsselaer, A., Becquart, J., and Vuilhorgne, M. (1994) Primary Structure Control of Recombinant Proteins Using High-Performance Liquid Chromatography, Mass Spectrometry and Microsequencing. *J. Chromatogr., B: Biomed. Appl.* 662, 245–259.
- (34) Patterson, S. D., and Katta, V. (1994) Prompt Fragmentation of Disulfide-Linked Peptides during Matrix-Assisted Laser Desorption Ionization Mass Spectrometry. *Anal. Chem.* 66, 3727–3732.
- (35) Pedersen, A. O., and Jacobsen, J. (1980) Reactivity of The Thiol Group in Human and Bovine Albumin at pH 3–9, As Measured by Exchange with 2,2'-dithiodipyridine. *Eur. J. Biochem.* 106, 291–295.

BC970038+

Electrospray Mass Spectrometry of α and β Chains of Selected Hemoglobins and Their TNBA and TNB Conjugates

Maciej Adamczyk* and John C. Gebler

Department of Chemistry (D9NM), Abbott Laboratories, Diagnostics Division, Building AP-20, 100 Abbott Park Road, Abbott Park, Illinois 60064. Received December 4, 1996[®]

The molecular weights of α and β hemoglobin chains from 15 different vertebrate animal sources and 2 common human variants were determined by electrospray mass spectrometry and compared to the calculated masses based on published amino acid sequences. Conjugates were prepared for 14 of the globins using 2 traditional colorimetric derivatizing reagents, 5,5'-dithiobis(2-nitrobenzoic acid) (DTNB) and trinitrobenzenesulfonic acid (TNBS), and the mass of each conjugate was determined by mass spectrometry.

INTRODUCTION

Hemoglobin (Hb)¹ is the major interplasmic protein of vertebrate red blood cells. Its primary function is O₂ and CO₂ transport (1). In its native state, Hb from vertebrates is a tightly folded tetrameric protein comprised of the noncovalent association of two similar chains (2 α 2 β) and heme (2). Typical denaturing conditions such as heat, acid, or organic solvents will dissociate Hb into the individual components (heme, α and β globins). Due to its critical biological function, high abundance, and ease of isolation, Hb is one of the most intensely studied proteins.

The most fundamental characteristic of Hb is its primary amino acid sequence which corresponds to a specific molecular weight. Primary sequences for many Hbs were determined by polypeptide degradation/peptide sequencing or DNA/RNA sequencing. Reported molecular weights for α and β Hb chains were calculated from the amino acid sequences. Traditionally, gel electrophoresis has been used to verify Hb molecular weight; however, its limited resolution (~5%) is not suitable for primary sequence verification (3). Moreover, detailed studies of mutations, amino acid modifications, or protein homogeneity cannot be accurately examined by electrophoresis.

Over the past several years, electrospray ionization mass spectrometry (ESI-MS) has become a powerful means of determining the molecular weight of peptides and proteins to ~200 kDa with a precision $\leq 0.01\%$. ESI-MS is a nondestructive ionization technique which typically gives only ions of the intact parent compound. The principle of ionization and mass analysis by ESI-MS is described in several excellent review articles (4). ESI-MS along with other mass spectrometry techniques has been utilized for detailed studies of human Hbs and their variants (5).

In this work, we describe the use of ESI-MS for the characterization of α and β Hb chains from selected species. In addition, we demonstrate the usefulness of ESI-MS to assess the effects of two traditional derivatizing reagents, DTNB and TNBS, used for the colorimetric quantification of cysteines and lysines. We prepared thionitrobenzoic acid (TNBA) and trinitrobenzene (TNB) conjugates with 14 of the Hbs and measured the molecular weight of each new conjugate by ESI-MS. This information allowed us to determine the number of TNBA or TNB groups attached to each globin.

MATERIALS AND METHODS

Hemoglobins from baboon, bovine, cat, dog, garter snake, goat, horse, human A₀,² human A₂,³ human S,⁴ mouse, pig, pigeon, rabbit, rat, sheep, and turkey, and BSA and horse heart myoglobin were obtained from Sigma (St. Louis, MO). 5,5'-Dithiobis(2-nitrobenzoic acid) was purchased from Pierce (Rockford, IL), and 2,4,6-trinitrobenzenesulfonic acid, sodium salt, was from Aldrich Chemical Co. (Milwaukee, WI). All other chemicals and solvents were of the highest purity available. HPLC was carried out on a Microtech Scientific (Sunnyvale, CA) binary microbore LC system employing a Polymer Laboratories (Amherst, MA) PLRP-S 8 μ m 1000 Å 50 \times 2.1 mm column. Mass spectra were recorded on a Perkin Elmer Sciex API 100 single quadrupole mass spectrometer equipped with a heated pneumatically-assisted ion source (TurboIonSpray). The ESI-MS was calibrated just prior to analysis using the manufacturer's protocols and calibration solutions (0.1 mM PPG 1000, 0.2 mM PPG 2000, 0.1% formic acid, and 2 mM ammonium acetate in 1:1 water/methanol). The calibration solutions provide ions throughout the mass range from 350 to 2400 amu. Accuracy and precision were determined using horse heart myoglobin and BSA by infusion of each protein (0.1 mg/mL in 0.1% formic acid, 2 mM ammonium formate, and 20% acetonitrile) directly into the instrument's ion source at a flow rate of 50 μ L/min. All spectra were collected using multi-scan-averaging (10 scans for myoglobin and 20 scans for BSA).

Spectra for each Hb were obtained on 2 μ L of a 1 mg/mL solution (~125 pmol) in 0.1% formic acid. Samples were injected into the HPLC column and eluted with a

* Correspondence should be addressed to this author. Telephone: (847) 937-0225. Fax: (847) 938-8927. E-mail: adamczykkm@apmac.abbott.com.

[®] Abstract published in *Advance ACS Abstracts*, May 1, 1997.

¹ Abbreviations: BSA, bovine serum albumin; CZE, capillary zone electrophoresis; DTNB, 5,5'-dithiobis(2-nitrobenzoic acid); ESI-MS, electrospray ionization mass spectrometry; Hb, hemoglobin; Hbs, hemoglobins; HPLC, high-performance liquid chromatography; LC, liquid chromatography; PPG, poly(propylene glycol); SDS, sodium salt of dodecyl sulfate; TNB, trinitrobenzene; TNBA, thionitrobenzoic acid; TNBS, trinitrobenzenesulfonic acid.

² Normal human Hb.

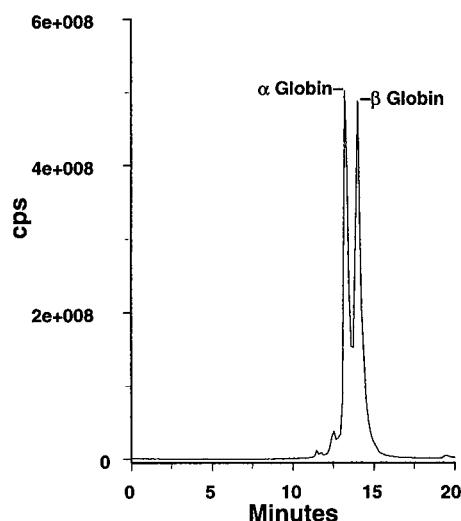
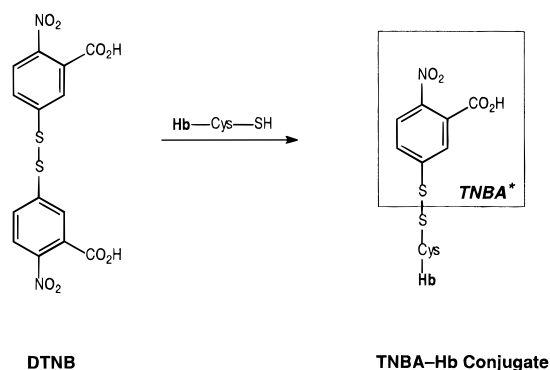
³ Purified minor human Hb A₂ comprised of (2 α 2 δ).

⁴ Purified Hb from humans with sickle cell disease (β chain mutation A6T).

Table 1. Calculated versus Observed Molecular Weights of α and β Globins of Various Hemoglobins

source (references)	calculated ^a		observed by ESI-MS	
	α globin	β globin	α globin	β globin
baboon (24, 25)	15435.7	15895.2	15435.4 \pm 1.0	15894.1 \pm 1.2
bovine (26, 27)	15053.1	15954.4	15053.5 \pm 1.1	15954.9 \pm 1.5
cat (21)	15305.4	(β -A) 15926.2 (β -B) 15943.1	15305.7 \pm 1.9	(β -A) 15924.9 \pm 2.1 (β -B) 15941.6 \pm 2.5
dog (28)	(α -I) 15217.3 (α -II) 15247.3	15996.3	(α -I) 15217.8 \pm 1.8 (α -II) 15247.2 \pm 1.0	15995.8 \pm 1.0
garter snake	na ^b	na	15445.4 \pm 1.9 15802.6 \pm 0.6	16028.3 \pm 1.6
goat (29, 30)	(α -I) 15033.1 (α -II) 15060.1	16021.4	(α -I) 15033.3 \pm 1.2 (α -II) 15060.0 \pm 2.0	16021.8 \pm 1.0
horse (31)	15114.3	16008.3	15115.1 \pm 1.2	16008.2 \pm 0.6
human A ₀ (32)	15126.3	15867.2	15126.7 \pm 1.4	15867.4 \pm 0.7
human A ₂ (33)	15126.3	(δ) 15924.3	15126.8 \pm 0.9	15922.8 \pm 1.3
human S (34)	15126.3	15837.2	15126.0 \pm 1.0	15836.4 \pm 0.5
mouse (35)	14995.0	(major) 15616.8 (minor) 15709.0	14995.9 \pm 1.5	(major) 15617.2 \pm 1.3 (minor) 15708.3 \pm 1.7
pig (36)	15039.1	16035.3	15040.2 \pm 1.2	16035.6 \pm 1.3
pigeon (14, 15, 16)	15123.2	16152.6	15117.1 \pm 0.6 15150.2 \pm 1.2	16164.0 \pm 0.3
rabbit (37, 38)	15457.6	16001.3	15458.5 \pm 0.9	16006.2 \pm 1.6
rat (39)	15197.3	15848.2	15197.6 \pm 1.1	15848.7 \pm 1.3
sheep (40, 41)	15047.1	16073.4	15047.0 \pm 0.6	16074.2 \pm 1.0
turkey (17)	(α^A) 15309.7 (α^D) 15649.8	16306.8	(α^A) 15308.5 \pm 2.1 (α^D) 15767.0 \pm 1.0	16304.7 \pm 1.3

^a Molecular weights were determined from primary amino acid sequences downloaded from electronic databases (see footnotes 5 and 6). ^b na, not available.

**Figure 1.** Total ion count (TIC) chromatograph from LC/ESI-MS of bovine Hb.**Scheme 1**

linear gradient of 10% acetonitrile in 0.1% TFA to 100% acetonitrile in 20 min at a flow rate of 100 μ L/min. The column output was directly linked to the ESI-MS ion source. ESI-MS operating parameters were as follows: interface auxiliary air flow of 4–5 L/min at 350 $^{\circ}$ C and

nebulizer air flow 1.5 L/min; ion spray 4500 V; counter-electrode (curtain plate) 1000 V; and orifice-to-skimmer potential difference 30 V. The instrument scanned a range of 650–1450 m/z in 0.1 amu steps for a total scan time of 8 s. The resulting spectra were “reconstructed” (deconvoluted) based on the Bayesian statistical analysis of the entire spectrum using the manufacturer’s software (BioMultiview version 1.2) which gave the results as true mass. No other data manipulation such as smoothing, noise filtering, or enhancement was employed. For presentation of spectra, files worked up in BioMultiview were imported as ASCII text files and then graphed and labeled using Axum (version 5.0 for Windows, Math Soft, Cambridge, MA).

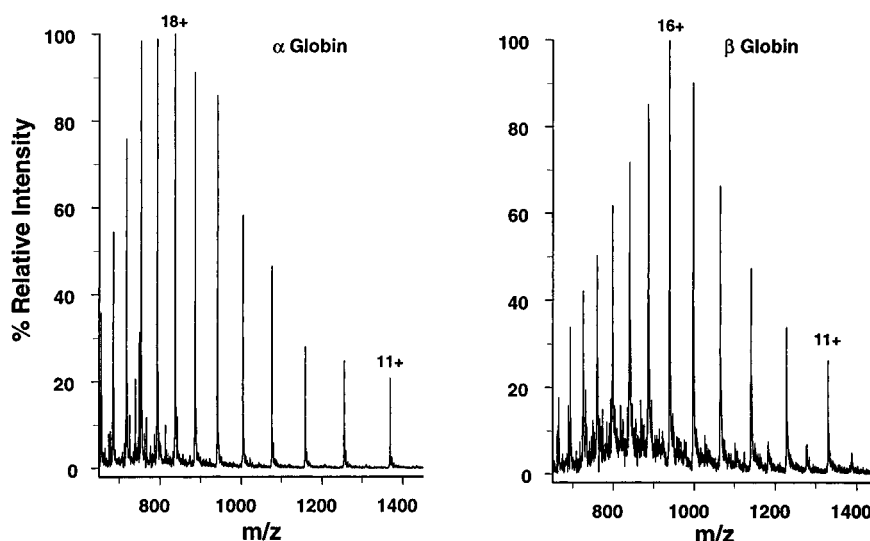
Conjugation with DTNB was carried out using a modified method of Ellman (6). To Hb solutions (50 μ L of 1 mg/mL in 100 mM phosphate buffer, pH 8.0) was added a solution of DTNB (50 μ L of 4 mg/mL in H₂O). The reaction mixture was incubated for 15 min at ambient temperature and then directly analyzed by LC-ESI-MS using the protocol for unmodified Hbs described earlier. The number of attached TNBA groups was determined from the equation:

$$\text{no. of TNBA groups in conjugate} = \frac{\text{TNBA conjugate mol wt} - \text{native Hb mol wt}}{\text{mol wt of TNBA group}}$$

Conjugation with TNBS was based on a modified method of Kakade et al. (7). To Hb solutions (100 μ L of \sim 1 mg/mL in 4% aqueous sodium bicarbonate) was added a solution of TNBS (100 μ L of 1 mg/mL in water). The reaction mixture was incubated at 37 $^{\circ}$ C for 2 h and then treated with hydrochloric acid (100 μ L, 1 N) and SDS solution (100 μ L, 10% w/v). The reaction mixture was directly analyzed by LC/ESI-MS using the protocol for unmodified Hbs previously described. The number of attached TNB groups was determined from the equation:

$$\text{no. of TNB groups in conjugate} = \frac{\text{TNB conjugate mol wt} - \text{native Hb mol wt}}{\text{mol wt of TNB group}}$$

A.



B.

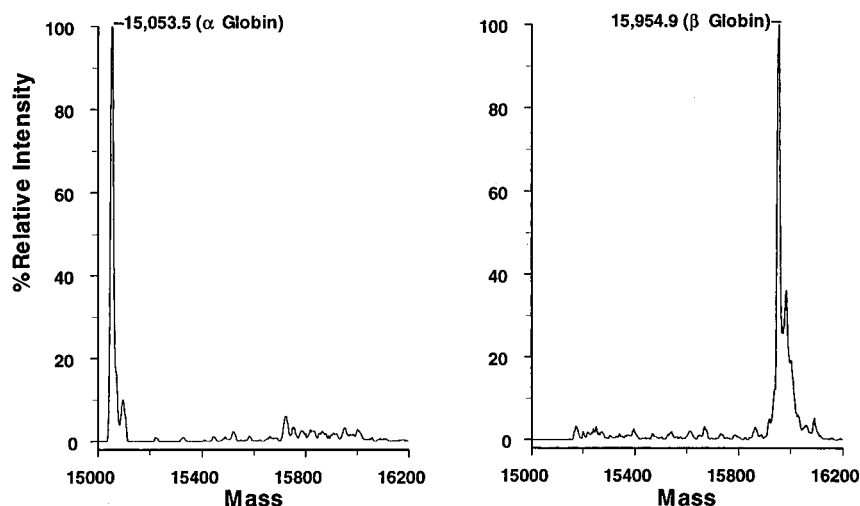


Figure 2. (A) Mass spectra for bovine Hb α and β globins. (B) Deconvoluted mass spectra for bovine Hb α and β globins.

RESULTS AND DISCUSSION

Molecular weight estimation was carried out on a single quadrupole electrospray mass spectrometer equipped with a heated pneumatically-assisted ion source interfaced with a microbore HPLC system. Typical ESI-MS instrumentation has a precision of $\leq 0.01\%$. Adopting the method of Feng et al. (8), we calibrated the instrument with a mixture of two poly(propylene glycol) solutions (average molecular weight of 1000 and 2000) employing multichannel averaging to improve signal-to-noise and reduce minor random peak position drifting between scans. As a result, we routinely achieved a precision of $<0.01\%$ for the protein standards myoglobin from horse heart, calculated molecular weight 16 951.5 (9), observed mass $16\,951.2 \pm 0.6$ (0.0018%), and bovine serum albumin, calculated molecular weight 66 430.3 (10), observed mass $66\,430.7 \pm 0.9$ (0.0006%).

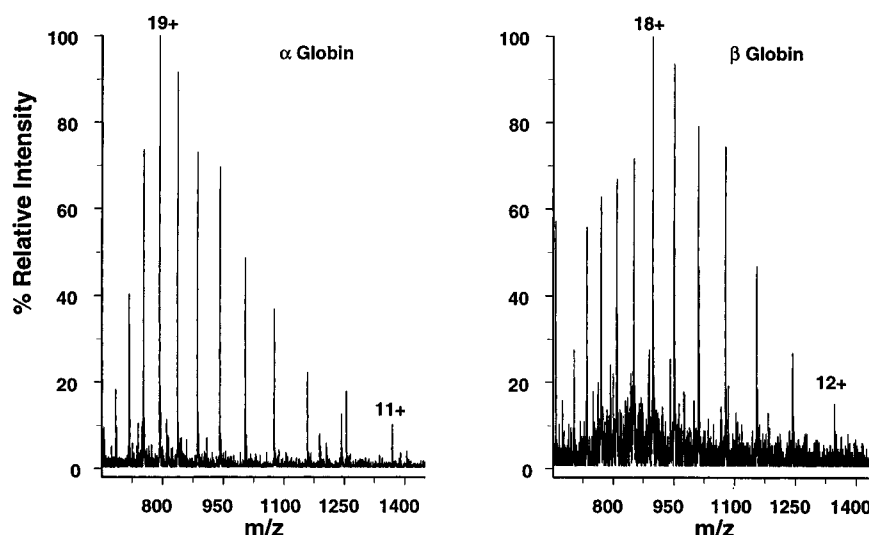
We selected 17 commercially available Hbs for ESI-MS characterization (see Table 1). Complete amino acid sequences for each Hb, except garter snake, have been published, and the most current sequences were down-

loaded via the internet.^{5,6} For analysis, Hb solutions were freshly prepared with acidic buffer and immediately injected into the mass analyzer via HPLC. The employed buffer dissociated the Hb tetramer into its primary constituents, α and β globins, and heme (11). Acidic dissociation of Hb has been exploited for the quantification of Hb constituents by reversed-phase HPLC. Typically C_{18} or C_4 columns employing an acidic mobile phase and extended gradient times (60–90 min) have provided the separation necessary for accurate quantification (12). We utilized a short polymer-based reversed-phase column which provided an adequate hydrophobic environment to ensure complete separation of the globins from salts, buffers, and/or impurities in ~ 20 min (Figure 1). The column and conditions employed resulted in separation of the α and β globins in some cases, but the lack of chromatographic resolution had no impact on ESI-MS

⁵ Sequences were obtained from NIH Protein databases, gopher.nih.gov/7mindex%3a/molbio/all.mindex.

⁶ Average molecular weight of each polypeptide was determined from the primary sequence using PAWS (Protein Analysis Worksheet) v.6.1 for Windows, Freeware software by Ronald Beavis, [ftp: mcphar01.med.nyu.edu](http://mcphar01.med.nyu.edu).

A.



B.

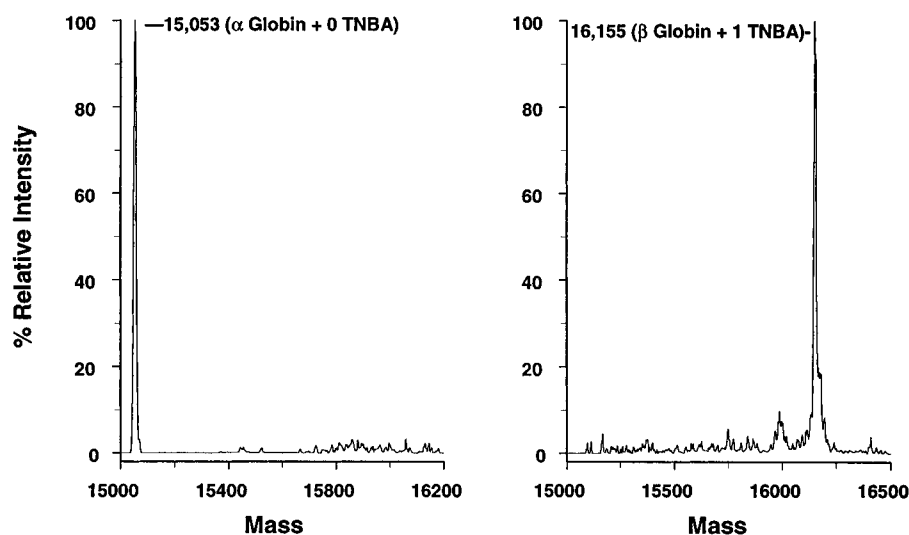


Figure 3. (A) Mass spectra for TNBA conjugates from bovine Hb α and β globins. (B) Deconvoluted mass spectra for TNBA conjugates from bovine Hb α and β globins.

data analysis. Hbs had retention times of 12–15 min and peak widths of 1–2 min depending on whether α and β globins eluted individually (narrower peaks) or coeluted (wider peaks). The use of HPLC interfaced into the ion source was not essential for ESI-MS analysis but was employed as a general method which would accommodate samples of unknown purity or origin.

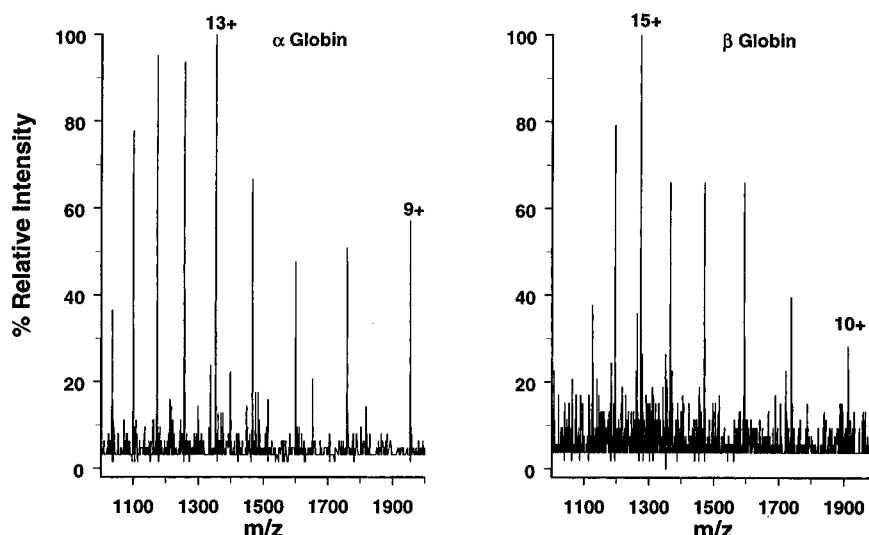
Mass analyses were carried out under the positive ion mode which resulted in spectra for the globins recorded as a series of protonated species, typically having 11–22 positive charges. Figure 2A shows the ESI-MS spectra for the α and β globins of bovine Hb. All of the tested Hbs, except cat Hb, provided well-resolved spectra and demonstrated similar ion count intensities and charge state arrays. Molecular weights of the examined globins were obtained by deconvolution of each multiion spectrum using the software provided from the instrument manufacturer. Upon deconvolution of the spectra, the predominate peaks observed were for the α and β globins (Figure 2B). All of the tested Hbs contained additional low-abundance peaks. Since the samples were not freshly drawn, it was not possible to determine if the

minor components were naturally part of a specific Hb or were formed during isolation, purification, or storage.

Table 1 lists the calculated and observed molecular weights for each investigated globin. The average deviation ranged from ± 0.3 for pigeon β globin to ± 2.5 for cat β -B globin. All of the recorded masses were within 2 daltons of the calculated molecular weights except for pigeon, turkey α^D globin, and rabbit β globin. The possible causes for these discrepancies could be errors in the reported primary sequences or *in vitro/in vivo* posttranslational modifications. Amino acid variations and posttranslational modifications have been reported for many Hbs. Genetic variations for the primary structure of rabbit β globin have been published (13). The number of literature reports of sequence analysis for turkey and pigeon is limited, and no reports were found addressing genetic, allelic, or translational variations (14, 15, 16, 17).

In a second set of experiments, the Hbs were reacted with two commonly used protein derivatizing reagents, DTNB and TNBS. DTNB specifically reacts with the free thiol group of cysteine, resulting in a mixed disulfide

A.



B.

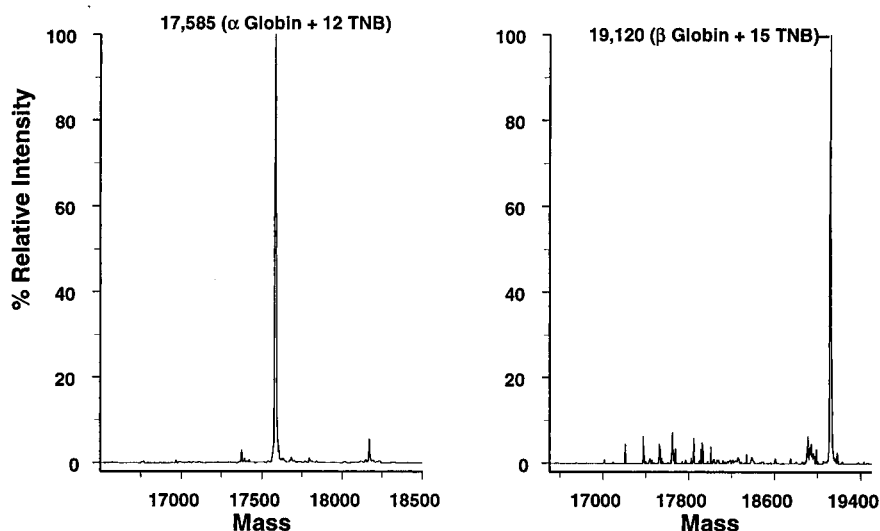


Figure 4. (A) Mass spectra for TNB conjugates from bovine Hb α and β chains. (B) Deconvoluted mass spectra for TNB conjugates from bovine Hb α and β chains.

which can be observed as a specific mass increase of 198 for each thiol derivative present (Scheme 1). Thus, 14 Hb samples were placed in phosphate buffer containing DTNB and incubated for 15 min at ambient temperature (18). The resulting reaction mixture was directly injected into the mass analyzer via HPLC using the same protocol as for unmodified Hbs. Figures 3A and 3B represent the mass spectra and deconvoluted spectra for α and β bovine globins after derivatization. The recorded mass for α globin of bovine Hb–TNBA conjugate is identical to the native α globin since there are no cysteines present in this polypeptide. The number of TNBA groups attached is presented in Table 2 and is in good agreement with the published sequence data.

Conjugation with TNBS to 14 Hbs followed the method of Kakade et al. (Scheme 2). Therefore, Hb and TNBS were incubated for 2 h at 37 °C in a sodium bicarbonate buffer and then directly injected into the mass analyzer via HPLC. This derivatization would result in a mass increase of 211 daltons for each TNB group attached (19). Figures 4A and 4B represent the mass spectra and deconvoluted spectra of TNB-derivatized α and β bovine globins. Table 3 reports the number of available nucleophilic

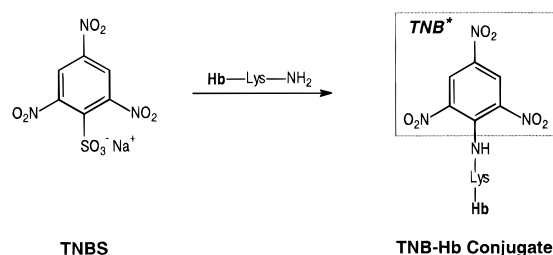
groups (free amines and thiols) on each Hb globin versus the number of TNB attached. The results indicated that the free thiol of cysteine, in addition to amino lysine side chains and the terminal amines, was derivatized by TNBS. This is in contrast to published accounts on the use of TNBS reagent for the specific quantification of lysines and N-terminal amines of polypeptides (18). We also observed that the globin–TNB conjugates did not ionize efficiently. Therefore, some spectra could not be deconvoluted (see Table 3). Derivatization of primary amines with an aromatic group containing electron-withdrawing substituents lowers the basicity of the amine and consequently suppresses protonation of that amine (20).

We observed that turkey α^D globin had one additional TNB derivative than expected and produced a mass of 117 daltons more than calculated. These results would indicate that a lysine is possibly unaccounted for in the primary sequence.

TNB and TNBA conjugates of cat Hb did not give ESI-MS spectra of suitable quality to determine the number of derivatives bound to each globin. The recorded spectra were low in ion intensities and had many overlapping

Table 2. Number of Cysteines Reported for Various Hemoglobins versus Number of Cysteines Detected after TNBA Derivatization

source ^a	reported number of thiols (cysteines)		number of TNBA groups attached	
	α globin	β globin	α globin	β globin
baboon	1	2	1	2
bovine	0	1	0	1
cat	4	2 (β -A) 2 (β -B)	b	b
dog	2 (α -I) 2 (α -II)	2	2 (α -I) 2 (α -II)	2
goat	1 (α -I) 1 (α -II)	1	1 (α -I) 1 (α -II)	1
horse	1	1	1	1
human	1	2	1	2
mouse	1	2 (major) 1 (minor)	1	2 (major) 1 (minor)
pigeon	1 2	3	1 2	3
pig	1	1	1	1
rabbit	1	1	1	1
rat	3	2	3	2
sheep	1	1	1	1
turkey	2 (α^A) 1 (α^D)	3	2 (α^A) 1 (α^D)	3

^a References noted in Table 1. ^b Spectra uninterpretable.**Scheme 2****Table 3. Number of Available Nucleophiles^b Reported versus Number of TNB Groups Attached As Determined by ESI-MS**

source ^a	reported ^b		number of TNB groups attached	
	α globin	β globin	α globin	β globin
baboon	15	15	15	15
bovine	12	15	12	15
cat	15	15 (β -A) 14 (β -B)	c	c
dog	14 (α -I) 14 (α -II)	17	14 (α -I) 14 (α -II)	17
goat	13 (α -I) 13 (α -II)	14	13 (α -I) c (α -II)	14
horse	13	13	13	13
human	13	14	13	14
mouse	13	13 (major) 14 (minor)	13	13 (major) c (minor)
pigeon	15	12	15	c
pig	13	13	13	13
rabbit	14	14	14	14
rat	16	14	16	14
sheep	13	14	13	14
turkey	15 (α^A) 12 (α^D)	14	c (α^A) 13 (α^D)	14

^a References noted in Table 1. ^b Total free amines and free thiols (lysines, N-terminal amine, and cysteines). ^c Unable to determine.

peaks (congested). Underivatized cat Hb produced a spectrum which was congested and lower in ion intensity when compared to the other Hbs. It is reported that Hbs from healthy cats have several variants and posttranslational modifications which would result in poor spectra quality (21).

In this paper, we have demonstrated the usefulness of ESI-MS for rapid, reliable, and accurate molecular weight determination of several hemoglobins and their TNBA and TNB conjugates. Masses were recorded in ~20 min with ~125 pmol (2 μ g) of sample with a minimum of sample handling. Direct characterization of TNBA/TNB-Hb conjugates by ESI-MS avoids possible misassignment inherent with these classical biochemical analyses (22, 23).

LITERATURE CITED

- (1) Bunn, F. H., and Forget, B. G. (1986) *Hemoglobin: Molecular, Genetic and Clinical Aspects*, Chapter 5, W. B. Saunders Company, New York.
- (2) Bunn, H. F., and Forget, B. G. (1986) *Hemoglobin: Molecular, Genetic and Clinical Aspects*, Chapter 2, W. B. Saunders Company, New York.
- (3) Barinaga, M. (1989) Protein chemists gain a new analytical tool. *Science* 246, 32.
- (4) Loo, J. A. (1996) Bioanalytical mass spectrometry: Many flavors to choose. *Bioconjugate Chem.* 6, 644, and references cited therein.
- (5) Shackleton, C. H. L., and Witkowska, H. E. (1996) Characterizing abnormal hemoglobin by MS. *Anal. Chem.* 68, 29A, and references cited therein.
- (6) Ellman, G. L. (1965) Tissue sulfhydryl groups. *Arch. Biochem. Biophys.* 82, 70.
- (7) Kakade, M. L., and Liener, I. E. (1969) Determination of available lysine in proteins. *Anal. Biochem.* 27, 273.
- (8) Feng, R., Konishi, Y., and Bell, A. W. (1991) High accuracy molecular weight determination and variation characterization of proteins up to 80 Ku by ionspray mass spectrometry. *J. Am. Soc. Mass Spectrom.* 2, 387.
- (9) Zaia, J., Annan, R. S., and Biemann, K. (1992) The correct molecular weight of myoglobin, a common calibrant for mass spectrometry. *Rapid Commun. Mass Spectrom.* 6, 32.
- (10) Hirayama, K., Akashi, S., Furuya, M., and Fukuhara, K.-I. (1990) Rapid confirmation and revision of the primary structure of bovine serum albumin by ESIMS and FRIT-FAB LC/MS. *Biochem. Biophys. Res. Commun.* 173, 639.
- (11) Masala, B., and Manca, L. (1994) Detection of globin chains by reversed-phase high-performance liquid chromatography. *Methods Enzymol.* 231, 21.
- (12) Shelton, J. B., Shelton, J. R., and Schroeder, W. A. (1984) High performance liquid chromatographic separation of globin chains on a large-pore C₄ column. *J. Liq. Chromatogr.* 7, 1969.
- (13) Garrick, M. D., Hafner, R., Bricker, J., and Garrick, L. M. (1974) Genetic variation in the primary structure of the beta chain of rabbit hemoglobin. *Ann. N.Y. Acad. Sci.* 241, 436.
- (14) Eguchi, Y., Nakashima, Y., Oshiro, M., and Takei, H. (1990) Complete nucleotide sequence of a pigeon alpha-globin cDNA. *Nucleic Acids Res.* 18, 7135.
- (15) Sultana, C., Abbasi, A., and Zaidi, Z. H. (1989) Primary structure of hemoglobin α -chain of *Columba livia* (Gray Wild Pigeon). *J. Protein Chem.* 8, 629.
- (16) Sultana, C., Abbasi, A., and Zaidi, Z. H. (1991) Primary structure of hemoglobin β -chain of *Columba livia* (Gray Wild Pigeon). *J. Protein Chem.* 10, 145.
- (17) Eguchi, Y., Ikehara, T., Kayo, S., Eguchi, T., and Takei, H. (1995) Amino acid sequence of α - and β -polypeptide chains of turkey (*Meleagris gallopavo*) hemoglobin. *Biol. Chem. Hoppe-Seyler* 376, 437.
- (18) Riddles, P. W., Blankeley, R. L., and Zerner, B. (1983) Reassessment of Ellman's reagent. *Methods Enzymol.* 91, 49.
- (19) Sashidhar, R. B., Capoor, A. K., and Ramana, D. (1994) Quantitation of ϵ -amino group using amino acids as reference standards by trinitrobenzene sulfonic acid. *J. Immunol. Methods* 167, 121.
- (20) March, J. (1992) *Advanced organic chemistry reactions, mechanisms, and structure*, 4th ed., Chapter 8, John Wiley & Sons, New York.
- (21) Abbasi, A., and Braunitzer, G. (1985) The primary structure of hemoglobins from the domestic cat (*Felis catus*, Felidae). *Biol. Chem. Hoppe-Seyler* 366, 699.

- (22) Adamczyk, M., Buko, A., Chen, Y.-Y., Fishpaugh, J. R., Gebler, J. C., and Johnson, D. (1995) Characterization of protein-hapten conjugates. 1. Matrix-assisted laser desorption ionization mass spectrometry of immuno BSA-hapten conjugates and comparison with other characterization methods. *Bioconjugate Chem.* 4, 631.
- (23) Adamczyk, M., Gebler, J. C., and Mattingly, P. G. (1996) Characterization of protein-hapten conjugates. 2. Electrospray mass spectrometry of bovine serum albumin-hapten conjugates. *Bioconjugate Chem.* 7, 475.
- (24) Nute, P. E., and Mahoney, W. C. (1979) Complete primary structure of the beta chain from the hemoglobin of a baboon, *Papio cynocephalus*. *Hemoglobin* 4, 109.
- (25) Mahoney, W. C., and Nute, P. E. (1980) Amino acid sequence of the hemoglobin α chain from a baboon (*Papio cynocephalus*): A product of gene fusion? *Biochemistry* 19, 1529.
- (26) Schroeder, W. A., Shelton, J. R., Shelton, J. B., Robberson, B., and Babin, D. R. (1967) Amino acid sequence of the α -chain of bovine fetal hemoglobin. *Arch. Biochem. Biophys.* 120, 1.
- (27) Schroeder, W. A., Shelton, J. R., Shelton, J. B., Robberson, B., and Babin, D. R. (1967) A comparison of amino acid sequences in the β -chains of adult bovine hemoglobins A and B. *Arch. Biochem. Biophys.* 120, 124.
- (28) Brimhall, B., Duerst, M., and Jones, R. T. (1977) The amino acid sequence of dog (*Canis familiaris*) hemoglobin. *J. Mol. Evol.* 9, 231.
- (29) Huisman, T. H. J., Brandt, G., and Wilson, J. B. (1968) The structure of goat hemoglobins II. Structural studies of the α chains of the hemoglobins A and B. *J. Biol. Chem.* 243, 3675.
- (30) Huisman, T. H. J., Adams, H. R., Dimmock, M. O., Edwards, W. E., and Wilson, J. B. (1967) The structure of goat hemoglobins I. Structural studies of the β chains of the hemoglobins of normal and anemic goats. *J. Biol. Chem.* 242, 2534.
- (31) Matsuda, G., Maita, T., Braunitzer, G., and Schrank, B. (1980) Hämoglobins, XXXIII. Notiz zur Sequenz der Hämoglobin des Pferdes. *Hoppe-Seyler's Z. Physiol. Chem.* 361, 1107.
- (32) Braunitzer, G., Gehring-Müller, R., Hilschmann, H., Hilse, K., Hobom, G., Rudloff, V., and Wittmann-Liebold, B. (1961) Die Konstitution des normalen Adulten Humanhämoglobins. *Hoppe-Seyler's Z. Physiol. Chem.* 325, 283.
- (33) Braunitzer, G., Schrank, B., Stangl, A., and Grillemeier, M. (1978) Hämoglobin, XXIII. Notiz zur Sequenz der delta Ketten der menschlichen Hämoglobin (Hb A₂ = $\alpha_2\delta_2$). *Hoppe-Seyler's Z. Physiol. Chem.* 359, 777.
- (34) Kan, Y. W., and Dozy, A. M. (1978) Polymorphism of DNA sequence adjacent to human β -globin structural gene: Relationship to sickle mutation. *Proc. Natl. Acad. Sci. U.S.A.* 75, 5631.
- (35) Popp, R. A., Bailiff, E. G., Skow, L. C., and Whitney, J. B., III (1982) The primary structure of genetic variants of mouse hemoglobin. *Biochem. Genet.* 20, 199.
- (36) Braunitzer, G., Schrank, B., Stangl, A., and Scheithauer, U. (1978) Hämoglobin, XXI: Die Sequenzanalyse des Hämoglobins des Schweines. *Hoppe-Seyler's Z. Physiol. Chem.* 359, 137.
- (37) Best, J. S., Flamm, U., and Braunitzer, G. (1969) Haemoglobins, XVII: The primary structure of the β -chain of rabbit haemoglobin. *Hoppe-Seyler's Z. Physiol. Chem.* 350, 563.
- (38) Braunitzer, G., Flamm, U., Best, J. S., and Schrank, B. (1968) Zur Phylogenie des Hämoglobinmoleküls. Die Konstitution der α -Ketten des Hämoglobins des Kaninchens (*Caniculus*). *Hoppe-Seyler's Z. Physiol. Chem.* 349, 1073.
- (39) Satoh, H., Fujii, H., and Okazaki, T. (1987) Molecular cloning and sequence analysis of two rat major globin cDNAs. *Biochem. Biophys. Res. Commun.* 146, 618.
- (40) Wilson, J. B., Brandt, G., and Huisman, T. H. J. (1968) The structure of sheep hemoglobins. III. Structural studies of the α chain of hemoglobin A. *J. Biol. Chem.* 243, 3687.
- (41) Garner, K. J., and Lingrel, J. B. (1989) A comparison of the β^A - and β^B -globin gene clusters of sheep. *J. Mol. Evol.* 28, 175.

BC9700392

Preparation, Characterization, and Biological Evaluation of Technetium(V) and Rhenium(V) Complexes of Novel Heterocyclic Tetradentate N₃S Ligands

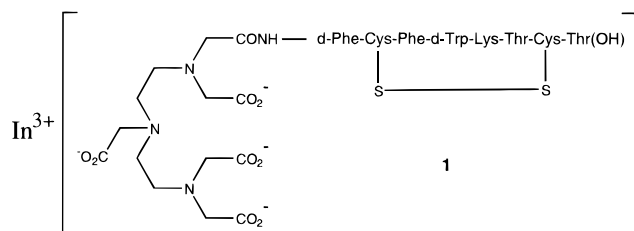
Raghavan Rajagopalan,* Glenn D. Grummon, Joseph Bugaj, Lynn S. Hallemann, Elizabeth G. Webb, Mary E. Marmion, Jean-Luc Vanderheyden, and Ananthachari Srinivasan

Mallinckrodt Medical Inc., St. Louis, Missouri 63134. Received October 3, 1996[®]

Various tetradentate N₃S ligands which contain pyridyl, morpholino, or imidazolyl moieties were prepared and labeled with technetium and rhenium. Metal complexation of the ligands occurred efficiently over the pH range from 2 to 11. Ligands possessing the *S*-THP (tetrahydropyranyl)-protected mercapto group labeled efficiently even under alkaline conditions, and among the three types of heterocyclic metal complexes, a marked difference in stability was observed; rhenium complexes decomposed to ReO₄[−] whereas technetium complexes decomposed to TcO₂/TcO₄[−]. In general, imidazolyl complexes of both technetium and rhenium were very stable in saline; less than 10% decomposition after 24 h. The technetium histidyl complex and technetium pyridyl complex were quite stable even under cysteine challenge; less than 10% decomposition after 24 h. The rhenium and technetium morpholino complexes were very unstable; greater than 10% decomposition after only 1 h in saline and greater than 25% decomposition in 1 h under cysteine challenge. Profound pharmacokinetic differences among these metal complexes were also observed in rat biodistribution studies. The neutral pyridyl complexes exhibited high blood and liver uptake and slow clearance from these tissues. The replacement of a hydroxyl group by a carboxyl group, which resulted in an anionic complex at physiological pH, resulted in a dramatic decrease in blood and liver uptake. The neutral imidazolyl complex exhibited marked reduction in blood uptake and much faster clearance from blood and liver compared to the neutral pyridyl complex. Finally, the anionic histidyl complex, which contains both the imidazolyl and carboxyl groups, had the most favorable pharmacokinetic properties in that it exhibited very low blood, liver, and kidney uptakes and a rapid clearance from the body via the renal system. The combination of the high stability and favorable pharmacokinetic properties of the imidazolyl complexes should render them useful for targeted delivery of the medically important isotopes.

INTRODUCTION

Small peptides and peptidomimetics are becoming increasingly useful for selective delivery of diagnostic and therapeutic radionuclides to target tissues (1–5). Currently, ¹¹¹In-labeled octreotide (**1**), a truncated cyclic



octapeptide analog of somatostatin, is being used for scintigraphic imaging of primary and metastatic neuroendocrine tumors bearing somatostatin receptors (6). Due to the well-recognized, ideal imaging properties of ^{99m}Tc, there is considerable interest in imaging biological receptors for neurological, oncological, and cardiovascular applications using bifunctional ^{99m}Tc chelates (7). Furthermore, for oncological applications, the similarity of technetium and rhenium chemistry may also permit the use of the same bifunctional chelates for radiotherapeutic procedures based on ¹⁸⁶Re or ¹⁸⁸Re.

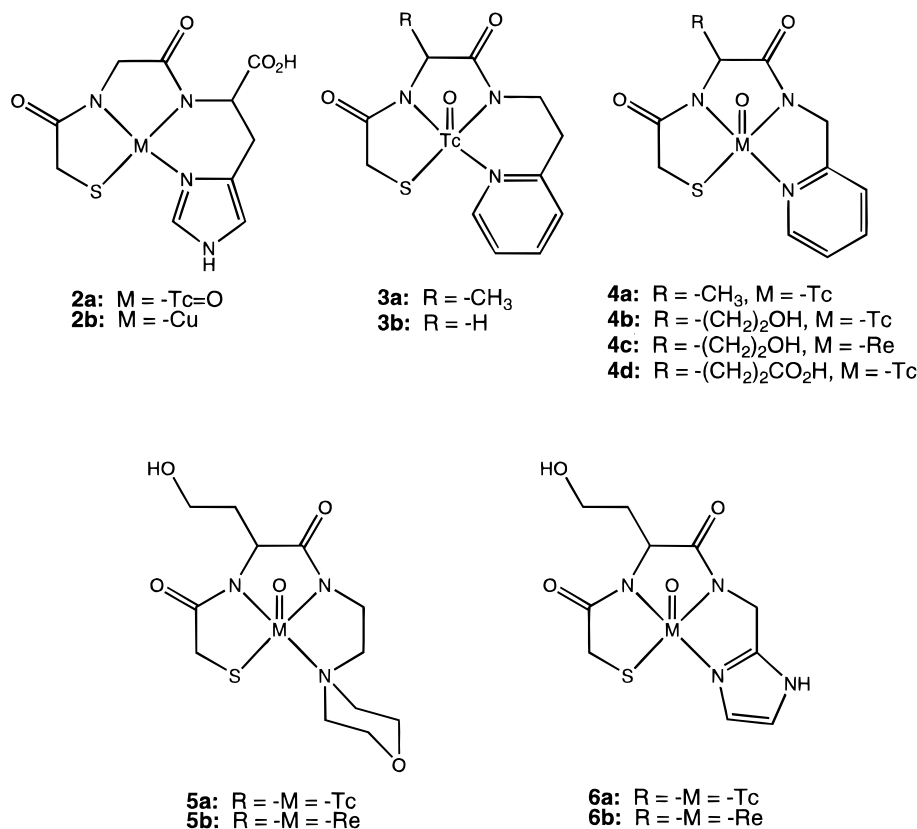
The two key requirements for designing bifunctional chelates are (a) high thermodynamic and kinetic stability of the metal complex and (b) rapid clearance of the

complex from critical nontarget organs such as blood, liver, and kidneys. Although the former requirement can be met by the rational design of ligand systems and by the knowledge of coordination chemistry, the latter is much more challenging. Pharmacokinetic information pertaining to various metal complexes still remains empirical, and a unified theory to explain existing pharmacological data remains elusive. Nevertheless, some design criteria such as size, charge, and the type of functional group required for clearance of metal complexes can be extracted from the vast amount of existing information. Accordingly, as part of our continuous efforts directed toward diagnosis and treatment of tumors using small peptides and peptidomimetics as carriers, herein we report our recent progress on the development of novel technetium and rhenium metal complexes that satisfy the key physicochemical and pharmacokinetic properties mentioned above (8).

Polyaminocarboxylate moieties such as diethylenetriaminepentaacetic acid (DTPA) used in octreotide (**1**) are very good chelators for lanthanides and some transition metal ions, including manganese (II) and indium (III), but are not optimal ligands for technetium and rhenium. The type of coordinating groups which bind tightly to these transition metal ions depends greatly on the oxidation state of the metal. In general, Tc^V and Re^V are readily accessible oxidation states which can be stabilized by coordination to a combination of amino, amido, and mercapto functionalities (9). Tetradentate amine thiol or amide thiol ligands are known to form very stable,

[®] Abstract published in *Advance ACS Abstracts*, May 1, 1997.

Chart 1



square pyramidal, mono-oxo Tc^V and Re^V complexes, and these ligands have been attached to bioactive molecules to generate bifunctional chelates (10–13). However, nitrogen sulfur-based ligands containing a heterocyclic moiety have not been studied extensively with regard to targeted delivery of ^{99m}Tc and ¹⁸⁶Re even though the copper imidazole complex **2b** and technetium pyridyl complex **3b** have been reported previously (14, 15; Chart 1). In this paper, we present the preparation, characterization, and biological evaluation of several novel diamide thiolate ^{99m}Tc=O and ¹⁸⁶Re=O complexes which contain pyridyl, morpholino, and imidazolyl moieties.

EXPERIMENTAL PROCEDURES

General. Unless otherwise noted, all starting materials and solvents were obtained from commercially available sources (Sigma/Aldrich Chemical Co., St. Louis, MO, or Bachem Co., Torrance, CA) and used without further purification. Catalytic hydrogenations were carried out using a Parr hydrogenation apparatus (Parr Instrument Co., Moline, IL). NMR spectra were obtained using Varian Gemini 300 300 MHz spectrometer. The mass spectra were obtained using Finnigan TSQ 700 triple-quadrupole mass spectrometer configured for either fast atom bombardment (FAB) or electrospray ionization (ESI) techniques. Elemental analyses were performed by Atlantic Microlabs, Norcross, GA. Melting points were determined using a Thomas Hoover capillary melting point apparatus and are reported uncorrected. ^{99m}Tc generator and Na¹⁸⁶ReO₄ solution were obtained from Mallinckrodt, Inc., St. Louis, MO. Electrophoresis (phosphate buffer, pH 6.4, 300 volts) was performed on a Gilman electrophoresis apparatus, Gillman Sciences, Ann Arbor, MI.

General Procedure for Preparation of Pyridyl Ligands 11a,b. A mixture of the pyridyl amines **7a** or **7b** (20 mmol) and *N*-Cbz-alanine *N*-succinimido esters

8a,b (20 mmol) in acetonitrile (30 mL) was stirred at ambient temperature for 4 h and then poured onto ice-cold water (150 mL). The gummy residues solidified overnight. The colorless solids were filtered, washed with water, and dried to give the 5.4–5.6 g (82–85%) of the *N*-Cbz derivatives which were sufficiently pure for use in the next step.

A solution of each of the Cbz derivatives (10 mmol) in methanol (20 mL) was carefully treated with 0.5 g of 10% Pd-C catalyst (added in small portions under a slow, steady stream of nitrogen). Thereafter, the mixture was hydrogenated at 50 psi (~3.5 atm) for 2 h. The catalyst was removed by filtration over Celite, and the filtrate was evaporated under reduced pressure to give the pyridyl amines **9a** and **9b** as a pale tan gum, which was used immediately in the next step.

A mixture of the amines **9a** or **9b** (5 mmol) and the active ester **10** (**16**) (5 mmol) in acetonitrile (10 mL) was stirred at ambient temperature for 2 h and poured onto ice-cold water (100 mL). The precipitates were collected by filtration, washed with water, dried, and recrystallized from acetonitrile to give the desired ligands **11a** and **11b** as colorless solids.

Ligand 11a. Yield, 1.4 g (78%); mp 150–152 °C. ¹H-NMR (CDCl₃) δ 8.41 (d, 1H), 7.90 (d, 2H), 7.55 (m, 2H), 7.40 (m, 3H), 7.18 (d, 1H), 7.10 (m, 2H), 4.55 (m, 3H), 3.75 (s, 2H), 1.40 (d, 3H). ¹³C-NMR (CDCl₃) δ 191.7, 172.2, 168.2, 156.6, 149.2, 137.0, 136.1, 134.2, 128.9, 127.6, 122.4, 121.8, 49.3, 44.4, 32.6, 18.1. Anal. Calcd for C₁₈H₁₉N₃O₃S: C, 60.49; H, 5.36; N, 11.76; S, 8.97. Found: C, 60.53; H, 5.40; N, 11.67; S, 9.04.

Ligand 11b. Yield, 1.6 g (84%); mp, 165–167 °C. ¹H-NMR (CDCl₃) δ 8.45 (d, 1H), 7.90 (m, 2H), 7.55 (m, 2H), 7.42 (t, 2H), 7.10 (m, 4H), 4.40 (m, 1H), 3.72 (s, 2H), 3.59 (m, 2H), 2.82 (t, 2H), 1.30 (d, 3H). ¹³C-NMR (CDCl₃) δ 191.5, 172.0, 167.9, 159.5, 149.3, 136.8, 136.1, 134.2, 128.9, 127.7, 123.6, 121.7, 49.2, 38.7, 36.6, 32.6, 18.1.

Anal. Calcd for C₁₉H₂₁N₃O₃S: C, 61.44; H, 5.70; N, 11.31; S, 8.63. Found: C, 61.54; H, 5.77; N, 11.34; S, 8.73.

Preparation of the Carboxyl Ligand 11c. A mixture of **7a** (1.2 g, 10 mmol) and the active ester **8c** (4.1 g, 10 mmol) in acetonitrile (25 mL) was stirred at ambient temperature for 4 h. The reaction mixture was poured onto water and extracted with methylene chloride (3 × 25 mL). The combined organic layers were washed with brine, dried (MgSO₄), and filtered, and the filtrate was evaporated under reduced pressure to give 4.0 g (85%) of the Cbz derivative as an off-white solid which was pure enough for use in the next step.

A solution of the Cbz derivative (10 mmol) in methanol (20 mL) was carefully treated with 0.5 g of 10% Pd-C catalyst (added in small portions under a slow, steady stream of nitrogen). Thereafter, the mixture was hydrogenated at 50 psi (~3.5 atm) for 2 h. The catalyst was removed by filtration over Celite, and the filtrate was evaporated under reduced pressure to give **9c** as pale tan gum. This amine turns dark on standing and, hence, was used immediately in the next step.

A mixture of the amine **9c** (2.8 g, 10 mmol) and the active ester **10** (2.9 g, 10 mmol) in acetonitrile (25 mL) was stirred at ambient temperature for 4 h. The reaction mixture was poured onto water and extracted with methylene chloride (3 × 25 mL). The combined organic extracts were washed with water, dried (MgSO₄), and filtered, and the filtrate was evaporated under reduced pressure. The waxy solid was then treated with trifluoroacetic acid (10 mL) and kept at ambient temperature for 1 h. The solution was poured onto water (200 mL), and the precipitate was collected by filtration, washed well with water, dried, and recrystallized from isopropyl alcohol to give 2.6 g (63%) of the ligand **11c** as colorless solid, mp 195–197 °C. ¹H-NMR (CDCl₃) δ 8.65 (m, 1H), 8.55 (m, 2H), 7.95 (m, 1H), 7.90 (m, 2H), 7.65 (m, 1H), 7.55 (m, 2H), 7.45 (m, 2H), 4.48 (d, 2H), 4.30 (m, 1H), 3.80 (s, 2H), 2.30 (m, 2H), 2.00 (m, 1H), 1.80 (m, 1H). ¹³C-NMR (CDCl₃) δ 191.1, 174.4, 172.0, 167.7, 157.5, 146.7, 140.3, 136.3, 134.5, 129.5, 127.2, 123.5, 122.5, 52.7, 42.9, 32.6, 30.1, 27.0. Anal. Calcd for C₂₀H₂₁N₃O₅S: C, 57.82; H, 5.09; N, 10.11; S, 7.72. Found: C, 57.71; H, 5.14; N, 10.00; S, 7.80.

N-Cbz-Homoserine Lactone (12). Benzyl chloroformate (9.4 g, 50 mmol) was added dropwise to a vigorously stirring solution of *L*-homoserine lactone hydrochloride (9.1 g, 50 mmol) and sodium carbonate (15.9 g, 150 mmol) in a biphasic mixture of methylene chloride and water (1:1, 200 mL). After the addition, the mixture was stirred at ambient temperature for 16 h. The organic layer was separated, dried (MgSO₄), and filtered, and the filtrate was evaporated under reduced pressure. Recrystallization of the resulting solid from ethyl acetate afforded 12.0 g (96%) of lactone **12** as colorless needles, mp 123–125 °C. ¹H-NMR (CDCl₃) δ 7.33 (bs, 6H), 5.10 (s, 2H), 4.40 (m, 2H), 4.21 (m, 1H), 2.72 (m, 1H), 2.20 (m, 1H). ¹³C-NMR (CDCl₃) δ 175.3, 156.4, 136.1, 128.7, 128.5, 128.3, 67.3, 65.7, 50.3, 30.1.

Pyridyl Amino Alcohol (15). A mixture of **7a** (4.32 g, 40 mmol) and the lactone **12** (8.40 g, 40 mmol) in glyme (30 mL) was heated under reflux for 2 h. The reaction mixture was poured onto ice-cold water (200 mL). The solid was filtered, washed with water, and recrystallized from hot water to give 8.8 g (70%) of the Cbz derivative as a colorless solid, mp 154–156 °C. ¹H-NMR (CDCl₃) δ 8.45 (d, 1H), 7.61 (t, 1H), 7.45 (bt, 1H), 7.10–7.40 (m, 8H), 6.05 (d, 1H), 5.05 (s, 2H), 4.50 (m, 3H), 3.67 (m, 2H), 2.00 (m, 1H), 1.87 (m, 1H). ¹³C-NMR (CDCl₃) δ 172.1, 157.0, 156.5, 149.2, 137.2, 136.3, 128.7, 128.5, 128.2, 122.7, 122.2, 67.1, 58.4, 52.5, 44.1, 35.8.

A solution of the above Cbz derivative (20 mmol) in methanol (30 mL) was carefully treated with 1.0 g of 10% Pd-C catalyst (added in small portions under a slow, steady stream of nitrogen). The mixture was hydrogenated at 50 psi (~3.5 atm) for 2 h. The catalyst was removed by filtration and the filtrate was evaporated under reduced pressure to give the pyridyl amino alcohol **15** as a pale yellow gum, which was used immediately in the next step. ¹H-NMR (CDCl₃) δ 8.42 (d, 1H), 8.28 (bt, 1H), 7.58 (m, 1H), 7.20 (m, 1H), 7.10 (m, 1H), 4.47 (d, 2H), 3.70 (t, 2H), 3.55 (dd, 1H), 2.80 (broad, 3H), 1.90 (m, 1H), 1.70 (m, 1H). ¹³C-NMR (CDCl₃) δ 176.0, 157.0, 149.1, 137.0, 122.5, 122.1, 59.7, 53.7, 44.0, 37.3.

Morpholino Amino Alcohol (16). A mixture of the amine **13** (5.60 g, 40 mmol) and the lactone **12** (8.36 g, 40 mmol) in glyme (30 mL) was heated under reflux for 2 h. The reaction mixture was poured onto ice-cold water (200 mL). The solvent was evaporated under reduced pressure, and the pale yellow gum (13.5 g) was kept under high vacuum for 72 h by which time the Cbz derivative solidified (mp 83–86 °C) and was used as such. ¹H-NMR (CDCl₃) δ 7.30 (bs, 5H), 6.89 (bt, 1H), 5.95 (d, 1H), 5.05 (dd, 2H), 4.35 (m, 1H), 3.62 (m, 4H), 3.40 (m, 4H), 1.95 (m, 1H), 1.78 (m, 1H). ¹³C-NMR (CDCl₃) δ 172.0, 157.0, 136.3, 128.7, 128.4, 128.1, 66.6, 58.3, 56.9, 53.2, 52.1, 35.7.

Hydrogenolysis of this Cbz derivative was carried out in the same manner as that described for compound **15**. The morpholino amino alcohol **16** was obtained as a pale yellow gum. ¹H-NMR (CDCl₃) δ 3.02 (m, 5H), 3.25 (m, 4H), 3.00 (m, 2H), 2.60 (t, 1H), 2.15 (m, 6H), 1.45 (m, 1H), 1.35 (m, 1H). ¹³C-NMR (CDCl₃) δ 176.8, 65.2, 57.4, 55.5, 51.6, 35.4, 34.7.

Imidazolyl Amino Alcohol (17). A mixture of 2-aminomethylimidazole dihydrochloride **14** (**17**) (3.40 g, 20 mmol), the lactone **12** (4.2 g, 20 mmol), and triethylamine (5.05 g, 50 mmol) in glyme (30 mL) was heated under reflux for 48 h. The reaction mixture was poured onto ice-cold water (200 mL). The solid was filtered, washed with water, and recrystallized from hot water to give 4.1 g (53%) of **17** as an off-white solid. ¹H-NMR (DMSO-*d*₆) δ 8.28 (t, 1H), 7.42 (d, 1H), 7.31 (m, 5H), 6.90 (s, 2H), 4.95 (dd, 2H), 4.35 (m, 2H), 4.08 (m, 1H), 3.40 (m, 3H), 1.78 (m, 1H), 1.68 (m, 1H). ¹³C-NMR (DMSO-*d*₆) δ 172.5, 156.4, 145.0, 137.3, 128.7, 125.9, 121.0, 65.5, 57.5, 52.2, 36.5, 34.9.

Hydrogenolysis of this Cbz derivative was carried out in the same manner as that described for compound **15**. The imidazolyl amino alcohol **17** was obtained as a pale yellow gum. ¹H-NMR (D₂O) δ 6.89 (s, 2H), 4.30 (s, 2H), 3.50 (t, 2H), 3.35 (t, 1H), 1.74 (m, 1H), 1.65 (m, 1H). ¹³C-NMR (D₂O) δ 177.9, 145.0, 122.2, 58.1, 51.9, 48.7, 36.2.

General Procedure for Preparation of Ligands 19–21. A solution of the amines **15**, **16**, or **17** (5 mmol) in acetonitrile (10 mL) was treated with the active ester **18** (**18**) (5 mmol) and stirred at ambient temperature for 4 h. The solvent was removed under reduced pressure, and the residue was worked up as described below for the individual ligands.

Ligand 19. The residue was dissolved in methylene chloride (20 mL), washed with water (2 × 20 mL), dried (MgSO₄), and filtered, and the filtrate was taken to dryness under reduced pressure. The gummy residue was purified by column chromatography over silica gel (Merck, 230–400 mesh, 40 g). Elution with chloroform/methanol (93:7) gave 1.1 g (74%) of the desired ligand **19** as an off-white solid, mp 86–88 °C. ¹H-NMR (CDCl₃) δ 8.48 (d, 1H), 7.90 (dd, 1H), 7.65 (m, 2H), 7.19 (m, 2H), 4.75 (m, 2H), 4.55 (m, 2H), 4.30 (broad, 1H), 3.95 (m, 1H), 3.67 (m, 2H), 3.42 (m, 1H), 3.35 (dd, 1H), 3.20 (dd, 1H),

2.05 (m, 1H), 1.40–1.90 (m, 7H). ^{13}C -NMR (CDCl_3) δ 172.0, 170.8, 156.7, 149.2, 137.1, 122.6, 122.0, 83.5, 65.7, 58.3, 51.0, 44.3, 35.8, 34.6, 30.9, 25.0, 21.6. Anal. Calcd for $\text{C}_{17}\text{H}_{25}\text{N}_3\text{O}_4\text{S}$: C, 55.59; H, 6.81; N, 11.44; S, 8.72. Found: C, 55.66; H, 6.87; N, 11.45; S, 8.70. Thermal spray mass spectrum, m/Z 368 [M + H].

Ligand 20. The gummy residue was purified by flash chromatography over C-18 reverse phase sorbent (20 g). Elution with pure water removed *N*-hydroxysuccinimide and other low molecular weight impurities. Elution with water/methanol (7:3) followed by evaporation of the solvent afforded 0.82 g (42%) of the desired ligand **20** as a pale greenish-yellow gum. ^1H -NMR (CDCl_3) δ 6.91 (m, 1H), 3.85 (m, 1H), 3.60 (m, 1H), 3.31 (t, 4H), 2.90–3.35 (m, 8H), 2.15 (m, 6H), 1.10–1.70 (m, 7H). ^{13}C -NMR (CDCl_3) δ 173.0, 172.5, 82.1, 76.8, 65.2, 57.0, 55.4, 51.6, 50.8, 35.0, 32.5, 32.3, 29.8, 23.8, 20.5. Thermal spray mass spectrum, m/Z 390 [M + H].

Ligand 21. The gummy residue was purified by flash chromatography over using C-18 reverse phase sorbent (20 g). Elution with pure water removed *N*-hydroxysuccinimide and other low molecular weight impurities. Elution with water/methanol (7:3) followed by evaporation of the solvent afforded 0.56 g (31%) of the desired ligand **21** as a pale tan foam. ^1H -NMR (D_2O) δ 6.67 (bs, 2H), 4.05 (broad, 3H), 3.55 (m, 1H), 3.35 (m, 2H), 2.90–3.20 (m, 3H), 1.05–1.80 (m, 7H). ^{13}C -NMR (D_2O) δ 173.4, 172.7, 143.9, 121.1, 82.2, 77.0, 65.2, 65.9, 50.7, 35.4, 32.6, 29.7, 23.8, 20.4. Anal. Calcd for $\text{C}_{15}\text{H}_{24}\text{N}_4\text{O}_4\text{S} \cdot 0.1 \text{ H}_2\text{O}$: C, 50.30; H, 6.76; N, 15.65; S, 8.94. Found: C, 50.00; H, 6.82; N, 15.32; S, 8.92. Thermal spray mass spectrum, m/Z 357 [M + H].

General Procedure for Preparation of $^{99\text{m}}\text{Tc}$ Complexes. To a solution of sodium gluconate (51 mg) in water (1 mL) and 1.0 M carbonate/bicarbonate buffer (200 μL) at the desired pH was added 1.9 mg of the appropriate ligand dissolved in water (280 μL). After the solution was purged with nitrogen for 10 min, 1.1 μL of stannous chloride stock solution (10 mg/mL) followed by 0.4 mL of sodium pertechnetate solution (5 mCi) were added and the container was sealed with a rubber septum (crimp-sealed) under nitrogen. The mixture was then heated in a boiling water bath for 15 min, and the crude reaction products were purified as described below.

General Procedure for Preparation of ^{186}Re Complexes. To a lyophilized preparation of stannous citrate (20 mg of lactose, 25 mg of citric acid, 2 mg of gentisic acid, and 1 mg of stannous chloride) in a closed 10 mL vial was added 450 μL of nitrogen-purged water and 50 μL of sodium perrhenate solution (14.4 mCi). After 5 min, 8.1 μL of appropriate ligand stock solution (22 mg/mL) was added and the container was sealed with a rubber septum (crimp-sealed) under nitrogen. The mixture was then heated in a boiling water bath for 15 min.

General Procedure for Complexation of Ligands **19 and **21** with Nonradioactive ("Cold") Rhenium.** To a lyophilized preparation of stannous citrate (20 mg of lactose, 25 mg of citric acid, 2 mg of gentisic acid, and 1 mg of stannous chloride) in a closed 10 mL vial was added 951 μg of sodium perrhenate in 400 μL of nitrogen-purged water. After 5 min, a solution of 2.1 mg of the ligand **19** or **21** in 133 μL of water was added and the mixture heated in a boiling water bath for 15 min. Thereafter, the reaction mixture was purified by HPLC under the following conditions.

General Procedure for Purification of Technetium and Rhenium Complexes. The reaction mixtures were purified by gradient HPLC using a Waters NovaPak C-18 column (15 cm). Solvent conditions varied

depending on the complex. The following six different conditions were used.

Condition 1. Solvent A, 0.1% aqueous trifluoroacetic acid; solvent B, 80% acetonitrile/20% 0.1% aqueous trifluoroacetic acid; linear gradient (100% solvent A to 50% solvent A, 50% solvent B in 15 min), flow rate, 1 mL/min.

Condition 2. Solvent A, 0.1% aqueous trifluoroacetic acid; solvent B, 80% acetonitrile/20% 0.1% aqueous trifluoroacetic acid; linear gradient (100% solvent A to 50% solvent A, 50% solvent B in 25 min), flow rate, 1 mL/min.

Condition 3. Solvent A, 5 mM NaH_2PO_4 ; solvent B, 5 mM NaH_2PO_4 , in 80% ethanol; linear gradient (100% solvent A to 50% solvent A, 50% solvent B in 15 min), flow rate, 1 mL/min.

Condition 4. Solvent A, 0.5 mM NaH_2PO_4 ; solvent B, 0.5 mM NaH_2PO_4 , in 80% ethanol; linear gradient (100% solvent A to 50% solvent A, 50% solvent B in 15 min), flow rate, 1 mL/min.

Condition 5. Solvent A, 5 mM KH_2PO_4 ; in 2% aqueous acetonitrile; solvent B, 5 mM NaH_2PO_4 , in 70% aqueous acetonitrile; linear gradient (100% solvent A to 50% solvent A, 50% solvent B in 15 min), flow rate, 1 mL/min.

Condition 6. Solvent A, 5 mM NaH_2PO_4 in 10% ethanol; solvent B, 5 mM NaH_2PO_4 , in 60% ethanol; linear gradient (100% solvent A to 50% solvent A, 50% solvent B in 15 min), flow rate, 1 mL/min.

Complex 2a. Condition 1, retention time, 8.74 min.

Complex 4b. Condition 5, retention time, 9.86 min.

Complex 4c. Condition 4, retention time, 9.94 min. FAB mass spectrum, m/Z 482 and 484 (relative intensity of 1:2).

Complex 4d. Condition 2, retention time, 11.53 min.

Complex 5a. Condition 1, retention time, 9.83 min.

Complex 5b. Condition 3, retention time, 8.77 min.

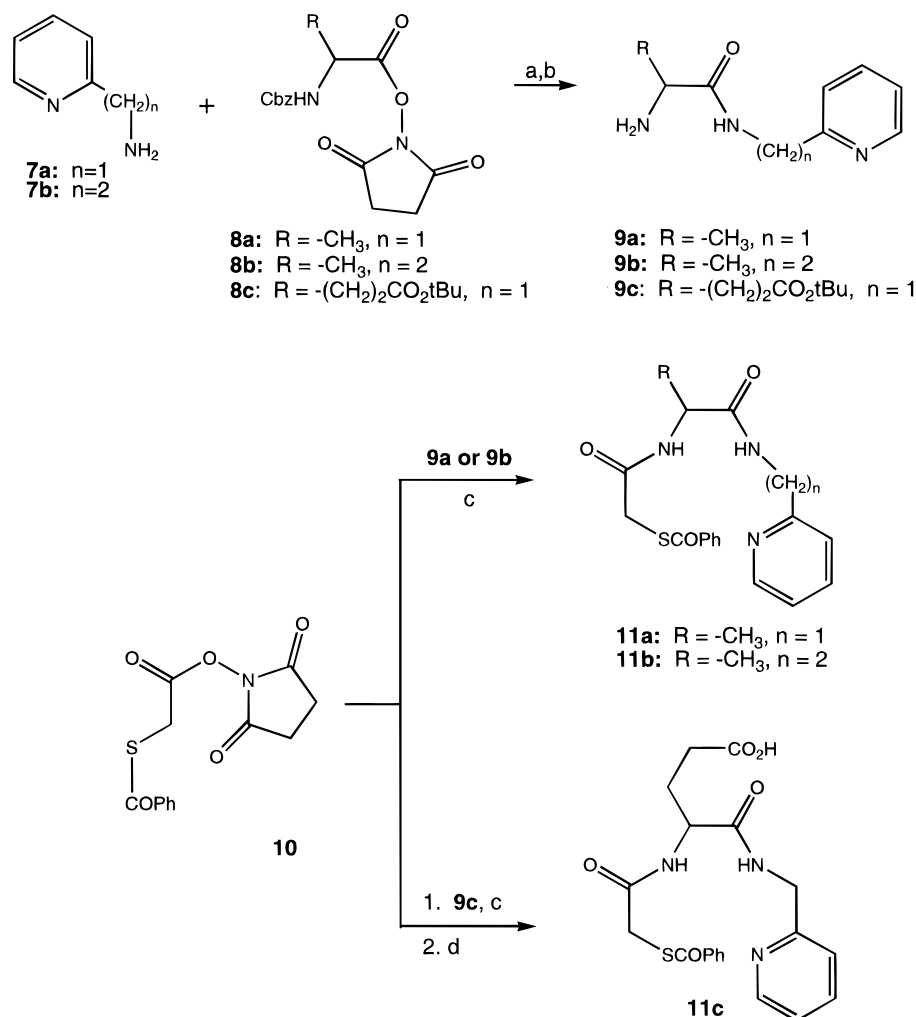
Complex 6a. Condition 1, retention time, 9.61 min.

Complex 6b. Condition 4, retention time, 11.47 min.

FAB mass spectrum, m/Z 471 and 473 (relative intensity of 1:2).

General Procedure for Stability Studies. Ligands **19**–**21** were radiolabeled with technetium and were purified by HPLC using Condition 6 described above. The purified fractions of complexes **2a**, **4b**, **5a,b**, and **6a,b** (2 mL) were collected, partitioned into two 1 mL portions, and then mixed either with physiological saline (1 mL) or with 1 mL of 0.01 M aqueous cysteine stock solution. The solutions were kept at ambient temperature, and the purity of the complex as well as the levels of $\text{TcO}_2/\text{TcO}_4^-$ or of ReO_4^- was monitored by HPLC (Condition 1) and paper chromatography at four time points (initial and 1, 4, and 24 h).

Biodistribution Studies. Biodistribution studies were performed on selected pyridyl and imidazolyl complexes, **2a**, **4b**–**d**, and **6b**, but were not carried out for the morpholino complexes **5a** and **5b** due to *in vitro* instability of these complexes. Male Sprague-Dawley rats weighing ~220 g were used to obtain the biodistribution data on these complexes. Each animal received 300 μL of HPLC-purified test article containing 10 μCi of radioactivity and 0.07 μg of material via the tail vein. The animals ($n = 3$) were sacrificed at 20', 60', and 120' post injection and ($n = 2$) at 24 h post injection. Selected tissue samples of blood, liver, kidney, and muscle were excised and rinsed with saline. These organs and tissues were assayed for percent injected dose per organ from standards prepared from the initial dosing material. For determining percent injected dose in the urine and feces, animals were housed in metabolism cages overnight. The

Scheme 1^a

^a Legend: (a) CH₃CN, room temperature. (b) H₂, 10% Pd-C, MeOH. (c) CH₃CN, room temperature. (d) CF₃CO₂H.

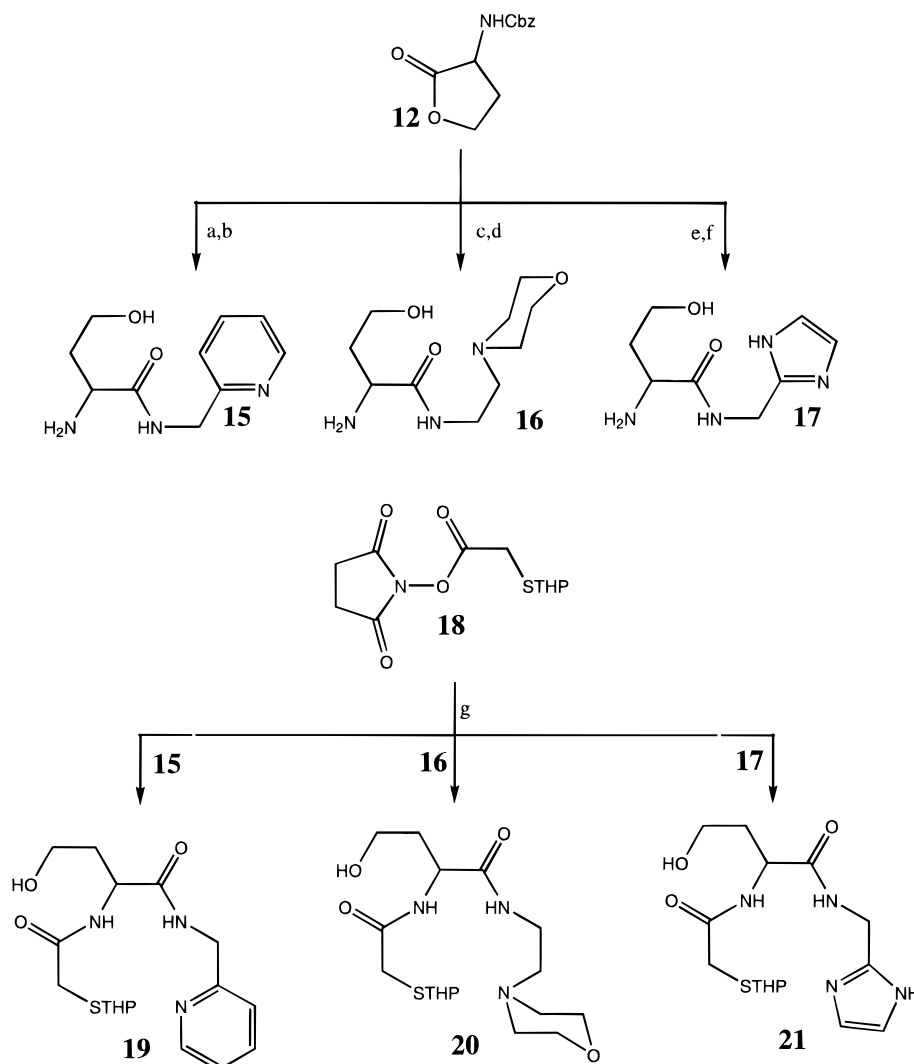
urine and feces samples were collected separately and counted against the prepared standards as noted previously.

RESULTS AND DISCUSSION

Ligand Syntheses. All ligands contain either a benzoyl- or a THP-protected mercapto group. Protection of the thiol functionality is always desirable, and often necessary, because the technetium and rhenium labeling of ligands which contain unprotected thiols frequently leads to poor yields and undesirable byproducts. The pyridyl ligands **11a,b** were prepared in three steps with the overall yield of about 70% (Scheme 1): (a) the reaction of pyridyl amines **7a** or **7b** with the alaninyl active ester **8a** or **8b**; (b) hydrogenolysis of the resulting Cbz derivatives; and (c) the reaction of the amines **9a,b** with the succinimido ester (**10**). It may be noted that compound **10** undergoes aminolysis chemoselectively at the succinimido ester center and not at the thiocarbonyl center. However, under the same conditions, the *S*-acetyl analog of **10** (*N*-succinimidyl *S*-acetylmercaptoacetate) undergoes aminolysis at *both* positions giving a mixture of products. For example, when *N*-succinimidyl *S*-acetylmercaptoacetate is reacted with triglycine, both *N*-acetyltriglycine and *N*-(*S*-acetylmercapto)acetamidotriglycine were obtained (R. Rajagopalan, unpublished results). The carboxy ligand **11c** was prepared in four steps with the overall yield of about 55% (Scheme 1): (a) reaction of **7a** with the glutamyl active ester **8c**; (b)

hydrogenolysis of the resulting Cbz derivative; (c) condensation of the amine **9c** with the active ester **10**; and (d) deprotection of the *tert*-butyl group with trifluoroacetic acid. The hydroxy ligands **19–21** were prepared in three steps (Scheme 2): (a) ring opening of *N*-Cbz-homoserine lactone (**12**) with the heterocyclic amines **7a**, **13**, or **14**; (b) hydrogenolysis of the resulting Cbz derivatives; and (c) condensation of the amino alcohols **15–17** with the active ester **18**. The overall yields of **19**, **20**, and **21** were 50%, 41%, and 20%, respectively. The histidyl ligand, *N*-[(*S*-benzoyl)mercapto]acetylglucylhistidine (**22**), for the preparation of technetium imidazolyl complex **2a**, was prepared according to the published procedure (14).

Radiolabeling, Characterization, and Stability. Technetium labeling of all the ligands **11a–c** and **19–21** was generally achieved by heating a mixture of ^{99m}Tc-gluconate and the ligand at 100 °C in an inert atmosphere at pH 2–12 for about 15 min. The rhenium complexes of the same ligands were prepared by heating a mixture of ¹⁸⁶Re citrate and the ligand at 100 °C in an inert atmosphere at pH 2–3 for about 15 min. The ligand to metal ratio used in rhenium labeling was 1.6:1. HPLC retention times of the major peak resulting from radiolabeling of a particular ligand at various pH conditions were identical, indicating that the same product is formed under different pH conditions. Furthermore, the HPLC retention times of the technetium and rhenium complexes derived from the same ligand differed by only about 1 min, indicating a strong structural similarity between

Scheme 2^a

^a Legend: (a) **7a**, DME, Δ . (b) H_2 , 10% Pd-C, MeOH. (c) 4-(2-Amino)ethylmorpholine (**13**), DME, Δ . (d) H_2 , 10% Pd-C, MeOH. (e) 2-Aminoethylimidazole dihydrochloride (**14**), DME, Δ . (f) H_2 , 10% Pd-C, MeOH. (g) CH_3CN , Δ .

^{99m}Tc and ^{186}Re complexes. FAB mass spectrum of nonradioactive rhenium complexes prepared from the pyridyl ligand **19** showed a pair of $[M + 1]$ signals, m/Z 482 and 484, in the ratio of 1:2, characteristic of ^{185}Re and ^{187}Re patterns associated with the complex **4c**. Similarly, the FAB mass spectrum of nonradioactive rhenium complexes prepared from the imidazolyl ligand **21** showed a pair of $[M + 1]$ signals, m/Z 471 and 473, in the ratio of 1:2, characteristic of ^{185}Re and ^{187}Re pattern associated with the complex **6b**. These data, along with the previous X-ray crystallographic study (15) on an analogous pyridyl complex, provide support for the structures designated as **4c** and **6b**.

Paper electrophoresis indicated that the complexes **3a,b**, **4a–c**, and **5a,b** were neutral; complexes **2a** and **4d** were anionic due to the presence of a carboxyl group; and complex **6a** was neutral below pH 11 but anionic above pH 11, indicating that the imidazolyl proton is being ionized only above this pH. The morpholino complexes **5a** and **5b** were too unstable for complete characterization. However, the similarity of HPLC retention times and the neutral charge of the complex suggest structural similarity with the pyridyl and imidazolyl complexes.

Table 1 shows the radiochemical yield of various heterocyclic metal complexes formed under various pH conditions. All ligands labeled efficiently under a wide

Table 1. Radiolabeling of Ligands with ^{99m}Tc and ^{186}Re at Various pH

ligand	metal ion	complex	pH	percent RCY ^{a,b}
11a	^{99m}Tc	4a	12.0	82
11b	^{99m}Tc	3a	12.0	96
11c	^{99m}Tc	4d	9.5	88
19	^{186}Re	4c	2.2	94
19	^{99m}Tc	4b	7.5	91
19	^{99m}Tc	4b	9.0	80
20	^{186}Re	5b	2.2	98
20	^{99m}Tc	5a	5.6	69
20	^{99m}Tc	5a	7.4	55
20	^{99m}Tc	5a	9.0	95
21	^{99m}Re	6b	2.2	94
21	^{99m}Tc	6a	2.2	61
21	^{99m}Tc	6a	4.0	75
21	^{99m}Tc	6a	7.5	47
21	^{99m}Tc	6a	9.0	54
22	^{99m}Tc	2a	11.0	75

^a RCY, radiochemical yield. ^b All values represent initial radiochemical yield and are unoptimized.

range of pH values. Ligands **19–21** labeled efficiently even at pH 9 despite the fact that the THP group is expected to be inert toward hydrolysis above pH 7. Although the *S*-THP group had been known to hydrolyze under alkaline conditions with mercury salts (19), such cleavage under technetium or rhenium labeling conditions had not been observed previously. Previous work

Scheme 3

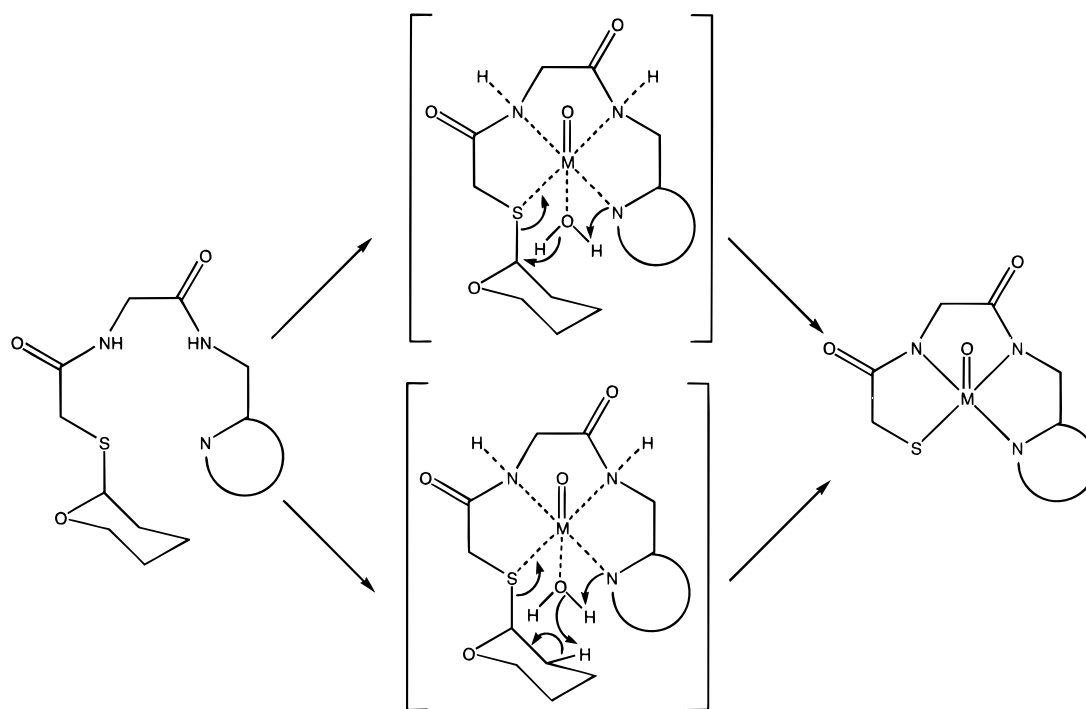


Table 2. Stability of Technetium and Rhenium Complexes

complex	initial		1 h		4 h		24 h	
	saline	cysteine	saline	cysteine	saline	cysteine	saline	cysteine
2a	98.9	99.4	99.1	96.1	99.5	96.2	83.7	89.5
4b	98.8	98.8	98.8	98.7	98.8	98.8	93.7	97.5
5a	98.7	69.2	90.0	72.8				
5b	97.6		83.2					
6a	96.3	76.8	96.3	60.3	93.6	60.5	95.2	47.5
6b	99.8		99.2		99.4		98.8	

on the labeling of triamide thiolate ligands containing *S*-THP group required strong acidic conditions (ca. pH < 3) to bring about the hydrolysis of the THP group with concomitant metal complexation; no radiolabeling was achieved under neutral or basic conditions (20). In the case of heterocyclic N₃S ligands, it is clear that both the metal ion and the amine are required for the hydrolysis of the *S*-THP protecting group. Although the precise mechanism for this reaction is not yet established, two possible pathways can be envisioned as illustrated in Scheme 3. In the transition state, the metal ion, the ligand, and a water molecule may organize in such a manner that the heterocyclic amine can act as a general base to deprotonate the coordinated water molecule and deliver the hydroxide ion to the highly polarized carbon-sulfur bond. Alternatively, the heterocyclic bases may remove the proton from the β position to eliminate the coordinated sulfur atom. Such eliminations have been known to occur during ruthenium and rhodium metal complexation reactions with macrocyclic crown thioether ligands (21). These reactions are possible because the acidity of water is greatly enhanced when attached to metal ions; the first pK_a 's of water bound to Tc(V) and Re(V) oxo species are 2.90 and 1.31, respectively (22, 23). Thus, at any given pH, a higher concentration of hydroxide should be present in the presence of metal ion compared to pure water to catalyze the displacement or elimination reactions. Other reactions, such as the hydrolysis of amides, esters, and phosphate esters via such an organized water molecule that is coordinated at the primary coordination sphere of a transition metal ion, have been postulated previously (24–26).

Although all ligands labeled well initially with technetium and rhenium, there were considerable differences in the stability of the metal complexes (Table 2). The desired HPLC fractions were collected for each selected sample and mixed with equal volumes of either physiological saline or with stock cysteine solution. The solutions were kept at ambient temperature, and the purity was monitored over time. The technetium pyridyl and imidazolyl complexes **2a** and **4b**, respectively, were very stable even when subjected to cysteine challenge. Both morpholino complexes **5a,b** were unstable. In fact, as soon as the desired HPLC fractions of **5a,b** are isolated, the solution seemed to degrade rapidly, and the resulting HPLC profiles of these complexes were so broad and complex that it was not possible to record the purity accurately. After about 2 h, the main peaks corresponding to **5a,b** were not present in the chromatograms. Although both the technetium and rhenium imidazolyl complex **6a,b** were quite stable in saline, **6a** underwent substantial decomposition under cysteine challenge.

Biological Properties. The biodistribution results of this series of metal chelates reveal a strong correlation with the polarity of the ligands. The stepwise modifications beginning with the lipophilic, neutral pyridine moiety culminating in the polar, anionic imidazole functionalities resulted in significantly increased blood clearances and decreased soft tissue retentions that translate to improved imaging quality for these metal complexes. The biodistribution studies were not carried out on the morpholino complexes **5a,b** due to their instability.

Tables 3 and 4 show the biodistribution data for the neutral ^{99m}Tc pyridyl complex **4b** and ¹⁸⁶Re pyridyl

Table 3. Normal Rat Biodistribution of Technetium Complex 4b

organ	percent injected dose per organ (mean \pm SE) ^a			
	20 min	1 h	2 h	24 h
blood	29.0 \pm 0.6	20.4 \pm 1.6	17.5 \pm 0.7	4.4 \pm 0.4
liver	17.6 \pm 2.4	24.9 \pm 1.6	25.5 \pm 2.1	9.2 \pm 1.1
kidneys	5.4 \pm 0.7	7.0 \pm 0.7	7.9 \pm 0.7	3.3 \pm 0.2
spleen	0.61 \pm 0.02	0.52 \pm 0.03	0.47 \pm 0.02	0.19 \pm 0.01
muscle	11.3 \pm 0.7	9.6 \pm 0.3	8.6 \pm 0.3	2.6 \pm 0.1
urine ^b				24.5 \pm 3.0
feces ^b				16.9 \pm 1.0
total excreted				41.4 \pm 4.0
percent recovered				88.6 \pm 6.0

^a SE, standard error. ^b Urine and fecal values were obtained only at 24 h.

Table 4. Normal Rat Biodistribution of Rhenium Complex 4c

organ	percent injected dose per organ (mean \pm SE) ^a			
	20 min	1 h	2 h	24 h
blood	45.6 \pm 0.3	26.8 \pm 3.7	20.5 \pm 0.6	0.40 \pm 0.21
liver	10.8 \pm 0.2	11.9 \pm 2.9	10.1 \pm 1.3	0.25 \pm 0.15
kidneys	5.5 \pm 0.7	7.7 \pm 0.2	8.5 \pm 0.7	0.51 \pm 0.15
muscle	14.9 \pm 0.5	13.5 \pm 0.3	10.2 \pm 0.6	0.30 \pm 0.12
urine ^b				35.2 \pm 2.9
feces ^b				51.5 \pm 5.3
total excreted				86.8 \pm 2.3
percent recovered				88.5 \pm 1.7

^a SE, standard error. ^b Urine and fecal values were obtained only at 24 h.

complex **4c**. These compounds exhibit elevated soft tissue retention and slower blood clearance rates, with predominately hepatobiliary clearance as indicated by the high fecal excretion. The type of the coordinating metal atom did have a significant effect on the biodistribution and excretion patterns despite identical overall charge and very similar molecular structures. The Tc complex **4b** clears significantly slower compared to the Re analogue **4c** and exhibits significantly higher retention in the liver (9% ID/organ vs 0.25% ID/organ) at 24 h; the Tc complex is retained in all of the tissues at a significantly greater level. At 24 h post dosing, 41% of the injected complex was still retained *in vivo*, with urinary excretion accounting for only 24% of the material. The difference in biodistribution between **4b** and **4c** may be attributed to the relative instability of pyridyl complexes compared to the imidazole complexes and to the very sensitive nature of Re^V species with respect to oxidative decomposition to perrhenate, which generally clears via the renal system.

The first structural modification of the complex involved the replacement of the OH group by a more polar COOH moiety while maintaining the Tc as the central metal atom (compound **4d**). At physiological pH, the carboxyl group should be fully ionized to give an anionic complex. The result of this modification is a large decrease in the soft tissue retention at all time points assayed (cf. Table 5). The clearance from the liver and the whole blood was most affected by this structural change. For this complex, the kidneys accounted for 16% of the initial dose which rapidly declined to 0.5% after only 2 h. Clearance of this compound was still predominately hepatobiliary with 62% in the feces and 32% in the urine. This functional group modification also resulted in 95% overall recovery of **4d**, representing a

Table 5. Normal Rat Biodistribution of Technetium Complex 4d

organ	percent injected dose per organ (mean \pm SE) ^a			
	20 min	1 h	2 h	24 h
blood	0.44 \pm 0.04	0.23 \pm .01	0.12 \pm 0.01	<0.1 \pm 0.01
liver	1.05 \pm 0.21	0.21 \pm .01	0.09 \pm .01	<0.1 \pm 0.01
kidneys	16.1 \pm 2.3	1.9 \pm 0.2	0.51 \pm 0.03	<0.1 \pm 0.01
muscle	5.7 \pm 0.4	0.53 \pm 0.32	0.09 \pm 0.01	<0.1 \pm 0.01
urine ^b				32.5 \pm 0.9
feces ^b				62.6 \pm 2.3
total excreted				95.1 \pm 3.2
percent recovered				95.2 \pm 3.2

^a SE, standard error. ^b Urine and fecal values were obtained only at 24 h.

Table 6. Normal Rat Biodistribution of Rhenium Complex 6b

organ	percent injected dose per organ (mean \pm SE) ^a			
	20 min	1 h	2 h	24 h
blood	1.31 \pm 0.08	0.41 \pm 0.02	0.25 \pm 0.03	<0.1 \pm 0.01
liver	35.1 \pm 0.9	13.9 \pm 1.3	5.0 \pm 0.5	0.24 \pm 0.01
kidneys	1.84 \pm 0.02	0.58 \pm 0.03	0.32 \pm 0.06	<0.1 \pm 0.01
muscle	2.14 \pm 0.16	0.60 \pm 0.05	0.34 \pm 0.04	0.05 \pm 0.05
urine ^b				44.4 \pm 6.9
feces ^b				46.3 \pm 7.2
total excreted				90.6 \pm 0.3
percent recovered				90.8 \pm 0.2

^a SE, standard error. ^b Urine and fecal values were obtained only at 24 h.

Table 7. Normal Rat Biodistribution of Technetium Complex 2a

organ	percent injected dose per organ (mean \pm SE) ^a			
	20 min	1 h	2 h	24 h
blood	0.78 \pm 0.11	0.13 \pm 0.02	<0.1 \pm 0.01	<0.1 \pm 0.01
liver	5.44 \pm 0.32	0.68 \pm 0.10	0.15 \pm 0.03	<0.1 \pm 0.01
kidneys	2.36 \pm 0.18	0.30 \pm 0.04	<0.1 \pm 0.01	<0.1 \pm 0.01
muscle	3.27 \pm 0.21	1.24 \pm 0.13	0.30 \pm 0.03	<0.1 \pm 0.01
urine ^b				49.8 \pm 0.07
feces ^b				46.1 \pm 0.1
total excreted				95.9 \pm 0.8
percent recovered				96.1 \pm 0.6

^a SE, standard error. ^b Urine and fecal values were obtained only at 24 h.

significant improvement over the OH analogue (**4c**), of which 45% of the injected dose was retained *in vivo*.

In the second modification, the pyridine ring is replaced with a more polar imidazole ring (compound **6b**). The central metal was retained as Re during radiolabeling for direct comparison with the pyridine analogue. This change resulted in a significant decrease in soft tissue retention and increased blood clearance (cf. Table 6). Clearance from the blood and liver was affected most by the modification, resulting in dramatic change in the metabolism of the chelate. Initial blood uptake was only 1% ID/organ compared to 46% for **4c**, while the liver value was decreased by a factor of 3, and at 24 h was a negligible 0.05% ID/organ. More importantly, the urinary and fecal excretion rates were virtually identical at 24 h, accounting for 44% and 46%, respectively, with the remaining soft tissues contributing a negligible percentage to the overall recovery of the compound.

In the final modification, both imidazole and COOH functionalities were incorporated. The corresponding Tc

complex exhibited a very rapid clearance from all tissues assayed (cf. Table 7). Blood, liver, and kidney clearances were more rapid compared to the other complexes evaluated. At 24 h post dosing the radioactivity was equally divided between the urine and feces, indicating increased renal clearance as a result of the increased polarity of the complex and only negligible amounts of material retained *in vivo*.

Conclusions. Ligands containing unsaturated heterocycles such as the pyridyl and the imidazolyl moieties have been shown to form stable technetium and rhenium complexes. The differences in stability between these heterocyclic complexes as well as the subtle difference in kinetic stability between the two imidazolyl complexes **2a** and **6a** cannot be simply explained in terms of σ basicity or π back-bonding capability; further theoretical investigation is being pursued and will be reported elsewhere. The presence of the imidazolyl moiety results in marked improvement in blood and liver clearances compared to those containing the pyridyl moiety. In addition, the presence of a carboxyl functionality also reduces liver and blood uptake substantially and induces more rapid clearance from these tissues. The combined effect of imidazolyl and carboxyl functionalities resulted in very low uptake in, and rapid clearance from, the critical nontarget organs, liver, blood, and kidneys and should render complexes such as **2a** and **4d** useful for bioconjugation purposes.

ACKNOWLEDGMENT

We thank Dr. T. Jeffrey Dunn and Dr. Karen F. Deutsch for support and encouragement of this work and Dr. William B. Jones, Dr. Stephen R. Cooper, and Dr. Edward Deutsch for their helpful discussions and suggestions.

LITERATURE CITED

- (1) Tenenbaum, F., Lumbroso, J., Schlumberger, M., Caillou, B., Fragu, P., and Paremntier, C. (1995) Radiolabeled Somatostatin Analog Scintigraphy in Differentiated Thyroid Carcinoma. *J. Nucl. Med.* **36**, 807–810.
- (2) Lipp, W. R., Silly, H., Ranner, G., Dobnig, H., Passath, A., Leb, G., and Krejs, G. J. (1995) Radiolabeled Octreotide for the Demonstration of Somatostatin Receptors in Malignant Lymphoma and Lymphadenopathy. *J. Nucl. Med.* **36**, 13–18.
- (3) Haldemann, A. R., Rosler, H., Barth, A., Waser, B., Geiger, L., Godoy, N., Markwalder, V., Seiler, R. W., Sulzer, M., and Reubi, J. C. (1995) Somatostatin Receptor Scintigraphy in Central Nervous System Tumors: Role of Blood-Brain Barrier Permeability. *J. Nucl. Med.* **36**, 403–410.
- (4) Knight, L. C., Radcliffe, R., Maurer, A. H., Rodwell, J. D., and Alvarez, V. L. (1994) Thrombus Imaging with Technetium-99m Synthetic Peptides Based upon the Binding Domain of a Monoclonal Antibody to Activated Platelets. *J. Nucl. Med.* **35**, 282–288.
- (5) Babich, J. W., Graham, W., Barrow, S. A., Dragotakes, S. C., Tompkins, R. G., Rubin, R. H., and Fischman, A. J. (1993) Technetium-99m-Labeled Chemotactic Peptides: Comparison with Indium-111-Labeled White Blood Cells for Localizing Acute Bacterial Infection in the Rabbit. *J. Nucl. Med.* **34**, 2176–2181.
- (6) Krenning, E., Kwekkeboom, D. J., and Bakker, W. H., et al. (1993) Somatostatin Receptor Scintigraphy with [111-In-DTPA-*d*-Phe]- and [123-Tyr3]-Octreotide: The Rotterdam Experience with More than 1000 Patients. *Eur. J. Nucl. Med.* **20**, 716–731.
- (7) Jurisson, S., Berning, D., Jia, W., and Ma, D. (1993) Coordination Compounds in Nuclear Medicine. *Chem. Rev.* **93**, 1137–1156.
- (8) Rajagopalan, R., Schmidt, M. A., Grummon, G. D., Marmion, M. E., LaFourniere, L., Vanderheyden, J.-L., Deutsch, K. F., Dunn, T. J., and Srinivasan, A. (1992) in *Abstracts of Papers*, 47th Annual Meeting of the Society of Nuclear Medicine, Toronto, Ontario, Canada, Society of Nuclear Medicine, New York.
- (9) Schwochau, K., and Pleger, U. (1993) Basic Coordination Chemistry of Technetium. *Radiochim. Acta* **63**, 103–110.
- (10) Johannsen, B., Noll, B., Leibnitz, P., Reck, G., Noll, St., and Spies, H. (1993) Occurrence and Nature of Different Tc(V) and Re(V) Complexes with Mercapto/Amide Ligands. *Radiochim. Acta* **63**, 133–137.
- (11) Gustavson, L. M., Rao, T. N., Jones, D. S., Fritzberg, A. R., and Srinivasan, A. (1991) Synthesis of a New Class of Tc Chelating Agents: N₂S₂ Monoamine–Monoamide (MAMA) Ligands. *Tetrahedron Lett.* **32**, 5485.
- (12) Weiden, P. L., Breitz, H. B., Seiler, C. A., Bjorn, M. J., Ratliff, B. A., Mallett, R., Beaumier, P. L., Appelbaum, J. W., Fritzberg, A. R., and Salk, D. (1993) Rhenium-186-Labeled Chimeric Antibody NR-LU-13: Pharmacokinetics, Biodistribution, and Immunogenicity Relative to Murine Analog NR-LU-10. *J. Nucl. Med.* **34**, 2111–2119.
- (13) Kasina, S., Rao, T. N., Srinivasan, A., Sanderson, J. A., Fitzner, J. N., Reno, J. M., Beaumier, P. L., and Fritzberg, A. R. (1991) Development and Biologic Evaluation of a Kit for Preformed Chelate Technetium-99m Radiolabeling of an Antibody Fab Fragment Using a Diamide Dimercaptide Chelating Agent. *J. Nucl. Med.* **32**, 1445–1451.
- (14) Sugiura, Y. (1978) Newly Synthesized Sulfhydryl- and Imidazole-Containing Tripeptides with a Specific Copper-Binding Site. *Inorg. Chem.* **17**, 2176–2182.
- (15) Bryson, N., Lister-James, J., Jones, A. G., Davis, W. M., and Davidson, A. (1990) *Inorg. Chem.* **29**, 2948.
- (16) Schneider, R. F., Subramanian, G., Feld, T. A., McAfee, J. G., Zapf-Longo, C., Palladino, E., and Thomas, F. D. (1984) *N,N*-Bis(*S*-benzoylmercaptoacetamido)ethylenediamine and Propylenediamine Ligands as Renal Function Imaging Agents. 1. Alternate Synthetic Methods. *J. Nucl. Med.* **25**, 223–229.
- (17) Bastiaansen, L. A. M., and Godefroi, E. F. (1978) 2-Aminomethylimidazole and Imidazole-2-Carboxaldehyde: Two Facile Syntheses. *J. Org. Chem.* **43**, 1603–1604.
- (18) Fritzberg, A. R., Kasina, S., Rao, T. N., VanderHeyden, J. L., and Srinivasan, A. (1990) U.S. Patent 4 965 392.
- (19) Green, T. W., and Wuts, P. G. M. (1991) Protection for the Thiol Group, in *Protective Groups, in Organic Synthesis*, pp 277–308, John Wiley and Sons, Inc., New York.
- (20) Rao, T. N., Gustavson, L. M., Srinivasan, A., Kasina, S., and Fritzberg, A. R. (1992) Kinetics and Mechanism of Reaction of S-Protected Dithiol Monoamine-monoamide (MAMA) Ligands with Technetium: Characterization of a Technetium Thiolate–Thioether–MAMA Complex, a Kinetic Intermediate of the Reaction. *Nucl. Med. Biol.* **19**, 889.
- (21) Blake, A. J., Holder, A. J., Hyde, T. I., Kuppers, H. J., Schroder, M., Stoetzel, S., and Wieghardt, K. J. (1989) *J. Chem. Soc., Chem. Commun.* 1600.
- (22) Roodt, A., Leipoldt, J. G., Helm, L., and Merbach, A. E. Equilibrium Behavior and Proton Transfer Kinetics of the Dioxotetracyanometalate Complexes of Molybdenum(IV), Tungsten(IV), Technetium(V), and Rhenium(V): Carbon-13 and Oxygen-17 NMR Study.
- (23) Fothergill, M., Goodman, M. F., Petruska, J., and (1995) Warshel, A. Structure–Energy Analysis of the Role of Metal Ions in Phosphodiester Bond Hydrolysis by DNA Polymerase I. *J. Am. Chem. Soc.* **117**, 11619–11627.
- (24) Chapman, W. H., and Breslow, R. (1995) Selective Hydrolysis of Phosphate Esters, Nitrophenyl Phosphates, and UpU by Dimeric Zinc Complexes Depends the Spacer Length. *J. Am. Chem. Soc.* **117**, 5462–5469.
- (25) Chin, J. (1991) Developing Artificial Hydrolytic Metalloenzymes by a Unified Mechanistic Approach. *Acc. Chem. Res.* **24**, 145.
- (26) Tsubouchi, A., and Bruice, T. C. (1995) Phosphate Ester Hydrolysis Catalyzed by Two Lanthanum Ions. Intramolecular Nucleophilic Attack of Coordinated Hydroxide and Lewis Acid Activation. *J. Am. Chem. Soc.* **117**, 7399–7411.

Use of Designed Peptide Linkers and Recombinant Hemoglobin Mutants for Drug Delivery: *In Vitro* Release of an Angiotensin II Analog and Kinetic Modeling of Delivery

S. P. Trimble,[†] D. Marquardt,[†] and D. C. Anderson^{*,‡}

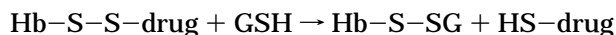
Somatogen Inc., Boulder, Colorado 80026, and Rigel Inc., Sunnyvale, California 94086. Received December 20, 1996[®]

We have designed and tested specific peptide linkers for the glutathione-mediated reductive release of the angiotensin II analog *N*-acetyl-CGDKVYIHPF attached to recombinant human hemoglobin mutants by a disulfide bond. Inclusion of negatively charged residues decreased the rate of release by as much as 5-fold for the N-terminal linker DCD when compared to that of the control linker CG. Two different surface cysteine mutants in the second domain of the $\alpha_1\alpha_2$ -chain of recombinant human hemoglobin, D75C and K16C, were examined for their effect on the release of peptide by reduced glutathione. The reaction of the D75C-peptide conjugate with glutathione for release of the peptide is slow, with a second-order rate constant of $2.1 \text{ M}^{-1} \text{ s}^{-1}$, allowing the possibility of long term delivery. The rate of peptide release from the K16C vs the D75C mutant was decreased 15-fold. Thus, different peptide release rates can be obtained by changing both peptide linker residues and the surface location of peptide attachment. Kinetic modeling of this release using either measured or literature values for different parameters suggests boundary conditions for application to the *in vivo* release of peptidomimetics, small molecules, or other drugs bound to the hemoglobin surface.

INTRODUCTION

The delivery of peptides, peptidomimetics, or small proteins may represent a more challenging goal than delivery of small molecules due to their short serum half-life, susceptibility to proteases, and first pass metabolism in the liver (1). As a consequence of the lack of oral bioavailability and sensitivity to proteases in the digestive tract of peptides larger than di- or tripeptides, parenteral delivery of peptides and small proteins may be preferred in some situations (2, 3). Thus, these molecules, or drugs for which compliance with frequent oral dosage schedules might be difficult to achieve, such as antibiotics used on an outpatient basis to treat diseases for which drug resistance is a problem such as tuberculosis (4), may represent one class of targets for an injectable multiweek timed release system.

A method of attaching a drug of interest with slow desorption under physiological conditions might allow the use of proteins with a long serum half-life as a drug delivery system. One such mechanism might utilize small molecule reducing agents such as serum endogenous thiols, which include GSH,¹ in the range of $10 \text{ }\mu\text{M}$ in human plasma (5), free reduced homocysteine ($0.1\text{--}0.35 \text{ }\mu\text{M}$) (6) and free cysteine (ca. $5 \text{ }\mu\text{M}$) (7). This method is designed to function by reductive cleavage of disulfide-linked drugs or peptides from a protein carrier such as hemoglobin by GSH.



Recombinant human hemoglobin has been the subject of extensive development over the last 12 years, beginning with the work of Nagai and Thøgersen (8–13), and

has been used in clinical trials for the delivery of oxygen as a blood substitute in humans in doses of up to 100 g. The crystal structures of both the oxy and deoxy forms are known, enabling rational design of this protein for a variety of purposes. These results present the opportunity to use mutants of native human hemoglobin as a model system for delivery of molecules other than oxygen.

In this paper, we discuss the development and *in vitro* testing of different peptide linkers, consisting of two or three amino acids inserted between hemoglobin and the peptide to be released, which are designed to allow peptide attachment via a disulfide bond and to control the reductive release of a peptide or drug by glutathione. We also examine the use of different surface cysteine mutants of recombinant hemoglobin which might be useful for this purpose, $\alpha_1\alpha_2$ -chain D75C and K16C. On the basis of the results of *in vitro* peptide release experiments presented here, and on the basis of known or determinable parameters for steps which might be important in the release and pharmacokinetics of peptides and drugs, we also explore a kinetic model of this timed release system to examine the most critical parameters which require further optimization. The model yields predictions of the time frame within which controlled release could occur, and thus the system's potential utility.

EXPERIMENTAL PROCEDURES

Peptide Design, Synthesis, and Radiolabeling. Angiotensin II (DRVYIHPF) was modified to include an N-terminal [^{14}C]acetyl group to allow *in vitro* measurements of free and attached peptide, a lysine replacing arginine 2 of native angiotensin II to avoid tachyphylaxis in animal studies (14), and with the dipeptide CG appended to the N terminus of angiotensin II to allow attachment to hemoglobin via a disulfide bond. The glycine acts as a spacer between the angiotensin II residues and cysteine. The N-terminal cysteine was protected with the *S*-nitropyridine sulfonyl group (15) to

* To whom reprint requests should be addressed.

[†] Somatogen Inc.

[‡] Rigel Inc.

[®] Abstract published in *Advance ACS Abstracts*, May 1, 1997.

¹ Abbreviations: GSH, reduced glutathione; IHP, inositol hexaphosphate; PBS, phosphate-buffered saline; EC₅₀, concentration required to half-activate a response; *t*_{1/2}, half-life.

allow direct coupling to hemoglobin thiols and to avoid disulfide formation between peptides (16, 17). The cysteine was added to the N and not to the C terminus since the C-terminal carboxylate and C-terminal six or seven residues are important for the receptor binding and activity of this peptide (18, 19).

[14C]-*N*-Acetylangiotensin II analogs were synthesized using standard butyloxycarbonyl (boc)-benzyl solid phase synthesis methodology on an Applied Biosystems 431A synthesizer (20). The peptides were *N*-acetylated on the resin with [¹⁴C]acetic anhydride, cleaved from the resin with hydrofluoric acid in the presence of anisole as a scavenger using the high protocol of Tam and Merrifield (21), which was required by the nitropyridinesulfonyl protection of the cysteine, and purified by reversed phase chromatography on a Vydac 4.6 × 250 mm C4 column. All analogs have been tested and were found to be active as vasoconstrictors in rats, with *EC*₅₀'s in the low nanomolar range (unpublished observations). For comparison, free angiotensin II contracts isolated rabbit aorta with an *EC*₅₀ of 1.9 nM (22).

Hemoglobin Mutants. Hemoglobin mutants were expressed in *Escherichia coli* and their sequences verified by DNA sequencing (10). Besides the use of a glycine to fuse the termini of the two α -chains to give a single α,α -chain which limits renal filtration of hemoglobin (12), the hemoglobin mutants also contain the β -chain Presbyterian mutation N108K, N-terminal Val to Met mutations for the α,α - and β -chains and a single cysteine in the C terminus of the two α -domains of the fused α,α -chain. The mutants were purified in a manner similar to described methods (23), using a Pharmacia Q-Sepharose column to capture bacterial contaminants while hemoglobin flows through and a second Q-Sepharose column to resolve the hemoglobin. A butyl hydrophobic interaction replaced the S-sepharose column for greater resolution. A G-25 or Sephacryl S-200 gel filtration column equilibrated with PBS at pH 7.4 was used after conjugate formation to separate unattached peptide from conjugate.

Peptide Conjugation to Hemoglobin. Conjugation of free peptide to hemoglobin was followed by the disappearance of free peptide counts and appearance of bound hemoglobin counts after gel filtration and was done under argon at pH 7.8–8.0 in the presence of 1–2 mM IHP. In the absence of oxygen, IHP binds to deoxyhemoglobin with a *K*₄ of 4 μ M while binding to oxyhemoglobin ca. 2500-fold more weakly (24). IHP was included to shift oxygen saturation curves to the right and maintain hemoglobin in the deoxy conformation. Argon was gently bubbled through a solution of IHP, buffer and peptide for 25 min before addition of hemoglobin through a septum. Typically, 50 mg/mL hemoglobin was reacted with a 20–100% molar excess of peptide under a gentle argon sparge for 2–3 h. Lower levels of hemoglobin gave substoichiometric peptide incorporation. Conjugate formation was checked by the ratio of hemoglobin-bound counts to total hemoglobin and by electrospray mass spectrometry on a VG BioQ apparatus by F. Bitsch and C. Shackleton (Children's Hospital Oakland Research Institute, Oakland, CA). All reactions of hemoglobin–peptide conjugates with GSH were under anoxic conditions at pH 7.4 in PBS, to avoid concurrent oxidation of GSH.

Curve Fitting and Modeling of Peptide Release Kinetics. Peptide release time courses were fit to a first order equation using the Levenberg–Marquard algorithm contained in the program PEAKFIT (Jandel Scientific, San Rafael, CA). Modeling of the free peptide time course in serum used the program MSIMPC, obtained from the Quantum Chemistry Program Ex-

change (25). This program uses stochastic methods to model the kinetics of chemical reactions and has been applied to a number of systems (see ref 26 for examples). After a reaction scheme and rate laws (in this case, a second-order reaction), rate constants, initial concentrations, the total number of molecules reacting in a fixed volume ($1-2 \times 10^5$), and the time of reaction ($1-2 \times 10^5$ events) were specified, a random number is assigned, causing selection of one reaction event. The resulting probability of reaction is based on the rate law. This is repeated for different times on the basis of the selected random number, generating a progress curve, which has random statistical noise and is thus not smooth. The results are then converted to concentrations and time and plotted.

The standard values used in the simulations were experimentally determined with our system (*k*_{2nd}, peptide half-life) or taken from the literature (hemoglobin half-life, glutathione concentration) or are well within the range of hemoglobin levels already used in humans (conjugate concentration). Values used for simulation were varied around these parameters to examine their importance in peptide delivery and, except as noted, are not meant to imply that they occur *in vivo*.

Molecular Modeling of Peptide Conjugates. Molecular modeling of the hemoglobin–peptide conjugates was based on the structure of deoxyhemoglobin (27) and was achieved Insight II v. 2.3.5 and Discover v. 2.9 or 2.9.6 (Biosym Inc., San Diego, CA). Hemoglobin was altered to include the Presbyterian mutation in both beta chains (N108K), a Gly fusing the C terminus of one α -chain with the N terminus of the second, creating a " α,α " chain, a Val to Met mutation at the N termini of the α,α - and β -chains, and changing either Lys 16 or Asp 75 to Cys in the second domain of the α,α -chain for attachment of the peptide. Each mutant used had only a single surface cysteine; all other cysteines are buried and inaccessible to water (27). Heme parameters were supplied by Biosym for use with the cvff force field and were based on those of Karplus (28). A nonbonded cutoff of 21 Å with a 1.5 Å switching distance was used to avoid program termination errors, and an explicit dielectric of 1.0 was used since the structure was hydrated. All ionizable residues were assigned the charge state they would have at pH 7.4. The heme rings were altered to create partial double bonds throughout the tetrapyrrole structure. After the peptide of interest in a β -sheet, α -helix, or extended conformation to hemoglobin was attached via a disulfide bond, the resulting structure was soaked in a 32 Å sphere of water centered on C α of residue 4 of the attached peptide. The sphere covered a circle of ca. 19 Å radius on the hemoglobin surface around the attachment site. The peptide–hemoglobin conjugate was then minimized for 100 steps of the steepest descent algorithm and enough steps of the conjugate gradient algorithm that the gradient of the energy was less than 0.001 kcal/Å. The system was minimized as above, fixing all heavy atoms beyond 27 Å from peptide residue 4, allowing at least 5 Å of mobile water beyond the end of the peptide.

RESULTS

Characterization of Peptide–Hemoglobin Conjugates. Angiotensin II analogs were attached to recombinant human hemoglobin mutants as described in Experimental Procedures, and stoichiometries of attachment were measured by counting ¹⁴C from the attached labeled peptide. Electrospray mass spectrometry was used to further examine the resulting conjugates for the

Table 1. Electrospray Mass Spectrometry of Hemoglobin–Angiotensin II Analog Conjugates

molecule	molecular weight (expected ^a)	molecular weight (observed)	
D75C β chain ^b	15 914.40	15 915.7 \pm 1.3	(<i>n</i> = 9)
in peptide conjugate	(no reaction)	Δ = 1.3	
D75C α , α -chain	30 312.96	30 341.4 \pm 21.3	(<i>n</i> = 4)
unconjugated		Δ = 28	
D75C α , α -chain	31 532.38	31 554.1 \pm 18.3	(<i>n</i> = 4)
Ac-CGDKVYIHPF		Δ = 22	
K16C β -chain ^b	15 914.40	15 914.5	(<i>n</i> = 1)
in peptide conjugate		Δ = 0.1	
K16C α , α -chain	30 299.87	30 304.1	(<i>n</i> = 1)
unconjugated		Δ = 4.2	
K16C α , α -chain	31 519.29	31 527.6	(<i>n</i> = 1)
AcCGDKVYIHPF		Δ = 8.3	

^a The calculated molecular weight is an average molecular weight; Δ refers to the difference between the observed and expected molecular weights. ^b The β -chains in both D75C and K16C are identical to the wild type β -chain.

distribution of attached peptides on α , α - and β -globin chains. The results are shown in Table 1.

The β -chains of both the D75C and K16C mutants appear to be identical, which is expected as there are no mutations introduced into these chains, and the weights are very close to those predicted on the basis of the sequence. No peptides were observed attached to the β -chains. This observation is consistent with the lack of reaction of this peptide with β -Cys 93, which can be derivatized by glutathione (29–31). The unconjugated α , α -chains either are very close to their predicted molecular weight (K16C mutant) or are almost within experimental error of the predicted weight (D75C mutant); thus, the difference between the expected and observed weight is difficult to interpret. Upon derivatization with peptide, the α , α -chain shifts for both the D75C and K16C mutants to a weight consistent with the addition of one peptide per chain. No additional peaks at higher weight were observed, suggesting that only one peptide per α , α -chain was attached. A control reaction of peptide with hemoglobin with no surface cysteine did not result in incorporation of ¹⁴C counts per minute into either globin chain.

GSH Dependence of Release of Peptide from D75C Hemoglobin. To examine the reductive release of peptide from hemoglobin mutants, the GSH dependence of the rate of peptide release was determined. Figure 1A shows the time course of peptide release as measured by gel filtration. Each curve, representing a different concentration of GSH injected at zero time, was well fit as a first-order process. The half-lives are shown in the figure legend. A linear plot of the first-order rate constants vs [GSH] in Figure 1B gave a second-order rate constant of 2.1 M⁻¹ s⁻¹ (32).

Control of the Peptide Release Rate by Peptide Linker Design and the Peptide Attachment Site. Figure 2 compares the rate of peptide release, using 0.5 mM GSH, from both the D75C and K16C mutants. This concentration of GSH was chosen to give a reasonable time frame for the experiment. The rate of release from D75C was roughly 15-fold faster than that from K16C hemoglobin.

The effect of different peptide linkers between the hemoglobin Cys and angiotensin II analog on peptide release rates from D75C hemoglobin was also examined. The linkers were designed to include different numbers of negatively charged residues around the cysteine attached to the hemoglobin surface cysteine. Increased negative charge density might be expected to slow attack

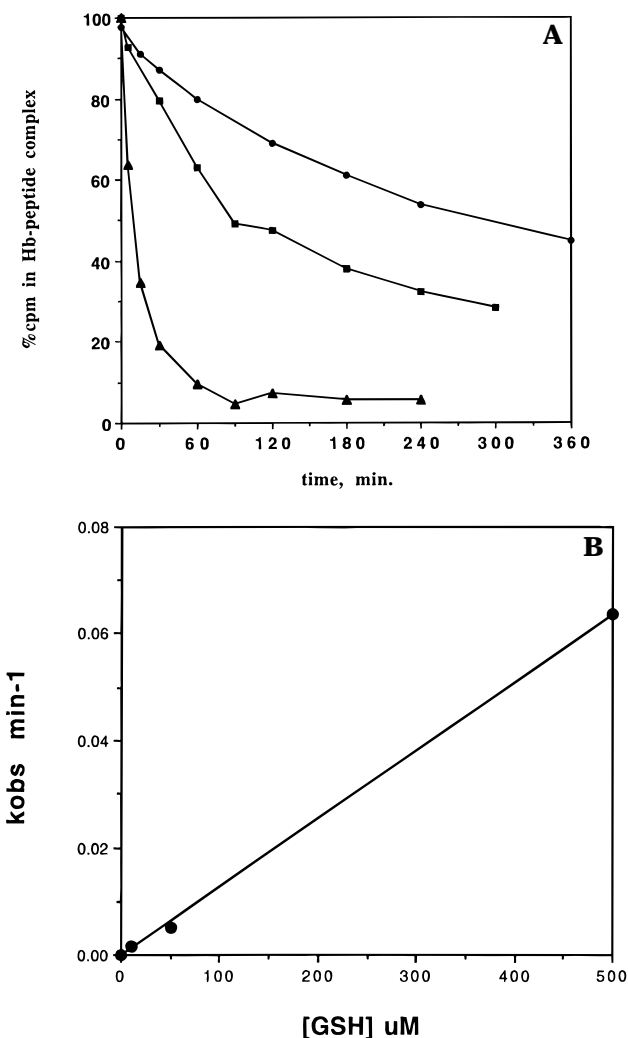


Figure 1. GSH dependence of the release of [¹⁴C]-*N*-acetyl-CGDKVYIHPF from D75C hemoglobin. (A) Time course of peptide release from the conjugate at three different levels of GSH. Each time course was well fit as a (pseudo) first-order kinetic process. The concentrations of GSH are as follows: filled circles (10 μM GSH), filled squares (50 μM GSH), and filled triangles (500 μM GSH). (B) Determination of the second-order rate constant from the slope of the plot of the pseudo-first-order rate constant *k*_{obs} vs [GSH] (32).

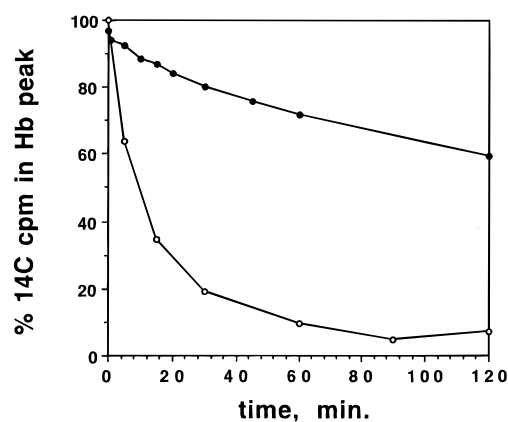


Figure 2. Release of [¹⁴C]-*N*-acetyl-CGDKVYIHPF from D75C and K16C hemoglobin by GSH. The half-lives for release from the two different hemoglobins are 165 min for K16C (filled circles) and 10.9 min for D75C (open circles).

by and thus reductive release by a thiolate anion, by electrostatic repulsion.

Table 2 shows the results of this experiment. Addition of a single Asp to the peptide sequence decreased the rate

Table 2. Release of Peptide Analogs with Different Linkers from D75C Hemoglobin^a

peptide	$t_{1/2}$ (min)
N-Ac-CGDKVYIHPF-COO ⁻	8.4
N-Ac-DCGDKVYIHPF-COO ⁻	9.8
N-Ac-GCDDKVYIHPF-COO ⁻	15.6
N-Ac-DCDDKVYIHPF-COO ⁻	45.3

^a Reduction of 3 μ M D75C hemoglobin-peptide (1:1) conjugate by 0.5 mM GSH at pH 7.4 and 37 °C in PBS under anoxic conditions as measured by gel filtration of free and bound peptide. The $t_{1/2}$ is calculated from a first-order fit of the data.

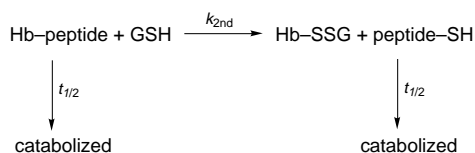
Table 3. Effect of Varying Kinetic Parameters on Predicted Peptide Serum Levels

parameter	standard value	range for kinetic modeling
Hb-peptide conjugate half-life (h)	6	1.5–48 (32)
k_{2nd} ($M^{-1} s^{-1}$)	2.1	0.2–18
[Hb]	22 μ M ^a	2.75–40 g
peptide half-life (min)	3 ^b	1–96
[GSH] (μ)	10	1–100

^a This concentration corresponds to ca. 22 μ M of conjugate injected into a person with a 7 L blood volume. ^b This half-life is approximately that of the angiotensin analog in rats.

of release 2-fold when it is immediately C-terminal to the Cys but had no effect when it is N-terminal to the Cys. Addition of an Asp on both sides of the Cys decreased the rate of release 5-fold relative to the linker CG.

Modeling of Peptide Release Rates. To examine the effect of pharmacokinetic parameters on how peptide release might occur *in vivo*, and thus which parameters might be most important for extended delivery with this system, stochastic modeling of peptide release kinetics was used (25, 26). The modeling allows simulation of free peptide concentrations based on a kinetic scheme describing release of peptide from its hemoglobin conjugate.



The reductive release of peptide was assumed to be a second-order reaction (Figure 1B), as this fits the experimental data and conjugate and free serum glutathione concentrations are likely to be similar. Hemoglobin disappearance from the circulation was simplified to be first-order, and peptide loss from blood was also assumed to be first-order. The ranges of individual parameters examined, and experimentally determined standard values or values taken from the literature, are shown in Table 3. A broad range was chosen for each parameter to examine its importance in delivery of free peptide into serum.

Figure 3 shows results from the kinetic modeling of the effect of the serum half-lives of the hemoglobin-peptide (or drug) conjugate and of the free peptide (drug). Each of the five parameters was independently varied around its standard value while the other values were kept constant. The predicted time course of free peptide in serum is shown for each varied parameter, with the illustrated concentration range of free peptide being up to 20–100 nM. Such a range might be desirable for potent drugs in serum.

The time course of free peptide at or above 10 nM is extended with increases in conjugate half-life (Figure 3A) from 1.5 to 48 h. A similar effect is seen with peptide

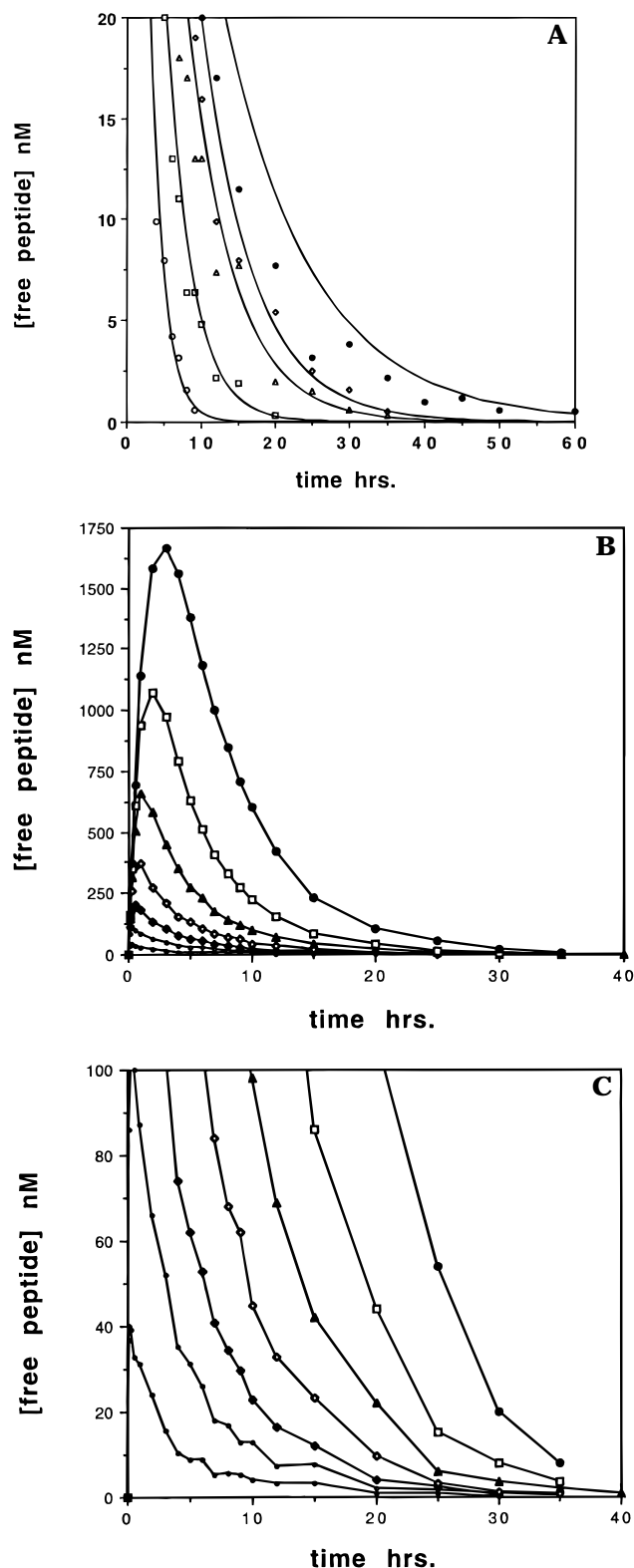


Figure 3. Predicted serum time courses of free peptide as a function of conjugate and free peptide serum half-lives. (A) Dependence of the free peptide time course on the serum half-life of the peptide-hemoglobin conjugate. The different half-lives simulated are 1.5 h (open circles), 3 h (open squares), 6 h (open triangles), 12 h (open diamonds), and 96 h (filled circles). (B) Dependence of the free peptide time course on the serum half-life of free peptide, which are 1 min (small filled circle), 3 min (small open square), 6 min (filled diamond), 12 min (open diamond), 24 min (filled triangle), 48 min (open square), and 96 min (large filled circle). The entire time course is shown in the upper panel, and the time course between 0 and 100 nM peptide is shown in the lower panel.

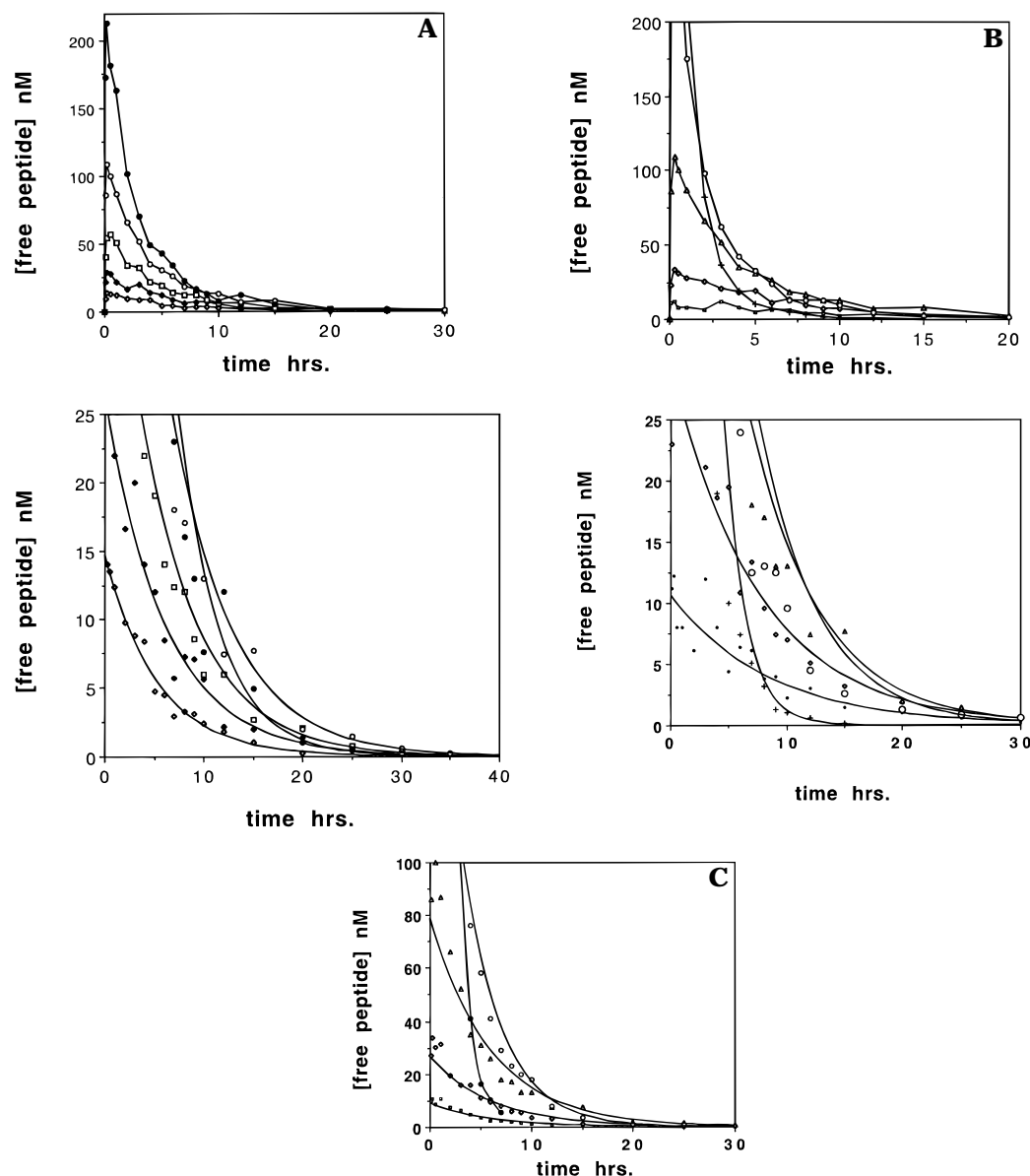


Figure 4. Predicted time courses of free serum peptide as a function of initial levels of peptide–hemoglobin conjugate, the second-order rate constant for peptide release, and levels of GSH. (A) Dependence of free peptide on initial serum conjugate concentration. Different serum conjugate levels simulated are 2.75 μM (open diamonds), 5.5 μM (filled diamonds), 11 μM (open squares), 22 μM (open circles), and 44 μM (filled circles). The full time course is shown in the top panel and is expanded to the region below 25 nM peptide in the bottom panel. (B) Dependence of free serum peptide on the second-order rate constant for the reaction of GSH with conjugated peptide. Different values for k_{2nd} are 0.2 $\text{M}^{-1} \text{s}^{-1}$ (small open circles), 0.6 $\text{M}^{-1} \text{s}^{-1}$ (open diamonds), 2.1 $\text{M}^{-1} \text{s}^{-1}$ (open triangles), 6 $\text{M}^{-1} \text{s}^{-1}$ (large open circles), and 18 $\text{M}^{-1} \text{s}^{-1}$ (crosses). The full time course is shown in the top panel and is expanded to the region below 25 nM peptide in the bottom panel. (C) Dependence of the free serum peptide time course on serum GSH levels. Different levels used are 1 μM (small open square), 3 μM (open diamond), 10 μM (open triangle), 30 μM (open circle), and 100 μM (filled circle).

half-life (Figure 3B). This half-life is normally ca. 3 min. for free angiotensin analogs in rat serum (data not shown); the angiotensin II analog has not been optimized to increase its serum half-life. Increasing this value to 96 min dramatically extends the predicted time course of free peptide in serum. Increases in the initial amount of hemoglobin–peptide conjugate also extend the time course of free peptide (Figure 4A), but at higher levels (44 μM conjugate), a shorter time course is observed, due to depletion of GSH. A steady state production of free GSH has not been incorporated into this model. The second-order rate constant for reaction of conjugate with GSH, which can be controlled by the location of the peptide attachment site and/or the peptide linker composition, is also important for peptide release (Figure 4B). With the standard parameters shown in Table 3, the

highest predicted serum peptide levels occur with a k_{2nd} of 2.1 $\text{M}^{-1} \text{s}^{-1}$. A higher value depletes conjugated peptide, while lower values appear to release peptide too slowly relative to the half-life of the peptide conjugate. Likewise, an optimal level of GSH for long term peptide release also exists; under these conditions, it is in the range of 10 μM GSH (Figure 4C). Higher levels deplete conjugated peptide more rapidly, while lower levels release less peptide.

When the individually optimized parameters are combined (Figure 5), the predicted time course of free serum peptide is significantly prolonged with free peptide remaining above 20 nM for over 10 days. Varying the second-order rate constant significantly affects the maximal concentration of peptide, which rises and falls in concentration in a fashion similar to that of a chemical

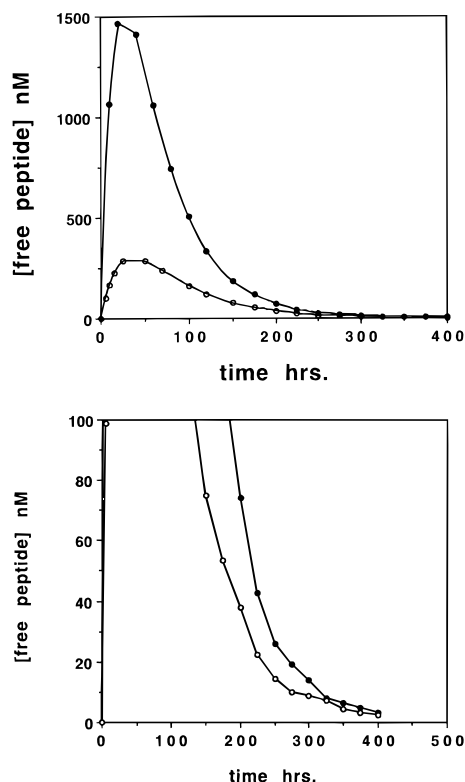


Figure 5. Predicted time courses of free serum peptide when individual kinetic parameters giving the longest serum peptide delivery are combined in the kinetic model. The parameters used are conjugate concentration ($22 \mu\text{M}$), conjugate half-life (48 h), peptide half-life (96 min), GSH concentration ($10 \mu\text{M}$), and second-order rate constant for peptide release [$0.03 \text{ M}^{-1} \text{ s}^{-1}$, (open circles) and $0.2 \text{ M}^{-1} \text{ s}^{-1}$ (filled circles)]. The full peptide time course is shown in the top panel, while that between 0 and 100 nM peptide is shown in the bottom panel.

reaction intermediate (34). After 400 h, the predicted serum concentration of GSH is $8.5 \mu\text{M}$, 15% below the starting level.

Molecular Modeling of Peptide Conjugates. Peptide (*N*-Ac-CGDKVYIHPF) conjugates with the D75C and K16C mutations were constructed and minimized in water for the deoxyhemoglobin structure. In the absence of an experimentally determined structure of the conjugate, modeling was done to examine the local environment around the disulfide bond, for comparison with peptide release data. The starting peptide conformation after attachment to hemoglobin was varied to examine the effect on the minimized structure. Table 4 shows the results from the minimizations of extended, α -helical, and β -sheet peptides attached to D75C and K16C mutants. The distance from the nearest charged residue is listed in the table. Minimization of the different conjugates shows that, in the K16C mutant, the charged residue nearest to the sulfurs composing the disulfide bond attaching the peptide is Glu 116, while the imidazole of His 72 is the (partially) charged residue nearest to Cys 75 in the D75C mutant.

DISCUSSION

In this paper, we have initiated the characterization of recombinant hemoglobin as a model system for the timed release of peptides, peptidomimetics, small molecules, or small proteins. To cleanly construct conjugates with a test peptide, which can be difficult when using chemical cross-linkers (20), we have used hemoglobin mutants with only a single surface cysteine and peptides containing a single cysteine in a noncritical part of their

sequence (18). The hemoglobin mutants are different from those used for oxygen delivery experiments or for clinical trials; we did not observe unusual effects of the mutant hemoglobin with its single surface cysteine on blood pressure in rats. The angiotensin II analogs are active as vasoconstrictors, with an EC_{50} in the range of 2 nM (unpublished data). Electrospray mass spectrometry shows that peptide-hemoglobin conjugate formation occurs cleanly on the α , α -chain with only one peptide attached. The use of a small molar excess of peptide during conjugation, a somewhat bulky cysteine protecting group, and a peptide significantly larger than the tripeptide glutathione results in a selective derivatization of the hemoglobin surface cysteine and no reaction with the β -cysteines 93.

This controlled release system is intended to function by reductive release of disulfide-attached peptides, drugs, or small proteins; thus, it is important to establish control over the rate of reductive release of a test peptide using a physiologically relevant reductant such as reduced glutathione. Other small molecule thiols such as cysteine and homocysteine could also reductively release peptide from the conjugate *in vivo*, but would be less important than reduced glutathione due to their lower serum concentrations (5–7). We have achieved control over the peptide release rate in two ways. First, by varying the site of attachment on the hemoglobin surface, we have seen a 15-fold slower rate of peptide release with the K16C vs the D75C mutant. Second, using the D75C mutant, we have observed a 5-fold range of release rates by varying the aspartate content of the peptide linker region.

All of the experimental peptide release results have been obtained with deoxyhemoglobin. Minimization of the deoxyhemoglobin conjugates in water with different peptide starting conformations was done to examine the environment around the peptide attachment site. Although the results are for single starting conformations in a situation where the peptide probably undergoes significant motion and conformational flexibility due to its attachment to the hemoglobin surface at only one terminus, they allow speculation regarding the fact that the slower release rate for K16C than for D75C could be due at least in part to the presence of a nearby negative charge on Glu 116 in the K16C mutant, and perhaps to a nearby partial positive charge on the imidazole ring of α -His 72 in the D75C mutant, depending on the pK_a of this histidine. The nearby negative charge could decrease the rate of reductive cleavage of the disulfide by the glutathiolate anion by charge repulsion. The effect of the peptide linker DCD in the D75C mutant, placing two aspartates near the disulfide, is consistent with this possibility. A steric contribution to occluding attack by glutathione cannot be completely ruled out, although addition of an Asp in the linker DCG did not change the rate of release relative to the control linker CG. Results similar to those discussed above may occur for oxyhemoglobin, as the nearest charged residues in the oxy structure are the same ones found for the deoxyhemoglobin mutants discussed above. These results suggest that several peptides or drugs could be attached to a protein carrier with surface cysteine mutations at different locations, potentially providing both short- and longer-lasting release times as well as enhanced amounts of released drug.

To assess the importance of the experimentally determined release rate constants, and which other parameters might be important for a multiday sustained release system, we simulated the time dependence of free peptide in serum by modeling the evolution of the second-order

Table 4. Results of Minimizations of Hemoglobin-Peptide Conjugates^a

peptide conformation before minimization	nearest charge for D75C	nearest charge for K16C
extended	α -His 72 imidazole nitrogen: 5.6 Å from peptide Cys 1 S _γ	none closer than 6 Å
β -sheet	α -His 72 imidazole nitrogen: 5.1 Å from Cys 75 S _γ	α -Glu 116 carboxylate oxygen: 5.5 Å from Cys 16 S _γ
right-handed α -helix	none closer than 6 Å	α -Glu 116 carboxylate oxygen: 3.56 Å from Cys 16 S _γ ; peptide Asp 3 carboxylate oxygen: 3.40 Å from peptide Cys 1 S _γ

^a In all of the calculations, the dielectric constant was 1, and the deoxyhemoglobin structure was used.

reaction with GSH. For release resulting in sustained free peptide or drug concentrations in the range of 10 nM, individual species (the carrier, its peptide conjugate, and the free peptide) cannot have short half-lives. Extending the half-life of the most transient species, in this case free peptide or free drug, gives the greatest improvement in delivery time. For a system giving timed release on a multiweek time scale, a long carrier half-life, as long or longer than that for dextran-hemoglobin of 2.4 days (33),² may also be important. Given defined values for the other variables, the initial conjugate concentration, k_{2nd} , and GSH concentration all had optimal values within a defined range. Combining individually optimized parameters, each of which is in an experimentally determined range or within a range of values reported in the literature, results in a prediction which holds that sustained release at or above 10 nM serum levels could occur for ca. 2 weeks.

The pharmacokinetic modeling-derived dependence of predicted serum peptide levels on variations in GSH, shown in Figure 4C, also serves as a rough guide for predicting the effect on free serum peptide levels of variations in serum GSH. If one takes the variation within individual studies as a guide to variation in humans, this variation is on the order of 15–30% between normal individuals (7, 35, 36). These individual differences will cause only a relatively small change in the rate of free peptide production. Differences in plasma GSH levels in different tissues may also affect drug release. For example, higher levels of GSH are found in rat hepatic vein plasma, and lower levels are found in renal vein plasma (37), suggesting that a higher rate of peptide or drug release might be found in the hepatic vein. In either case, the effect of small or large changes in GSH can be modeled using this methodology to predict potential problems due either to very low or very high peptide levels in different compartments or individuals.

The reliance on serum thiols for peptide release from hemoglobin conjugates has the potential to reduce plasma levels of GSH, which are coupled to cellular levels. In extreme circumstances, the loss of intracellular GSH to levels 20% of normal may allow cellular injury from oxidants (38). When the parameters individually optimized for the longest delivery are combined in a kinetic simulation, the predicted serum GSH levels are decreased only 15% after 400 h. This decrease may be overestimated, since it does not take into account the normal efflux of GSH into the blood from the liver (39), and that loss of GSH due to oxidizers results in enhanced synthesis and increased GSH, which may exceed initial levels (40). Thus, in the absence of use during conditions of severe oxidative stress, this system may not cause harmful sustained decreases in cellular GSH. This suggests that protein carriers utilizing this method of attachment and release may have utility for multiweek

release. Possible uses for such a system could include dosing with drugs on a similar time scale for which patient compliance is a problem, such as antibiotics treating tuberculosis (4).

LITERATURE CITED

- Edgington, S. M. (1991) The anatomy of access: peptide drug delivery. *Bio/Technology* 9, 1327.
- Sanders, L. (1992) Controlled delivery systems for peptides. In *Peptide and Protein Drug Delivery*. (V. H. L. Lee, Ed.) pp 785–807, Marcel Dekker Inc., New York.
- Lee, V. H. L. (1992) Changing needs in drug delivery in the era of peptide and protein drugs (V. H. L. Lee, Ed.) 1–57, Marcel Dekker Inc., New York.
- Yew, W., and Chau, C. (1995) Drug-resistant tuberculosis in the 1990's. *Eur. Respir. J.* 8, 1184–1192.
- Meister, A. (1991) Glutathione deficiency produced by inhibition of its synthesis, and its reversal; applications in research and therapy. *Pharmacol. Ther.* 51, 155–194.
- Araki, A., and Sako, Y. (1987) Determination of free and total homocysteine in human plasma by high-performance liquid chromatography with fluorescence detection. *J. Chromatogr.* 422, 43–52.
- Burgunder, J., Nelles, J., Bilzer, M., and Lauterburg, B. (1988) Ethanol decreases plasma sulphhydryls in man: effect of disulfiram. *Eur. J. Clin. Invest.* 18, 420–424.
- Nagai, K., and Thogersen, H. C. (1984) Generation of beta globin by sequence-specific proteolysis of a hybrid protein produced in *Escherichia coli*. *Nature* 309, 810–812.
- Nagai, K., Perutz, M. F., and Poyart, C. (1985) Oxygen binding properties of human mutant hemoglobins synthesized in *Escherichia coli*. *Proc. Natl. Acad. Sci. USA* 82, 7252–7255.
- Hoffman, S. J., Looker, D., Roehrich, J. M., Cozart, P. E., Durfee, S. L., Tedesco, J., and Stetler, G. (1990) Expression of fully functional tetrameric human hemoglobin in *Escherichia coli*. *Proc. Natl. Acad. Sci. U.S.A.* 87, 8521–8525.
- Snyder, S., and Walder, J. A. (1991) Chemically modified and recombinant hemoglobin blood substitutes. *Bio/Technology* 9, 101–116.
- Looker, D., Abbott-Brown, D., Cozart, P., Durfee, S., Hoffman, S., Mathews, A., Miller-Roehrich, J., Shoemaker, S., Trimble, S., Fermi, G., Komiyama, N., Nagai, K., and Stetler, G. (1992) A human recombinant haemoglobin designed for use as a blood substitute. *Nature* 356, 258–260.
- Bunn, H. F. (1993) The use of hemoglobin as a blood substitute. *Am. J. Hematol.* 42, 112–117.
- Miasiro, N., Oshiro, M., Paiva, T. B., and Paiva, A. (1983) Role of the two N-terminal residues of angiotensin II in the production of tachyphylaxis. *Eur. J. Pharmacol.* 87, 397–406.
- Matsueda, R., Kimura, T., Kaiser, E. T., and Matsueda, G. R. (1981) 3-Nitro-2-pyridinesulfonyl group for protection and activation of the thiol function of cysteine. *Chem. Lett.* 737–740.
- Bernatowicz, M. S., Matsueda, R., and Matsueda, G. (1986) Preparation of boc[S-(3-nitro-2-pyridinesulfonyl)]-cysteine and its use for unsymmetrical disulfide bond formation. *Int. J. Pept. Protein Res.* 28, 107–112.
- Drijfhout, J. W., Perdijk, E. W., Weijer, W. J., and Bloemhoff, W. (1988) Controlled peptide-protein conjugation by means of 3-nitro-2-pyridinesulfonyl protection-activation. *Int. J. Pept. Protein Res.* 32, 161–166.

² Hemoglobin half-life has been reported to be as long as 2.4 days for dextran-hemoglobin conjugates.

- (18) Khosla, M. C., Smeby, R., and Bumpus, F. (1974) in *Handbook of Experimental Physiology* (I. Page and F. Bumpus, Eds.) Vol. 37, pp 126–161, Springer-Verlag, Heidelberg.
- (19) Pendleton, R., Gessner, G., and Horner, E. (1989) Studies defining minimal receptor domains for angiotensin II. *J. Pharmacol.* 250, 31–36.
- (20) Anderson, D. C., Manger, R., Schroeder, J., Woodle, D., Barry, M., Morgan, A., and Fritzberg, A. R. (1993) Enhanced in vitro tumor cell retention and internalization of antibody derivatized with synthetic peptides. *Bioconjugate Chem.* 4, 10–18.
- (21) Tam, J. P., Heath, W. F., and Merrifield, R. B. (1983) SN₂ deprotection of synthetic peptides with a low concentration of HF in dimethyl sulfide: evidence and application in peptide synthesis. *J. Am. Chem. Soc.* 105, 6442.
- (22) Oshiro, M., Miasiro, N., Paiva, T., and Paiva, A. (1984) Angiotensin tachyphylaxis in the isolated rabbit aorta. *Blood Vessels* 21, 72–79.
- (23) Looker, D., Mathews, A., Neway, J., and Stetler, G. (1994) Expression of recombinant human hemoglobin in *Escherichia coli*. *Methods Enzymol.* 231, 364–374.
- (24) Robert, C. H., Fall, L., and Gill, S. J. (1988) Linkage of organic phosphates to oxygen binding in human hemoglobin at high concentrations. *Biochemistry* 27, 6835–6843.
- (25) Houle, F. A., and Bunker, D. L. (1981) Simulation methods in kinetics courses. *J. Chem. Educ.* 58, 405–407.
- (26) Bunker, D. L., Garrett, B., Kleindienst, T., and Long, G. S. (1974) Discrete simulation methods in combustion kinetics. *Combust. Flame* 23, 373–379. Davis, J. H., Shea, K. J., and Bergman, R. G. (1977). Stereochemistry of the Cope rearrangement and mechanism of thermal aromatization of 3,3'-bicyclopropenyls. *J. Am. Chem. Soc.* 99, 1499–1507.
- (27) Fermi, G., Perutz, M. F., Shaanan, B., and Fourme, R. (1984) The crystal structure of human deoxyhaemoglobin at 1.74 Å resolution. *J. Mol. Biol.* 175, 159–174.
- (28) Gelin, B. R., Lee, W. M. A., and Karplus, M. (1983) Hemoglobin tertiary structural change on ligand binding: its role in the co-operative mechanism. *J. Mol. Biol.* 171, 489–559.
- (29) Garel, M.-C., Domenget, C., Caburi-Martin, J., Prehu, C., Galacteros, F., and Beuzard, Y. (1986) Covalent binding of glutathione to hemoglobin. I. Inhibition of hemoglobin S polymerization. *J. Biol. Chem.* 261, 14704–14709.
- (30) Craescu, C. T., Poyart, C., Schaeffer, C., Garel, M. C., Kister, J., and Beuzard, Y. (1986) Covalent binding of glutathione to hemoglobin. II. Functional consequences and structural changes reflected in nmr spectra. *J. Biol. Chem.* 261, 14710–14716.
- (31) Wodak, S., De Coen, J.-L., Edelstein, S. J., Demarne, H., and Beuzard, Y. (1986) Modification of human hemoglobin by glutathione. III. Perturbations of hemoglobin conformation analyzed by computer modeling. *J. Biol. Chem.* 261, 14717–14724.
- (32) Jencks, W. P. (1969) *Catalysis in Chemistry and Enzymology*, pp 564–565, McGraw-Hill, New York.
- (33) Tam, S.-C., Blumenstein, J., and Wong, J. T.-F. (1978) *Can. J. Biochem.* 56, 981–984.
- (34) Frost, A. A., and Pearson, R. G. (1961) *Kinetics and Mechanism*, p 167, John Wiley & Sons, New York.
- (35) Mills, B. J., Richie, J. P., and Lang, C. A. (1994) Glutathione disulfide variability in normal human blood. *Anal. Biochem.* 222, 95–101.
- (36) Martensson, J. (1987) Method for determination of free and total glutathione and γ -glutamylcysteine concentrations in human leukocytes and plasma. *J. Chromatogr.* 420, 152–157.
- (37) Anderson, M. E., and Meister, A. (1980) Dynamic state of glutathione in blood plasma. *J. Biol. Chem.* 255, 9530–9533.
- (38) Reed, D. J. (1990) Review of the current status of calcium and thiols in cellular injury. *Chem. Res. Toxicol.* 3, 495–502.
- (39) Kretzschmar, M., and Klinger, W. (1990) The hepatic glutathione system-influences of xenobiotics. *Exp. Pathol.* 38, 145–164.
- (40) Meister, A. (1991) Glutathione deficiency produced by inhibition of its synthesis, and its reversal; applications in research and therapy. *Pharmacol. Ther.* 51, 155–194.

BC970037H

Peptomer Aluminum Oxide Nanoparticle Conjugates as Systemic and Mucosal Vaccine Candidates: Synthesis and Characterization of a Conjugate Derived from the C4 Domain of HIV-1_{MN} Gp120

Andreas Frey,^{†,‡} Marian R. Neutra,[†] and Frank A. Robey^{*,§}

Department of Pediatrics, Harvard Medical School, and GI Cell Biology Research Laboratory, Children's Hospital, Boston, Massachusetts 02115, and Oral and Pharyngeal Cancer Branch, The National Institute of Dental Research, National Institutes of Health, Bethesda, Maryland 20892. Received January 30, 1997[®]

Peptomers are polymers composed of peptides that are specifically cross-linked in a head-to-tail fashion. Recently, a peptomer composed of an amphipathic peptide from the C4 domain of HIV-1_{MN} gp120 was shown to display a prominent α -helical conformation that, as an immunogen, elicited rabbit antibodies recognizing native and recombinant gp120 [Robey et al. (1995) *J. Biol. Chem.* 270, 23918–23921]. For the present study, we synthesized a conjugate composed of the C4 peptomer covalently linked to calcinated aluminum oxide nanoparticles. The nanoparticles were first reacted with (3-aminopropyl)-triethoxysilane to provide an amine load of 15.9 mmol of R-NH₂/g of solid. The amine-modified aluminum oxide nanoparticles then were reacted with *N*-acetylhomocysteine thiolactone at pH 10 to place a reactive thiol on the nanoparticles. A bromoacetylated C4 peptomer, modified at the ϵ -amines of lysine residues, then was reacted with the thiolated nanoparticles to give the peptomer covalently linked to aluminum oxide via a thioether bond. The peptomer load was determined to be 16 mg of peptomer/g of particles, a 55% theoretical yield. Particle shape and size of the peptomer-conjugated alumina were analyzed by electron microscopy and displayed a mean maximum diameter of 355 nm and a mean minimum diameter of 113 nm, well within the desired size range of 300 nm believed to be optimal for mucosal immunization purposes. Experimentally determined values of mean particle diameters, specific surface area, and specific peptomer load provided the information necessary to calculate the mean antigen load, which was determined to be $53\,000 \pm 42\,000$ peptomer epitopes per particle. Peptomer–alumina conjugates, such as that described here, could form the basis of a new class of biomaterial that combines a chemically defined organic immunogen with a nontoxic chemically defined inorganic adjuvant.

INTRODUCTION

Human immunodeficiency virus type 1 (HIV-1) is a pathogen that is transmitted across the mucosal surfaces of the urogenital tract and the rectum (DeSchryver and Meheus, 1990; Amerongen et al., 1991). To intercept the virus on this route of infection, vaccines must be developed that induce a mucosal immune response against HIV-1 (Forrest, 1992; Marx et al., 1993). An important component of mucosal immune protection is antigen-specific secretory immunoglobulin A (sIgA), dimeric or polymeric molecules that are secreted onto mucosal surfaces where they bind pathogens, trap them in mucus, and prevent their further progression (Neutra et al., 1994). Nevertheless, an HIV vaccine should also be able to induce strong systemic humoral and cell-mediated immunity to arm the body against the virus if it breaches the mucosal barrier.

A sIgA response is induced only when the vaccine is delivered to the immune system via mucosal surfaces. In the intestine and rectum, antigens, particles, and pathogens are taken up by M cells, a specialized epithelial cell type that occurs exclusively in the epithelium over organized mucosa-associated lymphoid tissue. Selective uptake by M cells is enhanced when the antigen is formulated as a micro- or nanoparticulate material

ideally of 0.05–1 μ m diameter, since only M cells are able to translocate particles of such a size across the tight epithelial barrier (Neutra et al., 1996a,b; Frey et al., 1996). Soluble antigens in the size range of oligopeptides and small proteins are less desirable since they may be taken up by epithelial lining cells and give rise to a state of immunological unresponsiveness that is called oral tolerance (Bland and Warren, 1986). Formulating the antigen in particulate form also is beneficial for systemic vaccinations since mononuclear phagocytes, like macrophages and Kupffer cells, efficiently phagocytose, process, and present antigens that appear in such a particulate form.

When antibody-mediated protection against intact pathogens is desired, as for the protection of the mucosal surfaces by sIgA, it is essential that the vaccine be formulated to closely resemble the native structure and conformation of the antigen targets. The native structure and conformation of protein antigens can be altered by aggregation, improper folding, and defects in glycosylation of recombinant proteins or synthetic peptides as well as denaturation and breakdown during the formulation procedure. In addition, antigenic variation in the wild-type pathogen may reduce the efficacy of a vaccine based on protein antigens generated in the laboratory.

The development of an effective vaccine against HIV-1 hinges on all of these factors. For effective protection against HIV-1, the antibody response must be directed against the viral envelope glycoproteins gp120 or gp41. Antibodies directed against certain epitopes within the HIV-1 gp120 and gp41, however, were shown to enhance infection of macrophages and monocytes in culture

* Address correspondence to this author. Telephone: 301-496-4779; fax: 301-402-0823; e-mail: robey@yoda.nid.nih.gov.

[†] Harvard Medical School and Children's Hospital.

[‡] Present address: Center for Molecular Biology of Inflammation, University of Muenster, D-48129 Muenster, FRG.

[§] National Institutes of Health.

[®] Abstract published in *Advance ACS Abstracts*, May 1, 1997.

(Takeda et al., 1988) and to cross-react with immune-relevant host proteins such as HLA-DR (Lasky et al., 1987; Golding et al., 1988) and certain immunoglobulin subclasses (Bjork, 1991). Furthermore, both envelope proteins evade the immune surveillance of the body by continuous variation of their antigenic sites (Starcich et al., 1986; Gurgo et al., 1988). On the virus surface, the envelope proteins gp120/41 are assembled in complex oligomeric structures (Earl et al., 1990) in which the second and third variable regions (V2 and V3) and a segment of the fourth constant region (C4) of gp120 are exposed (Moore et al., 1994). Among those, C4 is of particular importance for the virulence of the virus because it is part of the binding site that interacts with the viral receptor CD4 (Lasky et al., 1987; Cordonnier et al., 1989). As numerous monoclonal antibodies against C4 are neutralizing and broadly cross-reactive between different HIV-1 isolates (Sun et al., 1989; Nakamura et al., 1993), this region appears to be an attractive candidate for an HIV-1 subunit vaccine.

However, synthetic C4 peptides do not bind CD4 without being in a solution containing helix-inducing substances such as certain nonionic detergents (Robey et al., 1996), and antibodies raised against monomeric C4 peptides (Robey et al., 1995) do not recognize native or recombinant gp120 glycoprotein. The reason for this is because monomeric C4 peptides display a random coil or β -sheet. Polymerizing the monomer head-to-tail in a coordinate manner renders the product predominantly α -helical and, with the proper adjuvant, enables it to induce antibodies that recognize recombinant as well as native gp120 (Robey et al., 1995). In contrast, polymerizing the monomer randomly (head-to-tail/tail-to-head) and immunizing in Freund's adjuvant, which could denature secondary structures (Scibienski, 1973; Robey et al., 1995), did not produce antibodies that recognized intact gp120 (Sastry and Arlinghaus, 1991). Thus, if C4 is used in a vaccine formulation, it should not only be polymeric but also be delivered in a nondenaturing environment in order to maintain its α -helical conformation.

Aluminum oxohydroxide, phosphate, and hydroxyphosphate compounds are hydrophilic, particulate adjuvants with a long history of safety and efficacy for systemic vaccination (Hem and White, 1995; Gupta et al., 1995). However, the drawbacks of these substances for oral administration are their pH lability and the noncovalent adsorption of the antigen to their surfaces. Thus, the antigen may readily dissociate during gastrointestinal passage, rendering the vaccine ineffective.

To circumvent the problems associated with the gel-type aluminum compounds, we designed a candidate vaccine in which the antigen is an HIV-1_{MN} gp120 C4 domain peptomer that is covalently conjugated onto the surface of calcinated aluminum oxide nanoparticles. In the present paper, we describe the synthesis and characterization of this conjugate with special emphasis on its immunologically relevant properties, such as particle diameter, antigen load, and degree of polymerization of the individual C4 domain oligopeptide units.

EXPERIMENTAL PROCEDURES

Materials. *Reagents for Particle, Peptide, and Peptomer Synthesis.* α -Aluminum oxide nanoparticles were purchased from Fluka (Ronkonkoma, NY). (3-Aminopropyl)triethoxysilane (98%), nitric acid, anhydrous toluene, toluene, and acetone (all ACS grade) were from Aldrich Chemical (Milwaukee, WI). Deionized ultrapure water was prepared using a Millipore water purification system (Millipore, Bedford, MA). All chemicals used for

peptide synthesis were from Applied Biosystems (Foster City, CA). Bromoacetic acid (99+%) and *N*-acetylhomocysteine thiolactone (99%) were obtained from Aldrich Chemical. *N*-succinimidyl bromoacetate was synthesized as described previously (Bernatowicz and Matsueda, 1986).

Materials and Reagents for Amino Acid Analysis, SDS-PAGE Analysis, and Electron Microscopy. Chemicals for the preparation of aqueous buffers and solutions were obtained from various sources in the highest quality commercially available (Sigma Chemical, St. Louis, MO; Fisher Scientific, Pittsburgh, PA; Aldrich Chemical; Calbiochem-Novabiochem, San Diego, CA). Tris-tricine 10–20% polyacrylamide gels were from Novex (San Diego, CA), and prestained low range protein molecular weight standards were from Gibco-BRL (Gaithersburg, MD). Poly(vinyl formal) (Formvar 15/95) and 150 square mesh copper grids were purchased from Polysciences Inc. (Warrington, PA).

Synthetic Procedures. *Synthesis of the HIV_{MN} gp120 C4 Domain Peptomer.* The general methods for preparing peptomers and their monomeric peptide building blocks have been described in detail previously (Robey and Fields, 1989; Robey, 1994). In brief, cysteine-containing peptide monomers were synthesized on *p*-methyl-PAM resin using the standard BOC technology on an Applied Biosystems Model 430 A automated peptide synthesizer on a 0.5 mmol scale. In the last step of the synthesis of the peptide chain, bromoacetic acid anhydride was reacted with the amino terminal amino acid to form the *N*- α -bromoacetyl-derivatized, fully protected peptide. Deprotection and release of the bromoacetylated peptide from the resin were accomplished by treating the resin with anhydrous hydrogen fluoride containing 10% (v/v) *m*-cresol. After evaporation of the hydrogen fluoride, the residual resin-peptide mixture was extracted with ethyl acetate followed by extraction of the peptide in 0.1 M acetic acid. The peptide solution was separated from the resin by filtration and dried by lyophilization. Purification of the peptide was accomplished by preparative reversed-phase HPLC on a Vydac C18 column using a 0.1% aqueous trifluoroacetic acid/acetonitrile gradient. The purified peptide was lyophilized and stored at room temperature in the dark. The *N*- α -bromoacetyl-derivatized HIV_{MN} gp120 C4 domain peptide was obtained in yields between 50 and 70%.

To form the HIV_{MN} gp120 C4 domain peptomer, typically 10 mg of purified *N*- α -bromoacetyl-derivatized peptide were dissolved in 1 mL of deoxygenated 10 mM Tris-HCl and 1 mM EDTA, pH 8.0, and allowed to autopolymerize for 21 h at room temperature under continuous stirring. The reaction was terminated by dialysis against water followed by dialysis against 0.1 M sodium bicarbonate, both at 4 °C using 15 000 MWCO dialysis tubing (Spectrum, Houston, Texas). The peptomer was then end-capped by first reacting it with 10 μ L/mL (143 mM) β -mercaptoethanol followed by 32 mg/mL (173 mM) iodoacetamide, each for 1 h at room temperature under continuous stirring. The end-capped peptomer was dialyzed against 0.1 M sodium acetate followed by deionized water, both at 4 °C. At that stage, the peptomer solution was either used directly for bromoacetylation of lysines with *N*-succinimidyl bromoacetate or lyophilized for long-term storage. When lyophilized, the sodium acetate form of the peptomer was a dry white powder that was stored desiccated at room temperature. Typical yields were 80–90% (referring to the initial amount of *N*- α -bromoacetyl-derivatized peptide).

Bromoacetylation of the HIV_{MN} gp120 C4 Domain Peptomer. A total of 12.4 mg (52.5 μ mol) *N*-succinimidyl bromoacetate was dissolved in 124 μ L of DMF, and 22.4

μL (~ 9 mmol of ester) of this solution was added to a solution of 20 mg of HIV_{MN} gp120 C4 domain peptomer (~ 26 mmol of free side chain amine) in 20 mL of water. After 15 min incubation at room temperature, the reaction was terminated by extensively dialyzing against O_2 -free deionized water at room temperature. The resulting 20 mL 1 mg/mL of bromoacetylated peptomer in water was used directly to react with the thiol-derivatized particles: derivatization yield, 28% of the free side chain amine ($\sim 80\%$ of the theoretical value referring to the amount of *N*-succinimidyl bromoacetate).

Surface Activation of the Aluminum Oxide Nanoparticles. The cleaning and surface activation of the alumina was carried out as recommended by Lynn (1975) and Weetall (1976). In a 2-L Erlenmeyer flask, 126.7 g (1.24 mol) of α -aluminum oxide nanoparticles (300 nm nominal diameter, calcinated at 1300 °C, 99.99% pure, >95% α -form) was suspended in 1140 mL of 5% (w/v) nitric acid and heated under swirling for 90 min at 88 °C. The slurry then was allowed to cool to 0 °C in an ice-water bath for 90 min before it was transferred into polyallomer centrifuge bottles, it was centrifuged at 1500g for 10 min at 4 °C, and the supernatant was aspirated. To wash the particles, they were resuspended mechanically in deionized ultrapure water at room temperature and centrifuged at 9500g for 15 min at 4 °C, and the supernatant was removed by aspiration. After a total of 10 washes in 440 mL of deionized ultrapure water each, the particle sediment was transferred into a nitric acid-cleaned glass beaker, dried at 250 °C until the weight was constant (21 h), pulverized in a nitric acid-cleaned mortar, and stored desiccated at room temperature in a nitric acid-cleaned glass bottle: yield, 112.2 g (88.6%).

Amine Modification of the Activated Aluminum Oxide Nanoparticles. The amine modification of the alumina was adapted from the procedures described by Lynn (1975) and Weetall (1976). In a 2-L round-bottom flask, 50.2 g (0.49 mol) of surface-activated, dry aluminum oxide nanoparticles was suspended in 450 mL of anhydrous toluene; 50 mL (0.21 mol) of (3-aminopropyl)triethoxysilane was added; and the mixture was refluxed under anhydrous conditions for 23 h at 135 °C in an oil bath. Then the suspension was allowed to cool to ambient temperature over 3 h before it was transferred into polyallomer centrifuge bottles and centrifuged at 200g for 5 min; the supernatant was aspirated. To wash the particles, they were resuspended mechanically in 450 mL of fresh toluene at room temperature and centrifuged, and the supernatant was removed by aspiration. After five washes in toluene, 450 mL each (centrifugation conditions: 200g, 5 min, 4 °C), followed by three washes in acetone, 450 mL of each (centrifugation conditions: 5000g, 20 min, 4 °C), the particle sediment was transferred to a nitric acid-cleaned glass beaker and dried for 17 h under vacuum at room temperature followed by 22 h at 115 °C and normal pressure. Then the sediment was pulverized in a nitric acid-cleaned mortar and the amine-modified nanoparticles were stored desiccated at room temperature in an amber bottle: yield, 48.1 g (96% referring to the weight of the underivatized surface activated particles); amine load, 15.9 mmol of $\text{R-NH}_2/\text{g}$ of solid.

Thiol Derivatization of the Amine-Modified Aluminum Oxide Nanoparticles. A 250-mg sample (1.57 mmol) of *N*-acetylhomocysteine thiolactone was added to 1 g of amine-modified aluminum oxide nanoparticles (15.9 mmol R-NH_2) in 10 mL of O_2 -free 0.1 M sodium borate buffer, pH 10, in a 13-mL polypropylene tube. The tube was placed on a rotator, and the reaction was allowed to proceed at room temperature for 45 min under constant

rotation at 30 rpm. The particles were then washed by centrifuging the buffer-particle mixture at 300g for 5 min at room temperature and resuspending the sediment in O_2 -free phosphate-buffered saline (PBS). This washing procedure was repeated twice, and the particles were finally suspended in 1 mL O_2 -free PBS.

Coupling of Bromoacetylated HIV_{MN} gp120 C4 Domain Peptomer to Thiol-Derivatized Aluminum Oxide Nanoparticles. A total of 20 mL of a solution of 1 mg/mL bromoacetylated peptomer (~ 7.3 mmol bromoacetyl residues) in water was added to 1 mL of thiol-derivatized particles suspended in PBS (700–800 mg of solids) in a 50-mL conical polypropylene tube. The mixture was placed on a rotator and mixed at room temperature for 1 h under constant rotation at 30 rpm. Then, 1 mL of O_2 -free 0.1 M sodium bicarbonate was added, and the reaction was allowed to proceed for another 65 h. The suspension was then centrifuged at 3000g for 20 min at room temperature and the resulting sediment was washed three times in PBS and five times in deionized water by resuspending and then centrifugating at 4 °C. The final sediment was lyophilized and stored desiccated at room temperature: yield, 684 mg of peptomer nanoparticles containing 16 mg of peptomer/g of particles (55% of the theoretical value).

Analytical Procedures. Analysis of the Aluminum Oxide Nanoparticle Derivatives. The amount of free amine that was covalently linked to the aluminum oxide particles was determined with the ninhydrin method of Sarin *et al.* (1981). The presence of free sulfhydryl groups on the modified aluminum oxide that was formed after the reaction of the free amine with *N*-acetylhomocysteine thiolactone was determined using Ellman's reagent (Ellman, 1959), and the amount of peptide conjugated to the aluminum oxide particles was determined by amino acid analysis using the Waters Picotag HPLC system (Waters Corp., Milford, MA).

SDS-Polyacrylamide Gel Analysis of Peptomer Preparations. Peptomer in sample buffer [2% (w/v) sodium dodecylsulfate, 10% (v/v) glycerol, 20% (v/v) β -mercaptoethanol, 0.01% (w/v) bromophenol blue] was denatured for 4 min at 100 °C, loaded (1–1.5 mg/lane) onto tris-tricine 10–20% polyacrylamide gradient/SDS gels, and run for 2 h at 40–50 mA in tris-tricine electrophoresis buffer (12.1 g/L tris base, 17.9 g/L tricine, 1 g/L sodium dodecyl sulfate). Gels were fixed for 3.5 h in 10% (v/v) acetic acid and 30% (v/v) methanol, and silver-stained according to the method of Oakley *et al.* (1980).

Circular Dichroism of Peptomer Preparations. CD spectra of the peptides, peptomers, and *N*- ϵ -bromoacetylated peptomers were studied using a Jasco Model J-500A/DP-501N CD spectropolarimeter with peptides and peptomers in 10 mM phosphate buffer pH 7.2. Details were described previously (Robey *et al.*, 1995).

Densitometry. To determine the relative amounts of individual peptide oligomers in the peptomer preparations, a photographic reproduction of a silver-stained peptomer polyacrylamide gradient gel was scanned with a Microtek Scanmaker III scanner (Microtek Lab Inc., Redondo Beach, CA) at 600 \times 600 dpi and analyzed with the NIH Image software package (National Institutes of Health, Bethesda, MD) after one-dimensional vertical background subtraction on an Apple Power PC 7100/66 computer (Apple Inc., Cupertino, CA).

Electron Microscopy and Particle Size Determination. A 5-mg sample of surface-activated aluminum oxide nanoparticles, amine-modified nanoparticles, or peptomer-conjugated nanoparticles was suspended in 1 mL of deionized water by agitation and brief sonication (1–2 \times 5 s) in a water bath sonicator (Sonorex RK510S,

Bandelin Electronic, Berlin, FRG). The suspensions were serially diluted to concentrations of 500, 50, and 5 mg/mL particles in water, with sonication between each dilution step.

For transmission electron microscopy (TEM), 10 mL of each diluted particle suspension was placed on formvar-coated copper grids, allowed to settle, and dried overnight. Particles were photographed at 14000 \times and 31000 \times magnification in a Philips EM 410 transmission electron microscope (Philips Electron Optics, Eindhoven, The Netherlands) using a magnification standard.

For scanning electron microscopy (SEM), a drop of each particle suspension was placed on a glass slide precoated with 3 nm of platinum/carbon, allowed to settle, drained, and air-dried overnight before it was coated with platinum/carbon at an angle of 65° under continuous rotation of the sample. The particles were photographed at 6000 \times to 60000 \times magnification in a Hitachi S-5000 field emission scanning electron microscope (Hitachi Instruments Inc., San Jose, CA) using a magnification standard. Particle sizes were determined by measuring the diameters of 125 randomly selected particles of each type on TEM photographs.

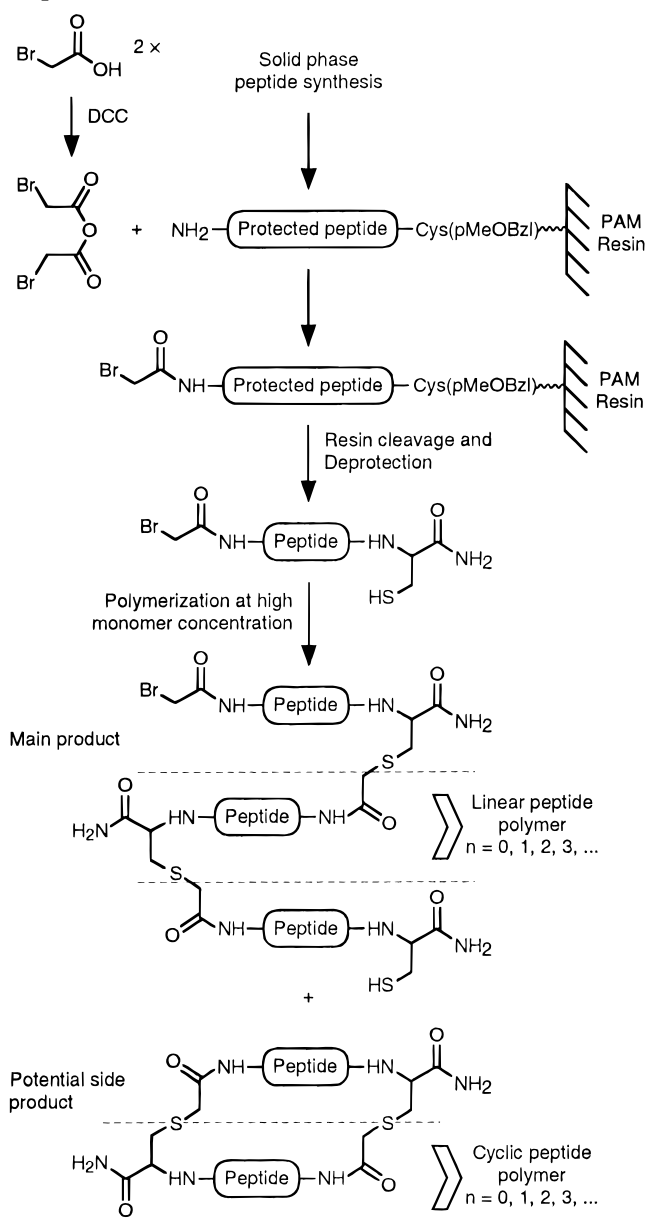
Determination of Nanoparticle Surface Area and Porosity. The specific surface area of the aluminum oxide nanoparticles was determined by nitrogen adsorption using the multipoint BET method (Brunauer et al., 1938) on a Quantachrome Autosorb 1 automated gas sorption system and by mercury porosimetry on a Quantachrome Autoscan 60 mercury porosimeter. Pore size, pore volume, and pore surface area were determined by mercury porosimetry (mercury intrusion analysis) (Washburn, 1921). Both analyses were performed by Quantachrome Corp. (Boynton Beach, FL).

RESULTS

Peptomers are polymers composed of head-to-tail linked synthetic peptides. The peptomer designed for this candidate HIV vaccine is a homopolymer of 18-mer oligopeptides comprised by the amino acid sequence: KIKQIINMWQEVGKAMYAC. The first 17 amino acids of this sequence motif represent amino acids 419–436 of gp120, the HIV-1_{MN} gp120 precursor protein (Gurgo et al., 1988). The sequence is a highly conserved linear epitope in the fourth constant region (C4) of gp120 (between hypervariable regions V4 and V5) (Starich et al., 1986). It is an essential part of the CD4 receptor binding site of gp120 (Lasky et al., 1987), and it was shown to give rise to virus-neutralizing antibodies (Sun et al., 1989; Nakamura et al., 1993).

Synthesis of the HIV_{MN} gp120 C4 Domain Peptomer Aluminum Oxide Nanoparticles. The HIV_{MN} gp120 C4 domain peptomer aluminum oxide nanoparticles were prepared by separately synthesizing the peptomer antigen and the particulate carrier and conjugating both compounds in a terminal step, as outlined in Schemes 1 and 2. First, the peptide monomer for the preparation of the peptomer was synthesized as C-terminal amide on an automated peptide synthesizer. To allow subsequent head-to-tail polymerization via thioether linkages, an additional cysteine, not present in HIV-1_{MN} gp120 at this position, was placed at the carboxy terminal end of the peptide chain. At the amino terminus, a bromoacetyl moiety was introduced by reacting the N-terminal amine of the immobilized, side-chain-protected peptide with bromoacetic acid anhydride (Scheme 1). The entire bifunctional peptide was then deprotected and released from the resin by anhydrous hydrogen fluoride, conditions that had been shown previously not to affect the integrity of the *N*- α -bromoacetyl

Scheme 1. Synthesis of HIV_{MN} gp120 C4 Domain Peptomer^a

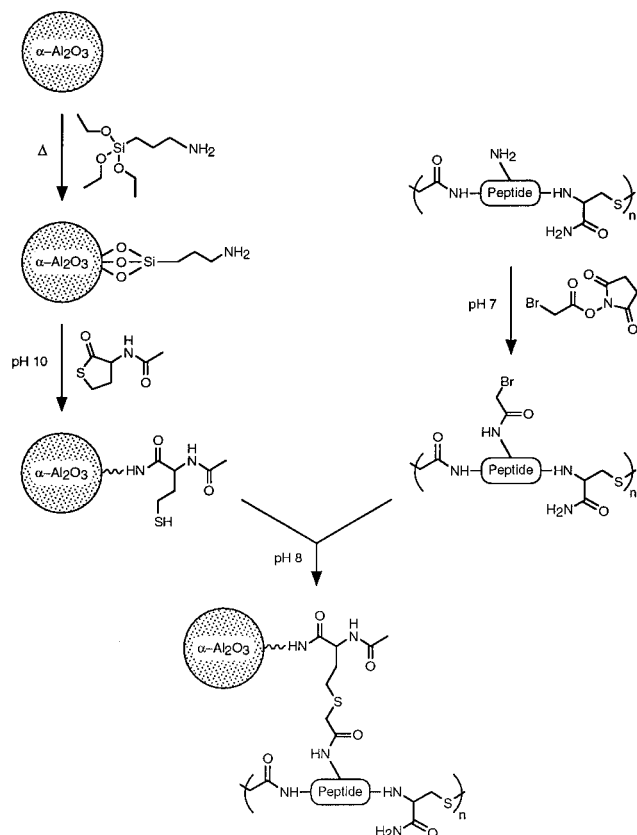


^a The C4 peptide used here and before (Robey et al., 1995, 1996) has the amino acid sequence, KIKQIINMWQEVGKAMYAC-NH₂.

moiety (Robey and Fields, 1989). To prevent premature polymerization or cyclization after removal of the sulfhydryl protecting group, all subsequent steps involving the monomeric peptide were carried out under acidic conditions. Typical yields of crude *N*- α -bromoacetyl-derivatized cysteine-containing peptide were between 50 and 70%. After preparative HPLC, 30% of the expected pure peptide was obtained.

Autopolymerization of the *N*- α -bromoacetyl-derivatized, cysteine-containing peptide was initiated by dissolving the purified peptide in aqueous buffer at slightly alkaline pH (pH 8.0). The reaction was performed at a high monomer concentration (≥ 10 mg/mL) to minimize cyclization reactions (Scheme 1). Under such conditions, the reaction was almost complete after 3 h, at which time most of the detectable free thiols had been consumed. However, as longer polymer chains may be formed preferentially toward the end of the reaction, a prolonged reaction time of 21 h was allowed. As expected, the

Scheme 2. Synthesis of HIV_{MN} gp120 C4 Domain Peptomer Nanoparticles



resulting product was not a homogeneous polymer of distinct molecular weight but rather a mixture of peptide oligomers of different chain length (Figure 1; Table 1). This mixture was used for the preparation of the conjugate without further size fractionation or enrichment for a particular oligomer species.

Initial attempts to utilize the *N*- α -bromoacetyl groups that were remaining after termination of the autopolymerization reaction for conjugating the peptomer onto the thiol-modified aluminum oxide nanoparticles were not successful. To generate reproducible conditions, the peptomer was therefore end-capped by completely removing the reactive groups at the head and tail of the polymer chain before it was prepared for "side on" conjugation by *N*- ϵ -bromoacetylation of the lysine side chains (Scheme 2). Bromoacetylation of the lysines was carried out with a 3-fold molar excess of ϵ -amino groups to *N*-succinimidyl bromoacetate in order to guarantee that the labeling occurred statistically in only one out of the three lysines present in a peptide unit. *N*- ϵ -Bromoacetylation of the lysines with the activated ester proceeded smoothly, consuming $\sim 84\%$ of the derivatizable amine (28% of the total ϵ -amino groups) within 15 min. The randomly bromoacetylated peptomer was then used without further purification for reaction with the thiol-modified particles.

Bromoacetylation of the peptomer did not effect the amount of α -helix that was in the peptomer as compared with the non-bromoacetylated peptomer, and the CD spectrum (Figure 2) of the bromoacetylated peptomer looked virtually identical to the nonbromoacetylated peptomer shown in the earlier publication (Robey et al., 1995). For comparison and as shown before (Robey et al., 1995), the monomeric peptide CD spectrum is given as the broken line in Figure 2 and shows that the peptide itself has very little, if any, helical conformation in the phosphate buffer, pH 7.2.

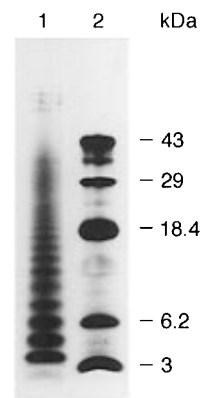


Figure 1. Gel analysis of the HIV_{MN} gp120 C4 domain peptomer. Silver stained, reducing 10–20% polyacrylamide/SDS gel. Lane 1: Peptomer of the large-scale preparation used for conjugate preparation. Lane 2: Molecular weight standards.

Table 1. Degree of Polymerization of HIV_{MN} gp120 C4 Domain Peptomer

chain length	% product formed ^a	chain length	% product formed ^a
monomer	1.7	octamer	4.7
dimer	22.3	nonamer	3.5
trimer	12.9	decamer	2.7
tetramer	10.8	undecamer	2.2
pentamer	8.0	dodecamer	1.6
hexamer	6.2	> dodecamer	17.7
heptamer	5.7		

^a Data are derived from a 600 \times 600 dpi scan of a silver-stained SDS–PAA gradient gel. Results are given as means of two measurements. Individual measurements differed less than 5% from the given means.

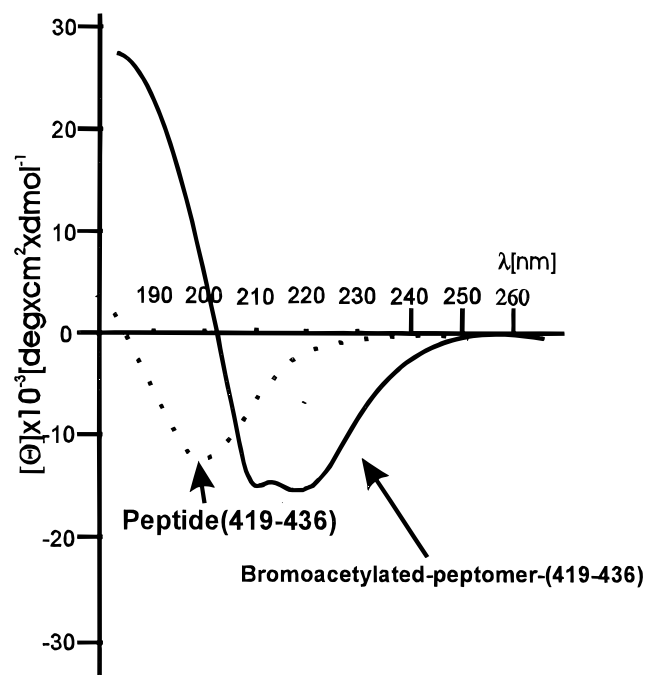


Figure 2. Conformational study of *N*- ϵ -bromoacetylated C4 peptide constructs. CD spectra of *N*-Ac-peptide-(419–436) (---) and *N*- ϵ -bromoacetylated peptomer-(419–436) (—).

The thiol-modified particles were prepared from plain α -aluminum oxide nanoparticles as depicted in Scheme 2. First, the surface of the corundum powder was cleaned and activated for subsequent derivatization by treatment with hot dilute nitric acid. To introduce a primary amino function onto the surface of the cleaned aluminum oxide nanoparticles, they were reacted with (3-aminopropyl)-

Table 2. Properties of Aluminum Oxide Nanoparticle Conjugates

particle type	diameter ^a				surface area ^b		conjugate load ^c (μmol/g)
	maximum diameter		minimum diameter		by MP (m ² /g)	by BET (m ² /g)	
	mean ± SD (nm)	range (nm)	mean ± SD (nm)	range (nm)			
surface-activated	394 ± 140	143–871	131 ± 52	39–358	11.9	11.9	n/a
amino-derivatized	430 ± 154	163–813	125 ± 50	47–325	nd	nd	15.9
peptomer-derivatized	355 ± 108	158–675	113 ± 43	42–269	nd	nd	7.0

^a Particle diameters were determined by transmission electron microscopy. As most particles were of nonspherical shape, the minimum and maximum diameters and the size ranges are given. ^b Particle surface area was determined after drying the sample at 300 °C either by mercury porosimetry (MP) or by nitrogen adsorption/desorption (multipoint BET method). Due to the high drying temperature for sample preparation, the procedure could not be used for amino- and peptomer-derivatized particles. ^c Conjugate loads were determined by ninhydrin assay (amino-derivatized particles) or Picotag amino acid analysis (peptomer-derivatized particles). For the peptomer-derivatized particles the molar amounts of peptide units on the particles are given. ^d n/a, not applicable. ^e nd, not determined.

triethoxysilane (Scheme 2). Assuming that a surface load of 2 mmol/m² is characteristic for a silane monolayer on a ceramic surface (Larsson, 1983) and the specific surface area of the aluminum oxide nanoparticles is 12 m²/g (Table 2), the silanizing reagent was applied in a 175-fold molar excess. The high particle dispersity [2.5% (v/v) alumina in solvent], in combination with the vast excess of silanizing reagent, effectively prevented cross-linking of the particles as evidenced by the less than 10% increase of the mean particle diameters from before to after the silanization (Table 2). After the surface attached (3-aminopropyl)triethoxysilane was sintered onto the particles, the amount of covalently attached 3-aminopropyl moieties was determined to be 15.9 mmol/g particles, which is equivalent to 1.3 mmol of amine/m². The modification proved to be largely resistant to mechanical stress because no significant amine loss could be detected after a total of 10 min sonication of a particle suspension in a bath sonicator.

To allow conjugation of the *N*- ϵ -bromoacetylated peptomer onto the particles via thioether linkages, the amine-modified alumina was reacted at pH 10 with a 100-fold molar excess of *N*-acetylhomocysteinethiolactone (Scheme 2). The formation of free thiol groups was assayed every 15 min with Ellman's reagent. After 45 min of reaction, the quantity of free thiol no longer increased and the reaction was terminated. However, though the kinetics of the derivatization could be monitored, it was impossible to determine the absolute amount of free thiol formed because part of the 2-nitro-5-thiobenzoic acid that was released through reaction with the free thiols was nonspecifically adsorbed to the particles.

The thiol-derivatized aluminum oxide nanoparticles then were reacted with the *N*- ϵ -lysyl-bromoacetylated peptomer until no more free sulfhydryl groups were detectable in the reaction mixture. Due to the high particle dispersity of 1% (v/v) solids in the reaction mixture, no cross-linking of the particles was observed. Instead, the mean particle diameters decreased by 10–20% when compared to the surface-activated and amine-modified alumina. We attribute this decrease in particle size to abrasion or splitting of the alumina because of mechanical stress during the synthesis. Amino acid analysis of the final conjugate revealed a 55% coupling yield for the peptomer leading to a specific antigen load of 16 mg of peptomer/g of aluminum oxide nanoparticles.

Characterization of the HIV_{MN} gp120 C4 Domain Peptomer Aluminum Oxide Nanoparticles. For use of the peptomer alumina as systemic or mucosal vaccines, the most important characteristics are particle size, porosity, and antigen load as well as the chain length of the attached peptomer and its stable covalent coupling to the carrier.

Particle shape and size of the surface-activated, amine-modified, and peptomer-conjugated alumina were ana-

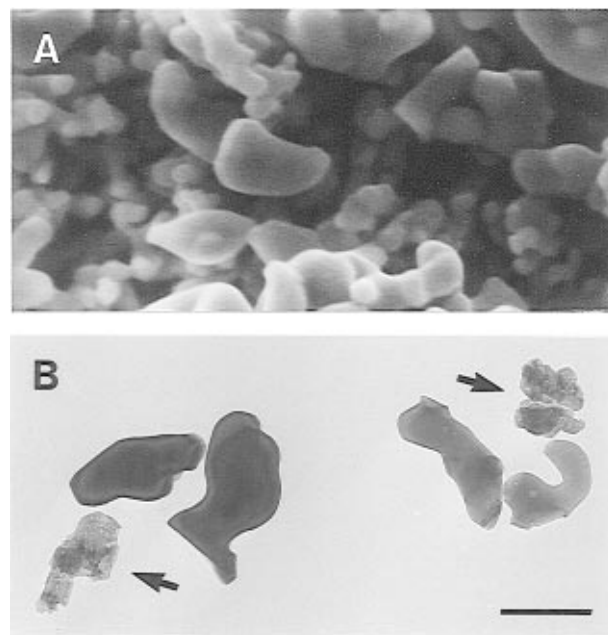


Figure 3. HIV_{MN} gp120 C4 domain peptomer-derivatized aluminum oxide nanoparticles. Representative electron micrographs depicting the peptomer-derivatized aluminum oxide nanoparticles. Scanning electron microscopy (A) at high particle density reveals the smooth surface texture that most of the nanoparticles displayed. Transmission electron microscopy (B) at low particle density demonstrates the predominantly elongated shape of the particles and the existence of a "crystalline" subpopulation (arrows) with rugged edges. Scale bar, 250 nm.

lyzed by electron microscopy (Figure 3). There was no evident difference in shape or size between the surface-activated starting material and the final peptomer conjugate. However, within each sample, two distinct particle populations were observed. Most of the particles were of ellipsoid or cylindrical shape and displayed a smooth surface texture without sharp corners and edges (Figure 3A). A minor fraction of particle consisted of generally smaller, rugged particles, mostly of non-spherical, irregular shape (Figure 3B, arrows). Because of the elongated shape of all the particles, the particle size is reported as minimum and maximum diameters (Table 2). The final product exhibited a mean maximum diameter of 355 nm and a mean minimum diameter of 113 nm, consistent with the desired size of 300 nm.

The porosity and surface area of the particles was determined by mercury intrusion and nitrogen adsorption, respectively. Both techniques require the sample to be completely dry. To meet that requirement, samples have to be heated to 300 °C under high vacuum, conditions under which a peptomer or γ -aminopropyl coating is likely to decompose. As the size, shape, and surface texture of all samples appeared identical when analyzed

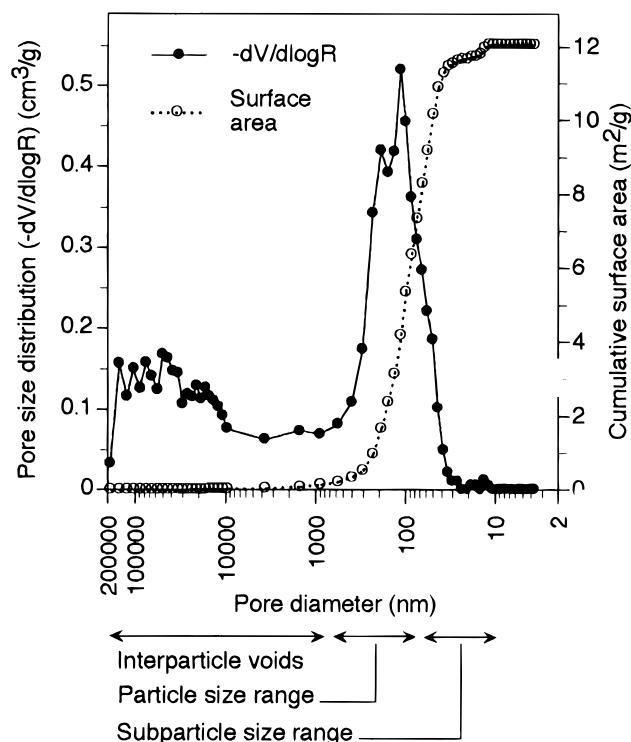


Figure 4. Pore size analysis of the surface-activated aluminum oxide nanoparticles. The differential pore size distribution and the cumulative surface area were obtained from mercury porosimetry. The analysis was carried out with intrusion pressures ranging from 0 to 42 000 N/cm². The data were calculated assuming a mercury contact angle of 140° and a surface tension of 480 erg/cm². For greater clarity, only every 20th measured point is shown.

by EM, we considered the underivatized, surface-activated alumina as representative for all particle types in terms of porosity and surface area. The porosity of the surface-activated alumina was determined by mercury intrusion analysis employing the Washburn relationship (Washburn, 1921) (Figure 4). When applying this technique, the interparticle voids as well as every concave surface curvature of the particles, no matter whether it is a shallow indentation, a deep cavity, or a channel, are regarded as pores. In the mercury intrusion analysis of the surface-activated alumina, 40% of the mercury-occupied interparticle voids (≥ 900 nm) were not included in the pore size analysis. The remainder intruded into pores between 12 and 900 nm without revealing any distinct pore classes. Instead, a nonparametric pore size distribution was observed with the most frequent pore diameter being 115 nm. Seventy-eight percent of the mercury intruded into pores of 76–575 nm and 13% into pores of 12–66 nm diameter. As the 76–575 nm range corresponds to the mean sizes of the particles themselves, these “pores” must be indentations or bulges on the surface of the alumina rather than true holes or channels and, therefore, must represent the outer surface of the particles. They provide 7.2 m²/g or 60% of the total specific surface area. The pores of 12–66 nm diameter can be considered true pores or holes representing the inner surface of the particles. They provide 4.7 m²/g or 40% of the total specific surface area of the particles. This pore diameter also corresponded well with the size of the center holes of some donut-shaped particles that were occasionally observed by EM.

The antigen load of individual particles was not directly measurable. However, the mean particle diameters, the specific surface area, and the specific peptomer load were determined experimentally, and with the aid

of these data the antigen load could be estimated. The estimation is based on the assumption that the mean particle is of cylindrical shape with hemispherical ends, a model that is the best possible approximation for the heterogeneous population of elongated particles which was observed by EM (Figure 3). For a population of such particles the specific surface area (SSA) is given by

$$\text{SAA} = \frac{4d_{\max}}{\rho d_{\min}(d_{\max} - 1/3d_{\min})} \quad (1)$$

where ρ is the density of the alumina as provided by the manufacturer (3.95 g/cm³) and d_{\max} and d_{\min} are the mean maximum and minimum particle diameters (Table 2), respectively. Using eq 1, the specific surface area of the surface-activated alumina was calculated to be 8.7 ± 3.5 m²/g. This result is in good agreement with the outer surface area of the particles (7.2 m²/g) as determined by mercury intrusion analysis, and the total surface area as determined by nitrogen adsorption or mercury intrusion (Table 2) also lies within the margins of error. We are therefore confident that the assumption of a cylindrical form with hemispheres on each end is an adequate model for the mean particle shape. Assuming such a particle shape, the number of peptide epitopes per mean particle (n_e) is given by

$$n_e = 1/4\rho\pi d_{\min}^2(d_{\max} - 1/3d_{\min})\text{SCL } N_A \quad (2)$$

where ρ is the density of the alumina, d_{\max} and d_{\min} are the mean maximum and minimum diameter, SCL is the specific conjugate load (Table 2), and N_A is the Avogadro constant (6.023×10^{23} mol⁻¹). With eq 2, n_e was calculated to be $53\,000 \pm 42\,000$.

Neither the chain length nor the conformation of the peptomer could be obtained experimentally when it was conjugated to the particle surface. These properties can therefore only be estimated on the basis of the chain length distribution in the peptomer solutions and the conformation of the *N*- ϵ -bromoacetylated peptomer prior to conjugation. Assuming that no steric constraints or differences in reactivity between peptomer molecules of different chain length exist, the chain length distribution of the immobilized peptomer would be identical to that of the soluble peptomer preparation. The soluble parent peptomer contained polymerization products ranging from the monomeric starting material to dodecamers and higher with a median chain length of 5 peptide units, the monomer made up only 1.7% of that preparation (Table 1). Even if a preference for smaller molecules prevailed in the conjugation reaction, the coupling yield of 55% implies that at least ~97% of the conjugate consist of dimers and larger molecules.

DISCUSSION

Both systemic and mucosal immunization strategies are needed to prevent HIV infection. In this paper, we describe the design, synthesis, and characterization of a nanoparticulate candidate vaccine against HIV-1 that can be adapted for mucosal and systemic administration and that may give rise to broadly cross-reactive, neutralizing antibodies against the viral envelope glycoprotein gp120.

To obtain a nanoparticle vaccine of defined particle size and high stability, we chose α -aluminum oxide nanoparticles of 300 nm diameter as antigen carrier. Gel-type aluminum oxohydroxide adjuvants have been licensed for decades for use in humans, and α -aluminum oxide has an excellent record of biocompatibility and safety in dentistry and orthopedics (Christel, 1992;

Fairhurst, 1992). Inhaled or ingested corundum powder (α - Al_2O_3) has been shown to be nontoxic and does not cause granuloma formation, chronic inflammatory reactions, or cancer as is the case for silica dust (Lindenschmidt, 1990). The benefit of a tight, preferably covalent, attachment of the antigen to a particulate carrier was emphasized by the work of Skea and Barber (1993), who bound influenza virus hemagglutinin by a noncovalent antibody bridge to alum gel and achieved a 1500-fold increase in immunogenicity. Likewise, Kossovsky et al. (1995) were able to dramatically enhance the immunogenicity of mussel adhesive protein by coupling it onto surface-modified diamond nanoparticles. Derivatization of macroparticulate silica by epoxy- or aminoalkyl silanes for use as high-performance affinity chromatography supports is well documented (Sportsman and Wilson, 1980; Larsson et al., 1983; Anspach et al., 1988; Huisden et al., 1990), but to date there have been no reports of a covalent surface modification and bioconjugation of Al_2O_3 nanoparticles. As aluminosilicates like garnet or zeolites are very stable compounds and silica atoms are readily replaced by aluminum in the silicate crystal lattice, we decided to covalently couple our antigen onto the surface of the alumina particles by a (3-aminopropyl)siloxane linker. An amino-derivatization was preferred over a mercaptopropyl or glycidoxypopyl silanization to allow the construction of an *N*-acetylhomocysteinyamidopropylsiloxane bridge, which should facilitate subsequent release of the antigen in the target cells. The risk of bridging the nanoparticles during silanization to clusters too big to be phagocytosed was anticipated, but it was avoided by using a 175-fold excess of silane and a high particle dispersity throughout the coupling procedure. The increase in particle diameter conferred by silanization, though statistically significant ($p < 0.05$; one factor ANOVA, Fisher PLSD), was only 10% (data not shown). Thus, the particles still matched the desired size for M cell uptake and phagocytosis by antigen presenting cells. As expected, the silanization product was base-labile but surprisingly sonication/abrasion-resistant, which facilitated handling and dispersion of the particles by sonication. The silanization yield of 1.3 mmol/m^2 was 12 times higher than that which we obtained previously with (3-mercaptopropyl)trimethoxysilane on glass cover slips (Ivanov et al., 1995). Theoretically, a surface load of 2.4 mmol/m^2 is achievable for a (3-aminopropyl)siloxane coat when allowing free rotation of the aminopropyl moiety around the Si-C bond (rotation radius: 450 pm). The dramatic increase in derivatization yield as compared to our previous experiments may be explained either by the use of a different silane reagent and a glass support or by the oxidative surface activation and cleaning procedure we applied in this study.

Though we did not achieve a complete surface coverage by aminopropylsiloxane, the amine load turned out to be ample for immobilizing the antigen, as only 0.61 mmol of HIV-1_{MN} gp120 C4 domain peptide units/ m^2 bound to the particle surface. With a median chain length of 5 peptide units/peptomer molecule, the average peptomer surface load was 0.123 mmol of peptomer/ m^2 , which is in good correlation with a surface saturation of 0.121 mmol/m^2 reported for oligopeptides coupled onto tresyl-activated glass (Massia and Hubbell, 1990). With regard to individual peptide units, we therefore achieved a peptide load five times that of a saturated peptide monolayer.

The complete coverage of the particles by antigen also circumvented potential problems associated with the analysis of the thiol-derivatized alumina. When moni-

toring the thiol derivatization of the amine-modified alumina with Ellman's reagent, part of the reaction product bound to the particles and rendered a quantitative detection of the thiol load impossible. However, in light of the fact that a complete surface coverage of the particles with antigen required only 10% of the amine anchors and that the thiolating *N*-acetylhomocysteine thiolactone was applied in a 100-fold molar excess, it is unlikely that the thiolation reaction was a yield limiting factor in the conjugation procedure.

The particles also interfered with the Picotag amino acid analysis of the immobilized peptomer. While the total antigen load could be determined reliably based on the absolute aliphatic amino acid contents, all dicarboxylic acids like glutamic acid, aspartic acid, *S*-carboxymethylcysteine, and *S*-carboxymethylhomocysteine were underrepresented (data not shown). We attribute this phenomenon to the release of aluminum cations from the alumina carrier. Al^{3+} could have chelated the diacids and thus prevented their labeling by phenylisothiocyanate or changed their motility in the subsequent chromatographic analysis. It is well-known that aluminum ions are able to chelate dicarboxylic acids (Yokel, 1994), but we did not expect the 6 N hydrochloric acid used in the conjugate hydrolysis to liberate Al^{3+} from the calcinated α - Al_2O_3 , which, in contrast to γ - Al_2O_3 , is considered to be acid resistant. Since *S*-carboxymethylcysteine is a marker for the polymeric nature of the peptomer and *S*-carboxymethylhomocysteine is a measure for its covalent coupling to the particle surface, the lack of reliable values for these amino acids forced us to estimate the chain length of the immobilized peptomer on the basis of its soluble unconjugated form.

In our view, the problems in obtaining accurate values for *S*-carboxymethylcysteine and -homocysteine were still outweighed by the biological benefits of the thioether linker technology. First, peptomers are fully biodegradable and their metabolites are predictable, a feature not all synthetic antigens can offer. The biodegradability usually hinges on the nature of the chemical cross-linker. The *S*-carboxymethylcysteine/homocysteine cross-linkers that are formed in the preparation of a peptomer vaccine are potential substrates for the mercapturic acid pathway of detoxification in which *S*-substituted cysteines are formed from halogenated xenobiotics and glutathione. The *S*-substituted cysteine is then *N*-acetylated to form a mercapturic acid before it is released into the bile and the urine (Jacoby et al., 1984). The *S*-carboxymethylcysteine and/or *S*-carboxymethylhomocysteine can join in that pathway before the *N*-acetylation step and will be readily excreted. Second, we demonstrated previously that HIV-1_{MN} gp120 C4 domain peptomers more closely resemble the native structure of that epitope than individual peptides do (Robey et al., 1995), a finding which should be exploited in designing an HIV-1 gp120 C4 domain vaccine.

The polymerization technology also provides additional, immunological benefits for a vaccine. Small oligopeptides are poorly immunogenic because they generally lack repetitive epitopes for T-cell-independent (TI-2) immune responses, and they are not large enough to contain additional helper T-cell epitopes that are essential for immunoglobulin class switches and the induction of immunologic memory. To overcome that problem without using a carrier protein or attaching a synthetic T-cell epitope, oligomerization of haptenic peptide anti-

gens was proposed as a means to enhance their immunogenicity.

For the study reported previously (Robey et al., 1995), the polymerization of the amphipathic C4 peptide resulted in the peptide assuming an α -helical conformation, and it allowed for the preparation of antibodies that appear to be directed toward the helix. In this case, antibody production may be only B-cell-dependent and T-cell-independent. Therefore, maintaining the helical conformation is most important since this sequence of amino acids is probably in a helical conformation in the parent protein, and it is the parent protein that we are targeting with these antibodies. Although modification of the central W in the C4 peptide (KIKQIINMWQEYVGKAMYA) resulted in a loss of helix in the peptomer, it appears that modification of the hydrophilic amino acids in C4 will not influence the ability of C4 to remain helical. The C4 from HIV-1 as compared with the C4 from HIV-2 differs on the hydrophilic face of the helix (Robey et al., 1996), and peptomers from both C4's display greater than 50% helical content, a property necessary for C4 to bind CD4, the cell receptor for HIV (Robey et al., 1996). It therefore comes as no surprise that the *N*- ϵ -bromoacetylation of the peptomer did not change the amount of helix in the peptomer since the bromoacetylation was being performed on the lysine residues, which are assumed to be on the hydrophilic face of the amphipathic helix.

Tam (1988) developed the multiple antigenic peptides (MAPs), which consist of a 4- or 8-branch dendritic lysine core onto which four or eight oligopeptide antigens are synthesized colinearly. The MAPs found widespread use and often outperformed the classical peptide carrier protein conjugates (Tam, 1988), but a major drawback of the MAP technology is the limited space on the lysine core. Steric hindrance can occur during the synthesis of long peptides (>10–15 aa) on 8-branch MAP cores, and the tightly packed peptide chains often prevent an antibody response to the more C-terminal amino acids toward the center of the MAP (Francis et al., 1991). As an alternative to the dendritic MAPs, linear head-to-tail peptide polymers have been described. They consisted of 20–30 peptide units prepared either by direct carboxy diimide coupling (Borras-Cuesta et al., 1988) or by applying the peptomer technology (Hillman et al., 1990). Both constructs gave rise to antibodies that recognized the native parent protein and did not require cognate T-cell help for induction of the class switch to the IgG isotype. The extent of polymerization that is necessary to achieve such an immunogenicity remains to be determined as both constructs were heterogeneous with respect to their chain length. The studies of Del Giudice et al. (1986) on polymerized NANP peptides from the *Plasmodium falciparum* CS protein indicate that the immunogenicity of peptide polymers increases with increasing chain length.

In light of that observation, we are confident that our HIV-1_{MN} gp120 C4 domain peptomer nanoparticle conjugate is immunogenic even in the absence of T-cell help as it combines the benefits of a linear peptide polymer with the dendritic, collinear peptide organization of a MAP. A summary of the immunogenicity studies will be forthcoming in a future publication.

ACKNOWLEDGMENT

We want to thank Dr. R. Reichelt, University of Muenster, Muenster, FRG, for his help with the scanning electron microscopy. We appreciate the professional work of Quantachrome Inc. in analyzing the particle

surface area and porosity. This work was supported by NIH Research Grants HD17557 and AI34757 to M.R.N. and by NIH Center Grant DK-34854 to the Harvard Digestive Diseases Center.

LITERATURE CITED

- Amerongen, H. M., Weltzin, R. A., Farnet, C. M., Michetti, P., Haseltine, W. A., and Neutra, M. R. (1991) Transepithelial transport of HIV-1 by intestinal M cells: a mechanism for transmission of AIDS. *J. Acquired Immune Defic. Syndr.* 4, 760–765.
- Anspach, B., Unger, K. K., Davies, J., and Hearn, M. T. W. (1988) Affinity chromatography with triazine dyes immobilized onto activated non-porous monodisperse silicas. *J. Chromatogr.* 457, 195–204.
- Bernatowicz, M. S., and Matsueda, G. R. (1986) Preparation of peptide-protein immunogens using N-succinimidyl bromoacetate as a heterobifunctional crosslinking reagent. *Anal. Biochem.* 155, 107–112.
- Bjork, R. L., Jr. (1991) HIV-1: seven facets of functional molecular mimicry. *Immunol. Lett.* 28, 91–96.
- Bland, P. W., and Warren, L. G. (1986) Antigen presentation of epithelial cells of the rat small intestine. II. Selective induction of suppressor T cells. *Immunology* 58, 9–14.
- Borras-Cuesta, F., Fedon, Y., and Petit-Camurdan, A. (1988) Enhancement of peptide immunogenicity by linear polymerization. *Eur. J. Immunol.* 18, 199–202.
- Brunauer, S., Emmet, P. H., and Teller, E. (1938) Adsorption of gases in multimolecular layers. *J. Am. Chem. Soc.* 60, 309–319.
- Christel, P. S. (1992) Biocompatibility of surgical-grade dense polycrystalline alumina. *Clin. Orthop.* 282, 10–18.
- Cordonnier, A., Montagnier, L., and Emerman, M. (1989) Single amino-acid changes in HIV envelope affect viral tropism and receptor binding. *Nature (London)* 340, 571–574.
- Del Giudice, G., Cooper, J. A., Merino, J., Verdini, A. S., Pessi, A., Togna, A. R., Engers, H. D., Corradin, G., and Lambert, P.-H. (1986) The antibody response in mice to carrier-free synthetic polymers of *Plasmodium falciparum* circumsporozoite repetitive epitope is I-Ab-restricted: possible implications for malaria vaccines. *J. Immunol.* 137, 2952–2955.
- DeSchryver, A., and Meheus, A. (1990) Epidemiology of sexually transmitted diseases: the global picture. *Bull. W. H. O.* 68, 639–654.
- Earl, P. L., Doms, R. W., and Moss, B. (1990) Oligomeric structure of the human immunodeficiency virus type 1 envelope glycoprotein. *Proc. Natl. Acad. Sci. U.S.A.* 87, 648–652.
- Ellman, G. L. (1959) Tissue sulfhydryl groups. *Arch. Biochem. Biophys.* 82, 70–77.
- Fairhurst, C. W. (1992) Dental ceramics: the state of science. *Adv. Dent. Res.* 6, 78–81.
- Forrest, B. D. (1992) The need for consideration of mucosal immunity in vaccine approaches to AIDS. *Vaccine Res.* 1, 137–142.
- Francis, M. J., Hastings, G. Z., Brown, F., McDermed, J., Lu, Y.-A., and Tam, J. P. (1991) Immunological evaluation of the multiple antigen peptide (MAP) system using the major immunogenic site of foot-and-mouth disease virus. *Immunology* 73, 249–254.
- Frey, A., Giannasca, K. T., Weltzin, R., Giannasca, P. J., Reggio, H., Lencer, W. I., and Neutra, M. R. (1996) Role of the glycocalyx in regulating access of microparticles to apical plasma membranes of intestinal epithelial cells: implications for microbial attachment and oral vaccine targeting. *J. Exp. Med.* 184, 1045–1059.
- Golding, H., Robey, F. A., Gates, F. T., 3rd, Linder, W., Beining, P. R., Hoffman, T., and Golding, B. (1988) Identification of homologous regions in human immunodeficiency virus 1 gp41 and human MHC class II beta 1 domain. *J. Exp. Med.* 167, 914–923.
- Gupta, R. K., Rost, B. E., Relyveld, E., and Siber, G. R. (1995) Adjuvant properties of aluminum and calcium compounds. *Pharm. Biotechnol.* 6, 229–248.
- Gurgo, C., Guo, H.-G., Franchini, G., Aldovini, A., Collalti, E., Farrell, K., Wong-Staal, F., Gallo, R. C., and Reitz, M. S., Jr.

- (1988) Envelope sequences of two new United States HIV-1 isolates. *Virology* 164, 531–536.
- Hem, S. L., and White, J. L. (1995) Structure and properties of aluminum-containing adjuvants. *Pharm. Biotechnol.* 6, 249–276.
- Hillman, K., Shapiro-Nahor, O., Blackburn, R., Hernandez, D., and Golding, H. (1991) A polymer containing a repeating peptide sequence can stimulate T-cell-independent IgG antibody production in vivo. *Cell. Immunol.* 134, 1–13.
- Huisden, R. E., Kraak, J. C., and Poppe, H. (1990) Modification of silica with glucose for the separation of proteins by high-performance liquid chromatography. *J. Chromatogr.* 508, 289–299.
- Ivanov, B., Grzesik, W., and Robey, F. A. (1995) Synthesis and use of a new bromoacetyl-derivatized heterotrifunctional amino acid for conjugation of cyclic RGD-containing peptides derived from human bone sialoprotein. *Bioconjugate Chem.* 6, 269–277.
- Jakoby, W. B., Stevens, J., Duffel, M. W., and Weisiger, R. A. (1984) The terminal enzymes of mercapturate formation and the thiomethyl shunt. *Rev. Biochem. Toxicol.* 6, 97–115.
- Kossovsky, N., Gelman, A., Hnatyszyn, H. J., Rajguru, S., Garrell, R. L., Torbati, S., Freitas, S. S. F., and Chow, G.-M. (1995) Surface-modified diamond nanoparticles as antigen delivery vehicles. *Bioconjugate Chem.* 6, 507–511.
- Larsson, P.-O., Glad, M., Hansson, L., Mansson, M.-O., Ohlson, S., and Mosbach, K. (1983) High performance liquid affinity chromatography. *Adv. Chromatogr.* 21, 41–85.
- Lasky, L. A., Nakamura, G., Smith, D. H., Fennie, C., Shimasaki, C., Patzer, E., Berman, P., Gregory, T., and Capon, D. J. (1987) Delineation of a region of the human immunodeficiency virus type 1 gp120 glycoprotein critical for interaction with the CD4 receptor. *Cell* 50, 975–985.
- Lindenschmidt, R. C., Driscoll, K. E., Perkins, M. A., Higgins, J. M., Maurer, J. K., and Belfiore, K. A. (1990) The comparison of a fibrogenic and two nonfibrogenic dusts by bronchoalveolar lavage. *Toxicol. Appl. Pharmacol.* 102, 268–281.
- Lynn, M. (1975) Inorganic support intermediates: covalent coupling of enzymes on inorganic supports. In *Immobilized enzymes, antigens, antibodies and peptides* (H. H. Weetall, Ed.) pp 1–48, Marcel Dekker, New York, NY.
- Marx, P. A., Compans, R. W., Gettie, A., Staas, J. K., Gilley, R. M., Mulligan, M. J., Yamschikov, G. V., Chen, D., and Eldridge, J. H. (1993) Protection against vaginal SIV transmission with microencapsulated vaccine. *Science* 260, 1323–1327.
- Massia, S. P., and Hubbell, J. A. (1990) Covalent surface immobilization of Arg-Gly-Asp- and Tyr-Ile-Gly-Ser-Arg-containing peptides to obtain well-defined cell-adhesive substrates. *Anal. Biochem.* 187, 292–301.
- Moore, J. P., Sattentau, Q. J., Wyatt, R., and Sodroski, J. (1994) Probing the structure of the human immunodeficiency virus surface glycoprotein gp120 with a panel of monoclonal antibodies. *J. Virol.* 68, 469–484.
- Nakamura, G. R., Byrn, R., Wilkes, D. M., Fox, J. A., Hobbs, M. R., Hastings, R., Wessling, H. C., Norcross, M. A., Fendly, B. M., and Berman, P. W. (1993) Strain specificity and binding affinity requirements of neutralizing monoclonal antibodies to the C4 domain of gp120 from human immunodeficiency virus type 1. *J. Virol.* 67, 6179–6191.
- Neutra, M. R., Michetti, P., and Kraehenbuhl, J.-P. (1994) Secretory immunoglobulin A: induction, biogenesis, and function. In *Physiology of the gastrointestinal tract*, 3rd ed. (L. R. Johnson, Ed.) pp 685–708, Raven Press, New York, NY.
- Neutra, M. R., Frey, A., and Kraehenbuhl, J.-P. (1996a) Epithelial M cells: gateways for mucosal infection and immunization. *Cell* 86, 345–348.
- Neutra, M. R., Pringault, E., and Kraehenbuhl, J.-P. (1996b) Antigen sampling across epithelial barriers and induction of mucosal immune responses. *Annu. Rev. Immunol.* 14, 275–300.
- Oakley, B. R., Kirsch, D. R., and Morris, N. R. (1980) A simplified ultrasensitive silver stain for detecting proteins in polyacrylamide gels. *Anal. Biochem.* 105, 361–363.
- Robey, F. A. (1994) Bromoacetylated synthetic peptides: Starting materials for cyclic peptides, peptomers and peptide conjugates. In *Methods in Molecular Biology* (M. Pennington, and B. Dunn, Eds.) Vol. 35, pp 73–91, Humana Press, Inc., Totowa, NJ.
- Robey, F. A., and Fields, R. L. (1989) Automated synthesis of N-bromoacetyl-modified peptides for the preparation of synthetic peptide polymers, peptide-protein conjugates, and cyclic peptides. *Anal. Biochem.* 177, 373–377.
- Robey, F. A., Kelson-Harris, T., Roller, P. P., and Robert-Guroff, M. (1995) A helical epitope in the C4 domain of HIV glycoprotein 120. *J. Biol. Chem.* 270, 23918–23921.
- Robey, F. A., Harris-Kelson, T., Robert-Guroff, M., Batinic, D., Ivanov, B., Lewis, M. S., and Roller, P. P. (1996) A synthetic conformational epitope from the C4 domain of HIV gp120 that binds CD4. *J. Biol. Chem.* 271, 17990–17995.
- Sarin, Y. K., Kent, S. B. H., Tam, J. P., and Merrifield, R. B. (1981) Quantitative monitoring of solid-phase peptide synthesis by the ninhydrin reaction. *Anal. Biochem.* 117, 147–157.
- Sastry, K. J., and Arlinghaus, R. B. (1991) Identification of T-cell epitopes without B-cell activity in the first and second conserved regions of the HIV env protein. *AIDS* 5, 699–707.
- Scibienski, R. J. (1973) Denaturation of lysozyme by Freund's complete adjuvant. *J. Immunol.* 111, 114–120.
- Skea, D. L., and Barber, B. H. (1993) Adhesion-mediated enhancement of the adjuvant activity of alum. *Vaccine* 11, 1018–1026.
- Sportsman, J. R., and Wilson, G. S. (1980) Chromatographic properties of silica-immobilized antibodies. *Anal. Chem.* 52, 2013–2018.
- Starich, B. R., Hahn, B. H., Shaw, G. M., McNeely, P. D., Modrow, S., Wolf, H., Parks, E. S., Parks, W. P., Josephs, S. F., Gallo, R. C., and Wong-Staal, F. (1986) Identification and characterization of conserved and variable regions in the envelope gene of HTLV-III/LAV, the retrovirus of AIDS. *Cell* 45, 637–648.
- Sun, N.-C., Ho, D. D., Sun, C. R. Y., Liou, R.-S., Gordon, W., Fung, M. S. C., Li, X.-L., Ting, R. C., Lee, T.-H., Chang, N. T., and Chang, T.-W. (1989) Generation and characterization of monoclonal antibodies to the putative CD4-binding domain of human immunodeficiency virus type 1 gp120. *J. Virol.* 63, 3579–3585.
- Takeda, A., Tuazon, C. U., and Ennis, F. A. (1988) Antibody-enhanced infection by HIV-1 via Fc receptor-mediated entry. *Science* 242, 580–583.
- Tam, J. P. (1988) Synthetic peptide vaccine design: Synthesis and properties of a high-density multiple antigenic peptide system. *Proc. Natl. Acad. Sci. U.S.A.* 85, 5409–5413.
- Washburn, E. W. (1921) Note on a method of determining the distribution of pore sizes in a porous material. *Proc. Natl. Acad. Sci. U.S.A.* 7, 115–116.
- Weetall, H. H. (1976) Covalent coupling methods for inorganic support materials. *Methods Enzymol.* 44, 134–148.
- Yokel, R. A. (1994) Aluminum chelation: chemistry, clinical, and experimental studies and the search for alternatives to desferrioxamine. *J. Toxicol. Environ. Health* 41, 131–174.

Peptide Targeting and Delivery across the Blood–Brain Barrier Utilizing Synthetic Triglyceride Esters: Design, Synthesis, and Bioactivity

Dinesh Patel,[†] Brian D. McKinley,[†] Thomas P. Davis,[‡] Frank Porreca,[‡] Henry I. Yamamura,[‡] and Victor J. Hruby^{*,†}

Departments of Chemistry and Pharmacology, University of Arizona, Tucson, Arizona 85721.
Received October 6, 1996[©]

As an approach to the development of therapeutically useful peptide pharmaceuticals that can penetrate the blood–brain barrier, we have designed and demonstrated the application of a carrier-targeting system. We have developed a prodrug design strategy that is designed to utilize membrane-bound enzymes whereby release of a bioactive peptide from a highly lipophilic triglyceride peptide-carrier is achieved *in situ*, thus attaining high localized concentrations of the bioactive peptide. Following localization of such a system, normal peptidase and lipase action is utilized to release the active peptide (deltorphin II) intact and in high concentration. At present, the exact mechanisms are unclear, but the observed results in which analgesia is observed following peripheral administration suggest that the active peptide is able to cross the blood–brain barrier and sustain prolonged periods of analgesia as determined by antinociception tests by release of the bioactive peptide. *In vitro* tests of binding and bioactivity by the peptide conjugate show essentially no potency in either target or control analogues, but potent antinociceptive effects are observed following peripheral administration.

INTRODUCTION

The *in vivo* site-specific delivery of bioactive analgesic peptides has been a challenging objective for medicinal chemists who strive to utilize the ever-increasing database of highly potent/selective opioid peptide sequences. Ever since the identification of the endogenous enkephalins, numerous successful studies have been reported on the design of highly potent opioid receptor ligands [the reader is referred to a few excellent reviews and the references therein (1–3)]. Very few studies, however, have been reported where attempts have been made to specifically site deliver these peptide analgesics. Those that have been reported have shown varying modest degrees of success (e.g., refs 4–7).

A major barrier must be overcome before the promise of these potent and selective ligands can be realized. The blood–brain barrier (BBB) is a unique membrane barrier that tightly segregates the brain interstitial fluid bathing the synapses from the circulating blood. With the exception of the brain and spinal cord, all organs are perfused by capillaries lined with endothelial cells that have small pores for the rapid movement of drugs and solutes into the organ interstitial fluid from the circulation. However, the capillary endothelium of the mammalian brain and spinal cord lack these pores, and therefore drugs can cross the BBB and enter the brain only via two principal mechanisms, either by carrier-mediated, catalyzed transport or by free diffusion. Peptides generally do not cross the BBB well because these highly polar compounds are not very lipid soluble and often do not have access to specialized BBB receptor-mediated transport systems. In principle, a peptide neuropharmaceutical that does not cross the BBB may be transported through the BBB by first coupling the active peptide to a BBB transport vector, i.e., a peptide

or modified plasma protein that is capable of transversing the BBB via receptor-mediated or absorptive mediated transcytosis through the brain capillary endothelial cell cytoplasm (8–11).

The primary aim in any site-specific delivery must be to ensure a selective deposition of the active species at the site of interest. This will in itself ensure a decrease in side effects brought about due to general administration of the drug, and furthermore, this will also decrease the overall dose required since general circulatory loss/absorption will be lower. Other factors that must be considered in the design of such a species include the prevention of self loss through self-aggregation or micellar formation. In principle, controlled deposition can be achieved by masking or prodrug design, so long as the active molecule remains masked while in circulation, and deposition is accomplished by release of the prodrug enzymatically at or near its site of action. Furthermore, the carrier for such a prodrug complex should have physicochemical properties that make it unique in its carrying capacity, in the sense that when bound to the efficacious component it masks the activity of said component without itself demonstrating undesired side effects. Site-specific delivery of such a prodrug carrier complex is a further complication in the design of such a species. It is perhaps fortunate that endothelial cell membranes are heterogeneous with respect to their content of membrane-bound enzymes distributed around the body (10, 11). Specifically, endopeptidases are localized with respect to their substrate specificity and also in their distribution around blood vessels of the brain. Utilizing the endopeptidase substrate specificity allows for the design of a targeting principal to be incorporated into the prodrug carrier complex. Activation of the complex is accomplished *in vivo* by removal of a mask by the endothelial membrane-bound enzymes in the locality of interest. Thus, the now-activated carrier complex is available for adsorption into the lipid environment of the cell in this locality.

* Author to whom correspondence should be addressed.

[†] Department of Chemistry.

[‡] Department of Pharmacology.

[©] Abstract published in *Advance ACS Abstracts*, May 1, 1997.

Peptides, both naturally occurring and designed, often can be highly efficacious and increasingly can be designed to be highly specific in their actions, with few demonstrated undesired side effects. The aim of the present study is to overcome what is probably the one major drawback of using peptides as drugs, and that is their poor ability to cross lipid membranes, specifically the blood–brain barrier. Peptide analgesics that have been found to be super-agonists when administered intracerebro ventricularly (i.c.v.) can show poor activity when administered intravenously (i.v.). It is generally thought that one of the primary reasons for this is their poor ability to cross the BBB even when they are relatively stable to degradation by peptidases. We believe that if the concentration of peptide can be maintained while in circulation, and if the peptide can be delivered into or onto the cell membranes at or near their desired site of action, then there is a higher probability that one would see a greater biological action of the peptide through the simple property of mass action.

In this present study, we demonstrate the design, synthesis, and bio-evaluation of a triglyceride peptide carrier prodrug complex that shows greatly improved analgesic activity of a heptapeptide deltorphin over administration of the free peptide.

EXPERIMENTAL PROCEDURES

Mouse Vas Deferens (MVD) and Guinea Pig Ileum (GPI) Bioassays. Electrically induced smooth muscle contraction of MVD and strips of GPI longitudinal muscle, myenteric plexus, were used as bioassays (12). In these assays, opioid agonists inhibit the electrically induced smooth muscle contractions in a dose-related manner in both smooth muscle systems. Percent inhibition of electrically induced muscle twitch was calculated as the average contraction height for 1 min preceding the addition of the agonist divided by the contraction height 3 min after exposure to the agonist. IC_{50} values represent the mean of not less than four tissue samples. IC_{50} values, relative potency estimates, and their associated standard errors were determined by fitting the mean data to the Hill equation with a nonlinear least-squares method (13).

Radioligand Binding. Membranes were prepared from whole brains taken from adult male Sprague–Dawley rats (250–300 g). All radioligand displacement experiments were run against the 3H -labeled ligands [p CIPhe 4]DPDPE and CTOP as previously described (14, 15). A minimum of three experiments were conducted for each radioligand. Data obtained from independent measurements were represented as the arithmetic mean \pm SEM.

Antinociception Studies. Male ICR mice (20–30 g) were used throughout these studies. They were housed in groups of four in Plexiglas boxes, maintained in a light- and temperature-controlled environment, with food and water available *ad libitum* until the time of antinociceptive testing. The peptide carrier complex and controls were dissolved in a few microliters of methanol and then diluted into physiological saline for peripheral administration via an intraperitoneal (i.p.) route. At the level of methanol used no toxicity is observed. All testing was performed in accordance with the recommendations and policies of the International Association for the Study of Pain, the National Institutes of Health, and the University of Arizona guidelines for the care and use of laboratory animals.

Antinociception was assessed in mice by the hot-plate assay, an assay known to be mediated by central receptors (16, 17). In the hot-plate assay, mice were placed

on a 55 °C surface, and the mean time to lick the back paws or escape jump was recorded. Percent antinociception was calculated as $100\% \times (\text{test latency} - \text{control latency}) / (60 \text{ s} - \text{control latency})$, with a cutoff latency of 20 s (baseline).

Data are presented as the mean \pm SEM for groups of 10 mice. Regression lines, ED_{50} and AD_{50} values, and their 95% confidence limits were calculated using individual data points.

Brain and Serum Stability Incubations. Aliquots (180 μ L) of resuspended, twice washed 15% mouse brain homogenates or mouse serum were placed into 1.5-mL centrifuge tubes. The tubes were prepared in triplicate for each time point (0, 10, 15, 30, 60, 120, and 240 min). An additional set of triplicate tubes were incubated with 50 mM Tris-HCl (pH 7.4) and served as buffer controls. Twenty microliters of 1 mM peptide triglyceride complex dissolved in methanol was added to each tube, which was agitated briefly by vortex. Incubation was begun immediately at 37 °C in a rolling water-bath incubator. Enzyme activity was terminated at the end of the each incubation by adding 200 μ L of CH_3CN and placing the tube on ice. Each tube was centrifuged at 3000g, and 300 μ L of the supernatant was transferred to a clean 1.5-mL tube. An equal volume of H_2O was added, and the sample was mixed for HPLC analysis.

Synthetic Methods. Thin layer chromatography (TLC) was done on silica gel G plates using the following solvent systems: (A) 1-butanol/acetic acid/pyridine/water (5:5:1:4); (B) ammonium hydroxide/water/2-propanol (1:1:3); (C) ethyl acetate/acetic acid/pyridine/water (5:5:1:4). The compounds were visualized on the TLC plate using UV light and iodine vapor. Analytical high-performance liquid chromatography (HPLC) was performed on a Hewlett Packard 1090 II instrument with a reversed-phase C4 or C18 Vydac column eluted with a linear gradient 0–90% CH_3CN (0.1% TFA) in 50 min. $HPLC\ k' = [(\text{compound retention time} - \text{solvent retention time}) / \text{solvent retention time}]$. 1H and ^{13}C NMR spectra were recorded on a Varian Gemini 200 or Bruker AM 500 spectrometer in $CDCl_3$ unless otherwise noted. Mass spectra were obtained on a MALDI Nicolet FT-MS with a CO_2 laser excitation source and hydroxy benzoic acid as the thermal matrix. Amino acid analysis was performed on a Beckman 7300 amino acid analyzer, after acid hydrolysis with 4 M methanesulfonic acid for 24 h.

2-Hydroxy-1,3-propan-2-yl Dibenzoate (II). Propane-1,2,3-triol (**I**) (2.0 g) was added to benzoyl chloride (6.6 g) (2.2 equiv) and refluxed for 4 h; after cooling, the mixture was poured onto ice water (200 mL) whereupon a white precipitate formed that was filtered and washed with small portions of ice cold water. The solid was recrystallized from aqueous ethanol to yield **II** as long white needles (5.54 g, 85%); mp, 137.2 °C. MS, m/z 300.09821 found (m/z 300.09976 calcd); C, H, N, 67.96, 5.32, 0.00, (calcd 67.97, 5.33, 0.00); TLC, R_f (a) 0.72, (b) 0.48, (c) 0.31; HPLC, $C_{18}\ k'$ 2.26.

2-Keto-1,3-propanyl Dibenzoate (III). **II** (5.0 g) was added slowly to Jones reagent (1 M in acetone:water (1:1), 20 mL) and stirred for 30 min. Propan-2-ol (50 mL) was added dropwise, and the reaction was stirred for 30 min. The resulting product was extracted with ethyl acetate (3 \times 50 mL); the combined extracts were washed with water (3 \times 100 mL), saturated $NaHCO_3$ (3 \times 100 mL), and saturated $NaCl$ (3 \times 100 mL), dried over $MgSO_4$, and evaporated *in vacuo*. The resulting solid was decolorized with activated carbon and recrystallized with aqueous ethanol to yield **III** (3.62 g, 73%); mp, 162.6 °C; MS, m/z 298.08612 found (m/z 298.08411 calcd); C, H, N,

68.40, 4.67, 0.00 (calcd 68.44, 4.69, 0.00); TLC, R_f (a) 0.53, (b) 0.68, (c) 0.71; HPLC, C_{18} K' 5.82.

2-(*N,N*-Diisopropylamino)-2-hydroxy-1,3-propan-2-yl Dibenzoate (IV). **III** (2.60 g) was dissolved in freshly distilled dry THF (50 mL) while under an inert atmosphere. Diisopropylethylamine (0.90 g, gold label, 1 equiv) was added very slowly via syringe pump (12 h). After a further 12 h of stirring, the mixture was evaporated to dryness *in vacuo*. The oily residue was purified by kieselgur distillation under vacuum. The desired product was obtained at 185–190 °C at 0.1 mmHg, which upon cooling gave a white waxy solid, to yield **IV** (1.21 g, 35%); mp, 86.2 °C; MS, m/z 399.20441 found (m/z 399.20455 calcd); C, H, N, 69.10, 7.29, 3.58 (calcd 69.14, 7.26, 3.50); TLC, R_f (a) 0.38, (b) 0.42, (c) 0.56; HPLC, C_{18} K' 3.94.

2-(*N,N*-Diisopropylamino)-1,2,3-propanetriol (V). **IV** (1.15 g) dissolved in THF (50 mL) with a few drops of HCl (12 M) was subjected to hydrogenation over Pd (5%) on carbon at 30 psi for 4 h. Following safe removal of the residual hydrogen, the catalyst was filtered and the solvent was removed *in vacuo*. The crude product **V** was found to be of sufficient purity to proceed with the following reaction (0.46 g, 84%); mp, 31.5 °C; MS, m/z 191.167124 found (m/z 191.15213 calcd); C, H, N, 56.38, 10.96, 7.29 (calcd 56.40, 10.98, 7.32); TLC, R_f (a) 0.83, (b) 0.53, (c) 0.46; HPLC, C_{18} K' 2.81.

2-(*N,N*-Diisopropylamino)-1,2,3-propan-2-yl Tris(octadecanoyl benzoate ester) (VI). **V** (0.45 g) was dissolved in dry THF (50 mL) under a nitrogen atmosphere, isobutyl chloroformate (1.0 g, 3.1 equiv) was added, and the mixture was stirred for 30 min. Octadecanedioic acid monobenzyl ester **XII** (2.95 g, 3.1 equiv) dissolved in dry THF (50 mL) was added via syringe pump over 12 h. Ice water (100 mL) was added slowly; the organic layer was extracted with ethyl acetate (3 × 100 mL); the combined extracts were washed with water (3 × 100 mL), saturated NaHCO_3 (3 × 100 mL), and saturated NaCl (3 × 100 mL), dried over MgSO_4 , and evaporated *in vacuo* to yield **VI** as a white waxy solid that was considered to be of sufficient purity to proceed with the following reaction (2.26 g, 70%); mp, 75.8 °C; MS, m/z 1349.99128 found (m/z 1349.99836 calcd); C, H, N, 74.67, 10.03, 1.02 (calcd 74.66, 10.00, 1.03); TLC, R_f (a) 0.36, (b) 0.52, (c) 0.61; HPLC, C_{18} K' 6.91.

2-(*N,N*-Diisopropylamino)-1,2,3-propan-2-yl Tris(octadecanedioic acid monoester) (VII). **VI** (1.90 g) dissolved in THF (50 mL) with a few drops of HCl (12 M) was subjected to hydrogenation over Pd (5%) on carbon at 30 psi for 4 h. Following safe removal of the residual hydrogen, the catalyst was filtered and the solvent was removed *in vacuo*. The crude product **VII** was found to be of sufficient purity to proceed with the following reaction (1.25 g, 82%); mp, 53.1 °C; MS, m/z 1079.84953 found (m/z 1079.85752 calcd); C, H, N, 70.04, 10.85, 1.33 (calcd 70.00, 10.83, 1.29); TLC, R_f (a) 0.59, (b) 0.51, (c) 0.41; HPLC, C_{18} K' 3.49.

2-(*N,N*-Diisopropylamino)-1,2,3-propan-2-yl Tris(octadecanedioic acid monoamide (arginyl(*N*-Pmc)-c)proline-*tert*-butyl ester) monoester) (VIII). Arginyl(*N*-Pmc)proline-*tert*-butyl ester **XIII** (3.5 g, 6.2 equiv) was dissolved in acetonitrile (50 mL). **VII** (1.02 g), BOP reagent (2.9 g, 6.2 equiv), and DIEA (1.8 g, 9.3 equiv) were added, and the solution was stirred for 6 h. Water (50 mL) was added; the organic layer was extracted with ethyl acetate (3 × 100 mL); the combined extracts were washed with water (3 × 100 mL), saturated NaHCO_3 (3 × 100 mL), and saturated NaCl (3 × 100 mL), dried over MgSO_4 , and evaporated *in vacuo* to yield **VIII** as a white waxy solid that was found to be of sufficient purity to

proceed with the following reaction (2.41 g, 91%); mp, decomp.; MS, m/z 2805.78973 found (m/z 2805.79986 calcd); TLC, R_f (a) 0.27, (b) 0.36, (c) 0.61; C_{18} K' 5.91; $[\alpha]^{20}_D$ 59.3° (c = 1.20 MeOH).

2-Amino-1,2,3-propan-2-yl Tris(octadecanedioic acid monoamide (arginyl(*N*-Pmc)proline-*tert*-butyl ester) monoester) (IX). **VIII** (2.10 g) was dissolved in freshly distilled tetrahydrofuran (50 mL) under an inert atmosphere at –78 °C. DIBAL-H (1.0 M in THF, 2.8 mL) was slowly added via a syringe pump over 12 h. The reaction was stirred for a further 12 h at room temperature. Acetone (20 mL) was slowly added to consume any unreacted reducing agent. Solvents were removed *in vacuo*, and the resulting solid was purified by reversed-phase HPLC (C_{18} preparative column, 0–90% acetonitrile with 0.1% trifluoroacetic acid in 50 min) to yield **IX** as a white waxy solid (1.36, 67%); mp, decomp.; MS, m/z 2721.71643 found (m/z 2721.70597 calcd); TLC, R_f (a) 0.34, (b) 0.42, (c) 0.49; HPLC, C_{18} K' 2.94; $[\alpha]^{20}_D$ 21.6° (c = 1.45 MeOH).

(*N*-(*tert*-Butyloxycarbonyl)tyrosyl(*O*-*tert*-butyl)-D-alanyl-phenylalanyl-glutamyl(γ -*tert*-butyl)-valinyl-valinyl-glycinamide)-1,2,3-propan-2-yl Tris(octadecanedioic acid monoamide (arginyl(*N*-Pmc)proline-*tert*-butyl ester) monoester) (X). **IX** (1.25 g) was dissolved in acetonitrile (50 mL). *N*-(*tert*-Butyloxycarbonyl)tyrosinyl(*O*-*tert*-butyl)-D-alanyl-phenylalanyl-glutamyl(γ -*tert*-butyl)-valinyl-valinyl-glycine (**XIV**) (0.65 g, 1.5 equiv), BOP reagent (0.34 g, 1.5 equiv), and DIEA (0.24 g, 2.5 equiv) were added, and the reaction was stirred at room temperature for 15 h. Water (50 mL) was added, and the organic layer was extracted with ethyl acetate (3 × 100 mL); the combined extracts were washed with water (3 × 100 mL), saturated NaHCO_3 (3 × 100 mL), and saturated NaCl (3 × 100 mL), dried over MgSO_4 , and evaporated *in vacuo*. The crude material was purified by reversed-phase HPLC (C_{18} preparative column, 0–90% acetonitrile with 0.1% trifluoroacetic acid in 50 min) to yield **X** as a white waxy solid (1.24 g, 73%); mp, decomp.; MS, m/z 3699.24697 found (m/z 3699.25330 calcd); TLC, R_f (a) 0.21, (b) 0.39, (c) 0.69; HPLC, C_{18} K' 4.38; $[\alpha]^{20}_D$ 53.6° (c = 1.31 MeOH).

(Tyrosyl-D-alanyl-phenylalanyl-glutamyl-valinyl-valinyl-glycinamide)-1,2,3-propan-2-yl Tris(octadecanedioic acid monoamide (arginylproline) ester) (XI). **X** (1.24 g) was dissolved in dichloromethane (50 mL) and trifluoroacetic acid (50 mL) and stirred at ambient temperature for 1 h. After removal of the solvents *in vacuo*, the crude product was purified by reversed-phase HPLC on a C_4 semi-preparative column eluted with a gradient of 0–90% acetonitrile in 0.1% trifluoroacetic acid over 50 min. The corresponding collected fractions were pooled and lyophilized to yield **XI** as a white waxy solid (0.74 g, 88%); mp, decomp.; MS, m/z 2529.66891 found (m/z 2529.66533 calcd); TLC, R_f (a) 0.25, (b) 0.42, (c) 0.59; HPLC, C_{18} K' 3.91; $[\alpha]^{20}_D$ 42.8° (c = 1.19 MeOH).

Octadecanedioic Acid Monobenzyl Ester (XII). Benzyl alcohol (1.03 g) was dissolved in freshly distilled tetrahydrofuran (50 mL) under an inert atmosphere, isobutyl chloroformate (1.43 g, 1.1 equiv) was added, and the mixture stirred for 30 min. Octadecanedioic acid (3.0 g) dissolved in dry THF (20 mL) was added slowly via a syringe pump over 12 h. Ice water (100 mL) was added, and the organic layer was extracted with ethyl acetate (3 × 100 mL); the combined extracts were washed with water (3 × 100 mL), saturated NaHCO_3 (3 × 100 mL), and saturated NaCl (3 × 100 mL), dried over MgSO_4 , and evaporated *in vacuo*. Purification on flash silica (500 g) using methanol/chloroform (1:3) yielded **XII** as a white

waxy solid (3.25 g, 85%); mp, 46.8 °C; MS, m/z 404.30221 found (m/z 404.29363 calcd); C, H, N, 74.28, 9.95, 0.00 (calcd 74.25, 9.90, 0.00); TLC, R_f (a) 0.39, (b) 0.48, (c) 0.62; HPLC, C_{18} k' 2.51.

Arginyl(*N*-Pmc)proline-*tert*-butyl Ester (XIII). Proline-*tert*-butyl ester hydrochloride (2.0 g) was dissolved in acetonitrile (50 mL). N^{ϵ} (Fmoc)Arginine (*N*-PMC)-OH (6.0 g, 1.1 equiv), BOP reagent (4.2 g, 1.1 equiv), and DIEA (2.1 g, 3.1 equiv) were added, and the solution was stirred for 6 h. Water (50 mL) was added; the organic layer was extracted with ethyl acetate (3 × 100 mL); the combined extracts were washed with water (3 × 100 mL), saturated NaHCO_3 (3 × 100 mL), and saturated NaCl (3 × 100 mL), dried over MgSO_4 , and evaporated *in vacuo* to an off white solid that was to be of sufficient purity to use without further purification. Piperidine 20% in DMF (50 mL) was added, and the reaction was stirred for 30 min at room temperature. The solvents were removed *in vacuo*. Water (50 mL) was added and adjusted to pH 8.5 with aqueous ammonia. The aqueous solution was extracted with ethyl acetate (3 × 100 mL); the combined extracts were washed with water (3 × 100 mL), saturated NaHCO_3 (3 × 100 mL), and saturated NaCl (3 × 100 mL), dried over MgSO_4 , and evaporated *in vacuo* to yield **XIII** (3.6 g, 89%); mp, 84.8 °C as a white solid. MS, m/z 727.70221 found (m/z 727.69614 calcd); TLC, R_f (a) 0.50, (b) 0.43, (c) 0.30. HPLC, C_{18} k' 3.10. $[\alpha]_D^{20}$ 37.9° (c = 1.24 MeOH).

N^{ϵ} -*tert*-Butoxycarbonyl-tyrosyl(*O*-*tert*-butyl)-D-alanyl-phenylalanyl-glutamyl(γ -*tert*-butyl)-valinyl-valinyl-glycine (XIV). Prepared by standard solid-phase peptide chemistry employing N^{ϵ} -Fmoc protection, with HBTU/HOBt activation on a super acid labile Rink resin (18). Cleavage of the protected peptide was achieved using 2% trifluoroacetic acid. The protected peptide was purified by size exclusion chromatography on a Sephadex G15 support employing 10% acetic acid in water as the eluting solvent. Lyophilization of pooled fraction yielded **XIV** (0.72 g, 71%); mp, decomp. MS, m/z 992.04596 found (m/z 992.00712 calcd); TLC, R_f (a) 0.52, (b) 0.48, (c) 0.34. HPLC, C_{18} k' 6.91. $[\alpha]_D^{20}$ 56.1° (c = 1.14 MeOH).

2-Amino-1,2,3-propan-2-yl Tris(octadecanoyl benzoylate ester) (XV). **VI** (1.05 g) was dissolved in freshly distilled tetrahydrofuran (50 mL) under an inert atmosphere at -78 °C. DIBAL-H (1.0 M in THF, 1.4 mL) was slowly added via a syringe pump over 12 h. The reaction was stirred for a further 12 h at room temperature. Acetone (20 mL) was slowly added to consume any unreacted reducing agent. Solvents were removed *in vacuo*, and the resulting solid was purified by reversed-phase HPLC (C18 preparative column, 0–90% acetonitrile with 0.1% trifluoroacetic acid in 50 min) to yield **XV** as a white waxy solid (0.68 g, 69%); mp, 56.2 °C; MS, m/z 1265.89947 found (m/z 1265.90446 calcd); C, H, N, 73.96, 9.72, 1.13 (calcd 73.93, 9.71, 1.10); TLC, R_f (a) 0.45, (b) 0.38, (c) 0.31; HPLC, C_{18} k' 2.68.

(N^{ϵ} -(*tert*-Butoxycarbonyl)tyrosinyl(*O*-*tert*-butyl)-D-alanyl-phenylalanyl-glutamyl(γ -*tert*-butyl)-valinyl-valinyl-glycinamide)-1,2,3-propan-2-yl Tris(octadecanoyl benzoylate ester) (XVI). **XV** (0.62 g) was dissolved in acetonitrile (50 mL). N^{ϵ} -(*tert*-butoxycarbonyl)tyrosyl(*O*-*tert*-butyl)-D-alanyl-phenylalanyl-glutyl-(γ -*tert*-butyrate)-valinyl-valinyl-glycine (**XIV**) (0.36 g, 1.5 equiv), BOP reagent (0.17 g, 1.5 equiv), and DIEA (0.12 g, 2.5 equiv) were added, and the reaction was stirred at room temperature for 15 h. Water (50 mL) was added, and the organic layer was extracted with ethyl acetate (3 × 100 mL); the combined extracts were washed with water (3 × 100 mL), saturated NaHCO_3 (3 × 100 mL), and saturated NaCl (3 × 100 mL), dried over MgSO_4 , and

evaporated *in vacuo*. The crude material was purified by reversed-phase HPLC (C18 preparative column, 0–90% acetonitrile with 0.1% trifluoroacetic acid in 50 min) to yield **XVI** as a white waxy solid, (0.77 g, 71%); mp, decomp.; MS, m/z 2228.30843 found (m/z 2228.33442 calcd); TLC, R_f (a) 0.21, (b) 0.45, (c) 0.68; C_{18} k' 5.94. $[\alpha]_D^{20}$ 48.5° (c = 1.82 MeOH).

2-(Tyrosyl-D-alanyl-phenylalanyl-glutamyl-valinyl-valinyl-glycinamide)-1,2,3-propan-2-yl tris(octadecanoyl benzoylate ester) (XVII). **XVI** (0.62 g) was dissolved in dichloromethane (50 mL) and trifluoroacetic acid (50 mL) and stirred at ambient temperature for 1 h. After removal of the solvents *in vacuo*, the crude product was purified by reversed-phase HPLC on a C4 semi-preparative column eluted with a gradient of 0–90% acetonitrile in 0.1% trifluoroacetic acid over 50 min. The corresponding collected fractions were pooled and lyophilized to yield **XVII** as a white waxy solid (0.49 g, 88%); mp, decomp.; MS, m/z 2040.33948 found (m/z 2040.34459 calcd); TLC, R_f (a) 0.34, (b) 0.39, (c) 0.52; HPLC, C_{18} k' 3.26. $[\alpha]_D^{20}$ 47.1° (c = 1.04 MeOH).

2-(Tyrosyl-D-alanyl-phenylalanyl-glutamyl-valinyl-valinyl-glycinamide)-1,2,3-propan-2-yl tris(octadecanedioic acid monoester) (XVIII). **XVII** (0.45 g) dissolved in THF (50 mL) with a few drops of HCl (12 M) was subjected to hydrogenation over Pd (5%) on carbon at 30 psi for 4 h. Following safe removal of the residual hydrogen, the catalyst was filtered. After removal of the solvents *in vacuo*, the crude product was purified by reversed-phase HPLC on a C4 semi-preparative column eluted with a gradient of 0–90% acetonitrile in 0.1% trifluoroacetic acid over 50 min. The corresponding collected fractions were pooled and lyophilized to yield **XVIII** as a white waxy solid (0.35 g, 90%); mp, decomp.; MS, m/z 1770.20981 found (m/z 1770.20375 calcd); TLC, R_f (a) 0.41, (b) 0.34, (c) 0.28; HPLC, C_{18} k' 3.10. $[\alpha]_D^{20}$ 51.3° (c = 1.61 MeOH).

2-(*N,N*-Diisopropylamino)-1,2,3-propan-2-yl Tris(octadecanoyl ester) (XIX). **V** (0.15 g) was dissolved in dry THF (50 mL) under a nitrogen atmosphere, isobutyl chloroformate (0.35 g, 3.1 equiv) was added, and the mixture was stirred for 30 min. Octadecanoic acid (0.85 g, 3.1 equiv) dissolved in dry THF (50 mL) was added via syringe pump over 12 h. Ice water (100 mL) was added slowly, and the organic layer extracted with ethyl acetate (3 × 100 mL); the combined extracts were washed with water (3 × 100 mL), saturated NaHCO_3 (3 × 100 mL), and saturated NaCl (3 × 100 mL), dried over MgSO_4 , and evaporated *in vacuo* to yield **XIX** as a white waxy solid that was considered to be of sufficient purity to proceed with the following reaction (0.50 g, 65%); mp, 74.9 °C; MS, m/z 989.94625 found (m/z 989.93498 calcd); C, H, N, 76.38, 12.46, 1.41 (calcd 76.36, 12.42, 1.41); TLC, R_f (a) 0.32, (b) 0.51, (c) 0.64; HPLC, C_{18} k' 5.37.

2-Amino-1,2,3-propan-2-yl Tris(octadecanoyl ester) (XX). **XIX** (0.50 g) was dissolved in freshly distilled tetrahydrofuran (50 mL) under an inert atmosphere at -78 °C. DIBAL-H (1.0 M in THF, 0.7 mL) was slowly added via a syringe pump over 12 h. The reaction was stirred for a further 12 h at room temperature. Acetone (20 mL) was slowly added to consume any unreacted reducing agent. Solvents were removed *in vacuo*, and the resulting solid was purified by reversed-phase HPLC (C18 preparative column, 0–90% acetonitrile with 0.1% trifluoroacetic acid in 50 min) to yield **XX** as a white waxy solid (0.25 g, 56%); mp, 89.4 °C; MS, m/z 905.84681 found (m/z 905.84108 calcd); C, H, N, 75.54, 12.27, 1.56 (calcd 75.50, 12.25, 1.54); HPLC, R_f (a) 0.35, (b) 0.39, (c) 0.42; HPLC, C_{18} k' 3.68.

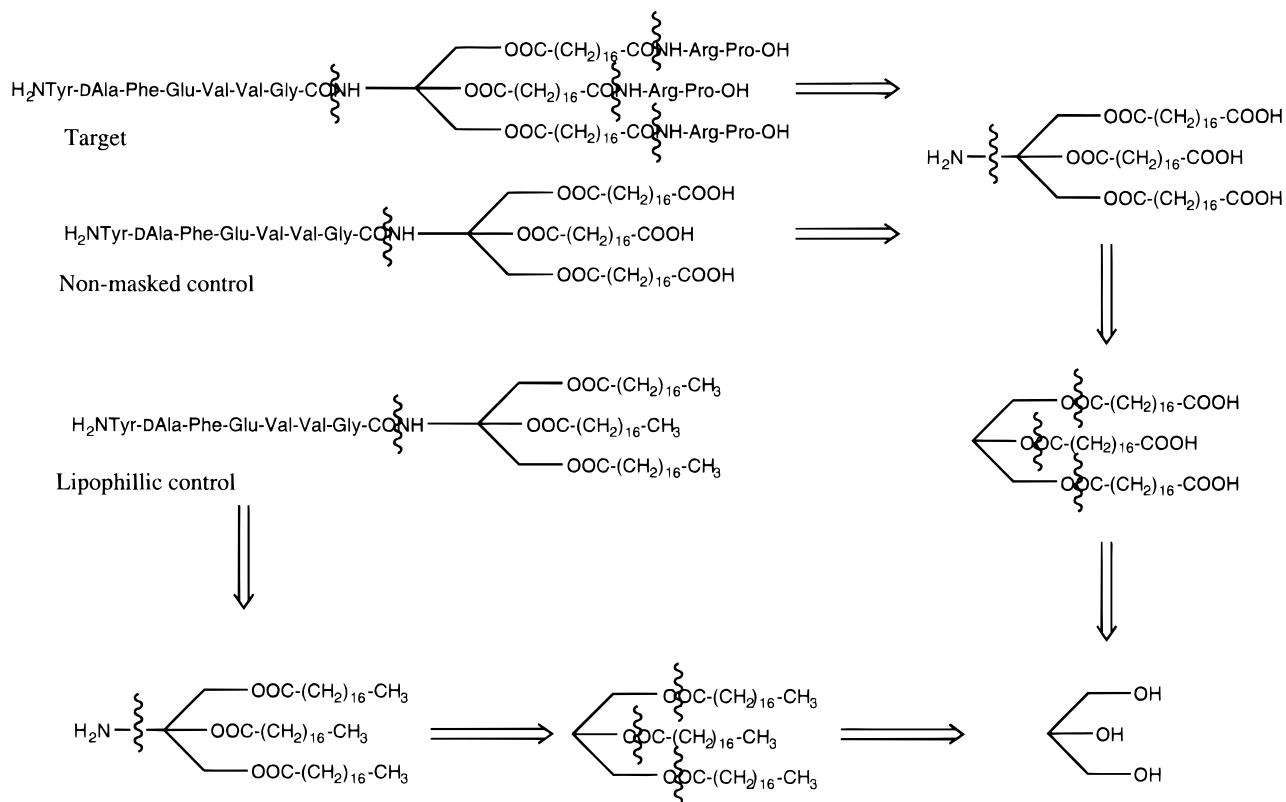


Figure 1. Retrosynthetic analysis of target and control molecules.

(*N*^t-(*tert*-Butyloxycarbonyl)tyrosyl(*O*-*tert*-butyl)-D-alanyl-phenylalanyl-glutamyl(γ -*tert*-butyl)-valinyl-valinyl-glycinamide)-1,2,3-propan-2-yl Tris(octadecanoyl ester) (XXI). **XX** (0.25 g) was dissolved in acetonitrile (50 mL). *N*^t-(*tert*-butyloxycarbonyl)tyrosyl(*O*-*tert*-butyl)-D-alanyl-phenylalanyl-glutamyl(γ -*tert*-butyl)-valinyl-valinyl-glycine (**XIV**) (0.13 g, 1.5 equiv), BOP reagent (0.07 g, 1.5 equiv), and DIEA (0.05 g, 2.5 equiv) were added, and the reaction was stirred at room temperature for 15 h. Water (50 mL) was added, and the organic layer was extracted with ethyl acetate (3 \times 100 mL); the combined extracts were washed with water (3 \times 100 mL), saturated NaHCO₃ (3 \times 100 mL), and saturated NaCl (3 \times 100 mL), dried over MgSO₄, and evaporated *in vacuo*. The crude material was purified by reversed-phase HPLC (C18 preparative column, 0–90% acetonitrile with 0.1% trifluoroacetic acid in 50 min) to yield **XXI** as a white waxy solid (0.37 g, 71%); mp, decomp.; MS, *m/z* 1889.42918 found (*m/z* 1889.43536 calcd); TLC, *R*_f (a) 0.31, (b) 0.45, (c) 0.56; HPLC, C₁₈ *K'* 4.29. [α]_D²⁰ 72.5° (*c* = 1.18 MeOH).

2-(Tyrosyl-D-alanyl-phenylalanyl-glutamyl-valinyl-valinyl-glycinamide)-1,2,3-propan-2-yl Tris(octadecanoyl ester) (XXII). **XXI** (0.30 g) was dissolved in dichloromethane (50 mL) and trifluoroacetic acid (50 mL) and stirred at ambient temperature for 1 h. After removal of the solvents *in vacuo*, the crude product was purified by reversed-phase HPLC on a C4 semi-preparative column eluted with a gradient of 0–90% acetonitrile in 0.1% trifluoroacetic acid over 50 min. The corresponding collected fractions were pooled and lyophilized to yield **XXII** as a white waxy solid (0.20 g, 78%); mp, decomp.; MS, *m/z* 1680.29063 found (*m/z* 1680.28121 calcd); TLC, *R*_f (a) 0.33, (b) 0.41, (c) 0.47; HPLC, C₁₈ *K'* 3.82. [α]_D²⁰ 60.2° (*c* = 1.37 MeOH).

RESULTS

The choice of the carrier molecule was based on the system for which the application was to be made, i.e., the mammalian system. Whereas a monoglyceride peptide conjugate might form micelles that would be stable at mammalian body temperature, thus resulting in a circulatory loss of the peptide prodrug, a triglyceride carrier, having a far greater critical micelle concentration at mammalian body temperature, would minimize such a loss. Based on these considerations, the proposed target and control molecules were analyzed by a retrosynthetic process (Figure 1) to arrive at a suitable starting point for the synthesis.

The masked peptide carrier conjugate was assembled by fragment condensation of the peptide, the carrier molecule, and the hydrophilic dipeptide mask. Condensation was achieved by classical solution phase amide bond formation of suitably protected fragments. The synthesis of the carrier molecule was accomplished as depicted in Figure 2, and the control molecules were accomplished as depicted in Figure 3. Briefly, the synthesis consisted of a series of protection/deprotection strategies while forming a quaternary substituted carbon center suitably functionalized to enable the final fragment condensations to be accomplished under mild conditions. The lipophilic tethers were attached **V** \rightarrow **VI** (Figure 2) as part of the synthesis by formation of ester linkages to mono-protected dicarboxylic fatty acids; this also acted as part of the protection strategy. The control carriers were similarly formed from the glycerol template utilizing monocarboxylic fatty acids, **V** \rightarrow **XIX** (Figure 3). The free acid triglycerides were protected prior to attachment of the deltorphin peptide. The peptide was attached to the carrier (**IX** \rightarrow **X**, Figure 2) as a semi-protected analogue that could be deprotected using mild conditions. Following selective deprotection of the triglyceride free acids, the preformed semi-protected dipep-

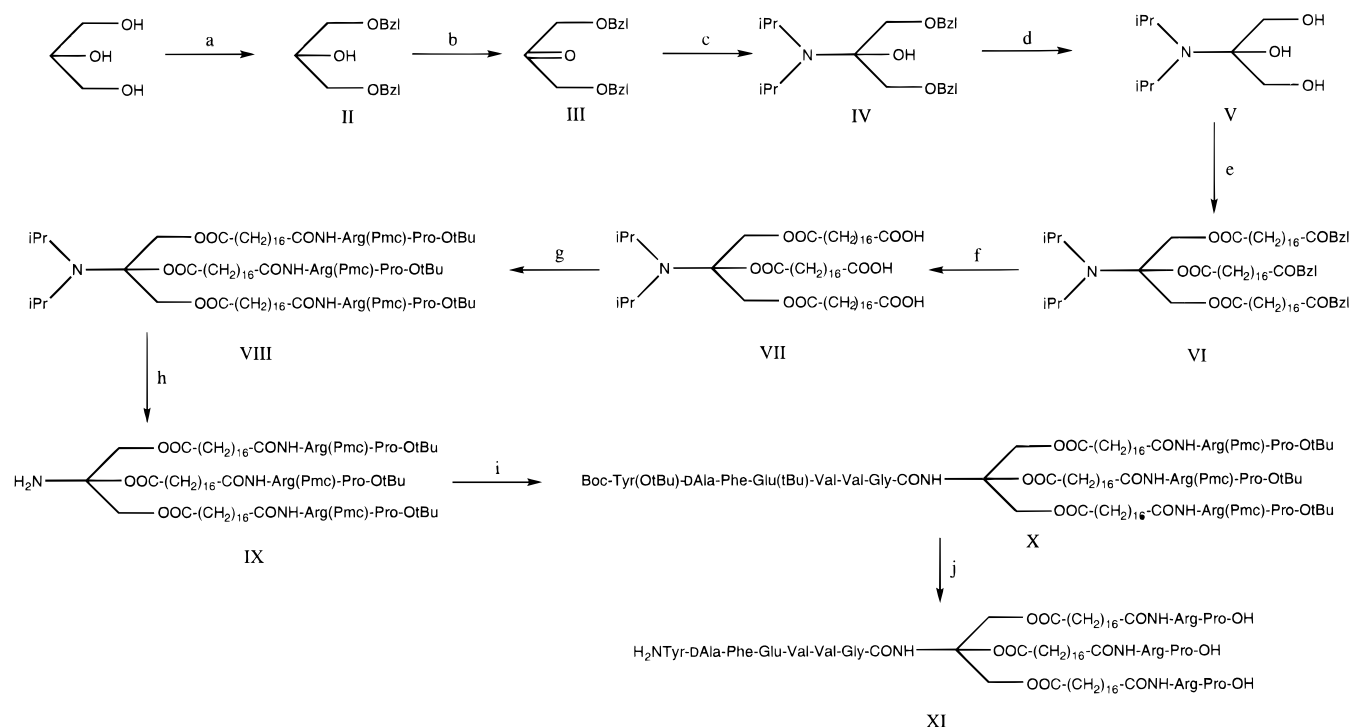


Figure 2. Synthetic route toward the target peptide carrier complex (XI): (a) benzoyl chloride, reflux; (b) Jones reagent, dropwise; (c) THF/diisopropylamine, N₂; (d) 5% Pd/CH₂; (e) N₂, isobutyl chloroformate, fatty acid; (f) 5% Pd/CH₂; (g) Arg-Pro-OtBu/BOP/DIEA; (h) DIBAL-H, THF, N₂; (i) protected peptide/BOP/DIEA; (j) TFA/DCM.

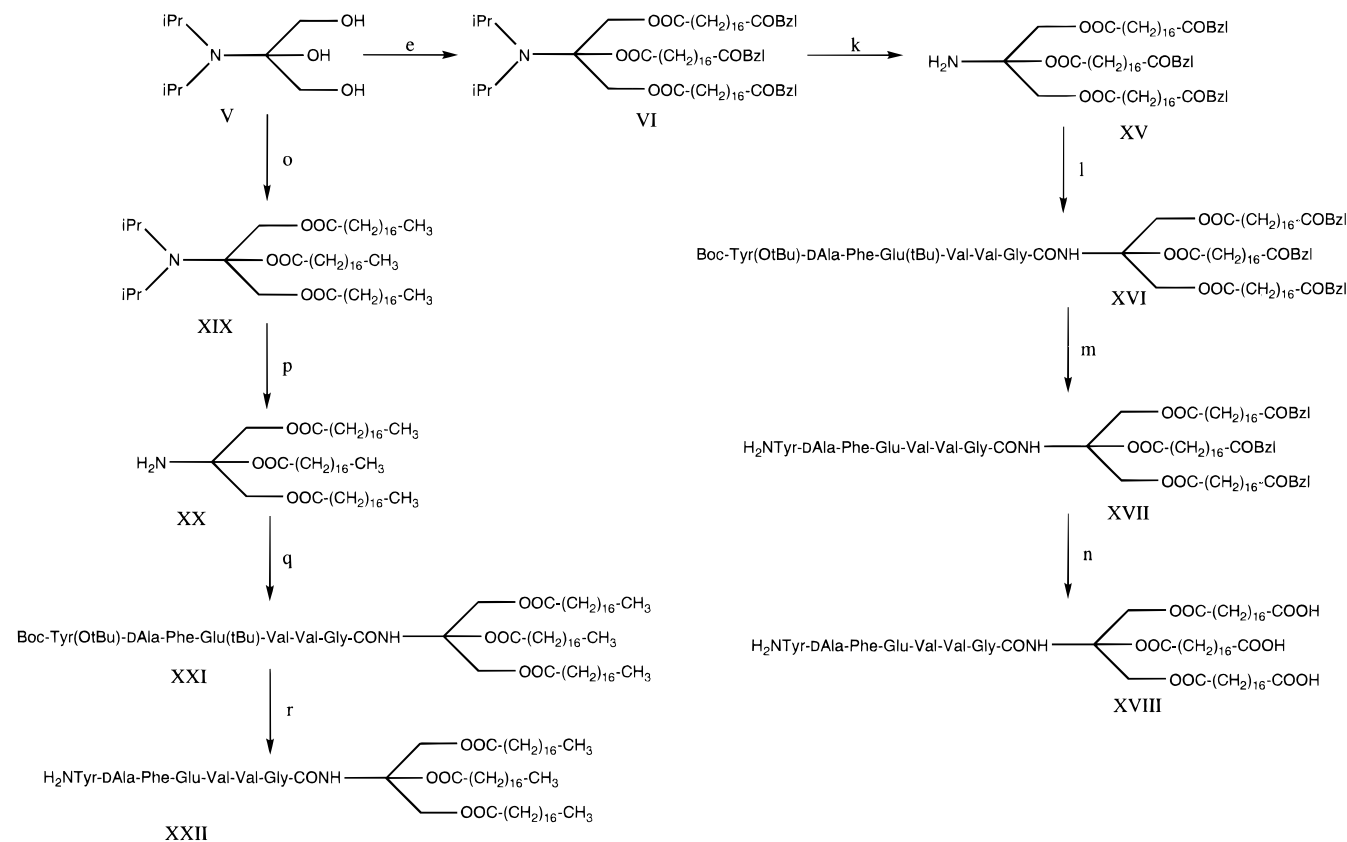


Figure 3. Synthetic route toward the control carrier complexes (XVIII and XXII): (e) N₂, isobutyl chloroformate, fatty acid; (k) DIBAL-H, THF, N₂; (l) protected peptide/BOP/DIEA; (m) TFA/DCM; (n) 5% Pd/CH₂; (o) N₂, isobutyl chloroformate, fatty acid; (p) DIBAL-H, THF, N₂; (q) protected peptide/BOP/DIEA; (r) TFA/DCM.

tide was condensed onto the peptide carrier complex. A further deprotection yielded the desired final target molecule XI (Figure 2). The protected deltorphin peptide was synthesized by a solid-phase strategy on a highly acid labile resin using *N*^t-Fmoc protection; side chain protection of the tyrosine and glutamic acid residues were

chosen so as to be stable to hydrogenation. The arginyl-proline dipeptide was synthesized by solution phase methods; the side chain and C-terminal protection groups were chosen so as to be removed in the final deprotection strategy of the whole complex. The target molecule was purified by reversed-phase high-pressure liquid chroma-

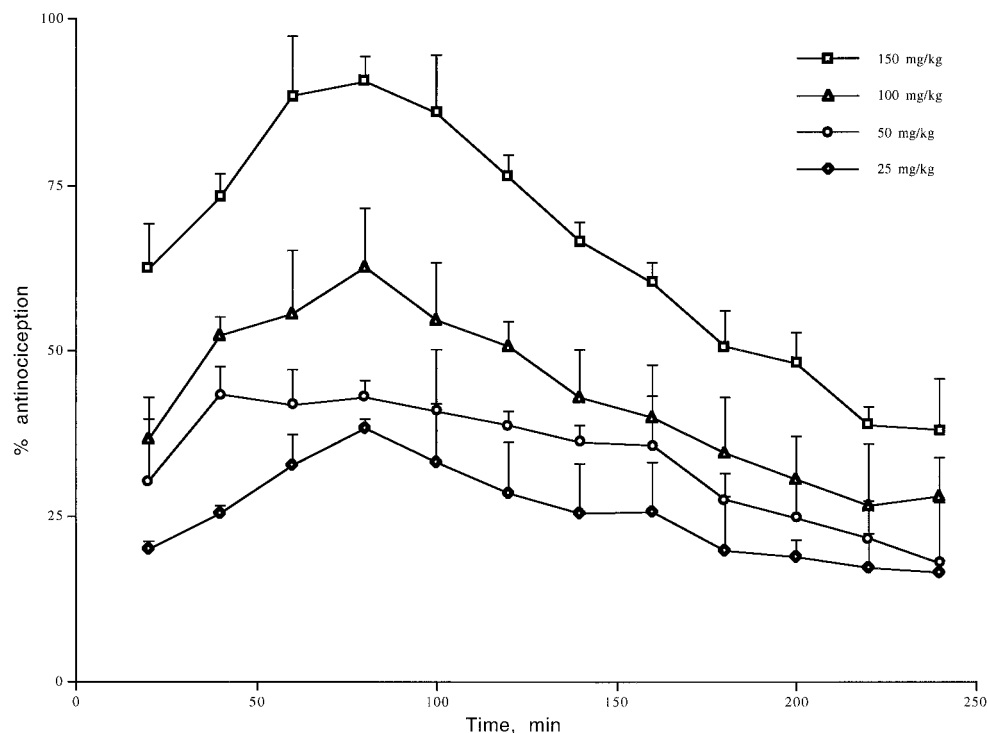


Figure 4. Antinociception as observed in the hot plate assay.

tography. The purity and properties of the target molecule and of the control molecules were assessed by a combination of high-resolution MALDI mass spectrometry, HPLC, elemental analysis, ^1H and ^{13}C NMR, optical rotation, and amino acid analysis (see Experimental Procedures).

The peptide carrier complex was evaluated for analgesic efficacy following i.p. administration in the mouse hot-plate test (Figure 4). This test measures the amount of time required to react to a standardized noxious stimulus. Substances that increase the reaction time are said to display antinociceptive effects, which may be interpreted as a measure of analgesia. It is important to note that the peptide carrier complex itself is inactive in the hot-plate test when given directly into the brain (not shown) but is highly potent and prolonged acting when given peripherally (i.p., Figure 4). The results depicted in Figure 4 show that the peptide carrier complex mediated analgesia is of very long duration. The rate of decline for the observed analgesia for the carrier is much slower than that observed for non-carrier mediated analgesia when deltorphin is given directly into the brain (not shown).

In vitro binding and bioassays showed little or no evidence of affinity or efficacy for the peptide carrier complex **XI** (Figure 2) with opioid receptors in binding experiments in rat brain homogenates or in bioassay experiments using the electrically stimulated mouse vas deferens and guinea pig ileum assays respectively (>10 mM). The free deltorphin peptide of course is well known to be highly potent in these systems with values obtained corresponding well with literature values (19, 20). It is interesting to note that both control molecules (Figure 3) gave results similar to those of the target molecule in *in vivo* studies, but yet when tested for analgesia did not show any activity.

The stability of the peptide carrier conjugate **XI** and the controls **XVIII** and **XXII** was determined in mouse serum ($t_{1/2} \approx 82, 61,$ and 63 min, respectively) and in the mouse brain ($t_{1/2} \approx 4.5, 5,$ and 6 h, respectively) by HPLC analysis. These results show that the masked peptide

carrier conjugate demonstrates greatly improved serum stability over the control molecules, but the mouse brain homogenates appear to have a greater degradative effect upon the masked molecule (compared to the control molecules), probably due to endopeptidase action upon the dipeptide. In the mouse brain homogenates, the $t_{1/2}$ times are of such length that they do not merit problematic effects over the duration of observed analgesia. Peptidase action upon the active peptide-carrier bond appears to be far less destructive in the brain homogenates and yet is the primary degradative site in serum. Analysis of the products generated from these assays (results not shown) suggest that incubation with mouse serum initially results in cleavage of the peptide carrier bond, and only upon further prolonged incubation is the dipeptide-carrier bond hydrolyzed.

DISCUSSION

The major goal of this study was to develop an approach by which a CNS efficacious bioactive peptide could be administered via an intravenous or other peripheral route and for this peptide to overcome the problems of enzymatic degradation and inability to cross the BBB into the brain. The unique approach undertaken here relied upon utilizing biophysical and physicochemical properties of the mammalian system, together with fundamental mass action principles.

The fact that the conjugate we designed was not active in the MVD and GPI assays and has very weak binding to the δ or μ opioid receptors in rat brain membrane but had potent analgesic activity when given peripherally (i.p.) suggests that the approach design has validity. A basic premise of our design was that first the dipeptide mask must be removed by protease activity before or during absorption of the circulating complex at the BBB. Then this would be followed by hydrolysis of the lipid bonds by lipases during or after transmission of the unmasked peptide complex through the BBB. The fact that both of these degradation reactions must occur before the bioactive peptide is released in the brain is consistent with the relatively slow onset of analgesia, and

perhaps can also account for the prolonged activity that occurs after peripheral administration. The apparent serum stability of the complex also suggests that the conjugates can remain in circulation for long periods of time to account for the prolonged analgesic activity observed. Whether the peptide crosses the BBB by active transport, by transcytosis, or by absorption-elimination across the lipid bilayer lies outside the scope of this present study. These questions and a careful evaluation of the mechanism(s) of release of the bioactive peptide from the complex will require the preparation and extensive examination of radiolabeled analogues of these conjugates. In the meantime, the results reported here provide an important new opportunity to further explore approaches to getting peptides or peptide conjugates that will cross the blood-brain barrier.

Finally, the opioid receptors affected by the deltorphin peptides are of practical importance to medicine. It has been hypothesized that, if an effective δ -selective agonist can be developed, such drugs might produce analgesia with limited tolerance and addiction liability (1, 21).

ACKNOWLEDGMENT

We thank Peg Davis, Ed Bilsky, Elizabeth Brownson, and Katherine B. Lee for their help in setting up the assays. This work was supported by a grant from the U.S. Public Health Service, National Institute of Drug Abuse, DA-06284.

LITERATURE CITED

- (1) Hruby, V. J., and Gehrig, C. C. (1989) Recent Developments in the Design of Receptor Specific Opioid-Peptides. *Med. Res. Rev.* 9, 343-401.
- (2) Knapp, R. J., Vaughn, L. K., and Yamamura, H. I. (1995) Selective Ligands for μ and δ Opioid Receptors. *The Pharmacology of Opioid Peptides* (L. F. Tseng, Ed.) pp 1-27, Harwood Academic Publishers, New York.
- (3) Schiller, P. W. (1993) Development of Receptor-Selective Opioid Peptide Analogs as Pharmacological Tools and As Potential Drugs. *Handbook of Experimental Pharmacology, Vol. 104/1 (Opioids I)*, pp 681-710, Springer-Verlag, Berlin.
- (4) Bickel, U., Yoshiwawa, T., Landaw, E. M., Faull, K. F., and Pardridge, W. M. (1993) Pharmacological Effects In Vivo in Brain by Vector-Mediated Peptide Drug Delivery. *Proc. Natl. Acad. Sci. U.S.A.* 90, 2618-2622.
- (5) Bongaard, H. (1992) Prodrugs as a Means to Improve the Delivery of Peptide Drugs. *Adv. Drug Delivery Rev.* 8, 1-38.
- (6) Kreuter, J., Alyautdin, R. N., Kharkevich, D. A., and Ivanov, A. A. (1995) Passage of Peptides Through the Blood-Brain-Barrier with Colloidal Polymer Particles (Nanoparticles). *Brain Res.* 674, 171-174.
- (7) Fukuta, M., Okada, H., Iinuma, S., Yanai, S., and Toguchi, H. (1994) Insulin Fragments as a Carrier for Peptide Delivery Across the Blood-Brain-Barrier. *Pharm. Res.* 11, 1681-1688.

- (8) Sakata, A., Tamai, I., Kawazu, K., Deguchi, Y., Ohnishi, T., Saheki, A., and Tsuji, A. (1994) In-Vivo Evidence for Atp-Dependent and P-Glycoprotein-Mediated Transport of Cyclosporine-A at the Blood-Brain-Barrier. *Biochem. Pharmacol.* 48 (10), 1989-1992.
- (9) Pardridge, W. M. (1991) *Peptide Drug Delivery to the Brain*, Raven Press, New York.
- (10) Risau, W., Dingler, A., Albrecht, U., Dehouck, M.-P., and Cecchelli, R. (1992) Blood-Brain-Barrier Pericytes are the Main Source of Gamma-Glutamyl-Transpeptidase Activity in Brain Capillaries. *J. Neurochem.* 58, 667-672.
- (11) Vorbodt, A. W., Lossinsky, A. S., and Wisniewski, H. M. (1986) Characterization of Endothelial-Cell Transport in the Developing Mouse Blood-Brain-Barrier. *Dev. Neurosci.* 8, 1-13.
- (12) Shook, J. E., Pelton, J. T., Wire, W. S., Hirning, L. D., Hruby, V. J., and Burks, T. F. (1987) Pharmacologic Evaluation of a Cyclic Somatostatin Analog with Antagonist Activity at Mu Opioid Receptors In Vitro. *J. Pharmacol. Exp. Ther.* 240, 772-777.
- (13) Statistical Consultants. (1986) *Am. Stat.* 40, 52-60.
- (14) Hawkins, K. N., Knapp, R. J., Lui, G. K., Guyla, K., Kazmierski, W., Wan, Y.-P., Pelton, J. T., Hruby, V. J., and Yamamura, H. I. (1989) [3 H]-[H-D-Phe-Cys-Tyr-D-Trp-Orn-Thr-Pen-Thr-NH $_2$](3 H)CTOP. A Potent and Highly Selective Peptide for Mu-Opioid Receptors in Rat-Brain. *J. Pharmacol. Exp. Ther.* 248, 73-80.
- (15) Vaughn, L. K., Knapp, R. J., Toth, G., Wan, Y.-P., Hruby, V. J., and Yamamura, H. I. (1989) A High-Affinity, Highly Selective Ligand for the Delta Opioid Receptor-[3 H][D-Pen 2 , pCl-Phe 4 , D-Pen 5]Enkephalin. *Life Sci.* 45, 1001-1008.
- (16) Horan, P., Mattia, A., Bilsky, E. J., Weber, S., Davis, T. P., Yamamura, H. I., Malatynsk, E., Appleyard, S. M., Slaninova, J., Misicka, A., Lipkowski, A. W., Hruby, V. J., and Porreca, F. (1993) Antinociceptive Profile of Biphalin, A Dimeric Enkephalin Analog. *J. Pharmacol. Exp. Ther.* 265, 1446-1454.
- (17) Heyman, J. S., Mulvaney, S. A., Mosberg, H. I., and Porreca, F. (1987) Opioid δ Receptor Involvement in Supraspinal and Spinal Antinociception in Mice. *Brain Res.* 420, 100-108.
- (18) Rink, H. (1987) Solid-Phase Synthesis of Protected Peptide-Fragments Using a Trialkoxy-Diphenyl-Methylester Resin. *Tetrahedron Lett.* 28, 3787-3791.
- (19) Erspamer, V., Melchiorri, P., Falconieri-Erspamer, G., Negri, L., Corsi, R., Sererini, C., Barra, D., Simmaco, M., and Kriegl, G. (1989) Deltorphins: A Family of Naturally Occurring Peptides With High Affinity and Selectivity for δ Opioid Binding Sites. *Proc. Natl. Acad. Sci. U.S.A.* 86, 5188-5192.
- (20) Amiche, M., Sagan, S., Mor, A., Delfour, A., and Nicholas, P. (1989) Dermenkephalin (Tyr-D-Met-Phe-His-Leu-Met-Asp-NH $_2$)-A Potent and Fully Specific Agonist for the Delta-Opioid Receptor. *Mol. Pharmacol.* 35, 774-779.
- (21) Rapaka, R. S., and Porreca, F. (1992) Lack of Antinociceptive Efficacy of Intracerebroventricular [D-Ala 2 , Glu 4]-Deltorphin, But Not [D-Pen 2 , D-Pen 5]Enkephalin In the Mu-Opioid Receptor Deficient Cx36 Mouse. *Pharm. Res.* 8, 1-8.

BC970027G

TECHNICAL NOTES

Conventional and High-Yield Synthesis of DTPA-Conjugated Peptides: Application of a Monoreactive DTPA to DTPA-D-Phe¹-octreotide Synthesis[†]

Yasushi Arano,^{*,‡} Hiromichi Akizawa,[‡] Takashi Uezono,[‡] Kenichi Akaji,[§] Masahiro Ono,[‡] Susumu Funakoshi,[‡] Mitsuru Koizumi,^{||} Akira Yokoyama,[‡] Yoshiaki Kiso,[§] and Hideo Saji[‡]

Department of Radiopharmaceutical Chemistry, Faculty of Pharmaceutical Sciences, Kyoto University, Sakyo-ku, Kyoto 606-01, Japan; Department of Medicinal Chemistry, Kyoto Pharmaceutical University, Yamashina-ku, Kyoto 607, Japan; and Cancer Institute Hospital, Toshima-ku, Tokyo 170, Japan.

Received October 31, 1996[⊗]

Successful imaging of somatostatin receptor-positive tumors with ¹¹¹In-DTPA-D-Phe¹-octreotide has stimulated development of peptide radiopharmaceuticals using DTPA as the chelating agent. However, use of cyclic DTPA dianhydride (cDTPA) resulted in low synthetic yields of DTPA-peptide by either solution or solid-phase syntheses. This paper reports a novel high-yield synthetic procedure for DTPA-D-Phe¹-octreotide that is applicable to other peptides of interest using a monoreactive DTPA derivative. A monoreactive DTPA that possesses one free terminal carboxylic acid along with four carboxylates protected with *tert*-butyl ester (mDTPA) was synthesized. Fmoc-Thr(^tBu)-ol, prepared from Fmoc-Thr(^tBu)-OH, was loaded onto 2-chlorotriyl chloride resin. After construction of the peptide chains by Fmoc chemistry, mDTPA was coupled to the α amine group of the peptide on the resin in the presence of 1,3-diisopropylcarbodiimide and 1-hydroxybenzotriazole. Treatment of the mDTPA-peptide-resin with trifluoroacetic acid–thioanisole removed the protecting groups and liberated [Cys(Acm)^{2,7}]-octreotide-D-Phe¹-DTPA from the resin. Iodine oxidation of the DTPA-peptide, followed by the reversed-phase HPLC purification, produced DTPA-D-Phe¹-octreotide in overall 31.8% yield based on the starting Fmoc-Thr(^tBu)-ol-resin. The final product gave a single peak on analytical HPLC, and amino acid analysis and mass spectrometry confirmed the integrity of the product. ¹¹¹In radiolabeling of the product provided ¹¹¹In-DTPA-D-Phe¹-octreotide with >95% radiochemical yield, as confirmed by analytical reversed-phase HPLC, TLC, and CAE. These findings indicated that use of mDTPA during solid-phase peptide synthesis greatly increased the synthetic yield of DTPA-D-Phe¹-octreotide, due to the absence of nonselective reactions that are unavoidable when cDTPA is used. These results also suggested that mDTPA would be a versatile reagent to introduce DTPA with high yield into peptides of interest.

INTRODUCTION

Low molecular weight peptides such as octreotide (1, 2), chemotactic peptides (3, 4), RGD-peptides (5, 6), and vasoactive intestinal peptide (7, 8) have attracted strong attention as new vehicles to deliver radioactivity to target tissues in diagnostic nuclear medicine, due to their reduced immunogenicity and rapid distribution pharmacokinetics when compared with murine antibodies. Since localization of these peptides involves specific binding to receptors expressed on the target cells, these peptides should be radiolabeled at high specific activities for clinical application (4). Radiolabeling of these peptides with metallic radionuclides such as technetium-99m (^{99m}Tc) and indium-111 (¹¹¹In) is important for clinical application of radiopharmaceuticals.

For radiolabeling with ¹¹¹In, diethylenetriaminepentaacetic acid (DTPA) is usually attached to peptide molecules to provide an ¹¹¹In chelating site. The resulting ¹¹¹In-labeled peptides possess specific activities and *in vivo* stabilities sufficient for clinical application (2). Indeed, recent clinical studies have demonstrated high target-to-nontarget ratios of radioactivity even at early postinjection times (9, 10). Furthermore, attachment of hydrophilic ¹¹¹In-DTPA chelate to peptides altered the excretion pathway from hepatobiliary to urinary excretion, which reduced abdominal radioactivity levels, as has been successfully observed with ¹¹¹In-DTPA-D-Phe¹-octreotide (Figure 1) (1, 9, 11). These findings indicate that DTPA would be a suitable chelating agent for ¹¹¹In radiolabeling of peptides for receptor scintigraphy.

For incorporation of a DTPA chelating site into peptides, cyclic DTPA dianhydride (cDTPA; Figure 2A) is used as the bifunctional chelating agent of choice, due to its simple conjugation reactions with peptides and ready availability from commercial sources. However, since cDTPA possesses two anhydride groups, formations of inter- and intramolecular cross-linkings are inevitable in its conjugation reactions with peptides (2, 3). Formation of ester bonds between DTPA and tyrosine residues

* Author to whom correspondence should be addressed [telephone 81-75-753-4566; fax 81-75-753-4568; e-mail arano@pharm.kyoto-u.ac.jp].

[†] This work is dedicated to the late Dr. Funakoshi.

[‡] Kyoto University.

[§] Kyoto Pharmaceutical University.

^{||} Cancer Institute Hospital.

[⊗] Abstract published in *Advance ACS Abstracts*, April 15, 1997.

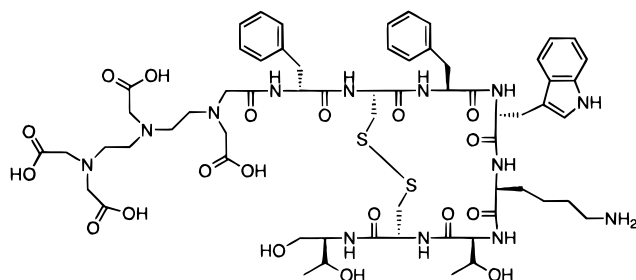


Figure 1. Chemical structure of DTPA-D-Phe¹-octreotide.

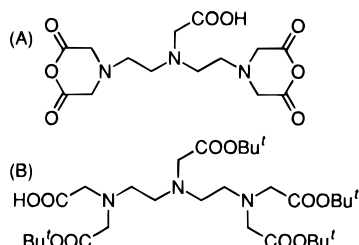


Figure 2. Chemical structures of cyclic DTPA dianhydride (A) and mDTPA (B).

of peptides has also been reported (12). Such undesirable side reactions along with a requirement of repeated purification result in low synthetic yield of DTPA-conjugated peptides when cDTPA is used as the bifunctional chelating agent. Since radiolabeling of peptides with ¹¹¹In-DTPA is useful not only for diagnostic applications but also for screening peptides for use in nuclear medicine, new synthetic procedures are warranted for preparation of DTPA-conjugated peptides with high synthetic yields.

Recently, we developed a monocarboxylic acid derivative of DTPA, with the rest of the four carboxylates being protected with acid-removable *tert*-butyl esters (mDTPA) as illustrated in Figure 2B (13). Since mDTPA possesses only one free carboxylic acid, formation of inter- and intramolecular cross-linking would be prevented during conjugation reactions with peptides. mDTPA also provides a coordination geometry similar to that of cDTPA when cDTPA is conjugated with peptides without any side reactions. The high solubilities of mDTPA in various organic solvents make this reagent versatile for either liquid- or solid-phase syntheses. In the present study, a simple and high-yield synthetic procedure for DTPA-conjugated peptides was designed with mDTPA using an octapeptide, octreotide, as a model.

MATERIALS AND METHODS

General. Amino acid analyses were performed with a Hitachi L8500 amino acid analyzer (Hitachi Co. Ltd., Tokyo, Japan) utilizing postcolumn ninhydrin detection. Optical rotations were measured with SEPA-300 (Horiba Co. Ltd., Kyoto, Japan). Analytical HPLC characterization of DTPA-conjugated peptides was performed on a YMC AM302 column (4.6 × 150 mm; YMC Co. Ltd., Kyoto, Japan), eluted with a linear gradient of acetonitrile (20–80%, 30 min) in 0.1% aqueous trifluoroacetic acid (TFA) at a flow rate of 0.9 mL/min. The eluent was monitored by measuring the UV absorption at both 230 and 254 nm. FPLC (Pharmacia, Uppsala, Sweden) was carried out with a YMC ODS-AQ300 column (1.5 × 50 cm) eluted with a linear gradient of 60% acetonitrile–0.1% aqueous TFA (0–100%, 400 min) in 0.1% aqueous TFA at a flow rate of 3 mL/min. The eluent was monitored by measuring the UV absorption at 254 nm.

Preparative HPLC purification was carried out on a YMC SH-343-5AM column (20 × 250 mm), which was eluted with a linear gradient of acetonitrile (20–80%, 60 min) in 0.1% aqueous TFA at a flow rate of 5 mL/min. The eluent was monitored by measuring the UV absorption at 254 nm. Fast atom bombardment mass spectra (FAB-MS) were obtained on a JMS-HX110 spectrometer equipped with a JMA-DA5000 (JEOL Ltd., Tokyo, Japan). Proton nuclear magnetic resonance (¹H-NMR) spectra were recorded on an AC 300 (300 MHz) spectrometer (Bruker), and the chemical shifts are reported in parts per million downfield from an internal tetramethylsilane standard. Melting points are reported uncorrected. Analytical HPLC characterization of ¹¹¹In-DTPA-D-Phe¹-octreotide was performed on a Cosmosil 5C₁₈-MS column (4.6 × 150 mm, Nacalai Tesque, Kyoto, Japan), eluted with a linear gradient of 40–80% MeOH in 0.05 M acetate buffer (pH 5.5) in 20 min at a flow rate of 1 mL/min. The final solvent composition was maintained for another 5 min, as reported (2). Radiochemical purities of ¹¹¹In-DTPA-D-Phe¹-octreotide were also determined by TLC and cellulose acetate electrophoresis (CAE). TLC (Merck Art. 5553) was developed with a 10% aqueous solution of ammonium chloride–methyl alcohol (1:1), while CAE was run at an electrostatic field of 0.8 mA/cm for 40 min in veronal buffer (*I* = 0.06, pH 8.6).

9-Fluorenylmethoxycarbonyl (Fmoc) amino acid derivatives and 2-chlorotrityl chloride resin were purchased from Nova Biochem (Läufelfingen, Switzerland). ¹¹¹InCl₃ was supplied by Nihon Medi-Physics Co. Ltd. (Tokyo, Japan).

Preparation of mDTPA. mDTPA was synthesized as reported previously (13). Briefly, one terminal amine of diethylenetriamine was trifluoroacetylated with ethyl trifluoroacetate, and the unprotected amines were alkylated with *tert*-butyl bromoacetate. After alkylation of amide nitrogen by *tert*-butyl bromoacetate in the presence of sodium hydride, the trifluoroacetyl protecting group was removed with anhydrous hydrazine in *tert*-butyl alcohol. The resulting secondary amine was alkylated with benzyl bromoacetate in the presence of *N,N*-diisopropylethylamine. mDTPA was then obtained in an almost quantitative yield by catalytic hydrogenation with Pd/C in ethyl acetate.

Fmoc-Thr(^tBu)-ol. This compound was synthesized according to the procedure of Rodriguez et al. (14). To a chilled (–15 °C) solution of Fmoc-Thr(^tBu)-OH (1.99 g, 5 mmol) in 5 mL of ethylene glycol dimethyl ether were added *N*-methylmorpholine (0.56 mL, 5 mmol) and isobutyl chloroformate (0.65 mL, 5 mmol) while the reaction temperature was maintained. After 1 min of stirring, the precipitate was removed, and a suspension of NaBH₄ (0.57 g, 15 mmol) in 15 mL of water was added at the same temperature. After 30 s, 125 mL of water was then added. The reaction solution was extracted with ethyl acetate (50 mL × 3), and the combined organic layers were washed with 5% aqueous NaHCO₃, followed by brine. The combined organic layers were dried over anhydrous Na₂SO₄, and the solvent was removed *in vacuo*. Fmoc-Thr(^tBu)-ol was obtained as a white solid (1.36 g, 70.9%) with a mp of 42–45 °C after column chromatography on silica gel using chloroform as an eluent: ¹H-NMR (CDCl₃) δ 1.16 (3H, d, *J* = 6.2 Hz, CHCH₃), 1.20 (9H, s, ^tBu), 2.88 (1H, broad, OH), 3.61 (1H, broad, CHCH₂OH), 3.66 (2H, broad, CHCH₂OH), 3.94 (1H, m, CHCH₃), 4.22 (1H, t, *J* = 6.8 Hz, CHCH₂CO), 4.40 (2H, m, CHCH₂CO), 5.28 (1H, d, *J* = 7.5 Hz, NH), 7.30 (2H, d, *J* = 7.4 Hz, aromatics), 7.38 (2H, t, *J* = 7.2 Hz, aromatics), 7.59 (2H, d, *J* = 7.4 Hz, aromatics), 7.74 (2H, d, *J* = 7.4 Hz, aromatics); FAB-MAS calcd for C₂₃H₂₉–

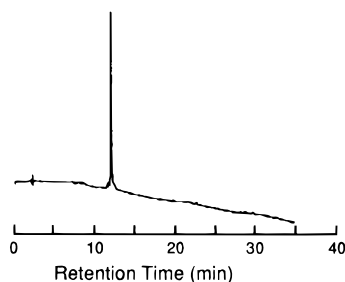


Figure 3. Analytical HPLC profile of DTPA-D-Phe-Cys(Acm)-Phe-D-Trp-Lys-Thr-Cys(Acm)-Thr-ol.

NO_4 $[\text{M} + \text{H}]^+$ m/z 384.2175, found 384.2159; $[\alpha]_{\text{D}}^{26} = +0.017$ (5.08 mg/mL, CH_3OH).

Loading of 2-Chlorotrityl Chloride Resin with Fmoc-Thr(^tBu)-ol. Fmoc-Thr(^tBu)-ol was linked to 2-chlorotrityl chloride resin as described (15). 2-Chlorotrityl chloride resin (393 mg, 1.5 mmol/g), Fmoc-Thr(^tBu)-ol (679 mg, 1.77 mmol), and pyridine (0.286 mL, 3.54 mmol) were stirred for 21 h in a mixed solution of dichloromethane (2.89 mL) and dimethylformamide (DMF, 2.89 mL). After the resin was washed with DMF, methanol (5 mL) was added and the mixture was stirred for 30 min to remove any remaining reactive chloro functionality. The loaded resin was successively washed with DMF and dichloromethane and desiccated to provide a substitution level of 0.287 mmol/g of resin as determined according to the method of Meienhofer (16).

Elongation. All amino acids were protected with N^α -Fmoc. Side-chain protecting groups were Cys(Acm), Lys(Boc), Thr(^tBu) (where Acm is acetamidomethyl). The peptide chain was constructed manually according to the published cycle consisting of (I) 20 min of deprotection with 20% piperidine–DMF and (II) 2 h of coupling of the Fmoc amino acid derivative (2.5 equiv) with 1,3-diisopropylcarbodiimide (DIPCDI, 2.5 equiv) and 1-hydroxybenzotriazole hydrate (HOBt, 2.5 equiv) in DMF (17). The coupling reaction was repeated when the resin became positive to the Kaiser test (18). The satisfactory incorporation of the respective amino acids was further confirmed by amino acid analysis after acid hydrolysis of the assembled peptide resin.

mDTPA Conjugation. After construction of the peptide chain on the resin, the Fmoc protecting group was removed by treating with 20% piperidine–DMF, and a mixture of mDTPA, DIPCDI, and HOBt (2.5 equiv each) in DMF was added and reacted for 2 h, as described above.

Cleavage of Peptide from the Resin and Deprotection. Thioanisole (0.5 mL) and TFA (5 mL) were added to fully protected peptide resin [mDTPA-D-Phe-Cys(Acm)-Phe-D-Trp-Lys(Boc)-Thr(^tBu)-Cys(Acm)-Thr(^tBu)-ol-resin, 200 mg] at 0 °C, and the mixture was stirred at room temperature for 2 h. After the mixture had cooled to 0 °C, dry ether was then added to precipitate crude peptide, and the peptide was extracted with 6 M aqueous guanidine hydrochloride (5 mL). After the resin was removed by filtration, the crude product was purified by FPLC. Fractions containing the peptide were collected, and the solvent was removed by lyophilization to afford 51.89 mg [58.8% from Fmoc-Thr(^tBu)-ol-resin] of DTPA-D-Phe-Cys(Acm)-Phe-D-Trp-Lys-Thr-Cys(Acm)-Thr-ol as a white powder. The purified peptide gave a single peak at a retention time of 11.95 min on HPLC, as shown in Figure 3. Amino acid ratios of the peptide after 6 N HCl hydrolysis: Thr \times 1, 0.90; Phe \times 2, 2.00; Lys \times 1, 1.07; FAB-MAS calcd for $\text{C}_{69}\text{H}_{100}\text{N}_{15}\text{O}_{21}\text{S}_2$ $[\text{M} + \text{H}]^+$, m/z 1538.6660, found 1538.6713.

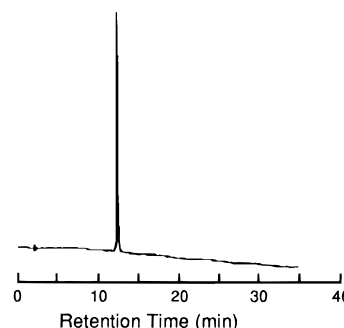


Figure 4. Analytical HPLC profile of DTPA-D-Phe¹-octreotide.

Disulfide Bond Formation. The S-protected peptide (10 mg, 6.5 μmol) was dissolved in 80% aqueous methanol (10 mL). To this solution was added 217.6 μL of 20% iodine in methanol in one portion, and the mixture was stirred at room temperature for 1 h. The excess iodine was reduced with 1 M ascorbic acid in water. This solution was subjected to FPLC and HPLC purifications, and fractions containing the desired product were collected and lyophilized to afford 4.90 mg (54.1%) of DTPA-D-Phe¹-octreotide as a white powder. This peptide showed a single peak at a retention time of 12.50 min on HPLC, as shown in Figure 4. Amino acid ratios after 6 N HCl hydrolysis: Thr \times 1, 0.87; Phe \times 2, 2.00; Lys \times 1, 1.15; FAB-MAS calcd for $\text{C}_{63}\text{H}_{88}\text{N}_{13}\text{O}_{19}\text{S}_2$ $[\text{M} + \text{H}]^+$, m/z 1394.5761, found 1394.5789.

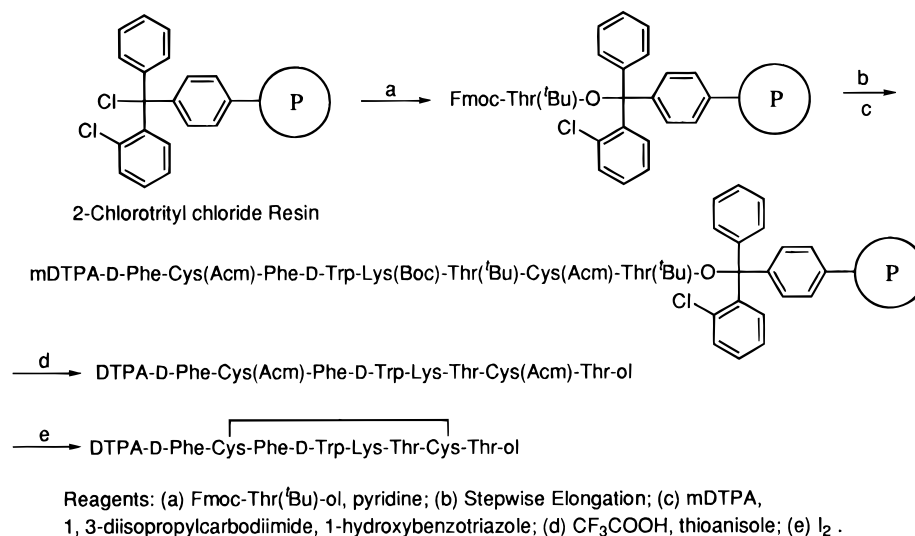
Radiolabeling of DTPA-D-Phe¹-octreotide with ¹¹¹In. ¹¹¹In radiolabeling of DTPA-D-Phe¹-octreotide was performed according to the procedure of Bakker (2) with slight modifications as follows: To 20 μL of DTPA-D-Phe¹-octreotide (0.05 mg/mL) in 0.1 M acetic acid was added 58 μL of a solution of ¹¹¹InCl₃ (74 MBq/mL) in 0.02 M HCl. The reaction mixture was then incubated at room temperature for 30 min.

RESULTS AND DISCUSSION

DTPA-D-Phe¹-octreotide was originally synthesized by protecting the N^ϵ -amine group of the lysine residue of octreotide with a Boc group, followed by condensation of the unprotected N^ϵ -amine group with cDTPA (2). However, the synthetic yield of the final product was rather low, which had been caused by the nonselective reaction procedure. Since the reaction of octreotide with $(\text{Boc})_2\text{O}$ forms a mixture of N^ϵ -Boc-, N^ϵ -Boc-, and N^ϵ , N^ϵ -di-Boc-octreotide as well as unreactive octreotide (19), separation of the desired N^ϵ -protected product from the mixture was required before conjugation reaction with cDTPA. Furthermore, since cDTPA possesses two anhydride moieties, formation of intermolecular cross-linking is unavoidable during the conjugation reaction, as also observed with cDTPA conjugation of chemotactic peptides (3).

Recently, Edwards et al. used solid-phase peptide synthesis to prepare DTPA-D-Phe¹-octreotide (20). They reacted cDTPA with protected octreotide precursor on resin before aminolysis with threoninol, followed by deprotection of Boc groups of D-Trp⁴, Lys⁵, and ^tBu group of Thr with TFA. The overall synthetic yield of DTPA-D-Phe¹-octreotide by this protocol was 5%, although this procedure excluded one of the two nonselective reactions (Boc protection reaction) of the original procedure. They concluded that the rather low synthetic yield of the final product, DTPA-D-Phe¹-octreotide, is attributed to formations of intermolecular cross-linking during the cDTPA conjugation reaction.

These findings strongly suggested that DTPA-D-Phe¹-octreotide would be synthesized in higher yields if the

Scheme 1. Synthetic Procedure for DTPA-D-Phe¹-octreotide Using a Monoreactive DTPA Derivative, mDTPA

DTPA conjugation reaction could be performed without inducing intermolecular cross-linking. Thus, we designed a new synthetic procedure for DTPA-conjugated peptides using a monoreactive derivative of DTPA, mDTPA, as outlined in Scheme 1. Fmoc-Thr(ᵀBu)-ol, prepared according to the method of Rodriguez (14), was loaded on the 2-chlorotrityl chloride resin with a substitution level of 0.29 mmol/g of resin. After the remaining chloride function was inactivated with MeOH, the combination of piperidine treatment and DIPCDI plus HOBt procedure (17) served to elongate the peptide chain manually to prepare D-Phe-Cys(Acm)-Phe-D-Trp-Lys(Boc)-Thr(ᵀBu)-Cys(Acm)-Thr(ᵀBu)-ol-resin. mDTPA was then coupled to the N^ε-amine group of the peptide in the presence of HOBt and DIPCDI, and mDTPA-conjugated peptide-resin was treated with TFA–thioanisole to liberate the peptide from the resin. During this treatment, the Boc and ᵀBu protecting groups of the peptide and DTPA were simultaneously removed. After HPLC purification, DTPA-D-Phe-Cys(Acm)-Phe-D-Trp-Lys-Thr-Cys(Acm)-Thr-ol was obtained as a white solid with an overall yield of 58.8% based on the starting Fmoc-Thr(ᵀBu)-ol-resin. The product gave a single peak on analytical HPLC (Figure 3). Integrity of the purified product was further determined by amino acid analyses and FAB-MS.

Formation of disulfide bonds in the S-protected DTPA-peptide was then performed in the presence of iodine. After the reaction was quenched with ascorbic acid, DTPA-D-Phe¹-octreotide was obtained with a yield of 54.1% after FPLC and HPLC purifications. The final product showed a single peak on analytical HPLC (Figure 4). Although DTPA-D-Phe¹-octreotide had a retention time very close to that of its precursor, DTPA-D-Phe-Cys(Acm)-Phe-D-Trp-Lys-Thr-Cys(Acm)-Thr-ol, on the analytical HPLC (12.50 vs 11.95 min), as shown in Figures 3 and 4, coelution of the two compounds indicated two separated peaks on the same HPLC system (data not shown). A similar phenomenon was observed in the previous study (21). Amino acid analyses and FAB-MS further confirmed the integrity of the final product. The low synthetic yield in this step might have been due to the interference of Trp residue during the formation of the intramolecular disulfide bonds (20). Despite this, the overall synthetic yield of DTPA-D-Phe¹-octreotide based on the starting Fmoc-Thr(ᵀBu)-ol-resin was 31.8%, which is much higher than those of previously reported procedures. The integrity of the DTPA chelating group of DTPA-D-Phe¹-octreotide was confirmed by the ¹¹¹In ra-

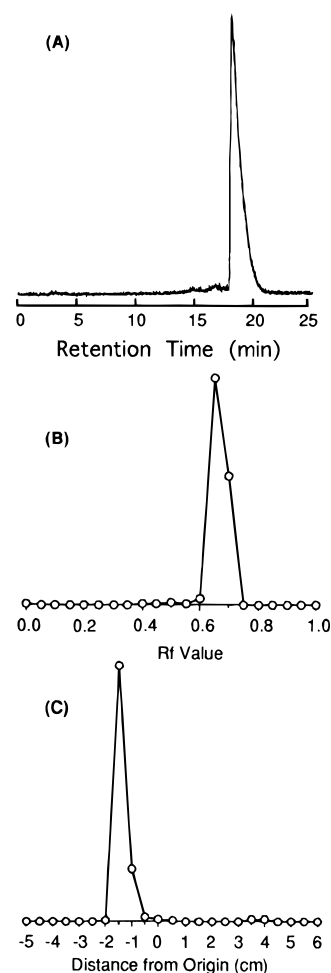


Figure 5. Radioactivity profiles of ¹¹¹In-DTPA-D-Phe¹-octreotide on analytical HPLC (A), TLC (B), and CAE (C).

diolabeling of DTPA-D-Phe¹-octreotide, where ¹¹¹In-DTPA-D-Phe¹-octreotide was obtained with >95% radiochemical yield at a specific activity of 4.3 MBq/μg when analyzed by HPLC, TLC, and CAE (Figure 5).

CONCLUSIONS

The findings of this study indicated that an application of mDTPA to solid-phase peptide synthesis of octreotide provides DTPA-D-Phe¹-octreotide with a high overall synthetic yield, due to the absence of nonselective reac-

tions during synthesis. Furthermore, the present procedure can be applied to the incorporation of a DTPA chelating moiety into various peptides of interest. Thus, use of mDTPA during solid-phase peptide syntheses is a convenient method for preparing DTPA-conjugated peptides in high yield.

ACKNOWLEDGMENT

We thank Nihon Medi-Physics Co. Ltd. for their kind gift of $^{111}\text{InCl}_3$. This work was supported in part by Grants-in-Aid for Developing Scientific Research (07672419 and 08557135) from the Ministry of Education, Science and Culture of Japan.

LITERATURE CITED

- (1) Bakker, W. H., Krenning, E. P., Breeman, W. A., Koper, J. W., Kooij, P. P., Reubi, J.-C., Klijn, J. G., Visser, T. J., Docter, R., and Lamberts, S. W. (1990) Receptor scintigraphy with a radiolabeled somatostatin analogue: radiolabeling, purification, biologic activity, and in vivo application in animals. *J. Nucl. Med.* **31**, 1501–1509.
- (2) Bakker, W. H., Albert, R., Bruns, C., Breeman, W. A. P., Hofland, L. J., Marbach, P., Pless, J., Pralet, D., Stolz, B., Koper, J. W., Lamberts, S. W. J., Visser, T. J., and Krenning, E. P. (1991) [^{111}In -DTPA-D-Phe 1]-octreotide, a potential radiopharmaceutical for imaging of somatostatin receptor-positive tumors: synthesis, radiolabeling and in vitro validation. *Life Sci.* **49**, 1583–1591.
- (3) Fischman, A. J., Pike, M. C., Kroon, D., Fucello, A. J., Rexinger, D., tenKate, C., Wilkinson, R., Rubin, R. H., and Strauss, H. W. (1991) Imaging focal sites of bacterial infection in rats with indium-111-labeled chemotactic peptide analogs. *J. Nucl. Med.* **32**, 483–491.
- (4) Fischman, A. J., Babich, J. W., and Strauss, H. W. (1993) A ticket to ride: peptide radiopharmaceuticals. *J. Nucl. Med.* **34**, 2253–2263.
- (5) Knight, L. C., Radcliffe, R., Maurer, A. H., Rodwell, J. D., and Alvarez, V. L. (1994) Thrombus imaging with technetium-99m synthetic peptides based upon the binding domain of a monoclonal antibody to activated platelets. *J. Nucl. Med.* **35**, 282–288.
- (6) Lister-Jones, J., Knight, L. C., Maurer, A. H., Bush, L. R., Moyer, B. R., and Dean, R. T. (1996) Thrombus imaging with a technetium-99m-labeled, activated platelet receptor-binding peptide. *J. Nucl. Med.* **37**, 775–781.
- (7) Virgolini, I., Kurtaran, A., Raderer, M., Leimer, M., Angelberger, P., Havlik, E., Li, S., Scheithauer, W., Niederle, B., Valent, P., and Eichler, H. G. (1995) Vasoactive intestinal peptide receptor scintigraphy. *J. Nucl. Med.* **36**, 1732–1739.
- (8) Virgolini, I., Raderer, M., Kurtaran, A., Angelberger, P., Banyai, S., Yang, Q., Li, S., Banyai, M., Pidlich, J., Niederle, B., Scheithauer, W., and Valent, P. (1994) Vasoactive intestinal peptide-receptor imaging for the localization of intestinal adenocarcinomas and endocrine tumors. *N. Engl. J. Med.* **331**, 1116–1121.
- (9) Krenning, E. P., Bakker, W. H., Kooij, P. P. M., Breeman, W. A. P., Oei, H. Y., de Jong, M., Reubi, J. C., Visser, T. J., Bruns, C., Kwekkeboom, D. J., Reijts, A. E. M., van Hagen, P. M., Koper, J. W., and Lamberts, S. W. J. (1992) Somatostatin receptor scintigraphy with indium-111-DTPA-D-Phe 1 -octreotide in man: metabolism, dosimetry and comparison with iodine-123-Tyr 3 -octreotide. *J. Nucl. Med.* **33**, 652–658.
- (10) Krenning, E. P., Kwekkeboom, D. J., Bakker, W. H., Breeman, W. A. P., Kooij, P. P. M., Oei, H. Y., Hagen, M. v., Postema, P. T. E., de Jong, M., Reubi, J. C., Visser, T. J., Reijts, A. E. M., Hofland, L. J., Koper, J. W., and Lamberts, S. W. J. (1993) Somatostatin receptor scintigraphy with [^{111}In -DTPA-D-Phe 1]- and [^{123}I -Tyr 3]-octreotide: the Rotterdam experience with more than 1000 patients. *Eur. J. Nucl. Med.* **20**, 716–731.
- (11) Marbach, P., Andres, H. A., Azria, M., Bauer, W., Briner, U., Buchheit, K.-H., Doepfner, W., Lemaire, M., Petcher, T. J., Pless, J., and Reubi, J.-C. (1987) Chemical structure, pharmacodynamic profile and pharmacokinetics of SMS 201–995 (Sandostatine®). *Sandostatine® in the Treatment of Acromegaly* (S. W. J. Lamberts, Ed.) pp 53–60, Springer-Verlag, Berlin.
- (12) Maisano, F., Gozzini, L., and de Haën, C. (1992) Coupling of DTPA to proteins: A critical analysis of the cyclic dihydride method in the case of insulin modification. *Bioconjugate Chem.* **3**, 212–217.
- (13) Arano, Y., Uezono, T., Akizawa, H., Ono, M., Wakisaka, K., Nakayama, M., Sakahara, H., Konishi, J., and Yokoyama, A. (1996) Reassessment of diethylenetriaminepentaacetic acid (DTPA) as a chelating agent for indium-111 labeling of polypeptides using a newly synthesized monoreactive DTPA derivative. *J. Med. Chem.* **39**, 3451–3460.
- (14) Rodriguez, M., Llinares, M., Doulet, S., Heitz, A., and Martinez, J. (1991) A facile synthesis of chiral N-protected β -amino alcohols. *Tetrahedron Lett.* **32**, 923–926.
- (15) Wenschuh, H., Beyermann, M., Haber, H., Seydel, J. K., Krause, E., and Bienert, M. (1995) Stepwise automated solid phase synthesis of naturally occurring peptaibols using Fmoc amino acid fluorides. *J. Org. Chem.* **60**, 405–410.
- (16) Meienhofer, J., Waki, M., Heimer, E. P., Lambros, T. J., Makofske, R. C., and Chang, C.-D. (1979) Solid phase synthesis without repetitive acidolysis. Preparation of leucyl-alanyl-glycyl-valine using 9-fluorenylmethoxycarbonyl-amino acids. *Int. J. Pept. Protein Res.* **13**, 35–42.
- (17) Akaji, K., Fujii, N., Tokunaga, F., Miyata, T., Iwanaga, S., and Yajima, H. (1989) Studies on peptides. CLXVIII. Syntheses of three peptides isolated from horseshoe crab hemocytes, Tachyplesin I, Tachyplesin II, and Polyphemusin I. *Chem. Pharm. Bull.* **37**, 2661–2664.
- (18) Kaiser, E., Collescott, R. L., Bossinger, C. D., and Cook, P. I. (1970) Color test for detection of free terminal amino groups in the solid-phase synthesis of peptides. *Anal. Biochem.* **34**, 595–598.
- (19) Smith-Jones, P. M., Stolz, B., Bruns, C., Albert, R., Reist, H. W., Fridrich, R., and Mäcke, H. R. (1994) Gallium-67/gallium-68-[DFO]-octreotide—a potential radiopharmaceutical for PET imaging of somatostatin receptor-positive tumors: Synthesis and radiolabeling in vitro and preliminary in vivo studies. *J. Nucl. Med.* **35**, 317–325.
- (20) Edwards, W. B., Fields, C. G., Anderson, C. J., Pajean, T. S., Welch, M. J., and Fields, G. B. (1994) Generally applicable, convenient solid-phase synthesis and receptor affinities of octreotide analogs. *J. Med. Chem.* **37**, 3749–3757.
- (21) Akaji, K., Fujino, K., Tatsumi, T., and Kiso, Y. (1993) Total synthesis of human insulin by regioselective disulfide formation using the silyl chloride-sulfoxide method. *J. Am. Chem. Soc.* **115**, 11384–11392.

BC970023B

Heterobifunctional Cross-Linkers Containing 4,9-Dioxa-1,12-dodecanediamine Spacers

Gary M. Johnson,^{*,†} James P. Albarella,[†] and Christoph Petry[‡]

Organic Chemistry Group, Bayer Corporation, P.O. Box 70, Elkhart, Indiana 46515, and Bayer AG ZF-FDM, Krefeld-Uerdingen, Germany. Received August 31, 1996[§]

A series of heterobifunctional linker arms has been prepared by functionalization of (*tert*-butoxycarbonyl)-4,9-dioxa-1,12-dodecanediamine [tBOC-HN(CH₂)₃O(CH₂)₄O(CH₂)₃NH₂] with anhydrides or acid chloride.

INTRODUCTION

Heterobifunctional cross-linkers are commonly used in bioconjugation technologies to prepare antibody–enzyme conjugates for use in enzyme immunoassays. Possible drawbacks can include instability and incomplete, oligomeric, and polymeric reactions, which frequently occur with commercially available cross-linkers. As part of a program to develop new reagents with enhanced stability and reactivity, 4,9-dioxa-1,12-dodecanediamine [H₂N(CH₂)₃O(CH₂)₄O(CH₂)₃NH₂] heterobifunctional cross-linkers were synthesized. This (3,4,3) extended spacer was readily available and inexpensive and had good water solubility. It has been postulated that extended length cross-linkers would reduce steric crowding between the enzyme and antibody and increase stability and may provide enhanced biochemical properties relative to those presently being used.

CHEMISTRY

Synthesis of the cross-linkers began by coupling the known¹ (*tert*-butoxycarbonyl)-4,9-dioxa-1,12-dodecanediamine [tBOC(343)NH₂] to anhydrides² **1–3** or acid chloride **4**, providing carboxy-functionalized intermediates **5–8** in near quantitative yields (see Scheme 1 and Table 1). Treatment with trimethylsilyl iodide (TMSI)³ in CHCl₃ followed by methanol quench furnished quantitative crude yields of amino acids **9** and **11–13**. In the case of intermediate **6**, the cyclic imide analog **10** was obtained via intramolecular cyclization. Compound **13** was obtained in 92% yield by treatment of **8** with NaOH in aqueous ethanol. Coupling of amino acids **9** and **11–13** with succinimidyl 4-(*N*-maleimidomethyl)cyclohexane-1-carboxylate (SMCC)⁴ in dimethylformamide/triethylamine (DMF/TEA) provided the heterobifunctional cross-linkers (**14–17**) in 67, 7, 32, and 30% yields,⁵ respectively.

N-Succinimidyl 3-(2-pyridyldithio)propionate (SPDP) analogs⁴ were also developed as thiol-functionalized cross-linkers. These were prepared by treating an amino acid with SPDP in DMF/TEA, as shown by the example

in Scheme 2 where intermediate **5** was converted into cross-linker **18** in 17% yield⁵ via amino acid **9**.

The linkers were activated as *N*-hydroxysuccinimidyl (NHS) esters before coupling to alkaline phosphatase, which in turn was then coupled to 2-iminothiolane (2IT)-activated antibody.⁴ Activation was performed *in situ* with NHS in DMF/TEA as the resultant esters were unstable. In the case of linkers **10** and **14**, intramolecular cyclizations to imides were determined to be significant side reactions.

To overcome these problems, heterobifunctional linker **17** was modified to the very stable hydrazide **19**, shown in Scheme 3. This modification used (*tert*-butoxycarbonyl)hydrazine (tBOCNHNH₂) and dicyclohexylcarbodiimide (DCC) in DMF (61%), followed by trifluoroacetic acid (TFA) for 2 h (31% yield).⁵ This stable, crystalline cross-linkers binds covalently to aldehyde sites on the antibody.

RESULTS AND DISCUSSION

A high-performance liquid chromatography (HPLC) profile of the crude reaction mixture, prepared with linker **19**, of a polyclonal anti-myoglobin antibody conjugated to alkaline phosphatase (AP) is shown in Figure 1. The new conjugate (overall yield of ~60%) was exchanged for and tested using the same procedure and conditions as the anti-myoglobin–AP conjugate normally used in the Technicon IMMUNO 1 myoglobin assay (product T01-3653-51) commercialized by Bayer Corp.

In that assay, magnetic particles carrying antibodies against fluorescein, a fluoresceinated monoclonal anti-myoglobin antibody, and an alkaline phosphatase-labeled polyclonal anti-myoglobin antibody are incubated for 15 min together with 3 μ L of a sample containing an unknown amount of myoglobin. During the course of the incubation, the two different antibody conjugates form a sandwich complex with the myoglobin–antigen. This complex is captured by the magnetic particles via the fluorescein moiety on the monoclonal antibody. The supermolecule thus formed is then precipitated by an external magnetic field and washed. Any antibody–AP conjugate present in the mixture is removed unless bound to the immobilized supermolecule. The amount of antibody–AP conjugate remaining in the assay is directly proportional to the amount of myoglobin in the sample. The kinetics of *p*-nitrophenyl phosphate hydrolysis is

[†] Bayer Corp.

[‡] Bayer AG ZF-FDM.

[§] Abstract published in *Advance ACS Abstracts*, April 15, 1997.

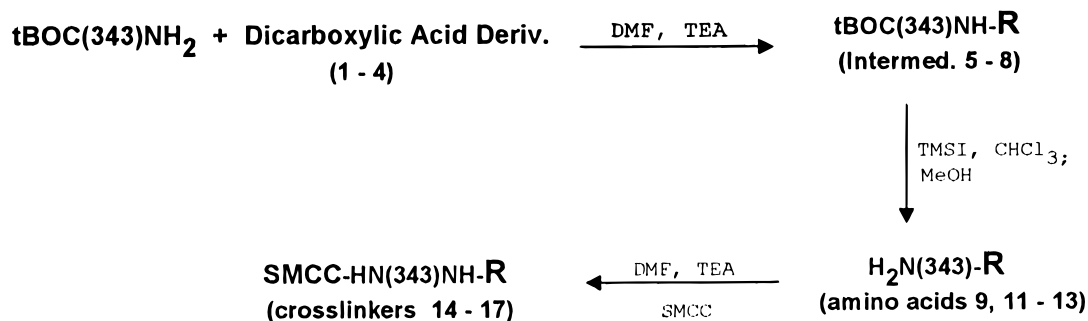
¹ Reference 1a was used to prepare tBOC(343)NH₂. Patent references 1b–d give other preparations and some uses of this linker.

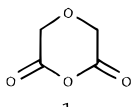
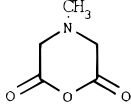
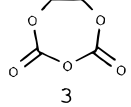
² Anhydride **2** from ref 2a. Anhydride **3** from ref 2b.

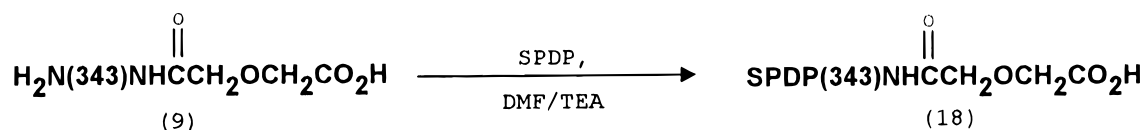
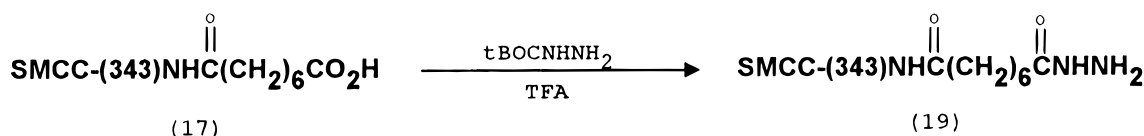
³ As described in ref 3.

⁴ These reagents were purchased from Pierce Co. (P.O. Box 17, Rockford, IL, 61105). General procedures other than those listed herein, additional examples, and relevant references may be found in their catalogs.

⁵ All isolated products exhibited spectroscopic (IR, MS, ¹H NMR, and ¹³C/D NMR) and analytical data which are fully consistent with the assigned structures. Yields are unoptimized in that good recoveries of crude product were generally obtained, but due to expediency, the preparative thin layer chromatography (TLC) plate purification method employed sacrificed quantity for purity.

Scheme 1**Table 1**

DICARBOXYLIC ACID DERIV.	INTERMEDIATES	AMINO ACIDS	HETEROBIFUNCTIONAL CROSSLINKERS
 1	$\text{tBOC(343)HNC(O)CH}_2\text{OCH}_2\text{CO}_2\text{H}$ 5	$\text{H}_2\text{N(343)HNC(O)CH}_2\text{OCH}_2\text{CO}_2\text{H}$ 9	$\text{SMCC(343)HNC(O)CH}_2\text{OCH}_2\text{CO}_2\text{H}$ 14
 2	$\text{tBOC(343)HNC(O)CH}_2\text{N(CH}_3\text{)CH}_2\text{CO}_2\text{H}$ 6	$\text{H}_2\text{N(343)N-C(O)CH}_2\text{N(CH}_3\text{)CH}_2\text{CO}_2\text{H}$ 10	
 3	$\text{tBOC(343)HNC(O)CH}_2\text{OCH}_2\text{CH}_2\text{OCH}_2\text{CO}_2\text{H}$ 7	$\text{H}_2\text{N(343)HNC(O)CH}_2\text{OCH}_2\text{CH}_2\text{OCH}_2\text{CO}_2\text{H}$ 11	$\text{SMCC(343)HNC(O)CH}_2\text{OCH}_2\text{CH}_2\text{OCH}_2\text{CO}_2\text{H}$ 15
$\text{EtO}_2\text{C(CH}_2\text{)}_6\text{C(O)Cl}$ 4	$\text{tBOC(343)HNC(O)(CH}_2\text{)}_6\text{CO}_2\text{Et}$ 8	$\text{H}_2\text{N(343)HNC(O)(CH}_2\text{)}_6\text{CO}_2\text{Et}$ 12	$\text{SMCC(343)HNC(O)(CH}_2\text{)}_6\text{CO}_2\text{Et}$ 16
		$\text{H}_2\text{N(343)HNC(O)(CH}_2\text{)}_6\text{CO}_2\text{H}$ 13	$\text{SMCC(343)HNC(O)(CH}_2\text{)}_6\text{CO}_2\text{H}$ 17

Scheme 2**Scheme 3**

measured to quantify the antibody-AP conjugate present and hence the amount of myoglobin in the sample.

The new antibody-AP conjugate synthesized with linker **19** was tested in the assay after substitution for the standard antibody-AP conjugate, and all other parameters and buffers remained unchanged (Technicon IMMUNO 1, protocol 5; fluoresceinated conjugate, 2.6 $\mu\text{g/mL}$, 65 μL of solution; antibody-AP conjugate, 6.5 $\mu\text{g/mL}$, 65 μL of solution; magnetic particles, 10 μL of suspension; sample volume, 3 μL , 15 min of simultaneous incubation, four washes).

The activity of the enzyme in the antibody-AP conjugate was measured as follows. One tablet of *p*-nitrophenyl phosphate (Sigma N2640) was dissolved into 15 mL of glycine buffer (1.88 g of glycine/L, pH 9.6). The antibody-AP conjugate was diluted to a concentration of 2.5 $\mu\text{g/mL}$ in AP reaction buffer (1.88 g of glycine, 0.2 g of magnesium chloride, 13 mg of zinc chloride, and 100 mL of glycerine). Five microliters of the diluted conjugate, 0.5 mL of a 0.05 M magnesium chloride solution, and 2.5 mL of a substrate solution were then mixed in a

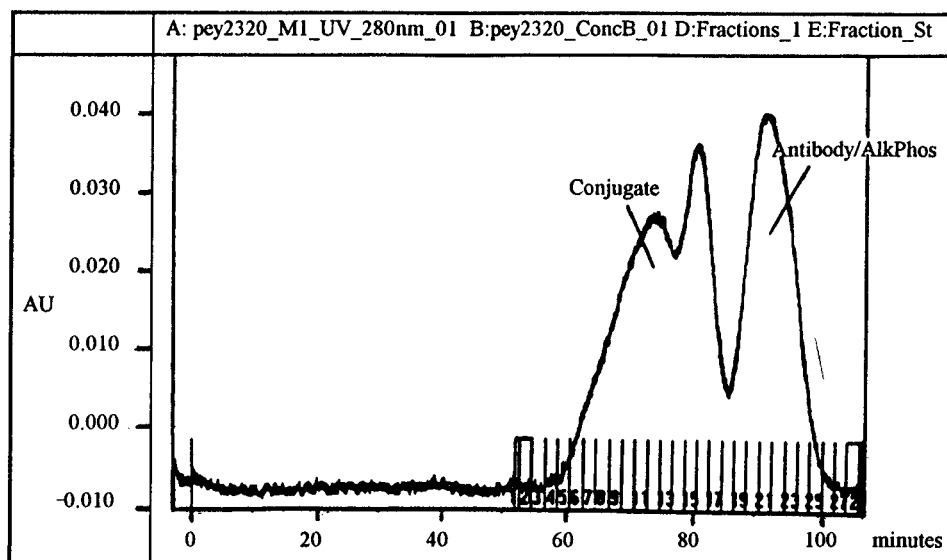


Figure 1. HPLC profile of the crude reaction mixture, prepared with linker **19**, of a polyclonal anti-myoglobin antibody conjugated to alkaline phosphatase.

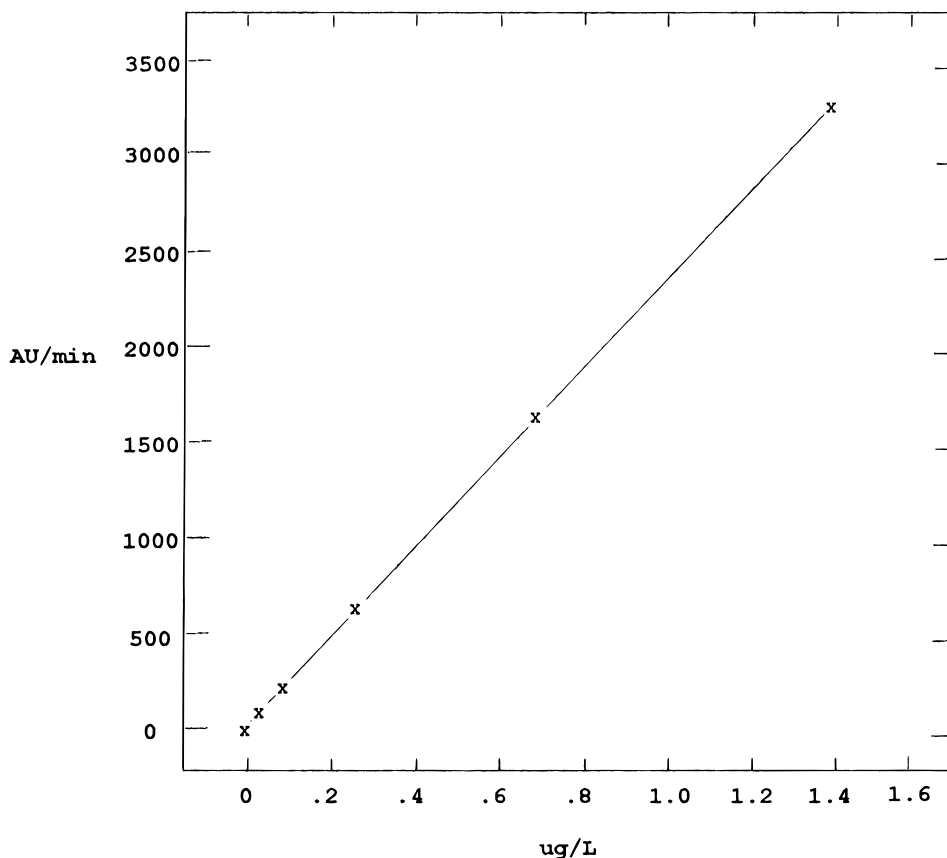


Figure 2. Dose-response curve of the myoglobin assay using linker **19**.

cuvette with a 1 cm path length, and the absorption increase of the solution was monitored at 25 °C and 400 nm.

A typical enzyme activity for an antibody-AP conjugate was 580 units/mg, where 1 unit of alkaline phosphatase digests 1 μ mol of substrate per second, and the extinction coefficient of *p*-nitrophenolate at 400 nm is 18.7 cm²/ μ mol. Conjugates prepared by procedures using shorter linkers directed against amino groups had typical enzyme activities of 400–650 units/mg, depending on the amount of NH-derivatizing agent used.

Figure 2 shows a dose-response curve of the myoglobin assay using linker **19** on the Technicon IMMUNO 1

assay. The dose-response curve depicted (using a six-point cubic-fit-through-zero calculation) was nearly identical with the optimized standard curve obtained using the regular antibody-AP conjugate. The instrument was calibrated using six myoglobin investigational calibrators having concentrations of 0, 63, 186, 619, 1552, and 3193 ng/mL. The reaction rates measured on the Technicon IMMUNO 1 assay for the calibrators were 3.5, 29.0, 78.0, 254.0, 638.6, and 1238.2 mA/min, respectively, and the dose-response curve using a six-point cubic-fit-through-zero calculation was constructed. As controls, three serum pools with assigned concentrations of 15, 75, and 667 ng/mL were run. Using this calibration, the controls

(reaction rates of 9.2, 33.7, and 284.3 mA/min) were recovered as 14.4 (−4%), 76.2 (+1.5%), and 691.6 (+3.7%), showing the versatility of the newly prepared reagent.

SUMMARY

This paper describes the synthesis and preliminary testing of heterobifunctional linkers containing an extended spacer unit. A new enzyme–antibody conjugate prepared in acceptable yield with highly stable linker **19** demonstrates that new linkers of this type can be used as versatile agents to prepare fully functional antibody–AP conjugates. Linker **19** is particularly useful in that coupling can be performed in the presence of the protein's surface amino groups.

MATERIALS AND METHODS

IR spectra were recorded on a Perkin-Elmer 710B spectrophotometer. NMR spectra were recorded on a GE 300 MHz spectrometer. Mass spectra were determined by fast atom bombardment (FAB) on a HP 5985A apparatus, FAB source with direct introduction. Thin layer chromatography was carried out on Merck GF 254 silica plates. HPLC separations were performed with a Pharmacia FPLC system on Pharmacia Superdex 200 columns. Protein concentrations were determined on a HP 8452A diode array spectrophotometer by measuring the absorbance at 280 nm. Performance testing was done on a Technicon IMMUNO 1 immunoanalyzer. All isolated products exhibited spectroscopic data (IR, MS, ^1H NMR, ^{13}C NMR, and ^{13}CD NMR) and analytical data which are fully consistent with the assigned structures.

EXPERIMENTAL PROCEDURES

Preparation (1a) of tBOC-HN(CH₂)₃O(CH₂)₄-O(CH₂)₃NH₂. To *tert*-butyl *S*-(4,6-dimethylpyrimidin-2-yl)thiocarbonate (35.3 g, 0.147 mmol, 0.6 equiv) in 1,4-dioxane (100.0 mL) under argon was added dropwise via cannula a solution of H₂N(CH₂)₃O(CH₂)₄O(CH₂)₃NH₂ (50.0 g, 0.245 mmol) in 1,4-dioxane (200.0 mL) over 60 min. The reaction mixture was stirred for 24 h and was filtered of precipitated solid, and the crude product solution was concentrated *in vacuo* under high vacuum in a water bath at about 50 °C. The compound was purified via flash chromatography (7.5 × 60 cm column, 800 g of 230–400 mesh silica gel-60), eluting with 100 mL fractions of 90/20/2 CHCl₃/CH₃OH/NH₄OH. TLC in 90/20/2 CHCl₃/CH₃OH/NH₄OH revealed an orange-colored product spot after iodine spray solution with an *R_f* value of about 0.35. Product fractions were combined and concentrated *in vacuo* at about 45 °C and then dissolved into CHCl₃/ether (1/1, 300 mL). The organics were washed with 50 mL of water, separated, and dried with granular MgSO₄. The solution was filtered and concentrated *in vacuo* to a pale yellow product oil (~14–18 g, 40–60%).

^1H NMR (300 MHz, CD₃OD, ppm): 1.42 (s, 9H), 1.62 (m, 4H), 1.72 (m, 4H), 1.75 (t, 2H), 3.12 (t, 2H), 3.46 (m, 8H).

General Synthetic Method for Preparation of Intermediates 5–7. Triethylamine (TEA, 5.34 mmol, 1.3 equiv) was added in one portion to a solution of tBOC-(343)NH₂ (4.11 mmol, 1 equiv) in DMF (anhydrous, 10 mL, 2.5 equiv) under argon. A solution of anhydride, or acid chloride (5.0 mmol, 1.2 equiv), in dimethylformamide (DMF, anhydrous, 2.0 mL) was added to the flask dropwise via syringe over 5 min. The reaction mixture was stirred under argon for 24 h. A white TEA·HCl precipitate was then removed by filtration, and the resultant solution was concentrated *in vacuo* under high

vacuum at about 50 °C. The crude material was then purified by flash column chromatography to provide the clean product.

5. ^1H NMR (300 MHz, DMSO-*d*₆, ppm): 1.36 (s, 9H), 1.5 (m, 4H), 1.6 (m, 4H), 2.95 (qrt, 2H), 3.15 (qrt, 2H), 3.35 (m, 8H), 3.78 (s, 2H), 3.88 (s, 2H), 6.75 (NH). ^{13}C NMR (75 MHz, DMSO-*d*₆, ppm): 26.1, 28.3 (tBOC), 29.4, 29.8, 35.7, 37.3, 67.7, 67.9, 69.9, 71.3, 71.5, 77.4, 155.6, 169.8, 172.9. EI-DIP/MS: 347 (M – tBOC:73, 2.7), 301 (5.5), 264 (18.5), 246 (14.1), 231 (16.2), 190 (43.3), 174 (73.4), 156 (83.6), 146 (base), 130 (17.5), 114 (25.7), 102 (37.8), 74 (65.6), 57 (34.4). IR (neat, cm^{−1}): 3700–3000, 1710, 1690, 1650, 1580, 1530, 1450, 1420, 1270, 1170.

6. ^1H NMR (300 MHz, CD₃OD, ppm): 1.42 (s, 9H), 1.61 (m, 4H), 1.65–1.81 (m, 4H), 2.78 (s, 3H), 3.1 (t, 2H), 3.31–3.5 (m, 10H), 3.58 (s, 2H), 3.76 (s, 2H). ^{13}C NMR (75 MHz, CD₃OD, ppm): 27.5 (methylenes), 28.8 (methyls, tBOC), 30.4 (methylene), 31.0 (methylene), 37.9 (methylene), 38.9 (methylene), 43.1 (quat, tBOC), 42.9 (*N*-methyl), 58.7 (methylene), 59.6 (methylene), 69.3 (methylene), 69.5 (methylene), 71.7 (methylene), 71.8 (methylene), 167.9 (C=O), 170.9 (C=O). FAB/MS: 334 [(M + H) – tBOC]. IR (neat, cm^{−1}): 3700–3130, 3130–2600, 1800–1600, 1550, 1530, 1390, 1250, 1175.

7. ^1H NMR (300 MHz, CD₃OD, ppm): 1.36 (brs, 9H), 1.58 (m, 4H), 1.65 (qnt, 2H), 1.75 (qnt, 2H), 3.05 (s, 2H), 3.28 (m, 2H), 3.4 (m, 8H), 3.71 (m, 4H), 3.95 (m, 4H). ^{13}C NMR (75 MHz, CD₃OD, ppm): 27.5, 28.8, 30.5, 37.9, 38.9, 69.2, 69.6, 69.9, 71.2, 71.4, 71.8, 71.9, 71.93, 79.4. FAB/MS: 365 [(M + H) – tBOC]. IR (neat, cm^{−1}): 3350, 2940, 1710, 1670, 1535, 1450, 1275.

Preparation of Intermediate 8. Pyridine (10.0 mmol, 2.0 equiv) was added in one portion to a solution of tBOC-4,9-dioxa-1,12-dodecanediamine (**1a**), tBOC(343)-NH₂ (5.0 mmol, 1 equiv), in CH₂Cl₂ (20 mL, 4 equiv) under argon at 0 °C. A solution of acid chloride (5.0 mmol, 1.0 equiv) in CH₂Cl₂ (5 mL, 1 equiv) was added to the flask, dropwise via cannula over 5 min. The reaction mixture was allowed to warm to room temperature over 2 h and stirred under argon for 24 h. The resultant solution was diluted with CH₂Cl₂ (50 mL) and then washed consecutively with saturated NaHCO₃, 1 M HCl, brine, and water (50 mL each). The organic phase was then dried and concentrated *in vacuo* under high vacuum at about 35 °C. The clean crude product was then used directly in the next step.

8. ^1H NMR (300 MHz, CD₃OD, ppm): 1.21 (t, 3H), 1.32 (m, 4H), 1.41 (s, 9H), 1.6 (m, 8H), 1.72 (m, 4H), 2.16 (t, 2H), 2.3 (t, 2H), 3.11 (m, 2H), 3.22 (m, 2H), 3.42 (m, 6H), 4.1 (qnt, 2H), 6.5 (NH). ^{13}C NMR (75 MHz, CD₃OD, ppm): 14.5, 25.9, 26.8, 27.5, 28.3, 29.4, 29.8, 29.9, 30.6, 31.0, 35.0, 37.1, 37.8, 38.9, 61.4, 69.5, 71.77, 71.8, 158.4, 175.5, 176.1. FAB/MS: 389 [(M + H) – tBOC:73], 242 (base). IR (neat, cm^{−1}): 2945, 1735, 1720, 1650, 1540, 1460, 1255, 1175.

General Synthetic Method for Preparation of Amino Acids 9 and 11–13. To R-(343)tBOC (**5–8**, 1.00 g, 2.05 mmol) in a solution of CDCl₃ (15 mL, 7.5 equiv) under argon was added TMSI (7.2 mmol, ~3.5 equiv). The reaction mixture was stirred for 20 min and then the reaction quenched with CD₃OD (1.5 mL), stirring 2 min. The reaction mixture was then concentrated *in vacuo*. The residue in the flask was then taken up in a 4.0 mL solution of water/acetic acid/ethyl ether (1.7/0.3/2.0); the organic phase were separated, and the aqueous phase was extracted with ethyl ether (three times). The combined organic phase was washed once with 2.0 mL of aqueous acetic acid (1.7/0.3), dried, and concentrated *in vacuo*. The crude product (quantitative yield) was

used directly in the next step, or it was used after preparative TLC plate purification.

9. ^1H NMR (300 MHz, CD_3OD , ppm): 1.60 (m, 4H), 1.75 (qnt, 2H), 1.88 (qnt, 2H), 3.0 (t, 2H), 3.31 (t, 2H), 3.45 (m, 6H), 3.55 (t, 2H), 4.03 (brs, 2H), 4.22 (brs, 2H). ^{13}C NMR (75 MHz, CD_3OD , ppm): 27.5 (two Cs), 28.5, 30.4, 37.7, 39.4, 69.1, 69.3, 69.7, 71.5, 72.1, 71.78. EI-DIP/MS: 303 (M - OH), 261 (M - $\text{CH}_2\text{CO}_2\text{H}$), 145 (base). IR (neat, cm^{-1}): 3700–2700, 1740, 1645, 1555, 1440, 1380, 1245.

11. ^1H NMR (300 MHz, CD_3OD , ppm): 1.62 (m, 4H), 1.78 (qnt, 2H), 1.9 (qnt, 2H), 3.05 (t, 2H), 3.36 (m, 2H), 3.4–3.55 (m, 6H), 3.57 (t, 2H), 3.71 (m, 2H), 3.73 (s, 2H), 3.98 (m, 2H), 4.01 (s, 2H). ^{13}C NMR (75 MHz, CD_3OD , ppm): 27.5 (two CH_2s), 28.5, 30.5, 37.8, 39.5, 69.2, 69.3, 69.6, 69.7, 71.2, 71.3, 71.8, 72.1. FAB/MS: 365 (M + H), 173 (base). IR (neat, cm^{-1}): 3600–2700, 1710, 1640, 1450, 1375.

12. ^1H NMR (300 MHz, CD_3OD , ppm): 1.21 (t, 3H), 1.33 (m, 4H), 1.6 (m, 8H), 1.74 (qnt, 2H), 1.9 (qnt, 2H), 2.16 (t, 2H), 2.3 (m, 2H), 3.02 (t, 2H), 3.22 (t, 2H), 3.45 (m, 6H), 3.55 (t, 2H), 4.1 (qnt, 2H). ^{13}C NMR (75 MHz, CD_3OD , ppm): 14.5, 25.9, 26.8, 27.5, 28.5, 29.8, 29.9, 30.6, 35.0, 37.0, 37.8, 39.5, 61.4 (quat), 69.3, 69.4, 71.8, 72.1. FAB/MS: 389 (M + H, base). IR (neat, cm^{-1}): 3300, 2940, 1735, 1640, 1555, 1465, 1280.

13. ^1H NMR (300 MHz, CD_3OD , ppm): 1.33 (m, 4H), 1.6 (m, 8H), 1.75 (qnt, 2H), 1.9 (qnt, 2H), 3.03 (t, 2H), 3.21 (t, 2H), 3.42 (m, 6H), 3.55 (t, 2H). ^{13}C NMR (75 MHz, CD_3OD , ppm): 25.9, 26.9, 27.5 (two Cs), 28.6, 29.9 (two Cs), 30.6, 34.7, 37.1, 37.8, 39.5, 69.3, 69.4, 71.8, 72.1, 176 (C=O). FAB/MS: 361 (M + H), 228 (base). IR (neat, cm^{-1}): 3700–3200, 3200–3000, 1730, 1630, 1550, 1450, 1370.

General Synthetic Method for Preparation of Cross-Linkers 14–18. TEA (1–1.3 equiv) was added in one portion to a solution of amino acid (1.5 mmol, 1 equiv) in DMF (anhydrous, 10 mL, ~7 equiv) under argon at 0 °C. SMCC or SPDP (1.5 mmol, 1.2 equiv) was added in one portion, and the reaction mixture was stirred under argon for 3–24 h, until complete via TLC monitoring. The reaction mixture was allowed to warm to room temperature if it was stirred for more than 6 h. The solution was then concentrated *in vacuo* under high vacuum at about 50 °C. The crude product was purified on preparative TLC plates to provide the desired cross-linker in 7–67% unoptimized⁵ yields.

14. ^1H NMR (300 MHz, CD_3OD , ppm): 1.0 (m, 4H), 1.4 (m, 4H), 1.62 (m, 4H), 1.75 (m, 6H), 2.1 (m, 2H), 3.22 (t, 2H), 3.35 (t, 2H), 3.45 (m, 4H), 3.5 (t, 2H), 4.04 (s, 2H), 4.22 (s, 2H), 6.8 (s, 2H), 7.75 (NH), 7.85 (NH). ^{13}C NMR (75 MHz, CD_3OD , ppm): 27.5 (methylenes), 30.0 (methylenes), 30.5 (methylenes), 30.96 (methylenes), 37.8 (methylenes), 44.5 (methylene), 45.6 (methine), 46.2 (methine), 69.1 (methylene), 69.6 (methylene), 69.9 (methylene), 71.5 (methylene), 71.8 (methylene), 71.9 (methylene), 135.2 (methines). FAB/MS: 617 ($\text{MNH}_4^+ + \text{Na} + \text{K}$), 579 ($\text{MNH}_4^+ + \text{Na}$), 557 (MNH_4^+ base). IR (neat, cm^{-1}): 3440, 3010, 1740, 1705, 1670, 1535, 1450, 1370, 1220.

15. ^1H NMR (300 MHz, CD_3OD , ppm): 1.0 (m, 4H), 1.4 (m, 4H), 1.6 (m, 4H), 1.7–1.9 (m, 10H), 2.1 (dt, 2H), 3.25 (m, 4H), 3.5 (m, 8H), 3.71 (m, 4H), 3.95 (s, 2H), 4.19 (s, 2H), 6.8 (s, 2H), 7.75 (NH), 7.88 (NH). ^{13}C NMR (75 MHz, CD_3OD , ppm): 27.6 (methylenes), 30.1 (methylenes), 30.5 (methylenes), 31.0 (methylene), 37.7 (methylene), 37.84 (methylene), 44.5 (methylene), 46.2 (methines), 69.1 (methylene), 69.6 (methylene), 69.8 (methylene), 71.2 (methylene), 71.8 (methylene), 71.9

(methylene), 135.2 (methines). FAB/MS: 602 [(M + H + HOH) or M + H, OH addition with ring opening of maleimide], 307 (base, matrix).

16. ^1H NMR (300 MHz, CD_3OD , ppm): 0.99 (m, 4H), 1.21 (t, 3H), 1.21–1.5 (m, 8H), 1.5–1.95 (m, 14H), 2.05–2.1 (dt, 2H), 2.1–2.35 (m, 4H), 3.25 (m, 4H), 3.45 (m, 8H), 4.1 (qnt, 2H), 6.8 (s, 2H), 7.75 (NH), 7.85 (NH). ^{13}C NMR (75 MHz, CD_3OD , ppm): 14.2 (methyl), 25.9 (methylene), 26.9 (methylene), 27.6 (methylenes), 29.9 (methylenes), 30.1 (methylenes), 30.6 (methylene), 31.0 (methylene), 35.0 (methylene), 37.1 (methylene), 37.8 (methylenes), 44.5 (methylene), 46.2 (methines), 61.4 (methylenes), 69.5 (methylene), 69.6 (methylene), 71.8 (methylenes), 135.3 (methines). FAB/MS: 608 (M + H), 115 (base). IR (neat, cm^{-1}): 3500–3300, 3020, 1710, 1645, 1520, 1450, 1370, 1280.

17. ^1H NMR (300 MHz, CD_3OD , ppm): 1.0 (m, 4H), 1.32 (m, 4H), 1.4 (m, 4H), 1.6 (m, 8H), 1.73 (m, 6H), 2.05–2.11 (dt, 2H), 2.15–2.25 (dt, 2H), 3.22 (m, 4H), 3.63 (m, 8H), 6.79 (s, 2H). ^{13}C NMR (75 MHz, CD_3OD , ppm): 26.3 (methylene), 26.9 (methylene), 27.6 (methylenes), 29.99 (methylene), 30.1 (methylene), 30.6 (methylene), 31.0 (methylene), 35.9 (methylene), 37.1 (methylene), 37.8 (methylene), 37.9 (methylene), 44.5 (methylene), 46.2 (methines), 69.6 (methylenes), 71.8 (methylenes), 135.3 (methines). FAB/MS: 602 (M + Na), 580 (M + H), 154 (base, matrix). IR (neat, cm^{-1}): 3300, 3100, 1725, 1640, 1550, 1450, 1370.

18. ^1H NMR (300 MHz, CD_3OD , ppm): 1.62 (m, 4H), 1.78 (m, 4H), 2.6 (t, 2H), 3.1 (t, 2H), 3.2–3.6 (m, 12H), 4.02 (s, 2H), 4.21 (s, 2H), 7.22 (m, 1H), 7.82 (m, 2H), 8.4 (m, 1H). ^{13}C NMR (75 MHz, CD_3OD , ppm): 27.6 (methylenes), 30.4 (methylene), 30.5 (methylene), 35.5 (methylene), 36.1 (methylene), 37.9 (methylenes), 69.2 (methylene), 69.4 (methylene), 69.9 (methylene), 71.5 (methylene), 71.8 (methylenes), 71.9 (methylene), 121.2 (methine), 122.4 (methine), 139.1 (methine), 150.4 (methine). FAB/MS: 573 ($\text{MNH}_4^+ + \text{K}$), 557 ($\text{MNH}_4^+ + \text{Na}$), 535 (MNH_4^+). IR (neat, cm^{-1}): 3310, 3080, 1750, 1665, 1540, 1420, 1370.

Preparation of Hydrazide 19. Compound **17** (300 mg, 0.518 mmol) was stirred in CH_2Cl_2 (5.0 mL) with DCC (107 mg, 1 equiv) and tBOC hydrazide (68.4 mg, 1 equiv) at 0 °C for 1 h and then allowed to warm to room temperature, stirring for a total of ~20 h. The precipitated urea was removed by filtration; the reaction products were concentrated *in vacuo* and purified on a preparative TLC plate (1 mm), eluting with 9/1 $\text{CHCl}_3/\text{MeOH}$, providing 220 mg (61%) of intermediate product. To this material (185 mg, 0.267 mmol) in CH_2Cl_2 (2.0 mL) was added TFA (2.5 mL), and the reaction mixture was stirred at room temperature, for 3 h. The reaction mixture was diluted with CH_2Cl_2 (50.0 mL), neutralized with NaHCO_3 , and the organic phase was separated, dried, and concentrated *in vacuo*. The crude reaction mixture was placed on a preparative TLC plate (1 mm), eluting with 90/10/1 $\text{CHCl}_3/\text{MeOH}/\text{NH}_4\text{OH}$ to provide 49 mg of compound **19** in a 31% unoptimized yield.

19. ^1H NMR (300 MHz, CD_3OD , ppm): 1.1 (m, 4H), 1.4 (m, 8H), 1.65 (m, 8H), 1.77 (m, 6H), 2.15–2.21 (m, 4H), 3.2 (m, 4H), 3.51 (m, 8H), 6.85 (s, 2H), 7.85 (NH), 7.95 (NH). ^{13}C NMR (75 MHz, CD_3OD , ppm): 26.7, 26.9, 27.6, 29.9, 30.1, 30.6, 31.0, 34.9, 37.1, 37.8, 37.9, 44.5, 46.2, 69.5, 69.6, 71.8, 135.3. FAB/MS: 634 (M + K), 616 (M + Na), 594 (M + H), 154 (base, matrix). IR (neat, cm^{-1}): 3700–3150, 3000–2850, 1710, 1650, 1540, 1410, 1370.

Preparation of NHS-Activated Cross-Linkers. About 5 mg of maleimido carboxylic acid was dissolved in 50 μL of dry DMF. In a thoroughly dried glass flask,

a 3-fold excess of dicyclohexylcarbodiimide (DCC) in 25 μ L of dry DMF was added followed by *N*-hydroxysuccinimide (NHS, 3-fold excess). The mixture was stirred overnight and was then filtered through a piece of tissue paper (ca. 4 mm²) placed into a Pasteur pipette. The product formed was detected by TLC (CHCl₃/MeOH, 9/1, visualized with iodine vapor). The *R_f* value of the compounds investigated is about 0.9 and can be easily distinguished from those of the starting materials (carboxylic acids, ca. 0.3–0.6, NHS near the baseline with excessive tailing).

Preparation of Antibody–AP Conjugates. The antibody was activated with Traut's reagent in triethanolamine buffer following Pierce's Technical Bulletin 26101X (P.O. Box 117, Rockford, IL 61105). The activated antibody was purified on a Pharmacia PD 10 column in pH 7.3 buffer and stored at 4 °C prior to use.

A solution of alkaline phosphatase (12 mg/mL) in glycerol/water (1/1) was incubated with the 10-fold stoichiometric excess of the crude activated cross-linker (**14–17**). After 25 min at 25 °C, a 1000-fold stoichiometric excess of 1 M glycine solution was added. The activated protein was purified on a Pharmacia PD 10 column with pH 7.3 buffer and stored at 4 °C prior to use. The two solutions of activated proteins were mixed in stoichiometric amounts (1/1) and kept at 25 °C for at least 3 h. The conjugate mixture obtained was fractionated by gel permeation chromatography.⁶

⁶ These reagents (Superdex resins, using standard conditions and techniques) were purchased from Pharmacia Biotech Inc. (800 Centennial Ave., P.O. Box 1327, Piscataway, NJ 08855-1327). General procedures other than those listed herein, additional examples, and relevant references may be found in their catalogs.

Preparation of the Antibody–AP Conjugate Using Linker 19. The enzyme was activated as described above. A solution of the antibody in 100 mM acetate buffer, (pH 5, 6 mg/mL) was incubated with a 1000-fold excess of sodium perchlorate in water (0.1 M, 1 h, 25 °C, darkness). The oxidation was then stopped by adding 0.3 M ethylene glycol solution in a 100-fold excess over perchlorate. After 5 min at room temperature, the mixture was buffer exchanged (100 mmol of acetate buffer at pH 5) and adjusted to 5 mg/mL. Cross-linker **19** was dissolved in DMF (20 mM) and added to the oxidized antibody in a 70-fold excess. The mixture was incubated for 3.5 h at room temperature. The activated antibody was buffer exchanged into the pH 7.3 conjugation buffer.

Stoichiometric amounts (1/1) of the activated antibody and the activated enzyme were incubated overnight. The conjugate mixture obtained was fractionated by gel permeation chromatography.⁶

LITERATURE CITED

- (1) (a) Nagasawa, T., et al. (1973) New Agents for t-Butyloxy-carbonylation and Methoxybenzyloxycarbonylation of Amino Acids. *Bull. Chem. Soc. Jpn.* 46, 1269–1272. (b) Sheldon, E. L., Levenson, C. H., Mullis, K. B., and Rapoport, H. (1989) N-Substituted 4,9-Dioxo-1,2-dodecane Diamines Useful for Preparing Nucleic Acid Intercalators. EP 0 309 006 A1. (c) Baer, B. W., Groves, E. S., Houston, L. L., and Levenson, C. H. (1989) Conjugates of Antisense Oligonucleotides & Therapeutic Uses Thereof. WO 91/04753. (d) Houston, L. L., Aldwin, L., and Nitecki, D. E. (1991) Thioether Linked Immunotoxin Conjugates. U.S. 5,024,834.
- (2) (a) Henry, D. W. (1966) *Heterocycl. Chem.*, 503–511. (b) Voerman, M. G. L. (1904) *Rec. Trav. Pays Bas*, 265–282.
- (3) Greene, T. W. (1981) *Protecting Groups in Organic Synthesis: tBOC Deprotection*, John Wiley & Sons, New York.

BC9700260

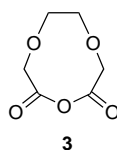
CORRECTIONS

Volume 8, Number 3, May/June 1997.

Gary M. Johnson,* James P. Albarella, and
Christoph Petry

HETEROBIFUNCTIONAL CROSS-LINKERS
CONTAINING 4,9-DIOXA-1,12-DODECANE-
DIAMINE SPACERS

Page 448. Structure **3** in Table 1 was incorrectly
depicted and should be shown as the structure below:



Page 450. The description of the preparation of **1a** should read as follows. *tert*-Butyl-*S*-(4,6-dimethylpyrimidin-2-yl)thiocarbonate (35.3 g, 0.147 mmol, 0.6 equiv) in 1,4-dioxane (100.0 mL) under argon was added dropwise via cannula to a solution of H₂N(CH₂)₃O(CH₂)₄O(CH₂)₃NH₂ (50.0 g, 0.245 mmol) in 1,4-dioxane (200.0 mL) over 60 min.

BC9800062

Published on Web 02/12/1998

ARTICLES

Synthesis and Characterization of the New Cytostatic Complex *cis*-Diammineplatinum(II)–Chlorocholylglycinate

Julio J. Criado,^{*,†} Rocio I. R. Macias,[‡] Manuel Medarde,[§] Maria J. Monte,[‡] Maria A. Serrano,^{||} and Jose J. G. Marin^{*,‡}

Departments of Inorganic Chemistry, Physiology and Pharmacology, Organic Chemistry, and Biochemistry and Molecular Biology, University of Salamanca, 37007 Salamanca, Spain. Received October 30, 1996[®]

Owing to the high efficiency of hepatocytes to take up bile acids, these endogenous compounds or their analogues can be considered as potential shuttles for delivering drugs to the liver. With the aim of using this strategy to target platinum(II)-related cytostatic drugs toward the hepatobiliary system, a cholylglycinate (CG) derivative of *cis*-diammineplatinum(II) has been synthesized by treatment of *cis*-diammineplatinum(II) dichloride with sodium cholylglycinate. The complex, named Bamet-R2, was characterized by spectroscopy and elemental analysis. Results obtained in these studies together with conductivity measurements, which pointed to nonelectrolyte behavior, allowed the structure of the complex to be identified as $C_{26}H_{48}N_3O_6ClPt$. The compound was found to be soluble (up to 3 mM) in water and was highly soluble (more than 10 mM) in ethanol, methanol, and dimethyl sulfoxide. Its stability in solution was monitored by HPLC analysis. In deionized water, the compound remains >90% pure in solution for up to 7 days and >80% for up to 28 days. However, in 150 mM NaCl it remains as >90% pure compound in solution for only 1 day. By contrast with the parent compound CG, Bamet-R2 was found to significantly inhibit the growth of rat hepatocytes in primary culture and L1210 murine leukemia cells, although in a less marked way than that observed for cisplatin. The cytostatic effect of Bamet-R2 was particularly strong against human colon adenocarcinoma LS174T cells. The results point to the potential usefulness of Bamet-R2 in the antitumoral therapy of enterohepatic-derived neoplasias.

INTRODUCTION

Considerable efforts have been devoted to the search for new chemotherapeutic agents with antitumoral activ-

ity. However, for several reasons such efforts have been only partially successful. The main drawbacks of currently available chemotherapy are toxicity for extratumoral tissues and the pre-existing or developed resistance of cancer cells to cytostatic agents. Several attempts have been made to circumvent resistance (1) and to improve the vectoriality of such drugs (2). In this sense, the marked organotropism of bile acids toward the hepatobiliary system has been proposed as an interesting characteristic for use of these endogenous compounds or their analogues as shuttles for delivering drugs to the liver. Some examples of this approach are the binding

* Address correspondence to these authors at Universidad de Salamanca Campus Miguel de Unamuno Edificio Departamental, Room S-09 37007, Salamanca, Spain (telephone 34-23-294674; fax 34-23-294669; e-mail jjgmarin@gugu.usal.es).

[†] Department of Inorganic Chemistry.

[‡] Department of Physiology and Pharmacology.

[§] Department of Organic Chemistry.

^{||} Department of Biochemistry and Molecular Biology.

[®] Abstract published in *Advance ACS Abstracts*, June 1, 1997.

of inhibitors of hydroxymethylglutaryl CoA (HMG-CoA) reductase (3) or the cytostatic compound chlorambucyl (4) to bile acids.

Since its introduction into clinical trials in 1972, the widespread success of *cis*-diamminedichloroplatinum(II) (cisplatin) and its analogues in the treatment of a variety of solid tumors (5) has encouraged the search for new cisplatin derivatives with a view to reducing its dose-limiting side effects, namely nephrotoxicity, myelotoxicity, neurotoxicity, nausea, and vomiting (6). Although many different cisplatin analogues have been synthesized, few of them are currently used in clinical practice (6). This is probably because the achieved reductions in extratumoral toxicity are only partial and are often accompanied by a loss of tumoricidal activity. Two interesting second-generation cisplatin analogues are *cis*-diammine(1,1-cyclobutanedicarboxylate)platinum(II) (carboplatin) and 1,2-cyclohexanediammineplatinum(II) (DACH-Pt) and their derivatives. These are not organotropic compounds, although changes in the physical-chemical properties of the resulting molecules do enhance their excretion. They are less nephrotoxic than cisplatin, although other side effects, such as myelotoxicity and neurotoxicity, have been reported to be similar or even greater than that of the parent drug (7). On the basis of the amphipathic properties of these steroids (8), previous DACH-Pt complexes with bile acids have been synthesized in attempts to obtain derivatives with both lipophilicity and water miscibility (9, 10). However, although promising results regarding the antitumoral activity of these complexes have emerged, no further investigations in this direction have been undertaken. Perhaps the large size of the complexes, containing a DACH-Pt moiety together with two bile acid molecules, excludes the possibility of their being transported by carrier proteins located in the basolateral and canalicular membrane of hepatocytes. These proteins are responsible for the selective and efficient clearance of bile acids from systemic blood, where these compounds are maintained at very low concentrations (11). The rationale of the present work was that cisplatin analogues with molecular structures closer to that of a natural bile acid might be recognized by transmembrane bile acid carrier proteins, which would enhance their vectoriality toward the hepatobiliary system. With this aim, *cis*-diammineplatinum(II) chlorocholylglycinate was synthesized and characterized. Preliminary results on the liver organotropism and *in vivo* antitumoral activity of this compound—named Bamet-R2—have been reported elsewhere (12, 13).

MATERIALS AND METHODS

Chemicals. *cis*-Diammineplatinum(II) dichloride [$\text{Pt}(\text{NH}_3)_2\text{Cl}_2$] was purchased from Fluka Quimica (Madrid, Spain). Sodium cholylglycinate (NaCG; >95% by thin-layer chromatography) and 3 α -hydroxysteroid dehydrogenase were obtained from Sigma Quimica (Madrid, Spain). All other reagents were of high purity and were used as purchased without any further purification.

Analytical Methods. 3 α -Hydroxysteroid concentrations were measured according to the classic method of Talalay (14). Chemical analyses for C, H, and N were performed on a Perkin-Elmer 2400 elemental analyzer (Perkin-Elmer Hispania SA, Madrid, Spain). Platinum was determined by atomic absorption in a flameless graphite furnace spectrophotometer Z-8100 Hitachi (Hitachi, Tokyo, Japan), set at a wavelength of 265.9 nm and using the following temperature program: 90 °C (20 s), 100 °C (20 s), 800 °C (20 s), 1600 °C (30 s), 2800 °C (5 s), and 3000 °C (4 s). Infrared (IR) spectra were recorded

in the 4000–200 cm^{-1} range on a Perkin-Elmer FT-IR 17300 instrument coupled to a Perkin-Elmer 3600 data station. KBr pellets and spectrophotometric grade Nujol (Fluka, Quimica) or polyethylene (Aldrich, Madrid, Spain) disks were used to record spectra above and below 400 cm^{-1} , respectively. Mass spectrometry studies were carried out on a VG-Autospec (Universidad Autonoma, Madrid, Spain), using L-SIMS ionization in the FAB⁺ mode (Cs ion emission) and m-NBA as matrix. Electrical conductivity in solution was measured using a CDM2e conductimeter (Radiometer, Copenhagen, Denmark), with a CDC104 immersion cell. Temperature was controlled in a Unitherm water bath (Selecta, Barcelona, Spain) with a precision of ± 0.01 °C. Nuclear magnetic resonance (NMR) spectra of ¹H (400 MHz) and ¹³C (102.6 MHz) were obtained in CD₃OD solutions, with TMS as internal standard using a Bruker DX400 instrument (Karlsruhe, Germany). Carbon resonances were distinguished in DEPT-90 and DEPT-135 experiments.

Synthesis. The platinum complex, named Bamet-R2 [$\text{Pt}(\text{NH}_3)_2\text{CGCl}$], was obtained according to the following procedure: A 3 mM $\text{Pt}(\text{NH}_3)_2\text{Cl}_2$ solution in water (100 mL) was prepared at room temperature and filtered onto paper. Then, an aqueous solution of NaCG (1.5 mM, 100 mL) was added. To prevent physicochemical effects due to the presence of bile acid micelles in the reaction mixture, attempts were made to keep the concentrations of free NaCG in the reaction mixture below the critical micellar concentration (cmc) for this bile acid. The NaCG solution was therefore added dropwise (1 mL/min) by means of a peristaltic pump to the continuously stirred $\text{Pt}(\text{NH}_3)_2\text{Cl}_2$ solution, which was maintained in the dark at 80 °C. This procedure takes about 1.5 h. The final pH was 6.0. The reaction mixture was allowed to reach room temperature for approximately 2 h, before undergoing solid-liquid extraction. The final product was obtained as a yellow solid after evaporation to dryness in a desiccator containing P₄O₁₀.

Purification. Reaction products were separated from the excess of unreacted platinum by solid-liquid extraction in octadecylsilane cartridges (C₁₈, Sep-Pak, Waters Cromatografia SA, Madrid, Spain) following a classical procedure (15). The retained compounds were recovered from the cartridges with methanol. The extract was then concentrated for thin-layer chromatography (TLC) on silica gel plates (60 F254, Merk, Darmstadt, Germany) using butyl acetate/methanol 30:70 (v/v) as the solvent system. Two major bands, one of them corresponding to unreacted CG ($R_f = 0.71$) and the other corresponding to Bamet-R2 ($R_f = 0.36$) were obtained. The latter band was scraped off and extracted with methanol. The resulting solution was further purified by semipreparative high-performance liquid chromatography (HPLC) in reversed phase, using a Waters C₁₈ RCM column (5 μm , 10 mm \times 25 cm) with a gradient pump module (Model 126, Beckman, Madrid, Spain) and a photodiode array detector (Model 168, Beckman) set simultaneously at 205 and 250 nm. The system was controlled by an IBM computer (Model 30286, IBM Corp., Portsmouth, U.K.) using System Gold software from Beckman. The column was equilibrated with 10 mM KH₂PO₄/methanol 25:75 (v/v), pH 7.02 (solvent A), and eluted with an isocratic system with solvent A for 5 min and then with a linear gradient from 100% solvent A to 20% solvent A and 80% methanol over 15 min. The solvent rate was 10 mL/min. In this HPLC system the retention time for CG was 4.8 min and that for Bamet-R2 was 11.2 min. During the semipreparative HPLC, fractions were collected automatically every 0.5 min. Those corresponding to the Bamet-R2 elution time, taking into account a 1 min time

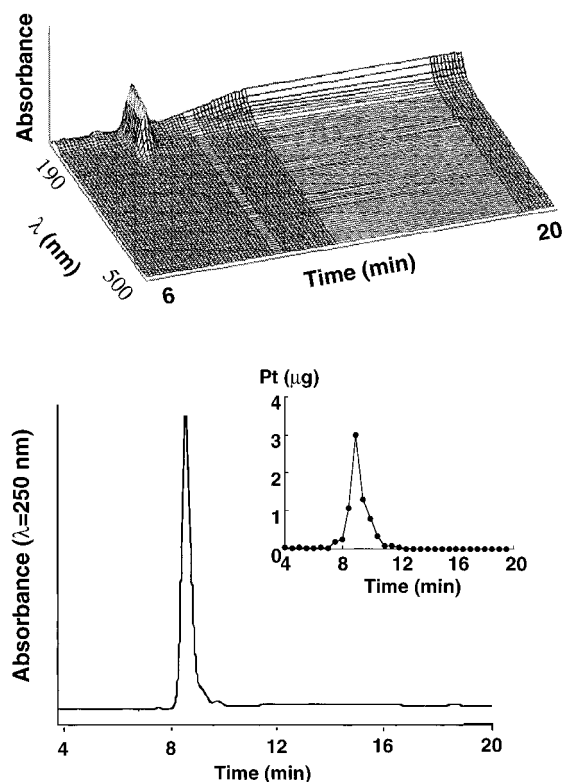


Figure 1. Reversed phase HPLC of purified Bamet-R2 as recorded by using photodiode array detector in scan mode from 190 to 500 nm wavelength (upper panel) and at 250 nm wavelength (lower panel). Inset represents the results of flameless atomic absorption spectroscopy measurement of platinum contents in samples collected every 0.5 min during HPLC of pure Bamet-R2. The delay from the detector to the fraction collector was approximately 1 min.

lapse between the detector and the fraction collector, were pooled together and dried. The result was desalted by methanolic extraction in C_{18} cartridges and dried again. With this procedure, highly pure (>95%) Bamet-R2 was obtained as a yellowish solid in 40% yield from the starting NaCG. The results of purity control by analytical HPLC (column, Beckman Ultrasphere C_{18} ODS, 5 μ m, 4.6 mm \times 250 mm; flow, 1 mL/min) carried out at the end of the purification process are shown in Figure 1. In this HPLC system the Bamet-R2 retention time was 9 min.

Stability in Solution. Bamet-R2 was dissolved (100 μ M) in ultrapure deionized water or in saline solution (150 mM NaCl). These solutions were maintained in the dark at 4 °C. After vigorous stirring, samples were collected periodically for immediate analysis by HPLC according to the analytical adaptation of the semi-preparative procedure described above. The concentration of Bamet-R2 in solution was calculated from the height of the absorbance peak (250 nm wavelength) eluted at 9 min (Figure 2).

In Vitro Cytostatic Studies. The complex was evaluated for *in vitro* cytostatic activity against murine lymphocytic leukemia L1210 and human colon adenocarcinoma LS174T cells, obtained from the American Type Culture Collection (ATCC, Rockville, MD), and rat hepatocytes in primary culture, obtained by an adaptation of the two-step collagenase perfusion method (16). Cells were grown in a humidified atmosphere of 95% air/5% CO_2 at 37 °C using minimum essential medium Eagle (MEM, Sigma, for LS174T cells) or Dulbecco's modified Eagle's medium (DMEM, Sigma, for L1210 cells) supplemented with 2 mM glutamine, 26.2 mM $NaHCO_3$, 25 mM

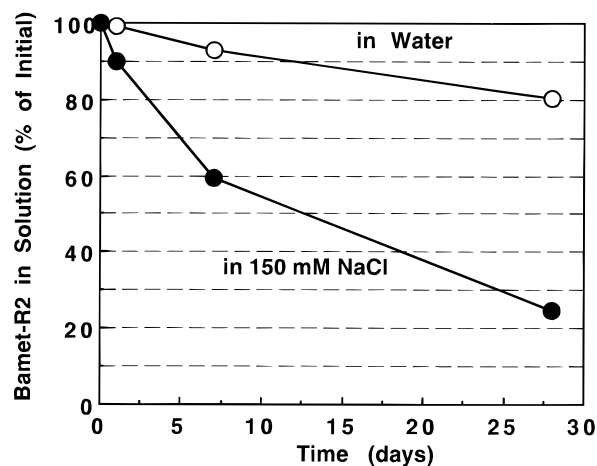


Figure 2. Time-course of Bamet-R2 stability in water or saline (150 mM NaCl) solution. Bamet-R2 solution (100 μ M) was maintained in the dark at 4 °C. After vigorous stirring, samples were collected at the indicated times for immediate HPLC analysis. Bamet-R2 concentrations were calculated from the height of the absorbance peak (250 nm wavelength) eluted at 9 min.

Hepes, and 10% horse (L1210 cells) or fetal bovine (LS174T cells) serum in the culture of cell lines and serum-free Williams' Medium E (Sigma) supplemented with 26.2 mM $NaHCO_3$, 10 mM Hepes, 100 nM Na_2SeO_3 , 30 nM dexamethasone, 100 nM insulin, 5 nM EGF, 11.1 mM galactose, 1 μ M ethanolamine, 5 μ g/mL transferrin, 5 μ g/mL linoleic acid, 5 μ g/mL albumin, 10 mM nicotinamide, and 6 mM ornithine in the culture of rat hepatocytes. On the basis of preliminary studies on the time course of cell growth, the following protocols were carried out for testing purposes. LS174T and L1210 cells were harvested during the exponential growth phase, diluted 1/20 with culture medium, seeded into 3 cm diameter cell culture dishes, and exposed to the tested compound for 72 h. Hepatocytes were allowed to become attached to the dish and start proliferation. The compounds were added to the culture at 24 h, and the liver cells were exposed for up to 72 h of culture. Studies comparing the cytostatic activity of cisplatin and Bamet-R2 were carried out using eight different concentrations (from 0.063 to 100 or 200 μ M) of the desired compound in the culture medium. At the end of the culture period, the culture medium and cell debris were removed and attached cells were washed and digested using Lowry solution (100 mM NaOH and 189 mM Na_2CO_3), after which DNA was determined fluorometrically using Hoechst-33258 (17). The trypan blue exclusion test performed on some dishes that were not subjected to digestion confirmed that the viability of remaining cells in the culture dishes was close to 100%.

Statistical Analysis. Results are expressed as means \pm SE. To calculate the statistical significance of differences among the groups, the Bonferroni method of multiple-range testing was used. Comparison between two means was carried out by Student *t*-test. Values for IC_{50} were calculated from nonlinear regression analysis using Ultrafit software (Biosoft, Cambridge, U.K.). Statistical analysis was performed on a Macintosh LC-III computer (Apple Computer, Inc., Cupertino, CA) with programs supplied by Apple Computer, Inc.

RESULTS AND DISCUSSION

Chemical Characterization. The pure complex [named Bamet-R2 (Ba stands for bile acid and -met stands for metal)] is a solid that has a melting point with

decomposition at 189 °C. The compound was found to be soluble (up to 3 mM) in water and was highly soluble (more than 10 mM) in ethanol, methanol, and dimethyl sulfoxide (DMSO). Its stability in solution was measured by HPLC analysis. In deionized water the compound remained >90% pure in solution for up to 7 days and >80% for up to 28 days. However, in 150 mM NaCl it remains in solution as >90% pure compound for only 1 day (Figure 2).

Bamet-R2 elemental analysis (EA) revealed a 1:1 ratio between the cholyglycinate residue and platinum in the complex, in agreement with the molecular formula $C_{26}H_{48}N_3O_6ClPt$, ruling out other combinations containing higher or lower numbers of nitrogen atoms and cholyglycinate residues (calcd: C, 42.82; H, 6.63; N, 5.76; Pt, 26.75. Found by EA: C, 43.01; H, 6.59; N, 5.80; Pt, 26.68).

The stoichiometry of the bile acid moieties and platinum atoms was also assessed by enzymatically measuring concentrations of 3 α -hydroxysteroid groups (3 α -HS) in a pure solution of Bamet-R2 using the 3 α -hydroxysteroid dehydrogenase assay. Platinum concentrations were measured in the same solution by flameless atomic absorption. The result also indicated a 3 α -HS-to-platinum ratio of 1:1.

The complex was characterized by a combination of spectroscopic methods. These allowed us to propose its structure in the absence of X-ray diffraction studies. The latter were not carried out because it was not possible to crystallize the compound under any of the large list of solvents and conditions assayed (data not shown).

In the IR spectrum there are no great differences between the cholyglycinate ligand and the complex. Both showed the stretching vibrational modes of NH and OH bonds as a broad band with a maximum at 3408 cm^{-1} in the ligand and as a split band in the complex, with a maximum at 3434 cm^{-1} , a small peak at 3521 cm^{-1} , and a shoulder at 3311 cm^{-1} . Major differences are expected to appear in the part of the ligand nearest to the metal or directly bonded to it. Thus, the carboxylate in the free CG shows characteristic bands at 1603 cm^{-1} (ν_{as}) and 1400 cm^{-1} (ν_{as}). By contrast, in the complex, the asymmetric vibration band appears at 1638 cm^{-1} , with an increase of 35 cm^{-1} (18, 19). The remaining absorption peaks appear without changes in the complex because they are related to unmodified skeletal vibrations (20, 21). Finally, in the far infrared the pronounced sharp absorption at 320 cm^{-1} of the vibration ν (Pt-Cl) appears at the same wavelength, although with much lower intensity than that observed in the case of pure cisplatin (22).

In the mass spectrum the molecular ion was not observed. Instead, a group of ions around m/z 693.3 had the highest value. These can be interpreted as $[M - Cl]^+$ produced by the ions containing different platinum isotopes, as suggested by their intensities, which match the natural abundance of platinum ions and the pattern displayed in a computer simulation of $[M - Cl]^+$ (m/z 693.3 calcd). The loss of Cl^- from this type of complex when it is analyzed by this technique is well documented (23). Other ions found at m/z 413, 289, and 176 can be considered as the result of typical fragmentation of the cholyglycinate moiety (24, 25).

Nuclear magnetic resonance (NMR) spectra of the complex confirmed the presence of only one type of cholyglycinate residue, which in comparison with the spectra of the free ligand is slightly modified in some of its signals by the effect of the association around the metal ion. The presence of the metal, two ammonia ligands, and the chlorine produces variations in the

Table 1. NMR Analysis of ^{13}C and 1H for NaCG and Bamet-R2 in CD_3OD^a

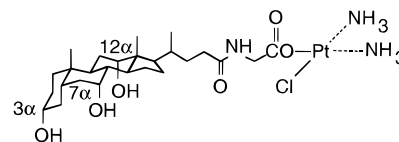
C	NaCG	Bamet-R2	H	NaCG	Bamet-R2
1	36.5	36.5	18	0.71 s	0.71 s
2	31.3	31.3			
3	72.9	72.9	19	0.92 s	0.91 s
4	40.5	40.6			
5	43.0	43.0	21	1.03 d	1.04 s
6	35.9	35.9			
7	69.1	69.1	other	1.30–2.35 m	1.25–2.35 m
8	41.1	41.1			
9	27.7	27.7	3	3.38 m	3.38 m
10	35.9	35.9			
11	29.6	29.6	25	3.74 s	4.05 s
12	74.0	74.1			
13	47.5	47.6			
14	43.2	43.3	7	3.80 bs	3.79 bs
15	24.2	24.2			
16	28.7	28.7	12	3.95 bs	3.94 bs
17	48.1	47.7			
18	13.0	13.0			
19	23.2	23.2			
20	37.0	37.3			
21	17.6	18.0			
22	34.2	*			
23	33.1	33.1			
24	176.3	182.7			
25	44.6	56.0			
26	176.5	189.4			

^a Numbering of the positions for C is the usual one for a bile acid structure of cholanoic acid type. Numbering of H is that of the carbon to which H is bound. *, no signal found masked by others in the spectrum.

signals of closer atoms: hydrogen atoms at position 25 and the glycinate methylene, in the 1H NMR spectrum, and C-24 to C-26 in the ^{13}C NMR spectrum. The observed values are shown in Table 1 in comparison with the chemical shifts of the NaCG free ligand (26–28).

All these data are in agreement with the presence of only one type of cholyglycinate ligand in the complex, because the simultaneous existence of a monodentate and a bidentate ligand would produce duplicate sets of signals in the NMR spectra. Furthermore, the elemental analysis and mass spectrum clearly support the presence of two amino, one chloride, and one cholyglycinate ligand in the complex.

The conductivity measurements carried out in water and methanol are consistent with the rest of the data obtained from Bamet-R2. In water, the Bamet-R2 concentration used was 0.87 mM and the observed conductivity was $\Lambda_M = 50.5 \Omega^{-1} cm^2 mol^{-1}$. In methanol, the conductivity displayed by a 0.85 mM Bamet-R2 solution was $\Lambda_M = 33.17 \Omega^{-1} cm^2 mol^{-1}$. These results confirmed the absence of ions in both solutions, further supporting the structure proposed for this complex. Therefore, the isolated Bamet-R2 is assumed to be a neutral complex, the platinum charge being compensated by both a cholyglycinate and a chloride, carrying two additional ammonia ligands to complete the coordination sphere, as represented below. The geometry of the complex



presumably is of the planar-quadrant type usually displayed by this kind of Pt(II) derivative.

Cytostatic Activity. According to the results of previous *in vivo* studies (29), we have reported that unlike the taurine-amidated cholic acid and similarly to

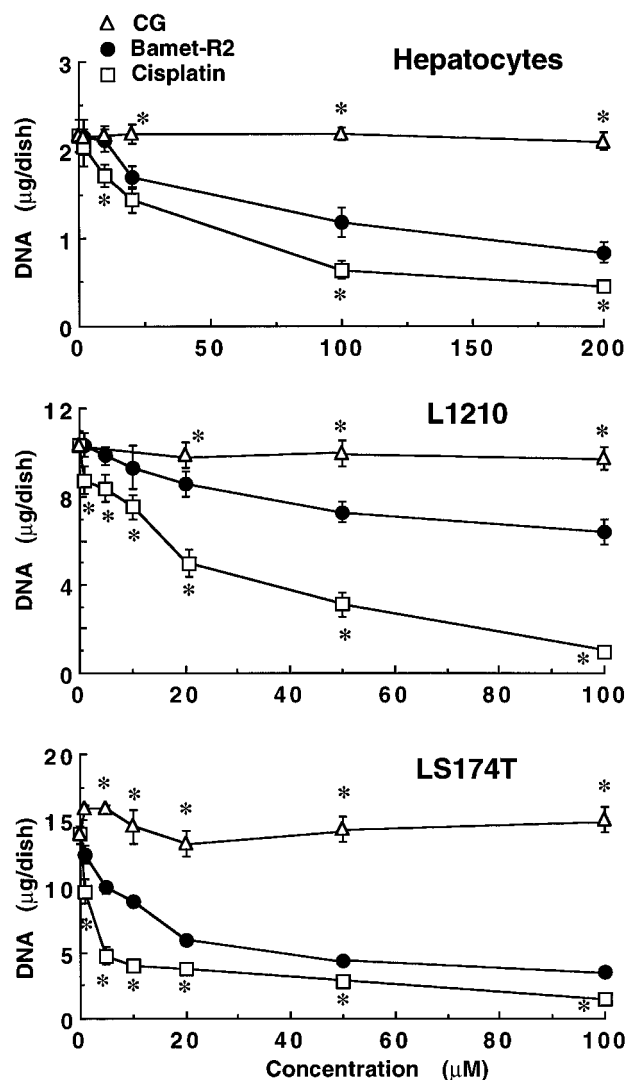


Figure 3. Effect of CG, cisplatin, and Bamet-R2 on cell growth as revealed by measurement of the amount of DNA in primary culture of rat hepatocytes, mouse lymphocytic leukemia L1210, and human colon adenocarcinoma LS174T cells. Cultures involved incubation with one of the above-mentioned compounds at the indicated concentrations from the beginning of the culture, in the case of cell lines, or after replacing the initial culture medium at 24 h from seeding in the case of rat hepatocytes to the end of the culture at 72 h, when the viability of the cells was tested and DNA contents in the dishes measured. Values are means \pm SE of three different cultures carried out in triplicate. *, $p < 0.05$ as compared with cultures incubated with Bamet-R2 by the Bonferroni method of multiple-range testing.

other different glycine-conjugated bile acids, NaCG does not seem to be able to affect the rate of liver cell proliferation. The present work confirms this point for rat hepatocytes in primary cultures (Figure 3). A similar absence of effect of NaGC on L1210 and LS174T cells was found (Figure 3). Cisplatin, which presumably enters the cells through a nonspecific pathway (probably by diffusion through the plasma membrane), was found to exert cytostatic activity against all of the cell types studied (Figure 3). Growth of the culture, as measured by the amount of DNA in the dishes at the end of the exposure period (72 h), was significantly reduced by incubation in the presence of cisplatin. Calculation of the concentration required to reduce the cell population by 50%, or inhibitory concentration 50 (IC_{50}), indicated that the sensitivity to cisplatin was higher for tumoral cell lines (L1210, $IC_{50} = 18 \pm 3 \mu M$; LS174T, $IC_{50} = 3.3 \pm 0.5 \mu M$) than for rat hepatocytes ($IC_{50} = 56 \pm 7 \mu M$).

Conversely, hepatocytes were more sensitive to Bamet-R2 ($IC_{50} = 131 \pm 20 \mu M$) than L1210 ($IC_{50} = 170 \pm 20 \mu M$). This difference makes sense because hepatocytes, but not L1210 cells, were expected to be able to take up Bamet-R2 more efficiently than cisplatin, provided that this bile acid derivative is indeed transported across the plasma membrane by the specific carrier proteins responsible for liver bile acid uptake (11). Efficient bile acid intestinal absorption, mainly in the ileum, also occurs via both passive and active transport processes, the latter involving specific carrier proteins located at the basal and apical membranes of ileocytes. Although there are no available data on the ability of LS174T cells to take up these compounds, this possibility cannot be ruled out and thus, very interestingly, we found that this human colon cancer-derived cell line was highly sensitive to Bamet-R2 ($IC_{50} = 17 \pm 2 \mu M$). In summary, these results show a strong cytostatic ability of Bamet-R2 on rat hepatocytes in primary culture and L1210 cells, which was significantly higher ($p < 0.05$) against LS174T cells. Moreover, they suggest that the potential interest of this new complex would be based on a combination of its cytostatic ability, which is lower than that of cisplatin, and the markedly enhanced enterohepatic organotropism as compared with cisplatin, which has been reported in preliminary studies (12, 13).

ACKNOWLEDGMENT

This study was supported in part by the Ministerio de Educacion y Ciencia (Grants SAF94-0693 and SAF96-0146), Spain. We thank Ms. M. I. Hernandez Rodriguez for secretarial help, Mr. M. Fernandez Gutierrez for technical assistance, and Mr. J. F. Martin Martin for caring for the animals. We also thank Nicholas Skinner for revising the English version of the manuscript.

LITERATURE CITED

- (1) Canon, J. L., Humblet, Y., and Symann, M. (1990) Resistance to cisplatin—How to deal with the problem. *Eur. J. Cancer* 26, 1–3.
- (2) Konno, T. (1992) Targeting chemotherapy for hepatoma - Arterial administration of anticancer drugs dissolved in Lipiodol. *Eur. J. Cancer* 28, 403–409.
- (3) Kramer, W., Wess, G., Enhsen, A., Bock, K., Falk, E., Hoffmann, A., Neckermann, G., Gantz, D., Schulz, S., Nickau, L., Petzinger, E., Turley, S., and Dietschy, J. M. (1994) Bile acid-derived HMG-CoA reductase inhibitors. *Biochim. Biophys. Acta* 1227, 137–154.
- (4) Kramer, W., Wess, G., Schubert, G., Bickel, M., Hoffmann, A., Baringhaus, K.H., Enhsen, A., Glombik, H., Mullner, S., Neckermann, G., Schulz, S., and Petzinger, E. (1993) Bile Acids as Carrier for Drugs. In *Bile Acids and the Hepatobiliary System. From the Basic Science to the Clinical Practice* (G. Paumgartner, A. Stiehl, and W. Gerok, Eds.) pp 161–176, Kluwer Academic Publishers, Dordrecht, The Netherlands.
- (5) Loeher, P. J., and Einhorn, L. H. (1984) Cisplatin. *Ann. Int. Med.* 100, 704–713.
- (6) Bradner, W. T., Rose, W. C., and Huftalen, J. B. (1980) Antitumor Activity of Platinum Analogs. In *Cisplatin: Current Status and New Developments* (A. W. Prestayko, S. T. Crooke, and S. K. Carter, Eds.) pp 171–182, Academic Press, New York.
- (7) Christian, M. C. (1992) The current status of new platinum analogs. *Semin. Oncol.* 19, 720–733.
- (8) Carey, M. C. (1985) Physical-Chemical Properties of Bile Acids and their Salts. In *Sterols and Bile Acids* (H. Danielsson and J. Sjovall, Eds.) pp 345–403, Elsevier Science Publishers, Amsterdam.
- (9) Maeda, M., Suga, T., Takasuka, N., Hoshi, A., and Sasaki, T. (1990) Effect of bis(bilato)-1,2-cyclohexanediammineplati-

- num(II) complexes on lung metastasis of B16-F10 melanoma cells in mice. *Cancer Lett.* 55, 143–147.
- (10) Maeda, M., Takasuka, N., Suga, T., and Sasaki, T. (1990) New antitumor Platinum(II) complexes with both lipophilicity and water miscibility. *Jpn. J. Cancer Res.* 81, 567–569.
 - (11) Hofmann, A. F. (1994). Biliary Secretion and Excretion—The Hepatobiliary Component of the Enterohepatic Circulation of Bile Acids. In *Physiology of the Gastrointestinal Tract* (L. R. Johnson, Ed.) pp 1555–1576, Raven Press, New York.
 - (12) Marin, J. J. G., Macias, R. I. R., Herrera, M. C., Palomero, M. F., Monte, M. J., Villanueva, G. R., El-Mir, M. Y., Criado, J. J., and Serrano, M. A. (1996) Liver and ileum transport of cytostatic platinated bile acids. *Hepatology* 24, 543A.
 - (13) Marin, J. J. G., Herrera, M. C., Palomero, M. F., Macias, R. I. R., Monte, M. J., Villanueva, G. R., El-Mir, M. Y., Serrano, M. A., and Criado, J. J. (1996) "In vivo" distribution, toxicity and cytostatic capacity of platinated bile acid analogs. *Hepatology* 24, 372A.
 - (14) Talalay, P. (1960) Enzymatic analysis of steroid hormones. *Methods Biochem. Anal.* 8, 119–143.
 - (15) Setchell, K. D. R., and Worthington, J. (1982) A rapid method for the quantitative extraction of bile acids and their conjugates from serum using commercially available reverse phase octadecylsilane-bonded silica cartridges. *Clin. Chim. Acta* 125, 135–144.
 - (16) Berry, M. N., and Friend, D. S. (1969) High-yield preparation of isolated rat liver parenchymal cells. *J. Cell Biol.* 43, 506–520.
 - (17) Labarca, C., and Paigen, K. (1980) A simple, rapid, and sensitive DNA assay procedure. *Anal. Biochem.* 102, 344–352.
 - (18) Paul, A. K., Mansuri-Torshizi, H., Srivastava, T. S., Chavan, S. J., and Chitnis, M. P. (1993) Some potential antitumor 2,2'-dipyridylamine Pt(II)/Pd(II) complexes with amino acids: Their synthesis, spectroscopy, DNA binding, and cytotoxic studies. *J. Inorg. Biochem.* 50, 9–20.
 - (19) Kieft, J. A., and Nakamoto, K. (1967) Infrared spectra of some platinum(II) glycine complexes. *J. Inorg.-Nucl. Chem.* 29, 2561–2568.
 - (20) Hanessian, S., and Wang, J. (1993) Design and synthesis of a cephalosporin-carboplatinum prodrug activatable by a β -lactamase. *Can. J. Chem.* 71, 896–906.
 - (21) Khokhar, A. R., Xu, Q., and al-Baker, S. (1991) Synthesis and characterization of highly lipophilic antitumor platinum(II) complexes. *J. Coord. Chem.* 24, 77–82.
 - (22) Altman, J., Castrillo, T., Beck, W., Bernhardt, G., and Schönenberger, H. (1991) Metal complexes with biologically important ligands. 62. Platinum(II) complexes of 3-(2-aminoethoxy)strone and estradiol. *Inorg. Chem.* 30, 4085–4088.
 - (23) Minghetti, G., Cinellu, M. A., Stoccoro, S., Zucca, A., and Manassero, M. (1995) Cyclometallated derivatives of Platinum(II) derived from 6-(tert-butyl)-2,2'-bipyridine (HL). Crystal and molecular structure of [Pt(L)Cl]. *J. Chem. Soc., Dalton Trans.* 7, 777–779.
 - (24) Wood, K. V., Sun, Y., and Elkin, R. G. (1991) Differentiation of isomeric conjugated bile acids using positive-ion B/E linked scans. *Anal. Chem.* 63, 247–250.
 - (25) Mingrone, G., Greco, A. V., Boniforti, L., and Passi, S. (1983) Analysis of conjugate bile acids by high performance liquid chromatography and mass spectrometry. *Lipids* 18, 90–95.
 - (26) Watabe, M., Takayama, T., Kuwahara, A., Kawahashi, T., Koike, Y., Horiuchi, A., Suzuki, M., Watanabe, T., Mikami, K., Matsumoto, T., and Narusawa, Y. (1995) Preparation and ¹³C and ¹⁹⁵Pt spectra of Platinum(II) peptide complexes and their growth-inhibitory activity against mouse meth A solid tumor in vivo. *Bull. Chem. Soc. Jpn.* 68, 2559–2565.
 - (27) Lee, Y. A., Jung, O. S., Lee, C. O., Choi, S. U., Jun, M. J., and Sohn, Y. S. (1995) Cationic diammineplatinum(II) complexes of nalidixic acid. *Inorg. Chim. Acta* 239, 133–138.
 - (28) Lee, Y. A., Jung, O. S., and Sohn, Y. S. (1995) Synthesis and properties of diammine(isopropylidemalonato) platinum(II): Crystal structure of O(CH₂CH₂)₂C(CH₂NH₂)₂Pt-(OOC)₂C=C(CH₃)₂. *Polyhedron* 14, 2099–2106.
 - (29) Barbero, E. R., Herrera, M. C., Monte, M. J., Serrano, M. A., and Marin, J. J. G. (1995) Role of amidation in bile acid effect on DNA synthesis by regenerating mouse liver. *Am. J. Physiol.* 31, G1051–G1059.

BC970061V

Interaction of a Novel Fluorescent Analog of Interferon- γ with Transformed Cells

Ayala Falach,[†] Ilana Nathan,[‡] Stavanit Baram,[†] Nurith Porat,[†] Alexander Dvilansky,[‡] and Abraham H. Parola^{*,†}

Department of Chemistry, Faculty of Natural Sciences, and Unit of Hematology, Faculty of Medical Sciences, Ben-Gurion University of the Negev, Beer-Sheva 84105, Israel. Received September 30, 1996[®]

A fluorescent analog of human recombinant interferon- γ (IFN- γ) was prepared for the first time. The recovered pyrene-labeled IFN- γ (py-IFN- γ), with an estimated seven pyrene molecules per IFN- γ , retained over half of its original biological activity. Binding of py-IFN- γ to human amnion WISH cells showed appreciable enhancement in fluorescence polarization from 0.055 to 0.215 and in fluorescence lifetime from 56 to 80 ns. The ratio of the vibronic peaks did not change, indicating that the pyrene molecules remained in water environment even after binding. Py-IFN- γ provides a novel tool for unraveling the mechanism of the initial interaction between this antiproliferative lymphokine and its target, cancer cell membrane receptors. Its fluorescence could provide the means to follow receptor recycling when it occurs.

INTRODUCTION

IFN- γ ¹ is a glycoprotein, produced by T lymphocytes after stimulation with mitogens or antigens, which exerts pleiotropic biological effects. In addition to its antiviral properties, it has antiproliferative, differentiating, and immunoregulatory activities (De Maeyer and De Maeyer-Guignard, 1988; Kalvakolanu and Borden, 1996). Of great interest is the antiproliferative activity of IFN- γ , which has been shown to be more potent than that of other interferons in blocking the growth of several tumor cells *in vivo* and *in vitro* (Rubin and Gupta, 1980). Two IFN- γ polypeptides self-associate to form noncovalent antiparallel homodimers with an apparent molecular mass of 34 kDa (Ealick, 1991).

To elicit cell responses, the initial interaction between IFN- γ and the target cell occurs at specific membranal receptors (Farrar and Schreiber, 1993). The functionally active IFN- γ receptor is composed of at least two species-specific components, a ligand binding subunit, α chain, and an additional subunit, β chain, that were cloned (Hemmi *et al.*, 1994; Soh *et al.*, 1994; Lundell and Narula, 1994).

Ligand binding provokes increased phosphorylation on serines, threonine (Mao *et al.*, 1990), and tyrosine of the receptor chains and regulates the association of the α and β receptor subunits with the tyrosine kinases JAK-1 and JAK-2 (Igarashi *et al.*, 1994; Darnell *et al.*, 1994; Kaplan *et al.*, 1996) and the transcription factor p91 (Greenlund *et al.*, 1994). The role of the JAK-STAT pathway in the signaling mechanism of IFN- γ was described (Heim *et al.*, 1995).

Although progress was made in the study of the signal transduction cascade, operating after ligand binding, the mechanism underlying the initial step of interaction

between IFN- γ and target cell membranes is not yet clear. Thus, association of the two receptor subunits upon exposure to the ligand was recently described, but the detailed initial cell surface events that initiate signaling are still unresolved (Marsters *et al.*, 1995).

IFN- γ labeled with radioactive iodine (¹²⁵I) was used to study binding to its receptor in intact human cells (Rubinstein *et al.*, 1987; Branca and Baglioni, 1981; Finbloom *et al.*, 1985). The number of binding sites per WISH cell was shown to be 50 000–70 000 with a K_d value of 7.3×10^{-9} M at 4 °C (Sarkar and Gupta, 1984). We thought that fluorescent-labeled IFN- γ would be a promising tool for studying these initial steps. It, together with other lipid specific membranal probes, would report on dynamical responses of various membrane components and provide an opportunity to study lipid–lipid and lipid–protein interactions in the IFN- γ activated membrane (Parola, 1993). In particular, IFN- γ , which is labeled by a microenvironmentally sensitive fluorescent probe, should be able to report both on its immediate surroundings and on dynamical changes in the receptor after binding IFN- γ (*e.g.* receptor recycling through the membrane). Such information cannot be obtained by radioactive reporters. To this end we have prepared a fluorescent-labeled IFN- γ and characterized its specific interaction with membranal receptors, using both steady-state and dynamic fluorescence. The label was a pyrene derivative, having a relatively long lifetime and vibronic peaks sensitive to its environment.

MATERIALS AND METHODS

Preparation of Pyrene-Labeled IFN- γ . Recombinant IFN- γ , 10^8 units/mg (Mory *et al.*, 1986; Novick *et al.*, 1982), was graciously donated by D. Novick, The Weizmann Institute of Science, Rehovot, Israel. In a typical labeling experiment, 2.4×10^5 units of IFN- γ in 0.1 M bicarbonate buffer, pH 9.2, was mixed with pyrenesulfonyl chloride (3.12×10^{-4} M) in ethylene glycol at a 3:1 ratio. This mixture was incubated for 3 h with stirring at room temperature. The reaction was terminated by incubation with 0.2 M lysine for 30 min at room temperature. Excess free label was removed on a Sephadex G-25 column, with PBS containing 0.1% gelatin as an elution buffer. The fluorescent-labeled fractions of IFN- γ (py-IFN- γ) were collected. For preparation of py-

* Author to whom correspondence should be addressed [telephone (972) 7 6472454; fax (972) 7 6472943; e-mail aparola@bgumail.bgu.ac.il].

[†] Department of Chemistry.

[‡] Unit of Hematology.

[®] Abstract published in *Advance ACS Abstracts*, June 1, 1997.

¹ Abbreviations: IFN- γ , interferon- γ ; py-IFN- γ , pyrenesulfonyl chloride labeled IFN- γ ; VSV, vesicular stomatitis virus; BSA, bovine serum albumin; PBS, phosphate-buffered saline (154 mM NaCl/10 mM sodium phosphate buffer, pH 7.4); SDS–PAGE, sodium dodecyl sulfate polyacrylamide gel electrophoresis.

IFN- γ for amino acid analysis the labeling procedure had the following modifications in the final stage of purification: (1) Excess free lysine and pyrenesulfonyl chloride were removed by ultrafiltration, using a Centricon filter with 10 000 molecular mass cutoff. (2) Alternatively, to avoid the presence of residual lysine, ethanolamine was used for termination of the pyrenesulfonyl chloride labeling of IFN- γ . Excess ethanolamine, free and bound to the fluorescent label, was removed either by repetitive extractions or by precipitation with TCA. Aqueous solutions of labeled and control IFN- γ were lyophilized and redissolved in 70 μ L of sodium citrate buffer, pH 2.2, at room temperature. Fifty microliters was injected to the amino acid analyzer.

Amino Acid Analysis. Amino acid analyses of unlabeled and pyrenesulfonyl chloride labeled IFN- γ were carried out on Dionex Bio LC at the Weizmann Institute of Science, Rehovot, Israel.

Protein Assay. Protein was determined according to the Bio-Rad method; absorption at 595 nm was read on a Gilford spectrophotometer (Sedmak and Grossberg, 1977).

IFN- γ Assay. Antiviral activity was determined in duplicates with a microtiter inhibition-of-cytopathic-effect assay against VSV on monolayers of WISH cells. Titers are reported as antiviral units, based on the National Institute of Health Human IFN- γ reference reagent Go-23-901-530 (Eppstein *et al.*, 1985).

SDS-PAGE. Special steps were undertaken in the preparation procedure of py-IFN- γ to be able to detect its band(s) on the SDS-PAGE. Higher initial concentration of protein (Reprogene, Rehovot), 0.5 μ g/ μ L, was used in the labeling step. To avoid the dilution encountered by gel filtration, py-IFN- γ was either loaded on 2 mL Sephadex G-25 columns, and the void volume collected following centrifugation (1400g, 2 min) or directly analyzed by 15% SDS-PAGE, following boiling in Laemmli buffer.

Fluorescence Measurements. Fluorescence spectra were taken on a Perkin-Elmer MPF-44 spectrofluorometer. Steady-state fluorescence polarization was measured on MPF-44, SLM 4800, and Gregg-MM spectrofluorometers (Parola, 1993). Unless otherwise indicated, all measurements were carried out at 4 °C. Fluorescence lifetime was measured on the SLM 4800 (Lakowicz *et al.*, 1979) or the Gregg-MM (an ISS upgrade of the SLM 4800). Data obtained on the SLM 4800 were analyzed in terms of two lifetimes; both lifetime and differential phase studies were carried out on the Gregg-MM system as described in detail before (Porat *et al.*, 1988; Parola *et al.*, 1994). The data were analyzed using the ISS187 decay analysis software.

Membrane Purification. WISH cell cultures (human amnion cell line), grown in MEM medium containing 10% fetal calf serum, were collected by scrapping with a rubber policeman on ice and centrifuged twice at 800g for 7 min at room temperature, and the pellet was washed twice with Hank's buffer (Ip and Cooper, 1980). The cells were resuspended in HEPES (2 mM) buffer, pH 7.2, containing 0.25 M sucrose (10^6 cells/mL). The cells were subjected to homogenization (7 s, setting of 5–6, 10 times) by Polytron (Kinematica GndH), and Na₂EDTA (0.5 mM) was added. The suspension was centrifuged twice at 5500g for 15 min at 4 °C. The supernatants were subsequently pelleted at 100000g for 60 min at 4 °C. This membrane-enriched fraction was resuspended in 0.3 mL of HEPES buffer, pH 7.2, containing 25% sucrose and kept frozen at –70 °C.

Binding of Py-IFN- γ to Membranes. WISH cell membranes (10 mg/mL) were washed with PBS, sus-

pended in 0.5 mL of PBS, and then incubated for 1 h with py-IFN- γ (6000 units) in the presence of BSA, 3 mg/mL. Control membranes incubated without interferon and membranes labeled in the presence of large excess (500 times) of unlabeled IFN- γ were similarly set in parallel. The latter sample served to determine nonspecific labeling of membranes by py-IFN- γ . Following incubation, the samples were centrifuged at 100000g for 30 min and the supernatants collected. The membranes were washed with PBS and finally suspended in 0.5 mL of PBS.

Binding of Py-IFN- γ to WISH Cells. WISH cells, harvested at confluency, were suspended in 0.3 mL of buffer, 1×10^7 cells/mL, and incubated for 1 h at 4 °C with py-IFN- γ (5000 units) in the presence of BSA, 3 mg/mL. The extent of nonspecific binding was determined by incubating the cells in the presence of an excess (500 times) of unlabeled IFN- γ . At the end of the incubation, cells were centrifuged at 1000g for 5 min. Cells were washed twice with PBS and resuspended in 1 mL of PBS containing 1% NP-40.

RESULTS

Labeled IFN- γ . *a. Preparation and Biological Activity.* The reaction of pyrenesulfonyl chloride with IFN- γ requires basic pH. At these conditions IFN- γ retains most of its biological activity. The reaction started at pH 9.2 and dropped to 8.5 at the end. Optimal incubation temperature and time were employed. Excess label was treated with lysine to prevent reaction with gelatin, which was used to prevent the adsorption of IFN- γ to the Sephadex G-25 column. The activity yields were checked during the labeling procedure. Optimal recovery results indicated 33% loss in activity at the end of the labeling, after the addition of lysine. Another 13% loss was noticed after the separation of labeled IFN- γ on the Sephadex G-25 column, resulting in a total activity loss of 46%. A similar loss in activity was encountered by IFN- γ subjected to the same labeling conditions in the absence of label molecules. Since there is no change in the amount of protein during the labeling step, the only protein loss could occur at the separation step, due to the trapping of IFN- γ molecules in the column. If this is true, the loss in activity resulting from IFN- γ inactivation is only 33%.

Figure 1 shows good correlation between the fluorescence emission and the biological activity of the eluted fractions of pyrene-labeled IFN- γ . The insert in Figure 1 shows good separation of the labeled IFN- γ from free pyrenesulfonyl chloride bound to lysine. Gel electrophoresis analysis of the labeled as compared with the unlabeled IFN- γ on SDS-PAGE resulted in a single band of both labeled and unlabeled IFN- γ (Figure 2). A single band was obtained when excess py-IFN- γ was removed either by Sephadex G-25 columns or by the 15% SDS-polyacrylamide gel. This result indicates a rather homogeneous population of labeled protein. It excludes the presence of two kinds of protein molecules, labeled and unlabeled, which should render two separate bands; in the case of heterogeneous labeling, band broadening should have resulted.

b. Fluorescence Characteristics. The emission spectra of diluted pyrene solutions depend on the nature of the solvent. Comparison between polar and nonpolar solvents shows a relative rise in the emission intensity of the symmetry forbidden vibronic transitions, which results in remarkably altered fluorescence emission profiles of the pyrene moiety (Lianos and Georgiou, 1979a).

To verify this phenomenon in pyrenesulfonyl chloride, we studied its spectra in various solvents. Marked

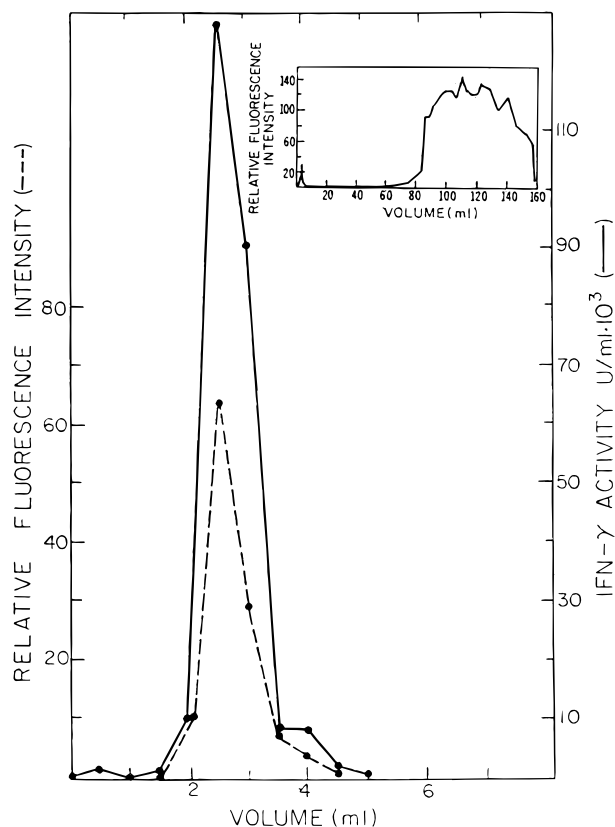


Figure 1. Elution profile of pyrene-labeled IFN- γ on Sephadex G-25 column (0.8 \times 14 cm). Elution buffer consisted of 0.1% gelatin in PBS. Fractions containing 0.5 mL were collected at a flow rate of 6 mL/h. Fluorescence was measured at $\lambda_{\text{max}}(\text{ex}) = 346$ nm; $\lambda_{\text{max}}(\text{em}) = 376$ nm. IFN- γ activity was measured as described under Materials and Methods. Insert shows separation of free excess label from py-IFN- γ .

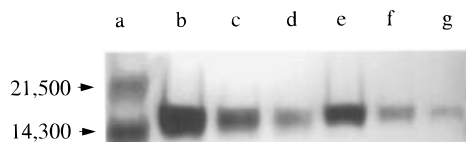


Figure 2. SDS-PAGE analysis of py-IFN- γ . Recombinant IFN- γ was labeled with pyrenesulfonyl chloride as described under Materials and Methods. For comparison, IFN- γ was treated similarly without label molecules. IFN- γ was separated on 15% SDS-polyacrylamide gel and stained with Coomassie blue. Lane a, M_r markers; lanes b-d, unlabeled IFN- γ ; lanes e-g, py-IFN- γ : lanes b and e, 6 μg ; lanes c and f, 2 μg ; lanes d and g, 1 μg of protein.

differences in the vibronic profile of the fluorescence emission of pyrenesulfonyl chloride are noted (Figure 3). Table 1 shows a summary of all the solvents studied, indicating both spectral shifts and changes in the two major emission peaks ratio. While spectral maxima slightly shifted, the ratio among the three major vibronic peaks varied markedly in the solvents. In THF, the major vibronic band appears at 420 nm; in ethylene glycol, ethanol, and water, the major bands are at 377 and 395 nm. The ratio among these peaks generally increases in more polar solvents, *e.g.*, solvent basicity (hydroxyl nature), may contribute to this ratio too. In American white oil, which is used to estimate the viscosity of biomembranes, the ratio between the first two vibronic modes of pyrene is 1.25, although the dielectric constant is very low. The range between the ratio of 1.25 in American white oil and 1.98 in water is wide enough to report on environmental changes upon binding to membrane receptors. Py-IFN- γ

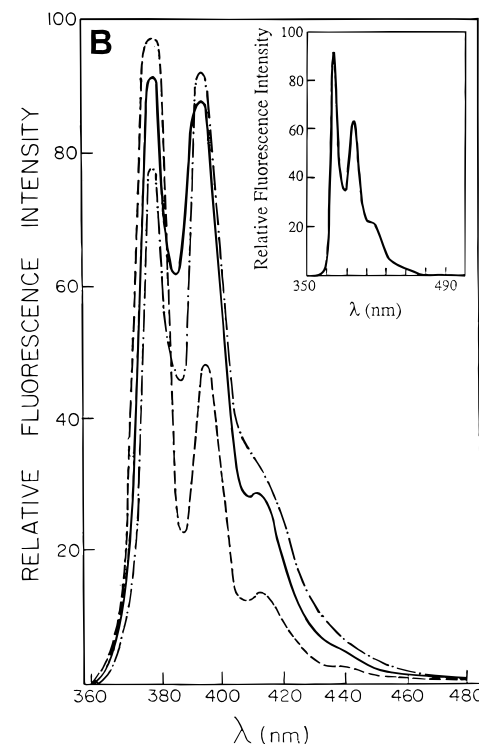
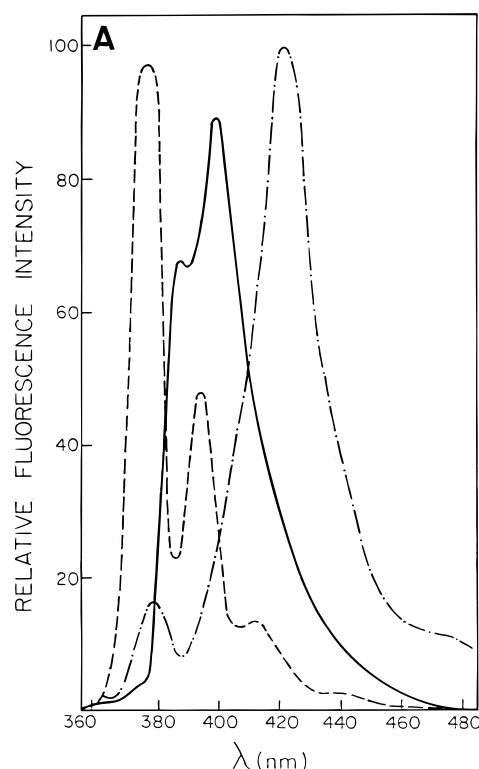


Figure 3. Fluorescence emission spectra of py-SO₂Cl (1×10^{-6} M) in various solvents: A, water (---), ethylene glycol (—), tetrahydrofuran (— · —); B, water (---), ethanol/water 1:1 ratio (— · —), ethanol (—); insert, American white oil. All uncorrected spectra were taken on the same MPF-44 spectrofluorometer.

in PBS containing 0.1% gelatin shows a fluorescence spectrum similar to that of pyrenesulfonyl chloride dissolved in water, with a peak ratio of 1.77 (Figure 4), which is remarkably different from that obtained for pyrenesulfonyl chloride in ethylene glycol (see Table 1). Excimer emission at 480 nm, with an intensity of 8.5% of the major monomer emission at 376 nm, is noted (not shown). Steady-state fluorescence polarization (Table 2)

Table 1. Vibronic Fluorescence Structure of Py-SO₂Cl in Various Solvents: Comparison with Free and Membrane-Bound Py-IFN- γ

solvent	dielectric constant	ratio of major emission peaks of pyrene-SO ₂ -X ^a	$\lambda_{\max}^1/\lambda_{\max}^2$ ^b (nm)
American white oil ^c	~2–2.40	1.25	377/398
		1.21 ^d	377/398
THF	2.95	0.16	380/430
		0.93	380/395
ethylene glycol	32.00	0.76	386/402
ethanol	24.30	0.85	377/395
ethanol/water 1:1		1.04	377/395
water	81.00	1.98	377/392
py-IFN- γ in buffer	ND	1.77	376/395
py-IFN- γ bound to membranes	ND	1.75	376/395
py-SS-ADA	ND	1.70	377/395

^aX is Cl for free label in various solvents and IFN- γ . ^bUsually (and as shown in Figure 2), pyrene exhibits three vibronic peaks: (1) at ~380, (2) at ~395, and (3) at ~420; (1) and (2) denote the first ones. ^cRange of values for various alkanes with C₈–C₁₂. ^dObtained on the Gregg-MM; all other values were recorded on the MPF-44 spectrofluorometer.

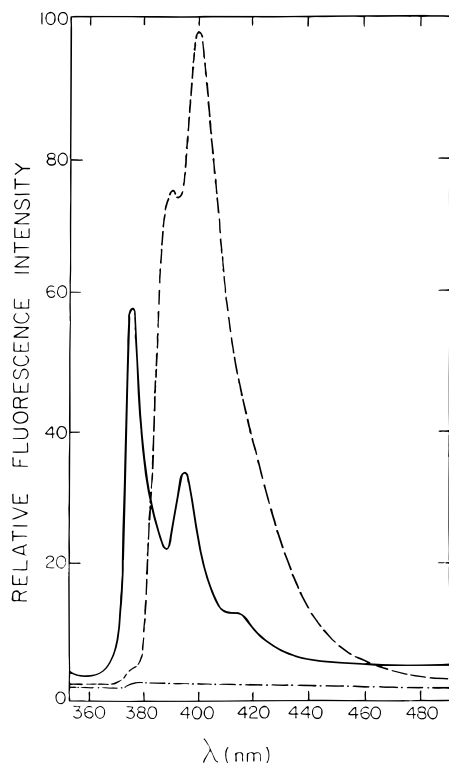


Figure 4. Emission spectra of py-IFN- γ (—) in PBS containing 0.1% gelatin, py-SO₂Cl in ethylene glycol (---), and unlabeled IFN- γ (- · -) in PBS. Fluorescence intensity was measured at $\lambda_{\max}(\text{ex}) = 346$ nm. Excitation and emission slits were 2 and 4 nm, respectively.

revealed increased polarization values upon binding to IFN- γ .

Amino Acid Analysis. Py-IFN- γ for amino acid analysis was carefully purified from excess pyrenesulfonyl chloride and, in addition, ethanolamine was substituted for lysine in the termination step of the reaction, as described under Materials and Methods. Amino acid hydrolysis profiles obtained by HPLC, for both unlabeled and pyrenesulfonyl chloride labeled IFN- γ , revealed the content of each amino acid in nanomoles. The nanomoles of each residue analyzed was normalized to that of either alanine or glycine, and the ratios between labeled and unlabeled samples were determined. The comparison among three repeats of such data, obtained for labeled

and unlabeled IFN- γ , revealed that pyrenesulfonyl chloride labeling resulted in the elimination of 7 of the 21 lysine residues. No other amino acid residue was affected.

Binding of Py-IFN- γ to Purified WISH Cell Membranes and Intact WISH Cells. The fluorescence of py-IFN- γ after binding to purified WISH cell membranes is shown in Figure 5. Binding specificity is evident from binding studies of py-IFN- γ in the presence of excess unlabeled IFN- γ . The specificity of binding averaged at $77.1 \pm 5.5\%$. Figure 6 shows the same experiment with whole cells. Because of increased scattering, the fluorescence spectra had to be taken after extraction with NP-40. Again, binding specificity was proved.

Table 2 shows fluorescence properties of py-IFN- γ after binding to the membranes. Fluorescence polarization increased 4-fold relative to free py-IFN- γ , indicating immobilization. Figure 7 is a representative phase and modulation lifetime analysis for py-IFN- γ in buffer, assuming a three-lifetime model. The long lifetime component, 56.3 ns, is the major contributor ($\alpha = 0.56$) and should be considered the most relevant in data analysis, since unlabeled cells have autofluorescence with two-lifetime components which coincide with the short and middle lifetime values of pyrene, *i.e.* 10.8 ns ($\alpha = 0.55$) and 1.5 ns ($\alpha = 0.45$). The increased pyrene fluorescence lifetime, in accord with Perrin's formula, supports our assignment of the rise in fluorescence polarization to the immobilization of py-IFN- γ . Rotational correlation times show the same trend (Table 2): Binding of py-IFN- γ to its receptor lengthens rotational correlation times.

DISCUSSION

The present work was aimed at obtaining a biologically active fluorescent lymphokine, *e.g.* IFN- γ , which would be used to study the dynamical consequences of binding to its receptor on target cells. Fluorescently tagged IFN- γ would shed light both on the initiation of the signaling process at the membrane level and on the phenomenon of receptor recycling, when it occurs (Uzgiris *et al.*, 1982). Others reported on internalization and translocation of IFN- γ , even into the nucleus (Bader and Wietzerbin, 1994). Fluorescently tagged IFN- γ would reveal such phenomena by reporting the change in the receptor's rotational correlation time. A prerequisite is the preparation of a fluorescently modified but still selectively binding and biologically active IFN- γ . To the best of our knowledge, this was not hitherto reported in the literature.

Pyrenesulfonyl chloride was chosen as a suitable probe for the following reasons: (1) It has a relatively long fluorescence lifetime (>20 ns). (2) The excitation maximum of pyrene (346 nm) is beyond the range of tryptophan excitation (280–290 nm). (3) Pyrene has a relatively high quantum yield, 0.7–0.8 (Turro, 1978), and a relatively large absorptivity coefficient ($40\,000\text{ M}^{-1}\text{ cm}^{-1}$) (Knopp and Weber, 1967), allowing its detection even at very low concentrations (10^{-8} M). (4) It has a large Stokes shift, which is particularly important for scattering biological systems. (5) The pyrene molecule has an appreciable environmental sensitivity, which is expressed in the variability of fluorescence lifetime and in the variable ratio of the vibrational emission bands (Lianos and Georgiou, 1979a,b; Lianos *et al.*, 1980). (6) The pyrene moiety is known for its excimer emission, which enables determination of adjacent pyrene labeling sites on proteins. Thus, while in py-SS-ADA with 1:1 molar ratio of pyrene to protein no excimer emission was observed (Porat *et al.*, 1988), in py-IFN- γ with seven

Table 2. Fluorescence Parameters of Free and Membrane-Bound Py-IFN- γ ^a

sample	polarization	lifetimes (ns)		χ^2	rotational correlation time (ns)	χ^2
py-SO ₂ Cl in ethylene glycol ^b	0.000	$\tau_1 = 18.50$ $\tau_2 = 5.00$	$\alpha_1 = 0.95$ $\alpha_2 = 0.05$	ND ^c	ND	ND
py-SO ₂ Cl in American white oil	0.025 ± 0.001	$\tau_1 = 30.89 \pm 1.49$ $\tau_2 = 5.17 \pm 1.20$ $\tau_3 = 1.14 \pm 0.26$	$\alpha_1 = 0.891 \pm 0.006$ $\alpha_2 = 0.061 \pm 0.007$ $\alpha_3 = 0.048 \pm 0.006$	5.4	5.00 ± 0.33^c	1.7
py-IFN- γ in buffer	0.055 ± 0.010	$\tau_1 = 56.35 \pm 1.07$ $\tau_2 = 13.88 \pm 0.30$ $\tau_3 = 1.95 \pm 0.06$	$\alpha_1 = 0.561 \pm 0.002$ $\alpha_2 = 0.323 \pm 0.002$ $\alpha_3 = 0.116 \pm 0.002$	0.6	8.24 ± 0.35	1.5
py-IFN- γ bound to membranes	0.215 ± 0.110	$\tau_1 = 80.40 \pm 5.22$ $\tau_2 = 16.16 \pm 1.07$ $\tau_3 = 1.94 \pm 0.10$	$\alpha_1 = 0.327 \pm 0.009$ $\alpha_2 = 0.308 \pm 0.011$ $\alpha_3 = 0.365 \pm 0.009$	2.3	$44.97 \pm 13.25^{c,d}$	2.2

^a All measurements, except *b*, were done on the upgraded Gregg-MM multifrequency phase modulation spectrofluorometer, using He-Cd laser [$\lambda_{\max}(\text{ex}) = 325 \text{ nm}$], L shape, and two Pyrex filters in the emission; the polarization results are the mean of at least four independent measurements; the results of lifetime and rotational correlation time are of at least eight frequencies, except *d*, which represents the analysis of only four frequencies; analysis was based on $\sigma_{\text{phase}} = 0.400$ and $\sigma_{\text{mod}} = 0.008$, except *c*, for which $\sigma_{\text{phase}} = 0.600$; lifetime was measured using the magic angle against POPOP as a reference; rotational correlation time was determined by analysis of phase only, using the long lifetime and a linear combination of the two shorter lifetimes. Standard deviation is shown. ^b Polarization was measured on the MPF-44 Perkin-Elmer spectrofluorometer; lifetime was measured on the SLM 4800 phase modulation spectrofluorometer using a combination of two filters: bandpass and Pyrex, at the excitation and emission maxima. ^c ND, not determined.

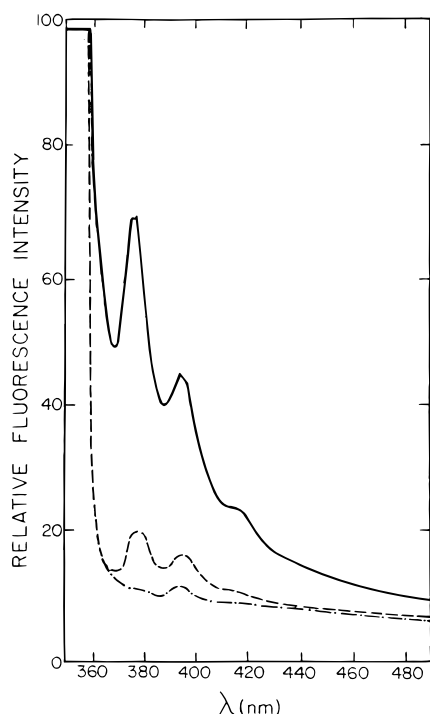


Figure 5. Binding of pyrene-labeled IFN- γ to WISH cell membranes: total binding of py-IFN- γ (—); nonspecific binding done in the presence of excess IFN- γ (---); unlabeled membranes (— · —). Fluorescence intensity was measured at $\lambda_{\max}(\text{ex}) = 346 \text{ nm}$.

pyrene moieties bound to one protein (see below) the excimer emission is seen.

The reaction between pyrenesulfonyl chloride and an amine moiety (*e.g.* lysine side chain) yields a sulfonamide bond, which is stable in both acidic and basic conditions (Porat *et al.*, 1988). The amino acid sequence of IFN- γ (Gray *et al.*, 1982; Rinderknecht *et al.*, 1984) shows numerous NH₂ moieties, potentially capable of binding pyrenesulfonyl chloride. Amino acid analysis indicated that seven lysine residues of IFN- γ were covalently bound to the labels. We attempted to verify the number of pyrenesulfonyl chloride molecules bound to IFN- γ by spectroscopic measurements. The difficulty in estimating this number arises from the low quantity of IFN- γ available, even at high level of activity. We could not detect either the protein or the attached pyrene in py-IFN- γ in the UV absorbance spectrum of the finally

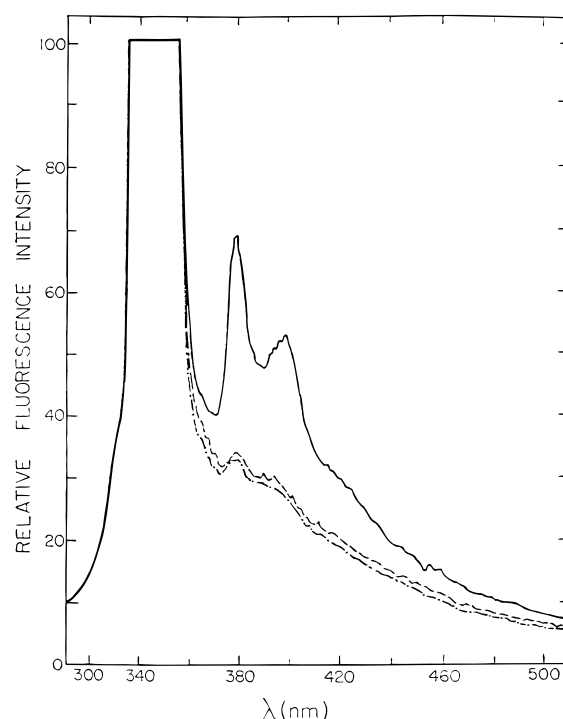


Figure 6. Binding of pyrene-labeled IFN- γ to WISH cells: total binding of py-IFN- γ (—); nonspecific binding done in the presence of excess IFN- γ (---); unlabeled cells (— · —). Fluorescence intensity was measured at $\lambda_{\max}(\text{ex}) = 346 \text{ nm}$.

labeled product, which was further diluted in the last step of column separation. Accordingly, the number of pyrene moieties was estimated by comparing the relative pyrene fluorescence of the labeled IFN- γ with that of pyrene-labeled adenosine deaminase of a similar, 45 000, molecular mass. The calculation is based on the assumption of similar fluorescence quantum yields of pyrene, when attached to either one of these proteins (in both proteins, pyrene fluorescence emission had similar lifetimes and emission profiles). On the basis of the molar extinction coefficient of the pyrene-labeled adenosine deaminase, $\epsilon = 40\,000 \text{ M}^{-1} \text{ cm}^{-1}$ (Knopp and Weber, 1967) at $\lambda_{\text{ex}}(\text{max}) = 346 \text{ nm}$, and the protein assay, the number of pyrene molecules attached to adenosine deaminase was experimentally determined. From the relative fluorescence of the two pyrene-labeled proteins and the ratio of protein concentration (calculated for IFN- γ from its specific activity after labeling), we estimated that about eight

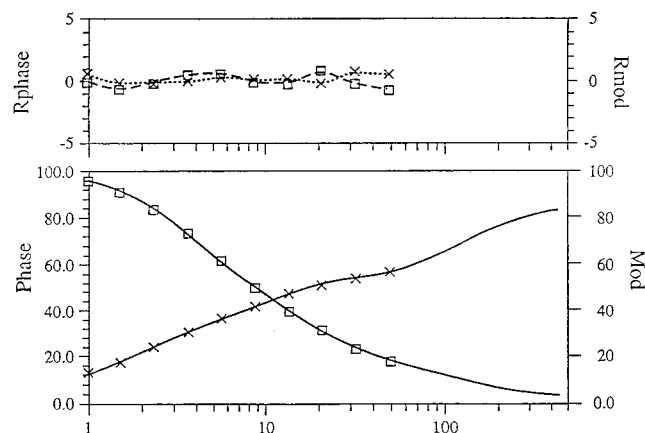


Figure 7. Fluorescence lifetime of py-IFN- γ bound to WISH cell membranes. Measurements were done on the upgraded Gregg-MM multifrequency phase modulation spectrofluorometer, using He-Cd laser [$\lambda_{\text{max}}(\text{ex}) = 325 \text{ nm}$], L shape, and two Pyrex filters. Lifetime was measured using the magic angle against POPOP as a reference.

pyrene moieties were attached to each IFN- γ molecule, in agreement with the amino acid analysis. Obviously, this number is based on gross assumptions. The binding of seven to eight pyrene moieties to each molecule of IFN- γ accounts for our ability to detect the fluorescence of IFN- γ even at the very low protein level. In spite of the large molar ratio of pyrene per IFN- γ , over 50% of its activity is retained. A similar loss in activity was encountered by IFN- γ subjected to the same labeling conditions in the absence of label molecules, indicating that the labeling *per se* did not cause the loss in activity. Statistically, it is inconceivable that half of the protein was labeled by 14 pyrene moieties while the other half, which remained unlabeled, is the one responsible for the observed 54% remaining activity. This was further verified by the SDS-PAGE studies exhibiting only a single band for both the labeled and the unlabeled IFN- γ .

Excessive labeling was avoided because it resulted in reduced IFN- γ activity; the activity of py-IFN- γ with a 3-fold increase in fluorescence intensity was about 25% of the activity of py-IFN- γ labeled by "only" seven to eight probe molecules. With about seven pyrene molecules attached to each IFN- γ , the observed excimer emission at 480 nm is caused by intramolecular interaction between pyrene molecules attached to adjacent lysine residues: there are at least 10 loci of two to four adjacent lysine residues in each IFN- γ molecule (Rinderknecht *et al.*, 1984).

Py-IFN- γ binding to its membranal receptors has two consequences: (I) specificity and (II) a high degree of py-IFN- γ immobilization. We found that pyrene-labeled IFN- γ specifically binds to its receptor on membranes purified from WISH cells. Competition experiments with excess (500-fold) unlabeled IFN- γ indicated $77.1 \pm 5.5\%$ specific binding (Figure 5). Thus, the fluorescent modification of IFN- γ did not alter its ability to recognize specifically its binding site on both membrane preparation as well as intact WISH cells (Figure 6). While additional quantitative binding studies would further characterize this fluorescently labeled IFN- γ , its spectroscopic potential is already evident. Binding of labeled IFN- γ to the receptor is also reflected in its spectroscopic characteristics. Steady-state fluorescence polarization increased 4-fold when compared to free py-IFN- γ (Table 2), indicating reduction in rotational motion. Differential phase studies revealed longer rotational correlation times in bound py-IFN- γ . The enlarged pyrene fluorescence

lifetime supports the assignment of enhanced fluorescence polarization and rotational correlation times to immobilization.

As indicated in Table 2 and already shown by others (Lianos and Georgiou, 1979a), pyrene lifetime depends strongly on the polarity, hydroxylic nature, and viscosity of the solvent. Thus, pyrenesulfonyl chloride in the more viscous (resulting in reduced diffusional quenching), nonhydroxylic, and apolar American white oil has longer lifetimes than in the more polar, less viscous, and hydroxylic ethylene glycol: $\tau_1 = 30$ and 18.5 ns, respectively. When bound to IFN- γ , τ_1 rises to 56.4 ns, indicative of the pyrene being buried in the protein in a hydrophobic enclave. The binding of py-IFN- γ to the cell membrane receptors results in a further increase in fluorescence lifetime to $\tau_1 = 80$ ns, presumably reflecting its location in a collision-free environment. The observation of the dramatic rise in steady-state polarization from 0.06 to 0.22, the rise in the rotational correlation time from 8 to 45 ns, and the longer lifetime are all indicative of intimate, tight binding of py-IFN- γ to a hydrophobic enclave of the membrane receptor.

The vibronic peak ratio was, however, nearly equal in py-IFN- γ in buffer solution and when bound to membranes. It thus lacks environmental sensitivity, probably because of the heterogeneity in the pyrene-labeled sites. It is possible that the pyrene moieties were in touch with water even after py-IFN- γ was bound to the receptor. Change in the vibronic ratio might occur on sinking from the initial water phospholipids-head-group interface into the hydrophobic core of the lipid bilayer. The preparation of a homogeneous py-IFN- γ with a 1:1 molar ratio of pyrene to IFN- γ would have been advantageous in detecting its immediate environment through the vibronic peak ratio. To detect it at the minute concentrations involved in biological activity, laser excitation would be required and irreversible photobleaching might result.

In summary, py-IFN- γ shows specific binding and immobilization and seems to meet the expected requirements essential for examining the dynamics of IFN- γ and its complex with the receptor, for which it was designed. This can be done by monitoring fluorescence polarization and lifetime following the interaction of target cell with IFN- γ . It is still anticipated that receptor recycling, which is associated with its sinking from the initial water phospholipids-head-group interface into the hydrophobic core of the lipid bilayer, would be detected through the expected change in the vibronic peak ratio.

ACKNOWLEDGMENT

We are most indebted to Dr. D. Novick for her gracious donation of recombinant IFN- γ . We thank Prof. D. Gill and Dr. R. Cohen-Luria for critical comments. We are grateful for the technical assistance of Ms. Zipora Zolotov and Ms. Liana Shkolnik. This work was supported in part by the Israel Cancer Research Fund and the Office of Naval Research (A.H.P.).

LITERATURE CITED

- Aguet, M. (1980) High affinity binding of ^{125}I -labeled mouse interferon to a specific cell surface receptor. *Nature* 284, 459–461.
- Bader, T., and Wietzerbin, J. (1994) Nuclear accumulation of interferon gamma. *Proc. Natl. Acad. Sci. U.S.A.* 91, 11831–11835.
- Branca, A. A., and Baglioni, C. (1981) Evidence that type I and II interferons have different receptors. *Nature* 294, 768–770.
- Darnell, J. E., Jr., Kerr, I. M., and Stark, G. R. (1994) Jak-STAT pathways and transcriptional activation in response to IFNs and other extracellular signalling proteins. *Science* 264, 1415–1421.

- De Maeyer, E., and De Maeyer-Guignard, J. (1988) *Interferons and Other Regulatory Cytokines*, Wiley, New York.
- Ealick, S. E., Cook, W. J., Vijay-Kumar, S., Carson, M., Nagabhushan, T. L., Trotta, P. P., and Bugg, C. E. (1991) Three-dimensional structure of recombinant human interferon- γ . *Science* 252, 698–702.
- Eppstein, D. A., Marsh, Y. V., van der Pas, M., Felgner, P. L., and Schreiber, A. B. (1985) Biological activity of liposome-encapsulated murine interferon mediated by a cell membrane receptor. *Proc. Natl. Acad. Sci. U.S.A.* 82, 3688–3692.
- Farrar, M. A., and Schreiber, R. D. (1993) The molecular cell biology of interferon-gamma and its receptor. *Annu. Rev. Immunol.* 11, 571–611.
- Finbloom, D. S., Hoover, D. L., and Wahl, L. M. (1985) The characteristics of binding of human recombinant interferon- γ to its receptor on human monocytes and human monocyte-like cells. *J. Immunol.* 135, 300–305.
- Greenlund, A. C., Farrar, M. A., Viviano, B. L., and Schreiber, R. D. (1994) Ligand induced IFN- γ receptor tyrosine phosphorylation couples the receptor to its signal transduction system (p91). *EMBO J.* 13, 1591–1600.
- Heim, N. H., Kerr, I. M., Stark, G. R., and Darnell, J. E., Jr. (1995) A novel member of the interferon receptor family complements functionality of the murine interferon- γ receptor in human cells. *Science* 267, 1347–1349.
- Hemmi, S., Bohni, R., Stark, G., Di Marco, G., and Auget, M. (1994) A novel member of the interferon receptor family complements functionality of the murine interferon- γ receptor in human cells. *Cell* 76, 803–810.
- Igarashi, K., Garotta, G., Ozmen, L., Ziemiecki, A., Wilks, A. F., Harpur, A. G., Larner, A. C., and Finbloom, D. S. (1994) Interferon- γ induces tyrosine phosphorylation of interferon- γ receptor and regulated association of protein tyrosine kinases, Jak1 and Jak2, with its receptor. *J. Biol. Chem.* 269, 14333–14336.
- Ip, S. H., and Cooper, R. A. (1980) Decreased membrane fluidity during differentiation of human promyelocytic leukemia cells in culture. *Blood* 56, 227–232.
- Kalvakolanu, D. V., and Borden, E. C. (1996) An overview of the interferon system: Signal transduction and mechanisms of action. *Cancer Invest.* 14, 25–53.
- Kaplan, D. H., Greenlund, A. C., Tanner, J. W., Shaw, A. S., and Schreiber, R. D. (1996) Identification of an interferon-gamma receptor alpha chain sequence required for JAK-1 binding. *J. Biol. Chem.* 271, 9–12.
- Knopp, J. A., and Weber, G. (1967) Fluorescence depolarization measurements of pyrene butyric-bovine serum albumin conjugates. *J. Biol. Chem.* 242, 1353–1354.
- Lakowicz, J. R., Prendergast, F. G., and Hogen, D. (1979) Differential polarized phase fluorometric investigations of diphenylhexatriene in lipid bilayers. Quantitation of hindered depolarizing rotations. *Biochemistry* 18, 508–519.
- Lianos, P., and Georghiou, S. (1979a) Complex formation between alcohols and the aromatic hydrocarbons pyrene and 1-methylpyrene. *Photochem. Photobiol.* 29, 843–846.
- Lianos, P., and Georghiou, S. (1979b) Solute-solvent interaction and its effect on the vibronic and vibrational structure of pyrene spectra. *Photochem. Photobiol.* 30, 355–362.
- Lianos, P., Mukhopadhyay, A. K., and Georghiou, S. (1980) Microenvironment of aromatic hydrocarbons employed as fluorescent probes of liposomes. *Photochem. Photobiol.* 32, 415–419.
- Lundell, D. L., and Narula, S. K. (1994) Structural elements required for receptor recognition of human interferon-gamma. *Pharmacol. Ther.* 64, 1–21.
- Mao, C., Merlin, G., Ballotti, R., Metzler, R. M., and Aguet, M. (1990) Rapid increase of the human IFN- γ receptor phosphorylation in response to human IFN- γ and phorbol myristate acetate. *J. Immunol.* 145, 4257–4264.
- Marsters, S. A., Pennica, D., Bach, E., Schreiber, R. D., and Shkenazi, A. (1995) Interferon gamma signals via a high-affinity multisubunit receptor complex that contains two types of polypeptide chain. *Proc. Natl. Acad. Sci. U.S.A.* 92, 5401–5405.
- Mory, Y., Ben-Barak, J., Segev, D., Cohen, B., Novick, D., Fischer, D. G., Rubinstein, M., Kargman, S., Zilberstein, A., Vigneron, M., and Revel, M. (1986) Efficient constitutive production of human IFN- γ in Chinese hamster ovary cells. *DNA* 5, 181–193.
- Novick, D., Eshhar, Z., and Rubinstein, M. (1982) Monoclonal antibodies to human α -interferon and their use for affinity chromatography. *J. Immunol.* 129, 2244–2247.
- Parola, A. H. (1993) Membranes lipid-protein interactions. In *Biomembranes, Physical Aspects* (M. Shinitzky, Ed.) Vol. 2, pp 159–277, Balaban Publishers, New York, VCH Weinheim.
- Parola, A. H., Porat, N., and Keisow, L. A. (1994) Chick Embryo Fibroblasts Exposed to Time-Varying Weak Magnetic Fields Share Cell Proliferation, Adenosine Deaminase Activity and Membrane Characteristics of Transformed Cells. *Bioelectromagnetics* 14, 215–228.
- Porat, N., Gill, D., and Parola, A. H. (1988) Adenosine deaminase in cell transformation: Biophysical manifestation of membrane dynamics. *J. Biol. Chem.* 263, 14608–14611.
- Rinderknecht, E., O'Conner, B. H., and Rodriguez, H. (1984) Natural human interferon- γ . Complete amino-acid sequence and determination of sites of glycosylation. *J. Biol. Chem.* 259, 6790–6797.
- Rubin, B. Y., and Gupta, S. L. (1980) Differential efficacies of human type I and type II interferons as anti-viral and anti-proliferative agents. *Proc. Natl. Acad. Sci. U.S.A.* 77, 5928–5932.
- Rubinstein, M., Novick, D., and Fischer, D. G. (1987) The human interferon- γ receptor system. *Immunol. Rev.* 97, 29–50.
- Sarkar, F. H., and Gupta, S. L. (1984) Receptors for human γ -interferon: binding and crosslinking of 125 I-labeled recombinant human γ -interferon to receptors on WISH cells. *Proc. Natl. Acad. Sci. U.S.A.* 81, 5160–5164.
- Sedmak, J. J., and Grossberg, S. E. (1977) A rapid, sensitive and versatile assay for protein using Coomassie brilliant blue. *Anal. Biochem.* 79, 544–552.
- Soh, J., Donnelly, R. J., Kotenko, S., Mariano, T. M., Cook, J. R., Wang, N., Emanuel, N., Schwartz, B., Miki, T., and Pestka, S. (1994) Identification and sequence of an accessory factor required for activation of the human γ -interferon. *Cell* 76, 793–802.
- Turro, N. J. (1978) *Modern Molecular Photochemistry*, p 351, Benjamin/Cumming, New York.
- Uzgiris, E. E., Lockwood, S. H., and Kaplan, J. H. (1982) Oscillation of cell surface charge of human peripheral blood lymphocytes after stimulation with concanavalin A. *J. Immunol.* 128, 1975–1978.

Immobilization of Reducing Sugars as Toxin Binding Agents

U. J. Nilsson,[†] L. D. Heerze,[‡] Y.-C. Liu,[†] G. D. Armstrong,[‡] M. M. Palcic,[†] and O. Hindsgaul^{*,†}

Departments of Chemistry and Medical Microbiology and Immunology, University of Alberta, Edmonton, Alberta T6G 2G2, Canada. Received December 12, 1996[®]

A simple and economical procedure for the attachment of reducing sugars to aminated solid supports has been developed. Reaction of the amino groups on the solid support with *p*-nitrophenyl chloroformate, followed by 1,6-hexanediamine, yields a chain-extended amine to which reducing sugars can be attached while remaining accessible to macromolecules. Immobilization of the reducing sugars involves a simple incubation followed by trapping of the resulting glycosylamine with acetic anhydride and recovery of the unreacted sugar by filtration. This technique was used to immobilize lactose and sialyllactose onto silylated Chromosorb P, producing solid supports that effectively neutralized the activity of cholera toxin from *Vibrio cholerae* and heat-labile enterotoxin of enterotoxigenic *Escherichia coli*. The general applicability of such solid supports for toxin neutralization was further demonstrated by immobilization of the enzymatically synthesized α Gal(1–3) β Gal(1–4)Glc trisaccharide, which produced a support that efficiently neutralized toxin A of *Clostridium difficile*. The results from this study suggest that these solid supports have the potential to serve as inexpensive therapeutics for bacterial toxin-mediated diarrheal diseases.

INTRODUCTION

The recognition of oligosaccharide receptors on host cells by pathogenic microorganisms or their toxins is a crucial event in causing disease in humans (1). One potential therapeutic approach to prevent disease in humans is to inhibit the attachment of the pathogens or their toxins to carbohydrate receptors on host cells using oligosaccharide receptor analogs that have the capability of binding bacteria or toxin. This approach has been utilized in two gastroenteric applications in which synthetic oligosaccharide sequences were immobilized onto a nondegradable diatomaceous earth, silylated Chromosorb P (2). These glycosylated solid supports possess the ability to bind shiga-like toxin produced by enterohemorrhagic *Escherichia coli* (the causative agent of hemorrhagic colitis and hemolytic-uremic syndrome), as well as toxin A from *Clostridium difficile*, which plays a major role in causing antibiotic-associated diarrhea (3–5). While these affinity supports were efficient at toxin neutralization, their preparation involves multistep chemical synthesis of 8-(methoxycarbonyl)octyl glycosides followed by their immobilization using coupling procedures that are very labor intensive. If potential therapeutics for third-world diseases such as cholera are being considered, the solid supports become prohibitively expensive.

This paper describes a simple and economical procedure for immobilization of commercially available reducing oligosaccharides onto an inert matrix to produce solid supports (termed SYNSORB's), for use as toxin binding agents. Commercial Chromosorb P was conventionally silylated using 3-(triethoxysilyl)propylamine (2). Reducing oligosaccharides were then coupled to the silylated Chromosorb P via a chain-extended glycosylamide linkage using inexpensive reagents and simple chemistry. The resulting solid supports were then

screened for their ability to bind cholera toxin (CT) from *Vibrio cholerae*, heat-labile enterotoxin (LT) from enterotoxigenic *Escherichia coli*, a common cause of bacteria-induced traveler's diarrhea, and toxin A from *C. difficile*. The oligosaccharides used in this investigation represent components of the pentasaccharide ganglioside GM₁ structure, the primary receptor for both CT and LT (6), and the trisaccharide recognized by toxin A of *C. difficile*, α Gal(1–3) β Gal(1–4)Glc (5). The α Gal(1–3) β Gal(1–4)Glc trisaccharide was obtained by enzymatic glycosylation of lactose using calf thymus α (1–3)-galactosyltransferase.

EXPERIMENTAL PROCEDURES

Materials. Calf thymus was obtained from Pel-Freeze Biologicals, UDP-Gal and alkaline phosphatase were from the Sigma Chemical Co., and *E. coli* β -galactosidase was from Boehringer Mannheim. AG 1 X8 and Bio-Gel P-2 were obtained from Bio-Rad. α (1–3)-Galactosyltransferase was isolated from calf thymus glands by extraction and chromatography on a UDP-hexanolamine Sepharose column as described by Blanken and van den Eijnden (7) using sodium cacodylate buffer instead of Tris-maleate buffer. After chromatography, the enzyme was concentrated by ultrafiltration, dialyzed against 30 mM sodium cacodylate buffer, pH 6.5, containing 20 mM MnCl₂ and 0.1% Triton X-100, and stored at 4 °C. Galactosyltransferase activity was monitored by incubation with 540 μ M β Gal(1–4) β GlcNAcO(CH₂)₈COOCH₃, 1 mM UDP-Gal, 35 000 dpm UDP-[³H]-Gal, 1 mg/mL bovine serum albumin, 0.8% Triton X-100, 50 mM MnCl₂, and 100 mM sodium cacodylate buffer, pH 6.1, in a total volume of 20 μ L. After reaction for 30 min at 37 °C, products were isolated on a reversed phase C₁₈ cartridge as previously described (8).

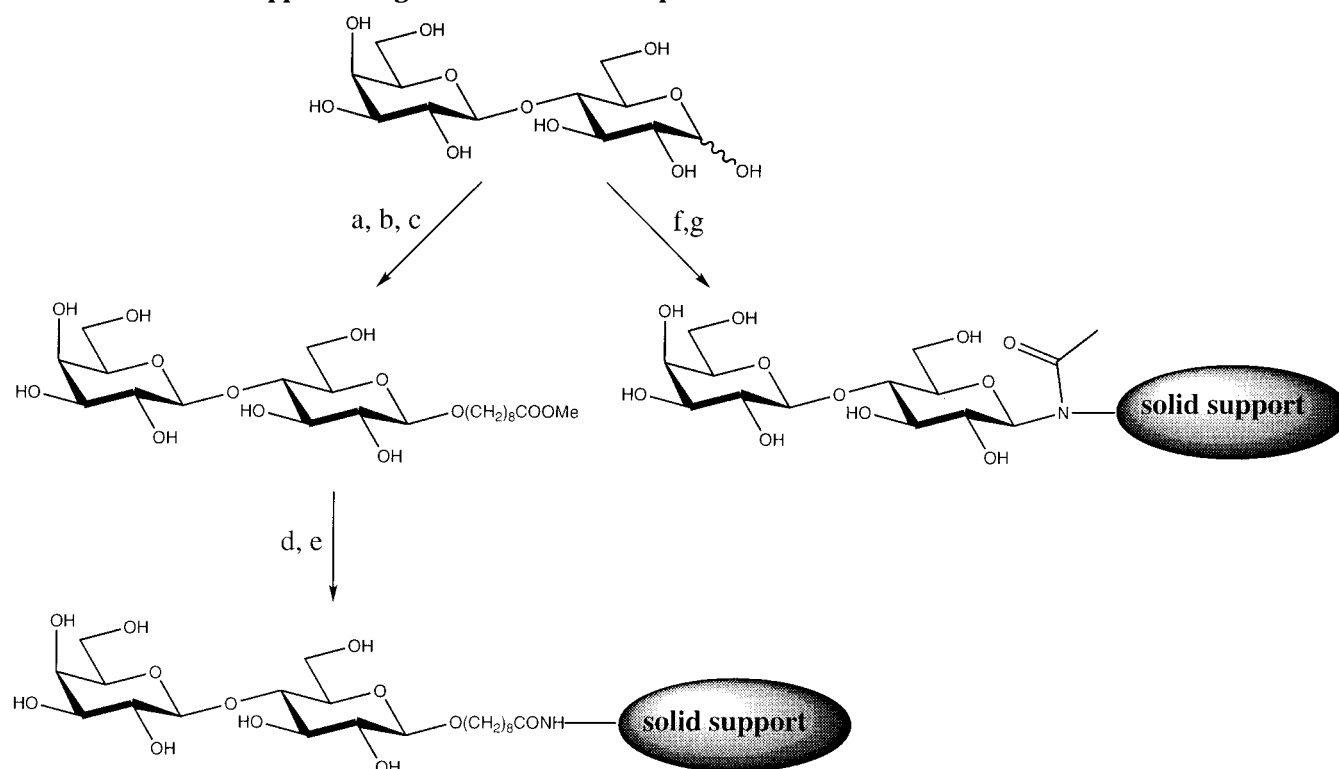
Typical Procedure for Immobilizing Reducing Sugars on Silylated Chromosorb P. To silylate Chromosorb P (20 g) and *p*-nitrophenyl chloroformate (15 g, 75 mmol) in dry tetrahydrofuran (80 mL) and dry dichloromethane (80 mL) was added diisopropylethylamine (13.1 mL, 75 mmol). The mixture was shaken occasionally for 3 h, after which time the resulting

* Author to whom correspondence should be addressed [telephone (403) 492-4171; fax (403) 492-7705; e-mail Ole.Hindsgaul@UAlberta.Ca].

[†] Department of Chemistry.

[‡] Department of Medical Microbiology and Immunology.

[®] Abstract published in *Advance ACS Abstracts*, June 1, 1997.

Scheme 1. Comparison of Traditional Organic Synthesis and Direct Coupling of Reducing Oligosaccharides to an Aminated Solid Support Using Lactose as the Example

^a Reagents: (a) Ac_2O , NaOAc ; (b) SnCl_4 , $\text{HO}(\text{CH}_2)_8\text{COOEt}$; (c) NaOMe/MeOH ; (d) H_2NNH_2 ; (e) HONO , $\text{H}_2\text{N-solids support}$; (f) MeOH , $\text{H}_2\text{N-solids support}$, 60°C ; (g) Ac_2O .

resin was filtered, washed with dichloromethane/tetrahydrofuran (1:1, $5 \times 100\text{ mL}$), and dried under vacuum. To the resulting dried resin was added 1,6-hexanediamine (8.7 g, 75 mmol) in dry dimethylformamide (200 mL) containing triethylamine (10.5 mL, 75 mmol). The reaction was allowed to proceed for 90 min with occasional shaking. The resin was then removed by filtration, washed successively with water ($3 \times 300\text{ mL}$), dimethylformamide ($3 \times 300\text{ mL}$), and dichloromethane/tetrahydrofuran (1:1, $5 \times 100\text{ mL}$), and dried under vacuum to give 22 g of resin. A portion of the resin (2.0 g), lactose (27.4 mg, 80 μmol), and acetic acid (40 μL) in dry methanol (6.5 mL) were heated to 60°C in a sealed flask for 47 h. The mixture was then cooled on ice ($\sim 5^\circ\text{C}$) and acetic anhydride (2.1 mL) was added. The mixture was shaken occasionally for 12 h, and the resin was recovered by filtration and then washed with water ($3 \times 50\text{ mL}$) and methanol ($3 \times 50\text{ mL}$). Fine particles were removed by suspending the resin in methanol and decanting the supernatant until it became clear. Drying the resin under vacuum gave 1.95 g of SYNSORB 260. Analysis of the product according to the phenol-sulfuric acid assay indicated an oligosaccharide incorporation of $1.24\text{ }\mu\text{mol/g}$ of resin (9).

Synthesis of $\alpha\text{Gal}(1\text{--}3)\beta\text{Gal}(1\text{--}4)\text{Glc}$. A reaction mixture containing lactose (50 mg), UDP-Gal (20 mg), $\alpha(1\text{--}3)$ -galactosyltransferase (60 milliunits), alkaline phosphatase (20 units), 20 mM MnCl_2 , and 0.1% Triton X-100 in 50 mM sodium cacodylate buffer (3 mL) at pH 6.5 was incubated at 37°C . Additional UDP-Gal was added to the mixture after 24 h (20 mg) and 48 h (50 mg). After 120 h, fresh $\alpha(1\text{--}3)$ -galactosyltransferase (20 milliunits) and UDP-Gal (10 mg) were added to the mixture, which was incubated for an additional 72 h, at which point very little unreacted lactose remained as estimated by TLC [SiO_2 , 0.1 M sodium borate/2-propanol 1:4, $R_f(\text{lactose}) = 0.60$, $R_f[\alpha\text{Gal}(1\text{--}3)\beta\text{Gal}(1\text{--}4)\text{Glc}] =$

0.51]. The reaction mixture was filtered through a $0.2\text{ }\mu\text{m}$ Nalgene nylon filter, the filtrate was applied to a Bio-Rad AG 1X8 column (Cl^- form, $2.5 \times 20\text{ cm}$, 0.6 mL/min), and the column was eluted with water. Saccharide fractions were combined and lyophilized. The dry residue was dissolved in 50 mM potassium phosphate buffer, pH 7.5, β -galactosidase (150 milliunits) was added to the mixture to destroy unreacted lactose, and the sample was left at ambient temperature (24°C) for 18 h. The mixture was boiled for 2 min, filtered through a $0.2\text{ }\mu\text{m}$ filter, and divided into three portions, each of which was loaded onto a C_{18} silica gel column (20 g). The columns were washed with water (200 mL), and the aqueous eluents were concentrated to dryness under reduced pressure. The residue was dissolved in water (5 mL) and applied to a Bio-Gel P-2 column ($2.5 \times 100\text{ cm}$, H_2O , 0.2 mL/min). Fractions that contained the trisaccharide were combined and lyophilized, to give 10.5 mg of $\alpha\text{Gal}(1\text{--}3)\beta\text{Gal}(1\text{--}4)\text{Glc}$ trisaccharide: $^1\text{H NMR}$ (500 MHz, D_2O) δ 5.22 (d, 0.36 H, $J = 3.6\text{ Hz}$, H-1 α), 5.14 (d, 1 H, $J = 3.0\text{ Hz}$, H-1'), 4.66 (d, 0.64 H, $J = 8.0\text{ Hz}$, H-1 β), 4.51 (d, 1 H, $J = 8.0\text{ Hz}$, H-1').

Assay of Toxin Activity Using Tissue Culture Cells. The cytotoxic activity of CT and LT was measured by using Chinese hamster ovary cells (CHO) maintained in Hams F12 medium supplemented with 10% fetal bovine serum (FBS) in an atmosphere of 5% CO_2 at 37°C . Toxin samples were diluted 1:5 in Hams media and filter sterilized through $0.22\text{ }\mu\text{m}$ syringe filters, the sterilized samples were serially 5-fold diluted in media, and 100 μL of each dilution was added to wells with confluent monolayers of CHO cells and incubated for 24 h at $37^\circ\text{C}/5\%\text{ CO}_2$. Each sample was analyzed two times. Cytotoxic effects were readily visible after 24 h of incubation by comparing wells with controls that did not contain toxin. After 24 h, the cells were fixed with 95% methanol and stained with Geimsa stain. Toxin-contain-

Table 1. SYNSORB Derivatives Used in Toxin Neutralization Experiments

Structure	SYNSORB designation	Oligosaccharide Incorporation ($\mu\text{mol/g}$)
	16	0.97
	89	1.0
	343	0.98
	260	0.37
	364	0.64
	366	1.0
	368	2.4
	370	2.1
	374	2.4
	376	0.9
	90	1.2

ing samples from neutralization experiments were treated in an analogous fashion except that the percent neutralization was determined by comparing the endpoint dilutions of samples with and without SYNSORB.

Screening of Immobilized Lactose, Sialyllactose, Maltose, and Cellobiose for the Ability To Neutralize CT and LT Activity. A solution containing purified CT or LT (Sigma, 2 μg in 1 mL of PBS) was added to

various SYNSORB derivatives (20 mg, SYNSORBs 16 and 89 were provided by D. Rafter, SYNSORB Biotech. Inc., Calgary, AB, Canada) in 1.5 mL microcentrifuge tubes and incubated at room temperature for 1 h on an end-over-end rotator. After incubation, the SYNSORB was allowed to settle to the bottom of the tubes and the supernatants were carefully removed by aspiration. Serial 5-fold dilutions of the supernatants were prepared and the cytotoxic endpoints determined as described above. The extent of reduction in the endpoint in the presence of SYNSORB was determined by comparing with controls in which SYNSORB was not added.

C. *difficile* Toxin A SYNSORB Neutralization Assays.

Toxin A was purified from a toxin producing strain of *C. difficile* (ATCC 43255, VPI strain 10463) as described (10). Solutions containing purified toxin A (1 mL) were added to 20 mg samples of either SYNSORB 364 (prepared by chemical and enzymatic synthesis), 374, 376, or 90 (provided by D. Rafter, SYNSORB Biotech. Inc.) in 1.5 mL microcentrifuge tubes and processed as described for CT and LT.

Hemagglutination Assays Using Rabbit Erythrocytes. Fresh rabbit erythrocytes were washed once in phosphate-buffered saline (PBS) and resuspended at a concentration of 2% (v/v) in cold PBS. Serial 2-fold dilutions (50 μ L) of toxin A containing solutions were made in cold PBS in U-shaped microtiter wells. An equal volume (50 μ L) of rabbit erythrocytes was then added to each well, and the microtiter plate was mixed gently. After the plate had been incubated for 4 h at 4 °C, the hemagglutination titer was assessed visually. All assays were done in duplicate.

RESULTS AND DISCUSSION

The broad application of immobilized oligosaccharides as bacterial toxin binding agents is hampered by the requirement of labor-intensive synthesis to produce complex oligosaccharides carrying a functionalized spacer arm that is suitable for coupling to a solid support. Immobilization of a synthetic lactoside typically involves five chemical reaction steps (11), even beginning with the commercially available inexpensive disaccharide (Scheme 1). Blomberg *et al.* (12) have, however, described an attractive alternative involving the coupling of reducing sugars to immobilize amines via a glycosylamine linkage to yield a stable glycosylamide.

To determine the feasibility of the immobilization strategy based on reducing sugars to form materials suitable for use in gastroenteric applications, lactose was immobilized onto silylated Chromosorb P. The procedure, adapted from that of Blomberg *et al.*, involves simply incubating the resin with a methanolic solution of lactose at 60 °C for 2 days. Addition of acetic anhydride, followed by filtration, then yielded the corresponding lactosyl acetamide (SYNSORB 343, Table 1). The resulting lactose conjugate was compared with SYNSORB 16, which carries lactose coupled via a chemically synthesized 8-(methoxycarbonyl)octyl linker, for the ability to neutralize CT and LT activity (13). SYNSORB 16 was used as the control, since we have previously demonstrated CT and LT binding to this support (unpublished results). The results from these experiments (Figure 1) indicate that lactose immobilized directly onto silylated Chromosorb P (SYNSORB 343) provided poor inhibitors of CT and LT binding as compared to SYNSORB 16. This is probably due to the close proximity of the sugar with the support, making it less accessible for toxin binding. To increase the accessibility of the sugar, an extended spacer carrying a primary amine at

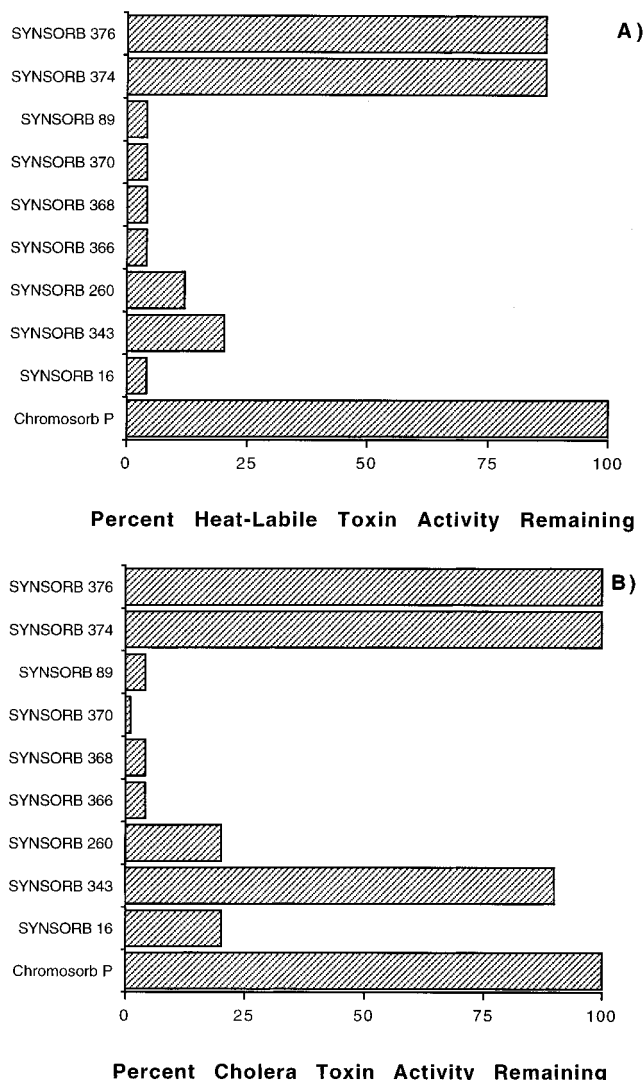
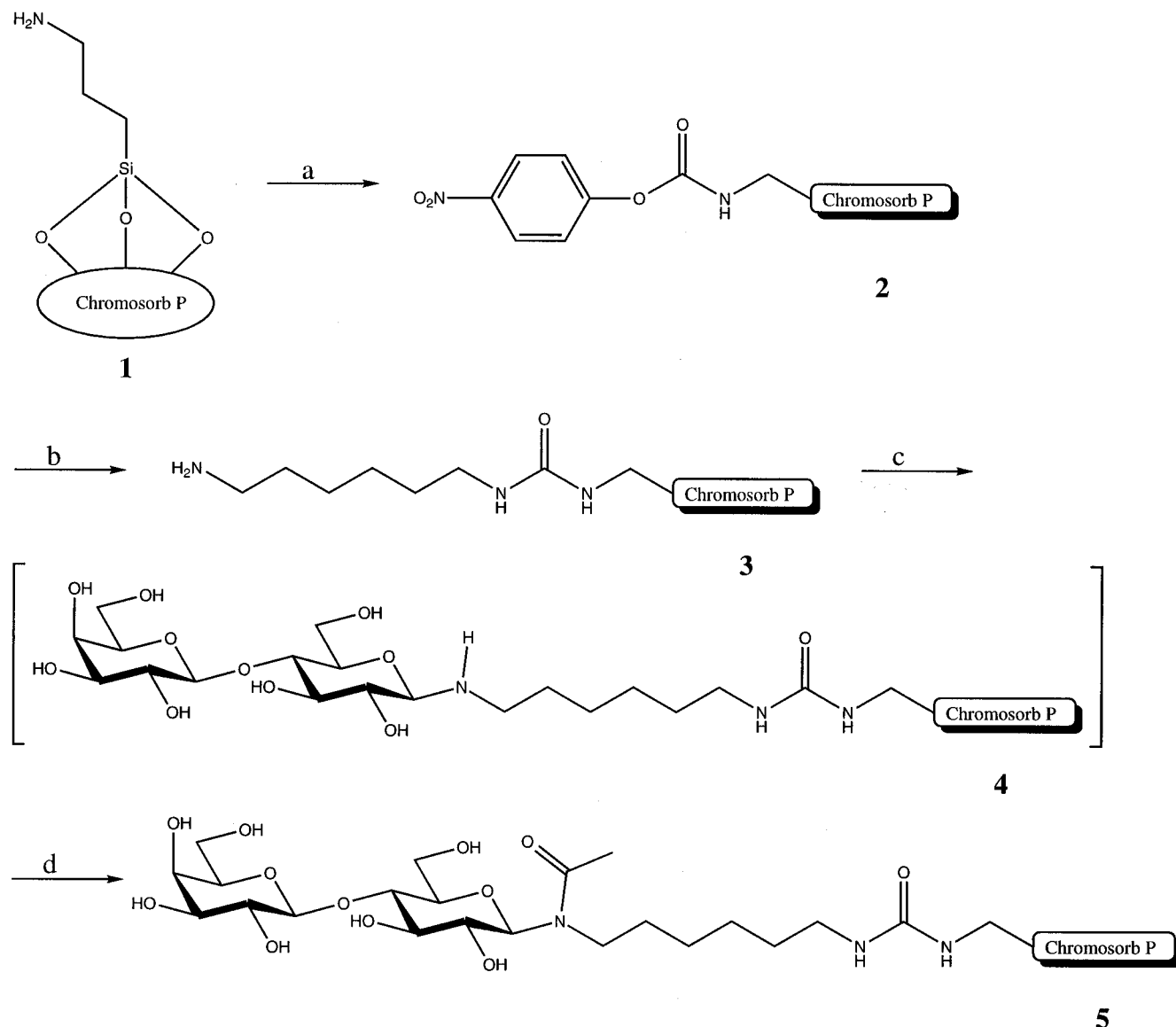


Figure 1. Neutralization of purified heat-labile toxin (A) and cholera toxin (B) cytotoxic activity using a panel of SYNSORB derivatives shown in Table 1.

the distal end was therefore introduced onto the silyl-aminated Chromosorb P as shown in Scheme 2 (14).

Silylated Chromosorb P (1) was treated with *p*-nitrophenyl chloroformate to give the Chromosorb P (2) activated as a *p*-nitrophenyl urethane. This activated Chromosorb P (2) was then treated with 1,6-hexanedi-amine to give the Chromosorb P (3) carrying a primary amine on an extended spacer. Oligosaccharides were immobilized on this derivatized Chromosorb P (3) by simply stirring the reducing sugar and silylated Chromosorb P in methanol containing 0.6% acetic acid at 60 °C and then trapping the glycosyl amine as a glycosyl acetamide (4) with acetic anhydride. The presence of acetic acid significantly increased the incorporation yield of the reducing sugar when compared to the original procedure (12). The amount of reducing sugar in the immobilization step had to exceed 40 μ mol of oligosaccharide/g of 3 to give a high incorporation of oligosaccharide. The excess reducing sugar could easily be recovered after removal of the resin by filtration and concentration of the mother liquor. Using this method, several commercially available oligosaccharides (Table 1) that resemble components of the ganglioside GM₁ structure were immobilized onto silylated Chromosorb P, giving incorporation yields ranging from 0.37 to 2.4 μ mol of sugar/g of Chromosorb P.

Scheme 2^a

^a (a) *p*-Nitrophenyl chloroformate, diisopropylethylamine, THF, CH₂Cl₂; (b) 1,6-hexanediamine, Et₃N, DMF; (c) MeOH, AcOH, lactose, 60 °C; (d) Ac₂O.

The results from the toxin neutralization experiments (Figure 1) indicated that the extent of neutralization with SYNSORBs 260, 366, 368, and 370 (Table 1) were comparable with control SYNSORBs 16 and 89. The maltose and cellobiose containing SYNSORBs (374 and 376) were not efficient at neutralizing either CT or LT, indicating carbohydrate-specific recognition. The conclusions from the toxin neutralization experiments are that the 8-(methoxycarbonyloctyl) linker arm can be replaced with a much more cost-effective alternative. In addition, simple commercially available oligosaccharides readily isolated from natural sources can serve as receptor analogs that effectively bind CT and LT activity.

To further demonstrate the generality of this method, it was applied to toxin A from *C. difficile*, which is unrelated to LT and CT. Toxin A from *C. difficile* recognizes the trisaccharide α Gal(1-3) β Gal(1-4)Glc (**5**) which, unlike lactose, is not readily available from natural sources. We chose to enzymatically galactosylate lactose in one step using calf thymus α (1-3)-galactosyltransferase to yield the reducing trisaccharide α Gal(1-3) β Gal(1-4)Glc on a 10 mg scale. Immobilization of this trisaccharide as described for lactose then gave SYNSORB 364 (Table 1). SYNSORB 364 neutralized the

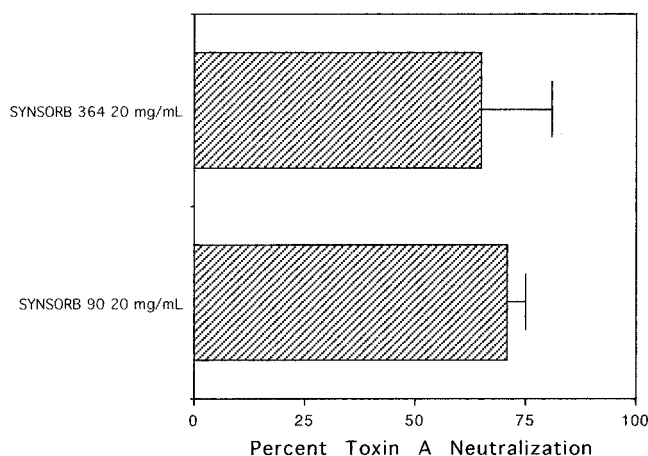


Figure 2. Neutralization of purified toxin *C. difficile* A hemagglutination activity using SYNSORBs 364 and 90 ($n = 5$). SYNSORBs 374 (maltose) and 376 (cellobiose) did not neutralize toxin A activity.

hemagglutination of rabbit erythrocytes by toxin A from *C. difficile* (Figure 2) as efficiently as SYNSORB 90 [carrying the α Gal(1-3) β Gal(1-4)Glc trisaccharide syn-

thesized in a traditional manner and linked via a 8-(methoxycarbonyl)octyl spacer]. Neither SYNSORB carrying maltose (374) nor SYNSORB carrying cellobiose (376) neutralized the hemagglutination activity of toxin A of *C. difficile* (data not shown).

The results from this study suggest that immobilization of simple oligosaccharides on a chain-extended inert support using inexpensive reagents provide cost-effective SYNSORB alternatives that could serve as potential therapeutics for diarrheal diseases that affect third-world countries. Additional investigations are underway to further refine the production of these toxin binding agents to a point where cost of production would be favorable for developing therapeutics for diseases such as cholera.

ACKNOWLEDGMENT

This work was supported by an industrial contract from SYNSORB Biotech. Inc., 201, 1204 Kensington Rd. NW, Calgary, AB, Canada T2N 3P5. We thank Sheila Hubscher for technical assistance.

LITERATURE CITED

- (1) Karlsson, K.-A. (1989) Animal glycosphingolipids as membrane attachment sites for bacteria. *Annu. Rev. Biochem.* 58, 309–350.
- (2) Lemieux, R. U., Baker, D. A., Weinstein, W. M., and Switzer C. M. (1981) Artificial antigens. Antibody preparations for the localization of Lewis determinants in tissues. *Biochemistry* 20, 199–205.
- (3) Armstrong, G. D., Fodor, E., and Vanmaele R. (1991) Investigation of shiga-like toxin binding to chemically synthesized oligosaccharide sequences. *J. Infect. Dis.* 164, 1160–1167.
- (4) Armstrong, G. D., Rowe, P. C., Goodyer, P., Orrbine, E., Klassen, T. P., Wells, G., MacKenzie, A., Lior, H., Blanchard, C., Auclair, F., Thompson, B., Rafter, D. J., and McLaine, P. N. (1995) A phase I study of chemically synthesized verotoxin (Shiga-like toxin) Pk-trisaccharide receptors attached to Chromosorb for preventing hemolytic-uremic syndrome. *J. Infect. Dis.* 171, 1042–1045.
- (5) Heerze, L. D., Kelm, M. A., Talbot, J. A., and Armstrong G. D. (1994) Oligosaccharide sequences attached to an inert support (SYNSORB) as potential therapy for antibiotic-associated diarrhea and pseudomembranous colitis. *J. Infect. Dis.* 169, 1291–1296.
- (6) Fishman, P. H., Pacuszka, T., and Orlandi, P. A. (1993) Gangliosides as receptors for bacterial enterotoxins. *Adv. Lipid Res.* 25, 165–187.
- (7) Blanken, W. M., and Van den Eijnden, D. H. (1985) Biosynthesis of terminal Gal α 1–3Gal β 1–4GlcNAc oligosaccharide sequences on glycoconjugates. *J. Biol. Chem.* 260, 12927–12934.
- (8) Palcic, M. M., Heerze, L. D., Pierce, M., and Hindsgaul, O. (1988) The use of hydrophobic synthetic glycosides as acceptors in glycosyltransferase assays. *Glycoconjugate J.* 5, 49–63.
- (9) Dubois, M., Gilles, K. A., Hamilton, J. K., Rebers, P. A., and Smith, F. (1979) Colorimetric method for determination of sugars and related substances. *Anal. Chem.* 28, 350–356.
- (10) Sullivan, N. M., Pellet, S., and Wilkins T. D. (1982) Purification and characterization of toxin A and B from *Clostridium difficile*. *Infect. Immunol.* 35, 1032–1040.
- (11) Banoub, J., and Bundle, D. R. (1979) Stannic tetrachloride catalysed glycosylation of 8-ethoxycarbonyloctanol by cellobiose, lactose, and maltose octaacetates; synthesis of α - and β -glycosidic linkages. *Can. J. Chem.* 57, 2085–2090.
- (12) Blomberg, L., Wieslander, J., and Norberg, T. (1993) Immobilization of reducing oligosaccharides to matrices by a glycosylamide linkage. *J. Carbohydr. Chem.* 12, 265–276.
- (13) Lemieux, R. U., Bundle, D. R., and Baker, D. A. (1975) The properties of a "synthetic" antigen related to the human blood-group Lewis a. *J. Am. Chem. Soc.* 97, 4076–4083.
- (14) Hutchins, S. M., and Chapman, K. T. (1995) A strategy for urea linked diamine libraries. *Tetrahedron Lett.* 36, 2583–2586.

BC9700603

Nicotinic Acetylcholine Receptor Labeled with a Tritiated, Photoactivatable Agonist: A New Tool for Investigating the Functional, Activated State[†]

Florence Kotzyba-Hibert,^{*,‡} Pascal Kessler,[§] Vincent Zerbib,[‡] Thomas Grutter,[‡] Christian Bogen,^{||} Kenneth Takeda,^{||} Akli Hammadi,[§] Laurent Knerr,[§] and Maurice Goeldner[‡]

Laboratoire de Chimie Bioorganique-URA 1386 CNRS and Laboratoire de Pharmacologie et Physiopathologie Cellulaires-URA 600 CNRS, Université Louis Pasteur Strasbourg, B.P. 24, 67401 Illkirch, France, and Département d'Ingénierie et d'Etudes des Protéines, CEA/Saclay, 91191 Gif-sur-Yvette, France. Received December 6, 1996[®]

Upon agonist activation, the nicotinic acetylcholine receptor undergoes allosteric transitions leading to channel opening and sodium ion influx. The molecular structure of the agonist binding site has been mapped previously by photoaffinity labeling, but most photosensitive probes used for this purpose interact only with closed receptor states (resting or desensitized). We have synthesized two novel photoactivatable 4-diazocyclohexa-2,5-dienone derivatives as cholinergic agonist candidates, with the objective of identifying structural changes at the acetylcholine binding site associated with receptor activation. One of these ligands, **9b**, is a functional agonist at muscle acetylcholine receptors in human TE 671 cells. In photolabeling experiments with **9b**, up to 35% inactivation of agonist binding sites was observed at *Torpedo* acetylcholine receptors. Tritiated **9b** was synthesized, and photolabeling was found to occur mainly on the α -subunit in a partially protectable manner. This novel radiolabeled photoprobe appears to be suitable for future investigation of the molecular dynamics of allosteric transitions occurring at the active acetylcholine receptor binding site.

INTRODUCTION

Using a fluorescent agonist (Dns-C₆-Cho),¹ it was shown that the activated nicotinic acetylcholine receptor (AChR) cycles between at least four discrete interconvertible conformational states [resting, R; active, A; intermediate, I; and desensitized, D (Heidmann and Changeux, 1979; Heidmann et al., 1983)]. Channel opening rapidly follows agonist binding (R to A state, microsecond to millisecond time scale) with slower successive transitions toward the intermediate (millisecond to second time scale) and the desensitized states (second to minute time scale).

The molecular structure of the acetylcholine (ACh) binding site has been probed by site-directed labels and by mutagenesis. For instance, residues contributing to the ACh binding site of *Torpedo* AChR were topographi-

cally mapped (Dennis et al., 1988; Galzi et al., 1990) to three different loops (loop A, Trp-86 and Tyr-93; loop B, Trp-149 and Tyr-151; and loop C, Tyr-190, Cys-192, Cys-193, and Tyr-198) on the α -subunit NH₂-terminal domain using the photosensitive antagonist [³H]DDF [*p*-(*N,N*-dimethylamino)benzene]diazonium fluoroborate]. DDF and other photosensitive antagonist labels have also provided information on the ACh binding site in closed states of AChR (Galzi et al., 1991; Kotzyba-Hibert et al., 1995). As the transition from the resting (R) to the active state (A) takes place on a millisecond time scale, photosensitive agonists that have high quantum yields and generate reactive species with short lifetimes are required in order to label specifically the functional state (A) of the AChR.

The previously described dynamic mapping of the ACh binding site by the agonist [³H]nicotine (Middleton and Cohen, 1991) suffers from extremely low labeling efficiency (around 1%) following an undefined photocoupling process. Therefore, we developed a new set of photoactivatable ligands displaying agonist activity at the AChR that allowed very efficient labeling of *Torpedo marmorata* AChR (Chatrenet et al., 1992). These aryl-diazonium salts photogenerated a highly reactive species, the aryl cation, having a $t_{1/2}$ of $<10^{-10}$ s (Gasper et al., 1995) and being able to react with any amino acid side chains defining a given binding site. However, the size and flexibility of the probe (14.5 Å in the extended conformation) did expand the labeling area beyond the ACh binding site.

Thus, in order to address the molecular changes occurring at the cholinergic agonist binding site during functional activation and upon desensitization, we recently developed a novel family of photosensitive agonists of adapted size and reactivity (Kotzyba-Hibert et al., 1996) designed to incorporate instantaneously and covalently, upon irradiation, in surrounding residues. One of these photoactivatable ligands (**1**), carrying a highly photosensitive 4-diazocyclohexa-2,5-dienone moiety (Ar-

[†] This work is dedicated to the memory of Prof. Christian Hirth.

[‡] Laboratoire de Chimie Bioorganique-URA 1386 CNRS, Université Louis Pasteur Strasbourg.

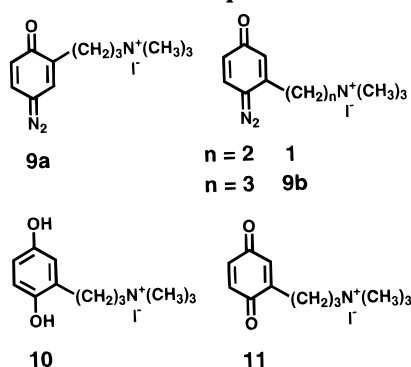
[§] CEA/Saclay.

^{||} Laboratoire de Pharmacologie et Physiopathologie Cellulaires-URA 600 CNRS, Université Louis Pasteur Strasbourg.

* To whom correspondence should be addressed at Laboratoire de Chimie Bioorganique-URA CNRS 1386, B.P. 24, 74 route du Rhin, F-67401 Illkirch, France. Telephone: (33) 3 88 67 68 38. Fax: (33) 3 88 67 88 91. E-mail: kotzyba@aspirine.u-strasbg.fr.

[®] Abstract published in *Advance ACS Abstracts*, June 15, 1997.

¹ Abbreviations: Dns-C₆-Cho, dansyl-C₆-choline; AChR, nicotinic acetylcholine receptor; ACh, acetylcholine; DDF, [*p*-(*N,N*-dimethylamino)benzene]diazonium fluoroborate; NCB, noncompetitive blocker; α -BuTX, α -bungarotoxin; PCP, phencyclidine; Carb, carbamylcholine; R_f , retention frontal; t_R , retention time; PBS, phosphate-buffered saline; $t_{1/2}$, half-life; λ_{max} , maximum absorbance wavelength; ϵ_{max} , molar extinction coefficient; M_p , melting point; K_p , protection constant; K_i , inhibition constant; d-Tubo, *d*-tubocurarine; ET, energy transfer; EtOAc, ethyl acetate.

Scheme 1. Structure of Photoactivatable Ligands 1, 9a, and 9b and Derived Compounds 10 and 11

nold et al., 1992) in addition to the quaternary ammonium group necessary for cholinergic recognition (Scheme 1), was shown to be a functional agonist (Kotzyba-Hibert et al., 1996). However, we did not succeed in isolating the corresponding radiolabeled analog of **1** because of its instability.

We describe here the synthesis of two novel ligands of this family, **9a** and **9b**, including the radioactive analog [**³H]-**9b**, and their binding properties at *Torpedo* AChR. One of these compounds, **9b**, was found to be a functional agonist in patch-clamp experiments, and in photolabeling experiments, [**³H]-**9b** was predominantly incorporated into the α -subunit.****

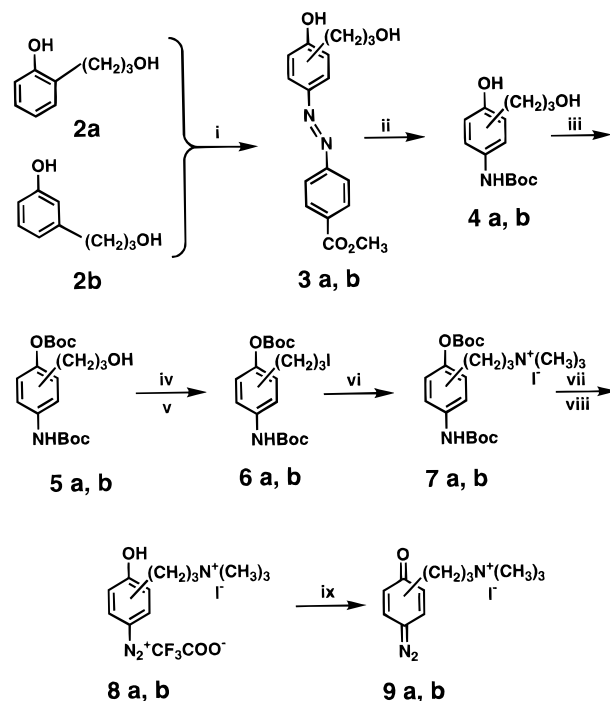
EXPERIMENTAL PROCEDURES

Materials. Bungarus [**¹²⁵I]- α -bungarotoxin (α -BuTX) and [**³H]-phenylcyclidine (PCP) were purchased from NEN, and carbamylcholine (Carb) was from Sigma and proadifen from SKF. *Naja nigricollis* [**³H]- α -neurotoxin was a generous gift from Prof. A. Ménez. Live *T. marmorata* specimens were purchased from the Station Biologique de Roscoff (France). All other commercial reagents were of the highest purity available. All solvents used were reagents of HPLC grade. 3-(2-Hydroxyphenyl)-1-propionic acid and 3-(3-hydroxyphenyl)-1-propionic acid were purchased from Aldrich. Literature procedures were used to prepare 3-(2-hydroxyphenyl)-1-propanol and 3-(3-hydroxyphenyl)-1-propanol (Smith, 1965).******

³H-NMR spectra were recorded at 250 MHz on a Bruker WM 250 spectrometer with tetramethylsilane as the internal standard. NMR spectra were recorded for a CDCl₃ solution except when indicated with a Bruker WM 250 or a AC300 spectrometer. Chemical shifts (δ in parts per million) are reported for ¹H at 250 and 300 MHz and for ¹³C at 61 and 75 MHz. Coupling constants are given in hertz. Mass spectra were acquired on a VG 7035E spectrometer, unless otherwise stated, by direct introduction and electron impact (EI) mode (reference = perfluorokerosene). Melting points were determined on a Kofler system. Tritium determinations were made in a SL 3000 Intertechnique liquid scintillation counter. The automatic gas transfer unit used for catalytic tritiation has been previously described (Morgat et al., 1975). Carrier-free tritium gas was obtained from Commissariat à l'Energie Atomique (France).

Synthesis of *p*-Diazocyclohexadienones 9a and 9b (Scheme 2). General Procedure for the Synthesis of Precursors 8a and 8b. Alcohols **2a** and **2b** were synthesized as previously described (Smith, 1965) (90 and 84% overall yield, respectively).

4-[[4-Hydroxy-3-(3-hydroxypropyl)phenyl]azo]benzoic Acid Methyl Ester **3a** and 4-[[4-Hydroxy-2-(3-hydroxypropyl)phenyl]azo]benzoic Acid Methyl Ester **3b**. A diazo-

Scheme 2. Syntheses of Diazo Compounds 9a and 9b^a

^a (i) CH₃CO₂C₆H₄N₂⁺/borate buffer at pH 10.3; yields, 90% **3a**, 88% **3b**. (ii) H₂, PtO₂/MeOH-BOC₂O; yields, 99% **4a**, 97% **4b**. (iii) NaH/DMF-BOC₂O; yields, 94% **5a**, 75% **5b**. (iv) CH₃SO₂Cl/Et₃N/THF. (v) NaI/acetone; yields in two steps, 85% **6a**, 89% **6b**. (vi) Et₃N (saturated/toluene); yields, 89% **7a**, 97% **7b**. (vii) TFA. (viii) Isoamyl nitrite/CH₃COOH. (ix) Physiological pH of 7.2; yields in three steps, 62% **9a**, 80% **9b**.

nium coupling was achieved on phenols **2a** and **2b** (34 mM solution) with *p*-(methoxycarbonyl)phenyldiazonium in sodium tetraborate buffer (93 mM, pH 10.3) at 0 °C, in the dark. The azo compounds were precipitated at acidic pH (addition of aqueous HCl), filtered, and recrystallized in MeOH/H₂O. The yields of orange powders were 90 and 88%, respectively. **3a**: *R*_f = 0.29 in 95:5 CH₂Cl₂/MeOH. **3b**: *R*_f = 0.17 in 96:4 CH₂Cl₂/MeOH.

3a. *M*_p = 183 °C. ¹H-NMR (acetone-*d*₆): δ 1.86–1.94 (m, 2H), 2.82 (t, *J* = 8.1 Hz, 2H), 3.63 (t, *J* = 6.3 Hz, 2H), 3.92 (s, 3H), 7.04 (d, *J* = 8.5 Hz, 1H), 7.75 (dd, *J*₁ = 8.5 Hz, *J*₂ = 2.4 Hz, 1H), 7.83 (d, *J* = 2.4 Hz, 1H), 7.92 (dd, *J*₁ = 6.8 Hz, *J*₂ = 2.0 Hz, 2H), 8.16 (dd, *J*₁ = 6.8 Hz, *J*₂ = 2.0 Hz, 2H). ¹³C-NMR (DMSO-*d*₆): δ 26.5, 32.6, 52.7, 60.8, 115.8, 122.5, 124.1, 124.7, 129.9, 130.6, 130.8, 145.6, 155.2, 160.2, 166.1. MS (high-resolution): *m/z* = 314.1222 (M)⁺ corresponds to C₁₇H₁₈N₂O₄ (314.1264).

3b. *M*_p = 162 °C. ¹H-NMR (acetone-*d*₆): δ 1.86–1.93 (m, 2H), 2.91 (s_{broad}, 1H), 3.22 (t, *J* = 8.8 Hz, 2H), 3.62 (t, *J* = 5.9 Hz, 2H), 3.91 (s, 3H), 6.81 (dd, *J*₁ = 8.9 Hz, *J*₂ = 2.6 Hz, 1H), 6.92 (d, *J* = 2.6 Hz), 7.75 (d, *J* = 8.9 Hz, 1H), 7.95 (d, *J* = 8.5 Hz, 2H), 8.15 (d, *J* = 8.5 Hz, 2H), 9.15 (s_{broad}, 1H). ¹³C-NMR (DMSO-*d*₆): δ 27.9, 35.3, 52.6, 60.7, 114.6, 116.7, 117.3, 122.6, 130.6, 130.7, 143.2, 146.6, 155.5, 162.1, 166.1. MS (high-resolution): *m/z* = 314.1279 (M)⁺ corresponds to C₁₇H₁₈N₂O₄ (314.1264).

[[4-Hydroxy-3-(3-hydroxypropyl)phenyl]carbamoyl]carbamoyl-*tert*-Butyl Ester **4a** and [[4-Hydroxy-2-(3-hydroxypropyl)phenyl]carbamoyl]carbamoyl-*tert*-Butyl Ester **4b**. The azo compounds **3a** and **3b** were reduced (H₂, 4 bar) over PtO₂ (10% w/w) in methanol, in the presence of di-*tert*-butyl dicarbonate (1.1 equiv) overnight. The carbamates thus obtained were purified by silica gel chromatography using 5:5 hexane/EtOAc and obtained in 99 and 97% yields, respectively, as colorless oils. **4a**: *R*_f = 0.22. **4b**: *R*_f = 0.16 in 6:4 hexane/EtOAc.

4a. $^1\text{H-NMR}$: δ 1.49 (s, 9H), 1.73–1.79 (m, 2H), 2.63 (t, J = 7.3 Hz, 2H), 3.52 (t, J = 6.6 Hz, 2H), 6.65 (d, J = 8.5 Hz, 1H), 6.70 (d, J = 1.9 Hz, 1H), 6.93 (dd, J_1 = 8.5 Hz, J_2 = 1.9 Hz, 1H), 7.06 (s_{broad} , 1H). $^{13}\text{C-NMR}$: δ 25.4, 28.3, 32.1, 60.8, 80.3, 116.1, 119.2, 122.2, 128.1, 130.6, 150.8, 153.8. MS (high-resolution): m/z = 267.1496 (M^+) corresponds to $\text{C}_{14}\text{H}_{21}\text{NO}_4$ (267.1468).

4b. $^1\text{H-NMR}$: δ 1.45 (s, 9H), 1.65–1.70 (m, 2H), 2.49 (t, J = 7.2 Hz, 2H), 3.45 (t, J = 6.0 Hz, 2H), 4.01 (s_{broad} , 1H), 6.53 (m, 2H), 6.97 (s_{broad} , 1H), 7.11 (d, J = 8.8 Hz, 1H), 8.37 (s_{broad} , 1H). $^{13}\text{C-NMR}$: δ 26.8, 28.2, 31.9, 60.9, 80.1, 113.5, 115.9, 127.0, 127.3, 137.0, 154.1, 155.4. MS (high-resolution): m/z = 267.1475 (M^+) corresponds to $\text{C}_{14}\text{H}_{21}\text{NO}_4$ (267.1468).

Carbonic Acid 4-[(tert-Butoxycarbonyl)amino]-2-(3-hydroxypropyl)phenyl Ester tert-Butyl Ester 5a and Carbonic Acid 4-[(tert-Butoxycarbonyl)amino]-3-(3-hydroxypropyl)phenyl Ester tert-Butyl Ester 5b. Phenols **4a** and **4b** were reacted with NaH (1 equiv) in dry DMF and protected with di-*tert*-butyl dicarbonate (1.1 equiv) to give carbonates **5a** and **5b**, which were chromatographed on silica using 7:3 hexane/EtOAc. The respective yields were 94 and 75%. **5a** was a white solid and **5b** a colorless oil **5a**: R_f = 0.42 in 6:4 hexane/EtOAc. **5b**: R_f = 0.55 in 5:5 hexane/EtOAc.

5a. M_p = 126 °C. $^1\text{H-NMR}$: δ 1.45 (s, 9H), 1.49 (s, 9H), 1.72–1.80 (m, 2H), 2.55 (t, J = 7.2 Hz, 2H), 2.71 (s_{broad} , 1H), 3.54 (t, J = 6.3 Hz, 2H), 6.93 (d, J = 8.7 Hz, 1H), 7.10 (d, J = 3.2 Hz, 1H), 7.12 (dd, J_1 = 8.7 Hz, J_2 = 3.2 Hz, 1H), 7.26 (s_{broad} , 1H). $^{13}\text{C-NMR}$: δ 26.0, 27.5, 28.1, 32.4, 61.4, 76.5, 77.0, 77.5, 80.1, 83.3, 117.1, 120.0, 122.1, 134.0, 136.3, 144.3, 152.1, 152.9. MS (low-resolution): m/z = 367 (M^+) and m/z = 267 ($\text{M} - \text{Boc} + \text{H}^+$). MS (high-resolution): m/z = 267.1428 ($\text{M} - \text{Boc} + \text{H}^+$) corresponds to $\text{C}_{14}\text{H}_{21}\text{NO}_4$ (276.1468).

5b. $^1\text{H-NMR}$: δ 1.49 (s, 9H), 1.54 (s, 9H), 1.74–1.85 (m, 2H), 2.67 (t, J = 7.1 Hz, 2H), 3.52 (t, J = 5.4 Hz, 2H), 6.96 (d, J = 2.6 Hz, 1H), 6.97 (dd, J_1 = 8.2 Hz, J_2 = 2.6 Hz, 1H), 7.41 (s_{broad} , 1H), 7.67 (d, J = 8.2 Hz, 1H). $^{13}\text{C-NMR}$: δ 26.4, 27.5, 28.2, 31.9, 60.2, 80.1, 83.2, 119.1, 121.8, 123.6, 133.5, 133.9, 147.1, 151.8, 153.8. MS (low-resolution): m/z = 367 (M^+) and m/z = 267 ($\text{M} - \text{Boc} + \text{H}^+$). MS (high-resolution): m/z = 267.1462 ($\text{M} - \text{Boc} + \text{H}^+$) corresponds to $\text{C}_{14}\text{H}_{21}\text{NO}_4$ (267.1468).

Carbonic Acid 4-(tert-Butoxycarbonyl)amino-2-(3-iodopropyl)phenyl Ester tert-Butyl Ester 6a and Carbonic Acid 4-(tert-Butoxycarbonyl)amino-3-(3-iodopropyl)phenyl Ester tert-Butyl Ester 6b. The remaining alcohols **5a** and **5b** were then mesylated in dry THF with methanesulfonyl chloride (1.5 equiv) in the presence of Et_3N (1.5 equiv). The nucleophilic displacement of the mesylate by the iodide ion (NaI, 10 equiv) in refluxing acetone for 2 h afforded the iodides which were purified by chromatography on silica using 9:1 hexane/EtOAc. The overall respective yields were 85 and 89% as white powders. **6a**: R_f = 0.33 in 9:1 hexane/EtOAc. **6b**: R_f = 0.22 in hexane/EtOAc.

6a. M_p = 83 °C. $^1\text{H-NMR}$: δ 1.50 (s, 9H), 1.55 (s, 9H), 2.04–2.13 (m, 2H), 2.63 (t, J = 7.1 Hz, 2H), 3.16 (t, J = 6.7 Hz, 2H), 6.72 (s, 1H), 6.98 (d, J = 8.7 Hz, 1H), 7.14 (dd, J_1 = 8.7 Hz, J_2 = 2.9 Hz, 1H), 7.31 (d, J = 2.9 Hz, 1H). $^{13}\text{C-NMR}$: δ 6.0, 27.6, 28.2, 31.0, 33.4, 80.4, 83.3, 117.4, 120.0, 122.5, 132.9, 136.2, 144.4, 152.1, 152.7. Elemental analysis in percent (theoretical): C, 47.93 (47.80); H, 5.94 (5.91); N, 2.72 (2.93); O, 16.61 (16.76). MS (low-resolution): m/z = 377 ($\text{M} - \text{Boc} + \text{H}^+$) and m/z = 277 ($\text{M} - 2\text{Boc} + 2\text{H}^+$). MS (high-resolution): m/z = 377.0443 ($\text{M} - \text{Boc} + \text{H}^+$) corresponds to $\text{C}_{14}\text{H}_{20}\text{INO}_3$ (377.0488).

6b. M_p = 91 °C. $^1\text{H-NMR}$: δ 1.51 (s, 9H), 1.55 (s, 9H), 2.03–2.15 (m, 2H), 2.69 (t, J = 7.1 Hz, 2H), 3.22 (t, J = 6.5 Hz, 2H), 6.31 (s_{broad} , 1H), 6.99 (d, J = 2.7 Hz, 1H), 7.02 (dd, J_1 = 8.5 Hz, J_2 = 2.7 Hz, 1H), 7.70 (d, J = 8.5 Hz, 1H). $^{13}\text{C-NMR}$: δ 6.3, 27.7, 28.3, 31.6, 32.9, 80.6, 83.4, 119.8, 122.0, 124.0, 132.4, 133.3, 147.4, 151.8, 153.4. Elemental analysis in percent (theoretical): C, 47.61 (47.80); H, 5.84 (5.91); N, 2.69 (2.93); O, 16.58 (16.76). MS (low-resolution): m/z = 377 ($\text{M} - \text{Boc} + \text{H}^+$) and m/z = 277 ($\text{M} - 2\text{Boc} + 2\text{H}^+$). MS (high-resolution): m/z = 377.0484 ($\text{M} - \text{Boc} + \text{H}^+$) corresponds to $\text{C}_{14}\text{H}_{20}\text{INO}_3$ (377.0488).

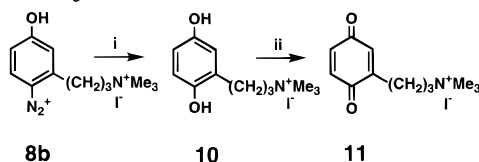
[3-[5-[(tert-Butoxycarbonyl)amino]-2-[(tert-butoxycarbonyl)oxy]phenyl]propyl]trimethylammonium **7a** and [3-[2-[(tert-Butoxycarbonyl)amino]-5-[(tert-butoxycarbonyl)oxy]phenyl]propyl]trimethylammonium **7b**. Finally, the trimethylammonium was obtained by substitution of the iodide in a saturated solution of trimethylamine in dry toluene. After 1 day at room temperature, the white precipitate was centrifuged, washed with dry toluene, and dried under reduced pressure to give the diazo precursors **7a** and **7b**, with 89 and 97% yields, respectively.

7a. M_p = 184 °C (dec). $^1\text{H-NMR}$: δ 1.40 (s, 9H), 1.45 (s, 9H), 2.02–2.15 (m, 2H), 2.57 (t, J = 7.4 Hz, 2H), 3.24 (s, 9H), 3.51 (t, J = 8.2 Hz, 2H), 6.96 (d, J = 8.7 Hz, 1H), 7.36 (dd, J_1 = 8.7 Hz, J_2 = 2.3 Hz, 1H), 7.45 (d, J = 2.3 Hz, 1H). $^{13}\text{C-NMR}$: δ 23.5, 26.6, 27.5, 28.2, 53.6, 66.4, 80.2, 84.0, 118.1, 120.2, 123.0, 133.0, 138.0, 144.7, 152.7, 153.9. Elemental analysis in percent (theoretical): C, 49.05 (49.25); H, 6.92 (6.95); N, 5.07 (5.22); O, 14.75 (14.91). MS (electrospray) (low-resolution): m/z = 409.02 (M^+).

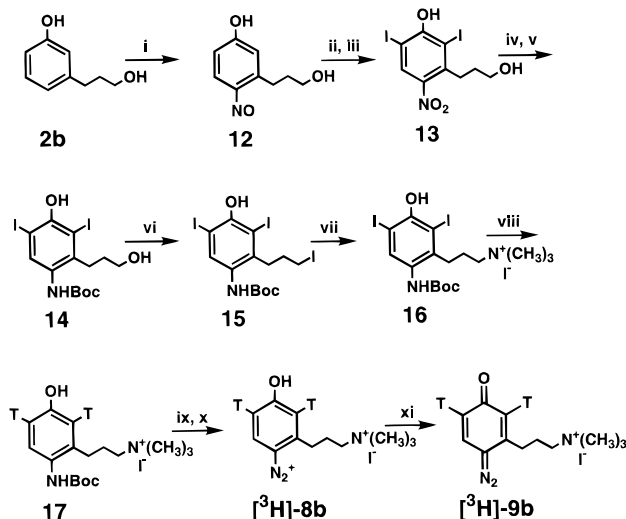
7b. M_p = 150 °C. $^1\text{H-NMR}$ (CD_3OD): δ 1.53 (s, 9H), 1.55 (s, 9H), 2.04–2.10 (m, 2H), 2.70 (t, J = 7.5 Hz, 2H), 3.14 (s, 9H), 3.43 (t, J = 8.3 Hz, 2H), 7.03 (dd, J_1 = 8.7 Hz, J_2 = 2.5 Hz, 1H), 7.19 (d, J = 2.5 Hz, 1H), 7.37 (d, J = 8.7 Hz, 1H). $^{13}\text{C-NMR}$ (CD_3OD): δ 23.1, 26.9, 27.3, 27.7, 52.8, 65.9, 80.1, 83.5, 119.9, 122.3, 133.6, 136.9, 148.9, 152.4, 155.6. MS (electrospray) (low-resolution): m/z = 409.08 (M^+).

3-(3-Diazo-6-oxocyclohexa-1,4-dienyl)propyl]trimethylammonium **9a** and 3-(3-Diazo-6-oxocyclohexa-1,4-dienyl)propyl]trimethylammonium **9b**. The diazotization step was performed as follows. The *tert*-butoxycarbonyl protecting groups of compounds **7a** and **7b** (20–50 μmol) were removed by stirring for 30 min in TFA at room temperature. After removal of TFA, the aminophenols were solubilized in acetic acid and 1.1 equiv of isoamylnitrite was added in small amounts in the dark at room temperature, over a period of 30 min. Diazonium salts **8a** and **8b** were purified by HPLC (C18 $\mu\text{Bondapak}$ semipreparative column; flow rate, 3 mL/min; solvent A, 0.03% TFA in H_2O ; solvent B, CH_3CN ; isocratic 0% B for 5 min, linear gradient from 0 to 50% B over 15 min, and then from 50 to 100% B over 8 min) and characterized by their retention time (t_R = 6 min) and their ^1H - and ^{13}C -NMR spectra. Diazo derivatives **9a** and **9b** were obtained from **8a** and **8b** by raising the pH to physiological conditions (pH 7.2; PBS) and were characterized by their UV spectra. For **9a**, λ_{max} = 355 nm and ϵ_{max} = 36 500 $\text{M}^{-1} \text{cm}^{-1}$. For **9b**, λ_{max} = 349 nm and ϵ_{max} = 26 500 $\text{M}^{-1} \text{cm}^{-1}$. In the absence of light, derivatives **9a** and **9b** were stable in PBS for days ($t_{1/2}$ = 333 h for **9b** at 15 °C). They were also characterized by their HPLC retention times with the same gradient as that for **8a** and **8b** (t_R = 14 min).

9a. $^1\text{H-NMR}$ (D_2O , reference = *tert*-BuOH): δ 1.98–2.12 (m, 2H), 2.63 (t, J = 7.4 Hz, 2H), 3.08 (s, 9H), 3.33 (t, J = 8.4 Hz, 2H), 6.75 (d, J = 9.2 Hz, 1H), 7.95 (d, J = 2.7 Hz, 1H), 8.0 (dd, J_1 = 9.2 Hz, J_2 = 2.7 Hz, 1H). ^{13}C -

Scheme 3. Syntheses of 8b Derivatives 10 and 11^a

^a (i) Photolysis in H₂O; yield, 79%. (ii) H₂O, room temperature, 24 h, yield, 50%.

Scheme 4. Synthesis of Radiolabeled Probe [³H]-9b^a

^a (i) NaNO₂/7.5 N HCl; yield, 50%. (ii) HNO₃/MeOH. (iii) ICl/MeOH/H₂O at pH 12, two-step quantitative yield. (iv) Na₂S₂O₄/10 N NaOH. (v) BOC₂O/HCl/MeOH/H₂O; yield in two steps, 46%. (vi) Triphenylphosphine/imidazole/I₂; yield, 60%. (vii) Me₃N/toluene, quantitative yield. (viii) T₂/PdO/Et₃N. (ix) TFA. (x) Isoamyl nitrite/CH₃COOH; yield in three steps, 69%. (xi) PBS, quantitative yield.

NMR (D₂O, reference = *tert*-BuOH): δ 23.1, 27.9, 54.3, 71.2, 88.6, 123.3, 133.8, 135.2, 135.4, 178.7.

9b. ¹H-NMR (D₂O, reference = *tert*-BuOH): δ 2.16–2.26 (m, 2H), 2.86 (t, J = 7.6 Hz, 2H), 3.13 (s, 9H), 3.43 (t, J = 8.3 Hz, 2H), 6.71–6.78 (m, 2H), 8.07 (dd, J_1 = 9.9 Hz, J_2 = 1.1 Hz, 1H). ¹³C-NMR (D₂O, reference = *tert*-BuOH): δ 24.4, 32.6, 56.0, 67.8, 89.7, 125.1, 129.6, 137.9, 152.7, 188.2.

Photolysis of 8b. Synthesis of 10 and 11 (Scheme 3). For the synthesis of **10**, **8b** (53.5 mg, 150 μ mol) was photolyzed in a pyrex reactor (3 mM in H₂O, pH 3, 125 W Phillips lamp, 4 min). The photolyzed derivative was collected, concentrated, and purified by HPLC (C18 300 \times 7.5 Bondasorb column). The column was eluted at 3 mL/min with isocratic 100% A (0.1% TFA in H₂O) for 5 min, a linear gradient from 0 to 100% B (CH₃CN) for 25 min, and isocratic 100% B for 5 min. Hydroquinone **10** was characterized by a t_R of 13 min, a λ_{max} of 290 nm, and an ϵ_{max} of 3100 M⁻¹ cm⁻¹ and stored as a solid under nitrogen below -20 °C (38.5 mg, 79% yield).

The oxidation of **10** to **11** occurs spontaneously by stirring an aqueous solution of hydroquinone **10** (38.5 mg, 119 μ mol) in 1 mL of H₂O at room temperature for a few hours. The mixture was purified by HPLC (same conditions as for **10**), and **11** was identified by a t_R of 16 min, a λ_{max} of 250 nm, and an ϵ_{max} of 8500 M⁻¹ cm⁻¹ (18.8 mg, 50% yield). ¹H-NMR (acetone-*d*₆): δ 2.08–2.28 (m, 2H), 2.40–2.60 (m, 2H), 3.55–3.75 (m, 2H), 6.70 (d, J = 10.3 Hz, 2H), 6.78 (s_{broad}, 1H).

Synthesis of 16, the Precursor of [³H]-8b (Scheme 4). 3-(3-Hydroxypropyl)-4-nitrosophenol **12**. Diol **2b** (5 g, 33 mmol) was dissolved in 150 mL of HCl (7.5 N) at 5 °C, and 1.1 equiv of NaNO₂ (2.75 g, 36.3 mmol) was added

during 20 min and stirred for 30 min. After extraction with EtOAc, the mixture was separated by chromatography on silica using 8:2 hexane/EtOAc to yield the nitrosophenol **12** (3 g, 50% yield, R_f = 0.30 in 95:5 CH₂Cl₂/MeOH). M_p = 90–92 °C. ¹H-NMR: δ 1.85–1.93 (m, 2H), 2.72 (t, J = 8.7 Hz, 2H), 3.69 (t, J = 7.4 Hz, 2H), 6.37 (d, J = 1.5 Hz, 1H), 6.46 (dd, J_1 = 8.5 Hz, J_2 = 1.5 Hz, 1H), 7.80 (d, J_1 = 8.5 Hz, 1H).

3-(3-Hydroxypropyl)-2,6-diiodo-4-nitrophenol **13**. Concentrated HNO₃ (54 mL) was added with care to nitrosophenol **12** (3 g, 16.7 mmol) in 70 mL of MeOH at room temperature until the solution turned red (30 min). The reaction was followed by TLC (95:5 CH₂Cl₂/MeOH). After reaction, the mixture was diluted with 100 mL of H₂O and solid Na₂CO₃ was added to reach pH 12. The reaction mixture was then concentrated under vacuum to a final volume of 100 mL (**caution**: do not evaporate to dryness since the residues might be explosive). The obtained nitrophenol solution was directly iodinated by addition of ICl (2 mL, 36.7 mmol, 2.2 equiv) in 20 mL of MeOH. After 5 min, the unreacted excess of ICl was destroyed by addition of sodium thiosulfate and 10% citric acid. The solid diiodonitrophenol **13** was obtained after extraction with EtOAc and concentrated under vacuum (5.6 g, quantitative yield, R_f = 0.30 in 9:1 CH₂Cl₂/MeOH). M_p = 90 °C. ¹H-NMR: δ 1.87–1.90 (m, 2H), 2.73 (t, J = 7.1 Hz, 2H), 3.65–3.69 (m, 2H), 7.21 (s, 1H).

[4-Hydroxy-2-(3-hydroxypropyl)-3,5-diiodophenyl]carbamate *tert*-Butyl Ester **14**. Diiodonitrophenol **13** (5.6 g, 16.7 mmol) was reduced in the presence of Na₂S₂O₄ (23 g, 132 mmol) in 100 mL of 10 N NaOH, 200 mL of MeOH, and 400 mL of H₂O at room temperature. After 15 min, the pH was lowered to 7.4 by addition of concentrated HCl. Di-*tert*-butyl dicarbonate (7.2 g, 31.7 mmol, 1.9 equiv) was added in 200 mL of MeOH/THF (1:1) and refluxed for 12 h. The mixture was chromatographed on silica using 8:2 hexane/EtOAc to yield the NHBoc-protected diiodoaminophenol **14** (4 g, 46% yield, R_f = 0.33 in 7:3 hexane/EtOAc). M_p = 133 °C. ¹H-NMR: δ 1.49 (s, 9H), 1.85–1.89 (m, 2H), 2.94 (t, J = 6.9 Hz, 2H), 3.57 (t, J = 5.6 Hz, 2H), 5.77 (s_{broad}, 1H), 7.83 (s, 1H), 8.04 (s, 1H).

[4-Hydroxy-2-(3-iodopropyl)-3,5-diiodophenyl]carbamate *tert*-Butyl Ester **15**. Triphenylphosphine (758 mg, 2.89 mmol, 3 equiv) and imidazole (197 mg, 2.89 mmol, 3 equiv) were dissolved at 0 °C in 13 mL of 8:2 Et₂O/MeCN under argon. Iodine (733 mg, 2.89 mmol, 3 equiv) was added rapidly. A solution of compound **14** (500 mg, 0.96 mmol, 1 equiv) in 3 mL of MeCN was then added very slowly at 0 °C. The reaction was followed by TLC with the eluent 8:2 hexane/EtOAc. After addition, the mixture was left at room temperature for 2 h and chromatographed on silica gel (7:3 hexane/EtOAc). The diiodo-protected aminophenol **15** was obtained (360 mg, 60% yield, R_f = 0.34 in 8:2 hexane/EtOAc). M_p = 144 °C. ¹H-NMR: δ 1.52 (s, 9H), 1.98–2.03 (m, 2H), 2.91 (t, J = 5.5 Hz, 2H), 3.30 (t, J = 6.5 Hz, 2H), 5.84 (s_{broad}, 1H), 6.29 (s_{broad}, 1H), 7.94 (s, 1H). ¹³C-NMR: δ 6.4, 28.5, 31.9, 38.0, 81.1, 89.8, 129.6, 135.2, 142.5, 151.6, 153.9. Elemental analysis in percent (theoretical): C, 26.72 (26.73); H, 2.97 (2.88); N, 2.21 (2.22). MS (low-resolution): m/z = 629 (M)⁺, m/z = 573 (M - *tert*-Bu + H)⁺, and m/z = 529 (M - Boc + H)⁺. MS (high-resolution): m/z = 572.7792 (M - *tert*-Bu + H)⁺ corresponds to C₁₀H₁₀I₃NO₃ (572.7798).

[4-Hydroxy-2-[3-(trimethylammonio)propyl]-3,5-diiodophenyl]carbamate *tert*-Butyl Ester **16**. Compound **15** (8.6 mg) dissolved in 1 mL of toluene was added to a saturated solution of gaseous trimethylamine in anhydrous toluene. After 24 h at room temperature, the

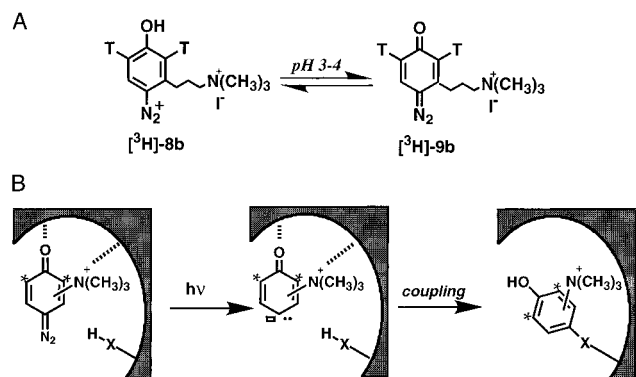


Figure 1. (a) Diazocyclohexadienone **[3H]-9b** was obtained with a quantitative yield from **[3H]-8b** by raising the pH to 7.2 (PBS). (b) Hypothetical mechanism for rapid coupling of photogenerated carbene from diazocyclohexadienone **[3H]-9b** with AChR. The carbonyl group and the charged quaternary ammonium mimic the pharmacophore, assuring cholinergic recognition. X-H represents any amino acid belonging to the ACh binding site.

mixture was centrifuged at 4000 rpm and the precipitate was washed with anhydrous toluene and dried under vacuum to yield 8 mg of a white solid identified as **16**. It was purified on a C18 reversed-phase column (Hyperbond, 300×3.9) equilibrated with 100% solvent A (0.01% TFA in H_2O) and eluted at 1.5 mL/min with isocratic 100% A for 5 min, a linear gradient from 0 to 100% B (CH_3CN) for 55 min, and isocratic 100% B for 5 min (8 mg, quantitative yield, $t_R = 30$ min, $R_f = 0.50$ in 6:2:1 EtOAc/ CH_3COCH_3/H_2O /acetic acid). $M_p = 136$ °C. 1H -NMR (acetone- d_6): δ 1.47 (s, 9H), 2.15–2.18 (m, 2H), 2.94 (t, $J = 7.9$ Hz, 2H), 3.42 (s, 9H), 3.73 (t, $J = 8.3$ Hz, 2H), 7.71 (s, 1H), 7.71 (s, 1H). ^{13}C -NMR (acetone- d_6): δ 22.4, 27.9, 33.7, 52.9, 65.9, 79.2, 93.1, 137.8, 140.7, 154.9. FABMS⁺ (thioglycerol): m/z 561 ($M + H^+$, 90%), 505 [$M^+ - C(CH_3)_3$, 100%], 435 ($M + H^+ - I$, 30%), 379 [$M + H^+ - I - C(CH_3)_3$, 40%].

Synthesis of [3H]-9b (Scheme 4). PdO (20 mg, 163.4 μ mol) was added to a solution of **16** (4 mg, 5.8 μ mol) in 1 mL of CH_3OH and 4 mL of Et_3N . The vial was connected to the tritiation apparatus. The solution was frozen in liquid N_2 . Carrier-free tritium gas was introduced and compressed to 2.4 bar. After thawing, the reaction mixture was kept at 20 °C and stirred for 30 min. Labile tritium atoms were exchanged by successive flash evaporations with 150 mL of MeOH. Crude product **17** was dissolved in 4 mL of MeOH (total radioactivity of 110 mCi) and analyzed by reverse-phase HPLC as for **16** ($t_R = 23$ min, $R_f = 0.20$ in 6:2:1:1 EtOAc/ CH_3COCH_3/H_2O /acetic acid). 1H -NMR (CD_3OD): δ 1.50 (s, 9H), 2.03–2.13 (m, 2H), 2.65 (t, $J = 7.4$ Hz, 2H), 3.1 (s, 9H), 3.29–3.34 (m, 2H), 7.03 (d, $J = 9$ Hz, 1H). 3H -NMR (CD_3OD): δ 6.63 (dd, $J_1 = 2.7$ Hz, $J_2 = 8.4$ Hz, 3H), 6.69 (d, $J = 2.7$ Hz, 3H).

The diazotization step was performed as follows. Six and six-tenths micromoles of radioactive precursors (1 μ mol of **17**, 24 Ci/mmol, mixed with 5.6 μ mol of nonradioactive **7b**) was deprotected from the *tert*-butoxycarbonyl moiety by stirring with 300 μ L of TFA for 40 min at room temperature, under N_2 . After removal of TFA and one-step freeze-drying (200 μ L of H_2O added to the residue), the obtained aminophenol was dissolved in 300 μ L of acetic acid and diazotized by adding in one step 7.4 μ mol of isoamyl nitrite (1.2 equiv) under N_2 at room temperature. After 30 min at room temperature, acetic acid was evaporated under reduced pressure, freeze-dried twice (300 μ L of H_2O added to the residue), and purified by reverse-phase HPLC (Hyperbond 300×3.9 C18

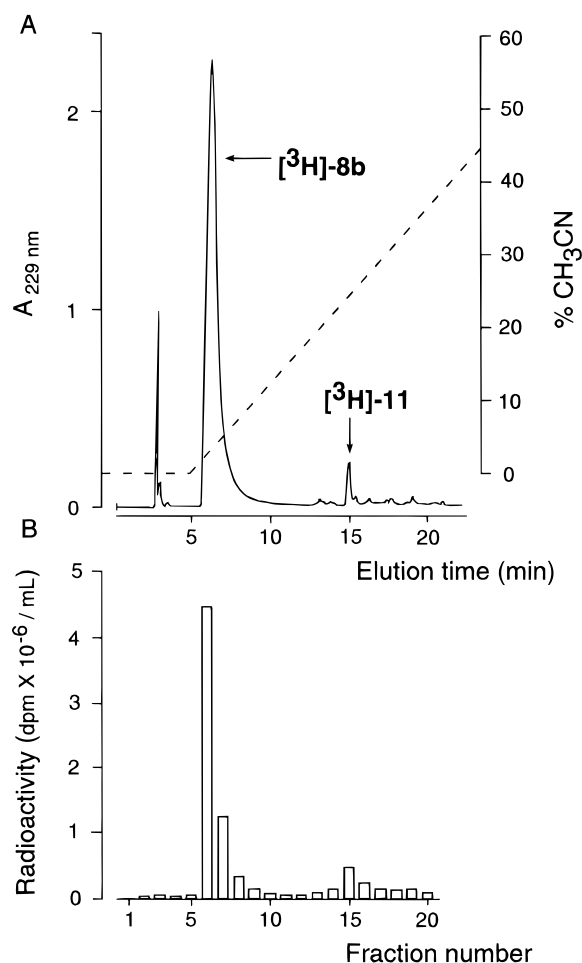


Figure 2. Reverse-phase HPLC analysis of **[3H]-8b** with UV (229 nm) (A) and radioactivity detection (B). Forty microliters of the diazotization crude reaction mixture was injected on the C18 column and eluted at 1.5 mL/min with the following gradient (isocratic 100% H_2O , 0.1% TFA for 5 min, linear gradient from 0 to 100% CH_3CN for 45 min, isocratic 100% CH_3CN for 5 min). Fractions (1.5 mL) were collected and counted (2 μ L aliquots) for radioactivity. Ten injections were needed to purify the total amount of crude product. Fractions 6–9 were pooled together to give 4.5 μ mol of pure diazonium **[3H]-8b** (3.7 Ci/mmol), and fractions 15 were pooled to obtain 0.32 μ mol of quinone **[3H]-11** (3.7 Ci/mmol).

reversed-phase column equilibrated with 100% solvent A and 0.1% TFA). The column was eluted at 1.5 mL/min [isocratic 100% A for 5 min, a linear gradient from 0 to 100% B (CH_3CN) for 45 min, and isocratic 100% B for 5 min], and **[3H]-8b** was characterized by a t_R of 6 min. The fractions containing the diazonium salt (UV characterization, $\lambda_{max} = 313$ nm) were collected, and radioactivity was counted (Figure 2). Compound **[3H]-8b** (4.5 μ mol, 69% yield, 3.7 Ci/mmol) was obtained and stored at -80 °C in H_2O (1 mM, pH 2) for several months without degradation. One byproduct formed during the diazotization step was isolated and identified as the tritiated analog of quinone **11** (0.32 μ mol, 4.8% yield, 4.4 Ci/mmol, $t_R = 15$ min, $\lambda_{max} = 250$ nm). The diazo derivative **[3H]-9b** was obtained from **[3H]-8b** by raising the pH to 7.2 in PBS for binding and photolabeling experiments (Figure 1A).

Binding Experiments. AChR-rich membrane fragments from *T. marmorata* were prepared (Saitoh and Changeux, 1980), and the concentration of ACh binding sites was measured at equilibrium by [^{125}I]- α -BuTX binding (Schmidt and Raftery, 1973). Ligand dissociation constants at the agonist binding site (Table 1) were determined (Weber and Changeux, 1974a,b) in the dark

Table 1. Protection (K_p) and Inhibition (K_i) Constants of Compounds **1, **9a**, **9b**, and **11** for the ACh and Noncompetitive Blocker (NCB) Binding Sites^a**

compound	agonist binding site K_p (μ M) ^b		NCB binding site K_i (μ M) ^c
	native form	with proadifen	with Carb
1	44 \pm 6	6.0 \pm 0.6	500 \pm 70
9a	44 \pm 2.5	6.0 \pm 1.0	190 \pm 40
9b	70 \pm 10	6.0 \pm 0.9	850 \pm 150
11	70 \pm 8	6.5 \pm 0.5	nd

^a All photosensitive ligands were fairly stable under the experimental binding conditions with a half-time of longer than 40 h. ^b For the agonist binding site, AChR-rich *Torpedo* membranes (4 nM α -BuTX binding site) were incubated with various concentrations of each compound (0.5 μ M to 1 mM) and *N. nigricollis* [³H]- α -neurotoxin (2 nM). The K_p values of the ligands reflect the ligand protection against the association of α -neurotoxin to its specific binding site. Native (75% R) and mostly desensitized (90% D; preincubation with 15 μ M proadifen) AChRs were used. ^c For the NCB binding site, K_i values were determined at equilibrium (45 min preincubation), using [³H]-PCP (1 nM) and ligand (10 μ M at 4 mM) on desensitized AChRs (64 nM α -BuTX binding sites, 30 min preincubation with 0.1 mM Carb at 25 °C). Values shown are mean \pm SEM from two to four experiments.

from the decrease in the initial binding rate of *N. nigricollis* [³H]- α -neurotoxin to AChRs (2–4 nM [¹²⁵I]- α -BuTX binding sites), in both their native and desensitized forms (\approx 90% D; pretreatment with 15 μ M proadifen). Following simultaneous addition of [³H]- α -neurotoxin (1 nM) and ligand (0.5 μ M to 1 mM), 0.3 mL aliquots were rapidly filtered (Millipore HAWP) at different times and counted. Dissociation constants of ligands for the NCB binding site (Table 1) were calculated (Eldefrawi et al., 1982) from competition experiments between [³H]PCP (1 nM) and ligand (10 μ M to 4 mM) at equilibrium using AChR-rich membranes (68 nM [¹²⁵I]- α -BuTX binding sites). The suspensions were filtered (Whatman GF/B) and counted.

Photochemical Properties of **9a and **9b**.** The photosensitivity of **9a** and **9b** was examined by sequential irradiation in PBS at 290 nm, in the presence of AChR (0.5 μ M [¹²⁵I]- α -BuTX binding sites) and an incident light energy of 50 μ V. The stability of the probe in the dark was determined by hourly sequential UV measurement over 10 h in PBS (20 °C) and calculated using $A = A_0 e^{-kt}$ (where A_0 is the initial absorbance at λ_{\max} of the probe and A the absorbance measured at time t). The half-life of ligands **9a** and **9b** was obtained from $t_{1/2} = \ln 2/k$.

Photochemical Labeling of AChR with **9b and [³H]-**9b**.** A monochromatic light beam from a 1000 W Xe-Hg lamp (Hanovia) was focused on a quartz cell (1 cm path length) to form a spot that was 10 mm high and 2 mm wide. Irradiation experiments were carried out at 290 nm for energy transfer (ET) conditions (Goeldner and Hirth, 1980) under magnetic stirring. Aliquots (600 μ L) of AChR-rich *Torpedo* membranes (280 pmol of [¹²⁵I]- α -BuTX binding sites) in PBS degassed with N₂ were mixed with probes [³H]-**9b** (0.1–20 μ M) after incubation with 15 μ M proadifen (50 min at room temperature) and irradiated at 290 nm (incident intensity of 50 μ V for 45 min at 10 °C). Protection experiments were carried out with prior addition of *d*-tubocurarine (10 μ M, 30 min at room temperature). Dithiothreitol (10 mM final concentration) was added after AChR photocoupling for 30 min at 30 °C to prevent protein aggregation. Before electrophoresis analysis, the amount of protein was determined using the microbradford assay (Bradford, 1976) which revealed that more than 50% (62% in the experiments described here) of the starting material was lost, probably due to nonspecific adsorption of alkylated proteins on

tubes. An aliquot of the remaining photolabeled AChR was solubilized and analyzed on 10% SDS-PAGE (Laemmli, 1970). The radioactivity incorporated into each polypeptide chain was quantified after gel slicing, digestion, and counting (Langenbuch-Cachat et al., 1988).

Electrophysiology. Conventional patch-clamp recordings were made and analyzed as described recently (Kotzyba-Hibert et al., 1996) on human TE 671 cells which express the embryonic form of peripheral (muscle-like) nicotinic AChR (Schoepfer et al., 1988; Sine, 1988; Luther et al., 1989). The bath solution contained (in millimolar) 140 NaCl, 5 KCl, 2 CaCl₂, 2 MgCl₂, 10 HEPES, and 11 glucose at pH 7.3 with NaOH. Cell-attached recordings were made with the external solution (in some cases, with 1 mM CsCl) in the pipette and various concentrations of drugs. The pipette solution for whole-cell recording contained (in millimolar) 140 CsCl, 2 MgCl₂, 1 CaCl₂, 11 EGTA, and 20 HEPES at pH 7.3 with CsOH. Drugs were locally applied with puffer pipettes. Photosensitive compounds were protected from ambient light. Experiments were carried out at room temperature.

RESULTS AND DISCUSSION

Synthesis and Properties of Photosensitive Probes

****9a** and **9b**.** The synthesis of probes **9a** and **9b** is summarized in Scheme 2 and used usual transformations characterized by satisfactory overall reaction yields (35 and 37%, respectively). The diazocyclohexadienone moieties were generated by diazotization of the *p*-aminophenol precursors and subsequent neutralization of the obtained diazonium salts.

[³H]-**9b** required the synthesis of iodinated precursor **16** (Scheme 4) using a synthetic pathway different from the general procedure (Scheme 2). The formation of the triiodide **15** was best achieved by the phosphine method (Lange and Gottardo, 1990). The diazotization of **17** gave [³H]-**8b**, and the diazo [³H]-**9b** was obtained by raising the pH to physiological conditions (Figure 1A).

All of the tested 4-diazocyclohexa-2,5-dienone derivatives (Scheme 1) are fairly stable in the dark under physiological conditions ($t_{1/2} > 1$ day, pH 7.2) (Kessler et al., 1990) and show spectral characteristics that are appropriate for energy transfer photoactivation (Goeldner and Hirth, 1980).

Binding Properties of 4-Diazocyclohexa-2,5-dienones. Ligands **9a** and **9b** have micromolar affinities for the ACh binding site in the D state (after proadifen preincubation) with a 10-fold decrease in affinity for the native form, as expected for cholinergic ligands (Table 1). These affinities are similar to those reported previously for **1** (K_p was 6 μ M for both **1** and **9b**; see Table 1). The probes are highly selective for the ACh binding site compared to the NCB site (Table 1), showing a difference in their respective affinities of \approx 2 orders of magnitude (D state). It was not possible to test the affinity of the hydroquinone **10** as oxidation to **11** occurs rapidly, especially in diluted solutions, even at low temperatures. However, **11** was stable and shared an affinity for the ACh binding site, similar to that of **9a** and **9b** (the K_p value for **11** was 6.5 μ M). From these data, it appears that the quaternary ammonium and the quinonoid-like ring constitute the pharmacophore necessary for cholinergic binding.

Photolabeling of the ACh Binding Site with [³H]-9b**.** The diazo photoprobes are stable in the absence of light and generate upon irradiation extremely reactive carbenic species that should be able to react efficiently with the nonactivated C–H bond of the ACh binding site, as schematically represented in Figure 1. We have previously described this interaction of carbenes

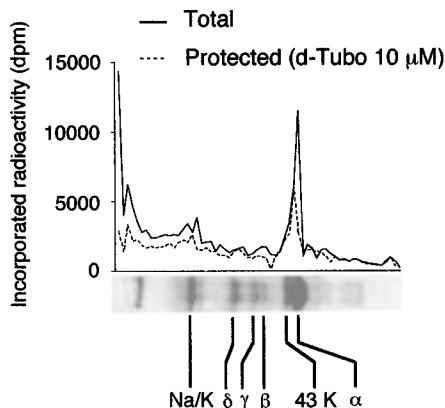


Figure 3. Photoincorporation of [^3H]-**9b** into the different subunits (α , β , γ , and δ) of the desensitized *Torpedo* AChR. Receptor-rich membranes (220 pmol) were irradiated at 290 nm for 45 min, in the presence of 1 μM [^3H]-**9b** (3.7 Ci/mmol) and 15 μM proadifen (to obtain the desensitized AChR state). Sixteen picomoles of solubilized photoalkylated AChR was loaded per well and analyzed on 10% SDS-PAGE. Distribution of the radioactivity in the four subunits was measured after gel slicing, digestion, and counting. Photoincorporation was determined without and with a protecting ligand (10 μM *d*-tubocurarine).

generated from 4-diazocyclohexa-2,5-dienones (Alcaraz et al., 1996).

In the dark, **9b** is very stable, while upon irradiation, it is very photosensitive, leading to efficient photodecomposition as described previously for similar compounds (Alcaraz et al., 1996). Photolysis of [^3H]-**9b** with *Torpedo* AChR under ET conditions allowed us to quantify the radioactivity incorporated specifically into the different subunits. As for DDF (Langenbuch-Cachat et al., 1988), the α -subunits were predominantly labeled (Figure 3), with minor contributions of the other subunits (less than 8% for β , γ , or δ). The yield of photoincorporation into the α -subunits using 1 μM [^3H]-**9b** was 6.6% of the total amount of ACh binding sites [6.6%; i.e. 1 pmol alkylated (8700 dpm) per 16 pmol of ACh binding sites loaded on SDS-PAGE per lane]. This 6.6% value is in fact largely underestimated if one takes into account the actual binding site occupancy (14%) in the used experimental conditions (Bayley, 1983). A series of controls were performed to ensure that the observed radioactivity pattern was due to the photolabeling of [^3H]-**9b**; no affinity labeling (identical experimental conditions but in the absence of irradiation) was detected on gels with [^3H]-**9b**, and photoaffinity labeling was negligible with the quinone [^3H]-**11**, showing that covalent labeling is due to diazo coupling and not radical photoreaction from the quinone. Partial protection was observed with 10 μM *d*-tubocurarine (50% with 1 μM [^3H]-**9b**, $n = 2$, Figure 3). A maximum of 34.5% of the ACh binding sites involved in the photocoupling were labeled specifically with 20 μM [^3H]-**9b** (Figure 4). Higher probe concentrations lead to increased nonspecific labeling. The limited photoincorporation might be due to a protector effect of quinone **11** which is formed during irradiation experiments (by oxidation of **10**) and which shows a good affinity for the ACh binding site (K_p values of 6.5 and 6 μM for **11** and **9b**, respectively).

Electrophysiology. ACh-activated single-channel and whole-cell currents in TE 671 cells have been recently described by Kotzyba-Hibert et al. (1996), and our data are in agreement with previous reports (Sine, 1988; Luther et al., 1989). Briefly, single-channel currents observed with 50–500 nM ACh had a mean elementary conductance γ of 31.3 ± 1.9 pS ($n = 8$) and a

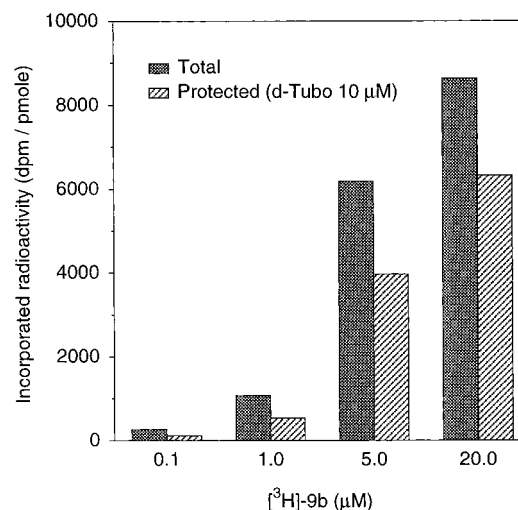


Figure 4. Concentration dependence of [^3H]-**9b** photoincorporation (0.1–20 μM) into the α -subunits without and with 10 μM *d*-tubocurarine expressed in disintegrations per minute per mole of AChR loaded on the gel.

mean open time τ of 4.8 ± 0.4 ms ($n = 4$). The interpolated zero-current potential was close to 0 mV, as expected for a nonselective cationic channel (Grassi et al., 1993). For desensitizing ACh concentrations (> 1 μM), characteristic clusters of burst-like single-channel openings separated by long-duration closures (Sakmann et al., 1980) were observed, and whole-cell inward currents showed rapid decay (Feltz and Trautmann, 1980) during maintained agonist exposure (not shown).

9b Is a Functional Cholinergic Agonist. Single-channel currents having characteristics essentially similar to those found for ACh were recorded from cell-attached patches on TE 671 cells when **9b** was included in the pipette at both 6.5 μM ($n = 7$, Figure 5A) and 65 μM ($n = 5$, Figure 5B). A full dose–response relationship was not established, but clearly, the threshold **9b** concentration for noticeable channel activity was higher (≥ 1 μM) compared to that for ACh. No channel activity was observed in the absence of agonist. The current–voltage relationship for **9b** was linear (Figure 5C), with an average slope conductance of 30.5 ± 1.7 pS ($n = 5$), again with an interpolated reversal potential near 0 mV. In the whole-cell recording configuration, macroscopic inward currents were obtained for 15 s applications of 65 μM **9b** ($n = 5$, Figure 6A). Such inward currents were maintained throughout the application of 65 μM **9b**, showing little or no signs of desensitization, unlike the rapid decay observed during exposure to high ACh concentrations (Kotzyba-Hibert et al., 1996). A complete block of macroscopic currents to 65 μM **9b** was produced within 1–2 min following bath application of 50 μM *d*-tubocurarine, with recovery after a 5 min washout ($n = 5$, Figure 6B).

The α -substituted compound **9a** was also tested at 50 μM in TE 671 cells. No single-channel activity was observed in cell-attached patches ($n = 10$, not shown). Similarly, macroscopic, inward whole-cell currents were not elicited by 15 s applications of 50 μM **9a** ($n = 10$, not shown). Thus, the position of the ammonium–methylene side chain relative to the carbonyl moiety, going from the α -position in **9a** to the β -position in **9b**, appears to be determinant for agonist activity, with only the β -substituted ligand **9b** being a functional agonist. This was also observed with the first cyclohexadienone series (Kotzyba-Hibert et al., 1996).

Several characteristics of **9b**-activated channels (linear current–voltage, reversal potential, and single-channel

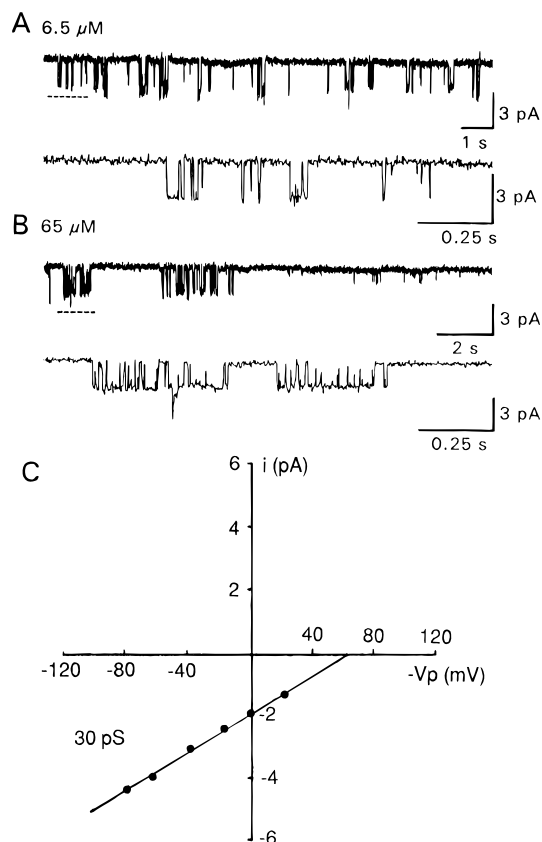


Figure 5. Single-channel currents activated by **9b** at 6.5 μM (A) and 65 μM (B) recorded from cell-attached patches of TE 671 cells. The pipette potential was 70 mV. The dashed lines indicate current segments shown below on a faster time scale. Data were filtered at 1 kHz. Inward currents are downward. (C) Current–voltage relationship for **9b**-activated single-channel currents from a cell-attached patch. The voltage axis is plotted as $-V_{\text{pipette}}$.

conductance) are quite close to those found for ACh. A notable difference was the apparent lack of desensitization for whole-cell currents during maintained (15 s) applications of 65 μM **9b**. Nevertheless, the block of **9b**-induced whole-cell current by *d*-tubocurarine together with the single-channel data is highly consistent with **9b** activating AChRs on TE 671 cells.

CONCLUSION

From both the binding and photolabeling data obtained on *Torpedo* AChR and the electrophysiological studies on TE 671 cells, we conclude that [**³H]-**9b** is a good candidate for exploring the active state of AChR at the molecular level. [**³H]-**9b** acts as a functional agonist of AChR that irreversibly labels the ACh binding site with efficiency. In photolabeling experiments, over 60% of the radioactivity was located on the α -subunit, as previously found for [**³H]-DDF (Langenbuch-Cachat et al., 1988).******

The uncharged photosensitive part of **9b** seems not to be critical for cholinergic recognition, unlike [**³H]-DDF (Langenbuch-Cachat et al., 1988; Dennis et al., 1988; Galzi et al., 1990). Thus, covalent labeling with **9b** might occur in different molecular regions of the ACh binding site, thereby providing new insight into the structural basis underlying the functional, activated state of AChR. Along these lines, on the basis of mutations of the δ Asp-180 and γ Asp-174 residues (which are thought to be at an appropriate distance from α Cys-192/193 to interact electrostatically with the positively charged ammonium of cholinergic ligands during agonist binding), it was recently concluded that these residues are involved in**

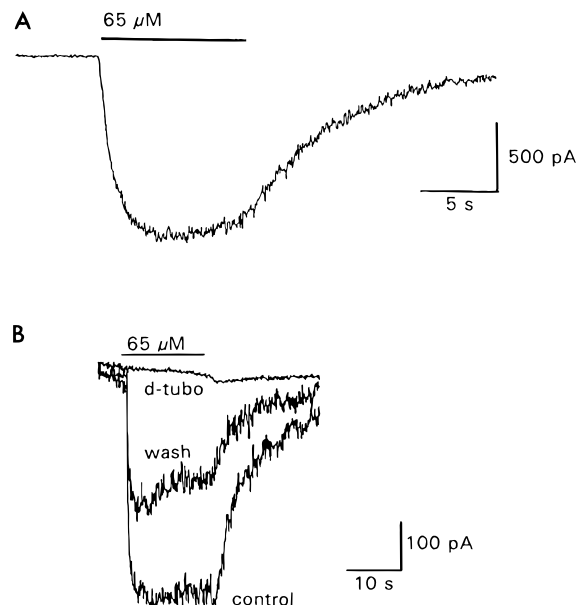


Figure 6. Macroscopic **9b**-activated inward currents from TE 671 cells obtained in the whole-cell recording configuration. (A) The current evoked by 65 μM **9b** was maintained during a 15 s application, showing negligible signs of desensitization. **9b** was locally microperfused using a pressurized puffer pipette. The holding potential was -70 mV. (B) Block of **9b**-activated current by bath application of 50 μM *d*-tubocurarine and partial recovery after a 5 min washout. The holding potential was -70 mV.

the conformational changes whereby receptor subunits move closer to bound agonist in the activated (A) state (Martin et al., 1996). Structural transitions associated with ACh binding have also been described using analysis of electron images of crystallized *Torpedo* AChR (Unwin, 1995). Upon binding, a cavity (thought to represent the ACh binding site) in the $\alpha\delta$ -subunit (α -subunit in contact with δ) disappears in the activated structure, while the β -subunit moves away from the $\alpha\delta$ -subunit toward the $\alpha\gamma$ -subunit. This coordination of structural responses of the two α -subunits is proposed to be central to the cooperative mechanism responsible for channel opening (Unwin, 1995). Also, new information obtained with **9b** should allow us to better understand how the transition between the active (A) and desensitized (D) states occurs at the molecular level. From labeling studies with DDF, it was shown that upon desensitization the contribution to the agonist binding site was increased for the δ -subunit and decreased for the γ -subunit (Galzi et al., 1991).

Functionally, **9b** activates currents through AChR as does ACh, with the exception that essentially no desensitization of whole-cell currents was observed at 65 μM **9b**, similar to our recently reported results for **1** (Kotzyba-Hibert et al., 1996). This should be useful for photolabeling the open channel A state of AChR with adapted flash-photolysis techniques. Because **9b** seems to modify the allosteric pathway for AChR reactivation, and given that desensitization is kinetically limiting (minute time range), photocoupling of **9b** to the A state of AChR may be greatly increased, and thus, very rapid photolabeling may be unnecessary.

We intend to use [**³H]-**9b** in photolabeling experiments to characterize the radiolabeled amino acids after purification and sequencing. This molecular investigation of the ACh binding site will first be carried out on the desensitized (D) state. Such characterization of the open channel A state will then be attempted by labeling the receptor using rapid mixing techniques. A more precise molecular understanding of conformational changes un-**

derlying the dynamic structural processes regulating cholinergic neurotransmission should be possible by comparing the topography of the ACh binding site before, during, and after AChR activation.

ACKNOWLEDGMENT

We thank Prof. A. Ménez (CEA/Saclay) for ^3H -labeled *N. nigricollis* α -neurotoxin, S. Braun and P. Poindron (Laboratoire d'Immunologie, Université Louis Pasteur Strasbourg) for providing the TE 671 cell line, and E. Krempp for technical support. Financial support was from CNRS (Centre National de la Recherche Scientifique), AFM (Association Française contre les Myopathies), and Naturalia and Biologia.

LITERATURE CITED

- Alcaraz, M. L., Peng, L., Klotz, P., and Goeldner, M. (1996) Synthesis and properties of photoactivatable phospholipid derivatives designed to probe the membrane-associated domains of proteins. *J. Org. Chem.* **61**, 192–201.
- Arnold, B. R., Sciaiano, J. C., Bucher, G. F., and Sander, W. W. (1992) Laser flash photolysis studies on 4-oxocyclohexa-2,5-dienylidenes. *J. Org. Chem.* **57**, 6469–6474.
- Bayley, H. (1983) in *Photogenerated reagents in biochemistry and molecular biology* (T. S. Work and R. H. Burdon, Eds.) p 97, Elsevier, Amsterdam.
- Bradford, M. M. (1976) A rapid and sensitive method for the quantitation of microgram quantities of protein utilizing the principle of protein-dye binding. *Anal. Biochem.* **72**, 248–254.
- Chatrenet, B., Kotzyba-Hibert, F., Mülle, C., Changeux, J.-P., Goeldner, M. P., and Hirth, C. (1992) Photoactivatable agonist of the nicotinic acetylcholine receptor: potential probe to characterize the structural transitions of the acetylcholine binding site in different states of the receptor. *Mol. Pharmacol.* **41**, 1100–1106.
- Dennis, M., Giraudat, J., Kotzyba-Hibert, F., Goeldner, M., Hirth, C., Chang, J. Y., Lazure, C., Chrétien, M., and Changeux, J.-P. (1988) Amino acids of the *Torpedo marmorata* acetylcholine receptor α -subunit labeled by a photoaffinity ligand for the acetylcholine binding site. *Biochemistry* **27**, 2346–2357.
- Eldefrawi, A. T., Miller, E. R., Murphy, D. L., and Eldefrawi, M. E. (1982) [^3H]Phencyclidine interactions with the nicotinic acetylcholine receptor channel and its inhibition by psychotropic, antipsychotic, opiate, antidepressant, antibiotic, antiviral and antiarrhythmic drugs. *Mol. Pharmacol.* **22**, 72–81.
- Feltz, A., and Trautmann, A. (1982) Desensitization at the frog neuromuscular junction: a biphasic process. *J. Physiol. (London)* **331**, 257–272.
- Galzi, J.-L., Revah, F., Black, D., Goeldner, M., Hirth, C., and Changeux, J.-P. (1990) Identification of a novel amino acid α -Tyr 93 within the cholinergic ligands-binding sites of the acetylcholine receptor by photoaffinity labeling: additional evidence for a three-loop model of the cholinergic ligands-binding sites. *J. Biol. Chem.* **265**, 10430–10437.
- Galzi, J.-L., Revah, F., Bouet, F., Ménez, A., Goeldner, M., Hirth, C., and Changeux, J.-P. (1991) Allosteric transitions of the acetylcholine receptor probed at the amino acid level with a photolabile cholinergic ligand. *Proc. Natl. Acad. Sci. U.S.A.* **91**, 5051–5056.
- Gasper, S. M., Devadoss, C., and Schuster, G. B. (1995) Photolysis of substituted benzenediazonium salts: spin-selective reactivity of aryl cations. *J. Am. Chem. Soc.* **117**, 5206–5211.
- Goeldner, M. P., and Hirth, C. G. (1980) Specific photoaffinity labeling induced by energy transfer: application to irreversible inhibition of acetylcholinesterase. *Proc. Natl. Acad. Sci. U.S.A.* **77**, 6439–6442.
- Grassi, F., Giovannelli, A., Fucile, S., Mattei, E., and Eusebi, F. (1993) Cholinergic responses in cloned human TE 671/RD tumour cells. *Pfluegers Arch.* **425**, 117–125.
- Heidmann, T., and Changeux, J.-P. (1979) Fast kinetic studies on the interaction of a fluorescent agonist with the membrane-bound acetylcholine receptor from *Torpedo marmorata*. *Eur. J. Biochem.* **94**, 255–279.
- Heidmann, T., Bernhardt, J., Newmann, E., and Changeux, J.-P. (1983) Rapid kinetics of agonist binding and permeability response analyzed in parallel on acetylcholine receptor rich membranes from *Torpedo marmorata*. *Biochemistry* **22**, 5452–5459.
- Kessler, P., Ehret-Sabatier, L., Goeldner, M., and Hirth, C. (1990) 4-Diazocyclohexa-2,5-dienones as photoaffinity reagents for proteins. *Tetrahedron Lett.* **31**, 1275–1278.
- Kotzyba-Hibert, F., Kapfer, I., and Goeldner, M. (1995) Recent trends in photoaffinity labeling. *Angew. Chem., Int. Ed. Engl.* **34**, 1296–1312.
- Kotzyba-Hibert, F., Kessler, P., Zerbib, V., Bogen, C., Snetkov, V., Takeda, K., Goeldner, M., and Hirth, C. (1996) Novel photoactivatable agonist of the nicotinic acetylcholine receptor of potential use for exploring the functional, activated state. *J. Neurochem.* **67**, 2557–2565.
- Laemmli, U. K. (1970) Cleavage of structural proteins during the assembly of the head of bacteriophage T4. *Nature* **227**, 680–685.
- Lange, G. L., and Gottardo, C. (1990) Facile conversion of primary and secondary alcohols to alkyl iodides. *Synth. Commun.*, 1473–1479.
- Langenbuch-Cachat, J., Bon, C., Mülle, C., Goeldner, M., Hirth, C., and Changeux, J.-P. (1988) Photoaffinity labeling of the acetylcholine binding sites on the nicotinic receptor by an aryldiazonium derivative. *Biochemistry* **27**, 2337–2345.
- Luther, M., Schoepfer, R., Whiting, P., Casey, B., Blatt, Y., Montal, M. S., Montal, M., and Lindstrom, J. (1989) A muscle acetylcholine receptor is expressed in the human cerebellar medulloblastoma cell line TE 671. *J. Neurosci.* **9**, 1082–1096.
- Martin, M., Czajkowski, C., and Karlin, A. (1996) The contribution of aspartyl residues in the acetylcholine receptor γ and δ subunits to the binding of the agonists and competitive antagonists. *J. Biol. Chem.* **271**, 13497–13503.
- Middleton, R. E., and Cohen, J. B. (1991) Mapping of the acetylcholine binding site of the nicotinic acetylcholine receptor: [^3H]nicotine as an agonist photoaffinity label. *Biochemistry* **30**, 6987–6997.
- Morgat, J.-L., Demares, J., and Cornu, M. (1975) Dispositif automatique de transfert de gaz (tritium, deutérium, hydrogène) (Automatic gas transfer apparatus for tritium, deuterium, and hydrogen). *J. Labelled Compd.* **11**, 257–264.
- Saitoh, T., and Changeux, J.-P. (1980) Phosphorylation *in vitro* of membrane fragments from *Torpedo marmorata* electric organ. *Eur. J. Biochem.* **105**, 51–62.
- Sakmann, B., Patlak, J., and Neher, E. (1980) Single acetylcholine-activated channels show burst-kinetics in the presence of desensitizing concentrations of agonist. *Nature* **286**, 71–73.
- Schmidt, T. J., and Raftery, M. A. (1973) A simple assay for the study of solubilized acetylcholine receptors. *Anal. Biochem.* **52**, 349–354.
- Schoepfer, R., Luther, M., and Lindstrom, J. (1988) The human medulloblastoma cell line TE 671 expresses a muscle-like acetylcholine receptor: cloning of the α subunit cDNA. *FEBS Lett.* **226**, 235–240.
- Sine, S. M. (1988) Functional properties of human skeletal muscle acetylcholine receptors expressed by the TE 671 cell line. *J. Biol. Chem.* **263**, 18052–18062.
- Smith, H. (1965) Intermediates in steroid synthesis. *Chem. Abstr.* **62**, 7692–7693.
- Unwin, N. (1995) Acetylcholine receptor channel imaged in the open state. *Nature* **373**, 37–43.
- Weber, M., and Changeux, J.-P. (1974a) Binding of *Naja nigricollis* [^3H]- α -toxin to membrane fragments from *Electrophorus* and *Torpedo* electric organs. Binding of the tritiated α -neurotoxin in the absence of effector. *Mol. Pharmacol.* **10**, 1–14.
- Weber, M., and Changeux, J.-P. (1974b) Binding of *Naja nigricollis* [^3H]- α -toxin to membrane fragments from *Electrophorus* and *Torpedo* electric organs. Effect of cholinergic agonists and antagonists on the binding of the tritiated α -neurotoxin. *Mol. Pharmacol.* **10**, 15–34.

Synthesis and Characterization of a Peptide Nucleic Acid Conjugated to a D-Peptide Analog of Insulin-like Growth Factor 1 for Increased Cellular Uptake

Soumitra Basu[†] and Eric Wickstrom*

Department of Microbiology and Immunology and Kimmel Cancer Center, Thomas Jefferson University, Philadelphia, Pennsylvania 19107. Received January 27, 1997[®]

DNA therapeutics show great potential for gene-specific, nontoxic therapy of a wide variety of diseases. The deoxyribose phosphate backbone of DNA has been modified in a number of ways to improve nuclease stability and cell membrane permeability. Recently, a new DNA derivative with an amide backbone instead of a deoxyribose phosphate backbone, peptide nucleic acid (PNA), has shown tremendous potential as an antisense agent. Although PNAs hybridize very strongly and specifically to RNA and DNA, they are taken up by cells very poorly, limiting their potential as nucleic acid binding agents. To improve cellular uptake of a PNA sequence, it was conjugated to a D-amino acid analog of insulin-like growth factor 1 (IGF1), which binds selectively to the cell surface receptor for insulin-like growth factor 1 (IGF1R). The IGF1 D-peptide analog was assembled on (4-methylbenzhydryl)amine resin, and then the PNA was extended as a continuation of the peptide. The conjugate and control sequences were radiolabeled with ¹⁴C or fluorescently labeled with fluorescein isothiocyanate. Cellular uptake of the PNA-peptide conjugate, a control with two alanines in the peptide, and a control PNA without the peptide segment were studied in murine BALB/c 3T3 cells, which express low levels of murine IGF1R, in p6 cells, which are BALB/c 3T3 cells which overexpress a transfected human IGF1R gene, and in human Jurkat cells, which do not express IGF1R, as a negative control. The specific PNA-peptide conjugate displayed much higher uptake than the control PNA, but only in cells expressing IGF1R. This approach may allow cell-specific and tissue-specific application of PNAs as gene-regulating agents *in vivo*.

INTRODUCTION

Targeting oligonucleotides to a particular gene, or messenger RNA of the gene, to specifically inhibit the expression of that gene has developed into an attractive therapeutic strategy in recent years, especially for treating cancers and viral diseases (1–3). Novel oligonucleotide analogs have been synthesized to act as antisense/antigene agents, to improve the biological stability, solubility, cellular uptake, and ease of synthesis. One of the recent additions to this group of modified oligonucleotide analogs is the peptide nucleic acid (PNA)¹ (Figure 1) (4). In these compounds, the entire deoxyribose phosphate backbone has been replaced with a structurally homomorphous polyamide (peptide) backbone composed of (2-aminoethyl)glycine units, leaving the oligomer uncharged. This synthetic DNA mimic exhibits enhanced affinity and specificity for its complementary nucleic acid target sequence.

* Address correspondence to this author at the Department of Microbiology and Immunology, Thomas Jefferson University, 1025 Walnut St., Suite 420, Philadelphia, PA 19107 [telephone (215) 955-4578; fax (215) 955-4580; e-mail ewick@lac.jci.tju.edu].

[†] Present address: Department of Molecular Biophysics and Biochemistry, Yale University School of Medicine, New Haven, CT 06520.

[®] Abstract published in *Advance ACS Abstracts*, June 15, 1997.

¹ Abbreviations: Boc, *tert*-butyloxycarbonyl; Bzl, benzyl; DMEM, Dulbecco's modified Eagle's medium; FITC, fluorescein isothiocyanate; Fmoc, fluorenylmethoxycarbonyl; HPLC, high-performance liquid chromatography; IGF1, insulin-like growth factor; IGF1R, insulin-like growth factor 1 receptor; Mob, 4-methoxybenzyl; PNA, peptide nucleic acid; SDS, sodium dodecyl sulfate; SEM, standard error of the means; *T*_m, melting temperature; Z, benzyloxycarbonyl.

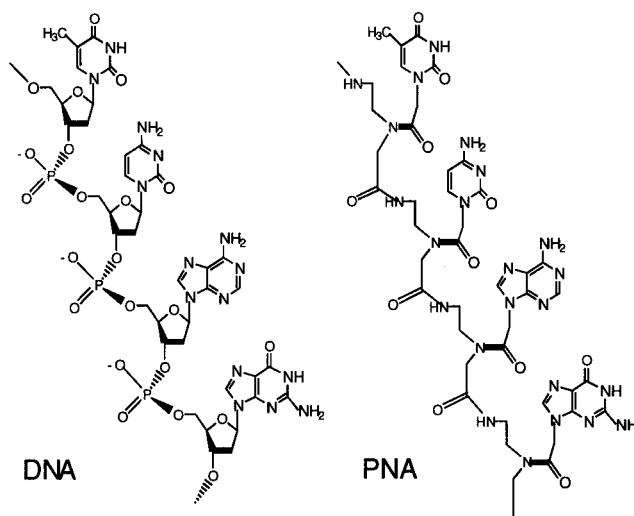


Figure 1. Structure of PNA and DNA. PNAs are peptide-based analogs of DNA in which the phosphate sugar backbone is replaced by (2-aminoethyl)glycine.

The PNAs have clear advantages over a variety of oligonucleotide analogs in several properties that are critical for antigene/antisense activity. Compared with other oligonucleotide derivatives, PNAs display the highest *T*_m values for duplexes formed with single-stranded DNA or RNA (5). PNAs are also resistant to both proteases and nucleases (6). Another major advantage is that PNAs can strand-invade duplex DNA, resulting in the formation of D-loops (7). This characteristic may make it possible to manipulate gene expression at the level of transcription. These complexes mediate the antigene/antisense effects of PNAs by steric hindrance

of enzyme complexes responsible for DNA transcription, cDNA synthesis, and RNA translation.

PNA activity as an antisense agent has been demonstrated *in vitro* and by microinjecting individual cells in culture (8). Microinjection of PNAs into cells was necessary because of poor cellular uptake (9) which was found to be 10 times less efficient than uptake of phosphorothioates in a variety of mammalian cells (10). One of the primary requirements for an oligonucleotide analog to be successful as an antigene/antisense agent is for it to be taken up by the cells in reasonable quantity so that it can reach its target in sufficient concentration. Since the PNAs suffer from poor cellular uptake, they have not been developed as an antigene/antisense therapeutic agent. To alleviate this situation, a strategy was developed to improve cellular uptake as well as to target the PNAs to specific cell types. A previous attempt was made to deliver PNA specifically through the blood-brain barrier (BBB) by binding a biotinylated PNA to streptavidin conjugated to a monoclonal antibody against transferrin receptor (11), to take advantage of the relatively high level of transferrin receptor at the BBB. The strategy was to have the PNAs cross the BBB via transferrin receptor mediated endocytosis. Though accumulation of the intravenously administered PNA-biotin-streptavidin-antibody inside the brain was 28-fold greater than accumulation of unmodified control PNA, no evidence was presented for cellular uptake of these large, complex conjugates.

Recent investigations have revealed that the insulin-like growth factor 1/insulin-like growth factor 1 receptor (IGF1/IGF1R) system plays major regulatory roles in development, cell cycle progression, and the early phase of tumorigenicity (12). Small peptides have been designed by molecular modeling as analogs of natural IGF1. The most effective peptide analog, JB3, D-Cys-Ser-Lys-Ala-Pro-Lys-Leu-Pro-Ala-Ala-Tyr-Cys, inhibits growth of certain cancer cell lines and competes with the natural ligand for binding to the IGF1R (13). Thus, we hypothesized that conjugation of the D-peptide analog with an antisense PNA against an effective target sequence of IGF1R mRNA (14) would provide cell-type specificity, and increased cellular uptake, by those cells overexpressing IGF1R. The rationale behind this strategy is the prediction that the peptide moiety would specifically bind the cell surface receptor, in this case IGF1R, to concentrate the conjugates on the specific cells, and then the conjugate would get taken up by receptor mediated endocytosis (15). In the case of PNAs, a study of cellular uptake demonstrated active endocytosis, with 13% of the internalized radiolabel localized to the nuclei after 8 h (10). No toxicity was evident over 24 h of observation. Once inside the cell, some fraction of internalized PNA may then interact with its target nucleic acid in the cytoplasm or nucleus.

The JB3 peptide has two Cys residues, one at each terminus, which are disulfide linked to form a loop with limited flexibility, favoring a conformation for binding to the receptor. The use of D-amino acids gave the peptide stability against cellular proteases. A reverse sequence was synthesized with respect to the normal L-amino acid sequence to account for the reversal of chirality (13). To reduce the complexity of the synthesis, a smaller version of JB3, called JB9, D-Cys-Ser-Lys-Cys, was selected for conjugation with the PNA. The peptide segment was synthesized automatically using standard Fmoc coupling, after which the PNA moiety was extended from the N terminus of the peptide by manual Boc coupling (16).

Cellular uptake of the PNA-peptide conjugate, a control with two D-Ala residues in the peptide in place

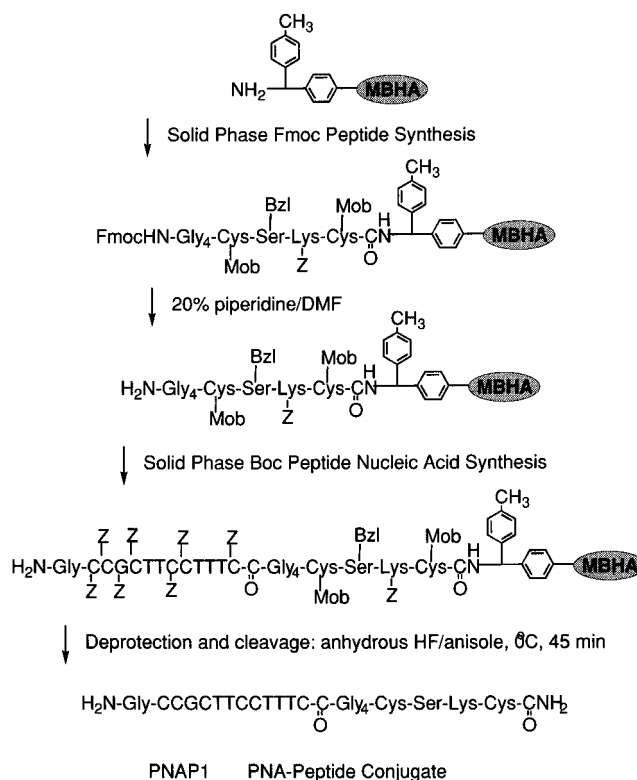


Figure 2. Synthetic scheme for assembly of PNA-peptide conjugates.

of D-Ser-Lys, and a control PNA without a peptide adduct were studied in murine BALB/c 3T3 cells, which express low levels of murine IGF1R, in p6 cells, which are BALB/c 3T3 cells, which overexpress a transfected human IGF1R gene (13), and in human Jurkat cells, which do not express IGF1R (17), as a negative control. In cells expressing IGF1R, the specific PNA-peptide conjugate displayed significantly higher uptake than the control PNA or the control PNA-peptide. This approach may allow cell-specific and tissue-specific application of PNAs as gene-regulating agents *in vivo*.

MATERIALS AND METHODS

Assembly of PNA-Peptide Conjugates. The IGF1R-targeted PNA-peptide (PNAP1) synthesized was H-Gly-CCGCTTCCTTTC-Gly4-Cys-Ser-Lys-Cys-NH₂ (Figure 2). The PNA dodecamer, CCGCTTCCTTTC, is complementary to nucleotides 2251–2262, codons 706–709, of human IGF1R mRNA, corresponding to the putative precursor processing site (18). The four glycines at the N terminus of the peptide adduct serve as a spacer between the peptide and the PNA moieties to minimize mutual interference, as these two segments by design have independent functions.

The peptide portion of the conjugate was synthesized automatically on *p*-methylbenzhydrylamine-HCl (1% divinyl polystyrene cross-linked) resin on an Applied Biosystems 331 peptide synthesizer at 0.10 mmol scale (250 mg) with a standard HBTU coupling protocol using Fmoc-D-Cys (Mob)-OH (Bachem Biosciences, Inc., King of Prussia, PA), Fmoc-D-Ser (Bzl)-OH (Bachem Biosciences), Fmoc-D-Lys (Z)-OH (Novabiochem, San Diego, CA), and Fmoc-Gly-OH (Applied Biosystems, Foster City, CA). After assembly of the complete peptide, the N-terminal Fmoc group was removed. Thus, the amino terminus became available for assembling the PNA chain as a continuation of the protected D-peptide segment, H₂N-Gly-Gly-Gly-Gly-D-Cys(Mob)-D-Ser(Bzl)-D-Lys(Z)-D-

Cys(Mob)–resin. The Boc-protected PNA monomers (PerSeptive Biosystems, Framingham, MA) were coupled manually essentially as described (16).

In short, 1.5 mL solutions of 0.10 M Boc-protected monomer (0.15 mmol) were preactivated for 2 min with 0.08 M HBTU and 0.20 M DIEA (base) in pyridine/DMF (1:1 v/v) and then coupled to 0.040 mmol (200 mg) of H-Gly-Gly-Gly-Gly-D-Cys(Mob)-D-Ser(Bzl)-D-Lys(Z)-D-Cys(Mob)–resin for 20 min. Qualitative ninhydrin analysis was conducted on an aliquot of the growing Boc-PNA–peptide–resin to determine the presence of free amines (19). The resin was washed twice with 3 mL of pyridine for 2 min. The free amines were capped with a mixture of acetic anhydride/pyridine/CH₂Cl₂ (10:12:78, v/v/v) for 5 min. Any acetyl esters formed by the capping step were removed by treatment with 3 mL of piperidine/CH₂Cl₂ for 5 min. The resin was then washed three times with 3 mL of DMF/CH₂Cl₂ (1:1, v/v), followed by washing three times with 3 mL of neat CH₂Cl₂, three times, for 2 min per wash step. The terminal Boc group was removed by treating the resin twice with TFA/*m*-cresol (95:5, v/v) for 2 min. The PNA–peptide–resin was washed three times with DMF/CH₂Cl₂ (1:1, v/v) for 2 min each, followed by two washes with neat pyridine for 2 min each. The coupling/deprotection cycle with Boc-PNA monomers was repeated until the entire PNA sequence was assembled. Ninhydrin analysis was repeated and proved to be negative. The completed PNA–peptide conjugate was deprotected and cleaved from the resin with anhydrous HF/anisole at 0 °C for 45 min. A control PNA (PNA1) without a peptide, Gly-CCGCTTCCTTTC-CONH₂, and a peptide sequence control (PNAP2), Gly-CCGCTTCCTTTC-CONH-Gly₄-Cys-Ala-Ala-Cys-CO₂H, were custom synthesized by PerSeptive Biosystems.

Purification of PNA–Peptide Conjugates. The two cysteine side chains in the peptide were cyclized by dissolving the conjugate in 0.01 M NaHCO₃, pH 8.5, at 5.0 g/L, and stirring for 24 h at room temperature in the presence of atmospheric oxygen to allow formation of disulfide linkages. The lyophilized conjugate was assayed for free sulfhydryl groups by Ellman's reagent (DTNB assay) (20). The cyclized crude product was purified by HPLC on a 10 × 250 mm C₁₈ Econosil column (Alltech Associates, Deerfield, IL) eluted over 40 min from 10% to 80% acetonitrile in water containing 0.1% TFA, at 4 mL/min, on a Waters 600 multisolvent delivery system coupled with a temperature controller maintaining the column at 50 °C and a Waters 486E variable-wavelength detector, monitoring eluent absorbance at 260 nm.

Characterization of PNA–Peptide Conjugates by Mass Spectroscopy. The conjugate was also characterized by MALDI-TOF mass spectroscopy (21) on a Hewlett-Packard 1700 LDI calibrated with a standard peptide mixture supplied by the manufacturer. Equal volumes of a 0.5 mM solution of the conjugate in 20% methanol, 80% water, and a solution of sinapinic acid (3,5-dimethoxy-4-hydroxycinnamic acid; Aldrich, Milwaukee, WI) were mixed well. Then, 1 µL of the solution was placed on the tip of the probe, and the sample was allowed to crystallize under vacuum and then analyzed to obtain the mass of the conjugate. A PNA1 sample was similarly analyzed.

Characterization of PNA–Peptide Conjugates by SDS–Polyacrylamide Gel Electrophoresis. The PNA–peptide conjugate was also characterized by SDS–polyacrylamide gel electrophoresis. The samples were electrophoresed on 4–20% acrylamide gradient gels (Bio-Rad, Hercules, CA), on a Bio-Rad Mini-Protean II Cell apparatus. Gel electrophoresis was conducted at 100 V,

in Laemmli buffer, pH 8.3 (22), calibrated with low-range prestained protein molecular mass standards, 3–43 kDa (Life Technologies, Gaithersburg, MD). The gels were stained with Coomassie brilliant blue to visualize the bands.

Synthesis of [¹⁴C]PNA–Peptide and [¹⁴C]PNA Conjugates. PNA1, PNAP1, and PNAP2 were radioactively labeled by reductive methylation with [¹⁴C]formaldehyde as described (10, 23). Briefly, PNA and PNA–peptides (100 nmol) were dissolved in 0.1 mL of 0.2 M Na₂HPO₄, pH 7.5 (to minimize lysine methylation), with 500 nmol of [¹⁴C]formaldehyde (NEC-039H, 40–60 Ci/mol, New England Nuclear, Boston, MA) and incubated for 2 h at room temperature with periodic vortexing. Sodium cyanoborohydride (0.1 mL of a fresh 100 mM solution) was then added to the mixture to reduce the Schiff base, and the incubation was continued for an additional 4 h with periodic vortexing. The [¹⁴C]PNA derivatives were purified by gel filtration on NAP10 G-25 Sephadex columns (17-0854-01, Pharmacia Biotech Inc., Piscataway, NJ). Homogeneity was evaluated by TLC of a small aliquot on cellulose plates (1366061, Eastman Kodak, Rochester, NY) developed with *n*-butanol/glacial acetic acid/H₂O (4:1:5). Specific activities of the labeled PNAs were estimated by measuring concentrations from A₂₆₀ in UV-absorbing TLC bands extracted with water and ¹⁴C radioactivity using liquid scintillation counting at 75% counting efficiency. The specific activities of several preparations ranged from 5.3 to 11 Ci/mol.

Synthesis of PNA–Peptide–Fluorescein and PNA–Fluorescein Conjugates. Purified PNAP1 and PNA1 were fluoresceinated with a 20-fold excess of FITC in 0.2 M Na₂HPO₄ buffer, pH 8.5 (to minimize lysine fluoresceinylation), for 2 h with constant stirring. The products were purified from free FITC by preparative chromatography on a NAP10 G-25 Sephadex column and further purified on a G-50 Sephadex column (Pharmacia Biotech Inc.). Fluorescein conjugates were then analyzed by SDS–polyacrylamide gel electrophoresis as above.

Thermal Denaturation of PNA–DNA Duplexes. Thermal denaturation profiles of an equimolar mixture of the purified PNAP1 conjugate or PNA1 control, and their complementary DNA target, were performed in 10 mM Tris-HCl, pH 8.0, 100 mM NaCl, on a Cary 3E spectrophotometer equipped with a multicell holder and a temperature controller (Varian, Palo Alto, CA). The rate of increase of the temperature was 1 °C/min, from 10 to 90 °C. All *T_m* values were calculated from the first derivative of the melting curve, and the reported values are the average of three experiments.

Serum Stability of the PNA–Peptide Conjugate. An aliquot of PNAP1 conjugate was incubated in 10% fetal bovine serum/PBS for 12 and 24 h at 37 °C. After incubation, 1 volume of acetonitrile was added to each sample to precipitate serum proteins, which were pelleted by centrifugation (24). Free conjugate in the supernatant was evaporated *in vacuo*. It was then analyzed by reversed phase HPLC as described above.

Cellular Uptake Studies with [¹⁴C]PNA and [¹⁴C]PNA–Peptide Conjugates. Cellular uptake studies with radiolabeled PNA derivatives were carried out as described previously (10). p6 cells, which are murine BALB/c 3T3 cells transfected with human IGF1R gene, and nontransfected murine BALB/c 3T3 cells were plated in DMEM with 10% FBS in 12.5 cm² flasks and then allowed to attach and grow for 2 days in a humidified cell incubator with 5% CO₂ at 37 °C, reaching 50–80% confluence, on the order of 10⁶ cells per flask. The medium was then removed and replaced with fresh medium containing 1 µM of the various [¹⁴C]PNA deriva-

tives, prewarmed to 37 °C; background cells received medium with no [14 C]PNA derivatives. After incubation for various times, attached cells were washed directly in the flasks using four washes: once with fresh medium, once with PBS, once with 1.0 M NaCl/0.4 M NaOAc, pH 3.3, and once with PBS. This procedure had the advantage of removing both noninternalized oligomer and any dead cells, which can accumulate large amounts of labeled oligomer and thereby skew any uptake measurements (10). Human Jurkat cells, which lack IGF1R (17), were used as a negative control. They were grown in suspension in RPMI 1640 with 10% FBS in a humidified cell incubator with 5% CO₂ at 37 °C. The Jurkat cells were treated in the same manner as the attached cells, except that they were incubated and washed in centrifuge tubes, rather than on plates, because they grow in suspension.

After the final wash, the cells were lysed in 1 mL of 1% SDS in H₂O, and the samples were processed for total protein measurement and liquid scintillation counting as described before (10). Fifty microliters of the lysate was allocated for total protein measurement, and 14 C activity in the remaining lysate was measured by liquid scintillation counting, from which background counts were subtracted. Background samples from control lysates not treated with [14 C]PNA derivatives typically yielded 12–15 cpm, corresponding to <1 pmol even at 10 Ci/mol or 0.2 pmol at a typical specific activity of 40 Ci/mol. Thus, an experimental sample with twice the background counts per minute would contain 0.2–1 pmol, depending on the specific activity, which may be considered the limit of detection.

Control samples of varying confluence were trypsinized following the last wash, resuspended in PBS for cell counting, and then lysed to obtain total protein values. This allowed the generation of a standard curve corresponding to total protein vs cell number. The curve was used to estimate cell counts from the total protein measurements of treated cells, and [14 C]PNA counts were used to calculate picomoles of oligomer using the specific activity of each labeled preparation. Values for cell number and picomoles of cell-associated oligomer were therefore obtained for each treated sample. Estimates of cell volume were obtained by microscopic evaluation of cell diameters using a micrometer and subsequent calculation of an average cell volumes, as described (10).

Cellular Uptake Studies with PNA–Fluorescein and PNA–Peptide–Fluorescein Conjugates. Cellular uptake studies with fluorescein conjugates of PNA1 and PNAP1 were conducted with p6 cells and Jurkat cells. P6 cells were plated on LAB TEK 8 well tissue culture Chamber Slides (Nunc, Naperville, IL) in DMEM with 10% FBS at a concentration of 20 000 cells/chamber. The cells were allowed to attach and grow for 24 h in a humidified cell incubator with 5% CO₂ at 37 °C. The attached cells were then washed with serum-free DMEM and PBS. The cells were incubated for 4 h at 37 °C with 1 μ M of the fluoresceinated PNAP1 in PBS. Human Jurkat cells, the negative control, were treated in the same manner as the p6 cells, except that they were incubated and washed in centrifuge tubes rather than on plates, because they grow in suspension. At the conclusion of the incubation period the cells were washed with serum-free DMEM once followed by three washings with PBS. Then the cells were fixed with 1% paraformaldehyde/PBS for 1 h and washed once with buffer from an ANTI-FADE kit (Molecular Probes, Eugene, OR). The chambers were removed and excess liquid drained off. One drop of the ANTI-FADE reagent was sufficient to cover the cells on the slides, which were covered with

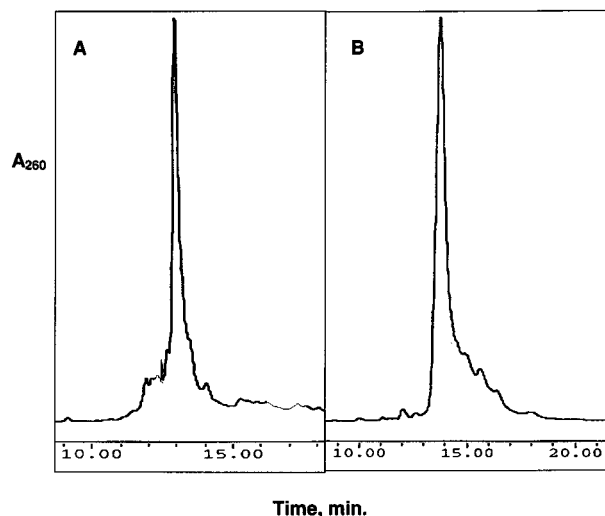


Figure 3. Analytical HPLC of purified, cyclized PNA–peptide conjugate PNAP1, on 4.6 \times 250 mm Econosil C₁₈ column eluted over 40 min from 12% to 76% acetonitrile in water containing 0.1% TFA, at 1 mL/min, at 50 °C: (A) following purification; (B) extracted from serum after 24 h of incubation. Eluent absorbance was monitored at 260 nm.

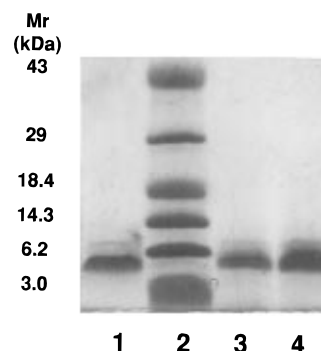


Figure 4. SDS–PAGE of the PNA–peptide conjugate: lanes 1 (0.5 nmol), 3 (0.75 nmol), and 4 (1.5 nmol) are the conjugate; lane 2 contains the molecular mass markers. The gel was stained with Coomassie brilliant blue. The conjugate (3.85 kDa) migrates between the 6.2 and the 3.0 kDa markers.

coverslips and sealed. The fixed slides were examined on a Bio-Rad MRC-600 laser scanning confocal microscope, interfaced to a Zeiss Axiovert 100 with a Plan-Apo 63X 1.40NA oil-immersion lens, using fluorescence microscopy and phase contrast microscopy to observe cellular uptake of the fluorescent oligomers.

RESULTS

Assembly, Chromatography, and Mass Spectroscopy of the PNA–Peptide Conjugate. The PNA–peptide conjugate PNAP1, 5'-CCGCTTCCTTTC-3'-N-(Gly)₄-D-(Cys-Ser-Lys-Cys)-C, was synthesized on a solid phase support with a blend of automatic and manual syntheses (Figure 2). The conjugate was deprotected and cleaved from the solid support, yielding 140 mg (0.0364 mmol) of crude linear product, a 91% yield by mass, which could be an overestimate, due to the potential inclusion of nonpeptide impurities. Analytical HPLC displayed a main product peak including almost 90% of the total area under the peaks. Thus, the product of 91% crude yield with 90% full-length product in that material gives a maximum estimated yield of 82%. The linear PNAP1 was then cyclized and purified by reversed phase HPLC. Analytical HPLC after purification (Figure 3A) displayed a single peak. This is the first demonstration of a partially automated synthesis of a PNA–peptide

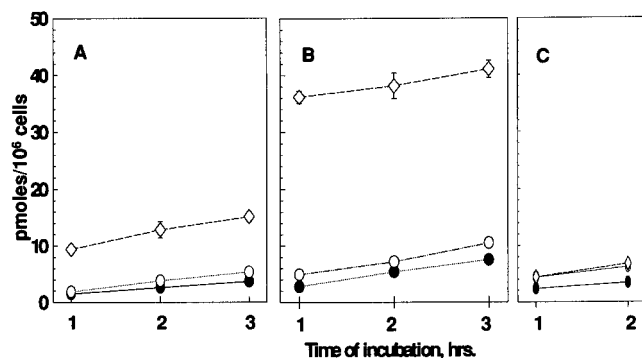


Figure 5. Cellular uptake of radiolabeled PNA and PNA-peptides by mammalian cells as a function of incubation time at 37 °C: (A) BALB/c 3T3 cells; (B) p6 cells; (C) Jurkat cells. Cells were incubated in the presence of 1 μ M [¹⁴C]PNA1 (●), [¹⁴C]PNAP1 (◇), and [¹⁴C]PNAP2 (○) for varying lengths of time and processed for measurement of cell-associated radioactivity. Data are presented in terms of picomoles of oligonucleotide per 10⁶ cells. Each data point in (A) and (B) represents the mean \pm SEM of three replicates. Each data point in (C) represents the mean \pm variance of two replicates.

conjugate. Two different coupling chemistries were utilized: the more widely used Fmoc coupling for the peptide segment and Boc coupling for the PNA segment. The purified cyclized PNAP1 peak provided a MALDI-TOF mass spectrum with a prominent peak at 3854.5 amu, close to the calculated mass (3850.7 amu) of the intended PNAP1 conjugate. A negative result from the DTNB assay of purified, cyclized PNAP1 implied absence of free sulfhydryl groups, confirming the completeness of disulfide cyclization. A single peak in the HPLC chromatogram, as well as a single peak in the mass spectrum corresponding to the monomeric mass of

PNAP1-peptide, indicated that the peptide portion was indeed cyclized, rather than dimerized or oligomerized. PNA1 was assembled, purified by HPLC, and analyzed by mass spectrum in the same fashion. PNAP2 from PerSeptive Biosystems was also homogeneous after cyclization and purification.

Electrophoretic Analysis of the PNA–Peptide Conjugate. To further characterize the conjugate, it was analyzed by denaturing SDS–polyacrylamide gel electrophoresis (22), used regularly for sizing of polypeptides. Previously, it has been possible to analyze complexes of PNAs hybridized to charged nucleic acids by nondenaturing gel electrophoresis (5). However, free PNAs have not been analyzed previously by gel electrophoresis, due to their lack of charge. The SDS-denatured conjugate migrated as predicted according to its molecular mass, compared to the standard peptide molecular mass markers (Figure 4). This is the first demonstration that PNA–peptide conjugates could be analyzed for their homogeneity and molecular mass by denaturing gel electrophoresis. Fluorescein conjugates were also analyzed by SDS–polyacrylamide gel electrophoresis and displayed single bands of lower mobility (not shown).

Thermal Denaturation of PNA–DNA Duplexes. The PNA–peptide conjugate includes a Gly₄ spacer between the dodecamer PNA segment and the tetrapeptide IGF1 analog. Despite the presence of the spacer section, it is plausible that the peptide might interfere with PNA hybridization to a complementary target. Therefore, a thermal denaturation study was undertaken to determine whether the peptide moiety might lower the *T_m* of the PNA/DNA hybrid. The two melting curves were identical, yielding a *T_m* of 60 \pm 1 °C. These results imply that the peptide moiety on the C terminus of the PNA

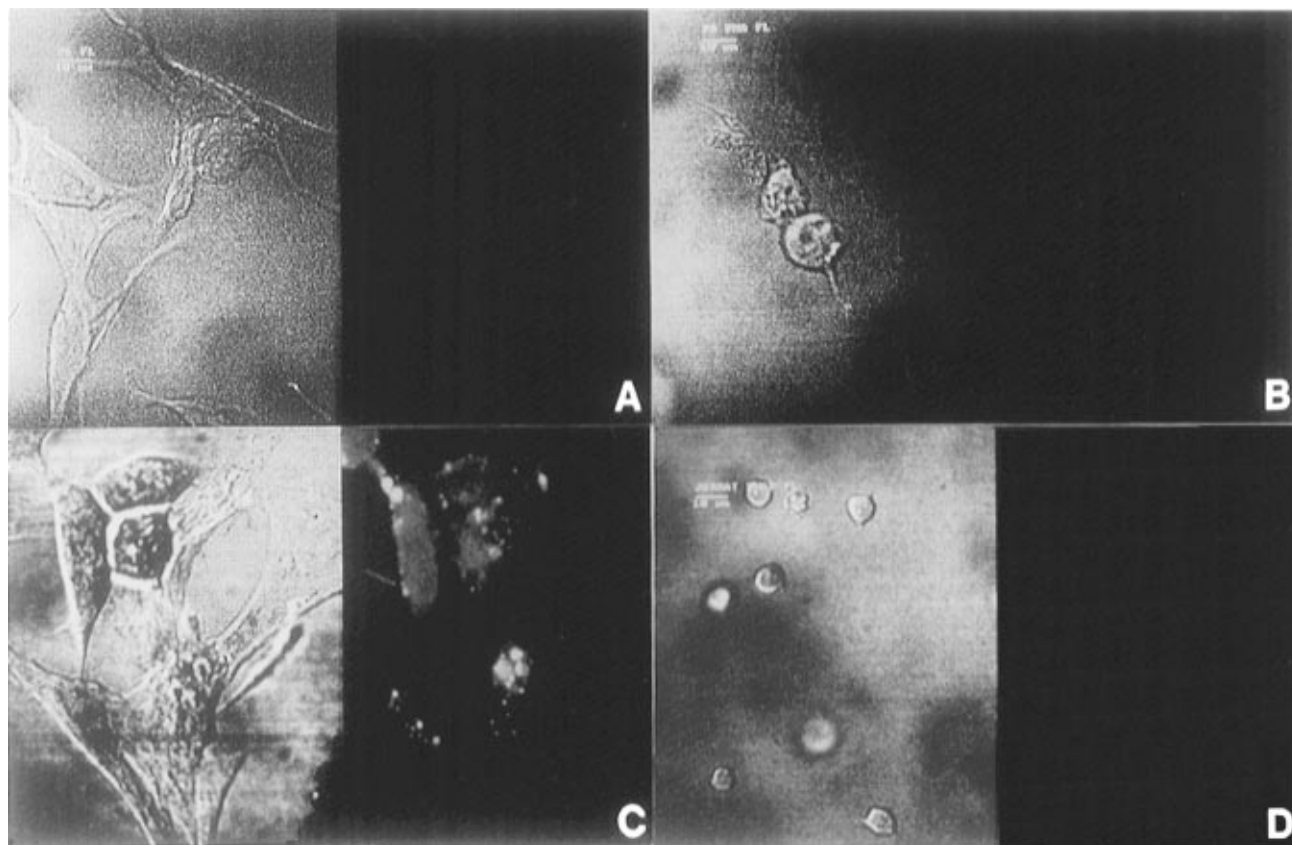


Figure 6. Confocal microscopy of mammalian cells incubated with 1 μ M fluorescein derivatives for 4 h at 37 °C: (A) p6 cells incubated with fluorescein alone; (B) p6 cells incubated with fluoresceinated PNA1; (C) p6 cells incubated with fluoresceinated PNAP1 peptide conjugate; (D) Jurkat cells incubated with fluoresceinated PNAP1 peptide conjugate. The right-hand side is the fluorescence image, and the left-hand side is the phase contrast image of the same field.

sequence did not adversely affect the hybridization efficiency of the PNA molecule to its complementary DNA target, in agreement with previous findings (25, 26).

Serum Stability of the PNA–Peptide Conjugate. The conjugate was designed to be resistant to both proteases and nucleases, as the PNAs are not degraded by either the proteases or the nucleases (6), and D-peptides are also resistant to proteases (13). Samples of PNAP1 incubated in serum were extracted at various times and analyzed by HPLC. As hypothesized in the design of PNAP1, the 24 h chromatogram displayed no detectable degradation (Figure 3B).

Cellular Uptake Studies with [14 C]PNA and [14 C]-PNA–Peptide Conjugates. The rationale behind the construction of the conjugate was that the peptide part would bind to IGF1R, a cell surface receptor which is overexpressed in a variety of oncogenic cell lines, and that would lead to internalization of the molecule via an endocytotic mechanism. Once inside the cells, the PNA may then find its target nucleic acid and hybridize. Therefore, cellular uptake of PNA–peptide conjugates was compared among nontransfected BALB/c 3T3 murine cells, which express modest levels of murine IGF1R, p6 cells, which are BALB/c 3T3 murine cells that overexpress human IGF1R (14), and human Jurkat cells, which display very low expression of IGF1R (17), as a negative control. BALB/c 3T3 cells, the parental line from which p6 cells were derived, displayed low uptake of [14 C]-PNAP1, which was still 4-fold more than BALB/c 3T3 uptake of [14 C]PNAP2 and [14 C]PNA1 controls (Figure 5A). Uptake measurements with p6 cells showed much greater uptake than observed with BALB/c 3T3 cells, with 5-fold greater uptake of [14 C]PNAP1 than of [14 C]-PNAP2 or [14 C]PNA1 controls (Figure 5B). In contrast, uptake experiments with Jurkat cells, which express virtually no IGF1R, displayed low uptake, with little preferential uptake of [14 C]PNAP1 relative to the controls (Figure 5C).

Cellular Uptake Studies with PNA–Fluorescein and PNA–Peptide–Fluorescein Conjugates. When the PNAP1 conjugate and the control PNA1 sequence were fluoresceinated, cellular uptake could be studied by fluorescence under a laser confocal microscope. The fields observed for fluorescence signals were also observed under phase contrast settings. Confocal microscopy allowed observation of different planar sections of the cells, which distinguished between intracellular fluorescence and cell surface fluorescence. This constitutes a significant advantage over conventional fluorescence microscopy, which cannot differentiate between signals inside vs outside the cells. Incubation of p6 cells with fluorescein (hydrolyzed FITC) alone (Figure 6A) or with fluoresceinated PNA1 (Figure 6B) showed only very weak cell-associated fluorescence, demonstrating that these molecules were negligibly taken up by p6 cells. This observation implies that uptake was not mediated by the fluorescein moiety. In contrast, incubation of p6 cells with fluoresceinated PNAP1 conjugate showed bright fluorescence signals associated with intracellular structures, including the nuclei (Figure 6C). Since the observed field was a planar section from inside of the cells, the PNAP1 conjugate was presumed to have been internalized. Finally, when Jurkat cells were exposed to the fluoresceinated PNA–peptide conjugate, negligible cell-associated fluorescence signals were observed (Figure 6D), consistent with the hypothesis that the uptake of the PNA–peptide conjugate PNAP1 would be mediated by the JB9 peptide moiety. Figure 7 shows the fluorescence image from the right side of Figure 6C cells superimposed upon the phase contrast image from the

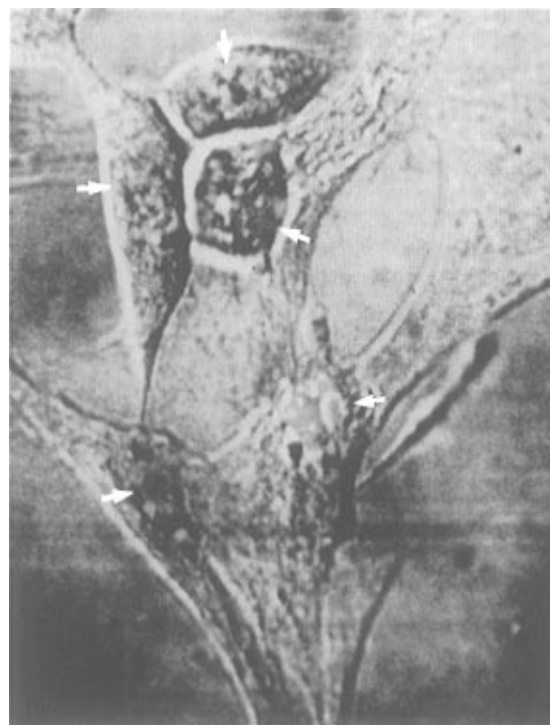


Figure 7. Confocal microscopy of p6 cells incubated with fluoresceinated PNAP1 peptide conjugate. The fluorescence image and the phase contrast image of the same fields shown in Figure 6C are superimposed to illustrate the location of the fluorescence signals within the cellular boundaries. Nuclei are indicated by arrows.

left side of Figure 6C, illustrating that the fluorescein signals came from compartments within the cells themselves.

DISCUSSION

The potential of antisense/antigene oligonucleotides as a novel class of therapeutic agents lies in the predictability and specificity of the complementary binding between the intracellular target RNA or DNA and the exogenously applied oligonucleotides by hydrogen bonding. The development of antisense/antigene oligonucleotides as therapeutic agents has focused on chemically modifying the oligonucleotides with the aim of enhancing biological stability and intracellular uptake, without compromising the hybridization efficiency or the binding specificity.

The JB9 peptide moiety, modeled to imitate an IGF1R binding domain of IGF1 (13), was hypothesized to enable cell specific targeting of an oligonucleotide, followed by receptor-mediated endocytosis, for the purpose of significantly increasing internalization. Previously, this rationale led us to synthesize a phosphorothioate DNA–JB3 conjugate (27). However, PNAs fit the criteria for therapeutic oligonucleotides better than phosphorothioates, with the exception of poor cellular uptake (9, 10). To solve this problem, a PNA–IGF1 analog conjugate was synthesized, which resulted in targeted and elevated cellular uptake.

For therapeutic application of oligonucleotide based agents, it is essential to develop an automated synthetic protocol. PNAs are typically synthesized on polystyrene-based solid supports, utilizing Boc protection, similar to what was developed for normal peptide synthesis (16, 28). Alternatively, a PNA synthesis has been reported utilizing Fmoc protection (29). Manual assembly of a PNA–peptide conjugate on a solid support has been described before, utilizing Boc protection for both segments (25).

The peptide segment, containing naturally occurring L-amino acids, was designed to be a substrate for protein kinase A, which phosphorylates the serine residue. Since PNAs have potential for application as antigene/antisense agents against many genetic targets, and PNA–peptide conjugates might overcome the problem of poor cellular uptake, it would be much more efficient to synthesize them automatically.

As a significant step in that direction a semiautomated synthesis protocol has been developed. The synthesis of the conjugate was achieved by integration of Fmoc chemistry to assemble the peptide moiety on a solid support and then Boc chemistry to extend the PNA segment. The other significant improvement was the use of D-amino acids for the peptide section, so that the IGF1 D-analog domain of the conjugate would be as resistant to degradation as the PNA segment, for optimum bioavailability.

The key problem in achieving solid phase synthesis of a biologically stable conjugate was finding the right combinations of protecting groups, so that the two synthetic strategies would be compatible. This task was made more difficult by the inclusion of D-amino acids, as commercially available choices for them are narrow. Utilization of Mob, Bzl, and Z protecting groups was found to be mutually compatible for synthesis of the two segments, resulting in an excellent yield of deprotected, cyclized conjugate. A cyclized peptide domain is essential in the conjugate to limit the flexibility of the JB9 segment, optimizing binding to the cell surface IGF1 receptor. The presence of the cyclized PNA–peptide conjugate was demonstrated by the negative DTNB assay, a homogeneous peak in the analytical HPLC chromatogram, a single peak of predicted molecular mass in the MALDI-TOF mass spectrum, and a single band on a denaturing SDS–polyacrylamide gel, used for the first time to characterize a PNA–peptide conjugate.

Measurements of cellular uptake and compartmentalization demonstrated specificity for the IGF1 analog, and elevated uptake of the PNA–IGF1 analog conjugate was dependent on the level of IGF1R expression. The conjugate was stable in serum over 24 h, which is essential for bioavailability. Furthermore, the peptide adduct did not inhibit hybridization of the PNA segment to complementary DNA. Finally, neither the radiolabeled nor the fluorescent conjugates were toxic to the cell lines tested. This is the first effective demonstration of cell specific targeting and delivery of PNAs.

For oligonucleotides to be applied successfully as antisense/antigene therapeutics, intracellular delivery is essential. Among the available assortment of modified oligonucleotide analogs, PNAs look very promising due to their favorable hybridization characteristics and biological stability. The successful delivery of the PNA–peptide conjugate inside cells without the need for microinjection opens up the opportunity for developing these oligonucleotide analogs as therapeutic agents. The next logical step is to evaluate their antisense efficacy in cell culture. This delivery strategy may be further improved with more potent ligands to achieve better cellular uptake, and other disease-related or tissue-specific cell surface receptors may be targeted in the future to concentrate PNA conjugates into other cell and tissue types.

ACKNOWLEDGMENT

We thank Dr. Michael Kligshiteyn for synthesis of DNA analogs, Dr. Rolf Berg for synthesis of peptide nucleic acids, and Dr. Janet Smith for a critical reading of the

manuscript. The p6 cell line was kindly supplied by Dr. Christopher Sell, while Dr. Danuta Kozbor provided the Jurkat cell line. This research was supported by National Institutes of Health Grants CA42960 and CA60139 to E.W.

LITERATURE CITED

- (1) Wickstrom, E., Ed. (1991) *Prospects for Antisense Nucleic Acid Therapy of Cancer and AIDS*, Wiley-Liss, New York.
- (2) Crooke, S. T., and Lebleu, B., Eds. (1993) *Antisense Research and Applications*, CRC Press, Boca Raton, FL.
- (3) Agrawal, S., Ed. (1996) *Antisense Therapeutics*, Humana Press, Totowa, NJ.
- (4) Nielsen, P. E., Egholm, M., Berg, R. H., and Buchardt, O. (1991) Sequence-selective recognition of DNA by strand displacement with a thymine-substituted polyamide. *Science* 254, 1497–1500.
- (5) Egholm, M., Buchardt, O., Christensen, L., Behrens, C., Freier, S. M., Driver, D. A., Berg, R. H., Kim, S. K., Norden, B., and Nielsen, P. E. (1993) PNA hybridizes to complementary oligonucleotides obeying the Watson-Crick hydrogen-bonding rules. *Nature* 365, 566–568.
- (6) Demidov, V. V., Potaman, V. N., Frank-Kamenetskii, M. D., Egholm, M., Buchardt, O., Sonnichsen, S. H., and Nielsen, P. E. (1994) Stability of peptide nucleic acids in human serum and cellular extracts. *Biochem. Pharmacol.* 48, 1310–1313.
- (7) Møllegaard, N. E., Buchardt, O., Egholm, M., and Nielsen, P. E. (1994) Peptide nucleic acid-DNA strand displacement loops as artificial transcription promoters. *Proc. Natl. Acad. Sci. U.S.A.* 91, 3892–3895.
- (8) Hanvey, J. C., Pfeffer, N. J., Bisi, J. E., Thomson, S. A., Cadilla, R., Josey, J. A., Ricca, D. J., Hassman, C. F., Bonham, M. A., Au, K. G., Carter, S. G., Bruckenstein, D. A., Boyd, A. L., Noble, S. A., and Babiss, L. E. (1992) Antisense and antigene properties of peptide nucleic acids. *Science* 258, 1481–1485.
- (9) Bonham, M. A., Brown, S., Boyd, A. L., Brown, P. H., Bruckenstein, D. A., Hanvey, J. C., Thomson, S. A., Pipe, A., Hassman, F., and Bisi, J. E. (1995) An assessment of the antisense properties of RNase H-competent and steric-blocking oligomers. *Nucleic Acids Res.* 23, 1197–1203.
- (10) Gray, G. D., Basu, S., and Wickstrom, E. (1997) Transformed and immortalized cellular uptake of oligodeoxynucleoside phosphorothioates, 3' alkylamino oligodeoxynucleotides, 2'-O-methyl oligoribonucleotides, oligodeoxynucleoside methylphosphonates, and peptide nucleic acids. *Biochem. Pharmacol.* 48, 1465–1476.
- (11) Pardridge, W. M., Boado, R. J., and Kang, Y.-S. (1995) Vector-mediated delivery of a polyamide ("peptide") nucleic acid analogue through the blood-brain barrier *in vivo*. *Proc. Natl. Acad. Sci. U.S.A.* 92, 5592–5596.
- (12) Baserga, R. (1995) The insulin-like growth factor 1 receptor: a key to tumor growth? *Cancer Res.* 55, 249–252.
- (13) Pietrzkowski, Z., Wernicke, D., Porcu, P., Jameson, B. A., and Baserga, R. (1992) Inhibition of cellular proliferation by peptide analogues of insulin-like growth factor 1. *Cancer Res.* 52, 6447–6451.
- (14) Pietrzkowski, Z., Sell, C., Lammers, R., Ullrich, A., and Baserga, R. (1992) Roles of insulinlike growth factor 1 (IGF-1) and the IGF-1 receptor in epidermal growth factor-stimulated growth of 3T3 cells. *Mol. Cell. Biol.* 12, 3883–3888.
- (15) Wagner, E., Zenke, M., Cotten, M., Beug, H., and Birnstiel, M. L. (1990) Transferrin-polycation conjugates as carriers of DNA uptake into cells. *Proc. Natl. Acad. Sci. U.S.A.* 87, 3410–3414.
- (16) Christensen, L., Fitzpatrick, R., Gildea, B., Petersen, K. H., Hansen, H. F., Koch, T., Egholm, M., Buchardt, O., Nielsen, P. E., Coull, J., and Berg, R. (1995) Solid-phase synthesis of peptide nucleic acids. *J. Pept. Sci.* 3, 175–183.
- (17) Lal, R. B., Rudolph, D. L., Folks, T. M., and Hooper, W. C. (1993) Over expression of insulin-like growth factor receptor type-1 in T-cell lines infected with human T-lymphotropic virus types-I and -II. *Leukemia Res.* 17, 31–35.
- (18) Ullrich, A., Gray, A., Tam, A. W., Yang-Feng, T., Tsubokawa, M., Collins, C., Henzel, W., Bon Le, T., Katchuria,

- S., Chen, E., Jacobs, S., Francke, D., Ramachandran, J., and Fujita-Yamaguchi, Y. (1986) Insulin-like growth factor 1 receptor primary structure: comparison with insulin receptor suggests structural determinations that define functional specificity. *EMBO J.* 5, 2503–2512.
- (19) Sarin, V. K., Kent, B. H., Tam, J. P., and Merrifield, R. B. (1981) Quantitative monitoring of solid phase peptide synthesis by the ninhydrin reaction. *Anal. Biochem.* 117, 147–157.
- (20) Ellman, G. L. (1959) Tissue sulfhydryl groups. *Arch. Biochem. Biophys.* 82, 70–77.
- (21) Piesles, U., Zurcher, W., Schar, M., and Moser, H. E. (1993) Matrix-assisted laser desorption ionization time-of flight mass spectrometry: a powerful tool for the mass and sequence analysis of natural and modified oligonucleotides. *Nucleic Acids Res.* 21, 3191–3196.
- (22) Laemmli, U. (1970) Cleavage of structural proteins during the assembly of the head of bacteriophage T4. *Nature* 227, 680–685.
- (23) Hughes, J. A., Avrutskaya, A. V., Brouwer, K. L. R., Wickstrom, E., and Juliano, R. L. (1995) Radiolabeling of methylphosphonate and phosphorothioate oligonucleotides and evaluation of their transport in everted rat jejunum sacs. *Pharm. Res.* 12, 817–824.
- (24) Wickstrom, E., Bacon, T. A., and Wickstrom, E. L. (1992) Down-regulation of c-myc antigen expression in lymphocytes of E μ -c-myc transgenic mice treated with anti-c-myc DNA methylphosphonate. *Cancer Res* 52, 6741–6745.
- (25) Koch, T., Naesby, M., Wittung, P., Jørgensen, M., Larsson, C., Buchardt, O., Stanley, C. J., Nordén, B., Nielsen, P. E., and Ørum, H. (1995) PNA-peptide chimeras. *Tetrahedron Lett.* 36, 6933–6936.
- (26) Soukchareun, S., Tregear, G. W., and Haralambidis, J. (1995) Synthesis and evaluation of nuclear targeting peptide-antisense oligodeoxynucleotide conjugates. *Bioconjugate Chem.* 6, 43–53.
- (27) Basu, S., and Wickstrom, E. (1995) Solid phase synthesis of a D-peptide-phosphorothioate oligodeoxynucleotide conjugate from two arms of a polyethylene glycol-polystyrene support. *Tetrahedron Lett.* 36, 4943–4946.
- (28) Erickson, B. W., and Merrifield, R. B. (1976) Solid phase peptide synthesis. In *The Proteins*, 3rd ed. (H. Neurath and R. L. Hill, Eds.) pp 255–257, Academic Press, New York.
- (29) Thomson, S. A., Josey, J. A., Cadilla, R., Gaul, M. D., Hassman, C. F., Luzzio, M. J., Pipe, A. J., Reed, K. L., Ricca, D. J., Wiethe, R. W., and Noble, S. A. (1995) Fmoc mediated synthesis of peptide nucleic acids. *Tetrahedron* 51, 6179–6194.

BC9700650

Cyclopentadienyl Iron Dicarbonyl (η^1 -*N*-Phthalimidato) Complexes Containing an Isothiocyanate Function: Synthesis and Application to Protein Side-Chain Selective Labeling

Anna Kazimierczak,[†] Janusz Zakrzewski,^{*,†} Michèle Salmain,[‡] and Gérard Jaouen^{*,‡}

Department of Organic Chemistry, University of Lodz, Narutowicza 68, 90-136 Lodz, Poland, and Ecole Nationale Supérieure de Chimie, Laboratoire de Chimie Organométallique, URA CNRS 403, 11 rue Pierre et Marie Curie, F-75231 Paris Cedex 05, France. Received February 25, 1997[®]

The two first transition metal carbonyl isothiocyanates were prepared in high yield within two steps from photolysis of $\text{CpFe}(\text{CO})_2\text{I}$ and 3- or 4-aminophthalimide in the presence of diisopropylamine followed by reaction with thiophosgene/triethylamine. Their reaction with a model amino acid, i.e. β -alanine, was performed and led to the expected thioureas. When reacted with bovine serum albumin in aqueous medium, conjugates bearing 6–10 iron–carbonyl fragments were obtained and characterized by Fourier transform infrared spectroscopy, thus demonstrating the usefulness of these reagents for the selective and covalent labeling of proteins.

INTRODUCTION

Organotransition metal complexes having substituents able to react selectively at functional groups present in biomolecules currently attract a great deal of attention as labeling reagents (Furuya et al., 1988; Carver et al., 1993; Wang et al., 1993; Anson et al., 1994; Dalla Riva Toma et al., 1994; Krämer, 1996). During the past few years, we have focused our interest on the use of transition metal carbonyl complexes as reporter groups for the labeling of biologically active molecules (Jaouen et al., 1993). These complexes can be detected in a sensitive and univoque manner by mid-IR¹ spectroscopy thanks to their ν_{CO} vibration modes that appear in the 1800–2150 cm^{-1} spectral region. Owing to the fact that quantities of complex in the order of magnitude of the picomole (10^{-12} mol) can be routinely detected and quantified by current FT spectrometers (Salmain et al., 1991), a new competitive immunological method, coined carbonyl metallo immunoassay (CMIA) has been elaborated for hapten assay (Salmain et al., 1992; Philomin et al., 1994; Varenne et al., 1995).

The labeling of high molecular weight antigens or antibodies, which is a prerequisite to the extension of CMIA to proteic antigens, poses new problems as compared to the labeling of haptens, owing to the polyfunctional character of proteins and their tendency to denaturation. These problems have been solved by preparing a series of metal carbonyl complexes containing an *N*-hydroxysuccinimide (NHS) ester function, which reacts with amino groups at the N-terminal position and the lysine residues of proteins (Varenne et al., 1993; Salmain et al., 1994; Gorfti et al., 1996). Other studies dealt with organometallic reagents containing a pyrylium group (Salmain et al., 1994; Malisza et al., 1995), reactive

toward amino groups. Recently, an organometallic complex containing an *N*-maleimide function, $\text{CpFe}(\text{CO})_2(\eta^1$ -*N*-maleimidato), has been synthesized (Rudolf and Zakrzewski, 1994). Although it is believed that this function reacts selectively with sulfhydryl groups (cysteines), it has been demonstrated that this complex can also react with amino groups or imidazole rings (histidines) (Rudolf and Zakrzewski, 1996). However, the coupling selectivity can be tuned by changing the reaction conditions (pH) (unpublished work).

Isothiocyanates have found numerous applications in peptide and protein chemistry to date (Wong, 1991). The best known examples include the Edman method of protein amino acid sequence determination by means of phenyl isothiocyanate (Cohen and Strydom, 1988) and the use of fluoresceine isothiocyanate (FITC) for fluorescent labeling of proteins [see, for example, Oshita and Katunuma (1993) and references cited therein]. Ferrocene–methyl isothiocyanate was also used to prepare immunogens so as to eventually produce anti-ferrocene polyclonal antibodies (Gill and Mann, 1966).

In this paper, we report the synthesis of two iron carbonyl complexes containing an isothiocyanate function. Their reactivity toward amino groups was checked using β -alanine and a model protein, bovine serum albumin (BSA), which we had previously chosen for NHS esters and pyrylium salt reactivity studies. Their preparation took advantage of the photochemical approach to the synthesis of $\text{CpFe}(\text{CO})_2(\eta^1$ -*N*-imidato) complexes ($\text{Cp} = \eta^5$ -cyclopentadienyl) (Zakrzewski, 1989). The idea was to synthesize complexes containing a phthalimidato ligand substituted by an amino function at the aromatic ring and then convert this amino group into an isothiocyanate function.

EXPERIMENTAL PROCEDURES

Materials. All chemical reactions were carried out under argon. Column chromatographies were performed with silica gel 60 (230–400 mesh ASTM, Merck). Benzene was distilled over sodium/benzophenone, and dichloromethane and chloroform were distilled over calcium hydride. Diisopropylamine and triethylamine (Aldrich) were stored over KOH. Other analytical grade solvents were used without purification. $\text{CpFe}(\text{CO})_2\text{I}$ was synthesized according to a published procedure (King, 1965).

* Author to whom correspondence should be addressed.

[†] University of Lodz.

[‡] Ecole Nationale Supérieure de Chimie.

[®] Abstract published in *Advance ACS Abstracts*, June 15, 1997.

¹ Abbreviations: BSA, bovine serum albumin; Cp, η^5 -cyclopentadienyl; CR, coupling ratio; DMF, dimethylformamide; ESI-MS, electrospray ionization spectroscopy; FT-IR, Fourier transform infrared; mid-IR, mid-infrared; NHS, *N*-hydroxysuccinimide; TLC, thin-layer chromatography; TMS, tetramethylsilane; TNBS, trinitrobenzenesulfonic acid.

Aminophthalimides (Kodak), thiophosgene, and β -alanine (Aldrich) were used as received. Photolyses were carried out by illuminating the solutions with visible light produced by four 150 W domestic tungsten lamps and simultaneous external cooling with a mixture of ice and water. Borate and phosphate buffers were prepared from demineralized water. Protein conjugations were performed with undistilled solvents at room temperature.

^1H NMR spectra were recorded on a Gemini 200BB apparatus (200 MHz for ^1H , Varian) and were referenced to the internal standard TMS (0.00 ppm). Mass spectra were recorded in the electronic impact mode at 15 eV with a 2091 GCMS spectrometer (LKB). Qualitative IR characterizations were performed on a 75IR spectrometer (Specord). Quantitative IR analyses were performed by depositing 10 μL samples on 9 mm diameter nitrocellulose membranes (Alltech), and spectra were recorded on a MB-100 FT spectrometer (Bomem) equipped with a liquid nitrogen-cooled InSb detector as described (Salmann et al., 1993). UV-vis spectra were recorded on a UV-mc² spectrometer (Safas).

Methods. *CpFe(CO)₂(η^1 -(N-1)(3-aminophthalimidato) (1a).* A mixture of *CpFe(CO)₂I* (1.2 g, 3.9 mmol), 3-aminophthalimide (0.52 g, 3.2 mmol), and diisopropylamine (4 mL) in benzene (50 mL) was photolyzed for 12 h. The black color turned yellow during the photolysis. The reaction course was followed by TLC using chloroform/methanol 95:5 as eluent. The solid was filtered off, and the filtrate was concentrated to ca. one-fourth of its original volume. After addition of pentane (50 mL) and cooling to -5°C , the solid formed was filtered off and dried, and **1a** was purified by column chromatography, eluted by chloroform, and crystallized from dichloromethane/pentane: yield 0.99 g (91%); ^1H NMR (CDCl_3) δ 7.20 (t, $J = 7$ Hz, partially obscured by the solvent signal, 1H, H-5), 6.95 (d, $J = 7.0$ Hz, 1H, H-4), 6.67 (d, $J = 7.0$ Hz, 1H, H-6), 5.11 (s, 5H, Cp), 5.06 (bs, 2H, NH_2); IR (CHCl_3) ν (in cm^{-1}) 3360, 3270 (NH_2), 2055, 1990 (Fe-CO), 1640 (imide CO); MS, m/e (assignment) (% intensity) 338 (M) (7), 310 (M - CO) (4), 282 (M - 2CO) (9), 186 (ferrocene?) (100). Anal. Calcd for $\text{C}_{15}\text{H}_{10}\text{N}_2\text{O}_4\text{Fe}$: C, 53.25; H, 2.96; N, 8.28. Found: C, 52.98; H, 2.82; N, 8.43.

CpFe(CO)₂(η^1 -(N-1)(4-aminophthalimidato) (1b). The procedure was similar to the synthesis of **1a**. After the photolysis, pentane (50 mL) was added to the photolyte, and after cooling to -5°C , the solid was filtered off, washed with pentane, triturated with 10% aqueous Na_2CO_3 (5 mL) and then with water, and dried. The crude product was purified by column chromatography, and **1b** was eluted by chloroform and crystallized from dichloromethane/ether: yield 0.71 g (71%); ^1H NMR (CDCl_3) δ 7.38 (d, $J = 6.9$ Hz, 1H, H-6), 6.87 (d, $J = 1.2$ Hz, 1H, H-3) and 6.64 (d, $J = 6.9$ Hz, $J = 1.2$ Hz, 1H, H-5), 5.09 (s, 5H, Cp), 4.16 (bs, 2H, NH_2); IR (CHCl_3) ν (in cm^{-1}) 3410, 3360 (NH_2), 2055, 2000 (Fe-CO), 1665, 1635 (imide CO); MS, m/e (assignment) (% intensity) 338 (M) (1), 310 (M - CO) (4), 282 (M - 2CO) (9), 186 (ferrocene?) (100). Anal. Calcd for $\text{C}_{15}\text{H}_{10}\text{N}_2\text{O}_4\text{Fe}$: C, 53.25; H, 2.96; N, 8.28. Found: C, 53.29; H, 2.98; N, 8.17.

CpFe(CO)₂(η^1 -(N-1)(3-isothiocyanatophthalimidato) (2a). A magnetically stirred solution of **1a** (700 mg, 2.07 mmol) and triethylamine (0.4 mL) in dichloromethane (33 mL) was treated with thiophosgene (0.207 mL, 2.71 mmol) at room temperature. After 1.5 h, the solvent was evaporated and the residue chromatographed on a short column. **2a** was eluted by chloroform and crystallized from dichloromethane/pentane: yield 630 mg (80%); dec 130 – 140°C ; ^1H NMR (CDCl_3) δ 7.4–7.55 (m, 3H, aromatic ring protons), 5.12 (s, 5H, Cp); IR (CHCl_3) ν (in cm^{-1}) 2100 (br) (NCS), 2050, 2005 (Fe-CO), 1655 (imide

CO); UV-vis (ethanol) λ_{max} (in nm) (ϵ) 275 (15070), 320 (4170); MS, m/e (assignment) (% intensity) 380 (M) (4), 352 (M - CO) (5), 324 (M - 2CO) (100). Anal. Calcd for $\text{C}_{16}\text{H}_8\text{N}_2\text{O}_4\text{SFe}$: C, 50.53; H, 2.11; N, 7.37; S, 8.42. Found: C, 50.22; H, 2.03; N, 7.36; S, 8.47.

CpFe(CO)₂(η^1 -(N-1)(4-isothiocyanatophthalimidato) (2b). A magnetically stirred solution of **1b** (850 mg, 2.51 mmol) and triethylamine (0.5 mL) in dichloromethane (40 mL) was treated with thiophosgene (0.25 mL, 3.28 mmol) at room temperature. After 1.5 h, the solvent was evaporated and the residue chromatographed on a short column. **2b** was eluted by chloroform and crystallized from dichloromethane/ether: yield 880 mg (92%); dec 150 – 160°C ; ^1H NMR (CDCl_3) δ 7.42 (d, $J = 1.6$ Hz, 1H, H-3), 7.57 (d, $J = 6.5$ Hz, 1H, H-6), 7.29 (dd, $J = 6.5$ Hz, $J = 1.6$ Hz, 1H, H-5), 5.12 (s, 5H, Cp); IR (CHCl_3) ν (in cm^{-1}) 2120 (br) (NCS), 2055, 2005 (Fe-CO), 1660 (imide CO); UV-vis (ethanol) λ_{max} (in nm) (ϵ) 264 (18160), 290 (18960); MS, m/e (assignment) (% intensity) 380 (M) (5), 352 (M - CO) (4), 324 (M - 2CO) (100). Anal. Calcd for $\text{C}_{16}\text{H}_8\text{N}_2\text{O}_4\text{SFe}$: C, 50.53; H, 2.11; N, 7.37; S, 8.42. Found: C, 50.50; H, 2.10; N, 7.29; S, 8.11.

Reaction of 2a with β -Alanine. **2a** (60 mg, 0.16 mmol) and β -alanine (60 mg, 0.67 mmol) were dissolved in pyridine (2 mL). To this solution were added 10% aqueous Na_2CO_3 (5 mL) and some water to obtain a homogeneous solution and pH 9–10. This solution was allowed to stand at room temperature in the dark for 24 h. The solvents were evaporated to dryness, and the residue was dissolved in water (5 mL) and extracted three times with dichloromethane. Then the water layer was acidified with HCl to pH 3–4. The precipitated yellow solid **3a** was filtered off, washed with water, and dried under vacuum: yield 64.5 mg (86% calculated from **2a**); dec 148°C ; ^1H NMR (CDCl_3) δ 10.14 (bs, 1H, COOH), 9.32 (d, $J = 8.3$ Hz, 1H, NH), 8.61 (bs, 1H, NH), 7.45–7.30 (m, 3H, benzene ring H's), 5.10 (s, 5H, Cp), 4.03 (m, 2H, CH_2), and 3.00 (m, 2H, CH_2); IR (CDCl_3) ν (in cm^{-1}) 2055, 1990 (Fe-CO), 1720 (COOH), 1640 (imide CO); UV-vis (ethanol) λ_{max} (in nm) (ϵ) 255 (23020), 275 (18900), 355 (5250). Anal. Calcd for $\text{C}_{19}\text{H}_{15}\text{N}_3\text{O}_6\text{SFe}$: C, 48.63; H, 3.23; N, 8.95; S, 6.83. Found: C, 48.34; H, 3.45; N, 9.15; S, 7.08.

Reaction of 2b with β -Alanine. The same procedure as in the preceding reaction was applied. However, after acidification, the product **3b** did not crystallize. Instead, it was extracted with dichloromethane: yield 33.7 mg (45%); dec 165 – 170°C ; ^1H NMR (CDCl_3) δ 10.31 (bs, 1H, COOH), 8.6 (bs, 1H, NH), 7.7–7.3 (m, 3H benzene ring H's), 7.2 (bs, 1H, NH), 5.11 (s, 5H, Cp), 3.95 (m, 2H, CH_2), and 2.78 (m, 2H, CH_2); IR (CDCl_3) ν (in cm^{-1}) 2050, 1990 (Fe-CO), 1720 (COOH), 1635 (imide CO); UV-vis (methanol) λ_{max} (in nm) (ϵ) 275 (15070), 320 (4170). Anal. Calcd for $\text{C}_{19}\text{H}_{15}\text{N}_3\text{O}_6\text{SFe}$: C, 48.63; H, 3.23; N, 8.95; S, 6.83. Found: C, 48.60; H, 3.50; N, 8.82; S, 6.88.

Reaction of 2a,b with BSA. To 2.7 mL of a 50 μM BSA solution in borate buffer pH 9.5 was added 0.3 mL of a 27 mM **2a,b** solution in DMF (i.e. 60 molar equiv). Partial precipitation of the organometallic reagent was noticed as soon as both solutions were mixed. The suspension was stirred for one night at room temperature. After centrifugation at 4000 rpm for 15 min, the supernatant was chromatographed on a prepacked gel filtration column (Econopac 10DG, Bio-Rad). Ten 1-mL fractions were collected and spectrophotometrically analyzed. The first four fractions were pooled. The concentration of protein [P] was measured according to the Coomassie blue method (Bradford, 1978) and by UV spectrophotometry at 280 nm ($\epsilon_{280} = 35700$), after subtraction of the contribution of the label to the total

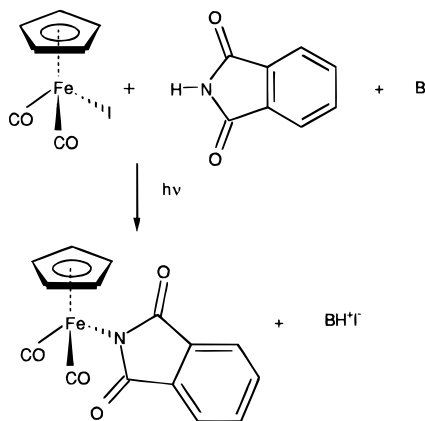


Figure 1. Synthetic scheme of $\text{CpFe(CO)}_2-(\eta^1\text{-}N\text{-phthalimidato})$ complexes. B = diisopropylamine.

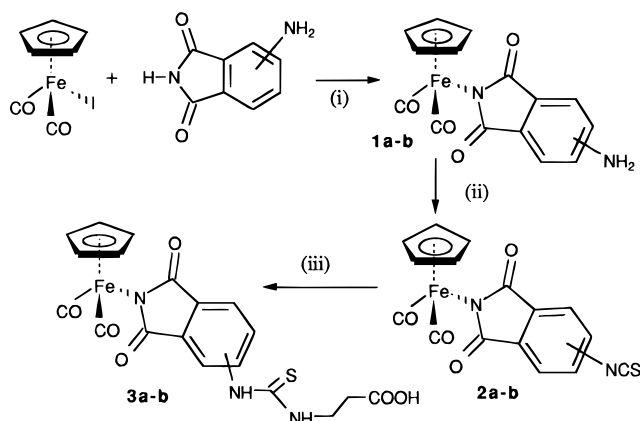


Figure 2. Synthetic route to compounds **1a,b**, **2a,b**, and **3a,b**: (a) 3-isomer, (b) 4-isomer; (i) diisopropylamine/ $h\nu$; (ii) CSeCl_2 /triethylamine; (iii) β -alanine/pH 9–10.

absorbance. The concentration of CpFe(CO)_2 groups [M] was measured by UV spectroscopy at 350 nm [ϵ_{350} (**3a**) = 5250; ϵ_{350} (**3b**) = 3780] and by IR spectroscopy on nitrocellulose membranes ($k = 18.2$) as described (Salmann et al., 1993). The concentration of free protein amino groups was measured according to the TNBS method (Snyder and Sobocinski, 1975).

RESULTS

We had earlier reported that irradiation with visible light of $\text{CpFe(CO)}_2\text{I}$ ($\text{Cp} = \eta^5\text{-C}_5\text{H}_5$) in the presence of phthalimide and diisopropylamine in benzene led to the efficient substitution of iodide by the phthalimide anion (Figure 1) (Zakrzewski, 1989; Bukowska-Strzyzewska et al., 1994). Other “N–H acidic” compounds such as pyrrole, indole (Zakrzewski, 1987; Zakrzewski and Giannotti, 1990), and uracils (Zakrzewski et al., 1995) react similarly.

In this paper, we used this photochemical reaction for synthesis of 3- and 4-amino derivatives of $\text{CpFe(CO)}_2(\eta^1\text{-}N\text{-phthalimidato})$. We found that $\text{CpFe(CO)}_2\text{I}$ reacted with 3- or 4-aminophthalimide and diisopropylamine in benzene, under irradiation with visible light, and yielded the yellow, air-stable complexes **1a,b** (Figure 2).

However, due to rather poor solubility of the starting aminophthalimides in the reaction medium (and their anticipated lower N–H acidity in comparison to the parent, unsubstituted phthalimide), these reactions required much longer photolysis times than the reaction with phthalimide (12 h vs 2 h). Nevertheless, the yields of isolated compounds **1a,b** were relatively high (91 and 71% for **1a** and **1b**, respectively), and no other reaction

products were detected in the photolysates by TLC. The presence of the amino substituents on the aromatic ring of phthalimide did not impair the photochemical reaction with the $\text{CpFe(CO)}_2\text{I}$ /diisopropylamine/ $h\nu$ system, which invariably involves coordination of the CpFe(CO)_2 moiety to the deprotonated imide nitrogen.

The IR spectra of **1a,b** displayed two bands in the region of the stretching N–H vibrations, which confirmed the presence of the primary amino function (NH_2 symmetric and antisymmetric vibrations). The imide carbonyl stretching frequencies were shifted toward lower wavenumbers (ca. $70\text{--}80\text{ cm}^{-1}$) in comparison to the parent N–H imides. The same shift was observed on going from phthalimide to $\text{CpFe(CO)}_2(\eta^1\text{-}N\text{-phthalimidato})$, suggesting the same coordination mode of the deprotonated phthalimide ligand to the CpFe(CO)_2 moiety.

Aromatic amines are versatile starting materials for the synthesis of aromatic isothiocyanates (Rifai and Wong, 1989). We found that **1a,b** react with thiophosgene in the presence of triethylamine at room temperature to afford the corresponding isothiocyanates **2a,b** (Figure 2). These complexes were isolated in 80% (**2a**) and 92% (**2b**) yields as yellow, air-stable crystalline solids, readily obtained in the pure form by chromatography and crystallization from CH_2Cl_2 /pentane or CH_2Cl_2 /diethyl ether mixtures. Their structure was confirmed by IR spectroscopy. No absorption in the region of the N–H stretching vibrations was noticed, whereas a relatively strong broad band at ca. 2100 cm^{-1} (NCS stretching vibration mode) was detected for both compounds.

The reactivity of **2a,b** toward an amine was checked using β -alanine. Coupling reactions were performed at room temperature for 24 h, in the pyridine/ H_2O / K_2CO_3 system. We obtained the expected thioureas **3a,b** in 86 and 45% yields, respectively (Figure 2). Interestingly, their formation was ascertained by the disappearing of the ν_{NCS} band at ca. 2100 cm^{-1} .

Having demonstrated the reactivity of both isothiocyanates with a model amino acid, we tried to label a model protein, i.e., bovine serum albumin (BSA), which is a well-characterized, low-cost protein. The primary sequence of BSA contains 60 amino groups, i.e., 60 potential sites of conjugation for isothiocyanates.

Conjugation of BSA was carried out in the presence of 60 molar equiv of isothiocyanates **2a,b**, in pH 9.5 borate buffer containing 10% of DMF so as to improve solubility of the iron–carbonyl reagents in the reaction medium. After one night at room temperature, the excess reagent was separated from the protein by centrifugation and gel filtration chromatography. Figure 3 shows the chromatograms obtained by plotting the absorbance of each fraction at 350 nm vs the elution volume. Each chromatogram presents two peaks at ca. 2–3 and 6–7 mL. The first eluted peak was readily assigned to the labeled protein, whereas the second was assigned to the unbound label. The whole-range IR spectrum of one of the protein conjugates was recorded and compared to the IR spectrum of native BSA (Figure 4). While the main features are conserved for the conjugate, two new bands are clearly detected in the ν_{CO} region (at 2048 and 2002 cm^{-1}) and assigned to the stretching vibration modes of the metal–carbonyl graft. As for the β -alanine conjugate, effective conjugation can be ascertained by the absence of the ν_{NCS} band at 2100 cm^{-1} .

To characterize both labeled protein samples, we measured the number of coupled CpFe(CO)_2 entities per protein molecule, CR, with $\text{CR} = [\text{M}]/[\text{P}]$, where [M] is the concentration of CpFe(CO)_2 entities and [P] the

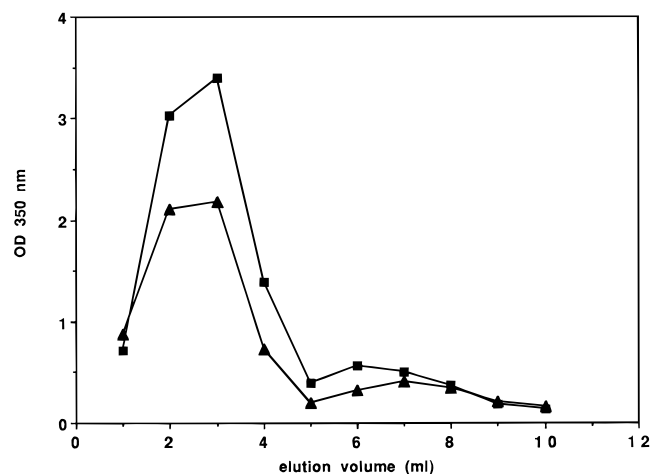


Figure 3. Gel filtration chromatography of BSA-[CpFe(CO)₂]_n conjugates: (■) reagent = **2a**; (▲) reagent = **2b**.

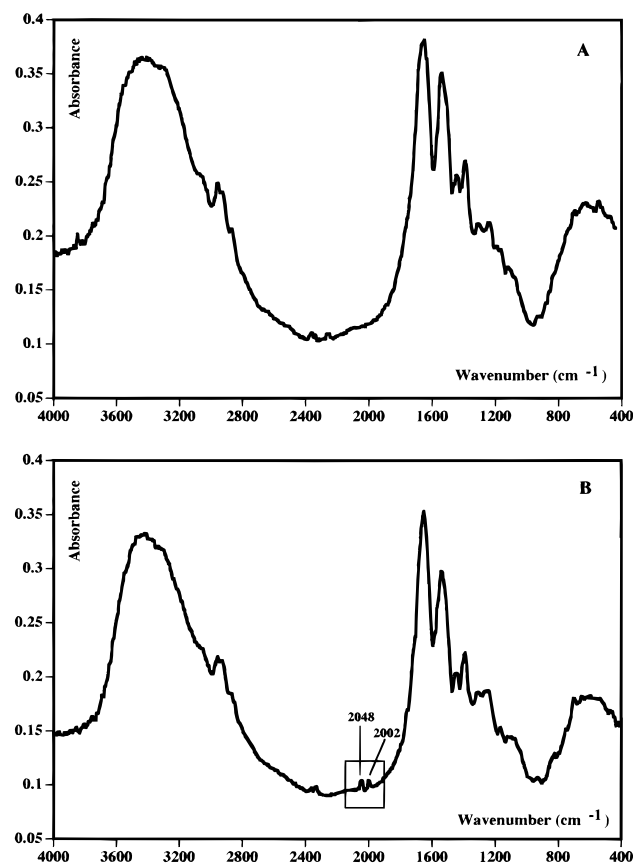


Figure 4. (A) IR spectrum of BSA; 13-mm KBr pellet of lyophilized protein. (B) IR spectrum of BSA-**3b** conjugate; 13-mm KBr pellet of lyophilized protein.

concentration of protein. Numerous methods have been described to date. The oldest one takes advantage of the UV-vis absorption properties of the introduced chromophore (Erlanger, 1980). More recently, the TNBS assay was used for titration of unreacted protein amino functions (Sashidhar et al., 1994). The most recent and widely applicable method exploits the change of molecular mass resulting from the conjugation of several haptens, which can be accurately detected by electrospray ionization mass spectroscopy (ESI-MS) (Adamczyk et al., 1996).

For simplicity reasons, we selected three classical methods further described. The first one is based on the indirect titration of free amino groups according to the TNBS assay. The two others take advantage of the

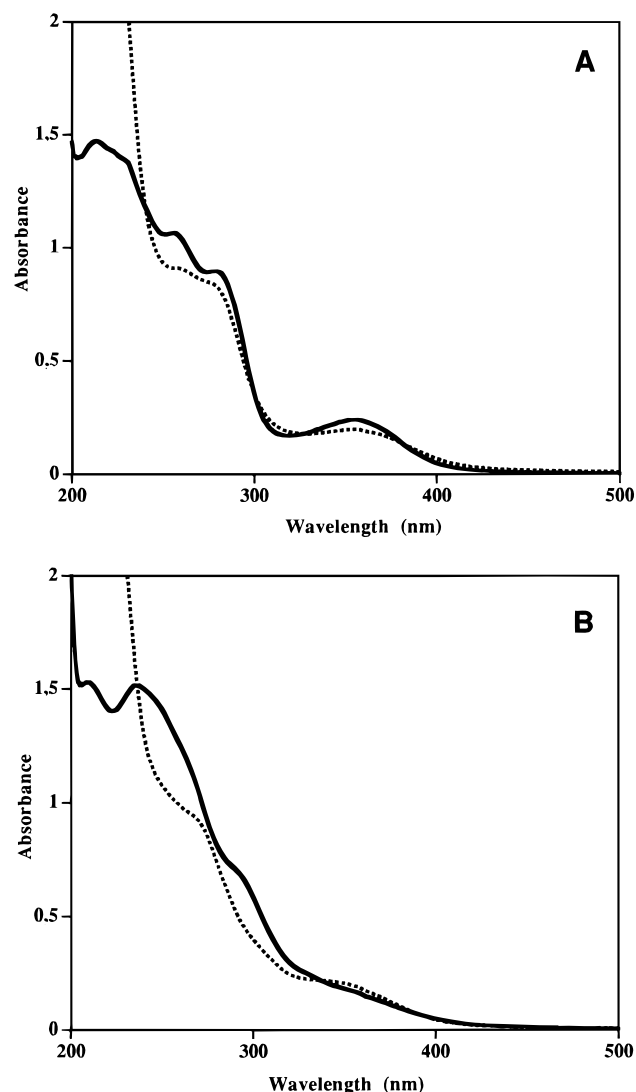


Figure 5. Comparison of the UV-vis spectra of BSA-[CpFe(CO)₂]_n conjugates (dotted line) with thioureas **3a** and **3b** (solid line): (A) 3-isomer; (B) 4-isomer.

spectroscopic properties of the metal-carbonyl graft. Indeed, compounds **3a,b** absorb above 300 nm (Figure 5). It was then expected that protein conjugates would also absorb in the same range. This allowed us to quantify the concentration of metal carbonyl haptens [M] by direct absorbance measurement at 350 nm. Protein concentration [P] was then deduced by differential spectroscopy at 280 nm. On the other hand, it was also possible to measure [M] by IR spectroscopy according to a previously described method (Salmain et al., 1993). Concentration [P] was this time measured according to a classical colorimetric method (Bradford, 1978). Results are gathered in Table 1.

It appears that the coupling ratios calculated from IR spectroscopic measurements are very close to the number of modified amino groups assayed by TNBS titration. Both are in the range of 6–10. This indicates in turn that [M] and [P] are overestimated by UV spectrophotometry.

DISCUSSION

Isothiocyanates are useful reagents for the selective modification of protein amino groups. When reacted at basic pH, thiourea bonds are formed, which are stable under normal physiological conditions. Examples of isothiocyanates among organometallic compounds are

Table 1. Analysis of Conjugated BSA Samples

	labeling reagent	
	2a	2b
Differential UV Spectroscopy		
[M] (μ M)	377 ^a	542 ^b
[P] (μ M)	31 ^c	43 ^d
CR	12.2	12.6
IR Spectroscopy		
[M] ^e (μ M)	242	176
[P] ^f (μ M)	25	27
CR	9.7	6.5
TNBS Assay		
no. of free amino groups per protein	49.3	52.1
CR ^g	10.7	7.9

^a [M] = $A_{350}/5250$. ^b [M] = $A_{350}/3780$. ^c [P] = $(A_{280} - [M] \times 16900)/35700$. ^d [P] = $(A_{280} - [M] \times 16350)/35700$. ^e [M] = $A_{2052}/18.2$. ^f Measured according to the Bradford assay. ^g CR = $60 - (\text{number of free amino groups})$.

rare and nonexistent in the transition metal–carbonyl series. Two examples of cyclopentadienyl iron dicarbonyl isothiocyanates have been presented herein. Their synthesis took advantage of the easy photolytically induced substitution of iodide and addition of 3- or 4-amino-phthalimide anion, then transformation of the amine into an isothiocyanate. Both isomers reacted with an amino acid to form the expected isothioureas. Similarly, they reacted with a model protein to give conjugates bearing several iron–carbonyl moieties per protein molecule.

Quantitation of the number of conjugated entities was performed according to several spectroscopic methods. IR spectroscopy and titration of the free amino groups by TNBS assay gave corroborating results. However, UV spectrophotometry gave overestimated measurements even if **3a,b** were chosen as standards for [M] determination as they were supposed to best mimic the organometallic label structure bound to the protein.

Indeed, a careful comparison between the UV spectra of compounds **3a,b** and their protein counterparts in the 250–400 nm region is necessary at this point (Figure 5). In the 3-substituted derivative series, both **3a** and the protein conjugate present a maximum at 355 nm but the protein conjugate does not show any maximum at 255 nm. In the 4-substituted derivative series, the protein conjugate presents a shoulder at 320 nm, while **3b** shows a shoulder at 290 nm. We then conclude that iron carbonyl entities and protein concentrations are inaccurately measured by UV spectrometry because **3a,b** are not appropriate standards. Such a discrepancy had been previously reported in the literature for studies dealing with the characterization of hapten–protein conjugates (i.e. immunogens) (Sashidhar et al., 1994). Very recently, ESI-MS appeared as a reference method, obviating the need of choosing standards, to perform accurate measurements of the degree of conjugation of hapten–protein conjugates (Adamczyk et al., 1996). Thanks to the particular nature of the reporter group, IR spectroscopy of ν_{CO} bands also appears as an accurate analytical tool for quantitation of conjugated metal–carbonyl species as ν_{CO} band intensities are relatively insensitive to chemical structural changes (Salmain et al., 1991).

Under identical reaction conditions, metal–carbonyl NHS esters give slightly higher coupling ratios, ranging from 13 to 30 (Varenne et al., 1992; Salmain et al., 1993; Gorfti et al., 1996). The slightly lower reactivity of isothiocyanates could be explained by their much lower solubility in aqueous medium. Isothiocyanates would eventually require a higher percentage of organic cosolvent (here 10% DMF) to be fully reactive, but one should keep in mind that this could lead to protein denaturation.

Finally, it bears noticing that while assay sensitivities using such reporter groups are theoretically proportional to the number of conjugated species, too high incorporation could be detrimental to the conservation of a high affinity of the conjugates toward their biological target (for example, in antibody–antigen reactions). Thus, by giving less conjugated proteins, metal carbonyl isothiocyanates could be an interesting alternative to NHS esters.

ACKNOWLEDGMENT

This work was financially supported by the Polish State Committee for Scientific Research (KBN), Grant 9T09A 008 08, and a Centre National de la Recherche Scientifique (CNRS) research grant.

LITERATURE CITED

- Adamczyk, M., Gebler, J. C., and Mattingly, P. G. (1996) Characterization of protein-hapten conjugates. 2. Electrospray mass spectrometry of bovine serum albumin-hapten conjugates. *Bioconjugate Chem.* 7, 475–481.
- Anson, C. E., Creaser, C. S., Egyed, O., Fey, M. A., and Stephenson, G. R. (1994) FTIR detection of an enzyme-bound organometallic carbonyl probe in the presence of the unbound probe molecule. *J. Chem. Soc., Chem. Commun.*, 39–40.
- Bradford, M. M. (1976) A rapid and sensitive method for the quantitation of microgram quantities of protein utilizing the principle of protein-dye binding. *Anal. Biochem.* 72, 248–254.
- Bukowska-Strzyzewska, M., Tosik, A., Wodka, D., and Zakrzewski, J. (1994) The X-ray crystal structure, ¹³C and ¹⁵N NMR spectra of $(\eta^5\text{-C}_5\text{H}_5)\text{Fe}(\text{CO})_2(\eta^1\text{-N-phthalimidato})$. *Polyhedron* 13, 1689–1694.
- Carver, J. A., Fates, B., and Kane-Maguire, L. A. P. (1993) Selective labelling of peptides using (dienyl)iron tricarbonyl cations. *J. Chem. Soc., Chem. Commun.*, 928–929.
- Cohen, S. A., and Strydom, D. J. (1988) Amino acid analysis utilizing phenylisothiocyanate derivatives. *Anal. Biochem.* 174, 1–16.
- Dalla Riva Toma, J. M., and Bergstrom, D. E. (1994) Transition metal labeling of oligodeoxyribonucleotides: synthesis and characterization of (pentacarbonyl)tungsten(0) nucleoside phosphites. *J. Org. Chem.* 59, 2418–2422.
- Erlanger, B. F. (1980) The preparation of antigenic hapten-carrier conjugates: a survey. *Methods Enzymol.* 70, 85–97.
- Furuya, F. R., Miller, L. L., Hainfeld, J. F., Christopfel, W. C., and Kenny, P. W. (1988) Use of $\text{Ir}_4(\text{CO})_{11}$ to measure the lengths of organic molecules with a scanning transmission electron microscope. *J. Am. Chem. Soc.* 110, 641–643.
- Gill, T. J., III, and Mann, L. T. (1966) Studies on synthetic polypeptide antigens XV. The immunochemical properties of ferrocenyl-poly Glu58Lys36Tyr6 (N°2) conjugates. *J. Immunol.* 96, 906–912.
- Gorfti, A., Salmain, M., Jaouen, G., McGlinchey, M. J., Benouna, A., and Mousser, A. (1996) Covalent and selective labeling of proteins with heavy metals. Synthesis, X-ray structure and reactivity studies of N-succinimidyl and N-sulfosuccinimidyl ester organotungsten complexes. *Organometallics* 15, 142–151.
- Jaouen, G., Vessières A., and Butler, I. S. (1993) Bioorganometallic chemistry: a future direction for transition metal organometallic chemistry? *Acc. Chem. Res.* 26, 361–369.
- King, R. B. (1965) Cyclopentadienyl iron dicarbonyl iodide. In *Organometallic Syntheses*, Academic Press, New York.
- Krämer, R. (1996) Application of π -arene-ruthenium complexes in peptide labeling and peptide synthesis. *Angew. Chem., Int. Ed. Engl.* 35, 1197–1199.
- Maliszka, K. L., Top, S., Vaissermann, J., Caro, B., Sénéchal-Tocquer, M.-C., Sénéchal, D., Saillard, J.-Y., Triki, S., Kahlal, S., Britten, J. F., McGlinchey, M. J., and Jaouen, G. (1995) Organometallics as potential protein labels: Pyrylium and pyridinium salts bearing $(\text{C}_6\text{H}_5)\text{Cr}(\text{CO})_3$, $(\text{C}_5\text{H}_4)\text{Mn}(\text{CO})_3$ and ferrocenyl substituents. *Organometallics* 14, 5273–5280.
- Oshita, T., and Katunuma, N. (1993) Analysis of lysosomal degradation of fluorescein isothiocyanate-labelled proteins by

- Toyaparl HW-40 affinity chromatography. *J. Chromatogr.* 633, 28–286.
- Philomin, V., Vessièrès, A., and Jaouen, G. (1994) New applications of carbonylmetalloimmunoassay (CMIA): a non-radioisotopic approach to cortisol assay. *J. Immunol. Methods* 171, 201–210.
- Rifai, A., and Wong, S. S. (1986) Preparation of phosphorylcholine-conjugated antigens. *J. Immunol. Methods* 94, 25–30.
- Rudolf, B., and Zakrzewski, J. (1994) (η^5 -cyclopentadienyl)Fe(CO)₂ - complex of maleimide anion: An organometallic carbonyl probe for biomolecules containing SH groups. *Tetrahedron Lett.* 35, 9611–9612.
- Rudolf, B., and Zakrzewski, J. (1996) Addition of imidazoles and aminoacids to the ethylenic bond in (η^5 -C₅H₅)Fe(CO)₂(η^1 -N-imidato). *J. Organomet. Chem.* 522, 313–315.
- Salmain, M., Vessièrès, A., Jaouen, G., and Butler, I. S. (1991) Fourier transform infrared spectroscopic technique for the quantitative analysis of transition metal carbonyl-labeled bioligands. *Anal. Chem.* 63, 2323–2329.
- Salmain, M., Vessièrès, A., Brossier, P., Butler, I. S., and Jaouen, G. (1992) Carbonylmetalloimmunoassay (CMIA), a new type of non-radioisotopic immunoassay. I. Principles and application to phenobarbital assay. *J. Immunol. Methods* 148, 65–75.
- Salmain, M., Gunn, M., Gorfti, A., Top, S., and Jaouen, G. (1993) Labeling of proteins by organometallic complexes of rhenium (I). Synthesis and biological activity of the conjugates. *Bioconjugate Chem.* 4, 425–433.
- Salmain, M., Malisza, K. L., Top, S., Jaouen, G., Sénéchal-Tocquer, M.-C., Sénéchal, D., and Caro, B. (1994) [η^5 -cyclopentadienyl] metal tricarbonyl pyrylium salts: novel reagents for the specific conjugation of proteins with transition organometallic labels. *Bioconjugate Chem.* 5, 655–659.
- Sashidhar, R. B., Capoor, A. K., and Ramana, D. (1994) Quantitation of ϵ -amino group using amino acids as reference standards by trinitrobenzene sulfonic acid. *J. Immunol. Methods* 167, 121–127.
- Snyder, S. L., and Sobocinski, P. Z. (1975) An improved 2,4,6-trinitrobenzene sulfonic acid method for the determination of amines. *Anal. Biochem.* 64, 284–288.
- Varenne, A., Salmain, M., Brisson, C., and Jaouen, G. (1992) Transition metal carbonyl labeling of proteins. A novel approach to a solid phase two-site immunoassay using Fourier transform infrared spectroscopy. *Bioconjugate Chem.* 3, 471–476.
- Varenne, A., Vessièrès, A., Salmain, M., Brossier, P., and Jaouen, G. (1995) Production of specific antibodies and development of a non-isotopic immunoassay for carbamazepine by the Carbonyl metallo immunoassay (CMIA) method. *J. Immunol. Methods* 186, 195–204.
- Wang, Z., Roe, B. A., Nicholas, K. M., and White, R. L. (1993) Metal carbonyl labels for oligonucleotide analysis by Fourier transform infrared spectroscopy. *J. Am. Chem. Soc.* 115, 4399–4400.
- Wong, S. S. (1991) *Chemistry of Protein Conjugation and Cross-Linking*, CRC Press, Boca Raton, FL.
- Zakrzewski, J. (1987) The photochemical reaction of (η^5 -C₅H₅)Fe(CO)₂-diisopropylamine system with pyrrole and indole. *J. Organomet. Chem.* 327, C41–C42.
- Zakrzewski, J. (1989) The photosubstitution of iodide in (η^5 -C₅H₅)Fe(CO)₂I. Synthesis of cyclopentadienyliron dicarbonyl- and carbonyl-phosphine complexes containing η^1 -N-imidato (1-) ligands. *J. Organomet. Chem.* 359, 215–219.
- Zakrzewski, J., and Giannotti, C. (1990) An improved photochemical synthesis of azaferrocene. *J. Organomet. Chem.* 388, 175–179.
- Zakrzewski, J., Tosik, A., and Bukowska-Strzyzewska, M. (1995) Photochemical reactions of (η^5 -cyclopentadienyl) dicarbonyl-iron iodide with 1-substituted uracils in the presence of diisopropylamine: Crystal structure of the (η^5 -C₅H₅)Fe(CO)₂ complex of deprotonated 5-fluoro-1-(tetrahydro-2-furyl)uracil (Ftorafur). *J. Organomet. Chem.* 495, 83–90.

BC970081X

Practical Method for the Multigram Separation of the 5- and 6-Isomers of Carboxyfluorescein

Francis M. Rossi[†] and Joseph P. Y. Kao^{*}

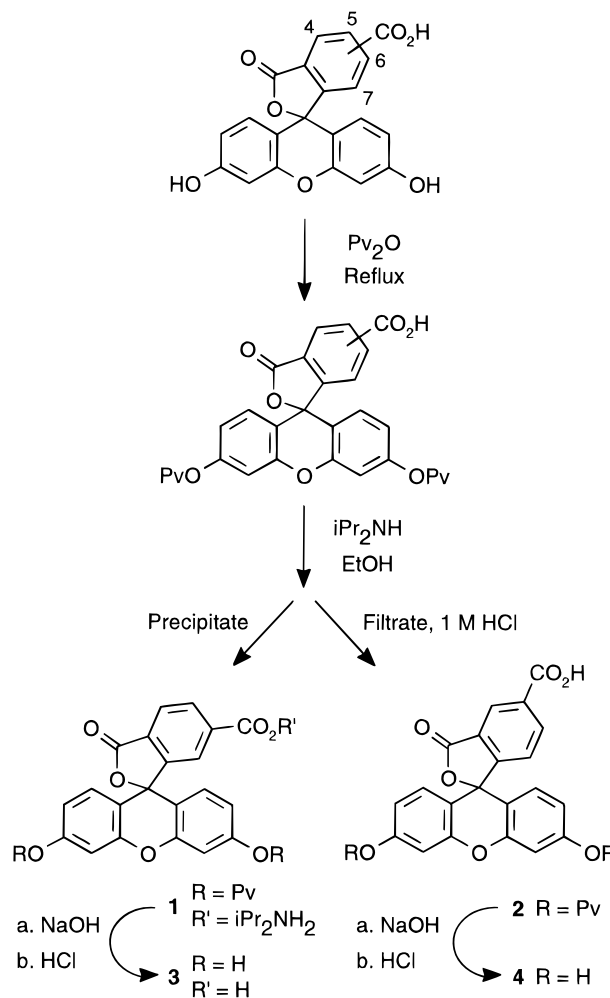
Medical Biotechnology Center and Department of Physiology, School of Medicine, University of Maryland, Baltimore, Maryland 21201. Received April 9, 1997[®]

An efficient preparative method for separating 5- and 6-carboxyfluorescein is presented. 6-Carboxyfluorescein dipivalate is isolated as its diisopropylamine salt, which can be converted to the free acid or used directly in coupling reactions. The 5-isomer is isolated from the acidified mother liquor. Isomerically pure carboxyfluoresceins are prepared by hydrolysis of the corresponding dipivalates.

Fluorescently labeled biologically active molecules have many important analytical and biochemical applications (1–5). Carboxyfluorescein is a useful reagent for the preparation of hydrolytically stable fluorescent conjugates and is a useful starting material for the synthesis of other fluorescein-derived reagents (1, 4–7). It is prepared as a mixture of roughly equal amounts of the 5- and 6-isomers by the reaction of benzene tricarboxylic acid anhydride with resorcinol and zinc chloride (8, 9). Although these isomers have nearly identical properties, when conjugated to other molecules, differences have been observed in conjugate polarity, internal fluorescence quenching, and, for the case of a related rhodamine labeling reagent, labeling specificity (10, 11). Moreover, multistep synthetic preparations of fluorescein derivatives require isomerically pure starting material so that reaction products can be easily purified and identified. Although isomerically pure carboxyfluorescein is commercially available in milligram quantities (12), we are aware of no published method for the separation of these isomers that is simple and does not require extensive chromatography.

With this in mind, we set out to develop a practical method for separating 5- and 6-isomers of carboxyfluorescein as shown in Scheme 1.¹ The poor solubility of fluorescein derivatives and their existence as either lactone or free acid tautomers complicate isomeric separation. Both of the problems were circumvented by heating carboxyfluorescein in pivalic anhydride to give a crude mixture of dipivalates. When this mixture was dissolved in ethanol and treated with various amines, an insoluble salt selectively formed between the 6-isomer and hindered amines such as diisopropylamine and diisopropylethylamine. When other solvents were ex-

Scheme 1



amined, e.g. methanol, isopropyl alcohol, acetonitrile, and acetone, no precipitate formed. NMR analysis of the diisopropylamine salt (1) indicated that the isomeric purity was >95%. The 5-isomer of carboxyfluorescein dipivalate (2) was crystallized from a nitromethane solution of the acidified mother liquor left from the preparation of 1. NMR analysis showed that it also had an isomeric purity >95%. Attempts to apply this method to separate the isomers of carboxyfluorescein diacetate failed to give an isomerically pure precipitate in all examined combinations of amines and solvents.

From the separated dipivalates, the corresponding carboxyfluoresceins (3 and 4) were prepared as shown

* Address correspondence to this author at the Medical Biotechnology Center and Department of Physiology, School of Medicine, University of Maryland, 725 W. Lombard St., Baltimore, MD 21201 [telephone (410) 706-4167; fax (410) 706-8184; e-mail jkao@umabnet.ab.umd.edu].

[†] Present address: Department of Chemistry, Santa Clara University, Santa Clara, CA 95053 (e-mail frossi@scuacc.scu.edu).

[®] Abstract published in *Advance ACS Abstracts*, June 15, 1997.

¹ Two numbering schemes for fluorescein coexist in the literature. The numbering convention adopted here is based on the lactone form of fluorescein (see Scheme 1), with the spiro carbon being position 1. An alternate numbering convention is based on the ring-opened free acid form of fluorescein, with the point of attachment of the phenyl ring to the xanthene chromophore being position 1. In the latter convention, 4- and 5-carboxyfluorescein, respectively, correspond to 5- and 6-carboxyfluorescein in the lactone convention used here.

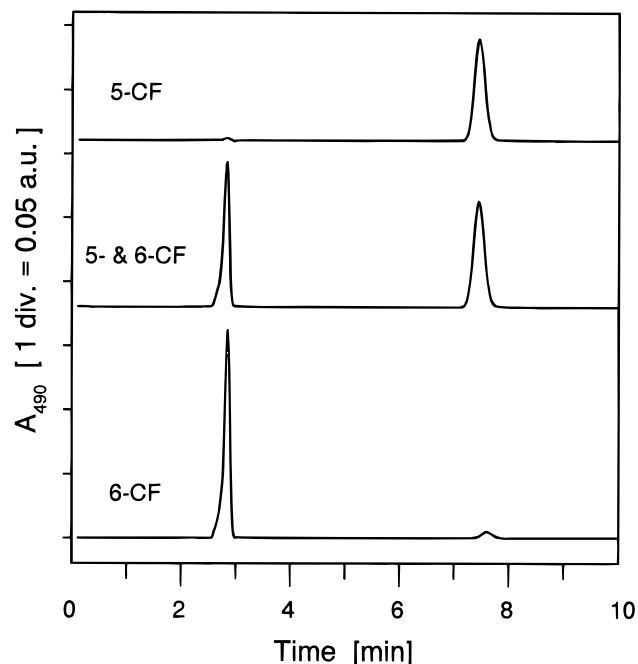


Figure 1. HPLC analysis of 5- and 6-carboxyfluoresceins as shown by elution profiles of 5- and 6-carboxyfluoresceins, prepared according to the method of Scheme 1, and the parent isomeric mixture, prepared as previously described (8, 9). Mobile phase for isocratic elution was an 8:2 mixture of 10 mM sodium phosphate (pH 7.05) and methanol. Approximately 25–50 nmol of sample was injected for each run. Samples were prepared as described under Experimental Procedures.

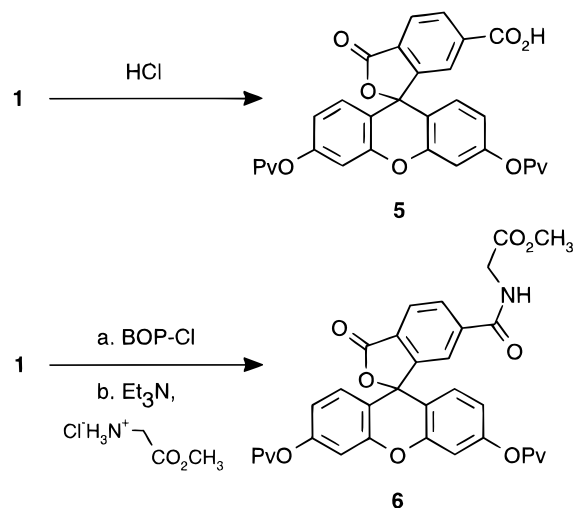
in Scheme 1. To assess the effectiveness of the separation procedure more quantitatively, we analyzed the resulting 5- and 6-carboxyfluoresceins by HPLC. The results are shown in Figure 1. Peak integration revealed that the 5-carboxyfluorescein sample contained 1.4% 6-carboxyfluorescein, whereas the 6-carboxyfluorescein sample contained 4.6% 5-carboxyfluorescein. The percentages given are based on total carboxyfluorescein in each sample and are not relative percentages. Thus, HPLC analysis confirmed that the procedure we have described is quite efficient for separating the two positional isomers of carboxyfluorescein.

Carboxyfluorescein dipivalates are useful synthetic intermediates in themselves (*1*), in addition to being precursors to carboxyfluoresceins **3** and **4**. For example, the diisopropylamine salt (**1**) was converted to the carboxylic acid (**5**) by treatment with HCl or was used directly in reactions that normally require an equivalent of base, as shown in Scheme 2. Thus, when salt **1** was treated with bis(2-oxo-3-oxazolidinyl)phosphinic chloride (BOP-Cl) and glycine methyl ester hydrochloride, amide conjugate **6** was isolated.

EXPERIMENTAL PROCEDURES

General. Reagents and solvents used were of ACS or HPLC grade and used as received from Aldrich or Fisher. All oxygen and water-sensitive reactions were performed under a dry argon atmosphere. For water-sensitive reactions, glassware was dried at 130 °C for at least 3 h and cooled under a stream of argon gas or in a desiccator prior to use. Silica gel 60 (230–400 mesh, E. Merck) was used for compounds purified by chromatography. Melting points were recorded on a Melt-temp II (Laboratory Devices) apparatus coupled to an Omega (Omega Engineering) HH23 digital thermometer and are uncorrected. The structures of all purified products were established by NMR spectral analysis. Spectra were recorded on a

Scheme 2



General Electric QE-300 (300 MHz) NMR spectrometer. Samples were dissolved in CDCl_3 (0.03% TMS), unless otherwise stated, and were referenced to tetramethylsilane (TMS). Samples dissolved in solvents other than CDCl_3 were referenced to the residual solvent peak. High-resolution mass spectral analysis was performed at the University of Maryland, College Park, on a Model VG707E spectrometer (VG Analytical).

HPLC Analyses. HPLC analyses were performed on a Waters chromatograph (Waters Corp.) consisting of a Model 600E multisolvent delivery system coupled to a Model 996 photodiode array detector. An Inertsil ODS-2 column (250 \times 4.6 mm, 5 μm particle size; MetaChem Technologies, Inc.) was used for analytical separations. The mobile phase for isocratic elution was an 8:2 mixture of 10 mM sodium phosphate (pH 7.05) and methanol. All elutions were performed at a flow rate of 1 $\text{mL} \cdot \text{min}^{-1}$, at room temperature. Millennium 2010 software (Waters Corp.) was used for data acquisition and analysis. All samples were made by mixing 1 mg of carboxyfluorescein with 2 equiv of 1 M NaOH and diluting the mixture with 10 mM sodium phosphate buffer (pH 7.05) to yield 10 mM carboxyfluorescein. Aliquots of 2.5–5 μL were injected for analysis.

Preparation of 6-Carboxyfluorescein Dipivalate Diisopropylamine Salt (1**).** 5(6)-Carboxyfluorescein (5.00 g, 13 mmol) was refluxed in trimethylacetic anhydride (10 mL, 49 mmol) for 2 h. The reaction mixture was cooled to room temperature and diluted with tetrahydrofuran (THF; 10 mL) and water (10 mL). After 2 h of vigorous stirring, ether (50 mL) was added and the aqueous layer was removed. The organic layer was washed with phosphate buffer (3 \times 25 mL, 1.4 M, pH 7.0), aqueous HCl (50 mL, 1 M), and saturated NaCl and dried with MgSO_4 . The solvent was removed by evaporation, and the resulting yellow syrup was taken up in absolute ethanol (50 mL). Diisopropylamine (5.0 mL, 36 mmol) was added, and the solution was cooled to -20 °C. The resulting solid was removed by filtration and washed with cold ethanol and acetone to give 2.39 g (28%) of **1**, which had an isomeric purity >95% as determined by proton NMR analysis: ^1H NMR δ 1.23 (d, J = 6.35 Hz, 12 H), 1.35 (s, 18 H), 3.21 (a quintet, J = 6.35 Hz, 2 H), 6.75 (dd, J = 1.95, 8.79 Hz, 2 H), 6.84 (d, J = 8.79 Hz, 2 H), 7.03 (d, J = 1.95 Hz, 2 H), 7.69 (s, 1 H), 7.99 (d, J = 7.81 Hz, 1 H), 8.26 (d, J = 7.81 Hz, 1 H); ^{13}C NMR δ 19.0, 27.0, 39.1, 46.3, 110.1, 116.3, 117.6, 124.3, 124.5, 126.7, 129.0, 131.1, 145.5, 151.4, 152.4, 152.9, 169.2, 169.8, 176.5; FABMS ($\text{M} + \text{H}^+$) 646; HRMS(EI) calcd for $\text{C}_{31}\text{H}_{29}\text{O}_9$ (carboxylate + 2H^+) 545.1812, observed 545.1835.

Preparation of 5-Carboxyfluorescein Dipivalate (2). The solvent was evaporated from the filtrate obtained in the preparation of **1**. The resulting syrup was diluted with ether (50 mL) and extracted with water (4 × 25 mL) and aqueous HCl (1 M, 25 mL). The organic layer was dried with MgSO₄, and the solvent was evaporated. The resulting foam was dissolved in nitromethane (10 mL) and cooled to -20 °C. A solid formed and was isolated by filtration and washed with a small amount of cold nitromethane to give 1.39 g (19%) of **2** that was isomerically pure by proton NMR analysis: mp 220–222 °C; ¹H NMR δ 1.36, (s, 18 H), 6.82, (s, 4 H), 7.08 (s, 2 H), 7.30 (d, *J* = 8.3 Hz, 1 H), 8.41 (d, *J* = 8.8 Hz, 1 H), 8.78 (s, 1H); ¹³C NMR δ 27.0, 39.1, 110.5, 115.3, 117.9, 124.4, 126.6, 127.6, 128.7, 131.7, 136.7, 151.4, 152.8, 157.5, 168.0, 169.7, 176.5; HRMS(CI) calcd for C₃₁H₂₉O₉ (M + H⁺) 545.1812, obsd 545.1804.

Preparation of 6-Carboxyfluorescein (3). Sodium hydroxide (1 M, 1.5 mL, 1.5 mmol) was added to a solution of pivalate **1** (0.161 g, 0.25 mmol) in methanol (3 mL). The colorless solution became orange on addition of the base. After 30 min of stirring, the solvent was evaporated, and the residue was dissolved in water and acidified with HCl (1 M, 1.5 mL, 1.5 mmol). The resulting solid was isolated by filtration and washed with water and ether to give 0.071 g (75%) of **3**: purity 95.4% by HPLC; mp 352–356 °C; ¹H NMR (NaOD/D₂O) δ 6.50 (m, 4 H), 7.18 (d, *J* = 9.8 Hz, 2 H), 7.83 (d, *J* = 1.5 Hz, 1 H), 7.86 (d, *J* = 8.3 Hz, 1 H), 8.09 (dd, *J* = 1.5, 7.8 Hz, 1 H); ¹³C NMR δ 106.1, 114.4, 125.2, 130.4, 132.1, 132.9, 133.3, 133.4, 133.7, 139.6, 144.4, 159.9, 160.6, 176.8, 177.4; HRMS(CI) calcd for C₂₁H₁₃O₇ (M + H⁺) 377.0661, obsd 377.0648.

Preparation of 5-Carboxyfluorescein (4). Sodium hydroxide (1 M, 3 mL, 3 mmol) was added to a solution of **2** (0.272 g, 0.50 mmol) in THF (3 mL). After 15 min, the solvent was evaporated and the resulting foamy residue was dissolved in water. The solution was acidified with concentrated HCl, giving a precipitate that was isolated by filtration, washed with water, and air-dried to give 0.185 g (98%) of **4** as an orange solid: purity 98.6% by HPLC; mp 368–372 °C; ¹H NMR (NaOD/D₂O) δ 6.46 (d, *J* = 1.96 Hz, 2 H), 6.52 (dd, *J* = 1.96, 9.27 Hz, 2 H), 7.05 (d, *J* = 9.28 Hz, 2 H), 7.11 (d, *J* = 8.30 Hz, 1 H), 7.93 (d, *J* = 9.28 Hz, 1 H), 8.16 (s, 1 H); ¹³C NMR δ 106.3, 114.3, 125.4, 130.9, 131.8, 132.5, 133.6, 136.3, 139.8, 142.2, 160.38, 160.39, 176.9, 177.2, 183.0; HRMS(EI) calcd for C₂₁H₁₂O₇ (M⁺) 376.0583, obsd 376.0590.

Preparation of 6-Carboxyfluorescein Dipivalate (5). Carboxyfluorescein salt **1** (1.50 g, 2.32 mmol) was dissolved in dichloromethane (25 mL) and extracted with aqueous HCl (1 M, 2 × 25 mL). The organic layer was dried with MgSO₄, and the solvent was evaporated to give 1.20 g (95%) of **5**: mp 198–200 °C; ¹H NMR δ 1.36 (s, 18 H), 6.79 (s, 4 H), 7.08 (s, 2 H), 7.86 (s, 1 H), 8.13 (d, *J* = 7.81 Hz, 1 H), 8.35 (d, *J* = 7.81 Hz, 1 H); ¹³C NMR δ 27.0, 39.1, 110.4, 115.3, 117.8, 125.4, 125.8, 128.6, 130.1, 131.7, 135.8, 151.5, 152.7, 153.1, 168.1, 169.2, 176.4; HRMS(CI) calcd for C₃₁H₂₉O₉ (M + H⁺) 545.1812, obsd 545.1784.

Preparation of N-(Dipivaloylfluorescein-6-ylcarbonyl)glycine Methyl Ester (6). BOP-Cl (0.280 g, 1.10 mmol) was added to a suspension of fluorescein salt **1**

(0.323 g, 0.50 mmol) in dichloromethane (3 mL). After 10 min, glycine methyl ester hydrochloride (0.138 g, 1.10 mmol) was added followed by triethylamine (0.17 mL, 1.10 mmol). The reaction mixture was stirred overnight, taken up in ethyl acetate (25 mL), and extracted with water and 1 M HCl. The organic layer was dried with MgSO₄, and the solvent was evaporated. The resulting solid was chromatographed with hexane/ethyl acetate (1:1) to give 0.169 g (55%) of **6**: ¹H NMR δ 1.36 (s, 18 H), 3.71 (s, 3 H), 4.19 (d, *J* = 4.9 Hz, 2 H), 6.68 (br s, 1 H), 6.80 (s, 4 H), 7.07 (s, 2 H), 7.52 (s, 1 H), 8.10 (s, 2 H); ¹³C NMR δ 27.0, 39.1, 41.7, 52.4, 110.4, 115.4, 117.8, 122.5, 125.6, 128.4, 128.8, 129.5, 140.3, 151.4, 152.7, 153.4, 165.6, 168.2, 169.9, 176.5; HRMS(CI) calcd for C₃₄H₃₄NO₁₀ (M + H⁺) 616.2183, obsd 616.2164.

ACKNOWLEDGMENT

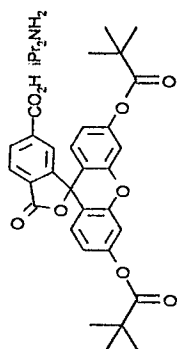
This work was supported by NIH Grant GM46956 to J.P.Y.K.

Supporting Information Available: ¹H-NMR spectra of compounds **1–6** (8 pages). Ordering information is given on any current masthead page.

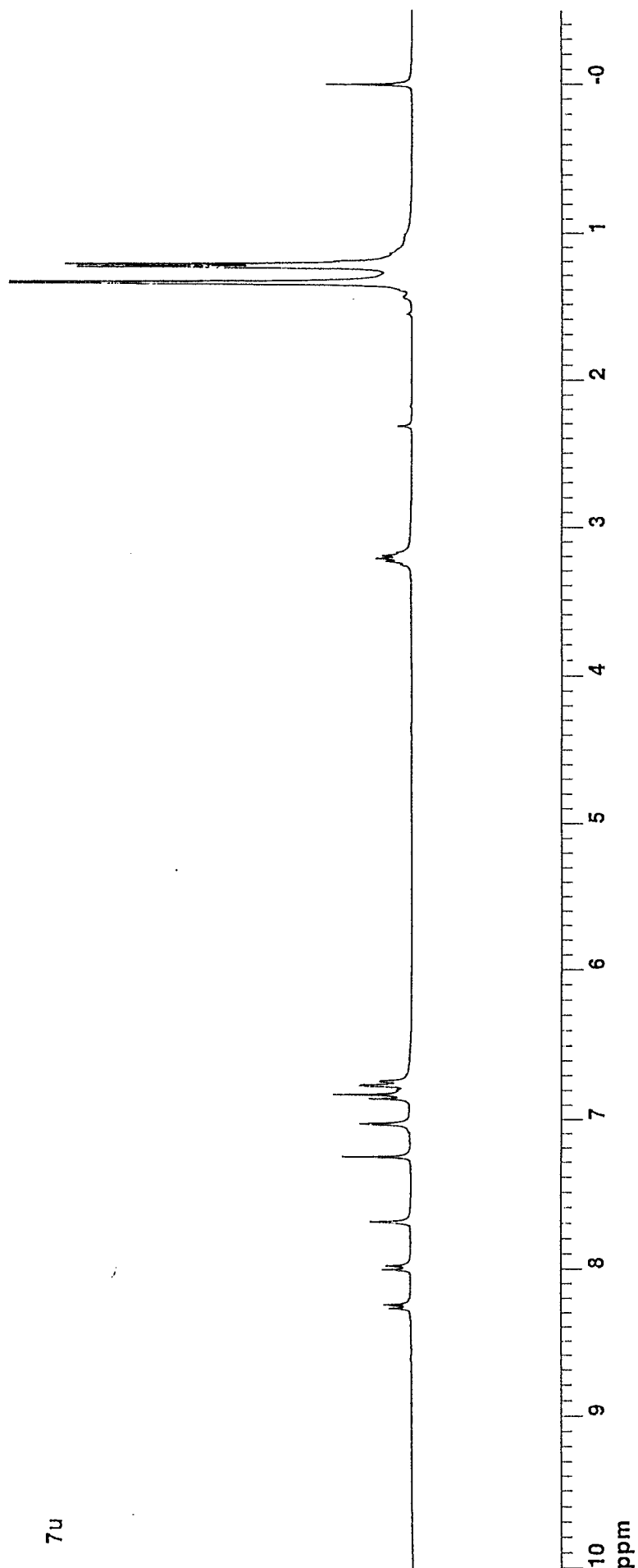
LITERATURE CITED

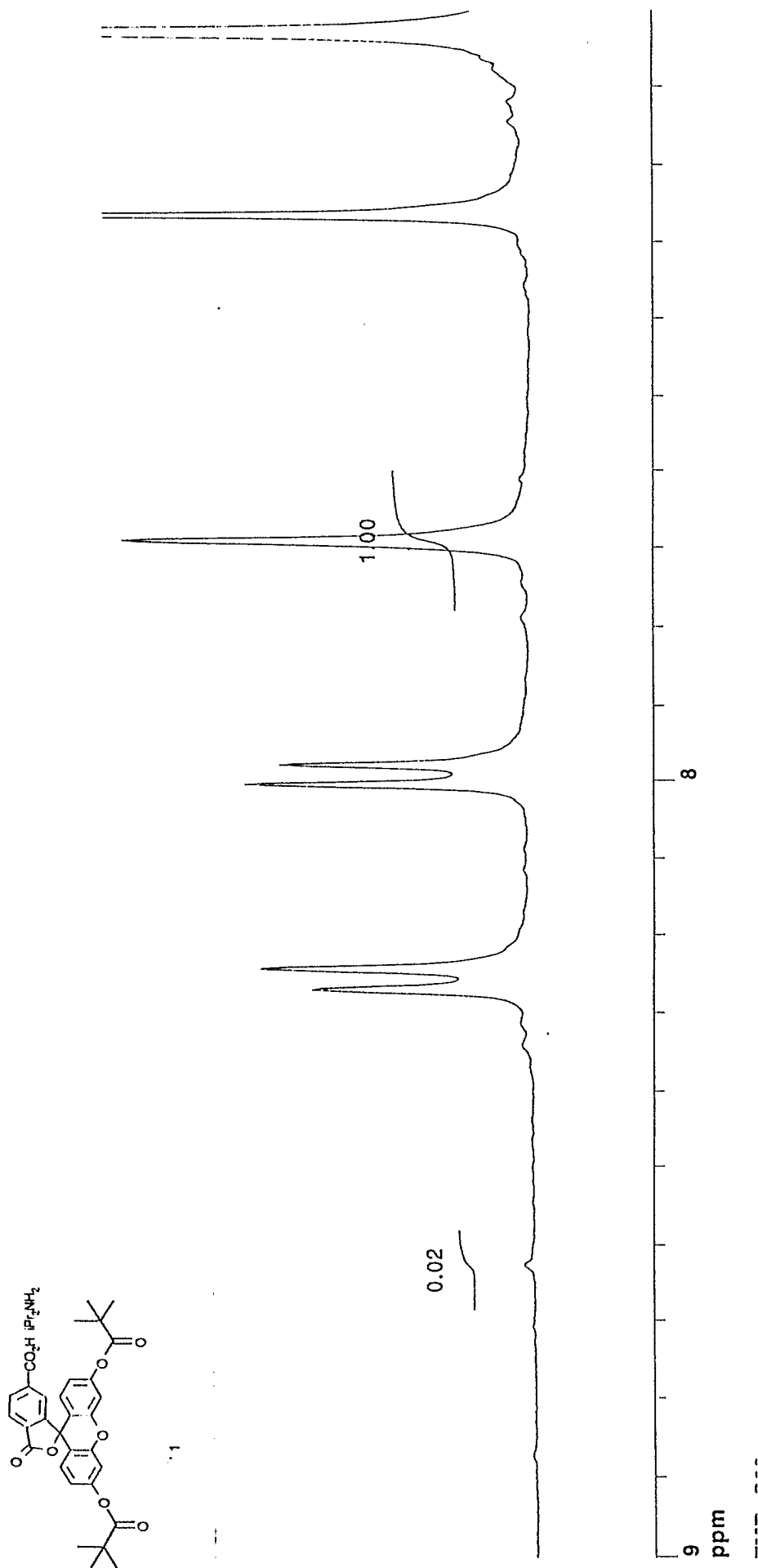
- (1) Theisen, P., McCollum, C., Upadhyaya, K., Jacobson, K., Vu, H., and Andrus, A. (1992) Fluorescent dye phosphoramidite labelling of oligonucleotides. *Tetrahedron Lett.* 33, 5033–5036.
- (2) Goodchild, J. (1990) Conjugates of oligonucleotides and modified oligonucleotides: a review of their synthesis and properties. *Bioconjugate Chem.* 1, 165–187.
- (3) Brinkley, M. (1992) A brief survey of methods for preparing protein conjugates with dyes, haptens, and cross-linking reagents. *Bioconjugate Chem.* 3, 2–13.
- (4) Mattingly, P. (1992) Preparation of 5- and 6-(aminomethyl)-fluorescein. *Bioconjugate Chem.* 3, 430, and ref 2 of this paper.
- (5) Souto, A. A., Acuña, U. A., Andreu, J. M., Barasoain, I., Abal, M., and Amat-Guerri, F. (1995) New fluorescent water-soluble taxol derivatives. *Angew. Chem., Intl. Ed. Engl.* 34, 2710–2712.
- (6) Fiechtner, M., Wong, M., Bieniarz, C., and Shipchandler, M. T. (1989) Hydrophilic fluorescent derivatives: useful reagents for liposome immunolytic assays. *Anal. Biochem.* 180, 140–146.
- (7) Bertrand, R., Derancourt, J., and Kassab, R. (1995) Production and properties of skeletal myosin subfragment 1 selectively labeled with fluorescein at lysine-553 proximal to the strong actin binding site. *Biochemistry* 34, 9500–9507.
- (8) Chen, C.-S., and Poenie, M. (1993) New fluorescent probes for protein kinase C. *J. Biol. Chem.* 268, 15812–15822.
- (9) Orndorff, W. R., and Hemmer, A. J. (1927) Fluorescein and some of its derivatives. *J. Am. Chem. Soc.* 49, 1272–1280.
- (10) Ajtai, K., Ringler, D., Toft, D., Hellen, E. H., Ilich, P. J., and Burghardt, T. P. (1992) Stereospecific reaction of muscle fiber proteins with the 5' or 6' iodoacetamido derivative of tetramethylrhodamine: Only the 6' isomer is mobile on the surface of S1. *Biophys. J.* 61, A287, Abstract 1647.
- (11) Buolamwini, J. K., Craik, J. D., Wiley, J. S., Robins, M. J., Gati, W. P., Cass, C. E., and Paterson, A. R. P. (1994) Conjugates of fluorescein and SAENTA (5'-S-(2-aminoethyl)-N⁶-(4-nitrobenzyl)-5'-thioadenosine): flow cytometry probes for the ES nucleoside transport elements of the plasma membrane. *Nucleosides Nucleotides* 13, 737–751.
- (12) Molecular Probes, Eugene, OR.

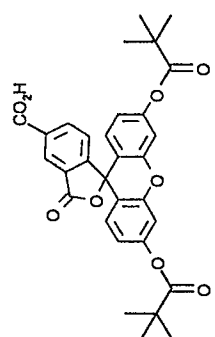
BC970078D



7u

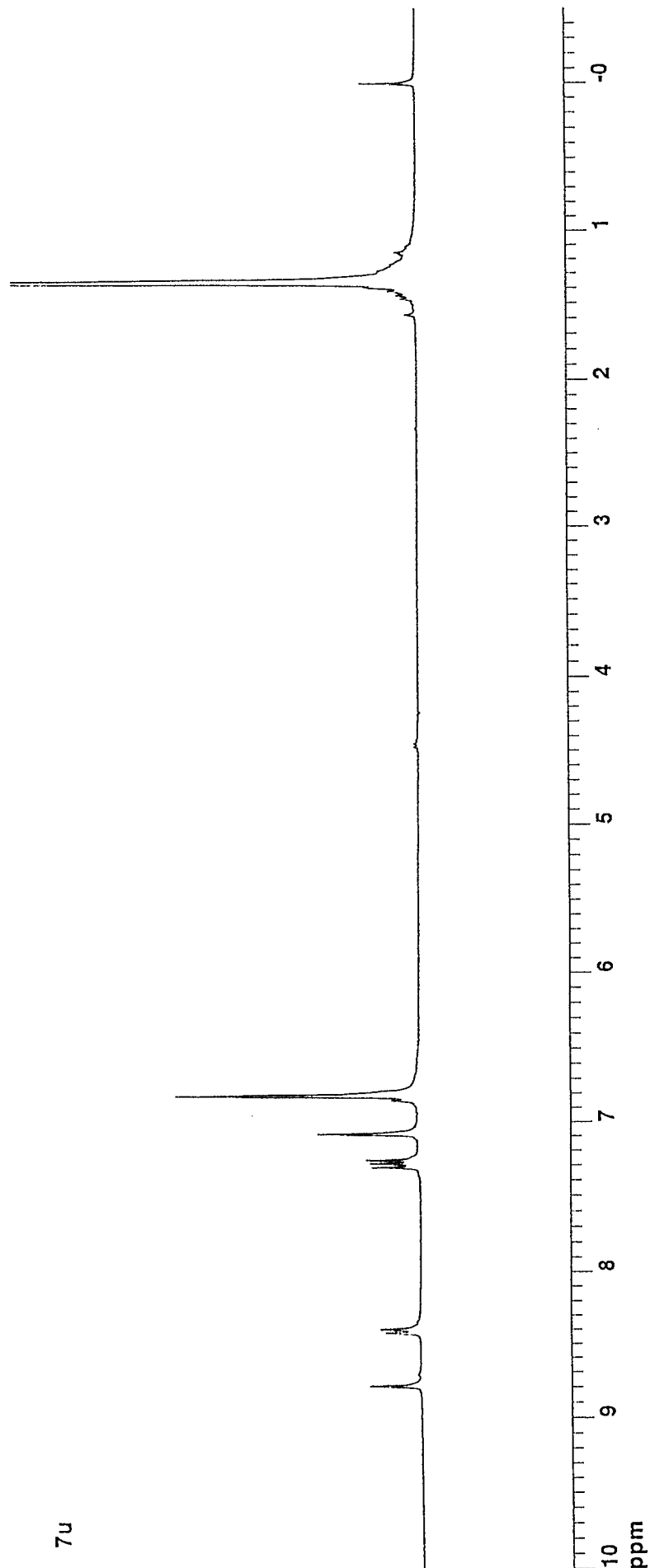


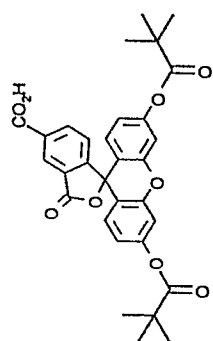




2

7u



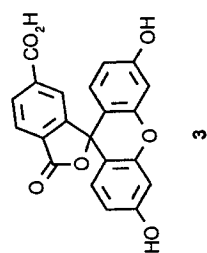


2

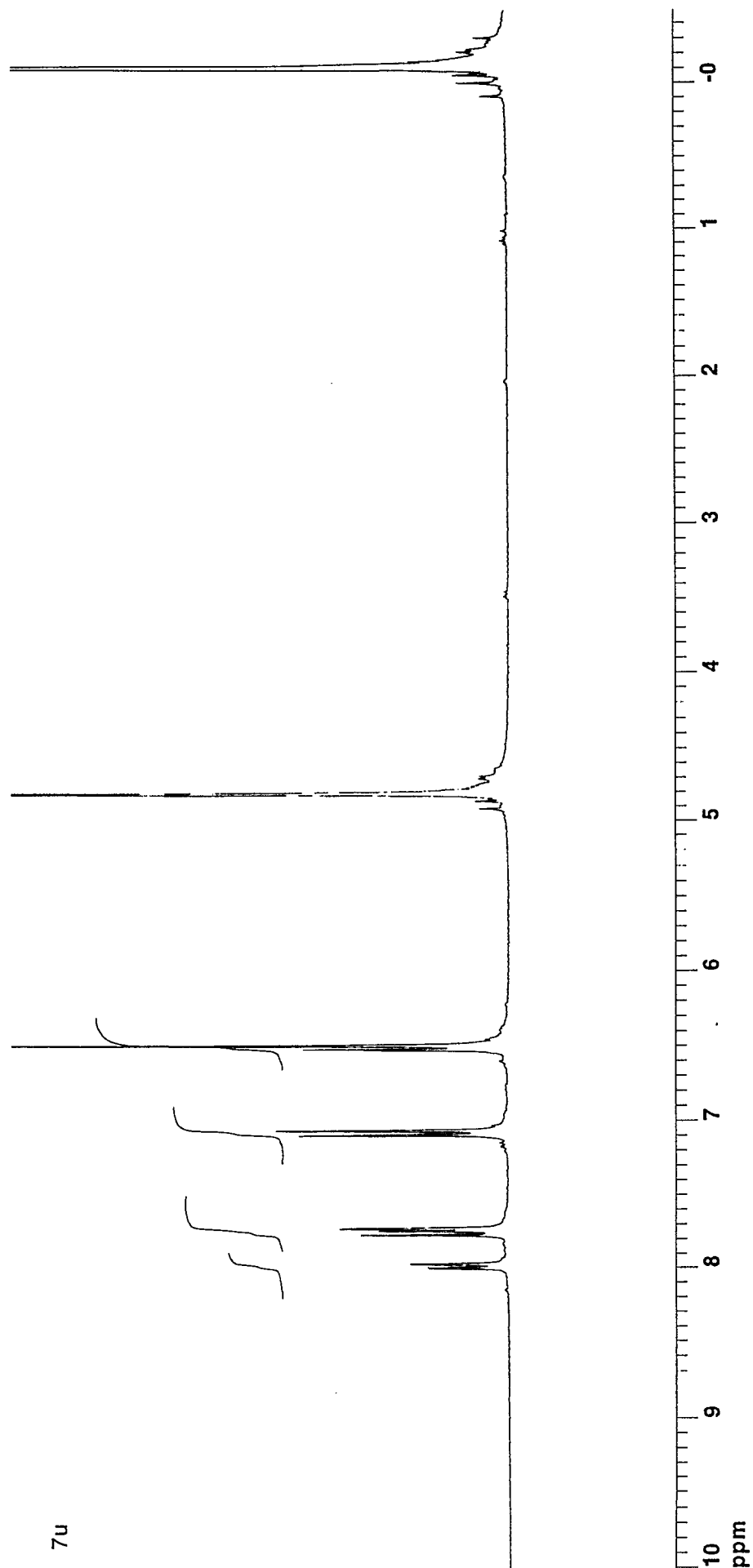
7u

8

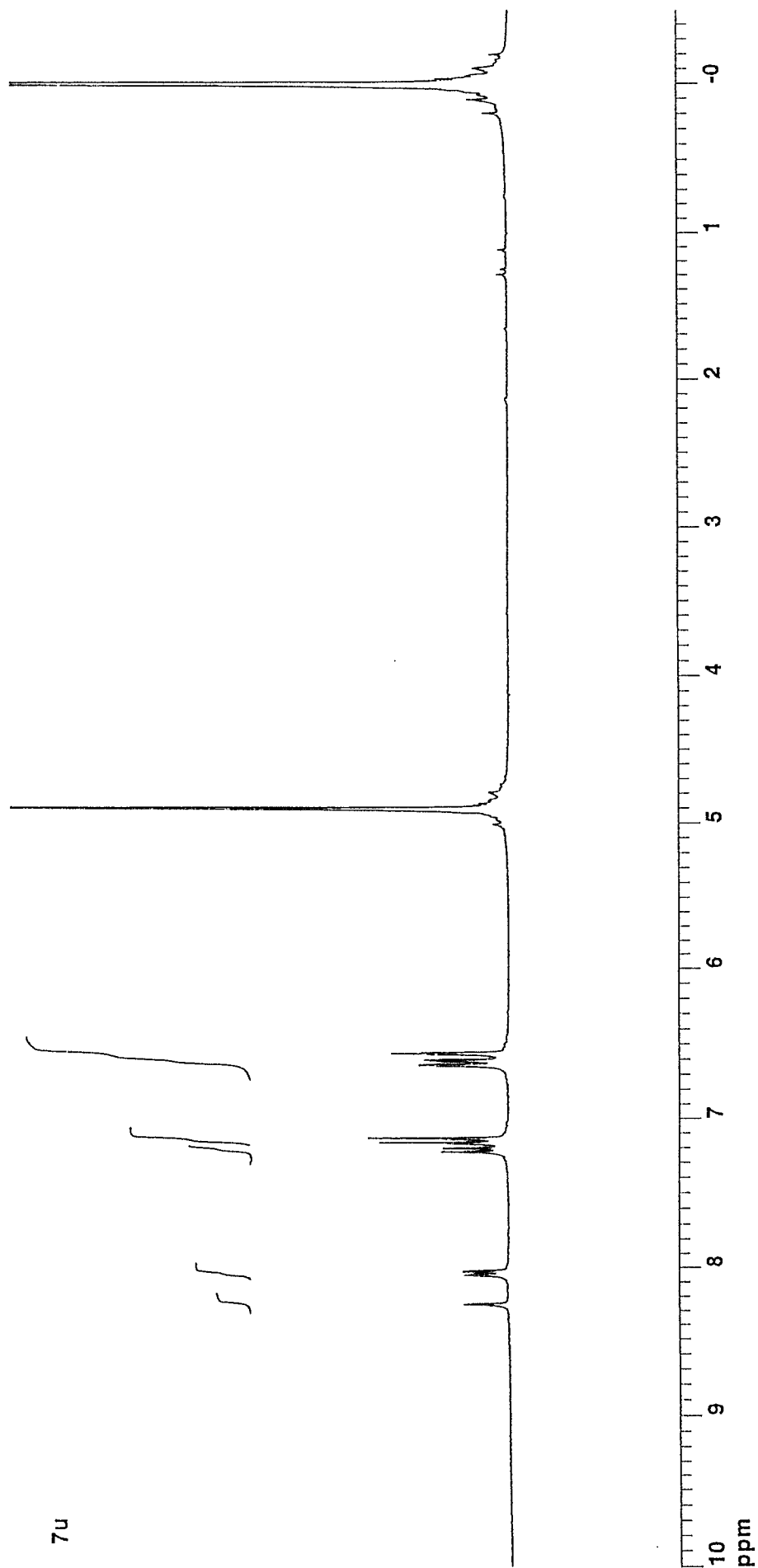
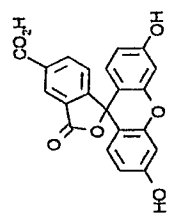
9 ppm

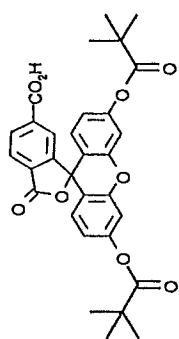


3



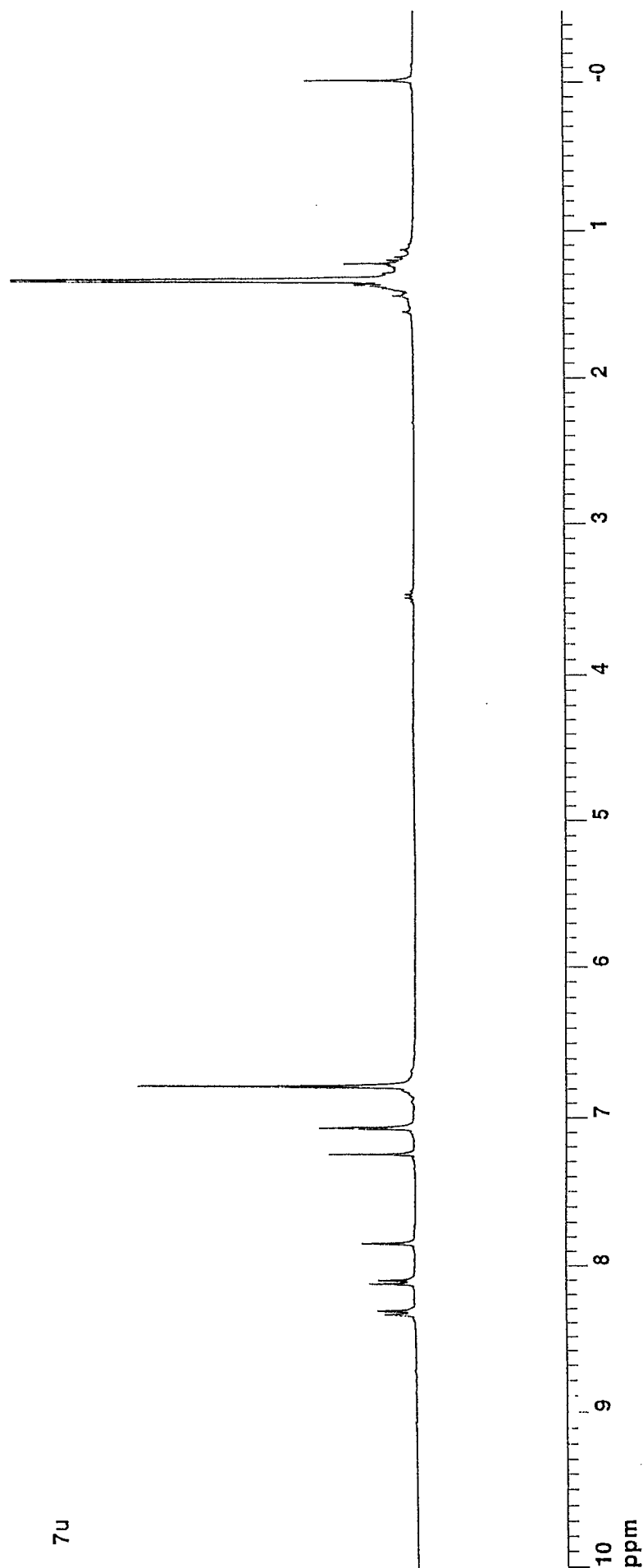
7u

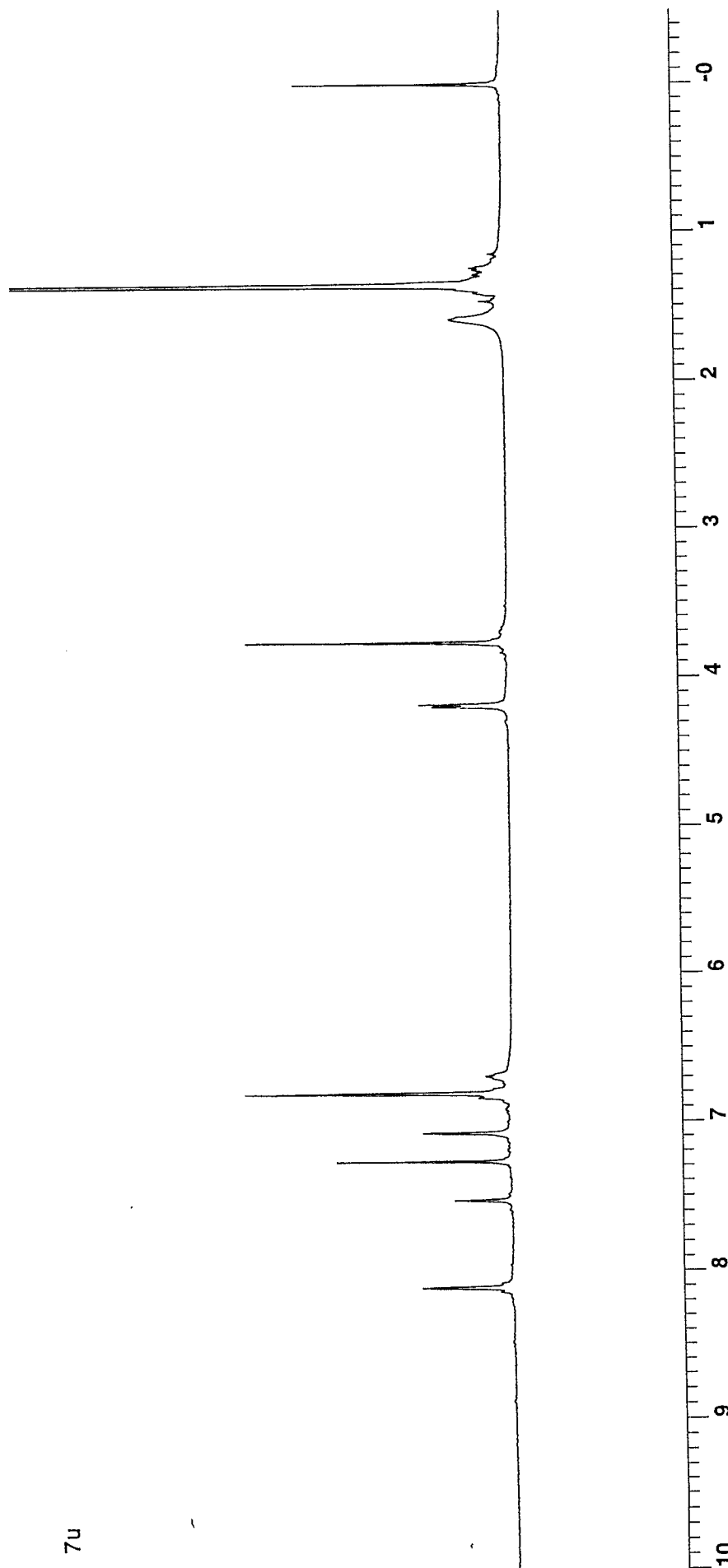
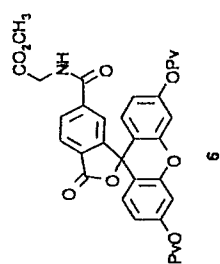




5

7u





ppm

FMR B274

File created:
Friday, July 5, 1996
9:34 AM

Sonolysis Promotes Indirect Co–C Bond Cleavage of Alkylcob(III)alamin Bioconjugates

W. Allen Howard, Jr.,^{†,§} Ashraf Bayomi,[§] Ettaya Natarajan,[§] Mohsen A. Aziza,[‡] Omar El-Ahmady,[‡] Charles B. Grissom,^{*,§} and Frederick G. West^{*,§}

Department of Chemistry, University of Utah, Salt Lake City, Utah 84112, and Faculty of Pharmacy, Al-Azhar University, Naser City, Cairo, Egypt. Received December 13, 1996[®]

Sonolysis of aqueous solutions produces H^\cdot and HO^\cdot that lead to Co–C bond cleavage in methylcob-(III)alamin (CH_3-Cbl^{III}) and 2-[4-[4'-[bis(2-chloroethyl)amino]phenyl]butyroxyl]ethylcob(III)alamin (Chl-HE-Cbl^{III}). Under anaerobic conditions, H^\cdot reduces CH_3-Cbl^{III} to the unstable $19 e^- CH_3-Cbl^{II}$ that dissociates to the alkane and Cbl^{II} . Under aerobic conditions, O_2 scavenges H^\cdot and Co–C bond cleavage occurs via a HO^\cdot -mediated process along with modification of the corrin ring by HO^\cdot . When H^\cdot and HO^\cdot are scavenged, there is no evidence of Co–C bond cleavage. This suggests no direct sonolysis of the Co–C bond occurs, in spite of the fact that the Co–C bond is 80 kcal/mol weaker than the H–OH bond. A bioconjugate of cob(III)alamin and the alkylating agent chlorambucil has been synthesized to give 2-[4-[4'-[bis(2-chloroethyl)amino]phenyl]butyroxyl]ethylcob(III)alamin. The chlorambucil–cobalamin complex also undergoes Co–C bond cleavage in a manner similar to that of methylcob-(III)alamin. Sonorelease of an active alkylating agent from the bioconjugate may provide a new method for the selective release of anticancer drugs and thus potentially reduce systemic toxicity.

The Co–C bond dissociation energies of adenosylcob-(III)alamin and methylcob(III)alamin (CH_3-Cbl^{III}) are about 31 and 37 kcal/mol, respectively (1–3), making this bond one of the weakest covalent linkages that is kinetically stable in aqueous solution (4, 5). Homolytic cleavage of the Co–C bond can be promoted by photolysis, thermolysis, or reducing conditions to produce cob(II)-alamin and the corresponding alkyl radical or closed-shell alkane (1–5). Herein, we report the use of ultrasound to cleave the Co–C bond of alkylcob(III)alamins by an indirect process that is mediated by H^\cdot and HO^\cdot . As an example of the possible utility of ultrasound-induced cleavage of alkylcob(III)alamins, we have tethered chlorambucil, a bisalkylating nitrogen mustard, to cob-(III)alamin. Sonolysis of aqueous 2-[4-[4'-[bis(2-chloroethyl)amino]phenyl]butyroxyl]ethylcob(III)alamin (Chl-HE-Cbl^{III}) produces aquocob(III)alamin and 2-[4-[4'-[bis(2-chloroethyl)amino]phenyl]butyroxyl]ethan-1-ol or 2-[4-[4'-[bis(2-chloroethyl)amino]phenyl]butyroxyl]ethane, depending on reaction conditions.

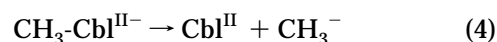
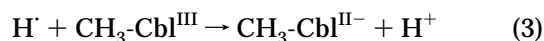
High-frequency sound waves (20 kHz–10 MHz) produce extreme conditions of high temperature (>5000 °C) and pressure (>500 atm) as they initiate bubble formation (cavitation) and collapse in solution (6, 7). In the transient gas phase of these bubbles, water dissociates into hydroxyl radicals (HO^\cdot) and hydrogen atoms (H^\cdot), as shown in eq 1 (8). The bubbles collapse quickly, but the radicals persist. Since hydrogen atoms exist in equilibrium with solvated electrons in alkaline solution (eq 2), all sonolysis experiments reported herein were carried out under neutral or slightly acidic conditions to prevent direct reduction of alkylcob(III)alamin by the solvated

electron.



Even the low-intensity and high-frequency conditions of diagnostic ultrasound can produce radical species (9, 10). The ESR spectrum of a spin-trapped radical that is generated by ultrasound is consistent with the products of eq 1 and H_2O_2 that is a product of HO^\cdot dimerization (11). Under aerobic conditions, O_2 scavenges H^\cdot , and all reactions occur via oxidative processes. Under anaerobic conditions in the presence of an organic compound with abstractable hydrogen atoms, HO^\cdot is depleted and all reactions occur through reductive pathways that are initiated by H^\cdot .

In this paper, we show that sonolysis of anaerobic solutions of CH_3-Cbl^{III} generates sufficient $[H^\cdot]$ to reduce CH_3-Cbl^{III} to the unstable $19 e^- CH_3-Cbl^{II}$ species, followed by loss of the alkyl ligand to return the system to the more stable $18 e^- Cbl^{II}$ species (eqs 3 and 4). Reductive Co–C bond scission is irreversible because a closed-shell alkane is produced (eq 5). This is in contrast to photochemically or thermally induced Co–C bond cleavage that leads to the formation of a radical pair that can undergo recombination (eq 6).



To demonstrate the possible utility of ultrasound to trigger ligand release from a cobalamin bioconjugate *in vivo*, the nitrogen mustard chlorambucil was attached to

* Address correspondence to either of these authors [C.B.G., (801) 581-4153, fax (801) 581-8433, e-mail grissomc@chemistry.chem.utah.edu; F.G.W., (801) 581-4954, fax (801) 581-8433, e-mail west@chemistry.chem.utah.edu].

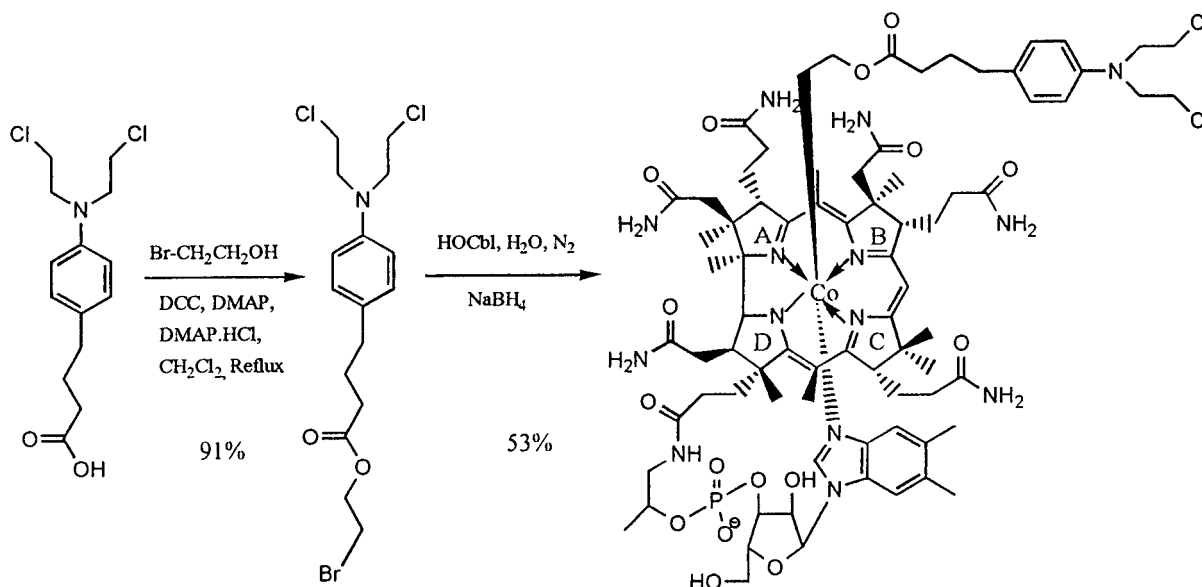
[†] Present address: Parke-Davis Pharmaceutical Research, 2800 Plymouth Rd., Ann Arbor, MI 48105.

[§] University of Utah.

[‡] Al-Azhar University.

[®] Abstract published in *Advance ACS Abstracts*, June 15, 1997.

Scheme 1



cobalamin through a hydroxyethyl linker and the products of sonochemical release have been characterized.

EXPERIMENTAL PROCEDURES

Preparation of 1-Bromo-2-[4-[4'-[bis(2-chloroethyl)amino]phenyl]butyroxylethane (Scheme 1). Twenty-five milliliters of freshly distilled CH_2Cl_2 , 0.343 g of dicyclohexylcarbodiimide (1.66 mmol), 0.305 g of 4-(dimethylamino)pyridine (2.5 mmol), and 0.263 g of 4-(dimethylamino)pyridinium chloride (1.66 mmol) were added to a flame-dried 50 mL round bottom flask equipped with a stir bar, reflux condenser, and Ar inlet (12). The solution was purged with argon and brought to reflux.

While refluxing, a solution of 0.304 g of chlorambucil (1.0 mmol) and 0.125 g of 2-bromoethanol (1.0 mmol) in 5 mL of CH_2Cl_2 (purged under argon for 30 min) was transferred via cannula to the refluxing solution over a period of 30 min. After addition was complete, the reaction mixture was stirred for 2 h at room temperature. Precipitated dicyclohexylurea was removed by filtration, and the solution was concentrated by rotary evaporation. The resulting residue was taken up in CH_2Cl_2 , filtered, and purified by flash silica column chromatography. The desired product was eluted using 1:9 ethyl acetate/hexanes (v/v) to give 0.374 g of a yellow oil in 91% yield: ^1H NMR (CDCl_3 , 300 MHz) δ 7.06 (d, 2 H, J = 8.4 Hz), 6.60 (d, 2 H, J = 8.7 Hz), 4.35 (t, 2 H, J = 6.2 Hz), 3.56–3.72 (m, 8 H), 3.48 (t, 2 H, J = 6.2 Hz), 2.56 (t, 2 H, J = 7.7 Hz), 2.35 (t, 2 H, J = 7.4 Hz), 1.91 (quintet, 2 H, J = 7.6 Hz); ^{13}C NMR (CDCl_3 , 75 MHz ^1H decoupled) δ 173.05, 144.35, 130.37, 129.75 (2), 112.12 (2), 63.68, 53.55 (2), 40.60 (2), 33.94, 33.41, 29.05, 26.72.

Preparation of 2-[4-[4'-[Bis(2-chloroethyl)amino]phenyl]butyroxylethylcob(III)alamin (Chl-HE-Cbl^{III}). Two hundred milligrams of hydroxocob(III)alamin (0.15 mmol) was dissolved in 10 mL of water and purged with Ar under stirring (13). The exiting gas was conducted in sequence through (1) a flask containing 0.025 g of NaBH_4 (0.66 mmol), (2) a flask containing 5 mL of H_2O , and (3) a flask containing 0.226 g of ester (0.55 mmol) in 5 mL of CH_3OH . After deaerating for 1 h, 0.5 mL of the water from flask 2 was transferred to flask 1 containing NaBH_4 via cannula and swirled to promote dissolution. This solution was transferred via cannula to the aqueous cobalamin solution. Reduction

was allowed to proceed for 20 min, after which time the chlorambucil bromoethyl ester was added to the solution. The reaction mixture was allowed to stir for an additional 5 min and then 0.2 mL of acetone was added to destroy the excess borohydride. All of the subsequent purification steps were carried out at 4 °C in a cold room. The solution was concentrated to approximately 2 mL by lyophilization, and the resulting solution was applied to a 2.5 × 30 cm column of Amberlite XAD-2 resin. The column was washed with 1 L of H_2O to desalt, and the cobalamin was eluted with 50% aqueous acetonitrile (v/v). The eluent was reduced to approximately 2 mL by rotary evaporation, and the solution was applied to a 1 × 40 cm column of SP-Sephadex C25 (Na^+ form). Elution with water removed the major red band, which was reduced to a minimal volume. Acetone was added until faint turbidity persisted after swirling. The solution was allowed to stand for 1 h at 0 °C, and excess acetone was added to promote further crystallization. The crystals were collected by vacuum filtration and dried *in vacuo*. Chl-HE-Cbl^{III} was obtained as red crystals (122.5 mg) with a yield of 53%: MS (FAB⁺) calcd for $\text{C}_{78}\text{H}_{111}\text{N}_{14}\text{O}_{16}\text{CoPCl}_2$, 1661.6; found 1663.6.

Sonolysis. Sonolysis was carried out with a Branson ultrasonic bath (Model 3200) operating at 47 kHz. The correct placement of the reaction vessel at a focal point of high-intensity ultrasound was determined by the oxidation of iodide to iodine in the presence of starch (14), and the temperature of the bath was maintained at 21 °C by a constant-temperature circulator. Aerobic sonolysis was typically carried out in a test tube or Erlenmeyer flask, whereas anaerobic sonolysis was carried out in a closed reaction vessel fitted with a sidearm and quartz cuvette. Anaerobic conditions were produced by sparging with Ar for 30 min prior to sonolysis. The role of the dissolved inert gas (argon vs nitrogen) was determined by comparing the results of sonolysis under air (80% N_2 /20% O_2) to an artificial mixture of 80% Ar/20% O_2 . The efficiency of sonolysis under 100% O_2 was also examined. In some experiments, the pH was buffered by the use of 100 mM phosphate (aerobic experiments) or 100 mM *N*-(2-hydroxyethyl)piperazine-*N*'-2-ethanesulfonate (Hepes) (anaerobic experiments), as specified. All procedures were carried out in the absence of light to prevent photolytic cleavage of the Co–C bond.

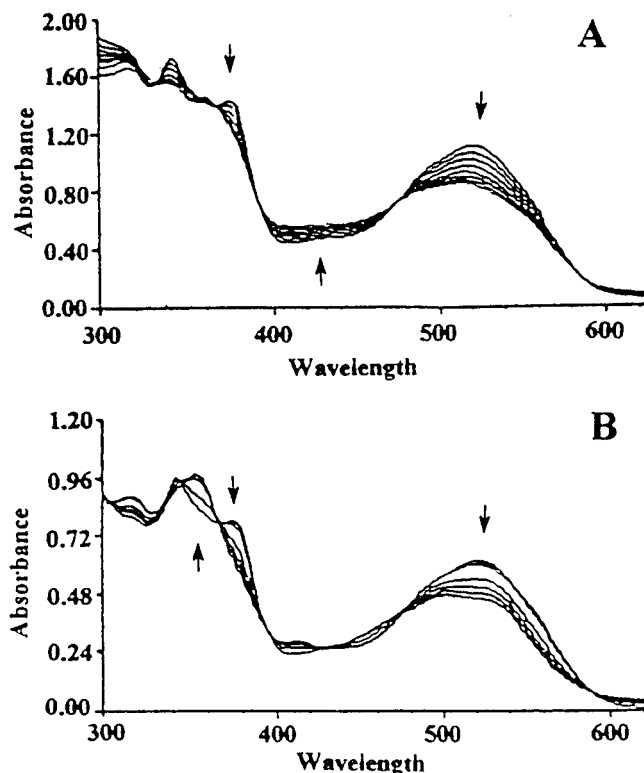


Figure 1. Sequential absorbance spectra of methylcob(III)alamin as a function of sonolysis time: (A) anaerobic conditions (100 mM Hepes, pH 7.4, 0.164 mM $\text{CH}_3\text{-Cbl}^{\text{III}}$, 21 °C, 6.5 h; the absorbance at 316 and 420 nm increases linearly with respect to sonolysis time); (B) aerobic conditions (pH 7.0, 0.164 mM $\text{CH}_3\text{-Cbl}^{\text{III}}$, 21 °C, 6 h).

Identification of Sonolysis Products. Absorption spectra were recorded on a diode array spectrophotometer (HP 8452A). The solutions were transferred to a quartz cuvette with a 1 cm light path for all optical measurements, and care was exercised to ensure that insignificant photolysis occurred during the 1 s measurement time. The products released by exhaustive sonolysis of $\text{Chl-HE-Cbl}^{\text{III}}$ were isolated by reversed-phase HPLC (Rainin Microsorb C_{18}). Elution and separation of the sonolysis products were carried out with an increasing gradient of acetonitrile (A) and 0.05 M phosphoric acid that was adjusted to pH 3.0 by the addition of NH_4OH (B). A mixture of 5:95 A/B was maintained for 2 min following injection, followed by a linear increase to 30:70 A/B over 10 min, maintained for an additional 2 min, and followed by a linear increase to 70:30 A/B over the next 10 min (15). The solvent was removed from each fraction, and the products were extracted with CH_2Cl_2 and characterized by ^1H and ^{13}C NMR.

RESULTS AND DISCUSSION

Sonolysis of Methylcob(III)alamin. Sequential absorption spectra of aqueous $\text{CH}_3\text{-Cbl}^{\text{III}}$ as a function of anaerobic sonolysis (pH 7.4, 100 mM Hepes, saturating Ar) are shown in Figure 1A. The absorbance value at 340, 374, and 520 nm decreases linearly as a function of sonolysis time, and the absorbance value at 316 and 420 nm increases linearly, thereby indicating the reaction is zero order in substrate concentration. The isosbestic points at 336, 390, and 585 nm are in agreement with those obtained through anaerobic photolysis of $\text{CH}_3\text{-Cbl}^{\text{III}}$. Under the conditions of anaerobic sonolysis, an additional isosbestic point occurs at 476 nm, rather than at 486 nm, as typically observed in the course of photolysis. This slight shift in the isosbestic point is caused by a minor

product that has an absorbance maximum near 490 nm. This may be cob(I)alamin that has a sufficient lifetime ($\tau_{1/2} = 22$ min at pH 6) to be observed spectrophotometrically. The absorption band at 374 nm is characteristic of a C–Co bond, and its disappearance unambiguously indicates displacement of the axial carbon ligand.

Under aerobic conditions, molecular oxygen scavenges H^\cdot and prevents the reduction of $\text{CH}_3\text{-Cbl}^{\text{III}}$ via eq 3. In the absence of an organic buffer with abstractable hydrogen atoms, reaction via HO^\cdot remains to be a viable process.



Figure 1B shows the change in absorbance spectra following aerobic sonolysis (air; 80% N_2 /20% O_2) in the absence of organic buffer. The decrease in absorbance at 340 and 374 nm is linear with increasing sonolysis time, indicating the reaction is zero order in substrate concentration, but the unexpected decrease in absorbance at 520 nm indicates the stable product of cobalamin sonolysis is not hydroxocob(III)alamin, as would be expected if molecular oxygen were to reoxidize cob(II)alamin to cob(III)alamin. This difference suggests that HO^\cdot is able to displace the alkyl ligand from Co^{III} , but other HO^\cdot reactions also occur (perhaps through the secondary products HOO^\cdot and $\cdot\text{O}_2^-$) to oxidize the corrin ring. Similar absorbance spectra are obtained from sonolysis of an aerated aqueous solution containing 100 mM phosphate buffer. The spectral changes produced are the same, but the rate of change in absorbance is higher in the artificial gas mixture of 80% Ar/20% O_2 or 100% O_2 owing to the greater efficiency of sonolysis and higher temperature of the collapsing bubble that is produced following cavitation (16).

Pulse radiolysis of aqueous $\text{CH}_3\text{-Cbl}^{\text{III}}$ produces similar spectral changes that are attributed to reaction by H^\cdot and HO^\cdot (17). The reducing species H^\cdot reacts to produce the same spectral changes shown in Figure 1A. Multiple oxidizing species (HOO^\cdot and $\cdot\text{O}_2^-$) can react with $\text{CH}_3\text{-Cbl}^{\text{III}}$ to cleave the Co–C bond, but these species also lead to irreversible degradation of the corrin ring, as evidenced by spectral changes that are strikingly similar to those seen in Figure 1B. A precedent for irreversible oxidation of the corrin ring also exists in the photooxygenolysis of alkylcobalamins by singlet oxygen (18).

Aerobic sonolysis of solutions containing 100 mM Hepes or 100 mM *tert*-butyl alcohol produces no change in the absorption spectra over comparable time (see Supporting Information). This is because molecular oxygen quenches the H^\cdot reaction pathway, and *tert*-butyl alcohol quenches the HO^\cdot reaction pathway. Although Hepes has not previously been reported to be a scavenger of HO^\cdot , many studies indicate that organic solute molecules, such as formate, can inhibit the reaction of HO^\cdot (19). The absence of any spectral changes under these conditions (see Supporting Information) suggests that direct sonolysis of the Co–C bond is not an important reaction pathway.

Sonolysis of 2-[4-[4'-[Bis(2-chloroethyl)amino]phenyl]butyroxylethylcob(III)alamin. Sequential absorption spectra of aqueous $\text{Chl-HE-Cbl}^{\text{III}}$ as a function of anaerobic sonolysis at pH 7.4, 100 mM Hepes, and saturating Ar, are shown in Figure 2A. The absorbance values at 374 and 520 nm decrease linearly as a function of sonolysis time, and the absorbance values at 316 and 420 nm increase linearly, thereby indicating the reaction is zero order in substrate concentration. The isosbestic points at 336, 390, 486, and 585 nm are in agreement with those obtained through anaerobic photolysis of $\text{CH}_3\text{-HE-Cbl}^{\text{III}}$.

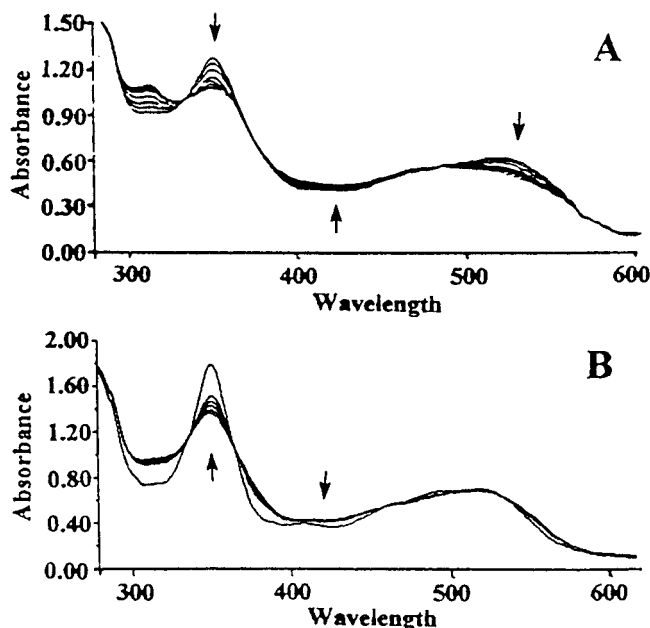


Figure 2. Sequential absorbance spectra of 2-[4-[4'-bis(2-chloroethyl)amino]phenyl]butyroxyl]ethylcob(III)alamin (Chl-HE-Cbl^{III}) as a function of sonolysis time: (A) anaerobic conditions (100 mM HEPES, pH 7.4, 0.065 mM Chl-HE-Cbl^{III}, 21 °C; the absorbance at 316 and 420 nm increases linearly with respect to sonolysis time); (B) aerobic conditions (100 mM phosphate, pH 7.0, 0.065 mM Chl-HE-Cbl^{III}, 21 °C).

The absorption band at 374 nm is characteristic of a Co–C bond, and its disappearance unambiguously indicates displacement of the axial carbon ligand.

Figure 2B shows the change in absorbance spectra following aerobic sonolysis of a Chl-HE-Cbl^{III} solution containing phosphate buffer. Different stable products are obtained under aerobic conditions. Because of the presence of molecular oxygen, the released product was shown by NMR to be 2-[4-[4'-bis(2-chloroethyl)amino]phenyl]butyroxyl]ethan-1-ol: ¹H NMR (CDCl₃, 300 MHz) δ 9.59 (s, 1 H), 7.08 (d, 2 H, J = 2.9 Hz), 6.62 (d, 2 H, J = 2.9 Hz), 4.67 (s, 2 H), 3.73–3.59 (m, 8 H), 2.60 (t, 2 H, J = 7.5 Hz), 2.45 (t, 2 H, J = 7.4 Hz), 1.95 (quintet, 2H, J = 7.4); ¹³C NMR (CDCl₃, 75 MHz ¹H decoupled) δ 195.85, 173.09, 144.54, 130.43, 129.92 (2), 112.29 (2), 68.73, 53.74 (2), 40.69 (2), 33.99, 33.13, 26.79. The decrease in absorbance at 374 nm is linear with increasing sonolysis time, indicating the reaction is zero order in substrate concentration.

The Co–C bond of CH₃-Cbl^{III} can be cleaved by sonolysis in aqueous solutions to produce the alkane and cob(II)alamin under anaerobic conditions or to produce the aldehyde and hydroxocob(III)alamin under aerobic conditions. Unlike photolysis and thermolysis that lead to direct Co–C bond cleavage, the predominant pathway for Co–C bond cleavage by sonolysis is through H[•]-mediated reduction of CH₃-Cbl^{III} to the labile 19 e[−] CH₃-Cbl^{II•} species followed by dissociation to the closed-shell alkane and Cbl^{II}, as shown in eqs 4 and 5, or through the reaction of HO[•] with CH₃-Cbl^{III} that leads to formation of hydroxocob(III)alamin as well as degradation of the corrin ring.

A parallel exists between the reactions of alkylcob(III)alamin under the conditions of sonolysis and pulse radiolysis (17), but without the need for expensive equipment. Although the violent cavitation during sonolysis has sufficient energy to break the Co–C bond to produce the {R[•] Cbl^{II}} radical pair by a dissociative pathway analogous to the photolysis of CH₃-Cbl^{III} (20–22), alkylcob(III)alamins are not sufficiently volatile to

be found in the extreme environment of the collapsing bubbles. Therefore, *direct* Co–C bond cleavage by sonolysis is not possible in spite of the >80 kcal/mol difference in bond dissociation energy between Co–C and H–OH. Anaerobic sonolysis of the Co–C bond is irreversible because a closed-shell alkane is formed, as shown by eqs 4 and 5. Under aerobic conditions, the rate of H[•] reaction with O₂ is on the same order of magnitude as the reaction of H[•] with CH₃[•], thereby suggesting the closed-shell alkane, CH₄, should be one of the end products of CH₃-Cbl^{III} sonolysis (23, 24). In contrast, Co–C bond cleavage of CH₃-Cbl^{III}, via anaerobic photolysis, is reversible from the {CH₃[•] Cbl^{II}} radical pair.

In summary, the ability to form cob(II)alamin and the closed-shell alkane without the use of chemical reductants and without the use of electrochemical, photochemical, or pulse radiolysis equipment may be a useful method to promote activation of drug–cobalamin complexes *in vivo*.

ACKNOWLEDGMENT

This work was supported in part by grants from the National Institute of Environmental Health Sciences (ES05728 to C.B.G.), the National Institute of General Medical Sciences (GM 49991 to Janet W. Grissom), the Channel Program of the Arab Republic of Egypt (A.B.), the University of Utah Research Committee, and the Huntsman Cancer Institute.

Supporting Information Available: Sequential absorption spectra of methylcob(III)alamin with H[•] and HO[•] reaction pathways quenched (1 page). Ordering information is given on any current masthead page.

LITERATURE CITED

- (1) Hay, B. P., and Finke, R. G. (1988) Thermolysis of the Co–C Bond in Adenosylcobalamin (Coenzyme B₁₂) IV. Products, Kinetics, and Co–C Bond Dissociation Energy Studies in Ethylene Glycol. *Polyhedron* 7, 1469.
- (2) Martin, B. D., and Finke, R. G. (1990) Co–C Homolysis and Bond Dissociation Energy Studies of Biological Alkylcobalamins: Methylcobalamin, Including a $\geq 10^{15}$ Co–CH₃ Homolysis Rate Enhancement at 25 °C following One-Electron Reduction. *J. Am. Chem. Soc.* 112, 2419.
- (3) Halpern, J., Kim, S.-H., and Leung, T. W. (1984) Cobalt–Carbon Bond Dissociation Energy of Coenzyme B₁₂. *J. Am. Chem. Soc.* 106, 8317.
- (4) Hogencamp, H. P. C. (1986) Reaction of Alkyl Ligands Coordinated to Cobalamins and Cobaloximes. In *B₁₂* (D. Dolphin, Ed.) Vol. 1, Chapter 9, Wiley, New York.
- (5) Schneider, Z., and Stroinski, A. (1987) *Comprehensive B₁₂*; deGruyter, Berlin.
- (6) Suslick, K. S. (1990) Sonochemistry. *Science* 247, 1439.
- (7) Suslick, K. S. (1989) The Chemical Effects of Ultrasound. *Sci. Am.* 260, 80.
- (8) Makino, K., Mossaba, M. M., and Riesz, P. (1983) Chemical Effect of Ultrasound on Aqueous Solutions. Formation of Hydroxyl Radicals and Hydrogen Atoms. *J. Phys. Chem.* 87, 1369.
- (9) Makino, K., Mossoba, M. M., and Riesz, P. (1983) Formation of HO[•] and H[•] in Aqueous Solutions by Ultrasound Using Clinical Equipment. *Radiat. Res.* 96, 416.
- (10) Kondo, T., Krishna, C. M., and Riesz, P. (1990) Free Radical Formation by Ultrasound in Aqueous Solutions. A Spin Trapping Study. *Free Radical Res. Commun.* 10, 17.
- (11) Weissler, A. (1959) Formation of Hydrogen Peroxide by Ultrasonic Waves: Free Radicals. *J. Am. Chem. Soc.* 81, 1077.
- (12) Boden, E. P., and Keck, G. E. (1985) Proton Transfer Steps in Steglich Esterification: A Very Practical New Method for Macrolactonization. *J. Org. Chem.* 50, 2394.
- (13) Brown, K. L., and Peck, S. (1988) Organocobalt Corrins. *Organomet. Syn.* 4, 304.

- (14) Mason, T. J. (1991) *Practical Sonochemistry: Users Guide to Applications in Chemistry and Chemical Engineering*, Horwood, New York.
- (15) Jacobsen, D. W., Green, R., and Brown, K. L. (1986) Analysis of Cobalamin Coenzymes and Other Corrinoids by High-Performance Liquid Chromatography. *Methods Enzymol.* 123, 14.
- (16) McKee, J. R. (1977) Effects of Ultrasound on Nucleic Acid Bases. *Biochemistry* 16, 4651.
- (17) Blackburn, R., Cox, D. L., and Phillips, G. O. (1972) Effect of Gamma Radiation on Vitamin B₁₂ Systems. *J. Chem. Soc., Faraday Trans. 1*, 1687.
- (18) Krautler, B., and Stepanek, R. (1985) Photooxygenolysis of Vitamin B₁₂. *Angew. Chem., Int. Ed. Engl.* 24, 62.
- (19) Weissler, A. (1962) Ultrasonic Hydroxylation in a Fluorescence Analysis for Microgram Quantities of Benzoic Acid. *Nature* 193, 1070.
- (20) Endicott, J. F., and Netzel, T. L. (1979) Early Events and Transient Chemistry in the Photolysis of Alkylcobalamins. *J. Am. Chem. Soc.* 101, 4000.
- (21) Chagovetz, A. M., and Grissom, C. B. (1993) Magnetic Field Effects in Adenosylcob(III)alamin Photolysis: Relevance to B₁₂ Enzymes. *J. Am. Chem. Soc.* 115, 12152.
- (22) Natarajan, E., and Grissom, C. B. (1996) The Origin of Magnetic Field Dependent Recombination in Alkylcobalamin Radical Pairs. *Photochem. Photobiol.* 64, 286.
- (23) Buxton, G. V., Greenstock, C. L., Helman, W. P., and Ross, A. B. (1988) Critical Review of Rate Constants for Reactions of Hydrated Electrons, Hydrogen Atoms, and Hydroxyl Radicals ($\cdot\text{OH}/\text{O}^-$) in Aqueous Solution. *J. Phys. Chem. Ref. Data* 17, 513.
- (24) Baulch, D. L., Cobos, C. J., Cox, R. A., Esser, C., Frank, P., Just, Th., Kerr, J. A., Pilling, M. J., Treo, J., Walker, R. W., and Warnatz, J. (1992) Evaluated Kinetic Data for Combustion Modeling. *J. Phys. Chem. Ref. Data* 21, 411.

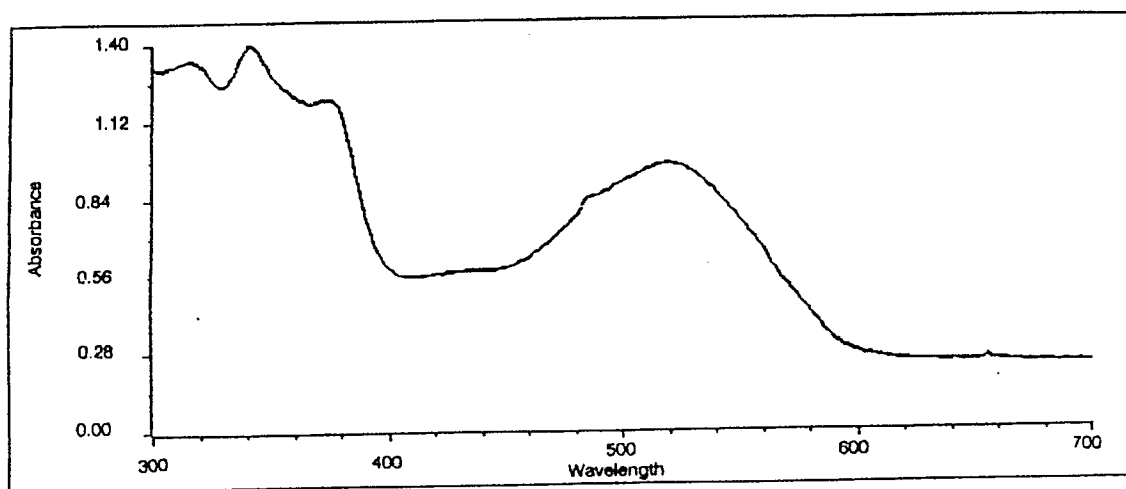
BC970077L

Supplementary Material for

Sonolysis Promotes Indirect C-Co Bond Cleavage of Alkylcob(III)alamin Bioconjugates

W. Allen Howard, Jr.;^{†§} Ashraf Bayomi;[‡] Ettaya Natarajan;[§] Mohsen A. Aziza;[‡]

Omar El-Ahmady;[‡] Charles B. Grissom^{§*}; Frederick G. West^{§*}



Aerobic sonolysis of methylcob(III)alamin with $H\bullet$ and $HO\bullet$ processes quenched.

Conditions: 100 mM Hepes, pH 7.0, 0.092 mM CH_3Cbl^{III} , 21 °C. Sonolysis was carried out over a period of 1.5 h. The sonication bath (not the reaction volume) was filled with deionized water and Alconox detergent was added as a surfactant to increase the reproducibility of sonic transduction from the stainless steel bath walls to the reaction vessel.

Fluorescein-Conjugated Lysine Monomers for Solid Phase Synthesis of Fluorescent Peptides and PNA Oligomers

Jesper Lohse,[†] Peter E. Nielsen,[‡] Niels Harrit,[†] and Otto Dahl^{*,†}

Department of Chemistry, The H. C. Ørsted Institute, University of Copenhagen, Universitetsparken 5, DK-2100 Ø Copenhagen, Denmark, and Center of Biomolecular Recognition, Department of Medical Biochemistry and Genetics, University of Copenhagen, The Panum Institute, Blegdamsvej 3c, DK-2200 N Copenhagen, Denmark. Received February 13, 1997[®]

Fluorescein ethyl ester, **I**, was used to prepare the fluorescent mixed ester/ether 6-*O*-(carboxymethyl)-fluorescein ethyl ester, **III**. Conjugation of **III** to the ϵ -amino group of α -*N*-Boc-L-lysine, via the *N*-hydroxysuccinimide ester, **IV**, gave the Boc-protected fluorescein-conjugated lysine monomer **V**. Removal of the Boc group, followed by reaction with Fmoc chloride, gave the Fmoc-protected monomer, **VI** (Figure 1). These Boc- and Fmoc-protected fluorescein-conjugated lysines were readily incorporated into peptides and PNA oligomers during solid phase synthesis to give fluorescent products. Mass spectroscopy and UV studies showed that the fluorophore remains unchanged during solid phase synthesis. In contrast to fluorescein, the photophysical properties of these derivatives are pH independent from pH 3 to 8, with a molar absorption coefficient, $\epsilon_{\max 456}$, of $2.9 \times 10^4 \text{ M}^{-1} \text{ cm}^{-1}$ and fluorescence quantum yield, ϕ_f , of 0.18.

INTRODUCTION

Merrifield solid phase synthesis (1, 2) is an area of increasing importance in organic chemistry. While originally developed for the synthesis of peptides from *tert*-butoxycarbonyl, Boc (2), or fluoren-9-yl-methoxycarbonyl, Fmoc (3), protected amino acids, it has since found many new applications. These include combinatorial libraries, peptidomimetics, and the peptide-based DNA analogue PNA, peptide nucleic acids (4). PNA has attracted much attention due to its high DNA and RNA affinity (5). Resistance toward enzymatic digestion (6) and its ability to efficiently and sequence specifically inhibit translation and translation *in vitro* (7) further make PNA oligomers prime candidates for antisense and antigene experiments. Fluorescence is a powerful and nondestructive method to study cell membrane penetration of PNA oligomers or other biologically active compounds, and fluorescent PNA oligomers have been prepared and used in photophysical experiments to elucidate PNA–DNA binding and structure (8).

It thus appeared desirable to prepare fluorescent Boc- and Fmoc-protected monomers that could be incorporated into PNA oligomers, peptides, and other compounds during solid phase synthesis. To our knowledge, such compounds have not previously been described in the literature, nor are they commercially available. Herein we describe the preparation of two such fluorescein monomers and their successful incorporation into PNA oligomers and peptides to produce fluorescent products.

EXPERIMENTAL PROCEDURES

Materials and Methods. Fluorescein (98%) was from Aldrich; α -*N*-(*tert*-butoxycarbonyl)- ϵ -*N*-(2-chlorobenzoyloxycarbonyl)-L-lysine, *N*-hydroxybenzotriazole uronium salt (HBTU), and MBHA and RINC resins were from Biochem; *N*-[2-(*tert*-butoxycarbonylamino)ethyl]glycine

ethyl ester was from Millipore; other reagents were from Sigma. Anhydrous HPLC grade solvents were from Labscan.

NMR spectra were recorded in DMSO-*d*₆ on a Varian 400 MHz Unity spectrometer, FAB mass spectra on a JEOL HX 110/110 mass spectrometer, MALDI-TOF mass spectra on a Kratos Compact Maldi II spectrometer, and UV–vis spectra on a Hewlett-Packard 8452 A spectrophotometer. Elementary analyses were performed by the Microanalysis Department of this Institute. Fluorescence emission and corrected excitation spectra were recorded at room temperature using a Perkin-Elmer LS-50B luminescence spectrometer.

Fluorescein Ethyl Ester, I [CAS Registry No. 72616-76-3]¹ (Figure 1). Fluorescein (16.6 g, 50 mmol) and concentrated H₂SO₄ (10 mL) were refluxed at 160–65 °C in diethyl oxalate (80 mL) for 80 min. Upon cooling, the reaction mixture was taken up in a mixture of CHCl₃ (500 mL) and MeOH (100 mL) and extracted with saturated NaHCO₃ (300 mL). The solvents were removed on a rotary evaporator, and the crude product was precipitated by addition of EtOH (25 mL) and ethyl acetate (275 mL). The precipitate was dissolved in boiling 96% EtOH (400 mL), and with boiling the volume was reduced to approximately 100 mL, whereby crystallization set in. Standing overnight at –20 °C gave 9.1 g (51%) of fluorescein ethyl ester, red-brown crystals with green luster: mp 241–242 °C [lit. (9) 242 °C]; ¹H NMR δ 0.83 (3 H, t), 3.94 (2 H, quart), 6.5–6.6 (3 H, overlapping m), 6.77 (1 H, s), 6.83 (1 H, s), 7.47 (1 H, dd), 7.7–7.9 (2 H, overlapping m), 8.16 (1 H, dd); ¹³C NMR δ 13.4, 60.96, 103.39, 114.82, 130.14, 130.16, 130.64, 130.72, 133.03, 133.67, 150.56, 156.15, 165.11; FAB⁺MS 361.2 HM⁺. Anal. Calcd for C₂₂H₁₆O₅: C, 73.32; H, 4.48. Found: C, 73.21; H, 4.47.

6-*O*-(*tert*-Butoxycarbonylmethyl)fluorescein Ethyl Ester, II. Fluorescein ethyl ester (5.8 g, 16 mmol) and bromoacetic acid *tert*-butyl ester (3.9 g, 20 mmol) in a mixture of DMF (20 mL) and diisopropylethylamine (10 mL) were refluxed at 100 °C for 1 h. The reaction mixture was taken up in ethyl acetate (100 mL) and

* Author to whom correspondence should be addressed (telephone 45 35320176; fax 45 35320212).

[†] Department of Chemistry.

[‡] Center of Biomolecular Recognition.

[®] Abstract published in *Advance ACS Abstracts*, June 15, 1997.

¹ CAS Registry Numbers were provided by the authors.

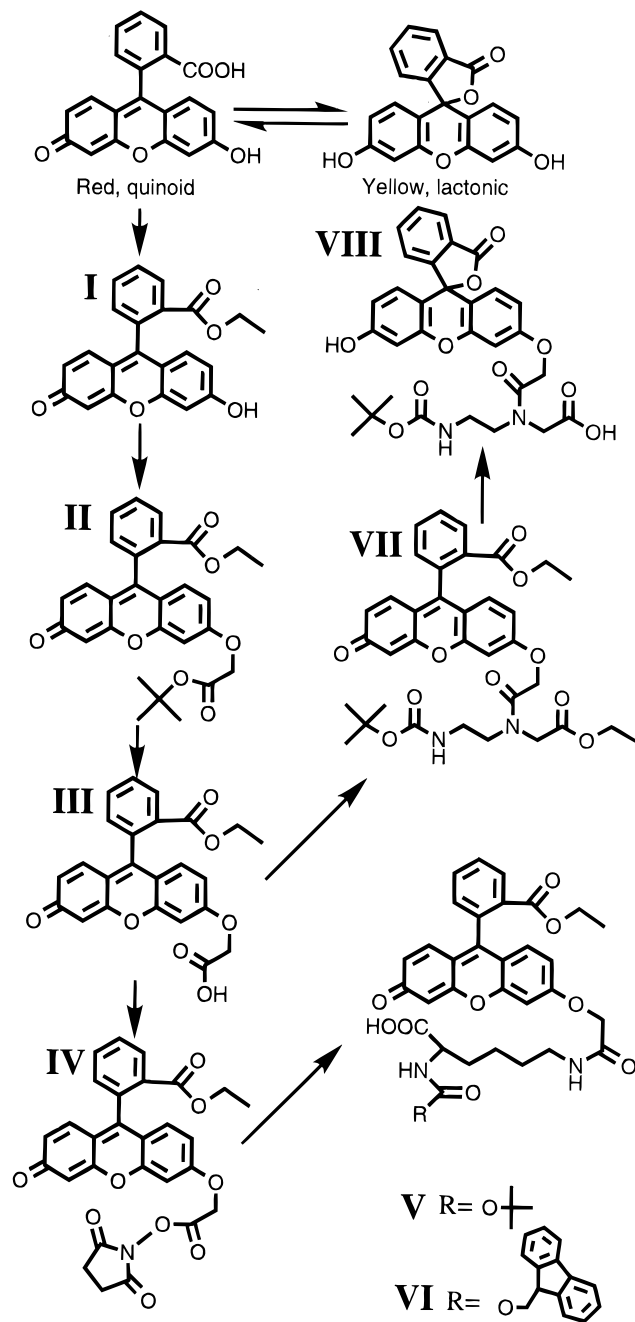


Figure 1. Synthesis and structures of I–VIII.

extracted with saturated NaHCO_3 (100 mL), 10% sodium citrate (pH 4.5, 100 mL), saturated NaHCO_3 (100 mL), and finally water (2×100 mL). The organic phase was dried over MgSO_4 , evaporated to a dark red tar, and dissolved in warm diethyl ether (15 mL). After 2 h at -20°C , the orange crystals (**II**) that had formed were filtered off and washed with ether/petroleum ether: yield 5.9 g (78%); mp $131\text{--}134^\circ\text{C}$; ^1H NMR δ 0.87 (3 H, t), 1.49 (9 H, s), 4.00 (2 H, d quart), 4.86 (2 H, s), 6.24 (1 H, d), 6.38 (1 H, dd), 6.8–6.9 (3 H, overlapping m), 7.19 (1 H, d), 7.50 (1 H, dd), 7.8 (2 H, overlapping m), 8.18 (1 H, dd); ^{13}C NMR δ 13.38, 27.74, 60.93, 65.48, 81.88, 101.49, 104.72, 113.56, 114.90, 117.10, 129.01, 130.05, 130.46, 130.64, 130.76, 133.10, 133.49, 149.76, 153.32, 158.34, 162.23, 164.98, 167.13, 183.95; FAB⁺MS 475.2 (HM^+). Anal. Calcd for $\text{C}_{28}\text{H}_{26}\text{O}_7$: C, 70.87; H, 5.52. Found: C, 70.68; H, 5.70.

6-O-(Carboxymethyl)fluorescein Ethyl Ester, III. **II** (7.8 g 16 mmol), in trifluoroacetic acid (40 mL), was refluxed at 75°C for 40 min. Most of the trifluoroacetic

acid was removed under reduced pressure, and a trifluoroacetate of the product was precipitated with diethyl ether and filtered off. It was dissolved in boiling 96% EtOH (350 mL), and with boiling the volume was reduced to 110 mL, whereby crystallization started. Overnight standing at -20°C produced orange crystals, which were filtered off, washed with a little ethanol, and dried at 100°C : yield 5.1 g (76%); mp $231\text{--}232^\circ\text{C}$; (Note: This compound and to some extent **V** and **VI** produced very broad NMR lines; to obtain good ^1H spectra, very dilute (0.1%), solutions had to be used) ^1H NMR δ 0.87 (3 H, t), 3.97 (2 H, m), 4.90 (2 H, s), 6.27 (1 H, s), 6.41 (1 H, d), 6.77–6.97 (3 H, overlapping m), 7.20 (1 H, s), 7.50 (d, 1 H), 7.79 (1 H, dd), 7.84 (1 H, dd), 8.19 (1 H, dd), 13.2 (1 H, br s); ^{13}C NMR δ 13.41, 60.98, 65.09, 101.35, 104.54, 113.68, 117.04, 130.65, 133.14, 169.5; FAB⁺MS 419.2 (HM^+). Anal. Calcd for $\text{C}_{24}\text{H}_{18}\text{O}_7\cdot\text{H}_2\text{O}$: C, 66.05; H, 5.52. Found: C, 65.67; H, 4.40.

6-O-[(1-Succinimidyl)oxycarbonylmethyl]-fluorescein Ethyl Ester, IV. **III** (6.3 g, 15 mmol), dicyclohexylcarbodiimide (3.7 g, 18 mmol), and *N*-hydroxysuccinimide (2.1 g, 18 mmol) in anhydrous DMF (40 mL) were stirred overnight at 40°C in a stoppered flask under N_2 . The reaction flask was placed for 3 h at -20°C , and the precipitated dicyclohexylurea was filtered off with suction and washed with 10 mL of anhydrous acetonitrile. Diethyl ether (100 mL) and petroleum ether [bp $60\text{--}80^\circ\text{C}$ (70 mL)] were added to the filtrate, and after approximately 15 min of vigorous stirring under N_2 , the phases combined under precipitation of the product. It was washed with 1:1 ether/petroleum ether (3×50 mL) and dried *in vacuo*, 0.1 mmHg. Yield was 5.7 g (74%) of **IV**, an orange powder. The product was contaminated with approximately 5% DMF (NMR and poor elemental analysis with low C/N ratio) and did not produce a sharp melting point. It is rapidly hydrolyzed when exposed to moisture and was prepared freshly for the subsequent reaction. ^1H NMR δ 0.87 (3 H, t), 2.82 (4 H, s), 3.95 (2 H, m), 5.54 (2 H, s), 6.24 (1 H, s), 6.38 (1 H, dd), 6.80 (1 H, dd), 6.87 (1 H, dd), 6.96 (1 H, dd), 7.31 (1 H, dd), 7.50 (1 H, d), 7.77 (1 H, dd), 7.84 (1 H, dd), 8.18 (1 H, d); ^{13}C NMR δ 13.42, 25.58, (weak signals at 30.84 and 35.84 from DMF), 61.01, 63.51, 101.71, 104.81, 113.79, 115.46, 117.47, 129.11, 129.73, 130.13, 130.53, 130.68, 130.81, 133.16, 133.46, 149.64, 153.24, 158.35, 161.27, 162.38, 164.99, 169.96, 184.06; FAB MS 516.3 (HM^+). Elem. Anal. Calcd for $\text{C}_{28}\text{H}_{21}\text{NO}_9$: C, 65.24; H, 4.11; N, 2.71. Found: C, 63.30; H, 4.48; N, 3.63.

6-O-[N-(5-Boc-amino-5-carboxypentyl)carbamoylmethyl]fluorescein Ethyl Ester, V. α -*N*-(*tert*-Butoxycarbonyl)- ϵ -*N*-(2-chlorobenzyloxycarbonyl)-L-lysine (7.8 g, 18 mmol) was dissolved in MeOH (50 mL), and 10% Pd/C (1.5 g) was added. The mixture was hydrogenated under atmospheric pressure for 4 h, consuming 430 mL (18 mmol) of H_2 . The solution was filtered through Celite to remove Pd/C and evaporated to dryness. The residue was taken up in anhydrous acetonitrile (50 mL) and again evaporated to form a white foam of α -*N*-Boc-L-lysine, which was used without further purification. It was taken up in dry acetonitrile (100 mL), and **IV** (5.8 g, 11.3 mmol) was added together with triethylamine (3 mL). The mixture was stirred overnight (an orange precipitate formed), evaporated to dryness, and triturated thoroughly with ice-cold 10% sodium citrate (100 mL, pH 4.5). This produced an orange powder that was washed repeatedly with cold water and then dried over NaOH in a desiccator: yield 6.0 g (82%); mp $159\text{--}161^\circ\text{C}$ (dec); ^1H NMR δ 0.87 (3 H, t), 1.3–4 (11 H, br s), 1.52–1.58 (4 H, m), 3.10 (2 H, m), 3.95 (2 H, m), 4.65 (2 H, s), 6.26 (1 H, s), 6.39 (1 H, d), 6.79–7.02 (3 H, overlapping m), 7.18 (1 H, s),

7.50 (1 H, d), 7.78–86 (2 H, overlapping m), 8.19 (1 H, d), 11–13 (1 H, s); ^{13}C NMR δ 13.43, 23.07, 28.28, 28.73, 30.63, 38.27, 53.59, 60.97, 67.44, 77.96, 101.50, 104.75, 113.97, 114.89, 117.10, 129.03, 129.55, 130.07, 130.48, 130.66, 130.81, 133.13, 133.54, 149.92, 153.37, 155.65, 158.39, 162.32, 165.01, 166.59, 174.37, 184.01; FAB⁺MS 647.3 (HM⁺). Anal. Calcd for $\text{C}_{35}\text{H}_{38}\text{N}_2\text{O}_{10}\cdot\text{H}_2\text{O}$: C, 63.24; H, 5.82; N, 4.21. Found: C, 63.22; H, 6.06; N, 4.11.

6-O-[N-(5-Fmoc-amino-5-carboxypentyl)carbamoylmethyl]fluorescein Ethyl Ester, VI. **V** (1.3 g, 2.0 mmol) was dissolved in trifluoroacetic acid (10 mL) and stirred at room temperature for 10 min. Trifluoroacetic acid was removed on a rotary evaporator, and the residue was dissolved in saturated Na_2CO_3 (15 mL). Fluoren-9-ylmethoxycarbonyl chloride (620 mg, 2.4 mmol) in dioxane (10 mL) was added and the mixture stirred for 16 h. It was diluted with dichloromethane (100 mL) and extracted with 10% sodium citrate (100 mL, pH 4.5) and then with water (2×100 mL). The organic phase was reduced to dryness and the residue purified on a silica column. The product was eluted with a mixture of acetic acid, methanol, and dichloromethane (2:8:90). Residual acetic acid was removed by repeated evaporation from 20% methanol in benzene, to give 980 mg (64%) of **VI** as a dark orange powder: ^1H NMR δ 0.86 (3 H, t), 1.23–1.43 (6 H, overlapping m), 3.11 (2 H, quart.), 3.80 (1 H, m), 3.95 (2 H, m), 4.64 (2 H, s), 6.24 (1 H, m), 6.39 (1 H, dd), 6.78–6.93 (3 H, overlapping m), 7.16 (1 H, m), 7.27–7.49 (7 H, overlapping m), 7.67–7.8 (6 H, overlapping m), 8.16–8.23 (2 H, overlapping m); ^{13}C NMR δ 13.42, 22.96, 28.88, 31.5, 46.78, 54.7, 60.95, 65.50, 67.40, 101.46, 104.75, 113.96, 114.84, 117.06, 120.13, 121.45, 125.32, 127.11, 127.65, 128.39, 128.99, 129.55, 130.05, 130.46, 130.63, 130.79, 133.11, 140.77, 149.89, 153.53, 155.91, 158.37, 162.3, 164.99, 166.57, 183.99; FAB⁺MS 767.4 (M – H). Anal. Calcd for $\text{C}_{45}\text{H}_{40}\text{N}_2\text{O}_{10}\cdot\text{H}_2\text{O}$: C, 68.69; H, 5.38; N, 3.56. Found: C, 68.98; H, 5.23; N, 3.38.

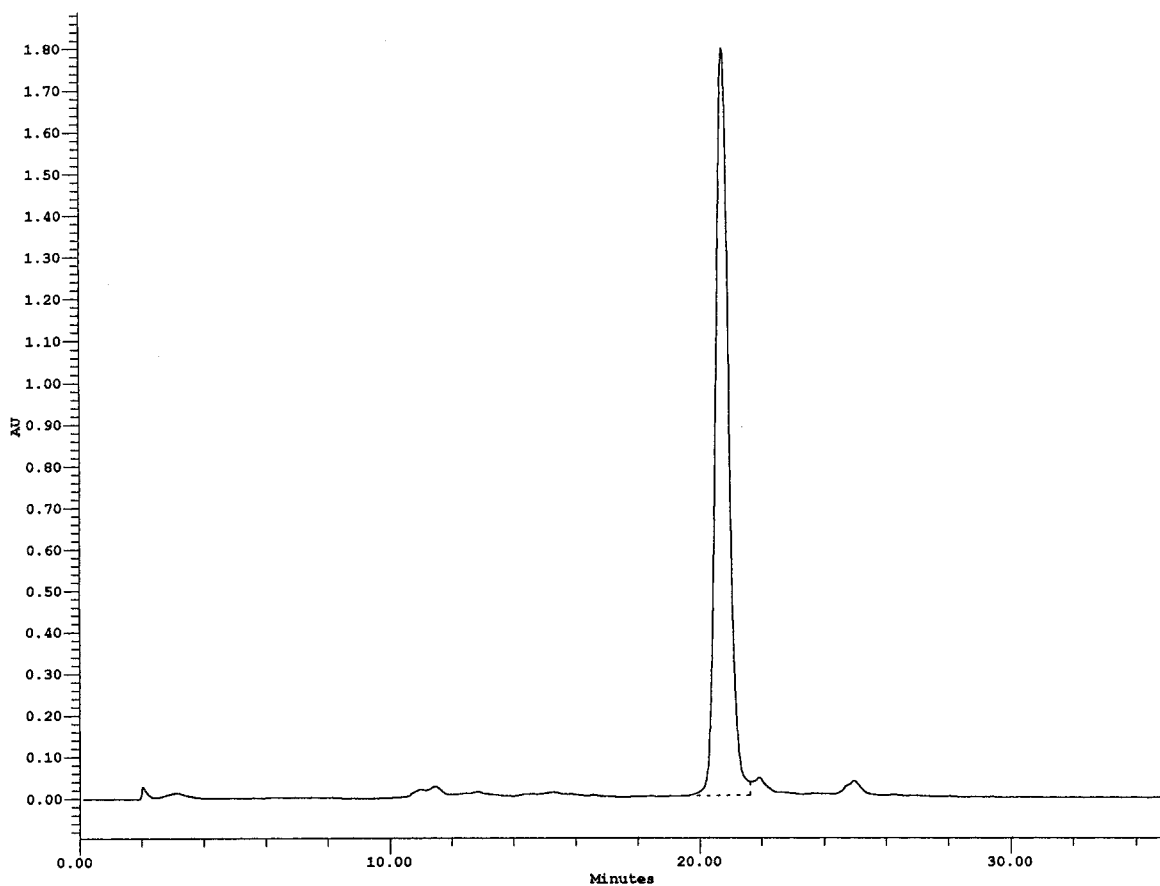
Fluorescein-PNA-Monomer Ethyl Ester, VII. **6-O**-(Carboxymethyl)fluorescein ethyl ester (500 mg, 1.2 mmol), dicyclohexylcarbodiimide (246 mg, 1.2 mmol), HBTU (195 mg, 1.2 mmol), and *N*-[2-(*tert*-butoxycarbonylamino)ethyl]glycine ethyl ester (290 mg, 1.2 mmol) were dissolved in DMF (5 mL) and diisopropylethylamine (1 mL). After 2 h at 70 °C, the mixture was cooled to room temperature, and dichloromethane (30 mL) was added. Standing overnight at 0 °C caused DCU to precipitate, the filtered solution was evaporated to dryness, and the residue was purified by column chromatography on silica with a gradient of 0–15% methanol in ethyl acetate. Removal of the solvent gave a red oil, which was triturated with diethyl ether to produce an orange-red powder, fluorescein-PNA-monomer ethyl ester, **VII**: yield 450 mg (58%); (Note: Since two conformations of the amide bond are present, several lines in the NMR spectra are doubled, representing the two different conformers; this is also the case for **VIII**): ^1H NMR δ 0.8–0.9 (3 H, two t), 1.1–1.3 (3 H, two t), 1.33 and 1.35 (9 H, two s), 3.0–3.5 [multiplets from PNA-backbone methylenes and strong singlet from water (3.32)], 4.0–4.2 (4 H, several overlapping quart.), 4.92 and 5.11 (2 H, two s), 6.22 (1 H, dd), 6.39 (1 H, dd), 6.8–6.9 (3 H, overlapping m), 7.02 (1 H, t), 7.16 (1 H, s), 7.5 (1 H, d), 7.7–7.9 (2 H, overlapping m), 8.19 (1 H, d); ^{13}C NMR δ 13.41, 14.07, 28.18, 37.73, 46.81, 47.49, 48.84, 60.60, 60.95, 61.28, 65.51, 66.20, 77.80, 78.15, 101.44, 104.58, 113.85, 114.66, 116.94, 128.80, 129.49, 130.06, 130.48, 130.63, 130.77, 133.12, 133.55, 149.94, 153.34, 155.90, 158.41, 162.72, 164.96, 166.97, 167.21, 169.07, 169.61, 183.93; FAB⁺MS 647.2 (HM⁺). Anal. Calcd for $\text{C}_{35}\text{H}_{38}\text{N}_2\text{O}_{10}$: C, 65.00; H, 4.33; N, 5.92. Found: C, 64.90; H, 4.38; N, 6.10.

Fluorescein-PNA-Monomer, VIII. **VII** (1.7 g, 2.6 mmol) was taken up in THF (6 mL), and 2.00 M LiOH (20.0 mL) was added. The mixture was stirred for 80 min, the THF was removed on a rotary evaporator, and to the ice-cooled solution was added 2.00 M HCl (20.0 mL). This produced a pale yellow precipitate, which was washed repeatedly with water: yield 1.2 g (78%); ^1H NMR δ 1.3–1.5 (9 H, s), 3.2 (2 H, m), 3.4 (2 H, m), 3.9 and 4.1 (2 H, two s), 4.8 and 5.0 (2 H, two s), 6.1 (1 H, s), 6.3–6.7 (3 H, overlapping m), 6.85 (1 H, d), 6.95 (1 H, d), 7.2–7.4 (2 H, overlapping m), 7.6–7.8 (2 H, m), 7.9 (1 H, m), 12.2 (1 H, br s); ^{13}C NMR δ 28.22, 37.77, 46.77, 47.29, 48.92, 65.25, 65.38, 65.98, 77.85, 78.17, 82.61, 101.46, 101.90, 102.18, 102.34, 107.55, 107.80, 109.41, 110.43, 111.46, 112.06, 112.29, 112.96, 114.58, 118.04, 119.12, 124.13, 124.76, 124.87, 125.79, 126.19, 127.36, 128.83, 129.13, 129.53, 129.92, 130.06, 130.26, 130.43, 132.46, 134.05, 135.76, 140.01, 143.78, 151.96, 152.58, 153.58, 155.74, 155.91, 159.78, 159.97, 163.95, 164.07, 164.58, 166.72, 167.01, 167.35, 167.68, 168.71, 170.67, 171.24; FAB⁺MS 589.2 (M – H). Anal. Calcd for $\text{C}_{31}\text{H}_{30}\text{N}_2\text{O}_{10}\cdot\text{H}_2\text{O}$: C, 61.20; H, 5.30; N, 4.60. Found: C, 61.18; H, 5.50; N, 4.38.

Solid Phase Synthesis. PNA oligomers were synthesized on a substituted polyethylene glycol MBHA-resin. In a typical procedure, **V** (32 mg, 0.05 mmol), *N*-cyclohexyldiethylamine (8 mg, 0.05 mmol), and HBTU (19 mg, 0.05 mmol) were dissolved in DMF (0.375 mL) and pyridine (0.125 mL). After 3 min of preactivation, the reaction mixture was applied to 100 mg of resin, and the coupling was allowed to proceed for 20 min. Prior to the next coupling step, the Boc-protected amino terminus was deprotected with *m*-cresol (5%) in trifluoroacetic acid (2×4 min). To cleave the finished oligomer from the resin, the resin was dried and treated twice with a mixture of trifluoroacetic acid (0.3 mL), trifluoromethanesulfonic acid (0.1 mL), *m*-cresol (0.05 mL), and thioanisole (0.05 mL) for 1 h. The combined cleavage mixtures were drained into diethyl ether (4 mL, at –80 °C), causing the PNA oligomer to precipitate. It was spun down, washed with cold ether (3×4 mL), and finally dried in a stream of nitrogen to produce a bright yellow fluorescent powder. To demonstrate the compatibility with the other PNA monomers, the PNA oligomer Ac-T-Lys^F-C-G-T-A-Lys-NH₂ (Ac denotes the acylated amino terminus of the oligomer, NH₂ the amidated carboxy terminus, and Lys^F the lysine-fluorescein conjugate) was synthesized this way. Analytical RP-HPLC (0.1% trifluoroacetic acid buffer, with a gradient of 0–50% acetonitrile in water on a C₁₈ column) revealed an essentially pure crude product (Figure 2A), and the identity was confirmed with MALDI-TOF mass spectroscopy, MH⁺: calcd 2022.8, found 2023.3 (Figure 2B).

The fluorescein-PNA-monomer, **VIII**, was coupled in the same way to PNA oligomers. In this case a brownish nonfluorescent oligomer was obtained, and while HPLC revealed one major product, the identity of which was confirmed by MALDI-TOF MS, several significant byproducts were also present.

Peptides were synthesized on a RINC resin. In a typical procedure **VI** (115 mg, 0.15 mmol), *N*-cyclohexyldiethylamine (24 mg, 0.15 mmol), and HBTU (57 mg, 0.15 mmol) were dissolved in DMF (1.5 mL). After 3 min of preactivation, the reaction mixture was applied to 100 mg of resin, and the coupling was allowed to proceed for 60 min. Prior to the next coupling step, the Fmoc-protected amino terminus was deprotected with 20% piperidine in DMF (5 min + 15 min). To cleave the finished peptide from the resin, the resin was dried and treated with 20% trifluoroacetic acid in dichloromethane



fl-test JL raw

Data: SAS20650.2 29 May 96 7:16 Cal: Lone290596 29 May 96 7:25
 Kratos Kompact MALDI 2 V4.0.0: + Linear High Power: 51

%Int. 100% = 23 mV [sum= 2322 mV] Shots 1-100 Smooth Av 22
 2023.3

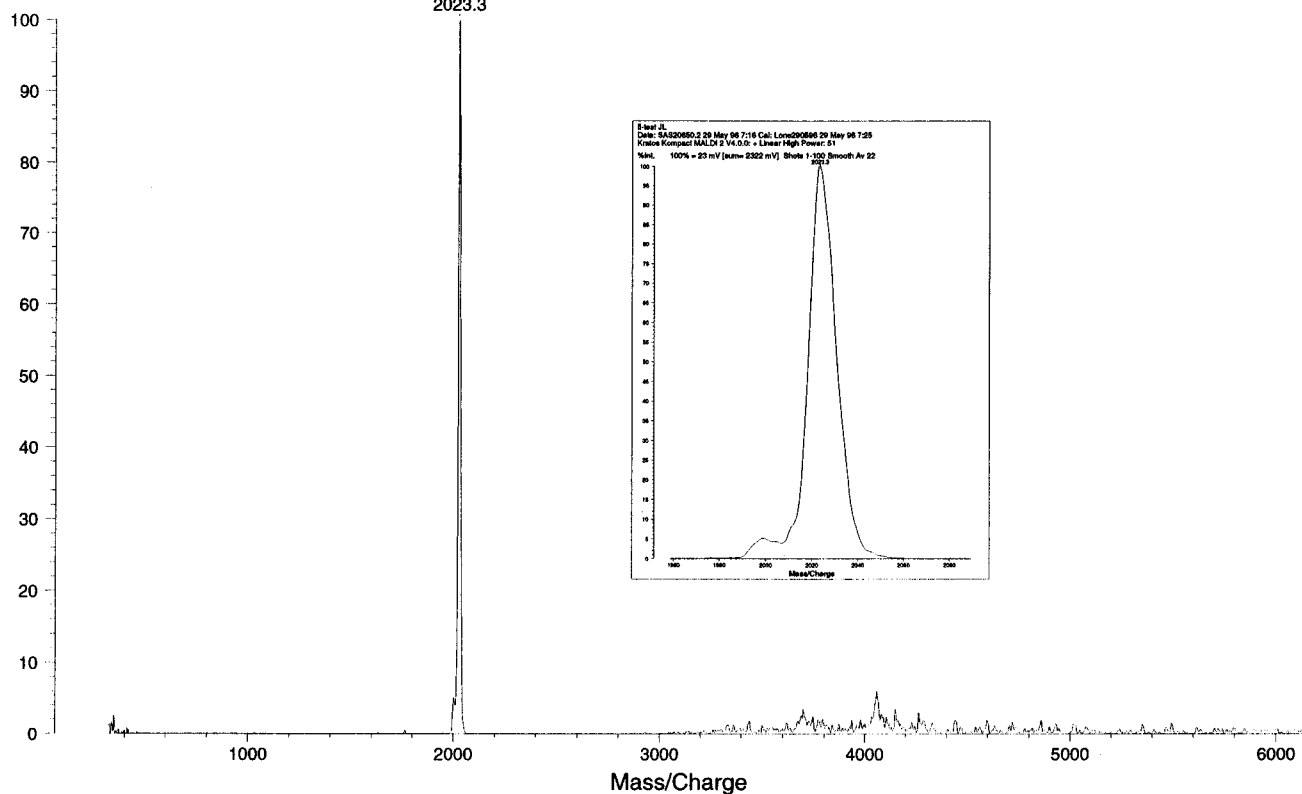


Figure 2. (A, top) RP-HPLC chromatogram (0.1% trifluoroacetic acid buffer, with a gradient of 0–50% acetonitrile in water on a C₁₈ column) of the crude PNA oligomer Ac-T-Lys_F-C-G-T-A-Lys-NH₂; (B) MALDI-TOF mass spectrum of the crude PNA oligomer Ac-T-Lys_F-C-G-T-A-Lys-NH₂ (calcd 2022.8).

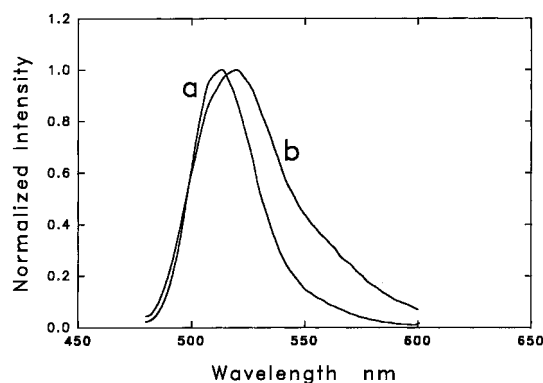


Figure 3. Normalized fluorescence emission spectra: (a) 860 nM fluorescein in 10 mM NaOH in 20% MeOH in water; (b) 860 nM peptide **IX** in 10 mM ammonium acetate in 20% MeOH in water. The samples were excited at 456 nm, at which they showed identical absorbencies. Bandwidth of excitation and emission slits: 2.5 nm.

(1 mL) for 20 min, and the peptide was isolated by evaporation of the solvent. The pentapeptide H-Gly-Lys^F-Leu-Phe-Gly-NH₂, **IX** (H denoting the free amino terminus, NH₂ the amidated carboxy terminus), was synthesized this way. Analytical RP-HPLC revealed an essentially pure crude product, and the identity was confirmed with MALDI-TOF mass spectroscopy, MH⁺: calcd 920.0, found 919.7. The peptide was purified by preparative RP-HPLC (0.1% trifluoroacetic acid buffer, with a gradient of 0–50% acetonitrile in water on a C₁₈ column) to >99% purity (UV at 230 nm). Elemental analysis of the purified product was in agreement with a hydrated trifluoroacetate. Anal. Calcd for C₄₉H₅₇N₇O₁₁·H₂O·(CF₃COOH)_{2.5}: C, 52.97; H, 5.40; N, 8.02. Found: C, 52.70; H, 5.20; N, 7.99.

Fluorescence Studies. Analytically pure samples of **V** and the pentapeptide **IX** were used for photophysical studies. In 10 mM aqueous ammonium acetate (pH 6.8), containing 20% methanol, **V** and **IX** have identical absorption spectra above 300 nm with maxima at 456 nm, $\epsilon = 2.9 \times 10^4 \text{ M}^{-1} \text{ cm}^{-1}$, and 484 nm, $\epsilon = 2.3 \times 10^4 \text{ M}^{-1} \text{ cm}^{-1}$, showing that the fluorophore remains unchanged during oligomerization and purification. The fluorescence spectrum of **IX** resembles that of dianionic fluorescein, though it is broadened and redshifted approximately 5 nm to $\lambda_{\text{em}} = 520 \text{ nm}$ (Figure 3). To measure the fluorescence quantum yield of **IX**, 860 nM solutions were prepared in eight different buffers [all 10 mM, 20% methanol in water, made up from trifluoroacetic acid (pH 2.1), acetic acid (pH 3.1), mixtures of acetic acid and ammonia with total concentration of 10 mM, and ammonia (pH 10.8)]. As reference was used 860 nM fluorescein in 10 mM aqueous NaOH, $\phi_f = 0.92$ (10, 11). This standard was chosen since its fluorescence spectrum almost coincides with that of **IX**, making instrumental corrections unnecessary. The samples were excited at 456 nm, at which they showed identical absorbencies, with excitation and emission slits of 2.5 nm. From pH 3.1 to 8.3 the fluorescence intensity of the peptide is constant, $\phi_f = 0.18 \pm 0.02$. In trifluoroacetic acid buffer at pH 2.1 the value drops to $\phi_f = 0.14 \pm 0.02$. Above pH 8 the intensity decreases, reaching a minimum level $\phi_f = 0.10 \pm 0.01$ above pH 9.8 (Figure 4).

RESULTS AND DISCUSSION

Our initial goal was to prepare an acetic acid derivative of fluorescein that could be conjugated to a Boc-protected amino acid, in analogy to the preparation of PNA-monomers (12). An extensive chemistry has been devel-

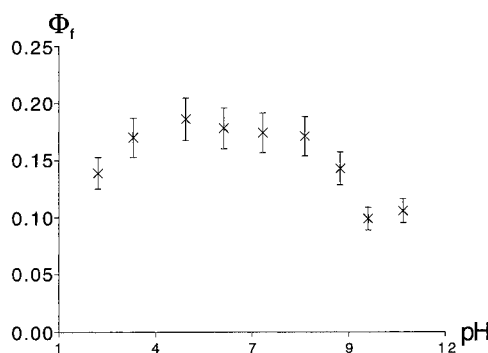


Figure 4. Fluorescence quantum yield vs pH for 860 nM solutions of the peptide **IX** in various 10 mM buffers in 20% MeOH in water.

oped to convert nitrofluoresceins via amines (13) to iso- or isothiocyanates (13, 14), but this strategy involves *de novo* synthesis of the entire ring system as well as extensive workup to separate isomers. While highly purified isothiocyanates of fluorescein are commercially available, they are prohibitively expensive as starting materials in a multistep synthesis. Other fluorescein derivatives for bioconjugation include active esters of carboxyfluoresceins or dichlorotriazine derivatives of aminofluoresceins, and comparative studies of the various reagents have recently been published (15, 16).

Apart from difficult synthesis, another common drawback of these derivatives is that they, as fluorescein, are free to assume either a nonfluorescent lactone form or a fluorescent quinoid structure (17, 18) as well as various ionic forms depending on pH and solvent (19, 20). This poses problems for both preparative work and especially structural assignment, a matter of controversy for more than a century (18, 21).

In the solid phase synthesis of DNA–fluorescein conjugates, this obstacle has been overcome by the synthesis of phosphoramidites conjugated to 3-*O*,6-*O*-dipivaloyl- or -diacetyl-protected fluoresceins. In this way the fluorophore is locked and protected in the lactone form during solid phase synthesis, until it is converted to the fluorescent form during the final basic deprotection. As PNA oligomers and peptides are cleaved from the solid support with strong acid (1) rather than base, this approach was not suitable. Instead, we chose to exploit the fact that quinoid fluorescein esters can be selectively 6-*O*-alkylated, to give well-defined, fluorescent mixed ester/ethers (18, 22–24).

Fluorescein ethyl ester was used as the starting material. This compound was first described more than a century ago, being prepared either directly from fluorescein in hot acidic ethanol (9) or in three steps via esterification of dihydrofluorescein (18), but in neither case are yields reported. More recent work on fluorescein esters (25) demonstrates that elevated temperatures are needed to obtain direct esterification of fluorescein, and moderate yields are reported for esters of low-boiling alcohols. To overcome this problem, we used diethyl oxalate as a high boiling and reactive ethyl donor. The H₂SO₄-catalyzed transesterification was essentially complete after 80 min at 160 °C, and following workup, a macrocrystalline product was obtained in 50% yield.

The following alkylation with bromoacetic acid *tert*-butyl ester and subsequent trifluoroacetic acid deprotection both proceeded without difficulty, and the product 6-*O*-(carboxymethyl)fluorescein ethyl ester, **III**, was obtained without resorting to chromatographic workup.

Initially, DCC coupling of **III** and *N*-[2-(*tert*-butoxycarbonylamino)ethyl]glycine ethyl ester was used to

prepare the PNA-fluorescein-monomer ester, **VII**, which was isolated by column chromatography. Subsequent basic deprotection of the two ethyl ester moieties produced the free PNA-fluorescein monomer, **VIII**. This product was isolated in a weakly fluorescent pale yellow modification, apparently predominantly as a lactonic or zwitterionic tautomer. This assignment is supported by the literature, in which 6-*O*-fluorescein ethers are described as pale yellow and weakly fluorescent (18, 24). We had anticipated that the strongly acidic conditions present during cleavage of the oligomers from the resin might convert the fluorescein moiety into its fluorescent quinoid form. This was, however, not the case; the oligomers prepared from **VIII** remained only weakly fluorescent and did not show any significant absorption above 300 nm.

Thus, to avoid removing the ester moiety on fluorescein, the active *N*-hydroxysuccinimide ester, **IV**, was prepared. Although NMR and elemental analyses of the product revealed a slight contamination with DMF, this did not interfere in the subsequent reaction with α -*N*-Boc-L-lysine, which produced **V** in 62% overall yield from **III**. In this procedure, which avoids chromatographic workup, it is essential that dry glassware and anhydrous solvents are used in order to avoid the formation of **III**, which will terminate the oligomer during solid phase synthesis.

Attempts to prepare **VI** directly from **III** and α -*N*-Fmoc-L-lysine did not produce a product of satisfactory purity. Rather, we chose to deprotect the readily prepared Boc-protected monomer **V** followed by introduction of the Fmoc protecting group with Fmoc chloride and achieved a yield of 64% for the two steps.

Oligomerization of both the Boc- and Fmoc-protected L-lysine monomers proceeded without problems using the described standard coupling and deprotection procedures. The ethyl ester protection group on fluorescein remained stable toward both the moderately basic conditions used to deprotect the Fmoc group of **VI** and the strongly acidic conditions used to cleave the PNA oligomers from the solid support. The importance of this is demonstrated by the lack of fluorescence of oligomers prepared from the PNA-fluorescein monomer **VIII**; that is, removal of the ester moiety on fluorescein results in tautomerization and loss of fluorescence.

An attractive feature of these monomers is that they can be incorporated anywhere in a peptide or PNA oligomer, allowing precise positioning of the fluorophore within the oligomers. The amino terminus remains available for further modifications such as conjugation to other compounds of biological or analytical interest. Thus, with the exception of cases in which strong base is employed, the monomers **V** and **VI** could find broad application in solid phase synthesis.

The photophysical properties of these fluorescein derivatives compare favorably with those of the usual fluorescein conjugates. The fact that they are mixed ester/ethers of fluorescein unambiguously locks the compounds in a fluorescent quinoid form. This is in agreement with other studies of 6-*O*-ethers of fluorescein esters, such as 6-*O*-ethylfluorescein ethyl ester (24), which exhibits almost pH-independent absorption from pH 4 to 9.3. Only at very acidic pH (pH 1.2) does the absorbance decrease and shift to lower wavelengths, a fact ascribed to protonization of the ring system.

As we observed for the peptide **IX**, largely pH-independent fluorescence quantum yields around $\phi_f = 0.13 \pm 0.01$ have been reported (23) for several lipophilic esters of 6-*O*-methylfluorescein in neutral or moderately acidic ethanol. Since these derivatives and **IX** have

coinciding absorption maxima (455 vs 456 nm for **IX**) and absorption coefficients (2.8×10^4 vs $2.9 \times 10^4 \text{ M}^{-1} \text{ cm}^{-1}$ for **IX**), we ascribe the somewhat higher quantum yield of $\phi_f = 0.18 \pm 0.02$ that we observed for **IX** to different solvents. The observed attenuation of fluorescence at extreme pH values is presumably due to protonization at acidic pH and quenching by OH^- under basic conditions, though the matter deserves further investigation.

Free fluorescein only exhibits an almost quantitative fluorescence quantum yield under nonbiological strong basic conditions in which the dianion is the only significant species (20). Thus, the pH-independent fluorescence of the fluorescein derivatives described herein is advantageous, as it allows direct quantification of fluorophore present in different environments such as various intracellular compartments, including acidic lysosomes, where fluorescein is almost devoid of fluorescence (23). The uncharged and relative lipophilic nature of the fluorophores described might further enhance cellular uptake.

ACKNOWLEDGMENT

We gratefully acknowledge Ulla Henriksen for valuable advice on the synthesis. We thank Margit Jørgensen, Jolanta Ludvigsen, and Lone Larsen for skilled technical support in the preparation of PNA oligomers. This study was supported by a grant from the Danish Natural Research Foundation.

LITERATURE CITED

- (1) Merrifield, R. B. (1963) Solid Phase Peptide Synthesis. I. The Synthesis of a Tetrapeptide. *J. Am. Chem. Soc.* **85**, 2149–2154.
- (2) Merrifield, R. B. (1986) Solid Phase Synthesis. *Science* **232**, 341–347.
- (3) Carpino, L. A., and Han, G. Y. (1972) The 9-Fluorenylmethoxycarbonyl Amino-Protecting Group. *J. Org. Chem.* **37**, 3404–3409.
- (4) Nielsen, P. E., Egholm, M., Berg, R. H., and Buchardt, O. (1991) Sequence-Selective Recognition of DNA by Strand Displacement with a Thymine-Substituted Polyamide. *Science* **254**, 1497–1500.
- (5) Egholm, M., Buchardt, O., Christensen, L., Behrens, C., Freier, S. M., Driver, D. A., Bergh, R. H., Kim, S. K., Norden, B., and Nielsen, P. E. (1993) PNA hybridizes to complementary oligonucleotides obeying the Watson-Crick hydrogen-bonding rules. *Nature* **365**, 566–568.
- (6) Demidov, V., Frank-Kamenetskii, M. D., Buchardt, O., Egholm, M., and Nielsen, P. E. (1994) Stability of peptide nucleic acids in human serum and cellular extracts. *Biochem. Pharmacol.* **48**, 1309–1313.
- (7) Hyrup, B., and Nielsen, P. E. (1996) Peptide Nucleic Acids (PNA). Synthesis, Properties and Potential Applications. *Bioorg. Biomed. Chem.* **4**, 5–23.
- (8) Ratilainen, T., Holmen, A., Nielsen, P. E., and Norden, B. (1996) Fluorescently Labelled Peptide Nucleic Acids: An Energy Transfer Study. In *Abstract Book*, Poster Abstract 30, Therapeutic oligonucleotides, Rome June 9–12, Accademia Nazionale di Medicina, Italy.
- (9) Feurstein, W., and Wallach, J. (1901) Ueber die directe Veresterung des Fluoresceins. *Ber. Dtsch. Chem. Ges.* **34**, 2641–2642.
- (10) Flemming, G. R., Knight, A. W. E., Morris, J. M., Morrison, R. J. S., and Robinson, G. W. (1977) Picosecond Fluorescence Studies of Xanthene Dyes. *J. Am. Chem. Soc.* **99**, 4306–4311.
- (11) Demas, J. N., and Crosby, G. A. (1971) The Measurement of Photoluminescence Quantum Yields. A Review. *J. Phys. Chem.* **75**, 991–1024.
- (12) Egholm, M., Buchardt, O., Nielsen, P. E., and Berg, R. H. (1992) Peptide Nucleic Acids (PNA). Oligonucleotide Analogues with an Achiral Peptide Backbone. *J. Am. Chem. Soc.* **114**, 1895–1897.
- (13) Coons A. H., and Kaplan, M. H. (1950) Localization of antigen in tissue cells. II. Improvements in a method for the

- detection of antigen by means of fluorescent antibody. *J. Exp. Med.* 91, 1–13.
- (14) Burckhalter, J. H., and Seiwald, J. R. (1960) Isothiocyanate compounds. U.S. Pat. 2937186.
- (15) Brinkley, M. (1992) A Brief survey of Methods for Preparing Protein Conjugates with Dyes, Haptens and Cross-Linking Reagents. *Bioconjugate Chem.* 3, 2–13.
- (16) Banks, P. R., and Paquette, D. M. (1995) Comparison of Three Common Amine Reactive Fluorescent Probes Used for Conjugation to Biomolecules by Capillary Zone Electrophoresis. *Bioconjugate Chem.* 6, 447–458.
- (17) Orndorff, W. R., and Hemmer, A. J. (1927) Fluorescein And Some Of Its Derivatives. *J. Am. Chem. Soc.* 49, 1272–1280.
- (18) Nietzki, R., and Schröter, P. (1895) Ueber die Constitution des Fluoresceins. *Ber. Dtsch. Chem. Ges.* 28, 44–56.
- (19) Zanker, V., and Peters, W. (1958) Die prototropen Formen des Fluoresceins. *Ber. Dtsch. Chem. Ges.* 91, 572–580.
- (20) Yguerabide, J., Talavera, E., Alvarez, J. M., and Quintero, B. (1994) Steady-State Fluorescence Method For Evaluating Excited State Proton Reactions: Applications to Fluorescein. *Photochem. Photobiol.* 60, 435–441.
- (21) Anthoni, U., Christophersen, C., Nielsen, P. H., Püschl, A., and Schaumburg, K. (1995) Structure of red and Orange Fluorescein. *Struct. Chem.* 6, 161–165.
- (22) Hurd, C. D., and Schmerlin, L. (1937) Alkenyl Derivatives of Fluorescein. *J. Am. Chem. Soc.* 59, 112–117.
- (23) Falck, J. R., Krieger, M., Goldstein, J. L., and Brown, M. S. (1981) Preparation and Spectral Properties of Lipophilic Fluorescein Derivatives: Application to Plasma Low-Density Lipoproteins. *J. Am. Chem. Soc.* 103, 7396–7398.
- (24) Zhao, Z.-G., Shen, T., and Xu, H.-J. (1989) The absorption and structure of fluorescein and its ethyl derivatives in various solutions. *Spectrochem. Acta* 45A, 1113–1116.
- (25) Brown, L., Halling P. J., Johnston, G. A., Suckling, C. J., and Valivety, R. H. (1990) The Synthesis of some Water Insoluble Dyes for the Measurement of pH in Water Immiscible Solvents. *J. Chem. Soc., Perkin Trans. 1*, 3349–3353.

BC9700704

Construction, Expression, and Activities of L49-sFv- β -Lactamase, a Single-Chain Antibody Fusion Protein for Anticancer Prodrug Activation

Nathan O. Siemers, David E. Kerr, Susan Yarnold, Mark R. Stebbins, Vivekananda M. Vrudhula, Ingegerd Hellström, Karl Erik Hellström, and Peter D. Senter*

Bristol-Myers Squibb Pharmaceutical Research Institute, 3005 First Avenue, Seattle, Washington 98121. Received February 11, 1997[©]

The L49 (IgG₁) monoclonal antibody binds to p97 (melanotransferrin), a tumor-selective antigen that is expressed on human melanomas and carcinomas. A recombinant fusion protein, L49-sFv-bL, that contains the antibody binding regions of L49 fused to the *Enterobacter cloacae* r2-1 β -lactamase (bL) was constructed, expressed, and purified to homogeneity in an *Escherichia coli* soluble expression system. The variable regions of L49 were cloned by reverse transcription–polymerase chain reaction from L49 hybridoma mRNA using signal sequence and constant region primers. Construction of the gene encoding L49-sFv-bL was accomplished by hybridization insertion of V_H, V_L, and sFv linker sequences onto a pET phagemid template containing the bL gene fused to the pelB leader sequence. Optimal soluble expression of L49-sFv-bL in *E. coli* was found to take place at 23 °C with 50 μ M isopropyl β -D-thiogalactopyranoside induction and the use of the nonionic detergent Nonidet P-40 for isolation from the bacteria. Construction and expression of a soluble form of the p97 antigen in Chinese hamster ovary cells allowed affinity-based methods for analysis and purification of the fusion protein. Surface plasmon resonance, fluorescent activated cell sorting, and Michaelis–Menten kinetic analyses showed that L49-sFv-bL retained the antigen binding capability of monovalent L49 as well as the enzymatic activity of bL. *In vitro* experiments demonstrated that L49-sFv-bL bound to 3677 melanoma cells expressing the p97 antigen and effected the activation of 7-(4-carboxybutanamido)cephalosporin mustard (CCM), a cephalosporin nitrogen mustard prodrug. On the basis of these results, L49-sFv-bL was injected into nude mice with subcutaneous 3677 tumors, and localization was determined by measuring bL activity. Tumor to blood conjugate ratios of 13 and 150 were obtained 4 and 48 h post conjugate administration, respectively, and the tumor to liver, spleen, and kidney ratios were even higher. A chemically produced L49-Fab'-bL conjugate yielded a much lower tumor to blood ratio (5.6 at 72 h post administration) than L49-sFv-bL. Therapy experiments established that well-tolerated doses of L49-sFv-bL/CCM combinations resulted in cures of 3677 tumors in nude mice. The favorable pharmacokinetic properties of L49-sFv-bL allowed prodrug treatment to be initiated 12 h after the conjugate was administered. Thus, L49-sFv-bL appears to have promising characteristics for site-selective anticancer prodrug activation.

INTRODUCTION

A considerable amount of attention has been directed toward the use of monoclonal antibody–enzyme conjugates in combination with suitable prodrugs for the selective delivery of chemotherapeutic agents to tumors (1–3). The monoclonal antibody (mAb¹) portions of these immunoconjugates recognize tumor-selective antigens and are capable of delivering the enzymes to tumor cell surfaces. Once tumor localization and systemic conjugate clearance have taken place, a prodrug form of a chemotherapeutic agent is administered, which is converted into an active drug by the targeted enzyme. This leads to the selective delivery of anticancer drugs to sites of neoplasia. Pharmacokinetic studies have shown that the

intratumoral drug concentrations resulting from mAb–enzyme/prodrug combinations can be significantly greater than that achieved by systemic drug administration (4–6). This probably accounts for the observed antitumor activities, which include complete tumor regressions and cures in a number of different models for human cancer (7–10).

Our recent research has focused on the use of antibodies against the human p97 (melanotransferrin) tumor antigen for the delivery of β -lactamase (bL) to tumor cells (10). This antigen has been found to be overexpressed on a majority of clinical melanoma isolates and is also observed on human carcinomas (11–14). Significant antitumor activities have been obtained using the combination of a chemically conjugated anti-p97 Fab'-bL and CCM (10), a cephalosporin containing prodrug of PDM (Figure 1). These effects were observed in a melanoma tumor model that was resistant to the activities of PDM.

A critical aspect of this targeting strategy surrounds the ability of the mAb to selectively deliver the enzyme to tumor cells and then clear from the systemic circulation before the prodrug is administered. The pharmacokinetics of the immunoconjugate can be greatly influenced by the nature, valency, and molecular weight of the mAb and also by the way that the enzyme is attached. Typically, mAb–enzyme conjugates are prepared using

* Author to whom correspondence should be addressed.

[©] Abstract published in *Advance ACS Abstracts*, June 15, 1997.

¹ Abbreviations: bL, β -lactamase; CHO, Chinese hamster ovary; CCM, 7-(4-carboxybutanamido)cephalosporin mustard; FITC, fluorescein isothiocyanate; IMDM, Iscove's Modified Dulbecco's Medium; IPTG, isopropyl β -D-thiogalactopyranoside; mAb, monoclonal antibody; PBS, 10 mM Na₂HPO₄, 1 mM KH₂PO₄, 137 mM NaCl, 2.7 mM KCl, pH 7.4; PCR, polymerase chain reaction; PDM, phenylenediamine mustard; SDS–PAGE, sodium dodecyl sulfate polyacrylamide gel electrophoresis; sp97, soluble p97 antigen; Tris, tris(hydroxymethyl)aminomethane.

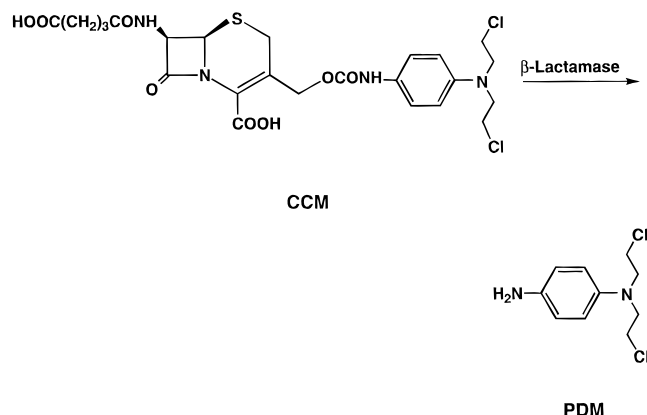


Figure 1. Structures of the cephalosporin mustard prodrug CCM and the parent drug phenylenediamine mustard PDM.

bifunctional cross-linking reagents that react with exposed amino acid residues on the individual proteins. Immunoconjugates produced in this manner are heterogeneous due to the inherent lack of regiospecificity of the cross-linking reagents. In addition, these conjugates are typically isolated in low yields. Although recent papers describe alternative coupling chemistries that can afford higher yields of more homogeneous immunoconjugates (15–17), these methods still involve chemical modification steps that contribute to product heterogeneity.

Recombinant technology offers an alternative method for producing homogeneous mAb–enzyme fusion proteins that can be designed to have appropriate pharmacokinetic properties for prodrug activation. There have recently been reports of the production, characterization, and activities of recombinant Fab, sFv, and disulfide-stabilized Fv–enzyme fusion proteins (4, 18–20). In this paper, we describe the construction, expression, and characteristics of L49-sFv-bL, an antibody β -lactamase fusion protein that binds to the p97 antigen. We also detail the construction and expression of sp97, a soluble form of the p97 antigen that has proven to be useful for conjugate analysis and purification. *In vitro* and *in vivo* experiments are presented that illustrate the ability of L49-sFv-bL to activate the phenylenediamine mustard prodrug CCM on p97 positive human melanoma cells, selectively localize in human tumor xenografts in nude mice, and induce regressions and cures of established tumors when combined with CCM.

MATERIALS AND METHODS

Materials. The *Enterobacter cloacae* P99 bL gene was obtained from the plasmid pNU363 (21) and subjected to codon-based mutagenesis at the nucleotides corresponding to amino acids 286–290. The r2-1 bL mutant, which has the sequence TSFGN at positions 286–290, was selected from the resulting library and displayed greater enzymatic activity than the wild type enzyme using cephalosporin doxorubicin as the substrate (22). L49-Fab'-bL was prepared as previously described by combining thiol-containing Fab' fragments of the antibodies with maleimide-substituted bL, forming a thioether link between the two proteins (23). CCM (24) and PDM (25) were prepared as previously described.

Isolation and Characterization of the L49 mAb. The L49-producing hybridoma was developed using standard techniques as previously described for the isolation of other hybridomas (26). Balb/C mice were immunized repeatedly with the H2981 (lung carcinoma), CH3 (lung carcinoma), and W56 (melanoma) cell lines, all of which were derived from human tumors. Spleen

cells from immunized mice were fused with the cell line P3X63-Ag8.563 (26) that was transfected with the neomycin resistance gene. Standard selection and cloning yielded a hybridoma producing the L49 IgG₁ mAb.

Scatchard analysis of L49 binding was performed by radiolabeling the mAb with [¹²⁵I]iodogen to a specific activity of 0.3 mCi/mg of protein. 3677 melanoma cells (10) in 96-well plates (13 000 cells/well) were incubated with 0.03–10 nM [¹²⁵I]L49 for 30 min on ice, and then the cells were separated from unbound radioactivity by centrifugation through silicon oil. The tubes were frozen, the cell pellet was cut from the supernatant, and both fractions were counted in a gamma counter. Binding affinity and the number of sites per cell were determined by Scatchard analysis (27).

Soluble p97 (sp97). A secreted form of p97 (sp97) was made utilizing PCR-based mutagenesis to introduce a stop codon after cysteine 709 (14), three amino acids upstream of the glycosylphosphatidylinositol anchor domain (28, 29). The 3' oligonucleotide used in the PCR reaction contained the mutation changing the S710 codon to a stop codon. Coding sequences for 29 amino acids, including the membrane anchor region, were deleted from the carboxyl terminus of wild type p97. Cloning and expression of sp97 were accomplished using a glutamine synthetase gene as an amplifiable marker in CHO cells (30). The sp97 gene was cloned into pEE14 (31) and transfected into CHO-K1 cells by calcium phosphate coprecipitation. Transformants were initially selected for resistance to 25 μ M methionine sulfoximine, and sp97-secreting colonies were selected for amplification at drug concentrations of 100, 250, and 500 μ M. The selection and amplification medium used was Glasgow Minimum Essential Medium without L-glutamine, tryptose phosphate broth, or sodium bicarbonate supplemented with 10% dialyzed fetal bovine serum.

A cloned CHO cell line secreting sp97 was cultured in 10 shelf cell factories. Soluble p97 was isolated from the medium on a 96.5 immunoaffinity chromatography column as described previously for the purification of wild type p97 from melanoma cells (32). Small amounts of residual contaminants were removed by gel filtration on a Sephacryl S300 HR column (Pharmacia LKB) using PBS as eluant. Solutions containing sp97 were concentrated by ultrafiltration to 1–5 mg/mL, sterilized by passage through a 0.1 μ m filter, and stored at 2–8 $^{\circ}$ C for up to 6 months without noticeable loss of biochemical or biological activity.

Cloning of L49 Variable Regions and sFv Construction. Construction of L49-sFv-bL by hybridization insertion was performed with materials and protocols from the Bio-Rad M13 mutagenesis kit, except for isolation of single-stranded phagemid template (Qiagen M13 kit, M13K07 helper phage). The variable regions of the L49 mAb were cloned from the corresponding hybridoma mRNA by RT-PCR (Perkin-Elmer GeneAmp reagents and Model 9600 thermal cycler), using random hexamer primed reverse transcription reactions and signal sequence and constant region PCR primers (33). Construction of L49-sFv-bL began with a single-stranded template of the pET-26b phagemid containing the r2-1 mutant of the *E. cloacae* P99 bL gene (22) fused to the pelB leader sequence. Hybridization mutagenesis was used to insert the 218 linker sequence (34) (chemically synthesized oligonucleotide, 5'-TTCTGACACTGGCGTGCCCTTGGTAGAGCCTTCGCCAGAGCCCGGTTTGCCA-GAGCCGGACGTCGAGCCGGCCATCGCCGGCTG-3') and full V_H and V_L region sequences (oligonucleotides produced by asymmetric PCR; V_H forward primer, 5'-CCAGCCGGCGATGGCCGAGGTGCAGCTTCAGGAGT-

3'; V_H reverse primer, 5'-AGAGCCGGACGTCGAGCCT-GAGGAGACGGTGACAGAGG-3'; V_L forward primer, 5'-AGGCTCTACCAAGGGCGATTTTGTGATGACCCAAAC-3'; V_L reverse primer, 5'-TTCTGACACTGGCGTC-CGTTTGATTCCAGCTTGG-3') in three consecutive insertion reactions between the pelB leader sequence and bL in a 5'-pelB-V_H-218-V_L-bL-3' orientation.

Expression, Purification, and Characterization of L49-sFv-bL. L49-sFv-bL was expressed as a soluble protein in *E. coli* strain BL21(λDE3) at 23 °C in 4 L baffled shake flasks. T-broth (1 L) containing 30 μg/mL kanamycin was inoculated with several colonies of freshly transformed BL21(λDE3) cells. The flasks were shaken (200 rpm) at 37 °C until the absorbance at 660 nm reached 0.8, the culture was cooled to 23 °C, and IPTG (50 μM) was added. Incubation at 23 °C with shaking was continued for an additional 16 h, at which time the absorbance at 660 nm was between 8 and 15. The cells were pelleted by centrifugation and resuspended in 30 mM Tris, 2 mM EDTA, and 0.3% (v/v) Nonidet P-40 at pH 8.5 and 4 °C. The mixture was stirred gently for 1 h and repelleted, and the supernatant was decanted and filtered (0.2 μm).

Purification of L49-sFv-bL was accomplished according to a two-step affinity purification. The above supernatant was first applied to a Sepharose column of immobilized sp97 antigen. The column was washed with PBS until the absorbance at 280 nm reached the baseline level, and bound protein was eluted with 50 mM sodium phosphate and 100 mM NaCl at pH 11.2. Fractions containing the bound protein were neutralized with 1:10 v/v of 3 M sodium phosphate, pH 7. This material was then subjected to Sepharose 4B *m*-aminophenylboronic acid affinity chromatography (35) using washing and pH 11.2 elution conditions described above. The resulting preparation was dialyzed against PBS, filtered (0.2 μm), and stored at 4 °C (0.1–1.1 mg/mL).

Competition binding experiments were performed as described earlier (10, 36). Immunoassays were performed by coating polystyrene 96-well plates with sp97 (0.1 mL, 2 μg/mL in PBS, overnight, 4 °C). The plates were blocked by adding specimen diluent (Genetic Systems Corp.) for 1 h at 22 °C, and the diluent was then removed. Fresh specimen diluent (0.1 mL) containing serial dilutions of the samples was added. After 1 h at 22 °C, the plates were washed and developed for 15 min at room temperature with 0.1 mL of a nitrocefin solution (37) at 0.1 mM in PBS containing 1% dimethylformamide. Absorbance measurements were read in an ELISA plate reader using a 490 nm filter with 630 nm as the reference wavelength.

Surface plasmon resonance experiments were performed on a BIAcore 2000 instrument (Pharmacia) at 25 °C. p97 was immobilized on a research grade CM5 sensor chip (Pharmacia) using the recommended *N*-ethyl-*N'*-(dimethylaminopropyl)carbodiimide/*N*-hydroxysuccinimide coupling conditions. Before use, the sensor surface was subjected to several rounds of analyte binding, followed by regeneration to ensure a stable level of derivatization. The mobile phase buffer for immobilization was PBS containing 0.005% P20 surfactant (Pharmacia). For binding studies, 0.2 mg/mL bovine serum albumin was added to the buffer.

In Vitro Cytotoxicity. 3677 melanoma cells were plated into 96-well microtiter plates (10⁴ cells/well in 100 μL of IMDM with 10% fetal bovine serum, 60 μg/mL penicillin, and 0.1 mg/mL streptomycin) and allowed to adhere overnight. For blocking experiments, the cells were incubated with unconjugated L49 at 1 μM for 30 min prior to treatment with the L49 conjugates. The cells

were treated with L49-sFv-bL or L49 Fab'-bL at 10 nM. After 30 min at 4 °C, the plates were washed three times with antibiotic-free RPMI 1640 medium (Gibco) with 10% fetal bovine serum, and then various concentrations of CCM were added. CCM and PDM were also added to cells treated with medium alone. After 1 h at 37 °C, cells were washed three times with IMDM and incubated for approximately 18 h at 37 °C. The cells were then pulsed for 12 h with [³H]thymidine (1 μCi/well) at 37 °C, detached by freezing at -20 °C and thawing, and harvested onto glass fiber filter mats using a 96-well harvester. Radioactivity was counted using a LKB Wallac β-plate counter.

Conjugate Localization. Subcutaneous 3677 melanoma tumors were established in female athymic nu/nu mice (8–12 weeks old, Harlan Sprague-Dawley, Indianapolis, IN) by transplanting tumors that had been previously passaged as previously described (10). Tumor-bearing mice were injected iv with L49-sFv-bL (1 or 4 mg of mAb component/kg) or with L49-Fab'-bL (1.8 mg/kg). At various time intervals, the mice were anesthetized, bled through the orbital plexus, and sacrificed. Tissues were removed and homogenized in PBS containing 15 μg/mL aprotinin (2 mL/g of tissue). To the homogenate was added 50 mM sodium phosphate containing 100 mM NaCl at pH 11.2 (10 mL/g of tissue), and the suspension was mixed. After 20 min at room temperature, 3 M sodium phosphate at pH 7.0 was added (2 mL/g of tissue), and the mixture was mixed and centrifuged.

Quantification of conjugate concentrations was accomplished using a direct enzyme immunoassay. Polystyrene 96-well microtiter plates were coated with an affinity-purified rabbit polyclonal antiserum to wild type *E. cloacae* bL (1 μg/mL) and were then blocked with specimen diluent (Genetic Systems Corp.). Serially diluted tissue extracts or purified samples (L49-sFv-bL as a standard for the fusion protein samples, L49-Fab'-bL as a standard for the L49-Fab'-bL samples) were added to the wells and allowed to bind for 3 h at room temperature. The plates were washed and developed by the addition of 0.1 mL of nitrocefin (37) at 0.1 mM in PBS containing 1% dimethylformamide. Absorbance measurements were read in an ELISA plate reader using a 490 nm filter with 630 nm as the reference wavelength.

In Vivo Therapy Experiments. 3677 tumor-bearing mice (subcutaneous implants, six animals/group, average tumor volume 130 mm³) were injected with L49-sFv-bL (iv, 7–8 days post tumor implant), followed 12–48 h later by CCM using doses of fusion protein and prodrug as indicated under Results. Treatment with L49-sFv-bL + CCM was repeated 1 week later. Animals were monitored 1–2 times/week for body weight, general health, and tumor growth. Tumor volume was estimated using the following formula: longest length × perpendicular dimension² ÷ 2. Cures were defined as an established tumor that, after treatment, was not palpable for ≥10 tumor volume doubling delays (≥40 days in the 3677 tumor model). Maximum tolerated doses led to <20% weight loss and no treatment-related deaths and were within 50% of the dose at which such events took place.

RESULTS

Characterization of the L49 MAb. The L49 mAb (IgG₁) binds to the p97 antigen, which has been shown to be present on most human melanomas and many carcinomas (11–13). Scatchard analysis of the binding of radiolabeled L49 to the 3677 human melanoma cell line indicated that the mAb bound with a dissociation constant of 1.0 nM (Figure 2). At saturation, there were approximately 2.1 × 10⁴ molecules of L49 bound/cell.

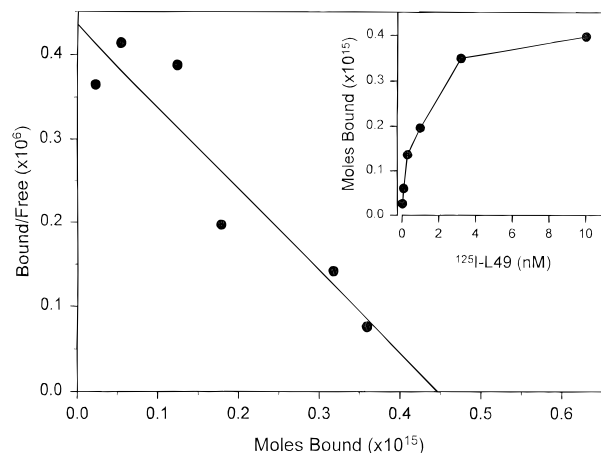


Figure 2. Scatchard analysis of L49 mAb binding to 3677 melanoma cells.

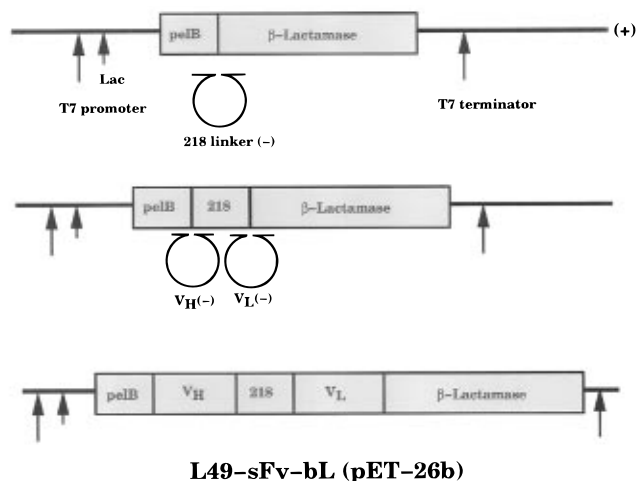


Figure 3. Construction of L49-sFv-bL. Three successive hybridization insertion reactions were used to install the 218 linker, variable heavy, and variable light chain sequences into a pET phagemid containing the r2-1 mutant of the *E. cloacae* bL. Single-stranded (+) phagemid DNA was produced by infection of XL-1 Blue carrying the pET phagemids with M13K07 helper phage. An oligonucleotide coding for the 218 linker sequence (– strand), with complementary regions to the 3' end of the pelB sequence and the 5' end of the bL gene was prepared by chemical synthesis. Corresponding V_H and V_L sequences (– strand) were generated by asymmetric PCR.

These values are very similar to those obtained for the 96.5 mAb (10), which also binds to p97 but to an epitope different from the one that L49 binds to (unpublished data).

Cloning and Expression of L49-sFv-bL. The variable region genes for the L49 mAb heavy and light chains were cloned from the L49 hybridoma line by reverse transcription PCR of hybridoma mRNA and amplification of the corresponding cDNA. A consensus sequence was determined by examining several clones from independent reverse transcription reactions to reduce the possibility of reverse transcription or PCR-derived errors. The PCR primers used were complementary to the signal sequence and constant region of the mAb. Thus, the entire variable regions were obtained.

L49-sFv-bL was constructed in a stepwise fashion by hybridization insertion of the sFv linker, V_H , and V_L region sequences onto a single-stranded pET phagemid template containing the pelB leader sequence and bL gene (Figure 3). The particular bL gene used coded for a mutant of the *E. cloacae* P99 bL (r2-1) that contained the amino acids TSFGN at positions 286–290. This

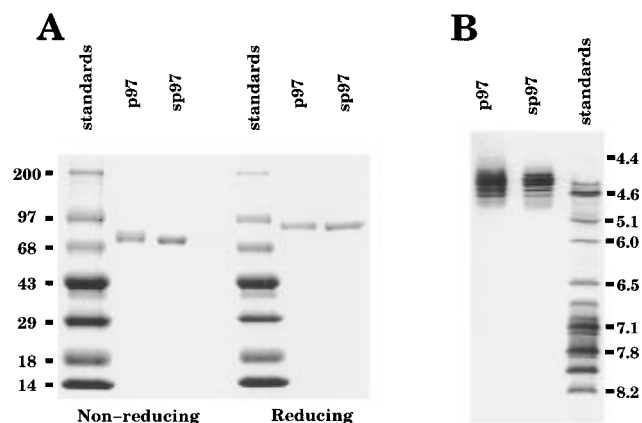


Figure 4. (A) SDS–PAGE (4–20%) and (B) isoelectric focusing analyses (pH 3–10) of recombinant sp97 and wild type p97 antigen.

mutated bL has been shown to have greater activity than the wild type enzyme toward hydrolysis of some cephalosporin prodrugs (22). The 218 linker sequence corresponds to amino acids GSTSGSGKPGSGEGSTKG and was used as the sFv linker on the basis of its ability to reduce sFv protein aggregation (34). An oligonucleotide coding for the 218 linker (– strand, produced by chemical synthesis) was first annealed to the phagemid template, resulting in a pelB-218-bL construct. V_H and V_L region segments (produced by asymmetric PCR) were then inserted into the intermediate construct in two separate steps to generate the final L49-sFv-bL gene in an pelB- V_H -218- V_L -bL orientation. The pelB leader sequence results in transport of the protein into the periplasmic space of *E. coli*. No additional linker was placed between V_L and the bL enzyme.

To facilitate the isolation and characterization of L49-containing fusion proteins, a soluble form of the p97 antigen was developed. This was made by truncating the p97 gene at a site upstream of the region encoding the membrane-anchoring domain. The soluble antigen (sp97) was expressed in CHO-K1 cells and purified by affinity chromatography. SDS–PAGE analysis of recombinant sp97 indicated that it was slightly lower in molecular weight than p97 (Figure 4A). Isoelectric focusing revealed little difference between p97 and sp97 (Figure 4B), a result that was anticipated, since only a single charged residue is lost in the sp97 construct. The multiple bands observed in the isoelectric focusing gel are due to charge heterogeneity in the expressed proteins.

L49-sFv-bL was expressed in soluble form in an *E. coli* strain that was transformed with the plasmid shown in Figure 3. Quantitation of L49-sFv-bL-containing samples was performed using an immunoassay in which the fusion protein was captured onto microtiter plates that were coated with sp97. The bL enzyme activity was then determined using nitrocefin as a colorimetric indicator (37). Thus, only bifunctional fusion protein was measured. Under the transcriptional control of the T7 promoter and lac operon, fusion protein expression could be detected by SDS–PAGE analyses of cell pellets in cultures that were induced with IPTG at concentrations as low as 1.6 μ M (Figure 5A). Significant levels of toxicity were observed when the IPTG concentration exceeded 90 μ M, resulting in inhibition of cell growth and in the eventual outgrowth of cell populations that did not express fusion protein. Typically, 50 μ M IPTG induction was used for large scale experiments, since this led to higher levels of fusion protein expression without significant levels of cytotoxicity. It was also found that expression of L49-sFv-bL was enhanced at lower tem-

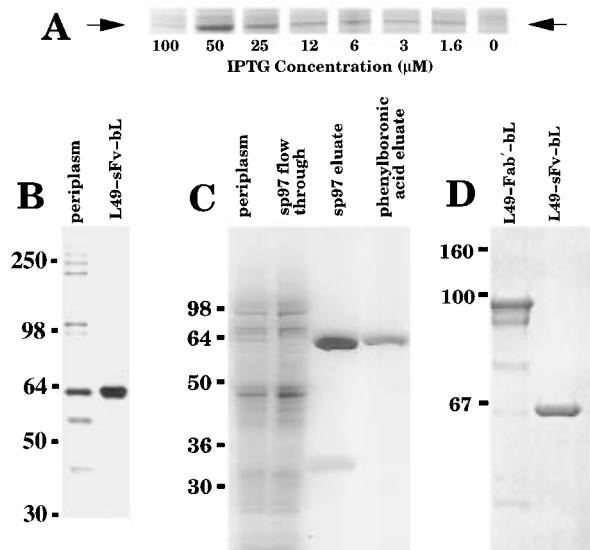


Figure 5. SDS-PAGE analyses of L49-sFv-bL expression and purification. (A) Induction of L49-sFv-bL at various IPTG concentrations (30 °C, total cellular protein, 12% Tris-glycine SDS-PAGE, Coomassie staining, nonreducing conditions). The band corresponding to L49-sFv-bL is indicated with arrows. (B) Western analysis with rabbit polyclonal anti-bL: (lane 1) periplasm; (lane 2) L49-sFv-bL standard (12% Tris-glycine SDS-PAGE, nonreducing conditions). (C) Purification of L49-sFv-bL: (lane 1) periplasm; (lane 2) flow through from the sp97 affinity column; (lane 3) material that eluted from the sp97 column at pH 11; (lane 4) material that bound and eluted off the phenylboronic acid column (12% Tris-glycine SDS-PAGE, Coomassie staining, nonreducing conditions). (D) Comparison of L49-sFv-bL to chemically prepared L49-Fab'-bL: (lane 1) L49-Fab'-bL; (lane 2) L49-sFv-bL (10% Tris-glycine SDS-PAGE, Coomassie staining, nonreducing conditions).

peratures, such that protein yields were higher at 23 or 30 °C compared to 37 °C. Similar results have been noted for the expression of antibody fragments and other recombinant proteins in *E. coli* (38).

In shake flask cultures, 80% of active material was present in the periplasm of the bacterial cells, with the remainder present in the culture supernatant. Conventional techniques for releasing the periplasmic contents, such as sucrose/lysozyme spheroplasting or osmotic shock, resulted in only a limited release of the available protein. Freeze-thawing or sonication of cells to release total cytoplasmic material did not result in an increased yield of functional fusion protein. It was found that a higher yield of fusion protein could be obtained by treating cell pellets with a solution of the detergent Nonidet-P-40. The levels of L49-sFv-bL in samples that were treated with this detergent ranged from 2.5 to 8 mg/L culture, approximately 4 times the amount extracted by other techniques. Western analysis (Figure 5B) with rabbit polyclonal antiserum raised to bL showed that most of the bL-containing protein in the preparation was approximately 63 kDa in molecular mass (theoretical molecular mass 66.5 kDa). Small amounts of truncated fragments and aggregated material were also detected.

Purification of L49-sFv-bL. The purification of L49-sFv-bL was achieved according to a two-step affinity chromatography procedure. Periplasmic preparations from shake flask cultures were first applied to an immobilized sp97 affinity column that could bind the L49 portion of the fusion protein. After extensive washing, bound material was eluted at pH 11.2 (Figure 5C). Acidic pH conditions (pH 2.2) also eluted the fusion protein, but caused protein precipitation. The sp97 chromatography purified material was approximately 70% pure by size exclusion HPLC and SDS-PAGE, with the contaminants

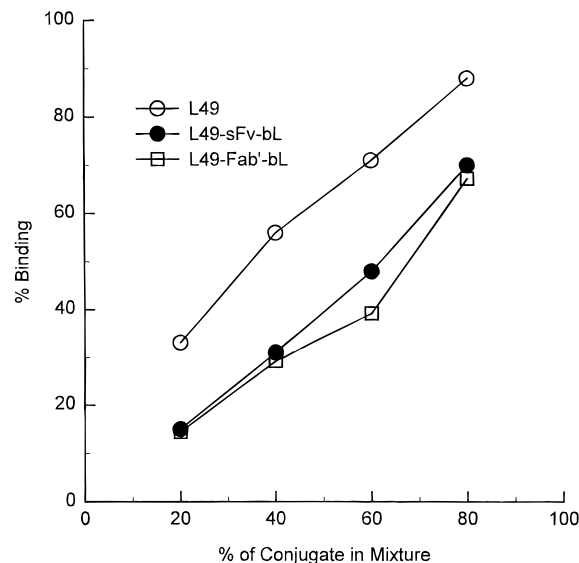


Figure 6. Competition binding assay. 3677 cells were incubated with various combinations of the test samples (L49, L49-sFv-bL, L49-Fab'-bL, and FITC-modified whole L49), keeping the total mAb concentration (test sample + L49-FITC) constant at 400 nM. Fluorescence intensity was determined by fluorescence activated cell sorter analysis.

consisting of two bands of approximately 33 kDa molecular mass. The second step of the purification involved binding the material to immobilized phenylboronic acid, a resin that binds to the active sites of β -lactamases. This led to the recovery of protein that was pure by SDS-PAGE analysis (Figure 5C,D). Size exclusion chromatographic analysis of the fusion protein indicated the presence of a single component that eluted in the expected molecular mass range (data not shown). In contrast, L49-Fab'-bL, which was prepared by combining maleimide-substituted bL with L49-Fab'-SH according to previously described methods (10, 23), displayed significant levels of heterogeneity by SDS-PAGE (Figure 5D).

L49-sFv-bL Characterization and Activity. In view of the detergent-based release of L49-sFv-bL from the bacteria, it was important to demonstrate that isolated fusion protein had been correctly processed and transported into the periplasm, such that the pelB leader sequence was cleaved from the amino terminus of the V_H region. This was determined by subjecting the purified fusion protein to N-terminal amino acid sequence analysis. The sequence obtained (EVQLQES) was identical to the expected V_H amino terminal sequence, indicating that the leader sequence was proteolytically clipped, as designed.

The binding characteristics of the sFv portion of the fusion protein were determined using a fluorescence-activated cell sorting assay in which fusion protein and FITC-modified whole L49 competed for binding to cell-surface antigens on SK-MEL 28 melanoma cells. L49-sFv-bL and the L49 Fab'-bL chemical conjugates bound equally well to the cell line, but not as well as bivalent whole L49 mAb (Figure 6). More detailed information about binding was obtained using surface plasmon resonance, which allowed the measurement of the on and off rates of L49-sFv-bL binding to the p97 antigen immobilized on a gold surface (Table 1). This assay established that the binding affinity of the fusion protein to the p97 antigen ($K_D = 1.0$ nM) was comparable to those of L49 Fab' ($K_D = 0.73$ nM) and chemically produced L49-Fab'-bL conjugate ($K_D = 1.3$ nM).

Enzymatic activity assays of the bL portion of L49-sFv-bL were undertaken using nitrocefin as the substrate

Table 1. Binding and Enzyme Kinetic Parameters of L49- and bL-Containing Proteins^a

sample	k_{on} ($M^{-1}\cdot s^{-1}$)	k_{off} (s^{-1})	K_D (nM)	k_{cat} (s^{-1})	K_m (μM)
L49 Fab'	2.3×10^5	1.7×10^{-4}	0.73	na ^b	na
r2-1 bL ^c	na	na	na	261	19
L49-Fab'-bL ^d	1.8×10^5	2.4×10^{-4}	1.3	nd ^e	nd
L49-sFv-bL ^c	4.1×10^5	4.2×10^{-4}	1.0	232	19

^a Values shown are the average of a minimum of two independent experiments, except for L49-Fab'-bL (binding experiment performed once). The range of values obtained in Michaelis-Menten kinetic analyses was within 5% of the means. Nitrocefin was used as an enzyme substrate. ^b Not applicable. ^c The r2-1 bL contains mutations at positions 286–290 compared to the wild type enzyme (22). ^d Chemically prepared conjugate containing the wild type enzyme. ^e Not determined.

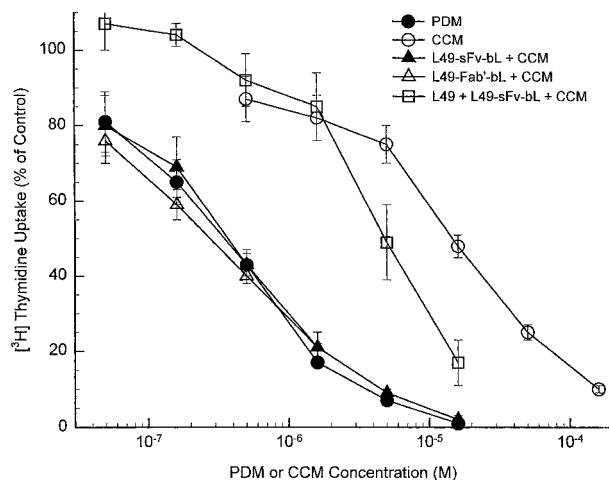


Figure 7. Cytotoxic effects of mAb-bL + CCM combinations on 3677 melanoma cells as determined by the incorporation of [³H]thymidine into DNA. 3677 cells were incubated with the mAb-bL conjugates, washed, and treated with CCM for 1 h. The effects were compared to cells treated with CCM or PDM for 1 h without prior conjugate exposure and to cells that were treated with saturating amounts of unconjugated L49 prior to conjugate treatment.

(Table 1). Michaelis-Menten kinetic analyses confirmed that the fusion protein retained the full enzymatic activity of the mutant bL enzyme from which it was derived (22). Thus, both the binding of the L49 mAb and the enzymatic activity of the *E. cloacae* r2-1 bL were preserved in the fusion protein.

The cytotoxic effects of L49-sFv-bL in combination with CCM were determined on 3677 human melanoma cells, which express the p97 antigen (Figure 7). The experiments were performed by treating the cells with the conjugates, washing off unbound material, adding various concentrations of CCM, and using [³H]thymidine incorporation as a measure of cytotoxic activity. The prodrug CCM ($IC_{50} = 16 \mu M$) was approximately 50-fold less toxic to 3677 cells than the drug PDM ($IC_{50} = 0.3 \mu M$). As expected, L49-sFv-bL and L49-Fab'-bL were equally effective at prodrug activation, and the combinations were equivalent in activity to PDM. This indicates that prodrug conversion by both conjugates was efficient under the conditions tested. In addition, it was found that activation was immunologically specific, since L49-sFv-bL did not activate CCM on cells that were saturated with unconjugated L49 before being exposed to the fusion protein.

In Vivo Localization. Biodistribution studies of L49-sFv-bL and L49-Fab'-bL were carried out in nude mice bearing sc 3677 melanoma tumor xenografts. The conjugates were injected iv, and at various time points

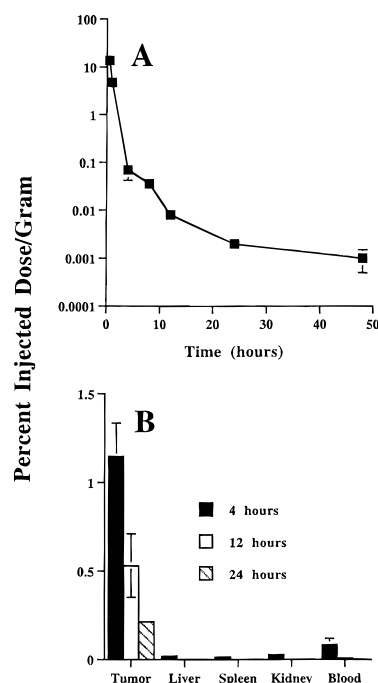


Figure 8. Pharmacokinetics of L49-sFv-bL in nude mice (three animals/group). L49-sFv-bL was injected intravenously, tissues were removed and extracted at the indicated times, and the β -lactamase activity was determined using nitrocefin as a substrate. (A) Clearance of L49-sFv-bL from the blood. Injected dose was 4 mg/kg. (B) L49-sFv-bL levels in subcutaneous 3677 melanoma tumors and in normal tissues. Injected dose was 1 mg/kg.

tissues were removed and extracted under alkaline conditions to disrupt antigen-antibody interactions. The samples were then trapped with polyclonal antiserum to bL, and bL activity was measured using nitrocefin as a colorimetric indicator (37). Control experiments in which L49-sFv-bL was directly injected into excised tumors and tissues indicated that this extraction procedure recovered 90% of the injected bL activity.

L49-sFv-bL cleared very rapidly from the blood (Figure 8A). The initial and terminal clearance half-lives ($t_{1/2\alpha}$ and $t_{1/2\beta}$, respectively) were 0.3 and 2.5 h, respectively, leading to a 10^4 reduction of L49-sFv-bL blood levels within 24 h of conjugate administration. In spite of this rapid clearance, relatively high intratumoral levels of L49-sFv-bL were measured compared to normal tissues, and the ratio remained high for 24 h (Figure 8B). At 4 h post L49-sFv-bL administration, the tumor to blood ratio was 13:1. The ratio increased substantially with time and was 105:1 within 24 h of conjugate administration (Table 2). Similar results were obtained using L49-sFv-bL doses of 4 mg/kg. At this dose, very high tumor to blood ratios (141–150:1) were measured 24–48 h after the conjugate was administered. Interestingly, chemically produced L49-Fab'-bL cleared quite slowly from the blood and had only a 5.6:1 tumor to blood ratio 72 h after administration. Thus, L49-sFv-bL localizes in tumors, clears rapidly from the systemic circulation, and has significantly improved pharmacokinetic properties compared to the chemically produced L49-Fab'-bL conjugate.

Therapeutic Activity. *In vivo* therapy experiments were performed using the L49-sFv-bL/CCM combination in nude mice with established sc 3677 tumors. This particular tumor model has previously been shown to be resistant to treatment with doxorubicin, PDM, and CCM (10). In the experiments reported here, conjugate treatment was initiated 7–8 days after tumor implant, at which time the tumors were approximately 130 mm³ in

Table 2. Tissue Distribution of Immunoconjugates

treatment ^a	time (h)	% injected dose/g (SD)				
		tumor	liver	spleen	kidney	blood
L49-sFv-bL, 1 mg/kg	4	1.1 (0.2)	0.021 (0.002)	0.014 (0.008)	0.027 (0.015)	0.084 (0.04)
tumor/tissue ratios		1	52	79	41	13
L49-sFv-bL, 1 mg/kg	12	0.53 (0.17)	<0.003	<0.003	<0.003	0.008 (0.001)
tumor/tissue ratios		1	>177	>177	>177	66
L49-sFv-bL, 1 mg/kg	24	0.21 (0.01)	<0.003	<0.003	<0.003	0.002 (0.001)
tumor/tissue ratios		1	>70	>70	>70	105
L49-sFv-bL, 4 mg/kg	12	0.73 (0.02)	<0.003	<0.003	<0.003	0.009 (0.001)
tumor/tissue ratios		1	>240	>240	>240	81
L49-sFv-bL, 4 mg/kg	24	0.29 (0.05)	<0.001	<0.001	<0.001	0.002 (0.0002)
tumor/tissue ratios		1	>290	>290	>290	141
L49-sFv-bL, 4 mg/kg	48	0.15 (0.07)	nd ^b	nd	nd	0.001 (0.0002)
tumor/tissue ratios		1				150
L49-Fab'-bL, 1.8 mg/kg	72	0.28 (0.26)	0.015 (0.003)	0.010 (0.006)	0.016 (0.005)	0.05 (0.015)
tumor/tissue ratios		1	19	28	18	5.6

^a Mice (three animals/group) were injected with conjugates, and at the times indicated, tissues were excised and extracted to remove the conjugate. The percent injected dose was based on the measured bL activity compared to standard curves obtained from extracted tissues that were spiked with known amounts of L49-sFv-bL or L49-Fab'-bL. ^b Not determined.

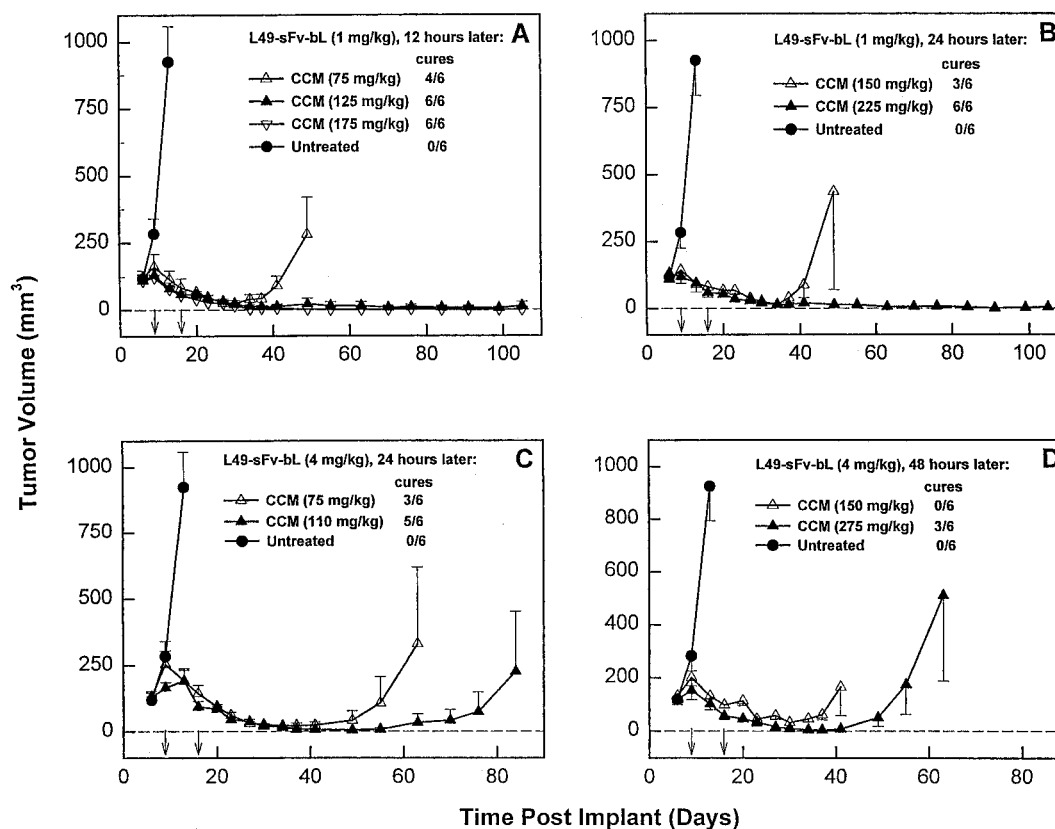


Figure 9. Therapeutic effects of L49-sFv-bL/CCM combinations in nude mice (six mice/group) with sc 3677 melanoma xenografts. Conjugates were injected, followed at various times by CCM (arrows on the X-axis). The average tumor volumes are reported until most or all of the animals were cured (tumors that became nonpalpable for ≥ 10 tumor volume doubling times) or until an animal was removed from the experiment due to tumor outgrowth. (A) L49-sFv-bL (1 mg/kg/injection) 12 h before CCM; (B) L49-sFv-bL (1 mg/kg/injection) 24 h before CCM; (C) L49-sFv-bL (4 mg/kg/injection) 24 h before CCM; (D) L49-sFv-bL (4 mg/kg/injection) 48 h before CCM.

volume. CCM was then administered 12, 24, or 48 h later, and the treatment protocol was repeated after 1 week. Maximum tolerated doses are defined as those that led to $<20\%$ weight loss and no treatment-related deaths and were within 50% of the dose at which such events took place. A tumor was considered as having been cured once it was not palpable for at least 10 tumor volume doubling times, based on the tumor growth of untreated animals (tumor volume doubling time was 4 days). If an animal was removed from the experiment because of tumor growth, the data from the entire group were no longer plotted, but the remaining animals were followed for tumor size and general health.

The maximum tolerated doses of CCM (300 mg/kg/injection) and PDM (3 mg/kg/injection) when administered weekly for three rounds induced 2 and 6 day delays in tumor outgrowth, respectively (data not shown). In contrast, pronounced antitumor activity was obtained in mice that received L49-sFv-bL prior to treatment with CCM (Figure 9). Therapeutic efficacy was schedule and dose dependent. Tumor cures were obtained in all of the animals that received CCM (125 and 175 mg/kg/injection) 12 h after treatment with L49-sFv-bL (Figure 9A). In this dosing schedule, significant antitumor activity including four cures in the group of six mice was obtained when the CCM dose was reduced to 75 mg/kg/injection.

The remaining two animals in this group had tumors that underwent partial regressions but eventually began to grow after the last prodrug treatment. There were no apparent toxicities in any of these treatment groups.

Significant antitumor activity could also be achieved when the prodrug was administered 24 h post conjugate administration, either by increasing the prodrug dose and keeping the conjugate dose constant at 1 mg/kg/injection (Figure 9B) or by increasing the conjugate dose to 4 mg/kg/injection (Figure 9C). In both cases, the majority of tumors were cured, again with no evidence of toxicity. Finally, therapeutic efficacy was also obtained with a 48 h interval between conjugate and prodrug administration (Figure 9D). Tumor regressions were obtained in all of the mice in these groups, and three of six animals that received 275 mg/kg/injection CCM were cured. Thus, the antitumor activities of L49-sFv-bL in combination with CCM were pronounced, and therapeutic efficacy was achieved in a variety of dosing schedules.

DISCUSSION

We have previously demonstrated that mAb-bL conjugates activate cephalosporin-containing prodrugs in an immunologically specific manner and such combinations lead to regressions and cures of established tumors in mice (6, 10, 24, 36). These conjugates were prepared by combining maleimide-substituted bL with thiol-containing mAbs and then subjecting the resulting mixtures to purification procedures that involved affinity and size exclusion chromatographic steps. Although care was taken to control the degree of protein modification and to isolate principally monomeric material, SDS-PAGE analysis generally has indicated the presence of aggregates, dimers and lower molecular mass components in the conjugate preparations. This is exemplified in Figure 5D, which shows that chemically produced L49-Fab'-bL contains several species besides the expected product at 92 kDa. Such heterogeneity is most likely due to the lack of specificity inherent in the reagents used for protein modification (39). While a number of elegant methods, such as reverse proteolysis (16, 40-42) and terminal amino acid group modification (43), have been devised to overcome this problem, these techniques can still lead to considerable product heterogeneity.

An alternative approach toward the preparation of uniform and well-defined antibody-enzyme immunoconjugates has involved recombinant technology for the production of fusion proteins. This has led to the development of L6-sFv-*Bacillus cereus* β -lactamase (19) and anti-p185HER2-Fv-*E. coli* β -lactamase (20) fusion proteins, both of which were capable of effecting prodrug activation *in vitro*. More detailed biological studies have been reported with a recombinant anti-CEA-Fab- β -glucuronidase fusion protein, which activated a doxorubicin prodrug *in vitro* and *in vivo* (4). The distinguishing features of these fusion proteins are that they are homogeneous and potentially can be made in reproducible and economical manners. In the work described here, we have utilized recombinant methodology for the production of L49-sFv-bL. It was possible to express soluble fusion protein in *E. coli* such that denaturation or refolding was not required for activity. L49-sFv-bL was purified using a two-stage affinity chromatography method leading to the isolation of a homogeneous product that was fully active with respect to both the L49 and bL components. As expected, the fusion protein was able to bind to melanoma cells that expressed the p97 antigen and activate a cephalosporin mustard in an immunologically specific manner.

To minimize systemic, nontargeted drug release *in vivo*, a high mAb-enzyme tumor to normal tissue ratio is needed before the prodrug is administered. To attain the required localization index in mice, the time between conjugate and prodrug administration has varied significantly from one system to another. For example, the delay between conjugate and prodrug was 3 days for 96.5-Fab'-bL (molecular mass 92 kDa) (10), 1 week for the anti CEA-Fab- β -glucuronidase fusion protein (molecular mass 250 kDa) (4), and 2 weeks for the ICR12-carboxypeptidase G2 conjugate (molecular mass range of 233-316 kDa) (9). In some cases, it has even been necessary to accelerate systemic conjugate clearance in a separate step involving the formation of immune complexes before prodrug could be administered (5, 44, 45). Here, we have shown that L49-sFv-bL not only clears very rapidly from the systemic circulation (Figure 8A) but also preferentially localizes into subcutaneous tumor xenografts (Figure 8B; Table 2). The very high tumor to nontumor fusion protein ratios obtained within 4-12 h of conjugate treatment would lead to the prediction that, in contrast to other enzyme/prodrug systems (4, 9, 10), therapeutic efficacy would not require protracted time intervals between conjugate and prodrug administration. This has now been experimentally confirmed, since cures of established tumors were obtained when CCM was administered 12 h following the conjugate (Figure 9A).

It is noteworthy that a correlation can be made between the outcome in the therapy experiments (Figure 9) and the pharmacokinetic data (Figure 8; Table 2). At a given conjugate dose, the intratumoral concentration decreased with a half-life of approximately 8 h (Table 2). This may be due to a variety of factors such as dissociation of the conjugate from the antigen, membrane recycling, enzyme metabolism, and rapid tumor growth. The net result is that longer time intervals between conjugate and prodrug administration require that the amount of either prodrug or conjugate be increased to maintain therapeutic efficacy (Figure 9).

In conclusion, we have shown that recombinant L49-sFv-bL has properties that are well suited for site-selective anticancer prodrug activation. The fusion protein is homogeneous, localizes in solid tumor masses, and clears very rapidly from the systemic circulation. In these respects, L49-sFv-bL has significant advantages over the L49-Fab'-bL chemically produced conjugate. Finally, we have shown that L49-sFv-bL/CCM combinations lead to cures of established melanoma tumors without toxic side effects. Currently, we are optimizing the treatment protocols and are investigating the effects of L49-sFv-bL/prodrug combinations in several carcinoma tumor models.

ACKNOWLEDGMENT

We thank William Bear, Joseph Cook, Wes Cosand, John Emswiler, Perry Fell, Deb Mahan, Hans Marquardt, Michael Neubauer, Hong Nguyen, Clay Siegall, Joseph Sundstrom, Håkan Svensson, and Trent Youngman for expert advice and assistance.

LITERATURE CITED

- (1) Senter, P. D., Wallace, P. M., Svensson, H. P., Vrduhula, V. M., Kerr, D. E., Hellström, I., and Hellström, K. E. (1993) Generation of cytotoxic agents by targeted enzymes. *Bioconjugate Chem.* 4, 3-9.
- (2) Jungheim, L. N., and Shepherd, T. A. (1994) Design of anticancer prodrugs: substrates for antibody targeted enzymes. *Chem. Rev.* 94, 1553-1566.
- (3) Bagshawe, K. D., Sharma, S. K., Springer, C. J., and Rogers, G. T. (1994) Antibody directed enzyme prodrug therapy

- (ADEPT). A review of some theoretical, experimental and clinical aspects. *Ann. Oncol.* 5, 879–891.
- (4) Bosslet, K., Czech, J., and Hoffmann, D. (1994) Tumor-selective prodrug activation by fusion protein-mediated catalysis. *Cancer Res.* 54, 2151–2159.
- (5) Wallace, P. M., MacMaster, J. F., Smith, V., Kerr, D. E., Senter, P. D., and Cosand, W. L. (1994) Intratumoral generation of 5-fluorouracil mediated by an antibody-cytosine deaminase conjugate in combination with 5-fluorocytosine. *Cancer Res.* 54, 2719–2723.
- (6) Svensson, H. P., Vruthula, V. M., Emswiler, J. E., MacMaster, J. F., Cosand, W. L., Senter, P. D., and Wallace, P. M. (1995) In vitro and in vivo activities of a doxorubicin prodrug in combination with monoclonal antibody β -lactamase conjugates. *Cancer Res.* 55, 2357–2365.
- (7) Springer, C. J., Bagshawe, K. D., Sharma, S. K., Searle, F., Boden, J. A., Antoni, P., Burke, P. J., Rogers, G. T., Sherwood, R. F., and Melton, R. G. (1991) Ablation of human choriocarcinoma xenografts in nude mice by antibody-directed enzyme prodrug therapy (ADEPT) with three novel compounds. *Eur. J. Cancer* 27, 1361–1366.
- (8) Meyer, D. L., Jungheim, L. N., Law, K. L., Mikolajczyk, S. D., Shepherd, T. A., Mackensen, D. G., Briggs, S. L., and Starling, J. J. (1993) Site-specific prodrug activation by antibody- β -lactamase conjugates: regression and long-term growth inhibition of human colon carcinoma xenograft models. *Cancer Res.* 53, 3956–3963.
- (9) Eccles, S. A., Court, W. J., Box, G. A., Dean, C. J., Melton, R. G., and Springer, C. J. (1994) Regression of established breast carcinoma xenografts with antibody-directed enzyme prodrug therapy against c-erbB2 p185. *Cancer Res.* 54, 5171–5177.
- (10) Kerr, D. E., Schreiber, G. L., Vruthula, V. M., Svensson, H. P., Hellström, I., Hellström, K. E., and Senter, P. D. (1995) Regressions and cures of melanoma xenografts following treatment with monoclonal antibody β -lactamase conjugates in combination with anticancer prodrugs. *Cancer Res.* 55, 3558–3563.
- (11) Woodbury, R. G., Brown, J. P., Yeh, M.-Y., Hellström, I., and Hellström, K. E. (1980) Identification of a cell surface protein, p97, in human melanomas and certain other neoplasms. *Proc. Natl. Acad. Sci. U.S.A.* 77, 2183–2187.
- (12) Brown, J. P., Nishiyama, K., Hellström, I., and Hellström, K. E. (1981) Structural characterization of human melanoma-associated antigen p97 with monoclonal antibodies. *J. Immunol.* 127, 539–545.
- (13) Brown, J. P., Woodbury, R. G., Hart, C. E., Hellström, I., and Hellström, K. E. (1981) Quantitative analysis of melanoma-associated antigen p97 in normal and neoplastic tissues. *Proc. Natl. Acad. Sci. U.S.A.* 78, 539–543.
- (14) Rose, T. M., Plowman, G. D., Teplow, D. B., Dreyer, W. J., Hellström, K. E., and Brown, J. P. (1986) Primary structure of the human melanoma-associated antigen p97 (melanotransferrin) deduced from the mRNA sequence. *Proc. Natl. Acad. Sci. U.S.A.* 83, 1261–1265.
- (15) Mikolajczyk, S. D., Meyer, D. L., Starling, J. J., Law, K. L., Rose, K., Dufour, B., and Offord, R. E. (1994) High yield, site-specific coupling of N-terminally modified β -lactamase to a proteolytically derived single-sulfhydryl murine Fab'. *Bioconjugate Chem.* 5, 636–646.
- (16) Werlen, R. C., Lankinen, M., Rose, K., Blakey, D., Shuttleworth, H., Melton, R., and Offord, R. E. (1994). Site-specific conjugation of an enzyme and an antibody fragment. *Bioconjugate Chem.* 5, 411–417.
- (17) Werlen, R. C., Lankinen, M., Smith, A., Chernushevich, I., Standing, K. G., Blakey, D. C., Shuttleworth, H., Melton, R. G., Offord, R. E., and Rose, K. (1995) Site-specific immunoconjugates. *Tumor Targeting* 1, 251–258.
- (18) Bosslet, K., Czech, J., Lorenz, P., Sedlacek, H. H., Shuermann, M., and Seemann, G. (1992) Molecular and functional characterization of a fusion protein suited for tumor specific prodrug activation. *Br. J. Cancer* 65, 234–238.
- (19) Goshorn, S. C., Svensson, H. P., Kerr, D. E., Somerville, J. E., Senter, P. D., and Fell, H. P. (1993) Genetic construction, expression, and characterization of a single chain anti-carcinoma antibody fused to β -lactamase. *Cancer Res.* 53, 2123–2127.
- (20) Rodrigues, M. L., Presta, L. G., Kotts, C. F., Wirth, C., Mordenti, J., Osaka, G., Wong, W. L. T., Nuijens, A., Blackburn, B., and Carter, P. (1995) Development of a humanized disulfide-stabilized anti-p185 HER2 Fv- β -lactamase fusion protein for activation of a cephalosporin doxorubicin prodrug. *Cancer Res.* 55, 63–70.
- (21) Galleni, M., Lindberg, F., Normark, S., Cole, S., Honore, N., Joris, B., and Frère, J. M. (1988) Sequence and comparative analysis of three *Enterobacter cloacae* ampC β -lactamase genes and their products. *Biochem. J.* 250, 753–760.
- (22) Siemers, N. O., Yelton, D. E., Bajorath, J., and Senter, P. D. (1996) Modifying the specificity and activity of the *Enterobacter cloacae* P99 β -lactamase by mutagenesis within an M13 phage vector. *Biochemistry* 35, 2104–2111.
- (23) Svensson, H. P., Wallace, P. M., and Senter, P. D. (1994) Synthesis and characterization of monoclonal antibody- β -lactamase conjugates. *Bioconjugate Chem.* 5, 262–267.
- (24) Vruthula, V. M., Svensson, H. P., Kennedy, K. A., Senter, P. D., and Wallace, P. M. (1993) Antitumor activities of a cephalosporin prodrug in combination with monoclonal antibody- β -lactamase conjugates. *Bioconjugate Chem.* 4, 334–340.
- (25) Everett, J. L., and Ross, W. C. R. (1949) Aryl-2-haloalkylamines. Part II. *J. Chem. Soc.*, 1972–1983.
- (26) Yeh, M. Y., Hellström, I., Brown, J. P., Warner, G. A., Hansen, J. A., and Hellström, K. E. (1979) Cell surface antigens of human melanoma identified by monoclonal antibody. *Proc. Natl. Acad. Sci. U.S.A.* 76, 2927–2931.
- (27) Trucco, M., and dePetris, S. (1981) Determination of equilibrium binding parameters of monoclonal antibodies specific for cell surface antigens. *Immunological Methods* (I. Lefkovits and B. Pernis, Eds.) pp 1–26, Academic Press, New York.
- (28) Alemany, R., Rosa Vila, M., Franci, C., Egea, G., Real, R. X., and Thomson, T. M. (1993) Glycosyl phosphatidylinositol membrane anchoring of melanotransferrin (p97): apical compartmentalization in intestinal epithelial cells. *J. Cell Sci.* 104, 1155–1162.
- (29) Food, M. R., Rothenberger, S., Gabathuler, R., Haidl, I. D., Reid, G., and Jefferies, W. A. (1994) Transport and expression in human melanomas of a transferrin-like glycosylphosphatidylinositol-anchored protein. *J. Biol. Chem.* 269, 3034–3040.
- (30) Cockett, M. I., Bebbington, C. R., and Yarranton, G. I. (1990) High level expression of tissue inhibitor of metalloproteinases in Chinese hamster ovary cells using glutamine synthetase gene amplification. *Biotechnology* 8, 662–667.
- (31) Stephens, P. E., and Cockett, M. I. (1989) The construction of a highly efficient and versatile set of mammalian expression vectors. *Nucleic Acids Res.* 17, 7110.
- (32) Baker, E. N., Baker, H. M., Smith, C. A., Stebbins, M. R., Kahn, M., Hellström, K. E., and Hellström, I. (1992) Human melanotransferrin (p97) has only one functional binding site. *FEBS Lett.* 298, 215–218.
- (33) Jones, S. T., and Bendig, M. M. (1991) Rapid PCR-cloning of full-length mouse immunoglobulin variable regions. *Biotechnology* 9, 88–92.
- (34) Whitlow, M., Bell, B. A., Feng, S.-L., Fipula, D., Hardman, K. D., Hubert, S. L., Rollence, M. L., Wood, F. F., Schott, M. E., Milenic, D. E., Yokota, T., and Schlom, J. (1993) An improved linker for single-chain Fv with reduced aggregation and enhanced proteolytic stability. *Protein Eng.* 6, 989–995.
- (35) Cartwright, S. J., and Waley, S. G. (1984) Purification of β -lactamases by affinity chromatography on phenylboronic acid-agarose. *Biochem. J.* 221, 505–512.
- (36) Svensson, H. P., Kadow, J. F., Vruthula, V. M., Wallace, P. M., and Senter, P. D. (1992) Monoclonal antibody- β -lactamase conjugates for the activation of a cephalosporin mustard prodrug. *Bioconjugate Chem.* 3, 176–181.
- (37) O'Callaghan, D. E., Morris, A., Kirby, S., and Shingler, A. H. (1972) Novel method for detection of β -lactamases by using a chromogenic cephalosporin substrate. *Antimicrob. Agents Chemother.* 1, 283–288.
- (38) Plückthun, A. (1992) Mono- and bivalent antibody fragments produced in *E. coli*: engineering, folding, and antigen binding. *Immunol. Rev.* 130, 151–188.

- (39) Adamczyk, M., Gebler, J. C., and Mattingly, P. G. (1996) Characterization of protein-hapten conjugates. 2. Electrospray mass spectrometry of bovine serum albumin-hapten conjugates. *Bioconjugate Chem.* 7, 475–481.
- (40) Chang, T. K., Jackson, D. Y., Burnier, J. P., and Wells, J. A. (1994) Subtiligase: a tool for semisynthesis of proteins. *Proc. Natl. Acad. Sci. U.S.A.* 91, 12544–12548.
- (41) Jackson, D. Y., Burnier, J., Quan, C., Stanley, M., Tom, J., and Wells, J. A. (1994) A designed peptide ligase for total synthesis of ribonuclease A with unnatural catalytic residues. *Science* 266, 243–247.
- (42) Schwarz, A., Wandrey, C., Bayer, E. A., and Wilchek, M. (1991) Enzymatic C-terminal biotinylation of proteins. *Methods Enzymol.* 184, 160–162.
- (43) Rose, K., Vilaseca, L. A., Werlen, R., Meunier, A., Fisch, I., Jones, R. M. L., and Offord, R. E. (1991) Preparation of well-defined protein conjugates using enzyme-assisted reverse proteolysis. *Bioconjugate Chem.* 2, 154–159.
- (44) Kerr, D. E., Garrigues, U. S., Wallace, P. M., Hellström, K. E., Hellström, I., and Senter, P. D. (1993) Application of monoclonal antibodies against cytosine deaminase for the *in vivo* clearance of a cytosine deaminase immunoconjugate. *Bioconjugate Chem.* 4, 353–357.
- (45) Rogers, G. T., Burke, P. J., Sharma, S. K., Koodie, R., and Boden, J. A. (1995) Plasma clearance of an antibody-enzyme conjugate in ADEPT by monoclonal anti-enzyme: its effect on prodrug activation in vivo. *Br. J. Cancer* 72, 1357–1363.

BC9700751

Enhanced Transepithelial Transport of Peptides by Conjugation to Cholic Acid

Peter W. Swaan,[†] Kathleen M. Hillgren,[‡] Francis C. Szoka, Jr., and Svein Øie*

Department of Biopharmaceutical Sciences, University of California at San Francisco, California 94143-0446.
Received November 5, 1996[®]

The potential of the intestinal bile acid transporter to serve as a shuttle for small peptide molecules was investigated. Eleven peptides with a 2–6 amino acid backbone were conjugated to the 24-position of 3 α ,7 α ,12 α -trihydroxy-5 β -cholan-24-oic acid (cholic acid) via an amide bond using an automated peptide synthesizer. In a human intestinal cell line (CaCo-2), cholic acid–peptide conjugates were able to inhibit the transepithelial transport of [³H]taurocholic acid, a natural substrate for the bile acid carrier, at a 100:1 conjugate/substrate ratio. Affinity for the carrier decreased significantly when the conjugate in the 24-position increased from 1 to 2 amino acids. Further increase in the amino acid chain length caused only minor decrease in affinity. A tetrapeptide–bile acid conjugate, [³H]-ChEAAA (Ch = cholic acid), was transported by the bile acid transporter, showing markedly higher apical (AP)-to-basolateral (BL) compared to BL-to-AP transport and inhibition by a 100-fold excess taurocholic acid. Another conjugate with 6 amino acids (ChEASASA) was transported by a passive diffusion pathway but still showed higher transport rates than the passive permeability marker mannitol, suggesting the possibility that the cholic acid moiety aids the passive membrane transfer of peptide molecules by increasing its lipophilicity. Metabolism of bile acid–peptide conjugates in CaCo-2 cells was 3% over 3 h. In conclusion, these studies show that the coupling of peptides to the 24-position of the sterol nucleus in cholic acid results in a combination of decreased metabolism and increased intestinal absorption, either by a carrier-mediated pathway or by accelerated passive diffusion.

INTRODUCTION

The use of peptides as therapeutic entities is constrained by their poor oral absorption. This is due to a combination of low cellular penetration and metabolism in the intestinal tract. Approaches to enhance the oral absorption of peptide drugs include (a) the concomitant administration of protease inhibitors or permeation enhancers; (b) drug delivery methods to increase retention time of the drug at the absorption site (e.g. polymer systems); and (c) strategies to increase metabolic resistance by structural alterations (e.g. prodrugs, stable peptide bonds, etc.). Targeting to carrier-mediated transport mechanisms is another promising tactic to enhance intestinal absorption of poorly absorbable compounds (1, 2). In this approach, a drug substance is chemically coupled to an actively absorbed compound and the resulting complex is recognized and transported by the carrier system. Although many transport systems are known to exist in the small intestine, only those having a high capacity and low substrate specificity are suitable targets for intestinal drug delivery. A transporter that seems ideal for this approach is the bile acid transporter, which facilitates the daily absorption of 10–20 g of bile salts at a >95% efficiency. Besides transporting its natural substrates, conjugated and unconjugated bile acids, the bile acid carrier allows chemical modifications

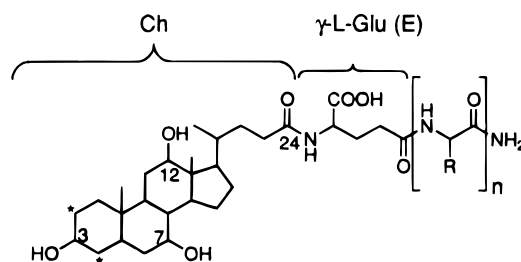


Figure 1. General structural formula of bile acid–peptide conjugates; cholic acid is indicated by “Ch”. Important carbon atoms in the sterol nucleus are numbered. Asterisks represent the position of the ³H isotope in radiolabeled compounds. All terminal amino acids are amide esters, except for ChDF, which is the methyl ester.

at the 3- and 24-positions of the sterol nucleus (Figure 1) (2, 3). Ho (2) showed that cholic acid, modified at the 3-position with tosyl or benzoyl groups, is transported by the bile acid transporter. Kim and colleagues (4) used the 3-position to enhance the intestinal absorption of renin-inhibitory peptides. They showed that their conjugates were able to bind to the intestinal bile acid transporter but were not transported *in vivo*. More recently, Kramer and colleagues used modifications at the 3-position for liver specific targeting of chlorambucil (5), HMG-CoA reductase inhibitors (6), and small peptides up to 4 amino acids (7). The essential molecular requirement for active bile acid absorption is the retention of an acidic moiety around the 24-position on the sterol nucleus. As an alternative to modifications at the 3-position, a number of groups (8–10) have shown that the 24-position of cholic acid can be modified so that conjugates maintain affinity for the intestinal bile acid transporter. In the present study we examined the influence of side-chain length (i.e. number of amino acids that can be coupled to the 24-position) and lipophilicity on the carrier affinity by coupling small model peptides

* Address correspondence to this author at the Department of Biopharmaceutical Sciences, University of California at San Francisco, Box 0446, San Francisco, CA 94143-0446 [telephone (415) 476-3180; fax (415) 476-0688; e-mail soie@itsa.ucsf.edu].

[†] Present address: Department of Pharmaceutics and Pharmaceutical Chemistry, The Ohio State University, Columbus, OH 43210.

[‡] Present address: Department of Drug Metabolism and Pharmacokinetics, Rhône-Poulenc Rohrer, Collegeville, PA 19426.

[®] Abstract published in *Advance ACS Abstracts*, June 15, 1997.

of increasing chain length to the 24-position of cholic acid. We show that peptides with 4 amino acid residues are transported by the intestinal bile acid carrier and that 6 amino acid peptides still have moderate affinity for this transporter.

MATERIALS AND METHODS

Cholic acid was obtained from Fluka BioChemika (Buchs, Switzerland). [2,4-³H]Cholic acid, D-[1-³H(N)]-mannitol, and [24-¹⁴C]taurocholic acid were from Dupont NEN (Wilmington, DE). 2-(1*H*-Benzotriazol-1-yl)-1,1,3,3-tetramethyluronium hexafluorophosphate (HBTU) was obtained from Advanced ChemTech (Louisville, KY). All Fmoc-protected amino acids and amino acid analogs were purchased from Bachem California (Torrance, CA) and are L-enantiomers, unless noted otherwise. Fmoc-L-Ala-dimethoxyalkoxybenzylamine resin was obtained from Peninsula Laboratories (Belmont, CA). All other chemicals were from Sigma (St. Louis, MO).

General Procedure for the Preparation of Bile Acid–Peptide Conjugates. Bile acid–peptide conjugates were synthesized on a Protein Technologies Model PS3 automated peptide synthesizer (Rainin Instrument Co., Woburn, MA) applying FastMoc chemistry (11) using HBTU as a coupling agent. For a 0.5 mmol scale synthesis approximately 0.75 g of Fmoc-L-Ala-dimethoxyalkoxybenzylamine resin was used. Coupling time was generally set to 40 min with a coupling volume of 15 mL of *N,N*-dimethylformamide. To provide the required negative charge around the 24-position of the sterol nucleus, Fmoc-L- γ -glutamic acid was coupled to the peptide prior to coupling to cholic acid. Conjugates were deprotected and cleaved from the resin with TFA containing 5% water as a scavenger.

Synthesis of Radiolabeled Bile Acid–Peptide Conjugates. Syntheses of tritiated compounds were carried out in microreaction vials. Presynthesized and deprotected EAAA-amide resin or EASASA-amide resin was allowed to swell in DMF. [³H]Cholic acid (500 μ Ci) was added to the reaction vial and allowed to react for 30 min. After cleaving the conjugates from the resin, the raw material was spotted on TLC plates (Whatman PE SIL G/UV, 250 μ m layer) and developed with a mixture of 1-butanol/acetic acid/water (10:1:1). Places with *R_f* values corresponding to ChEAAA and ChEASASA were scraped off, and the radiolabeled compounds were collected by extraction with ethanol and stored at 4 °C.

Analytical Methods. Analytical RP-HPLC was carried out on a Merck LiChrospher 100 C₁₈ (5 μ m) column using a Perkin-Elmer Series 4 liquid chromatograph, a Shimadzu SPD-6A UV detector operating at 230 nm, and a Waters Associates WISP 710A automated injector. The column was developed with a linear gradient of 0–100% acetonitrile over 30 min. Conjugates were purified by preparative HPLC on a Rainin Dynamax MicroSorb (8 μ m beads, 21.4 \times 250 mm) column with a guard module (21.4 \times 50 mm). The column was eluted at room temperature at 8 mL/min using a linear gradient of 0–100% acetonitrile containing 0.1% TFA. Peptide–bile acid conjugates were dissolved in DMSO and loaded on the column in 500 μ L batches. The mass of the compounds was determined by positive and negative FAB-MS. ¹H NMR spectra were acquired on a General Electric (300 MHz) instrument. The chemical shifts are expressed as parts per million (ppm) using tetramethylsilane as an internal standard (δ = 0.0 ppm).

Cell Culture. CaCo-2 cells were grown in 175 cm² culture flasks (Costar Corp.) in culture medium consisting of high-glucose (4.5 g/L) DMEM supplemented with FBS (10%), NEAAs (1%), penicillin (100 units/mL), and

streptomycin (100 μ g/mL). The cells were maintained at 37 °C in an atmosphere of 5% CO₂. At approximately 80% confluence, cells were trypsinized and plated at a density of 64 000 cells/cm² on Costar Transwell polycarbonate membranes, previously coated with rat tail collagen (Collagen Corp., Palo Alto, CA). The cell culture medium, 1.5 mL of apical side and 2.5 mL of basolateral side, was replaced every other day for the first week and daily thereafter. Experiments were performed 21–28 days after seeding. The integrity of the cell monolayers was determined by checking the paracellular transport of 1 μ Ci of [³H]mannitol. If transfer of mannitol reached values of 0.5%/h, the results were not included in the analysis due to the possibility of membrane leakage.

Biological Properties. Inhibition Studies in CaCo-2 Cells. Cell monolayers were rinsed and preincubated as described above for transport studies. Studies were initiated by replacing the solution on the apical side with 1.5 mL of 4 μ M [¹⁴C]taurocholic acid (TCA) in the presence or absence (control) of a 100-fold excess of a bile acid conjugate (\pm 400 μ M). The concentrations of the bile acid analogs [³H]ChEAAA and [³H]ChEASASA were 20 and 30 μ M, respectively. The percent inhibition of transepithelial transport was calculated by comparing the apparent transport rate in the presence of an inhibitor against the control.

Transport Mechanism of Bile Acid–Peptide Conjugates in CaCo-2 Cells. The transepithelial transport of [³H]choly-L- γ -Glu-L-Ala-L-Ala-L-Ala-amide (ChEAAA) and [³H]choly-L- γ -Glu-L-Ala-L-Ser-L-Ala-L-Ser-L-Ala-amide (ChEASASA) was determined in CaCo-2 cells at 37 °C. Cell monolayers were washed twice with modified HBSS (containing 25 mM glucose and 10 mM Hepes buffer; pH 7.4) and allowed to equilibrate for 20 min at 37 °C. Studies were initiated by replacing the solution on the apical side with 1.5 mL of test solution in HBSS 20 μ M radiolabeled compound. Samples of 100 μ L were taken from the basolateral side at designated times and replaced with fresh 100 μ L transport solution. The amount of radiolabeled material in the samples was determined using a Beckman LS-5801 liquid scintillation counter. The transport rate was calculated by linear regression from the amount of recovered compound on the basolateral side during the experiment.

Stability and Metabolism of [³H]ChEAAA and [³H]ChEASASA in CaCo-2 Cells. The stability of the two radiolabeled cholic acid–peptide conjugates was checked during and after transport experiments in CaCo-2 cells. Detection of metabolism on the apical and basolateral side of the cell monolayers was carried out by TLC and HPLC analysis.

TLC Analysis. At 30, 60, 90, and 120 min, 50 μ L of the apical and basolateral solution was spotted on a TLC plate and immediately developed in 1-butanol/acetic acid/water (10:1:1). Dry plates were sprayed with surface autoradiography enhancer (En³Hance spray; DuPont Biotechnology Products, Boston, MA) and exposed to film at –80 °C for 2 weeks.

HPLC Analysis. A Shimadzu chromatography system, consisting of two LC-6A pumps, an SCL-6A gradient controller, and an SPD-6AV UV detector (λ 230 nm), was coupled in series to a Packard Radiomatic 500 TR Series flow scintillation analyzer. The column, a Merck LiChrospher 100 C₁₈ (5 μ m), was eluted at 0.8 mL/min with 55% acetonitrile/water containing 0.1% TFA. On this system, [³H]cholic acid, [³H]ChEASASA, and [³H]ChEAAA had retention times of 2.8, 1.8, and 1.95 min, respectively.

Characterization of Conjugates. The bile acid–peptide conjugates prepared for this study are detailed in Table 1. They were characterized by analytical RP-

Table 1. Physicochemical Characteristics of Bile Acid–Peptide Conjugates

compd	chain length (<i>n</i> + <i>E</i>)	<i>M_w</i> ^a		¹ H-NMR ^b (DMSO- <i>d</i> ₆)	retention time ^c (min)
		calcd	exptl		
cholic acid	0	409			15.50
ChDF	2	684.4	683.5 [M + H]	4.05 (m, 1H, α); 4.25 (m, 1H, α); 7.05–7.35 (m, 5H, Ø)	14.62
ChEA	2	607.4	608.3 [M + H]	4.3–4.5 (m, 2H, α)	12.69
ChEAA	3	678.4	679.4 [M + H]	4.2–4.4 (m, 3H, α)	13.56
ChEAAA	4	749.5	750.4 [M + H]/ 748.3 [M – H]	4.1–4.5 (m, 4H, α)	13.99
ChEASA	4	765.5	766.5 [M + H]	4.15–4.4 (m, 4H, α)	9.52
ChEAYA	4	841.5	840.5 [M – H]	4.1–4.4 (m, 4H, α); 6.6 (d, 2H, <i>J</i> = 8 Hz, Ø); 7.0 (d, 2H, <i>J</i> = 8 Hz, Ø)	13.67
ChEFSA	4	841.5	840.4 [M – H]	4.25–4.8 (m, 3H); 7.2–7.4 (m, 3H); 7.95–8.2 (m, 2H)	13.03
ChEASAA	5	836.5	835.4 [M – H]	4.15–4.35 (m, 5H, α)	12.40
ChEFSSA	5	929.5	928.5 [M – H]	4.2–4.6 (m, 5H, α); 7.1–7.3 (m, 5H, Ø)	8.09
ChEASASA	6	923.5	922.5 [M – H]	4.05–4.35 (m, 6H, α)	8.49
ChEASPSA	6	949.5	948.4 [M – H]	4.1–4.8 (m, 6H, α)	7.53

^a Monoisotopic mass. ^b Only characteristic peaks are shown; δ values are in ppm relative to TMS; α indicates assignment to α-proton peaks in amino acid residues; Ø indicates assignment to aromatic protons in Phe and Tyr residues. ^c Retention time of the conjugate on a 10 cm RP C₁₈ column eluted with a gradient of 0–100% acetonitrile in 20 min.

HPLC, ¹H-NMR, and FAB-MS. Analytical HPLC confirmed that the compounds did not contain any cholic acid and that the purity of the product peak was >98%. The FAB mass spectra in all cases gave a molecular ion in agreement with the calculated mass of the conjugates. It should be noted that negative FAB is more successful (i.e., gives better results) for this class of compounds than positive FAB. The analytical HPLC, ¹H-NMR, and MS results are compiled in Table 1.

Statistical Analysis. Biological data from quadruplicate samples were subjected to one-way analysis of variance and were considered to be significantly different at a probability level of *P* < 0.05.

RESULTS

Synthesis of Bile Acid–Peptide Conjugates. The synthetic strategy of coupling peptides to 3α,7α,12α-trihydroxy-5β-cholan-24-oic acid (cholic acid) was based on the relative ease of coupling the carboxyl group at the C24 position of the cholane D-ring (Figure 1) to the terminal amino group of a peptide via an amide linkage. The negative moiety around the C24-position was retained, since this moiety is required for affinity to the intestinal bile acid transporter (12). Using an automated peptide synthesizer, bile acid–peptide conjugates were obtained with a general structure as depicted in Figure 1. In the structural formulas presented in the subsequent figure, Ch represents the cholic acid moiety, coupled at the 24-position via an amide bond to L-γ-glutamic acid. In our syntheses, we chose to use an FMOC-L-Ala-dimethoxyalkoxybenzylamine resin as the solid support, since this resin produces the amino acid amide after treatment with 95% TFA. It should be noted that the cleavage time of the conjugates from the solid support turned out to be critical. Cleavage times longer than 30 min caused TFA to react with the hydroxyl groups on the sterol nucleus, which afforded the mono- and ditrifluoroacetoxy esters of the conjugates, as observed by mass spectrometry. The cholic acid–peptide conjugates were obtained in good yield by this method after chromatographic purification on preparative RP-HPLC. To investigate the influence of side-chain (amino acid) length on carrier affinity, we started with a homologous series of alanine residues before coupling L-γ-glutamic acid and cholic acid. Because conjugates with more than 4 alanine residues showed poor aqueous solubility, more hydrophilic serine residues were incorporated in the peptide side chain.

Inhibition of [¹⁴C]TCA Transport by Bile Acid–Peptide Conjugates. The CaCo-2 cell system was

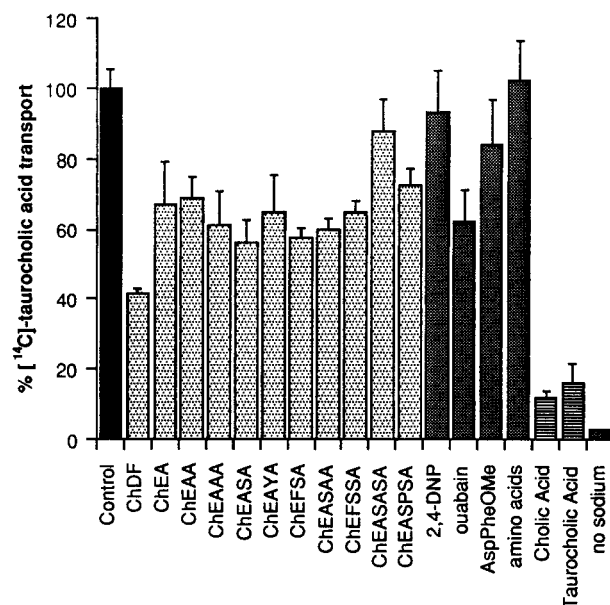


Figure 2. Relative transport of 4 μM [¹⁴C]taurocholic acid (control) in CaCo-2 cells in the presence of a 100-fold excess concentration of bile acid–peptide conjugates (±400 μM) and natural substrates (horizontally striped bars) and in the absence of sodium (dotted bars); values are presented as the mean ± SEM, *n* = 4–8.

chosen for this study because these cells functionally express the bile acid transporter (7, 13). Since maximal expression of this carrier occurs after 21 days after seeding on transwell membranes, all experiments were carried with cells cultured for 21–28 days. Since bile acids have detergent-like properties, control experiments were carried out to assess the effect of bile acid–peptide conjugates on the transepithelial transport of the paracellular absorption marker [³H]mannitol. Mannitol is normally transported across CaCo-2 cell monolayers at rates <0.5%/h. The permeability of mannitol was not affected (data not shown) by TCA or cholic acid–peptide conjugates at concentrations up to 400 μM (the inhibitor concentration used in inhibition studies), suggesting that the integrity of CaCo-2 cell monolayers remained intact after exposure to these compounds.

The affinity of bile acid–peptide conjugates for the bile acid transporter was measured by their ability to inhibit transepithelial transport of [¹⁴C]TCA at a 100-fold excess concentration (Figure 2). Control experiments with the natural substrates cholic acid and taurocholic acid inhibit [¹⁴C]TCA transport to 12.1 (±1.8) and 16.2 (±5.2)% of

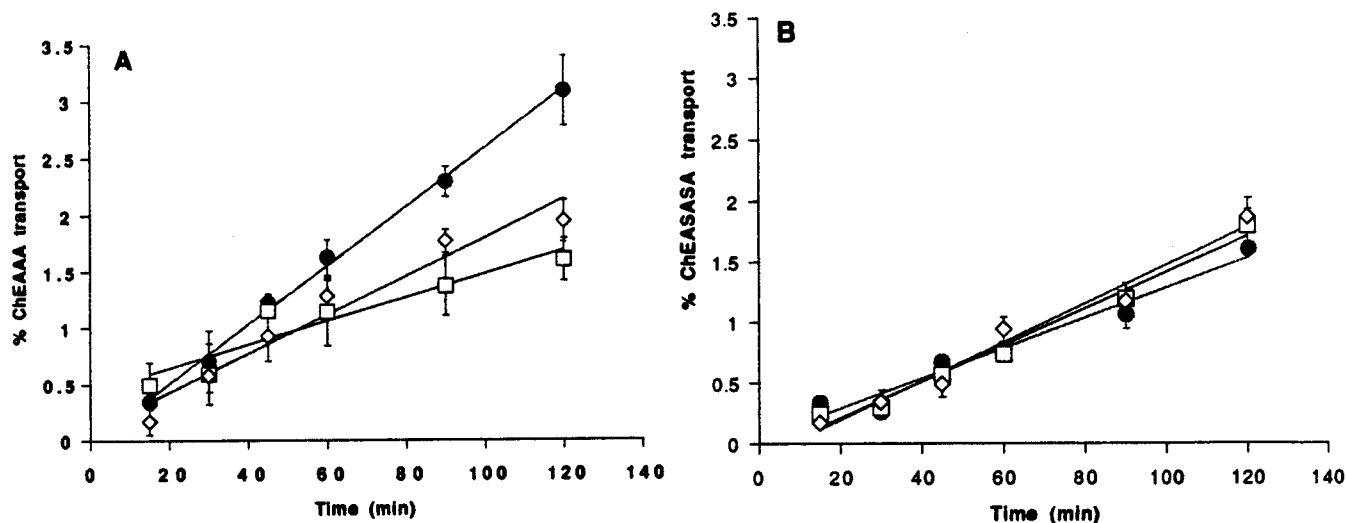


Figure 3. Apical to basolateral (circles) and basolateral to apical (diamonds) transport of 4 μ M [3 H]ChEAAA (A) and 4 μ M [3 H]ChEASASA (B) in CaCo-2 cells. Transepithelial transport is plotted relative to the concentration on the donor side. The transport of both conjugates in the presence of a 100-fold excess of taurocholic acid is indicated by squared symbols. Values are presented as the mean \pm SEM, $n = 4-8$.

transport in the absence of inhibitors, respectively, which is in good agreement with previous studies (10, 13, 14). Removal of sodium from the incubation almost completely inhibits ($2.6 \pm 0.3\%$ of control) TCA transport. The protonophore 2,4-dinitrophenol does not inhibit transport of TCA, indicating that TCA transport is not affected by a H^+ gradient. TCA transport is not influenced by amino acids (a cocktail of Pro, Phe, Lys, and Glu) or the dipeptide L-Asp-L-Phe-O-Me. The Na^+/K^+ ATPase-inhibitor ouabain (0.1 mM at the basolateral side of the monolayers) indirectly inhibits TCA transport by 38% (± 9.2). The affinity of cholic acid-peptide conjugates for the bile acid transporter decreases with increasing peptide length, although the relationship between chain length and inhibitory activity was relatively weak ($r^2 = 0.38$; $p = 0.05$). Lowering the hydrophilicity of the peptide chain by incorporation of a hydrophobic residue (Phe) in the peptide chain does not seem to influence affinity for the carrier.

Transport of [3 H]ChEAAA and [3 H]ChEASASA in CaCo-2 Cells. Parts A and B of Figure 3 show the relative transepithelial transport of [3 H]ChEAAA and [3 H]ChEASASA, respectively, in CaCo-2 cell monolayers. The apical (AP) to basolateral (BL) transport rate for [3 H]ChEAAA amounts to $1.56 \pm 0.04\%/h$, while the BL-AP transport rate is only $0.63 \pm 0.10\%/h$. AP-BL transport of [3 H]ChEAAA is suppressed to $1.03 \pm 0.11\%/h$ in the presence of a 100-fold excess of taurocholic acid. AP-BL and BL-AP transport rates for [3 H]ChEASASA are 0.75 ± 0.08 and $0.90 \pm 0.06\%/h$, respectively, while the AP-BL transport rate in presence of sodium amounts to $0.93 \pm 0.08\%/h$.

Metabolism of ChEAAA and ChEASASA in CaCo-2 Cells. After transport studies, the apical and basolateral solutions were collected and either injected on an HPLC system with radiometric detection or spotted on TLC plates. On the HPLC system, the injection peak eluted after 1.00 min, as detected by UV at 230 nm. Cellular debris and buffer components eluted around 1.50 min. A steady baseline (UV) was acquired after 1.75 min. Under these conditions, ChEASASA and ChEAAA had retention times of 1.8 and 1.9 min, well before cholic acid eluted at 3.2–3.3 min. Figure 4 shows a chromatogram of a basolateral sample of ChEASASA after 120 min. A small peak can be detected at the same time cholic acid elutes but represents only 3% of total peak area.

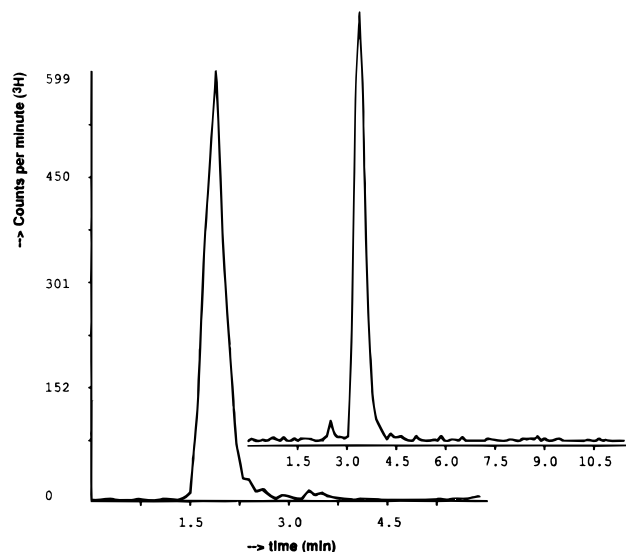


Figure 4. Metabolism of [3 H]ChEASASA in CaCo-2 cells. A basolateral sample after a 2 h transport study was analyzed by HPLC with radiometric detection as described under Materials and Methods. The inset shows the chromatogram of [3 H]cholic acid.

DISCUSSION

The use of carrier-mediated transport systems in the gut to increase the oral absorption of drugs has received increased attention over the past decade. From a pharmaceutical point of view, the coupling of drugs to natural substrates for endogenous carriers in the gut opens the possibility of efficient drug delivery for poorly absorbable compounds, such as peptides. To evaluate the potential of the intestinal bile acid pathway as a drug delivery system for peptidic molecules, we have coupled small model peptides—up to 6 amino acids—via an amide bond to the 24-position of 3 α ,7 α ,12 α -trihydroxy-5 β -cholan-24-oic acid. Using an automated peptide synthesizer, we created a series of conjugates of general formula ChEX_{*n*} (where Ch corresponds to cholic acid, E to γ -L-Glu, and X to any amino acid) in good yield. To conserve the specific interaction of these conjugates with the bile acid transporter, we incorporated a γ -L-glutamic acid, which carries a free α -carboxylic acid, providing the required negative charge around the 24-position. γ -Glutamic acid

was chosen over α -glutamic acid, since the former contains only one carbon atom between the α -carbon atom and the free carboxylic acid group (compared to two carbon atoms in α -Glu), thus allowing less flexibility in the relative position of this moiety. Even though we observed high affinity for cholic acid–aspartic acid–benzyl esters in our preliminary studies (10), we avoided the inclusion of aspartyl residues in the peptide backbone because of the common instability (peptide bond cleavage) associated with this residue under acidic conditions and at elevated temperatures. The peptide chain was subsequently elongated with a series of L-alanine residues, the smallest amino acid still demonstrating stereoisomerism. The L-enantiomer was chosen over the D-form, since most biologically active peptides contain L-amino acids, even though these compounds are generally less stable against proteolytic attacks. Peptides with more than 4 Ala residues had very poor aqueous solubility and, therefore, the more hydrophilic Ser residues were incorporated. Phenylalanine residues were incorporated to examine the influence of side-chain lipophilicity on carrier affinity and because our previous studies (10) showed that side chains containing a six-membered ring had high affinity for the bile acid carrier. The position of the various residues was varied in the peptide backbone to assess the influence of amino acid position and affinity for the transporter. To limit the overall negative charge to 1, we chose to use an Fmoc-L-Ala-dimethoxyalkoxybenzylamine resin which produces an electroneutral endstanding amide group after cleavage of the peptide from the resin with 95% TFA.

The potential of these conjugates to interact with the intestinal bile acid transporter is reflected by their ability to inhibit the transport of [14 C]TCA in the human intestinal cell line CaCo-2. The bile acid carrier is functionally expressed in this cell line, as illustrated by a decrease in AP–BL transport of [14 C]TCA across CaCo-2 monolayers in the presence of the natural substrates TCA and cholic acid (Figure 2). This process is energy and sodium dependent on the basis of inhibition by the Na^+/K^+ -ATPase inhibitor ouabain and reduced [14 C]TCA transport rates in the absence of sodium. In contrast, AP–BL transport of [3 H]TCA was not altered in the presence of amino acids or a small peptide (AspPheOMe), indicating that [14 C]TCA is transported solely by the bile acid transporter. The protonophore 2,4-DNP did not alter transport of [14 C]TCA, indicating that intestinal bile acid transport is not influenced by a proton gradient over the CaCo-2 monolayer membrane.

Bile salts are known to form micelles in water when present at concentrations above the critical micelle concentration (cmc). Using the fluorescent probe 8-anilino-naphthalene-1-sulfonate (ANS) (15), we estimated the cmc of ChEASASA to be approximately 5 mM (data not shown). This is in good agreement with studies by Mills and colleagues (16), who found cmc's between 2 and 10 mM for various bile acid–amino acid derivatives. Since we used concentrations up to 400 μ M in our inhibition studies, we were always well below the cmc of our conjugates. At a 100-fold excess, conjugates with a peptide side chain of up to 6 amino acids significantly inhibited [14 C]TCA transport, although one of the conjugates with a peptide chain of 6 amino acids (ChEASASA) had limited inhibitory capacity (Figure 2). This decrease in affinity for the carrier when the peptide side chains exceeds 5 amino acids suggests that the cutoff size for transport of compounds conjugated to the 24-position has been reached. However, further studies are required to learn if peptide length or some other feature such as

structure of the peptide chain is responsible for the loss of inhibitory activity.

The dipeptide analog AspPheOMe, which comprises the side chain of the conjugate ChDF, does not inhibit [3 H]TCA transport, whereas ChDF in its entirety does. Thus, the free peptide is not responsible for carrier affinity. Although inhibition studies are a good indicator for the ability of a conjugate to bind to the bile acid transporter, it fails to predict the ability of a conjugate to transfer across the enterocyte by means of the transporter. Therefore, we synthesized two radiolabeled conjugates, [3 H]ChEAAA and [3 H]ChEASASA, and studied their transepithelial transport across CaCo-2 cell monolayers. Active bile acid transport is a monodirectional process (13), i.e. AP–BL transport is higher than BL–AP transport, since the carrier only transports substrates from the AP side of the membrane to the BL side. As shown in Figure 3, the total AP–BL flux of ChEAAA is markedly higher than the corresponding BL–AP flux, which indicates that ChEAAA is partly transported by an active transport pathway. Furthermore, ChEAAA transport is inhibited by TCA (Figure 3), indicating that these compounds share a similar intestinal transport pathway, most probably the sodium-dependent bile acid transporter. Since BL–AP ChEAAA flux is substantially higher than 0 and a 100-fold excess of TCA is not sufficient to completely inhibit ChEAAA transport, a second pathway for transepithelial flux, possibly passive diffusion, exists for this compound. Contrarily, the AP–BL and BL–AP transport rates of ChEASASA are identical and its transport is not inhibited by TCA. Thus, ChEASASA does not appear to be transported by the bile acid carrier and most probably crosses the intestinal epithelium via passive routes.

From these studies we conclude that bile acid conjugates with up to 6 amino acids show affinity for the intestinal bile acid transporter. However, whether compounds with 6 amino acids or more can be transported is not clear. ChEASASA was found not to be transported by the bile acid carrier, but whether ChEASPSA, which has a higher affinity for the bile acid transporter on the basis of inhibition studies, may be transported was not tested.

Even though ChEASASA does not appear to be transported by the bile acid transporter, it still shows a relatively high passive permeability ($\sim 0.9\%/h$) compared to the transepithelial transport of mannitol ($< 0.5\%/h$), which is generally considered to indicate the lower limits of passive diffusion in the gut—irrespective of transport pathway—and, thus, poor bioavailability. Since active transport is unidirectional, the passive component of ChEAAA transport is reflected by its BL–AP permeability constant ($\sim 1.0\%/h$), which is also twice that of mannitol. Small peptides such as EASASA and EAAA generally have poor intestinal absorption (0–5% bioavailability) (17). Thus, conjugation with cholic acid seems to aid the passive transport of this compound across the intestinal epithelium. The question arises as to how and to what relative extent side-chain length and lipophilicity influence carrier affinity. Although the current experiments cannot resolve this issue, it is part of our continuing effort to resolve the quantitative structure–transport relationship for the intestinal bile acid transporter.

The CaCo-2 cell line is also a useful model for studying peptide metabolism (14, 18). After 21 days in culture, these cells express most endo-, trans-, amino-, carboxy- and dipeptidyl peptidases also found in human enterocytes (19). Since only 3% [3 H]cholic acid can be found on either side of the membrane after 2 h of incubation

(Figure 4), the metabolism of both conjugates is minimal in cell culture and presumably also in the gut. Normally, peptides are rapidly metabolized when exposed to the enzymes present in the brush-border membrane in CaCo-2 cells. For example, Augustijns and Borchardt (20) showed that 91% of the nonapeptide WAGGDASGE was metabolized after 2 h of incubation on the basolateral membrane of CaCo-2 monolayers. Although we have not tested the stability of all peptides with the exact composition of those in our conjugates, it seems that by coupling small peptides to cholic acid the metabolic degradation of these conjugates is reduced.

In summary, we have shown an easy and straightforward strategy to synthesize bile acid-peptide conjugates using an automated peptide synthesizer. Within certain structural limits, the resulting conjugates show moderate affinity for and are transported by the intestinal bile acid carrier. Overall, this approach has the potential to increase intestinal absorption of otherwise poorly absorbed peptide molecules, either by a carrier-mediated pathway or by increasing the passive membrane permeability. Furthermore, the conjugates are slowly metabolized in the intestinal cell line model, CaCo-2, which indicates that the metabolic stability of these small peptides is increased by coupling them to cholic acid. Currently we are investigating the absorption and stability of radiolabeled peptide-bile acid conjugates *in vivo* to learn if oral absorption is improved by this bioconjugation strategy.

ACKNOWLEDGMENT

This work was supported in part by the University of California Universitywide AIDS Research Program (Grant UARP R93SF061) to S.Ø., a UARP Fellowship (F95SF036 to P.W.S.), an FIP Fellowship to P.W.S., and a PhRMA Fellowship to K.M.H. The UCSF Mass Spectrometry Facility (A. L. Burlingame, Director) is supported by the Biomedical Research Technology Program of the National Center for Research Resources RR01614 and National Science Foundation DIR 8700766. We thank the UCSF Computer Graphics Laboratory (NIH P41-RR01081) for their computing support. We also thank Dr. Deanna Kroetz for the kind use of the Packard Radiometric detector.

LITERATURE CITED

- (1) Swaan, P. W., Øie, S., and Szoka, F. C., Jr. (1996) Carrier-mediated oral drug delivery—preface. *Adv. Drug Delivery Rev.* 20, 1–3.
- (2) Ho, N. (1987) Utilizing bile acid carrier mechanisms to enhance liver and small intestine absorption. *Ann. N.Y. Acad. Sci.* 507, 315–329.
- (3) Swaan, P. W., Øie, S., and Szoka, F. C., Jr. (1996) Use of the bile acid transporter for drug delivery. *Adv. Drug Delivery Rev.* 20, 59–82.
- (4) Kim, D. C., Harrison, A. W., Ruwart, M. J., Wilkinson, K. F., Fisher, J. F., Hidalgo, I. J., and Borchardt, R. T. (1993) Evaluation of the bile acid transporter in enhancing intestinal permeability to renin-inhibitory peptides. *J. Drug Targeting* 1, 347–359.
- (5) Kramer, W., Wess, G., Schubert, G., Bickel, M., Girbig, F., Gutjahr, U., Kowalewski, S., Baringhaus, K.-H., Enhnen, A., Glombik, H., Müllner, S., Neckermann, G., Schulz, S., and Petzinger, E. (1992) Liver-specific drug targeting by coupling to bile acids. *J. Biol. Chem.* 267, 18598–18604.
- (6) Kramer, W., Wess, G., Enhnen, A., Bock, K., Falk, E., Hoffmann, A., Neckermann, G., Gantz, D., Schulz, S., Nickau, L., Petzinger, E., Turley, S., and Dietschy, J. M. (1994) Bile acid derived HMG-CoA reductase inhibitors. *Biochim. Biophys. Acta* 1227, 137–154.
- (7) Kramer, W., Wess, G., Neckermann, G., Schubert, G., Fink, J., Girbig, F., Gutjahr, U., Kowalewski, S., Baringhaus, K. H., Böger, G., Enhnen, A., Falk, E., Friedrich, M., Glombik, H., Hoffmann, A., Pittius, C., and Urmann, M. (1994) Intestinal absorption of peptides by coupling to bile acids. *J. Biol. Chem.* 269, 10621–10627.
- (8) Stephan, Z., Yurachek, E., Sharif, R., Wasvary, J., Steele, R., and Howes, C. (1992) Reduction of cardiovascular and thyroxine-suppressing activities of L-T₃ by liver targeting with cholic acid. *Biochem. Pharmacol.* 43, 1969–1974.
- (9) Mills, C. O., and Elias, E. (1992) Biliary excretion of chenodeoxychollysilyl rhodamine in Wistar rats: a possible role of a bile acid as a carrier for drugs. *Biochim. Biophys. Acta* 1126, 35–40.
- (10) Kagedahl, M., Swaan, P. W., Redemann, C. T., Tang, M., Craik, C. S., Szoka, F. C., Jr., and Øie, S. (1997) Use of the intestinal bile acid carrier for the transport of HIV-1 protease inhibitors. *Pharm. Res.* 14, 176–180.
- (11) Knorr, R., Trzeciak, A., Bannwarth, W., and Gillesen, D. (1989) New coupling reagents in peptide chemistry. *Tetrahedron Lett.* 30, 1927–1930.
- (12) Lack, L., and Weiner, I. M. (1966) Intestinal bile salt transport: structure-activity relationships and other properties. *Am. J. Physiol.* 210, 1142–1152.
- (13) Hidalgo, I. J., and Borchardt, R. T. (1990) Transport of bile acids in a human intestinal epithelial cell line, CaCo-2. *Biochim. Biophys. Acta* 1035, 97–103.
- (14) Chandler, C. E., Zaccaro, L. M., and Moberly, J. B. (1993) Transepithelial transport of cholytaurine by CaCo-2 cell monolayers is sodium dependent. *Am. J. Physiol.* 264, G1118–G1125.
- (15) Biaselle, C. J., and Millar, D. B. (1975) Studies on Triton X-100 detergent micelles. *Biophys. Chem.* 3, 355–361.
- (16) Mills, C. O., Martin, G. H., and Elias, E. (1986) The effect of tyrosine conjugation on the critical micellar concentration of free and glycine-conjugated bile salts. *Biochim. Biophys. Acta* 876, 677–683.
- (17) M. D. Taylor and G. L. Amidon, Eds. (1995) *Peptide-based Drug Design: Controlling Transport and Metabolism*, pp 1–567, American Chemical Society, Washington, DC.
- (18) Jumarie, C., and Malo, C. (1994) Alkaline phosphatase and peptidase activities in CaCo-2 cells: differential response to triiodothyronine. *In Vitro Cell. Dev. Biol.* 30A, 753–760.
- (19) Howell, S., Kenny, A. J., and Turner, A. J. (1992) A survey of membrane peptidases in two human colonic cell lines, CaCo-2 and HT-29. *Biochem. J.* 284, 595–601.
- (20) Augustijns, P. F., and Borchardt, R. T. (1995) Transport and metabolism of delta sleep-inducing peptide in cultured human intestinal epithelial cell monolayers. *Drug Metab. Dispos.* 23, 1372–1378.

BC970076T

Bivalent Hapten-Bearing Peptides Designed for Iodine-131 Pretargeted Radioimmunotherapy

E. Janevik-Ivanovska,^{†,‡} E. Gautherot,[§] M. Hillairet de Boisferon,[†] M. Cohen,[†] G. Milhaud,[‡] A. Tartar,^{||} W. Rostene,[†] J. Barbet,[§] and A. Gruaz-Guyon^{*,†}

INSERM U.339 and Service de Biophysique, Faculté de Médecine Saint Antoine, 27 Rue Chaligny, 75012 Paris, France; IMMUNOTECH S.A., 130 Avenue de Lattre de Tassigny, B.P. 176, 13276 Marseille Cedex 9, France; and URA 1309 CNRS, Institut Pasteur de Lille, 1 Rue du Pr. Calmette, B.P. 245, 59019 Lille Cedex, France. Received November 15, 1996[®]

Pretargeting with bispecific antibodies has been used successfully for tumor detection and is now considered for radioimmunotherapy. The advantages of bivalent haptens have been demonstrated in this context. A series of bivalent molecules allowing efficient labeling with radioactive iodine has been designed for use with this new technology. They were based on the histamine–hemisuccinate hapten and prepared by solid phase peptide synthesis. Simultaneous binding of two antibody molecules to one bivalent hapten was possible with low steric hindrance when the two hapten groups were attached to the lateral chains of lysine residues separated by a single amino acid. Bispecific antibodies to the hapten and to carcinoembryonic antigen were shown to mediate specific binding of the haptens to tumor cells *in vitro*. These experiments demonstrated that the bivalent hapten AG3.0, with a lysyl-D-tyrosyl-lysine connecting chain, possessed the best binding properties. This peptide was used to target iodine-125 to human colon cancer xenografts in nude mice. High tumor uptake and tumor to normal tissue ratios were observed. This peptide thus appears as a good candidate for further development. Asymmetric bivalent haptens, with one histamine–hemisuccinate and one diethylenetriaminepentaacetic acid group, have also been prepared and shown to be capable of binding simultaneously two specific antibody molecules. These peptides should be useful to target radioiodine to cells characterized by the expression of two different antigenic markers.

INTRODUCTION

During the past 15 years, radionuclides have been targeted to tumors by means of monoclonal antibodies for diagnostic imaging and radioimmunotherapy [for reviews see Mach et al. (1991) and Goldenberg (1993)]. To increase the targeting specificity, two- and three-step pretargeting techniques have been proposed (Goodwin et al., 1986, 1988; Stickney et al., 1989, 1991; Lollo et al., 1994; Santos et al., 1995). We have worked on an improved two-step pretargeting technique (Le Doussal et al., 1989), which we refer to as the “affinity enhancement system” (AES). The AES uses a bispecific antibody (BsmAb) (anti-tumor antigen \times anti-hapten) to target a radiolabeled bivalent hapten. The bivalent hapten exhibits preferential binding to cell-bound BsmAb, as opposed to excess circulating BsmAb, due to the formation of stable cyclic complexes at the cell surface (cell antigen–BsmAb–bivalent hapten–BsmAb–cell antigen). This technique affords high tumor to normal tissue ratios in animal models (Le Doussal et al., 1990). The advantages of bivalent haptens in this context have also been independently recognized by Goodwin et al. (1992). The efficacy of the AES technique has been established for the detection of tumors expressing the carcinoembryonic antigen (CEA) such as colon carcinoma (Le Doussal et al., 1993; Chetanneau et al., 1994) and medullary thyroid

carcinoma (MTC) (Peltier et al., 1993) in the clinic. Very small MTC occult metastases (2 mm in diameter) have been localized by peroperative detection and resected, demonstrating the accuracy and specificity of the method (de Labriolle-Vaylet et al., 1993).

In clinical trials the diethylenetriaminepentaacetic acid (DTPA)–indium complex has been used as a hapten because indium-111 is well suited to tumor scintigraphy and peroperative detection. Radioimmunotherapy should also be markedly improved by targeting β -emitting isotopes to tumors using BsmAb and a bivalent hapten. We introduced a tyrosine residue in the peptide sequence of the bivalent hapten designed for ¹¹¹In-labeling to allow also iodine-125 or iodine-131 labeling (Gruaz-Guyon et al., 1991). Nevertheless, new bivalent haptens, with improved targeting efficiency, specifically designed for use in radioimmunotherapy with iodine-131 would be of major interest. Here we report the synthesis of a series of bivalent haptens in which the histamine–hemisuccinate hapten (Morel et al., 1990) has been coupled to peptide connecting chains of various lengths and structures. The resulting bivalent haptens have been investigated for their ability to simultaneously bind, with high affinity, two anti-histamine–hemisuccinate antibody molecules. One bivalent hapten has been selected on this basis and studied for its ability to bind to BsmAb-pretargeted tumor cells *in vitro* and *in vivo*.

MATERIALS AND METHODS

Haptens and Antibodies. The hapten 3-[[[2-(4-imidazolyl)ethyl]amino]carbonyl]propionylglycine has been coupled to a series of peptide chains. This hapten will be referred to as histamine-succinyl-glycyl (HSG). The anti-HSG monoclonal antibody (mAb) 679.1MC7 (IgG_{1,k}) has already been described (Morel et al., 1990).

* Author to whom correspondence should be addressed [telephone (33) 01 40 01 14 66; fax (33) 01 43 43 89 46; e-mail rostene@idf.ext.jussieu.fr].

[†] INSERM.

[‡] Service de Biophysique.

[§] IMMUNOTECH.

^{||} URA 1309 CNRS.

[®] Abstract published in *Advance ACS Abstracts*, June 15, 1997.

Table 1. Synthesized Peptides and Equilibrium Affinity Constants of HSG-DTPA and HSG Haptens for Anti-HSG Antibody Fab' Fragment^a

Bivalent HSG-haptens	HSG-DTPA haptens	Monovalent HSG haptens
$\text{Ac-Lys-GABA-DTyr-GABA-Lys-NH}_2$ AG 3.1	$\text{Ac-Lys-GABA-DTyr-GABA-Lys-NH}_2$ AG 5.1 $K_a = 2.6 \pm 0.2 \times 10^9 \text{ M}^{-1}$	$\text{Ac-Lys-GABA-DTyr-GABA-Lys-NH}_2$ AG 4.1 $K_a = 3.8 \pm 0.1 \times 10^9 \text{ M}^{-1}$
$\text{Ac-Lys-DTyr-Lys-NH}_2$ AG 3.0	$\text{Ac-Lys-DTyr-Lys-NH}_2$ AG 5.0 $K_a = 2.9 \pm 0.1 \times 10^9 \text{ M}^{-1}$	$\text{Ac-Lys-DTyr-Lys-NH}_2$ AG 4.0 $K_a = 6.8 \pm 0.2 \times 10^9 \text{ M}^{-1}$
HSG-Lys-DTyr-NH_2 AG 3.2	HSG-Lys-DTyr-NH_2 AG 5.2 $K_a = 4.1 \pm 0.1 \times 10^8 \text{ M}^{-1}$	HSG-Lys-DTyr-NH_2 AG 4.2 $K_a = 3.2 \pm 0.1 \times 10^8 \text{ M}^{-1}$
HSG-DTyr-Lys-NH_2 AG 3.3	HSG-DTyr-Lys-NH_2 AG 5.3 $K_a = 2.2 \pm 0.1 \times 10^7 \text{ M}^{-1}$	HSG-DTyr-Lys-NH_2 AG 4.3 $K_a = 1.1 \pm 0.1 \times 10^7 \text{ M}^{-1}$

^a HSG, histamine-succinyl-glycyl; GABA, γ -aminobutyric acid; DTPA, diethylenetriaminepentaacetic acid.

DTPA was also coupled to a series of peptides bearing the HSG hapten. The 734 monoclonal antibody ($\text{IgG}_{1,\lambda}$), with specificity to the DTPA-indium complex, has been described previously (Le Doussal et al., 1990).

F6 is a mouse $\text{IgG}_{1,\kappa}$ antibody specific for human CEA. The antibodies were produced in tissue culture, purified, and fragmented by pepsin digestion according to standard procedures. The F(ab')_2 fragments were reduced with 2-mercaptoethylamine for 1 h at 37 °C and alkylated with *N*-ethylmaleimide to prepare the monovalent tracers or with maleimidobiotin to prepare the antibody-coated solid phases, using avidin-coated tubes (Immunotech S.A., Marseille, France). The anti-CEA \times anti-HSG BsmAb was prepared by chemical coupling of the two reduced Fab' fragment using *o*-phenylenedimaleimide according to the procedure of Glennie et al. (1987).

Peptides. We synthesized peptides bearing one HSG hapten (mono-HSG peptides, the AG4 series), two HSG haptens (di-HSG peptides, the AG3 series), and one DTPA and one HSG hapten (DTPA-HSG peptides, the AG5 series) as listed in Table 1. *N*- α -DTPA-tyrosyl-*N*- ϵ -DTPA-lysine dipeptide (di-DTPA-TL) was synthesized as described previously (Le Doussal et al., 1990).

Synthesis of Mono-HSG and Di-HSG Peptides. Mono-HSG and di-HSG peptides were synthesized manually by the stepwise solid phase method. The protected amino acids (1.57 mmol) (Bachem, Switzerland) were sequentially coupled to *p*-methylbenzhydrylamine resin (0.63 mmol of active groups) after activation with dicyclohexylcarbodiimide and 1-hydroxybenzotriazole (HOBT) to synthesize the backbone. The tyrosine side chain was protected with the 2,6-dichlorobenzyl group. *tert*-Butyloxycarbonyl (tBoc), fluorenylmethyloxycarbonyl (Fmoc), and 2-chlorobenzyloxycarbonyl (2-ClZ) were used to protect either α or ϵ amino groups, as shown in Figure 1, depending on in which position the hapten HSG was to be synthesized. We used for AG3.0 and AG4.0 the same protections as for AG3.1 and AG4.1. Each coupling step was repeated twice. After synthesis of the backbone, the desired NH_2 groups were deprotected and *N*- α -protected glycine (tBoc-Gly or Fmoc-Gly) was coupled under the conditions described above for backbone synthesis. After deprotection, a 3-fold molar excess of succinic anhydride was coupled in the presence of diiso-

propylethylamine (DIEA) (3-fold molar excess) (Aldrich, France). Histamine dihydrochloride (3-fold molar excess) (Aldrich) in solution in dimethyl sulfoxide/dimethylformamide (5:2, v/v) was coupled using benzotriazol-1-yloxytris(dimethylamino)phosphonium (BOP) and HOBT (3-fold molar excess) in the presence of DIEA (15-fold molar excess). Then 600 mg of the dried peptide resin was treated by liquid hydrogen fluoride (6 mL) in the presence of *p*-cresol (750 μL) for 1 h at 4 °C. After evaporation *in vacuo*, the crude peptide was precipitated in cold diethyl ether and extracted with 10% acetic acid. The peptide was purified by gel permeation chromatography and C_{18} reversed phase chromatography (Nucleosil, Shandon, France) with a gradient (A = 0.5% trifluoroacetic acid in water and B = 0.5% trifluoroacetic acid in water/acetonitrile, 50:50, v/v) from 0% B to 40% B in 70 min. The purity of each peptide ($\geq 95\%$) was checked by C_{18} reversed phase HPLC (Nucleosil) in two different solvent systems: system 1 (A = 0.5% trifluoroacetic acid in water; B = acetonitrile; gradient = isocratic 0% B for 5 min, to 30% B in 30 min, then to 60% in 10 min) and system 2 (A = heptafluorobutyric acid 0.5% in water; B = acetonitrile; gradient = isocratic 0% B for 5 min, to 50% B in 30 min, then to 60% in 10 min). UV absorbance was monitored at 210 and 280 nm. The amino acid ratios determined after total acid hydrolysis for the HSG and DTPA-HSG series were consistent with theoretical results. We further characterized the peptides by plasma desorption mass spectrometry using a Bio-Ion mass spectrometer (Uppsala, Sweden).

AG4.1 ($\text{M} + \text{H}$)⁺: 899.8 found, 899.8 calcd. AG4.0 ($\text{M} + \text{H}$)⁺: 729.6 found, 729.6 calcd.

AG4.2 ($\text{M} + \text{H}$)⁺: 559.4 found, 559.6 calcd. AG4.3 ($\text{M} + \text{H}$)⁺: 559.4 found, 559.4 calcd.

AG3.1 ($\text{M} + \text{H}$)⁺: 1149.6 found, 1149.11 calcd. AG3.0 ($\text{M} + \text{H}$)⁺: 980.1 found, 979.7 calcd.

AG3.2 ($\text{M} + \text{H}$)⁺: 809.6 found, 809.5 calcd. AG3.3 ($\text{M} + \text{H}$)⁺: 809.9 found, 809.5 calcd.

2D NMR spectrometry (in DMSO at 313 K with a Bruker 400 MHz AMX spectrometer) confirmed the structure of the compound AG3.0 (Figure 2) selected for *in vivo* studies: ^1H NMR ($\text{DMSO}-d_6$) δ CH_3CO 1.90; Lys¹ (NH 8.00, H α 3.66, H β 1.40, H β' 1.43, H γ 0.95, H γ' 1.00, H $\delta\delta'$ 1.45, H $\epsilon\epsilon'$ 3.05, N ϵ H 7.80); Tyr² (NH 8.17, H α 4.46,

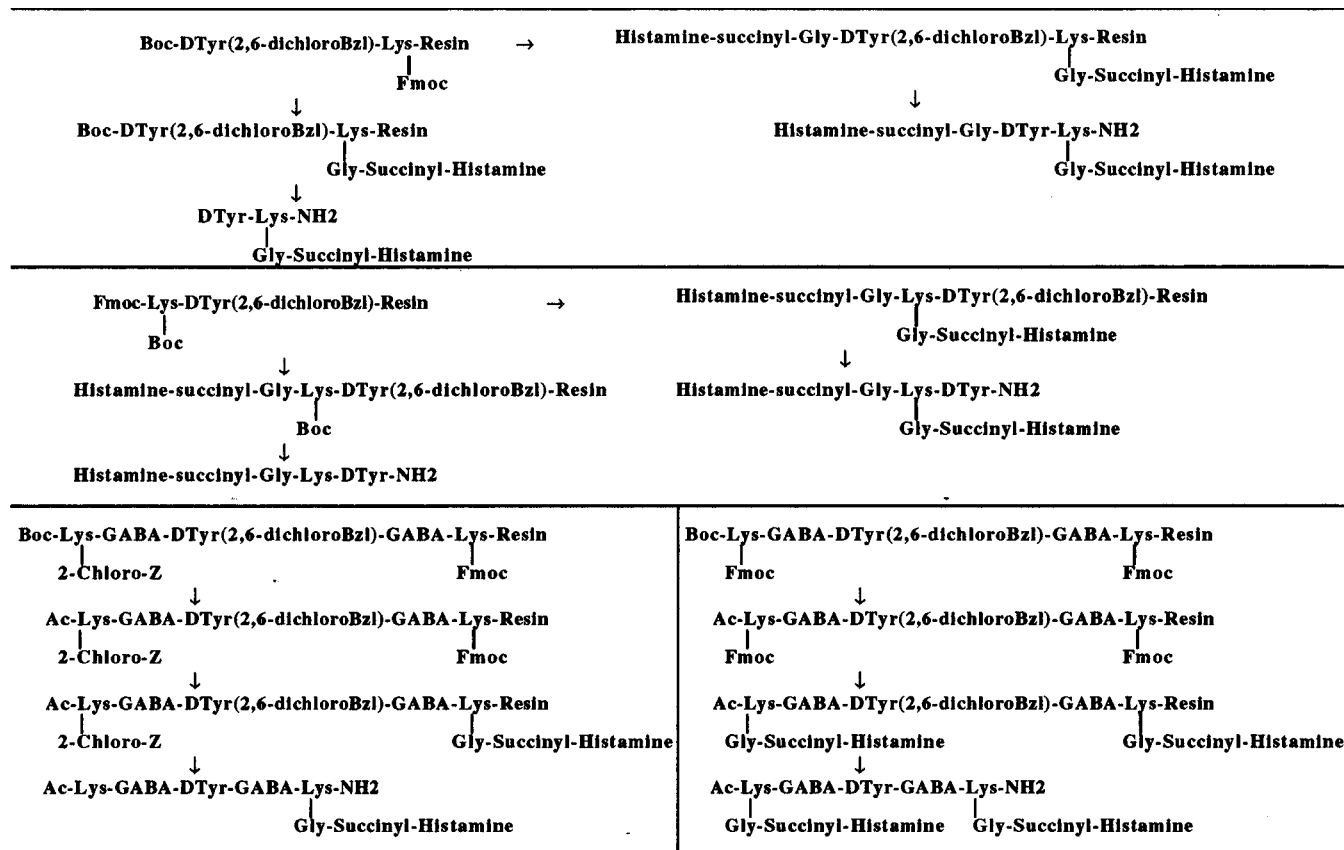


Figure 1. Synthesis of mono-HSG and di-HSG haptens. Resin, *p*-methylbenzhydrylamine resin; tBoc, *tert*-butoxyloxycarbonyl; Fmoc, fluorenylmethyloxycarbonyl; 2-chloro-Z, 2-chlorobenzoyloxycarbonyl; 2,6-dichloroBzl, 2,6-dichlorobenzyl.

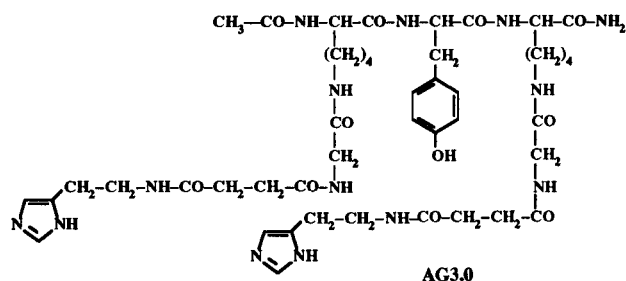


Figure 2. Structure of the AG3.0 bivalent hapten.

H β 3.02, H β' 2.74, H-3,5 6.70, H-2,6 7.10; Lys³ (NH 7.95, H α 4.20, H β 1.72, H β' 1.57, H $\gamma\gamma'$ 1.25, H $\delta\delta'$ 1.45, H $\epsilon\epsilon'$ 3.10, N ϵ H 7.80); CONH₂ 7.05, 7.25; Gly (NH 8.03, H α 3.02); succinyl(CH₂)₂ 2.43; histamine (NH 7.96, N-CH₂ 3.38, CH₂-Im 2.75, imidazole H-2 8.45, H-4 7.10).

Synthesis of DTPA-HSG Peptides. DTPA was coupled to the mono-HSG peptide as follows. Briefly, 25 μ mol of a peptide solution (5 mM) in HEPES buffer (1 M, pH 8.2) was added with stirring to 150 μ mol of DTPA dianhydride (Aldrich) in solution in DMSO (150 mM). The pH was maintained at 8.2 until the reaction was completed. After evaporation of the solvents, the crude product was dissolved in water and trifluoroacetic acid added to reach pH 2. The solution was filtered through Chelex 100 (Bio-Rad, France). The resulting peptide was purified by C₁₈ reversed phase preparative HPLC (Nucleosil) as described above for di-HSG peptides. The solvents were filtered through Chelex 100 (Bio-Rad). The purity \geq 95% was checked by HPLC in systems 1 and 2.

AG5.1 (M + H)⁺: 1275.7 found, 1275.0 calcd. AG5.0 (M + H)⁺: 1104.9 found, 1104.6 calcd.

AG5.2 (M + H)⁺: 934.7 found, 934.4 calcd. AG5.3 (M + H)⁺: 934.4 found, 934.4 calcd.

The measured UV molar absorbance at 280 nm (pH 7) for a solution of each purified peptide was consistent with the peptide concentration (determined after total acid hydrolysis and amino acid analysis) and the tyrosine content (molar extinction coefficient = 1300). This value was used to determine the concentration of the peptides in all experiments.

Radiolabeling. Iodination of AG3.0 (2 nmol) was performed using Na¹²⁵I (18.5 MBq) and chloramine T (10 μ g) for 2 min at room temperature and stopped with 100 μ g of sodium disulfide. The monoiodinated peptide was purified by reversed phase C₁₈ HPLC. Antibodies (25 μ g) were iodinated with Na¹²⁵I (18.5 MBq) using iodogen (Salacinsky et al., 1981).

Labeling with indium-111 (37 MBq InCl₃) of DTPA peptides (250 pmol) was performed in citrate buffer (pH 5.0) for 24 h, and then 10 nmol of unlabeled InCl₃ was added to saturate free DTPA groups. Free indium-111 was determined after chromatography on a Sep-Pak C₁₈ cartridge (Waters, Milford, MA), and maximal immunoreactivity (\geq 95%) was evaluated from binding experiments of trace amounts of ¹¹¹In-labeled peptide to 734 antibody-coated tubes.

Binding Experiments. *Equilibrium Affinity Constant Determination.* For *K_a* determination of mono-HSG and DTPA-HSG peptide binding to anti-HSG mAb, trace amounts of ¹¹¹In-labeled AG5.1 were incubated for 2.5 h under shaking in 679.1MC7 mAb-coated tubes in the presence of increasing amounts of competitors at 37 °C (pH 7.4) in 1 mL (final volume) of PBS-0.2% BSA (four experiments in triplicate). Nonspecific binding was evaluated in the presence of excess unlabeled AG5.1 (2 \times 10⁻⁷ M). *K_a* values were fitted from four experimental competition curves in triplicate (Barbet et al., 1993).

For K_a determination of (In)DTPA-bearing peptide binding to anti-(In)DTPA, mAb was determined in similar experiments using 734 mAb-coated tubes and competition between ^{111}In labeled AG5.0 and unlabeled AG5.1.

Sandwich experiments with DTPA-HSG peptides were performed in 679.1MC7 antibody-coated tubes at 37 °C and pH 7.4. The coated antibody concentration (about 3×10^{-9} M) was determined from competition binding experiments as described above with unlabeled AG5.1 as competitor. Increasing concentrations of unlabeled DTPA-HSG peptides were incubated in the presence of trace amounts of labeled ^{125}I -734 Fab' (alkylated with *N*-ethylmaleimide) for 2.5 h under shaking in a final volume of 1 mL of PBS-0.2% BSA. Nonspecific binding (1.2%) was determined in the absence of bivalent hapten. Di-HSG peptides sandwich experiments were performed as for DTPA-HSG peptides, except for the antibody-coated tube concentration (about 5×10^{-10} M), and the use of ^{125}I -labeled 679.1MC7 Fab' antibody fragment.

Cell binding experiments were performed on LS 174 T colorectal carcinoma strain cell (ATCC). One hundred microliters of suspension (2×10^7 cells/mL), 100 μL of bispecific anti-CEA \times anti-histamine BsmAb (F6 \times 679.1MC7) dilutions, 150 μL of ^{125}I -labeled AG3.0 (4.6×10^{-10} M final, specific activity = 2.3×10^{18} cpm/mol) were incubated together in PBS-0.2% BSA supplemented with NaN_3 (0.02%). After 2.5 h under shaking, 100 μL of the suspensions was centrifuged in triplicate tubes for 30 s through a phthalate mixture (Dower et al., 1981). Aliquots of supernatants and the bottom of each tube (containing the cell pellet) were counted. Binding studies of trace amounts of ^{125}I -labeled BsmAb in the presence of increasing concentrations of unlabeled BsmAb were performed according to the same procedure.

In Vivo Experiments. *Animals.* Female BALB/c-nu/nu mice, 6–8 weeks old (Iffa-Credo, France) were grafted by sc injection in the flank with 2×10^6 LS174T human colorectal carcinoma cells. In some experiments a control tumor (2×10^6 A375 human melanoma cells) was grafted in the other flank. Immunoscintigraphy and biodistribution studies were performed 2 weeks later.

Biodistribution. Triplicate mice were given 2 μg (in 50 μL of PBS) of F6 \times 679.1MC7 (anti-CEA \times anti-HSG) BsmAb by iv injection under light ether anesthesia. Seventeen hours later ^{125}I -labeled AG3.0 (1 pmol, 2.7×10^{18} cpm/mol) was injected iv. Mice were weighed and sacrificed with ether at selected time intervals (1–168 h). Blood was collected on heparin after heart puncture. Actual injected doses were estimated by subtraction of noninjected and sc-injected material from the total dose. Data from mice injected with <80% efficiency were discarded. Control mice were injected with 10^7 cpm of ^{125}I -labeled F6 F(ab')₂ and 20 μg of unlabeled F6 F(ab')₂.

Similar experiments were performed to compare ^{125}I - and ^{111}In -labeled bivalent hapten biodistribution. Pretargeting was performed by injection of 2 μg of F6 \times 734 (anti-CEA \times anti-DTPA) BsmAb. Seventeen hours later ^{111}In -labeled *N*- α -DTPA-tyrosyl-*N*- ϵ -DTPA-lysine (1 pmol 5×10^{18} cpm/mol) was injected.

Plasma Chromatography. Plasma samples collected 1 h after administration of the labeled hapten were chromatographed on a Superdex 200 gel filtration column (Pharmacia, France).

RESULTS

Synthesis. Di(histamine-succinyl-glycyl) peptides (bivalent haptens) and the mono(histamine-succinyl-glycyl) peptides (monovalent haptens) were synthesized manually according to the solid phase method. The HSG

hapten was built by coupling a glycine residue to a deprotected $-\text{NH}_2$ group, succinylation, and coupling histamine to the free hemisuccinates using BOP and HOBT. DTPA-HSG haptens (bearing a chelating agent for ^{111}In labeling) were obtained by coupling DTPA to the respective monovalent HSG haptens. Appropriate protection/deprotection strategies using tBoc, Fmoc, and 2-ClZ protecting groups were designed to afford the various isomers (Figure 1). All of them were purified to at least 95% purity (by HPLC) and identified by mass spectrometry and amino acid analysis after total acid hydrolysis.

For ^{125}I -labeling of AG3.0, about 60% iodine was incorporated in the peptide and about 60% of the labeled peptide was monoiodinated. The monoiodinated ^{125}I -labeled AG3.0 was purified by HPLC. The maximal binding of trace amounts of this purified fraction to anti-histamine-coated tubes was >90%.

^{111}In labeling of DTPA peptides led to 95% chelation of ^{111}In (<5% free ^{111}In was eluted from Sep-Pak C₁₈ cartridges). The maximal binding ($\geq 95\%$) of trace amounts of ^{111}In -labeled peptides to anti-DTPA-coated tubes is in accordance with this result, and the ^{111}In -labeled peptides were used without purification.

The ^{125}I -radiolabeling yields of antibodies ranged from 30% to 70% and immunoreactivity was always >60%.

Equilibrium Affinity Constant Determination. The equilibrium affinity constants (K_a) for the binding of the mono-HSG (AG4 series) and the DTPA-HSG (AG5 series) peptides (Table 1) were determined from competition binding curves with ^{111}In -labeled AG5.1, run in triplicate. To allow comparisons with cell binding and *in vivo* experiments, all measurements were performed at 37 °C with physiological salt concentration. Nonlinear least-squares regression (Barbet et al., 1993) was used to identify the equilibrium parameters (affinity constant, number of binding sites). The affinity of the HSG hapten depends on its position on the peptide chain. The highest K_a value is observed for HSG coupled to the lateral chain of lysine [AG4.0 $K_a = (6.8 \pm 0.2) \times 10^9 \text{ M}^{-1}$]. The K_a value for the homologous peptide in the DTPA-HSG series is lower [AG5.0 $K_a = (2.9 \pm 0.1) \times 10^9 \text{ M}^{-1}$]. The presence of a γ -aminobutyric acid (GABA) next to the lysine also decreases K_a in the HSG series [AG4.1 $K_a = (3.8 \pm 0.1) \times 10^9 \text{ M}^{-1}$].

The affinity constant [$K_a = (1.8 \pm 0.2) \times 10^9 \text{ M}^{-1}$] of the anti-DTPA indium antibody to (In)DTPA coupled to the ϵ - NH_2 of a lysine was determined from similar competition binding experiments, using ^{111}In -labeled and unlabeled AG5.0.

Sandwich Experiments. DTPA-HSG peptides were tested for simultaneous binding to two anti-hapten antibodies. Then, increasing concentrations of peptides were incubated in anti-HSG antibody-coated tubes (about 3×10^{-9} M) in the presence of trace amounts of ^{125}I -labeled anti-DTPA antibody. The results of two experiments (in triplicate tubes) were fitted to the calculated equilibrium isotherms by nonlinear least-squares regression (Barbet et al., 1993). A coefficient (σ) was introduced in the calculation to express the steric hindrance for the simultaneous binding of two antibodies to the bivalent hapten: if K_a is the affinity constant for the first binding event, then the affinity for the binding of a second antibody to the bivalent hapten is σK_a . The σ parameter and the immunoreactivity of the labeled antibody were highly correlated, and as a consequence they could not be adjusted simultaneously. However, assuming 70% immunoreactivity in all calculations, comparison of σ values showed that the hapten accessibility depends on the length of the peptide chain. Very similar σ values

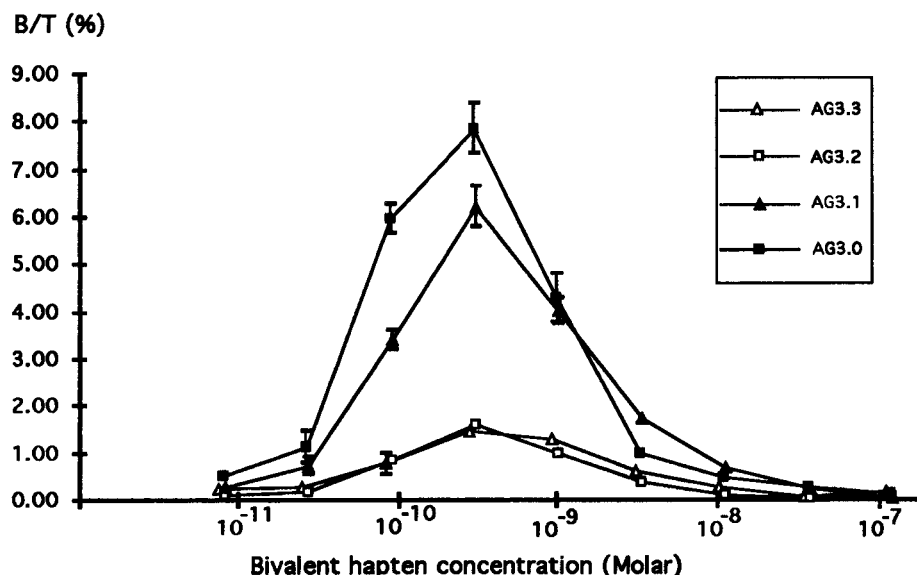


Figure 3. di-HSG hapten mediated binding of anti-HSG ^{125}I -Fab' to anti-HSG Fab'-coated solid phase: the tracer antibody was incubated for 2.5 h at 37 °C in anti-HSG-coated tubes in the presence of increasing concentrations of di-HSG hapten. Then aliquots of supernatant were counted (F), and the tubes were emptied, washed, and counted again (B). Mean B/F \pm SD bars are given unless smaller than point plotted ($n = 6$).

were evaluated for the two longest peptides AG5.1 and AG5.0, 0.6 and 0.5 respectively. For the shortest peptide AG 5.2, σ was found lower than 0.1.

With bivalent di-HSG haptens (the AG3 series), cross-linking of two antibodies coated on the tube must be avoided to allow binding analysis. Thus, a 6×10^{-10} M concentration of coated antibody was determined as appropriate to minimize this cross-linking phenomenon (data not shown). The accessibility of bivalent HSG haptens to two anti-HSG antibodies was then evaluated using 6×10^{-10} M anti-HSG antibody-coated tubes (Figure 3). Assuming that the immunoreactivity of the labeled antibody was 70%, the accessibility coefficients σ for AG3.1 and AG3.0 were 0.4 and 0.3, respectively.

Equilibrium Binding to Tumor Cells *in Vitro*.

The ability of the anti-CEA \times anti-HSG BsmAb to target ^{125}I -labeled AG3.0 to CEA-expressing cells was studied in binding experiments using LS174T human colorectal carcinoma cells. The binding of the labeled hapten to the target cells was monitored in the presence of increasing concentrations of BsmAb. At the optimal BsmAb concentration (3.2×10^{-9} M), 59% of the hapten was bound. The binding parameters of the BsmAb (immunoreactivity = 50%), $K_a = (2.1 \pm 0.3) \times 10^8 \text{ M}^{-1}$ and binding site concentration = $(3.3 \pm 0.4) \times 10^5$ sites per cell, were calculated from binding studies of trace amounts of ^{125}I -labeled BsmAb in the presence of increasing concentrations of unlabeled BsmAb in a parallel experiment.

***In Vivo* Targeting of AG3.0 to Human Colon Carcinoma Grafted in Nude Mice.** Tumor-bearing (from 0.15 to 1.3 g) mice were given an injection of BsmAb (anti-CEA \times anti-HSG) and, 17 h later, ^{125}I -labeled AG3.0. The targeted activity at 3 h was 15.6 ± 1.0 of the injected dose per gram of tumor (% ID/g) and remained stable until 6 h. Then it decreased slowly to reach 6% ID/g at 24 h and 2% ID/g at 96 h ($T_{1/2} = 54.2 \pm 0.2$ h, Figure 4). High tumor to normal tissue contrast ratios were observed as soon as 3 h after tracer injection: tumor/plasma = 1.7 ± 0.2 , tumor/liver = 7.9 ± 2.5 , tumor/kidney = 4.0 ± 1.1 as shown in Figure 4, tumor/heart = 14.1 ± 3.8 , tumor/gastrointestinal tract = 12.7 ± 0.8 , tumor/lung = 6.0 ± 0.5 , tumor/spleen = 11.7 ± 2.8 . They all increased with time. Similar tumor uptake

was observed with the directly labeled F(ab')_2 , but maximum uptake was reached around 48 h. Tumor wash-out was slow and approximately parallel to that of pretargeted AG3.0. Tumor to plasma ratios were always significantly higher with the pretargeted hapten, whereas in other tissues the contrast ratios were higher with the pretargeted hapten for 24 h (kidneys) to 48 h (liver) and then plateaued at longer time intervals (Figure 4).

Control experiments in mice bearing two grafted tumors showed that hapten pretargeting was specific: as soon as 1 h after tracer injection, the contrast between the CEA positive target tumor (LS174T) and the control tumor (A375) (CEA negative) was 2.0 ± 0.2 ; it was 7.3 ± 1.6 at 3 h and reached 31.2 ± 8.0 at 24 h.

When compared to *in vivo* targeting of the ^{111}In -labeled hapten, the ^{125}I -labeled AG3.0 exhibited comparable tumor uptake but higher tumor to blood contrast ratios and tumor to other organs contrast ratios 24 h after tracer injection (Figure 5).

Analysis of Plasma and Urine Samples. Mice were injected with BsmAb and then 17 h later with the labeled bivalent hapten. Plasma samples were collected 1 h later. The samples were submitted to gel filtration chromatography. Two peaks of activity were observed at 13 and 16 mL corresponding to 200 and 100 kDa (Figure 6), respectively. This demonstrated that most hapten remained bivalent and circulated bound to one (100 kDa) or two BsmAb (200 kDa) (the free hapten would elute around 22 mL under these conditions). In addition, urine samples were tested for immunoreactivity, which was found better than 90% up to 24 h after injection.

DISCUSSION

We have demonstrated in previous studies that pretargeted AES immunodetection affords improved tumor detection sensitivity as compared to other imaging techniques such as magnetic resonance imaging, ultrasonography, computed tomography, and classical immunoscintigraphy with directly labeled antibodies. This technique is based on the formation of cyclic complexes at the cell surface between two BsmAb molecules and one bivalent hapten-bearing peptide. Our previous work

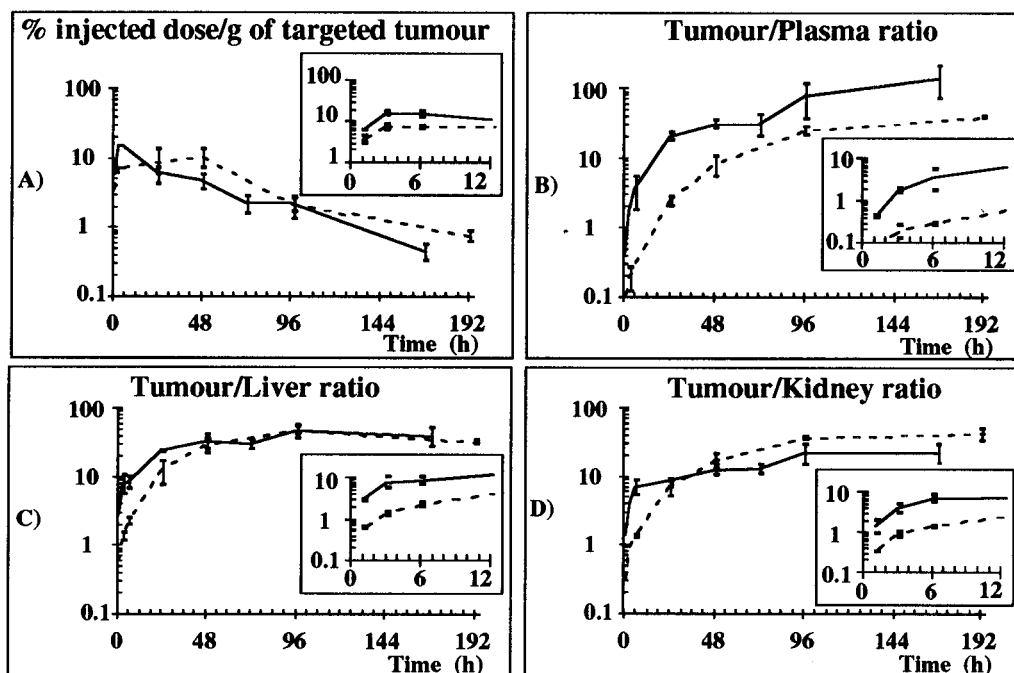


Figure 4. Tumor localization (A), tumor/organ ratios (B, C, D) time course: nude mice bearing LS174T tumor (CEA positive) in the flank were injected in triplicate with $20\ \mu\text{g}$ of ^{125}I -labeled $\text{F}(\text{ab}')_2$ (dashed lines) or with $2\ \mu\text{g}$ of anti-CEA \times anti-HSG BsmAb and 17 h later with ^{125}I -labeled AG3.0 (solid lines). Groups of three mice were sacrificed at selected time intervals, and dissected organs were counted. Mean \pm SD are plotted. In each panel an insert shows the kinetics over the first 12 h after activity injection.

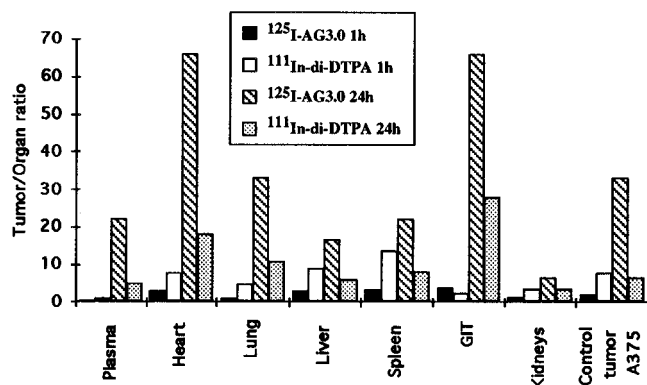


Figure 5. Biodistribution of ^{125}I - and ^{111}In -labeled bivalent haptens: nude mice bearing LS174T tumor (CEA-positive) in one flank and A375 (CEA-negative) tumor in the other were injected with $2\ \mu\text{g}$ of the BsmAb and 17 h later with the labeled bivalent hapten, anti-ACE \times anti-HSG BsmAb and ^{125}I -labeled AG3.0, or anti-ACE \times anti-indium-DTPA BsmAb and ^{111}In -di-DTPA. Groups of three mice were sacrificed and dissected at 1 and 24 h, and the organs were counted.

concerning tumor and metastasis detection has been performed with the ^{111}In -labeled $N\text{-}\alpha$ -DTPA-tyrosyl- $N\text{-}\epsilon$ -DTPA-lysine dipeptide. The high tumor to normal tissue ratios and the amount of injected dose localized in tumors, observed in animals and in the clinic, should allow radioimmunotherapy with this technique, and experiments are in progress to demonstrate this possibility. However, to use iodine-131, a β -emitting isotope useful for therapy, the DTPA-indium hapten required the development of specific labeling and purification techniques because indium must be complexed to DTPA before or after labeling with iodine. In addition, chemical syntheses with DTPA, a pentavalent carboxylic acid, are difficult and usually afford complex mixtures containing polymeric contaminants. The aim of this work was thus to synthesize new bivalent hapten-bearing peptides, suitable for radioimmunotherapy using the AES technique, with improved antibody-binding and targeting

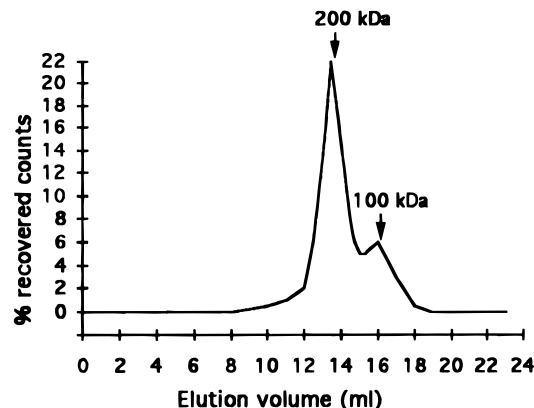


Figure 6. Gel filtration radioactivity elution profile of plasma: the sample was collected 1 h after ^{125}I -labeled AG3.0 injection to a mouse preinjected 17 h before with BsmAb.

efficiency characteristics. These hapten-bearing peptides were also designed to allow fast and easy radiolabeling with iodine-131. The other characteristics of an ideal hapten are low toxicity, high-affinity binding to available antibodies, and no cross-reactivity or nonspecific binding with body components. The histamine-succinyl-glycine hapten was chosen for these reasons.

A first bivalent HSG peptide was synthesized. Although able to target radioactivity to tumors, it was rapidly degraded *in vivo* (Gruaz-Guyon et al., 1991). We therefore synthesized more stable compounds (Gruaz-Guyon et al., 1993). A D-tyrosine was introduced in the backbone for iodine labeling. The C-terminal end was amidated, the N-terminal was acetylated, and lysine side chains were substituted. As a result, the bivalent HSG peptide AG 3.0 should be extremely resistant to proteases. In plasma most of the activity recovered 1 h after injection circulated bound to two bispecific antibody molecules (Figure 6), and in the urine 90% of the radioactivity is able to bind to anti-HSG antibody 24 h after injection. In addition, the stability of this hapten-

bearing peptide after internalization by target cells *in vitro* has recently been demonstrated (Manetti et al., 1995).

To determine the peptide chain providing the optimal distance between the two haptens, we synthesized a series of bivalent haptens listed in Table 1 and studied *in vitro* their ability to cross-link two antibodies. The HSG hapten equilibrium affinity constants have been measured for monohistamine derivatives and, as expected, the K_a depends on the hapten position in the peptide chain. Coupling the hapten to the lateral chain of lysine affords the highest affinity. This is consistent with the observation of Morel et al. (1990) that optimum binding affinity is obtained only when the hapten closely mimics the immunogen. We then studied the binding of a labeled anti-hapten Fab fragment to a solid phase coated with anti-hapten Fab fragment in the presence of increasing concentrations of bivalent haptens. As a model, we studied several peptides bearing two different haptens: DTPA-indium and HSG (Table 1). The equilibrium binding curves of ^{125}I -labeled anti-DTPA-indium antibody to anti-HSG-coated tubes in the presence of increasing concentrations of peptide were fitted using a simple computer program (Barbet et al., 1993). As expected, the bivalent haptens AG5.0 and AG5.1 with the longest connecting peptide chain exhibited the best accessibility to two antibodies. The accessibilities for the bivalent HSG haptens AG3.0 and AG3.1 were found very close. It is remarkable that maximum cross-linking ability is obtained with rather short peptide chains (2 to 3 residues), in agreement with early work by Valentine and Green (1967).

As the hapten affinity was higher for the AG3.0 peptide, it was selected for further studies as the most appropriate hapten-bearing peptide in this series. As expected, ^{125}I -labeled AG 3.0 can be efficiently targeted to cultured colorectal cells (LS174T) in the presence of anti-CEA \times anti-HSG BsmAb. *In vivo*, the BsmAb was used to target ^{125}I -labeled AG 3.0 to LS174T tumor cells grafted in nude mice. The fraction of dose localized per gram of tumor was similar to the one observed with the directly labeled F(ab')_2 (Figure 4) or the ^{111}In -labeled bivalent hapten (Figure 5), and it decreased very slowly with time ($T_{1/2} = 54.2 \pm 0.2$ h, Figure 4). The targeting of AG 3.0 was specific as high tumor to control tumor ratios were observed. Tumor uptake was equivalent to what was observed with a directly labeled F(ab')_2 , but maximum uptake was obtained more rapidly and tumor to nontumor contrast ratios were higher in plasma at all times and in other tissues in the first 24–48 h after hapten injection (Figure 4). The iodine-labeled hapten also afforded higher contrasts than the ^{111}In -labeled DTPA hapten. As a result, the more favorable biodistribution of ^{131}I -labeled AG3.0 should translate into better dosimetry: it is indeed very important to minimize bone marrow stem cell exposure by circulating activity and to rapidly deliver the activity to the tumor. Further studies are in progress to evaluate the respective effects of the radioisotope and of the hapten–antibody system to explain the observed differences.

The asymmetric haptens should be useful in designing more specific targeting reagents when no tumor-specific marker is available, as for example in the treatment of lymphomas. We have already shown, in a lymphocyte model, that tracers bearing two different haptens (DNP and DTPA), in combination with two different BsmAb, each directed to a different cellular antigen (mouse CD22 or MHC class II I-E^k) and to one of the haptens, provide a very efficient way of targeting with high specificity cells bearing simultaneously the two antigens (Le Doussal,

1991). The peptides AG5.1 and AG5.0 of the DTPA–HSG series should be especially well suited to this approach since they do not contain the hydrophobic hapten DNP. They will now be tested in a tumor model in which target cells will be differentiated from normal cells by the simultaneous expression of two differentiation antigens otherwise expressed independently in different normal cell types.

CONCLUSION

AES immunoscintigraphy and radioimmunoguided surgery enable the detection of very small pathologic lymph nodes and their resection (de Labriolle-Vaylet et al., 1993). However, detecting lymph nodes smaller than 2 mm in diameter and micrometastases remains impractical. The management of these extremely small tumors should benefit from radioimmunotherapy with α - or β -emitting isotopes. The specificity of ^{125}I -labeled AG 3.0 targeting, the low background, and the persistence of the tumor-bound activity for extended periods of time are very strong arguments in favor of the use of AG3.0 as a tracer for targeting iodine-131 tumor cells. Further studies are now in progress to determine the doses of radiation delivered to tumors and normal organs using this molecule (Manetti et al., 1997). In addition, new hapten-bearing peptides derived from AG3.0 have been synthesized with attached chelating agents capable of binding other radioisotopes of interest for scintigraphy (technetium-99m) or therapy (rhenium-186 or rhenium-188).

ACKNOWLEDGMENT

The chemical syntheses were performed by A.G.G. in the U.113 INSERM, Faculté de Médecine Saint-Antoine, Paris, France, and URA 1309 CNRS, Institut Pasteur, Lille, France. We thank Dr. D. Marion for nuclear magnetic resonance spectroscopy (Institut de Biologie Structurale, Grenoble, France), Pr. G. C. Gesquiere and Pr. C. Sergherardt for helpful discussions, Pr. S. Askienazy for constant support, and Pr. P. Sautière for amino acid analysis. We are grateful to our colleagues at Immunotech E. Rouvier for fruitful discussions and to M. Martin and C. Manetti for the generous supply of indispensable antibody reagents. This work was supported in part by the Association pour la Recherche contre le Cancer through Grant 6073 allocated to G.M. We gratefully acknowledge Pr. M. Delaage, who pioneered the AES technology.

LITERATURE CITED

- Barbet, J., Le Doussal, J. M., Gruaz-Guyon, A., Martin, M., Gautherot, E., and Delaage, M. (1993) Computer simulation of multiple binding equilibrium isotherms: application to the binding of bivalent ligands to antibodies interacting with cell surface Fc-receptors. *J. Theor. Biol.* 165, 321–340.
- Chetanneau, A., Barbet, J., Peltier, P., Le Doussal, J. M., Gruaz-Guyon, A., Bernard, A. M., Resche, I., Rouvier, E., Bourguet, P., Delaage, M., and Chatal, J. F. (1994) Pretargeted imaging of colorectal cancer recurrences using an ^{111}In -labeled bivalent hapten and a bispecific antibody conjugate. *Nucl. Med. Commun.* 15, 972–980.
- De Labriolle-Vaylet, C., Gruaz-Guyon, A., Wioland, M., Sarfati, E., Mensch, B., Delaage, M., Barbet, J., and Milhaud, G. (1993) Radioimmunodetection de métastases du cancer médullaire de la thyroïde (CMT) à l'aide d'une nouvelle méthode en deux temps. *J. Med. Nucl.* 7/8, 318.
- Dower, S. K., DeLisi, C., Titus, J., and Segal, D. M. (1981) Mechanism of binding of multivalent immune complexes to Fc receptors. I. Equilibrium binding. *Biochemistry* 20, 6326–6334.

- Glennie, M. J., McBride, H. M., Worth, A. T., and Stevenson, G. T. (1987) Preparation and performance of bispecific F(ab')₂ antibody containing thioether-linked Fab'γ fragments. *J. Immunol.* **139**, 2367–2375.
- Goldenberg, D. M. (1993) Monoclonal antibodies in cancer detection and therapy. *Am. J. Med.* **94**, 297–312.
- Goodwin, D. A., Meares, C. F., McTigue, M., and David, G. S. (1986) Monoclonal antibodies as reversible equilibrium carriers of radiopharmaceuticals. *Int. J. Nucl. Med. Biol.* **7**, 569–580.
- Goodwin, D. A., Meares, C. F., McCall, M. J., McTigue M., and Chaovapong, W. (1988) Pre-targeted immunoscintigraphy of murine tumors with indium-111-labelled bifunctional haptens. *J. Nucl. Med.* **29**, 226–234.
- Goodwin, D. A., Meares, C. F., McTigue, M., Chaovapong, W., Diamanti, C. I., Ransone, C. H., and McCall, M. J. (1992) Pretargeted immunoscintigraphy: effect of hapten valency on murine tumour uptake. *J. Nucl. Med.* **33**, 2006–2013.
- Gruaz-Guyon, A., Gras-Masse, H., and Le Doussal, J. M. (1991) Radiolabelled hapten derivatized peptides for tumour imaging with bispecific antibody conjugates. In *Peptides 1990* (E. Giraldo and D. Andreu, Eds.) pp 822–825, ESCOM, Leiden, The Netherlands.
- Gruaz-Guyon, A., Gautherot, E., Martin, M., Le Doussal, J. M., Barbet, J., Delaage, M., and Milhaud, G. (1993) Haptènes bivalents marqués à l'iode et au technetium pour l'immunoscintigraphie de tumeurs avec des anticorps bi-spezifiques. *J. Med. Nucl.* **7/8**, 328.
- Le Doussal, J. M., Martin, M., Gautherot, E., Delaage, M., and Barbet, J. (1989) *In vitro* and *in vivo* targeting of radiolabelled monovalent and divalent haptens with dual specificity monoclonal antibody conjugates: enhanced divalent hapten affinity for cell-bound antibody conjugate. *J. Nucl. Med.* **30**, 1358–1366.
- Le Doussal, J. M., Gruaz-Guyon, A., Martin, M., Gautherot, E., Delaage, M., and Barbet, J. (1990) Targeting of indium-111-labelled bivalent hapten to human melanoma mediated by bispecific monoclonal antibody conjugates: imaging of tumors hosted in nude mice. *Cancer Res.* **50**, 3445–3452.
- Le Doussal, J. M., Gautherot, E., Martin, M., Barbet, J., and Delaage, M. (1991) Enhanced *in vivo* targeting of an asymmetric bivalent hapten to double-Ag-positive mouse B cells, using mAb conjugate cocktails. *J. Immunol.* **146**, 169–175.
- Le Doussal, J. M., Chetanneau, A., Gruaz-Guyon, A., Martin, M., Gautherot, E., Lehur, P. A., Chatal, J. F., Delaage, M., and Barbet, J. (1993) Bispecific (anti-CEA, anti-In-DTPA) monoclonal antibody-mediated targeting of an Indium-111-labelled DTPA dimer to primary colorectal tumors: pharmacokinetics, biodistribution, scintigraphy and immune response. *J. Nucl. Med.* **34**, 1662–1671.
- Lollo, C., Halpern, S., Bartholomew, R., David, G., and Hagan, P. (1994) Non-covalent antibody-mediated drug delivery. *Nucl. Med. Commun.* **15**, 483–491.
- Mach, J. P., Pèlegri, A., and Buchegger, F. (1991) Imaging and therapy with monoclonal antibodies in non-hematopoietic tumors. *Curr. Opin. Immunol.* **3**, 685–693.
- Manetti, C., Le Doussal, J. M., Rouvier, E., Gruaz-Guyon, A., and Barbet, J. (1995) Intracellular uptake and catabolism of anti-IgM antibodies and bispecific-antibody-targeted hapten by B lymphoma cells. *Int. J. Cancer* **63**, 250–256.
- Morel, A., Darmon, M., and Delaage, M. (1990) Recognition of imidazole and histamine derivatives by monoclonal antibodies. *Mol. Immunol.* **27**, 995–1000.
- Peltier, P., Curtet, C., Chatal, J. F., Le Doussal, J. M., Daniel, G., Aillet, G., Gruaz-Guyon, A., Barbet, J., and Delaage M. (1993) Radioimmunodetection of medullary thyroid cancer using a bispecific anti-CEA/anti-Indium-DTPA antibody and an indium-111-labelled DTPA dimer. *J. Nucl. Med.* **34**, 1267–1273.
- Salacinsky, P. R. P., McLean, P., Sykes, J. E. C., Clement-Jones, V. V., and Lowry, P. J. (1981) Iodination of proteins and peptides using a solid phase oxidizing agent 1,3,4,6-tetrachloro-3,6-diphenylglycoluril (Iodogen). *Anal. Biochem.* **117**, 136–141.
- Santos, O., Payne, J. K., Domitrowsky, J. B., Berkeley C., and Mackensen D. G. (1995) A two-step delivery system utilizing a bi-specific monoclonal antibody for radioimmunotherapy. *Antibody Immunoconjugate Radiopharm.* **8**, 93–109.
- Stickney, D. R., Slater, B., Kirk, A., Ahlem, C., Chang, C., and Frincke, J. M. (1989) Bifunctional antibody: ZCE/CHA 111In BLEDTA-IV clinical imaging in colorectal carcinoma. *Antibody Immunoconjugate Radiopharm.* **2**, 1–13.
- Stickney, D. R., Anderson, L. D., Slater, J. B., Ahlem, C. N., Kirk, G. A., Schweighardt, S. A., and Frincke, J. M. (1991) Bifunctional antibody: a binary radiopharmaceutical delivery system for imaging colorectal carcinoma. *Cancer Res.* **51**, 6650–6655.
- Valentine, R. C., and Green, N. M. (1967) Electron microscopy of an antibody-hapten complex. *J. Mol. Biol.* **27**, 615–623.

BC970083H

Properties of and Oxygen Binding by Albumin–Tetraphenylporphyrinatoiron(II) Derivative Complexes

Eishun Tsuchida,^{*,†} Katsutoshi Ando, Hiromitsu Maejima, Noriyuki Kawai, Teruyuki Komatsu, Shinji Takeoka, and Hiroyuki Nishide

Department of Polymer Chemistry, Advanced Research Institute for Science and Engineering, Waseda University, Tokyo 169, Japan. Received December 23, 1996[®]

A hydrophobic tetraphenylporphyrinatoiron(II) derivative bearing a covalently bound axial imidazole [Fe(II)P] was efficiently and noncovalently bound into human serum albumin (HSA) up to an average of eight Fe(II)P molecules per HSA molecule. The aqueous solutions of the HSA–Fe(II)P complex provided a reversible and relatively stable oxygen adduct under physiological conditions (pH 7.4 and 37 °C). The half-life of the oxygen adduct ($\tau_{1/2}$) was 1 h at 37 °C in an air atmosphere. With Fe(II)-TpivPP (the so-called “picket-fence heme”) having no axial base, an oxygenated HSA–Fe(II)TpivPP complex was obtained using a 20-fold molar excess of 1,2-dimethylimidazole, but the $\tau_{1/2}$ was very short (ca. 10 min at 37 °C). The oxygen affinity [$P_{1/2}(\text{O}_2)$] and oxygen transporting efficiency (OTE) of HSA–Fe(II)P at 37 °C were 30 Torr and 22%, respectively. Furthermore, the oxygen-binding and dissociation rate constants (k_{on} and k_{off}) are extremely high in comparison with those of hemoglobin. The HSA molecule binding eight Fe(II)P molecules can transport about 3.4 mL/dL of oxygen under physiological conditions, corresponding to about 60 % of the oxygen transporting amount of human blood.

INTRODUCTION

Human serum albumin (HSA)¹ is the second major protein, following hemoglobin, of the proteins in blood. Its molecular mass is 66.5 kDa, which is similar to that of hemoglobin (64.5 kDa). HSA maintains the colloidal osmotic pressure of blood and transports nutritional and metabolic products, physiologically active compounds, toxic materials, heavy metals, and so on. For example, heme released from hemoglobin by hemolysis is trapped by HSA in plasma and is transported to the liver for metabolic processing. The formation of the HSA–heme complex has been widely studied (Beaven et al., 1974; Adams & Berman, 1980; Morgan et al., 1980; Lamola et al., 1981; Hrkal & Klementova, 1983; Kodicek et al., 1983; Moehring et al., 1983); however, there has been no report on the reduction of heme to heme and the oxygenation of the heme bound to HSA. Marden et al. (1989) determined the carbonylation of a deoxyheme–HSA complex in an aqueous solution, and Bonaventura et al. (1994) preliminarily reported the reversible spectral change of HSA binding a heme derivative in presence of a large molar excess of axial imidazole upon exposure to dioxygen but did not succeed in obtaining a stable oxygen adduct.

* Author to whom all correspondence should be addressed. Fax: +81 3-3209-5522. Phone: +81 3-3209-8895.

[†]CREST investigator, JST.

[®] Abstract published in *Advance ACS Abstracts*, July 1, 1997.

¹ Abbreviations: Fe(II)P, 2-[[[8-[N-(2-methylimidazolyl)]octanoyl]oxy]methyl]-5,10,15,20-tetrakis($\alpha,\alpha,\alpha,\alpha$ -*o*-pivalamido)phenylporphyrinatoiron(II); Fe(II)TpivPP, 5,10,15,20-tetrakis($\alpha,\alpha,\alpha,\alpha$ -*o*-pivalamido)phenylporphyrinatoiron(II); HSA, human serum albumin; r-HSA, recombinant human serum albumin; HSA–Fe(II)P, Fe(II)P bound to HSA; Asb, L-ascorbic acid; DMF, *N,N*-dimethylformamide; DMSO, dimethyl sulfoxide; $\tau_{1/2}$, half-life of the oxygen adduct; $P_{1/2}(\text{O}_2)$, oxygen affinity; OTE, oxygen transporting efficiency; BCG, bromocresol green; k_{on} , rate constant of oxygen binding; k_{off} , rate constant of oxygen dissociation; $P_{1/2}(\text{CO})$, carbon monoxide affinity; 1,2-Me₂Im, 1,2-dimethylimidazole; SOD, superoxide dismutase; lipidheme, tetraphenylheme derivative having four alkylphosphocholine groups; LH-V, lipidheme vesicle; LH-M, lipidheme microsphere.

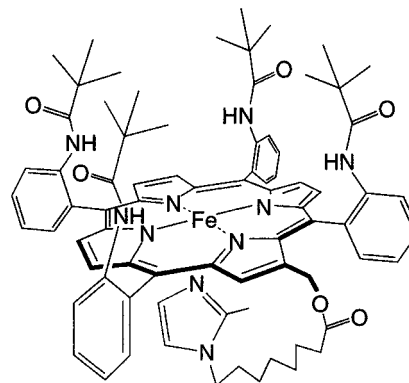


Figure 1. Structure of Fe(II)P.

We have synthesized 2-[[[8-[N-(2-methylimidazolyl)]octanoyl]oxy]methyl]-5,10,15,20-tetrakis($\alpha,\alpha,\alpha,\alpha$ -*o*-pivalamido)phenylporphyrinatoiron(II) [Fe(II)P with a molecular mass of 1.3 kDa] which has an axial base covalently bound to the porphyrin ring (Figure 1). The axial base coordinates to the fifth coordination site of the central iron of the porphyrin and permits dioxygen coordination at the sixth site. We confirmed that Fe(II)P complexed with oxygen in organic solvents such as toluene or *N,N*-dimethylformamide (DMF) without adding imidazole derivatives for axial bases. Recently, we have found that the injection of a Fe(III)P/dimethyl sulfoxide (DMSO) solution into an HSA aqueous solution leads to a 1/1 complex of Fe(III)P and HSA (Komatsu et al., 1995), which gave a stable oxygen adduct even in the aqueous phase after its reduction by sodium dithionite ($\text{Na}_2\text{S}_2\text{O}_4$) to Fe(II)P. Since then, the preparation procedure has been significantly improved to make more concentrated solutions of complex and to bind a greater number of Fe(II)P molecules into one HSA molecule so as to make the oxygen transporting ability comparable to that of hemoglobin. This paper reports on a new preparation procedure of HSA–Fe(II)P complexes binding one, four, and eight Fe(II)P molecules and also

describes the characteristics and oxygen-binding properties of the resulting complexes.

EXPERIMENTAL PROCEDURES

Materials. Fe(III)P was synthesized according to our previous paper (Tsuchida et al., 1995). Tetrapivalamidophenylporphyrinatoiron(III) [Fe(III)TpivPP, the so-called “picket-fence heme”] without an axial base was also synthesized according to the method reported by Collman et al. (1973). An HSA solution was purchased from Bayer Co., Ltd. (Albumin Cutter, 5 wt %), and the recombinant HSA solution (r-HSA, 25 wt %) was a gift from Green Cross Co., Ltd. Pure water (Otsuka Pharmaceutical Co., Ltd.) was used for dilution of HSA, and high-grade ethanol (purity, >99.5%; Kanto Chemical Co., Ltd.) was for the Fe(II)P solvent.

Preparation of HSA–Fe(II)P. A brown-red Fe(III)P ethanol solution [$[\text{Fe(III)P}] = 0.15 \text{ mM}$] was prepared by dissolving Fe(III)P (39.1 mg) into 200 mL of ethanol. An HSA aqueous solution ($[\text{HSA}] = 18.8 \text{ }\mu\text{M}$) was prepared by diluting 10 mL of HSA (5 wt %) 40 times with pure water. L-Ascorbic acid (Asb, 104 mg) was completely dissolved into 2 mL of pure water under a N_2 atmosphere, and 100 μL of the Asb solution was added to the Fe(III)P ethanol solution after bubbling CO through it for 10 min. The color of the Fe(III)P solution immediately changed to red, indicating reduction to Fe(II)P. A 200 mL aliquot of the Fe(II)P(CO) solution was dropped into 400 mL of the HSA solution and vigorously stirred, giving an Fe(II)P/HSA ratio of 4. The resulting red transparent mixture (600 mL) was evaporated down to 300 mL at 35 $^\circ\text{C}$ for 3 h and further concentrated to 7 mL by ultrafiltration (cutoff MW of 50 000, N_2 pressure of 5 kg/cm^2 , 2 h, 4 $^\circ\text{C}$). The remaining or oxidized Asb molecules were also removed during this procedure. The solution diluted 10 times was freeze-dried to obtain a reddish-white powder for long-term storage. The powder was redispersed by dissolving it in phosphate-buffered saline (300 mM, pH 7.4). After the dialysis against a saline solution for 15 h, the concentration of the sample was adjusted to 3 mM Fe(II)P for the complex where Fe(II)P/HSA = 4. The HSA–Fe(II)P solution which bound eight Fe(II)P molecules to one HSA was also prepared using the same procedure. In this case, the HSA concentration was decreased to half ($[\text{HSA}] = 9.4 \text{ mM}$), and the Fe(II)P concentration after preparation was adjusted to 6 mM.

Determination of the Half-Life of the Oxy State of HSA–Fe(II)P and Its O_2 Affinity. One milliliter of the HSA–Fe(II)P(CO) solution in a 1 cm quartz cuvette was converted to the oxygenated state (oxy state) by irradiating with visible light from a halogen lamp (500 W) under flowing O_2 . The cuvette was constantly cooled in an ice bath. The conversion to the oxy state was completed within 6 min, and the oxy state identified in the change of the maximum absorption wavelength (λ_{max}) from 540 to 548 nm (Q-band). The half-life of the oxy state ($\tau_{1/2}$) at 37 $^\circ\text{C}$ was determined from a decrease in the Q-band peak at 548 nm. The oxygen-binding and dissociation equilibrium curve was plotted from the visible spectral change after the complex was saturated with O_2/N_2 mixed gases in which the oxygen partial pressure decreased from 760 Torr (pure O_2 gas) to zero. The 100% oxy state and the 100% deoxy state were determined from the spectra after the solution was saturated with 100% O_2 gas and 100% N_2 gas, respectively. The oxygen affinity was evaluated as $P_{1/2}(\text{O}_2)$, the oxygen partial pressure where 50% of Fe(II)P was oxygenated.

Quantitative Analysis of HSA and Fe(II)P. The HSA concentration in a HSA–Fe(II)P(CO) solution was determined using a bromocresol green method (BCG

method, A/G-B test wako, Wako Pure Chemical Industries). The absorption at 630 nm was measured after reacting BCG with HSA. A calibration curve was obtained by diluting a standard HSA solution ($[\text{HSA}] = 1\text{--}5 \text{ g/dL}$). To avoid the influence of Fe(II)P(CO) absorption, the difference spectra between the HSA–Fe(II)P(CO)/BCG solution and HSA–Fe(II)P(CO)/pure water were recorded.

After the injection of the ethanolic Fe(II)P(CO) solution into water, the suspended Fe(II)P(CO) can be completely extracted with chloroform because of its low solubility into water, whereas Fe(II)P(CO) in HSA dissolved in aqueous solutions cannot be extracted with chloroform. The amount of Fe(II)P bound to HSA can therefore be determined by extracting the Fe(II)P with a chloroform/methanol (1/1) mixture. After the complete drying of the extracted solution, it was redissolved in methanol, and its concentration was determined from the molar absorption coefficient of Fe(II)P(CO) ($\epsilon_{417\text{nm}}$ in methanol = $2.0 \times 10^5 \text{ M}^{-1} \text{ cm}^{-1}$). The binding ratio of Fe(II)P to HSA was determined from the quantitative analyses of Fe(II)P and HSA.

Viscosity of HSA–Fe(II)P. The viscosity of the HSA–Fe(II)P solution was measured using a cone plate rotatory viscometer (Shibaura System VSA-K).

Kinetic Parameters of O_2 and CO Binding to HSA–Fe(II)P. The binding (k_{on}) and dissociation (k_{off}) rate constants of O_2 and CO for HSA–Fe(II)P in aqueous solutions ($[\text{Fe(II)P}] = 20 \text{ }\mu\text{M}$) were determined by laser flash photolysis spectroscopy (Gibson, 1970; Traylor et al., 1985) using an UNISOKU TSP-601 spectrometer. CO affinity [$P_{1/2}(\text{CO})$] was determined from the visible absorption spectral change for various partial pressures of CO.

RESULTS AND DISCUSSION

The oxygen-binding properties of Fe(II)P having an intramolecular axial base and Fe(II)TpivPP with no covalently bound axial base were compared in toluene solutions. Fe(III)TpivPP and Fe(III)P were reduced in toluene by aqueous $\text{Na}_2\text{S}_2\text{O}_4$. When a large molar excess of the axial base [1,2-dimethylimidazole (1,2-Me₂Im)] was coexisting, the Fe(II)TpivPP formed a stable oxygen adduct, which was confirmed by the visible absorption spectrum ($\lambda_{\text{max}} = 421$ and 544 nm). On the other hand, Fe(II)P gave an oxygen adduct without adding 1,2-Me₂Im. The coordination of oxygen to the sixth coordination site of Fe(II)P was also confirmed from the visible absorption spectrum ($\lambda_{\text{max}} = 422$ and 549 nm). $P_{1/2}(\text{O}_2)$ of Fe(II)P in toluene was 38 Torr at 25 $^\circ\text{C}$. No difference in $P_{1/2}(\text{O}_2)$ between Fe(II)P and Fe(II)TpivPP was observed in the toluene solution. After carbonylation under a 20-fold molar excess of 1,2-Me₂Im in ethanol, the CO adduct of Fe(II)TpivPP was mixed with HSA, and then an oxygenated HSA–Fe(II)TpivPP complex was obtained by irradiating with visible light under an oxygen atmosphere. Nevertheless, the half-life of the oxygen adduct was only about 10 min at 37 $^\circ\text{C}$. The coordination of the histidine residues of HSA to protoheme and deuteroheme was reported by Casella et al. (1993). The histidine residues of HSA do not however allow axial coordination to Fe(II)P, since complexation with histidine residues and oxygen binding was not observed for a Fe(II)TpivPP/HSA system. This result might be due to the binding of Fe(II)P to HSA by the hydrophobic interaction between the polypeptide chain and *tert*-butyl groups of Fe(II)P so that no histidine residue of HSA can coordinate to the central iron of Fe(II)P. Furthermore, the excess imidazole would cause unfavorable problems by binding to the site of the oxygen coordination, binding to HSA, or being toxic through intravenous injection. On the other hand, because Fe(II)P possesses only the intramolecular imi-

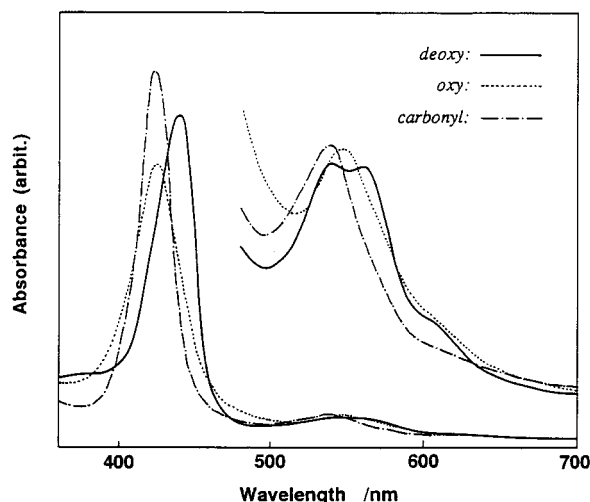


Figure 2. Visible absorption spectral change after O_2 and CO binding to HSA-Fe(II)P in an aqueous medium (pH 7.4 and 25 °C).

dazole, and carbonylation in the ethanol solution allows 100% coordination at the fifth coordinated site of Fe(II)P. Fe(II)P can be bound to HSA without changing the coordination structure.

Figure 2 shows the visible absorption spectra of HSA-Fe(II)P in aqueous solutions. When a reducing agent such as Asb was added to Fe(III)P bound to HSA under a N_2 atmosphere, only four-coordinated Fe(II)P ($\lambda_{max} = 438$ and 560 nm) was observed. In contrast, carbonylation was once carried out in an organic solution, the intramolecular coordination of the imidazole to the fifth coordinated site was confirmed. After the incorporation of Fe(II)P(CO) into HSA, five-coordinated deoxy-Fe(II)P ($\lambda_{max} = 439$, 542, 563, and 605 nm) was obtained by irradiating HSA-Fe(II)P(CO) with visible light under a N_2 atmosphere. The oxy state ($\lambda_{max} = 424$ and 548 nm) was confirmed after passing oxygen gas over the solution of the deoxy state. This conversion is reversible, and the degree of oxygenation corresponds to the oxygen partial pressure. The carbonyl state ($\lambda_{max} = 424$ and 540 nm) was also immediately generated upon exposure to carbon monoxide gas with either the deoxy or oxy state. The molar absorption coefficients (ϵ at λ_{max} of the Soret band) of HSA-Fe(II)P were $1.1 \times 10^5 \text{ M}^{-1} \text{ cm}^{-1}$ (deoxy state), $9.8 \times 10^4 \text{ M}^{-1} \text{ cm}^{-1}$ (oxy state), and $1.3 \times 10^5 \text{ M}^{-1} \text{ cm}^{-1}$ (carbonyl state).

The solution of HSA-Fe(II)P having four Fe(II)P molecules was prepared by mixing an Fe(II)P ethanol solution (0.15 mM) with a diluted HSA aqueous solution (18.8 μM). The evaporation of ethanol, the concentration by ultrafiltration, and the dialysis could be carried out with no degradation of HSA and Fe(II)P. HSA-Fe(II)P binding eight Fe(II)P molecules was also prepared when the concentration of Fe(II)P was reduced to half during the sample preparation.

The preparation procedure as described above has been improved in comparison with the former reported method (Komatsu et al., 1995) in the following points. (1) Asb and ethanol were used instead of $Na_2S_2O_4$ and DMSO. These chemicals are relatively harmless. (2) The ferric state of the iron-porphyrin derivative can be reduced to the ferrous state by the addition of 1 molar equiv of Asb in ethanol. (3) HSA-Fe(II)P(CO) can be stored as a freeze-dried powder under long-term storage (2 years), and the concentration can be adjusted by redissolving it in a given amount of pure water. There was no difference in the turbidity, the Fe(II)P incorporation ratio, and the filter permeability for the HSA-Fe(II)P solution before

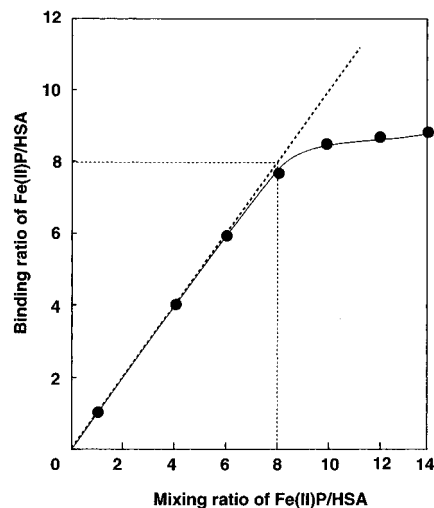


Figure 3. Relationship between mixing ratio and binding ratio of Fe(II)P/HSA.

Table 1. Comparison of Solution Properties at 37 °C

solutions	specific gravity	viscosity (cP at 230 s^{-1})
HSA-Fe(II)P	1.013–1.021	1.3
serum	1.027	1.3
human blood	1.055–1.063	4.4–5.0

and after redissolution of the freeze-dried powder. HSA-Fe(II)P(CO) could be stored at 4 °C for more than 1 month even in the solution state. The carbonyl state was easily converted to the oxy state by the irradiation of visible light under an oxygen atmosphere.

The quantitative analyses of the free Fe(II)P after the preparation of HSA-Fe(II)P disclosed an incorporation ratio of 100% for Fe(II)P/HSA = 1, 99% for 4, 94% for 8, but only 60% for 14 as shown in Figure 3. The concentration of HSA after sample preparation was 5.0 g/dL for Fe(II)P/HSA = 1, 5.1 g/dL for 4, and 4.9 g/dL for 8, indicating no loss of HSA during the sample preparation. Figure 3 indicates a possible binding ratio of Fe(II)P to one HSA molecule of about eight. Interestingly, the molar absorption coefficients of the Fe(II)P(CO) in HSA were constant ($\epsilon_{540nm} = 1.2 \times 10^4 \text{ M}^{-1} \text{ cm}^{-1}$ in phosphate-buffered saline at pH 7.4 and 25 °C) versus the Fe(II)P/HSA ratio (=1, 4, and 8).

The solution properties of HSA-Fe(II)P are summarized in Table 1. The specific gravity varies from 1.013 [Fe(II)P/HSA = 0] to 1.021 [Fe(II)P/HSA = 8]. The viscosity of HSA-Fe(II)P was the same as that of HSA (1.3 cP at a high shear rate of 230 s^{-1}), which was much lower than that of human blood (4.4–5.0 cP). There is no indication of aggregation even when eight Fe(II)P molecules are bound to one HSA, indicating its excellent dispersion stability with high oxygen transporting ability.

Figure 4 shows the spectral change of the Q-band for the HSA-Fe(II)P(O_2) incubated at 37 °C in air. The absorption maxima at 548 nm just before or after incubation of the oxygenated complex for up to 17 h gave Fe(II)P percentages of 0 or 100%, respectively. The half-life of the oxygen adduct ($\tau_{1/2}$) at 37 °C was about 1 h. This value was constant for HSA-Fe(II)P at different ratios (Table 2). A stable $\tau_{1/2}$ was obtained when an equimolar amount of Asb was added to Fe(II)P. The addition of superoxide dismutase and catalase did not improve the lifetime, indicating that there was no influence of active oxygen species generated from the oxidation of Fe(II)P(O_2) on the half-life. A significantly short $\tau_{1/2}$ was observed when an excess amount of Asb was added to the Fe(II)P for reduction to Fe(II)P, and the effect of superoxide dismutase and catalase confirmed at

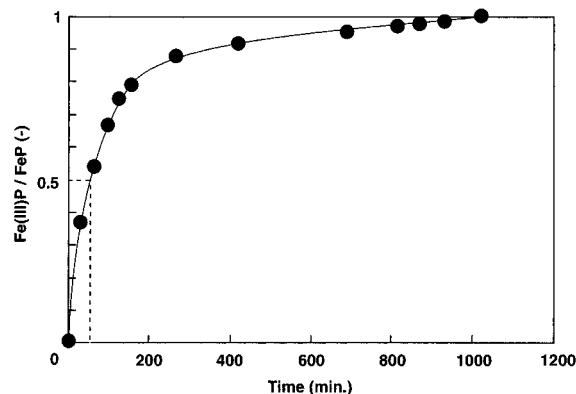


Figure 4. Oxidation of Fe(II)P(O₂) bound to HSA. Fe(II)P/HSA = 4 mol/mol. [HSA]: 5 wt %, under air, at pH 7.4 and 37 °C.

Table 2. $\tau_{1/2}$ of Oxygenized HSA–Fe(II)P Prepared in Various Conditions^a

samples	[HSA] (mM)	[Fe(II)P] (mM)	Fe(II)P/ HSA	O ₂ transport ^b (mL/L)	$\tau_{1/2}$ (min)
HSA–Fe(II)P	0.750	0.75	1/1	4.2	60
	0.025	0.10	4/1	0.6	63
	0.050	0.20	4/1	1.1	69
	0.125	0.50	4/1	2.8	65
	0.750	3.00	4/1	17.0	62
	0.750	6.00	8/1	34.0	59
blood	—	9.2 ^c	4/1 ^d	59	—

^a In phosphate-buffered saline at pH 7.4 and 37 °C. ^b O₂ transport = OTE (percent)/100 × [heme] (molar) × 22.4 L/mol × 310 K/273 K. ^c [heme]. ^d Heme/Hb.

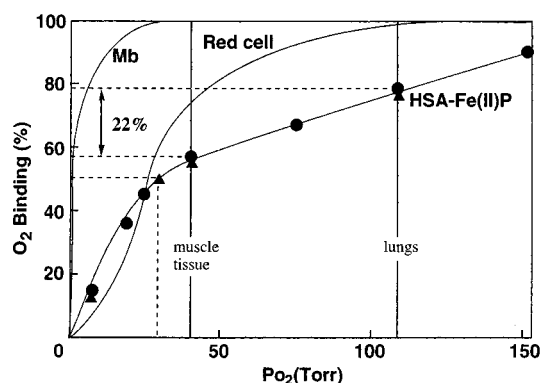


Figure 5. O₂ binding equilibrium curve of HSA–Fe(II)P (pH 7.4 and 37 °C): (●) Fe(II)P/HSA = 4 mol/mol, (▲) Fe(II)P/HSA = 8 mol/mol.

the time indicated the generation of active oxygen species from the autooxidation of Asb, and their oxidation of Fe(II)P to Fe(III)P.

Figure 5 shows the oxygen-binding and dissociation equilibrium curves of HSA–Fe(II)P [Fe(II)P/HSA = 4] obtained from its saturated spectrum at each oxygen partial pressure. From this figure, the oxygen affinity [$P_{1/2}(\text{O}_2)$] was estimated to be about 30 Torr, and it was expected that HSA–Fe(II)P would release 22% of the

bound oxygen, if it circulated between the lung ($P_{\text{O}_2} = 110$ Torr) and mixed venous ($P_{\text{O}_2} = 40$ Torr). The same results were obtained for HSA–Fe(II)P having eight Fe(II)P. The Hill coefficient was calculated to be 1.0 from the curve, and no allostericity was observed.

The half-lives ($\tau_{1/2}$) of the Fe(II)P(O₂) at 1, 4, 25, and 37 °C were 7 days, 5 days, 7 h, and 1 h, respectively. The activation energy was calculated as 89 kJ/mol. The $\tau_{1/2}$ was increased by raising the oxygen partial pressure (e.g., $\tau_{1/2}$ was 140 min at 37 °C in a pure oxygen atmosphere). This is the same profile as that of hemoglobin (Sakai et al., 1994). Deoxyhemoglobin, to which H₂O is weakly coordinated, reacts with oxygen more rapidly to form methemoglobin than does oxyhemoglobin (Brantley et al., 1993).

The O₂ and CO binding parameters are summarized in Table 3. The $P_{1/2}(\text{O}_2)$ of HSA–Fe(II)P in an aqueous solution is 8.0 Torr at 25 °C and 30 Torr at 37 °C. The $P_{1/2}(\text{O}_2)$ of Fe(II)P in toluene is 38 Torr at 25 °C. The low $P_{1/2}(\text{O}_2)$ of Fe(II)P in HSA means that the oxygen affinity is higher than that of Fe(II)P in the solution state. This might be due to the existence of polar amide groups of HSA around the oxygen coordination site of Fe(II)P (Springer et al., 1989). Furthermore, k_{on} and k_{off} are extremely high in comparison with those of red blood cells ($1.1 \times 10^4 \text{ M}^{-1} \text{ s}^{-1}$, 0.16 s^{-1}) and hemoglobin ($3.3 \times 10^7 \text{ M}^{-1} \text{ s}^{-1}$, 13 s^{-1}).

Because no difference in the $\tau_{1/2}$ of HSA–Fe(II)P with different binding ratios of Fe(II)P was observed, hydrophobicity should originate from the *tert*-butyl groups of Fe(II)P, not from the hydrophobic pocket of HSA. Therefore, we expect to improve the half-life of the oxygen adduct as an oxygen carrier by designing the molecular structure of the heme derivative to be more hydrophobic such as a double-sided porphyrin which has four alkyl chains on both sides of the porphyrin plane (Tsuchida et al., 1993).

We have been developing artificial red cells using totally synthetic heme derivatives (lipidheme) (Kobayashi & Tsuchida, 1995). The heme derivatives were amphiphiles and were incorporated into the hydrophobic region of the bilayer of phospholipid vesicles (LH-V) or onto the surface of a triglyceride microsphere (LH-M). The $P_{1/2}(\text{O}_2)$ values of these oxygen carriers at 37 °C were 43 and 38 Torr, respectively. These are higher than that of red blood cells (27 Torr). Their $\tau_{1/2}$ values at 37 °C were 24 and 12 h, respectively. In the case of Fe(II)P, it could not form a stable oxygen adduct in the phospholipid bilayer membrane because it does not have alkylphosphocholine groups which provide a high affinity with the phospholipid bilayer membrane and fix the iron–porphyrin at the hydrophobic center of the bilayer membrane. However, Fe(II)P can easily bind to HSA, and the advantages of HSA are considered to be its low toxicity and long circulation lifetime in comparison with the others.

The rate constants of oxygen binding (k_{on}) of LH-V and LH-M were 9.8×10^7 and $9.6 \times 10^7 \text{ M}^{-1} \text{ s}^{-1}$, respectively.

Table 3. O₂ and CO Binding Parameters of the HSA–Fe(II)P in an Aqueous Medium at 25 °C

samples	solutions	O ₂			CO		
		$P_{1/2}$ (Torr)	$10^{-7}k_{\text{on}}$ (M ⁻¹ s ⁻¹)	$10^{-3}k_{\text{off}}$ (s ⁻¹)	$10^2P_{1/2}$ (Torr)	$10^{-6}k_{\text{on}}$ (M ⁻¹ s ⁻¹)	10^2k_{off} (s ⁻¹)
HSA–Fe(II)P	pb ^d (pH 7.4)	8.0 (30) ^f	24	3.2	1.4	4.4	8
r-HSA–Fe(II)P ^a	pb ^d (pH 7.4)	11 (33) ^f	23	4.2	1.7	4.4	9
Fe(II)P ^b	toluene	38	16	46	0.6	2.9	17
Hb (R state) ^c	pb ^d (pH 7.0)	0.22 (0.82) ^f	3.3	0.013	0.14	4.6	0.9
red cell ^d	pb ^d (pH 7.4)	8.8 (27) ^f	0.0011	0.00016	57	0.014	1

^a r-HSA, recombinant HSA. ^b Measured by Tsuchida (1995). ^c Measured by Gibson (1970). ^d Measured by Tsuchida (1985). ^e pb, phosphate buffer. ^f $P_{1/2}$ values in parentheses were measured at 37 °C.

k_{on} and k_{off} are quite high relative to those of hemoglobin, indicating its fast oxygen binding and dissociation. This would be due to the easily accessible pathway to the central iron of lipidheme through four alkylphosphocholine groups rather than through the folded polypeptide main chain of hemoglobin. In the case of red blood cells, the kinetic parameters are apparent and very slow because of the small surface area for oxygen transport and low diffusion of the viscous and concentrated hemoglobin solution inside the cell. In the case of HSA-Fe(II)P, k_{on} is significantly high ($2.4 \times 10^8 \text{ M}^{-1} \text{ s}^{-1}$) compared with that of hemoglobin. There is no steric hindrance of the peptide chain around the oxygen binding sites like a heme pocket of hemoglobin, but the environment around them is kept hydrophobic.

The k_{off} of HSA-Fe(II)P is $3.2 \times 10^3 \text{ s}^{-1}$, which is about $1/3$ that of LH-V ($8.2 \times 10^3 \text{ s}^{-1}$) and LH-M ($1.0 \times 10^4 \text{ s}^{-1}$). This would be due to the vicinity of the oxygen binding site of Fe(II)P having a higher polarity than the hydrophobic region of LH-V and LH-M. This was supported by the result that Fe(II)P in toluene showed a k_{off} ($4.6 \times 10^4 \text{ s}^{-1}$) 10 times higher in comparison with that in HSA.

It is quite remarkable that eight Fe(II)P molecules can be bound to HSA. The hydrophobic interaction of the four *tert*-butyl groups of Fe(II)P with the hydrophobic region of the HSA surface enables the binding of Fe(II)P onto the surface. Because all Fe(II)P bound onto the surface would have the same chemical environment that comes from the hydrophobicity of the four *tert*-butyl groups, the molar absorption coefficient, the binding parameters of oxygen and carbon monoxide, and the half-life of the oxygen adduct do not depend on the binding ratio of Fe(II)P.

From the oxygen transporting efficiency (22%) in Figure 5, the transporting amount of oxygen was calculated as shown in Table 2. The concentration of HSA in an HSA-Fe(II)P solution was adjusted to that in blood (5 wt %; 0.75 mM) to control the colloidal osmotic pressure of the solution. When a 5 wt % HSA-Fe(II)P [Fe(II)P/HSA = 8] solution is prepared, it can transport 3.4 mL/dL of oxygen during the circulation between lung ($P_{\text{O}_2} = 110 \text{ Torr}$) and mixed venouses ($P_{\text{O}_2} = 40 \text{ Torr}$). This corresponds to about 60% of the oxygen transporting amount of human blood (5.9 mL/dL), because the heme concentration of the HSA-Fe(II)P solution is low (6.0 mM) in comparison with that (9.2 mM) of blood ([hemoglobin] = 15 g/dL). Furthermore, the value of OTE can be increased by using other heme derivatives having a lower $P_{1/2}(\text{O}_2)$ than that of Fe(II)P, and the transporting amount of oxygen can be improved by increasing the HSA concentration from 5 wt % for *in vivo* use.

Recently, recombinant HSA (r-HSA) has been manufactured by gene cloning and expression in *Saccharomyces cerevisiae* or *Escherichia coli*, etc. (Sumi et al., 1993). The same results were obtained using r-HSA-Fe(II)P as a totally synthetic oxygen carrier as shown in Table 3. Animal tests are now being undertaken by the authors.

ACKNOWLEDGMENT

This work was partially supported by Grants-in-Aid from the Ministry of Education, Science, and Culture, Japan (05403028 and 07508005) and a Waseda University Grant for Special Research Projects.

LITERATURE CITED

- Adams, P. A., and Berman, M. C. (1980) Kinetics and Mechanism of the Interaction between Human Serum Albumin and Monomeric Haemin. *Biochem. J.* 191, 95–102.
- Beaven, G. H., Chen, S.-H., D'Albis, A., and Gratzer, W. B. (1974) A Spectroscopic Study of the Haemin-Human-Serum-Albumin System. *Eur. J. Biochem.* 41, 539–546.
- Bonaventura, J., Brouwer, M., Brouwer, T., Cashion, B., and Cameron, S. (1994) presented in part at the 11th Congress ISABI, Boston, MA.
- Brantley, R. E., Jr., Smerdon, S. J., Wilkinson, A. J., Singleton, E. W., and Olson, J. S. (1993) The Mechanism of Autooxidation of Myoglobin. *J. Biol. Chem.* 268, 6995–7010.
- Casella, L., Gullotti, M., Poli, S., and Gioia, L. D. (1993) Haem-Protein Interactions. The Binding of Haem Complexes to Serum Albumin. *Gazz. Chim. Ital.* 123, 149–154.
- Collman, J. P., Gagne, R. R., Halbert, T. R., Marchon, J. C., and Reed, C. A. (1973) Reversible Oxygen Adduct Formation in Ferrous Complexes Derived from a Picket Fence Porphyrin. Model for Oxy-myoglobin. *J. Am. Chem. Soc.* 95, 7868–7870.
- Gibson, Q. H. (1970) The Reaction of Oxygen with Hemoglobin and the Kinetic Basis of the Effect of Salt on Binding of Oxygen. *J. Biol. Chem.* 245, 3285–3288.
- Hrkál, Z., and Klementova, S. (1984) Bilirubin and Haeme Binding to Human Serum Albumin Studied by Spectroscopy Methods. *J. Biochem.* 16 (7), 799–804.
- Kobayashi, K., and Tsuchida, E. (1995) Totally Synthetic Hemes: Their Characteristics and Oxygen-Carrying Capacity in Dogs. In *Artificial Red Cells* (E. Tsuchida, Ed.) pp 93–116, John Wiley and Sons, New York.
- Kodicek, M., Hrkál, Z., and Vodrazka, Z. (1983) Kinetics of Haem Binding to Human Albumin and Haemopexin: Non-specific Interactions of Haem with Proteins. *Int. J. Biol. Macromol.* 5, 194–198.
- Komatsu, T., Ando, K., Kawai, N., Nishide, H., and Tsuchida, E. (1995) O_2 -Transport Albumin: A New Hybrid-Haemoprotein Incorporating Tetraphenylporphyrinatoiron(II) Derivative. *Chem. Lett.*, 813–814.
- Lamola, A. A., Asher, I., Muller-Eberhard, U., and Poh-Fitzpatrick, M. (1981) Fluorimetric Study of Binding of Protoporphyrin to Haemopexin and Albumin. *Biochem. J.* 196, 693–698.
- Marden, M. C., Hazard, E. S., Leclerc, L., and Gibson, Q. H. (1989) Flash Photolysis of the Serum Albumin-Heme-CO Complex. *Biochemistry* 28, 4422–4426.
- Moehring, G. A., Chu, A. H., Kulansik, L., and Williams, T. J. (1983) Heterogeneity of Albumin As Detected by Its Interactions with Deuteroporphyrin IX. *Biochemistry* 22, 3381–3386.
- Morgan, W. T., Smith, A., and Koskelo, P. (1980) The Interaction of Human Serum Albumin and Hemopexin with Porphyrins. *Biochim. Biophys. Acta* 624, 271–285.
- Sakai, H., Takeoka, S., Seino, Y., and Tsuchida, E. (1994) Suppression of Methemoglobin Formation by Glutathione in a Concentrated Hemoglobin Solution and in a Hemoglobin-Vesicle. *Bull. Chem. Soc. Jpn.* 67, 1120–1125.
- Springer, B. A., Egeberg, K. D., and Sligar, S. G. (1989) Discrimination between Oxygen and Carbon Monoxide and Inhibition of Autooxidation by Myoglobin. *J. Biol. Chem.* 264, 3057–3060.
- Sumi, A., Ohtani, W., Kobayashi, K., Ohmura, T., Yokoyama, K., Nishida, M., and Suyama, T. (1993) Purification and Physicochemical Properties of Recombinant Human Serum Albumin. *Colloq. INSERM* 227, 293–298.
- Traylor, T. G., Tsuchiya, S., Campbell, D., Mitchell, M., Styne, D., and Koga, N. (1985) Anthracene Heme Cyclophanes: Steric Effect in CO , O_2 , and RNC Binding. *J. Am. Chem. Soc.* 107, 604–614.
- Tsuchida, E., Nishide, H., Yuasa, M., Hasegawa, E., Matsushita, Y., and Eshima, K. (1985) Phosphocholine-substituted 5,10,15,20-Tetraphenylporphyrinatoiron(II): Oxygen Carrier under Physiological Conditions. *J. Chem. Soc., Dalton Trans.*, 275–278.
- Tsuchida, E., Komatsu, T., Arai, K., and Nishide, H. (1993) Synthesis and Dioxygen-binding Properties of Double-sided Porphyrinatoiron(II) Complexes bearing Covalently Bound Axial Imidazole. *J. Chem. Soc., Dalton Trans.*, 2465–2469.
- Tsuchida, E., Komatsu, T., Kumamoto, S., Ando, K., and Nishide, H. (1995) Synthesis and O_2 -binding Properties of Tetraphenylporphyrinato-iron(II) Derivatives Bearing a Proximal Imidazole Covalently Bound at the β -pyrrolic Position. *J. Chem. Soc., Perkin Trans. 2*, 747–753.

Methemoglobin Formation in Hemoglobin Vesicles and Reduction by Encapsulated Thiols

Shinji Takeoka, Hiromi Sakai, Takehiro Kose, Yuichi Mano, Yuriko Seino, Hiroyuki Nishide, and Eishun Tsuchida^{*†}

Department of Polymer Chemistry, Advanced Research Institute for Science and Engineering, Waseda University, Tokyo 169, Japan. Received December 23, 1996[®]

The hemoglobin vesicle (HbV) is a red cell substitute encapsulating purified concentrated Hb in a phospholipid vesicle. In order to suppress metHb formation or autoxidation, for the long-term maintenance of the oxygen transporting capability, a series of thiols (cysteine, Cys; glutathione, GSH; homocysteine, Hcy; and acetylcysteine, Acy) were studied as reductants of metHb. Hcy and GSH showed a good suppressive effect on metHb formation, while Cys adversely accelerates the metHb formation at a rate twice that of the Hb solution without any reductants and Acy showed no change. The significant suppression by the coaddition of superoxide dismutase (SOD) and catalase to Cys indicated that Cys was easily oxidized by oxygen and simultaneously generates a large amount of active oxygens. The effective suppression of metHb formation by SOD and catalase was not observed for HbV containing no reductants, indicating that the generation of active oxygens from Hb itself is not significant. The coencapsulation of Hcy with Hb resulted in a low rate of metHb formation in HbV (initial rate, 1%/h) *in vitro* at an oxygen partial pressure (P_{O_2}) of 142 Torr. The rate increased with decreasing P_{O_2} , showed a maximum (2.2%/h) around $P_{O_2} = 23$ Torr, and then decreased to 0%/h at 0 Torr. From these results, it is suggested that the fast metHb formation rate in the blood circulation of Wistar rats injected with 20 vol % of the HbV solution would be mainly caused by the exposure of HbV to the low P_{O_2} .

INTRODUCTION

The hemoglobin vesicle (HbV)¹ or liposome-encapsulated hemoglobin (LEH), which have the cellular structure of a phospholipid vesicle encapsulating a concentrated Hb solution, is expected as one candidate for red cell substitutes for transfusion (Djordjeovich & Miller, 1980; Hunt et al., 1985; Rudolph, 1995; Tsuchida & Takeoka, 1995). HbV with excellent physicochemical properties was prepared (Sakai et al., 1996; Takeoka et al., 1996), and a 90% blood exchange transfusion was carried out with the HbV using rats (Izumi et al., 1997; Sakai et al., 1997). On the other hand, acellular Hb solutions such as chemically modified Hb or recombinant Hb are now under clinical trials (Winslow, 1995); however, some side effects were reported such as vasoconstriction causing transient hypertension, which were considered to be induced by the trapping of nitric oxide generated from endothelial cells by acellular Hb (Vandegriff & Winslow, 1995; Tsai et al., 1996; Olsen et al., 1996). They will be solved by encapsulating Hb with a membrane.

The common issue of Hb-based red cell substitutes is the relatively rapid metHb formation during blood circulation (Yang & Olsen, 1989; Stratton et al., 1988) due to the absence of metHb reduction systems originally present in a red blood cell. The systems include NADH–

cytochrome b_5 , NADPH–flavin, direct reduction by glutathione (GSH) and ascorbic acid, and scavengers for active oxygens such as superoxide dismutase (SOD) for O_2^- and catalase for H_2O_2 . Hb in a ferrous state is autoxidized to the ferric state (metHb) and loses its oxygen binding ability. It is well-known that HbO_2 dissociates into metHb and O_2^- (Brunori et al., 1975; Tomoda et al., 1981; Wallace et al., 1982; Shikama, 1984; Watkins et al., 1985); however, the percentage of metHb in RBC is maintained at less than 0.5% of the total Hb by the systematic reduction.

Preservation of the native enzyme activities in RBC is one method of reducing the metHb formation in HbV (Ogata et al., 1995); however, their activity would change with the conditions of outdated red blood cells and the amounts of remaining substances, and virus inactivation using heat treatment is impossible in this case. Moreover, the mechanism of metHb reduction is complicated and influenced by many unknown factors. In the case of modified Hb solutions, direct conjugation with catalase and superoxide dismutase to suppress the metHb formation was reported by Quebec and Chang (1995); however, diminution of active oxygens is not sufficient to maintain the low metHb content. Especially in our case, these chemicals and enzymes are denatured and completely removed during the purification of Hb from RBC (Sakai et al., 1993) and the preparation of HbV; the construction of a metHb reduction system by coencapsulation of an appropriate amount of reductants is required.

There are many reductants which can reduce the metHb to deoxyHb under anaerobic conditions. However, a few of them can suppress the metHb formation of Hb vesicles; nevertheless, some enhance the metHb formation. It is because under aerobic conditions there is no metHb to be reduced in the Hb vesicle at the beginning, and encapsulated reductants are autoxidized generally faster than the rate of metHb formation. Furthermore, active oxygens generated from the autoxidation of the

^{*} To whom all correspondence should be addressed. Fax: +813-5286-3120. Phone: +813-3205-4740.

[†] CREST investigator, JST.

[®] Abstract published in *Advance ACS Abstracts*, July 1, 1997.

¹ Abbreviations: Hb, hemoglobin; HbV, hemoglobin vesicles; RBC, red blood cell; metHb, methemoglobin; HbCO, carbonyl-hemoglobin; DPPC, 1,2-dipalmitoyl-*sn*-glycero-3-phosphatidylcholine; DPPG, 1,2-dipalmitoyl-*sn*-glycero-3-phosphatidylglycerol; PBS, phosphate-buffered saline; P_{O_2} , oxygen partial pressure; Cys, L-cysteine; Hcy, DL-homocysteine; GSH, glutathione; Acy, N-acetyl-L-cysteine.

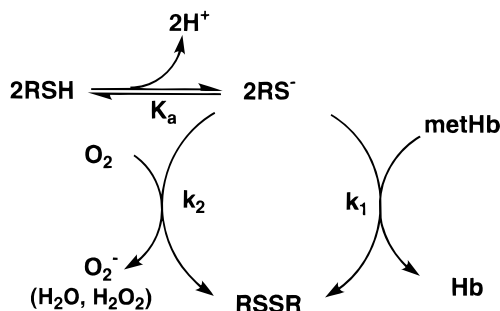


Figure 1. Estimated elemental reactions in the mixture of Hb and thiols.

reductant oxidize the Hb to metHb (Sampath & Caugey, 1985; Eyer et al., 1975). Therefore, a relatively high stability under aerobic condition is desired for reductants. Farivre et al. (1994) reported the coinjection of reductants such as ascorbic acid and methylene blue with modified Hb solutions; however, such small molecules are rapidly excreted from the kidney. Glutathione (GSH), a kind of thiol compound, is a representative reductant for reducing metHb nonenzymatically (12 mM in a red blood cell). We found that GSH had the effective activity to suppress the metHb formation in the Hb vesicle (Sakai et al., 1994).

In this paper, the encapsulation effect of a series of thiols, including GSH, on the reduction of metHb was studied from the view point of their structures and the elemental reactions in terms of active oxygens and oxygen partial pressures. The metHb formation of HbV during blood circulation was also studied to confirm the effectiveness of the selected reductant for the suppression of metHb formation in HbV *in vivo*.

EXPERIMENTAL PROCEDURES

Purification of Hemoglobin from Outdated Red Blood Cells. Hemoglobin was simply isolated from outdated red blood cells (Hokkaido Red Cross Blood Center) using our original processes (Sakai et al., 1993): (1) stabilization of Hb using carbonylation, (2) solvent treatment for hemolysis and removal of stromata, (3) removal of residual solvent with active carbon, (4) heat treatment (60 °C for 10 h), (5) dialysis to remove the small molecules, and (6) ultrafiltration (cutoff MW of 30 000). The profile of the obtained HbCO solution is as follows: [Hb], 40 g/dL; [metHb], <1%; protein purity, 99.95%; residual phospholipids, <0.2%; and residual organic solvent, <0.1 ppm.

Rate Constants of Elemental Reactions of Thiols. Thiols used are L-cysteine (Cys, Kanto Chemical Co.), glutathione (GSH, Kanto Chemical Co.), DL-homocysteine (Hcy, Aldrich), and N-acetyl-L-cysteine (Acy, Merck Co.), which are different in the dissociation degrees of the thiol group. The elemental reactions in the mixture of Hb and thiols are estimated as shown in Figure 1. The apparent rate constants of metHb reduction by thiols (k_1^{app}) were measured by an absorbance increase at 430 nm in the Soret band (deoxyHb) during the incubation of the metHb solution (10 μ M) with each thiol compound (20–60 mM) at 37 °C and pH 7.0 in 50 mM HEPES buffer. The apparent rate constants for thiol oxidation by oxygen (k_2^{app}) during incubation of the thiol solution (15 mM) at an oxygen partial pressure (P_{O_2}) of 713 Torr at 37 °C and pH 7.0 in 50 mM HEPES buffer were calculated from the decrease in the amount of SH group quantitatively measured using an N-ethylmaleimide method (Morell et al., 1964).

Suppression of MetHb Formation in Hb Solutions Using Thiols. To the Hb solutions (10 g/dL, pH 7.0)

containing pyridoxal 5'-phosphate (PLP, 4.7 mM, Merck Co.) as an allosteric effector of oxygen affinity of Hb were added 10 mM thiols, and then they were incubated at a P_{O_2} of 142 Torr and 37 °C. The metHb content was periodically measured using a standard cyanomethemoglobin method (Van Assendelft, 1970).

Preparation of Hb Vesicles (HbV). HbV were prepared in the same manner as previously reported (Sakai et al., 1996). The encapsulated HbCO (ca. 38 g/dL) contained PLP (18 mM, Merck Co.) and a reductant (5 mM). Catalase (from bovine liver, Merck, 10^5 units/mL) and/or superoxide dismutase (SOD, from bovine RBC, Wako Chemical Co., 10^3 units/mL) were added to the HbCO as scavengers for active oxygens. The lipid bilayer was composed of Presome PPG-I [a mixture of 1,2-dipalmitoyl-*sn*-glycero-3-phosphatidylcholine (DPPC), cholesterol, 1,2-dipalmitoyl-*sn*-glycero-3-phosphatidylglycerol (DPPG) (Nippon Fine Chem Co.), and α -tocopherol (Merck Co.) at a molar composition of 5/5/1/0.1]. The HbCO solution and the lipids were mixed and stirred for 36 h at 4 °C. After sizing with an extrusion method (4 °C; final pore size of membrane filters, 0.2 μ m) and the removal of unencapsulated Hb using ultracentrifugation (50 000g, 40 min), the resulting HbV was diluted with phosphate-buffered saline (PBS) at an Hb concentration of 0.5 g/dL, and HbCO was converted to oxyhemoglobin by illumination with visible light under an O_2 atmosphere (Chung et al., 1995). Finally, the Hb concentration of the HbV suspension was adjusted to 10 g/dL.

MetHb Content in HbV *in Vitro* and *in Vivo*. As for the *in vitro* measurements, the HbV suspensions were incubated at pH 7.4 and 37 °C at a constant P_{O_2} . The P_{O_2} was varied from 142 to 0 Torr. About 5 μ L of the sample was periodically pipetted out and added in a UV cuvette with 3 mL of PBS. The deoxygenation of the sample using N_2 bubbling resulted in the presence of only deoxyHb and metHb. The percentage of metHb was calculated from the calibration curve: the ratio of absorbance at 405 nm (metHb) and 430 nm (deoxyHb) in the Soret band without HbV destruction and the mixing ratio of deoxyHbV and metHbV (Hamada et al., 1995).

For the *in vivo* measurements, about 20 vol % HbV of the estimated total blood of Wistar rats [$n = 5$; body weight of 360 ± 13 g (mean \pm SD); total blood of ca. 58 mL/kg] was intravenously overdosed into the cervical vena cava, or 90% of the estimated total blood was exchanged with HbV at 2 mL withdrawal (via the common carotid artery)/2 mL infusion (via the right atrium) cycles at a rate of 2 mL/min after anesthesia (Izumi et al., 1997; Sakai et al., 1997). Venous blood was periodically withdrawn with a heparinized syringe and then transferred into a glass capillary for a hematocrit measurement. The centrifugation of the capillary at 10 000g produced separated layers of RBC and HbV. The HbV layer was collected and dispersed in PBS in a UV cuvette. The measurement of the metHb percentage was obtained in the same manner as already mentioned.

RESULTS AND DISCUSSION

MetHb Reduction by Thiols. The metHb reduction by thiols proceeds as a pseudo-first-order reaction in a nitrogen atmosphere as shown in Figure 2. Table 1 lists the reduction rate constants of the thiols. Hcy showed a high rate constant almost the same as that of Cys, whereas GSH and Acy showed ca. $1/10$ of that of Cys. Therefore, the order is Cys > Hcy > GSH > Acy. The thiol group dissociates to a thiolate anion, and one electron transfers from it to metHb, resulting in the production of deoxyHb and disulfide. On the other hand, the apparent rate constants of thiol oxidation by oxygen

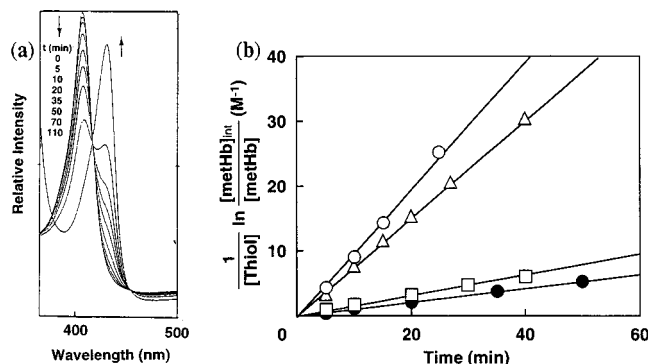


Figure 2. (a) Representative visible spectral change of metHb after the addition of thiol (Acy, 63 mM) under anaerobic conditions $[\text{metHb}] = 8 \mu\text{M}$ in HEPES buffer (50 mM, pH 7.0). (b) Kinetic analysis of metHb reduction rates $[\text{metHb}] = 10 \mu\text{M}$, $[\text{thiols}] = 20\text{--}60 \text{ mM}$ in HEPES buffer (50 mM, pH 7.0): (○) Cys, (△) Hcy, (□) GSH, (●) Acy, and $[\text{metHb}]_{\text{int}}$ initial concentration of metHb.

(k_2^{app}) were measured using an *N*-ethylmaleimide method and are also listed in Table 1. Cys showed the highest value, and the order is $\text{Cys} \gg \text{Hcy} > \text{Acy} > \text{GSH}$. It is generally expected that the thiol with the higher dissociation degree leads to the higher reactivity. However, it is difficult to obtain the dissociation constant of the thiol group, because pH titration is also accompanied by the deprotonation of the ammonium group. The obtained equilibrium constant contains both the proton dissociation of the thiol group and the deprotonation of the ammonium group.

The partial charge of hydrogen in an SH group of the thiols was calculated because the higher value indicates the higher tendency of the proton dissociation. First, the structures of Cys, Hcy, GSH, and Acy were optimized on the basis of molecular force field calculations using the MM2 parameter. The molecular orbital was calculated by a semiempirical method using the PM3 parameter, and then the partial charge was calculated. This calculation was performed using CAChe Mechanics (version 3.8) and MOPAC 94 (version 3.8) (Sony Tektronix Co.). Figure 3 shows the rate of metHb reduction (k_1^{app}) and the rate of thiol autooxidation (k_2^{app}) plotted versus the calculated partial charge. In this figure, the partial charge of Acy was very low (-0.005) and could not be depicted. The order of the partial charge is $\text{Cys} > \text{Hcy} > \text{GSH} \gg \text{Acy}$. Interestingly, the effect of the partial charge is more significant for thiol autooxidation than for metHb reduction. Since the order of the dissociation constant from the literature is $\text{Cys} > \text{GSH} > \text{Hcy} > \text{Acy}$ (Friedman et al., 1965), the order of the rate constants for metHb reduction and the thiol oxidation agrees well with the order of the dissociation constants except for GSH. From the view point of molecular structure, it is supposed that the dissociation of the thiol group of Cys is promoted by the existence of the ammonium group which shields the electrostatic repulsion between the thiolate anion and carboxylate anion, while the thiol dissociation of Acy is quite low because such an amino group is acetylated. In the case of Hcy, the shielding effect of the ammonium group is lower than that of Cys. GSH shows the slower rate of metHb reduction in spite of its dissociation rate being higher than that of Hcy. The thiolate anion of GSH would be stabilized by the neighboring electrophilic carbonyl group, and reactions with both metHb and oxygen would be restricted.

Figure 4 shows the time courses of metHb formation in 40 g/dL Hb solutions in the presence of thiols. The addition of Cys (10.0 mM) to the Hb solution (6.2 mM) promoted metHb formation and showed an initial rate

of metHb formation 6 times higher in comparison with that of the Hb solution without Cys. Acy does not show the ability to reduce metHb. Both GSH and Hcy showed the effective suppression of metHb formation for the Hb solution without reductants (Table 1). Considering the balance of the Cys contribution toward metHb reduction and autooxidation by oxygen, it is postulated from Figure 4 that the generation of active oxygens such as O_2^- and H_2O_2 during the autooxidation of Cys would adversely convert Hb to metHb because the autooxidation rate is high (Misra, 1974). This has been confirmed by the addition of superoxide dismutase (SOD) and catalase with Cys, after which the rate of metHb formation dramatically decreased from 7.5 to 0.9 $\text{M}^{-1} \text{min}^{-1}$ (Table 1). This addition effect is due to the quenching of the active oxygens such as O_2^- and H_2O_2 generated from Cys. On the other hand, Hcy and GSH showed the effective suppression of metHb formation because their low rates of autooxidation exceed the low rate of metHb reduction. The fact that the rate of metHb formation slightly decreased from 0.7 to 0.6 $\text{M}^{-1} \text{min}^{-1}$ even in the presence of SOD and catalase was supported. GSH showed a suppressive effect of metHb formation lower than that of Hcy; however, the effect was maintained for a longer time than that of Hcy because GSH is less reactive. The above-mentioned results suggest that it is important to consider both the metHb reduction and the autooxidation of the reductants. Because the metHb concentration to be reduced by reductants is small at the initial stage, most of the reductants should be autooxidized accordingly. A suitable reductant should possess a small rate of autooxidation but a high efficiency of metHb reduction. This can be expressed from $k_2^{\text{app}}/k_1^{\text{app}}$, and its order is $\text{Acy} > \text{Cys} > \text{GSH} > \text{Hcy}$ (Table 1). From the above results, we selected Hcy as a reductant in HbV to effectively suppress metHb formation.

In order to determine the appropriate concentration of Hcy in the inner Hb solution of HbV, the rate of metHb formation was studied for Hb solutions with various Hcy concentrations. The results are shown in Figure 5. The rate of metHb formation decreases with increasing Hcy concentration and then shows a minimum at around 5–10 mM. In the high Hcy concentration region, the active oxygens generated by the autooxidation of Hcy should accelerate metHb formation, and this effect exceeds the effect of metHb reduction. Therefore, an Hb solution containing 5 mM Hcy was used for encapsulation. However, in the presence of SOD and catalase, the decrease in the metHb percentage was observed for the higher concentration of Hcy because the active oxygens from the autooxidation of Hcy would be diminished by SOD and catalase. In this case, over 10 mM Hcy is effective, and the rate of metHb formation was 0.1%/h at 37 °C. There is no significant difference between the SOD- and catalase-coadded system and the catalase-added one, indicating that Hcy does not generate O_2^- but H_2O_2 .

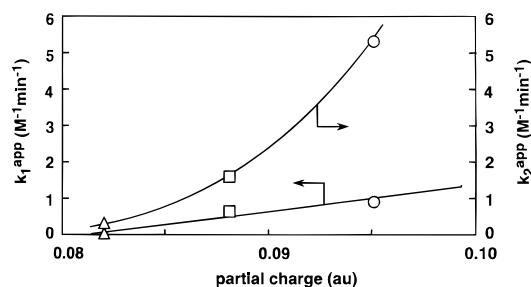
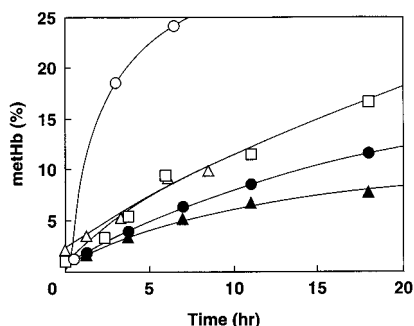
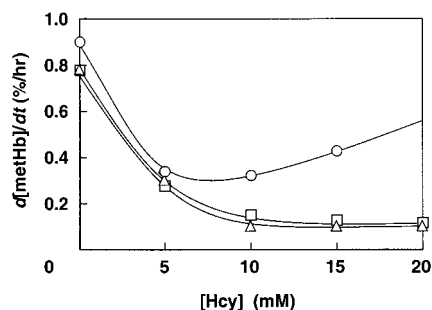
Effect of Hcy and Catalase on the MetHb Formation in HbV *in Vitro*. The metHb formation in HbV containing 5 mM Hcy was studied *in vitro* at a P_{O_2} of 143 Torr and 37 °C, and the metHb content was 23% after 24 h (Figure 6, ◇). This rate was 60% of the rate in the case of HbV without Hcy (35% after 24 h). As for the modified Hb solutions, chemical modification sometimes decreases the stabilization of Hb against oxidation; e.g., polymerized Hb shows 80% metHb after 24 h (Quebec & Chang, 1995). The advantage of HbV is coencapsulation

Table 1. Dissociation Constants (pK_a) and Rate Constants of Elemental Reactions of Thiols and Their Influence on the Rate of MetHb Formation^a

thiol	$pK_a^{b,c}$	metHb reduction k_1^{app} ($M^{-1} min^{-1}$)	thiol oxidation k_2^{app} ($M^{-1} min^{-1}$)	k_2^{app}/k_1^{app}	$\frac{d[metHb]}{dt_{t=0}}$ ($M min^{-1}$)	$\frac{d[metHb]}{dt_{t=0}}$ ($M min^{-1}$)
L-cysteine (Cys)	8.15	1.0	5.4	5.4	7.5	0.9
glutathione (GSH)	8.56	0.15	0.37	2.5	0.9	—
homocysteine (Hcy)	8.70	0.78	1.7	2.2	0.7	0.6
N-acetylcysteine (Acy)	9.52	0.11	0.73	6.6	1.3	—
control	—	—	—	—	1.2	—

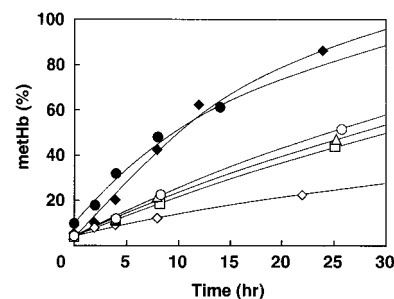
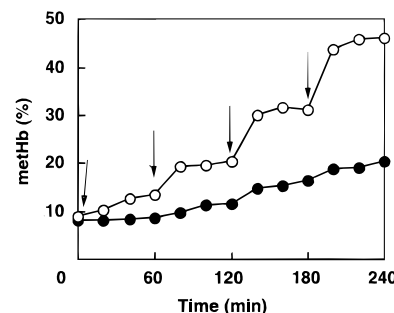
^a [Hb] = 6.2 mM. [thiol] = 10 mM. [PLP] = 18.6 mM in HEPES buffer (50 mM, pH 7.0). P_{O_2} = 142 Torr at 37 °C.

^b $NH_3^+-R-COO^- \rightleftharpoons NH_3^+-R-COO^-$. ^c Friedman et al. (1965). ^d With SOD/catalase.

**Figure 3.** Relationship between the hydrogen partial charge of the mercapto group and the rate constants of metHb reduction (k_1^{app}) and thiol oxidation (k_2^{app}): (Δ) glutathione (GSH), (\square) DL-homocysteine (Hcy), and (\circ) L-cysteine (Cys).**Figure 4.** Time course of the metHb percentage in an Hb solution. [Hb] = 6.2 mM, [thiols] = 10 mM, and [PLP] = 18.6 mM, in HEPES buffer (50 mM, pH 7.0) with P_{O_2} = 142 Torr: (\circ) Cys, (Δ) Hcy, (\bullet) GSH, (\square) Acy, and (\square) without thiols.**Figure 5.** Influence of the concentration of Hcy on the rate of metHb formation in Hb solution ([Hb] = 5.1 mM, [PLP] = 15.3 mM, pH 7.4, P_{O_2} = 142 Torr, and 37 °C): (\circ) without catalase, (\square) with catalase, and (Δ) with SOD/catalase.

of various reagents without the chemical modification of Hb. It was also confirmed by study *in vivo* (20% overdose). The rate of metHb of HbV containing 5 mM Hcy was 50% after 24 h, which is 60% lower than that of HbV without Hcy *in vivo* (83% after 24 h). Therefore, the coencapsulation of Hcy is expected to show high efficiency.

When H_2O_2 was progressively added to the HbV suspension, the metHb percentage increased in response to the addition (Figure 7). H_2O_2 easily diffuses through

**Figure 6.** Time course of the metHb percentage of HbV *in vitro* (\diamond) at P_{O_2} = 142 Torr and 37 °C and *in vivo* after 90 vol % exchange transfusion or 20 vol % overdose into anesthetized Wistar rats ([Hcy] = 5 mM, [SOD] = 10^3 units/mL, and [catalase] = 10^5 units/mL): 20 vol % overdose with (\bullet) HbV without Hcy, (\circ) HbV with Hcy, (Δ) HbV with Hcy and catalase, and (\square) HbV with Hcy and SOD/catalase, and 90 vol % exchange transfusion (\bullet).**Figure 7.** Time course of the metHb percentage of HbV after the stepwise addition of H_2O_2 ([Hb] = 0.78 mM, [catalase] = 10^5 units/mL, and 3.1 mM of H_2O_2 was added after 0, 60, 120, and 180 min).

the bilayer membrane and generates hydroxyl radicals by a Fenton reaction in the presence of a trace amount of free iron inside the HbV (Gutteridge, 1986). They convert Hb to metHb. However, the addition of H_2O_2 to the Hb solution purified by dialysis does not induce the metHb formation because of the absence of free iron or heme. This indicates that, even though the highly purified Hb solution was used for HbV preparation, a small amount of free iron or heme would be released from Hb during the preparation of HbV by extrusion. On the other hand, HbV coencapsulated with catalase did not show such a response to H_2O_2 addition and maintained a low metHb content (Figure 7), indicating that catalase in HbV diminishes not only H_2O_2 generated from Hcy oxidation but also H_2O_2 invading from the outer phase through the bilayer membranes.

Effect of Hcy and Oxygen Partial Pressure on the MetHb Formation of HbV *in Vivo*. After the intravenous injection of HbV into rats at a 20 vol % overdose, the rate of metHb formation was about twice as high in comparison with that measured under physiological conditions *in vitro* at a P_{O_2} of 142 Torr (Figure 6).

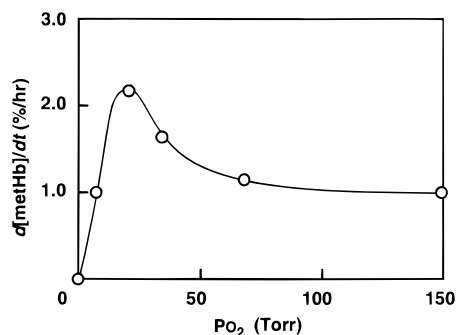


Figure 8. P_{O_2} dependence of the initial rate of metHb formation in HbV ([Hb] = 0.78 mM and pH 7.4).

Furthermore, at a 90% exchange transfusion, the rate was four times as high. Though the coencapsulation of active oxygen scavengers such as SOD and catalase is thought to suppress metHb formation, the coencapsulation had a little effect on metHb suppression *in vivo*. This indicates that the main reason of the difference in the data between *in vitro* and *in vivo* would be due to the ratio of deoxyHb which is oxidized more easily than oxyHb if the appropriate reductant like Hcy is used in the appropriate amount, and the injection amount is 20 vol %. This can be supported by the fact that the addition of H_2O_2 did not accelerate metHb formation as shown in Figure 7.

The influence of P_{O_2} on the rate of metHb formation in HbV was studied and is shown in Figure 8. The rate increases with decreasing P_{O_2} . After showing a maximum at a P_{O_2} of 23 Torr, the rate decreases to zero at a P_{O_2} of 0 Torr. It was reported that deoxyHb, to which H_2O was weakly coordinated, reacted with oxygen to form metHb more rapidly than did HbO_2 (Brantley et al., 1993). When P_{O_2} is higher than 100 Torr, the rate of metHb formation is constant because the degree of oxygen saturation is ca. 100%. The increase in the rate of metHb formation at a P_{O_2} lower than 100 Torr is due to the increase in the amount of the more reactive deoxyHb. The subsequent decrease is due to the lower oxygen concentration which reacts with deoxyHb. The rate at the maximum was almost the same as that *in vivo* as shown in Figure 6. During blood circulation, HbV is continuously exposed to different P_{O_2} s. Usually, P_{O_2} in arterial blood and mixed venous blood is estimated to be 100 and 40 Torr, respectively. That in tissue capillaries is estimated to be 25–30 Torr. Therefore, the reason to accelerate the metHb formation of HbV *in vivo* would be due to the increased ratio of deoxyHb at a lower P_{O_2} . There have been some papers which report the P_{O_2} dependence on the rate of metHb formation in Hb solutions (Levy et al., 1988; Mansouri & Winterhalter, 1973). Of course, active oxygens, including nitric oxide, would cause metHb formation under more severe conditions such as a 90% exchange transfusion or hemorrhagic shock. In this case, coencapsulation of SOD and/or catalase would be effective.

From these results, it is apparent that the generation of active oxygens from Hb autoxidation is low when the purity of Hb is high. Because the active oxygens are generated from the autoxidation of reductants, reductants should be selected for a low autoxidation rate. In this sense, Hcy should be the best reductant for HbV. The autoxidation of Hcy *in vivo* should be slower than that in air because of the low oxygen partial pressure *in vivo*. Therefore, the higher rate of metHb formation during blood circulation was effectively suppressed by the addition of Hcy.

ACKNOWLEDGMENT

This work was supported in part by Grants-in-Aid from the Ministry of Education, Science, and Culture, Japan (07508005 and 08680940), the Ogasawara Foundation for the Promotion of Science and Engineering, and the Kawakami Memorial Foundation. The authors thank Drs. Y. Izumi, A. Yoshizu, and K. Kobayashi (Department of Medicine, Keio University) for their experimental cooperation in animal tests and discussions.

LITERATURE CITED

- Brantley, R. E., Smerdon, S. J., Wilkinson, A. J., Singleton, E. W., and Olson, J. S. (1993) The Mechanism of Autoxidation of Myoglobin. *J. Biol. Chem.* 268, 6995–7010.
- Brunori, M., Falcioni, G., Giardina, B., and Rotilio, G. (1975) Formation of Superoxide in the Autoxidation of the Isolated α and β Chains of Human Hemoglobin and Its Involvement in Hemichrome Precipitation. *Eur. J. Biochem.* 53, 99–104.
- Chung, J. E., Hamada, K., Sakai, H., Takeoka, S., and Tsuchida, E. (1995) Ligand Exchange Reaction of Carboxylhemoglobin to Oxyhemoglobin in a Hemoglobin Liquid Membrane. *Nihonkagaku kaishi* 2, 123–127.
- Djordjević, L., and Miller, I. F. (1980) Synthetic Erythrocytes from Lipid Encapsulated Hemoglobin. *Exp. Hematol. (Charlottesville, Va.)* 8, 584–592.
- Eyer, P., Hertle, H., Kiese, M., and Klein, G. (1975) Kinetics of Ferrihemoglobin Formation by some Reducing Agents, and the Role of Hydrogen Peroxide. *Mol. Pharmacol.* 11, 326–334.
- Faivre, B., Menu, P., Labrude, P., Grandgeorge, M., and Vigneron, C. (1994) Methemoglobin Formation after Administration of Hemoglobin Conjugated to Carboxylate Dextran in Guinea Pigs. Attempts to Prevent the Oxidation of Hemoglobin. *Artif. Cells, Blood Substitutes, Immobilization Biotechnol.* 22, 551–558.
- Friedman, M., Cavins, J. F., and Wall, J. S. (1965) Relative Nucleophilic Reactivities of Amino Groups and Mercaptide Ions in Addition Reactions with α,β -Unsaturated compounds. *J. Am. Chem. Soc.* 87, 3672–3682.
- Gutteridge, J. M. C. (1986) Iron Promoters of the Fenton Reaction and Lipid Peroxidation can be Released from Hemoglobin by Peroxides. *FEBS Lett.* 201, 291–295.
- Hamada, K., Kose, T., Ohgushi, T., Sakai, H., Takeoka, S., Nishide, H., and Tsuchida, E. (1995) Assay Systems for the Components of Red Cell Substitutes (NRC). *Artif. Blood* 3, 96–101.
- Hunt, C. A., Burnette, R. R., MacGregor, R. D., Strubbe, A. E., Lau, D. T., Taylor, N., and Kawada, H. (1985) Synthesis and Evaluation of a Prototypal Artificial Red Cell. *Science* 230, 1165–1168.
- Izumi, Y., Sakai, H., Hamada, K., Takeoka, S., Yamahata, K., Katoh, H., Nishide, H., Tsuchida, E., and Kobayashi, K. (1996) Physiological Responses to Exchange Transfusion with Hemoglobin Vesicles as an Artificial Oxygen Carrier in Anesthetized Rats: Changes in Mean Arterial Pressure and Renal Cortical Tissue Oxygen Tension. *Crit. Care Med.* 24, 1869–1873.
- Izumi, Y., Sakai, H., Takeoka, S., Kose, T., Hamada, K., Yoshizu, A., Nishide, H., Tsuchida, E., and Kobayashi, K. (1997) Evaluation of the Capabilities of Hemoglobin Vesicles as Artificial Oxygen Carriers in a Rat Exchange Transfusion Model. *ASAIO J.* 43 (in press).
- Levy, A., Zhang, L., and Rifkin, J. M. (1988) Hemoglobin: A Source of Superoxide Radical under Hypoxic Conditions. *Oxygen Radicals Mol. Biol. Pathol., Proc. Upjohn-UCLA Symp.*, 11–25.
- Mansouri, A., and Winterhalter, H. (1973) Nonequivalence of Chains in Hemoglobin Oxidation. *Biochemistry* 12, 4946–4949.
- Misra, H. P. (1974) Generation of Superoxide Free Radicals during the Autoxidation of Thiols. *J. Biol. Chem.* 249, 2151–2155.
- Morell, S. A., Ayers, V. E., Grenwalt, T. J., and Hoffman, P. (1964) Thiols of the Erythrocyte. *J. Biol. Chem.* 239, 2696–2705.

- Ogata, Y., Okamoto, T., Suzuki, K., and Kamitani, T. (1994) The Development of Neo Red Cells (NRC) with Enzymatic Reduction System of the Methemoglobin. *Artif. Blood* 2, 62–66.
- Olsen, S. B., Tang, D. B., Jackson, M. R., Gomez, E. R., Ayala, B., and Alving, B. M. (1996) Enhancement of Platelet Deposition by Cross-linked Hemoglobin in a Rat Carotid Endarterectomy Model. *Circulation* 93, 327–332.
- Quebec, E. A., and Chang, T. M. S. (1995) Superoxide Dismutase and Catalase Cross-linked to Polyhemoglobin Reduces Methemoglobin Formation *in vitro*. *Artif. Cells, Blood Substitutes, Immobilization Biotechnol.* 23, 693–705.
- Rudolph, A. S. (1995) Encapsulation of Hemoglobin in Liposomes. In *Blood Substitutes: Physiological Basis of Efficacy* (R. M. Winslow, K. D. Vandegriff, and M. Intaglietta, Eds.) pp 90–104, Birkhauser, Boston.
- Sakai, H., Takeoka, S., Yokohama, H., Seino, Y., Nishide, H., and Tsuchida, E. (1993) Purification of Concentrated Hemoglobin Using Organic Solvent and Heat Treatment. *Protein Expression Purif.* 4, 563–569.
- Sakai, H., Takeoka, S., Seino, Y., and Tsuchida, E. (1994) Suppression of Methemoglobin Formation by Glutathione in a Concentrated Hemoglobin Solution and in a Hemoglobin Vesicle. *Bull. Chem. Soc. Jpn.* 67, 1120–1125.
- Sakai, H., Hamada, K., Takeoka, S., Nishide, H., and Tsuchida, E. (1996) Physical Characteristics of Hemoglobin Vesicles as Red Cell Substitutes. *Biotechnol. Prog.* 12, 119–125.
- Sakai, H., Takeoka, S., Park, S. I., Kose, T., Hamada, K., Izumi, Y., Yoshizu, A., Nishide, H., Kobayashi, K., and Tsuchida, E. (1997) Surface Modification of Hemoglobin Vesicles with Poly(ethylene glycol) and Effects on Aggregation, Viscosity, and Blood Flow during 90% Exchange Transfusion in Anesthetized Rats. *Bioconjugate Chem.* 8, 23–30.
- Sampath, V., and Caughey W. S. (1985) Prooxidant Effects of Glutathione in Aerobic Hemoglobin Solutions. Superoxide Generation from Uncoordinated Dioxygen. *J. Am. Chem. Soc.* 107, 4076–4078.
- Shikama, K. (1984) A Controversy on the Mechanism of Autoxidation of Oxy myoglobin and Oxyhemoglobin: Oxidation, Dissociation, or Displacement? *Biochem. J.* 223, 279–280.
- Stratton, L. P., Rudolph, A. S., Knoll, W. K., Jr., Bayne, S., and Farmer, M. C. (1988) The Reduction of Methemoglobin Levels by Antioxidants. *Hemoglobin* 12, 358–368.
- Takeoka, S., Ohgushi, T., Ohmori, T., Terase, K., Nishide, H., and Tsuchida, E. (1996) Layer Controlled Hemoglobin Vesicles by Interaction of Hemoglobin with Phospholipid Assembly. *Langmuir* 12, 1775–1779.
- Tomoda, A., Yoneyama, T., and Tsuji, A. (1981) Changes in Intermediate Haemoglobins during Autoxidation of Haemoglobin. *Biochem. J.* 195, 485–492.
- Tsai, A. G., Kerger, H., and Intaglietta, M. (1996) Microvascular Oxygen Distribution: Effects due to Free Hemoglobin in Plasma. In *Blood Substitutes: New Challenges* (R. M. Winslow, K. D. Vandegriff, and M. Intaglietta, Eds.) pp 124–131, Birkhauser, Boston.
- Tsuchida, E., and Takeoka, S. (1995) Stabilized Hemoglobin Vesicles. In *Artificial Red Cells* (E. Tsuchida, Ed.) pp 35–64, John Wiley and Sons, New York.
- Van Assendelft, O. W. (1970) *Spectrophotometry of Haemoglobin Derivatives*, pp 128–129, Royal Vangorcun Ltd., Assen, The Netherlands.
- Vandegriff, K. D., and Winslow, R. M. (1995) The Theoretical Analysis of Oxygen Transport: A New Strategy for the Design of Hemoglobin-based Red Cell Substitutes. In *Blood Substitutes: Physiological Basis of Efficacy* (R. M. Winslow, K. D. Vandegriff, and M. Intaglietta, Eds.) pp 143–154, Birkhauser, Boston.
- Wallace, W. J., Houtchens, R. A., Maxwell, J. C., and Caughey, W. S. (1982) Mechanism of Autoxidation for Hemoglobins and Myoglobins. *J. Biol. Chem.* 257, 4966–4977.
- Watkins, J. A., Kawanishi, S., and Caughey, W. S. (1985) Autoxidation Reactions of Hemoglobin A Free from Other Red Cell Components: A Minimal Mechanism. *Biochem. Biophys. Res. Commun.* 132, 742–748.
- Winslow, R. M. (1995) Blood Substitutes: A Moving Target. *Nature Med.* 1, 1212–1215.
- Yang, T., and Olsen, K. W. (1989) The Effect of Crosslinking by Bis(3,5-dibromosalicyl) Fumarate on the Autoxidation of Hemoglobin. *Biochem. Biophys. Res. Commun.* 163, 733–738.

BC970091Y

Basic Studies on Heterobifunctional Biotin–PEG Conjugates with a 3-(4-Pyridyldithio)propionyl Marker on the Second Terminus

Karl Kaiser, Markus Marek, Thomas Haselgrübler, Hansgeorg Schindler, and Hermann J. Gruber*

Institute of Biophysics, J. Kepler University, Altenberger Strasse 69, A-4040 Linz, Austria. Received February 14, 1997[⊗]

Heterobifunctional poly(ethylene glycol) (PEG) derivatives with a biotin terminus have been synthesized and characterized with respect to avidin binding. Unambiguous measurement of biotinyl and pyridyldithiopropionyl end groups was established by selecting suitable assays and introducing necessary modifications. Functional studies on the binding of biotin–PEG conjugates to avidin tetramers revealed much similarity to known biotin–spacer–peptide conjugates with 7–27 atom spacers: dissociation kinetics of the initially formed 4:1 complexes were multiexponential, the complex with 2 ligands per avidin dissociating rather slowly with half-times of ~2 days at 25 °C. The observed stability of 3:1 and 2:1 complexes with avidin is particularly significant since it allows exploitation of the additional advantages of PEG spacers, i.e. reduced steric strain in biotin–avidin–biotin bridges, reduced nonspecific adsorption of biotinylated probes and markers, and, especially, uncomparable fluorescence intensities of biotin–PEG–fluorophore conjugates as is demonstrated in the accompanying study (second of three papers in this issue).

INTRODUCTION

Avidin–biotin technology is an indispensable tool in modern bioscience (Wilchek and Bayer, 1990a). In most bioanalytical applications a probe molecule (antibody, hormone, etc.) is connected to a marker molecule (fluorophore, marker enzyme, nanogold, etc.) by a biotin–avidin–biotin (B–A–B)¹ bridge or a B–A bridge, and analogous configurations occur in biochemical and biotechnological applications (Wilchek and Bayer, 1990b). In any case, biotin residues must be covalently linked to markers and/or probes. Such biotin derivatives, however, regularly showed greatly reduced affinities for avidin/streptavidin, due to steric hindrance (Finn et al., 1980; Lavielle et al., 1983; Romovacek et al., 1983), yet high affinity and metastability of avidin–biotin interaction could be restored when 7–27 atom spacers were introduced between biotin and peptid hormones (Finn et al., 1984; Finn and Hofmann, 1985) or fluorophores (Chu et al., 1994; Schray et al., 1988).

Besides local strain of the avidin–biotin interaction, two other types of steric hindrance are to be expected in B–A–B and in B–A bridges between probes and markers: First, the four biotin binding sites on avidin/

streptavidin are organized in two pairs on opposite sides of the receptor protein (Green et al., 1971), and steric repulsion between adjacent biotinylated probes/markers allows the exploitation of only one site per pair in practice (Green, 1990). Second, the recognition site of a biotinylated probe molecule (e.g. an antibody) will frequently be impaired upon B–A–B or B–A bridge formation, especially when using large markers. Such long-range steric hindrances will not be relieved by 7–27 atom spacers, and longer spacer chains are desirable.

PEG spacers appear as ideal candidates to further optimize avidin–biotin technology: (i) Any chain length can be chosen for the long-range separation of probe, avidin/streptavidin, and marker. (ii) The well-known flexibility of the PEG chains will further reduce steric interaction of all interconnected elements. (iii) As an additional benefit, PEG chains will not increase but decrease nonspecific binding of attached markers (e.g. fluorophores), due to their antiadsorptive behavior (Lim and Herron, 1992).

The crucial criterion for the usefulness of biotin–PEG conjugates was the unknown magnitude of PEG–PEG repulsion in complexes of avidin with four, three, or two biotin–PEG conjugates. To solve this question, we have synthesized heterobifunctional biotin–PEG conjugates with a reliable chromogenic marker and tested for stoichiometry and stability of avidin binding. The results demonstrated the potential of heterobifunctional biotin–PEG conjugates.

EXPERIMENTAL PROCEDURES²

Materials. P.a. grade materials were used as far as commercially available. Affinity-purified avidin was prepared as described (Fudem-Goldin and Orr, 1990) or obtained from Sigma (A-9271). Biotin, Boc₂O, DACA, 2,2'-dithiodipyridine, 3-mercaptopropionic acid, NHS, and 2-thiopyridone were obtained from Sigma. Biotin–NHS was prepared as described (Wilchek and Bayer, 1990c). 4,4'-Dithiodipyridine and 4-thiopyridone were obtained

* Author to whom correspondence should be addressed [telephone +43 (732) 2468-9271; fax +43 (732) 2468-822; e-mail hermann.gruber@jk.uni-linz.ac.at].

[⊗] Abstract published in *Advance ACS Abstracts*, June 15, 1997.

¹ Abbreviations: ANS, 2-anilinonaphthalene-6-sulfonic acid; B–A bridge, biotin–avidin bridge; B–A–B bridge, biotin–avidin–biotin bridge; biotin, biotinoyl group; biotin–NHS, succinimidyl ester of biotin; Boc₂O, di-*tert*-butyl pyrocarbonate; Boc-, *tert*-butoxycarbonyl group; DACA, *p*-(dimethylamino)-cinnamaldehyde; DMF, *N,N*-dimethylformamide; DTSP, 3,3'-dithio(succinimidyl)propionate; DTT, 1,4-dithiothreitol; EDTA, ethylenediamine-*N,N,N,N*-tetraacetic acid; Et₃N, *N,N,N*-triethylamine; 2-ME, 2-mercaptoethanol; NH₂-PEG₈₀₀-NH₂, *O,O*-bis(2-aminopropyl)poly(ethylene glycol) 800; NH₂-PEG₁₉₀₀-NH₂, *O,O*-bis(2-aminopropyl)poly(ethylene glycol) 1900; NHS, *N*-hydroxysuccinimide; PDP, 3-(4-pyridyldithio)propionyl group; PDP-OH, 3-(4-pyridyldithio)propionic acid; PEG, poly(ethylene glycol); RT, room temperature; SPDP, *N*-succinimidyl 3-(2-pyridyldithio)propionate; THF, tetrahydrofuran.

² Detailed procedures, NMR data, and a systematic comparison of different biotin end group assays can be found in the Supporting Information.

from Aldrich. 2,2'-Dithiodipyridine, DMF, DTSP, DTT, Et₃N, 2-ME, NH₂-PEG₈₀₀-NH₂, and NH₂-PEG₁₉₀₀-NH₂ were purchased from Fluka. NaCl, methanol, and 2-propanol were obtained from Riedel de Haen. Acetic acid and chloroform were purchased from Baker. ANS was obtained from Molecular Probes. Sephadex-based gels were obtained from Pharmacia. All other materials were purchased from Merck. Absolute DMF was prepared according to a standard procedure.

Buffers. Buffer A contained 100 mM NaCl, 50 mM NaH₂PO₄, and 1 mM EDTA, adjusted to pH 7.5 with NaOH. Buffer B contained 100 mM NaCl and 20 mM sodium acetate, adjusted to pH 4.5 with HCl. Buffer C contained 0.4 M Na₂HPO₄, adjusted to pH 11 with NaOH. Buffer D contained 0.2 M boric acid, adjusted to pH 9.0 with NaOH. Buffer E contained 0.6 M NaH₂PO₄, adjusted to pH 6.0 with NaOH. Polybuffer contained 20 mM citric acid and 20 mM NaH₂PO₄, adjusted to the desired pH by addition of HCl or NaOH, as required.

Synthesis of CH₃COOH·NH₂-PEG₈₀₀-NH-Boc. Boc₂O (55 mmol in 50 mL of methanol) was slowly added to NH₂-PEG₈₀₀-NH₂ (55 mmol in 150 mL of methanol) and stirred overnight. After addition of acetic acid (3 mL) and toluene, the solvent was removed (60 g of crude product). Three grams of crude product was purified by silica chromatography in chloroform/methanol/acetic acid (90:10:0.1 and 70:30:5), yielding 1.25 g (1.17 mmol) of product, pure by TLC.

Synthesis of HCl·NH₂-PEG₁₉₀₀-NH-Boc. The procedure was the same as for the PEG₈₀₀ homologue except that ion exchange chromatography was used because of too much peak tailing on the silica column. Fifty grams (25 mmol) of NH₂-PEG₁₉₀₀-NH₂ was reacted with 5.5 g (25 mmol) of Boc₂O, resulting in 53 g of crude product. Three grams of the crude product was purified by ion exchange chromatography on SP Sephadex C-25 (sodium form, using distilled water for loading and washing and eluting with 20 mM NaCl). After volume reduction and saturation with NaCl, the product was extracted into chloroform, evaporated, redissolved with a minimal amount of methylene chloride, and precipitated with peroxide-free diethyl ether. Yield = 0.82 g (0.38 mmol), pure by TLC.

Synthesis of Biotin-NH-PEG₈₀₀-NH-Boc. Boc-NH-PEG₈₀₀-NH₂·CH₃COOH (0.90 g, 0.83 mmol) was reacted with 0.39 g of biotin-NHS (0.39 g, 1.14 mmol) in absolute DMF/Et₃N for 24 h at RT. Unreacted biotin-NHS was hydrolyzed with water. After evaporation, the residue was dissolved in 10 mL of 200 mM Na₂CO₃ and filtered through paper. The filtrate was saturated with NaCl, extracted with methylene chloride, and dried at 1–10 Pa for 1 h. Yield = 637 mg (0.51 mmol), pure by TLC.

Synthesis of Biotin-NH-PEG₁₉₀₀-NH-Boc. The procedure was the same as for the PEG₈₀₀ homologue: 1.9 g of Boc-NH-PEG₁₉₀₀-NH₂·HCl (0.90 mmol) was reacted with 0.46 g of biotin-NHS (1.41 mmol) and 0.22 mL of Et₃N. Yield = 1.92 g (0.82 mmol), pure by TLC.

Synthesis of Biotin-NH-PEG₈₀₀-NH₂·HCl. Biotin-NH-PEG₈₀₀-NH-Boc (528 mg, 0.42 mmol) was deprotected in 98% formic acid (4 h at RT). After solvent removal, the crude product was purified on SP Sephadex C-25 and isolated in a similar way as HCl·NH₂-PEG₁₉₀₀-NH-Boc (see above). Yield = 389 mg (330 μmol), pure by TLC.

Synthesis of Biotin-NH-PEG₁₉₀₀-NH₂·HCl. The procedure was the same as for the PEG₈₀₀ homologue: 1.5 g of biotin-NH-PEG₁₉₀₀-NH-Boc (0.64 mmol) was deprotected, yielding 1.18 g of crude product. Five hundred milligrams of crude product was purified on SP Sephadex C-25, yielding 407 mg (178 μmol) of product, pure by TLC.

Synthesis of Biotin-PEG₈₀₀-PDP. Biotin-NH-PEG₈₀₀-NH₂·HCl (93 mg, 78 μmol) was reacted with 80 mg of DTSP (200 μmol) in 10 mL of peroxide-free THF plus 50 μL of Et₃N under Ar. After overnight stirring, the solvent was removed. The residue was dissolved in buffer A (5 mL) and reduced with excess DTT (62 mg, 400 μmol) under Ar. After 15 min, the pH was lowered to 4.5 with 0.5 M acetic acid and pure biotin-NH-PEG₈₀₀-NHCOCH₂CH₂SH was isolated by gel filtration on Sephadex G-25 in buffer B under Ar.

For synthesis of the final product, 4,4'-dithiodipyridine (35 mg, 160 μmol) was dissolved in 3.4 mL of 120 mM HCl and the column fractions containing biotin-NH-PEG₈₀₀-NHCOCH₂CH₂SH were added under Ar. Then the pH was raised to 4.4 by addition of buffer C (~0.4 mL). After 15 min of Ar bubbling at RT, the solution was lyophilized, redissolved in water (8 mL), and filtered through paper, and pure biotin-PEG₈₀₀-PDP was isolated by gel filtration on Sephadex in distilled water. Yield = 19 μmol according to biotin end group titration, 99% pure by TLC.

Synthesis of Biotin-PEG₁₉₀₀-PDP. Synthetic steps, procedures, and precautions were the same as for the corresponding PEG₈₀₀ derivative (see above): 224 mg of biotin-NH-PEG₁₉₀₀-NH₂·HCl (98 μmol), 112 mg of DTSP (280 μmol), and 125 μL of Et₃N were reacted in 8 mL of peroxide-free THF. The resulting disulfide product was reduced with 430 mg of DTT (2.8 mmol). After acidification with acetic acid and chromatography on Sephadex G-25 M, the void peak (20 mL) containing biotin-NH-PEG₁₉₀₀-NHCOCH₂CH₂SH was added to a solution of 220 mg of 4,4'-dithiodipyridine in 2 mL of distilled water plus 220 μL of HCl concentrate. The pH was raised to 4.5 by addition of buffer C under constant bubbling with Ar. After 15 min, the mixture was lyophilized, redissolved in water, and filtered, and the filtrate was subjected to gel filtration in water as above, yielding 39 μmol of biotin-PEG₁₉₀₀-PDP in the void peak, 99% pure by TLC.

Synthesis of 3-(4-Pyridyldithio)propionic Acid. 3-Mercaptopropionic acid (4.25 mmol; dissolved in 20 mL of methanol plus 1 mL of acetic acid) was slowly added to a solution of 4.36 mmol of 4,4'-dithiodipyridine in methanol/water/acetic acid (10 mL:10 mL:2 mL) at -10 °C, whereupon highly pure product precipitated. The crystals were successively washed with methanol/water/acetic acid, with THF, and with ethyl acetate. Drying gave 2.72 mmol of PDP-OH, pure by TLC (in chloroform/methanol/acetic acid, 70:30:0.1). The original motivation had been the synthesis of succinimidyl 3-(4-pyridyldithio)propionate, in analogy to the commercially available cross-linker SPDP. Unfortunately, the formation of succinimidyl ester was always accompanied by rapid decomposition of the 4-pyridyldithio group, the main reason being the poor solubility of the free carboxylic acid under the conditions of any known method of succinimidyl ester formation. In the present study the pure crystalline PDP-OH served as an ideal standard for the determination of ε₃₂₄ of 4-thiopyridone, which is released upon addition of a slight excess of a mercaptan such as 2-ME (4.5 < pH < 6.5).

Quantitative Assay for 3-(4-Pyridyldithio)propionyl Groups. PDP groups were determined by quantitative release of 4-thiopyridone upon reduction with 2-ME. Typically, 300 μL of sample (containing <40 μM PDP groups in water or buffer A) was mixed with 1.2 mL of buffer E, and 25 μL of 2-ME reagent was added from an Eppendorf Multipette. Absorbance was read at 324 nm against a reagent blank. The 2-ME reagent contained 0.5 M 2-ME (3.50 mL per 50 mL) and 5 mM acetic acid

(14.3 μL per 50 mL) in distilled water. It could be stored at 4 °C at ambient atmosphere for several weeks without losing activity or producing increasing background absorbance at 324 nm, in contrast to DTT. Moreover, reaction kinetics with DTT are not as instantaneous as with 2-ME and a gas mask is required when using DTT (but not 2-ME) for this type of assay to prevent severe irritation (noticed by all personnel after several hours of exposure). PDP terminus concentrations were calculated from A_{324} by assuming a molar extinction coefficient of 24 000 $\text{M}^{-1} \text{cm}^{-1}$, as argued under Results.

Quantitative Assay for Biotin End Groups. A published fluorescence assay for avidin-biotin interaction (Mock and Horowitz, 1990) was modified. Typically, 2 mL of buffer A containing 2 μM affinity-purified avidin was mixed with 25 μL of 5 mM ANS in DMSO, and fluorescence was monitored at 328 nm excitation (slit = 10 nm) and 408 nm emission (slit = 10 nm). Refined protocols can be found in the Supporting Information.

Quantitative Assay for Empty Biotin Binding Sites in Avidin Partially Occupied with Biotin-PEG-PDP. Solutions with partially saturated avidin were obtained from gel filtrations in the course of binding studies (see below) and usually contained <1 μM unoccupied receptor sites. Two milliliters of such a solution was mixed with 25 μL of 5 mM ANS, and ANS fluorescence was monitored during titration with 5–10 μL aliquots of exactly 40 μM *d*-biotin standard as described above.

Gel Filtration Assay for Binding of Biotin-PEG-PDP to Avidin. To test for metastable binding of biotin-PEG-PDP to avidin, 0.5 mL samples of buffer A containing 50 μM "functional" avidin (as determined by titration with *d*-biotin while monitoring ANS fluorescence, see above) and various amounts of biotin-PEG-PDP were incubated for 1 h at 25 °C and subjected to gel filtration on a 1 \times 48 cm column of Sephadex G-100 at RT. Samples were loaded rather quantitatively by rinsing the loading reservoir with another 200 μL of buffer A. Elution was at 0.25 mL/min with buffer A; fractions were collected at 5 min intervals. All fractions were assayed for PDP group concentrations as described above. From the resulting PDP profile the "avidin peak" and the "free PEG peak" could be identified to pool corresponding fractions (see Figure 3).

Total avidin in the peak was determined from A_{282} using the known absorbance of 1.54 at 1 mg/mL of avidin and the molecular mass 67 000 g/mol (Green, 1990) and correcting for the functional purity of 98–99% as determined by the ANS fluorescence method (which always confirmed batch specifications by Sigma). It was also demonstrated that gel filtration did not change the functional purity of avidin in control runs without ligand. Empty receptor sites on partially occupied avidin were assayed as described above.

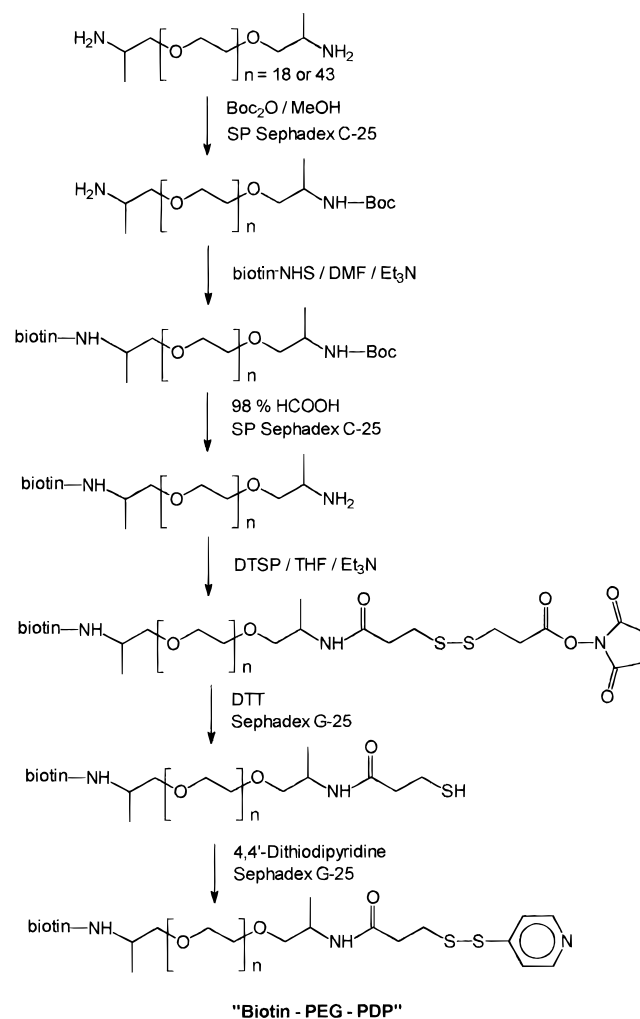
PDP group concentrations in the "avidin peak" and in the "PEG peak" were determined as described above. Biotin terminus concentrations in the PEG peak were determined according to the "mixed ANS titration method" described above.

All assays on pooled peaks were done in triplicate. Free *d*-biotin, free PDP-OH, or free 4-thiopyridone was never observed at the elution volume typical for small volumes, in spite of routine checks.

RESULTS² AND DISCUSSION

Synthetic Route to Biotin-PEG-PDP. The starting materials $\text{NH}_2\text{-PEG}_{800}\text{-NH}_2$ and $\text{NH}_2\text{-PEG}_{1900}\text{-NH}_2$ contained sizable fractions with one or no primary amino group, as judged from TLC in chloroform/methanol/acetic

Scheme 1. Synthesis of Biotin-PEG₈₀₀-PDP and Biotin-PEG₁₉₀₀-PDP



acid and from chromatography on SP Sephadex C-25 with salt gradient elution. The sequence of steps in Scheme 1 was devised to get rid of these impurities and to arrive at maximum purity of biotin-PEG-PDP. The mono-Boc derivative collected from the first SP Sephadex C-25 column was still contaminated with monoamine impurities from the starting materials, and these amines were also biotinylated in the following step. However, after deprotection of biotin-NH-PEG-NH-Boc only the correct product biotin-NH-PEG-NH₂·HCl was retained on SP Sephadex C-25.

Having arrived at pure heterobifunctional biotin-NH-PEG-NH₂·HCl, it was essential to prevent deterioration of end group purity because further product isolations on Sephadex G-25 only selected for PEG derivatives as opposed to small molecules but not for PEGs with different end groups. It was, therefore, necessary (i) to provide for quantitative end group conversion in every subsequent step and (ii) to prevent NH₂ or SH oxidation by rigorous application of Ar atmosphere, especially for the switch to basic reaction conditions. Consequently, it was possible to synthesize biotin-PEG₈₀₀-PDP and biotin-PEG₁₉₀₀-PDP with exactly 1 biotin residue on each chain and with 96% or 89%, respectively, of the expected PDP group contents. Such heterobifunctional purity favorably compares with the 15% PDP group content of CH₃-O-PEG-NH-PDP recently synthesized according to a different procedure (Woghiren et al., 1993).

The overall yields of biotin-PEG-PDP could certainly be optimized if larger amounts of such products are

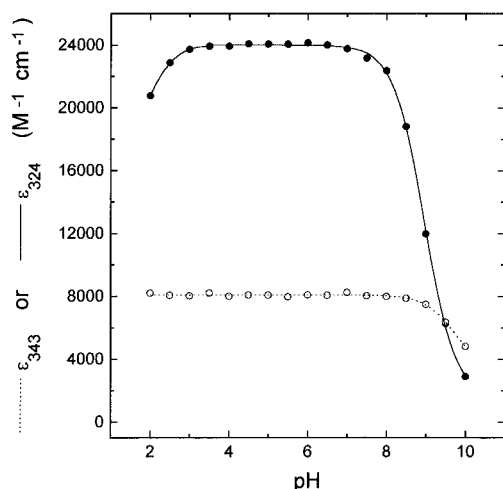


Figure 1. pH dependence of molar extinction coefficients of 4- and 2-thiopyridone. To 2 mL of polybuffer with the indicated pH value was added 50 μ L of 2 mM 4-thiopyridone or 2-thiopyridone (in water), and A_{324} or A_{343} , respectively, were read against a water reference. Background absorbance of relevant reagent blanks was subtracted.

desired. The main losses occurred during the two filtration steps (after reaction with DTSP and after lyophilization/redissolution in the final step) in which product was probably occluded in the precipitates formed by excess of reagents and/or byproducts. However, the primary goal of the present study was successfully reached, i.e. to arrive at biotin-PEG-PDP with sufficient purity for the functional experiments reported below.

Use of 3-(4-Pyridyldithio)propionyl as a Marker for Biotin-PEG Elements. PDP groups are well-known and widely used for specific coupling to free SH groups (Carlsson et al., 1978; Woghiren et al., 1993). Of course, it is implied that biotin-PEG-PDP should be useful to attach biotin-PEG elements to biomolecules with SH groups. For the purpose of this study, however, the PDP group was strictly viewed as a stoichiometric marker for biotin-PEG conjugates. The special advantage of the PDP group lies in the fact that the chromophoric marker is not the PDP group itself but free 4-thiopyridone, which is released from the PDP group after thiol addition (Grassetti and Murray, 1967), thereby eliminating any unpredictable influence of the PEG chain upon the UV-vis absorbance of a covalently attached chromophore. Such an influence has indeed been observed in subsequent studies with some biotin-PEG-dye conjugates (see the second of three papers in this issue). While the need for PDP cleavage required much pipetting (e.g. to measure the PDP profiles in Figure 3), the payoff was the unambiguous quantitation of biotin-PEG conjugates, whether bound to avidin or not.

The 4-pyridyldithio group was far more attractive than the 2-pyridyldithio function because of its much higher UV absorbance after cleavage (Grassetti and Murray, 1967). Unfortunately, conflicting values have been given in the literature for the molar extinction coefficients of 4- and 2-thiopyridone (Carlsson et al., 1978; Grassetti and Murray, 1967; Jou et al., 1983; Leserman et al., 1984). Figure 1 shows a re-examination, as well as the pH dependence of, the UV absorbance of 4- and 2-thiopyridone.

For 4-thiopyridone, $\epsilon_{324} = 24\,000\text{ M}^{-1}\text{ cm}^{-1}$ was obtained in the plateau region ($3.5 \leq \text{pH} \leq 6.5$). In parallel, 25 300 and 22 500 $\text{M}^{-1}\text{ cm}^{-1}$ were measured for 4-thiopyridone released from known concentrations of 4,4'-dithiodipyridine and from newly synthesized PDP-OH, respectively. Thus, the values from all available stan-

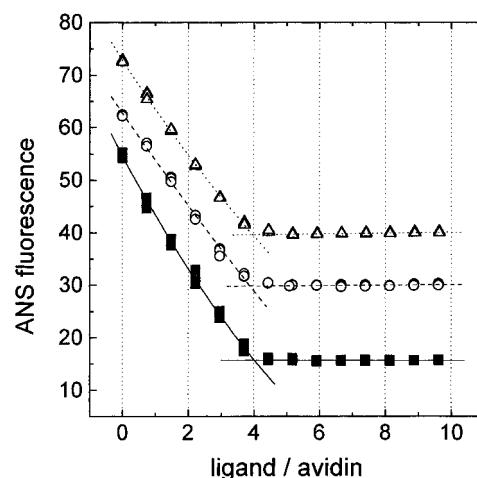


Figure 2. Demonstration of 4:1 stoichiometries in saturated complexes of biotin-PEG conjugates with avidin. Avidin with 99% functional purity was titrated with known solutions of *d*-biotin (■), biotin-NH-PEG₁₉₀₀-NH₂·HCl (○), or biotin-PEG₁₉₀₀-PDP (△). The latter two curves were displaced by +10 and +20 fluorescence units, respectively, to improve legibility of the plot.

dards closely agreed, and the average value $\epsilon_{324} = 24\,000\text{ M}^{-1}\text{ cm}^{-1}$ was chosen for determination of PDP concentrations.

The UV absorbance of 2-thiopyridone was re-examined by DTT-induced cleavage of 2,2'-dithiodipyridine preparations from Fluka and Sigma and of crystalline 3-(2-pyridyldithio)propionic acid synthesized in the course of a preceding study (Haselgrübler et al., 1995). Obtained values for ϵ_{343} were 8040, 8050, and 8150 $\text{M}^{-1}\text{ cm}^{-1}$, respectively. The pH profile was measured with 2-thiopyridone from Sigma, which initially gave 8600 $\text{M}^{-1}\text{ cm}^{-1}$ in the plateau region ($\text{pH} \leq 7.5$) when 100% purity was assumed. The plateau in Figure 1 was set to 8080 $\text{M}^{-1}\text{ cm}^{-1}$ to compensate for impurities and to comply with the best possible estimate.

Figure 1 shows that the less common 4-isomer of the PDP group is a 3-fold better chromogenic marker than the 2-isomer, but knowledge of pH dependence is even more critical because absorbance becomes pH-dependent at $\text{pH} \geq 6.5$, rather than at $\text{pH} \geq 7.5$, respectively. Fortunately, cleavage of the 4-isomer by DTT or 2-ME under typical assay conditions is rapid or instantaneous, respectively, even at pH 6.0 (data not shown).

Quantitative Determination of Biotin End Group Content. As shown below, the functional characterization of biotin-PEG-PDP required accurate determination of the PDP marker functions, as well as of the biotin termini. In a systematic investigation² the ANS assay (Mock and Horowitz, 1990) was found to yield unambiguous results if complete titrations were performed, as shown in Figure 2. In the absence of a biotin derivative (= ligand) the pseudoligand ANS weakly binds to all four functional biotin binding sites on avidin, resulting in high ANS fluorescence. Successive addition of *d*-biotin (solid squares, calibration), biotin-PEG₁₉₀₀-PDP (open circles), or biotin-NH-PEG₁₉₀₀-NH₂·HCl (open triangles) results in displacement of weakly bound ANS, with concomitant loss of ANS fluorescence. The breakpoint unequivocally corresponds to saturation of avidin with exactly 4 biotin derivatives per functional avidin tetramer. Such titration method is very robust, i.e. insensitive to the second functional group on the PEG chain, because only the breakpoint in the titration profile and not the magnitude of the fluorescence signal is used for quantitative evaluation. Thus, even intensely colored biotin-PEG-fluorophore conjugates could be characterized according to

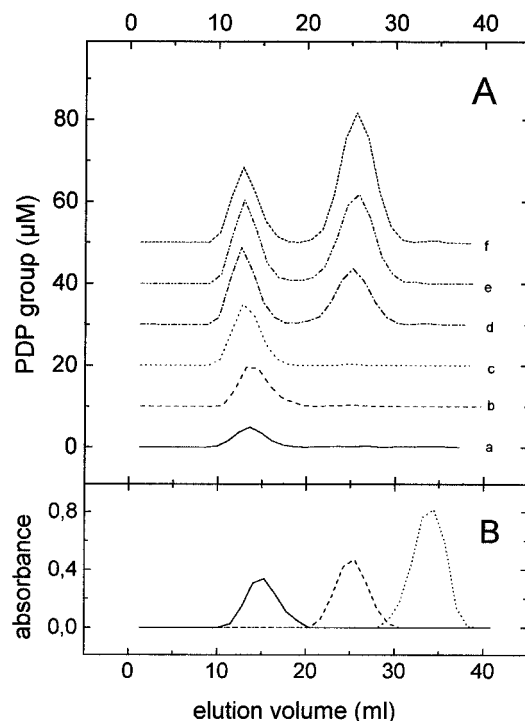


Figure 3. Chromatography of avidin complexes with biotin-PEG₁₉₀₀-PDP on Sephadex G-100: (A) loaded samples contained 1, 2, 3, 6, 8, or 10 ligands per avidin tetramer, yielding PDP profiles a, b, c, d, e, or f, respectively; (B) control of nonspecific binding and of column performance. Avidin (—, A_{282}) had been blocked with *d*-biotin (177 mol/mol of avidin) before the usual incubation with biotin-PEG₁₉₀₀-PDP (---, PDP profile, A_{324} after thiopyridone release) and chromatography. In a parallel run, 0.5 mL of 4 mM NaN₃ was eluted (· · ·) to mark the peak of small molecules. Virtually identical results (as shown in panels A and B) were seen in fully equivalent series with biotin-PEG₈₀₀-PDP except that the free PEG₈₀₀ derivative eluted slightly later than the free PEG₁₉₀₀ derivative, yet the PEG₈₀₀ peak was still well resolved from the salt peak marked by NaN₃.

this method (see the second of three papers in this issue). The same biotin end group contents as with the ANS assay were also found with other methods,² albeit less clear-cut and with much less convenience.

Assessment of Purity of Heterobifunctional Biotin-PEG-PDP Conjugates. For a final assessment the following findings had to be taken into account: (i) The biotin/PDP ratios in biotin-PEG₈₀₀-PDP and in biotin-PEG₁₉₀₀-PDP were 100:96 and 100:89, respectively, when assayed as described above. (ii) All biotin and PDP termini were covalently linked to PEG molecules since they coeluted in the void volume of Sephadex G-25 in the final synthetic step (see Experimental Procedures). (iii) According to TLC, both the immediate precursors and the two products were homogeneous, by all specific staining criteria.² (iv) Most importantly, the "bindability" of biotin-PEG₈₀₀-PDP and biotin-PEG₁₉₀₀-PDP toward slight excess of avidin was $\geq 99\%$, while nothing was bound to avidin preblocked with *d*-biotin (see Figure 3). Taken together, the data consistently indicate that every PEG chain had exactly one biotin terminus, while the slight imperfection on the PDP side may in part be due to residual uncertainty about ϵ_{324} of 4-thiopyridone and/or a small percentage of symmetric disulfides (biotin-NH-PEG-NHCOCH₂CH₂S₂).

Proof of 4:1 Stoichiometry and Measurement of Metastability in the Complex of Avidin with Biotin-PEG-PDP. The main idea of this study was to test whether four biotin-PEG conjugates can bind to avidin tetramers in a stoichiometric way, in spite of

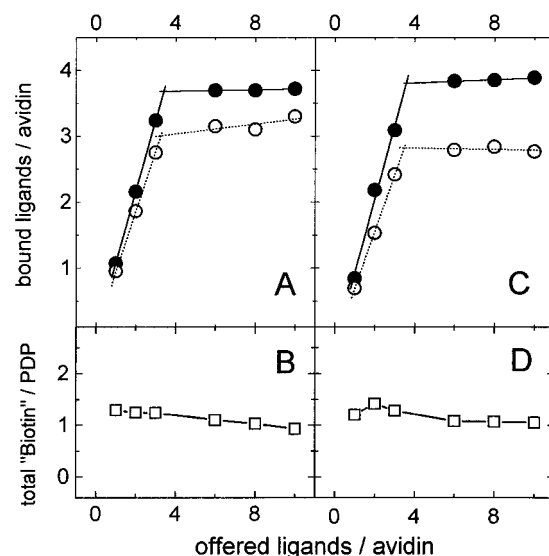


Figure 4. Stoichiometric ratios of biotin-PEG-PDP/avidin after chromatography on Sephadex G-100: (A) binding of biotin-PEG₁₉₀₀-PDP to avidin [eluted avidin peaks from Figure 3 were analyzed for occupied sites/avidin (●) or for PDP markers/avidin (○; before plotting, the numbers were multiplied by 100/89 to account for those 11% of PEG₁₉₀₀ molecules which had a biotin end group while lacking the PDP terminus)]; (B) "biotin" groups in the total chromatograms of Figure 3 were calculated by adding the number of occupied sites on avidin to the number of biotin groups seen in the PEG₁₉₀₀ peak (PDP groups in the total chromatograms of Figure 3 were calculated by adding the number of PDP markers in the avidin peak to the PDP groups in the PEG₁₉₀₀ peak; the ratio of total "biotin"/total PDP is plotted); (C) binding of biotin-PEG₈₀₀-PDP to avidin, analogous to panel A (the number of PDP markers/avidin were corrected for those 4% of biotin-PEG conjugates which lacked the PDP terminus); (D) ratio of "biotin"/PDP in experiments with biotin-PEG₈₀₀-PDP, analogous to panel B.

possible PEG-PEG repulsion, and how stable such complexes would be. This implied the use of 98–99% functionally pure avidin tetramers for all relevant studies. The ANS assay (Figure 2) clearly demonstrated that biotin-NH-PEG₁₉₀₀-NH₃⁺ Cl[−] (open triangles) and biotin-PEG₁₉₀₀-PDP (open circles) bind to intact avidin tetramers in the same 4:1 ratio as does *d*-biotin (solid squares) under equilibrium conditions.

Metastability and specificity of binding was tested by gel filtration on Sephadex G-100 (Figure 3), by which three well-resolved peaks were obtained for avidin, for free PEG molecules, and for small molecules (see Figure 3B and legend to Figure 3). Speaking in the terminology of receptor pharmacologists, we tested for "bindability", "saturation", and "displacement".

Bindability was 1 because all PDP marker groups comigrated with avidin at excess of receptor sites/ligands (traces a–c in Figure 3A).

Saturation was tested at excess of ligand/receptor sites (traces d–f in Figure 3A). As expected, a constant amount of PDP marker groups comigrated with avidin, while the variable excess of PDP markers was eluted at the position of free PEG molecules.

Quantitative evaluation of ligand/avidin stoichiometry after gel filtration is shown in parts A and C of Figure 4 for biotin-PEG₁₉₀₀-PDP and biotin-PEG₈₀₀-PDP, respectively. As expected, avidin appeared to be occupied by almost 4 ligands/tetramer when judged by measurement of occupied and empty binding sites (solid circles). In contrast, maximum ligand binding appeared to be only ~3 (open circles) when PDP markers per avidin were counted. Obviously, PDP markers had been lost during

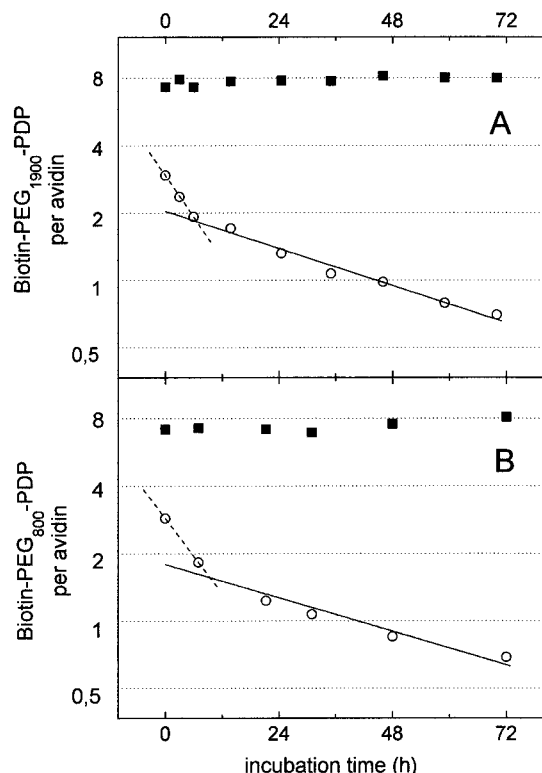


Figure 5. Displacement of biotin-PEG-PDP from complexes with avidin. See text for details.

gel filtration, while biotin endings had been retained in the receptor sites of avidin.

Loss of *small* PDP fragments could be ruled out by the absence of small PDP-containing molecules in the Sephadex G-100 chromatograms (see Figure 3A and legend to Figure 3). Loss of *full-sized* PEG-PDP elements, however, was clearly observed because the "free PEG peak" in Figure 3A always contained an excess of biotin-free PEG-PDP elements in addition to intact biotin-PEG-PDP. This excess quantitatively corresponded to the "missing" PDP markers in the avidin peak. In other words, the total "biotin" (= measured *occupied* sites in the avidin peak plus measured biotin groups in the free PEG peak) nicely fitted with the total eluted PDP markers within experimental uncertainty (see Figure 4B,D).

The observed phenomenon necessarily means that $\sim 1/2$ or ~ 1 mol of PEG-PDP element per mole of avidin had been lost from saturated complexes with biotin-PEG₁₉₀₀-PDP (solid circles minus open circles in Figure 4A) or biotin-PEG₈₀₀-PDP (solid circles minus open circles in Figure 4C), respectively, and that the missing biotin termini appeared stuck in their original receptor site on avidin. Here it seems appropriate to speculate that PEG chain crowding might provide the driving force and some nucleophilic group on avidin might provide the catalysis for "de-biotinylation" of bound biotin-PEG-PDP. At least, any alternate explanation seems even less acceptable.

Dissociation kinetics were analyzed over long time periods as shown in parts A and B of Figure 5 for biotin-PEG₁₉₀₀-PDP and biotin-PEG₈₀₀-PDP, respectively. Mixtures (8:1) of ligand/avidin were subjected to active ligand displacement by adding *d*-biotin (340 mol/mol of avidin) at zero incubation time. After the indicated incubation times (at 25 °C), aliquots were gel filtered on Sephadex G-100 as before. Recovery of protein and of biotin-PEG-PDP was almost quantitative (the small losses being due to imperfect loading). In particular, the

PDP/avidin ratios in the total elution volumes ($\sim 8:1$, solid squares in Figure 5A,B) were equivalent to those of the loaded samples; that is, no selective adsorption of any component had occurred. Bound ligands/avidin in the protein peak were determined from the ratio of PDP marker groups/avidin (open circles in Figure 5A,B).

The time course of biotin-PEG-PDP displacement by *d*-biotin was very similar for biotin-PEG₁₉₀₀-PDP (Figure 5A) and for biotin-PEG₈₀₀-PDP (Figure 5B), and both were apparently biphasic.

The starting point at "zero time" (no addition of *d*-biotin) always showed ~ 3 PEG-PDP markers bound per avidin tetramer, mainly due to *chemical* loss of PEG-PDP elements (as argued above) and partly due to physical dissociation of intact biotin-PEG-PDP molecules during the 1 h elution time.

Displacement by *d*-biotin of biotin-PEG-PDP from the 3:1 complex with avidin then proceeded with a half-times of ~ 10 and ~ 11 h for PEG₁₉₀₀ and PEG₈₀₀, whereas the 2:1 complexes showed much slower dissociation kinetics, the half-times being ~ 44 and ~ 48 h, respectively.

Thus, the measured dissociation kinetics of biotin-PEG conjugates represent no exception to the rule that biotin derivatives with bulky residues display biexponential time courses (Finn and Hofmann, 1985; Hofmann et al., 1982). The longevity of the 2:1 complexes is known to originate from the actual geometry of the avidin tetramer: The pairwise arrangement of receptor sites renders the *trans* complex with one ligand in each pair of sites most stable (Green, 1990).

Displacement of biotin-PEG-PDP by excess of *d*-biotin was inapplicable for testing the *specificity* of ligand binding because complete dissociation would have taken weeks at room temperature. Instead, avidin was irreversibly blocked by a large excess of *d*-biotin [dissociation half-time of 200 days according to Green (1990)] before addition of biotin-PEG-PDP and loading on Sephadex G-100. As shown by the results in Figure 3B, there was absolutely no nonspecific binding between avidin (solid lines) and biotin-PEG₁₉₀₀-PDP (dashed lines) or biotin-PEG₈₀₀-PDP (equal results, not shown).

Conclusions. The goal of this study was to test the practical potential of heterobifunctional biotin-PEG conjugates. Basic steps were to synthesize biotin-PEG-PDP and to establish analytical procedures for unequivocal counting of biotin and PDP termini in aqueous samples. Consequently, it was necessary to analyze the stoichiometry and metastability of avidin binding by such novel biotin-PEG ligands.

The results showed that avidin indeed binds 4 biotinylated PEG chains per protein tetramer and that the dissociation kinetics are slow enough to utilize 3:1 complexes (~ 10 h half-life) and 2:1 complexes (~ 2 day half-life) in typical applications. Similar biphasic dissociation kinetics and half-lives have been reported for biotin derivatives with 7–27 atom spacers (Finn et al., 1984; Finn and Hofmann, 1990; Hofmann et al., 1982). In the accompanying study with biotin-PEG-fluorophore conjugates it is shown that even 4:1 complexes are sufficiently stable for the minute time scale of most applications (see the second of three papers in this issue).

The essential point of the present study, however, does not depend on any gradual advantage/disadvantage of PEG spacers as opposed to conventional 7–27 atom spacers! Most important is the mere fact that biotin-PEG conjugates are indeed good ligands for avidin—and thus allow exploitation of all other advantages of PEG spacers: (i) minimized steric strain on probe molecules (e.g. antibodies) in B–A–B or B–A bridges, (ii) reduced

nonspecific adsorption of markers (e.g. fluorophores) to biological specimen, and (iii) virtually unquenched fluorescence in avidin/streptavidin-bound biotin-PEG-fluorophore conjugates, as demonstrated in the accompanying study (see the second of three papers in this issue).

ACKNOWLEDGMENT

We are indebted to Prof. Dr. H. Falk and his staff for helpful advice and use of spectrometer facilities, to Mag. J. Theiner for careful elemental analyses of the hygroscopic materials, and to S. Buchegger and B. Kenda for technical assistance. This work was supported by the Austrian Research Funds (Project S-6607 to H.S.).

Supporting Information Available: Detailed procedures, NMR data, and a systematic comparison of different biotin end group assays (20 pages). Ordering information is given on any current masthead page.

LITERATURE CITED

- (1) Carlsson, J., Drevin, H., and Axen, R. (1978) Protein thiolation and reversible protein-protein conjugation: *N*-Succinimidyl 3-(2-pyridyldithio)propionate, a new heterobifunctional reagent. *Biochem. J.* 173, 723–737.
- (2) Chu, Y.-H., Lees, W. J., Stassinopoulos, A., and Walsh, Ch. T. (1994) Using affinity capillary electrophoresis to determine binding stoichiometries of protein-ligand interactions. *Biochemistry* 33, 10616–10621.
- (3) Finn, F. M., and Hofmann, K. H. (1985) Synthesis of biotinyl derivatives of peptide hormones and other biological materials. *Methods Enzymol.* 109, 418–445.
- (4) Finn, F. M., Titus, G., Montibeller, J. A., and Hofmann, K. (1980) Hormone-receptor studies with avidin and biotinylinsulin-avidin complexes. *J. Biol. Chem.* 255, 5742–5746.
- (5) Finn, F. M., Titus, G., and Hofmann, K. (1984) Ligands for insulin receptor isolation. *Biochemistry* 23, 2554–2558.
- (6) Fudem-Goldin, B., and Orr, G. A. (1990) 2-Iminobiotin-containing reagent and affinity columns. *Methods Enzymol.* 184, 167–173.
- (7) Grassetti, D. R., and Murray, J. F., Jr. (1967) Determination of sulfhydryl groups with 2,2'- or 4,4'-dithiodipyridine. *Arch. Biochem. Biophys.* 119, 41–49.
- (8) Green, N. M. (1990) Avidin and Streptavidin. *Methods Enzymol.* 184, 51–67.
- (9) Green, N. M., Konieczny, L., Toms, E. J., and Valentine, R. C. (1971) The use of bifunctional biotinyl compounds to determine the arrangement of subunits in avidin. *Biochem. J.* 125, 781–791.
- (10) Haselgrübler, Th., Amerstorfer, A., Schindler, H., and Gruber, H. J. (1995) Synthesis and application of a new poly(ethylene glycol) derivative for the crosslinking of amines with thiols. *Bioconjugate Chem.* 6, 242–248.
- (11) Hofmann, K., Titus, G., Montibeller, J. A., and Finn, F. M. (1982) Avidin binding of carboxyl-substituted biotin and analogues. *Biochemistry* 21, 978–984.
- (12) Jou, Y.-H., Mazzaferro, P. K., Mayers, G. L., and Bankert, R. B. (1983) Methods for the attachment of haptens and proteins to erythrocytes. *Methods Enzymol.* 92, 257–276.
- (13) Lavielle, S., Chassaing, G., and Marquet, A. (1983) Avidin binding of biotinylated analogues of substance P. *Biochim. Biophys. Acta* 759, 270–277.
- (14) Leserman, L. D., Machy, P., and Barbet, J. (1984) Covalent coupling of monoclonal antibodies and protein A to liposomes: Specific interaction with cells in vitro and in vivo. *Liposome Technology* (G. Gregoriadis, Ed.) Vol. III, pp 29–40, CRC, Boca Raton, FL.
- (15) Lim, K., and Herron, J. N. (1992) Molecular simulation of protein-PEG interaction. In *Poly(ethylene glycol) chemistry: Biotechnical and biomedical applications* (J. M. Harris, Ed.) pp 29–56, Plenum Press, New York.
- (16) Mock, D. M., and Horowitz, P. (1990) Fluorometric assay for avidin-biotin interaction. *Methods Enzymol.* 184, 234–240.
- (17) Romovacek, H., Finn, F. M., and Hofmann, K. (1983) Avidin binding of biotinylated corticotropins. *Biochemistry* 22, 904–909.
- (18) Schray, K. J., Artz, P. G., and Hevey, R. C. (1988) Determination of avidin and biotin by fluorescence polarization. *Anal. Chem.* 60, 853–855.
- (19) Wilchek, M., and Bayer, E. A. (1990a) Introduction to avidin-biotin technology. *Methods Enzymol.* 184, 5–13.
- (20) Wilchek, M., and Bayer, E. A. (1990b) Applications of avidin-biotin technology: Literature Survey. *Methods Enzymol.* 184, 14–45.
- (21) Wilchek, M., and Bayer, E. A. (1990c) Biotin-containing reagents. *Methods Enzymol.* 184, 123–138.
- (22) Woghiren, C., Sharma, B., and Stein, S. (1993) Protected thiol-polyethylen glycol: A new activated polymer for reversible protein modification. *Bioconjugate Chem.* 4, 314–318.

BC970086U

Methods. Thin Layer Chromatography. Plastic sheets, precoated with 0.2 mm silica gel 60 without fluorescent indicator (Merck) were used. Eluent I, II, and III contained chloroform/methanol/acetic acid (80/20/2, 100/30/2, and 70/30/5, respectively). Besides nonspecific staining with iodine vapor, amines were specifically detected with ninhydrin (Schuurmans-Stekhoven et al., 1992) and biotin derivatives were visualized by color reaction with DACA (McCormick & Roth, 1970). Boc-protected amines responded to ninhydrin after ~1 min delay at 100 °C, due to thermal deprotection.

Syntheses. General Precautions. All essential precautions are being summarized in advance to avoid reiteration. Oxidation of primary amines and thiols by atmospheric oxygen was significant unless properly suppressed. Whenever amines were in the deprotonated state air was rigorously excluded by purging all solutions with Ar and by maintaining Ar superpressure in the reaction vessel with an Ar bubbler. Whenever possible, amines and thiols were kept in the protonated state by addition of acid. This induced a secondary problem in the case of NH₂-PEG-NH-Boc where the NH₂ group had to be protected from oxidation with acetic acid while at the same time Boc cleavage by acid was to be avoided when removing the solvents from solutions in chloroform/methanol/acetic acid. This was accomplished by including toluene and by attaching the rotavap to a vacuum source strong enough for rapid evaporation at 25-30 °C bath temperature. Even in the protonated state traces of amines were oxidized unless stored under slight Ar superpressure at -25 °C. Chromatography of amines and thiols on different Sephadex columns was also performed under rigorous air exclusion: Buffers were constantly bubbled with Ar, column outlets were equipped with hypodermic needles, and vessels or tubes for

collection of eluting fractions were sealed with rubber septa and pre-rinsed with Ar. For detection of eluting peaks a few drops between consecutive fractions were collected and assayed immediately.

Another regular problem besides autoxidation was hydrolysis of amide bonds between -NH-PEG-NH- and the terminal acyl groups which was unanticipated in the extent observed. Paradoxically, no such hydrolysis was observed in aqueous solutions buffered at neutral pH but in *p.a.* chloroform and in the dry films obtained after evaporation of *p.a.* chloroform such hydrolysis was detectable after a week of storage at -25 °C (the extent being ~3% and ~30% for biotin- and PDP-group, respectively, after one year at -25 °C). Amide cleavage was avoided by pre-treatment of chloroform with basic alumina immediately before use (also for silica chromatography). For long term storage, however, PEG derivatives were dissolved in plenty of water and lyophilized.

Synthesis of CH₃COOH·NH₂-PEG₈₀₀-NH-Boc. 50 g (55 mmol) of NH₂-PEG₈₀₀-NH₂ were crushed and dissolved in 150 ml methanol (see above for general precautions). 12g (55 mmol) of Boc₂O were dissolved in 50 ml methanol, added over a 30 min period, and the reaction mixture was stirred overnight. After addition of 3 ml acetic acid and 100 ml toluene the solution was concentrated to ~50 ml by rotary evaporation, addition of toluene and concentration to ~50 ml was repeated, and after the third addition of toluene rotary evaporation was completed. The crude product (60 g) was stored at -25°C. 3 g of crude product were subjected to chromatography on silica 60 (50 g). Elution with chloroform/methanol/acetic acid (250 ml 90/10/0.1 and 300 ml 70/30/5) gave the product which was taken to dryness by the "toluene procedure" as described above. For removal of silica, the residue was dissolved in 30 ml water, saturated with NaCl (11 g) and extracted 3 x with 20 ml chloroform. The organic layers were dried with Na₂SO₄, evaporated, and dried at 1-10 Pa for 1 h, yielding 1.25 g (1.17 mmol) of product. Pure by TLC: R_f^{II} (product) = 0.29-0.40, R_f^{II} (di-*t*-

Boc) = 0.78, R_f^{II} (diamine) = 0.06-0.18. $^1\text{H-NMR}$ (CDCl_3 , 200 MHz) δ : 1.06 (6H, m, CH_3 , aminopropyl termini of PEG) 1.34 (9H, s, *t*-butyl) 3.20-3.93 (~72H, m, $\text{OCH}_2\text{CH}_2\text{O}$, PEG chain) 3.32-3.42 (5H, m, 2 x OCH_2 and 1 x NCH , aminopropyltermini of PEG) 3.71 (1H, q, $J = 4$ Hz, NH_3^+CH) 4.86 (1H, broad s, Boc-NH).

Synthesis of $\text{HCl}\cdot\text{NH}_2\text{-PEG1900-NH-Boc}$. The procedure was the same as for the PEG800 homologue except that ion exchange chromatography was used because of too much peak tailing on the silica column. 50 g (25 mmol) of $\text{NH}_2\text{-PEG1900-NH}_2$ were reacted 5.5g (25 mmol) of Boc_2O . The crude product (53 g) was stored at -25°C . 3 g of the crude product were dissolved in 50 ml water and residual toluene was removed by short rotary evaporation. The solution was applied to a 5 x 16 cm column of SP Sephadex C-25 (Na^+ form, pre-equilibrated in water) at 8 ml/min and after washing with 500 ml water the product was eluted with 20 mM NaCl while monitoring amine elution with a fluorescamine assay (see below). Pooled fractions with product were reduced to 100 ml by rotary evaporation at 25°C under strong vacuum, saturated with NaCl, and extracted 4 x with 30 ml of chloroform. After drying with Na_2SO_4 the solvent was removed. The residue was dissolved in 1 ml CH_2Cl_2 and 25 ml of ether (pre-filtered through 0.3 volumes of basic alumina) were slowly added under stirring. After 30 min of stirring at 4°C the precipitate was isolated by suction filtration and washed with 5 ml of ether. Drying at 1-10 Pa for 1 h gave 0.82 g of product (0.38 mmol). The product was pure by TLC ($R_f^{\text{III}} = 0.24\text{-}0.46$). $^1\text{H-NMR}$ (CDCl_3 , 200 MHz) δ : 0.86 (6H, m, CH_3 , aminopropyl termini of PEG) 1.34 (9H, s, *t*-butyl) 3.20-3.90 (~172H, m, $\text{OCH}_2\text{CH}_2\text{O}$, PEG chain) 3.31-3.47 (5H, m, 2 x OCH_2 and 1 x NCH , aminopropyltermini of PEG) 3.82 (1H, q, $J = 4$ Hz, NH_3^+CH) 4.9 (1H, broad s, Boc-NH) 7.85 (3H, broad s, NH_3^+).

Synthesis of biotin-NH-PEG800-NH-Boc. 0.90 g Boc-NH-PEG800- $\text{NH}_2\cdot\text{CH}_3\text{COOH}$ (0.83 mmol) were dissolved in 8 ml absolute DMF, 0.39 g

biotin-NHS (1.14 mmol) and 0.2 ml Et₃N were added (see above for general precautions). Stirring was continued at RT for 24 h. Unreacted biotin-NHS was destroyed by addition of 8 ml water and stirring for 2 hours. After evaporation the residue was dissolved in 10 ml 200 mM Na₂CO₃ and filtered through paper. The filtrate was saturated with NaCl, extracted with CH₂Cl₂ and dried at 1-10 Pa for 1h. Yield: 637 mg (0.51 mmol). TLC and staining with iodine, ninhydrin, or DACA showed pure product ($R_f^I = 0.40-0.50$). ¹H-NMR: (CDCl₃, 200 MHz) δ : 1.07 (6H, m, 2 x CH₃, aminopropyltermini of PEG), 1.38 (9H, s, *t*-butyl) 1.30-1.75 (6H, m, CH₂CH₂CH₂CH₂CONH, biotin side chain) 2.13 (2H, t, *J* = 7 Hz, CH₂CONH, biotin side chain) 2.69 ppm (1H, d, *J*_{gem} = 13 Hz, SCH₂ (I), biotin) 2.82 (1H, q, *J*_{1gem} = 13 Hz, *J*_{2vic} = 5 Hz, SCH₂ (II), biotin) 3.09 (1H, m, SCH, biotin) 3.20-3.95 (~72H, m, OCH₂CH₂O, PEG chain) 3.31-3.47 (6H, m, 2 x OCH₂CH(CH₃)NH, aminopropyltermini of PEG) 4.04 (1H, broad s, OCH₂CH(CH₃)NH-biotin, amide bond between PEG and biotin) 4.25 (1H, m, NCH, biotin) 4.44 (1H, m, NCH, biotin) 5.08 (1H, broad s, OCH₂CH(CH₃)NH-Boc) 6.27-6.81 (2H, m, NHCONH in biotin).

Synthesis of biotin-NH-PEG₁₉₀₀-NH-Boc. The procedure was the same as for the PEG₈₀₀ homologue. 1.9 g Boc-NH-PEG₁₉₀₀-NH₂·HCl (0.90 mmol) were reacted with 0.46 g biotin-NHS (1.41 mmol) and 0.22 ml Et₃N. Yield: 1.92 g (0.82 mmol). TLC and staining with iodine, ninhydrin, and DACA showed pure product ($R_f^I = 0.38-0.50$). ¹H-NMR: (CDCl₃, 200 MHz) δ : 1.07 (6H, m, 2 x CH₃, aminopropyltermini of PEG), 1.37 (9H, s, *t*-butyl) 1.24-1.66, (6H, m, CH₂CH₂CH₂CH₂CONH, biotin side chain) 2.13 (2H, t, *J* = 7 Hz, CH₂CONH, biotin side chain) 2.68 ppm (1H, d, *J*_{gem} = 13 Hz, SCH₂ (I), biotin) 2.84 (1H, q, *J*_{1gem} = 13 Hz, *J*_{2vic} = 5 Hz, SCH₂ (II), biotin) 3.08 (1H, m, SCH, biotin) 3.20-3.93 (~172H, m, OCH₂CH₂O, PEG chain) 3.31-3.47 (6H, m, 2 x OCH₂CH(CH₃)NH, aminopropyltermini of PEG) 4.04 (1H, broad s, OCH₂CH(CH₃)NH-biotin, amide bond between PEG and biotin) 4.24 (1H, q, *J*₁ = 5 Hz, *J*₂ = 8 Hz, NCH, biotin), 4.44 (1H, q, *J*₁ = 5 Hz, *J*₂ = 8 Hz, NCH, biotin)

4.84 (1H, broad s, $\text{OCH}_2\text{CH}(\text{CH}_3)\text{NH-Boc}$) 6.17-6.72 (2H, m, NHCONH in biotin).

Synthesis of biotin-NH-PEG800-NH₂·HCl. 528 mg biotin-NH-PEG800-NH-Boc (0.42 mmol) were dissolved in 8 ml formic acid and 0.2 ml water were added (see above for general precautions). After stirring for 4 h formic acid was azeotroped 2 x with 20 ml portions of toluene on the rotavap. The crude product was dissolved in 5 ml water and loaded onto a 2.5 x 15 cm column of SP Sephadex C-25 (Na^+ form, pre-equilibrated in water) at 0.7 ml/min. After washing with 150 ml water the product was eluted with 180 ml 50 mM NaCl. Fractions containing amine (detected by fluorescamine assay, see below) were pooled, concentrated to 10 ml by rotary evaporation, saturated with NaCl, and extracted 3 x with 50 ml portions of chloroform. After drying with Na_2SO_4 the product was taken to dryness (1h at 10 Pa). Yield 389 mg (330 μmol). TLC showed a single spot ($R_f^{\text{II}} = 0.11-0.44$) with positive response to ninhydrin and DACA. $^1\text{H-NMR}$: (CDCl_3 , 200 MHz) δ : 1.07 (6H, m, 2 x CH_3 , aminopropyltermini of PEG) 1.27-1.77 (6H, m, $\text{CH}_2\text{CH}_2\text{CH}_2\text{CH}_2\text{CONH}$, biotin side chain) 2.13 (2H, t, $J = 7$ Hz, CH_2CONH , biotin side chain) 2.69 ppm (1H, d, $J_{\text{gem}} = 13$ Hz, SCH_2 (I), biotin) 2.81 (1H, q, $J_{1\text{gem}} = 13$ Hz, $J_{2\text{vic}} = 5$ Hz, SCH_2 (II), biotin) 3.10 (1H, m, SCH , biotin) 3.19-3.94 (~172H, m, $\text{OCH}_2\text{CH}_2\text{O}$, PEG chain) 3.31-3.47 (5H, m, 2 x OCH_2 and 1 x NCH , aminopropyltermini of PEG) 3.77 (1H, q, $J = 4$ Hz, CHNH_3^+) 4.04 (1H, broad s, $\text{OCH}_2\text{CH}(\text{CH}_3)\text{NH}$ -biotin, amide bond between PEG and biotin) 4.24 (1H, m, NCH , biotin), 4.45 (1H, m, NCH , biotin) 6.25-6.78 (2H, m, NHCONH in biotin) 7.86 (3H, broad s, NH_3^+).

Synthesis of biotin-NH-PEG1900-NH₂·HCl. The procedure was the same as for the PEG800 homologue. 1.5 g biotin-NH-PEG1900-NH-Boc (0.64 mmol) were deprotected, yielding 1.18 g of crude product. 500 mg crude product were dissolved in 10 ml water and loaded onto a 2.5 x 15 cm column of SP Sephadex

C-25 (Na^+ form, pre-equilibrated in water) at 0.3 ml/min. After washing with 150 ml water the product was eluted with 150 ml 20 mM NaCl. Fractions containing amine (fluorescamine assay, see below) were pooled, saturated with NaCl, and extracted 4 x with 50 ml portions of CH_2Cl_2 . After drying with Na_2SO_4 the product was taken to dryness (1.5 h at 1-10 Pa). Yield 407 mg (178 μmol). TLC showed a single spot ($R_f^{\text{II}} = 0.08-0.37$) with positive response to ninhydrin and DACA. $^1\text{H-NMR}$: (CDCl_3 , 200 MHz) δ : 1.07 (6H, m, 2 x CH_3 , aminopropyltermini of PEG) 1.24-1.75 (6H, m, $\text{CH}_2\text{CH}_2\text{CH}_2\text{CH}_2\text{CONH}$, biotin side chain) 2.13 (2H, t, $J = 7$ Hz, CH_2CONH , biotin side chain) 2.69 ppm (1H, d, $J_{\text{gem}} = 13$ Hz, SCH_2 (I), biotin) 2.82 (1H, q, $J_{1\text{gem}} = 13$ Hz, $J_{2\text{vic}} = 5$ Hz, SCH_2 (II), biotin) 3.10 (1H, m, SCH , biotin) 3.17-3.93 (~172H, m, $\text{OCH}_2\text{CH}_2\text{O}$, PEG chain) 3.31-3.47 (5H, m, 2 x OCH_2 and 1 x NCH , aminopropyltermini of PEG) 3.78 (1H, q, $J = 4$ Hz, CHNH_3^+) 4.04 (1H, broad s, $\text{OCH}_2\text{CH}(\text{CH}_3)\text{NH}$ -biotin, amide bond between PEG and biotin) 4.24 (1H, m, NCH , biotin), 4.44 (1H, m, NCH , biotin) 6.20-6.71 (2H, m, NHCONH in biotin) 7.90 (3H, broad s, NH_3^+). Elemental analysis after 3 d drying over P_2O_5 (average of duplicates): C: calc. 53.56%, found 53.34%; H: calc. 8.85%, found 9.07%; N: calc. 2.85%, found 2.51%; S: calc. 1.40%, found 1.29%; Cl: calc. 1.55%, found 1.52%.

Synthesis of Biotin-PEG800-PDP. 93 mg biotin-NH-PEG800-NH $_2$ ·HCl (78 μmol), 80 mg DTSP (200 μmol), and 50 μl of Et_3N were reacted in 10 ml peroxide-free THF (see above for general precautions!). After overnight stirring the solvent was evaporated. From TLC (and subsequent staining with iodine, ninhydrine, and DACA) it was concluded that all of the amine had reacted with DTSP. The residue was dissolved in 5 ml buffer A and residual solid was removed by filtration through paper. The filtrate was replenished to 5 ml with buffer A and bubbled with Ar for 2 min. 62 mg DTT (400 μmol) were added at once (without stirring) and Ar bubbling was continued for 15 min in a good hood. Then 0.75 ml of 0.5 M acetic acid were added to lower the pH to ~4.5. The reaction mixture was loaded on a 1.5 x 48 cm column of Sephadex G-25M (pre-

equilibrated in buffer B, see above for general precautions). The product was eluted with buffer B at 1 ml/min while collecting 5 ml fractions. The product biotin-NH-PEG800-NH-CO-CH₂-CH₂-SH was found in # 7-11, absolutely no thiol was observed in # 12 and 13, whereas all small thiols eluted in # 14-18. Thiols were detected by reaction with 4,4'-dithiodipyridine (Grasseti & Murray, 1967).

For synthesis of the final product, 35 mg of 4,4'-dithiodipyridine (160 μ mol) were dissolved in 3 ml water plus 420 μ l 1 M HCl, and throughout the experiment the pH was controlled with a glass electrode under constant bubbling with Ar, rather than stirring. The column fractions containing biotin-NH-PEG800-NH-CO-CH₂-CH₂-SH were added, and subsequently the pH was raised to 4.4 by addition of buffer C (~0.4 ml). After 15 min of Ar bubbling at RT the solution was frozen and lyophilized. The residue was dissolved in 8 ml of water, filtered through paper, and the filtrate (~6 ml) was applied to a 1.5 x 48 cm column of Sephadex G-25M. Elution was at 1 ml/min with distilled water. The column was not identical with the first Sephadex column to avoid any possible contact between the final product and contaminating DTT. Peaks were detected by reduction with 2-ME (see below). As in the preceeding step, the PEG derivative (19 μ mol product) in the void peak was well separated from all small molecules by 10 ml of elution volume containing neither product nor by-products. For functional experiments with avidin the product peak was stored frozen at -25 °C. For NMR and TLC analysis, an aliquot of the product was lyophilized and redissolved in CDCl₃ or chloroform, respectively. TLC gave a homogeneous main spot at $R_f^{\text{II}} = 0.55-0.78$ (DACA-positive, ninhydrin-negative). A DACA-positive trace impurity with ~1% stain intensity was seen at $R_f^{\text{II}} = 0.91$. ¹H-NMR: (CDCl₃, 200 MHz) δ : 0.99-1.07 (6H, m, 2 x CH₃, aminopropyltermini of PEG) 1.30-1.62 (6H, m, CH₂CH₂CH₂CH₂CONH, biotin side chain) 2.26 (2H, t, J = 7 Hz, CH₂CONH, biotin side chain) 2.45 (2H, t, J = 7 Hz, NH-COCH₂CH₂SS, PDP group) 2.71-2.89 (2H, d and q, J_{gem} = 12 Hz, J_{vic} = 5 Hz,

SCH₂ (I), biotin) 2.95 (2H, t, J = 7 Hz, COCH₂CH₂SS) 3.03-3.10 (1H, m, SCH, biotin) 3.54 (~172H, broad s, OCH₂CH₂O, PEG chain) 3.27-3.44 (6H, m, 2 x OCH₂CH(CH₃)NH, aminopropyltermini of PEG) 4.00 (1H, broad s, OCH₂CH(CH₃)NH-biotin, amide bond between PEG and biotin) 4.22 (1H, m, NCH, biotin), 4.42 (1H, m, NCH, biotin) 5.65 (1H, broad s, NH-COCH₂CH₂SS, amide bond between PEG and PDP) 6.14-6.61 (2H, m, NHCONH in biotin) 7.36 and 8.38 (each 2H, AA'BB'-system of a *p*-substituted aromat, 4-pyridyl). ¹³C-NMR (50,3 MHz, CDCl₃) δ: Biotin: 25.36, 27.92, 28.07, 33.84, 40.24 (CH₂); 55.33, 59.95, 61.58 (CH); 163.6, 172.1 (C=O); PDP group: 149.22 (C2 and C6), 119.73 (C3 and C5), 169.34 (C=O); PEG: 17.43 (aminopropyl), 70.31 (OCH₂CH₂O).

Synthesis of Biotin-PEG₁₉₀₀-PDP. Synthetic steps, procedures, and precautions were the same as for the corresponding PEG₈₀₀ derivative (see above). 224 mg biotin-NH-PEG₁₉₀₀-NH₂·HCl (98 μmol), 112 mg DTSP (280 μmol), and 125 μl Et₃N were reacted in 8 ml peroxide-free THF. The disulfide product was reduced with 430 mg DTT (2.8 mmol). After acidification with acetic acid and chromatography on Sephadex G-25 M the void peak (20 ml) containing biotin-NH-PEG₁₉₀₀-NH-CO-CH₂-CH₂-SH was added to a solution of 220 mg 4,4'-dithiodipyridine in 2 ml of distilled water plus 220 μl HCl conc. The pH was raised to 4.5 by addition of buffer C under constant bubbling with Ar. After 15 min the mixture was lyophilized, redissolved in water, filtered, and the filtrate subjected to gel filtration in water as above, yielding 39 μmol Biotin-PEG₁₉₀₀-PDP in the void peak. TLC gave a homogeneous main spot at R_F^{II} = 0.43-0.57 (DACA-positive, ninhydrin-negative). ¹H-NMR: (CDCl₃, 200 MHz) δ: 1.04 (6H, m, 2 x CH₃, aminopropyltermini of PEG) 1.24-1.70 (6H, m, CH₂CH₂CH₂CH₂CONH, biotin side chain) 2.08 (2H, t, J = 7 Hz, CH₂CONH, biotin side chain) 2.45 (2H, t, J = 7 Hz, NH-COCH₂CH₂SS, PDP group) 2.69 (1H, d, J_{gem} = 13 Hz, SCH₂ (I), biotin) 2.82 (1H, q, J_{1gem} = 13 Hz, J_{2vic} = 5 Hz, SCH₂ (II), biotin) 2.95 (2H, t, J = 7 Hz, NH-COCH₂CH₂SS) 3.02 (1H, q, J

= 5 Hz, SCH, biotin) 3.16-3.92 (~172H, m, OCH₂CH₂O, PEG chain) 3.27-3.44 (6H, m, 2 x OCH₂CH(CH₃)NH, aminopropyltermini of PEG) 4.00 (1H, broad s, OCH₂CH(CH₃)NH-biotin, amide bond between PEG and biotin) 4.22 (1H, m, NCH, biotin), 4.42 (1H, m, NCH, biotin) 5.65 (1H, broad s, NH-COCH₂CH₂SS, amide bond between PEG and PDP) 6.14-6.61 (2H, m, NHCONH in biotin) 7.36 and 8.38 (each 2H, AA'BB'-system of a *p*-substituted aromat, 4-pyridyl). Elemental analysis after 3 d drying over P₂O₅ (average of duplicates): C: calc. 53.97%, found 53.11%; H: calc. 8.52%, found 8.66%; N: calc. 2.86%, found 2.73%; S: calc. 3.93%, found 3.64%.

Synthesis of 3-(4-Pyridyldithio)propionic acid. 4,4'-Dithiodipyridine (0.96 g, 4.36 mmol) was dissolved in a solvent mixture of methanol (10 ml), water (10 ml), and acetic acid (2 ml), and cooled to -10 °C. 3-Mercaptopropionic acid (0.37 ml, 4.25 mmol) dissolved in a mixture of methanol (20 ml) and acetic acid (1 ml) was added dropwise to the vigorously stirred solution of 4,4'-dithiodipyridine at -10 °C over a period of 20 minutes. A white precipitate formed. The mixture was allowed to react at -10 °C for 1 h and then at RT for an additional 3 h. The precipitate was filtered off, washed twice with 4 ml of the solvent mixture methanol/water/acetic acid (30/10/3), twice with 10 ml of THF, and twice with 20 ml of ethyl acetate. Drying in the desiccator overnight gave 587 mg (64 %) of the product. The product was readily soluble in DMSO, N-methylpyrrolidone, and pyridine, sparingly soluble at RT in DMF, and nonsoluble in all other common organic solvents. TLC solvent: chloroform/methanol/acetic acid (70/30/0.1); R_f (product) = 0.43; R_f (4,4'-dithiodipyridine) = 0.81; R_f (3,3'-dithio-bis[propionic acid]) = 0.17-0.35; R_f (4-thiopyridone) = 0.61. ¹H-NMR (DMSO-d₆, 200 MHz) δ: 2.62 (2H, t, J = 7 Hz, -COCH₂CH₂S-) 2.99 (2H, t, J = 7 Hz, -COCH₂CH₂S-) 7.56 (2H, dd, J = 1.5 and 5 Hz, NCHCHCS) 8.50 (2H, dd, J = 1.5 and 6 Hz, NCHCHCS).

Quantitative Assay for Primary Amino Groups. Chromatography of amine derivatives on SP-Sephadex C-25 required monitoring of primary amino groups in eluting fractions. A modified fluorescamine assay (Gruber et al., 1995; Udenfriend et al., 1972) was best suited because the strongly non-linear dose response affords a dynamic concentration range of 2-3 orders of magnitude. Typically, 100 μ l of sample (between 10 μ M and \sim 1 mM in amino groups) were mixed with 1 ml of water and 100 μ l of buffer D, and 25 μ l of 10 mM fluorescamine in DMSO were added from an Eppendorf Multipipette *while* vortexing. Fluorescence was read after > 2 min at 390 nm excitation (slit 5 nm) and 475 nm emission wavelength (slit 5 nm). Calibration was done with known standards containing $\text{NH}_2\text{-PEG-NH}_2$.

Quantitative Assays for Biotin End Groups. A published fluorescence assay for avidin-biotin interaction (Mock & Horowitz, 1990) was modified. Typically, 2 ml of buffer A containing 2 μ M affinity-purified avidin were mixed with 25 μ l 5 mM ANS in DMSO and fluorescence was monitored at 328 nm excitation (slit 10 nm) and 408 nm emission wavelength (slit 10 nm).

In the "uniform titration method", 5-10 μ l aliquots of \sim 400 μ M biotin derivative (in water or buffer A) were added at 0.5 min intervals from a Hamilton syringe while stirring, thereby displacing the pseudo-ligand ANS from the biotin sites in avidin and reducing ANS fluorescence until all biotin sites were saturated with biotin derivative.

In the "mixed titration method", enough of the biotin-PEG conjugate was added at once to saturate approximately half of the biotin binding sites on avidin, and titration was continued with 5-10 μ l aliquots of exactly 400 μ M *d*-biotin in buffer A while stirring.

In both methods, the exact concentration of the 2 μ M avidin solution was standardized by uniform titration with exactly 400 μ M *d*-biotin. Aliquots of

standardized stock solutions of 5 mM ANS, 400 μ M *d*-biotin, and 2 μ M avidin were stored at -25 °C. Loss of avidin function was observed after >1 month at -25 °C but no denaturation was observed when refreezing \leq 2 times within this period. Exposure of ANS to light was minimized to avoid decomposition.

Quenching of Trp fluorescence in avidin (Lin & Kirsch, 1979) by biotin-PEG conjugates was tested also. Typically, 2 ml 80 nM avidin in buffer A were titrated in 5-10 μ l steps with \sim 20 μ M biotin derivative (or with *d*-biotin standard) while stirring and monitoring Trp fluorescence at 290 nm excitation (slit 10 nm) and 340 nm emission (slit 10 nm).

Alternatively, biotin termini were assayed by chemical reaction with DACA (McCormick & Roth, 1970). A 50 μ M standard solution of *d*-biotin in absolute ethanol was prepared by dilution of 80 mM *d*-biotin in DMSO (DMSO was shown not to interfere). For calibration, a concentration series was prepared by mixing 0, 0.25, 0.50, 0.75, 1.00, or 1.25 ml of 50 μ M *d*-biotin solution with complementary amounts of absolute ethanol to give 1.25 ml final volumes. 150 μ l 2% H₂SO₄ in absolute ethanol and 150 μ l 0.2% DACA in the same solvent were added, and after 1 h incubation at RT A₅₃₃ was read against a reagent blank. Eppendorf Multipettes were used for all pipetting steps. Solutions with \sim 50 μ M biotin-PEG conjugates were prepared by lyophilizing defined aliquots of aqueous stock solutions and dissolving the residues in absolute ethanol under minimal evaporation of the solvent. Concentration series with these unknowns were performed as above.

Optimization of Biotin End Group Determination and Demonstration of High Purity of Biotin-PEG-PDP. Published biotin group assays are literally unnumerable - but none was found that guaranteed unperturbed quantitation of biotin residues on PEG. Moreover, heterobifunctional biotin-PEG conjugates have so far appeared in a commercial catalogue only (Shearwater Polymers) but not in scientific literature.

A reliable procedure could be established by comparing elemental analysis, spectrophotometry after reaction with DACA (McCormick & Roth, 1970), and titration of avidin while monitoring the fluorescence either of avidin's tryptophans (Lin & Kirsch, 1979) or of the pseudoligand ANS (Mock & Horowitz, 1990), for the two compounds biotin-NH-PEG₁₉₀₀-NH₂·HCl and Biotin-PEG₁₉₀₀-PDP. All assays essentially agreed - but the ANS assay turned out to be the most convenient, accurate, and sensitive method, with the additional advantage of being insensitive to the second functional group on the PEG chain.

Elemental analysis after 3 d vacuum drying over P₂O₅ confirmed both the 1:1 ratios of the two corresponding terminal groups and the average chain length with 43 repeat units as stated by Fluka for NH₂-PEG₁₉₀₀-NH₂ (see Experimental section). However, rapid re-uptake of water was observed with such rigorously dried products.

All other assays were performed on aliquots from a single stock solution (for each of the two compounds) which was obtained by redissolving lyophilized product (dried by pumping for 1 h at ~1-10 Pa after disappearance of ice) at known mg/ml concentrations in water. Nominal molar concentrations of biotin-NH-PEG₁₉₀₀-NH₂·HCl and Biotin-PEG₁₉₀₀-PDP were calculated from the nominal molecular masses of 2269 and 2494 g/mol, respectively, as expected for 43 repeat units and as confirmed by elemental analysis within experimental uncertainty.

Biotin end group determination by the ANS fluorescence assay is shown in Figure 6A. Displacement of the pseudoligand ANS by *d*-biotin ended at 17.3 nmol *d*-biotin (solid squares). This allowed to calculate a "functional" concentration of 2.16 μ M for avidin in the initial assay volume (2 ml) which implied a functional purity of 85.4% for this batch of affinity-purified avidin. The same amount of avidin *appeared* to bind nominal amounts of 22.7 nmol or 22.8 nmol of biotin-NH-PEG₁₉₀₀-NH₂·HCl (open circles) or Biotin-PEG₁₉₀₀-PDP

(open triangles), respectively. However, avidin cannot be expected to *specifically* bind more biotin derivative than it binds *d*-biotin (i.e. 4 per protein tetramer), and the inflection points in Figure 6A necessarily always meant saturation of avidin by 17.3 nmol *d*-biotin or biotin derivative. From this followed that the biotin terminus concentrations of biotin-NH-PEG₁₉₀₀-NH₂·HCl and of Biotin-PEG₁₉₀₀-PDP were 0.55 mM (nominally 0.72 mM) and 0.40 mM (nominally 0.53 mM), respectively, the discrepancies being due to the unknown water contents of the lyophilized products.

The ANS method shown in Figure 6A correctly measured biotin end group concentrations, and these were identical with the concentrations of *all* PEG derivatives in the same samples, for the following reasons: (i) Equivalent biotin terminus concentrations were obtained from the final inflection points of Trp quenching titrations (see Figure 7B, solid squares and triangles). (ii) Identical concentration values were also obtained for Biotin-PEG₁₉₀₀-PDP when using the DACA assay (see open triangles in Figure 8). The minor discrepancy for biotin-NH-PEG₁₉₀₀-NH₂·HCl (open circles) is not unexpected for this chemical assay (McCormick & Roth, 1970). (iii) According to TLC, products were homogeneous, by all staining criteria. (iv) Biotin-NH-PEG₁₉₀₀-NH₂·HCl had a 1:1 end group ratio as judged from the S:Cl ratio in elemental analysis. (v) The biotin/PDP ratios in Biotin-PEG₁₉₀₀-PDP and in Biotin-PEG₈₀₀-PDP were 100/89 and 100/96, respectively. (vi) All biotin and PDP termini were covalently linked to the PEG molecules since they strictly co-migrated with PEG on Sephadex G-25 (see descriptions of syntheses) and on Sephadex G-100 (see Figure 3 in the Results section). (vii) Most importantly, all PEG molecules in preparations of Biotin-PEG-PDP were bound to excess of avidin while nothing was bound to avidin pre-blocked with *d*-biotin (see Results section).

Taken together the data consistently indicate that the ANS assay correctly measured biotin termini on PEG, that every PEG in Biotin-PEG-PDP had exactly

one biotin terminus, and that Biotin-PEG₈₀₀-PDP and Biotin-PEG₁₉₀₀-PDP had the expected molecular weights with ~18 and ~43 repeat units on average, respectively.

The sensitivity of the ANS method for measuring biotin-PEG conjugates could greatly be increased when using a "mixed titration method". Thus it was possible to work at 80 nM avidin (Figure 6B), rather than at 2 μ M avidin (Figure 6A). For a demonstration, avidin was saturated with exactly 2 moles of biotin-NH-PEG₁₉₀₀-NH₂·HCl (open circles in Figure 6B) or 2 moles of Biotin-PEG₁₉₀₀-PDP (open triangles in Figure 6B) per protein tetramer, and titration was continued with a standard solution of *d*-biotin. As expected, the inflection points now occurred after addition of 2.0 moles of *d*-biotin per protein tetramer, the intercept of the two linear portions being very pronounced. Uniform titration of such dilute avidin with biotin-NH-PEG₁₉₀₀-NH₂·HCl (solid circles in Figure 6B) or Biotin-PEG₁₉₀₀-PDP (solid triangles in Figure 6B) failed to give a clear inflection point, in contrast to uniform titration at 2 μ M avidin (Figure 6A, open circles and triangles).

Not surprisingly, titration curves were also "smeared out" when using avidin's tryptophans instead of ANS as fluorescence reporters while titrating at the same low avidin concentration with biotin-NH-PEG₁₉₀₀-NH₂·HCl (open circles in Figure 7A) or Biotin-PEG₁₉₀₀-PDP (open triangles in Figure 7A). The problem clearly originated from too slow on-kinetics at such low reactant concentrations because when the time intervals between successive additions were raised from 0.5 min (in Figure 7A) to 15 min (in Figure 7B) the titration curves for Biotin-PEG₈₀₀-PDP (solid squares in Figure 7B) and Biotin-PEG₁₉₀₀-PDP (solid triangles in Figure 7B) showed a more pronounced inflection at the expected value of 4 ligands per protein tetramer.

In contrast to the ANS method, the Trp quenching method could not be improved by "mixed titration" (see lines without symbols in Figure 7B), due to the complex

nature of the Trp quenching curves. So far only monotonic decreases have been reported (Chignell et al., 1975; Lin & Kirsch, 1979) as shown for *d*-biotin (solid squares in Figure 7A). While the problem seems interesting, selection among reasonable explanations for the biphasic Trp quenching curves will require a broader data set than presently available (compare Kurzban et al., 1989).

LITERATURE CITED in the Supplements only:

- Chignell, C. F., Starkweather, D. K., and Sinha B. K. (1975) A spin label study of egg white avidin. *J. Biol. Chem.* 250, 5622-5630.
- Gruber, H. J., Wilmsen, H. U. Schurga, A., and Schindler, H. (1995) Measurement of intravesicular volumes by salt entrapment. *Biochim. Biophys. Acta* 1240, 266-276.
- Kurzban, G. P., Gitlin, G., Bayer, E. A., Wilchek, M., and Horowitz, P. M. (1989) Shielding of tryptophan residues of avidin by the binding of biotin. *Biochemistry* 28, 8537-8542.
- Lin, H. J., and Kirsch, J. F. (1979) A rapid, sensitive fluorometric assay for avidin and biotin. *Methods Enzymol.* 62, 287-289.
- McCormick, D. B., and Roth, J. A. (1970) Colorimetric determination of biotin and analogs. *Methods Enzymol.* 18, 383-385.
- Schuurmans-Stekhoven, F.M.A.H., Tesser, G.I., Ramsteyn, G., Swarts, H.G.P., and De Pont, J.J.H.H.M. (1992) Binding of ethylenediamine to phosphatidylserine is inhibitory to Na^+/K^+ -ATPase. *Biochim. Biophys. Acta* 1109, 17-32.
- Udenfriend, S., Stein, S., Böhlein, P., and Dairman, W. (1972) Fluorescamine: Reagent for assay of amino acids, peptides, proteins, and primary amines in the picomole range. *Science* 178, 871-872.

Figure 6: Biotin end group assay by the ANS method. *A:* 2 ml of affinity-purified avidin (2.53 μ M avidin concentration according to A₂₈₂) were titrated with 0.40 mM *d*-biotin (solid squares, standardization), or with nominally 0.72 mM biotin-NH-PEG₁₉₀₀-NH₂·HCl (open circles), or with nominally 0.53 mM Biotin-PEG₁₉₀₀-PDP (open triangles), while monitoring the fluorescence of 62.5 μ M ANS. For better legibility, curves for the amino and PDP-derivative were vertically displaced by +10 or +20 fluorescence units, respectively. *B:* 2 ml 80 nM avidin (functional concentration as determined in panel A) were titrated with increments of 16 μ M biotin-NH-PEG₁₉₀₀-NH₂·HCl (solid circles) or with increments of Biotin-PEG₁₉₀₀-PDP (solid triangles) while monitoring the fluorescence of 25 μ M ANS. Alternatively, avidin was "semi-saturated" by exactly 2 biotin-NH-PEG₁₉₀₀-NH₂·HCl (open circles) or by exactly 2 Biotin-PEG₁₉₀₀-PDP (open triangles) per avidin tetramer, and titration was continued with increments of exactly 16 μ M *d*-biotin.

Figure 7: Biotin end group assay by the Trp quenching method. *A:* 2 ml of 216 nM avidin (according to ANS assay) were titrated with 5 μ l steps of 40 μ M *d*-biotin (solid squares) while monitoring the Trp fluorescence of avidin. Alternatively, titration was with biotin-NH-PEG₁₉₀₀-NH₂·HCl (open circles, 55 μ M titrant according to ANS assay) or with Biotin-PEG₁₉₀₀-PDP (open triangles 40 μ M titrant according to ANS assay). Time intervals per addition were 0.5 min in all cases. For disentangling of overlapping curves, +10 and +30 fluorescence units were added to the actual values for amine and for the PDP derivative, respectively. *B:* Slow titration of avidin at 15 min intervals per addition of Biotin-PEG₁₉₀₀-PDP (solid triangles) or Biotin-PEG₈₀₀-PDP (solid squares). All concentrations were already known from ANS assays. For "mixed titration", avidin was partially saturated with 1.0 (—) or 2.0 (- - -) or 3.0 (. . . .)

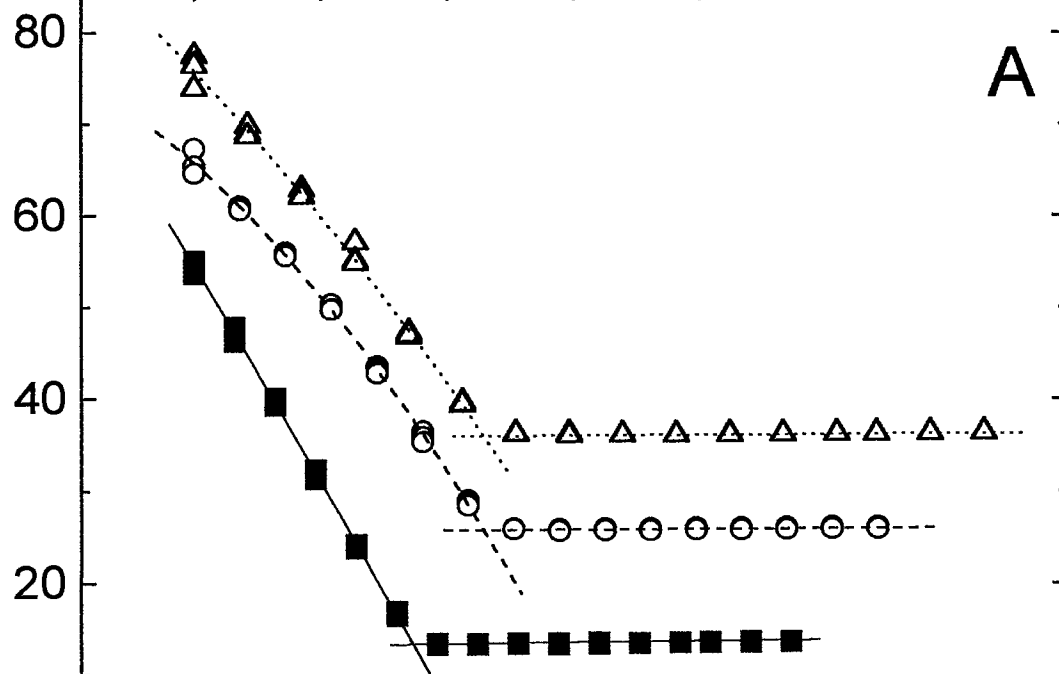
moles of Biotin-PEG₈₀₀-PDP per mole of avidin, and titration was continued with *d*-biotin.

Figure 8: DACA assay for biotin end groups. Samples with the indicated concentrations of *d*-biotin (solid squares) or biotin-NH-PEG₁₉₀₀-NH₂·HCl (open circles) or Biotin-PEG₁₉₀₀-PDP (open triangles) were reacted with DACA and sulfuric acid in absolute ethanol. Concentrations of biotin-PEG conjugates were known from ANS assays.

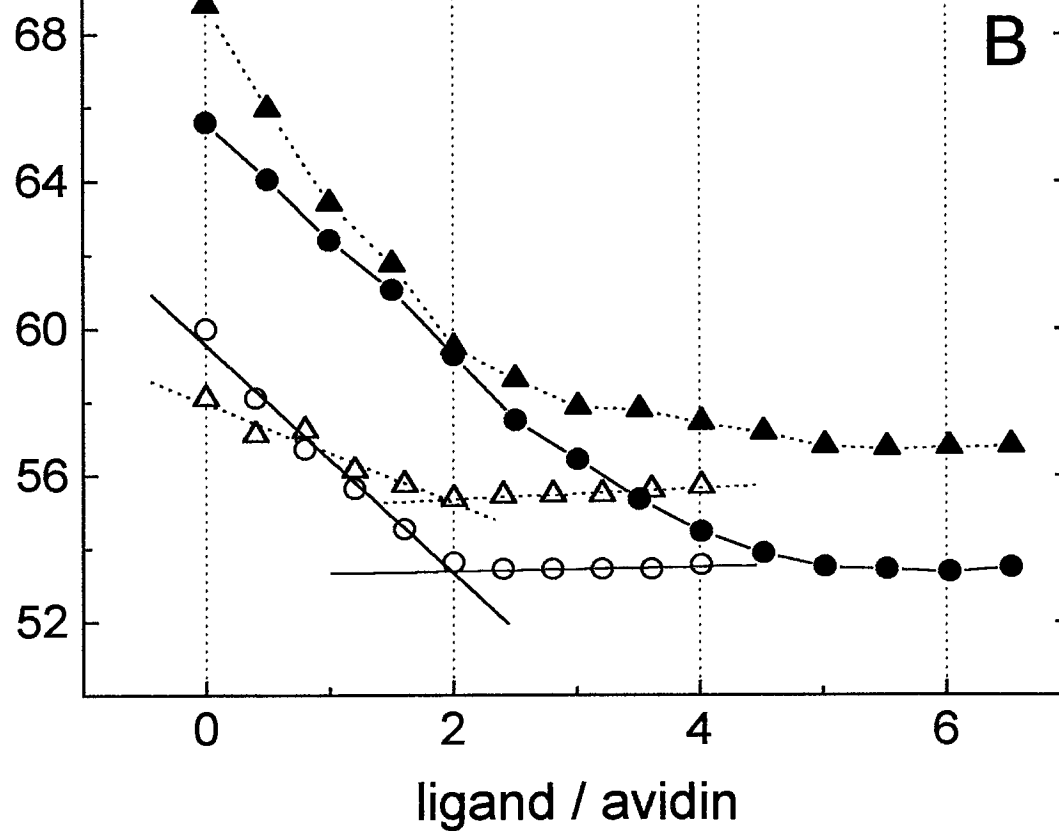
nmol ligand (nominal values by weight)

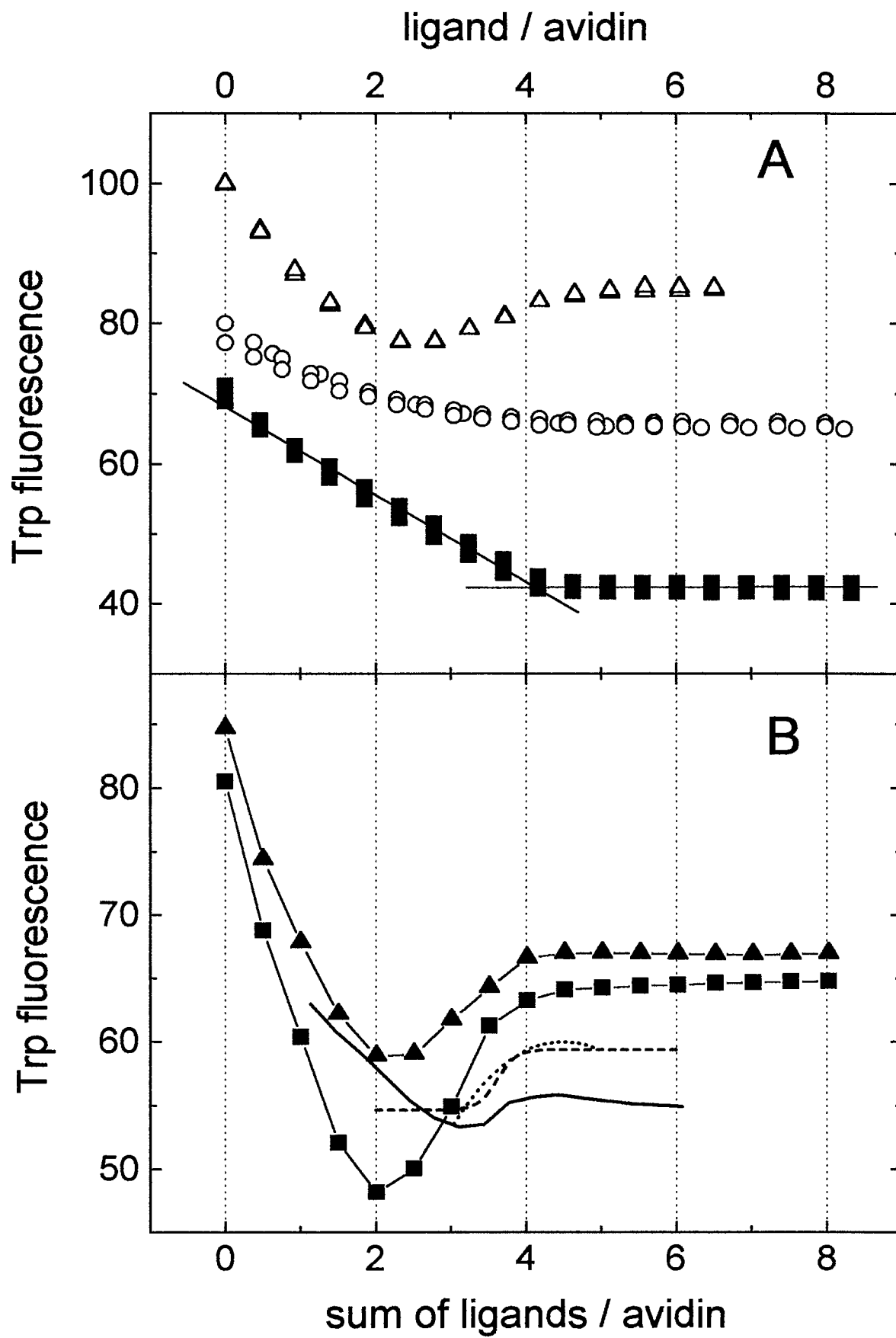
0 10 20 30 40 50 60

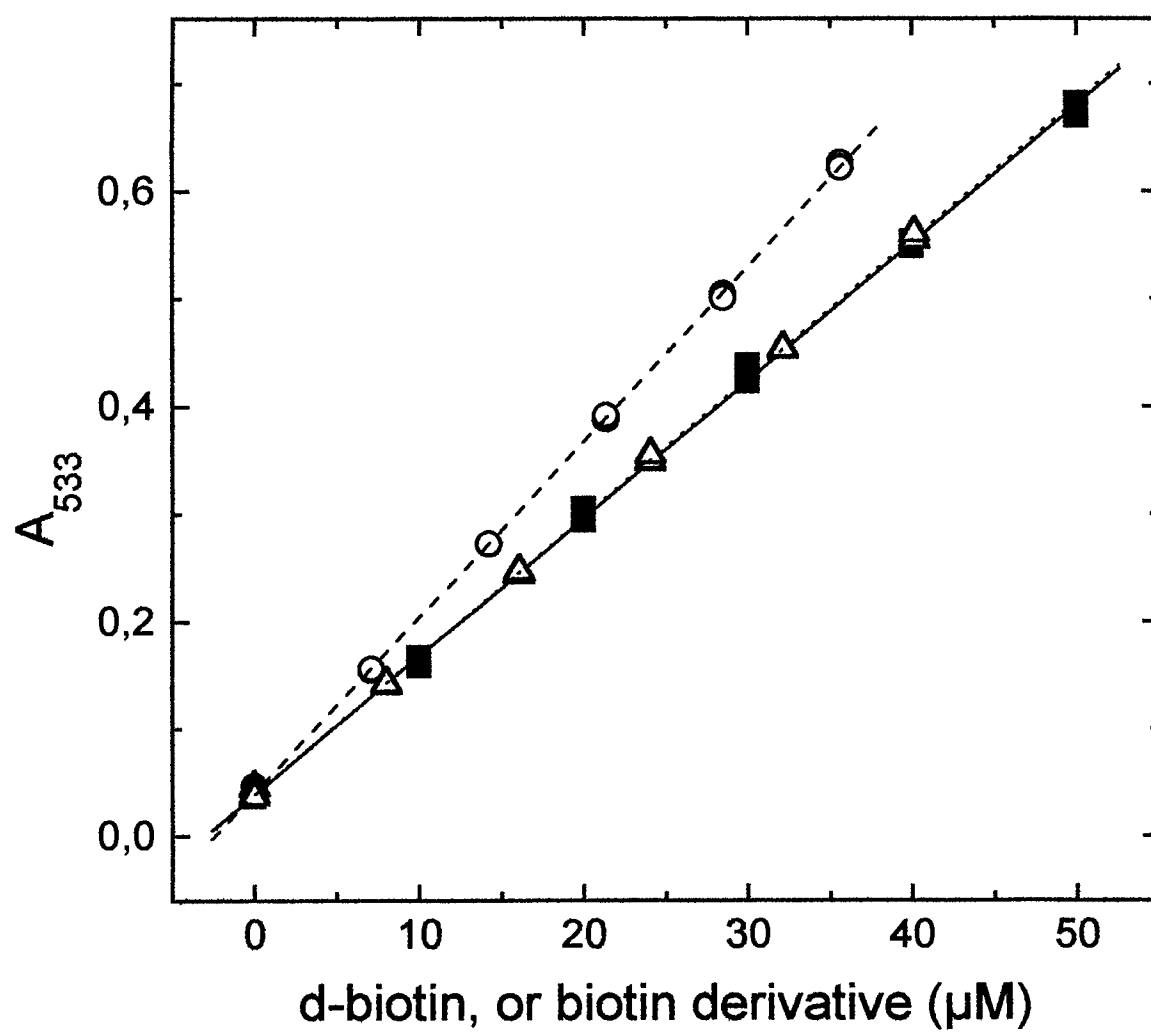
ANS fluorescence



ANS fluorescence







Biotin–Fluorophore Conjugates with Poly(ethylene glycol) Spacers Retain Intense Fluorescence after Binding to Avidin and Streptavidin

Hermann J. Gruber,* Markus Marek, Hansgeorg Schindler, and Karl Kaiser

Institute of Biophysics, J. Kepler University, Altenberger Strasse 69, A-4040 Linz, Austria. Received February 14, 1997[§]

Conventional biotin–fluorophore conjugates with ~14 atom spacers lose most of their fluorescence when binding to avidin or streptavidin, as is demonstrated in the present study. This explains the unusual fact that only biotinylated marker enzymes, but not fluorescent biotins, are regularly used in bioanalytic assays. Novel biotin–spacer–fluorophore conjugates are presented that retain intense fluorescence when binding to avidin or streptavidin. Preservation of fluorescence depends upon the use of poly(ethylene glycol) (PEG) spacers, which are shown not to interfere with biotin function. The observed absence of nonspecific interactions may also be attributed to the PEG chain. These novel fluorescent biotins are expected to be excellent new tools in fluorescence microscopy and related techniques.

INTRODUCTION

Specific detection of immobilized biomolecules is a standard task in modern bioscience. Generally target molecules are recognized by specific probe molecules (antibodies, oligonucleotides, etc.) which are labeled for detection (Wilchek and Bayer, 1990a). Direct labeling of a probe with a marker function (fluorophore, enzyme, etc.) implies an irreversible restriction to a single detection method. Biotinylation of a probe, however, allows the use of the same probe in combination with almost any known detection method because a wide variety of biotinylated markers or (strept)avidin–marker conjugates is commercially available for the postlabeling of biotinylated probes via biotin–(strept)avidin–biotin bridges or via biotin–(strept)avidin bridges, respectively (Wilchek and Bayer, 1988, 1990b).

Fluorescent markers play a pre-eminent role in bioanalytic assays; therefore, it seems logical to expect extensive use of fluorescent biotins. However, conventional biotin–fluorophore conjugates (with ~14 atom spacers) lose most of their fluorescence when binding to (strept)avidin, as is demonstrated in the present study. This adverse effect explains why only two fluorescent biotins are commercially available—and mostly used for purposes other than postlabeling of biotinylated probes (Chu et al., 1994; Schray et al., 1988; Shah et al., 1994).

In the present study a series of novel biotin–spacer–fluorophore conjugates is presented that retain intense fluorescence after binding to (strept)avidin. Preservation of fluorescence depends on the use of PEG₁₉₀₀¹ or PEG₈₀₀ as spacer elements: The PEG chains minimize dye–dye and dye–protein interactions, which cause the quenching in complexes of conventional fluorescent biotins with (strept)avidin.

While PEG spacers in biotin–PEG–fluorophore conjugates are beneficial to the fluorophore function, the question remained to be answered whether the PEG spacers would hinder the biotin terminus from binding

to (strept)avidin. In the preceding study with nonfluorescent biotin–PEG conjugates (see the first of three papers in this issue) it has been demonstrated that 4:1 complexes with (strept)avidin were indeed formed and that at least three biotin–PEG elements per tetrameric receptor protein were bound on a time scale of hours. The present study shows that nearly four biotin–PEG–fluorophore ligands/protein remain bound on a time scale of minutes, as is desired in bioanalytic fluorescence detections.

EXPERIMENTAL PROCEDURES²

Materials. P.a. grade materials were used as far as commercially available. Affinity-purified avidin and streptavidin, *d*-biotin, Boc₂O, and DACA were obtained from Sigma. DMF and Et₃N were purchased from Fluka. NaCl and methanol were obtained from Riedel de Haen. 1,12-diamino-4,9-dioxadodecane was obtained from Aldrich. Acetic acid and chloroform were purchased from Baker. fluorescein–biotin (see footnote 1 for full structure), ANS, 5-(and 6)-carboxyfluorescein succinimidyl ester, and 5-(and 6)-carboxytetramethylrhodamine succinimidyl ester were obtained from Molecular Probes. Cy3

¹ Abbreviations: ANS, 2-anilinonaphthalene-6-sulfonic acid; biotin, biotinoyl group; biotin–NHS, succinimidyl ester of biotin; biotin–dode–TMR, 5-(and 6)-[[*N*-(12-biotinamido-4,9-dioxadodecyl)]aminocarbonyl]tetramethylrhodamine; biotin–NH–PEG₈₀₀ or 1900–NH₂·HCl, *N*-biotinoyl-*O*,*O'*-bis(2-aminopropyl)poly(ethylene glycol)₈₀₀ or 1900 hydrochloride; biotin–PEG₈₀₀ or 1900–dye, see Scheme 1; biotin–PEG₈₀₀ or 1900–Flu, see Scheme 1; biotin–PEG₈₀₀ or 1900–TMR, see Scheme 1; biotin–PEG₈₀₀ or 1900–Cy3, see Scheme 1; biotin–PEG₈₀₀ or 1900–Cy5, see Scheme 1; Boc₂O, di-*tert*-butyl pyrocarbonate; Boc, *tert*-butoxycarbonyl group; DACA, *p*-(dimethylamino)cinnamaldehyde; DMF, *N,N*-dimethylformamide; EDTA, ethylenediamine-*N,N,N,N*-tetraacetic acid; Et₃N, *N,N,N*-triethylamine; Flu, 5-(and 6)-carboxyfluorescein residue; fluorescein–biotin, 5-[[*N*-[5-[*N*-(6-biotinoyl)amino]hexanoyl]amino]pentyl]thioureydyl]fluorescein; (strept)avidin, streptavidin and/or avidin; FRET, fluorescence resonance energy transfer; NHS, *N*-hydroxysuccinimide; PEG, poly(ethylene glycol); RT, room temperature; TMR, 5-(and 6)-carboxytetramethylrhodamine residue.

² Detailed procedures and NMR data can be found in the Supporting Information.

* Author to whom correspondence should be addressed [telephone +43 (732) 2468-9271; fax +43 (732) 2468-822; e-mail hermann.gruber@jk.uni-linz.ac.at].

[§] Abstract published in *Advance ACS Abstracts*, June 15, 1997.

and Cy5 monofunctional dyes (succinimidyl esters) were purchased from Amersham. Sephadex-based gels were obtained from Pharmacia. All other materials were purchased from Merck. Biotin-NHS was prepared as described (Wilchek and Bayer, 1990c). Absolute DMF was prepared according to a standard procedure. Biotin-NH-PEG₈₀₀-NH₂·HCl and biotin-NH-PEG₁₉₀₀-NH₂·HCl were synthesized as described before (see the first of three papers in this issue).

Buffers. Buffer A contained 100 mM NaCl, 50 mM NaH₂PO₄, and 1 mM EDTA, adjusted to pH 7.5 with NaOH. Buffer B contained 1 mM NaH₂PO₄ (adjusted to pH 7.5 with NaOH) and variable NaCl concentrations (as specified).

Methods. *Synthesis of N-Boc-4,9-dioxo-1,12-diaminododecane·CH₃COOH.* 4,9-Dioxo-1,12-diaminododecane (29.4 mmol) in methanol was reacted with 28.4 mmol of Boc₂O under Ar. After addition of toluene and 5 mL of acetic acid, the mixture was taken to dryness (10.5 g of crude product). Silica chromatography of 3 g of crude product in chloroform/methanol/acetic acid mixtures (90:10:0.1 and 70:30:5) gave 3.20 mmol of product, which was pure by TLC.

Synthesis of N-Boc-N-biotin-4,9-dioxo-1,12-diaminododecane. N-Boc-4,9-dioxo-1,12-diaminododecane·HCl (1.8 mmol) was reacted with 2.7 mmol of biotin-NHS and 240 μ L of Et₃N in 10 mL of absolute DMF. Excess biotin-NHS was hydrolyzed with water. After solvent removal, the crude product was purified on silica 60 (eluent chloroform/methanol/acetic acid 120:30:0.5), resulting in 1.11 mmol of product (pure by TLC).

Synthesis of N-Biotin-4,9-dioxo-1,12-diaminododecane·HCl. N-Boc-N-biotin-4,9-dioxo-1,12-diaminododecane (1.11 mmol) was deprotected with 98% formic acid, and the crude product was purified by ion exchange chromatography on SP Sephadex C-25. Salt was removed by extracting deprotonated product into chloroform. Drying and lyophilization from dilute HCl gave 0.64 mmol of product (pure by TLC).

Synthesis of Biotin-dode-TMR. N-Biotin-4,9-dioxo-1,12-diaminododecane·HCl (19 μ mol) was reacted with 30 μ mol of 5-(and 6)-carboxytetramethylrhodamine succinimidyl ester and 10 μ L of Et₃N in chloroform under Ar. TLC showed quantitative labeling of the primary amine. The mixture was taken to dryness and purified by chromatography on silica 60 (chloroform/methanol/water 70:26:4). In spite of using 100 g of silica 60 it was impossible to remove those two TMR derivatives, which were already present in the commercial TMR reagent and whose *R_f* values were just below (0.45) or above (0.56) that of the product (0.51). For characterization, TLC spots were harvested quantitatively, extracted with chloroform/ethanol/water (10:15:2), clarified by centrifugation, and checked for TMR contents by their UV-vis spectra. The two byproducts together gave rise to 17% of the absorption at 550 nm, while the correct main product contributed with 83% to *A*₅₅₀. From determination of biotin end group contents (by the ANS method, see below) a similar estimate of purity was obtained (87% as compared to the TMR group contents estimated from UV-vis absorption).

Synthesis of Biotin-PEG₈₀₀-TMR. Biotin-NH-PEG₈₀₀-NH₂·HCl (8.4 μ mol) was quantitatively labeled with 23 μ mol of 5-(and 6)-carboxytetramethylrhodamine succinimidyl ester in chloroform/Et₃N under Ar. After evaporation, the crude product was gel filtered on Sephadex G-25 in distilled water, yielding 4.8 μ mol of biotin-PEG₈₀₀-TMR according to biotin end group assay (see below). Quantitative TLC (as performed with biotin-dode-TMR,

see above) showed that free TMR gave rise to 2% of the absorption at 550 nm, while the product contributed 98% to *A*₅₅₀.

Synthesis of Biotin-PEG₁₉₀₀-TMR. The procedure was the same as for the PEG₈₀₀ derivative. Forty-three milligrams of biotin-NH-PEG₁₉₀₀-NH₂·HCl (nominally 18.7 μ mol, ~20% water content) was reacted with 36 μ mol of 5-(and 6)-carboxytetramethylrhodamine succinimidyl ester. Yield = 12.8 μ mol of biotin-PEG₁₉₀₀-TMR according to biotin end group assay (see below). Quantitative TLC (as performed with biotin-dode-TMR, see above) showed that free TMR gave rise to 3% of the absorption at 550 nm, while the product contributed 97% to *A*₅₅₀.

Synthesis of Biotin-PEG₈₀₀-Flu. Twenty-two micromoles of biotin-NH-PEG₈₀₀-NH₂·HCl was labeled with 43 μ mol of 5-(and 6)-carboxyfluorescein succinimidyl ester in DMF/Et₃N under Ar. After solvent removal, the residue was dissolved in chloroform and successively washed with 200 mM Na₂CO₃ (saturated with NaCl) and with dilute acetic acid (saturated with NaCl). The organic layer was dried, evaporated, redissolved in 2 mL of 3 mM Na₂CO₃, and chromatographed on QAE Sephadex A-25 using buffer B with increasing NaCl concentrations. Salt was removed by extraction into chloroform. Yield = 18 μ mol, pure by TLC.

Synthesis of Biotin-PEG₁₉₀₀-Flu. Fifty milligrams of biotin-NH-PEG₁₉₀₀-NH₂·HCl (22 μ mol) was reacted with 15.5 mg of 5-(and 6)-carboxyfluorescein succinimidyl ester (33 μ mol). The procedure was the same as for the PEG₈₀₀ homologue, except that 50 mM instead of 150 mM NaCl in buffer B was used to elute the product from QAE-Sephadex A-25. Yield = 12 μ mol product, pure by TLC.

Synthesis of Biotin-PEG₈₀₀-Cy3. Biotin-NH-PEG₈₀₀-NH₂·HCl (1.7 μ mol) was reacted with one vial of Cy3 monofunctional dye ("reactive dye to label 1 mg of antibody" according to Amersham) in absolute DMF/Et₃N. After solvent removal, the residue was dissolved in buffer B and chromatographed on QAE Sephadex A-25, using 125 mM NaCl in buffer B for product elution. Yield = 63 nmol determined from *A*₅₅₀ (ϵ ₅₅₀ = 150 000 M⁻¹ cm⁻¹ for Cy3 according to Amersham) or 54 nmol according to biotin end group assay with ANS (see below). The uncoupled dye was eluted from QAE-Sephadex A-25 with 1 M NaCl and amounted to 74 nmol according to *A*₅₅₀.

Synthesis of Biotin-PEG₁₉₀₀-Cy3. The procedure was the same as for the PEG₈₀₀ derivative, except that 0.44 μ mol of biotin-NH-PEG₁₉₀₀-NH₂·HCl was reacted, and 75 mM NaCl in buffer B was used for elution from the ion exchange column. Yield = 55 nmol determined from *A*₅₅₀ or 52 nmol according to biotin end group assay with ANS (see below).

Synthesis of Biotin-PEG₁₉₀₀-Cy5. The procedure was the same as for the corresponding Cy3 analogue, except that 5 mg of biotin-NH-PEG₁₉₀₀-NH₂·HCl (2.2 μ mol) was reacted with one vial of Cy5 monofunctional dye. Yield = 55 nmol determined from *A*₆₄₇ (ϵ ₆₄₇ = 250 000 M⁻¹ cm⁻¹ for Cy5 according to Amersham) or 39 nmol according to biotin end group assay with ANS (see below).

Quantitative Assay for Biotin End Groups and for Biotin Binding Sites. A published fluorescence assay for avidin-biotin interaction (Mock and Horowitz, 1990) was modified as described before (see the first of three papers in this issue). Typically, 2 mL of buffer A containing 1 nmol of avidin was mixed with 20 μ L of 5 mM ANS, and ~2 nmol (estimated from UV-vis absorption) of a biotin-fluorophore conjugate was added to saturate about half of the receptor sites on avidin. The unoccupied sites were then titrated with 5 μ L increments of exactly 100 μ M

d-biotin in buffer A while the fluorescence of the pseudoligand ANS was monitored at 328 nm excitation (10 nm slit) and 408 nm emission wavelength (10 nm slit). The inflection point in the titration curve indicated saturation of all biotin binding sites (determined by parallel standardization of the avidin stock solution with *d*-biotin alone). Fortunately, none of the biotin–fluorophore conjugates caused significant background fluorescence under these assay conditions.

The ANS assay was also used to determine functional biotin binding sites in avidin stock solutions as described before (see the first of three papers in this issue), whereas streptavidin was functionally characterized by titration with biotin–PEG₈₀₀–pyrene (see the third of three papers in this issue) because streptavidin is known not to bind the pseudoligand ANS (Mock and Horowitz, 1990).

Gel Filtration Assay for Binding of Biotin–PEG–Dye to Avidin and Streptavidin. Specificity and metastability of biotin–PEG–dye binding to avidin or streptavidin was tested by gel filtration as previously described (see the first of three papers in this issue). Typically, 0.5 mL samples of buffer A containing 50 μ M “functional” avidin (see above) or 2 μ M “functional” streptavidin (see above) and various amounts of biotin–PEG–dye were incubated for 1 h at 25 °C and subjected to gel filtration on a 1 \times 48 cm column of Sephadex G-100 at RT. Elution was at 0.25 mL/min with buffer A while fractions were collected at 5 min intervals. All fractions were assayed for avidin or streptavidin by A_{282} (corrected for $\epsilon_{282} = 0.08\epsilon_{550}$ or $0.20\epsilon_{550}$ or $0.18\epsilon_{496}$ in the case of Cy3–, TMR–, and Flu–PEG conjugates, respectively) and for dye contents by UV–vis absorbance at λ_{\max} . Molar extinction coefficients for avidin and streptavidin were taken from the literature (Green, 1990).

Measurement of Fluorescence in Complexes of Biotin–PEG–Dye with Avidin and Streptavidin. In a “forward titration” 2 mL of receptor protein (≤ 80 nM) in buffer A was titrated with a stock solution of biotin–PEG–dye (7–15 μ M). In the “reverse titration” mode 2 mL of fluorescent ligand (≤ 320 nM) in buffer A was titrated with stock solutions of avidin or streptavidin (2–4 μ M). All fluorescence signals were corrected for the small dilution factors. Time intervals were 3–5 min as required for equilibration at RT (except for titration of streptavidin with fluorescein–biotin, for which 10 min intervals were required). The concentrations of receptor proteins and ligands refer to biotin binding sites and biotin termini, respectively, as determined by functional titrations (see above).

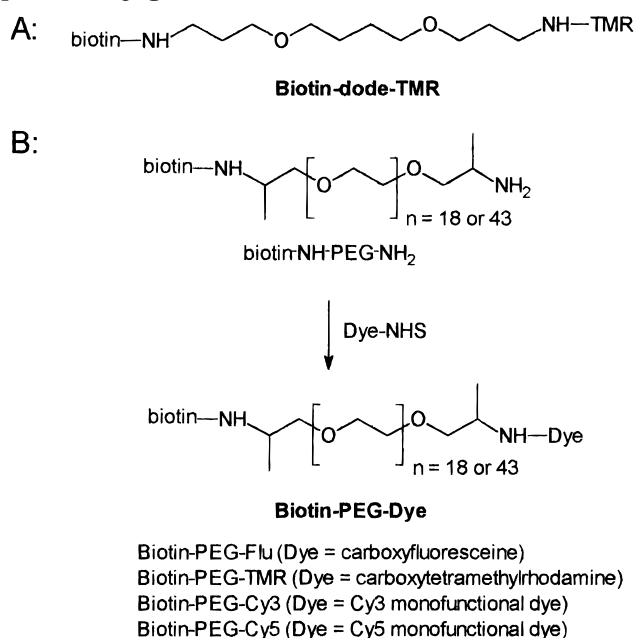
RESULTS

Syntheses of Biotin–Spacer–Dye Conjugates.

The goal of the present study was the identification of biotin–spacer–fluorophore structures that retain high fluorescence yield when binding to avidin or streptavidin. PEG₁₉₀₀, PEG₈₀₀, and a 14-atom homologue were chosen as spacers, and the most popular/promising fluorochrome labels were tested (see Scheme 1).

Biotin–PEG–dyes with anionic fluorophores could be subjected to ion exchange chromatography, resulting in homogeneous products as evidenced by TLC. In contrast, special precautions were necessary to arrive at 97–98% purity with the zwitterionic TMR derivatives (see Experimental Procedures). Purity and 1:1 ratios of biotin/fluorophore end groups were also confirmed by ¹H NMR. Virtually noise-free single-pulse spectra were recorded at 500 MHz to obtain correct integrals from unsaturated signals. Moreover, the specific bindability of all biotin–PEG–dyes to (strept)avidin was close to 100%, as determined by gel filtration assays (compare Figure 5) which

Scheme 1. Synthesis and Structure of Biotin–Fluorophore Conjugates



further excluded the presence of fluorescent molecules without a biotin terminus.

One short fluorescent biotin (fluorescein–biotin) with a 14-atom spacer was commercially available. For a more systematic study a second example was synthesized in which biotin is linked to TMR via a 14-atom spacer also (see Scheme 1). In spite of moderate purity the product fully served its intended role as a poor fluorescent ligand for avidin and streptavidin (see Figures 2 and 9).

Fluorescence Properties of Biotin–Spacer–Fluorophore Conjugates before/after Binding to Avidin or Streptavidin. The superiority of novel biotin–PEG–dyes over conventional fluorescent biotins is demonstrated in Figures 1 and 2. Short fluorescein–biotin is highly quenched when binding to avidin (Figure 1B, open squares) or streptavidin (Figure 1C, open squares), and the same is true for short biotin–dodecyl–TMR (Figure 2C, circles). Avidin and streptavidin are tetravalent receptor proteins for biotin; therefore, the abrupt rise in fluorescence at ligand/receptor ratios $> 4:1$ indicates stoichiometric binding, and the absence of nonspecific binding is evidenced by the strictly parallel nature of this linear rise with the linear dose response in the absence of receptor protein. Saturation at 4:1 stoichiometry and absence of further binding were also observed with biotin–PEG–dyes (see Figures 1, 2A,B, and 3A) except for the Cy3 derivatives (see Figures 3B,C and 4).

In contrast to short fluorescein–biotin, the long biotin–PEG₁₉₀₀–Flu showed little quenching when bound to avidin (Figure 1A). More quenching was observed with the intermediate conjugate biotin–PEG₈₀₀–Flu when bound to avidin (Figure 1B, circles) or streptavidin (Figure 1C, circles), but the fluorescence signals in 4:1 complexes with receptor protein were still very intense in comparison to those of short fluorescein–biotin (Figure 1B,C, open squares).

Biotin–PEG–TMR conjugates (Figure 2A,B) differ from corresponding fluorescein analogues in two aspects: The effect of PEG chain length is much less pronounced, and the fluorescence quenching in the bound state is increased, reaching $\sim 50\%$ in the 4:1 complexes with avidin and streptavidin. Taking into account the zwitterionic nature of TMR and the smaller Stokes shift as compared to fluorescein, it is not surprising that self-

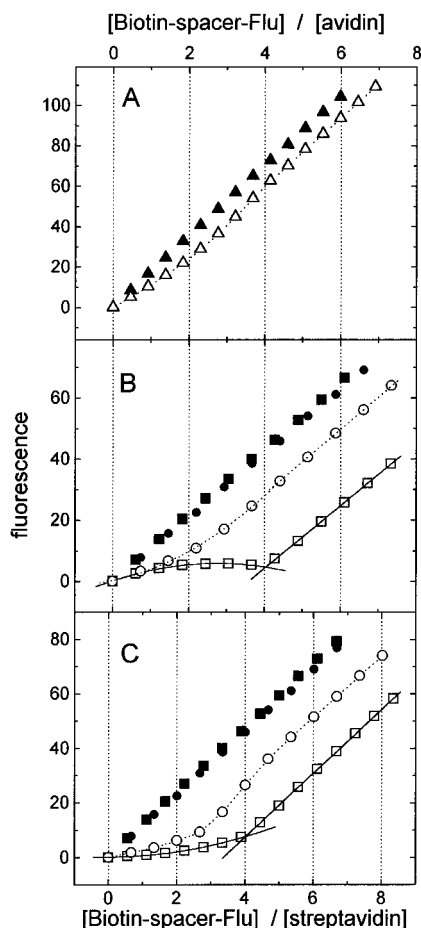


Figure 1. Fluorescence of biotin-spacer-fluorescein conjugates in the presence (open symbols) and absence (controls, solid symbols) of avidin or streptavidin. Excitation was at 485 nm (5 nm slit), and emission was at 525 nm (5 nm slit). (A) 50 nM avidin was titrated with 9.2 μ M biotin-PEG₁₉₀₀-Flu. (B) 50 nM avidin was titrated with 14.7 μ M biotin-PEG₈₀₀-Flu (circles) or with 12.2 μ M fluorescein-biotin (squares). (C) 55 nM streptavidin was titrated with 14.7 μ M biotin-PEG₈₀₀-Flu (circles) or with 12.2 μ M fluorescein-biotin (squares). In the presence of 4 μ M *d*-biotin neither avidin nor streptavidin had an effect on any of the biotin-spacer-fluorescein conjugates (not shown to avoid overloading of the figures).

association and/or self-quenching by FRET will be favored in TMR. Nevertheless, biotin-PEG-TMR conjugates (Figure 2A,B) compare well with short fluorescent biotins (open squares in Figure 1B,C, circles in Figure 2C).

The dark red-emitting conjugate biotin-PEG₁₉₀₀-Cy5 showed much similarity with biotin-PEG₁₉₀₀-Flu in that fluorescence was mostly preserved after binding to avidin (Figure 3A). The small reduction just allowed visualization of the 4:1 complex formation.

Best results were obtained with biotin-PEG-Cy3 conjugates (Figures 3B,C and 4). The optimal case is represented by biotin-PEG₁₉₀₀-Cy3, where fluorophore performance was virtually independent from binding to avidin (Figure 3B) while biotin-PEG₈₀₀-Cy3 seemed "more than optimal" because binding to avidin enhanced fluorescence yields above the control values observed in the absence of avidin (Figure 3C). This enhancement was further verified by inverse titration of a constant fluorescent ligand concentration with a concentrated avidin stock solution (Figure 3D). In contrast to avidin, streptavidin caused little increase in the fluorescence of biotin-PEG₈₀₀-Cy3 (Figure 4).

Specificity of Biotin-PEG-Dye Binding to Avidin and Streptavidin. While emphasizing the out-

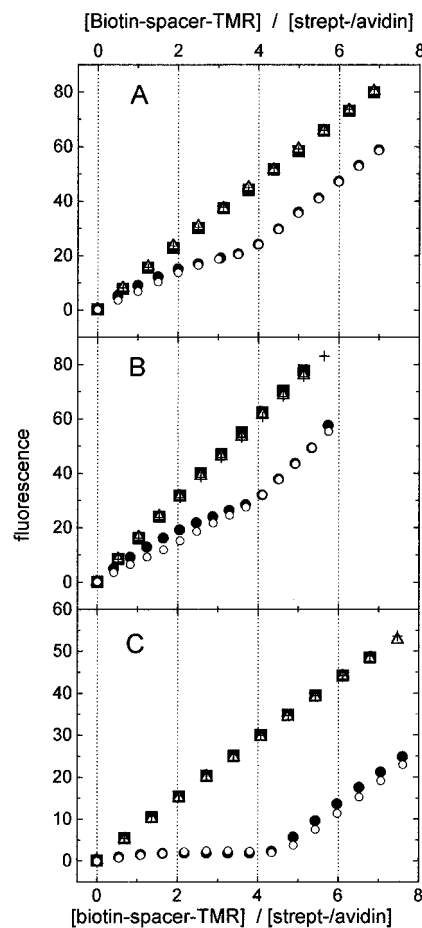


Figure 2. Fluorescence of biotin-spacer-TMR conjugates in the presence and absence (controls, ■) of avidin or streptavidin. Excitation was at 540 nm (5 nm slit) and emission at 580 nm (slit 5 nm except for biotin-dode-TMR, for which a 10 nm slit was used). 80 nM avidin (●) or streptavidin (○) was titrated with 10.0 μ M biotin-PEG₁₉₀₀-TMR (A), 8.2 μ M biotin-PEG₈₀₀-TMR (B), or 22 μ M biotin-dode-TMR (C; 17% of the TMR labels had no biotin terminus—see Experimental Procedures—therefore, 17% of the corresponding control signal in the absence of protein was subtracted from the signal in the presence of protein to estimate the fluorescence that originates from biotin-dode-TMR). In the presence of 8 μ M *d*-biotin neither avidin (Δ) nor streptavidin (+) had an effect on any of the biotin-spacer-fluorescein conjugates.

standing fluorescence properties of biotin-PEG₈₀₀-Cy3, we have so far ignored a puzzling feature of the titration curves in Figures 3C and 4: They are obviously triphasic. At ligand/receptor ratios <4:1 the slopes are steeper than normal, between 4 and 8 ligands/receptor protein the slopes are flatter than normal, and above 8 ligands/receptor the linear increases appear parallel to control series in the absence of protein (see lines in Figure 4). We are thus confronted with an apparent 8:1 stoichiometry between biotin-PEG₈₀₀-Cy3 and avidin (Figure 3C) or streptavidin (Figure 4), which has never been reported for any other biotin derivative. Yet binding of all 8 ligands fully depends on specific interaction with biotin end groups, as is evidenced by complete block with *d*-biotin (see triangles in Figures 3C and 4).

Fortunately, ligands 5–8 are easily removed by "washing", and only ligands 1–4 stay tightly bound to the tetravalent receptor protein as demonstrated by gel filtration of a 8:1 mixture of biotin-PEG₈₀₀-Cy3 and streptavidin (Figure 5C). Specificity of binding is further proven by complete bindability in the absence of *d*-biotin (Figure 5B) and by complete absence of binding in the presence of *d*-biotin (Figure 5A).

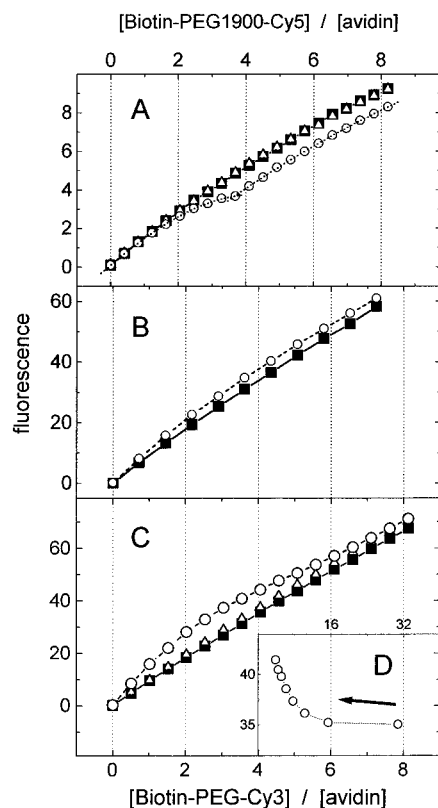


Figure 3. Fluorescence of biotin-PEG-cyanine conjugates in the presence (○) and absence (controls, ■) of avidin. Excitation/emission was at 650 nm/670 nm for Cy5 labels (A) and at 550 nm/570 nm for Cy3 labels (B–D); excitation slits were 5 nm and emission slits 10 nm. (A) 80 nM avidin was titrated with 6.6 μ M biotin-PEG₁₉₀₀-Cy5 (○). In a parallel run, avidin had been blocked with 10 μ M *d*-biotin (△) before titration with fluorescent ligand. (B) 80 nM avidin was titrated with 11.0 μ M biotin-PEG₁₉₀₀-Cy3 (○). (C) 80 nM avidin was titrated with 7 μ M biotin-PEG₈₀₀-Cy3 (○). In a parallel run, avidin had been blocked with 10 μ M *d*-biotin (△) before titration with fluorescent ligand. (D) Inverse titration of 320 nM biotin-PEG₈₀₀-Cy3 with 2.08 μ M avidin stock solution; the arrow indicates starting point and direction of the titration experiment.

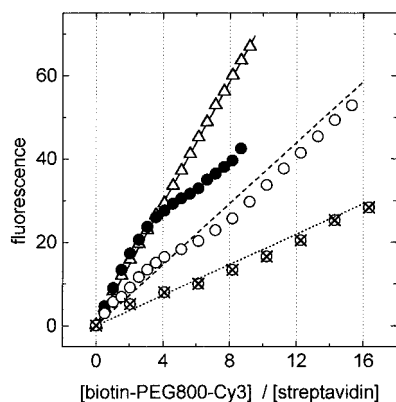


Figure 4. Fluorescence of biotin-PEG₈₀₀-Cy3 in the presence or absence of streptavidin. 40 (●), 20 nM (○), or 10 nM streptavidin (⊗) were titrated with 7.0 μ M biotin-PEG₈₀₀-Cy3 while fluorescence was monitored at 550 nm excitation (5 nm slit) and 570 nm emission wavelength (10 nm slit). In parallel control experiments (—, ---, ···, respectively) the receptor protein was absent. Specificity was tested by blocking 40 nM streptavidin with 4 μ M *d*-biotin (△) before titration with fluorescent ligand.

Unequivocal proof that only specific binding occurs in spite of the unexpected 8:1 stoichiometry was obtained from measurement of Cy3 label fluorescence polarization (Figure 6B). When avidin was blocked with *d*-biotin

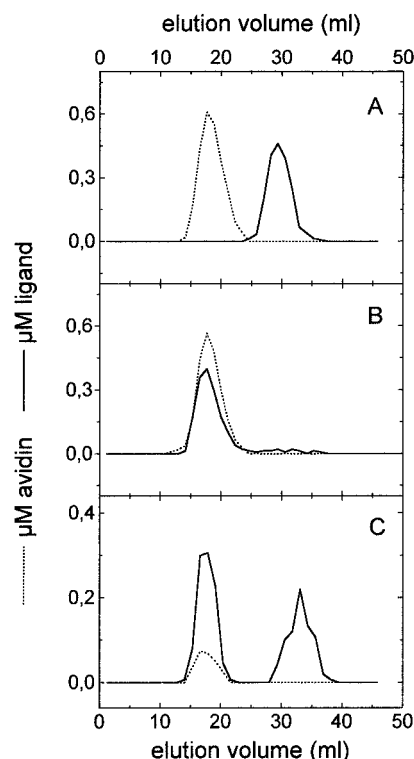


Figure 5. Gel filtration assay for the binding of biotin-PEG₁₉₀₀-Cy3 to avidin or streptavidin. (A) 3.1 nmol of avidin was blocked with 400 nmol of *d*-biotin, and 3.1 nmol of biotin-PEG₁₉₀₀-Cy3 was added before gel filtration (see Experimental Procedures). (B) 3.1 nmol of avidin and 3.1 nmol of biotin-PEG₁₉₀₀-Cy3 were equilibrated before gel filtration. (C) 0.5 nmol of streptavidin and 4 nmol of biotin-PEG₁₉₀₀-Cy3 were equilibrated before gel filtration.

(triangles), it had as little effect on the mobility of biotin-PEG₈₀₀-Cy3 as if it were completely absent (squares). In contrast, Cy3 labels were immobilized in complexes with <4 ligands/avidin, whereas unusual enhancement of average mobility is seen when ligands 5–8 bind to avidin (circles). Beyond 8:1 ratios the average fluorescence polarization obviously increased because free ligands with somewhat higher polarization contributed to the average values.

Fluorescence polarization also served to verify that the unexpected 8:1 stoichiometry only occurred with Cy3 labels (Figure 6B) and not with Cy5 labels (Figure 6A), where saturation was reached at the normal 4:1 ratio, in agreement with the fluorescence titration curve in Figure 3A. Such delicate influence of only two methine groups in the fluorophore fits in with the picture of a weak interaction between ligands 5–8 and (strept)avidin.

It can be summarized that binding of biotin-PEG₈₀₀-Cy3 to (strept)avidin is only specific, in spite of the unusual 8:1 stoichiometry. Yet for practical purposes it is not necessary to resolve the paradox because ligands 5–8 bind with much lower affinity and metastability and will be washed away in typical applications.

Mobility of Fluorochrome Labels in Complexes of Biotin-PEG-Dye and Avidin or Streptavidin.

Above it has been shown that fluorescence polarization can be used as a sensitive empirical parameter to monitor ligand/receptor stoichiometries. In this sense Figures 7 and 8 generally confirm 4:1 complex formation in the case of all biotin-spacer-fluorescein and biotin-spacer-TMR conjugates, respectively. No sharp inflection points can be expected at the 4:1 ratios because average polarization in 4:1 complexes is slightly higher than in the unbound state, and further addition of free ligands will necessarily

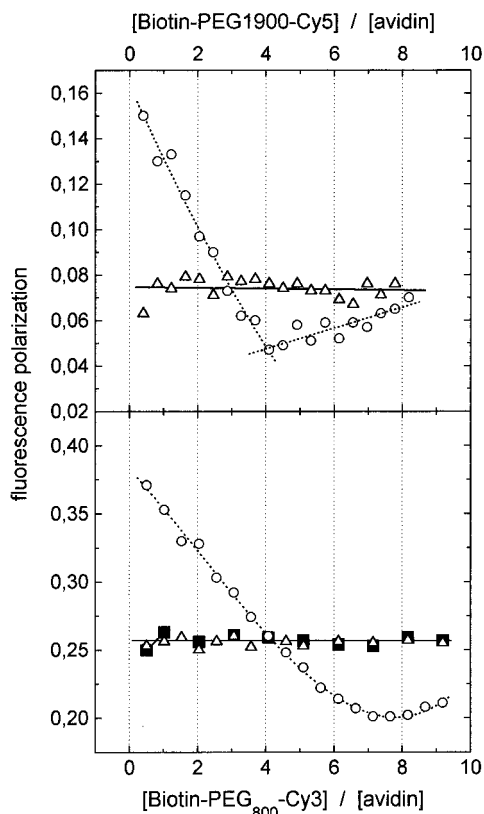


Figure 6. Fluorescence polarization in complexes of biotin-PEG₁₉₀₀-Cy5 or biotin-PEG₈₀₀-Cy3 with avidin. (A) 80 nM avidin was titrated with 6.6 μ M biotin-PEG₁₉₀₀-Cy5 (○) while fluorescence polarization was monitored at 650 nm excitation (10 nm slit) and 670 nm emission wavelength (10 nm slit). In a parallel run, avidin was specifically blocked with 10 μ M *D*-biotin (Δ , —) before titration with fluorescent ligand. (B) 80 nM avidin was titrated with 8.2 μ M biotin-PEG₈₀₀-Cy3 (○) while fluorescence polarization was monitored at 550 nm excitation (10 nm slit) and 570 nm emission (10 nm slit). In a parallel control experiment, the receptor protein was omitted. In another control experiment, avidin was specifically blocked with 10 μ M *D*-biotin (Δ) before titration with fluorescent ligand.

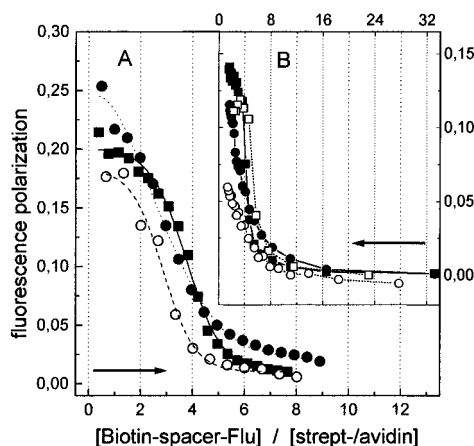


Figure 7. Fluorescence polarization in complexes of fluorescein-biotin (squares) or biotin-PEG₈₀₀-Flu (circles) with avidin (solid symbols) or streptavidin (open symbols). Excitation was at 485 nm (5 nm slit) and emission at 525 nm wavelength (5 nm slit). (A) Forward titration of avidin (80 nM) with fluorescent ligand; (B) reverse titration of fluorescent ligand (320 nM) with avidin or streptavidin. The arrows indicate starting points and directions of the titration experiments in each panel.

cause asymptotic approximation of the average value to free state polarization.

Magnitude and direction of fluorescence polarization provide a rough picture of dynamics and interactions

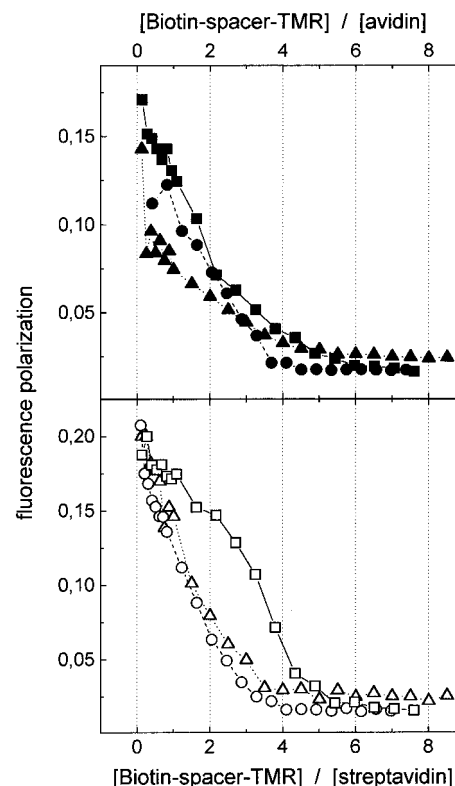


Figure 8. Fluorescence polarization in complexes of biotin-spacer-TMR conjugates with avidin (A) or streptavidin (B). 80 nM receptor protein was titrated with 27 μ M biotin-dodecyl-TMR (squares) or 8.2 μ M biotin-PEG₈₀₀-TMR (circles) or 10.0 μ M biotin-PEG₁₉₀₀-TMR (triangles). Excitation was at 540 nm (10 nm slit) and emission at 580 nm wavelength (20 nm slit).

within the ligand/receptor associates. Average mobility of fluorescent labels was always maximally reduced at the lowest ligand/receptor ratios (see Figures 6–8), and mobility rapidly increased at higher ratios. Label mobilities in 4:1 complexes of fluorescein derivatives (Figure 7) and TMR derivatives (Figure 8) were still somewhat lower than in the unbound state, as would be anticipated. In 4:1 complexes of biotin-PEG₁₉₀₀-Cy5 (Figure 6A) and in the 8:1 complexes of biotin-PEG₈₀₀-Cy3 (Figure 6B) with avidin, however, fluorophore mobility was higher than in free solution. Obviously PEG-PEG repulsion in the crowded complexes had a mobilizing effect on the free ends of the PEG chains.

Thermodynamics and Kinetics of Binding of Fluorescent Biotins to Avidin and Streptavidin.

Preservation of high fluorescence after binding to (strept)avidin is a necessary but insufficient criterion for fluorescent biotins that are to be used as markers. In addition, binding must be fast, specific, tight, and metastable on the time scale of typical applications. All biotin-PEG-dyes were tested by gel filtration experiments, such as shown in Figure 5: Absence of nonspecific binding (Figure 5A), full bindability to excess of receptor (Figure 5B), and good metastability of the 4:1 complexes on a 1 h time scale (Figure 5) were verified without exception.

In the accompanying study (see the third of three papers in this issue) the association/dissociation kinetics of (strept)avidin and biotin-PEG-pyrene conjugates were studied by suitable fluorescence methods. These assays were extended to the series of biotin-spacer-TMR conjugates, which generally showed about 3-fold higher affinities and about 2-fold slower dissociation as compared to pyrene-labeled analogues. All details are included in the pyrene study (see the third of three papers

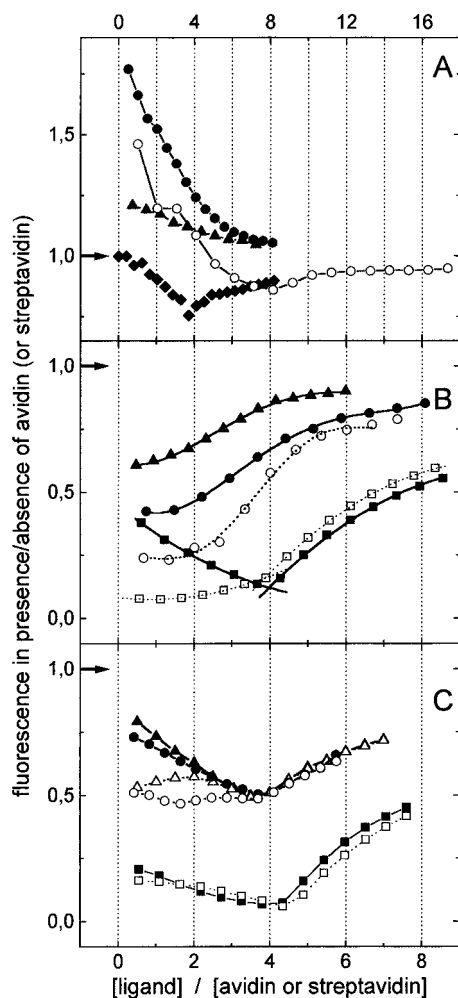


Figure 9. Persistence of biotin-PEG-dye fluorescence after binding to avidin (solid symbols) or streptavidin (open symbols). PEG₁₉₀₀ spacers are indicated by triangles and diamonds, PEG₈₀₀ spacers by circles, and 14 atom spacers by squares. (A) Cy3 derivatives (calculated from Figure 3B,C and from the 20 nM streptavidin titration in Figure 4) and Cy5 derivative (diamonds, calculated from Figure 3A); (B) fluorescein derivatives (calculated from Figure 1); (C) TMR derivatives (calculated from Figure 2). The arrow in each panel indicates a "relative fluorescence" of 1.0; that is, the fluorescence of the label is not altered when the biotin terminus binds to avidin or streptavidin.

in this issue) to avoid splitting of coherent data (for practical relevance of these results, see below).

DISCUSSION

The aim of this study was identification of biotin-spacer-fluorophore conjugates that can serve as intense fluorescence markers for immobilized avidin or streptavidin. Three criteria were to be met simultaneously: (i) high affinity of the biotin termini for avidin and streptavidin, (ii) absence of nonspecific binding, and (iii) high fluorescence yield, i.e. minimal quenching of the ligands in the bound state. These criteria were fulfilled by biotin-PEG-fluorophore conjugates with a number of fluorescent labels (see Scheme 1).

Binding of biotin-PEG-dyes (and of nonfluorescent biotin-PEG conjugates, see the first of three papers in this issue) is not essentially different from that of previously known biotin derivatives containing ≥ 7 atom spacers with respect to affinities and biphasic dissociation kinetics (Finn et al., 1985; Hofmann et al., 1982; Lavielle et al., 1983; Romovacek et al., 1983). This and two other studies (see the first and third of three papers in this issue) have consistently shown that avidin and strepta-

vidin bind four biotin-PEG conjugates with <3 nM affinity. These four ligands stay largely bound on a time scale of minutes—but at least three ligands/protein are bound with much higher affinity and stay associated for hours.

Nonspecific binding of biotin-PEG conjugates was never detected (see also the first and third of three papers in this issue) as expected for PEG derivatives (Lim and Herron, 1992).

The main result of the present study, however, was the preservation of high fluorescence yield in biotin-PEG-dyes after binding to (strept)avidin. The contrast between conventional and novel fluorescent biotins and the gradual differences among the latter are demonstrated by the normalized plots in Figure 9.

Cy3 and Cy5 derivatives are the obvious champions because relative fluorescence in the bound state versus unbound state is ~ 1 or even higher (Figure 9A). This is particularly fortunate because Cy3 is the "brightest fluorophore" (Wessendorf, 1992) and less sensitive to bleaching than any other fluorochrome label (unpublished observation). Yet Cy5 derivatives seem even more promising because a standard diode laser can be used for excitation at 650 nm and, most of all, background fluorescence of biomatter was seen to be lower by orders of magnitude in comparison to excitation at any shorter wavelength with an argon ion laser.

Nevertheless, biotin-PEG-Flu and biotin-PEG-TMR are highly useful fluorescent ligands (see Figure 9B,C), and the relative drawbacks are compensated by prices that allow the synthesis of reasonable quantities and not just tiny test samples. Moreover, the fluorescence intensity of biotin-PEG₁₉₀₀-TMR was fully sufficient for resolution of "local stoichiometries determined by counting individual molecules" (Schmidt et al., 1996).

In conclusion, the novel biotin-PEG-dyes combine all aspects of good fluorescent ligands and thus appear ready for use in fluorescence microscopy and related techniques involving specific detection of biomolecules.

ACKNOWLEDGMENT

We are indebted to Prof. Dr. H. Falk and his staff for helpful advice and use of spectrometer facilities. This work was supported by the Austrian Research Funds (Project S-6607 to H.S.).

Supporting Information Available: Detailed procedures and NMR data (7 pages). Ordering information is given on any current masthead page.

LITERATURE CITED

- Chignell, C. F., Starkweather, D. K., and Sinha, B. K. (1975) A spin label study of egg white avidin. *J. Biol. Chem.* **250**, 5622–5630.
- Chu, Y.-H., Lees, W. J., Stassinopoulos, A., and Walsh, Ch. T. (1994) Using affinity capillary electrophoresis to determine binding stoichiometries of protein-ligand interactions. *Biochemistry* **33**, 10616–10621.
- Finn, F. M., and Hofmann, K. H. (1985) Synthesis of biotinyl derivatives of peptide hormones and other biological materials. *Methods Enzymol.* **109**, 418–445.
- Green, N. M. (1990) Avidin and Streptavidin. *Methods Enzymol.* **184**, 51–67.
- Hofmann, K., Titus, G., Montibeller, J. A., and Finn, F. M. (1982) Avidin binding of carboxyl-substituted biotin and analogues. *Biochemistry* **21**, 978–984.
- Kurzban, G. P., Gitlin, G., Bayer, E. A., Wilchek, M., and Horowitz, P. M. (1989) Shielding of tryptophan residues of avidin by the binding of biotin. *Biochemistry* **28**, 8537–8542.

- Lavielle, S., Chassaing, G., and Marquet, A. (1983) Avidin binding of biotinylated analogues of substance P. *Biochim. Biophys. Acta* 759, 270–277.
- Lim, K., and Herron, J. N. (1992) Molecular simulation of protein-PEG interaction. In *Poly(ethylene glycol) chemistry: Biotechnical and biomedical applications* (J. M. Harris, Ed.) pp 29–56, Plenum Press, New York.
- Mock, D. M., and Horowitz, P. (1990) Fluorometric assay for avidin-biotin interaction. *Methods Enzymol.* 184, 234–240.
- Romovacek, H., Finn, F. M., and Hofmann, K. (1983) Avidin binding of biotinylated corticotropins. *Biochemistry* 22, 904–909.
- Schmidt, Th., Schütz, G. J., Gruber, H. J., and Schindler, H. (1996) Local stoichiometries determined by counting individual molecules. *Anal. Chem.* 68, in press.
- Schray, K. J., Artz, P. G., and Hevey, R. C. (1988) Determination of avidin and biotin by fluorescence polarization. *Anal. Chem.* 60, 853–855.
- Shah, D., Salbilla, V., Richerson, R., and Brown, W., III (1994) Determination of biotin in biotin-conjugated protein by measuring fluorescence polarization. *Clin. Chem.* 40, 2112–2113.
- Wessendorf, M. W. (1992) Which fluorophore is brightest? A comparison of staining obtained using fluorescein, tetramethylrhodamine, lissamine rhodamine, Texas Red, and cyanine 3.18. *Histochemistry* 98, 81–86.
- Wilchek, M., and Bayer, E. A. (1988) The avidin-biotin complex in bioanalytical applications. *Anal. Biochem.* 171, 1–32.
- Wilchek, M., and Bayer, E. A. (1990a) Introduction to avidin-biotin technology. *Methods Enzymol.* 184, 5–13.
- Wilchek, M., and Bayer, E. A. (1990b) Applications of avidin-biotin technology: Literature Survey. *Methods Enzymol.* 184, 14–45.
- Wilchek, M., and Bayer, E. A. (1990c) Biotin-containing reagents. *Methods Enzymol.* 184, 123–138.

BC970087M

Thin Layer Chromatography. Plastic sheets, precoated with 0.2 mm silica gel 60 without fluorescent indicator (Merck) were used. Eluents I, II and III contained chloroform/methanol/acetic acid (70/30/5, 70/26/4, and 100/30/2, respectively), eluent IV contained chloroform/methanol/water (70/26/4), and eluents V and VI contained chloroform/methanol/ammonia (70/26/4 and 100/30/2, respectively). Besides nonspecific staining with iodine vapor, amines were specifically detected with ninhydrin (Schuurmans-Stekhoven et al., 1992) and biotin derivatives were visualized by color reaction with DACA (McCormick & Roth, 1970). Boc-protected amines responded to ninhydrin after ~1 min delay at 100 °C, due to thermal deprotection.

Syntheses. General Precautions. Autoxidation of the primary amines used in this study had to be avoided by rigorous exclusion of ambient air and/or use of acidic conditions whenever possible. The second problem regularly encountered was hydrolysis of the amide bond between PEG and fluorophore residues as previously observed between PEG and the 3-(4-pyridyldithio)propionyl group (see manuscript #1). Paradoxically amide cleavage did not occur in water at pH ~7 but was very significant in chloroform solutions or in films dried from this solvent during storage at -25 °C. Pre-treatment of *all* chloroform quantities with basic alumina cured the problem. For long term storage, however, the biotin-PEG-fluorophore conjugates were lyophilized from dilute aqueous solutions. Fluorophores were protected from light as much as possible.

Synthesis of N-Boc-4,9-dioxa-1,12-diaminododecane-CH₃COOH. 6 g 4,9-dioxa-1,12-diaminododecane (29.4 mmol) were dissolved in 50 ml methanol and a solution of 6.2 g (28.4 mmol) Boc₂O in 20 ml methanol was slowly added while stirring (see above for general precautions). After overnight stirring under Ar 5 ml acetic acid and 100 ml toluene were added. The solution was concentrated to ~50 ml at 25 °C bath temperature, and toluene addition was

repeated twice before the mixture was taken to dryness. Only in this way was cleavage of the Boc group completely suppressed. Yield: 10.5 g of crude product. 3 g of crude product were purified by chromatography on silica 60 (50 g), using chloroform/methanol/acetic acid mixtures for elution (250 ml 90/10/0.1 and 400 ml 70/30/5). Product fractions were taken to dryness by the "toluene procedure" as described above. In order to remove silica, the residue was redissolved in 15 ml water, saturated with NaCl, and extracted with chloroform (3 x 15 ml). The organic layers were dried with Na₂SO₄ and the solvent was removed. Yield 1.09 g (3.20 mmol), pure by TLC (R_f^I = 0.41, ninhydrin, iodine). ¹H-NMR (CDCl₃, 200 MHz) δ : 1.41 (9H, s, t-butyl) 1.59 (4H, t, OCH₂CH₂CH₂CH₂O) 1.65-1.78 (2H, m, CH₂CH₂NH-Boc) 1.94-2.07 (2H, m, CH₂CH₂NH₃⁺) 3.10-3.23 (2H, m, CH₂NH-Boc) 3.38-3.48 (8H, m, 2 x CH₂OCH₂) 3.56 (2H, t, CH₂NH₃⁺) 4.95 (1H, broad s, NH-Boc) 6.7 (3H, broad s, NH₃⁺).

Synthesis of N-Boc-N'-biotin-4,9-dioxa-1,12-diaminododecane. 627 mg N-Boc-4,9-dioxa-1,12-diaminododecane-HCl (1.8 mmol) were dissolved in 10 ml absolute DMF, 882 mg biotin-NHS (2.7 mmol) and 240 μ l Et₃N were added (see above for general precautions). After overnight stirring 10 ml water were added and stirring was continued for 3 h. The solvent was removed at 1-10 Pa and the dry product was subjected to chromatography on silica 60 (eluent chloroform/methanol/acetic acid 120/30/0.5). Product fractions were taken to dryness by the "toluene procedure" (see above). Dry product was redissolved in chloroform and silica was removed by centrifugation. Yield: 590 mg (1.11 mmol), pure by TLC (R_f^I = 0.64, DACA, iodine, ninhydrin response after ~1min delay at 100 °C). ¹H-NMR (CDCl₃, 200 MHz) δ : 1.41 (9H, s, t-butyl) 1.60-1.77 (12H, m, OCH₂CH₂CH₂CH₂O + CH₂CH₂NH-Boc + CH₂CH₂CH₂CH₂CONH from biotin side chain) 2.18 (2H, t, CH₂CONH, biotin side chain) 2.72 and 2.9 (2H, d and q, J_{gem} = 12 Hz, J_{vic} = 5 Hz, SCH₂) 3.12-3.18 (1H, m, SCH) 3.28-3.51 (12H, m, 2 x CH₂N and 2 x CH₂OCH₂) 4.30-4.49 (2H, m, 2 x CHNH in biotin) 5.01 (1H, broad s, NH amide) 6.29 and 6.54 (2H, broad s, NH in biotin).

Synthesis of N-biotin-4,9-dioxa-1,12-diaminododecane-HCl. 590 mg N-Boc-N'-biotin-4,9-dioxa-1,12-diaminododecane (1.11 mmol) were dissolved in 6 ml 98 % formic acid and stirred at RT for 8 h. Formic acid was removed by azeotropeing with several portions of toluene. The crude product was dissolved in 2 ml water, clarified by centrifugation and loaded on a 1.5 x 14 cm column of SP-Sephadex C-25 (Na-form) at 0.5 ml/min. After washing with 15 ml water the product was eluted with 500 mM ammonium acetate. Pooled product fractions were adjusted to pH = 12 by addition of NaOH while bubbling with Ar (no stirring) and extracted with chloroform (3 x 15 ml) under Ar. The organic layers were taken to dryness, the residue was dissolved in 0.1 M HCl and lyophilized. Yield 300 mg (0.64 mmol), pure by TLC ($R_f^I = 0.15$, positive with iodine, DACA, and ninhydrin). $^1\text{H-NMR}$ (CDCl_3 , 200 MHz) δ : 1.60-1.77 (12H, m, $\text{OCH}_2\text{CH}_2\text{CH}_2\text{CH}_2\text{O} + \text{CH}_2\text{CH}_2\text{NH}_3^+ + \text{CH}_2\text{CH}_2\text{CH}_2\text{CH}_2\text{CONH}$, biotin side chain) 2.18 (2H, t, CH_2CONH , biotin side chain) 2.72 and 2.90 (2H, d and q, $J_{\text{gem}} = 12 \text{ Hz}$, $J_{\text{vic}} = 5 \text{ Hz}$, SCH₂) 3.12-3.18 (1H, m, SCH) 3.28-3.51 (12H, m, 2 x CH_2N and 2 x CH_2OCH_2) 4.30-4.49 (2H, m, 2 x CHNH in biotin) 5.01 (1H, broad s, NH, amide) 6.29 and 6.54 (2H, broad s, NHCONH in biotin).

Synthesis of Biotin-dode-TMR. 9 mg N-biotin-4,9-dioxa-1,12-diaminododecane-HCl (19 μmol) were dissolved 2 ml chloroform, 16 mg 5-(and-6)-carboxytetramethylrhodamine succinimidyl ester and 10 μl Et_3N were added (see above for general precautions). TLC analysis proved quantitative conversion of the ninhydrin- and DACA-positive educt ($R_f^V = 0.48$, $R_f^{IV} = 0.16$, $R_f^{II} = 0.25$) into TMR-labeled product ($R_f^V = 0.84$, $R_f^{IV} = 0.51$, $R_f^{II} = 0.64$). The mixture was taken to dryness and chromatographed on silica 60 (chloroform/methanol/water 70/26/4), yielding 83 % pure product with a 17 % content of free TMR (see Experimental Procedures). $^1\text{H-NMR}$ (CDCl_3 , 200 MHz) δ : 1.25-1.70 (14H, m, $\text{OCH}_2\text{CH}_2\text{CH}_2\text{CH}_2\text{O} + 2 \times \text{CH}_2\text{CH}_2\text{N} + \text{CH}_2\text{CH}_2\text{CH}_2\text{CH}_2\text{CONH}$, biotin side chain) 1.96 (12H, m, 4 x NCH_3 in TMR) 2.12 (2H, t, $J = 7 \text{ Hz}$, CH_2CONH , biotin side chain) 2.72 and 2.87 (2H, d and q,

$J_{\text{gem}} = 12 \text{ Hz}$, $J_{\text{vic}} = 5 \text{ Hz}$, SCH₂) 3.10 (1H, m, SCH) 3.31-3.74 (13H, m, 2 x CH₂N and 2 x CH₂OCH₂, biotinoyl-NHCH₂) 4.27 and 4.48 (2H, m, CHNH in biotin) 5.59 and 5.65 (together 1H, broad s, NH-TMR, 5-and-6 isomer) 6.42-6.70 (8H, 6 H from TMR xanthene moiety and 2 H from NHCONH in biotin).

Synthesis of Biotin-PEG800-TMR. 10 mg biotin-NH-PEG800-NH₂·HCl (nominally 8.4 μmol) were dissolved in 0.5 ml chloroform, 12 mg 5-(and-6)-carboxytetramethylrhodamine succinimidyl ester (23 μmol , dissolved in 1 ml chloroform) and 20 μl Et₃N were added (see above for general precautions). After 2 h of stirring TLC showed quantitative conversion of biotin-NH-PEG800-NH₂·HCl into TMR-labeled product. The mixture was taken to dryness, redissolved in 3 ml water and loaded on a 1.5 x 48 cm column of Sephadex G-25 M at 1.0 ml/min. Elution with water resulted in complete separation of the PEG derivative (eluting shortly after the void volume) from all by-products. Yield: 4.8 μmol of Biotin-PEG800-TMR according to biotin end group assay (see Experimental Procedures). TLC indicated near purity, besides the product ($R_f^{\text{IV}} = 0.56\text{-}0.81$) traces of biotin-NH-PEG800-NH₂·HCl ($R_f^{\text{IV}} = 0.85$) and of free TMR ($R_f^{\text{IV}} = 0.22$) were visible. ¹H-NMR: (CDCl₃, 200 MHz) δ : 1.09 (6H, m, 2 x CH₃, aminopropyltermini of PEG) 1.17-1.63 (6H, m, CH₂CH₂CH₂CH₂CONH, biotin side chain) 2.03 (12H, m, 4 x NCH₃ in TMR) 2.12 (2H, t, $J = 7 \text{ Hz}$, CH₂CONH, biotin side chain) 2.68 ppm (1H, d, $J_{\text{gem}} = 13 \text{ Hz}$, SCH₂ (I), biotin) 2.84 (1H, q, $J_{1\text{gem}} = 13 \text{ Hz}$, $J_{2\text{vic}} = 5 \text{ Hz}$, SCH₂ (II), biotin) 3.08 (1H, m, SCH, biotin) 3.20-3.93 (~72H, m, OCH₂CH₂O, PEG chain) 3.38-3.47 (6H, m, 2 x OCH₂ and 2 x NCH, aminopropyltermini of PEG) 4.03 (1H, broad s, biotinoyl-NH) 4.28 (1H, m, NCH, biotin), 4.44 (1H, m, NCH, biotin) 4.83 and 5.46 (together 1H, broad s, NH-TMR, 5-and-6 isomer) 6.33, 6.42, 6.50 (each 2H, TMR xanthene moiety) 6.13-6.82 (2 H, NHCONH in biotin) 7.16, 7.53, 7.98, 8.16, 8.34 (together 3H, TMR phthalide residue, 5-and-6 isomer).

Synthesis of Biotin-PEG1900-TMR. The procedure was the same as for the PEG800 derivative. 43 mg biotin-NH-PEG1900-NH₂·HCl (nominally 18.7 μ mol, ~20% water content) were reacted with 19 mg 5-(and-6)-carboxytetramethylrhodamine succinimidyl ester (36 μ mol). The product eluted as sharp void peak from Sephadex G-25 M. Yield: 12.8 μ mol of Biotin-PEG1900-TMR according to biotin end group assay (see Experimental Procedures). TLC indicated near purity, besides the product ($R_f^{IV} = 0.53-0.80$) traces of biotin-NH-PEG800-NH₂·HCl ($R_f^{IV} = 0.86$) and of free TMR ($R_f^{IV} = 0.21$) were visible. ¹H-NMR: (CDCl₃, 200 MHz) δ : 1.11 (6H, m, 2 x CH₃, aminopropyltermini of PEG) 1.21-1.67 (6H, m, CH₂CH₂CH₂CH₂CONH, biotin side chain) 2.05 (12H, m, 4 x NCH₃ in TMR) 2.15 (2H, t, J = 7 Hz, CH₂CONH, biotin side chain) 2.69 ppm (1H, d, J_{gem} = 13 Hz, SCH₂ (I), biotin) 2.84 (1H, q, J_{1gem} = 13 Hz, J_{2vic} = 5 Hz, SCH₂ (II), biotin) 3.12 (1H, m, SCH, biotin) 3.22-3.95 (~172H, m, OCH₂CH₂O, PEG chain) 3.42-3.50 (6H, m, 2 x OCH₂ and 2 x NCH, aminopropyltermini of PEG) 4.07 (1H, broad s, biotinoyl-NH) 4.30 (1H, m, NCH, biotin), 4.45 (1H, m, NCH, biotin) 4.89 and 5.51 (together 1H, broad s, NH-TMR, 5-and-6 isomer) 6.35, 6.43, 6.53 (each 2H, TMR xanthene moiety) 6.20-6.90 (2 H, NHCONH in biotin) 7.18, 7.56, 8.00, 8.17, 8.36 (together 3H, TMR phthalide residue, 5-and-6 isomer).

Synthesis of Biotin-PEG800-Flu. 50 mg biotin-NH-PEG800-NH₂·HCl (22 μ mol) and 20 mg 5-(and-6)-carboxyfluoresceine succinimidyl ester (43 μ mol) were dissolved in 1 ml DMF and 15 μ l Et₃N were added (see above for general precautions). After 2 h of stirring the mixture was cooled and evaporated at 1-10 Pa with stirring. The residue was dissolved in 5 ml chloroform and washed with 20 ml 0.2 M Na₂CO₃ saturated with NaCl. The strongly colored aqueous phase was re-extracted 4 x with 10 ml chloroform. All 5 organic phases were pooled and washed with 10 ml of saturated NaCl solution containing 15 μ l acetic acid (to remove traces of Et₃N). Drying of the chloroform solution with Na₂SO₄ and evaporation yielded 51 mg crude product which was dissolved in 2 ml water and

30 μ l 0.2 M Na_2CO_3 and loaded on a 2.5 x 17 cm column of QAE-Sephadex A-25 (pre-equilibrated in buffer B) at 1 ml/min. After washing with 90 ml of buffer B the product was eluted with 200 ml 150 mM NaCl in buffer B. The volume was reduced to \sim 20 ml on a rotavap at $\sim 10^2$ Pa, saturated with NaCl, extracted 4 x with chloroform, the organic layers were dried with Na_2SO_4 , taken to dryness and dried at 1-10 Pa for 1 h. Yield 27 mg (18 μ mol) highly viscous oil. Pure by TLC: $R_f^{\text{III}} = 0.46$ -0.65, $R_f^{\text{VI}} = 0.04$ -0.28, typical PEG tails, fluorescent, positive stain with DACA. $^1\text{H-NMR}$: (CDCl_3 , 200 MHz) δ : 1.09 (6H, m, 2 x CH_3 , aminopropyltermini of PEG) 1.27-1.73 (6H, m, $\text{CH}_2\text{CH}_2\text{CH}_2\text{CH}_2\text{CONH}$, biotin side chain) 2.14 (2H, t, $J = 7$ Hz, CH_2CONH , biotin side chain) 2.67 ppm (1H, d, $J_{\text{gem}} = 13$ Hz, SCH_2 (I), biotin) 2.81 (1H, q, $J_{1\text{gem}} = 13$ Hz, $J_{2\text{vic}} = 5$ Hz, SCH_2 (II), biotin) 3.07 (1H, m, SCH , biotin) 3.18-3.91 (\sim 72H, m, $\text{OCH}_2\text{CH}_2\text{O}$, PEG chain) 3.31-3.47 (6H, m, 2 x OCH_2 and 2 x NCH , aminopropyltermini of PEG) 4.04 (1H, broad s, biotinoyl-NH) 4.24 (1H, m, NCH , biotin), 4.40 (1H, m, NCH , biotin) 4.75 and 5.64 (together 1H, broad s, NH-fluoresceine, 5-and-6 isomer) 6.52 (4H, fluoresceine xanthene moiety) 6.66 (2H, fluoresceine xanthene moiety) 6.10-6.85 (2 H, NHCONH in biotin) 7.64, 7.97, 8.07, 8.12, 8.43, 8.84 (together 3H, fluoresceine phthalide residue, 5-and-6 isomer).

Synthesis of Biotin-PEG₁₉₀₀-Flu. 50 mg biotin-NH-PEG₁₉₀₀-NH₂·HCl (22 μ mol) were reacted with 15.5 mg 5-(and-6)-carboxyfluoresceine succinimidyl ester (33 μ mol). The procedure was the same as for the PEG₈₀₀ homologue, except that 50 mM NaCl in buffer B was used to elute the product from QAE-Sephadex A-25. Yield: 31.5 mg (12 μ mol). Pure by TLC: ($R_f^{\text{III}} = 0.55$ -0.88, $R_f^{\text{VI}} = 0.04$ -0.38). $^1\text{H-NMR}$: (CDCl_3 , 200 MHz) δ : 1.07 (6H, m, 2 x CH_3 , aminopropyltermini of PEG) 1.25-1.69 (6H, m, $\text{CH}_2\text{CH}_2\text{CH}_2\text{CH}_2\text{CONH}$, biotin side chain) 2.12 (2H, t, $J = 7$ Hz, CH_2CONH , biotin side chain) 2.67 ppm (1H, d, $J_{\text{gem}} = 13$ Hz, SCH_2 (I), biotin) 2.82 (1H, q, $J_{1\text{gem}} = 13$ Hz, $J_{2\text{vic}} = 5$ Hz, SCH_2 (II), biotin) 3.08 (1H, m, SCH , biotin) 3.21--3.91 (\sim 172H, m, $\text{OCH}_2\text{CH}_2\text{O}$, PEG chain) 3.31-3.47 (6H, m, 2 x OCH_2 and 2 x NCH ,

aminopropyltermini of PEG) 4.04 (1H, broad s, biotinoyl-NH) 4.24 (1H, m, NCH, biotin), 4.42 (1H, m, NCH, biotin) 4.76 and 5.35 (together 1H, broad s, NH-fluoresceine, 5-and-6 isomer) 6.50 (4H, fluoresceine xanthene moiety) 6.69 (2H, fluoresceine xanthene moiety) 5.77-6.45 (2 H, NHCONH in biotin) 7.57, 7.68, 7.97, 8.07, 8.15, 8.38, 8.86 (together 3H, fluoresceine phthalide residue, 5-and-6 isomer).

Synthesis of Biotin-PEG₈₀₀-Cy3. One vial Cy3 monofunctional dye ("reactive dye to label 1 mg of antibody" according to Amersham) was dissolved in 1 ml absolute DMF. 2 mg biotin-NH-PEG₈₀₀-NH₂-HCl (1.7 μ mol) and 5 μ l Et₃N were added (see above for general precautions). After 2 h the mixture was cooled and evaporated at 1-10 Pa with stirring. TLC (eluent V) indicated that all of the succinimidyl ester component (~1/2 of the commercial reagent) had reacted with the primary amine while the other dye components (mostly free carboxylic acid of Cy3) remained unchanged. The dry residue was dissolved in 2 ml buffer B and loaded on a 1 x 10 cm column QAE-Sephadex A-25 at 0.16 ml/min. After washing with 30 ml of the same buffer the product band was eluted with 125 mM NaCl in buffer B. Yield: 63 nmol determined from A₅₅₀ (ϵ_{550} = 150000 M⁻¹ cm⁻¹ for Cy3 according to Amersham) or 54 nmol according to biotin end group assay with ANS (see Experimental Procedures).

LITERATURE CITED in the Supplements only

- McCormick, D. B., and Roth, J. A. (1970b) Colorimetric determination of biotin and analogs. *Methods Enzymol.* 18, 383-385.
- Schuermans-Stekhoven, F.M.A.H., Tesser, G.I., Ramsteyn, G., Swarts, H.G.P., and De Pont, J.J.H.H.M. (1992) Binding of ethylenediamine to phosphatidylserine is inhibitory to Na⁺/K⁺-ATPase. *Biochim. Biophys. Acta* 1109, 17-32.

Biotin–Pyrene Conjugates with Poly(ethylene glycol) Spacers Are Convenient Fluorescent Probes for Avidin and Streptavidin

Markus Marek, Karl Kaiser, and Hermann J. Gruber*

Institute of Biophysics, J. Kepler University, Altenberger Strasse 69, A-4040 Linz, Austria. Received February 14, 1997[§]

Conventional biotin–fluorophore conjugates with ~14 atom spacers are strongly quenched when bound to avidin or streptavidin, whereas fluorescence becomes insensitive to receptor binding if typical fluorophores are linked to biotin via poly(ethylene glycol) (PEG) chains (Gruber et al., see the second of three papers in this issue). In the present study the antagonism between PEG–PEG repulsion and fluorophore interaction was examined more closely, using biotin–PEG–pyrene conjugates as model compounds. The antagonistic tendencies between hydrophilic PEG chains and hydrophobic pyrene labels were about balanced in the PEG₁₉₀₀ derivative since quenching was ~50% in 4:1 complexes with avidin or streptavidin. In contrast, strong quenching and concomitant excimer fluorescence was seen with the biotin–PEG₈₀₀–pyrene conjugate, providing for a new fluorescence assay to accurately measure avidin and streptavidin concentrations at ≥ 40 and ≥ 10 nM, respectively. Association/dissociation kinetics were analyzed from pyrene fluorescence changes, and dissociation constants were deduced. About 3-fold affinities were observed for streptavidin as compared to avidin, and little influence of PEG chain length was seen. All affinities were increased by a factor of ~3 when biotin–PEG–tetramethylrhodamine conjugates were used. The observed effect of fluorophore variation upon biotin binding is unexpectedly small; thus, the kinetic/thermodynamic data appear to be representative for biotin–PEG conjugates in general.

INTRODUCTION

In the preceding study a series of novel biotin–PEG¹–fluorophore conjugates has been presented that retain intense fluorescence after binding to avidin or streptavidin (see the second of three papers in this issue). The implications for bioanalytic applications are obvious (Wilchek and Bayer, 1990a,b) and have been discussed (see the second of three papers in this issue). All fluorescent marker groups in the above series are very polar and electrically charged, which helps to explain their low tendency of self-association and self-quenching in 4:1 complexes with (strept)avidin.

At this point it was an irresistible temptation to synthesize a biotin–PEG conjugate with a very hydrophobic fluorophore and see what happens: Would the product be soluble in water? Would PEG–PEG repulsion in 4:1 complexes with (strept)avidin be strong enough to prevent self-association and self-quenching of the hydrophobic fluorophores? What would be the possible use of such amphiphilic fluorescent biotin derivatives?

* Author to whom correspondence should be addressed [telephone +43 (732) 2468-9271; fax +43 (732) 2468-822; e-mail hermann.gruber@jk.uni-linz.ac.at].

[§] Abstract published in *Advance ACS Abstracts*, June 15, 1997.

¹ Abbreviations: ANS, 2-anilinonaphthalene-6-sulfonic acid; biotin, biotinoyl group; biotin–NH–PEG₈₀₀ or ₁₉₀₀–NH₂·HCl, *N*-biotinoyl-*O*,*O*'-bis(2-aminopropyl)poly(ethylene glycol)₈₀₀ or ₁₉₀₀ hydrochloride; biotin–fluorescein, 5-[[*N*-(2-biotinoylamino)ethyl]-thioureidyl]fluorescein; biotin–PEG₈₀₀ or ₁₉₀₀–pyrene, see Scheme 1; BODIPY, 4,4-difluoro-4-bora-3a,4a-diaza-*s*-indacene; DACA, *p*-(dimethylamino)cinnamaldehyde; DMF, *N,N*-dimethylformamide; EDTA, ethylenediamine-*N,N,N,N*-tetraacetic acid; Et₃N, *N,N,N*-triethylamine; fluorescein–biotin, 5-[[*N*-[5-[*N*-[6-(biotinoyl)amino]hexanoyl]amino]pentyl]thioureidyl]fluorescein; FRET, fluorescence resonance energy transfer; HABA, 4-hydroxyazobenzene-2'-carboxylic acid; PEG, poly(ethylene glycol); RT, room temperature; (strept)avidin, streptavidin and/or avidin; TMR, tetramethylrhodamine.

Pyrene was selected as the ideal label for this purpose because self-association can unequivocally be detected via excimer fluorescence (Galla and Hartmann, 1980). The results more than satisfied the expectations: Biotin–PEG–pyrene conjugates are water soluble as free monomers; long biotin–PEG₁₉₀₀–pyrene retains about half of its fluorescence in complexes with (strept)avidin, whereas fluorescence of the shorter homologue biotin–PEG₈₀₀–pyrene is reduced by a factor of ~10, providing for new and easy ways to measure (strept)avidin concentrations and to study the kinetics of association and dissociation.

EXPERIMENTAL PROCEDURES²

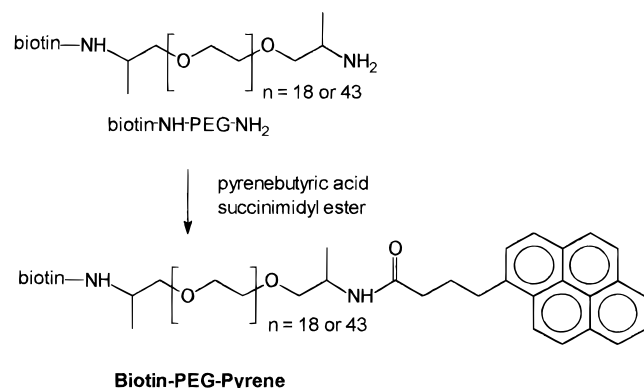
Materials. P.a. grade materials were used as far as commercially available. Affinity-purified avidin and streptavidin, *d*-biotin, DACA, and *N*-hydroxysuccinimide were obtained from Sigma. 4-(1-Pyrene)butyric acid was obtained from Aldrich. ANS and fluorescein–biotin were obtained from Molecular Probes. *N,N*-dicyclohexylcarbodiimide and buffer components were purchased from Merck. Absolute DMF was prepared according to a standard procedure. Biotin–NH–PEG₈₀₀–NH₂·HCl, biotin–NH–PEG₁₉₀₀–NH₂·HCl, and their TMR derivatives were synthesized as described before (see the first and second of three papers in this issue).

Methods. *Buffer.* Buffer A contained 100 mM NaCl, 50 mM NaH₂PO₄, and 1 mM EDTA, adjusted to pH 7.5 with NaOH.

Synthesis of Biotin–PEG₈₀₀–Pyrene and Biotin–PEG₁₉₀₀–Pyrene (Scheme 1). One millimole of 4-(1-pyrene)butyric acid was activated with 1 mmol of *N,N*-dicyclohexylcarbodiimide and 1 mmol of *N*-hydroxysuccinimide in 6 mL of absolute DMF, filtered from byproduct, and taken to dryness. Seventeen micromoles of biotin–NH–PEG₈₀₀–NH₂·HCl was reacted with 39 μ mol

² Detailed procedures and NMR data can be found in the Supporting Information.

Scheme 1. Synthesis and Structure of Biotin–PEG–Pyrene Conjugates



of succinimidyl 4-(1-pyrene)butyrate in 2 mL of absolute DMF and 20 μ L of Et₃N for 2 h under Ar. After evaporation, the product was isolated by preparative TLC in chloroform/methanol (9:1), yielding 8.5 μ mol of pure product as determined from UV absorption [assuming a molar extinction coefficient of 40 000 M⁻¹ cm⁻¹, in analogy to free 4-(1-pyrene)butyric acid, see Haugland (1992a)]. This estimate of pyrene termini agreed well with the amount of biotin termini found in functional experiments with avidin and streptavidin (see Results). For synthesis of the PEG₁₉₀₀ analogue, 10 μ mol of biotin–NH–PEG₁₉₀₀–NH₂·HCl was reacted with 26 μ mol of succinimidyl ester and 10 μ L of Et₃N, resulting in 2.7 μ mol of pure biotin–PEG₁₉₀₀–pyrene. Again, the biotin/pyrene ratio was 1:1 within error limit (<5%).

RESULTS

Fluorescence Properties of Biotin–PEG–Pyrene after Binding to Avidin or Streptavidin. The pyrene label is uniquely suited to report on the association of molecules in microphases, such as biomembranes, because dimeric association is accompanied by the appearance of excimer fluorescence at 480 nm and by a strong decrease of normal fluorescence in the UV region (Galla and Hartmann, 1980). Association of biotin–PEG–pyrene in aqueous solution is anticipated to occur by two different mechanisms: (i) At sufficiently high concentrations micellization should be induced by the large hydrophobic pyrene residues. (ii) Even at low concentrations of biotin–PEG–pyrene the probability of pyrene–pyrene dimer formation will greatly be enhanced upon specific binding of two, three, or four biotin–PEG–pyrene molecules to a single avidin molecule. Fortunately no micelles were formed at the submicromolar concentrations used in this study as is concluded from the absence of excimer fluorescence in avidin-free aqueous solutions containing 320 nM biotin–PEG–pyrene (solid lines in Figure 1). Even at 16 μ M biotin–PEG₈₀₀–pyrene no micelle formation was observed (not shown). Addition of avidin, however, caused significant excimer fluorescence at 480 nm, with concomitant quenching of normal pyrene fluorescence at 380 nm (dashed and dotted lines in Figure 1). At a 4:1 ratio of ligand/avidin all ligands were bound by the tetravalent receptor protein, giving rise to maximal quenching and maximal excimer fluorescence (dotted lines), while at a 8:1 ratio of ligand/avidin only half of the ligands were bound and fluorescence properties were intermediate (dashed lines). Thus, the linear response to titration with avidin can easily be understood in terms of complementary fractions of ligand which either take part in 4:1 complexes with avidin or stay unbound (see Figure 4 for the corresponding linear titration profiles).

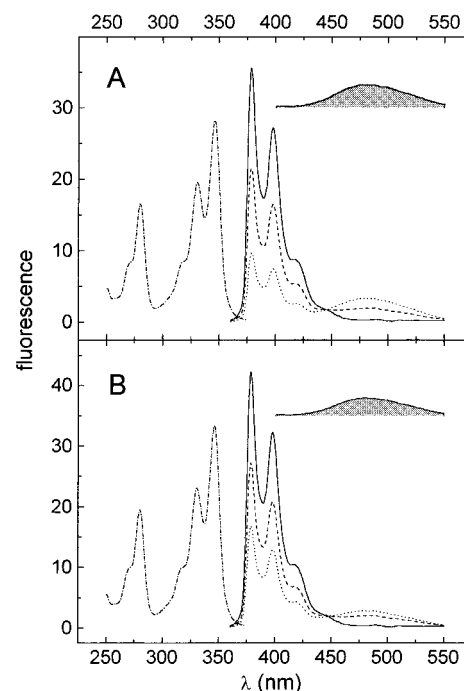


Figure 1. Fluorescence of biotin–PEG₈₀₀–pyrene (A) and biotin–PEG₁₉₀₀–pyrene (B) in the absence and presence of avidin. Excitation spectra (– · –) were measured at 380 nm emission wavelength and emission spectra at 345 nm excitation wavelength. Both slits were set to 5 nm. Emission of 320 nM biotin–PEG–pyrene in buffer A was recorded in the absence of avidin (—), after addition of 40 nM avidin (– –), and after addition of 80 nM avidin (· · ·). Pure excimer spectra at 80 nM avidin (shaded areas) were calculated and plotted with vertically displaced baselines.

For characterization of pyrene fluorescence in complexes with <4 ligands per tetravalent receptor protein, constant amounts of avidin or streptavidin were titrated with increasing amounts of biotin–PEG–pyrene (Figure 2). The nonlinear titration profiles meet expectation because the probability of pyrene–pyrene interaction, and thus the extent of fluorescence quenching, will necessarily increase with the number of ligands bound per receptor protein. The data also reflect enhanced pyrene–pyrene association in complexes with PEG₈₀₀ chains (circles) as compared to PEG₁₉₀₀ chains (triangles). The steep increase in fluorescence with >4 ligands per tetravalent receptor protein was always exactly parallel to the control profile obtained in the absence of protein (squares). This strongly suggests that biotin–PEG–pyrene does not bind to avidin or streptavidin in a nonspecific way.

Normalized representation of the data in Figure 2B allowed for a direct comparison with other known fluorescent biotin derivatives (see Figure 9 in the second of three papers in this issue) from which biotin–PEG₈₀₀–pyrene emerged as the most sensitive fluorescent probe for avidin and streptavidin, with the sharpest inflection point at 4 ligands per tetravalent receptor protein.

The usefulness of biotin–PEG₈₀₀–pyrene to measure concentrations of functional streptavidin and avidin was critically tested as shown in Figures 3 and 4, respectively. Identical results in this respect were obtained whether normal fluorescence (Figures 3A and 4A) or excimer fluorescence (Figures 3B and 4B) was used for the monitoring of receptor–ligand titrations. “Forward titration” of streptavidin with ligand is shown in Figure 3, yielding nonlinear titration curves as argued above. At the lowest concentration of streptavidin (5 nM) in appears as if 5 ligands per streptavidin tetramer was necessary to saturate all binding sites. This indicates

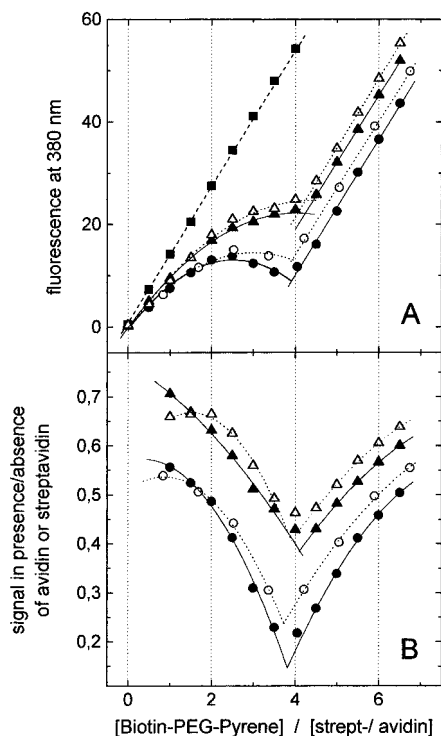


Figure 2. Titration of avidin and streptavidin with biotin-PEG-pyrene. (A) 2 mL of 80 nM avidin (solid symbols, solid lines) or 80 nM streptavidin (open symbols, dotted lines) in buffer A was titrated with 5 μ L increments of 16 μ M biotin-PEG₈₀₀-pyrene (circles) or biotin-PEG₁₉₀₀-pyrene (triangles) from a Hamilton syringe while fluorescence was monitored at 345 nm excitation and 380 nm emission wavelength. Both slit widths were 5 nm. Interval times of 8 min were necessary at 26 °C to obtain stable signals when titrating from 2 to 4 ligands per protein. In a control run (squares) protein was omitted. Fluorescence data were corrected for sample dilution. (B) Fluorescence data from panel A were divided by the corresponding signal in the absence of receptor protein.

incomplete binding and a K_D value in the nanomolar range as confirmed below (see Figure 6). Thus, biotin-PEG₈₀₀-pyrene can measure streptavidin only at ≥ 10 nM protein concentration.

The detection limit of the biotin-PEG₈₀₀-pyrene assay for avidin was found at 40 nM protein concentration, as can be seen from Figure 4. Here "reverse titration" of ligand with receptor protein was chosen because the linear titration profiles gave more clearly defined inflection points at which all ligands *appeared* to be bound to avidin. At 10 nM avidin (inflection point of the triangle series in Figure 4) 8 ligands/avidin seemed to be necessary for saturation, whereas at 40 nM avidin (inflection point of the square series in Figure 4) 4 ligands/avidin was sufficient for saturation, as expected for this tetra-valent receptor protein. Obviously the K_D value of the 4:1 complex is too high for stoichiometric binding of biotin-PEG₈₀₀-pyrene at < 40 nM avidin (see below).

Thermodynamics and Kinetics of Binding between Biotin-PEG₈₀₀-Pyrene and Avidin or Streptavidin. The association and dissociation reactions between biotin-PEG-pyrene and avidin or streptavidin could be measured in a very convenient way because (i) the fluorescence yield of pyrene labels strongly depends on ligand/receptor stoichiometry (see Figure 2B) and (ii) the typical half-times for the association and dissociation of the fourth ligand were in the order of minutes when using 80 nM receptor protein (see Figure 5A).

Measurement of on- and off-rate constants is exemplified in Figure 5. The initial signal in Figure 5A corre-

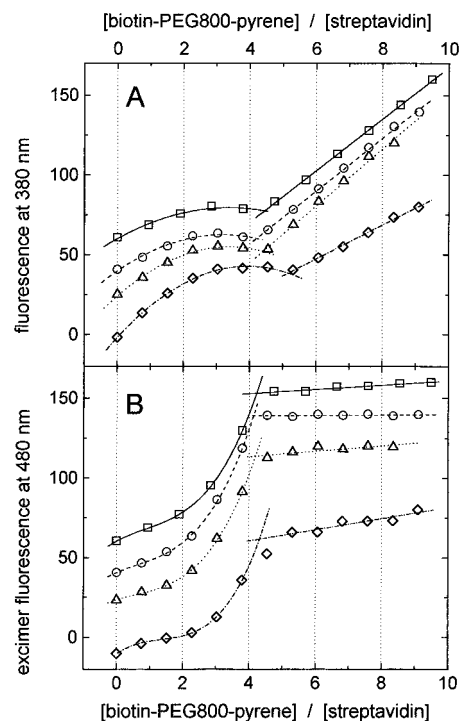


Figure 3. Comparison of normal pyrene fluorescence and excimer fluorescence for the monitoring of streptavidin titration with biotin-PEG₈₀₀-pyrene. 40 (squares), 20 (circles), 10 (triangles), or 5 nM (diamonds) streptavidin in buffer A was titrated with successive increments of biotin-PEG₈₀₀-pyrene (see legend to Figure 2) and both 380 nm fluorescence (A) and excimer fluorescence (B) were recorded at 345 nm excitation wavelength after each titration step. 2 min intervals were required at 36 °C to obtain stable signals. For easier comparison all titration profiles were normalized to identical overall fluorescence increase, and overlap of profiles was avoided by serial vertical displacement.

sponds to unquenched biotin-PEG₁₉₀₀-pyrene in the absence of receptor protein. Then exactly 160 pmol of tetrameric avidin were added to bind all of the 640 pmol of biotin-PEG₁₉₀₀-pyrene and the signal dropped by $\sim 55\%$ within minutes, as expected from Figure 2B (triangles). The initial period of fluorescence quenching was too fast for this manual assay, but the slower relaxation was assumed to reflect the binding of the "fourth ligand" to the 3:1 complex with avidin. According to this idealization 160 pmol of ligand was assumed to react with 160 pmol of 3:1 complex in a bimolecular reaction:

$$q/(a - q) = (a/V)k_{on}t$$

Hereby q denotes the moles of 4:1 complex that have formed within the time t , $a = 160$ pmol = initial amount of both reactants, and $V = 2$ mL. The fluorescence F is assumed to change from F_3' to F_4' in a linear way (see Figure 5A):

$$\frac{F_3' - F}{F - F_4'} = \frac{(F_3' - F_4') - (F - F_4')}{F - F_4'} = (a/V)k_{on}t$$

Rearrangement gives a linear equation:

$$\frac{1}{F - F_4'} = \frac{1}{F_3' - F_4'} + \frac{1}{F_3' - F_4'}(a/V)k_{on}t$$

In practice F_4' was varied until the plot of $1/(F - F_4')$ versus t was linear (see Figure 5B). From the ordinate

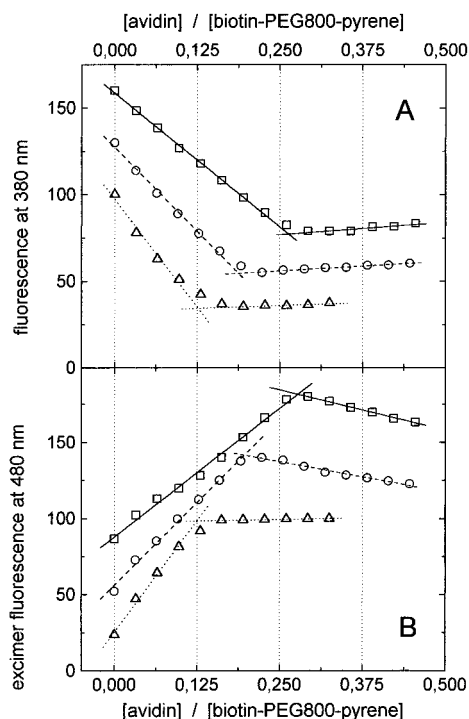


Figure 4. Reverse titration of biotin-PEG₈₀₀-pyrene with avidin at different absolute concentrations of the ligand. 2 mL samples of buffer A containing either 160 (squares), 80 (circles), or 40 nM (triangles) biotin-PEG₈₀₀-pyrene were titrated with stock solutions of avidin (2, 1, and 0.5 μ M, respectively) while both 380 nm fluorescence (A) and excimer fluorescence (B) were recorded after each titration step. Intervals of 3–5 min were required at 36 °C to obtain stable signals. For easier comparison all titration profiles were normalized to identical overall fluorescence increase, and overlap of profiles was avoided by serial vertical displacement.

$A = 1/(F_3' - F_4')$ and the slope $B = (F_3' - F_4')^{-1}(a/V)k_{on}$ the on-rate constant could be calculated.

The dissociation of biotin-PEG₁₉₀₀-pyrene from the 4:1 complex was induced by addition of an excess of *d*-biotin (second spike in Figure 5A). The subsequent slow increase in fluorescence was pseudolinear and could be interpreted in terms of a monomolecular reaction (dissociation of the fourth ligand from the 4:1 complex):

$$\frac{F - F_3}{F_4 - F_3} = \frac{\Delta q}{q} = -k_{off}\Delta t$$

For minimization of model assumptions, $F_3 - F_4$ was set to one-fourth of the total quenching effect of avidin (see Figure 5A), which is not unjustified in the light of Figure 2B.

The same procedure was used to estimate the on-rate constants (Figure 6A) and off-rate constants (Figure 6B) for the binding of biotin-PEG₈₀₀-pyrene (circles) or biotin-PEG₁₉₀₀-pyrene (triangles) toward avidin (solid symbols) or streptavidin (open symbols), and the equilibrium constants K_D were calculated as k_{off}/k_{on} (Figure 6C). It should be noted that the underlying model assumptions may introduce a systematic error amounting up to a factor of 2 in the kinetic constants. Direction and magnitude of this systematic misinterpretation, however, should be rather uniform; thus, the relative trends and patterns are well represented in Figure 6.

The on-rate constants were hardly dependent on PEG chain length, temperature, and the type of receptor protein (see Figure 6A). As a consequence, the equilibrium dissociation constants (Figure 6C) followed the same pattern as the off-rate constants (Figure 6B): The

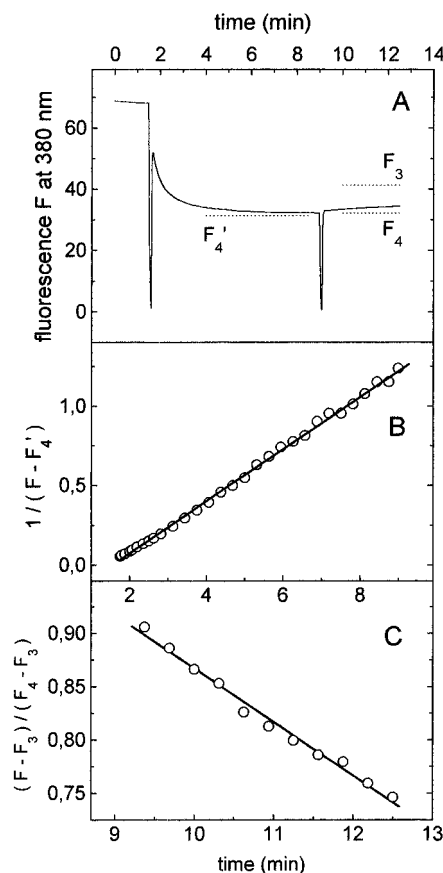


Figure 5. Formation and dissociation of the 4:1 complex between biotin-PEG₁₉₀₀-pyrene and avidin. (A) 2 mL of buffer A containing 320 nM biotin-PEG₁₉₀₀-pyrene was stirred at 16 °C, and fluorescence was monitored at 345 nm excitation and 380 nm emission wavelength (both slits were 5 nm). The first spike indicates the moment when the cover was opened and avidin was quickly added at a final concentration of 80 nM. The second spike marks the moment when excess of *d*-biotin was added (4 μ M final concentration). (B) Linearization of the association time course in terms of a bimolecular reaction (see text for details). (C) Analysis of dissociation in terms of a monomolecular reaction (see text for details).

affinities for streptavidin were generally about 3-fold higher than for avidin, and the enhanced dissociation at 36 °C caused a significant reduction in affinity. Very surprisingly, no significant influence of PEG chain length on any kinetic parameter has been observed, in good agreement with earlier results (see Figure 5 in the first of three papers in this issue).

Formation of 4:1 complexes between biotin-PEG-pyrene and avidin (or streptavidin) is expected to be disfavored by PEG-PEG repulsion. Figure 6 gives a pessimistic picture of the affinities between biotin-PEG conjugates and avidin (or streptavidin) because it deals with association/dissociation of the fourth ligand only.

Much higher stabilities were observed in complexes with ≤ 3 biotin-PEG-pyrene bound per avidin molecule, as is shown in Figure 7. A similar procedure as in Figure 5 was used to measure association and dissociation, but the latter was monitored over a 15 h period after which time most of the fluorescent ligands had been replaced by *d*-biotin, as is obvious from recovery of the fluorescence signal (Figure 7A). For meaningful analysis, the time course of fluorescence recovery in Figure 7A had to be converted into a time course of fluorescence ligand displacement, as shown in Figure 7B. The problem was solved by taking resort to Figure 2B (solid circles), which shows the correlation between the average number n of biotin-PEG₈₀₀-pyrene molecules bound per avidin and

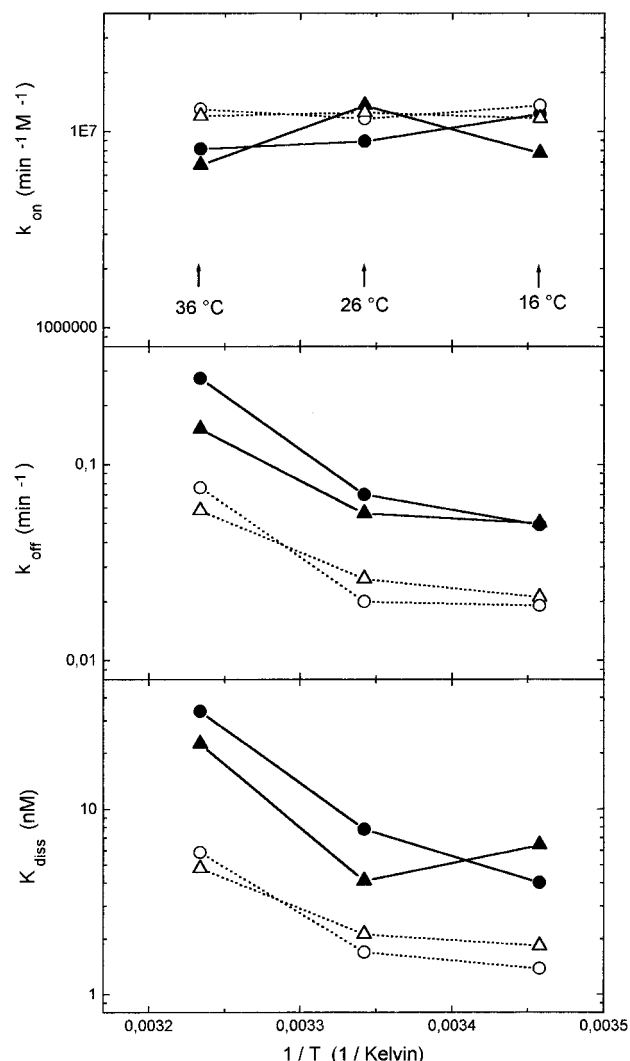


Figure 6. Estimated rate constants and dissociation constants of the 4:1 complexes between biotin-PEG₈₀₀-pyrene (circles) or biotin-PEG₁₉₀₀-pyrene (triangles) with avidin (solid symbols) or streptavidin (open symbols). The fluorometric assay shown in Figure 5 was used to estimate the rate constants for the association (A) and dissociation (B) of the fourth ligand. The equilibrium constants for dissociation of the fourth ligand (C) were calculated from k_{off}/k_{on} .

the relative fluorescence F/F_0 (as compared to the unbound state):

$$F/F_0 = 0.57 + 0.026n - 0.036n^2$$

Figure 2B, however, refers to a situation in which all fluorescent ligands were bound (as long as $n \leq 4$), whereas the displacement curve in Figure 7A refers to a situation with a constant overall ratio of $n = 4$ fluorescent ligands/avidin, of which N are still bound to avidin while $4 - N$ have already been displaced by excess of *d*-biotin. The relative fluorescence, therefore, is a weighted average of both states:

$$4(F/F_0)_N = (4 - N) + N(0.57 + 0.026N - 0.026N^2)$$

Inversion gave the empirical expression

$$N = 4.18 - 1.61(F/F_0) - 2.46(F/F_0)^2 + 3.72(F/F_0)^3 - 3.82(F/F_0)^4$$

which served to calculate the time course of fluorescent

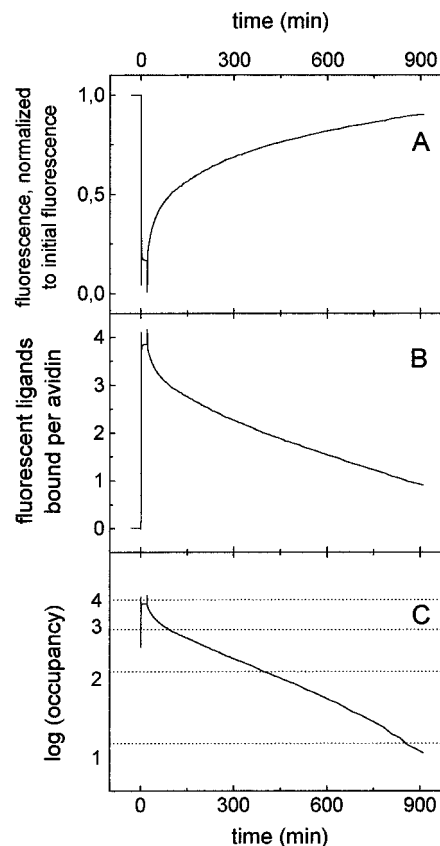


Figure 7. Multistep displacement of biotin-PEG₈₀₀-pyrene from the 4:1 complex with avidin. (A) 2 mL of buffer A containing 320 nM biotin-PEG₈₀₀-pyrene was stirred at 26 °C, and fluorescence was recorded at 345 nm excitation and 380 nm emission wavelength. Addition of avidin at 80 nM final concentration caused an 83% signal drop. After 15 min, the signal was stable and excess of *d*-biotin was added (final concentration 4 μ M). The sample was covered to prevent evaporation, and the excitation slit was set to 2 nm to minimize bleaching during the long observation time. (B) The fluorescence profile in panel A was analyzed in terms of fluorescent ligand displacement via reasonable model assumptions (see text for details). (C) Semilogarithmic representation of panel B.

ligand displacement (Figure 7B) from the time course of fluorescence recovery (Figure 7A). The semilogarithmic representation in Figure 7C clearly shows biphasic behavior, with a half-time of ~ 11 min for rapid initial dissociation from the 4:1 complex and slow further dissociation with a half-time of ~ 7 h. Most surprising is the complete absence of a breakpoint in dissociation kinetics at the 2:1 ratio of ligand/avidin, which has been observed with virtually any biotin derivative (Chu et al., 1994; Finn et al., 1984; Green, 1990; Hofmann et al., 1982; Lavielle et al., 1983; Romovacek et al., 1983) and even with another biotin-PEG conjugate (see the first of three papers in this issue). This peculiarity must relate to accidental balancing between the favorable effect of enhanced pyrene-pyrene interaction and the unfavorable effect of enhanced PEG-PEG repulsion in the 3:1 complex as compared to the 2:1 complex.

Comparison of Biotin-PEG-Pyrene with Other Biotin-Fluorophore Conjugates. Once the specific binding of biotin-PEG-pyrene toward avidin and streptavidin had been characterized, the question arose whether these findings were representative for biotin-PEG conjugates in general or whether the pyrene residues imposed serious effects on the receptor-ligand interaction. This was examined by exchanging pyrene labels for TMR labels and running the same experiments as shown in Figure 5.

Table 1. Dissociation Equilibrium Constants^a and Half-Lives of 4:1 Complexes between Various Biotin–Spacer–Fluorophore Conjugates and Avidin or Streptavidin at 26 °C

receptor	spacer	fluorophore		
		pyrene	TMR	fluorescein
avidin	14 atoms ^b		2.6 nM (29 min) ^c	0.2 nM (240 min)
	PEG ₈₀₀	7.8 nM (10 min)	1.7 nM (21 min)	
	PEG ₁₉₀₀	4.1 nM (12 min)	1.3 nM (19 min)	
streptavidin	14 atoms ^b		1.3 nM (55 min)	0.5 nM (165 min)
	PEG ₈₀₀	1.7 nM (35 min)	0.6 nM (71 min)	
	PEG ₁₉₀₀	2.1 nM (26 min)	0.7 nM (34 min)	

^a Dissociation constants of biotin–PEG–pyrene conjugates were taken from Figure 6 and included for comparison. Kinetic and equilibrium constants of the other biotin–PEG–fluorophore conjugates were measured according to the same experimental procedure as shown in Figure 5. ^b See the second of three papers in this issue for molecular structures. ^c Half-lives are shown in parentheses and refer to the dissociation of the fourth ligand in a 4:1 complex, the other three ligands dissociating much more slowly (compare Figure 7C).

The results are summarized in Table 1. Affinities of the TMR analogues are generally about 3-fold higher and half-lives about 2-fold longer in comparison to those of biotin–PEG₈₀₀–pyrene and biotin–PEG₁₉₀₀–pyrene. Thus, it can be concluded that the pyrene residues have a minor influence on the binding of biotinylated PEG chains to avidin or streptavidin and that the overall pattern in Figure 6 is informative on biotin–PEG conjugates in general.

Unfortunately, the biotin–PEG–fluorescein conjugates could not be characterized in the same way because displacement of one fluorescent ligand from the 4:1 complex with avidin caused a slight overall fluorescence decrease, and only further displacement by *d*-biotin caused fluorescence recovery, in contrast to the steady increase observed with TMR and pyrene derivatives (see Figure 7A).

It should be emphasized that the “conventional” biotin–fluorescein or biotin–TMR conjugates with 14 atom spacers are quenched by 84–88% or 94%, respectively, upon binding to avidin/streptavidin, while the corresponding PEG analogues retain most of their fluorescence in the bound state (see Figure 9 in the second of three papers in this issue). Obviously PEG spacers are highly advantageous to the fluorescence function while not disturbing (even slightly favoring) the biotin function, as can be seen from the series of TMR derivatives in Table 1.

DISCUSSION

Novel biotin–PEG–pyrene conjugates have been synthesized to test the consequences of a hydrophobic label in a biotin–PEG–fluorophore conjugate. The effect of variable hydrophilic–lipophilic balance was assessed by comparing the PEG₈₀₀ with the PEG₁₉₀₀ homologue.

In the preceding study (see the second of three papers in this issue) biotin–PEG–fluorophore conjugates with electrically charged, polar fluorophores were identified as excellent fluorescent markers for (strept)avidin. Binding to the receptor proteins caused little or no fluorescence quenching, in contrast to conventional fluorescent biotins with ≤14 atom spacers (see the second of three papers in this issue). Surprisingly, even biotin–PEG₁₉₀₀–pyrene proved to be a better fluorescence marker than conventional ligands because the PEG₁₉₀₀–PEG₁₉₀₀ repulsion was strong enough to oppose pyrene–pyrene association and preserve nearly half of the unbound state fluorescence intensity (see Figure 2B). In biotin–PEG₈₀₀–pyrene, however, the PEG₈₀₀ chains no longer impede pyrene–pyrene association in 4:1 complexes with (strept)avidin, as is obvious from ~10-fold fluorescence reduction (see Figure 2B). Here, the PEG₈₀₀ chain only serves the purpose to “solubilize” this biotin–fluorophore conjugate as monomer in the unbound state.

The significance of the present study is threefold: (i) By comparison with the previous study on hydrophilic conjugates and the present study on hydrophobic biotin–PEG–fluorophore conjugates, it is now possible to roughly predict the fluorescence properties of hypothetical biotin–PEG–fluorophore conjugates. To give an example, biotin–PEG–BODIPY conjugates should lose most of their fluorescence after binding to (strept)avidin because hydrophobicity and self-association tendency should be similar to that of pyrene and the much smaller Stokes shift should lead to strong self-quenching (Haugland, 1992b).

(ii) The interaction between (strept)avidin and biotin–PEG–pyrene could be studied in great detail (see Figures 5–7), the results being representative for biotin–PEG conjugates in general (see Table 1; compare the first of three papers in this issue). In other words, the fluorescence properties of pyrene labels strongly respond to receptor binding, but the latter is not much influenced by the pyrene labels.

(iii) A practical consequence of this study was the discovery of a new fluorescence assay for avidin and streptavidin, with distinct advantages, as demonstrated and tested in Figures 4 and 3, respectively: Sensitivity is 10²-fold in comparison to ANS fluorescence titration (Mock and Horowitz, 1990) and HABA absorbance titration (Green, 1970). Second, the quantitative information is calculated from distinct breakpoints in titration curves, whereas estimation of avidin via biotin–fluorescein polarization is only semiquantitative, albeit at lower detection limit (Schray et al., 1988). Most importantly, both avidin and streptavidin can be titrated with biotin–PEG₈₀₀–pyrene, whereas HABA and ANS do not recognize streptavidin (Green, 1990; Mock and Horowitz, 1990) and the polarization method has not been tested.

It can be concluded that biotin–PEG–pyrene conjugates not only figure as hydrophobic model compounds in the series of novel biotin–PEG–fluorophore conjugates but are unique fluorescent probes for avidin and streptavidin with broad application potential.

ACKNOWLEDGMENT

We are indebted to Prof. Dr. H. Falk and his staff for helpful advice and use of spectrometer facilities. This work was supported by the Austrian Research Funds (Project S-6607).

Supporting Information Available: Detailed procedures and NMR data (3 pages). Ordering information is given on any current masthead page.

LITERATURE CITED

- Chu, Y.-H., Lees, W. J., Stassinopoulos, A., and Walsh, Ch. T. (1994) Using affinity capillary electrophoresis to determine binding stoichiometries of protein–ligand interactions. *Biochemistry* 33, 10616–10621.

- Finn, F. M., Titus, G., and Hofmann, K. (1984) Ligands for insulin receptor isolation. *Biochemistry* 23, 2554–2558.
- Galla, H.-J., and Hartmann, W. (1980) Excimer-forming lipids in membrane research. *Chem. Phys. Lipids* 27, 199–219.
- Green, N. M. (1970) Spectrophotometric determination of avidin and biotin. *Methods Enzymol.* 18A, 418–424.
- Green, N. M. (1990) Avidin and Streptavidin. *Methods Enzymol.* 184, 51–67.
- Haugland, R. P. (1992a) *Handbook of fluorescent probes and research chemicals*, pp 249–259.
- Haugland, R. P. (1992b) *Handbook of fluorescent probes and research chemicals*, pp 24–27.
- Hofmann, K., Titus, G., Montibeller, J. A., and Finn, F. M. (1982) Avidin binding of carboxyl-substituted biotin and analogues. *Biochemistry* 21, 978–984.
- Lavielle, S., Chassaing, G., and Marquet, A. (1983) Avidin binding of biotinylated analogues of substance P. *Biochim. Biophys. Acta* 759, 270–277.
- McCormick, D. B., and Roth, J. A. (1970b) Colorimetric determination of biotin and analogs. *Methods Enzymol.* 18, 383–385.
- Mock, D. M., and Horowitz, P. (1990) Fluorometric assay for avidin-biotin interaction. *Methods Enzymol.* 184, 234–240.
- Romovacek, H., Finn, F. M., and Hofmann, K. (1983) Avidin binding of biotinylated corticotropins. *Biochemistry* 22, 904–909.
- Schray, K. J., Artz, P. G., and Hevey, R. C. (1988) Determination of avidin and biotin by fluorescence polarization. *Anal. Chem.* 60, 853–855.
- Schuurmans-Stekhoven, F. M. A. H., Tesser, G. I., Ramsteyn, G., Swarts, H. G. P., and De Pont, J. J. H. H. M. (1992) Binding of ethylenediamine to phosphatidylserine is inhibitory to Na^+/K^+ -ATPase. *Biochim. Biophys. Acta* 1109, 17–32.
- Wilchek, M., and Bayer, E. A. (1990a) Introduction to avidin-biotin technology. *Methods Enzymol.* 184, 5–13.
- Wilchek, M., and Bayer, E. A. (1990b) Applications of avidin-biotin technology: Literature Survey. *Methods Enzymol.* 184, 14–45.

BC970088E

Thin Layer Chromatography. Plastic sheets, precoated with 0.2 mm silica gel 60 without fluorescent indicator (Merck) were used. Eluents I, II, and III contained 70/26/4 ratios of chloroform/methanol/x (x = conc. ammonia or water or acetic acid, respectively). Eluent IV contained chloroform/methanol (90/10). Besides nonspecific staining with iodine vapor, amines were specifically detected with ninhydrin (Schuurmans-Stekhoven et al., 1992) and biotin derivatives were visualized by color reaction with DACA (McCormick & Roth, 1970). Most pyrene derivatives were visible under UV illumination (366 nm).

Synthesis of Biotin-PEG800-Pyrene. 289 mg 4-(1-pyrene)butyric acid (1 mmol), 206 mg N,N'-dicyclohexylcarbodiimide (1 mmol), and 115 mg N-hydroxysuccinimide (1 mmol) were dissolved in 6 ml absolute DMF and stirred for 6 h at RT. Precipitated N,N'-dicyclohexylurea was removed by filtration, the filtrate was cooled and evaporated at 1-10 Pa, yielding almost pure succinimidyl ester ($R_f^I = 0.69$, $R_f^{II} = 0.58$, $R_f^{III} = 0.83$) with traces of free 4-(1-pyrene)butyric acid ($R_f^I = 0.20$, $R_f^{II} = 0.56$, $R_f^{III} = 0.75$) and N-hydroxysuccinimide ($R_f^I = 0.04$). 20 mg biotin-NH-PEG800-NH₂·HCl (16.8 μ mol) and 15 mg succinimidyl 4-(1-pyrene)butyrate (39 μ mol) were dissolved in 2 ml absolute DMF, oxygen was removed by Ar perfusion and 20 μ l Et₃N were added. After 2 h of stirring under Ar the mixture was cooled and evaporated at 1-10 Pa with stirring. TLC analysis showed quantitative conversion of biotin-NH-PEG800-NH₂·HCl into product ($R_f^{II} = 0.64$, $R_f^{IV} = 0.33$). The crude product was dissolved in chloroform and applied to preparative TLC (20 cm x 20 cm, 2 mm silica 60 layer with fluorescent indicator because the pyrene-PEG conjugate shows no autofluorescence on the plate, eluent IV). A small strip of the preparative TLC plate was subjected to staining with DACA to confirm the

product band which was harvested and extracted with chloroform/methanol/water (2/7/1). The extract was taken to dryness, redissolved in 7 ml of water, frozen, thawed slowly at 4 °C, and silica particles were removed by ultracentrifugation (3 h at 60000 g_{\max}). Yield: 8.5 μmol according to UV absorption (assuming a molar extinction coefficient of 40000 $\text{M}^{-1} \text{cm}^{-1}$, in analogy to free 4-(1-pyrene)butyric acid, see Haugland, 1992a). For TLC (which showed pure product) and NMR analysis aliquots of the aqueous stock solution were lyophilized and redissolved in CHCl_3 or CDCl_3 , respectively, both of which had been pre-treated with basic alumina immediately before use. ^1H -NMR: (CDCl_3 , 200 MHz) δ : 1.05 (6H, m, 2 x CH_3 , aminopropyltermini of PEG) 1.23-1.68 (10H, m, $\text{CH}_2\text{CH}_2\text{CH}_2\text{CH}_2\text{CONH}$, biotin side chain, $\text{CH}_2\text{CH}_2\text{CH}_2\text{CONH}$, pyrene side chain) 2.05-2.23 (4H, m, CH_2CONH , biotin side chain and pyrene side chain) 2.62 ppm (1H, d, $J_{\text{gem}} = 13 \text{ Hz}$, SCH_2 (I), biotin) 2.84 (1H, q, $J_{1\text{gem}} = 13 \text{ Hz}$, $J_{2\text{vic}} = 5 \text{ Hz}$, SCH_2 (II), biotin) 3.08 (1H, m, SCH , biotin) 3.11-3.83 (~78H, m, $\text{OCH}_2\text{CH}_2\text{O}$, 2 x OCH_2 , and 2 x NCH , PEG chain) 4.03 (1H, broad s, biotinoyl-NH) 4.15 (1H, m, NCH , biotin), 4.30 (1H, m, NCH , biotin) 6.35 and 6.42 (2 H, NHCONH in biotin) 7.96-8.40 (9H, pyrene residue).

Synthesis of Biotin-PEG1900-Pyrene. 23 mg biotin-NH-PEG1900- $\text{NH}_2\cdot\text{HCl}$ (10 μmol) were reacted with 10 mg succinimidyl 4-(1-pyrene)butyrate (26 μmol) and 10 μl Et_3N . The procedure was the same as for the PEG800 homologue. Yield: 2.7 μmol of pure product. ^1H -NMR: (CDCl_3 , 200 MHz) δ : 1.07 (6H, m, 2 x CH_3 , aminopropyltermini of PEG) 1.20-1.72 (8H, m, $\text{CH}_2\text{CH}_2\text{CH}_2\text{CH}_2\text{CONH}$, biotin side chain, $\text{CH}_2\text{CH}_2\text{CONH}$, pyrene side chain) 2.08-2.26 (4H, m, CH_2CONH , biotin side chain and pyrene side chain) 2.51-2.65 ppm (3H, m, SCH_2 (I), biotin, and $\text{CH}_2\text{CH}_2\text{CH}_2\text{CONH}$, pyrene side chain) 2.81 (1H, q, $J_{1\text{gem}} = 13 \text{ Hz}$, $J_{2\text{vic}} = 5 \text{ Hz}$, SCH_2 (II), biotin) 3.05-3.85 (~179H, m, $\text{OCH}_2\text{CH}_2\text{O}$, 2 x OCH_2 , and 2 x NCH , PEG chain; SCH , biotin) 4.05 (1H, broad s, biotinoyl-NH) 4.17 (1H, m, NCH , biotin), 4.32 (1H, m, NCH , biotin) 6.38 and 6.44 (2 H, NHCONH in biotin) 7.98-8.43 (9H, pyrene residue).

LITERATURE CITED in the Supplements only:

McCormick, D. B., and Roth, J. A. (1970b) Colorimetric determination of biotin and analogs. *Methods Enzymol.* 18, 383-385.

Schuurmans-Stekhoven, F.M.A.H., Tesser, G.I., Ramsteyn, G., Swarts, H.G.P., and De Pont, J.J.H.H.M. (1992) Binding of ethylenediamine to phosphatidylserine is inhibitory to Na^+/K^+ -ATPase. *Biochim. Biophys. Acta* 1109, 17-32.

Neoglycophospholipids with Alkyl Spacers: Synthesis via an Improved Reductive Amination and Monolayer Properties

Lijun Sun and Elliot L. Chaikof*

Laboratory for Biomolecular Materials Research, Department of Surgery, Emory University School of Medicine, Atlanta, Georgia 30322. Received February 10, 1997*

An efficient synthesis of neoglycophospholipids with variable length alkyl spacer chains is described. Neoglycophospholipids tethered by alkyl chains of 3, 5, 7, 10, and 16 methylene units were synthesized in good overall yields in four steps. The key intermediates, ω -oxoalkyl glycopyranosides, were synthesized in two steps by glycosidation of chloro (or ethylthio) glycosides with a diol followed by oxidation of the remaining hydroxy group to an aldehyde functionality. Conjugation of the ω -glycoalkyl aldehyde with distearoylphosphatidylethanolamine via an improved reductive amination procedure significantly enhanced efficiency and yields with respect to those from traditional procedures. The amphiphilic properties of the neoglycophospholipids were characterized at the air–water interface. While the carbohydrate head group had relatively little effect, the length of the alkyl spacer profoundly influenced surface area–pressure isotherms.

INTRODUCTION

Glycolipids, a class of liposome-forming amphiphiles, have generated great interest in both basic science and medicine (1–4). The importance of glycolipids and glycopospholipids in living systems is demonstrated not only by their ubiquitousness as components of cell membranes but also by their role in intercellular recognition processes, the control of cell growth and tumor formation, and their interaction with biologically active factors such as enzymes, hormones, bacteriotoxins, and viruses (5–7). The diversity and complexity of natural glycolipids require a wide range of analytical and biochemical techniques in order to determine their structure–function relationships. In this respect, a powerful approach is the use of synthetic glycolipids (neoglycolipids) which mimic the behavior of the natural glycoconjugate but with structurally defined carbohydrate units. Neoglycolipids have been widely used in the characterization of carbohydrate–protein interactions and in the identification and purification of lectins. In addition, they are invaluable as antigens for generating anti-carbohydrate antibodies and as artificial vaccines and hold significant promise for receptor-targeted drug delivery and gene therapy as well as for the study of cell–tissue interactions. Another potential application of glycolipids is in the formation of biomimetic functionalized membranes on solid supports (8–10). Over the last decade, many oligosaccharide sequences have been identified which mimic functions of the parent polysaccharides. Thus, incorporation of a carbohydrate functionality into supported membranes via neoglycolipids provides opportunities to develop advanced biomedical materials and biosensors. While several methods have been described for covalently conjugating saccharides to lipids, current synthetic methods appear to be inefficient. Furthermore, the utilization of a spacer arm to enhance the bioactivity of a given lipid conjugate remains a challenging objective, with only limited success having been reported (11–18).

We describe herein a general protocol for the construction of glycopospholipids with alkyl spacer arms through a modified reductive amination and their monolayer behavior at an air–water interface.

EXPERIMENTAL PROCEDURES

Representative procedures for the synthesis of **2–5** are provided in this section. The synthesis of all new compounds and their structural characterization, spectral data, and general experimental methods can be found in the Supporting Information. Starting materials **1a–f** were prepared according to known methods (see the Supporting Information for references and procedures). The phosphatidylethanolamine used in this study was purchased from Avanti Polar Lipids (Alabaster, AL). All other chemicals, reagents, and solvents were purchased from Aldrich (Milwaukee, WI) and used as received. Anhydrous solvents were dried over molecular sieves and stored under argon.

Synthesis of 1-(10-Hydroxy-*n*-decanyl)-2,3,4,6-tetra-*O*-benzyl- α -D-galactopyranoside (2d**).** A mixture of 1-chloro-2,3,4,6-tetra-*O*-benzyl- α -D-galactopyranoside (**1a**) (0.560 g, 1.00 mmol), 1,10-decanediol (1.50 g, 8.61 mmol), CdCO_3 (0.20 g, 1.15 mmol), and CaSO_4 (0.50 g) was stirred in dry acetonitrile/toluene (1:2, 15 mL) at 65 °C under a nitrogen atmosphere. TLC analysis of the reaction mixture indicated complete consumption of the carbohydrate starting material and the formation of a new carbohydrate derivative after 1.5 h. The reaction mixture was allowed to cool to room temperature. The organic layer was filtered with a toluene wash (20 mL), diluted with ethyl acetate (10 mL), washed with water (3 \times 25 mL), dried over MgSO_4 , and concentrated to an oil. Chromatographic purification (silica gel, 20% ethyl acetate in hexane) afforded 0.570 g (0.818 mmol, 82%) of **2d** as a clear oil. R_f = 0.44 (silica gel, 30% ethyl acetate in hexanes). ^1H NMR (CDCl_3 , 300 MHz): δ 7.32 (m, 20H), 4.98 (dd, J = 12.0, 4.5 Hz, 2H), 4.80 (d, J = 10.5 Hz, 1H), 4.77 (d, J = 4.8 Hz, 1H), 4.66 (d, J = 11.8 Hz, 1H), 4.47 (d, J = 4.5 Hz, 2H), 4.39 (d, J = 10.5 Hz, 1H), 4.00 (m, 2H), 3.85 (dt, J = 10.8, 1.8 Hz, 1H), 3.64 (t, J = 6.9 Hz, 4H), 3.54 (m, 3H), 1.65 (m, 2H), 1.57 (m, 4H), 1.30 (br m, 12H). ^{13}C NMR (CDCl_3 , 75 MHz): δ 138.7,

* Address correspondence to Professor Elliot L. Chaikof, 1364 Clifton Road, N.E., Box M-11, Laboratory for Biomolecular Materials Research and Department of Surgery, Emory University, Atlanta, GA 30322. Phone: (404) 727-8413. Fax: (404) 727-3660. E-mail: echaikof@surgery.eushc.org.

† Abstract published in *Advance ACS Abstracts*, July 1, 1997.

138.6, 138.5, 137.9, 128.32, 128.25, 128.15, 128.05, 127.83, 127.78, 127.73, 127.67, 127.62, 127.58, 127.4, 103.9, 82.1, 79.5, 75.1, 74.4, 73.4, 73.3, 72.9, 69.9, 68.8, 62.9, 32.7, 29.6, 29.44, 29.40, 29.3, 26.1, 25.6. HRMS¹ (FAB⁺) calcd for C₄₄H₅₆O₇ + Li⁺ 703.4186, found 703.4197.

Synthesis of 1-(10-Oxo-*n*-decanyl)-2,3,4,6-tetra-*O*-benzyl-*D*-galactopyranoside (3d). Under an atmosphere of nitrogen, pyridinium dichromate (460 mg, 1.222 mmol) was added to a dry methylene chloride solution (10 mL) of **2d** (570 mg, 0.818 mmol). The resulting brown slurry was stirred at room temperature under nitrogen. TLC analysis (visualization by UV and char with 10% sulfuric acid in ethanol) of the reaction mixture indicated complete consumption of the starting material and the formation of a new compound after 20 h. The reaction mixture was treated with ether (10 mL), filtered through silica gel and Celite with an ether wash (25 mL), and concentrated to an off-white oil. Chromatographic purification (silica gel, 20% ethyl acetate in hexane) afforded 374 mg (0.539 mmol, 66%) of **3d** as a clear oil. *R*_f = 0.61 (silica gel, 30% ethyl acetate in hexanes). ¹H NMR (CDCl₃, 300 MHz): δ 9.77 (t, *J* = 1.5 Hz, 1H), 7.30 (m, 20H), 4.97 (dd, *J* = 12.0, 2.7 Hz, 2H), 4.78 (d, *J* = 11.1 Hz, 1H), 4.77 (d, *J* = 4.5 Hz, 1H), 4.65 (d, *J* = 12 Hz, 1H), 4.46 (d, *J* = 4.2 Hz, 2H), 4.38 (d, *J* = 7.8 Hz, 1H), 3.95 (m, 1H), 3.84 (dt, *J* = 10.2, 1.8 Hz, 1H), 3.50 (m, 7H), 2.40 (dt, *J* = 7.5, 1.8 Hz, 2H), 1.65 (m, 6H), 1.30 (m, 8H). ¹³C NMR (CDCl₃, 75 MHz): δ 202.8, 138.9, 138.6, 138.5, 137.9, 128.4, 128.3, 128.2, 128.1, 127.9, 127.8, 127.7, 127.6, 127.5, 127.3, 127.2, 103.9, 82.2, 79.6, 75.1, 74.4, 73.5, 73.4, 73.3, 73.0, 70.0, 68.9, 43.8, 29.7, 29.3, 29.2, 26.1, 22.0. HRMS (FAB⁺) calcd for C₄₄H₅₄O₇ + Li⁺ 701.4030, found 701.4051.

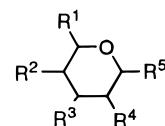
Synthesis of the Perbenzylated Galactopyranoside-*n*-Decanyl-DSPE Conjugate 4d. Under a nitrogen atmosphere, sodium cyanoborohydride (20 mg, 0.318 mmol) was added in its solid form to a white slurry of distearoylphosphatidylethanolamine (DSPE) (200 mg, 0.267 mmol) in methanol and chloroform (10 mL, 1:1 by volume) in the presence of molecular sieves (3 Å, 800 mg). The mixture was stirred at 50 °C for 15 min to form a cloudy solution, while gas was liberated from the reaction solution. To the above solution stirred at 50 °C was added dropwise **3d** (120 mg, 0.173 mmol) dissolved in methanol and chloroform (1:1, 5 mL). The clear solution was stirred for another 2 h, while TLC analysis (visualization by UV, molybdenum blue reagent and char with 10% sulfuric acid in ethanol) indicated the complete consumption of the decanal starting material and the formation of a new compound. The reaction mixture was cooled to room temperature, filtered, and concentrated to give a white solid. Chromatographic purification (silica gel, 150:12 CHCl₃/MeOH) afforded 228 mg (0.160 mmol, 92%) of the perbenzylated decanyl-DSPE-galactopyranoside conjugate **4d** as a waxy solid. *R*_f = 0.47 (silica gel, 1:10 methanol/chloroform). ¹H NMR (CDCl₃, 300 MHz): δ 10.20 (br s, 2H), 7.25 (m, 20H), 5.22 (m, 1H), 4.91 (dd, *J* = 11.7, 2.7 Hz, 2H), 4.71 (m, 3H), 4.60 (q, *J* = 11.7 Hz, 1H), 4.40 (d, *J* = 4.8 Hz, 2H), 4.33 (m, 2H), 4.20 (m, 3H), 4.00 (m, 2H), 3.88 (m, 2H), 3.78 (t, *J* = 7.8 Hz, 1H), 3.50 (m, 5H), 3.11 (br s, 2H), 2.85 (m, 2H), 2.27 (q, *J* = 6.0 Hz, 4H), 1.70 (br s, 2H), 1.59 (br m, 6H),

1.24 (s, 68H), 0.86 (t, *J* = 6.0 Hz, 6H). ¹³C NMR (CDCl₃, 75 MHz): δ 173.2, 172.9, 138.7, 138.6, 138.5, 137.9, 128.3, 128.2, 128.1, 128.0, 127.83, 127.79, 127.7, 127.6, 127.4, 127.3, 103.9, 82.2, 79.5, 75.1, 74.4, 73.4, 73.3, 73.2, 73.0, 70.0, 68.8, 64.0, 63.9, 62.5, 60.7, 49.2, 48.1, 34.2, 34.0, 31.9, 29.7, 29.5, 29.3, 29.1, 29.08, 26.6, 26.1, 26.0, 24.9, 24.8, 22.6, 14.1. HRMS (FAB⁺) calcd for C₈₅H₁₃₆NO₁₄P + H⁺ 1426.9777, found 1426.9740.

Preparation of *D*-Galactopyranoside-Decanyl-DSPE 5d. Perbenzylated galactopyranoside-decanyl-DSPE conjugate **4d** (100 mg, 0.0701 mmol) was dissolved in chloroform (3 mL) and methanol (12 mL). The solution was stirred at room temperature in the presence of 10% Pd-C (200 mg) under a hydrogen atmosphere (balloon). TLC analysis (visualization by UV, molybdenum blue reagent and char with 10% sulfuric acid in ethanol) of the reaction mixture indicated the complete consumption of the perbenzylated starting material and the formation of a new compound after 1 h. The reaction mixture was filtered through Celite with a chloroform/methanol (1:1, 10 mL) wash. Concentration and chromatographic purification (silica gel, 150:30:1 CHCl₃/MeOH/H₂O) afforded 56 mg (0.0525 mmol, 75%) of **5d** as a white solid. *R*_f = 0.33 (silica gel, 150:30:1 CHCl₃/MeOH/H₂O). ¹H NMR [CDCl₃/CD₃OD (2:1 v/v), 300 MHz]: δ 5.00 (m, 1H), 4.18 (dd, *J* = 11.7, 3.0 Hz, 1H), 3.99 (d, *J* = 6.9 Hz, 1H), 3.95 (m, 1H), 3.90 (m, 2H), 3.78 (t, *J* = 6.0 Hz, 2H), 3.68 (m, 1H), 3.55 (d, *J* = 6.0 Hz, 1H), 3.30 (m, 4H), 2.95 (br m, 2H), 2.74 (br t, *J* = 7.8 Hz, 2H), 2.10 (q, *J* = 7.2 Hz, 4H), 1.48 (m, 2H), 1.37 (m, 6H), 1.03 (s, 70H), 0.65 (t, *J* = 6.6 Hz, 6H). ¹³C NMR [CDCl₃/CD₃OD (2:1 v/v), 75 MHz]: δ 174.4, 174.1, 103.9, 75.3, 74.1, 71.9, 70.8, 70.7, 70.4, 69.3, 64.4, 63.0, 61.7, 61.1, 34.7, 34.6, 32.4, 30.2, 30.1, 30.0, 29.8, 29.7, 29.6, 29.5, 29.4, 26.9, 26.5, 26.2, 25.4, 25.3, 23.2, 14.4. HRMS (FAB⁺) calcd for C₅₇H₁₁₂NO₁₄P + H⁺ 1066.7899, found 1066.7880.

RESULTS AND DISCUSSION

Synthesis. Our approach to the synthesis of neoglycophospholipid conjugates was based on the finding of Feizi and colleagues (19, 20), who demonstrated that oligosaccharides, when treated with an excess amount (10–50 equiv) of a phosphatidylethanolamine (PE) in the presence of sodium cyanoborohydride (NaBH₃CN), could be conjugated to a PE via a reductive amination reaction. A significant drawback of this method is the fact that the reducing end of the oligosaccharide thus conjugated is inevitably destroyed, potentially diminishing the biological activity of smaller carbohydrates. For the same reason, the method is also inapplicable to monosaccharides and synthetic oligosaccharides. In order to circumvent these limitations, methodology was developed for glycolipid conjugation using a spacer arm inserted on the saccharide and possessing the required carbonyl functionality for reductive amination. In view of the requirement for a general method, different monosaccharides (**1**) were used to initiate this investigation.



- 1a: R¹=β-BnOCH₂, R²=β-BnO, R³=β-BnO, R⁴=α-BnO, R⁵=α-Cl
 1b: R¹=β-BnOCH₂, R²=α-BnO, R³=β-BnO, R⁴=α-BnO, R⁵=α-Cl
 1c: R¹=α-CH₃, R²=α-BnO, R³=α-BnO, R⁴=β-BnO, R⁵=α-Cl
 1d: R¹=β-BnOCH₂, R²=α-BnO, R³=β-BnO, R⁴=β-BnO, R⁵=α-Cl
 1e: R¹=β-BnOCH₂, R²=α-BnO, R³=β-BnO, R⁴=β-BnO, R⁵=α-SEt
 1f: R¹=β-BnOCH₂, R²=α-BnO, R³=β-BnO, R⁴=α-NHAc, R⁵=α-SEt

¹ Abbreviations: Galp, *D*-galactopyranoside; Glcp, *D*-glucopyranoside; Fucp, *L*-fucopyranoside; Manp, *D*-mannopyranoside; GlcpNAc, 2-acetamido-2-deoxy-*D*-glucopyranoside; DSPE, distearoylphosphatidylethanolamine; PDC, pyridinium dichromate; TBPA⁺, tris(4-bromophenyl)aminium hexachloroantimonate(V); NIS, *N*-iodosuccinimide; COSY, correlated spectroscopy; HRMS, high-resolution mass spectroscopy.

Table 1. Syntheses of Neoglycophospholipid Conjugates^a

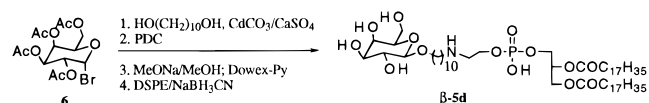
<p>a: HO(CH₂)_nOH; b: PDC; c: DSPE/NaBH₃CN; d: H₂, 10% Pd-C</p>							
Entry	Carbohydrate, 1	n	β : α	2 (Yield)	3 (Yield)	4 (Yield)	5 (Yield)
1	Galp, 1a	3	85:15	2a (87%)	3a (63%)	4a (83%)	5a (82%)
2	Galp, 1a	5	84:16	2b (89%)	3b (72%)	4b (82%)	5b (69%)
3	Galp, 1a	7	88:12	2c (81%)	3c (69%)	4c (84%)	5c (72%)
4	Galp, 1a	10	88:12	2d (82%)	3d (66%)	4d (92%)	5d (75%)
5	Galp, 1a	16	88:12	2e (90%)	3e (76%)	4e (95%)	5e (81%)
6	GlcP, 1b	7	86:14	2f (75%)	3f (74%)	4f (95%)	5f (72%)
7	GlcP, 1b	10	89:11	2g (86%)	3g (74%)	4g (85%)	5g (75%)
8	Fucp, 1c	10	88:12	2h (81%)	3h (69%)	4h (82%)	5h (71%)
9	Manp, 1e	7	10:90	2i (41%)	3i (63%)	4i (90%)	5i (62%)
10	Manp, 1e	10	10:90	2j (65%)	3j (71%)	4j (89%)	5j (72%)
11	GlcPNAc, 1f	10	>95:5	2k (84%)	3k (73%)	4k (85%)	5k (78%)

^a All yields are isolated yields after flash silica gel chromatography purification.

Table 1 summarizes our strategy and results according to this protocol. Perbenzylated α -glycopyranosyl chlorides (**1a–d**) reacted with alkyldiols of 3, 5, 7, 10, and 16 methylene units, respectively, in the presence of CdCO₃ and CaSO₄ and in mixed solvents of 2:1 toluene/acetonitrile. In most synthetic schemes, CdCO₃ is predominantly utilized as an acid scavenger and its application as a glycosylation catalyst has been limited (21, 22). Nonetheless, Conrow and Bernstein have observed that CdCO₃ could catalyze the synthesis of steroid conjugates of aryl glucuronides, providing improved overall results when compared with the results with traditional heavy metal catalysts (23). Similarly, in the synthesis of compounds **2**, CdCO₃ resulted in better yields and satisfied β -anomeric selectivity in contrast to AgClO₄, HgBr₂, and AgOTf. Compounds **2a–h** were produced in excellent isolated yields with anomeric selectivity ranging from 84:16 to 89:11 in favor of the β -anomer as determined by HPLC or ¹H NMR. The β -anomeric stereochemistry of the major isomers in **2a–h** was characterized by a larger coupling constant ($J = 7.8–10.0$ Hz) of the anomeric proton with chemical shifts at $\delta = 4.35–4.40$ ppm. The unambiguous assignments of the anomeric protons were achieved by COSY which correlated the anomeric protons to other protons on the carbohydrate rings rather than to the protons of the methylene

protons of the benzyl groups. Further, the anomeric carbons of the major isomers of **2a–h** were observed at about 103–104 ppm while the minor isomers at 98–99 ppm.² Optimized reaction conditions for obtaining high yields and good anomeric selectivity include carrying out the glycosidation reactions at 60–65 °C in a mixed solvent system of toluene and acetonitrile and using an excess amount of the diol. The anomeric selectivity was also substrate controlled as glucosyl, fucosyl, and galactosyl chlorides (**1a–c**) showed good β -selectivity, while mannosyl chloride (**1d**) did not demonstrate any selectivity. Thus, under the same reaction conditions, a 50:50 mixture of α/β anomers (**2i**) was obtained in 86% yield from α -mannopyranosyl chloride (**1d**) when it was treated with 1,7-heptanediol.³ On the other hand, the corresponding α -thiomannopyranoside (**1e**), when treated with either 1,7-heptanediol or 1,10-decanediol under the reac-

² Amphiphile β -**5d** was prepared as shown below from aceto-bromo galactoside (**6**) and has the same spectral behavior as the major anomer of **5d**. Detailed study will be reported in due course.



tion conditions developed by Sinay (24, 25) (-40 to -20 °C in acetonitrile with TBPA^{+} as the initiator), could be transformed to desired products **2i** and **2j** in moderate to good yields with high α -selectivity (90:10).⁴ Because of the existence of a neighboring participating group in thioglycoside **1f**, its reaction with 1,10-decanediol under the Fraser-Reid protocol (26) (NIS/TfOH) proceeded with high β -selectivity ($>95:5$ by ^1H NMR) to afford **2k** in 84% yield. The nonseparable anomeric mixtures of **2** were used directly in subsequent reactions. Transformation of the primary hydroxy group in compounds **2** to an aldehyde via PDC oxidation in methylene chloride (27) produced compounds **3** in good yields.

Disappointing results were obtained under standard reductive amination conditions when aldehydes **3** were reacted with DSPE using NaBH_3CN as the reducing agent (28–30). Thus, compound **3b** was first mixed with 10 equiv of distearoylphosphatidylethanolamine (DSPE) in a 1:1 mixed solvent of methanol and chloroform in the presence of 3 Å molecular sieves. The reaction mixture then was treated with NaBH_3CN at 50 °C. Under this procedure, only 10–30% of the desired reductive amination product **4b** was isolated after the reaction mixture was stirred for over 72 h. However, it was found that, by reversing the order of addition of the reagents, a much more efficient reductive amination procedure was discovered. NaBH_3CN was added to DSPE in a mixed solvent of methanol and chloroform (1:1) at 50 °C and allowed to be stirred for about 10 min. A methanol/chloroform (1:1) solution of aldehydes **3** (1:1.3–1.5 **3**/DSPE) was then added dropwise to the above reaction mixture. TLC analysis indicated a very clean reaction with complete conversion of the aldehyde to the corresponding conjugates **4** in about 30 min after addition. The reaction was allowed to proceed for 1–1.5 h to ensure quantitative conversion of the aldehyde. All compounds **3** underwent efficient reaction with 1.3–1.5 equiv of DSPE to afford conjugates **4** in 80–95% yields. The possible byproduct formed by dialkylation of the primary amino group of DSPE was not detected. It is noteworthy that, with this improved procedure for reductive amination, the amount of DSPE used in the reaction was reduced from 10 equiv to about 1.3–1.5 equiv; the reaction time was reduced from 72 to 0.5–1.5 h, and most importantly, the yields were improved from 10–30 to 80–95%.

The perbenzylated conjugates **4**, which were easily isolated as a mixture of anomers from excess DSPE/ NaBH_3CN via flash column chromatography, were subjected to the condition of hydrogenation (H_2 balloon, 2.0 equiv of 10% Pd-C by weight) to furnish the desired amphiphiles **5** in good to excellent yields. We found that using an excess amount of the Pd-C catalyst significantly improved the reaction efficiency by shortening the reaction time and improving the reaction yields. Using <1 equiv of the catalyst occasionally resulted in a long reaction time and some decomposition; thus, a low reaction yield was observed. The use of a minimal amount of chloroform to assist dissolving the starting materials also improved the hydrogenation reaction. Under these conditions, all benzylated conjugates **4** underwent clean deprotection to furnish the corresponding amphiphiles **5** in good to excellent yields.

As shown in Table 1, the method is general to spacer arms of 3, 5, 7, 10, and 16 methylene units and to a

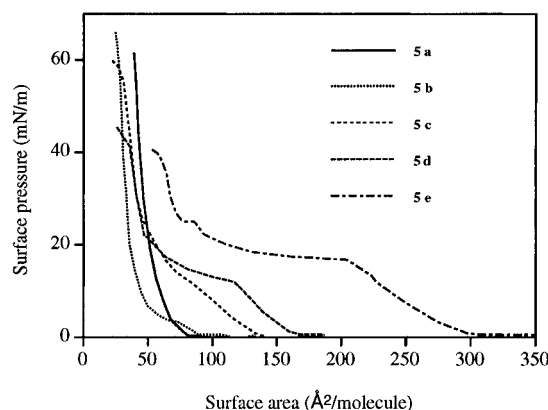


Figure 1. π - A isotherms of galactosyl amphiphiles with C3–C16 spacers.

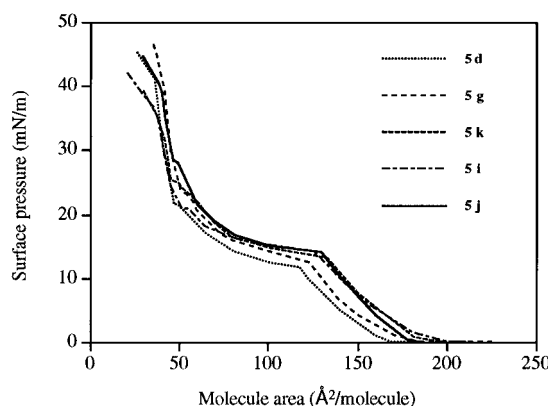


Figure 2. π - A isotherms of amphiphiles with C10 spacers.

variety of simple and functionalized saccharides. To our knowledge, the galactopyranoside–hexadecanyl-DSPE conjugate (**5e**) represents a bioconjugate of its class with the longest (C16) alkyl spacer arm reported in the literature to date.

Amphiphilic Properties. The amphiphilic properties of neoglycoconjugates **5** were investigated at the air–water interface using a Langmuir–Blodgett trough. All amphiphiles **5a–k** formed stable monolayers with intriguing properties. Figure 1 illustrates the effect of the alkyl spacer arm on the monolayer behavior of the galactopyranoside–alkyl-phospholipid conjugates **5a–e**. The molecular areas at monolayer collapse of **5a–d** were in the range of 35–45 Å²/molecule. Compound **5e**, however, exhibited a higher molecular area of approximately 70 Å²/molecule, indicative of less compacted packing at the collapse point. When the spacer length increases, the transition region from expanded to condensed phases increases in both the range of molecular area and surface pressure. Significantly, compounds **5d** and **5e** have well-developed transition regions with **5e** having the highest surface pressure (24–25 mN/m) and a range extending between 120 and 200 Å²/molecule. The pressure–area (π - A) isotherms of glycopospholipids with different carbohydrate head groups, all having a 10-methylene spacer arm, are presented in Figure 2. Well-developed expanded to condensed phase transition regions were observed. However, the carbohydrate head group had little influence on either the collapse area, the collapse pressure, or the shape of the isotherm. While a recent report has documented that oligosaccharides may influence the phase transition of nonphospholipidic glycolipids in the absence of a spacer arm, in our system, the stereochemistry and presence of functional groups on the carbohydrate ring appear to have little effect on monolayer packing (31).

³ The synthesis of this mixture and their spectroscopic data are included in the Supporting Information.

⁴ The α -stereochemistry of the major anomer was determined spectroscopically and confirmed by a synthesis of α -**5j** similar to that of β -**5d**. Detailed study will be reported in due course.

CONCLUSION

In conclusion, we have developed an efficient protocol for the synthesis of glycophospholipids. The key to this protocol is the conjugation of PE to a saccharide via an alkyl spacer with a terminal aldehyde using an improved reductive amination procedure. In this manner, the structural integrity of the saccharide is maintained and alkyl spacer arms of different lengths can be incorporated into the neoglycophospholipid. Optimization of carbohydrate binding to specific peptides or cell surface receptors may lead to the discovery of novel liposome-based cell- and tissue-targeted drug and gene delivery systems. Studies in this matter are currently under investigation and will be reported in due course.

ACKNOWLEDGMENT

The authors are grateful for the financial support provided by the ONR, the Whitaker Foundation, and NIH Grant HL56819. E.L.C. is a Clinician Scientist of the American Heart Association. NMR and MS facilities used in this study were purchased through grants from NIH and NSF.

Supporting Information Available: Experimental details for the synthesis of all compounds and their characterization data are provided (25 pages). Ordering information is given on any current masthead page.

LITERATURE CITED

- (1) Lee, Y. C., and Lee, R. T., Eds. (1994) in *Neoglycoconjugates*, Academic Press, San Diego.
- (2) Wong, S. Y. C. (1995) Neoglycoconjugates and their applications in glycobiology. *Curr. Opin. Struct. Biol.* 5, 599–604.
- (3) Ahlers, M., Muller, W., Reichert, A., Ringsdorf, H., and Venzmer, J. (1990) Specific interactions of proteins with functional lipid monolayers—Ways of simulating biomembrane processes. *Angew. Chem., Int. Ed. Engl.* 29, 1269–1285.
- (4) Dwek, R. A. (1996) Glycobiology—toward understanding the function of sugars. *Chem. Rev.* 96, 683–720.
- (5) Giannis, A. (1994) The sialyl lewis(x) group and its analogs as ligands for selectins—chemoenzymatic syntheses and biological functions. *Angew. Chem., Int. Ed. Engl.* 33, 178.
- (6) Varki, A. (1993) Biological roles of oligosaccharides—all of the theories are correct. *Glycobiology* 3, 97–130.
- (7) Garegg, P. J. (1996) Some contributions of chemical synthesis to glycobiology: an organic chemist's point of view. *Med. Res. Rev.* 16, 345–364.
- (8) Ulman, A. (1996) Formation and structure of self-assembled monolayers. *Chem. Rev.* 96, 1533–1554.
- (9) Sackmann, E. (1996) Supported membranes—scientific and practical applications. *Science* 271, 43–48.
- (10) Muller, W., Ringsdorf, H., Rump, E., Zhang, X., Angermaier, L., Knoll, W., and Spinke, J. (1994) Formation of protein multilayers and their competitive replacement based on self-assembled biotinylated phospholipids. *J. Biomater. Sci., Polym. Ed.* 6, 481–495.
- (11) Biessen, E. A. L., Beuting, D. M., Rolen, H. C. P., van de Marel, G. A., van Boom, J. H., and van Berkel, T. J. C. (1995) Synthesis of cluster galactosides with high-affinity for the hepatic asialoglycoprotein receptor. *J. Med. Chem.* 38, 1538–1546.
- (12) Kuhlenschmidt, T. B., and Lee, Y. C. (1984) Specificity of chicken liver carbohydrate binding protein. *Biochemistry* 23, 3569.
- (13) Gabius, H.-J. (1990) Influence of type of linkage and spacer on the interaction of β -galactoside-binding proteins with immobilized affinity ligands. *Anal. Biochem.* 189, 91–94.
- (14) Haensler, J., and Schuber, F. (1991) Influence of the galactosyl ligand structure on the interaction of galactosylated liposomes with mouse peritoneal macrophages. *Glycoconjugate J.* 8, 116–124.
- (15) Defrees, S. A., Phillips, L., Guo, L., and Zalipsky, S. (1996) Sialyl-lewis-x liposomes as a multivalent ligand and inhibitor of E-selectin mediated cellular adhesion. *J. Am. Chem. Soc.* 118, 6101–6104.
- (16) Wang, P., Schuster, M., Wang, Y.-F., and Wong, C.-H. (1993) Synthesis of phospholipid-inhibitor conjugates by enzymatic transphosphatidylation with phospholipase D. *J. Am. Chem. Soc.* 115, 10487.
- (17) Schmidt, R. R. (1989) Recent development in the synthesis of glycoconjugates. *Pure Appl. Chem.* 61, 1257–1270.
- (18) Schmidt, R. R. (1986) New methods for the synthesis of glycosides and oligosaccharides—are there alternatives to the Koenigs-Knorr methods. *Angew. Chem., Int. Ed. Engl.* 25, 212.
- (19) Pang, P. W., Gooi, H. C., Hardy, M., Lee, Y. C., and Feizi, T. (1985) Novel approach to the study of the antigenicities and receptor functions of carbohydrate chains of glycoproteins. *Biochem. Biophys. Res. Commun.* 132, 474–480.
- (20) Stoll, M. S., Mizuochi, T., Childs, R. A., and Feizi, T. (1988) Improved procedure for the construction of neoglycolipids having antigenic and lectin-binding activities, from reducing oligosaccharides. *Biochem. J.* 256, 661–664.
- (21) Toshima, K., and Tatsuta, K. (1993) Recent progress in O-glycosylation methods and its application to natural products synthesis. *Chem. Rev.* 93, 1503–1531.
- (22) Paulsen, H. (1982) Advances in selective chemical syntheses of complex oligosaccharides. *Angew. Chem., Int. Ed. Engl.* 21, 115–224.
- (23) Conrow, R. B., and Bernstein, S. (1971) Steroid conjugates. VI. An improved Koenigs-Knorr synthesis of aryl glucuronides using cadmium carbonate, a new and effective catalyst. *J. Org. Chem.* 36, 863–870.
- (24) Sinay, P. (1991) Recent advances in glycosylation reactions. *Pure Appl. Chem.* 63, 519.
- (25) Marra, A., Mallet, J.-M., Amatore, C., and Sinay, P. (1990) Glycosylation using a one-electron-transfer homogeneous reagent: A novel and efficient synthesis of β -linked disaccharides. *Syntlett*, 572.
- (26) Knoradsson, P., Mootoo, D. R., McDevitt, R. E., and Fraser-Reid, B. (1990) Iodonium ion generated *in situ* from *N*-iodosuccinimide and trifluoromethanesulphonic acid promotes direct linkage of 'disarmed' pent-4-enyl glycosides. *J. Chem. Soc., Chem. Commun.*, 270–272.
- (27) Corey, E. J., and Schmidt, G. (1979) Useful procedures for the oxidation of alcohols involving pyridinium dichromate in aprotic media. *Tetrahedron Lett.*, 399–402.
- (28) Borch, R. F., Bernstein, M. D., and Durst, H. S. (1971) The cyanohydridoborate anion as a selective reducing agent. *J. Am. Chem. Soc.* 93, 2897–2904.
- (29) Abdel-Magid, A., Carson, K. G., Harris, B. D., Maryanoff, C. A., and Shah, R. D. (1996) Reductive amination of aldehydes and ketones with sodium triacetoxyborohydride—studies on direct and indirect reductive amination procedures. *J. Org. Chem.* 61, 3849–3862, and references cited therein.
- (30) Zhao, H., and Mootoo, D. R. (1996) Triple reductive amination approach to polyhydroxyindolizidine alkaloids—a total synthesis of castanospermine. *J. Org. Chem.* 61, 6762–6763, and references cited therein.
- (31) Tamada, K., Minamikawa, H., Hato, M., and Miyano, K. (1996) Phase-transition in glycolipid monolayers induced by attractions between oligosaccharide head groups. *Langmuir* 12, 1666, and references cited therein.

BC9700897

Supporting Information to

Neoglycophospholipids with Alkyl Spacers: Synthesis via an Improved Reductive Amination and Monolayer Properties

Lijun Sun and Elliot L. Chaikof*

Laboratory for Biomolecular Materials Research, Emory University School of Medicine,
Department of Surgery, Atlanta, GA 30322

General Methods

^1H and ^{13}C NMR spectra were recorded on a General Electric QE-300 (300 MHz ^1H , 75.5 MHz ^{13}C) spectrometer in either deuteriochloroform (CDCl_3) with chloroform (7.26 ppm ^1H , 77.00 ppm ^{13}C) as an internal reference or a mixture of deuteriochloroform and deuteriomethanol (2:1 in volume) with methanol (3.10 ppm ^1H , 49.00 ppm ^{13}C) as an internal reference unless otherwise stated. Data are reported in the following order: chemical shifts are given (δ , ppm); multiplicity is indicated (s (singlet), d (doublet), t (triplet), q (quartet), hex (hextet), hept (heptet), m (multiplet)); coupling constants, J , are reported (Hz); and integration is provided. Only the signals corresponding to the major anomers were reported, because most of the signals corresponding to the minor anomers were overlapped by the major ones. High resolution mass spectra were recorded on a Joel mass spectrometer. Monolayer isotherms were measured using a NIMA 2000 Langmuir-Blodgett trough. Amphiphiles were spread from chloroform/methanol (5:1 by wt) solutions. Barrier movement was initiated 10-15 min after spreading. Isotherms were recorded with the barrier moving at constant speed of $20\text{ cm}^2/\text{min}$.

Analytical thin-layer chromatography (TLC) was performed on Merck silica gel plates with F-354 indicator. Visualization was accomplished by one or more of the following methods: UV light, char with 10% H_2SO_4 in ethanol, and Molybdenum blue. Solvents for extraction and chromatography were reagent grade and used as received. Flash column chromatography was conducted using 32 - 63 μm flash silica gel obtained from EM. Solvents (chloroform, toluene, acetonitrile, THF, methylene

chloride, dichloroethane) used as reaction media were dried over freshly regenerated 4Å molecular sieves before use. Methanol was dried over 3Å molecular sieves before use. Reagents purchased from commercial source were used directly without further purification. All reactions were performed under a dry argon or nitrogen atmosphere in base-washed, oven-dried (230 °C) glassware.

Starting materials

The following compounds were prepared according to literature procedures: 1-chloro-2,3,4,6-tetra-*O*-benzyl- α -D-galactopyranoside (**1a**)¹; 1-chloro-2,3,4,6-tetra-*O*-benzyl- α -D-glucopyranoside(**1b**);² 1-chloro-2,3,4-tri-*O*-benzyl- α -L-fucopyranoside (**1c**);³ 1-chloro-2,3,4,6-tetra-*O*-benzyl- α -D-mannopyranoside(**1d**);⁴ 1-ethyl-2,3,4,6-tetra-*O*-benzyl- α -D-thiomannopyranoside (**1e**).⁵

Synthesis of 2-Acetamido-2-deoxy-1-ethyl-3,4,6-tri-*O*-benzyl- α -D-thioglucopyranoside (1f). A white slurry of 2-acetomido-2-deoxy-1-ethyl-3,4,6-tri-*O*-acetyl- α -D-thioglucopyranoside (Toronto Research) (2.00 g, 5.12 mmol) in MeOH (20 mL) was treated with MeONa (25% wt in MeOH, 10 drops) at room temperature for 1.0 h. The reaction mixture was neutralized with pyridinium-Dowex ion exchange resin, filtered and concentrated to a white solid. The crude product was dissolved in DMF (15 mL) and then treated with BnBr (3 mL) and NaH (0.92 g) at room temperature overnight. The reaction mixture was poured into ice and extracted with ether (3 x 50 mL). The combined organic layer was dried over, concentrated and purified by partition with ether and hexanes to give 2.47 g (4.64 mmol, 90%) of **1f** as an off-white solid. ¹H NMR (CDCl₃, 300 MHz) δ : 7.38-7.24 (m, 15H), 6.69 (d, *J*= 8.4 Hz, 1H), 4.88 (d, *J*= 11.7 Hz, 1H), 4.4.83 (d, *J*= 11.1 Hz, 1H), 4.70 (m, 2H), 4.63 (m, 2H), 3.9-3.6 (m, 5H), 3.85 (m, 1H), 2.75 (dt, *J*= 7.5, 4.8 Hz, 2H), 1.90 (s, 3H), 1.29 (t, *J*= 7.5 Hz, 3H); ¹³C NMR (CDCl₃, 75 MHz) δ :170.3, 138.2, 138.0, 137.9, 128.3, 128.2, 127.9, 127.8, 127.60, 127.55, 127.4, 83.7, 83.0, 79.0, 78.4, 74.7, 74.6, 73.6, 68.9, 54.9, 24.0, 23.4, 14.9.

Synthesis of ω -Hydroxyalkylglycopyranosides, 2.

Typical example for the synthesis of ω -hydroxyalkylglycopyranosides (2) from glycosyl chlorides (1a-c) and alkyldiols: Synthesis of 1-(10-hydroxy-*n*-decanyl)-2,3,4,6-tetra-*O*-benzyl-D-galactopyranoside (2d). A mixture of 1-chloro-2,3,4,6-tetra-*O*-benzyl- α -D-galactopyranoside (**1a**) (0.560 g, 1.00 mmol), 1,10-decanediol (1.50 g, 8.61 mmol), CdCO₃ (0.20 g, 1.15 mmol) and CaSO₄ (0.50 g) was stirred in dry acetonitrile/toluene (1:2, 15 mL) at 65 °C under a nitrogen atmosphere. TLC analysis of the reaction mixture indicated complete consumption of the carbohydrate starting material and the formation of a new carbohydrate derivative after 1.5 h. The reaction mixture was allowed to cool to rt. The organic layer was filtered with a toluene wash (20 mL), diluted with ethyl acetate (10 mL), washed with water (3 x 25 mL), dried over MgSO₄ and concentrated to an oil. Chromatographic purification (silica gel, 20% ethyl acetate in hexanes) afforded 0.570 g (0.818 mmol, 82%) of **2d** as a clear oil. *R*_f = 0.44 (silica gel, 30% ethyl acetate in hexanes); ¹H NMR (CDCl₃, 300 MHz) δ : 7.32 (m, 20 H), 4.98 (dd, *J* = 12.0, 4.5 Hz, 2H), 4.80 (d, *J* = 10.5 Hz, 1H), 4.77 (d, *J* = 4.8 Hz, 1H), 4.66 (d, *J* = 11.8 Hz, 1H), 4.47 (d, *J* = 4.5 Hz, 2H), 4.39 (d, *J* = 10.5 Hz, 1H), 4.00 (m, 2H), 3.85 (dt, *J* = 10.8, 1.8 Hz, 1H), 3.64 (t, *J* = 6.9 Hz, 4H), 3.54 (m, 3H), 1.65 (m, 2H), 1.57 (m, 4H), 1.30 (br m, 12 H); ¹³C NMR (CDCl₃, 75 MHz) δ : 138.7, 138.6, 138.5, 137.9, 128.32, 128.25, 128.15, 128.05, 127.83, 127.78, 127.73, 127.67, 127.62, 127.58, 127.4, 103.9, 82.1, 79.5, 75.1, 74.4, 73.4, 73.3, 72.9, 69.9, 68.8, 62.9, 32.7, 29.6, 29.44, 29.40, 29.3, 26.1, 25.6. HRMS (FAB+) calcd for C₄₄H₅₆O₇ + Li⁺: 703.4186; Found: 703.4197.

2a. According to the representative procedure for the synthesis of **2d**, alcohol **2a** was prepared as a white oil in 87% yield (0.520 g, 0.870 mmol) from **1a** (0.560 g, 1.00 mmol), 1,3-propanediol (0.760 g, 10.00 mmol), CdCO₃ (0.20 g, 1.15 mmol) and CaSO₄ (1.0 g) by stirring in dry acetonitrile/toluene (1:2, 15 mL) at 50 °C for 2.0 h. Chromatographic purification (silica gel, 30-50% ethyl acetate in hexanes); *R*_f = 0.21 (silica gel, 50% ethyl acetate in hexanes); ¹H NMR (CDCl₃, 300 MHz) δ : 7.30 (m, 20H), 4.96 (d, *J* = 11.7 Hz, 1H), 4.83 (m, 1H), 4.75 (d, *J* = 2.7 Hz, 2H), 4.63 (d, *J* = 11.7 Hz, 1H), 4.42 (d, *J* = 8.7 Hz, 1H), 4.38 (d, *J* = 8.1 Hz, 1H), 4.05 (dt, *J* = 9.6, 6.3 Hz, 1H), 3.90 (m, 2H), 3.84

(m, 1H), 3.73 (m, 4H), 3.56 (m, 4H), 2.43 (br s, 1H), 1.85 (sept, $J = 6.3$ Hz, 2H); ^{13}C NMR (CDCl_3 , 75 MHz) δ : 138.5, 138.4, 138.3, 137.7, 128.3, 128.26, 128.19, 128.1, 128.0, 127.9, 127.8, 127.5, 127.4, 127.3, 103.8, 82.2, 79.3, 75.1, 74.4, 73.4, 73.3, 72.8, 68.8, 67.4, 60.0, 32.3. HRMS (FAB+) calcd for $\text{C}_{37}\text{H}_{42}\text{O}_7 + \text{Li}^+$: 605.3091; Found 605.3101.

2b. According to the representative procedure for the synthesis of **2d**, alcohol **2b** was prepared as a white oil in 89% yield (0.560 g, 0.894 mmol) from **1a** (0.560 g, 1.00 mmol), 1,5-pentanediol (1.00 g, 10.00 mmol), CdCO_3 (0.20 g, 1.15 mmol) and CaSO_4 (1.0 g) by stirring in dry acetonitrile/toluene (1:2, 15 mL) at 50 °C for 1.75 h. Chromatographic purification (silica gel, 30-50% ethyl acetate in hexanes); $R_f = 0.58$ (silica gel, 50% ethyl acetate in hexanes); ^1H NMR (CDCl_3 , 300 MHz) δ : 7.30 (m, 20H), 4.95 (d, $J = 5.9$ Hz, 1H), 4.91 (d, $J = 5.1$ Hz, 1H), 4.77 (d, $J = 10.8$ Hz, 1H), 4.73 (d, $J = 4.2$ Hz, 1H), 4.61 (m, 2H), 4.43 (d, $J = 4.2$ Hz, 1H), 4.35 (d, $J = 10.8$ Hz, 1H), 3.91 (m, 2H), 3.81 (dt, $J = 8.7, 1.5$ Hz, 1H), 3.35 (m, 8 H), 1.6-1.4 (m, 7H); ^{13}C NMR (CDCl_3 , 75 MHz) δ : 138.8, 138.6, 138.5, 137.9, 128.4, 128.3, 128.27, 128.24, 128.1, 127.8, 127.7, 127.5, 127.4, 127.3, 103.9, 82.2, 79.6, 75.1, 74.5, 73.5, 73.4, 73.0, 69.8, 68.9, 62.7, 32.4, 29.4, 22.3. HRMS (FAB+) calcd for $\text{C}_{39}\text{H}_{46}\text{O}_7 + \text{Li}^+$: 633.3404; Found: 633.3423.

2c. According to the representative procedure for the synthesis of **2d**, alcohol **2c** was prepared as a white oil in 81% yield (0.520 g, 0.795 mmol) from **1a** (0.550 g, 0.984 mmol), 1,7-heptanediol (1.30 g, 9.84 mmol), CdCO_3 (0.20 g, 1.15 mmol) and CaSO_4 (1.0 g) by stirring in dry acetonitrile/toluene (1:2, 15 mL) at 50 °C for 1.75 h. Chromatographic purification (silica gel, 30-50% ethyl acetate in hexanes); $R_f = 0.65$ (silica gel, 50% ethyl acetate in hexanes); ^1H NMR (CDCl_3 , 300 MHz) δ : 7.30 (m, 20H), 4.95 (dd, $J = 10.2, 1.8$ Hz, 2H), 4.8-4.7 (m, 3H), 4.64 (q, $J = 11.7$ Hz, 1H), 4.45 (d, $J = 4.5$ Hz, 2H), 4.37 (d, $J = 7.8$ Hz, 1H), 3.99-3.86 (m, 3H), 3.83 (dt, $J = 8.7, 1.8$ Hz, 1H), 3.60 (m, 7H), 1.68 (m, 2H), 1.50 (m, 2H), 1.31 (m, 6H); ^{13}C NMR (CDCl_3 , 75 MHz) δ : 138.7, 138.5, 138.4, 137.8, 128.3, 128.2, 128.1, 128.0, 127.9, 127.8, 127.7, 127.6, 127.5, 127.4, 127.3, 103.9, 82.1, 79.5, 75.0, 74.4, 73.4, 73.2, 72.9, 69.8, 68.8, 62.7, 32.5, 29.5, 29.1, 26.0, 25.5. HRMS (FAB+) calcd for $\text{C}_{41}\text{H}_{50}\text{O}_7 + \text{Li}^+$: 661.3717; Found: 661.3687.

2e. According to the representative procedure for the synthesis of **2d**, alcohol **2e** was prepared as a white oil in 90% yield (0.455 g, 0.583 mmol) from **1a** (0.360 g, 0.644 mmol), 1,16-hexadecanediol (1.00 g, 3.87 mmol), CdCO₃ (0.19 g, 1.09 mmol) and CaSO₄ (1.0 g) by stirring in dry acetonitrile/toluene (1:2, 15 mL) at 60 °C for 22 h. Chromatographic purification (silica gel, 20% ethyl acetate in hexanes); *R_f* = 0.45 (silica gel, 30% ethyl acetate in hexanes); ¹H NMR (CDCl₃, 300 MHz) δ: 7.35 (m, 20H), 4.96 (d, *J* = 11.1 Hz, 2H), 4.85 (m, 1H), 4.75 (d, *J* = 6.0 Hz, 1H), 4.64 (d, *J* = 11.7 Hz, 1H), 4.45 (d, *J* = 4.8 Hz, 2H), 4.38 (d, *J* = 7.8 Hz, 1H), 4.0-3.8 (m, 4H), 3.7-3.5 (m, 7H), 1.79 (br s, 1H), 1.65 (m, 2H), 1.56 (m, 2H), 1.28 (m, 24 H); ¹³C NMR (CDCl₃, 75 MHz) δ: 138.7, 138.5, 138.4, 137.8, 128.3, 128.2, 128.1, 128.04, 128.02, 127.8, 127.7, 127.6, 127.4, 127.3, 103.9, 82.1, 79.5, 75.1, 74.4, 73.4, 73.3, 73.2, 72.9, 69.9, 68.8, 62.8, 32.7, 29.6, 29.55, 29.51, 29.37, 29.35, 26.1, 25.7. HRMS (FAB+) calcd for C₅₀H₆₈O₇+Li⁺: 787.5125; Found: 787.5132.

2f. According to the representative procedure for the synthesis of **2d**, alcohol **2f** was prepared as a white oil in 75% (0.482 g, 0.735 mmol) from **1b** (0.55 g, 0.984 mmol), 1,7-heptanediol (1.30 g, 9.84 mmol), CdCO₃ (0.20 g, 1.15 mmol) and CaSO₄ (1.0 g) by stirring in dry acetonitrile/toluene (1:2, 15 mL) at 50 °C for 1.0 h. Chromatographic purification (silica gel, 30% ethyl acetate in hexanes); *R_f* = 0.30 (silica gel, 50% ethyl acetate in hexanes); ¹H NMR (CDCl₃, 300 MHz) δ: 7.25 (m, 20H), 4.93 (d, *J* = 9.3 Hz, 1H), 4.89 (d, *J* = 9.0 Hz, 1H), 4.77 (d, *J* = 9.6 Hz, 1H), 4.74 (d, *J* = 10.5 Hz, 1H), 4.68 (d, *J* = 10.8 Hz, 1H), 4.52 (t, *J* = 8.4 Hz, 2H), 4.36 (t, *J* = 6.0 Hz, 1H), 4.35 (d, *J* = 7.8 Hz, 1H), 3.93 (dt, *J* = 9.6, 6.3 Hz, 1H), 3.69 (t, *J* = 9.6 Hz, 1H), 3.62 (d, *J* = 9.6 Hz, 1H), 3.56 (m, 1H), 3.53 (m, 4H), 3.41 (m, 2H), 1.64 (m, 2H), 1.47 (m, 3H), 1.29 (m, 6H); ¹³C NMR (CDCl₃, 75 MHz) δ: 138.5, 138.4, 138.2, 138.0, 128.3, 128.0, 127.9, 127.7, 127.6, 127.5, 103.5, 84.6, 82.2, 77.9, 75.6, 74.9, 74.8, 74.7, 73.4, 70.0, 69.0, 62.8, 32.6, 29.6, 29.1, 26.1, 25.6. HRMS (FAB+) calcd for C₄₁H₅₀O₇+Li⁺: 661.3717; Found: 661.3705.

2g. According to the representative procedure for the synthesis of **2d**, alcohol **2g** was prepared as a white oil in 86% (0.324 g, 0.465 mmol) from **1b** (0.300 g, 0.537 mmol), 1,10-decanediol (1.00 g, 5.74 mmol), CdCO₃ (0.10 g, 0.575 mmol) and CaSO₄ (0.50 g) by stirring in dry acetonitrile/toluene (1:2, 15 mL) at 65 °C for 1.5 h. Chromatographic purification (silica gel, 30% ethyl acetate in hexanes);

$R_f = 0.25$ (silica gel, 30% ethyl acetate in hexanes); ^1H NMR (CDCl_3 , 300 MHz) δ : 7.36 (m, 20H), 5.02 (t, $J = 10.5$ Hz, 2H), 4.89 (d, $J = 9.0$, 1H), 4.86 (d, $J = 9.0$ Hz, 1H), 4.80 (d, $J = 10.8$ Hz, 1H), 4.66 (d, $J = 8.4$ Hz, 1H), 4.58 (dd, $J = 6.9$, 4.8 Hz, 1H), 4.47 (d, $J = 7.8$ Hz, 1H), 4.05 (m, 1H), 3.9-3.5 (m, 10H), 1.70 (m, 2H), 1.57 (m, 2H), 1.35 (m, 13H); ^{13}C NMR (CDCl_3 , 75 MHz) δ : 138.5, 138.4, 138.1, 138.0, 128.2, 127.9, 127.7, 127.6, 127.55, 127.51, 127.45, 103.5, 84.6, 82.2, 77.8, 75.6, 74.9, 74.7, 74.6, 73.3, 70.0, 68.9, 62.8, 32.6, 29.7, 29.43, 29.39, 29.30 (2C), 26.1, 25.6. HRMS (FAB+) calcd for $\text{C}_{44}\text{H}_{56}\text{O}_7 + \text{Li}^+$: 703.4186; Found: 703.4182.

2h. According to the representative procedure for the synthesis of **2d**, alcohol **2h** was prepared as a white oil in 85% (0.668 g, 1.131 mmol) from **1c** (0.60 g, 1.324 mmol), 1,10-decanediol (1.75 g, 10.00 mmol), CdCO_3 (0.24 g, 1.395 mmol) and CaSO_4 (1.70 g) by stirring in dry acetonitrile/toluene (1:2, 15 mL) at 55-60 °C for 15 h. Chromatographic purification (silica gel, 30% ethyl acetate in hexanes); $R_f = 0.58$ (silica gel, 50% ethyl acetate in hexanes); ^1H NMR (CDCl_3 , 300 MHz) δ : 7.35 (m, 15H), 4.99 (d, $J = 6.3$ Hz, 1H), 4.95 (d, $J = 5.4$ Hz, 1H), 4.75 (m, 4H), 4.32 (d, $J = 7.8$ Hz, 1H), 3.95 (m, 1H), 3.82 (dd, $J = 9.6$, 7.8 Hz, 1H), 3.7-3.4 (m, 6H), 1.62 (m, 2H), 1.55 (m, 3H), 1.28 (s, 12H), 1.19 (d, $J = 6.3$ Hz, 3H); ^{13}C NMR (CDCl_3 , 75 MHz) δ : 138.7, 138.5, 128.3, 128.2, 128.1, 128.0, 127.9, 127.8, 127.7, 127.3, 127.2, 103.6, 82.3, 79.3, 76.1, 74.9, 74.3, 72.9, 70.0, 69.6, 62.6, 32.5, 29.6, 29.4, 29.3, 29.2, 26.0, 25.6; 16.7. HRMS (FAB+) calcd for $\text{C}_{37}\text{H}_{50}\text{NO}_6 + \text{Li}^+$: 597.3767; Found: 597.3753.

2i. According to the representative procedure for the synthesis of **2d**, alcohol **2i** was prepared as a white oil in 86% ($\beta:\alpha = 50:50$; 0.556 g, 1.131 mmol) from **1c** (0.56 g, 1.00 mmol), 1,7-heptanediol (1.00 g, 5.75 mmol), CdCO_3 (0.20 g, 1.395 mmol) and CaSO_4 (1.70 g) by stirring in dry acetonitrile/toluene (1:2, 15 mL) at 50 °C for 24 h. Chromatographic purification (silica gel, 30% ethyl acetate in hexanes); $R_f = 0.27$ (silica gel, 30% ethyl acetate in hexanes); ^1H NMR (CDCl_3 , 300 MHz) δ : 7.4-7.2 (m, 40H), 5.05 (t, $J = 10.2$ Hz, 2H), 4.86 (d, $J = 10.2$ Hz, 2H), 4.75-4.70 (m, 6H), 4.6-4.4 (m, 6H), 4.0-3.9 (m, 4H), 3.9-3.75 (m, 4H), 3.64 (m, 6H), 3.6-3.4 (m, 8H), 1.60 (m, 4H), 1.50 (m, 4H), 1.33 (m, 12H); ^{13}C NMR (CDCl_3 , 75 MHz) δ : 138.6, 138.2, 138.1, 128.4, 128.3, 127.9, 127.8, 127.7, 127.67, 127.62, 127.58, 127.5, 127.4, 127.3, 127.2, 101.6, 97.7, 82.2, 80.1, 78.2,

76.5, 75.8, 75.2, 75.0, 74.9, 74.8, 74.7, 74.5, 73.9, 73.6, 73.5, 73.3, 73.2, 72.4, 72.3, 72.0, 71.6, 71.3, 69.8, 69.6, 69.2, 67.4, 64.4, 62.8, 62.7, 62.6, 32.5, 32.4, 29.5, 29.2, 28.9, 28.4, 25.9, 25.6, 25.5.

Synthesis of 7-(2,3,4,6-tetra-*O*-benzyl-D-mannopyranosyloxy)-*n*-heptanol (2i).

Into an acetonitrile (50 mL) slurry of 1-ethyl-2,3,4,6-tetra-*O*-benzyl- α -D-thiomannopyranoside (1.20 g, 2.103 mmol) and 1,7-heptanediol (1.40 g, 10.61 mmol) held at -40 °C under argon was added tris(*p*-bromophenyl)aminium hexachloroantimonate (2.58 g, 1.80 mmol). The resulting blue mixture was stirred for 3.0 h while the temperature was kept between -40 to -25 °C. The resulting brown mixture was warmed to room temperature and then filtered with an acetonitrile wash (10 mL), concentrated and purified by chromatography (silica gel, 30% ethyl acetate in hexanes) to afford 0.554 g (0.847 mmol, 41%) of **2i** as a clear oil. R_f = 0.60 (silica gel, 50% ethyl acetate in hexanes); ^1H NMR (CDCl_3 , 300 MHz) δ : 7.27 (m, 20H), 4.86 (d, J = 10.2 Hz, 2H), 4.72 (d, J = 2.7 Hz, 2H), 4.64 (d, J = 12.0 Hz, 1H), 4.61 (m, 1H), 4.51 (dd, J = 11.7, 10.5 Hz, 2H), 4.03 (t, J = 6.9 Hz, 2H), 3.95 (d, J = 9.0 Hz, 1H), 3.89 (dd, J = 9.3, 2.7 Hz, 1H), 3.75 (m, 3H), 3.65 (m, 1H), 3.57 (q, J = 6.6 Hz, 2H), 3.34 (dt, J = 9.6, 6.3 Hz, 1H), 1.91 (br s, 1H), 1.60 (m, 2H), 1.50 (m, 2H), 1.33 (m, 6H); ^{13}C NMR (CDCl_3 , 75 MHz) δ : 138.2, 128.1, 128.0, 127.9, 127.8, 127.6, 127.5, 127.4, 127.3, 127.2, 97.7, 80.1, 75.0, 74.9, 73.2, 72.4, 72.0, 71.6, 69.2, 67.4, 64.4, 62.6, 32.5, 28.9, 28.4, 25.9, 25.5. HRMS (FAB+) calcd for $\text{C}_{41}\text{H}_{50}\text{O}_7 + \text{Li}^+$: 661.3717; Found: 661.3726.

Synthesis of 1-(10-hydroxy-*n*-decanyl)-2,3,4,6-tetra-*O*-benzyl-D-

mannopyranoside (2j). Into an acetonitrile (50 mL) slurry of 1-ethyl-2,3,4,6-tetra-*O*-benzyl- α -D-thiomannopyranoside (1.20 g, 2.103 mmol) and 1,10-decanediol (1.80 g, 11.10 mmol) held at -40 °C under argon was added tris(*p*-bromophenyl)aminium hexachloroantimonate (2.58 g, 1.80 mmol). The resulting blue mixture was stirred for 2.0 h while the temperature was gradually warmed to 0 °C. The resulting brown mixture was then filtered with an acetonitrile wash (10 mL), concentrated and purified by chromatography (silica gel, 30% ethyl acetate in hexanes) to afford 0.950 g (1.365 mmol, 65%) of **2j** as a clear oil. R_f = 0.25 (silica gel, 30% ethyl acetate in hexanes); ^1H NMR (CDCl_3 , 300 MHz) δ : 7.40-7.15 (m, 20H), 4.89 (dd, J = 10.2, 1.8 Hz, 2H), 4.74 (d, J = 1.8 Hz, 1H), 4.68 (d, J = 12.0 Hz, 1H),

4.63 (m, 2H), 4.53 (dd, J = 12.0, 11.1 Hz, 2H), 4.05 (t, J = 6.9 Hz, 1H), 3.98 (d, J = 9.0 Hz, 1H), 3.90 (dd, J = 9.0, 3.0 Hz, 1H), 3.78 (m, 3H), 3.66 (m, 1H), 3.59 (m, 3H), 3.45 (m, 1H), 1.52 (m, 5H), 1.29 (m, 12H); ^{13}C NMR (CDCl_3 , 75 MHz) δ : 138.5, 138.3, 128.3, 128.2, 128.1, 127.9, 127.7, 127.64, 127.60, 127.5, 127.4, 127.3, 127.2, 97.7, 80.2, 75.0, 74.7, 73.2, 72.4, 72.0, 71.6, 69.2, 67.5, 64.5, 62.7, 32.6, 29.4, 29.33, 29.29, 29.1, 28.5, 26.0, 25.6. HRMS (FAB+) calcd for $\text{C}_{44}\text{H}_{56}\text{O}_7 + \text{Li}^+$: 703.4186; Found 703.4177.

Synthesis of 1-(10-hydroxy-*n*-decanyl)-2-acetamido-2-deoxy-3,4,6-tri-*O*-benzyl- β -D-glucopyranoside (2k). THF (6 mL) was added to a dichloroethane (24 mL) slurry of 1,10-decanediol (540 mg, 3.10 mmol) and ethyl 2-acetamido-2-deoxy-3,4,5-tribenzyl- α -thioglucopyranoside (1e) (330 mg, 0.616 mmol) to form a clear solution in the presence of MS (3A, 0.8 g). NIS (180 mg, 0.800 mmol) was then added to the above solution followed immediately by dropwise addition of a methylene chloride (2 mL) solution of TfOH (120 mg, 0.800 mmol). The resulting red mixture was stirred at room temperature for 5 min, filtered, diluted with methylene chloride (10 mL), washed with $\text{Na}_2\text{S}_2\text{O}_5$ (10 mL), NaHCO_3 (25 mL), H_2O (3 x 25 mL), dried over Na_2SO_4 and concentrated to an off-white solid. Flash chromatography purification (silica gel, 150:10 of $\text{CHCl}_3/\text{MeOH}$) afforded 335 mg (0.496 mmol, 83%) of **2k** as a white solid. R_f = 0.39 (silica gel, 100:10 of $\text{CHCl}_3/\text{MeOH}$); ^1H NMR (CDCl_3 , 300 MHz) δ : 7.30 (m, 15 H), 5.80 (d, J = 7.8 Hz, 1H), 4.80 (m, 2H), 4.78 (d, J = 6.3 Hz, 1H), 4.67 (d, J = 12.0 Hz, 1H), 4.58 (m, 2H), 4.11 (dd (J = 9.3, 7.8 Hz, 1H), 3.85 (q, J = 6.6 Hz, 1H), 3.75 (m, 1H), 3.73 (d, J = 6.6 Hz, 1H), 3.61 (m, 6H), 3.44 (m, 2H); 2.09 (br s, 1H); 1.85 (s, 3H), 1.79 (br s, 1H), 1.55 (m, 4H), 1.27 (s, 12H); ^{13}C NMR (CDCl_3 , 75 MHz) δ : 170.3, 138.4, 138.1, 138.0, 128.4, 128.3, 128.2, 127.9, 127.8, 127.7, 127.6, 127.5, 99.8, 80.3, 78.6, 74.9, 74.5, 73.3, 69.5, 69.0, 62.8, 56.9, 32.7, 29.4, 29.3, 29.24, 29.20, 25.8, 25.6, 23.4. HRMS (FAB+) calcd for $\text{C}_{39}\text{H}_{53}\text{NO}_7 + \text{Li}^+$: 654.3982; Found: 654.3999.

Synthesis of ω -Glycopyranosyloxyalkyl Aldehydes, 3.

Typical example for the synthesis of ω -glycopyranosyloxyalkyl aldehydes (3) via PDC oxidation of 2: The synthesis of 10-(2,3,4,6-tetra-*O*-benzyl-D-

galactopyranosyloxy)-*n*-decanal (3d). Under an atmosphere of nitrogen, pyridinium dichromate (460 mg, 1.222 mmol) was added to a dry methylene chloride solution (10 mL) of 10-(2,3,4,6-tetra-*O*-benzyl-D-galactopyranosyloxy)-*n*-decanol (570 mg, 0.818 mmol). The resulting brown slurry was stirred at room temperature under nitrogen. TLC analysis (visualization by UV and char with 10% sulfuric acid in ethanol) of the reaction mixture indicated complete consumption of the starting material and the formation of a new compound after 20 h. The reaction mixture was treated with ether (10 mL), filtered through silica gel and Celite with an ether wash (25 mL) and concentrated to an off-white oil. Chromatographic purification (silica gel, 20% ethyl acetate in hexanes) afforded 374 mg (0.539 mmol, 66%) of **3d** as a clear oil. R_f = 0.61 (silica gel, 30% ethyl acetate in hexanes); ^1H NMR (CDCl_3 , 300 MHz) δ : 9.77 (t, J =1.5 Hz, 1H), 7.30 (m, 20 H), 4.97 (dd, J =12.0, 2.7 Hz, 2H), 4.78 (d, J =11.1 Hz, 1H), 4.77 (d, J =4.5 Hz, 1H), 4.65 (d, J =12 Hz, 1H), 4.46 (d, J =4.2 Hz, 2H), 4.38 (d, J =7.8 Hz, 1H), 3.95 (m, 1H), 3.84 (dt, J =10.2, 1.8 Hz, 1H), 3.50 (m, 7H), 2.40 (dt, J =7.5, 1.8 Hz, 2H), 1.65 (m, 6H), 1.30 (m, 8 H); ^{13}C NMR (CDCl_3 , 75 MHz) δ : 202.8, 138.9, 138.6, 138.5, 137.9, 128.4, 128.3, 128.2, 128.1, 127.9, 127.8, 127.7, 127.6, 127.5, 127.3, 127.2, 103.9, 82.2, 79.6, 75.1, 74.4, 73.5, 73.4, 73.3, 73.0, 70.0, 68.9, 43.8, 29.7, 29.3, 29.2, 26.1, 22.0. HRMS (FAB+) calcd for $\text{C}_{44}\text{H}_{54}\text{O}_7 + \text{Li}^+$: 701.4030; found 701.4051.

3a. According to the representative procedure for the synthesis of **3d**, aldehyde **3a** was prepared in 63% (330 mg, 0.554 mmol) by stirring a mixture of **2a** (520 mg, 0.870 mmol) and PDC (600 mg, 1.595 mmol) in dry methylene chloride (10 mL) at room temperature for 24 h. Chromatographic purification (silica gel, 20% ethyl acetate in hexanes); R_f = 0.55 (silica gel, 30% ethyl acetate in hexanes); ^1H NMR (CDCl_3 , 300 MHz) δ : 9.82 (t, J = 1.5 Hz, 1H), 7.35 (m, 20H), 5.00 (A of ABq, J = 11.7 Hz, 1H), 4.88 (A of ABq, J = 10.8 Hz, 1H), 4.77 (m, 2H), 4.70 (B of ABq, J = 10.8 Hz, 1H), 4.48 (m, 1H), 4.43 (b of ABq, J = 11.7 Hz, 1H), 4.25 (dt, J = 9.9, 6.0 Hz, 1H), 3.95 (m, 2H), 3.85 (m, 1H), 3.60 (m, 6H), 2.75 (m, 2H); ^{13}C NMR (CDCl_3 , 75 MHz) δ : 200.8, 138.5, 138.4, 138.3, 137.7, 128.3, 128.2, 128.17, 128.07, 128.04, 127.8, 127.7, 127.5, 127.4, 127.3, 103.8, 82.0, 79.3, 75.1, 74.4, 73.4, 73.3, 73.28, 73.24, 72.9, 68.7, 63.4, 43.7. HRMS (FAB+) calcd for $\text{C}_{37}\text{H}_{40}\text{O}_7 + \text{Li}^+$: 603.2934; Found 603.2932.

3b. According to the representative procedure for the synthesis of **3d**, aldehyde **3b** was prepared in 72% (404 mg, 0.647 mmol) by stirring a mixture of **2b** (560 mg, 0.897 mmol) and PDC (600 mg, 1.595 mmol) in dry methylene chloride (10 mL) at room temperature for 16 h. Chromatographic purification (silica gel, 20% ethyl acetate in hexanes); R_f = 0.50 (silica gel, 30% ethyl acetate in hexanes); ^1H NMR (CDCl_3 , 300 MHz) δ : 9.68 (t, J = 1.5 Hz, 1H), 7.31 (m, 20H), 4.93 (t, J = 12.0 Hz, 2H), 4.80 (m, 1H), 4.74 (d, J = 3.0 Hz, 1H), 4.64 (m, 1H), 4.43 (m, 2H), 4.35 (d, J = 7.8 Hz, 1H), 3.93 (m, 2H), 3.83 (dt, J = 8.7, 0.9 Hz, 1H), 3.58 (m, 6H), 2.42 (m, 2H), 1.69 (m, 4H); ^{13}C NMR (CDCl_3 , 75 MHz) δ : 202.3, 138.7, 138.5, 138.4, 137.8, 128.3, 128.27, 128.20, 128.1, 127.9, 127.8, 127.79, 127.70, 127.5, 127.4, 103.8, 82.2, 79.5, 75.1, 74.4, 73.4, 73.3, 72.9, 69.2, 68.8, 43.4, 29.0, 18.8. HRMS (FAB+) calcd for $\text{C}_{39}\text{H}_{44}\text{O}_7 + \text{Li}^+$: 631.3247; Found: 631.3226.

3c. According to the representative procedure for the synthesis of **3d**, aldehyde **3c** was prepared in 69% (1.11 g, 1.70 mmol) by stirring a mixture of **2c** (1.62 g, 2.477 mmol) and PDC (1.50 g, 4.00 mmol) in dry methylene chloride (20 mL) at room temperature for 16 h. Chromatographic purification (silica gel, 20% ethyl acetate in hexanes); R_f = 0.74 (silica gel, 30% ethyl acetate in hexanes); ^1H NMR (CDCl_3 , 300 MHz) δ : 9.73 (d, J = 1.5 Hz, 1H), 7.34 (m, 20H), 4.98 (d, J = 5.7 Hz, 1H), 4.94 (d, J = 4.8 Hz, 1H), 4.82 (m, 1H), 4.76 (d, J = 4.2 Hz, 1H), 4.63 (q, J = 12.0 Hz, 1H), 4.50 (m, 1H), 4.46 (d, J = 3.9 Hz, 1H), 4.37 (d, J = 7.8 Hz, 1H), 3.92 (m, 3H), 3.84 (dt, J = 8.7, 2.1 Hz, 1H), 3.6-3.5 (m, 5H), 2.38 (dt, J = 7.2, 1.8 Hz, 2H), 1.65 (m, 4H), 1.40 (m, 4H); ^{13}C NMR (CDCl_3 , 75 MHz) δ : 202.7, 138.9, 138.7, 138.6, 138.0, 128.4, 128.36, 128.27, 128.24, 128.16, 128.0, 127.9, 127.8, 127.5, 127.4, 104.0, 82.2, 79.6, 75.1, 74.5, 73.6, 73.4 (2C), 73.0, 69.8, 68.9, 43.8, 29.5, 29.0, 26.0, 22.0. HRMS (FAB+) calcd for $\text{C}_{41}\text{H}_{48}\text{O}_7 + \text{Li}^+$: 659.3650; Found: 659.3541.

3e. According to the representative procedure for the synthesis of **3d**, aldehyde **3e** was prepared in 76% (345 mg, 0.443 mmol) by stirring a mixture of **2e** (455 mg, 0.583 mmol) and PDC (320 mg, 0.851 mmol) in dry methylene chloride (6 mL) at room temperature for 17 h. Chromatographic purification (silica gel, 10% ethyl acetate in hexanes); R_f = 0.72 (silica gel, 30% ethyl acetate in hexanes); ^1H NMR (CDCl_3 , 300 MHz) δ : 9.75 (t, J = 1.5 Hz, 1H), 7.30 (m, 20H), 4.95 (d, J = 11.7 Hz, 2H), 4.75 (m, 2H), 4.63 (d, J = 11.7 Hz, 1H), 4.43 (d, J = 4.5 Hz, 2H), 4.36 (d, J = 7.8 Hz, 1H), 3.65 (m,

2H), 3.62 (dt, J = 8.7, 1.5 Hz, 1H), 3.56 (m, 6H), 2.40 (dt, J = 7.5, 1.5 Hz, 2H), 1.60 (m, 4H), 1.26 (m, 22 H); ^{13}C NMR (CDCl_3 , 75 MHz) δ : 202.9, 138.8, 138.7, 138.6, 138.0, 128.4, 128.36, 128.26, 128.2, 128.0, 127.9, 127.8, 127.7, 127.6, 127.5, 104.0, 82.3, 79.6, 75.2, 74.5, 73.6, 73.5, 73.4, 73.1, 70.1, 68.9, 43.9, 29.8, 29.7, 29.6, 29.5, 29.46, 29.39, 29.2, 26.2, 22.1. HRMS (FAB+) calcd for $\text{C}_{50}\text{H}_{66}\text{O}_7 + \text{Li}^+$: 785.4969; Found: 785.4979.

3f. According to the representative procedure for the synthesis of **3d**, aldehyde **3f** was prepared in 74% (358 mg, 0.549 mmol) by stirring a mixture of **2f** (482 mg, 0.737 mmol) and PDC (420 mg, 1.117 mmol) in dry methylene chloride (5 mL) at room temperature for 17 h. Chromatographic purification (silica gel, 20% ethyl acetate in hexanes); R_f = 0.58 (silica gel, 50% ethyl acetate in hexanes); ^1H NMR (CDCl_3 , 300 MHz) δ : 9.75 (t, J = 1.8 Hz, 1H), 7.35 (m, 20H), 5.00 (dd, J = 11.1, 6.3 Hz, 2H), 4.85 (t, J = 9.6 Hz, 2H), 4.77 (d, J = 11.1 Hz, 1H), 4.62 (m, 2H), 4.55 (dd, J = 5.7, 4.5 Hz, 1H), 4.43 (d, J = 7.8 Hz, 1H), 4.01 (dt, J = 9.3, 6.3 Hz, 1H), 3.79 (dd, J = 10.2, 1.5 Hz, 1H), 3.74 (d, J = 4.8 Hz, 1H), 3.68 (d, J = 8.4 Hz, 1H), 3.65 (d, J = 9.3 Hz, 1H), 3.59 (m, 1H), 3.50 (m, 2H), 2.40 (dt, J = 7.5, 1.5 Hz, 2H), 1.68 (m, 4H), 1.41 (m, 4H); ^{13}C NMR (CDCl_3 , 75 MHz) δ : 202.5, 138.5, 138.4, 138.2, 138.1, 128.3, 127.9, 127.8, 127.7, 127.6, 127.5, 103.5, 84.6, 82.2, 77.8, 75.6, 74.9, 74.8, 74.7, 73.4, 69.8, 68.9, 43.7, 29.5, 28.8, 25.9, 21.9. HRMS (FAB+) calcd for $\text{C}_{41}\text{H}_{48}\text{O}_7 + \text{Li}^+$: 659.3560; Found: 659.3569.

3g. According to the representative procedure for the synthesis of **3d**, aldehyde **3g** was prepared in 74% (204 mg, 0.294 mmol) by stirring a mixture of **2g** (275 mg, 0.395 mmol) and PDC (220 mg, 0.585 mmol) in dry methylene chloride (6 mL) at room temperature for 16 h. Chromatographic purification (silica gel, 20% ethyl acetate in hexanes); R_f = 0.40 (silica gel, 30% ethyl acetate in hexanes); ^1H NMR (CDCl_3 , 300 MHz) δ : 9.75 (t, J = 1.8 Hz, 1H), 7.32 (m, 20H), 4.98 (dd, J = 10.8, 9.6 Hz, 2H), 4.84 (t, J = 10.5 Hz, 2H), 4.75 (d, J = 10.8 Hz, 1H), 4.61 (d, J = 8.4 Hz, 1H), 4.56 (dd, J = 10.8, 6.0 Hz, 1H), 4.43 (d, J = 7.8, 1H), 4.00 (m, 1H), 3.8-3.4 (m, 8H), 2.40 (dt, J = 7.2, 1.5 Hz, 2H), 1.70 (m, 6H), 1.31, (m, 8H); ^{13}C NMR (CDCl_3 , 75 MHz) δ : 202.7, 138.5, 138.4, 138.1, 138.0, 128.2, 128.0, 127.8, 127.7, 127.6, 127.5, 127.4, 103.5, 84.6, 82.2, 77.8, 75.5, 74.9, 74.7, 74.6,

73.3, 70.0, 68.9, 43.8, 29.7, 29.2, 29.19, 29.0, 26.0, 21.9. HRMS (FAB+) calcd for $C_{44}H_{54}O_7+Li^+$: 701.4030; Found: 701.4052.

3h. According to the representative procedure for the synthesis of **3d**, aldehyde **3h** was prepared in 71% (410 mg, 0.697 mmol) by stirring a mixture of **2h** (580 mg, 0.982 mmol) and PDC (550 mg, 1.424 mmol) in dry methylene chloride (20 mL) at room temperature for 18 h. Chromatographic purification (silica gel, 20% ethyl acetate in hexanes); R_f = 0.50 (silica gel, 30% ethyl acetate in hexanes); 1H NMR ($CDCl_3$, 300 MHz) δ : 9.76 (t, J = 1.8 Hz, 1H), 7.35 (m, 15H), 5.02 (d, J = 8.1 Hz, 1H), 4.98 (d, J = 7.2 Hz, 1H), 4.81 (m, 2H), 4.76 (d, J = 5.7 Hz, 1H), 4.72 (d, J = 5.7 Hz, 1H); 4.34 (d, J = 7.8 Hz, 1H), 3.97 (dt, J = 9.6, 6.0 Hz, 2H), 3.84 (dd, J = 9.6, 7.8 Hz, 1H), 3.65-3.40 (m, 3H), 2.41 (dt, J = 7.2, 1.5 Hz, 2H), 1.65 (m, 4H), 1.31 (s, 10H), 1.21 (d, J = 6.3 Hz, 3H); ^{13}C NMR ($CDCl_3$, 75 MHz) δ : 202.7, 138.8, 138.5, 138.4, 128.33, 128.25, 128.18, 128.07, 127.9, 127.8, 127.4, 127.3, 103.7, 82.4, 79.3, 76.2, 74.9, 74.4, 73.0, 70.1, 69.6, 43.7, 29.6, 29.2, 29.19, 29.12, 29.0, 26.0, 21.9, 16.7. HRMS (FAB+) calcd for $C_{37}H_{48}NO_6+Li^+$: 595.3611; Found: 595.3605.

3i. According to the representative procedure for the synthesis of **3d**, aldehyde **3i** was prepared in 63% (188 mg, 0.288 mmol) by stirring a mixture of **2i** (300 mg, 0.459 mmol) and PDC (260 mg, 0.691 mmol) in dry methylene chloride (6 mL) at room temperature for 16 h. Chromatographic purification (silica gel, 10-20% ethyl acetate in hexanes); R_f = 0.74 (silica gel, 30% ethyl acetate in hexanes); 1H NMR ($CDCl_3$, 300 MHz) δ : 9.73 (m, 1H), 7.30 (m, 20H), 4.87 (d, J = 10.5 Hz, 2H), 4.73 (d, J = 2.7 Hz, 2H), 4.63 (m, 2H), 4.52 (dd, J = 12.0, 10.1 Hz, 2H), 4.04 (t, J = 6.6 Hz, 2H), 3.96 (d, J = 9.3 Hz, 1H), 3.89 (dd, J = 9.3, 3.0 Hz, 1H), 3.76 (m, 3H), 3.64 (dt, J = 9.3, 6.9 Hz, 1H), 3.34 (dt, J = 9.3, 6.3 Hz, 1H), 2.36 (m, 2H), 1.60 (m, 4H), 1.30 (m, 4H); ^{13}C NMR ($CDCl_3$, 75 MHz) δ : 202.5, 138.5, 138.3, 128.2, 128.1, 127.9, 127.7, 127.6, 127.5, 127.4, 127.3, 97.8, 80.2, 75.0, 74.9, 74.7, 73.2, 72.5, 72.0, 71.7, 69.2, 67.3, 64.2, 43.7, 28.7, 28.3, 25.8, 21.8. HRMS (FAB+) calcd for $C_{41}H_{48}O_7+Li^+$: 659.3560; Found: 659.3575.

3j. According to the representative procedure for the synthesis of **3d**, aldehyde **3j** was prepared in 77% (345 mg, 0.497 mmol) by stirring a mixture of **2j** (450 mg, 0.646 mmol) and PDC (400 mg, 1.036 mmol) in dry methylene chloride (10 mL) at room temperature for 15 h. Chromatographic

purification (silica gel, 20% ethyl acetate in hexanes); $R_f = 0.50$ (silica gel, 30% ethyl acetate in hexanes); ^1H NMR (CDCl_3 , 300 MHz) δ : 9.76 (dt, $J = 5.1, 1.5$ Hz, 1H), 7.31 (m, 20H), 4.93 (d, $J = 6.6$ Hz, 1H), 4.91 (d, $J = 2.4$ Hz, 1H), 4.78 (d, $J = 2.1$ Hz, 1H), 4.72 (d, $J = 12.0$ Hz, 1H), 4.67 (m, 2H), 4.57 (dd, $J = 12.0, 10.8$ Hz, 2H), 4.09 (t, $J = 6.9$ Hz, 1H), 4.03 (d, $J = 9.3$ Hz, 1H), 3.96 (dd, $J = 12.0, 2.7$ Hz, 1H), 3.82 (m, 3H), 3.68 (m, 1H), 3.40 (dt, $J = 9.6, 6.6$ Hz, 2H), 2.41 (dt, $J = 7.2, 1.8$ Hz, 2H), 1.64 (m, 4H), 1.32 (m, 10H); ^{13}C NMR (CDCl_3 , 75 MHz) δ : 202.6, 138.4, 138.3, 128.2, 128.13, 128.09, 127.9, 127.6, 127.58, 127.54, 127.43, 127.40, 127.37, 127.33, 127.2, 97.7, 80.2, 75.0, 74.9, 74.7, 73.1, 72.4, 71.9, 71.6, 69.2, 67.4, 64.4, 43.7, 29.2, 29.1, 29.0, 28.4, 25.9, 25.7, 21.9. HRMS (FAB+) calcd for $\text{C}_{44}\text{H}_{54}\text{O}_7 + \text{Li}^+$: 701.4030; Found: 701.4031.

3k. According to the representative procedure for the synthesis of **3d**, aldehyde **3k** was prepared in 73% (225 mg, 0.349 mmol) by stirring a mixture of **2k** (310 mg, 478 mmol) and PDC (270 mg, 0.718 mmol) in dry methylene chloride (10 mL) at room temperature for 17 h. Chromatographic purification (silica gel, 100:2.5 of chloroform and methanol); $R_f = 0.65$ (silica gel, 100:10 of chloroform and methanol); ^1H NMR (CDCl_3 , 300 MHz) δ : 9.71 (t, $J = 3.0$ Hz, 1H), 7.28 (m, 15H), 5.94 (d, $J = 7.8$ Hz, 1H), 4.77 (m, 3H), 4.54 (m, 3H), 4.06 (t, $J = 7.8$ Hz, 1H), 3.82 (m, 1H), 3.71 (m, 2H), 3.56 (m, 2H), 3.40 (m, 2H), 2.44 (m, 2H), 1.84 (s, 3H), 1.53 (m, 5H), 1.25 (s, 10H); ^{13}C NMR (CDCl_3 , 75 MHz) δ : 202.9, 170.2, 138.4, 138.1, 138.0, 128.4, 128.3, 128.2, 128.19, 128.10, 127.9, 127.8, 127.7, 127.5, 99.8, 80.4, 78.6, 74.7, 74.5, 73.4, 69.5, 69.0, 57.0, 43.8, 29.5, 29.3, 29.2, 29.0, 25.8, 23.5, 22.0. HRMS (FAB+) calcd for $\text{C}_{39}\text{H}_{51}\text{NO}_7 + \text{Li}^+$: 652.3852; Found: 652.3849.

Synthesis of Perbenzylated Glycopyranside-*n*-alkyl-DSPE Conjugates, **4**.

Typical example for the synthesis of benzyl protected glycoconjugates **4 via reductive amination of aldehydes **3** with DSPE: The synthesis of **4d**.** Under a nitrogen atmosphere, sodium cyanoborohydride (20 mg, 0.318 mmol) was added in its solid form to a white slurry of DSPE (200 mg, 0.267 mmol) in methanol and chloroform (10 mL, 1:1 by volume) in the presence of molecular sieves (3Å, 800 mg). The mixture was stirred at 50 °C for 15 min to form a cloudy solution while gas was liberated from the reaction solution. To the above solution stirred at 50 °C

was added dropwise **3d** (120 mg, 0.173 mmol) dissolved in methanol and chloroform (1:1, 5 mL). The clear solution was stirred for another 2 h while TLC analysis (visualization by UV, molybdenum blue reagent and char with 10% sulfuric acid in ethanol) indicated the complete consumption of the decanal starting material and the formation of a new compound. The reaction mixture was cooled to room temperature, filtered and concentrated to give a white solid. Chromatographic purification (silica gel, 150:12 of CHCl₃/MeOH) afforded 228 mg (0.160 mmol, 92%) of the perbenzylated DSPE-decanyl-galactopyranoside conjugate (**4d**) as a waxy solid. R_f = 0.47 (silica gel, 1:10 of methanol and chloroform); ¹H NMR (CDCl₃, 300 MHz) δ : 10.20 (br s, 2H), 7.25 (m, 20H), 5.22 (m, 1H), 4.91 (dd, J = 11.7, 2.7 Hz, 2H), 4.71 (m, 3H), 4.60 (q, J = 11.7 Hz, 1H), 4.40 (d, J = 4.8 Hz, 2H), 4.33 (m, 2H), 4.20 (m, 3H), 4.00 (m, 2H), 3.88 (m, 2H), 3.78 (t, J = 7.8 Hz, 1H), 3.50 (m, 5H), 3.11 (br s, 2H), 2.85 (m, 2H), 2.27 (q, J = 6.0 Hz, 4H), 1.70 (br s, 2H), 1.59 (br m, 6H), 1.24 (s, 68H), 0.86 (t, J = 6.0 Hz, 6H); ¹³C NMR (CDCl₃, 75 MHz) δ : 173.2, 172.9, 138.7, 138.6, 138.5, 137.9, 128.3, 128.2, 128.1, 128.0, 127.83, 127.79, 127.7, 127.6, 127.4, 127.3, 103.9, 82.2, 79.5, 75.1, 74.4, 73.4, 73.3, 73.2, 73.0, 70.0, 68.8, 64.0, 63.9, 62.5, 60.7, 49.2, 48.1, 34.2, 34.0, 31.9, 29.7, 29.5, 29.3, 29.1, 29.08, 26.6, 26.1, 26.0, 24.9, 24.8, 22.6, 14.1. HRMS (FAB+) calcd for C₈₅H₁₃₆NO₁₄P+H⁺: 1426.9777; Found: 1426.9740.

4a. According to the representative procedure for the synthesis of **4d**, conjugate **4a** was prepared in 83% (195 mg, 0.147 mmol) by stirring at 50 °C a chloroform-methanol (15 mL, 1:1) solution **3a** (105 mg, 0.176 mmol), DSPE (190 mg, 0.254 mmol), and sodium cyanoborohydride (20 mg, 0.318 mmol) in the presence of molecular sieves (3Å, 1.0 g) for 1.0 h. Chromatographic purification (silica gel, 150:12 of chloroform and methanol); R_f = 0.50 (silica gel, 1:10 of methanol and chloroform); ¹H NMR (CDCl₃, 300 MHz) δ : 9.50 (br s, 2H), 7.38 (m, 20 H), 4.89 (br m, 1H), 4.92 (d, J = 11.7 Hz, 1H), 4.80 (m, 2H), 4.70 (m, 2H), 4.60 (d, J = 11.7 Hz, 1H), 4.47 (m, 1H), 4.42 (d, J = 9.9 Hz, 2H), 4.35 (m, 1H), 4.11 (m, 2H), 3.95 (m, 4H), 3.77 (dd, J = 9.3, 8.1 Hz, 1H), 3.57 (m, 6H), 2.97 (br s, 2H), 2.90 (br s, 2H), 2.25 (q, J = 7.5 Hz, 4H), 2.10 (br m, 2H), 1.55 (br m, 4H), 1.25 (s, 56 H), 0.89 (t, J = 7.2 Hz, 6H); ¹³C NMR (CDCl₃, 75 MHz) δ : 173.3, 173.1, 138.7, 138.6, 138.4, 137.8, 128.4, 128.29, 128.26, 128.1, 128.0, 127.8, 127.78, 127.72, 127.5, 127.4, 103.6, 82.3, 79.3, 75.0, 74.5,

73.4, 73.3, 73.1, 72.9, 70.3, 68.4, 66.8, 64.0, 62.6, 61.0, 48.4, 46.0. HRMS (FAB+) calcd for $C_{78}H_{122}NO_{14}P+H^+$: 1328.8681; Found: 1328.8668.

4b. According to the representative procedure for the synthesis of **4d**, conjugate **4b** was prepared in 82% (115 mg, 0.0847 mmol) by stirring at 50 °C a chloroform-methanol (11 mL, 1:1) solution of **3b** (64 mg, 0.103 mmol), DSPE (115 mg, 0.154 mmol), and sodium cyanoborohydride (20 mg, 0.318 mmol) in the presence of molecular sieves (3Å, 1.0 g) for 1.5 h. Chromatographic purification (silica gel, 150:12 of chloroform and methanol); R_f = 0.50 (silica gel, 1:10 of methanol and chloroform); 1H NMR ($CDCl_3$, 300 MHz) δ : 10.28 (br s, 2H), 7.32 (m, 20H), 5.27 (m, 1H), 4.97 (d, J = 11.7 Hz, 1H), 4.92 (d, J = 11.1 Hz, 1H), 4.83 (m, 2H), 4.76 (d, J = 3.3 Hz, 1H), 4.67 (t, J = 12.0 Hz, 1H), 4.40 (m, 2H), 4.36 (d, J = 7.8 Hz, 1H), 4.20 (m, 3H), 4.07 (m, 3H), 3.92 (m, 1H), 3.82 (dt, J = 8.7, 1.8 Hz, 1H), 3.50 (m, 6H), 3.10 (br m, 2H), 2.75 (br m, 2H), 2.32 (dt, J = 7.2, 4.5 Hz, 4H), 1.95 (br m, 2H), 1.75 (br m, 2H), 1.63 (m, 4H), 1.42 (m, 2H), 1.29 (s, 56H), 0.92 (t, J = 6.6 Hz, 6H); ^{13}C NMR ($CDCl_3$, 75 MHz) δ : 173.3, 172.9, 138.8, 138.6, 138.4, 137.8, 128.32, 128.25, 128.20, 128.1, 128.0, 127.8, 127.7, 127.6, 127.4, 127.3, 103.8, 82.1, 79.4, 75.0, 74.4, 73.4, 73.3, 73.2, 72.9, 70.1, 70.0, 69.3, 68.6, 63.9, 62.5, 60.5, 49.2 (br), 47.9, 34.2, 34.0, 31.9, 29.6, 29.5, 29.48, 29.3, 29.1, 24.84, 24.81, 23.3, 22.6, 14.1. HRMS (FAB+) calcd for $C_{80}H_{126}NO_{14}P+H^+$: 1356.8994; Found: 1356.9032.

4c. According to the representative procedure for the synthesis of **4d**, conjugate **4c** was prepared in 84% (282 mg, 0.204 mmol) by stirring at 50 °C a chloroform-methanol (16 mL, 1:1) solution of **3c** (158 mg, 0.242 mmol), DSPE (250 mg, 0.334 mmol), and sodium cyanoborohydride (40 mg, 0.636 mmol) in the presence of molecular sieves (3Å, 1.0 g) for 1.0 h. Chromatographic purification (silica gel, 150:10 of chloroform and methanol); R_f = 0.55 (silica gel, 1:10 of methanol and chloroform); 1H NMR ($CDCl_3$, 300 MHz) δ : 10.04 (br s, 2H), 7.27 (m, 20H), 5.25 (m, 1H), 4.90 (dd, J = 11.7, 5.4 Hz, 2H), 4.75 (m, 2H), 4.56 (m, 1H), 4.45-4.30 (m, 5H), 4.15 (br m, 3H), 4.0-3.85 (m, 4H), 3.77 (dt, J = 8.4, 1.2 Hz, 1H), 3.6-3.4, (m, 5H), 3.15 (br m, 2H), 2.90 (br m, 2H), 2.27 (q, J = 7.8 Hz, 4H), 1.67 (m, 2H), 1.60 (m, 4H), 1.24 (s, 64H), 0.86 (t, J = 6.9 Hz, 6H); ^{13}C NMR ($CDCl_3$, 75 MHz) δ : 173.4, 173.0, 138.8, 138.7, 138.6, 137.9, 128.4, 128.3, 128.2, 128.1, 128.0, 127.9, 127.8,

127.7, 127.6, 127.5, 127.4, 104.0, 82.2, 79.6, 75.1, 74.5, 73.5, 73.3, 73.2, 73.0, 70.1, 69.8, 68.8, 64.1, 62.6, 60.8, 48.1, 34.3, 34.1, 31.9, 29.7, 29.68, 29.61, 29.56, 29.4, 29.19, 29.17, 29.0, 26.7, 26.1, 26.0, 24.92, 24.89, 22.7, 14.1. HRMS (FAB+) calcd for $C_{80}H_{130}NO_{14}P+H^+$: 1384.9307; Found: 1384.9270.

4e. According to the representative procedure for the synthesis of **4d**, conjugate **4e** was prepared in 95% (184 mg, 0.122 mmol) by stirring at 50 °C a chloroform-methanol (15 mL, 1:1) solution of **3e** (100 mg, 0.128 mmol), DSPE (150 mg, 0.201 mmol), and sodium cyanoborohydride (20 mg, 0.318 mmol) in the presence of molecular sieves (3Å, 1.0 g) for 1.5 h. Chromatographic purification (silica gel, 150:12 of chloroform and methanol); R_f = 0.44 (silica gel, 1:10 of methanol and chloroform); 1H NMR ($CDCl_3$, 300 MHz) δ : 9.80 (br s, 2H), 7.28 (m, 20H), 5.22 (m, 1H), 4.92 (dd, J = 12.0, 1.5 Hz, 2H), 4.72 (m, 3H), 4.60 (d, J = 11.7 Hz, 1H), 4.40 (d, J = 4.8 Hz, 2H), 4.33 (d, J = 7.8 Hz, 1H), 4.15 (m, 3H), 3.95 (m, 4H), 3.78 (dd, J = 9.6, 7.8 Hz, 1H), 3.6-3.4 (m, 6H), 3.13 (br s, 2H), 2.87 (br m, 2H), 2.27 (q, J = 7.2 Hz, 4H), 1.72 (br m, 2H), 1.57 (br m, 4H), 1.24 (s, 82H), 0.86 (t, J = 6.9 Hz, 6H); ^{13}C NMR ($CDCl_3$, 75 MHz) δ : 173.2, 172.9, 138.7, 138.6, 138.5, 137.9, 128.3, 128.2, 128.13, 128.06, 128.03, 127.8, 127.7, 127.6, 127.4, 127.3, 103.9, 82.1, 79.5, 75.2, 74.5, 73.5, 73.4, 73.2, 73.0, 70.1, 70.0, 68.9, 63.9, 62.5, 60.8, 49.1, 48.2, 34.3, 34.1, 31.9, 29.7, 29.6, 29.5, 29.4, 29.2, 29.1, 26.8, 26.2, 26.0, 24.93, 24.91, 22.7, 14.1. HRMS (FAB+) calcd for $C_{91}H_{148}NO_{14}P+H^+$: 1511.0716; Found: 1511.0733.

4f. According to the representative procedure for the synthesis of **4d**, conjugate **4f** was prepared in 95% (202 mg, 0.146 mmol) by stirring at 50 °C a chloroform-methanol (15 mL, 1:1) solution of **3f** (100 mg, 0.153 mmol), DSPE (175 mg, 0.234 mmol), and sodium cyanoborohydride (25 mg, 0.398 mmol) in the presence of molecular sieves (3Å, 1.0 g) for 1.5 h. Chromatographic purification (silica gel, 200:10 to 100:10 of chloroform and methanol); R_f = 0.60 (silica gel, 1:10 of methanol and chloroform); 1H NMR ($CDCl_3$, 300 MHz) δ : 10.28 (br s, 2H), 7.29 (m, 20H), 5.25 (m, 1H), 4.94 (dd, J = 11.1, 5.7 Hz, 2H), 4.80 (t, J = 10.5 Hz, 2H), 4.72 (d, J = 11.1 Hz, 1H), 4.58 (q, J = 12.0 Hz, 2H), 4.52 (d, J = 10.8 Hz, 1H), 4.40 (m, 2H), 4.20 (m, 3H), 4.00 (m, 2H), 3.94 (m, 1H), 3.72 (m, 2H), 3.62 (t, J = 8.7 Hz, 2H), 3.55 (d, J = 8.4 Hz, 1H), 3.45 (q, J = 8.4 Hz, 2H), 3.12 (br m, 2H),

2.83 (br m, 2H), 2.80 (q, $J = 6.3$ Hz, 4H), 1.72 (m, 2H), 1.60 (m, 4H), 1.26 (s, 64 H), 0.89 (t, $J = 6.3$ Hz, 6H); ^{13}C NMR (CDCl_3 , 75 MHz) δ : 173.4, 173.0, 138.6, 138.5, 138.2, 138.1, 128.3, 128.0, 127.9, 127.8, 127.7 (2C), 127.6, 127.5, 103.7, 84.7, 82.3, 77.9, 75.7, 75.0, 74.8, 74.7, 73.5 (2C), 70.1, 70.0, 69.9, 69.0, 64.1, 62.5, 49.4 (br), 48.1, 34.3, 34.1, 31.9, 29.7, 29.5, 29.4, 29.2, 29.1, 28.9, 26.6, 26.1, 26.0, 24.92, 24.89, 22.7, 14.1. HRMS (FAB+) calcd for $\text{C}_{82}\text{H}_{130}\text{NO}_{14}\text{P}+\text{H}^+$: 1384.9307; Found: 1384.9274.

4g. According to the representative procedure for the synthesis of **4d**, conjugate **4g** was prepared in 85% (158 mg, 0.111 mmol) by stirring at 50 °C a chloroform-methanol (15 mL, 1:1) solution of **3g** (90 mg, 0.130 mmol), DSPE (150 mg, 0.201 mmol), and sodium cyanoborohydride (20 mg, 0.318 mmol) in the presence of molecular sieves (3Å, 1.0 g) for 1.5 h. Chromatographic purification (silica gel, 150:12 of chloroform and methanol); $R_f = 0.33$ (silica gel, 1:10 of methanol and chloroform); ^1H NMR (CDCl_3 , 300 MHz) δ : 10.05 (br s, 2H), 7.28 (m, 20H), 5.25 (m, 1H), 4.95 (d, $J = 8.4$ Hz, 1H), 4.91 (d, $J = 8.1$ Hz, 1H), 4.78 (t, $J = 10.2$ Hz, 2H), 4.70 (d, $J = 11.1$ Hz, 1H), 4.57 (d, $J = 9.9$ Hz, 1H), 4.50 (m, 1H), 4.39 (m, 1H), 4.20 (m, 3H), 4.00 (m, 3H), 3.8-3.4 (m, 9H), 3.12 (br m, 2H), 2.85 (br m, 2H), 2.27 (q, $J = 7.5$ Hz, 4H), 1.73 (m, 2H), 1.58 (m, 4H), 1.24 (s, 70 H), 0.86 (t, $J = 6.6$ Hz, 6H); ^{13}C NMR (CDCl_3 , 75 MHz) δ : 173.2, 172.9, 138.5, 138.4, 138.1, 138.0, 128.2, 128.0, 127.9, 127.8, 127.7, 127.65, 127.61, 127.5, 127.4, 103.6, 84.6, 82.2, 77.8, 77.2, 75.6, 74.9, 74.8, 74.7, 73.4, 70.0, 68.9, 63.9, 63.8, 62.5, 60.7 (br), 48.1, 34.2, 34.0, 31.8, 29.6, 29.5, 29.3, 29.1, 26.7, 26.1, 26.0, 24.83, 24.81, 22.6, 14.0. HRMS (FAB+) calcd for $\text{C}_{85}\text{H}_{136}\text{NO}_7\text{P}+\text{H}^+$: 1426.9777; Found: 1426.9750.

4h. According to the representative procedure for the synthesis of **4d**, conjugate **4h** was prepared in 82% (184 mg, 0.140 mmol) by stirring at 50 °C a chloroform-methanol (15 mL, 1:1) solution of **3h** (100 mg, 0.170 mmol), DSPE (170 mg, 0.227 mmol), and sodium cyanoborohydride (20 mg, 0.318 mmol) in the presence of molecular sieves (3Å, 1.0 g) for 1.0 h. Chromatographic purification (silica gel, 150:10 of chloroform and methanol); $R_f = 0.23$ (silica gel, 1:10 of methanol and chloroform); ^1H NMR (CDCl_3 , 300 MHz) δ : 10.05 (br s, 2H), 7.27 (m, 15H), 5.23 (m, 1H), 4.95 (d, $J = 9.6$ Hz, 1H), 4.91 (d, $J = 8.4$ Hz, 1H), 4.8-4.6 (m, 4H), 4.37 (dd, $J = 12.0, 3.0$ Hz, 1H), 4.28 (d, $J = 7.5$ Hz, 1H),

4.18 (m, 3H), 3.98 (m, 2H), 3.88 (m, 1H), 3.70 (dd, J = 9.3, 8.1 Hz, 1H), 3.6-3.5 (m, 4H), 3.11 (br s, 2H), 2.85 (br m, 2H), 2.26 (q, J = 6.3 Hz, 4H), 1.70 (br s, 2H), 1.58 (br m, 4H), 1.23 (s, 70H), 1.50 (d, J = 5.3 Hz, 3H), 0.86 (t, J = 6.3 Hz, 6H); ^{13}C NMR (CDCl_3 , 75 MHz) δ : 173.2, 172.9, 138.8, 138.6, 138.5, 128.4, 128.3, 128.2, 128.1, 128.0, 127.9, 127.8, 127.4, 103.4, 82.4, 79.4, 77.2, 76.2, 74.9, 74.4, 73.1, 70.1, 69.7, 63.9, 62.4, 60.8, 48.8, 48.0, 34.1, 33.0, 31.8, 29.6, 29.4, 29.3, 29.0, 26.6, 26.1, 25.8, 24.8, 24.7, 22.6, 16.8, 14.0. HRMS (FAB+) calcd for $\text{C}_{78}\text{H}_{130}\text{NO}_{13}\text{P}+\text{Li}^+$: 1326.9440; Found: 1326.9475.

4i. According to the representative procedure for the synthesis of **4d**, conjugate **4i** was prepared in 90% (124 mg, 0.0895 mmol) by stirring at 50 °C a chloroform-methanol (10 mL, 1:1) solution of **3i** (65 mg, 0.100 mmol), DSPE (110 mg, 0.147 mmol), and sodium cyanoborohydride (20 mg, 0.318 mmol) in the presence of molecular sieves (3Å, 1.0 g) for 1.5 h. Chromatographic purification (silica gel, 150:10 of chloroform and methanol); R_f = 0.50 (silica gel, 1:10 of methanol and chloroform); ^1H NMR (CDCl_3 , 300 MHz) δ : 10.25 (br s, 2H), 7.32 (m, 20H), 5.24 (m, 1H), 4.88 (m, 2H), 4.74 (m, 2H), 4.63 (m, 2H), 4.51 (dd, J = 12.0, 6.6 Hz, 2H), 4.40 (d, J = 10.8 Hz, 1H), 4.19 (m, 4H), 4.00 (m, 4H), 3.90 (dd, J = 9.3, 2.7 Hz, 1H), 3.76 (m, 3H), 3.63 (m, 1H), 3.35 (m, 1H), 3.15 (br m, 2H), 2.92 (br m, 2H), 2.28 (q, J = 6.9 Hz, 4H), 1.75 (m, 2H), 1.57 (m, 6H), 1.26 (s, 62H), 0.89 (t, J = 6.6 Hz, 6H); ^{13}C NMR (CDCl_3 , 75 MHz) δ : 173.3, 173.0, 138.5, 138.4, 138.34, 138.33, 128.2, 127.9, 127.6, 127.5, 127.4, 127.3, 97.8, 80.3, 77.2, 75.1, 74.8, 73.3, 72.5, 72.0, 71.7, 70.3, 69.2, 67.4, 64.3, 63.9, 62.0, 61.3, 48.2, 48.1, 34.2, 34.0, 31.8, 29.7, 29.59, 29.57, 29.37, 29.33, 29.29, 29.15, 29.13, 29.0, 26.7, 26.1, 25.7, 24.9, 24.8, 22.6, 14.0. HRMS (FAB+) calcd for $\text{C}_{82}\text{H}_{130}\text{NO}_{14}\text{P}+\text{K}^+$: 1422.8866; Found: 1422.8815.

4j. According to the representative procedure for the synthesis of **4d**, conjugate **4j** was prepared in 89% (182 mg, 0.127 mmol) by stirring at 50 °C a chloroform-methanol (15 mL, 1:1) solution of **3j** (100 mg, 0.144 mmol), DSPE (170 mg, 0.227 mmol), and sodium cyanoborohydride (20 mg, 0.318 mmol) in the presence of molecular sieves (3Å, 1.0 g) for 1.5 h. Chromatographic purification (silica gel, 150:10 of chloroform and methanol); R_f = 0.30 (silica gel, 1:10 of methanol and chloroform); ^1H NMR (CDCl_3 , 300 MHz) δ : 9.50 (br s, 2H), 7.4-7.1 (m, 20H), 5.25 (m, 1H), 4.88 (d, J = 6.6 Hz,

1H), 4.87 (d, J = 3.0 Hz, 1H), 4.74 (d, J = 2.4 Hz, 1H), 4.68 (d, J = 12.0 Hz, 1H), 4.63 (m, 1H), 4.55 (d, J = 10.5 Hz, 1H), 4.51 (d, J = 10.5 Hz, 1H), 4.41 (m, 2H), 4.20 (m, 3H), 4.00 (d, J = 9.0 Hz, 3H), 3.93 (m, 1H), 3.76 (m, 3H), 3.65 (m, 2H), 3.36 (m, 2H), 3.12 (br m, 2H), 2.90 (br m, 2H), 2.29 (q, J = 7.5 Hz, 4H), 1.76 (m, 2H), 1.26 (s, 74H), 0.89 (t, J = 6.3 Hz, 6H); ^{13}C NMR (CDCl_3 , 75 MHz) δ : 173.3, 173.0, 138.5, 138.4, 138.3, 128.3, 128.2, 127.9, 127.8, 127.7, 127.5, 127.47, 127.42, 127.3, 97.8, 80.3, 75.1, 74.9, 74.8, 73.6, 73.3, 72.5, 72.1, 71.7, 70.2, 69.2, 67.6, 63.9 (br), 62.6, 61.1 (br), 48.2 (br), 34.2, 34.0, 31.9, 29.6, 29.5, 29.49, 29.42, 29.35, 29.31, 29.2, 26.8, 26.1, 25.8, 24.9, 24.8, 22.6, 14.1. HRMS (FAB+) calcd for $\text{C}_{85}\text{H}_{136}\text{NO}_{14}\text{P}+\text{H}^+$: 1426.9777; Found: 1426.9794.

4k. According to the representative procedure for the synthesis of **4d**, conjugate **4k** was prepared in 85% (182 mg, 0.132 mmol) by stirring at 50 °C a chloroform-methanol (10 mL, 1:1) solution of **3k** (100 mg, 0.155 mmol), DSPE (150 mg, 0.201 mmol), and sodium cyanoborohydride (20 mg, 0.318 mmol) in the presence of molecular sieves (3Å, 1.0 g) for 1.0 h. Chromatographic purification (silica gel, 150:10 to 150:15 of chloroform and methanol); R_f = 0.24 (silica gel, 1:10 of methanol and chloroform); ^1H NMR (CDCl_3 , 300 MHz) δ : 10.05 (br s, 1H), 7.26 (m, 15H), 6.00 (d, J = 7.5 Hz, 1H), 5.22 (m, 1H), 4.78 (m, 3H), 4.55 (m, 3H), 4.38 (dd, J = 12.0, 2.7 Hz, 1H), 4.18 (m, 4H), 4.00 (m, 2H), 3.85 (m, 1H), 3.72 (m, 2H), 3.58 (m, 2H), 3.44 (m, 2H), 3.10 (br s, 2H), 2.85 (br s, 2H), 2.27 (q, J = 6.6 Hz, 4H), 1.85 (s, 3H), 1.72 (m, 2H), 1.57 (m, 4H), 1.25 (s, 68 H), 0.87 (t, J = 6.6 Hz, 6H); ^{13}C NMR (CDCl_3 , 75 MHz) δ : 173.3, 172.9, 170.2, 138.4, 138.1, 138.0, 128.3, 128.27, 128.22, 127.9, 127.8, 127.7, 127.6, 127.5, 127.4, 99.9, 80.6, 78.6, 74.7, 74.5, 73.3, 70.2, 70.1, 69.4, 69.0, 63.9, 62.5, 56.9, 48.1, 34.2, 34.0, 31.8, 29.7, 29.6, 29.5, 29.3, 29.1, 26.6, 25.9, 25.8, 25.7, 24.84, 24.81, 23.4, 22.6, 14.0. HRMS (FAB+) calcd for $(\text{C}_{80}\text{H}_{133}\text{N}_2\text{O}_{14}\text{P}+2\text{Li}-\text{H})^+$: 1389.9736; Found: 1389.9681.

Synthesis of Glycopyranside-*n*-alkyl-DSPE Amphiphiles, 5.

Typical example for the synthesis of amphiphilic glycopospholipids **5** by hydrogenation of **4**: Preparation of D-galactopyranoside-decanyl distearoyl

phosphoethanolamine 5d: Perbenzylated galactopyranoside-decanyl-DSPE conjugate **4d** (100 mg, 0.0701 mmol) was dissolved in chloroform (3 mL) and methanol (12 mL). The solution was stirred at room temperature in the presence of 10% Pd-C (200 mg) under a hydrogen atmosphere (balloon). TLC analysis (visualization by UV, molybdenum blue reagent and char with 10% sulfuric acid in ethanol) of the reaction mixture indicated the complete consumption of the perbenzylated starting material and the formation of a new compound after 1 h. The reaction mixture was filtered through Celite with a chloroform/methanol (1:1, 10 mL) wash. Concentration and chromatographic purification (silica gel, 150:30:1 of CHCl₃:MeOH:H₂O) afforded 56 mg (0.0525 mmol, 75%) of **5d** as a white solid. R_f = 0.33 (silica gel, 150:30:1 of CHCl₃:MeOH:H₂O); ¹H NMR (CDCl₃/CD₃OD (v/v=2/1), 300 MHz) δ : 5.00 (m, 1H), 4.18 (dd, J = 11.7, 3.0 Hz, 1H), 3.99 (d, J = 6.9 Hz, 1H), 3.95 (m, 1H), 3.90 (m, 2H), 3.78 (t, J = 6.0 Hz, 2H), 3.68 (m, 1H), 3.55 (d, J = 6.0 Hz, 1H), 3.30 (m, 4H), 2.95 (br m, 2H), 2.74 (br t, 7.8 Hz, 2H), 2.10 (q, J = 7.2 Hz, 4H), 1.48 (m, 2H), 1.37 (m, 6H), 1.03 (s, 70H), 0.65 (t, J = 6.6 Hz, 6H); ¹³C NMR (CDCl₃/CD₃OD (v/v=2/1), 75 MHz) δ : 174.4, 174.1, 103.9, 75.3, 74.1, 71.9, 70.8, 70.7, 70.4, 69.3, 64.4, 63.0, 61.7, 61.1, 34.7, 34.6, 32.4, 30.2, 30.1, 30.0, 29.8, 29.7, 29.6, 29.5, 29.4, 26.9, 26.5, 26.2, 25.4, 25.3, 23.2, 14.4. HRMS (FAB+) calcd for C₅₇H₁₁₂NO₁₄P+H⁺: 1066.7899; Found: 1066.7880.

5a. According to the representative procedure for the synthesis of **5d**, **5a** was prepared as a white solid in 81% (38 mg, 0.0393 mmol) by hydrogenation of **4a** (65 mg, 0.0489 mmol) with 10% Pd-C (140 mg) in chloroform (2 mL) and methanol (8 mL) for 2.0 h. Chromatographic purification (silica gel, 150:30:1 of CHCl₃:MeOH:H₂O); R_f = 0.21 (silica gel, 150:30:1 of CHCl₃:MeOH:H₂O); ¹H NMR (CDCl₃/CD₃OD (v/v=2/1), 300 MHz) δ : 5.16 (m, 1H), 4.06 (br m, 4H), 3.93 (br m, 2H), 3.75 (br m, 4H), 3.46 (br m, 2H), 3.25 (br m, 4H), 2.46 (br s, 1H), 2.42 (br m, 4H), 2.00 (br m, 2H), 1.50 (br s, 4H), 1.17 (s, 56H), 0.79 (t, J = 6.0 Hz, 6H); ¹³C NMR (CDCl₃/CD₃OD (v/v=2/1), 75 MHz) δ : 173.9, 173.6, 103.4, 79.0, 74.3, 73.3, 70.9, 70.5, 70.3, 69.5, 69.2, 62.6, 61.5, 61.4, 34.2, 34.0, 31.8, 29.6, 29.1, 29.0, 24.7, 24.5, 22.5, 13.7. HRMS (FAB+) calcd for C₅₀H₉₈NO₁₄P+Na⁺: 990.6623; Found: 990.6597.

5b. According to the representative procedure for the synthesis of **5d**, **5b** was prepared as a white solid in 69% (51 mg, 0.0562 mmol) by hydrogenation of **4b** (100 mg, 0.0737 mmol) with 10% Pd-C (200 mg) in chloroform (2 mL) and methanol (8 mL) for 2.0 h. Chromatographic purification (silica gel, 150:50:2 of CHCl₃:MeOH:H₂O); *R_f* = 0.18 (silica gel, 150:50:2 of CHCl₃:MeOH:H₂O); ¹H NMR (CDCl₃/CD₃OD (v/v=2/1), 300 MHz) δ: 5.20 (m, 1H), 4.38 (dd, *J* = 12.0, 1.2 Hz, 2H), 4.24 (d, *J* = 6.6 Hz, 1H), 4.12 (m, 4H), 4.00 (br s, 1H), 3.95 (m, 4H), 3.79 (m, 4H), 3.60 (m, 4H), 3.47 (m, 1H), 3.28 (m, 2H), 3.20 (m, 2H), 3.00 (m, 2H); 2.20 (q, *J* = 7.8 Hz, 4H), 1.70 (m, 2H), 1.60 (m, 2H), 1.48 (m, 4H), 1.14 (s, 58H), 0.75 (t, *J* = 6.9 Hz, 6H); ¹³C NMR (CDCl₃/CD₃OD (v/v=2/1), 75 MHz) δ: 174.8, 174.5, 104.2, 75.2, 74.5, 72.1, 71.4, 71.3, 71.2, 70.5, 64.9, 64.8, 63.5, 62.4, 61.6, 35.0, 34.9, 32.8, 30.5, 30.4, 30.3, 30.2, 30.1, 30.0, 28.7, 25.8, 25.7, 23.9, 23.5, 14.5. HRMS (FAB+) calcd for C₅₂H₁₀₂NO₁₄P+Cs⁺: 1128.6092; Found: 1128.6053.

5c. According to the representative procedure for the synthesis of **5d**, **5c** was prepared as a white solid in 72% (54 mg, 0.0527 mmol) by hydrogenation of **4c** (100 mg, 0.0723 mmol) with 10% Pd-C (200 mg) in chloroform (4 mL) and methanol (16 mL) for 0.75 h. Chromatographic purification (silica gel, 150:30:1 of CHCl₃:MeOH:H₂O); *R_f* = 0.21 (silica gel, 150:30:1 of CHCl₃:MeOH:H₂O); ¹H NMR (CDCl₃/CD₃OD (v/v=2/1), 300 MHz) δ: 5.16 (m, 1H), 4.30 (d, *J* = 2.7 Hz, 1H), 4.15 (d, *J* = 2.4 Hz, 1H), 4.07 (m, 3H), 3.92 (br m, 2H), 3.85 (m, 1H), 3.72 (m, 3H), 3.50 (m, 2H), 4.30 (m, 2H), 3.15 (br m, 2H), 2.92 (br m, 2H), 2.24 (q, *J* = 7.5 Hz, 4H), 1.68 (m, 2H), 1.53 (m, 6H), 1.33 (m, 6H), 1.18 (s, 56H), 0.80 (t, *J* = 6.6 Hz, 6H); ¹³C NMR (CDCl₃/CD₃OD (v/v=2/1), 75 MHz) δ: 174.5, 174.2, 103.9, 74.8, 74.2, 71.8, 71.0, 70.9, 70.0, 69.8, 64.5, 64.4, 63.2, 61.8, 61.5, 34.8, 34.6, 32.5, 30.2, 30.10, 30.08, 30.03, 30.0, 29.9, 29.70, 29.67, 29.5, 28.3, 25.7, 25.5, 25.4, 23.2, 14.4. HRMS (FAB+) calcd for C₅₄H₁₀₆NO₁₄P+H⁺: 1024.7429; Found: 1024.7434.

5e. According to the representative procedure for the synthesis of **5d**, **5e** was prepared as a white solid in 81% (62 mg, 0.0539 mmol) by hydrogenation of **4e** (100 mg, 0.071 mmol) with 10% Pd-C (200 mg) in chloroform (3 mL) and methanol (12 mL) for 0.5 h. Chromatographic purification (silica gel, 150:30:1 of CHCl₃:MeOH:H₂O); *R_f* = 0.30 (silica gel, 150:30:1 of CHCl₃:MeOH:H₂O); ¹H NMR (CDCl₃/CD₃OD (v/v=2/1), 300 MHz) δ: 5.17 (m, 1H), 4.33 (dd, *J* = 12.0, 3.3 Hz, 1H), 4.14 (d, *J* =

6.9 Hz, 1H), 4.08 (dd, J = 12.0, 6.9 Hz, 1H), 4.00 (m, 2H), 3.92 (t, J = 6.0 Hz, 2H), 3.81 (dt, J = 6.0, 2.7 Hz, 2H), 3.69 (d, J = 6.3 Hz, 2H), 3.45 (m, 4H), 3.10 (br m, 2H), 2.89 (dd, J = 8.1, 8.1 Hz, 2H), 2.25 (q, J = 8.4 Hz, 4H), 1.60 (m, 2H), 1.53 (m, 4H), 1.18 (s, 82H), 0.80 (t, J = 6.9 Hz, 6H); ^{13}C NMR ($\text{CDCl}_3/\text{CD}_3\text{OD}$ (v/v=2/1), 75 MHz) δ : 174.6, 174.2, 104.0, 75.4, 74.3, 72.0, 70.9, 70.6, 69.5, 64.4, 64.3, 63.2, 61.8, 61.2, 61.1, 34.8, 34.7, 32.5, 30.3, 30.2, 30.14, 30.12, 30.0, 29.9, 29.7, 27.1, 26.7, 26.5, 25.50, 25.47, 23.2, 14.4. HRMS (FAB+) calcd for $\text{C}_{63}\text{H}_{124}\text{NO}_{14}\text{P}+\text{H}^+$: 1150.8838; Found: 1150.8881.

5f. According to the representative procedure for the synthesis of **5d**, **5f** was prepared as a white solid in 72% (16 mg, 0.0156 mmol) by hydrogenation of **4f** (30 mg, 0.0220 mmol) with 10% Pd-C (60 mg) in chloroform (2 mL) and methanol (8 mL) for 1.0 h. Chromatographic purification (silica gel, 150:50:1 of CHCl_3 :MeOH:H₂O); R_f = 0.17 (silica gel, 150:30:1 of CHCl_3 :MeOH:H₂O); ^1H NMR ($\text{CDCl}_3/\text{CD}_3\text{OD}$ (v/v=2/1), 300 MHz) δ : 5.20 (m, 1H), 4.36 (dd, J = 12.0, 3.0 Hz, 1H), 4.22 (d, J = 7.8 Hz, 1H), 4.12 (dd, J = 9.9, 6.9 Hz, 2H), 4.08 (m, 2H), 3.94 (t, J = 6.0 Hz, 2H), 3.80 (m, 2H), 3.70 (dd, J = 12.0, 4.8 Hz, 2H), 3.50 (m, 1H), 3.35 (m, 2H), 3.22 (m, 2H), 3.15 (br m, 2H), 2.94 (br t, J = 7.2 Hz, 2H), 2.26 (dq, J = 7.5, 4.5 Hz, 4H), 1.67 (m, 2H), 1.55 (m, 4H), 1.36 (m, 6H), 1.21 (s, 56 H), 0.82 (t, J = 6.9 Hz, 6H); ^{13}C NMR ($\text{CDCl}_3/\text{CD}_3\text{OD}$ (v/v=2/1), 75 MHz) δ : 174.6, 174.2, 103.5, 78.2, 77.2, 76.7, 74.3, 71.0, 70.9, 70.8, 70.2, 64.4, 63.2, 62.3, 61.2, 34.8, 34.6, 32.5, 30.3, 30.2, 30.1, 29.9, 29.8, 29.7, 28.9, 26.5, 26.2, 25.8, 25.5, 25.4, 23.2, 14.4. HRMS (FAB+) calcd for $\text{C}_{54}\text{H}_{106}\text{NO}_{14}\text{P}+\text{H}^+$: 1024.7429; Found: 1024.7445.

5g. According to the representative procedure for the synthesis of **5d**, **5g** was prepared as a white solid in 75% (56 mg, 0.0525 mmol) by hydrogenation of **4g** (100 mg, 0.0701 mmol) with 10% Pd-C (200 mg) in chloroform (3 mL) and methanol (12 mL) for 1.0 h. Chromatographic purification (silica gel, 150:30:1 of CHCl_3 :MeOH:H₂O); R_f = 0.27 (silica gel, 150:30:1 of CHCl_3 :MeOH:H₂O); ^1H NMR ($\text{CDCl}_3/\text{CD}_3\text{OD}$ (v/v=2/1), 300 MHz) δ : 5.15 (m, 1H), 4.30 (d, J = 2.1 Hz, 1H), 4.20 (d, J = 7.8 Hz, 1H), 4.08 (m, 3H), 3.91 (m, 2H), 3.79 (m, 1H), 3.7-3.5 (m, 2H), 3.46 (m, 1H), 3.36 (m, 2H), 3.20 (m, 2H), 3.15 (br s, 2H), 2.92 (br t, J = 7.8 Hz, 2H), 2.24 (q, J = 7.2 Hz, 4H), 1.69 (m, 2H), 1.78 (s, 74H), 0.79 (t, J = 6.9 Hz, 6H); ^{13}C NMR ($\text{CDCl}_3/\text{CD}_3\text{OD}$ (v/v=2/1), 75 MHz) δ : 174.4, 174.1,

103.4, 77.1, 76.5, 74.1, 70.9, 70.8, 70.7, 70.5, 64.5, 64.4, 63.2, 62.2, 61.4, 34.7, 34.5, 32.4, 30.2, 30.1, 30.0, 29.88, 29.86, 29.74, 29.67, 29.60, 29.5, 27.0, 26.30, 26.28, 25.5, 25.4, 23.2, 14.4. HRMS (FAB+) calcd for $C_{57}H_{112}NO_7P+H^+$: 1066.7899; Found: 1066.7903.

5h. According to the representative procedure for the synthesis of **5d**, **5h** was prepared as a white solid in 71% (56 mg, 0.0532 mmol) by hydrogenation of **4h** (100 mg, 0.0750 mmol) with 10% Pd-C (200 mg) in chloroform (4 mL) and methanol (12 mL) for 1.5 h. Chromatographic purification (silica gel, 150:50:1 of $CHCl_3$:MeOH:H₂O); R_f = 0.25 (silica gel, 150:30:1 of $CHCl_3$:MeOH:H₂O); 1H NMR ($CDCl_3/CD_3OD$ (v/v=2/1), 300 MHz) δ : 5.19 (m, 1H), 4.36 (dd, J = 12.0, 2.7 Hz, 1H), 4.13 (m, 4H), 3.95 (m, 2H), 3.80 (m, 1H), 3.70 (m, 1H), 3.55 (m, 2H), 3.46 (m, 2H), 3.17 (br s, 2H), 3.44 (br t, J = 8.1 Hz, 2H), 2.27 (q, J = 6.9 Hz, 4H), 1.70 (m, 2H), 1.55 (m, 4H), 1.25 (d, J = 6.9 Hz, 3H), 1.24 (s, 70H), 0.83 (t, J = 6.9 Hz, 6H); ^{13}C NMR ($CDCl_3/CD_3OD$ (v/v=2/1), 75 MHz) δ : 174.5, 174.2, 103.8, 74.5, 72.3, 71.7, 71.2, 71.1, 71.0, 70.5, 64.6, 64.5, 63.3, 61.5, 34.8, 34.7, 32.5, 30.3, 30.2, 30.0, 29.9, 29.8, 29.7, 29.6, 27.1, 26.5, 26.4, 25.6, 25.5, 23.3, 16.6, 14.5. HRMS (FAB+) calcd for $(C_{57}H_{112}NO_{13}P+2Li-H)^+$: 1062.8113; Found: 1062.8099.

5i. According to the representative procedure for the synthesis of **5d**, **5i** was prepared as a white solid in 62% (49 mg, 0.0479 mmol) by hydrogenation of **4i** (100 mg, 0.0773 mmol) with 10% Pd-C (200 mg) in chloroform (4 mL) and methanol (16 mL) for 0.75 h. Chromatographic purification (silica gel, 150:50:1 of $CHCl_3$:MeOH:H₂O); R_f = 0.37 (silica gel, 150:50:2 of $CHCl_3$:MeOH:H₂O); 1H NMR ($CDCl_3/CD_3OD$ (v/v=2/1), 300 MHz) δ : 5.20 (m, 1H), 4.36 (dd, J = 12.3, 2.7 Hz, 1H), 4.12 (d, J = 6.9 Hz, 2H), 4.09 (d, J = 7.5 Hz, 1H), 3.96 (br t, J = 6.0 Hz, 2H), 3.89 (m, 1H), 3.85 (dd, J = 12.3, 3.6 Hz, 1H), 3.77 (d, J = 8.4 Hz, 2H), 3.73 (m, 2H), 3.64 (dt, J = 9.3, 6.0 Hz, 1H), 3.50 (m, 1H), 3.39 (dt, J = 9.6, 6.0 Hz, 1H), 3.21 (br s, 2H), 2.98 (br t, J = 7.5 Hz, 2H), 2.27 (q, J = 7.5 Hz, 4H), 1.75 (br m, 2H), 1.55 (br m, 4H), 1.26 (br s, 4H), 1.21 (s, 60H), 0.83 (t, J = 6.9 Hz, 6H); ^{13}C NMR ($CDCl_3/CD_3OD$ (v/v=2/1), 75 MHz) δ : 174.6, 174.3, 100.2, 72.9, 72.0, 71.7, 71.1, 71.0, 68.1, 67.5, 64.6, 64.5, 63.3, 61.7, 61.6, 34.9, 34.8, 32.6, 30.3, 30.26, 30.19, 30.02, 29.99, 29.8, 29.6, 29.1, 26.8, 26.32, 26.27, 25.6, 25.5, 25.2, 23.3, 14.5. HRMS (FAB+) calcd for $C_{54}H_{106}NO_{14}P+H^+$: 1024.7429; Found: 1024.7435.

5j. According to the representative procedure for the synthesis of **5d**, **5j** was prepared as a white solid in 72% (43 mg, 0.0403 mmol) by hydrogenation of **4j** (80 mg, 0.0561 mmol) with 10% Pd-C (160 mg) in chloroform (3 mL) and methanol (12 mL) for 0.75 h. Chromatographic purification (silica gel, 150:50:1 of CHCl₃:MeOH:H₂O); R_f = 0.32 (silica gel, 150:30:1 of CHCl₃:MeOH:H₂O); ¹H NMR (CDCl₃/CD₃OD (v/v=2/1), 300 MHz) δ: 5.16 (m, 1H), 4.42 (m, 1H), 4.36 (dd, *J* = 12.0, 2.7 Hz, 1H), 4.06 (m, 3H), 3.92 (m, 2H), 3.78 (m, 2H), 3.69 (m, 3H), 3.60 (m, 1H), 3.45 (m, 1H), 3.33 (m, 1H), 3.14 (br m, 2H), 2.92 (br t, *J* = 7.8 Hz, 2H), 2.25 (q, *J* = 6.0 Hz, 4H), 1.60 (m, 2H), 1.52 (m, 4H), 1.19 (s, 70H), 0.80 (t, *J* = 6.3 Hz, 6H); ¹³C NMR (CDCl₃/CD₃OD (v/v=2/1), 75 MHz) δ: 174.5, 174.2, 100.6, 73.2, 72.1, 71.6, 71.0, 70.9, 68.2, 67.4, 64.5, 64.4, 63.2, 61.8, 61.5, 34.8, 34.7, 32.5, 30.3, 30.2, 30.0, 29.8, 29.7, 29.5, 27.1, 26.5, 25.5, 25.4, 23.3, 14.5. HRMS (FAB+) calcd for C₅₇H₁₁₂NO₁₄P+H⁺: 1066.7899; Found: 1066.7909.

5k. According to the representative procedure for the synthesis of **5d**, **5k** was prepared as a white solid in 78% (63 mg, 0.0570 mmol) by hydrogenation of **4k** (100 mg, 0.0727 mmol) with 10% Pd-C (200 mg) in chloroform (4 mL) and methanol (8 mL) for 1.0 h. Chromatographic purification (silica gel, 150:40:1 of CHCl₃:MeOH:H₂O); R_f = 0.40 (silica gel, 150:50:2 of CHCl₃:MeOH:H₂O); ¹H NMR (CDCl₃/CD₃OD (v/v=2/1), 300 MHz) δ: 5.16 (m, 1H), 4.35 (dd, *J* = 8.1, 4.2 Hz, 2H), 4.11 (m, 3H), 3.96 (m, 2H), 3.80 (m, 3H), 3.64 (t, *J* = 8.7 Hz, 1H), 3.43 (m, 3H), 3.29 (m, 1H), 3.26 (m, 2H), 2.97 (br t, *J* = 7.2 Hz, 2H), 2.28 (q, *J* = 7.2 Hz, 4H), 1.99 (s, 3H), 1.72 (m, 2H), 1.50 (m, 4H), 1.22 (m, 70 H), 0.83 (t, *J* = 6.9 Hz, 6H); ¹³C NMR (CDCl₃/CD₃OD (v/v=2/1), 75 MHz) δ: 173.6 (2C), 173.2, 100.7, 77.2, 75.4, 74.4, 70.1, 70.0, 69.9, 69.6, 63.5, 63.4, 62.2, 61.00, 60.95, 60.5, 60.4, 55.5, 33.8, 33.6, 31.5, 29.2, 29.09, 29.06, 28.91, 28.88, 28.68, 28.63, 28.59, 28.56, 28.4, 28.3, 26.0, 25.3, 24.5, 24.4, 22.2, 22.1, 13.4. HRMS (FAB+) calcd for (C₅₉H₁₁₅N₂O₁₄P+2Li-H)⁺: 1119.8328; Found: 1119.8278.

References

- Iversen, T.; Bundle, D. R. *Carbohydr. Res.* **1982**, *103*, 29

2. Pougny, J.-R.; Jacquinet, J.-C.; Nassr, M.; Duchet, D.; Milat, M.-L.; Sinay, P. (1977) A novel synthesis of 1,2-cis-disaccharides. *J. Am. Chem. Soc.* 99, 6763
3. Jacquinet, J.-C., Sinay, P. (1979) Synthesis of blood-group substances. Part 8. A synthesis of the branched trisaccharide 2-acetamido-2-deoxy-4-O-(α -L-fucopyranosyl)-3-O-(β -D-galactopyranosyl)-D-glucopyranose. *J. Chem. Soc. Perkin I*, 319.
4. Perdomo, G. R.; Krepinsky, J. (1987) A glycosidation reaction: conversion of methyl glycosides to glycosyl chlorides by boron trichloride. *Tetrahedron Lett.* 28, 5595.
5. Dasgupta, F., Garegg, P. J. (1989) Synthesis of ethyl and phenyl 1-thio-2-trans-D-glycopyranosides from the corresponding per-O-acetylated glycopyranoses having a 1,2-trans-configuration using anhydrous ferric chloride as a promoter. *Acta Chem. Scandinavica*, 3, 471.

Biotin Reagents for Antibody Pretargeting. Synthesis, Radioiodination, and *in Vitro* Evaluation of Water Soluble, Biotinidase Resistant Biotin Derivatives

D. Scott Wilbur,* Donald K. Hamlin, Pradip M. Pathare, and S. Ananda Weerawarna

Department of Radiation Oncology, University of Washington, Seattle, Washington 98195. Received January 21, 1997[®]

As part of our development of antibody pretargeting for cancer therapy, an investigation has been conducted to examine the stability of water solubilized, radioiodinated biotin derivatives toward biotinidase degradation in mouse and human serum. Eight new biotin derivatives were synthesized to conduct the study. The biotin derivatives synthesized contained (1) the biotin moiety, (2) a water solubilizing linker moiety, (3) *p*-iodobenzoate or *p*-tri-*n*-butylstannylbenzoate moieties, and (4) in some of the compounds, N-methyl or α -methyl containing moieties were added to block biotinidase activity. The linker moiety, 4,7,10-trioxa-1,13-tridecanediamine, **5**, was included in the biotin derivatives to improve their water solubility, and it also functioned as a 17 Å spacer between the biotin and the benzoyl moieties. Four of the new biotin derivatives (**12**, **14**, **22**, and **23**) contained a *p*-tri-*n*-butylstannylbenzoyl moiety as precursors which could be radioiodinated in the last synthetic step. The other four biotin derivatives (**13**, **15**, **24**, and **25**) contained *p*-iodobenzoyl moieties and were used as HPLC reference standards. Initial studies involved radioiodination of **12** to yield [¹²⁵I]**13**. Radioiodinated **13**, which did not contain a moiety for blocking biotinidase activity, was found to be rapidly degraded in both mouse and human serum at 37 °C. Derivatives which were designed to be stable to biotinidase incorporated N-methyl and α -methyl moieties adjacent to the biotin carboxylate group. In one set of biotin derivatives (**14** and **15**), the N-methyl moiety was obtained by incorporating *N,N*-dimethyl-4,7,10-trioxa-1,13-tridecanediamine, **9**, as a linker in the place of **5**. In the second set of biotin derivatives (**22** and **24**), the N-methyl moiety was introduced by incorporating a sarcosine (*N*-methylglycine) moiety between biotin and **5**. The radioiodinated N-methyl containing biotin derivatives [¹²⁵I]**15** and [¹²⁵I]**24** were found to be very stable to biotinidase degradation. An α -methyl group was obtained in a pair of biotin derivatives (**23** and **25**) by incorporating a 3-aminobutyric acid moiety between biotin and **5**. The radioiodinated α -methyl containing derivative, [¹²⁵I]**25**, was found to have an intermediate stability with regards to biotinidase degradation.

INTRODUCTION

The very strong binding of biotin (vitamin H; coenzyme R) with the proteins avidin (**1**) and streptavidin (**2**) have made compounds containing biotin attractive for *in vitro* bioassays (**3**, **4**) and *in vivo* medical applications. One important application under investigation by a number of research groups is the use of "pretargeted" monoclonal antibody conjugates with the biotin/(strept)avidin technology for imaging and therapy of cancer (**5-7**). A focus of our studies is the investigation of antibody conjugates with recombinant streptavidin (r-streptavidin)¹ and radiolabeled biotin derivatives in tumor pretargeting protocols as a method of amplifying the amount of radioactivity delivered to cancer cells (**8**). We have hypothesized that the amount of radioactivity attached to a cancer cell which has been pretargeted with a biotinylated antibody might be increased by repeated administration of radio-

labeled biotin dimers or trimers that are capable of cross-linking streptavidin. To investigate this hypothesis, new biotin derivatives had to be prepared. Quite early in our studies in the preparation of new biotin derivatives, it became apparent that there were two problems, serum stability and aqueous solubility of biotin derivatives, that had to be surmounted before they could be applied to tumor pretargeting.

In our initial design of biotin derivatives for pretargeting and in derivatizing other molecules (**9**), alkyl diamine linking moieties were used to conjugate biotin to the molecules of interest. However, low water solubility of biotin derivatives caused problems in their evaluation. For example, in one (unreported) study, a biotin dimer designed for use in cross-linking streptavidin on cancer cells was synthesized by conjugating two biotin moieties with *p*-iodobenzoyl-5-aminoisophthalate ditetrafluorophenyl ester (**10**) using two diaminopropane linkers. The biotin dimer obtained had very low water solubility (e.g., <1 µg/mL), which made cross-linking studies difficult to conduct. Although low aqueous solubility of biotin derivatives had not previously been reported as a problem in the synthesis of monomeric radiohalogenated biotin derivatives (**11-17**), it was apparent that for our application this was a problem that needed to be addressed. Even though our desire to obtain water solubilized derivatives was ultimately directed at obtaining radiolabeled biotin dimers and trimers, we were also interested in obtaining a water soluble monomeric radioiodinated biotin derivative for our studies.

* Address correspondence to Department of Radiation Oncology, University of Washington, 2121 N. 35th Street, Seattle, WA 98103-9103. Phone: 206-685-3085. Fax: 206-685-9630. E-mail: dswilbur@u.washington.edu.

[®] Abstract published in *Advance ACS Abstracts*, July 1, 1997.

¹ Abbreviations: ChT, chloramine-T; cpm, counts per minute; DIP, direct insertion probe, EDC, 1-(3-dimethylaminopropyl)-3-ethylcarbodiimide hydrochloride; EI, electron impact, 2-HEDS, 2-hydroxyethyl sulfide; HOHgBz, hydroxymercuribenzoic acid; *nca*, no-carrier-added; NCS, *N*-chlorosuccinimide; r-streptavidin, recombinant streptavidin; rt, room temperature; TFP, tetrafluorophenyl; TFP-OH, tetrafluorophenol; TFP-OTFA, tetrafluorophenyl trifluoroacetate.

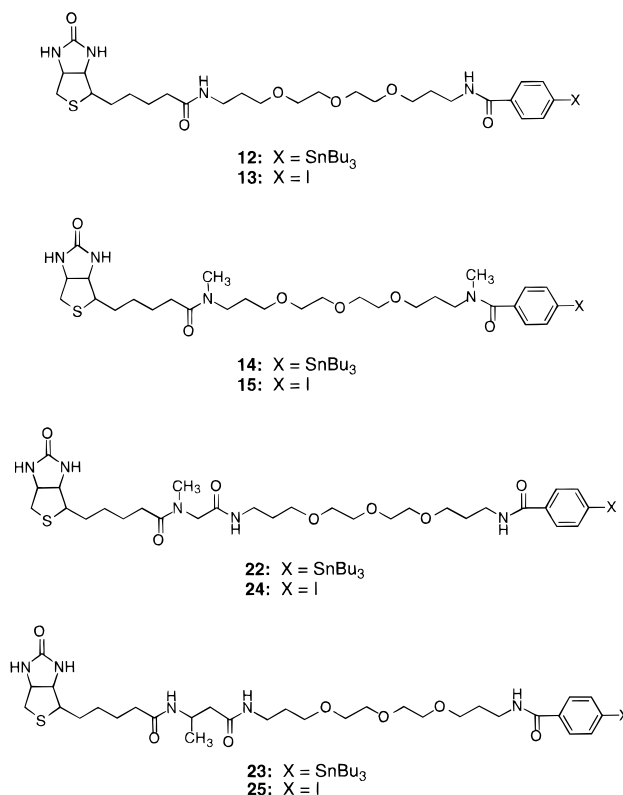
Results of studies involving binding of a radioiodinated biotin derivative with r-streptavidin in phosphate buffer and mouse serum suggested that there was a problem with its stability in serum. Inspection of the literature pointed to the serum enzyme biotinidase (18–24) as the most likely cause for the instability. Indeed, human serum contains large quantities of biotinidase (25 nM), with the concentration being some 12 times higher than both free and bound biotin (24). Although the presence of biotinidase in serum has been known for over four decades (25), until recently (26–29), it had been generally overlooked in the design of biotin derivatives for *in vivo* use. This is very important as any instability toward biotinidase cleavage of biotin from radiolabeled biotin derivatives used in pretargeting studies will result in diminished binding. Even though some of the biotin derivatives under development have two or three biotin moieties, high serum stability is considered critical since removal of only one biotin from a biotin dimer or trimer could result in an inability to cross-link streptavidin. Thus, the instability of radioiodinated biotin derivatives in serum led us to consider the changes in the design of the biotin derivatives such that amide cleaving action of the enzyme biotinidase was blocked.

Reported herein is an investigation of the serum stability of four radioiodinated biotin derivatives. The biotin derivatives synthesized were made more water soluble² with an ether containing linking moiety, 4,7,10-trioxa-1,13-tridecanediamine. Additionally, functional groups were incorporated into some of the biotin derivatives to block biotinidase activity. The functional groups incorporated were based on previous literature reports indicating stability of certain biotin derivatives to biotinidase activity (18, 22, 26–29). Thus, two biotin derivatives incorporated N-methyl functionalities (compounds 15 and 24) similar to those reported by Gustavson et al. (28, 29) and another incorporated an α -methyl group (compound 25) similar to the α -carboxylate reported by Rosebrough (26, 27). *In vivo* diagnostic or therapeutic applications of biotin derivatives in pretargeting requires having a radiolabel attached. In this investigation, radioiodination was important as the radiolabel made it possible to follow the fate of the biotin derivatives in serum. Our desire to introduce the radioiodine into the biotin derivatives in the last synthetic step, and a requirement for high specific activity radioiodinated biotin derivatives for *in vivo* application led to the use of aryltrialkylstannane derivatives for introducing the radioiodine into the molecules under study (31–33). On the basis of the foregoing considerations, the biotin derivatives shown in Chart 1 were targeted for synthesis and radioiodination. The stability of the radioiodinated biotin derivatives synthesized was evaluated in mouse and human serum using an assay employing ultrafiltration centrifugation. Biotinidase contains a sulfhydryl group in its active site, and its hydrolase activity can be blocked by treatment with sulfhydryl reactive agents such as iodoacetamide and hydroxymercuribenzoic acid (HOHgBz) (34). Therefore, HOHgBz was used in this investigation to block the biotinidase activity at specified time points and in controls wherein serum activity was blocked prior to incubation.

EXPERIMENTAL PROCEDURES

General. All chemicals purchased from commercial sources were analytical grade or better and were used

Chart 1. Biotinidase Stabilized, Water Solubilized, Biotin Derivatives Targeted for Synthesis



without further purification unless noted. Most of the reagents used were obtained from Aldrich Chemical Co. (Milwaukee, WI). Biotin was obtained from Sigma Chemicals (St. Louis, MO). 4,7,10-Trioxa-1,13-tridecanediamine, 5, and sarcosine methyl ester were obtained from Fluka (St. Louis, MO). 2,3,5,6-Tetrafluorophenyl trifluoroacetate, TFP-OTFA, was prepared as previously described (35). Solvents for HPLC analysis were obtained as HPLC grade and were filtered (0.2 μ m) prior to use. Silica gel chromatography was conducted with 70–230 mesh 60 Å silica gel (Aldrich Chemical Co.). Centricon-10 and Microcon-30 centrifugation concentrators were obtained from Amicon (Beverly, MA). Melting points were obtained in open capillary tubes on a Mel-Temp II apparatus with a Fluke 51 K/J electronic thermometer and are uncorrected.

Radioactive Materials. Standard safety methods for using radionuclides of iodine were employed (8). Na[¹²⁵I]I and Na[¹³¹I]I were purchased from NEN/Dupont (Billerica, MA) as high pH, high concentration solutions in 0.1 N NaOH. Measurement of ¹²⁵I and ¹³¹I was accomplished on the Capintec CRC-15R or a Capintec CRC-6A Radioisotope Calibrator. Radioactive samples were counted in a LOGIC Model 111B Gamma Counter (Abbott Laboratories, Chicago, IL).

Spectral Analyses. ¹H NMR were obtained on Bruker AC-200 (200 MHz) instrument, and chemical shifts are expressed as parts per million using tetramethylsilane as internal standard (δ = 0.0 ppm). IR data were obtained on a Perkin-Elmer 1420 infrared spectrophotometer. Mass spectral data (both low and high resolution) were obtained on a VG Analytical (Manchester, England) VG-70 SEQ mass spectrometer with associated 11250J Data System. Most mass spectral data were obtained by fast atom bombardment (FAB⁺) in a matrix of 2-hydroxyethyl disulfide (2HEDS) and polyethylene glycol 300 or 600 containing thioglycolate. Some mass spectral data were obtained by electron impact (EI) on

² Water solubilization can be obtained with linkers containing oxygen, nitrogen, or fluorine through hydrogen bonding with those atoms (30).

the sample introduced by the direct insertion probe (DIP), and this is noted with those mass spectral data. High-resolution mass spectral data were used for compound identification. Most compounds containing Sn isotopes had five matching isotopic masses, but only one is provided as identification. ^1H NMR and HPLC were used to assess compound purity (these data are provided in the Supporting Information).

Chromatography. HPLC separations of nonradioactive compounds were obtained on Hewlett-Packard quaternary 1050 gradient pumping system with a variable wavelength UV detector (254 nm) and a Vares ELSD MKIII evaporative light-scattering detector. Analysis of the HPLC data were conducted on Hewlett-Packard HPLC ChemStation software. All reactions were monitored by HPLC. Reverse-phase HPLC chromatography was carried out using an Alltech Altima C-18 column (5 μm , 250 mm \times 4.6 mm) using a gradient solvent system at a flow rate of 1 mL/min. Three different separation systems were used. Gradient I was a gradient using MeOH and 1% aqueous HOAc. Starting with 40% MeOH, the initial solvent mixture was held for 2 min, then the gradient was increased to 100% MeOH over the next 10 min, then held at 100% MeOH for 5 min. Retention times (t_R) under these conditions for biotin conjugates were as follows: **8** = 12.9 min; **9** = 2.5 min; **10** = 2.5 min; **11** = 9.7 min; **12** = 16.8 min; **13** = 11.9 min; **14** = 16.8 min; **15** = 12.0 min; **16** = 5.1 min; **17** = 4.6 min; **18** = 11.4 min; **19** = 11.7 min; **21** = 3.8 min; **22** = 16.7 min; **23** = 15.9 min; **24** = 11.8 min; **25** = 11.9 min. Gradient II was the same as gradient I, except the gradient starting solvent mixture began at 70% MeOH/30% 1% aqueous HOAc: t_R : **3** = 13.8 min; **4** = 20.7 min. Gradient III was a gradient using MeOH and 1% aqueous Et_3NHOAc (pH 4.4). Starting with 40% MeOH, the initial solvent mixture was held for 2 min, then the gradient was increased to 100% MeOH over the next 13 min, then held at 100% MeOH for 5 min. Retention times under these conditions for conjugates were: t_R : **6** = 10.5 min; **7** = 18.4 min.

HPLC separations of radioiodinated biotin derivatives were conducted using a gradient system which consisted of two Beckman model 110B pumps, a Beckman 420 controller, a Beckman model 153 UV detector (254 nm), and a Beckman model 170 radioisotope detector. The separations were obtained using HPLC conditions described for gradient I, except water was used in the place of 1% aqueous HOAc.

4-Iodobenzoate Tetrafluorophenyl ester (3). To 16 g (64.5 mmol) of 4-iodobenzoic acid, **1**, suspended in 100 mL of anhydrous EtOAc was added 21 g (126 mmol) of 2,3,5,6-tetrafluorophenol, **2**, in 50 mL of anhydrous EtOAc. To that mixture was added 18.6 g of EDC, rinsing the weighing vessel with an additional 50 mL of EtOAc. The mixture was allowed to stir overnight at rt, and the EtOAc was removed by rotary evaporation, resulting in an oily solid. The residue was dissolved in 350 mL CH_3Cl , washed with 10% sodium bicarbonate (2 \times 100 mL), dried over anhydrous MgSO_4 , and concentrated to a tacky solid. The solid was recrystallized from acetonitrile to yield 22.1 g (87%) of **3** as an off white solid, mp = 148–149 $^\circ\text{C}$; ^1H NMR (CDCl_3): δ 7.84 (s, 4H), 6.96 (m, 1H). IR (nujol, cm^{-1}): 1748, 1510, 1489, 1277, 1250, 1173, 1094, 940. HRMS (EI, DIP): mass calcd for $\text{C}_{13}\text{H}_5\text{F}_4\text{IO}_2$ (M) $^+$, 395.9270; found, 395.9275.

4-Tri-*n*-butylstannylbenzoate Tetrafluorophenyl Ester (4). To 10 g (25.2 mmol) of **3** dissolved in 250 mL anhydrous toluene was added 25 mL (50 mmol) of bis-(tributyltin) followed by 500 mg of tetrakis(triphenylphosphine)palladium(0). The reaction was heated to reflux

for 6 h, then cooled, and the toluene was removed under vacuum by rotary evaporation. The resultant thick oil was adsorbed onto 10 g of silica gel and added to a 260 g silica gel 60 column that was equilibrated in hexanes. The mixture was then eluted with hexanes (75 mL fractions) until the excess bis(tributyltin) came off the column. At that point, the solvent was changed to 10% EtOAc in hexanes. The desired compound was in fractions 33–40. Evaporation of the solvent yielded 10.3 g (73%) of **4** as a colorless oil. ^1H NMR (CDCl_3): δ 8.10 (d, J = 3.9 Hz, 2H), 7.70 (m, 1H), 7.65 (d, J = 3.9 Hz, 2H), 1.53 (m, 6H), 1.33 (q, J = 3.6 Hz, 6H), 1.11 (t, J = 8.2 Hz, 6H), 0.88 (t, J = 7.2 Hz, 9H). IR (neat, cm^{-1}): 1787, 1555, 1510, 1304, 1271, 1260, 1208, 1200, 1110, 1022, 980, 970. HRMS (EI, DIP): mass calcd for $\text{C}_{21}\text{H}_{23}\text{F}_4\text{O}_2\text{-Sn}$ ($\text{M} - \text{Bu}$) $^+$, 503.0656; found, 503.0667.

***N*-(13'-Amino-4',7',10'-trioxatridecanyl)-4-iodobenzamide (6).** A 2.0 g (5.05 mmol) quantity of **3** dissolved in 100 mL of anhydrous DMF was added dropwise over 1 h to a mixture of 11 g (50 mmol) of 4,7,10-trioxa-1,13-tridecanediamine, **5**, and 2 mL of Et_3N . The reaction was stirred at rt for 30 min and solvent was removed under vacuum with rotary evaporation. The resulting oil was triturated in 200 mL of ether. The product was extracted with CH_3Cl (2 \times 100 mL). The combined CH_3Cl extracts were washed with H_2O (2 \times 50 mL), dried over anhydrous Na_2SO_4 , and CH_3Cl was removed under vacuum. The semisolid was then loaded onto a silica column (2.5 cm \times 35 cm), eluting with EtOAc, then EtOAc/MeOH. The product was eluted with EtOAc:MeOH (7:3). The solvent was removed under vacuum to yield 1 g (44%) of **6** as a light yellow solid, mp 117–119 $^\circ\text{C}$. ^1H NMR (CDCl_3): δ 7.65 (d, J = 8.4 Hz, 2H), 7.4 (d, J = 8.8 Hz, 3H), 6.4 (s, 2H), 3.4–3.6 (m, 14H), 2.9 (t, J = 6.3 Hz, 2H), 1.6–1.8 (m, 4H). IR (KBr, cm^{-1}): 3340, 1630, 1585, 1530, 1460, 1110. HRMS: mass calcd for $\text{C}_{17}\text{H}_{28}\text{IN}_2\text{O}_4$ ($\text{M} + \text{H}$) $^+$, 451.1096; found, 451.1083.

***N*-(13'-Amino-4',7',10'-trioxatridecanyl)-4-tributylstannylbenzamide (7).** A 2.0 g quantity (3.57 mmol) of **4** dissolved in 50 mL of anhydrous DMF was added dropwise over 1 h to a mixture containing 8 g (35.7 mmol) of 4,7,10-trioxa-1,13-tridecanediamine, **5**, and 1 mL of Et_3N . The reaction mixture was stirred at rt for 30 min, and the solvent was removed under vacuum. The resulting oil was triturated in 200 mL of ether. The product was extracted with CH_3Cl (2 \times 100 mL). The combined CH_3Cl extracts were washed with (2 \times 50 mL) H_2O , dried over anhydrous Na_2SO_4 , and the CH_3Cl was removed under vacuum. The resultant oil was dried under vacuum to yield 2.2 g (99%) of **6**. ^1H NMR (CDCl_3): δ 7.7 (d, J = 7.8 Hz, 2H), 7.5 (d, J = 8.0 Hz, 3H), 3.4–3.6 (m, 14H), 2.7 (t, J = 6.7 Hz, 2H), 0.6–1.8 (m, 33H). IR (KBr, cm^{-1}): 3340, 1630, 1585, 1530, 1460, 1110. HRMS: mass calcd for $\text{C}_{29}\text{H}_{55}\text{N}_2\text{O}_4\text{Sn}$ (120) ($\text{M} + \text{H}$) $^+$, 615.3184; found, 615.3159.

Biotin Tetrafluorophenyl Ester (8). This compound was prepared as previously described (8).

***N,N*-Dimethyl-4,7,10-trioxa-1,13-tridecanediamine (9).** A 50.8 g (231 mmol) quantity of 4,7,10-trioxa-1,13-tridecanediamine, **5**, was dissolved in 300 mL of ethyl formate at ambient temperature and was stirred under argon for 14 h. Excess ethyl formate was removed under vacuum and the remaining oil was dissolved in 500 mL CH_3Cl . The CH_3Cl solution was washed with H_2O (2 \times 100 mL), dried over anhydrous Na_2SO_4 , and evaporated to give 62.2 g (97%) of 4,7,10-trioxa-1,13-tridecanediamine-*N,N*-diformamide as an oil. ^1H NMR (CDCl_3): δ 8.12 (s, 2H), 3.45–3.75 (m, 12H), 3.25–3.45 (m, 4H), 1.70–1.92 (m, 4H).

A 50 g quantity (181 mmol) of the crude diformamide was dissolved in 200 mL of anhydrous THF under argon. The solution was cooled in an ice–H₂O bath and 750 mL (1500 mmol) of 2 M borane–methyl sulfide in THF was added dropwise. After the addition was complete, the mixture was allowed to warm to rt, then was heated to reflux for 1 h. THF (~750 mL) was removed by distillation, and the reaction mixture was cooled with an ice–H₂O bath. A solution of 14 g of anhydrous HCl in 300 mL of MeOH was (very cautiously) added dropwise to the cooled reaction mixture. The reaction mixture was allowed to warm to rt, then heated to reflux for 30 min. The solvent and excess HCl were removed by rotary evaporation. The solid obtained was triturated in ether, filtered, and dried to give 56.4 g (97%) of a tacky white solid.

The crude product was dissolved in MeOH:H₂O (1:1, 500 mL) and was filtered. The filtrate was neutralized with 1 N NaOH and evaporated to dryness. The solid obtained was dissolved in CHCl₃, washed with H₂O, and dried over anhydrous Na₂SO₄. The CHCl₃ solution was evaporated to give 40 g (92%) of **9** as a white solid, mp 102–104 °C. ¹H NMR (CD₃OD): δ 3.69 (m, 12H), 3.16 (m, 4H), 2.73 (s, 6H), 2.01 (m, 4H). ¹H NMR (free base, CDCl₃): δ 3.65 (m, 12H), 2.77 (t, *J* = 6.8 Hz, 4H), 2.49 (s, 6H), 1.85 (m, 4H). IR (KBr, cm⁻¹): 3400, 2470, 2410, 1620, 1460, 1340, 1100. HRMS: mass calcd for C₁₂H₂₉N₂O₃ (M + H)⁺, 249.2178; found, 249.2167.

***N*-(13-Amino-4,7,10-trioxatridecanyl)biotinamide (10).** This compound was prepared as previously described (**8**).

***N*-(13-(*p*-tri-*n*-butylstannylbenzamido)-4,7,10-trioxatridecanyl)biotinamide (12).** A 0.628 g (1.12 mmol) quantity of **4** dissolved in 10 mL of anhydrous DMF was added dropwise over 10–15 min to a mixture of 0.5 g (1.12 mmol) of **10** in 25 mL of DMF and 0.4 mL of Et₃N. The reaction was stirred at rt for 2 h and solvent was removed under vacuum. The residue was extracted with CH₃Cl (200 mL), washed with saturated sodium bicarbonate solution (3 × 15 mL), then with H₂O (2 × 50 mL), and dried over anhydrous Na₂SO₄. The CH₃Cl was removed under vacuum with rotary evaporation to yield 0.75 g (80%) of **12** as a light yellow oil after drying under vacuum. ¹H NMR (CD₃OD): δ 7.7 (d, *J* = 8 Hz, 2H), 7.4 (d, *J* = 8 Hz, 2H), 4.35 (m, 1H), 4.2 (m, 1H), 3.34–3.5 (m, 12H), 3.05–3.2 (m, 3H), 2.7–2.9 (m, 3H), 2.6 (d, *J* = 13 Hz, 1H), 2.08 (t, *J* = 7.3 Hz, 2H), 1.0–1.8 (m, 32H), 0.8 (m, 9H). IR (KBr, cm⁻¹): 3280, 2910, 2850, 1690, 1640, 1580, 1110. HRMS: mass calcd for C₃₉H₆₉N₄O₆SSn(120) (M + H)⁺, 841.3925; found, 841.3960.

***N*-(13-(*p*-Iodobenzamido)-4,7,10-trioxatridecanyl)biotinamide (13).** To a 0.5 g (1.12 mmol) quantity of **10** dissolved in 25 mL of anhydrous DMF was added 0.4 mL of Et₃N (4 mmol) followed by 0.44 g (1.1 mmol) of **3**. The reaction mixture was stirred at rt for 0.5 h, and the solvent was removed under vacuum by rotary evaporation. The residue was extracted into CH₃Cl (200 mL). The CH₃Cl was washed with H₂O (2 × 15 mL), dried over anhydrous Na₂SO₄, and removed under vacuum. The resultant product was dried under vacuum to yield 0.6 g (80%) of **13** as a white solid, mp 107–109 °C. ¹H NMR (CD₃OD): δ 7.8 (d, *J* = 9 Hz, 2H), 7.5 (d, *J* = 8.7 Hz, 2H), 4.5 (m, 1H), 4.3 (m, 1H), 3.4–3.6 (m, 14H), 3.2–3.3 (m, 4H), 2.80–2.95 (m, 3H), 2.7 (d, *J* = 13.2 Hz, 1H), 2.2 (t, *J* = 7.3 Hz, 2H), 1.6–1.9 (m, 9H), 1.46 (m, 2H). IR (KBr, cm⁻¹): 3280, 2910, 2850, 1690, 1640, 1580, 1110. HRMS: mass calcd for C₂₇H₄₁N₄O₆SI (M + H)⁺, 677.1869; found, 677.1865.

1,13-*N,N*-Dimethyl-*N*-(13-(*p*-tri-*n*-butylstannylbenzamido)-4,7,10-trioxatridecanyl)biotinamide (14).

A 2.0 g (5.1 mmol) quantity of **8** in 50 mL of anhydrous DMF was added dropwise to a mixture of 12.65 g (51 mmol) of *N,N*-dimethyl-4,7,10-trioxa-1,13-tridecanediamine and 2 mL of Et₃N over 1 h. The reaction was stirred at rt for 2 h, and the solvent was removed under vacuum. The oil obtained was extracted in acetonitrile and filtered. The solvent was removed by distillation, and the resultant oil was loaded onto a silica column (2.5 cm × 35 cm). The column was first eluted with EtOAc and then with EtOAc:MeOH. The product eluted with MeOH. The solvent was removed from the collected fractions under vacuum. The isolated product was dried under high vacuum to yield 600 mg (25%) of **11** as an oily solid. ¹H NMR (CDCl₃): δ 6.6 (m, 2H), 4.2–4.6 (m, 2H), 1.2–3.7 (m, 38H).

To a solution containing 0.23 g (0.49 mmol) **11** and 17 μL of Et₃N in 5 mL of DMF was added 0.302 g (0.54 mmol) of **4**. The reaction mixture was stirred at rt for 14–16 h and then evaporated to dryness. The product was extracted with CH₃Cl (2 × 100 mL). The combined CH₃Cl extracts were washed with (2 × 50 mL) H₂O, dried over anhydrous Na₂SO₄, and the CH₃Cl was removed under vacuum. The product was triturated with ether, collected, and dried under vacuum to yield 0.18 g (74%) of **14** as an oil. ¹H NMR (CDCl₃): δ 7.2–7.5 (m, 2H), 6.0–6.5 (m, 3H), 4.1–4.5 (m, 2H), 0.7–3.7 (m, 65H). IR (KBr, cm⁻¹): 1695, 1640, 1455, 1300, 1120. HRMS: mass calcd for C₄₁H₇₃N₄O₆SSn(120) (M + H)⁺, 869.4289; found, 869.4273.

1,13-*N,N*-Dimethyl-*N*-(13-(*p*-iodobenzamido)-4,7,10-trioxatridecanyl)biotinamide (15). To a solution containing 0.18 g (0.38 mmol) of **11** and 14 μL Et₃N in 5 mL of DMF was added 0.166 g (0.42 mmol) of **3**. The reaction was stirred at rt for 14–16 h and then evaporated to dryness. The product was loaded onto a silica column (2.5 cm × 35 cm). The column was first eluted with CH₃CN, then with increasing percentage of MeOH in CH₃CN. The product eluted with a 3:7 mixture of MeOH/CH₃CN. The solvent was removed under vacuum and the residue was dried under vacuum to yield 0.12 g (74%) of **15** as an oil. ¹H NMR (CDCl₃): δ 7.7 (d, *J* = 8.2 Hz, 1H), 7.2 (d, *J* = 8.2 Hz, 1H), 6.4 (m, 1H), 6.0 (m, 1H), 4.2–4.6 (m, 2H), 1.2–3.7 (m, 39H). IR (KBr, cm⁻¹): 1695, 1640, 1455, 1300, 1120. HRMS: mass calcd for C₂₉H₄₆IN₄O₆S (M + H)⁺, 705.2183; found, 705.2167.

***N*-Methylglycylbiotinamide (16).** A 2.5 g (6.4 mmol) quantity of **8** dissolved in 30 mL of DMF under argon atmosphere was added to a mixture of (1.075 g, 7.68 mmol) *N*-methylglycine methyl ester hydrochloride dissolved in 10 mL of DMF and 1.25 mL (9.0 mmol) of Et₃N. The reaction mixture was stirred at rt for 2–3 h, then the solvent was removed under vacuum. The residue was extracted into CH₃Cl (2 × 100 mL). The CH₃Cl extract was washed with H₂O (2 × 25 mL), dried over anhydrous Na₂SO₄. The CH₃Cl was removed under vacuum, and the residue was dried under high vacuum to yield 2.1 g (99.7%) of methyl ester of *N*-methylglycine biotinamide as a semisolid. ¹H NMR (CD₃OD): δ 4.5 (m, 1H), 4.3 (m, 1H), 3.7 (d, *J* = 9.6 Hz, 2H), 3.1–3.2 (m, 3H), 2.8–3.0 (m, 6H), 2.7 (d, *J* = 12.6 Hz, 1H), 2.2–2.5 (m, 2H), 1.4–1.8 (m, 6H). HPLC: *t*_R = 6.6 min (gradient I).

N-Methylglycylbiotinamide methyl ester was hydrolyzed in a mixture of 31.5 mL of MeOH and 10.5 mL of 1 N NaOH solution at rt for 1 h. Methanol was removed by distillation, and the aqueous solution remaining was stirred with ether (100 mL). This resulted in precipitation of a solid. The solid was filtered and dried under vacuum to yield 1.2 g (60%) of **16** as a colorless solid, mp 190–192 °C. ¹H NMR (DMSO-*d*₆): δ 6.2 (d, *J* = 15.6 Hz, 2H), 3.7–4.2 (m, 4H), 2.7–2.9 (m, 3H), 2.6 (m, 2H), 2.35

(m, 2H), 2.0 (m, 2H), 1.0–1.5 (m, 6H). IR (KBr, cm^{-1}): 3320, 3280, 2910, 1695, 1650, 1480, 1120, 880. HRMS: mass calcd for $\text{C}_{13}\text{H}_{22}\text{N}_3\text{O}_4\text{S}$ ($\text{M} + \text{H}$)⁺, 316.1331; found, 316.1321.

***N*-(13-(*p*-tri-*n*-butylstannylbenzamido)-4,7,10-trioxatridecanyl)-*N*-methylglycylbiotinamide (22).** To a 0.25 g (0.8 mmol) quantity of **16** dissolved in 15 mL of DMF under argon atmosphere was added 0.25 g (0.96 mmol) of 2,3,5,6-tetrafluorophenyl trifluoroacetate, TFP-OTFA, followed by 0.119 mL (0.96 mmol) of Et_3N . The reaction mixture was stirred at rt for 20 min to obtain **18**. To the solution containing **18** was added 0.491 g (0.8 mmol) of **7** in 5 mL of DMF. That mixture was stirred at rt for 0.5 h, and the solvent was removed under vacuum. The residue was triturated with ether, and the solid was filtered. The isolated solid was dried under high vacuum to yield 0.5 g (69%) of **22** as colorless solid, mp 89–91 °C. ^1H NMR (CD_3OD): δ 7.7 (d, $J = 7.4$ Hz, 2H), 7.5 (d, $J = 7.4$ Hz, 2H), 4.5 (m, 1H), 4.3 (m, 1H), 4.0 (d, $J = 8.4$ Hz, 2H), 2.9–3.8 (m, 25H), 2.7 (d, $J = 12.6$ Hz, 2H), 2.4 (m, 2H), 0.8–2.0 (m, 36H). IR (KBr, cm^{-1}): 3280, 2920, 2860, 1695, 1650, 1450, 1120, 1000. HRMS: mass calcd for $\text{C}_{42}\text{H}_{74}\text{N}_5\text{O}_7\text{SSn}(120)$ ($\text{M} + \text{H}$)⁺, 912.4308; found, 912.4331.

***N*-(13-(*p*-iodobenzamido)-4,7,10-trioxatridecanyl)-*N*-methylglycylbiotinamide (24).** To a 0.15 g (0.48 mmol) quantity of **16** dissolved in 12 mL of DMF under argon atmosphere was added 0.15 g (0.576 mmol) of TFP-OTFA and 71 μL (0.576 mmol) of Et_3N . The reaction mixture was stirred at rt for 20 min to form **18**. To the solution of **18** was added 0.216 g (0.48 mmol) of **6** in 5 mL of DMF. The reaction mixture was stirred at rt for 0.5 h, then the solvent was removed by distillation, and the residue was loaded onto a silica gel column. The column was eluted with EtOAc then with increasing amounts of MeOH in EtOAc. The fractions containing the product were evaporated to dryness to yield 0.22 g (61%) of **24** as a colorless solid after drying under high vacuum, mp 114–116 °C. ^1H NMR (CD_3OD): δ 7.8 (d, $J = 8.6$ Hz, 2H), 7.6 (d, $J = 8.8$ Hz, 2H), 4.4 (m, 1H), 4.3 (m, 1H), 4.0 (d, $J = 10$ Hz, 2H), 2.9–3.6 (m, 22H), 2.9 (m, 2H), 2.7 (d, $J = 12.6$ Hz, 1H), 2.4 (m, 2H), 1.3–1.9 (m, 11H). IR (KBr, cm^{-1}): 3280, 2920, 2860, 1695, 1650, 1450, 1120, 1000. HRMS: mass calcd for $\text{C}_{30}\text{H}_{46}\text{IN}_5\text{O}_7\text{SSNa}$ ($\text{M} + \text{Na}$)⁺, 770.2060; found, 770.2086.

3-(Biotinamido)butyric Acid (17). To a 1.32 g (12.76 mmol) quantity of 3-aminobutyric acid dissolved in 200 mL of DMF under argon atmosphere was added 3.6 mL (25.5 mmol) of Et_3N , followed by 5 g (12.76 mmol) of **8**. The reaction was stirred at rt for 24 h, and the solvent was removed under vacuum. The residue was triturated with acetonitrile and filtered. The isolated solid was dried under high vacuum to yield 4.8 g (98%) of **17** as a colorless solid, mp 161–163 °C. ^1H NMR ($\text{DMSO}-d_6$): δ 7.6 (m, 1H), 6.2 (d, $J = 11.2$ Hz, 2H), 3.9–4.2 (m, 3H), 2.6 (m, 2H), 2.35 (d, $J = 12.6$ Hz, 1H), 1.7–2.1 (m, 4H), 0.7–1.5 (m, 10H). IR (KBr, cm^{-1}): 3280, 3060, 2920, 2840, 1695, 1640, 1540, 1260, 1080. HRMS: mass calcd for $\text{C}_{14}\text{H}_{24}\text{N}_3\text{O}_4\text{S}$ ($\text{M} + \text{H}$)⁺, 330.1488; found, 330.1479.

3-(Biotinamido)butyrate Tetrafluorophenyl Ester (19). To a 4.0 g (12.16 mmol) quantity of **17** dissolved in 100 mL of DMF under argon atmosphere was added 3.8 g (14.6 mmol) of TFP-OTFA, followed by 0.2 mL of Et_3N . The reaction mixture was stirred at rt for 1 h, and the solvent was removed under vacuum. The residue was extracted into CH_3Cl (4 \times 100 mL). The combined CH_3Cl extracts were washed with saturated aqueous NaHCO_3 (2 \times 50 mL) and H_2O (2 \times 50 mL). The CH_3Cl solution was dried over anhydrous Na_2SO_4 , and the CH_3Cl

was removed under vacuum. The isolated product was dried under high vacuum to yield 4.7 g (81%) of **19** as a colorless solid, mp 137–139 °C. ^1H NMR ($\text{DMSO}-d_6$): δ 7.7 (m, 2H), 6.2 (d, $J = 13.2$ Hz, 2H), 3.9–4.2 (m, 3H), 2.5–2.7 (m, 4H), 2.35 (d, $J = 12.6$ Hz, 1H), 1.85 (t, $J = 7.0$ Hz, 2H), 0.7–1.5 (m, 10H). IR (KBr, cm^{-1}): 3280, 3060, 2920, 2840, 1780, 1695, 1640, 1520, 1260, 1080. HRMS: mass calcd for $\text{C}_{20}\text{H}_{24}\text{F}_4\text{N}_3\text{O}_4\text{S}$ ($\text{M} + \text{H}$)⁺, 478.1424; found, 478.1424.

1-*N*-(13-Amino-4,7,10-trioxatridecanyl)-3-(biotinamido)butyramide (21). To a 4.0 g (8.39 mmol) quantity of **19** dissolved in 50 mL of anhydrous DMF was added dropwise over 1 h a mixture of 18.5 g (83.9 mmol) of **5** and 3 mL of Et_3N . The reaction was stirred at rt for 30 min, and the solvent was removed under vacuum. The resulting oil was triturated in 200 mL of ether, stirred for 30 min, and the solid was collected. The semisolid was dissolved in MeOH:EtOAc (3:7) and loaded onto a silica column (2.5 cm \times 35 cm). The column was eluted with the same solvent mixture, with increasing concentration of MeOH. The product eluted with MeOH. The solvent was removed under vacuum from the fractions containing **21**. The isolated solid was dried under high vacuum to yield 4.0 g (90%) of **21** as a colorless solid, mp 154–156 °C. ^1H NMR (CD_3OD): δ 4.5 (m, 1H), 4.2–4.3 (m, 2H), 3.4–3.7 (m, 15H), 3.2 (m, 4H), 2.9 (dd, $J = 3.2$ Hz, $J = 8.2$ Hz, 1H), 2.7–2.8 (m, 3H), 2.1–2.4 (m, 5H), 1.4–1.9 (m, 11H), 1.2 (d, $J = 4.6$ Hz, 3H). IR (KBr, cm^{-1}): 3280, 3060, 2920, 2840, 1695, 1640, 1540, 1260, 1100. HRMS: mass calcd for $\text{C}_{24}\text{H}_{46}\text{N}_5\text{O}_6\text{S}$ ($\text{M} + \text{H}$)⁺, 532.3169; found, 532.3154.

1-*N*-(13-(*p*-Tri-*n*-butylstannylbenzamido)-4,7,10-trioxatridecanyl)-3-(biotinamido)butyramide (23). To a solution containing 0.5 g (0.942 mmol) of **21** and 20 μL of Et_3N in 20 mL of DMF was added 0.528 g (0.942 mmol) of **4** over a period of 5–10 min. The reaction was stirred at rt for 1 h and evaporated to dryness. The product was crystallized from MeOH/EtOAc and dried under high vacuum to yield 0.63 g (72%) of **23** as a yellowish solid, mp 158–159 °C. ^1H NMR (CD_3OD): δ 7.75 (d, $J = 5.2$ Hz, 2H), 7.5 (d, $J = 5.6$ Hz, 2H), 4.5 (m, 1H), 4.2–4.3 (m, 2H), 3.4–3.7 (m, 16H), 3.2 (m, 4H), 2.9 (dd, $J = 3.2$ Hz, $J = 8.4$ Hz, 1H), 2.7 (d, $J = 8.6$ Hz, 1H), 2.1–2.4 (m, 5H), 0.8–1.9 (m, 41H). IR (KBr, cm^{-1}): 3280, 3060, 2920, 2840, 1695, 1640, 1540, 1260, 1100. HRMS: mass calcd for $\text{C}_{43}\text{H}_{76}\text{N}_5\text{O}_7\text{SSn}(120)$ ($\text{M} + \text{H}$)⁺, 926.4478; found, 926.4487.

1-*N*-(13-(*p*-Iodobenzamido)-4,7,10-trioxatridecanyl)-3-(biotinamido)butyramide (25). To a solution containing 0.5 g (0.942 mmol) of **21** and 20 μL of Et_3N in 20 mL of DMF was added 0.373 g (0.942 mmol) of **3** over a period of 5–10 min. The reaction was stirred at rt for 1 h and evaporated to dryness. The product was crystallized from MeOH/EtOAc and dried under high vacuum to yield 0.4 g (56%) of **25** as a yellowish solid, mp 155–157 °C. ^1H NMR (CD_3OD): δ 7.85 (d, $J = 5.6$ Hz, 2H), 7.55 (d, $J = 6.0$ Hz, 2H), 4.5 (m, 1H), 4.2–4.3 (m, 2H), 3.4–3.7 (m, 16H), 3.2 (m, 4H), 2.9 (dd, $J = 3.2$ Hz, $J = 8.4$ Hz, 1H), 2.7 (d, $J = 8.6$ Hz, 1H), 2.1–2.4 (m, 5H), 1.4–1.9 (m, 11H), 1.2 (d, $J = 6.6$ Hz, 3H). IR (KBr, cm^{-1}): 3280, 3060, 2920, 2840, 1695, 1640, 1540, 1260, 1100. HRMS: mass calcd for $\text{C}_{31}\text{H}_{49}\text{IN}_5\text{O}_7\text{S}$ ($\text{M} + \text{H}$)⁺, 761.2397; found, 762.2366.

General Procedure for Iodination of 12, 14, 22, 23. Iodinations were performed on the stannylbenzoyl-biotin derivatives **12**, **14**, **22**, and **23** to confirm that the reaction gives the corresponding iodobenzoyl-biotin derivatives **13**, **15**, **24**, and **25**. A typical reaction was conducted as follows: To a 500 μL aliquot of a 2 mg/mL solution of stannylbenzoyl-biotin derivative in 1% HOAc/

Table 1. Radioiodinated Biotin Derivative Binding^a with r-Streptavidin

radioiodinated biotin derivative	quantity added (nmol)	with r-streptavidin ^b (% activity filtered)	without r-streptavidin ^c (% activity filtered)
^{[125]I} 13	3.6	2.9 ± 0.1	99.5 ± 0.1
	7.1	3.1 ± 0.0	
	10.6	30.2 ± 1.5	
^{[125]I} 24	3.2	3.1 ± 0.1	99.4 ± 0.1
	6.4	3.3 ± 0.0	
	9.7	23.0 ± 1.1	

^a Values represent the percentage of radioactivity filtered in a Microcon-30 centrifugation unit (i.e., not retained by binding with r-streptavidin or nonspecifically bound to membrane or plastic apparatus). ^b Values represent percentage of radioactivity that was filtered when a known quantity of the biotin derivative was added to 2.0 nmol of r-streptavidin (8 nmol biotin binding capacity); average of two analyses ± SD. ^c Values represent percentage of radioactivity filtered when the biotin derivative was added to solutions without r-streptavidin; average of two analyses ± SD. The nonspecific binding with the Microcon-30 unit is obtained by subtracting the values shown from 100%.

MeOH was added the appropriate amount of a 22 mg/mL aqueous solution of NaI to obtain 0.75 equiv (relative to **12**, **14**, **22**, or **23**), followed by addition of the appropriate amount of a 22 mg/mL MeOH solution of *N*-chlorosuccinimide (NCS) to provide 1 equiv. The mixture turned dark upon addition of the NCS, but became colorless within 2 min. After 2 min, 1 equiv of an aqueous sodium metabisulfite solution (22 mg/mL) was added to mimic the quench step used in the radioiodination reaction. The reactions were followed by HPLC.

General Procedure for Radioiodination of **12, **14**, **22**, and **23**.** To 50 µL of a 1 mg/mL solution of **12**, **14**, **22**, or **23** was added 1–5 µL of Na^{[125]I} in 0.1 N NaOH, followed by 10 µL of a 1 mg/mL solution of NCS in MeOH. After 2 min, 10 µL of a 1 mg/mL aqueous sodium metabisulfite solution was added. The reaction mixture was then drawn into a syringe for purification by HPLC. The radioiodinated compounds were obtained from the HPLC effluent. Radiochemical yields of the isolated (purified) biotin derivatives were [^{125]I}**13** (50%); [^{125]I}**15** (24%); [^{125]I}**24** (37%, 39%); and [^{125]I}**25** (66%, 76%). Portions of the isolated radioiodinated biotin compounds were used for biotinidase activity experiments, and the remainder was stored (in the eluant solvent) in the refrigerator to determine the radiochemical/chemical stability over time.

Streptavidin Binding of **13 and **24**.** A 1.0 mg/mL solution of the iodobenzoyl-biotin derivative (**13** or **24**) in 10% aqueous MeOH was diluted to 1:1 with the corresponding radioiodinated biotin derivative ([^{125]I}**13** or [^{125]I}**24**) in aqueous MeOH (from HPLC) to give a final concentration of 0.50 mg/mL. Two, four, and six aliquots of 2.4 µL each (**13** = 1.77 nmol; **24** = 1.61 nmol) were added to three Eppendorf tubes containing 100 µL of a 1 mg/mL solution of r-streptavidin (100 µg; 2.0 nmol). The mixtures were incubated at rt for 1 h, then the contents of the tubes were transferred to Microcon-30 concentrators, and the samples were reduced in volume by centrifugation at 7500 rpm to approximately 50 µL. The residual protein solution in the Microcon-30 were rinsed and concentrated three times with 200 µL of 20 mM phosphate buffer, pH 6.8. The top and bottom (containing filtrate and three rinses) of the Microcon-30 were counted in a well counter, and the percent of nonretained radioactivity was calculated by dividing the amount of radioactivity in the bottom by the total amount (top and bottom) times 100. The data obtained are listed in Table 1.

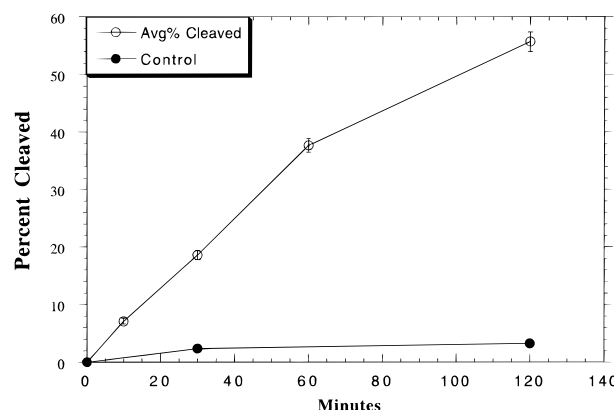


Figure 1. Graphical presentation of the data obtained at various time points after incubation of [^{125]I}**13** in mouse serum at 37 °C. Each point represents the average ± standard deviation of triplicate experiments.

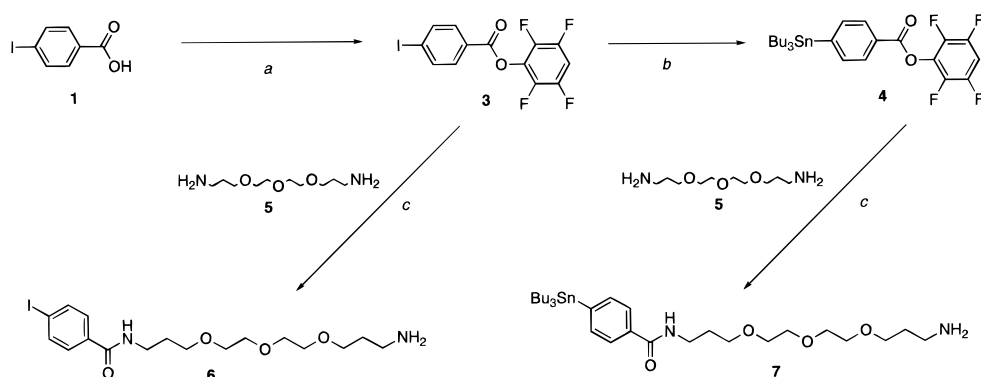
Table 2. Biotinidase Activity with Radioiodinated Derivatives Incubated in Diluted (10%) Mice and Human Serum at 37 °C for 2 h^a

radioiodinated biotin derivative	group 1 without HOHgBz ^b	group 2 with HOHgBz ^c	group 3 no streptavidin ^d
mouse serum ^e			
13	60.5 ± 1.9	3.0 ± 0.1	
15	1.1 ± 0.1	0.9 ± 0.1	
24	1.5 ± 0.6	1.3 ± 0.1	
25	5.2 ± 0.4	2.7 ± 0.1	
human serum ^e			
13	88.0 ± 1.1	1.1 ± 0.2	76.1 ± 2.0
15	1.2 ± 0.1	1.3 ± 0.1	79.6
24	1.0 ± 0.1	0.4 ± 0.1	86.0 ± 0.3
25	34.0 ± 0.7	2.0 ± 0.2	86.9 ± 0.2

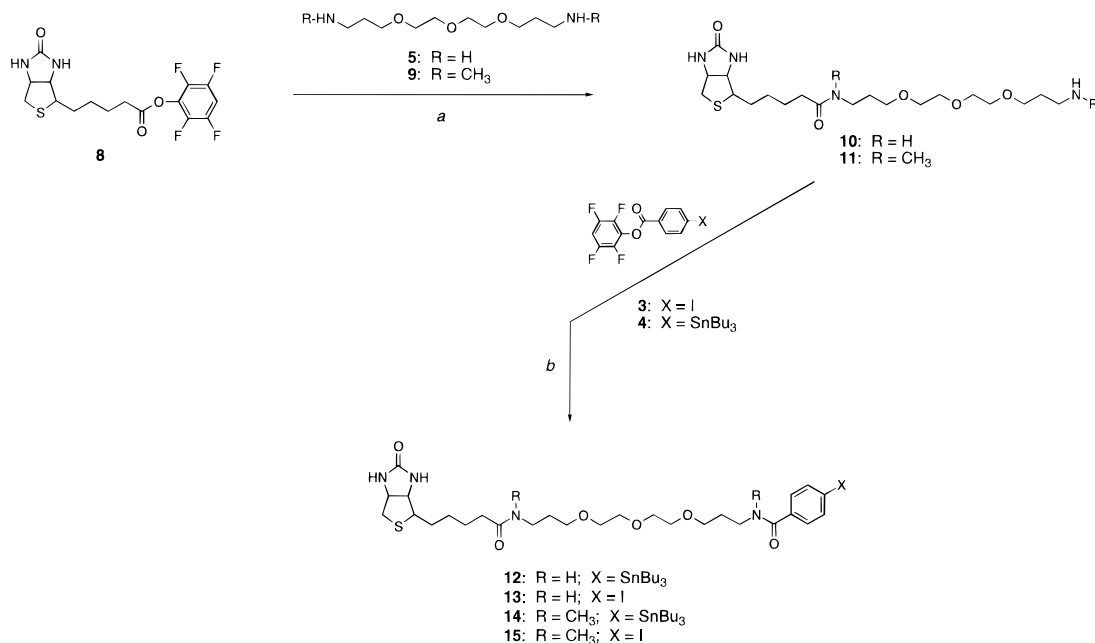
^a All values represent the percentage of radioactivity filtered in a Centricon-10 centrifugation unit (i.e., not retained by binding with r-streptavidin or nonspecifically bound). ^b Group 1 values represent percent of radioactivity filtered from diluted, but untreated, serum after an excess of r-streptavidin was added; average of three analyses ± SD. ^c Group 2 values represent activity filtered from diluted and HOHgBz treated serum after an excess of r-streptavidin was added. HOHgBz deactivates biotinidase, thus these values represent amounts not bound to streptavidin or nonspecifically bound; average of three analyses ± SD. ^d Group 3 values represent percent of radioactivity filtered from HOHgBz treated serum when no streptavidin was added; average of two analyses ± SD except for **15**. The nonspecific binding (that retained when streptavidin is not present) is obtained by subtracting the filtered values from 100%. ^e Mouse serum had been frozen and thawed twice, and human serum was fresh (refrigerated at 4 °C).

Measurement of Biotinidase Cleavage. Two separate experiments were conducted, one evaluated the degradation of [^{125]I}**13** with time (Figure 1) and the other evaluated the amount of degradation that had occurred after incubation of the radioiodinated biotin derivative for 2 h in serum (Table 2). The following general procedure was employed for both experiments. The same conditions were used when the compounds were evaluated in mice or human serum. Triplicate runs were conducted.

Biotinidase cleavage of [^{125]I}**13**, [^{125]I}**15**, [^{125]I}**24**, and [^{125]I}**25** was evaluated using the following procedure. The radiolabeled biotin derivative (in MeOH/H₂O) was diluted with H₂O to obtain approximately 3500 cpm per 10 µL in a well counter. To a tube containing 500 µL of diluted serum (1:10 with 20mM phosphate buffer, pH 6.8) was added 10 µL of the radiolabeled biotin derivative. The tube was lightly vortexed and placed in a 37 °C heating block. After the desired time (e.g., 2 h), 40 µL of 2 mM 4-(hydroxymercuri)benzoic acid (HOHgBz) sodium salt

Scheme 1. Synthesis of Tetrafluorophenyl Esters of *p*-Iodobenzoic Acid and *p*-Tri-*n*-butylstannylbenzoic acid, and Their Reaction with 4,7,10-Trioxa-1,13-tridecanediamine


^a **1**, EtOAc, EDC, TFP-OH, rt, 16–24 h, 87%. ^b **3**, toluene, (Bu₃Sn)₂, [(C₆H₅)₃P]₄Pd(0), Δ, 6 h, 73%. ^c **3** or **4**, DMF, **5**, Et₃N, 1.5 h, 44/99%.

Scheme 2. Synthesis of Benzoyltrioxadamine-Biotin Derivatives


^a **9**, DMF, Et₃N, 2 h, 25%. ^b **3** or **4**, DMF, Et₃N, 2–16 h, rt, 74–80%.

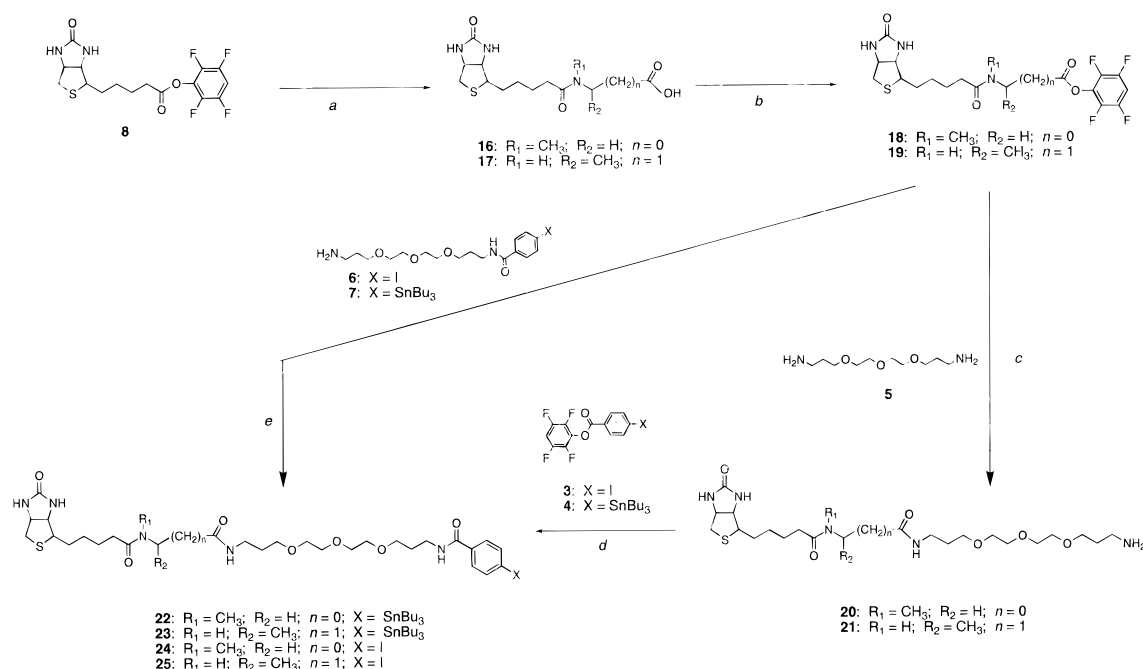
in H₂O was added to inhibit biotinidase. Following this, an excess of streptavidin (40 μL; 0.24 mg) was added, and the mixture in serum was incubated at 37 °C for another 30 min. The solution was transferred to a Centricon-10, which had been prerinsed with 20 mM phosphate buffer and was centrifuged at 3000g for 30 min. The nonfiltered material was washed with 0.5 mL of phosphate buffer, followed by 3 × 0.2 mL of H₂O, concentrating by centrifugation each time. The top and bottom (containing filtrate and washes) of the Centricon-10 were counted in a well counter after each washing to determine that no further rinsing of radioactivity was occurring. The ratio of nonbound counts (bottom) to the total counts (top and bottom) was calculated to determine the percent of the biotin derivative that had been cleaved. As a control, this procedure was repeated as above except that the HOHgBz was added prior to the radiolabeled biotin derivative to inhibit biotinidase activity.

Nonspecific binding of the radiolabeled biotin derivatives in human serum was also determined using Centricon-10 concentrators. In that evaluation, each of the radioiodinated biotin derivatives [i.e., [¹²⁵I]**13**, [¹²⁵I]**15**, [¹²⁵I]**24**, and [¹²⁵I]**25**] was diluted to give approximately 5000 counts/10 μL solution. The experimental procedure

was the same as described above, except the serum was deactivated with HOHgBz prior to addition of the radioiodinated biotin derivative and no streptavidin was added. The percentages of radioactivity filtered (i.e., not retained) in deactivated human serum without adding streptavidin are listed in Table 2 (group 3). Nonspecific binding (amount retained) is calculated by subtracting the values in Table 2, group 3, from 100%.

RESULTS

Synthesis of Biotin Derivatives. The biotin derivatives shown in Chart 1 were synthesized as outlined in Schemes 2 and 3. The *p*-tri-*n*-butylstannylbenzoyl derivatives **12**, **14**, **22**, and **23** were prepared as precursors to the radioiodinated biotin derivatives and the *p*-iodobenzoyl derivatives **13**, **15**, **24**, and **25** were prepared for use as HPLC reference standards. Incorporation of the *p*-tri-*n*-butylstannylbenzoyl- and *p*-iodobenzoyl moieties into the biotin derivatives required a fair quantity of these materials. While *p*-iodobenzoyl chloride was commercially available, the stannylbenzoate was not available from commercial sources. We had previously

Scheme 3. Synthesis of Benzoyltrioxadiazine-Sarcosine-Biotin Derivatives and Benzoyltrioxadiazine-Amino-butyryl-Biotin Derivatives

^a(**16**) sarcosine methyl ester, DMF, Et₃N, rt, 2–3 h, 1 N NaOH/MeOH, rt, 1 h, 60%; ^a(**17**) 3-aminobutyric acid, DMF, Et₃N, rt, 24 h, 98%. ^b(**18**) TFP-OTFA, Et₃N, 20 min, not isolated; ^b(**19**) TFP-OTFA, DMF, Et₃N, rt, 1 h, 81%. ^c(**21**) **5**, DMF, rt, 1.5 h, 90%. ^d(**23**, **25**) **3** or **4**, DMF, Et₃N, rt, 1 h, 72%, 56%. ^e(**22**, **24**) **18**, **6**, or **7**, rt, 0.5 h, 69%, 61%.

prepared the *N*-hydroxysuccinimidyl (NHS) and tetrafluorophenyl (TFP) (**36**) esters of *p*-tri-*n*-butylstannylbenzoate by a synthesis that employed the methyl ester of *p*-bromobenzoate (**37**). For the syntheses of biotin derivatives, the TFP ester was preferred as it is more stable to hydrolysis and provided good aminolysis yields. Rather than using the method employing stannylation of the methyl ester followed by hydrolysis and re-esterification with tetrafluorophenol (TFP-OH), we investigated the stannylation reaction with the TFP ester of *p*-iodobenzoate, **3**, as shown in Scheme 1. This approach had been described previously (**38**), but experimental methods were not reported. Preparation of **4** was accomplished on a large scale in 64% overall yield from *p*-iodobenzoic acid.

Preparation of the stannylbenzoylbiotin derivative **12** and its iodinated counterpart **13** were accomplished in three synthetic steps in 62 and 69% (respectively) overall yields as shown in Scheme 2. Synthesis of the *N,N*-dimethyl counterparts to **12** and **13**, biotin derivatives **14** and **15**, were not as facile, most likely due to the lower reactivity of the secondary amines in the aminolysis reactions. To prepare biotin derivatives **14** and **15**, a synthesis of the dimethyl analog of commercially available 4,7,10-trioxo-1,13-tridecanediamine, **5**, was required. Methylation was accomplished by reaction of **5** with ethyl formate to prepare the *N,N*-trioxatridecane diformamide, followed by subsequent reduction of the formamide groups with borane-methyl sulfide to yield **9**.

The synthesis of the *N*-methylglycine (sarcosine) containing biotin derivatives **22** and **24** is depicted in Scheme 3. Direct coupling of biotin with sarcosine was attempted under a number of reaction conditions, but low yields were obtained. In contrast to this, the methyl ester of sarcosine gave very good yields in the coupling reaction. Once coupled, the methyl ester was readily hydrolyzed with 1 N NaOH in MeOH, providing an overall yield of the sarcosine-biotin adduct **16** of about 60%. The next synthetic step, preparation of the TFP ester of **16** was also fraught with difficulties. Monitoring the reaction

by HPLC showed that a single new species was prepared when the transesterification reagent **2** was added, but upon removal of the solvent, a mixture of compounds was obtained in which the initially formed species was a minor component. On the basis of those results, coupling of the trioxadiazine **5** without isolation of the TFP ester **18** was attempted. To avoid making the biotin dimer in the coupling reaction of **18** with **5**, a large excess of **5** was used. Although the conjugation reaction was high yielding (by HPLC analysis), separation of the excess **5** from the desired biotin adduct **20** proved to be difficult. Therefore, it was decided that the trioxadiazine **5** might be coupled with the iodobenzoate **3** and stannylbenzoate **4** to form **6** and **7** (Scheme 1) prior to conjugation with **18**. Preparation of **6** was accomplished in low yield (44%) due to difficulties of separating **5** from **6**, but an excellent yield (99%) of **7** was obtained due to the relative ease of separating the more lipophilic tri-*n*-butylstannyl derivative from **5**. Conjugation of **6** and **7** with *in situ* generated **18** was facile, resulting in 61–69% isolated yields of **24** and **22**.

Synthesis of biotin derivatives **23** and **25** which contain an α -methyl adjacent to the biotin carboxamide group is also depicted in Scheme 3. Unlike the reactions with sarcosine, synthesis of **23** and **25** were straightforward, being synthesized in five synthetic steps to give 40–51% overall yields. Reaction of 3-aminobutyric acid with the TFP ester of biotin **8** resulted in nearly quantitative yield of **17**. The TFP ester **19** was formed in high yield and could be isolated without difficulty. Coupling of **19** with **5** was facile and purification of the resultant **21** was readily achieved. Reaction of **21** with the TFP benzoate esters **3** and **4** gave **25** and **23** in good yields.

Iodination/Radioiodination of Biotin Derivatives. Iodination reactions were conducted with the stannylbenzoylbiotin derivatives **12**, **14**, **22**, and **23** prior to conducting the radioiodination reactions. Upon iodination, all of the stannylbenzoatebiotin derivatives provided only one new peak on the HPLC chromatograms. In each case, the new peak coeluted with the iodobenzoate-biotin

derivative (**13**, **15**, **24**, or **25**) corresponding to the starting stannylbenzoylbiotin used.

Radioiodinations of the stannylbenzoylbiotin derivatives, **12**, **14**, **22**, and **23** were conducted at no-carrier-added (*nca*) levels of Na^{125}I in MeOH using *N*-chlorosuccinimide (NCS) as the oxidant. In the initial studies, *nca* radioiodinations were carried out on >98% pure stannylbenzoylbiotin derivatives. Interestingly, the radioiodination reactions of **12**, **14**, and **22** resulted in radioiodinated compounds that had retention times which were close to the iodinated standards, but did not coelute with them. Further, the initial radioactive peaks seen on HPLC analysis were transformed to more hydrophilic species within 30 min of isolation (as observed when reinjected onto the HPLC).³ We felt that there were a number of possible explanations for the apparent instability of radioiodinated material, but it seemed most likely that a radioiodinated impurity had been isolated rather than the desired product(s). The radioiodination of **22** gave a product which coeluted with the iodinated standard, but the yield was uncharacteristically low. Subsequently, 1 mg quantities of stannylbenzoate derivatives were highly purified (>99.5%) by multiple injections/isolations from an analytical HPLC column and were used in the radioiodination reactions. Use of the highly purified stannylbenzoylbiotin derivatives resulted in obtaining reasonable yields (24–76%) of *nca* radioiodinated products which coeluted with the iodobenzoylbiotin standards. The radioiodinated compounds obtained from the highly purified stannylbenzoylbiotin derivatives were stored at 4 °C for several weeks. In general, the compounds were found to be stable during storage. However, in one preparation of ^{125}I **24**, another compound slowly grew in with time. The new radioiodinated species formed had a HPLC retention time that indicated it might be the biotin sulfoxide.

Streptavidin Binding. An evaluation of the binding of two radioiodinated biotin derivatives, **13** and **24**, with streptavidin was conducted to demonstrate that 4 equiv bound, and to determine if nonspecific binding would be a problem in the biotinidase assay. Only biotin derivatives **13** and **24** were investigated as it was thought that the binding of the α -methyl biotinamide **25** should be similar to **13**, and the *N*-methyl biotinamide **15** should be similar to **24**. In the experiment, solutions of the nonradioactive biotin derivative (**13** or **24**) were mixed with tracer quantities of the same radioiodinated biotin derivative. From these stock solutions, varying quantities of the biotin derivative were added to three tubes containing a set amount of streptavidin. Quantities of the biotin derivative that were less than required to saturate the biotin binding sites on streptavidin were placed in two of the three tubes, and an excess of the biotin derivative was added to the third tube. The tubes were incubated for 1 h at room temperature, then the contents of each tube was transferred to a centrifuge filtration tube. After concentration and three washes with phosphate buffer, the top and bottom of the cen-

trifugation filter were counted separately in a well counter. The results, expressed as percent activity filtered (i.e., activity in filtrate plus three washes) are shown in Table 1. Since less than 4 equiv of each biotin derivative were added to some of the tubes containing r-streptavidin, it was expected in those examples that very little activity would pass through the centrifugation membrane. Indeed, in each tube containing less than the quantity of biotin derivative necessary for saturation of streptavidin (i.e., 8 nmol), only 3% of the activity passed through the membrane filter. Importantly, in those examples where an excess of biotin derivative was added, the amount in excess of 4 equiv filtered readily. The calculated excess percentages (33% for **13** and 21% for **24**) were very close to the amounts filtered, indicating that there was very little if any nonspecific binding with streptavidin or the filtration membrane. The lack of nonspecific binding to the centrifugation filtration membrane and plastic parts was dramatically shown in that less than 0.5% of **13** and **24** were retained when centrifuged without streptavidin.

Biotinidase Assay. Biotinidase activity results in cleavage of the amide bond linking biotin with the portion of the molecule containing the radiolabel. Therefore, biotinidase activity can be measured by evaluation of the amount of radioactivity that binds with an excess quantity of r-streptavidin after incubation in serum. In the initial experiment examining biotinidase activity, the biotin derivative **13**, which did not contain a biotinidase blocking group, was incubated in dilute (10%) mouse serum at 37 °C for 2 h. Aliquots were taken at various time points and biotinidase activity was stopped with the addition of hydroxymercuribenzoic acid (HOHgBz), a chemical which is known to deactivate biotinidase (**32**). As a control, an equivalent sample of **13** was incubated in mouse serum that had been pretreated with HOHgBz. The results of a triplicate analyses for those studies are shown graphically in Figure 1. The results indicated that the biotinidase activity in mouse serum increased almost linearly over the 2 h period.

Following the initial study with **13**, evaluations of the stability of the water solubilized, *N*-methyl and α -methyl containing biotin derivatives **15**, **24**, and **25** toward biotinidase degradation were conducted. Since the most important issue to be determined was whether complete blocking of biotinidase activity could be obtained in the derivatives, it was only necessary to evaluate the biotinidase cleavage reaction (e.g., amount of radioactivity that did not bind with r-streptavidin) at a single time point. We chose to incubate for 2 h since over 50% specific cleavage⁴ had been seen at 2 h when **13** was incubated in dilute serum. In the analysis of each biotin derivative (i.e., **15**, **24**, and **25**), equivalent samples of nonstabilized biotin derivative **13** and the biotin derivative being tested in serum pretreated with HOHgBz were also examined. All of the biotin derivatives were evaluated in human serum as well as mouse serum. We felt that it was important to evaluate the stability in mouse serum as our preclinical studies involving radiolabeled biotin derivatives in tumor pretargeting use athymic mice containing human tumor xenografts. It seemed equally important to evaluate the derivatives in human serum as the biotin derivatives are ultimately being developed for use in applications of human cancer therapy. The results of triplicate bioassays involving biotin derivatives

³ The radioactivity peak on the HPLC had a shorter retention time (t_R) than expected in each radioiodination reaction. For example, in the radioiodination of **12** the iodo standard, **13**, had a $t_R = 7.0$ min by UV detection, whereas the major radioactive peak had a $t_R = 7.1$ min. Due to the distance between the UV detector and the radioactivity detector on the HPLC used, the t_R should be 0.3 min longer for the radioactive peak than the UV peak (previously determined). Reinjection of the isolated radioactivity (from peak at 7.1 min) after 30 min showed that the radioactive material had changed to one that eluted at $t_R = 2.0$ min. This change in t_R most likely indicated that the radioiodine was not stably attached to the compound isolated.

⁴ Specific cleavage is defined as the amount of radioactivity not bound with r-streptavidin after incubation for 2 h minus the amount of radioactivity not bound with r-streptavidin when HOHgBz is added prior to incubation.

13, **15**, **24**, and **25** are provided in Table 2. The nonspecific binding of radioiodinated biotin derivatives in serum was assessed by the measuring the quantity of radioiodinated derivative retained when no r-streptavidin is present. That value is obtained by subtracting the amount filtered (from Table 2) from 100%.

DISCUSSION

The primary purpose of this study was to gain information that would aid our development of radioiodinated biotin derivatives for application to radiotherapy of cancer using an antibody tumor "pretargeting" approach (8). It was apparent from initial studies that the biotin derivatives being developed needed to have improved water solubility. It also became apparent that the biotin derivatives synthesized needed to be designed in a manner that blocked the serum enzyme biotinidase (18, 22). Thus, the design of new biotin derivatives to be used in our studies had to incorporate functional groups which (1) permitted radioiodination, (2) improved water solubility, and (3) blocked biotinidase activity.

An important consideration in the design of the new biotin derivatives was the functionality to be used to introduce radioiodine. As with all radioiodination reactions, it was desired that the radioiodine be introduced into the biotin derivatives in the last synthetic step, which meant that a iodine reactive intermediate had to be prepared. Some investigators have used biotin derivatives which contained phenolic moieties, such as tyrosine or tyramine, to allow incorporation of radioiodine (12). However, concern that mixtures of mono- and diiodo biotin derivatives would be obtained and concern that *in vivo* deiodination of phenolic biotin compounds would occur led us to choose an alternate labeling moiety. Our, and other investigators', studies have shown that radioiodinated compounds containing iodophenyl derivatives are resistant to *in vivo* deiodination (31–33), so iodoaryl-biotin derivatives were chosen. Introduction of high specific activity radioiodine into a biotin derivative through the use of a triazenyl intermediate had been reported (15), but the radiochemical yields were low. An alternative, more facile and higher yielding reactive intermediate was desired. Stannylbenzoyl intermediates were chosen for radioiodination of biotin because these intermediates had been used previously in many other applications and had proven to be facile and high yielding in radioiodination reactions. In the initial experiments with the stannylbenzoate derivatized biotin derivatives, radioiodinated products were obtained which appeared (by HPLC retention times) to be unstable. The identity of the unstable compounds were not determined because purification of the stannylbenzoate precursors resulted in obtaining the desired radioiodinated biotin derivatives. We were concerned about the potential for oxidation of the biotin thioether (to sulfoxide or sulfone) in the iodination reactions, but this had not been reported as a problem in a previous investigation using tri-*n*-butylstannyl-anilide as the moiety for radioiodination (17). To assure ourselves that the sulfoxide derivatives were not formed under the conditions of radioiodination, oxidation of **13** was conducted in HOAc with H₂O₂ to provide a biotin sulfoxide standard for HPLC analysis.⁵ Indeed, the HPLC retention time for the biotin sulfoxide derivative clearly ruled out formation of the sulfoxide in the iodination reaction. After purification of the stannylbenzoate intermediates, radioiodinated biotin derivatives were obtained which coeluted with the iodinated standards. Although the radiochemical yields were lower than anticipated, radioiodination of tri-*n*-butylstannylbenzoate derivatives, **12**, **14**, **22**, and **23**, resulted in

acceptable yields (24–76%) of isolated biotin derivatives ([¹²⁵I]**13**, [¹²⁵I]**15**, [¹²⁵I]**24**, and [¹²⁵I]**25**).

Although water solubilization of biotin derivatives had been largely ignored in previously reported radiohalogenated biotin derivatives, we felt that this was a very important aspect of the design of new derivatives. Many different water solubilizing linkers can be envisioned, however, we addressed the issue of increasing the water solubility by incorporating a neutral, nonionic, ether containing linker between the biotin moiety and the aryl moiety in the biotin derivatives of interest. In addition to providing water solubilizing properties, the linker (4,7,10-trioxa-1,13-tridecanediamine) provided a 17 Å spacer⁶ between the biotin carboxylate and the radioiodination moiety. There have been many examples demonstrating that the binding avidity of biotin derivatives with avidin and streptavidin remains high when a linking molecule is used between the biotin carboxylate and the coupled compound (40).

The most important aspect of the design of new biotin derivatives is modification such that serum biotinidase does not cleave biotin from the rest of the molecule. The new biotin derivatives could not be used for *in vivo* applications without being stable in the presence of biotinidase. Literature reports provided insight into the types of modifications that might be used to make water solubilized, radioiodinated biotin derivatives stable to biotinidase activity. It is important to note that biotinidase is not confined to a particular tissue, rather it is found in many tissues, with its activity being high in liver, kidney, adrenal glands, and serum (18, 22). Biotinidase appears to be involved in the transport and cellular uptake of biotin, and may function as a biotinyl transferase to biotinylate specific proteins or small molecules (24), but the function that is important in developing new biotin derivatives is its role in conserving biotin in the body by cleaving biotin from its lysine adduct, biocytin. Biocytin is produced upon catabolism of the four biotin-dependent enzymatic peptide carboxylases which utilize it in their catalytic active site (41). It has been reported that human serum biotinidase is specific for cleavage of the lysine portion of biocytin, and the fact that other biotin derivatives such as biotinylphenylalanine, biotinyl- ϵ -aminocaproic acid, and biotinyl- γ -amino-*n*-butyric acid were not cleaved (22) tends to support this concept. However, the amide cleaving action of biotinidase cannot be truly specific to lysine since cleavage is observed with conjugated *p*-aminobenzoic acid and iodotyramine (42), as well as with L-lysine. Thus, it seems unlikely that simply changing the lysine to another amine containing molecule would block the action of biotinidase. Importantly, other investigators have re-

⁵ Formation of the biotin sulfoxide of **13** was accomplished using the reaction conditions reported by Melville (39). The H₂O₂ oxidation reaction with **13** resulted in formation of a single product; *t*_R = 11.0 min using Gradient I (*t*_R = 11.9 min for **13**). The retention difference of **13** and the oxidized product (i.e., biotin sulfoxide) using the HPLC conditions for radioiodinated biotin derivatives was much more pronounced: **13**, *t*_R = 10.7 min and oxidized product, *t*_R = 6.3 min. Investigation of the oxidation of **13** with NCS was also conducted. After 24 h with 1 equiv of **13** and NCS in MeOH/HOAc, there was about 22% of the same oxidized product (by coinjection on HPLC) as formed with H₂O₂. In the time period similar to the radioiodination reaction (i.e., 10 min), none of the oxidized product was seen.

⁶ This value is the distance between the two nitrogen atoms in the fully linearized 4,7,10-trioxa-1,13-tridecanediamine. The distance was obtained from the computer program ChemDraw 3D (CambridgeSoft Corp.) after structural and energy minimization.

ported that some simple modifications of biotin derivatives block biotinidase activity. For example, amide cleavage appears to be sensitive to steric encumbrance near the biotin carboxylate. Biotin conjugated with the amine of *p*-aminobenzoic acid (PABA) is readily cleaved by biotinidase, but *m*-aminobenzoic acid is cleaved at only 10% of the rate of PABA, and *o*-aminobenzoic acid does not appear to be cleaved (22). Other parameters such as the distance from the ring structures of biotin to the carboxylate amide appear to also be important as shortening the aliphatic side chain decreases the activity to 2% of the unaltered rate when PABA conjugates are studied (22).

Three of the new radioiodinated biotin derivatives were chemically modified near the biotin carboxylate to block the amidase action of biotinidase. Although it was known that alterations in the biotin moiety would decrease biotinidase activity, we chose to leave biotin unaltered with the exception of conjugation of the carboxylate with an amine containing moiety. It was felt that modification of biotin would likely result in a decreased binding with streptavidin. The early studies of Rosebrough indicated that an α -carboxylate group (from a cysteinyl linked biotin) was efficient at blocking cleavage of defero-acetyl-cysteinyl-biotin by biotinidase (26, 27). However, our desire to use the water solubilizing trioxatridecanediamine linker made the cysteinyl derivative unattractive for our studies. We felt that an α -methyl group from the biotin adduct with 3-aminobutyric acid might provide similar steric hindrance to that of an α -carboxyl group, so biotin derivative **25** was targeted for synthesis and evaluation. The results obtained suggest that the α -methyl group does not provide enough steric hindrance to completely block biotinidase activity. For the purposes of these studies we chose to limit the number of biotin derivatives synthesized. However, based on the results with the α -methyl substituted biotin adduct **25**, it would be of interest to synthesize and compare a biotin-aspartic acid adduct, which would be equivalent to **25**, except it would have an α -carboxylate group.

The reports that the sarcosine (*N*-methylglycine) adduct of biotin completely blocked biotinidase activity (28, 29) led to targeting the radioiodinated biotin derivative **24** for synthesis and evaluation. Although **24** was prepared, the difficulties encountered in that synthesis led to the desire to prepare an additional *N*-methyl biotin derivative. From a limited survey of commercial sources, it appeared that there were very few commercially available *N*-methyl compounds that could be used as linkers. The *N*-methyl compounds that were available from commercial sources were not attractive for our studies as we felt that they would not provide enough water solubilization for the biotin derivatives, nor did they provide the spacer distance we were seeking. This led to consideration of synthesizing a *N*-methylamine or *N,N*-dimethyldiamine derivative for use as a linker molecule. Interestingly, synthesis of a biotin-psoralen adduct containing a *N,N*-dimethylhexanediamine linker had been previously reported (43), but it was thought that such an aliphatic linker would decrease water solubility of biotin derivatives. These considerations prompted us to synthesize *N,N*-dimethyl-4,7,10-trioxa-1,13-tridecanediamine, **9**, and to use it in the synthesis of radioiodinated biotin derivative **15**.

Biotinidase activity was measured utilizing centrifugation concentrators which retain molecules with a molecular mass over 10 kDa. Incubation of the radioiodinated biotin derivative [¹²⁵I]**13** at 37 °C in 10% mouse serum displayed nearly linear cleavage by biotinidase over a 2 h time period (Figure 1). Deactivation of biotinidase with

HOHgBz prior to incubation showed that the cleavage was specific. To measure biotinidase stability of biotin derivatives [¹²⁵I]**13**, [¹²⁵I]**15**, [¹²⁵I]**24**, and [¹²⁵I]**25**, each was incubated in diluted mouse or human serum at 37 °C for 2 h. After incubation in serum, an excess of streptavidin was added to bind with biotin. The assay solutions containing serum, streptavidin, and radiolabeled biotin were then filtered through a size exclusion centrifugation membrane and rinsed with PBS and water. The radioactivity that went through the membrane represents that activity which was no longer attached to biotin. To demonstrate that the activity penetrating the membrane was due to biotinidase cleavage, pretreatment with HOHgBz was conducted. Additionally, to examine whether the biotin derivatives might bind nonspecifically in serum and/or on the membrane, centrifugation without added streptavidin was conducted. The results of the biotinidase activity assay are provided in Table 2. It is apparent that the radioiodinated biotin derivative which had no functional group for blocking serum biotinidase (i.e., **13**) was rapidly degraded by biotinidase. It was equally apparent that the biotin derivatives containing *N*-methylbiotinamide functionalities (i.e., **15** and **24**) were very stable to biotinidase degradation. Interestingly, the α -methyl biotinamide functionality (i.e., **25**) was found to be relatively stable in mouse serum, but was cleaved at an intermediate rate in human serum. It is not known why there is such a difference in rate of cleavage in the two types of serum, but it may be due to differences in the way the serum was handled. It has been reported that mouse serum biotinidase is less active than human serum biotinidase (18), but perhaps more important is the fact that the mouse serum used was frozen and thawed twice whereas the human serum was fresh (refrigerated). Freeze-thawing is reported to decrease biotinidase activity (22).

In addition to the biotin derivatives prepared and evaluated in this study, a large number of other biotin derivatives can be envisioned which are likely to block biotinidase activity *in vivo*. It seemed obvious that biotinidase activity could be completely blocked if the biotin amide were reduced to an amine. Therefore, as part of this investigation, the biotin-trioxadamine adduct **10** was reduced with borane-methyl sulfide to give the secondary amino derivative. That compound was subsequently reacted with the TFP esters, iodobenzoate, **3**, and stannylbenzoate, **4** (unreported results). Although these biotin derivatives had improved water solubility, they were difficult to purify and were found to be unstable upon storage, so this derivative was not investigated further. The literature also suggests that shortening the pentanoic acid side chain in biotin will cause a blockage of biotinidase activity (22). Therefore, compounds such as the norbiotinamine and its isothiocyanato derivative (44) might be used to prepare compounds that are stable to biotinidase activity.

The goal of these studies was to obtain information with regards to biotin modifications and biotinidase stability, but it is also important to consider how modifications to biotin derivatives affect their binding with streptavidin or avidin. Since bulky substituents attached directly to the biotin carboxylate decrease binding with avidin, it might be expected that biotin derivatives containing bulky substituents adjacent to the carbonyl group, such as *N*-methyl derivatives and α -methyl groups, could result in decreased binding. Therefore, we are planning to evaluate the dissociation kinetics (44) of the compounds described herein to determine the effect on binding with r-streptavidin brought about by the modi-

fications. If the binding is greatly decreased, then additional biotin derivatives designed to block biotinidase activity will be prepared and evaluated.

Summary. In this study, four radioiodinated, water solubilized, biotin derivatives were evaluated for their stability toward degradation in serum by the enzyme biotinidase. The biotin derivative which had a simple amido bonded biotin, **13**, was found to be unstable in both mouse and human serum when incubated at 37 °C. Two biotin derivatives, **15** and **24**, which contained *N*-methyl-amido bonded biotin were found to be very stable toward degradation of biotinidase, similar to other previously reported biotin derivatives. In contrast to the *N*-methyl derivatives, a biotin derivative, **25**, which contained a methyl group α to the biotin amido linkage was not stable to biotinidase, but was degraded at a slower rate than **13**. The use of high specific activity radioiodinated biotin derivatives (^{125}I **13**, ^{125}I **15**, ^{125}I **24**, and ^{125}I **25**) made the evaluation of their *in vitro* stability relatively easy. The radioiodinated biotin derivatives were readily prepared from *p*-tri-*n*-butylstannylbenzoyl biotin derivatives (**12**, **14**, **22**, and **23**), but not without being highly purified on the HPLC. In addition to the biotinidase stabilizing functionalities in the biotin derivatives studied, a water solubilizing linker moiety was incorporated into each compound.

ACKNOWLEDGMENT

We thank Dr. Robert Vessella and Kent Buhler for providing the mouse and human serum used in these studies. We thank Dr. Patrick Stayton and Lisa Klumb for providing r-streptavidin used in the studies and for their helpful comments on the manuscript. We are grateful for the generous financial support provided by the Department of Energy, Medical Applications and Biophysical Research Division, Office of Health and Environmental Research under Grant DE-FG06-95ER62029.

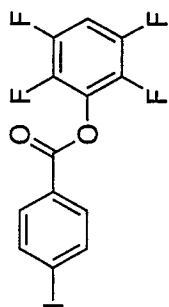
Supporting Information Available: HPLC chromatograms and ^1H NMR spectra of the new compounds prepared in the research described in this manuscript (34 pages). Ordering information is given on any current masthead page.

LITERATURE CITED

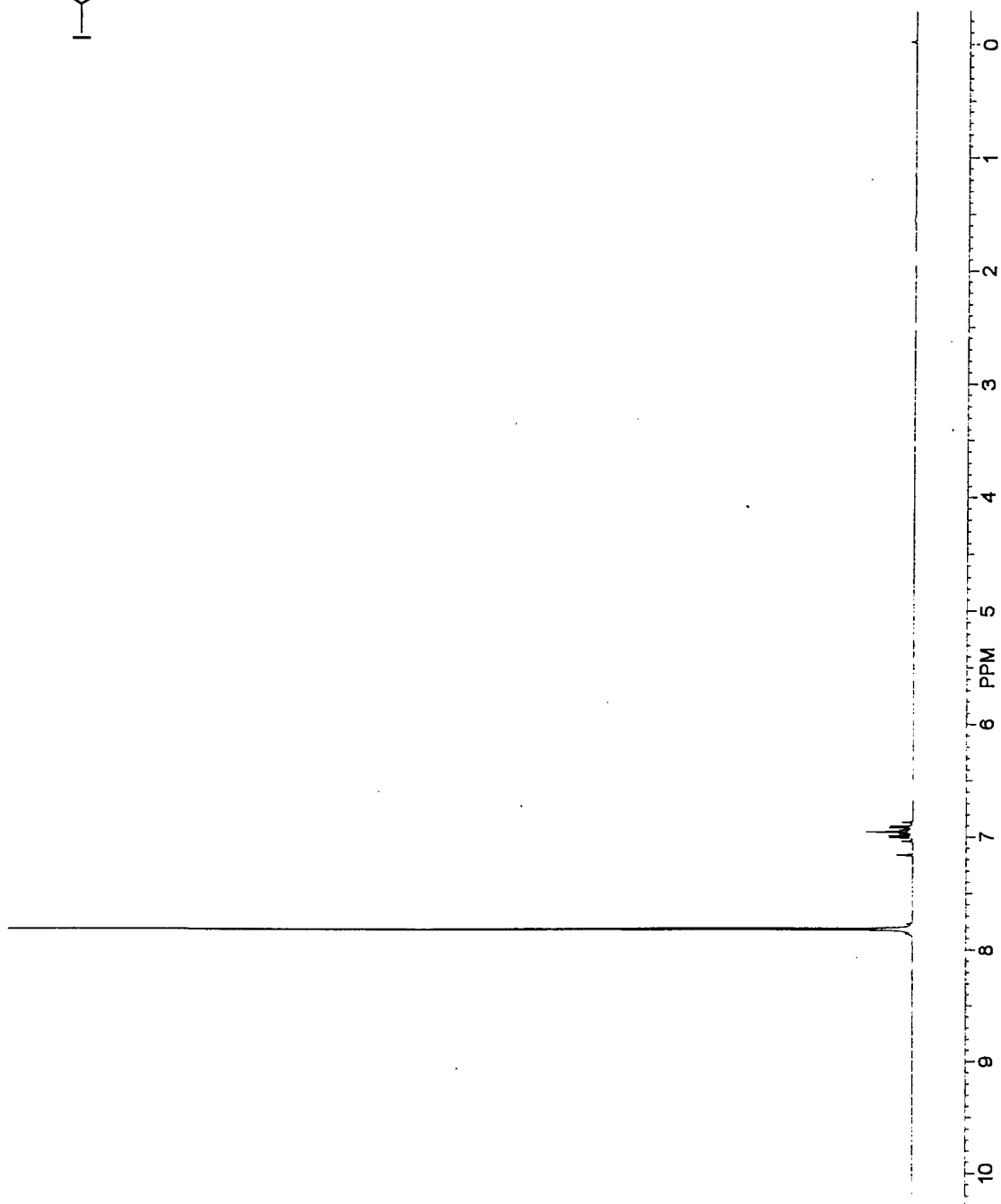
- (1) Green, N. M. (1975) Avidin. *Adv. Protein Chem.* **29**, 85–133.
- (2) Green, N. M. (1990) Avidin and Streptavidin. *Methods Enzymol.* **184**, 51–67.
- (3) Diamandis, E. P., and Chrostopoulos, T. K. (1991) The Biotin-(Strept)Avidin System: Principles and Applications in Biotechnology. *Clin. Chem.* **37**, 625–636.
- (4) Wilchek, M., and Bayer, E. A. (1988) The Avidin-Biotin Complex in Bioanalytical Applications. *Anal. Biochem.* **171**, 1–32.
- (5) Hnatowich, D. J., Virzi, F., and Rusckowski, M. (1987) Investigations of Avidin and Biotin for Imaging Applications. *J. Nucl. Med.* **28**, 1294–1302.
- (6) Goodwin, D. A. (1995) Tumor Pretargeting: Almost the Bottom Line. *J. Nucl. Med.* **36**, 876–879.
- (7) Paganelli, G., Malcovati, M., and Fazio, F. (1991) Monoclonal antibody pretargeting techniques for tumor localization: the avidin-biotin system. *Nucl. Med. Commun.* **12**, 211–234.
- (8) Wilbur, D. S., Hamlin, D. K., Vessella, R. L., Stray, J. E., Buhler, K. R., Stayton, P. S., Klumb, L. A., Pathare, P. M., and Weerawarna, S. A. (1996) Antibody Fragments in Tumor Pretargeting. Evaluation of Biotinylated Fab' Colocalization with Recombinant Streptavidin and Avidin. *Bioconjugate Chem.* **7**, 689–702.
- (9) Pathare, P. M., Wilbur, D. S., Heusser, S., Quadros, E. V., McLoughlin, P., and Morgan, A. C. (1996) Synthesis of Cobalamin-Biotin Conjugates That Vary in the Position of Cobalamin Coupling. Evaluation of Cobalamin Derivative Binding to Transcobalamin II. *Bioconjugate Chem.* **7**, 217–232.
- (10) Pathare, P. M., Wilbur, D. S., Hamlin, D. K., Heusser, S., Quadros, E. V., McLoughlin, P., and Morgan, A. C. (1996) Synthesis of Cobalamin Dimers Using Isophthalate Cross-Linking of Corrin Ring Carboxylates and Evaluation of Their Binding to Transcobalamin II. *Bioconjugate Chem.* **8**, 161–172.
- (11) Livaniou, E., Evangelatos, G. P., and Ithakissios, D. S. (1987) Radioiodinated Biotin Derivatives for *In Vitro* Radioassays. *J. Nucl. Med.* **28**, 1430–1434.
- (12) Groman, E. V., Rothenberg, J. M., Bayer, E. A., and Wilchek, M. (1990) Enzymatic and Radioactive Assays for Biotin, Avidin, and Streptavidin. *Methods Enzymol.* **184**, 208–217.
- (13) Khawli, L. A., and Kassis, A. I. (1992) *m*- ^{125}I Iodoaniline: a Useful Reagent for Radiolabeling Biotin. *Nucl. Med. Biol.* **19**, 297–301.
- (14) Najafi, A., and Peterson, A. (1993) Preparation and *In Vitro* Evaluation of "No-carrier-added" ^{18}F -labeled Biotin. *Nucl. Med. Biol.* **20**, 401–405.
- (15) Kortylewicz, Z. P., Baranowska-Kortylewicz, J., Adelstein, S. J., Carmel, A. D., and Kassis, A. I. (1994) Radiolabeled Biotin Amides from Triazene Precursors: Synthesis, Binding, and *In-Vivo* Properties. *J. Labelled Compd. Radiopharm.* **34**, 1129–1146.
- (16) Shoup, T. M., Fischman, A. J., Jaywook, S., Babich, J. W., Strauss, H. W., and Elmaleh, D. R. (1994) Synthesis of Fluorine-18-Labeled Biotin Derivatives: Biodistribution and Infection Localization. *J. Nucl. Med.* **35**, 1685–1690.
- (17) Foulon, C. F., Adelstein, S. J., and Kassis, A. I. (1996) One-Step Synthesis of Radioiodinated Biotin Derivatives. *Bioorg. Med. Chem. Lett.* **6**, 779–784.
- (18) Pispas, J. (1965) Animal Biotinidase. *Ann. Med. Exp. Biol. Fenn.* **43** (Suppl 5), 4–39.
- (19) Chauhan, J., Ebrahim, H., Bhullar, R. P., and Dakshinamurti, K. (1985) Human Serum Biotinidase. *Ann. NY Acad. Sci.* **447**, 386–388.
- (20) Craft, D. V., Goss, N. H., Chandramouli, N., and Wood, H. G. (1985) Purification of Biotinidase from Human Plasma and Its Activity on Biotinyl Peptides. *Biochemistry* **24**, 2471–2476.
- (21) Chauhan, J., and Dakshinamurti, K. (1986) Purification and Characterization of Human Serum Biotinidase. *J. Biol. Chem.* **261**, 4268–4275.
- (22) Wolf, B., Hymes, J., and Heard, G. S. (1990) Biotinidase. *Methods Enzymol.* **184**, 103–111.
- (23) Cole, H., Reynolds, T. R., Lockyer, J. M., Bucks, G. A., Denson, T., Spence, J. E., Hymes, J., and Wolf, B. (1994) Human Serum Biotinidase. cDNA Cloning, Sequence, and Characterization. *J. Biol. Chem.* **269**, 6566–6570.
- (24) Hymes, J., and Wolf, B. (1996) Biotinidase and its role in biotin metabolism. *Clin. Chim. Acta* **255**, 1–11.
- (25) Thoma, R. W., and Peterson, W. H. (1954) The enzymatic degradation of soluble bound biotin. *J. Biol. Chem.* **210**, 569–579.
- (26) Rosebrough, S. F. (1993) Plasma Stability and Pharmacokinetics of Radiolabeled Deferoxamine-Biotin Derivatives. *J. Pharmacol. Exp. Ther.* **265**, 408–415.
- (27) Hashmi, M., and Rosebrough, S. F. (1995) Synthesis, Pharmacokinetics, and Biodistribution of ^{67}Ga Deferoxamine-acetyl-cysteinylbiotin. *Drug Metab. Disposition* **23**, 1362–1367.
- (28) Gustavson, L. M., Su, F.-M., Reno, J. M., Axworthy, D. B., Lyen, L. J., Fritzberg, A. R., and Theodore, L. J. (1995) Design and Synthesis of Metabolically Stable Chelate-Biotin Conjugates for Pretargeted Tumor Radioimmunotherapy. Proceedings of 209th American Chemical Society Meeting, Anaheim, CA., *Med. Chem. Abstract* 010.
- (29) Su, F.-M., Gustavson, L. M., Axworthy, D. B., Lyen, L. J., Theodore, L. J., Fritzberg, A. R., and Reno, J. M. (1995)

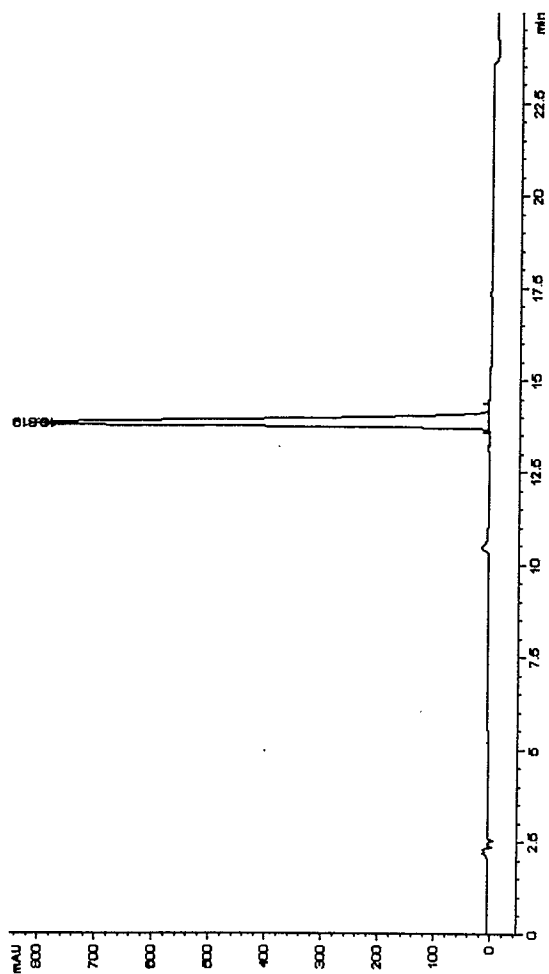
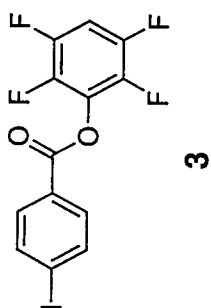
- Characterization of a New Y-90 Labeled DOTA-Biotin for Pretargeting. *J. Nucl. Med.* 36, 154P (abstract).
- (30) March, J. (1985) *Advanced Organic Chemistry: Reactions Mechanisms, and Structure*, 3rd ed., Chapter 3, pp 71–74, John Wiley & Sons, New York.
- (31) Kabalka, G. W., and Varma, R. S. (1989) The Synthesis of Radiolabeled Compounds Via Organometallic Intermediates. *Tetrahedron* 45, 6601–6621.
- (32) Wilbur, D. S. (1992) Radiohalogenation of Proteins: An Overview of Radionuclides, Labeling Methods, and Reagents for Conjugate Labeling. *Bioconjugate Chem.* 3, 433–470.
- (33) Ali, H., and van Lier, J. E. (1996) Synthesis of Radiopharmaceuticals via Organotin Intermediates. *Synthesis* 423–445.
- (34) Wolf, B., and McVoy, J. S. (1983) A sensitive radioassay for biotinidase activity: deficient activity in tissues of serum biotinidase-deficient individuals. *Clin. Chim. Acta* 135, 275–281.
- (35) Gamper, H. B., Reed, M. W., Cox, T., Viroso, J. S., Adams, A. D., Gall, A. A., Scholler, J. K., and Meyer, R. B. (1993) Facile preparation of nuclease resistant 3' modified oligodeoxynucleotides. *Nucleic Acids Res.* 21, 145–150.
- (36) Hadley, S. W., Grant, L. M., and Wilbur D. S. (1987) Evaluation of Radioiodinations and Conjugations of 4-Iodobenzoates for Protein Labeling. *J. Nucl. Med.* 28, 725 (abstract).
- (37) Wilbur, D. S., Hadley, S. W., Hylarides, M. D., Abrams, P. G., Beaumier, P. A., Morgan, A. C., Reno, J. M., and Fritzberg, A. R. (1989) Development of a Stable Radioiodinating Reagent to Label Monoclonal Antibodies for Radiotherapy of Cancer. *J. Nucl. Med.* 30, 216–226.
- (38) Shen, X., Hanson, R. N., and Elmaleh, D. R. (1991) Synthesis and Evaluation of Radioiodinated Tetrafluorophenyl m-Iodobenzoate and Tetrafluorophenyl-5-iodopentenoates as Conjugation Agents for Proteins and Antibodies. *J. Labelled Compd. Radiopharm.* 30, 222–223 (abstract).
- (39) Melville, D. B. (1954) Biotin Sulfoxide. *J. Biol. Chem.* 208, 495–501.
- (40) Wilchek, M., and Bayer, E. A. (1990) Biotin-Containing Reagents. *Methods Enzymol.* 184, 123–138.
- (41) Bonjour, J. (1985) Biotin in Human Nutrition. *Ann. NY Acad. Sci.* 447, 97–104.
- (42) Evangelatos S. A., Kakabakos S. E., Evangelatos G. P., and Ithakissios D. S. (1993) Determination of Serum Biotinidase Activity with Biotinyl Derivatives of Iodotyramines as Substrates. *J. Pharm. Sci.* 82, 1228–1231.
- (43) Elsner, H. I., and Mouritsen, S. (1994) Use of Psoralens for Covalent Immobilization of Biomolecules in Solid Phase Assay. *Bioconjugate Chem.* 5, 463–467.
- (44) Szalecki, W. (1996) Synthesis of Norbiotinamine and Its Derivatives. *Bioconjugate Chem.* 7, 271–273.
- (45) Chilkoti, A., and Stayton, P. S. (1995) Molecular Origins of the Slow Streptavidin-Biotin Dissociation Kinetics. *J. Am. Chem. Soc.* 117, 10622–10628.

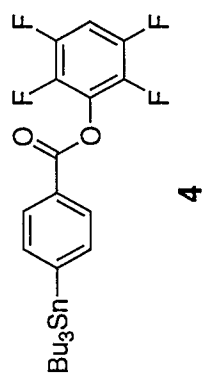
BC9700852



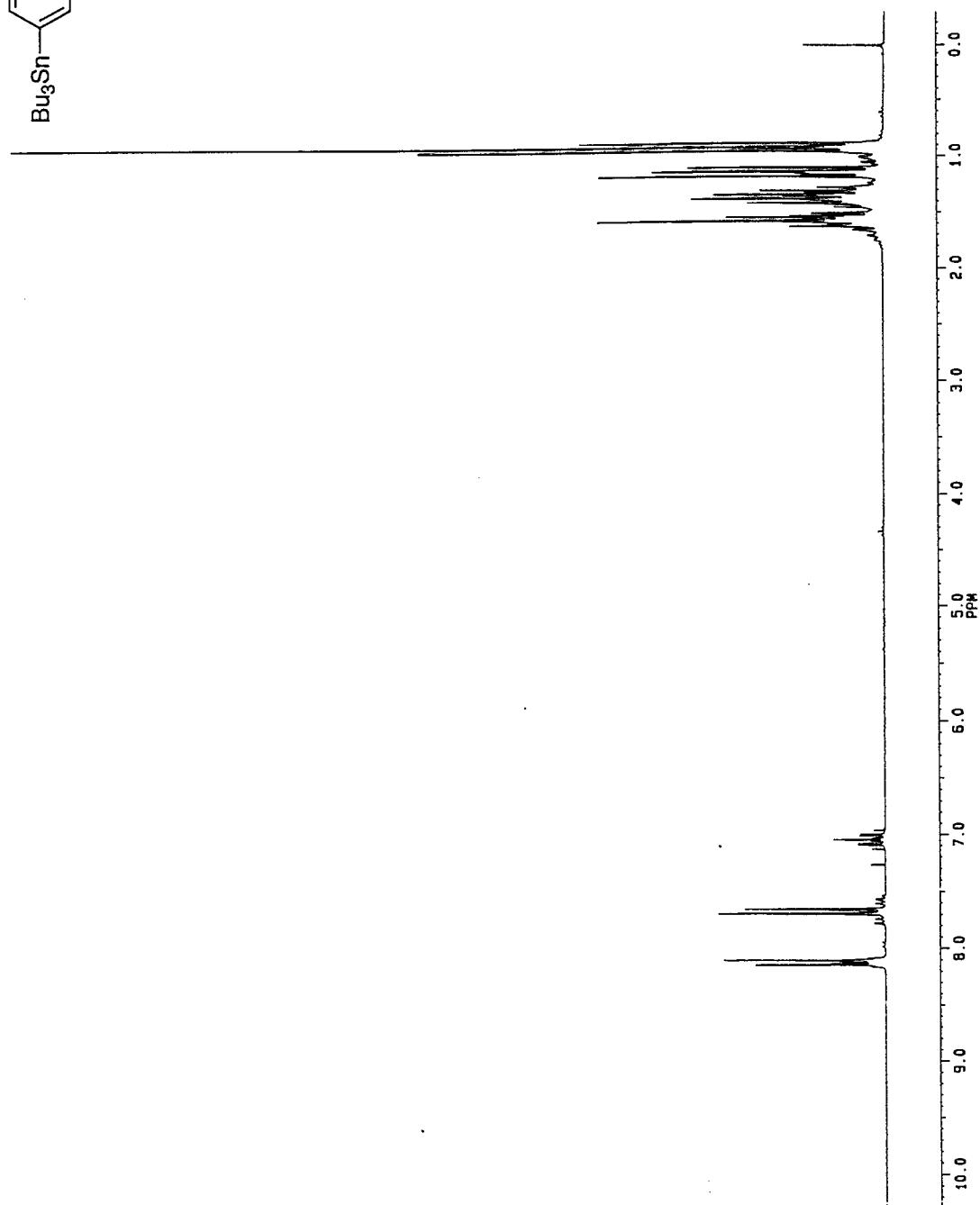
3

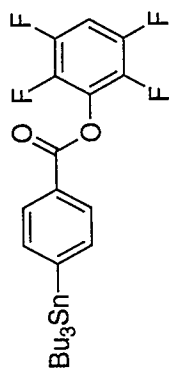




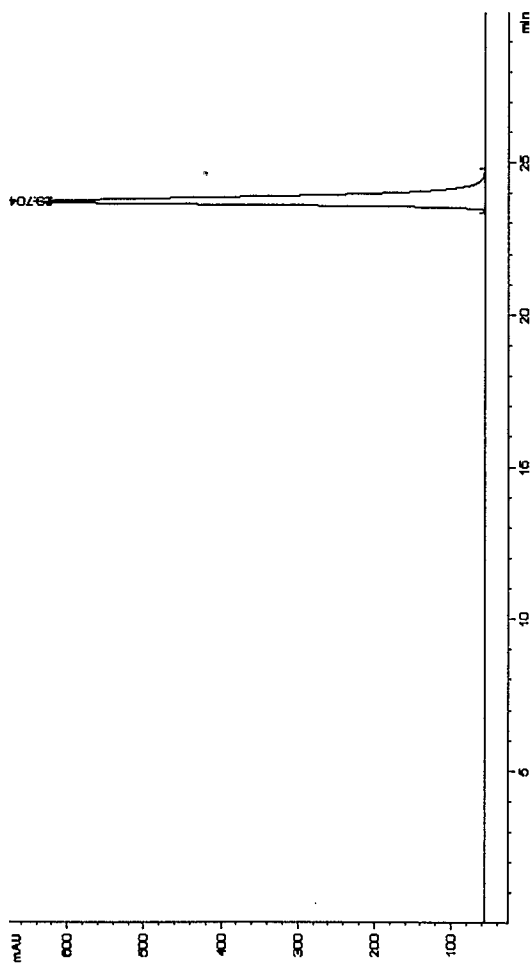


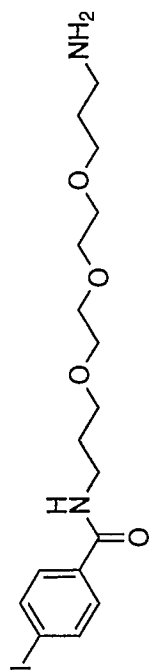
4



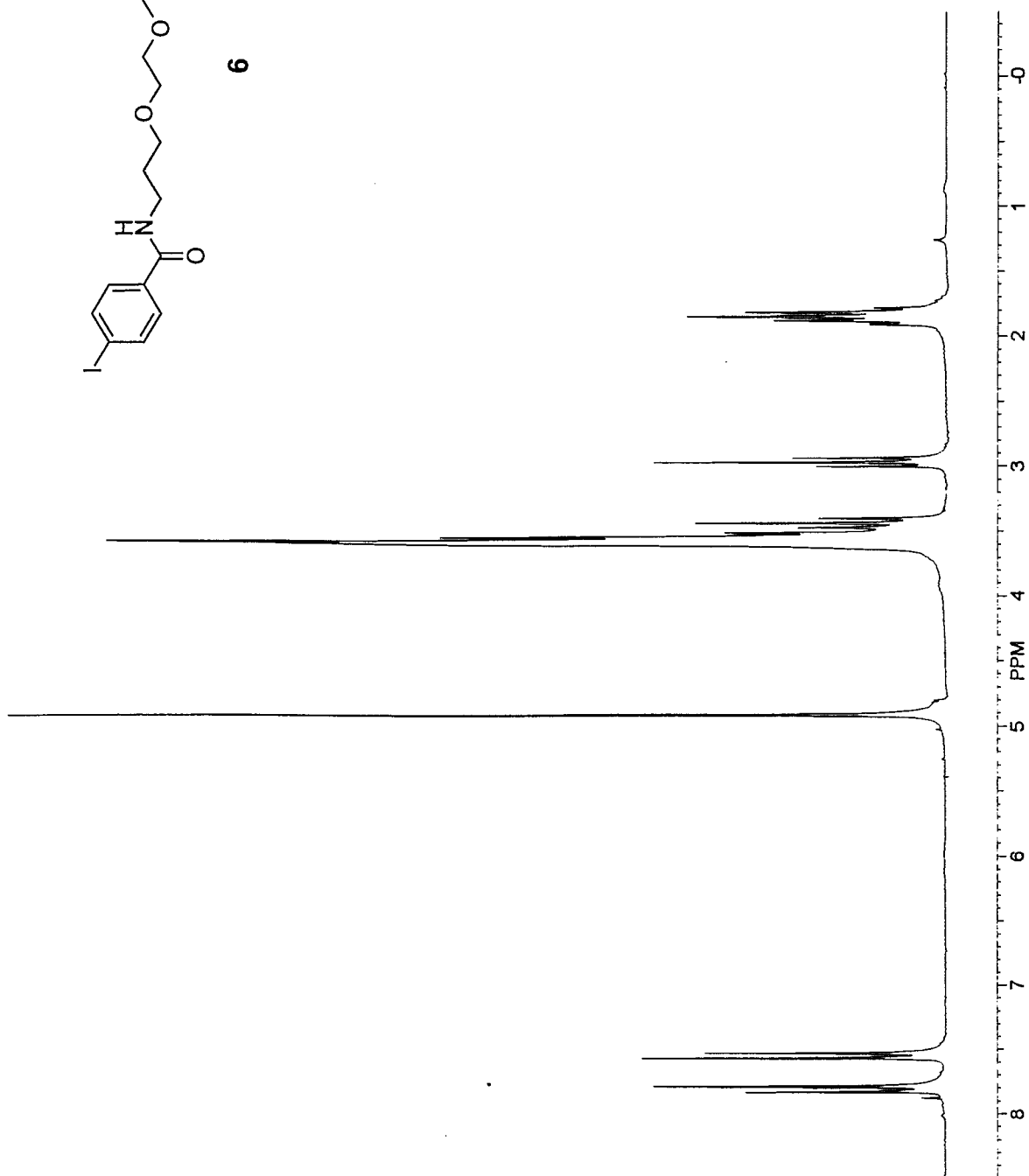


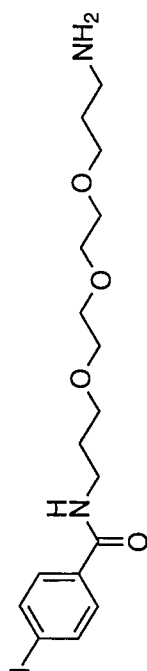
4



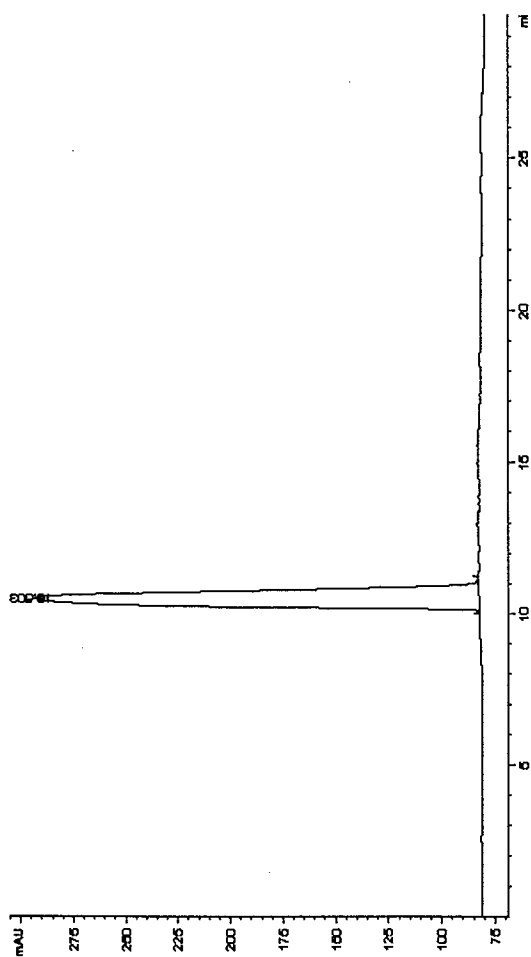


6

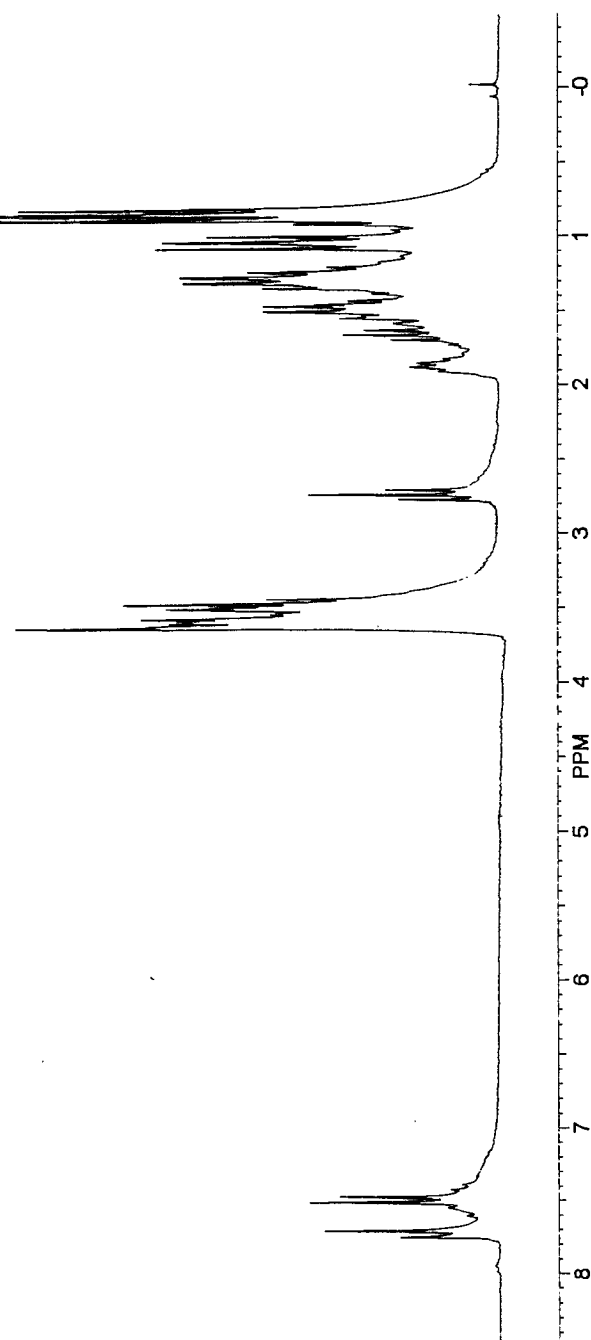


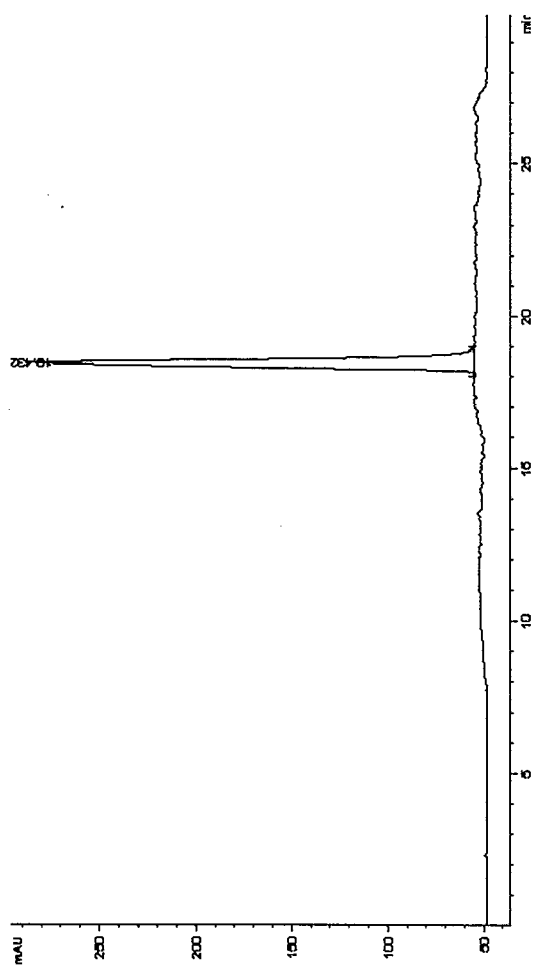


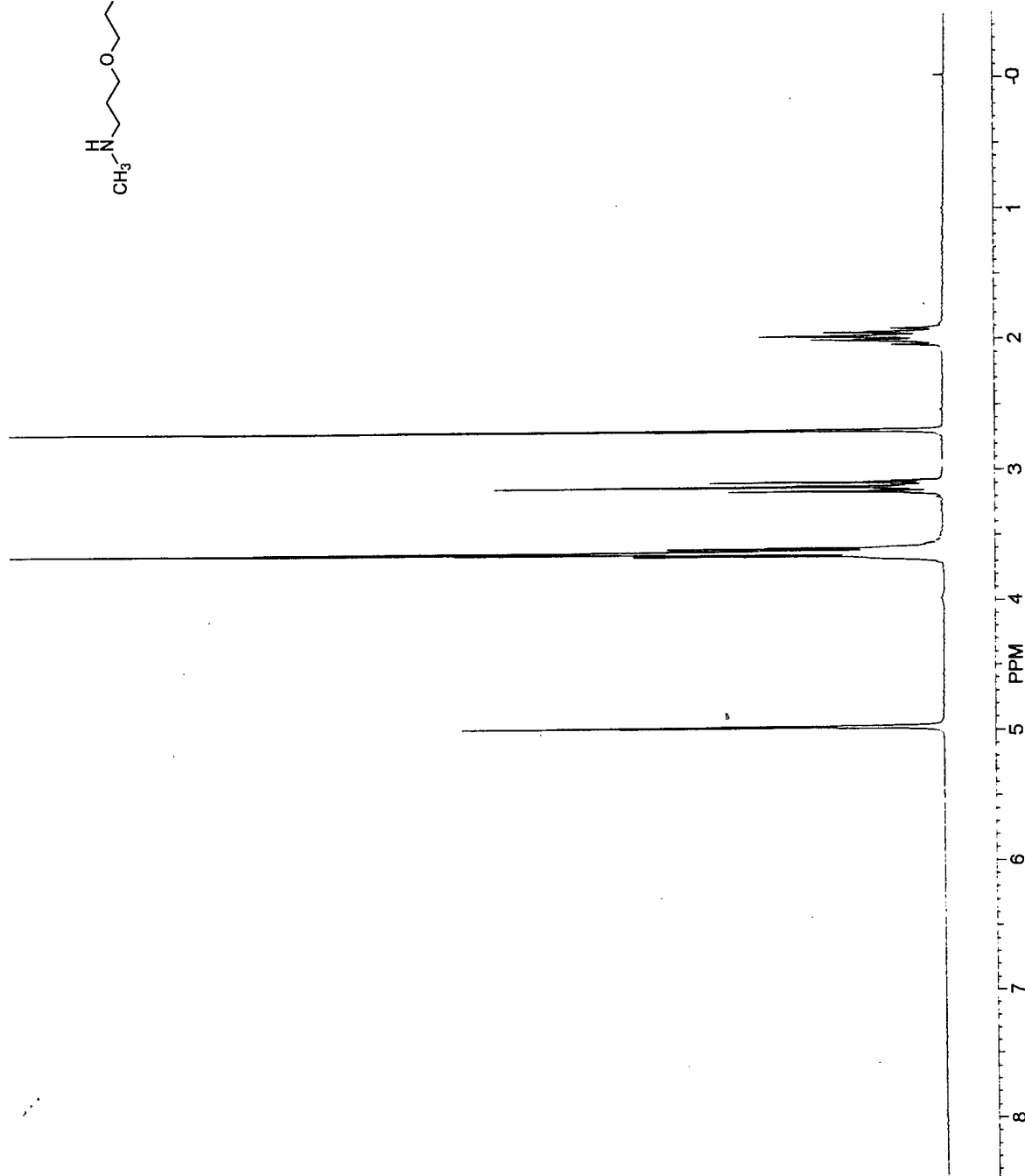
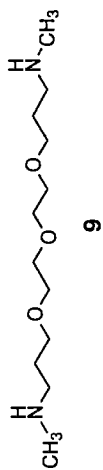
6

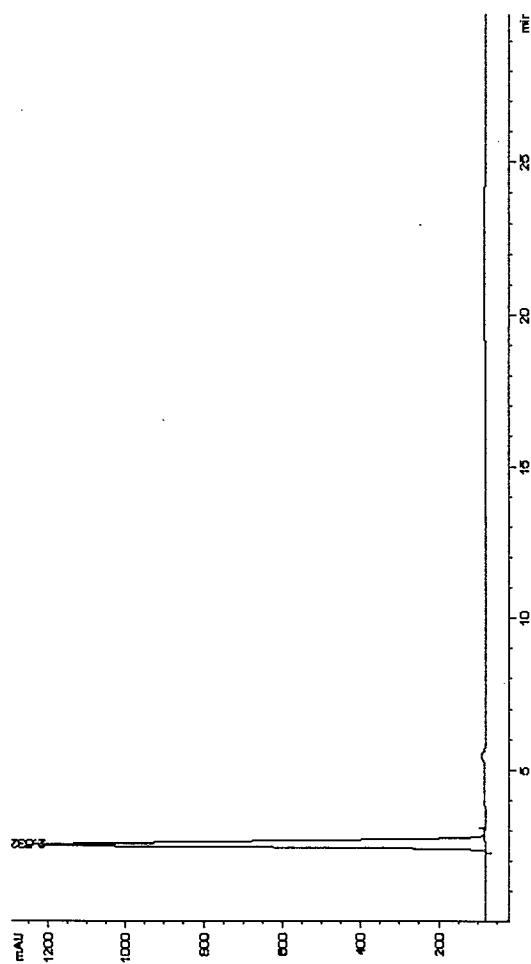
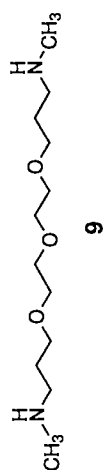


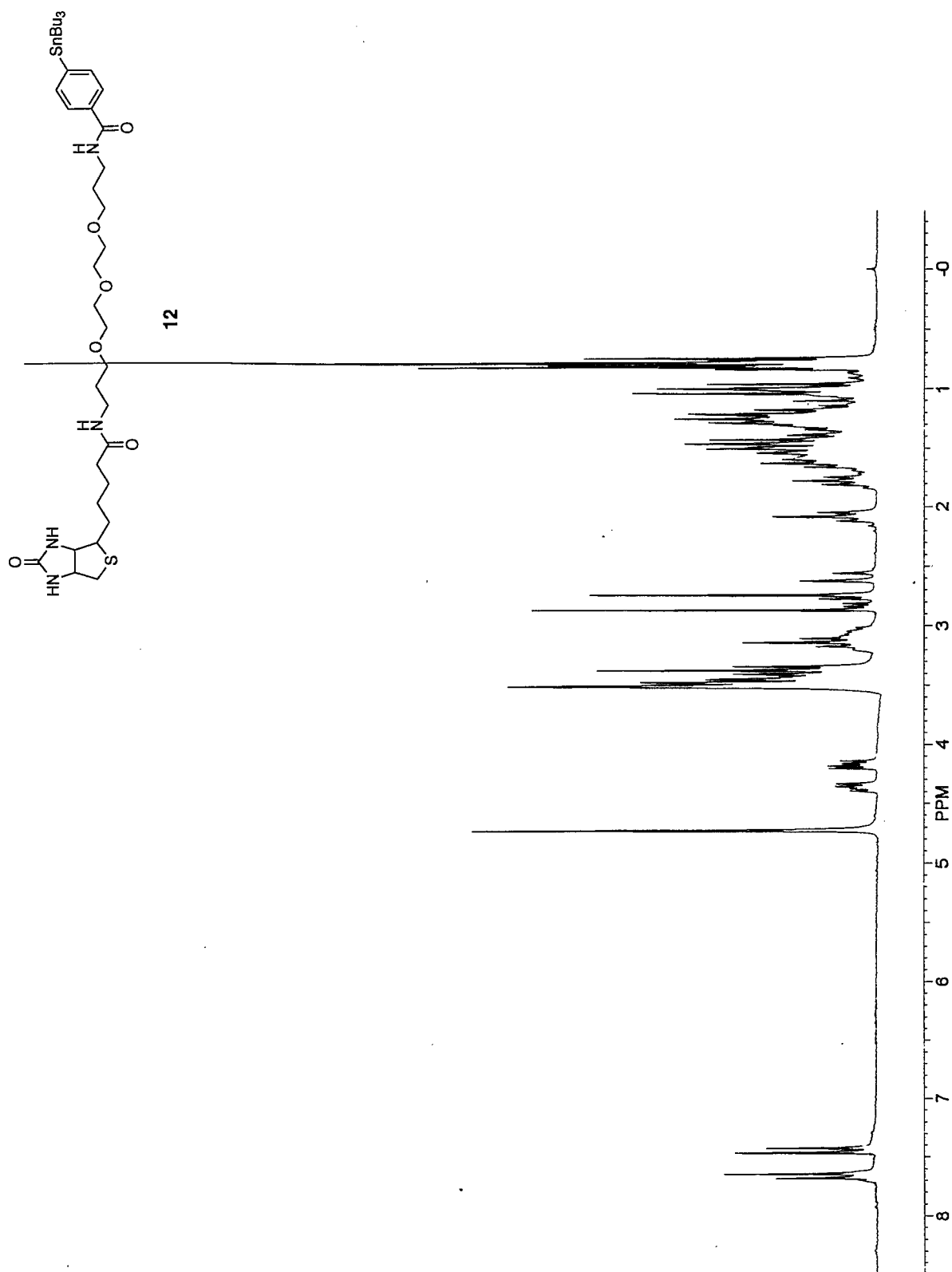
2

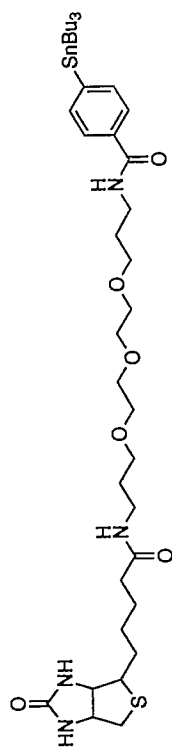




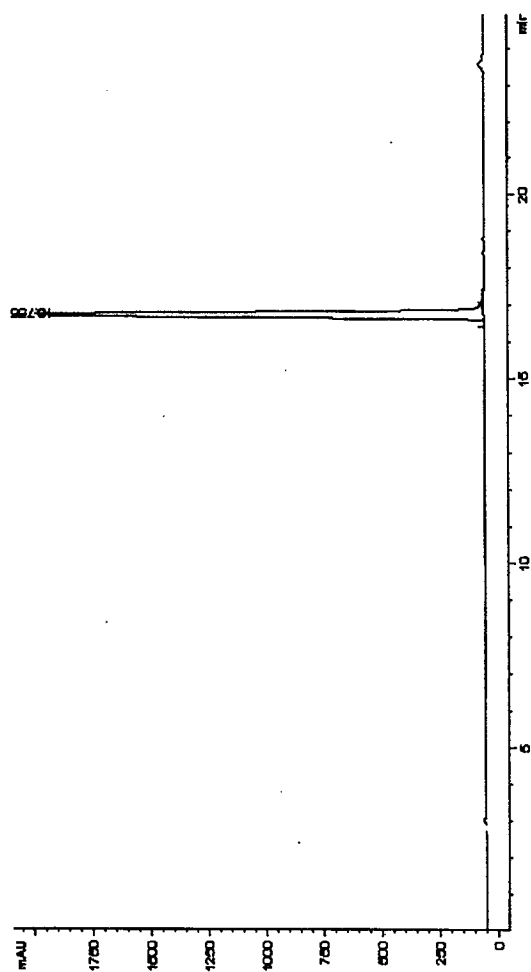


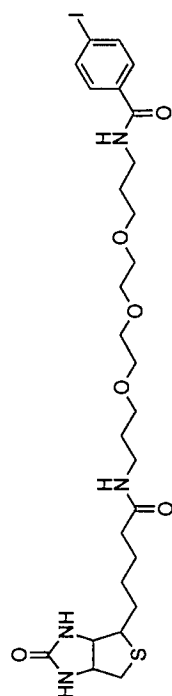




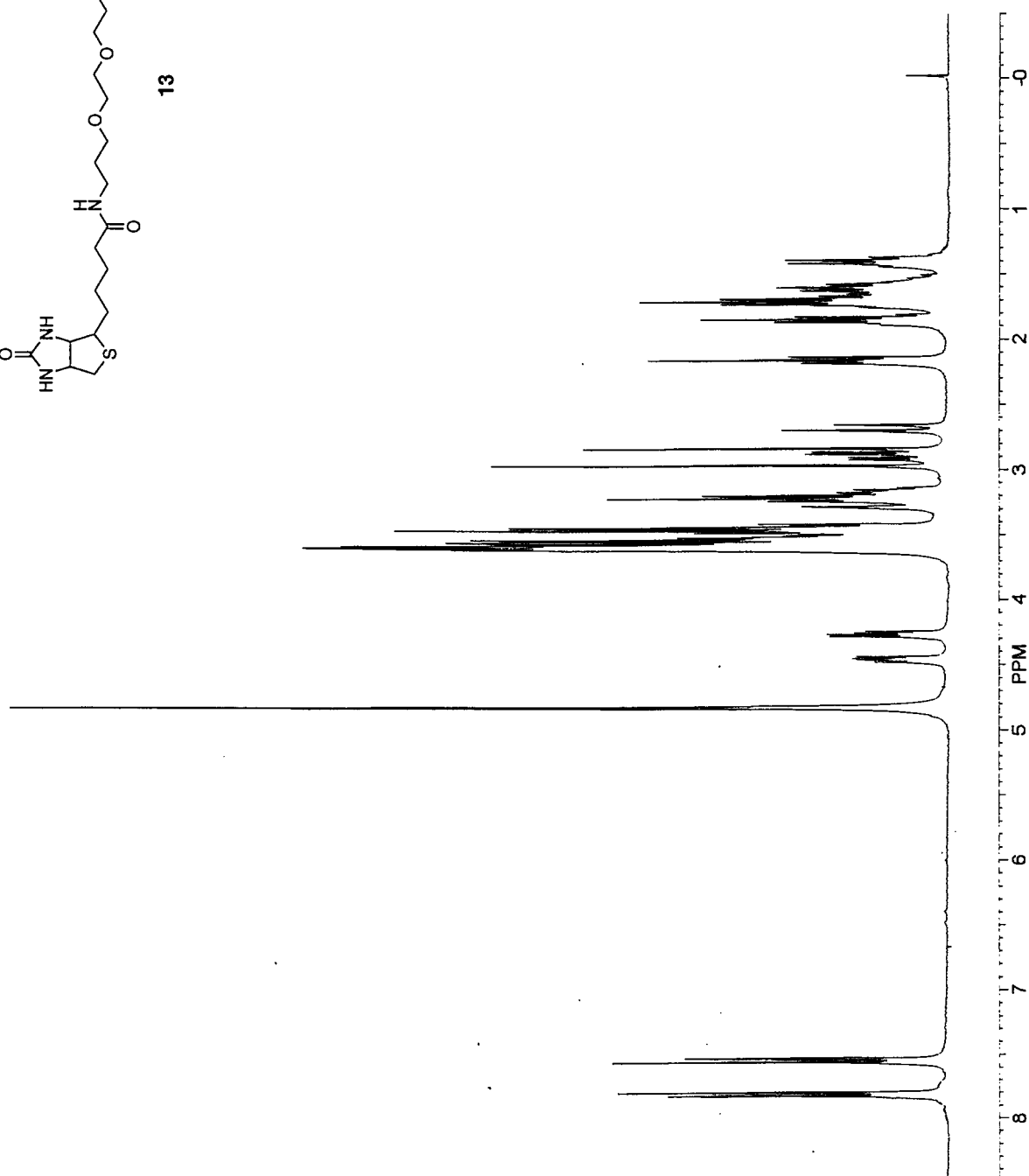


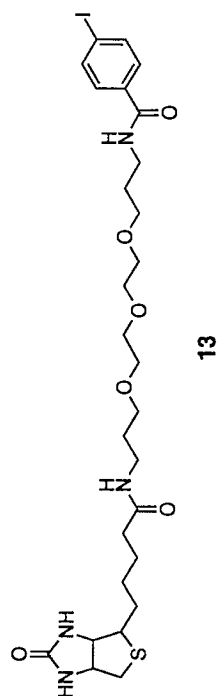
12



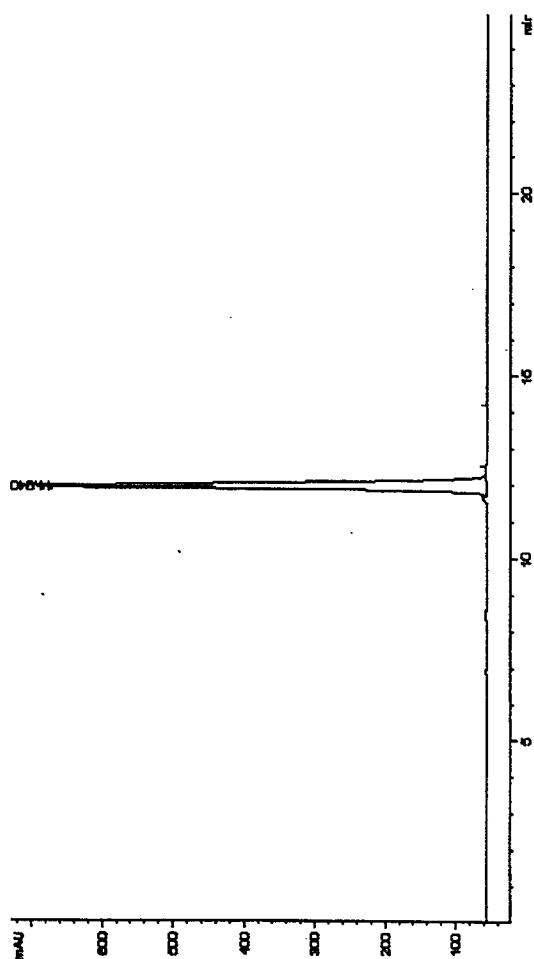


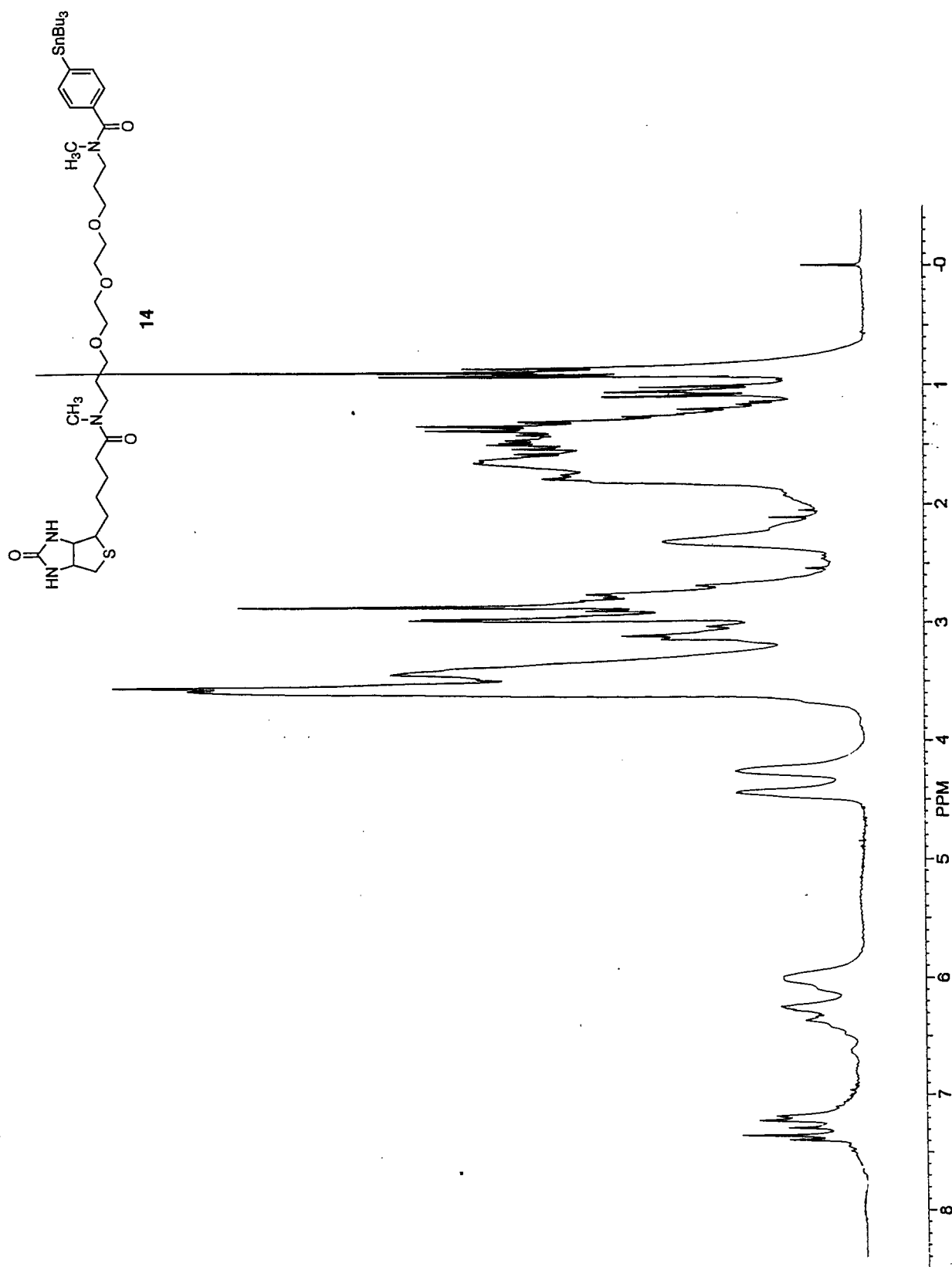
13

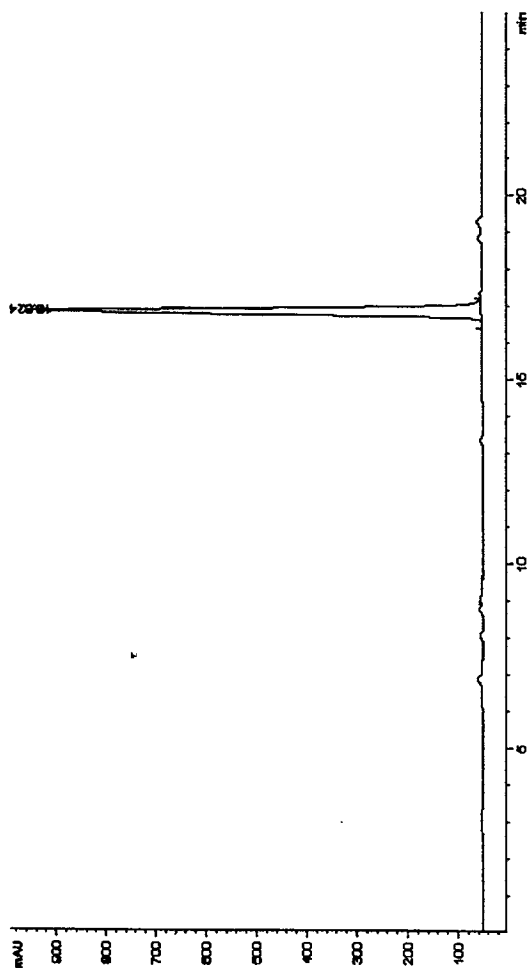
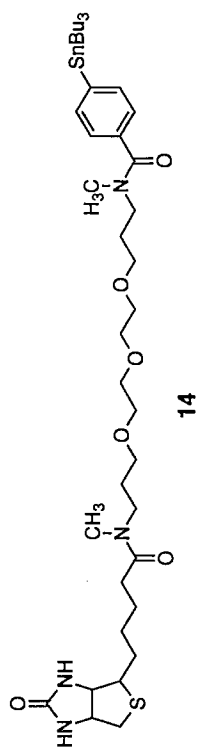


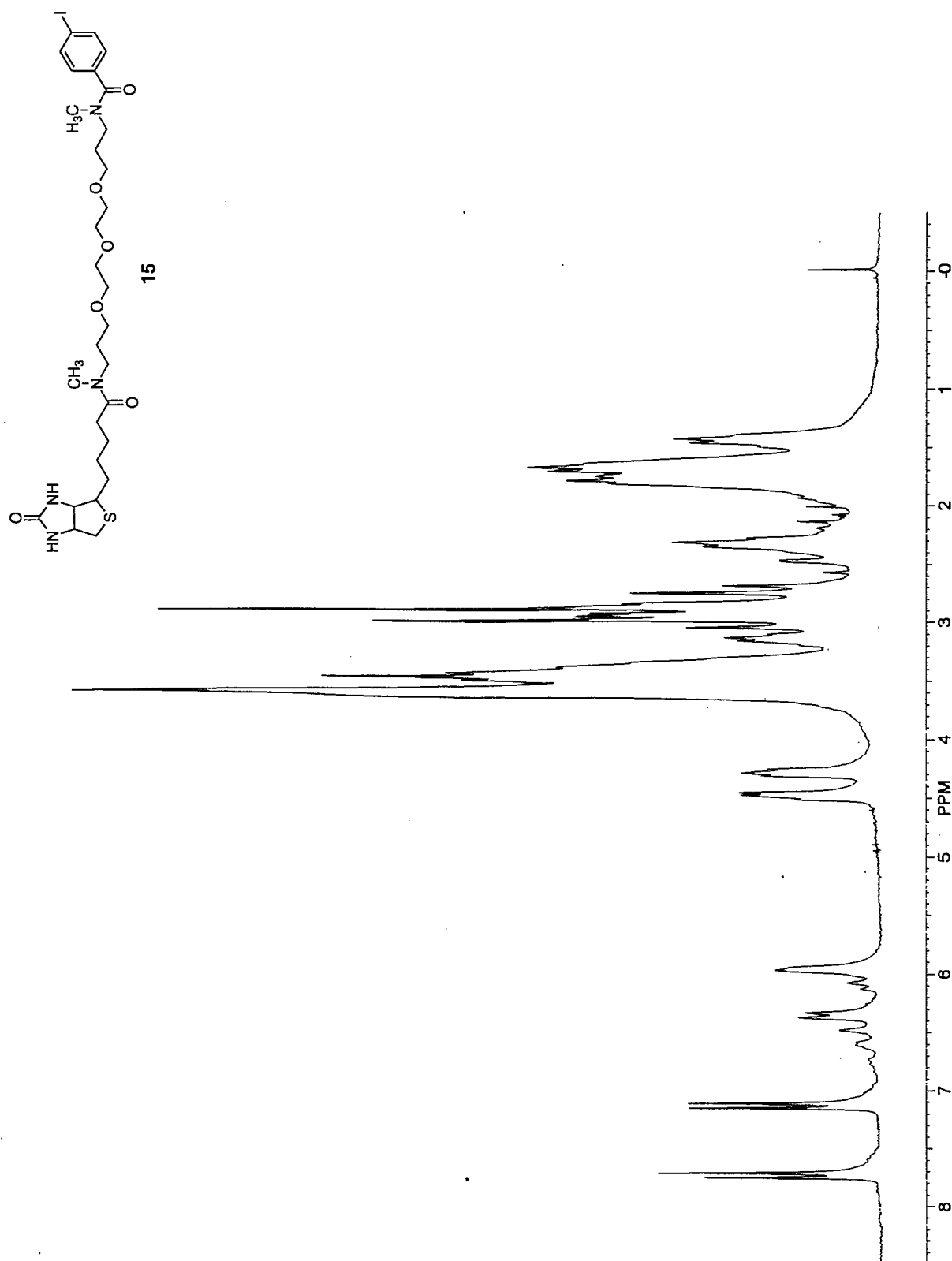


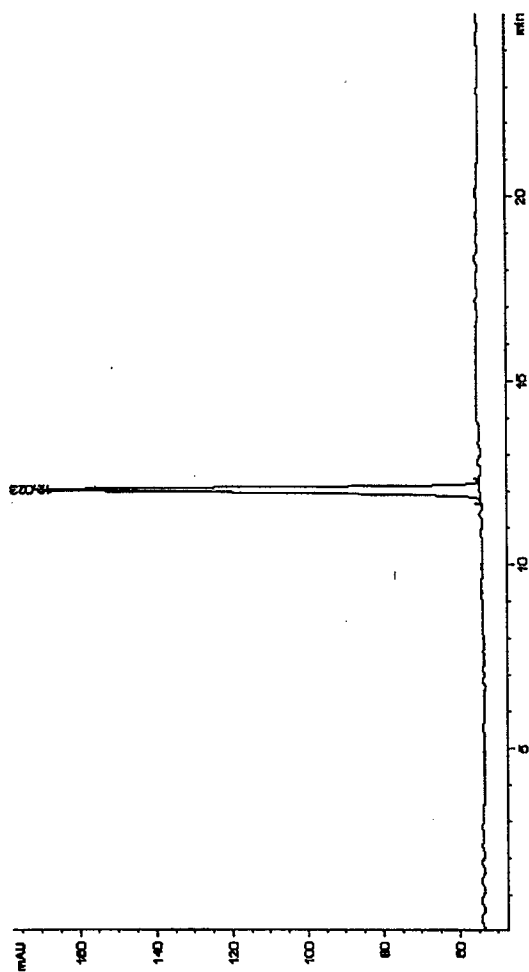
13

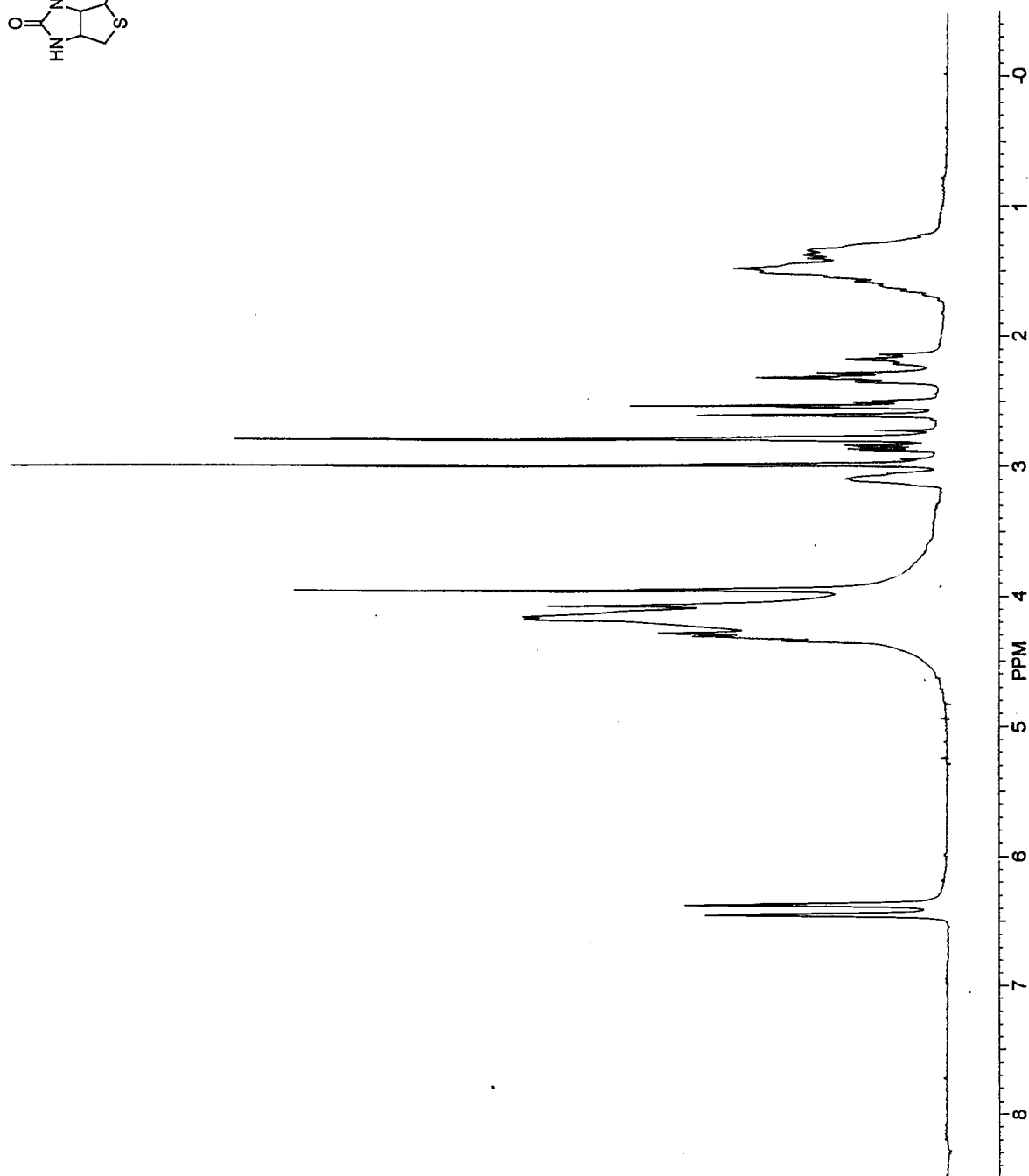
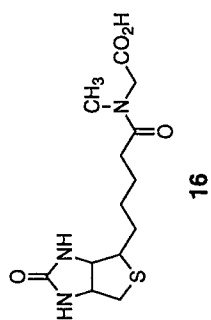


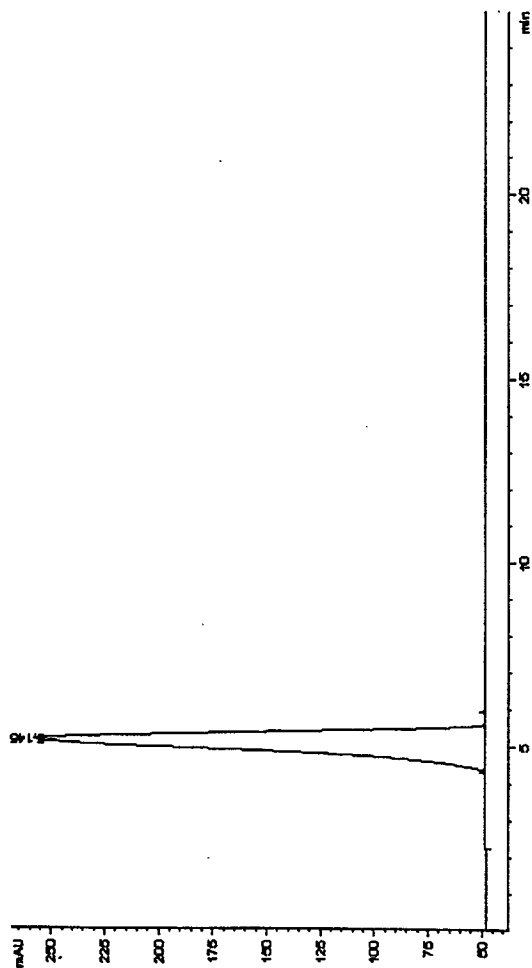
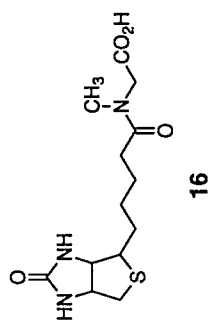


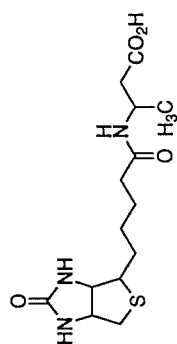




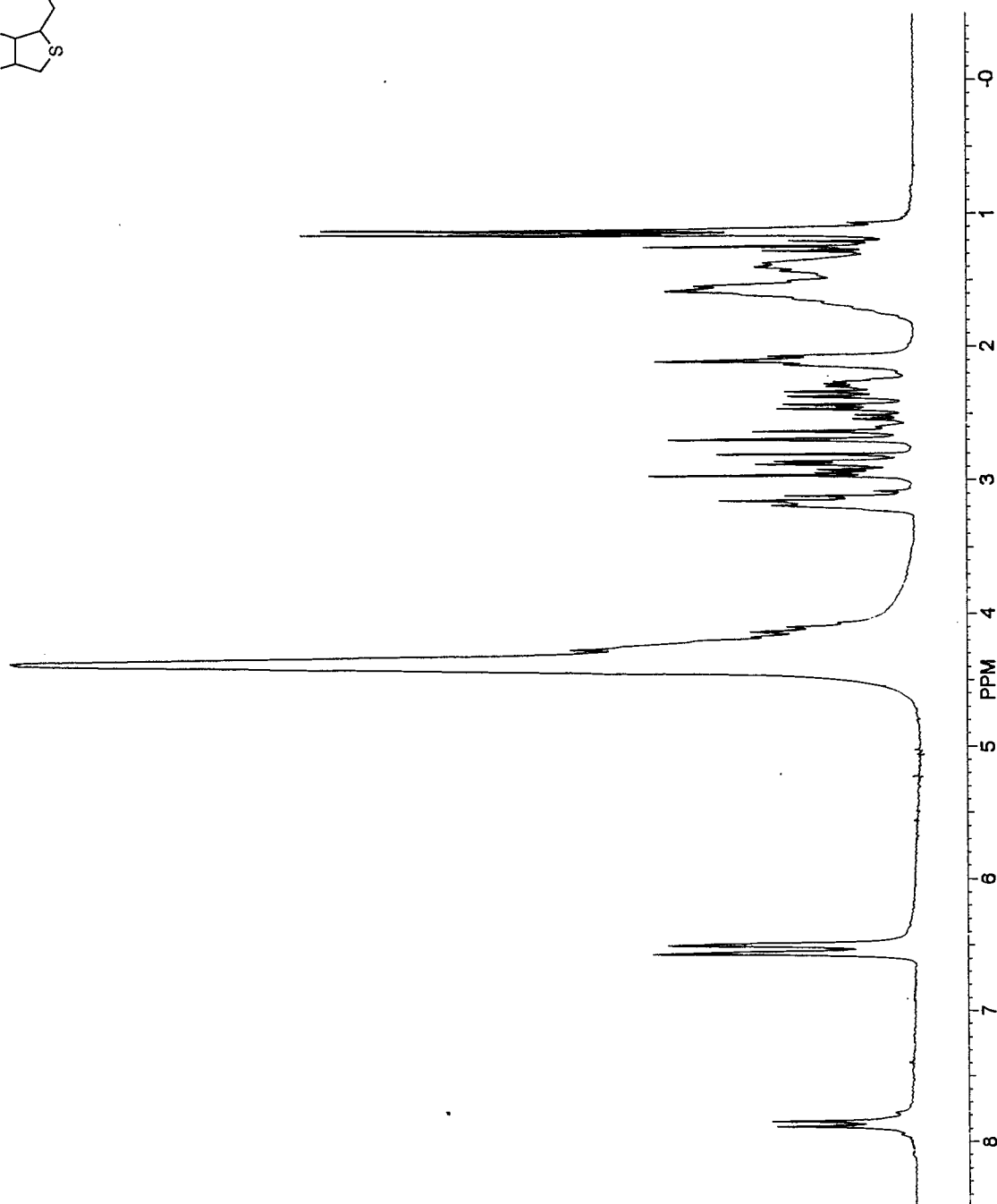


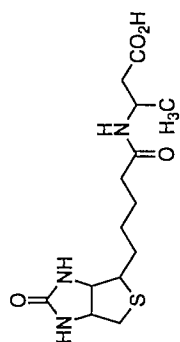




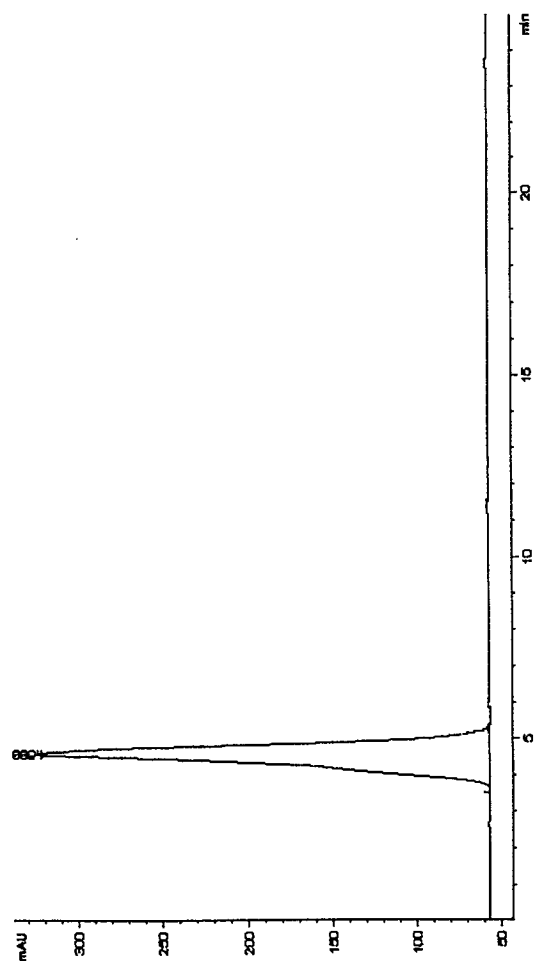


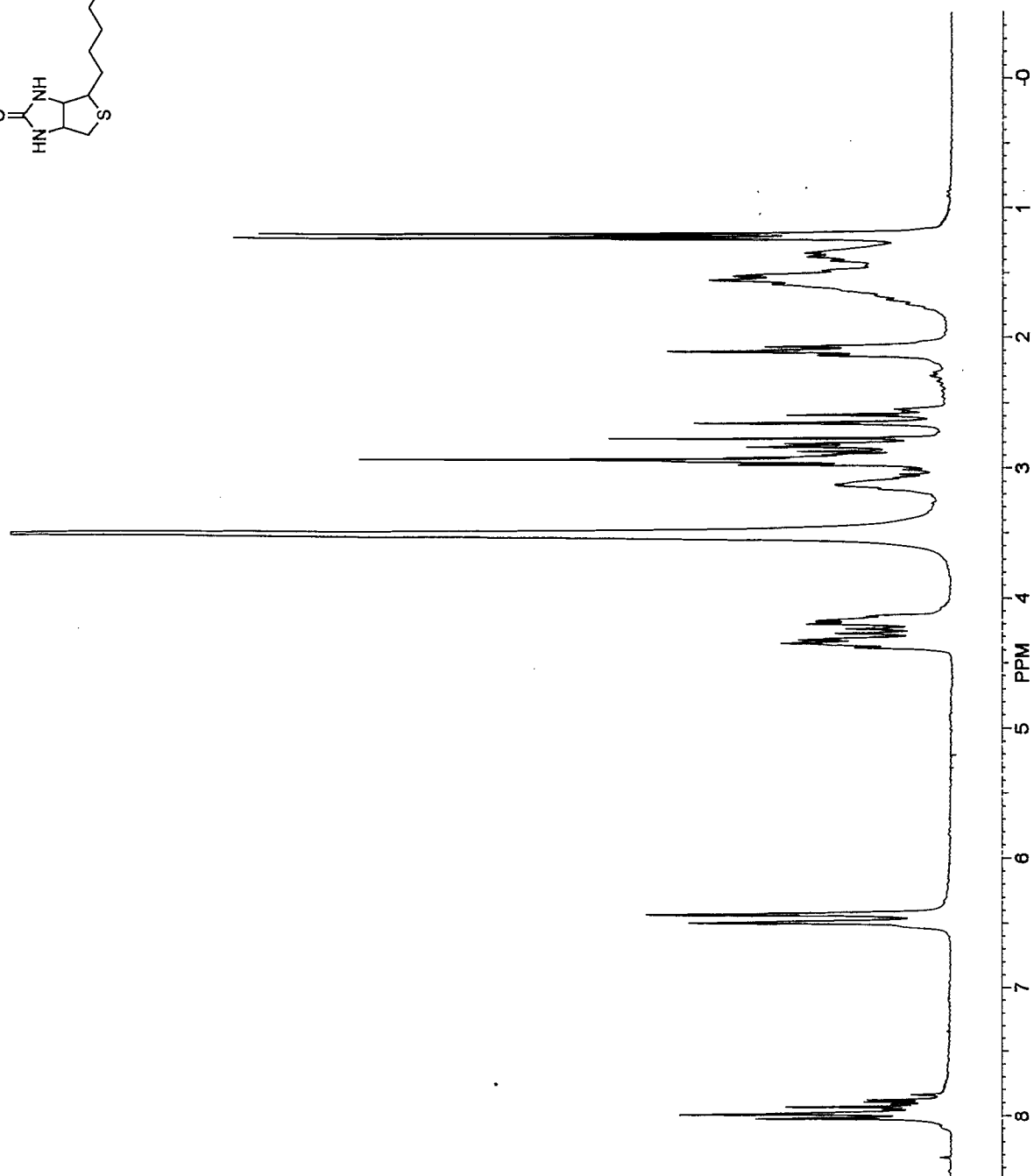
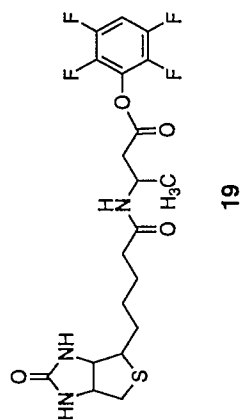
17

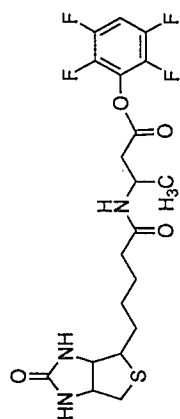




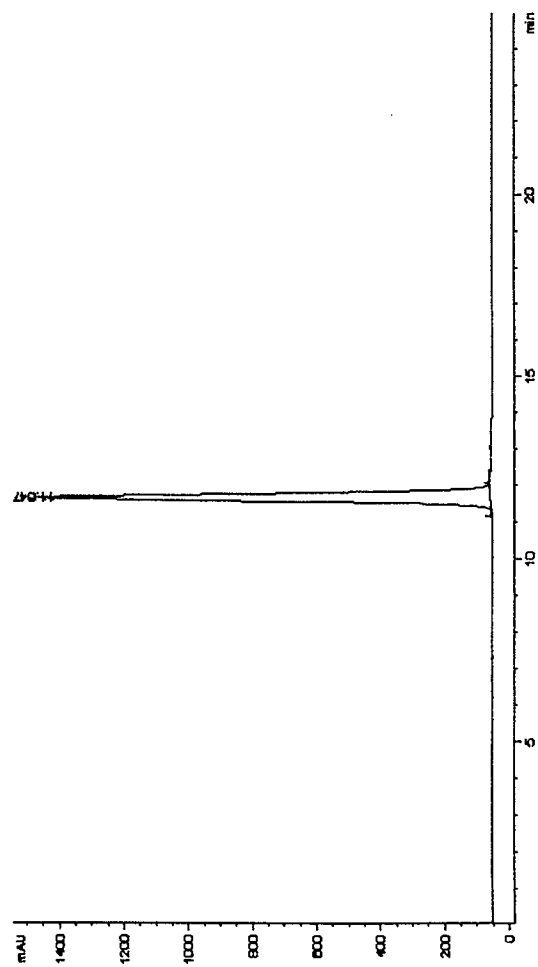
17

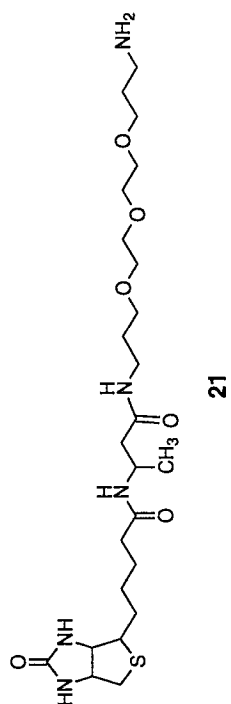




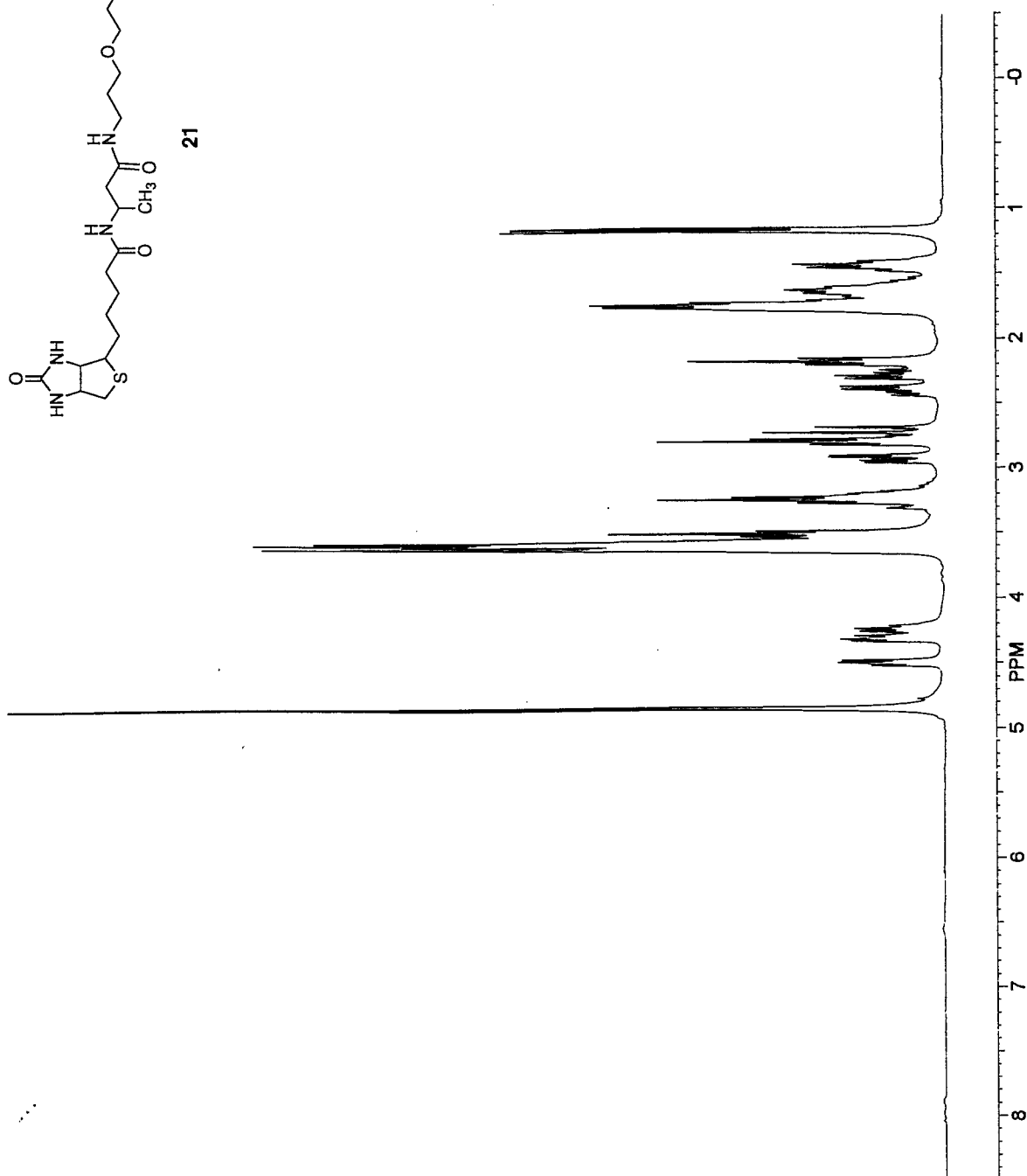


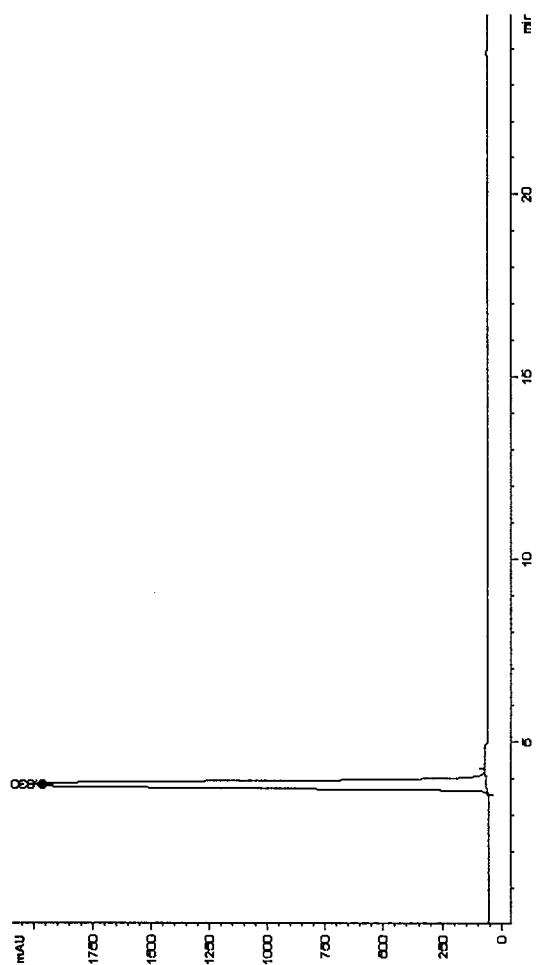
19

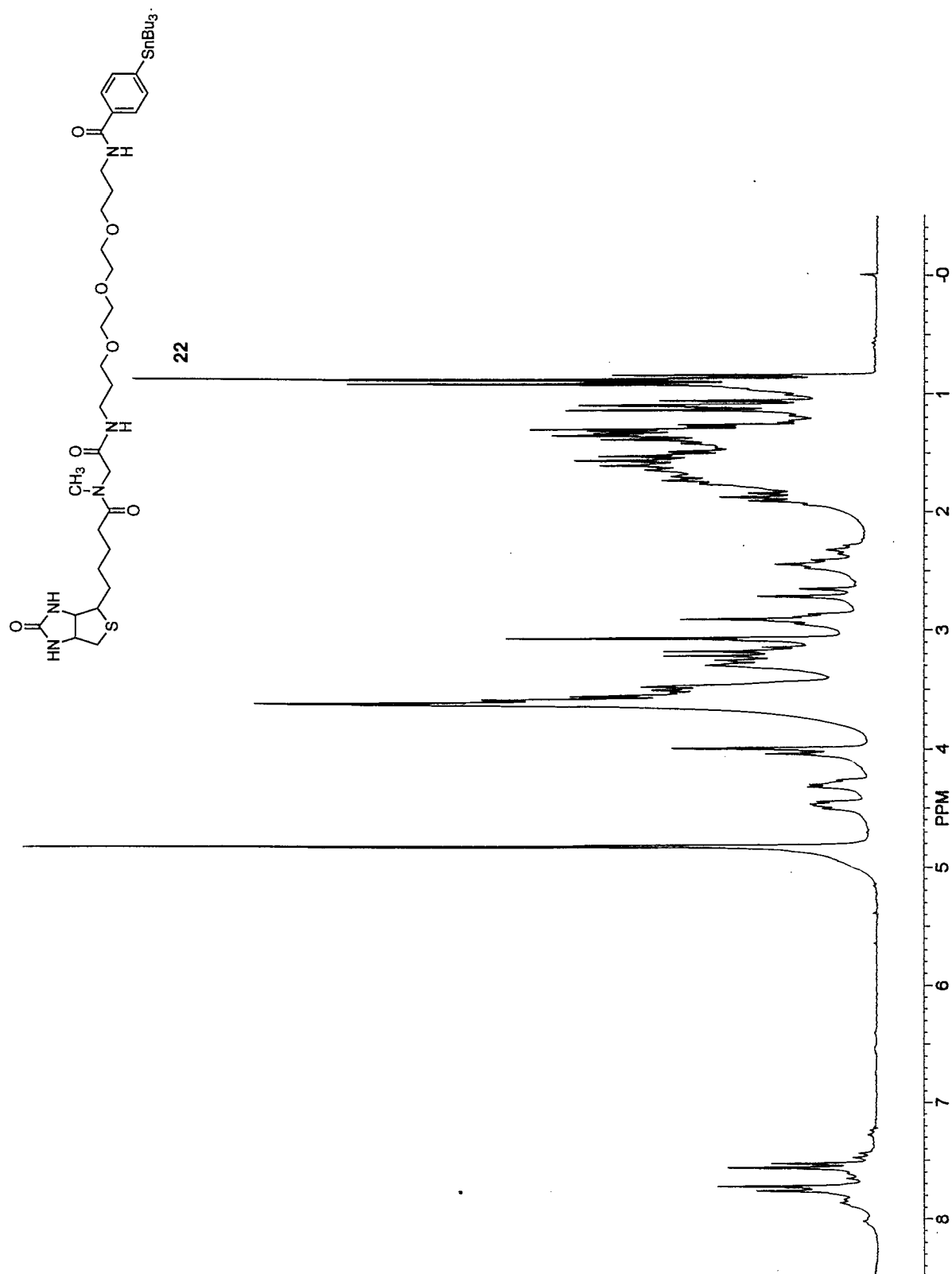


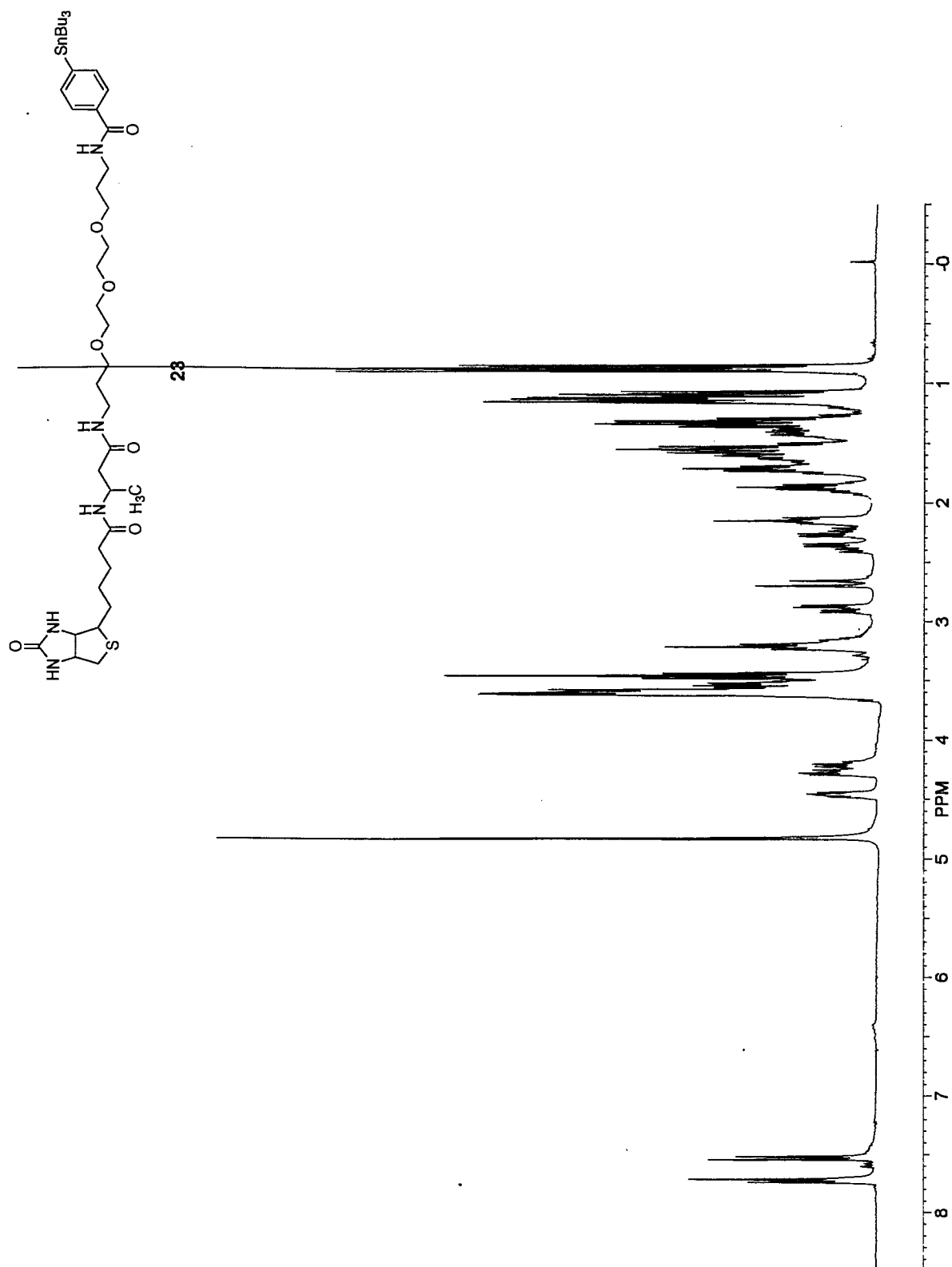


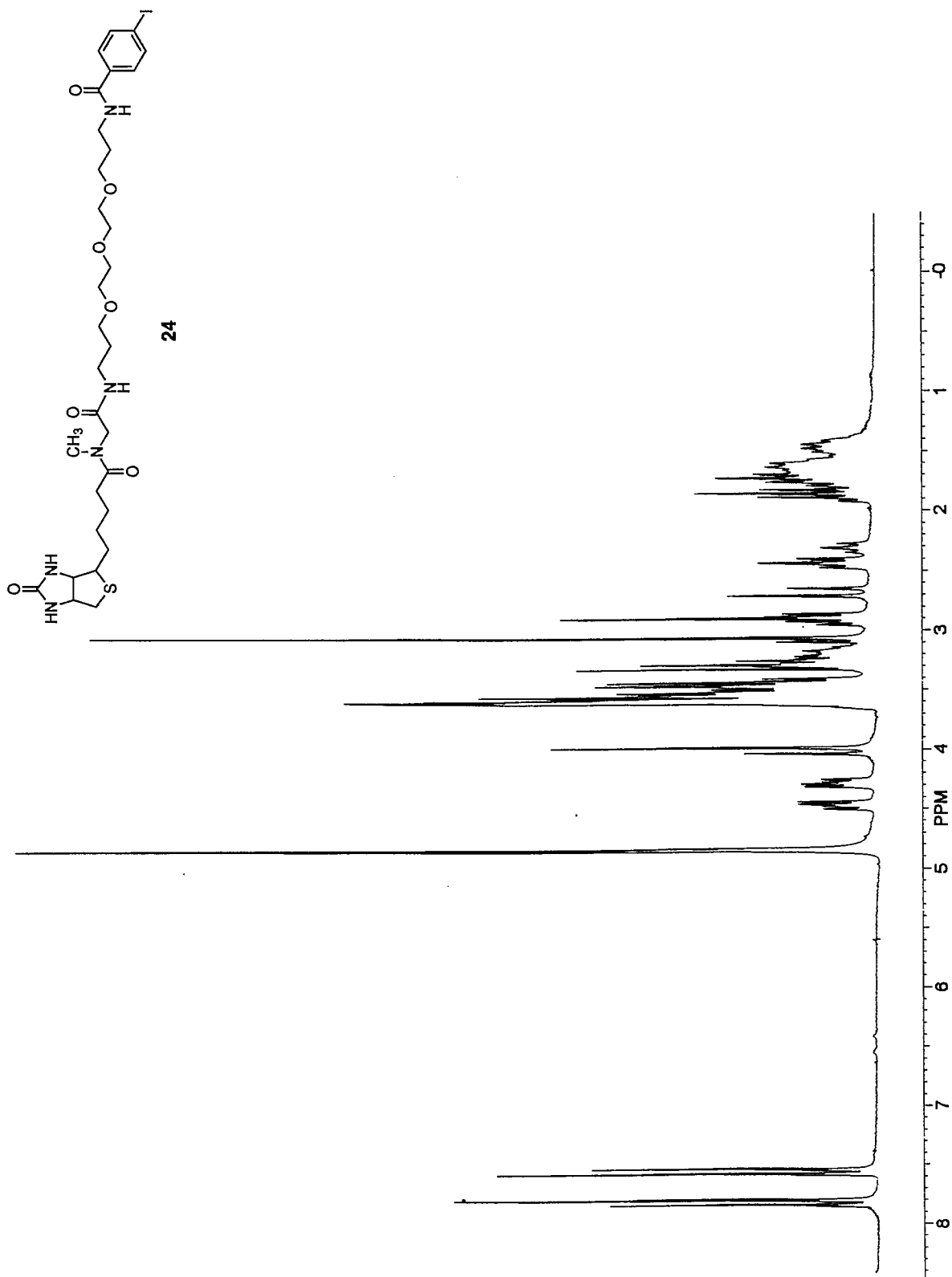
21

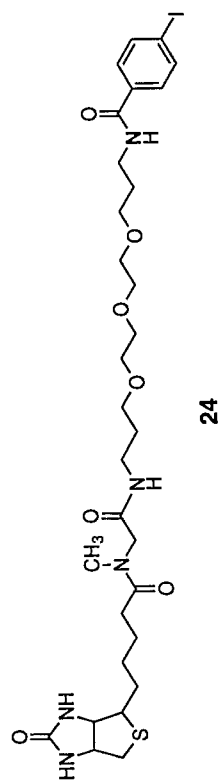




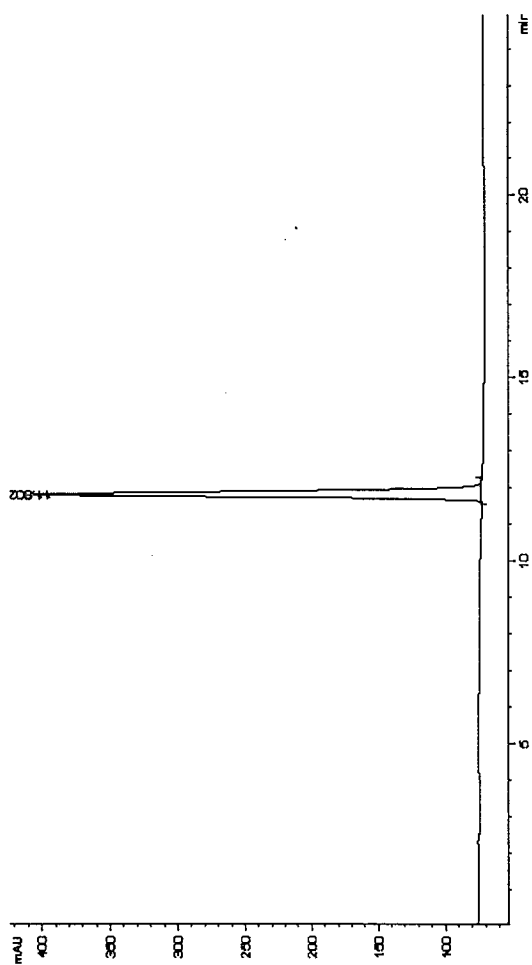


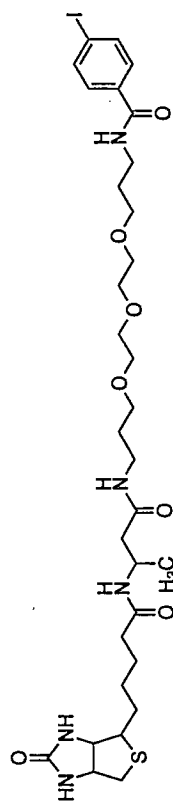




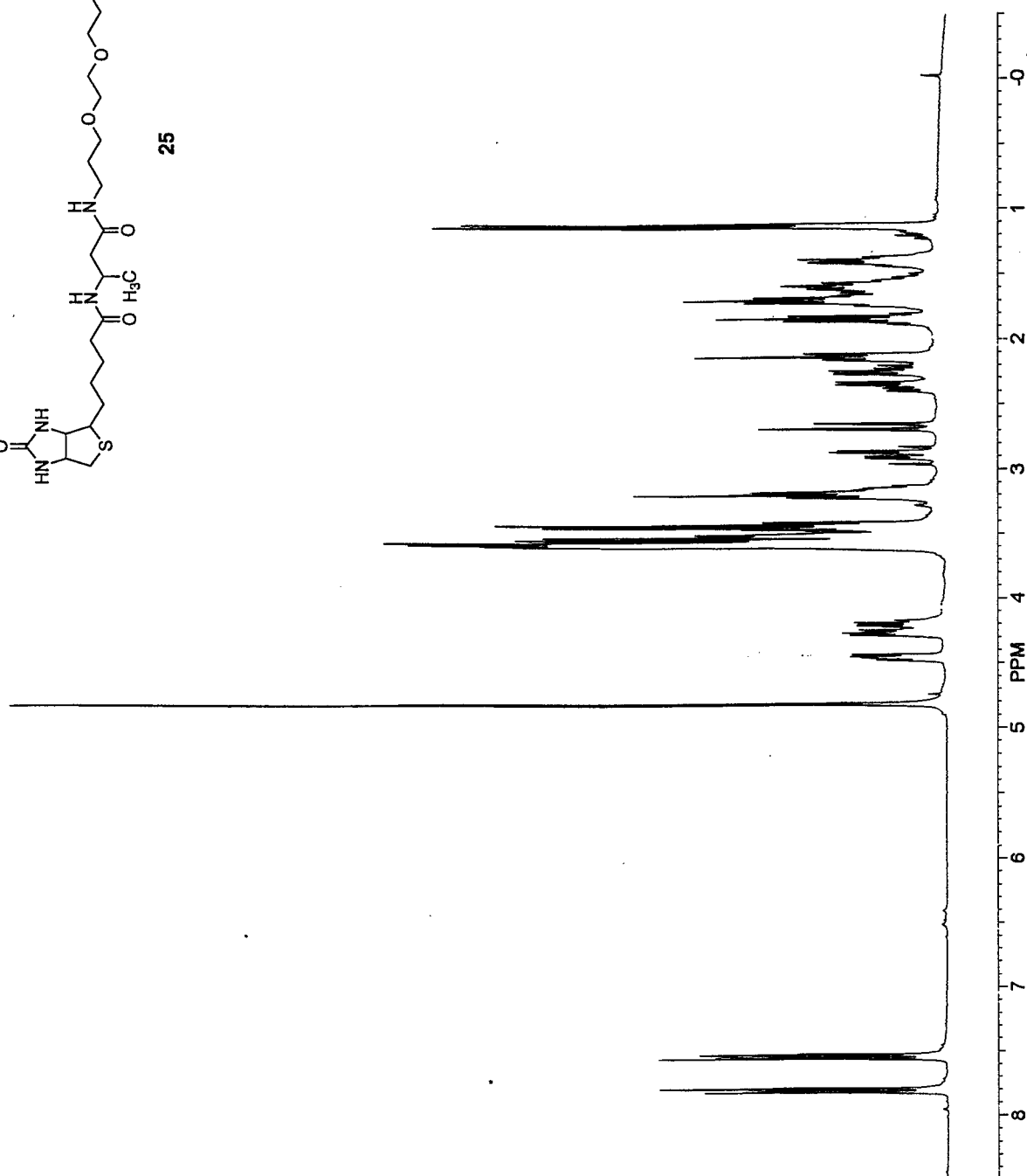


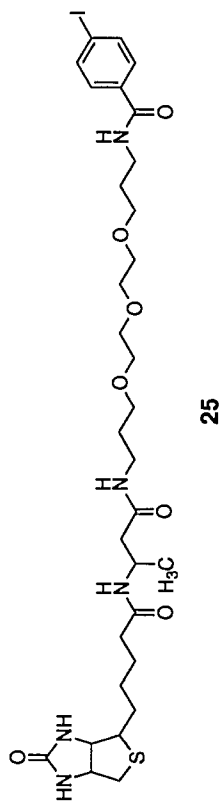
24



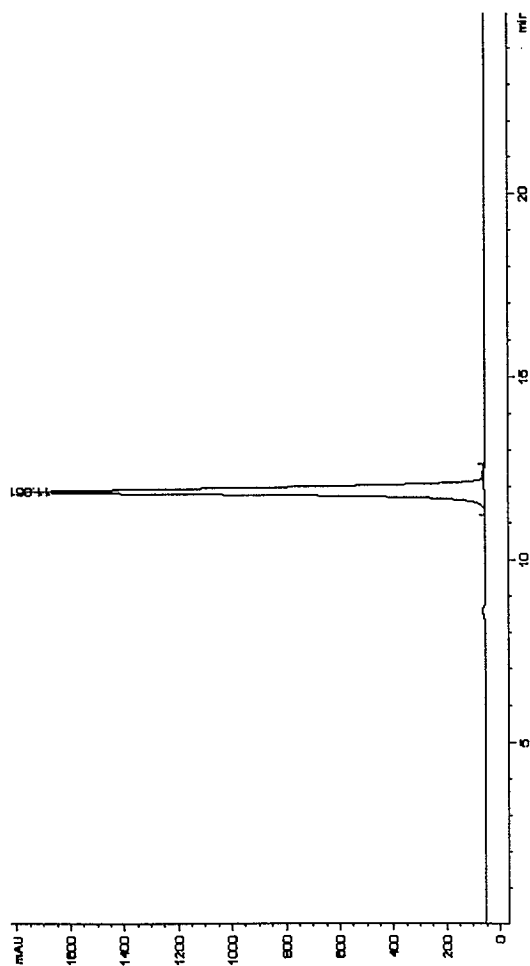


25





25



Development of a Streptavidin–Anti-Carcinoembryonic Antigen Antibody, Radiolabeled Biotin Pretargeting Method for Radioimmunotherapy of Colorectal Cancer. Reagent Development[†]

Habibe Karacay,^{*,‡} Robert M. Sharkey,[§] Serengulam V. Govindan,[‡] William J. McBride,[‡] David M. Goldenberg,[§] Hans J. Hansen,[‡] and Gary L. Griffiths[‡]

Immunomedics, Inc., Morris Plains, New Jersey 07950, and Garden State Cancer Center, Belleville, New Jersey 07109. Received February 25, 1997[®]

With pretargeting, radioisotope delivery to tumor is decoupled from the long antibody localization process, and this can increase tumor:blood ratios dramatically. Several reagents were prepared for each step of a "two-step" pretargeting method, and their properties were investigated. For pretargeting tumor, streptavidin–monoclonal antibody (StAv–mab) conjugates were prepared by cross-linking sulfo-SMCC-derivatized streptavidin to a free thiol (SH) group on MN-14 [a high-affinity anti-carcinoembryonic antigen (CEA) mab]. Thiolated mabs were generated either by reaction of 2-iminothiolane (2-IT) with mab lysine residues or by reduction of mab disulfide bonds with (2-mercaptoethyl)amine (MEA). Both procedures gave protein–protein conjugates isolated in relatively low yields (20–25%) after preparative size-exclusion (SE) chromatography purification with conservative peak collection. Both StAv–MN-14 conjugates retained their ability to bind to CEA, to an anti-idiotypic antibody to MN-14 (WI2), and to biotin, as demonstrated by SE-HPLC. Two clearing agents, WI2 mab and a biotin–human serum albumin (biotin–HSA) conjugate, were developed to remove excess circulating StAv–MN-14 conjugates in animals. Both clearing proteins were also modified with galactose residues, introduced using an activated thioimide derivative, to produce clearing agents which would clear rapidly and clear primary mab rapidly. At least 14 galactose residues on WI2 were required to reduce blood levels to $5.9 \pm 0.7\%$ ID/g in 1 h. Faster blood clearance ($0.7 \pm 0.2\%$ ID/g) was observed in 1 h using 44 galactose units per WI2. For the delivery of radioisotope to tumor, several biotinylated conjugates consisting of biotin, a linker, and a chelate were prepared. Conjugates showed good *in vitro* and *in vivo* stability when D-amino acid peptides were used as linkers. biotin–peptide–DOTA–indium-111 had a slightly longer blood circulation time ($0.09 \pm 0.02\%$ ID/g in 1 h) than biotin–peptide–DTPA–indium-111 ($0.05 \pm 0.03\%$ ID/g in 1 h) in nude mice. A longer circulation time with the neutral DOTA complex might allow higher tumor uptake.

INTRODUCTION

The concept of monoclonal antibody (mab)-directed pretargeting for the delivery of radioimmunotherapy (RAIT) to target cells *in vivo* has received considerable attention in the last few years. A significant advantage of using this approach is the fact that the lengthy antibody-to-target localization phase occurs with the mab not carrying a radiotoxic nuclide. Instead, the mab carries a secondary recognition moiety, which itself is later targeted with a radiolabeled hapten recognizing that secondary recognition moiety. A number of such systems have been described (1–5), with the best known being the one based on the high-affinity interaction between avidin (or streptavidin) and biotin (6–12). Basically, two biotin–avidin pretargeting approaches have been described. The "two-step" method involves administration of a mab–avidin (–streptavidin) conjugate followed by a biotin–nuclide conjugate. In the "three-step" method, mab–biotin is administered first, followed by an avidin (which acts as a mab–biotin clearing agent and biotin–nuclide bridging agent), and

third a biotin–nuclide conjugate. In both methods, additionally administered agents which remove residual primary conjugate from the blood have been described (13, 14).

Perhaps because of the highly interdisciplinary nature of this field, many publications only deal with the chemistry involved in reagent preparation in a peripheral manner. However, since the reagents necessitated by the approach include protein–protein conjugates, protein–carbohydrate conjugates, biotinylated proteins, radiolabeled proteins, biotin–chelate conjugates, and radiolabeled biotin–chelate conjugates, the required supporting chemistry is neither obvious nor trivial. Aside from synthetic chemistry and bioconjugate chemistry work, methods of purification and analysis also need to be developed for each prospective agent prior to embarking on expensive *in vivo* experimentation. A number of articles have appeared which outline various methodologies in this area, but these methodologies are often incompletely developed, sometimes appear less than satisfactory in terms of analytical characterization, and, in any case, are scattered across the scientific literature (15–28). In this paper, we concentrate on chemical considerations related to preclinical two-step pretargeting studies, and we identify and describe useful preparative and analytical methods for this purpose.

The reagents described herein are for evaluation of two-step pretargeting, using appropriate radiolabeled derivatives, although more than two steps are used.

[†] Presented in part at the Sixth Conference on Radioimmunodetection and Radioimmunotherapy of Cancer in Princeton, NJ, on October 10–12, 1996.

* Address correspondence to this author at Immunomedics, Inc., 300 American Rd., Morris Plains, NJ 07950. Telephone: (201) 605-8200. Fax: (201) 605-1103.

[‡] Immunomedics, Inc.

[§] Garden State Cancer Center.

[®] Abstract published in *Advance ACS Abstracts*, July 1, 1997.

Tumor is pretargeted with StAv–MN-14, a streptavidin–anti-carcinoembryonic (CEA) mab conjugate, and after allowing 2 days for maximizing tumor uptake, a clearing agent is injected to remove non-tumor-bound, circulating StAv–MN-14. A clearing agent is used to remove extraneous conjugate from the blood and achieve high tumor:blood ratios of StAv–MN-14 in a short time. An alternative approach would be to allow a longer time for the conjugate to clear from blood without the aid of a clearing agent, as has been described (26). This approach requires that the StAv–mab conjugate remain at the tumor for a long period of time either without internalization or without losing its biotin binding capacity due to endogenous biotin-saturating StAv binding sites. Thus, a clearing agent is used to reduce the time between the targeting by the mab and the injection of the labeled biotin. Clearance mechanisms to be tested are based on anti-idiotypic binding to the antigen-binding part of StAv–MN-14 or biotin binding to the StAv part of the StAv–MN-14 conjugate. In addition, clearing agents substituted with carbohydrate moieties are examined, since these agents themselves are rapidly cleared from the blood and localized into hepatocytes by specific receptors (29).

Radiometal-labeled biotinylated chelate is administered in the final step 2–24 h after the clearing agent. Requirements for a useful biotinylated chelate include *in vivo* stability, since serum biotinidase is known to cleave biotinylated substrates (30). A final requirement is the fact that the radiometal–chelate–biotin must have a reasonably short serum half-life in order to minimize normal tissue radiotoxicity upon therapy; yet at the same time, it must remain in circulation long enough to allow for adequate tumor accretion.

MATERIALS AND METHODS

The murine anti-CEA antibody, MN-14, has been described previously (31), as has the rat anti-MN-14 idiotype antibody WI2 (32). Streptavidin (StAv) and avidin were purchased from Pierce (Rockford, IL) and Sigma Chemical Co. (St. Louis, MO), respectively, and used without purification. Human serum albumin (HSA) (catalog no. A 3782) was from Sigma and was purified on a preparative size-exclusion HPLC column to remove a large molecular weight contaminant prior to its modification. CEA was obtained from Scripps (San Diego, CA). 1,4,7,10-Tetraazacyclododecane-*N,N,N',N'*-tetraacetic acid (DOTA) was obtained from Parish Chemicals (Orem, UT). (2-Mercaptoethyl)amine (MEA) and cyanomethyl 2,3,4,6-tetra-*O*-acetyl-1-thio- β -D-galactopyranoside (CTTG) were from Sigma, and [5-(biotinamido)-pentyl]amine was from Pierce. The remaining chemicals, including 2-iminothiolane, were purchased from Pierce or Aldrich (Milwaukee, WI). All were used without further purification. *N,N,N,N',N'*-Pentakis(carboxymethyl)-2-(*p*-aminobenzyl)diethylenetriamine (amino-benzyl-DTPA) was prepared according to literature methods (33) and converted to *N,N,N,N',N'*-pentakis(carboxymethyl)-2-(*p*-isothiocyanatobenzyl)diethylene-triamine (ITC-Bz-DTPA) as described (34).

Protein solutions were sterile-filtered using Millipore (Marlborough, MA) Millex-GV 0.22 μ m filter units. Centrifuged spin columns were prepared according to published procedures (34, 35). The gel, Sephadex G-50–80 (Sigma), was hydrated in the appropriate buffer and washed with 7 buffer volumes before storage at 4 °C. Analytical protein analyses were performed on a Bio-Sil SEC-250 SE-HPLC column (Bio-Rad, Richmond, CA) equipped with an in-line absorbance detector (Waters 486 or Beckman 167), set at 280 nm, and an in-line radiation

detector (Packard Radiomatic Flo-One). Columns were eluted at 1 mL/min with 0.2 M sodium phosphate and 0.02% sodium azide at pH 6.8. Preparative protein purifications were carried out by fractionation on a Waters 650 HPLC system using a 60 \times 21.5 cm TSK-gel G3000SW column (TosoHaas, Montgomeryville, PA), eluted with 0.2 M sodium phosphate, 0.15 M sodium chloride, and 0.02% sodium azide at pH 6.8 at 1.5 mL/min. Concentrations of StAv–MN-14 were determined from a calibration curve (concentration vs absorbance) constructed using absorbance readings from equimolar solutions of StAv and MN-14 at 280 nm. The curve was constructed by mixing 10–45 μ L of 1.25×10^{-5} M solutions of StAv and MN-14 in 0.1 M sodium phosphate at pH 7 to a final volume of 555 μ L. The slope and intercept were determined to be 3.95×10^5 M⁻¹ L and –0.0217, respectively.

Biotin analyses were performed using a published spectrophotometric procedure (4'-hydroxyazobenzene-2-carboxylic acid; HABA) (36, 37). The biotinylated peptides and chelates were analyzed on a Waters 4000 HPLC system using a reverse-phase Waters 8 \times 100 mm radial pak cartridge filled with C-18 Nova-Pak 4 μ m stationary phase where the column was eluted at 3 mL/min with a linear gradient of 100% A [0.1% trifluoroacetic acid (TFA) in water] to 100% B (0.1% TFA in 90% acetonitrile/10% water) over 10 min. At 10 min, the flow rate was increased to 5 mL/min and remained at 100% B for 5 min before the re-equilibration to initial conditions began. The purifications of the peptides and chelating agents were performed on preparative C-18 column, Waters PrepPack RCM Base, using gradients of the above eluents at 75 mL/min. A Waters 486 absorbance detector set at 220 nm was used for both analytical and preparative HPLC systems involving biotinylated peptides.

Mass spectral analyses were performed by Mass Consortium Corp. (San Diego, CA) using electrospray ionization (ESI) and matrix-assisted laser desorption ionization (MALDI) mass spectrometry methods for small molecular weight compounds and antibodies, respectively.

For *in vitro* stability studies, blood drawn from healthy volunteers was allowed to clot at room temperature, centrifuged, and sterile-filtered. Serum aliquots (250 and 500 μ L) were stored frozen at 4 °C until needed. Approximately 45 min before use, serum vials were thawed and equilibrated at 37 °C under a humidified 5% CO₂ atmosphere. Mouse serum was isolated from non-tumor-bearing 5–8-week-old athymic nude mice (Taconic Farms, Germantown, NY). Mice were first anesthetized with sodium pentobarbital and bled by cardiac puncture. Blood was allowed to clot and serum collected after centrifugation. The GW-39 animal xenograft (human colonic carcinoma) model is described in detail elsewhere (38). All experiments involving animals were carried out using AAALAC-recognized standard procedures for the humane use of such animals.

StAv–MN-14 with StAv Appended to mab Lysine Residues. Streptavidin (20 mg, 3.3×10^{-7} mol) in 1.9 mL of 0.1 M sodium borate (pH 8.3) containing 10 mM ethylenediaminetetraacetic acid (EDTA) was treated with 80 μ L of an aqueous solution of sulfosuccinimidyl 4-(*N*-maleimidomethyl)cyclohexane-1-carboxylate (sulfo-SM-CC, 0.8 mg, 1.8×10^{-6} mol) and stirred at room temperature for 1 h. The modified streptavidin (StAv–SMCC) was purified on 4 \times 3 mL centrifuged spin columns in 0.1 M PBS and 10 mM EDTA at pH 6.4. To 6.6 mL of MN-14 (47.6 mg, 3.1×10^{-7} mol) in 0.1 M PBS at pH 7.4 was added 600 μ L of 0.5 M borate buffer at pH 8.5. A fresh solution of 0.1 M 2-IT in H₂O was prepared, and 16 μ L of this (1.6×10^{-6} mol) was added to the MN-

14 solution. The mixture was stirred at room temperature for 50 min and the thiolated mab was purified on 8×3 mL spin columns in 0.1 M PBS and, 10 mM EDTA at pH 6.4. This effluent was added to the purified StAv-SMCC solution and stirred at room temperature for 1 h. After this time, *N*-ethylmaleimide (10 mg, 8×10^{-5} mol) dissolved in 50 μ L of *N,N*-dimethylformamide (DMF) was added to the conjugation reaction mixture and incubated for 30 min at 37 °C to block residual mab thiol groups. The StAv-MN-14 conjugate was purified on a preparative size-exclusion HPLC column, as described above.

StAv-MN-14 with StAv Appended to mab Cysteine Residues. Streptavidin (25 mg, 4.2×10^{-7} mol) in 2.5 mL of 0.1 M sodium phosphate at pH 7.3 was treated with 208 μ L of 10 mM sulfo-SMCC in H₂O (2.1×10^{-6} mol) and incubated at room temperature for 45 min. The modified StAv was purified on 4×3 mL spin columns in 0.1 M sodium phosphate at pH 7, and its concentration was determined by UV absorbance ($1\% E_{280} = 32$). MN-14 (60 mg, 3.9×10^{-7} mol) in 3 mL of 0.1 M sodium phosphate at pH 7.3 was treated with 600 μ L of 0.1 M MEA in 5 mM EDTA. The reduction was carried out for 45 min at room temperature. Reduced MN-14 was purified on two successive sets of 5×3 mL spin columns with 0.1 M sodium phosphate and 5 mM EDTA at pH 7, and its final concentration was determined by UV absorbance at 280 nm. The number of free SH groups per mab was determined by Ellman reaction by reference to a standard curve (39). The StAv-MN-14 conjugate was prepared by simultaneous addition of 3.35 mL of MN-14 (IgG-SH) (3.05×10^{-7} mol) and 3.35 mL of StAv-SMCC (3.05×10^{-7} mol) in 5 equal portions over 10 min to 6 mL of 0.1 M sodium phosphate at pH 7.0 while stirring. After 1 h at room temperature under an argon atmosphere, solid sodium tetrathionate was added to a final concentration of 5 mM and the solution was stirred for an additional 5 min. The reaction mixture was first purified on 16×3 mL spin columns in 0.1 M sodium phosphate at pH 7.3 and then as above on a preparative SE-HPLC column. Retention times on analytical size-exclusion HPLC columns were as follows: streptavidin, 11.5 min; MN-14, 10.0 min; and StAv-MN-14, 9.3 min.

For radiolabeling purposes, both conjugates were substituted with the strong chelating agent, Bz-DTPA. Briefly, to a solution of StAv-MN-14 (325 μ L, 4.6 mg, 2.15×10^{-8} mol) in 0.1 M sodium phosphate at pH 8.1 was added 4.1 μ L of ITC-Bz-DTPA (1.4×10^{-7} mol). The pH of the reaction mixture was raised to 8.4 with 5–10 μ L of a saturated solution of tribasic sodium phosphate, and the mixture was left at 37 °C for 90 min. The product was isolated following purification on two consecutive 3 mL spin columns in 0.1 M sodium acetate at pH 6.5.

StAv-MN-14 Prepared Using Biotin. This conjugate was prepared according to a published procedure (40). MN-14 was first biotinylated by treating MN-14 (17 mg, 1.1×10^{-7} mol, 18.1 mg/mL) in 0.1 M sodium phosphate at pH 8.6 with 12 μ L of 1 mg/100 μ L solution of sulfo-NHS-LC-biotin (2.2×10^{-7} mol). After 2 h at 4 °C, the biotinylated mab was purified on two consecutive 3 mL spin columns packed in 0.1 M sodium phosphate at pH 7. HABA analysis demonstrated 0.8 biotin per MN-14. This mab (10.9 mg in 800 μ L) was added to 1 mL of streptavidin (21 mg, 3.51×10^{-7} mol) in 0.1 M sodium phosphate at pH 7 in 5×200 μ L portions. After a further 30 min, the StAv-biotin-MN-14 conjugate was purified by SE-HPLC, as described above.

For each conjugate, retention of the biotin binding capacity was determined by mixing 10 μ L aliquots of the

StAv-MN-14 conjugate (1.2×10^{-7} M in 0.1 M sodium phosphate at pH 7.3) with 10 μ L of ^{111}In -bio-DTPA or bio-peptide-DOTA (0.3 μ Ci, 6×10^{-12} mol) (see below) in 0.1 M sodium acetate at pH 6.5 and determining the percentage of radioactivity associated with the conjugate by SE-HPLC. Values obtained were compared to those for free streptavidin (i.e., four biotin binding sites).

Galactosylation of Proteins. These compounds were prepared using published methods (29, 41). Briefly, CTTG (0.23 g, 5.7×10^{-4} mol) was dissolved in 6.2 mL of anhydrous methanol. Sodium methoxide, 0.5 M in methanol (115 μ L, 5.75×10^{-5} mol), was added to the above solution under argon and stirred at room temperature for 18 h. The imidate was used immediately, or unused portions were stored at 4 °C. Stored solutions were discarded upon the appearance of precipitate.

To galactosylate lysine residues on WI2, imidate corresponding to various imidate:WI2 molar ratios was evaporated in individual vials using a stream of argon. WI2 mab was added to each, the final protein concentration adjusted to 8.4 mg/mL by addition of 0.1 M sodium phosphate at pH 8.1, and the final pH adjusted to 8.5–8.6 with a saturated solution of tribasic sodium phosphate. Reaction mixtures were stirred at room temperature for 2 h, and the modified WI2s were purified on two consecutive sets of centrifuged spin columns packed with Sephadex G-50–80 in 0.1 M sodium phosphate at pH 7.3. Initially, the level of galactose modification was determined indirectly by analyzing the degree of modification of protein primary amines using a published fluorometric assay (42). Galactosylated WI2 samples were later analyzed by MALDI-MS to determine the exact number of galactose residues present.

HSA was biotinylated by treating 37.7 mg of purified HSA (5.54×10^{-7} mol) in 0.1 M sodium phosphate at pH 8.1 with 1.6 mg of sulfo-NHS-LC-biotin (2.88×10^{-6} mol) at a final protein concentration and pH of 15.6 mg/mL and 8.4, respectively. After 1 h at room temperature, the reaction mixture was applied to three sets of consecutive centrifuged spin columns to remove unreacted biotin. Biotin analysis by HABA showed 2.5 biotins per HSA. Several batches of biotinylated HSA were galactosylated with 100- and 300-fold molar excesses of dried imidate. Each reaction was performed at a final protein concentration of 10 mg/mL in 0.1 M sodium phosphate at pH 8.7, adjusted thereto with a saturated solution of tribasic sodium phosphate. After 2 h at room temperature with occasional vortexing, the conjugates were purified on two consecutive sets of spin columns with 0.1 M sodium phosphate at pH 7.5.

[5-(Biotinamido)pentyl]amidyl-Bz-DTPA (Bio-DTPA). This reagent was prepared by incubating [5-(biotinamido)pentyl]amine (86.3 mg, 2.63×10^{-4} mol) and ITC-Bz-DTPA (6.39×10^{-5} mol) in 1.2 mL of sodium phosphate at 37 °C for 1 h while the pH was maintained at 9.2 by occasional addition of saturated tribasic sodium phosphate. RP-HPLC analysis indicated completion of the reaction by consumption of ITC-Bz-DTPA. The product was isolated in 68–83% yield following purification on a preparative C-18 column using a step gradient of 0% B for 10 min and 20% B for 9 min, followed by a linear gradient of 20 to 30% B over 30 min at a constant flow rate of 75 mL/min. The retention time on an analytical C-18 column was 6.29 min. The identity of the product was confirmed by ESI mass spectrometry [m/e 869 ($M + H$)⁺].

[(Biotinamido)pentyl]-DOTA Monoamide. DOTA was activated using a published procedure (43). Briefly, DOTA (81.5 mg, 0.2 mmol) was suspended in 10 mL of DMF/triethylamine (Et₃N) (4:1 v/v) and stirred at room

temperature under argon for 18 h. The almost clear solution was cooled at 4 °C (ice bath) and was treated, under stirring, with a dropwise addition of isobutyl chloroformate (26.5 μ L, 0.2 mmol) using an Eppendorf pipette. After 15 min, [5-(biotinamido)pentyl]amine (65.7 mg, 0.2 mmol) was added. The reaction mixture was stirred for 5 h at room temperature. The solvents were evaporated using a high-vacuum pump, and the residue was dissolved in 8 mL of water and injected onto a preparative reverse-phase HPLC column. The HPLC conditions were as follows: elution with 0% B for 10 min, followed by a linear gradient of 0 to 100% B over 60 min, with the solvent flow constant at 75 mL/min. Mono-biotinylated DOTA (29 mg, 20.3% yield) was isolated as a white solid with a retention time of 5.57 min on the analytical RP-HPLC column; ESI mass spectrometry yielded a value of m/e 715 [M + H].

Biotin-D-Peptide-DTPAs. Peptides (1) biotin-D-Lys-NH₂, (2) biotin-D-Phe-D-Lys-NH₂, and (3) biotin-D-Phe-D-Phe-D-Lys-NH₂ were synthesized either manually or on an automated peptide synthesizer (Advanced Chemtech 348 MPS) by the standard solid-phase methodology (44) on a Rink resin (Advanced ChemTech; 0.56 mmol/g) in which the *N*- α -amino groups were Fmoc-protected. After the last amino acid was attached, biotin was coupled using *O*-benzotriazole-*N,N,N,N*-tetramethyluronium hexafluorophosphate (HBTU) (0.15 M), 1-hydroxybenzotriazole (HOBT) (0.15 M), and *N,N*-diisopropylethylamine (DIPEA) (0.75 M) in DMF. A minimal amount of *N*-methylpyrrolidinone was added to aid in solubilization. The peptides were cleaved from the resin with a solution of 91% TFA/4.5% water/4.5% ethylmethyl sulfide. Subsequent to removal of the solvents, the crude peptides (1–3) were treated with a 0.3–0.5:1 molar ratio of ITC-Bz-DTPA/peptide in water at pH 8.6 and 37 °C until all of the ITC-Bz-DTPA was determined to be consumed by monitoring with RP-HPLC. The peptide bio-D-Phe-D-Phe-D-Lys-NH₂ required 20% acetonitrile for solubilization in water. The unreacted peptides and the biotin-peptide-DTPAs were isolated by preparative RP-HPLC purification using a linear gradient from 0 to 70% B over 40 min at 75 mL/min. Yield: peptides, 59–64%; peptide-DTPA, 68–76%. Mass spectrum m/z (M + H)⁺: peptide 1 not isolated; peptide 2 (C₂₅H₃₈N₆O₄S), calcd 519, found 519; peptide 3 (C₃₄H₄₆N₇O₅S), calcd 666, found 666; peptide-DTPA 1 (C₃₈H₅₇N₉O₁₃S₂), calcd 912, found 912; peptide-DTPA 2 (C₄₇H₆₆N₁₀O₁₄S₂), calcd 1059, found 1059; peptide-DTPA 3 (C₅₆H₇₅N₁₁O₁₅S₂), calcd 1206, found 1206.

Biotin-D-Peptide-DOTAs. DOTA was activated as its *N*-hydroxysuccinimide ester according to a published procedure (45). To a solution of 450 mg (960 μ mol) of DOTA and 208 mg (960 μ mol) of sulfo-NHS in 1 mL of water, cooled to 4 °C, was added 503 μ L (91.5 mg, 477 μ mol) of 1-ethyl-3-[3-(dimethylamino)propyl]carbodiimide hydrochloride (EDC), freshly prepared in water at 4 °C. The reaction mixture was stirred at 4 °C for 30 min, after which it was used immediately, without purification. Crude biotinyl-D-peptide (~320 μ mol of biotin-D-Lys-NH₂, biotin-D-Phe-D-Lys-NH₂, or biotin-D-Ser-D-Lys-NH₂) dissolved in 500 μ L of acetonitrile and 2 mL of water was added to the active ester and the pH of the reaction adjusted to 8.5 with 6 N NaOH. The mixture was stirred for 15 h at 4 °C and purified on a preparative RP-HPLC column with a gradient system of 0 to 15% B over 40 min at 75 mL/min. For biotinylated DOTA chelating agents, yields, retention times on an analytical RP-HPLC col-

umn, and ESI-MS data are as follows.

	yield (mg)	ret. time (min)	m/z (M + H) ⁺	
			calcd	found
bio-D-Lys-(DOTA)-NH ₂ (C ₃₂ H ₅₅ N ₉ O ₁₀ S)	40	5.45	758	758
bio-D-Phe-D-Lys-(DOTA)-NH ₂ (C ₄₁ H ₆₄ N ₁₀ O ₁₁ S)	87	6.3	905	905
bio-D-Ser-D-Lys-(DOTA)-NH ₂ (C ₃₅ H ₆₀ N ₁₀ O ₁₂ S)	50	5.63	845	845

Radiolabeling. MN-14, streptavidin, and StAv-MN-14 were radioiodinated by the chloramine-T method (46). The StAv-MN-14-Bz-DTPA conjugate was radiolabeled with ⁸⁸Y (Los Alamos National Laboratory, Los Alamos, NM). Briefly, ⁸⁸YCl₃ was neutralized with 3 volumes of 0.5 M sodium acetate at pH 6.1 and mixed with the StAv-MN-14-Bz-DTPA conjugate at a specific activity of 0.1 mCi/mg. After 1 h at room temperature, 0.1 M DTPA was added to a final concentration of 10 mM and the mixture was left for an additional 10 min before applying to two consecutive spin columns of Sephadex G-50-80 in 0.1 M sodium acetate at pH 6.5. Purified yields ranged from 70 to 90%. All radiolabeled conjugates were analyzed by SE-HPLC. The immunoreactive fraction of radiolabeled MN-14 and StAv-MN-14 was estimated from the percentage of radioactivity shifting to an earlier HPLC retention time after complexation with an 10–80-fold molar excess of CEA for 5 min at room temperature.

Biotinylated chelating agents were radiolabeled with ¹¹¹In. Biotinylated DTPAs (6.5 \times 10^{−9} mol) in 122 μ L of 0.5 M sodium acetate at pH 6.1 were added to 2.3 mCi ¹¹¹InCl₃ (received in 0.05 M HCl and was then diluted with 3 volumes of 0.5 M sodium acetate at pH 6.1 before use) and incubated at room temperature for 1 h. The labeling yield was determined by analytical size-exclusion HPLC and by instant thin layer chromatography (ITLC) where approximately 0.2 μ Ci of the sample was applied to ITLC strips (Gelman Sciences) prespotted with 5 μ L of 1% HSA and developed in a 5:2:1 water/ethanol/ammonium hydroxide solvent system. In this ITLC system, unchelated ¹¹¹In remains at the origin while the chelated ¹¹¹In migrates with the solvent front. Radiolabeling of biotin-chelate was confirmed by HPLC analysis of the radiolabeled sample both before and after mixing with streptavidin, with successful radiolabeling indicated by a complete shift of retention time of the radioactive biotin-chelate (14–15 min) to the retention time of streptavidin (11.5 min). For biotinylated DOTA chelating agents, 2.4 mCi of InCl₃ in 3 volumes of 0.5 M ammonium acetate at pH 5.5 was mixed with 21.5 μ L of biotin-peptide-DOTA (4.7 \times 10^{−8} mol) in 0.5 M ammonium acetate at pH 5.5. Mixtures were held for 2 h at 42–45 °C in a preheated block, and radiolabeling (\geq 97%) was confirmed as for the DTPA-biotin-chelates.

For *in vitro* stability studies, chelates were labeled with either ¹¹¹In or ⁹⁰Y as described and diluted in 250 μ L of human serum to 1.2 \times 10^{−7} to 2.1 \times 10^{−6} M. Serum samples were incubated at 37 °C under a 5% CO₂ atmosphere, and 5–10 μ L aliquots were analyzed by HPLC before and after mixing with excess streptavidin (1–200-fold). The *in vitro* stability of biotinylated HSA was studied by incubating 20 μ g of bio₃-HSA-gal₃₉ in 500 μ L of mouse serum at 37 °C under 5% CO₂. Samples (20 μ L at 1 and 4 h) were mixed with ¹¹¹In-Bz-DTPA-StAv-MN-14 and analyzed by SE-HPLC.

RESULTS

StAv-MN-14 Conjugates. StAv-MN-14 conjugate preparation using both methods (Figure 1) resulted in

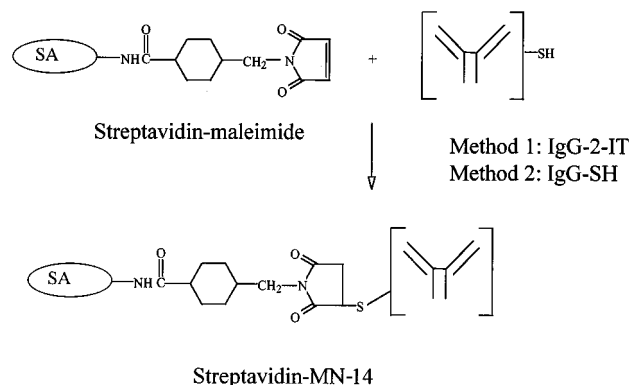


Figure 1. StAv-MN-14 (IgG) was prepared by covalent attachment of activated streptavidin to thiolated IgG (IgG-2IT, method 1) or MEA-reduced IgG (IgG-SH, method 2).

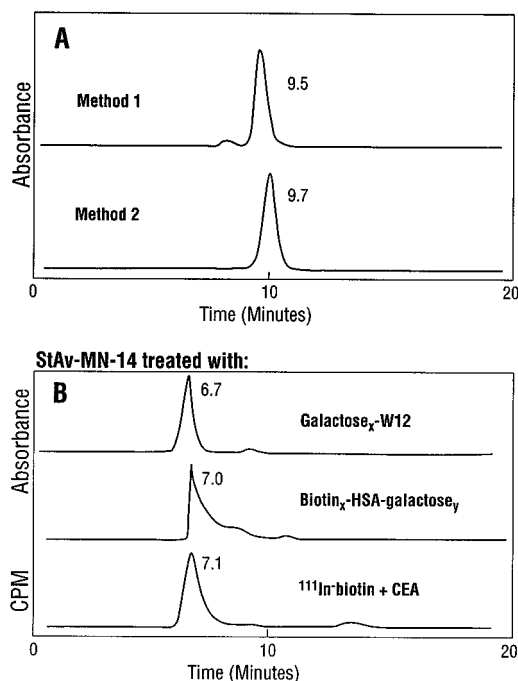


Figure 2. (A) HPLC chromatograms of StAv-MN-14 (IgG) conjugates prepared by 2-IT (method 1) and MEA (method 2) on an analytical size-exclusion HPLC column. (B) Characterization of StAv-MN-14. Retention of its binding properties with gal-WI2 (1:1), bio₃-HSA-gal₃₉ (1:1), and ¹¹¹In-bio plus CEA (20 × excess of CEA) as indicated by elution near the void volume on an analytical size-exclusion HPLC apparatus. Retention times: gal-WI2 (9.3 min), bio₃-HSA-gal₃₉ (11 min), and ¹¹¹In-bio-DTPA (15 min).

relatively low product yields, ~20–25% after preparative HPLC, when peaks were collected conservatively, as just the central peak fraction. Aggregates (~12%) were observed in the conjugate prepared by the 2-IT method during long term storage (50 days) at 4 °C, whereas no aggregation was observed in conjugate prepared by the MEA method during storage. Interestingly, monomeric conjugate prepared using the 2-IT method eluted at an earlier HPLC retention time (9.5 min) than conjugate prepared using MEA (9.7 min) (Figure 2A), suggesting formation of an apparently larger molecular weight or differently shaped compound using the 2-IT method.

To prove binding properties of StAv-MN-14s were retained, unlabeled conjugates were separately treated with WI2, bio-HSA-gal, and ¹¹¹In-bio-DTPA followed by CEA. In each instance, the StAv-MN-14 showed complexation to these agents with the formed complexes eluting at appropriate retention times on SE-HPLC (Figure 2B). Retention of full biotin binding capacity was

Table 1. Biotin Binding Capacity of Streptavidin and StAv-MN-14 Conjugates

protein	biotin binding capacity
streptavidin	4
StAv-MN-14 (2-IT method)	4 ± 0.3
StAv-MN-14 (MEA method)	4 ± 0.3
StAv-biotin-MN-14	3 ± 0.5

Table 2. Determination of Galactose Levels on mab WI2 by MALDI-MS

imide:protein ratio in galactosylation	MW by MALDI-MS	no. of galactose/WI2
0	149 562	0
15	149 830	1.1
30	150 517	4.0
75	153 012	14.6
400	157 740	34.7
400	160 000	44

shown by reference to unsubstituted streptavidin. Conjugates prepared by both the 2-IT and MEA reactions showed retention of four biotin binding sites (Table 1), whereas the StAv-biotin-MN-14 conjugate prepared using one of the biotin binding sites on streptavidin to link to biotinylated MN-14 showed 3 ± 0.5 biotin binding sites remaining, as would be expected (40). StAv-MN-14 conjugate (25 μg) incubated in 250 μL of mouse serum also showed full retention of biotin binding capacity by SE-HPLC when aliquots of it at 0, 1, and 24 h were mixed with excess ¹¹¹In-bio-peptide-DTPA.

The biodistribution of StAv-MN-14 (prepared with MEA) was compared to that of MN-14 in GW-39 tumor-bearing animals. Both were radioiodinated using the chloramine-T procedure and shown to bind to WI2 and CEA at 90–100% levels *in vitro* (data not shown). ¹²⁵I-StAv-MN-14 (10 μCi, 1 μg) and ¹³¹I-MN-14 (25 μCi, ~2 μg) were coinjected into groups of tumor-bearing nude mice with major organs obtained 3, 24, and 72 h postinjection (Figure 3). Similar, but not identical, biodistributions for MN-14 and StAv-MN-14 were seen.

Clearing Agents. The percentage of protein lysine residues that were modified with galactose was determined using a fluorescamine assay. Fluorometric analyses showed >81% modification of the available lysine residues on HSA with a 300-fold molar excess of thioimide and 37–52% modification with a 100-fold molar excess of thioimide. The WI2 samples were analyzed by MALDI-MS to determine the average level of modification per WI2. To determine the number of galactose residues attached to WI2, the molecular mass difference between the modified and unmodified WI2 was determined and divided by 236 (galactose residue formula weight). Results are shown in Table 2. HPLC analyses of mixtures of galactose_x-WI2 (where x = 0, 1, 4, 14.6, 35, and 44 residues) and MN-14 at a 1:1.6 molar ratio showed complete binding of galactosylated WI2 with MN-14 (results not shown). Galactosylated WI2 also showed complete binding to the StAv-MN-14 conjugate, as did biotin-HSA-galactose, a third possible clearing agent (Figure 2B).

In order to correlate the level of galactose substitution with blood clearance, WI2s with various galactose substitutions (0, 1, 4, 14.6, and 44) were radioiodinated and injected into BALB/c mice. Blood was drawn 1 h postinjection, and animals were sacrificed at 24 h for organ distribution studies. The results (Figure 4) showed rapid blood clearance of WI2 at galactose levels of >14. At these higher levels, the WI2 that was cleared from blood was taken up in the liver. At the highest galactose substitution, 44 per WI2, the blood level at 1 h was reduced to 0.7 ± 0.2% ID/g. Since high galactose

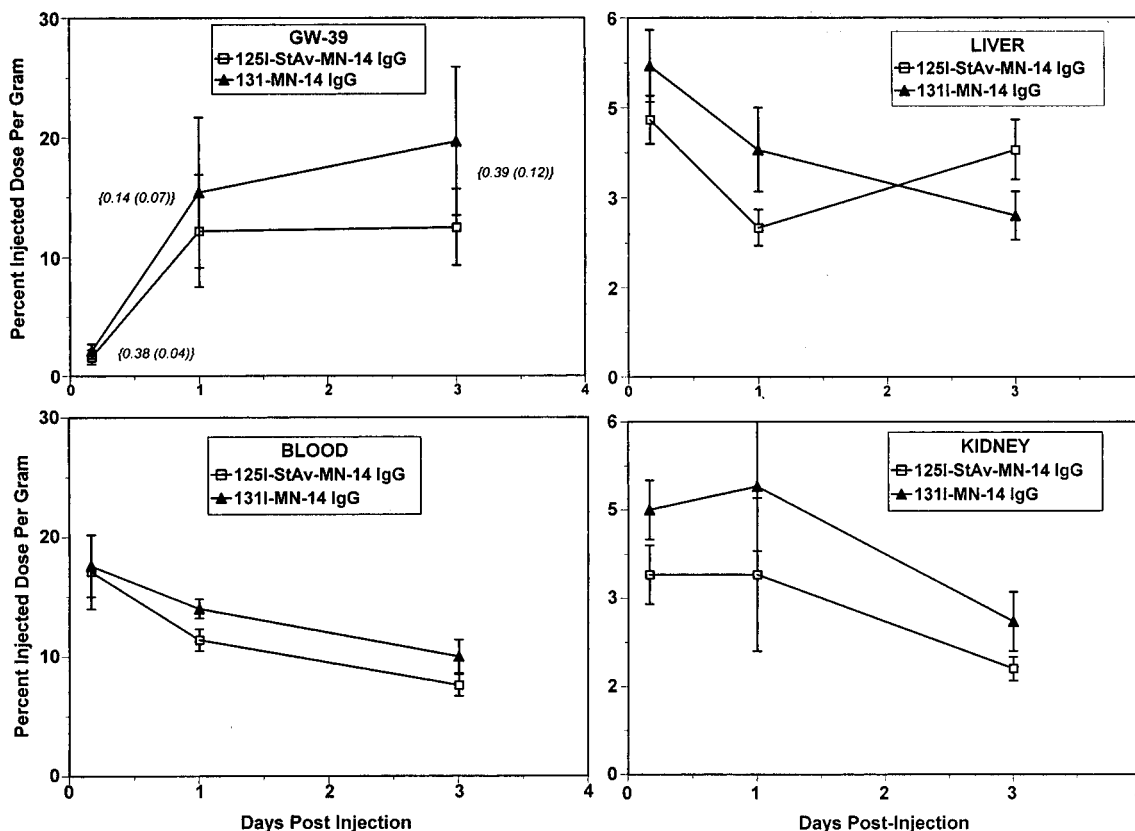


Figure 3. Comparison of the biodistribution of ^{125}I -StAv-MN-14 (IgG) and ^{131}I -MN-14 (IgG) in tumor-bearing mice in major organs: tumor, significant differences at all time points ($p < 0.02$); liver, significant differences at 4 and 72 h ($p < 0.006$); blood, significant differences at 24 and 72 h ($p < 0.05$); and kidney, significant differences at all time points ($p < 0.02$). Tumor sizes and standard deviations are shown in braces, and parentheses, respectively.

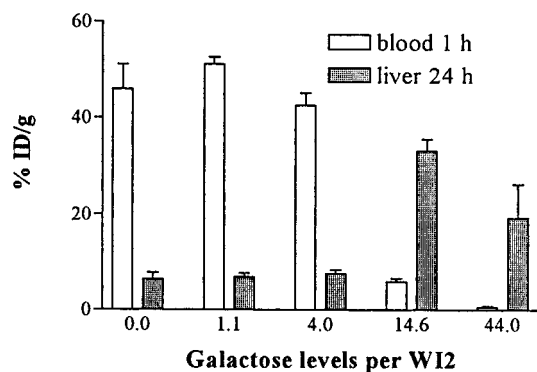


Figure 4. Effect of galactose levels on clearance of ^{125}I -gal-WI2. Higher galactose levels correspond to faster blood clearance.

substitutions did not effect WI2 binding to StAv-MN-14, but provided faster clearance from the blood, the higher substitution level was used for the pretargeting studies in animals.

The stability of the linkage between biotin and HSA toward mouse serum enzymes was examined *in vitro* and *in vivo*. ^{111}In -Bz-DTPA-StAv-MN-14 showed a shift to a higher MW on a SE-HPLC column when biotin₃-HSA-gal₃₉ incubated for 4 h in nude mouse serum was mixed with it, indicating the stability of biotin(s) on HSA to serum enzymes. One group of nude mice were injected with 200 μg of biotin₃-HSA-gal₃₉ and the other with 200 μg of biotin-HSA. Serum collected from the nude mice 1 and 8 h later was incubated with ^{111}In -Bz-DTPA-StAv-MN-14. HPLC analysis showed no binding with the biotin₃-HSA-gal at 1 and 8 h, suggesting rapid blood clearance of the agent reduced its concentration in the blood to undetectable levels. Thus it was not possible to

test the *in vivo* stability of the biotin-HSA-gal. However, ^{111}In -Bz-DTPA-StAv-MN-14 mixed with serum samples from mice given nongalactosylated biotin-HSA, at both 1 and 8 h, showed a shift to a higher molecular weight, thus demonstrating *in vivo* stability of at least one biotin-HSA linkage. These results suggest that the biotin-HSA-gal was also stable in the blood, particularly given its very short blood half-life.

Biotinylated Chelating Agents. Biotinylated chelating agents were radiolabeled with ^{111}In and mixed with unlabeled streptavidin prior to SE-HPLC to prove the presence of covalently attached biotin. Radiolabeled biotin-chelates eluted at 14–15 min, and streptavidin eluted at 11.5 min. Binding to streptavidin was demonstrated when the streptavidin and biotin-chelate mixture eluted at 11.5 min. Our first biotinylated chelate, biotin-DTPA, although stable in aqueous media, showed instability toward serum enzymes such that after 10 min in human serum only 58% of the radiolabeled chelate could still bind to streptavidin. At 21 h, no binding to streptavidin was observed. ITLC analysis of the serum sample at 21 h showed that the radiolabel was still bound to a chelate but had lost its biotin binding function. A similar behavior was observed with the first biotin-DOTA derivative. In contrast, *in vitro* stability studies of biotinylated DOTA and Bz-DTPAs, wherein the biotin and chelate are linked through D-amino acids, consistently showed serum stability for 48 h (data not shown). *In vivo* stability was shown by examining the excreted product in the urine taken from tumor-bearing mice given 200 μg of StAv-MN-14 followed 48 h later by a clearing agent, 200 μg of biotin₃-HSA-gal₃₉, and then given 40 μCi (6 μg) of biotin-D-Phe-D-Lys- ^{111}In -Bz-DTPA-NH₂ 2 h later. Urine was collected 4 h after biotin-D-Phe-D-Lys- ^{111}In -Bz-DTPA-NH₂ injection and analyzed by HPLC

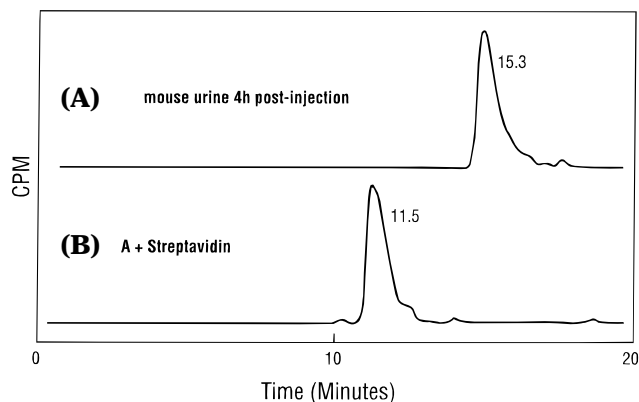


Figure 5. *In vivo* stability of ^{111}In -bio-D-Phe-D-Lys(ITC-Bz-DTPA)- NH_2 . (A) HPLC of mouse urine collected 4 h after injection of ^{111}In -labeled biotin in tumor-bearing mice pretargeted with StAv-MN-14 and cleared with $\text{bio}_3\text{-HSA-gal}$ 48 h later. ^{111}In -labeled biotin was injected 2 h after the clearing agent. (B) The same mouse urine treated with streptavidin.

before and after mixing with streptavidin. A shift in the retention time from that of radiolabeled peptide (15 min) to that of the radiolabeled peptide-streptavidin complex (11.5 min) was observed (Figure 5).

The biodistributions of two different biotinylated chelates were compared. ^{111}In -labeled DOTA and Bz-DTPA derivatives of bio-D-Phe-D-Lys- NH_2 ($40\ \mu\text{Ci}$; 5.8×10^{-9} moles of each) were injected intravenously in female nude mice bearing 5-day-old GW-39 tumors (average weight of 0.04–0.05 g). Figure 6 shows the biodistribution of these agents over a 48 h time period with five animals per group per time interval. Each conjugate was cleared from the blood very rapidly with less than 0.1% per gram at 1 h. The DOTA complex was 2-fold higher ($p < 0.05$)

in the blood than the DTPA complex at 1, 3, and 24 h. Most of the normal tissues had similar uptake with both complexes, except the liver and spleen. For example, at 24 h, the DOTA complex was about 3-fold higher ($p = 0.0028$) in the liver (0.03 ± 0.006 vs 0.01 ± 0.002). Tumor uptake was higher than that in most organs, except the kidney. Even without pretargeting, tumor:blood ratios were as high as 10.6 ± 2.8 for the DTPA complex at 1 h but decreased to about 4:1 at 3 and 24 h. The tumor:blood ratio for the DOTA complex was about 5:1 at each time point over the first 24 h.

DISCUSSION

This article describes reagent validation work which we considered essential before formal two-step pretargeting studies using a biotin/streptavidin recognition system, due to the complexities involved in the system. Certain potential pitfalls were expected prior to embarking on the work, and the importance of others became apparent as we proceeded. Some of these primarily involve biological aspects such as doses and timings and will be discussed elsewhere (38). Chemistry considerations included the simple ability to separate a pure sample of StAv-MN-14 for testing, a demonstration (qualitative and quantitative) that it retained its binding capacities and that it targeted tumor, choice of clearing and biotin chelating agents, and suitable stability studies, prior to embarking on more expensive preclinical *in vivo* studies.

For the first step, streptavidin conjugates of the MN-14 mab were prepared after streptavidin was derivatized with sulfo-SMCC to introduce maleimide groups. In one method, lysine residues of MN-14 were modified with 2-IT to introduce free SH groups, and in the other, disulfide bonds on IgG were reduced with MEA. In both

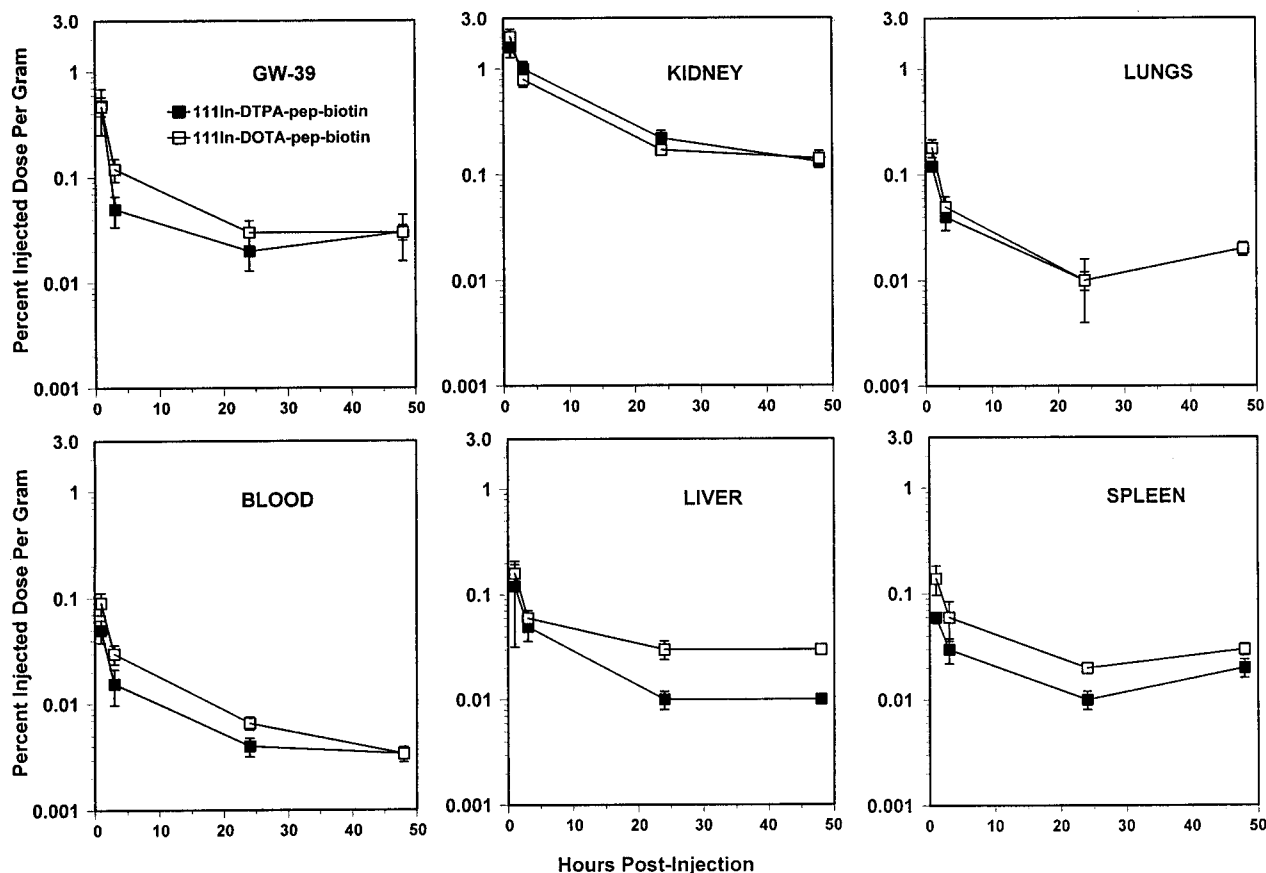


Figure 6. Comparison of the bioistribution of ^{111}In -labeled biotinylated chelates bio-D-Phe-D-Lys(DOTA)- NH_2 and bio-D-Phe-D-Lys(Bz-DTPA)- NH_2 in GW-39 tumor-bearing nude mice.

cases, varying reaction conditions were examined to improve conjugate yield, but conditions such as pH (5.1–7.4), concentration (4.6–11 mg/mL), temperature (4–37 °C), and reaction ratios (IgG:SA molar ratios of 0.5–4:1) did not improve yields significantly with either method. This is almost certainly due to the rapid kinetics of the thiol reaction with the maleimide under the range of conditions studied. Somewhat higher conjugate yields could be obtained, but these reactions invariably were accompanied by higher aggregate formation. To limit aggregate formation and protein losses, we chose to use a low number of sulfhydryl groups (2 ± 0.3 SH/IgG) generated on MN-14 using MEA, and the unused IgG-SH/IgG was collected during purification and recycled. Aggregate formation was minimized, but never eliminated. Others (16, 28) have claimed high yields of streptavidin–mab conjugates, but only low yields were observed with both methods described here. No attempt was made to improve yields for StAv–biotin–MN-14, prepared according to the method of Hnatowich *et al.* (40). The difference in retention times (apparent MWs) of StAv–MN-14 conjugates prepared by the two methods could be due to the linkage chemistry (Figure 1). We speculate that conjugates prepared via internal mab disulfide bonds must be approached more closely by the reacting SA than those prepared using 2-IT. In either case, non-radiolabeled StAv–MN-14 conjugates retained binding properties to CEA, to all possible clearing agents (WI2, galactosylated WI2, and biotinylated HSA), and to the biotin–chelate conjugates prepared as final step agents.

An important aspect of using StAv–MN-14 to pretarget tumors is the potential to increase uptake of radioactivity localized at tumor 4-fold due to the four biotin binding sites on streptavidin. For this to occur, it is essential that the biotin binding capacity on streptavidin be preserved after covalent attachment to MN-14. Biotin binding was found to be quantitative for both conjugates prepared with SMCC. In addition to stability in aqueous media, StAv–MN-14 conjugates were shown to retain biotin binding capacity in mouse serum *in vitro* for 24 h. StAv–MN-14 conjugate prepared using MEA was selected since it was found to be more resistant to aggregate formation during storage than the conjugate prepared using 2-IT.

Radiiodinated StAv–MN-14 prepared using the chloramine-T procedure did retain binding to CEA and WI2 (90–100%) *in vitro*, but it showed a partial loss (20–90%) of biotin binding capability to biotinylated HSA and other biotin compounds (results not shown), probably due to oxidation of biotin–binding tryptophan residues of the StAv, and made this type of agent unsuitable for dual radiolabel pretargeting work. Other iodination methods such as the Bolton–Hunter method were briefly investigated but discarded primarily due to unsatisfactory radioiodination yields. Instead, for radiotracer purposes, Bz-DTPA was attached to lysine residues of StAv–MN-14, radiolabeled with ^{89}Y without loss of binding characteristics, and used for targeting agent biodistributions.

Clearance agents based on biotin and anti-idiotypic recognition of StAv–MN-14 were developed and were further modified with galactose for rapid blood clearance (29). Studies with galactosylated WI2s showed faster blood clearance at higher galactose substitutions (Figure 4). In the case of HSA, stable biotin(s) also needed to be attached as a recognition system, and our *in vitro* and *in vivo* stability studies showed the stability of at least one biotin–HSA linkage toward serum enzymes, such as biotinidases. We cannot rule out the fact that some biotin(s) might have been cleaved from the HSA, since

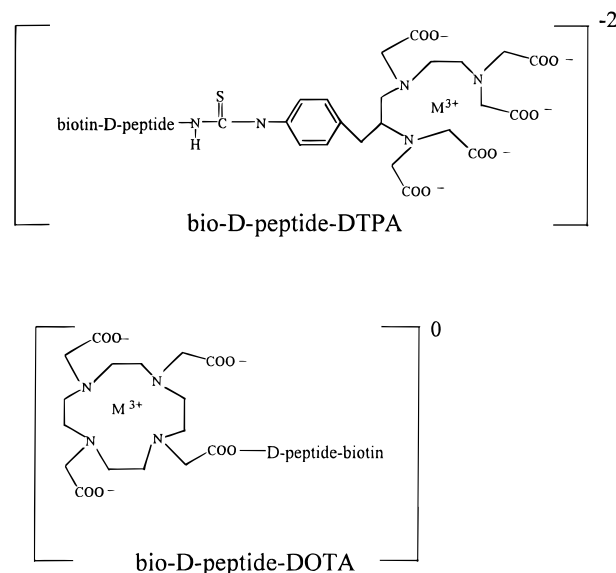


Figure 7. Metal complexes of biotinylated peptide chelating agents.

no effort was made to quantitate the biotins remaining bound on injected HSA.

The galactosylation reaction was somewhat inconsistent, because different levels of galactose modification were observed with the same ratios of activated thioimide:protein (Table 2). Thus, proteins were analyzed for galactose content after each such modification. Most interestingly, the level of galactose substitutions on either WI2 or HSA had no apparent effects on their respective ligand binding properties. A high galactosylation level was critical for fast blood clearance of either clearing agent (≥ 35 galactose residues per WI2). We have decided to concentrate on WI2, thinking that anti-idiotypic clearance will be a superior mechanism due to its lack of competitive binding to the tumor-targeted first-step agent, lack of potential for blocking to StAv binding sites, and more complete serum clearance.

For the final step, biotin–chelate conjugates consisting of biotin, a linker, and a chelating agent were prepared, first using commercially available [5-(biotinamido)pentyl]amine. Biotin–chelate conjugates with both DOTA and Bz-DTPA directly attached to this agent were found to be unstable toward serum enzymes. D-Amino acid peptides were selected as biotin–to–chelate linkers on the basis that they might offer stability toward serum enzymes and also later allow synthesis of reagents with variable hydrophobicities and serum clearance rates (hence, more tumor passes and higher tumor uptake). DOTA and Bz-DTPA were attached to a D-lysine side chain of the peptides and biotin to the α -amino terminus. All corresponding ^{111}In -labeled species then showed good *in vitro* and *in vivo* stability. When ^{111}In -labeled biotin-peptide–Bz-DTPA and bio-peptide–DOTA were compared for clearance in tumor-bearing mice (Figure 6), the former, containing a negatively charged ^{111}In –DTPA complex (Figure 7), cleared blood faster.

The first step in developing a complex delivery system such as this is to ensure that reagents are suitably characterized, functional, and stable under expected *in vivo* conditions, and this has been done. Investigation of a two-step pretargeting approach using the agents selected through these studies will be described elsewhere (38). Within this work, other issues then have to be considered, including the timing and dose of each reagent, the specific activity of the radiolabeled biotin–

chelate, and the effect of competition from endogeneous biotin for targeted StAv-MN-14 biotin-binding sites.

ACKNOWLEDGMENT

We acknowledge Agatha Sheerin for assisting in reagent preparation and Rosarito Aninipot for animal biodistribution studies. This work was supported in part by U.S. Public Health Service Grants CA-37895 and CA-39841 from the NIH.

LITERATURE CITED

- (1) Bamias, A., and Epenetos, A. A. (1992) Two-step strategies for the diagnosis and treatment of cancer with bioconjugates. *Antibody, Immunoconjugates, Radiopharm.* 5, 385–395.
- (2) Goodwin, D. A., Meares, C. F., McCall, M. J., McTigue, M., and Chaovapong, W. (1988) Pre-targeted immunoscintigraphy of murine tumors with indium-111-labeled bifunctional haptens. *J. Nucl. Med.* 29, 226–234.
- (3) Stickney, D. R., Anderson, L. D., Slater, J. B., Ahlem, C. N., Kirk, G. A., Schweighardt, S. A., and Frincke, J. M. (1991) Bifunctional antibody: A binary radiopharmaceutical delivery system for imaging colorectal carcinoma. *Cancer Res.* 51, 6650–6655.
- (4) Hawkins, G. A., McCabe, R. P., Kim, C.-H., Subramanian, R., Bredehorst, R., McCullers, G. A., Vogel, C.-W., Hanna, M. G., Jr., and Pomata, N. (1993) Delivery of radionuclides to pretargeted monoclonal antibodies using dihydrofolate reductase and methotrexate in an affinity system. *Cancer Res.* 53, 2368–2373.
- (5) Bos, E. S., Kuijpers, W. H. A., Meesters-Winters, M., Pham, D. T., deHaan, A. S., van Doormalen, A. M., Kaspersen, F. M., van Boeckel, C. A. A., and Gougeon-Bertrand, F. (1994) *In vitro* evaluation of DNA-DNA hybridization as a two-step approach in radioimmunotherapy of cancer. *Cancer Res.* 54, 3479–3486.
- (6) Hnatowich, D. J., Virzi, F., and Rusckowski, M. (1987) Investigations of avidin and biotin for imaging applications. *J. Nucl. Med.* 28, 1294–1302.
- (7) Paganelli, G., Pervez, S., Siccardi, A. G., Rowlinson, G., Deleide, G., Chiolerio, F., Malcovati, M., Scasellati, G. A., and Epenetos, A. A. (1990) Intraperitoneal radiolocalization of tumors pre-targeted by biotinylated monoclonal antibodies. *Int. J. Cancer* 45, 1184–1189.
- (8) Axworthy, D. B., Theodore, L. J., Gustavson, L. M., and Reno, J. M. (1993) Pretargeting methods and compounds. International Patent Application WO 93/25240.
- (9) Axworthy, D. B., Fritzberg, A. R., Hylarides, M. D., Mallet, R., Theodore, L. J., Gustavson, L., Su, F.-M., Beaumier, P. L., and Reno, J. M. (1995) Durable complete remissions of breast, lung and colon tumor xenografts with a single dose of pretargeted Y-90 in a mouse model. *J. Nucl. Med.* 36, 217P (abstract).
- (10) Saga, T., Weinstein, J. N., Jeong, J. M., Heya, T., Lee, J. T., Le, N., Paik, C. H., Sung, C., and Neuman, R. D. (1994) Two-step targeting of experimental lung metastases with biotinylated antibody and radiolabeled streptavidin. *Cancer Res.* 54, 2160–2165.
- (11) Sung, C., van Osdol, W. W., Saga, T., Neumann, R. D., Dedrick, R. L., and Weinstein, J. L. (1994) Streptavidin distribution in metastatic tumors pretargeted with a biotinylated monoclonal antibody: Theoretical and experimental pharmacokinetics. *Cancer Res.* 54, 2166–2175.
- (12) Marshall, D., Pedley, R. B., Melton, R. G., Boden, R., and Begent, R. H. J. (1995) Galactosylated streptavidin for improved clearance of biotinylated intact and F(ab)₂ fragments of an anti-tumor monoclonal antibody. *Br. J. Cancer* 71, 18–24.
- (13) Paganelli, G., Chinol, M., Grana, C., De Cicco, C., Cremonesi, M., Meares, C. F., Franceschini, R., Tarditi, L., and Siccardi, A. G. (1995) Optimization of the three-step pretargeting approach for diagnosis and therapy in cancer patients. *J. Nucl. Med.* 36, 225P (abstract).
- (14) Breitz, H., Ratliff, B., Reno, J., Axworthy, D., Fritzberg, A., Su, F.-M., Appelbaum, J., Kunz, S., Seiler, C., and Weiden, P. (1995) Performance of antibody streptavidin pretargeting in patients: Initial results. *J. Nucl. Med.* 36, 225P (abstract).
- (15) Pimm, M. V., Fells, H. F., Perkins, A. C., and Baldwin, R. W. (1988) Iodine-131 and indium-111 labeled avidin and streptavidin for pre-targeted immunoscintigraphy with biotinylated anti-tumor monoclonal antibody. *Nucl. Med. Commun.* 9, 931–941.
- (16) Sheldon, K., Baumal, R., and Marks, A. (1992) Targeting of [¹¹¹In]biocytin to cultured ovarian adenocarcinoma cells using covalent monoclonal antibody-streptavidin conjugates. *Appl. Radiat. Isot.* 43, 1399–1402.
- (17) Virzi, F., Fritz, B., Rusckowski, M., Gionet, M., Misra, H., and Hnatowich, D. J. (1991) New indium-111 labeled biotin derivatives for improved immunotargeting. *Nucl. Med. Biol.* 18, 719–726.
- (18) Del Rosario, R. B., Baron, L. E., Lawton, R. G., and Wahl, R. (1992) Streptavidin-biotinylated IgG conjugates: A simple procedure for reducing polymer formation. *Nucl. Med. Biol.* 19, 417–421.
- (19) Rosebrough, S. F. (1993) Pharmacokinetics and biodistribution of radiolabeled avidin, streptavidin and biotin. *Nucl. Med. Biol.* 20, 663–668.
- (20) Khawli, L. A., Alauddin, M. M., Miller, G. K., and Epstein, A. L. (1993) Improved immunotargeting of tumors with biotinylated monoclonal antibodies and radiolabeled streptavidin. *Antibody, Immunoconjugates, Radiopharm.* 6, 13–27.
- (21) Hnatowich, D. J., Fritz, B., Virzi, F., Mardirossian, G., and Rusckowski, M. (1993) Improved tumor localization with (strept)avidin and labeled biotin as a substitute for antibody. *Nucl. Med. Biol.* 20, 189–195.
- (22) Kang, Y.-S., and Pardridge, W. M. (1994) Use of neutral avidin improves pharmacokinetics and brain delivery of biotin bound to an avidin-monoclonal antibody conjugate. *J. Pharmacol. Exp. Ther.* 269, 344–350.
- (23) Kobayashi, H., Sakahara, H., Hosono, M., Yao, Z.-S., Toyama, S., Endo, K., and Konishi, J. (1994) Improved clearance of radiolabeled biotinylated monoclonal antibody following the infusion of avidin as a “chase” without decreased accumulation in the target tumor. *J. Nucl. Med.* 35, 1677–1684.
- (24) Kobayashi, H., Sakahara, H., Endo, K., Hosono, M., Yao, Z.-S., Toyama, S., and Konishi, J. (1994) Comparison of the chase effects of avidin, streptavidin, neutravidin, and avidin-ferritin on a radiolabeled biotinylated anti-tumor monoclonal antibody. *Jpn. J. Cancer Res.* 86, 310–314.
- (25) Kassis, A. I., Jones, P. L., Matalka, K. Z., and Adelstein, S. J. (1996) Antibody-dependent signal amplification in tumor xenografts after pretreatment with biotinylated monoclonal antibody and avidin or streptavidin. *J. Nucl. Med.* 37, 343–352.
- (26) Alvarez-Diez, T. M., Polihronis, J., and Reilly, R. M. (1996) Pretargeted tumor imaging with streptavidin immunoconjugates of monoclonal antibody CC49 and ¹¹¹In-DTPA-biocytin. *Nucl. Med. Biol.* 23, 459–466.
- (27) Rusckowski, M., Fogarasi, M., Virzi, F., and Hnatowich, D. J. (1995) Influence of endogeneous biotin on the biodistribution of labelled derivatives in mice. *Nucl. Med. Commun.* 16, 38–46.
- (28) Ngai, W. M., Reilly, R. M., Polihronis, J., and Shpitz, B. (1995) *In vitro* and *in vivo* evaluation of streptavidin immunoconjugates of the second generation TAG-72 monoclonal antibody CC49. *Nucl. Med. Biol.* 22, 77–86.
- (29) Mattes, M. J. (1987) Biodistribution of antibodies after intraperitoneal or intravenous injection and effects of carbohydrate modifications. *J. Natl. Cancer Inst.* 79, 855–863.
- (30) Chauhan, J., and Dakshinamurti, K. J. (1986) Purification and characterization of human serum biotinidase. *J. Biol. Chem.* 261, 4268–4275.
- (31) Hansen, H. J., Goldenberg, D. M., Newman, E. S., Grebenau, R., and Sharkey, R. M. (1993) Characterization of second-generation monoclonal antibodies against carcinoembryonic antigen. *Cancer* 71, 3478–3485.
- (32) Losman, M. J., Novick, K. E., Goldenberg, D. M., and Monestier, M. (1994) Mimicry of a carcinoembryonic antigen epitope by a rat monoclonal anti-idiotypic antibody. *Int. J. Cancer* 56, 580–584.

- (33) Cummins, C. H., Rutter, E. W., and Fordyce, W. A. (1991) A convenient synthesis of bifunctional chelating agents based on diethylenetriaminepentaacetic acid and their coordination chemistry. *Bioconjugate Chem.* 2, 180–186.
- (34) Meares, C. F., McCall, M. J., Reardon, D. T., Goodwin, D. A., Diamanti, C. I., and McTigue, M. (1984) Conjugation of antibodies with bifunctional chelating agents: Isothiocyanate and bromoacetamide reagents, methods of analysis, and subsequent addition of metal ions. *Anal. Biochem.* 142, 68–78.
- (35) Penefsky, H. S. (1979) A centrifuged column procedure for the measurement of ligand binding by beef heart F1. Part G. *Methods Enzymol.* 56, 527–530.
- (36) Green, N. M. (1965) A spectrophotometric assay for avidin and biotin based on binding of dyes by avidin. *Biochem. J.* 94, 23c–24c.
- (37) Savage, M. D., Mattson, G., Desai, S., Nielander, G. W., Morgensen, S., and Conklin, E. J. (1994) Assays for biotin and avidin. In *Avidin-Biotin Chemistry: A Handbook*, 2nd ed., pp 14–21, Pierce Chemical Co., Rockford, IL.
- (38) Sharkey, R. M., Karacay, H., Griffiths, G. L., Behr, T. M., Blumenthal, R., Mattes, M. J., Hansen, H. J., and Goldenberg, D. M. (1997) Development of a two-step avidin-biotin pretargeting method for radioimmunotherapy of colorectal cancer. *Bioconjugate Chem.* 8, 595–604.
- (39) Ellman, G. L. (1959) Tissue sulfhydryl groups. *Arch. Biochem. Biophys.* 82, 70–77.
- (40) Rowlinson-Busza, G., Hnatowich, D. J., Ruszkowski, M., Snook, D., and Epenetos, A. A. (1993) Xenograft localization using pretargeted streptavidin-conjugated monoclonal antibody and ^{111}In -labeled biotin. *Antibody, Immunoconjugates, Radiopharm.* 6, 97–109.
- (41) Lee, Y.-C., Stowell, C. P., and Krantz, M. J. (1976) 2-Imino-2-methoxyethyl-1-thioglycosides: New reagents for attaching sugars to proteins. *Biochemistry* 15, 3956–3963.
- (42) Stocks, S. J., Jones, A. J. M., Ramey, C. W., and Brooks, D. E. (1986) A fluorometric assay of the degree of modification of protein primary amines with polyethylene glycol. *Anal. Biochem.* 154, 232–234.
- (43) Li, M., and Meares, C. F. (1993) Synthesis, metal chelate stability studies, and enzyme digestion of a peptide-linked DOTA derivative and its corresponding radiolabeled immunoconjugates. *Bioconjugate Chem.* 4, 275–283.
- (44) Bodansky, M. (1993) *Principles of Peptide Synthesis*, 2nd ed., pp 1–329, Springer-Verlag, Berlin.
- (45) Lewis, M. R., Raubitschek, A., and Shively, J. E. (1994) A facile, water-soluble method for modification of proteins with DOTA. Use of elevated temperature and optimized pH to achieve high specific activity and high chelate stability in radiolabeled immunoconjugates. *Bioconjugate Chem.* 5, 565–576.
- (46) Greenwood, F. C., and Hunter, W. M. (1963) The preparation of I-131 labeled human growth hormone of high specific radioactivity. *Biochem. J.* 89, 114–123.

BC970102N

Development of a Streptavidin–Anti-Carcinoembryonic Antigen Antibody, Radiolabeled Biotin Pretargeting Method for Radioimmunotherapy of Colorectal Cancer. Studies in a Human Colon Cancer Xenograft Model[†]

Robert M. Sharkey,^{*,‡} Habibe Karacay,[§] Gary L. Griffiths,[§] Thomas M. Behr,[‡] Rosalyn D. Blumenthal,[‡] M. Jules Mattes,[‡] Hans J. Hansen,[§] and David M. Goldenberg[‡]

Garden State Cancer Center, Belleville, New Jersey 07109, and Immunomedics, Inc., Morris Plains, New Jersey 07950. Received February 25, 1997[®]

Pretargeting methodologies can produce high tumor:blood ratios, but their role in cancer radioimmunotherapy (RAIT) is uncertain. A pretargeting method was developed using a streptavidin (StAv) conjugate of MN-14 IgG, an anti-carcinoembryonic antigen (CEA) murine monoclonal antibody (mab) as the primary targeting agent, an anti-idiotypic antibody (WI2 IgG) as a clearing agent, and DTPA- or DOTA-conjugated biotin as the radiolabeled targeting agent. A variety of reagents and conditions were examined to optimize this method. At 3 h, ¹¹¹In–DTPA–peptide-biotin tumor uptake was 3.9 ± 0.8 % per gram and tumor:blood ratios were >11:1. By 24 h, this ratio was 178:1, but tumor accretion declined in accordance with the gradual loss of StAv–MN-14 from the tumor. Tissue retention was highest in the liver and kidneys, but their tumor:organ ratios were >2:1. Dosimetry predicted that radiolabeled MN-14 alone would deliver higher tumor doses than this pretargeting method. Increasing the specific activity and using DOTA–biotin in place of DTPA increased tumor uptake nearly 2-fold, but analysis of StAv–MN-14's biotin-binding capacity indicated over 90% of the initial biotin-binding sites were blocked within 24 h. Animals fed a biotin-deficient diet had 2-fold higher ¹¹¹In–DOTA–biotin uptake in the tumor, but higher uptake also was observed in all normal tissues. Although exceptionally adept at achieving high tumor:blood ratios rapidly, the tumor uptake of radiolabeled biotin with this pretargeting method is significantly ($p < 0.0001$) lower than that with a radiolabeled antibody. Endogenous biotin and enhanced liver and kidney uptake may limit the application of this method to RAIT, especially when evaluating the method in animals, but with strategies to overcome these limitations, this pretargeting method could be an effective therapeutic alternative.

INTRODUCTION

Improving the therapeutic window for RAIT requires either increasing the amount and duration of radiolabeled antibody delivered to the tumor or decreasing the amount and residence time in normal tissues. Maximum tumor accretion is observed with whole IgG, but with a blood clearance time of 2–3 days in patients, the red marrow also is exposed to a substantial radiation dose. Bivalent and monovalent antibody fragments are cleared more rapidly from the blood with higher tumor:blood ratios, and thus, a higher radiation dose can be given. For example, nude mice can survive 275 μ Ci of ¹³¹I-labeled IgG, but with F(ab')₂ fragments, the dose can be escalated to 1.0–1.2 mCi (1). However, antibody fragments have lower tumor uptake and a shorter half-life in the tumor than IgG (2). There have been reports in some animal models of improved antitumor effects with F(ab')₂ fragments over whole IgG (3), but we could not observe an appreciable advantage of a single injection of an antibody fragment in comparison to whole IgG in animals (4). Fab and even single-chain antibodies (scFv) have not been widely used for therapy due to their low tumor and high renal uptake. Renal accretion of fragments can be reduced substantially by basic amino acids

(5–7), and Behr *et al.* (8) showed that ⁹⁰Y-labeled Fab fragments have antitumor effects rivaling that of whole IgG. Thus, with their smaller size enabling them to penetrate tumors more uniformly than whole IgG (9, 10), antibody fragments may yet become highly effective radiotherapeutics.

Other approaches to retaining high tumor uptake while reducing blood concentrations of radiolabeled antibody have been explored. Our studies (11, 12), as well as those of others (13–15), showed that the administration of anti-antibodies can reduce blood concentrations of radiolabeled antibodies very quickly. The rapid clearance of the antibody from the blood also reduces the level of antibody in the tumor, but it usually takes 1–2 days before tumor levels decrease substantially. Early indications suggest that ¹³¹I–NP-4 anti-carcinoembryonic antigen (CEA)¹ IgG combined with an anti-idiotypic antibody given at 24 h improves antitumor activity in tumor-bearing nude mice (16). Since the anti-antibody and radiolabeled antibody complexes are cleared predominantly by the liver, this procedure is ideally suited only for radioiodinated and not radiometal-labeled (i.e., ⁹⁰Y) antibodies. Extracorporeal removal of radiolabeled antibodies from the blood is also possible (17, 18). This procedure allows antibodies with any radiolabel to be used. One clinical study suggested that this method reduced tumor uptake by only 10% while decreasing blood pool by 59%, but other studies have shown a 20–25% loss from the tumor (17).

[†] Presented at the Sixth Conference on Radioimmunodetection and Radioimmunotherapy of Cancer in Princeton, NJ, on October 10–12, 1996.

* Address for correspondence and reprints: Robert M. Sharkey, Ph.D., GSCC, 520 Belleville Ave., Belleville, NJ 07109.

[‡] Garden State Cancer Center.

[§] Immunomedics, Inc.

[®] Abstract published in *Advance ACS Abstracts*, July 1, 1997.

¹ Abbreviations: Av, avidin; CEA, carcinoembryonic antigen; gal, galactose; DTPA–peptide-biotin, DTPA–D-Phe-D-Lys-biotin; i.v., intravenous; % ID/g, percent injected dose per gram; MIRD, medical internal radiation dose; StAv, streptavidin.

Pretargeting approaches dissociate the radiolabel from the large, slow-clearing antibody to a small, extremely fast-clearing compound. The radiolabeled carrier also is designed to pass freely from the kidneys, thereby avoiding high renal retention. Several pretargeting approaches have been described (19), and each reportedly produces high tumor:blood ratios within hours. The avidin (or streptavidin)–biotin procedures are of particular interest due to the exceptionally high affinity of biotin for avidin, and with up to four potential biotin-binding sites per avidin molecule, the amount of radioactivity targeted to the tumor may be amplified. Several approaches have been used: pretarget with biotin-conjugated mab, followed by radiolabeled avidin (Av) or more commonly streptavidin (StAv); pretarget with biotin-conjugated mab followed by StAv or Av clearance/bridging, and then target with radiolabeled biotin; or pretarget with StAv-conjugated mab followed by targeting with radiolabeled biotin. Although sometimes referred to as two- or three-step procedures, these methods commonly require a minimum of three, and as many as five, separate injections, each one being precisely timed and with carefully determined dosages. On the basis of the findings of Axworthy *et al.* (20), who showed similar tumor accretion of labeled biotin in comparison to a whole IgG, we decided to investigate a streptavidin mab, radiolabeled biotin pretargeting method. Our purpose in developing this technology was to determine if a pretargeting approach could be an effective therapeutic method. This report, and that of Karacay *et al.* (21), describe our initial investigation of this approach and examine the prospects for its development as a viable approach for the therapy of cancer.

MATERIALS AND METHODS

Reagents. All reagents used in these studies were described in detail by Karacay *et al.* (21). Briefly, the studies were conducted with a StAv–MN-14 anti-CEA IgG conjugate prepared by mixing StAv (Pierce, Rockford, IL) that was modified with sulfosuccinimidyl 4-(*N*-maleimidomethyl)cyclohexane-1-carboxylate and mercaptoethylamine (SMCC)-reduced murine MN-14 anti-CEA IgG mab (22) (method 2 in Karacay *et al.* (21)). In most instances, the conjugate administered to the animals contained a tracer quantity ($<2\ \mu\text{g}$) of either radioiodinated or ^{88}Y -labeled StAv–MN-14. Each radiolabeled conjugate was tested by size-exclusion high-pressure liquid chromatography (HPLC) and instant thin-layer chromatography (ITLC). The immunoreactive fraction was determined by mixing the labeled conjugate with a molar excess of CEA (Scripps, San Diego, CA) and observing a shift in the sizing profile by size-exclusion HPLC. The rat monoclonal WI2 IgG was produced in a bioreactor and then purified by protein A. It was used without modification or after galactosylation (21). Biotinylated DTPA and DOTA were prepared with a peptide spacer (e.g., DTPA–D-Phe–D-Lys–biotin or DTPA–peptide–biotin) to eliminate cleavage by serum enzymes (21). The chelated biotin was radiolabeled with ^{111}In (New England Nuclear, North Bellerica, MA) according to Karacay *et al.* (21).

Animal Studies. Studies were conducted in 5–8-week-old, female BALB/c or athymic nude mice (CR-Nu-Nu; Taconic, Germantown, NY). All animals were watered and fed *ad libitum* a standard lab chow (autoclavable Rodent Lab Chow, PMI Feed, Inc., St. Louis, MO) or a biotin-deficient diet (with 30% egg white solids; Harlan Teklad, Madison, WI). Whenever radioiodinated agents were administered, water was supplemented with Lugol's

iodine solution (1 mL/500 mL). The GW-39 human colonic tumor cell line (23), serially propagated in nude mice, was used for tumor targeting. Tumors were removed aseptically from mice bearing stock cultures and placed in Hank's balanced salt solution (HBSS; Gibco, Life Technologies, Grand Island, NY). Tumors were weighed, and the tumor of the desired weight was placed in a petri dish with HBSS, finely minced with scissors, and then passed through a 40-mesh wire screen to obtain a uniform cell suspension. The tumor was rinsed in a sterile beaker with a volume of HBSS equal to 10 times the tumor weight (i.e., a 10% w/v cell suspension). Animals were inoculated subcutaneously with 0.2 mL of the tumor suspension. The injection of the primary antibody occurred 5–6 days later, when tumors were about 0.05 g. Since a majority of the studies were completed within 3–4 days thereafter, the tumor size at the termination of most studies ranged from 0.05 to 0.12 g. The actual average tumor size for each study is given in the figure legends. These small-sized tumors minimized the amount of StAv–MN-14 IgG necessary to saturate antigen-binding sites in the GW-39 tumors. Such conservative measures were taken because of the relatively low yields obtained during StAv–MN-14 production (21).

All agents were injected intravenously in the lateral tail vein in a volume of 0.05–0.2 mL of buffer. In most instances, dual tracers were utilized to monitor two of the injected agents. In order to determine more precisely the amount of StAv–MN-14 IgG in the blood prior to administering a clearing agent, three to five mice were bled immediately before the pending injection of the clearing agent (actual number for each study given in the figure legend). Using the specific activity of the radiolabeled StAv–MN-14 IgG (including total unlabeled StAv–MN-14 injected), the molar concentration of conjugate in the total blood volume was determined. A total blood volume of 1.5 mL (approximately 7.4% of a 20 g mouse) was assumed per animal, and thus, the final mole ratio of clearing agent was adjusted accordingly. At the designated time, three to seven animals were selected from their respective treatment groups, anesthetized with sodium pentobarbital, bled by cardiac puncture, and then euthanized by cervical dislocation. Tumors and major organs (liver, spleen, kidneys, and lung) were removed and weighed. Tissues, including weighed blood, were placed in 4 mL vials and counted in a γ scintillation counter using channels appropriate for the individual or paired isotopes. With paired isotopes, windows were set to eliminate dual-channel crossover. Channel crossover was determined by counting a series of standards containing increasing levels of radioactivity from the single radionuclide. Each group of tissues was also counted with standards prepared from the stock agent(s) injected into the respective animals. Commonly, 10 μCi of ^{125}I -, 25 μCi of ^{131}I -, 1 μCi of ^{88}Y -, and 40 μCi of ^{111}In -labeled agents were injected with the prescribed amount of total agent. The Results and figure legends contain more details for each experiment. Dosimetry calculations were based on extended biodistribution studies using the specified agent (e.g., labeled antibody or biotin). The methodology used to calculate radiation doses in mice has been reported (24). Briefly, time–activity curves for tumors were fit by trapezoidal modeling, whereas most normal tissues were fit to exponential functions, with the exception of the case when the activity in a tissue failed to decline over time or the r coefficient was <0.9 for the exponential fit. Under these circumstances, a trapezoidal function was used. Time–activity curves were extrapolated to infinity, using the last two time points to define the remaining portion of the curve, and integrated to

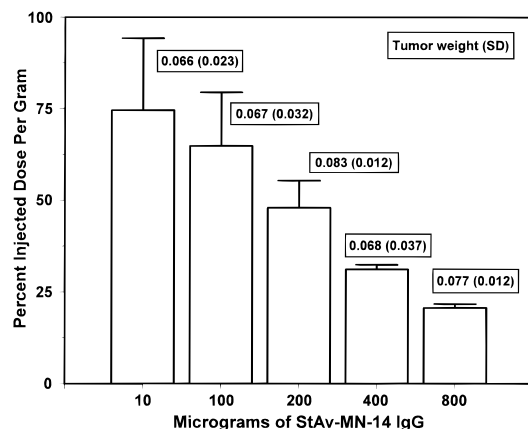


Figure 1. Determinations of optimal protein dose for saturating small GW-39 tumors with StAv–MN-14 IgG. Nude mice ($n = 5$ /group) were injected intravenously with ^{131}I –StAv–MN-14 IgG ($2 \mu\text{g}/25 \mu\text{Ci}$) containing the prescribed dose of unlabeled StAv–MN-14. Animals were necropsied 2 days later. The average tumor weight for each group of animals is shown in the bar with their corresponding SD.

obtain cumulated activity. S factors were derived previously for small volumes. The cumulated activity was converted to absorbed radiation dose according to standard medical internal radiation dose (MIRD) schema.

RESULTS

Development of the Targeting Approach. This pretargeting approach is divided into three separate steps: the pretargeting of the StAv–MN-14 IgG conjugate, the clearance of residual StAv–MN-14 from the blood, and finally the injection of the radiolabeled biotin. Each of these steps was evaluated independently and optimized on the basis of the considerations described below.

As shown by Karacay *et al.* (21), the StAv–MN-14 IgG and MN-14 IgG had similar biodistribution properties. For pretargeting approaches, sufficient quantities of the primary StAv–antibody conjugate should be given to provide adequate numbers of surrogate binding sites for the biotin. We had shown previously that a protein dose of nearly 1.0 mg was required to saturate CEA-binding sites in relatively small (~ 0.2 g) GW-39 tumor xenografts grown in the hamster cheek pouch (25). In nude mice bearing small GW-39 tumors, lower protein doses could be used, but doses of 0.4 mg were still necessary (26). As shown in Figure 1, the percent uptake of StAv–MN-14 in tumors of 0.06–0.08 g was approximately 70% of the injected dose per gram at a protein dose level of $10 \mu\text{g}$. In comparison to the uptake seen at $10 \mu\text{g}$, a significant decrease in the percent uptake, signifying saturation of antigen-binding sites, did not occur until protein doses of $200 \mu\text{g}$ and higher were used ($p < 0.022$). Thus, 200 – $400 \mu\text{g}$ of StAv–MN-14 IgG was considered the optimal dosage for pretargeting procedures. A dosage of $200 \mu\text{g}$ was used in most studies.

Given our experience using anti-antibodies as clearing agents (11, 12, 16), the anti-idiotypic WI2 antibody was the primary clearing agent of interest. However, two options were considered: use of the WI2 antibody alone or a galactosylated conjugate of WI2 (gal–WI2). Galactosylating antibodies accelerate an IgG's clearance from the blood (27), and Karacay *et al.* (21) showed that >14 galactose residues per WI2 were required to accelerate its clearance from the blood. For pretargeting applications, WI2 was galactosylated with >36 galactose per WI2. In order to determine a suitable protein dose for the WI2 clearing agent, clearance studies were first

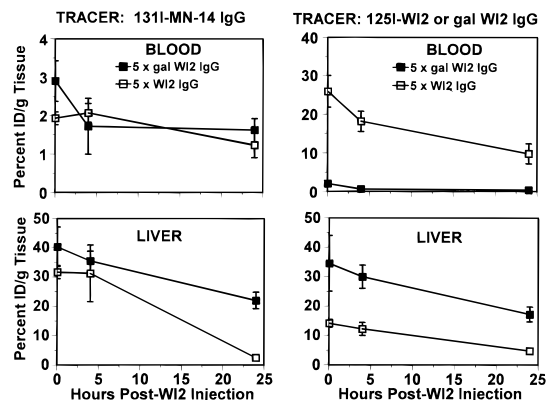


Figure 2. Assessment of primary antibody clearance by the WI2 or gal–WI2 anti–MN-14 idiotype IgG clearing agent in BALB/c mice. Animals were injected intravenously with $25 \mu\text{Ci}$ ($2 \mu\text{g}$) of ^{131}I –MN-14 IgG. Three days later, groups of animals ($n = 3$) were given increasing doses of either WI2 or gal–WI2 IgG, starting at 5 times the molar amount of MN-14 remaining in the blood at the time of WI2 injection, and increasing 10, 50, and 100 times. The clearing agent contained ^{125}I –WI2 or gal–WI2 so the distribution of the clearing agent could be monitored. The left panels show the distribution of ^{131}I –MN-14 at the designated times after the injection of the clearing agent, while the right panels show the corresponding WI2 or gal–WI2 distribution in these same animals. Data are shown only for the group of animals given 5 times the amount of WI2 or gal–WI2, since no differences were seen between these groups and those with the higher concentrations of clearing agents. Values represent the means, and the bars are the SD for each observation.

conducted in BALB/c mice injected with ^{131}I –MN-14 IgG ($2 \mu\text{g}$), followed 72 h later by WI2 or gal–WI2. The amount of WI2 was adjusted to prescribed molar excesses in relationship to the amount of MN-14 IgG remaining in the entire blood pool, on the basis of the specific activity of the radiolabeled MN-14 conjugate. WI2 or gal–WI2 in molar excesses of 5-, 10-, 50-, and 100-fold were tested. ^{125}I -labeled WI2 or gal–WI2 was added to the WI2 or gal–WI2, respectively, as a tracer dose. The blood concentration of ^{131}I –StAv–MN-14 IgG was reduced as effectively with a 5-fold molar excess as with higher molar concentrations of either WI2 or gal–WI2 (data not shown), indicating that this lower molar excess was sufficient for clearing StAv–MN-14 from the blood for either agent. As seen in Figure 2 (left panel), the StAv–MN-14 blood concentration was reduced from 23.3 ± 2.6 % per gram to between 2 and 4 % within just 15 min of the WI2 or gal–WI2 injection, respectively. There appeared to be a more rapid blood clearance of the MN-14 with the WI2, but within 4 h of their injection, no differences were seen between the concentrations of MN-14 remaining in the blood, regardless of which clearing agent was used. As expected, the gal–WI2, as reflected by the ^{125}I -labeled tracer (Figure 2, right panel), was itself cleared from the blood very quickly, with 2.0 ± 0.6 % of the injected dose per gram in the blood within 15 min. A separate group of BALB/c mice which were coinjected with an identical concentration of only radiolabeled gal–WI2 and WI2 (i.e., no preinjection of MN-14) showed identical blood clearance kinetics for gal–WI2 and WI2 (not shown). This further illustrated the fact that there was an abundant molar excess of gal–WI2 and WI2 to affect the clearance of MN-14 without affecting their own clearance.

Regardless of the clearing agent used, MN-14 was cleared primarily into the liver, with the liver concentration of MN-14 increasing from 3.2 % injected dose per gram to between 30 and 40% within 15 min of the WI2 or gal–WI2 injection, respectively (Figure 2, left panel). An interesting difference was found between gal–WI2

and WI2 in relationship to the amount of radiolabeled MN-14 remaining in the liver. Within 24 h of the unconjugated WI2 injection, the concentration of MN-14 in the liver had decreased to $2.4 \pm 0.5\%$, whereas the amount of MN-14 in the liver of animals who received gal-WI2 had decreased to only $22.0 \pm 2.9\%$. As shown previously (27), galactosylated proteins are taken up in the liver, but unlike antigen-antibody complexes that are removed predominantly by the reticuloendothelial (RE) cells in the liver, galactosylated proteins are removed by galactose receptors on hepatocytes. This was observed in a separate group of animals (three animals per time point) that received a mixture of ^{131}I - and ^{125}I -labeled gal-WI2 and unconjugated WI2 (not shown). In these animals, $63.3 \pm 3.0\%$ of the gal-WI2 was in the liver within 15 min, with only $1.2 \pm 0.1\%$ remaining in the blood. This compares to $20.0 \pm 1.6\%$ in the liver for unconjugated WI2 alone with a blood concentration of $28.8 \pm 5.3\%$ at the same time point. The level of gal-WI2 in the liver even in these animals remained significantly higher than that of WI2 alone for the 24 h this study was monitored (at 24 h, 19.2 ± 7.0 vs $6.2 \pm 0.5\%$ for gal-WI2 vs WI2, respectively; $n = 3$, $p = 0.033$). Thus, the slower rate of MN-14 clearance from the liver in animals given gal-WI2 as the clearing agent was probably due to its association with gal-WI2.

The clearance properties of StAv-MN-14 with either unconjugated WI2 or gal-WI2 was identical to that described above for MN-14, regardless of the StAv-MN-14 protein dose administered, as long as the dose of the WI2 was given in the prescribed 5-fold molar excess. Despite the differences in how gal-WI2 and WI2 are distributed, the most important finding was the fact that the MN-14 cleared by the gal-WI2 was retained in the liver at a higher level than that seen when WI2 alone was used. This suggests that agents cleared via the hepatocytes may not be catabolized from the liver as rapidly as when they are cleared by the RE cells. Studies in nude mice bearing GW-39 xenografts showed more WI2 in the tumor (3.0 ± 1.0 and $4.2 \pm 0.3\%$ at 4 and 24 h after WI2 injection, respectively) than gal-WI2 (2.0 ± 0.9 and $0.03 \pm 0.1\%$ at 4 and 24 h after gal-WI2 injection, respectively). Even though earlier studies had discounted the possibility that an anti-idiotypic antibody was the cause of reduced levels of radiolabeled primary antibody in a tumor (12), gal-WI2 was selected as a clearing agent in the ensuing studies.

The next important step in the development of the two-step pretargeting approach was determining an optimal time for administering the radiolabeled biotin. A major consideration here is the fact that the concentration of StAv-MN-14 in the blood must be reduced sufficiently to avoid binding the radiolabeled biotin to the StAv in the blood before it has an opportunity to localize to the StAv targeted to the tumor via the MN-14. Experiments were conducted in tumor-bearing nude mice to evaluate administration of ^{111}In -DTPA-peptide-biotin given 2 and 24 h after gal-WI2 injection. Figures 3 and 4 show the results from the group that received ^{111}In -DTPA-peptide-biotin 2 h after the gal-WI2 injection. In comparison, animals given radiolabeled biotin 24 h after the gal-WI2 had identical tumor:nontumor ratios, but the percentage of labeled biotin in all of the tissues, and most importantly in the tumor, was reduced about 5-fold (not shown). This result may be related to the lower amount of StAv-MN14 in the various tissues between the 2 and 24 h periods. Since successful therapy depends on not only the tumor:nontumor ratio but also the absolute amount of radioactivity in the tumor, it was

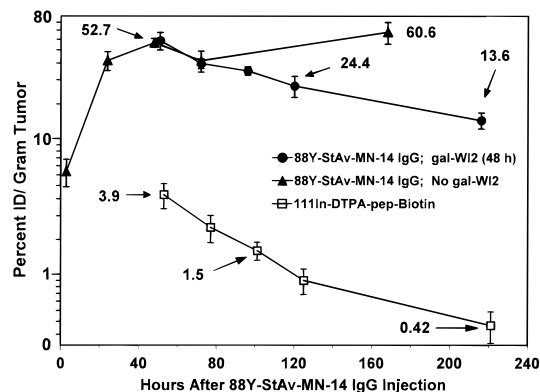


Figure 3. GW-39 uptake of pretargeted ^{111}In -DTPA-peptide biotin and ^{88}Y -StAv-MN-14 IgG with or without clearance with gal-WI2. All animals were given $200\text{ }\mu\text{g}$ of StAv-MN-14 IgG intravenously containing $2\text{ }\mu\text{Ci}$ of ^{88}Y -StAv-MN-14 IgG. One group of animals received no further injections and were necropsied 3 h and 1, 2, 3 and 7 days later ($n = 5/\text{time}$) to determine tumor uptake and organ distribution. The remaining animals received i.v. injections of gal-WI2 (5 times the molar concentration of StAv-MN-14 in the blood) 48 h after the StAv-MN-14 injection. Two hours later, all animals were injected with ^{111}In -DTPA-peptide-biotin [$6\text{ }\mu\text{g}$ ($5.7 \times 10^{-9}\text{ mol}$)/ $40\text{ }\mu\text{Ci}$] 2 h after the gal-WI2 injection. At 3, 24, 48, 72, and 168 h after the ^{111}In -DTPA-peptide-biotin injection, five animals were necropsied. Average tumor sizes ($\pm\text{SD}$) were 0.052 ± 0.009 , 0.055 ± 0.016 , 0.086 ± 0.019 , 0.109 ± 0.028 , and $0.199 \pm 0.029\text{ g}$ for the first group at 3 h and 1, 2, 3, and 7 days, respectively. The second group had values of 0.092 ± 0.023 , 0.102 ± 0.02 , 0.106 ± 0.041 , 0.137 , 0.038 , and $0.184 \pm 0.038\text{ g}$ at 3 h and 1, 2, 3, and 7 days after the ^{111}In -DTPA-peptide-biotin injection (i.e., 51, 72, 96, 120, and 216 h after ^{88}Y -StAv-MN-14 injection). The arrows indicate the mean percent of injected dose per gram in the tumor at the times shown.

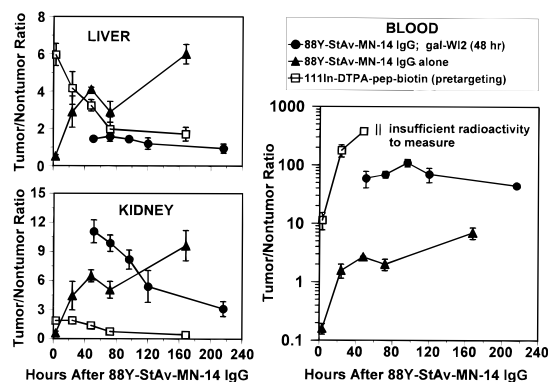


Figure 4. Tumor:nontumor ratios from the data shown in Figure 2 for the blood, liver, and kidneys.

determined that the earlier administration of the radiolabeled biotin was favored over delaying its injection.

Figures 3 and 4 also show the biodistribution of ^{88}Y -StAv-MN-14 IgG used as a tracer in the pretargeting method, as well as in a separate group of animals that received only the ^{88}Y -labeled StAv-MN-14 IgG. These three situations illustrate the results that may be obtained if ^{90}Y -labeled MN-14 was used alone (^{88}Y -StAv-MN-14 alone) or in combination with a second antibody (^{88}Y -StAv-MN-14 cleared by gal-WI2 in the pretargeting approach) or the pretargeting of ^{90}Y -DTPA-peptide-biotin was used (as modeled by the ^{111}In -DTPA-peptide-biotin in these biodistribution studies). As seen in Figure 3, the percent injected dose of ^{88}Y -StAv-MN-14 alone is sustained at a level of 50–60% for 5 days after taking 2 days to reach the maximum tumor uptake level. Administration of gal-WI2 causes a slow but steady decline of the ^{88}Y -StAv-MN-14 in the tumor, taking 48 h before the level in the tumor was lower than the ^{88}Y -

Table 1. Prediction of Maximum Radiation Dose Delivered to the Tumor Based on the Biodistribution of Each of the Listed Radiolabeled Materials^a

method	maximum tumor dose (cGy)	MTD (mCi)	dose-limiting organ (absorbed dose in cGy)
¹³¹ I–MN-14 IgG alone	16716	0.275	red marrow (2500)
¹³¹ I–MN-14 IgG/gal–WI2 at 24 h	20824	0.877	red marrow (2400) liver (7000)
⁹⁰ Y–StAv–MN-14 IgG alone	4264	0.126	red marrow (2500)
pretargeting/ ⁹⁰ Y–biotin	2349	1.0	liver (7000) red marrow (176) kidney (2574)

^a ¹¹¹In–DTPA–peptide–biotin was used to predict the behavior of ⁹⁰Y.

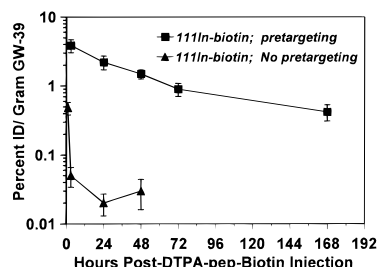


Figure 5. Comparison of ¹¹¹In–DTPA–peptide–biotin uptake in GW-39 with and without pretargeting. The data for the StAv–MN-14 pretargeting group were taken from Figure 2. A separate group of nude mice ($n = 5$ /observation) bearing small GW-39 tumors (0.03 ± 0.01 , 0.044 ± 0.017 , 0.057 ± 0.015 , and 0.048 ± 0.02 g at 1, 3, 24, and 48 h, respectively) were injected intravenously with $40 \mu\text{Ci}/6 \mu\text{g}$ of ¹¹¹In–DTPA–peptide–biotin. Due to the very rapid clearance of this agent, monitoring was only possible over 48 h given the injected activity.

StAv–MN-14 alone. For pretargeting, $200 \mu\text{g}$ of StAv–MN-14 IgG was given, followed 48 h later with gal–WI2 (5-fold molar excess), and then 2 h later, $40 \mu\text{Ci}$ (5.7×10^{-9} mol) was given. Three hours after ¹¹¹In–DTPA–peptide–biotin injection, tumor uptake was $3.9 \pm 0.8\%$ per gram, but it too declined over time at a rate analogous to the decline of StAv–MN-14 in the tumor. Tumor:blood ratios (Figure 4) for the pretargeting method were excellent, reaching 11.3 ± 3.7 just 3 h after the injection of the ¹¹¹In–DTPA–peptide–biotin to 178 ± 42 within 1 day. The level of ¹¹¹In–DTPA–peptide–biotin in the blood became too low to monitor accurately after 48 h, confirming the very rapid blood clearance of this small molecule. Tumor:blood ratios for ⁸⁸Y–StAv–MN-14 were less than 2:1 for a period of 3 days. However, if cleared by gal–WI2, tumor:blood ratios for ⁸⁸Y–StAv–MN-14 increased to 59 ± 19 within just 5 h of the gal–WI2 injection. In the pretargeting method, the liver and kidney had the highest uptake of ¹¹¹In–DTPA–peptide–biotin and the lowest tumor:nontumor ratios of all of the times tested. Tumor:liver ratios for the ¹¹¹In–DTPA–peptide–biotin started at a level of 6.0 ± 0.6 but within 3 days had decreased to 2:1. Tumor:kidney ratios were 1.9 ± 0.04 just 3 h after ¹¹¹In–DTPA–peptide–biotin injection, remaining greater than 1:1 for 48 h, but by 72 h, it decreased to 0.8 ± 0.3 . Tumor:lung and spleen ratios were between 15 and 30:1 over the first 72 h (not shown).

In order to affirm the fact that the tumor uptake of the ¹¹¹In–DTPA–peptide–biotin was due to specific binding by the StAv localized in the tumor, the biodistribution of ¹¹¹In–DTPA–peptide–biotin alone was evaluated. As shown in Figure 5, the percent uptake of ¹¹¹In–DTPA–peptide–biotin alone was only a fraction of that achieved if the tumor had been pretargeted with the StAv–MN-14. Three hours after injection, only 0.05 ± 0.016 of the ¹¹¹In–DTPA–peptide–biotin was in the tumor. This was nearly 80-fold less than that achieved with the pretargeting method shown earlier, supporting the specific

targeting of ¹¹¹In–DTPA–peptide–biotin to the StAv in the pretargeting approach.

Dosimetry. In order to predict the therapeutic potential for pretargeting, these extended biodistribution studies were used to calculate radiation-absorbed doses to the tissues and tumors if ⁹⁰Y-labeled biotin was used. Table 1 shows the maximum tumor dose projected to be delivered at the maximum tolerated dose (MTD). Included in the table also are projections for ⁹⁰Y–MN-14 IgG without second antibody clearance, using the data from the ⁸⁸Y–StAv–MN-14. In addition, radiation dose estimates are provided from biodistribution studies conducted in nude mice bearing size-matched GW-39 tumors that were given ¹³¹I–MN-14 IgG with and without blood clearance by gal–WI2 given at 24 h after the ¹³¹I–MN-14 was administered. The MTD for ⁹⁰Y–MN-14 IgG and ¹³¹I–MN-14 IgG without second antibody clearance has been determined empirically to be 120 and 275 μCi , respectively (4). However, without an empirical determination of the MTD for the other procedures, the following assumptions were made to estimate a possible MTD. For ¹³¹I–MN-14 IgG cleared by a second antibody, tumor doses were normalized to a maximum blood dose of 2500 cGy, which represented the blood dose delivered at the MTD for each agent alone. Secondly, the absorbed dose could not exceed 7000 cGy to either the liver or kidney. This limit is based on studies performed in nude mice with ⁹⁰Y-labeled MN-14 Fab fragments, which showed animals tolerating this absorbed dose level (8).

The data indicate that ¹³¹I–MN-14 IgG cleared with the gal–WI2 at 24 h would achieve the highest tumor dose at the projected MTD, followed by ¹³¹I–MN-14 IgG alone. Since the gal–WI2 clearance mechanism resulted in sustained liver retention of the ¹³¹I–MN-14 IgG, liver doses were determined to be dose-limiting before the 2500 cGy dose to the red marrow (as estimated from the blood doses) could be achieved. Doses to the red marrow for the pretargeting approach were the lowest of all methods, being only 176 cGy. However, projected maximum tumor doses for the pretargeting approach were nearly 8-fold lower than that using ¹³¹I–MN-14 alone. Some of the differences in tumor dose can be attributed to the very small size of these tumors (i.e., ~ 0.1 g), and thus, a large portion of the radiation dose for a long-range β -emitting particle such as ⁹⁰Y would be lost to the surrounding tissue. In addition, there are other inherent difficulties in determining dosimetry for internally administered radionuclides, and there is incomplete information regarding the relationship of toxicity to these radiation dose estimates. Therefore, these dose estimates should be interpreted cautiously. Nevertheless, the data suggest that, in order for the pretargeting approach to compete with a radiolabeled antibody with or without the second antibody method for blood clearance, either the amount of radiolabel delivered to the tumor needs to be increased, doses to the normal tissues (notably liver and then

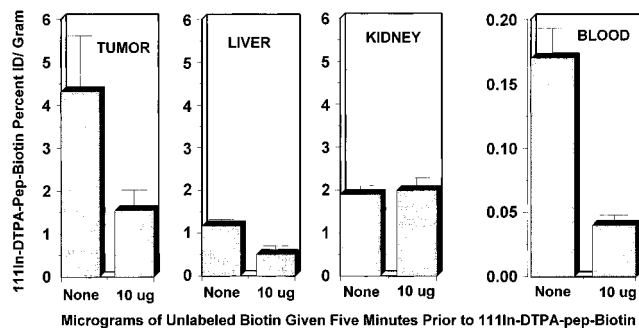


Figure 6. Effect of preinjection of unlabeled biotin on the biodistribution of pretargeted ^{111}In -DTPA-peptide-biotin. Animals bearing GW-39 tumors (0.087 ± 0.038 and 0.098 ± 0.03 g for $10 \mu\text{g}$ of unlabeled biotin and none, respectively) were given $400 \mu\text{g}$ of StAv-MN-14 IgG (contains the ^{88}Y -StAv-MN-14 tracer). Two days later, $5 \times$ gal-WI2 was given. Two hours thereafter, one group of animals ($n = 5$) was injected intravenously with $10 \mu\text{g}$ of unlabeled biotin and then 5 min later received ^{111}In -DTPA-peptide-biotin ($6 \mu\text{g}/40 \mu\text{Ci}$), while the other group received only the radiolabeled biotin ($n = 5$). All animals were necropsied 3 h after the ^{111}In -biotin injection. Note the scale difference for the blood data.

kidney) need to decrease further, or a combination of both needs to be used.

Attempts To Optimize the Pretargeting Approach. Initially, strategies to optimize the pretargeting approach focused on reducing uptake in the liver. Due to its accessibility to blood-borne agents, it was possible that the liver may be acting as a sink for the ^{111}In -DTPA-peptide-biotin, thereby reducing the supply of biotin able to reach the tumor. Thus, the first approach that was evaluated involved a preinjection of unlabeled biotin, the rationale being that a brief exposure of unlabeled biotin may bind the StAv-biotin binding sites in the liver, giving the radiolabeled biotin more opportunity to localize to StAv in the tumor. Nude mice bearing GW-39 tumors were first pretargeted with $400 \mu\text{g}$ of StAv-MN-14 and cleared with gal-WI2 48 h later. Two hours after the gal-WI2 injection, animals were injected intravenously with $10 \mu\text{g}$ of unlabeled biotin, followed 5 min later with the radiolabeled biotin. A separate group was given the radiolabeled biotin without preinjection of unlabeled biotin. Preinjection of unlabeled biotin had the desired effect of reducing liver uptake of the radiolabeled biotin, but there was also a significant decrease in the amount of radiolabeled biotin targeted to the tumor compared to tumor uptake seen when unlabeled biotin was not preadministered ($p = 0.005$, Figure 6). The end result was that most tumor:nontumor ratios remained unchanged (except tumor:kidney which decreased). This study is important also because it shows that binding of the radiolabeled biotin to the tumor can be inhibited, thereby further supporting the possibility that a specific interaction between biotin and StAv in the tumor is occurring. In a separate study, animals were pretargeted in an identical fashion but were given 1, 10, or $100 \mu\text{g}$ of unlabeled biotin 5 min before the radiolabeled biotin (not shown). This study indicated that $10 \mu\text{g}$ of biotin had sufficiently inhibited the biotin-binding sites in the tissues, since no further reduction in normal tissue uptake (or tumor) was seen with the $100 \mu\text{g}$ of unlabeled biotin dose. However, since this procedure did not enhance tumor uptake or tumor:nontumor ratios, other strategies were pursued.

The next attempt was to use a different clearing agent. Axworthy *et al.* (20) had used galactosylated, biotinylated human serum albumin (HSA) as their clearing agent. Although using an inert carrier, such as HSA, requires biotinylation for the clearing agent to form a complex

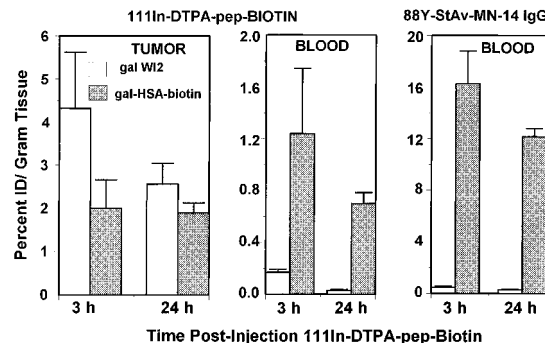


Figure 7. Evaluation of galactosylated, biotinylated HSA as a clearing agent for the pretargeting approach. Nude mice bearing GW-39 tumors (0.098 ± 0.03 and 0.118 ± 0.03 g at 3 and 24 h for the gal-WI2 group and 0.078 ± 0.023 and 0.145 ± 0.079 g for the HSA group, respectively) were injected intravenously with $400 \mu\text{g}$ of StAv-MN-14 IgG (containing ^{88}Y -StAv-MN-14). Forty-eight hours later, $200 \mu\text{g}$ of the gal-HSA-biotin was given intravenously, and then 2 h later, the ^{111}In -DTPA-peptide-biotin was injected. Animals ($n = 5/\text{group}$) were necropsied 3 and 24 h after the radiolabeled biotin injection.

with the circulating StAv-mab conjugate, this conjugate configuration can also have a dual role by blocking StAv-biotin binding sites in the tissues prior to the addition of the radiolabeled biotin. Two groups of nude mice bearing GW-39 tumors were pretargeted with $400 \mu\text{g}$ of StAv-MN-14 IgG, and after 48 h, gal-HSA-biotin₃ (81% of the available lysines were modified with galactose) or gal-WI2 was given at a 5-fold molar excess in relationship to the amount of StAv-MN-14 in the blood. Two hours later, ^{111}In -DTPA-peptide-biotin was given. These dosages and timing were consistent with that reported by Axworthy *et al.* (20). Unlike the StAv-MN-14 that was easily cleared by gal-WI2 to $0.5 \pm 0.08\%$ in the blood within 5 h of the gal-WI2 injection, there was a negligible effect on the clearance of StAv-MN-14 from the blood with the gal-HSA-biotin, with ^{88}Y -StAv-MN-14 IgG blood concentrations at $16.3 \pm 2.5\%$ at 5 h after the biotinylated HSA clearing agent was given (Figure 7). Tumor uptake and tumor:blood ratios for ^{111}In -DTPA-peptide-biotin were not improved and in fact were much lower than that achieved using gal-WI2 as the clearing agent. Low tumor:blood ratios for the ^{111}In -DTPA-peptide-biotin (only 2.8 ± 0.6 at 24 h) were caused primarily by the higher concentration of ^{111}In -DTPA-peptide-biotin in the blood compared to the levels seen in the pretargeting approach, when gal-WI2 was used as a clearing agent (0.7 ± 0.08 vs $0.03 \pm 0.007\%$ for gal-HSA-biotin vs gal-WI2 at 24 h, respectively). The higher concentration of ^{111}In -biotin in the blood is most likely due to its association with residual StAv-MN-14. Another experiment was performed with a 10-fold excess of gal-HSA-biotin with similar results. The failure of the HSA clearing agent to remove the StAv-MN-14 conjugate could be explained by three possibilities: the biotin on the HSA was unable to bind to the StAv-MN-14 conjugate, it was cleaved by biotinidases, or the StAv biotin-binding sites on the MN-14 conjugate were already bound with biotin from endogenous supplies. *In vitro* and *in vivo* data showed quantitative complexation of StAv-MN-14 with gal-HSA-biotin₃ or HSA-biotin conjugates prepared for these studies (21), suggesting the biotin was accessible. Thus, it was likely that the StAv-MN-14 already had a portion of its biotin binding sites occupied due to endogenous biotin. Given the implications that endogenous biotin would have on this type of pretargeting approach, additional studies were designed to elucidate the nature of this problem.

Table 2. Effect of Endogenous Biotin on the Biotin-Binding Ability of StAv–MN-14 after i.v. Injection in Tumor-Bearing Nude Mice^a

condition	percent free biotin-binding sites remaining on StAv–MN-14		
	1 h after StAv–Mn-14 injection	24 h after StAv–Mn-14 injection	48 h after StAv–Mn-14 injection
standard lab chow	100	2	2.4–2.9
StAv predose	ND ^b	ND	3.3
biotin-deficient diet	ND	ND	100

^a Animals were injected intravenously with 200 μ g of StAv–MN-14 IgG. At the times indicated, two mice were bled and the serum was either pooled or evaluated separately. Animals pre-dosed with StAv had received a single injection of 500 μ g of StAv 1 day prior to StAv–MN-14 injection, whereas animals which were placed on a biotin-deficient diet were fed this diet for 7 days prior to the StAv–MN-14 IgG injection. ^b ND, not determined.

In order to investigate this possibility, nude mice were injected with 200 μ g of StAv–MN-14 IgG containing a trace of ⁸⁸Y–StAv–MN-14. At 1, 24, and 48 h later, the mice were bled. Serum was collected and then mixed with varying amounts of the radiolabeled DTPA–peptide-biotin. After incubation for 5 min at room temperature, the samples were run over a size-exclusion HPLC column, and profiles were evaluated for the amount of radiolabeled biotin associated with the high-molecular weight StAv–MN-14 peak. Knowing the specific activity of the StAv–MN-14 and the known amount of biotin added to each sample, the number of biotin binding sites remaining on the StAv–MN-14 was determined. Values were compared to those of the same batch of StAv–MN-14 that was not injected *in vivo*. The results, shown in Table 2, indicate that StAv–MN-14 taken at 1 h retained nearly 100% of its original biotin-binding capacity, whereas StAv–MN-14 taken from animals after 24 and 48 h had lost over 90% of its biotin-binding capacity. Since our earlier findings showed complete retention of StAv–MN-14 in binding biotin when incubated *in vitro* in serum over a 24 h period (21), these *in vivo* results suggest that continued exposure to body fluids provides greater opportunity for blockade of the biotin-binding sites. Indeed, considering that the published serum level of biotin in rats is 3.1×10^{-8} M (28) (4.5×10^{-11} mol in a mouse assuming a 1.5 mL blood volume) and that 200 μ g of StAv–MN-14 contains 4.3×10^{-10} mol of StAv with its full biotin-binding capacity (i.e., four binding sites/molecule), there should have been sufficient biotin-binding capacity to avoid this problem. Thus, with evidence that a majority of the biotin-binding sites were blocked, studies were designed to investigate the pretargeting method in animals with diminished levels of biotin.

Rosebrough and Hartley (28) showed that endogenous stores of biotin could be reduced in rabbits and dogs by administering avidin. In order to investigate this procedure, nude mice bearing GW-39 tumors were given i.v. injections of 20, 100, or 500 μ g of StAv 24 h before the administration of 200 μ g of StAv–MN-14 IgG. Another group of animals received 100 μ g of StAv at the same time that the StAv–MN-14 was given. After waiting 48 h, gal–W12 was given, followed 2 h later with ¹¹¹In–DTPA–peptide-biotin. The animals were then necropsied 3 h later. The results shown in Figure 8 indicate no improvement in tumor retention compared to the results from animals that did not receive additional StAv, and in fact, at the higher StAv doses, increased uptake of ¹¹¹In–DTPA–peptide-biotin was seen in the liver and blood, but more notably, in the kidneys, the major organ where StAv is known to accrete (30). This also occurred in animals that were coinjected with 100 μ g of StAv on

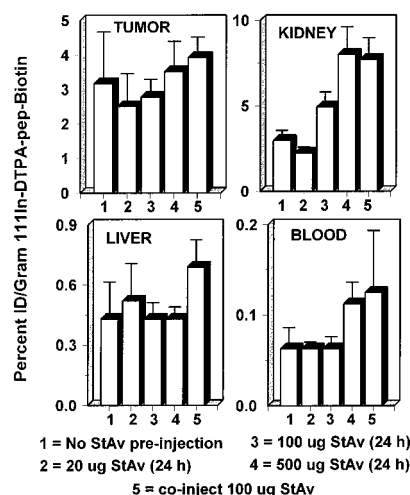


Figure 8. Effect of StAv pretreatment to reduce endogenous biotin levels on the biodistribution of ¹¹¹In–DTPA–peptide-biotin in nude mice. Animals in groups 1–4 were given varying amounts of StAv and 1 day later given 200 μ g of StAv–MN-14. Group 5 received 100 μ g of StAv on the same day the StAv–MN-14 was given. Two days later, the StAv–MN-14 was cleared with gal–W12; 2 h later, the ¹¹¹In–DTPA–peptide-biotin was given, followed by necropsy at 3 h. Each group of animals contained three or four animals with an average tumor size of 0.042 ± 0.027 , 0.038 ± 0.017 , 0.068 ± 0.012 , 0.035 ± 0.010 , and 0.036 ± 0.01 g for groups 1–5, respectively.

the day of the StAv–MN-14 injection. Measurement of StAv–MN-14's ability in the blood at 48 h to bind biotin showed that the StAv pretreatment did not reduce endogenous biotin blockade of the conjugate (Table 2).

Prior to examination the use of a biotin-deficient diet to reduce endogenous biotin stores, studies were conducted to determine how the specific activity of the labeled biotin affected its biodistribution, and to assess if DOTA would provide an advantage over DTPA. *In vivo* studies with ¹¹¹In–DOTA–peptide-biotin suggested that this conjugate has slower blood clearance than DTPA–peptide-biotin (21) and that perhaps slowing the blood clearance of the labeled biotin might provide a greater opportunity for tumor binding. Four separate groups of tumor-bearing nude mice were selected. Each animal received 200 μ g of StAv–MN-14 followed 2 days later with gal–W12. Two hours later, the animals received an i.v. injection of either DTPA- or DOTA-conjugated biotin labeled at either a high (1.2×10^{-9} mol of the labeled biotin) or low (5.7×10^{-9} mol of the labeled biotin) specific activity. Only the high-specific activity DOTA showed a significant increase in tumor uptake, and this was apparent only 3 h after injection ($p < 0.01$, Figure 9). By 24 h after the biotin injection, all of the groups had similar amounts of labeled biotin in the tumor. The high-specific activity DOTA also had a higher level of radioactivity in the blood, compared to the lower specific activity DOTA or the DTPA-conjugated biotin. These results were also most pronounced at 3 rather than at 24 h. However, since increasing the specific activity and changing the chelate improved tumor uptake from 4 to approximately 8% of the injected dose per gram, this combination was used in the next study to determine the effects of biotin-deficient diets.

Two groups of animals were initiated on either biotin-deficient or standard lab chow diets immediately upon receipt from the vendor. Within 2 days, a GW-39 tumor suspension was given to initiate tumor growth, and then on day 7, all animals were given 200 μ g of StAv–MN-14. Two days later, gal–W12 was given, and 2 h later, ¹¹¹In–DOTA–peptide-biotin (1.2×10^{-9} mol) was ad-

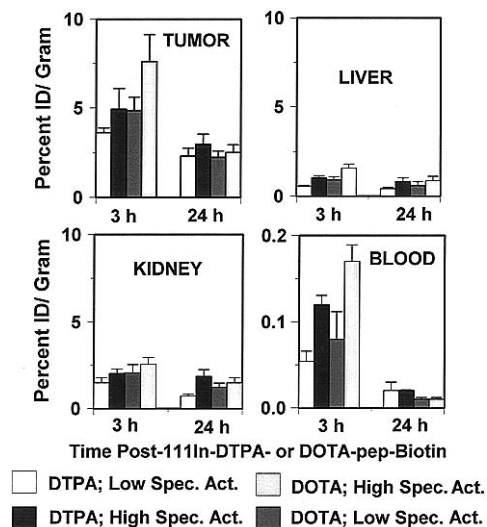


Figure 9. Comparison of DTPA-peptide-biotin and DOTA-peptide-biotin at low and high specific activities in the two-step pretargeting approach. Nude mice bearing GW-39 tumors were divided into four groups as indicated (tumor sizes were 0.11 ± 0.019 and 0.127 ± 0.082 , 0.104 ± 0.022 and 0.137 ± 0.056 , 0.113 ± 0.035 and 0.147 ± 0.027 , and 0.122 ± 0.031 and 0.101 ± 0.064 g for groups 1–4 at 3 and 24 h, respectively). All animals received an initial injection of 200 μ g of StAv-Mn-14 IgG followed 2 days later with clearance by gal-WI2, and then 2 h later, the radiolabeled biotin was given. The low specific activity contained 5.7×10^{-9} mol of radiolabeled chelate-peptide-biotin (approximately 6 μ g each), whereas the high specific activity contained only 1.2×10^{-9} mol of radiolabeled chelate-peptide-biotin. Animals were necropsied 3 and 24 h after the biotin injection.

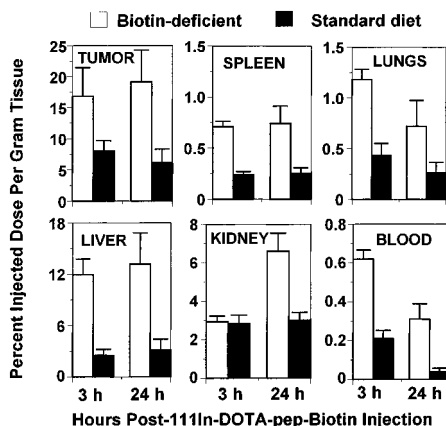


Figure 10. Effect of biotin-deficient diet on the biodistribution of pretargeted ^{111}In -DOTA-peptide-biotin. Nude mice were fed standard autoclavable lab chow or a biotin-deficient diet (supplemented with 30% egg solids). On day 2, animals were inoculated with GW-39 tumors, and on day 7, 200 μ g of StAv-MN-14 was injected. Gal-WI2 was given 2 days later, with ^{111}In -DOTA-peptide-biotin (1.2×10^{-9} mol) injected intravenously 2 h thereafter. Animals were necropsied 3 and 24 h after the radiolabeled biotin was given ($n = 5/\text{group}$). Tumor sizes at 3 and 24 h were 0.052 ± 0.011 and 0.072 ± 0.016 g, respectively, for the animals given the biotin-deficient diet and 0.71 ± 0.018 and 0.88 ± 0.033 g for the animals fed the normal rodent diet, respectively.

ministered. The animals were necropsied 3 and 24 h after the radiolabeled biotin injection. Under these conditions, tumors taken from animals given biotin-deficient diets had a nearly 2-fold higher (16.9 ± 4.6) tumor uptake than animals fed the standard lab chow (Figure 10). This level of ^{111}In -DOTA-peptide-biotin in the tumor was sustained over the 24 h monitoring period. Although tumor uptake was increased, uptake in all normal tissues also increased. Interestingly, tumor:liver and kidney

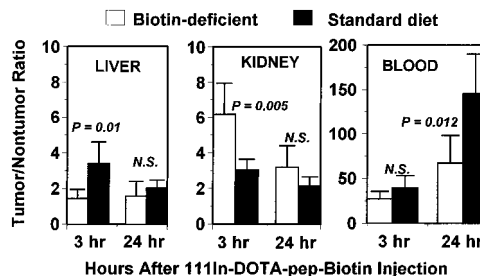


Figure 11. Tumor:nontumor ratios for the study described in Figure 10. Statistical evaluation was performed by a general Student's *t* test with *p* values given in the figure. N.S. means not significant at a *p* < 0.05 level.

ratios in animals given the biotin-deficient diet were not significantly different at 24 h (Figure 11). Although tumor:blood ratios were significantly lower in animals given the biotin-deficient diet on day 1, the actual ratios exceeded 50:1. Thus, even under these conditions, the pretargeting method maintained its tumor:blood advantage compared to a radiolabeled antibody alone. Analysis of serum taken from these mice 48 h prior to administration of gal-WI2 revealed the conjugate had retained 100% of its original biotin-binding capacity (Table 2).

DISCUSSION

Pretargeting approaches are very attractive for use with radiolabeled antibodies because they offer exceptional tumor:blood ratios. This property is highly desirable for imaging and therapeutic applications. For imaging, the simple use of an antibody fragment may be preferred over the multiple steps involved in a pretargeting approach. The same can be said for therapy, where the simplest approach will prevail over those requiring multiple steps, unless these alternative approaches improve the therapeutic outcome.

The work presented herein, and in a companion article (21), illustrates some of the complexities involved in developing a two-step, streptavidin-biotin pretargeting method. Multiple agents need to be prepared and tested, dosages optimized, and appropriate dosing schedules evaluated. After evaluation of a number of different agents and parameters, a successful two-step pretargeting approach was established that produced excellent tumor:blood ratios within a few hours. The liver and kidney were the major organs for retention of the radiolabeled biotin, but even this uptake produced tumor:nontumor ratios in excess of 2:1, which is acceptable for imaging applications but may need to be improved for therapy. A major concern for the pretargeting approach was the fact that the percentage of radiolabeled biotin targeted to the tumor was much lower than that observed with a radiolabeled antibody alone. This may present a problem for therapeutic applications that will require a critical concentration of radioactivity in order to effect changes in tumor growth. However, the primary issue is not the percent of injected radioactivity delivered to the tumor but the absolute amount of radioactivity that can be delivered at the maximum tolerated dose for each procedure in combination with the longevity of tumor binding. Dosimetry estimates suggest that, with the current pretargeting approach and 4% of the injected dose per gram tumor, approximately 40 μCi could be delivered (assuming 1 mCi is the MTD). At a 60% injected dose per gram, an antibody labeled with ^{90}Y could deliver 72 $\mu\text{Ci/g}$ to the tumor (MTD of 120 μCi), whereas an ^{131}I -labeled antibody could deliver 165 $\mu\text{Ci/g}$. From this perspective, the pretargeting approach would need to increase the percentage delivered to the tumor at least

2-fold, or if liver and kidney were reduced at least 2-fold and this allowed a doubling in the administered dose, then the pretargeting approach would be more competitive with other forms of RAIT.

By itself, the labeled biotin is cleared very quickly from all tissues. Our studies showed that, within 1 day, only 0.004 and 0.01% per gram of ^{111}In -DTPA-peptide and DOTA-peptide-biotin, respectively, remained in the blood (21). The kidney was the organ with the highest uptake, but it was as low as 0.22 and 0.17% per gram 1 day after the biotin injection. In animals given StAv-MN-14 IgG, there were higher levels of radiolabeled biotin in all the major organs. Thus, the altered distribution was due to the radiolabeled biotin binding to the StAv contained in these normal tissues. Indeed, it was possible to show that, within just 5 min, biotin-binding sites could be saturated with a preinjection of 10 μg of unlabeled biotin.

Several approaches were examined to increase tumor uptake or to reduce normal tissue uptake. Tumor uptake was increased somewhat by raising the specific activity of the labeled biotin and by using DOTA rather than DTPA. Trying to inhibit biotin binding in tissues selectively is difficult. In most instances, inhibition of residual StAv biotin-binding sites caused a concomitant reduction in the level of radiolabeled biotin targeted to the tumor, thereby negating the value of the procedure. Another important finding was the fact that endogenous biotin levels in the mouse seriously inhibit this approach. Hnatowich *et al.* (30) had brought this problem to attention earlier, but it has not been studied in detail in the literature. On the basis of published levels of biotin in mouse serum, and our *in vitro* studies showing the full biotin-binding capability of the conjugates, it was assumed that there would be abundant biotin-binding sites on the StAv with the doses administered. It was interesting to discover that problems with endogenous biotin could not be appreciated by incubating the conjugate in serum *in vitro*, but rather, the conjugate needed to be injected in the mice and then assayed over time. Our experience showed that, within 1 day, the vast majority of biotin-binding sites on the conjugate were blocked. Since tumor localization in nude mice generally requires 2 days to achieve optimal tumor accretion, this is a serious disadvantage for assessing this methodology preclinically. The fact that ^{111}In -biotin uptake in the tumor and normal tissues could be reduced by a preinjection of unlabeled biotin clearly showed that not all biotin-binding sites were blocked by endogenous biotin. Fortunately, feeding animals a biotin-free diet can reduce endogenous biotin levels, and temporary reductions in biotin do not have a serious impact on the health of the animals. Using this approach, unfortunately, exacerbates the problem of residual StAv in the tissues capable of binding the radiolabeled biotin. Although biotin levels in humans are reported to be more than 10-fold lower than those in mice (28), it is still uncertain whether endogenous biotin will play an equally important role in humans because these measurements only account for serum levels and do not account for other storage sites. Thus, it is not merely a question of serum biotin levels but a test subject's capacity to restore serum biotin homeostasis, either by liberation of biotin from intracellular stores or by an increase in absorption of dietary biotin. Kalofonos *et al.* (31) showed that, 3 days after the injection of only 1.0 mg of StAv-conjugated antibody, the antibody in the blood of patients still retained its ability to bind biotin. However, the precise number of biotin-binding sites remaining was not reported. Nevertheless, this result is encouraging, especially since

higher conjugate dosages will further reduce the influence of endogenous biotin in patients. At least in animal models, which may predict whether human studies are warranted, endogenous biotin is a serious problem.

We elected to evaluate the StAv-antibody, radiolabeled biotin approach on the basis of early reports by Axworthy *et al.* (20), who stated that they were able to achieve > 20% injected dose per gram ^{111}In -biotin tumor uptake, similar to the level obtained with their radiolabeled antibody alone. If identical tumor uptake with markedly improved tumor:blood ratios is possible with this pretargeting approach, as compared to the radiolabeled antibody, then improved antitumor effects should also be possible. Indeed, Axworthy *et al.* (32) have reported improved therapeutic effects in animals with this pretargeting approach. If a tumor uptake can be achieved with this pretargeting approach identical to that seen with the radiolabeled antibody, it would be most encouraging. As pointed out by O'Connor and Bale (33), only a small portion of an antibody will have an opportunity to pass through a tumor. With an agent that is rapidly cleared from the blood, the portion passing through the tumor would be substantially lower than a substance that is cleared from the blood more slowly. This relationship is evident when comparing tumor uptake of whole IgG to antibody fragments; the uptake is always substantially higher with the whole IgG. However, the pretargeting approach offers other advantages that could alter this relationship, namely an increase in the number (maximum of four biotins/StAv) and affinity of the binding sites in the tumor (i.e., StAv-biotin vs antibody-antigen). Combined with the fact that, as a small molecule, biotin is able to be distributed more quickly and uniformly throughout the tumor than a large macromolecule, this pretargeting approach has the potential to compete effectively with directly radiolabeled antibodies. However, the complexity of these procedures in comparison to using radiolabeled antibodies, coupled with the possibility of increased immunogenicity of StAv-mab conjugates, makes it necessary that these procedures exceed the therapeutic ability of the simpler approach. Clinical trials will ultimately be required to make this determination.

Despite some of the problems cited herein, we have yet to investigate further modifications that could either improve the total amount of radioactivity delivered to the tumor or reduce the level in normal tissues. For example, using WI2 in place of gal-WI2 may reduce the quantity of StAv-MN-14 available in the liver, and perhaps waiting 4–8 h between the injection of the clearing agent until the labeled biotin is given will further reduce the potential for high liver accretion. Once fully optimized, it will also be important to establish empirically a maximum tolerated dose level for the pretargeting approach rather than depending on dosimetry to decide the fate of this promising procedure. Given the relatively surprising finding that a single injection of ^{90}Y -labeled MN-14 Fab may have a therapeutic benefit comparable to that of ^{90}Y -IgG (8), we are encouraged to further explore the potential therapeutic benefit that may be afforded by such pretargeting approaches.

ACKNOWLEDGMENT

The authors thank Ms. Rosarito Aninipot for her technical assistance in performance of the animal studies and Mr. Mark Prysbylowski for the purification of the antibodies. This study was supported in part by U.S. Public Health Service Grants CA-37895 and CA-39841.

LITERATURE CITED

- (1) Blumenthal, R. D., Sharkey, R. M., Haywood, L., Natale, A. M., Wong, G. Y., Siegel, J. A., Kennel, S. J., and Goldenberg, D. M. (1992) Targeted therapy of athymic mice bearing GW-39 human colonic cancer micrometastases with ^{131}I -labeled monoclonal antibodies. *Cancer Res.* **52**, 6036–6044.
- (2) Sharkey, R. M., Blumenthal, R. D., Hansen, H. J., and Goldenberg, D. M. (1990) Biological considerations for radioimmunotherapy. *Cancer Res.* **50** (Suppl.) 964s–969s.
- (3) Buchegger, F., Pèlegri, A., Delaloye, B., Bischof-Delaloye, A., and Mach, J.-P. (1990) Iodine-131-labeled MAb F(ab')₂ fragments are more efficient and less toxic than intact anti-CEA antibodies in radioimmunotherapy of large colon carcinoma grafted in nude mice. *J. Nucl. Med.* **31**, 1035–1044.
- (4) Sharkey, R. M., Blumenthal, R. D., Behr, T. M., Wong, G., Haywood, L., Forman, D., Griffiths, G., and Goldenberg, D. M. (1997) Selection of radioimmunconjugates for the therapy of well-established or micrometastatic colon carcinoma. *Int. J. Cancer* (in press).
- (5) Behr, T. M., Sharkey, R. M., Juweid, M. E., Blumenthal, R. D., Dunn, R. M., Griffiths, G. L., Wolf, F. G., Becker, W. S., and Goldenberg, D. M. (1995) Reduction of the renal uptake of radiolabeled monoclonal antibody fragments by cationic amino acids and their derivatives. *Cancer Res.* **55**, 3825–3834.
- (6) DePalatis, L. R., Frazier, K. A., Cheng, R. C., and Kotite, N. J. (1995) Lysine reduces renal accumulation of radioactivity associated with injection of the [^{177}Lu] α -[2-(4-aminophenyl)ethyl]-1,4,7,10-tetraaza-cyclodecane-1,4,7,10-tetraacetic acid-CC49 Fab radioimmunoconjugate. *Cancer Res.* **55**, 5288–5295.
- (7) Kobayashi, H., Yoo, T. M., Kim, I. S., Kim, M.-K., Le, N., Webber, K. O., Pastan, I., Paik, C. H., Eckelman, W. C., and Carrasquillo, J. A. (1996) L-lysine effectively blocks renal uptake of ^{125}I - or $^{99\text{m}}\text{Tc}$ -labeled anti-Tac disulfide-stabilized Fv fragment. *Cancer Res.* **56**, 3788–3795.
- (8) Behr, T. M., Sharkey, R. M., Sgouros, G., Blumenthal, R. D., Dunn, R. M., Kolbert, K., Griffiths, G. L., Siegel, J. A., Becker, W. S., and Goldenberg, D. M. (1997) Improved cancer therapy by overcoming nephrotoxicity of radiometal-labeled immunoconjugates and peptides: biological effects in relation to internal radiation dosimetry in a human colon cancer model. *Cancer* (in press).
- (9) Blumenthal, R. D., Fand, I., Sharkey, R. M., Boerman, O. C., Kashi, R., and Goldenberg, D. M. (1991) The effect of antibody protein dose of tumor distribution of radiolabeled antibodies: an autoradiographic study. *Cancer Immunol. Immunother.* **33**, 351–358.
- (10) Fujimori, K., Covell, D. G., Fletcher, J. E., and Weinstein, J. N. (1989) Modeling analysis of the global and microscopic distribution of immunoglobulin G, F(ab')₂, and Fab in tumors. *Cancer Res.* **49**, 5656–5663.
- (11) Sharkey, R. M., Primus, F. J., and Goldenberg, D. M. (1984) Second antibody clearance of radiolabeled antibody in cancer radioimmunodetection. *Proc. Natl. Acad. Sci. U.S.A.* **81**, 2843–2846.
- (12) Sharkey, R. M., Boerman, O. C., Natale, A., Pawlyk, D., Monestier, M., Losman, M. J., and Goldenberg, D. M. (1992) Enhanced clearance of radiolabeled murine monoclonal antibody by a syngeneic anti-idiotypic antibody in tumor-bearing nude mice. *Int. J. Cancer* **51**, 266–273.
- (13) Goodwin, D., Meares, C., Diamanti, C., McCall, M., Lai, C., Torti, F., McTigue, M., and Martin, B. (1984) Use of specific antibody for rapid clearance of circulating blood background from radiolabeled tumor imaging proteins. *Eur. J. Nucl. Med.* **29**, 226–243.
- (14) Begent, R. H. J., Ledermann, J. A., Green, A. J., Bagshawe, K. D., Riggs, S. J., Searle, F., Keep, P. A., Adam, T., Dale, R. G., and Glaser, M. G. (1989) Antibody distribution and dosimetry in patients receiving radiolabelled antibody therapy for colorectal cancer. *Br. J. Cancer* **60**, 406–412.
- (15) Pedley, R. B., Dale, R., Boden, J. A., Begent, R. H. J., Keep, P. A., and Green, A. J. (1989) The effect of second antibody clearance on the distribution and dosimetry of radiolabelled anti-CEA antibody in a human colonic tumor xenograft model. *Int. J. Cancer* **43**, 713–718.
- (16) Blumenthal, R. D., Sharkey, R. M., and Goldenberg, D. M. (1995) Overcoming Dose-Limiting, Radioantibody-Induced Myelotoxicity. In *Cancer Therapy with Radiolabeled Antibodies* (D. M. Goldenberg, Ed.) pp. 295–314, CRC Press, Boca Raton, FL.
- (17) Norrgren, K., Strand, S.-E., Nilsson, R., Lindgren, L., and Sjögren, H.-O. (1993) A general, extracorporeal immunoadsorption method to increase the tumor-to-normal tissue ratio in radioimaging and radioimmunotherapy. *J. Nucl. Med.* **34**, 448–454.
- (18) Lear, J. L., Kasliwal, R. K., Feyerabend, A. J., Pratt, J. P., Bunn, P. A., Dienhar, D. G., Gonsaly, R., Johnson, T. K., Bloedow, D. C., Maddock, S. W., and Glenn, S. D. (1991) Improved tumor imaging with radiolabeled monoclonal antibodies by plasma clearance of unbound antibody with anti-antibody column. *Radiology* **179**, 509–512.
- (19) Goodwin, D. A., and Meares, C. F. (1997) Pretargeting: General principles. *Cancer* (in press).
- (20) Axworthy, D. B., Fritzberg, A. R., Hylarides, M. D., Mallet, R. W., Theodore, L. J., Gustavson, L. M., Su, F.-M., Beaumier, P. L., and Reno, J. M. (1994) Preclinical evaluation of an anti-tumor monoclonal antibody/streptavidin conjugate for pre-targeted ^{90}Y radioimmunotherapy in a mouse xenograft model. *J. Immunother.* **16**, 158 (abstract).
- (21) Karacay, H., Sharkey, R. M., Griffiths, G. L., Govindan, S. V., McBride, W. J., Goldenberg, D. M., and Hansen, H. J. (1997) Development of a streptavidin–anti-carcinoembryonic antigen antibody, Radiolabeled Biotin pretargeting method for radioimmunotherapy of colorectal cancer. Reagent Development. *Bioconjugate Chem.* **8**, 585–594.
- (22) Hansen, H. J., Goldenberg, D. M., Newman, E. S., Grebenau, R., and Sharkey, R. M. (1993) Characterization of second-generation monoclonal antibodies against carcinoembryonic antigen. *Cancer* **71**, 3478–3485.
- (23) Goldenberg, D. M., and Hansen, H. J. (1972) Carcinoembryonic antigen present in human colonic neoplasms serially propagated in hamsters. *Science* **175**, 1117–1118.
- (24) Sharkey, R. M., Motta-Hennessy, C., Pawlyk, D., Siegel, J. A., and Goldenberg, D. M. (1990) Biodistribution and radiation dose estimates for yttrium- and iodine-labeled monoclonal antibody IgG and fragments in nude mice bearing human colonic tumor xenografts. *Cancer Res.* **50**, 2330–2336.
- (25) Sharkey, R. M., Primus, F. J., and Goldenberg, D. M. (1987) Antibody protein dose and radioimmunodetection of GW-39 human colon tumor xenografts. *Int. J. Cancer* **39**, 611–617.
- (26) Boerman, O. C., Sharkey, R. M., Wong, G. Y., Blumenthal, R. D., Aninipot, R. L., and Goldenberg, D. M. (1992) Influence of antibody protein dose on therapeutic efficacy of radioiodinated antibodies in nude mice bearing GW-39 human tumors. *Cancer Immunol. Immunother.* **35**, 127–134.
- (27) Mattes, M. J. (1987) Biodistribution of antibodies after intraperitoneal or intravenous injection and effect of carbohydrate modification. *J. Natl. Cancer Inst.* **79**, 855–863.
- (28) Rosebrough, S. F., and Hartley, D. F. (1995) Quantification and lowering of serum biotin. *Lab. Anim. Sci.* **45**, 554–557.
- (29) Rosebrough, S. F. (1993) Pharmacokinetics and biodistribution of radiolabeled avidin, streptavidin, and biotin. *Nucl. Med. Biol.* **20**, 663–668.
- (30) Hnatowich, D. J. (1994) The *in vivo* uses of streptavidin and biotin: a short progress report. *Nucl. Med. Commun.* **15**, 575–577.
- (31) Kalofonos, H. P., Rusckowski, M., Siebecker, D. A., Sivolapenko, G. B., Snook, D., Lavender, J. P., Epenetos, A. A., and Hnatowich, D. J. (1990) Imaging of tumor in patients with indium-111-labeled biotin and streptavidin-conjugated antibodies: Preliminary communication. *J. Nucl. Med.* **31**, 1791–1796.
- (32) Axworthy, D. B., Beaumier, P. L., Bottino, S., Goshorn, R. W., Mallett, R. W., Stone, D. M., Su, F.-M., Theodore, L. J., Yau, E. K., and Reno, J. M. (1996) Preclinical optimization of pretargeted radioimmunotherapy components: High efficiency, curative ^{90}Y delivery to mouse tumor xenografts. *Tumor Targeting* **2**, 156–157 (abstract).
- (33) O'Connor, S. W., and Bale, W. F. (1984) Accessibility of circulating immunoglobulin G to the extravascular compartment of solid rat tumors. *Cancer Res.* **44**, 3719–3723.

TECHNICAL NOTES

Polymeric Conjugates of Gd^{3+} –Diethylenetriaminepentaacetic Acid and Dextran. 1. Synthesis, Characterization, and Paramagnetic Properties

Richard Rebizak,[†] Michel Schaefer,[‡] and Édith Dellacherie^{*,†}

Laboratoire de Chimie-Physique Macromoléculaire, URA CNRS 494, ENSIC-INPL, B.P. 451, 54001 Nancy Cedex, France, and Guerbet-GCA, B.P. 15, 93601 Aulnay-sous-Bois, France. Received August 5, 1996[®]

Macromolecular conjugates of dextran and diethylenetriaminepentaacetic acid (DTPA), aimed to complex gadolinium, were synthesized to obtain contrast agents for nuclear magnetic resonance imaging with good paramagnetic properties and long intravascular persistence. These conjugates were prepared from dextran 40 ($M_n = 38$ kg/mol and $M_w = 43$ kg/mol), which was first carboxymethylated. Then amines were introduced by reacting ethylenediamine with dextran carboxylic acid groups in the presence of 2-ethoxy-1-(ethoxycarbonyl)-1,2-dihydroquinoline. DTPA was then covalently linked to aminated dextran by using three different coupling procedures (DTPA bisanhydride, dicyclohexylcarbodiimide/*N*-hydroxysuccinimide, and isobutyl chloroformate). The different final products were compared in terms of DTPA contents, molecular masses, and sizes, and it was proved that the last synthesis step led to a small fraction of cross-linked chains as M_n was between 128 and 166 kg/mol and M_w between 332 and 371 kg/mol. In spite of this partial cross-linking which theoretically decreases the complexation capacity of the dextran-linked DTPA molecules, the Gd^{3+} -complexed conjugates exhibited relaxivities at 20 MHz/mol of gadolinium—2.5 times as great as that of free GdDTPA^{2-} .

INTRODUCTION

Today, the complexes most commonly used in humans for nuclear magnetic resonance imaging are small molecules such as gadolinium–diethylenetriaminepentaacetic acid (GdDTPA^{2-}) and gadolinium–tetraazacyclododecanetetraacetic acid (GdDOTA^-) (1). These complexes are very strong, and their thermodynamic stability constants are, respectively, $10^{22.5}$ (2) and 10^{28} L mol⁻¹ (3). This high stability hampers the release in body, of gadolinium, Gd^{3+} , which is a very toxic ion. However, because of their molecular size, these complexes are totally and rapidly excreted via urine. In man, GdDTPA^{2-} has a 90 min biological half-life, and 5 min after its injection, its blood concentration is only about 30% of the initial dose (4). Therefore, for prolonged clinical tests, injection of several doses of GdDTPA^{2-} is necessary.

Recently, a number of investigations have aimed to bind GdDTPA^{2-} and GdDOTA^- to polymers or macromolecules such as proteins (albumin, immunoglobulins) (5–8), polylysine (8), or polysaccharides such as dextran (9–13). The use of polymers as carriers of gadolinium complexes has two advantages. The first is that, by influencing the complex rotation speed, the r_1 longitudinal and r_2 transversal relaxivities are increased. For example, GdDTPA^{2-} r_1 relaxivity is 3.7 mM⁻¹ s⁻¹ at 20 MHz, while for polymers, r_1 relaxivity can be > 10 mM⁻¹ s⁻¹ (14). The second advantage is the increase in the plasma persistence. A polylysine– GdDTPA^{2-} , studied by

Schuhmann-Giampieri et al. (15), exhibited a rabbit plasma half-life of 1.9 h against 0.6 h for GdDTPA^{2-} . These new macromolecular contrast agents can thus be used as blood pool tracers.

This paper describes the synthesis and properties of dextran-linked DTPA. Dextran 40 (Figure 1, M_w about 40 kg/mol) was chosen because of its biocompatibility and biodegradability. It is commonly used as a plasma expander to improve blood circulation and to prevent blood platelet aggregation and as the basis of oxygen-carrier blood substitutes (16). Different syntheses were investigated to bind DTPA to previously aminated dextran 40 (Figure 1), and the resulting DTPA-containing polymers were compared in terms of molecular mass and DTPA content. The aim was to obtain highly substituted polymers with molecular mass as low as possible, because high molecular mass polymers remain a long time in the intravascular space before being excreted, which can produce allergies. To limit the molecular mass, it was important to hamper the cross-linking reactions between amines of different polysaccharide chains and several carboxylic groups of one DTPA molecule. Furthermore, this reaction is also undesirable because the stability constant of the gadolinium–DTPA complex decreases when the number of DTPA carboxylic groups substituted by amine functions increases (17–19).

EXPERIMENTAL PROCEDURES

Syntheses. *Synthesis of Carboxymethyldextran (CMD).* Ten grams of dextran 40 (Pharmacia LKB, Uppsala, Sweden) was dissolved in 82.5 mL of 6 N NaOH previously cooled in an ice bath. Then, 20.4 g (0.216 mol) of chloroacetic acid (Aldrich-France, St Quentin-Fallavier, France) was introduced. The mixture was maintained at 60 °C for 50 min and then cooled at room temperature.

* Author to whom correspondence should be addressed [telephone (33) 383 17 52 21; fax (33) 383 37 99 77; e-mail e.dellacherie@kekule.ensic.u-nancy.fr].

[†] ENSIC-INPL.

[‡] Guerbet-GCA.

[®] Abstract published in *Advance ACS Abstracts*, June 1, 1997.

Then the polymer was precipitated with methanol. CMD was recovered by filtration and dried under vacuum at 50 °C.

Synthesis of Aminated Carboxymethyldextran (CMDA) by Means of 2-Ethoxy-1-(ethoxycarbonyl)-1,2-dihydroquinoline (EEDQ). Ten grams of CMD (31 mmol of COONa) was dissolved in 100 mL of water and the pH was adjusted to 3 with 1 N HCl. Then an EEDQ solution prepared with 15.4 g (62 mmol) of EEDQ (Fluka, Buchs, Switzerland) and 233 mL of methanol was added dropwise. The resulting solution was added to 20.7 mL (310 mmol) of ethylenediamine (Aldrich) under stirring. After 4 h, CMDA was precipitated with methanol, then recovered by filtration, and finally dried under vacuum at 50 °C.

Coupling of DTPA to Aminated Carboxymethyldextran (CMDA–DTPA). (a) *Method Using DTPA Bisanhydride (DTPAba).* DTPAba was previously prepared according to a method deriving from that of Eckelman et al. (20). One gram of CMDA (1.7 mmol of NH₂) was dissolved in 10 mL of water. Then, 1/20 of this CMDA solution and 1/20 of the total DTPAba amount to be used (11 g, 30.8 mmol) were successively added to 20 mL of water. This step was carried out by keeping the pH constant at 10 with 6 N NaOH. This operation was repeated until consumption of all the reagents. The final mixture was stirred for 4 h and then dialyzed against water for 3 days. Finally, the polymer was recovered by freeze-drying. The cellulosic dialysis tubes employed (Polylabo, Paris, France) had a molecular mass cutoff of 6000–8000 g/mol.

(b) *Method Using DTPA Succinimide Ester (DTPA-ONSu).* One gram (2.54 mmol) of DTPA (Aldrich) was dissolved in 10 mL of acetonitrile in the presence of triethylamine (Aldrich) at 55 °C. After DTPA was completely dissolved, the solution was cooled at room temperature and then 0.371 g (1.80 mmol) of dicyclohexylcarbodiimide (DCC; Aldrich) and 0.207 g (1.80 mmol) of *N*-hydroxysuccinimide (HONSu; Aldrich) were simultaneously added. The DCC/HONSu and DTPA/DCC molar ratios were, respectively, 1 and 1.4. The solution was stirred for 90 min. The precipitated urea was removed by filtration, and the resulting solution containing DTPA-ONSu was dropped into a solution prepared with 1 g of CMDA (1.7 mmol of NH₂/g) and 10 mL of water. This operation was carried out by maintaining a constant pH of 10. The solution was stirred for 24 h, and then acetonitrile was removed by rotative evaporation. Finally, the solution was dialyzed against water for 3 days, and the final polymer was recovered by freeze-drying.

(c) *Method Using DTPA Mixed Anhydride.* First of all, 6.7 g (17 mmol) of DTPA was dissolved in 10 mL of acetonitrile at 55 °C in the presence of triethylamine. The solution was cooled at –10 °C and then dropped into 1.12 mL (8.6 mmol) of isobutyl chloroformate (IBCF; Aldrich). This mixture was stirred for only 1 min and then was added to a CMDA solution composed of 1 g of CMDA (1.7 mmol of NH₂/g) and 10 mL of carbonate buffer (0.1 M, pH 8.4) at room temperature. After 4 h at room temperature, acetonitrile was removed by rotative evaporation. The resulting solution was dialyzed against water for 3 days, and the final polymer was recovered by freeze-drying.

Preparation of CMDA–GdDTPA[–] from CMDA–DTPA. CMDA–GdDTPA[–] was prepared as follows: CMDA–DTPA was mixed at pH 6.5 with GdCl₃·6H₂O (Aldrich) using a molar ratio Gd³⁺/DTPA = 1. Residual uncomplexed CMDA–DTPA (or Gd³⁺) concentration was determined, and when it was >1% of the CMDA–GdDTPA[–] concentration, further GdCl₃·6H₂O (or CMDA–DTPA)

was added. Gd³⁺ concentration was determined following a colorimetric titration method with arsenazo, a compound that leads to a complex with Gd³⁺ absorbing at 654 nm (21). The concentration of uncomplexed CMDA–DTPA was determined using the potentiometric titration method described in the next part for the measurement of the DTPA content of CMDA–DTPA samples.

Physicochemical Methods. The carboxylate content of CMD and the carboxylate and amine contents of CMDA were determined according to a pH-metric method. The equipment was composed of a titroprocessor (Metrohm E636, Herisau, Switzerland) coupled to a silver–glass combined electrode.

DTPA contents were obtained by a complexometric reverse dosage. CMDA–DTPA was dissolved in distilled water with an excess of Gd³⁺ with respect to the expected DTPA concentration. Then, the amount of uncomplexed Gd³⁺ was dosed with EDTA. During this operation, the potential fluctuations between a copper electrode and a glass one were registered.

The substitution of CMDA amines by DTPA carboxylic groups was checked by ¹³C NMR chemical shifts of amino α -carbon upon being converted to an amido α -carbon. The ¹³C NMR spectra were recorded in a water–D₂O mixture (90/10 mL/mL) at room temperature on a Bruker AM 200 MHz spectrometer (Karlsruhe, Germany) with sodium 3-(trimethylsilyl)-1-propanesulfonate (DSS) as internal reference.

\bar{M}_n and \bar{M}_w were determined by size exclusion chromatography coupled to low-angle laser light scattering (SEC-LALLS). The LALLS detector was a Chromatix KMX6 (Milton Roy, Riviera Beach, FL). The refractometric detector was a Waters R 410 (Milford, MA). The SEC columns were TSK PW G 4000 and G 6000 (Touzart et Matignon, Courtaboeuf, France; 7.8 mm × 30 cm), connected in series, and the eluent was a 0.15 M NaNO₃ water solution.

The polymer hydrodynamic size distribution profiles were determined by high-performance size exclusion chromatography (HP-SEC). The experiments were carried out on a system equipped with a refractometric detector (Waters R 410) and with a 500 Ultrahydrogel column (Waters; 7.8 mm × 30 cm). Eluent was a 0.05 M phosphate buffer, pH 7.2.

Longitudinal (r_1) relaxivity values were determined in water at 10 and 20 MHz, at 37 °C with an IBM Research field cycling relaxometer (Mons University, Belgium) using an inversion recovery pulse sequence.

RESULTS AND DISCUSSION

Synthesis. The CMDA–DTPA synthesis was carried out in three steps (Figure 1). The first step consisted of introducing carboxylic functions on dextran 40 to obtain carboxymethyldextran (CMD) without degrading the polysaccharidic backbone. For this purpose, chloroacetic acid, which can react with one (or more) of the three hydroxylic groups of the glucopyranose unit, was used. In the second step, the CMD carboxylic groups were allowed to react with ethylenediamine by means of a coupling agent, 2-ethoxy-1-(ethoxycarbonyl)-1,2-dihydroquinoline (EEDQ), to give aminated carboxymethyldextran (CMDA). Finally, three different experimental procedures were investigated to activate one of the DTPA carboxylic functions so that it could react with CMDA amines. The most commonly used method consists of using DTPA bisanhydride (DTPAba). However, in most cases, the reaction of DTPAba with aminated polymers leads to polymers with a high molecular mass (22, 23). DTPA can also be activated in the form of succinimide ester (DTPA-ONSu) by employing both dicyclohexylcar-

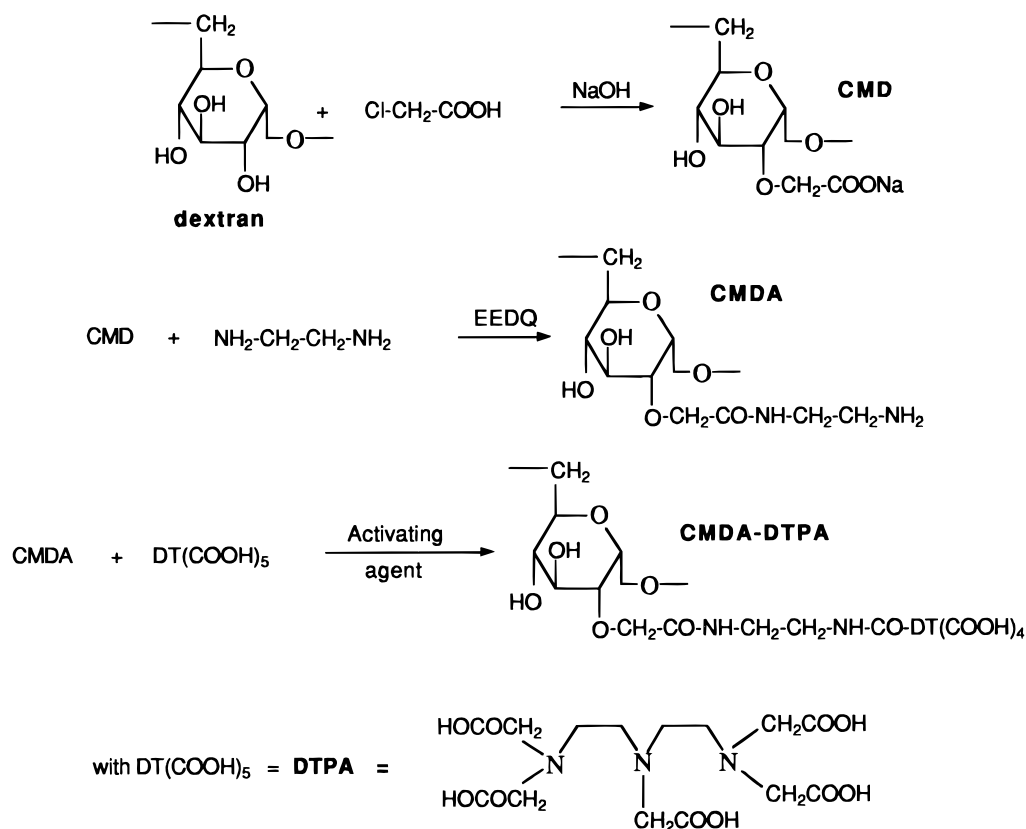


Figure 1. Synthesis of CMDA–DTPA. EEDQ, 2-ethoxy-1-(ethoxycarbonyl)-1,2-dihydroquinoline.

Table 1. Influence of the EEDQ/COONa Molar Ratio on the Amine Content of CMDA

molar ratio EEDQ/COONa	CMDA composition			
	NH ₂ content		COONa content	
	mmol/g	mol/mol of glucose	mmol/g	mol/mol of glucose
0.5	1.0	0.15	2.0	0.44
1	1.3	0.27	1.5	0.31
2	1.7	0.37	1.0	0.21

^a Initial CMD contained 0.59 mol of COONa/mol of glucose unit. The COONa and NH₂ contents were determined by a pH-metric measurement.

bodiimide (DCC) and *N*-hydroxysuccinimide (HONSu) (8, 24) or in the form of a mixed anhydride by means of IBCF (25, 26).

CMD was prepared according to the literature (27) from dextran 40. At 60 °C, in one step and for a 50 mn reaction time, a carboxymethylated polymer was obtained that contained 2.8 mmol of COONa/g, i.e. 0.59 mol of COONa/mol of glucose unit.

In the synthesis of CMDA, an increase in the amine content was observed when the EEDQ/COONa molar ratio increased (Table 1). However, the anhydride resulting from the reaction between EEDQ and CMD carboxylic groups is sensitive to hydrolysis. This side reaction consumes reagents and hampers the synthesis of highly aminated polymers. Accordingly, it can be seen in Table 1 that an excess of EEDQ with regard to COONa did not lead to the amidification of all the COONa functions. Indeed, the CMDA sample prepared with EEDQ/COONa = 2 mol/mol still contained residual unsubstituted COONa groups (0.21 mol of COONa/mol of glucose unit).

The ¹³C NMR spectrum of CMDA (not shown) exhibited two peaks at 39 and 41.7 ppm, corresponding to, respectively, the amino α-carbon and the amido α-carbon, while,

Table 2. DTPA Contents of CMDA–DTPA Samples Synthesized According to Three Different Methods^a

no.	nature of the activated DTPA	activated DTPA/NH ₂ molar ratio used in the reaction	DTPA content of polymer (mmol/g)
1	DTPAba	17	0.74
2	DTPA succinimide ester	8	0.76
3	DTPA mixed anhydride	5	0.74

^a The DTPA contents were determined by complexometric titration. The initial CMDA contained 0.35 mol of NH₂/mol of glucose unit.

in the case of CMDA–DTPA and whatever the synthesis procedure (DTPA bisanhydride, activated ester, or mixed anhydride), the peak corresponding to the amino α-carbon disappeared. It can thus be concluded that all of the CMDA amino groups were substituted by DTPA.

To obtain a high substitution rate of CMDA amines by DTPA in spite of the reagent hydrolysis (coupling agent and activated DTPA), an excess of activated DTPA with regard to the amine concentration was used. This excess was different depending on the synthesis procedure (Table 2). Under these conditions, the three CMDA–DTPA samples, synthesized from the same CMDA (0.35 mol of NH₂/mol of glucose unit), exhibited about the same DTPA content, i.e. 0.75 mmol of DTPA/g (Table 2). This value corresponds only to the dextran-monoamidified DTPA since it was determined by a back-titration procedure using EDTA. In fact, the constant of complexation of EDTA with Gd³⁺ is about 10¹⁷ L mol⁻¹ (28), i.e. 100 times smaller than that of monoamidified DTPA [about 10¹⁹ L mol⁻¹ (5, 17)], and the complex of Gd³⁺ with dextran-monoamidified DTPA cannot be dissociated by a low concentration of EDTA. On the other hand, it is not the same situation with Gd³⁺ complexed to dextran-diamidified DTPA, since the complex stability constant is only about 10¹⁶ L mol⁻¹ (17), i.e. smaller than that of EDTA-complexed Gd³⁺, which leads to the removal of

Table 3. Average Molecular Masses of Successive Polymeric Derivatives^a

polymer	\bar{M}_n (kg/mol)		\bar{M}_w (kg/mol)		polydispersity index, I	
	measd	calcd	measd	calcd	measd	calcd
dextran 40	38		43		1.1	
CMD	45	49	56	56	1.2	1.1
CMDA	45	50	67	57	1.5	1.1
CMDA-DTPA 1 ^b	128		345		2.7	
CMDA-DTPA 2 ^b	166	95	332	142	2.0	1.5
CMDA-DTPA 3 ^b	137		371		2.7	

^a Molecular masses were determined by SEC-LALLS as described under Experimental Procedures. The CMDA-DTPA numbers refer to those of Table 2. The theoretical CMD and CMDA molecular masses (\bar{M}_n and \bar{M}_w) were calculated using those of initial dextran and the experimental chemical compositions of CMD (0.59 mol of COONa/mol of glucose unit) and CMDA (0.24 mol of COONa and 0.35 mol of NH₂/mol of glucose unit). ^b The theoretical molecular masses of CMDA-DTPA samples were calculated using those of parent CMDA and the COONa, amine, and DTPA contents as determined by the CMDA-DTPA analysis.

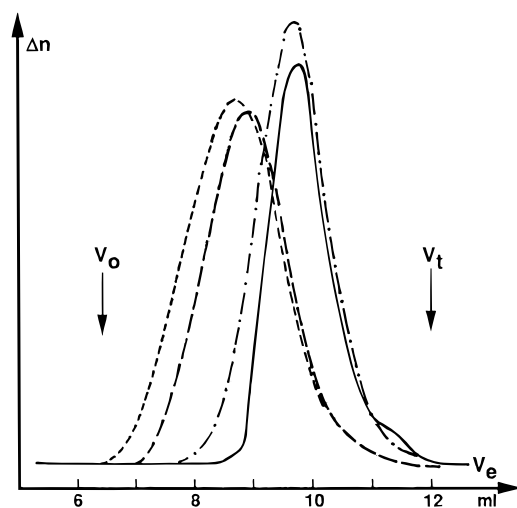


Figure 2. HP-SEC elution profiles of dextran (---), CMD (—), CMDA (···), and CMDA-DTPA **1** (- · -) prepared by means of DTPAba (see Table 2), on a 500 Ultrahydrogel column: eluent, 0.05 M phosphate buffer, pH 7.2; refractometric detection; flow rate, 0.7 mL/min; void volume, $V_0 = 6.4$ mL; total permeation volume, $V_t = 12$ mL.

Gd³⁺ from its complex with dextran-diamidified DTPA upon addition of EDTA.

Hydrodynamic Volumes and Average Molecular Masses (\bar{M}_n and \bar{M}_w). The average molecular masses of different polymeric derivatives of the same family are shown in Table 3, and their hydrodynamic volume distributions are presented in Figure 2.

As expected, CMD has average molecular masses higher than those of initial dextran (Table 3) as a result of the coupling of carboxymethyl groups, and the experimental values are close to those that can be theoretically calculated. Moreover, the experimental polydispersity index is similar to that of dextran 40. These results prove that the CMD chains are statistically substituted. The CMD hydrodynamic volume estimated by HP-SEC (Figure 2) is higher than that of dextran 40. By using the calibration plot of a 500 Ultrahydrogel column, obtained with dextrans of known \bar{M}_w , the CMD hydrodynamic volume was found to be close to that of a dextran with a \bar{M}_w of 100 kg/mol. The great difference between the molecular size of dextran 40 and that of CMD can be explained by the fact that, under the applied ionic strength conditions (0.05 M phosphate buffer, pH 7.2),

many repulsive electrostatic interactions exist inside the polysaccharidic chains between the anionic groups.

During the CMDA synthesis, some cross-linking mechanisms can take place. Indeed, at the pH of CMDA synthesis (pH 11), a part of the ethylenediamine molecules is totally nonprotonated ($pK_a^1 = 7.5$ and $pK_a^2 = 10.7$) and can react with two activated carboxylic groups of two different CMD chains. Therefore, to limit these undesirable side reactions, an excess of ethylenediamine with respect to COONa concentration (diamine/COONa = 10 mol/mol) was used. Table 3 shows that the CMDA molecular masses as measured by SEC-LALLS are a little higher than those which can be theoretically calculated from the CMDA composition. Moreover, the experimental polydispersity index of CMDA ($I = 1.5$) is slightly greater than that of the parent CMD ($I = 1.2$) and its molecular mass distribution profile is a little less symmetrical than that of CMD (not shown). All of these results prove that the CMDA sample is cross-linked. The CMDA average hydrodynamic molecular size as illustrated by the HP-SEC profile (Figure 2) is much smaller than that of CMD and close to that of initial dextran, although the CMDA \bar{M}_w value is higher. In fact, the replacement of some CMD carboxylate groups by amines leads, under the experimental conditions at which the polymers are studied (0.05 M phosphate buffer, pH 7.2), to attractive electrostatic interactions between NH₃⁺ and COO⁻ inside the CMDA chains, which results in a shrinkage of the polymer chains.

The last step of this synthesis concerned the coupling of DTPA with CMDA. As DTPA possesses five carboxylic acid functions, there was a risk that more than one of them would have been activated in the presence of a coupling agent. In this case one DTPA molecule could react with two (or more) amine functions carried by two (or more) different CMDA chains. Therefore, the coupling procedures (DTPAba, DCC/HONSu, and IBCF) were optimized to limit these cross-linking reactions. In the DTPAba procedure, to limit the probability that one DTPAba molecule would react with two CMDA amines, a very low molar amine concentration of about 3.4×10^{-3} mol/L was used. Concerning the procedures using both HONSu and DCC, Spanoghe et al. (8) and Paxton et al. (24) showed that it was possible to prepare a monoactivated DTPA by using DCC/DTPA and HONSu/DTPA molar ratios, respectively, of 1 and 0.7. These conditions were applied for the synthesis of CMDA-DTPA by means of DCC/HONSu. In the IBCF procedure, a IBCF/DTPA molar ratio of 0.5 mol/mol was used. The other reaction parameters (molar ratios of activated DTPA/NH₂) are those given in Table 2.

Theoretical \bar{M}_n , \bar{M}_w , and polydispersity index values of, respectively, 95 and 142 kg/mol and 1.5 were calculated for a CMDA-DTPA containing 0.35 mol of DTPA and 0.24 mol of COONa/mol of glucose unit. The theoretical DTPA content was assumed to be 0.35 mol/mol of glucose unit since the parent CMDA contained 0.35 mol of NH₂/mol of glucose unit and since according to the ¹³C NMR spectra all of the NH₂ functions were substituted. The content in COONa was that of the parent CMDA. As shown in Table 3, the \bar{M}_n and \bar{M}_w experimental values of the three CMDA-DTPA samples are higher than those theoretically calculated. The same remark can be made for the polydispersity indices, which are >2 while that of the parent CMDA is 1.5. These results lead to the conclusion that, whatever the experimental procedure carried out to prepare the CMDA-DTPA samples, a part of the DTPA molecules is polyactivated, which gives rise to a few cross-linking reactions and therefore to a fraction of high molecular mass

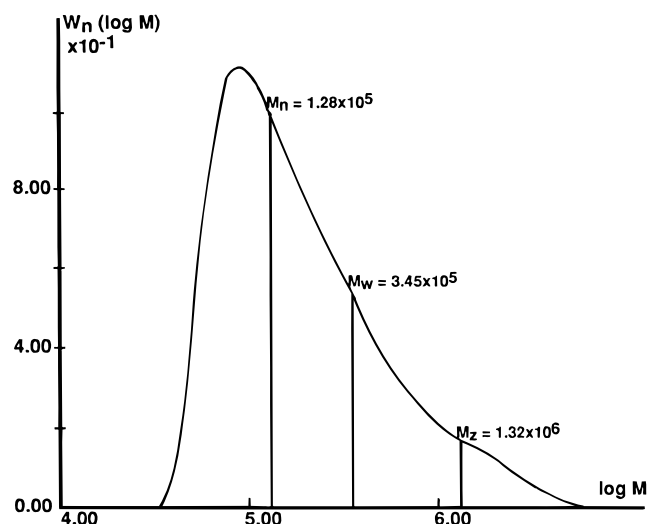


Figure 3. Molecular mass distribution profile (logarithmic normal distribution) of CMDA-DTPA **1** (cf. Figure 2) obtained by SEC-LALLS: columns used, TSK PW G 6000 and 4000; eluent, 0.1 M NaNO₃ aqueous solution.

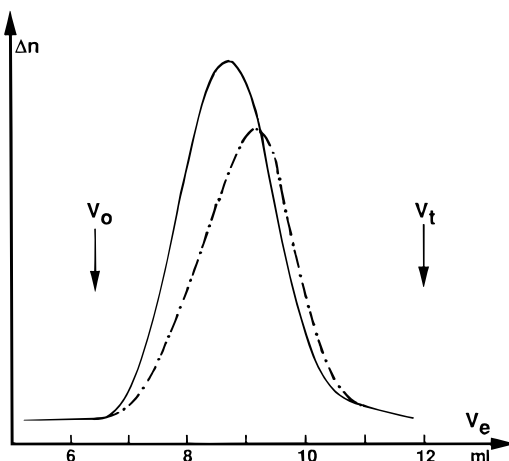


Figure 4. HP-SEC elution profiles of CMDA-DTPA **1** (—) (cf. Figure 2) and of corresponding CMDA-GdDTPA²⁻ (---), on a 500 Ultrahydrogel column. Conditions were as in Figure 2.

molecules. This cross-linking phenomenon is clearly proved in the CMDA-DTPA molecular mass distribution profiles. One example of these CMDA-DTPA profiles is given in Figure 3 (sample 1 synthesized by means of DTPAba), and it can be seen that the profile is widened toward the high molecular masses.

The fact that all of the CMDA-DTPA samples present some cross-linked chains proves that the monoamidification is not the only reaction whatever the coupling procedure and conditions employed. Among the four types of polymers studied—dextran, CMD, CMDA, and CMDA-DTPA—the last one has, by far, the largest average hydrodynamic volume (Figure 2). For example, the CMDA-DTPA sample **1** (prepared by means of DTPAba) has a molecular size close to that of a dextran with a M_w of 140 kg/mol. This large increase in the molecular size results of course from the cross-linking reactions but above all from the presence on the polysaccharidic chains of a great amount of COO⁻ groups (residual carboxymethyl and DTPA) which, in the used HP-SEC eluent, strongly extends the polymer structure.

Figure 4 presents the HP-SEC profile of CMDA-DTPA **1** compared to that of CMDA-GdDTPA²⁻ obtained after complexation of the DTPA carboxylate functions with Gd³⁺. It shows that the Gd³⁺ complexation produces a decrease in the polymer molecular size. Indeed, while

the molecular size of CMDA-DTPA can be compared to that of a 140 kg/mol dextran, CMDA-GdDTPA²⁻ is now comparable to a 77 kg/mol dextran. This result confirms that uncomplexed CMDA-DTPA is really subjected to repulsive electrostatic interactions which can no longer exist in the final complex with Gd³⁺.

Paramagnetic Properties. As CMDA-GdDTPA²⁻ has to be used as a contrast agent in NMR imaging, its capacity in enhancing contrast was estimated by determining its r_1 relaxivity at 10 and 20 MHz, at 37 °C. For CMDA-GdDTPA²⁻ **1** (obtained from CMDA-DTPA **1**, Table 2), the r_1 values at 10 and 20 MHz were, respectively, 8.9 and 9.8 mM⁻¹ s⁻¹. These values are thus, respectively, 1.9 and 2.5 times as great as those of molecular complexes GdDTPA²⁻ that are commonly used in NMR imaging. This enhancement of the r_1 value of a paramagnetic element when bound to a macromolecule has been already described and explained (14, 29). This increase is caused by a "changeover" in the values of correlation times, τ_R (rotation correlation time) and τ_S (electron spin relaxation time), when the paramagnetic species becomes bound to a macromolecule, which brings about an increase in τ_C (effective correlation time) (14).

CONCLUSION

Polymeric conjugates of Gd³⁺-DTPA and dextran described in this paper present some differences with those already reported elsewhere: first, they are more substituted than almost all of the dextran conjugates described in the literature (10–13). The possibility of using highly substituted polymers is important as it allows one to inject small amounts of polymer while achieving a good contrast and thus to limit the risks of allergies. Only the conjugates presented by Armitage et al. (9) possessed DTPA contents similar to those of this paper, but in Armitage's work, DTPA was linked directly to the polysaccharide via an ester function, while in the conjugates here described, a short spacer arm was used and DTPA was linked to aminated dextran by an amide function.

According to the analysis of the synthesized conjugates, a small fraction of polymeric chains is cross-linked, which means that a part of the dextran-linked DTPA molecules is diamidified. This could lead to *in vivo* toxicity because of the decrease of the complexation constant between Gd³⁺ and DTPA due to the decrease of the number of free carboxylate groups. In fact, while the thermodynamic stability constant of GdDTPA²⁻ is 10^{22.5} L mol⁻¹ (2), that of Gd³⁺-complexed monoamidified DTPA as determined by Lauffer et al. (5) and Sherry et al. (17) is, respectively, 10^{19.1} and 10^{19.7} L mol⁻¹ and that of Gd³⁺-complexed diamidified DTPA is 10^{16.2} L mol⁻¹ (17). To overcome the difficulty caused by the potential *in vivo* Gd³⁺ release from diamidified DTPA, the high molecular mass fraction of conjugates should be removed, for example, by ultrafiltration. Such experiments are now under investigation.

Finally, the CMDA-GdDTPA²⁻ r_1 relaxivity values at 10 and 20 MHz are higher, per mole of Gd, than those of free ligand. Thus, during a clinical examination, the gadolinium concentration needed to obtain contrast will be lower with CMDA-GdDTPA²⁻ than with GdDTPA²⁻. Moreover, as CMDA-GdDTPA²⁻ has an average molecular size bigger than that of dextran 40, it is likely that its plasma half-life will be greater than that of dextran, which will be another advantage over GdDTPA²⁻.

ACKNOWLEDGMENT

This work was supported by a CIFRE grant (Société Guerbet-GCA, Aulnay-sous-Bois, France, and ANRT,

France). We thank Mrs. T. Geoffroy and Mr. A. Vicherat for helpful technical assistance, respectively, in LALLS and RMN analyses. We also thank Prof. R. N. Muller (Mons University, Belgium) for helpful discussions on the interpretation of relaxivities.

LITERATURE CITED

- (1) Niendorf, H. P., Alhassan, A., Haustein, J., Clauss, W., and Cornelius, I. (1993) Safety and risk of gadolinium-DTPA: extended clinical experience after more than 5,000,000 applications. *Adv. MRI Contrast* 2, 12.
- (2) Martell, A. E., and Smith, R. M. (1986) *Critical Stability Constants*, Vol. 6, Plenum Press, New York.
- (3) Desreux, J. F. (1980) Nuclear magnetic resonance spectroscopy of lanthanide complexes with a tetraacetic tetraaza macrocycle. Unusual conformation properties. *Inorg. Chem.* 19, 1319.
- (4) Schmiedl, U., Moseley, M. E., Ogan, M. D., Chew, W. D., and Brasch, R. C. (1987) Comparison of initial biodistribution patterns of Gd-DTPA and albumin-(Gd-DTPA) using rapid spin echo MR imaging. *J. Comput. Assist. Tomogr.* 11, 306.
- (5) Lauffer, R. B., Brady, T. J., Brown III, R. D., Baglin, C., and Koenig, S. H. (1986) 1/T1 NMRD profiles of solutions of Mn²⁺ and Gd³⁺ protein-chelate conjugates. *Magn. Reson. Med.* 3, 541.
- (6) Paaanen, H., Reisto, T., Hemmila, I., Komu, M., Niemi, P., and Kormano, M. (1990) Proton relaxation enhancement of albumin, immunoglobulin G and fibrinogen labeled with Gd-DTPA. *Magn. Reson. Med.* 13, 38.
- (7) Niemi, P., Reisto, T., Hemmila, I., and Kormano, M. (1991) Magnetic field dependence of longitudinal relaxation rates of solutions of various protein-gadolinium³⁺ chelate conjugates. *Invest. Radiol.* 26, 820.
- (8) Spanoghe, M., Lanens, D., Dommissie, R., Van Der Linden, A., and Alderweireldt, F. (1992) Proton relaxation enhancement by means of serum albumin and poly-L-lysine labeled with DTPA-Gd³⁺: relaxivities as a function of molecular weight and conjugation efficiency. *Magn. Reson. Imaging* 10, 913.
- (9) Armitage, F. E., Richardson, D. E., and Li, K. C. P. (1990) Polymeric contrast agents for magnetic resonance imaging: synthesis and characterization of gadolinium diethylenetriaminepentaacetic acid conjugated to polysaccharides. *Bioconjugate Chem.* 1, 365.
- (10) Wang, S. C., Wikstroem, M. G., White, D. L., Klaveness, J., Holtz, E., Rongved, P., Moseley, M. E., Michael, E., and Brash, R. C. (1990) Evaluation of the gadolinium-DTPA-labeled dextran as an intravascular MR contrast agent: imaging characteristics in normal rat tissues. *Radiology* 175, 483.
- (11) Bligh, S. W. A., Harding, C. T., Sadler, P. J., Bulman, R. A., Bydder, G. M., Pennoock, J. M., Kelly, J. D., Latham, I. A., and Marriott, J. A. (1991) Use of paramagnetic chelated derivatives of polysaccharides and spin-labeled polysaccharides as contrast agents in magnetic resonance imaging. *Magn. Reson. Med.* 17, 516.
- (12) Rongved, P., and Claveness, J. (1991) Water soluble polysaccharides as carriers of paramagnetic contrast agents for magnetic resonance imaging: Synthesis and relaxation properties. *Carbohydr. Res.* 214, 315.
- (13) Brash, R. C. (1991) Rationale and applications for macromolecular Gd-based contrast agent. *Magn. Reson. Med.* 22, 282.
- (14) Lauffer, R. B., and Brady, T. J. (1985) Preparation and water relaxation properties of proteins labeled with paramagnetic metal chelates. *Magn. Reson. Imaging* 3, 11.
- (15) Schuhmann-Giampieri, G., Schmitt-Willich, H., Frenzel, T., Press, W.-R., and Weinmann, H.-J. (1991) In vivo and in vitro evaluation of Gd-DTPA-polylysine as a macromolecular contrast agent for resonance magnetic imaging. *Invest. Radiol.* 26, 969.
- (16) Dellacherie, É. (1996) Polysaccharides in oxygen-carrier blood substitutes. In *Polysaccharides in Medicinal Applications* (S. Dumitriu, Ed.) p 525, Marcel Dekker, New York.
- (17) Sherry, A. D., Cacheris, W. P., and Kuan, K.-T. (1988) Stability constants for Gd³⁺ binding to model DTPA-conjugates and DTPA-proteins: implications for their use as magnetic resonance contrast agents. *Magn. Reson. Med.* 8, 180.
- (18) Aime, S., Anelli, P. L., Botta, M., Fedeli, F., Grandi, M., Paoli, P., and Ugeri, F. (1992) Synthesis, characterization, and 1/T1 NMRD profiles of gadolinium(III) complexes of monoamide derivatives of DOTA-like ligands. X-ray structure of the 10-[2-[[2-hydroxy-1-(hydroxymethyl)ethyl]amino]-1-[(phenylmethoxy)methyl]-2-oxoethyl]-1,4,7,10-tetra-azacyclododecane-1,4,7-triacetic acid-gadolinium(III) complex. *Inorg. Chem.* 31, 2422.
- (19) Konings, M. S., Dow, W. C., Love, D. B., Raymond, K. N., Quay, S. C., and Rocklage, S. M. (1990) Gadolinium complexation by a new DTPA-amide ligand. Amide oxygen coordination. *Inorg. Chem.* 29, 1488.
- (20) Eckelman, W. C., Karesh, S. M., and Reba, R. C. (1975) New compounds: fatty acid and long chain hydrocarbon derivatives containing a strong chelating agent. *J. Pharm. Sci.* 64, 704.
- (21) Onishi, H., and Sekine, K. (1972) Reagent for the determination of Th, U, Zr and rare earth metals. *Talanta* 19, 473.
- (22) Paik, C. H., Ebbert, M. A., Murphy, P. R., Lassman, C. R., Reba, R. C., Eckelman, W. C., Pak, K. Y., Powe, J., Steplewski, Z., and Koprowski, H. (1983) Factors influencing DTPA conjugation with antibodies by cyclic DTPA anhydride. *J. Nucl. Med.* 24, 1158.
- (23) Maisano, F., Gozzini, L., and de Haen, C. (1992) Coupling of DTPA to proteins: a critical analysis of the cyclic dianhydride method in the case of insulin modification. *Bioconjugate Chem.* 3, 212.
- (24) Paxton, R. J., Jakowatz, J. G., Beatty, J. D., Beatty, B. G., Vlahos, W. G., Williams, L. E., Clark, B. R., and Shively, J. E. (1985) High-specific-activity ¹¹¹In-labeled anticarcinoma embryonic antigen monoclonal antibody: improved method for the synthesis of diethylenetriaminepentaacetic acid conjugates. *Cancer Res.* 45, 5694.
- (25) Li, M., and Meares, C. F. (1993) Synthesis, metal chelate stability studies and enzyme digestion of a peptide-linked DOTA derivative and its corresponding radiolabeled immunoconjugates. *Bioconjugate Chem.* 4, 275.
- (26) Sieving, P. F., Watson, A. D., and Rocklage, S. M. (1990) Preparation and characterization of paramagnetic polychelates and their protein conjugates. *Bioconjugate Chem.* 1, 65.
- (27) Bouttemy, M. (1960) Contribution à l'étude des carboxyméthylcelluloses. Préparation des carboxyméthylcelluloses de hauts degrés de substitution (Contribution to the study of carboxyméthylcelluloses. Preparation of carboxyméthylcelluloses with a high degree of substitution). *Bull. Soc. Chim. Fr.* 1750.
- (28) Cacheris, W. P., Nickle, S. K., and Sherry, A. D. (1987) Thermodynamic study of lanthanide complexes of 1,4,7-triazacyclononane-*N,N,N'*-triacetic acid and 1,4,7,10-tetraazacyclododecane-*N,N,N',N''*-tetraacetic acid. *Inorg. Chem.* 26, 958.
- (29) Lauffer, R. B. (1987) Paramagnetic metal complexes as water proton relaxation agents for NMR imaging: theory and design. *Chem. Rev.* 87, 901.

BC970062N

8-(ω -Aminoalkyl)theophyllines and Their Use in Preparing Fluorescently Labeled Derivatives for Applications in Immunoassay

Fulya Yahioğlu,[†] Colin W. Pouton, and Michael D. Threadgill*

School of Pharmacy and Pharmacology, University of Bath, Claverton Down, Bath BA2 7AY, United Kingdom.
Received September 10, 1996[⊗]

Reaction of alkane-1, ω -diamines with 6-chloro-1,3-dimethylpyrimidine-2,4-dione under carefully controlled conditions gives 6-(ω -aminoalkylamino)-1,3-dimethylpyrimidine-2,4-diones, which can be readily separated from traces of products of disubstitution after benzyloxycarbonyl protection. A sequence of nitrosation at the pyrimidine 5-position, thermal cyclization, and deprotection affords 8-(ω -aminoalkyl) derivatives of theophylline, an important drug in the treatment of asthma and related diseases. These 8-(ω -aminoalkyl)theophyllines can be coupled to fluorescein-5-isothiocyanate and to dansyl chloride, giving fluorescent derivatives of theophylline with applications in automated immunoassay of the drug in biofluids using the fluorescence capillary fill device.

INTRODUCTION

Theophylline (**1**; Scheme 1) is a drug that is commonly used as a bronchospasmolytic agent in the prevention and treatment of asthma, apnoea, and obstructive lung diseases and is an inhibitor of cyclic nucleotide phosphodiesterases (1–3). Drug-induced toxicity occurs at plasma concentrations not far above those required for therapy, and plasma concentrations vary greatly among individuals given the same dose. Rapid and accurate measurement of its concentration in biofluids is therefore necessary (2, 3). Current methods for the determination of theophylline in blood include ELISA (4), radioimmunoassay (5), and HPLC (6), although not all of these completely fulfill criteria of speed, ease, and low cost of assay. The fluorescence capillary fill device (FCFD) (7–10) overcomes these drawbacks. To develop an immunoassay for theophylline in whole blood using this device, we required fluorescent derivatives of theophylline that have good immunoreactivity with appropriate anti-theophylline antibodies. To be able to optimize both the photoproperties of the fluorophore and the length and lipophilicity of the link between theophylline and the fluorophore, a series of 8-(ω -aminoalkyl)theophyllines and related ethers was sought. Thus, a variety of widely used fluorescent groups bearing isothiocyanate and sulfonyl chloride electrophiles could be attached.

EXPERIMENTAL PROCEDURES

Chemical Synthesis. IR spectra were recorded on a Perkin-Elmer 782 spectrophotometer as potassium bromide disks, unless otherwise stated. NMR spectra were recorded using JEOL JNM GX270 and JNM EX400 spectrometers of samples in (CD₃)₂SO, except where stated. Chemical shifts were measured relative to tetramethylsilane as internal standard. Mass spectra were obtained using a VG7070E analytical mass spectrometer using electron impact (EI) or fast atom bombardment (FAB) techniques in the positive ion mode. Melting points are uncorrected. Dioxane refers to 1,4-dioxane. Chromatographic separations were carried out using

Sorbisil C60 (0.040–0.063) silica gel. Solvents were evaporated under reduced pressure. Solutions in organic solvents were dried over magnesium sulfate. Experiments were conducted at ambient temperature unless otherwise stated. Chemicals were purchased from Aldrich Chemical Co. (Gillingham, U.K.), Sigma Chemical Co. (Gillingham, U.K.), and Maybridge Chemicals (Tintagel, U.K.).

Phenylmethyl N-[[[6-(1,1-Dimethylethoxy)carbonyl]amino]hexyl]carbamate (3). Phenylmethyl chloroformate (610 mg, 3.6 mmol) in CH₂Cl₂ (6 mL) was added during 30 min to 1,1-dimethylethyl *N*-(6-aminoethyl)carbamate hydrochloride (**2**) (900 mg, 3.6 mmol) and Et₃N (720 mg, 7.1 mmol) in CH₂Cl₂ (12 mL). The mixture was stirred for 24 h and was filtered. The filtrate was washed twice with water and once with hydrochloric acid (2 M) and dried. The solvent was evaporated to afford **3** as a white crystalline solid (960 mg, 77%): mp 190 °C; IR 3340, 1680, 1550 cm⁻¹; NMR δ (CDCl₃) 1.44 (17 H, m, CH₂CH₂CH₂CH₂CH₂CH₂ + Bu⁺), 1.85 (1 H, br, NH), 3.11 (2 H, q, *J* = 6 Hz, CH₂N), 3.17 (2 H, m, CH₂N), 4.85 (1 H, br, NH), 5.09 (2 H, s, PhCH₂), 7.35 (5 H, s, Ar-H₅); MS (EI) 350 (M). Anal. Calcd for C₁₉H₃₀N₂O₄: C, 65.12; H, 8.63; N, 7.99. Found: C, 65.41; H, 8.61; N, 8.17.

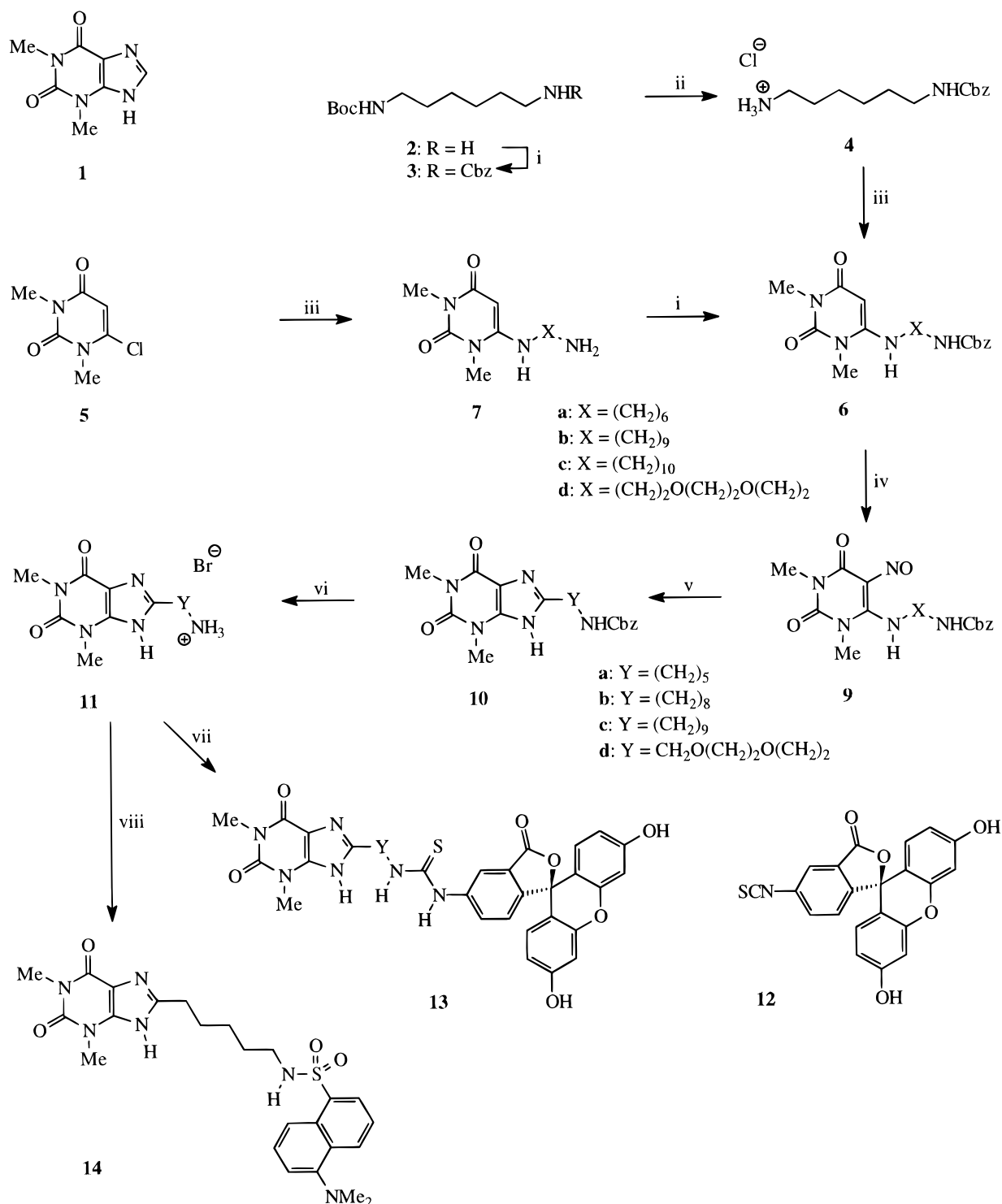
Phenylmethyl N-(6-Aminoethyl)carbamate Hydrochloride (4). HCl was passed through **3** (960 mg, 2.7 mmol) in CH₂Cl₂ (100 mL) for 1 h. The solvent and excess reagent were evaporated to afford **4** as white crystals (680 mg, 99%): mp 177–178 °C [lit. (11) mp 177–178 °C]; IR 3470, 3340–3280, 1700, 1630 cm⁻¹; NMR δ (CDCl₃) 1.18 (4 H, m, 2 \times CH₂), 1.35 (4 H, m, 2 \times CH₂), 2.93 (2 H, t, *J* = 6 Hz, CH₂N⁺H₃), 3.08 (2 H, q, *J* = 6 Hz, CH₂NH), 3.61 (3 H, br, N⁺H₃), 5.07 (2 H, s, PhCH₂), 7.39 (5 H, s, Ar-H₅); MS (EI) 287 (M).

1,3-Dimethyl-6-[[[6-(phenylmethoxy)carbonyl]amino]hexyl]aminopyrimidine-2,4-dione (6a). 1,3-Dimethyl-6-chloropyrimidine-2,4-dione (**5**) (490 mg, 2.8 mmol), **4** (840 mg, 3.7 mmol), and Na₂CO₃ (600 mg, 5.7 mmol) were boiled under reflux in dioxane (8 mL) for 4 h. The cooled mixture was diluted with CHCl₃, and the solution was washed twice with water and once with saturated brine and was dried. The evaporation residue was recrystallized (EtOH) to give **6a** as yellow crystals (600 mg, 54%): mp 128–130 °C; IR 3360, 3280, 1700, 1630 cm⁻¹; NMR δ 0.90 (4 H, m, 2 \times CH₂), 1.23 (4 H, m, 2 \times CH₂), 3.15 (2 H, t, *J* = 6 Hz, CH₂N), 3.17 (2 H, t, *J* = 6 Hz, CH₂N), 3.06 (3 H, s, NMe), 3.23 (3 H, s, NMe), 4.21 (2 H,

* Author to whom correspondence should be addressed (e-mail m.d.threadgill@bath.ac.uk).

[†] Present address: Department of Clinical Biochemistry, The London Hospital Medical College, Turner Street, London E1 2AD, U.K.

[⊗] Abstract published in *Advance ACS Abstracts*, June 1, 1997.

Scheme 1. Structures of Theophylline 1 and Fluorescein-5-isothiocyanate 12 and Synthetic Routes to the Fluorescent Theophylline Derivatives 13a–d and 14a

^a Reagents: i, CbzCl, Et₃N, CH₂Cl₂; ii, HCl, CH₂Cl₂; iii, **5**, 1,4-dioxane, Na₂CO₃, Δ; iv, C₅H₁₁ONO, HCl, EtOH; v, BuOH, Δ; vi, HBr, HOAc; vii, **12**, K₂CO₃, dioxane, water, pH 9.0 ± 0.2; viii, 5-(dimethylamino)naphthalene-1-sulfonyl chloride, Na₂CO₃, dioxane, water, pH 9.5–10.0.

m, pyrimidine 5-H + NH), 4.69 (2 H, s, PhCH₂), 6.79 (5 H, m, Ph-H₅), 7.70 (1 H, br, NH); *m/z* (EI) 388 (M), 91 (100%). Anal. Calcd for C₂₀H₂₈N₄O₄: C, 61.82; H, 7.27; N, 14.43. Found: C, 61.85; H, 7.36; N, 14.3.

1,3-Dimethyl-6-[[[9-(phenylmethoxy)carbonyl]amino]nonyl]amino]pyrimidine-2,4-dione (6b). The chloropyrimidine **5** (1.00 g, 5.7 mmol) was boiled under reflux with nonane-1,9-diamine (1.81 g, 11 mmol) and Na₂CO₃ (1.21 g, 1.4 mmol) in EtOH (40 mL) for 3 h. The mixture was filtered and the solvent was evaporated. Recrystal-

lization (EtOH) afforded 1,3-dimethyl-6-[(9-aminononyl)-amino]pyrimidine-2,4-dione (**7b**) as a white solid (1.09 g, 65%); mp 210–212 °C; IR 3500, 1660 cm⁻¹; NMR δ 1.29 [14 H, m, (CH₂)₇], 2.54 (2 H, m, CH₂NH₂), 3.03 (2 H, m, NHCH₂), 3.03 (3 H, s, NMe), 3.26 (3 H, s, NMe), 4.65 (1 H, br, NH), 6.72 (1 H, s, pyrimidine 5-H); *m/z* (EI) 297 (M), 159 (100%). This material (3.16 g, 11 mmol) was stirred with phenylmethyl chloroformate (1.91 g, 11 mmol) and Et₃N (2.16 g, 21 mmol) in CH₂Cl₂ (150 mL) for 24 h. The suspension was filtered, and the filtrate

was washed twice with water and once with hydrochloric acid (2 M) and was dried. Evaporation and chromatography ($\text{CHCl}_3/\text{EtOAc}$ 4:1 \rightarrow EtOAc) gave **6b** as white crystals (2.02 g, 43%): mp 105–106 °C; IR 3420, 1700, 1680 cm^{-1} ; NMR δ (CDCl_3) 1.30 (4 H, br, $2 \times \text{CH}_2$), 1.50 (2 H, quintet, $J = 7.3$ Hz, CH_2), 1.66 (8 H, m, $4 \times \text{CH}_2$), 3.09 (2 H, q, $J = 7.3$ Hz, NCH_2), 3.18 (2 H, q, $J = 6.3$ Hz, NCH_2), 3.31 (3 H, s, NMe), 3.39 (3 H, s, NMe), 4.35 (1 H, br, NH), 4.79 (1 H, br, NH), 4.86 (1 H, s, 5-H), 5.09 (2 H, s, PhCH_2), 7.35 (5 H, s, Ph-H_5); MS (EI) 431 (M), 336 (M – PhCH_2OH), 91 (100%). Anal. Calcd for $\text{C}_{20}\text{H}_{28}\text{N}_4\text{O}_4$: C, 61.84; H, 7.27; N, 14.42. Found: C, 61.9; H, 7.35; N, 14.39.

1,3-Dimethyl-6-[[[10-(phenylmethoxy)carbonyl]amino]decyl]aminopyrimidine-2,4-dione (6c). The chloropyrimidine **5** (1.35 g, 7.7 mmol) was treated with decane-1,10-diamine (1.60 g, 9.3 mmol) as for the synthesis of **7b**, except that recrystallization was omitted, to give crude 1,3-dimethyl-6-[(10-aminodecyl)aminopyrimidine-2,4-dione (**7c**) (1.24 g, 52%) as a white solid: mp 72–74 °C; IR 3400, 1660 cm^{-1} ; NMR δ ($\text{CF}_3\text{CO}_2\text{D}$) 1.41 [16 H, m, $(\text{CH}_2)_8$], 1.82 (2 H, m, CH_2N), 3.28 (2 H, m, CH_2N), 3.60 (3 H, s, NMe), 3.69 (3 H, s, NMe); MS (EI) 310 (M), 173. The amine **7c** (800 mg, 2.6 mmol) was treated with phenylmethyl chloroformate (440 mg, 2.6 mmol) as for the synthesis of **6b**, except that the chromatographic eluant was $\text{CHCl}_3/\text{MeOH}$ 10:1, to afford **6c** as white crystals (620 mg, 54%): mp 100–102 °C; IR 3360, 3280, 1700, 1640 cm^{-1} ; NMR δ (CDCl_3) 1.29 [12 H, m, $(\text{CH}_2)_6$], 1.49 (2 H, m, CH_2), 1.65 (2 H, quintet, $J = 6.8$ Hz, CH_2), 3.08 (2 H, dt, $J = 5.1, 7.1$ Hz, CH_2), 3.18 (2 H, q, $J = 6.6$ Hz, NCH_2), 3.31 (3 H, s, NMe), 3.39 (3 H, s, NMe), 4.40 (1 H, br, NH), 4.81 (1 H, s, pyrimidine 5-H), 5.09 (2 H, s, PhCH_2), 7.35 (5 H, m, Ph-H_5); MS (EI) 444 (M), 336 (M – PhCH_2OH), 91 (100%). Anal. Calcd for $\text{C}_{24}\text{H}_{36}\text{N}_4\text{O}_4$: C, 64.82; H, 8.17; N, 12.61. Found: C, 65.1; H, 8.14; N, 12.65.

1,3-Dimethyl-6-[[[2-[2-(2-(phenylmethoxy)carbonyl]amino]ethoxyethoxyethyl]amino]pyrimidine-2,4-dione (6d). The chloropyrimidine **5** (2.82 g, 16 mmol) was treated with 3,6-dioxaoctane-1,8-diamine (6.0 g, 40 mmol) as for the synthesis of **7b**, except that recrystallization was omitted, to give crude 1,3-dimethyl-6-[[[2-[2-(2-aminoethoxy)ethoxy]ethyl]amino]pyrimidine-2,4-dione (**7d**) (3.03 g, 69%). This material was treated with phenylmethyl chloroformate (1.90 g, 11 mmol), as for the synthesis of **6b**, except that the chromatographic eluant was $\text{EtOAc} \rightarrow \text{EtOAc}/\text{MeOH}$ 6:1, to afford **6d** as a colorless gum (2.04 g, 44%): IR 3400–3280, 1740–1670 cm^{-1} ; NMR δ (CDCl_3) 3.24 (2 H, q, $J = 6$ Hz, NCH_2), 3.31 (3 H, s, NMe), 3.36 (3 H, s, NMe), 3.40 (2 H, q, $J = 5.3$ Hz, NCH_2), 3.58 (2 H, t, $J = 6$ Hz, NCH_2CH_2), 3.62 (4 H, s, $\text{OCH}_2\text{CH}_2\text{O}$), 3.68 (2 H, t, $J = 6$ Hz, NCH_2CH_2), 4.83 (1 H, s, pyrimidine 5-H), 5.00 (1 H, br, NH), 5.09 (2 H, s, PhCH_2), 5.29 (1 H, br, NH), 7.35 (5 H, s, Ph-H_5); MS (EI) 421 (M), 91 (100%). Anal. Calcd for $\text{C}_{20}\text{H}_{28}\text{N}_4\text{O}_6$: C, 57.12; H, 6.72; N, 13.33. Found: C, 56.95; H, 6.78; N, 13.39.

1,3-Dimethyl-8-[[[5-(phenylmethoxy)carbonyl]amino]pentyl]purine-2,6-dione (10a). Pentyl nitrite (410 mg, 3.5 mmol) was added carefully to **6a** (550 mg, 1.4 mmol) in EtOH (25 mL) at 40 °C, and the solution was stirred for 10 min. Hydrochloric acid (9 M, 0.3 mL) was added, and the mixture was stirred at ambient temperature for 16 h. The solvent was evaporated to afford crude **9a** as a red gum (430 mg, 73%). This material was boiled under reflux in BuOH (3 mL) for 45 min until decolorization had occurred. The evaporation residue was washed with Et_2O and recrystallized (BuOH) to give **10a** as off-white crystals (400 mg, 71% from **6a**): mp 182–184 °C; IR 3300, 1700, 1680, 1660 cm^{-1} ; NMR δ 1.55 (2 H, quintet,

$J = 7.0$ Hz, CH_2), 1.67 (2 H, quintet, $J = 7$ Hz, CH_2), 1.90 (2 H, quintet, $J = 7.3$ Hz, CH_2), 1.92 (2 H, t, $J = 7.3$ Hz, CH_2), 3.23 (2 H, q, $J = 6.4$ Hz, CH_2N), 3.45 (3 H, s, NMe), 3.59 (3 H, s, NMe), 5.23 (2 H, br, PhCH_2), 7.54 (1 H, br, CbzNH), 7.58 (5 H, m, Ph-H_5); MS (EI) 400 (M), 292 (M – PhCH_2OH), 91 (100%). Anal. Calcd for $\text{C}_{20}\text{H}_{25}\text{N}_5\text{O}_4$: C, 60.14; H, 6.31; N, 17.53. Found: C, 60.09; H, 6.34; N, 17.50.

1,3-Dimethyl-8-[[[8-(phenylmethoxy)carbonyl]amino]octyl]purine-2,6-dione (10b). The pyrimidine **6b** was treated with pentyl nitrite as for the synthesis of **9a**, to give crude **9b** as a purple gum. This material was heated, as for the synthesis of **10a**, to give **10b** as a cream solid (26%): mp 145–147 °C; IR 3320, 1740, 1680 cm^{-1} ; NMR δ 1.24 (8 H, m, $4 \times \text{CH}_2$), 1.38 (2 H, quintet, $J = 6$ Hz, CH_2), 1.65 (2 H, quintet, $J = 6$ Hz, CH_2), 2.65 (2 H, t, $J = 6.2$ Hz, CH_2), 2.95 (2 H, q, $J = 6.2$ Hz, NCH_2), 3.21 (3 H, s, NMe), 3.41 (3 H, s, NMe), 4.99 (2 H, s, PhCH_2), 7.22 (1 H, br, NH), 7.33 (5 H, m, Ph-H_5), 13.15 (1 H, s, NH); MS (EI) 442 (M), 334 (M – PhCH_2OH), 91 (100%). Anal. Calcd for $\text{C}_{23}\text{H}_{31}\text{N}_5\text{O}_4$: C, 62.57; H, 7.08; N, 15.86. Found: C, 62.99; H, 7.35; N, 15.79.

1,3-Dimethyl-8-[[[9-(phenylmethoxy)carbonyl]amino]nonyl]purine-2,6-dione (10c). The 10-Cbz-aminodecyl-aminopyrimidine **6c** was treated with pentyl nitrite, as for the synthesis of **9a**, to afford crude **9c** as a red-purple oil. This material was boiled under reflux for 40 min in BuOH , and the solvent was evaporated. Recrystallization (BuOH) gave **10c** as pale buff crystals (300 mg, 45%): mp 95–96 °C; IR 3300, 1730, 1700, 1650 cm^{-1} ; NMR δ 1.24 [10 H, m, $(\text{CH}_2)_5$], 1.38 (2 H, t, $J = 6$ Hz, CH_2), 1.67 (4 H, m, $2 \times \text{CH}_2$), 2.66 (2 H, q, $J = 7.6$ Hz, NCH_2), 2.97 (2 H, q, $J = 6.4$ Hz, CH_2), 3.22 (3 H, s, NMe), 3.41 (3 H, s, NMe), 4.99 (2 H, s, PhCH_2), 7.22 (1 H, t, $J = 6$ Hz, NH), 7.34 (5 H, m, Ph-H_5); MS (EI) 455 (M), 347 (M – PhCH_2OH), 194 (100%). Anal. Calcd for $\text{C}_{24}\text{H}_{33}\text{N}_5\text{O}_4$: C, 63.26; H, 7.31; N, 15.38. Found: C, 63.6; H, 7.28; N, 15.4.

1,3-Dimethyl-8-[2-[2-(phenylmethoxy)carbonyl]ethoxyethoxymethyl]purine-2,6-dione (10d). The pyrimidine **6d** was treated with pentyl nitrite, as for the synthesis of **9a**, to give **9d** as a purple gum (97%). This material was heated as for the synthesis **10a**, to give **10d** as a yellow gum (66%): IR 3420, 3250, 1740, 1680 cm^{-1} ; NMR δ 3.15 (2 H, q, $J = 5.9$ Hz, NCH_2), 3.23 (3 H, s, NMe), 3.40 (2 H, m, NCH_2CH_2), 3.42 (3 H, s, NMe), 3.55 (2 H, m) and 3.59 (2 H, m) ($\text{OCH}_2\text{CH}_2\text{O}$), 4.53 (2 H, s, CH_2), 5.00 (2 H, s, PhCH_2), 7.33 (6 H, m, $\text{Ph-H}_5 + \text{NH}$), 13.57 (1 H, br, purine-NH); m/z (EI) 431 (M), 91 (100%). Anal. Calcd for $\text{C}_{20}\text{H}_{25}\text{N}_5\text{O}_6$: C, 55.68; H, 5.84; N, 16.23. Found: C, 55.40; H, 5.72; N, 16.39.

8-(5-Aminopentyl)-2,4-dimethylpurine-1,3-dione Hydrobromide (11a). The Cbz-protected amine **10a** (230 mg, 0.58 mmol) was stirred with HBr in AcOH (30%, 0.8 mL) for 15 min. Dry Et_2O (10 mL) was added, the suspension was stirred vigorously for 5 min, and the Et_2O was decanted. This washing procedure was repeated five times, and the solid was dried to afford **11a** as an off-white powder (200 mg, 100%); mp 250–252 °C; IR 3500–3400, 3240, 1740, 1680 cm^{-1} ; NMR δ 1.31 (2 H, quintet, $J = 6.7$ Hz, CH_2), 1.56 (2 H, quintet, $J = 7.3$ Hz, CH_2), 1.70 (2 H, quintet, $J = 7.3$ Hz, CH_2), 2.70 (2 H, t, $J = 7.7$ Hz, CH_2), 2.75 (2 H, t, $J = 7.7$ Hz, NCH_2), 3.22 (3 H, s, NMe), 3.41 (3 H, s, NMe), 7.74 (3 H, br, N^+H_3); MS (FAB) 266 (M + H), 180 (100%). Anal. Calcd for $\text{C}_{12}\text{H}_{20}\text{BrN}_5\text{O}_2$: C, 41.63; H, 5.82; N, 20.23. Found: C, 41.57; H, 5.77; N, 20.22.

8-(8-Amino-octyl)-2,4-dimethylpurine-1,3-dione Hydrobromide (11b). The Cbz-protected amine **10b** was treated with HBr , and the solid was washed with Et_2O , as for

the synthesis of **11a**, to give **11b** as a white powder (100%): mp 239–241 °C; IR 3440, 3200, 1760, 1680 cm^{-1} ; NMR δ 1.27 [8 H, m, $(\text{CH}_2)_4$], 1.52 (2 H, m, CH_2), 1.67 (2 H, quintet, $J = 6.7$ Hz, CH_2), 2.68 (2 H, t, $J = 7.6$ Hz, purine- CH_2), 2.76 (2 H, sextet, $J = 6.4$ Hz, NCH_2), 3.22 (3 H, s, NMe), 3.41 (3 H, s, NMe), 7.72 (3 H, br, N^+H_3); MS (FAB) 308 ($\text{M} + \text{H}$), 180 (100%). Anal. Calcd for $\text{C}_{15}\text{H}_{26}\text{BrN}_5\text{O}_2$: C, 46.42; H, 6.75; N, 18.04. Found: C, 46.41; H, 6.67; N, 18.10.

8-(9-Aminononyl)-2,4-dimethylpurine-1,3-dione Hydrobromide (11c). The Cbz-protected amine **10c** was treated with HBr, and the solid was washed with Et_2O , as for the synthesis of **11a**, to give **11c** as an off-white powder (87%): mp 218–219 °C; IR 3160, 1720, 1680 cm^{-1} ; NMR δ 1.25 (10 H, br, $\text{CH}_2\text{CH}_2\text{CH}_2\text{CH}_2\text{CH}_2\text{CH}_2\text{CH}_2\text{CH}_2$), 1.51 (2 H, m, CH_2), 1.67 (2 H, m, CH_2), 2.68 (2 H, t, $J = 7.5$ Hz, purine- CH_2), 2.75 (2 H, m, NCH_2), 3.22 (3 H, s, NMe), 3.41 (3 H, s, NMe), 7.71 (3 H, s, N^+H_3); MS (FAB) 322 ($\text{M} + \text{H}$), 180 (100%). Anal. Calcd for $\text{C}_{16}\text{H}_{28}\text{BrN}_5\text{O}_2$: C, 47.77; H, 7.01; N, 17.41. Found: C, 47.84; H, 7.11; N, 17.22.

8-[2-(2-Aminoethoxy)ethoxymethyl]-2,4-dimethylpurine-1,3-dione Hydrobromide (11d). The Cbz-protected amine **10d** was treated with HBr, and the solid was washed with Et_2O , as for the synthesis of **11a**, to give **11d** as a pale yellow solid (100%): mp 220–221 °C; NMR δ 2.97 (2 H, sextet, $J = 6$ Hz, NCH_2), 3.23 (3 H, s, NMe), 3.43 (3 H, s, NMe), 3.62 (6 H, m, $\text{OCH}_2\text{CH}_2\text{OCH}_2$), 4.55 (2 H, s, purine- CH_2), 7.83 (3 H, br, N^+H_3); m/z (FAB) 298 ($\text{M} + \text{H}$), 180 (100%). Anal. Calcd for $\text{C}_{12}\text{H}_{20}\text{N}_5\text{O}_4\text{Br}$: C, 38.11; H, 5.33; N, 18.52. Found: C, 38.15; H, 5.27; N, 18.46.

5-[N-[5-(2,4-Dimethyl-1,3-dioxopurin-8-yl)pentyl]thio]ureido]-3',6'-dihydroxy-5-isothiocyanatospiro[isobenzofuran-1(3H),9'-(9H)xanthen]-3-one (13a). 3',6'-Dihydroxy-5-isothiocyanatospiro[isobenzofuran-1(3H),9'-(9H)xanthen]-3-one (fluorescein-5-isothiocyanate; **12**) (340 mg, 870 μmol) was suspended in water (12 mL) and brought to pH 9.0 by dropwise addition of aqueous K_2CO_3 (1 M). To this stirred solution was added **11b** (300 mg, 870 μmol) in water (6.7 mL) and dioxane (3.3 mL) during 30 min. The mixture was stirred for 3 h. During this time, the pH was maintained at 9.0 ± 0.2 by dropwise addition of aqueous K_2CO_3 (1 M). The solution was acidified to pH 6.0 by dropwise addition of hydrochloric acid (2 M). Water (200 mL) was added, and the mixture was freeze-dried for 24 h to reveal an orange fluffy solid. Chromatography ($\text{EtOAc} \rightarrow \text{EtOAc/MeOH}$ 10:1) gave **13a** as an orange-yellow solid (280 mg, 50%): mp 197–198 °C; IR 3480, 1710, 1660 cm^{-1} ; NMR δ 1.37 (2 H, m, CH_2), 1.62 (2 H, m, NCH_2CH_2), 1.76 (2 H, m, purine- CH_2CH_2), 2.73 (2 H, t, $J = 7.7$ Hz, purine- CH_2), 3.24 (3 H, s, NMe), 3.40 (3 H, s, NMe), 3.53 (2 H, m, NCH_2), 6.56 (2 H, dd, $J = 8.8, 2.2$ Hz, xanthene 2',7'- H_2), 6.61 (2 H, d, $J = 8.8$ Hz, xanthene 1',8'- H_2), 6.70 (2 H, d, $J = 2.2$ Hz, xanthene 4',5'- H_2), 7.20 (1 H, d, $J = 8.2$ Hz, Ar 3-H), 7.73 (1 H, m, Ar 4-H), 8.25 (1 H, br, NH), 8.27 (1 H, br, Ar 6-H), 9.93 (1 H, br, NH), 10.13 (2 H, s, $2 \times \text{OH}$), 13.21 (1 H, br, purine NH); MS (FAB) 655 ($\text{M} + \text{H}$). Anal. Calcd for $\text{C}_{33}\text{H}_{30}\text{N}_6\text{O}_7\text{S}$: C, 60.53; H, 4.62; N, 12.84. Found: C, 60.61; H, 4.57; N, 12.72.

5-[N-[8-(2,4-Dimethyl-1,3-dioxopurin-8-yl)octyl]thio]ureido]-3',6'-dihydroxy-5-isothiocyanatospiro[isobenzofuran-1(3H),9'-(9H)xanthen]-3-one (13b). The 8-(8-amino-octyl)purine salt **11b** was treated with **12**, as for the synthesis of **13a**, to give **13b** as an orange-yellow solid (72%): mp 182–183 °C; IR 3500–3100, 1710, 1660 cm^{-1} ; NMR δ 1.30 (8 H, m, $4 \times \text{CH}_2$), 1.55 (2 H, m, NCH_2CH_2), 1.66 (2 H, m, purine- CH_2CH_2), 2.67 (2 H, t, $J = 7.3$ Hz, purine- CH_2), 3.22 (3 H, s, NMe), 3.41 (3 H, s, NMe), 3.49 (2 H, m,

NCH_2), 6.53 (2 H, dd, $J = 8.8, 2.2$ Hz, xanthene 2',7'- H_2), 6.58 (2 H, d, $J = 8.8$ Hz, xanthene 1',8'- H_2), 6.68 (2 H, d, $J = 2.2$ Hz, xanthene 4',5'- H_2), 7.19 (1 H, d, $J = 8.4$ Hz, Ar 3-H), 7.70 (1 H, m, Ar 4-H), 8.27 (1 H, br, Ar 6-H), 10.23 (2 H, s, $2 \times \text{OH}$); m/z (FAB) 697 ($\text{M} + \text{H}$). Anal. Calcd for $\text{C}_{36}\text{H}_{36}\text{N}_6\text{O}_7\text{S}$: C, 62.05; H, 5.21; N, 12.01. Found: C, 62.11; H, 5.27; N, 12.02.

5-[N-[9-(2,4-Dimethyl-1,3-dioxopurin-8-yl)nonyl]thio]ureido]-3',6'-dihydroxy-5-isothiocyanatospiro[isobenzofuran-1(3H),9'-(9H)xanthen]-3-one (13c). The 8-(9-aminononyl)purine salt **11c** was treated with **12**, as for the synthesis of **13a**, to give **13c** as an orange-yellow solid (68%): mp 178–179 °C; IR 3400–3000, 1740, 1700, 1650 cm^{-1} ; NMR δ 1.29 (10 H, br, $5 \times \text{CH}_2$), 1.56 (2 H, m, NHCH_2CH_2), 1.68 (2 H, m, purine- CH_2CH_2), 2.67 (2 H, t, $J = 7.5$ Hz, purine- CH_2), 3.22 (3 H, s, NMe), 3.41 (3 H, s, NMe), 3.48 (2 H, m, NCH_2), 6.56 (2 H, dd, $J = 8.8, 2.2$ Hz, xanthene 2',7'- H_2), 6.59 (2 H, d, $J = 8.8$ Hz, xanthene 1',8'- H_2), 6.67 (2 H, d, $J = 2.2$ Hz, xanthene 4',5'- H_2), 7.17 (1 H, d, $J = 8.4$ Hz, Ar 3-H), 7.70 (1 H, m, Ar 4-H), 8.06 (1 H, br, CH_2NH), 8.22 (1 H, brs, Ar 6-H), 9.86 (1 H, br, Ar-NH), 10.18 (2 H, s, $2 \times \text{OH}$), 13.35 (1 H, purine NH); MS (FAB) 711 ($\text{M} + \text{H}$). Anal. Calcd for $\text{C}_{37}\text{H}_{38}\text{N}_6\text{O}_7\text{S}$: C, 62.52; H, 5.39; N, 11.82. Found: C, 62.45; H, 5.41; N, 11.75.

5-[N-[2-[2-(2,4-Dimethyl-1,3-dioxopurin-8-yl)methoxy]ethoxyethyl]thio]ureido]-3',6'-dihydroxy-5-isothiocyanatospiro[isobenzofuran-1(3H),9'-(9H)xanthen]-3-one (13d). The purine derivative salt **11d** was treated with **12**, as for the synthesis of **13a**, to give **13d** as an orange-yellow solid (77%): mp 1971–1998 °C; IR 3400–3200, 1740, 1700, 1650 cm^{-1} ; δ 3.22 (3 H, s, NMe), 3.41 (3 H, s, NMe), 3.63 (8 H, m, $\text{OCH}_2\text{CH}_2\text{OCH}_2\text{CH}_2$), 4.54 (2 H, s, purine- CH_2), 6.56 (2 H, dd, $J = 8.8$ and 2.2 Hz, xanthene 2',7'- H_2), 6.59 (2 H, d, $J = 8.8$ Hz, xanthene 1',8'- H_2), 6.66 (2 H, d, $J = 2.2$ Hz, xanthene 4',5'- H_2), 7.18 (1 H, d, $J = 8.4$ Hz, Ar 3-H), 7.73 (1 H, brd, $J = 8.5$ Hz, Ar 4-H), 8.1 (1 H, br, NH), 8.26 (1 H, br, Ar 6-H), 10.05 (1 H, br, NH), 10.14 (2 H, s, $2 \times \text{OH}$), 13.6 (1 H, purine NH); MS (FAB) 687 ($\text{M} + \text{H}$). Anal. Calcd for $\text{C}_{33}\text{H}_{30}\text{N}_6\text{O}_9\text{S}$: C, 57.71; H, 4.41; N, 12.24. Found: C, 57.61; H, 4.45; N, 12.22.

2,4-Dimethyl-8-[5-[5-(dimethylamino)naphthalene-1-sulfonylamino]pentyl]purine-1,3-dione Hydrobromide (14). The aminopentylpurine salt **11a** (200 mg, 580 μmol) in water (8 mL) and dioxane (4 mL) was brought to pH 9.5 by addition of aqueous Na_2CO_3 (0.5 M). 5-(Dimethylamino)naphthalene-1-sulfonyl chloride (160 mg, 580 μmol) in dioxane (10 mL) was added. The mixture was stirred for 3 h. During this time, the pH was maintained at 9.5–10.0 by dropwise addition of aqueous Na_2CO_3 (0.5 M). The solution was neutralized to pH 7.0 by addition of hydrochloric acid (2 M). Water (25 mL) was added and the mixture was freeze-dried for 24 h to reveal an orange fluffy solid. The residue, in ethyl acetate, was washed with water and dried. The solvent was evaporated, and the residue was recrystallized (EtOH) to give **14** as a green-yellow solid (160 mg, 55%): mp 183–185 °C; NMR δ 1.14 (2 H, quintet, $J = 7$ Hz, $\text{CH}_2\text{CH}_2\text{CH}_2\text{CH}_2\text{CH}_2$), 1.29 (2 H, quintet, $J = 7$ Hz, $\text{CH}_2\text{CH}_2\text{N}$), 1.46 (2 H, quintet, $J = 7$ Hz, purine- CH_2CH_2), 2.76 (2 H, t, $J = 5.9$ Hz, purine- CH_2), 2.81 (6 H, s, NMe_2), 3.22 (3 H, s, NMe), 3.39 (5 H, m, $\text{NMe} + \text{CH}_2\text{N}$), 7.24 (1 H, d, $J = 7.3$ Hz, naphthalene 6-H), 7.58 (1 H, t, $J = 8.1$ Hz, naphthalene 3-H or 6-H), 7.61 (1 H, d, $J = 7.7$ Hz, naphthalene 8-H), 7.87 (1 H, t, $J = 7.9$ Hz, naphthalene 6-H or 3-H), 8.08 (1 H, d, $J = 7.3$ Hz, naphthalene 4-H), 8.29 (1 H, d, $J = 8.4$ Hz, naphthalene 2-H), 13.1 (1 H, br, purine-NH); MS (FAB) 531.2020 ($\text{M} + \text{H}$) ($\text{C}_{24}\text{H}_{31}\text{N}_6\text{O}_4\text{S}$ requires 531.2026).

Immunoassay. The FCFD devices were fabricated according to the method of Badley *et al.* (7). The lower base plate was activated with (3-aminopropyl)trimeth-

Table 1. Binding Affinities of the Theophylline–Fluorescein Conjugates **13a–d to the Antibody Immobilized in the FCFD Device**

conjugate	linker unit	binding affinity K_a (M^{-1})
theophylline (1)		$(0.06 \pm 0.02) \times 10^6$
13a	$(CH_2)_5$	$(3.1 \pm 1.5) \times 10^6$
13b	$(CH_2)_8$	$(1.4 \pm 0.6) \times 10^6$
13c	$(CH_2)_9$	$(3.2 \pm 1.8) \times 10^6$
13d	$CH_2O(CH_2)_2O(CH_2)_2$	$(1.0 \pm 0.4) \times 10^6$

oxysilane. Anti-theophylline IgA mouse monoclonal antibody was dissolved in HEPES buffer (0.1 M) containing NaCl (0.2 M) to a final concentration of $200 \mu g mL^{-1}$. Aliquots of this solution ($15 \mu L$) were used for coupling of the antibody to the lower plate according to a carbonyldiimidazole method. The plates were then assembled in the usual way. Solutions of the theophylline–fluorescein conjugates **13a–d** were prepared in Tris-HCl buffer at pH 8.8. All assays using the FCFDs were performed in duplicate following incubation at ambient temperature for 20 min to ensure that the system had come fully to equilibrium. Total binding of **13a–d** to the antibody was measured by incubating the FCFDs with concentrations of conjugates from 0 to $5 \mu M$. Nonspecific binding of **13a–d** to the antibody-loaded devices was measured in the presence of theophylline (1 mM). The specific binding isotherms were constructed by plotting (total fluorescence signal observed minus signal in the presence of excess theophylline) vs concentration of **13a–d**. From these plots (not shown) were obtained the binding affinities of each conjugate for the immobilized antibody (Table 1).

RESULTS AND DISCUSSION

Chemistry. Synthesis of 8-(2-aminoethyl)theophylline has been reported (12) involving acylation of 5,6-diamino-1,3-dimethylpyrimidine-2,4-dione (a relatively unstable compound) with *N*-protected 3-aminopropanoic acid, followed by cyclization under drastic conditions. We sought to develop a method that started with more readily available 1, ω -diamines and which did not use vigorous conditions for cyclization. Fuchs *et al.* (12) have suggested that treatment of 6-chloro-1,3-dimethylpyrimidine (**5**) with 1, ω -diamines would give the products of 1, ω -disubstitution. Thus, our initial approach involved setting up a synthon for hexane-1,6-diamine, which is protected at one amine only. Exchange of protecting groups on the commercially available mono-Boc hexane-1,6-diamine (**2**) was achieved by benzyloxycarbonylation at the free amine to give the orthogonally protected biscarbamate **3**, followed by acidolytic removal of Boc in excellent yield. The Cbz protection in **4** was designed to survive the reaction conditions in later steps, which would cleave Boc. Substitution of the chlorine of the 6-chloropyrimidinedione **5** with the amine **4** was effected in boiling 1,4-dioxane in the presence of inorganic base to give **6a** in satisfactory yield, as shown in Scheme 1. An attempt to raise the yield by use of refluxing ethanol as the reaction medium gave only a small amount of **6a** but encouraged substitution of chlorine by the solvent to give largely 1,3-dimethyl-6-ethoxypyrimidine-2,4-dione. Following the general method of Goldner *et al.* (13), nitrosation at C-5 of the pyrimidine was carried out with pentyl nitrite, in a reaction catalyzed by a small quantity of acid. Thermal cyclization/condensation of the brightly colored 5-nitrosopyrimidine **9a** to the Cbz-protected 8-(5-aminopentyl)theophylline **10a** was rapid and high yielding in boiling butanol. Deprotection using hydrogen bromide in acetic acid was virtually quantitative in furnishing the 8-(5-aminopentyl)theophylline salt **11a**,

which carries the required link and nucleophilic amine for attachment of electrophilically substituted fluorophores.

Selective monoprotection of longer chain alkane-1, ω -diamines, particularly 3,6-dioxaoctane-1,8-diamine, proved to be troublesome. However, by careful selection of reacting quantities and conditions, it proved possible to obtain good yields of the unprotected 6-[ω -amino(oxa)alkylamino]pyrimidines **7b–d**, which could be separated with difficulty from traces of the products of 1, ω -disubstitution. Nevertheless, direct reaction of the crude product mixture with benzyl chloroformate gave the easily purified Cbz-protected 6-[ω -amino(oxa)alkylamino]pyrimidines **6b–d**. As before, the sequence of nitrosation, thermal cyclization, and deprotection furnished the required 8-[ω -amino(oxa)alkylamino]theophylline salts **11b–d**.

The aminoalkyltheophyllines **11a–c** enabled study of the effect of the length of the link between hapten and fluorophore on the immunoreactivity of the final derivatives, whereas comparison of these with the diether linked compounds derived from **11d** indicated the importance of hydrophilicity of the link.

Fluorescein has absorption and fluorescence emission maxima at wavelengths that are appropriate for the FCFD device, with a large Stokes shift and a high quantum yield. The 5-isothiocyanate or mixtures of the 4- and 5-isothiocyanates have frequently been used for fluorescent labeling of amino groups of biological molecules in aqueous media (15, 16). Fluorescein also confers aqueous solubility on its derivatives, a factor important for the target fluorescent theophylline derivatives. To have a chemically defined system, the 5-isothiocyanate was used to thiocarbamoylate the amines **11a–d**. It was found necessary to control closely the pH of the aqueous reaction mixture in the range 9.0 ± 0.2 to ensure that the amine was not protonated and that the isothiocyanate was not subject to base-catalyzed hydrolysis. To provide an alternative fluorescent derivative of theophylline for our studies with different wavelength maxima for excitation and fluorescence, 8-(5-aminopentyl)theophylline (**11a**) was also coupled with dansyl chloride [5-(dimethylamino)naphthalene-1-sulfonyl chloride] under aqueous basic conditions, although this reaction tolerated a higher pH (9.5–10.0), owing to the lower lability of dansyl chloride to hydrolysis. The dansylaminopentyltheophylline **14** was formed in good yield.

The 1H NMR spectra of the fluorescein–theophylline derivatives **13a–d** were examined in solution in deuteriodimethyl sulfoxide. The signals for the xanthene moiety show considerable symmetry, in which H-1' and H-8' are magnetically equivalent, as are H-2' and H-7' and H-4' and H-5', respectively. Most interestingly, the phenolic OH signal appears as a 2 H singlet at δ 10.2, confirming that the fluorescein is present in this solvent as the tautomer shown, rather than the lactone-opened carboxylate tautomer.

Straightforward syntheses of a range of 8-[ω -amino(oxa)alkyl]theophyllines have been achieved, providing convenient access to fluorescent derivatives with applications in automated immunoassays for theophylline.

Immunoassay. The initial requirement of the study was to determine the antibody-binding affinities of the fluorescent theophylline conjugates **13a–d**, and it was sensible to carry out these experiments on the immobilized antibody within the FCFD by introducing the conjugates in solution to the FCFD in the presence and absence of excess theophylline. The FCFD reader was able to determine the relative intensity of surface fluo-

rescence, and the antibody-bound fluorescence was determined by subtracting the nonspecific fluorescence, in the presence of excess theophylline, from the total fluorescence. Initial experiments were conducted to establish the equilibration time of the system, by recording the total fluorescence at 30 s intervals over a 30 min period. Binding equilibrium was achieved within approximately 10 min, and a standard incubation time of 20 min was adopted for further studies. Specifically bound fluorescence was plotted against concentration of each conjugate, according to the Langmuir equation, to allow determination of the binding affinities of **13a–d** (Table 1). The binding affinity of theophylline could then be determined by competition with a fluorescent derivative, in this case with **13a** (Table 1). The binding affinities of the conjugates compared well with that of theophylline, indicating that this antibody could tolerate substitution of theophylline at position 8. The affinities were almost independent of the length $[(CH_2)_5 \text{ vs } (CH_2)_9]$ or the hydrophobic/hydrophilic nature of the link $[(CH_2)_9 \text{ vs } CH_2O(CH_2)_2O(CH_2)_2]$ between the theophylline hapten and the fluorophore. Compound **13a** was identified by a small margin as being the conjugate of choice and was selected for further testing and development of assay procedures. Briefly, it was established that the fluorescent conjugates had the appropriate antibody-binding properties for development of an FCFD-based assay for theophylline, within a concentration range which would be useful for clinical use (0–300 μM theophylline). Compound **13a** was used at a concentration of 10^{-6} M within the FCFD device, with low levels of interference from nonspecific surface-bound fluorescence. Theophylline competed with **13a** such that the signal recorded by the FCFD reader decreased from maximum to minimum levels between theophylline concentrations of 5 and 500 μM . Precision was determined at theophylline concentrations of 25, 50, and 125 μM , the coefficients of variation being 6.5%, 6.0%, and 5.2% (within-assay) and 8.0%, 7.5%, and 5.0% (between-assay), respectively. This concentration range corresponded to a useful clinical range, although the precision of the assay in estimating the concentration of theophylline was compromised by insufficient total fluorescence. This total fluorescence could be increased by immobilizing a higher mass of antibody to the bottom plate of the FCFD. Nevertheless, the FCFD devices studied here would be capable of distinguishing between low (5 μM) and high (250 μM) clinical levels of theophylline, which could be useful in acute conditions to establish whether a patient is presenting with overdose or underdose of theophylline.

Preliminary experiments were carried out to test the cross-reactivity of the system with other xanthines, including caffeine, theobromine, and metabolites of theophylline. Initial results suggested that the concentration of each xanthine required to displace **13a** was at least 100 times greater than that for theophylline. Thus, little interference can be expected from other blood-borne xanthines. It was also established that the assay worked as well in the presence of 5 mg mL^{-1} human serum albumin, with a slight loss of sensitivity presumably due to interactions between xanthines and albumin, which reduced the effective concentration of free xanthines in the FCFD.

The results of further studies on the development and validation of the immunoassays will be reported in full elsewhere.

ACKNOWLEDGMENT

We thank Dr. G. Robinson and Dr. J. Deacon (Serono Diagnostics) for helpful discussions, Mr. R. R. Hartell and Mr. D. Wood (University of Bath) for the NMR spectra, Mr. C. Cryer (University of Bath) for the mass spectra, and Serono Diagnostics for financial support. F.Y. held an EPSRC CASE studentship.

LITERATURE CITED

- (1) Hendeles, L., and Weinberger, M. (1983) Theophylline: a "state of the art review". *Pharmacotherapy* 3, 2.
- (2) Bierman, C. W., and Williams, P. V. (1989) Therapeutic monitoring of theophylline—rationale and current status. *Clin. Pharmacokinetics* 17, 377.
- (3) Self T., and Abou-Shala, N. (1994) Theophylline. *Lancet* 343, 1226.
- (4) Danilova, N. D., and Vasilov, R. G. (1991) Production and characterisation of anti-theophylline monoclonal antibodies suitable for immunoassay. *Immunol. Lett.* 28, 79.
- (5) Neese, A. L., and Soyka, L. F. (1977) Development of a radioimmunoassay for theophylline. Application to studies in premature infants. *Clin. Pharmacol. Ther.* 21, 633.
- (6) Kester, M. B., Saccar, C. L., Rocci, M. L., and Mansmann, H. C. (1986) New simplified microassay for the quantitation of theophylline and its major metabolites in serum by high performance liquid chromatography. *J. Chromatogr.* 380, 99.
- (7) Badley, R. A., Drake, R. A. L., Shanks, I. A., and Smith, A. M. (1987) Optical biosensors for immunoassays: the fluorescence capillary-fill device. *Philos. Trans. R. Soc. London* 312, 143.
- (8) Parry, R. P., Love, C., and Robinson, G. A. (1990) Detection of rubella antibody using an optical immunosensor. *J. Virol. Methods* 27, 39.
- (9) Robinson, G. A. (1991) Optical immunosensing systems—meeting the market needs. *Biosensors Bioelectronics* 6, 183.
- (10) Deacon, J. K., Thomas, A. M., Page, A. L., Stops, J. E., Roberts, P. R., Whiteley, S. C., Attridge, J. W., Love, C. A., and Robinson, G. A. (1991) An assay for human chorionic gonadotrophin using the capillary fill immunosensor. *Biosensors Bioelectronics* 6, 193.
- (11) Jeno, K. (1978) Synthesis of 8-aminomethyl- and 8-aminoethyl-theophylline. *Juhász Gyula Tanárképző Főiskola Tud. Kozl.* 133; *Chem. Abstr.* 93, 239365.
- (12) Fuchs, H., Gottlieb, M., and Pfeleiderer, W. (1978) Purine, XII—Über die Cyclisierung von 4-Alkylamino-5-nitroso-uracilen und die Synthese von 8-substituierten Xanthenen und Bis(theophylline-8-yl)-alkan-Derivaten. *Chem. Ber.* 111, 982.
- (13) Goldner, H., Dietz, G., and Carstens, E. (1966) Eine neue Xanthin-Synthese. *Liebigs Ann. Chem.* 692, 134.
- (14) Mann, K. G., and Fish, W. W. (1972) Protein polypeptide chain molecular weights by gel chromatography in guanidinium chloride. *Methods Enzymol.* 26, 28.
- (15) Miller, L., Phillips, M., and Riesler, E. (1988) Polymerisation of actin modified with fluorescein isothiocyanate. *Eur. J. Biochem.* 174, 23.
- (16) Atwell, G. J., and Denny, W. A. (1984) Monoprotection of α,ω -alkanediamines with the benzyloxycarbonyl group. *Synthesis*, 1032.

BC9700648

COMMUNICATIONS

Identification of Preferred Distamycin–DNA Binding Sites by the Combinatorial Method REPSA

Paul Hardenbol,[†] Jo C. Wang, and Michael W. Van Dyke*

Department of Tumor Biology, The University of Texas M. D. Anderson Cancer Center, Houston, Texas 77030.
Received April 21, 1997[®]

The combinatorial method restriction endonuclease protection, selection, and amplification (REPSA) was used to determine the preferred duplex DNA binding sites of the peptide *N*-methylpyrrolicarboxamide antibiotic distamycin A. After 12 rounds of REPSA, several sequences were identified that bound distamycin with an apparent affinity of 2–20 nM. Among these, the highest-affinity sites averaged 10 bp in length, suggesting that these sites may be occupied by multiple, cooperatively interacting distamycin molecules. Presently, REPSA is the only combinatorial approach that allows the identification of preferred DNA targets for small molecule ligands at physiologically relevant concentrations in solution. As such, it should prove useful in the design and screening of sequence-specific DNA-binding molecules.

Many drugs important in anticancer chemotherapy bind duplex DNA noncovalently and with some sequence specificity (1). Their mechanisms of action, while not fully elucidated, are thought to rely on the strength and selectivity of these interactions. Considerable efforts have been made to identify the preferred binding sites of these small molecules, primarily employing either chemical or enzymatic cleavage protection methods (2, 3). Such “footprinting” methods, while capable of defining a drug-binding site down to base pair resolution, typically only survey 100–200 bp per experiment. Sur-

veys of several million base pairs, however, are required to identify their hypothetical best binding sites, those presumably recognized at physiological drug concentrations.

To survey large numbers of potential binding sites, combinatorial methods involving multiple rounds of ligand–nucleic acid complex selection and PCR amplification are usually employed. These methods have succeeded in identifying preferred duplex DNA binding sites for many proteins and triplex-forming oligonucleotides (4, 5). The methods all relied on a physical separation of ligand–DNA complexes from free DNAs, either as a result of altered chemical properties of the ligand–DNA complex (e.g., increased mass-to-charge ratio and reduced electrophoretic mobility) or through the use of affinity methods (e.g., ligand-specific antibodies). However, such methods cannot be used to selectively isolate drug–DNA complexes; thus, no combinatorial method has as yet been available for their study.

We have recently described a combinatorial method,

* Address correspondence to this author at Department of Tumor Biology, Box 79, The University of Texas M. D. Anderson Cancer Center, 1515 Holcombe Blvd., Houston, TX 77030. Telephone: (713) 792-8954. Fax: (713) 794-4784. E-mail: mishko@odin.mdacc.tmc.edu.

[†] Present address: Department of Biochemistry, Stanford University, Stanford, CA 94305-5307.

[®] Abstract published in *Advance ACS Abstracts*, August 15, 1997.

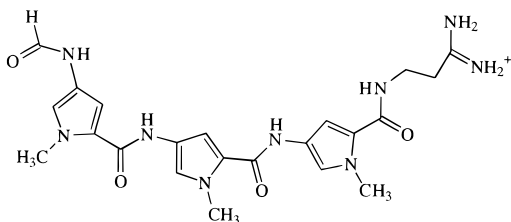


Figure 1. Structure of the DNA-binding antibiotic distamycin A.

restriction endonuclease protection selection and amplification (REPSA), for the identification of preferred nucleic acid and protein binding sites on duplex DNA (6). Unlike conventional methods, REPSA relies on the inhibition of an enzymatic process, DNA cleavage by a type IIS restriction endonuclease (IISRE), in selecting complexed DNAs. Thus, potentially, any ligand capable of being investigated by footprinting should also be amenable to analysis by REPSA.

As a test of REPSA's applicability to the identification of preferred small molecule–DNA binding sites, the method was used to investigate the sites recognized by the natural product antibiotic distamycin A. Distamycin A, a tripeptide tri-*N*-methylpyrrolicarboxamide (Figure 1), binds as a 1:1 ligand–DNA complex in the minor groove of duplex DNA, preferentially at AT-rich sequences 4–5 bp in length (7, 8). For a series of (A/T)₄ sequences, distamycin demonstrated binding affinities ranging from 0.1 to 1.0 μ M (9). Numerous studies have shown that distamycin effectively inhibits DNA cleavage by both nonspecific endonucleases and restriction endonucleases (reviewed in ref 10) and that higher-affinity, multimeric distamycin binding sites exist in heterogeneous DNA (11). Taken together, these findings suggest that distamycin would provide an ideal test for REPSA.

A round of REPSA involves three steps: complex formation between a ligand and a subpopulation of DNAs, preferential cleavage of the uncomplexed DNAs, and PCR amplification of the uncleaved templates (Figure 2). Selection of bound DNAs is made possible through the use of IISREs, restriction endonucleases that cleave duplex DNA not at a specific sequence but rather at a fixed distance from their recognition sites (12). Given the proper ligand/IISRE combination, it is possible to efficiently cleave uncomplexed DNAs while maintaining the complexed DNAs intact. These intact DNAs then serve as templates for PCR amplification, thereby increasing the representation of these sequences within the pool. These steps can then be repeated for a number of rounds, until a desired population of ligand-binding sequences emerges.

Central to REPSA is the design of a selection template, which allows the probing of a region of randomized sequence by IISREs. The selection template used in this analysis, ST3, is shown schematically in Figure 3. ST3 incorporates a central 21 bp cassette of randomized sequence, flanked by defined sequences containing different IISRE recognition sites. This length of random sequence is many times that of an individual distamycin binding site (5 bp). Thus, ST3 allows screening for multimeric distamycin binding sites, which are believed to have higher affinities (11). The flanking sequences were designed to allow interconversion of the IISRE sites, from *BpmI* to *BsgI* or *Eco57I*, depending on the primers used. Such a design provides greater flexibility with this template and allows the rotation of IISREs in different REPSA rounds, which can be essential for preventing artifact selection (e.g., selection of sequences bound by proteins present in the commercial restriction endonu-

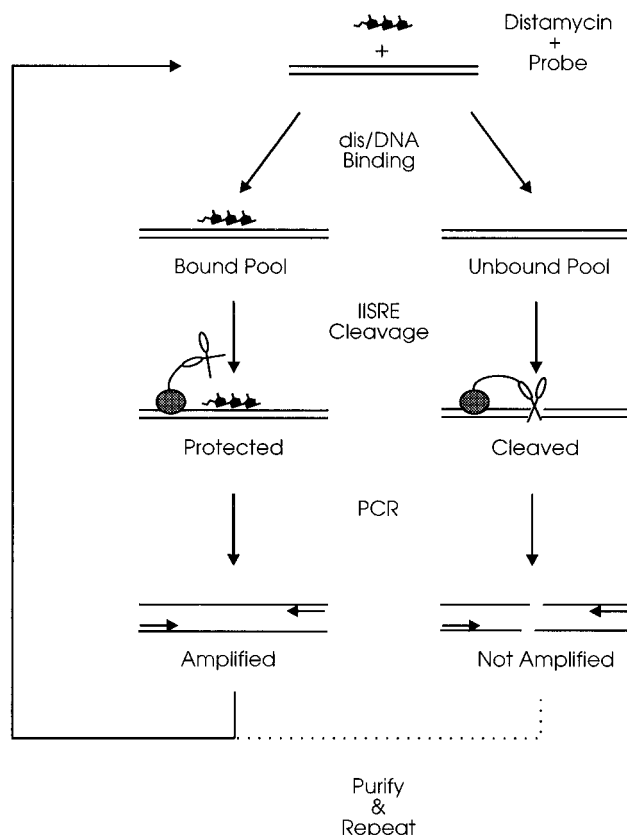


Figure 2. Flow chart for the combinatorial method restriction endonuclease protection, selection, and amplification (REPSA). The tricyclic ligand represents the DNA-binding drug distamycin A; a type IIS restriction endonuclease is represented by a scissors (nonspecific cleaving domains) attached to gray ovals (sequence-specific DNA-binding domains).



Figure 3. Design of the selection template, ST3, used for the identification of preferred distamycin–DNA binding sites by REPSA. Locations of restriction endonuclease binding (brackets) and cleavage (arrows) sites are indicated. Long horizontal arrows correspond to the sequences of the PCR amplimers indicated. N represents random nucleotides.

lease preparations) (6). Each of the IISREs has an identical span (16 nucleotides in the top strand, 14 nucleotides in the bottom strand) between binding and cleavage sites. Also, having identical IISRE sites on both flanks increased the efficiency of template probing by some of the less efficient IISREs (e.g., *BsgI*) (6).

To initiate REPSA, 1 ng of ST3 was incubated (30 min, 25 °C) with 0.1 μ M distamycin in 10 μ L of a buffer suitable for subsequent IISRE cleavage. The amount of selection template used (25 fmol) was optimal for subsequent manipulations and provided a good representation of all possible 17-mer sequences; the concentration of distamycin corresponded to its lowest dissociation constant reported for binding to a 4 bp A/T-rich sequence (9). After drug binding, 2 units of *BpmI* (New England Biolabs) was added and cleavage allowed to proceed for an additional 30 min at 37 °C. Afterward, the entire

Table 1. REPSA-Selected Distamycin Binding Sequences

clone	sequence ^a	K_{app} (nM) ^b
1	TATAAAAGTCTATCTATAATT	20
2	TAAATATAAATTATTCTTTAA	4
3	TATAATTAGTTACATAATATT	6
4	AAGTAAGATTTTTATCACAA	5
5	AATGGTTCATTATTTTGACT	6
6	CTTAATTAAATATTAATTATA	5
7	ATTAATTAGCTATATATATAA	8
8	ATATAAATAAATTATCTTATA	7
9	CATCAGAAAATATTAACAC	4
10	TCAGTAAATATAAAAGGATTA	2
11	TTATCATCTAATATAGACATA	7
12	TATATAATAGAATATATTATG	2
13	GTTTGAATACTAGATGAAACC	15
14	ATAGATAGTATACCATTAAAT	4
15	TGGTGGGAATTTATTGGAGT	2

^a Sequences obtained following 12 rounds of REPSA with 0.1 mM distamycin. Distamycin binding sites, as determined by DNase I footprinting, are underlined. ^b Concentrations of distamycin that afforded 50% DNase I cleavage protection.

mixture was added to a standard PCR reaction mixture (6) containing 200 ng each of *BsgI*(L) and *BsgI*(R) primers and amplified for 6, 9, and 12 cycles with a profile of 94 °C for 1 min of denaturation, 25 °C for 3 min of annealing, and 50 °C for 2 min of elongation. The annealing step was added to facilitate hybridization between the *BsgI* primers and the *BpmI* site-containing ST3, given the two base mismatches. After PCR, an aliquot of each reaction mixture was analyzed by PAGE to determine relative levels of amplification; the remainder was purified by phenol extraction and ultrafiltration, essentially as previously described (6). Selections in subsequent rounds were with *BsgI* (rounds 2, 5, 8, and 11), *Eco57I* (rounds 3, 6, 9, and 12), or *BpmI* (rounds 1, 4, 7, and 10), with the appropriate amplimers being used in the preceding round of PCR.

After 12 rounds of REPSA, the selected DNAs were subcloned into pUC19 and individual colonies sequenced. Sequences of 15 clones containing the entire 21 bp cassette were obtained (Table 1). These selected sequences were substantially enriched in A's and T's with respect to the starting distribution (83.2 versus 58.5%). Using a χ^2 analysis, we identified possible consensus distamycin binding sequences. For each possible 4, 5, and 6 bp combination, only the sequences TATA, ATATA, and AATTAT occurred with substantially higher than expected frequencies ($P < 0.05$). Most notably, the 9 bp sequence ATAAATTAT was found twice among these 15 sequences ($P < 0.01$), suggesting this could be a highly preferred distamycin binding site under our experimental conditions.

To better ascertain the exact distamycin binding sites and their relative binding affinities, a DNase I footprinting analysis was performed. An autoradiogram of a footprinting analysis for clone 2 (Table 1) is shown in Figure 4. DNase I cleavage protection was first observed when 3 nM distamycin was present, with cleavage protection occurring over an 11 bp region centered on the

Distamycin (nM)

0 1 3 10 30 100 A

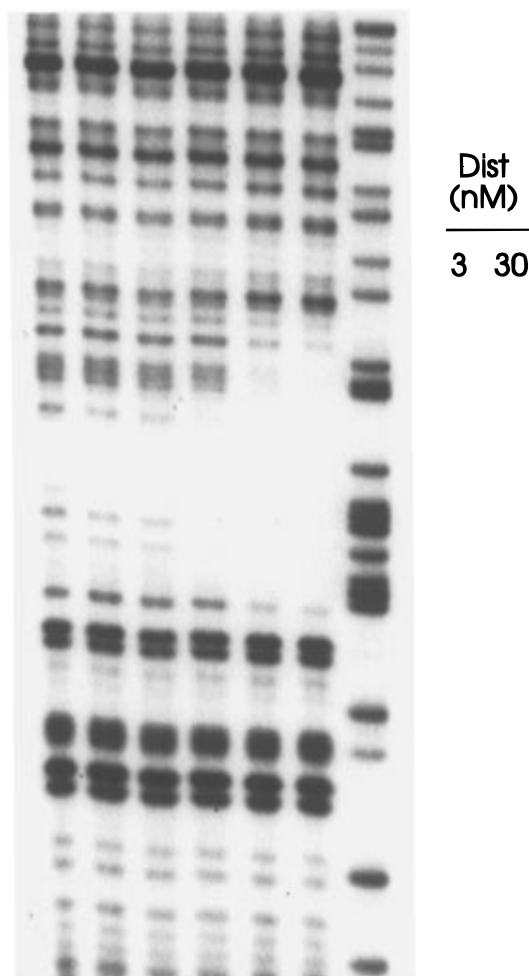


Figure 4. DNase I footprinting analysis of distamycin A binding to REPSA-selected clone 2. A 160 bp footprinting probe was generated by PCR using the pUC sequencing primers TGTGTGTGGAATTGTG and CAAGGCGATTAAGTTGG, the latter being end-labeled with [γ -³²P]ATP and T4 kinase. Footprinting reactions were performed essentially as previously described, except with the addition of 50 mM KCl in the binding reaction (13). The extents of the DNase I protection afforded by 3 and 30 nM distamycin are indicated at the right of the figure.

sequence ATAAATTAT (Table 1, underlined). At a 10-fold higher distamycin concentration, cleavage protection extended over the entire 21 bp cassette. Note that, under these conditions, the more extensive cleavage protection most likely reflected the binding of multiple distamycin molecules to the DNA. Using densitometry, it was possible to estimate the concentration of distamycin necessary to afford 50% DNase I protection. This value corresponded to the apparent binding affinity of distamycin for this sequence. Similar footprinting analyses were performed for the other REPSA-selected sequences; initial distamycin-binding sites (underlined) and binding affinities are presented in Table 1. From this analysis, we found that the distamycin binding affinity of these sequences ranged from 2 to 20 nM and that the initial protections typically incorporated the consensus sequences identified by statistical means. Noticeably, these binding affinities are 10–100-fold greater than those previously described for most distamycin binding sites (9), indicative of the preferred nature of REPSA-selected sequences. Also note that these initial binding sites are

larger than those typically described for distamycin (averaging 10 bp for the highest-affinity sites). This suggests that these preferred sites may actually be bound by multiple, cooperatively interacting distamycin molecules. Alternatively, these sites could be composed of several overlapping subsites with the sum of their protections yielding an apparently higher-affinity site. However, the relatively uniform DNase I protection observed throughout each site would argue against the latter hypothesis.

These studies demonstrate that REPSA can be used to identify the preferred DNA-binding sequences of small molecule ligands such as distamycin. Binding sites in the nanomolar range were obtained, and possible consensus sequences were identified. The observed clustering of binding affinities (13 of the 15 sequences had affinities in the range of 2–8 nM) could reflect the actual limit for distamycin binding, though it may instead reflect a limitation of the selection conditions used (e.g., 100 nM final distamycin concentration). Further REPSA with this selected population at a reduced distamycin concentration should help to address this question. Similarly, identification of a single consensus sequence was not possible with this limited data set. Upon identification of a selected population possessing maximal affinity, and with a sufficiently large number of sequences, it should be possible to define a best binding sequence for this molecule. Nonetheless, the sequences identified by REPSA are a considerable improvement over prior defined sequences and should be of great utility in many future studies on this class of molecules. (e.g., for better understanding of DNA recognition by minor groove-binding ligands; to test for direct regulation of specific gene transcription by DNA-binding drugs).

Beyond being the only combinatorial approach suitable for investigating drug-binding sites on duplex DNA, REPSA possesses the additional benefits of being suitable for studies with complex mixtures of relatively uncharacterized ligands. This fact was demonstrated in our REPSA investigation of purine-motif triplex-forming sequences, in which consensus sequences for proteins present in the IISRE preparation were also identified (6). Thus, it is conceivable that a combinatorial method like REPSA could be used to survey a library of compounds and identify a series of preferred binding sites. These selected sequences could then be back-selected against an array of these compounds, thereby identifying the sequence recognized by a particular compound. Indeed, it may be possible to use a combinatorially derived series of compounds to ascertain the range of sequences recognized by a series of related compounds. Such a two-dimensional combinatorial study could be especially useful in the development of small molecules with defined sequence specificities, e.g., the *N*-methylpyrrole/2-methylimidazole polyamides (14, 15), these being potentially useful for catalyzing gene replacements or for a pharmacological regulation of specific gene expression.

ACKNOWLEDGMENT

We thank Christine Hoover and Jing Shen for their participation on this project and Michèle Sawadogo for

critical reading of the manuscript. This research was supported by grants from the Welch Foundation (G-1199) and the American Cancer Society (RPG-97-028-01-DHP) and by a Physicians' Referral Service research award. P.H. was the recipient of a National Research Service Award predoctoral traineeship from the National Cancer Institute (T32 CA60440).

LITERATURE CITED

- (1) Neidle, S., and Waring, M. J. (1993) *Molecular Aspects of Anticancer Drug-DNA Interactions*, Macmillan, London.
- (2) Van Dyke, M. W., Hertzberg, R. P., and Dervan, P. B. (1982) Map of distamycin, netropsin, and actinomycin binding sites on heterogeneous DNA: DNA cleavage inhibition patterns with methidiumpropyl-EDTA-Fe(II). *Proc. Natl. Acad. Sci. U.S.A.* 79, 5470–5474.
- (3) Lane, M. J., Dabrowiak, J. C., and Vournakis, J. N. (1983) Sequence specificity of actinomycin D and netropsin binding to pBR322 DNA analyzed by protection from DNase I. *Proc. Natl. Acad. Sci. U.S.A.* 80, 3260–3264.
- (4) Szostak, J. W. (1992) In vitro genetics. *Trends Biochem. Sci.* 17, 89–93.
- (5) Wright, W. E., and Funk, W. D. (1993) CASTing for multicomponent DNA-binding complexes. *Trends Biochem. Sci.* 18, 77–80.
- (6) Hardenbol, P., and Van Dyke, M. W. (1996) Sequence specificity of triplex DNA formation: analysis by a combinatorial approach restriction endonuclease protection selection and amplification. *Proc. Natl. Acad. Sci. U.S.A.* 93, 2811–2816.
- (7) Coll, M., Fredrick, C. A., Wang, A. H. J., and Rich, A. (1987) A bifurcated hydrogen-bonded conformation in the d(A·T) base pairs of the DNA dodecamer d(CGCAAATTTGCG) and its complex with distamycin. *Proc. Natl. Acad. Sci. U.S.A.* 84, 8385–8389.
- (8) Pelton, J. G., and Wemmer, D. E. (1988) Structural modeling of the distamycin A-d(CGCGAATTCGCG)₂ complex using 2D NMR and molecular mechanics. *Biochemistry* 27, 8088–8096.
- (9) Abu-Daya, A., Brown, P. M., and Fox, K. R. (1995) DNA sequence preferences of several AT-selective minor groove binding ligands. *Nucleic Acids Res.* 23, 3385–3392.
- (10) Dabrowiak, J. C. (1983) Sequence specificity of drug-DNA interactions. *Life Sci.* 32, 2915–2931.
- (11) Samuelson, P., Jansen, K., and Kubista, M. (1994) Long-range interactions between DNA-bound ligands. *J. Mol. Recognit.* 7, 233–241.
- (12) Szybalski, W., Kim, S. C., Hasan, N., and Podhajski, A. J. (1991) Class-IIS restriction enzymes—a review. *Gene* 100, 13–26.
- (13) Musso, M., and Van Dyke, M. W. (1995) Polyamine effects on purine-purine-pyrimidine triple helix formation by phosphodiester and phosphorothioate oligodeoxyribonucleotides. *Nucleic Acids Res.* 23, 2320–2327.
- (14) Geierstanger, B. H., Mrksich, M., Dervan, P. B., and Wemmer, D. E. (1996) Extending the recognition site of designed minor groove binding molecules. *Nat. Struct. Biol.* 3, 321–324.
- (15) Trauger, J. W., Baird, E. E., and Dervan, P. B. (1996) Recognition of DNA by designed ligands at subnanomolar concentrations. *Nature* 382, 559–561.

BC970066S

REVIEWS

^{99m}Tc Labeling of Highly Potent Small Peptides

Shuang Liu,* D. Scott Edwards, and John A. Barrett

Radiopharmaceuticals Division, The DuPont Merck Pharmaceutical Company, 331 Treble Cove Road, North Billerica, Massachusetts 01862. Received April 21, 1997

INTRODUCTION

Peptides are compounds that contain amino acids (α -aminocarboxylic acids) linked by amide (peptide) bonds. Designed by nature for stimulating, inhibiting, or regulating numerous life functions, peptides for a long time have been considered ideal agents for therapeutic applications (1). Although the ¹¹¹In-labeled peptide was first explored for use in nuclear medicine in 1981 (2), it was not until recently that ^{99m}Tc-labeled peptides have emerged as an important class of radiopharmaceuticals in diagnostic nuclear medicine. Of particular interest are ^{99m}Tc-labeled chemotactic peptides (3–11), small peptides based on platelet factor 4 (12), and tuftsin receptor antagonists (13–15) for imaging focal sites of infection, somatostatin analogs for imaging tumors (16–20), and platelet glycoprotein IIb/IIIa (GPIIb/IIIa) receptor antagonists for imaging thrombi (21–34).

In the past two decades, monoclonal antibodies (MAbs) or their fragments, F(ab') or F(ab')₂, have been widely used as vehicles to carry radionuclides of diagnostic or therapeutic characteristics to a specific target such as a tumor (35–40). Although considerable progress has been made in this area (40–43), clinical studies with radiolabeled MAbs have often demonstrated limited accumulation in the tumor, and relatively slow blood clearance due to their high molecular weight, resulting in only modest target-to-background ratios. The poor match between the pharmacokinetics and the physical half-life of ^{99m}Tc has limited the development of ^{99m}Tc-labeled MAbs and their fragments as commercial target-specific radiopharmaceuticals.

The difference between proteins and peptides is their sizes. The term "peptides" is usually used to refer to those compounds containing fewer than 100 amino acids with a molecular mass of about 10 000 Da (44). Small peptides refers to peptides with fewer than 30 amino acids or molecular mass of <3500 Da. Compared to antibodies, small peptides offer several advantages. Peptides are necessary elements in more fundamental biological processes than any other class of molecule, and in many cases the affinities of small peptides for their receptors are significantly greater than that of antibodies or their fragments (7). Small peptides are easy to synthesize and modify, are less likely to be immunogenic, and can have rapid blood clearance. The faster blood clearance results in adequate target-to-background ratios (T/B) earlier so that it is practical to use ^{99m}Tc, which is the preferred radionuclide for diagnostic nuclear medicine. All of these factors make small peptides excellent candidates for the development of target-specific radiopharmaceuticals.

This review is intended to address some important issues associated with the ^{99m}Tc labeling of highly potent

small peptides. Instead of covering all of the ^{99m}Tc-labeled peptides, which have been reviewed recently (1, 7, 44, 45), it will focus on the following topics: clinical requirements for new ^{99m}Tc radiopharmaceuticals, various radiolabeling approaches, different chelating systems and their ^{99m}Tc-labeling kinetics, and examples of ^{99m}Tc-labeled peptides as radiopharmaceuticals.

REQUIREMENTS FOR NEW ^{99m}Tc-BASED RADIOPHARMACEUTICALS

In the development of a new ^{99m}Tc-based radiopharmaceutical several factors need to be considered to satisfy the clinical requirements. First, the new radiopharmaceutical has to demonstrate its biological efficacy (high uptake in the target organ, high T/B, and favorable pharmacokinetics). Second, a kit formulation is required due to the 6 h half-life of ^{99m}Tc. A kit contains the substance to be labeled [a ligand for the technetium complex radiopharmaceutical or a bifunctional chelating agent (BFCA) derivatized peptide conjugate for the peptide-based radiopharmaceutical], a reducing agent such as stannous chloride, if necessary, and other components such as a bulking agent or a weak transfer ligand. Kits can be purchased and stored for daily preparation. In many cases, the ^{99m}Tc labeling can be accomplished simply by adding [^{99m}Tc]pertechnetate to the kit. Third, the new radiopharmaceutical should have high radiochemical purity (RCP \geq 90%) and high solution stability with a shelf life preferably \geq 6 h. Finally, the ^{99m}Tc-labeling should be accomplished in 10–30 min, preferably at room temperature.

TECHNETIUM-99m AND TECHNETIUM CHEMISTRY

^{99m}Tc is the metastable nuclear isomer of the long-lived ⁹⁹Tc ground state. Nearly 80% of all radiopharmaceuticals used in nuclear medicine are ^{99m}Tc-labeled compounds. The reason for such a preeminent position of ^{99m}Tc in clinical use is its extremely favorable physical and nuclear characteristics. The 6 h half-life is long enough to allow a radiochemist to carry out radiopharmaceutical synthesis and for nuclear medicine practitioners to collect useful images. At the same time, it is short enough to permit the administration of millicurie amounts of ^{99m}Tc radioactivity without significant radiation dose to the patient. The monochromatic 140 keV photons are readily collimated to give images of superior spatial resolution. Furthermore, ^{99m}Tc is readily available from commercial ⁹⁹Mo–^{99m}Tc generators at low cost.

^{99m}Tc is produced from a parent radionuclide, ⁹⁹Mo, a fission product with a half-life of 2.78 days. In a ⁹⁹Mo–^{99m}Tc generator, [⁹⁹Mo]molybdate is adsorbed to an alumina column and ^{99m}Tc is formed by decay of ⁹⁹Mo. The ^{99m}Tc in the form of [^{99m}Tc]pertechnetate is eluted from the column with saline. ^{99m}Tc produced by the generator is never carrier-free. Fifteen percent of ⁹⁹Mo

* Author to whom correspondence should be addressed [telephone (508) 671-8696; fax (508) 436-7500].

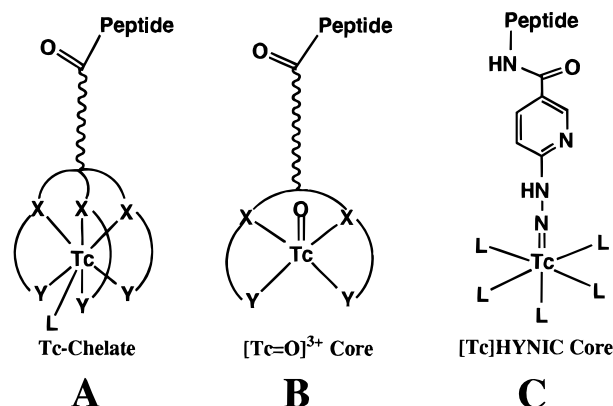
Table 1. Oxidation States and Stereochemistry of Technetium^a

oxidn state	example	coord geometry	coord no.	magnetic moment (μ B)
+7 (d ⁰)	[TcH ₉] ²⁻	trig prismatic	9	diamagnetic
	TcO ₄ ⁻	tetrahedral	4	diamagnetic
+6 (d ¹)	TcO ₄ ²⁻	tetrahedral	4	1.60
+5 (d ²)	[Tc(NCS) ₆] ⁻	octahedral	6	diamagnetic
	[Tc(Diars) ₂ Cl ₄] ⁺	dodecahedral	8	0.9 (?)
	TcOCl ₄ ⁻	sq pyramidal	5	diamagnetic
	[TcO(ECD)]	sq pyramidal	5	diamagnetic
	[TcO(<i>d,l</i> -HM-PAO)]	sq pyramidal	5	diamagnetic
	[TcO ₂ (tetrofosmin)] ⁺	octahedral	6	diamagnetic
+4 (d ³)	[TcCl ₆] ²⁻	octahedral	6	4.05
+3 (d ⁴)	[Tc(Diars) ₂ Cl ₂] ⁺	octahedral	6	diamagnetic
+2 (d ⁵)	[TcCl ₂ (PhP(OEt) ₂) ₄]	octahedral	6	1.4
+1 (d ⁶)	[Tc(CNC(CH ₃) ₃) ₆] ⁺	octahedral	6	diamagnetic
0 (d ⁷)	[Tc ₂ (CO) ₁₀]	octahedral	6	diamagnetic
-1 (d ⁸)	[Tc(CO) ₅] ⁻	trig bipyramidal	5	diamagnetic

^a Examples of technetium complexes are selected from the following two references: (1) N. N. Greenwood and Earnshaw, Eds. (1984) *Chemistry of the Elements*, p 1217, Pergamon Press, New York. (2) Tisato, F., Refosco, F., and Bandoli, G. (1994) Structural survey of technetium complexes. *Coord. Chem. Rev.* 135/136, 325–394.

decays directly to the long-lived isotope ⁹⁹Tc (*t*_{1/2} = 2.13 × 10⁵ y), which is also the single decay product of ^{99m}Tc. The specific activity of eluted ^{99m}Tc is dependent upon the prior elution time because the longer the time between generator elutions, the more ^{99m}Tc decays to ⁹⁹Tc. The mole fraction of ^{99m}Tc to total technetium (^{99m}Tc and ⁹⁹Tc) present in the generator eluent varies from 0.836 at 0.5 h postelution to 0.277 at 24 h postelution and to 0.077 at 72 h postelution. The concentration of total technetium (^{99m}Tc and ⁹⁹Tc) in the ⁹⁹Mo–^{99m}Tc generator eluent is in the range of 10⁻⁷–10⁻⁶ M. The exact value depends on factors such as the generator age and prior elution time.

Diverse Redox Chemistry of Technetium. The two isotopes (^{99m}Tc and ⁹⁹Tc) of technetium have identical chemical properties. ^{99m}TcO₄⁻ is negatively charged and no effective chemistry exists that can be used to attach the negatively charged pertechnetate anion to a small peptide. Therefore, it is necessary to reduce Tc(VII) in ^{99m}TcO₄⁻ to a lower oxidation state to produce a stable ^{99m}Tc–peptide complex or to a reactive intermediate complex from which ^{99m}Tc can be easily transferred to a BFCA–peptide conjugate. When ^{99m}TcO₄⁻ is reduced, the oxidation state of technetium in the complex formed depends upon the nature of the reducing agent, the ligand(s) available, and the reaction conditions employed in the synthesis. The following examples illustrate this quite dramatically. On the macroscale (using ⁹⁹TcO₄⁻) the brown-black insoluble TcO₂·2H₂O is readily produced in an aqueous solution when Na₂S₂O₄ is used as the reducing agent (46). If ethane-1,2-dithiol is present, an orange Tc(V) complex, [TcO(SCH₂CH₂S)₂]⁻, is obtained (47). If pentane-2,4-dione is used as a ligand, the red Tc(III) complex, [Tc(acac)₃], results (48), while the N-substituted pyridinone ligands form very stable tris-ligand Tc(IV) complexes [Tc(L)₃]⁺ (L = N-substituted pyridinone) (49). If the ligand contains P donors, Tc(IV), Tc(III), and Tc(I) complexes are isolated depending on the number of P donors and coligands in the complex (50–52). Isonitrile ligands form colorless Tc(I) complexes, [Tc(CNR)₆]⁺, almost quantitatively (53). Table 1 summarizes various oxidation states and coordination geometries of technetium. The rich and diverse redox chemistry of technetium makes it difficult to control the oxidation state and the stability of the Tc complex. At the same time, it provides more opportunities to modify the structure and properties (such as the overall complex

**Figure 1.** Three technetium cores for ^{99m}Tc labeling.

charge and lipophilicity) of Tc complexes by the choice of the ligand system or through the use of donor atoms having high affinity for a specific oxidation state of the Tc, as well as by the introduction of nondonating functional groups.

Isomerism in Technetium Complexes. Another aspect of technetium chemistry is isomerism. Isomers are compounds having the same chemical composition but different structures. These include geometric isomers, epimers, enantiomers, and diastereomers. Epimers are often found in square pyramidal or octahedral oxotechnetium complexes containing chelating ligands with functional groups on the ligand backbone or a tertiary amine-N donor atom (54–79). The formation of these isomers is due to the relative orientation (*anti* and *syn*) of the functional groups to the Tc=O core. One of the two epimers is often predominant. Enantiomers are often found in oxotechnetium complexes such as [TcO(MAG₃)]⁻ because of the asymmetrical bonding of MAG₃⁴⁻ to the Tc=O core even though the free ligand H₄MAG₃ does not have a chiral center. If a technetium complex contains two or more chiral centers, diastereomers may be formed. These chiral centers can be on the ligand backbone or one on the ligand backbone and the other on the Tc center. Diastereomers can often be separated using appropriate HPLC methods.

Isomers often have different lipophilicities and biodistributions in biological systems. This has been well documented (54–59, 74, 75) and is particularly true for technetium complex radiopharmaceuticals as their biological properties are determined exclusively by the physical and chemical characteristics of the technetium complex. For example, the complex [TcO(map)]⁻ [map = 2,3-bis(mercaptoacetamido)propanoate], has two epimers (*anti* and *syn*) due to the disposition of the COOH group on the chelate ring relative to the Tc=O core. It was reported that in humans 58% of the *syn* isomer was excreted at 30 min as compared to only 19% of the *anti* isomer (74). For receptor-based radiopharmaceuticals, the target uptake is largely dependent on the receptor binding affinity of the peptide and the blood clearance, which is determined by the physical properties of both the peptide and technetium chelate. Therefore, the formation of isomers can have significant impact on the biological properties of a radiopharmaceutical.

TECHNETIUM CORES FOR ^{99m}Tc LABELING

The technetium core determines the design of the BFCA framework and the choice of donor atoms. Figure 1 shows three different technetium cores, which can be used for ^{99m}Tc labeling. In Figure 1A, the technetium core is a “naked” Tc atom, which is completely wrapped

by a hexadentate BFCA. The oxidation state for the Tc can be 3+ or 4+, and the donor atoms can be all imine nitrogens such as those in BATOs (80–82) or a combination of amine nitrogens and phenolate oxygens (83). Because of the chelate or macrocyclic effect, technetium complexes of this type are stable. The use of a polydentate chelate is also beneficial for minimizing isomerism. BATOs (boronic acid adducts of technetium dioximes) (84, 85) and DTPA (86) have been used as BFCAs for the ^{99m}Tc labeling of antibodies.

Since the $[\text{Tc}=\text{O}]^{3+}$ core is very stable in the presence of a strong chelating ligand in aqueous media, it has become the most frequently used technetium core in ^{99m}Tc radiopharmaceuticals. The $[\text{Tc}=\text{O}]^{3+}$ core forms square pyramidal oxotechnetium complexes, often with tetradentate ligands, which include N_4 propylene amine oxime (87), N_3S triamidethiols (24, 54, 55, 57–59), N_2S_2 diamidedithiols (24, 31, 32, 54, 74), N_2S_2 monoamidemonoaminedithiols (69, 77, 79), and N_2S_2 diaminedithiols (61–65). Functionalization on the ligand backbone of these chelators results in *syn* and *anti* isomers due to the relative orientation of the functional group to the $\text{Tc}=\text{O}$ core (58–79).

The $[\text{O}=\text{Tc}=\text{O}]^+$ core forms octahedral technetium complexes with polydentate ligands with either amine N/thioether S donors (88) or phosphine P donor atoms (89). An example of a technetium radiopharmaceutical using the $[\text{O}=\text{Tc}=\text{O}]^+$ core is $[\text{O}=\text{Tc}=\text{O}_2(\text{tetrofosmin})_2]^+$ [tetrofosmin = 1,2-bis[bis(2-ethoxyethyl)phosphino]ethane], in which the two bidentate phosphine ligands bind to the Tc at the four equatorial positions and the oxo O donors at the two apical positions (89). This complex was developed as a heart-imaging agent because of its cationic character (90–92). The $[\text{O}=\text{Tc}=\text{O}]^+$ core has also been used in ^{99m}Tc labeling of a macrocyclic tetraamine-derivatized somatostatin analog (19).

Recently, Abrams and co-workers (93, 94) reported the use of the $[\text{Tc}]\text{HYNIC}$ core (Figure 1C) in the ^{99m}Tc labeling of polyclonal IgG. The $[\text{Tc}]\text{HYNIC}$ core was also used for the ^{99m}Tc labeling of chemotactic peptides (4–11). The HYNIC group is of particular interest because it can be easily labeled with very high efficiency (rapid and high yield radiolabeling). Since the HYNIC can only occupy one or two coordination sites, a coligand such as glucoheptonate is required to complete the square pyramidal or octahedral coordination sphere of the technetium. Tricine was also used as a coligand in the ^{99m}Tc labeling of a HYNIC-conjugated polyclonal IgG (95, 96) and a HYNIC-modified cyclic platelet GPIIb/IIIa receptor antagonist (24, 27). The success of using HYNIC as a bonding group for the ^{99m}Tc clearly demonstrates that a BFCA does not have to be a polydentate chelating agent as long as it can form a stable bond with Tc.

THREE RADIOLABELING APPROACHES

A large number of radiolabeling techniques have been developed and extensively reviewed (97–110). They can be classified into three main categories: direct labeling, the preformed chelate approach, and the indirect labeling approach. The direct labeling approach (Chart 1) usually uses a reducing agent to convert a number of disulfide linkages in a protein into free thiols, which are able to bind the Tc very efficiently. The advantage of this approach is that it is easy to carry out. It has been reported that both thiolate sulfur and imidazole nitrogen are involved in bonding to the Tc (111). However, very little is known about the number of these donor atoms and the coordination geometry around the Tc center. There is little control over the stability of the ^{99m}Tc complex or the nonspecific binding. In addition, this

Chart 1. Direct Labeling Approach

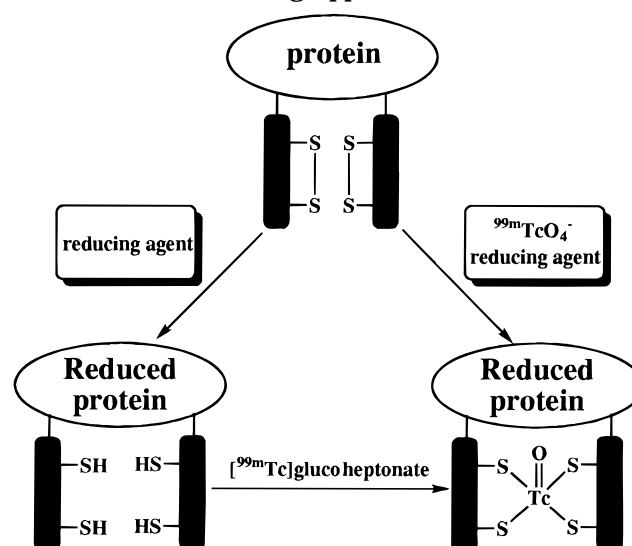
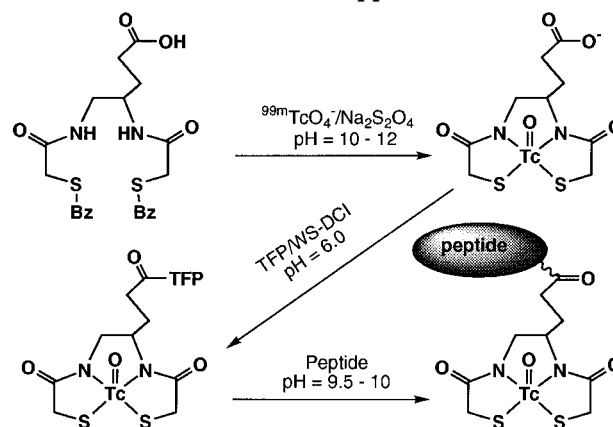


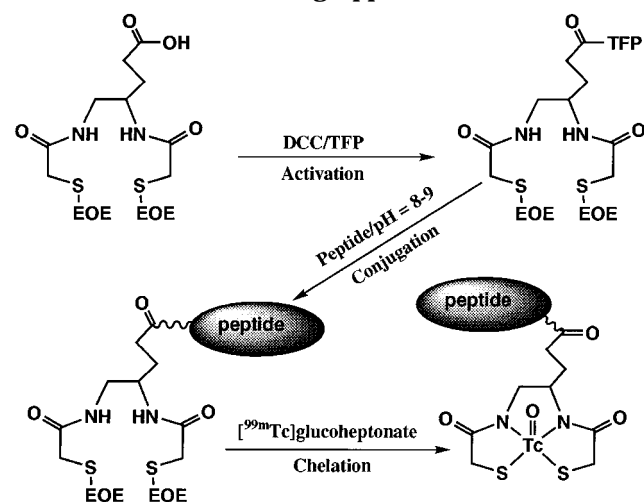
Chart 2. Preformed Chelate Approach



method applies only to proteins or their fragments because many small peptides do not have any disulfide bonds, or in some cases the disulfide bond is too critical for maintaining their biological properties to be reduced.

The preformed chelate approach, an example of which is shown in Chart 2, involves formation of the ^{99m}Tc complex with a BFCA and conjugation of the ^{99m}Tc –BFCA complex to a protein or peptide in a separate step on the tracer level. Several thiol-containing BFCAs such as mapt [4,5-bis(mercaptoacetamido)pentanoic acid] and MeMAG₂-gaba [*N*-[2-(mercapto)propionyl]glycylglycyl- γ -aminobutyric acid] have been used in ^{99m}Tc labeling of proteins (112–115) and small peptides (25, 116). In this approach, the chemistry is better defined, and the peptide or protein is not exposed to the sometimes forcing conditions used in the chelation step. However, this approach is too complex and time-consuming for routine clinical use. The multiple-step tracer level synthesis makes it very difficult to develop an instant kit formulation.

In the indirect labeling approach (Chart 3), a BFCA is first attached to the peptide or protein to form a BFCA–peptide (protein) conjugate. The BFCA can be attached to the C terminus or N terminus via a linker, if needed. It can also be attached to the side chain of the peptide or incorporated in the peptide backbone (31–34) provided that incorporation of the BFCA does not significantly affect the receptor binding affinity of the peptide. The radiolabeling can be achieved either by direct reduction of $^{99m}\text{TcO}_4^-$ in the presence of a BFCA–peptide conjugate

Chart 3. Indirect Labeling Approach

or by ligand exchange with an intermediate ^{99m}Tc complex such as $[\text{}^{99m}\text{Tc}]\text{glucoheptonate}$. This approach combines the ease of direct labeling with the well-defined chemistry of the preformed chelate approach. Therefore, the indirect labeling is the most practical approach for the development of peptide-based target-specific radiopharmaceuticals.

BIFUNCTIONAL CHELATORS AND THEIR ^{99m}Tc -LABELING KINETICS

In simple technetium complex radiopharmaceuticals such as $[\text{}^{99m}\text{Tc}]\text{sestamibi}$, $[\text{}^{99m}\text{Tc}(\text{MIBI})_6]^+$ and $[\text{}^{99m}\text{Tc}]\text{-bicisate}$, $[\text{}^{99m}\text{TcO}(\text{ECD})]$, the ligand (MIBI and ECD, respectively) is always present in large excess. The main factor influencing the ^{99m}Tc -labeling kinetics is the nature of the donor atoms and the radiolabeling conditions. For receptor-based peptide radiopharmaceuticals, however, the use of large amount of BFCAs-peptide may result in receptor site saturation, blocking the docking of the ^{99m}Tc -labeled BFCAs-peptide conjugate, as well as unwanted side effects. To avoid these problems, the concentration of the BFCAs-peptide conjugate in each kit has to be very low (usually 5–20 $\mu\text{g/mL}$, corresponding to 5×10^{-6} to 2×10^{-5} M for a BFCAs-peptide conjugate with molecular mass of 1000 Da and IC_{50} values in the nanomolar range). Otherwise, a postlabeling purification is often needed to remove excess unlabeled peptide, which is time-consuming and thus not amenable for clinical use. Compared to the total technetium concentration ($\sim 5 \times 10^{-7}$ M) in 100 mCi of $[\text{}^{99m}\text{Tc}]\text{pertechnetate}$ eluate (24 h prior elution), the BFCAs-peptide conjugate is not in overwhelming excess. In this situation, the ^{99m}Tc -labeling yield and the labeling kinetics may be affected by the amount of both BFCAs-peptide conjugate and total technetium (^{99m}Tc and ^{99}Tc) in the kit. Therefore, the BFCAs attached to the peptide must have very high radiolabeling efficiency. The design of new and efficient BFCAs systems provides a challenge for inorganic chemists interested in ^{99m}Tc labeling of highly potent small peptides.

A BFCAs can be divided into three parts: a binding unit, a conjugation group, and a spacer (if necessary). An ideal BFCAs is that which is able to form a stable ^{99m}Tc complex in high yield at very low concentration of the BFCAs-peptide conjugate. There are several requirements for an ideal BFCAs. First, the binding unit can selectively stabilize an intermediate or lower oxidation state of Tc so that the ^{99m}Tc complex is not subject to redox reactions; oxidation state changes are often accompanied by transchelation of ^{99m}Tc from a $[\text{}^{99m}\text{Tc}]\text{-}$

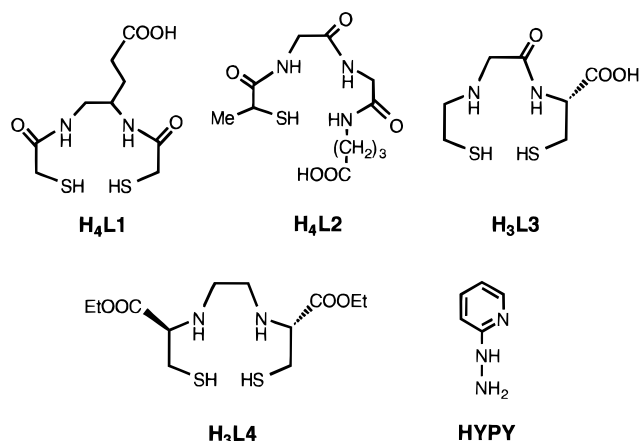


Figure 2. Unprotected thiol-containing chelators and 2-hydrazinopyridine.

BFCAs-peptide complex to the native chelating ligands in biological systems. Second, the BFCAs forms a ^{99m}Tc complex that has thermodynamic stability and kinetic inertness with respect to dissociation. Third, the BFCAs forms a ^{99m}Tc complex with a minimum number of isomers since different isomeric forms of the ^{99m}Tc -labeled chelate may have significant impact on the biological and pharmacokinetic characteristics of the $[\text{}^{99m}\text{Tc}]\text{BFCAs-peptide}$ complex. Finally, the conjugation group can be easily attached to the peptide.

Various chelators have been used as BFCAs in labeling proteins, peptides, and other biologically active molecules with ^{99m}Tc . These include N_3S triamidedithiols (25, 116), N_2S_2 diamidedithiols (112–115, 117), N_2S_2 monoamidodithiols (77), N_2S_2 diaminedithiols (114–123), PnAO (propyleneamine oxime) (16), tetraamines (17), BATOs (84, 85), and HYNIC (4–6, 8–11, 24, 27). However, there are very few comparative data on these chelators obtained under similar controlled conditions. Recently, we studied the relative labeling efficiency of several potentially tetradentate thiol-containing chelators (Figure 2) by competing them with glucoheptonate in $[\text{}^{99m}\text{Tc}]\text{glucoheptonate}$ (128). We also studied the labeling efficiency of 2-hydrazinopyridine (HYPY), which was used as a model compound for HYNIC.

There are several factors that influence the labeling efficiency of a chelator. These include the identity of donor atoms, the chelator concentration, the presence of protecting groups, and reaction conditions such as temperature, time, and pH. If the chelator concentration is fixed, the conditions used for the ^{99m}Tc labeling are largely dependent upon the nature of donor atoms. For example, high pH and heating at 100 $^\circ\text{C}$ for 30 min are required for the successful ^{99m}Tc labeling of N_3S triamidedithiol ($\text{H}_4\text{L1}$) and N_2S_2 diamidedithiol ($\text{H}_4\text{L2}$), while the N_2S_2 monoamidodithiol ($\text{H}_3\text{L3}$) can be well labeled under milder conditions. For the N_2S_2 diaminedithiol ($\text{H}_3\text{L4}$), the ligand exchange can be completed within 60 min at room temperature. It is obvious that substitution of an amine-N for an amide-N enhances the rate of ^{99m}Tc labeling.

Unlike tetradentate thiol-containing chelators ($\text{H}_4\text{L1}$ – $\text{H}_3\text{L4}$), which replace the glucoheptonate in $[\text{}^{99m}\text{Tc}]\text{glucoheptonate}$, HYPY reacts with the $[\text{Tc}=\text{O}]^{3+}$ core and bonds to the Tc as a mono- or bidentate ligand. The radiolabeling efficiency of HYPY using glucoheptonate as coligand is better than that of $\text{H}_4\text{L1}$ or $\text{H}_4\text{L2}$, slightly better than that of $\text{H}_3\text{L3}$, and comparable to that of $\text{H}_3\text{L4}$. Therefore, HYNIC and N_2S_2 diaminedithiols are better candidates as BFCAs in labeling small peptides with very high potency.

It should be noted that the ^{99m}Tc -labeling efficiency of a BFCA is also affected by the presence of protecting groups on the donor atom(s) and the identity of the exchange ligand (coligand for HYNIC). For example, it has been reported that tricine as a coligand gives much better radiolabeling efficiency and higher specific activity for the ^{99m}Tc -labeled HYNIC-IgG than glucoheptonate (94–96). The use of protecting group(s) for thiol-containing chelators (129, 130) usually slows down the rate of radiolabeling. The use of the appropriate combination of BFCA and exchange ligand (or coligand) is needed for the successful ^{99m}Tc labeling of biologically active small peptides.

^{99m}Tc -LABELED PEPTIDES AS PHARMACEUTICALS

Thrombus Imaging. Venous and arterial thrombus formations are common and potentially life-threatening events. It has been estimated that in United States approximately 5 million patients experience one or more episodes of deep vein thrombosis (DVT) per year and that over 500 000 cases of pulmonary embolism occur, resulting in 100 000 deaths (131). It also has been estimated that >70% of pulmonary emboli arise from DVT in the lower extremities (132). However, existing diagnostic modalities are inadequate to diagnose and determine the morphology of the evolving thrombus (133–137). Thus, the development of agents that will not only detect the location but, in addition, determine the age of the thrombi is a critical unmet need in diagnostic nuclear medicine.

A venous thrombus is an intravascular deposit predominantly comprising fibrin, and aggregates of platelets and red blood cells. Platelet aggregation is mediated by fibrinogen, which binds via the Arg-Gly-Asp (RGD) tripeptide sequence to the GPIIb/IIIa receptor expressed on activated platelets. Much of the early work in thrombus imaging was focused on the radiolabeling of fibrinogen (138, 139). In 1976, it was reported that platelets can be labeled very efficiently with [^{111}In]oxine (140). Since then, ^{111}In -labeled platelets have been used to detect left ventricular thrombi (141, 142), pulmonary emboli (143), and DVT (144, 145). However, imaging using ^{111}In -labeled platelets suffers from several limitations. The technique is too complex and time-consuming for routine clinical use (146). It usually takes 24–72 h to get useful images. The ^{111}In -labeled platelets cannot detect small thrombi such as coronary artery thrombi due to the relatively high background (blood pool) activity (147). The slow blood clearance and poor T/B severely limit the use of ^{111}In -labeled platelets.

Platelet activation and deposition are the initial events in acute thrombus formation and may continue for a variable period as thrombus organization proceeds (31). Activated platelets express the GPIIb/IIIa receptor, which recognizes proteins and peptides bearing the RGD tripeptide sequence, while nonactivated platelets express virtually none of the receptor in its active conformation. A number of RGD-containing small peptides (33, 148–151), which are antagonists of the platelet GPIIb/IIIa receptor, have been synthesized and studied for their antithrombotic activities. These small peptides represent a rapidly growing class of antithrombotics.

Recently, DeGrado and co-workers (152–155) reported a series of very potent cyclic GPIIb/IIIa receptor antagonists, two (I and II) of which are shown in Figure 3. Peptides I and II have very high selectivity and binding affinity for the GPIIb/IIIa receptor, with IC_{50} values in the nanomolar range for inhibition of both platelet aggregation and fibrinogen binding (153). This makes them candidates of choice as targeting molecules to carry

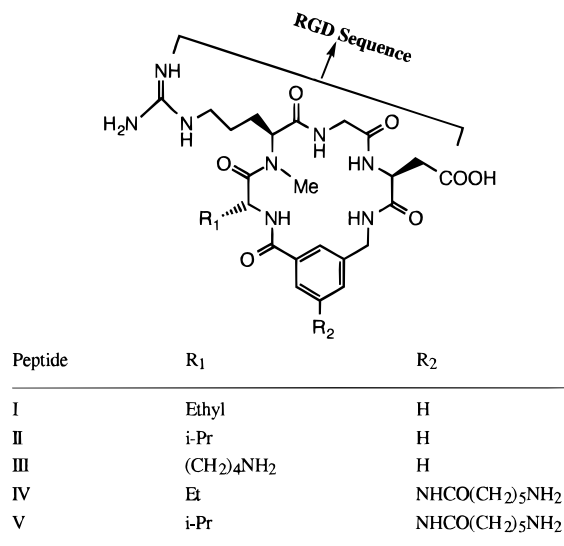
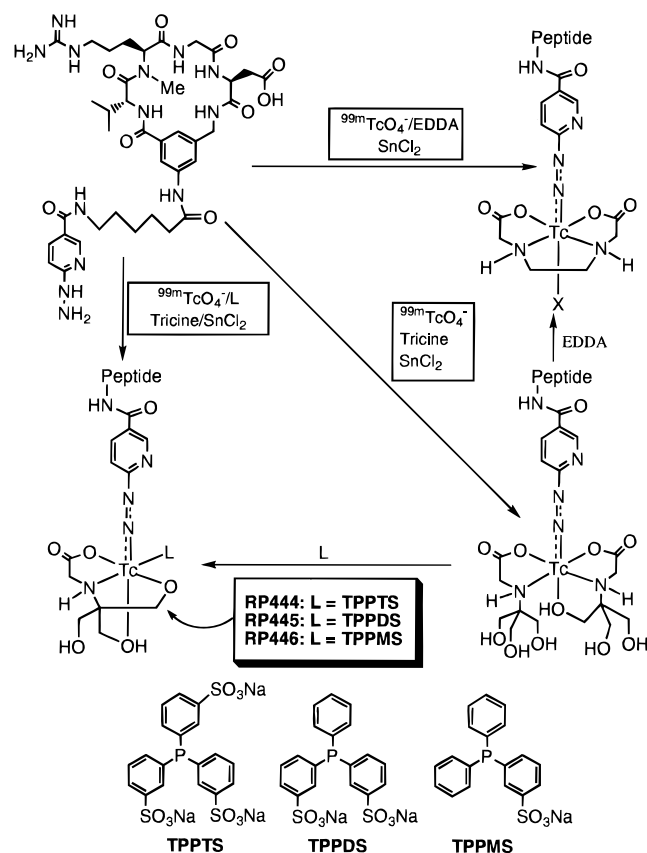


Figure 3. Cyclic GPIIb/IIIa receptor antagonists.

the radionuclide (^{99m}Tc) to thrombi. Since the RGD tripeptide sequence is vital for maintaining biological activity, the functionalized cyclic peptides III–V were prepared by incorporation of a lysine residue between the arginine residue and the Mamb [mamb = *m*-(aminomethyl)benzoic acid] or by attachment of a 6-aminocaproic acid linker on the benzene ring of the Mamb moiety (156, 157). The use of the 6-aminocaproic acid linker keeps the Tc center far from the RGD sequence to minimize the effect of ^{99m}Tc labeling on the receptor binding affinity. Since the GPIIb/IIIa receptor is expressed only on activated platelets, the ^{99m}Tc -labeled cyclic GPIIb/IIIa receptor antagonists should only be bound to platelets intimately involved in the thrombotic event. The rapid blood clearance of small peptides allows the use of ^{99m}Tc and permits earlier imaging of rapidly growing thrombi.

The preformed chelate approach has been used to label several cyclic GPIIb/IIIa receptor antagonists with ^{99m}Tc (25). It was found that both the cyclic peptide and the BFCA contribute to the differences in physical and biological properties of the [^{99m}Tc]BFCA-peptide complex (25, 26). In a canine arteriovenous shunt (AV shunt) model four complexes, [$^{99m}\text{TcO}(\text{L1-III})$][−], [$^{99m}\text{TcO}(\text{L2-III})$][−], [$^{99m}\text{TcO}(\text{L1-V})$][−], [$^{99m}\text{TcO}(\text{L2-V})$][−], were found to be incorporated into the growing thrombus under both arterial and venous conditions. The differences in the uptake of these complexes under both arterial and venous conditions are related to the receptor binding affinity of the peptide and the rate of clearance of technetium complexes from the blood circulation. In a canine DVT model, the complex [$^{99m}\text{TcO}(\text{L1-V})$][−] was incorporated in the growing thrombus with images clearly detectable within 15 min postinjection. At 2 h postinjection, thrombus-to-blood and thrombus-to-muscle ratios were approximately 7:1 and 10:1, respectively. This clearly demonstrated that the complex [$^{99m}\text{TcO}(\text{L1-V})$][−] has the potential for rapid diagnosis of thromboembolic events occurring under both arterial and venous conditions.

The indirect labeling approach (Chart 3) has been used to synthesize the complex [$^{99m}\text{TcO}(\text{L1-V})$][−] (117). The synthesis of the complex [$^{99m}\text{TcO}(\text{L1-V})$][−] was carried out using the ligand exchange method, in which the (EOE)₂H₂L1-V conjugate was allowed to react with [^{99m}Tc]glucoheptonate. It usually requires at least 200 μg of (EOE)₂H₂L1-V conjugate in each reaction vial to achieve a successful ^{99m}Tc labeling. This is consistent with the low labeling efficiency of N₂S₂ diamidedithiols.

Chart 4. ^{99m}Tc Labeling of HYNIC-V

HYNIC was also used to label the peptide **V** with ^{99m}Tc (24) (Chart 4). The advantage of using HYNIC as the BFCA is its high labeling efficiency and the choice of various coligands, which allows control of the hydrophilicity and pharmacokinetics of the ^{99m}Tc -labeled small peptides. Among various coligands, tricine gives the best radiolabeling efficiency. For example, very high specific activity ($\leq 20\,000\text{ Ci}/\mu\text{mol}$) can be achieved for the complex $[^{99m}\text{Tc}(\text{HYNIC-V})(\text{tricine})_2]$. However, it was found that the complex $[^{99m}\text{Tc}(\text{HYNIC-V})(\text{tricine})_2]$ is not stable, particularly in dilute solutions, and exists as multiple species, which we have attributed to different bonding modalities of the hydrazine moiety of the HYNIC-V and the tricine coligands. Although the animal studies in a canine arteriovenous (AV) shunt and a DVT model show that $[^{99m}\text{Tc}(\text{HYNIC-V})(\text{tricine})_2]$ is able to image both arterial and venous thrombi (23, 29), it would still be difficult to develop for clinical use because of the solution instability and the presence of the many isomeric forms.

To prepare $[^{99m}\text{Tc}]\text{HYNIC-V}$ complexes with higher solution stability and less isomerism, EDDA (ethylene-diamine-*N,N*-diacetic acid), which is more symmetrical and potentially tetradentate, was used as the coligand for the radiolabeling (Chart 4). It was found that EDDA forms a complex, $[^{99m}\text{Tc}(\text{HYNIC-V})(\text{EDDA})]$, with much higher solution stability and less isomerism (24). However, the HPLC data showed that the complex $[^{99m}\text{Tc}(\text{HYNIC-V})(\text{EDDA})]$ exists in at least three isomeric forms.

In an alternative approach (Figure 4), a water soluble phosphine (TPPTS, TPPDS, and TPPMS) is used as an additional coligand to form a ternary ligand system (27). These monodentate phosphines react readily with $[^{99m}\text{Tc}(\text{HYNIC-V})(\text{tricine})_2]$, replace one of its two tricine coligands, and form complexes, $[^{99m}\text{Tc}(\text{HYNIC-V})(\text{tricine})(\text{L})]$ (RP444, L = TPPTS; RP445, L = TPPDS; RP446, L =

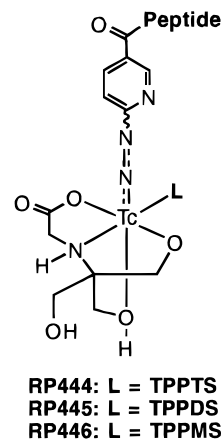


Figure 4. Proposed structures for ternary ligand technetium complexes.

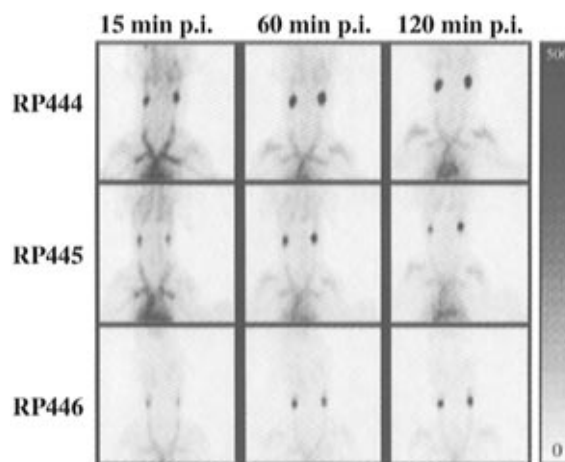


Figure 5. Representative DVT images of complexes RP444, RP445, and RP446 at 15, 60, and 120 min postinfusion. The bar to the right of the images indicates the scale from 0 (white) to 506 (greatest/black). The images have not been filtered.

TPPMS) in high yield and high specific activity ($\geq 20\,000\text{ Ci}/\text{mmol}$). RP444, RP445, and RP446 are formed as equal mixtures of two isomeric forms, which is due to the resolution of diastereomers resulting from the chiral centers on the peptide backbone and the chirality of the technetium chelate (158). The composition of these complexes was determined to be 1:1:1 for Tc:HYNIC-V:L:tricine through a series of mixed ligand experiments on the tracer (^{99m}Tc) level. This composition is maintained over a wide range of relative ligand ratios.

In the canine AV shunt model (28), RP444, RP445, and RP446 were adequately incorporated into the arterial and venous portions of the growing thrombus (7.8–9.9 and 0.2–3.7% ID/g, respectively). Figure 5 shows representative unfiltered images of RP444, RP445, and RP446 in the DVT imaging model at 15, 60, and 120 min postinfusion. All three complexes had thrombus uptake (%ID/g = 2.86 ± 0.4 , 3.4 ± 0.9 , 3.38 ± 1.1 for RP444, RP445, and RP446, respectively) that far exceeded that of the negative control, $[^{99m}\text{Tc}]\text{albumin}$. They also show similar blood clearance with a $t_{1/2}$ values of approximately 90 min. Visualization of DVT can be as early as 15 min postinjection and improves over time with the thrombus/muscle ratios of 9.7 ± 1.9 , 13.8 ± 3.6 , and 9.4 ± 2 for RP444, RP445, and RP446, respectively, at 120 min postinjection. The administration of RP444, RP445, and RP446 did not alter platelet function, hemodynamics, or the coagulation cascade. Therefore, all three complexes have the capability to detect rapidly growing venous and arterial thrombi. RP444 was selected for clinical studies

as a new thrombus imaging agent for both arterial thrombi and DVT.

Obviously, the use of this new ternary ligand system offers several major advantages. First, bonding of the phosphine coligand to the Tc dramatically reduces the number of isomeric forms of the [^{99m}Tc]HYNIC-V complexes. Second, the solution stability of [^{99m}Tc]HYNIC-V complexes is dramatically improved. RP444 was found to be stable for at least 6 h under dilute conditions, while the HPLC-purified corresponding ^{99}Tc analog, [^{99}Tc -(HYNIC-V)(tricine)(TPPTS)], remains stable in aqueous solution for more than 6 months without any decomposition (158). It is amazing that three different ligands (HYNIC-V, tricine, and phosphine) combine with Tc and form technetium complexes with only two detectable isomers and with extremely high solution stability. Finally, the hydrophilicity of [^{99m}Tc]HYNIC-V complexes with this ternary ligand system can be tuned either by altering the number of sulfonato groups or by using water soluble phosphines with other polar functionality. The tricine coligand can also be substituted by other potentially tetradentate aminocarboxylates such as dicine [*N*-bis(hydroxymethyl)methylglycine] and bicine [*N,N*-bis(hydroxyethyl)glycine]. However, the specific activity of [^{99m}Tc]HYNIC-V complexes using dicine and bicine as coligands is not as high as that of the corresponding tricine complexes. This is consistent with the literature results reported by Abrams and co-workers (93–96), who found that the [^{99m}Tc]tricine precursor complex has the highest reactivity with hydrazines. Using the combination of a polydentate aminocarboxylate and a phosphine ligand, HYNIC-conjugated peptides and other HYNIC-derivatized small molecules can be readily labeled with ^{99m}Tc in high specific activity and high stability for potential use as radiopharmaceuticals.

The technetium oxidation state and the exact nature of bonding between these three ligands (HYNIC, tricine, and phosphine) and the Tc are not yet clear. It has been proposed that the technetium oxidation state in the [^{99m}Tc]tricine complex is 5+ (92, 93). However, the oxidation state might change when the HYNIC group and phosphine coligand are bonded to the Tc center. Furthermore, the technetium oxidation state largely depends on how the HYNIC group binds to the Tc and how one counts the charge on the HYNIC ligand.

Complexes containing Tc–hydrazido and Tc–diazenido bonds have been previously reported and characterized by X-ray crystallography (159–165). Recently, Davison and co-workers (166, 167) reported a series of technetium-(III) and rhenium(III) complexes of 2-hydrazinopyridine. It was found that unlike phenylhydrazine, 2-hydrazinopyridine has several bonding modalities: neutral bidentate pyridyldiazene (166, 167), neutral monodentate pyridiniumdiazenido (166), and anionic monodentate pyridyldiazenido (167). Various Tc/Re complexes can be prepared depending upon the starting material and reaction conditions. For example, the reaction of $\text{NH}_4[\text{TcO}_4]$ with 2-hydrazinopyridine dihydrochloride gives $[\text{TcCl}_3(\text{HN}=\text{NC}_5\text{H}_4\text{N})(\text{N}=\text{NC}_5\text{H}_4\text{NH})]$. The reaction of $[\text{ReCl}_3(\text{HN}=\text{NC}_5\text{H}_4\text{N})(\text{N}=\text{NC}_5\text{H}_4\text{NH})]$ with triphenylphosphine (PPh_3) in the presence of a base such as diisopropylethylamine produces the complex $[\text{ReCl}_2(\text{PPh}_3)(\text{N}=\text{NC}_5\text{H}_4\text{N})(\text{N}=\text{NC}_5\text{H}_4\text{NH})]$, in which the $\text{N}=\text{NC}_5\text{H}_4\text{N}$ moiety was found to be an anionic monodentate pyridyldiazenido (166). We also found that $\text{NH}_4[\text{TcO}_4]$ or $[\text{n-Bu}_4\text{N}][\text{TcOCl}_4]$ reacts with $\text{HYPY}\cdot 2\text{HCl}$ in the presence of excess PPh_3 to give the complex $[\text{Tc}(\text{N}=\text{NC}_5\text{H}_4\text{N})(\text{PPh}_3)_2\text{Cl}_2]$. The NMR data suggest that the $\text{N}=\text{NC}_5\text{H}_4\text{N}$ moiety is likely bidentate pyridyldiazenido (158).

When the HYNIC binds to the Tc, it likely forms either

a terminal Tc–diazenido or Tc–hydrazido bond. If one assumes that the coordination geometry around the Tc in the ternary ligand complexes is distorted octahedral, the tricine coligand is expected to be tetradentate with the carboxylate O, amine N, and hydroxy O occupying equatorial positions and one of the two remaining hydroxy O's occupying the apical site of the Tc (Figure 4). Efforts are continuing to better understand the coordination chemistry of this unique, versatile, and complex ternary ligand system.

Lister-James and co-workers (31–34) also used ^{99m}Tc -labeled IIb/IIIa receptor antagonists for the development of new thrombus imaging agents. P280 is a small oligopeptide made of two identical, linked, cyclic 13 amino acid monomers. Each monomer contains a (*S*-aminopropylcysteine)-Gly-Asp tripeptide sequence, which is mimetic of the RGD sequence found in molecules such as fibrinogen and fibronectin. P280 has high affinity for the GPIIb/IIIa receptor with an IC_{50} of 87 nM for inhibition of human platelet aggregation (31). Each monomer contains a Cys(Acm)-Gly-Cys(Acm) tripeptide sequence, which forms an N_2S_2 diamidedithiol bonding unit for ^{99m}Tc labeling. Because of the low labeling efficiency of N_2S_2 diamidedithiols and the presence of protecting group on the two thiol groups, the ^{99m}Tc labeling of P280 requires the use of a large amount of peptide ($\geq 250 \mu\text{g}$) and heating at 100 °C for 15 min when prepared by ligand exchange with [^{99m}Tc]glucoheptonate. The specific activity for the [^{99m}Tc]P280 complex is low (60 mCi/ μmol) compared to that of RP444 ($\geq 20\,000$ mCi/ μmol). [^{99m}Tc]P280 was reported to give excellent images of DVT in a canine DVT model. However, the thrombus uptake at 4 h postinjection is only $0.0059 \pm 0.0025 \text{ \%ID/g}$ (31), which is much lower than that of RP444 ($2.8 \pm 0.4 \text{ \%ID/g}$) (28). The low thrombus uptake is most likely related to the lower binding affinity of P280 ($\text{IC}_{50} = 87 \text{ nM}$) for the GPIIb/IIIa receptor and faster blood clearance ^{99m}Tc –P280 ($t_{1/2\alpha} = 1.6 \text{ min}$ and $t_{1/2\beta} = 20 \text{ min}$) as compared to the binding affinity of peptide V ($\text{IC}_{50} = 6 \text{ nM}$) and the blood clearance of RP444 ($t_{1/2} = 90 \text{ min}$).

P748 is another platelet GPIIb/IIIa receptor antagonist under investigation for imaging pulmonary embolism (33, 44). P748 has a higher receptor binding affinity ($\text{IC}_{50} = 28 \text{ nM}$ against aggregation of human platelets) than P280 ($\text{IC}_{50} = 87 \text{ nM}$), and [^{99m}Tc]P748 has slower blood clearance with $t_{1/2\alpha} = 9.6 \text{ min}$ and $t_{1/2\beta} = 145 \text{ min}$. It is not surprising that [^{99m}Tc]P748 shows a higher uptake ($\text{\%ID/g} = 0.018 \pm 0.0068$ at 4 h postinjection) and a higher T/B than [^{99m}Tc]P280. Unlike P280, P748 uses an N_3S aminediamidethiol chelating unit. Because of the asymmetric character of the chelator, two epimers are seen, one of which is predominant. It was reported that P748 can be easily labeled by ligand exchange with [^{99m}Tc]glucoheptonate at room temperature. The reported highest specific activity for [^{99m}Tc]P748 is about 2000 mCi/ μmol . Apparently, the presence of the amine N donor and a unprotected thiol in the chelator dramatically improves the radiolabeling efficiency.

Infection/Inflammation Imaging. Imaging focal sites of infection or inflammation using radiolabeled peptides is another important area in diagnostic nuclear medicine. Accurate and rapid localization of infectious and inflammatory foci facilitate elucidation of the cause of disease and the implementation of a tailored therapeutic regimen (169). Current imaging procedures such as X-ray computed tomography (CT), ultrasound (US), conventional radiography, and magnetic resonance imaging (MRI) rely primarily on focal changes in tissue density to define lesions. In the early stage of an inflammatory lesion, lesion localization using these pro-

cedures may be difficult because the tissue changes associated with necrosis have not occurred (6).

For a number of years, imaging of inflammation and infection has been performed using either [^{67}Ga]citrate or [^{111}In]-labeled white blood cells (WBCs) (170, 171). $^{99\text{mTc}}$ -labeled nonspecific polyclonal IgG's were also used for detection of infection foci (92, 94, 172–177). Although these agents are well-accepted and efficacious, it usually takes 24 h to obtain diagnostically useful images. Recently, two new radiopharmaceuticals were introduced for imaging sites of infection: [$^{99\text{mTc}}$]hexamethylpropylene amine oxime (HMPAO)-WBCs (178–180) and [$^{99\text{mTc}}$]albumin colloid-WBCs (181). Imaging using both agents can be completed on the same day, but these procedures may impose significant risks to laboratory personnel and patients, particularly with the increasing prevalence of human immunodeficiency virus in the population (6, 182, 183).

WBCs, particularly polymorphonuclear leukocytes (PMNLs) and monocytes, accumulate in high concentrations at sites of infection. Therefore, most attention has been directed toward radiolabeling small molecules that bind to both circulating granulocytes and leukocytes. These include chemotactic peptides, analogs of *N*-formyl-methionylleucylphenylalanine (fMLF) (3–11), small peptides based on platelet factor 4 (12), and tuftsin receptor antagonists (13–15).

The chemotactic peptide fMLF is a bacterial product that initiates leukocyte chemotaxis by binding to high-affinity receptors on inflammatory cells. Fischman and co-workers (4–11) have investigated a series of radiolabeled chemotactic peptides as infection/inflammation imaging agents. These peptides were modified with HYNIC (for $^{99\text{mTc}}$ labeling) or DTPA (for [^{111}In] labeling) at the C terminus. The $^{99\text{mTc}}$ labeling of HYNIC-modified chemotactic peptides can be achieved using various coligands such as glucoheptonate, mannitol, and glucamine (5). It was reported that very high specific activity ($\geq 20\,000\text{ mCi}/\mu\text{mol}$) could be achieved using glucoheptonate as the coligand. Different biodistributions were observed for various coligands (5). Animal studies have shown evidence of binding to leukocytes in vivo and localization at sites of infection (6–11). In a rabbit infection model, a $^{99\text{mTc}}$ -labeled fMLF analog gave a target to background ratio greater than or equal to that achieved with [^{111}In]WBCs (11).

We also labeled a chemotactic peptide–HYNIC conjugate (fMLFK–HYNIC) using tricine or glucoheptonate as coligand (183). It was found that tricine and glucoheptonate form technetium complexes, [$^{99\text{mTc}}$](fMLFK–HYNIC)(L)₂ (L = tricine and glucoheptonate), with many isomeric forms. These technetium complexes are not stable in the absence of excess coligand. The combination of tricine and TPPTS forms a stable ternary ligand complex [$^{99\text{mTc}}$](fMLFK–HYNIC)(tricine)(TPPTS)], which was evaluated in two animal (guinea pig and rabbit) models of focal infection. It was found that the ternary ligand complex was superior with a T/B of 5–7:1 at 4 h postinjection, reflecting an increased clearance from the normal muscle. In the rabbit infection model a transient decrease in WBC count of 35% was observed in all three groups during the first 30 min postinjection (183). A similar neutropenic response was also reported for the $^{99\text{mTc}}$ -labeled chemotactic peptides, [$^{99\text{mTc}}$]RP050 and [$^{99\text{mTc}}$]RP056 (184).

Apparently, the $^{99\text{mTc}}$ labeling of these highly potent agonists suffers a drawback, severe reduction of peripheral leukocyte count because of the unlabeled peptide even at very low doses. There are two approaches to avoid this problem. The first approach is to separate the

radiolabeled peptide from the excess unlabeled peptide using HPLC. This results in a product almost at its theoretical specific activity but is inconvenient for routine clinical use. The alternative approach is to use antagonist peptides, which bind to the receptor but do not trigger the neutropenic effect, as targeting molecules. However, the receptor binding affinities of the antagonists tested to date appear to be much lower than that of the agonists (185).

Platelet factor 4 (PF-4) is a 29 kDa homotetrameric protein for which receptors have been identified on PMNLs, monocytes, endothelium, fibroblasts, and hepatocytes. Peptide P483 (acetyl-Lys-Lys-Lys-Lys-Lys-Cys-Gly-Cys-Gly-Gly-Pro-Leu-Tyr-Lys-Lys-Ile-Ile-Lys-Lys-Leu-Leu-Glu-Ser) is an analog of the C-terminal tridecapeptide of human PF-4. It contains a Cys-Gly-Cys tripeptide chelating unit for $^{99\text{mTc}}$ labeling and a pentylsine sequence on the N terminus to promote renal clearance (12). It was reported that complexation of [$^{99\text{mTc}}$]P483 with heparin substantially enhanced the binding to WBCs and resulted in improved uptake in sites of infection in a rabbit infection model (12). The in vitro distribution in human blood suggests that [$^{99\text{mTc}}$]P483H associates with specific WBCs, particularly monocytes. In the rabbit infection model, [$^{99\text{mTc}}$]P483H showed slightly higher infection uptake ($0.062 \pm 0.022\text{ \%ID/g}$) than [^{111}In]oxine–WBCs ($0.051 \pm 0.008\text{ \%ID/g}$), and a 6-fold higher T/B, probably due to the rapid blood clearance (12).

Tuftsin is a tetrapeptide (TKPR) derived from the Fc portion of IgG. It promotes phagocytosis and chemotaxis of neutrophils and monocyte/macrophages. Recently, a $^{99\text{mTc}}$ -labeled tuftsin receptor antagonist [Pic-SC(Acm)G-TKPPR; Pic = picolinic acid] was used for imaging inflammation (13). The Pic-SC(Acm)G sequence forms an N₃S chelating unit for $^{99\text{mTc}}$ bonding. Radiolabeling was achieved by ligand exchange with [$^{99\text{mTc}}$]glucoheptonate. In rats with infectious (*Escherichia coli*) inflammation (13), the $^{99\text{mTc}}$ -labeled tuftsin antagonist was able to give excellent images with the T/B of 3.6, 5.0, and 16.2 at 0.5, 3, and 17 h postinjection, respectively. Another $^{99\text{mTc}}$ -labeled tuftsin receptor antagonist is [$^{99\text{mTc}}$]RP128 [RP128 = dimethylGSC(Acm)G-TKPPR]. In an inflammatory bowel disease (IBD) model, [$^{99\text{mTc}}$]RP128 showed much better imaging quality than [^{111}In]oxine–WBCs (14). The target (inflamed terminal colon) to background (proximal noninflamed colon) ratios of 2.14, 2.51, 2.90, and 1.90 were obtained at 0.5, 1, 3, and 18 h postinjection, respectively. Both agents were rapidly excreted via the renal system.

Tumor Imaging. There is an unmet need for the development of new target-specific tumor-imaging agents. Radiolabeled receptor-based biomolecules such as small peptides are of particular interest because they have the potential to detect primary sites, identify occult metastatic lesions, guide surgical intervention, stage tumors, and predict efficacy of therapeutic agents. When labeled with a suitable radionuclide, they can also be used as radiotherapeutic agents.

The peptide that has attracted greatest interest is somatostatin, a tetradecapeptide which exhibits an inhibitory effect on the secretion of numerous hormones, including growth hormone, thyrotrophin, insulin, glucagon, vasoactive intestinal peptide (VIP), and secretin. Somatostatin receptors are overexpressed on a number of human tumors and their metastases (186–189), thereby serving well as the target for tumor imaging. Although the first report of in vivo imaging with a somatostatin analog appeared in 1976 (190), further development was hampered due to rapid degradation of the native peptide

by plasma and tissue proteases (191). For this reason, analogs of somatostatin have been synthesized using D-amino acids to prolong the in vivo half-life by inhibiting the action of amino and carboxypeptidases. Octreotide (Sandostatin, SMS 201-995) is a metabolically stable analog of somatostatin and has been successfully used for the treatment of acromegaly and GEP tumors (192–194).

Derivatives of octreotide have been radiolabeled with γ -emitting radionuclides such as ^{123}I (195, 196) and ^{111}In (197–204), and these radiotracers have been successfully used to detect somatostatin receptor-positive tumors by γ -scintigraphy. [^{111}In]DTPA-octreotide (OctreoScan) has been approved in many countries in Europe and North America and has become one of the most commonly used radiopharmaceuticals in clinical tumor imaging. However, this agent suffers several drawbacks such as the long half-life ($t_{1/2} = 67\text{ h}$, $\gamma = 173\text{ keV}$, 89%, and 247 keV, 94%) and the high cost of ^{111}In . For diagnostic purposes, $^{99\text{m}}\text{Tc}$ is more desirable because of its low cost, easy availability, and ideal nuclear characteristics, which better match the rapid blood clearance and fast tumor accumulation of octreotide.

In the past several years, various somatostatin analogs have been labeled with $^{99\text{m}}\text{Tc}$ using different BFCAs, including N_2S_2 diamidedithiols (19, 20), N_3S triamidedithiols (19, 20), N_3S aminediamidedithiols (19, 20), PnAO (propyleneamine oxime) (16), and tetraamines (17). Of particular interest are $^{99\text{m}}\text{Tc}$ -labeled peptides P587 and P829. Both peptides contain the Tyr-(D-Trp)-Lys-Val sequence, which is responsible for somatostatin receptor binding. The cyclic peptide backbone does not contain the S–S disulfide linkage and is not susceptible to reductive cleavage. In P587, the Gly-Gly-Cys tripeptide constitutes an N_3S triamidedithiol chelator for $^{99\text{m}}\text{Tc}$ bonding, while P829 uses the (β -Dap)-Lys-Cys tripeptide sequence to form an N_3S aminediamidedithiol chelating unit. Studies in CA20948 tumor-bearing rats showed that the tumor uptake of [$^{99\text{m}}\text{Tc}$]P587 and [$^{99\text{m}}\text{Tc}$]P829 is comparable to or better than that of [^{111}In]DTPA-octreotide (19). [$^{99\text{m}}\text{Tc}$]P829 is excreted predominantly through the renal system and has been selected for clinical trials.

HYNIC was also used to label somatostatin analogs with $^{99\text{m}}\text{Tc}$ (205, 206). It was conjugated to the N terminus of octreotide either directly or via a β -alanine or diaminobutanesuccinyl linker. The use of tricine as coligand produced a very high specific activity ($\sim 6000\text{ mCi}/\mu\text{mol}$). In a tumor bearing mouse model (AR4-2J), all three $^{99\text{m}}\text{Tc}$ -labeled HYNIC-octreotide conjugates showed comparable tumor uptake to [^{111}In]DTPA-octreotide (205, 206). The observed high blood activity is probably related to the instability of [$^{99\text{m}}\text{Tc}$]HYNIC-octreotide-tricine complexes and plasma protein binding.

Somatostatin analogs (e.g. BIM-23014, RC-160, and Sandostatin), which contain a S–S disulfide bond in the cyclic peptide backbone, have also been radiolabeled by the direct labeling approach (1, 18, 207, 208). It is believed that when the S–S bond is reduced, the thiolate S atoms bond to the Tc center and form stable $^{99\text{m}}\text{Tc}$ complexes (18). It was also reported that these $^{99\text{m}}\text{Tc}$ -labeled somatostatin analogs have not shown any apparent loss of biological activity, nor have they shown any abnormal blood clearance in experimental animals compared to that with [^{111}In]DTPA-octreotide (1, 207, 208). However, several critical questions remain to be answered for this approach. First, how many peptides are bonded to the Tc center? If only one peptide binds to the Tc, which tripeptide sequence (Cys-AA-AA or AA-AA-Cys) is involved in Tc bonding? How many $^{99\text{m}}\text{Tc}$

species are in the radiolabeled kit? What is the impact of $^{99\text{m}}\text{Tc}$ labeling on the receptor binding affinity of the cyclic peptide?

CONCLUSIONS

From the discussion above, it is apparent that significant progress has been made in the development of peptide-based target specific radiopharmaceuticals. $^{99\text{m}}\text{Tc}$ labeling of biologically active peptides stemmed from the studies of $^{99\text{m}}\text{Tc}$ -labeled antibodies for diagnosis or therapy of various tumors. In a very short period of time, $^{99\text{m}}\text{Tc}$ -labeled peptides have become an important class of imaging agents for the detection of not only tumors but also thrombosis and infection/inflammation. $^{99\text{m}}\text{Tc}$ -labeled peptides such as RP444, [$^{99\text{m}}\text{Tc}$]P280, [$^{99\text{m}}\text{Tc}$]P483H, [$^{99\text{m}}\text{Tc}$]P748, [$^{99\text{m}}\text{Tc}$]P829, and [$^{99\text{m}}\text{Tc}$]RP128 are now being evaluated in clinical trials. Results from preclinical studies have lived up to their expectations: high specificity, high uptake in the target organ, and high T/B due to rapid blood clearance of the $^{99\text{m}}\text{Tc}$ -labeled small peptides. Hopefully, some of these $^{99\text{m}}\text{Tc}$ -labeled small peptides will soon become commercial products and serve the nuclear medicine community for decades.

Radiolabeled small peptides continue to attract interest because of their favorable physical and chemical characteristics compared to antibodies and their fragments. Small peptides, once the receptor binding sequence is identified, can be easily synthesized and modified according to their pharmacokinetic requirements. Ideally, a peptide-based radiopharmaceutical should have the following characteristics: rapid uptake by target tissues, metabolic stability, and fast renal clearance. This is particularly important for infection and tumor imaging because rapid renal clearance minimizes the accumulation of radioactivity in the abdominal area and results in improved T/B. The isotope of choice for radiolabeling will continue to be $^{99\text{m}}\text{Tc}$ rather than ^{111}In for diagnostic radiopharmaceuticals because of cost and convenience. The experience learned from $^{99\text{m}}\text{Tc}$ labeling of small peptides can be applied to other highly potent receptor binding small molecules. In addition, these biologically active small peptides can also be used for the development of therapeutic radiopharmaceuticals when labeled with appropriate radionuclides such as ^{186}Re .

In the area of tumor imaging, $^{99\text{m}}\text{Tc}$ -labeled substance P (SP) and vasoactive intestinal peptide (VIP) as well as their analogs may become new classes of tumor-imaging agents. [^{111}In -DTPA-Arg¹]SP has been successfully used to visualize SP-positive processes such as adjuvant arthritis and atransplantable pancreatic tumor (209). Studies using [^{123}I]VIP have clearly demonstrated its utility in localizing intestinal adenocarcinoma and endocrine tumors as well as metastatic tumor sites in humans (210). Of course, the next logical step is $^{99\text{m}}\text{Tc}$ labeling of substance P (SP) and vasoactive intestinal peptide (VIP) analogs with favorable pharmacokinetics.

$^{99\text{m}}\text{Tc}$ labeling of highly potent small peptides is different from that of simple organic chelators. Because of the possible side-effects, the BFCA-peptide conjugate has to be labeled at very low concentrations (usually $5\text{--}20\text{ }\mu\text{g/mL}$, corresponding to 5×10^{-6} to $2 \times 10^{-5}\text{ M}$ for a BFCA-peptide conjugate with molecular mass of 1000 Da and IC_{50} values in the nanomolar range) to achieve high specific activity. One of the challenges for inorganic chemists is to design new ligand systems that have very high labeling efficiency and form technetium complexes with minimal isomerism.

It should be noted that the development of new $^{99\text{m}}\text{Tc}$ -labeling technologies and synthesis of new biologically active peptides with high receptor binding affinities are

equally important. Improvement of the pharmacokinetics of ^{99m}Tc -labeled peptides can be achieved by modification of both the peptide and the Tc chelate. The development of ^{99m}Tc -labeled peptide radiopharmaceuticals is a multidisciplinary effort and requires the collaboration from scientists in several areas, including organic chemistry, inorganic chemistry, biochemistry, biology, formulation chemistry, and nuclear medicine. As Jurriss (211) stated: "Without their joint efforts nuclear medicine would not be where it is today, nor will it progress".

ACKNOWLEDGMENT

We give special thanks to Dr. Joseph L. Glajch and Dr. Steven B. Haber for helpful discussions.

LITERATURE CITED

- Thakur, M. L. (1995) Radiolabeled peptides: now and future. *Nucl. Med. Commun.* 6, 724–732.
- Zoghbi, S. S., Thakur, M. L., and Gottschalk, A. (1981) Selective cell labeling: a potential radioactive agent for labeling of human neutrophils. *J. Nucl. Med.* 22, P32 (abstract).
- Baidoo, K. E., Stathis, M., Scheffiel, U., Lever, S. Z., and Wagner, H. N., Jr. (1993) High affinity Tc-labeled chemotactic peptides. *J. Nucl. Med.* 34, 18P (abstract 62).
- Babich, J. W., Solomon, H., Pike, M. C., Kroon, D., Graham, W., Abrams, M. J., Tompkins, R. G., Rubin, R. H., and Fischman, A. J. (1993) Technetium-99m-labeled hydrazino nicotinamide derivatized chemotactic peptide analogs for imaging focal sites of bacterial infection. *J. Nucl. Med.* 34, 1967–1974.
- Babich, J. W., and Fischman, A. J. (1995) Effect of "coligand" on the biodistribution of ^{99m}Tc -labeled hydrazino nicotinic acid derivatized chemotactic peptides. *Nucl. Med. Biol.* 22, 25–30.
- Fischman, A. J., Babich, J. W., and Rubin, R. H. (1994) Infection imaging with technetium-99m-labeled chemotactic peptide analogs. *Semin. Nucl. Med.* 24, 154–168, and references cited therein.
- Fischman, A. J., Babich, J. W., and Strauss, H. W. (1993) A ticket to ride: peptide radiopharmaceuticals. *J. Nucl. Med.* 34, 2253–2263.
- Fischman, A. J., Rauh, D., Solomon, H., Babich, J. W., Tompkins, R. G., Kroon, D., Strauss, H. W., and Rubin, R. H. (1993) In vivo bioactivity and biodistribution of chemotactic peptide analogs in nonhuman primates. *J. Nucl. Med.* 34, 2130–2134.
- Babich, J. W., Graham, W., Barrow, S. A., and Fischman, A. J. (1995) Comparison of the infection imaging properties of a ^{99m}Tc labeled chemotactic peptide with ^{111}In IgG. *Nucl. Med. Biol.* 22, 643–648.
- Babich, J. W., Solomon, H., Pike, M. C., Kroon, D., Graham, W., Abrams, M. J., Tompkins, R. G., Rubin, R. H., Barrow, S. A., and Fischman, A. J. (1993) Technetium-99m-labeled hydrazino nicotinamide derivatized chemotactic peptide analogs for imaging focal sites of bacterial infection. *J. Nucl. Med.* 34, 1964–1974.
- Babich, J. W., Graham, W., Barrow, S. A., Dragotakes, S. C., Tompkins, R. H., Rubin, R. H., and Fischman, A. J. (1993) Technetium-labeled chemotactic peptides: comparison with Indium-111-labeled white blood cells for localizing acute bacterial infection in the rabbit. *J. Nucl. Med.* 34, 2176–2181.
- Moyer, B. R., Vallabhajosula, S., Lister-James, J., Bush, L. R., Cyr, J. E., Snow, D. A., Bastidas, D., Lipszyc, H., and Dean, R. T. (1996) Technetium-99m-white blood cell-specific imaging agent developed from platelet factor 4 to detect infection. *J. Nucl. Med.* 37, 673–679.
- Goodbody, A. E., Ballinger, J., Tran, L. L., Sumner-Smith, M., Lau, F., Meghji, K., and Pollak, A. (1994) A new Tc-99m labeled peptide inflammation imaging agent. *Eur. J. Nucl. Med.* 21, 790 (abstract 262).
- Cavelier, V., Goodbody, A. E., Tran, L. L., Bossuyt, A., and Thornback, J. (1996) Human dosimetry of Tc99m-RP128, a potential inflammation imaging agent. *Eur. J. Nucl. Med.* 23, 1131 (abstract OMO398).
- Peers, S. H., Tran, L. L., Eriksson, S. J., Ballinger, J., and Goodbody, A. E. (1995) Imaging a model of colitis with RP128, a Tc-99m-chelated tuftsin Antagonist. *J. Nucl. Med.* 36, 114P (abstract 465).
- Maina, T., Stolz, B., Albert, R., Bruns, C., Koch, P., and Mäcke, H. (1994) Synthesis, radiochemistry and biological evaluation of a new somatostatin analogue (SDZ 219-387) labeled with technetium-99m. *Eur. J. Nucl. Med.* 21, 437–444.
- Maina, T., Stolz, B., Albert, R., Nock, B., Bruns, C., and Mäcke, H. (1995) Synthesis, radiochemical and biological evaluation of ^{99m}Tc [N4-(D)PHE¹]-octreotide, a new octreotide derivative with high affinity for somatostatin receptors. *Technetium and Rhenium in Chemistry and Nuclear Medicine 4* (M. Nicolini, G. Banoli, and U. Mazzi, Eds.) pp 395–400, SGEEditoriali, Padova.
- Kolan, H., Li, J.-H., and Thakur, M. L. (1996) Sandostatin[®] labeled with ^{99m}Tc : In vitro stability, in vivo validity and comparison with ^{111}In -DTPA-octreotide. *Pept. Res.* 9, 144–150.
- Vallabhajosula, S., Moyer, B. R., Lister-James, J., McBride, W. J., Lipszyc, H., Lee, H., Bastidas, D., and Dean, R. T. (1996) Preclinical evaluation of technetium-99m-labeled somatostatin receptor binding peptides. *J. Nucl. Med.* 37, 1016–1022.
- Pearson, D. A., Lister-James, J., McBride, W. J., Wilson, D. M., Martel, L. J., Civitello, E. R., Taylor, J. E., Moyer, B. R., and Dean, R. T. (1996) Somatostatin receptor-binding peptides labeled with technetium-99m: chemistry and initial biological studies. *J. Med. Chem.* 39, 1361–1371.
- Barrett, J. A., Heminway, S. J., Damphousse, D. J., Thomas, J. R., Looby, R. J., Edwards, D. S., Harris, T. D., Rajopadhye, M., Liu, S., and Carroll, T. R. (1994) Platelet GP IIb/IIIa antagonists in the canine arteriovenous shunt: potential thrombus imaging agents. *J. Nucl. Med.* 35, 52P (abstract 202).
- Harris, T. D., Barrett, J. A., Bourque, J. P., Carroll, T. R., Damphousse, P. R., Edwards, D. S., Glowacka, D., Liu, S., Looby, R. J., Poirier, M. J., Rajopadhye, M., and Yu, K. (1994) Design and synthesis of radiolabeled GPIIb/IIIa receptor antagonists as potential thrombus imaging agents. *J. Nucl. Med.* 35, 245P (abstract 1005).
- Barrett, J. A., Bresnick, M. R., Crocker, A. C., Damphousse, D. J., Hampson, J. R., Heminway, S. J., Mazaika, T. J., Kagan, M., Lazewatsky, J. L., Edwards, D. S., Liu, S., Harris, T. D., Rajopadhye, M., and Carroll, T. R. (1995) RP-431: a potential thrombus imaging agent. *J. Nucl. Med.* 36, 16P (abstract 55).
- Liu, S., Edwards, D. S., Looby, R. J., Harris, A. R., Poirier, M. J., Barrett, J. A., Heminway, S. J., and Carroll, T. R. (1996) Labeling a hydrazino nicotinamide-modified cyclic IIb/IIIa receptor antagonist with ^{99m}Tc using aminocarboxylates as coligands. *Bioconjugate Chem.* 7, 63–71.
- Liu, S., Edwards, D. S., Looby, R. J., Harris, A. R., Poirier, M. J., Rajopadhye, M., and Bourque, J. P. (1996) Labeling cyclic IIb/IIIa receptor antagonists with ^{99m}Tc by the pre-formed chelate approach: effects of chelators on properties of [^{99m}Tc]chelator-peptide conjugate. *Bioconjugate Chem.* 7, 196–202.
- Barrett, J. A., Damphousse, D. J., Heminway, S. J., Liu, S., Edwards, D. S., Looby, R. J., and Carroll, T. R. (1996) Biological evaluation of ^{99m}Tc -labeled cyclic GPIIb/IIIa receptor antagonists in the canine arteriovenous shunt and deep vein thrombosis models: effects of chelators on biological properties of [^{99m}Tc]chelator-peptide conjugates. *Bioconjugate Chem.* 7, 203–208.
- Edwards, D. S., Liu, S., Harris, A. R., Looby, R. J., Ziegler, M. C., Heminway, S. J., Barrett, J. A., and Carroll, T. R. (1997) A new and versatile ternary ligand system for technetium radiopharmaceuticals: water soluble phosphines and tricine as coligands in labeling a hydrazino nicotinamide-modified cyclic glycoprotein IIb/IIIa receptor antagonist with ^{99m}Tc . *Bioconjugate Chem.* 8, 146–154.
- Barrett, J. A., Crocker, A. C., Damphousse, D. J., Heminway, S. J., Liu, S., Edwards, D. S., Harris, A. R., Looby, R. J., Lazewatsky, J. L., Kagan, M., Mazaika, T. J., Carroll, T. R. (1997) Biological evaluation of thrombus imaging agents

- utilizing water soluble phosphines and tricine as coligands to label a hydrazinonicotinamide-modified cyclic glycoprotein IIb/IIIa receptor antagonist with ^{99m}Tc . *Bioconjugate Chem.* 8, 155–160.
- (29) Barrett, J. A., Bresnick, M., Crocker, A. C., Damphousse, D. J., Heminway, S. J., Mazaika, T. J., Kagan, M., Lazewatsky, J. L., Edwards, D. S., Liu, S., Harris, T. D., Rajpladhye, M., and Carroll, T. R. (1997) RP431: a technetium-99m-labeled platelet GP IIb/IIIa receptor antagonist as a thrombus imaging agent. *J. Nucl. Med.* (in press).
- (30) Knight, L. C., Radcliffe, R., Maurer, A. H., Rodwell, J. D., and Alvarez, V. L. (1994) Thrombus imaging with technetium-99m synthetic peptides based upon the binding domain of a monoclonal antibody to activated platelets. *J. Nucl. Med.* 35, 2842–288.
- (31) Lister-James, J., Knight, L. C., Mauer, A. H., Bush, L. R., Moyer, B. R., and Dean, R. T. (1996) Thrombus imaging with technetium-99m-labeled, activated platelet receptor binding peptide. *J. Nucl. Med.* 37, 775–781.
- (32) Muto, P., Lastoria, S., Varrella, P., Vergara, E., Salvatore, M., Morgano, G., Lister-James, J., Bernardy, J. D., Dean, R. T., Wencker, D., and Boer, J. S. (1995) Detecting deep venous thrombosis with technetium-99m-labeled synthetic peptide P280. *J. Nucl. Med.* 36, 1384–1391.
- (33) Pearson, D. A., Lister-James, J., McBride, W. J., Wilson, D. M., Martel, L. J., Civitello, E. R., and Dean, R. T. (1996) Thrombus imaging using technetium-99m labeled high potency GPIIb/IIIa receptor antagonists. Chemistry and initial biological studies. *J. Med. Chem.* 39, 1372–1382.
- (34) Lister-James, J., Vallabhajosula, S., Moyer, B. R., Pearson, D. A., McBride, B. J., De Rosch, M. A., Bush, L. R., Machac, J., and Dean, R. T. (1997) Pre-clinical evaluation of technetium-99m platelet receptor-binding peptide. *J. Nucl. Med.* 38, 105–111.
- (35) Goldenberg, D. M. (1989) Future role of radiolabeled monoclonal antibodies in oncological diagnosis and therapy. *Semin. Nucl. Med.* 19, 332–339.
- (36) Parker, D. (1990) Tumor targeting with radiolabeled macrocycle-antibody conjugates. *Chem. Soc. Rev.* 19, 271–291.
- (37) Keenan, A. M., Harbert, J. C., and Larson, S. M. (1985) Monoclonal antibodies in nuclear medicine. *J. Nucl. Med.* 26, 532–537.
- (38) Verbruggen, A. M. (1990) Radiopharmaceuticals: state of the art. *Eur. J. Nucl. Med.* 17, 346–364.
- (39) Buchsbaum, D. J., and Lawrance, T. S. (1991) Tumor therapy with radiolabeled monoclonal antibodies. *Antibody, Immunoconjugates, Radiopharm.* 4, 245–272.
- (40) Serafini, A. N. (1993) From monoclonal antibodies to peptides and molecular recognition units: an overview. *J. Nucl. Med.* 34, 533–536.
- (41) Huston, J. S., George, A. J. T., Adams, G. P., Stafford, W. F., Jamar, F., Tai, M.-S., McCartney, J. E., Oppermann, H., Heelan, B. T., Peters, A. M., Houston, L. L., Bookman, M. A., Wolf, E. J., and Weiner, L. M. (1996) Single-chain Fv radioimmunotargeting. *Q. J. Nucl. Med.* 40, 320–333.
- (42) Delaloye, A. B., and Delaloye, B. (1995) Radiolabeled monoclonal antibodies in tumor imaging and therapy: out of fashion? *Eur. J. Nucl. Med.* 22, 571–580.
- (43) Behr, T. M., and Goldenberg, D. M. (1996) Improved prospects for cancer therapy with radiolabeled antibody fragments and peptides. *J. Nucl. Med.* 37, 834–836 (Editorial).
- (44) Lister-James, J., Moyer, B. R., and Dean, R. T. (1996) Small peptides radiolabeled with ^{99m}Tc . *Q. J. Nucl. Med.* 40, 221–233.
- (45) McAfee, J. G., and Neumann, R. D. (1996) Radiolabeled peptides and other ligands for receptors overexpressed in tumor cells for imaging neoplasms. *Nucl. Med. Biol.* 23, 673–676.
- (46) Jones, A. G., Orvig, C., Trop, H. S., Davison, A., and Davis, M. A. (1980) A survey of reducing agents for the synthesis of tetraphenylarsonium oxotechnetiumbis(ethanedithiolate) from ^{99}Tc pertechnetate in aqueous solution. *J. Nucl. Med.* 21, 279–281.
- (47) Davison, A., Jones, A. G., Orvig, C., and Sohn, M. (1981) A new class of oxotechnetium (5+) chelate complexes containing a TcON_2S_2 core. *Inorg. Chem.* 20, 1629–1632.
- (48) Abrams, M. J., Davison, A., Jones, A. G., and Costello, C. E. (1983) Synthesis and characterization of new Tc(IV) cation: $\text{Tris}(\text{acetylacetonato})\text{-technetium(IV)}$ tetrafluoroborate. *Inorg. Chim. Acta* 77, L235–L236.
- (49) Edwards, D. S., Liu, S., Poirier, M. J., Zhang, Z., Webb, G. A., and Orvig, C. (1994) Characterization of $\text{tris}(\text{N-substituted-2-methyl-3-hydroxy-4-pyridinonato})\text{technetium(IV)}$ cations. *Inorg. Chem.* 33, 5607–5609.
- (50) Deutsch, E., Vanderheyden, J.-L., Gerundini, P., Libson, K., Hirth, W., Colombo, F., Savi, A., and Fazio, F. (1987) Development of nonreducible technetium-99m(III) cations as myocardial perfusion imaging agents: initial experience in humans. *J. Nucl. Med.* 28, 1870–1880.
- (51) Vanderheyden, J.-L., Libson, K., Nosco, D. L., Katering, A. R., and Deutsch, E. (1983) Preparation and characterization of $^{99m}\text{Tc}(\text{DMPE})_2\text{X}_2^{+}$, $\text{X} = \text{Cl}, \text{Br}$ (DMPE = 1,2-bis-(dimethylphosphino)ethane). *Int. J. Appl. Radiat. Isot.* 34, 1611–1618.
- (52) Doyle, M. N., Libson, K., Woods, M., Sullivan, J. C., and Deutsch, E. (1986) Electron transfer reactions of technetium complexes. 1. Rate of the self-exchange reaction of the Tc(I)/Tc(II) couple $[\text{Tc}(\text{DMPE})_3]^{+2+}$, where DMPE = 1,2-bis-(dimethylphosphino)ethane). *Inorg. Chem.* 25, 3367–3371.
- (53) Abrams, M. J., Davison, A., Jones, A. G., Costello, C. E., and Pang, H. (1983) Synthesis and characterization of hexakis(alkyl isocyanide) and hexakis(aryl isocyanide) complexes of technetium (I). *Inorg. Chem.* 22, 2798–2800.
- (54) Rao, T. N., Adhikesavalu, D., Camerman, A., and Fritzberg, A. R. (1990) Technetium(V) and rhenium(V) complexes of 2,3-bis(mercaptoacetamido)-propanoate. Chelate ring stereochemistry and influence on chemical and biological properties. *J. Am. Chem. Soc.* 112, 5798–5804.
- (55) Eshima, D., Taylor, A., Jr., Fritzberg, A. R., Kasina, S., Hansen, L., and Sorenson, J. F. (1987) Animal evaluation of technetium-99m triamide mercaptide complexes as potential renal imaging agents. *J. Nucl. Med.* 28, 1180–1186.
- (56) Vanbilloen, H. P., De Roo, M. J., and Verbruggen, A. M. (1996) Complexes of technetium-99m with tetrapeptides containing one alanyl and three glycyl moieties. *Eur. J. Nucl. Med.* 23, 40–48.
- (57) Subhani, M., Cleynhens, B., Bormans, G., Hoogmartens, M., De Roo, M., and Verbruggen, A. M. (1989) Complexes of technetium-99m with mercaptoacetyltri-peptides: labeling characteristics and biodistribution in mice. *Technetium and Rhenium in Chemistry and Nuclear Medicine 3* (M. Nicolini, G. Banoli, and U. Mazzi, Eds.) pp 453–461, Cortina International, Verona.
- (58) Bormans, G., Cleynhens, B., Hoogmartens, M., De Roo, M., and Verbruggen, A. M. (1989) Synthesis and biological evaluation of L-alanyl derivatives of $^{99m}\text{Tc-MAG}_3$. *Technetium and Rhenium in Chemistry and Nuclear Medicine 3* (M. Nicolini, G. Banoli, and U. Mazzi, Eds.) pp 661–666, Cortina International, Verona.
- (59) Bormans, G., Cleynhens, B., Adriaens, P., De Roo, M., and Verbruggen, A. M. (1993) Synthesis and labeling characteristics of ^{99m}Tc -mercaptoacetyltri-peptides. *J. Labelled Compounds Radiopharm.* 33, 1065–1078.
- (60) Vanbilloen, H. P., Bormans, G. M., De Roo, M. J., and Verbruggen, A. M. (1996) Complexes of technetium-99m with tetrapeptides, a new class of ^{99m}Tc -labelled agents. *Nucl. Med. Biol.* 22, 325–338.
- (61) Edwards, D. S., Cheesman, E. H., Watson, M. W., Maheu, L. J., Nguyen, S. A., Dimitre, L., Nason, T., Watson, A. D., and Walovitch, R. (1990) Synthesis and characterization of technetium and rhenium complexes of N, N'-1,2-ethylenediylbis-L-cysteine. Neurolite® and its metabolites. *Technetium and Rhenium in Chemistry and Nuclear Medicine 3* (M. Nicolini, G. Banoli, and U. Mazzi, Eds.) pp 431–444, Cortina International, Verona.
- (62) Oya, S., Kung, M.-P., Frederick, D., and Kung, H. F. (1995) New bisaminoethanethiol (BAT) ligands which form two interconvertible Tc-99m complexes. *Nucl. Med. Biol.* 22, 749–757.

- (63) Kung, H. F., Guo, Y. Z., Yu, C. C., Billings, J., Subramanyam, V., and Calabrese, J. C. (1989) New brain perfusion imaging agents based on ^{99m}Tc -bis(aminoethanethiol) complexes: stereoisomers and biodistribution. *J. Med. Chem.* 32, 433–437.
- (64) Mach, R. H., Kung, H. F., Guo, Y. Z., Yu, C. C., Subramanyam, V., and Calabrese, J. C. (1989) Synthesis, characterization and biodistribution of neutral M^{VO} ($\text{M} = \text{Tc}$, Re) Amine-thiol complexes containing a pendant phenylpiperidine group. *Inorg. Chem.* 32, 3114–3124.
- (65) Francesconi, L. C., Graczyk, G., Wehrli, S., Shaikh, S. N., McClinton, D., Liu, S., Zubietta, J., and Kung, H. F. (1993) Synthesis and characterization of neutral M^{VO} ($\text{M} = \text{Tc}$, Re) Amine-thiol complexes containing a pendant phenylpiperidine group. *Inorg. Chem.* 32, 3114–3124.
- (66) Meegalla, S., Plüssl, K., Kung, M.-P., Chumpradit, S., Stevenson, D. A., Frederick, D., and Kung, H. F. (1996) Tc-99m-labeled tropanes as dopamine transporter imaging agents. *Bioconjugate Chem.* 7, 421–429.
- (67) O'Neil, J. P., Wilson, S. R., and Katzenellenbogen, J. A. (1994) Preparation and structural characterization of monoamine-monoamide bis(thiol) oxo complexes of technetium(V) and rhenium(V). *Inorg. Chem.* 33, 319–323.
- (68) Lever, S. Z., Baidoo, K. E., and Mahmood, A. (1990) Structure proof of *syn/anti* isomerism in N-alkylated diaminedithiol (DADT) complexes of technetium. *Inorg. Chim. Acta* 176, 183–184.
- (69) Marchi, A., Marvelli, L., Rossi, R., Magon, L., Bertolasi, V., Ferretti, V., and Gilli, P. (1992) Nitrido- and oxotechnetium(V) chelate complexes with N_2S_2 ligands: Synthesis and crystal structures. *J. Chem. Soc., Dalton Trans.*, 1485–1490.
- (70) Spyriounis, D. M., Pelecanou, M., Stassinopoulou, C. I., Raptopoulou, C. P., Terzis, A., and Chiotellis, E. (1995) Synthesis and characterization of oxotechnetium(V) complexes with aza-substituted 2,6-dimethyl-4-azaheptane-2,6-dithiol ligands and benzyl mercaptan as coligand. *Inorg. Chem.* 34, 1077–1082.
- (71) Mastrostamatis, S. G., Papadopoulos, M. S., Pirmettis, I. C., Paschali, E., Varvarigou, A. D., Stassinopoulou, C. I., Raptopoulou, C. P., Terzis, A., and Chiotellis, E. (1994) Tridentate ligands containing the SNS donor atom set as a novel backbone for the development of technetium brain-imaging agents. *J. Med. Chem.* 37, 1077–1082.
- (72) Pirmettis, I. C., Papadopoulos, M. S., Mastrostamatis, S. G., Raptopoulou, C. P., Terzis, A., and Chiotellis, E. (1996) Synthesis and characterization of oxotechnetium(V) mixed-ligand complexes containing a tridentate N-substituted bis-(2-mercaptoethyl)amine and a monodentate thiol. *Inorg. Chem.* 35, 1685–1691.
- (73) Papadopoulos, M. S., Pelecanou, M., Pirmettis, I. C., Spyriounis, D. M., Raptopoulou, C. P., Terzis, A., Stassinopoulou, C. I., and Chiotellis, E. (1996) A new donor system [(SNN)(S)] for the synthesis of oxotechnetium(V) mixed-ligand complexes. *Inorg. Chem.* 35, 4478–4483.
- (74) Klingensmith III, W. C., Fritzberg, A. R., Spitzer, V. M., Johnson, D. L., Kuni, C. C., Williamson, M. R., Washer, G., and Weil III, R. (1984) Clinical evaluation of Tc-99m N,N'-bis(mercaptoacetyl)-2,3-diaminopropanoate as a replacement for I-131 hippurate: concise communication. *J. Nucl. Med.* 25, 42–48.
- (75) Walovitch, R. C., Cheesman, E. H., Maheu, L. J., and Hall, K. M. (1994) Studies of the retention mechanism of the brain perfusion imaging agent ^{99m}Tc -Bicisate (^{99m}Tc -ECD). *J. Cerebral Blood Flow Metab.* 14, S4–S11.
- (76) Harris, T. D., Edwards, D. S., and Platts, S. H. (1992) Synthesis and characteristics of isomers L,L, D,D, and D,L of Tc-99m-ECD in monkeys. *J. Nucl. Med.* 33, 979–980.
- (77) Kung, H. F., Bradshaw, J. E., Chumpradit, S., Zhang, Z. P., Kung, M. P., Mu, M., and Frederick, D. (1995) New TcO(III) and ReO(III) N_2S_2 complexes as potential CNS 5-HT_{1A} receptor imaging agents. In *Technetium and Rhenium in Chemistry and Nuclear Medicine 4* (M. Nicolini, G. Banoli, and U. Mazzi, Eds.) pp 293–298, SGEEditoriali, Padova.
- (78) Meegalla, S., Plüssl, K., Kung, M.-P., Stevenson, D. A., Liable-Sand, L. M., Rheingold, A. L., and Kung, H. F. (1995) First example of a ^{99m}Tc complex as a dopamine transporter imaging agent. *J. Am. Chem. Soc.* 117, 11037–11038.
- (79) Meegalla, S., Plüssl, K., Kung, M.-P., Chumpradit, S., Stevenson, D. A., Kushner, S. A., McElgin, W. T., Mozley, P. D., and Kung, H. F. (1997) Synthesis and characterization of technetium-99m-labeled tropanes as dopamine transporter-imaging agents. *J. Med. Chem.* 40, 9–17.
- (80) Treher, E. N., Francesconi, L. C., Gougoutas, J. Z., Malley, M. F., and Nunn, A. D. (1989) Monocapped tris(dioxime) complexes of technetium(III): synthesis and structural characterization of $\text{TcX}(\text{dioxime})_3\text{B-R}$ ($\text{X} = \text{Cl}$, Br ; dioxime = dimethylglyoxime, cyclohexanedione dioxime; $\text{R} = \text{CH}_3$, and C_4H_9). *Inorg. Chem.* 28, 3411–3416.
- (81) Linder, K. E., Malley, M. F., Gougoutas, J. Z., Unger, S. E., and Nunn, A. D. (1990) Neutral, seven-coordinated dioxime complexes of technetium(III): synthesis and characterization. *Inorg. Chem.* 29, 2428–2434.
- (82) Linder, K. E., Nowotnik, D. P., Malley, M. F., Gougoutas, J. Z., and Nunn, A. D. (1991) An unexpected by-product obtained during the preparation of technetium(III) boronic acid adducts of dioximes. The single crystal structure of $\text{TcCl}(\text{DMG})_2(\text{BDI})\text{BET}$ ($\text{DMG} = \text{dimethylglyoxime}$, $\text{BDI} = \text{butane-2,3-dione imine-oxime}$). *Inorg. Chim. Acta* 190, 249–255.
- (83) Marmion, M. E., Woulfe, S. R., Newmann, W. L., Pilcher, G., and Nosco, D. L. (1996) Synthesis and characterization of novel N_3O_3 -Schiff base complexes of ^{99g}Tc , and in vivo imaging studies with analogous ^{99m}Tc complexes. *Nucl. Med. Biol.* 23, 567–584.
- (84) Linder, K. E., Wen, M. D., Nowotnik, D. P., Malley, M. F., Gougoutas, J. Z., Nunn, A. D., and Eckelman, W. C. (1991) Technetium labeling of monoclonal antibodies with functionalized BATO's: 1. $\text{TcCl}(\text{DMG})_3\text{PITC}$. *Bioconjugate Chem.* 2, 160–170.
- (85) Linder, K. E., Wen, M. D., Nowotnik, D. P., Ramalingam, K., Sharkey, R. M., Yost, F., Narra, R. K., Nunn, A. D., and Eckelman, W. C. (1991) Technetium labeling of monoclonal antibodies with functionalized BATO's: 2. $\text{TcCl}(\text{DMG})_3\text{CPITC}$ labeling of B72.3 and NP-4 whole antibodies and NP-4 F(ab')₂. *Bioconjugate Chem.* 2, 407–414.
- (86) Lanteingne, D., and Hnatowich, D. J. (1984) The labeling of DTPA coupled proteins. *Int. J. Radiat. Isot.* 35, 617–621.
- (87) Jurisson, S., Aston, K., Fair, C. K., Schlemper, E. O., Sharp, P. R., and Troutner, D. E. (1987) Effect of ring size on properties of technetium amine oxime complexes. X-ray structures of $\text{TcO}_2\text{Pent}(\text{AO})_2$, which contains an unusual eight-membered chelate ring, and of $\text{TcOEn}(\text{AO})_2$. *Inorg. Chem.* 26, 3576–3582.
- (88) Ianoz, E., Mantegazzi, D., and Lerch, P. (1989) Preparation, crystal and molecular structure of *trans*-dioxo(1,4-dithia-8,11-diazacyclotetradecane)-technetium(V) hexafluorophosphate. *Inorg. Chim. Acta* 156, 235–239.
- (89) Kelly, J. D., Forster, A. M., Archer, C. M., Booker, F. S., Canning, L. R., Chiu, K. W., Edwards, B., Gill, H. K., McPartlin, M., Nagle, K. R., Latham, I. A., Pickett, R. D., Storey, A. E., and Webbon, P. M. (1993) Technetium-99m-tetrofosmin as a new radiopharmaceutical for myocardial perfusion imaging. *J. Nucl. Med.* 34, 222–227.
- (90) Higley, B., Smith, F. W., Gemmell, H. G., Gupta, P. D., Gvozdanovic, D. V., Graham, D., Hinge, D., Davidson, J., and Lahiri, A. (1993) Technetium-99m1,2-bis[bis(2-ethoxyethyl)-phosphino]ethane: human biodistribution, dosimetry and safety of a new myocardial perfusion imaging agent. *J. Nucl. Med.* 34, 30–38.
- (91) Jones, S., and Hendel, R. C. (1993) Technetium-99m tetrofosmin: a new myocardial perfusion agent. *J. Nucl. Med. Technol.* 21, 191–195.
- (92) Schwochau, K. (1994) Technetium radiopharmaceuticals-fundamentals, synthesis, structure, and development. *Angew. Chem., Int. Ed. Engl.* 33, 2258–2267.
- (93) Abrams, M. J., Juweid, M., tenKate, C. I., Schwartz, D. A., Hauser, M. M., Gaul, F. E., Fuccello, A. J., Rubin, R. H., Strauss, H. W., and Fischman, A. J. (1990) Technetium-99m-human polyclonal IgG radiolabeled via the hydrazino nicotinamide derivative for imaging focal sites of infection in rats. *J. Nucl. Med.* 31, 2022–2028.
- (94) Schwartz, D. A., Abrams, M. J., Hauser, M. M., Gaul, F. E., Larsen, S. K., Rauh, D., and Zubietta, J. A. (1991)

- Preparation of hydrazino-modified proteins and their use for the synthesis of ^{99m}Tc -protein conjugates. *Bioconjugate Chem.* 2, 334–336.
- (95) Larson, S. K., Abrams, M. J., Higgins III, J. D., Solomon, H. F., Babich, J. W., and Fischman, A. J. (1994) Technetium complexes of tricine: useful precursor for the ^{99m}Tc labeling of hydrazino nicotinamide modified human polyclonal IgG. *J. Nucl. Med.* 35, 105P.
- (96) Larson, S. K., Solomon, H. F., Caldwell, G., and Abrams, M. J. (1995) [^{99m}Tc]tricine: a useful precursor complex for the radiolabeling of hydrazinonicotinate protein conjugates. *Bioconjugate Chem.* 6, 635–638.
- (97) Eckelman, W. C., Paik, C. H., and Steigman, J. (1989) Three approaches to radiolabeling antibodies with ^{99m}Tc . *Nucl. Med. Biol.* 16, 171–176.
- (98) Fritzberg, A. R., Berninger, R. W., Hadley, S. W., and Wester, D. W. (1988) Approaches to radiolabeling of antibodies for diagnosis and therapy of cancer. *Pharm. Res.* 5, 325–334.
- (99) Otsuka, F. L., and Welch, M. J. (1987) Methods to label monoclonal antibodies for use in tumor imaging. *Nucl. Med. Biol.* 14, 243–249.
- (100) Hnatowich, D. J. (1990) Antibody radiolabeling, problems and promises. *Nucl. Med. Biol.* 17, 49–55.
- (101) Hnatowich, D. J. (1990) Recent developments in radiolabeling of antibodies with iodine, indium, and technetium. *Semin. Nucl. Med.* 20, 80–91.
- (102) Srivastava, S. C., and Mease, R. C. (1991) Progress in research on ligands, nuclides and techniques for labeling monoclonal antibodies. *Nucl. Med. Biol.* 18, 589–603.
- (103) Delmon-moingeon, L. I., Mahmood, A., Davison, A., and Jones, A. G. (1991) Strategies for labeling monoclonal antibodies and antibody-like molecules with technetium-99m. *J. Nucl. Biol. Med.* 35, 47–59.
- (104) Rhodes, B. A. (1991) Direct labeling of proteins with ^{99m}Tc . *Nucl. Med. Biol.* 18, 667–676.
- (105) Eckelman, W. C., and Steigman, J. (1991) Direct labeling with ^{99m}Tc . *Nucl. Med. Biol.* 18, 3–7.
- (106) Liu, Y.-F., and Wu, C.-C. (1991) Radiolabeling of monoclonal antibodies with metal chelates. *Pure Appl. Chem.* 63, 427–463.
- (107) Griffiths, G. L., Goldenberg, D. M., Jones, A. L., and Hansen, H. J. (1992) Radiolabeling of monoclonal antibodies and fragments with technetium and rhenium. *Bioconjugate Chem.* 3, 91–99.
- (108) Bhargava, K. K., and Acharya, S. A. (1989) Labeling of monoclonal antibodies with radionuclides. *Semin. Nucl. Med.* 19, 187–201.
- (109) Wolf, W., and Shani, J. (1986) Criteria for the selection of the most desirable radionuclide for radiolabeling monoclonal antibodies. *Nucl. Med. Biol.* 13, 319–324.
- (110) Gansow, O. A. (1991) Newer approaches to the radiolabeling of monoclonal antibodies by use of metal chelates. *Nucl. Med. Biol.* 18, 269–281.
- (111) Zamora, P. O., and Rhodes, B. A. (1992) Imidazoles as well as thiolates in proteins bind technetium-99m. *Bioconjugate Chem.* 3, 493–498.
- (112) Fritzberg, A. R., Abrams, P. G., Beaumier, P. L., Kasina, S., Morgan, A. C., Rao, T. N., Reno, J. M., Sanderson, J. A., Srinivasan, A., and Wilbur, D. S. (1988) Specific and stable labeling of antibodies with technetium-99m with a diamide dithiolate chelating agent. *Proc. Natl. Acad. Sci. U.S.A.* 85, 4025–4029.
- (113) Eary, J. F., Schroff, R. W., Abrams, P. G., Fritzberg, A. R., Morgan, A. C., Kasina, S., Reno, J. M., Srinivasan, A., Woodhouse, C. S., Wilbur, D. S., Natale, R. B., Collins, C., Stehlin, J. S., Mitchell, M., and Nelp, W. B. (1989) Successful imaging of malignant melanoma with technetium-99m-labeled monoclonal antibodies. *J. Nucl. Med.* 30, 25–32.
- (114) Kasina, S., Rao, T. N., Srinivasan, A., Sanderson, J. A., Fitzner, J. N., Reno, J. M., Beaumier, P. L., and Fritzberg, A. R. (1991) Development and biological evaluation of a kit for preformed chelate technetium-99m radiolabeling of an antibody Fab fragment using a diamide dimercaptide chelating agent. *J. Nucl. Med.* 32, 1445–1451.
- (115) Majocha, R. E., Reno, J. M., Friedland, R. P., VanHaight, C., Lyle, L. R., and Marotta, C. A. (1992) Development of a monoclonal antibody specific for βA4 amyloid in Alzheimer's disease brain for application to in vivo imaging of amyloid angiopathy. *J. Nucl. Med.* 33, 2184–2189.
- (116) Liu, S., and Edwards, D. S. (1995) New N_2S_2 diamidedithiol and N_3S triamidethiols as bifunctional chelating agents for labeling small peptides with technetium-99m. In *Technetium and Rhenium in Chemistry and Nuclear Medicine 4* (M. Nicolini, G. Banoli, and U. Mazzi, Eds.) pp 383–393, SGE-ditorali, Padova.
- (117) Rajopadhye, M., Edwards, D. S., Bourque, J. P., and Carroll, T. R. (1996) Synthesis and technetium-99m labeling of cyclic GPIIb/IIIa receptor antagonists conjugated to 4,5-bis(mercaptoacetyl-amido)pentanoic acid (mapt). *Bioorg. Med. Chem. Lett.* 6, 1737–1740.
- (118) Baidoo, K. E., and Lever, S. Z. (1990) Synthesis of a diaminedithiol bifunctional chelating agent for incorporation of technetium-99m into biomolecules. *Bioconjugate Chem.* 1, 132–137.
- (119) Lever, S. Z., Baidoo, K. E., Mahmood, A., Matsumura, K., Scheffel, U., and Wagner, H. N., Jr. (1994) Novel technetium ligand with affinity for muscarinic cholinergic receptor. *Nucl. Med. Biol.* 21, 157–164.
- (120) Lever, S. Z., Sun, S.-Y., Scheffel, U. A., Kaltovich, F. A., Baidoo, K. E., Goldfarb, H., and Wagner, H. N., Jr. (1994) Pulmonary accumulation of neutral diamine dithiol complexes of technetium-99m. *J. Pharm. Sci.* 84, 802–809.
- (121) Del Rosario, R. B., Jung, Y.-W., Baidoo, K. E., Lever, S. Z., and Wieland, D. M. (1994) Synthesis and in vivo evaluation of a $^{99m/99}\text{Tc}$ -DADT-Benzovesamicol: a potential marker for cholinergic neurons. *Nucl. Med. Biol.* 21, 197–203.
- (122) O'Neil, J. P., Anderson, C. J., Carlson, K. E., Welch, M. J., and Katzenellenbogen, J. A. (1993) An improved progesterone-technetium complex as a potential imaging agent for steroid receptors. *J. Nucl. Med.* 33, 18P (abstract 61).
- (123) Eisenhut, M., Mißfeldt, M., Lehmann, W. D., and Karas, M. (1991) Synthesis of a bis(aminoethanethiol) ligand with an activated ester group for protein conjugation and ^{99m}Tc -labeling. *J. Labelled Comp. Radiopharm.* 29, 1283–1291.
- (124) Eisenhut, M., Lehmann, W. D., Becker, W., Elser, H., Strittmatter, W., Baum, R. P., Valerius, T., Repp, R., and Deo, Y. (1996) Bifunctional NHS-BAT ester for antibody conjugation and stable technetium-99m labeling: conjugation chemistry, immunoreactivity and kit formulation. *J. Nucl. Med.* 37, 362–370.
- (125) DiZio, J. P., Fiashi, R., Davison, A., Jones, A. G., and Katzenellenbogen, J. A. (1991) Progesterone-rhenium complexes: metal labeled steroids with high receptor binding affinity, potential receptor-directed agents for diagnostic imaging or therapy. *Bioconjugate Chem.* 2, 352–366.
- (126) O'Neil, J. P., Carlson, K. E., Anderson, C. J., Welch, M. J., and Katzenellenbogen, J. A. (1994) Progesterone radiopharmaceuticals labeled with technetium and rhenium: synthesis, binding affinity, and in vivo distribution of a new progesterone N_2S_2 -metal conjugate. *Bioconjugate Chem.* 5, 182–193.
- (127) DiZio, J. P., Anderson, C. J., Davison, A., Ehrhardt, G. J., Carlson, K. E., Welch, M. J., and Katzenellenbogen, J. A. (1992) Technetium- and rhenium-labeled progestins: synthesis, receptor binding and in vivo distribution of an β -substituted progesterone labeled with technetium-99m and rhenium-186. *J. Nucl. Med.* 33, 558–569.
- (128) Liu, S., Edwards, D. S., Harris, A. R., and Singh, P. R. (1997) ^{99m}Tc -labeling kinetics of four thiol-containing chelators and 2-hydrazinopyridine: factors influencing their radiolabeling efficiency. *Appl. Radiat. Isot.* (in press).
- (129) Bryson, N., Lister-Jones, J., Jones, A. G., Davis, W. M., and Davison, A. (1990) Protecting groups in the preparation of thiolate complexes of technetium. *Inorg. Chem.* 29, 2948–2951.
- (130) Bryson, N., Dewan, J. C., Lister-Jones, J., Jones, A. G., and Davison, A. (1988) Neutral technetium(V) complexes with amide-thiol-thioether chelate ligands. *Inorg. Chem.* 27, 2154–2161.
- (131) Anderson, F. A., Wheeler, H. B., Goldberg, R. T., Hosner, D. W., Patwardhar, N. A., Jovanovic, B., Forcier, A., and Dalen, J. E. A. (1991) A population-based perspective of the

- hospital incidence and case facility rates of deep vein thrombosis and pulmonary embolism. *Ann. Intern. Med.* 151, 933–938.
- (132) Hull, R. D., Hirsh, J., Carter, D. J., Jay, R. M., Dodd, P. E., Ockelford, P. A., Coates, G., Gill, G. J., Turpie, A. G., Dayle, D. J., Buller, H. R., and Raskob, G. E. (1983) Pulmonary angiography, ventilation lung scanning and venography for clinically suspected pulmonary embolism with abnormal perfusion lung scan. *Ann. Intern. Med.* 98, 891–938.
- (133) Knight, L. C. (1990) Radiopharmaceuticals for thrombus detection. *Semin. Nucl. Med.* 20, 52–67.
- (134) Knight, L. C. (1993) Scintigraphic methods for detecting vascular thrombus. *J. Nucl. Med.* 34, 554–561.
- (135) Wasser, M. N. J. M., and Pauwels, E. K. J. (1990) Immunoscintigraphy of thrombosis. *Eur. J. Nucl. Med.* 16, 583–585 (Editorial).
- (136) Loscalzo, J., and Rocco, T. P. (1992) Imaging arterial thrombi: an elusive goal. *Circulation* 85, 382–384.
- (137) Som, P., and Oster, Z. H. (1994) Thrombus-specific imaging: approaching the elusive goal. *J. Nucl. Med.* 35, 202–203 (Editorial).
- (138) Flank, C., Kakkar, V. V., and Clarke, M. B. (1968) The detection of venous thrombosis of the legs using ^{125}I -labelled fibrinogen. *Br. J. Surg.* 55, 742–747.
- (139) Negus, D., Pinto, D. J., LeQuensne, L. P., Brown, N., and Chapman, M. (1968) ^{125}I -labelled fibrinogen in diagnosis of deep-vein thrombosis and its correlation with phlebography. *Br. J. Surg.* 55, 835–839.
- (140) Thakur, M. L., Welch, M. J., Joist, J. H., and Coleman, R. E. (1976) Indium-111-labeled platelets: studies on preparation and evaluation of in vitro and in vivo functions. *Thromb. Res.* 9, 345–357.
- (141) Ezekowitz, M. D., Leonard, J. C., Smith, E. O., Allen, E. W., and Taylor, F. B. (1981) Identification of left ventricular thrombi in man using indium-111-labeled autologous platelets. *Circulation* 63, 801–810.
- (142) Stratton, J. R., Ritchie, J. L., Hamilton, G. W., Hammermeister, K. E., and Harker, L. A. (1981) Left ventricular thrombi: in vivo detection by indium-111 platelet imaging and two dimensional echocardiography. *Am. J. Cardiol.* 47, 874–881.
- (143) Ezekowitz, M. D., Eichner, E. R., Scatterday, R., and Elkins, C. R. (1982) Diagnosis of a persistent pulmonary embolus by indium-111 platelet scintigraphy with angiography and tissue confirmation. *Am. J. Med.* 72, 839–842.
- (144) Davis, H. H., II, Siegel, B. A., Sherman, L. A., Heaton, W. A., and Welch, M. J. (1980) Scintigraphy with ^{111}In -labeled autologous platelets in venous thromboembolism. *Radiology* 136, 203–207.
- (145) Fenech, A., Hussey, J. K., Smith, F. W., Dendy, P. P., Bennett, B., and Douglas, A. S. (1981) Diagnosis of deep vein thrombosis using autologous indium-111-labeled platelets. *Br. Med. J.* 282, 1020–1022.
- (146) Stratton, J. R. (1991) Thrombosis imaging with indium-111-labeled platelets. *Cardiac Imaging—Principles and Practice* (M. L. Marcus, H. R. Schelbert, D. J. Skorton, and D. J. Wolf, Eds.) pp 1121–1134. W. B. Saunders, New York.
- (147) Stratton, J. R., Cerqueira, M. D., Dewhurst, T. A., and Kohler, T. R. (1994) Imaging arterial thrombosis: comparison of technetium-99m-labeled monoclonal antifibrin antibodies and indium-111-platelets. *J. Nucl. Med.* 35, 1731–1737.
- (148) Ali, F. E., Bennett, D. B., Calvo, R. R., Elliott, J. D., Hwang, S. M., Ku, T. W., Lago, M. A., Nichols, A. J., Romoff, T. T., Shah, D. H., Vasko, J. A., Wong, A. S., Yellin, T. O., Yuan, C.-K., and Samanen, J. M. (1994) Conformationally constrained peptides and semipeptides derived from RGD as potent inhibitors of the platelet fibrinogen receptor and platelet aggregation. *J. Med. Chem.* 37, 769–780, and references cited therein.
- (149) Cheng, S., Craig, W. S., Mullen, D., Tschopp, J. F., Dixon, D., and Pierschbacher, M. D. (1994) Design and synthesis of novel cyclic RGD-containing peptides as highly potent and selective integrin $\alpha_{\text{IIb}}\beta_3$ antagonists. *J. Med. Chem.* 37, 1–8, and references cited therein.
- (150) Teng, W., Rose, J. W., Phillips, D. R., Nannizzi, L., Arsen, A., Campbell, A. M., and Charo, I. F. (1993) Design of potent and specific integrin antagonists. *J. Biol. Chem.* 268, 1066–1073.
- (151) Zablocki, J. A., Miyano, M., Garland, R. B., Pireh, D., Schretzman, L., Rao, S. N., Lindmark, R. J., Panzer-Knodle, S. G., Nicholson, N. S., Taite, B. B., Salyers, A. K., King, L. W., Campion, J. G., and Feigen, L. P. (1993) Potent *in vitro* and *in vivo* inhibitors of platelet aggregation based upon the Arg-Gly-Asp-Phe sequence of fibrinogen. A proposal on the nature of the binding interaction between the Arg-guanidine of RGD mimetics and the platelet GP IIb/IIIa receptor. *J. Med. Chem.* 36, 1811–1919.
- (152) Bach, A. C., II, Eyermann, C. J., Gross, J. D., Bower, M. J., Harlow, R. L., Weber, P. C., and DeGrado, W. F. (1994) Structural studies of a family of high affinity ligands for GPIIb/IIIa. *J. Am. Chem. Soc.* 116, 3207–3219.
- (153) Jackson, S., DeGrado, W. F., Dwivedi, A., Parthasarathy, A., Higley, A., Krywko, J., Rockwell, A., Markwalder, J., Wells, G., Wexler, R., Mousa, S., and Harlow, R. L. (1994) Template-constrained cyclic peptides: design of high-affinity ligands for GPIIb/IIIa. *J. Am. Chem. Soc.* 116, 3220–3230.
- (154) Xue, C.-B., and DeGrado, W. F. (1995) An efficient synthesis of glycoprotein IIb/IIIa inhibitor DMP728. A novel synthesis of N^{α} -methylarginine-containing peptide. *J. Org. Chem.* 60, 946–952.
- (155) Wityak, J., Fevig, J. M., Jackson, S. A., Johnson, A. L., Mousa, S. A., Parthasarathy, A., Wells, G. J., DeGrado, W. F., and Wexler, R. R. (1995) Synthesis and antiplatelet activity of DMP757 analogs. *Bioorg. Med. Chem. Lett.* 5, 2097–2100.
- (156) Harris, T. D., Rajopadhye, M., Damphousse, P. R., Glowacka, D., Yu, K., Bourque, J. P., Barrett, J. A., Damphousse, D. J., Heminway, S. J., Lazewatsky, J. L., Mazaika, T., and Carroll, T. R. (1996) Tc-99m-labeled fibrinogen receptor antagonists: design and synthesis of cyclic RGD peptides for the detection of thrombi. *Bioorg. Med. Chem. Lett.* 6, 1741–1746.
- (157) Rajopadhye, M., Harris, T. D., Yu, K., Glowacka, D., Damphousse, P. R., Barrett, J. A., Heminway, S. J., Edwards, D. S., and Carroll, T. R. (1997) Synthesis, evaluation and Tc-99m complexation of a hydrazinonicotinyl conjugate of a GP IIb/IIIa antagonist cyclic peptide for the detection of deep vein thrombosis. *Bioorg. Med. Chem. Lett.* 7, 955–960.
- (158) Liu, S., and Edwards, D. S. Unpublished results.
- (159) Abrams, M. J., Larsen, S. K., Shaikh, S. N., and Zubieta, J. (1991) Investigation of technetium-organohydrazine coordination chemistry. The crystal and molecular structures of $[\text{TcCl}_2(\text{C}_6\text{H}_5\text{N}_4)(\text{PPh}_3)_2] \cdot 0.75\text{C}_7\text{H}_8$ and $[\text{TcNCl}_2(\text{PPh}_3)_2] \cdot 0.25\text{CH}_2\text{Cl}_2$. *Inorg. Chim. Acta* 185, 7–15.
- (160) Archer, C. M., Dilworth, J. R., Jobanputra, P., Thompson, R. M., McPartlin, M., Povey, D. C., Smith, G. W., and Kelly, J. D. (1990) Development of new technetium cores containing technetium-nitrogen multiple bonds. Synthesis and characterization of some diazenido-, hydrazido- and imido- complexes of technetium. *Polyhedron* 9, 1497–1502.
- (161) Dilworth, J. R., Jobanputra, P., Thompson, R. M., Archer, C. M., Povey, D. C., Kelly, J. D., and Hiller, W. (1992) Crystal structure of a diazenido- dithiocarbamate complex of technetium, $[\text{Tc}(\text{NNC}_6\text{H}_4\text{Cl})((\text{CH}_3)_2\text{NCS}_2)_2(\text{PPh}_3)]$. *Z. Naturforsch.* 46, 449–452.
- (162) Archer, C. M., Dilworth, J. R., Jobanputra, P., Thompson, R. M., McPartin, M., and Hiller, W. (1993) Technetium diazenido complexes. Part 1. Synthesis and structures of $[\text{TcCl}(\text{NNC}_6\text{H}_4\text{Cl}-4)_2(\text{PPh}_3)_2]$ and $[\text{TcCl}(\text{NNPh})(\text{Ph}_2\text{PCH}_2\text{CH}_2\text{PPh}_2)_2][\text{PF}_6] \cdot \text{H}_2\text{O}$. *J. Chem. Soc., Dalton Trans.*, 897–904.
- (163) Dilworth, J. R., Jobanputra, P., Thompson, R. M., Povey, D. C., Archer, C. M., and Kelly, J. D. (1994) Technetium diazenido complexes. Part 2. Substitution chemistry of structures of $[\text{TcCl}(\text{NNC}_6\text{H}_4\text{Cl}-4)_2(\text{PPh}_3)_2]$ and the synthesis of technetium diazenido-complexes directly from $[\text{NH}_4][\text{TcO}_4]$. *J. Chem. Soc., Dalton Trans.*, 1251–1256.
- (164) Nicholson, T., de Vries, N., Davison, A., and Jones, A. G. (1989) Synthesis and characterization of aryldiazenido technetium complexes and their protonation reactions. The X-ray structure of $[\text{TcCl}(\text{PPh}_3)_2(\text{NNC}_6\text{H}_4\text{Br})_2]$. In *Technetium and Rhenium in Chemistry and Nuclear Medicine 3* (M. Nicolini,

- G. Bandoli, and U. Mazzi, Eds.) pp 95–108, Cortina International, Verona.
- (165) Cook, J., Davison, A., Jones, A. J., and Davis, W. M. (1990) The reaction chemistry of $\text{HTc}(\text{CO})_3(\text{PPh}_3)_2$. In *Technetium and Rhenium in Chemistry and Nuclear Medicine 3* (M. Nicolini, G. Bandoli, and U. Mazzi, Eds.) pp 65–68, Cortina International, Verona.
- (166) Nicholson, T., Cook, J., Davison, A., Rose, D. J., Maresca, K. P., Zubieta, J. A., and Jones, A. J. (1996) The synthesis and characterization of $[\text{MCl}_3(\text{N}=\text{NC}_5\text{H}_4\text{NH})(\text{HN}=\text{NC}_5\text{H}_4\text{N})]$ from $[\text{MO}_4]^-$ (where M = Re, Tc) organodiazenido, organodiazene-chelate complexes. The X-ray structure of $[\text{ReCl}_3(\text{N}=\text{NC}_5\text{H}_4\text{NH})(\text{HN}=\text{NC}_5\text{H}_4\text{N})]$. *Inorg. Chim. Acta* 252, 421–426.
- (167) Nicholson, T., Cook, J., Davison, A., Rose, D. J., Maresca, K. P., Zubieta, J. A., and Jones, A. J. (1996) The synthesis, characterization and X-ray crystal structure of the rhenium organodiazenido, organodiazene complex of $[\text{ReCl}_2(\text{PPh}_3)(\text{N}=\text{NC}_5\text{H}_4\text{N})(\text{HN}=\text{NC}_5\text{H}_4\text{N})]$. *Inorg. Chim. Acta* 252, 427–430.
- (168) Oyen, W. J. G., Boerman, O. C., van der Laken, C. J., Claessens, R. A. M. J., van der Meer, J. W. M., and Corsten, F. H. M. (1996) The uptake mechanisms of inflammation- and infection-localizing agents. *Eur. J. Nucl. Med.* 23, 459–465.
- (169) Boxen, I., and Ballinger, J. R. (1991) Nuclear Medicine detection of inflammation and infection. *Curr. Opin. Radiol.* 3, 840–850.
- (170) McAfee, J. G. (1990) What is the best method for imaging focal infections? *J. Nucl. Med.* 31, 413–416 (Editorial).
- (171) Claessens, R. A. M. J., Koenders, E. B., Oyen, W. J. G., and Corstens, F. H. M. (1996) Retention of technetium-99m in infectious foci in rats after release from technetium-99m labelled human non-specific polyclonal immunoglobulin G: a dual-label study with hydrazinonicotinamido and iminothiolano immunoglobulin. *Eur. J. Nucl. Med.* 23, 1536–1539.
- (172) Buscombe, J. R., Lui, D., Ensing, G., de Jong R., and Ell, P. J. (1990) $^{99\text{m}}\text{Tc}$ -human immunoglobulin (HIG)-first results of a new agent for the localization of infection and inflammation. *Eur. J. Nucl. Med.* 16, 649–655.
- (173) Lei, K., Rusckowski, M., Chang, F., Qu, T., Mardirosian, G., and Hnatowich, D. J. (1996) Technetium-99m antibodies labeled with MAG_3 and SHNH: an in vitro and animal in vivo comparison. *Nucl. Med. Biol.* 23, 917–922.
- (174) Barrow, S. A., Graham, W., Jyawook, S., Dragotakes, S. C., Solomon, H. F., Babich, J. W., Rubin, R. H., and Fischman, A. J. (1993) Localization of indium-111-immunoglobulin G, technetium-99m-immunoglobulin G and indium-111-labeled white blood cells at sites of acute bacterial infection in rabbits. *J. Nucl. Med.* 34, 1975–1979.
- (175) Callahan, R. J., Barrow, S. A., Abrams, M. J., Rubin, R. H., and Fischman, A. J. (1996) Biodistribution and dosimetry of technetium-99m-hydrazino nicotinamide IgG: comparison with indium-111-DTPA-IgG. *J. Nucl. Med.* 37, 843–846.
- (176) Fischman, A. J., Solomon, H. F., Babich, J. W., Abrams, M. J., Callahan, R. J., and Strauss, H. W. (1994) Imaging of focal sites of inflammation in rhesus monkeys with $^{99\text{m}}\text{Tc}$ -labeled human polyclonal IgG. *Nucl. Med. Biol.* 21, 111–116.
- (177) Peters, A. M., Danpure, H. J., Osman, S., Halker, R. J., Henderson, B. L., Hodgson, H. J., Kelly, J. D., Neirinckx, R. D., and Lavender, J. P. (1986) Clinical experience with $^{99\text{m}}\text{Tc}$ -hexamethylpropyleneamineoxime for labeling leukocytes and imaging inflammation. *Lancet* 2, 946–949.
- (178) Vorne, M., Soini, I., Lantto, T., and Paakkinen, S. (1989) Technetium-99m-HM-PAO-labeled leukocytes in detection of inflammatory lesions: comparison with gallium-67 citrate. *J. Nucl. Med.* 30, 1332–1336.
- (179) Charron, M., Orenstein, S. R., and Bhargava, S. (1994) Detection of inflammatory bowel disease in pediatric patients with technetium-99m-HMPAO-labeled leukocytes. *J. Nucl. Med.* 35, 451–455.
- (180) Peters, A. M. (1996) The choice of an appropriate agent for imaging inflammation. *Nucl. Med. Commun.* 17, 455–458.
- (181) Lange, J. M. A., Boucher, C. A. B., Hollak, C. E. M., Wiltink, E. H. H., Reiss, P., van Royen, E. A., Roos, M., Danner, S. D., and Goudsmit, J. (1990) Failure of zidovudine prophylaxis after accidental exposure to HIV-1. *N. Engl. J. Med.* 322, 1375–1377.
- (182) Rojas-Burke, J. (1990) Health officials reacting to infection mishaps. *J. Nucl. Med.* 33, 13–27.
- (183) Edwards, D. S., Barrett, J. A., Liu, S., Ziegler, M. C., Mazaika, T., Vining, M., Bridger, G., Higgins, III, J., and Abrams, M. J. (1996) A stabilized Tc-99m complex of a chemotactic peptide-HYNIC conjugate for imaging infection. *Eur. J. Nucl. Med.* 23, 1142 (abstract Omo440).
- (184) Pollak, A., Goodbody, A. E., Ballinger, J. R., Duncan, G. S., Tran, L. L., Dunn-Dufault, R., Meghji, K., Lau, F., Andrey, T. W., Boxen, I., and Sumner-Smith, M. (1996) Imaging inflammation with $^{99\text{m}}\text{Tc}$ -labelled chemotactic peptides: analogues with reduced neutropenia. *Nucl. Med. Commun.* 17, 132–139.
- (185) Solomon, H. F., Derlan, C. K., Beblavy, M., Jester, D., Santull, R., Pike, M., Kroon, D., Hoey, K., and Fischman, A. J. (1994) Focal infection imaging using an In-111 labeled antagonist chemotactic peptide. *J. Nucl. Med.* 35, 45P (abstract 172).
- (186) Reubi, J. C. (1993) The role of peptides and their receptors as tumor markers. *Endocrinol. Metab. Clin. North Am.* 22, 917–939.
- (187) Virgolini, I., Pangerl, T., Bischof, C., Leimer, M., Kartaran, A., Yang, Q., Peck-Radosavjevic, M., Kaserer, K., Niederle, B., Angelberger, P., Gangl, A., and Valent, P. (1996) Somatostatin (SST) and vasoactive intestinal peptide (VIP) receptor[®] subtype expression. *Eur. J. Nucl. Med.* 23, 1101 (abstract Omo274).
- (188) Maini, C. L., Tofani, A., Scuito, R., Carapella, C., Cioffi, R., and Crecco, M. (1993) Somatostatin receptors in meningiomas: a scintigraphic study using ^{111}In -DTPA-Phe-1-octreotide. *Nucl. Med. Commun.* 14, 550–558.
- (189) Reubi, J. C. (1995) Neuropeptide receptors in health and disease: the molecular basis for in vivo imaging. *J. Nucl. Med.* 36, 1825–1835.
- (190) Bardfeld, P. A., Chervu, L. R., and Myrty, D. R. K. (1976) The organ distribution of ^{131}I -tyrosyl somatostatin. *Br. J. Radiol.* 49, 381–382.
- (191) Wangberg, B., Nilsson, O., Theodorsen, E., Dahlström, A., and Ahlman, H. (1991) The effect of a somatostatin analog on the release of hormones from human midgut carcinoid tumor cells. *Br. J. Cancer* 64, 23–28.
- (192) Lamberts, S. W. J. (1988) The role of somatostatin in the regulation of anterior pituitary hormone secretion and the use of its analogues in the treatment of human pituitary tumors. *Endocrinol. Rev.* 9, 417–436.
- (193) Bauer, W., Briner, U., Doepfner, W., Haller, R., Huguenin, R., Marbach, P., Petcher, T. J., and Pless, J. (1982) SMS 201-995: a very potent and selective octapeptide analogue of somatostatin with prolonged action. *Life Sci.* 31, 1133–1140.
- (194) Weckbecker, G., Liu, R., Tolcsvai, L., and Bruns, C. (1992) Antiproliferative effects of octreotide (SMS 201-995) on ZR-75-1 human breast cancer cells in vivo and in vitro. *Cancer Res.* 52, 4973–4978.
- (195) Bakker, W. H., Krenning, E. P., Breeman, W. A. P., Koper, J. W., Kooij, P. P. M., Reubi, J. C., Klijn, J. G., Visser, T. J., Docter, R., and Lamberts, S. W. J. (1990) Receptor scintigraphy with a radioiodinated somatostatin analogue: radio-labeling, purification, biologic activity and in vivo application in animals. *J. Nucl. Med.* 31, 1501–1509.
- (196) Krenning, E. P., Breeman, W. A., Bakker, W. H., Koper, J. W., Kooij, P. P., Ansema, L., Lamberts, S. W. J., and Reubi, J. C. (1989) Localization of endocrine-related tumors with radioiodinated analogue of somatostatin. *Lancet* 1, 242–243.
- (197) Bakker, W. H., Krenning, E. P., Reubi, J. C., Breeman, W. A. P., SelyonoHan, B., de Jong, M., Kooij, P. P. M., Bruns, C., van Hagen, P. M., Marbach, P., Visser, T. J., Pless, J., and Lamberts, S. W. J. (1991) In vivo application of [^{111}In -DTPA-DPhe¹]-octreotide for detection of somatostatin receptor-positive tumors in rats. *Life Sci.* 49, 1593–1601.
- (198) Lipp, R. W., Silly, H., Ranner, G., Dobnig, H., Passath, A., Leb, G., and Krejs, G. J. (1995) Radiolabeled octreotide for the demonstration of somatostatin receptors in malignant lymphoma and lymphadenopathy. *J. Nucl. Med.* 36, 13–18.
- (199) Moretti, J. L., Caglar, M., Boaziz, C., Caillat-Vigneron, N., and Morere, J. F. (1995) Sequential functional imaging with technetium-99m hexakis-2-methoxy-isobutylisonitrile and indium-111 octreotide: can we predict the response to

- chemotherapy in small cell lung cancer? *Eur. J. Nucl. Med.* 22, 177–180.
- (200) Tenebaum, F., Lumbroso, J., Schlumberger, M., Mure, A., Plouin, P. F., Cailou, B., and Parmentier, C. (1995) Comparison of radiolabeled octreotide and meta-iodobenzylguanidine (MIBG) scintigraphy in malignant pheochromocytoma. *J. Nucl. Med.* 36, 1–6.
- (201) Haldemann, A. R., Rösler, H., Barth, A., Waser, B., Geiger, L., Godoy, N., Markwalder, R. V., Seiler, R. W., Sutzer, M., and Reubi, J. C. (1995) Somatostatin receptor scintigraphy in central nervous system tumors: role of blood-brain barrier permeability. *J. Nucl. Med.* 36, 403–410.
- (202) Maini, C. L., Cioffi, R. P., Tofani, A., Sciuto, R., Fontana, M., and Carapella, C. M. (1995) Indium-111 octreotide scintigraphy in neurofibromatosis. *Eur. J. Nucl. Med.* 22, 201–206.
- (203) Duet, M., Mundler, O., Ajzenberg, C. A., Berolatti, B., Chedin, P., Duranteau, L., and Warnet, A. (1994) Somatostatin receptor imaging in non-functioning pituitary adenomas: value of an uptake index. *Eur. J. Nucl. Med.* 21, 647–650.
- (204) Breeman, W. A. P., Hofland, L. J., van der Pluijm, M., van Koetsveld, P. M., de Jong, M., Setyono-Han, B., Bakker, W. H., Kwekkeboom, D. J., Visser, T. J., Lamberts, S. W. J., and Krenning, E. P. (1994) A new radiolabeled somatostatin analogue [¹¹¹In-DTPA-DPhe¹]RC-160: preparation, biological activity, receptor scintigraphy in rats and comparison with [¹¹¹In-DTPA-DPhe¹]octreotide. *Eur. J. Nucl. Med.* 21, 328–335.
- (205) Mäcke, H. R., and Behe, M. (1996) New octreotide derivatives labelled with technetium-99m. *J. Nucl. Med.* 37, 29P (abstract 107).
- (206) Behe, M., and Mäcke, H. R. (1995) New somatostatin analogues labelled with technetium-99m. *Eur. J. Nucl. Med.* 22, 791 (abstract 267).
- (207) Thakur, M. L., John, E., Li, J., Reddy, H. R., Halmos, G., and Schally, A. V. (1995) Tc-99m-RC-160: a somatostatin analog for imaging prostate cancer—comparison with I-125-RC-160, and In-111-octreotide. *J. Nucl. Med.* 36, 92P (abstract 374).
- (208) Thakur, M. L., Halmos, G., and Jan, J. (1994) Technetium-99m-RC-160: a somatostatin analog. *J. Nucl. Med.* 35, 259P (abstract 1063).
- (209) Breeman, W. A. P., VanHagen, M. P., Visser-Wisselaar, H. A., van der Pluijm, M. E., Koper, J. W., Setyono-Han, B., Bakker, W. H., Kwekkeboom, D. J., Hazenberg, M. P., Lamberts, S. W. J., Visser, T. J., and Krenning, E. P. (1996) In vitro and in vivo studies of substance P receptor expression in rats with the new analog [Indium-111-DTPA-Arg¹]substance P. *J. Nucl. Med.* 37, 108–117.
- (210) Virgolini, I., Raderer, M., Kurtaran, A., Angelberger, P., Yang, Q., Radosavljevic, M., Leimer, M., Kaserer, K., Li, S. R., Kornek, G., Hübsch, Niederle, B., Pidlich, J., Scheithauer, W., and Valent, P. (1996) ¹²³I-vasoactive intestinal peptide (VIP) receptor scanning: update of imaging results in patients with adenocarcinomas and endocrine tumors of the gastrointestinal tract. *Nucl. Med. Biol.* 23, 685–692.
- (211) Jurisson, S., Berning, D., Jia, W., and Ma, D.-S. (1993) Coordination compounds in nuclear medicine. *Chem. Rev.* 93, 1137–1156.

BC970058B

ARTICLES

Protein Conjugates with Water-Soluble Poly(alkylene oxide)s Entrapped in Hydrated Reversed Micelles

Boris I. Kurganov,^{*,†} Irina N. Topchieva,[‡] and Nadezhda V. Efremova[†]

A. N. Bach Institute of Biochemistry, Russian Academy of Sciences, Leninsky Prospekt 33, Moscow 117071, Russia, and Department of Chemistry, M. V. Lomonosov Moscow State University, Lenin Hills, Moscow 119899, Russia. Received October 23, 1996[®]

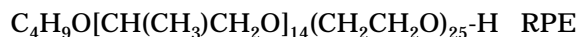
Conjugates of α -chymotrypsin (ChT) with poly(ethylene glycol) (PEG) and block copolymers of ethylene and propylene oxides (proxanols) have been synthesized. The molecular mass of the polymers used was 2 kDa. The conjugates contained five to seven polymer chains per enzyme molecule. Hydrolysis of *N-trans*-cinnamoylimidazole catalyzed by the conjugates of ChT with poly(alkylene oxide)s was studied in 0.05 M Tris-HCl buffer at pH 8.0 and in the system of the hydrated reversed micelles of aerosol OT (AOT) in octane at 25 °C. The deacylation rate constant k_3 for the conjugates in buffer solution was 1.5–1.8-fold higher than that for native ChT. The value of the $[H_2O]:[AOT]$ ratio corresponding to the maximum on k_3 versus $[H_2O]:[AOT]$ curves for the conjugates (ca. 16) allows the dimensions of their molecules to be evaluated. The radius of the conjugate molecules was found to be about 2.8 nm. The value of k_3 for the conjugate of ChT with PEG, as in the case of native ChT, remains constant when the concentration of AOT is varied. However, the deacylation rate constant for the conjugates of ChT with proxanols decreases with the increase in AOT concentration, which indicates that these conjugates are able to interact with the micellar matrix and therefore may be considered membranotropic compounds.

INTRODUCTION

Modification of proteins with hydrophilic polymers, e.g. poly(ethylene glycol), is widely used to impart new useful properties to proteins: solubility in organic solvents, protracted retention in blood circulation, reduced immunogenicity and antigenicity, etc. (1–5). We were pioneers in applying block copolymers of ethylene and propylene oxides (proxanols) to modification of proteins; conjugates of proxanols with α -chymotrypsin, BSA, cytochrome *c*, and superoxide dismutase were synthesized (6–10). The modification of proteins with proxanols allows products with new properties stemming from the amphiphilic nature of polymer–modifier to be obtained. In particular, conjugates with membranotropic properties were prepared (6, 7).

The structures of protein conjugates with poly(alkylene oxide)s are presented in Figure 1. Poly(alkylene oxide)s with a molecular mass of 2 kDa were used for protein modification. The relative dimensions of the protein molecule in the scheme correspond to those of the ChT¹ molecule. Conjugate **I** is a product of modification of a protein by PEG. Proxanols of types RPE and REP (R is

a starting radical, P is propylene oxide, and E is ethylene oxide) used for the modification had identical compositions but differed in the position of blocks toward the end functional group:



Conjugates **IIa** and **IIb** differ in the type of polymer chain distribution on the surface of the protein globule. Conjugates **IIa** are characterized by a clustered distribution of polymer chains, whereas a statistical distribution of polymer chains is characteristic of conjugates **IIb**. In conjugate **III**, the hydrophobic poly(propylene oxide) block is directly attached to protein, whereas the hydrophilic poly(ethylene oxide) block is located at the periphery of the conjugate molecule.

In previous papers (6, 7), the membranotropic properties of protein conjugates with proxanols were studied by their effect on the rate of oxygen consumption by thymus lymphocytes. On the basis of the results obtained, we proposed that conjugates of type **IIa** are capable of translocation across the membrane of T-lymphocytes. Conjugates of the other types do not exhibit such properties.

In order to obtain additional information about the physicochemical properties of protein conjugates with poly(alkylene oxide)s, in the present work, we used the micellar systems containing hydrated reversed micelles of aerosol OT (AOT) in octane. Previously, Levashov and co-workers (11–14) substantiated the possibility of application of hydrated reversed micelles to the detection of the ability of proteins and its derivatives to interact with biological membranes.

* Address correspondence to this author at A. N. Bach Institute of Biochemistry, Russian Academy of Sciences, Leninsky Prospekt 33, Moscow 117071, Russia. Telephone: (007-095) 952-30-66. Fax: (7-095) 954-27-32.

[†] Russian Academy of Sciences.

[‡] M. V. Lomonosov Moscow State University.

[®] Abstract published in *Advance ACS Abstracts*, June 1, 1997.

¹ Abbreviations: AOT, Aerosol OT [sodium salt of bis(2-ethylhexyl)sulfosuccinic acid]; ChT, α -chymotrypsin; PEG, poly(ethylene glycol); (RPE)₅-ChT(statist) and (RPE)₇-ChT(clust), conjugates of ChT with proxanols of type RPE with a statistical or clustered distribution of polymer chains on the surface of the protein globule, respectively.

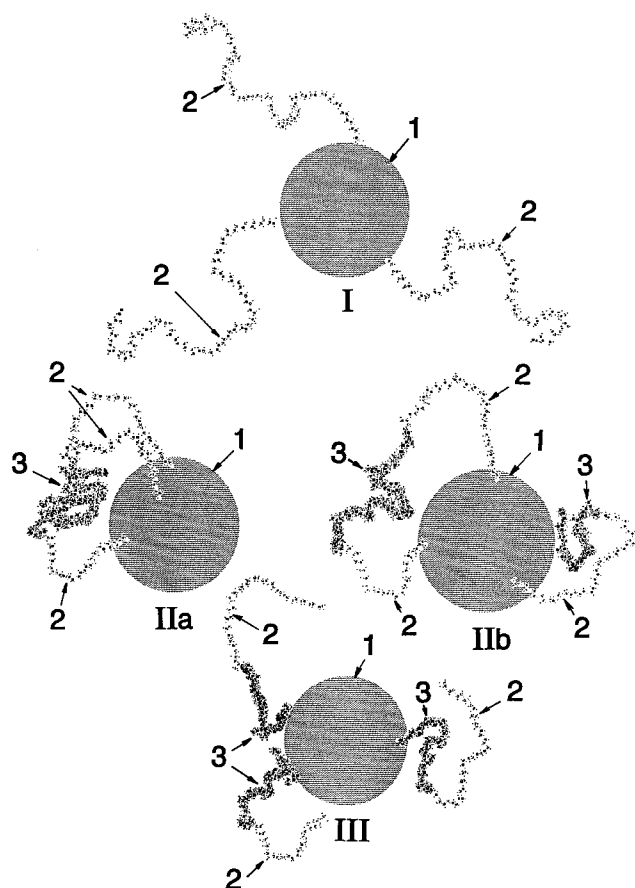


Figure 1. Molecular models of protein conjugates (9): (I) with PEG, (II) with propanols of type RPE, and (III) with propanols of type REP. The poly(propylene oxide) blocks of the polymer chains are shaded.

In recent years, much attention has been focused on the formation of nonlinear lipid structures in biomembranes, built like the reversed micelles or close to them (hexagonal phase H_{II}) (15–17). Such structures can participate in many cellular processes, such as fusion of membranes, formation of the intercellular contacts, the transmembrane transfer of low- and high-molecular weight substances, and regulation of the activity of membrane-bound enzymes. Integral membrane-bound proteins are assumed to be able to distort the bilayer organization of biomembrane with formation of the structures of the type of reversed micelles. For instance, De Kruijff et al. (18) suggested that incorporation of cytochrome *c* in an intramembrane reversed micelle allows it to contact cytochrome *c* oxidase embedded in the membrane. Interactions of integral membrane-bound proteins of photosynthetic membranes mediated by the formation of nonbilayer structures were presumed by Murphy (19). Thus, the protein-containing hydrated micelles may be considered models of the structural organization of certain membrane-bound proteins, producing local disturbances in the lipid bilayer (20–22).

Besides, the systems of hydrated reversed micelles may be a useful source of information about the dimensions of conjugate supramolecules in aqueous solutions and hence the structural organization of conjugates, namely the character of disposition of polymer chains near the protein globule.

EXPERIMENTAL PROCEDURES

Chemicals. Crystalline α -chymotrypsin (ChT, EC 3.4.21.1) from bovine pancreas with an activity of 40–60 IU/mg and *N-trans*-cinnamoylimidazole were pur-

chased from Sigma. Monomethyl ether of poly(ethylene glycol) with a molecular mass of 1.9 kDa was purchased from Serva. Proxanols, block copolymers of ethylene and propylene oxides, differing in the type of arrangement of poly(ethylene oxide) and poly(propylene oxide) blocks (molecular mass of 2 kDa; both containing 40 wt % propylene oxide), were purchased from the Scientific Manufacturing Association "NIOPIK" (Russia). The sodium salt of bis(2-ethylhexyl)sulfosuccinic acid (AOT, Merck, Germany) was used without additional purification. According to infrared spectroscopy data, the content of water in the AOT preparation was 0.85 mol of H_2O per mole of AOT. This water content was taken into account when calculating the degree of hydration of reversed micelles of AOT in organic solvent. Hydrated reversed micelles of AOT were obtained in *n*-octane ("Reakhim", Russia). Tris (Reanal, Hungary) was used for preparation of buffer solutions.

Synthesis of Conjugates. The procedure proposed in ref 9 was used for modification of ChT with monoaldehyde derivatives of PEG and proxanols. The content of protein in conjugates and the amount of attached polymer chains were measured as described in ref 9. The content of the active sites in conjugates was calculated from the data on the titration by *N-trans*-cinnamoylimidazole (23). The content of the active enzyme in the preparation of ChT was 70%.

Enzymatic Assay. The enzymatic activity of ChT and its conjugates with proxanols was measured with the nonspecific substrate, *N-trans*-cinnamoylimidazole, by the spectrophotometric method. The time course of the change in optical absorbance at 335 nm has a two-phase character, indicating that the acylation step proceeds essentially faster than the deacylation step. The slope of the steady-state part of the kinetic curve (after the completion of the fast stage) gives the rate of deacylation of *N-trans*-cinnamoyl-ChT. In the kinetic experiments, 5 μ L of a 0.1 M solution of *N-trans*-cinnamoylimidazole in acetonitrile and 0–160 μ L of a buffer solution (0.05 M Tris-HCl at pH 8.0) were added to 2 mL of a 0.03–0.3 M solution of AOT in octane. After vigorous shaking, a 10–15 μ L aliquot of the enzyme solution in buffer was added, and the mixture was shaken again. The rate of the enzymatic reaction was measured in the system formed, which was optically transparent. The rates of the enzymatic hydrolysis of *N-trans*-cinnamoylimidazole were corrected for nonenzymatic hydrolysis. The final concentrations of the enzyme and substrate in the reaction mixture were 2.5×10^{-6} and 2.5×10^{-4} M, respectively. Spectrophotometric measurements were performed at 25 $^{\circ}$ C in an Ultraspec spectrophotometer (LKB, Sweden) equipped with the thermostated cell holder. When calculating the rate of the enzymatic reaction, we take into account the fact that the molar extinction coefficient of *N-trans*-cinnamoylimidazole in the system AOT–water–octane differs from the corresponding value in water (9370 $M^{-1} cm^{-1}$) and varies from 2200 $M^{-1} cm^{-1}$ in practically dry micelles to 3600 $M^{-1} cm^{-1}$ when $[H_2O]:[AOT] = 20$ (24).

Sedimentation Analysis. Sedimentation of the reversed micelles containing ChT and its conjugates with poly(alkylene oxide)s was studied using a Spinco model E analytical ultracentrifuge (Beckman, Austria), equipped with an absorption optical system, a monochromator, and a photoelectric scanner. Assays were carried out at 25 $^{\circ}$ C. We used 12 mm bisection cells and an An-G-Ti rotor in the sedimentation experiments. The rotor speed was 40 000 rpm. Scanning was performed at 300 nm (empty micelles were not registered at this wavelength).

Table 1. Properties of Conjugates of ChT with Poly(alkylene oxide)s

no.	polymer	wt % of ChT	molar ratio of polymer to ChT	content of active sites	designation of conjugate
1	PEG	69	5:1	41	(PEG) ₅ -ChT
2	REP	67	6:1	62	(REP) ₆ -ChT
3	RPE	61	7:1	73	(RPE) ₇ -ChT(clust)
4	RPE	70	5:1	62	(RPE) ₅ -ChT(statist)

Table 2. Properties of Micellar Systems Containing ChT and Its Conjugates with Poly(alkylene oxide)s^a

ChT and its conjugates	$\left(\frac{[\text{H}_2\text{O}]}{[\text{AOT}]}\right)_{\text{opt}}$	$k_{3,\text{max}} \times 10^3, \text{s}^{-1}$	$k_3 \times 10^3, \text{s}^{-1}$ (for buffer)
ChT	11	7.4	5.0
(PEG) ₅ -ChT	16	7.3	7.8
(REP) ₆ -ChT	16	7.6	7.7
(RPE) ₇ -ChT(clust)	16	7.9	7.8
(RPE) ₅ -ChT(statist)	16	8.7	8.9

^a 0.05 M Tris-HCl buffer at pH 8.0 and 25 °C.

RESULTS AND DISCUSSION

The characteristics of the protein-polymer conjugates synthesized are given in Table 1. As has been shown previously (9), conjugates **3** and **4** synthesized from proxanol RPE in media with different polarity differ in the type of polymer chain distribution on the surface of the protein globule. Conjugate **3** synthesized in aqueous solution is characterized by a clustered distribution of amphiphilic polymer chains, whereas synthesis in water-organic medium gives conjugate **4** with a statistical distribution of polymer chains (designations clust and statist are used, respectively).

When studying the catalytic properties of native ChT and its conjugates with poly(alkylene oxide)s, we found that the rate constant for deacylation of *N-trans*-cinnamoyl-ChT (k_3) for all the conjugates studied is higher than that for native enzyme (see Table 2, last column). It should be noted that we also observed an enhancement of the catalytic constant in comparison with that of native ChT, when enzymatic hydrolysis of the *N*-benzoyl-L-tyrosine ethyl ester catalyzed by such conjugates was studied (9). The effect, however, was markedly less than that in the case with *N-trans*-cinnamoylimidazole as a substrate.

Figure 2 shows the results of measuring the catalytic activity of native ChT and its conjugates with poly(alkylene oxide)s entrapped in hydrated reversed micelles of AOT in octane at different values of water content in the micellar system. The deacylation rate constant k_3 for native ChT reaches a maximum when the $[\text{H}_2\text{O}]:[\text{AOT}]$ ratio is equal to approximately 11. This finding is in line with the data reported by other investigators (24, 25). According to the concept developed by Levashov and his colleagues, the position of the optimum on the catalytic activity versus $[\text{H}_2\text{O}]:[\text{AOT}]$ curve corresponds to the conditions under which the dimensions of the inner cavity of the micelle coincide with those of the molecule of solubilized protein. The molecule of ChT measures $4 \times 4 \times 5$ nm (26) and may be approximated to a sphere with a radius of 2.15 nm. The inner cavity of the reversed micelle has the same radius when $[\text{H}_2\text{O}]:[\text{AOT}] = 11.6$ (27).

It is worth noting that at the optimum $[\text{H}_2\text{O}]:[\text{AOT}]$ ratio the value of k_3 for ChT is significantly higher (by a factor of 1.5) than the corresponding value measured in buffer solution. On the basis of the spin-label studies, Levashov and co-workers (25) concluded that the increase in the catalytic activity of ChT in micelles of the optimum

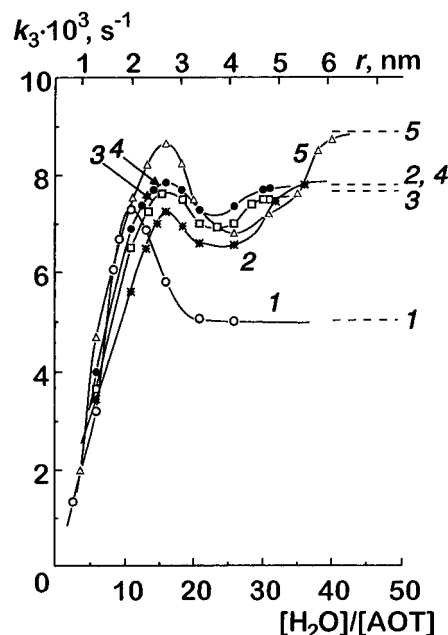


Figure 2. Dependences of the rate constant for deacylation of *N-trans*-cinnamoyl-ChT (k_3) on the content of water solubilized in the system AOT (concentration in octane is 0.1 M)-0.05 M Tris-HCl buffer (pH 8.0)-octane for native ChT (1) and its conjugates (PEG)₅-ChT (2), (REP)₆-ChT (3), (RPE)₇-ChT-clust (4), and (RPE)₅-ChT-statist (5) (25 °C). The upper scale is the radius of the inner aqueous cavity of a micelle. Dashed horizontal lines are the values of k_3 measured for ChT and its conjugates in buffer solution.

size was due to the enhancement of the rigidity of the enzyme active site.

Previously, we studied the physicochemical properties of protein-proxanol conjugates by the methods of sedimentation analysis, differential scanning calorimetry, and hydrophobic chromatography and concluded that the conjugates were peculiar intramolecular micelles, in which polymer chains "enveloped" the protein globule (9). It is of interest that this conclusion is also valid for protein-PEG conjugates. The proposed structure of protein-PEG conjugates may be explained on the basis of the concept of poly(alkylene oxide) solubility in water (28), according to which the solubility of PEG in water is due to its ability to fix into the crystal structure of water. The fragments of the PEG molecule located near the protein globule lose this ability and in consequence become hydrophobic.

The position of the maximum on k_3 versus $[\text{H}_2\text{O}]:[\text{AOT}]$ curves for all the conjugates studied is shifted toward higher degrees of micelle hydration ($[\text{H}_2\text{O}]:[\text{AOT}]_{\text{opt}} \approx 16$) compared with that of native ChT. Knowing the optimum value of the $[\text{H}_2\text{O}]:[\text{AOT}]$ ratio and the data on the dimensions of the inner cavity of reversed micelles (27), the dimensions of the conjugate molecules may be estimated; the radius of the molecule for all the conjugates studied is about 2.8 nm. Thus, the thickness of the polymer layer in the conjugates is 0.65 nm. From the comparison of this value with the undisturbed dimensions of isolated polymer chains, namely with the root-mean-square end-to-end distance [3.4 nm for PEG (29) and 3.2 nm for proxanols], it may be concluded that the polymer chains in conjugates are highly packed and form a dense polymer layer near the surface of the protein globule.

The value of k_3 for conjugates of ChT with proxanols reaches the limiting value corresponding to that for buffer solution with the increase in the $[\text{H}_2\text{O}]:[\text{AOT}]$ ratio in a more complex manner than in the case of native ChT.

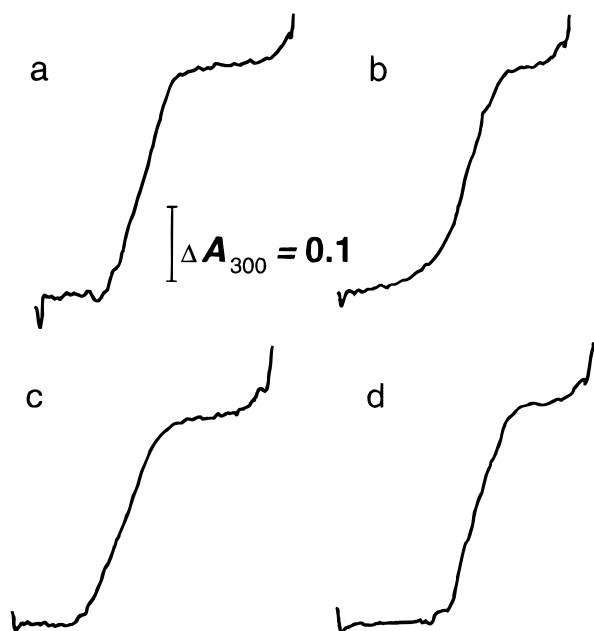


Figure 3. Sedimentation of (PEG)₅-ChT (a and b) and (RPE)₅-ChT(statist) (c and d) entrapped in hydrated reversed micelles of AOT in octane. The [H₂O]:[AOT] ratios are 15.8 (a and c), 22.5 (d), and 30.0 (b). The concentration of conjugates was 1.5 mg/mL (calculated on ChT). The rotor speed was 40 000 rpm. The times of sedimentation (minutes) were 28 (a), 30 (b), 32 (c), and 33 (d).

As seen from Figure 2, when [H₂O]:[AOT] \approx 25, the dependence of k_3 on [H₂O]:[AOT] passes through the minimum. The following explanation may be given for the increase in the value of k_3 for conjugates when [H₂O]:[AOT] > 25. When the content of water in the system rises, both the protein globule and polymer chains are hydrated. The ability of poly(ethylene oxide)s to bind water and modify its structure is well-known (28). Therefore, one would expect that in the case of conjugates the k_3 value will reach the limiting value corresponding to that for buffer solution with the increasing [H₂O]:[AOT] ratio at a higher content of water in the micellar system. This feature of conjugates manifests itself as a minimum following a maximum on k_3 versus [H₂O]:[AOT] curves.

The increase in the catalytic activity of conjugates at a [H₂O]:[AOT] ratio of higher than \sim 25 may be connected with association of ChT conjugates, as happens, for example, with glycosylated ChT (13). In order to check this suggestion, we studied sedimentation of conjugates of ChT entrapped in reversed micelles using an analytical ultracentrifuge. Figure 3 shows the results of sedimentation studies for (PEG)₅-ChT and (RPE)₅-ChT(statist) conjugates. As illustrated in Figure 3, at the [H₂O]:[AOT] values corresponding to the maximum on k_3 versus [H₂O]:[AOT] curves and at a higher content of water in the micellar system, the sedimentation boundaries are symmetrical, suggesting that the conjugates entrapped in reversed micelles do not tend to aggregate. The sedimentation coefficients for the reversed micelles containing the (PEG)₅-ChT conjugate were 19.7, 20.7, and 24.4 S with [H₂O]:[AOT] ratios of 15.8, 22.5, and 30.0, respectively. In the case of the micelles containing the (RPE)₅-ChT(statist) conjugate, the sedimentation coefficients were 18.5 and 25.0 S with [H₂O]:[AOT] ratios of 15.8 and 22.5, respectively. The sedimentation coefficients for the reversed micelles containing conjugates of ChT are close to those for the micelles containing native ChT (30). This fact is not surprising since previously we showed that the sedimentation coefficients for

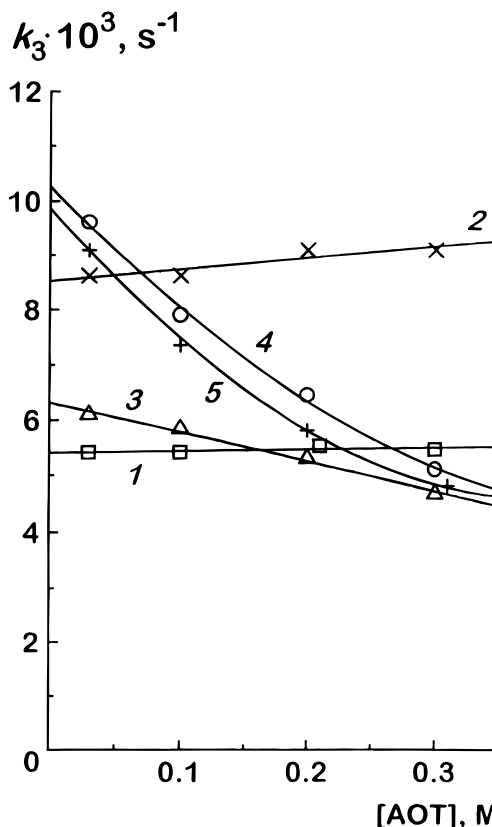


Figure 4. Dependences of the rate constant for deacylation of *N-trans*-cinnamoyl-ChT (k_3) on AOT concentration in the micellar system AOT-Tris-HCl buffer-octane for ChT (1) and its conjugates (PEG)₅-ChT (2), (REP)₆-ChT (3), (RPE)₇-ChT-(clust) (4), and (RPE)₅-ChT(statist) (5). [H₂O]:[AOT] = 16 at 25 °C.

conjugates of ChT with poly(alkylene oxide)s and for native ChT were practically identical (9).

Membranotropic properties of enzymes entrapped in reversed micelles may be demonstrated through the study of their catalytic activity at various concentrations of surfactant (11–14). The catalytic activity of the enzymes which are able to interact with biological membranes changes when the concentration of surfactant is varied (in such experiments, the [H₂O]:[surfactant] ratio is held constant). Such an effect was observed, for example, for horseradish peroxidase (EC 1.11.1.7), prostaglandin H synthetase (EC 1.14.99.1) from vesicular glands of ram, acid phosphatase (EC 3.1.3.2) from wheat germs, and laccase (EC 1.10.3.2) from *Coriolus versicolor*. Therefore, we expected that the study of the catalytic properties of different conjugates in the system of hydrated reversed micelles of AOT-octane would allow us to reveal the membranotropic properties of conjugates.

Figure 4 shows the dependences of the k_3 value on the concentration of AOT when [H₂O]:[AOT] = 16. The value of k_3 for native ChT remains constant on variation of [AOT]. This fact is consistent with the results obtained in refs 11–14 and indicates that the native enzyme does not exhibit membranotropic properties. The same behavior is observed for conjugates of ChT with PEG. However, in the case of (REP)₆-ChT, (RPE)₇-ChT-(clust), and (RPE)₅-ChT(statist) conjugates, the value of k_3 decreases markedly with increasing AOT concentration. These results suggest that the conjugates studied interact with the micellar matrix. Membranotropic properties of the (RPE)₇-ChT-(clust) conjugate coincide with its capability of translocation across the membrane of T-lymphocytes (6, 7). (RPE)₅-ChT(statist) and (REP)₆-ChT con-

jugates, as was demonstrated previously (7), do not pass through the cell membrane. However, their membranotropic properties established in the system of hydrated reversed micelles suggest that such conjugates are able to interact with biological membranes, for example, by incorporating in the lipid bilayer.

It is worth noting that the use of the system of hydrated reversed micelles allows the membranotropic properties of ChT modified with stearic acid (12) and D-glucosamine (13) to be demonstrated.

Variations in the concentration of AOT in octane at a fixed degree of micelle hydration ($[H_2O]:[AOT] = \text{constant}$) result in a change in the concentration of reversed micelles (31). At the same time, the average radius of the inner cavity of a micelle and the width of distribution over the micelle size remain practically unchanged. Therefore, one can expect that the catalytic activity of solubilized enzymes at a fixed degree of hydration must be independent of the concentration of surfactant. In order to explain the experimentally obtained dependences of the catalytic activity of solubilized enzymes on the concentration of surfactant, it was assumed that empty micelles were able to interact with enzyme-containing micelles with the formation of "deformed" micelles, in which the enzyme loses the catalytic activity (12, 14).

Thus, hydrated reversed micelles may serve as a simple and very informative tool in the study of the physicochemical properties of polymer-protein conjugates. The dimensions of protein conjugates with poly(alkylene oxide)s determined using this approach allowed us to describe their morphological structure which is consistent with the micellar model for conjugates of such a type proposed in our previous works (9). The ability of conjugates of ChT with proxanols to interact with the micellar matrix may be considered a manifestation of their membranotropic properties.

ACKNOWLEDGMENT

We thank P. V. Kalmykov for the help in obtaining sedimentation coefficients of the conjugates. The study was funded by Grant 93-2223 from the INTAS and a grant from State Research Program 08.05 Newest Methods of Bioengineering, subprogram Engineering in Enzymology.

LITERATURE CITED

- Abuchowski, A., McCoy, I. R., Palczuk, N. C., and Davis, F. F. (1977) Effect of covalent attachment of polyethylene glycol on immunogenicity and circulating time of bovine liver catalase. *J. Biol. Chem.* 252, 3582–3586.
- Abuchowski, A., Van Es, T., Palczuk, N. C., and Davis, F. F. (1977) Alteration of immunological properties of bovine serum albumin by covalent attachment of polyethylene glycol. *J. Biol. Chem.* 252, 3578–3582.
- Harris, J. M., Ed. (1992) *Poly(ethylene glycol) Chemistry: Biotechnical and Biomedical Applications*, Plenum Press, New York.
- Matsushima, A., Okada, M., and Inada, Y. (1984) Chymotrypsin modified with polyethylene glycol catalyzes peptide synthesis reaction in benzene. *FEBS Lett.* 178, 275–282.
- Takahashi, K., Kodera, Y., Yoshimoto, T., Ajima, A., Matsushima, A., and Inada, Y. (1985) Ester-exchange catalyzed by lipase modified with polyethylene glycol. *Biochem. Biophys. Res. Commun.* 131, 532–538.
- Kirillova, G. P., Mokhova, E. N., Deduchova, V. I., Tarakanova, A. N., Ivanova, V. P., Efremova, N. V., and Topchieva, I. N. (1993) The influence of pluronics and their conjugates with proteins on the rate of oxygen consumption by liver mitochondria and thymus lymphocytes. *Biotechnol. Appl. Biochem.* 18, 329–339.
- Topchieva, I. N., Mokhova, E. N., Kirillova, G. P., and Efremova, N. V. (1994) Membranotropic properties of protein conjugates with block copolymers of ethylene oxide and propylene oxide. *Biokhimiya* 59, 16–22; *Biochemistry (Moscow)* 59, 11–15.
- Topchieva, I. N., and Efremova, N. V. (1994) Conjugates of proteins with block copolymers of ethylene and propylene oxides. *Biotechnol. Genet. Eng. Rev.* 12, 357–382.
- Topchieva, I. N., Efremova, N. V., Khvorov, N. V., and Magretova, N. N. (1995) Synthesis and physicochemical properties of protein conjugates with water-soluble poly(alkylene oxides). *Bioconjugate Chem.* 6, 360–368.
- Topchieva, I. N., and Efremova, N. V. (1995) Conjugates of proteins with poly(alkylene oxides). In *Modern Enzymology: Problems and Trends* (B. I. Kurganov, S. N. Kochetkov, and V. I. Tishkov, Eds.) pp 599–605, Nova Science Publishers, New York.
- Klyachko, N. L., Levashov, A. V., Kabanov, A. V., Khmel'nitsky, Yu. L., and Martinek, K. (1991) Catalysis by enzymes entrapped in hydrated surfactant aggregates having various structures in organic solvents. In *Kinetics and Catalysis in Microheterogeneous Systems* (M. Gratzel and K. Kalyanasundaram, Eds.) pp 135–181, Marcel Dekker, New York.
- Kabanov, A. V., Levashov, A. V., Klyachko, N. L., Nametkin, S. N., Pshezhetsky, A. V., and Martinek, K. (1988) Enzymes entrapped in reversed micelles of surfactants in organic solvents: a theoretical treatment of the catalytic activity regulation. *J. Theor. Biol.* 133, 327–343.
- Levashov, A. V., Rariy, R. V., Martinek, K., and Klyachko, N. L. (1993) Artificially glycosylated α -chymotrypsin in reversed micelles of Aerosol OT in octane. *FEBS Lett.* 336, 385–388.
- Khmel'nitsky, Yu. L., Kabanov, A. V., Klyachko, N. L., Levashov, A. V., and Martinek, K. (1989) Enzymatic catalysis in reversed micelles. In *Structure and Reactivity in Reversed Micelles* (M. P. Pileni, Ed.) pp 230–261, Elsevier, Amsterdam.
- De Kruijff, B., Cullis, P. R., Verkleij, A. J., Hope, M. J., van Echteld, C. J. A., and Taraschi, T. E. (1985) Lipid polymorphism and membrane functions. In *The Enzymes of Biological Membranes* (A. N. Martonosi, Ed.) pp 131–204, Plenum Press, New York.
- Cullis, P. R., De Kruijff, B., Hope, M. J., Verkleij, A. J., Nayar, R., Farreu, S. B., Tilcock, C., Madden, T. D., and Bally, B. (1985) Structural properties of lipids and their functional roles in biological membranes. In *Membrane Fluidity in Biology* (R. C. Aloia, Ed.) pp 39–81, Academic Press, New York.
- De Kruijff, B. (1987) Polymorphic regulation of membrane lipid composition. *Nature* 329, 587–588.
- De Kruijff, B., Verkleij, A. J., van Echteld, C. J. A., Gerritsen, W. J., Noordam, P. C., Mombers, C., Rietveld, A., de Gier, J., Cullis, P. R., Hope, M. J., and Nayar, R. (1980–1981) Non-bilayer lipids and the inner mitochondrial membrane. In *International Cell Biology* (H. G. Schwinger, Ed.) pp 559–571, Springer, Berlin.
- Murphy, D. Y. (1982) The importance of non-planar bilayer regions in photosynthetic membranes and their stabilization by galactolipids. *FEBS Lett.* 150, 19–26.
- Klyachko, N. L., Levashov, A. V., Pshezhetsky, A. V., Bogdanova, N. G., Berezin, I. V., and Martinek, K. (1986) Catalysis by enzymes entrapped into hydrated surfactant aggregates having lamellar or cylindrical (hexagonal) or ball-shaped (cubic) structure in organic solvents. *Eur. J. Biochem.* 161, 149–154.
- Kabanov, A. V., Nametkin, S. N., Evtushenko, G. N., Chernov, N. N., Klyachko, N. L., Levashov, A. V., and Martinek, K. (1989) A new strategy for the study of oligomeric enzymes: γ -glutamyltransferase in reversed micelles of surfactants inorganic solvents. *Biochim. Biophys. Acta* 996, 147–162.
- Kurganov, B. I., Shkarina, T. N., Malakhova, E. A., Davydov, D. R., and Chebotareva, N. A. (1989) Kinetics of soybean lipoxygenase reaction in hydrated reversed micelles. *Biokhimiya* 71, 573–578.

- (23) Schonbaum, G. R., Zerner, B., and Bender, M. L. (1961) The spectrophotometric determination of the operational normality of an α -chymotrypsin solution. *J. Biol. Chem.* 236, 2430–2435.
- (24) Levashov, A. V., Klyachko, N. L., and Martinek, K. (1981) Catalysis by enzymes entrapped in reversed micelles of surfactants in organic solvents. 3. The influence of the hydration of Aerosol OT in octane on the rate of cinnamoyl- α -chymotrypsin hydrolysis. *Bioorg. Khim.* 7, 670–679; *Russ. J. Bioorg. Chem.* 7, 581–589.
- (25) Belonogova, O. V., Likhtenstein, A. V., Levashov, A. V., Khmelnitsky, Yu. L., Klyachko, N. L., and Martinek, K. (1983) A spin-label study of the state of the active center and microenvironment of α -chymotrypsin solubilized in octane using the surfactant Aerosol OT. *Biokhimiya* 48, 379–386; *Biochemistry (Moscow)* 48, 329–335.
- (26) Squire, P. G., and Himmel, M. E. (1979) Hydrodynamics and protein hydration. *Arch. Biochem. Biophys.* 196, 165–177.
- (27) Eicke, H.-F., and Rehak, J. (1976) On the formation of water/oil microemulsions. *Helv. Chim. Acta* 59, 2883–2891.
- (28) Kjellander, R., and Florin, E. (1981) Water structure and changes in thermal stability of the system poly(ethylene oxide)–water. *J. Chem. Soc., Faraday Trans.* 77, 2053–2077.
- (29) Bailey, F. E., Jr., and Koleske, J. V. (1966) Configuration and hydrodynamic properties of the polyoxyethylene chain in solution. In *Nonionic Surfactants* (M. Schnick, Ed.) Chapter 23, Marcel Dekker Inc., New York.
- (30) Khmelnitsky, Yu. L., Levashov, A. V., Klyachko, N. L., Chernyak, V. Ya., and Martinek, K. (1983) Enzymes entrapped in reversed micelles of surfactants in organic solvents. The study of the system protein–Aerosol OT–H₂O by the sedimentation method. *Biokhimiya* 47, 86–99; *Biochemistry (Moscow)* 47, 75–86.
- (31) Zulauf, M., and Eicke H.-F. (1979) Inverted micelles and microemulsions in the ternary system H₂O/Aerosol OT/isooctane as studied by photon correlation spectroscopy. *J. Phys. Chem.* 83, 480–486.

BC970041T

Induced Thermostability of Poly(ethylene oxide)-Modified Hemoglobin in Glycols

Natsue Y. Kawahara and Hiroyuki Ohno*

Department of Biotechnology, Tokyo University of Agriculture & Technology, Koganei, Tokyo 184, Japan.
Received August 12, 1996[®]

The thermostability and redox activity of poly(ethylene oxide) (PEO)-modified human hemoglobin in PEO₂₀₀ (PEO containing KCl, average MW of 200, <0.3% H₂O) were investigated by UV-vis spectroscopy, by circular dichroism spectroscopy, and by cyclic voltammetry. Using PEO oligomers as a solvent, PEO-modified hemoglobin was reduced and oxidized at an indium tin oxide glass electrode in the temperature range of -10 to 120 °C. The thermostability of PEO-modified hemoglobin was affected by the molecular weight of the solvent PEO. In lower-molecular weight glycols (MW of <150), PEO-modified hemoglobin was denatured within a few minutes at 80 °C. On the other hand, the absorbance at the Soret band for PEO-modified hemoglobin was unchanged for 2 h at 80 °C in PEO₂₀₀. A decrease in the water content of solvent PEO₂₀₀ also improved the thermostability of PEO-modified hemoglobin. Improvement in the thermostability was attributed to physicochemical characteristics such as the relatively low molecular motion of PEO oligomers used as a solvent.

INTRODUCTION

We use poly(ethylene oxide) (PEO)¹ oligomers as a nonaqueous medium for heme proteins. PEO has been used as a key material in preparing ion conductive polymers. Since PEO can dissolve inorganic salts by its large dipole moment and can transport the dissociated ions through segmental motion, it shows a high bulk ionic conductivity (1–3). PEO has recently been applied as a polymer solvent for electrochemical reactions of many substrates, including heme proteins (4–8). Although native heme proteins are insoluble and redox inactive in dehydrated PEO oligomers, these heme proteins are soluble and show redox activity even in PEO oligomers when they are chemically modified with PEO (9–12).

PEO modification of proteins has already found an application, for example in suppressing antigenicity of medicinal materials (13–15). Similarly, PEO-modified human hemoglobin (PEO-Hb) has been developed as an artificial red blood cell, and the detailed bioactivity of PEO-Hb as an oxygen carrier has been studied (13, 16). However, there are only a few studies on the electrochemical redox reactions of hemoglobin in an aqueous medium at a chemically modified electrode (17), because hemoglobin shows no electron transfer reaction *in vivo*.

PEO modification of proteins also supports the solubility of proteins in nonaqueous media (13). Papers on the enzymatic activities (18, 19) and structure (20) of PEO-modified enzymes in homogeneous solutions of organic solvents such as benzene exist. The electrochemical characteristics of PEO-modified proteins in nonaqueous media have also been reported (21). These works studied nonaqueous biology in organic solvents only, and heme proteins were expected to exhibit both a redox activity and an excellent thermostability in the oligomers used as a solvent. With PEO as the solvent, PEO modification

onto the proteins was essential to improve their solubility while keeping their functions unchanged from those in organic solvents. PEO-Hb proved to be soluble in PEO oligomers and showed direct electron transfer reactions at an indium tin oxide glass electrode without any mediator (9, 10). The redox reaction has been reported for other PEO-modified heme proteins, such as myoglobin (11, 12), cytochrome *c* (22), and peroxidase (23), in PEO oligomers. Incorporated in a polymer matrix, PEO-modified proteins are expected to exhibit characteristic behavior even under severe conditions such as high temperatures. We studied PEO-Hb as a new redox active biomaterial in PEO oligomers at various temperatures. The thermostability of PEO-Hb in PEO oligomers has already been reported (24); however, a detailed study of the thermostability of PEO-Hb in PEO oligomers has not been carried out.

In the present study, the PEO-Hb/PEO oligomer system was used as a typical example of a new bioconjugate/nonaqueous system. Here, we show the effectiveness of the new PEO-heme protein conjugates/PEO oligomers system, which shows excellent thermostability through using the PEO-protein conjugate and the polymer solvent. The effects of several factors on the thermostability of PEO-Hb in PEO oligomers were also analyzed.

EXPERIMENTAL PROCEDURES

Materials. Human hemoglobin (Hb) and PEO-modified Hb pyridoxalated (PEO-Hb) were donated by Ajinomoto Co. Ltd. PEO activated with *N*-hydroxysuccinimide was in reaction with amino groups on the surface of Hb, according to the method reported previously (16). We used PEO-Hb having six PEO chains (average MW of 3000) on average (16) for all experiments.

PEO₂₀₀ (average MW of 200) containing no antioxidant additive was purchased from NOF Co. Ltd. Except where otherwise stated, PEO containing 0.50 M KCl was used as a solvent after drying *in vacuo* at 60 °C for 3 days. Ethylene glycol, di(ethylene glycol), and tri(ethylene glycol) were purchased from Kanto Chemical Co. Ltd. These glycols were dried *in vacuo* at room temperature for 3 days after mixing with 0.50 M KCl. All other

* To whom correspondence should be addressed. Phone: +81-423-88-7024. Fax: +81-423-88-7012. E-mail: ohnoh@cc.tuat.ac.jp.

[®] Abstract published in *Advance ACS Abstracts*, August 1, 1997.

¹ Abbreviations: PEO, poly(ethylene oxide); Hb, human hemoglobin; PEO-Hb, PEO-modified human hemoglobin; ITO, indium tin oxide; DSC, differential scanning calorimetry; CD, circular dichroism.

analytical grade reagents not noted here were purchased from Kanto Chemical Co. Ltd.

An indium tin oxide (ITO) glass electrode (ITO layer thickness of 130 nm, surface resistance of 30.9 Ω /square) was purchased from Oji Tobi Co. Ltd. This was used as a working electrode for both visible spectroscopy and cyclic voltammetry measurements after washing with acetone followed by chloroform.

Water Content Determination. The water content of the glycols used here was determined by the Karl Fischer titration method. The water content of every glycol used was calculated to be less than 0.2 wt % according to the Karl Fischer moisture titrator (Kyoto Electronics MKS-210). The water content was the average of at least three measurements for each sample. The total water content of every PEO-Hb/glycol solution containing KCl was determined to be less than 0.3 wt %.

Circular Dichroism Spectroscopy. Circular dichroism spectra were recorded at various temperatures with a JASCO J-720 spectropolarimeter. The protein solution, with a final concentration of 1.0×10^{-5} M, was placed in a quartz cuvette with a 1.00 mm light path length (JASCO 165-01). The sample temperature was controlled by a cell holder incorporating a Peltier device (JASCO PTC-343).

Differential Scanning Calorimetry Measurement. The thermodynamics of Hb and PEO-Hb denaturation in 0.10 M potassium phosphate buffer solution at pH 7.0 were studied using a high-sensitivity differential scanning calorimeter (Seiko Instrument Inc. DSC 120). The protein sample solution (0.2 g mL^{-1} , 70 μL), located in a Ag pan, was measured with a scanning rate of $1.0^\circ \text{C min}^{-1}$.

Cyclic Voltammetry Measurement. The redox reaction of PEO-Hb in PEO₂₀₀ was also analyzed by cyclic voltammetry (Fuso Seisakusho HECS 326PC) at various temperatures. The temperature was controlled as in UV-vis spectrophotometry. All measurements were carried out with the ITO electrodes as a working electrode (working area of 1 cm²) and as a counter electrode and Ag wire ($\phi = 0.5$ mm) as a reference electrode. Sufficient nitrogen gas was bubbled through to expel oxygen from the solutions in the electrochemical cell.

UV-Vis Spectroscopy under Potential. Glycol solutions of PEO-Hb with a final concentration of 1.0×10^{-4} M, containing 0.50 M KCl as a supporting electrolyte, were prepared by a gentle mixing of all components for 1 h at room temperature. UV-vis absorption spectra were recorded from -10 to 20°C with a Shimadzu UV-2200 A spectrophotometer under an applied potential (Nikko Keisoku, potentiostat NPOT-2501) using a thin layer cell system (11). A thin layer cell was used with light path length of 100 μm , constructed with the ITO electrode as a working electrode. Since an ITO electrode has little absorption in the visible spectrum, the visible spectral change of PEO-Hb was monitored under the given potential (-1.2 to ~ 1.2 V vs Ag). A homogeneous PEO solution of PEO-Hb was first put in a quartz cell. The thin layer cell was soaked in the quartz cell in order to raise the homogeneous PEO solution in the thin layer cell by capillarity. Ag and Pt wires were also introduced into the cell to act as reference and counter electrodes, respectively. This cell system was sealed under a nitrogen atmosphere before setting it in a UV-vis spectrometer. The temperature was controlled with a water-jacketed cell holder connected to a thermostated water bath (Tokyo Rika Kikai US-10S).

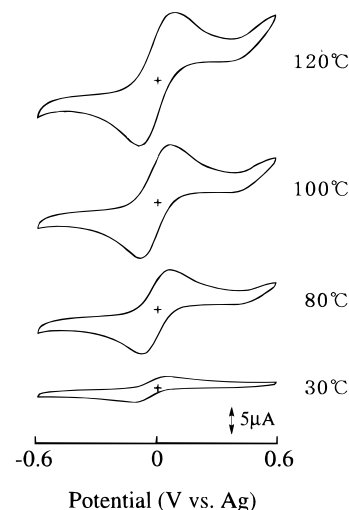


Figure 1. Cyclic voltammograms for PEO-Hb at an ITO electrode recorded with a scan rate of 33 mV s^{-1} in PEO₂₀₀ containing 0.50 M KCl at 30 – 120°C .

RESULTS AND DISCUSSION

Stability of PEO-Hb in PEO₂₀₀ at High Temperatures. Poly(ethylene oxide)-modified hemoglobin (PEO-Hb) was dissolved in PEO₂₀₀ (average MW of 200). The electrochemical redox reaction of PEO-Hb in PEO₂₀₀, which was analyzed with UV-vis spectrometry, has already been reported by the present authors (24). The electron transfer reaction of PEO-Hb with the ITO glass electrode in PEO₂₀₀ at temperatures of up to 120°C is confirmed by cyclic voltammetry as shown in Figure 1. Typical redox peaks of PEO-Hb were clearly observed in PEO₂₀₀ upon keeping the temperature settled for 20 min. The formal redox potential for PEO-Hb, calculated from the cathodic (48 mV vs Ag) and anodic (-110 mV vs Ag) peak potentials, was -31 mV vs Ag in PEO₂₀₀ at 30°C . The electrochemical response for PEO-Hb at the ITO glass electrode in PEO₂₀₀ was stable even under continuous potential cycling for at least 24 h at 30°C . The ratio of the anodic to cathodic peak current was almost unity at all temperatures (30 – 120°C). The peak potential separation of PEO-Hb in PEO₂₀₀ was also unchanged by alterations in this temperature range. However, the peak current and the charge for PEO-Hb in PEO₂₀₀ increased with increasing temperatures. PEO-Hb, solubilized in PEO₂₀₀, was stable and redox active up to 120°C . A redox response of PEO-Hb in PEO₂₀₀ was found even at 140°C , although the charge for PEO-Hb in PEO₂₀₀ at 140°C was smaller than that at 120°C . This observation suggests that PEO-Hb in PEO₂₀₀ was gradually denatured at 140°C . The thermostability of porcine pancreatic lipase in an organic medium was also reported by Klibanov's group (25). There is also a report on the thermostability of the membrane protein in two-dimensional films at 140°C (26). These results suggest that proteins themselves are thermally stable in the absence of water.

A detailed study was carried out to elucidate the factors responsible for this thermostability. The thermal response of Hb and PEO-Hb is first verified by differential scanning calorimetry (DSC). Both native Hb and PEO-Hb in 0.10 M potassium phosphate buffer (pH 7.0) showed a characteristic endothermic peak at 60°C as shown in Figure 2. This peak can be attributed to conformational change and especially to the unfolding of the polypeptide chain. Both Hb and PEO-Hb in a buffer solution were denatured and formed irreversible aggregates above 60°C . The DSC study clearly showed

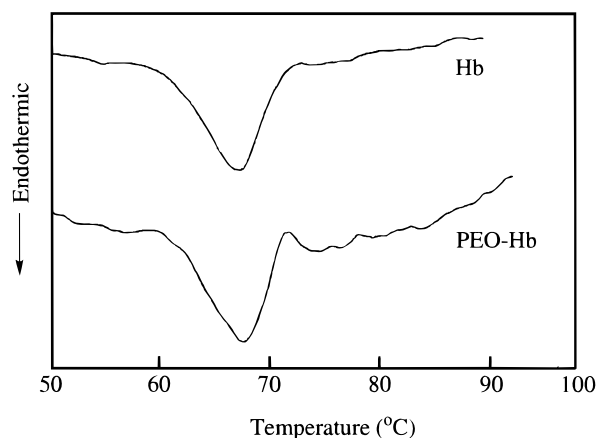


Figure 2. DSC thermograms for native Hb and PEO-Hb in 0.10 M potassium phosphate buffer at pH 7.0 with a scan rate of 1 °C min⁻¹. The protein concentration was 0.2 g mL⁻¹.

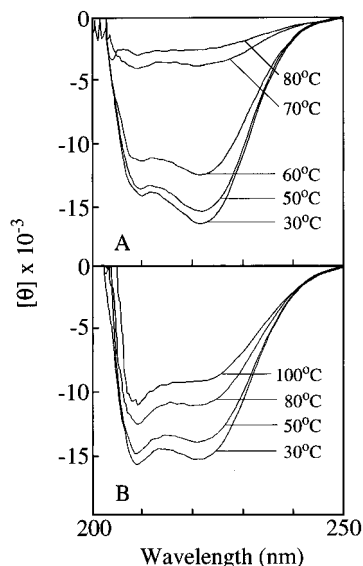


Figure 3. CD spectra for native Hb in 0.10 M potassium phosphate buffer at pH 7.0 (A) and PEO-Hb in PEO₂₀₀ containing 0.50 M KCl (B).

that PEO modification of Hb did not improve the thermostability in a buffer solution. These DSC results strongly suggest that the excellent thermostability is due to the use of PEO oligomers as a solvent.

Figure 3 shows circular dichroism (CD) spectra of native Hb in buffer (A) and PEO-Hb in PEO₂₀₀ (B) at various temperatures. It is known that native Hb shows about 75% α -helix content (27). Native Hb in 0.10 M potassium phosphate buffer at pH 7.0 showed two strong negative absorptions at 208 and 222 nm due to the α -helix structure at room temperature (Figure 3A). These were also observed for PEO-Hb in PEO₂₀₀ (Figure 3B). The α -helix content for PEO-Hb was confirmed to be reduced little even in PEO₂₀₀ with CD measurement. We have already reported that the α -helix content of PEO-modified myoglobin in PEO oligomers was almost the same as that in buffer (12). In a buffer solution at pH 7.0, the α -helix content of Hb decreased with increasing temperatures (Figure 3A). This change was irreversible, and the α -helix content was not recovered even after cooling. The α -helix content of PEO-Hb in PEO₂₀₀ also decreased with increasing temperatures, but only slightly (Figure 3B). This change was smaller than that in a buffer solution, and the α -helix content of PEO-Hb was mostly recovered by cooling. Although heating up to 100 °C induces a slight conformational change of PEO-Hb in

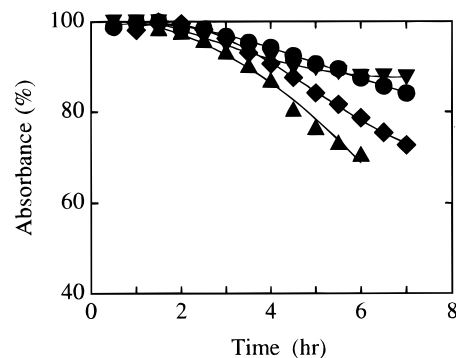


Figure 4. Absorbance changes at the λ_{\max} for oxidized PEO-Hb at 80 °C in PEO₂₀₀ under an applied potential of 0.5 V vs Ag. The concentrations of KCl were 0.05 (▲), 0.10 (▼), 0.20 (◆), and 0.50 M (●).

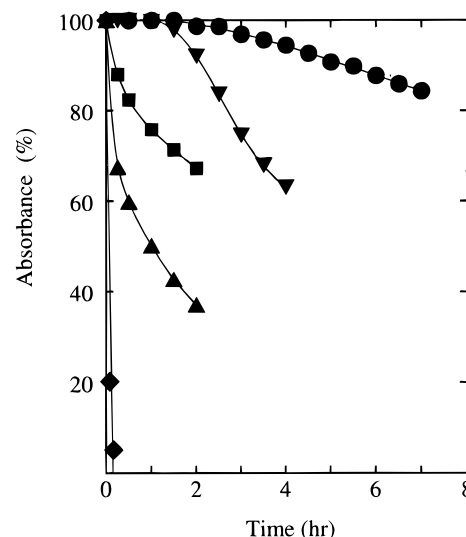


Figure 5. Absorbance changes at the λ_{\max} for oxidized PEO-Hb at 80 °C in different glycols under an applied potential of 0.5 V vs Ag. The solvents were PEO₂₀₀ (●), tri(ethylene glycol) (▼), di(ethylene glycol) (■), ethylene glycol (▲), and 0.10 M potassium phosphate buffer at pH 7.0 (◆). Every solvent contains 0.50 M KCl.

the PEO oligomer, this change is reversible and less dramatic. Thermal denaturation of PEO-Hb in PEO oligomers should differ from that in the phosphate buffer solution.

To confirm the effect of the KCl concentration on the thermal response of PEO-Hb in PEO₂₀₀, a series of experiments was carried out to compare certain physicochemical characteristics of the solvent. It is known that the ionic conductivity, the glass transition temperature, and the degree of crystallinity of the PEO matrix are considerably affected by the concentration of the supporting electrolytes (28). The absorbance at the λ_{\max} for oxidized PEO-Hb in PEO₂₀₀ solutions containing different concentrations of KCl was recorded at 80 °C under a constant potential of 0.5 V vs Ag, as shown in Figure 4. The absorbance for PEO-Hb in PEO₂₀₀ containing different concentrations of KCl was not changed at 80 °C for 2 h, indicating no dependence on the salt concentration. The effect of the concentration of supporting electrolytes in PEO₂₀₀ should be small in the concentration range of 0.05–0.50 M.

Figure 5 shows the effect of molecular weight of the solvent PEO on the thermostability of oxidized PEO-Hb at 80 °C under an applied potential of 0.5 V vs Ag. When tri(ethylene glycol) and PEO₂₀₀ were used as a solvent, the absorbance at the λ_{\max} for oxidized PEO-Hb was

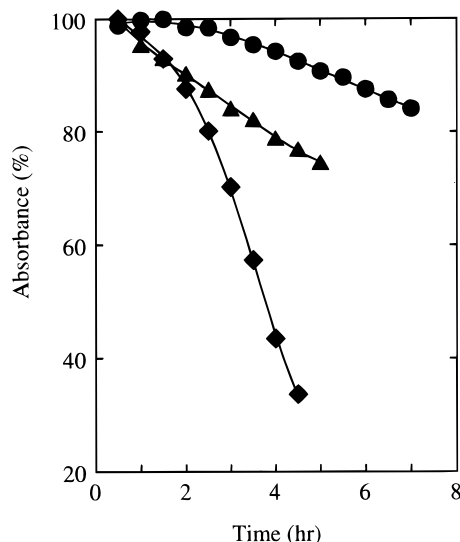


Figure 6. Absorbance changes at the λ_{\max} for oxidized PEO-Hb in PEO₂₀₀ containing 0.50 M KCl at 80 °C under an applied potential of 0.5 V vs Ag. The water contents were 0.3 (●), 10 (▲), and 20 wt % (◆).

constant at 80 °C for 2 h. After longer incubation times, PEO-Hb in PEO₂₀₀ was confirmed to be more stable upon heating than PEO-Hb in tri(ethylene glycol). However, in a phosphate buffer, ethylene glycol, and di(ethylene glycol), the absorbance of PEO-Hb decreased by more than 20% within a few minutes upon incubation at 80 °C. The decrease in the absorbance for PEO-Hb was more marked when glycols with smaller molecular weights and phosphate buffer were used as solvents. The molecular weight of PEO oligomers used as solvents considerably affected the thermostability of proteins. As mentioned above, an increase in the molecular weight of the solvent made protein more stable for several hours at 80 °C. The secondary structure of PEO-Hb is expected to be solvated with polar groups of the solvent glycols, such as the terminal OH groups. The segmental motion of the polypeptide chain itself is influenced by the surrounding molecular motion of the solvent molecules. This result suggests that the reduced thermal motion of the oligomer solvent at high temperatures should improve the thermostability of proteins.

There would also be reduced thermostability of proteins in a mixed PEO/water solvent system if the presence of a low-molecular weight solvent was the major factor causing reduced thermostability. The effect of the total water content for the PEO-Hb solution on the thermostability of PEO-Hb in PEO₂₀₀ is shown in Figure 6. PEO-Hb/PEO₂₀₀ solution containing KCl (<0.3% H₂O) was mixed with different amounts of water. The absorbance at the λ_{\max} for oxidized PEO-Hb decreased remarkably with the water content. This result suggests that the water in PEOs considerably reduces the thermostability of the proteins. Since mixed PEO/water solvent is known to be a precipitant for some proteins (29), there is a possibility of inducing a conformational change of the protein in such mixed solvents. We must therefore discuss the effect of water molecules in a mixed solvent. We observed no precipitation of PEO-Hb in mixed PEO/water solvent regardless the water content. A detailed discussion on the conformational characteristics of PEO-Hb in this mixed solution will be given elsewhere.

Characteristics of PEO-Hb in PEO₂₀₀ below the Physiological Temperature. Figure 7 shows UV-vis spectra of oxidized (Fe³⁺) and reduced (Fe²⁺) forms of deoxy-PEO-Hb in PEO₂₀₀ containing 0.50 M KCl below

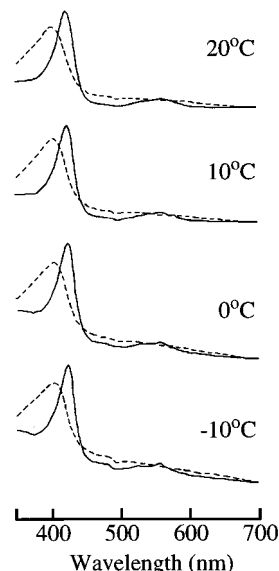


Figure 7. UV-vis spectra of PEO-Hb in PEO₂₀₀ at a temperature below the physiological temperature. The spectra of oxidized (---) and reduced (—) PEO-Hb were recorded under applied potentials of 0.5 and -1.2 V vs Ag, respectively.

the physiological temperature. Dashed and solid lines refer to data for oxidized and reduced PEO-Hb, respectively. These data were recorded under the fixed potentials of 0.5 and -1.2 V vs Ag, respectively. The oxidized PEO-Hb was reduced and reoxidized in PEO₂₀₀ even at -10 °C. The change in the UV-vis spectrum at -10 °C was similar to that at room temperature. Even below room temperature, no significant effects on the UV-vis spectra and redox activity for PEO-Hb were recognized in PEO₂₀₀ except for the apparent rate constant. Although an aqueous solution was not used as a solvent below 0 °C, this result clearly shows that protein is electrochemically active below 0 °C when PEO is used as a solvent. However, the electrochemical redox reaction requires a longer time at lower temperatures. This is due to a slow diffusion of PEO-Hb in PEO, which should be improved by the use of a less viscous matrix or another reaction system. No effect of PEO modification on the absorption maximum at the Soret band of PEO-Hb, arising from $\pi-\pi^*$ transitions of the heme active site, has been reported (24). The heme active site for Hb was therefore considered to be unchanged by PEO modification. In PEO₂₀₀, the absorption maximum at Soret bands of deoxy-PEO-Hb for both oxidized and reduced forms shifted slightly to a shorter wavelength compared to that in a buffer solution. This suggests little structural change around heme for PEO-Hb in PEO₂₀₀. For other PEO-modified heme proteins in nonaqueous media, a structural change of the heme active site has been reported (20, 22).

The maximum absorbance at a λ_{\max} of 423 nm for reduced PEO-Hb was altered by the polarity change of the given potential in PEO₂₀₀ at 80, 30, and -10 °C as shown in panels A-C of Figure 8, respectively. The absorbance at 423 nm increased upon applying negative potential and decreased with positive potential in PEO₂₀₀ at all temperatures examined. The rates of oxidation and reduction of PEO-Hb increased with elevating temperature as is clearly seen in Figure 8, suggesting the diffusion control systems. Supporting evidence for the redox activity of PEO-Hb in PEO₂₀₀ at -10 °C is provided by the cyclic voltammetry observations as shown in Figure 9. Typical redox responses of PEO-Hb were also obtained in PEO₂₀₀ below room temperature. Both the peak current and the charge for PEO-Hb decreased with

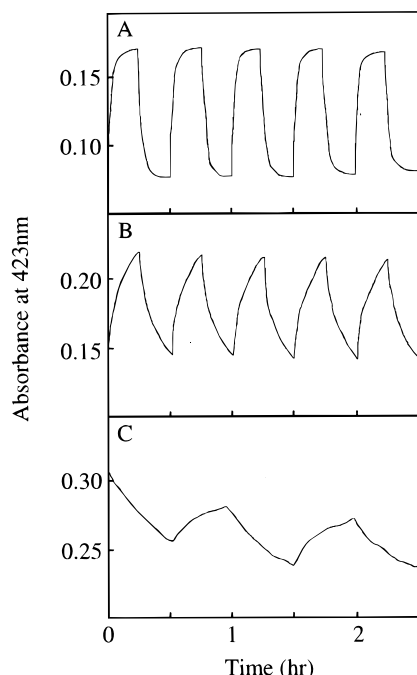


Figure 8. Absorbance changes at the λ_{\max} for reduced PEO-Hb in PEO₂₀₀ containing 0.50 M KCl under potential switching (± 1.2 V vs Ag) at 80 (A), 30 (B), and -10 °C (C).

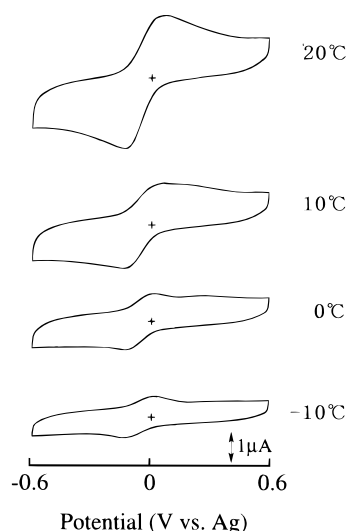


Figure 9. Cyclic voltammograms for PEO-Hb at an ITO electrode recorded with a scan rate of 33 mV s^{-1} in PEO₂₀₀ containing 0.50 M KCl at -10 to 20 °C.

decreasing temperatures. This may be due to the reduced ionic conductivity of PEO oligomer as a solvent, and slow diffusion of PEO-Hb, at lower temperatures. However, the peak separation at -10 °C, which was estimated from the cathodic (17 mV vs Ag) and anodic (-127 mV vs Ag) peak potentials, was almost the same as that at 30 °C in PEO₂₀₀. This observation suggests that the rate of redox reaction of PEO-Hb in the vicinity of the ITO electrode below 0 °C was almost the same as that at room temperature.

CONCLUSION

We have found that PEO-Hb showed quasi-reversible direct electron transfer in PEO₂₀₀ at -10 to 120 °C. The molecular weight and water content of solvent PEO strongly affected the thermostability of PEO-Hb. Both a high molecular weight and a decrease in the water content of the solvent improved the thermostability of

PEO-Hb in PEO₂₀₀. The use of dehydrated polyethers allowed the preparation of protein redox systems that proved to be highly stable against heating.

ACKNOWLEDGMENT

The authors thank Dr. Yuji Iwashita (Central Research Center, Ajinomoto Co. Ltd.) for supplying Hb and PEO-Hb. The present study was supported by a Grant-in-Aid for Scientific Research from the Ministry of Education, Science, Sports and Culture, Japan (08246101).

LITERATURE CITED

- (1) MacCallum, J. R., and Vincent, C. A., Eds. (1987) *Polymer Electrolyte Reviews-1*, Elsevier Applied Science, London.
- (2) MacCallum, J. R., and Vincent, C. A., Eds. (1989) *Polymer Electrolyte Reviews-2*, Elsevier Applied Science, London.
- (3) Gray, F. M. (1991) *Solid Polymer Electrolytes*, VCH Publishers Inc., New York.
- (4) Oliver, B. N., Egekeze, J. O., and Murray, R. W. (1988) "Solid-state" voltammetry of a protein in a polymer solvent. *J. Am. Chem. Soc.* **110**, 2321–2322.
- (5) Ohno, H. (1992) Applications of polymer electrolytes: electrochromics, sensors and biology. *Electrochim. Acta* **37**, 1649–1651.
- (6) Ohno, H., and Satoh, H. (1993) Solubility, diffusion coefficient and ionic conductivity of alkyl viologens in poly(ethylene oxide) and its derivatives. *J. Electroanal. Chem.* **360**, 27–37.
- (7) Ohno, H. (1994) Polymer solvents for electrochemical reactions. *J. Macromol. Sci., Pure Appl. Chem.* **A31**, 1881–1891.
- (8) Ohno, H., Yoshida, H., and Ohtsuka, M. (1994) Effect of salt species on the electrochemical p-doping of poly(pyrrole) films in poly(ethylene oxide) oligomers. *Solid State Ionics* **68**, 125–131.
- (9) Ohno, H., Yamaguchi, N., and Watanabe, M. (1993) Electron transfer reaction of poly(ethylene oxide)-modified hemoglobin on the ITO electrode in solid polymer electrolytes. *Polym. Adv. Technol.* **4**, 133–138.
- (10) Ohno, H., and Kawahara, N. Y. (1995) Electron transfer of heme proteins on the ITO electrode in polymer solvents. *Polym. Adv. Technol.* **6**, 185–189.
- (11) Ohno, H., and Tsukuda, T. (1992) Electron-transfer reaction of polyethylene oxide-modified myoglobin in polyethylene oxide oligomers. *J. Electroanal. Chem.* **341**, 137–149.
- (12) Ohno, H., Ohkubo, W., and Yamaguchi, N. (1994) Conformation and electrochemical reduction of myoglobin in PEO oligomers. *Polym. Adv. Technol.* **5**, 411–415.
- (13) Harris, J. M., Ed. (1992) *Poly(ethylene glycol) Chemistry: Biotechnical and Biomedical Applications*, Plenum Press, New York.
- (14) Inada, Y., Matsushima, A., Kodera, Y., and Nishimura, H. (1990) Polyethylene glycol (PEG)-protein conjugates: application to biomedical and biotechnological processes. *J. Bioact. Compat. Polym.* **5**, 343–364.
- (15) Kamisaki, Y., Wada, H., Yagura, T., Matsushima, A., and Inada, Y. (1981) Reduction in immunogenicity and clearance rate of *Escherichia coli* L-asparaginase by modification with monomethoxy polyethylene glycol. *J. Pharmacol. Exp. Ther.* **216**, 410–414.
- (16) Iwashita, Y. (1991) Pyridoxalated hemoglobin-polyoxyethylene conjugate (PHP) as an oxygen carrier. *Artif. Organs Today* **1**, 89–114.
- (17) Ye, J., and Baldwin, R. P. (1988) Catalytic reduction of myoglobin and hemoglobin at chemically modified electrodes containing methylene blue. *Anal. Chem.* **60**, 2263–2268.
- (18) Takahashi, K., Yoshimoto, T., Ajima, A., Tamaura, Y., and Inada, Y. (1984) Modified lipase catalyzes ester synthesis in benzene. *Enzyme* **32**, 235–240.
- (19) Matsushima, A., Okada, M., and Inada, Y. (1984) Chymotrypsin modified with polyethylene glycol catalyzes peptide synthesis reaction in benzene. *FEBS Lett.* **178**, 275–277.
- (20) Mabrouk, P. A. (1995) The use of nonaqueous media to probe biochemically significant enzyme intermediates: The generation and stabilization of horseradish peroxidase com-

- pound II in neat benzene solution at room temperature. *J. Am. Chem. Soc.* 117, 2141–2146.
- (21) Ohsaka, T., Shintani, Y., Matsumoto, F., Okajima, T., and Tokuda, K. (1995) Mediated electron transfer of polyethylene oxide-modified superoxide dismutase by methyl viologen. *Bioelectrochem. Bioenerg.* 37, 73–76.
- (22) Kurusu, F., Kawahara, N. Y., and Ohno, H. (1996) Electron transfer of PEO-modified cytochrome *c* in PEO oligomers. *Solid State Ionics* 86–88, 337–340.
- (23) Kawahara, N. Y., Muneyasu, K., and Ohno, H. (1997) Conformation and redox reaction of poly(ethylene oxide)-modified horseradish peroxidase in poly(ethylene oxide) oligomers. *Chem. Lett.* 381–382.
- (24) Ohno, H., and Yamaguchi, N. (1994) Redox reaction of poly(ethylene oxide)-modified hemoglobin in poly(ethylene oxide) oligomers at 120 °C. *Bioconjugate Chem.* 5, 379–381.
- (25) Zaks, A., and Klivanov, A. M. (1984) Enzymatic catalysis in organic media at 100 °C. *Science* 224, 1249–1251.
- (26) Shen, Y., Safinya, C. R., Liang, K. S., Ruppert, A. F., and Rothschild, K. J. (1993) Stabilization of the membrane protein bacteriorhodopsin to 140 °C in two-dimensional films. *Nature* 366, 48–50.
- (27) Colowic, S. P., and Kaplan, N. O., Eds. (1981) Hemoglobin. *Methods in Enzymology*, Vol. 76, Academic Press, San Diego.
- (28) Ohno, H., Inoue, Y., and Wang, P. (1993) Temperature-controlled ionic conductivity switching in poly[oligo(oxyethylene)methacrylate]/poly(ethylene oxide) layered film. *Solid State Ionics* 62, 257.
- (29) Ingham, K. C. (1984) Protein precipitation with polyethylene glycol. *Methods Enzymol.* 104, 351–356.

BC9701196

Interactions of Pluronic Block Copolymers with Brain Microvessel Endothelial Cells: Evidence of Two Potential Pathways for Drug Absorption

Donald W. Miller,^{*,†} Elena V. Batrakova,[†] Timothy O. Waltner,[†] Valery Yu. Alakhov,[‡] and Alexander V. Kabanov[†]

Department of Pharmaceutical Sciences, University of Nebraska Medical Center, 600 South 42nd Street, Omaha, Nebraska 68198, and Supratek Pharma Inc., c/o Institute Armand-Frappier, 513 Boulevard des Prairies, Case Postale 100, Laval, Quebec, Canada H7N 4Z3. Received March 7, 1997[®]

Pluronic block copolymers have been previously reported to increase the delivery of agents to the brain [Kabanov *et al.* (1992) *J. Controlled Release* 22, 141–158]. In the present study, primary cultured bovine brain microvessel endothelial cells (BBMEC) were used as an *in vitro* model of the blood–brain barrier to examine the membrane interactions of Pluronic P85 (P85) and potential mechanisms for drug absorption. At concentrations below the critical micelle concentration (cmc), P85 enhanced the accumulation of the fluorescent probe rhodamine 123 (R123) in BBMEC through inhibition of P-glycoprotein (P-gp)-mediated drug efflux. The effects of P85 on the cellular accumulation of R123 were also observed in KBv cells (P-gp positive) but not in human umbilical vein endothelial cells (P-gp negative). In contrast to the effects with P85 below the cmc, the enhanced absorption of R123 observed with Pluronic micelles was transient and not dependent on P-gp. A transient increase in R123 accumulation was observed in both P-gp positive cells (brain microvessel endothelial cells and KBv) and P-gp negative cells (human umbilical vein endothelial cells). Therefore, it appears that P85 affects the absorption of drugs in brain microvessel endothelial cells through (1) inhibition of the P-gp-mediated drug efflux at low concentrations of the copolymer and (2) increased vesicular transport at higher concentrations of the copolymer. Furthermore, both interactions of P85 with the brain endothelial cells appear to be energy-dependent as demonstrated by the inhibitory effects of the metabolic inhibitor 2-deoxyglucose.

INTRODUCTION

Amphiphilic block copolymers, such as Pluronic copolymers with the basic poly(ethylene oxide)_a–poly(propylene oxide)_b–poly(ethylene oxide)_a structure, are of interest as potential drug delivery and drug targeting systems due to their ability to form self-assembling micelles (1–7). However, little is known about the interactions of the block copolymers with cellular membranes. Studies in Jurkat T lymphoma cells and MDCK cells suggest that the micelles of Pluronic copolymers are absorbed through an endocytic pathway (8). In addition, recent studies suggest that Pluronic copolymers can increase drug absorption in multiple-drug-resistant cancer cells by inhibition of the P-glycoprotein (P-gp¹) drug efflux system in cells (9, 10). Together these studies indicate that Pluronic copolymers may enhance drug absorption in the cell through separate and distinct pathways.

The present study examines the interactions of Pluronic copolymers with brain microvessel endothelial cells

that form the blood–brain barrier (BBB). Pluronic P85 (P85) micelles have been previously reported to enhance the delivery of haloperidol to the brain, resulting in a significant increase in neuroleptic activity of the drug (2, 4). The mechanisms for the enhanced brain delivery of haloperidol with P85 are unknown. Brain microvessel endothelial cells have reduced levels of vesicular activity compared to peripheral endothelial cells (11), as well as increased expression of P-gp (12, 13). Thus, the enhanced delivery of haloperidol to the brain observed with P85 may be attributable to enhanced endocytosis and/or inhibition of P-gp in the brain endothelial cells.

Using primary cultured bovine brain microvessel endothelial cells (BBMEC) as an *in vitro* model of the BBB, we report that P85 can affect the absorption of drugs in brain microvessel endothelial cells through (1) inhibition of P-gp at low concentrations of the copolymer and (2) increased vesicular transport at higher concentrations of the copolymer. Furthermore, both interactions of P85 with the brain endothelial cells appear to be energy-dependent processes. Understanding the properties of the Pluronic copolymers that are required to interact with the two absorption pathways may allow further development of more effective approaches for enhancing drug delivery to the brain.

MATERIALS AND METHODS

Cell Isolation and Culturing. BBMEC were isolated from fresh cow brains using a combination of enzymatic digestion and density centrifugation as described previously (14). The BBMEC were seeded at a density of 50 000 cells/cm² onto collagen-coated, fibronectin-treated 24-well plates using MEM:F12 culture media supplemented with 10% horse serum, heparin sulfate

* Author to whom correspondence should be addressed.

[†] University of Nebraska Medical Center.

[‡] Supratek Pharma Inc.

[®] Abstract published in *Advance ACS Abstracts*, August 1, 1997.

¹ Abbreviations: BBB, blood–brain barrier; BBMEC, bovine brain microvessel endothelial cells; cmc, critical micelle concentration; CSA, cyclosporin A; DG, 2-deoxyglucose; DMEM, Dulbecco's modified essential medium; EO, ethylene oxide; FBS, fetal bovine serum; HLB, hydrophilic–lipophilic balance; HUVEC, human umbilical vein endothelial cells; LY, Lucifer Yellow; P85, Pluronic P85, EO₂₅–PO₃₉–EO₂₅; PBS, phosphate-buffered saline; PO, propylene oxide; P-gp, P glycoprotein; R110, rhodamine 110; R123, rhodamine 123.

(100 $\mu\text{g/mL}$), amphotericin B (2.5 $\mu\text{g/mL}$), and gentamicin (50 $\mu\text{g/mL}$). Medium was replaced every other day, and studies were performed on confluent BBMEC monolayers (10–13 days). To examine the P-gp-mediated responses with P85, two additional cell types were also used. Human umbilical vein endothelial cells (HUVEC) were isolated and cultured as described by Kasakoff and colleagues (15). Both functional and biochemical studies with HUVEC indicate that these cells express little, if any, P-gp (12, 13). The multidrug-resistant KBv cell line, which expresses high levels of P-gp, was also used (16). To maintain the high expression of P-gp in the KBv cells, the cells were cultured in DMEM supplemented with 10% FBS and 1 $\mu\text{g/mL}$ vinblastine. Both the HUVEC and KBv cells were grown in 24-well culture plates and used in accumulation experiments after reaching confluency. Confluency of all the cell monolayers was determined by visual inspection using an inverted light microscope.

Preparation of Pluronic Block Copolymer Solutions. The present study uses P85, a poly(ethylene oxide)-*block*-poly(propylene oxide)-*block*-poly(ethylene oxide) copolymer provided by BASF Co. (Parisspany, NJ). The molecular mass of the propylene oxide segment in this sample was 2500, and the content of ethylene oxide chains was 50% w/w. P85 solutions were prepared on a percent weight basis by dissolving various amounts of the copolymer in assay buffer. At concentrations above the critical micelle concentration (cmc) (0.03% w/v) P85 self-assembles into micelles of approximately 15 nm in diameter (4). The rhodamine compounds, R123 and R110, were added to the P85 solutions and incubated at 37 °C for at least 1 h prior to use in the experiments.

Cellular Accumulation of R123, R110, and LY. The cellular accumulation of the fluorescent dyes (R123, R110, and LY) was used to examine the effects of Pluronic copolymers on the cell monolayers. Previous studies with R123 (13) and LY (17) in BBMEC monolayers indicate that these fluorescent markers are good probes for examining P-gp and fluid-phase endocytic activity, respectively. Furthermore, compared to R123, the structural analog R110 has little interaction with P-gp (18). Cell monolayers were washed and preincubated for 30 min at 37 °C with assay buffer. After this, the assay buffer was removed and the cells were exposed to R123 (3.2 μM), R110 (3.2 μM), or LY (0.5 μM) in either assay buffer or assay buffer containing various concentrations of Pluronic copolymers (BASF). The cells were incubated with dye solutions for up to 120 min at 37 °C. After that, the dye solutions were removed and cell monolayers were washed three times with ice-cold PBS. The cells were then solubilized in 1.0% Triton X-100, and aliquots (0.25 mL) were removed for determination of cellular dyes using a Shimadzu RF5000 fluorescent spectrophotometer: λ_{ex} = 505 nm, λ_{em} = 540 nm for R123 and R110; λ_{ex} = 430 nm, λ_{em} = 540 nm for LY. Samples were also taken for protein determination using the Pierce BCA method. In separate experiments, the cellular accumulation of R123 or LY was determined using the metabolic inhibitor, 2-deoxyglucose (DG). For these experiments, the cells were preincubated for 60 min at 37 °C in assay buffer containing DG (40 mM). Cellular accumulation of R123 (3.2 μM) or LY (0.5 mg/mL) was then performed in assay buffer or in P85 solutions containing 40 mM DG.

In separate studies, BBMEC were grown on collagen-coated, fibronectin-treated chamber slides (Fisher, St. Louis, MO) for examining R123 cellular accumulation using fluorescent microscopy. The BBMEC were exposed to the various R123 solutions for either 15 or 90 min at 37 °C. After this incubation period, the R123 solutions were removed and the BBMEC were washed a total of

three times with ice-cold PBS and examined using a Leitz fluorescent microscope.

Cellular Accumulation of [^3H]P85. [^3H]P85 with specific radioactivity of 0.3 Ci/mmol was provided by the Faculty of Chemistry, Moscow State University (Russia). The uptake of [^3H]P85 was examined in confluent BBMEC monolayers at 37 °C for 0–90 min time intervals. For these studies, the culture medium was removed from the BBMEC monolayers and replaced with assay buffer. After a 30 min preincubation at 37 °C, the assay buffer was removed and 0.5 mL of 0.5 $\mu\text{Ci/mL}$ (1.6 nM) [^3H]P85 solution was added to the monolayers. The cellular accumulation of [^3H]P85 was done in the presence and absence of the metabolic inhibitor, DG. For this study, BBMEC monolayers were pretreated with 40 mM DG as described in the previous section. After the pretreatment, BBMEC monolayers were exposed to [^3H]P85 with 40 mM DG. The uptake experiments were stopped by removing the radiolabeled copolymer solutions and washing the BBMEC monolayers three times with 0.5 mL of ice-cold PBS. The BBMEC monolayers were solubilized in 1.0% Triton X-100 (0.5 mL), and aliquots were taken for determining (1) cell-associated radioactivity using a Hewlett-Packard liquid scintillation counter and (2) protein content using the Pierce BCA method. Data from the [^3H]P85 uptake studies were expressed as amount of cell-associated copolymer per milligram of protein.

Determination of R123 and R110 Partitioning in P85 Micelles. The partitioning coefficients of R123 and R110, P , were determined as previously described for daunorubicin (9) from the dependence of drug fluorescence at λ_{ex} = 512 nm and λ_{em} = 540 nm on P85 concentration

$$\frac{I_{\text{max}} - I}{I - I_0} = \frac{119}{P([\text{P85}] - \text{cmc})} - \frac{1}{P} \quad (1)$$

where I_0 is the fluorescence intensity in the absence of P85, I is the fluorescence at the given P85 concentration, $[\text{P85}]$, and I_{max} is the fluorescence at a "saturating" concentration of P85 (when fluorescence reaches the maximal value). The value of P was 110 for R123 and 32 for R110. The fractions of drug that is incorporated into the micelles were determined from the equation

$$\alpha = \frac{P([\text{P85}] - \text{cmc})}{119 + (P - 1)([\text{P85}] - \text{cmc})} \quad (2)$$

where the cmc was determined using a fluorescent probe (pyrene) technique as previously described (19).

RESULTS

Concentration-Dependent Effects of P85 on R123 Accumulation. The cellular accumulation of R123 in BBMEC monolayers was examined in the presence of various concentrations of P85 (Figure 1). The effects of P85 on R123 accumulation in BBMEC monolayers were concentration-dependent. At concentrations below the cmc (0.03%) there was a steady increase in cell-associated R123, with both 0.001 and 0.01% P85 causing a significant increase in R123 accumulation in the BBMEC monolayers. The increase in cellular R123 occurring with concentrations of P85 below the cmc was comparable with that observed following treatment with the P-gp inhibitor, CSA (Figure 1). In contrast, at concentrations of P85 above the cmc (0.1–5% P85), there was a significant decrease in R123 accumulation in the BBMEC monolayer-

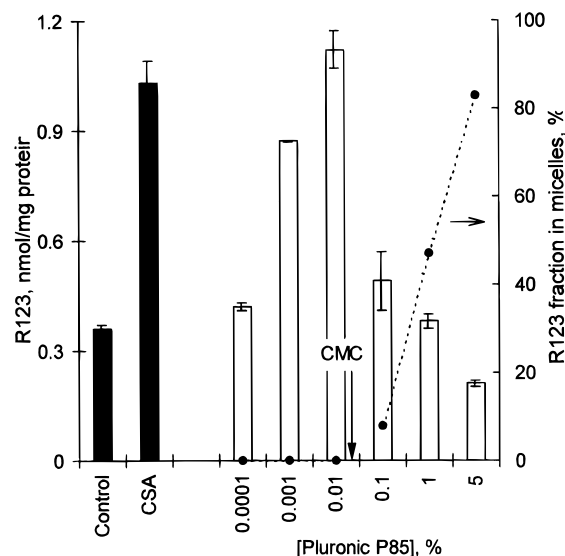


Figure 1. Concentration-dependent effects of P85 on R123 accumulation in BBMEC monolayers. Accumulation of R123 in BBMEC monolayers (60 min, 37 °C) was examined under control conditions, in the presence of 2 μ g/mL CSA, and in the presence of various concentrations of P85. Values represent the mean \pm SEM of four monolayers per treatment group. The solid circles show the fraction of R123 solubilized into micelles at the various concentrations of P85. The cmc of the P85 solution is shown by the vertical arrow.

ers. The decreased accumulation of R123 in BBMEC monolayers observed with the higher concentrations of P85 was inversely correlated with the extent of R123 partitioning into P85 micelles.

Cellular Interactions with P85 Unimers. To further examine the mechanism of the concentration-dependent responses with P85, the cellular accumulation of R123 was examined using a concentration of P85 below (unimer) the cmc. In the BBMEC monolayers, R123 accumulation was increased significantly with 0.001% P85 compared to that in the control group (Figure 2A). The effects of 0.001% P85 on R123 accumulation in the BBMEC monolayers were observed after approximately 15 min. The greatest increases in R123 accumulation in BBMEC monolayers treated with 0.001% P85 occurred at the later time points (60–90 min; Figure 2A). A similar enhancement of R123 accumulation was also observed in the P-gp expressing KBv cell monolayers in the 0.001% P85 treatment group (Figure 2B). In contrast, R123 accumulation was not increased in HUVEC and only slightly increased in the KB monolayers following treatment with 0.001% P85 (Figure 2C,D).

Studies comparing the cellular accumulation of the non-P-gp substrate, R110, were also performed in the presence and absence of 0.001% P85 in BBMEC monolayers (Figure 3). Unlike the studies with R123, the amount of cell-associated R110 in BBMEC monolayers was low and only slightly affected by 0.001% P85. The P-gp modifying agent CSA also had no significant effect on R110 accumulation in BBMEC monolayers. In contrast, CSA exposure increased R123 accumulation by approximately 2-fold over a 2 h time period compared to control monolayers receiving only R123 (Figure 3).

Cellular Interactions with P85 Micelles. The effects of P85 at concentrations above the cmc were also evaluated. In the BBMEC monolayers, treatment with 1.0% P85 caused an initial increase in the amount of cell-associated R123 compared to control monolayers receiving assay buffer (Figure 4A). This effect was transient and peaked within 15 min. At time points >15 min, the amount of cell-associated R123 began to decline, reaching

levels near control values within 60 min (Figure 4A). Although smaller in magnitude, a qualitatively similar pattern of cellular accumulation of R123 was also observed in KBv monolayers treated with 1.0% P85 (Figure 4B). The transient increase in R123 accumulation produced by P85 micelles was not confined to only the P-gp positive cells, as both HUVEC and KB monolayers showed an initial enhancement of R123 accumulation when treated with 1.0% P85 (Figure 4C,D). Furthermore, enhanced accumulation of R110 was also observed in BBMEC monolayers following treatment with 1.0% P85 (Figure 5).

Fluorescent Microscopy Studies in BBMEC Monolayers. Fluorescence microscopy studies confirm the time-dependent effect of P85 unimers and micelles on R123 accumulation in BBMEC (Figure 6). Following a 15 min exposure to R123, there is a clear increase in cellular fluorescence in the P85 unimer and micelle treatment groups, compared to control groups receiving assay buffer (Figure 6A–C). The fluorescence is highest at 15 min in the P85 micelle treatment group as an increase in R123 is seen throughout the entire cell. In contrast, the enhanced accumulation of R123 in the P85-unimer-treated cells at 15 min appears to be confined to the cytosol (Figure 6). At the 90 min R123 exposure period, there is an increase in R123 accumulation in the BBMEC treated with P85 unimers compared to control BBMEC. The increased accumulation of R123 in the P85 unimer treatment group at the 90 min time appears as an increased fluorescence in the cytosol of the cell (Figure 6D,E). In contrast, the fluorescence observed in the P85-micelle-treated BBMEC following 90 min exposure to R123 is substantially less than that of either the 90 min control or the 15 min P85 micelle treatment groups (Figure 6).

Role of Endocytosis in Interactions of P85 with BBMEC Monolayers. The possible involvement of endocytosis in the interactions of P85 with BBMEC monolayers was examined. As shown in Figure 7, cellular accumulation of the fluid phase endocytosis marker, LY, in BBMEC monolayers is time-dependent. Furthermore, exposure to the metabolic inhibitor, DG, resulted in a significant decrease in cell-associated LY in BBMEC monolayers (Figure 7A). In contrast, at the concentrations used in the present study, DG had no significant effect on R123 accumulation in BBMEC monolayers in the absence of P85 (Figure 7B).

The effect of DG on R123 accumulation in BBMEC monolayers exposed to P85 micelles is shown in Figure 8A. Within the first hour of exposure, there was a significant increase in cell-associated R123 in BBMEC monolayers treated with 1.0% P85 compared to control. Pretreatment of the BBMEC monolayers with DG resulted in a significant decrease in the amount of cell-associated R123 in the 1.0% P85 treatment group (Figure 8A). Exposure to DG had a similar inhibitory effect on R123 accumulation in BBMEC monolayers in the 0.001% P85 treatment group (Figure 8B).

The effects of DG on P85 unimer interactions with the BBMEC monolayers were further examined using [3 H]-P85. At concentrations of [3 H]P85 below the cmc (0.0007%) the accumulation of [3 H]P85 was time-dependent (Figure 9). Addition of DG resulted in a significant decrease in the amount of [3 H]P85 accumulating in the BBMEC monolayers at all time points above 15 min (Figure 9).

DISCUSSION

The results of the present study provide evidence supporting at least two potential pathways for enhancing

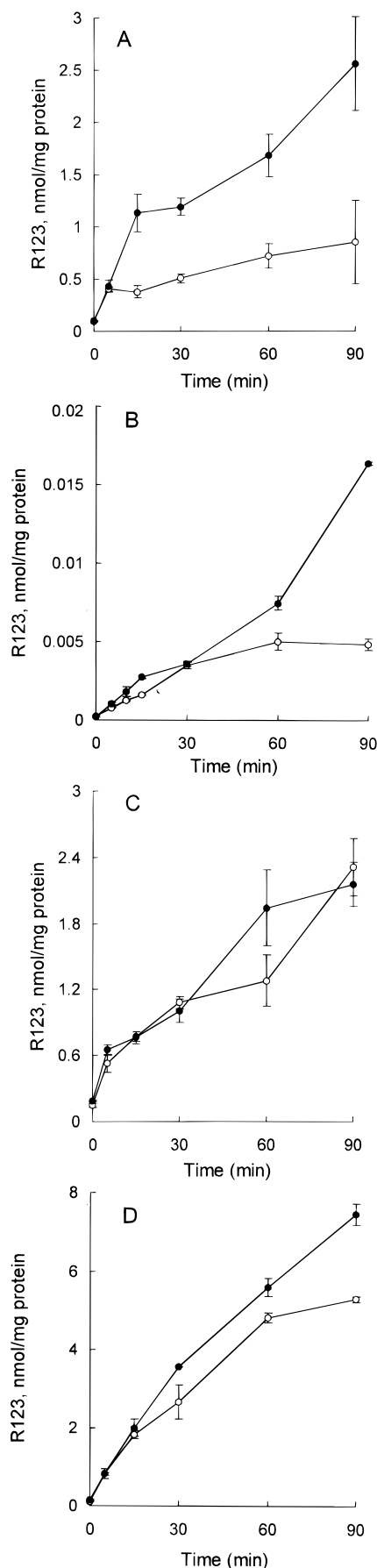


Figure 2. Effects of P85 unimers on R123 accumulation in various cells. Accumulation of R123 ($3.2 \mu\text{M}$) was examined using assay buffer (open circles) and 0.001% P85 (solid circles) in BBMEC (A), KBv (B), HUVEC (C), and KB monolayers (D). Values represent the mean \pm SEM of four monolayers.

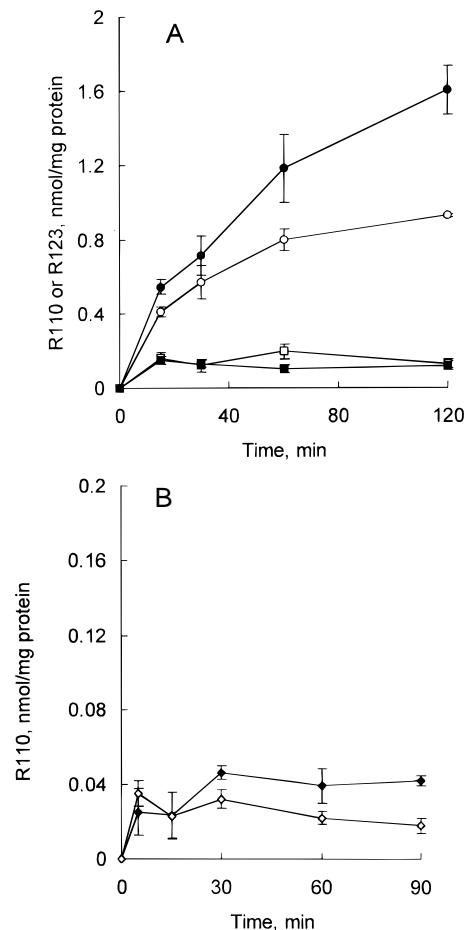


Figure 3. Accumulation of R123 and R110 in BBMEC monolayers. The accumulation of R123 (\circ , \bullet) and R110 (\square , \blacksquare) was examined in BBMEC monolayers over a 2 h period in the presence (solid symbols) and absence (open symbols) of $2 \mu\text{g/mL}$ CSA (A). The accumulation of R110 in BBMEC monolayers using assay buffer (\diamond) and 0.001% P85 (\blacklozenge) was also examined (B). Values shown represent the mean \pm SEM of three monolayers per treatment group.

drug absorption in the brain microvessel endothelial cells with P85 block copolymer. At concentrations below the cmc, P85 apparently inhibits P-gp function, thereby reducing drug efflux out of the brain microvessel endothelial cells. At concentrations above the cmc, P85 appears to increase vesicular transport of the drug into the brain microvessels.

There are several pieces of evidence supporting inhibition of P-gp as the cellular mechanism responsible for the enhanced absorption of R123 observed with unimer concentrations of P85 in BBMEC monolayers. First, the increased accumulation of R123 in BBMEC monolayers treated with P85 unimers resembles the increases in cell-associated R123 observed following exposure to CSA, a known inhibitor of P-gp function (13, 20). Under the conditions of the present study, inhibition of a drug efflux system, such as P-gp, would result in an increase in the amount of substrate in the cell. Therefore, the similarities in the effects of CSA and P85 unimers are consistent with the inhibition of P-gp-mediated removal of R123 from BBMEC.

Additional evidence supporting P-gp inhibition by P85 unimers can be found in the studies examining R123 accumulation in KBv, KB, and HUVEC monolayers. In KBv cells, a cancer cell line that overexpresses P-gp (16), the P85 unimers produced an increase in cell-associated R123 similar to that observed in the BBMEC monolayers. Furthermore, in HUVEC monolayers, which express little

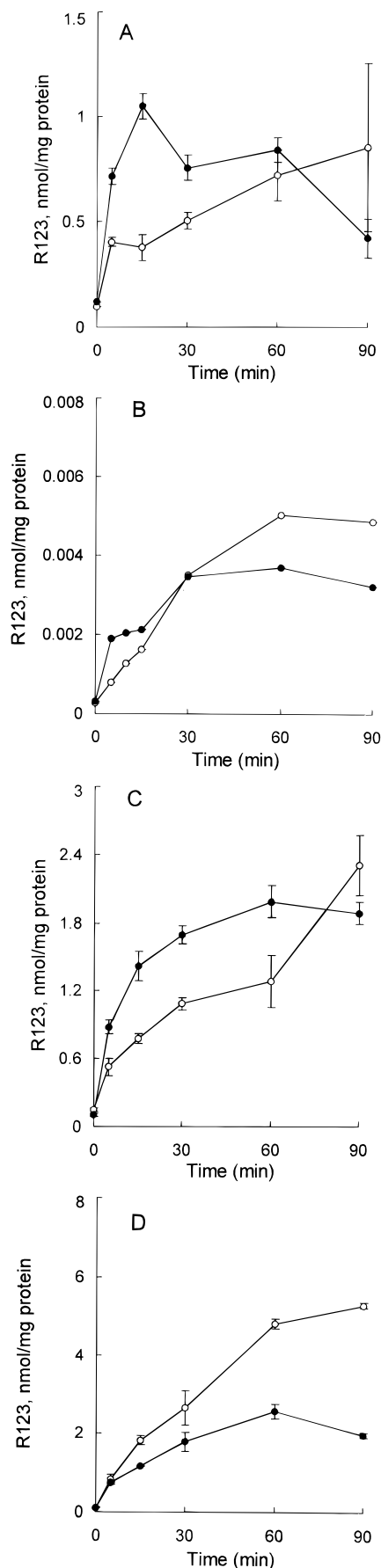


Figure 4. Effects of P85 micelles on R123 accumulation in various cells. Accumulation of R123 ($3.2 \mu\text{M}$) was examined using assay buffer (open circles) and 1.0% P85 (solid circles) in BBMEC (A), KBv (B), HUVEC (C), and KB monolayers (D). Values represent the mean \pm SEM of four monolayers.

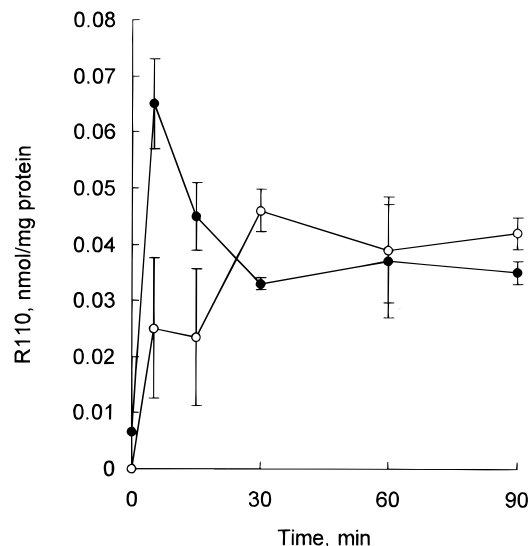


Figure 5. Effects of P85 micelles on the cellular accumulation of R110 in BBMEC monolayers. The accumulation of R110 in BBMEC monolayers was examined using assay buffer (open circles) and 1.0% P85 (solid circles) over a 90 min period. Values represent the mean \pm SEM of three monolayers.

if any P-gp (12), there was no enhancement of the cellular accumulation of R123 with the P85 unimers. While there was a small but significant enhancement of R123 accumulation with P85 unimers in the KB cells, this is probably due to inhibition of P-gp that may be expressed at a low intrinsic level in these cells. The fact that R123 is a substrate for P-gp (13, 21, 22) and the fact that its cellular accumulation is enhanced by the unimers of P85 in those cells expressing the protein suggest that P85 is inhibiting the function of P-gp. The minimal effects of 0.001% P85 on R123 accumulation in the KB and HUVEC monolayers also argues against a nonspecific increase in membrane permeability as the mechanism for the enhanced absorption observed with the unimers in BBMEC monolayers.

The final evidence supporting specific interactions of P85 unimers with P-gp are the studies with the zwitterionic analog of R123, R110. In the present studies, 0.001% P85 had little effect on R110 accumulation in BBMEC monolayers. Likewise, the P-gp inhibitor, CSA, had no significant effect on R110 accumulation in BBMEC monolayers. Despite structural similarities, R123 and R110 have significantly different transport capacities with respect to the P-gp drug efflux system (18). The reduction in P-gp activity with R110 appears to result from the electroneutrality of R110 compared to the positive charge associated with R123. The ability of the P85 unimers to selectively enhance R123 accumulation in the BBMEC monolayers is consistent with inhibition of P-gp-mediated transport out of the cells.

Previous studies have reported that various surfactants can inhibit P-gp-related drug efflux in cells (23–25). Furthermore, Pluronic copolymers have been shown to reverse multidrug resistance in cancer cells through what appears to be inhibition of P-gp-mediated drug efflux out of the cell (9, 10). On the basis of the results of the present study, it would appear that it is the unimer form of P85 that inhibits P-gp. Similar unimer effects were reported previously for Pluronic copolymers in multidrug-resistant cancer cells (9). It is also interesting to note that studies by Nerurkar *et al.* (23) report inhibition of drug efflux transport systems in Caco-2 cell monolayers with various surfactants at concentrations below the cmc.

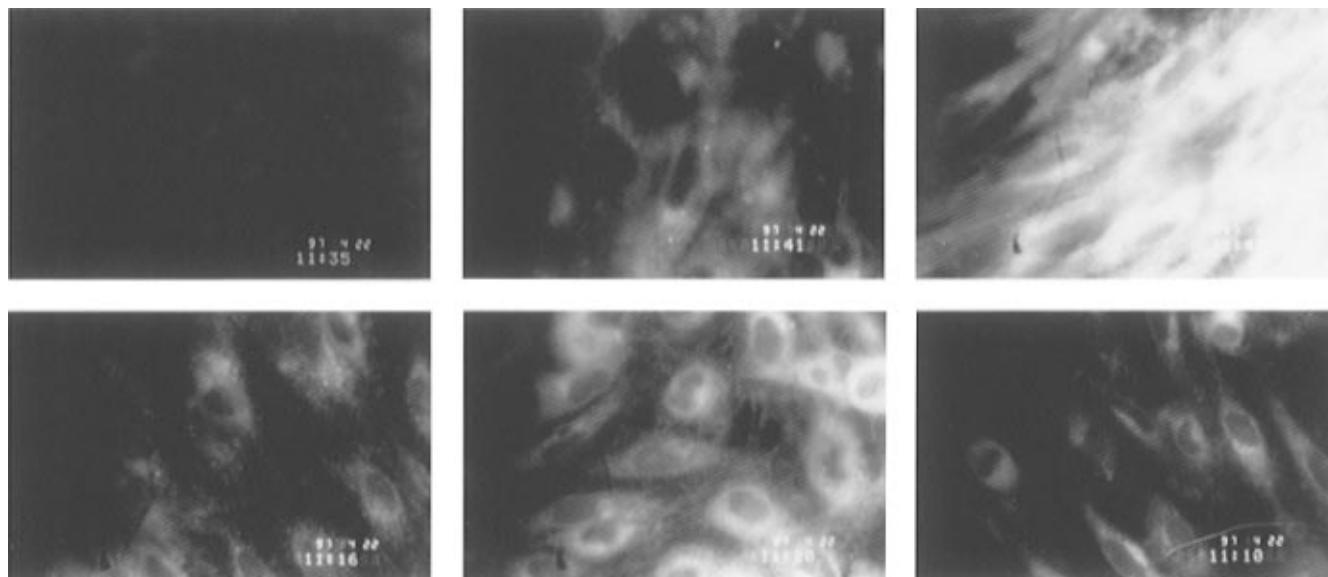


Figure 6. Fluorescent microscopy of R123 accumulation in BBMEC. The BBMEC were exposed to R123 in either assay buffer [A (top left), D (bottom left)], 0.01% P85 [B (top middle), E (bottom middle)], or 1.0% P85 [C (top right), F (bottom right)] for 15 min [A–C (top row)] or 90 min [D–F (bottom row)]. The cellular fluorescence was determined at 100 \times magnification using a Leitz fluorescent microscope. (The figure is reproduced here at 47% of the original.)

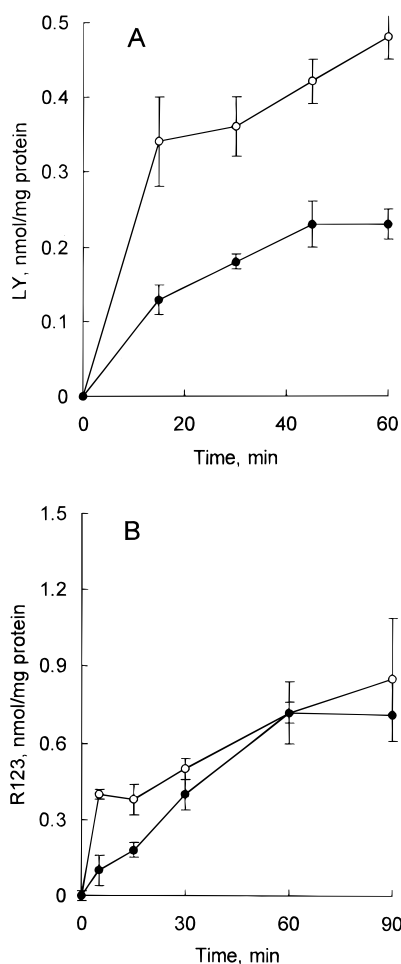


Figure 7. Energy dependency of LY and R123 accumulation in BBMEC monolayers. Accumulation of LY (A) and R123 (B) in BBMEC monolayers was examined in the presence (●) and absence (○) of 40 mM DG. Values represent the mean \pm SEM of four monolayers.

The fact that the apparent effects of P85 on P-gp-mediated transport systems are seen at concentrations below the cmc implies that the unimer is interacting either directly with the protein or with the lipid mem-

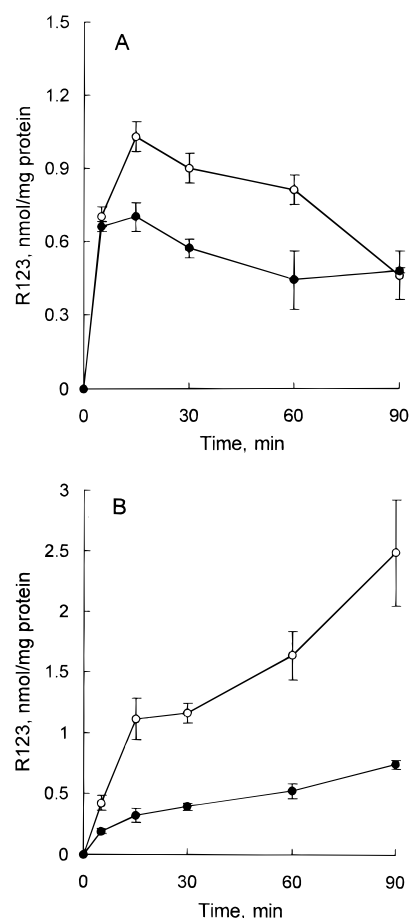


Figure 8. Energy dependency of P85 effects on R123 accumulation in BBMEC monolayers. The effects of 1.0% (A) and 0.001% P85 (B) on R123 accumulation in BBMEC monolayers was examined in the presence (solid circles) and absence (open circles) of 40 mM DG. Values represent the mean \pm SEM of four monolayers per treatment group.

brane microenvironment surrounding the protein. Regardless of the exact mechanism, it appears that the inhibition of P-gp with P85 unimers is related to vesicular transport since the effect of the unimers is completely abolished when endocytosis is inhibited with DG. The

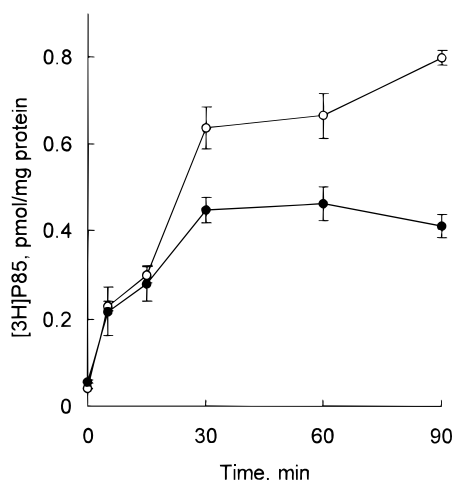


Figure 9. Energy dependency of $[^3\text{H}]\text{P85}$ accumulation in BBMEC monolayers. Accumulation of R123 in BBMEC monolayers was examined in the presence (●) and absence (□) of 40 mM DG. Values represent the mean \pm SEM of three monolayers per treatment group.

likely explanation is that to reach the site of action within the membrane, the P85 unimers must first undergo endocytic transport into the cell. This conclusion is also supported by the observation that DG inhibits the accumulation of the $[^3\text{H}]\text{P85}$ unimers in BBMEC cells. Internalization of the unimers through endocytic pathways may help explain the effects on R123 accumulation observed with the unimers, as there would be a lag time required for the unimer to undergo vesicular transport and be subsequently released from the endosome prior to interaction with P-gp.

The presence of P-gp in brain capillary endothelial cells and in cultured brain microvessel endothelial cells has been well-documented (12, 13, 26). The expression of the protein in the BBB is important in limiting the passage of potential neurotoxins from the blood to the central nervous system (27). However, recent studies suggest that the presence of P-gp in the endothelial cells that form the BBB may also influence the delivery, and ultimately the biological activity, of various central nervous system drugs (28). The results of the present study suggest that Pluronic copolymers, at concentrations below the cmc, may be useful for increasing the brain delivery of selective neuroleptic agents that interact with the P-gp drug efflux system. Indeed, given the recent studies suggesting haloperidol is a weak substrate for P-gp (28), inhibition of P-gp in the BBB may explain, in part, the enhanced brain delivery of haloperidol observed previously in mice treated with P85 (2, 4).

In addition to the effects of P85 unimers on P-gp, there appears to be another pathway that is involved with R123 accumulation in BBMEC monolayers at concentrations of P85 above the cmc. The kinetics associated with this pathway is markedly different from that observed with P85 unimers or free R123. Furthermore, the R123 accumulation in the cells following treatment with 1.0% P85 does not appear to be dependent on the presence of P-gp. The transient and rapid increase in cell-associated R123 in BBMEC monolayers treated with 1.0% P85 was also observed in HUVEC and to a lesser extent in KB cells. Furthermore, in contrast to P85 unimers, the accumulation of the P-gp-sensitive R123 and P-gp-insensitive R110 were similar with P85 micelles. Taken together, these experiments suggest a major difference in the transport mechanisms observed with the P85 unimers and micelles.

One possible route for R123 absorption in BBMEC monolayers in the presence of P85 micelles is through endocytosis. Previous studies have shown that block copolymers can direct vesicular transport of solubilized drugs into cells (8). In the present study, there were some qualitative similarities in the initial uptake kinetics associated with R123 in the presence of 1.0% P85 and that observed with the fluid phase endocytosis marker, LY, in BBMEC monolayers. While the cell-associated R123 in the P85 micelle study could represent cell-polymer interactions on the extracellular surface of the BBMEC, the fluorescent microscopy studies indicate that R123 is found throughout the cytosol of the cell, with some fluorescence even observed in the nucleus. Furthermore, the decreased accumulation of R123 in the micelle treatment group following exposure to the metabolic inhibitor, DG, provides additional evidence supporting the presence of R123 within the cell. The use of DG as an inhibitor of endocytosis in BBMEC monolayers has been reported previously (17). In the present study, DG inhibited uptake of the fluid phase endocytosis marker, LY, in BBMEC monolayers. The inhibition of cell-associated R123 in the presence of P85 micelles following treatment with DG suggests endocytosis of the micelle-solubilized R123 is also occurring in the BBMEC monolayers. Together, these findings suggest that the P-gp-independent absorption process observed with micelle concentrations of P85 in BBMEC monolayers is due to endocytosis.

Compared to the absorption of R123 and R110 in assay buffer, the enhanced absorption observed with the P85 micelles was transient, reaching a maximum within the first 15 min of exposure. The reason for the transient increase in absorption produced by the P85 micelles is unclear. However, the fluorescence microscopy studies indicate that the transient increases in cell-associated R123 are due to changes within the cell and not merely changes in binding or association of the micelles with the plasma membrane.

Potential toxicity issues concerning the P85 micelles do not appear to be involved in the transient increase in R123 absorption observed as previous cytotoxicity studies have shown no significant toxicity to cells within the concentration range of P85 used in the present study (9). Furthermore, if the micelles were killing the cells, one would not expect DG, the metabolic inhibitor, to produce such a dramatic decrease in R123 accumulation in the P85 micelle treatment group. Indeed, if the micelles were toxic to the cells, then the R123 accumulating in the cells would be anticipated to steadily increase throughout the time course of the experiments due to the loss of membrane integrity.

An alternative explanation of the transient effects of P85 micelles on R123 accumulation may involve a change in the endocytic rate of the BBMEC during exposure to the micelles. Previous studies indicate that endocytic activity can be influenced by Pluronic copolymers (unpublished results). Whether such a mechanism is involved in the transient increase in absorption with the P85 micelles in the current study is under investigation.

In summary, the present studies indicate that Pluronic copolymers interact with the brain microvessel endothelial cells that form the BBB in two distinct ways. The copolymer unimers increase the uptake of the drug through the P-gp-dependent pathway. As a result of the effects of the unimers on drug efflux systems in the BBB, the permeability of selective drugs that are P-gp substrates may be enhanced. Alternatively, at concentrations of P85 above the cmc, drugs that are solubilized within the copolymer micelles may penetrate the BBB

through vesicular transport within the brain microvessel endothelial cells. Since the unimer effects on P-gp are dependent on the amount of free drug, the contribution of the P-gp pathway will diminish as the copolymer concentration reaches the cmc and the drug begins to solubilize into micelles. Both the interactions of the unimers and the micelles of P85 are energy-dependent, suggesting that the membrane interactions with P85 have an initial endocytic component.

ACKNOWLEDGMENT

We thank Drs. T. McGuire and E. Hoie (Department of Pharmacy Practice, University of Nebraska Medical Center) for providing the HUVEC. Pluronic copolymers were a kind gift from BASF Co. This work was supported by a Nebraska Research Initiative and Nebraska Department of Health Smoking and Cancer Diseases Research Grant as well as the Industrial Research Assistance Program (IRAP) Grant 14113Q from the National Research Council of Canada.

LITERATURE CITED

- (1) Bader, H., Ringsdorf, H., and Schmidt, B. (1984) Water soluble polymers in medicine. *Angew. Macromol. Chem.* 123/124, 457–485.
- (2) Kabanov, A. V., Chekhonin, V. P., Alakhov, V. Yu., Batrakova, E. V., Lebedev, A. S., Melik-Nubarov, N. S., Arzhakov, S. A., Levashov, A. V., Morozov, G. V., Severin, E. S., and Kabanov, V. A. (1989) The neuroleptic activity of haloperidol increases after its solubilization in surfactant micelles. Micelles as microcontainers for drug targeting. *FEBS Lett.* 258, 343–345.
- (3) Yokoyama, M., Miyauchi, M., Yamada, N., Okano, T., Sakurai, Y., Kataoka, K., and Inoue, S. (1990) Characterization and anticancer activity of the micelle-forming polymeric anticancer drug adriamycin-conjugated poly(ethylene glycol)-poly(aspartic acid) block copolymer. *Cancer Res.* 50, 1693–1700.
- (4) Kabanov, A. V., Batrakova, E. V., Melik-Nubarov, N. S., Fedoseev, N. A., Dorodnich, T. Yu., Alakhov, V. Yu., Chekhonin, V. P., Nazarova, I. R., and Kabanov, V. A. (1992) A new class of drug carriers: micelles of poly(oxyethylene)-poly(oxypropylene) block copolymers as microcontainers for drug targeting from blood in brain. *J. Controlled Release* 22, 141–158.
- (5) Hagan, S. A., Coombes, G. A., Garnett, M. C., Dunn, S. E., Davies, M. C., Illum, L., Davis, S. S., Harding, S. E., Purkiss, S., and Gellert, P. R. (1996) Polylactide-poly(ethylene glycol) copolymers as drug delivery systems. 1. Characterization of water dispersible micelle-forming systems. *Langmuir* 12, 2153–2161.
- (6) La, S. B., Okano, T., and Kataoka, K. (1996) Preparation and characterization of the micelle-forming polymeric drug indomethacin-incorporated poly(ethylene oxide)-poly(β -benzyl L-aspartate) block copolymer micelles. *J. Pharm. Sci.* 85, 91–95.
- (7) Batrakova, E. V., Dorodnich, T. Yu., Klinskii, E. Yu., Kliushnenkova, E. N., Shemchukova, O. B., Goncharova, O. N., Arjakov, S. A., Alakhov, V. Yu., and Kabanov, A. V. (1996) Anthracycline antibiotics non-covalently incorporated into micelles of Pluronic block copolymers: activity against drug sensitive and resistant tumors. *Br. J. Cancer* 74, 1545–1552.
- (8) Kabanov, A. V., Slepnev, V. I., Kuznetsova, L. E., Batrakova, E. V., Alakhov, V. Yu., Melik-Nubarov, N. S., Sveshnikov, P. G., and Kabanov, V. A. (1992) Pluronic micelles as a tool for low-molecular compound vector delivery into a cell: effect of *Staphylococcus aureus* enterotoxin B on cell loading with micelle incorporated fluorescent dye. *Biochem. Int.* 26, 1035–1042.
- (9) Alakhov, V. Y., Moskaleva, E. Yu., Batrakova, E. V., and Kabanov, A. V. (1996) Hypersensitization of multidrug resistant human ovarian carcinoma cells by Pluronic P85 block copolymer. *Bioconjugate Chem.* 7, 209–216.
- (10) Venne, A., Li, S., Mandeville, R., Kabanov, A. V., and Alakhov, V. Yu. (1996) Hypersensitizing effects of Pluronic L61 on cytotoxic activity, transport, and subcellular distribution of doxorubicin in multiple drug-resistant cells. *Cancer Res.* 56, 3626–3629.
- (11) Audus, K. L., Chikhale, P. J., Miller, D. W., Thompson, S. E., and Borchardt, R. T. (1992) Brain uptake of drugs: The influence of chemical and biological factors. *Adv. Drug Res.* 23, 3–64.
- (12) Hegmann, E. J., Bauer, H. C., and Kerbel, B. S. (1992) Expression and functional activity of P-glycoprotein in cultured cerebral capillary endothelial cells. *Cancer Res.* 52, 6969–6975.
- (13) Fontaine, M., Elmquist, W. F., and Miller, D. W. (1996) Use of rhodamine 123 to examine the functional activity of P-glycoprotein in primary cultured brain microvessel endothelial cell monolayers. *Life Sci.* 59, 1521–1531.
- (14) Miller, D. W., Audus, K. L., and Borchardt, R. T. (1992) Application of cultured bovine brain endothelial cells of the brain microvasculature in the study of the blood-brain barrier. *J. Tissue Cult. Methods* 14, 217–224.
- (15) Kazakoff, P. W., McGuire, T. R., Hoie, E. B., Cano, M., and Iversen, P. L. (1995) An in vitro model for endothelial cell permeability and assessment of monolayer multiplicity. *In Vitro Cell. Dev. Biol.* 31, 846–852.
- (16) Gervasoni, J. E., Fields, S. Z., Krishna, S., Baker, M. A., Rosado, M., Thuraishamy, K., Hindenburg, A. A., and Taub, R. N. (1991) Subcellular distribution of daunorubicin in P-glycoprotein-positive and -negative drug-resistant cell lines using laser-assisted confocal microscopy. *Cancer Res.* 51, 4955–4964.
- (17) Guillot, F. L., Audus, K. L., and Raub, T. J. (1990) Fluid-phase endocytosis by primary cultures of bovine brain microvessel endothelial cell monolayers. *Microvascular Res.* 39, 1–14.
- (18) Lampidis, T. J., Castello, C., Del Giglio, A., Pressman, B. C., Viallet, P., Trevorow, K. W., Valet, G. K., Tapiero, H., and Savaraj, N. (1989) Relevance of the chemical charge of rhodamine dyes to multiple drug resistance. *Biochem. Pharmacol.* 38, 4267–4271.
- (19) Kabanov, A. V., Nazarova, I. R., Astafieva, I. V., Batrakova, E. V., Alakhov, V. Yu., Yaroslavov, A. A., and Kabanov, V. A. (1995) Micelle formation and solubilization of fluorescent probes in poly(oxyethylene-b-oxypropylene-b-oxyethylene) solutions. *Macromolecules* 28, 2303–2314.
- (20) Zacherl, J., Hamilton, G., Thalhammer, T., Riegler, M., Cosentini, E. P., Ellinger, A., Bischof, G., Schweitzer, M., Teleky, B., Koperna, T., and Wenzl, E. (1994) Inhibition of P-glycoprotein-mediated vinblastine transport across HCT-8 intestinal carcinoma monolayers by verapamil, cyclosporine A and SDZ PSC 833 in dependence on extracellular pH. *Cancer Chemother. Pharmacol.* 34, 125–132.
- (21) Wigler, P. W., Lyon, K. L., Patterson, F. K., Laloggia, A. J., Dia-Arauzo, H., Reddy, M. S., and Cook, J. M. (1994) Epoxide metabolite of quinine and inhibition of the multidrug resistance pump in human leukemic lymphoblasts. *Mol. Pharmacol.* 46, 563–567.
- (22) Jancis, E. M., Carbone, R., Loechner, K. J., and Dannies, P. S. (1993) Estradiol induction of rhodamine 123 efflux and multidrug resistance pump in rat pituitary tumor cells. *Mol. Pharmacol.* 43, 51–56.
- (23) Nerurkar, M. M., Burton, P. S., and Borchardt, R. T. (1996) The use of surfactants to enhance the permeability of peptides through Caco-2 cells by inhibition of an apically polarized efflux system. *Pharm. Res.* 13, 528–534.
- (24) Dudeja, P. K., Anderson, K. M., Harris, J. S., Buckingham, L., and Coon, J. S. (1995) Reversal of multidrug resistance phenotype by surfactants: relationship to membrane lipid fluidity. *Arch. Biochem. Biophys.* 319, 309–315.
- (25) Zordan-Nudo, T., Ling, V., Liu, Z., and Georges, E. (1993) Effects of nonionic detergents on P-glycoprotein drug binding and reversal of multidrug resistance. *Cancer Res.* 53, 5994–6000.
- (26) Hunter, P. N., Scheutjens, J. M. H. M., and Hatton, T. A. (1993) Molecular modeling of micelle formation and solubi-

- lization in block copolymer micelles. 1. A self-consistent mean-field lattice theory. *Macromolecules* 26, 5592–5601.
- (27) Schinkel, A. H., Smit, J. J. M., van Tellingen, O., Beijnen, J. H., Wagenaar, E., van Deemter, L., Mol, C. A. A. M., van der Valk, M. A., Robanus-Maandag, E. C., te Riele, H. P. J., Berns, A. J. M., and Borst, P. (1994) Disruption of the mouse *mdr1a* P-glycoprotein gene leads to a deficiency in the blood-brain barrier and to increased sensitivity to drugs. *Cell* 77, 491–502.
- (28) Schinkel, A. H., Wagenaar, E., Mol, C. A. A. M., and van Deemter, L. (1996) P-glycoprotein in the blood-brain barrier of mice influences the brain penetration and pharmacological activity of many drugs. *J. Clin. Invest.* 97, 2517–2524.

BC970118D

Formation of Microscale Gradients of Protein Using Heterobifunctional Photolinkers

Claire L. Hypolite,[†] Terri L. McLernon,[‡] Derek N. Adams,[†] Kenneth E. Chapman,[†] Curtis B. Herbert,[†] C. C. Huang,[§] Mark D. Distefano,^{*,‡} and Wei-Shou Hu[†]

Department of Chemical Engineering and Materials Science, Department of Chemistry, and School of Physics and Astronomy, University of Minnesota, Minneapolis, Minnesota 55455-0132. Received February 21, 1997[®]

Gradients of biological molecules on a microscale have been postulated to elicit cellular responses, such as migration. However, it has been difficult to prepare such gradients for experimental testing. A means for producing such gradients has been developed using a heterobifunctional photolinking agent with laser light activation. The photolinking agent synthesized includes an *N*-hydroxysuccinimide group and a photoreactive benzophenone (BP) separated by a tetraethylene glycol (TEG) spacer. The presence of the tetraethylene glycol spacer renders the photolinker hydrophilic, a desirable trait for conjugation in aqueous solutions. The linker was then conjugated to R-phycoerythrin (R-PE), a fluorescent protein. The resulting photolinker–R-phycoerythrin conjugate (BP–TEG–PE) was then immobilized onto a polystyrene surface by laser irradiation on a motorized stage. By varying exposure time of the sample to the beam, the amount of BP–TEG–PE immobilized on the surface was changed over an order of magnitude over a distance of 250 μm . This method can be applied to prepare gradients of proteins that elicit biological responses, such as extracellular matrix proteins or growth factors, and to study the biological effects of such gradients.

INTRODUCTION

Immobilizing proteins and peptides on surfaces is a powerful method for studying the response of cells to these molecules. Growth factors, cell adhesion molecules, and peptides have all been immobilized on surfaces in a variety of means for that purpose (1–3). Of particular interest is the patterning of molecules that promote the adhesion of cells to a surface. For instance, nerve cells have been shown to preferentially attach to and extend neurites along pathways of adhesion that have been patterned using lithographic techniques (4–8). The sizes and shapes of these patterns have also been shown to influence cell behavior (9–11). One goal of this research has been to find ways to control cell behavior, in particular, migration, by manipulating the adhesiveness of a substrate. A deeper understanding of cell migration could allow researchers to construct paths through matrices for cell migration and the formation of innervated, vascularized tissue.

Formation of tissues *in vitro* will require a better understanding of the means by which the cells native to these tissues migrate. In many cases, gradients of various molecules have been speculated to be the directing force in the migration of cells from one location in a tissue to another. For example, neuronal cells extend neurites on laminin, but what are the necessary signals for migration of the growth cone to a specific target? Halfter reported that axons from chick retinal explants show directional migration up both steep and shallow gradients of basal lamina or merosin (12). Additionally,

Snow and Letourneau studied the response of three types of neuronal cells to a step gradient of chondroitin sulfate proteoglycan (CS-PG) on laminin. The number of neurites extending into each region of the gradient decreased as the concentration of CS-PG increased (13). In contrast, McKenna and Raper found that shallow gradients of laminin did not confer any directionality to neurite extension (14). Although direct comparison of the results from Halfter and McKenna and Raper is difficult because of the differences in gradient analysis (one quantitative, one qualitative), it can be speculated that the gradient profile (how steep or shallow) may be a key factor in determining the effects of these gradients on cell behavior. Since cells may only be capable of detecting differences in molecule concentrations through receptors located in the cell membrane, it may be necessary for the gradients to have sufficient change in concentration within those dimensions to elicit a cellular response. Unfortunately, investigating this hypothesis has proved to be difficult because a reproducible and quantifiable method for producing microscale gradients *in vitro* to study cell response has yet to be developed. Lithography offers the ability to produce patterns with submillimeter dimensions (5, 10, 15, 16), but its use for the preparation of immobilized gradients has not been reported. To overcome this limitation, we have investigated the possibility of creating microscale gradients using photoreactive cross-linking agents, with activation through laser light exposure. This method offers a flexible means of controlling the amount of protein or peptide immobilized on a surface because the exposure time of the sample to the laser is easily varied during substrate processing. By focusing the laser, the dimensions of the patterns produced can be controlled to submillimeter dimensions. Gradients can be prepared by a raster pattern of irradiation in which the laser moves over the surface at progressively faster speeds.

In this paper, we describe the preparation of stable gradients using the above approach. A conjugation reagent containing a photoactivatable benzophenone

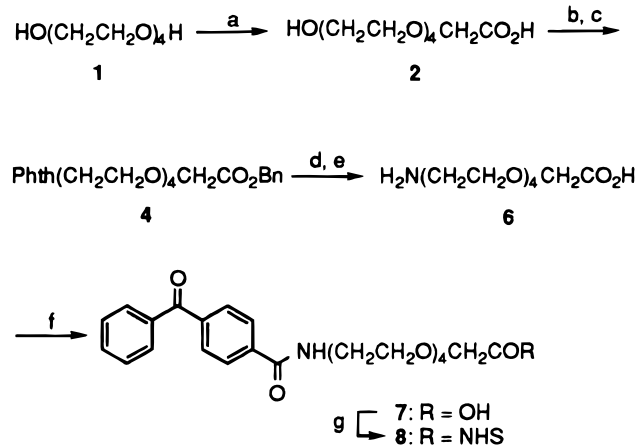
* Address correspondence to this author at the Department of Chemistry, University of Minnesota, 207 Pleasant St. S.E., Minneapolis, MN 55455 (e-mail distefan@chemsun.chem.umn.edu).

[†] Department of Chemical Engineering and Materials Science.

[‡] Department of Chemistry.

[§] School of Physics and Astronomy.

[®] Abstract published in *Advance ACS Abstracts*, August 1, 1997.

Scheme 1. Preparation of Linker (BP-TEG-NHS)^a

Reagents: (a) Na⁺, ClCH₂CO₂H; (b) BnBr, KHCO₃, DMF; (c) Phthalimide, PPh₃, DEAD, THF; (d) H₂, Pd/C, abs EtOH; (e) H₂NNH₂, EtOH; (f) 4-Benzoylbenzoic acid NHS ester, DMF; (g) DCC, NHS, CH₂Cl₂:EtOAc (1:1)

^a Linker based on benzophenone, tetraethylene glycol, and NHS.

(BP), a water-soluble tetraethylene glycol (TEG) spacer, and an amine reactive *N*-hydroxysuccinimide (NHS) ester was prepared and used to derivatize R-phycoerythrin (R-PE). This conjugate was then cross-linked to a polystyrene surface using a focused laser and a programmable stage. The resulting cross-linked patterns and gradients were visualized by measuring the intrinsic phycoerythrin fluorescence that remained on the surface after extensive washing.

MATERIALS AND METHODS

General Procedures. Tetrahydrofuran (THF) was dried over sodium benzophenone ketyl, and *N,N*-dimethylformamide (DMF) was dried over 4 Å molecular sieves. Analytical TLC was performed on precoated Polygram Sil G/UV₂₅₄ plates from Macherey-Nagel and visualized under UV irradiation or by staining with iodine. Flash column chromatography was performed on silica gel (230–400 mesh) (Merck/Bodman, Aston Township, PA). Reversed phase chromatography was performed on C₁₈ Sep-Pak cartridges (Waters Corp., Milford, MA). NMR spectra were obtained on a Varian 300 MHz spectrometer. Coupling constants are reported in hertz.

Linker Synthesis. A heterobifunctional photoreactive cross-linking agent containing the reactive BP and NHS moieties with a TEG spacer was synthesized (Scheme 1). All materials were obtained from Aldrich Chemical Co., Inc. (Milwaukee, WI) unless otherwise specified. Compound 2 was prepared according to the literature (17).

Benzyl 14-Hydroxy-3,6,9,12-tetraoxatetradecanoate (3). 14-Hydroxy-3,6,9,12-tetraoxatetradecanoic acid (2) (2.01 g, 7.99 mmol) in dry DMF (31 mL) under N₂ was combined with KHCO₃ (973.0 mg, 9.72 mmol) and benzyl bromide (1.15 mL, 9.67 mmol). The mixture was stirred at 23 °C for 22 h, and the solvent was removed by vacuum distillation. The resulting dark yellow oil was dissolved in CH₂Cl₂, and the solids were removed by filtration. Purification by flash column chromatography (SiO₂, MeOH/CH₂Cl₂) gave a very light-colored yellow oil (959 mg; *R*_f = 0.63, SiO₂, 10% MeOH/CH₂Cl₂). A second fraction was obtained (539 mg; *R*_f = 0.72), which was indistinguishable from the slower moving fraction (*R*_f = 0.63) by ¹H NMR:¹ combined yield, 55%; ¹H NMR (CDCl₃,

300 MHz) δ 7.34–7.31 (m, 5H), 5.16 (s, 2H), 4.18 (s, 2H), 3.74–3.64 (m, 6H), 3.63 (br s, 8H), 3.58–3.55 (m, 2H), 2.84 (br t, *J* = 5.7, 1H); ¹³C NMR (CDCl₃, 75 MHz) δ 170.23, 135.29, 128.48, 128.30, 72.43, 70.81, 70.47, 70.41, 70.38, 70.16, 68.52, 66.41, 61.57; HRFABMS calcd for C₁₇H₂₇O₇ [M + H]⁺ 343.1757, found 343.1741.

Benzyl 14-*N*-Phthalimido-3,6,9,12-tetraoxatetradecanoate (4). To PPh₃ (1.31 g, 5.00 mmol) and phthalimide (1.10 g, 7.46 mmol) under N₂ at 23 °C was added benzyl 14-hydroxy-3,6,9,12-tetraoxatetradecanoate (3) (0.84 g, 2.47 mmol, *R*_f = 0.63 as noted above) dissolved in 10 mL of THF. The mixture was diluted with 20 mL of THF to completely dissolve all solids. Diethyl azodicarboxylate (DEAD; 800 μL, 5.08 mmol) was added, and the mixture was stirred for 4 days. The solvent was removed under reduced pressure and the crude oil partially purified by flash column chromatography (EtOAc/hexanes, 1:1 v/v) to give 4 contaminated with a significant amount of triphenylphosphine oxide (TPPO). The material was used without further purification.² A sample of pure 4 was obtained by rebenzylation of the purified free acid 5. To 5 (28 mg, 0.073 mmol) in dry DMF at 23 °C under N₂ was added KHCO₃ (22 mg, 0.22 mmol) and benzyl bromide (12 μL, 0.10 mmol). The mixture was stirred for 3 days, and the solvent was removed by vacuum distillation. The residue was dissolved in CH₂Cl₂, filtered through Celite, and purified by flash column chromatography (0–75% EtOAc/hexanes) to give 4 as a very light-colored yellow oil (*R*_f = 0.42, SiO₂, 75% EtOAc/hexanes): ¹H NMR (CDCl₃, 300 MHz) δ 7.83 (dd, *J* = 5.2, 3.1, 2H), 7.70 (dd, *J* = 5.5, 3.0, 2H), 7.34 (br s, 5H), 5.18 (s, 2H), 4.18 (s, 2H), 3.88 (t, *J* = 5.7, 2H), 3.74–3.70 (m, 4H), 3.66–3.61 (m, 4H), 3.59–3.57 (m, 6H); ¹³C NMR (CDCl₃, 75 MHz) δ 170.31, 168.20, 135.39, 133.87, 132.08, 128.56, 128.37, 123.18, 70.87, 70.55, 70.52, 70.49, 70.02, 68.62, 67.85, 66.45, 37.19; HRFABMS calcd for C₂₅H₃₀NO₈ [M + H]⁺ 472.1971, found 472.1985.

14-*N*-Phthalimido-3,6,9,12-tetraoxatetradecanoic Acid (5). Compound 4, contaminated with TPPO, was dissolved in absolute EtOH (50 mL), 10% Pd/C (0.25 g) was added, and the mixture was stirred under 1 atm of H₂ at 23 °C for 23 h. The catalyst was removed by filtration through Celite and the filtrate concentrated under reduced pressure. Purification by flash column chromatography (0–2% MeOH/CH₂Cl₂ and then 2% MeOH/CH₂Cl₂ containing 0.03% HOAc) gave a liquid containing very slight impurities, which was used without further purification (343 mg, 36% yield from compound 3).² A small sample was repurified by flash column chromatography to give a yellow, crystalline solid: ¹H NMR (CDCl₃, 300 MHz) δ 8.55 (br s, 1H), 7.83 (dd, *J* = 5.4, 3.0, 2H), 7.70 (dd, *J* = 5.4, 3.0, 2H), 4.13 (s, 2H), 3.89 (t, *J* = 5.7, 2H), 3.74–3.70 (m, 4H), 3.66–3.62 (m, 4H), 3.60–3.56 (m, 6H); ¹³C NMR (CDCl₃, 75 MHz) δ 172.96, 172.62, 168.27, 133.92, 132.03, 123.21, 71.17, 70.48, 70.38, 70.32, 70.18, 70.12, 68.82, 67.94, 37.20; HRFABMS calcd for C₁₈H₂₄NO₈ [M + H]⁺ 382.1502, found 382.1520.

¹ Both fractions are believed to be compound 3. One fraction may contain materials complexed as a potassium salt. See ref 17.

² Another 110 mg of 5 was obtained by eluting the SiO₂ column used for the purification of 4 with 10% MeOH/CH₂Cl₂ to provide a second more crude fraction of 4. This material was subjected to hydrogenation as described for the preparation of compound 5. The crude orange oil isolated contained 54.5% of 5 by weight (as estimated by NMR). Combined yield of 5: 48% from compound 3.

14-Amino-3,6,9,12-tetraoxatetradecanoic Acid (6). To 14-*N*-phthalimido-3,6,9,12-tetraoxatetradecanoic acid (**5**) (228 mg, 0.598 mmol) in absolute EtOH (6 mL) under N₂ was added NH₂NH₂·H₂O (50 μ L, 1.03 mmol). The mixture was refluxed for 5 h, cooled in an ice bath, and filtered, and the filtrate was concentrated under reduced pressure. The residue was dissolved in a small amount of absolute EtOH and water added to give a cloudy suspension. After further filtration and concentration, water was again added. After a third filtration and concentration of the filtrate with absolute EtOH, a viscous yellow oil was obtained, which crystallized on standing (94% purity by NMR; 93% yield). This material was further purified by reversed phase chromatography (H₂O/MeOH): ¹H NMR (CDCl₃, 300 MHz) δ 7.96 (br s, 3H), 3.86 (s, 2H), 3.79 (t, *J* = 4.6, 2H), 3.66–3.54 (m, 12H), 3.06 (t, *J* = 4.8, 2H); ¹³C NMR (CDCl₃, 75 MHz)³ δ 175.50, 71.28, 70.35, 69.78, 69.51, 69.43, 69.36, 69.26, 67.04, 39.62; HRFABMS calcd for C₁₀H₂₂NO₆ [M + H]⁺ 252.1447, found 252.1448.

14-(4-Benzoylbenzamido)-3,6,9,12-tetraoxatetradecanoic Acid (7). To 14-amino-3,6,9,12-tetraoxatetradecanoic acid (**6**) (95 mg, 0.38 mmol) in dry DMF (8 mL) under N₂ was added 4-benzoylbenzoic acid *N*-hydroxysuccinimide ester (298 mg, 0.92 mmol). The temperature was raised to 73 °C and the reaction stirred for 25 h. After vacuum distillation to remove the solvent, the crude material was purified by flash chromatography to remove excess NHS ester (100% CH₂Cl₂). The product **7** and *N*-hydroxysuccinimide were then eluted from the column with 50% MeOH/CH₂Cl₂ containing HOAc (~0.5%). Removal of the solvents gave a viscous orange residue. Water was added to the residue to give a cloudy suspension. The precipitate (4-benzoylbenzoic acid) was removed by centrifugation and the supernatant (a precipitate forms on standing) concentrated. The residue was dissolved in CH₂Cl₂/H₂O, the layers were separated, and the aqueous layer was extracted twice more with CH₂Cl₂. The combined CH₂Cl₂ layers were washed once with saturated NaCl, decanted into a dry flask, and concentrated. Further purification by flash column chromatography (using 2% MeOH/CH₂Cl₂ to remove residual 4-benzoylbenzoic acid) gave a very light-colored yellow oil (81 mg; 46.5% yield): ¹H NMR (CDCl₃, 300 MHz)⁴ δ 9.22 (br s, 1H), 8.16 (d, *J* = 7.8, 2H), 7.76–7.72 (m, 4H), 7.57 (tt, *J* = 7.4, 1.6, 1H), 7.45 (dd, *J* = 7.5, 7.5, 2H), 3.84 (s, 2H), 3.66–3.52 (m, 16H); ¹³C NMR (CDCl₃, 75 MHz)⁵ δ 196.30, 175.25, 166.88, 139.45, 137.86, 137.12, 132.70, 130.00, 129.75, 128.34, 127.72, 70.82, 70.21, 69.52, 69.28, 69.01, 68.63, 39.73; HRFABMS calcd for C₂₄H₂₈NO₈Na₂ [M – H + 2Na]⁺ 504.1610, found 504.1626.

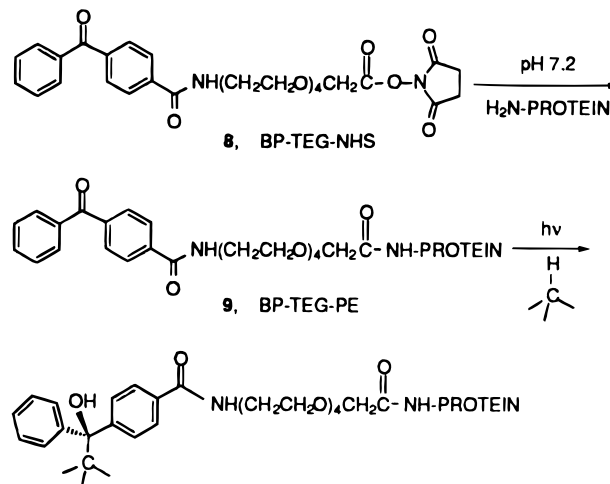
14-(4-Benzoylbenzamido)-3,6,9,12-tetraoxatetradecanoic Acid *N*-Hydroxysuccinimide Ester (8). To 14-(4-benzoylbenzamido)-3,6,9,12-tetraoxatetradecanoic acid (**7**) (59.0 mg, 0.13 mmol) in 4 mL of EtOAc (material is not completely soluble) was added *N*-hydroxysuccinimide (16.4 mg, 0.14 mmol) and dicyclohexylcarbodiimide (DCC) (26.9 mg, 0.13 mmol). CH₂Cl₂ (5 mL) was then added to completely dissolve the solids. The

³ The ¹³C NMR spectrum is concentration dependent. The four resonances from δ 69.51 to 69.26 coalesce to two peaks at δ 69.57 and 69.47 upon dilution.

⁴ The ¹H NMR spectrum of the free acid **7** is also concentration dependent. The aromatic resonance at δ 8.01 and the α -CH₂ resonance at δ 4.06 shift to δ 8.11 and 3.92, respectively, upon dilution.

⁵ In the ¹³C spectrum of **7**, the methylene carbons of the TEG unit show a decrease in intensity relative to that of the aromatic and carbonyl carbons when compared to other spectra in the series.

Scheme 2. Conjugation of BP-TEG-NHS to R-PE



^a Reaction scheme resulting in formation of BP-TEG-PE and subsequent immobilization to dish surface through C–H bond.

mixture was stirred at 23 °C for 17.5 h, and the solvents were removed under reduced pressure. A small amount of CH₂Cl₂ was added to the residue and the mixture cooled to 0 °C under N₂. The precipitate was removed by filtration and the filtrate concentrated (precipitation and filtration performed twice) to give a yellow-brown oil containing impurities (84.7 mg; theoretical yield = 71.2 mg; purity \leq 85%): ¹H NMR (CDCl₃, 300 MHz) δ 7.98–7.89 (m, 2H), 7.82–7.74 (m, 4H), 7.59 (tt, *J* = 7.5, 1.9, 1H), 7.47 (dd, *J* = 7.5, 7.5, 2H), 4.46 (s, 2H), 3.74–3.60 (m, 16H), 2.82 (s, 4H); ¹³C NMR (CDCl₃, 75 MHz) δ 196.01, 168.78, 166.76, 165.88, 139.85, 137.72, 136.96, 132.78, 130.00, 129.95, 128.35, 127.06, 71.15, 70.73, 70.45, 70.41, 70.35, 70.12, 69.55, 66.39, 39.92, 33.58.

Reaction of BP-TEG-NHS, **8, with Alanine.** To the photolinker **8** as an oily residue was added excess alanine (racemic) as a cold aqueous solution. The mixture was stirred at 0 °C for 1.5 h (all materials dissolve). Excess alanine was removed by CH₂Cl₂ extraction (three times) of any TEG-containing compounds. Purification by multiple elution (six times) of a preparative TLC plate (SiO₂, dipped first in 2% HOAc/MeOH and dried, then loaded and eluted with 5% MeOH/CH₂Cl₂ containing 0.05% HOAc) and extraction of the band at *R*_f = 0.30 gave a white solid.⁶ The crude material was dissolved in MeOH/H₂O, excess disodium EDTA·2H₂O was added, the MeOH was removed under reduced pressure, and the sample was warmed to completely dissolve the EDTA. The aqueous solution was extracted with CH₂Cl₂ (three times) to remove the Ala-linker adduct, and the CH₂Cl₂ layers were concentrated. ¹H NMR (CDCl₃, 300 MHz) δ 7.97 (ddd, *J* = 8.4, 1.8, 1.8, 2H), 7.84 (ddd, *J* = 8.4, 1.8, 1.8, 2H), 7.80 (ddd, *J* = 6.9, 1.6, 1.6, 2H), 7.65–7.56 (m, 3H), 7.50 (ddt, *J* = 7.5, 7.5, 1.6, 2H), 4.66 (quintet, *J* = 7.5, 1H), 4.07 (d, *J* = 16.2, 1H), 3.94 (d, *J* = 15.9, 1H), 3.83–3.58 (m, 16H), 1.46 (d, *J* = 7.2, 3H); ¹H NMR (CD₃OD, 300 MHz) δ 7.97 (ddd, *J* = 8.4, 1.9, 1.9, 2H), 7.84 (ddd, *J* = 8.4, 1.8, 1.8, 2H), 7.79 (ddd, *J* = 6.9, 1.6, 1.6, 2H), 7.66 (tt, *J* = 7.2, 1.6, 1H), 7.54 (ddt, *J* = 7.3, 7.3, 1.5, 2H), 4.31 (q, *J* = 7.2, 1H), 3.97 (s, 2H), 3.74 (s, 2H), 3.71–3.58 (m, 14H), 1.38 (d, *J* = 7.2, 3H).

Conjugation of Phycoerythrin to BP-TEG-NHS, **8 (Scheme 2).** R-Phycoerythrin (Molecular Probes, Eugene, OR) was pelleted by centrifugation from a

⁶ The product is believed to bind Ca²⁺ (a binding material contained within the preparative plates). See ref 17.

suspension of 4 mg/mL in 60% ammonium sulfate, pH 7, and resuspended in 0.1 M NaCl/0.1 M Na₂HPO₄, as suggested by the supplier. For conjugation, 2 mL of R-PE at a concentration of 0.2 mg/mL was combined with 100 μ L of BP-TEG-NHS, **8**, at 5 mg/mL in distilled water to achieve a final molar ratio of 1:500 R-PE:BP-TEG-NHS. The reaction was carried out at 4 °C in darkness for 24 h. The solution was then dialyzed against approximately 750 mL of 0.1 M NaCl/0.1 M Na₂HPO₄, pH 7.0, overnight at 4 °C, with two changes of the dialysis solution. After dialysis, the BP-TEG-PE was aliquoted and stored at 4 °C.

Immobilization of BP-TEG-PE, 9. The BP-TEG-PE solution was diluted to a final concentration of 400 ng/mL in 0.1 M NaCl/0.1 M Na₂HPO₄. A 60 μ L drop of this solution was placed onto a 35 mm Petri dish (Falcon, Becton Dickinson Labware, Lincoln Park, NJ) and allowed to air-dry at room temperature. The Petri dish was then placed on the stage and irradiated using a Cd/He laser (4 mW, 325 nm, Model 3056-4, Omnichrome Corp., Chino, CA). The laser beam passes through a computer-controlled electronic shutter (Newport/Klinger, Garden City, NY), followed by a 190 μ m pinhole and a 5 \times objective lens before reaching the sample on the stage. Stage motion was mediated through the use of three mutually perpendicular 850-B actuators (Newport/Klinger). The actuators and shutter were controlled with the Motion Master 2000 system (Newport/Klinger). The pattern of irradiation was generated by controlling the direction and the speed of stage movement during laser exposure. The focal point of the laser beam has a width of approximately 20 μ m. Patterns of immobilized PE were generated by manipulating the path of laser irradiation. The exposure time of the laser at any given point along the path was controlled by the speed of movement of the stage on which the sample was placed. Lines of uniform exposure to laser irradiation can be created readily by maintaining a constant stage velocity. Lines with varying exposure are produced by changing the speed of the stage movement during exposure to laser irradiation. A shutter is used to block out laser irradiation to create discrete patterns. An irradiated area greater than the width of the laser beam was created using repetitive line scans with the laser. To minimize the possibility of a gap or a low irradiation region between lines, the irradiated area in two consecutive line scans was allowed to overlap by a distance smaller (typically about half) than the width of laser beam. An area with a gradient of laser exposure was created by gradually changing the exposure time in the consecutive lines.

After irradiation, the Petri dishes were sonicated for 5 min at room temperature in each of the following five solutions: ethanol; methanol; 1:1 (v/v) methanol/distilled water; distilled water; methanol.

Fluorescence Detection. An epifluorescence inverted microscope (Nikon Diaphot, Nikon Inc., Melville, NY) equipped with a confocal scanning laser system (Multiprobe 2001, Molecular Dynamics, Sunnyvale, CA) was used to detect fluorescence from the immobilized BP-TEG-PE. Samples were excited at 488 nm with an argon laser light source, and emission wavelengths above 510 nm were collected using a long-pass filter and a pinhole aperture of 100 μ m. The voltage of the photomultiplier tube for fluorescence intensity was kept constant for all scans. The acquired images (512 \times 512, pixel size 1.3 or 0.6 μ m) were collected on a Silicon Graphics Indigo workstation (Iris, Silicon Graphics, Inc., Mountain View, CA) using ImageSpace software (Molecular Dynamics). The resulting images were stored as two-

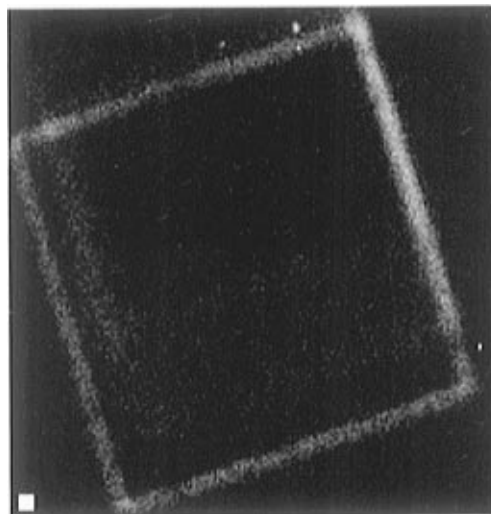


Figure 1. Square of immobilized BP-TEG-PE; fluorescent confocal image of the square outline. Image was created using black-to-white (low intensity to high intensity) gray-scale palette. Box = 20 μ m.

dimensional arrays of pixel intensity and position. Plots of fluorescence intensities were generated for each image by determining the average intensity for each column of pixels. These averages were normalized on the basis of the highest fluorescence intensity of the image. The background intensity (determined from each image) was subtracted, and these values were plotted against their position in the image. The levels of background fluorescence for irradiated samples were comparable to levels found in the control dish.

RESULTS

Synthesis of Photolinker. A new water soluble heterobifunctional cross-linking agent **8** was synthesized which incorporates a TEG spacer and the photoreactive BP group. The synthesis of **8** was accomplished in seven steps from TEG (Scheme 1). Compound **2** was prepared according to the literature (17). After protection of **2** as its benzyl ester **3**, conversion of the free alcohol to the phthalimide **4**, and complete deprotection (compounds **5** and **6**), the desired spacer **6** was obtained. Incorporation of the BP moiety was accomplished by acylation of **6** with 4-benzoylbenzoic acid NHS ester to give **7**. Activation of the free acid **7** as its NHS ester gave photolinker **8**. All compounds were characterized by ¹H and ¹³C NMR and HRMS. It is interesting to note that although these compounds are water soluble, they are readily soluble in chlorinated solvents. These unusual solubility properties manifest themselves as peculiarities in their CDCl₃ ¹H and ¹³C spectra.³⁻⁵ To demonstrate the solubility and reactivity of our new photolinker under mild conditions compatible with proteins, **8** was treated with alanine in aqueous solution and the adduct isolated and characterized by ¹H NMR. Compound **8** was then used to attach the BP-TEG moiety to R-PEphycoerythrin. The resulting conjugate was purified by dialysis and then used in subsequent photoimmobilization experiments.

Immobilization of BP-TEG-PE. BP-TEG-PE was immobilized onto a polystyrene surface by irradiation with a Cd/He laser. Four lines, each 500 μ m in length, were scanned to generate the pattern of a square. After unbound BP-TEG-PE was washed off, the pattern of immobilized phycoerythrin was visualized with a microscope. Figure 1 shows the image of a square produced in this fashion. The width of the fluorescent path of the outline is approximately 20 μ m. The pattern is clearly

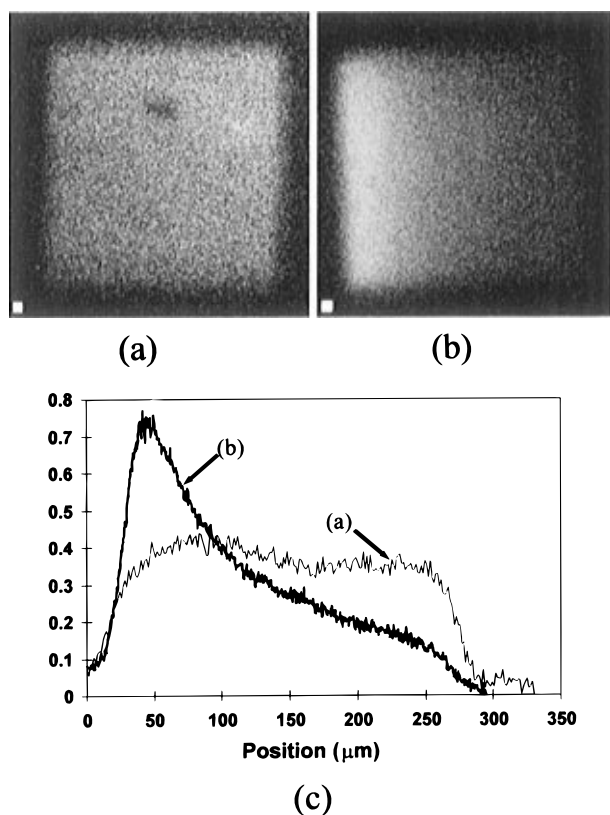


Figure 2. Comparison of uniform and gradient squares; comparison of fluorescent confocal images of solid square (a) and gradient (b). Graph (c) shows normalized average fluorescence intensity for both (a) and (b). A black-to-white palette was used. Box = 10 μm.

visible over the background fluorescence. A control was also included in which the surface was irradiated using unmodified phycoerythrin (instead of BP-TEG-PE) on the surface. The fluorescent intensity of this control was identical to the background level (data not shown). Thus, the background fluorescence is attributed in part to residual BP-TEG-PE that remained adsorbed to the surface after extensive washing. Clearly, the square pattern as shown in Figure 1 is due to the immobilization of phycoerythrin on the surface.

Gradient of Phycoerythrin. A surface with a concentration gradient of phycoerythrin was created by scanning the Cd/He laser across the surface in a raster pattern but with increasing scanning speed in consecutive lines. The width of the laser beam, i.e., the width of each scanned line, was approximately 20 μm. In the rastering process, each line was moved 10 μm down from the previous one and scanned in a parallel direction. The scanning speed along each single line was kept constant. Two types of scans were used. In the first the scanning speed for all rasters was invariant; in the other, the scanning speed was increased by 40% in each consecutive line. The lowest scanning speed used was 1/11 of the highest one. A square of 250 μm × 250 μm was irradiated to create a patch of immobilized phycoerythrin with a decreasing concentration from one end to the other. Figure 2 shows the images of a solid square with uniform irradiation and one irradiated with a varying scanning speed. The square generated by uniform irradiation shows a relatively uniform fluorescence intensity above the background level (Figure 2a). The second surface, irradiated with an increasing speed of laser scanning, shows a gradual decrease in fluorescence (Figure 2b). The average fluorescence intensity of all pixels along the direction of line scan was calculated and plotted along

the direction of adjacent lines of scanning. The results are shown in Figure 2c. This difference between the uniform surface and the surface with a gradient is evident. In one, the fluorescence intensity varied little over the 250 μm distance, while in the other it decreased approximately 1 order of magnitude over the same distance.

DISCUSSION

A wide range of heterobifunctional cross-linking agents for protein conjugation has been reported in the literature, many of which are commercially available (18, 19). Most of these compounds contain aryl azides as the photoreactive component. BP-containing reagents, however, are also being used (7, 20, 21), and are attractive alternatives. BPs can be manipulated in ambient light and are activated at wavelengths that are less damaging to proteins. Most importantly, BPs cross-link with higher efficiency than other photoreactive functionalities (22). This can be attributed to the reversible nature of the photoexcited state of BP.

The photoreactive cross-linking agent used in this study incorporates a BP unit (present as a benzoylbenzamide) and an NHS ester as the reactive groups, coupled with a TEG spacer. The NHS ester was chosen as the protein reactive group because of previous evidence that reactions between the R-PE and NHS esters do not result in a loss of intrinsic R-PE fluorescence (15). TEG is hydrophilic, in contrast to the alkane-based spacers used in many cross-linking agents, and was used to produce a linker that had an increased solubility in the aqueous solutions used for reactions with proteins. This modular design of the linker allows the properties of the linker to be systematically varied in future experiments with other proteins.

By combining photoreactive cross-linking agents and laser scanning, we have developed a method of creating a surface with a gradient of immobilized protein molecules. Increasing the exposure time of the surface to the laser beam increased the amount of BP-TEG-PE immobilized on the surface. Higher laser scanning velocities (shorter exposure times) resulted in lower concentrations of immobilized protein than at slower velocities. It is important to note that R-PE alone was not immobilized after laser exposure. Therefore, it is the modification of the R-PE with the photolinker that allows us to produce the patterns visualized. This method now serves as a model for future experiments involving other proteins or peptides.

Immobilization of proteins and peptides using bifunctional cross-linking agents has been accomplished by a number of researchers (7, 23–25). In many cases, these techniques have been combined with lithography to pattern proteins on surfaces. This is an effective means for immobilization, and the use of lithography allows for the production of patterns with dimensions on the order of micrometers (subcellular). However, lithographic techniques alone do not provide a means for immobilizing proteins and peptides with a gradient of density at a microscale distance. The results presented here demonstrate the ability to produce gradients of molecules on surfaces using heterobifunctional photoreactive cross-linking agents and laser light activation. This method provides a means for testing current hypotheses on the effects of gradients in cell behavior. ECM proteins, growth factors, and even peptides can be immobilized as gradients to determine the effects of these gradients on cell behavior.

ACKNOWLEDGMENT

This work was supported in part by grants from the National Science Foundation (BES-9308527) and the Center for Interfacial Engineering at the University of Minnesota. C.L.H. was supported by a fellowship from the National Science Foundation. Both C.L.H. and D.N.A. were recipients of a traineeship from the National Institute of Health. C.B.H. and T.L.M. were supported by a postdoctoral fellowship from a training grant from the National Science Foundation (NSF\BIR-9413241).

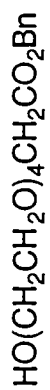
Supporting Information Available: ^1H and ^{13}C NMR spectra of compounds **1–8** and the photolinker–alanine conjugate (15 pages). Ordering information is given on any current masthead page.

LITERATURE CITED

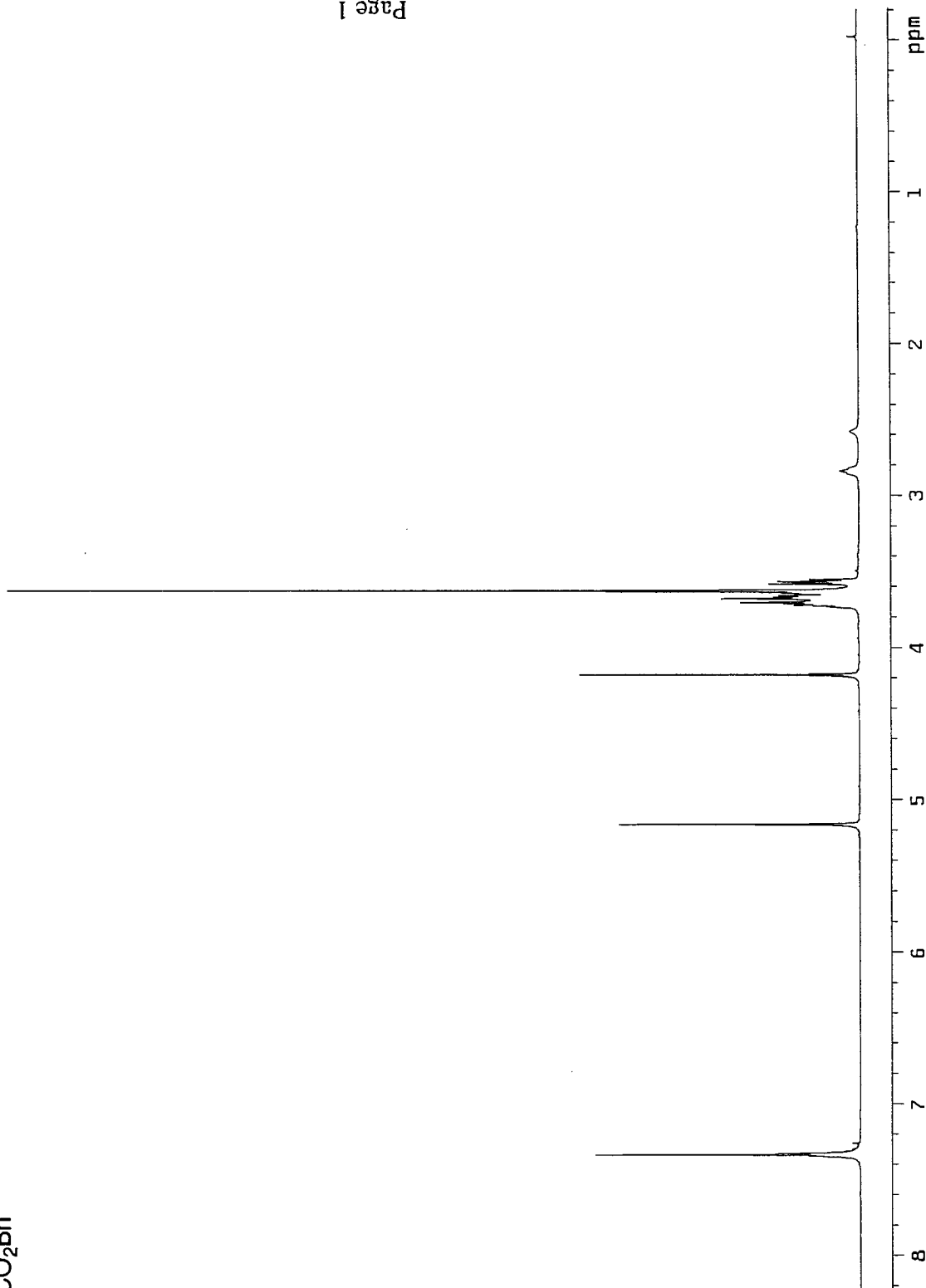
- (1) Massia, S. P., and Hubbell, J. A. (1991) Human endothelial cell interactions with surface-coupled adhesion peptides on a nonadhesive glass substrate and two polymeric biomaterials. *J. Biomed. Mater. Res.* 25, 223–242.
- (2) Kang, I.-K., Kwon, B. K., Lee, J. H., and Lee, H. B. (1993) Immobilization of proteins on poly(methyl methacrylate) films. *Biomaterials* 14, 787–792.
- (3) Liu, S. Q., Ito, Y., and Imanishi, Y. (1993) Cell growth on immobilized cell growth factor. 9. Covalent immobilization of insulin, transferrin, and collagen to enhance growth of bovine endothelial cells. *J. Biomed. Mater. Res.* 27, 909–915.
- (4) Hammarback, J. A., McCarthy, J. B., Palm, S. L., Furcht, L. T., and Letourneau, P. C. (1988) Growth cone guidance by substrate-bound laminin pathways is correlated with neuron-to-pathway adhesivity. *Dev. Biol.* 126, 29–39.
- (5) Hickman, J. J., Bhatia, S. K., Quong, J. N., Shoen, P., Stenger, D. A., Pike, C. J., and Cotman, C. W. (1994) Rational pattern design for in vitro cellular networks using surface photochemistry. *J. Vac. Sci. Technol. A* 12, 607–616.
- (6) Ranieri, J. P., Bellamkonda, R., Bekos, E. J., Gardella, J. A. J., Mathieu, H. J., Ruiz, L., and Aebischer, P. (1994) Spatial control of neuronal cell attachment and differentiation on covalently patterned laminin oligopeptide substrates. *Int. J. Dev. Neurosci.* 12, 725–735.
- (7) Clemence, J.-F., Ranieri, J. P., Aebischer, P., and Sigrist, H. (1995) Photoimmobilization of a bioactive laminin fragment and pattern-guided selective neuronal cell attachment. *Bioconjugate Chem.* 6, 411–417.
- (8) Kleinfeld, D., Kahler, K. H., and Hockberger, P. E. (1988) Controlled outgrowth of dissociated neurons on patterned substrates. *J. Neurosci.* 8, 4098–4120.
- (9) Berggren, K. K., Bard, A., Wilbur, J. L., Gillaspay, J. D., Helg, A. G., McClelland, J. J., Rolston, S. L., Phillips, W. D., Prentiss, M., and Whitesides, G. M. (1995) Microlithography by using neutral metastable atoms and self-assembled monolayers. *Science* 269, 1255–1257.
- (10) Singhvi, R., Kumar, A., Lopez, G. P., Stephanopoulos, G. N., Wang, D. I. C., Whitesides, G. M., and Ingber, D. E. (1994) Engineering cell shape and function. *Science* 264, 696–698.
- (11) Ireland, G. W., Dopping-Hepenstal, P., Jordan, P., and O'Neill, C. (1987) Effect of patterned surfaces of adhesive islands on the shape, cytoskeleton, adhesion and behavior of Swiss Mouse 3T3 fibroblasts. *J. Cell Sci. Suppl.* 8, 19–33.
- (12) Halfter, W. (1996) The behavior of optic axons on substrate gradients of retinal basal lamina proteins and merosin. *J. Neurosci.* 16, 4389–4401.
- (13) Snow, D. M., and Letourneau, P. C. (1992) Neurite outgrowth on a step gradient of chondroitin sulfate proteoglycan (CS-PG). *J. Neurobiol.* 23, 322–336.
- (14) McKenna, M. P., and Raper, J. A. (1988) Growth cone behavior on gradients of substratum bound laminin. *Dev. Biol.* 130, 232–236.
- (15) Bhatia, S. K., Hickman, J. J., and Ligler, F. S. (1992) New approach to producing patterned biomolecular assemblies. *J. Am. Chem. Soc.* 114, 4432–4433.
- (16) Clark, P., Connolly, P., and Moores, G. R. (1992) Cell guidance by micropatterned adhesiveness in vitro. *J. Cell Sci.* 103, 287–292.
- (17) Yamaguchi, K., Kuboniwa, H., Murakami, N., Hirao, A., Nakahama, S., and Yamazaki, N. (1989) Studies on synthetic ionophores. VIII. Transport of alkaline earth metal ions by polyether carboxylic acids through liquid membrane. *Bull. Chem. Soc. Jpn.* 62, 1097–1101.
- (18) Brunner, J. (1993) New photolabeling and crosslinking methods. *Annu. Rev. Biochem.* 62, 483–514.
- (19) Ji, T. H. (1979) The application of chemical crosslinking for studies on cell membranes and the identification of surface reporters. *Biochim. Biophys. Acta* 559, 39–69.
- (20) Olszewski, J. D., Dorman, G., Elliott, J. T., Hong, Y., Ahern, D. G., and Prestwich, G. D. (1995) Tethered benzophenone reagents for the synthesis of photoactivatable ligands. *Bioconjugate Chem.* 6, 395–400.
- (21) Rozsnyai, L. F., Benson, D. R., Fodor, S. P. A., and Schultz, P. G. (1992) Photolithographic immobilization of biopolymers on solid supports. *Angew. Chem., Int. Ed. Engl.* 31, 759–761.
- (22) Dorman, G., and Prestwich, G. D. (1994) Benzophenone photophores in biochemistry. *Biochemistry* 33, 5661–5673.
- (23) Ito, Y., Chen, G., and Imanishi, Y. (1996) Photoimmobilization of insulin onto polystyrene dishes for protein-free cell culture. *Biotechnol. Prog.* 12, 700–702.
- (24) Sigrist, H., Collioud, A., Clemence, J.-F., Gao, H., Luginbuhl, R., Sanger, M., and Sundarababu, G. (1995) Surface immobilization of biomolecules by light. *Opt. Eng.* 34, 2339–2348.
- (25) Bhatia, S. K., Shriver-Lake, L. C., Prior, K. J., Georger, J. H., Calvert, J. M., Bredehorst, R., and Ligler, F. S. (1989) Use of thiol-terminal silanes and heterobifunctional crosslinkers for immobilization of antibodies on silica surfaces. *Anal. Biochem.* 178, 408–413.

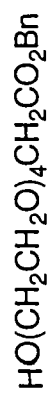
BC9701252

Compound 3
Benzyl 14-hydroxy-3,6,8,12-tetraoxatetradecanoate

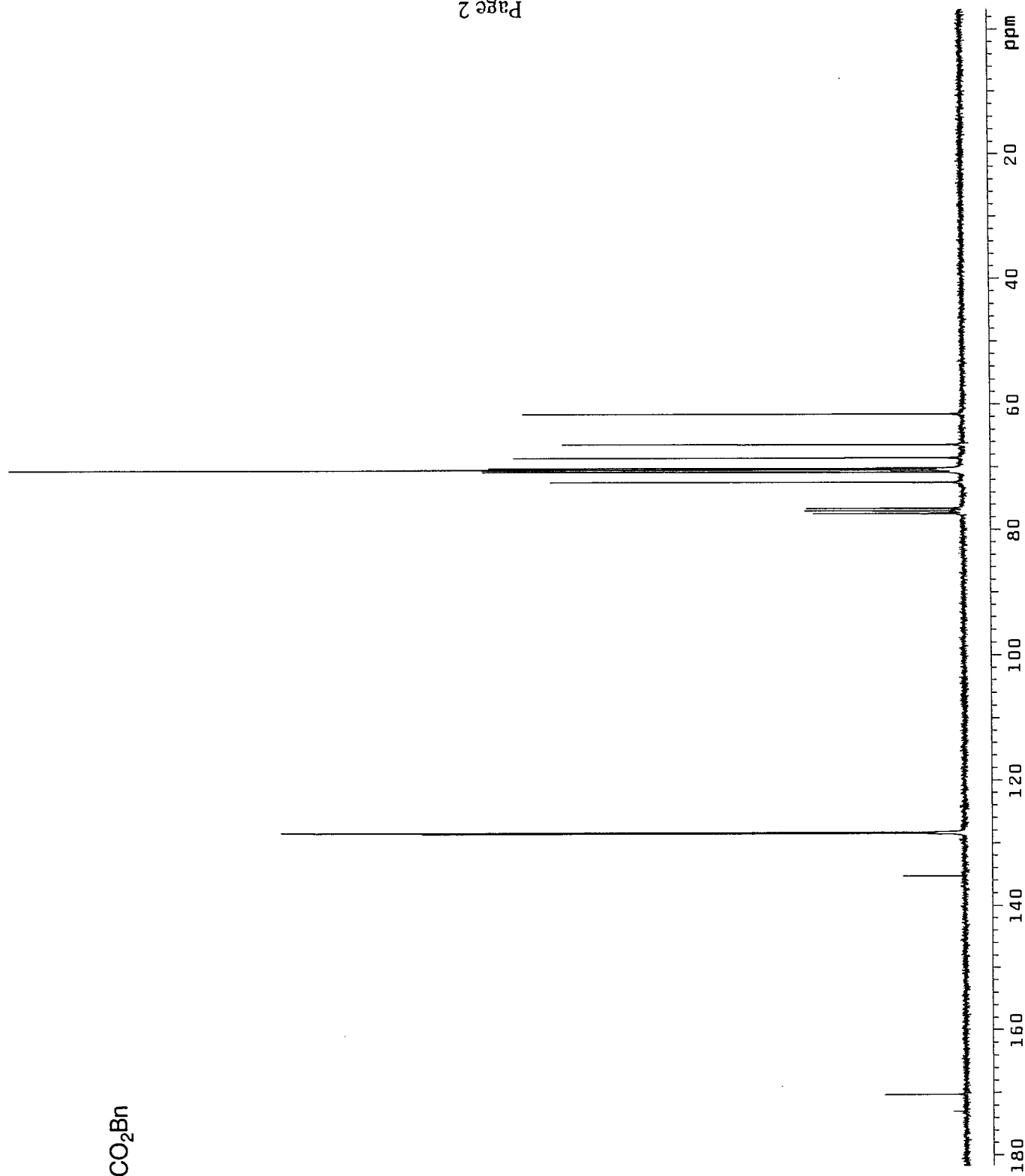


3





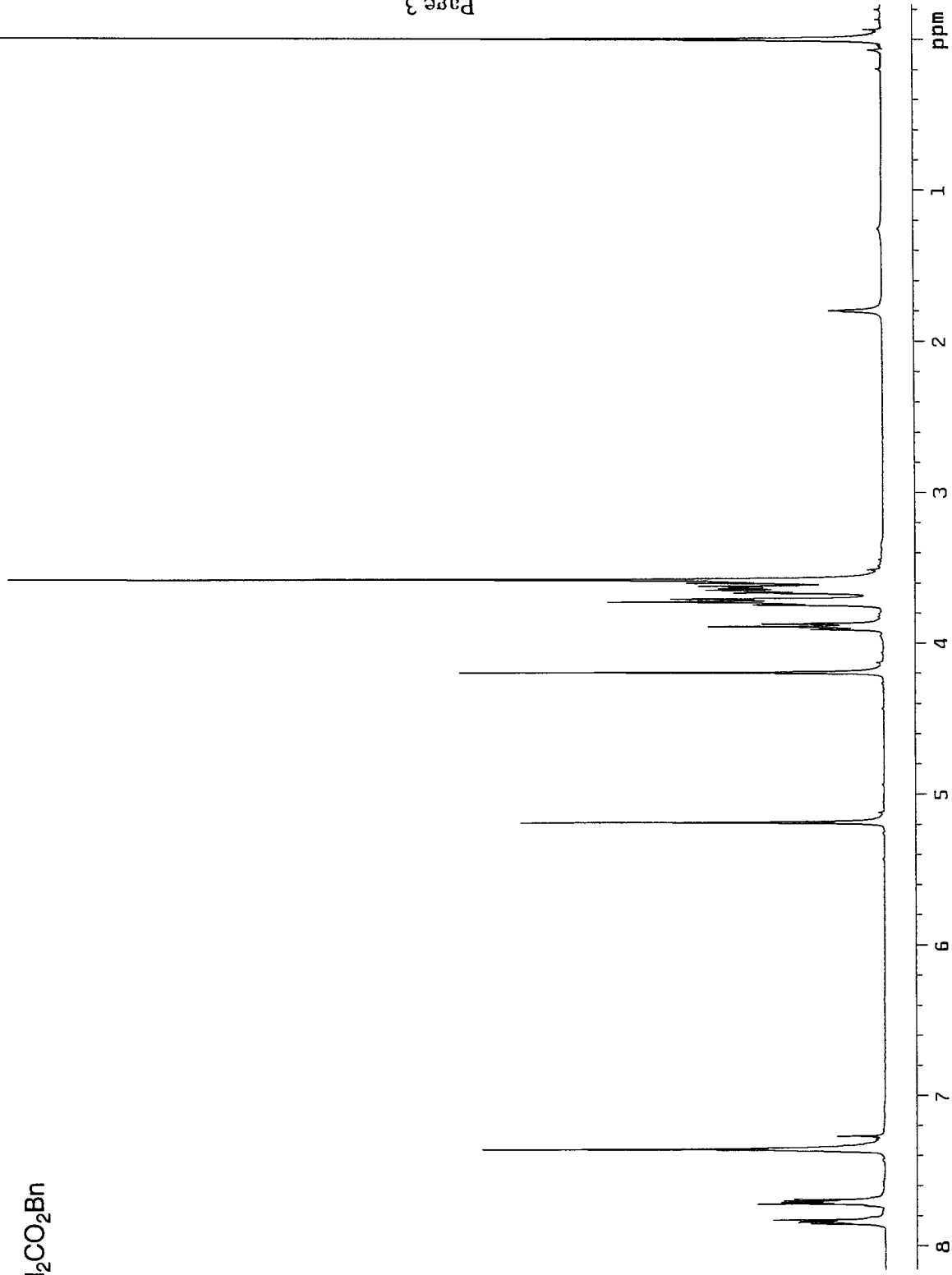
3





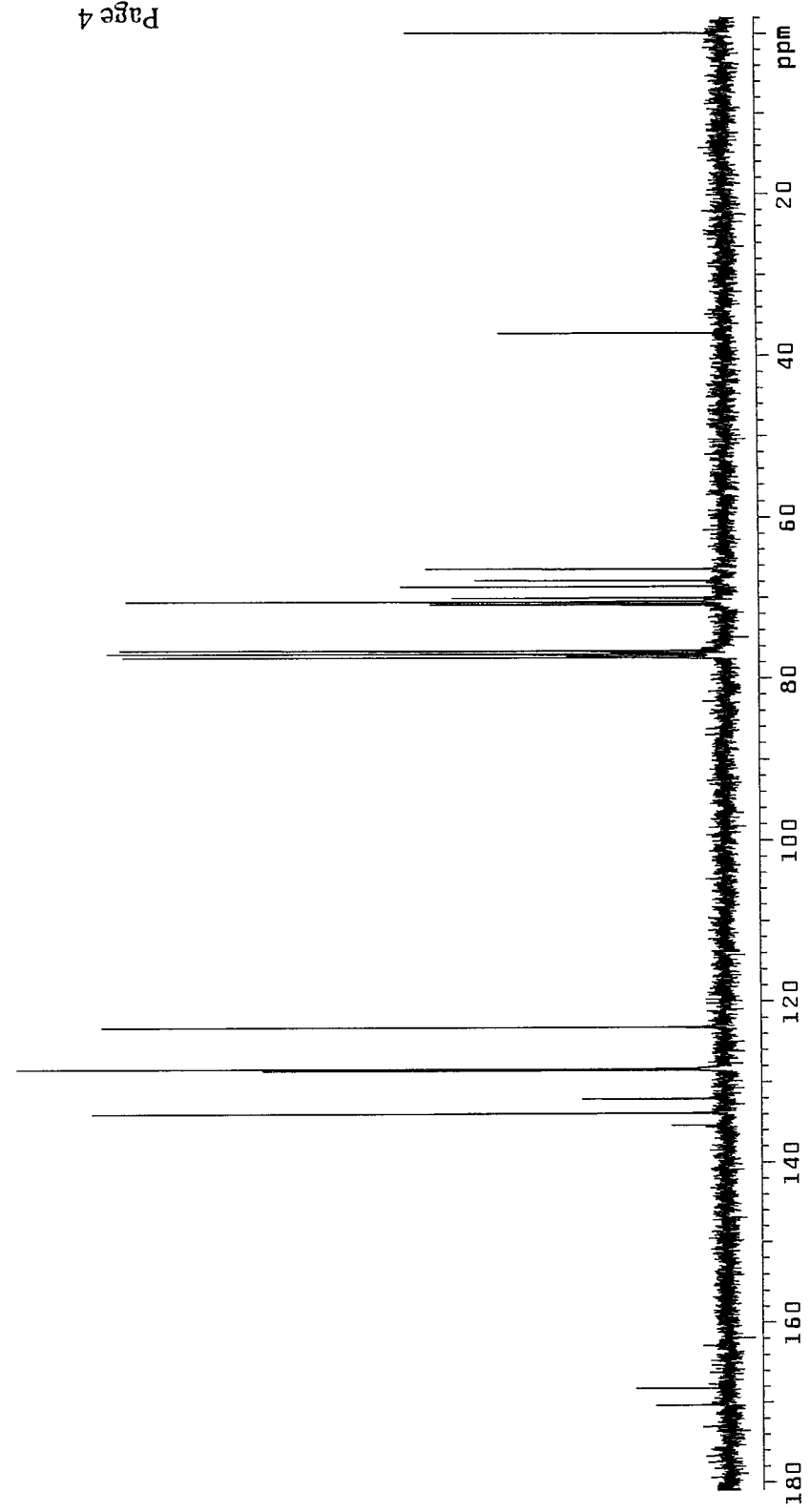
4

Page 3

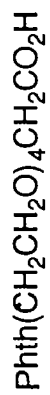




4

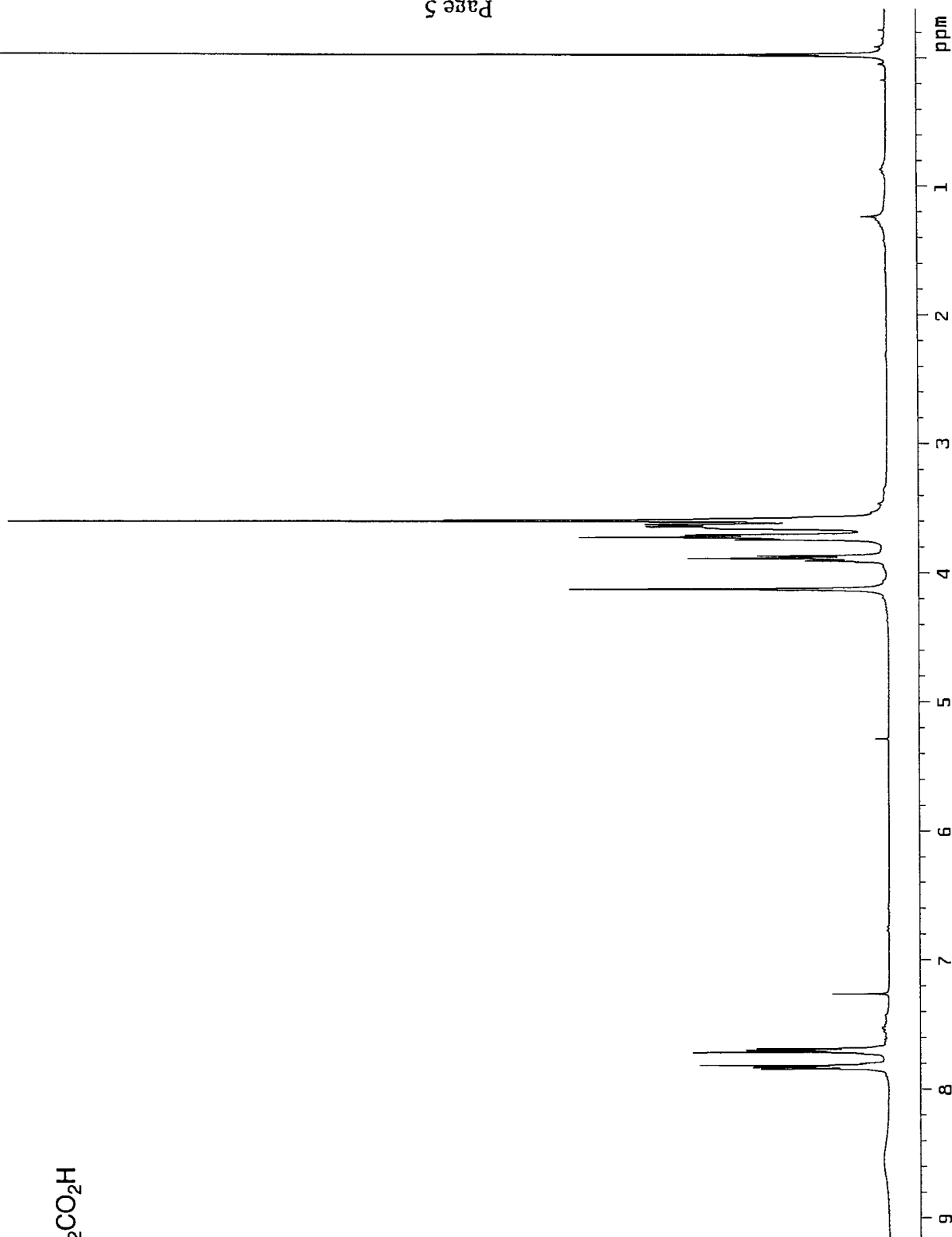


Compound 5
14-N-Phthalimido-3,6,9,12-tetraoxatetradecanoic acid



5

Page 5

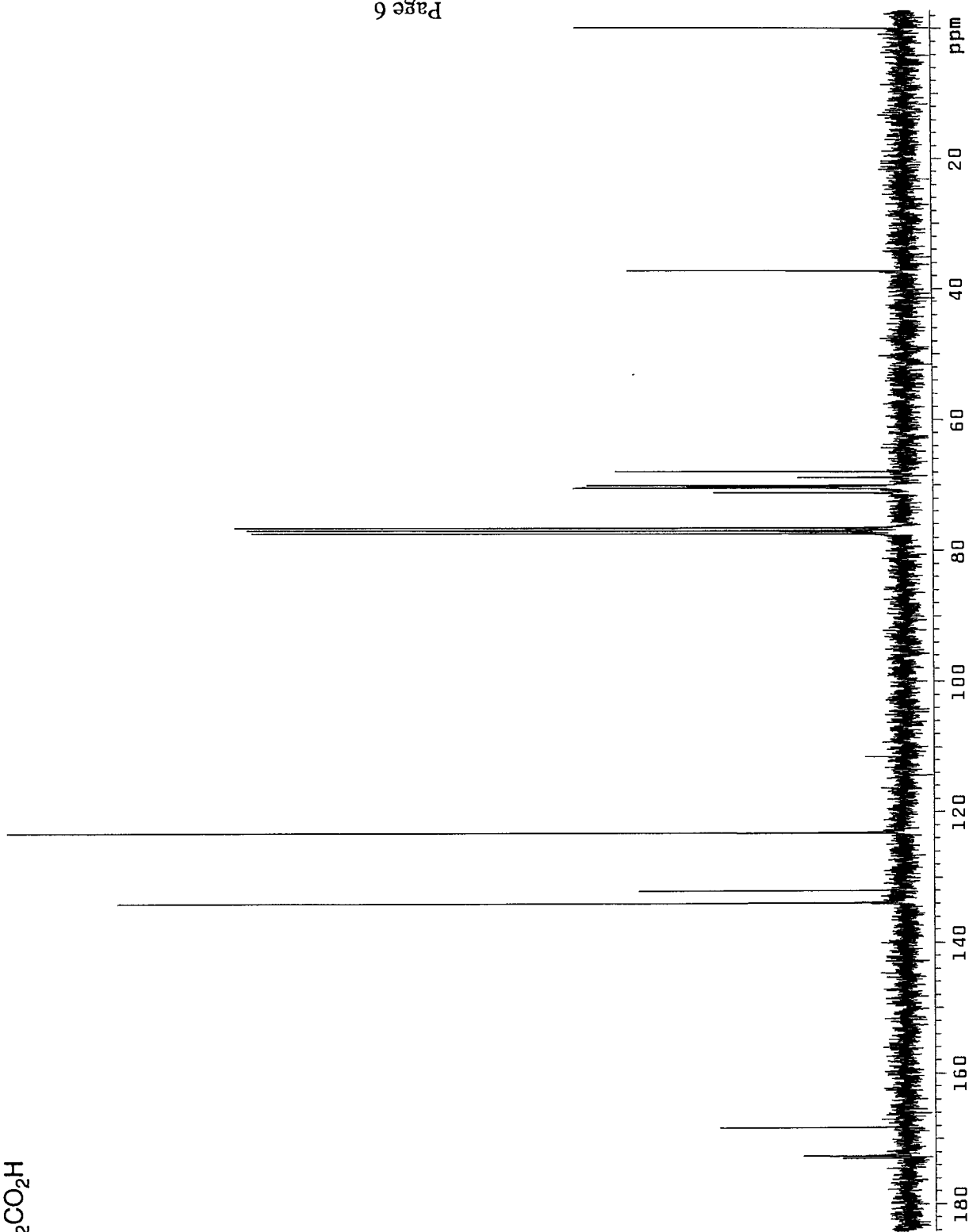


Compound 5
1,4-N-Phthalimido-3,6,9,12-tetraoxatetradecanoic acid

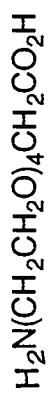


5

Page 6



Compound 6
1,4-Amino-3,6,9,12-tetraoxatetradecanoic acid



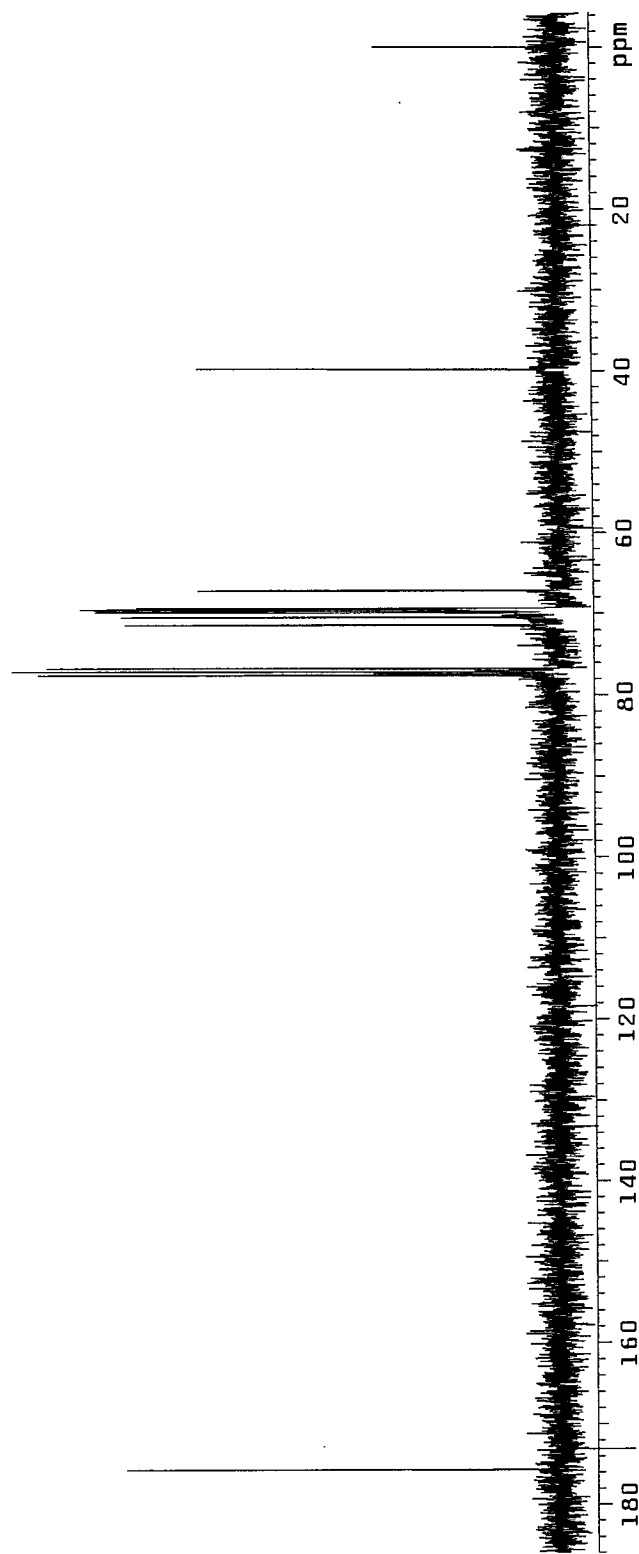
6

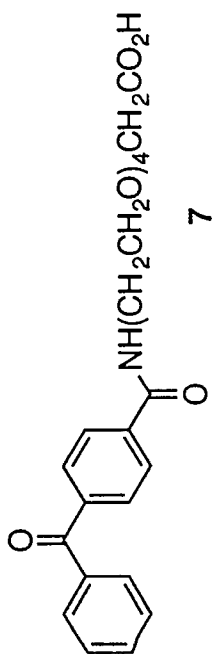
Page 7



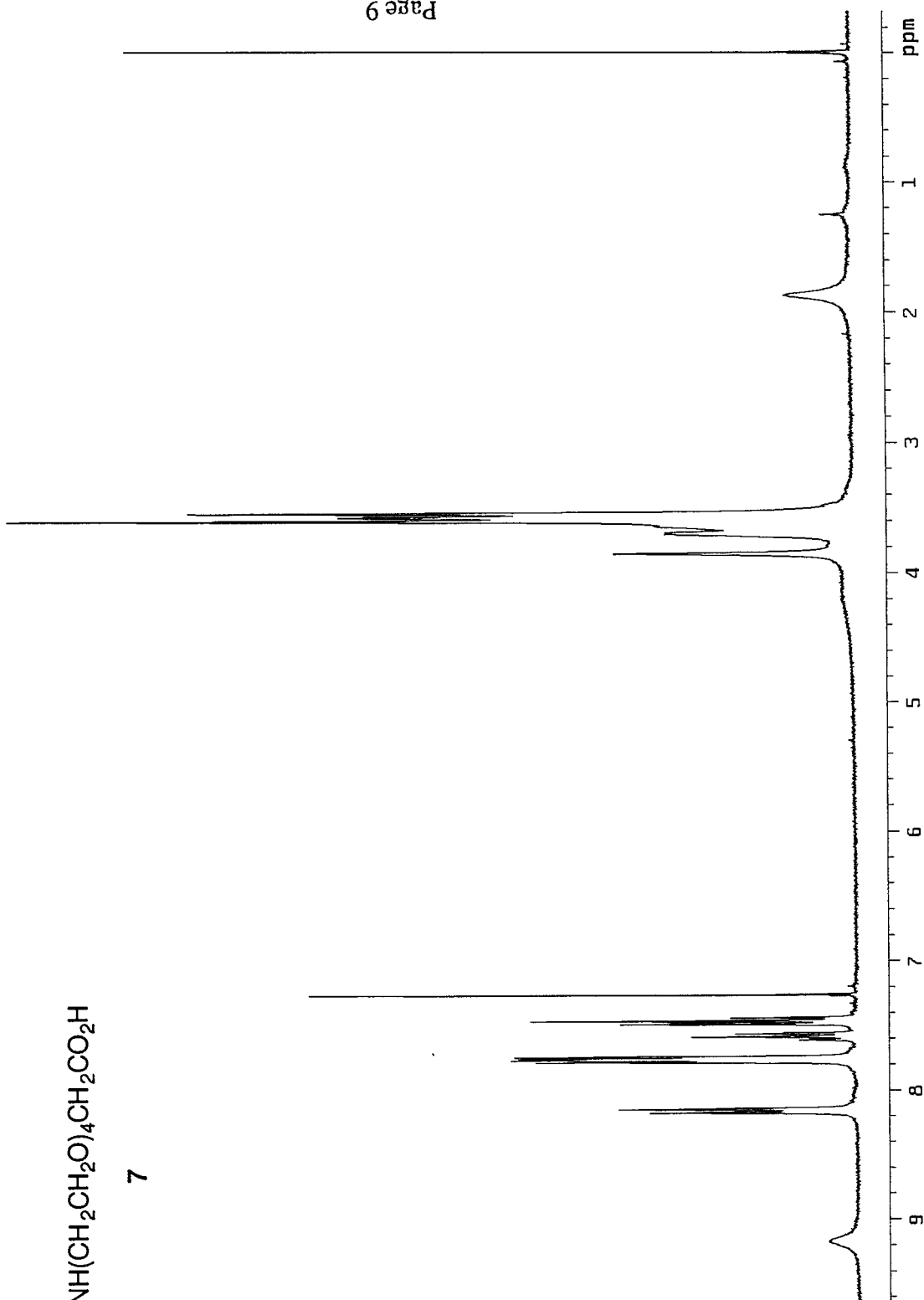


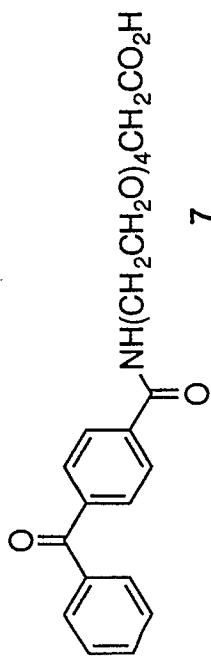
6



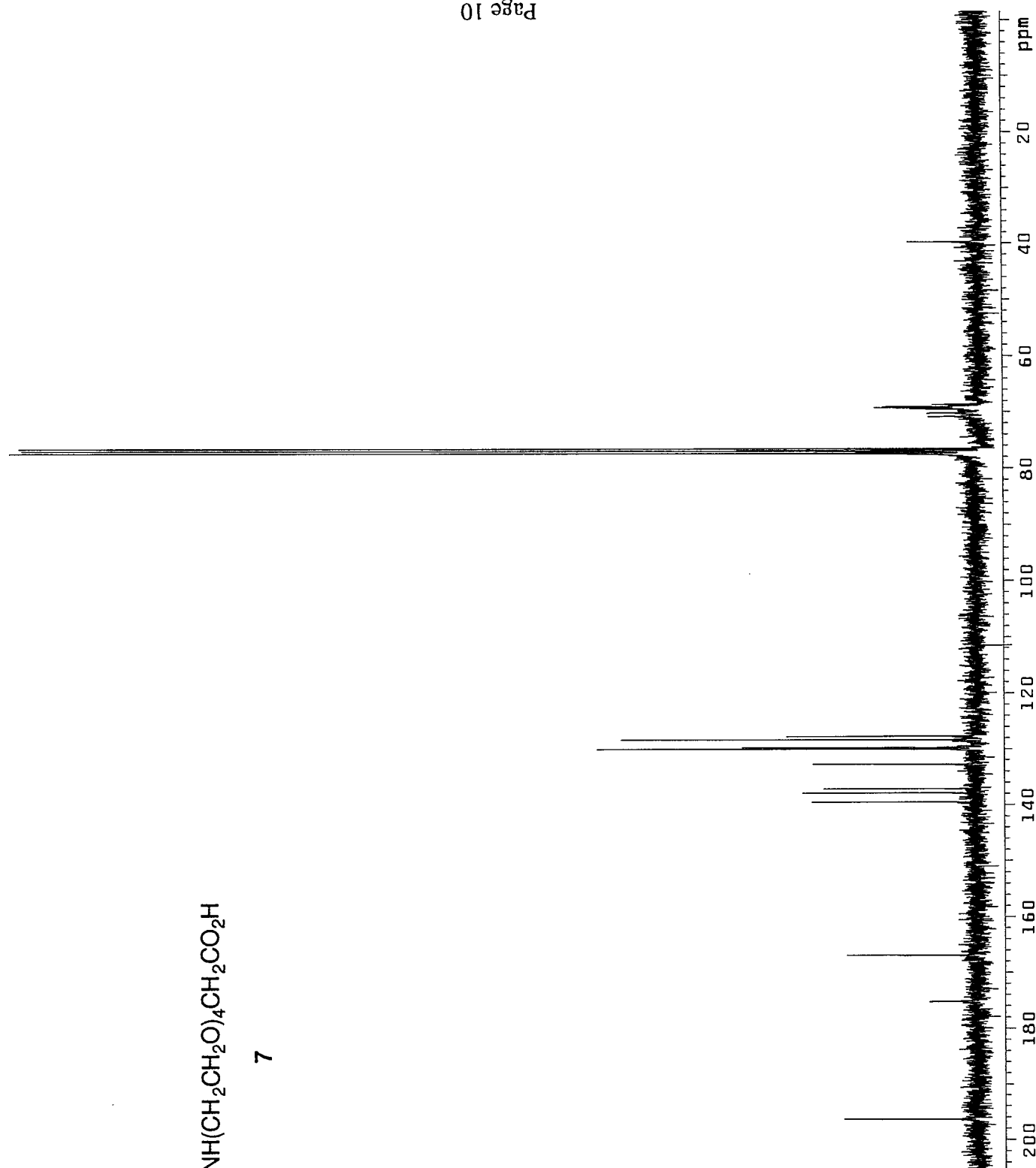


7





7



Compound 8 - Sample #1



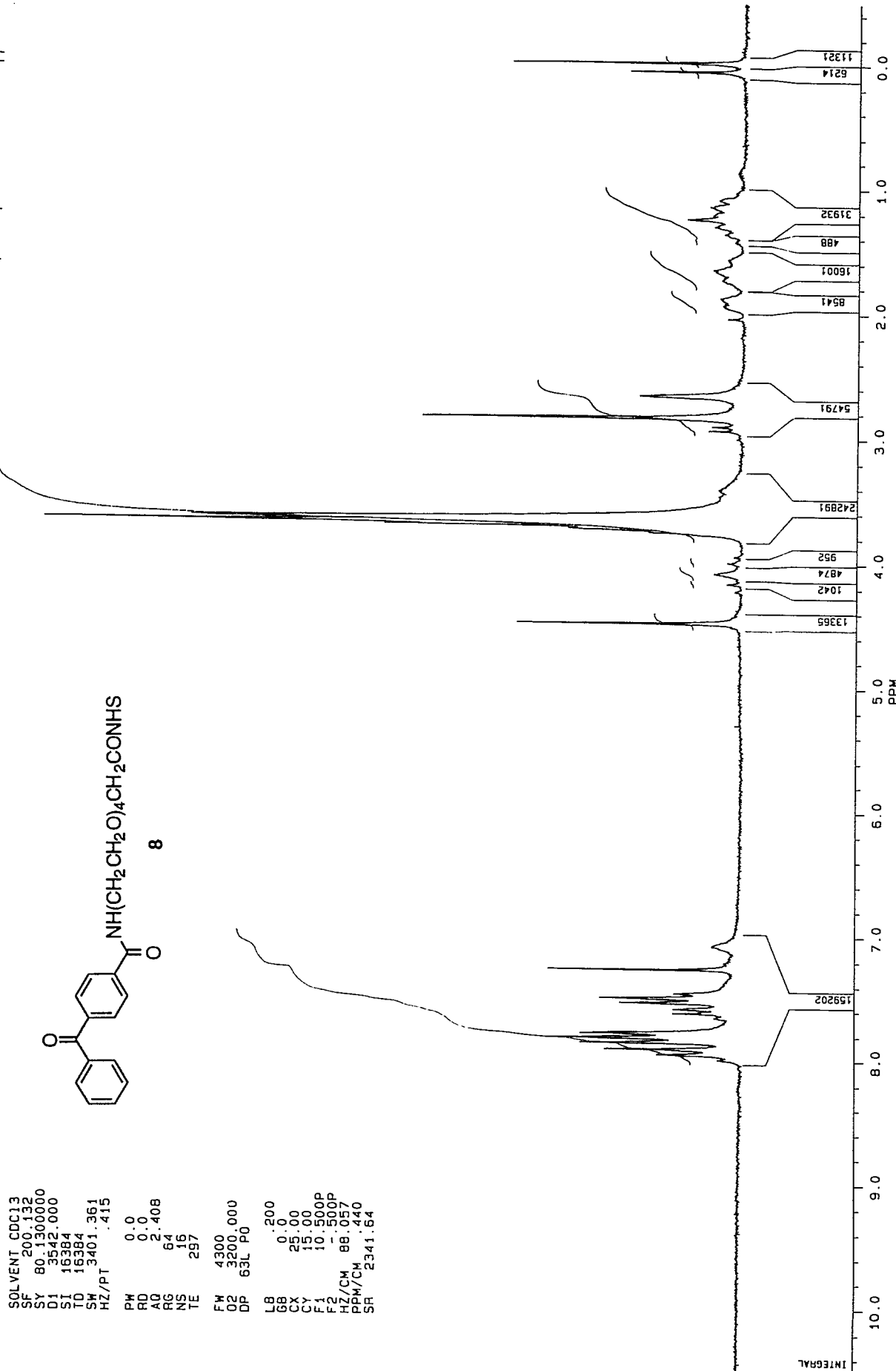
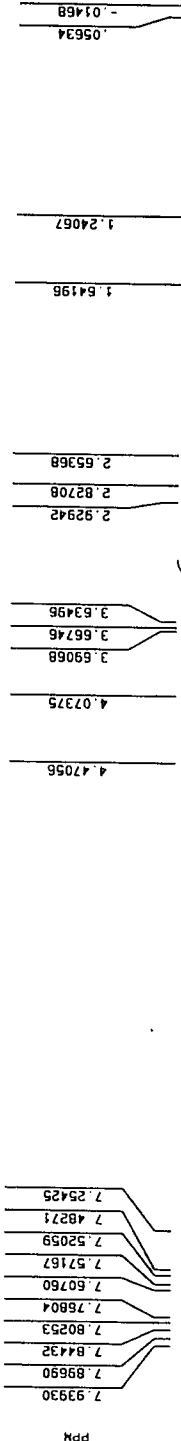
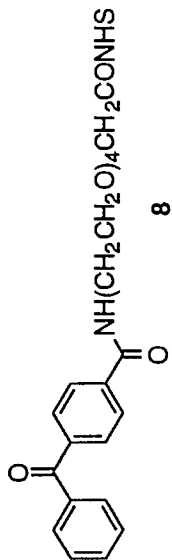
AP030S:102
AU PROG:
X75-AU
DATE 3-4-96
TIME 10:36

SOLVENT CDCl3
SF 200.132
SY 80.1300000
D1 3542.000
SI 16384
TD 16384
SW 3401.361
HZ/PT .415

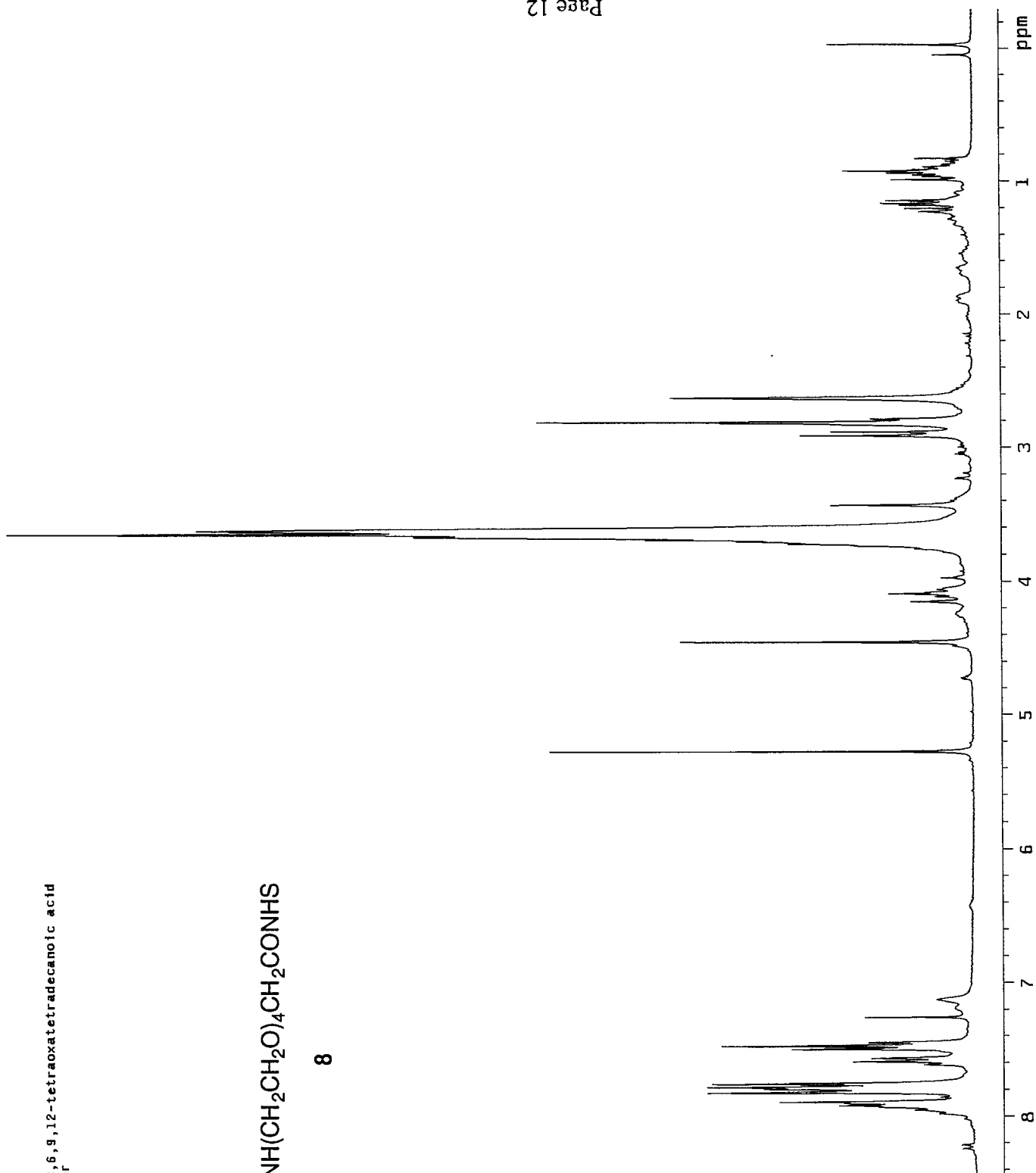
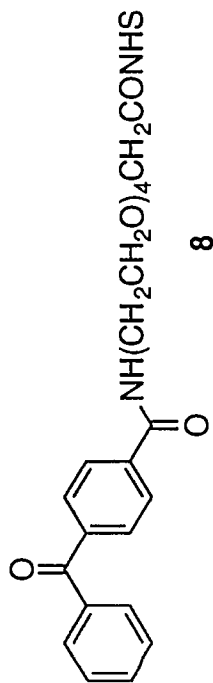
PW 0.0
RD 0.0
AQ 2.408
RG 64
NS 16
TE 297

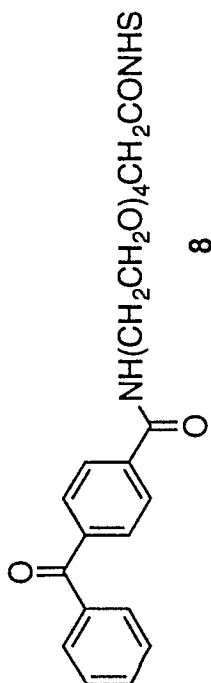
FW 4300
O2 3200.000
DP 63L P0

LB .200
GB 0.0
CX 25.00
CY 15.00
F1 10.500P
F2 -500P
HZ/CM 88.057
PPM/CM 88.440
SR 2341.64

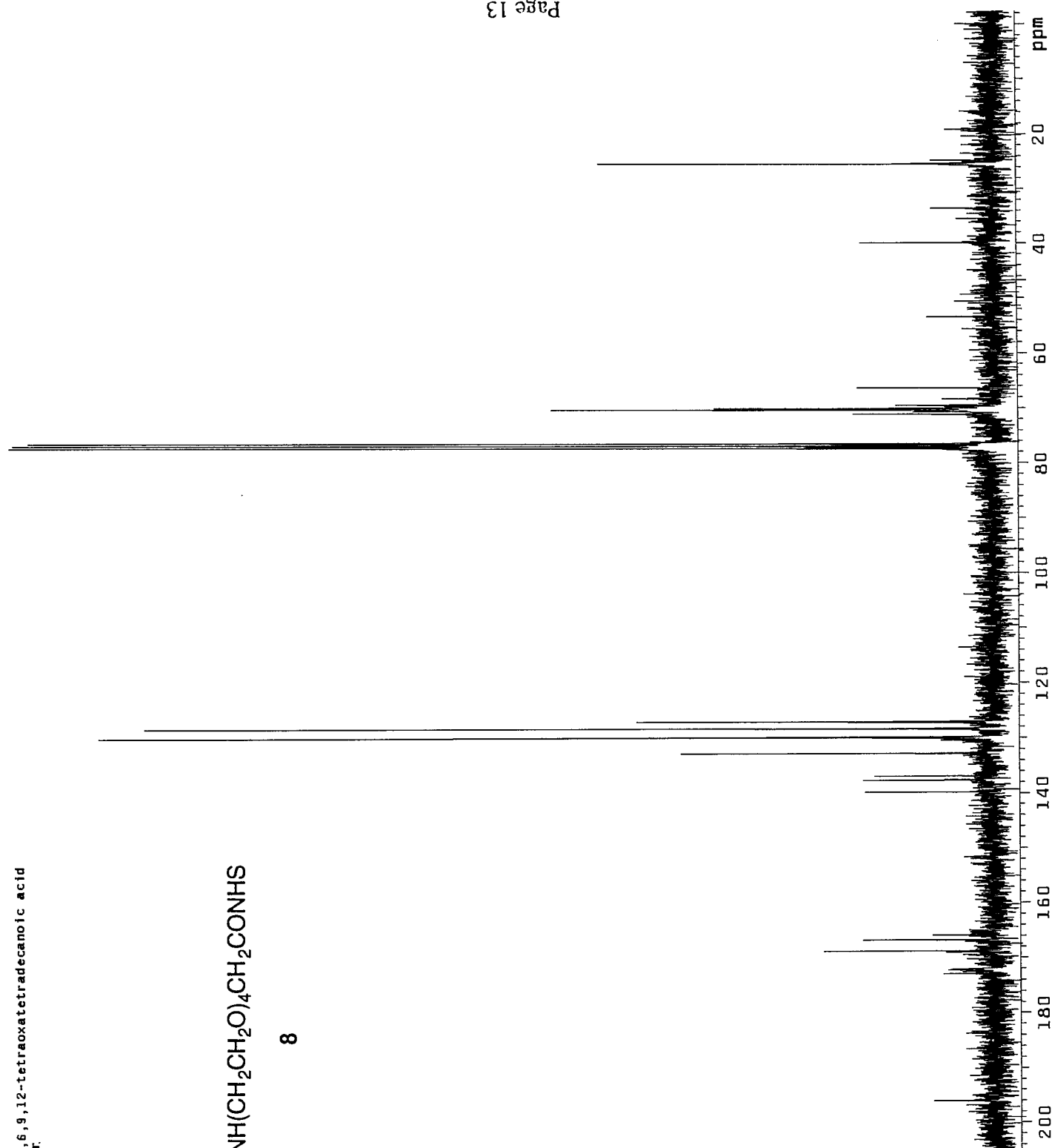


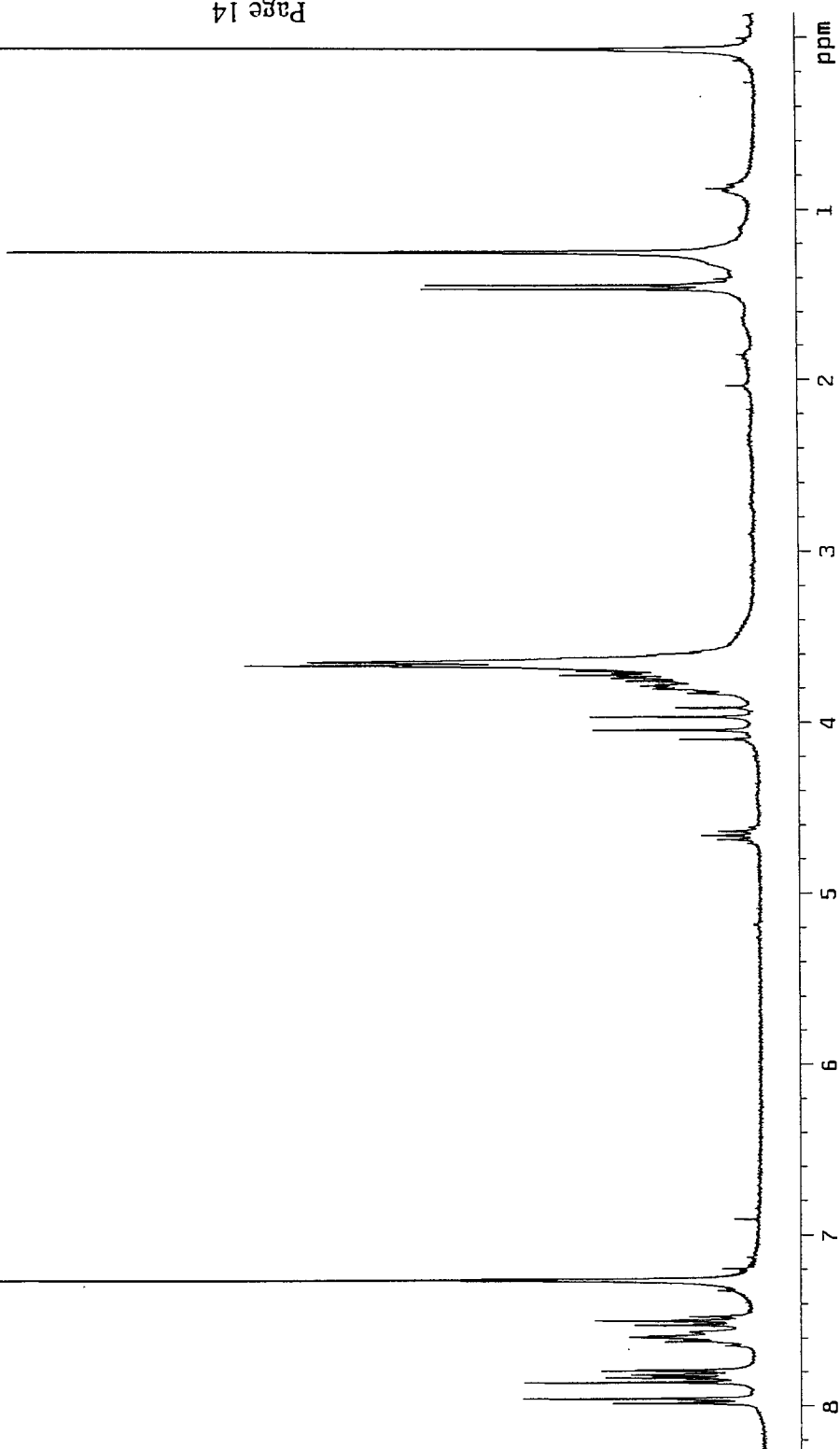
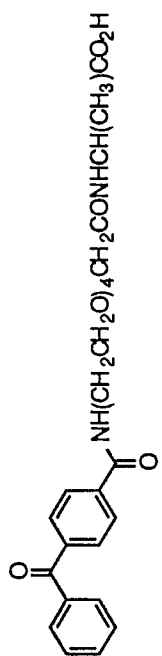
Compound 8
1,4-(4-Benzoylbenzamido)-3,6,9,12-tetraoxatetradecanoic acid
N-hydroxysuccinimide ester



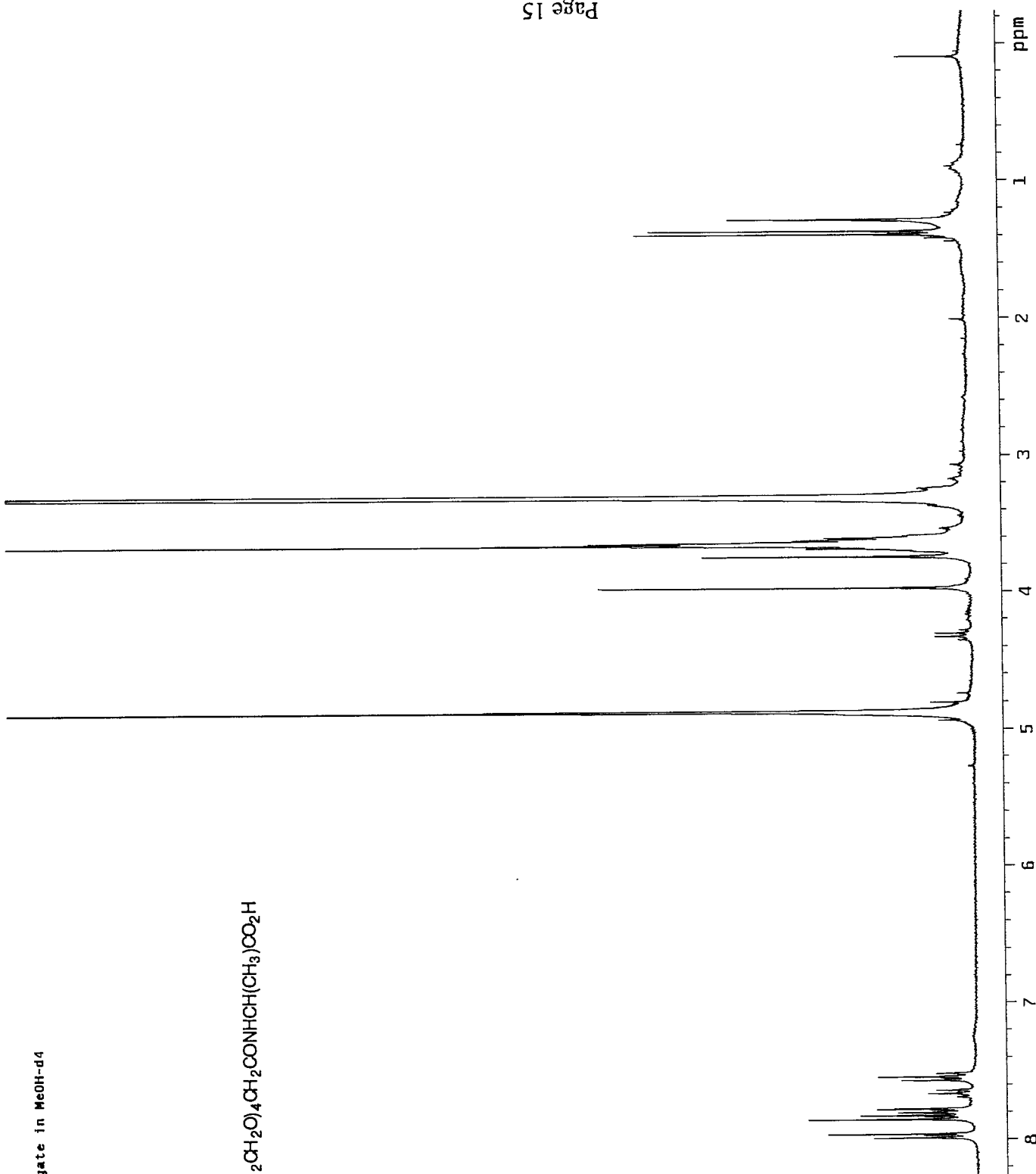


8





Alanine-Photolinker conjugate in MeOH-d₄



Glucose-Induced Release of Glycosylpoly(ethylene glycol) Insulin Bound to a Soluble Conjugate of Concanavalin A

Feng Liu,[†] Soo Chang Song,[†] Don Mix, Miroslav Baudyš, and Sung Wan Kim*

Department of Pharmaceutics and Pharmaceutical Chemistry/Center for Controlled Chemical Delivery, Biomedical Polymers Research Building, Room 205, University of Utah, Salt Lake City, Utah 84112. Received February 3, 1997*

Treatment of diabetes mellitus by insulin injections provides long-term control of the disease but lacks any feedback response to glucose concentration changes, which finally leads to a number of life-threatening conditions. The purpose of this study was to improve and optimize an implantable, concanavalin A (Con A) based, glucose-responsive insulin delivery system studied earlier [Jeong, S. Y., Kim, S. W., Holmberg, D. L., and McRea, J. C. (1985) *J. Controlled Release* 2, 143–152], which can be used for long-term diabetes treatment. To optimize the “insulin component” of the delivery system, we prepared PheB1 insulin amino group monosubstituted monoglucosylpoly(ethylene glycol) (G-PEG) insulin conjugates (PEG M_r 600 or 2000), which showed preserved bioactivity, significantly improved solubility and solution stability at neutral pH, and substantially suppressed hexamerization/dimerization. To improve the delivery system further, we synthesized and characterized a conjugate of Con A and monomethoxypoly(ethylene glycol) (mPEG, M_r 5000) grafted hydrophilic poly(vinylpyrrolidone-*co*-acrylic acid) (PVPAA) with M_r of 250 000. The optimal conjugate contained around eight PEG chains and two to three Con A tetramers attached through the amide bonds to the PVPAA chain. The Con A sugar binding characteristics were preserved, and, more importantly, Con A solubility at pH 7.4 substantially increased. This also holds true for a complex formed by the Con A conjugate and G-PEG insulin, which is soluble and does not precipitate under the physiologically relevant conditions under which the complex formed by the Con A conjugate and glycosyl insulin immediately precipitates. Finally, no leakage of the Con A conjugate from a membrane device was detected. Preliminary *in vitro* release experiments with Con A conjugate and G-PEG insulin complex enclosed in the membrane device showed a pulsative, reversible release pattern for G-PEG insulin in response to glucose challenges of 50–500 mg/dL, demonstrating the feasibility of the release system for use in planned, chronic *in vivo* studies with diabetic (pancreatectomized) dogs.

INTRODUCTION

The need to improve the control of glucose homeostasis and to avoid frequent chronic hyperinsulinemic episodes caused by conventional parenteral insulin injections in the treatment of diabetes led in the late 1970s to the development of different continuous insulin delivery systems (1). However, most of these systems suffered from the lack of feedback regulation utilizing some kind of glucose level monitoring *in vivo*; therefore, new approaches have been used to develop glucose-responsive insulin delivery systems (2–8). Our group has been working for a long time on a unique delivery system based on competitive binding (9), namely the displacement of glycosylated insulin by glucose from concanavalin

A (Con A).¹ The system is enclosed in a polymeric membrane device that is permeable to glucose and glycosylated insulin and nonpermeable to Con A. The current version of the system is a rechargeable pouch that can be implanted into the peritoneal cavity and then be refilled from the outside (10). Nevertheless, the performance of such a device is hampered by the limited solubility of glycosylated insulin–Con A complex, which causes a long unwanted lag phase for the onset of release of glycosylated insulin derivative when the device is challenged by high glucose concentration (11). The physicochemical basis for this phenomenon is the tetrameric nature of the Con A molecule (12) and the limited, yet partially preserved, ability of glycosylated insulin derivatives to form dimers and hexamers (13). This especially holds true for GlyA1 substituted derivatives that comprise the major component in glycosylated insulin preparations used in the release studies so far (14).

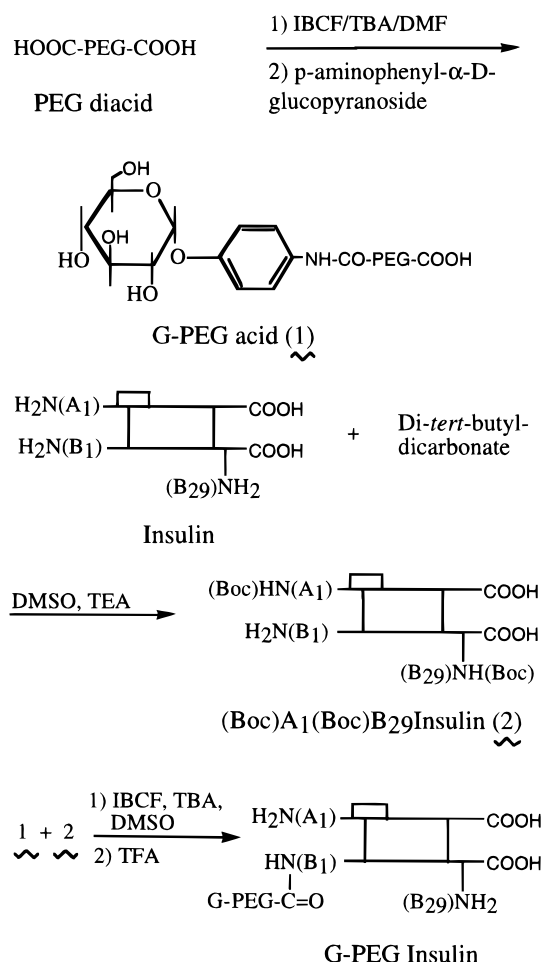
Recently, we worked out a new synthetic scheme for glycosylated insulins enabling us to attach a sugar moiety specifically to the PheB1 amino group (15). Generally, this site-specific modification does not have a negative impact on the binding of such derivatives to insulin receptors, and thus their biological activity is more or less preserved (16). We have also shown that these glycosylated derivatives are predominantly dimeric over the considered concentration range (15). We hypothesized that by placing a sufficiently long poly(ethylene glycol) (PEG) spacer between the sugar moiety and the above specified amino group of the insulin molecule (Scheme 1), we would achieve further reduction in the

* Author to whom correspondence should be addressed [telephone (801) 581-6654; fax (801) 581-7848; e-mail rburns@pharm.utah.edu].

[†] Both contributed equally to the project.

© Abstract published in *Advance ACS Abstracts*, August 15, 1997.

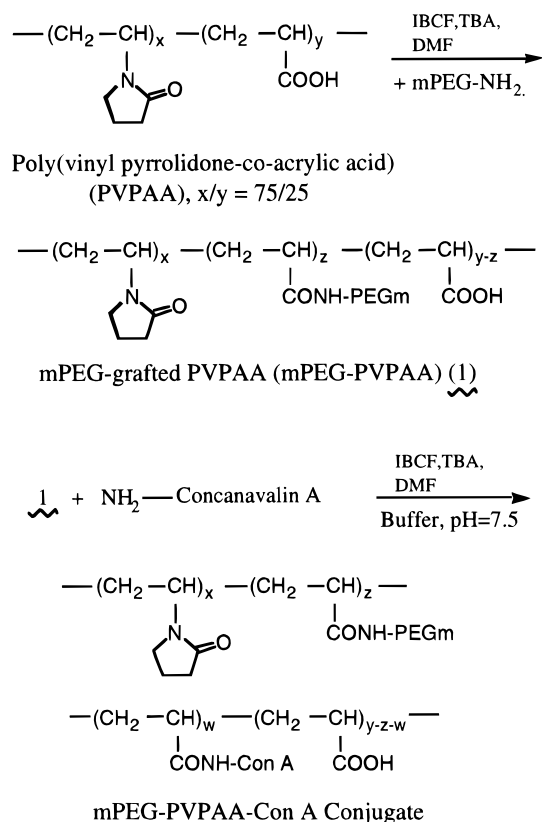
¹ Abbreviations: Con A, concanavalin A; PEG, poly(ethylene glycol); G-PEG, glycosyl(glucosyl)poly(ethylene glycol); mPEG, monomethoxypoly(ethylene glycol); mPEG-NH₂, aminomethoxypoly(ethylene glycol); PVPAA, poly(vinyl pyrrolidone-*co*-acrylic acid); mPEG-PVPAA, mPEG-grafted PVPAA; mPEG-PVPAA-Con A, conjugate of Con A and mPEG-PVPAA; Hepes, 4-(2-hydroxyethyl)-1-piperazineethanesulfonic acid; AcOH, acetic acid; TFA, trifluoroacetic acid; TBA, tributylamine; TEA, triethylamine; IBCF, isobutylchloroformate; Boc, *tert*-butoxy-carbonyl; DMF, dimethylformamide; DMSO, dimethyl sulfoxide; MWCO, molecular weight cutoff; AUC, area under the curve; SEC, size exclusion chromatography.

Scheme 1. Preparation of PheB1-Substituted Mono-glycosyl Poly(ethylene glycol) Insulin

dimerization of glycosylpoly(ethylene glycol) insulin (G-PEG insulin), thus preventing precipitation of its complex with Con A and improving its release profile from a pouch.

Moreover, the attachment of PEG chain(s) to the insulin molecule should have a beneficial impact on several important characteristics of the hormone, such as diminished immunogenicity and antigenicity, as has already been demonstrated for PEG insulin conjugates (17), reduced susceptibility to proteolysis, and increased plasma half-life as well as significantly improved physical stability, as has been shown for many pharmaceutically relevant proteins (18). The last feature is especially important for the pouch design since insulin solutions at elevated temperature (37 °C) and constant irregular motions (hydrodynamic stress) tend to form insoluble fibrils with negligible bioactivity (19–22).

To further optimize physicochemical and biological features of the glucose-responsive insulin delivery system described above for *in vivo* use, unsolved problems associated with Con A had to be also addressed. Originally, unmodified Con A was used, which was slowly leaking from a pouch (23). To prevent the leakage, new insoluble Con A systems were designed based on Con A immobilized onto a solid support (24) or Con A cross-linked as microspheres (14), which had the disadvantage that the beads or microspheres settled to the bottom of the pouch, preventing reliable and reproducible insulin release during glucose challenge experiments. Thus, soluble Con A oligomer ($M_r > 300\,000$) was prepared by glutaraldehyde cross-linking (25). Still, reproducibility problems persisted because of limited solubility of Con

Scheme 2. Preparation of mPEG-NH₂ Grafted Poly(vinylpyrrolidone-co-acrylic acid) and Conjugation of Concanavalin A

A oligomer and the insolubility of Con A oligomer-glycosylated insulin complex. To increase Con A solubility and prevent Con A leakage from the pouch as well as precipitation of the complex, we decided to synthesize a conjugate of Con A and hydrophilic copolymer poly(vinylpyrrolidone-co-acrylic acid) (PVPAA) with high M_r of 250 000 (Scheme 2). Grafting of mPEG-NH₂ molecules to PVPAA before Con A conjugation should further increase the solubility of Con A and its complex with glycosylated insulin and especially with G-PEG insulin.

This paper describes the synthesis, purification, and chemical, physical, and biological characterization of G-PEG insulin derivatives with various lengths of PEG spacer. Preparation and characterization of a high M_r and soluble Con A conjugate with mPEG-grafted PVPAA (mPEG-PVPAA) are also described. Finally, the release behavior of G-PEG insulin from mPEG-PVPAA-Con A conjugate enclosed within a porous polymer membrane device at various glucose concentrations was studied to demonstrate the feasibility of using this system for self-regulating insulin delivery *in vivo*.

EXPERIMENTAL PROCEDURES

Materials. Poly(ethylene glycol) diacid (PEG diacid, M_r 600 and 2000) was purchased from Fluka (Ronkonkoma, NY), and aminomethoxypoly(ethylene glycol) (mPEG-NH₂) of M_r 5000 was obtained from Shearwater Polymers (Huntsville, LA) and dried over P₂O₅ under vacuum before use. Human crystalline Zn-insulin was obtained from Bayer Corp. (Kankakee, IL). *p*-Aminophenyl α -D-glucopyranoside, methyl α -D-mannopyranoside, dansyl chloride, ammonium bicarbonate, anisole, urea, Trizma base, Hepes, and concanavalin A-Sepharose were purchased from Sigma Chemical Co. (St. Louis, MO). Concanavalin A (Sigma) was purified by precipitation of the fragmented fraction in ammonium bicarbonate (12).

Acetic (AcOH), trifluoroacetic (TFA), and sulfuric acids, isobutylchloroformate (IBCF), tributylamine (TBA), triethylamine (TEA), di-*tert*-butyl dicarbonate (Boc dicarbonate), and all other reagents as well as all organic solvents used were at least ACS grade and purchased from Aldrich Chemical Co. (Milwaukee, WI). Spectra/Por dialysis tubing (MWCO 1000 and 3500) and Spectra/Por RC DispoDialyzer (1 mL, MWCO 10 000, 25 000, 50 000) were purchased from Spectrum Medical Industries (Houston, TX). Ultrafiltration membranes (PCMK regenerated cellulose disks) with MWCO 300 000 were from Millipore (Bedford, MA). Poly(vinylpyrrolidone-co-acrylic acid) (PVPA) (M_r 250 000, VP/AA molar ratio = 75/25) was obtained from ISP Technologies, Inc. Insulin radioimmunoassay kits from ICN Micromedics, Horsham, PA, were used.

Synthesis of Glucosyl-PEG Diacid (G-PEG Diacid). The mixed anhydride method of amide bond formation was used to couple one of the carboxylic groups of PEG diacid to the amino group of glucoside (26). A 1 g (1.67 mmol) portion of PEG diacid (M_r 600) containing 3.34 mmol of free carboxyl groups was dissolved in 3 mL of dry dimethylformamide (DMF) containing 1.83 mmol of TBA in an ice bath under N_2 . IBCF (1.83 mmol) dissolved in 1 mL of dry DMF was added and the mixture stirred for 15 min. *p*-Aminophenyl α -D-glucoside (1.67 mmol) dissolved in 3 mL of dry DMF was added dropwise, and the mixture was stirred for an additional 15 min in an ice bath and for 3 h at room temperature. The product was precipitated in an excess of dry ether (200 mL). The precipitate was dissolved in 20 mL of distilled water, dialyzed against distilled water (tubing with MWCO 1000), and freeze-dried. The unreacted PEG diacid was removed from the mixture on a Con A-Sepharose column under conditions described later (see G-PEG Insulin Synthesis). The fraction eluted by 0.1 M methyl α -D-mannopyranoside was collected, dialyzed extensively against water, and freeze-dried. Alternatively, PEG diacid (M_r 2000) was used and an identical procedure followed.

Synthesis and Purification of PheB1-Substituted G-PEG Insulins. Di-*N*^t-Boc-GlyA1, *N*^t-Boc-LysB29 insulin was synthesized and purified as described earlier (27). DiBoc-GlyA1, LysB29 insulin derivative (26 μ mol) was dissolved in 6 mL of dry dimethyl sulfoxide (DMSO) and activated G-PEG diacid (M_r 600) added. To prepare activated G-PEG diacid, 173 mg of the G-PEG diacid mixture containing 130 μ mol of free carboxyl groups was dissolved in 3 mL of dry DMF containing 130 μ mol of TBA and 130 μ mol of IBCF and stirred for 15 min under N_2 in an ice bath. Finally, the reaction mixture was stirred for 3 h at room temperature under N_2 and the reaction stopped by the addition of excess of aminoethanol (1.3 mmol). The resulting insulin derivative was precipitated in excess of dry acetone (100 mL) containing 65 μ L of 6 N HCl. The precipitate was washed with 10 mL of ethanol twice, dissolved, dialyzed against 0.01% NH_4HCO_3 , and finally lyophilized. This material was dissolved in 5 mL of anhydrous TFA with 5% anisole as a scavenger and kept under N_2 at 0 °C for 1 h to remove Boc groups. Deprotected insulin derivative was precipitated in an excess of dry ether, dissolved, dialyzed against 0.01% NH_4HCO_3 , and lyophilized. Alternatively, PEG diacid (M_r 2000) was used and an identical procedure followed.

Purification of G-PEG insulin derivatives (PEG 600, PEG 2000) was achieved first using FPLC on a Mono S preparative column (Pharmacia AB) using 1 M AcOH and 7 M urea as eluent and a gradient of NaCl as described earlier (13, 15). In each case, only the major peak was

collected, dialyzed, and lyophilized. Final purification was achieved by affinity chromatography on a Con A-Sepharose column. The lyophilisate (40 mg) was dissolved in 40 mL of 0.02 M Tris buffer, pH 7.4, containing 0.5 M NaCl, 3 mM $CaCl_2$, and 3 mM $MnCl_2$ and loaded on a Con A-Sepharose column (40 mL) at a flow rate 0.15 mL/min. The column was eluted until absorbance at 280 nm (A_{280}) dropped below 0.01 value, and then identical buffer containing 0.1 M methyl α -D-mannopyranoside was applied. The specifically eluted peak of G-PEG insulin derivative was detected by monitoring A_{280} , collected, dialyzed against water and 0.01% NH_4HCO_3 , and finally lyophilized.

Characterization of G-PEG Insulins. To assess physical stability, G-PEG insulin derivatives were dissolved in 0.01 M PBS (0.15 M NaCl, 0.01% sodium azide), pH 7.4, at 80 μ M concentration and filtered through a 0.22 μ m filter. Zn-Insulin, as well as Zn-free insulin solutions prepared in the same manner were used as controls. The aggregation was evaluated in 5 mL of borosilicate glass vials (1.2 mL filling volume) at 37 °C, 100 strokes/min. Individual vials ($n = 12$) were periodically withdrawn at preselected periods of time, and the remaining soluble fraction of insulin derivative was determined after filtration (PVDF membrane, 0.22 μ m) using ultraviolet spectroscopy or HPLC.

The biological activity of insulin derivatives was tested in a rat model (male Sprague-Dawley rats, 250 ± 50 g) by measuring blood glucose depression levels. All procedures in handling animals adhered to the "Principles of Laboratory Animal Care" (NIH Publication 85-23, revised 1985). The animals were fasted overnight (16 h) prior to the experiment. In the morning, the rats were anesthetized with sodium pentobarbital intraperitoneally. Each animal received an intravenous (iv) injection (tail vein) of the particular insulin derivative [3.4 nmol (mL of NS)⁻¹/kg⁻¹]. Blood samples were taken from the jugular vein 15 and 5 min before injection and 15, 30, 60, 90, 120, 180, and 240 min after injection. Blood glucose levels were measured with an Accucheck III blood glucose monitor (Boehringer Mannheim). Bioactivities of insulin derivatives were calculated from area under the curve (AUC) values and the AUC value for the same dose of unmodified human insulin.

Synthesis of Comb-Type Graft Copolymer of PVPA and mPEG-NH₂. One gram of PVPA was dissolved in 20 mL of dry DMF containing 0.48 mL of TEA in an ice-water bath. The solution was purged with dry nitrogen for 10 min. IBCF (18, 36, or 72 μ mol, respectively) was added to the above solution with stirring. After 5 min, 90, 180, or 360 mg (18, 36, or 72 μ mol) of mPEG-NH₂ respectively, dissolved in 5 mL of dry DMF was added dropwise. The mixture was kept at 0 °C for 30 min and at room temperature for an additional 30 min. The reaction solution was then poured into 500 mL of ethyl ether, and the precipitate was collected and washed with ethyl ether. mPEG-PVPA was purified by ultrafiltration using membrane with MWCO of 300 000 until no mPEG-NH₂ was detected in the ultrafiltrate by the ninhydrin method (28). Finally, the product was dialyzed against distilled water and lyophilized. The amount of grafted mPEG in the copolymer was analyzed by ¹H-NMR spectroscopy (200 MHz, D₂O) through the integration of PEG polymer signal (δ 3.62).

Synthesis and Characterization of mPEG-PVPA-Con A Conjugate. mPEG-PVPA copolymer (50 mg) was dissolved in 1.0 mL of DMSO containing 140 μ L of TEA and the solution purged with nitrogen. IBCF (1 μ mol) was added and the mixture stirred for 5 min at room temperature. The activated polymer solution was

then added to 20 mL of Hepes buffer (0.05 M, pH 7.4, 3 mM CaCl_2 , 3 mM MnCl_2 , and 0.9% NaCl) containing 100 mg of Con A at 0 °C. The reaction was allowed to proceed for 30 min at 0 °C and then for 30 min at ambient temperature. The product was purified by ultrafiltration using membrane with MWCO of 300 000 until no A_{280} was detected in the ultrafiltrate. Traces of turbidity were removed by centrifugation (5000 rpm, 4 °C, 30 min). The Con A content in the final concentrated solution of the conjugate was assayed by A_{280} (25).

To compare the binding characteristics of conjugated Con A with that of free Con A, a glycogen precipitation assay was employed. Glycogen in the Hepes buffer (see above, 100 μL) was added to a 1 mL stirred UV cuvette containing mPEG-PVPAA-Con A or Con A in the same buffer (900 μL). The final concentrations of Con A (in both free and conjugated forms) and glycogen were 200 and 60 $\mu\text{g/mL}$, respectively. The increase in turbidity was monitored continuously through absorbance changes at 480 nm (29).

Solubility of complexes formed by mPEG-PVPAA-Con A or free Con A and glycosyl insulin or G-PEG insulin was also investigated. Known amounts of Con A or mPEG-PVPAA-Con A and insulin derivatives in Hepes buffer were mixed in a 1 mL UV cuvette and incubated at 37 °C for 10 min. The concentration of free Con A or Con A in the polymer conjugate was 1 mg/mL; the concentration of insulin derivatives varied from 4 to 40 μM . The solubility of complexes was assayed by turbidity measurements at 480 nm.

Preliminary *in Vitro* G-PEG Insulin Release Experiments. One milliliter of Hepes buffer containing mPEG-PVPAA-Con A conjugate (4 mg/mL of Con A) and appropriate insulin derivative (500 $\mu\text{g/mL}$) was transferred into a DispoDialyzer with a sample volume of 1 mL (membrane MWCO 25 000). The loaded microdialyzer was placed into a small column (inner volume of 6 mL) equipped with a water jacket. The temperature was maintained at 37 °C. The column with microdialyzer was washed upward at a constant flow rate of 9 mL/h with Hepes buffer containing glucose. The glucose concentration changed every 4 h between 50 and 500 mg/dL. Sixty minute fractions of the eluent were collected and assayed for G-PEG insulin using RIA commercial kit (Coat-A-Count) according to the manufacturer's instructions. An RIA standard curve was constructed using G-PEG insulin samples of known concentrations.

Analytical Methods. Quantitative analysis of sugar residue (hexose type) content in the conjugates was performed by using the phenol/sulfuric acid method (30). *p*-Aminophenyl α -D-glucopyranoside was used to construct calibration curves. Alternatively, a UV spectrophotometric assay was used taking advantage of the strong chromophoric acylamidophenoxy group presence in the PEG conjugates. *p*-Succinamidophenyl α -D-glucopyranoside (15) was used as a standard to the construct calibration curve at 244 nm ($\epsilon_{\lambda\text{max}} = 1.02 \times 10^4 \text{ M}^{-1} \text{ cm}^{-1}$).

Free N-terminal amino acids in insulin derivatives were determined by the N-terminal dansylation technique. Released dansyl amino acids were identified after acid hydrolysis (6 N HCl, 105 °C, 8 h) by two-dimensional TLC (31).

UV absorption spectra were obtained on a Perkin-Elmer UV-vis Lambda 19 spectrophotometer. CD absorption spectra for G-PEG insulin derivatives were obtained by the use of a JASCO J-720 spectropolarimeter. In this case, samples (0.5 mg/mL or lower) were dissolved in phosphate-buffered saline (0.01 M phosphate; 0.15 M NaCl) (PBS), pH 7.4, containing 0.01% azide, and the

ellipticity of the solution was measured in a cylindrical quartz cell (0.1 cm optical path length).

Analytical Chromatographic Procedures. The concentration dependence of the elution volume for G-PEG insulins was examined by size exclusion chromatography (SEC) on a Superose 12 (10 mm \times 30 cm) column (Pharmacia AB) using FPLC. The column was eluted with 0.05 M Tris/HCl, pH 8.0, at a flow rate 0.4 mL/min at 22 °C. A 0.2 mL sample was injected, and the eluent was continuously monitored at 280 nm. The column was calibrated with molecular weight standards to generate a calibration curve ($\log M_r$ vs V_e/V_0) to enable calculation of the apparent M_r of insulin derivatives.

Homogeneity and concentration of insulin derivatives in solution were determined using reversed phase HPLC (Waters modular system with Waters Model 745 integrator). The Vydac C_4 column (4.6 mm \times 25 cm) was equilibrated with 0.1% TFA and 20% acetonitrile (solvent A) at a flow rate of 1 mL/min. A 100 μL volume of each sample was injected, and a linear gradient of solvent B (0.1% TFA in 90% acetonitrile) with a slope of 2% B/min was applied. A_{280} of the eluent was recorded and processed to evaluate insulin derivative content. Alternatively, homogeneity was examined on analytical Mono S HR 5/5 column (Pharmacia AB) equilibrated with 1 M AcOH, 7 M urea, and 0.01 M NaCl under conditions described earlier (15).

RESULTS AND DISCUSSION

G-PEG Diacid Synthesis and Characterization.

To achieve specific binding of PEG insulin derivative to concanavalin A, an aminophenyl glucopyranosyl moiety had to be first attached to PEG diacid (Scheme 1). A mixed anhydride method to activate carboxylic groups of PEG diacid was used. The molar chloroformate/PEG diacid ratio used was kept slightly over 1.0 (exactly 1.1:1) because of the traces of water from PEG diacid preparation that were very difficult to remove. These conditions resulted in quantitative coupling and preferential formation of monoglucosyl-PEG (monoG-PEG) diacid conjugate. As expected according to the statistical nature of the reaction, however, diglucosyl-PEG (diG-PEG) diacid conjugate, as well as unreacted PEG diacid, was also present in the mixture. The molar ratio of the three components comprising the mixture was 2 (monoG-PEG diacid):1 (diG-PEG diacid):1 (PEG diacid). This was indirectly shown by volumetric titration analysis, which revealed that $51 \pm 3 \text{ mol } \%$ of carboxylic groups were no longer available, and by glucose content determination (phenol/sulfuric acid destruction method and UV spectrophotometric method; see Experimental Procedures), which was $1.05 \pm 0.09 \text{ mol/mol}$ of conjugate. In both cases, the M_r of the conjugate was considered to be equal to the M_r of monoG-PEG diacid.

Unreacted PEG diacid was removed from the mixture by affinity chromatography on a Con A-Sepharose column (unbound fraction). The specifically eluted fraction was a mixture of monoG-PEG diacid and diG-PEG diacid conjugates at a molar ratio 2:1, again as determined through glucose residues quantitation (1.3 mol of glucose/mol of PEG diacid) and titration of carboxylic groups (0.7 mol of COOH/mol of PEG diacid). The presence of disubstituted PEG diacid derivative does not interfere with insulin modification, and unreacted PEG diacid, the presence of which would result in formation of covalent insulin dimers (through PEG chain spacer), has been removed. Thus, the Con A-Sepharose-purified G-PEG diacid fraction was used directly for insulin modification. The overall yield was 30%.

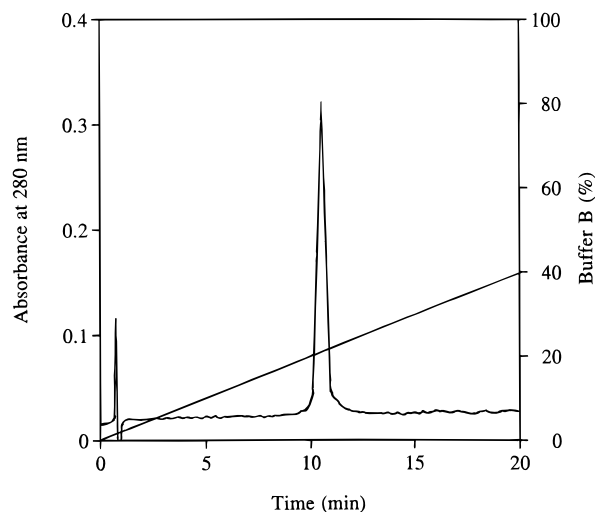


Figure 1. Analytical cation exchange chromatography of G-PEG(600) insulin on a Mono S HR 5/5 column (Pharmacia AB). The column was equilibrated with buffer A (1 M AcOH, 7 M urea, 0.01 M NaCl) at a flow rate 1 mL/min. Sample (200 μ L, 1 mg/mL buffer A) was injected and the column eluted with a linear gradient of buffer B (1 M AcOH, 7 M urea, 0.3 M NaCl) with a slope 2% B/min.

PheB1-Substituted G-PEG Insulin Synthesis and Purification. It is a well-documented fact that the reactivity of the PheB1 amino group of insulin toward an electrophilic substitution group is low compared to that of the GlyA1 and LysB29 amino groups (32). We previously overcame this problem by the reversible protection of GlyA1 and LysB29 amino groups by a Boc group and synthesizing diBoc-GlyA1, LysB29 insulin derivative. Using this intermediate (Scheme 1), specific modification reaction on the PheB1 amino group can be accomplished. Specifically, a 5 molar excess of activated monoG-PEG diacid (M_r 600 or 2000) over diBoc-insulin (taking into account 33 mol % contamination with diG-PEG diacid, see above) had to be used to achieve quantitative modification of the PheB1 amino group. After the removal of Boc groups with TFA, PheB1-substituted G-PEG insulin was purified by two-step chromatography on Mono S and concanavalin A columns to separate residual unreacted G-PEG derivatives and other impurities. The 5 molar excess of activated monoG-PEG diacid could result not only in the specific acylation of the only available insulin PheB1 amino group but also in side reactions, specifically O-acylation of insulin molecule through insulin hydroxyl groups. However, if any esters of monoG-PEG diacid and insulin were formed, they were later hydrolyzed by very extensive dialysis in ammonium bicarbonate under basic conditions. The overall yield was about 25%, and homogeneity of synthesized G-PEG insulins was established by analytical ion exchange (Figure 1) and reversed phase chromatography (Figure 2).

Characterization of G-PEG Insulins. The PheB1 amino group of insulin as the site of attachment of G-PEG moiety was confirmed by N-terminal group analysis. Only dansylglycine and dansyl- ϵ -lysine, which corresponds to a single inner-chain lysine residue, were detected by two-dimensional TLC. No dansylphenylalanine was found (Table 1). Glucose content also pointed to the presence of exactly one G-PEG moiety in both conjugates. Moreover, the retention time of G-PEG insulins on an analytical Mono S column coincided exactly with that of other monosubstituted (monoamidated) insulin derivatives (15). To have further proof that only one G-PEG moiety was attached to the insulin molecule and, thus, no G-PEG

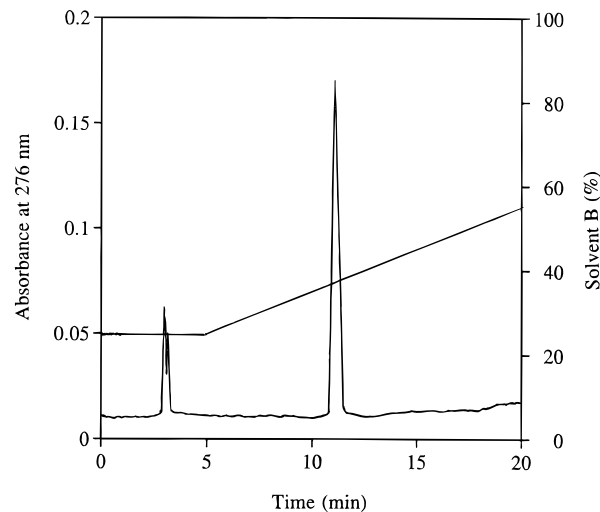


Figure 2. Analytical reversed phase HPLC of G-PEG(600) insulin on a Vydac C_4 column (Separations Group). The column was equilibrated with buffer A (0.1% TFA, 20% acetonitrile) at a flow rate 1 mL/min. Sample (100 μ L, 1 mg/mL solvent A) was injected and the column washed isocratically for 5 min. A linear gradient of solvent B (0.1% TFA, 90% acetonitrile) with a slope 2% B/min was then applied.

Table 1. Characterization of Glucosyl-PEG Insulins

derivative	N-terminal amino acid	glucose content (mol/mol)	biol. act. ^a \pm SD (IU/mg)	fibrillation period \pm SD (days)
insulin	Gly, Phe	0.05	25.2 ± 4.7	0.5 ± 0.2
G-PEG(600) ^b insulin	Gly	1.05	21.2 ± 4.2	26.4 ± 5.4
G-PEG(2000) ^b insulin	Gly	0.89	15.2 ± 3.6	32.3 ± 4.3

^a The biological activity of each derivative was determined with at least six animals. ^b The site of G-PEG attachment is PheB1 amino group.

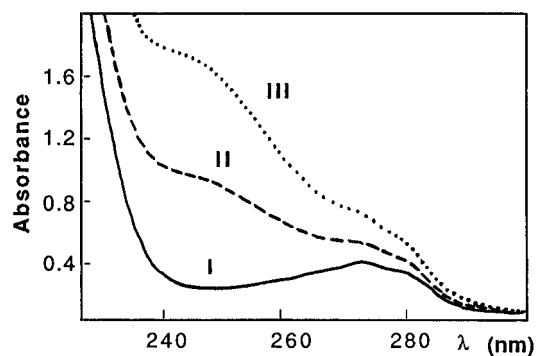


Figure 3. UV spectra of Zn-free insulin (I), G-PEG(600) insulin (II), and PheB1-LysB29-diglucosyl insulin (III) at concentration 68 μ M. UV spectra of G-PEG(2000) insulin and PheB1-mono-glucosyl insulin overlapped with that of G-PEG(600) derivative and therefore have not been included.

moieties were coupled to the insulin molecule through O-acylation, UV spectra of G-PEG insulins were examined. The UV spectrum of G-PEG(600) insulin is shown in Figure 3 and compared to the UV spectrum of Zn-free insulin and PheB1-LysB29-diglucosyl insulin that contains two succinamidophenyl α -D-glucopyranoside moieties coupled to the insulin molecule (15). Not shown, for visual clarity, are the UV spectra of PheB1-mono-glucosyl insulin, containing one succinamidophenyl α -D-glucopyranoside group, and G-PEG(2000) insulin, which both coincided with the UV spectrum of G-PEG(600) insulin. It is evident that the region between 240 and 260 nm is very sensitive to the number of succinamidophenyl α -D-glucopyranoside groups coupled to the insulin molecule. Thus, identical spectra of PheB1-G-

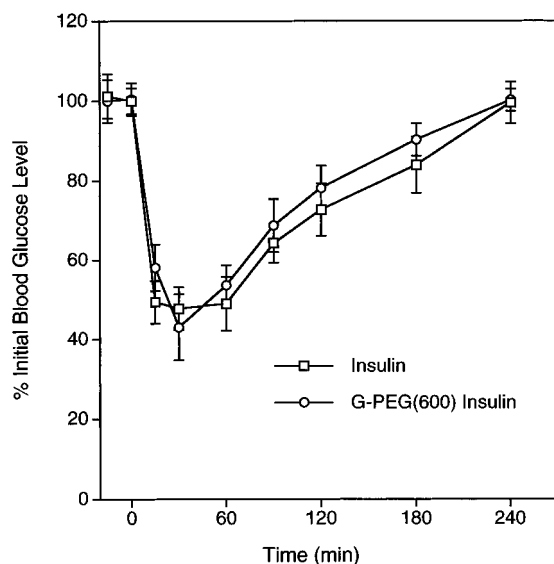


Figure 4. Effect of insulin and G-PEG(600) insulin on blood glucose levels *in vivo*. The peptides were administered to fasted rats by intravenous injection of a dose of 3.4 nmol/kg. Vertical bars represent standard deviation ($n \geq 6$). See Experimental Procedures for further details.

PEG insulins and PheB1-monoglucosyl insulin, together with a failure to detect any trace of dansyl-Phe, can be taken as a direct proof that only one G-PEG moiety is attached specifically to the insulin PheB1 amino group.

The bioactivity of the conjugates was tested *in vivo* by blood glucose depression test in rats using an iv dose of 3.4 nmol kg⁻¹ mL⁻¹ of a specific derivative (Table 1; Figure 4). It can be concluded that the bioactivity of the G-PEG insulin derivative with lower M_r of attached PEG-(600) has slightly lower bioactivity than insulin, but this difference is not statistically significant (Student's *t*-test, $p > 0.2$), which agrees with the findings of Neubauer et al. (33). As the M_r of attached PEG is increased (2000), the bioactivity decreases further and the difference becomes significant ($p < 0.002$). To exclude the possibility that changes in secondary/tertiary structure of the insulin molecule occurred because of modification, CD spectra of G-PEG insulins were compared to that of Zn-free insulin (Figure 5). The spectra practically overlap, indicating that no spatial structural changes occurred. Previously, PheB1-substituted high M_r PEG (5500) insulin conjugate was synthesized and found to be practically devoid of any biological activity (34). Its CD spectrum, contrary to our findings, was substantially changed. It has been well established that PheB1 and its vicinity are not involved in the binding to insulin receptor (16, 35). Thus, in our case, the negative effect of PEG moiety attached to PheB1 on bioactivity of G-PEG insulins can be most likely explained by nonspecific steric hindrance to the receptor binding by the PEG moiety, caused by its large hydrodynamic volume (36). Also, as the attached PEG moiety M_r is increasing further and becoming comparable to insulin (34), it has a direct negative effect on the insulin conformation, thus decreasing the conjugate bioactivity further.

The long-term physical stability of PheB1-substituted G-PEG insulins was investigated by assessing their ability to form fibrils in an accelerated shaking test (19, 22). Insulin aggregation constitutes a major problem in a long-term steady insulin administration by insulin pumps (1). Solutions of G-PEG insulins (80 μ M) were vigorously shaken at 37 °C for extended periods of time. Samples were periodically withdrawn and filtered, and the residual concentration of insulin derivative was

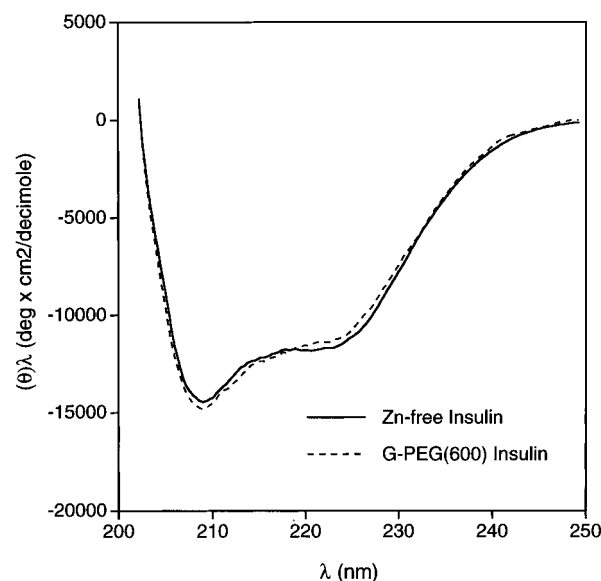


Figure 5. Far-UV CD spectra of Zn-free insulin and G-PEG-(600) insulin in PBS, pH 7.4, at a concentration of 75 μ M. Mean residual ellipticity $(\theta)_i$ was calculated using the expression $(\theta)_i = \theta_i M_0 / 10^4 Cl$, where θ_i is the observed ellipticity at wavelength λ , M_0 is the mean residue molecular weight, which for G-PEG-(600) insulin was calculated to be 132, C is the protein concentration in g/mL, and l is the optical path length in cm. The CD spectrum of G-PEG(2000) insulin overlapped with that of G-PEG(600) derivative and therefore has not been included.

Table 2. Concentration Dependence of Association State of G-PEG Insulins As Determined by SEC^a

derivative	association state (M_r app/ M_r monomer)			
	$c = 0.17$ mM	$c = 0.43$ mM	$c = 0.87$ mM	$c = 1.73$ mM
2Zn-insulin	2.0	3.4	4.2	4.6
G-PEG(600) insulin	1.2	1.6	1.9	2.2
G-PEG(2000) insulin	1.1	1.6	2.2	2.3

^a On Superose 12 column.

measured by UV or HPLC. In parallel, CD spectra for these samples were recorded to ensure that no conformational changes took place in the soluble fractions of the samples. Zn-insulin and Zn-free insulin were used as controls (Table 1). G-PEG insulins showed excellent physical stability, even 2–3 times higher than that of PheB1-substituted glycosylated insulins (15). Also, some effect of PEG spacer length was observed, even though the difference was not significant.

Since insulin forms dimers and hexamers depending on its concentration, association properties of G-PEG insulins were evaluated using SEC on a Superose 12 column (Table 2). It is evident that attachment of PEG derivative chains to PheB1 has the same effect as was observed in the case of glycosylated insulins (13, 15), significantly suppressing hexamer formation without having a large impact on dimer formation. This can be taken as an independent indication that the spatial structure of G-PEG insulin derivatives is preserved. It also indicates, however, that the G-PEG coupling to PheB1 insulin amino group did not sufficiently suppress the dimerization ability of these insulin derivatives. Indeed, when G-PEG(600) insulin solution (1 mg/mL) was intermixed with Con A solution (4 mg/mL), precipitate formed instantly (see further).

In general, G-PEG insulin with the smaller M_r PEG spacer of 600 (hereafter, G-PEG insulin) seemed to be suitable for use in a self-regulated insulin delivery system based on concanavalin A, because of its preserved bio-

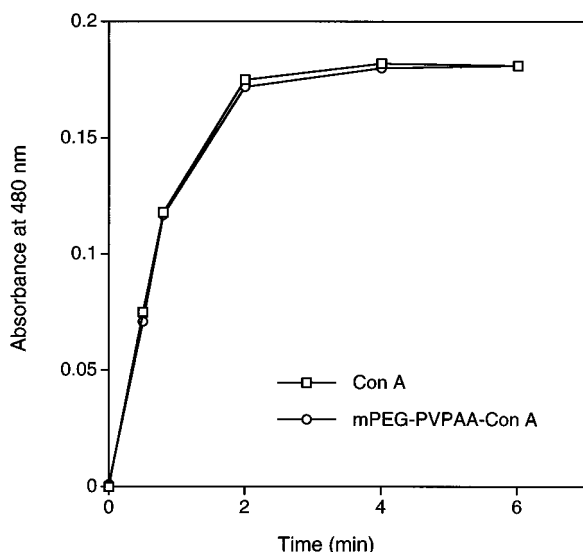


Figure 6. Time course of turbidity formation for free Con A and mPEG-PVPAA-Con A conjugate in glycogen precipitation test. Concentration of free Con A or Con A in the conjugate was 200 $\mu\text{g/mL}$, and concentration of glycogen was 60 $\mu\text{g/mL}$ in 0.05 M HEPES buffer, pH 7.4, containing 3 mM CaCl_2 and MnCl_2 and 0.9% NaCl.

activity and increased solution stability, and was used exclusively in further studies. However, its partially preserved dimerization ability causing precipitation of G-PEG insulin-Con A complex still hampered its use in this specific delivery system (see below). Therefore, our efforts then concentrated on improving the solubility of Con A, and especially its complex with G-PEG insulin, through Con A covalent conjugation to mPEG-grafted hydrophilic polymer PVPAA.

mPEG-PVPAA-Con A Conjugate Synthesis and Characterization. At first, we intended to synthesize a simple conjugate of Con A and PVPAA to prevent Con A leakage from the pouch and increase solubility of Con A and especially of Con A-G-PEG insulin complex. It turned out, however, that this was not feasible because the high degree of cross-linking resulted in an insoluble conjugate (data not shown). Thus, to limit or prevent cross-linking, we decided to graft mPEG-NH₂ chains onto a PVPAA backbone (Scheme 2). Three different molar ratios of mPEG-NH₂ to PVPAA, 17:4, 34:4, and 68:4, were used, which resulted in grafting 4.2, 7.8, and 16.1 PEG chains to one molecule of PVPAA, respectively, as demonstrated by ¹H NMR spectroscopy. Using these grafted copolymers for Con A conjugation (see Experimental Procedures for details), we discovered that the low-degree PEGylated PVPAA still gave rise to a cross-linked, mostly insoluble, material, while the high-degree PEGylated PVPAA reacted with Con A with very low efficiency. Only mPEG-PVPAA graft copolymer with a medium degree of substitution (7.8 mol of PEG/mol of PVPAA) gave an mPEG-PVPAA-Con A complex that was soluble. This complex contained about 2.5 mol of Con A tetramer per mole of mPEG-PVPAA copolymer. No leakage of Con A or the conjugate was detected from Spectra/Por DispoDialyzers (with different MWCO of up to 50 000) over a 1 week period, as assayed by UV spectroscopy of surrounding dialyzate (5 mL) under static conditions (no flow, see further). This conjugate was used in further studies.

The rate of appearance of turbidity resulting from the reaction of glycogen and Con A reflects the state of saccharide-binding activity of Con A in mPEG-PVPAA-Con A conjugate. As shown in Figure 6, the time courses of precipitation with glycogen for mPEG-PVPAA-Con

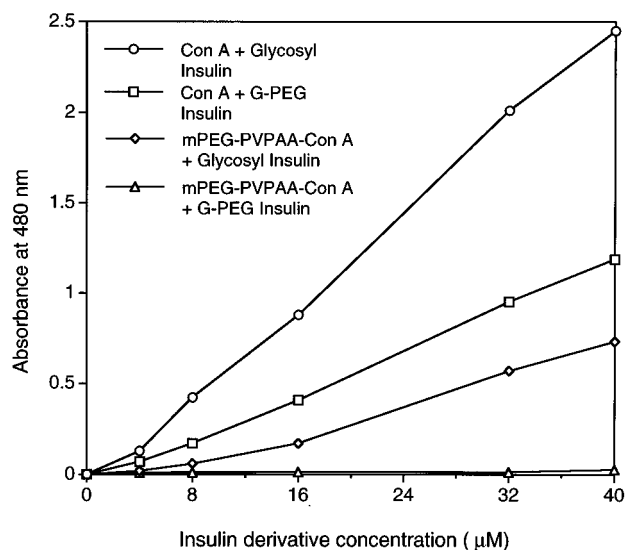


Figure 7. Solubility of complexes formed by free Con A or mPEG-PVPAA-Con A conjugate and glucosyl insulin or G-PEG(600) insulin. Concentration of Con A or Con A in the conjugate was 1 mg/mL in 0.05 M HEPES buffer, pH 7.4. The concentration of insulin derivatives was varied, and turbidity formed was measured by absorbance increase at 480 nm, 10 min after mixing.

A conjugate or free Con A do not differ significantly, which indicates that the coupling reaction of Con A and mPEG-PVPAA did not occur within the saccharide binding sites of Con A. The glycogen turbidity curve (see Figure 6 for conditions) after 1 week of preincubation of the conjugate in the precipitation buffer (HEPES buffer, pH 7.4, 37 °C) was identical to the turbidity curve obtained with mPEG-PVPAA-Con A conjugate freshly dissolved in the precipitation buffer and incubated with glycogen, indicating that the Con A binding activity in the conjugate is preserved for at least 7 days.

Having established that the binding characteristics of Con A in the conjugate are preserved, we investigated the solubility of complexes formed by mPEG-PVPAA-Con A and glucosyl-PheB1-insulin (15) or G-PEG insulin as a function of the insulin derivatives' concentrations (Figure 7). For comparison, turbidity measurements for free Con A and glucosyl insulin or G-PEG insulin complexes are also included. It is evident that the solubility of the complex formed by mPEG-PVPAA-Con A conjugate and G-PEG insulin is superior to those of other complexes formed, even though for high G-PEG insulin concentration a very slight turbidity was detected (Figure 7). Insulin replacement therapy usually requires administration of 1–2 mg of insulin per day per patient. Thus, to be closer to therapeutically relevant conditions, we also investigated long-term solubility/stability of mPEG-PVPAA-Con A conjugate and G-PEG insulin mixture at concentrations 4 and 0.5 mg/mL, respectively. No precipitate was detected at 37 °C for at least 7 days. In contrast, if glucosyl insulin at the same concentration was used, macroscopic precipitate formed sediment in <1 h. Using free Con A (4 mg/mL) and glucosyl or G-PEG insulin (0.5 mg/mL), the precipitate formed instantly or in a matter of minutes. In summary, it is evident that the novel self-regulated insulin delivery system based on G-PEG insulin and mPEG-PVPAA-Con A conjugate is superior to Con A based insulin delivery systems designed previously (10, 11, 14, 25), from both points of view of solubility/stability and prevention of Con A leakage.

In Vitro Release of G-PEG Insulin in Response to Glucose Stimulus. The feasibility of the new system was tested using a DispoDialyzer with a 1 mL sample

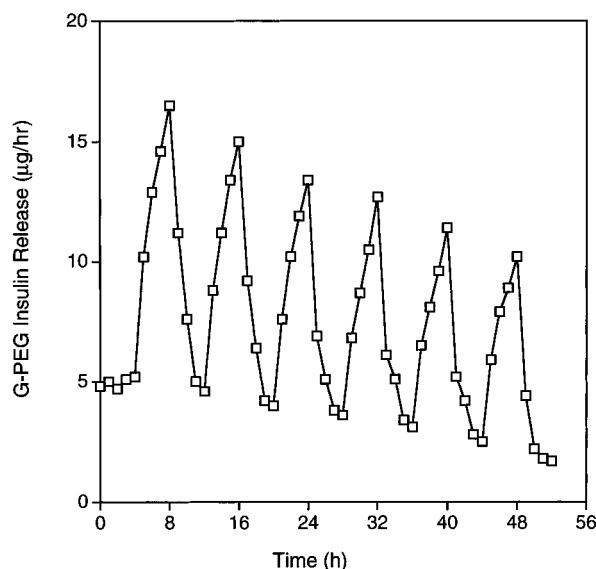


Figure 8. Release rate of G-PEG(600) insulin in a flow-through cell (6 mL inner volume) containing DispoDialyzer membrane device with 1 mL sample volume, loaded with mPEG-PVPAA-Con A conjugate (4 mg/mL) and G-PEG insulin (0.5 mg/mL) in Hepes buffer, pH 7.4, in response to a periodic (4 h), stepwise challenge of glucose (50 and 500 mg/mL) in the same buffer. The challenge buffer was pumped through the cell at 9 mL/h flow rate, and 60 min fractions of the eluent were collected and assayed for G-PEG insulin concentration by RIA insulin kit.

volume and membrane MWCO 25 000. Using this MWCO guaranteed that no leakage of the conjugate (Con A) occurred, while the membrane was freely permeable to G-PEG insulin. A flow-through experimental setup was used. The loaded microdialyzer was placed in a cylindrical flow cell, and release buffer containing low glucose concentration (50 mg/mL) was pumped through the cell at a flow rate of 9 mL/h to establish the baseline G-PEG insulin release from the system (Figure 8). After 4 h, the glucose concentration in the eluent was changed to 500 mg/mL, which resulted in increased G-PEG insulin release. When glucose concentration was brought back to 50 mg/mL after 4 h, the insulin release rate returned to the original baseline levels. The system is fully reversible as demonstrated by alternation of glucose concentration six different times over a 2 day period. In addition, the relative release rate of G-PEG insulin decreases as a function of time due to the depletion of loaded G-PEG insulin. The relatively large delay in G-PEG insulin release in response to stepwise changes of the glucose concentration is predominantly caused by the large dead volume and long diffusional distances of the current experimental system used.

In general, *in vitro* release data for the described system are very encouraging. Future studies will focus on optimization of G-PEG insulin release using an implantable, rechargeable pouch for which transport-related phenomena should be negligible; thus, the G-PEG insulin release in response to glucose challenges will be prompt. We also plan to use a new type of biocompatible membrane (P. Tresco, unpublished data), which will enable chronic *in vivo* studies using pancreatectomized dogs.

ACKNOWLEDGMENT

We thank Takashi Uchio for assistance and valuable discussions. This work was supported by NIH Grant DK 36598-10 and by MacroMed, Inc.

LITERATURE CITED

- (1) Brange, J. (1987) *Galénics of Insulin*, Springer-Verlag, Berlin.
- (2) Brownlee, M., and Cerami, A. (1979) A glucose-controlled insulin delivery system: Semisynthetic insulin bound to lectin. *Science* 206, 1190–1191.
- (3) Lim, F., and Sun, A. M. (1980) Microencapsulated islets as bioartificial endocrine pancreas. *Science* 210, 908–910.
- (4) Fischel-Ghodsian, F., Brown, L., Mathiowitz, E., Brandenburg, D., and Langer, R. (1988) Enzymatically controlled drug delivery. *Proc. Natl. Acad. Sci. U.S.A.* 85, 2403–2406.
- (5) Brown, L. R., Edelman, E. R., Fischel-Ghodsian, F., and Langer, R. (1996) Characterization of glucose-mediated insulin release from implantable polymers. *J. Pharm. Sci.* 85, 1341–1345.
- (6) Ito, Y., Chung, D. J., and Imanishi, Y. (1994) Design and synthesis of a protein device that releases insulin in response to glucose concentration. *Bioconjugate Chem.* 5, 84–87.
- (7) Nakamae, K., Miyata, T., Jikihara, A., and Hoffman A. S. (1994) Formation of poly(glucosyloxyethyl methacrylate)-concanavalin A complex and its glucose-sensitivity. *J. Biomater. Sci. Polym. Ed.* 6, 79–90.
- (8) Obaidat, A. A., and Park, K. (1996) Characterization of glucose dependent gel-sol phase transition of the polymeric glucose-concanavalin A hydrogel system. *Pharm. Res.* 13, 989–995.
- (9) Jeong, S. Y., Kim, S. W., Eenink M. J. D., and Feijen, J. (1984) Self-regulating insulin delivery systems: I. Synthesis and characterization of glycosylated insulin. *J. Controlled Release* 1, 57–66.
- (10) Kim, S. W., and Jacobs, H. A. (1994) Self-regulated insulin delivery—Artificial pancreas. *Drug Dev. Ind. Pharm.* 20, 575–580.
- (11) Jeong, S. Y., Kim, S. W., Holmberg D. L., and McRea, J. C. (1985) Self-regulating insulin delivery systems: III. *In vivo* studies. *J. Controlled Release* 2, 143–152.
- (12) Cunningham, A., Wang, J. L., Pflumm, M. N., and Edelman, G. M. (1972) Isolation and proteolytic cleavage of the intact subunit of concanavalin A. *Biochemistry* 11, 3233–3239.
- (13) Baudyš, M., Uchio, T., Hovgaard, L., Zhu, E. F., Avramoglou, T., Jozefowicz, M., Říhová, B., Park, J. Y., Lee, H. K., and Kim, S. W. (1995) Glycosylated insulins. *J. Controlled Release* 36, 151–157.
- (14) Pai, C. M., Bae, Y. H., Mack, E. J., Wilson, D. E., and Kim, S. W. (1992) Concanavalin A micropheres for a self-regulating insulin delivery system. *J. Pharm. Sci.* 81, 532–536.
- (15) Baudyš, M., Uchio, T., Mix, D., Wilson, D., and Kim, S. W. (1995) Physical stabilization of insulin by glycosylation. *J. Pharm. Sci.* 84, 28–33.
- (16) Murray-Rust, J., McLeod, A. N., Blundell, T. L., and Wood, S. P. (1992) Structure and evolution of insulins: Implications for receptor binding. *BioEssays* 14, 325–330.
- (17) Liu, F., Baudyš, M., Mix, D., Hinds, K., and Kim, S. W. (1997) Bioactive polyethylene glycol–insulin conjugates with enhanced stability. *Polym. Prepr. (Am. Chem. Soc., Div. Polym. Chem.)* 38, 595–596.
- (18) Francis, G. E., Delgado, C., and Fisher, D. (1993) PEG-modified proteins. *Stability of Protein Pharmaceuticals: Part B, In vivo pathways of Degradation and Strategies for Protein Stabilization* (T. J. Ahern and M. C. Manning, Eds.) pp 235–263, Plenum Press, New York.
- (19) Brange, J., and Langkjaer, L. (1993) Insulin structure and stability. *Stability and Characterization of Protein and Peptide Drugs: Case Histories* (Y. J. Wang and R. Pearlman, Eds.) pp 315–350, Plenum Press, New York.
- (20) Hovgaard, L., Mack, E. J., and Kim, S. W. (1992) Insulin stabilization and GI absorption. *J. Controlled Release* 19, 99–109.
- (21) Sluzky, V., Tamada, J. A., Klibanov, A. M., and Langer, R. (1991) Kinetics of insulin aggregation in aqueous solutions upon agitation in the presence of hydrophobic surfaces. *Proc. Natl. Acad. Sci. U.S.A.* 88, 9377–9381.
- (22) Waugh, D. F., Wilhelmson, D. F., Commerford, S. L., and Sackler, M. L. (1953) Studies of the nucleation and growth reactions of selected types of insulin fibrils. *J. Am. Chem. Soc.* 75, 2592–2600.

- (23) Sato, S., Jeong, S. Y., McRea, J. C., and Kim, S. W. (1984) Self-regulating insulin delivery systems. II. *In vitro* studies. *J. Controlled Release* 1, 67–77.
- (24) Kim, S. W., Pai, C. M., Makino, K., Seminoff, L. A., Holmberg, D. L., Gleeson, J. M., Wilson, D. E., and Mack, E. J. (1990) Self-regulated glycosylated insulin delivery. *J. Controlled Release* 11, 193–201.
- (25) Pai, C. M., Jacobs, H., Bae, Y. H., and Kim, S. W. (1993) Synthesis and characterization of soluble concanavalin A oligomer. *Biotechnol. Bioeng.* 41, 957–963.
- (26) Vaughan, J. R. (1951) Acylalkylcarbonates as acylating agents for the synthesis of peptides. *J. Am. Chem. Soc.* 73, 3547–3550.
- (27) Markussen, J., Halstrøm, J., Wiberg, F. C., and Schaffer, L. (1991) Immobilized insulin for high capacity affinity chromatography of insulin receptors. *J. Biol. Chem.* 266, 18814–18818.
- (28) Kim, H. R., Rho, H. W., Park, J. W., Park, B. H., Kim, J. S., and Lee, M. W. (1994) Assay of ornithine aminotransferase with ninhydrin. *Anal. Biochem.* 223, 205–207.
- (29) Poretz, R. D., and Goldstein, I. J. (1968) Protein–carbohydrate interaction. XI. A study of turbidity as it relates to concanavalin A–glycan interaction. *Immunology* 14, 165–174.
- (30) Dubois, M., Gilles, K. A., Hamilton, J. K., Roberts, P. A., and Smith, F. (1956) Colorimetric method for determination of sugars and related substances. *Anal. Chem.* 28, 350–357.
- (31) Baudyš, M., and Kostka, V. (1983) Covalent structure of chicken pepsinogen. *Eur. J. Biochem.* 139, 89–99.
- (32) Blundell, T. L., Dodson, G. G., Hodgkin, D. C., and Mercola, D. (1972) Insulin: The structure in the crystal and its reflection in chemistry and biology. *Adv. Protein Chem.* 26, 279–402.
- (33) Neubauer, H. P., Obermaier, R., and Schöne, H. H. (1983) Influence of polyethylene glycol insulin on lipid tissues of experimental animals. *Diabetes* 32, 953–958.
- (34) Ehrat, M., and Luisi, P. L. (1983) Synthesis and spectroscopic characterization of insulin derivatives containing one or two poly(ethylene oxide) chains at specific positions. *Biopolymers* 22, 569–573.
- (35) Brange, J., Owens, D. R., Kang, S., and Vølund, A. (1990) Monomeric insulins and their experimental and clinical applications. *Diabetes Care* 13, 923–954.
- (36) Harris, J. M. (1992) Introduction to biotechnical and biomedical applications of poly(ethylene glycol). *Poly(Ethylene Glycol) Chemistry: Biotechnical and Biomedical Applications* (J. M. Harris, Ed.) pp 1–12, Plenum Press, New York.

BC970128E

Design and Synthesis of [^{111}In]DTPA–Folate for Use as a Tumor-Targeted Radiopharmaceutical

Susan Wang,[†] Jin Luo,[†] Douglas A. Lantrip,[†] David J. Waters,[‡] Carla J. Mathias,[§] Mark A. Green,[§] Philip L. Fuchs,^{*,†} and Philip S. Low^{*,†}

Department of Chemistry, Department of Veterinary Clinical Sciences, and Department of Medicinal Chemistry and Molecular Pharmacology, Purdue University, West Lafayette, Indiana 47907. Received January 17, 1997[®]

Folate-conjugated metal chelates have been proposed as potential imaging agents for cancers that overexpress folate receptors. In a previous study, folic acid was linked through its γ -carboxyl group to deferoxamine (DF), and the ^{67}Ga -labeled complex (^{67}Ga]DF–folate) was examined for *in vivo* tumor targeting efficiency in athymic mice with a human tumor cell implant. Although superb tumor-to-background contrast was obtained, slow hepatobiliary clearance would compromise imaging of abdominal tumors such as ovarian cancer. In the present study, folic acid was conjugated to an alternative chelator, diethylenetriaminepentaacetic acid (DTPA), via an ethylenediamine spacer. The desired DTPA–folate(γ) regioisomer was synthesized by two different approaches, purified by reversed phase column chromatography, and characterized mainly by analytical HPLC, mass spectroscopy, and NMR. In cultured tumor cells, uptake of [^{111}In]DTPA–folate(γ) was found to be specific for folate receptor-bearing cells, and the kinetics of uptake were similar to those of free folate and other folate-conjugated molecules. In the normal rat, intravenously administered [^{111}In]DTPA–folate(γ) was found to be rapidly excreted into the urine, giving intestinal levels of radiotracer 10-fold lower than those observed with [^{67}Ga]DF–folate(γ) at 4 h. In a preliminary mouse imaging study, a folate receptor-positive KB cell tumor was readily visualized by γ scintigraphy 1 h following intravenous administration of [^{111}In]DTPA–folate(γ).

INTRODUCTION

The membrane-associated folate receptor is a tumor marker that is overexpressed on a variety of neoplastic tissues, including breast, cervical, ovarian, colorectal, renal, and nasopharyngeal tumors, but highly restricted in most normal tissues (Rettig et al., 1988; Campbell et al., 1991; Coney et al., 1991; Weitman et al., 1992; Garin-Chesa et al., 1993; Holm et al., 1994; Franklin et al., 1994; Ross et al., 1994; Stein et al., 1991; Li et al., 1996). Previously, it has been shown that the natural receptor-mediated endocytosis pathway for the vitamin folic acid can be exploited to selectively and nondestructively deliver folate-conjugated small molecules, macromolecules, and drug carriers such as liposomes into cultured tumor cells (Wang et al., 1996; Leamon and Low, 1991, 1993; Lee and Low, 1994). When folate is covalently linked to a molecule via its γ -carboxyl moiety, its affinity for its cell surface receptor ($K_d \sim 10^{-9}$ M; McHugh and Cheng, 1979; Antony et al., 1985; Kamen and Capdevila, 1986; Kane and Waxman, 1989; Luhrs et al., 1992; Matsue et al., 1992) remains essentially unaltered. Further, following binding to the cell surface receptor, the conjugated folate is internalized by the cell in much the same manner as the unmodified vitamin (Leamon and Low, 1991; Lee et al., 1996). Recycling of the folate receptor can then lead to further accumulation of the folate conjugates in such target cells.

To evaluate the potential of a radiolabeled folate conjugate in tumor diagnostic imaging, the metal chelator

deferoxamine (DF)¹ was linked to folic acid, labeled with ^{67}Ga , and imaging was performed in an athymic mouse tumor model using the [^{67}Ga]DF–folate radiopharmaceutical (Wang et al., 1996; Mathias et al., 1996a). The [^{67}Ga]DF–folate conjugate was found to afford excellent tumor/blood, tumor/muscle, and tumor/liver contrast (Mathias et al., 1996a,b). The greatly enhanced tumor/background contrast (tumor to blood ratio averaged 409 after 4 h and 1500 after 46 h postinjection) indicated the high specificity and efficiency of folate-targeted delivery, probably due to its small size, and therefore the very rapid clearance rate from blood and other nontarget tissues such as liver and muscle. However, it was also shown that approximately 30% of the administered [^{67}Ga]DF–folate was excreted via the hepatobiliary route into the intestines (Mathias et al., 1996b), making the clearance rate through the GI tract a major factor in determining the time frame over which imaging of abdominal tumors would be feasible.

Our goal in this study has been to optimize radiotracer performance for tumor imaging by development of a folate receptor-targeted agent that is cleared more rapidly and selectively from the body into the urine. Diethylenetriaminepentaacetic acid (DTPA) was chosen for this purpose because of its high water solubility, relatively simple conjugation chemistry (Hnatowich et al., 1983), and strong metal-chelating interaction with ^{111}In , a 67.4 h half-life γ -emitting radionuclide with nuclear properties desirable for tumor imaging.

EXPERIMENTAL PROCEDURES

Materials. Folic acid, dimethyl sulfoxide (DMSO), *N*-hydroxysuccinimide (NHS), carboxypeptidase G₂, fluo-

* To whom correspondence should be addressed. Phone: (317) 494-5273. Fax: (317) 494-0239.

[†] Department of Chemistry.

[‡] Department of Veterinary Clinical Sciences.

[§] Department of Medicinal Chemistry and Molecular Pharmacology.

[®] Abstract published in *Advance ACS Abstracts*, September 1, 1997.

¹ Abbreviations: DMSO, dimethyl sulfoxide; NHS, *N*-hydroxysuccinimide; FITC, fluorescein isothiocyanate; TFA, trifluoroacetic acid; EDA, ethylenediamine; DTPA, diethylenetriaminepentaacetic acid; DF, deferoxamine; PBS, phosphate-buffered saline; t_R , retention time.

rescein isothiocyanate (FITC), tetrabutylammonium phosphate, and cyclic DTPA dianhydride were purchased from Sigma Chemical Co. (St. Louis, MO). The bicinchoninic acid protein assay kit was obtained from Pierce (Rockford, IL). Acetonitrile (HPLC grade), dicyclohexylcarbodiimide, trifluoroacetic acid (TFA), and ethylenediamine (EDA) were purchased from Aldrich (Milwaukee, WI). [^{111}In]Indium(III) chloride was purchased from Mallinckrodt Medical, Inc. (St. Louis, MO). Tissue culture products were obtained from GIBCO (Grand Island, NY), and cultured cells were received as a gift from the Purdue Cancer Center (West Lafayette, IN).

Cell Culture. KB cells, a human nasopharyngeal epidermal carcinoma cell line that overexpresses the folate binding protein, and A549 cells, a human lung carcinoma cell line that expresses no detectable folate receptors, were cultured continuously as a monolayer at 37 °C in a humidified atmosphere containing 5% CO_2 in folate-deficient modified Eagle's medium as described previously (Wang et al., 1996). Forty-eight hours prior to each experiment, the cells were transferred to 35 mm culture dishes at 5×10^5 cells per dish and grown to ~80% confluence.

Synthesis and Purification of the EDA-Derivatized Folic Acid. (*Method A*) *Synthesis of a Mixture of EDA-Folate(α) and EDA-Folate(γ).* Folic acid (441 mg, 1 mmol) slowly dissolved in 20 mL of DMSO was reacted with 1.2 molar equiv of dicyclohexylcarbodiimide and 2.0 molar equiv of NHS at 50 °C for 6 h. The resulting folate-NHS was mixed with 10 molar equiv of EDA plus 100 μL of pyridine and allowed to react at 25 °C for ~5 h, by which time the reaction had reached completion by TLC analysis (silica gel plate, 2-propanol/chloroform = 7/3, R_f values for folic acid and the mixture of EDA isomers were 0.2 and 0.4, respectively). The crude product was precipitated by addition of 20 mL of acetonitrile, centrifuged, and then washed three times with diethyl ether before drying under vacuum. A fine dark yellow powder (390 mg) was obtained. The γ -isomer of EDA-folate (58 mg, 12% yield) was separated from the α -isomer and unreacted folic acid by HPLC on a Microsorb preparative C-18 reversed phase column (250 mm \times 21 mm) using a linear gradient (eluant A, water with 0.05% TFA at pH 3.5; eluant B, acetonitrile; gradient, 0 to 15% B over 20 min at a flow rate of 10 mL/min). The elution times for EDA-folate(γ) and EDA-folate(α) were 7.6 and 10.3 min, respectively.

The chemical purities and identities of the two EDA-folate monoisomers were examined by analytical HPLC on an Econosphere C-18 reversed phase column (150 mm \times 4.6 mm) [EDA-folate(α), t_R = 12.9 min; EDA-folate(γ), t_R = 15.0 min; eluent A, 5 mM phosphate buffer at pH 7; eluent B, acetonitrile; gradient, 1 to 10% B over 15 min at a flow rate of 0.7 mL/min]. Mass spectroscopic analysis and the carboxypeptidase G_2 hydrolysis assay were conducted as described previously (Wang et al., 1996).

(*Method B*) *Regiospecific Synthesis of EDA-Folate(γ)* (Figure 1). To 2.8 g of tetramethylguanidinium L-methyl folate(γ) [5.95 mmol, a new compound of which the synthesis was reported by Luo et al. (1997)] was added 20 mL of ethylenediamine (0.3 mol) with stirring at 25 °C. The solid gradually dissolved as it reacted with the diamine. The reaction was complete in 3 h as indicated by analytical HPLC under the same conditions described in method A, and filtration gave a clear solution which was then transferred to a well-stirred mixture of acetonitrile and diethyl ether (1/1 v/v, 500 mL). The precipitated solid was collected by centrifugation and redissolved in 500 mL of water, followed by addition of 5%

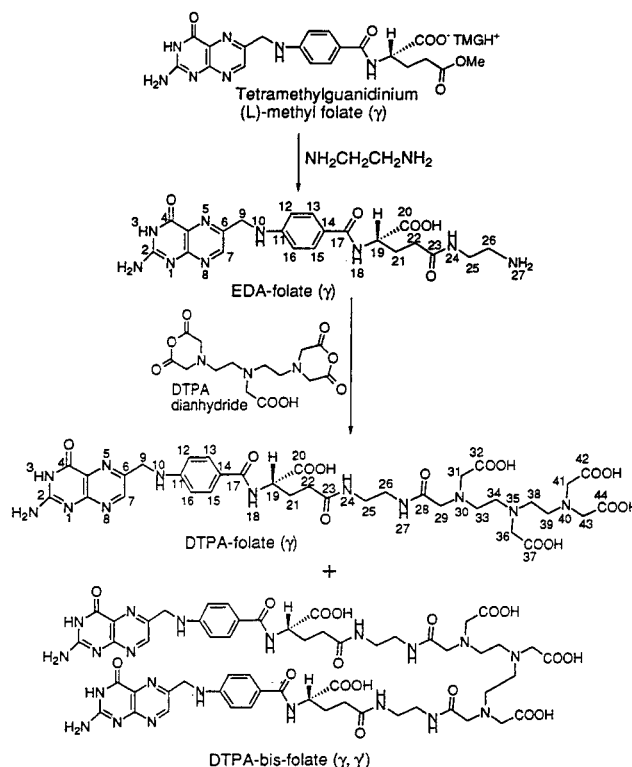


Figure 1. Regiospecific synthesis of the DTPA-folate conjugate.

hydrochloric acid until pH 7.0, which resulted in precipitation of the product. The solid was collected by centrifugation and washed thoroughly with 3×250 mL of water to remove any trace of ethylenediamine (^1H NMR was used to assay for the presence of the diamine). A yellow solid (2.1 g, 88% yield) was obtained after washing once with 100 mL of acetonitrile and 3×50 mL of diethyl ether and drying for 24 h under vacuum. Analytical HPLC showed a single peak at 15.2 min under the same analysis conditions as above or at 3.0 min using an ion-pair agent tetrabutylammonium phosphate (eluant A, 10 mM tetrabutylammonium phosphate buffer at pH 7; eluant B, acetonitrile; gradient, 15 to 50% B over 30 min at a flow rate of 0.7 mL/min). ^1H NMR (300 MHz, $\text{DMSO}-d_6/\text{CF}_3\text{CO}_2\text{D}$, ~10/1 v/v): δ 8.75 (s, 1H, C7-H), 7.66 (d, J = 8.6 Hz, 2H, Ar), 6.63 (d, J = 8.6 Hz, 2H, Ar), 4.57 (s, 2H, C9-H₂), 4.34 (dd, J = 4.0, 9.6 Hz, 1H, C19-H), 3.28–3.13 (m, 2H, C25-H₂), 2.80 (m, 2H, C26-H₂), 2.16 (m, 2H, C22-H₂), 2.15–1.85 (m, 2H, C21-H₂). ^{13}C NMR (75 MHz, $\text{D}_2\text{O}/\text{NaOD}$): δ 178.8 (C20), 176.0 (C23), 173.1 (C17), 169.5 (C2), 164.0 (C4), 155.5 (C8a), 151.1 (C11), 147.3 (C6), 147.2 (C7), 129.0 (C13 and C15), 128.2 (C4a), 121.4 (C14), 112.5 (C12 and C16), 55.3 (C19), 45.8 (C9), 42.0 (C25), 39.8 (C26), 32.8 (C22), 28.0 (C21) (see the Supporting Information). High-resolution MS (fast atom bombardment): $\text{C}_{21}\text{H}_{25}\text{N}_9\text{O}_5$ [$\text{M} + \text{H}$] $^+$ 484.2057, found 484.2062. Decomposition point: ~278 °C.

Evaluation of FITC-EDA-Folate Affinity for Cell Surface Receptors. Five milligrams of each of the α - and γ -isomers of EDA-folate from method A were dissolved in 1 mL of DMSO and reacted with 3 molar equiv of FITC at room temperature for 3 h. The folate-conjugated FITC was precipitated with 10 mL of cold acetone, after which unreacted FITC was removed by washing the pellet three times with cold acetone. Conjugation was confirmed by UV-visible spectroscopy of the product by demonstrating that the resulting spectrum approximated the sum of the spectra of folate and FITC. Affinities of the two folate derivatives for cell surface

folate receptors were determined by incubating KB cells with various concentrations of the conjugates at 4 °C for 30 min. The cells were then washed with 3 × 1 mL of phosphate-buffered saline (PBS, 136.9 mM NaCl, 2.68 mM KCl, 8.1 mM Na₂HPO₄, and 1.47 mM KH₂PO₄ at pH 7.4) and dissolved in 2 mL of 1% TX-100. Cell-associated fluorescence was measured on a Perkin-Elmer MPF-44A fluorescence spectrophotometer. Cellular protein was determined by the bicinchoninic acid assay (Lee and Low, 1994). Competition between the folate conjugates and free folic acid for cell surface receptors was examined by including 1 mM folic acid in the incubation medium.

Production of DTPA–Folate. One gram of EDA–folate(γ) (2.1 mmol) was dissolved in 50 mL of DMSO by bath sonication overnight. Then the dark yellow solution was slowly added to a stirring suspension of 2.0 g of DTPA dianhydride (5.6 mmol) in 10 mL of anhydrous DMSO. The mixture became homogeneous by the end of addition. Analytical HPLC showed the absence of the starting material EDA–folate after 30 min, at which time the reaction mixture was filtered through a pad of Celite to remove traces of solid residue. After the temperature of the reaction mixture was reduced with an ice bath, 10 mL of 2.5 N NaOH was added to quench the reaction and to neutralize the solution. The resulting precipitate containing the majority of the DTPA–folate(γ) produced was separated by centrifugation from the supernatant. The yellow pellet was then washed with 100 mL of acetonitrile and dissolved in 50 mL of water, and the pH of the solution was adjusted to 7 with concentrated HCl. After filtration to remove the solid residue, the clear orange solution was directly purified on a LiChroprep C-18 reversed phase MPLC column (310 mm × 25 mm, 45–60 μm) using 10 mM ammonium bicarbonate buffer as the eluant (*t_R* = 20–35 min, flow rate of 10 mL/min). The collected product was concentrated by vacuum and further purified by preparative HPLC on the Microsorb C-18 column with a gradient (eluant A, 10 mM ammonium bicarbonate buffer at pH 7.4; eluant B, acetonitrile; gradient, 0 min at 4% B, 10 min at 12% B, and 15 min at 15% B at a flow rate of 10 mL/min; *t_R* = 6.3 min) to remove residual bis-conjugated side product (Figure 1) and to obtain 0.85 g of DTPA–folate after lyophilization with a purity above 99% and a yield of 47%. Analytical HPLC on the Econosphere C-18 reversed phase column (150 mm × 4.6 mm) revealed a single peak with a retention time of 11.74 min (eluant, 10 mM tetrabutylammonium phosphate buffer (pH 7) at 75% and acetonitrile at 25%; flow rate of 0.7 mL/min). ¹H NMR (300 MHz, D₂O): δ 8.46 (s, 1H, C7-H), 7.41 (d, *J* = 8.3 Hz, 2H, Ar), 6.34 (d, *J* = 8.3 Hz, 2H, Ar), 4.24 (dd, *J* = 4.4, 8.4 Hz, 1H, C19-H), 4.15 (s, 2H, C9-H₂), 3.53 (s, 4H), 3.47 (s, 2H), 3.42 (s, 2H), 3.18–2.97 (overlap, 14H), 2.28 (m, 2H, C22-H₂), 2.28–1.83 (m, 2H, C21-H₂) (see the Supporting Information). ¹³C NMR (75 MHz, D₂O): δ 178.9, 178.0, 175.9, 175.7, 173.6, 173.2, 169.0, 164.8 (C4), 154.4 (C2), 152.8 (C8a), 150.2 (C11), 148.3, 148.2, 128.9 (C13 and C15), 126.5 (C4a), 120.7 (C14), 111.7 (C12 and C16), 58.6, 58.2, 57.9, 55.6, 55.4, 51.9, 51.6, 51.1, 50.6, 45.4 (C9), 38.8 (C25), 38.5 (C26), 32.8 (C22), 28.1 (C21) (also see the attached spectrum for assignment). Low-resolution MS (matrix-assisted laser desorption ionization): C₃₅H₄₅N₁₂O₁₄ [M – H][–] 857.3, found 857.8.

Radiotracer Synthesis. The [¹¹¹In]DTPA–folate radiopharmaceutical was obtained in high radiochemical yield by ligand exchange from [¹¹¹In]citrate. Briefly, ¹¹¹In³⁺ (0.2–5.4 mCi) in HCl (0.05 M, 2–55 μL) was transferred to a test tube and buffered by addition of 200 μL of 3% aqueous sodium citrate. The resulting [¹¹¹In]citrate was mixed with 300–350 μg of DTPA–folate in

water (2 mg/mL, pH 7–8). Two to 24 h later, the radiochemical purity of the [¹¹¹In]DTPA–folate was determined by TLC on C-18 reversed phase plates eluted with methanol and consistently found to exceed 98% ([¹¹¹In]DTPA–folate *R_f* = 0.8; [¹¹¹In]citrate *R_f* = 0.0). The [¹¹¹In]DTPA–folate product was diluted with normal saline, as needed, prior to use in the animal biodistribution experiments. [⁶⁷Ga]DF–folate was prepared as described previously (Mathias et al., 1996a).

Cellular Uptake of [¹¹¹In]DTPA–Folate. Cultured KB and A549 cells in 35 mm dishes were incubated with 100 nM [¹¹¹In]citrate or [¹¹¹In]DTPA–folate in 1 mL of folate-deficient medium at room temperature for various lengths of time. The cells were then washed with 3 × 1 mL of PBS and suspended in 1 mL of PBS by scraping. The amount of cell-associated radioactivity was determined using an automatic γ counter. Cellular protein content was measured by the bicinchoninic acid assay. In folate competition experiments, the same protocol was used except that 1 mM folic acid was included in the incubation medium.

Biodistribution and Imaging Studies with [¹¹¹In]DTPA–Folate. All animal studies were carried out in accordance with procedures approved by the Purdue Animal Care and Use Committee. The biodistributions of [¹¹¹In]DTPA–folate and [⁶⁷Ga]DF–folate were determined in normal male Sprague-Dawley rats following intravenous injection under diethyl ether anesthesia, as described previously (Tsang et al., 1994). In addition, a γ scintillation image of a female athymic mouse Nu/Nu (22 g) was obtained using a PhoGamma 37GP camera fitted with a 300 keV parallel hole collimator. The animal used for this imaging study was maintained for 3 weeks on a folate-free diet (to reduce its serum folate to a level near that of human serum) and had been implanted subcutaneously in the interscapular region with human KB tumor cells, as described previously (Mathias et al., 1996a). The tumor mass at the time of the imaging study was approximately 0.25 g. The animal was imaged for 1 h following intravenous administration of [¹¹¹In]DTPA–folate (200 μCi in 0.1 mL) via the femoral vein under diethyl ether anesthesia. To promote clearance of the radiotracer from the urinary bladder, 1.5 mL of sterile saline was administered by ip injection immediately following the intravenous radiotracer injection. For imaging, the mouse was re-anesthetized with ketamine (60 mg/kg) and xylazine (6 mg/kg) immediately prior to the image acquisition period. The total administered mass of the DTPA–folate conjugate was 13 μg (0.57 mg/kg).

RESULTS

Production of the EDA-Derivatized Folic Acid. Ethylenediamine (EDA) was conjugated to the γ-carboxyl of folic acid either by carbodiimide activation or by regioselective methyl folate synthesis (Figure 1) to serve as a linker between the vitamin and the metal chelator, DTPA. High-resolution FAB mass spectroscopic analysis showed the EDA–folate [M + H]⁺ parent ion peak at *m/e* = 484.2062 (calculated 484.2057), indicating the desired 1/1 conjugation ratio. The chemical purity and identity of EDA–folate(γ) was confirmed by analytical HPLC and NMR spectroscopy (see the Supporting Information). The ¹H NMR spectrum shows that one of the amine groups on EDA is conjugated to the γ-carboxylate of folic acid, shifting the protons on the ethylene group to a lower field. Derivatization of the folate at the γ-carboxyl, in contrast to the α-carboxyl, rendered the conjugate a substrate of the hydrolytic enzyme carboxypeptidase G₂ (Levy and Goldman, 1967; Fan et al., 1991).

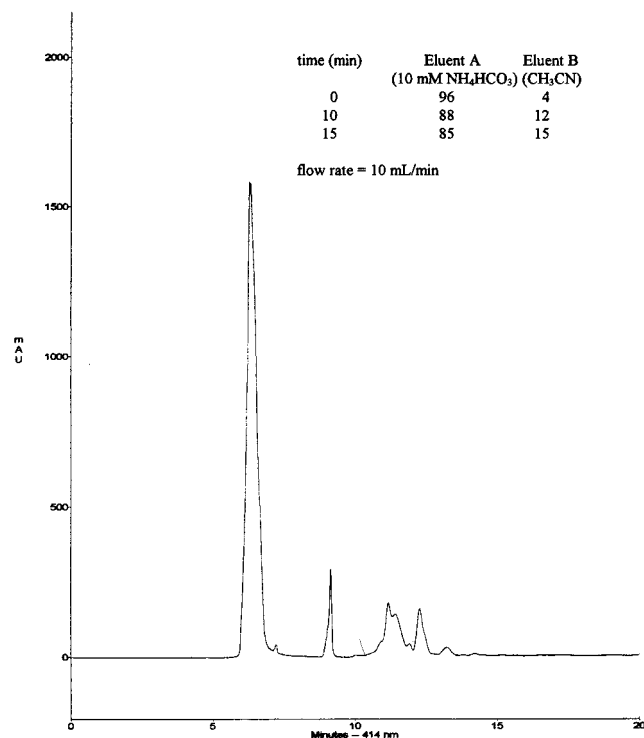


Figure 2. Purification of DTPA-folate(γ) by HPLC. Fifty milligrams of the reaction crude product dissolved in 0.5 mL of H₂O was loaded onto a Microsorb preparative C-18 reversed phase column and eluted with the gradient shown above the chromatogram. The desired DTPA-folate(γ) conjugate was eluted at 6.3 min, while the peak at 9.2 min was found to be the DTPA-bis-folate(γ,γ') side product. Other peaks were the impurities present in tetramethylguanidinium L- γ -methyl folate.

Synthesis of DTPA-Folate. The amide-linked DTPA-folate(γ) conjugate (Figure 1) was obtained by reaction of cyclic DTPA anhydride with the purified EDA-folate(γ), followed by chromatographic purification to remove the major side product DTPA-bis-folate(γ,γ') and other impurities (Figure 2). The chemical structure of purified DTPA-folate was characterized by MS and NMR (see the Supporting Information), and the purity was confirmed by analytical HPLC. The ion-pair agent in the mobile phase was found to be essential for a quantitative HPLC analysis, probably due to the complete neutralization of the multiple charges on DTPA-folate(γ) which allowed adequate interaction between the sample compound and the hydrocarbon stationary phase.

Affinities of FITC-EDA-Folate for Cell Surface Receptors. To determine the affinities of EDA-folate for cell surface folate receptors, the α - and γ -isomers were labeled with the fluorophore FITC and incubated with KB cells overexpressing the receptor. As shown in Figure 3, 1.6 nM FITC-EDA-folate(γ) isomer was required to reach 50% maximal binding, similar to that of folic acid and DF-folate(γ). Excess folic acid in the incubation medium effectively competed with the receptor binding of FITC-EDA-folate(γ). On the other hand, the α -isomer of FITC-EDA-folate had virtually no affinity for the cell surface receptors. The low level of nonspecific uptake observed with both isomers was probably due to the hydrophobicity of the FITC conjugates.

Cellular Uptake of [¹¹¹In]DTPA-Folate. The kinetics of the cellular uptake of the [¹¹¹In]DTPA-folate complex were evaluated by a time-dependent binding assay. As shown in Figure 4, the time needed to reach 50% saturation of available folate receptors was ~3 min at room temperature, similar to that observed for folic acid and folate conjugates such as [⁶⁷Ga]DF-folate (Wang

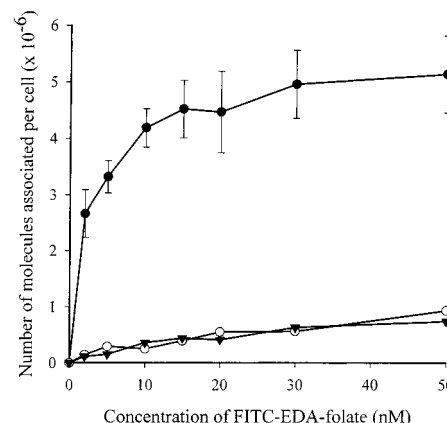


Figure 3. Determination of the affinities of FITC-EDA-folate isomers for cell surface folate receptors. KB cells were incubated with various concentrations of the α -isomer (○) or γ -isomer (●) of the conjugate at 4 °C for 30 min. Cell-associated fluorescence was measured as described in Experimental Procedures. Competition for the receptor binding of FITC-EDA-folate(γ) by excess folic acid (▼) was also evaluated.

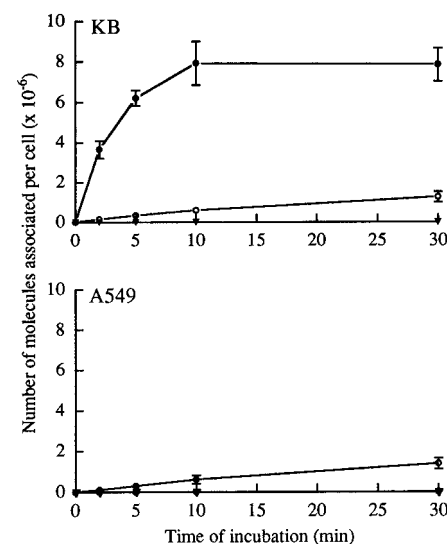


Figure 4. Cellular uptake of ¹¹¹In-labeled imaging agents. KB and A549 cells were treated with 100 nM [¹¹¹In]citrate (○) or [¹¹¹In]DTPA-folate(γ) with (▼) or without (●) competition by 1 mM folic acid for various lengths of time. Cell-associated radioactivity was measured by automated γ counting as described in Experimental Procedures.

et al., 1996) and [¹²⁵I]BSA-folate (Leamon et al., 1991). Coincubation with 1 mM free folic acid completely blocked conjugate uptake (Figure 4, inverted triangles), further confirming that cell association of the radioactivity was mediated by folate receptors. A549 cells which lack folate receptors did not show significant [¹¹¹In]DTPA-folate uptake at any time point. Nonspecific uptake of the complex was also not observed in either cell line, probably due to the sufficient hydrophilicity of the entire molecule. Cellular uptake of [¹¹¹In]citrate, on the other hand, was not saturable and virtually identical in the cell line expressing (KB cell) and not expressing (A549 cell) the folate receptor.

Biodistribution of [¹¹¹In]DTPA-Folate. Following intravenous administration to rats, the [¹¹¹In]DTPA-folate radiotracer was found to be efficiently cleared from the blood and primarily excreted into the urine (Table 1). Only $3.7 \pm 1.4\%$ of the injected ¹¹¹In dose was found in the intestines at 4 h postinjection (Table 1), a value 10-fold lower than the intestinal radioactivity observed with [⁶⁷Ga]DF-folate in the rat model at the same time

Table 1. Biodistribution of [¹¹¹In]DTPA–Folate in Normal Male Rats Following Intravenous Injection

	percentage of injected ¹¹¹ In dose per organ (tissue) ^a	
	4 h	24 h
blood	0.078 ± 0.005	0.029 ± 0.006
heart	0.021 ± 0.002	0.017 ± 0.002
lungs	0.024 ± 0.003	0.022 ± 0.001
liver	0.25 ± 0.01	0.17 ± 0.01
spleen	0.019 ± 0.004	0.017 ± 0.003
kidneys (two)	13.5 ± 1.4	12.1 ± 1.3
intestines and contents	3.7 ± 1.4	1.2 ± 0.3
bladder and contents	0.39 ± 0.63	0.09 ± 0.14

^a Values shown represent the mean ± standard deviation of data from three animals (188 ± 7 g). Blood was assumed to account for 7% of the total body mass. The DTPA–folate dose was 0.268 ± 0.021 mg/kg.

Table 2. Biodistribution of [⁶⁷Ga]Deferoxamine–Folate ([⁶⁷Ga]Df–Folate) in Normal Male Rats Following Intravenous Injection

	percentage of injected ⁶⁷ Ga dose per organ (tissue) ^a		
	5 min	4 h	24 h
blood	8.7 ± 0.2	0.072 ± 0.004	0.045 ± 0.019
heart	0.20 ± 0.01	0.020 ± 0.002	0.017 ± 0.001
lungs	0.51 ± 0.07	0.023 ± 0.004	0.016 ± 0.001
liver	8.1 ± 0.4	0.23 ± 0.03	0.203 ± 0.002
spleen	0.099 ± 0.012	0.007 ± 0.001	0.0075 ± 0.0017
kidneys (two)	8.63 ± 0.35	11.5 ± 1.0	10.2 ± 0.7
intestines and contents	10.3 ± 1.1	39.3 ± 1.3	2.7 ± 3.5
bladder and contents	12.6 ± 3.2	12.8 ± 3.2	0.02 ± 0.02

^a Values shown represent the mean ± standard deviation of data from three animals (186 ± 7 g). Blood was assumed to account for 7% of the total body mass. The Df–folate dose was 0.262 ± 0.012 mg/kg.

point (Table 2). Since it is clinically desirable to be able to initiate imaging as rapidly as possible following radiotracer injection, [¹¹¹In]DTPA–folate may offer advantages over [⁶⁷Ga]Df–folate for imaging abdominal tumors, due to a more favorable pattern of clearance from nontarget tissues. The [⁶⁷Ga]Df–folate and [¹¹¹In]DTPA–folate tracers also differ in the amount of radiotracer found in the “bladder and contents” at 4 h postinjection; however, this difference is of questionable significance, since no provision was made to prevent spontaneous voiding of the urinary bladder. By 24 h postinjection, both the [¹¹¹In]DTPA–folate and [⁶⁷Ga]Df–folate radiolabels are largely cleared from the body, with only the kidneys exhibiting substantial levels of radioactivity (Tables 1 and 2). This prolonged renal retention of a fraction of both agents probably reflects radiopharmaceutical binding to the folate receptor known to be present in the proximal tubules (Selhub and Franklin, 1984; Selhub et al., 1987a,b).

The ability of [¹¹¹In]DTPA–folate to target folate receptors *in vivo* also appears to be demonstrated in a preliminary imaging study with an athymic mouse bearing a subcutaneous folate receptor-positive human KB cell tumor. The KB cell tumor is readily apparent in the γ image obtained 1 h following intravenous administration of the [¹¹¹In]DTPA–folate radiopharmaceutical (Figure 5). While radiotracer uptake is also apparent in the kidneys, the tumor/background tissue contrast is otherwise quite good, even at this relatively short time postinjection.

DISCUSSION

The development of new and improved tumor-selective radiopharmaceuticals is clinically desirable as a means

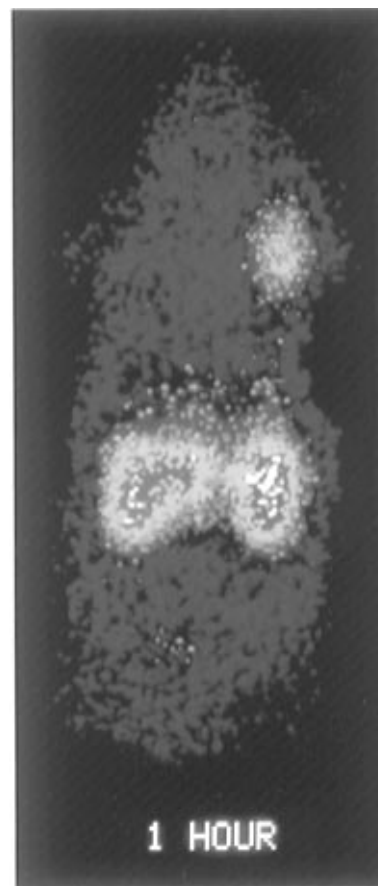


Figure 5. Whole body γ image (dorsal view; 200 000 counts) of a female athymic mouse with a subcutaneous folate receptor-positive tumor in the right shoulder 1 h following intravenous administration of [¹¹¹In]DTPA–folate(γ). Radiotracer uptake is apparent in both the tumor (upper right) and kidneys.

of (i) detecting and/or confirming the presence and location of primary and metastatic lesions, (ii) probing biochemical features of neoplastic tissue that have implications for tumor staging and/or subsequent treatment, and (iii) monitoring tumor response to treatment. If sufficiently high tumor specificity can be achieved, radiopharmaceuticals labeled with an appropriate α - or β -emitting nuclide could also provide an attractive means for site-selective delivery of radiation therapy.

It has been demonstrated that only those folate conjugates containing the adduct attached at the γ -carboxyl of folic acid retain the ability to bind to cell surface folate receptors with the same affinity as free folic acid (Wang et al., 1996). In this paper, two synthetic methods were employed to conjugate the EDA linker to folic acid. Although method A represents a relatively simple and fast synthetic route, its lack of regioselectivity yields both an inactive α -conjugate and the active γ -conjugate. Also, the requirement for HPLC purification to separate the two isomers and the poor water solubility of the EDA–folate intermediate severely limit large scale production of the desired product.

Regiospecific functionalization of the γ -carboxylate on folic acid was achieved, however, by converting folic acid to pteroyl azide and then attaching the commercially available 5-methyl glutamate to form γ -methyl folate (Luo et al., 1997). In this procedure (method B), production of large amounts of EDA–folate(γ) could be accomplished simply by dissolving the γ -methyl folate in EDA. The overall yield from folic acid to EDA–folate(γ) was 52%, and a chemical purity of above 90% was achieved without column purification. Importantly, this

unique regiospecific activation of the γ -carboxyl on folic acid can potentially be applied in the preparation of many folate-targeted anticancer agents.

Our previous imaging study with [^{67}Ga]DF-folate(γ) in the athymic mouse KB cell tumor model demonstrated the feasibility of targeting tumor folate receptors *in vivo* with simple folate-chelate conjugates (Mathias et al., 1996a). However, roughly 30% of the [^{67}Ga]DF-folate(γ) radiopharmaceutical was found to be excreted via the GI tract, where its presence could interfere with clear and rapid visualization of abdominal cancers. In order to overcome this obstacle, in the present study, [^{111}In]DTPA-folate(γ) was synthesized and shown to have affinity for the folate receptor *in vitro*. In preliminary rat and tumor-bearing mouse studies, the [^{111}In]DTPA-folate(γ) appears to afford targeting to folate receptors *in vivo*, while also providing reasonably selective clearance of unbound radiotracer into the urine. This second-generation folate-chelate imaging agent would appear to offer advantages over the previously reported folate-deferoxamine conjugate for imaging tumors in the abdominal region, where the intestinal levels of [^{67}Ga]DF-folate(γ) are expected to contribute undesirably high background activity. While further experiments will clearly be required to better define the suitability of [^{111}In]DTPA-folate(γ) as a radiopharmaceutical for imaging folate receptor-positive tumors and to prove the role of the folate receptor in mediating tumor uptake of the ^{111}In radiolabel, the reported imaging results with the athymic mouse tumor model (Figure 5) support the conclusion that this agent can provide tumor-selective radionuclide delivery *in vivo*.

ACKNOWLEDGMENT

This work was supported in part by a grant from the National Cancer Institute (R01-CA70845). The Purdue Athymic Mouse Facility and Cell Culture Facility are partially supported by Cancer Center (Core) Support Grant P30-CA23168 awarded by the National Cancer Institute.

Supporting Information Available: ^1H and ^{13}C NMR spectra of EDA-folate(γ), ^1H and ^{13}C NMR spectra of DTPA-folate(γ), analytical HPLC chromatograms of the two compounds with the conditions described in Experimental Procedures, and a table showing the biodistribution of [^{111}In]DTPA-folate and [^{67}Ga]DF-folate in rats calculated as a percentage of the injected dose per gram (%ID/g) of tissue wet weight (7 pages). Ordering information is given on any current masthead page.

LITERATURE CITED

- Antony, A. C., Kane, M. A., Portillo, R. M., Elwood, P. C., and Kolhouse, J. F. (1985) Study of the role of a particulate folate-binding protein in the uptake of 5-methyltetrahydrofolate. *J. Biol. Chem.* **260**, 14911–14917.
- Campbell, I. G., Jones, T. A., Foulkes, W. D., and Trowsdale, J. (1991) Folate-binding protein is a marker for ovarian cancer. *Cancer Res.* **51**, 5329–5338.
- Coney, L. R., Tomassetti, A., Carayannopoulos, L., Frasca, V., Kamen, B. A., Colnaghi, M. I., and Zurawski, V. R., Jr. (1991) Cloning of a tumor-associated antigen: MOv18 and MOv19 antibodies recognize a folate-binding protein. *Cancer Res.* **51**, 6125–6132.
- Doerr, R. J., Abdel-Nabi, H., Krag, D., and Mitchell, E. (1991) Radiolabeled antibody in the management of colorectal cancer. Results of a multicenter study. *Ann. Surg.* **214**, 118–124.
- Fischman, A. J., Khaw, B. A., and Strauss, H. W. (1989) Quo vadis radioimmune imaging. *J. Nucl. Med.* **30**, 1911–1915.
- Franklin, W. A., Waintrub, M., Edwards, D., Christensen, K., Prendegast, P., Woods, J., Bunn, P. A., and Kolhouse, J. F. (1994) New anti-lung-cancer antibody cluster 12 reacts with human folate receptors present on adenocarcinoma. *Int. J. Cancer* **8** (Suppl.), 89–95.
- Fritzberg, A. R., Berninger, R. W., Hadley, S. W., and Wester, D. W. (1988) Approaches to radiolabeling of antibodies for diagnosis and therapy of cancer. *Pharm. Res.* **5**, 325–334.
- Garin-Chesa, P., Campbell, I., Saigo, P., Lewis, J., Old, L., and Rettig, W. (1993) Trophoblast and ovarian cancer antigen LK26. Sensitivity and specificity in immunopathology and molecular identification as a folate-binding protein. *Am. J. Pathol.* **142**, 557–567.
- Goldenberg, D. M., Goldenberg, H., Higginbotham-Ford, E., Shochat, D., and Ruoslahti, E. (1987) Imaging of primary and metastatic liver cancer with ^{131}I monoclonal and polyclonal antibodies against alphafetoprotein. *J. Clin. Oncol.* **5**, 1827–1835.
- Griffiths, G. L., Goldenberg, D. M., Jones, A. L., and Hansen, H. J. (1992) Radiolabeling of monoclonal antibodies and fragments with technetium and rhenium. *Bioconjugate Chem.* **3**, 91–99.
- Halpern, S. E. (1986) The advantages and limits of indium-111 labeling of antibodies. Experimental studies and clinical applications. *Appl. Radiat. Isot.* **13**, 195–201.
- Hnatowich, D. J., Layne, W. W., Childs, R. L., and Davis, M. A. (1983) Radioactive labeling of antibody: a simple and efficient method. *Science* **220**, 613–615.
- Holm, J., Hansen, S. I., Hoier-Madsen, M., Sondergaard, K., and Bzorek, M. (1994) Folate receptor of human mammary adenocarcinoma. *APMIS* **102**, 413–419.
- Kairemo, K. J., Hopsu, E. V., Melartin, E. J., and Heikkilä, P. S. (1991) Imaging of a parapharyngeal hemangiopericytoma. Radioimmunosintigraphy (SPECT) with indium-111-labeled anti-CEA antibody, and comparison to digital subtraction angiography, computed tomography, and immunohistochemistry. *Cancer* **67**, 61–66.
- Kamen, B. A., and Capdevila, A. (1986) Receptor-mediated folate accumulation is regulated by the cellular folate content. *Proc. Natl. Acad. Sci. U.S.A.* **83**, 5983–5987.
- Kane, M. A., and Waxman, S. (1989) Role of folate binding proteins in folate metabolism. *Lab. Invest.* **60**, 737–746.
- Lamki, L. M. (1995) Tissue characterization in nuclear oncology: its time has come. *J. Nucl. Med.* **36**, 207–210.
- Laufer, I., Keenan, A. M., and Dinsmore, B. (1990) Advances in the diagnosis and imaging of gastrointestinal cancer. *Curr. Opin. Oncol.* **2**, 711–717.
- Leamon, C. P., and Low, P. S. (1991) Delivery of macromolecules into living cells: a method that exploits folate receptor endocytosis. *Proc. Natl. Acad. Sci. U. S. A.* **88**, 5572–5576.
- Leamon, C. P., and Low, P. S. (1993) Membrane folate-binding proteins are responsible for folate-protein conjugate endocytosis into cultured cells. *Biochem. J.* **291**, 855–860.
- Lee, R. J., and Low, P. S. (1994) Delivery of liposomes into cultured KB cells via folate receptor-mediated endocytosis. *J. Biol. Chem.* **269**, 3198–3204.
- Lee, R. J., Wang, S., and Low, P. S. (1996) Measurement of Endosomal pH Following Folate Receptor-Mediated Endocytosis. *Biochim. Biophys. Acta* **1312**, 237–242.
- Levy, C. C., and Goldman, P. (1967) The enzymatic hydrolysis of methotrexate and folic acid. *J. Biol. Chem.* **242**, 2933–2938.
- Li, P. Y., Del Vecchio, S., Fonti, R., Carriero, M. V., Potena, M. I., Botti, G., Miotti, S., Lastoria, S., Menard, S., Colnaghi, M. I., and Salvatore, M. (1996) Local concentration of folate binding protein GP38 in sections of human ovarian carcinoma by *in vitro* quantitative autoradiography. *J. Nucl. Med.* **37**, 665–672.
- Luo, J., Smith, M., Lantrip, D. A., Wang, S., and Fuchs, P. L. (1997) Efficient syntheses of pyrofolate and pteroylazine, reagents for the production of carboxyl differentiated derivatives of folic acid. *J. Am. Chem. Soc.* (submitted for publication).
- Mathias, C. J., Wang, S., Lee, R. J., Waters, D. J., Low, P. S., and Green, M. A. (1996a) Tumor selective radiopharmaceutical targeting via receptor-mediated endocytosis: evaluation of a gallium-67 labeled deferoxamine-folate conjugate. *J. Nucl. Med.* **37**, 1003–1008.

- Mathias, C. J., Wang, S., Waters, D. J., Low, P. S., and Green, M. A. (1996b). Ga-67 and In-111 labeled folate-chelate conjugates for targeting tumor-associated folate binding protein. *J. Nucl. Med.* 37, 347P–348P (abstract).
- Matsue, H., Rothberg, K. G., Takashima, A., Kamen, B. A., Anderson, R. G. W., and Lacey, S. W. (1992) Folate receptor allows cells to grow in low concentrations of 5-methyltetrahydrofolate. *Proc. Natl. Acad. Sci. U.S.A.* 89, 6006–6009.
- McHugh, M., and Cheng, Y. C. (1979) Demonstration of a high affinity folate binder in human cell membranes and its characterization in cultured human KB cells. *J. Biol. Chem.* 254, 11312–11318.
- Rettig, W., Garin-Chesa, P., Beresford, H., Oettgen, H., Melamed, M., and Old, L. (1988) Cell-surface glycoproteins of human sarcomas: differential expression in normal and malignant tissues and cultured cells. *Proc. Natl. Acad. Sci. U.S.A.* 85, 3110–3114.
- Ross, J. F., Chaudhuri, P. K., and Ratnam, M. (1994) Differential regulation of folate receptor isoforms in normal and malignant tissues in vivo and in established cell lines. Physiologic and clinical implications. *Cancer* 73, 2432–2443.
- Selhub, J., and Franklin, W. A. (1984) The folate-binding protein of rat kidney. *J. Biol. Chem.* 259, 6601–6606.
- Selhub, J., Emmanouel, D., Stavropoulos, T., and Arnold, R. (1987a) Renal folate absorption and the kidney folate binding protein. I. Urinary clearance studies. *Am. J. Physiol.* 252, F750–F756.
- Selhub, J., Nakamura, S., and Carone, F. A. (1987b) Renal folate absorption and the kidney folate binding protein. II. Micro-infusion studies. *Am. J. Physiol.* 252, F757–F760.
- Serafini, A. N., Ed. (1993) Monoclonal antibody imaging: crossing the research/clinical barrier. *Seminars in Nuclear Medicine*, Vol. 23, pp 87–179, Saunders, Orlando, FL.
- Stein, R., Goldenberg, D. M., and Mattes, J. (1991) Normal tissue reactivity of four anti-tumor monoclonal antibodies of clinical interest. *Int. J. Cancer* 47, 163–169.
- Tsang, B. W., Mathias, C. J., Fanwick, P. E., and Green, M. A. (1994) Structure-distribution relationships for metal-labeled myocardial imaging agents: comparison of a series of cationic gallium(III) complexes with hexadentate bis(salicylaldimine) ligands. *J. Med. Chem.* 37, 4400–4406.
- Wang, S., Lee, R. J., Cauchon, G., Gorenstein, D. G., and Low, P. S. (1995) Delivery of antisense oligonucleotides against the human epidermal growth factor receptor into cultured KB cells with liposomes conjugated to folate via polyethylene-glycol. *Proc. Natl. Acad. Sci. U.S.A.* 92, 3318–3322.
- Wang, S., Lee, R. J., Mathias, C. J., Green, M. A., and Low, P. S. (1996) Synthesis, purification, and tumor cell uptake of ⁶⁷Ga-deferoxamine-folate, a potential radiopharmaceutical for tumor imaging. *Bioconjugate Chem.* 7, 56–62.
- Weitman, S. D., Lark, R. H., Coney, L. R., Fort, D. W., Frasca, V., Zurawski, V. R., Jr., and Kamen, B. A. (1992) Distribution of the folate receptor (GP38) in normal and malignant cell lines and tissues. *Cancer Res.* 52, 3396–3401.
- Wilbur, D. S. (1992) Radiohalogenation of proteins: an overview of radionuclides, labeling methods, and reagents for conjugate labeling. *Bioconjugate Chem.* 3, 433–470.

BC9701297

Photoaffinity Analogue for the Anti-inflammatory Drug α -Trinositol: Synthesis and Identification of Putative Molecular Targets

Anu Chaudhary[†] and Glenn D. Prestwich^{*}

Department of Chemistry and Department of Biochemistry and Cell Biology, University at Stony Brook, Stony Brook, New York 11794-3400. Received March 27, 1997[©]

α -Trinositol (α T), or Ins(1,2,6)P₃, is a semisynthetic inositol trisphosphate produced commercially by the partial degradation of phytic acid with phytase. The molecular targets mediating the mechanism of action of this novel anti-inflammatory, analgesic, and antivasoconstrictive drug are unknown. A new photoaffinity analogue, 4-[³H]BZDC- α T, has been prepared in which the [³H]-*p*-benzoyldihydrocinnamoyl ([³H]BZDC) photophore is tethered through an *O*-(5-aminopentanoyl) linkage to the 4-OH of α T. Photoaffinity labeling experiments with two human tissues, umbilical cord vascular smooth muscle cells and platelet membranes, revealed proteins that were selectively labeled by 4-[³H]BZDC- α T. Thus, co-incubation with α T but not with Ins(1,3,4,5)P₄ during photolysis competitively displaced labeling of a 55 kDa platelet protein. In vascular epithelial cells, α T and Ins(1,3,4,5)P₄ both displaced labeling of a 55 and 43 kDa proteins. The identification of putative protein targets for α T in smooth vascular tissue may have important implications in elucidation of the mechanism of action of this unusual drug.

INTRODUCTION

D-*myo*-Inositol 1,4,5-trisphosphate, or Ins(1,4,5)P₃,¹ is released from phosphatidylinositol 4,5-bisphosphate by ligand-induced activation of phospholipase C and has multiple roles in cellular calcium signaling (1, 2). A regioisomeric inositol trisphosphate, α -trinositol (**1**) [Ins-(1,2,6)P₃, or α T] (Figure 1), has been synthesized in bulk by controlled hydrolysis of phytic acid with a specific phytase (3), and its physiological properties can be explored. Rather than acting simply as a mimic of Ins-(1,4,5)P₃, α T (**1**) exhibited a number of useful pharmacological properties, including inhibition of inflammation (4), inhibition of edema formation in skin burn injury (5), inhibition of vasoconstriction evoked by neuropeptide Y (NPY) and ATP (6), and prevention of diabetic complications (7). The vascular effects of *myo*-inositol and a series of D-*myo*-inositol phosphate derivatives have been studied in rat heart membranes, guinea pig basilar artery (*in vitro*), and pithed rats (8). Inhibition of the NPY-induced pressor response *in vivo* by α T was reminiscent of a new class of synthetic non-peptide drugs that inhibit the vascular effects of NPY without binding to the NPY receptor itself (9). Moreover, α T facilitated the flexor reflex but did not block the depressive effect of NPY (10). In rat aortal rings, α T acted on the plasmalemma and

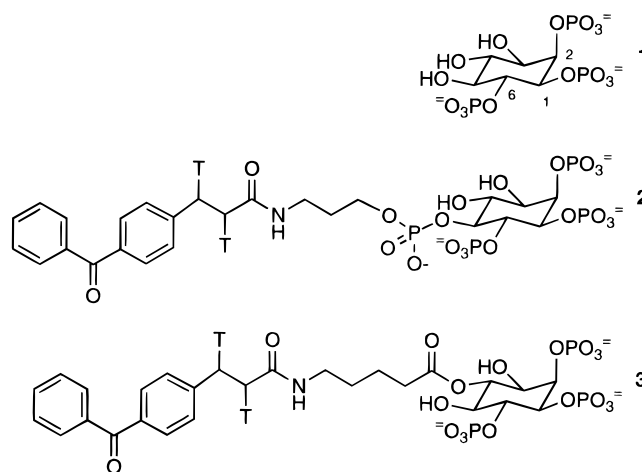


Figure 1. Structures of α T and photoaffinity analogues: **1**, α T [Ins(1,2,6)P₃]; **2**, [³H]BZDC-P-5-(*O*-aminopropyl) Ins(1,2,5,6)-P₄; **3**, [³H]BZDC-4-*O*-(5-aminopentanoate) Ins(1,2,6)P₃.

modulated Ca²⁺ influx from the extracellular space (11). Finally, the edema-preventing effects of α T may occur through modulation of β_1 -integrin function (12).

Despite this plethora of physiological data, neither the molecular target(s) nor the molecular mechanism of action of α T is known. To investigate potential molecular targets, a new photoaffinity analogue (**3**) of α T was prepared, in which the 4-OH was modified as the 5-aminopentanoate and then derivatized as the photoactivatable [³H]-*p*-benzoyldihydrocinnamoyl ([³H]BZDC) amide (13). We further describe the use of this photoaffinity label to identify putative target proteins for α T in human platelet membranes and umbilical cord vascular smooth muscle cells. Direct autoradiography using the latter cells had previously shown distinct and selective high-affinity binding sites for α T and Ins(1,3,4,5)P₄ (14).

EXPERIMENTAL PROCEDURES

Materials and Methods. All NMR spectral data were obtained on either QE-300 or AC-250 instruments.

^{*} Address correspondence to this author at the Department of Medicinal Chemistry, 308 Skaggs Hall, The University of Utah, Salt Lake City, UT 84112 [telephone (801) 585-9051; fax (801) 585-9053; e-mail gprestwich@deans.pharm.utah.edu].

[†] Present address: Department of Medicinal Chemistry, 308 Skaggs Hall, The University of Utah, Salt Lake City, UT 84112.

[©] Abstract published in *Advance ACS Abstracts*, August 1, 1997.

¹ Abbreviations: α T, α -trinositol [Ins(1,2,6)P₃]; DIBAL, diisobutyl aluminum hydride; EA, ethyl acetate; H, hexane; [³H]-BZDC, [³H]-*p*-benzoyldihydrocinnamoyl; Ins(1,4,5)P₃, D-*myo*-inositol 1,4,5-trisphosphate; InsP₄, D-*myo*-inositol 1,3,4,5-tetrakisphosphate; NPY, neuropeptide Y; PEG, poly(ethylene glycol); PMB, *p*-methoxybenzyl; rt, room temperature; SDS-PAGE, sodium dodecyl sulfate–polyacrylamide gel electrophoresis; TEAB, triethylammonium bicarbonate; TCA, trichloroacetic acid.

All reagents were obtained from Aldrich Chemical Co. (Milwaukee, WI). All solvents used were of reagent or HPLC grade. CH_2Cl_2 was distilled from CaH_2 , and DMF was dried by storage over molecular sieves. The normal workup procedure involved extraction three times with the appropriate solvent, washing the combined organic extracts once, drying over anhydrous MgSO_4 , filtration, and concentration by rotary evaporation. EN³HANCE was obtained from NEN Life Science Products (Boston, MA). Chromatographic purification was performed over "flash" grade SiO_2 using ethyl acetate (EA)/hexane (H) mixtures. HPLC retention times are denoted t_R . Only diagnostic NMR resonances are reported. Mass spectrometry analysis was performed at the Mass Spectrometry Laboratory in the Department of Chemistry at The University of Utah.

Methyl 2-*O*-Benzyl-4,6-*O*-(benzylidene)- α -D-glucopyranoside (5). Methyl 4,6-*O*-benzylidene- α -D-glucopyranoside (20 g, 0.06 mol), tetrabutylammonium hydrogen sulfate (4.07 g, 0.012 mol), and benzyl bromide (12.2 mL, 0.102 mol) were dissolved in 1000 mL of CH_2Cl_2 ; 100 mL of aqueous NaOH (5% w/v) was added, and the mixture was refluxed for 48 h. The mixture was then cooled, the layers were separated, and the organic layer was washed with water, dried (MgSO_4), and concentrated. The syrup obtained was triturated with hexane twice to give a white precipitate, which was dissolved in 2:1 EA/H ($R_f = 0.5$), filtered, and concentrated to yield 11.2 g of a white solid (50.4% yield, mp 121–122 °C): ^1H NMR (300 MHz, CDCl_3) δ 7.8–7.3 (10 H, phenyl CH, m), 5.4 (1H, CH, s), 4.8 (s, 2H), 4.6 (m, 1H), 4.4–4.2 (3H, m), 4.0–3.6 (3H, m), 3.4 (3H, OCH_3 , s), 2.68 (1H, bs); HRMS calcd for $\text{C}_{21}\text{H}_{24}\text{O}_6$ 372.1573, found 372.1572.

Methyl 2-*O*-Benzyl-4,6-*O*-(benzylidene)-3-*O*-(*p*-methoxybenzyl)- α -D-glucopyranoside (6). NaH (3 g, 2.3-fold excess) was washed (THF), suspended in 450 mL of DMF, and treated with a solution of **5** in 300 mL of DMF followed in 5 min by 16.5 mL of *p*-methoxybenzyl chloride. The mixture was stirred for 12 h at 45 °C, quenched (CH_3OH , then H_2O), extracted (ether), and purified on SiO_2 (50% EA/H, $R_f = 0.6$) to give **6** in 90% yield: ^1H NMR (300 MHz, CDCl_3) δ 7.4–7.1 (12H, phenyl CH, m), 6.7 (2H, d), 5.4 (1H, CH, s), 4.8–4.6 (m, 2H), 4.59 (1H, d), 4.25 (dd, 1H), 4.1 (m, 3H), 3.75 (s, 3H, $\text{PMB}-\text{OCH}_3$), 3.7–3.6 (4H, m), 3.3 (3H, OCH_3 , s); HRMS calcd for $\text{C}_{29}\text{H}_{32}\text{O}_7$ 492.2148, found 492.2153.

Methyl 2,4-Di-*O*-benzyl-3-*O*-(*p*-methoxybenzyl)- α -D-glucopyranoside (7). A solution of 1 g (1.86 mmol) of **6** in 100 mL of dry CH_2Cl_2 was cooled to –30 °C, and 9.3 mL of 1 M DIBAL-H (9.3 mmol) in CH_2Cl_2 was added dropwise. The solution was stirred at –30 °C for 0.5 h and quenched (CH_3OH , then 0.5 M aqueous NaHSO_4 at 0 °C). The organic layer was washed (H_2O , brine), dried (MgSO_4), concentrated, and purified on SiO_2 (25% EA/H, $R_f = 0.3$) to yield 0.5 g of a colorless oil (55% yield): ^1H NMR (300 MHz, CDCl_3) δ 7.4–7.1 (12H, phenyl CH, m), 6.7 (2H, d), 4.8–4.6 (m, 4H), 4.59 (2H, d), 4.25 (m, 1H), 3.75 (s, 3H, $\text{PMB}-\text{OCH}_3$), 3.7–3.6 (4H, m), 3.3 (3H, OCH_3 , s), 2.8 (1H, bs).

Methyl 2,4-Di-*O*-benzyl-3-*O*-(*p*-methoxybenzyl)- α -D-glucohexodialdo-1,5-pyranoside (8). A solution of 1.19 mL (6.81 mmol) of $(\text{COCl})_2$ in 75 mL of CH_2Cl_2 was cooled to –78 °C, and 2.0 mL of dry DMSO was added dropwise. The solution was stirred at –78 °C for 10 min, and then a solution of **7** (2.706 mmol, 3.5 g) in 25 mL of CH_2Cl_2 was added via cannula under argon. The mixture was stirred for 30 min, triethylamine (22 mmol, 6.1 mL) was added dropwise, and the solution was stirred, warmed to room temperature (rt), and worked up as described to give a near-quantitative yield of crude

aldehyde **8** (observed by TLC using 25% EA/H, $R_f = 0.7$) that was employed without further purification: ^1H NMR (250 MHz, CDCl_3) δ 9.8 (1H, s), 7.4–7.1 (12H, phenyl CH, m), 6.7 (2H, d), 4.59 (2H, d), 4.25 (dd, 1H), 4.1 (m, 3H), 3.75 (s, 3H, $\text{PMB}-\text{OCH}_3$), 3.7–3.6 (4H, m), 3.3 (3H, OCH_3 , s), 2.8 (1H, bs); HRMS calcd for $\text{C}_{29}\text{H}_{32}\text{O}_7$ 492.2148, found 492.2151.

Methyl (Z)-2,4-Di-*O*-benzyl-3-*O*-(*p*-methoxybenzyl)-6-*O*-acetyl- α -D-gluc-5-enopyranoside (9). Anhydrous K_2CO_3 (3.56 mmol, 0.49 g) was added to a stirred solution of compound **8** (0.539 mmol, 0.289 g) in 30 mL of dry CH_3CN and stirred for 10 min at rt. The solution was then treated with excess Ac_2O , refluxed at 80 °C for 8 h, cooled, quenched with H_2O , diluted with ether, and product isolated as usual with purification on SiO_2 (25% EA/H, $R_f = 0.43$) to give 0.2 g (70% yield) of enol acetate **9**: ^1H NMR (250 MHz, CDCl_3) δ 7.4–7.1 (12H, phenyl CH, m), 6.7 (2H, d), 4.59 (1H, m), 4.25 (dd, 1H), 4.1 (m, 3H), 3.75 (s, 3H, PMB/OCH_3), 3.7–3.6 (4H, m), 3.3 (3H, OCH_3 , s), 2.2 (3H, s); HRMS calcd for $\text{C}_{31}\text{H}_{34}\text{O}_8$ 534.2253, found 534.2280.

1-*O*-Acetyl-3,5-di-*O*-benzyl-4-*O*-(*p*-methoxybenzyl)-2-deoxy-2-oxo-*myo*-inositol (10). Mercury(II) acetate (4.58 mmol, 1.46 g) was added to a stirred solution of **9** (0.458 mmol, 0.264 g) in 25 mL of acetone/water (3:2); after 45 min at rt, 5 mL of saturated aqueous NaCl was added, and stirring was continued at rt for another 22 h. Product isolation as usual with purification on SiO_2 (40% EA/H, $R_f = 0.52$) gave 0.13 g of **10** (55% yield): ^1H NMR (250 MHz, CDCl_3) δ 7.4–7.1 (12H, phenyl CH, m), 6.7 (2H, d), 4.59 (1H, m), 4.25 (dd, 1H), 4.1 (m, 3H), 3.75 (s, 3H, PMB/OCH_3), 3.7–3.6 (4H, m), 2.2 (3H, s).

1-Acetyl-3,5-di-*O*-benzyl-4-*O*-(*p*-methoxybenzyl)-*myo*-inositol (11). Inosose **10** (0.188 mmol, 0.1 g) was dissolved in 7 mL of dry CH_3CN , and sodium triacetoxymethylborohydride (1.886 mmol, 0.399 g) was added. Glacial $\text{CH}_3\text{CO}_2\text{H}$ (1.3 mL) was then added dropwise. Product isolation as usual gave 60 mg of crude alcohol **11** (62%) that was used without further purification: ^1H NMR (250 MHz, CDCl_3) δ 7.4–7.1 (12H, phenyl CH, m), 6.7 (2H, d), 4.59 (1H, m), 4.25 (dd, 1H), 4.1 (m, 3H), 3.75 (s, 3H, $\text{PMB}-\text{OCH}_3$), 3.7–3.6 (4H, m), 2.5 (1H, bs), 2.2 (3H, s).

3,5-Di-*O*-benzyl-4-*O*-(*p*-methoxybenzyl)-*myo*-inositol (12). Acetate **11** (0.08 mmol, 46 mg) was saponified (3 mL of 0.35 M NaOH in CH_3OH solution, 1.5 h, 80 °C), and 30 mg of product **12** was isolated as usual (79%) and used without further purification: ^1H NMR (250 MHz, CDCl_3) δ 7.4–7.1 (12H, phenyl CH, m), 6.7 (2H, d), 4.59 (1H, m), 4.25 (dd, 1H), 4.1 (m, 3H), 3.75 (s, 3H, $\text{PMB}-\text{OCH}_3$), 3.7–3.6 (4H, m), 2.5 (2H, bs); HRMS calcd for $\text{C}_{28}\text{H}_{32}\text{O}_7$ 480.2448, found 480.2481.

Benzyl 1,2,6-[3,5-Di-*O*-benzyl-4-*O*-(*p*-methoxybenzyl)-*myo*-inosityl] Trisphosphate (13). To a stirred solution of 20 mg (0.038 mmol) of triol **12** and 27 mg (0.38 mmol) of 1*H*-tetrazole in 3 mL of dry CH_2Cl_2 was added a solution of 59 mg of (*N,N*-diisopropylamino)dibenzyl-oxyphosphine in 0.5 mL of dry CH_2Cl_2 . The reaction mixture was stirred overnight at rt and cooled to –40 °C, and then 43 mg (0.25 mmol) of *m*-chloroperbenzoic acid was added. The solution was stirred for 5 min at –40 °C, warmed to rt for 2 h, diluted with 10 mL of CH_2Cl_2 , and quenched with 10 mL of 10% Na_2SO_3 . The organic layer was washed (10% sodium sulfite, saturated aqueous NaHCO_3), dried (MgSO_4), filtered, concentrated *in vacuo*, and purified on SiO_2 using EA/H (1:2, $R_f = 0.3$) as eluant to give 32 mg (62%) of **13** as a syrup: ^1H NMR (250 MHz, CDCl_3) δ 7.4–7.1 (40H, phenyl CH, m), 6.7 (2H, d), 5.25 (m, 15H), 4.9 (6H, m), 3.9 (s, 3H, $\text{PMB}-\text{OCH}_3$); ^{31}P NMR (101 MHz, CDCl_3) 0.45 ppm; HRMS calcd for $\text{C}_{70}\text{H}_{71}\text{O}_{16}\text{P}_3$ 1260.3954, found 1260.3951.

3,5-Di-*O*-benzyl-1,2,6-tris(*O*-dibenzylphosphoryl)-*myo*-inositol (14). To 60 mg (0.05 mmol) of compound **13** was added 55 mg (0.09 mmol) of ceric ammonium nitrate in 6 mL of acetonitrile/water (9:1). The reaction mixture was stirred for 80 min at rt, quenched with 15 mL of saturated aqueous NaHCO₃, and diluted with 15 mL of CH₂Cl₂, and the organic layer was washed (saturated aqueous NaHCO₃, H₂O), dried (MgSO₄), concentrated *in vacuo*, and purified on SiO₂ with 75% EA/H (*R_f* = 0.6) as eluant to give 41 mg (75%) of **14** as an oil: ¹H NMR (250 MHz, CDCl₃) δ 7.4–7.1 (40H, phenyl CH, m), 5.25 (m, 16H), 4.2–3.6 (6H, m); ³¹P NMR (101 MHz, CDCl₃) 0.41 ppm; HRMS calcd for C₆₂H₆₃O₁₅P₃ 1140.3379, found 1140.3241.

***N*-Cbz-5-aminopentanoic Acid.** A solution of 5-aminopentanoic acid (0.5 g) and 1 g of *N*-(benzyloxycarbonyloxy)succinimide in dioxane/water/triethylamine (1:1:0.1) was heated at 90 °C for 72 h. The mixture was cooled to rt, extracted with EA, and evaporated to obtain a white powder. The solid was purified on SiO₂ using 2:1:1 EA/H/CH₂Cl₂ as eluant (*R_f* = 0.45): yield 78.5 mg (73%); ¹H NMR (250 MHz, CDCl₃) δ 7.4 (5H, m), 5.2 (2H, s), 3.2 (2H, t), 2.4 (2H, t), 1.6 (4H, m).

3,5-Di-*O*-benzyl-1,2,6-tris(dibenzylphosphoryl)-4-*O*-[5-(*N*-Cbz-aminopentanoyl)]-*myo*-inositol (15). A solution of 40 mg (0.03 mmol) of compound **14** in CH₂Cl₂, 5-*N*-Cbz-aminopentanoic acid (1.5 equiv), DCC (1.5 equiv), and DMAP (0.1 equiv) was stirred at rt overnight. The solution was filtered, concentrated *in vacuo*, and purified on SiO₂ with 2:1 EA/H (*R_f* = 0.6) as solvent to give 25 mg of **15** (55%): ¹H NMR (250 MHz, CDCl₃) δ 7.8–7.6 (45H, phenyl CH, m), 5.5 (m, 18H), 4.9 (6H, m), 3.2 (2H, t), 2.4 (2H, t), 1.6 (4H, m); ³¹P NMR (101 MHz, CDCl₃) 0.45 ppm (all three phosphates appear as a single broad resonance).

4-*O*-(5-Aminopentanoyl)-*myo*-inositol 1,2,6-Trisphosphate (16). Benzylated precursor **15** was dissolved in 25 mL of 95% ethanol and hydrogenated over 100 mg of 10% Pd-C catalyst at 45 psi overnight. The catalyst was removed by filtration through Celite, washed (95% ethanol, 2:1 ethanol/water, 30 mL of water), adjusted to pH 9.0 with concentrated NH₄OH, and concentrated *in vacuo*. The residue was dissolved in 3 mL of water and passed through an ion exchange column (Na⁺ form, Bio-Rad Chelex 100 resin). Elution with 25 mL of water and concentration *in vacuo* gave 24 mg (75%) of ester **16** as a colorless glass: ¹H NMR (250 MHz, D₂O) δ 4.2–3.8 (6H, m), 3.2 (2H, t), 2.4 (2H, t), 1.5 (4H, m); FAB-MS calcd C₁₁H₁₈NNa₆O₁₆P₃ 650.92, found 651.0; MALDI-TOF 671.08 (M⁺ – 3H + Na). Anal. Calcd C, 20.28; H, 2.77. Found: C, 20.32; H, 2.77.

4-*O*-[5-(*p*-Benzoyldihydrocinnamoyl)aminopentanoyl]-*myo*-inositol 1,2,6-Trisphosphate (3a). To a solution of the *p*-benzoyldihydrocinnamoyl *N*-hydroxysuccinimido ester (BZDC-NHS) in DMF was added the aminopentanoyl αT (**16**) in 0.25 M TEAB. A white suspension formed during the addition but then dissolved, and the solution was stirred overnight. The clear and homogeneous solution was concentrated *in vacuo* and evaporated three times with methanol. The resulting white solid was suspended in 0.2 mL of water and concentrated *in vacuo*. The solid was dissolved in 0.1 mL of water and applied to a column of DEAE-cellulose (HCO₃[−] form). The column was washed with 2 mL of water, 1 mL of 0.2 M TEAB, 1 mL of 0.3 M TEAB, 1 mL of 0.4 M TEAB, and 1 mL of 0.6 M TEAB. The fractions were chromatographed on a TLC plate using 4:1:1 butanol/acetic acid/water as eluant. The samples were analyzed on HPLC (RP-HPLC with a C₈ Brownlee RP-300 column, 250 mm × 4.6 mm, with 15% acetonitrile in

0.05 M KH₂PO₄ buffer at pH 4.5): ¹H NMR (250 MHz, D₂O) δ 7.7–7.4 (9H, m), 4.2–3.8 (6H, m), 3.2–2.7 (6H, m), 2.4 (2H, t), 1.6 (4H, m).

4-*O*-[*N*-(*p*-Benzoyl[³H]dihydrocinnamoyl)-5-aminopentanoyl]-*myo*-inositol 1,2,6-Trisphosphate (3b). Two stock solutions were prepared: (i) 2 mCi/mL [³H]-BZDC-NHS in ethyl acetate and (ii) 0.25 mg/mL 4-*O*-(5-aminopentanoyl)-*myo*-inositol 1,2,6-trisphosphate in 0.25 M TEAB buffer. A 0.5 mL (1 mCi) aliquot of [³H]BZDC-NHS ester stock was carefully evaporated under a stream of nitrogen, redissolved in 50 μL of DMF, and added to a stirred solution of aminopentanoate **16**. The reaction mixture was stirred for 48 h at rt in the dark and concentrated *in vacuo*, and the residue was taken up in 500 μL of water and reconstituted, redissolved in 500 μL of water, applied to a pipet column (4 × 0.5 cm; DEAE-cellulose HCO₃[−] form), and washed successively with water (1 mL), 0.1 M TEAB (1 mL), 0.2 M TEAB (2 mL), 0.3 M TEAB (2 mL), 0.4 M TEAB (2 mL), 0.5 M TEAB (2 mL), 0.6 M TEAB (2 mL), and 0.8 M TEAB (2 mL). The highest activity (cpm) fractions (0.3–0.5 M TEAB) were analyzed by HPLC (Aquapore RP C₈, 250 × 4.6 mm, isocratic elution with 15% acetonitrile in 0.05 M KH₂PO₄ buffer, pH 4.4, with monitoring at 280 nm and with a radiochemical detector). The net radiochemical yield was approximately 12% (specific activity = 42.5 Ci/mmol, *t_R* = 10 min).

Biochemical Experiments. Protein Preparation. Umbilical cords were thawed on ice, washed in incubation buffer (0.14 M NaCl, 1 mM KH₂PO₄, 11 mM glucose), and blood was squeezed out. The cords were cut into small pieces and dissected to remove the Wharton's jelly portion. Next, 7 g of the vasculature was homogenized with Polytron in 15 mL of prep buffer (250 mM Tris, pH 7.7, 1 mg of leupeptin, 1 mg of apoprotinin, 3 mg of pepstatin, 3 mg of collagenase). The suspension was centrifuged at 2000*g* (SS-34 rotor) for 15 min and the pellet discarded. The resultant supernatant was centrifuged at 100000*g* (37 000 rpm, rotor type 60 Ti) for 1.5 h. The pellet was washed three times by resuspension in prep buffer and centrifuged at 100000*g* (37 000 rpm, rotor type 60 Ti) for 15 min each. The extensively washed pellet was suspended in 3 volumes of prep buffer with 1% CHAPS and incubated on ice for 1 h. The suspension was centrifuged at 100000*g* for 30 min, and the pellet was discarded. Protein concentration was determined by dye binding prior to photoaffinity labeling and protein separation by SDS-PAGE.

Photoaffinity Labeling. Protein samples (20 μg) were incubated on ice with 0.5 μCi (0.25 μM) of 4-[³H]BZDC-αT (**3b**) in the presence (1000-fold excess) or absence of competing ligand for 10 min. The samples were then photolyzed at 360 nm (1900 μW/cm²) for 45 min at 4 °C. Proteins were precipitated with 10% cold trichloroacetic acid and centrifuged (14000*g*, 15 min), the pellet was washed with 100 μL of cold acetone, and 5 × sample buffer was added. The sample was boiled for 5 min, and proteins were separated by SDS-12.5% PAGE. The gel was Coomassie blue stained, destained, incubated in EN³-HANCE for 1 h, miniaturized with 50% PEG, dried, and exposed to XAR-5 X-ray film for 14 days at −80 °C (15).

RESULTS AND DISCUSSION

Photoaffinity Analogues of α-Trinositol. Benzophenone-containing photoaffinity analogues (**16**) have been prepared for Ins(1,4,5)P₃, Ins(1,2,4,5)P₄, Ins(1,3,4,5)-P₄, Ins(1,2,3,4,5,6)P₆, PtdIns(4,5)P₂, and PtdIns(3,4,5)P₃ by preparing an ω-aminoalkyl ester of one of the phosphates (17–22), followed by amidation using [³H]BZDC-NHS ester (13). Thus, we initially prepared [³H]BZDC-

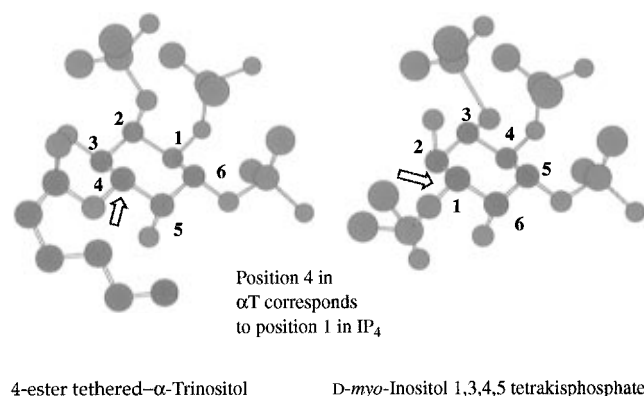


Figure 2. Comparison of energy-minimized structures of 4-ester-tethered α T and Ins(1,3,4,5) P_4 . Superposition of structures of α T and Ins(1,3,4,5) P_4 suggests that the 4-position of α T could be modified without loss of biological activity.

P-5-(*O*-aminopropyl) Ins(1,2,5,6) P_4 (**2**), a phosphate-tethered analogue of **1** (**23**) (Figure 1), to identify molecular targets for α T. However, only nonspecific photolabeling (i.e., no competition by α T using a 2000-fold molar excess) was observed using either soluble or membrane protein preparations from rat heart, rat brain, pig aorta, and human vascular smooth muscle cells (A. Chaudhary, H. Yoo, and G. D. Prestwich, unpublished results). Moreover, unlabeled BZDC-P-5 Ins(1,2,5,6) P_4 (**2**) failed to displace [3 H] α T in rat heart or pig aorta binding assays (**24**) or in autoradiographic studies in human umbilical vasculature (**14**) (A. Chaudhary, H. Yoo, and D. A. Walsh, unpublished results).

High-affinity [3 H] α T binding can be readily displaced from rat heart membranes by Ins(1,2,5,6) P_4 and by Ins(1,3,4,5) P_4 , but not by Ins(1,4,5) P_3 (**24**). Thus, in analogy to the mimicry of Ins(1,4,5) P_3 by Ins(1,2,4,5) P_4 (**25**), we noted that α T and Ins(1,3,4,5) P_4 could be partially superimposed (**23**). The structures were minimized in SYBYL using a TRIPOS force field with manual parametrization of the pentavalent phosphorus atoms. Figure 2 shows 3D structures for the modified α T and Ins(1,3,4,5) P_4 , suggesting that the axial P-2 phosphate of the α T is not superimposable with the equatorial P-5 phosphate in Ins(1,3,4,5) P_4 . However, on the basis of this model, the 4-hydroxyl position of α T appeared to be suitable for introduction of a tethered photoaffinity label. This proposal was further strengthened by the observation that the 2,3,4-trihexanoate and tridecanoate esters were physiologically active (**3**).

Synthesis. The synthesis of enantiomerically pure 4-tethered α T (**3**) was accomplished via the Ferrier rearrangement (**26**, **27**), which allows the conversion of carbohydrates into cyclitols via a ring opening–ring closure process. Indeed, this method mimics the biosynthesis of inositol monophosphate from D-glucose 6-phosphate. We have now applied the Ferrier route (**28**) to the synthesis of a comprehensive series of inositol polyphosphate and phosphoinositide polyphosphate affinity reagents (**29**). For the synthesis of the desired 4-tethered α T derivative **3**, the 4-position of glucose must be protected uniquely relative to the other hydroxyl groups.

The synthesis is shown in Figure 3. Selective 3-benzoylation of methyl 4,6-*O*-benzylidene- α -D-glucopyranoside (**4**) under phase transfer conditions gave **5**, and protection of the 4-OH gave *p*-methoxybenzyl (PMB) ether **6** (**22**). Regioselective reductive cleavage of the benzylidene acetal with DIBAL in CH_2Cl_2 at $-30^\circ C$ gave primary alcohol **7**. Swern oxidation of **7** to aldehyde **8**, followed by formation of the *Z*-enol acetate **9** and Ferrier rearrangement using mercuric acetate and aqueous sodium

chloride, yielded the inosose skeleton **10** possessing the desired C-2 axial stereochemistry. Stereoselective reduction of the β -hydroxy ketone with sodium triacetoxyborohydride gave **11**, and hydrolysis provided the 1,2,6-triol **12**. Phosphitylation/oxidation of the triol gave protected trisphosphate **13**. Oxidative cleavage of the PMB group gave alcohol **14**, which was acylated with 4-*N*-Cbz-aminopentanoic acid to give the fully protected precursor **15**. Hydrogenation at 45 psi quantitatively removed all benzyl groups to give the 4-ester α T **16**, which was purified and converted into the Na^+ form by passage through Chelex (Na^+ form). The primary amine was amidated with [3 H]BZDC-NHS ester in 1.25 M TEAB/DMF to give tritiated probe **3b** (specific activity = 42.5 Ci/mmol as determined by the activity of the [3 H]BZDC-NHS ester employed); unlabeled BZDC- α T (**3a**) was also prepared. Photoaffinity analogues **3b** and **3a** were purified on DEAE cellulose (HCO_3^- form) and analyzed by HPLC.

Photoaffinity Labeling. Thin-section autoradiographic studies (**14**) had shown specific high-affinity binding for [3 H] α T localized to specific areas of human umbilical cord vascular smooth muscle tissue. Thus, fresh human umbilical cords were obtained, and membranes were prepared from dissected vascular tissue. The membrane pellet was solubilized with 1% CHAPS and photoaffinity labeled with 4-[3 H]BZDC- α T (**3b**). To determine the specificity of binding, 0.25 mM α T or 0.25 mM Ins(1,3,4,5) P_4 was included in the solution. Samples were incubated on ice for 10 min and irradiated (45 min at 360 nm), and proteins were separated by denaturing electrophoresis (SDS–PAGE). The gels were impregnated with a fluor to enhance tritium detection, dried, and exposed to X-ray film at $-80^\circ C$. Despite the number and abundance of proteins visible by Coomassie blue staining (Figure 4A), only very few proteins were covalently modified by **3b** (Figure 4B). Indeed, the fluorogram shows selective labeling of CHAPS-solubilized human vascular cell membrane proteins at 55 and 43 kDa; a 1000-fold excess of either α T or Ins(1,3,4,5) P_4 competitively displaced the labeling of these bands. In addition, a third band that shows specific displacement by Ins(1,3,4,5) P_4 is evident at 40 kDa. No competition for any of these proteins was observed when 1000-fold excesses of Ins(1,4,5) P_3 or adenophostin A [an Ins(1,4,5)- P_3 hyperagonist] (**30**) or Ins P_6 were used as competing ligands (data not shown). In addition, as with earlier photoprobe **2**, the new probe **3b** failed to exhibit any specific labeling of proteins from rat heart membranes; that is, no competitive displacement of photolabeling was observed with either excess α T or Ins(1,3,4,5) P_4 .

Potential molecular targets in platelet membranes were also investigated. Thus, platelet membranes were incubated and photoaffinity labeled following the same protocols used for the umbilical cord vascular membranes. Figure 5A shows that despite a high protein loading as seen by Coomassie blue staining of the gel, only very few proteins were covalently modified by the α T analogue **3b** (Figure 5B). In platelet membranes, a tritium-labeled protein band at 55 kDa shows unambiguous competitive displacement by a 1000-fold excess of α T, but much weaker displacement by Ins(1,3,4,5) P_4 .

The selective labeling of signaling proteins by BZDC derivatives of inositol polyphosphates and polyphosphoinositides has now been observed in many crude preparations. This selectivity can be attributed to the high efficiency of the benzophenone photophore for modification of hydrophobic regions of proteins and the lack of nonspecific interception of the reactive ketyl/diradicaloid by solvent or protein nucleophilic groups (**14**, **20**). The

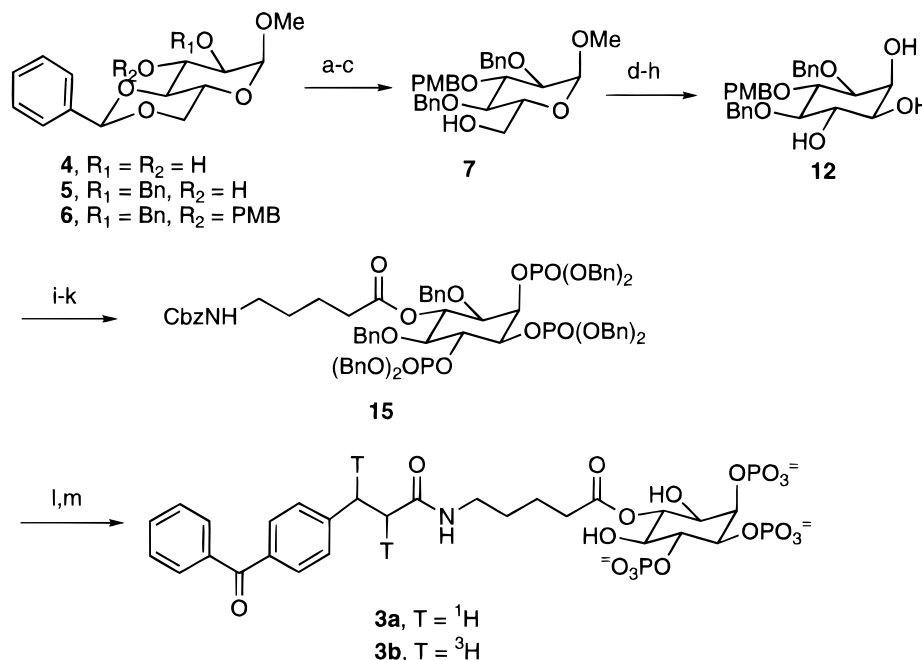


Figure 3. Synthesis of 4-acyl-BZDC- α T (**3a** and **3b**). Reagents and conditions: (a) Bu_4NHSO_4 , $BnBr$, CH_2Cl_2 , aqueous $NaOH$, 48 h, 50%; (b) $PMB-Cl$, NaH , DMF , $45^\circ C$, 90%; (c) $DIBAL$, CH_2Cl_2 , $-30^\circ C$, 30 min, 55%; (d) $(COCl)_2$, $DMSO$, Et_3N , CH_2Cl_2 , $-78^\circ C$, 25 min, 98%; (e) Ac_2O , anhydrous K_2CO_3 , $MeCN$, $80^\circ C$, 8 h, 70%; (f) $Hg(OAc)_2$, Me_2CO/H_2O (3:2), $NaCl$, rt, 22 h, 55%; (g) $NaBH-(OAc)_3$, $AcOH$, 40 min, rt, 62%; (h) 0.35 M $NaOH$ in $MeOH$, $80^\circ C$, 90 min, 79%; (i) $(BnO)_2PN/Pr_2$, tetrazole, CH_2Cl_2 , rt, 5 h, and then $mCPBA$, $-40^\circ C$, 0.5 h, 62%; (j) $(NH_4)_2Ce(NO_3)_6$, $MeCN/H_2O$ (9:1), rt, 40 min, 75%; (k) $CbzNH(CH_2)_4COOH$, DCC , $DMAP$, rt, overnight, 55%; (l) 10% $Pd-C$ in 95% $EtOH$, H_2 gas, 45 psi, overnight, and then Chelex resin (Na^+ form); (m) T-BZDC-NHS ester, 1.25 M $TEAB$, DMF , 24 h, and then DEAE-cellulose (HCO_3^- form).

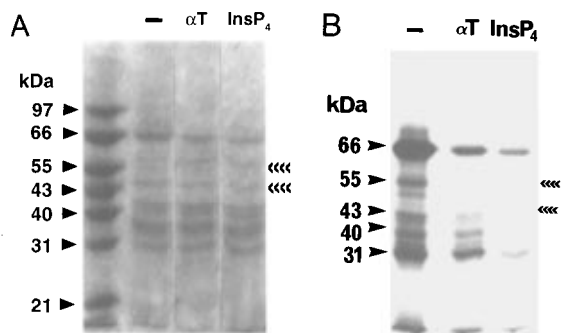


Figure 4. Photoaffinity labeling of CHAPS-solubilized human umbilical cord membrane proteins with probe **3b**: (A) 12.5% SDS-PAGE gel stained with Coomassie blue (arrows indicate positions of labeled proteins); (B) corresponding fluorogram of **3b** labeled proteins. The fluorogram shows αT - and $Ins(1,3,4,5)P_4$ -displaceable bands at 55 and 43 kDa. A third band at 40 kDa shows competition only with excess $Ins(1,3,4,5)P_4$. Other proteins show evidence of nonspecific labeling. The proteins were labeled (45 min, $4^\circ C$, 360 nm) with $0.5 \mu Ci$ ($0.25 \mu M$) of **3b** in the absence (-) or presence of $0.25 mM$ αT or $0.25 mM$ $Ins(1,3,4,5)P_4$ as competing ligands.

selective labeling occurs at 40–80% efficiency as seen recently for the rat cerebellar inositol trisphosphate receptor (18), rat clathrin assembly protein, AP-2 (31, 32), rat brain phosphoinositide (3–5) trisphosphate receptor, centaurin- α (21), and C2B domain of synaptotagmin II (33).

In summary, we report the asymmetric total synthesis of a novel photoaffinity analogue of α -trinositol and demonstrate its application in identifying putative target proteins having molecular masses of 55, 43, and 40 kDa in the membranes of vascular smooth muscle cells from human umbilical cords. The presence of selectively labeled 55 kDa protein in human platelets further implicates this protein as a potential molecular target for this drug. The photoaffinity probe **3b** labels relatively few proteins, and the selective, drug-compatible binding

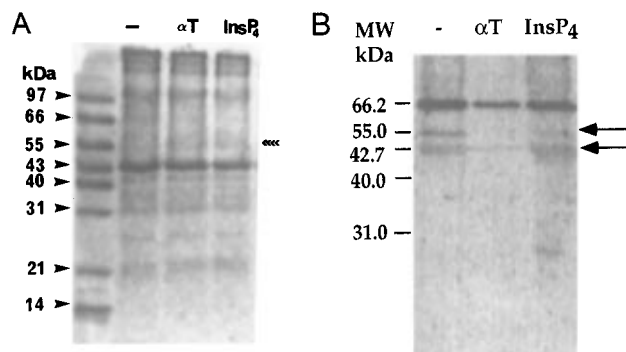


Figure 5. Photoaffinity labeling of detergent-solubilized human platelet membrane pellet with **3b**: (A) 12.5% SDS-PAGE gel stained with Coomassie blue (arrow indicates labeled protein); (B) corresponding fluorogram of labeled proteins. A protein at 55 kDa labeled by probe **3b** shows clear displacement of labeling by 1000-fold excess αT and weaker displacement by $Ins(1,3,4,5)P_4$. Other bands exhibit nonspecific labeling. The proteins were labeled (45 min, $4^\circ C$, 360 nm) with $0.5 \mu Ci$ ($0.25 \mu M$) of **3b** in the absence (-) or presence of $0.25 mM$ αT or $0.25 mM$ $Ins(1,3,4,5)P_4$ as competing ligands.

for these proteins is highly suggestive of a role in the mechanism of action for this drug. Thus, this paper exemplifies the utility of the photoaffinity labeling technique in identifying unknown target proteins for new drugs, a first step in determining the biochemical basis for their physiological activities.

ACKNOWLEDGMENT

We thank Perstorp Pharma and the NIH (NS 29632) for financial support, Dr. D. A. Walsh (London Hospital Medical College) and Dr. H. Yoo (Perstorp) for sharing unpublished results, and Drs. J. D. Olszewski (Stony Brook) and D. G. Ahern of NEN Life Science Products (Boston, MA) for providing [3H]BZDC-NHS ester. We are grateful to Mr. J. T. Elliott (Stony Brook) for providing the platelet membranes.

LITERATURE CITED

- (1) Berridge, M. J. (1994) The biology and medicine of calcium signalling. *Mol. Cell. Endocrinol.* **98**, 119–124.
- (2) Furuichi, T., and Mikoshiba, K. (1995) Inositol 1,4,5-trisphosphate receptor-mediated Ca^{2+} signaling in the brain. *J. Neurochem.* **64**, 953–960.
- (3) Blum, C., Karlsson, S., Schlewer, G., Spiess, B., and Rehnberg, N. (1995) Synthesis of optically active (+)-D-3,4,5-tri-*O*-phenylcarbamoyl myo-inositol from phytic acid. *Tetrahedron Lett.* **36**, 7239–7242.
- (4) Woie, K., and Reed, R. K. (1994) Neurogenic inflammation and lowering of interstitial fluid pressure in rat trachea is inhibited by α -trinositol. *Am. J. Respir. Crit. Care Med.* **150**, 924–928.
- (5) Nakazawa, H., Gustafsson, T. O., Traber, L. D., Herndon, D. N., and Traber, D. L. (1994) α -Trinositol decreases lung edema formation after smoke inhalation in an ovine model. *J. Appl. Physiol.* **76**, 278–282.
- (6) Wahlestedt, C., Reis, D. J., Yoo, H., Adamsson, M., Andersson, D., and Edvinsson, L. (1992) A novel inositol phosphate selectively inhibits vasoconstriction evoked by the sympathetic co-transmitters neuropeptide Y (NPY) and adenosine triphosphate (ATP). *Neurosci. Lett.* **143**, 123–126.
- (7) Siren, M., Linne, L., and Persson, L. (1991) Pharmacological effects of D-myo-inositol 1,2,6-trisphosphate. In *Inositol Phosphates and Derivatives* (A. B. Reitz, Ed.) Vol. 463, pp 103–110, American Chemical Society, Washington, DC.
- (8) Sun, X. Y., Edvinsson, L., Yoo, H., Wahlestedt, C., and Hedner, T. (1995) Effects of some novel D-myo-inositol-phosphate derivatives on binding and sympathetic transmission. *J. Cardiovasc. Pharmacol.* **25**, 696–704.
- (9) Sun, X. Y., You, J. P., Hedner, T., Erlinge, D., Fellstrom, B., Yoo, H. Y., Wahlestedt, C., and Edvinsson, L. (1996) α -Trinositol: a functional (non-receptor) neuropeptide Y antagonist in vasculature. *J. Pharm. Pharmacol.* **48**, 77–84.
- (10) Xu, X. J., and Wiesenfeld-Hallin, Z. (1995) Intrathecal α -trinositol facilitates the flexor reflex but does not block the depressive effect of NPY. *Eur. J. Pharmacol.* **272**, 219–222.
- (11) Brailoiu, E., Baltatu, O., Costuleanu, M., Slatineanu, S., Filipeanu, C. M., and Brtanisteanu, D. D. (1995) Effects of α -trinositol administered extra- and intra-cellularly (using liposomes) on rat aorta rings. *Eur. J. Pharmacol.* **281**, 209–212.
- (12) Rodt, S. A., Reed, R. K., Ljungstrom, M., Gustafsson, T. O., and Rubin, K. (1994) The anti-inflammatory agent α -trinositol exerts its edema-preventing effects through modulation of beta-1 integrin function. *Circ. Res.* **75**, 942–948.
- (13) Olszewski, J. D., Dormán, G., Elliott, J. T., Hong, Y., Ahern, D. G., and Prestwich, G. D. (1995) Tethered benzophenone reagents for the synthesis of photoactivatable ligands. *Bioconjugate Chem.* **6**, 395–400.
- (14) Walsh, D. A., Mapp, P. I., Polak, J. M., and Blake, D. R. (1995) Autoradiographic localization and characterization of [^3H]- α -trinositol binding sites in human and mammalian tissues. *J. Pharmacol. Exp. Ther.* **273**, 461–469.
- (15) Mohamed, M. A., Lerro, K. A., and Prestwich, G. D. (1989) Polyacrylamide gel miniaturization improves protein visualization and autoradiographic detection. *Anal. Biochem.* **177**, 287–290.
- (16) Dormán, G., and Prestwich, G. D. (1994) Benzophenone photophores in biochemistry. *Biochemistry* **33**, 5661–5673.
- (17) Chen, J., Dormán, G., and Prestwich, G. D. (1996) Asymmetric total synthesis of D-myo-inositol 1,2,4,5-tetrakisphosphate and its P-2-(*O*-aminopropyl) derivative. *J. Org. Chem.* **61**, 393–397.
- (18) Mourey, R. J., Estevez, V. A., Marecek, J. F., Barrow, R. K., Prestwich, G. D., and Snyder, S. H. (1993) Inositol 1,4,5-trisphosphate receptors: mapping the inositol 1,4,5-trisphosphate binding site with photoaffinity ligands. *Biochemistry* **32**, 1719–1726.
- (19) Prestwich, G. D., Marecek, J. F., Mourey, R. J., Theibert, A. B., Ferris, C. D., Danoff, S. K., and Snyder, S. H. (1991) Tethered IP_3 . Synthesis and biochemical applications of the 1-*O*-(3-Aminopropyl) ester of inositol (1,4,5) trisphosphate. *J. Am. Chem. Soc.* **113**, 1822–1825.
- (20) Prestwich, G. D., Dormán, G., Elliott, J. T., Marecak, D. M., and Chaudhary, A. (1997) Benzophenone photoprobes for phosphoinositides, peptides, and drugs. *Photochem. Photobiol.* **65**, 222–234.
- (21) Hammonds-Odie, L. P., Jackson, T. R., Profit, A. A., Blader, I. J., Turck, C., Prestwich, G. D., and Theibert, A. B. (1996) Identification and cloning of centaurin: A novel phosphatidylinositol 3,4,5-trisphosphate binding protein from rat brain. *J. Biol. Chem.* **271**, 18859–18868.
- (22) Dormán, G., Chen, J., and Prestwich, G. D. (1995) Synthesis of D-myo-P-1-(*O*-aminopropyl)-inositol-1,4,5-trisphosphate affinity probes from α -D-glucose. *Tetrahedron Lett.* **36**, 8719–8722.
- (23) Chaudhary, A., Dormán, G., and Prestwich, G. D. (1994) Synthesis of P-5 tethered inositol-1,2,6-trisphosphate, an affinity reagent for α -trinositol receptors. *Tetrahedron Lett.* **35**, 7521–7524.
- (24) Yoo, H., Fallgren, B., Lindahl, A., and Wahlestedt, C. (1994) Characterization of specific binding sites for α -trinositol in rat tissues. *Eur. J. Pharmacol.* **268**, 55–63.
- (25) Ozaki, S., Kondo, Y., Siotani, N., Ogasawara, T., and Watanabe, Y. (1992) Synthesis and some properties of D-myo-inositol 1,4,5-tris(dihydrogen-phosphate). *J. Chem. Soc., Perkin Trans. 1*, 729–737.
- (26) Ferrier, R. J. (1979) Unsaturated carbohydrates: A carbocyclic ring closure of hex-5-enopyranoside derivative. *J. Chem. Soc., Perkin Trans. 1*, 1455–1458.
- (27) Ferrier, R. J., and Middleton, S. (1993) The conversion of carbohydrate derivatives into functionalized cyclohexanes and cyclopentanes. *Chem. Rev.* **93**, 2779–2831.
- (28) Estevez, V. A., and Prestwich, G. D. (1991) Synthesis of chiral, P-1 tethered inositol tetrakisphosphate affinity labels via a Ferrier rearrangement. *J. Am. Chem. Soc.* **113**, 9885–9887.
- (29) Prestwich, G. D. (1996) Touching all the bases: Synthesis of inositol polyphosphate and phosphoinositide affinity probes from glucose. *Acc. Chem. Res.* **29**, 503–513.
- (30) Chaudhary, A., and Prestwich, G. D. (1994) Adenophostins: Newly discovered metabolites of *Penicillium brevicompactum* as potent agonists of the inositol 1,4,5-trisphosphate receptor. *Chemtracts: Org. Chem.* **7**, 111–114.
- (31) Theibert, A. B., Estevez, V. A., Mourey, R. J., Marecek, J. F., Barrow, R. K., Prestwich, G. D., and Snyder, S. H. (1992) Photoaffinity labeling and characterization of isolated inositol 1,3,4,5-tetrakisphosphate- and inositol hexakisphosphate-binding proteins. *J. Biol. Chem.* **267**, 9071–9079.
- (32) Voglmaier, S. M., Keen, J. H., Murphy, J., Ferris, C. D., Prestwich, G. D., Snyder, S. H., and Theibert, A. B. (1992) Inositol hexakisphosphate receptor identified as the clathrin assembly protein AP-2. *Biochem. Biophys. Res. Commun.* **187**, 158–163.
- (33) Mehrotra, B., Elliott, J. T., Chen, J., Olszewski, J. D., Profit, A. A., Chaudhary, A., Fukuda, M., Mikoshiba, K., and Prestwich, G. D. (1997) Selective photoaffinity labeling of the inositol polyphosphate binding C2B domains of synaptotagmins. *J. Biol. Chem.* **272**, 4237–4244.

BC9700446

Synthesis and *in Vitro* Degradation of New Polyvalent Hydrazide Cross-Linked Hydrogels of Hyaluronic Acid

Koen P. Vercruysse,^{†,‡} Dale M. Marecak,^{†,‡} James F. Marecek,[‡] and Glenn D. Prestwich^{*,†,‡}

Department of Medicinal Chemistry, Room 201, The University of Utah, 30 South, 2000 East, Salt Lake City, Utah 84112-5820, and Department of Chemistry, The University at Stony Brook, Stony Brook, New York 11794-3400. Received June 5, 1997[®]

New polyvalent hydrazide cross-linkers were synthesized, characterized, and used to prepare hydrazide cross-linked hydrogels derived from hyaluronic acid (HA). First, the chemical synthesis and characterization of the di-, tri-, tetra-, penta-, and hexahydrazides are presented. Second, HA concentration, buffer type and concentration, and ratio of HA to carbodiimide to cross-linker were varied to obtain HA-hydrogels with different chemical and physical properties. Third, two new assays are described to monitor the stability of HA-hydrogels toward hyaluronidase (Hase) and other media. These assays were used to evaluate the stability of cross-linked HA-hydrogels to Hase solutions and different pH values. Hydrophobic cross-linkers gave the most stable gels, and the susceptibility of the gels to Hase was independent of cross-linker concentration. Hase does not significantly penetrate the HA-hydrogels and acts primarily at the gel–solution interface. The HA-hydrogels are stable in acid environments and dissolve gradually above pH 7.0.

INTRODUCTION

Hyaluronic acid (Figure 1) is a naturally occurring linear polysaccharide that is abundant in the vitreous and in synovial fluid and plays pivotal roles in wound healing, cell differentiation, and cell motility. In addition, aberrant HA¹ receptors are involved in cancer metastasis (1, 2). A component of the extracellular matrix, it is a fully biocompatible candidate for modification with drugs and other effector molecules. The use of biocompatible polymers in the treatment of various ailments has expanded rapidly in the past two decades (3). Moreover, derivatization of such polymers with reporter groups (4) and drugs (5, 6) has emerged as a powerful method for controlling delivery and release of these various compounds. Small drug molecules can be linked to the polymer by a method that allows controlled release of the free bioactive group. Highly water-soluble polymers are of added benefit in helping increase the amount of a hydrophobic drug that can be effectively delivered into a living system. The general features of these systems must therefore include complete biocompatibility, water solubility, ability to be chemically modified to allow high substrate loading with a designed release profile, and an economical, scalable process chemistry.

Hydrogels have many unique properties and advantages for the development of novel controlled drug delivery systems (7). HA and its derivatives have been used as drug delivery systems with a wide variety of drugs (8, 9). To extend the utility of HA hydrazide derivatives (10–12) to include hydrogels with selected physical properties, we required a selection of polyfunc-

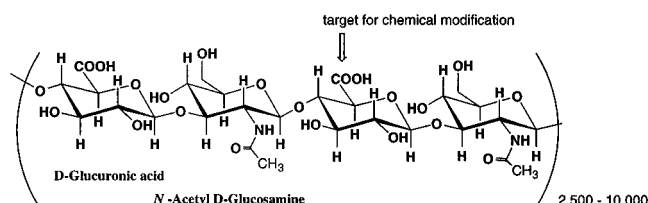


Figure 1. Structure of native hyaluronic acid.

tional cross-linking agents (13, 14). Herein we describe the synthesis and applications of hydrazide-containing cross-linkers in which the length, hydrophilicity, and number of functional groups have been varied. We also describe the effects of varying pH, buffer type, HA concentration, and cross-linker/carbodiimide/HA ratios to obtain hydrogels with desired physicochemical properties.

In vivo, enzymes play a major role in the biodegradation process of biomaterials. Even the most inert polymers can undergo some degradation under physiological conditions (7). *In vivo*, HA is degraded by Hase, which is ubiquitous in cells and in serum (15, 16). *In vitro*, the biodegradation of hydrogels has been studied by monitoring the release of microspheres from a matrix (17), by monitoring the release of radiolabeled compounds (18, 19), by monitoring the loss of weight or swelling properties (20, 21), or by visual inspection (22–25). In this paper, we also describe the biodegradation of new cross-linked HA-hydrogels. Two new methods for monitoring the degradation of the HA-hydrogels by Hase were developed and used to examine the effect of the chemical composition of the gels upon their degradation.

MATERIALS AND METHODS

General. Fermentation-derived hyaluronan (HA, sodium salt) was provided by Clear Solutions Biotechnology, Inc. (Stony Brook, NY). 1-Ethyl-3-[3-(dimethylamino)propyl]carbodiimide (EDC), succinic dihydrazide, fastgreen FCF, and carboxylic acids and esters for the hydrazide syntheses (used without purification) were purchased from Aldrich Chemical Co. (Milwaukee, WI). Bovine testicular hyaluronidase (Hase; 880–1000 units/mg) and bis-tris hydrochloride were obtained from Sigma Chemi-

* Author to whom correspondence should be addressed [telephone (801) 585-9051; fax (801) 585-9053; e-mail gprestwich@deans.pharm.utah.edu].

[†] The University at Stony Brook

[‡] The University of Utah.

[®] Abstract published in *Advance ACS Abstracts*, August 15, 1997.

¹ Abbreviations: EDC, 1-ethyl-3-[3-(dimethylamino)propyl]carbodiimide; CAS-RN, Chemistry Abstracts Service Registry Number; HA, hyaluronic acid; Hase, hyaluronidase; PEG, poly(ethylene glycol); XL, cross-linker.

cal Co. (St. Louis, MO). Coomassie Brilliant blue R250 was obtained from Fisher Scientific Co. (Santa Clara, CA). Adipic dihydrazide was obtained from Eastman Kodak Co. (Rochester, NY). Suberic and terephthalic dihydrazide were obtained from Lancaster Synthesis, Inc. (Windham, NH). Methyl acrylate, ethylenediamine, and 1,4-butanedi-amine were purified by distillation under nitrogen. Other amines were used as received. The $\text{H}_2\text{N}-(\text{CH}_2\text{CH}_2\text{O})_n-\text{CH}_2\text{CH}_2\text{NH}_2$ was purchased from Shearwater Polymers, Inc. (Huntsville, AL) and had a nominal molecular weight of 3400. All other chemicals used were of analytical grade.

Analytical Instrumentation. ^1H -NMR spectra were obtained on either a Bruker AC-250 or a GE QE-300 spectrometer at 250 or 300 MHz, respectively. ^{13}C -NMR spectra were measured using a Bruker AM-300 spectrometer at 75 MHz. IR spectra were recorded using a Mattson Galaxy Model 3000 FTIR spectrometer.

General Procedure for the Preparation of Hydrazides. Free carboxylic acid (5 g) was dissolved in dry alcohol (methanol or ethanol) (50 mL) containing 1–3 drops of concentrated H_2SO_4 , refluxed under nitrogen for 1 h, concentrated under reduced pressure to <20 mL volume, and transferred to a separatory funnel using 60 mL of EtOAc or Et_2O . The organic layer was washed (2×30 mL H_2O) and concentrated *in vacuo* to yield the crude oily ester, which was used without further purification.

A solution of the ester (5 g) in 15 mL of alcohol was added dropwise into a stirred solution of 4–8 equiv of hydrazine hydrate per ester group in 10 mL of alcohol. The stirred reaction was warmed and reacted until the ester was fully consumed, as determined by TLC. Hydrazide products were precipitated either by cooling of the reaction mixture or by cooling combined with the addition of 10–20 mL of hexanes. The filtered and washed crystals were dried under vacuum (0.1 Torr, 24–48 h, 20–30 °C) to remove excess hydrazine hydrate.

For 3-mercaptopropionic hydrazide, the commercially available methyl ester was converted as described above with strict exclusion of oxygen from the system. The oily product obtained by concentration *in vacuo* was recrystallized at low temperature.

3,3'-Dithiobis(propionic dihydrazide) (6): 84%, two steps; CAS-RN 50906-77-9;² ^1H NMR (D_2O) δ 4.70 (br s, 5H, HOD, NH_2), 2.90 [t, 2H, $\text{CH}_2\text{C}(\text{O})$], 2.58 (t, 2H, SCH_2); mp 125–126 °C; FAB-MS ($\text{M} + \text{H}^+$) 239.

3,3'-Thiodipropionic Dihydrazide (7): 38%, two steps; CAS-RN 6292-68-8; ^1H NMR (D_2O) δ 4.70 (br s, 4H, with HOD, NH_2), 2.69 [t, 2H, $\text{CH}_2\text{C}(\text{O})$], 2.38 (t, 2H, SCH_2); mp 151–152 °C; FAB-MS ($\text{M} + \text{H}^+$) 207.

3-Mercaptopropionic Hydrazide (8): 100%; CAS-RN 689-02-1; ^1H NMR (CDCl_3 , 300 MHz) δ 7.88 (br s, 1H, NH), 3.2 (br s, 2H, NH_2 and SH), 2.72 [t, 2H, $\text{CH}_2\text{C}(\text{O})$], 2.40 (t, 2H, SCH_2); ^{13}C NMR (CDCl_3) δ 173, 38, 21; mp 0–5 °C; FAB-MS ($\text{M} + \text{H}^+$) 121.

Tartaric Dihydrazide [2,3-Dihydroxybutanedioic Dihydrazide] (9): prepared from the commercially available ethyl ester (100%); mp 183–188 °C [lit. mp 183 °C (26)]; CAS-RN 54789-92-3.

Trimesic Trihydrazide [1,3,5-Benzene(tricarboxylic trihydrazide)] (10): 38%, two steps; ^1H NMR ($\text{DMSO}-d_6$) δ 9.7 (s, 1H, NH), 8.2 (s, 1H, Ph), 4.5 (br s, 2H, NH_2); mp >265 °C; EI-MS (M^+) 252; CAS-RN 36997-31-6.

Tri(methyl propanoate)amine [β -Alanine, *N,N*-Bis(3-methoxy-3-oxopropyl)-methyl ester] (11): CAS-RN 3330-09-4. This ester was prepared in the same manner as

the first stage of the starburst dendrimer synthesis as described by Tomalia (27, 28).

General Procedure for the Preparation of the Tetramethyl α,ω -Alkyldiaminotetrapropanoates. Methyl acrylate (12.9 g, 150 mmol, 13.5 mL) was dissolved in 30 mL of methanol and cooled (4 °C) under nitrogen. The diamine (30 mmol), dissolved in 5–20 mL of methanol depending on its solubility, was added dropwise over 5 min to the stirred acrylate solution. The ice was allowed to melt, and the solution was stirred at room temperature overnight. The solvent and excess methyl acrylate were evaporated under reduced pressure, and the oil remaining was stirred *in vacuo* for a few hours to remove any residual volatiles. The crude colorless oily products were isolated in essentially quantitative yield and used without further purification for conversion to the hydrazide (26, 29).

Tetramethyl 1,2-Ethanediyldiamino-*N,N,N,N*-tetrapropanoate (12): ^1H NMR (CDCl_3) δ 3.58 (s, 12H, CH_3), 2.68 (t, 8H, $J = 7.9$ Hz, CH_2), 2.40 (s, 4H, CH_2), 2.35 (t, 8H, $J = 7.9$ Hz, CH_2); ^{13}C NMR (CDCl_3) δ 172.7, 52.1, 51.3, 49.6, 32.5.

Tetramethyl 1,4-Butanediyldiamino-*N,N,N,N*-tetrapropanoate (13): ^1H NMR (CDCl_3) δ 3.58 (s, 12H, CH_3), 2.67 (t, 8H, $J = 11.4$ Hz, CH_2), 2.36 (t, 8H, $J = 11.4$ Hz, CH_2), 2.32 (m, 4H, CH_2), 1.30 (m, 4H, CH_2); ^{13}C NMR (CDCl_2) δ 172.9, 53.5, 51.3, 49.1, 32.4, 24.9.

Tetramethyl 1,6-Hexanediyldiamino-*N,N,N,N*-tetrapropanoate (14): ^1H NMR (CDCl_3) δ 3.49 (s, 12H, CH_3), 2.58 (t, 8H, $J = 7.2$ Hz, CH_2), 2.26 (t, 8H, $J = 7.2$ Hz, CH_2), 2.19 (t, 4H, $J = 7.2$ Hz, CH_2), 1.23 (m, 4H, CH_2), 1.07 (m, 4H, CH_2); ^{13}C NMR (CDCl_3) δ 172.7, 53.5, 51.2, 49.0, 32.3, 27.0, 26.9.

Tetramethyl 1,12-Dodecanediyldiamino-*N,N,N,N*-tetrapropanoate (15): ^1H NMR (CDCl_3) δ 3.63 (s, 12H, CH_2), 2.73 (t, 8H, $J = 7.2$ Hz, CH_2), 2.40 (t, 8H, $J = 7.2$ Hz, CH_2), 2.36 (t, 4H, $J = 7.3$ Hz, NCH_2), 1.37 (m, 4H, CH_2), 1.22 (m, 16H, CH_2); ^{13}C NMR (CDCl_3) δ 172.9, 53.7, 51.3, 49.1, 32.4, 29.5, 29.45, 29.4, 27.2, 27.0.

Tetramethyl 1,2-Dihydroxyethanediyldiethylamino-*N,N,N,N*-tetrapropanoate (16): ^1H NMR (CDCl_3) δ 3.51 (s, 12H, CH_3), 3.42 (s, 4H, $\text{OCH}_2\text{CH}_2\text{O}$), 3.37 (t, 4H, $J = 6.8$ Hz, OCH_2), 2.67 (t, 8H, $J = 8.0$ Hz, CH_2), 2.52 (t, 4H, $J = 6.8$ Hz, OCH_2), 2.30 (t, 8H, $J = 8.0$ Hz, CH_2); ^{13}C NMR (CDCl_3) δ 172.7, 70.2, 69.4, 53.0, 51.3, 49.7, 32.4.

Pentamethyl Spermidine-*N,N,N,N',N'*-pentapropanoate [Pentamethyl (*N*-(3-Aminopropyl)-1,4-butanedi-amine)-*N,N,N,N',N'*-pentapropanoate] (17): Methyl acrylate (4.30 g, 50 mmol) was dissolved in 10 mL of methanol and cooled in an ice bath under nitrogen. Spermidine (1.09 g, 7.5 mmol) in 3 mL of methanol was added dropwise over 2 min to the stirred solution. Stirring was continued at ice bath temperature for 1 h and then at room temperature for 16 h. The solvent and excess methyl acrylate were removed *in vacuo* to give 4.06 g (96%) of a colorless oil: ^1H NMR (CDCl_3) δ 3.49 (s, 15H, CH_3), 2.58 (t, 10H, $J = 7.8$ Hz, CH_2), 2.26 (t, 10H, $J = 7.8$ Hz, CH_2), 2.21 (m, 8H, N-CH_2), 1.37 (m, 2H, CH_2), 1.20 (m, 4H, CH_2); ^{13}C NMR (CDCl_3) δ 172.96, 172.74, 53.51, 53.48, 51.54, 51.22, 51.19, 49.10, 49.04 (probably two overlapping peaks), 32.34, 32.28, 32.07, 24.80, 24.68, 24.64.

Hexamethyl Cascade 6 Aza(3):1-azapropane:propanoate (18): Methyl acrylate (18.1g, 210 mmol, 19 mL) was dissolved in 40 mL of methanol and cooled at 4 °C under nitrogen. Tris(2-aminoethyl)methane (4.39 g, 30 mmol) dissolved in 3 mL of methanol was added with stirring for 3 min. Stirring was continued at 4 °C for 2 h and at room temperature overnight, and then solvent and excess methyl acrylate were removed *in vacuo* at

² All CAS-RN have been provided by the author.

room temperature to give 19.6 g (98%) of a yellow oil: ^1H NMR (CDCl_3) δ 3.58 (s, 18H, CH_3), 2.70 (t, 12H, $J = 7.1$ Hz, CH_2), 2.42 (bs, 12H, $-\text{NCH}_2\text{CH}_2\text{N}-$), 2.36 (t, 12H, $J = 7.1$ Hz, CH_2); ^{13}C NMR (CDCl_3) δ 172.6, 53.2, 52.0, 51.2, 49.5, 32.3.

Tetramethyl PEG–Diamine-*N,N,N,N*-tetrapropanoate (19). PEG-diamine (1.02 g, 0.3 mmol) was dissolved in 5 mL of dry methanol with gentle warming. The solution was cooled to room temperature under nitrogen and methyl acrylate (0.16 g, 1.8 mmol, 0.17 mL) added. The solution was stirred under nitrogen at room temperature for 18 h, and then the solvent and excess methyl acrylate were evaporated *in vacuo* at room temperature to give 1.1 g of a white solid. ^1H -NMR (CDCl_3) showed two triplets at 2.82 and 2.45 ppm, indicating that the propanoate was present.

Tris(propanoic hydrazide)amine (20; CAS-RN 91933-31-2 (β -Alanine, *N,N*-Bis(3-hydrazino-3-oxopropyl)-, Hydrazide). To a 40 °C solution of hydrazine hydrate (40 mL, 0.80 mol) in methanol (30 mL) was slowly added a solution of tris(methyl propanoate) amine (40 mmol, 12.4 g) in methanol (30 mL). The solution was stirred at 40 °C for 1 h, then cooled to room temperature for 1 h, concentrated *in vacuo* to 20 mL, and recrystallized from isoamyl alcohol at 0 °C to give 12.0 g (97%) of a crystalline white solid, mp 56–57 °C.

General Procedure for the Preparation of Acyl Hydrazides [1,2-Ethanediyldiamino-*N,N,N,N*-tetrakis(propanoic hydrazide) (21)]. Tetramethyl ethanediaminetetrapropanoate (12) (2.02 g, 5.0 mmol) was dissolved in 3 mL of absolute ethanol, and hydrazine hydrate (2.00 g, 40 mmol, 2.00 mL) was added. The solution was stirred under nitrogen at 45 °C for 2 h and then cooled to room temperature; ethanol and excess hydrazine were removed *in vacuo* to give a viscous syrup. The crude material was dissolved in 15 mL of boiling 2-propanol and cooled slowly to room temperature (fast cooling caused the product to oil out) to give a white crystalline solid, which was isolated by filtration and then vacuum dried to give 1.95 g (95%) of **21**: mp 140–141 °C (dec); ^1H NMR (D_2O) δ 2.74 (t, 8H, $J = 11.2$ Hz, CH_2), 2.52 (s, 4H, $\text{NCH}_2\text{CH}_2\text{N}$), 2.33 (t, 8H, $J = 11.2$ Hz, CH_2); ^{13}C NMR (D_2O) δ 174.5, 50.7, 49.7, 31.5; HRMS calcd for $\text{C}_{14}\text{H}_{32}\text{N}_{10}\text{O}_4$ 405.2686, found 405.2700.

1,4-Butanediyldiamino-*N,N,N,N*-tetrakis(propanoic hydrazide) (22) was prepared by the general procedure using 2.16 g (5.0 mmol) of tetraester **13** in 3 mL of ethanol. The product separated as a solid during the reaction. Evaporation of the solvent and excess hydrazine left a white powder that was crystallized from 100 mL of 2-propanol to give 2.13 g (98%) of **22**: mp 126–127 °C; ^1H NMR (D_2O) δ 2.64 (t, 8H, CH_2), 2.34 (bs, 4H, CH_2), 2.23 (t, 8H, CH_2), 1.29 (bs, 4H, CH_2); ^{13}C NMR (D_2O) δ 174.7, 53.3, 49.3, 31.4, 24.5; HRMS calcd for $\text{C}_{16}\text{H}_{36}\text{N}_{10}\text{O}_4$ 433.2999, found 433.2976.

1,6-Hexanediyldiamino-*N,N,N,N*-tetrakis(propanoic hydrazide) (23) was prepared by the general procedure using 2.30 g (5.0 mmol) of tetraester **14** in 4 mL of ethanol. Evaporation of the solvent and excess hydrazine left a viscous syrup that was dissolved in 5 mL of 2-propanol, concentrated *in vacuo*, redissolved in 30 mL of boiling 2-propanol, and cooled (4 °C) overnight. The mixture was then cooled to –10 °C for 2 h, and the solid was isolated by filtration and washed with cold 2-propanol to give 2.34 g of a sticky white solid. Recrystallization from 2-propanol gave 2.0 g (87%) of **23**: mp 105–108 °C (dec); ^1H NMR (D_2O) δ 2.65 (t, 8H, $J = 7.2$ Hz), 2.32 (m, 4H), 2.24 (t, 8H, $J = 7.2$ Hz), 1.32 (m, 4H), 1.15

(m, 4H); ^{13}C NMR (D_2O) δ 174.7, 53.3, 49.3, 31.3, 27.4, 26.2; HRMS calcd for $\text{C}_{18}\text{H}_{40}\text{N}_{10}\text{O}_4$ 461.3312, found 461.3297.

1,12-Dodecanediyldiamino-*N,N,N,N*-tetrakis(propanoic hydrazide) (24) was prepared from 1.36 g (2.5 mmol) of tetraester **15** and 1.00 g (20 mmol) of hydrazine hydrate in 2 mL of ethanol. After heating for 1 h, the solution set to a waxy solid; the solvent and excess hydrazine were removed *in vacuo* using 5 mL of 2-propanol. The crude product was dissolved in 50 mL of boiling 2-propanol, cooled slowly to room temperature (crystallization occurred), stored at 5 °C overnight, and filtered, and the solid was washed with 2×5 mL of propanol and vacuum dried to give 1.10 g of **24** (81%): mp 124–128 °C (dec); ^1H NMR (D_2O) δ 2.66 (t, 8H, $J = 7.7$ Hz, CH_2), 2.33 (m, 4H, NCH_2), 2.26 (t, 8H, $J = 7.7$ Hz, CH_2), 1.33 (m, 4H, CH_2), 1.16 (m, 16H, CH_2); ^{13}C NMR (D_2O) δ 174.5, 53.6, 49.4, 31.4, 29.7, 29.6, 27.8, 26.3; HRMS calcd for $\text{C}_{24}\text{H}_{52}\text{N}_{10}\text{O}_4$ 545.4251, found 545.4255.

1,2-Dihydroxyethanediyldiethyldiamino-*N,N,N,N*-tetrakis(propanoic hydrazide) (25) was prepared by the general procedure from 2.46 g (5.0 mmol) of tetraester **16** in 6 mL of ethanol. The crude product was crystallized twice from 25 mL of boiling 2-propanol by cooling to –20 °C to give 2.0 g (80%) of **25**, as a syrupy liquid at room temperature: ^1H NMR (D_2O) δ 3.53 (s, 4H, $\text{OCH}_2\text{CH}_2\text{O}$), 3.45 (t, 4H, CH_2O), 2.69 (t, 8H, CH_2), 2.55 (t, 4H, NCH_2), 2.23 (t, 8H, CH_2); ^{13}C NMR (D_2O) δ 174.5, 70.3, 68.8, 52.5, 49.8, 31.4; HRMS calcd for $\text{C}_{18}\text{H}_{40}\text{N}_{10}\text{O}_6$ 493.3211, found 493.3217.

Spermidine Pentapropanoic Pentahydrazide (26). A solution of pentamethyl spermidine pentapropanoate (**17**, 1.15g, 2.0 mmol) in 3 mL of ethanol containing hydrazine monohydrate (1.00 g, 20 mmol) was stirred at 45 °C for 2 h, ethanol and excess hydrazine were removed *in vacuo* at room temperature, and the syrup remaining was concentrated using 5 mL of 2-propanol. The crude product was dissolved in 12 mL of boiling 2-propanol and cooled to –10 °C; the solvent was decanted from the solid and the crystallization repeated. Solid **26** (1.0 g, 86%) was dried *in vacuo* at –10 °C, but was a syrup above 0 °C: ^1H NMR (D_2O) δ 2.60 (t, 10H, CH_2), 2.31 (m, 8H, NCH_2), 2.23 (t, 10H, CH_2), 1.48 (m, 2H, CH_2), 1.29 (m, 4H, CH_2); ^{13}C NMR (D_2O) δ 174.58, 53.51, 53.25, 51.69, 51.46, 49.41, 49.32, 31.41, 31.33, 30.97, 24.50, 24.27, 23.09; HRMS calcd for $\text{C}_{22}\text{H}_{49}\text{N}_{13}\text{O}_5$ 576.4058, found 576.4023.

Cascade 6 Aza(3):1-azapropane:propanoic Hexahydrazide (27). Hexamethyl cascade 6 aza(3):1-azapropane:propanoate (**18**, 3.31 g, 5.0 mmol) was dissolved in 5 mL of absolute ethanol, and hydrazine hydrate (3.00 g, 60 mmol, 3.0 mL) was added. The solution was stirred at 45 °C for 2 h, and the ethanol and excess hydrazine were removed *in vacuo*. The crude oil was dissolved in 30 mL of boiling 2-propanol, cooled to 40 °C, chilled quickly to –78 °C to give a filterable solid that was isolated by filtration through a prechilled funnel at –10 °C, and washed with cold 2-propanol. It was dried under vacuum at –10 °C to give 2.85 g (85%) of **27** (the material melted at temperatures above 0 °C): ^1H NMR (D_2O) δ 2.65 (t, 12H, $J = 7.1$ Hz, CH_2), 2.46 (bs, 12H, $\text{NCH}_2\text{CH}_2\text{N}$), 2.23 (t, 12H, $J = 7.1$ Hz, CH_2); ^{13}C NMR (D_2O) δ 173.6, 51.0, 49.7, 48.9, 30.6; HRMS calcd for $\text{C}_{24}\text{H}_{54}\text{N}_{16}\text{O}_6$ 663.4491, found 663.4469.

PEG–Diaminetetrapropanoic Tetrahydrazide (28). Tetramethyl PEG–diaminetetrapropanoate (**19**, 1.1 g, 0.3 mmol) was dissolved in 3 mL of absolute ethanol, and hydrazine hydrate (0.12 g, 2.4 mmol) was added. The

solution was stirred at 45 °C for 3.5 h and at room temperature overnight, and solvent and excess hydrazine were removed *in vacuo* to give 1.1 g as a white powder. The ¹H-NMR (CDCl₃) had two triplets at 2.39 and 2.75 ppm and two smaller triplets at 2.55 and 2.84 ppm (the large PEG peak was evident at 3.55 ppm as a broad absorption).

Cross-Linking of HA. The cross-linker (XL) was added to an aqueous solution of sodium hyaluronate. The pH was adjusted to the desired value by dissolving the appropriate amount of bis-tris HCl or by addition of 0.1 N HCl. EDC was dissolved in water and added to the mixture. After stirring vigorously for 1 min, the mixture was left at room temperature to gel. All XL equivalents (mol equiv) mentioned in this paper are expressed as the molar ratio of XL to the carboxylic functions present in the glucuronic acid subunits of HA.

Degradation of HA-Hydrogel by Hase: Plate Assay. After the reagents were mixed, the gelling solution was poured into a Petri dish and left at room temperature for 24 h to complete gelation. The gel was then washed with water, and six 0.5-cm-diameter wells were excised with a cork borer. One well was loaded with 25 μL of buffer (30 mM citric acid/150 mM Na₂HPO₄/150 mM NaCl; pH 6.3), and the other wells were loaded with 25 μL of Hase samples dissolved in the same buffer. The gel was incubated at 37 °C for 24 h, at which point the remaining gel was stained with a solution of fastgreen FCF. Clear rings of digested gel could be observed against a green background.

Degradation of HA-Hydrogel by Hase: Spectrophotometric Assay. The cross-linking of HA was performed in the presence of 40 μM Coomassie Brilliant blue R250. After all of the reagents were mixed, 1 mL of the gelling mixture was placed in a plastic cuvette such that the volume of gel did not block the light path. When gelation was complete (24 h of standing at room temperature), the gel was washed and 1 mL of enzyme solution was overlaid on top of the gel, in the light path of the spectrophotometer. The absorbance of the hyperphase solution was monitored at 590 nm as a function of the reaction time.

pH Stability Experiments. HA was cross-linked in the presence of 50 μM Coomassie Brilliant blue R250. Upon gelation, the gels were cut in pieces of approximately 2 g and washed several times with water (pH 5.6). After the last washing, the water was replaced by a 50 mM phosphate buffer solution (mono- or dibasic phosphate or a mixture of both) with a pH of 4.5, 6.5, 6.9, 7.25, 7.65, or 9.1. One piece of gel was stored in 0.1 N HCl solution (pH 1.3). All samples were incubated at 37 °C. At several time intervals, 2-mL samples were taken, the absorbance was measured at 590 nm, and the samples were returned to the solutions again.

RESULTS

Synthesis of Polyvalent Hydrazides. Mono-, di-, and trihydrazides (Figure 2) were prepared by esterification followed by reaction with excess hydrazine hydrate in alcohol by modification of standard procedures (29). The polyvalent hydrazides (Figure 3) were prepared by first reacting a polyamine with a 25% excess of methyl acrylate (26). The resulting polymethyl alkylpolyaminopolypropanoates were treated with an excess of hydrazine hydrate in absolute ethanol to yield the acyl hydrazides. The crude products could usually be crystallized from 2-propanol, albeit often at low temperature. Hydrazinolysis reactions proceeded in near quantitative yields, and recrystallization gave high recovery of purified

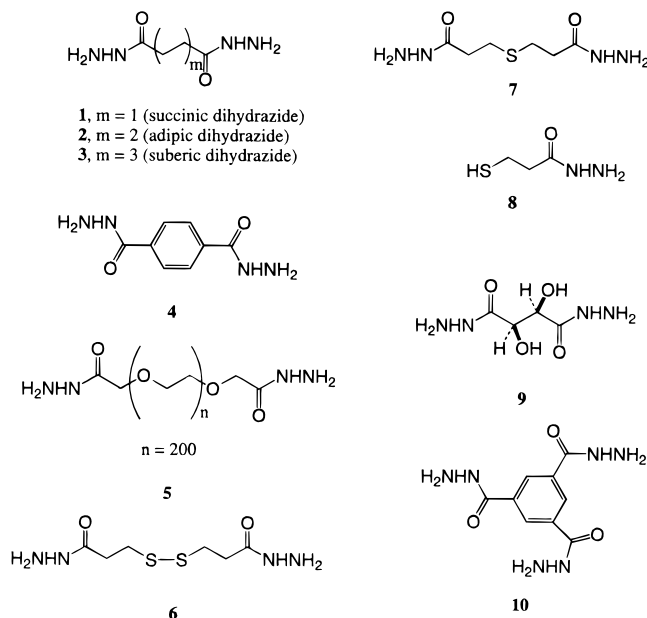


Figure 2. Selected commercially available hydrazides and synthetic mono-, di-, and trihydrazides.

Table 1. Limiting Reaction Parameters and Physicochemical Properties of Resulting HA-Hydrogels^a

reagents	pourable gels	solid gels
HA	2.5 mg/mL	8.0 mg/mL
0.1 N HCl	pH 4.7	pH 3.5
(fast reaction)		
bis-tris HCl, pH 4.75	100 mM	500 mM
(slow reaction)		
cross-linker (XL)	0.1 mol equiv	1.5 mol equiv
EDC	0.5 mol equiv	1.0 mol equiv
buffer	tris (pK _a = 8.1)	bis-tris (pK _a = 6.5)

^a A variety of gels were prepared with intermediate properties by varying the parameters indicated.

polyhydrazides. With the exception of trimesic trihydrazide, each of the polyhydrazides was water soluble and was readily employed for HA modification and gelation reactions.

Cross-Linking of HA. Depending on the reaction conditions, gels with physicochemical properties ranging from soft and pourable to solid and readily shattered were obtained. The pH of the reaction was maintained between 3.5 and 4.7 by addition of either 0.1 N HCl or 100–500 mM bis-tris HCl. Gels would form very rapidly (20–40 s) with HCl as the reaction initiator, but would solidify in 5–30 min when bis-tris HCl was used. Table 1 presents an overview of the limiting reaction parameters involved and their effect on the properties of the gels obtained. Hydrogels with properties ranging between both extremes given in Table 1 were obtained by varying the parameters between the values indicated.

Plate Assay for Degradation of HA-Hydrogels. Figure 4A illustrates diagrammatically the protocol for this assay. Following hydrogel formation, circular wells were excised and loaded with either buffer (= blank) or an Hase solution. After incubation at 37 °C for 24 h and staining with fastgreen FCF solution, clear rings of digested gel appear against the colored background (Figure 4B). Importantly, the assay is highly reproducible as seen in Figure 4B, which compares five wells containing identical Hase concentrations with a single blank. When using different amounts of Hase, the diameter of the digested rings can be plotted against the amount of enzyme added. A linear relationship was obtained, and the slope reflected the sensitivity of the

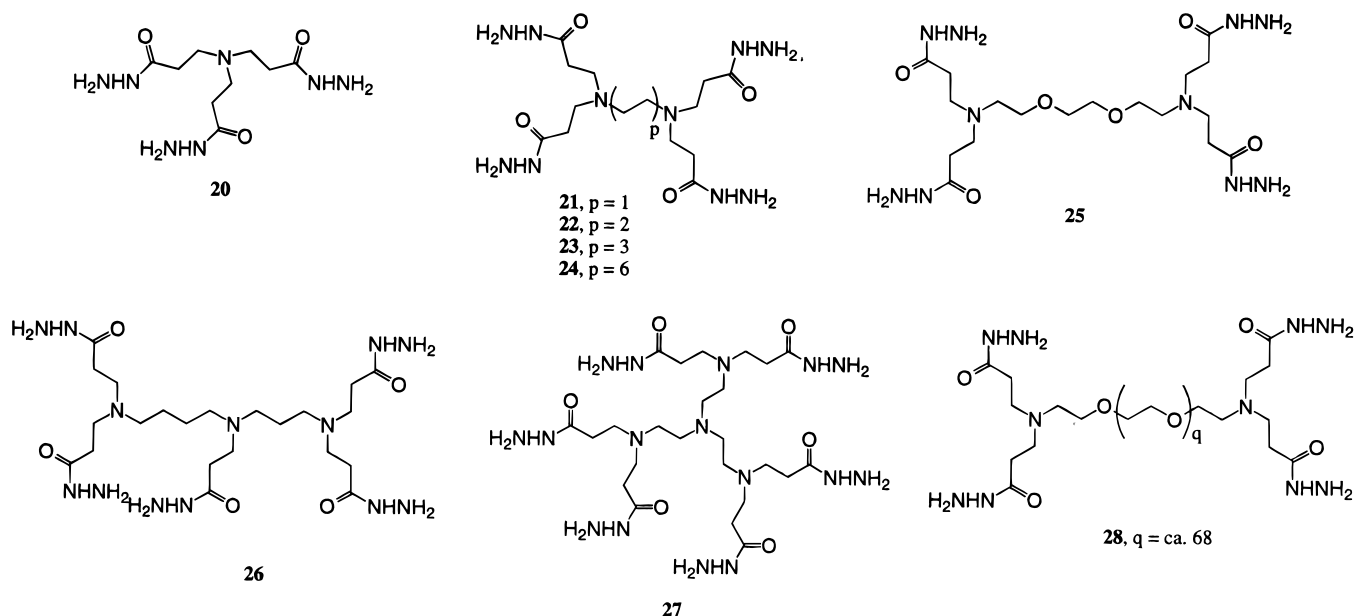


Figure 3. Structures of amine-based polyhydrazides.

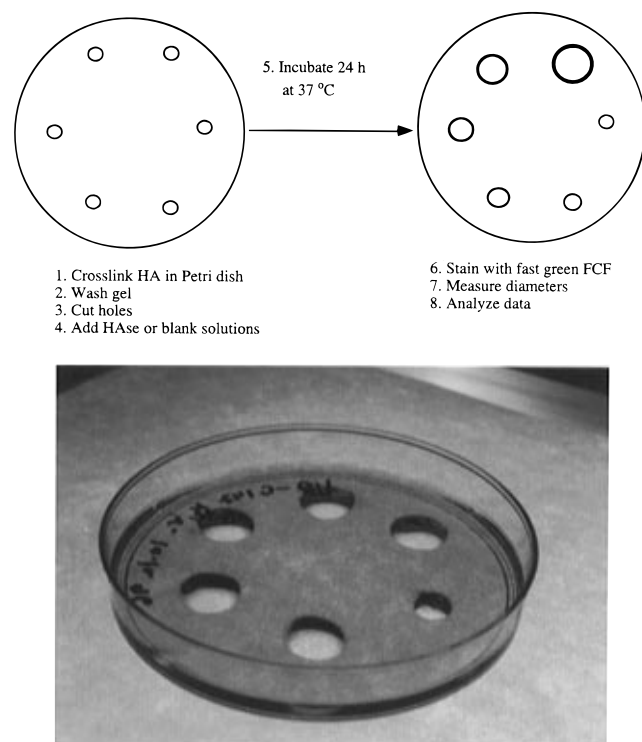


Figure 4. (A, top) Schematic representation of the plate assay for the investigation of the degradation of HA-hydrogels by Hase as described under Materials and Methods. (B, bottom) Photograph (side angle view) showing endpoint of representative plate assay with one blank (at right) and five identical Hase solutions.

gel toward Hase, with a larger slope indicating greater susceptibility to Hase digestion. Figure 5 illustrates a comparison of the degradation of two hydrogels (4.8 mg/mL HA) prepared using 0.3 mol equiv of cross-linker (XL) **6** or **23**. The diamine-derived tetrahydrazide **23** afforded a more readily degraded gel than the disulfide-containing dihydrazide **6**.

Next, using **XL-6**, the effects of the amount of cross-linker and the amount of HA in the gel on the degradation by Hase were examined. For each gel recipe, six Petri plates were prepared and the wells were loaded with different amounts of Hase, varying from 0 to 5.5 units. The average diameters of the digested rings

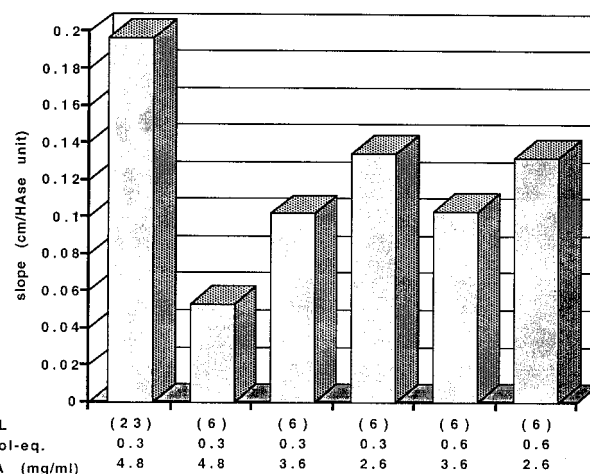


Figure 5. Degradation of HA-gels by Hase using the plate assay. Comparison of the degradation of gels made with **XL-6** and **XL-23** (see Figures 2 and 3) is shown by the effect of the amount of **XL-6** and the amount of HA in the gel upon their degradation by Hase. The slope of the plot of the average ($n = 6$) diameter (in cm) of the digested wells as a function of the amount of Hase (in units) is plotted against the type of gel investigated.

(standard deviations varied from 2.4 to 4.2%) were plotted as a function of the amount of Hase added; linear regressions (r^2 ranged from 0.93 to 0.99) were performed. Figure 5 summarizes the slope values obtained for the gel recipes investigated. Decreasing the HA concentration made the gels more susceptible to Hase degradation, but doubling the XL concentration at a given HA concentration had no effect on the gel degradation.

On the basis of these results, the degradation of HA-gels made with 10 different types of cross-linkers (**XL-1**, **-2**, **-3**, **-4**, **-6**, **-9**, **-21**, **-22**, **-23**, **-24**; see Figures 2 and 3) was investigated. Gels containing 4.8 mg/mL HA and 0.5 mol equiv cross-linker were prepared in Petri dishes. Six wells were excised, and 25 μ L of buffer (= blank) was added to one well, while 25 μ L of Hase solution (104 units/mL) was added (= addition of 2.6 units) to the other five wells. After incubation at 37 °C for 24 h, the gels were stained and the diameters of the wells were measured (see Figure 4B). The percentage increase in diameter vs the blank was averaged ($n = 5$) for each type

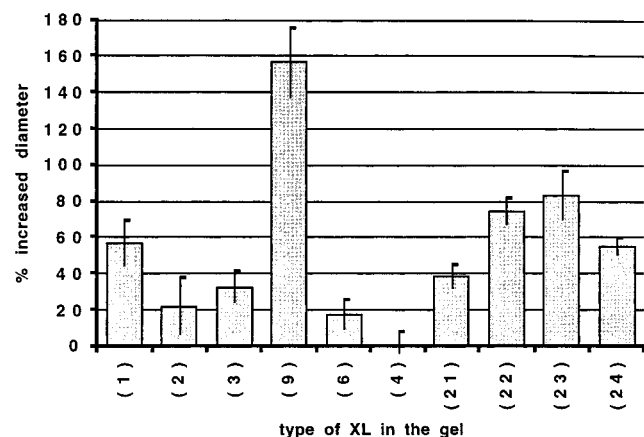


Figure 6. Degradation of HA-gels by Hase using the plate assay. A comparison of the effect of 10 different types of cross-linker on the degradation of the HA-gel by Hase is shown. Gels were made containing 4.8 mg/mL HA and 0.5 mol equiv cross-linker. The degradation was investigated at a single enzyme concentration (104 units/mL), and the average ($n = 5$) diameter of the digested rings was compared to the diameter of the blank (see Figure 4B). The percent increase in diameter is plotted as a function of the type of cross-linker. For chemical structures and numbering of the cross-linkers, see Figures 2 and 3.

of gel, and the results obtained are plotted in Figure 6. Hydrophobic cross-linkers such as XL-2, -3, and -4 and the disulfide XL-6 produced gels that showed the greatest resistance to degradation. Indeed, the terephthalic-derived material using XL-4 showed little or no degradation in 24 h. In contrast, the more hydrophilic dihydrazide and tetrahydrazide linkers showed higher susceptibility to Hase. The tartrate-derived linker XL-9 gave the least stable gel.

Spectrophotometric Assay for Degradation of HA-Hydrogels. Figure 7 illustrates the scheme for the basic assay as well as two modifications discussed below. The displacement technique described under Materials and Methods allows the transfer of reproducible amounts of gelling mixture on the bottom of the cuvettes. The average (\pm standard deviation; $n = 30$) weight of gel was 1.010 ± 0.003 g. No Coomassie Brilliant blue R250 leached out of the gels when only buffer was added above the gel. When Hase solution was added, the gel was digested at the surface and the dye was released, diffusing into the hyperphase (Figure 7A).

Figure 8 presents representative results obtained for the degradation of HA-gel prepared using 4 mg/mL HA and 0.45 mol equiv XL-23 and containing 40 μ M Coomassie Brilliant blue 250 by Hase (180 units/mL). The assay was run with one control and three replicates. Only buffer was added above the control gel, and the enzyme solution was added on top of the other three gels. The absorbance at 590 nm of the hyperphase was continuously monitored, averaged, and plotted as a function of the reaction time. This assay was not compatible with all cross-linkers. For example, the lower solubility of XL-6 resulted in precipitation during the degradation, thereby removing co-complexed Coomassie Brilliant blue R250. In these cases, no increase in absorbance could be detected as the degradation proceeded, unless the samples were mixed or shaken. Nonetheless, for the gels made with XL-23, reproducible release profiles could be obtained. Using this assay, the effect of the amount of this tetrafunctional cross-linker (0.15–0.60 mol equiv) on the degradation of the gel by Hase was investigated. Each experiment was performed in triplicate. Interestingly, the rate of degradation of the gels made with XL-23 appeared to be independent of cross-linker concentration

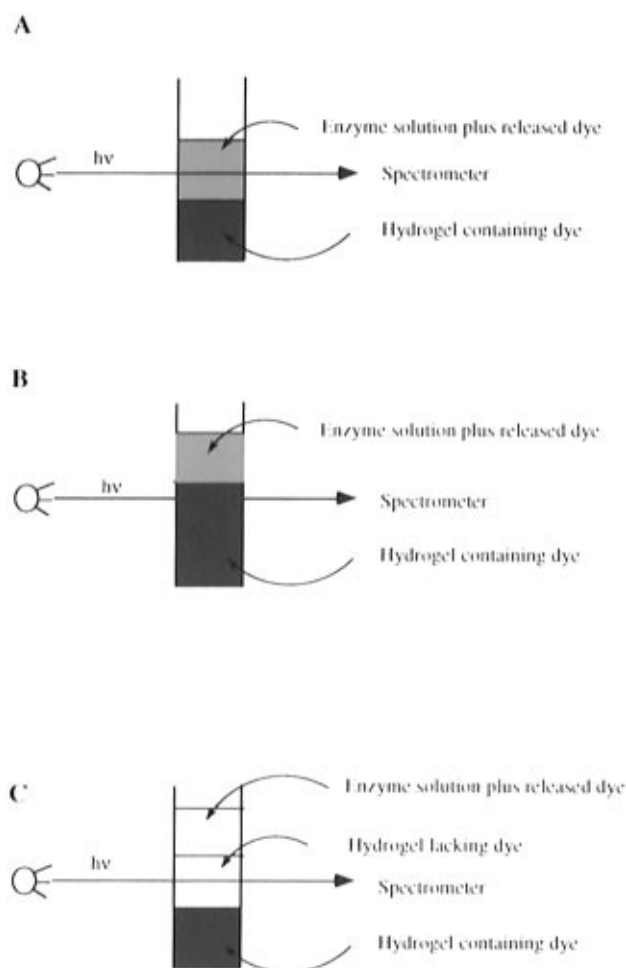


Figure 7. Degradation of HA-gels by Hase using the spectrophotometric assay. Panel A shows the basic assay configuration. Panels B and C illustrate two modifications employed to demonstrate the interfacial mode of degradation.

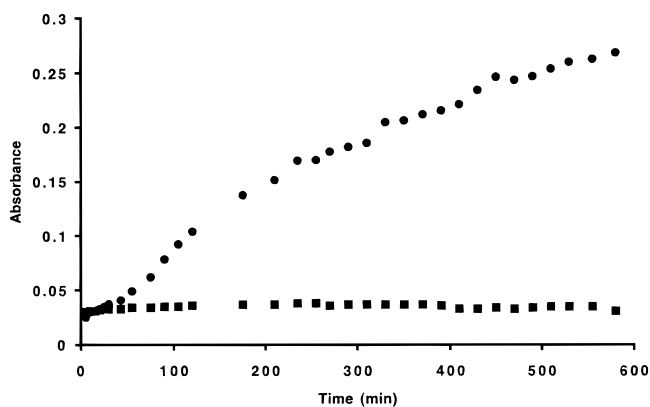


Figure 8. Degradation of HA-gels by Hase using the spectrophotometric assay. One milliliter of gel (containing 4 mg/mL HA, 0.45 mol equiv XL-23, and 40 μ M Coomassie Brilliant blue R250) was poured on the bottom of a plastic cuvette. One milliliter of Hase solution (180 units/mL) was added on top of the gel, and the release of Coomassie Brilliant blue R250 was monitored at 590 nm as a function of the reaction time. (■) Data points when only buffer is added on top of the gel; (●) average of data points ($n = 3$) when the Hase solution is added on top of the gel.

(results not shown), consistent with HA degradation occurring at the gel–solution interface.

pH Stability Experiments. During the water wash of the gels containing 4.8 mg/mL HA, 1 mol equiv of either XL-6 or XL-23, and 50 μ M Coomassie Brilliant blue R250, no dye leached out of the gels. The pieces of

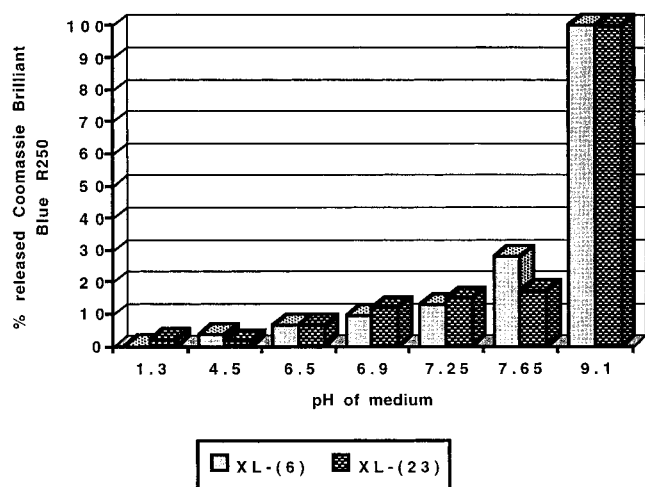


Figure 9. Release of Coomassie Brilliant blue R250 from HA-hydrogels at different pH values. Samples (2 g) of HA-hydrogel containing 4.8 mg/mL HA, 1 mol equiv XL-6 or XL-23, and 50 μ M Coomassie Brilliant blue R250 were stored in 0.1 N HCl (pH 1.3) or in 50 mM phosphate solutions pH 4.5, 6.5, 6.9, 7.25, 7.65, and 9.1. The percentage of dye released from both types of gel after 4 days of storage at 37 °C is plotted as a function of the pH of the medium.

tetrafunctional cross-linked gel kept their shape during the washing process, but the gel pieces from XL-6 exhibited considerable swelling during the wash. Gels were incubated for several days at pH values from 1.3 to 9.1. At pH 9.1, the gels steadily dissolved in the surrounding medium. Much less dissolution could be observed at pH 7.65, and virtually no released dye could be detected when the gels were stored in media with pH values below 7.0. The gels remained stable under acidic conditions. Within 4 days, both types of gels stored at pH 9.1 were completely dissolved in the medium (100% release). Figure 9 illustrates the percent dye released after 4 days of storage of the gel samples at different pH values.

DISCUSSION

Modification of carboxylic functions of small molecules and polymeric polycarboxylates as mediated by carbodiimides has been extensively investigated (30, 31). The extent of reaction is determined by the acid consumed; thus, the degree of cross-linking of HA is a function of reaction pH (see Table 1). The rapidity of the reaction is dependent on the amount of acid immediately available for the reaction. When the pH is adjusted with HCl (total dissociation), all of the acid is readily available for reaction, resulting in rapid, but often heterogeneous, gelation. When using buffer salts such as bis-tris HCl or tris HCl as the source of acid, the amount of acid available depends on the pH of the mixture and the pK_a of the buffer component. During the reaction, the free acid is consumed and this is counteracted by the release of some additional acid from the buffer components, leading to more controlled gelation and more homogeneous hydrogels in the presence of amine buffer salts.

The plate assay described in this paper was developed on the basis of the method of Richman and co-workers for the quantitation of Hase in biological samples (32). This approach allows comparison of different types of gels for their sensitivity toward Hase, or, in principle, in response to any other gel-degrading agent. The results presented in Figure 5 show a relative comparison of the degradation of gels made with two different types of cross-linker, different amounts of cross-linker, and different amounts of HA. The gel made with tetrahydrazide

XL-23 is more readily degraded by Hase than the gel made with disulfide dihydrazide XL-6. With XL-6, increasing the amount of cross-linker in the gel seemed not to affect the degradation, while decreasing the amount of HA in the gel seems to increase the extent of degradation by Hase.

When the type of cross-linker was varied (Figure 6), extensive degradation was observed for the gel cross-linked with the tartaric dihydrazide crosslinker XL-9, while no degradation could be observed with the terephthalic dihydrazide cross-linker XL-4. Again, very little degradation was observed for gels made with the disulfide dihydrazide XL-6. These results suggest that the degradation of the HA-gels is slower for more hydrophobic cross-linkers. Although most types of gels investigated showed clear signs of degradation by Hase, the enzyme concentrations used (30–200 units/mL) were much higher than the concentration of Hase in, e.g., pooled serum (reported to be 2.6 units/mL) (33). The action of Hase on native HA has been extensively investigated using Hase concentrations ranging from 0.3 to 6.6 units/mL (34–36). The large difference in Hase concentration used to monitor the degradation of native HA or cross-linked HA suggests that the cross-linking reaction dramatically reduces the degradability of HA by Hase. It would be anticipated, therefore, that many of the hydrogels from these studies would show *in vivo* half-lives of days or weeks at Hase concentrations 100-fold below those tested in this study.

The spectrophotometric assay (Figure 7) has two main advantages over the plate assay. First, it requires smaller amounts of material for testing, and, second, the time kinetics of the degradation process can be monitored. However, as described under Results, it was not applicable to all types of gels. In principle, this assay could be modified to be performed as a "tablet dissolution test". The release profiles of Coomassie Brilliant blue R250 (see Figure 8) can be approximated by a sigmoidal curve. This is probably due to the fact that the gel surfaces are not perfectly flat during the enzymatic degradation. As with the plate assay, no difference could be observed with different concentrations of the cross-linker XL-23 on the susceptibility of the gel to degradation by Hase.

Two explanations can be advanced for the independence of degradation on cross-linker concentration. First, the Hase assays employed might be insensitive toward the subtle changes in the different gels prepared with different amounts of cross-linker. Conceivably, we have not tested low enough or high enough cross-linker concentrations to see the effect. Moreover, the very high concentrations of Hase used to investigate the degradation of the gels yield a very vigorous attack on the gels. Second, the enzyme could act only at the surface of the gel and would therefore be unaffected by the bulk of the gel body. This would be consistent with both the lack of concentration dependence and the importance of the hydrophobicity or hydrophilicity of the cross-linker on the susceptibility of the gel to Hase degradation.

To test the second hypothesis, experiments were performed in which the cuvettes were filled with 2 mL of gelling mixture (Figure 7B) instead of the usual 1 mL. This amount of blue-stained gel blocks the light of the spectrophotometer, leading to continuous high absorbance readings. An Hase solution was added on top of the gel. It was reasoned that if the enzyme acted only on the surface of the gel, no change in absorbance readings would be observed until the gel was degraded, surface by surface, to a level that the light of the spectrophotometer was no longer blocked. If Hase dif-

fused into the gel body and acted within the gel, gradual changes in absorbance, due to the solubilization of the gel from below the interface, would be noticed before the level of the gel had regressed below the light of the spectrophotometer. The results observed (data not shown) were in agreement with surface erosion. That is, the change in absorbance was a sharp step function corresponding to solubilization until the level of the beam was reached.

A second modification of the spectrophotometric assay was set up to address the same question. A cuvette was filled with 1 mL of a gelling mixture containing Coomassie Brilliant blue as usual. After gelation, 1 mL of the same gelling mixture containing no dye was added on top and allowed to gel. This yielded a cuvette with a piece of blue gel on the bottom and a piece of clear gel on top, the latter in the light path of the spectrophotometer (Figure 7C). Since the top gel is transparent, continuous low absorbances were measured. On top of this "sandwich-type" of gel, the enzyme solution was added. If the enzyme acted only at the surface, nothing would be observed until the top gel was degraded and the enzyme reached the bottom gel. If the enzyme diffused into the gel bodies, dye would be released from the bottom gel and diffuse into the top gel, leading to differences in the absorbance readings. Again, the results (data not shown) were in agreement with surface erosion.

The results of the pH stability test (Figure 9) indicated that HA-hydrogels prepared with two different cross-linkers, disulfide dihydrazide XL-6 and diamine-based tetrahydrazide XL-23, were stable in solutions with pH values below 7.0. At pH values above 7.0, a gradual dissolution and consequent release of dye could be observed. Dye release was not due to an increased swelling of the gel but was solely due to a disintegration and dissolution of the gel. Despite the 3-fold difference of these two gels in susceptibility to Hase, the pH stability of the gels appeared to be independent of the nature of the cross-linker. This stability toward acid pH values and instability toward alkaline pH values could be exploited for transporting drugs, peptides, etc., safely through acid environments (e.g., the stomach) and subsequent release in more alkaline environments (e.g., the intestines).

In conclusion, the bioconjugate chemistry previously developed for the chemical modification of HA with hydrazide functionalities has been applied to the cross-linking of this biopolymer to form hydrogels. Cross-linking conditions have been varied so that gels with a broad range of physicochemical properties can be obtained. Two new approaches were developed to investigate the biodegradation of these gels *in vitro*. With these methods, we observed that hydrophobic linkers provided gels with considerable resistance to Hase. Interestingly, hydrogel degradation was independent of cross-linker concentration, suggesting that degradation occurs only at the gel interface. The stability of these HA-hydrogels in acidic media and their slow dissolution above pH 7.0 suggest potential uses for controlled drug delivery in alkaline environments.

ACKNOWLEDGMENT

We thank Collaborative Laboratories, Inc. (East Setauket, NY), Clear Solutions Biotechnology, Inc. (Stony Brook, NY), the U.S. Public Health Service, the Center for Biotechnology at The University at Stony Brook, and start-up funds from The University of Utah for financial support of this work. Pioneering contributions by Dr. T. Pouyani are gratefully acknowledged.

LITERATURE CITED

- (1) LeBoeuf, R. D., Raja, R. H., Fullert, G. M., and Wiegel, P. H. (1986) Human fibrinogen specifically binds hyaluronic acid. *J. Biol. Chem.* **261**, 12586–12592.
- (2) Turley, E. A., Austen, L., Moore, D., and Hoare, K. (1993) Ras-transformed cells express both CD44 and RHAMM hyaluronan receptors—only RHAMM is essential for hyaluronan-promoted locomotion. *Exp. Cell Res.* **207**, 277–282.
- (3) Duncan, R., Dimitrijevic, S., and Evagorou, E. G. (1996) The role of polymer conjugates in the diagnosis and treatment of cancer. *J. Ther. Polym. Pharm. Sci.* **6**, 237–263.
- (4) Brinkley, M. (1992) A brief survey of methods for preparing protein conjugates with dyes, haptens, and crosslinking agents. *Bioconjugate Chem.* **3**, 2–13.
- (5) Krinick, N. L., and Kopecek, J. (1991) Soluble polymers as targetable drug carriers. In *Targeted Drug Delivery. Handbook of Experimental Pharmacology* (R. L. Juliano, Ed.) pp 105–179, Springer Verlag, Berlin.
- (6) Puttnam, D., and Kopecek, J. (1995) Polymer conjugates with anticancer activity. *Adv. Polym. Sci.* **122**, 55–123.
- (7) Park, K., Shalaby, W. S. W., and Park, H. (1993) *Biodegradable Hydrogels for Drug Delivery*, 252 pp, Technomic Publishing, Lancaster, PA.
- (8) Larsen, N. E., and Balazs, E. A. (1991) Drug delivery systems using hyaluronan and its derivatives. *Adv. Drug Delivery Rev.* **7**, 279–293.
- (9) Drobnik, J. (1991) Hyaluronan in drug delivery. *Adv. Drug Delivery Rev.* **7**, 295–308.
- (10) Pouyani, T., and Prestwich, G. D. (1994) Functionalized derivatives of hyaluronic acid oligosaccharides—drug carriers and novel biomaterials. *Bioconjugate Chem.* **5**, 339–347.
- (11) Pouyani, T., and Prestwich, G. D. (1997) Functionalized derivatives of hyaluronic acid. U.S. Pat. 5,616,568, April 1, 1997.
- (12) Pouyani, T., Harbison, G. S., and Prestwich, G. D. (1994) Novel hydrogels of hyaluronic acid: synthesis, surface morphology, and solid-state NMR. *J. Am. Chem. Soc.* **116**, 7515–7522.
- (13) Prestwich, G. D., Marecak, D. M., Marecek, J. F., Ver-cruysse, K. P., and Ziebell, M. R. (1997) Controlled chemical modification of hyaluronic acid: Synthesis, applications and biodegradation of hydrazide derivatives. *J. Controlled Release* (in press).
- (14) Prestwich, G. D., Marecak, D. M., Marecek, J. F., Ver-cruysse, K. P., and Ziebell, M. R. (1997) Chemical modification of hyaluronic acid for drug delivery, biomaterials, and biochemical probes. In *The Chemistry, Biology, and Medical Applications of Hyaluronan and its Derivatives* (T. C. Laurent and E. A. Balazs, Eds.) Wenner-Gren Foundation, Stockholm, Sweden (in press).
- (15) Kreil, G. (1995) Hyaluronidases—a group of neglected enzymes. *Protein Sci.* **4**, 1666–1669.
- (16) Afify, A. M., Stern, M., Guntenhoner, M., and Stern, R. (1993) Purification and characterization of human serum hyaluronidase. *Arch. Biochem. Biophys.* **305**, 434–441.
- (17) Yui, N., Okano, T., and Sakurai, Y. (1992) Inflammation responsive degradation of crosslinked hyaluronic acid gels. *J. Controlled Release* **22**, 105–116.
- (18) Heller, J., Helwing, R. F., Baker, R. W., and Tuttle, M. E. (1983) Controlled release of water-soluble macromolecules from bioerodable hydrogels. *Biomaterials* **4**, 262–266.
- (19) Cartledge, S. A., Duncan, R., Lloyd, J. B., Rejmanova, P., and Kopecek, J. (1986) Soluble, crosslinked *N*-(2-hydroxypropyl)methacrylamide copolymers as potential drug carriers. 1. Pinocytosis by rat visceral yolk sacs and rat intestine cultured *in vitro*. Effect of molecular weight on uptake and intracellular degradation. *J. Controlled Release* **3**, 55–66.
- (20) Ratner, B. D., Gladhill, K. W., and Horbett, T. A. (1988) Analysis of *in vitro* enzymatic and oxidative degradation of polyurethanes. *J. Biomed. Mater. Res.* **22**, 509–527.
- (21) Shalaby, W. S. W., Blevins, W. E., and Park, K. (1991) Enzyme-degradable hydrogels. Properties associated with albumin-crosslinked polyvinylpyrrolidone hydrogels. In *Water-Soluble Polymers* (W. S. W. Shalaby, C. L. McCormick, and G. B. Butler, Eds.) ACS Symposium Series 467, pp 484–492, American Chemical Society, Washington, DC.

- (22) Ulbrich, K., Strohalm, J., and Kopecek, J. (1982) Polymers containing enzymatically degradable bonds. VI. Hydrophilic gels cleavable by chymotrypsin. *Biomaterials* 3, 150–154.
- (23) Pangburn, S. H., Trescony, P. V., and Heller, J. (1982) Lysozyme degradation of partially deacetylated chitin, its films and hydrogels. *Biomaterials* 3, 105–108.
- (24) Hennink, W. E., Franssen, O., Overbeek, A. V., van Steenberg, M. J., and Talsma, H. (1995) Enzymatic degradation of dextran hydrogels. *Proc. Int. Symp. Controlled Release Bioact. Mater.* 22.
- (25) Dickinson, H. R., and Hiltner, A. (1981) Biodegradation of a poly(α -amino acid) hydrogel. II. *In vitro*. *J. Biomed. Mater. Res.* 15, 591–603.
- (26) Lutter, L. C., Ortanderl, F., and Fasold, H. (1974) The use of a new series of cleavable protein-crosslinkers on the *Escherichia coli* ribosome. *FEBS Lett.* 48, 288–292.
- (27) Tomalia, D. A. (1993) StarburstTM/cascade dendrimers: Fundamental building blocks for a new nanoscopic chemistry set. *Aldrichim. Acta* 26, 91–101.
- (28) Tomalia, D. A., Baker, H., Dewald, J., Hall, M., Kallos, G., Martin, S., Roeck, J., Ryder, J., and Smith, P. (1986) Dendritic macromolecules: Synthesis of starburst dendrimers. *Macromolecules* 19, 2466–2468.
- (29) Smith, P. A. S. (1946) The Curtius Reaction. *Organic Reactions* (R. Adams, W. E. Bachmann, L. F. Fieser, J. R. Johnsons, and H. R. Snyder, Eds.) Vol. 3, pp 366–367, Wiley, New York.
- (30) Nakajima, N., and Ikada, Y. (1995) Mechanism of amide formation by carbodiimide for bioconjugation in aqueous media. *Bioconjugate Chem.* 6, 123–130.
- (31) Kuo, J.-w., Swann, D. A., and Prestwich, G. D. (1991) Chemical modification of hyaluronic acid by carbodiimides. *Bioconjugate Chem.* 2, 232–241.
- (32) Richman, P. G., and Baer, H. (1980) A convenient plate assay for the quantitation of hyaluronidase in Hymenoptera venoms. *Anal. Biochem.* 109, 376–380.
- (33) Delpech, B., Bertrand, P., and Chauzy, C. (1987) An indirect enzymeimmunoassay for hyaluronidase. *J. Immunol. Methods* 104, 223–229.
- (34) Vercruysse, K. P., Lauwers, A. R., and Demeester, J. M. (1994) Kinetic investigation of the degradation of hyaluronan by hyaluronidase using gel permeation chromatography. *J. Chromatogr. B: Biomed. Appl.* 656, 179–190.
- (35) Vercruysse, K. P., Lauwers, A. R., and Demeester, J. M. (1995) Absolute and empirical determination of the enzymic activity and kinetic investigation of the action of hyaluronidase on hyaluronan using viscosimetry. *Biochem. J.* 306, 153–160.
- (36) Vercruysse, K. P., Lauwers, A. R., and Demeester, J. M. (1995) Kinetic investigation of the action of hyaluronidase on hyaluronan using the Morgan-Elson and neocuproine assays. *Biochem. J.* 310, 55–59.

BC9701095

Genetic Construction and Characterization of an Anti-Monkey CD3 Single-Chain Immunotoxin with a Truncated Diphtheria Toxin

Shenglin Ma, Huaizhong Hu, Jerry Thompson, Scott Stavrou, Joshua Scharff, and David M. Neville, Jr.*

Section on Biophysical Chemistry, Laboratory of Molecular Biology, National Institute of Mental Health, National Institutes of Health, Bethesda, Maryland 20892-4034. Received February 3, 1997[®]

We have previously developed a chemically conjugated anti-rhesus monkey CD3 immunotoxin FN18–CRM9 that can deplete *in vivo* T cells and induce long term tolerance of mismatched renal allograft in rhesus monkeys. This immunotoxin is a monkey analogue of anti-human CD3 immunotoxin UCHT1–CRM9. In this study, we cloned the light and heavy chain variable regions of anti-monkey CD3 monoclonal antibody FN18 and constructed a single-chain Fv (sFv) by linking variable light and variable heavy regions with a (Gly₄Ser)₃ linker. The single-chain immunotoxin DT390–FN18sFv was constructed by ligating the sFv to the carboxyl terminus of DT390, a truncated form of diphtheria toxin. The DT390–FN18sFv fusion protein was expressed in *Escherichia coli* and purified with Ni-RTA affinity and anion exchange columns. Similar to the chemically conjugated immunotoxin FN18–CRM9, DT390–FN18sFv can also specifically inhibit protein synthesis in primary monkey T cells in a dose-dependent manner. DT390–FN18sFv at 10^{−7} mol/L or FN18–CRM9 at 10^{−8} mol/L is sufficient to reduce protein synthesis of monkey primary T cells to less than 5% of the control. The 50% inhibition dosage (IC₅₀) of FN18–CRM9 is 1 × 10^{−10} mol/L, while the IC₅₀ of DT390–FN18sFv is 1 × 10^{−8} mol/L, reflecting the lowered affinity of monovalent Fab' FN18 to its parental divalent antibody. The availability of functional FN18sFv will provide the basis for the construction of divalent anti-CD3 immunotoxins for preclinical studies on the induction of tolerance in organ transplantation and experimental autoimmune diseases.

INTRODUCTION

Diphtheria toxin (DT,¹ 535 amino acids, 59 kDa) is composed of three functionally distinct regions: an enzymatically active domain, a cell receptor binding domain, and a domain for translocation of the toxin across the cell membrane (1). Because of its efficiency at crossing eukaryotic cell membranes and initiating cell death, it has been used to construct immunotoxins (ITs) to target and kill specifically selected cells (2–5). ITs were initially generated by chemically conjugating the toxin to a targeting protein [such as a monoclonal antibody (mAb)]. But the ITs made in this mode are heterogeneous chimeric molecules, and it is difficult to produce ITs in large amounts because the antibody and toxin must be purified separately and then conjugated in a reaction that often has a low yield. More recently, ITs have been constructed by fusing DT toxin genes with those genes encoding targeting proteins (6–13) and expressing the recombinant fusion protein in *Escherichia coli*. The genetic engineering procedure has advantages in economy and the potential to optimize the construct with respect to efficacy and freedom of side effects.

FN18–CRM9 is an anti-rhesus monkey CD3 immunotoxin, which is chemically conjugated with an anti-

rhesus monkey CD3 mAb FN18 and a binding site mutant of diphtheria toxin, CRM9 (14, 15). This immunotoxin is a monkey analogue of anti-human CD3 immunotoxin (UCHT1–CRM9) which is capable of regressing established xenografted human T cell (Jurkat) tumors in nude mice (16). FN18–CRM9 can transiently deplete T cells to 1% of initial values in both the blood and lymph node compartments and can also induce long term tolerance of mismatched renal allografts in rhesus monkey models (15, 17).

In this study, we cloned and sequenced the light and heavy chain variable regions (V_L and V_H) of FN18 and created the anti-monkey CD3 single-chain immunotoxin DT390–FN18sFv. DT390–FN18sFv is composed of a truncated DT mutant DT390 and an anti-monkey CD3 single-chain Fv (FN18sFv). It is highly toxic to monkey primary T cells through the CD3 moiety.

EXPERIMENTAL PROCEDURES

Cloning of Anti-Monkey CD3 Variable Regions and Construction of the DT390–FN18sFv Gene Cassette. The hybridoma FN18 producing anti-monkey CD3 (Biomedical Research Primate Center, Rijswijk, The Netherlands) was used for extraction of mRNA. The genes encoding anti-CD3 variable domains were amplified by RT-PCR on mRNA of FN18. The sense strand PCR primers for amplification of anti-CD3 light and heavy chain variable regions were degenerated primers and designed upon consensus sequences of murine framework residues according to Kabat et al. (18). The antisense primers were designed upon constant region sequences of murine mAb. The primer sequences we used are the following: V_L sense, 5'-CATGCCATGGGACATTGTGATGTACAGTCTC; V_L antisense, 5'-cctccgagccaccgctccgctgctccgctccTTTGATTTCAGCTTGCTGCC; V_H sense, 5'-gcagcggaggcgggtggtcgggagggggagggtcgcAGGTCCAGCTGCAGCAGTCTG; and

* To whom reprint requests should be addressed. Phone: 301-496-6807. Fax: 301-402-0245. E-mail: davidn@helix.nih.gov.

[®] Abstract published in *Advance ACS Abstracts*, September 1, 1997.

¹ Abbreviations: DT, diphtheria toxin; ITs, immunotoxins; RT-PCR, reverse transcriptase polymerase chain reaction; PCR, polymerase chain reaction; IPTG, isopropyl β-D-thiogalactopyranoside; SDS–PAGE, sodium dodecyl sulfate–polyacrylamide gel electrophoresis; EF-2, elongation factor-2; NAD, nicotinamide adenine dinucleotide; TCA, trichloroacetic acid; FITC, fluorescein isothiocyanate; FACS, fluorescence-activated cell sorting; PMA, phorbol myristate acetate; PBS, phosphate-buffered saline; BSA, bovine serum albumin.

V_H antisense, 5'-CGGAATTCCTTATGAGGAGACGGT-GACCGAG. The restriction sites *Nco*I and *Eco*RI are underlined. The complementary tags in primers are in lowercase, which is designed for encoding a (Gly₄Ser)₃ linker. The PCR products for each variable domain were cloned into the PCR II vector (Invitrogen, San Diego, CA) and sequenced by using a double-stranded DNA sequencing kit (GIBCO/BRL, Gaithersburg, MD). The V_L and V_H regions were linked together by recombinant PCR to create a single-chain variable fragment (FN18sFv) (V_L-linker-V_H). The unique restriction sites *Nco*I and *Eco*RI were incorporated at the 5'-end of V_L and the 3'-end of V_H for directional cloning, respectively. The linker encodes a (Gly₄Ser)₃ peptide which should allow for proper folding of the individual variable domains for forming a functional antibody binding site. DT390, a truncated DT gene fragment, was amplified from the genomic DNA of DT mutant strain CRM9, and the *Nde*I and *Nco*I restriction sites were incorporated at the 5'- and 3'-ends of DT390 fragment, respectively (13). The restriction enzyme-digested DT390 and FN18sFv were subcloned into the *E. coli* expression plasmid pET27b (Novagen, Madison, WI) for expression of the immunotoxin fusion protein (Figure 2).

Immunotoxin Expression and Purification. The FN18-CRM9 immunotoxin was conjugated as previously described by thiolating both the mAb FN18 moiety and the toxin CRM9 moiety and then cross-linking with bis-(maleimido)hexane (5).

DT390-FN18sFv was expressed in *E. coli* and purified with a Ni-RTA affinity column and an anion exchange column. Briefly, *E. coli* BL21(DE3) (Novagen) cells transformed with pET27b-DT390-FN18sFv were propagated in 2 L of LB medium containing 50 µg/mL kanamycin. Production of DT390-FN18sFv was induced by the addition of IPTG (Sigma, St. Louis, MO) to a final concentration of 0.5 mmol/L, and cells were cultured at 30 °C for 2 h prior to harvesting by centrifugation. The cell pellet was resuspended in 10 mL of sonication buffer [50 mmol/L sodium phosphate (pH 8.0) and 100 mmol/L NaCl] and lysed by sonication. It was then centrifuged (30000g for 30 min at 4 °C) to collect the soluble proteins. The crude DT390-FN18sFv fusion protein was loaded onto an 8 mL Ni-RTA resin column (1.2 × 7 cm) (Qiagen Inc., Chatsworth, CA) and washed with sonication buffer until the OD₂₈₀ per centimeter approached 0.01. The fusion protein was eluted with a 0 to 0.5 mol/L imidazole gradient in sonication buffer. The peak fractions were pooled and further purified with a 12 mL Q-Sepharose column. The fusion protein was eluted with a 0 to 0.5 mol/L NaCl gradient in 20 mmol/L Tris buffer (pH 8.0). The purified immunotoxin was confirmed with SDS-PAGE and Western blotting analysis.

Western Blotting Analysis. The Western blotting procedure is the same as described (19). The DT390-FN18sFv proteins separated on 10% SDS-PAGE were transferred to nitrocellulose paper and probed with an anti-DT A chain mAb (DT4, produced in this laboratory). After the phosphatase-labeled goat anti-mouse antibody probing, the membrane was color developed.

ADP Ribosylation Assay. The trypsin-nicked DT390-FN18sFv and CRM9 were examined for their ADP-ribosyltransferase activity as previously described (20). Briefly, 5 µL of diluted toxin samples was added with 5 µL of 0.25 mol/L dithiothreitol, followed by 15 µL of 10 mmol/L Tris-HCl buffer containing 1 mmol/L EDTA (pH 8.0) and 25 µL of EF-2, which was isolated from rat liver homogenates and purified by (NH₄)₂SO₄ precipitation and DEAE-Sephadex chromatography. The reactions were initiated by the addition of 10 µL of a

nicotinamide adenine dinucleotide (NAD) mixture which delivered 1 µCi of [³²P]NAD (Dupont NEN, Boston) and 10 µmol/L of unlabeled NAD (Sigma). After incubation at room temperature for 18 min, samples from the reactions were quenched in 0.1 mL of 10% trichloroacetic acid (TCA). The precipitate was spotted onto glass microfiber filter paper (Whatman GF/C) (Whatman Lab-sales, Inc., Hillsboro, OR) that had been presoaked in 10% TCA and 10 mmol/L NAD. Filters were washed twice with 5 mL of 10% TCA and once with 5 mL of 100% ethyl alcohol. Standard liquid scintillation techniques were used to determine the amount of radioactivity.

Isolation of the CD3 Positive Monkey Primary Cells. The monkey mononuclear cells were isolated from monkey blood by density centrifugation over a Ficoll-Hypaque gradient. The CD3 positive cells were isolated with the magnetic Dynabeads technique as indicated in the product instructions (DynaL Inc., Lake Success, NY). Briefly, the monkey blood mononuclear cells were incubated with an excess amount of FN18 for 30 min with gentle shaking at 4 °C. The pretreated cells were collected by centrifugation at 800g for 10 min, resuspended, and washed twice with Hank's balanced salt solution (HBSS, pH 7.4) to remove all unbound antibody. The Dynabeads M-450 goat anti-mouse IgG1 was added to the pretreated monkey cells to a final concentration of 4 × 10⁷ Dynabeads per 8 × 10⁶ cells in 1 mL. After the mixture was incubated for 10 min under bidirectional rotation, the cells attached to Dynabeads were collected with a Dynal magnet and washed in PBS/BSA (containing 0.1% BSA) three times. Finally, the CD3 positive cells attached to Dynabeads were cultured directly in RPMI 1640 medium containing 20 units/mL IL-2 (GIBCO/BRL) and 10 ng/mL PMA (Sigma) for 4–5 days to obtain sufficient cells for further experiments (21). To determine the purity of the selected T cells, they were analyzed by fluorescence-activated cell sorting (FACS). Briefly, cells (1 × 10⁶) were incubated on ice for 30 min with FITC-conjugated FN18 in PBS. After washing twice with PBS/BSA, cells were resuspended in 0.5 mL of PBS containing 2.5 µg/mL propidium iodide. Cells were analyzed in a Becton Dickinson FACS scanner. Dead cells were gated out on the basis of propidium iodide uptake.

Antibody and Immunotoxin Affinity Estimation by FACS Analysis. FN18 was derivatized with FITC at a mole ratio of 5:1 FITC:protein by Chromaprobe Inc. (Mountain View, CA). The Fab' fragment of FN18 was prepared by pepsin digestion using a Pierce kit (Rockford, IL) and the manufacturer's instructions which followed reduction. The product was verified by HPLC over a Zorbax (Dupont Co., Wilmington, DE) GF250 column. The Fab' fragment was derivatized with maleimide-FITC (Molecular Probes, Inc., Eugene, OR) utilizing the Fab' hinge region thiols. The relative affinities of the derivatized intact and Fab' antibody were estimated by comparing the concentrations where the mean channel fluorescence of T cell-bound antibody failed to increase beyond 10% with a 3-fold increment in concentration utilizing a whole blood method by flow cytometry (15). The same method was used to estimate the relative affinity of DT390-FN18sFv for FN18-CRM9. FN18-FITC was used as a tracer at 4.8 × 10⁻⁹ mol/L which was just below the saturation concentration for monkey T cell FACS analysis (data not shown). DT390-FNsFv and FN18-CRM9 were added as competitors ranging from 4.8 × 10⁻⁹ to 4.8 × 10⁻⁷ mol/L. One hundred microliters of monkey blood was incubated with the tracer in the presence or absence of the competitors for 30 min at room temperature, and then red blood cells

were lysed with lysis solution (Becton Dickinson, San Jose, CA). White blood cells were washed three times by a 1 min centrifugation and resuspended in PBS for FACS acquisition. Only the lymphocyte population was gated for data analysis.

Cytotoxicity Assay. The purified DT390–FN18sFv was quantified by BCA protein assay (procedure per the product instructions, Pierce). BCA assay-determined immunotoxin concentrations were comparable within a factor of 2 to those determined by a cell-free ADP ribosylation assay (20).

The cytotoxic activity of FN18–CRM9 and DT390–FN18sFv was determined by their ability to inhibit protein synthesis in isolated monkey primary T cells (13, 21), and a CD3 negative B cell line Ramos (ATCC, Rockville, MD) was used as a control in this assay. Briefly, the immunotoxin was serially diluted in ice-cold leucine-free RPMI 1640 (GIBCO/BRL), and 10 μ L of such immunotoxin dilutions was added to each appropriate well of a 96-well microtiter plate, which contained 5×10^4 cells/well in leucine-free RPMI 1640. After the contents of each well were carefully mixed, the plate was then incubated for 20 h at 37 °C in 5% humidified CO₂. Each well was then pulsed for 4 h with 10 μ L of [³H]-leucine (3.3 μ Ci/mL). Cells were harvested onto filters with a Skatron harvester and were counted in a Beckman liquid scintillation counter. Results were expressed as a percentage of the control to which no toxin was added.

To demonstrate that the cytotoxic effect of the DT390–FN18sFv is specifically mediated through the monkey CD3 moiety, competitive cytotoxicity experiments were performed using increasing concentrations of anti-CD3 mAb FN18 as an inhibitor to block cytotoxic effects. An irrelevant IgG1 mAb UCHT1, not reactive with rhesus T cells, was included as a control.

RESULTS

Gene Cloning of the FN18 Variable Regions. The genes encoding V_L and V_H regions of anti-monkey CD3 mAb FN18 were amplified from mRNA by RT-PCR. The mRNA was isolated from FN18 hybridoma cells. The amplified V_L and V_H gene segments of FN18 were cloned into the PCR II vector. Four V_L and four V_H recombinants were individually sequenced. The sequences are shown in Figure 1. The V_L and V_H regions have 339 and 372 base pairs and 113 and 124 amino acids, respectively. The sequences were analyzed according to the scheme of Kabat et al. (18). The FN18 V_L belongs to the mouse κ -chain IV group, and the V_H belongs to the mouse heavy chain IIA subgroup. The complementary determining regions and frameworks are indicated in the sequences.

Expression and Purification of the Single-Chain Immunotoxin. The single-chain immunotoxin DT390–FN18sFv gene construct is illustrated in Figure 2. The gene segments were digested with suitable restriction enzymes and subcloned into the pET27b expression vector. The pel B sequence encoding a signal peptide was added at the 5'-end of the fusion gene to facilitate the secretion of DT390–FN18sFv. A gene segment encoding a six-histidine tag was added at the 3'-end of the fusion gene for purification of DT390–FN18sFv.

The DT390–FN18sFv immunotoxin was expressed in *E. coli* BL21(DE3) cells by induction with IPTG and purified with a Ni-RTA affinity column and an anion exchange column. The yield of purified product is about 0.5–1 mg/L. The crude soluble and purified fractions of DT390–FN18sFv were separated on SDS–PAGE under reducing and nonreducing conditions. The fusion immunotoxin appears as an expected 70 kDa band on a Coomassie blue-stained gel (Figure 3A) and Western

FN18–V_L DNA Sequence and Corresponding Protein Sequence

FR1	
D I V M S Q S P S S L A V S V G E K V T	20
GACATTGTGATGTCACAGTCTCCATCTCCCTAGCTGTGTCAGTTGGAGAGAAGGTACT	60
CDR1	
M S C K S S Q S L L Y S S N Q K N Y L Y	40
ATGAGCTGCAAGCTCAGTCAGAGCCTTTATATAGTAGTAATCAAAAGAACTACTTGCC	120
FR2	
W Y Q Q K P G Q S P K L L I N W A S T R	60
TGGTACCAAGCAGAAGCCAGGGCAGTCTCTAAATGTGTGATTAACATGGGCATCCACAGG	180
CDR2	
E S G V P D R F T G S G S R T D F T L T	80
GAATCTGGGGTCCCTGATCGCTTCACAGGCAGTGGATCTAGGACAGATTCTACTCTACC	240
FR3	
I S S V K A E D L A V Y F C Q Q F Y S Y	100
ATCAGCAGTGTGAAGCTGAAGACCTGGCAGTTTATTTCTGTGCAAGTTTATAGTTAT	300
FR4	
P P T F G G G T K L E I K	113
CCTCCGACGTTCGGTGGAGGCCACCAAGCTGGAAATCAAA	339

FN18–V_H DNA Sequence and Corresponding Protein Sequence

FR1	
Q V Q L Q Q S E A E L A R P G A S V K M	20
CAGGTCCAGCTGCAGCAGTCTGAAGCTGAAGTGGCAAGCTGGGGCTCAGTGAAGATG	60
CDR1	
S C K A S G Y T F T D Y T I H W L K Q R	40
TCCTGCAAGGCTTCTGGCTACACCTTTACTGACTACACGATACACTGGTTAAACAGAGG	120
FR2	
P G Q G L D W I G Y F N P S S E S T E Y	60
CCTGGACAGGGTCTGGACTGGATTGGATATTTAATCTAGCAGTGAATCTACTGTAATAC	180
CDR2	
N R K F K D R T I L L A D R S S T T A Y	80
AATCGAAATTCAGGACAGGACCATATGTAGTCGACAGATCTCAACACAGCCTAC	240
FR3	
M Q L S S L T S E D S A V Y Y C S R K G	100
ATGCAACTGAGCAGCTGACATCTGAGGACTCTGGGGTCTATTACTGTTCAGAAAGGG	300
CDR3	
E K L L G N R Y W Y F D V W G A G T S V	120
GAGAACTACTTGGTAACCGTTACTGGTACTTCGATGTCTGGGGCGCAGGAGCTCGGTC	360
FR4	
T V S S	124
ACCGTCTCTCA	372

Figure 1. Nucleotide sequences and derived amino acid sequences of V_L and V_H regions of mAb FN18. The positions of the frameworks (FRs) and complementary determining regions (CDRs) are indicated. The sequences of FN18 V_L and V_H genes have been submitted to GenBank, and the accession numbers are U83617 and U83618, respectively.

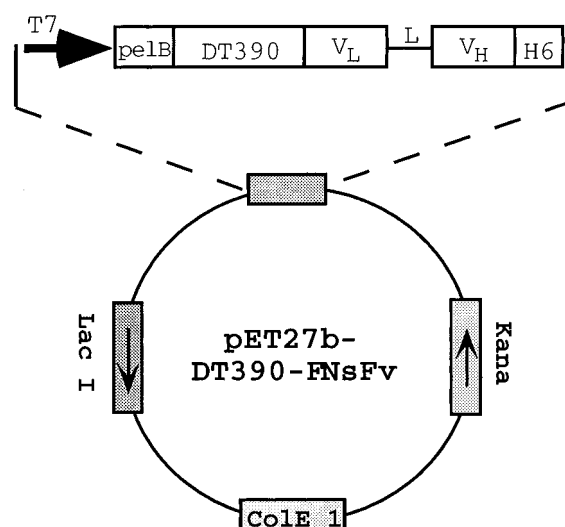


Figure 2. Schematic representation of the expression plasmid for single-chain immunotoxin DT390–FN18sFv. The single-chain immunotoxin gene DT390–FNsFv was constructed and cloned into vector pET27b for expression of the immunotoxin: T7, T7 promoter; pelB, signal sequence; DT390, truncated mutant of DT; V_L, light chain variable region of mAb FN18; L, (Gly₄Ser)₃ peptide linker; V_H, heavy chain variable region of mAb FN18; H6, six-histidine tag.

blotting membrane (Figure 3B). The soluble DT390–FN18sFv was enriched and partially purified by histidine tag affinity purification. Finally, the purified DT390–

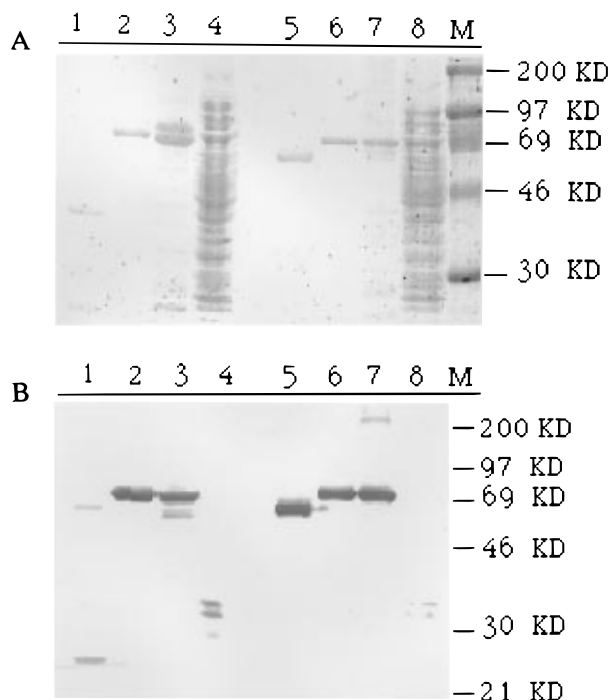


Figure 3. Analysis of DT390-FN18sFv protein purification. The protein samples were separated on 10% SDS-polyacrylamide gels under reduced (lanes 1–4) and nonreduced (lanes 5–8) conditions. (A) The protein bands were visualized with Coomassie Blue R250 staining. (B) An identical gel was transferred to a nitrocellulose membrane and detected using anti-A chain monoclonal antibody in Western blotting. Lanes 4 and 8 are crude DT390-FN18sFv before purification. Lanes 3 and 7 are partially purified fractions following a single step with a Ni-RTA affinity column. Lanes 2 and 6 are the final product obtained by anion exchange following the affinity step. Lanes 1 and 5 are pure CRM9 as controls.

FN18sFv was obtained by anion exchange chromatography, and it was shown as a single 70 kDa band on SDS-PAGE and the Western blotting assay by an anti-DT A chain mAb. The nicked CRM9 was used as a control. As we assumed, both the A (21 kDa) and B chain (37 kDa) were visualized under reducing condition. Additionally, only one band (59 kDa) for CRM9 was observed under nonreducing conditions. The CRM9 B chain was not detected in Western blotting because the probing antibody is directed against the DT A chain.

ADP Ribosylation Activity. The toxicity of diphtheria toxin is due to the ADP ribosylation of cytoplasmic EF-2 by DT A chain enzymatic activity, to further inhibit protein synthesis. A cell-free assay system was used to determine the enzymatic activity of DT390-FN18sFv. The serially diluted DT390-FN18sFv or CRM9 reacted with EF-2 in the presence of [32 P]nicotinamide adenine dinucleotide. The results showed that serially diluted DT390-FN18sFv and CRM9 produce a similar dose-dependent increase of 32 P radioactivity incorporation in the TCA-precipitated products (Figure 4). This confirms that DT390-FN18sFv possesses an ADP ribosylation activity similar to that of CRM9.

Antibody and Immunotoxin Affinity Estimation by FACS Analysis. The FACS analyses were performed to compare the specificity and affinity of the recombinant immunotoxin and the chemically conjugated immunotoxin (Figure 5). FN18-CRM9 and FN18 significantly inhibit the binding of FN18-FITC to monkey T cells at the same concentration of FN18-FITC (4.8×10^{-9} mol/L), and they largely replace the FN18-FITC binding to monkey T cells at a concentration 10–100 times higher. But the DT390-FN18sFv did not significantly inhibit the

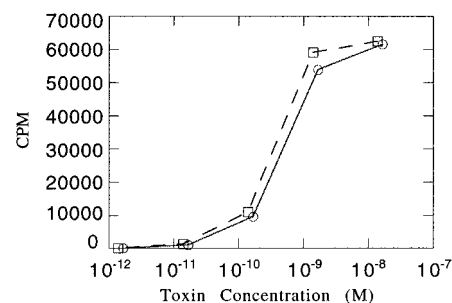


Figure 4. ADP ribosylation activity assay of DT390-FN18sFv. The ADP transferase activity of the nicked DT390-FN18sFv (○) and nicked CRM9 (□) was determined in a cell-free assay, which contained elongation factor-2 (EF-2) and [32 P]nicotinamide adenine dinucleotide. The counts of [32 P]ADP-ribose-associated EF-2 showed the enzymatic activity of the toxins. Data are expressed as mean counts versus concentration.

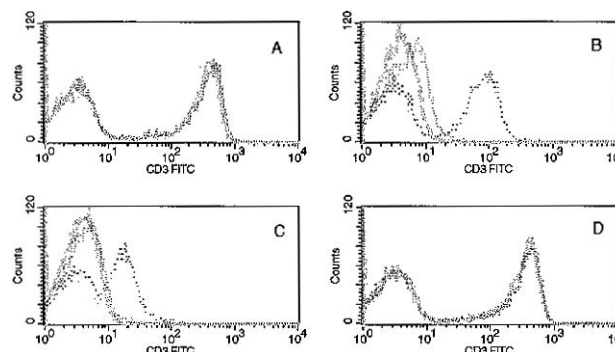


Figure 5. FACS analysis of competitive binding of the immunotoxins to monkey T cells. Monkey blood cells following RBC lysis were used as target cells and mixed with tracer FN18-FITC at 4.8×10^{-9} mol/L (orange curve) and competitors at 4.8×10^{-9} mol/L (black dot curve), 4.8×10^{-8} mol/L (green curve), and 4.8×10^{-7} mol/L (red curve). Competitors are DT390-FN18sFv (A), FN18-CRM9 (B), FN18 (C), and an irrelevant mAb UCHT1 (D). Fluorescent values below 10 are largely due to autofluorescence of cells. Both FN18 and FN18-CRM9 significantly compete with FN18-FITC at 4.8×10^{-9} mol/L (B and C), whereas DT390-FN18sFv fails to compete at 4.8×10^{-9} mol/L (A).

binding of FN18-FITC to monkey T cells at the same concentrations. These results indicate that the affinity of DT390-FN18sFv for the rhesus CD3 epitope is less than $1/100$ of that of the FN18. To determine if this affinity loss was due to the monovalency of the DT390-FN18sFv construct, we prepared Fab' FN18-FITC and compared its binding to monkey T cells with that of FN18-FITC under similar conditions. FN18-FITC binding was 90% saturated at 4.8×10^{-9} mol/L (data not shown). Over the concentration range of 0.5 – 5.0×10^{-6} mol/L, Fab' FN18-FITC displayed a hyperbolic binding curve; however, 90% saturation was not achieved in the 1 – 5×10^{-6} mol/L interval (data not shown). This indicates that the monovalent Fab' FN18-FITC has at least a $1/200$ reduction in affinity with respect to the divalent FN18-FITC.

Specific Cytotoxicity of the Anti-Monkey CD3 Single-Chain Immunotoxin. The CD3 positive monkey T cells used for the cytotoxicity assay were isolated from monkey mononuclear cells by the indirect magnetic Dynabeads method and stimulated with anti-monkey CD3 mAb FN18 in the presence of IL-2 and PMA. After 5 days of culture, 99% of live cells were CD3 positive as shown by FACS analysis (Figure 6).

The cytotoxic effects of DT390-FN18sFv and FN18-CRM9 were evaluated with these CD3 positive monkey T cells and the CD3 negative B cell line Ramos (Figure 7A). Both immunotoxins can inhibit the protein synthe-

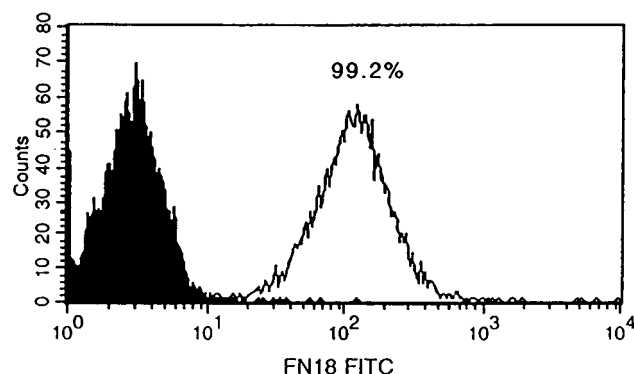


Figure 6. CD3 positive monkey primary T cells isolated by magnetic Dynabeads technique. The isolated T cells were subjected to FACS analysis with FITC-labeled anti-monkey CD3 mAb FN18. Dead cells were removed by gating. A negative control with unlabeled FN18 is shown as a filled curve; FN18-FITC binds to 99% of the live cells as indicated by the shift in relative fluorescence intensity.

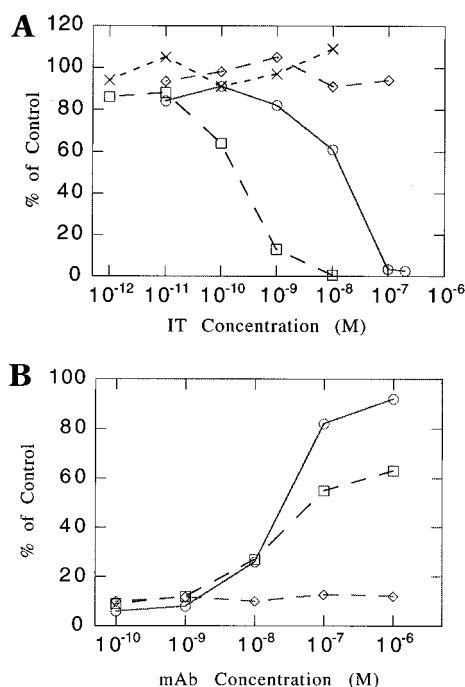


Figure 7. DT390-FN18sFv mediates the specific cytotoxicity to monkey primary T cells through the CD3 ϵ moiety in a dose-dependent way similar to that of FN18-CRM9. (A) Monkey T cells were incubated with increasing concentrations of DT390-FN18sFv (\circ) or FN18-CRM9 (\square) for 20 h in leucine-free medium in a 96-well plate. Cells were pulsed with [3 H]leucine and harvested for scintillation counting; the cytotoxicity of DT390-FN18sFv (\diamond) and FN18-CRM9 (\times) to CD3 negative B cell line Ramos was measured under the same conditions. (B) Increasing concentrations of mAb FN18 were mixed with 1×10^{-7} mol/L DT390-FN18sFv (\circ) or 1×10^{-9} mol/L FN18-CRM9 (\square) and then added to cells for the cytotoxicity assay. Results were expressed as a percentage of the control to which no toxin was added. The cytotoxicity blocking assay of 1×10^{-7} mol/L DT390-FN18sFv (\diamond) by an irrelevant antibody UCHT1 was also carried out under the same conditions.

sis of monkey primary T cells in a dose-dependent manner. After a 20 h incubation for cytotoxicity assay, about 10^{-8} mol/L FN18-CRM9 or 10^{-7} mol/L DT390-FN18sFv was sufficient to reduce protein synthesis of monkey CD3 positive cells to less than 5% of the control. The 50% inhibitory dosage (IC_{50}) of FN18-CRM9 is about 1×10^{-10} mol/L, and the IC_{50} of DT390-FN18sFv is about 1×10^{-8} mol/L. However, DT390-FN18sFv and FN18-CRM9 did not show any cytotoxicity to CD3

negative B cell line Ramos. The result shows that the fusion immunotoxin is specifically toxic to monkey T cells.

The competitive cytotoxicity experiments further demonstrated that the cytotoxic effect of DT390-FN18sFv is specifically mediated through the monkey CD3 moiety. The results of cytotoxicity blocking assay by parental mAb FN18 and an irrelevant mAb UCHT1 on monkey T cells are presented in Figure 7B. The parental mAb FN18 can block the cytotoxicity of FN18-CRM9 and DT390-FN18sFv in a dose-dependent way, and it needs more FN18 to block the cytotoxicity of FN18-CRM9 to the same level as that for DT390-FN18sFv. The toxicity of both constructs can be completely inhibited with an excess of FN18 ($>10^{-6}$ mol/L). However, the irrelevant mAb UCHT1 did not block the cytotoxicity of the fusion immunotoxin to monkey T cells in increasing concentrations. The result confirmed that DT390-FN18sFv was specifically toxic to monkey T cells and less toxic than FN18-CRM9 which contains divalent mAb FN18 as a binding moiety.

DISCUSSION

In this report, we cloned the light and heavy chain variable regions of anti-monkey CD3 mAb FN18 and constructed the anti-monkey CD3 single-chain immunotoxin DT390-FN18sFv. The monovalent single-chain Fv, FN18sFv, specifically recognizes the CD3 ϵ subunit of the monkey T cell receptor and can mediate DT390 entry into monkey T cells by an optimal intracellular routing (22). The fusion immunotoxin could specifically inhibit the protein synthesis of CD3 positive monkey T cells but was not toxic to CD3 negative cells, and its cytotoxicity can be blocked by the parental mAb FN18 in a dose-dependent mode, but not by an irrelevant antibody. Other studies have also demonstrated the relatively low nonspecific toxicity of DT390 fusion toxins (2, 9, 12, 13). The experiments confirmed that the toxic effect of DT390-FN18sFv on monkey T cells is specifically mediated through the CD3 moiety.

Intoxication of cells by immunotoxins can be subdivided into four general steps: (1) specific binding to the cell surface, (2) endocytosis into the cells, (3) translocation of the enzymatic domain of the toxin out of the endosome, and (4) enzymatic inactivation of the target molecule (13, 22). The single-chain immunotoxin DT390-FN18sFv is less toxic to monkey T cells than the chemically conjugated FN18-CRM9, but the ADP ribosylation assay demonstrated that DT390-FN18sFv possessed ADP-ribosyltransferase activity similar to that of FN18-CRM9. In the competitive cytotoxicity assay, more parental mAb FN18 was needed for blocking the cytotoxicity of 1×10^{-9} M FN18-CRM9 than for 1×10^{-7} M DT390-FN18sFv. The FACS competitive binding analysis indicated that DT390-FN18sFv possessed less than $1/100$ of the affinity to the monkey CD3 moiety compared to FN18-CRM9. We noted at least a $1/200$ loss in the T cell binding of monovalent Fab' FN18-FITC compared to that of the divalent FN18-FITC. Therefore, the $1/100$ reduction in potency of the engineered DT390-FN18sFv construct compared to the chemically coupled construct can be explained, at least in large part, by the $1/100$ reduction in affinity of the intoxication pathway cell surface receptor binding step secondary to monovalency. This indirectly suggests that the translocation step in the engineered immunotoxin pathway is largely intact. We are currently acquiring direct evidence on this point.

The large reduction in binding affinity between monovalent and divalent anti-CD3 ϵ and the rhesus T cell receptor indicates that divalent binding is the preferred binding mode. This may reflect the fact that each T cell

receptor complex contains two CD3 ϵ chains (23) so that divalent binding and ligation within a single T cell receptor can occur. Others have reported smaller reductions in binding on going from divalent to monovalent binding or binding mediated through Fv compared to Fab' (24–28). However, our data indicate that divalent immunotoxin binding for the CD3 ϵ is highly correlated with potency. This suggests to us that optimized engineered anti-CD3 ϵ immunotoxins will require a divalent construction. We have already constructed a single-chain divalent anti-human CD3 ϵ antibody that can serve as the basis for such an immunotoxin (19). The availability of cloned anti-rhesus anti-CD3 ϵ sFv should permit the construction of divalent anti-rhesus anti-CD3 ϵ immunotoxins.

FN18–CRM9 is highly efficacious for inducing organ transplantation tolerance and retarding the progress of experimental allergic encephalomyelitis in monkey models (17, 30). However, studies have also found that monkeys like humans can contain pre-existing anti-DT antibodies which can reduce the ability of anti-CD3–CRM9 immunotoxins to induce T cell depletion (15). Thompson et al. (13) investigated the inhibitory effect of the pre-existing anti-DT antibodies in human serum to anti-human CD3 immunotoxin UCHT1–CRM9 and a DT390 single-chain immunotoxin. The DT390 immunotoxin was only moderately inhibited by anti-DT antibodies in human serum under conditions resulting in complete neutralization of UCHT1–CRM9 (13). This suggests that DT390 immunotoxins will also reduce the inhibitory effect of the pre-existing anti-DT antibody in monkey studies and permit a preclinical evaluation of these immunotoxins for the induction of transplantation tolerance and the treatment of autoimmune disease and T cell leukemias.

In summary, this report describes a single-chain immunotoxin, DT390–FN18sFv. It has specific toxic effects on monkey primary T cells mediated through the CD3 ϵ moiety. It inhibits protein synthesis of monkey T cells in a manner similar to that of the chemically conjugated immunotoxin CRM9–FN18 that has efficient treatment effects for organ transplantation and autoimmune disease in monkey models (17, 30). Divalent forms of DT390–FN18sFv with enhanced binding affinity based on divalent single-chain antibodies (19) are currently under construction.

ACKNOWLEDGMENT

We thank Dr. Margaret Jonker for making the hybridoma-producing FN18 mAb available for this study.

LITERATURE CITED

- Nicholls, P. J., Johnson, V. G., Andrew, S. M., Hoogenboom, H. R., Raus, J. C. M., and Youle, R. J. (1993) Characterization of single-chain antibody (sFv)-toxin fusion proteins produced *in vitro* in rabbit reticulocyte lysate. *J. Biol. Chem.* **268**, 5302.
- Murphy, J. R., and van der Spek, J. C. (1995) Targeting diphtheria toxin to growth factor receptors. *Semin. Cancer Biol.* **6**, 259.
- Youle, R. J., Greenfield, L., and Johnson, V. G. (1988) Genetic engineering of immunotoxins. In *Immunotoxins* (A. E. Frankel, Ed.) pp 113–122, Kluwer Academic Publishers, Boston.
- Nicholls, P. J., and Youle, R. J. (1992) The Structure of diphtheria toxin as a guide to rational design. In *Genetically Engineered Toxins* (A. E. Frankel, Ed.) pp 339–363, Marcel Dekker Inc., New York.
- Neville, D. M., Jr., Srinivasachar, K., Stone, R., and Scharff, J. (1989) Enhancement of immunotoxin efficacy by acid-cleavable cross-linking agents utilizing diphtheria toxin and toxin mutants. *J. Biol. Chem.* **264**, 14653.
- Murphy, J. R., Bishai, W., Borowski, M., Miyanochara, A., Boyd, J., and Nagle, S. (1986) Genetic construction, expression, and melanoma-selective cytotoxicity of a diphtheria toxin-related alpha-melanocyte-stimulating hormone fusion protein. *Proc. Natl. Acad. Sci. U.S.A.* **83**, 8258.
- Williams, D. P., Parker, K., Bacha, P., Bishai, W., Borowski, M., Genbauffe, F., Strom, T. B., and Murphy, J. R. (1987) Diphtheria toxin receptor binding domain substitution with interleukin-2: genetic construction and properties of a diphtheria toxin-related interleukin-2 fusion protein. *Protein Eng.* **1**, 493.
- Jean, L. L., and Murphy, J. R. (1991) Diphtheria toxin receptor-binding domain substitution with interleukin 6: genetic construction and interleukin 6 receptor-specific action of a diphtheria toxin-related interleukin 6 fusion protein. *Protein Eng.* **4**, 989.
- Chaudhary, V. K., Gallo, M. G., FitzGerald, D. J., and Pastan, I. (1990) A recombinant single-chain immunotoxin composed of anti-Tac variable regions and a truncated diphtheria toxin. *Proc. Natl. Acad. Sci. U.S.A.* **87**, 9491.
- Batra, J. K., FitzGerald, D. J., Chaudhary, V. K., and Pastan, I. (1991) Single-chain immunotoxins directed at the human transferrin receptor containing *Pseudomonas* exotoxin A or diphtheria toxin: anti-TFR(Fv)-PE40 and DT388-anti-TFR(Fv). *Mol. Cell. Biol.* **11**, 2200.
- Chan, C. H., Blazar, B. R., Eide, C. R., Kreitman, R. J., and Valleria, D. A. (1995) A murine cytokine fusion toxin specifically targeting the murine granulocyte-macrophage colony-stimulating factor (GM-CSF) receptor on normal committed bone marrow progenitor cells and GM-CSF-dependent tumor cells. *Blood* **86**, 2732.
- Valleria, D. A., Panoskaltsis-Mortari, A., Jost, C., Ramakrishnan, S., Eide, C. R., Kreitman, R. J., Nicholls, P. J., Pennell, C., and Blazar, B. R. (1996) Anti-graft-versus-host disease effect of DT390-anti-CD3sFv, a single chain Fv fusion immunotoxin specifically targeting the CD3 ϵ moiety of the T-cell receptor. *Blood* **88**, 2342.
- Thompson, J., Hu, H. Z., Scharff, J., and Neville, D. M., Jr. (1995) An anti-CD3 single-chain immunotoxin with a truncated diphtheria toxin avoids inhibition by pre-existing antibodies in human blood. *J. Biol. Chem.* **270**, 28037.
- Greenfield, L., Johnson, V. G., and Youle, R. J. (1987) Mutations in diphtheria toxin separate binding from entry and amplify immunotoxin selectivity. *Science* **238**, 536.
- Neville, D. M., Jr., Scharff, J., Hu, H. Z., Rigaut, K., Shiloach, J., Slingerland, W., and Jonker, M. (1996) A new reagent for the induction of T-cell depletion, anti-CD3–CRM9. *J. Immunother.* **19**, 85.
- Neville, D. M., Scharff, J., and Srinivasachar, K. (1992) In vivo T-cell ablation by a holo-immunotoxin directed at human CD3. *Proc. Natl. Acad. Sci. U.S.A.* **89**, 2585.
- Knechtle, S., Vargo, D., Fechner, J., Zhai, Y., Wang, J., Hanaway, M. J., Scharff, J., Hu, H. Z., Knapp, L., Watkins, D., and Neville, D. M., Jr. (1997) FN18–CRM9 immunotoxin promotes tolerance in primate renal allografts. *Transplantation* **63**, 1.
- Kabat, E. A., Wu, T. T., Reid-Miller, M., and Gottesman, K. S. (1987) in *Sequences of Proteins of Immunological Interest*, U.S. Department of Health and Human Services, U.S. Government Printing Office, Washington, DC.
- Ma, S. L., Thompson, J., Hu, H. Z., and Neville, D. M., Jr. (1996) Expression and characterization of a divalent chimeric anti-human CD3 single chain antibody. *Scand. J. Immunol.* **43**, 134.
- Youle, R. J., and Neville, D. M., Jr. (1979) Receptor-mediated transport of the hybrid protein ricin diphtheria toxin fragment A with subsequent ADP-ribosylation of intracellular elongation factor II. *J. Biol. Chem.* **254**, 11089–11096.
- Rigaut, K. D., Scharff, J., and Neville, D. M., Jr. (1995) Selective killing of T cells by immunotoxins directed at distinct V β epitopes of the T cell receptor. *Eur. J. Immunol.* **25**, 2077.
- Neville, D. M., Jr., Scharff, J., and Srinivasachar, K. (1992) Anti-T cell immunotoxins: a look at post-endocytotic receptor-mediated routing. *J. Controlled Release* **24**, 133.

- (23) Blumberg, R. S., Ley, S., Sanch, J., Lonberg, N., Lacy, E., McDermott, F., Schad, V., Greenstein, J. L., and Terhorst, C. (1990) Structure of the T-cell antigen receptor: Evidence for two CD3 ϵ subunits in the T-cell receptor-CD3 complex. *Proc. Natl. Acad. Sci. U.S.A.* 87, 7220.
- (24) Anand, N. N., Mandal, S., Mackenzie, C. R., Sadowska, J., Sigurskjod, B., Young, N. M., Bundle, D. R., and Narang, S. A. (1991) Bacterial expression and secretion of various single-chain Fv genes encoding proteins specific for a *Salmonella* serotype B O-antigen. *J. Biol. Chem.* 266, 21874.
- (25) Condra, J. H., Sardana, V. V., Tomassini, J. E., Schlabach, A. J., Davies, M. E., Lineberger, D. W., Graham, D. J., Gotlib, L., and Colonna, R. J. (1990) Bacterial expression of antibody fragments that block human Rhinovirus infection of cultured cells. *J. Biol. Chem.* 265, 2292.
- (26) Bird, R. E., Hardman, K. D., Jacobson, J. W., Johnson, S., Kaufman, B. M., Lee, S. M., Lee, T., Pope, S. H., Riordan, G. S., and Whitlow, M. (1988) Single-chain antigen-binding proteins. *Science* 242, 423.
- (27) Chaudhary, V. K., Queen, C., Junghans, J. P., Waldmann, T. A., FitzGerald, D. J., and Pastan, I. (1989) A recombinant immunotoxin consisting of two antibody variable domains fused to *Pseudomonas* exotoxin. *Nature* 339, 394.
- (28) Batra, J. K., FitzGerald, D. J., Chaudhary, V. K., and Pastan, I. (1991) Single chain immunotoxin directed at the human transferrin receptor containing *Pseudomonas* exotoxin A or diphtheria toxin: anti-TFR (Fv). *Mol. Cell. Biol.* 11, 2200.
- (29) Huston, J. S., Levinson, D., Mudgett-Hunter, M., Tai, M.-S., Novotny, J., Margolies, M. N., Ridge, R. J., Brucoleri, R. E., Haber, E., Crea, R., and Oppermann, H. (1988) Protein engineering of antibody binding sites: recovery of specific activity in an anti-digoxin single chain Fv analogue produced in *Escherichia coli*. *Proc. Natl. Acad. Sci. U.S.A.* 85, 5879.
- (30) Hu, H. Z., Stavrou, S., Baker, B. C., Tornatore, C., Scharff, J., Okunieff, P., and Neville, D. M., Jr. (1997) Depletion of T lymphocytes with immunotoxin retards the progress of experimental allergic encephalomyelitis in rhesus monkeys. *Cell. Immunol.* 177, 26.

BC9701398

Water-Soluble Polyion Complex Associates of DNA and Poly(ethylene glycol)–Poly(L-lysine) Block Copolymer

Satoshi Katayose and Kazunori Kataoka*

Department of Materials Science and Technology and Research Institute for Biosciences, Science University of Tokyo, Yamazaki 2641, Noda-shi, Chiba 278, Japan. Received February 13, 1997[®]

Complex formation of poly(ethylene glycol)–poly(L-lysine) (PEG–PLL) AB type block copolymer with salmon testes DNA or Col E1 plasmid DNA in aqueous milieu was studied. The PLL segment of PEG–PLL interacts with nucleic acid through an electrostatic force to form a water-soluble complex associate with a diameter of ca. 50 nm. PEG segments surrounding the core of the polyion complex prevented the complex from precipitation even under stoichiometric conditions, at which the unit ratio of L-lysine in PEG–PLL and phosphate in the DNA is equal. The profile of the thermal melting curve revealed a higher stabilization of DNA structure in PEG–PLL/DNA complexes compared to that in the complex made from DNA and PLL homopolymer with the same molecular weight as the PLL segment in PEG–PLL. This stabilizing effect on the DNA structure may be due to the compartmentalization of DNA into the microenvironment of PEG with low permittivity. The reversible nature of the PEG–PLL/DNA complex was further verified through the addition of polyanion [poly(L-aspartic acid)]: Poly(L-aspartic acid) replaced DNA in the complex with PEG–PLL, resulting in the release of free DNA in the medium. Furthermore, the PEG–PLL/DNA complex showed high resistance against DNase I attack, suggesting DNA protection through the segregation into the core of the associate having PEG palisade.

INTRODUCTION

Polyion complexes between polyelectrolytes with an opposite charge have attracted wide attention in the fields of medicine and biology. For example, polyion complexes of a nucleotide with polycations are considered one of the promising systems for a gene vector (1–5). DNA has a polyanionic character and can be bound to polycations, e.g., poly(L-lysine), through electrostatic interaction. It is well-known that polylysine strongly binds to DNA to induce compaction of the DNA molecule (6–8). However, a soluble and electrically neutral (stoichiometric) complex consisting of poly(L-lysine) and DNA is hardly obtained because charge neutralization usually induces the formation of insoluble precipitates.

Recently, we have shown that complexation of DNA with a poly(ethylene glycol)–poly(L-lysine) block copolymer (PEG–PLL) led to the formation of water-soluble complex associates in aqueous milieu (9). Use of a cationic block copolymer with a PEG segment as the complexation partner of DNA was based on the results of our systematic study on polymeric micelle drugs (10, 11). Supramolecular association of a block copolymer consisting of PEG and polyamino acids through hydrophobic or electrostatic interaction leads to the formation of core-shell type nanoassociates or micelles in which drug molecules are hydrophobically or electrostatically included in the core of the micelle surrounded by the PEG outer shell (12–14). The proper micelle size, ca. ~50 nm, and high flexibility and hydrophilicity of the outer-shell PEG seem to contribute to the stability of the micelles. Indeed, both long circulation in the blood compartment and exceptionally high accumulation in a solid tumor were evidenced for block copolymer micelles with an entrapped anticancer drug (doxorubicin) (15, 16). These features of block copolymer micelles provide a rationale

for exploring the feasibility of polymeric micelles as a novel vector system for genes and oligonucleotides. It should be noted that water-soluble and narrowly distributed polyion complex micelles have recently been prepared from a pair of PEG–PLL and an oligonucleotide with antisense activity toward the oncogene (c-Ha-ras) by our group (17). Further, transfection activity of plasmid DNA/PEG–PLL was recently reported by Wolfert et al., indicating a promising feature of these block copolymer/nucleotide complexes as a novel vector system (18). PEG–PLL association with DNA is also interesting from the standpoint of modeling the interaction of cationic proteins with DNA through electrostatic interactions, which are responsible for the stability of the higher ordered chromatin structure. Particularly, study of the exchange reaction of complexed DNA with other polyanion compounds could provide a motivation for exploring a gene expression from the chemical point of view.

We report here the physicochemical characteristics of water-soluble nanoassociates formed between salmon testes DNA or Col E1 plasmid DNA and a PEG–PLL block copolymer. The stability of the complex is discussed on the basis of the results of melting curve measurements, which have been widely used to estimate the properties of polylysine/DNA complexes as a model for chromatin (19–29). Further, dissociation of the complex was evidenced through the exchange reaction of complexed DNA with a model polyanion [poly(aspartic acid)].

MATERIALS AND METHODS

Materials. High molecular weight poly(L-lysine) hydrobromide (H-PLL, DP = 927), low molecular weight poly(L-lysine) hydrobromide (L-PLL, DP = 19), poly(L-aspartic acid) sodium salt (DP = 105), and DNA (sodium salt from salmon testes) were purchased from Sigma Chemical Co. and used without further purification. Col E1 plasmid DNA (6646 bp, percentage of GC is 48%), which produces colicin E1, was purchased from Nippon Gene Co., Ltd., Japan. DNase I nuclease and *EcoRI* restriction nuclease were purchased from Takara Shuzo

* Author to whom correspondence should be addressed (telephone +81-471-23-9771; fax +81-471-23-9362).

[®] Abstract published in *Advance ACS Abstracts*, August 15, 1997.

Co., Ltd., Japan. Col E1 plasmid was linearized using *EcoRI* restriction nuclease through a standard protocol. α -Methyl- ω -amino poly(ethylene glycol) (MW = 4300) was a cordial gift from Nippon Oil & Fats Co., Ltd., Japan. The PEG-PLL block copolymer (average degree of PLL segment is 20) was prepared as described before (14). For other reagents, commercial special grade reagents were used without further purification.

Dynamic Light Scattering (DLS) and Laser-Doppler Electrophoresis Measurements of PEG-PLL/DNA Complex. DLS measurements were carried out using a DLS-700 instrument (Otuka Electronics Co, Ltd.). An Ar ion laser ($\lambda_0 = 488$ nm) was used as the incident beam. The sample was prepared by direct mixing of each solution of DNA (from salmon testes) and PEG-PLL in 10 mM sodium phosphate buffer (pH 7.4) containing 150 mM NaCl. PEG-PLL solution of a certain concentration was added to 1.0 mL of 50 μ g/mL (1.00 OD at 260 nm) DNA solution to completely compensate for the charge of the DNA (stoichiometric condition). The DNA concentration of the mixture was then adjusted to 25 μ g/mL for DLS measurement. Laser-Doppler electrophoresis measurements of the complex associates were carried out using an ELS-800 instrument (Otuka Electronics) in 10 mM phosphate buffer (pH 7.4). From the determined electrophoretic mobility, the zeta-potential (ζ) was calculated according to the Smoluchowski equation as

$$\zeta = 4\pi\eta u/\epsilon$$

where η is the viscosity of the solution, u is the electrophoretic mobility, and ϵ is the dielectric constant of the solvent.

Measurement of Melting Curve of PEG-PLL/DNA Complexes. DNA (from salmon testes) was dissolved at a concentration of 1.00 OD in 1 mM sodium phosphate buffer (pH 7.4). To a constant volume of DNA solution were added directly at once varying amounts of PEG-PLL, H-PLL, or L-PLL in an equivolume of phosphate buffer to form a solution with a DNA concentration of 0.50 OD. The ratio of lysine residue to the nucleotide in the mixed solution is designated r ($=$ [lysine residue]/[nucleotide]). After 2 h of incubation at room temperature, the same volume of methanol was added to each sample. The melting profiles of the complexes were then monitored by absorbance at 260 nm on a Jasco Ubest-50 spectrophotometer with a Peltier EHC363 type cell holder. Samples were heated from 30 to 76 $^{\circ}$ C. The scanning rate was 1.0 $^{\circ}$ C/min.

Differential Scanning Calorimeter (DSC) Measurement of DNA Complexes. The thermal behavior of the DNA complexes in 10 mM phosphate buffer (pH 7.4) (DNA concentrations were adjusted to 250 μ g/mL) was determined using a microdifferential scanning calorimeter (MC-2 differential scanning calorimeter, Microcal, Inc.). One milliliter of PEG-PLL solution with various concentrations was added dropwise to 1.0 mL of DNA solutions (DNA concentration was 500 μ g/mL) to form $r = 0.10$, 0.20, and 0.30 complexes with vortex stirring. Two hundred fifty micrograms of complexed DNA was used for DSC measurement. The samples were heated from 10 to 105 $^{\circ}$ C. The heating rate was 1.5 $^{\circ}$ C/min.

Exchange Reaction of PEG-PLL/Plasmid DNA (pDNA) Complex with Poly(aspartic acid). The PEG-PLL/pDNA complex ($r = 1.0$, DNA concentration was 33.3 μ g/mL) was prepared through a direct mixing of linearized Col E1 pDNA and PEG-PLL block copolymer in 10 mM phosphate-buffered saline (10 mM sodium phosphate buffer containing 150 mM NaCl, pH 7.4). The

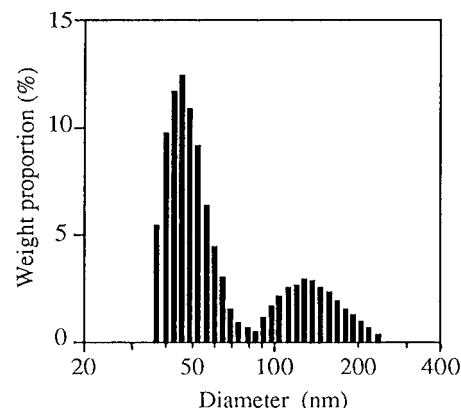


Figure 1. Size distribution of PEG-PLL/DNA complex determined from DLS measurement (weight-averaged scale).

complex was incubated for 2 h at room temperature, followed by the addition of poly(aspartic acid) [P(Asp)] solutions of various concentrations in 10 mM phosphate-buffered saline. The molar ratio of P(Asp) to DNA in the complexes was 0.50, 1.0, 2.0, 4.0, 10, and 20. The final concentration of pDNA was adjusted to 25 μ g/mL. After overnight incubation of the mixtures at room temperature, 25 μ L of each sample was analyzed by electrophoresis at 5.6 V/cm with a 0.6% agarose gel in Tris-HCl buffer (pH 7.4) (3.3 mM Tris, 1.7 mM sodium acetate). DNA was visualized by ethidium bromide (0.5 μ g/mL of gel). The same experiments were done for the H-PLL (DP = 927)/pDNA complex to compare the stability with PEG-PLL/pDNA complexes.

Nuclease Resistance of PEG-PLL/DNA Complex. Salmon testes DNA (0.8 OD) and an equimolar amount of PEG-PLL in 10 mM phosphate buffer (pH 7.4) containing 5 mM magnesium sulfonate were mixed directly to obtain a 0.4 OD solution of PEG-PLL/DNA complex ($r = 1.0$). After the addition of 10 units (10 μ L) of DNase I to 1 mL of PEG-PLL/DNA complex at 25 $^{\circ}$ C, the absorbance change at 260 nm was followed to estimate DNA degradation by DNase I.

RESULTS AND DISCUSSION

DLS Measurement of PEG-PLL/DNA Complex. On the addition of PEG-PLL to a 1.0 OD solution of DNA in 10 mM phosphate buffer containing 150 mM NaCl at pH 7.4 (phosphate-buffered saline), no turbidity was observed even under stoichiometric condition, when the unit ratio of L-lysine and phosphate was equal ($r = 1.0$). This is in sharp contrast to the mixture of H-PLL or L-PLL with DNA, which caused a precipitate regardless of the polymerization degree with increasing r to 1.0. In spite of the transparent appearance of the PEG-PLL/DNA solution, the light scattering intensity of the solution was increased about 10 times compared to that of the original DNA solution, suggesting the formation of water-soluble nanoassociates through a complexation of DNA with PEG-PLL. Indeed, this was verified by the histogram analysis of the DLS data. Figure 1 shows the weight-averaged size distribution analyzed by the histogram method for the PEG-PLL/DNA complex. Associates of 48.5 nm in diameter were observed with a small fraction of secondary aggregates in the 140 nm region. Size and distribution were similar for all of the associates prepared with varying salt concentration in the range between 0 and 300 mM NaCl in 10 mM phosphate buffer. Recently, atomic force microscope image of the PEG-PLL/DNA complex was reported by Wolfert et al. (18). Their result revealed that PEG-PLL/DNA complex mainly forms extended toroidal structure,

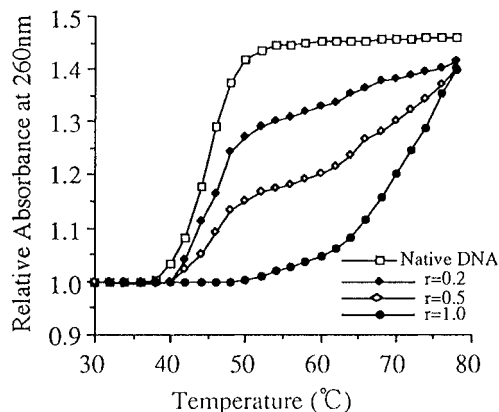


Figure 2. Melting curves of PEG-PLL/DNA complexes in 50% (v/v) methanol/1 mM phosphate buffer (pH 7.4).

which has a size exceeding 100 nm. In comparison, a smaller sized complex was dominant in our light scattering measurement. One possible reason for the inconsistency of the complex size might be a difference in the composition of the block copolymers. They used PEG-PLL with a longer chain length of PLL segment (DP = 78). It should be noted that complex size was correlated to PLL chain length in the case of DNA complex with PLL homopolymer (30).

The average ζ -potential of the associate was then calculated using the Smoluchowski equation from the value of the electrophoretic mobility [$(-0.890 \pm 0.321) \times 10^{-5} \text{ cm}^2/\text{V}\cdot\text{s}$ in 10 mM phosphate buffer, pH 7.4] measured by Laser-Doppler electrophoresis (ELS-800, Otsuka Electronics Co.). The ζ -potential thus calculated was $-1.12 \pm 0.40 \text{ mV}$ ($n = 3$). This small absolute value of the ζ -potential was consistent with the formation of a core-shell structure, in which the PEG corona surrounds the complexed DNA in the core to form a microenvironment with relatively low permittivity. Presumably, this local environment with lowered permittivity may facilitate the compaction of complexed DNA to form a collapsed core of the complexed associate. It should be noted that charge neutralization by polycations as well as lowered permittivity of the environment are both known to be essential factors for DNA compaction (8, 31).

Measurement of Melting Curve of PEG-PLL/DNA Complexes. The stability of the complex was then evaluated through melting curve measurement, which has been widely used for the characterization of DNA/polylysine complexes. Melting is conveniently monitored by an increase in absorbance (hyperchromic effect) that results from the disruption of base stacking in double-stranded DNA due to the breakage of hydrogen bonds. A biphasic melting profile has been shown for a DNA/polylysine complex system with an excess DNA ratio (22–28): One at a lower temperature is the melting of free DNA base pairs, and the other at higher temperature is that of base pairs in the region complexed with polylysine. Because the double-stranded structure of DNA is considerably stable under physiological condition, measurements were carried out in methanol-added buffer with low ionic strength (1 mM sodium phosphate buffer) to reduce the transition temperature of the complexed DNA to the measuring temperature range (30–78 °C) (24). Note that the melting temperature of DNA increases with lowered salt counterion due to an increase in electrostatic repulsion between phosphates as well as with methanol addition due to the destabilization of hydrogen bonding of the base pairs.

Figure 2 shows the melting profiles of DNA (from salmon testes) at various complex ratios of PEG-PLL

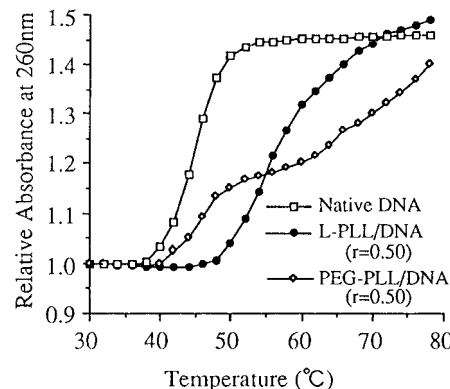


Figure 3. Melting curves of DNA complexes ($r = 0.50$) in 50% (v/v) methanol/1 mM phosphate buffer (pH 7.4).

to DNA in 1 mM phosphate buffer/methanol 50% (v/v). The melting temperature (T_m) of free DNA was observed at 44 °C. At $r = 1.0$, the transition of free DNA was no longer observed, and only the transition due to the denaturation of the complexed DNA was observed at higher temperature (ca. 70 °C), indicating that a stoichiometric complex was formed between DNA and PEG-PLL. In the $0 < r < 1$ region, the melting curve is biphasic. Contribution of the free DNA to hyperchromicity decreased with increases in the ratio of PEG-PLL, while the contribution of complexed DNA increased with increases in the ratio of PEG-PLL. These biphasic melting profiles demonstrate that the complexed and free parts of DNA in the PEG-PLL/DNA system could be clearly discriminated by the melting temperature. Thus, migration of PEG-PLL along/between DNA molecules should be extremely slow to observe free and complexed DNA separately in the melting profile.

It should be noted that only a single transition temperature was observed for the L-PLL/DNA system and that this averaged transition temperature shifted to a higher region with increasing ratio of L-PLL to DNA. As shown in Figure 3, L-PLL/DNA at $r = 0.5$ showed a single transition at the middle point of the transition temperature of free DNA ($r = 0$) and complexed DNA ($r = 1.0$). This result suggests the fast migration of the constituent molecules in the complex, resulting in the facile dissociation of the complex. That is, only an unstable complex is formed between L-PLL and DNA. The L-PLL molecule seems to be too short to form a stable polyion complex with DNA and may migrate along the DNA molecule like a low molecular weight counterion (24). Thus, the L-PLL/DNA complex ($r = 0.50$) is thought to form a so-called nonstoichiometric complex. Formation of a nonstoichiometric water-soluble complex occurs when a polyelectrolyte with relatively low molecular weight is mixed with an excess amount of an oppositely charged polyelectrolyte with higher molecular weight (32). Compared with the molecular weight of DNA, the polymerization degree of L-PLL is small enough to form a nonstoichiometric complex. In contrast, the PEG-PLL/DNA complex showed the features of a stoichiometric complex even though the length of the poly(lysine) segment in PEG-PLL is almost the same as that in L-PLL. The PEG segment of PEG-PLL contributes crucially to improve the stability as well as the solubility of the complex. One plausible factor for stabilizing the DNA complex with PEG-PLL may be a local decrease in permittivity around the DNA molecule due to the PEG chain. Indeed, PEG is known to induce a coil-globule transition of DNA due to decreased permittivity (33). However, to induce the transition of DNA, an extremely high concentration of PEG ($> 5 \text{ mol/L}$) should be required. In our system, the

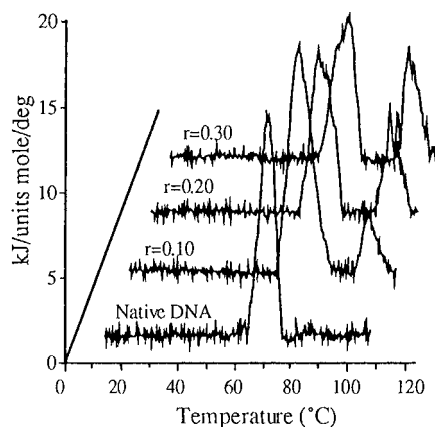


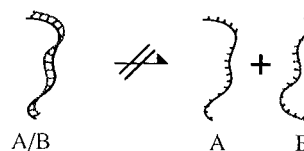
Figure 4. DSC curves of PEG-PLL/DNA complexes in 10 mM phosphate buffer (pH 7.4). Scan rate = 1.5 °C/min; DNA concentration = 250 µg/mL.

average PEG concentration in the complex solution was too low to change the bulk permittivity of the solution. Nevertheless, binding of the block copolymer to DNA through electrostatic interaction allows an increase in the local concentration of PEG around the DNA molecules to decrease the permittivity of the microenvironment. Charge neutralization of DNA by the poly(L-lysine) segment as well as compartmentalization of complexed DNA in the microenvironment of PEG may lead to the higher stability of the PEG-PLL/DNA complex compared to the corresponding L-PLL/DNA complex system. Although complex stabilization could be achieved by increasing the molecular weight of the poly(L-lysine) homopolymer in the PLL/DNA system, the resultant complex was too low in solubility in water to form a precipitate. This is in sharp contrast to the PEG-PLL/DNA complex system, which shows a high solubility in aqueous milieu.

DSC Measurements of DNA Complexes. As demonstrated in the melting curve experiments described above, stabilization of the double-stranded helical structure of DNA complexed with PEG-PLL or H-PLL is achieved through the neutralization of the phosphate group by the ϵ -NH₃⁺ group of the PLL segment. Further, the phase transition of DNA into a globule form may occur with the PEG-PLL/DNA complex because of the compartmentalization into the PEG atmosphere with low permittivity. However, methanol was added for the experiments in the melting curve measurements. Thus, the possibility that added methanol decreases the permittivity to induce coil-globule transition of DNA is not excluded. Therefore, to estimate the contribution of the PEG segment of the PEG-PLL block copolymer to DNA stabilization in aqueous milieu, DSC measurements were done in 10 mM phosphate buffer (pH 7.4) (34). The DSC curve of native DNA (from salmon testes) showed an endothermic peak at 69.4 °C (Figure 4). The DSC curves of PEG-PLL/DNA with various lysine/phosphate ratios (*r*) showed two endothermic peaks at around 70 and 95 °C, respectively. These peaks are thought to correspond to the denaturation of free and complexed DNA and are consistent with the biphasic melting profile shown in Figure 2. Note that the area of the peak corresponding to complexed DNA increased with an increase in *r*, which is in line with formation of a stoichiometric complex of DNA with PEG-PLL in a cooperative manner. Only a broad peak was obtained for the L-PLL/DNA complex (data not shown), reflecting fast migration of molecules in the complex between L-PLL and DNA.

The enthalpy of denaturation of the complexed DNA was roughly estimated from the area of the peak that appeared in the higher temperature region (second peak).

a) Dissociation reaction



b) Exchange reaction

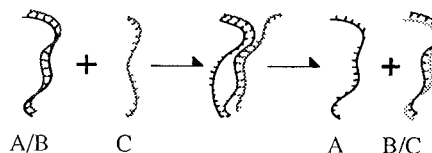


Figure 5. Schematic illustrations of dissociation (a) and exchange (b) of polyion complexes: (a) dissociation of the polyion complex scarcely occurs because of multisite binding; (b) exchange reaction of the polyion complex may occur through a cooperative exchange reaction.

The enthalpy change for denaturation of complexed DNA with PEG-PLL was estimated to be 50 kJ (bp mol)⁻¹ °C⁻¹ and that with H-PLL complex was 18 kJ (bp mol)⁻¹ °C⁻¹. This result indicates greater ability of PEG-PLL to stabilize the DNA double-helical structure than H-PLL even though the latter has a polymerization degree 50 times higher than the former, demonstrating the crucial role of the PEG segment in the stabilization process of the complex. PEG segments surrounding electrically neutralized DNA molecules allow formation of a microenvironment with relatively low permittivity. This local environment may facilitate the compaction of DNA to stabilize the complex structure.

Exchange Reaction of PEG-PLL/pDNA Complex on the Addition of Poly(aspartic acid). Simple dissociation of an ion complex between a pair of oppositely charged macromolecules with sufficient chain length is hardly believed to occur because of the integrated stabilization through multisite interaction (18, 22, 35). However, exchange reaction with other charged macromolecules is known to take place as schematically shown in Figure 5 (36). It is suggested that this type of exchange reaction may take place in the release of DNA from the complex with polycations and cationic polypeptides in intracellular environment because various types of anionically charged macromolecules, including mRNA, sulfated sugars, and nuclear chromatin, exist as essential cellular components (35). From these aspects, it may be worth estimating the exchange reaction of DNA in complexes with other polyanions. In this study, P(Asp) with a DP of 105 was used as the replacing polyanion. Figure 6 shows the results of the agarose gel electrophoresis for the PEG-PLL/pDNA complex after the addition of various amounts of P(Asp). As a model double-stranded DNA, linearized Col E1 plasmid DNA (6646 bp, 4.4 × 10⁶ Da) was used in the experiment shown in Figure 6 to omit the effect of molecular size distribution of DNA and to gain sensitivity in gel electrophoresis.

Linearized plasmid DNA mixed with PEG-PLL in an equimolar unit ratio (*r* = 1.0) showed no migration from the slot of the agarose gel because of the quantitative formation of a neutral complex (Figure 6, lane 2). This fact further confirms a stable complex formation between DNA and PEG-PLL block copolymer even in the solution with physiological salt concentration. Interestingly, pDNA in the complexes began to migrate with the addition of 10 times excess amounts of P(Asp), as shown in lane 7 of Figure 6. This is considered to be due to the cooperative exchange reaction of P(Asp) with pDNA in

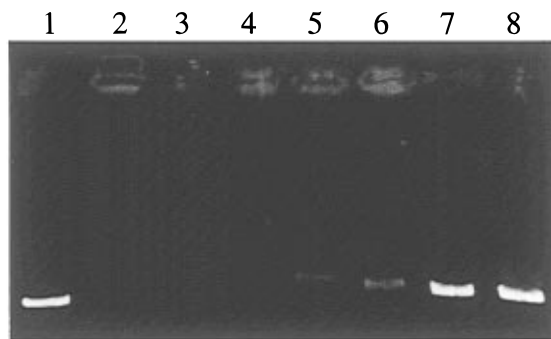


Figure 6. Effect of P(Asp) addition on the electrophoretic migration of pDNA from PEG-PLL/pDNA in 0.6% agarose gel: (lane 1) pDNA alone; (lane 2) PEG-PLL/pDNA complex; (lanes 3–8) PEG-PLL/pDNA complexes with progressively increasing proportions of P(Asp) [0.50, 1.0, 2.0, 4.0, 10, and 20 equiv of P(Asp) to pDNA].

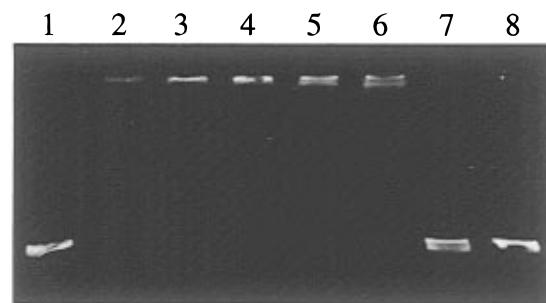
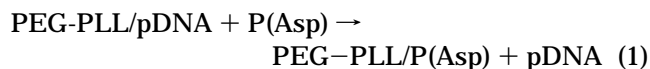


Figure 7. Effect of P(Asp) addition on the electrophoretic migration of pDNA from H-PLL/pDNA in 0.6% agarose gel: (lane 1) pDNA alone; (lane 2) H-PLL/pDNA complex; (lanes 3–8) H-PLL/pDNA complexes with progressively increasing proportions of P(Asp) [0.50, 1.0, 2.0, 4.0, 10, and 20 equiv of P(Asp) to pDNA].

the complex (eq 1), allowing the release of pDNA in the medium.



Worth mentioning are the facts that the PEG-PLL/pDNA complex formation is not irreversible in nature and that DNA in the complex can be substituted by an appropriate counterpolyanion. A similar phenomenon was also observed for the H-PLL/DNA system. pDNA in the H-PLL/pDNA complex was also substituted with a 10 times excess molar amount of P(Asp) (Figure 7, lane 7). Given that the stability of polyion complexes depends only on the molecular weight of the constituent polyelectrolytes, more P(Asp) should be required to release pDNA from the H-PLL/DNA complex compared to the PEG-PLL/DNA system because H-PLL (DP = 927) has an extremely higher degree of polymerization than PEG-PLL, having a PLL segment with a DP of only 20. Obviously, this is not the case, and both PEG-PLL/pDNA and H-PLL/pDNA complexes required the same amount of P(Asp) to release DNA. Thus, from the viewpoint of the exchange reaction, the PEG-PLL/pDNA complex is stable enough, as is the H-PLL/pDNA complex, in spite of the short PLL segment. In the case of the L-PLL/pDNA system, the L-PLL/pDNA complex was dissociated in the electrophoretic field under this buffer condition even without the addition of P(Asp), indicating its unstable nature.

From a practical viewpoint, the regulated release of DNA from the complex through replacement by the counterpolyanion is noteworthy because the restricted

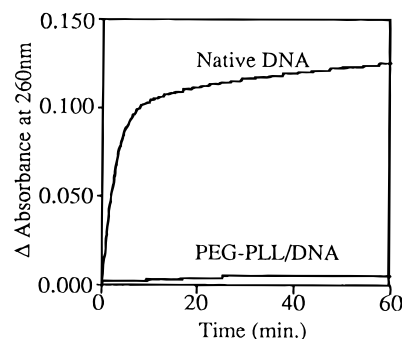


Figure 8. Degradation profile of DNA and PEG-PLL/DNA complex by DNase I.

release of free DNA is one of the problems of the conventional vector system based on a polyion complex. Decreased molecular weight of PLL may increase the release rate of DNA, yet it may also shift the nature of the complex to a nonstoichiometric one as shown in Figure 3. Use of the PEG-PLL block copolymer system seems to overcome this discrepancy by stabilizing the complex through the compartmentalization into the PEG microenvironment, yet, on the other hand, retaining the ability for replacement with a counterpolyanion.

Nuclease Resistance of PEG-PLL/DNA Complex.

Stabilization of DNA through PEG-PLL complexation was further studied from the viewpoint of nuclease resistance. By addition of DNase I to native DNA solution, absorbance of the solution was increased immediately due to the fragmentation of the DNA. However, no substantial increase in absorbance was observed for the PEG-PLL/DNA complex system (Figure 8). From a comparison of the slope of the curves reflecting the velocity of the degradation, it was calculated that the apparent activity of DNase I to degrade complexed DNA with PEG-PLL is only 1.5% of that for native DNA. This high nuclease resistance ability of the PEG-PLL/DNA system indicates the stable nature of the PEG-PLL/DNA complex in which the migration of the constituent polymer chain (PEG-PLL and DNA) is restricted. This feature of high resistance toward nuclease attack is surely an advantage of using the PEG-PLL/DNA complex as a reservoir for DNA under physiological circumstances when DNA degradation through nuclease attack readily takes place.

ACKNOWLEDGMENT

This research was supported by a Grant-in-Aid for Scientific Research (Priority Area Research Program: Supramolecular Structures), the Ministry of Education, Science, and Culture, Japan.

LITERATURE CITED

- (1) Wu, G. Y., and Wu, C. H. (1987) Receptor-mediated in vitro Gene Transformation by a soluble DNA carrier system. *J. Biol. Chem.* 262, 4429–4432.
- (2) Wagner, E., Zenke, M., Cotten, M., Beug, H., and Birnstiel, M. L. (1990) Transferrin-polycation conjugates as carriers for DNA uptake into cells. *Proc. Natl. Acad. Sci. U.S.A.* 87, 3410–3414.
- (3) Behr, J. P., Demeneix, B., Loeffler, J. P., and Perez-Mutul, J. (1989) Efficient gene transfer into mammalian primary endocrine cells with lipopolyamine-coated DNA. *Proc. Natl. Acad. Sci. U.S.A.* 86, 6982–6986.
- (4) Boussif, O., Lezoualc'h, F., Zanta, M. A., Mergny, M. D., Scherman, D., Demeneix, B., and Behr, J. P. (1995) A versatile vector for gene and oligonucleotide transfer into cells in culture and in vivo: Polyethyleneimine. *Proc. Natl. Acad. Sci. U.S.A.* 92, 7297–7301.

- (5) Zhou, X., Klivanov, A. L., and Huang, L. (1991) Lipophilic polylysines mediate efficient DNA transfection in mammalian cells. *Biochim. Biophys. Acta* 1065, 8–14.
- (6) Haynes, M., Garrett, R. A., and Gratzner, W. B. (1970) Structure of nucleic acid-poly base complexes. *Biochemistry* 9, 4410–4416.
- (7) Chatteraj, D. K., Gosule, L. C., and Schellman, J. A. (1978) DNA Condensation with polyamines II. Electron microscopic studies. *J. Mol. Biol.* 121, 327–337.
- (8) Manning, S. G. (1978) The molecular theory of polyelectrolyte solutions with application to the electrostatic properties of polynucleotides. *Q. Rev. Biophys.* 11, 179–246.
- (9) Katayose, S., and Kataoka, K. (1996) PEG-Poly(lysine) block copolymer as a novel type of synthetic gene vector with supramolecular structure. In *Advanced Biomaterials in Biomedical Engineering and Drug Delivery System* (N. Ogata, S. W. Kim, J. Feijin, and T. Okano, Eds.) pp 319–320, Springer-Verlag, Tokyo.
- (10) Kataoka, K., Kwon, G. S., Yokoyama, Y., Okano, T., and Sakurai, Y. (1993) Block copolymer micelles as vehicles for drug delivery. *J. Controlled Release* 24, 119–132.
- (11) Kwon, G. S., and Kataoka, K. (1995) Block copolymer micelles as long-circulating drug vehicles. *Adv. Drug. Deliv. Rev.* 16, 295–309.
- (12) Yokoyama, Y., Miyauchi, M., Yamada, N., Okano, T., Sakurai, Y., Kataoka, K., and Inoue, S. (1990) Polymer micelles as novel drug carrier: Adriamycin-conjugated poly(ethylene glycol)-poly(aspartic acid) block copolymer. *J. Controlled Release* 11, 269–278.
- (13) Kwon, G. S., Naito, N., Yokoyama, Y., Okano, T., Sakurai, Y., and Kataoka, K. (1995) Physical entrapment of adriamycin in AB block copolymer micelles. *Pharm. Res.* 12, 200–203.
- (14) Harada, A., and Kataoka, K. (1995) Formation of polyion complex micelles in an aqueous milieu from a pair of oppositely-charged block copolymers with poly(ethylene glycol) segments. *Macromolecules* 28, 5294–5299.
- (15) Yokoyama, M., Okano, T., Sakurai, Y., Ekimoto, H., Shibasaki, C., and Kataoka, K. (1991) Toxicity and antitumor activity against solid tumors of micelle-forming polymeric anticancer drug and its extremely long circulation in blood. *Cancer Res.* 51, 3229–3236.
- (16) Kwon, G. S., Suwa, S., Yokoyama, M., Okano, T., Sakurai, Y., and Kataoka, K. (1994) Enhanced tumor accumulation and prolonged circulation times of micelle-forming poly(ethylene oxide-aspartate) block copolymer-adriamycin conjugates. *J. Controlled Release* 29, 17–23.
- (17) Kataoka, K., Togawa, H., Harada, A., Yasugi, K., Matsumoto, T., and Katayose, S. (1996) Spontaneous formation of polyion complex micelles with narrow distribution from antisense oligonucleotide and cationic block copolymer in physiological saline. *Macromolecules* 29, 8556–8557.
- (18) Wolfert, M. A., Schacht, E. H., Toncheva, V., Ulbrich, K., Nazarova, O., and Seymour, L. W. (1996) Characterization of vector for gene therapy formed by self-assembly of DNA with synthetic block co-polymers. *Hum. Gene Ther.* 7, 2123–2133.
- (19) Shapiro, J. T., Leng, M., and Felsenfeld, G. (1969) Deoxyribonucleic acid-polylysine complexes. Structure and nucleotide specificity. *Biochemistry* 8, 3219–3232.
- (20) Carroll, D. (1972) Complexes of polylysine with polyuridylic acid and other polynucleotides. *Biochemistry* 11, 426–433.
- (21) Chang, C., Weiskopf, M., and Li, H. J. (1973) Conformation studies of nucleoprotein. Circular dichroism of deoxyribonucleic acid base pairs bound by polylysine. *Biochemistry* 12, 3028–3032.
- (22) Fasman, G. D., and Mandel, R. (1976) Chromatin models. Interaction between DNA and polypeptides containing L-Lysine and L-Valine: Circular dichroism and thermal denaturation studies. *Biochemistry* 15, 3122–3130.
- (23) Tuboi, M., Matsuo, K., and Ts'o, P. O. P. (1966) Interaction of poly-L-lysine and nucleic acids. *J. Mol. Biol.* 15, 256–267.
- (24) Leng, M., and Felsenfeld, G. (1966) The preferential interactions of polylysine and polyarginine with specific base sequences in DNA. *Proc. Natl. Acad. Sci. U.S.A.* 56, 1325–1332.
- (25) Olins, D. E., Olins, A. L., and Von Hippel, P. H. (1967) Model nucleoprotein complexes: Studies on the interaction of cationic homopolypeptides with DNA. *J. Mol. Biol.* 24, 157–176.
- (26) Shih, T. Y., and Bonner, J. (1970) Thermal denaturation and template properties of DNA complexes with purified histone fractions. *J. Mol. Biol.* 48, 469–487.
- (27) Li, H. J., Chang, C., Weiskopf, M., Brand, B., and Rotter, A. (1974) Helix-Coil transition in nucleoprotein: Renaturation of polylysine-DNA and polylysine-nucleohistone complexes. *Biopolymers* 13, 649–667.
- (28) Li, H. J., Brand, B., Rotter, A., Chang, C., and Weiskopf, M. (1974) Helix-Coil transition in nucleoprotein. Effect of ionic strength on thermal denaturation of polylysine-DNA complexes. *Biopolymers* 13, 1681–1697.
- (29) Weiskopf, M. (1977) Poly(L-Lysine)-DNA interaction in NaCl solutions: B→C and B→ψ transitions. *Biopolymers* 16, 669–684.
- (30) Wolfert, M. A., and Seymour, L. W. (1996) Atomic force microscopic analysis of the influence of the molecular weight of poly(L)lysine on the size of polyelectrolyte complexes formed with DNA. *Gene Ther.* 3, 269–273.
- (31) Yoshikawa, K. (1996) Kinetics of collapse and Decollapse of a single double-stranded DNA chain. *Macromol. Symp.* 106, 367–378.
- (32) Kabanov, V. A., and Zevin, A. B. (1982) Water-soluble nonstoichiometric polyelectrolyte complexes: A new class of synthetic polyelectrolytes. *Sov. Sci. Rev., Sect. B* 4, 207–282.
- (33) Evdokimov, Y. M., Akimenko, N. M., Glukhova, N. E., and Varshavskii, Y. M. (1974) Compact form of DNA in solution communication I. Feature of the absorption spectra of Polyribonucleotides and DNA in aqueous salt solutions containing polyethyleneglycol. *Mol. Biol. (Kiev)* 8, 396–405.
- (34) Fujioka, K., Baba, Y., and Kagemoto, A. (1979) Thermal properties of DNA-poly(L-lysine) system. *Polym. J.* 11, 509–513.
- (35) Erbacher, P., Roche, A. C., Monsigny, M., and Midoux, P. (1995) Glycosylated polylysine/DNA complexes: Gene transfer efficiency in relation with the size and the substitution level of glycosylated polylysines and with the plasmid size. *Bioconjugate Chem.* 6, 401–410.
- (36) Bakeev, K. N., Izumrudov, V. A., Kuchanov, S. I., Zevin, A. B., and Kabanov, V. A. (1992) Kinetics and mechanism of interpolyelectrolyte exchange and addition reactions. *Macromolecules* 25, 4249–4254.
- (37) Labrt-Moleur, F., Steffan, A. M., Brisson, C., Perron, H., Feugeas, O., Furstenberger, P., Oberling, F., Brambilla, E., and Behr, J. P. (1996) An electron microscopy study into the mechanism of gene transfer with lipopolyamines. *Gene Ther.* 3, 1010–1017.

BC9701306

Expression and Characterization of Bryodin 1 and a Bryodin 1-Based Single-Chain Immunotoxin from Tobacco Cell Culture

Joseph A. Francisco,[†] Susan L. Gawlak,[†] Michael Miller,[‡] Jessie Bathe,[‡] David Russell,[‡] Dana Chace,[†] Bruce Mixan,[†] Lei Zhao,[†] H. Perry Fell,[†] and Clay B. Siegall^{*,†}

Molecular Immunology Department, Bristol-Myers Squibb Pharmaceutical Research Institute, 3005 First Avenue, Seattle, Washington 98121, and Agracetus, Inc., 8520 University Green, Middleton, Wisconsin 53562. Received May 28, 1997; Revised Manuscript Received July 16, 1997[®]

Bryodin 1 (BD1) is a potent ribosome-inactivating protein (RIP) isolated from the plant *Bryonia dioica*. It is relatively nontoxic in rodents ($LD_{50} > 40$ mg/kg) and represents a potential improvement over other RIPs and bacterial toxins that have been used in immunotoxins. Recombinant BD1, expressed in *Escherichia coli*, localizes to insoluble inclusion bodies necessitating denaturation and refolding steps to generate active protein. In this report, BD1 was expressed as a soluble recombinant protein in tobacco cell culture (ntBD1) and purified to near homogeneity with yields of up to 30 mg/L of culture). The protein synthesis inhibition activity of ntBD1 was identical to that of both native BD1 isolated from the roots of *B. dioica* and recombinant BD1 expressed in *E. coli*. Toxicology analysis showed that ntBD1 was well tolerated in rats at doses that cannot be achieved with most other toxin components of immunotoxins. Additionally, a single-chain immunotoxin composed of BD1 fused to the single-chain Fv region of the anti-CD40 antibody G28-5 (ntBD1–G28-5 sFv) was expressed in tobacco tissue culture as a soluble protein and was specifically cytotoxic toward CD40 expressing non-Hodgkin's lymphoma cells *in vitro*. These data indicate that tobacco tissue culture is a viable system for soluble expression of BD1 and BD1-containing immunotoxins.

INTRODUCTION

Immunotoxins are bispecific proteins composed of an antibody binding domain chemically linked or genetically fused to a protein toxin (1–3). While the binding moiety directs the immunotoxin to the targeted cell surface antigen, it is the toxin domain that, once inside the cell, is responsible for killing the cell by enzymatically inhibiting protein synthesis. The toxin components of immunotoxins possess unique toxicity profiles that can significantly contribute to the dose-limiting toxicity in patient therapy. The plant ribosome-inactivating proteins (RIPs) ricin, pokeweed antiviral protein, and saporin, and the bacterial ADP-ribosylating toxins *Pseudomonas* exotoxin and diphtheria toxin, have been the most widely utilized toxin components of clinically tested immunotoxins (3, 4). However, even in the absence of a targeting domain, the native or nontargeted forms of these toxins are toxic with LD_{50} values (concentration lethal to 50% of the animals tested) of <5 mg/kg in rodents (5, 6). Dose escalations of immunotoxins in clinical trials to amounts that would be expected to result in significant therapeutic efficacy have been problematic. Even so, immunotoxins containing these toxins have shown some promise in the clinic for indications ranging from cancer to autoimmune disease (7–11).

The identification of toxins that have potent activity when targeted by an antibody binding domain but reduced nonspecific toxicity profiles could ultimately lead to the development of immunotoxins with broader therapeutic windows. One such toxin is the RIP bryodin 1

(BD1) which has been found to have potent cell-free protein synthesis inhibition activity while exhibiting approximately 10-fold less toxicity *in vivo* ($LD_{50} > 40$ mg/kg in rodents) than other toxins (5). The gene encoding BD1 was recently cloned and expressed in *Escherichia coli* as insoluble inclusion bodies which were refolded to yield protein that had activity *in vitro* and *in vivo* equivalent to that of native BD1 (nBD1) extracted from *Bryonia dioica* roots (6).

In this report, we describe the expression of BD1 in soluble form using a transgenic tobacco (*Nicotiana tabacum*) tissue culture system with yields of purified BD1 (ntBD1) of up to 30 mg/L. The *in vitro* and *in vivo* activities of ntBD1 were virtually identical to those of both nBD1 and *E. coli*-expressed rBD1. Additionally, a single-chain immunotoxin containing BD1 and the cloned variable regions of the anti-CD40 mAb G28-5 (ntBD1–G28-5 sFv) was constructed and expressed in transgenic tobacco cultures as a soluble fusion protein. ntBD1–G28-5 sFv was specifically cytotoxic toward CD40-expressing non-Hodgkin's lymphoma cells. These data indicate the utility of tobacco cell culture for the production of BD1 and BD1-based single-chain immunotoxins in soluble form and describe an immunotoxin which is being investigated for potential therapeutic applications.

EXPERIMENTAL PROCEDURES

Construction of Tobacco Culture Expression Plasmids Encoding BD1 and BD1–G28-5 sFv. A previously described rBD1 expression vector, pSE13.0 (6), encoding BD1 amino acid residues 1–247 was digested with *NcoI* and *EcoRI*. The *EcoRI* site was prepared as a blunt end using the Klenow fragment of DNA polymerase I, and the resulting 770 bp BD1 fragment was ligated into the plant expression vector WRG2481 that had been digested with *NcoI* and *SmaI*. The resulting plasmid, WRG5074, contained the gene encoding BD1 under control of the cauliflower mosaic virus (CaMV) 35S promoter (12) with the extensin leader sequence (13) to

* Address correspondence to Clay B. Siegall, Bristol-Myers Squibb Pharmaceutical Research Institute, 3005 First Ave., Seattle, WA 98121. E-mail: Clay B. Siegall@ccmail.bms.com. Phone: (206) 727-3542. Fax: (206) 727-3603.

[†] Bristol-Myers Squibb Pharmaceutical Research Institute.

[‡] Agracetus, Inc.

[®] Abstract published in *Advance ACS Abstracts*, September 1, 1997.

direct secretion of soluble protein into the media and the nopaline synthase poly(A) terminator for efficient transcription termination (14). A kanamycin resistance gene under the control of the nopaline synthase promoter was inserted as a selectable marker.

The expression plasmid containing the gene fusion BD1-G28-5 sFv was prepared by first PCR amplifying BD1-G28-5 sFv from pSE151 (15) using a 5' primer that introduced an *Nco*I site and sequences from WRG2481 and a 3' primer that introduced a *Sma*I site and sequences from WRG2481. Homologous recombination (16) assembled the *Nco*I- and *Sma*I-digested plant expression vector WRG2481 and the amplified PCR fragment containing BD1-G28-5 sFv following cotransformation in *E. coli* strain DH5 α . The resulting expression plasmid was designated WRG5293. Both WRG5074 (BD1) and WRG5293 (BD1-G28-5 sFv) constructs were confirmed by DNA sequencing.

Expression and Purification of ntBD1 and ntBD1-G28-5 sFv in Transgenic Tobacco Cell Culture. *Nicotiana tabacum* L. cell culture line NT-1 was obtained from D. Ellis (University of Wisconsin, Madison, WI). The cells were grown in tobacco suspension medium (TSM) or on solid tobacco culture medium (TCM; J. T. Cooley, J. H. Bathe, J. T. Fuller, L. Zhao, H. P. Fell, and D. R. Russell, in preparation). NT-1 suspension cultures were grown in the dark at 28 °C with constant shaking at 150 rpm. The cells were subcultured once per week.

NT-1 cells were transformed with gold particles coated with plasmid DNA using the Acell microparticle bombardment system (Agracetus, Madison, WI) as previously described (17). Briefly, 1 day after bombardment, the cells were transferred to reduced osmoticum (TCM containing 0.1 M mannitol and 0.1 M sorbitol) for 24 h and then transferred to TCM plates containing 350 μ g/mL kanamycin sulfate for selection. For growth of suspension cultures, kanamycin resistant calli approximately 1 in. in diameter were placed into TSM media containing kanamycin, shaken in the dark at 28 °C for 48 h, and then homogenized by repeat pipetting. Suspension cultures were maintained by subculturing every 10 days.

For purification, spent medium from suspension culture was filtered and concentrated 4-fold. ntBD1 was purified from the concentrate using Macrorep High S (BioRad, Hercules, CA) cation exchange chromatography. ntBD1-G28-5 sFv was purified by CM Sepharose Fast Flow (Pharmacia, Piscataway, NJ) cation exchange chromatography followed by purification over an immobilized CD40-Ig affinity column (18). The affinity eluate, which contained ntBD1-G28-5 sFv as well as free sFv, was subsequently purified by cation exchange chromatography using Poros HS resin (PerSeptive, Cambridge, MA).

Preliminary analysis of N-linked glycosylation was performed using the FACE N-linked oligosaccharide profiling system (Glyko Inc., Novato, CA) according to the manufacturer's instructions.

Cell-Free and Cell-Based Protein Synthesis Inhibition Assays. Cell-free inhibition of protein synthesis was analyzed using a rabbit reticulocyte lysate translation system (Promega, Madison, WI) as previously described (5). Various concentrations of ntBD1, ntBD1-G28-5 sFv, and rBD1 as a control were incubated at 30 °C with rabbit reticulocyte lysate, a mixture of amino acids without leucine, 0.5 mCi/mL [³H]leucine (Amersham, Arlington Heights, IL), and brome mosaic virus RNA as a template. The reaction proceeded for 1 h and was terminated by the addition of 1 M NaOH with 2% H₂O₂, and the translation product was precipitated with trichloroacetic acid. The radiolabeled proteins were

harvested on glass filters and quantitated using a scintillation counter. Samples were performed in triplicate. IC₅₀ was defined as the concentration that inhibited 50% of the cell-free protein synthesis.

Cell-based inhibition of protein synthesis assays was performed using JAR choriocarcinoma cells for ntBD1 and rBD1 and Raji or Daudi non-Hodgkin's lymphoma cells for ntBD1-G28-5 sFv. One hundred microliters of cells, diluted to 1 \times 10⁵ cells/mL in leucine-free RPMI 1640, was plated in 96-well cell culture plates and incubated for 48 h at 37 °C with various concentrations of ntBD1, rBD1, or ntBD1-G28-5 sFv. The samples were then pulsed with 1 μ Ci/well [³H]leucine and incubated at 37 °C for an additional 6 h, and radiolabeled protein was harvested onto filter mats using a Tomtec cell harvester (Orange, CT). The incorporation of [³H]leucine into cellular proteins was analyzed with an LKB Beta-Plate liquid scintillation counter (Wallac, Gaithersburg, MD).

Toxicity of ntBD1 in Rats. The acute toxicity of ntBD1 was determined in Wistar Furth rats (Harlan-Sprague Dawley, Indianapolis, IN). ntBD1 was administered as bolus intraperitoneal injections at doses of up to 60 mg/kg diluted in PBS. Animals were observed for at least 10 days to determine survival. Selected rats were sacrificed 24 h after administration of ntBD1 to perform comprehensive necropsy analysis.

CD40 Binding Analysis. CD40 binding activity was analyzed by ELISA essentially as previously described (18). Briefly, 96-well microtiter plates were coated overnight at 4 °C with 100 μ L of CD40-Ig at 0.5 μ g/mL. CD40-Ig consists of the extracellular domain of human CD40 fused to the Fc domain of human IgG1 (19). The plates were then blocked for 1 h with Specimen Diluent (Genetics Systems, Redmond, WA) and incubated for 1 h with dilutions of ntBD1-G28-5 sFv in the absence or presence of G28-5 IgG or an isotype-matched control antibody. After being washed three times with phosphate-buffered saline (PBS), the plates were incubated with rabbit polyclonal anti-BD1 antiserum followed by horseradish peroxidase-conjugated goat anti-rabbit Ig antiserum. Binding to immobilized CD40 was detected by the addition of TMB chromagen reagent (Genetic Systems) and analyzed on a microtiter plate reader at 450 nm.

RESULTS

Expression and Purification of ntBD1. The expression plasmid WRG5074 was constructed as described in Experimental Procedures and is shown schematically in Figure 1A. The plasmid contains the gene encoding BD1 under the control of the cauliflower mosaic virus (CaMV) 35s promoter (12). The extensin leader sequence (13) at the amino terminus of BD1 directs the secretion of the recombinant protein into the culture medium. WRG5074 was transfected into the tobacco cell line NT1 using the Acell electric discharge propulsion system (17), and callus samples were analyzed by SDS-PAGE and Western blotting to identify clones that expressed ntBD1. One clone which yielded qualitatively higher expression was further expanded, and after 10 days of growth, the culture supernatant was isolated and ntBD1 was purified by cation exchange chromatography. SDS-PAGE of the eluted peak (Figure 1B) revealed that ntBD1 was purified to near homogeneity and migrated at a molecular mass of approximately 28 kDa, slightly higher than rBD1 expressed in *Escherichia coli* (6), likely due to glycosylation of the plant-derived protein. Preliminary analysis confirmed the presence of N-linked oligosaccharides (data not shown), although further analysis will be necessary

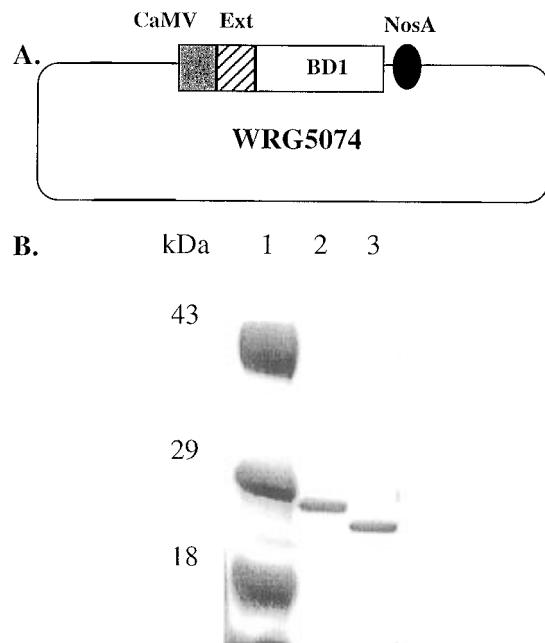


Figure 1. ntBD1 expression plasmid and SDS-PAGE of purified ntBD1. (A) Schematic diagram of the ntBD1 expression plasmid WRG5074. CaMV = the cauliflower mosaic virus 35S promoter. Ext = the extensin leader sequence. NosA = the Nos poly(A) transcription terminator. (B) SDS-PAGE (12%) of ntBD1 (lane 2) and rBD1 (lane 3). The molecular mass markers, in kilodaltons, are shown in lane 1. Samples were electrophoresed under nonreducing conditions.

to determine the extent of N-linked glycosylation as well as to analyze for the presence of O-linked oligosaccharides. The final yield of purified ntBD1 was 30 mg/L of starting culture).

In Vitro Activity of ntBD1. Both type I and type II RIPs catalytically inactivate the 60S subunit of eukaryotic ribosomes by cleaving the N-glycosidic bond of adenine 4324 in 28S rRNA, thereby halting protein synthesis (20). The protein synthesis inhibition activity of ntBD1 was investigated in a cell-free rabbit reticulocyte lysate system and compared to the activity of rBD1. Both ntBD1 and rBD1 inhibited protein synthesis equally with IC_{50} values (concentration that inhibited 50% of protein synthesis) of 0.5 ng/mL (Figure 2A). While BD1 does not contain a cell binding domain, it has previously been shown that type I RIPs such as BD1, saporin, and momorcharin are cytotoxic to trophoblasts and choriocarcinoma cells (21). Both ntBD1 and rBD1 were cyto-

Table 1. LD_{50} of ntBD1 Rats^a

amount injected (mg/kg)	no. surviving/no. injected
10	3/3
20	3/3
40	2/3
60	0/3

^a Groups of Wistar Furth rats were administered the indicated amount of ntBD1 via interperitoneal injection and were observed for 10 days to determine survival.

toxic to JAR choriocarcinoma cells with IC_{50} values of 10 ng/mL (Figure 2B). These data indicate that both sources of BD1 were identical in potency and that the glycosylation of ntBD1 did not interfere with the catalytic activity. The difference in IC_{50} values between the cell-free and cell-based protein synthesis inhibition assays reflects the fact that in the cell-based assay the toxin molecule must enter the cell and translocate into the cytosol before it can catalytically inactivate the rRNA.

Toxicity of ntBD1 in Rats. Vascular leak syndrome (VLS) has been the dose-limiting toxicity for a number of immunotoxins tested in the clinic (8–10, 22). While immunotoxin-induced VLS has not been seen in mice, it has been observed in rats given either *Pseudomonas* exotoxin-based immunotoxins or binding-defective forms of *Pseudomonas* exotoxin (23, 24). Since it was unknown whether the glycosylated state of ntBD1 would affect its toxicity *in vivo*, experiments were performed to investigate the toxicity of ntBD1 in rats. Pairs of female Wistar Furth rats were administered ntBD1 (up to 60 mg/kg) via intraperitoneal injection. No signs of toxicity were observed at ntBD1 doses of up to 20 mg/kg (Table 1). At 40 and 60 mg/kg, two out of three and zero out of three rats, respectively, survived, indicating that the LD_{50} of ntBD1 in rats was between 40 and 60 mg/kg. This is consistent with previous findings showing that the LD_{50} of rBD1 in rats was >25 mg/kg (6). In contrast, the LD_{50} values of PE40 and deglycosylated ricin A chain were 2.0 and 5 mg/kg, respectively (6).

Necropsy analysis of the animals 24 h after injection of ntBD1 (60 mg/kg) revealed that the toxicity was localized to the liver and lungs with the gastrointestinal tract, spleen, heart, uterus, brain, kidney, and pancreas all within normal histologic parameters. In the liver, hepatocytes were swollen and some were necrotic. These histologic changes are consistent with the clinical chemistry values obtained showing elevated liver transaminases, indicating liver injury. In the lungs, there was focal edema in the parenchyma and widened perivascular

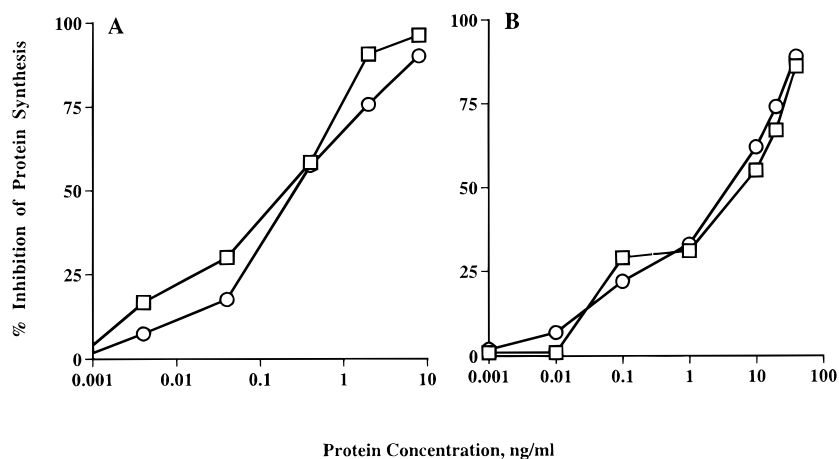


Figure 2. Comparison of the catalytic activity of ntBD1 versus rBD1. (A) Analysis of the cell-free protein synthesis inhibition activity of ntBD1 (○) and rBD1 (□) in the rabbit reticulocyte lysate system. (B) Cytotoxic activity of ntBD1 (○) and rBD1 (□) on JAR choriocarcinoma cells.

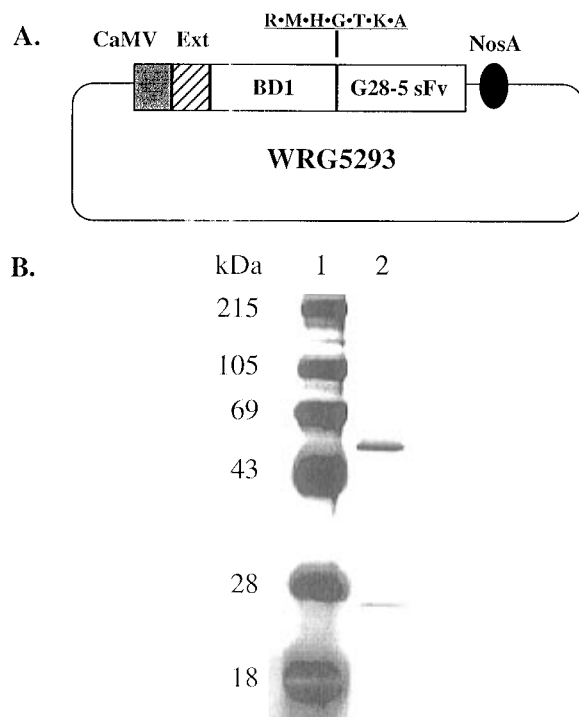


Figure 3. ntBD1-G28-5 sFv expression plasmid and SDS-PAGE. (A) Schematic diagram of ntBD1-G28-5 sFv expression plasmid WRG5293. CaMV = the cauliflower mosaic virus 35S promoter. Ext = the extensin leader sequence. NosA = the Nos poly(A) transcription terminator. The underlined sequence between the BD1 and sFv moieties is the amino acid sequence of the cloning linker. (B) SDS-PAGE (12%) of ntBD1-G28-5 sFv (lane 2) run under nonreducing conditions.

spaces containing scant inflammatory cells. The lung toxicities, indicative of VLS, were similar to those observed in rats 24 h after administration of 2 mg/kg of BR96 sFv-PE40 (23) or PE40 alone (24). Thus, ntBD1 was approximately 30-fold less toxic to rats than PE40 with the dose-limiting toxicity in both cases being VLS.

Construction, Expression, and Purification of BD1-G28-5 sFv. The use of tobacco cell culture for the production of a single-chain immunotoxin consisting of ntBD1 fused to the sFv region of the G28-5 mAb was investigated. G28-5 recognizes the human CD40 antigen (24), and we have previously shown that a single-chain immunotoxin targeted to CD40 (G28-5 sFv-PE40) specifically kills CD40-positive malignant cell lines both *in vitro* and *in vivo* (18, 26). Additionally, we have recently shown that BD1-G28-5 sFv expressed in *E. coli* was cytotoxic to CD40-expressing cells *in vitro* (15). Since the crystal structure of BD1 indicated that the N terminus was less solvent accessible than the C terminus (6), the C terminus of BD1 was fused to the N terminus of G28-5 sFv (BD1-G28-5 sFv) rather than in the opposite orientation (Figure 3A). This was the orientation of the fusion protein that yielded active material when refolded from inclusion bodies isolated from *E. coli*.

After expression of ntBD1-G28-5 sFv, encoded by WRG5293, the fusion protein was purified from tobacco cell culture supernatant by cation exchange followed by affinity chromatography using immobilized CD40-Ig. The affinity eluate was subsequently purified by an additional cation exchange step. Analysis of the purified sample by SDS-PAGE under nonreducing conditions showed two distinct proteins (Figure 3B), one migrating at 55 kDa, the expected size of the immunotoxin, and the second migrating at 27 kDa. Western blot analysis with anti-BD1 monoclonal antibodies and polyclonal anti-G28-5 idiotype antiserum revealed that the 55 kDa

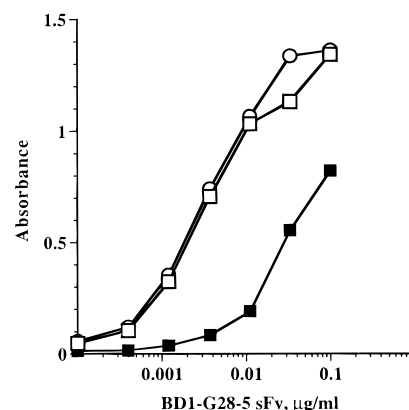


Figure 4. ELISA binding of ntBD1-G28-5 sFv to immobilized CD40-Ig. ntBD1-G28-5 sFv binding was analyzed without competitor (□) or in the presence of 10 mg/mL G28-5 IgG (■) or 10 μg/mL isotype-matched control antibody (○).

protein was ntBD1-G28-5 sFv (data not shown). The 27 kDa protein was recognized only by the anti-G28-5 antiserum and thus represents the sFv fragment, as confirmed by N-terminal protein sequencing (data not shown). The origin of the free sFv is not known, although it is likely the result of proteolysis, either during expression in tobacco cell culture or during purification. However, analysis of the peptide linker between the BD1 and G28-5 sFv moieties did not reveal any known protease cleavage sites that would yield the N-terminal sequence analysis obtained for this protein band (data not shown).

The difference in isoelectric points for G28-5 sFv and BD1-G28-5 sFv (theoretical values of 7.0 and 9.0, respectively) should have been sufficient to allow for separation by ion exchange chromatography. The fact that the sFv and ntBD1-G28-5 sFv molecules were readily separated on SDS-PAGE under non-reducing conditions but not by ion exchange chromatography suggests that the two molecules may have been noncovalently associated, although the exact nature of this association is unclear. In addition, the two protein species could not be separated by gel filtration (data not shown). Some sFv molecules have been shown to form dimers in solution with the V_H of one molecule associating with the V_L of a second molecule (27, 28), so it is possible that a similar dimerization occurred between the sFv of the fusion protein and the free sFv. Nevertheless, the resulting BD1-G28-5 sFv preparation was >90% pure.

Binding and Cytotoxic Activity of ntBD1-G28-5 sFv. ntBD1-G28-5 sFv bound to immobilized CD40-Ig as determined by an ELISA (Figure 4). This binding was specific since it could be blocked by the addition of the parental antibody G28-5 (10 μg/mL) but not by an isotype-matched control antibody. The ability of ntBD1-G28-5 sFv to inhibit protein synthesis in CD40-expressing cells, and therefore induce cytotoxicity, was examined. For this analysis, the Burkitt's lymphoma cell lines Raji and Daudi and the B lymphoblastoid line T51 were used, all of which were previously shown to express CD40 (18). The T cell leukemia line HPB-ALL, which does not express CD40, was used as a control. The three CD40-positive lines were sensitive to the cytotoxic activity of ntBD1-G28-5 sFv with IC_{50} values ranging from 0.2 to 1.0 ng/mL (Figure 5A). HPB-ALL cells were insensitive to this immunotoxin even at 1 μg/mL. ntBD1 by itself was not cytotoxic to any of the cell lines tested, indicating that the cytotoxic effect on the CD40-positive lines was a result of the immunotoxin being targeted to the receptor. Furthermore, the cytotoxic activity was specifically inhibited by the addition of 10 μg/mL G28-5 IgG

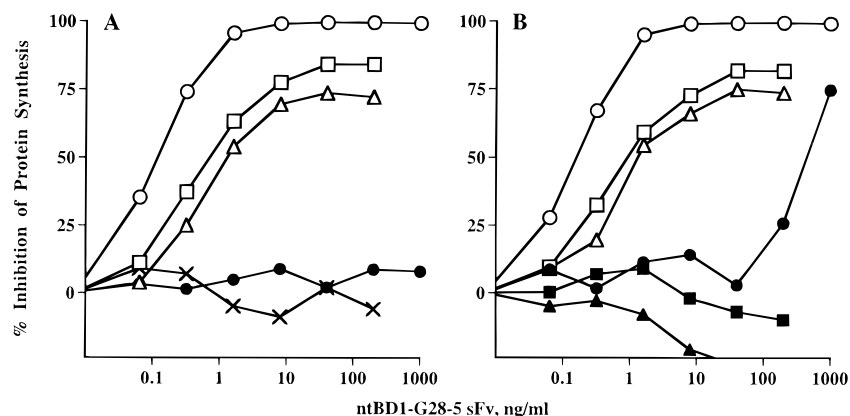


Figure 5. Protein synthesis inhibition activity of ntBD1-G28-5 sFv. (A) Activity of ntBD1-G28-5 sFv on the CD40-positive cell lines Daudi (□), T51 (○), and Raji (△) and the CD40-negative cell line HPB-ALL (×). Also shown is the activity of ntBD1 on T51 cells (●). (B) Activity of ntBD1-G28-5 sFv in the presence of 10 mg/mL G28-5 IgG or isotype-matched control antibody. Daudi: with G28-5 IgG (■) or with control antibody (□). T51: with G28-5 IgG (●) or with control antibody (○). Raji with G28-5 IgG (▲) or with control antibody (△).

but not by the addition of an isotype-matched control antibody (Figure 5B).

DISCUSSION

Immunotoxins can selectively eliminate malignant cells expressing specific surface antigens *in vivo*. However, the clinical utility of immunotoxins has been limited in large part by the nonspecific toxicities that are associated with the toxin moiety rather than cross-reactivities with normal tissues that express the target antigen. The reduced toxicity observed with BD1 (the LD₅₀ of BD1 in rodents is 10–30-fold higher than that of ricin A chain and PE40) indicates that this RIP represents an improvement over presently utilized toxins in immunotoxin development.

The use of transgenic tobacco cell culture offers an effective and robust means of producing BD1 and BD1-containing single-chain immunotoxins. Soluble ntBD1 was readily obtained from tobacco cell culture without refolding of denatured inclusion bodies as is required for many products expressed in *E. coli*. Tobacco culture-expressed ntBD1 was indistinguishable from rBD1 in protein synthesis inhibition activity, cytotoxicity, and rat toxicity, although ntBD1 migrated as a slightly larger molecule than rBD1 on nonreducing SDS-PAGE. Additionally, ntBD1-G28-5 sFv, a single-chain immunotoxin fusion protein targeted to the CD40 antigen, was solubly expressed in tobacco tissue culture. This fusion protein was specifically and potently cytotoxic to CD40-expressing non-Hodgkin's lymphoma cell lines *in vitro*, demonstrating that tobacco cell culture is a viable system for the production of RIP-based single-chain immunotoxins.

Plant cell culture offers an attractive alternative to bacterial, yeast, and mammalian cells for the production of heterologous proteins. It may also be possible to express BD1 fusion proteins in transgenic plants such as corn or soybean as a method for large scale production. In this report, we have shown that tobacco cell culture can be utilized to produce soluble forms of a plant ribosome-inactivating protein, ntBD1 and a single-chain immunotoxin containing BD1, ntBD1-G28-5 sFv. It is anticipated that BD1-containing immunotoxins will likewise be less toxic than analogous PE40-containing immunotoxins. Comparative efficacy and toxicity studies of the two single-chain anti-CD40 immunotoxins, ntBD1-G28-5 sFv and G28-5 sFv-PE40, will ultimately allow for determination of their relative therapeutic windows.

ACKNOWLEDGMENT

The authors thank Drs. J. Ledbetter and K. E. Hellström for helpful discussions and Dr. D. Liggitt for performing comprehensive necropsy analysis on the rats used in the toxicity studies.

LITERATURE CITED

- Vitetta, E. S., Thorpe, P. E., and Uhr, J. W. (1993) Immunotoxins: magic bullets or misguided missiles? *Immunol. Today* 14, 252–259.
- Siegall, C. B., Wolff, E. A., Gawlak, S. L., Paul, L., Chace, D., and Mixan, B. (1995) Immunotoxins as cancer chemotherapeutic agents. *Drug Dev. Res.* 34, 210–219.
- Pastan, I., Pai, L. H., Brinkmann, U., and FitzGerald, D. (1996) Recombinant immunotoxins. *Breast Cancer Res. Treat.* 38, 3–9.
- Press, O. W. (1991) Immunotoxins. *Biotherapy* 3, 65–76.
- Siegall, C. B., Gawlak, S. L., Chace, D., Wolff, E. A., Mixan, B., and Marquardt, H. (1994) Characterization of ribosome-inactivating proteins isolated from *Bryonia dioica* and their utility as carcinoma-reactive immunoconjugates. *Bioconjugate Chem.* 5, 423–429.
- Gawlak, S. L., Neubauer, M., Klei, H. E., Chang, C. Y., Einspahr, H. M., and Siegall, C. B. (1997) Molecular, biological, and preliminary structural analysis of bryodin 1, a ribosome-inactivating protein from the plant *Bryonia dioica*. *Biochemistry* 36, 3095–3103.
- Vitetta, E. S., Stone, M., Amlot, P., Fay, J., May, R., Till, M., Newman, J., Clark, P., Collins, R., Cunningham, D., Ghetie, V., Uhr, J. W., and Thorpe, P. E. (1991) Phase I immunotoxin trial in patients with B-cell lymphoma. *Cancer Res.* 51, 4052–4058.
- Amlot, P. L., Stone, M. J., Cunningham, D., Fay, J., Newman, J., Collins, R., May, R., McCarthy, M., Richardson, J., Ghetie, V., Ramilo, O., Thorpe, P. E., Uhr, J. W., and Vitetta, E. S. (1993) A phase I study of an anti-CD22-deglycosylated ricin A chain immunotoxin in the treatment of B-cell lymphomas resistant to conventional therapy. *Blood* 82, 2624–2633.
- Sausville, E. A., Headlee, D., Stetler-Stevenson, M., Jaffe, E. S., Solomon, D., Frigg, W. D., Herdt, J., Kopp, W. C., Rager, H., Steinberg, S. M., Ghetie, V., Schindler, J., Uhr, J., Wittes, R. E., and Vitetta, E. S. (1995) Continuous infusion of the anti-CD22 immunotoxin IgG-RFB4-SMPT-dgA in patients with B-cell lymphoma: a phase I study. *Blood* 85, 3457–3465.
- Pai, L. H., Wittes, R., Setser, A., Willingham, M. C., and Pastan, I. (1996) Treatment of advanced solid tumors with immunotoxin LMB-1: an antibody linked to *Pseudomonas* exotoxin. *Nat. Med. (N.Y.)* 2, 350–353.
- LeMaistre, C. F., Craig, F. E., Meneghetti, C., McMullin, B., Parker, K., Reuben, J., Boldt, D. H., Rosenblum, M., and Woodworth, T. (1993) Phase I trial of a 90-minute infusion

- f the fusion toxin DAB486IL-2 in hematological cancers. *Cancer Res.* 53, 3930–3934.
- (12) Gardner, R. C., Howarth, A. J., Hahn, P., Brown-Luedi, M., Shepherd, R. J., and Messing, J. (1981) The complete nucleotide sequence of an infectious clone of cauliflower mosaic virus by M13mp7 shotgun sequencing. *Nucleic Acids Res.* 9, 2871–2888.
 - (13) DeLoose, M., Gheysen, G., Tire, C., Gielen, J., Villarroel, R., Gentello, C., Van Montagu, M., Depicker, A., and Inze, D. (1991) The extensin signal peptide allows secretion of a heterologous protein from protoplasts. *Gene* 99, 95–100.
 - (14) Depicker, A., Stachel, S., Dhaese, P., Zambryski, P., and Goodman, H. M. (1982) Nopaline synthase: transcript mapping and DNA sequence. *J. Mol. Appl. Genet.* 1, 561–573.
 - (15) Francisco, J. A., Gawlak, S. L., and Siegall, C. B. (1997) Construction, expression and characterization of BD1-G28-5 sFv, a single-chain anti-CD40 immunotoxin containing the ribosome-inactivating protein Bryodin 1. *J. Biol. Chem.* (in press).
 - (16) Bubeck, P., Winkler, M., and Bautsch, W. (1993) Rapid cloning by homologous recombination in vivo. *Nucleic Acids Res.* 21, 3601–3602.
 - (17) McCabe, D. E., Swain, W. F., Martinell, B. J., and Christou, P. (1988) Stable transformation of soybean (*Glycine max*) by particle acceleration. *BioTechnology* 6, 923–926.
 - (18) Francisco, J. A., Gilliland, L. K., Stebbins, M. R., Norris, N. A., Ledbetter, J. A., and Siegall, C. B. (1995) Activity of a single-chain immunotoxin that selectively kills lymphoma and other B-lineage cells expressing the CD40 antigen. *Cancer Res.* 55, 3099–3104.
 - (19) Noelle, R. J., Roy, M., Shepherd, D. M., Stamenkovic, I., Ledbetter, J. A., and Aruffo, A. (1992) A 39-kDa protein on activated helper T cells binds CD40 and transduces the signal for cognate activation of B cells. *Proc. Natl. Acad. Sci. U.S.A.* 89, 6550–6554.
 - (20) Endo, Y., Mitsui, K., Motizuki, M., and Tsurugi, K. (1987) The mechanism of action of ricin and related toxic lectins on eukaryotic ribosomes: the site and the characteristics of the modification in 28 S ribosomal RNA caused by the toxins. *J. Biol. Chem.* 262, 5908–5912.
 - (21) Battelli, M. G., Montacuti, V., and Stirpe, F. (1992) High sensitivity of cultured human trophoblasts to ribosome-inactivating proteins. *Exp. Cell Res.* 201, 109–112.
 - (22) Conry, R. M., Khazaeli, M. B., Saleh, M. N., Ghetie, V., Vitetta, E. S., Liu, T., and LoBuglio, A. F. (1996) Phase I trial of an anti-CD19 deglycosylated ricin A chain immunotoxin in non-Hodgkin's lymphoma: effect of an intensive schedule of administration. *J. Immunother.* 18, 231–241.
 - (23) Siegall, C. B., Liggitt, D., Chace, D., Tepper, M. A., and Fell, H. P. (1994) Prevention of immunotoxin-mediated vascular leak syndrome in rats with retention of antitumor activity. *Proc. Natl. Acad. Sci. U.S.A.* 91, 9514–9518.
 - (24) Siegall, C. B., Liggitt, D., Chace, D., Mixan, B., Sugai, J., Davidson, T., and Steinitz, M. (1997) Characterization of vascular leak syndrome induced by the toxin component of *Pseudomonas* exotoxin-based immunotoxins and its potential inhibition with nonsteroidal anti-inflammatory drugs. *Clin. Cancer Res.* 3, 339–345.
 - (25) Clark, E. A., and Ledbetter, J. A. (1986) Activation of human B cells mediated through two distinct cell surface differentiation antigens, Bp35 and Bp50. *Proc. Natl. Acad. Sci. U.S.A.* 83, 4494–4498.
 - (26) Francisco, J. A., Schreiber, G. J., Comerkeski, C. R., Mezza, L. E., Warner, G. L., Davidson, T. J., Ledbetter, J. A., and Siegall, C. B. (1997) *In vivo* efficacy and toxicity of a single-chain immunotoxin targeted to CD40. *Blood* 89, 4493–4500.
 - (27) Schodin, B. A., and Kranz, D. M. (1993) Binding affinity and inhibitory properties of a single-chain anti-T cell receptor antibody. *J. Biol. Chem.* 268, 25722–25727.
 - (28) Griffiths, A. D., Malmqvist, M., Marks, J. D., Bye, J. M., Embleton, M. J., McCafferty, J., Maier, M., Holliger, K. P., Gorick, B. D., Hughes-Jones, N. C., Hoogenboom, H. R., and Winter, G. (1993) Human anti-self antibodies with high specificity from phage display libraries. *EMBO J.* 12, 725–734.

BC970107K

Synthesis and Biological Properties of Mannosylated Starburst Poly(amidoamine) Dendrimers

Daniel Pagé and René Roy*

Department of Chemistry, University of Ottawa, Ottawa, Ontario, Canada K1N 6N5. Received March 13, 1997[®]

Starburst PAMAM dendrimers ending with mannopyranoside residues were readily synthesized in large scale and good yields from commercially available dendrimers bearing high-density amine functionality on their surface and *p*-isothiocyanatophenyl 2,3,4,6-tetra-*O*-acetyl- α -D-mannopyranoside. The first four generations of this novel class of monodispersed neoglycoconjugates having up to 32 mannoside units were evaluated as ligands for the phytohemagglutinins from concanavalin A (Con A) and *Pisum sativum* (pea lectin) using enzyme-linked lectin assay (ELLA) and turbidimetric analyses. The binding properties of these glycodendrimers, together with reference monosaccharides, were determined using yeast mannan as a coating antigen and peroxidase-labeled lectins. These mannosylated dendrimers were demonstrated to be potent inhibitors with IC₅₀ values 400 times better than those of monomeric methyl α -D-mannopyranoside taken as a standard. Their lipophilic character was shown to be sufficient for their direct use as coating antigens in microtiter plate assays. Moreover, their ability to bind and form insoluble carbohydrate–lectin complexes was also demonstrated by radial double immunodiffusion and turbidimetric analyses. Furthermore, the ability of these ligands to selectively precipitate a mannose-binding protein (Con A) from a crude lectin mixture was also demonstrated using polyacrylamide gel electrophoresis (SDS–PAGE). These multivalent neoglycoconjugates were shown to constitute novel biochromatography materials of high affinity for the easy isolation of carbohydrate-binding proteins.

INTRODUCTION

The significant roles played by cell surface multiantennary glycoconjugates in mediating critical biological events at the cellular level are now well-established (1). Among known deleterious interactions, mannoside-ending glycoproteins that serve as high-affinity ligands for bacterial attachment to host tissues are of special interest (2–4). Protective immune responses against bacterial infections are mediated by serum mannose binding proteins (MBP)¹ (5, 6), followed by subsequent phagocytosis of the pathogens by macrophages (7, 8). Therefore, the study of such complex carbohydrate–cell surface interplay makes it challenging for both chemists and glycobiologists to design suitable glycomimetic inhibitors having similar or even enhanced binding properties with respect to those of naturally occurring multiantennary glycoproteins. Such multivalent neoglycoconjugates would have potential applications as antiadhesive agents or even as cell-targeting devices (9, 10).

Previous studies from our group and others have demonstrated the powerful protein binding properties of multivalent neoglycoconjugates (11). The arrangement of carbohydrate ligands into “clusters” can markedly increase their binding capacity, thus compensating for the relatively weak binding affinities of single monosac-

charide residues ($K_D \approx 0.1$ –1 mM) (12). Neoglycoproteins (13), telomers (14), and glycopolymers (15–17) nicely fulfill this multivalency criteria by providing up to 1000-fold increases in binding properties. However, the carbohydrate heterogeneity of these polydispersed macromolecules makes accurate biophysical measurements somewhat cumbersome. Thus, there is a need for multivalent ligands with better defined densities and geometrically well-organized scaffold.

Dendrimers (18–21), the first class of perfectly monodispersed synthetic macromolecules, are globular or tree-shaped molecules that truly resemble many biological components in their sizes, shapes, and geometries. Incorporation of terminal glycoside residues into these hyperbranched structures would create well-defined multiantennary glycoconjugates, mimicking the naturally occurring glycans found on cell surface glycoproteins. Such spherical and bidirectional “glycodendrimers” (22) have already been successfully prepared and demonstrated powerful inhibitory properties against their specific lectins. For instance, bidirectional poly(L-lysine) dendrimers with sialic acid ending residues were shown to strongly inhibit erythrocyte hemagglutination by influenza A viruses (23). Furthermore, similar glycodendrimers ending with α -D-mannopyranoside residues showed up to 2000-fold increased inhibitory properties toward concanavalin A and *Pisum sativum* (pea lectin) binding to yeast mannan (24). They also showed promising application as biochromatography adsorbents for the selective isolation of specific carbohydrate-binding proteins from crude mixtures (25). Another type of spheroid dendrimer ending with similar mannoside residues also showed improved binding properties with mannose-specific lectins (26). These encouraging results demonstrate the biological potential of such molecules as high-affinity ligands.

Tomalia and co-workers have synthesized poly(amidoamine) (PAMAM) dendrimers by a divergent growth

* Author to whom correspondence should be addressed. Telephone: (613) 562-5800 ext 6055. Fax: (613) 562-5170. E-mail: rroy@science.uottawa.ca

[®] Abstract published in *Advance ACS Abstracts*, September 1, 1997.

¹ Abbreviations: BSA, bovine serum albumin; Con A, concanavalin A; ELISA, enzyme-linked immunosorbent assays; ELLA, enzyme-linked lectin assays; FABMS, fast atom bombardment mass spectrometry; HRP, horseradish peroxidase; MBP, mannose binding protein; PAMAM, poly(amidoamine); PSA, *Pisum sativum* agglutinin; SDS–PAGE, sodium dodecyl sulfate–polyacrylamide gel electrophoresis; WGA, wheat germ agglutinin.

procedure (18, 27). These dendrimers can be produced in successive "generations" [G(0), G(1), G(2), ...] with well-defined size and valency. These attractive molecules have drawn a vast interest in many research areas, finding diversified applications such as linker molecules for radiolabeled antibodies (28), vectors in gene delivery systems (29), or even soluble supports in combinatorial chemistry (30). Interestingly, a recent study (31) demonstrated the lack of immunogenicity and toxicity that would preclude the use of PAMAM dendrimers in biological applications. PAMAM dendrimers with terminal Tn antigens (GalNAc α -Ser/Thr) (32), lactose and maltose derivatives (33), and mannositides (34) have recently been reported, but information about their physical and biological properties is scarce. We previously described the easy and efficient coupling of different polyamine molecules to *p*-isothiocyanatophenyl α -D-mannopyranoside (35). The resulting structures had enhanced binding properties compared to other α -substituted mannopyranosides (36–38). We therefore report herein the synthesis and biological properties of novel *p*-isothiocyanatophenyl α -D-mannopyranosyl-substituted PAMAM dendrimers using enzyme-linked lectin assays (ELLA), double immunodiffusion, and turbidimetric analyses. We also highlight for the first time the possible use of these dendritic molecules for the straightforward isolation and purification of phytohemagglutinins.

MATERIALS AND METHODS

General Methods. Melting points were determined on a Gallenkamp apparatus and are uncorrected. The ^1H and ^{13}C NMR spectra were obtained on a Brüker 500 MHz AMX NMR spectrometer. The proton chemical shifts (δ) are given with respect to internal chloroform (7.24 ppm) for CDCl_3 solutions and with respect to internal DMSO (2.49 ppm) for DMSO- d_6 solutions. The carbon chemical shifts are given relative to deuteriochloroform (77.0 ppm) and to DMSO- d_6 (39.5 ppm). The assignments were based on COSY, DEPT, and HMQC experiments. Optical rotations were measured on a Perkin-Elmer 241 polarimeter and were carried out at 23 °C. Mass spectra were recorded on a Kratos Concept ITH apparatus for FABMS using a glycerol matrix. Thin layer chromatography (TLC) was performed using silica gel 60 F-254 and column chromatography on silica gel 60. Optical densities (OD) for the ELLA tests and turbidimetric measurements were performed on a Dynatech MR 600 Microplate Reader.

Reagents. The lectins from *Triticum vulgaris* (wheat germ, WGA), *Canavalia ensiformis* (concanavalin A, Con A), and peroxidase-labeled concanavalin A, along with yeast mannan from *Saccharomyces cerevisiae* and bovine serum albumin (BSA), were purchased from Sigma (catalog numbers L 9640, C 2631, L 6397, M 7504, and A-7638, respectively). Pea lectin (*P. sativum*, PSA) and horseradish peroxidase-labeled pea lectin were obtained from EY Laboratories (catalog numbers L-2701–10 and H-2701–1, respectively). Methyl α -D-mannopyranoside was purchased from Aldrich (Madison, WI) and *p*-nitrophenyl α -D-mannopyranoside from Fluka. Monosaccharide **1** and divalent mannosylated ligand **3** were available from previous work (35). The Starburst PAMAM dendrimer cores [G(0)–G(3)] were kind gifts from R. Spindler of Dendritech, Inc. (Midland, MI).

Synthesis of Mannopyranosylated Starburst PAMAM Dendrimers. Divalent and trivalent ligands **3** and **5** (Figure 1) were synthesized from ethylenediamine and tris(2-aminoethyl)amine-based dendrimers and were included for comparison purposes. Divalent mannosylated ligand **3** was synthesized as previously described (35).

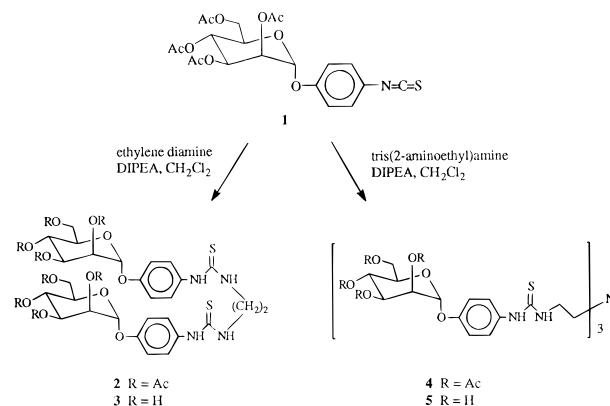


Figure 1. Structures of divalent (**3**) and trivalent (**5**) mannosylated ligands.

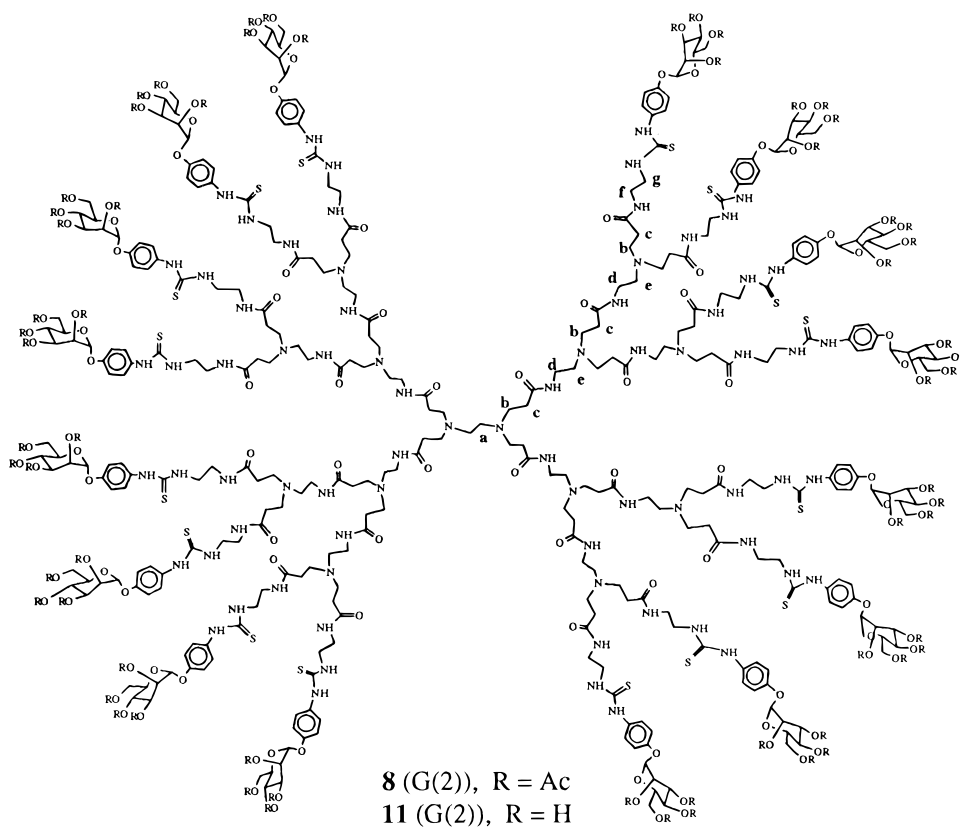
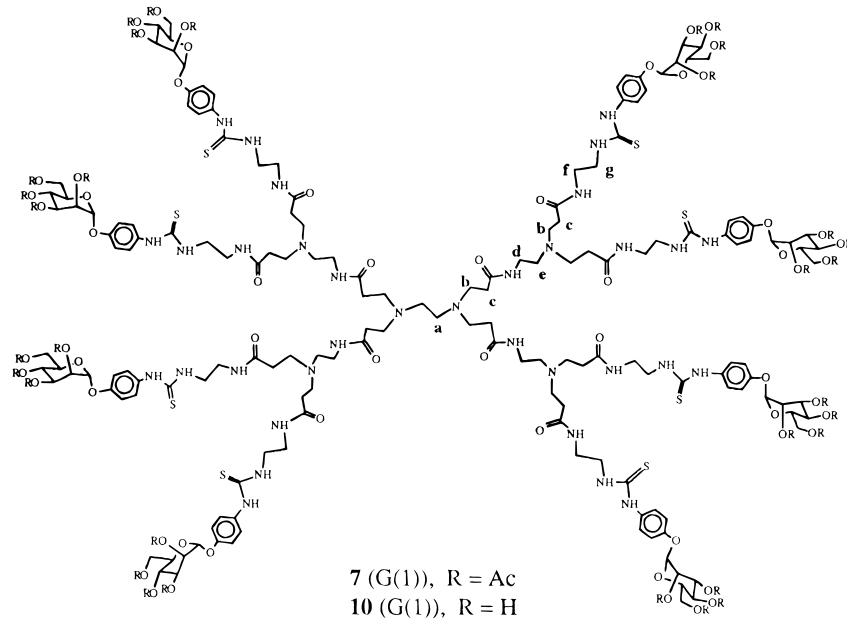
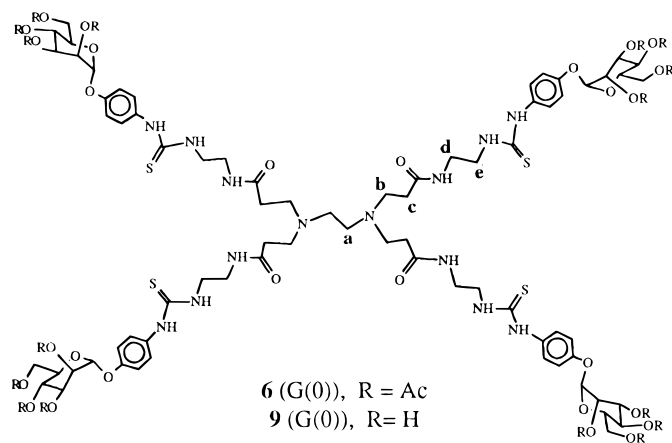
Briefly, *p*-isothiocyanatophenyl 2,3,4,6-tetra-*O*-acetyl- α -D-mannopyranoside (**1**) (2.4 equiv) was added to a CH_2Cl_2 solution containing ethylenediamine (1 equiv) and a catalytic amount of diisopropylethylamine (DIPEA). The solution was stirred at room temperature for 1 h, and the crude peracetylated ligand was purified by silica gel column chromatography. Standard Zemplén de-*O*-acetylation (MeOH, NaOMe, pH 8.5) afforded compound **3** in 98% overall yield (50 mg) as a white amorphous solid. Trivalent mannosylated ligand **5** was also obtained as an amorphous solid in 87% yield following the same procedure.

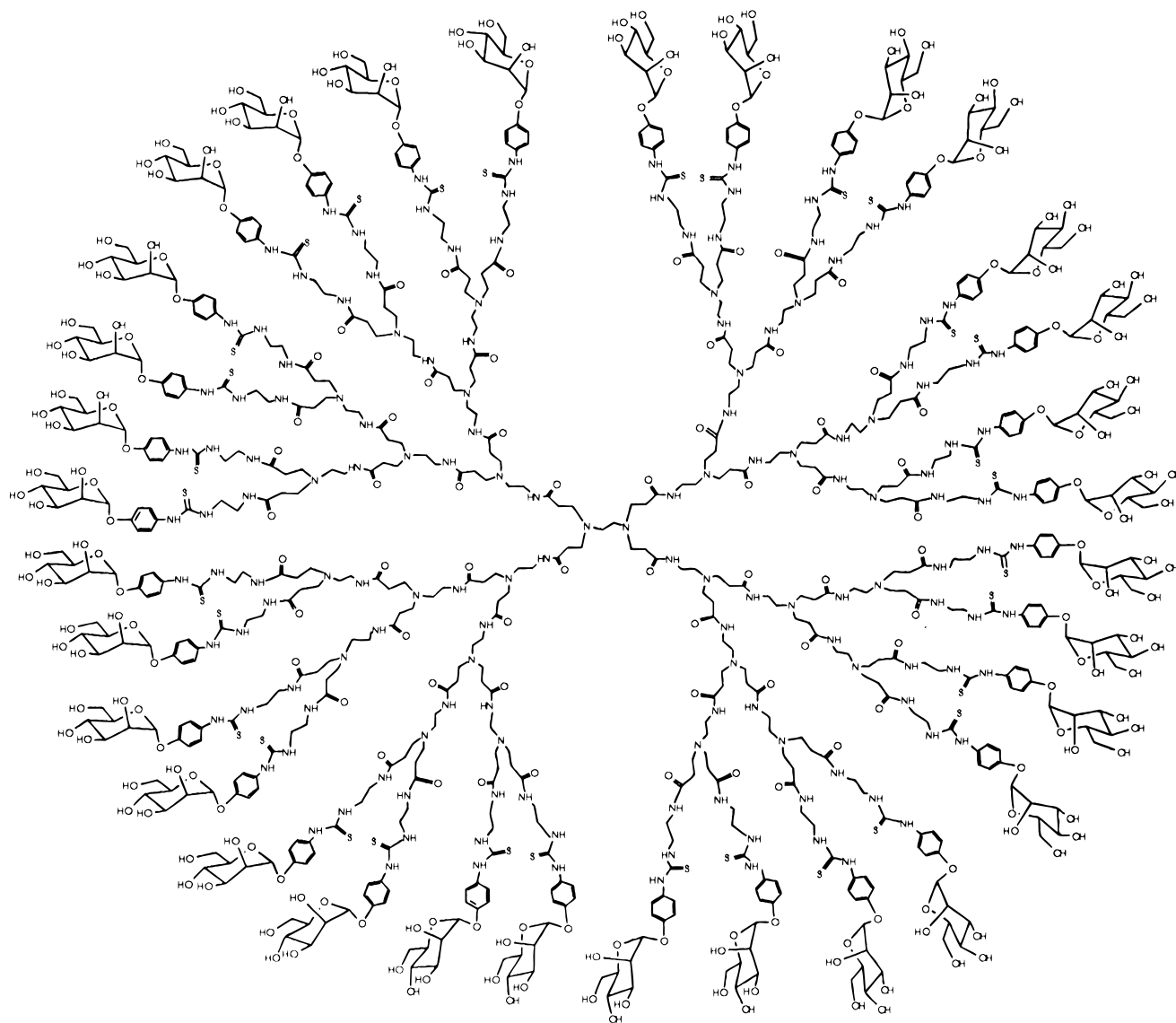
Mannopyranosylated PAMAM dendrimers **9–12** (Figure 2) were synthesized using a different approach. Methanolic PAMAM solutions G(0) and G(1) were evaporated and coevaporated with CH_2Cl_2 four times under reduced pressure. The residues obtained were dissolved in CH_2Cl_2 (5 mL) along with compound **1** (1.2 equiv per terminal amino group), and the solutions were refluxed for 3 h. The resulting acetylated glycodendrimers **6–8** were purified by silica gel column chromatography in 55–90% yields using the following eluent: **6** [G(0), 4-mer], 5:1 $\text{CHCl}_3/\text{MeOH}$; **7** [G(1), 8-mer], 3:1 $\text{CHCl}_3/\text{MeOH}$; **8** and [G(2), 16-mer], 10:6:1 $\text{CHCl}_3/\text{MeOH}/\text{H}_2\text{O}$. All products were obtained as foams.

De-*O*-acetylated glycodendrimers **9–13** were obtained by stirring compounds **6–8** in MeOH containing 1 M NaOMe (pH \approx 8.5) overnight at room temperature. Addition of an equal volume of cold ether precipitated the products which were filtered and rinsed with ether to afford products **9–11** in 60–95% (80–100 mg) yields as white powders.

Because of the lack of solubility of the G(3) PAMAM generation (32-mer) in CH_2Cl_2 , DMF was used as the solvent and the solution was stirred at room temperature for 48 h. The product was readily de-*O*-acetylated by the addition of an equal volume of MeOH containing a catalytic amount of 1 M NaOMe (pH \approx 8.5). The solution was stirred for 24 h, while maintaining the pH at \approx 8.5 by addition of 1 M NaOMe, and then dialyzed against 1:1 $\text{H}_2\text{O}/\text{DMSO}$ (MW cutoff of 2000). Lyophilization in water afforded glycodendrimer **12** in 55% yield as a white powder.

Analytical Data for Starburst PAMAM Glycodendrimers. Compound **4**: mp 108–111 °C dec; $[\alpha]_D^{25} = 66.8^\circ$ ($c = 0.50$, CHCl_3); ^1H NMR (CDCl_3) δ (ppm) 2.00 (2X), 2.01 and 2.16 (4s, 36 H, Ac), 2.64 (t, 6 H, $J = 0.7$ Hz, NCH_2), 3.61 (bs, 6 H, CH_2NH), 4.06 (m, 6 H, H-5 and H-6'), 4.21 (dd, 3 H, $J_{5,6} = 5.2$ Hz, $J_{6,6'} = 12.3$ Hz, H-6), 5.33 (dd, 3 H, $J_{3,4} = 9.9$ Hz, $J_{4,5} = 10.0$ Hz, H-4), 5.38 (bs, 3 H, H-2), 5.49 (dd, 3 H, $J_{2,3} = 3.1$ Hz, H-3), 5.50 (d, 3 H, $J_{1,2} = 1.5$ Hz, H-1), 6.65 (b, 3 H, CH_2NH), 7.04 (d, 6





12 (32-mer)

Figure 2. Structures of the G(0)–G(3) of mannopyranosylated PAMAM dendrimers [G(0)–G(2)].

H, $J_{o,m} = 8.8$ Hz, H-ortho), 7.20 (d, 6 H, H-meta), 8.15 (b, 3 H, NH aromatic); ^{13}C NMR (CDCl_3) δ (ppm) 20.7 (3C) and 20.9 (Ac), 43.2 (NCH_2), 53.4 (CH_2NH), 62.0 (C-6), 65.8 (C-4), 68.8 (C-3), 69.2 (C-2), 69.3 (C-5), 96.0 (C-1), 117.5 (C-ortho), 126.8 (C-meta), 154.1 (C-ipso), 169.9 (2C), 170.1 and 170.5 (C=O's), 181.2 (C=S); MS (positive FAB) calcd for $\text{C}_{69}\text{H}_{87}\text{N}_7\text{O}_{30}\text{S}_3$ 1589.5, found 1590.5 ($\text{M}^+ + 1$, 0.1%).

Compound 5: mp 149–151 °C dec; $[\alpha]_D = 112.2^\circ$ ($c = 1.00$, MeOH); ^1H NMR ($\text{DMSO}-d_6$) δ (ppm) 2.69 (t, 6 H, $J = 0.6$ Hz, NCH_2), 3.41–3.66 (m, 21 H, CH_2NH , H-3, H-4, H-5, H-6, and H-6'), 3.82 (bs, 3 H, H-2), 4.48 (m, 3 H, OH-6), 4.76 (d, 3 H, $J = 5.6$ Hz, OH-3), 4.84 (d, 3 H, $J = 4.8$ Hz, OH-4), 5.02 (d, 3 H, $J = 4.1$ Hz, OH-2), 5.32 (s, 3 H, H-1), 7.04 (d, 6 H, $J_{o,m} = 8.8$ Hz, H-ortho), 7.24 (d, 6 H, H-meta), 7.49 (bs, 3 H, CH_2NH), 9.48 (b, 3 H, NH aromatic); ^{13}C NMR ($\text{DMSO}-d_6$) δ (ppm) 42.0 (NCH_2), 52.3 (CH_2NH), 61.1 (C-6), 66.7 (C-4), 70.2 (C-3), 70.7 (C-2), 75.0 (C-5), 99.3 (C-1), 117.1 (C-ortho), 125.6 (C-meta), 153.6 (C-ipso), 180.5 (C=S); MS (positive FAB) calcd for $\text{C}_{45}\text{H}_{63}\text{N}_7\text{O}_{18}\text{S}_3$ 1085.3, found 1086.3 ($\text{M}^+ + 1$, 0.3%).

Compound 6: $[\alpha]_D = 52.3^\circ$ ($c = 1.00$, CHCl_3); ^1H NMR (CDCl_3) δ (ppm) 2.00, 2.01, 2.02, and 2.16 (4s, 48 H, Ac), 2.32 (bs, 8 H, Hb), 2.65 (bs, 8 H, Hc), 3.35 (d, 8 H, Hd),

3.70 (bs, 8 H, He), 4.06 (m, 8 H, H-5 and H-6'), 4.23 (dd, 4 H, $J_{5,6} = 5.4$ Hz, $J_{6,6'} = 12.9$ Hz, H-6), 5.34 (dd, 4 H, $J_{3,4} = 9.9$ Hz, $J_{4,5} = 10.0$ Hz, H-4), 5.38 (dd, 4 H, $J_{1,2} = 1.8$ Hz, $J_{2,3} = 3.5$ Hz, H-2), 5.48 (dd, 4 H, H-3), 5.49 (d, 4 H, H-1), 7.06 (d, 8 H, $J_{o,m} = 8.8$ Hz, H-ortho), 7.23 (d, 8 H, H-meta), 7.65 (bs, 4 H, NHC(O)), 8.42 (bs, 4 H, NH -aromatic); ^{13}C NMR (CDCl_3) δ (ppm) 20.7 (3C) and 20.9 (Ac), 34.0 (Cb), 39.5 (Cd), 44.6 (Ce), 49.9 (Cc), 50.6 (Ca), 62.1 (C-6), 65.8 (C-4), 68.9 (C-3), 69.3 (2C) (C-2 and C-5), 96.0 (C-1), 117.5 (C-ortho), 126.9 (C-meta), 132.0 (C-para), 154.1 (C-ipso), 169.7, 170.0 (2C) and 170.6 (C=O's, acetates), 173.4 (NHC=O's), 181.6 (C=S).

Compound 7: $[\alpha]_D = 47.1^\circ$ ($c = 1.50$, CHCl_3); ^1H NMR (CDCl_3) δ (ppm) 1.98, 1.99, 2.00, and 2.14 (4s, 96 H, Ac), 2.27 (bs, 24 H, Hb), 2.46 (bs, 8 H, He), 2.64 (bs, 24 H, Hc), 3.17 (bs, 8 H, Hd), 3.34 (bs, 16 H, Hf), 3.66 (bs, 16 H, Hg), 4.01–4.03 (m, 16 H, H-5 and H-6'), 4.21 (dd, 8 H, $J_{5,6} = 5.4$ Hz, $J_{6,6'} = 12.2$ Hz, H-6), 5.32 (dd, 8 H, $J_{3,4} = 10.0$ Hz, $J_{4,5} = 10.1$ Hz, H-4), 5.36 (dd, 8 H, $J_{1,2} = 1.6$ Hz, $J_{2,3} = 3.3$ Hz, H-2), 5.45 (dd, 8 H, H-3), 5.47 (d, 8 H, H-1), 7.02 (d, 16 H, $J_{o,m} = 8.5$ Hz, H-ortho), 7.23 (d, 16 H, H-meta), 7.70 (bs, 12 H, NHC(O)), 8.65 (bs, 8 H, NH -aromatic); ^{13}C NMR (CDCl_3) δ (ppm) 20.7 (3C) and 20.8

(Ac), 34.2 (Cb), 37.8 (Cd), 39.4 (Cf), 44.5 (Cg), 50.3 (Cc), 52.4 (Ce), 62.1 (C-6), 65.8 (C-4), 68.9 (C-3), 69.3 (2C) (C-2 and C-5), 96.0 (C-1), 117.3 (C-ortho), 126.8 (C-meta), 132.5 (C-para), 153.8 (C-ipso), 169.7, 170.0 (2C), and 170.6 (C=O's, acetates), 173.7 (NHC=O's), 181.6 (C=S).

Compound 8: $[\alpha]_D = 37.9^\circ$ ($c = 1.00$, CHCl₃); ¹H NMR (CDCl₃) δ (ppm) 1.96, 1.97, 1.99, and 2.12 (4s, 192 H, Ac), 2.26 (bs, 56 H, Hb), 2.46 (bs, 24 H, He), 2.63 (bs, 56 H, Hc), 3.18 (bs, 24 H, Hd), 3.33 (bs, 32 H, Hf), 3.64 (bs, 32 H, Hg), 4.02 (m, 32 H, H-5 and H-6'), 4.20 (d, 16 H, H-6), 5.31 (d, 16 H, H-4), 5.35 (s, 16 H, H-2), 5.45 (m, 32 H, H-3 and H-1), 7.00 (d, 32 H, $J_{o,m} = 8.5$ Hz, H-ortho), 7.21 (d, 32 H, H-meta), 7.70 (bm, 28 H, NHC(O)), 8.65 (bs, 16 H, NH-aromatic); ¹³C NMR (CDCl₃) δ (ppm) 20.7 (3C) and 20.8 (Ac), 34.1 (Cb), 37.7 (Cd), 39.4 (Cf), 44.5 (Cg), 50.3 (Cc), 52.4 (Ce), 62.0 (C-6), 65.8 (C-4), 68.9 (C-3), 69.2 (C-2), 69.3 (C-5), 96.0 (C-1), 117.3 (C-ortho), 126.7 (C-meta), 132.6 (C-para), 153.8 (C-ipso), 169.6, 170.0 (2C) and 170.6 (C=O's, acetates), 173.0 and 173.5 (NHC=O's), 181.6 (C=S).

Compound 9: $[\alpha]_D = 66.0^\circ$ ($c = 0.50$, DMSO); ¹H NMR (DMSO-*d*₆) δ (ppm) 2.20 (bs, 8 H, Hb), 2.43 (bs, 4 H, Ha), 2.63 (bs, 8 H, Hc), 3.21 (d, 8 H, Hd), 3.42–3.51 (m, 20 H, He, H-4, H-5, and H-6'), 3.59 (d, 4 H, $J_{6,6'} = 11.1$ Hz, H-6), 3.66 (dd, 4 H, $J_{2,3} = 2.5$ Hz, $J_{3,4} = 8.8$ Hz, H-3), 3.81 (s, 4 H, H-2), 4.40–5.00 (bm, 16 H, OH's), 5.30 (s, 4 H, H-1), 7.01 (d, 8 H, $J_{o,m} = 8.5$ Hz, H-ortho), 7.25 (d, 8 H, H-meta), 8.06 (bm, NH's); ¹³C NMR (DMSO-*d*₆) δ (ppm) 33.3 (Cb), 38.1 (Cd), 43.7 (Ce), 49.8 (Cc), 51.0 (Ca), 61.1 (C-6), 66.8 (C-4), 70.2 (C-2), 70.7 (C-3), 74.9 (C-5), 99.3 (C-1), 117.0 (C-ortho), 125.5 (C-meta), 133.3 (C-para), 153.5 (C-ipso), 172.0 (C=O), 181.9 (C=S); MS (positive FAB) calcd for C₇₄H₁₀₈N₁₄O₂₈S₄ 1768.7, found 1769.7 ($M^+ + 1$, 1.0%).

Compound 10: $[\alpha]_D = 54.4^\circ$ ($c = 0.50$, DMSO); ¹H NMR (DMSO-*d*₆) δ (ppm) 2.20 (bs, 24 H, Hb), 2.42 (bs, 12 H, Ha and He), 2.65 (bs, 24 H, Hc), 3.08 (bs, 8 H, Hd), 3.21 (bs, 16 H, Hf), 3.42–3.51 (m, 40 H, Hg, H-4, H-5, and H-6'), 3.59 (d, 8 H, $J_{6,6'} = 11.1$ Hz, H-6), 3.67 (d, 8 H, $J_{2,3} = 2.3$ Hz, H-3), 3.81 (s, 8 H, H-2), 4.40–5.00 (bm, 32 H, OH's), 5.30 (s, 8 H, H-1), 7.00 (d, 16 H, $J_{o,m} = 8.4$ Hz, H-ortho), 7.24 (d, 16 H, H-meta), 7.83 and 8.00 (2 bs, NH's); ¹³C NMR (DMSO-*d*₆) δ (ppm) 33.3 (Cb), 37.0 (Cd), 39.4 (Cf), 43.6 (Cg), 49.6 (Cc), 50.9 (Ca), 52.2 (Ce), 61.0 (C-6), 66.7 (C-4), 70.1 (C-2), 70.7 (C-3), 74.8 (C-5), 99.3 (C-1), 116.9 (C-ortho), 125.4 (C-meta), 133.3 (C-para), 153.5 (C-ipso), 171.5 and 171.9 (C=O's), 180.8 (C=S).

Compound 11: $[\alpha]_D = 57.5^\circ$ ($c = 0.40$, DMSO); ¹H NMR (DMSO-*d*₆) δ (ppm) 2.19 (bs, 56 H, Hb), 2.42 (bs, 28 H, Ha and He), 2.64 (bs, 56 H, Hc), 3.08 (bs, 24 H, Hd), 3.22 (bs, 32 H, Hf), 3.38–3.49 (m, 80 H, Hg, H-4, H-5, and H-6'), 3.58 (d, 16 H, $J_{6,6'} = 10.8$ Hz, H-6), 3.66 (bd, 16 H, H-3), 3.81 (s, 16 H, H-2), 4.45 (bs, 16 H, OH-6), 4.73 (bs, 16 H, OH-3), 4.82 (bs, 16 H, OH-4), 5.00 (bs, 16 H, OH-2), 5.30 (s, 16 H, H-1), 7.01 (d, 32 H, $J_{o,m} = 8.2$ Hz, H-ortho), 7.23 (d, 32 H, H-meta), 7.64, 7.78, 7.99, and 9.43 (4 bs, NH's); ¹³C NMR (DMSO-*d*₆) δ (ppm) 33.3 (Cb), 37.0 (Cd), 38.0 (Cf), 43.6 (Cg), 49.6 (Cc), 52.2 (Ce), 61.1 (C-6), 66.8 (C-4), 70.2 (C-2), 70.7 (C-3), 74.9 (C-5), 99.3 (C-1), 117.0 (C-ortho), 125.5 (C-meta), 133.2 (C-para), 153.6 (C-ipso), 171.4 and 171.9 (C=O's), 180.9 (C=S).

Compound 12: $[\alpha]_D = 58.6^\circ$ ($c = 0.50$, DMSO); ¹H NMR (DMSO-*d*₆) δ (ppm) 2.19 (bs, 120 H, Hb), 2.42 (bs, 60 H, Ha and He), 2.65 (bs, 120 H, Hc), 3.08 (bs, 56 H, Hd), 3.22 (bs, 64 H, Hf), 3.41–3.49 (m, 160 H, Hg, H-4, H-5, and H-6'), 3.58 (d, 32 H, $J_{6,6'} = 10.8$ Hz, H-6), 3.66 (bs, 32 H, H-3), 3.81 (bs, 32 H, H-2), 4.44 (bs, 32 H, OH-6), 4.73 (bs, 32 H, OH-3), 4.81 (bs, 32 H, OH-4), 4.99 (bs, 32 H, OH-2), 5.30 (s, 32 H, H-1), 7.01 (d, 64 H, $J_{o,m} = 8.0$ Hz, H-ortho), 7.23 (d, 64, H-meta), 7.62, 7.77, 7.99, and

9.41 (4 bs, NH's); ¹³C NMR (DMSO-*d*₆) δ (ppm) 33.2 (Cb), 36.9 (Cd), 38.0 (Cf), 43.6 (Cg), 49.5 (Cc), 52.2 (Ce), 61.0 (C-6), 66.7 (C-4), 70.1 (C-2), 70.7 (C-3), 74.9 (C-5), 99.2 (C-1), 116.9 (C-ortho), 125.4 (C-meta), 133.1 (C-para), 153.5 (C-ipso), 171.3 and 171.8 (C=O's), 180.8 (C=S).

Enzyme-Linked Lectin Assay (ELLA). Linbro (Titertek) microtitration plates were coated with yeast mannan (100 μ L/well) diluted from a stock solution of 10 μ g/mL in 0.01 M phosphate saline buffer (PBS, pH 7.3) at room temperature overnight for experiments done with Con A. Alternatively, a similar concentration of mannosylated copolyacrylamide copolymer (acrylamide: mannoside ratio of 37:1) (24) was used for pea lectin experiments. The wells were then washed three times with 300 μ L/well washing buffer [PBS containing 0.05% (v/v) Tween 20] (PBST). This washing procedure was repeated after each incubation throughout the assay. The wells were then blocked with 150 μ L/well BSA/PBS (1%) for 1 h at 37 $^\circ$ C. After washing, the wells were filled with 100 μ L/well serial dilutions of peroxidase-labeled concanavalin A (Con A-HRP) or lectin-peroxidase-labeled *P. sativum* (PSA-HRP) from 10⁻¹ to 10⁻⁵ mg/mL in PBS and incubated at 37 $^\circ$ C for 1 h. The plates were washed, and 50 μ L/well 2,2'-azinobis(3-ethylbenzothiazoline-6-sulfonic acid) diammonium salt (ABTS) (1 mg per 4 mL) in citrate/phosphate buffer (0.2 M, pH 4.0 with 0.015% H₂O₂) was added. The reaction was stopped after 20 min by adding 50 μ L/well H₂SO₄ (1 M), and the optical density (OD) was measured at 410 nm relative to 570 nm. Blank wells contained citrate/phosphate buffer. The concentration of each lectin-enzyme conjugate that had an OD between 0.8 and 1.0 was used for inhibition experiments.

Inhibition Experiments. Linbro microtiter plates were coated overnight at room temperature with yeast mannan (100 μ L of a 10 μ g/mL stock solution). The plates were then washed and blocked with BSA as described previously. The monomers (methyl α -D- and *p*-nitrophenyl α -D-mannopyranosides) and multivalent mannosylated ligands (**3**, **5**, and **9–12**) were used as stock solutions varying from 1 to 3 mg/mL PBS. Each inhibitor was added in serial 2-fold dilutions (60 μ L/well) in PBS with 60 μ L of the desired lectin-enzyme conjugate concentration on Nunclon (Delta) microtiter plates and incubated at 37 $^\circ$ C for 1 h. The above solutions (100 μ L) were then transferred to the antigen-coated plates which were incubated for an additional 1 h at 37 $^\circ$ C. The plates were washed as described above, and the ABTS substrate was added (50 μ L/well). Color development was stopped after 20 min, and the OD was measured at 410 nm relative to that at 570 nm. The data were plotted and analyzed using Graphpad Inplot Software, v. 4.03. The percent inhibitions were calculated as follows:

$$\% \text{ inhibition} = \frac{A_{(\text{no inhibitor})} - A_{(\text{with inhibitor})}}{A_{(\text{no inhibitor})}} \times 100$$

IC₅₀'s were reported as the concentration required for 50% inhibition of the coating antigen.

Mannosylated Starburst PAMAM Dendrimers as Coating Antigens in ELLA. PAMAM glycodendrimers **9–12** were coated overnight on microtiter plates in concentrations varying from 1 to 20 nmol/well. The wells were then washed and blocked following the procedure described above. Peroxidase-labeled concanavalin A was then added, and the plates were incubated at 37 $^\circ$ C for 1 h. After washing, the ABTS substrate solution was added, and color development was stopped after 20 min by the addition of 1 M H₂SO₄. The OD was then measured at 410 nm relative to 570 nm. Each test was done in triplicate.

Turbidimetric Analysis. Turbidimetry experiments were performed in Linbro (Titertek) microtitration plates where an 80 μ L/well stock lectin solution prepared from Con A (1 mg/mL PBS) was mixed with a volume PAMAM glycodendrimers **9–12** (stock solutions of 1 mg/mL PBS) corresponding to 10 nmol of mannoside residues. The total volume of each well was brought to 100 μ L by the addition of PBS. The solutions were diluted with PBS to obtain a final volume of 100 μ L per well and were then incubated at room temperature for 2–3 h. The turbidity of the solutions was monitored by reading the optical density (OD) at 490 nm at regular time intervals until no noticeable changes could be observed. Each test was done in triplicate.

Agar Gel Diffusion. Agar gel diffusion experiments were performed in 1% agarose containing 2% poly(ethylene glycol) (MW of 8000) in PBS buffer following a procedure described elsewhere (39). The lectin (Con A) and glycodendrimers tested (**11** and **12**) were used at a concentration of 1 mg/mL in PBS. The precipitin bands were allowed to form overnight at 4 °C and were stained with 0.1% Coomassie Brilliant Blue solution.

Lectin Precipitation by Dendrimers. PAMAM glycodendrimer **9** (20 μ L, 1 mg/mL PBS) was added to a Con A/WGA mixture (180 μ L, 1 mg/mL PBS) and was stirred overnight at room temperature. The insoluble lectin–dendrimer complex was removed by centrifugation (Fisher Micro-Centrifuge Model 235B, 14000*g*), and the supernatant was transferred into a new Eppendorf tube where another 20 μ L of dendrimer solution was added. The solution was stirred for 2 h and then centrifuged as before. The supernatant was decanted and saved for electrophoresis, whereas the pellets obtained from both precipitations were resuspended in PBS. D-Mannose (3.0 mg) was added, and the solution was stirred at room temperature for 1 h or until no more precipitate could be observed. This solution was also saved for the subsequent step.

Electrophoresis of Phytohemagglutinins. Sodium dodecyl sulfate–polyacrylamide gel electrophoresis (SDS–PAGE) was carried out by the method of Laemmli (40) using a Bio-Rad (Richmond, CA) Mini-PROTEAN II dual-slab cell apparatus. Stock solutions of the lectins (1 mg/mL for Con A and WGA) along with the lectin/dendrimer solutions were diluted 1-fold with the electrophoretic buffer [0.5 M Tris-HCl (pH 6.8) containing 10% (w/v) SDS, 10% (v/v) glycerol, 5% (v/v) 2-mercaptoethanol, and 0.05% (w/v) bromophenol blue]. Bovine serum albumin (BSA, 1 mg/mL) was used as a standard and also diluted 1-fold with the electrophoretic buffer. The samples were heated at 95 °C for 5 min, and 25 μ L portions were applied to the gel. Electrophoresis was performed on a 1.5 mm thick gel in 12% acrylamide as the separating slab gel (0.375 M Tris at pH 8.8) and in 4% acrylamide as the stacking gel (0.125 M Tris at pH 6.8) with a constant current of 50 mA until the tracking dye reached the bottom of the gel. The bands were then stained with 0.1% (w/v) Coomassie Brilliant Blue solution (10% aqueous acetic acid and 40% aqueous methanol) for 3 h and then destained (10% aqueous acetic acid and 40% aqueous methanol) overnight.

RESULTS AND DISCUSSION

Inhibitory Potency of Mannosylated Starburst PAMAM Dendrimers. The binding properties of dendritic PAMAM ending with aryl α -D-mannopyranoside residues were first established by enzyme-linked lectin assays (ELLA) using the two model plant lectins concanavalin A (Con A) and *P. sativum* (pea lectin). The α -anomeric configuration of the mannosides was chosen

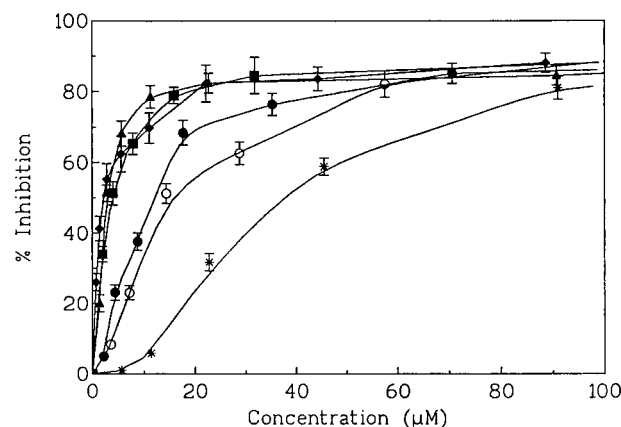


Figure 3. Results from the inhibition of binding of peroxidase-labeled Con A to yeast mannan by mannosylated ligands **3** (dimer) (*), **5** (trimer) (○), **9** (tetramer) (●), **10** (8-mer) (■), **11** (16-mer) (▲), and **12** (32-mer) (◆).

because these two lectins were shown to possess stronger binding affinity toward α -substituted D-mannopyranoside derivatives than toward free D-mannose. Moreover, mannopyranosides bearing aromatic α -aglycons also have higher affinities than those bearing aliphatic aglycons (36–38). Yeast mannan was used as the coating ligand in microtiter plates for studies involving the inhibition of HRP-labeled Con A binding. In the case of HRP-labeled pea lectin, a low-density mannosylated polymer (24) having an acrylamide:mannoside ratio of 37:1 was used as the coating antigen since the measured optical densities done with yeast mannan were too low. The results for the inhibition of binding of Con A to yeast mannan are shown in Figure 3 and Table 1. Methyl α -D-mannopyranoside (Me α -D-Man) and *p*-nitrophenyl α -D-mannopyranoside (*p*NO₂ α -D-Man) were used as reference monomers.

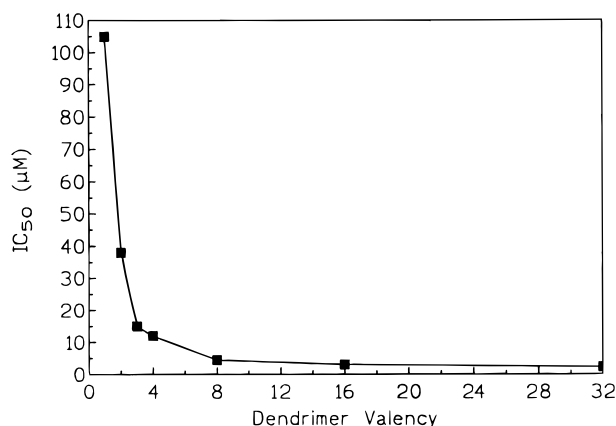
Di- and trivalent ligands **3** and **5**, where amine cores constitute starting materials for PAMAM dendrimers, were also included for comparison purposes. They respectively showed 24- and 63-fold increased binding potency when compared to Me α -D-Man in the inhibition of binding of yeast mannan to Con A. However, it has to be noticed that other divalent ligands with identical α -substituted mannopyranoside residues have already been reported to be almost 4 times more potent than ligand **3** (35). Striking increases in inhibitory potencies were achieved with mannosylated PAMAM dendrimers **9–12** which showed IC₅₀'s from 12.4 μ M (tetramer) to 2.3 μ M (32-mer) against Con A. When the IC₅₀'s for Con A were plotted as a function of dendrimer valencies (Figure 4), it is possible to observe a plateau of inhibition at dendrimer valencies of 4 (**9**) to 8 (**10**). This phenomenon has also been previously observed with mannosylated poly(L-lysine) dendrimers (24). When the values are expressed on a per-mannoside residue basis, the highest valency effect was obtained with octameric dendrimer **10** where each mannoside residue was 28 times more potent than monomeric Me α -D-Man.

The results for pea lectin inhibition of binding to mannosylated copolyacrylamide by the dendrimers are also reported in Table 1. Dimeric (**3**) and trimeric (**5**) ligands showed only slight improvements in inhibition with IC₅₀ values almost identical at 431 and 455 μ M, respectively. There was, however, a marked increase in inhibitory potencies arising from tetravalent and octavalent dendrimers **9** and **10** with IC₅₀'s of 34.0 and 17.5 μ M, respectively. When expressed on a monosaccharide basis, they both showed an approximate 28-fold increase in potency, making them the best inhibitors. The higher-

Table 1. Inhibition of Peroxidase-Labeled Concanavalin A and Pea Lectins by Mannopyranosylated PAMAM Dendrimers

compound	MW	IC ₅₀ (μM)	Con A relative potency ^a	ΔΔG° (kcal/mol)	IC ₅₀ (μM)	pea lectin relative potency ^a	ΔΔG° (kcal/mol)
Me α-D-Man	194.2	924	1.0	—	3850	1.0	—
pNO ₂ α-D-Man	301.3	105	3.5	-1.33	2489	1.5	-0.26
3 (dimer)	686.8	38.0	24.3 (12.2)	-1.93	431	8.9 (4.5)	-1.32
5 (trimer)	1086.7	14.7	62.9 (21.0)	-2.51	455	8.5 (2.8)	-1.29
9 (tetramer)	1770.3	12.4	75 (18.8)	-2.61	34.0	113 (28.3)	-2.87
10 (8-mer)	3936.6	4.1	224 (28.0)	-3.28	17.5	220 (27.5)	-3.27
11 (16-mer)	8269.3	3.1	301 (18.8)	-3.45	87.8	43.8 (2.7)	-2.29
12 (32-mer)	16 935.6	2.3	402 (12.6)	-3.63	36.2	106 (3.3)	-2.82

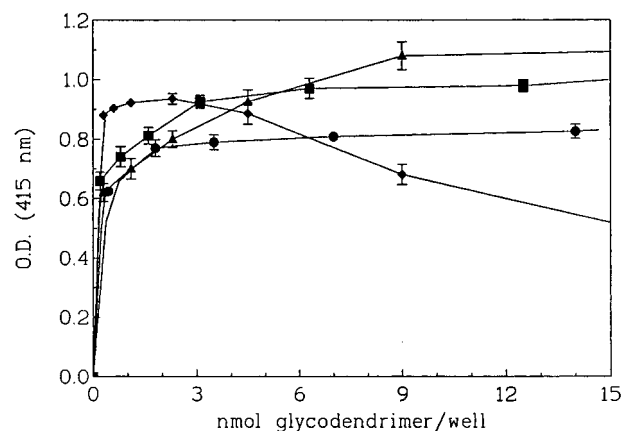
^a Values in parentheses are based on per-mannoside residues.

**Figure 4.** Effect of dendrimer valency on the inhibition of Con A to yeast mannan.

generation dendrimers **11** (16-mer) and **12** (32-mer) demonstrated somewhat lower inhibition, with IC₅₀'s of 87.8 and 36.2 μM, respectively. This represented only a 2.7–3.3-fold increase in inhibitory potency relative to that of Me α-D-Man.

The lowest relative potencies on a per-mannoside residue basis obtained with the higher dendrimer generations (dendrimers **11** and **12** with values of 18.8 and 12.6 for Con A and 2.7 and 3.3 for pea lectin, respectively) may result from inaccessible mannoside residues for binding due to steric crowding by bound lectin molecules. In the case of pea lectin, the drop of potency observed for the 16- and 32-mer (**11** and **12**) may also be attributed to other factors such as the poorer ability of this divalent lectin to form a well-organized cross-linked lattice with the multivalent glycodendrimers when compared to tetra-valent Con A. It is also conceivable that the relative molecular weights of the glycodendrimers (8300 for **11** and 16 900 for **12**) play a major role when compared to the size of the lectin themselves (102 000 for Con A and only 49 000 for pea lectin). It is also noteworthy to mention that low-valency dendrimers analogous to **3** (dimer) and **5** (trimer), which have less pronounced tendency to cross-link the lectins at lower concentrations, showed intrinsic affinities (*K_D*) somewhat identical to those of monosaccharides for Con A (R. Roy, D. Pagé, S. Dimick, and E. J. Toone, unpublished data). This issue raises some unresolved questions about the exact nature of the so-called "cooperative" multivalent carbohydrate–protein binding interactions.

The capacity of glycodendrimers **9–12** to act as coating antigens was next evaluated in similar ELLA experiments (Figure 5). From these results, it appeared that all dendrimers were lipophilic enough to adhere to the plastic wells, even in the range of 1–3 nmol per well, making them very potent coating multivalent ligands. This property may be particularly beneficial in direct binding experiments. The "prozone" effect observed for

**Figure 5.** Enzyme-linked lectin assays (ELLA) using mannosylated PAMAM glycodendrimers **9** (●), **10** (■), **11** (▲), and **12** (◆) as coating antigens for peroxidase-labeled Con A.

the larger dendrimer **12** (32-mer), which seems to "leak" the microtiter plate at high concentrations, may be a result of its more likely hydrophilic surface originating from a globular shape and its larger size when compared to smaller dendrimers.

Evidence for Direct Binding of Mannosylated Dendrimers to Lectins. The highest ligand affinity expressed by Con A relative to pea lectin can be explained by the difference in valency between these two lectins. At physiological pH, Con A exists as tetramers that may facilitate the formation of stable cross-linked lattices with mannosylated clusters (41), whereas the dimeric pea lectin cannot promote such highly cross-linked complexes. The ability of mannosylated dendrimers **11** (16-mer) and **12** (32-mer) to form such stable insoluble complexes with Con A was first illustrated by agar gel diffusion (Figure 6). Clear precipitin bands were formed overnight, proving the cross-linking properties of these novel neoglycoconjugates. Polyacrylamide copolymers with allyl α-D-mannopyranoside (top well) and with β-D-N-acetylglucosamine (42) (right well) were used as positive and negative controls, respectively.

The reactivity of all mannosylated PAMAM dendrimers (**9–12**) toward Con A was further substantiated by turbidimetric measurements as depicted in Figures 7 and 8. When glycodendrimers **9–12** were mixed with Con A (at concentrations equal to 10 nmol of mannoside residues), insoluble complexes could be clearly and readily visualized within a few minutes of mixing (Figure 7). Here again, octavalent glycodendrimer (**10**) proved to be the most efficient binder on a per-mannoside scale. The reversibility of the carbohydrate–lectin interaction was also demonstrated by the addition of a large excess of D-mannose which helped in resolubilizing the lectin into solution by an inhibition process (Figure 8). When the analyses were repeated with pea lectin, no substantial

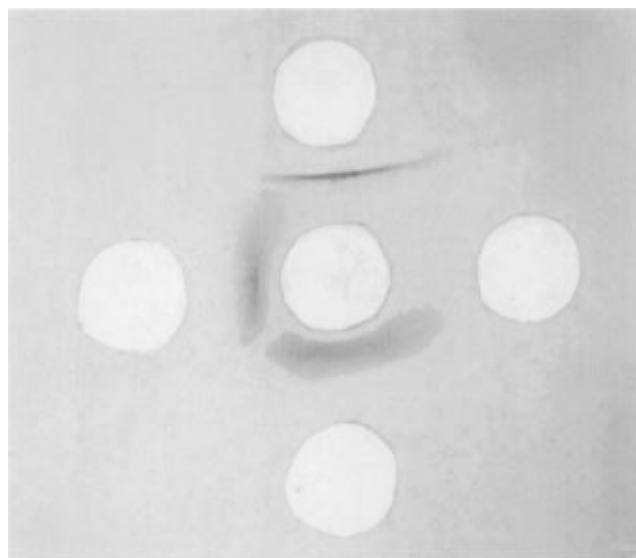


Figure 6. Agar gel diffusion of Con A (1 mg/mL, center well) against poly(acrylamide-co-allyl α -D-mannopyranoside) (positive control, top well), poly(acrylamide-co- β -D-N-acetylglucosamine) (negative control, right well), mannosylated PAMAM dendrimer **11** (bottom well), and mannosylated PAMAM dendrimer **12** (left well).

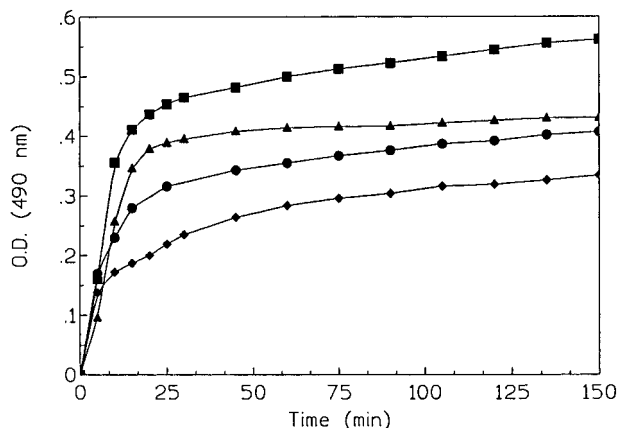


Figure 7. Time course for the turbidimetric analyses of Con A with mannosylated PAMAM dendrimers at concentrations corresponding to 10 nmol of mannoside residues: **9** (●), **10** (■), **11** (▲), and **12** (◆).

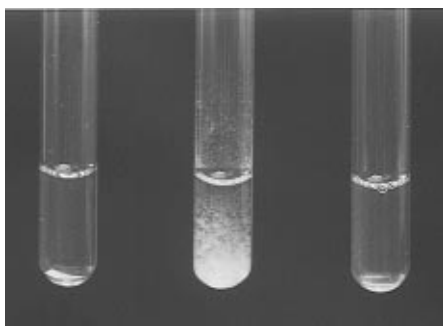


Figure 8. Precipitation of Con A with mannosylated PAMAM dendrimer **9**. From left to right: Con A (1 mg/mL, PBS), a solution of Con A and PAMAM dendrimer **9** (1 mg/mL), and a Con A/dendrimer solution after addition of D-mannose showing the reversibility of the precipitation reaction.

precipitation occurred even after a few hours (not shown), thus suggesting the higher solubility of the complex.

Starburst PAMAM Glycodendrimers as Chromatography Adsorbents. The turbidimetric analyses described above clearly demonstrated the ability of PAMAM glycodendrimers to precipitate lectins in solu-

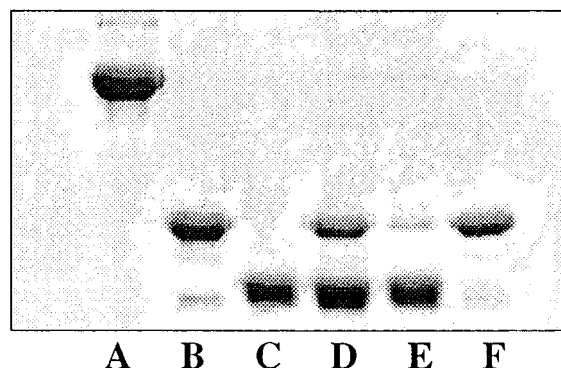


Figure 9. Electrophoresis of lectin/dendrimer **9** mixtures; (A) BSA (standard), (B) Con A, (C) WGA, (D) artificial Con A/WGA mixture, (E) Con A/WGA mixture after precipitation with mannosylated dendrimer **9** (supernatant), and (F) Con A/WGA mixture after precipitation with mannosylated dendrimer **9** (resuspended pellets, after two cycles of precipitation).

tion. Previous testings using similar types of mannosylated dendrimers (24) also proved the precipitation to be mannose-specific (Con A and pea lectins), whereas no binding interactions could be observed for other lectins (e.g. wheat germ agglutinin, WGA). These specific interactions were therefore exploited for the isolation and purification of such proteins from crude extracts. Selective isolation of Con A from crude mixtures has already been made possible with poly(L-lysine)-based glycodendrimers (25). Mannosylated PAMAM dendrimers with similar properties would represent useful chromatography adsorbents because of their easy preparation. Therefore, PAMAM glycodendrimer **9** was added to an artificial mixture of Con A and WGA, the first lectin being specific for D-mannose and the other specific for N-acetylglucosamine. When the mixture was stirred overnight, an insoluble lectin-carbohydrate precipitate formed. This Con A-dendrimer precipitate was removed from the supernatant by centrifugation and resuspended in PBS buffer where D-mannose was added to dissociate the complex to resolubilize Con A. Electrophoresis under reducing conditions (SDS-PAGE) of both supernatant and precipitate fractions showed that, from the previous Con A/WGA solution mixture (Figure 9, column D), only trace amounts of Con A were left in the supernatant, leaving WGA intact (column E), and that only Con A was selectively precipitated by glycodendrimer **9** (column F) with no trace of WGA. Modification of the terminal carbohydrate residues could also make possible the isolation of other types of lectins, showing the great versatility of PAMAM dendrimers. Work is already ongoing in order to reach these goals.

CONCLUSION

Starburst PAMAM dendrimers are multibranched spherical molecules with well-defined size, shapes, and geometries. The commercial availability of different generations (valencies) of aminated PAMAM dendrimers makes them useful precursor molecules for diverse biological and nonbiological applications. Their use in the synthesis of dendritic carbohydrate conjugates provides synthetic multiantennary glycan mimetics with powerful binding properties. Incorporation of terminal α -substituted mannoside residues furnished glycodendrimers showing an up to 400-fold increase in binding capacities. Even expressed on a monosaccharide basis, the relative inhibitory potencies are still high (up to 28 times more potent). They were also lipophilic enough to constitute useful coating antigens in microtiter plate assays even at concentrations as low as 1–3 nmol.

Furthermore, turbidimetric assays demonstrated the ability of these ligands having as low as four residues to bind and form stable cross-linked lattices with the lectins. Their capacity to selectively precipitate their homologous protein receptors from crude mixtures makes them convenient tools for the rapid and easy isolation of proteins. Other potential applications of such structures could span from cell-targeting devices to inhibition of bacterial adherence. The latest point is currently under investigations with mannoses and other carbohydrate ligands.

ACKNOWLEDGMENT

We are thankful to the Natural Sciences and Engineering Research Council of Canada (NSERC) for financial support and for a postgraduate scholarship to D. P. We are also thankful to Dendritech, Inc., for kindly providing Starburst PAMAM dendrimer cores G(0)–G(3). Starburst is a registered trademark of Dendritech, Inc.

LITERATURE CITED

- (1) Varki, A. (1993) Biological roles of oligosaccharides: all of the theories are correct. *Glycobiology* 3, 97–130.
- (2) Beachy, E. H. (1981) Bacterial adherence: adhesin-receptor interactions mediating the attachment of bacteria to mucosal surfaces. *J. Infect. Dis.* 143, 325–345.
- (3) Sharon, N. (1987) Bacterial lectins, cell-cell recognition and infectious disease. *FEBS Lett.* 217, 145–157.
- (4) Sharon, N., and Lis, H. (1989) Lectins as cell recognition molecules. *Science* 246, 227–246.
- (5) Lee, R. T., Ichikawa, Y., Kawasaki, T., Drickamer, K., and Lee, Y. C. (1992) Multivalent ligand binding by serum mannose-binding protein. *Arch. Biochem. Biophys.* 299, 129–136.
- (6) Weis, W. I., Drickamer, K., and Hendrickson, W. A. (1992) Structure of a C-type mannose-binding protein complexed with an oligosaccharide. *Nature* 360, 127–134.
- (7) Sharon, N. (1984) Carbohydrates as recognition determinants in phagocytosis and in lectin-mediated killing of target cells. *Biol. Cell.* 51, 239–246.
- (8) Ofek, I., and Sharon, N. (1988) Lectinophagocytosis: a molecular mechanism of recognition between cell surface sugars and lectins in the phagocytosis of bacteria. *Infect. Immun.* 56, 539–547.
- (9) Akhtar, S., Routledge, A., Patel, R., and Gardiner, J. M. (1995) Synthesis of mono- and dimannoside phosphoramidite derivatives for solid-phase conjugation to oligonucleotides. *Tetrahedron Lett.* 36, 7733–7736.
- (10) Wijsman, E. R., Filippov, D., Valentijn, A. R. P. M., van der Marel, G. A., and van Boom, J. H. (1996) Solid-support synthesis of di- and tetramannosylated tetrathymidylate acid. *Recl. Trav. Chim. Pays-Bas* 115, 397–401.
- (11) (a) Roy, R. (1996) Syntheses and some applications of chemically defined multivalent glycoconjugates. *Curr. Opin. Struct. Biol.* 6, 692–702. (b) Roy, R. (1997) Recent developments in the rational design of multivalent glycoconjugates. *Top. Curr. Chem.* 187, 241–274. (c) Matrosovich, M. N. (1989) Towards the development of antimicrobial drugs acting by inhibition of pathogen attachment to host cells: a need for polyvalency. *FEBS Lett.* 252, 1–4. (d) Kiessling, L. L., and Pohl, N. L. (1996) Strength in numbers: non-natural polyvalent carbohydrate derivatives. *Chem. Biol.* 3, 71–77.
- (12) Lee, Y. C. (1994) in *Neoglycoconjugates, Preparation and Applications* (Y. C. Lee and R. T. Lee, R. T., Eds.) pp 3–21, Academic Press, San Diego.
- (13) Roy, R. (1996) Design and synthesis of glycoconjugates. In *Modern Methods in Carbohydrate Synthesis* (S. H. Khan, S. H. and R. O'Neil, Eds.) pp 378–402, Harwood Academic, Amsterdam.
- (14) Park, W. K. C., Aravind, S., Romanowska, A., Renaud, J., and Roy, R. (1994) Synthesis of clustered lactosides by telomerization. *Methods Enzymol.* 242, 294–304.
- (15) Fan, J. Q., Quesenberry, M., Takegawa, K., Iwahara, S., Kondo, A., Kato, I., and Lee, Y. C. (1995) Synthesis of neoglycoconjugates by transglycosylation with *Arthrobacter protophormiae* endo- β -N-acetylglucosaminidase. *J. Biol. Chem.* 270, 17730–17735.
- (16) Bovin, N. V., and Gabius, H.-J. (1995) Polymer-immobilized carbohydrate ligands: versatile tools for biochemistry and medical sciences. *Chem. Soc. Rev.* 24, 413–421.
- (17) Roy, R. (1996) Blue-prints, synthesis and applications of glycopolymers. *Trends Glycosci. Glycotechnol.* 8, 79–99.
- (18) Tomalia, D. A. (1993) Starburst/cascade dendrimers: fundamental building blocks for a new nanoscopic chemistry set. *Aldrichim. Acta* 26, 91–101.
- (19) Ardoin, N., and Astruc, D. (1995) Molecular trees: from syntheses towards applications. *Bull. Soc. Chim. Fr.* 132, 875–909.
- (20) Astruc, D. (1996) Research avenues on dendrimers towards molecular biology: from biomimeticism to medical engineering. *C. R. Acad. Sci., Ser. IIB* 322, 757–766.
- (21) Dvornic, P. R., and Tomalia, D. A. (1996) Recent advances in dendritic polymers. *Curr. Opin. Colloid Interface Sci.* 1, 221–235.
- (22) (a) Roy, R. (1996) Glycodendrimers: a novel class of biopolymers. *Polym. News* 21, 226–232. (b) Zanini, D. and Roy, R. (1997) Synthesis of new α -thiosialodendrimers and their binding properties to the sialic acid specific lectin from *Limax flavus*. *J. Am. Chem. Soc.* 119, 2088–2095. (c) Zanini, D., and Roy, R. (1996) Novel dendritic α -sialosides: synthesis of glycodendrimers based on a 3,3'-iminobis(propylamine) core. *J. Org. Chem.* 61, 7348–7354.
- (23) Roy, R., Zanini, D., Meunier, S. J., and Romanowska, A. (1993) Solid-phase synthesis of dendritic sialoside inhibitors of Influenza A virus haemagglutinin. *J. Chem. Soc., Chem. Commun.*, 1869–1872.
- (24) Pagé, D., Zanini, D., and Roy, R. (1996) Macromolecular recognition: effect of multivalency in the inhibition of binding of yeast mannan to Concanavalin A and pea lectins by mannosylated dendrimers. *Bioorg. Med. Chem.* 4, 1949–1961.
- (25) Pagé, D., and Roy, R. (1997) Glycodendrimers as novel biochromatography adsorbents. *Int. J. Biochromatogr.* 3 (in press).
- (26) Pagé, D., Aravind, S., and Roy, R. (1996) Synthesis and lectin binding properties of dendritic mannopyranoside. *J. Chem. Soc., Chem. Commun.* 1913–1914.
- (27) Tomalia, D. A., Naylor, A. M., and Goddard, W. A., III (1990) Starburst dendrimers: molecular-level control of size, shape, surface chemistry, topology, and flexibility from atoms to macroscopic matter. *Angew. Chem., Int. Ed. Engl.* 29, 138–175.
- (28) Roberts, J. C., Adams, Y. E., Tomalia, D. A., Mercer-Smith, J. A., and Lavallée, D. K. (1990) Using Starburst dendrimers as linker molecules to radiolabeled antibodies. *Bioconjugate Chem.* 1, 305–308.
- (29) Tang, M. X., Redemann, C. T., and Szoka, F. C., Jr. (1996) In vitro gene delivery by degraded polyamidoamine dendrimers. *Bioconjugate Chem.* 7, 703–714.
- (30) Kim, R. M., Manna, M., Hutchins, S. M., Griffin, P. R., Yates, N. A., Bernick, A. M., and Chapman, K. T. (1996) Dendrimer-supported combinatorial chemistry. *Proc. Natl. Acad. Sci. U.S.A.* 93, 10012–10017.
- (31) Roberts, J. C., Bhalgat, M., and Zera, R. T. (1996) Preliminary biological evaluation of polyamidoamine (PAMAM) Starburst dendrimers. *J. Biomed. Mater. Res.* 30, 53–65.
- (32) Toyokuni, T., and Singhal, A. K. (1995) Synthetic carbohydrate vaccines based on tumor-associated antigens. *Chem. Soc. Rev.* 24, 231–242.
- (33) Aoi, K., Itoh, K., and Okada, M. (1995) Globular carbohydrate macromolecule "sugar balls". 1. Synthesis of novel sugar-persubstituted poly(amido amine) dendrimers. *Macromolecules* 28, 5391–5393.
- (34) Lindhorst, T. K., and Kieburg, C. (1996) Glycocoating of oligovalent amines: synthesis of thiourea-bridged cluster glycosides from glycosyl isothiocyanates. *Angew. Chem., Int. Ed. Engl.* 35, 1953–1956.
- (35) Pagé, D., and Roy, R. (1997) Optimizing lectin-carbohydrate interactions: improved binding of divalent α -mannosylated ligands towards Concanavalin A. *Glycoconjugate J.* 14, 345–356.

- (36) Sharon, N., and Lis, H. (1990) Legume lectins: a large family of homologous proteins. *FASEB J.* 4, 3198–3208.
- (37) Loontjens, F. G., Van Wauve, J. P., De Gussem, R., and De Bruyne, C. K. (1973) Binding of para-substituted phenyl glycosides to Concanavalin A. *Carbohydr. Res.* 30, 51–62.
- (38) Poretz, R. D., and Goldstein, I. J. (1971) Protein-carbohydrate interaction: on the mode of binding of aromatic moieties to Concanavalin A, the phytohemmagglutinin of the Jack bean. *Biochem. Pharmacol.* 20, 2727–2739.
- (39) Roy, R., Tropper, F. D., and Romanowska, A. (1992) New strategy in glycopolymer syntheses. Preparation of antigenic water-soluble poly(acrylamido-*co-p*-acrylamidophenyl β -lactoside). *Bioconjugate Chem.* 3, 256–261.
- (40) Laemmli, U. K. (1970) *Nature* 227, 680–685.
- (41) Brewer, C. F. (1996) Multivalent lectin-carbohydrate cross-linking interactions. *Chemtracts: Biochem. Mol. Biol.* 6, 165–179.
- (42) Roy, R., and Tropper, F. D. (1988) *Glycoconjugate J.* 5, 203–206.

BC970126U

Method for Radioiodination of Proteins Using *N*-Succinimidyl 3-Hydroxy-4-iodobenzoate

Ganesan Vaidyanathan,* Donna J. Affleck, and Michael R. Zalutsky

Department of Radiology, Duke University Medical Center, Durham, North Carolina, 27710. Received April 3, 1997[®]

A conjugation method has been developed for the radioiodination of proteins which should be adaptable to kit formulation. *m*-Hydroxybenzoic acid was converted to 3-hydroxy-4-^[131I]iodobenzoic acid in 65% radiochemical yield using Chloramine-T as the oxidant. This intermediate was then converted to *N*-succinimidyl 3-hydroxy-4-^[131I]iodobenzoate (^[131I]*m*SHIB) in 75% yield by reaction with *N*-hydroxysuccinimide and dicyclohexylcarbodiimide in a reaction time of only 10 min. Monoclonal antibody (mAb) 81C6 was labeled in 40–60% yield by reaction with ^[131I]*m*SHIB. Performing purifications of radioiodinated compounds using cartridges instead of HPLC did not alter conjugation efficiency, mAb immunoreactivity, or tissue distribution. Thyroid uptake of labeled mAb was low but up to 2.4 times higher than that seen when the mAb was labeled with *N*-succinimidyl 3-^[125I]iodobenzoate. These results suggest that ^[131I]*m*SHIB may be a useful reagent for the radioiodination of proteins, particularly in contexts when less complicated purification methods would be advantageous.

INTRODUCTION

For many years, radioiodinated proteins have served as valuable tools for basic biochemical research. An advantage of this approach for labeling proteins is the availability of multiple γ -emitting iodine radionuclides including ¹²⁵I and ¹³¹I, thus permitting direct comparisons, for example, of the tissue distribution of two proteins in the same animal. In the clinical sector, monoclonal antibodies (mAbs¹) labeled with ¹³¹I, ¹²³I, and ¹²⁴I have received considerable attention for the diagnosis and treatment of many types of cancer.

Because of its simplicity, the most common technique used for the radioiodination of proteins is direct iodination using an oxidant, which results in the introduction of iodine in the meta position of the benzene ring of tyrosine residues (Hunter and Greenwood, 1962; Fraker and Speck, 1978). Although these methods are easy to perform in high radiochemical yield, at least two problems have been associated with their use. First, the strong oxidizing conditions may compromise the biological function of proteins and alter the antigen binding capacity of mAbs (Hayes *et al.*, 1988). Second, the chemical similarity of the protein iodination site to thyroid hormones renders directly labeled proteins susceptible to dehalogenation *in vivo* due to endogenous deiodinases.

To circumvent these problems, conjugation labeling agents have been developed for the radioiodination of proteins; in general, these are reactive with the ϵ -amino group of lysine residues [reviewed in Wilbur (1992)]. The prototypical compound is the Bolton–Hunter reagent, *N*-succinimidyl 3-(4'-hydroxy-3'-iodophenyl)propionic acid

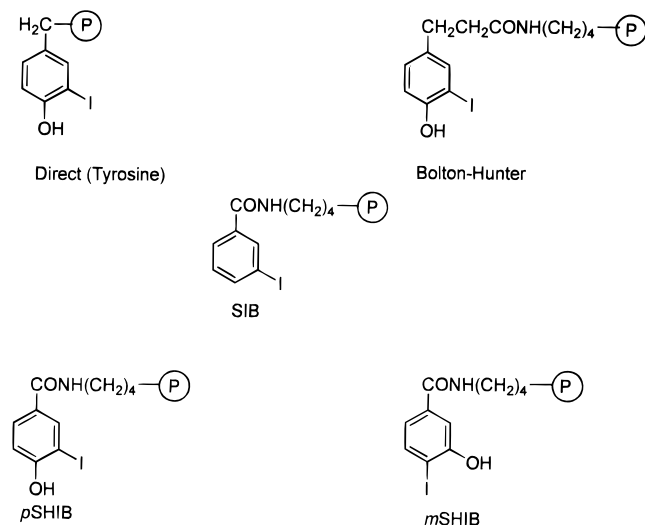
(Bolton and Hunter, 1973). Proteins and peptides labeled via the Bolton–Hunter reagent often have exhibited improved biological function as well as a lower degree of deiodination compared with directly radioiodinated proteins (Vaidyanathan and Zalutsky, 1990). On the other hand, conjugation efficiencies for the Bolton–Hunter reagent have been low, generally between 15 and 30% (Wood *et al.*, 1975; Bolton *et al.*, 1976; Vaidyanathan and Zalutsky, 1990). More recent approaches have utilized electrophilic destannylation to label a variety of *N*-succinimidyl esters, which are similar to the Bolton–Hunter reagent except that they lack a hydroxy group on the benzene ring (Wilbur *et al.*, 1989; Zalutsky and Narula, 1987; Zalutsky *et al.*, 1989). The absence of the hydroxy group ortho to the iodination site is thought to account for the up to 100-fold reduction in thyroid accumulation (an indicator of deiodination) achieved when mAbs are radioiodinated using these methods. Coupling of *N*-succinimidyl 3-iodobenzoate (SIB) to proteins proceeds in about 2-fold higher yield than the Bolton–Hunter reagent (Vaidyanathan and Zalutsky, 1990). However, the advantages of SIB and similar reagents have yet to be demonstrated in the clinical domain. Routine application of reagents such as SIB is hindered by the lack of commercial availability of its *N*-succinimidyl 3-(tri-*n*-butylstannyl)benzoate precursor and the need for HPLC purification of SIB to obtain maximum immunoreactivity and coupling efficiency (Garg *et al.*, 1989). HPLC purification of SIB would be particularly problematic for clinical radioimmunotherapy applications, for which preparation of hundreds of millicuries of ¹³¹I-labeled mAb frequently is required (Press *et al.*, 1993).

It is thus desirable to develop alternative protein radioiodination agents that can be prepared in high yield using simple procedures, while generating a labeled mAb with high immunoreactivity and substantial *in vivo* stability. With this goal in mind, the current study was undertaken to investigate the potential utility of *N*-succinimidyl 3-hydroxy-4-iodobenzoate (*m*SHIB) (Chart 1) for the radioiodination of proteins. This reagent could be prepared from commercially available starting materials without HPLC purification, and a mAb could be labeled using *m*SHIB in reasonable yield and with good *in vivo* stability.

* Address correspondence to this author at Box 3808, Department of Radiology, Duke University Medical Center, Durham, NC 27710 [telephone (919) 684-7811; fax (919) 684-7122; e-mail g405@acpub.duke.edu].

[®] Abstract published in *Advance ACS Abstracts*, August 15, 1997.

¹ Abbreviations: mAb, monoclonal antibody; SIB, *N*-succinimidyl 3-iodobenzoate; *p*HBA, *p*-hydroxybenzoic acid; *p*HIBA, 3-iodo-4-hydroxybenzoic acid; *p*SHIB, *N*-succinimidyl 3-iodo-4-hydroxybenzoate; *m*HBA, *m*-hydroxybenzoic acid; *m*HIBA, 4-iodo-3-hydroxybenzoic acid; *m*SHIB, *N*-succinimidyl 4-iodo-3-hydroxybenzoate; NHS, *N*-hydroxysuccinimide; DCC, *N,N*-dicyclohexylcarbodiimide; DCU, *N,N*-dicyclohexylurea.

Chart 1. Structure of Radioiodination Moiety/Site**EXPERIMENTAL PROCEDURES**

General. All reagents were purchased from Aldrich unless otherwise specified. Radioiodinated SIB was prepared from *N*-succinimidyl 3-(tri-*n*-butylstannyl)benzoate using previously described procedures (Zalutsky and Narula, 1987; Garg *et al.*, 1989). Sodium [¹²⁵I]iodide and sodium [¹³¹I]iodide were obtained from Du Pont-New England Nuclear (North Billerica, MA) in 0.1 N NaOH solution. Murine mAb 81C6, obtained as a gift from Dr. Darell Bigner (Department of Pathology, Duke University Medical Center), is of the IgG_{2b} isotype and reacts with an epitope of the extracellular matrix antigen tenascin (Bourdon *et al.*, 1983).

Melting points were determined on Fisher-Johns melting point apparatus and were uncorrected. NMR spectra were obtained with a General Electric Midfield GN-300 spectrometer. Tetramethylsilane ($\delta = 0$) was used as an internal reference. Mass spectra were obtained on a ZAB-E high-resolution mass spectrometer (VG, Manchester, England), on a Hewlett-Packard GC/MS/DS Model HP-5988A instrument, or on a JEOL SX-102 high-resolution mass spectrometer. HPLC was performed with two LKB Model 2150 pumps, an LKB Model 2152 control system, an LKB Model 2138 fixed-wavelength UV detector, and a Beckman Model 170 radioisotope detector. Peak analysis was performed with a Nelson Analytical software package on an IBM computer.

Preparation of *N*-Succinimidyl 3-Hydroxy-4-iodobenzoate. A solution of 9.2 g of potassium iodide and 2.92 g of iodine in 23 mL of water was added over a period of 10 min to a solution of *m*-hydroxybenzoic acid (3.3 g; 0.024 mol) in 545 mL of 30% ammonium hydroxide. The mixture was stirred at room temperature for about an hour and concentrated to about 80 mL by rotary evaporation. The pH of the solution was adjusted to 4 with concentrated hydrochloric acid, yielding a thick precipitate. This precipitate was extracted with ethyl acetate, and the ethyl acetate solution was washed with brine, dried, and evaporated to yield 1.7 g (27%) of a solid. An analytical sample was obtained by crystallization from a 1:1 mixture of ethanol and water: mp 225–226 °C (decomposes); TLC (86:1:5 chloroform/methanol/acetic acid) $R_f = 0.75$ vs 0.63 for starting material; NMR(CD₃CN) δ 7.24 (dd, 1H; H-6; $J_{\text{HH ortho}} = 8.25$ Hz, $J_{\text{HH meta}} = 1.65$ Hz), 7.43 (d, 1H; H-2; $J_{\text{HH meta}} = 1.8$ Hz), 7.83 (d, 1H; H-5; $J_{\text{HH ortho}} = 8.1$ Hz). Verification that this iodinated intermediate was 3-hydroxy-4-iodobenzoic acid was accomplished by heteronuclear multibond connectivity

(HMBC) NMR (Bax and Summers, 1986): MS (CI; NH₃) 282 [(M + NH₄)⁺], 265 (MH⁺), 246.

Dicyclohexylcarbodiimide (126 mg; 0.6 mmol) was added to a mixture of 3-hydroxy-4-iodobenzoic acid (134 mg; 0.51 mmol) and *N*-hydroxysuccinimide (67 mg; 0.58 mmol) in 5 mL of dry THF, and the mixture was stirred overnight at room temperature. The precipitated urea derivative was filtered off and washed with THF. The contents of the filtrate were adsorbed onto silica gel (1–2 g), and the product was isolated by silica gel chromatography using ethyl acetate as the eluent ($R_f = 0.61$ vs 0.2 for starting material in TLC using this eluent): yield 124 mg (68%); mp 195–197 °C; NMR (CD₃CN) δ 2.84 (s, 4H; –CH₂CH₂–), 7.34 (dd, 1H; H-6; $J_{\text{HH ortho}} = 8.10$ Hz, $J_{\text{HH meta}} = 1.5$ Hz), 7.18 (d, 1H; H-2; $J_{\text{HH meta}} = 1.8$ Hz), 7.96 (d, 1H; H-5; $J_{\text{HH ortho}} = 8.10$ Hz), 8.25 (br s, 1H; OH); HRMS (FAB⁺) calcd for C₁₁H₉INO₅ (MH⁺) 361.9525, found 361.9542.

***N*-Succinimidyl 3-Hydroxy-4-[^{125/131}I]iodobenzoate Preparation Using HPLC Purification.** To simplify purification, minimization of *m*HBA would be desirable, and so the yield for this reaction was studied as a function of *m*HBA concentration. Radiolabeling was performed as follows: To 0.1–2.1 mCi of [^{125/131}I] in 3 μ L or less of 0.1 N NaOH was added 5 μ L of *m*-hydroxybenzoic acid (*m*HBA) solution (final concentration 0.2–6.3 mM) in 0.05 N NaOH and 5 μ L of 0.04 M solution of Chloramine-T in 0.1 M borate, pH 8.5. The pH of this final mixture was 9.0–9.5. After 10 min of incubation at room temperature, the reaction was quenched by adding 7 μ L of 0.4 M sodium bisulfite in 0.1 M borate. The product was purified by reversed-phase HPLC using a Waters μ Bondapak C₁₈ column (3.9 \times 300 mm) eluted with 110:89:1 (v/v/v) methanol/water/acetic acid at a flow rate of 0.5 mL/min ($t_R = 17$ –19 min vs 8.5 min for *m*HBA). The HPLC fractions containing the product activity (70% radiochemical yield) were evaporated with an argon purge to remove most of the methanol and acidified with 1 N HCl to a pH of about 1. The radioactive product was extracted into ethyl acetate, and the ethyl acetate solution was washed with brine and dried with sodium sulfate. After being concentrated to a small volume, the solution containing the radioiodinated acid was transferred to a 0.5-dram vial and evaporated to dryness.

Esterification of [^{125/131}I]*m*HIBA was achieved by addition of 30 μ L each of 0.1 M solutions of *N*-hydroxysuccinimide and DCC in dry ethyl acetate (Sure seal, Aldrich). To minimize the duration of the labeling procedure, the yield for the esterification step was investigated as a function of incubation time. The product was purified by silica gel HPLC using an Alltech Partisil silica column (4.6 \times 250 mm) eluted with 70:30:2 (v/v/v) hexane/ethyl acetate/acetic acid at a flow rate of 1 mL/min ($t_R = 25$ min). The optimized radiochemical yield for this step based on HPLC was 85–90%.

***N*-Succinimidyl 3-Hydroxy-4-[^{125/131}I]iodobenzoate Preparation Using Solid-Phase Cartridge Purification.** About 2–3 mCi of [^{125/131}I] was evaporated to dryness in an Eppendorf tube, and 5 μ L of a 2.6 mM solution of *m*HBA in 0.05 N NaOH was added followed by 5 μ L of a 0.04 M solution of Chloramine-T in 0.1 M borate, pH 8.5. After 10 min of incubation at room temperature, the reaction was quenched by adding 7 μ L of 0.4 M sodium bisulfite in borate. For the purification of *m*HIBA, a Waters tC₁₈ ENV reversed-phase solid-phase cartridge activated with methanol and water (6 mL each) was used. The reaction mixture was loaded onto the cartridge and eluted in sequence with 0.5 mL of water, 2 mL of 5:95:1 methanol/water/acetic acid, 3.5 mL of 10:90:1 methanol/water/acetic acid, 2.5 mL of 50:50:1 methanol/water/acetic

acid, and finally, several 0.25 mL portions of methanol. The required [$^{125/131}\text{I}$]*m*HIBA generally eluted in the third through the sixth methanol fractions. The radiochemical yield was 65–70%, and the HPLC of an aliquot indicated a major single peak corresponding to *m*HIBA; no *m*HBA was detected. After these fractions were pooled and the methanol was evaporated, the [$^{125/131}\text{I}$]*m*HIBA was redissolved in ethyl acetate and dried with sodium sulfate and the esterification reaction was performed as described in the previous section. Purification of the ester was achieved by passing the reaction mixture through a silica Sep-Pak (Waters) activated with 2 mL each of ethyl acetate and hexane and then eluted with 2 mL of hexane, 5 mL of 5% ethyl acetate in hexane, 7 mL of 10% ethyl acetate in hexane, 2×2 mL of 50% ethyl acetate in hexane, and, finally, several 1 mL portions of ethyl acetate. The required activity generally eluted in the second 50% ethyl acetate/hexane and the first few ethyl acetate fractions. The radiochemical yield for esterification was 75–80%, and the product was >95% radiochemically pure by HPLC.

Radiolabeling of mAb 81C6 with [$^{125/131}\text{I}$]*m*SHIB. The HPLC or Sep-Pak fractions containing [$^{125/131}\text{I}$]*m*SHIB were evaporated with an argon stream to a small volume, transferred to a 0.5-dram vial, and evaporated further to dryness. A solution of 81C6 (5 mg/mL; 75 μL) in 0.2 M borate buffer, pH 9.0, was added, and the mixture was incubated for 15–20 min at room temperature. Unreacted [$^{125/131}\text{I}$]*m*SHIB was quenched by the addition of 0.3 mL of 0.2 M glycine in the above borate buffer, and the incubation was continued for another 5 min. The labeled mAb was purified by gel filtration using a Sephadex G-25 column and phosphate-buffered saline as the eluent. The protein-associated activity was determined by TCA precipitation, and the purity of the labeled protein was further assessed by gel filtration HPLC. For the latter, a Bio-Rad 600 mm \times 7.5 mm Bio-Sil SEC-250-10 column was eluted with phosphate-buffered saline, pH 7.14, at a flow rate of 1 mL/min.

Immunoreactive Fraction. The immunoreactive fraction of 81C6 labeled with HPLC-purified [^{131}I]*m*SHIB was compared in a paired-label format to mAb labeled with [^{125}I]*m*SHIB purified using the cartridge procedure. Approximately 100 ng of each preparation was incubated with serial dilutions of tenascin-positive D-54 MG human glioma homogenates at 4 $^{\circ}\text{C}$ for 18–20 h. The homogenates were washed three times with phosphate-buffered saline containing 2% human serum albumin, and the [^{125}I] and [^{131}I] activity in the homogenate and supernatant was counted in an automated gamma counter (LKB 1282, Wallac, Finland) using a dual-label protocol. The immunoreactive fraction was determined according to the method of Lindmo *et al.* (1984).

Tissue Distribution Measurements. These studies were performed in a paired-label format in male BALB/c mice weighing about 25 g. In the first study, the biodistribution of 81C6 labeled with HPLC-purified [^{131}I]*m*SHIB was compared with that labeled with [^{125}I]*SIB*. Mice were injected intravenously with 8 μCi (5 μg) of [^{125}I]*SIB*-labeled 81C6 and 6 μCi (5 μg) of [^{131}I]*m*SHIB-labeled 81C6. Groups of five animals were killed by halothane overdose at 24, 48, 120, 144, and 168 h. In the second study, the tissue distributions of 81C6 labeled with HPLC-purified and Sep-Pak-purified *m*SHIB were compared. Mice were injected with 7 μCi (10 μg) of 81C6 labeled with HPLC-purified [^{125}I]*m*SHIB and 5 μCi (10 μg) of Sep-Pak-purified [^{131}I]*m*SHIB, and tissue uptake was determined at 24, 48, 60, and 168 h postinjection. At necropsy, tissues of interest were isolated, washed, blot-dried, and weighed. Tissues were then counted for

^{125}I and ^{131}I in a gamma counter using a dual-label counting program. The percent injected dose per gram of tissue was calculated by comparison to standards of appropriate count rate. Since the tissue distribution was performed in a paired-label format, with each animal serving as its own control, a paired *t* test was used to determine the statistical significance of differences between the uptake of the two radionuclides.

RESULTS AND DISCUSSION

Direct radioiodination is an efficient, convenient approach for protein labeling and, as a result, is the most commonly used technique for basic and clinical applications. This remains the case despite its obvious drawbacks. Exposure of the protein to oxidants can compromise biological function and, for some mAbs, lower immunoreactivity (Hayes *et al.*, 1988). For *in vivo* applications, dehalogenation can result in loss of label from directly labeled proteins, decreasing their ability to deliver radiation to specific cell populations.

An alternative is to use the Bolton–Hunter reagent, which is commercially available labeled with ^{125}I and thus is only suitable for *in vitro* studies. The presence of the two methylene groups between the ester functionality and the iodine-substituted benzene ring decreases the hydrolytic stability of this reagent, resulting in only modest conjugation yields and, possibly, *in vivo* susceptibility to hydrolytic enzymes (Vaidyanathan and Zalutsky, 1990). While reagents such as SIB have shown encouraging results for the radioiodination of proteins (Zalutsky *et al.*, 1989; Wilbur *et al.*, 1989), their chemistry may not be readily adaptable for widespread use, particularly in centers without access to radio-HPLC.

Reagents such as SIB are synthesized via destannylation to avoid the need for a hydroxy group ortho to the iodination site to activate the ring toward electrophilic substitution. While this hydroxy group decreases the strength of the carbon–iodine bond, it does not always lead to rapid deiodination *in vivo*. For example, we have reported that a mAb labeled using the Bolton–Hunter reagent exhibited considerably lower thyroid accumulation than the same mAb labeled using Iodogen (Vaidyanathan and Zalutsky, 1990). This motivated us to investigate *p*SHIB, which is analogous to the Bolton–Hunter reagent except it does not contain the two intervening methylene groups (Vaidyanathan *et al.*, 1993). The deiodination of a mAb labeled using *p*SHIB was only slightly inferior to that of the same mAb labeled with SIB. Unfortunately, the yields for coupling *p*SHIB to mAbs were modest even with long reaction times. It was hypothesized that these poor coupling efficiencies were due to the presence of a hydroxy group at the para position of the carboxylic ester group. The current study was performed to investigate this possibility through the synthesis of the isomeric compound *m*SHIB in which the hydroxy group was moved to the meta position. In addition, the adaptability of *m*[^{131}I]*SHIB* for preparation by a kit method was studied.

HPLC standards of *m*HIBA and *m*SHIB were prepared following a procedure reported for the isomeric compound (Vaidyanathan *et al.*, 1993). Unlike the case for *p*HBA, iodination of *m*HBA can result in three different monoiodinated regioisomers. Proof that the iodinated product indeed was 3-hydroxy-4-iodobenzoic acid was provided by a HMBC NMR experiment (Bax and Summers, 1986).

Since the ultimate goal of this work is to develop a method that is adaptable to kit formulation, it is essential to minimize impurities that may have deleterious effects on the peptide or mAb. For example, the active ester of *m*-hydroxybenzoic acid itself could react with lysine

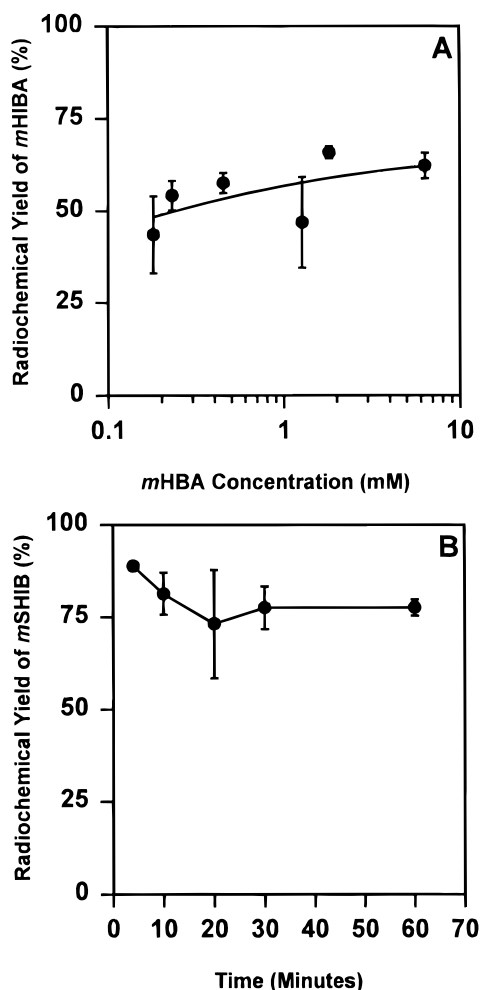


Figure 1. (A) Radiochemical yield for the preparation of $[^{131}\text{I}]\text{-mHIBA}$ as a function of *m*HBA concentration. (B) Temporal effect on the coupling efficiencies of $[^{131}\text{I}]\text{mSHIB}$ to 81C6.

ϵ -amino groups and, if present in considerable amounts, could alter its biological characteristics. To determine the minimum amount of *m*HBA needed to have a satisfactory radiochemical yield, the radioiodination of *m*HBA was studied as a function of *m*HBA concentration. The radiochemical yield for HIBA increased with *m*HBA concentration, but the concentration dependence was not dramatic (Figure 1A). While a yield of $43.5 \pm 10.5\%$ was obtained with 0.2 mM *m*HBA, a yield of $62.3 \pm 3.5\%$ was obtained when the concentration was 6.3 mM ($p < 0.05$). An *m*HBA concentration of 1.3 mM was chosen for subsequent radioiodinations, and this gave radiochemical

yields of 60–65%. In comparison, 3.9 mM *p*HBA had been used previously for the preparation of 4-hydroxy-3- $[^{131}\text{I}]\text{iodobenzoic acid}$ (Vaidyanathan *et al.*, 1993).

Conversion of 4-hydroxy-3- $[^{131}\text{I}]\text{iodobenzoic acid}$ to the corresponding NHS ester required 2–3 h (Vaidyanathan *et al.*, 1993). The esterification of 3-hydroxy-4- $[^{131}\text{I}]\text{iodobenzoic acid}$ was studied as a function of time. Radiochemical yields of $>75\%$ were obtained in as little as 5–10 min (Figure 1B). No further improvement in yield was achieved by increasing the reaction time up to 1 h. Although different solvents were used in the two studies (ethyl acetate, *m*HIBA; THF, *p*HIBA), the faster kinetics observed for the meta isomer may be a result of relatively higher susceptibility of carboxyl carbonyl in 3-hydroxy-4-iodobenzoic acid toward nucleophilic attack (*vide infra*).

One of the principal advantages of *m*HIBA compared with *p*HIBA is the possible higher reactivity of the active ester of the former with lysine ϵ -amino groups on proteins. As mentioned before, poor coupling yields were obtained for the conjugation of *p*SHIB to mAb 81C6, and this was attributed to the influence of the hydroxy group at the *para* position (Vaidyanathan *et al.*, 1993). On this basis, it was predicted that higher yields would be obtained with *m*SHIB, and, in fact, conjugation efficiencies of 40–60% were observed when mAb 81C6 was incubated with $[^{131}\text{I}]\text{mSHIB}$ for 20 min. Increasing the incubation time up to 1 h did not result in any significant increase in conjugation efficiency. In comparison, only 10–15% coupling yield was obtained at 1 h with *p*SHIB, confirming the prediction that *m*SHIB would offer better conjugation yields.

The characteristics of 81C6 labeled with *m*SHIB prepared and purified using HPLC were compared to those obtained using the cartridge procedure. Size exclusion HPLC demonstrated the presence of a single radioactive peak with an elution time corresponding to that of IgG. There was no shoulder on the peak, indicating the absence of higher molecular weight aggregates in the preparations. Previous studies with SIB have shown that it is important to minimize cold active ester impurities to maintain mAb immunoreactivity (Zalutsky and Narula, 1988). The immunoreactive fractions for the binding of 81C6 labeled to D-54 MG human glioma homogenates were excellent. When the mAb was reacted with *m*SHIB prepared using HPLC, an immunoreactive fraction of 95% was obtained compared with 91% with the cartridge procedure. This is consistent with mass spectroscopy and IR analyses which did not detect any NHS ester of *m*HBA in the *m*SHIB preparation (data not shown).

The tissue distribution of 81C6 mAb labeled with HPLC-purified $[^{131}\text{I}]\text{mSHIB}$ was compared in normal

Table 1. Paired-Label Tissue Distribution of Radioiodine in Normal Mice following Injection of 81C6 Labeled with $[^{125}\text{I}]\text{SIB}$ and with $[^{131}\text{I}]\text{mSHIB}$

tissue	% injected dose per organ ^a					
	1 day		5 days		6 days	
	SIB	<i>m</i> SHIB	SIB	<i>m</i> SHIB	SIB	<i>m</i> SHIB
liver	4.29 ± 0.51	4.10 ± 0.50	1.59 ± 0.18	3.24 ± 0.35	1.23 ± 0.11	3.08 ± 0.44
spleen	0.34 ± 0.04	0.29 ± 0.03	0.12 ± 0.02	0.19 ± 0.03	0.08 ± 0.01	0.17 ± 0.02
lungs	1.97 ± 0.46	2.26 ± 0.62^b	0.85 ± 0.38	2.08 ± 0.97	0.41 ± 0.06	1.16 ± 0.19
heart	0.53 ± 0.10	0.57 ± 0.11	0.19 ± 0.03	0.43 ± 0.05	0.12 ± 0.03	0.35 ± 0.10
kidneys	1.83 ± 0.18	1.77 ± 0.19^b	0.57 ± 0.07	1.21 ± 0.15	0.44 ± 0.04	1.15 ± 0.17
stomach	0.50 ± 0.07	0.48 ± 0.06^b	0.13 ± 0.01	0.26 ± 0.04	0.09 ± 0.01	0.23 ± 0.05
sm intest	2.39 ± 0.27	2.04 ± 0.24	0.78 ± 0.13	1.42 ± 0.22	0.59 ± 0.08	1.33 ± 0.22
lg intest	1.06 ± 0.13	1.00 ± 0.06^b	0.33 ± 0.04	0.65 ± 0.10	0.26 ± 0.04	0.62 ± 0.12
muscle	10.55 ± 1.67	10.72 ± 1.73^b	4.06 ± 0.64	8.56 ± 1.09	2.74 ± 0.26	7.23 ± 0.43
bone	5.55 ± 0.91	4.64 ± 0.76	$.88 \pm 0.27$	3.13 ± 1.57	1.26 ± 0.07	2.59 ± 0.20
blood	20.93 ± 1.62	26.82 ± 1.93	7.12 ± 0.84	18.99 ± 1.57	5.11 ± 0.48	16.82 ± 1.74
brain	0.17 ± 0.03	0.20 ± 0.03	0.06 ± 0.01	0.13 ± 0.02	0.04 ± 0.00	0.11 ± 0.02

^a Mean \pm SD ($n = 5$). ^b The difference between two values statistically not significant by a *t* test ($p > 0.05$).

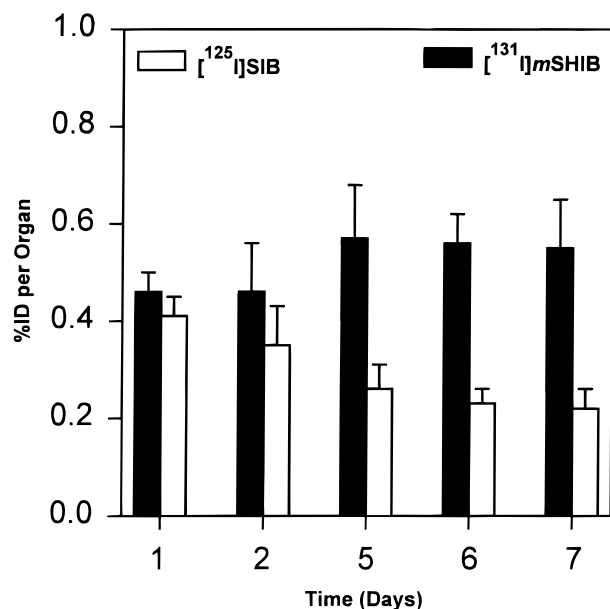


Figure 2. Paired-label thyroid uptake of ^{131}I and ^{125}I following injection of 81C6 labeled with [^{131}I]mSHIB and [^{125}I]SIB in normal mice.

mice with that for mAb labeled with [^{125}I]SIB. SIB was chosen for comparison because use of this reagent reduced dehalogenation and normal tissue levels and increased tumor uptake and therapeutic efficacy compared with mAb labeled via the Iodogen method (Zalutsky *et al.*, 1989; Schuster *et al.*, 1991). The paired-label thyroid uptake of 81C6 labeled with [^{131}I]mSHIB and with [^{125}I]SIB is shown in Figure 2. Initially, the difference in uptake of ^{131}I and ^{125}I was small but statistically significant ($p < 0.05$). With time the difference increased and by day 7, the percent injected dose (ID) of ^{131}I was 2.5-fold higher than that of ^{125}I . Nonetheless, thyroid accumulation of radioiodine from mAb labeled using mSHIB was $<0.6\%$ ID at all time points. These levels were similar to those observed with 81C6 labeled using [^{131}I]pSHIB and 10-fold lower than seen when this mAb was labeled using the Iodogen method (Vaidyanathan and Zalutsky, 1990, 1993).

The percent injected dose of radioiodine retained by other normal tissues at 1, 5, and 6 days after injection of 81C6 labeled with [^{131}I]mSHIB and with [^{125}I]SIB is summarized in Table 1 (data for other time points is provided in Supporting Information). On day 1, the distributions of the two radioiodine nuclides were quite similar with the exception of the blood, where significantly higher activity levels were observed for mAb labeled with [^{131}I]mSHIB ($26.82 \pm 1.93\%$ ID versus $20.93 \pm 1.62\%$ ID; $p < 0.05$). However, by day 5, significantly higher levels of ^{131}I were found in most normal tissues compared with ^{125}I . At this time, differences of about a factor of 2–3 were seen in liver, lungs, kidneys, and blood. It is interesting to note that when the tissue distributions of 81C6 labeled with [^{131}I]pSHIB and [^{125}I]SIB were compared, higher tissue levels were seen for the former (Vaidyanathan *et al.*, 1993); however, the magnitude of the difference was much higher in the present case.

The presence of impurities in mSHIB preparations could affect the distribution of mAbs labeled with this reagent. Previous studies have shown that higher levels of *N*-succinimidyl (tri-*n*-butylstannyl)benzoate precursor altered the distribution of a mAb F(ab')₂ fragment labeled using SIB preparations (Zalutsky and Narula, 1988). A second paired-label experiment was performed to determine whether the tissue distribution of 81C6 labeled with

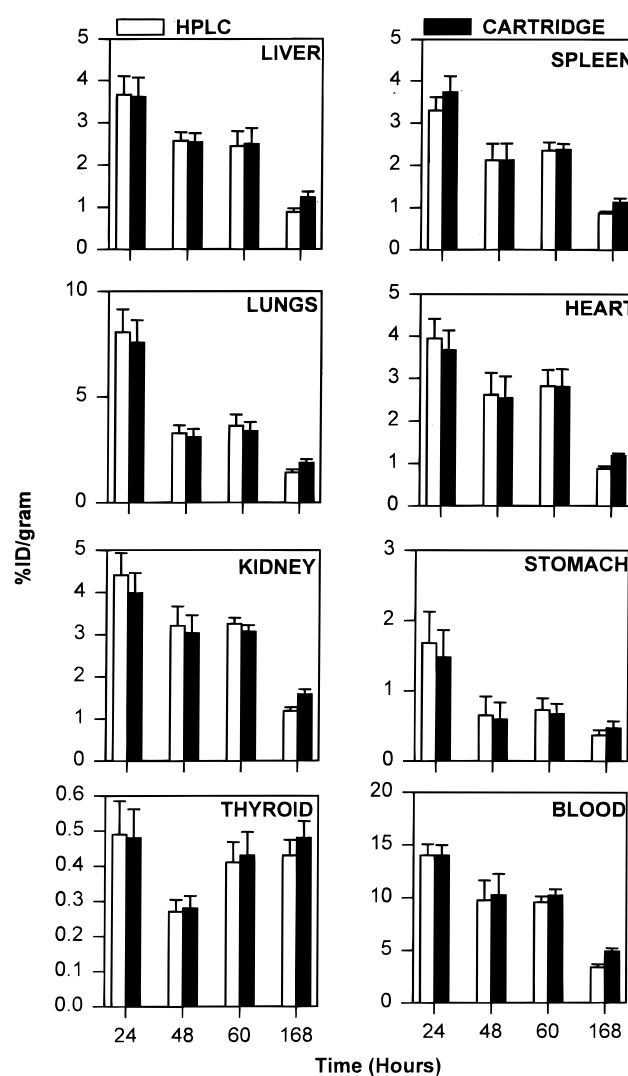


Figure 3. Paired-label tissue uptake of ^{131}I and ^{125}I following injection of 81C6 labeled with [^{131}I]mSHIB (cartridge) and [^{125}I]mSHIB (HPLC) in normal mice.

mSHIB prepared via the cartridge procedure was the same as that obtained when HPLC-purified mSHIB was used. As shown in Figure 3, no differences in tissue distribution of 81C6 mAb were seen when the simpler mSHIB purification procedure was used.

Although the normal tissue retention of radioiodine for mAb labeled with mSHIB was higher than that seen with SIB at later time points, the magnitude of normal tissue levels with mSHIB was not particularly high in any organ and is consistent with the anticipated distribution of an IgG molecule. The extent to which the normal tissue uptake of mAbs labeled with mSHIB would be problematic would depend on the nature of the application. Imaging protocols with 13-h ^{123}I generally focus on the first day after injection, during which the normal tissue uptake observed with mSHIB labeling was nearly identical to that seen with SIB. For radioimmunotherapeutic applications involving ^{131}I , the increased normal tissue levels observed at later time points with mSHIB might detract from the potential utility of this reagent. However, use of mAb fragments or use of nonintravenous routes of labeled mAb administration are approaches that might be particularly beneficial in tandem with mSHIB for reducing the radiation dose received by normal tissues.

Because the differences in uptake are apparent only at later time points, it appears likely that the higher

normal tissue retention for mAb labeled with *m*SHIB is related to either a slower rate of degradation to more rapidly clearing low molecular weight catabolites or the generation of catabolites with more prolonged normal tissue retention than those produced from mAbs labeled using SIB. Catabolites created in the degradation of mAbs labeled with SIB and *p*SHIB include the corresponding aromatic acids, iodobenzoic acid (IBA) and *p*HIBA, respectively (Vaidyanathan *et al.*, 1993; Garg *et al.*, 1995). It is known that serum protein binding and blood cell uptake of aromatic acids increase with lipophilicity (Lázníček and Lázníčková, 1995). However, *p*HIBA is less lipophilic than IBA, and hence one would expect less background due to binding to blood elements with the former. Although *m*HIBA would also be expected to be less lipophilic than IBA, it should be pointed out that salicylic acid (*o*-hydroxybenzoic acid) actually had a higher lipophilicity than benzoic acid (Lázníček and Lázníčková, 1995). An additional difference in catabolite behavior is that IBA is cleared rapidly from normal tissues as a glycine conjugate and *p*HIBA is not (Vaidyanathan *et al.*, 1993). The catabolism of mAbs labeled using *m*SHIB will be investigated in future experiments. A key objective of this study was to develop a method for preparing *m*SHIB that would be adaptable to kit formulation. The two HPLC purification procedures were replaced by solid-phase cartridges. After radioiodination, *m*HIBA was purified using a Waters tC₁₈ ENV cartridge, and after several trials, an elution protocol was identified that isolated [¹²⁵I/¹³¹I]*m*HIBA in good purity. The esterification reaction mixture was passed through a Waters silica solid-phase extraction cartridge using an optimized elution pattern. In the development of this elution protocol, care was taken to minimize the coelution of NHS, DCC, and the byproduct DCU. The success of the dual-cartridge approach is reflected by the fact that radiochemical yields for these two steps were comparable to those obtained with HPLC purification. More importantly, *m*SHIB so produced could be coupled to mAb 81C6 in high yield and excellent immunoreactivity.

In conclusion, a conjugation method that is adaptable for a kit preparation has been developed for labeling proteins. Compared with the Bolton–Hunter reagent, *m*SHIB offers the advantage of an approximately 2-fold higher protein coupling efficiency. Thyroid uptake in normal mice (a monitor of deiodination) for a mAb labeled using *m*SHIB was low, suggesting that this reagent may be useful for *in vivo* applications. This possibility will be pursued in future experiments, which will investigate the tissue distribution and catabolism of mAbs labeled with *m*SHIB in athymic mice with human tumor xenografts.

ACKNOWLEDGMENT

We thank Susan Slade for excellent technical assistance. This work was supported by Grants CA 42324 and NS 20023 from the National Institutes of Health and Grant FG02-96ER62148 from the Department of Energy.

Supporting Information Available: Paired-label tissue distribution of radioiodine in normal mice (1 page). Ordering information is given on any current masthead page.

LITERATURE CITED

- Bax, A., and Summers, M. F. (1986) ¹H and ¹³C assignments from sensitivity-enhanced detection of Heteronuclear Multiple-Bond Connectivity by 2D multiple quantum NMR. *J. Am. Chem. Soc.* 108, 2093–2094.
- Bolton, A. E., and Hunter, W. M. (1973) The labelling of proteins to high specific radioactivities by conjugation to a ¹²⁵I-containing acylating agent. *Biochem. J.* 133, 529–539.
- Bolton, A. E., Bennie, J. G., and Hunter, W. M. (1976) Innovations in labeling techniques for radiomunoassays. *Protides Biol. Fluids* 24, 687–693.
- Bourdon, M. A., Wikstrand, C. J., Furthmayr, H., Mathews, T. J., and Bigner, D. D. (1983) Human glioma-mesenchymal extracellular matrix defined by monoclonal antibody. *Cancer Res.* 43, 2796–2805.
- Fraker, P. J., and Speck, J. C. (1978) Protein and cell membrane iodinations with a sparingly soluble chloramide 1,3,4,6-tetrachloro-3a,6a-diphenylglycouril. *Biochem. Biophys. Res. Commun.* 80, 849–857.
- Garg, P. K., Archer, G. E., Jr., Bigner, D. D., and Zalutsky, M. R. (1989) Synthesis of radioiodinated *N*-succinimidyl iodobenzoate: optimization for use in antibody labelling. *Appl. Radiat. Isot.* 40, 485–490.
- Garg, P. K., Alston, K. L., and Zalutsky, M. R. (1995) Catabolism of radioiodinated murine monoclonal antibody F(ab)₂ fragment labeled using *N*-succinimidyl 3-iodobenzoate and iodogen methods. *Bioconjugate Chem.* 6, 493–501.
- Hayes, D. F., Noska, M. A., Kufe, D. W., and Zalutsky, M. R. (1988) Effect of radioiodination on the binding of monoclonal antibody DF3 to breast carcinoma cells. *Nucl. Med. Biol.* 15, 235–241.
- Hunter, W. M., and Greenwood, F. C. (1962) Preparation of iodine-131 labelled human growth hormone of high specific activity. *Nature* 194, 495–496.
- Lázníček, M., and Lázníčková, A. (1995) The effect of lipophilicity on the protein binding and blood cell uptake of some acidic drugs. *J. Pharm. Biomed. Anal.* 13, 823–828.
- Lindmo, T., Boven, E., Cuttitta, F., Fedorko, J., and Bunn, P. A., Jr. (1984) Determination of the immunoreactive fraction of radiolabeled monoclonal antibodies by linear extrapolation to binding at infinite antigen excess. *J. Immunol. Methods* 72, 77–89.
- Press, O. W., Eary, J. F., Appelbaum, F. R., Martin, P. J., Badger, C. C., Nelp, W. B., Glenn, S., Butchko, G., Fisher, D., Porter, B., Matthews, D. C., Fisher, L. D., and Bernstein, I. D. (1993) Radiolabeled-antibody therapy of B-cell lymphoma with autologous bone marrow support. *N. Engl. J. Med.* 329, 1219–1224.
- Schuster, J. M., Garg, P. K., Bigner, D. D., and Zalutsky, M. R. (1991) Improved therapeutic efficacy of a monoclonal antibody radioiodinated using *N*-succinimidyl-3-(tri-*n*-butylstannyl)-benzoate. *Cancer Res.* 51, 4164–4169.
- Vaidyanathan, G., and Zalutsky, M. R. (1990) Protein radiohalogenation: observations on the design of *N*-succinimidyl ester acylation agents. *Bioconjugate Chem.* 1, 269–273.
- Vaidyanathan, G., Affleck, D. J., and Zalutsky, M. R. (1993) Radioiodination of proteins using *N*-succinimidyl 4-hydroxy-3-iodobenzoate. *Bioconjugate Chem.* 4, 78–84.
- Wilbur, D. S. (1992) Radiohalogenation of proteins: an overview of radionuclides, labeling methods, and reagents for conjugate labeling. *Bioconjugate Chem.* 3, 433–470.
- Wilbur, D. S., Hadley, S. W., Hylarides, M. D., Abrams, P. G., Beaumier, P. A., Morgan, A. C., Reno, J. M., and Fritzberg, A. R. (1989) Development of a stable radioiodinating reagent to label monoclonal antibodies for radiotherapy of cancer. *J. Nucl. Med.* 30, 216–226.
- Wood, F. T., Wu, M. M., and Gerhart, J. C. (1975) The radioactive labeling of proteins with an iodinated amidation reagent. *Anal. Biochem.* 69, 339–349.
- Zalutsky, M. R., and Narula, A. S. (1987) A method for the radiohalogenation of proteins resulting in decreased thyroid uptake of radioiodine. *Int. J. Radiat. Appl. Instrum. A* 38, 1051–1055.
- Zalutsky, M. R., and Narula, A. S. (1988) Radiohalogenation of a monoclonal antibody using an *N*-succinimidyl 3-(tri-*n*-butylstannyl)benzoate intermediate. *Cancer Res.* 48, 1446–1450.
- Zalutsky, M. R., Noska, M. A., Colapinto, E. V., Garg, P. K., and Bigner, D. D. (1989) Enhanced tumor localization and *in vivo* stability of a monoclonal antibody radioiodinated using *N*-succinimidyl 3-(tri-*n*-butylstannyl)benzoate. *Cancer Res.* 49, 5543–5549.

Supporting Information

Paired-label tissue distribution of radioiodine in normal mice following injection of 81C6 labeled with [^{125}I]SIB and with [^{131}I]mSHIB

Tissue	Percent injected dose per organ ^a			
	2 days		7 days	
	SIB	mSHIB	SIB	mSHIB
Liver	3.83 ± 0.60	4.53 ± 0.83	1.06 ± 0.10	2.68 ± 0.25
Spleen	0.28 ± 0.02	0.29 ± 0.03 ^b	0.08 ± 0.01	0.16 ± 0.03
Lungs	1.57 ± 0.92	2.18 ± 1.38	0.60 ± 0.26	1.85 ± 0.67
Heart	0.45 ± 0.02	0.59 ± 0.04	0.13 ± 0.03	0.37 ± 0.06
Kidneys	1.60 ± 0.21	1.93 ± 0.24	0.40 ± 0.04	1.06 ± 0.13
Stomach	0.36 ± 0.03	0.42 ± 0.03	0.10 ± 0.02	0.26 ± 0.06
Sm. Int.	1.86 ± 0.21	1.96 ± 0.23 ^b	0.54 ± 0.08	1.25 ± 0.09
Lg. Int.	0.83 ± 0.21	0.92 ± 0.05	0.26 ± 0.05	0.67 ± 0.12
Muscle	9.18 ± 0.83	11.42 ± 1.23	2.49 ± 0.34	6.81 ± 0.73
Bone	4.09 ± 0.52	4.19 ± 0.49 ^b	1.19 ± 0.33	2.74 ± 0.67
Blood	16.75 ± 0.79	25.89 ± 1.12	4.70 ± 0.71	16.12 ± 0.85
Brain	0.13 ± 0.02	0.17 ± 0.02	0.04 ± 0.01	0.12 ± 0.01

^aMean ± S.D. (n = 5). ^bThe difference between two values statistically not significant by a *t* test (*p* > 0.05).

Photoimmobilization of Sulfated Hyaluronic Acid for Antithrombogenicity

Guoping Chen,[†] Yoshihiro Ito,^{*,†,‡} Yukio Imanishi,[†] Agnese Magnani,[§] Stefania Lamponi,[§] and Rolando Barbucci[§]

Department of Material Chemistry, Graduate School of Engineering, Kyoto University, Kyoto 606-01, Japan, PRESTO, JST, Keihanna Plaza, Hikaridai 1-7, Seika-cho, Kyoto 612-02, Japan, and CRISMA, Siena University, Via E. Bastianini n. 12, 53100 Siena, Italy. Received April 2, 1997; Revised Manuscript Received July 2, 1997[®]

Anticoagulant polymer sulfated hyaluronic acid was patterned immobilized on a poly(ethylene terephthalate) (PET) film in a specific pattern by photolithography. Hyaluronic acid was sulfated by a sulfur trioxide–pyridine complex. The polymer was coupled with azidoaniline. The derivatized polymer was cast on a PET film from aqueous solution. After drying, the film was photoirradiated in the presence or absence of a photomask. The micropatterning was confirmed by staining with a dye, brilliant green. Since the anticoagulant polymer has negative charges, the cationic dye was adsorbed on the regions where the anticoagulant polymer was immobilized. Platelet adhesion was reduced on the sulfated hyaluronic acid-immobilized areas. The immobilized sulfated hyaluronic acid significantly reduced thrombus formation.

INTRODUCTION

One of the most widely employed approaches in the synthesis of blood compatible materials is heparinization, in which synthetic polymers are coated or immobilized with heparin. Heparin is a natural polyanionic polysaccharide carrying sulfonate groups (1, 2). Therefore, several investigations using sulfonated polymers have been performed (3–13). Recently, it has been found that sulfated hyaluronic acid has a heparin-like property (14–17).

In the present study, the anticoagulant polymer was immobilized on a poly(ethylene terephthalate) (PET) film and its interaction with blood was investigated. In order to immobilize the polymer on the film surface, the photoimmobilization method developed by Matsuda and Sugawara (18–21) was used. Because the method does not need the presence of functional groups on the matrix surface to connect the functional unit with the polymer, it has been applied for surface functionalization of conventional polymers (22, 23). Micropatterning of anticoagulant polysaccharide by the photolithography technique allowed visualization of interactions with blood in the regions with or without immobilized polysaccharide.

MATERIALS AND METHODS

Materials. 4-Azidoaniline hydrochloride, 1-ethyl-3-[3-(dimethylamino)propyl]carbodiimide hydrochloride (water-soluble carbodiimide, WSC), Triton X-100, and brilliant green were purchased from Wako Pure Chemical Ind. Ltd. (Osaka, Japan). The photolithographic mask was purchased from Nippon Filcon Co., Ltd. (Osaka, Japan). Poly(ethylene terephthalate) (PET) film (diameter, 13.5 mm) was purchased from Akita Sumitomo Bake Co.

(Akita, Japan). Bovine serum albumin (BSA) was purchased from Interger Co. (Purchase, NY). Propidium iodide was purchased from Sigma Co. (St. Louis, MO). Vectashield mounting medium for fluorescence was purchased from Vector Laboratories, Inc. (Burlingame, CA).

Synthesis of the Photoreactive Polymer. The synthetic scheme of the photoreactive polymer is shown in Figure 1. Sulfated hyaluronic acid (SHyal) was prepared as previously reported (14–17). Briefly, a solution of tributylammonium hyaluronate in *N,N*-dimethylformamide (DMF) was mixed with a solution of the sulfur trioxide–pyridine complex in DMF under a nitrogen gas flow. The mixture was kept at 0 °C for 1 h. Then, double-distilled water and a 1 M NaOH solution were added. The sulfated hyaluronic acid was precipitated by an excess of ethanol. The product was separated by centrifugation (15 min at 1500 rpm) and dialyzed against double-distilled water in a dialysis tube with a cutoff MW of 12 000. The solution was then lyophilized. The purified product was referred to as SHyal. NMR analysis revealed that 87.5% of the OH groups were sulfated (14).

SHyal (18.20 mg), 4-azidoaniline (7.75 mg), and WSC (10 mg) were dissolved in deionized water (20 mL), and the pH of the solution was adjusted to 7.0. The solution was stirred at 4 °C for 24 h. Then, the solution was ultrafiltered (Millipore MoleCut II, filtration off below a MW 10 000) and the residue was repeatedly washed with distilled water until the absence of 4-azidoaniline in the filtrate was confirmed by ultraviolet absorption at 257 nm. The purified solution was then lyophilized. The photoreactive SHyal conjugate is referred to as AzPhS-Hyal. The content of azidophenyl groups in the copolymer was measured by ultraviolet absorption.

Photoimmobilization. The micropatterning procedure is shown in Figure 2. An aqueous solution of AzPhSHyal (1 mg/mL, 0.1 mL) was dropped onto a PET film and air-dried at room temperature. Subsequently, the film was irradiated with an ultraviolet lamp (Koala, 100 W) at a distance of 5 cm for 10 s in the presence or absence of a photomask. The film was washed with distilled water until the absence of AzPhSHyal in the wash was confirmed by ultraviolet spectroscopy. The

* Address correspondence to Yoshihiro Ito, Department of Material Chemistry, Graduate School of Engineering, Kyoto University, Kyoto 606-01, Japan. Telephone: 81-75-753-5638. Fax: 81-75-753-4911. E-mail: H51535@sakura.kudpc.kyoto-u.ac.jp.

[†] Kyoto University.

[‡] JST.

[§] Siena University.

[®] Abstract published in *Advance ACS Abstracts*, September 1, 1997.

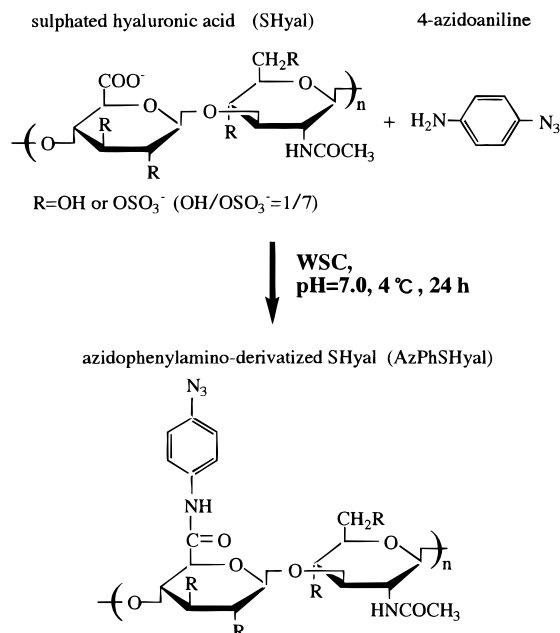


Figure 1. Preparation of azidophenylamino-derivatized sulfated hyaluronic acid.

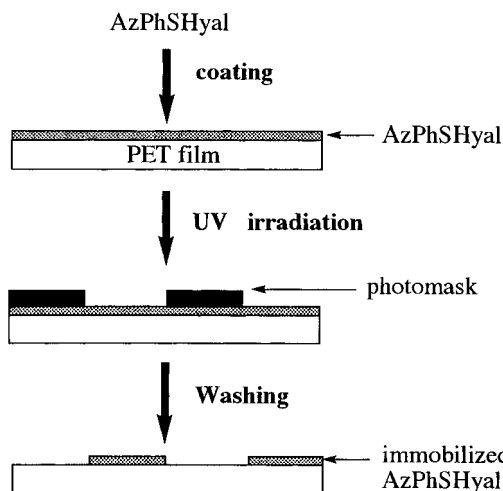


Figure 2. Photoimmobilization of azidophenylamino-derivatized sulfated hyaluronic acid. The photoimmobilization was carried out with or without a photomask.

PET film immobilized with AzPhSHyal in a specific pattern was immersed in an aqueous solution of brilliant green (1 mg/mL) for 5 min. After washing with distilled water, the stained film was observed using a microscope (Olympus Co., Tokyo, Japan).

Anticoagulant Activity Assays. Human blood was collected by gravity through a 19-gauge scalp vein needle into polypropylene tubes containing 1 part of ACD solution for 9 parts of blood. The ACD solution contains anhydrous D-glucose (2.45 g), sodium citrate dihydrate (2.20 g), and citric acid monohydrate (0.08 g) in distilled water (100 mL). The citrated blood was used for the following measurements: recalcification coagulation time, platelet adhesion, and *in vitro* thrombus formation.

The recalcification coagulation time was measured as follows. SHyal or AzPhSHyal (2.5 mg) was added in tubes containing 0.5 mL of citrated blood, and subsequently, 0.05 mL of 0.1 M CaCl_2 was added. The tubes were gently mixed until the thrombus was formed. The time required for thrombus formation was measured.

The platelet adhesion experiment was performed as follows. The citrated human blood was centrifuged at

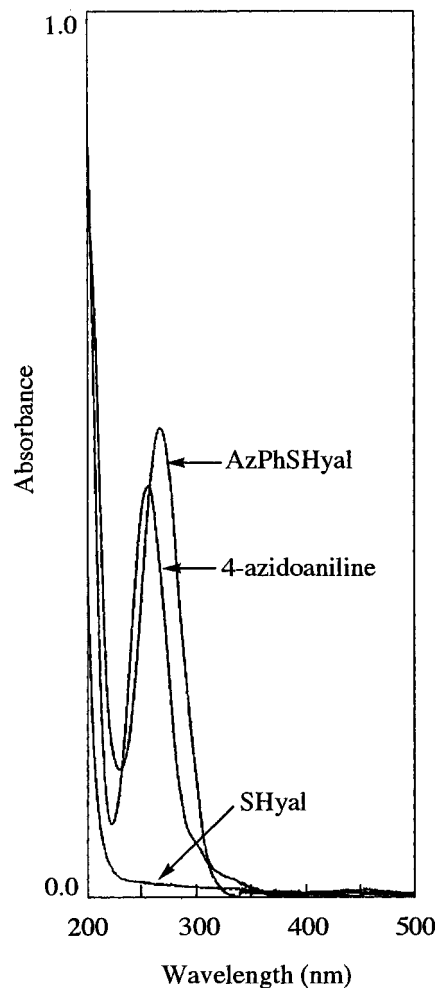


Figure 3. UV spectra of 4-azidoaniline (6.2 $\mu\text{g/mL}$), azidophenylamino-derivatized SHyal (34.0 $\mu\text{g/mL}$), and the original SHyal (34.0 $\mu\text{g/mL}$).

1200 rpm for 20 min at 4 $^\circ\text{C}$. The supernatant (0.2 mL), which is platelet-rich plasma, was added to the micro-processed PET film. After incubation at 37 $^\circ\text{C}$ for 2 h, the film was gently washed with distilled water and immersed in a phosphate-buffered saline (PBS) solution containing 3% paraformaldehyde for 10 min. The film was washed three times for 10 min each with PBS and treated with PBS containing 0.25% Triton X-100. After washing with PBS three times, the film was incubated in PBS containing 3% BSA at room temperature for 1 h. Subsequently, the film was incubated in PBS containing 0.1% BSA and 1 $\mu\text{g/mL}$ propidium iodide at room temperature for 1 h. The film was washed three times for 10 min each with PBS, briefly rinsed with distilled water, and then mounted in Vectashield mounting medium. The film adhered with platelets was observed by a fluorescence microscope (Olympus).

In vitro thrombus formation on the sample film was carried out as reported previously (24). The citrated blood (0.2 mL) was put to a sample film, and 0.02 mL of a 0.1 M CaCl_2 solution was added. After incubation at 37 $^\circ\text{C}$ for a prescribed period, the film was gently washed with distilled water and immersed in a PBS solution containing 3% paraformaldehyde for 10 min. Then, the formed thrombus was weighed after drying.

RESULTS

Synthesis and Activity of AzPhSHyal. Ultraviolet spectra of SHyal and AzPhSHyal are shown in Figure 3. In the spectrum of AzPhSHyal, an absorption at 268 nm

Table 1. Recalcification Coagulation Times of Sulfated Hyaluronic Acid

sample	time ^a (min)
nothing	20 ± 3
sulfated hyaluronic acid	> 120
azidophenylamino-derivatized sulfated hyaluronic acid	> 120

^a $n = 5$, \pm standard deviation.

which is assignable to the azidophenyl group was observed. The absorption was somewhat red-shifted from the corresponding absorption of 4-azidoaniline. This shift could be due to electron delocalization of the azidophenyl group by the amido bond formation. Assuming that the molecular absorption coefficient of azidophenyl group at 268 nm was the same as that of 4-azidoaniline at 257 nm, the content of azidophenyl groups in the copolymer was 1.01 ± 0.04 mol/mol of disaccharide unit of sulfated hyaluronic acid. It is known that one carboxyl group exists in a disaccharide unit of SHyal. Under the present reaction conditions, the carboxyl groups were fully coupled with the azidophenylamino group.

Table 1 shows the recalcification coagulation time of the two kinds of sulfated hyaluronic acids. The incorporation of the azidophenylamino group did not seem to affect the anticoagulant activity of SHyal. This result indicates that the availability of carboxylate groups, unlike that of heparin (25), is not indispensable for the anticoagulant activity of SHyal. In fact, in the case of SHyal, the anticoagulant activity is mainly based on its high density of negative charges as previously demonstrated (15). Since AzPhSHyal can elongate the coagulation time in the solution, the polymer was immobilized on a substrate.

Micropattern Immobilization of AzPhSHyal. AzPhSHyal was photoimmobilized in the presence of a photomask. Upon UV irradiation, the azidophenyl group was easily photolyzed to generate highly reactive nitrene, which spontaneously formed covalent bonds with the neighboring hydrocarbon in the PET film surface. After being thoroughly washed with distilled water, the immobilized polymer was exactly in the pattern of the photomask as shown in Figure 4. Since the polymer was anionic, the cationic dye, brilliant green, selectively stained the areas of AzPhSHyal immobilization.

Interaction with Blood. Platelet adhesion onto the micropattern of immobilized AzPhSHyal is shown in Figure 5. The adhered platelets were detected only in the regions without AzPhSHyal immobilization. It is visually shown that the micropatterning of sulfated hyaluronic acid reduced the interaction of the PET film with platelets.

Thrombus formation on the PET film with AzPhSHyal photoimmobilized in the absence of the photomask was investigated, and the result is shown in Figure 6. On the AzPhSHyal-immobilized film, the thrombus was not formed in the initial 20 min. The amount of thrombus formed on the AzPhSHyal-immobilized PET film in 1 h was about 25% of that formed on the PET film without immobilization.

We previously showed that no thrombus formation was found on the heparinized polyurethane over the course of 20 min by the same evaluation method (24). It was demonstrated that the antithrombogenic effect of immobilized sulfated hyaluronic acid corresponded to that of immobilized heparin.

DISCUSSION

Hyaluronic acid is a linear polysaccharide and consists of repeating disaccharide units of β -glucuronic acid and

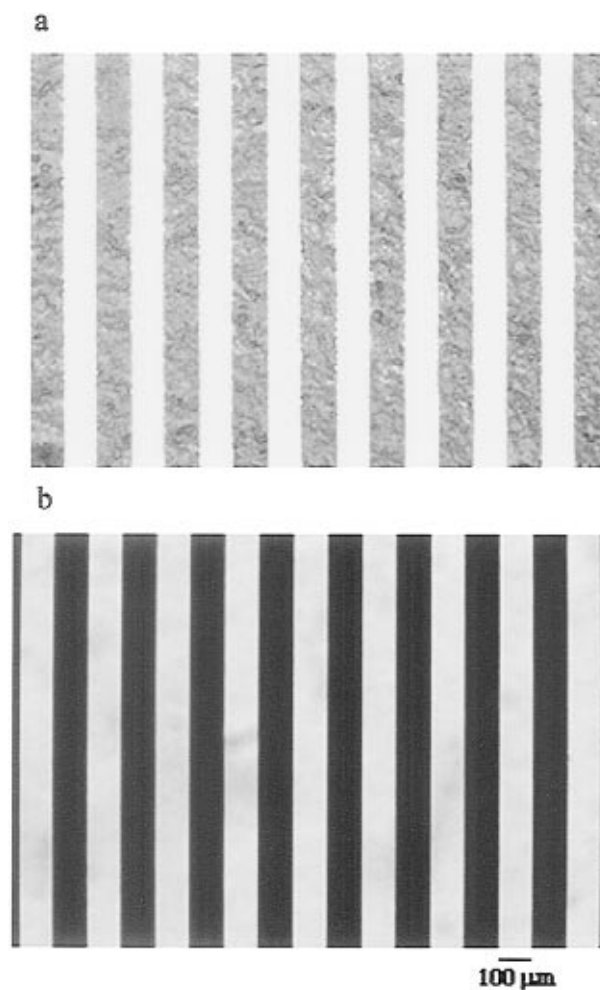


Figure 4. Micrographs of (a) an AzPhSHyal-immobilized film and (b) a photomask. AzPhSHyal was stained by brilliant green.

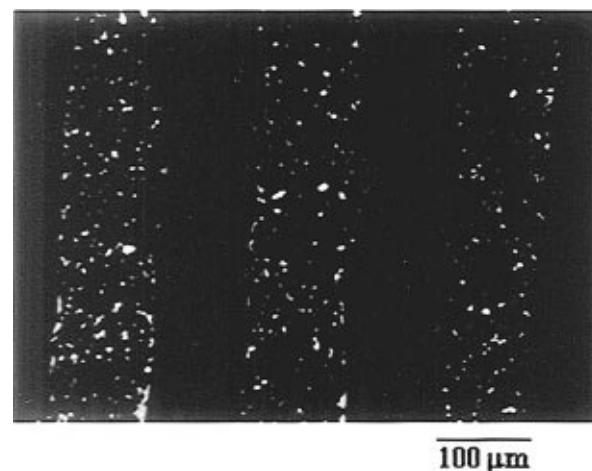


Figure 5. Fluorescence micrograph of platelets adhered onto a PET film micropattern-immobilized with AzPhSHyal. The adhered platelets were stained by fluorescent propidium iodide. *N*-acetyl- β -D-glucosamine. By itself, hyaluronic acid shows a growth-promotion effect, and investigations were carried out to enhance wound-healing properties, for instance, by culturing human keratinocytes on sponges and membranes composed of the benzyl ester of hyaluronic acid (26). Inoue and Katakami (27) reported that the hyaluronic acid stimulated proliferation of epithelial cells more than fibronectin and that as the result corneal epithelial wound healing was promoted. Hamann et al. (28) demonstrated that hyaluronic acid promoted proliferation of undifferentiated progenitor cells through the

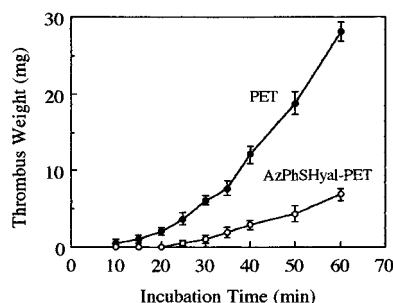


Figure 6. Time course of thrombus formation on a sulfated hyaluronic acid-immobilized PET film and a PET film without immobilization.

CD44 receptor on the surface of progenitor during eosinopoiesis *in vitro*. Recently, Rooney et al. (29) reviewed the role of hyaluronic acid in tumor neovascularization upon which tumor growth and metastasis are totally dependent. They suggested a model to account for hyaluronic acid of differing molecular mass being present, at different locations, within a single tumor and how this hyaluronic acid aids both general tumor growth and tumor metastasis (29). To endow the polymer with anticoagulant properties, hyaluronic acid was sulfated by Balazs et al. (30). The sulfated hyaluronic acid (SHyal) inactivated thrombin in a manner different from that of heparin. While heparin inhibits thrombin via antithrombin III, SHyal directly binds thrombin by specific electrostatic interactions (15).

To make conventional polymers antithrombogenic, several methods, including coating and immobilization of the anticoagulant, have been developed. Covalent immobilization is thought to be suitable for attaining a long-term antithrombogenicity. However, the presence of functional groups such as carboxyl groups and amino groups is needed on the matrix surface as a scaffold for covalent immobilization. The photoimmobilization method used in the present investigation does not need such functional groups. The photochemical method was used by Erdtmann et al. (31) to immobilize heparin, dermatan sulfate, and dextran sulfate. Kuijpers et al. (32) also photoimmobilized a small molecule, theophylline, on medical-grade polyurethane for inhibition of surface-induced activation of blood platelets by the same method in which a 4-azidophenylamino group is involved. Although they did not use a lithographic technique and did not investigate the interaction of photoimmobilized material with whole blood, they found that the theophylline-immobilized polyurethane reduced platelet adhesion by 1 order of magnitude. Considering no platelet adhesion on AzPhSHyal-immobilized regions, the immobilized AzPhSHyal was more effective than the immobilized theophylline.

In this investigation, it was shown that the polymer having anticoagulant activity in the solution was photoimmobilized on a conventional polymeric material to make the material antithrombogenic. In the case of heparinization of the material, the heparinized surface generally reduced platelet adhesion, although the effect of heparin on platelet is unclear in solution (1). On the other hand, some anticoagulants did not effectively reduce thrombus formation after immobilization. For synthesis of blood compatible materials, it is necessary to choose adequate anticoagulants and immobilization methods for them.

Well-known is the fact that the absence of platelets on the substrate surface following exposure to blood does not in itself indicate that the material possesses anticoagulant properties (33). However, the bioinertness of the

material surface is necessary to give biomaterials anti-thrombogenicity. Recently, various types of combinatorial approaches have been carried out for design of biomaterials (34, 35). The lithographic technique allowed visual evaluation of biological activities of the hybrid material under the same conditions as for nontreated material. The photoimmobilization or photolithographic method will be useful for design and synthesis of new biomaterials.

ACKNOWLEDGMENT

The authors thank Drs. T. Matsuda and Y. Nakayama at the National Cardiovascular Center Research Institute for their helpful suggestions on the photolithography technique. This work was partially supported by a Grant-in-Aid for scientific research from the Ministry of Education, Science and Culture of Japan and partially supported by the Nissan Science Foundation.

LITERATURE CITED

- (1) Ito, Y. (1987) Antithrombogenic heparin-bound polyurethanes. *J. Biomater. Appl.* 2, 235–265.
- (2) Ito, Y., Okuyama, T., Kashiwagi, T., and Imanishi, Y. (1994) Interaction of heparin with amphiphile assemblies and biocompatibility of the heparin complexes. *J. Biomater. Sci., Polym. Ed.* 6, 707–714.
- (3) Sederal, L. C., van der Does, L., van Doijl, J. F., Beugeling, T., and Bantjes, A. (1981) Anticoagulant activity of a synthetic heparinoid in relation to molecular weight and N-sulphate content. *J. Biomed. Mater. Res.* 15, 819–827.
- (4) Muzzarelli, R. A., Tanfani, F., Emanuelli, M., Pace, D. P., Chiurazzi, E., and Piani, M. (1984) Sulfated N-(carboxymethyl)-chitosans: novel blood anticoagulants. *Carbohydr. Res.* 126, 225–231.
- (5) Crassous, G., Harjanto, F., Mendjel, H., Sledz, J., and Schue F. (1985) A new symmetric membrane having blood compatibility. *J. Membr. Sci.* 22, 269–282.
- (6) Gebelein, C. G., and Murphy, D. (1987) The synthesis of some potentially blood compatible heparin-like polymeric materials. In *Advances in Biomedical Polymers* (C. G. Gebelein, Ed.) pp 277–284, Plenum Press, New York.
- (7) Ito, Y., Liu, L.-S., and Imanishi, Y. (1991) Interaction of poly(sodium vinyl sulfonate) and its surface graft with antithrombin III. *J. Biomed. Mater. Res.* 25, 99–105.
- (8) Ito, Y., Iguchi, Y., Kashiwagi, T., and Imanishi, Y. (1991) Synthesis and nontrombogenicity of polyetherurethaneurea film grafted with poly(sodium vinyl sulfonate). *J. Biomed. Mater. Res.* 25, 1347–1361.
- (9) Ito, Y., Iguchi, Y., and Imanishi, Y. (1992) Synthesis and nontrombogenicity of heparinoid polyurethanes. *Biomaterials* 13, 131–135.
- (10) Hergen, R. W., and Cooper, S. L. (1992) Improved materials for blood-contacting applications: blends of sulphonated and non-sulphonated polyurethanes. *J. Mater. Sci.: Mater. Med.* 3, 313–321.
- (11) Jozefonvicz, J., and Jozefowicz, M. (1994) Blood contacting polymers. In *Polymeric Materials* (S. Dumitriu, Ed.) pp 349–366, Marcel Dekker, New York.
- (12) Lim, F., and Cooper, S. L. (1995) Effect of sulphonate incorporation on *in vitro* leucocyte adhesion to polyurethanes. *Biomaterials* 16, 457–466.
- (13) Han, D. K., Lee, N. Y., Park, K. D., Kim, Y. H., Cho, H. I., and Miu, B. G. (1995) Heparin like anticoagulant activity of sulphonated poly(ethylene oxide) and sulphonated poly(ethylene oxide)-grafted polyurethane. *Biomaterials* 16, 467–471.
- (14) Barbucci, R., Magnani, A., Casolaro, M., Marchettini, N., Rossi, C., and Bosco, M. (1995) Modification of hyaluronic acid by insertion of sulfate groups to obtain a heparin-like molecule. Part I. Characterization and behaviour in aqueous solution towards H^+ and Cu^{2+} ions. *Gazz. Chim. Ital.* 125, 169–180.
- (15) Magnani, A., Albanese, A., Lamponi, S., and Barbucci, R. (1996) Blood-interaction performance of differently sulfated hyaluronic acids. *Thromb. Res.* 81, 383–395.

- (16) Barbucci, R., Magnani, A., Lamponi, S., and Casolaro, M. (1996) Different sulphation degree and biological performance of hyaluronic acid as heparin-like molecule. *Macromol. Symp.* 105, 1–8.
- (17) Barbucci, R., Cialdi, G., and Magnani, A. (1995) Noval heparin-like sulphated polysaccharides. PCT Int. Appl. WO 95/25751.
- (18) Sugawara, T., and Matsuda, T. (1994) Novel surface graft copolymerization method with micron-order regional precision. *Macromolecules* 27, 7809–7814.
- (19) Matsuda, T., and Sugawara, T. (1995) Development of surface photochemical modification method for micropatterning of cultured cells. *J. Biomed. Mater. Res.* 29, 749–756.
- (20) Matsuda, T., and Sugawara, T. (1995) Development of a novel protein fixation method with micron-order precision. *Langmuir* 11, 2267–2271.
- (21) Matsuda, T., and Sugawara, T. (1995) Photochemical protein fixation on polymer surfaces via derivatized phenyl azido group. *Langmuir* 11, 2272–2276.
- (22) Ito, Y., Chen, G., Guan, Y., and Imanishi, Y. (1997) Patterned immobilization of thermo-responsive polymer. *Langmuir* 13, 2756–2759.
- (23) Ito, Y., Kondo, S., Chen, G., and Imanishi, Y. (1997) Patterned artificial juxtacrine stimulation of cells by covalently immobilized insulin. *FEBS Lett.* 403, 159–162.
- (24) Ito, Y., Sisido, M., and Imanishi, Y. (1986) Synthesis and antithrombogenicity of polyurethaneurea containing quaternary ammonium groups in the side chains and of the polymer/heparin complex. *J. Biomed. Mater. Res.* 20, 1017–1033.
- (25) Casu, B. (1995) Structure and biological activity of heparin. *Adv. Carbohydr. Chem. Biochem.* 43, 51–134.
- (26) Andreassi, L., Casini, L., Trabucchi, E., Diamantini, S., Rastrelli, A., Donati, L., Tenchini, M. L., and Malcovati, M. (1991) Human keratinocytes cultured on membranes composed of benzyl ester of hyaluronic acid suitable for grafting. *Wound* 3, 116–126.
- (27) Inoue, M., and Katakami, C., (1993) The effect of hyaluronic acid on corneal epithelial cell proliferation. *Invest. Ophthalmol. Visual Sci.* 34, 2313–2315.
- (28) Hamann, K. J., Dowling, T. L., Neeley, S. P., Grant, J. A., and Leff, A. R. (1995) Hyaluronic acid enhances cell proliferation during eosinopoiesis through the CD44 surface antigen. *J. Immunol.* 154, 4073–4080.
- (29) Rooney, P., Kumar, S., Ponting, J., and Wang, M. (1995) The role of hyaluronan in tumour neovascularization. *Int. J. Cancer* 60, 632–626.
- (30) Balazs, E. A., Hogberg, B., and Laurent, T. C. (1951) The biological activity of hyaluronic sulfuric acid. *Acta Phys. Scand.* 23, 168–178.
- (31) Erdtmann, M., Keller, R., and Baumann, H. (1994) Photochemical immobilization of heparin, dermatan sulphate, dextran sulphate and endothelial cell surface heparan sulphate onto cellulose membranes for the preparation of athrombogenic and antithrombogenic polymers. *Biomaterials* 15, 1043–1048.
- (32) Kuijpers, J. M. H., Kardaum, G. A., Blezer, B., Pijpers, A. P., and Koole, L. H. (1995) Immobilization of theophylline on medical grade polyurethane inhibits surface-induced activation of blood platelets. *J. Am. Chem. Soc.* 117, 8691–8697.
- (33) Sefton, M. V. (1993) The good, the bad and the obvious: 1993 clemson award for basic research—Keynote lecture. *Biomaterials* 14, 1127–1134.
- (34) Ito, Y. (1996) Molecular shape recognition. In *Polymeric Materials Encyclopedia* (J. C. Salamone, Ed.) pp 4473–4481, CRC Press, Boca Raton, FL.
- (35) Brocchini, S., James, K., Tangpasuthadol, V., and Kohn, J. (1997) A combinatorial approach for polymer design. *J. Am. Chem. Soc.* 119, 4553–4554.

BC9700493

Nanoparticle DNA Carrier with Poly(L-lysine) Grafted Polysaccharide Copolymer and Poly(D,L-lactic acid)

Atsushi Maruyama,^{*,†} Tsutomu Ishihara,[†] Jin-Seok Kim,[‡] Sung Wan Kim,[‡] and Toshihiro Akaike[‡]

Department of Biomolecular Engineering, Faculty of Bioscience and Biotechnology, Tokyo Institute of Technology, 4259 Nagatsuta, Midori, Yokohama 226, Japan, and Department of Pharmaceutics and Pharmaceutical Chemistry, Center for Controlled Chemical Delivery, Biomedical Polymer Research Building, University of Utah, Salt Lake City, Utah 84112. Received March 17, 1997[®]

Biodegradable nanoparticles, which contain the sites for both polynucleotide adsorption and targeting ligand on their surfaces, were prepared as a novel carrier for genetic materials. The nanoparticles were obtained from poly(D,L-lactic acid) and poly(L-lysine)-*graft*-polysaccharide copolymers by using either a solvent evaporation method or a diafiltration method. The size of the particles prepared by the diafiltration method was controlled by varying the initial concentration of the graft copolymer. Nanoparticles as small as 60 nm in diameter were successfully obtained from the graft copolymers with high polysaccharide contents but not from the poly(L-lysine) homopolymer. Polysaccharide moieties on the surface of the nanoparticles were found to interact specifically with a particular lectin as verified by the aggregation assay. The polynucleotide adsorption capacity of the nanoparticles was increased with increasing polysaccharide contents in the graft copolymers, suggesting that the adsorption conformation of poly(L-lysine) moiety in the graft copolymer on the nanoparticle surface is different from that in poly(L-lysine) homopolymer. Moreover, the nanoparticles from the graft copolymer exhibited resistance against self-aggregation and nonspecific adsorption of serum proteins, presumably due to the *polymer brush effect* and/or *exclusion effect* from the polysaccharide graft chains. These results suggest that the nanoparticles prepared from poly(L-lysine)-*graft*-polysaccharide copolymer and poly(D,L-lactic acid) can serve as a good DNA carrier *in vivo*.

INTRODUCTION

During the past decade, new therapeutic approaches introducing genetic materials (i.e. genes, antisense oligonucleotides, ribozymes, and triple-helix-forming nucleotides) into the intact cells have shown rapid progress both fundamentally and clinically in gene therapy (1–5). Many types of synthetic carriers, including liposomes (6, 7), polymers (8), and particles (9–11), were studied to deliver exogenous genetic materials into cells in a cellular specific or nonspecific manner.

Recently, biodegradable nano(micro)particles have also been studied not only as sustained-release matrices of drug molecules (12–14) but as a potential carrier for genetic materials (9–11). Advantages of biodegradable particles as a gene delivery carrier include the following: (1) they are relatively inert and biocompatible; (2) their biological behavior can be regulated by controlling the size and surface properties; (3) preparation, storage, and handling are relatively easy; and (4) the release of genetic materials can also be controlled by changing the degradation rate of the matrix polymer.

Cortesi *et al.* (9) have encapsulated DNA into micro-particles by a coacervation method, although it was difficult to obtain small particles suitable for intravenous injection. In practice, genetic materials adsorbed on (not encapsulated in) the nano(micro)particles might be also convenient because only a simple mixing of particles with genetic materials is needed to form a genetic material-carrier complex. The size and shape of the resulting formulation can also remain homogeneous and uniform, compared to the formulations based on liposomes or

polycations. Bertling *et al.* (15) prepared nanoparticles from polycyanoacrylate in the presence of DEAE-dextran. These nanoparticles exhibited a strong DNA binding capacity and resistance against DNase I degradation, although the biological activity of the plasmid DNA was not observed presumably due to the strong binding of the DNA to particles. Poly(alkyl cyanoacrylate) nanoparticles were also evaluated as an oligonucleotide carrier, and their physical stability and biological efficacy of antisense oligonucleotides were found to be greatly enhanced in this formulation (11, 16). Poly(isohexyl cyanoacrylate) nanoparticles were used recently to adsorb cholesterol-oligonucleotide conjugates on their surface via hydrophobic interaction, where a sequence specific antisense effect was observed only when the oligonucleotide was associated with the nanoparticles (17). In the studies mentioned above, the majority of the surface of the particles was probably occupied by poly(oligo)nucleotides and it was difficult to modify their surfaces with functional molecules, such as ligand moieties, to modulate biodistribution.

We report here the preparation and characterization of polysaccharide-bearing bifunctional nanoparticles that have a polynucleotide adsorption capacity as well as carbohydrate-mediated recognition of specific receptor. Since carbohydrate moieties can serve as a targeting ligand for carbohydrate-binding proteins identified on the surface of mammalian cells (18–22), carriers containing carbohydrate moieties have proved to be delivered successfully to cells *in vitro* and *in vivo* (19, 23–26). Furthermore, some acidic carbohydrates, such as sialic acid, were reported to reduce the reticular endothelial system (RES) uptake (27–29). Therefore, carbohydrates are useful not only as a ligand moiety but also as a component to reduce nonspecific interaction of the formulates with proteins and cells, as well as other hydrophilic polymer chains (30–33). These nanoparticles were

* Author to whom correspondence should be addressed.

† Tokyo Institute of Technology.

‡ University of Utah.

® Abstract published in *Advance ACS Abstracts*, August 15, 1997.

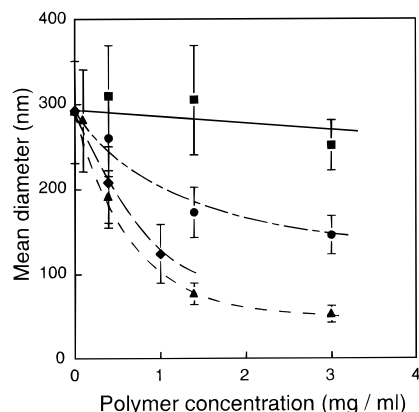


Figure 2. Effect of PLL (squares), PLL-Dex (4-5900) (circles), PLL-Dex (7-5900) (diamonds), or PLL-Dex (34-2600) (triangles) concentration in DMSO on the particle size. Weight-average diameters determined by DLS are shown. Error bars indicate standard deviation. Particles were prepared by the diafiltration method from 10 mL of DMSO solution containing 25 mg of PLA and various amounts of PLL or graft copolymers.

Nanoparticle Surfaces. Nanoparticle suspensions were fractionated by centrifugation (5600*g* for 10 min), and the pellets were washed three times with distilled water by repeated centrifugation (5600*g* for 10 min) and resuspension. The size of the fractionated nanoparticles was in the range from 200 to 300 nm as determined by DLS. The nanoparticles were finally obtained by lyophilization. The adsorption isotherm of plasmid DNA on the particle surfaces was analyzed as follows: The nanoparticles (0.5 mg) and the indicated amount of plasmid DNA (0–30 μ g) were mixed in PBS (180 μ L). After 1 h of incubation at 20 °C, the suspension was centrifuged at 5600*g* for 10 min to precipitate the nanoparticles. The amount of unadsorbed plasmid was determined fluorometrically by incubating 150 μ L of supernatant with 3 μ L of ethidium bromide solution (50 μ g/mL) using a microplate spectrofluorometer at $\lambda_{\text{ex}} = 490$ nm and $\lambda_{\text{em}} = 590$ nm (MTP-32, Corona Electric Co. Ltd., Ibaragi, Japan).

Adsorption of Fluorescein Isothiocyanate (FITC)-Labeled Bovine Serum Albumin (BSA) on Nanoparticle Surfaces. BSA (fraction V, Sigma, St. Louis, MO) was labeled with fluorescein isothiocyanate (FITC) by mixing 1.5 g of BSA and 30 mg of FITC in a 5 mL of phosphate buffer solution (0.1 M, pH 8.5) for 1 h at room temperature. FITC-labeled BSA free from the nonincorporated FITC was then purified by a gel filtration on a Sephadex G-50 column.

The adsorption isotherm of FITC-labeled BSA on the particle surfaces was analyzed as follows: The nanoparticles (0.5 mg) fractionated by centrifugation (5600*g* for 10 min) and the indicated amount of FITC-labeled BSA (0–10 μ g) were mixed in PBS (180 μ L). After 1 h of incubation at 20 °C, the suspension was centrifuged at 5600*g* for 10 min to precipitate the nanoparticles. The supernatant (150 μ L) was used to determine the amounts of unadsorbed FITC-BSA using a microplate spectrofluorometer at $\lambda_{\text{ex}} = 490$ nm and $\lambda_{\text{em}} = 530$ nm.

RESULTS AND DISCUSSION

Preparation of Nanoparticles. To develop a novel carrier for genetic materials, we have successfully prepared biodegradable nanoparticles from graft copolymers and poly(lactic acid). We found that the characteristics of nanoparticles prepared by a diafiltration method were affected by the polymer concentration. As shown in Figure 2, the initial polymer concentration had a profound effect on the size of the nanoparticles. When the

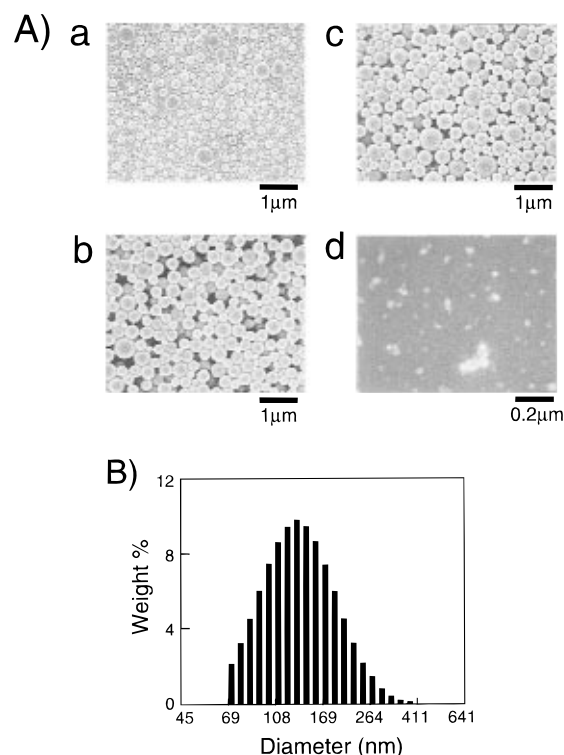


Figure 3. SEM view (A) and DLS profile (B) of nanoparticles. (A) a, PLL NPs prepared by the solvent evaporation method; b, PLL NPs prepared by the diafiltration method from 10 mL of DMSO solution containing 25 mg of PLA and 5 mg of PLL; c and d, PLL-Dex (34-2600) NPs prepared by the diafiltration method from 10 mL of DMSO solution containing 25 mg of PLA and (c) 4 or (d) 30 mg of PLL-Dex (34-2600). The NPs were not fractionated except for the NPs in (d), which were obtained by centrifugation at 160000*g*. (B) DLS profile of particles shown in view c of panel A.

concentration of graft copolymers (PLL-*graft*-dextran or PLL-*graft*-Dex) was increased, the mean diameter of the resulting nanoparticles decreased. At a concentration of 3 mg/mL of the PLL-*graft*-Dex (34-2600) copolymer, nanoparticles as small as 60 nm were obtained. On the contrary, the concentration of PLL homopolymer did not significantly affect the particle size. For example, the size of the nanoparticles prepared from 4 mg/mL PLL homopolymer was over 200 nm in diameter. It is probable that the polysaccharide in the graft copolymer might have decreased the interfacial energy at the water/PLA interface more effectively than PLL homopolymer, resulting in the formation of the smaller particles. The mean diameter of the nanoparticles prepared from PLL-*graft*-Dex (7-5900) was smaller than that of PLL-*graft*-Dex (4-5900), suggesting that the particle size is controllable either by changing the concentration of graft copolymer or by changing the polysaccharide content in the graft copolymers.

In addition, the shape of the nanoparticles was spherical regardless of the preparation methods, but the size distribution of the nanoparticles prepared by the diafiltration method was more homogeneous than that of the particles prepared by the solvent evaporation method (Figure 3A). A typical DLS profile of the PLL-*graft*-Dex (34-2600) nanoparticles is shown in Figure 3B.

Surface Characterization of Nanoparticles. Results from ζ -potential measurement of the nanoparticles prepared by the diafiltration method are summarized in Table 2. The nanoparticles prepared from PLA alone showed a highly negative ζ -potential in PBS. This negative value of the PLA nanoparticles is due to the terminal carboxyl groups of PLA and/or the hydrophobic

Table 2. ζ -Potential Measurement of Various Nanoparticles^a

code	none ^b	PLL	PLL-Dex (4-2600)	PLL-Dex (7-2600)	PLL-Dex (7-5900)
ζ -potential (mV)	-30.0	+14.3	+14.7	+6.8	+4.8

^a All samples were measured in phosphate-buffered saline (PBS). Nanoparticles were prepared by the diafiltration method from 10 mL of DMSO containing 25 mg of PLA and the indicated polymer (5 mg equivalent based on PLL). ^b Particles were prepared with PLA only.

characteristic of the nanoparticle surfaces. In contrast, the nanoparticles prepared from PLL homopolymer/PLA mixture showed a positive ζ -potential, leading to a 44 mV difference from that of PLA nanoparticles. The result indicates that the PLL moiety is stably associated with the surface of the nanoparticles. On the other hand, for the nanoparticles prepared from PLL-*graft*-Dex/PLA, the ζ -potential was decreased from +14 to +4.8 mV with increasing dextran contents in the graft copolymers. The nanoparticles prepared from PLL-*graft*-Dex with high dextran contents, however, still exhibited a positive ζ -potential, indicating the presence of the graft copolymers on the particle surfaces. The effect of dextran chains on the ζ -potential may be attributed to preferential distribution of dextran moieties over PLL chains in the outer surfaces of the nanoparticles, as will be discussed in the latter part of this paper.

A lectin-induced aggregation test confirmed the presence of polysaccharide on the nanoparticles. As shown in Figure 4, the nanoparticles prepared by the diafiltration method from PLL-*graft*-Dex (7-5900)/PLA aggregated by the addition of Con A, an α -glucose, and an α -mannose specific lectin (panel b). The aggregation was inhibited by glucose (panel c) but not by galactose (panel d), suggesting that the aggregation is caused by the Con A-specific recognition and cross-linking to dextran moieties on the nanoparticles. Finally, the carbohydrate specificity of the aggregation was verified by using Allo A, a β -galactose-specific lectin, that caused no aggrega-

tion (panel e). Taken together, these results confirmed that the surface of nanoparticles prepared from the copolymer was covered with the carbohydrate moieties which are recognized by specific carbohydrate-binding protein. The presence of polysaccharide was also confirmed on the nanoparticles prepared by the solvent evaporation method (data not shown).

For practical use, the nanoparticles should have a dispersive stability in an aqueous media and not aggregate during storage. The dispersive stability of the nanoparticles was analyzed from the change in turbidity of various nanoparticle suspensions. The suspension of the nanoparticles prepared with PLL/PLA or PLA alone exhibited a gradual decrease in turbidity during the time course of incubation at 37 °C (Figure 5), indicating an aggregate formation. In contrast, the suspension of the nanoparticles prepared with PLL-*graft*-Dex (7-5900) exhibited no significant change in turbidity even after 10 days of incubation, indicating excellent dispersiveness. Thus, the results suggest that the dextran chains on the nanoparticle surfaces were effective in preventing particle aggregation.

The surface property of the nanoparticles was also examined by analyzing the effect of multivalent anions on particle aggregation. As shown in Table 3, in phosphate buffer (20 mM, pH 7) without NaCl, the nanoparticles prepared from PLL homopolymer/PLA formed severe aggregates. This aggregation was formed presumably due to interparticle cross-linking of PLL moieties via multivalent phosphate anions. Such aggregation, however, was not observed for the nanoparticles prepared from PLL-*graft*-Dex/PLA with high dextran content, but a change in the length of the hydrophilic chain, like maltose on PLL backbone, failed to prevent aggregate formation.

DNA Adsorption onto the Particle Surfaces. The interaction of DNA with the nanoparticle was studied by a gel retardation assay as described under Materials and Methods. Plasmid DNA (1 μ g) was mixed with various amounts of nanoparticles and incubated for 1 h at room

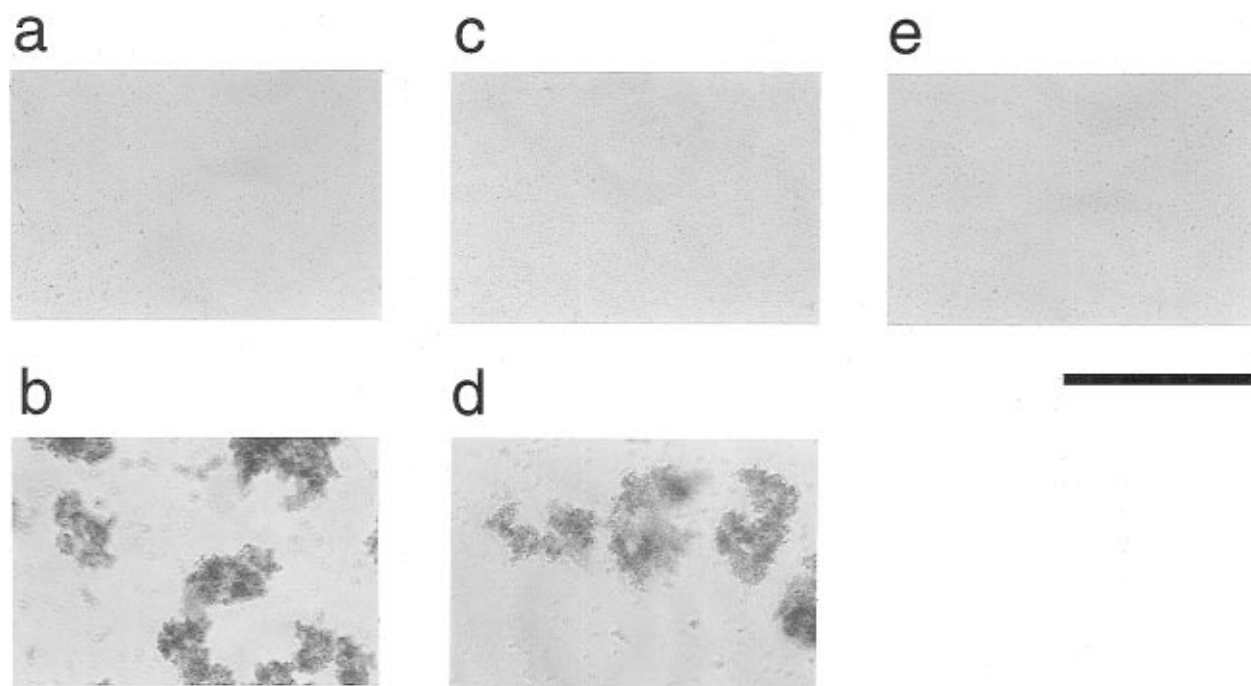


Figure 4. Lectin-induced aggregation of PLL-Dex NPs in PBS. PLL-Dex (7-5900) NPs (100 μ g) were suspended in 400 μ L of PBS (a) and added with 10 μ g of Con A (b), 1 mg of glucose and 10 μ g of Con A (c), 1 mg of galactose and 10 μ g of Con A (d), or 10 μ g of Allo A lectin (e). The NPs were prepared by the diafiltration method from 10 mL of DMSO solution containing 25 mg of PLA and the defined amount of the graft copolymers. (Scale bar, 200 μ m.)

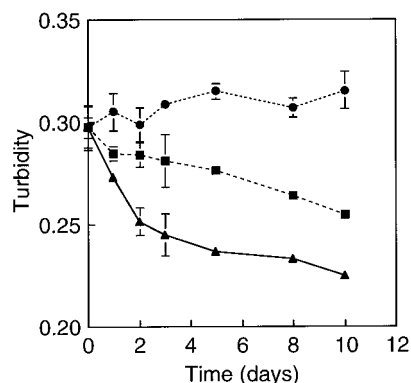


Figure 5. Dispersive stability of various nanoparticles. PLA NPs (triangles); PLL NPs (squares); PLL-Dex (7-5900) NPs (circles). NPs were prepared by the diafiltration method from 10 mL of DMSO solution containing 25 mg of PLA and the indicated polymers (5 mg equivalent based on PLL) and stored at 37 °C. PLA NPs were prepared with PLA only.

Table 3. Phosphate-Induced Aggregation of Nanoparticles

code	PLL	PLL-Mal (6-360)	PLL-Mal (12-360)	PLL-Dex (4-5900)	PLL-Dex (7-5900)
aggregation ^a	++	++	+	—	—

^a ++, hard aggregation or precipitation; +, weak aggregation; —, no aggregation. To a nanoparticle suspension in distilled water was added phosphate buffer (final concentration = 20 mM, pH 7.2).

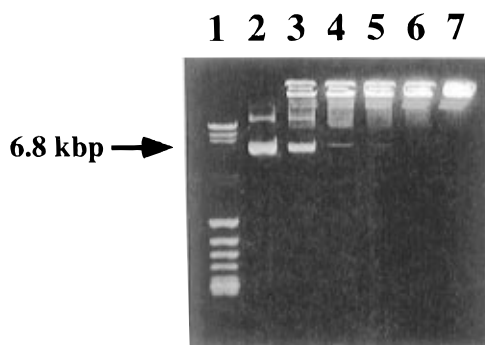


Figure 6. Gel electrophoresis of plasmid DNA (pSV) and NPs mixtures (1% agarose): (lane 1) MW marker; (lane 2) pSV alone (1 μg); (lanes 3–7) mixtures of pSV (1 μg) and increasing amounts of PLL-Dex (7-2600) NPs (10, 30, 50, 80, or 120 μg). Before electrophoresis, these mixtures were incubated in PBS for 1 h at room temperature. Plasmid DNA was detected as ultraviolet fluorescence after ethidium bromide staining. PLL-Dex (7-2600) NPs were prepared by the diafiltration method from 10 mL of DMSO solution containing 25 mg of PLA and 9 mg of PLL-Dex (7-2600).

temperature. Plasmid DNA was then resolved by electrophoresis on 1% agarose gel. As shown in Figure 6, an increase in particle amount caused a gradual disappearance of the plasmid DNA. At a weight ratio of over 80 of the nanoparticles to plasmid DNA, the plasmid DNA did not migrate at all into the gel, indicating that all of the plasmid DNA was trapped on the surface of the nanoparticles.

Figure 7 shows the adsorption isotherms of the plasmid DNA on various nanoparticles prepared by the diafiltration method. The adsorption of DNA on the surface of nanoparticles largely depends on the dextran contents in the graft copolymer. It was noteworthy that the DNA adsorption capacity of the nanoparticles increased significantly with the dextran contents of the graft copolymer. We found that nanoparticles prepared from PLL-*graft*-Dex (7-5900)/PLA adsorbed 3 times more DNA than

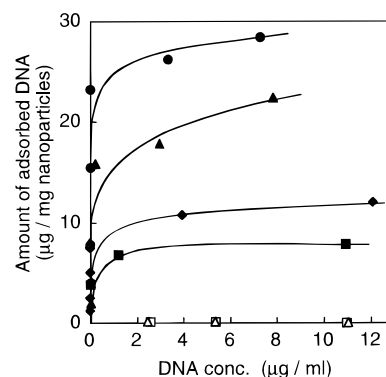
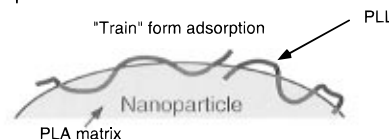


Figure 7. Adsorption isotherm for pSV plasmid to various nanoparticles at 25 °C. PLL NPs (solid squares), PLL-Dex (4-2600) NPs (solid diamonds), PLL-Dex (7-2600) NPs (solid triangles), and PLL-Dex (7-5900) NPs (solid circles) were measured in 1× PBS. PLL NPs (open squares) or PLL-Dex (7-2600) NPs (open triangles) were measured in 10× PBS. NPs were prepared by the diafiltration method from 10 mL of DMSO solution containing 25 mg of PLA and the indicated polymer (5 mg equivalent based on PLL).

PLL nanoparticle



PLL-*graft*-polysaccharide nanoparticle

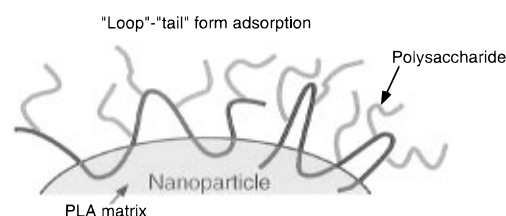


Figure 8. Schematic illustration of polymer structure on nanoparticle surface.

those prepared from PLL homopolymer/PLA. The similar adsorption profile was also obtained with the same nanoparticles prepared by the solvent evaporation method (data not shown). As the nanoparticles used in this experiment were fractionated to a homogeneous size of 250 ± 50 nm in diameter before the measurement, the difference in DNA adsorption capacity is presumably due to the differences in polymer density and its conformation on the nanoparticles. Since no DNA adsorption occurred in a high ionic strength buffer, the ionic interaction between DNA and PLL moieties on the nanoparticles is thought to be the main driving force for DNA adsorption. For the particles prepared from PLL homopolymer/PLA, the majority of the amino groups in PLL might be interacted with PLA, leading to "train"-form adsorption of PLL on the nanoparticle surfaces (Figure 8). The hydrophobic nature of PLL may facilitate the "train"-form adsorption. On the other hand, dextran graft chains partially disturb the ionic interaction between PLA and PLL segments. Therefore, PLL segments on the copolymer nanoparticle adopt the "loop" and "tail" forms as shown in Figure 8. The majority of the amino groups in PLL backbone were free with such adsorption forms, providing higher capacity of DNA adsorption. In addition to the polymer conformation, dextran chains might also modify interaction of DNA with PLL segments.

DNA adsorption behavior was further investigated by ζ -potential measurements. As summarized in Table 4, the surface charge of the nanoparticles became neutral

Table 4. ζ -Potentials of Nanoparticles Treated with pSV Plasmid^a

	NPs alone	+pSV (4.5 μ g)	+pSV (9 μ g)	+pSV (27 μ g)
ζ -potential (mV)	+4.8	+2.8	+0.8	-11.2

^a PLL-Dex (7-5900) nanoparticles shown in Table 2 were dispersed in PBS at 60 μ g/mL. To 5 mL of nanoparticle suspension was added the indicated amount of pSV plasmid or BSA from their stock solution. After 1 h of incubation, ζ -potential was measured.

as the amounts of adsorbed DNA increased. Treatment of the nanoparticles with an excess amount of DNA (90 μ g/mg of nanoparticles), however, resulted in a highly negative ζ -potential, which indicates that an electrostatically excess amount of DNA molecules remained on the surface of nanoparticles, leading to a negative ζ -potential.

Polycations such as DNA are liable to aggregate cationic particles. As shown in Figure 9b, plasmid DNA induced a slight aggregation of PLL-*graft*-Dex (4-2600) nanoparticles. The DNA-induced aggregation was, however, not observed for PLL-*graft*-Dex (7-5900) nanoparticles (Figure 9d), suggesting that dextran chains are also effective in avoiding polyanion-induced aggregation of the nanoparticles.

The capability of the polysaccharide chain on DNA-loaded nanoparticles to bind to lectins was evaluated. The nanoparticles mixed with 25 μ g of DNA/mg of nanoparticles formed aggregates by the addition of Con A (panel e) but not with 100 μ g of DNA/mg of nanoparticles (panel f). Thus, the excess amount of DNA on the surface of the nanoparticles inhibited the recognition of carbohydrate by lectin, resulting in less or no aggregate formation. Therefore, optimum DNA loading is necessary for the nanoparticles to preserve their carbohydrate specificity.

Interaction of Nanoparticles with BSA. The adsorption behavior of BSA on the nanoparticles is shown

in Figure 10. The adsorption of BSA on the nanoparticles was markedly reduced with an increase in carbohydrate contents in the graft copolymer. For the nanoparticles prepared from PLL-*graft*-amylose (15-3000), almost no adsorption of BSA was observed. The resistance of the nanoparticle surface to nonspecific BSA adsorption was also seen from the ζ -potential measurement as summarized in Table 5. As the BSA molecules have a negative surface charge at the physiological condition, positively charged nanoparticle surface electrostatically attracted the BSA molecules. The ζ -potential of nanoparticles prepared from PLL homopolymer was drastically reduced by addition of BSA, resulting from adsorption of BSA. On the contrary, nanoparticles prepared from PLL-*graft*-amylose (15-3000) and PLL-*graft*-Dex (7-5900) did not show a significant change in ζ -potential by the addition of BSA, indicating negligible interaction of BSA with these nanoparticles. Even though there should be a favorable electrostatic interaction between BSA and nanoparticles, polysaccharide chains on the surface of the nanoparticles effectively shield positive charges of PLL chains (Table 2) and keep BSA molecules away from nanoparticles by the exclusion effect (37), leading to a negligible interaction. This finding is very important and can be very useful for designing effective gene delivery systems *in vivo* since nonspecific interaction of the designed nanoparticles should be negligibly small.

CONCLUSION

Tissue-specific delivery of genetic materials is of great importance for gene therapeutic approaches. However, much progress has not been achieved so far, due to the lack of a suitable carrier to reach the goal. We prepared and characterized novel biodegradable nanoparticles by simple solvent evaporation and diafiltration methods, without using any emulsifier or surfactant. Though the nanoparticles from the diafiltration method exhibited narrower size distribution than that of the solvent

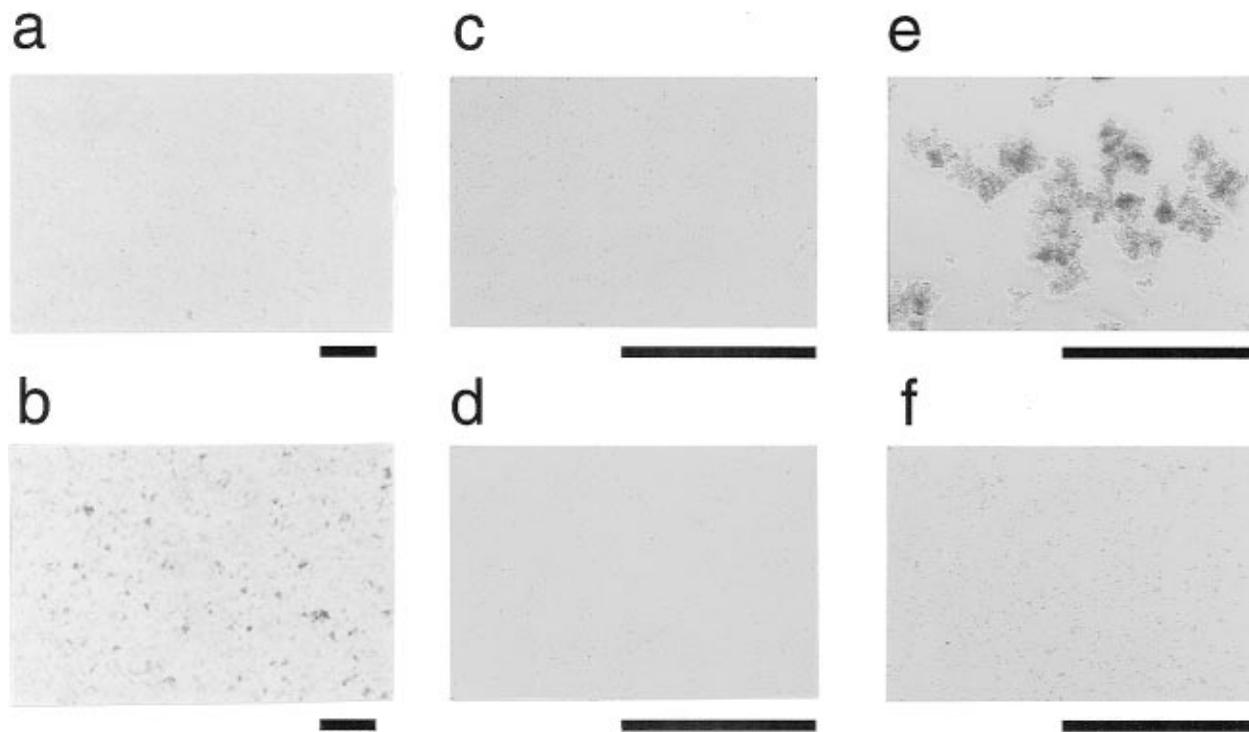


Figure 9. Effect of plasmid DNA on PLL-Dex NPs on lectin-induced aggregation. PLL-Dex (4-2600) NPs (100 μ g) were suspended in 400 μ L of PBS (a) and added with 1.2 μ g of plasmid DNA (b). PLL-Dex (7-5900) NPs (100 μ g) were suspended in 400 μ L of PBS (c) and added with 2.5 μ g of plasmid DNA (d), 2.5 μ g of plasmid DNA and 10 μ g of Con A (e), or 10 μ g of plasmid DNA and 10 μ g of Con A (f). The NPs were prepared by the diafiltration method from 10 mL of DMSO solution containing 25 mg of PLA and the defined amount of the graft copolymers. (Scale bar, 200 μ m.)

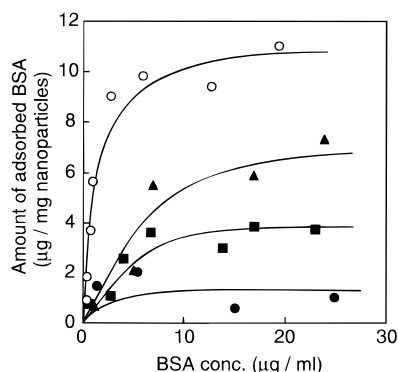


Figure 10. Adsorption profile of FITC-labeled BSA to various nanoparticles at 25 °C. PLL NPs (solid triangles), PLL-Amy (4-3000) NPs (solid squares), and PLL-Amy (15-3000) NPs (solid circles) were prepared by the solvent evaporation method as described under Materials and Methods. Polystyrene latex [mean diameter = 310 nm (open circles)] was measured as a control particle.

Table 5. ζ -Potentials of Nanoparticles Treated with BSA^a

code	NPs alone	+BSA
PLL	+27.0	-3.3
PLL-Amy (15-3000)	+3.3	+3.1
PLL-Dex (7-5900)	+4.8	+4.3

^a PLL and PLL-Amy (15-3000) nanoparticles were prepared by solvent evaporation method as described under Materials and Methods. PLL-Dex (7-5900) nanoparticles shown in Table 2 were used. Nanoparticles were dispersed in PBS at 60 μ g/mL. To 5 mL of nanoparticles suspension was added 1 mg of BSA from their stock solution. After 1 h of incubation, ζ -potential was measured.

evaporation method, the nanoparticles prepared by either method showed similar properties in terms of plasmid DNA adsorption and lectin-induced aggregation.

In addition to the targeting characteristic of carbohydrate chains, the hydrophilic nature of the chains was also found to be very important in several aspects.

First, the size of the nanoparticles is controllable either by changing the concentration of graft copolymer or by changing the polysaccharide content in the graft copolymers as shown in Figure 2. The nanoparticles as small as 60 nm in diameter were available with the PLL-*graft*-polysaccharide copolymers/PLA but not with PLL homopolymer/PLA. This strongly indicates that the hydrophilic moiety in the graft copolymer effectively reduces the interfacial energy between the particle surfaces and the aqueous media. In general, the size of a carrier is one of the major factors that significantly affects the *in vivo* pharmacokinetics of the drugs or genes, and smaller ones usually show a better therapeutic effect than larger ones, because of less uptake by the reticular endothelial system (RES) (38).

Secondly, grafting of carbohydrate chains to PLL increased adsorption capacity of the nanoparticles for DNA. As the PLL segments are the major adsorption site for DNA, it is assumed that the PLL backbone of the graft copolymer might adopt a different conformation on the particle surface compared to the PLL homopolymer, leading to an increase in the adsorption capacity, although the exact mechanism remains to be solved. Furthermore, our preliminary study indicated that the graft copolymer nanoparticles exhibited stable adsorption of oligonucleotides (20-mer) compared with PLL nanoparticles.

Third, nanoparticles prepared from the graft copolymers showed an excellent dispersive stability during

storage in PBS. Phosphate anion did not induce aggregation of the graft copolymer nanoparticles. The excellent dispersion property of the nanoparticles was maintained even after DNA loading. As summarized in Table 2, while the adsorption capacity of DNA increased with increasing dextran contents, positive values of the ζ -potentials observed for the nanoparticles decreased. The results strongly indicated that the positive charges of PLL chains were effectively shielded by dextran chains, implying preferential localization of dextran chains to the outermost surfaces over PLL chains (37, 39–41). Carbohydrate chains on the nanoparticle surfaces probably prevented the particle aggregation due to the so-called "exclusion effect" and/or "polymer brush effect" (37, 42, 43). The carbohydrate chains on the nanoparticle surfaces, which prefer the solvent of the suspension, resist overlapping and separating the particles to a distance at which attractive interaction is too weak to keep the particles together (42). Furthermore, the repulsive force between particles arises ultimately from the high osmotic pressure inside the carbohydrate chains (42). In a similar manner, the carbohydrate chains were shown to reduce the adsorption of BSA to the nanoparticles. This effect is expected to be important to minimize nonspecific interactions of nanoparticles with serum components.

The combination of poly(D,L-lactic acid) and PLL-*graft*-polysaccharide showed advantages as follows: (1) the ligand moiety could be introduced to the nanoparticles; (2) the size of the nanoparticles could be controlled; (3) there was a high DNA adsorption capacity; and (4) the nanoparticles had a high dispersive stability. Thus, the nanoparticles prepared from PLL-*graft*-polysaccharide and poly(D,L-lactic acid) fulfill several important requirements as a DNA carrier. Since the syntheses of the graft copolymers were simple and showed high coupling yielding (>90%) (44), the preparation of the nanoparticles with different types of carbohydrate chains is also possible. Different types of nanoparticle carriers for the targeting of genetic materials can be designed by modifying or replacing carbohydrate segments with other ligands or hydrophilic polymers.

LITERATURE CITED

- (1) Mulligan, R. C. (1993) The basic science of gene therapy. *Science* 260, 926–932.
- (2) Anderson, W. F. (1992) Human gene therapy. *Science* 256, 808–813.
- (3) Hanania, E. G., Kavanagh, J., Hortobagyi, G., Giles, R. E., Champlin, R., and Deisseroth, A. B. (1995) Recent advances in the application of gene therapy to human disease. *Am. J. Med.* 99, 537–552.
- (4) Scanlon, K. J., Ohta, Y., Ishida, H., Kijima, H., Ohkawa, T., Kaminski, A., Tsai, J., Horng, G., and Kashani-Sabet, M. (1995) Oligonucleotide-mediated modulation of mammalian gene expression. *FASEB J.* 9, 1288–1296.
- (5) Wagner, R. W. (1994) Gene inhibition using antisense oligodeoxynucleotides. *Nature* 372, 333–335.
- (6) Gao, X., and Huang, L. (1995) Cationic liposome-mediated gene transfer. *Gene Ther.* 2, 710–722.
- (7) Fraley, R., Straubinger, R. M., Rule, G., Spinger, E. L., and Papahadjopoulos, D. (1981) Liposome-mediated delivery of deoxyribonucleic acid to cells: enhanced efficiency of delivery related to lipid composition and incubation conditions. *Biochemistry* 20, 6978–6987.
- (8) Kabanov, A. V., and Kabanov, V. A. (1994) DNA complexes with polycations for the delivery of genetic material into cells. *Bioconjugate Chem.* 6, 7–19.
- (9) Cortesi, R., Esposito, E., Menegatti, E., Gambari, R., and Nastruzzi, C. (1994) Gelatin microspheres as a new approach for the controlled delivery of synthetic oligonucleotides and PCR-generated DNA fragments. *Int. J. Pharm.* 105, 181–186.

- (10) Alexakis, T., Boadi, D. K., Quong, D., Groboillot, A., O'Neill, I., Poncelet, D., and Neufeld, R. J. (1995) Microencapsulation of DNA within alginate microspheres and crosslinked chitosan membranes for in vivo application. *Appl. Biochem. Biotechnol.* **50**, 93–106.
- (11) Chavany, C., Doan, T. L., Couvreur, P., Puisieux, F., and Hélène, C. (1992) Polyalkylcyanoacrylate nanoparticles as polymeric carriers for antisense oligonucleotides. *Pharm. Res.* **9**, 441–449.
- (12) Alexakis, T., Boadi, K., Quong, D., Groboillot, A., and Washington, C. (1990) Drug release from microdisperse systems: a critical review. *Int. J. Pharm.* **58**, 1–12.
- (13) Hutchinson, F. G., and Furr, B. J. A. (1990) Biodegradable polymer system for sustained release of polypeptide. *J. Controlled Release* **13**, 279–294.
- (14) Okada, H., Heya, T., Ogawa, Y., and Shimamoto, T. (1987) One-month release injectable microcapsules of luteinizing hormone-releasing hormone agonist (Leuprolide acetate) for treating experimental endometriosis in rats. *J. Pharm. Exp. Ther.* **244**, 744–750.
- (15) Bertling, W. M., Gareis, M., Paspaleeva, V., Zimmer, A., Kreuter, J., Nürnberg, E., and Harrer, P. (1991) Use of liposomes, viral capsids, and nanoparticles as DNA carriers. *Biotechnol. Appl. Biochem.* **13**, 390–405.
- (16) Chavany, C., Saison-Behmoaras, T., Doan, T. L., Puisieux, F., Couvreur, P., and Hélène, C. (1994) Adsorption of oligonucleotides onto polyisohexylcyanoacrylate nanoparticles protects them against nucleases and increases their cellular uptake. *Pharm. Res.* **11**, 1370–1378.
- (17) Godard, G., Boutorine, A. S., Saison-Behmoaras, E., and Hélène, C. (1995) Antisense effects of cholesterol-oligonucleotide conjugates associated with poly(alkylcyanoacrylate) nanoparticles. *Eur. J. Biochem.* **232**, 404–410.
- (18) Ashwell, G., and Harford, J. (1982) Carbohydrate-specific receptors of the liver. *Annu. Rev. Biochem.* **51**, 531–554.
- (19) Walz, G., Aruffo, A., Kolanus, W., Bevilacqua, M., and Seed, B. (1990) Recognition by ELAM-1 of the sialyl-Lex determinant on myeloid and tumor cells. *Science* **250**, 1132–1135.
- (20) Phillips, M. L., Nudelman, E., Gaeeta, F. C. A., Perez, M., Singhal, A. K., Hakomori, S., and Paulson, J. C. (1990) ELAM-1 mediates cell adhesion by recognition of a carbohydrate ligand, sialyl-Le^x. *Science* **250**, 1130–1132.
- (21) Smedsrød, B., Pertoft, H., Gustafson, S., and Laurent, T. C. (1990) Scavenger functions of the liver endothelial cell. *Biochem. J.* **266**, 313–327.
- (22) Kolb, H., Vogt, D., Herbertz, L., Corfield, A., Schauer, R., and Schlepper-Schäfer, J. (1980) The galactose-specific lectins on rat hepatocytes and Kupffer cells have identical binding characteristics. *Hoppe-Seyler's Z. Physiol. Chem.* **361**, 1747–1750.
- (23) Haensler, J., and Szoka, F. C., Jr. (1993) Synthesis and characterization of a trigalactosylated bisacridine compound to target DNA to hepatocytes. *Bioconjugate Chem.* **4**, 85–93.
- (24) Plank, C., Zatloukal, K., Cotten, M., Mechtler, K., and Wagner, E. (1992) Gene transfer into hepatocytes using asialoglycoprotein receptor mediated endocytosis of DNA complexed with an artificial tetra-antennary galactose ligand. *Bioconjugate Chem.* **3**, 533–539.
- (25) Wu, G. Y., Wilson, J. M., Shalaby, F., Grossman, M., Shafritz, D. A., and Wu, C. H. (1991) Receptor-mediated gene delivery in vivo. *J. Biol. Chem.* **266**, 14338–14342.
- (26) Maruyama, A., Ishihara, T., Adachi, N., and Akaike, T. (1994) Preparation of nanoparticles bearing high density carbohydrate chains using carbohydrate-carrying polymers as emulsifier. *Biomaterials* **15**, 1035–1042.
- (27) Oku, N., Namba, Y., and Okada, S. (1992) Tumor accumulation of novel RES-avoiding liposomes. *Biochim. Biophys. Acta* **1126**, 255–260.
- (28) Gabizon, A., and Papahadjopoulos, D. (1988) Liposome formulations with prolonged circulation time in blood and enhanced uptake by tumors. *Proc. Natl. Acad. Sci. U.S.A.* **85**, 6949–6953.
- (29) Allen, T. M., Hansen, C., and Rutledge, J. (1988) Liposomes with prolonged circulation times: factors affecting uptake by reticuloendothelial and other tissues. *Biochim. Biophys. Acta* **981**, 27–35.
- (30) Maruyama, K., Okamoto, A., Ishida, O., Kojima, S., Suginaka, A., Huang, L., and Iwatsuru, M. (1994) Biodistribution and antitumor effect of adriamycin encapsulated in long-circulating liposomes containing amphipathic polyethylene glycol or ganglioside G-M1. *J. Liposome Res.* **4**, 701–723.
- (31) Yokoyama, M., Okano, T., Sakurai, Y., Ekimoto, H., Shibasaki, C., and Kataoka, K. (1991) Toxicity and antitumor activity against solid tumors of micelle-forming polymeric anticancer drug and its extremely long circulation in blood. *Cancer Res.* **51**, 3229–3236.
- (32) Verrecchia, T., Spenlehauer, G., Bazile, D. V., Murry-Brelier, A., Archimbaud, Y., and Veillard, M. (1994) Non-stealth (poly(lactic acid/albumin)) and stealth (poly(lactic acid-polyethylene glycol)) nanoparticles as injectable drug carriers. *J. Controlled Release* **36**, 49–61.
- (33) Gref, R., Minamitake, Y., Peracchia, T. M., Trubetskoy, V., Torchilin, V., and Langer, R. (1994) Biodegradable long-circulating polymeric nanospheres. *Science* **263**, 1600–1603.
- (34) Maruyama, A., Katoh, M., Ishihara, T., and Akaike, T. (1997) Comb-type polycations effectively stabilize DNA triplex. *Bioconjugate Chem.* **8**, 3–6.
- (35) Martinez-Fong, D., Mullersman, J. E., Purchio, A. F., Armendariz-Borunda, J., and Martinez-Hernandez, A. (1994) Nonenzymatic glycosylation of poly-L-lysine: A new tool for targeted gene delivery. *Hepatology* **20**, 1602–1608.
- (36) Cho, C. S., Jeong, Y. I., Ishihara, T., Park, J. U., Park, K. H., Maruyama, A., and Akaike, T. (1997) Simple preparation of nanoparticles coated with carbohydrate-carrying polymers. *Biomaterials* **18**, 323–326.
- (37) Fujimoto, K., Inoue, H., and Ikada, Y. (1993) Protein adsorption and platelet adhesion onto polyurethane grafted with methoxy-poly(ethylene glycol) methacrylate by plasma technique. *J. Biomed. Mater. Res.* **27**, 1559–1567.
- (38) Moghimi, S. M., Porter, C. J., Illum, L., and Davis, S. S. (1991) Non-phagocytic uptake of intravenously injected microspheres in rat spleen: Influence of particle size and hydrophilic coating. *Biochem. Biophys. Res. Commun.* **177**, 861–866.
- (39) Ohshima, H. (1993) Electrophoretic mobility of soft particles. *J. Colloid Interface Sci.* **130**, 281–282.
- (40) Ohshima, H., and Kondo, T. (1989) Approximate analytic expression for the electrophoretic mobility of colloidal particles with surface-charge layers. *J. Colloid Interface Sci.* **163**, 474–483.
- (41) Stolnik, S., Davies, M. C., Illum, L., Davis, S. S., Boustta, M., and Vert, M. (1994) The preparation of sub-200 nm biodegradable colloidal particles from poly(β -malic acid-co-benzyl malate) copolymers and their surface modification with poloxamer and poloxamine surfactants. *J. Controlled Release* **30**, 57–67.
- (42) Milner, S. T. (1991) Polymer brushes. *Science* **251**, 905–914.
- (43) Watanabe, H., and Tirrell, M. (1993) Measurement of Forces in symmetric and asymmetric interactions between diblock copolymer layers adsorbed on mica. *Macromolecules* **26**, 6455–6466.
- (44) Maruyama, A., Watanabe, H., Ferdous, A., Katoh, M., Ishihara, T., and Akaike, T. (1997) Characterization of inter polyelectrolyte complex between double stranded DNA and polylysine comb-type copolymer having hydrophilic side chains. *Bioconjugate Chem.* (submitted for publication).

BC9701048

Synthesis of Green Fluorescent Protein–Ricin and Monitoring of Its Intracellular Trafficking

Edward Tagge,[†] Billie Harris,[†] Chris Burbage,[‡] Philip Hall,[§] Joseph Vesely,^{||} Mark Willingham,^{||} and Arthur Frankel^{*‡}

Departments of Surgery, Pathology and Laboratory Medicine, Pharmacy, and Medicine, Medical University of South Carolina, Charleston, South Carolina 29425. Received May 8, 1997; Revised Manuscript Received July 23, 1997[©]

We performed genetic engineering to fuse enhanced green fluorescent protein (EGFP) to the N terminus of RTA, expressed the fusion protein in *Escherichia coli*, purified and reassociated EGFP–RTA with plant RTB, and purified EGFP–ricin by size exclusion HPLC. The fusion heterodimer was able to bind galactosides, intoxicate cells, and show strong fluorescence. Mammalian cells incubated with EGFP–ricin showed strong cell surface fluorescence at 4 °C and, on incubation at 37 °C, distributed initially to endosomes and then to Golgi vesicles. Variable sensitivity of mammalian cells to ricin and ricin fusion proteins may be due in part to different patterns of intracellular routing. Cells were incubated with ricin or EGFP–ricin, and inhibition of protein synthesis was measured. Human hepatocellular carcinoma Hep3B cells were 10-fold more sensitive to ricin and 85-fold more sensitive to EGFP–ricin than human epidermoid carcinoma KB cells. Epifluorescence microscopy of cells incubated with EGFP–ricin showed greater localization of the fluorescence signal in the Golgi compartments in Hep3B cells than in KB cells. These data support a model requiring a Golgi-dependent step in cell intoxication by ricin. The work further identifies the usefulness of green fluorescent protein fusions in the study of retrograde transport of internalized peptides.

INTRODUCTION

Ricin from the *Ricinus communis* plant is a frequently used component in antibody–toxin conjugates for therapy of cancer and autoimmune diseases. Thus, knowledge of its mechanism of action is important both for understanding structure–function relationships of toxic lectins and for improved design of human therapeutics.

The first necessary step in ricin intoxication is cell surface binding to galactose-terminated oligosaccharides on glycoproteins and glycolipids (1). The second step involves internalization from the cell surface to intracellular compartments. This step is energy-dependent (2) and leads to toxin localization in a compartment which avoids neutralization by anti-toxin antibodies added to the medium (3). Mutant cells resistant to ricin have been isolated with reduced internalization (4). Morphologic studies using ricin labeled with gold, ferritin, and horseradish peroxidase demonstrated endocytosis of ricin from clathrin-coated pits into endocytic vesicles (5–7).

The third step in ricin intoxication is transport to the Golgi. This hypothesis is supported by several experiments. Immunoelectron microscopy of cultured cells exposed to ricin showed uptake sequentially in endosomes and then the trans-Golgi network (8). Hybridoma cells producing anti-RTB antibodies were not intoxicated by ricin, suggesting neutralization in the trans-Golgi network, a major membrane compartment shared by the two pathways. Finally, at 19 °C, ricin failed to reach the

Golgi and cell death was not observed (9). The fourth intoxication step involves post-Golgi sorting of ricin to a translocation-competent compartment. Brefeldin A blocks ricin toxicity but does not alter trafficking of ricin to the trans-Golgi network (10), suggesting a critical distal compartment. After addition of the ER retention signal KDEL to the C terminus of RTA, both RTA and ricin cytotoxicity were markedly enhanced (11–13), supporting the ER as the distal translocation-competent organelle. Transient expression of transdominant mutants of GTPases involved in vesicular traffic followed by ricin exposure showed reduced intoxication when the GTPases which regulate ER–Golgi traffic (Rab1, ARF1, and Sar1) were modified but no change in ricin cytotoxicity when endosome-related GTPases (dynamin element 1, Rab5, and Rab9) were mutated (14). These results suggest that ricin reaches the Golgi system and yet must proceed further to the ER to produce cell toxicity. The penultimate step in intoxication is membrane translocation. This step requires reduction of the intersubunit disulfide bond (15) and unfolding of RTA (16), but little else is known regarding the molecular mechanism. The final step takes place in the cytosol where RTA catalytically inactivates protein synthesis by hydrolysis of a highly conserved adenosine at the elongation factor binding site on the 60S ribosome (17).

Variable sensitivity of tumor cell lines and fresh tumor cells to ricin and ricin-based targeted molecules may in part be due to altered intracellular trafficking. Measurements of premature transport of toxins to lysosomes with subsequent degradation and lack of cytotoxicity have been observed with anti-CD2–RTA, anti-CD3–RTA, and anti-CD5–RTA conjugates (18–20). In each case, the assays were indirect and detected release of free label in the media after incubation of cells with radiolabeled conjugate or increased label in lysosome-enriched sucrose gradient fractions of cell extracts. We sought a labeling method which would permit live cell measurements and not damage the ligand–receptor function of the molecule.

* Address correspondence to this author at the following address: Hollings Cancer Center, Rm 311, 86 Jonathan Lucas St., Charleston, SC 29425. Telephone: 803-792-1450. Fax: 803-792-3200.

[†] Department of Surgery.

[‡] Department of Medicine.

[§] Department of Pharmacy.

^{||} Department of Pathology and Laboratory Medicine.

[©] Abstract published in *Advance ACS Abstracts*, September 1, 1997.

Green fluorescent protein appeared to offer the ideal properties. Bioluminescent cnidaria, including *Aequorea victoria*, contain green fluorescent proteins (GFPs) which absorb radiative and nonradiative energy from the photoprotein aequorin and emit green light (21). GFP cDNA has been cloned and expressed in prokaryotic and eukaryotic cells and retains the fluorescent properties of the original compound (22). Recently, the three-dimensional structure of GFP has been solved (23), and chromophore mutants with increased fluorescence-enhanced green fluorescent proteins (EGFPs) have been identified (24). GFP has been fused to several proteins and expressed in mammalian cells (25, 26). Intracellular distributions of the fusion molecules have been measured and depended upon signal sequences in the mammalian peptide. To date, no investigators have reported attachment of GFPs to external proteins which undergo endocytosis and intracellular routing.

To obtain more accurate quantitative information on ricin intracellular trafficking, we now report the cloning, expression, and reassociation of an EGFP-ricin molecule and its chemical and biological properties. Our findings support the hypothesis that ricin must be routed to the Golgi network. In addition, the experiments document the ability of EGFP to serve as a tool for measuring the intracellular fate of imported molecules.

EXPERIMENTAL PROCEDURES

Construction of the Transfer Vector Encoding EGFP-RTA. The pEGFP-1 plasmid containing DNA encoding EGFP was obtained from Clontech Laboratories (Palo Alto, CA) and propagated in *Escherichia coli* INV α F' cells (Invitrogen, San Diego, CA). The plasmid was then prepared using the alkaline lysis method and cesium chloride density gradient centrifugation, and a *Bam*HI DNA cassette encoding EGFP was amplified by polymerase chain reaction (PCR) on a thermal cycler with Taq polymerase following the recommendations of the supplier (Perkin-Elmer, Foster City, CA). Oligonucleotides were synthesized on an Applied Biosystems 380B DNA synthesizer and desalted with butan-1-ol. The 5'-oligonucleotide contained nine nonsense bases, a *Bam*HI site, and 18 bases from the coding sequence for the N terminus of the EGFP gene. The 3'-oligo contained nine nonsense bases, a *Bam*HI site, and the reverse noncoding strand sequence for two stop codons and the C-terminal amino acid residues of EGFP. The PCR product was subcloned into pCR2.1 (Invitrogen) again as suggested by the manufacturer. PCR2.1-EGFP DNA was restricted with *Bam*HI, and the EGFP fragment was purified by agarose gel electrophoresis and a Prep-A-Gene matrix (BioRad, Hercules, CA). A cesium chloride-purified preparation of the pGEX2T-RTA plasmid (13) was restricted with *Bam*HI, treated with calf intestinal phosphatase (Boehringer Mannheim, Indianapolis, IN), purified with a Prep-A-Gene matrix, ligated with the EGFP DNA, and used to transform INV α F' cells. Transformants were analyzed by restriction enzyme digestions with *Bam*HI, *Eco*RI, and *Nco*I. The pGEX2T-EGFP-RTA plasmid was purified from the appropriate transformant and dideoxy sequenced using the Sequenase kit (U.S. Biochemicals, Cleveland, OH).

Expression of GST-EGFP-RTA. The pGEX2T-EGFP-RTA construct was transformed into JM105 *E. coli* cells (Pharmacia Biotech, Piscataway, NJ), and 1 L cultures were grown at 30 °C with 225 rpm in 2XYT broth containing 100 μ g/mL ampicillin induced with 1 mM IPTG (Gibco BRL, Grand Island, NY). After 4 h, the cells were harvested by centrifugation at 5000g for 10 min at 4 °C.

Purification of the EGFP-RTA Protein. Purification was accomplished by affinity chromatography utilizing a glutathione-Sepharose matrix and thrombin cleavage. Briefly, cells were resuspended in 50 mL of phosphate-buffered saline (PBS), homogenized three strokes in a glass homogenizer, sonicated for 5 min total in 30 s bursts, and adjusted to 1% Triton X-100. After gentle mixing on ice for 30 min, and centrifugation at 12000g for 10 min at 4 °C, 1 mL of a 50% slurry of glutathione-Sepharose 4B (Pharmacia) was added and incubation continued for 30 min. This suspension was centrifuged at 500g for 5 min and washed three times with 5 mL of PBS. The matrix was then resuspended in 475 μ L of PBS and 25 μ L of thrombin (1 IU/mL) added. After overnight cleavage at room temperature, the solution was centrifuged at 500g for 5 min and the supernatant saved.

Characterization of EGFP-RTA. The protein concentration was determined by optical density based on absorbance at 280 nm (OD of 1 mg/mL = 0.77) and a BCA (Pierce, Rockford, IL) protein assay. Tubes containing various stages of purification were subjected to imaging via a 302 nm UV transilluminator for fluorescence.

Aliquots of EGFP-RTA at various stages of purification and prestained low-molecular mass standards were subjected to 15% reducing SDS-PAGE, stained with Coomassie Blue R-250 (Sigma, St. Louis, MO), and scanned on an IBAS automatic image analysis system (Kontron, Germany). Additional aliquots of EGFP-RTA were run on 15% reducing SDS-PAGE and proteins transferred to nitrocellulose, blocked with 10% Carnation's nonfat dry milk/0.1% bovine serum albumin (BSA)/0.1% Tween20, washed with PBS plus 0.05% Tween 20, and reacted with either 1:400 rabbit antibody/ricin (Sigma) or 1:1000 rabbit antibody/EGFP (Clontech). The blots were rewashed, incubated with alkaline phosphatase-conjugated goat anti-(rabbit IgG), washed again, and developed with the Vectastain alkaline phosphatase kit (Vector Laboratories, Burlingame, CA) as described the manufacturer's recommendations.

The enzymatic activity of EGFP-RTA was quantitated by an *in vitro* protein synthesis inhibition assay. Dilutions of plant RTA or EGFP-RTA were added to a rabbit reticulocyte lysate protein translation mixture (Promega, Madison, WI) with [3 H]leucine (133 Ci/mmol, Du Pont, Wilmington, DE) and the brome mosaic virus mRNA model substrate as specified by the manufacturer. The mixtures were incubated at 4 °C for 30 min and then at 30 °C for 30 min. Protein translation was monitored by following [3 H]leucine incorporation into acid-precipitable product according to the manufacturer's instructions. A 50% inhibition of incorporation (ID₅₀) was determined for each protein.

Reassociation of EGFP-RTA with Plant RTB. EGFP-RTA (400 μ g) was mixed with a 3-fold molar excess of deglycosylated plant RTB (1.2 mg, Inland Laboratories, Austin, TX) in a total volume of 500 μ L of PBS. The excess RTB was added to ensure heterodimer formation of EGFP-RTA. After gentle rocking for 12 h at room temperature under oxidizing conditions that should lead to interchain disulfide bridge formation, aliquots were analyzed to determine heterodimer concentration by a modified ricin ELISA (27). Briefly, wells of an EIA plate (Costar, Cambridge, MA) were coated with 10 μ g/mL P2 anti-RTB monoclonal antibody in 100 μ L of PBS overnight at 4 °C. The wells were washed with PBS plus 0.1% Tween 20, blocked with 3% BSA in PBS plus 0.02% sodium azide, rewashed, incubated with 12 dilutions of plant ricin (Inland Laboratories) or reassociated heterodimers, washed again, incubated with biotin-

conjugated α BR12 anti-RTA monoclonal antibody at 5 μ g/mL in PBS/0.5% BSA/0.1% sodium azide, washed, incubated with alkaline phosphatase-conjugated streptavidin (Sigma) at 1:1000 in PBS/0.5% BSA/0.1% sodium azide, washed again, and developed with *p*-nitrophenyl phosphate (Sigma) at 1 mg/mL in 50 mM diethanolamine at pH 9.8. Absorbance at 405 nm was read on a microplate reader.

Excess RTB was removed from the EGFP–RTA–RTB by size exclusion chromatography on a Bio-Sil SEC 125 HPLC column with a Bio-Sil SEC Guard column (BioRad) on a Waters 510 pump and 486 absorbance detector using the PBS column eluant. Column fractions were stored at 4 °C.

Characterization of EGFP–Ricin. The protein concentration was again determined by absorbance at 280 nm and the BCA protein assay. Aliquots and prestained low-molecular mass protein standards were run on a nonreducing 15% SDS–PAGE and either stained with Coomassie blue R-250 or transferred to immunoblots for reaction with anti-ricin and anti-EGFP antibodies. Immunoblots were performed as described above. The nonreducing SDS–PAGE measured disulfide bond formation between EGFP–RTA and RTB. An asialofetuin ELISA was performed to measure the galactoside avidity of the heterodimer as previously described (27).

Cell Cytotoxicity Assays. KB human epidermoid carcinoma cells and Hep3B human hepatocellular carcinoma cells were obtained from the American Type Culture Collection (Rockville, MD) and grown in RPMI1640 with 10% fetal bovine serum (Irvine Scientific, Irvine, CA). Cells were trypsinized and seeded at 1.5×10^4 cells per well in 100 μ L of media in 96-well flat-bottomed plates. The cells adhered to plates after several hours of incubation. Fifty microliters of 12 different concentrations of castor bean ricin or EGFP–ricin was added in the same medium, and the cells were incubated at 37 °C in 5% CO₂ for 48 h. [³H]Leucine, (0.5 μ Ci per well, 133 Ci/mmol, Du Pont) in 50 μ L of the same medium was added and incubation continued for 4 h. Cells were then harvested with a Skatron cell harvester onto glass fiber mats, dried, mixed with 3 mL of liquid scintillation fluid, and counted in an LKB-Wallac liquid scintillation counter gated for ³H. Cells cultured with medium alone served as controls. All assays were performed in triplicate. The IC₅₀ was the concentration of protein which inhibited protein synthesis by 50% compared to control.

Cell Fluorescence Assays. Corning 35 mm dishes were seeded with 10^5 KB or Hep3B cells and the cells grown in RPMI1640 plus 10% fetal bovine serum at 37 °C in 5% CO₂ until 70% confluence. The medium was then aspirated, and dishes were blocked for 15 min with 1% BSA in PBS at 4 °C. Dishes were then incubated with 1% BSA in PBS alone or with EGFP–ricin at 10 μ g/mL in 1% BSA in PBS at 4 °C for 30 min, washed three times with PBS, fixed with 3.7% formaldehyde in PBS, washed and permeabilized with inclusion of 0.1% saponin in all subsequent incubations, incubated with 1:500 wheat germ agglutinin conjugated to rhodamine (WGA–TRITC, Sigma) in PBS/BSA/saponin, rewashed, mounted under a no. 1 coverslip in glycerol/PBS (90:10), and examined using a Zeiss Axioplan epifluorescence microscope with the fluorescein channel and Texas Red channel. Identical dishes were heated to 37 °C after the 4 °C incubation with EGFP–ricin and, after 30 or 60 min, washed three times with PBS, fixed in 3.7% formaldehyde, rewashed in saponin-containing buffer, incubated with or without WGA–TRITC in saponin/BSA/PBS,

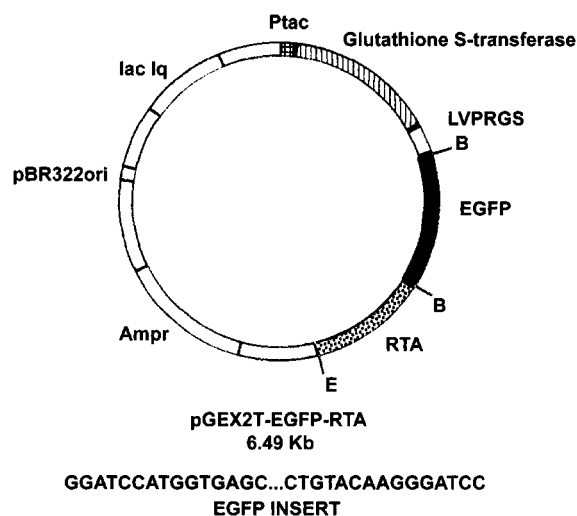


Figure 1. Schematic diagram of the pGEX2T–EGFP–RTA expression plasmid. In pGEX2T–EGFP–RTA, the coding region of GST–EGFP–RTA is under the control of the Ptac promoter (hatched box) and is followed by codons encoding glutathione S-transferase (striped box), a thrombin cleavable linker (LVPRGS) with a *Bam*HI site (white box), EGFP (black box), and RTA (dotted box). Amp^r denotes the β -lactamase gene. pBR322 ori is the high-copy number bacterial replicon. lacIq stands for the lac repressor gene. B = *Bam*HI. E = *Eco*RI. arrow = thrombin cleavage site. The 729 bp EGFP gene and the 810 bp RTA gene add to the 4948 bp pGEX2T vector to produce a total size of 6.487 kb.

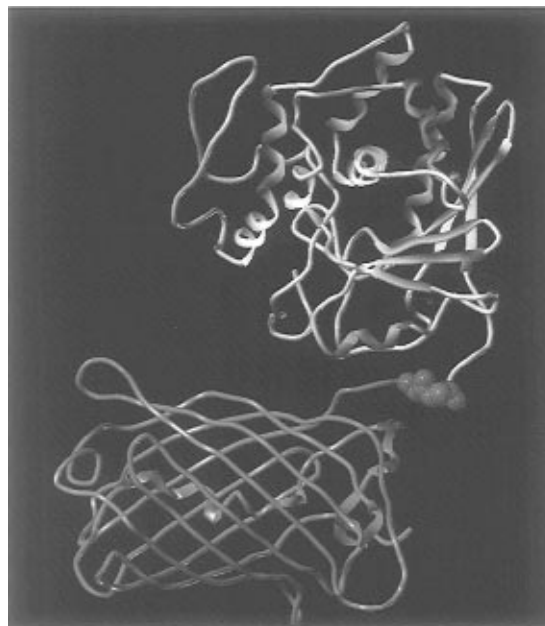


Figure 2. Model of EGFP–RTA showing α -carbon backbones of EGFP (bluegreen), junction amino acid residues of GS (purple), and RTA (yellow). All molecules depicted are based on coordinates read from Brookhaven Protein Data Bank files. The PDB abbreviations are 2aa1-ricin and 1-gfp. The MUSC BioMolecular Computing Resource SYBYL molecular modeling software was used to render the protein chains as shaded ribbons derived from cubic spline fits to the α -carbon backbone.

rewashed, mounted under glycerol/PBS, and examined for epifluorescence.

RESULTS

Construction of the EGFP–RTA-Encoding Bacterial Expression Plasmid. The EGFP-coding region from pEGFP-1 was modified to create a *Bam*HI cassette with the correct reading frame and subcloned in pGEX2T–

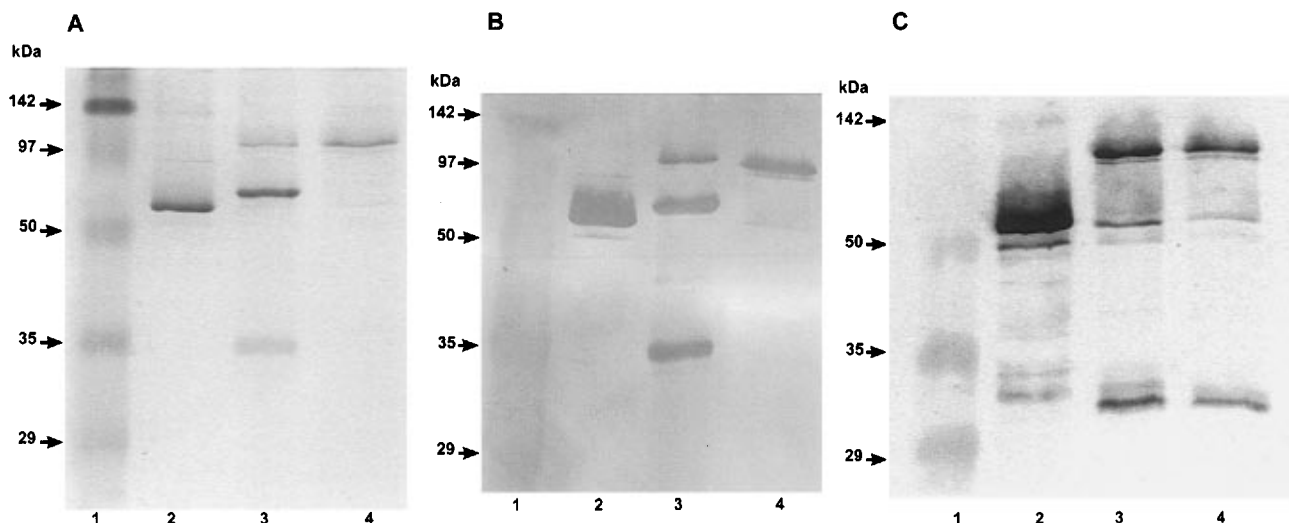


Figure 3. Nonreducing 15% SDS-PAGE of EGFP-RTA, an EGFP-RTA and RTB mixture, and purified EGFP-ricin. (A) Coomassie-stained gel. (B) Immunoblot using rabbit anti-ricin antibody. (C) Immunoblot using rabbit anti-EGFP antibody: lane 1, low-molecular mass prestained BioRad protein standards; lane 2, EGFP-RTA; lane 3, mixture of EGFP-RTA and plant RTB after 24 h incubation at room temperature; and lane 4, post-HPLC-purified EGFP-ricin. Bands are observed at 55 kDa (EGFP-RTA), 34 kDa (RTB), 65 kDa (RTB homodimers), and 90 kDa (EGFP-ricin). Arrows point to protein standards and show molecular masses in kilodaltons.

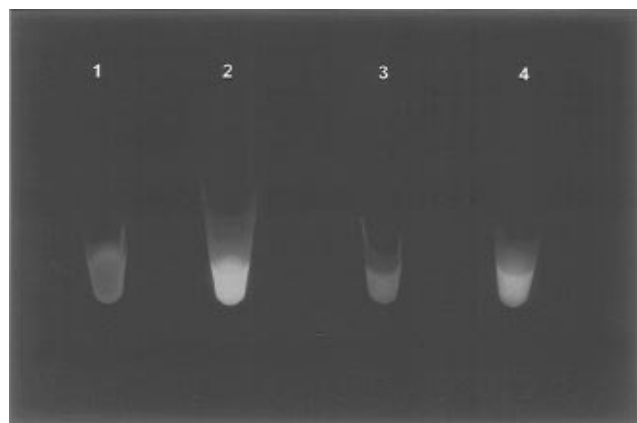


Figure 4. Fluorescence of EGFP-RTA. Eppendorf tubes (1.5 mL) containing 0.5 mL of various fractions with EGFP-RTA illuminated with a 302 nm UV light: tube number 1, induced *E. coli* pellet postsonication; tube number 2, glutathione-Sepharose matrix after binding-induced bacterial extract; tube number 3, eluant from matrix prior to thrombin cleavage; and tube number 4, thrombin-cleaved eluant containing EGFP-RTA.

RTA (Figure 1). The final construction was verified by sequencing.

Production of EGFP-RTA. Yields of 0.375 ± 0.025 mg/L of culture medium) were obtained on the basis of absorbance measurements and Bradford assays. The predicted folding of the molecule based on published coordinates in the Brookhaven Protein Data Bank is shown in Figure 2.

Characterization of EGFP-RTA. SDS-PAGE followed by Coomassie staining showed a single band of 55 kDa (Figure 3A). On the basis of densitometry of the Coomassie-stained gel, the purity was in excess of 90%. Immunoblots with rabbit anti-ricin and rabbit anti-EGFP showed similar reactivity (Figure 3B,C). Green light emission after UV illumination at 302 nm was observed in both the GST fusion and the final EGFP-RTA preparation (Figure 4).

The enzymatic activity of the EGFP-RTA was indistinguishable from that of previous preparations of bacterial RTA and plant RTA. All three proteins inhibited *in*

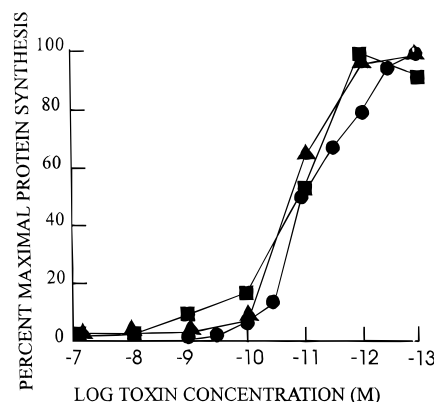


Figure 5. In vitro rabbit reticulocyte lysate protein synthesis inhibition assay. The assay was as described in text. Each experiment was performed in triplicate: (●) plant RTA, (▲) bacterial recombinant RTA, and (■) EGFP-RTA. $ID_{50} = 2 \times 10^{-11}$ M for each.

vitro protein synthesis of rabbit reticulocyte lysates with ID_{50} s of 2×10^{-11} M (Figure 5).

Reassociation of the Recombinant Protein with Plant RTB. After reassociation with a 3-fold molar excess of plant RTB, $31 \pm 6\%$ of the EGFP-RTA formed heterodimers, based on ricin ELISA and yields from HPLC. As shown in lane 3 of Figure 3C, no EGFP-RTA remained unreassociated after oxidation with excess RTB.

Properties of EGFP-Ricin. Size exclusion chromatography of the EGFP-RTA-RTB plus RTB mixture revealed a single fraction eluting at 90 kDa with green fluorescence (Figure 6). SDS-PAGE followed by Coomassie staining and immunoblots revealed a single band at 90 kDa which reacted with both anti-EGFP antibodies and anti-ricin antibodies (Figure 3).

The heterodimer bound asialofetuin with that same avidity as plant ricin ($K_{ds} = 10^{-9}$ M). The EGFP-ricin was cytotoxic to mammalian cells with IC_{50} s of 6×10^{-11} M on KB cells and 7×10^{-13} M on Hep3B cells (Figure 7). Plant ricin had IC_{50} s of 5×10^{-13} and 5×10^{-14} M on KB and Hep3B cell lines, respectively. Thus, the fusion protein is approximately 10-fold less cytotoxic for Hep3B and 100-fold less cytotoxic for KB cells than ricin.

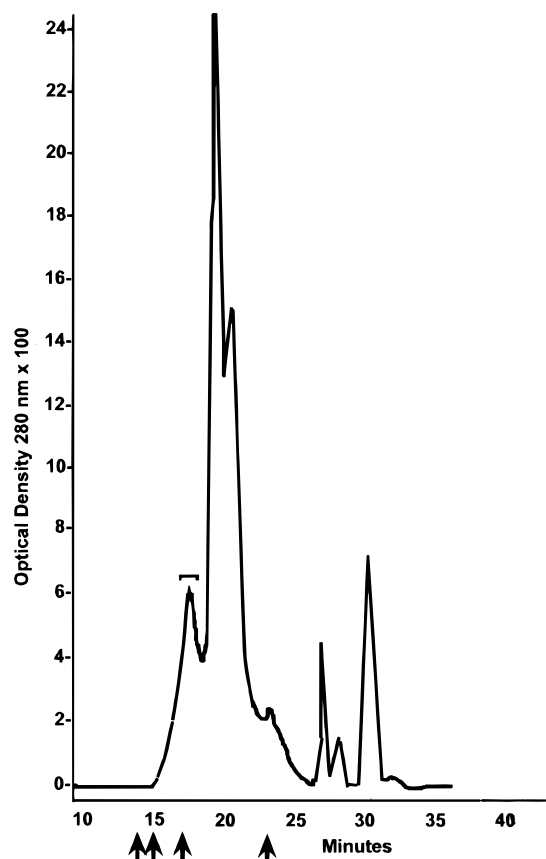


Figure 6. Elution profile from a HPLC Bio-sil SEC125 column with PBS elution. OD_{280} is on the y -axis, and the time for elution is in minutes on the x -axis. Elution times for BioRad gel filtration protein standards are shown as arrows, including thyroglobulin (670 kDa), bovine γ -globulin (158 kDa), chicken ovalbumin (44 kDa), and equine myoglobin (17 kDa). The pooled sample with fluorescence is shown in brackets. Delayed elution of EGFP-ricin and RTB fractions was observed.

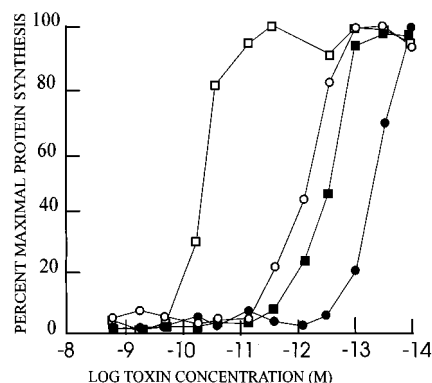


Figure 7. Cell cytotoxicity of ricin and EGFP-ricin. Cells were exposed at the dilutions indicated for 48 h at 37 °C in 5% CO_2 . Incorporation of [3H]leucine was assayed after a 4 h incubation and compared against untreated cell incorporation: (●) ricin on Hep3B cells, (■) EGFP-ricin on Hep3B cells, and (○) ricin on KB cells, (□) EGFP-ricin on KB cells.

Immunofluorescent Detection of EGFP-Ricin.

Cells incubated with EGFP-ricin at 4 °C showed diffuse plasma membrane fluorescence indicating surface localization (Figure 8). After the cells were warmed to 37 °C for 30 min, fluorescence on surface membranes decreased and an intracellular pattern of fluorescence was seen which was consistent with endosomes. After 1 h at 37 °C, EGFP-ricin was detected in both endosomes and in the Golgi network (Figure 8). Comparative studies were done with KB cells and Hep3B cells (Figure 9). After 1

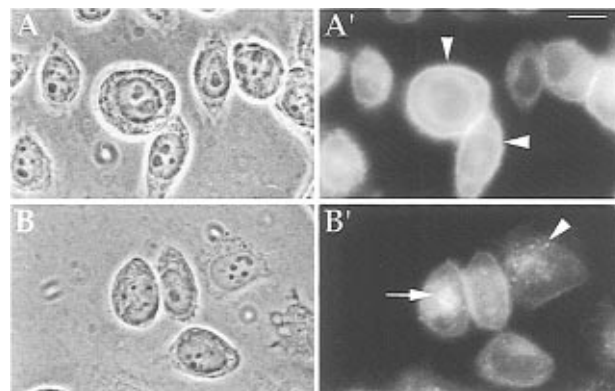


Figure 8. Fluorescence of the EGFP-ricin pathway in mammalian cells. KB cells were attached to tissue culture dishes, incubated with EGFP-ricin for varying times, fixed with 3.7% formaldehyde in PBS, and examined for fluorescence on the fluorescein channel. (A and A') Incubation at 4 °C for 30 min. (B and B') Incubation at 37 °C for 60 min. (A and B) Phase contrast. (A' and B') Fluorescein channel. The arrowhead in panel A' shows surface localization of fluorescence; the arrowhead in panel B' shows endosomal distribution, and the long arrow in panel B' shows Golgi localization. Magnification = 280 times; bar = 20 μm .

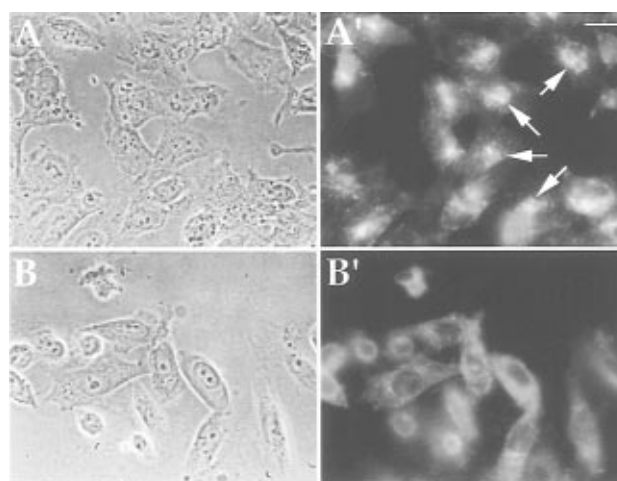


Figure 9. Fluorescence distribution of EGFP-ricin after 60 min of incubation at 37 °C in ricin-sensitive (Hep3B) and -resistant (KB) cell lines. (A and A') Hep3B. (B and B') KB. (A and B) Phase contrast. (A' and B') Fluorescence. Arrows = Golgi region fluorescence. Magnification = 202.5 times; bar = 25 μm .

h incubation of cells with EGFP-ricin at 37 °C, much more Golgi fluorescence was detected in Hep3B cells than in KB cells. Control experiments with wheat germ agglutinin conjugated to tetramethylrhodamine isothiocyanate (WGA-TRITC) confirmed colocalization with EGFP-ricin in Golgi organelles (Figure 10).

DISCUSSION

EGFP-RTA was produced in bacteria as a glutathione S -transferase (GST) fusion protein. The GST-EGFP-RTA lost fluorescence properties when bacteria were grown at 37 °C instead of at 30 °C. A similar loss in fluorescence was seen on lyophilization of EGFP-RTA-RTB. The sensitivity of the EGFP chromophore to temperature and high-ionic strength autooxidation has been previously reported (28).

The GST-EGFP-RTA produced in *E. coli* cells at 30 °C was soluble in the bacterial cell and readily released by sonication. After binding to glutathione-Sepharose

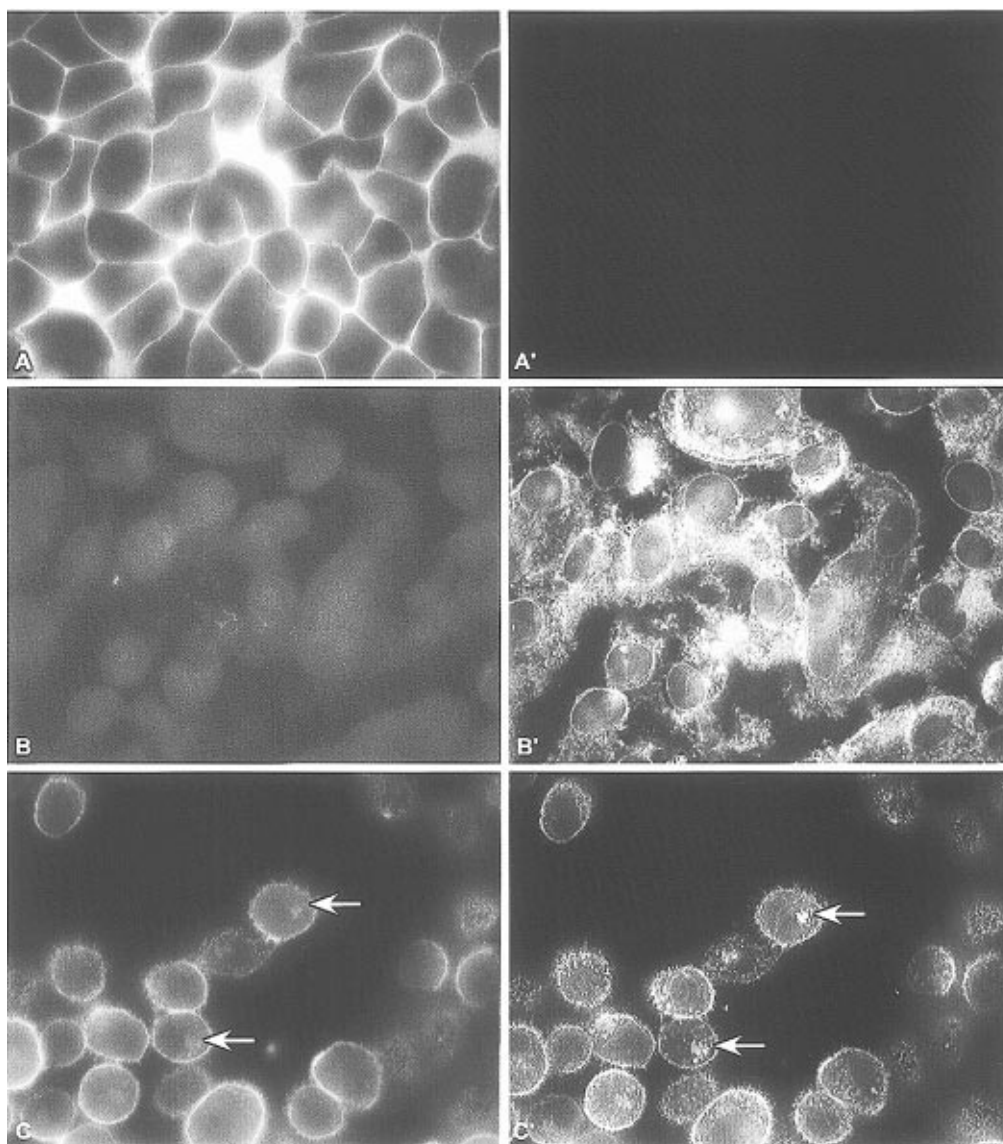


Figure 10. KB cells imaged in a Zeiss Axioplan epifluorescence microscope with a DAGE/MTI 100 integrating CCD with separate Texas Red and FITC filters (Chroma). Cells were magnified 100 times with a Plan-Neofluar NA1.3 objective lens. (A–C) FITC channel. (A'–C') Texas Red channel. Specimens were prepared as described in the text. Colocalization of EGFP–ricin and WGA–TRITC is shown with arrows. (A and A') At 4 °C, 30 min of incubation with EGFP–ricin at 10 $\mu\text{g/mL}$. (B and B') At 4 °C, 30 min of incubation with WGA–TRITC (1:500, Sigma). (C and C') At 37 °C, 20 min of incubation with EGFP–ricin and WGA–TRITC.

and cleavage with thrombin, reasonable yields of 0.35 mg/ (L culture medium) were obtained. These were 10-fold lower than that with RTA or RTA–KDEL reported previously with this expression vector and cell line (13), but well within the range of workable concentrations for purification and biological assays.

The observed extinction coefficient of 0.77 is similar to that of RTA alone (29) and suggests similar absorbance characteristics for the amino acid residues of EGFP and RTA at 280 nm.

The molecular mass of EGFP–RTA deduced from reducing SDS–PAGE was 55 kDa which is identical to that expected from the fusion of the 27 kDa Mr EGFP (22) and the 28 kDa Mr RTA peptides (13). The reactivity of the hybrid molecule with antibodies to EGFP and ricin suggests, epitopes for each domain are accessible on the molecular surface. This would be expected from the three-dimensional structure of each polypeptide. The C terminus of EGFP is freely mobile and remote from the β -barrel (23), and the N terminus of RTA also has significant mobility (30, see Figure 2). Thus, the individual domains should retain their native folding without steric hindrance from the other component. Further,

they should have multiple epitopes on each domain accessible to immunoglobulin in the solvent.

The ability of EGFP–RTA to reassociate with RTB was expected because of the extensive ionic and hydrophobic bonds in the RTA–RTB interface which promote reassociation and the disulfide bond between RTA Cys-259 and RTB Cys-4 (31). Our observation of 30% reassociation compares reasonably well with the 50% reassociation for plant RTA–RTB under identical conditions (32). The RTA amino acid residues which interact with RTB include H40, E41, Q182, Y183, L207, R234, R235, F240, I247, I249, P250, I251, I252, R258, C259, and A260, which are remote from the N terminus (31).

The purification of the EGFP–ricin by HPLC Bio-Sil SEC125 size exclusion chromatography yielded one-step removal of contaminating subunits with excellent recovery and maintenance of activities. We have observed a lack of detectable cell surface binding of EGFP–ricin in the presence of excess RTB ligand (unpublished observations); hence, the purification step was necessary for subsequent studies.

Cell fluorescence experiments required high EGFP–ricin concentrations (20 $\mu\text{g/mL}$ or 500 nM). This concen-

tration is 10-fold higher than the available receptor sites at 10⁷/cell and 40-fold above the K_d of 1 nM. Thus, a relatively weak signal was observed relative to immunofluorescence assays with ricin (27) where multiple antibody molecules each with several fluoresceins amplify the signal. Further, the fluorescein channel on the epifluorescence microscope (309 nm) is designed for fluorescein absorption and emission. We did not optimize the detection system for EGFP (489 nm).

The lower sensitivity of KB cells relative to Hep3B cells to ricin-based toxicity may be due to altered receptor density, altered intracellular compartmentalization, altered rates of degradation, different efficiencies of translocation, differing rates of cytosolic RTA metabolism, or varying ribosome inactivation. KB and Hep3B cells have different genetic backgrounds, and any of these events may, in principle, affect the sensitivity of these cells with respect to ricin. Nevertheless, our results of different accumulated concentrations of ricin in the Golgi network are consistent with observations from other laboratories. Antibody-RTA conjugates with similar cell surface binding to different epitopes on T cell antigens (CD2, CD3, and CD5) showed variable cytotoxicity with respect to T cells which was related to excessive lysosomal transport and degradation (18–20). Toxin routing in such cells should lead to reduced concentrations in the Golgi cisternae. Further, the reduced toxicity of ricin at 19 °C where Golgi uptake is blocked (9) and the reduced sensitivity of myeloid leukemia cell lines to antibody-RTA conjugates with increased lysosomal trafficking of ligands (33) are additional examples of the role of Golgi transport in ricin intoxication.

This report is the first demonstration of the use of EGFP in following the endocytic pathway of surface-bound polypeptide ligands.

ACKNOWLEDGMENT

We thank Starr Hazard for the molecular graphics analysis and James Nicholson for imaging analysis. This study was supported in part by NIH Grant R29CA74677 (E.T.).

LITERATURE CITED

- Baenziger, J., and Fiete, D. (1979) Structural determinants of Ricinus communis agglutinin and toxin specificity for oligosaccharides. *J. Biol. Chem.* 254, 9795–9799.
- Sandvig, K., and Olsnes, S. (1982) Entry of the toxic proteins abrin, modeccin, ricin and diphtheria toxin into cells. *J. Biol. Chem.* 257, 7504–7513.
- Olsnes, S., Refsnes, K., and Pihl, A. (1974) Mechanism of action of the toxic lectins abrin and ricin. *Nature* 249, 627–631.
- Ray, B., and Wu, H. (1982) Chinese hamster ovary cell mutants defective in the internalization of ricin. *Mol. Cell. Biol.* 2, 535–544.
- van Deurs, B., Pedersen, L., Sundan, A., Olsnes, S., and Sandvig, K. (1985) Receptor-mediated endocytosis of ricin-colloidal gold conjugate in Vero Cells. *Exp. Cell Res.* 159, 287–304.
- Nicholson, G. (1974) Ultrastructural analysis of toxin binding and entry into mammalian cells. *Nature* 251, 628–629.
- Gonatas, J., Stieber, A., Olsnes, S., and Gonatas, N. (1980) Pathways involved in fluid phase and adsorptive endocytosis in neuroblastoma. *J. Cell Biol.* 87, 579–588.
- van Deurs, B., Tonnessen, T., Petersen, O., Sandvig, K., and Olsnes, S. (1986) Routing of internalized ricin and ricin conjugates to the Golgi complex. *J. Cell Biol.* 102, 37–47.
- van Deurs, B., Petersen, O., Olsnes, S., and Sandvig, K. (1987) Delivery of internalized ricin from endosomes to cisternal Golgi elements is a discontinuous, temperature-sensitive process. *Exp. Cell Res.* 171, 137–152.
- Sandvig, K., Prydz, K., Hansen, S., and van Deurs, B. (1991) Ricin transport in Brefeldin A-treated cells: correlation between Golgi structure and toxic effect. *J. Cell Biol.* 115, 971–981.
- Wales, R., Chaddock, J., Roberts, L., and Lord, J. (1992) Addition of an ER retention signal to the ricin A chain increases the cytotoxicity of the holotoxin. *Exp. Cell Res.* 203, 1–4.
- Wales, R., Roberts, L., and Lord, J. (1993) Addition of an endoplasmic reticulum retrieval sequence to ricin A chain significantly increases its cytotoxicity to mammalian cells. *J. Biol. Chem.* 268, 23986–23990.
- Tagge, E., Chandler, J., Tang, B., Hong, W., Willingham, M., and Frankel, A. (1996) Cytotoxicity of KDEL-terminated ricin toxins correlates with distribution of the KDEL receptor in the Golgi. *J. Histochem. Cytochem.* 44, 159–165.
- Simpson, J., Dascher, C., Roberts, L., Lord, J., and Balch, W. (1995) Ricin cytotoxicity is sensitive to recycling between the endoplasmic reticulum and the Golgi complex. *J. Biol. Chem.* 270, 20078–20083.
- Masuh, Y., Kishida, K., Saito, M., Umemoto, N., and Hara, T. (1982) Importance of the antigen-binding valency and the nature of the cross-linking bond in ricin A-chain conjugates with antibody. *J. Biochem.* 91, 1583–1591.
- Argent, R., Roberts, L., Wales, R., Robertus, J., and Lord, J. (1994) Introduction of a disulfide bond into ricin A chain decreases the cytotoxicity of the ricin holotoxin. *J. Biol. Chem.* 269, 26705–26710.
- Szewczak, A., Moore, P., Chang, Y., and Wool, I. (1993) The conformation of the sarcin/ricin loop from 28S ribosomal RNA. *Proc. Natl. Acad. Sci. U.S.A.* 90, 9581–9585.
- Press, O., Vitetta, E., Farr, A., Hansen, J., and Martin, P. (1986) Evaluation of ricin A-chain immunotoxins directed against human T cells. *Cell. Immunol.* 102, 10–20.
- Oosterhout, Y., Preijers, F., Wessels, H., and Witte, T. (1992) Cytotoxicity of CD3-ricin A chain immunotoxins in relation to cellular uptake and degradation kinetics. *Cancer Res.* 52, 5921–5925.
- Manske, J., Buchsbaum, D., and Vallera, D. (1989) The role of ricin B chain in the intracellular trafficking of anti-CD5 immunotoxins. *J. Immunol.* 142, 1755–1766.
- Prasher, D. (1995) Using GFP to see the light. *Trends Genet.* 11, 320–323.
- Chalfie, M. (1995) Green fluorescent protein. *Photochem. Photobiol.* 62, 651–656.
- Ormo, M., Cubitt, A., Kallio, K., Gross, L., Tsien, R., Remington, S. (1996) Crystal structure of the Aequorea victoria green fluorescent protein. *Science* 273, 1392–1395.
- Cormack, B., Valdivia, R., and Falkow, S. (1996) FACS-optimized mutants of the green fluorescent protein (GFP). *Gene* 173, 33–38.
- Ludin, B., Doll, T., Meili, R., Kaech, S., and Matus, A. (1996) Application of novel vectors for GFP-tagging of proteins to study microtubule-associated proteins. *Gene* 173, 107–111.
- De Giorgi, F., Brini, M., Bastianutto, C., Marsault, R., Montero, M., Pizzo, P., Rossi, R., Rizzuto, R. (1996) Targeting aequorin and green fluorescent protein to intracellular organelles. *Gene* 173, 113–117.
- Frankel, A., Burbage, C., Fu, T., Tagge, E., Chandler, J., and Willingham, M. (1996) Ricin toxin contains at least three galactose-binding sites located in B chain subdomains 1 α , 1 β , and 2 γ . *Biochemistry* 35, 14747–14756.
- Heim, R., Prasher, D. C., and Tsien, R. Y. (1994) Wave-length mutations and posttranslational autooxidation of green fluorescent protein. *Proc. Natl. Acad. Sci. U.S.A.* 91, 12501–12504.

- (29) Olsnes, S., and Pihl, A. (1973) Different biological properties of the two constituent peptide chains of ricin, a toxic protein inhibiting protein synthesis. *Biochemistry* *12*, 3121–3126.
- (30) Bushuev, V., and Tonevitsky, A. (1989) High mobility of N-terminal parts of A and B subunits of ricin. *J. Biomol. Struct. Dynamics* *6*, 1061–1070.
- (31) Rutenber, E., and Robertus, J. (1991) Structure of ricin B-chain at 2.5 Ångstrom resolution. *Proteins* *10*, 260–269.
- (32) Frankel, A. E., Roberts, H., Afrin, L., Vesely, J., and Willingham, M. C. (1994) Expression of ricin B chain in *Spodoptera frugiperda*. *Biochem. J.* *303*, 787–794.
- (33) Engert, A., Brown, A., and Thorpe, P. (1991) Resistance of myeloid leukemia cell lines to ricin A-chain immunotoxins. *Leuk. Res.* *15*, 1079–1086.

BC9700749

Functionalized Tricarbocyanine Dyes as Near-Infrared Fluorescent Probes for Biomolecules

James H. Flanagan, Jr.,[†] Shaheer H. Khan,[‡] Steve Menchen,[‡] Steven A. Soper,[†] and Robert P. Hammer^{*,†}

Department of Chemistry, 232 Choppin Hall, Louisiana State University, Baton Rouge, Louisiana 70803-1804, and PE Applied Biosystems, 850 Lincoln Centre Drive, Foster City, California 94404. Received June 9, 1997; Revised Manuscript Received July 28, 1997[⊗]

The syntheses of three novel functionalized tricarbocyanine dyes are described. These dyes containing isothiocyanate and succinimidyl ester functional groups are reactive toward primary amines and can be used as fluorescent probes for biologically pertinent compounds such as amino acids and functionalized dideoxynucleotides. The absorption and fluorescence maxima occur in the near-IR region of the spectrum (770–810 nm). The succinimidyl ester proved to be very sensitive to hydrolysis and was generated *in situ* to label amino acids. The isothiocyanates were less susceptible to hydrolysis and were conjugated using organic modified [40% (v/v) acetonitrile] buffers to amino acids. A dye with an alkyl isothiocyanate moiety showed conjugation to amino-functionalized dideoxynucleotide triphosphates.

INTRODUCTION

There is increasing interest in the use of fluorescent probes as a means of detection of biological and organic compounds because of the sensitivity and ease of use compared to radiochemical methods. The dyes that are most commonly used fluoresce in the visible region of the spectrum where the background fluorescence of the matrix can cause considerable interference. In the near-IR region of the spectrum (750–1000 nm), very few molecules exhibit intrinsic fluorescence, and since Raman scattering shows a $1/\lambda^4$ dependence, the background can potentially be much lower in the near-IR than in the visible region. Thus, near-IR-fluorescence-based techniques have lower limits of detection relative to visible fluorescent methods, which has the added benefit of decreasing the quantity of reagents required for analysis (1). In addition, semiconductor devices such as diode lasers and avalanche diodes can be used as inexpensive excitation sources and detectors. The disadvantages are that there are very few near-IR chromophores with a functionality that can be used for the covalent labeling of analytes.

There are several factors which constitute an ideal fluorescent dye for the labeling of biomolecules. Generally, the fluorophore must be chemically and photochemically robust in solution and water-soluble, should have a large fluorescence quantum yield when bound to the analyte, must be specific for an analyte, and should minimize the interference with the analysis being performed (e.g. electrophoretic mobility shifts in capillary gel electrophoresis in DNA sequencing caused by differences in chromophore labels). Additionally, dyes that covalently bind to analytes of interest must possess reactive functional groups which are stable to long-term storage but also have high labeling efficiencies with minimal side reactions and produce a stable covalent

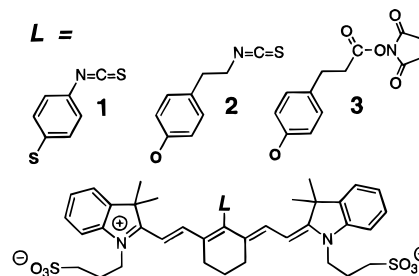


Figure 1. New water-soluble near-IR fluorescent dyes synthesized for covalent labeling of biomolecules.

bond (2). Representative labeling functionalities include isothiocyanates and succinimide esters for coupling with primary and secondary amines and iodoacetamides for reacting with thiols. Chromophores that noncovalently interact with analytes must possess a large fluorescence quantum yield enhancement upon interaction and a large binding constant with the analyte of interest.

Recently, there have been several reports on near-IR fluorophores that covalently and noncovalently label biological and organic compounds, including amino acids (3, 4), proteins (5, 6), nucleotides (7), DNA primers (1, 8), double-stranded DNA (9, 10), thiols (11, 12), and antibodies (13). The near-IR probes for covalent labeling are tricarbocyanine dyes containing an isothiocyanate or succinimidyl ester functional group for labeling of amines or an iodoacetamide group for labeling thiols. While these chromophores do not possess large fluorescence quantum yields in H₂O, the reduced background in the near-IR region results in an overall larger signal-to-noise ratio (1).

We describe the synthesis and properties of three new labeling tricarbocyanine dyes (1–3; Figure 1) containing either an isothiocyanate or a succinimidyl ester moiety attached to the chromophore through a phenyl thioether or phenyl ether linkage. All of these dyes show absorption and emission maxima in the near-IR region (770–810 nm), large extinction coefficients ($\sim 2 \times 10^6 \text{ cm}^{-1} \text{ M}^{-1}$), and excellent solubility in aqueous solution due to the negatively charged sulfopropyl groups on the nitrogen of the heteroaromatic rings. The potential of dyes 1–3 for use in bioanalytical applications has

* Author to whom correspondence should be addressed. Telephone: 504-388-4025. Fax: 504-388-3458. E-mail: chammer@chrs1.chem.lsu.edu.

[†] Louisiana State University.

[‡] PE Applied Biosystems.

[⊗] Abstract published in *Advance ACS Abstracts*, September 1, 1997.

been evaluated by conjugation reactions with amino acids and propargyl amine-functionalized dideoxynucleotides.

EXPERIMENTAL PROCEDURES

Chemicals. Aniline, cyclohexanone, *N,N*-dimethylformamide, 1,3-propane sultone, 4-aminothiophenol, thiophosgene, *N*-hydroxysuccinimide, 1,1-thiocarbonyldiimidazole, and sodium hydride were purchased from Aldrich Chemical Co. (Milwaukee, WI). Phosphorus oxychloride and 2,3,3-trimethylindolenine were purchased from Kodak Co. (Rochester, NY). Tyramine, glutamic acid, and tryptophan were purchased from Sigma Chemical Co. (St. Louis, MO). 3-(*p*-Hydroxyphenyl)propionic acid was purchased from Pfaltz and Bauer (Waterbury, CT). All other solvents were purchased from Fisher Scientific Co. (Pittsburgh, PA).

Purification and Spectroscopic Analysis. Unless otherwise specified, purification of the dyes was performed on a Rainin model Rabbit HP preparative HPLC apparatus using a Waters C18-RP preparative column (radial compression cartridge, 5 × 10 cm; flow rate = 5 mL/min) starting at 45:55 H₂O/MeOH for 5 min and then a linear gradient over 20 min to 20:80 H₂O/MeOH followed by washing with pure MeOH. Analytical separations were done using a Brownlee Spheri-5 ODS reversed-phase analytical column (0.46 × 10 cm). The HPLC detector was a Shimadzu absorbance detector which was set at 770 or 790 nm. H₂O/MeOH gradients were used in all experiments. Dyes were recovered from pooled, collected fractions, and the solvent was removed using a rotary evaporator at 40–45 °C. These dyes were dried overnight *in vacuo* (<0.1 Torr), suspended in Et₂O, and collected by filtration. Visible near-IR absorbance spectra were collected on a Perkin-Elmer Lambda 3 spectrophotometer. Fluorescence spectra were collected using a Spex fluorimeter. The proton NMR spectra were recorded in DMSO-*d*₆ or CD₃OD on a Bruker FT-NMR spectrometer. Mass spectral data were acquired using a Finnigan MAT 900 fast-atom bombardment instrument with glycerol as the sample matrix.

General Synthesis. The functionalized tricarbo-cyanine dyes were synthesized using modifications of previously described procedures (11, 14–21).

2,3,3-Trimethyl-1-(3-sulfopropyl)-3H-indolium, Inner Salt (4). Toluene (50 mL), 2,3,3-trimethylindolenine (10 mL, 0.0623 mol), and 1,3-propane sultone (8.2 mL, 0.0935 mol) were heated under reflux for 18 h. The reaction mixture was allowed to cool to room temperature. The resulting pink crystals were filtered and washed with acetone (3 × 10 mL). The filtered product was crystallized from a solution of MeOH and Et₂O. The crystals were collected and dried *in vacuo* to yield 14.88 g (85%): FAB-MS calcd for C₁₄H₂₀NO₃S 282.0 (M + H⁺), found 282.1; ¹H NMR (CD₃OD, 250 MHz) δ 8.06 (br dd, 1H), 7.85 (br dd, 1H), 7.62 (m, 2H), 4.75 (t, 2H, *J* = 7.2 Hz), 2.85 (s, 3H), 2.65 (t, 2H, *J* = 6.5 Hz), 2.17 (m, 2H), 1.54 (s, 6 H).

***N*-[5-Anilino-3-chloro-2,4-(propane-1,3-diyl)-2,4-pentadiene-1-ylidene]anilinium Chloride (5).** At 0 °C, phosphorus oxychloride (11 mL, 0.12 mol) was added dropwise from a pressure-equalizing addition funnel to anhydrous DMF (13 mL, 0.17 mol). After 30 min, cyclohexanone (5.5 mL, 0.053 mol) was added and the mixture was refluxed for 1 h. Next, with constant cooling at 20 °C, an aniline/EtOH [1:1 (v/v), 18 mL] mixture was added dropwise. Reaction was continued for an additional 30 min after aniline addition, and then the deep purple mixture was poured into ice cold H₂O/concentrated HCl (10:1, 110 mL). Crystals were allowed to form for 2 h in an ice bath, then filtered, washed with

cold H₂O and Et₂O, and then dried *in vacuo*: yield 15.41 g (87%): mp 220 °C: FAB-MS calcd for C₂₀H₂₀N₂Cl 323.1 (M⁺), found 323.3; ¹H NMR (DMSO-*d*₆, 200 MHz) δ 8.5 (s, 2H), 7.6–7.2 (m, 10H), 2.74 (t, 4H, *J* = 5.6 Hz), 1.85 (m, 2H).

Cy.7.Cl (6). A solution of **4** (1.69 g, 6 mmol), **5** (1.079 g, 3 mmol), and anhydrous sodium acetate (600 mg, 7 mmol) in absolute EtOH (60 mL) under a N₂ atmosphere was heated under reflux for 3.5 h. The EtOH was removed under reduced pressure, and the residue was purified by preparative RP-HPLC to afford 1.08 g (52%) of **6**: FAB-MS calcd for C₃₆H₄₄O₆N₂S₂Cl 699.2 (protonated form, M⁺), found 699.8, 721.8 (M – H + Na), 743.9 (M – 2H + 2Na); ¹H NMR (DMSO-*d*₆, 400 MHz) δ 8.26 (d, 4H, *J* = 14.1 Hz, *J* = 12.9 Hz), 7.62 (d, 2H, *J* = 7.4 Hz), 7.54 (d, 2H, *J* = 8.0 Hz), 7.42 (dd, 2H, *J* = 7.6 Hz), 7.27 (dd, 2H, *J* = 7.4 Hz), 6.53 (d, 2H, *J* = 14.2 Hz), 4.39 (t, 4H, *J* = 7.0 Hz), 2.75 (t, 4H, *J* = 5.2 Hz), 2.56 (br t, 4H), 2.03 (m, 4H, *J* = 7.1 Hz), 1.83 (m, 4H), 1.67 (s, 12H).

Cy.7.SPh.NCS (1). *Method A.* 4-Aminothiophenol (348 mg, 2.8 mmol) was dissolved in anhydrous DMF (30 mL) under a N₂ atmosphere. Chlorodye **6** (100 mg, 0.14 mmol) was added, and the mixture was stirred for 5 min. The DMF was removed under reduced pressure, and the residue was dissolved in 2 mL of DMF and precipitated with 10 mL of Et₂O. The solvents were removed, and the residue was washed with 20 mL of Et₂O and purified by reversed-phase HPLC. The fractions collected were concentrated and dried overnight *in vacuo* which gave 55 mg (50%) of Cy.7.SPh.NH₂ (**7**). This compound was not stable to storage and was used immediately for the preparation of the isothiocyanate. The aminothioether Cy.7.SPh.NH₂ (55 mg, 0.07 mmol) and anhydrous sodium carbonate (12 mg) were dissolved in anhydrous DMF (10 mL) under a N₂ atmosphere. At 0 °C, thiophosgene (11 μL, 0.14 mmol) was added with stirring. After 5 min, the mixture was taken off of the ice bath and allowed to react at room temperature for 1 h. The solution was filtered, and the precipitate was washed with DMF. The combined filtrate and washings were concentrated *in vacuo* at 40 °C. The resulting residue was dried *in vacuo* overnight to give 23 mg (39%) of **1**: FAB-MS calcd for C₄₃H₄₈N₃O₆S₄ 830.2 (protonated form, M⁺), found 830.3; ¹H NMR (CD₃OD, 250 MHz) δ 8.73 (d, 2H, *J* = 14.1 Hz), 7.1–7.4 (m, 12H), 6.48 (d, 2H, *J* = 14.0 Hz), 4.36 (br t, 4H), 2.95 (t, 4H, *J* = 6.5 Hz), 2.84 (br t, 4H), 2.23 (m, 4H), 2.02 (m, 4H), 1.50 (s, 12H); IR 2108 cm^{–1}.

Method B (Preferred). 4-Aminothiophenol (54 mg, 0.4 mmol) was dissolved in anhydrous DMF (10 mL) under a N₂ atmosphere. Chlorodye **6** (100 mg, 0.14 mmol) was added and the mixture stirred for 5 min. The reaction was quenched with dry ice. After the mixture was allowed to warm to room temperature (5 min), thiocarbonyldiimidazole (22–24) (210 mg, 1.0 mmol) was added with stirring. After 30 min, Et₂O (30 mL) was added to precipitate the dye. The resulting suspension was placed into a centrifuge for 30 s, and the supernatant was discarded. The precipitate was dissolved in H₂O/MeOH (1:1, 1.5 mL) and purified using five C18 Sep-Pak Plus cartridges in series using a MeOH/H₂O gradient (40:60, 3 mL; 60:40, 2 mL; 80:20, 4 mL). The fractions collected were concentrated and dried overnight under high vacuum which gave 34 mg (29%) of Cy.7.SPh.NCS.

2-(*p*-Hydroxyphenyl)ethylisothiocyanate. Tyramine (400 mg, 2.9 mmol) was dissolved in anhydrous DMF (10 mL) under a N₂ atmosphere. 1,1-Thiocarbonyldiimidazole (520 mg, 2.9 mmol) was added, and the pale yellow color of the solution turned an amber red color. After 30 min, the solvent was taken off by a rotary evaporator at 40 °C to afford an orange oil. The oil was

dissolved in 1 mL of MeOH, and 3 volumes of water were added to precipitate the isothiocyanate. The product was filtered and washed with cold water to afford 320 mg (62%). GC-EIMS calcd for C_9H_9NOS 180.0 (M^+), found 180.0; 1H NMR (DMSO- d_6 , 250 MHz) δ 7.67 (s, 1H), 7.05 (d, 2H, J = 8.1 Hz), 6.70 (d, 2H, J = 8.6 Hz), 3.80 (t, 2H, J = 6.6 Hz), 2.81 (t, 2H, J = 6.6 Hz); IR 2081 cm^{-1} .

Cy.7.OPhEt.NCS (2). A 60% oil dispersion of NaH (14 mg, 0.3 mmol) was added to anhydrous DMF (4 mL) under a N_2 atmosphere at 0 °C. In a separate flask, 2-(*p*-hydroxyphenyl)ethylisothiocyanate (58 mg, 0.3 mmol) was dissolved in anhydrous DMF (1 mL) under a N_2 atmosphere at 0 °C, and the solution was added to the slurry of NaH. After 30 min, the phenoxide isothiocyanate solution was added to chlorodye **6** (100 mg, 0.14 mmol) dissolved in anhydrous DMF (4 mL) under a N_2 atmosphere. The reaction was followed by HPLC. After 18 h, the reaction was quenched with dry ice and the solvent was removed on a rotary evaporator at 40 °C. The crude material was filtered and purified by preparative HPLC to afford 37 mg (32%) of **2**: FAB-MS calcd for $C_{45}H_{52}N_3O_7S_3$ 842.3 (protonated form, M^+), found 843.3; 1H NMR (CD_3OD , 400 MHz) δ 7.99 (d, 2H, J = 14.2 Hz), 7.04–7.38 (m, 12H), 6.31 (d, 2H, J = 14.1 Hz), 4.30 (t, 4H, J = 7.6 Hz), 3.76 (m, 4H), 2.79 (t, 4H, J = 5.8 Hz), 2.20 (m, 4H, J = 7.5 Hz), 2.03 (t, 2H, J = 5.7 Hz), 1.31 (s, 12H).

Cy.7.OPhEt.CO₂Su (3). 3-(*p*-Hydroxyphenyl)propionic acid (224 mg, 1.4 mmol) was dissolved in anhydrous DMF (10 mL) under a N_2 atmosphere. Sodium hydride (65 mg of a 60% oil dispersion, 2.7 mmol) was added and allowed to form the phenolate for 30 min under constant stirring. Chlorodye **6** (100 mg, 0.14 mmol) was added and allowed to react under N_2 with stirring for 30 min. The reaction was quenched with dry ice, and the DMF was taken off by a rotary evaporator. The residue was dissolved in $H_2O/MeOH$ (3:2, 3 mL), filtered, and purified by preparative HPLC. The collected fractions were concentrated on a rotary evaporator and dried *in vacuo* overnight to provide 35 mg (31%) of Cy.7.OPhEt.CO₂H (**8**): FAB-MS calcd for $C_{45}H_{53}N_2O_9S_2$ 829.3 (protonated form, M^+), found 829.6; 1H NMR (CD_3OD , 250 MHz) δ 8.00 (d, 2H, J = 14.2 Hz), 7.34–7.40 (m, 8H), 7.24 (m, 4H), 7.00 (d, 4H, J = 8.6 Hz), 6.30 (d, 2H, J = 14.2 Hz), 4.31 (br t, 4H), 2.95 (t, 2H, J = 6.6 Hz), 2.80 (br t, 4H), 2.35 (m, 2H), 2.21 (m, 4H), 2.09 (m, 2H), 1.34 (s, 12H).

N-Hydroxysuccinimide (7 mg, 60 μ mol) and Cy.7.OPhEt.CO₂H (**8**) (1 mg, 1.2 μ mol) were added sequentially to anhydrous DMF (100 μ L). After the free acid dye had dissolved, dicyclohexylcarbodiimide (DCC, 12 mg, 60 μ mol) was added and stirred overnight in the dark. The reaction was followed by analytical HPLC. The dye was then used without further purification. The synthesis afforded 85% conversion to Cy.7.OPhEt.CO₂Su (**3**) as determined by HPLC (remaining 15% of near-IR absorbing material was the starting free acid dye Cy.7.OPhEt.CO₂H). The succinate ester **3** could not be isolated, but the DMF solution was used directly for all conjugation reactions to primary amines.

Labeling of Amino Acids with Isothiocyanate Derivatives 1 and 2. A 10-fold excess of **1** or **2** in DMSO was dissolved in a 0.1 mM solution of amino acid in borate buffer [13 mM, pH 9.3, 40% (v/v) acetonitrile; 100 μ L of ~10:40:50 DMSO/acetonitrile/buffer], and the solution was shaken in the dark at room temperature. The reaction was analyzed by analytical HPLC after 12 h.

Labeling of Amino Acids with Succinimidyl Derivative 3. In the case of tryptophan, dye **3** was synthesized according to the procedure outlined earlier and the purity was assayed by HPLC. Aliquots of the

reaction solution were added in a 10-fold excess to 1 μ M solutions of tryptophan in carbonate/bicarbonate buffer (67 mM, pH 9.4). Reactions were followed by analytical HPLC. The reactions were determined to be complete within 20 min.

Labeling of 7-(3-Amino-1-propynyl)-2',3'-dideoxy-7-deazaadenosine 5'-Triphosphate (9a). 7-(3-Amino-1-propynyl)-2',3'-dideoxy-7-deazaadenosine 5'-triphosphate (ddATP) (0.16 μ mol) and **2** (1.4 mg, 1.6 μ mol) were dissolved in 67 mM sodium bicarbonate buffer (100 μ L, pH 9.3) and allowed to react in the dark at room temperature for 48 h. Diisopropylethylamine (100 μ L) was added and allowed to react for 24 h to form the conjugate. The reaction was followed by reverse-phase HPLC.

Labeling of 7-(3-Amino-1-propynyl)-2',3'-dideoxy-7-deazaguanosine 5'-Triphosphate (9b). 7-(3-Amino-1-propynyl)-2',3'-dideoxy-7-deazaguanosine 5'-triphosphate (ddGTP) was kindly provided by P. Cotofana of PE Applied Biosystems and was prepared by methods described by Prober *et al.* (25). The dye-ddGTP conjugate was prepared by optimization of a method described previously (25). In general, the purification required two steps. Anion exchange was used to separate free dye and the dye-labeled ddGTP. A subsequent, reverse-phase column was used to separate the ddGTP and the dye-labeled ddGTP. The final product was dried *in vacuo* and diluted with 50 mM CAPSO (750 μ L, pH 9.6) to a concentration of 1.7 μ M. The concentration of the formulated bulk is confirmed by absorbance spectroscopy at 765 nm.

Anion Exchange HPLC. Column: Aquapore AX-300, 7 μ m particle size, 220 \times 4.6 mm (PE Applied Biosystems). Gradient: 40% acetonitrile/60% triethylammonium bicarbonate (TEAB, 0.1 M) to 40% acetonitrile/60% TEAB (1.5 M) at 1.5 mL/min over 20 min, followed by isocratic elution.

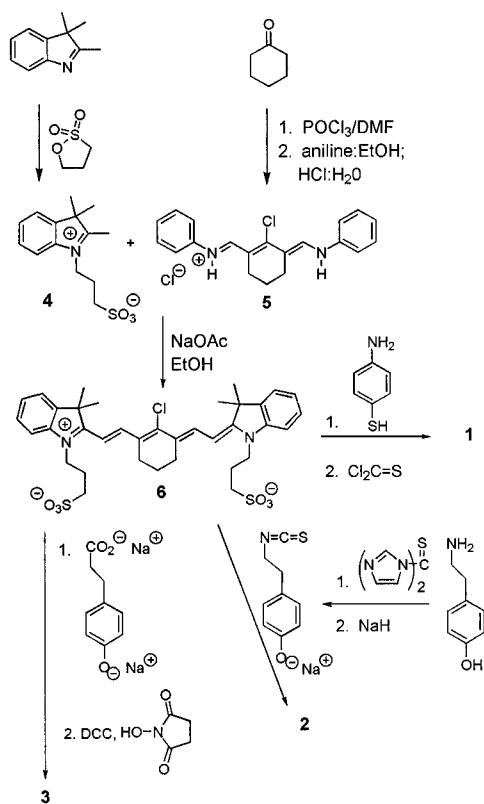
Reverse-Phase HPLC. Column: Spheri-5 RP-C18, 5 μ m particle size, 220 \times 4.6 mm (PE Applied Biosystems). Gradient: 100% triethylammonium acetate (TEAA, 0.1 M) to 40% acetonitrile/60% TEAA at 1.5 mL/min over 20 min followed by 40 to 100% acetonitrile at 1.5 mL/min over 5 min.

Detection. UV/vis: 260 nm.

RESULTS AND DISCUSSION

All three labeling dyes **1–3** (Figure 1, Scheme 1) were prepared from the base chlorocyanine dye **6** by nucleophilic substitution (via an $S_{RN}1$ mechanism) (17) of the chloride by phenolates or thiols. The heptamethine chain of chlorodye **6** is assembled from the aldol-like condensation of indolinium salt **4** and the iminium salt **5**. The inclusion of the sulfopropyl groups on the nitrogen of the indolenine ring of **4** (and subsequently **6**) gives all of the dyes (**1–3**, and **6**) excellent water solubility. However, the isothiocyanate dyes, **1** and **2**, show appreciable aggregation in aqueous solution as shown in Figure 2. The appearance of the absorption band at lower wavelength (~675 and ~650 nm in panels A and B of Figure 2, respectively) is indicative of the formation of higher-order aggregates (26). The addition of 40% organic modifier (methanol or acetonitrile) to this solution inhibits aggregation resulting in primarily the monomeric dye. The addition of *p*-aminothiophenol to chlorodye **6** to generate the aminothioether dye Cy.7.SPH.NH₂ (**7**, structure not shown) occurred with moderate yields. However, pure **7** was not stable at room temperature over long periods of time, so it was generally reacted with thiophosgene (or preferably thiocarbonyldiimidazole) immediately to provide the isothiocyanate. The preferred

Scheme 1



one-pot procedure for preparation of isothiocyanate dye **1** (method B) gave the best overall results in terms of time required and the resulting purity of **1**.

To obtain an isothiocyanate dye with a two-carbon longer linker arm, the addition of the phenolate of tyramine to chlorodye **6** was envisioned as a possible strategy. Attempts to use tyramine directly in this reaction led to complicated mixtures. Apparently, the free amine causes side reactions or decomposition of the dye (as in the case of free amine thioether dye **7** above). Thus, some sort of protection of the nitrogen is required, which would have to be removed and the isothiocyanate formed once the dye is assembled. Patonay and co-workers (21) have shown that the isothiocyanate group is stable under the moderately basic and nucleophilic reaction conditions required for the replacement of the Cl on dye **6**. This strategy is much more convergent and minimizes handling of dye-containing intermediates as it avoids the need for deblocking of the amine (usually protected with a Boc group) and subsequent formation of the isothiocyanate dye. Thus, the phenolate derivative of tyramine isothiocyanate (prepared from thiocarbonyl-diimidazole and tyramine) was directly added to the chlorodye **6** to provide the alkyl isothiocyanate dye **2** in moderate yield.

To compare the labeling efficiencies of different functional groups, the succinimide ester **3** was prepared. Again, the chlorodye reacts efficiently with the salt of 3-(*p*-hydroxyphenyl)propanoic acid to give the carboxylic acid dye Cy.7.OPhEt.COOH (**8**, structure not shown). The succinimide ester **3** was formed from **8**, *N*-hydroxy-succinimide, and dicyclohexylcarbodiimide; however, this compound was difficult to isolate because the ester was highly sensitive to hydrolysis even under neutral pH conditions. As a result, for purposes of labeling, active ester **3** was made just prior to use. All the dyes have a strong near-IR absorbance and a 20 nm Stokes shift of the fluorescence emission maxima (Table 1).

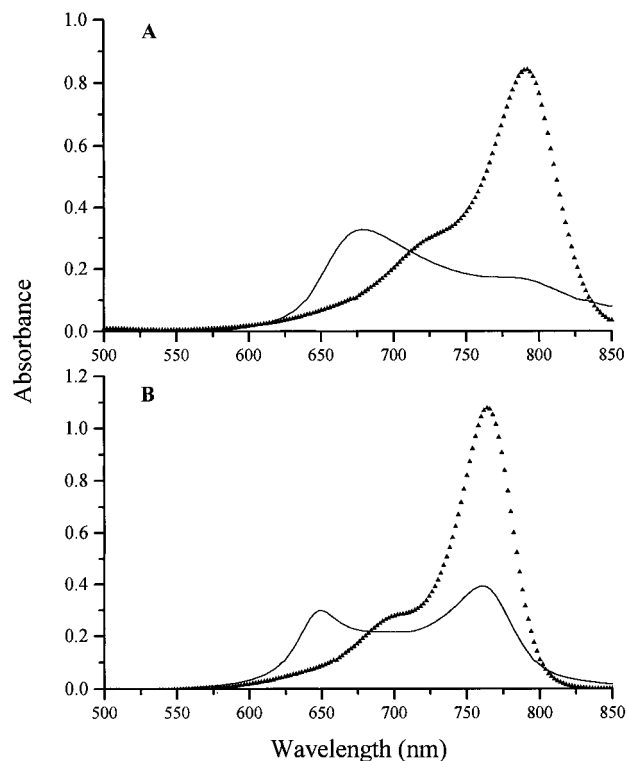


Figure 2. Absorbance spectrum of **1** (A) and **2** (B) in 13 mM borate (pH 9.3) (—) and 13 mM borate (pH 9.3) with 40% (v/v) methanol (▲). Concentration 5×10^{-6} M.

Table 1. Absorbance and Fluorescence Data of Near-IR Dyes

dye	name	absorbance maximum ^a	$\epsilon (\times 10^5 \text{ cm}^{-1} \text{ M}^{-1})^a$	fluorescence maximum ^a
6	Cy.7.Cl	778	1.8	802
7	Cy.7.SPh.NH ₂	791	1.7	810
1	Cy.7.SPh.NCS	791	1.7	810
2	Cy.7.OPhEt.NCS	768	2.0	791
8	Cy.7.OPhEt.COOH ^b	771	2.0	790

^a Measurements collected in methanol solutions. Concentration of 5×10^{-6} M. ^b The hydrolytic instability of Cy.7.OPhEt.COOSu (**3**) did not allow its full spectroscopic characterization.

Table 2. Conjugation Efficiencies of Dyes 1 and 2 with Respect to Amino Acids

buffer	tryptophan ^a		glutamic acid ^a	
	1	2	1	2
aqueous	35%	10%	nr ^b	4%
40% (v/v) acetonitrile	quant ^c	20%	80%	10%

^a The percent conjugation of reaction was determined from the following formula: $[(10 \times \text{the integrated area of the conjugate peak}) / (\text{total integrated area of all peaks in the chromatogram})] \times 100\%$. ^b No reaction. ^c Quantitative reaction.

Initially, aryl isothiocyanate **1** and alkyl isothiocyanate **2** were conjugated to tryptophan and glutamic acid using aqueous borate buffers (pH 9.3). Under these conditions, **1** exhibits moderate conjugation to tryptophan and does not conjugate to glutamic acid. Likewise, **2** shows poor conjugation to each amino acid (Table 2). However, the addition of organic modifier [40% (v/v) acetonitrile] improves the conjugation efficiency of both dyes. The increase in percent conjugation is most likely due to the decreased aggregation of the dyes in these buffers because of the organic modifier (Figure 2). Chromatograms of the conjugation of each labeling dye (**1** and **2**) to tryptophan under optimum conditions are shown in Figure 3. Thioether isothiocyanate dye **1** showed quantitative reaction with very little concomitant hydrolysis

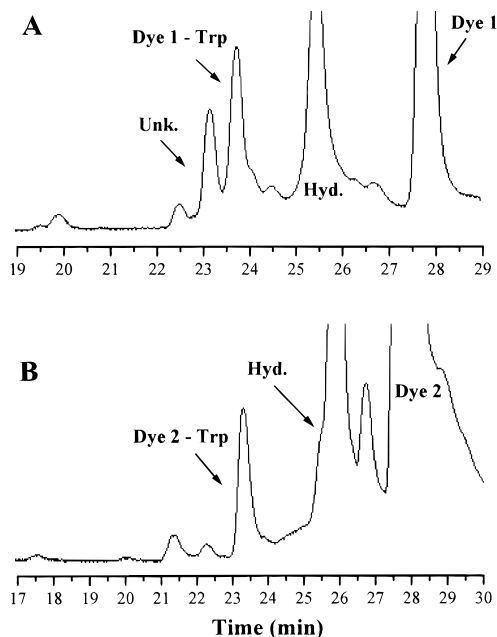
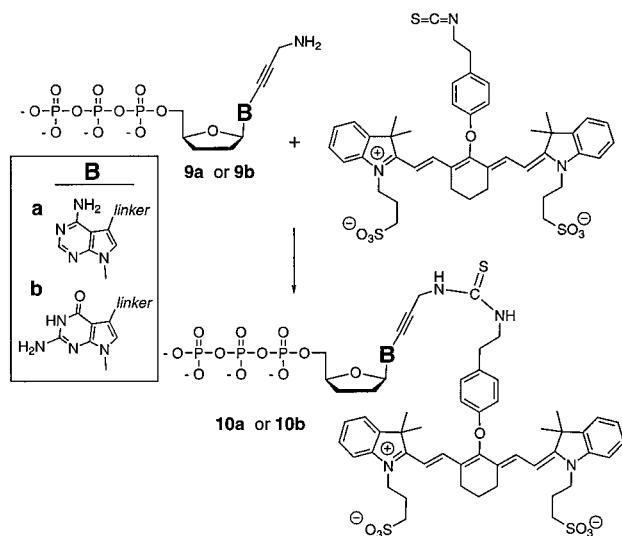


Figure 3. Reversed-phase HPLC chromatograms of tryptophan labeled with dye **1** (A) and **2** (B). Labeling and separation conditions are as stated in the text. Unk. (unknown) and Hyd. (hydrolysis products).

Scheme 2



of the functionalized chromophore. The phenethylisothiocyanate dye **2** showed poor conjugation efficiency toward tryptophan. This may be attributed to the slower reaction kinetics of alkyl isothiocyanates when compared to that of aryl isothiocyanates (27). The conjugation of the succinimidyl ester **3** to tryptophan produced several products due to the hydrolysis of the ester (data not shown) that obfuscated the positive identification of the tryptophan conjugate.

An attempt was made to conjugate each chromophore to propargyl amino-modified ddATP **9a** and ddGTP **9b** analogs. Arylisothiocyanate dye **1** and succinimide ester dye **3** showed no conjugation to the ddATP. The succinimide ester of **3** appears to be hydrolyzed before it can attach to the amino linker arm of the dideoxynucleotide. We have also seen this lack of conjugation to negatively charged amino acids with a closely related arylisothiocyanate cyanine dye (4). Successful conjugation to the ddATP and ddGTP (Scheme 2 and Figure 4) was achieved with alkylisothiocyanate dye **2**. Increasing the length of the chain which contains the isothiocyanate functional

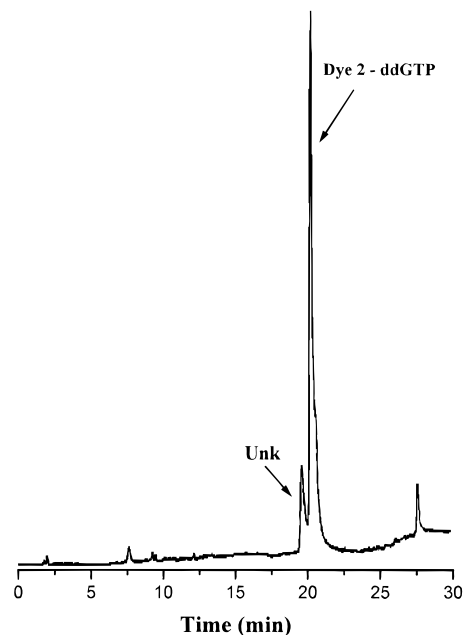


Figure 4. Reversed-phase HPLC chromatogram of ddGTP modified with a propargyl linker arm containing a primary amine covalently attached to **2**.

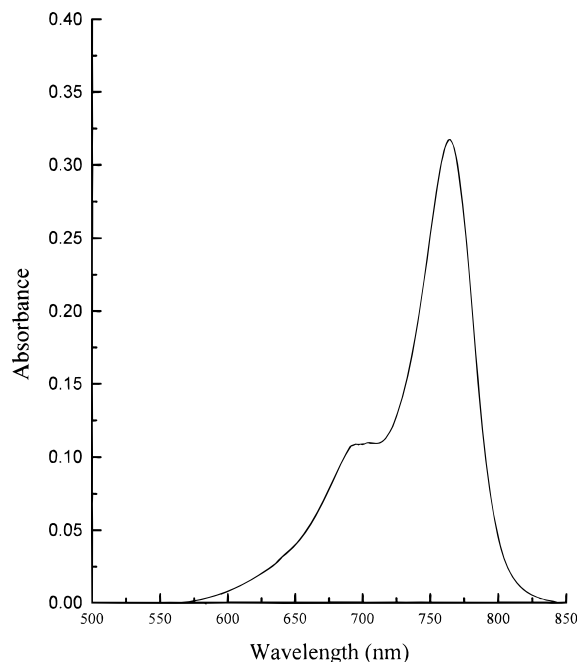


Figure 5. Absorbance spectrum of the **2**-ddGTP conjugate (**10b**) in triethylammonium bicarbonate buffer (~ 1.0 M, pH 7.0). Concentration of 1.7×10^{-5} M; path length of 1 mm.

group (**2** vs **1**) improved the efficiency of conjugation to the highly negatively charged nucleotides. This may be due to the increased distance of the isothiocyanate from the chromophore in tyramine-derived **2**, which decreases steric or electrostatic interactions that may occur between the analyte and dye. In addition, the use of an organic modifier, which inhibits aggregation of the dye, may be responsible for the more efficient conjugation of **2** with the nucleotides. The conjugates of dye **2** and ddNTP's **10a** and **10b** show no aggregation in aqueous buffer as demonstrated by absorption spectroscopy (Figure 5).

CONCLUSION

The preparation and application of three new tricarbocyanine dyes **1–3**, including functionalized groups, for

the derivatization of primary amines is described. The conjugation of these dyes with amino acids and triphosphate dideoxynucleotides is shown. These dyes show absorbance and fluorescence maxima in the near-IR region which allows for the use of inexpensive semiconductor devices such as diode lasers as excitation sources and avalanche diodes as detectors in a fluorescence detection assay. The conjugation of these dyes to primary amines allows their use as near-IR fluorescent labels for compounds such as proteins, amino acids, and antibodies. Dyes **1** and **2** contain an isothiocyanate functional group which conjugates specifically with primary amines, including amine-modified ddATP and ddGTP, with modest efficiency and only minor hydrolysis. We are currently exploring dye-ddNTP conjugates as terminators in a Sanger dideoxy sequencing protocol with a near-IR fluorescence detection scheme.

ACKNOWLEDGMENT

We would like to thank the National Institutes of Health (Grant HG00824) and the Louisiana Educational Quality Support Fund (LEQSF) for financial support of this work, PE Applied Biosystems for the donation of the ddGTP analog, and Dupont for the donation of the ddATP analog. We are particularly grateful to Dr. Tracy McCauley and Dr. Wenzhe Lu for expert assistance with mass spectrometric analysis.

LITERATURE CITED

- (1) Williams, D. C., and Soper, S. A. (1995) Ultrasensitive near-IR fluorescence detection for capillary gel electrophoresis and DNA sequencing applications. *Anal. Chem.* **67**, 3427–3432.
- (2) Waggoner, A. (1995) Covalent labeling of proteins and nucleic acids with fluorophores. In *Methods in Enzymology* (J. N. Abelson and M. I. Simon, Eds.) Vol. 246, pp 362–373, Academic Press, San Diego, CA.
- (3) Flanagan, J. H., Jr., Legendre, B. L., Jr., Hammer, R. P., and Soper, S. A. (1995) Binary solvent effects in capillary zone electrophoresis with ultrasensitive near-IR fluorescence detection of related tricarbocyanine dyes and dye-labeled amino acids. *Anal. Chem.* **67**, 341–347.
- (4) Legendre, B. L., Jr., Moberg, D. L., Williams, D. C., and Soper, S. A. (1997) Ultrasensitive near-IR laser induced fluorescence detection in capillary electrophoresis using a diode laser and avalanche photodiode. *J. Chromatogr. A* (in press).
- (5) Williams, R. J., Lipowska, M., Patonay, G., and Strekowski, L. (1993) Comparison of covalent and noncovalent labeling with near-infrared dyes for the high-performance liquid chromatographic determination of human serum albumin. *Anal. Chem.* **65**, 601–605.
- (6) Legendre, B. L., Jr., and Soper, S. A. (1996) Binding properties of near-IR dyes to proteins and separation of the dye/protein complexes using capillary electrophoresis with laser-induced fluorescence detection. *Appl. Spectrosc.* **50**, 1196–1202.
- (7) Steffens, D. L., Jang, G. Y., Sutter, S. L., Brumbaugh, J. A., Middendorf, L. R., Mühlegger, K., Mardis, E. R., Weinstein, L. A., and Wilson, R. K. (1995) An infrared fluorescent dATP for labeling DNA. *Genome Res.* **5**, 393–399.
- (8) Shealy, D. B., Lipowska, M., Lipowski, J., Narayanan, N., Sutter, S., Strekowski, L., and Patonay, G. (1995) Synthesis, chromatographic separation and characterization of near-infrared-labeled DNA oligomers for use in DNA sequencing. *Anal. Chem.* **67**, 247–251.
- (9) Owens, C. V., Davidson, Y. Y., Kar, S., and Soper, S. A. (1997) High-resolution separation of DNA restriction fragments using capillary electrophoresis with near-IR, diode-based, laser-induced fluorescence detection. *Anal. Chem.* **69**, 1256–1261.
- (10) Davidson, Y. Y., Gunn, B. M., and Soper, S. A. (1996) Spectroscopic and binding properties of near-infrared tricarbocyanine dyes to double-stranded DNA. *Appl. Spectrosc.* **50**, 211–221.
- (11) Ernst, L. A., Gupta, R. K., Mujumdar, R. B., and Waggoner, A. S. (1989) Cyanine dye labeling reagents for sulfhydryl groups. *Cytometry* **10**, 3–10.
- (12) Mank, A. J. G., Molenaar, E. J., Lingeman, H., Gooijer, C., Brinkman, U. A. T., and Velthorst, N. H. (1993) Visible diode laser induced fluorescence detection in liquid chromatography after precolumn derivatization of thiols. *Anal. Chem.* **65**, 2197–2203.
- (13) Williams, R. J., Narayanan, N., Casey, G. A., Lipowska, M., Strekowski, L., Patonay, G., Peralta, J. M., and Tsang, V. C. W. (1994) Instrument to detect near-infrared fluorescence in solid-phase immunoassay. *Anal. Chem.* **66**, 3102–3107.
- (14) Makin, S. M., Boiko, I. I., and Shavrygina, O. A. (1977) Synthesis and investigation of tricarbocyanines containing five- and six-membered rings in the chromophore. *J. Org. Chem. USSR* **13**, 2269–2271.
- (15) Mujumdar, R. B., Ernst, L. A., Mujumdar, S. R., and Waggoner, A. S. (1989) Cyanine dye labeling reagents containing isothiocyanate groups. *Cytometry* **10**, 11–19.
- (16) Southwick, P. L., Ernst, L. A., Tauriello, E. W., Parker, S. R., Mujumdar, R. B., Mujumdar, S. R., Clever, H. A., and Waggoner, A. S. (1990) Cyanine dye labeling reagents—Carboxymethylindocyanine succinimidyl esters. *Cytometry* **11**, 418–430.
- (17) Strekowski, L., Lipowska, M., and Patonay, G. (1992) Substitution reactions of a nucleofugal group in heptamethine cyanine dyes. Synthesis of an isothiocyanato derivative for labeling of proteins with a near-infrared chromophore. *J. Org. Chem.* **57**, 4578–4580.
- (18) Strekowski, L., Lipowska, M., and Patonay, G. (1992) Facile derivatizations of heptamethine cyanine dyes. *Synth. Commun.* **22**, 2593–2598.
- (19) Lipowska, M., Patonay, G., and Strekowski, L. (1993) New near-infrared cyanine dyes for labeling of proteins. *Synth. Commun.* **23**, 3087–3094.
- (20) Mujumdar, R. B., Ernst, L. A., Mujumdar, S. R., Lewis, C. J., and Waggoner, A. S. (1993) Cyanine dye labeling reagents: Sulfoindocyanine succinimidyl esters. *Bioconjugate Chem.* **4**, 105–111.
- (21) (a) Narayanan, N., and Patonay, G. (1995) A new method for the synthesis of heptamethine cyanine dyes: Synthesis of new near-infrared labels. *J. Org. Chem.* **60**, 2391–2395. (b) Narayanan, N., Strekowski, L., Lipowska, M., and Patonay, G. (1997) A new method for the synthesis of heptamethine cyanine dyes: Synthesis of new near-infrared labels. *J. Org. Chem.* (in press).
- (22) This reagent, which has been used to convert primary amines to their isothiocyanate derivatives, is a powder and thus less volatile and safer to handle than thiophosgene.
- (23) Staab, H. A., and Walther, G. (1962) Reaktionen von *N,N*-Thiocarbonyl-Di-Imidazol (Reactions with *N,N*-thiocarbonyl-di-imidazole). *Liebigs Ann. Chem.* **657**, 98–103.
- (24) Staab, H. A., and Walther, G. (1962) Synthese von Isothiocyanaten (Synthesis of isothiocyanates). *Liebigs Ann. Chem.* **657**, 104–107.
- (25) Prober, J. M., Dam, R. J., Robertson, C. W., Jr., Hobbs, F. W., Jr., and Trainor, G. L. (1988) Eur. Pat. Appl. 0 252 683.
- (26) Patonay, G., Antoine, M. D., Devanathan, S., and Strekowski, L. (1991) Near-infrared probe for determination of solvent hydrophobicity. *Appl. Spectrosc.* **45**, 457–461.
- (27) Drobnica, L., Kristian, P., and Augustin, J. (1977) The chemistry of the -NCS group. In *The Chemistry of Cyanates and their Thio Derivatives* (S. Patai, Ed.) pp 1003–1221, John Wiley & Sons, Chichester, England.

BC970113G

TECHNICAL NOTES

Preparation and Properties of Oligodeoxynucleotides Containing 5-Iodouracil and 5-Bromo- and 5-Iodocytosine

Elisenda Ferrer,[†] Marten Wiersma,[†] Bernard Kazimierczak,[‡] Christoph W. Müller,[‡] and Ramon Eritja*,[†]

European Molecular Biology Laboratory, Meyerhofstrasse 1, D-69117 Heidelberg, Germany, and European Molecular Biology Laboratory, Grenoble Outstation, c/o ILL, B.P. 156, 38042 Grenoble Cedex 9, France.
Received March 26, 1997[⊗]

The behavior of oligonucleotides containing 5-iodouracil, 5-bromocytidine, and 5-iodocytidine in concentrated ammonia is described. 5-Aminouracil and 5-aminocytidine are obtained as side products when deprotection is performed at 60 °C. Small amounts, if any, of side products are obtained when ammonia deprotection is performed at room temperature. The base-pairing properties of these 5-halopyrimidines including triple helix are described.

Oligonucleotides containing 5-halopyrimidines are important tools for research into nucleic acid and nucleic acid–protein interactions. Specifically, they are used in the following areas: (a) in structural elucidation of mispairs with natural bases to explain their mutagenic properties (1–3); (b) in the study of cytosine methyltransferases (4–6); (c) for photo-cross-linking with proteins which bind DNA and RNA (7–9); (d) in X-ray diffraction experiments of nucleic acids (10, 11) and nucleic acid binding proteins (12); (e) as nonradioactive labels (13) and as alternatives for mixed probes (14); (f) for triple-helix stabilization (15, 16); (g) as antisense oligonucleotides (17, 18); and (h) in the study of the restriction endonucleases cleavage mechanism (19, 20).

The preparation of these modified oligonucleotides can be performed by enzymatic methods (8, 9, 13) or preferably by chemical synthesis (1–7, 10, 14–20). Phosphoramidite derivatives of most of the 5-halopyrimidines are commercially available. The use of mild conditions during the ammonia treatment is recommended to avoid base modification (24–48 h, room temperature, refs 10 and 21), although, to our knowledge, there is no detailed study on these modifications. During the preparation of oligonucleotides containing 5-bromo-2'-deoxyuridine (2, Figure 1), a side product produced during the ammonia treatment was isolated and characterized as 5-amino-2'-deoxyuridine (4, Figure 1) (16). The degree of modification of 5-bromouracil during the standard ammonia treatment (16 h, 50 °C) was near 20%, and no side product was detected if the deprotection was performed at room temperature. To ensure complete deprotection of natural bases at room temperature, phosphoramidites carrying more labile protecting groups such as phenoxyacetyl (22), *tert*-butylphenoxyacetyl (23), or FOD (24) are recommended (3, 16). 5-Fluorouracil was found to be stable during ammonia deprotection (3).

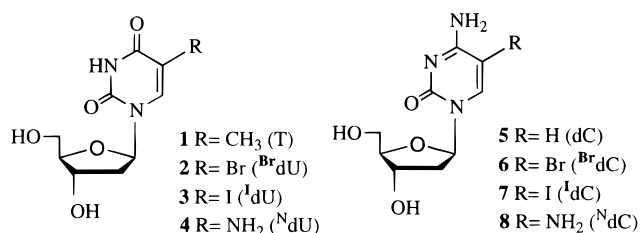


Figure 1. Chemical structures of 5-substituted pyrimidines.

In this paper we show that 5-iodo-2'-deoxyuridine (3), 5-bromo-2'-deoxycytidine (6), and 5-iodo-2'-deoxycytidine (7) (Figure 1) are also prone to ammonia degradation, giving 5-amino derivatives as described by 5-bromouracil. However, using optimal deprotection conditions, oligonucleotides containing these bases can be obtained with the high purity required for cocrystallization with proteins and subsequent X-ray diffraction studies.

RESULTS AND DISCUSSION

To assess the stability of 5-halopyrimidines to oligonucleotide deprotection conditions, the corresponding 2'-deoxypyrimidine nucleosides were treated with concentrated ammonia at 60 °C and analyzed by reversed-phase HPLC. 5-Bromo- (2) and 5-iodo-2'-deoxyuridine (3) gave, after ammonia treatment, a more polar product having the same retention time and the same UV absorption spectrum as 5-amino-2'-deoxyuridine (4) (25). The degree of base modification was more pronounced with 5-iodo-2'-deoxyuridine (3) than with 5-bromo-2'-deoxyuridine (2). After 24 h, nearly 50% of the 5-iodo-2'-deoxyuridine (3) is converted to 5-amino-2'-deoxyuridine (4), and in the case of the 5-bromo derivative 2, 50% of modification is observed after 3 days. Some minor products were also observed in the 5-iodo derivative (3) eluting very closely to the peak of 5-amino-2'-deoxyuridine (4). Treatment of the nucleosides with ammonia at room temperature did not give any detectable side products.

Similar results were obtained during the treatment of halogenated derivatives of 2'-deoxycytidine (6 and 7). A polar product appeared when 5-bromo- (6) and 5-iodo-2'-deoxycytidine (7) were treated with concentrated am-

* Address correspondence to this author at EMBL, Meyerhofstrasse 1, D-69117 Heidelberg, Germany (telephone 49-6221-387210; fax 49-6221-387306; e-mail eritja@embl-heidelberg.de).

[†] EMBL, Heidelberg.

[‡] EMBL, Grenoble.

[⊗] Abstract published in *Advance ACS Abstracts*, August 1, 1997.

Table 1. Modification of 5-Halogenated Pyrimidine Oligonucleotides in Concentrated Ammonia Solutions

oligonucleotide sequence	conditions	% 5-haloPyr oligonucleotide	HPLC retention time (min)	MS (Da)	% 5-aminoPyr oligonucleotide	HPLC retention time (min)	MS (Da)
⁵ IUT ³ '	60 °C, 16 h	53	21.2	658.1	47	9.4	547.2
⁵ IUT ³ '	RT, 24 h	100	21.2	658.1	none		
⁵ BrCT ³ '	60 °C, 16 h	67	18.5	608.9; 611.1	33	6.8	546.0
⁵ BrCT ³ '	RT, 24 h	100	18.5	608.9; 611.1	none		
⁵ ICT ³ '	60 °C, 16 h	35	18.4	656.9	38 ^a	7.0	546.1
⁵ ICT ³ '	RT, 24 h	93	18.4	656.9	1 ^a	7.0	

^a In the case of the dimer ¹CT two more side products were observed: compound **X**, retention time = 11.6 min, MS = 531 Da; compound **Y**, retention time = 13.9 min, MS = 546.1 Da. After 16 h at 60 °C, compound **X** is present at 10% and compound **Y** at 16%. After 24 h at RT, compound **X** is present at 2% and compound **Y** at 4%.

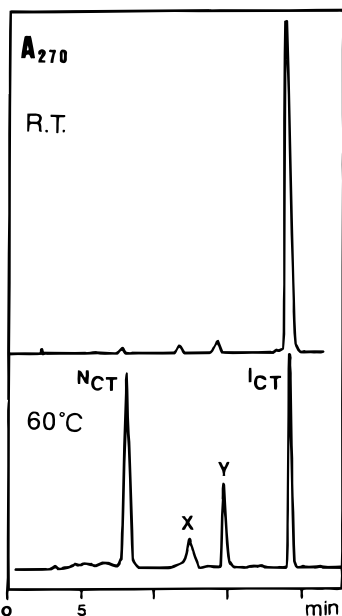


Figure 2. Analytical HPLC of dimer ¹CT after ammonia treatment at room temperature and at 60 °C. HPLC conditions are given under Experimental Procedures.

monia at 50 °C which had the same retention time and UV absorption spectrum as 5-amino-2'-deoxycytidine (**8**) (26). However, in this case the modification was more severe than with the halogenated uracils. After 24 h, 5-bromo-2'-deoxycytidine (**6**) yielded near 90% of the amino nucleoside (**8**) and more than 95% modification was observed with 5-iodo-2'-deoxycytidine (**7**). Some minor products were also observed in the 5-iodo derivative. Treatment of the cytidine derivatives with concentrated ammonia at room temperature yielded only small amounts of the amino derivatives (near 5%).

The behavior of oligonucleotides containing halogenated nucleosides in concentrated ammonia was studied on the dinucleotide 5'XT3'; X = 5-iodo-2'-deoxyuridine (**3**) and 5-bromo- (**6**) and 5-iodo-2'-deoxycytidine (**7**). Dinucleotides were prepared using standard phosphoramidite techniques and commercially available phosphoramidites (21). The amino group of 5-bromo- and 5-iodo-2'-deoxycytidine was protected with the benzoyl group (21). Oligonucleotides were prepared without the dimethoxytrityl group at the 5' end, and aliquots of the dinucleotide support were treated with concentrated ammonia at room temperature (24 h) and at 60 °C (16 h). Products were analyzed by reversed-phase HPLC, and the different products were analyzed by UV, enzyme digestion, and mass spectrometry. Results are shown in Table 1 and Figure 2. Similar to what has been found at the nucleoside level, 5-halopyrimidine oligonucleotides were partially decomposed to the corresponding 5-amino derivatives when ammonia treatment was performed at 60 °C.

The desired 5-halopyrimidine dimer had a larger retention time than the side products (Figure 2). The rate of modification at 60 °C was different for each dimer. One-third of the 5-bromocytosine dimer was transformed into 5-aminocytosine dimer (33%) after 16 h and, under the same conditions, half of the 5-iodouracil dimer was transformed into 5-aminouracil (47%). Base modification on 5-iodocytosine dimer was more complex. Only 35% of the UV-absorbing material was due to 5-iodocytosine dimer. The remaining 65% was divided in three different products. The major product was 5-aminocytosine dimer (38%), but two other minor products were observed. One of these side products (compound **Y**, 16%, retention time = 13.9 min) had a mass similar to that of the 5-aminocytosine dimer but had a different UV absorption spectrum. This side product can be assigned either to a dimer containing 6-aminocytosine or to a dimer containing 5-hydroxycytosine. Previous studies have shown that 6-aminocytosine is produced as minor product when 5-bromocytosine is treated with liquid ammonia (26). Alternatively, if water acts as a nucleophile, 5-hydroxycytosine may be obtained. The molecular weights of these products differ by only 1 mass unit of difference. Finally, the less abundant side product (compound **X**, 10%, 11.6 min) had a molecular mass of 531 Da, corresponding to a dimer without iodine. Enzyme digestion of this product gave two nucleoside peaks that eluted similarly to T and dC; therefore, this side product was assigned to the CT dimer. The replacement of a 5-iodo group by hydrogen by treatment with hot ammonia solutions has been previously described (27).

When deprotection was performed at room temperature for 24 h, complete elimination of the benzoyl group of BrC and ¹C was observed, as was the absence of base degradation. In the case of ¹C dimer it was possible to detect small amounts (1–4%) of base degradation products. The side products observed were the same as the products observed at high temperature, but the relative amounts were different. These results are in agreement with previous observations of degradation of 5-halopyrimidines during deprotection (10, 16, 21) and show the importance of using milder conditions for deprotection of these modified oligonucleotides.

Once the deprotection conditions were established on model dinucleotides, longer oligonucleotides were prepared and base-pairing properties of 5-halopyrimidine oligonucleotides were analyzed. For this purpose, the following oligonucleotide sequences were prepared: 15-mer, A, 5' TAG AGG XTC CAT TGC 3' (being X = ¹U, BrC and ¹C); and 11-mers, B, 5' CYY CCY CCY CT 3' (being Y = BrU and ¹U), and C, 5' ZTT ZTT ZTT ZT 3' (being Z = BrC and ¹C). Phosphoramidites protected with the more labile, *tert*-butylphenoxyacetyl protecting groups were used for the natural bases to ensure complete deprotection with concentrated ammonia at room temperature. Oligonucleotides were separated from trun-

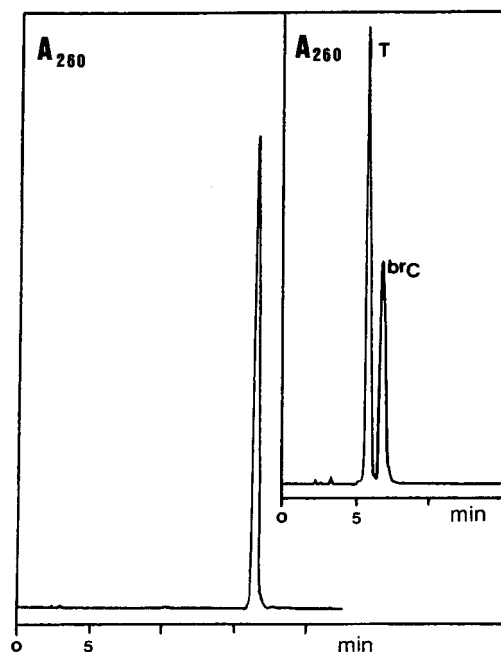


Figure 3. Analytical HPLC and enzyme digestion of purified 11-mer B 5' BrCTT BrC^{Br}CT BrC^{Br}CT TT 3'.

Table 2. Melting Temperatures^a (°C) of Duplexes Containing 5-Halopyrimidines and Related Compounds

5'TAG AGG XTC CAT TGC3'
3'ATC TCC YAG GTA ACG5'

X	G	Y A	C	T
C	59.3	47.1	44.7	45.7
BrC	63.6	49.3	44.0	47.6
¹ C	63.5	47.5	43.8	47.7
T	51.3	56.0	45.5	47.0
BrU	52.0	57.5	45.0	46.5
¹ U	53.1	56.0	45.7	46.9
^N U	51.6	56.1	43.2	48.3

^a 0.15 M NaCl, 0.05 N Tris-HCl buffer, pH 7.4.

cated sequences using COP reversed-phase cartridges or HPLC. Purified oligonucleotides were analyzed by reversed-phase and ion-exchange HPLC. In all cases a single peak was observed, which then was collected and characterized by mass spectrometry and/or enzyme digestion (Figure 3). The presence of 5-aminopyrimidine derivatives was not detected.

Melting curves of duplexes containing ¹U, BrC, and ¹C showed a single transition and melting temperatures were measured. Table 2 shows the values of melting temperatures. Small differences were observed when compared with the melting temperatures of natural base pairs. For the purpose of comparison, melting temperatures of duplexes containing 5-aminouracil (^NU) were also included (28). As a general trend, it is observed that the presence of the halogen slightly increases melting temperatures of the purine·pyrimidine base pairs, while pyrimidine·pyrimidine base pairs are not affected. Other investigators have reported similar results with duplexes containing ¹U·A and BrC·G base pairs (17).

Moreover, the influence of 5-halopyrimidines on triple-helix formation was studied with the sequence described by Xodo *et al.* (29). Triple helices were formed by mixing the hairpin molecule (h₂₆) with different all-pyrimidine single-stranded 11-mers (s₁₁) which contain 5-halopyrimidines substituting C or T. The UV absorbance at 270

Table 3. Melting Temperatures^a (°C) for the Triplex h₂₆:s₁₁ Containing 5-Halouracil and Related Compounds

h₂₆: 5'GAAGGAGGATTTTCTCTCCTTC3'
s₁₁-Y: 5'CYCCYCCYCT3'

X,Y	pH 5.5	pH 6.0	pH 6.5	pH 7.0
C,T	49	20		
C,BrU	53	33	26	
C, ¹ U	40	27		
C, ^N U	31	<20		

^a 1 M NaCl, 100 mM sodium phosphate/citric acid buffer. The duplex T_m values of h₂₆ occurred between 82 and 75 °C.

nm was then followed as a function of temperature at different pH values. As described previously, at acidic pH, two clear transitions were observed (16, 21). The first transition is due to dissociation of s₁₁ from h₂₆ (triplex to duplex) and the second transition to the denaturation of h₂₆ (duplex to single strand) (21). Melting temperatures for triple-helix dissociation of triplexes containing BrU and ¹U are shown in Table 3. Substitution of T for BrU stabilized triple helix but substitution of T for ¹U produced a slight destabilization of triple helix. Triple helices formed with the side product 5-aminouracil were less stable than the triple helix containing BrU and ¹U. Substitution of C for BrC and ¹C in s₁₁ abolished triple-helix formation. Only the duplex to single-strand transition was observed in the range from pH 5.5 to 7. The absence of triple-helix formation in 5-halocytosine derivatives is explained by the fact that cytosine should be protonated to form triple helix and 5-halocytidines have a much lower pK_a than cytidine (pK_a of cytidine = 4.6; pK_a of 5-bromocytidine = 3.8; pK_a of 5-iodocytidine = 3.5, ref 30).

Finally, oligonucleotides containing ¹U and ¹C at different sites were prepared for cocrystallization experiments. In sequences containing the palindromic binding site of the eukaryotic transcription factor T protein 5' AATTCACACCTAGGTGTCAAATT 3' nucleotides T and C were systematically substituted by ¹U and ¹C. Oligonucleotides were prepared on a 1 μmol scale as described and purified without the DMT on Mono Q columns using sodium chloride gradients. The resulting products were desalted by dialysis and cocrystallized with the DNA-binding domain of the T-protein. We were able to obtain cocrystals of a subset of the ¹U oligonucleotides, and the iodine positions in the crystal could be located by difference Patterson and difference Fourier techniques (data not shown). In contrast, cocrystals obtained with 5-iodouracil oligonucleotides prepared using standard deprotection conditions failed to show the iodine positions (data not shown). These results confirmed the importance of the use of mild conditions during the deprotection of oligonucleotides containing 5-halopyrimidines.

EXPERIMENTAL PROCEDURES

Abbreviations. ACN, acetonitrile; BrC, 5-bromocytosine; ¹C, 5-iodocytosine; ^NC, 5-aminocytosine; DMT, 4,4'-dimethoxytrityl; BrdC, 5-bromo-2'-deoxycytidine; ¹dC, 5-iodo-2'-deoxycytidine; ^NdC, 5-amino-2'-deoxycytidine; BrdU, 5-bromo-2'-deoxyuridine; ¹dU, 5-iodo-2'-deoxyuridine; ^NdU, 5-amino-2'-deoxyuridine; BrU, 5-bromouracil; ¹U, 5-iodouracil; ^NU, 5-aminouracil.

Materials. Reagents for oligonucleotide synthesis were obtained from Glen Research, Perkin-Elmer-ABI, and PerSeptive Biosystems. Oligonucleotide purification cartridges (COP) were obtained from Cruachem. Dry solvents were from SDS and Romil. HPLC grade solvents were from Romil and E. Merck. Snake venom

phosphodiesterase (from *Crotalus durissus*) and alkaline phosphatase were from Boehringer Mannheim. The rest of the reagents were from Aldrich and Fluka and were used without further purification. Oligonucleotide syntheses were performed on Applied Biosystems 394 and PerSeptive Biosystems Expedite instruments. Mass spectra were obtained on a API III SCIEX Perkin-Elmer instrument equipped with a triple-quadrupole detector.

Oligonucleotide Synthesis. The following sequences have been synthesized: dimers ${}^5\text{UT}^3$, ${}^5\text{BrCT}^3$, and ${}^5\text{LCT}^3$; 15-mers ${}^5\text{GCA ATG GAY CCT CTA}^3$, where $\text{Y} = \text{BrU}$, ${}^1\text{U}$, ${}^{\text{Br}}\text{C}$, ${}^1\text{C}$, T , C ; 11-mers $\text{s}_{11}\text{-Y}^5\text{CCY CCY CT}^3$, where $\text{Y} = \text{BrU}$, ${}^1\text{U}$, and T ; 11-mers $\text{s}_{11}\text{-Z}^5\text{ZTT ZTT ZTT ZT}^3$, where $\text{Z} = \text{BrC}$, ${}^1\text{C}$, and C ; 26-mer $\text{h}_{26}^5\text{GAA GGA GGA GAT TTT TCT CCT CCT TC}^3$; and 24-mer ${}^5\text{AAY YYZ AZA ZZY AGG YGY ZAA AY}^3$ with $\text{Y} = \text{T}$ and $\text{Z} = \text{C}$. T and C were substituted by ${}^1\text{U}$ and ${}^1\text{C}$, respectively, at up to two positions per oligonucleotide. Oligonucleotides were prepared on a DNA synthesizer using standard 2-cyanoethyl phosphoramidites and the modified phosphoramidites. ${}^{\text{Br}}\text{dC}$ and ${}^1\text{dC}$ phosphoramidites were protected with the benzoyl group (Glen Research). For the preparation of oligonucleotides containing ${}^{\text{Br}}\text{U}$, ${}^1\text{U}$, ${}^{\text{Br}}\text{C}$, and ${}^1\text{C}$, phosphoramidites protected with more labile *tert*-butylphenoxyacetyl groups (23) were used as described (3, 16). Complementary pentadecamers containing natural bases were also prepared using commercially available chemicals and following standard protocols.

Oligonucleotide supports containing ${}^{\text{Br}}\text{U}$, ${}^1\text{U}$, ${}^{\text{Br}}\text{C}$, and ${}^1\text{C}$ were treated with 32% aqueous ammonia at room temperature for 24 h. The remaining oligonucleotide supports were treated with 32% aqueous ammonia at 50 °C for 16 h. Ammonia solutions were concentrated to dryness, and the products were purified either by cartridge purification (COP) or by reversed-phase HPLC. Oligonucleotides were prepared on a 1 μmol scale. Dimers and 24-mers were prepared without the last DMT group (DMT-off protocol). The remaining oligonucleotides were synthesized, with the last DMT group at the 5' end (DMT-on protocol) to help reversed-phase purification. All purified products presented a major peak, which was collected and analyzed by snake venom phosphodiesterase and alkaline phosphatase digestion followed by HPLC analysis of the nucleosides (HPLC conditions B). The retention times of nucleosides obtained after enzyme digestion were as follows: dC, 2.8 min; dG, 5 min; T, 5.9 min; dA, 9 min; ${}^{\text{N}}\text{dU}$, 2.8 min; 5-amino-dC, 2.7 min; ${}^1\text{dU}$, 10.8 min; ${}^{\text{Br}}\text{dC}$, 7.2 min; ${}^1\text{dC}$, 8.4 min. Yields (OD units at 260 nm) were as follows: $\text{s}_{11}\text{-BrU}$, 46 OD; $\text{s}_{11}\text{-}^1\text{U}$, 31 OD; $\text{s}_{11}\text{-BrC}$, 25 OD; $\text{s}_{11}\text{-}^1\text{C}$, 27 OD; 15b- ${}^{\text{Br}}\text{U}$, 32 OD; 15b- ${}^1\text{U}$, 28 OD; 15b- ${}^{\text{Br}}\text{C}$, 31 OD; 15b- ${}^1\text{C}$, 26 OD. HPLC solutions are as follows: solvent A, 5% ACN in 100 mM triethylammonium acetate (pH 6.5); solvent B, 70% ACN in 100 mM triethylammonium acetate (pH 6.5). For analytical runs the following conditions were used: column, Nucleosil 120C18, 250 \times 4 mm; flow rate, 1 mL/min; conditions A, a 40 min linear gradient from 0 to 75% B; conditions B, a 20 min linear gradient from 0 to 20% B. For preparative runs the following conditions were used: columns, Nucleosil 120C18, 250 \times 10 mm; flow rate, 3 mL/min; a 20 min linear gradient from 15 to 60% B (DMT-on) or a 30 min linear gradient from 0 to 40% B (DMT-off). Analytical ion-exchange chromatography was performed on a Mono Q HR 5/5 (Pharmacia) column. A 50 min linear gradient from 0.4 M to 0.8 M NaCl in 10 mM NaOH (pH 12.5) and a flow rate 0.5 mL/min were used. For preparative runs a Mono Q HR 10/5 column with a flow rate of 4 mL/min was used.

Stability Studies of 5-Halopyrimidine Dimers in Concentrated Ammonia. Dinucleotide supports con-

taining ${}^1\text{U}$, ${}^{\text{Br}}\text{C}$, and ${}^1\text{C}$ (${}^5\text{XT}^3$) were treated with concentrated ammonia (a) at room temperature for 24 h and (b) at 60 °C for 16 h. The different ammonia solutions were concentrated to dryness and analyzed by HPLC. The column and solvents used were the same as described above but, in this case, a 30 min linear gradient from 0 to 50% B was used. Elution was followed at 270 nm.

Dimer ${}^1\text{UT}$: HPLC retention time, 21.2 min; UV max, 272; mass spectrum, 658.1. Side product: 5-amino-2'-deoxyuracil-T dimer; HPLC retention time, 9.4 min; UV max, 272, shoulder at 300 nm; mass spectrum, 547.2.

Dimer ${}^{\text{Br}}\text{CT}$: HPLC retention time, 18.5 min; UV max, 271; mass spectrum, 608.9, 611.1; two isotopes of Br. Side product: 5-amino-2'-deoxycytidine-T dimer; HPLC retention time, 6.8 min; UV max, 270, shoulder at 296 nm; mass spectrum, 546.0.

Dimer ${}^1\text{CT}$: HPLC retention time, 18.4 min; UV max, 270, shoulder at 290 nm; mass spectrum, 656.9. Side product 1: 5-amino-2'-deoxycytidine-T dimer; HPLC retention time, 7.0 min; UV max, 270, shoulder at 300 nm; mass spectrum, 546.1. Side product 2 (compound **X**): HPLC retention time, 11.6 min; UV max 268; mass spectrum, 531.1; enzyme digestion yields two nucleosides T and a second product eluting with the same retention time as dC. Side product 3 (compound **Y**): HPLC retention time, 13.9 min; UV max, 274 nm; mass spectrum, 546.1.

Melting Experiments. Melting experiments of pentadecamers (15b-Y) duplexes were carried out by mixing equimolar amounts of two pentadecamer strands dissolved in a solution containing 0.15 M NaCl and 0.05 N Tris-HCl buffer (pH 7.4). Duplexes were annealed by slow cooling from 80 to 4 °C. UV absorption spectra and melting curves (absorbance vs temperature) were recorded in 1-cm path-length cells using a Varian Cary 13 spectrophotometer having a temperature controller with a programmed temperature increase of 0.5 °C/min. Melts were run on duplex concentrations of 4 μM at 260 nm.

Melting experiments with triple helix were performed as follows: Solutions of equimolar amounts of the hairpin oligonucleotide (h_{26}) and the appropriate 11-mer ($\text{s}_{11}\text{-Y}$) were mixed in the appropriate buffer. The solutions were heated to 80 °C and allowed to cool slowly to room temperature, and then samples were kept in the refrigerator overnight. UV absorption spectra and melting experiments (absorbance vs temperature) were recorded in 1-cm path-length cells using a spectrophotometer, which has a temperature controller with a programmed temperature increase of 0.5 °C/min. Melts were run on duplex concentrations of 4 μM at 270 nm.

ACKNOWLEDGMENT

We thank Drs. Matthias Mann, Matthias Wilm, and Gitte Neubauer for obtaining the mass spectra of oligonucleotides.

LITERATURE CITED

- (1) Sowers, L. C., Goodman, L. C., Eritja, R., Kaplan, B., and Fazakerley, G. V. (1989) Ionized and wobble base-pairing for bromouracil-guanine base-pair as a function of pH. *J. Mol. Biol.* 205, 437-447.
- (2) Kremer, A. B., Mikita, T., and Beardsley, G. P. (1987) Chemical consequences of incorporation of 5-fluorouracil into DNA as studied by NMR. *Biochemistry* 26, 391-397.
- (3) Yu, H., Eritja, R., Bloom, L. B., and Goodman, M. F. (1993) Ionization of bromouracil and fluorouracil stimulates base mispairing frequencies with guanine. *J. Biol. Chem.* 268, 15935-15943.

- (4) MacMillan, A. M., Chen, L., and Verdine, G. L. (1992) Synthesis of an oligonucleotide suicide substrate for DNA methyltransferase. *J. Org. Chem.* 57, 2989–2991.
- (5) Friedman, S., and Ansari, N. (1992) Binding of the EcoRII methyltransferase to 5-fluorocytosine-containing DNA. Isolation of a bound peptide. *Nucleic Acids Res.* 20, 3241–3248.
- (6) Hanck, T., Schmidt, S., and Fritz, H. (1993) Sequence-specific and mechanism-based crosslinking of Dcm DNA cytosine-C5 methyltransferase of *E. coli* K-12 to synthetic oligonucleotides 5-fluoro-2'-deoxycytidine. *Nucleic Acids Res.* 21, 303–309.
- (7) Dong, Q., Blatter, E., Ebright, Y. W., Bister, K., and Ebright, R. H. (1994) Identification of amino acid-base contacts in the Myc-DNA complex by site-specific bromouracil mediated photocrosslinking. *EMBO J.* 13, 200–204.
- (8) Willis, M. C., Hicke, B. J., Uhlenbeck, O. C., Cech, T. R., and Koch, T. H. (1993) Photocrosslinking of 5-iodouracil-substitutes RNA and DNA to proteins. *Science* 262, 1255–1257.
- (9) Meisenheimer, K. M., Meisenheimer, P. L., Willis, M. C., and Koch, T. H. (1996) High yield photocrosslinking of a 5-iodocytidine (IC) substituted RNA to its associated protein. *Nucleic Acids Res.* 24, 981–982.
- (10) Sheardy, R. D., and Seeman, N. C. (1986) The synthesis of a deoxyoligonucleotide incorporating 5-iododeoxyuridine. *J. Org. Chem.* 51, 4301–4303.
- (11) Dickerson, R. E. (1992) DNA structure from A to Z. *Methods Enzymol.* 211, 67–110.
- (12) Nelson, H. C. M. (1995) Structure and function of DNA-binding proteins. *Curr. Opin. Genet. Dev.* 5, 180–189.
- (13) Seliger, H., Fröhlich, Gröger, G., Krist, B., Montenarh, M., Rösch, H., Rösch, R., and Ramalho Ortigao, F. (1991) Synthetic oligonucleotides for biomedical applications. *Nucleic Acids Res. Symp. Ser.* 24, 193–196.
- (14) Habener, J. F., Vo, C. D., Le, D. B., Gryan, G. P., Ercolani, L., and Wang, H.-J. (1988) 5-Fluorodeoxyuridine as an alternative to the synthesis of mixed hybridization probes for the detection of specific gene sequences. *Proc. Natl. Acad. Sci. U.S.A.* 85, 1735–1739.
- (15) Povsic, T. J., and Dervan, B. (1989) Triple helix formation by oligonucleotides on DNA extended to the physiological pH range. *J. Am. Chem. Soc.* 111, 3059–3061.
- (16) Ferrer, E., Fàbrega, C., Güimil-García, R., Azorín, F., and Eritja, R. (1996) Preparation of oligonucleotides containing 5-bromouracil and 5-methylcytidine. *Nucleosides Nucleotides* 15, 907–921.
- (17) Sanghvi, Y. S., Hoke, G. D., Freier, S. M., Zounes, M. C., Gonzalez, C., Cummins, L., Sasmor, H., and Dan Cook, P. (1993) Antisense oligonucleotides: synthesis, biophysical and biological evaluation of oligodeoxynucleotides containing modified pyrimidines. *Nucleic Acids Res.* 21, 3197–3203.
- (18) Kemal, O., Brown, T., Burgess, S., Bishop, J. D., and Leigh-Brown, A. J. (1991) *Nucleosides Nucleotides* 10, 555–561.
- (19) Hayakawa, T., Ono, A., and Ueda, T. (1988) Synthesis of decadeoxyribonucleotides containing 5-modified uracils and their interactions with restriction endonucleases BglII, Sau3AI and MboI. *Nucleic Acids Res.* 16, 4761–4776.
- (20) Fliess, A., Wolfes, H., Seela, F., and Pingoud, A. (1988) Analysis of the recognition mechanism involved in the EcoRV catalyzed cleavage of DNA using modified oligodeoxynucleotides. *Nucleic Acids Res.* 16, 11781–11793.
- (21) Glen Research 1996 catalog.
- (22) Schulhof, J. C., Molka, D., and Teoule, R. (1987) The final deprotection step in oligonucleotide synthesis is reduced to a mild and rapid ammonia treatment by using labile base-protecting groups. *Nucleic Acids Res.* 15, 397–416.
- (23) Sinha, N. D., Davis, P., Usman, N., Pérez, J., Hodge, R., Kremsky, J., and Casale, R. (1993) Labile exocyclic amine protection of nucleosides in DNA, RNA and oligonucleotide analog synthesis facilitating N-deacylation, minimizing depurination and chain degradation. *Biochemie* 75, 13–23.
- (24) Vu, Y., McColum, C., Jacobson, K., and Thiesen, P. (1990) Fast oligonucleotide deprotection phosphoramidite chemistry for DNA synthesis. *Tetrahedron Lett.* 31, 7269–7272.
- (25) Roberts, M., and Visser, D. W. (1952) Uridine and cytidine derivatives. *J. Am. Chem. Soc.* 74, 668–669.
- (26) Golman, D., and Kalman, T. I. (1983) Formation of 5- and 6-aminocytosine nucleosides and nucleotides from the corresponding 5-bromocytosine derivatives: synthesis and reaction mechanism. *Nucleosides Nucleotides* 2, 175–187.
- (27) Johnson, T. B., and Johns, C. O. (1906) Researches on pyrimidins: Some 5-iodopyrimidin derivatives; 5-iodocytosin. *J. Biol. Chem.* 1, 305–319.
- (28) Ferrer, E., Neubauer, G., Mann, M., and Eritja, R. (1997) Synthesis of oligodeoxynucleotides containing 5-amino-uracil and its N-acetyl derivative. *J. Chem. Soc., Perkin Trans. 1* (in press).
- (29) Xodo, L. E., Manzini, G., Quadrifoglio, F., van der Marel, G. A., and van Boom, J. H. (1991) Effect of 5-methylcytosine on the stability of triple-stranded DNA—a thermodynamic study. *Nucleic Acids Res.* 19, 5625–5631.
- (30) Massoulié, J., Michelson, A. M., and Pochon, F. (1966) *Biochim. Biophys. Acta* 114, 16–25.

BC970042L

Facile Synthesis of a High-Affinity Ligand for Mammalian Hepatic Lectin Containing Three Terminal *N*-Acetylgalactosamine Residues

Reiko T. Lee and Yuan C. Lee*

Department of Biology, Johns Hopkins University, Baltimore, Maryland 21218. Received May 13, 1997[®]

A simple cluster glycoside containing three residues of *N*-acetylgalactosamine with proper inter-residual distances can be a high-affinity ligand for asialoglycoprotein receptor of mammalian liver. YEE(ah-GalNAc)₃ [Lee, R. T., and Lee, Y. C. (1987) *Glycoconjugate J.* 4, 317–328] is such a ligand having a *K_d* in the subnanomolar range, and this high-affinity ligand has been successfully utilized in the delivery of gene to the parenchymal cells of the liver [Merwin, J. R., Noell, G. S., Thomas, W. L., Chiou, H. C., DeRome, M. E., McKee, T. D., Spitalny, G. L., and Findeis, M. A. (1994) *Bioconjugate Chem.* 5, 612–620; Hangeland, J. J., Levis, J. T., Lee, Y. C., and Ts'o, P. O. P. (1995) *Bioconjugate Chem.* 6, 695–701]. Reported here is a synthetic procedure for an equally effective, homologous trivalent ligand, YDD(G-ah-GalNAc)₃. The advantage offered by this new cluster glycoside is that the synthetic scheme accomplishes purification of reaction intermediates and the product without chromatographic separations. This greatly simplifies the procedure and allows scale-up of the operation at reduced cost of production.

INTRODUCTION

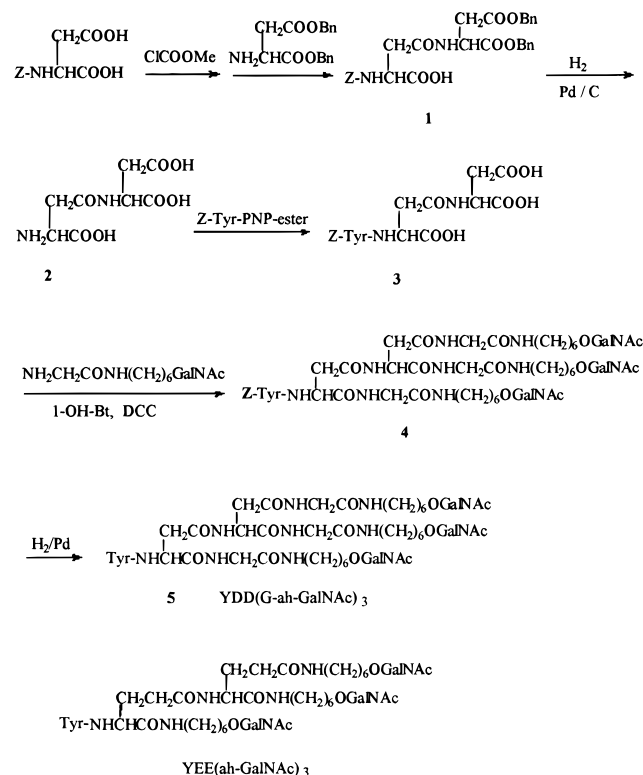
Mammalian hepatocytes contain on their surface a large number (ca. 200 000) of a recycling endocytotic receptor called asialoglycoprotein receptor (ASGP-R)¹ (1). ASGP-R, also known as hepatic lectin, recognizes terminal galactose (Gal) and *N*-acetylgalactosamine (GalNAc), and the affinity of a ligand for this receptor is highly dependent on the valency of Gal/GalNAc, as well as on the three-dimensional arrangement of the sugar residues (2).

Earlier we developed simple synthetic procedures for preparing high-affinity ligands of ASGP-R that contain two and three sugar residues (3, 4). These cluster glycosides were synthesized by attaching an ω -amino-terminated glycoside to each of the two and three carboxylic acid groups, respectively, of Asp (D) and γ -L-glutamyl-L-glutamic acid (γ -EE). Because GalNAc is bound to the receptor about 50-fold more tightly than Gal, a GalNAc-containing trivalent ligand, YEE(ah-GalNAc)₃ (see Scheme 1 for structure), has a particularly strong affinity to the receptor, its affinity being even superior to that of the best glycoprotein ligand, asialoorosomucoid (ASOR).

Although such ligands, after endocytosis, are targeted to lysosome and destined for degradation, this route of entry into hepatocytes has been used successfully for delivery of genes and drugs for therapeutic purposes (5, 6). Recent papers describe the successful use of YEE(ah-GalNAc)₃ as a vehicle for delivery of a gene (7) and an antisense oligodeoxynucleotide (8) to the liver.

Synthetically, the preparation of YEE(ah-GalNAc)₃ presents some practical problems, mainly due to poor

Scheme 1



solubility of the peptide backbone in aqueous as well as organic solvents. In this paper, we describe a facile synthesis of β -L-aspartyl-L-aspartic acid (β -DD), which is utilized instead of γ -EE to form a new trivalent ligand. The procedure represents much improvement over the previous method in terms of the overall ease of operation and the cost of production. The new trivalent ligand, YDD(G-ah-GalNAc)₃, was found to possess affinity for ASGP-R as high as that of YEE(ah-GalNAc)₃.

EXPERIMENTAL PROCEDURES

Materials. *N*-Benzyloxycarbonyl-L-aspartic acid (Z-D), L-aspartic acid dibenzyl ester *p*-toluenesulfonate,

* Author to whom correspondence should be addressed [telephone (410) 516-7041; fax (410) 516-8716; e-mail Bio_zycl@jhuvms.hcf.jhu.edu].

[®] Abstract published in *Advance ACS Abstracts*, August 1, 1997.

¹ Abbreviations: ASGP-R, asialoglycoprotein receptor; ASOR, asialoorosomucoid; Z-D, *N*-benzyloxycarbonyl L-aspartic acid; β -DD, β -L-aspartyl-L-aspartic acid; γ -EE, γ -L-glutamyl-L-glutamic acid; ah, 6-aminoethyl; DCC, dicyclohexylcarbodiimide; DMF, *N,N*-dimethylformamide; DMSO, dimethyl sulfoxide; TEA, triethylamine; NMM, *N*-methylmorpholine; 1-OH-Bt, 1-hydroxybenzotriazole; TNBS, trinitrobenzenesulfonic acid.

N-methylmorpholine, methyl chloroformate, and α -L-aspartyl-L-aspartic acid were obtained from Sigma Chemical Co. (St. Louis, MO). *p*-Nitrophenyl ester of *N*-benzyloxycarbonyl-L-tyrosine was obtained from Research Organics (Cleveland, OH). The preparation of 6-amino-hexyl 2-acetamido-2-deoxy- β -D-galactopyranoside (ah-GalNAc) has been reported (4). The aglycon of ah-GalNAc was extended by a glycyl residue to produce G-ah-GalNAc according to the method described for G-ah-GlcNAc (9). Crystalline G-ah-GalNAc had mp 163–164 °C. ^1H NMR spectrometry gave correct ratios for the anomeric H, *N*-acetyl H, and methylene H signals. Anal. Calcd ($\text{C}_{16}\text{H}_{31}\text{N}_3\text{O}_7$): C, 50.91; H, 8.28; N, 11.13. Found: C, 50.65; H, 8.17; N, 10.81.

Rat hepatocytes freshly isolated by liver perfusion method were kindly provided by The Center for Alternatives to Animal Testing's In Vitro Toxicology Laboratory (Johns Hopkins University, Baltimore, MD).

Methods. Iodination of ASOR using 0.5 mCi of carrier-free Na^{125}I (Amersham Corp., Arlington Heights, IL) was by the chloramine T method (10). The binding of [^{125}I]ASOR to rat hepatocyte surface and the inhibition assay for the assessment of the binding affinity of various ligands have been described (11). Briefly, hepatocytes were incubated in a pH 7.5 medium at 2 °C for 2 h with end-over-end tumbling (12 rpm) of the incubation tubes. A nonradiolabeled inhibitor at various concentrations was incubated together with [^{125}I]ASOR (ca. 1 nM) to determine the inhibitor concentration (I_{50}) at which [^{125}I]ASOR bound to the hepatocytes was decreased by 50%. The hepatocyte-bound radioactivity was separated from the bulk radioactivity by centrifuging the suspension through an oil layer (density slightly heavier than the medium). The tip of the microcentrifuge tube where cell pellet had been collected was cut off and counted in a gamma counter (MINAXIG, Packard). The I_{50} value of each test ligand was obtained from a plot of percent inhibition versus log[ligand concentration].

The amino group was quantified according to a trinitrobenzenesulfonic acid (TNBS) method (12). TLC was done with fluorescent silica gel plates coated on aluminum backing (E. Merck). Compounds on the plate were visualized by inspection under a UV lamp, by spraying with 15% sulfuric acid in 50% ethanol followed by heating on a hot plate (for sugars and certain peptide backbones) or by spraying with 0.5% ninhydrin in 95% ethanol and heating briefly (for amino groups). Amino acids and GalN were analyzed according to the Waters Picotag automated method (Waters Chromatography Division, Millipore Corp., Milford, MA). To separate GalN from amino acids, the initial eluting condition was held for 2 min before the gradient was initiated. NMR spectra were obtained with a Bruker AMX 300 spectrometer, and molecular weight was determined by FAB-MS (VG Instruments, Manchester, U.K.) using nitrobenzene or glycerol as matrix. Elemental analyses were done by Galbraith Labs (Knoxville, TN).

RESULTS

Synthesis of *N*-Benzyloxycarbonyl- β -L-aspartyl-L-aspartic Acid Dibenzy Ester (1). Z-D (1.34 g, 5 mmol) was dissolved in cold DMF (20 mL) and cooled in a dry ice–ethanol bath. To this solution were added methyl chloroformate (0.5 mL, 6.4 mmol) and *N*-methylmorpholine (NMM) (1.5 mL, 13.65 mmol) with stirring, which was continued for 20 min. A solution of L-aspartyl dibenzy ester *p*-toluenesulfonate (2.43 g, 5 mmol) and NMM (0.55 mL, 5 mmol) in DMF (10 mL) was added, and the reaction mixture was slowly brought to room temperature. After an overnight stirring at room tem-

perature, the precipitate was removed by filtration and the filtrate evaporated. Upon addition of water (30 mL) to the residue, the desired product, **1**, separated as a white precipitate, which was broken up into small pieces with a spatula, and the suspension was stirred overnight at room temperature. Yield of **1** (after filtration and drying) was 2.64 g (assumed as mono-NMM salt, 3.98 mmol, 80%). The product was purified by repeated crystallization from absolute ethanol, until a single UV-absorbing and charring spot was observed by TLC (R_f = 0.41 in ethyl acetate/acetic acid, 50:1); mp 126–127 °C. The ^1H NMR spectrum in CDCl_3 was consistent with the structure: δ 2.73–3.13 (2 Asp CH_2 ; each H, dd); 4.515 (Asp CH; dd); 4.874 (Asp CH, t); 5.064 (benzyl CH_2 , dd); 5.125 (2 benzyl CH_2 , dd); 7.274–7.350 (15 aromatic H, m). Anal. Calcd ($\text{C}_{30}\text{H}_{30}\text{N}_2\text{O}_9$): C, 64.05; H, 5.38; N, 4.98. Found: C, 63.99; H, 5.49; N, 4.94. The linkage between the two aspartic acid residues was determined to be β after deprotection of **1** (see below).

β -L-Aspartyl-L-aspartic Acid (β -DD) (2). The product (**1**) obtained above (0.85 g, 1.5 mmol) in 90% acetic acid (15 mL) was hydrogenated for 5 h in the presence of 10% palladium on carbon (100 mg) using a Brown hydrogenator (13). After filtration of the reaction mixture, the filtrate was evaporated to a syrup, which was then stirred in dry DMF (ca. 20 mL) to produce crystalline **2** in quantitative yield. Crystals were washed with DMF and ether and dried, mp 152–153 °C. TLC of **2** with ethyl acetate/acetic acid/water (3:2:1) showed a single ninhydrin-positive spot, which moved more slowly (R_f = 0.24) than Asp (R_f = 0.31). The amino group determined by TNBS method showed that, on a weight basis, **2** contained a correct amount of primary amino group (using Asp as standard), and the amino group content doubled upon acid hydrolysis. The acid hydrolysate contained only Asp (TLC).

The product was compared with authentic α -L-aspartyl-L-aspartic acid by ^1H NMR spectrometry. Spectra were taken in dimethyl- d_6 sulfoxide using the D_2O -exchanged samples. The α and β isomeric AspAsp each have a characteristic pattern of two well-separated methine signals. One of the two methine signals in each isomer is a broad, unresolved peak, while the other is a broad dd. The unresolved methine signal presumably belongs to the N-terminal Asp, since substituents on this methine C should have less freedom of rotation than that on the C-terminal Asp. α Isomer: δ 4.3 (unresolved broad peak, methine H of the N-terminal Asp); 4.0 (broad dd, 3.99 and 8.88 H_z , methine H of the C-terminal Asp). Product **2** (β isomer): δ 4.4 (broad dd, 5.7 and 14 H_z , methine H of the C-terminal Asp); 3.65 (unresolved broad peak, methine H or the N-terminal Asp).

***N*-Benzyloxycarbonyl-L-tyrosyl- β -L-aspartyl-L-aspartic Acid (Z-Yb-DD) (3).** To a solution of β -DD (300 mg, 0.86 mmol) in DMSO (10 mL) was added *p*-nitrophenyl ester of *N*-benzyloxycarbonyl-L-tyrosine (633 mg, 1.45 mmol) and triethylamine (0.5 mL, 3.6 mmol). The resulting yellow solution was left at room temperature overnight. After the removal of solvent, the resultant oil was diluted with ethyl acetate (ca. 2 mL), and ether (ca. 20 mL) was added with stirring. After the mixture was allowed to stand overnight at room temperature, the supernatant was decanted off and the precipitate was dissolved in 95% ethanol. Undissolved material was filtered, and the ethanolic solution was evaporated to yield **3** (450 mg, 0.7 mmol as mono TEA salt). TLC in ethyl acetate/isopropyl alcohol/water (4:2:1) indicated that the precipitate contained mostly a slow-moving material, which is UV-absorbing and charred weakly and was presumed to be **3**. The ethyl acetate/ether supernate

contained higher R_f , UV-absorbing, and noncharring spots (presumably *p*-nitrophenyl derivatives) and no desired product, **3**. Since **3** was difficult to redissolve once obtained in solid form, this preparation was used in the next reaction without further purification. For the product characterization, an accurately weighed sample of **3** was hydrolyzed by acid, and the hydrolysate was analyzed for amino acid composition and UV absorption spectrum. The ratio of Asp to Tyr was 2:1, and the tyrosine content was 98% of the theoretical amount on the basis of $\epsilon = 1500$ at 275 nm. ^1H NMR in $\text{DMSO}-d_6$ showed aromatic signals of benzyl and tyrosyl groups and three methine H signals.

Trivalent GalNAc Ligand, Z-YDD(G-ah-GalNAc)₃ (4). Coupling of carboxylic acid groups of Z-Y β -DD with G-ah-GalNAc was accomplished using the 1-hydroxybenzotriazole (1-OH-Bt) method (14). Z-Y β -DD (120 mg, ca. 0.185 mmol) and G-ah-GalNAc (250 mg, 0.66 mmol) were dissolved in DMSO (3 mL) and diluted with DMF (2 mL). To a slightly cooled solution (slight cloudiness remains) were added 1-OH-Bt (90 mg, 0.66 mmol), dicyclohexylcarbodiimide (DCC) (157 mg, 0.76 mmol), and NMM (24 mL, 0.22 mmol), and the mixture was stirred for 48 h at room temperature. The precipitated dicyclohexylurea was filtered, and a large excess of toluene was added to the filtrate to precipitate the product. After the mixture was allowed to stand overnight at room temperature, the supernate was decanted and the amorphous solid was dried briefly in a vacuum desiccator. TLC in ethyl acetate/acetic acid/water (3:2:1) showed the presence of two charring spots: a small amount of the remaining G-ah-GalNAc ($R_f = 0.17$) and the product, Z-YDD(G-ah-GalNAc)₃ ($R_f = 0.06$). The product **4** was crystallized from 50% ethanol. The mother liquor was evaporated, dissolved in 0.1 M acetic acid, and fractionated on a column of Sephadex G-15 (2.5 \times 140 cm) using 0.1 M acetic acid as eluant. The two components were totally separated, **4** being eluted much ahead of G-ah-GalNAc. Yield of **4** was 218 mg, 72.4%. ^1H NMR of the D_2O -exchanged **4** in $\text{DMSO}-d_6$ showed that it has correct ratios among aromatic H, methine H, anomeric H, and methyl H (*N*-acetyl group) of GalNAc. FAB-MS gave an $\text{M} + \text{Na}$ ion peak of 1645.8 ($\text{M} = 1622.78$).

Hydrogenolysis of 4 To Produce YDD(G-ah-GalNAc)₃ (5). The *N*-protecting group was removed by hydrogenolysis primarily for the purpose of improving solubility of the trivalent ligand in water. Hydrogenolysis in 60% acetic acid proceeded smoothly to produce **5** in quantitative yield. Upon TLC in ethyl acetate/acetic acid/water (3:2:1) the product barely moved from the origin ($R_f = 0.01$). The amino acid analysis showed the correct ratios of Y, D, G, and GalN. FAB-MS gave an $\text{M} + \text{H}$ ion peak of 1489.7 in the presence of trifluoroacetic acid ($\text{M} = 1488.74$).

Affinity of YDD(G-ah-GalNAc)₃ for ASGP-R on Rat Hepatocyte Surface. The affinity of YDD(G-ah-GalNAc)₃ and others to ASGP-R on rat hepatocytes was estimated using an inhibition assay as described under Methods. The I_{50} values of YDD(G-ah-GalNAc)₃ and YEE(ah-GalNAc)₃ were both 8 nM, while that of ASOR was 10 mM.

DISCUSSION

The reactions we adopted for the synthesis of a GalNAc-containing, high-affinity ligand for ASGP-R are shown in Scheme 1. In the first step, an amino-protected aspartic acid (e.g., Z-D) is activated with 1 equiv of methyl chloroformate and then reacted with aspartyl dibenzyl ester [$\text{D}(\text{OBn})_2$]. This produced exclusively

β -aspartylaspartic acid derivative. It is not clear if the β isomeric form is produced directly from a specifically β -activated Z-D or if the reaction proceeds through the cyclic anhydride of Z-D. Irrespective of the mechanism involved, the formation of a single isomer allows easy purification of the product by recrystallization. Thus, a gram quantity of β -AspAsp dipeptide [$\text{Z}-\beta\text{-DD}(\text{OBn})_2$] is produced without effort. $\text{Z}-\beta\text{-DD}(\text{OBn})_2$ was then converted to β -AspAsp (β -DD) by hydrogenolysis. β -DD was obtained in pure form by suspending the residue from the hydrogenolysis reaction in DMF. However, this reaction removed all of the protective groups, thus necessitating reprotection of the exposed amino group before the carboxylic acid groups can be utilized for conjugation to an amino-terminated glycoside (step 4, scheme 1). The reaction of β -DD with a commercially available reagent, PNP ester of Z-tyrosine, accomplished both the *N*-protection and the introduction of a radioiodinatable group. In the final step of conjugating an ω -amino-containing glycoside to the carboxylic acid groups of Z-Y β -DD, an *in situ* activation method using 1-OH-Bt and DCC (14) appears to give higher yields of the trivalent product than the previously used chloroformate method (4).

This synthetic scheme represents a considerable improvement over the synthetic scheme for YEE(ah-GalNAc)₃ (4), mainly in simplifying the operation by accomplishing purification by crystallization and precipitation rather than column chromatography, thus avoiding handling of a large volume of dilute solutions. Inexpensive starting materials and the simple operations also mean a lower cost of production. However, prior to arriving at the present scheme, we have tested the following alternative possibilities. First, *N*-BOC-aspartic acid was substituted for Z-D in the initial step, so that the deprotection of the product can be carried out stepwise, thus eliminating the necessity for reprotection of the amino group. Although the conjugation of *N*-BOC-Asp with $\text{D}(\text{OBn})_2$ appeared to proceed smoothly, the product *N*-BOC- β -DD($\text{OBn})_2$ could not be isolated as easily as $\text{Z}-\beta\text{-DD}(\text{OBn})_2$. Perhaps due to the fact that the BOC group is less hydrophobic than the Z group, the product, *N*-BOC- β -DD($\text{OBn})_2$, did not precipitate from water, so that an initial cleanup step of partition between aqueous and organic layers was adopted. This turned out to be quite tedious and gave an unsatisfactory result. It is also not certain whether this reaction produced a single isomeric form of DD or not. In another experiment, the benzyl esters of $\text{Z}-\beta\text{-DD}(\text{OBn})_2$ were removed by saponification instead of hydrogenolysis, so that the *N*-protecting group would be preserved in the product, $\text{Z}-\beta\text{-DD}$. Although the saponification appeared to have proceeded well, it is apparently difficult to regenerate all three carboxylic acid groups completely to the acidic form, since a trial conjugation of $\text{Z}-\beta\text{-DD}$ with G-ah-sugar produced a fair amount of divalent product.

The subunits of ASGP-R are known to be organized on the surface of rat hepatocytes in a rather rigid, lattice-like configuration (15). When a ligand can occupy two or more of the receptor binding sites simultaneously, its binding affinity increases tremendously. Therefore, an effective cluster glycoside must have a proper intersugar spacing, which is determined largely by the length of the aglycon. For the Asp-based cluster ligands, the optimal aglycon appears to be 6-(*N*-glycyl)aminohexyl for monosaccharides (Gal or GalNAc) and 6-aminohexyl (ah) for disaccharides (Lac). For the γ -EE-based ligands, aminohexyl appears to be suitable for both mono- and disaccharides. Since the new trivalent ligand is based

on an Asp dipeptide, we decided to use the longer aglycon, namely 6-(*N*-glycyl)aminohexyl, in the present synthetic scheme.

The I_{50} value of the new trivalent ligand YDD(G-ah-GalNAc)₃ is comparable to that of ASOR and YEE(ah-GalNAc)₃, compounds with proven effectiveness for delivery of their conjugates to the liver. Therefore, the new trivalent ligand should prove equally efficient in carrying out the delivery of its payload to the liver.

ACKNOWLEDGMENT

We acknowledge the help of Mrs. Joyce Lily for the analyses of amino acids and GalN and the help of Dr. J. L. Kachinski, Jr., for FAB-MS and Dr. L. X. Wang for NMR spectroscopy, performed at MS and NMR facilities of Department of Chemistry, Johns Hopkins University.

LITERATURE CITED

- (1) Ashwell, G., and Harford, J. (1982) Carbohydrate-specific receptors of the liver. *Annu. Rev. Biochem.* 51, 531–554.
- (2) Lee, Y. C. (1992) Biochemistry of carbohydrate-protein interaction. *FASEB J.* 6, 3193–3200.
- (3) Lee, R. T., Lin, P., and Lee, Y. C. (1984) New synthetic cluster ligands for galactose/*N*-acetylgalactosamine-specific lectin of mammalian liver. *Biochemistry* 23, 4255–4261.
- (4) Lee, R. T., and Lee, Y. C. (1987) Preparation of cluster glycosides of *N*-acetylgalactosamine that have subnanomolar binding constants towards the mammalian hepatic Gal/GalNAc-specific receptor. *Glycoconjugate J.* 4, 317–328.
- (5) Wu, G. Y., and Wu, C. H. (1987) Receptor-mediated in vitro gene transformation by a soluble DNA carrier system. *J. Biol. Chem.* 262, 4429–4432.
- (6) Plank, C., Zatloukal, K., Cotten, M., Mechtler, K., and Wagner, E. (1992) Gene transfer into hepatocytes using asialoglycoprotein receptor mediated endocytosis of DNA complexed with an artificial tetra-antennary galactose ligand. *Bioconjugate Chem.* 3, 533–539.
- (7) Merwin, J. R., Noell, G. S., Thomas, W. L., Chiou, H., C., DeRome, M. E., McKee, T. D., Spitalny, G. L., and Findeis, M. A. (1994) Targeted delivery of DNA using YEE(GalNAcAH)₃, a synthetic glycopeptide ligand for the asialoglycoprotein receptor. *Bioconjugate Chem.* 5, 612–620.
- (8) Hangeland, J. J., Levis, J. T., Lee, Y. C., and Ts'o, P. O. P. (1995) Cell-type specific and ligand specific enhancement of cellular uptake of oligodeoxynucleoside methylphosphonates covalently linked with a neoglycopeptide, YEE(ah-GalNAc)₃. *Bioconjugate Chem.* 6, 695–701.
- (9) Lee, R. T., Ichikawa, Y., Kawasaki, T., Drickamer, K., and Lee, Y. C. (1992) Multivalent ligand binding by serum mannose-binding protein. *Arch. Biochem. Biophys.* 299, 129–136.
- (10) Greenwood, F. C., Hunter, N. M., and Glover, J. S. (1963) The preparation of ¹³¹I-labelled human growth hormone of high specific radioactivity. *Biochem. J.* 89, 114–123.
- (11) Connolly, D. T., Townsend, R. R., Kawaguchi, K., Bell, W. R., and Lee, Y. C. (1982) Binding and endocytosis of cluster glycosides by rabbit hepatocytes. *J. Biol. Chem.* 257, 939–945.
- (12) McKelvy, J. F., and Lee, Y. C. (1969) Microheterogeneity of the carbohydrate group of *Aspergillus oryzae* α-amylase. *Arch. Biochem. Biophys.* 132, 99–110.
- (13) Brown, C. A., and Brown, H. C. (1966) Catalytic hydrogenation II. A new, convenient technique for laboratory hydrogenations. A simple, automatic device for atmospheric pressure hydrogenations. *J. Org. Chem.* 31, 3989–3995.
- (14) Johnson, T. B., and Coward, J. K. (1987) Synthesis of oligophosphopeptides and related ATP γ-peptide esters as probes for cAMP-dependent protein kinase. *J. Org. Chem.* 52, 1771–1779.
- (15) Lee, R. T. (1991) Ligand structural requirements for recognition and binding by the hepatic asialoglycoprotein receptor. In *Liver Diseases: Targeted Diagnosis and Therapy Using Specific Receptors and Ligands* (G. Y. Wu and C. H. Wu, Eds.) pp 65–86, Dekker, New York.

BC9700796

Conjugation of Unprotected Trisuccin, *N*-[Tris[2-[(*N*-hydroxyamino)carbonyl]ethyl]methyl]succinamic Acid, to Monoclonal Antibody CC49 by an Improved Active Ester Protocol

Ahmad Safavy,* Alicia Sanders,[†] Haoyu Qin, and Donald J. Buchsbaum

Department of Radiation Oncology, University of Alabama at Birmingham, Birmingham, Alabama 35294.

Received January 21, 1997[®]

For the conjugation of the trihydroxamate bifunctional chelating agent *N*-[tris[2-[(*N*-(benzyloxy)amino]carbonyl]ethyl]methyl]succinamic acid (trisuccin, **1**) to antibodies, we originally used the corresponding 2,3,5,6-tetrafluorophenyl active ester followed by the postconjugation removal of the benzyl protecting groups by catalytic hydrogenation. It was of interest to us to design a conjugation protocol capable of incorporating deblocked hydroxamates into peptides and proteins. Reported procedures that were expected to be compatible with the functionalities present in trisuccin were used with no success, as judged by the lack of ability of the products to radiolabel with ¹⁸⁸Re. A simple conjugation method was then developed utilizing the *o*-nitrophenol (ONP) activated ester of the unprotected trisuccin, *N*-[tris[2-[(*N*-hydroxyamino)carbonyl]ethyl]methyl]succinamic acid, **3**, which eliminates the need for the postconjugation deblocking. An assay for indirect estimation of the active ester content, based on the concentration of its decomposition byproduct, ONP-OH, was developed. Comparison of the indirectly estimated concentrations with those obtained directly from purified products showed >90% accuracy for this assay. This procedure has the advantage of rapidly using the unpurified active ester, eliminating the possibilities of its decomposition through solvolysis or self-condensation by the unprotected hydroxamate functions. A colorimetric assay was developed for estimation of the number of ligands per molecule of protein. This assay and the fact that all conjugates consistently radiolabeled with ¹⁸⁸Re show that this procedure conjugated the unprotected hydroxamate ligands to the CC49 monoclonal antibody. These results indicate the potential applicability of this technique to conjugation of unprotected hydroxamate derivatives with other proteins and peptides.

INTRODUCTION

Bifunctional chelating agents (BCAs¹) constitute an important class of organic molecules, used for radiometal labeling of molecules such as peptides and antibodies (*1*). Due to a great deal of interest developed in the application of radioactive metals toward "targeted" diagnosis and therapy of cancer, a variety of BCAs have been synthesized (*2–5*). We had identified hydroxamic acids as potential BCAs and reported on the synthesis of the first member of this class, *N*-[tris[2-[(*N*-(benzyloxy)amino]carbonyl]ethyl]methyl]succinamic acid (trisuccin, **1**) (*6*). Monoclonal antibody–trisuccin conjugates were synthesized and radiolabeled with ^{99m}Tc (*6*) and ¹⁸⁶Re (*7*). On the basis of these results and also the known affinity of

hydroxamic acids toward such metals as copper, iron, and cobalt (*8*), we regarded hydroxamic acids as potential BCA candidates and set out to develop and optimize protocols for their efficient and controlled conjugation to proteins, peptides, and other molecules of biological interest. In the original procedure, we used the benzyl-blocked trisuccin, in the form of its TFP active ester **2**, for conjugation to different MAb's followed by removal of the blocking groups by catalytic hydrogenation of the conjugate. This protocol was based on the available conjugation functionality (–COOH) of trisuccin, which had been designed as a hydroxamate-compatible, orthogonally protected group in the synthesis of this molecule (*6*). Although relatively high yields of radiolabeling were obtained and immunoreactivities of the conjugates were preserved to a good extent, it was of interest to us to develop a method that eliminated the need for the catalytic hydrogenation of the protein conjugate. This would be an important modification because some peptides and proteins may assume lower biological activities under the hydrogenation conditions. Furthermore, preconjugation removal of the blocking groups will ensure uniform availability of all incorporated hydroxamate functions for metal chelation and, thereby, eliminate any ambiguities about the nature of the conjugate. This paper describes the development of such a protocol, its application to radiometal (¹⁸⁸Re) labeling of MAb's, and a simple method for the quantitative measurement of the number of conjugated ligands per molecule of the antibody.

EXPERIMENTAL PROCEDURES

General. All reagents and solvents were obtained from commercial suppliers and were used as received.

* Address correspondence to this author at the University of Alabama at Birmingham, Department of Radiation Oncology, 1824 6th Ave. S., WTI 674, Birmingham, AL 35294-6832 [fax (205) 975-7060; e-mail radt004@uabdp.dpo.uab.edu].

[†] Present address: Department of Medical Genetics, 908 S. 20th St., Birmingham, AL 35294-2050.

[®] Abstract published in *Advance ACS Abstracts*, August 15, 1997.

¹Abbreviations: A/C, absorbance–concentration; BCA, bi-functional chelating agent; BSA, bovine serum albumin; DCC, dicyclohexylcarbodiimide; DCU, 1,3-dicyclohexylurea; DMF, *N,N*-dimethylformamide; DPBS, Dulbecco's phosphate-buffered saline; EDTA, ethylenediaminetetraacetic acid; HPLC, high-performance liquid chromatography; ITLC, instant thin-layer chromatography; L:P, ligand-to-protein; MAb, monoclonal antibody; MALDI-TOF MS, matrix-assisted laser desorption ionization-time of flight mass spectroscopy; NHS, *N*-hydroxysuccinimide; ONP, *o*-nitrophenyl; %PF, percent purity factor; PBS, phosphate-buffered saline; RP, reversed-phase; SEC, size exclusion chromatography; TCA, trichloroacetic acid; TFP, 2,3,5,6-tetrafluorophenyl; THF, tetrahydrofuran; *t*_R, retention time.

Benzyl-protected trisuccin, **1**, was prepared as described previously (6). HPLC analyses were carried out on a BioRad Model 5000 Titanium system (BioRad, Richmond, CA) equipped with a Model 1806 UV-vis detector and a Beckman Model 170 radioisotope detector, operated by ValueChrome software (BioRad). For analytical SEC, a Biosil-125, 7.5 × 600 mm (BioRad), column and for reversed-phase runs either a 4.6 × 250 mm analytical C₁₈ or a 10 × 250 mm C₄ semipreparative column (Vydac, Hesperia, CA) were used. HPLC solvents were as follows: SEC, 10 mM PBS containing 300 mM NaCl and 10% (v/v) DMSO at pH 6.8; RP, 0.1% TFA/H₂O (A), 57:43, CH₃CN:H₂O (v/v) containing 0.1% TFA (B), isocratic elution. Preparative SEC was carried out using Sephadex G-25 columns (PD-10, Pharmacia Biotech AB, Uppsala, Sweden) eluted with DPBS. UV-vis spectroscopy experiments were carried out by either a Gilford Response unit (Ciba Corning, Medfield, MA) or a Shimadzu UV-10-02 (Shimadzu Instruments, Columbia, MD). Mass spectra were run on an API VI triple-quadrupole mass spectrometer (PE-Sciex, Toronto, ON) in electrospray mode and PerSeptive Biosystems (Framingham, MA) Voyager Elite MALDI-TOF instruments. Microanalysis was performed by Galbraith Laboratories (Knoxville, TN). Metal-free purified water was obtained from a Milli-QF system (Millipore, Bedford, MA). ¹⁸⁸Re was produced by an in-house ¹⁸⁸W-¹⁸⁸Re generator (Oak Ridge National Laboratory, Oak Ridge, TN) eluted with normal saline. ITLC was carried out on silica gel-impregnated glass fiber slides (Gelman Sciences, Ann Arbor, MI).

N-[Tris[2-[(N-hydroxyamino)carbonyl]ethyl]methyl]succinamic Acid (3). Compound **1** (1 g, 1.51 mmol) was dissolved in methanol (Fisher, HPLC grade, 200 mL), and a slurry of Pd/C (10%, 80 mg, 0.075 mmol) in methanol (1 mL) was added. The flask was sealed with a rubber septum and evacuated for 10 min with stirring. Hydrogen gas was introduced through a needle at a pressure of about 8 atm from a balloon, and the stirring was continued for 65 h at room temperature. The solvent was concentrated *in vacuo* to 10 mL, and the catalyst was separated by an Acrodisc syringe-tip 0.2 μm filter. Evaporation of the solvent to dryness *in vacuo* afforded a white glassy solid (580 mg, 98%): mp 129.5–130.5 °C; RP-HPLC, *t*_R = 3.49 min; ¹H NMR (D₂O) δ 1.95 (m, 6H), 2.14 (m, 6H), 2.52 (m, 2H), 2.61 (m, 2H); ¹³C NMR (D₂O, 100.6 MHz) δ 26 (–CH₂–), 29 (–CH₂–), 30.5 (quat –CH₂–), 48 (Succ. C), 57.5 (Succ. –CH₂–), 172 (hydroxamic –CO–), 174 (Succ. –CO–), 177 (Succ. –CO–); MS (M + H) 393.

2-Nitrophenyl N-[Tris[2-[(N-hydroxyamino)carbonyl]ethyl]methyl]succinate (4). The solution of debenzylated trisuccin **3** (50 mg, 0.127 mmol) and ONP-OH (71 mg, 0.51 mmol) in dry DMF (400 μL) was cooled under argon to 0 °C. The solution of DCC (31.5 mg, 0.17 mmol) in DMF (50 μL) was added, and the reaction was allowed to stir for 16 h at 4 °C. The white solid precipitate was separated by centrifugation, and the supernatant was slowly dripped into a mixture of petroleum ether and dry THF (30:70 v/v, 50 mL) with vigorous stirring. The off-white solid precipitate was collected by centrifugation and washed with the same solvent mixture (3 × 50 mL) by successive vortexing and centrifugation followed by drying of the product in a vacuum desiccator over P₂O₅. Typically, about 40 mg of the product mixture was recovered: Anal. RP-HPLC *t*_R = 20.3 min (B: 5–60%/20 min); Prep. RP-HPLC *t*_R = 41 min (B: 5–75%/60 min); ¹H NMR (D₂O) δ 1.98 (m, 6H), 2.14 (m, 6H), 2.68 (m, 2H), 3.05 (m, 2H), 7.35 (d, *J* = 8 Hz, 1H), 7.55

(m, 1H), 7.82 (m, 1H), 8.2 (d, *J* = 8 Hz, 1H); ¹³C NMR (D₂O, 100.6 MHz) δ 24 (quat C), 26 (–CH₂–), 28 (–CH₂–), 58 (Succ. –CH₂–), 67 (Succ. –CH₂–), 124–135 (Arom. C), 171 (hydroxamic –CO–); MS (M + H) 514.

Methyl N-[Tris[2-[(N-hydroxyamino)carbonyl]ethyl]methyl]succinate (7). The same procedure as for the preparation of compound **3** was used. This product was recrystallized from methanol to obtain 42 mg (70%) of an analytical sample: mp 129.3–129.8 °C; RP-HPLC, *t*_R = 4.5 min; ¹H NMR (D₂O) δ 1.95 (m, 6H), 2.15 (m, 6H), 2.55 (m, 2H), 2.65 (m, 2H), 3.70 (s, 3H), 4.80 (broad singlet). Anal. Calcd for C₁₅H₂₆N₄O₉: C, 44.33%; H, 6.64%; N, 13.79%. Found: C, 44.20%; H, 6.62%; N, 13.73%.

Measurement of the Content of the Active Ester in the Reaction Mixture. A solution of ONP in 0.2 M sodium carbonate buffer (pH 9.5) was scanned in a spectrophotometer, in the 300–600 nm range to reveal a maximum absorption wavelength (λ_{max}) of 415 nm. This λ_{max} was stable after the sample was incubated at 55 °C for 2 h and was used for the construction of an A/C plot as follows: Stock solutions of nitrophenol were made by first dissolving this reagent in 10 mM KOH to obtain a 10 mM solution of ONP-OH, which was then diluted with 0.2 M carbonate buffer (pH 9.5) to a 1 mM working solution. At 415 nm, absorbances of increasing concentrations of ONP-OH, injected as 10 μL aliquots into a starting volume of 400 μL of the carbonate buffer, were measured. The values were then averaged and plotted against the molar concentrations. A concentration range of 2.44 × 10^{–5} M to 13.04 × 10^{–5} M was used for this plot in which a completely linear relationship (*r* = 0.9990) was observed.

A 12.7 mg/mL solution of the active ester **4** in carbonate buffer (0.2 M, pH 9.5) was allowed to decompose at 55 °C for at least 1 h, and 20–50 μL aliquots were withdrawn; absorbances were measured at 415 nm in 400 μL of the carbonate buffer. The corresponding molar concentrations of ONP-OH byproduct were then calculated from the plot as a measure of active ester content in the product mixture. For the active ester used in this work, and using the following equation, a chemical yield of 12.3%, based on a %PF of 20, was obtained.

$$\% \text{ chemical yield} = \frac{(\% \text{PF}) W_{\text{mix}}}{M_{\text{tris}}(\text{MW})_{\text{p}}}$$

*W*_{mix} is the total weight of the product mixture, *M*_{tris} is the number of moles of the starting material trisuccin, and (MW)_p is the molecular weight of the product ester.

Monoclonal Antibody Conjugation. To the solution of the CC49 MAAb (1 mg) in PBS (0.1 M, pH 7.1) at 0 °C was added the solution of **4** in DMF (50 μL) with gentle stirring. After 0.5 h, the mixture was stirred at 4 °C for an additional hour and then at room temperature for 0.5 h, and the reaction was quenched by addition of 20 μL of a 1 M solution of glycine in carbonate buffer (pH 9.5). The conjugate was purified on a PD-10 column using DPBS as the eluting buffer.

Measurement of Ligand-to-Protein Ratio (L:P). This assay was designed to estimate the number of molecules of hydroxamate ligands attached covalently to each molecule of protein. The well-known (8) burgundy red color of hydroxamate–ferric complexes was utilized in this assay as the chromophore handle. Mixing DMSO solutions of **7** (1.23 × 10^{–5} M) and Fe(NO₃)₃·9H₂O (1.98 × 10^{–5} M) provided a deep red solution of the complex with a final concentration of 4.92 × 10^{–4} M, which was used as the stock solution. A spectrophotometric scan of this complex in sodium acetate buffer (0.1 M, pH 5.3)

revealed a λ_{\max} of 386.5 nm. Ten-microliter aliquots of the complex solution were added to the sample cell containing 0.1 M acetate buffer (pH 5.3, starting volume 400 μ L), and absorbances were recorded in triplicate at 386.5 nm against the blank buffer. The averaged absorbances were then plotted against corresponding molar concentrations to afford a linear A/C plot with $r = 0.9998$. A complex concentration range of 7.93×10^{-5} to 32.74×10^{-5} M was used for this plot.

The conjugate prepared above was dialyzed in 0.1 M acetate buffer (pH 5.4), and the protein concentration was determined by Lowry assay (9). Fifty microliters of this conjugate solution was added to 400 μ L of the acetate buffer containing Fe^{3+} with a final concentration of 0.84 mM, and the absorbance was measured at 386.5 nm. Using this absorbance, the molarity of the ligand- Fe^{3+} complex was determined from the A/C plot, and the molarity of the protein in the sample was calculated from its Lowry concentration. The ligand-to-antibody ratio was then calculated by the following equation:

$$\text{L:P} = \text{Mc/Mp}$$

Mc is the molarity of the ferric complex, and Mp is the molarity of the MAB.

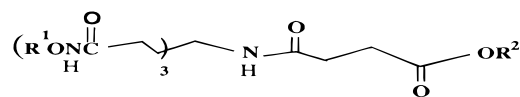
Radiolabeling of Trisuccin-MAB Conjugate. The $\text{Na}^{[188\text{Re}]}\text{-ReO}_4$ in saline (2–5 mCi/mL) was reduced with stannous chloride under argon at 90 °C, and the pH was raised to pH 7 by addition of 1 M carbonate buffer (pH 10). This solution was added at 0 °C to the solution of the conjugate, and the mixture was incubated at 40 °C for 30 min. Radiolabeling was monitored by radio-HPLC, and the radiolabeled conjugate was purified on a PD-10 column eluting with DPBS. Measurement of the radiolabeling yield and purity was done by ITLC using 12% (w/v) TCA (10, 11). In this analysis, radiolabeled protein remained at the origin and any unbound activity moved with the solvent front. Typically, radiolabeling yields of >80% with >95% purities were obtained through this procedure.

RESULTS AND DISCUSSION

The objective of this work was the development of a method which (1) allows the efficient attachment of molecules containing free (unprotected) hydroxamic acids to proteins, peptides, and other molecules with proper functionalities, (2) avoids any interaction between the free hydroxamates and the activated function of the BCA that is to undergo the conjugation reaction, and (3) ensures the availability of all hydroxamate groups in the molecule for further metal chelation.

On the basis of our previous experience with this molecule and its promising radiolabeling results, we focused on the hydroxamate-deprotected analogue of trisuccin for this work in which all benzyl groups are removed prior to attachment to another molecule. In a preliminary evaluation, a number of standard conjugation procedures, including that of Koizumi *et al.* (12), for conjugation of the natural hydroxamate, deferoxamine to antibodies, and reductive amination techniques (13, 14) were studied. Also attempted was a site-specific conjugation technique (15) utilizing MAB's *in situ*-generated aldehydes and an amine derivative of trisuccin.² On the basis of their inability to radiolabel and produce a

Scheme 1



- 1: $\text{R}^1 = \text{Benzyl}, \text{R}^2 = -\text{H}$
- 2: $\text{R}^1 = \text{Benzyl}, \text{R}^2 = 2,3,5,6\text{-tetrafluorophenyl}$
- 3: $\text{R}^1 = -\text{H}, \text{R}^2 = -\text{H}$
- 4: $\text{R}^1 = -\text{H}, \text{R}^2 = \text{ONP}$
- 6: $\text{R}^1 = -\text{Bn}, \text{R}^2 = -\text{OCH}_3$
- 7: $\text{R}^1 = -\text{H}, \text{R}^2 = -\text{OCH}_3$

positive ferric assay (see below), it was decided that none of these procedures were effective toward accomplishment of this goal. These procedures seemed to suffer from a range of shortcomings, including instability of intermediates and/or final product BCA, incompatibility in the nature of the synthetic schemes, and dimerization/polymerization of the activated molecules. We decided, therefore, to design a facile protocol that may effectively conjugate a free hydroxamate to proteins without any need for isolation and purification of intermediate(s) and is not ultimately affected by side reactions and any byproduct(s) formed during the course of the process.

Protein Conjugation. From the preliminary studies, we reasoned that an appropriate choice from the pool of conjugation chemistries would be the amide bond formation through activated esters. On the basis of two advantages associated with ONP esters, *i.e.*, their release of the easily detected ONP-OH on decomposition and maintenance of their activity under steric hinderance (16), we selected these derivatives for the conjugation protocol. Thus, the carboxylic acid **3** was esterified with ONP-OH at 0–4 °C and in the presence of DCC (Scheme 1) and the byproduct DCU and excess ONP-OH were extracted by centrifugation and THF wash, respectively. The off-white solid powder containing the product **4** was dried *in vacuo* and stored under argon at freezer temperature. We expected that any interaction of the hydroxamate moieties with the ONP ester in this unpurified product mixture should result in the formation of an easily detected yellow color and formation of the higher MW byproducts. A given reaction mixture could be expected to consist of unreacted **3**, unreacted DCC, traces of DCU, the desired product (**4**), and the high MW condensation byproducts, if any. Initially, we expected that a *head-to-tail* competing reaction between the activated ester and free hydroxamate functions of the molecule would result in the formation of polymeric byproducts. Interestingly however, the mass spectra showed the major byproduct to be a compound with m/z 748, to which we have tentatively assigned the cyclic dimer structure **5** (Figure 1). This compound has been formed only in small quantities, limiting its isolation as a single pure compound. The whole solid product mixture was readily soluble in aqueous buffers containing $\leq 10\%$ DMF, and only occasionally, with reaction times longer than 24 h, were small traces of water-insoluble solids, which might be due to polymeric byproducts, observed. Qualitatively, these components of the mixture

²Safavy *et al.*, unpublished data. The amine derivative was prepared by the DCC coupling of *N*-Boc-1,6-diaminohexane with compound **1** of Scheme 1 followed by catalytic hydrogenation and TFA deprotection of the adduct.

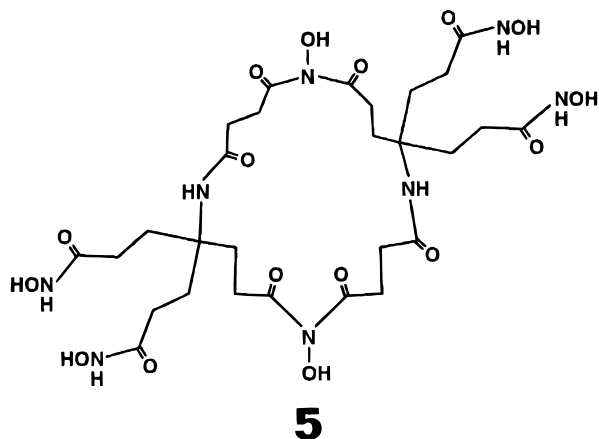


Figure 1. Proposed structure for a m/z 748 trace byproduct of the active ester **4** synthesis.

may be readily detectable by mass spectroscopy (see below). Quantitatively, however, only the concentration of the target active ester needs to be determined for conjugation purposes. On the basis of our mass spectral analyses, and under the conditions required for such conjugation, all other components of this mixture should be unreactive and only the decomposition of the active ester **4**, through hydrolysis or aminolysis, should generate the yellow ONP-OH. Therefore, a simple ONP-OH titration of the product mixture, decomposed by complete base hydrolysis, should indirectly reveal the active ester content in any given batch. The L:P molar ratio for any conjugation reaction would be readily adjusted through this technique, and all unwanted impurity byproducts and decomposition material should be eliminated at the same time during the conjugate purification step. A linear A/C plot of ONP-OH was therefore constructed at 415 nm and used for the measurement of the trisuccin ONP ester content of each batch of the product mixture. A weighed sample of the product mixture was hydrolyzed at a basic pH and elevated temperature, and the intensity of the yellow color was measured at equilibrium. Using the A/C plot, this intensity gave the amount of active ester **4** in the mixture from which a %PF could be calculated. It was found through this analysis that on proper handling and storage of these mixtures,³ ester **4** remained intact for periods >6 months and the same batch of the product could be used repeatedly for protein conjugation with reproducible results. For protein conjugation, the calculated weight of **4** in pure form was measured, immediately prior to the start of the reaction, by applying the %PF to the product mixture. For the active ester product used here, a %PF of 20 was obtained. To validate this technique, we considered a quantitative analysis of the ONP ester formation by standard analytical methods. One approach was to subject an aliquot of the reaction mixture to ¹H NMR spectrometry, assign the peaks, and simply use the integration ratios to estimate the ONP-ester content of the mixture. Also considered was a similar technique using HPLC. It turned out, however, that the unpurified reaction mixture resulted in an NMR pattern which was too crowded to be useful. This was particularly true within the δ 1.5–3.0 range, where most of the signals of this structure occur. A similar limitation was encountered with HPLC. We therefore decided to carefully purify the reaction mixtures

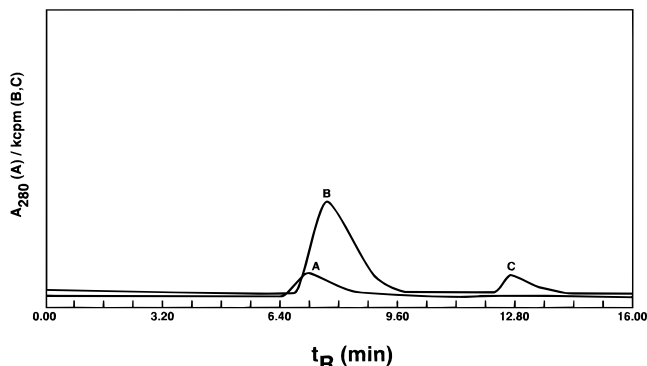


Figure 2. Size exclusion HPLC traces of a ¹⁸⁸Re-labeled trisuccin-CC49 conjugate: UV (A) and radioactivity (B) traces eluted with a short t_R difference due to a series connection of the detectors. Free, unbound radioactivity (C) is eluted with considerably longer t_R . The radioactivity scale is in 10^3 counts/min (kcpm).

and compare the weight of the recovered product with that estimated by the nitrophenol assay. Thus, the dry powder of the reaction mixture was purified on a semi-preparative RP-HPLC column, taking all necessary precautions to prevent loss of the product. Indeed, weights of HPLC-purified products agreed closely with that obtained by the assay. For two independently prepared batches, these values differed by $7.1 \pm 0.3\%$.

The relatively low yield of ester formation should not pose a significant problem since the quantities needed for conjugation are typically in the milligram range or lower. Using DMF as solvent the mixture resulted in a colorless homogeneous solution that turned pale yellow only slowly on standing at room temperature (after 24 h or longer depending on the purity and dryness of the DMF used). The fresh solution thus prepared was mixed with the buffered protein solution to form the homogeneous conjugation solution.

Rhenium-188 Radiolabeling. The MAb (CC49) conjugates prepared through this procedure were radiolabeled with ¹⁸⁸Re. The radio-HPLC trace of a typical ¹⁸⁸Re-radiolabeled antibody is shown in Figure 2. Peaks A and B, respectively, show the UV and radioactivity traces of [¹⁸⁸Re]trisuccin-CC49 conjugate, whereas peak C shows the free, unbound ¹⁸⁸Re. On the basis of this chromatogram, it was estimated that about 89% of the total radioactivity is protein-bound. It should be noted that once corrected for the loss of rhenium as unreduced perrhenate, the yield may even be higher. The radiolabeled conjugates were purified by gel chromatography, and the elution profile of a typical purification run is shown in Figure 3. The radiolabeled antibody conjugates were prepared in this way with preservation of immunoreactivities (17) and were used for animal biodistribution experiments. Details of these studies will be reported separately. Furthermore, a derivative of a gastrin-releasing peptide was conjugated to trisuccin through this protocol as recently reported (18).

L:P Ratio Evaluation. A colorimetric assay, based on the burgundy red color of hydroxamate-Fe³⁺ complex, was developed for the measurement of L:P ratio, to be used for evaluation of conjugation chemistries and final products. In this procedure, the methyl ester of hydroxamate-deblocked trisuccin (**7**) was complexed with ferric nitrate in DMSO and the λ_{\max} was determined in acetate buffer at 386.5 nm. An A/C plot for the complex at this wavelength was constructed which showed linearity ($r = 0.9998$) and was used for the later measurements of ligand concentrations in antibody conjugates. The choice of DMSO and acetate buffer (pH 5.4) was based on our

³Each batch of the product active ester was dried in a vacuum desiccator over P₂O₅ and stored under argon in sealed vials, at freezer temperatures of ≤ -20 °C.

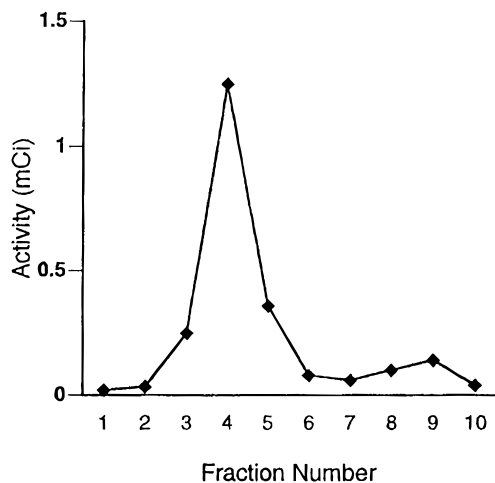


Figure 3. Gel column elution profile of a [^{188}Re]trisuccin-CC49 conjugate purified on a PD-10 column.

earlier studies: the trisuccin- Fe^{3+} compound had lower water solubility and precipitated as a red solid mass when a solution of the ligand in pure water was added to the solution of either ferric nitrate or ferric chloride in buffer, water, or methanol. DMSO, on the other hand, retained the homogeneity of the burgundy red solution with no precipitation on standing over extended periods of time. Similarly, the low-pH acetate buffer retained homogeneity of the solutions mainly through preserving the ferric reagent. In PBS, for instance, the ferric salts quickly hydrolyzed, resulting in precipitation of an insoluble colloid. The selection of the methyl ester of trisuccin, as opposed to that of the carboxylic acid **3**, was to eliminate possibilities of any interaction from the -COOH function with the metal chelation process. Samples of purified trisuccin-antibody conjugates with known concentrations were treated with ferric nitrate and incubated at 55 °C for 1 h, and the change in absorbance at the same wavelength was recorded. The absorbances thus obtained were used to calculate the L:P ratio through the A/C plot of the ferric complex. For the trisuccin-CC49 conjugate described in this paper, an active ester-to-MAb molar ratio of 5 was used, which resulted in a L:P ratio of 1.2. For validating this assay, we analyzed these conjugates with MALDI-TOF MS. Due to the apparent low stabilities of this ONP ester (**4**), we were limited to a maximum buffer pH of 7.1. Reactions at higher pH did not result in conjugation in any detectable extent, and below this pH, probably due to highly protonated protein $-\text{NH}_2$ groups, again no conjugation was observed. This may lead to the conclusion that, at least for this particular active ester,⁴ a low L:P may always result which, for radiolabeling experiments, poses no limitation as our radiolabelings proceeded smoothly and with good yields. However, for analytical experiments such as MALDI-TOF MS, this low L:P may fall beyond the sensitivity limits of the instrument and, therefore, not be easily detectable. Only in one conjugation, carried out under the described conditions, were we able to detect a L:P of about 0.65 by MALDI-TOF MS. If we consider the MS data a reliable tool for assessing the

L:P, we may conclude that the ferric assay reported here may overestimate this ratio. However, due to the simplicity of this assay and its cost-effectiveness, its application may be considered as a preliminary test of conjugation, particularly in experiments for which an exact value for L:P is not required.

These results indicate that the conjugation method described in this paper may be utilized as a general protocol for the covalent attachment of unprotected hydroxamic acids to molecules containing suitable nucleophilic functionalities.

ACKNOWLEDGMENT

This work was supported by NIH Grants CA62550, CA44173, and DOE DE-FG05-93ER61654. We acknowledge the assistance of the Comprehensive Cancer Center Mass Spectrometry (Mr. Marion Kirk) and Nuclear Magnetic Resonance Shared Facilities and also Kamellia Safavy for protein determinations and radioimmunoassays. We thank Sally Lagan for manuscript preparation.

LITERATURE CITED

- (1) Meares, C. F. (1986) Chelating agents for the binding of metal ions to antibodies. *Nucl. Med. Biol.* 13, 311.
- (2) Jurisson, S., Berning, D., Jia, W., and Ma, D. (1993) Coordination compounds in nuclear medicine. *Chem. Rev.* 93, 1137.
- (3) Baidoo, K. E., Scheffel, U., and Lever, S. Z. (1990) $^{99\text{m}}\text{Tc}$ labeling of proteins: Initial evaluation of a novel diaminedithiol bifunctional chelating agent. *Cancer Res. (Suppl.)* 50, 799s.
- (4) Schwartz, D. A., Abrams, M. J., Hauser, M. M., Gaul, F. E., Larsen, S. K., Rauth, D., and Zubieta, J. A. (1991) Preparation of hydrazine-modified proteins and their use for the synthesis of $^{99\text{m}}\text{Tc}$ -protein conjugates. *Bioconjugate Chem.* 2, 333.
- (5) Vanderheyden, J.-L., Gofinch, S., Srinivasan, A., Su, F. M., Venkatesan, P., Woodhouse, C., Sanderson, J., Woods, M., Wilkening, D., and Beaumier, P. (1989) Preparation and characterization of Re-188 NR-CO-O2 F(ab')₂: A new anti-CEA antibody fragment for radioimmunotherapy. *J. Nucl. Med.* 30, 793.
- (6) Safavy, A., Buchsbaum, D. J., and Khazaeli, M. B. (1993) Synthesis of *N*-[tris[2-[[*N*-(benzyloxy)amino]carbonyl]ethyl]methyl]succinamic acid, trisuccin. Hydroxamic acid derivatives as a new class of bifunctional chelating agents. *Bioconjugate Chem.* 4, 194.
- (7) Safavy, A., Khazaeli, M. B., and Buchsbaum, D. J. (1994) Rhenium-186 labeling of CC49 monoclonal antibody with *N*-[tris[2-[[*N*-(benzyloxy)amino]carbonyl]ethyl]methyl]succinamic acid, trisuccin, and biodistribution studies. *J. Nucl. Med.* 35, 258P.
- (8) Gagliardi, E., and Raber, H. (1962) Hydroxamsauren als analytische reagentien. *Monatsh. Chem.* 93, 360.
- (9) Lowry, O. H., Rosebrough, N. J., Farr, A. L., and Randall, R. J. (1951) Protein measurement with the Folin phenol reagent. *J. Biol. Chem.* 193, 265.
- (10) Griffiths, G. L., Goldenberg, D. M., Knapp, F. F., Jr., Callahan, A. P., and Chang, C.-H. (1991) Labeling and animal biodistribution studies. *Cancer Res.* 51, 4594.
- (11) Goldrosen, M. H., Biddle, W. C., Pancock, J., Bakshi, S., Vanderheyden, J.-L., Fritzberg, A. R., Morgan, A. C., Jr., and Foon, K. A. (1990) Biodistribution, pharmacokinetic, and imaging studies with ^{186}Re -labeled NR-LU-10 whole antibody in LS174T colonic tumor-bearing mice. *Cancer Res.* 50, 7973.
- (12) Koizumi, M., Endo, K., Kunitatsu, M., Sakahara, H., Nakashima, T., Kawamura, Y., Watanabe, Y., Saga, T., Konishi, J., Yamamuro, T., Hosoi, S., Toyama, S., Arano, Y., and Yokoyama, A. (1988) ^{67}Ga -labeled antibodies for immunoscintigraphy and evaluation of tumor targeting of drug-antibody conjugates in mice. *Cancer Res.* 48, 1189.
- (13) Jentoft, N., and Dearborn, D. G. (1979) Labeling of proteins by reductive methylation using sodium cyanoborohydride. *J. Biol. Chem.* 254, 4359.
- (14) Chamow, S. M., Kogan, T. P., Peers, D. H., Hastings, R. C., Byrn, R. A., and Ashkenazi, A. (1992) Conjugation of

⁴Other ONP esters may show higher stabilities under the conjugation conditions described here. We have recently synthesized a trisuccin derivative (data not shown) in which the 4-nitrophenyl moiety is a benzoate. Our preliminary results indicate that, under the same conditions, this ester has a higher stability than the lead trisuccin described here. Higher CC49 radiolabeling yields have been achieved with this compound, which may be due to a higher L:P.

- soluble CD4 without loss of biological activity via a novel carbohydrate-directed cross-linking reagent. *J. Biol. Chem.* 267, 15916.
- (15) Gaertner, H. F., Rose, K., Cotton, R., Timms, D., Camble, R., and Offord, R. E. (1992) Construction of protein analogs by site-specific condensation of unprotected fragments. *Bioconjugate Chem.* 3, 262.
- (16) Bodanszky, M., Fink, M. L., Funk, K. W., Kondo, M., Lin, C. Y., and Bodanszky, A. (1974) Rigid active esters in peptide synthesis. *J. Am. Chem. Soc.* 96, 2234.
- (17) Lindmo, T., Boven, E., Cuttitta, F., Fedorko, J., and Bunn, J., P. A. (1984) Determination of the immunoreactive fraction of radiolabeled monoclonal antibodies by linear extrapolation to binding at infinite antigen excess. *J. Immunol Methods.* 72, 77.
- (18) Safavy, A., Khazaeli, M. B., and Buchsbaum, D. J. (1997) Synthesis of bombesin analogues for radiolabeling with rhenium-188. *Cancer* (in press).

BC970127M

Synthesis of 17 β -Hydroxy Esters of 4-Estren-17 β -ol-3-one and Carbenicillin, Ticarcillin, or Functionalized Oxacillin: Potentially Useful Conjugates for β -Lactamase-Based Homogeneous Immunoassays

M. Kohl,* L. Thunus, and R. Lejeune

Institut de Pharmacie, Université de Liège, Service de Chimie analytique, rue Fusch, 3, B-4000 Liege, Belgium.
Received January 7, 1997[®]

On the basis of the large range of kinetic constants of their substrates, β -lactamases seem to be interesting enzymes for the development of homogeneous immunoassays. For this purpose, hapten–penicillin or –cephalosporin conjugates have to be prepared. The aim of this work is to couple the anabolizing steroid nandrolone to several penicillins characterized by extremely low K_m and k_{cat} values: ticarcillin, carbenicillin, and oxacillin. The easy decarboxylation of derivatives of phenylmalonic acid (carbenicillin) and thienylmalonic acid (ticarcillin) imposes the choice of very mild procedures which have been specifically adapted to each substance investigated. 4-Estren-17 β -ol-3-one hemi-phenylmalonate is conjugated to 6-aminopenicillanic acid after 1,1'-carbonyldiimidazole activation, while 4-estren-17 β -ol-3-one hemi(3-thiophene)malonate is coupled to 6-aminopenicillanic acid after activation using methanesulfonyl chloride. Before conjugation of oxacillin, a carboxylated analogue of its side chain has been prepared. A procedure resorting to *tert*-butyl ester protection of the carboxyl group present on the isoxazole ring allows the binding of nandrolone to the remaining carboxyl followed, after specific deprotection, by the conjugation to 6-aminopenicillanic acid giving the oxacillin derivative. In this way, conjugates retaining immunological properties of nandrolone and high inhibiting power of β -lactamases should be obtained.

INTRODUCTION

β -lactamases have never been used as a basis for the development of homogeneous immunoassays, although they display interesting properties in this field (1, 2): the formation of stable pseudocovalent enzyme–substrate complexes and the availability of powerful inhibitory substrates such as carbenicillin, ticarcillin, or oxacillin (Figure 1) as well as efficient colored reporter substrates such as nitrocefin.

When reporter substrates are mixed with inhibitory substrates in the presence of some class C β -lactamases, a modulation of β -lactamase activity is obtained depending on the relative concentration of the reporter substrate and the inhibitor. These characteristics could be exploited for the design of a homogeneous immunoassay if the inhibitor is conjugated to a hapten to be determined and if the addition of an antibody directed to the hapten results in a masking effect on the inhibitor activity.

Conjugation of penicillins to proteins or polymers has been carried out after activation of the carboxyl groups present on the thiazolidine ring or in the side chain (3, 4). In several procedures, native or introduced thiols have also been used for this purpose (5, 6). However, the best known reaction of penicillins is the hemisynthesis which is usually performed by enzymatic or chemical coupling of side chains to 6-aminopenicillanic acid (6 APA) (II) or 7-aminocephalosporanic acid (7 ACA) (7).

In this work, we have tried to prepare conjugates of β -lactamase inhibitors and of nandrolone (4-estren-17 β -ol-3-one) (I), an anabolizing steroid frequently determined using immunoassay techniques (8).

EXPERIMENTAL PROCEDURES

General Methods. All chemicals and solvents were commercial grade and of the highest purity. 4-Carboxy-

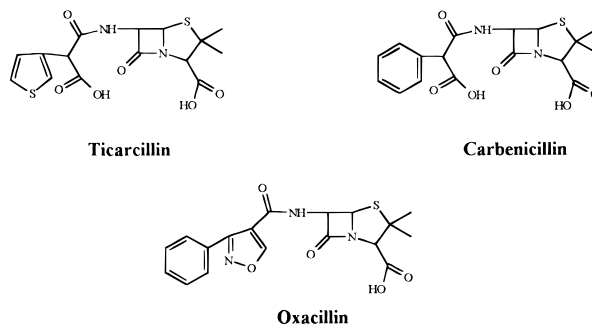


Figure 1. Penicillins characterized by interesting kinetic parameters.

benzaldehyde (>99%), ethyl acetoacetate sodium salt (98.5%), *tert*-butyl acetoacetate (98%), lithium iodide (99%), *p*-toluenesulfonic acid monohydrate (98.5%), and phenylmalonic acid (98%) were purchased from Aldrich Chemical Co. (Milwaukee, WI). 4-Estren-17 β -ol-3-one (nandrolone) was from Steraloids (Wilton, NH) and 3-thiophenemalonic acid (98%) from Acros Chimica (Geel, Belgium). Silica gel 60 (E-Merck, 230–400 mesh ASTM) (Merck, Darmstadt, Germany) was used for column chromatography. Thin layer Alugram Sil6/UV₂₅₄ plates (from Macherey-Nagel, Düren, Germany) with fluorescent indicator were used for thin layer chromatography (TLC). All the organic extracts are dried over anhydrous Na₂SO₄. All mixtures of solvents used either as mobile phases or as crystallization solvents are expressed in volume–volume proportions. Infrared (IR) spectra were recorded on a Perkin-Elmer (Beaconsfield, Bucks, England) spectrum 2000 Fourier transform infrared spectrophotometer. Spectra were obtained either after dissolving the compound at 0.1% in tetrachloroethylene or after mixing the compound at 0.4% in potassium bromide.

[®] Abstract published in *Advance ACS Abstracts*, August 15, 1997.

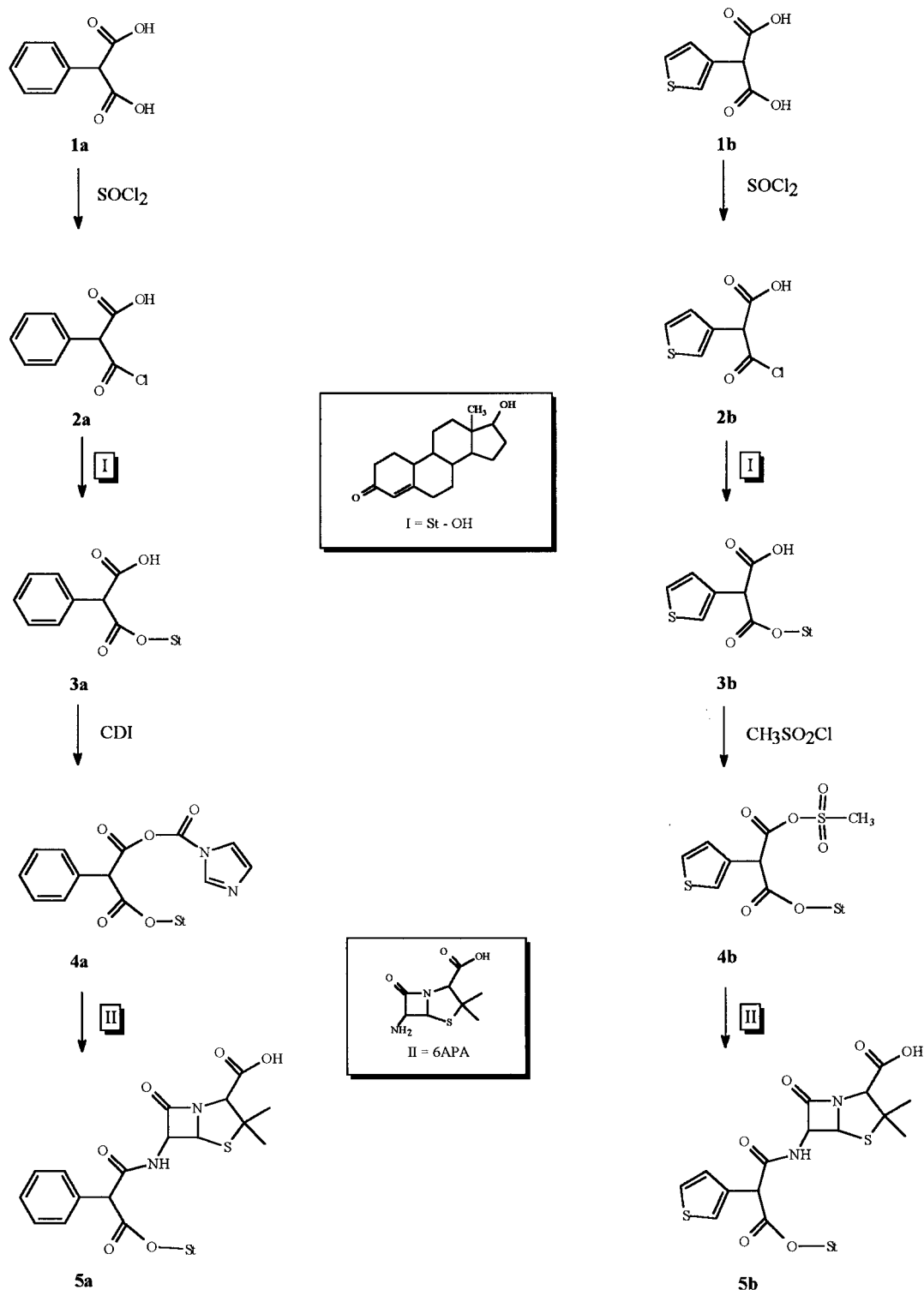


Figure 2. Synthesis of 6-[3-(4-estren-3-one-17 β -oxy)-3-oxo-2-phenylpropanamido]penicillanic acid and of 6-[3-(4-estren-3-one-17 β -oxy)-3-oxo-2-thienylpropanamido]penicillanic acid.

Solutions were scanned in a liquid transmission cell, with an internal volume of 200 μ L and a path length of 500 μ m.

Mass spectra (MS), by electrospray ionization (ES) using a mixture of acetonitrile/water (50/50) as the solvent and 30 V as the cone voltage and by liquid secondary ion ionization (20 kV) (LSI) using glycerol as a matrix, were obtained on a VG platform Fisons or on a Autospec Q VG analytical Fisons (Danvers, MA) mass spectrometer. Elemental analyses were accomplished on a Carlo Erba CHNS-O EA 1108 instrument (Rodano,

Milano, Italy). All obtained products have analytical data (C, H, and N), except for unstable products.

EXPERIMENTAL SYNTHESIS

(A) Conjugation of Nandrolone to Carbenicillin or Ticarcillin (Figure 2). (1) *Preparation of 4-Estren-17 β -ol-3-one Hemiphenylmalonate (3a).* To a solution of 2 g (11.2 mmol) of phenylmalonic acid (**1a**) in a mixture of dry ether (20 mL) and dry 1,4-dioxan (4 mL) are added 1 drop of dimethylformamide and 1.18 g (736 μ L \approx 10 mmol) of thionyl chloride. The solution is warmed to 45

°C for 2 h. The yellow solution obtained (**2a**) is cooled to -25°C . A solution of 2 g (7.2 mmol) of 4-estren-17 β -ol-3-one (**1**) is prepared in dry toluene (15 mL) and added to the acyl chloride solution. A triethylamine solution (2.26 g \approx 3.14 mL \approx 20 mmol) in dry toluene (10 mL) is slowly added dropwise to the combined solutions. The mixture is allowed to warm to room temperature for 1 h. The solution is then poured into 150 mL of a 0.1 M HCl/water solution. The organic phase is washed copiously with cold water and dried. The so-obtained organic solution is treated with charcoal. After filtration, the solution is partially evaporated under reduced pressure and the residue is purified by column chromatography (using the same mobile phase as for the TLC). The 4-estren-17 β -ol-3-one hemiphenylmalonate (**3a**) is crystallized from a mixture of toluene and petroleum ether: bp 100–140 °C (5–45); yield 42% IR (cm^{-1}) (KBr) 1738 ($\nu_{\text{estren ester}}^{\text{C=O}}$), 1716 ($\nu_{\text{malonic acid, C=O}}$), 1682 ($\nu_{\text{estren ketone, C=O}}$), MS (LSI) m/z 437 ($M + H^+$); TLC toluene/ethyl acetate/acetic acid (1/1/0.1) $R_f = 0.36$.

(2) *Preparation of 6-[3-(4-Estren-3-one-17 β -oxy)-3-oxo-2-phenylpropanamido]penicillanic Acid (**5a**)*. A solution of 50 mg (0.1 mmol) of 4-estren-17 β -ol-3-one hemiphenylmalonate (**3a**) and 16 mg (0.1 mmol) of 1,1'-carbonyldiimidazole is stirred at 0 °C for 4 h in dry tetrahydrofuran (6 mL). Forty milligrams (0.2 mmol) of 6-aminopenicillanic acid (**II**) is dissolved into a 2% NaHCO_3 /water solution (5 mL), diluted with acetone (4 mL), and cooled under stirring to 0 °C. The former solution containing the activated derivative of 4-estren-17 β -ol-3-one hemiphenylmalonate (**4a**) is added drop by drop to the latter solution. After 2 h, the mixture is diluted with a 2% NaHCO_3 /water solution (20 mL) and filtered. The filtrate is poured into ethyl acetate (10 mL) and acidified with a 0.1 M HCl/water solution to pH 2–3. The organic phase is washed three times with water and dried. The solvent is removed under reduced pressure. The oily yellow residue is crystallized from toluene and petroleum ether: bp 40 °C (5–25); yield 52%; IR (cm^{-1}) (KBr) 1740 ($\nu_{\text{estren ester, C=O}}$), 1676 ($\nu_{\text{malonic amide, C=O}}$), 1765 ($\nu_{\text{cyclic amide, C=O}}$), 1725 ($\nu_{\text{penicillanic acid, C=O}}$), MS (LSI) m/z 635 ($M + H^+$); TLC toluene/ethyl acetate/acetic acid (1/1/0.2) $R_f = 0.04$, chloroform/ethyl acetate/methanol/acetic acid (4/4/1/0.2) $R_f = 0.63$.

(3) *Preparation of 4-Estren-17 β -ol-3-one Hemi(3-thiophene)malonate (**3b**)*. To a solution of 2 g (10.75 mmol) of 3-thiophenemalonic acid (**1b**) in a mixture of dry ether (20 mL) and dry 1,4-dioxan (4 mL) are added 1 drop of dimethylformamide and 1.06 g (662 $\mu\text{L} \approx$ 9 mmol) of thionyl chloride. The solution is stirred at room temperature for 4 h. The resulting solution (**2b**) is cooled to -35°C . A cooled solution of 1.5 g (5.4 mmol) of 4-estren-17 β -ol-3-one (**1**) in dry acetone (10 mL) is added to the acyl chloride solution. A triethylamine solution (2.26 g \approx 3.14 mL \approx 20 mmol) in dry toluene is added slowly and by little portions to the combined solution. The mixture is allowed to warm to room temperature for 1 h. The solution is then poured into 150 mL of a cooled water solution of 0.1 M HCl. The organic phase is washed copiously with cold water and dried. The so-obtained organic solution is treated with charcoal. After filtration, the toluene is partially evaporated under reduced pressure and the residue is purified by column chromatography (using the same mobile phase as for the TLC). The 4-estren-17 β -ol-3-one hemi-(3-thiophene)malonate (**3b**) is crystallized from a mixture of toluene and petroleum ether: bp 100–140 °C (5–25); yield 31%, IR (cm^{-1}) (C_2Cl_4) 1743 ($\nu_{\text{estren ester, C=O}}$), 1715 ($\nu_{\text{thiophenemalonic acid, C=O}}$), 1682 ($\nu_{\text{estren ketone, C=O}}$); MS (ES^+)

m/z 443 ($M + H^+$); TLC toluene/ethyl acetate/acetic acid (1/1/0.1) $R_f = 0.38$.

(4) *Preparation of 6-[3-(4-Estren-3-one-17 β -oxy)-3-oxo-2-(3-thienyl)propanamido]penicillanic Acid (**5b**)*. A solution of 100 mg (0.276 mmol) of 4-estren-17 β -ol-3-one hemi(3-thiophene)malonate (**3b**) in dry tetrahydrofuran (5 mL) is treated with *N,N*-diisopropylethylamine (51 μL , 0.292 mmol) and then cooled to -50°C . Methanesulfonyl chloride (56 μL , 0.692 mmol) is added, and the solution is stirred at -50°C for a further 2 h. This mixture containing the mixed sulfonic acid anhydride (**4b**) is then added to a preformed solution of 6.3 mg (0.292 mmol) of 6-aminopenicillanic acid (**II**) in a 2% NaHCO_3 /water solution (5 mL) and acetone (4 mL) and cooled to 0 °C. After the mixture has been stirred for 1 h at 0 °C, ethyl acetate and water are added. The pH is adjusted to 3 with a 0.1 M HCl/water solution. The organic phase is washed with water. The solvent is removed under reduced pressure. The viscous yellow residue is purified on a precoated TLC plate sil 6–200 from Merck. The mixture toluene/ethyl acetate/acetic acid (1/1/0.1) is used as the mobile phase. The linear spot is scraped from the plate. The silica is washed with several ethyl acetate fractions. The resulting organic solution is washed with water and dried. The solvent is removed under reduced pressure. Crystallization from ethyl acetate and petroleum ether gave the product (**5b**): bp 40 °C (10–90); yield 21%; IR (cm^{-1}) (KBr) 1672 ($\nu_{\text{malonic amide, C=O}}$), 1767 ($\nu_{\text{cyclic amide, C=O}}$), 1724 ($\nu_{\text{penicillanic acid, C=O}}$); MS (ES^-) m/z 639 ($M - H^-$); TLC chloroform/ethyl acetate/methanol/acetic acid (4/4/1/0.02) $R_f = 0.64$.

(B) *Preparation of a Nandrolone–Oxacillin Conjugate (Figure 3)*. (5) *Preparation of 4-Carboxybenzal-doxime (7)*. A stirred solution of 10 g (65 mmol) of 4-carboxybenzaldehyde (**6**) and 9.1 g (130 mmol) of hydroxylamine hydrochloride in a mixture of methanol (100 mL)/water (100 mL) is brought up to pH 4.5 with a 1 M NaOH/water solution. The reaction mixture is then kept at 45 °C for 2 h. The starting reactive product (4-carboxybenzaldehyde, $R_f = 0.79$) (**6**) is gradually used up, and this is monitored by thin layer chromatography. The methanol is removed under reduced pressure when the reaction is over. To the so-obtained aqueous solution is added a water solution of 0.1 M HCl to pH 2. It gives a white precipitate. The suspension is then filtered. The solid residue is washed three times with water. It is then dissolved in a 5% NaHCO_3 /water solution and treated with charcoal. The aqueous mixture is filtered. The filtrate is acidified with a 0.1 M HCl/water solution to pH 2. The wished compound crystallizes from water. The carboxybenzaldehyde (**7**) is then filtered off, washed with water, and dried under reduced pressure: yield 89%, IR (cm^{-1}) (KBr) 1689 ($\nu_{\text{acid, C=O}}$), 1608 ($\nu_{\text{oxime, C=N}}$), 3585 ($\nu_{\text{oxime, N-OH}}$); MS (ES^+) m/z 166 ($M + H^+$); TLC chloroform/tetrahydrofuran/acetic acid (7/0.8/0.2) ($R_f^{\text{carboxybenzaldehyde}} = 0.76$). Anal. Calcd for $\text{C}_8\text{H}_7\text{O}_3\text{N}$: C, 58.19; H, 4.27; N, 8.48. Found: C, 58.29; H, 4.29; N, 8.46.

(6) *Preparation of 4-Carboxybenzohydroxamoyl Chloride (8)*. A stirred solution of 8 g (48 mmol) of 4-carboxybenzaldehyde (**7**) in anhydrous 1,4-dioxan (65 mL) and chloroform (20 mL) is cooled to -10°C . The solution is treated with 4 g (60 mmol) of chlorine in chloroform (150 mL). The mixture is left overnight at room temperature. After removal of the solvent under reduced pressure, crude 4-carboxybenzohydroxamoyl chloride (**8**) is obtained as an oil. This residue is crystallized from a mixture of ethanol and petroleum ether (bp of 40 °C; 5–65). The 4-carboxybenzohydroxamoyl chloride (**8**) is filtered off, washed with petroleum ether (bp of 40 °C), and dried under reduced pressure: yield 86%, IR (cm^{-1})

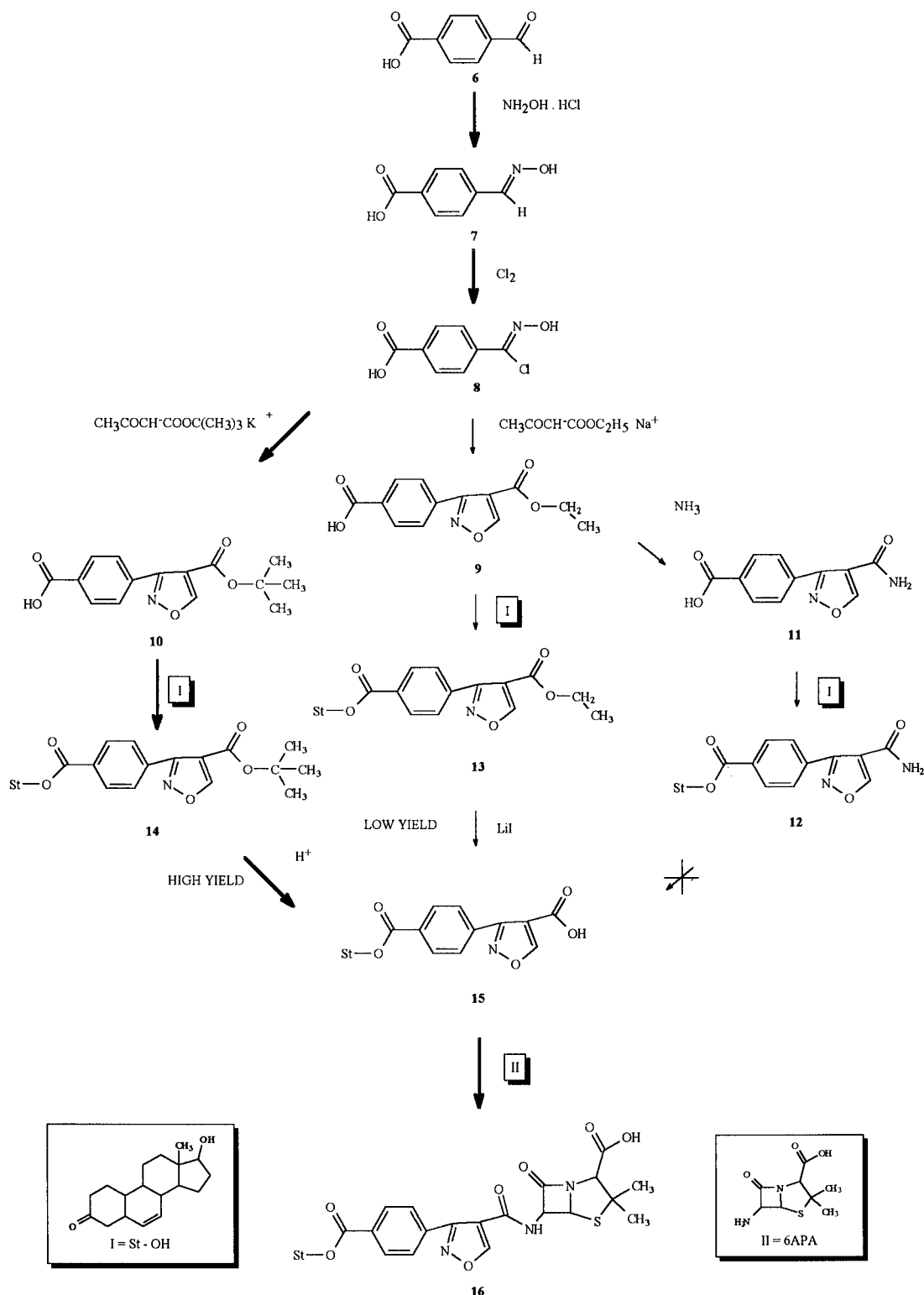


Figure 3. Synthesis of 6-[3-(4-estren-17 β -ol-3-one benzenecarboxyl-yl)-5-methylisoxazole-4-carboxamido]penicillanic acid.

(KBr) 1691 (ν_{acid} , C=O), 1610 (ν_{oxime} , C=N), 3581 (ν_{oxime} , N-OH); ES^- m/z 198 ($\text{M} - \text{H}$) $^-$; TLC chloroform/tetrahydrofuran/acetic acid (7/0.8/0.2) R_f = 0.86. Anal. Calcd for $\text{C}_{28}\text{H}_{36}\text{O}_3\text{NCl}$: C, 48.14; H, 3.03; N, 7.01. Found: C, 48.24; H, 3.15; N, 6.90.

(7) *Preparation of Ethyl 3-(4-Carboxyphenyl)-5-methylisoxazole-4-carboxylate (9).* A solution of 7 g (35.1 mmol) of 4-carboxybenzohydroxamic acid (8) in methanol (80 mL) and acetonitrile (80 mL) is chilled to -5°C . Then a solution of 10.7 g (70 mmol) of ethyl acetoacetate sodium salt in acetonitrile (60 mL) is slowly added. The

mixture is allowed to warm to room temperature overnight. The solvent is then evaporated under reduced pressure. The oily residue is shaken in a 0.1 M HCl/water solution (100 mL) and chloroform (200 mL). The aqueous phase is once again extracted with chloroform. The combined chloroform extracts are washed with water and dried. The solvent is removed under reduced pressure. The obtained residue is crystallized from a mixture of chloroform and petroleum ether (bp of 40°C ; 5–45). The ethyl 3-(4-carboxyphenyl)-5-methylisoxazole-4-carboxylate (9) is filtered off, washed with petroleum ether

(bp of 40 °C), and dried under reduced pressure: yield 70%; IR (cm⁻¹) (KBr) 1688 (ν_{acid} , C=O), 1720 (ν_{ester} , C=O); ES⁻ *m/z* 274 (M - H)⁻; TLC toluene/ethyl acetate/acetic acid (2/1/0.1) *R_f* = 0.42. Anal. Calcd for C₁₄H₁₃O₅N: C, 61.09; H, 4.76; N, 5.08. Found: C, 61.21; H, 4.95; N, 5.01.

(8) Preparation of *tert*-Butyl 3-(4-Carboxyphenyl)-5-methylisoxazole-4-carboxylate (**10**). This compound is prepared from 7 g (35.1 mmol) of 4-carboxybenzohydroxamoyl chloride (**8**) and 13.75 g (70 mmol) of *tert*-butyl acetoacetate potassium salt by a similar procedure used previously for ethyl 3-(4-carboxyphenyl)-5-methylisoxazole-4-carboxylate (**9**): yield 71.24%, IR (cm⁻¹) (C₂Cl₄) 1698 (ν_{acid} , C=O), 1614 (ν_{oxime} , C=N), 1714 ($\nu_{\text{tert-butyl ester}}$, C=O); ES⁻ *m/z* 301 (M - H)⁻; TLC toluene/ethyl acetate/acetic acid (2/1/0.1) *R_f* = 0.5. Anal. Calcd for C₁₆H₁₈O₅N: C, 61.85; H, 5.88; N, 5.08. Found: C, 61.68; H, 5.81; N, 4.96.

(9) Preparation of Ethyl 3-(4-Estren-17 β -ol-3-one-benzenecarboxylate-4-yl)-5-methylisoxazole-4-carboxylate (**13**). A solution of 1 g (3.6 mmol) of ethyl 3-(4-carboxyphenyl)-5-methylisoxazole-4-carboxylate (**9**), 4 mg of 4-dimethylaminopyridine, and 900 mg (3.28 mmol) of 4-estren-17 β -ol-3-one (**I**) in dry dichloromethane (25 mL) is cooled to 0 °C. A small excess of 1,3-dicyclohexylcarbodiimide (900 mg, 4.32 mmol) is added by little portions. This mixture is stirred for 2 h until room temperature is reached. The starting reactive product [ethyl 3-(4-carboxyphenyl)-5-methylisoxazole-4-carboxylate, *R_f* = 0.42] is gradually used up, and this is monitored by thin layer chromatography. After reaction, the solution is filtered. The filtrate is concentrated under reduced pressure, and the oily residue is dissolved in ethyl acetate. This ethyl acetate solution is cooled to 4 °C over 2 h. The cooled solution is then filtered in order to eliminate dicyclohexylurea. The filtrate is washed with a 5% NaHCO₃/water solution and then with water and dried. The solvent is removed under reduced pressure. The solid residue is purified by crystallization from a mixture of toluene and petroleum ether: bp 40 °C (10–90); yield 83%, IR (cm⁻¹) (C₂Cl₄) 1716 ($\nu_{\text{ethyl ester}}$, C=O), 1725 ($\nu_{\text{estren ester}}$, C=O), 1668 ($\nu_{\text{estren ketone}}$, C=O); ES⁺ *m/z* 532 (M - H)⁺; TLC toluene/ethyl acetate/acetic acid (2/1/0.1) *R_f* = 0.52. Anal. Calcd for C₃₂H₃₇NO₆: C, 72.30; H, 7.01; N, 2.63. Found: C, 72.61; H, 7.26; N, 2.72.

(10) Preparation of *tert*-Butyl 3-(4-Estren-17 β -ol-3-one-benzenecarboxylate-4-yl)-5-methylisoxazole-4-carboxylate (**14**). This compound is prepared from 1 g (3.43 mmol) of *tert*-butyl 3-(4-carboxyphenyl)-5-methylisoxazole-4-carboxylate (**10**) and 900 mg (3.28 mmol) of 4-estren-17 β -ol-3-one (**I**) by a similar procedure used for ethyl 3-(4-estren-17 β -ol-3-one benzenecarboxylate-4-yl)-5-methylisoxazole-4-carboxylate (**13**): yield 81%, IR (cm⁻¹) (C₂Cl₄) 1713 ($\nu_{\text{tert-butyl ester}}$, C=O), 1725 ($\nu_{\text{estren ester}}$, C=O), 1678 ($\nu_{\text{estren ketone}}$, C=O); ES⁺ *m/z* 561 (M - H)⁺; TLC toluene/ethyl acetate/acetic acid (2/1/0.1) *R_f* = 0.62. Anal. Calcd for C₃₄H₄₁NO₆: C, 72.90; H, 7.38; N, 2.50. Found: C, 72.59; H, 7.66; N, 2.63.

(11) Preparation of 3-(4-Estren-17 β -ol-3-one-benzenecarboxylate-4-yl)-5-methylisoxazole-4-carboxylic acid (**15**) (11.1) by LiI. Six hundred thirty milligrams mg (4.7 mmol) of dry LiI, 500 mg (0.94 mmol) of ethyl 3-(4-estren-17 β -ol-3-one benzenecarboxylate-4-yl)-5-methylisoxazole-4-carboxylate (**13**), and 77 mg (0.94 mmol) of anhydrous sodium acetate are dissolved in dry dimethylformamide. The solution is heated under a nitrogen stream in a thermostatically controlled oil bath for 32 h at 115 °C. The solution is then cooled to room temperature and poured into a mixture of a 0.1 M HCl/water solution (25 mL) and chloroform (25 mL). The organic phase is washed three times with water and dried. The solvent

is removed under reduced pressure. The desired compound is isolated by column chromatography using the same mobile phase as for TLC. The resulting organic solution is washed with water and dried. The solvent is removed under reduced pressure. The obtained residue is crystallized from a mixture of toluene and petroleum ether (bp of 40 °C; 5–75). The 3-(4-estren-17 β -ol-3-one-benzenecarboxylate-4-yl)-5-methylisoxazole-4-carboxylic acid (**15**) is filtered off, washed with petroleum ether (bp of 40 °C), and dried under reduced pressure: yield 3–16%, IR (cm⁻¹) (C₂Cl₄) 1698 (ν_{acid} , C=O); ES⁻ *m/z* 502 (M - H)⁻; TLC toluene/ethyl acetate/acetic acid (2/1/0.1) *R_f* = 0.44. Anal. Calcd for C₃₀H₃₃NO₆: C, 71.55; H, 6.60; N, 2.78. Found: C, 71.68; H, 6.87; N, 2.75.

(11.2) Preparation of **15** by *p*-Toluenesulfonic Acid. To a solution of 500 mg (0.9 mmol) of *tert*-butyl 3-(4-estren-17 β -ol-3-one benzenecarboxylate-4-yl)-5-methylisoxazole-4-carboxylate (**14**) in nitromethane (25 mL) and toluene (10 mL) is added a solution of 235 mg (1.35 mmol) of *p*-toluenesulfonic acid in nitromethane (10 mL) warmed to 50 °C. That mixture is kept at room temperature for 4 h. It is then diluted with chloroform. The organic phase is washed three times with water and dried. The solvent is removed under reduced pressure. The oily residue is purified by column chromatography using a mixture of toluene/ethyl acetate/acetic acid (2/1/0.1) as a mobile phase. After elimination of the solvent under reduced pressure, the resulting organic solution is washed with water and dried. The obtained white residue crystallized from a mixture of chloroform and petroleum ether (bp of 40 °C; 5–70). The 3-(4-estren-17 β -ol-3-one benzenecarboxylate-4-yl)-5-methylisoxazole-4-carboxylic acid (**15**) is filtered off and dried under reduced pressure: yield 56%; IR (cm⁻¹) (C₂Cl₄) 1696 (ν_{acid} , C=O); ES⁻ *m/z* 502 (M - H)⁻; TLC toluene/ethyl acetate/acetic acid (2/1/0.1) *R_f* = 0.44, chloroform/ethyl acetate/methanol/acetic acid (4/4/1/0.02) *R_f* = 0.88. Anal. Calcd for C₃₀H₃₃NO₆: C, 71.55; H, 6.60; N, 2.78. Found: C, 71.71; H, 6.87; N, 2.96.

(12) Preparation of 3-(4-Carboxyphenyl)-5-methylisoxazole-4-carboxamide (**11**). A solution of 4 g (14.5 mmol) of ethyl 3-(4-carboxyphenyl)-5-methylisoxazole-4-carboxylate (**9**) in 22 mL (0.29 mol) of a 25% ammonia/water solution cooled to 0 °C is put into a pressure-sealed reactor and autoclaved over 48 h at 50 °C. The solution is cooled to 0 °C and then transferred into a flask, and the excess of the ammonia water solution is removed under reduced pressure. The solution is acidified with a 1 M HCl/water solution to pH 2.5. The obtained residue is washed with water and then with ether and with chloroform. It is dried under reduced pressure: yield 65%, IR (cm⁻¹) (KBr) 1694 (ν_{acid} , C=O); ES⁻ *m/z* 245 (M - H)⁻; TLC chloroform/tetrahydrofuran/acetic acid (7/0.8/0.2) *R_f* = 0.47. Anal. Calcd for C₁₂H₁₀N₂O₄: C, 58.54; H, 4.09; N, 11.37. Found: C, 58.71; H, 4.38; N, 11.68.

(13) Preparation of 3-(4-Estren-17 β -ol-3-one-benzenecarboxylate-4-yl)-5-methylisoxazole-4-carboxamide (**12**). A solution of 1 g (4.06 mmol) of 3-(4-carboxyphenyl)-5-methylisoxazole-4-carboxamide (**11**), 4 mg of 4-dimethylaminopyridine, and 900 mg (3.28 mmol) of 4-estren-17 β -ol-3-one (**I**) in dry dichloromethane (25 mL) and dry dimethylformamide (6 mL) is cooled to 0 °C. A small excess of 1,3-dicyclohexylcarbodiimide (1 g, 4.86 mmol) is added by little portions. This mixture is stirred for 2 h; the starting reactive product [3-(4-carboxyphenyl)-5-methylisoxazole-4-carboxamide, *R_f* = 0.48] is gradually used up, and this is monitored by thin layer chromatography. The solution is filtered. The filtrate is concentrated under reduced pressure, and the oily residue is

dissolved in ethyl acetate. The ethyl acetate solution is cooled to 4 °C for 2 h. The solution is then filtered in order to eliminate dicyclohexylurea. The filtrate is washed with a 5% NaHCO₃/water solution and then with water and dried. The solvent is removed under reduced pressure. The solid residue is purified by column chromatography using the same mobile phase as above and by crystallization from a mixture of toluene and petroleum ether: bp 40 °C (5–45); yield 35%; IR (cm⁻¹) (C₂-Cl₄) 1713 ($\nu_{\text{ester}}^{\text{ester}}$, C=O), 1609 (ν_{oxime} , C=N), 1659 (ν_{amide} , C=O); ES⁺ *m/z* 503 (M - H)⁺; TLC chloroform/tetrahydrofuran/acetic acid (7/0.8/0.2) *R_f* = 0.63. Anal. Calcd for C₃₀H₃₄N₂O₅: C, 71.70; H, 6.82; N, 5.57. Found: C, 71.98; H, 7.01; N, 5.71.

(14) *Preparation of 6-[3-(4-Estren-17 β -ol-3-one-benzenecarboxylate-4-yl)-5-methylisoxazole-4-carboxamido]penicillanic Acid (16).* A solution of 100 mg (0.2 mmol) of 3-(4-estren-17 β -ol-3-one-benzenecarboxylate-4-yl)-5-methylisoxazole-4-carboxylic acid (15) in dry tetrahydrofuran (5 mL) is treated with *N,N*-diisopropylethylamine (46 μ L, 0.25 mmol) and then cooled to -50 °C. Methanesulfonyl chloride (40 μ L, 0.52 mmol) is added and the solution is stirred at -50 °C for a further 2 h. This mixture containing the mixed sulfonic acid anhydride is then added to a preformed solution of 6.3 mg (2.92×10^{-4} mol) of 6-aminopenicillanic acid (II) in a 2% NaHCO₃/water solution (5 mL) and acetone (4 mL) and cooled to 0 °C. After the mixture has been stirred for 1 h at 0 °C, ethyl acetate and water are added. The pH is adjusted to 3 with a 0.1 M HCl/water solution. The organic phase is washed with water and dried. The solvent is removed under reduced pressure. The oily white residue is purified by a precoated TLC plate sil 6–200 from Merck. The toluene/ethyl acetate/acetic acid (1/1/0.1) is used as the mobile phase (*R_f* = 0.1). The linear spot is scraped from the plate. Silice is washed with several ethyl acetate fractions. The resulting organic solution is washed with water and dried. The solvent is removed under reduced pressure. Crystallization from ethyl acetate and petroleum ether (bp of 40 °C; 5–55) gave the product (16): yield 42%; IR (cm⁻¹) (KBr) 1726 ($\nu_{\text{ester}}^{\text{ester}}$, C=O), 1767 ($\nu_{\text{cyclic amide}}$, C=O), 1717 ($\nu_{\text{penicillanic acid}}$, C=O), 1664 ($\nu_{\text{isoxazol amide}}$, C=O); ES⁻ *m/z* 699 (M - H)⁻; TLC chloroform ethyl acetate methanol-acetic acid (4/4/1/0.2) *R_f* = 0.71.

RESULTS AND DISCUSSION

(A) Conjugation of Nandrolone to Carbenicillin or Ticarcillin (Figure 2). The activation methods of penicillins or cephalosporins are carried out in order to bind them to various substances among others carrier proteins (9, 10). The functional groups born from the enzymatic or alkaline hydrolysis of the β -lactam cycle cannot be used because these reactions yield products which have lost all valuable properties in relation to the enzymes (β -lactamases) (4). Some studies on the active site of class A and C β -lactamases have shown that modified substrates where a free carboxylate group on C-3 of penicillins or C-4 of cephalosporins had been esterified does not impair much either acylation or deacylation steps for these compounds with the enzymes (11). We have been aware of keeping these original properties and of obtaining conjugates as similar as possible to the original antibiotics. So we considered chiefly the reactive functions which were located on the side chains. The two carboxylic acid functions on carbenicillin and ticarcillin have a real close reactivity (12) so that it seems rather difficult to make one react without any influence on the other. Therefore, a hemisynthesis of these substances has been tried using a modified side

chain by conjugation to nandrolone. The hemisynthesis of penicillin from a side chain and from 6-aminopenicillanic acid is often carried out in two steps (3, 7). The carboxylic acid function on the side chain is first activated into an acyl chloride or a mixed anhydride or by using a dioxanedione cycle (meldrum acid) (13), before coupling to 6-aminopenicillanic acid. Here, the side chain had to be first synthesized by reaction of the hydroxyl function on C-17 of nandrolone upon phenylmalonic and 3-thiophenemalonic acids. But these two acids are easily decarboxylated when one of the acid functions is activated (14).

Because it is difficult to obtain a monoactivated derivative from these two acids, through classical activators such as 1,3-dicyclohexylcarbodiimide (DCC), ethyl chloroformate, or 1,1'-carbonyldiimidazole (CDI), the old acylation techniques have been selected. By using a strong chlorinating agent such as thionyl chloride (SOCl₂) in an equivalent amount, monochlorides of phenylmalonic and 3-thiophenemalonic acids are obtained. By binding at low temperature these monoactivated derivatives to the slightly and not easily reachable hydroxyl of nandrolone, we were able to identify a nandrolone hemiphenylmalonate and a nandrolone hemi(3-thiophene)malonate. The binding of these substances to 6-aminopenicillanic acid could not be carried out by reagents classically used in the synthesis of carbenicillin or ticarcillin; conversion of malonate carboxyl into an acyl chloride using either thionyl chloride or phosphorus pentachloride or dichloromethyl methyl ether does not operate without any damage to the steroid. Moreover, the use of dioxanedione cycle (meldrum acid) is not possible, because the second acid function has been turned into a nandrolone ester. Enzymatic synthesis can no more be applied due to the hydrophobicity of a steroid-modified side chain. Among the mild coupling procedures, DCC or ethyl chloroformate leads to decarboxylation, giving nandrolone phenylacetate or 3-thiophenylacetate. However, a carbonyldiimidazole activation was partly successful.

A [(4-estren-3-one-17 β -oxy)-3-oxo-2-phenylpropanamido]penicillanic acid (5a) has been isolated with a 21% yield. We could not obtain a [(4-estren-3-one-17 β -oxy)-3-oxo-2-(3-thienyl)propanamido]penicillanic acid using the same procedure (5b), while this substance has been obtained in good yield by activating 4-estren-17 β -ol-3-one hemi(3-thiophene)malonate (3b) with methanesulfonyl chloride (CH₃SO₂Cl) into mixed sulfonic acid anhydride (3).

4-Estren-17 β -ol-3-one hemi(3-thiophene)malonate (3b) which seems more sensitive to decarboxylation does react upon addition of CH₃SO₂Cl. Probably this latter reagent provides a slighter electronic density on the oxygen constitutive of the mixed sulfonic acid anhydride. This reduced electronic mobility (in comparison with an usual mixed anhydride) decreases the trend toward decarboxylation.

(B) Preparation of a Nandrolone–Oxacillin Conjugate. Oxacillin is an antibiotic created by binding 6-aminopenicillanic acid to a phenyl isoxazole molecule (15). This substance cannot be coupled with nandrolone. In order to proceed to such coupling, a reactive group must be present on the phenyl cycle of phenylisoxazole. Knowing the reactivity of the hydroxyl function located on C-17 of nandrolone with a carboxylic acid function (16) on one hand and being aware of most techniques of synthesis of isoxazole nuclei on the other hand, we have been conveyed to synthesize a 3-(4-carboxyphenyl)-5-methylisoxazole-4-carboxylate derivative. Cycloaddition of an enamine to a benzonitrile oxide derivative (18) or

a dimethyl acetylenedicarboxylate derivative leads to phenylisoxazole products (19). Binding benzoyl chloride with ethyl 3-(methylamino)-2-butenate leads to phenylisoxazole derivatives as well (17). The last one can also be obtained by coupling ethyl acetoacetate sodium salt with either benzaldehyde chloroxime (benzohydroxamoyl chloride) or benzoyl chloride (20).

Only the last two techniques started from a commercial product. We chose the method described above with benzaldehyde and ethyl acetoacetate sodium salt and, from a commercial product (*p*-carboxybenzaldehyde), we were able to obtain ethyl 3-(4-carboxyphenyl)-5-methylisoxazole-4-carboxylate (**9**) (Figure 3).

The carboxylic acid function of the isoxazole cycle being so protected by an alkyl ester, nandrolone could react upon a mixed iminoanhydride derivative obtained by activating the carboxyphenyl group with DCC in contact with 4-dimethylaminopyridine (DMAP). The next synthesized molecule, ethyl 3-(4-estren-17 β -ol-3-one-benzenecarboxylate-4-yl)-5-methylisoxazole-4-carboxylate (**13**) displays an ester function at each of its terminals. We tried to eliminate the ethyl ester function in order to bind the molecule to 6-aminopenicillanic acid.

Alkaline reagents ($K_2CO_3/MeOH-H_2O$) induced preferential hydrolysis of the ester function of nandrolone less stable than the ethyl ester. We then tried to remove the ethyl ester function with lithium iodide in contact of pyridin and acetate or cyanide (21) (Figure 3). We obtained with this trial the end product we wanted, but the yield was weak and inconsistent (3–15%).

In order to overcome these problems of hydrolysis of the nandrolone ester, we turned the ethyl ester into an amide (Figure 3). Before we bound it to nandrolone, ethyl 3-(4-carboxyphenyl)-5-methylisoxazole-4-carboxylate (**9**) reacted upon ammonia under pressure. The binding of nandrolone to 3-(4-carboxyphenyl)-5-methylisoxazole-4-carboxamide (**11**) was carried out following the same route as for **9**. The splitting of the primary amide function did not give satisfactory results. We could not obtain the desired product. We were looking for it by using reagents like nitrite salts in a methanolic acid medium or N_2O_4 in contact with sodium acetate and CCl_4 (22, 23).

At this time, we tried to use a more unstable protection (Figure 3). *tert*-Butyl acetoacetate potassium salt was bound to 4-carboxybenzohydroxamoyl chloride (**8**). And so we could identify a *tert*-butyl 3-(4-carboxyphenyl)-5-methylisoxazole-4-carboxylate derivative (**10**). The binding to nandrolone was conducted according to the previous method. The *tert*-butyl ester was more easily removed by *p*-toluenesulfonic acid than by trifluoroacetic acid when solved into toluene and nitromethane without any conflict of ester hydrolysis (24, 25) (Figure 3).

The so-obtained 3-(4-estren-17 β -ol-3-one-benzenecarboxylate-4-yl)-5-methylisoxazole-4-carboxylic acid (**15**) was then connected to 6-aminopenicillanic acid by means of a mixed sulfonic anhydride at low temperature (3). An end product according to the expected formula has been isolated in good yield.

In conclusion, we succeeded in the preparation of these three penicillin conjugates. These products were obtained in good yields. So we set up an efficient preparation for coupling haptens to β -lactam derivatives.

ACKNOWLEDGMENT

We are grateful to the Fond National de la Recherche Scientifique (FNRS) for the support accorded to one of us (RL). The authors thank Prof. E. Depauw (service de

Chimie physique) and Dr. G. Ghitti (Biocode Biotechnologie) for taking and interpreting mass spectra.

LITERATURE CITED

- (1) Galleni, M., Frere, J. M. (1988) A survey of kinetic parameters of class C β -lactamases. *Biochem. J.* 255, 119–122.
- (2) Matagne, A., Misselyn-Bauduin, A.-M., Joris, B., Erpicum, T., Granier, B., and Frere, J. M. (1990) The diversity of catalytic properties of class A β -lactamases. *Biochem. J.* 265, 131–146.
- (3) Brown, P., Calvert, S. H., Chapman, P. C. A., Cosham, S. C., Eglinton, A. J., Elliot, R. L., Harris, M. A., Hinks, J. D., Lowther, J., Merrikin, D. J., Pearson, M. J., Ponsford, R. J., and Syms, J. V. (1991) β -lactamase-stable penicillins. Synthesis and structure-activity relationships of (Z)-alkyloxymino penicillins; Selection of BRL 44154. *J. Chem. Soc., Perkin Trans. 1*, 881–890.
- (4) Bondaruk, J., Curcio-Vonlanthen, V., and Schneider, C. H. (1995) Basic aspect related to penicillin-allergy skin testing: on variability of the hapten-paratope interaction. *Allergy* 50, 671–676.
- (5) Rose, B. G., Kampsholtzapapple, C., and Stanker, L. H. (1995) Competitive indirect elisa for ceftiofur sodium and the effect of different immunizing and coating antigen conjugates. *Bioconjugate Chem.* 6, 529–535.
- (6) Rose, B. G., Buckley, S. A., Kampsholtzapapple, C., Beier, R. C., Stanker, L. H. (1996) Ceftiofur sodium - monoclonal antibody development and cross-reactivity studies with structurally related cephalosporins. *J. Agric. Food Chem.* 44, 622–627.
- (7) Buckwell, S. C., and Page, M. I. (1988) Hydrolysis of 6-alkyl penicillins catalysed by β -lactamase I from *Bacillus cereus* and by hydroxide ion. *J. Chem. Soc., Perkin Trans. 2*, 1809–1813.
- (8) Van Look, L. J., Jansen, E. H., Van den Berg, R. H., Zomer, G., Vanoosthuyze, K. E., and Van Peteghem, Ch. (1991) Development of a competitive enzyme immunoassay for 17 α -19-nortestosterone. *J. Chromatogr.* 564 (2), 451–459.
- (9) Caneva, E., Di Gennaro, P., Farina, F., Orlandi, M., Rindone, B., and Falagiani, P. (1993) Synthesis and characterization of a penicillin-poly(L-lysine) which recognizes human IgE anti-penicillin antibodies. *Bioconjugate Chem.* 4, 309–313.
- (10) Eng, G. Y., Jones, L., and Medina, M. (1995) Characterization of an immobilized protein matrix for use in an affinity method for beta-lactam antibiotics. *Biotechnol. Appl. Biochem.* 22, 129–144.
- (11) Monnaie, D., Dubus, A., Cooke, D., Marchand-Brynaert, J., Normark, S., and Frere, J. M. (1994) Role of residue Lys315 in the mechanism of action of the *Enterobacter cloacae* 908R beta-lactamase. *Biochemistry* 33, 5193–5201.
- (12) Neise, B., and Steglich, W. (1978) Simple method for the esterification of carboxylic acids. *Angew. Chem., Int. Ed. Engl.* 17, 522–524.
- (13) Crooy, P., De Neys, R., Eliaers, J., Liveyns, R., Simonet, G., and Vandeveld, J. (1977) Use of meldrum's acids in the semi-synthesis of a carboxylated penicillins and cephalosporins. *Bull. Soc. Chim. Belg.* 86, 991–1002.
- (14) Brain, L., and Nayler, J. H. C. (1964) BE 646991; *Chem. Abstr.* 63, 13269.
- (15) Doyle, F. P., and Nayler, J. H. C. (1962) US 2996501; *Chem. Abstr.* 56, 5971.
- (16) Hassner, A., and Alexanian, V. (1978) Direct room temperature esterification of carboxylic acids. *Tetrahedron Lett.* 46, 4475–4478.
- (17) Chantegrel, B., Deshayes, Ch., and Pujol, B. (1990) Synthesis of isoxazolo[4,5-d]pyridazin-4(5H)-ones and 4-acyl-5-hydroxy-3(2H)-pyridazinones. *J. Heterocycl. Chem.* 27, 927–934.
- (18) Chantegrel, B., Nadi, A. I., and Gelin, S. (1984) Synthesis of [1]benzopyrano[3,4-d]isoxazol-4-ones from 2-substituted chromone-3-carboxylic esters. A reinvestigation of the reaction of 3-acyl-4-hydroxycoumarins with hydroxylamine. Synthesis of 4-(2-hydroxybenzoyl) isoxazol-5-ones. *J. Org. Chem.* 49, 4419–4424.
- (19) Farina, F., Fraile, T. M., Martin, M. R., Martin, M. V., and Martinez de Guerenú, A. (1995) Synthesis of isoxazoles

- bearing methoxycarbonyl and formyl groups by 1,3-dipolar cycloaddition of nitrile oxides to olefinic and acetylenic dipolarophiles. *Heterocycles* 40, 285–293.
- (20) Doyle, F. P., Hanson, J. C., Long, A. A. W., Naylor, J. H. C., and Stove, E. R. (1963) Derivatives of 6-aminopenicillanic acid. Part VI. Penicillins from 3- and 5-phenylisoxazole-4-carboxylic acid and their alkyl and halogen derivatives. *J. Chem. Soc.*, 5838–5976.
- (21) Mc Murry, J. E., and Wong, G. B. (1972) An improved method for the cleavage of methyl esters. *Synth. Commun.* 6, 389–394.
- (22) Woodward, R. B. (1973) The total synthesis of vitamin B₁₂. *Pure Appl. Chem.* 33, 145–148.
- (23) Kempe, U. M., Das Gupta, T. K., Blatt, K., Gygax, P., Felix, D., and Eschenmoser, A. (1972) α -Chlor-nitrone I: Darstellung und Ag induzierte reaktion mit olefinen. *Helv. Chim. Acta* 55, 2187–2198.
- (24) Pirotte, B., Dive, G., Delarge, J., Masereel, B., Dupont, L., Thunus, L., Schynts, M., Coyette, J., and Frere, J. M. (1992) Synthese, etude theorique et evaluation biologique de derives du amino 4h -1,2,4-triazole analogues des antibiotiques beta-lactamiques. *Eur. J. Med. Chem.* 27, 193–205.
- (25) Anderson, G. W., and Callahan, F. M. (1960) T-Butyl esters of amino acids and peptides and their use in peptide synthesis. *J. Am. Chem. Soc.* 82, 3359–3363.

BC970138F

COMMUNICATIONS

Listeriolysin O Potentiates Immunotoxin and Bleomycin Cytotoxicity

David E. Kerr,[†] George Y. Wu,[‡] Catherine H. Wu,[‡] and Peter D. Senter^{*,†}

Bristol-Myers Squibb Pharmaceutical Research Institute, 3005 First Avenue, Seattle, Washington 98121, and Division of Gastroenterology–Hepatology, Department of Medicine, University of Connecticut Health Center, 263 Farmington Avenue, Farmington, Connecticut 06030-1845. Received July 3, 1997[®]

Antitumor immunotoxins were formed by covalently attaching the ribosome-inactivating protein ricin A chain (RA) to the antitumor antibodies BR96 and L6. In vitro cytotoxicity assays established that BR96-RA was cytotoxic to H2987 human lung adenocarcinoma cells ($IC_{50} = 6$ nM), while L6-RA exhibited very low levels of cytotoxic activity (18% cell kill at 67 nM). The virulence factor from the intracellular pathogen *Listeria monocytogenes*, listeriolysin O (LLO), was able to potentiate the cytotoxicity of BR96-RA and L6-RA by 120- and >1340-fold, respectively, resulting in IC_{50} values of approximately 50 pM. LLO also potentiated the cytotoxicity of the peptide anticancer drug bleomycin by a factor of >2500 but had no effect on the cytotoxic activities of the anticancer drugs cytarabine and etoposide phosphate. In addition, LLO did not potentiate the cytotoxic activity of unconjugated ricin A chain or L6-RA on H2987 cells that were saturated with L6 prior to conjugate treatment. These results are attributed to LLO-induced alteration of the intracellular trafficking of molecules that are incorporated into acidic vesicles.

INTRODUCTION

A great deal of research has been directed toward the use of antitumor monoclonal antibodies (mAb¹) for the delivery of ricin A chain (RA) and other toxins to tumors (reviewed in refs 1–3). Therapeutic efficacy with such immunotoxins requires that sufficient quantities bind to cell surface receptors, undergo intracellular uptake, and

then access the cytosol where the toxin exerts its activity (4, 5). Entry into the cytosol has been identified as a common limitation in immunotoxin efficacy (4–6), and a number of methods have been described to enhance cytosolic delivery. These include the use of lysosomotropic amines such as ammonium chloride (7), ionophores such as monensin (8, 9), and, more recently, a 25 amino acid peptide derived from protein G of vesicular stomatitis virus (10). These agents reduce immunotoxin degradation by raising lysosomal pH (7), by altering protein trafficking within the cell (8), or by destabilizing intracellular membranes in lower pH environments (10). Thus, there is considerable evidence that improvements in immunotoxin activity can result if the process of cytosolic delivery is enhanced.

Listeriolysin O (LLO) is a major virulence factor from

* Author to whom correspondence should be addressed.

[†] Bristol-Myers Squibb.

[‡] University of Connecticut.

[®] Abstract published in *Advance ACS Abstracts*, October 15, 1997.

¹ Abbreviations: mAb, monoclonal antibody; RA, ricin A chain; IC_{50} , concentration resulting in 50% cell death; LLO, listeriolysin O.

the intracellular pathogen *Listeria monocytogenes*. Upon uptake of the bacteria into target cells, secreted LLO disrupts endosomes and lysosomes, allowing the bacteria to enter the cytoplasm and grow (11–14). One of the key differences between LLO and other hemolytic proteins is that its pH optimum is close to 5.5, and at pH 7 the activity is almost undetectable (11). For these reasons, it seemed reasonable that LLO might potentiate immunotoxin activity by facilitating its transport out of acidic vesicles. The same might be true for anticancer drugs that have restricted intracellular access. Here, we describe the activities of LLO in combination with immunotoxins and clinically approved anticancer drugs. We show that LLO can have a pronounced effect on the cytotoxic activities of selected antitumor agents.

EXPERIMENTAL PROCEDURES

Materials. The H2987 human lung carcinoma cell line has been described before (15). Bleomycin sulfate, cytarabine, bovine serum albumin, and dithiothreitol were purchased from Sigma (St. Louis, MO), and etoposide phosphate was provided by Bristol-Myers Squibb. The mAbs BR96 (16) and L6 (17) were conjugated to deglycosylated ricin A chain (Inland Laboratories, Austin, TX) through a disulfide bond using previously described methods (16).

Isolation of LLO. The hemolytic *L. monocytogenes* strain, MAC, a LLO hypersecretor, was a kind gift from Dr. Daniel A. Portnoy. MAC cells were grown overnight in 10 mL of brain heart infusion broth (Difco) at 37 °C, and the culture was continued in 1 L of LB medium at 37 °C with shaking until $A_{660\text{nm}}$ was ~0.6. After centrifugation (10000g, 15 min at 4 °C), the supernatant was concentrated at 4 °C to 200 mL using an Amicon CH2PRS-spiral cartridge concentrator with an Amicon S1Y30 spiral cartridge. The concentrated supernatant was applied to a 40 mL Macro-Prep ceramic hydroxyapatite column (80 μm particles, Bio-Rad) that was equilibrated with 10 mM potassium phosphate buffer at pH 6.8 at 4 °C. LLO was eluted with 400 mM potassium phosphate buffer at pH 6.8. The hemolysis assay on human erythrocytes at pH 6.0 was performed as previously described (11), and it was found that the purified protein contained 167 000 units/mg.

In Vitro Cytotoxicity. H2987 cells in Iscove's modified Dulbecco's medium supplemented with 10% fetal bovine serum containing penicillin (60 $\mu\text{g}/\text{mL}$) and streptomycin (100 $\mu\text{g}/\text{mL}$) were plated into 96-well-microtiter plates at 10^4 cells/well and allowed to adhere overnight at 37 °C. The cells (previously untreated or saturated with unconjugated L6 at 1 mg/mL) were then treated with L6-RA or BR96-RA at various concentrations at 37 °C in the presence or absence of LLO at 1 $\mu\text{g}/\text{mL}$. Control cells were treated with LLO or ricin A chain alone. After 18 h, the plates were washed three times with Iscove's modified Dulbecco's medium, incubated for an additional 8 h, and pulsed for 7 h with [^3H]thymidine (1 $\mu\text{Ci}/\text{well}$). The plates were frozen at -20 °C and thawed, and the cells were harvested on a Tomtec 96-well harvester. Radioactivity was counted on a Wallac beta plate counter. In a separate experiment, cells were treated with bleomycin, cytarabine, or etoposide phosphate in the presence or absence of 1 $\mu\text{g}/\text{mL}$ LLO. After 2 h, the plates were washed, incubated overnight at 37 °C, and pulsed for 7 h with [^3H]thymidine (1 $\mu\text{Ci}/\text{well}$). The plates were then treated as above.

RESULTS AND DISCUSSION

RA was conjugated to the antitumor antibodies L6 (17) and BR96 (16) through a disulfide-containing linker as previously described (16). The conjugates thus formed

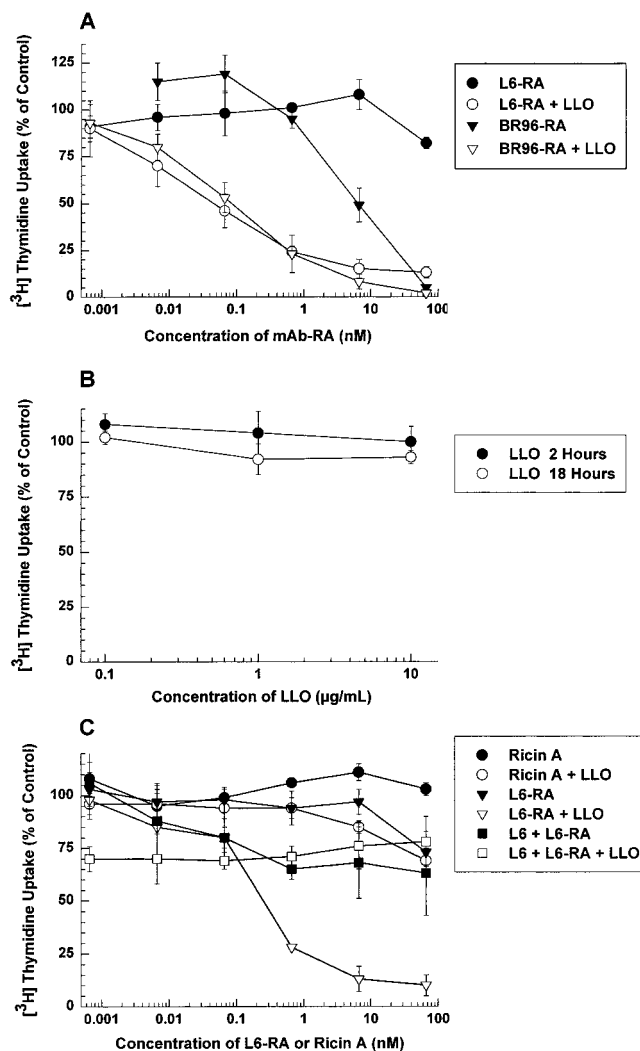


Figure 1. Cytotoxic effects of L6-RA and BR96-RA in the presence or absence of LLO as determined by the inhibition of [^3H]thymidine into DNA: (A) H2987 cells incubated for 18 h with L6-RA or BR96-RA \pm LLO at 1 $\mu\text{g}/\text{mL}$, washed, and pulsed with [^3H]thymidine; (B) cytotoxic effects of LLO without immunconjugate treatment; (C) H2987 cells incubated for 18 h with RA or L6-RA \pm LLO at 1 $\mu\text{g}/\text{mL}$ and treated as in (A). Some of the cells were treated with unconjugated L6 (1 mg/mL) and incubated at 4 °C for 30 min, followed by L6-RA \pm LLO. The data represent the mean of three samples \pm standard deviations.

were capable of binding to cell surface L6 and BR96 antigens, which are present in high density on the H2987 human lung adenocarcinoma cell line. These particular antibodies were selected for the studies described here since they display significantly different characteristics upon antigen binding. BR96 is known to be very rapidly internalized into cells (16), while L6 remains primarily extracellular but gradually internalizes and is degraded (18, 19). It was therefore not surprising to find that BR96-RA was cytotoxic to H2987 cells (IC_{50} = 6 nM), while L6-RA exhibited very low levels of activity (18% cell kill at 67 nM) (Figure 1A).

Once internalized into antigen-positive cells, the potency of immunotoxins is often limited by their ability to escape from acidic intracellular compartments to the cytosol. Agents that are capable of facilitating this transfer have been shown to lead to enhanced levels of cytotoxicity (7–10). Toward this end, we explored the activities of LLO, a 58 kDa protein that enables the pathogenic bacterium *L. monocytogenes* to escape from acidic vesicles into the cytosol of mammalian host cells

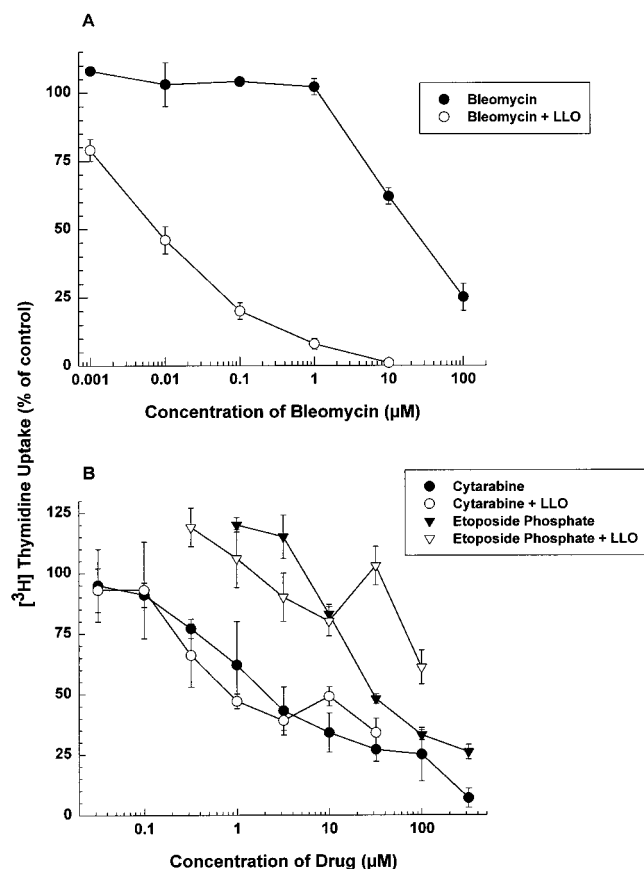


Figure 2. Cytotoxic effects of (A) bleomycin and (B) cytarabine and etoposide phosphate in the presence or absence of LLO as determined by the inhibition of [3 H]thymidine into DNA. H2987 cells were incubated for 2 h with bleomycin, cytarabine, or etoposide phosphate \pm LLO at 1 μ g/mL, washed, incubated further, and then pulsed with [3 H]thymidine.

(11–14). Purified LLO at 0.1, 1, and 10 μ g/mL was noncytotoxic to H2987 cells (Figure 1B). When LLO at 1 μ g/mL was combined with BR96-RA or L6-RA, the resulting activity far exceeded that of either immunotoxin alone (Figure 1A). In both cases, the IC_{50} was reduced to 50 pM, corresponding to 120- and >1340-fold increases in activity for BR96-RA and L6-RA activity, respectively.

LLO did not significantly enhance the activity of ricin A chain alone, a molecule that does not show detectable binding to H2987 cells (Figure 1C). In this same experiment, it was found that the effect of LLO on L6-RA cytotoxic activity could be abrogated by saturating the cells with unconjugated L6 prior to the addition of LLO and the L6-RA chain conjugate. LLO therefore appears to mediate its effects on molecules that bind to cell surface receptors and are then actively transported inside cells.

These results led us to explore whether LLO could potentiate the activity of some clinically approved anti-tumor agents. Bleomycin is used for the treatment of lymphoma, squamous cell carcinoma, and testicular cancer (20). The activity of this drug on mammalian cells has been attributed to the induction of DNA (20) and RNA (21) strand breaks. It has previously been reported that bleomycin binds in a saturable manner to a membrane protein that is thought to play a role in its internalization (22). This process is most likely inefficient, on the basis of the finding that bleomycin potency is greatly increased when target cell membranes are permeabilized by electroporation (23, 24).

In a 2 h exposure assay on H2987 lung adenocarcinoma cells, bleomycin had an IC_{50} value of 20 μ M (Figure 2A).

LLO at a completely nontoxic concentration (1 μ g/mL) was able to enhance the activity of bleomycin by 2500-fold, resulting in an IC_{50} of 8 nM. The effect of LLO was not general, in that the protein had no effect on the activities of etoposide phosphate and cytarabine (Figure 2B). Etoposide phosphate, being negatively charged, is expected to have limited intracellular access and has been shown to be significantly less cytotoxic than etoposide (25). These results, taken together with those shown in Figure 1, are therefore in general agreement with previously studies showing that LLO has an intracellular site of activity rather than a nonspecific mechanism involving disruption of the plasma membrane (11–14).

The data reported here indicate that LLO complements other known immunotoxin potentiators (7–10) and has the additional property of being able to significantly increase the potency of bleomycin, a clinically approved anticancer drug. It may be possible to exploit these activities by combining the RA conjugates, bleomycin, or other appropriate anticancer drugs with a mAb–LLO conjugate that binds to the target cell population of interest. Such studies will be the subject of future investigations.

ACKNOWLEDGMENT

We thank Nathan Siemers, Jacques Garrigues, and Cherie Walton for their valuable contributions to the research described here. This work was supported in part by the U.S. Public Health Service, NIDDK Grant DK-42182 (G.Y.W.), and a grant from TargeTech, Inc./Immune Response Corp. (C.H.W.). G.Y.W. and C.H.W. hold equity in the Immune Response Corp.

LITERATURE CITED

- Vitetta, E. S. (1994) From the basic science of B cells to biological missiles at the bedside. *J. Immunol.* 153, 1407–1420.
- Press, O. W. (1991) Immunotoxins. *Biotherapy* 3, 65–76.
- Pastan, I., Pai, L. H., Brinkmann, U., and FitzGerald, D. (1996) Recombinant immunotoxins. *Breast Cancer Res. Treat.* 38, 3–9.
- Byers, V. S., Pawluczyk, I. Z., Hooi, D. S., Price, M. R., Carroll, S., Embleton, M. J., Garnett, M. C., Berry, N., Robins, R. A., and Baldwin, R. W. (1991) Endocytosis of immunotoxin-791T/36-RTA by tumor cells in relation to its cytotoxic action. *Cancer Res.* 51, 1990–1995.
- Bilge, A., Howell-Clark, J., Ramakrishnan, S., and Press, O. W. (1994) Degradation of ricin A chain by endosomal and lysosomal enzymes—the protective role of ricin B chain. *Ther. Immunol.* 1, 197–204.
- Kornfeld, S. B., Leonard, J. E., Mullen, M. D., and Taetle, R. (1991) Assessment of ligand effects in intracellular trafficking of ricin A chain using anti-ricin hybridomas. *Cancer Res.* 51, 1689–1693.
- Carayon, P., Bord, A., Gaillard, J. P., Vidal, H., Gros, P., and Jansen, F. K. (1993) Ricin A-chain cytotoxicity depends on its presentation to the cell membrane. *Bioconjugate Chem.* 4, 146–152.
- Marsh, J. W. (1989) Cellular processing of a ricin-antibody conjugate. *J. Biol. Chem.* 264, 10405–10410.
- Dosio, F., Franceschi, A., Ceruti, M., Brusa, P., Cattell, L., and Colombatti, M. (1996) Enhancement of ricin toxin A chain immunotoxin activity: synthesis, ionophoretic ability, and in vitro activity of monensin derivatives. *Biochem. Pharmacol.* 52, 157–166.
- Chignola, R., Anselmi, C., Dalla Serra, M., Franceschi, A., Fracasso, G., Pasti, M., Chiesa, E., Lord, J. M., Tridente, G., and Colombatti, M. (1995) Self-potentialization of ligand-toxin conjugates containing ricin A chain fused with viral structures. *J. Biol. Chem.* 270, 23345–23351.
- Geoffroy, C., Gaillard, J. L., Alouf, J. E., and Berche, P. (1987) Purification, characterization, and toxicity of the

- sulphydryl-activated hemolysin listeriolysin O from *Listeria monocytogenes*. *Infect. Immun.* 55, 1641–1646.
- (12) Mengaud, J., Vincente, M. F., Chenvert, J., Pereira, J. M., Geoffrey, C., Gicquel-Sanzey, B., Baquero, F., Perez-Diaz, J.-C., and Cossart, P. (1988) Expression in *Escherichia coli* and sequence analysis of the listeriolysin O determinant of *Listeria monocytogenes*. *Infect. Immun.* 56, 766–772.
- (13) Cossart, P., Vicente, M. F., Mengaud, J., Baquero, F., Perez-Diaz, J.-C., and Berche, P. (1989) Listeriolysin O is essential for virulence of *Listeria monocytogenes*: direct evidence obtained by gene complementation. *Infect. Immun.* 57, 3629–3636.
- (14) Bielecki, J., Youngman, P., Connelly, P., and Portnoy, D. A. (1990) *Bacillus subtilis* expressing a haemolysin gene from *Listeria monocytogenes* can grow in mammalian cells. *Nature* 345, 175–176.
- (15) Svensson, H. P., Vruthula, V. M., Emswiler, J. E., MacMaster, J. F., Cosand, W. L., Senter, P. D., and Wallace, P. M. (1995) In vitro and in vivo activities of a doxorubicin prodrug in combination with monoclonal antibody β -lactamase conjugates. *Cancer Res.* 55, 2357–2365.
- (16) Hellström, I., Garrigues, H. J., Garrigues, U., and Hellström, K. E. (1990) Highly tumor-reactive, internalizing, mouse monoclonal antibodies to Le^y-related cell surface antigens. *Cancer Res.* 50, 2183–2190.
- (17) Hellström, I., Horn, D., Linsley, P., Brown, J. P., Brankovan, V., and Hellström, K. E. (1986) Monoclonal mouse antibodies raised against human lung carcinoma. *Cancer Res.* 46, 3917–3923.
- (18) Mattes, M. J., Griffiths, G. L., Diril, H., Goldenberg, D. M., Ong, G. L., and Shih, L. B. (1994) Processing of antibody-radioisotope conjugates after binding to the surface of tumor cells. *Cancer* 73, 787–793.
- (19) Schmidberger, H., King, L., Lasky, L. C., and Valleria, D. A. (1990) Antitumor activity of L6-ricin immunotoxin against the H2981-T3 lung adenocarcinoma cell line in vitro and in vivo. *Cancer Res.* 50, 3249–3256.
- (20) Chabner, B. A., and Myers, C. E. (1993) Antitumor antibiotics. *Cancer: Principles and Practice of Oncology* (V. T. J. DeVita, S. Hellman, and S. A. Rosenberg, Eds.) pp 374–376, J. B. Lippincott Co., Philadelphia.
- (21) Hecht, S. M. (1994) RNA degradation by bleomycin, a naturally occurring bioconjugate. *Bioconjugate Chem.* 5, 513–526.
- (22) Pron, G., Belehradek, J., Jr., and Mir, L. M. (1993) Identification of a plasma membrane protein that specifically binds bleomycin. *Biochem. Biophys. Res. Commun.* 194, 333–337.
- (23) Shimizu, N., and Kawazoe, Y. (1996) A new method for permeabilization of cultured cells without cell damage. *Biol. Pharm. Bull.* 19, 484–486.
- (24) Tounekti, O., Pron, G., Belehradek, J., Jr., and Mir, L. M. (1993) Bleomycin, an apoptosis-mimetic drug that induces two types of cell death depending on the number of molecules internalized. *Cancer Res.* 53, 5462–5469.
- (25) Senter, P. D., Saulnier, M. G., Schreiber, G. J., Hirschberg, D. L., Brown, J. P., Hellstrom, I., and Hellstrom, K. E. (1988) Anti-tumor effects of antibody-alkaline phosphatase conjugates in combination with etoposide phosphate. *Proc. Natl. Acad. Sci. U.S.A.* 85, 4842–4846.

BC970124+

Synthesis and Enzymatic Stability of Phosphodiester-Linked Peptide–Oligonucleotide Hybrids

Jordi Robles, Marta Maseda, Maite Beltrán, Maria Concernau, Enrique Pedroso, and Anna Grandas*

Departament de Química Orgànica, Facultat de Química, Universitat de Barcelona, Martí i Franquès 1-11, E-08028 Barcelona, Spain. Received March 21, 1997[®]

Nucleopeptides Ac-Tyr(p^{3'}dACGT)-Ala-Phe-Gly-NH₂, Ac-Thr(p^{3'}dACGT)-Ala-Phe-Gly-OH, Ac-Ser(p^{3'}dACGT)-Ala-Phe-Gly-OH, and Phac-Hse(p^{3'}dACGT)-Ala-Phe-Gly-OH, in which the 3'-end of a tetradeoxyribonucleotide is linked by a phosphodiester bond to a hydroxylated amino acid, were synthesized using a stepwise solid-phase methodology to study the influence of the linking amino acid on their stability to 3'-exonucleases. HPLC analysis of the reaction crudes after treatment of each nucleopeptide with snake venom phosphodiesterase showed that the lability of the amino acid–nucleoside linkage increases in the order Thr < Ser < Hse < Tyr.

The development of efficient and reliable synthetic methods has allowed differently modified nucleic acid fragments to be obtained, and it has opened the door to the exploration of new therapeutic alternatives based on the capacity of recognition of oligonucleotides (1). These oligonucleotide analogs are designed to inhibit gene expression by forming either a duplex with a complementary RNA sequence (antisense principle) or a triplex with a double-stranded DNA fragment (antigene therapy). The oligonucleotide modification is usually chosen to facilitate cell uptake and/or to increase the resistance of the oligonucleotide to the nucleases of biological fluids.

The covalent attachment of an oligonucleotide to a protein recognized by a specific cellular receptor has been shown to enhance the uptake of the oligonucleotide (2). Consequently, various peptide–oligonucleotide conjugates have been prepared to facilitate the penetration of the oligonucleotide into the cell. Polycationic (3), hydrophobic (4), viral (5, 6), and signal (7–10) peptides have been evaluated as transporting agents, but there is no general consensus yet as to which type of peptide is the best carrier. Attachment of the peptide to the 3'-end of the oligonucleotide has also been claimed to increase oligomer stability to the most ubiquitous exonucleases, 3'-exonucleases (4, 6, 11, 12), but little experimental evidence has been provided to support this assumption (4, 12). The covalent union between the peptide and the oligonucleotide is most often established through a linker (3–12), but direct phosphoramidate (13) or phosphate diester (14, 15) linkages may also be established between the two molecules. Nucleopeptides (peptide–oligonucleotide hybrids with a phosphodiester bond between the side-chain hydroxyl group of an amino acid and one of the terminal hydroxyl groups of an oligonucleotide) offer the advantage, with respect to other synthetic conjugates, that the linking amino acid can be placed at any position of the peptide sequence.

We report on the synthesis of four 3'-nucleopeptides, three of which contain proteinogenic amino acid–nucleoside phosphate diester linkages, and the fourth one incorporates a homoserine residue as the linking amino

acid (16): Ac-Tyr(p^{3'}dACGT)-Ala-Phe-Gly-NH₂ (1), Ac-Thr(p^{3'}dACGT)-Ala-Phe-Gly-OH (2), Ac-Ser(p^{3'}dACGT)-Ala-Phe-Gly-OH (3), and Phac-Hse(p^{3'}dACGT)-Ala-Phe-Gly-OH (4).¹ We have used these products to evaluate the effect of the linking amino acid on the relative enzymatic stability of the hybrids. If nucleopeptides are to be designed as antisense or antigene therapeutic agents, the peptide sequence must be chosen so as to facilitate polyanion uptake by the cell and to minimize degradation of the oligonucleotide by exonucleases before it can reach its target. To our knowledge, the only data available on the enzymatic lability of peptide–oligonucleotide phosphate linkages refer to tyrosine–phosphate bonds in nucleoproteins (17).

The four nucleopeptides were synthesized following a stepwise solid-phase methodology in which the peptide fragment is first built on a solid matrix and the oligonucleotide is lengthened at the side chain group of a hydroxylated amino acid (15, 18), as summarized in Figure 1. Fmoc-leucine was first incorporated as the internal reference amino acid onto an amine-functionalized polystyrene solid matrix (either aminomethylpolystyrene, in the case of 1 and 2, or a *p*-methylbenzhydrylamine resin for 3 and 4), and, after acetylation of the unreacted amine groups, the Fmoc group was eliminated and a hydroxy acid bifunctional handle was incorporated. 4-(2-Hydroxyethyl)-3-nitrobenzoic acid was used in the preparation of tyrosine- and threonine-nucleopeptides, as previously described (15, 18), whereas for the synthesis of nucleopeptides 3 and 4 we chose a handle that establishes a more base-labile ester bond with the C-terminal amino acid, *N*-[2-(9-hydroxymethylfluorenyl)]-succinamic acid (19). The glycine residue was attached to the resulting resins by reaction with DCC and a catalytic amount of dimethylaminopyridine.

The peptide chains were synthesized manually using the standard protocol for Boc-amino acids. The side-

* Author to whom correspondence should be addressed (telephone 34 3 4021263; fax 34 3 3397878; e-mail grandas@mafalda.qui.ub.es).

[®] Abstract published in *Advance ACS Abstracts*, September 1, 1997.

¹ Abbreviations: Ac, acetyl; Boc, *tert*-butoxycarbonyl; CNE, 2-cyanoethyl; DCC, *N,N*-dicyclohexylcarbodiimide; DCM, dichloromethane; DIEA, *N*-ethyl-*N,N*-diisopropylamine; DMF, *N,N*-dimethylformamide; DMT, 4,4'-dimethoxytrityl; Fmoc, 9-fluorenylmethoxycarbonyl; HOBt, 1-hydroxybenzotriazole; NMI, *N*-methylimidazole; oNPT, 5-(2-nitrophenyl)tetrazole; Phac, phenylacetyl; PS, polystyrene-*co*-1%-divinylbenzene; tBpa, 4-*tert*-butylphenoxyacetyl; TBAF, tetrabutylammonium fluoride; TCA, trichloroacetic acid; TFA, trifluoroacetic acid; THF, tetrahydrofuran.

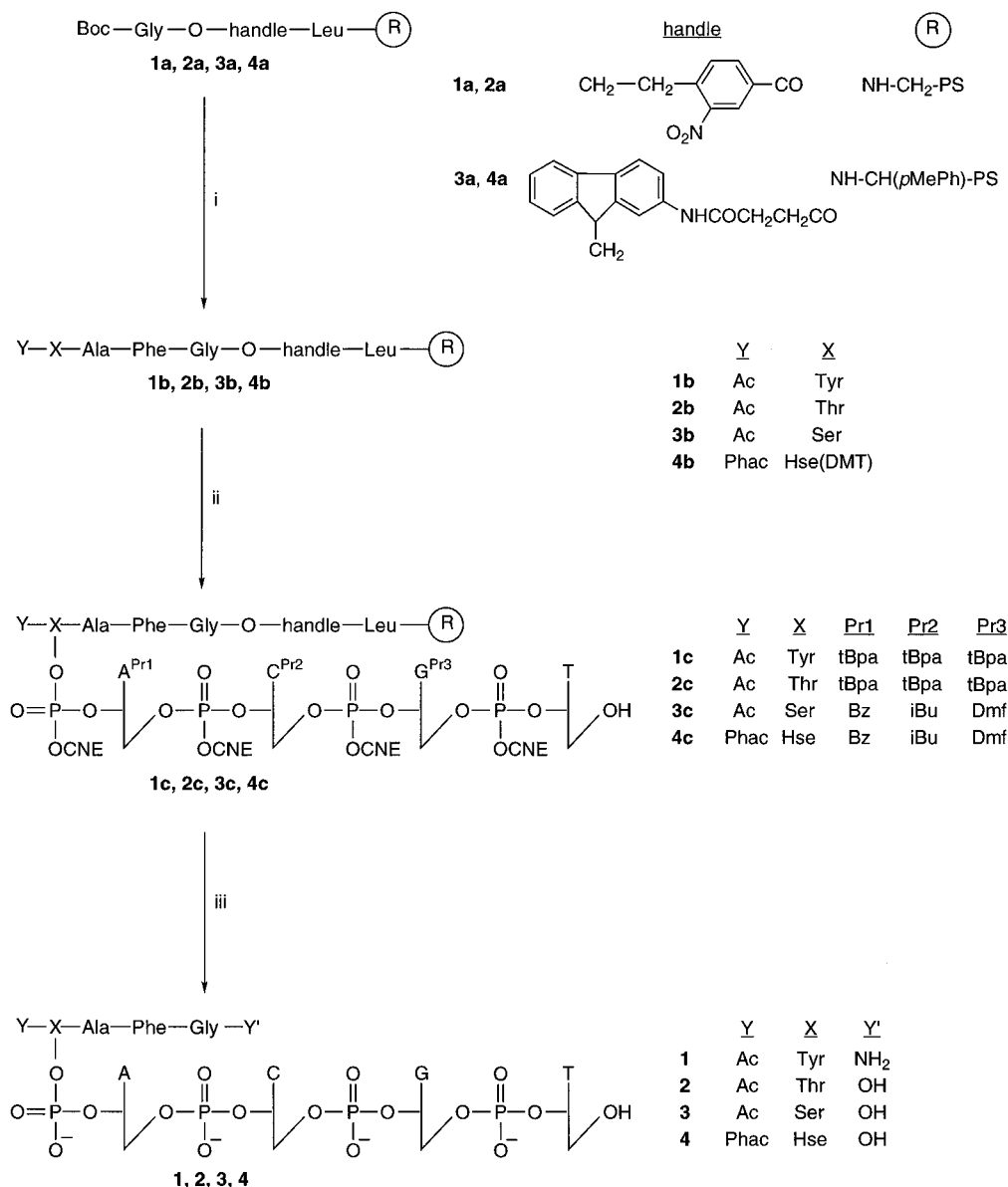


Figure 1. Stepwise solid-phase synthesis scheme of the four nucleopeptides: (i) peptide assembly [removal of the Boc group (TFA), neutralization (DIEA), DCC-mediated coupling of the amino acid]; (ii) elongation of the oligonucleotide chain [coupling of the DMT-nucleoside phosphoramidite (oNPT- or tetrazole-mediated), capping [(tBpa)₂O or Ac₂O + NMI], oxidation (aqueous I₂), detritylation (TCA)]; (iii) TBAF followed by concentrated aqueous NH₃/dioxane 1:1 at room temperature or concentrated aqueous NH₃/dioxane 1:1 at 55 °C (in the case of **1**).

chain hydroxyl groups of Boc-threonine, Boc-tyrosine, and Boc-serine were unprotected. After their incorporation and Boc removal, the terminal amine group was acylated by treatment with Ac₂O (10 equiv) in DMF for 0.5 h. In the synthesis of nucleopeptide **4**, the Phac-Hse(DMT)-O⁻ HTEA⁺ derivative of homoserine was coupled in the presence of DCC and HOBT (16).

The elongation of the oligonucleotide on peptide-resins was carried out on an automatic synthesizer using 5'-(dimethoxytrityl)-3'-phosphoramidite deoxynucleoside derivatives with the minor modifications that render the phosphite triester approach compatible with polystyrene supports (20). 5-(2-Nitrophenyl)tetrazole was used as the acid catalyst in the coupling step in the first two syntheses, but for the assembly of nucleopeptides **3** and **4** it was replaced by the standard catalyst, tetrazole, with similar results.

In the case of nucleopeptides **1** and **2**, *tert*-butylphenoxyacetyl groups (21) were used to protect the exocyclic amino groups of cytosine, adenine, and guanine, so unreacted hydroxyl groups were capped with *tert*-butyl

ylphenoxyacetic anhydride (21). An unexpectedly low value of DMT⁺ absorbance was found after the incorporation of the deoxyguanosine synthon, which approximately doubled after the incorporation of thymidine. Even though this surprising behavior was reproduced in different syntheses of the same products using commercial nucleosides from different batches, it did not seem to have any effect on the purity of the products (Figure 2). Nevertheless, we decided to change the base-protecting groups to benzoyl, isobutyryl, and (dimethylamino)-methylene (for adenine, cytosine, and guanine, respectively) in the assembly of nucleopeptides **3** and **4**.

Reaction with 0.05 M TBAF in anhydrous THF (1 h, room temperature) led to the detachment of nucleopeptides **2–4** from the resin and to their partial deprotection (74, 71, and 89% cleavage yields, respectively). Full deprotection was achieved by an overnight treatment with 1:1 concentrated aqueous NH₃/dioxane at room temperature. Nucleopeptide **1** cannot be obtained using these conditions, since the phenoxide ion is a fairly good leaving group and TBAF may also cleave the phosphodi-

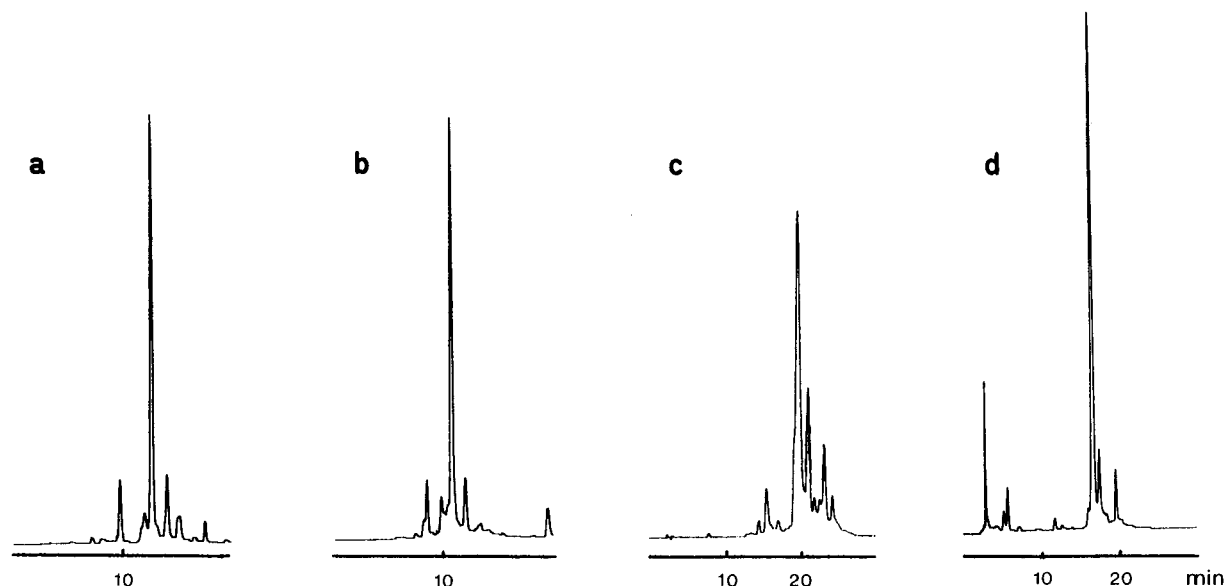


Figure 2. Reversed-phase HPLC profiles of crude nucleopeptides: (a) **1**, (b) **2** (Na^+ salt), (c) **3**, and (d) **4**. Analysis conditions (solvent A, 0.01 M triethylammonium acetate; solvent B, acetonitrile/ H_2O 1:1, 1 mL/min, 260 nm): linear gradients from 10 to 50% of solvent B in 20 min (chromatograms a and b) or 30 min (chromatograms c and d).

ester bond between tyrosine and the 3'-end of the oligonucleotide through attack at the phosphorus atom (22). Nucleopeptide **1** was shown to be compatible with an overnight treatment with 1:1 concentrated aqueous NH_3 /dioxane at 55 °C as the final cleavage and deprotection step, which, as expected (18), afforded the C-terminal carboxamide (66% cleavage yield).

After reversed-phase MPLC purification,² all nucleopeptides were shown to be homogeneous by analytical HPLC. The overall synthesis, cleavage, deprotection, and purification yields were 19, 15, 8, and 18% for nucleopeptides **1**, **2**, **3**, and **4**, respectively. It should be emphasized that no particular difficulties have been detected in the formation of a phosphodiester linkage between two secondary hydroxyl groups as in nucleopeptide **2**.

The expected composition in amino acids and nucleosides after acid hydrolysis and enzymatic digestion with snake venom phosphodiesterase and alkaline phosphatase, respectively, was confirmed for all products. The electrospray mass spectrometric analysis showed, in all cases, a series of peaks with an m/z ratio from which the calculated molecular mass was in accord with the expected mass.³

The relative stability of these four nucleopeptides in the presence of a 3'-exonuclease was evaluated by treating them with snake venom phosphodiesterase⁴ in the presence of an internal standard, Boc-Tyr-OH. This amino acid derivative was stable to the reaction conditions and did not coelute with any of the four nucleopeptides under the reversed-phase HPLC conditions used to analyze the reaction mixtures. The comparison of the relative areas of the nucleopeptide and the standard showed that, after 4 h, nucleopeptides **1** (Tyr), **2** (Thr), **3** (Ser), and **4** (Hse) were degraded by 70, 5, 25, and 55%, respectively. An enzyme-free control experiment showed

that all of the nucleopeptides are completely stable (6 h) under the reaction conditions used to evaluate their 3'-exonuclease stability.

It is not surprising that the tyrosine–nucleopeptide (**1**) is the least stable, since phosphodiesterases are able to hydrolyze phenyl–phosphate esters (23). With respect to the other nucleopeptides, there seems to be a correlation between steric hindrance and the lability of the nucleopeptide to the 3'-exonuclease. The most sterically hindered threonine–nucleoside bond (in **2**) is cleaved more slowly than the phosphodiester linkage to the primary hydroxyl group of an amino acid (Ser and Hse). The higher lability of the homoserine–nucleoside bond (in **4**) with respect to the serine–nucleoside linkage (in **3**) is probably due to the additional methylene group in the homoserine residue, which renders the 3'-end of the oligonucleotide more accessible.

The results described in this paper show, for the first

³ **1**: Gly 1.22, Ala 1.03, Tyr 0.80, Phe 0.97, dC 1.0, dG 1.2, T 1.0, dA 1.1; electrospray-MS m/z 576.3 $[\text{M} - 3\text{H}]^{3-}$, 583.9 $[\text{M} - 4\text{H} + \text{Na}]^{3-}$, 865.4 $[\text{M} - 2\text{H}]^{2-}$, 876.4 $[\text{M} - 3\text{H} + \text{Na}]^{2-}$; calcd mass for $\text{C}_{64}\text{H}_{80}\text{O}_{30}\text{N}_{20}\text{P}_4$ 1733.4, mass found 1732.6 ± 0.7 . **2**: Thr 0.87, Gly 1.24, Ala 1.03, Phe 0.97, dC 1.0, dG 1.2, T 1.0; electrospray-MS m/z 556.4 $[\text{M} - 3\text{H}]^{3-}$, 563.5 $[\text{M} - 4\text{H} + \text{Na}]^{3-}$, 835.2 $[\text{M} - 2\text{H}]^{2-}$, 845.7 $[\text{M} - 3\text{H} + \text{Na}]^{2-}$, 856.8 $[\text{M} - 4\text{H} + 2\text{Na}]^{2-}$; calcd mass for $\text{C}_{59}\text{H}_{77}\text{O}_{31}\text{N}_{19}\text{P}_4$ 1672.3, mass found 1671.8 ± 0.6 . **3**: Ser 0.39, Gly 1.45, Ala 1.02, Phe 0.98, dC 1.0, dG 1.1, T 1.0; electrospray-MS m/z 551.7 $[\text{M} - 3\text{H}]^{3-}$, 559.1 $[\text{M} - 4\text{H} + \text{Na}]^{3-}$, 828.1 $[\text{M} - 2\text{H}]^{2-}$, 839.1 $[\text{M} - 3\text{H} + \text{Na}]^{2-}$, 850.1 $[\text{M} - 4\text{H} + 2\text{Na}]^{2-}$; calcd mass for $\text{C}_{58}\text{H}_{75}\text{O}_{31}\text{N}_{19}\text{P}_4$ 1658.2, mass found 1658.0 ± 0.3 . **4**: Gly 1.39, Ala 1.05, Phe 0.96, dC 1.0, dG 1.0, T 1.0; electrospray-MS m/z 581.8 $[\text{M} - 3\text{H}]^{3-}$, 884.2 $[\text{M} - 3\text{H} + \text{Na}]^{2-}$; calcd mass for $\text{C}_{65}\text{H}_{81}\text{O}_{31}\text{N}_{19}\text{P}_4$ 1748.4, mass found 1748.9 ± 0.5 .

⁴ Fifty microliters of a solution 10 mM in MgCl_2 and 50 mM in Tris-HCl that contained 0.0076 unit of the enzyme (phosphodiesterase from *Crotalus durissus*, Boehringer Mannheim, approximately 0.003 unit/ μL) and 100 μL of an aqueous solution of Boc-tyrosine (8.5 mM) were added to each nucleopeptide (1 OD₂₆₀). The evolution of the enzymatic digestion mixture (pH 7.08, 36 °C) was monitored by HPLC analysis of aliquots of the mixture (10 μL , diluted with 50 μL of water) removed at different times. The samples were kept frozen while not analyzed (C_{18} Nucleosil, 1 mL/min, linear gradient from 15 to 45% of B in 20 min, where A = 0.01 M triethylammonium acetate and B = acetonitrile/ H_2O 1:1).

² Exchange of tetrabutylammonium ions for sodium ions by chromatography through Dowex 50Wx4 sometimes simplifies the HPLC traces of crude nucleopeptides and thus facilitates the MPLC purification step. Nucleopeptides were purified by reversed-phase MPLC (C_{18} Vydac), using a gradient from 15 to 45% of B, in the case of nucleopeptides **1** and **2**, and from 17 to 31% of B, for **3** and **4** (A = 0.05 M triethylammonium acetate, pH 7.0; B = acetonitrile/ H_2O 1:1; 150 mL of each solvent).

time, that the enzymatic stability of nucleoside-O-P(O)-(O⁻)-OR phosphodiester groups can vary significantly even with small changes in the structure of the "R" group. As a result, in the absence of any other experimental data that might clarify this point, the enzymatic stability of [oligonucleotide-linker-peptide] hybrids having a phosphodiester nucleoside-linker bond cannot be relied upon and should be tested.

In summary, the stepwise solid-phase synthetic method originally developed for serine-nucleopeptides has also been shown to be suitable for the preparation of peptide-oligonucleotide hybrids with different hydroxylated linking amino acids. Even though the stability of nucleopeptides should be evaluated in biological media, the preliminary results described in this paper indicate that their lability to 3'-exonucleases increases in the order threonine < serine < homoserine < tyrosine. The choice of one of the four residues to establish the phosphodiester bond with the oligonucleotide may thus depend on whether the target product is to reproduce a naturally occurring structure (homoserine is then excluded) or is designed to be used in structural studies or to be evaluated as a therapeutic agent. Homoserine-nucleopeptides are the most robust from the chemical point of view, but threonine is the amino acid of choice if exonuclease resistance is the main requirement.

ACKNOWLEDGMENT

We are grateful for the use of the facilities of the "Servei de RMN de la Universitat de Barcelona" and thank Dr. Irene Fernández for the electrospray mass spectrometric analysis. This work was supported by funds from the DGICYT (Grant PB94-0844) and the Generalitat de Catalunya (GRQ93-1094, SRG96-0001, and Centre de Referència de Biotecnologia).

LITERATURE CITED

- (1) Ratajczak, M. Z., and Gewirtz, A. M. (1994) Oligonucleotide-based therapeutics of human malignancies. *Nucleic Acids Mol. Biol.* 8, 298-326.
- (2) Lu, X.-M., Fischman, A. J., Jyawook, S. L., Hendricks, K., Tompkins, R. G., and Yarmush, M. L. (1994) Antisense DNA delivery in vivo: liver targeting by receptor-mediated uptake. *J. Nucl. Med.* 35, 269-275.
- (3) Leonetti, J.-P., Degols, G., and Lebleu, B. (1990) Biological activity of oligonucleotide-poly(L-lysine) conjugates: Mechanism of cell uptake. *Bioconjugate Chem.* 1, 149-153.
- (4) Juby, C. D., Richardson, C. D., and Brousseau, R. (1991) Facile preparation of 3' oligonucleotide-peptide conjugates. *Tetrahedron Lett.* 32, 879-882.
- (5) Bongartz, J.-P., Aubertin, A.-M., Milhaud, P. G., and Lebleu, B. (1994) Improved biological activity of antisense oligonucleotides conjugated to a fusogenic peptide. *Nucleic Acids Res.* 22, 4681-4688.
- (6) Soukchareun, S., Tregear, G. W., and Haralambidis, J. (1995) Preparation and characterization of antisense oligonucleotide-peptide hybrids containing viral fusion peptides. *Bioconjugate Chem.* 6, 43-53.
- (7) Eritja, R., Pons, A., Escarceller, M., Giralt, E., and Albericio, F. (1991) Synthesis of defined peptide-oligonucleotide hybrids containing a nuclear transport signal sequence. *Tetrahedron* 47, 4113-4120.
- (8) De la Torre, B. G., Aviñó, A., Tarrason, G., Piulats, J., Albericio, F., and Eritja, R. (1994) Stepwise solid-phase synthesis of oligonucleotide-peptide hybrids. *Tetrahedron Lett.* 35, 2733-2736.
- (9) Reed, M. W., Fraga, D., Schwartz, D. E., Scholler, J., and Hinrichsen, R. D. (1995) Synthesis and evaluation of nuclear targeting peptide-antisense oligodeoxynucleotide conjugates. *Bioconjugate Chem.* 6, 101-108.
- (10) Arar, K., Aubertin, A.-M., Roche, A.-C., Monsigny, M., and Mayer, R. (1995) Synthesis and antiviral activity of peptide-oligonucleotide conjugates prepared by using N_α-(bromoacetyl)-peptides. *Bioconjugate Chem.* 6, 573-577.
- (11) Basu, S., and Wickstrom, E. (1995) Solid phase synthesis of a D-peptide-phosphorothioate oligodeoxynucleotide conjugate from two arms of a polyethylene glycol-polystyrene support. *Tetrahedron Lett.* 36, 4943-4946.
- (12) Haralambidis, J., Duncan, L., and Tregear, G. W. (1987) The solid phase synthesis of oligonucleotides containing a 3'-peptide moiety. *Tetrahedron Lett.* 28, 5199-5202.
- (13) Bergmann, F., and Bannwarth, W. (1995) Solid phase synthesis of directly linked peptide-oligodeoxynucleotide hybrids using standard synthesis protocols. *Tetrahedron Lett.* 36, 1839-1842.
- (14) Dreef-Tromp, C. M., van der Maarel, J. C. M., van den Elst, H., van der Marel, G. A., and van Boom, J. H. (1992) Solid-phase synthesis of the nucleopeptide fragment H-Asp-Ser-[pAAAAGTAAGCC]-Glu-OH from the nucleoprotein of *Bacillus subtilis* phage ϕ 29. *Nucleic Acids Res.* 20, 4015-4020.
- (15) Robles, J., Pedroso, E., and Grandas, A. (1994) Stepwise solid-phase synthesis of the nucleopeptide Phac-Phe-Val-Ser-(p³ACT)-Gly-OH. *J. Org. Chem.* 59, 2482-2486.
- (16) Beltrán, M., Maseda, M., Robles, J., Pedroso, E., and Grandas, A. (1997) Synthesis of homoserine derivatives for the preparation of nucleopeptide analogues. *Lett. Pept. Sci.* (in press).
- (17) Juodka, B., Pfütz, M., and Werner, D. (1991) Chemical and enzymatic analysis of covalent bonds between peptides and chromosomal DNA. *Nucleic Acids Res.* 19, 6391-6398.
- (18) Robles, J., Pedroso, E., and Grandas, A. (1995) Solid-phase synthesis of a nucleopeptide from the linking site of adenovirus-2-nucleoprotein, -Ser(p⁵CATCAT)-Gly-Asp-. Convergent versus stepwise strategy. *Nucleic Acids Res.* 23, 4151-4161.
- (19) Rabanal, F., Giralt, E., and Albericio, F. (1992) A new fluorene-derived anchor for solid-phase synthesis of protected peptides. *Tetrahedron Lett.* 33, 1775-1778.
- (20) Montserrat, F. X., Grandas, A., Eritja, R., and Pedroso, E. (1994) Criteria for the economic large scale solid-phase synthesis of oligonucleotides. *Tetrahedron* 50, 2617-2622.
- (21) Sinha, N. D., Davis, P., Usman, N., Pérez, J., Hodge, R., Kremsky, J., and Casale, R. (1993) Labile exocyclic amine protection of nucleosides in DNA, RNA and oligonucleotide analog synthesis facilitating N-deacylation, minimizing depurination and chain degradation. *Biochimie* 75, 13-23.
- (22) Hydrolysis of phosphate esters. (1996) *Nucleic Acids in Chemistry and Biology* (G. M. Blackburn and M. J. Gait, Eds.) pp 101-107, Oxford University Press, Oxford, U.K.
- (23) Landt, M., and Buther, L. (1978) 5'-Nucleotide phosphodiesterase: isolation of covalently bound 5'-adenosine monophosphate, an intermediate in the catalytic mechanism. *Biochemistry* 17, 4130-4139.

BC970051U

Synthesis, DNA Binding, and Cleaving Properties of an Ellipticine–Salen–Copper Conjugate

Sylvain Routier,[†] Jean-Luc Bernier,[†] Jean-Pierre Catteau,[†] Pierre Colson,[‡] Claude Houssier,[‡] Christian Rivalle,[§] Emile Bisagni,[§] and Christian Bailly^{*,||}

Laboratoire de Chimie Organique Physique, URA 351 CNRS, USTL C3, 59655 Villeneuve d'Ascq, France, Laboratoire de Chimie Macromoléculaire et Chimie Physique, Université de Liège, 4000 Liège, Belgium, UMR 176 CNRS, Institut Curie, Université d'Orsay, Bât. 110–112, 91405 Orsay, France, and Laboratoire de Pharmacologie Moléculaire Antitumorale du Centre Oscar Lambret et INSERM U-124, 59045 Lille, France. Received July 16, 1997[®]

The synthesis of a DNA-cutting agent that conjugates an ellipticine chromophore and a copper complex of bis(salicylidene)ethylenediamine, referred to as a salen, is reported. The presence of the salen·Cu complex allows cleavage of DNA via oxygen-based radicals, and the ellipticine moiety serves as a DNA anchor. Spectroscopic measurements indicate that the intercalation geometry of the ellipticine chromophore is preserved with the hybrid. The cleavage is much more efficient with the conjugate than with the Schiff base copper complex alone.

Among the strategies available for the design of artificial nucleases is the use of metal complexes that create different types of DNA lesions (1). While considerable attention has been focused on the development of phenanthroline- and porphyrin-based metal complexes to tune the selectivity and reactivity of such chelates, few studies have sought to harness the potential of metal complexes of bis(salicylidene)ethylenediamine, usually referred to as salen. Complexes of tetradentate salen-type Schiff bases with Cu, Co, and Mn have proved useful as synthetic catalysts to investigate nucleic acids conformation (2). In recent studies, we have investigated the capacity of different types of salen–Cu^{II} complexes to cleave DNA. Initially, we reported that a functionalized salen–Cu^{II} complex is capable of triggering single-stranded and nonspecific DNA cleavage after activation with a reducing agent (3). Subsequently, we showed that the coupling of the salen moiety to anthraquinone derivatives significantly promotes their affinity for DNA but has no effect on the cleavage reaction (4). More recently, a DNA minor groove binding element was coupled to the salen moiety in an effort to increase the specificity of cleavage, but the cleavage remained relatively weak (5). Here we report the preparation of an ellipticine–salen·Cu conjugate (Figure 1) and its ability to bind and to cleave DNA. The appended ellipticine chromophore serves as a DNA anchor, and as such, it potentiates significantly the capacity of the salen moiety to cleave DNA.

The salen moiety functionalized with a butylamino side chain was synthesized directly as a copper complex as recently described (3). The ellipticine derivative bearing an aminopropylaminoethyl side chain (6) was first reacted with succinic anhydride to give the corresponding acid,¹ which was then condensed with the salen moiety via a conventional coupling procedure using dicyclohexylcarbodiimide and *N*-hydroxybenzotriazole.²

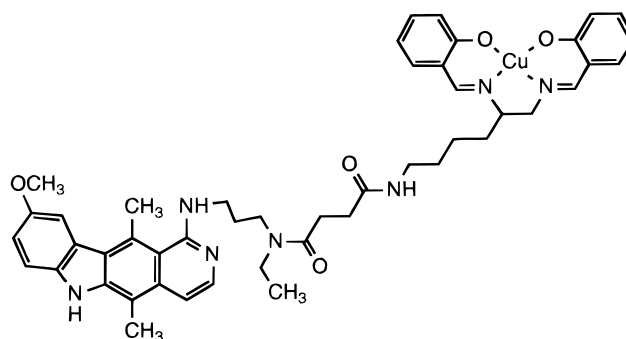


Figure 1. Structure of the ellipticine–salen·copper complex.

The absorption spectrum of the conjugate is significantly modified in the presence of DNA (Figure 2). The absorption band centered at 308 nm corresponding to the ellipticine moiety is shifted by 11 nm when the ligand is fully bound to DNA, and a marked hypochromism is observed. The interaction of the salen·Cu moiety with DNA causes a weak hypochromism in the 360 nm band.

Circular dichroism (CD) and electric linear dichroism (ELD) experiments were performed to define the orientation of the ligand chromophore with respect to the DNA helix. In contrast to what we previously reported with the functionalized salen·Cu complex (3), the CD spectra obtained with the ellipticine–salen·Cu hybrid in the presence of increasing DNA concentrations show no isodichroic point, indicating that the binding is geometrically heterogeneous (spectra not shown). The CD

* Author to whom correspondence should be addressed [fax (+33) 320 16 92 29; e-mail bailly@inserm.lille.fr].

[†] CNRS-USTL.

[‡] Université de Liège.

[§] Institut Curie.

^{||} COL-INSERM.

[®] Abstract published in *Advance ACS Abstracts*, November 1, 1997.

¹ The succinyl side chain was introduced by reacting 1-[(ethylamino)propyl]amino-9-methoxyellipticine (376 mg, 1 mmol) with succinic anhydride (100 mg, 1 mmol) in 200 mL of toluene for 5 h under reflux. After evaporation of the solvent, the functionalized ellipticine derivative was recrystallized in acetone. Yield: 310 mg, 63%, mp 150 °C; ¹H NMR (DMSO-*d*₆) δ 1.19 (t, 3H, *J* = 6.9 Hz, CH₃–CH₂), 1.88 (q, 2H, *J* = 6.8 Hz, CH₂–β), 2.67 (s, 3H, CH₃–5), 3.38 (s, 3H, CH₃–11), 3.4–3.5 (m, 10H, CH₂–α, CH₂–8, CH₂–CH₃, CO–CH₂, CH₂–CO₂H), 3.92 (s, 3H, OCH₃), 6.57 (s large, 1H, NH–1), 7.02 (d, 1H, *J* = 6.2 Hz), 7.16 (dd, 1H, *J* = 2.4 and 8.7 Hz), 7.47 (d, 1H, *J* = 8.7 Hz, H–7), 7.77 (d, 1H, *J* = 6.2 Hz, H–3), 7.79 (d, 1H, *J* = 2.4 Hz, H–10), 11.04 (s, 1H, NH–6). Anal. Calcd for C₂₇H₃₂N₄O₄·H₂O: C, 65.57; H, 6.93; N, 11.33. Found: C, 65.28; H, 6.88; N, 11.05.

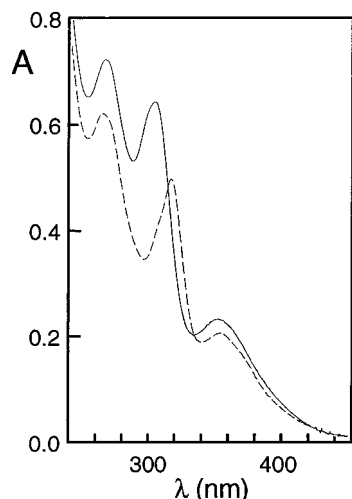


Figure 2. Absorption spectra of the ellipticine-salen-Cu^{II} hybrid (35 μ M) in the absence (full line) and presence (dashed line) of calf thymus DNA (175 μ M) in 1 mM sodium cacodylate buffer, pH 6.5. The spectrum corresponding to the drug bound to DNA was referenced against a DNA solution of exactly the same concentration and was adjusted to a common baseline.

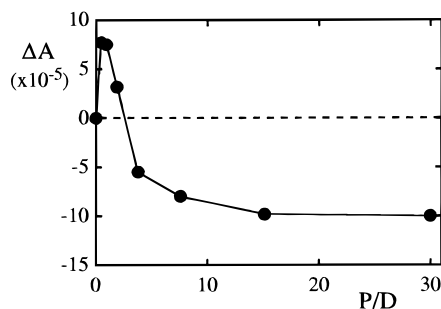


Figure 3. Dependence of the CD ΔA on the DNA-phosphate-to-drug ratio. The CD was monitored at 320 nm in the presence of 50 μ M drug and decreasing concentrations of calf thymus DNA in 1 mM sodium cacodylate buffer, pH 6.5.

signal monitored at 320 nm first increases with increasing P/D ratios, until a P/D value of 0.5–1 is reached, and then rapidly decreases to become negative at a P/D value >5 and remains constant at P/D >10 (Figure 3). The same biphasic evolution of the CD at 320 nm was previously reported with a structurally related ellipticine derivative (7). The decrease of the CD peak at P/D ratio ≥ 1 is attributable to decrease of excitonic coupling arising from a distance increase between adjacent intercalated molecules. Similar variation of molar dichroism with the P/D ratio has been reported with other typical intercalating agents such as ethidium bromide and acridine orange (8).

² *N,N*-Dicyclohexylcarbodiimide (7.6 mg, 36.8 mmol) and *N*-hydroxybenzotriazole (5.1 mg, 37.7 mmol) dissolved in 1 mL of DMF were added to a cold solution of the ellipticine acid (16 mg, 32.6 μ mol) in CH₂Cl₂. The mixture was stirred for 2 h at 0 °C before a solution containing the aminosalen-Cu complex (20.3 mg, 39.4 mmol) and triethylamine (6 μ L, 49.3 mmol) was added. The reaction was continued for 1 h at 0 °C and then for 4 days at room temperature. After evaporation of the solvent *in vacuo*, the crude residue is dissolved in pure CH₂Cl₂ and washed twice in turn with 10% citric acid (25 mL), 1 N sodium bicarbonate (10 mL), and water (20 mL). The organic layer is dried over Na₂SO₄ and evaporated under reduced pressure to yield the final product as a brown solid: 22 mg, 65%, mp 131–133 °C; IR ν 3400 (CONH), 2930 (CH₂, CH₃), 1730 (CONH), 1690 (CONH), 1620 (NH) cm⁻¹; MS (laser desorption) 859.3 ($M + 1$)⁺, 921.2 ($M + Cu$)⁺, 881.4 ($M + Na$)⁺. Anal. Calcd for C₄₇H₅₃N₇O₅·Cu: C, 65.71; H, 6.22; N, 11.42. Found: C, 65.80; H, 6.25; N, 11.35.

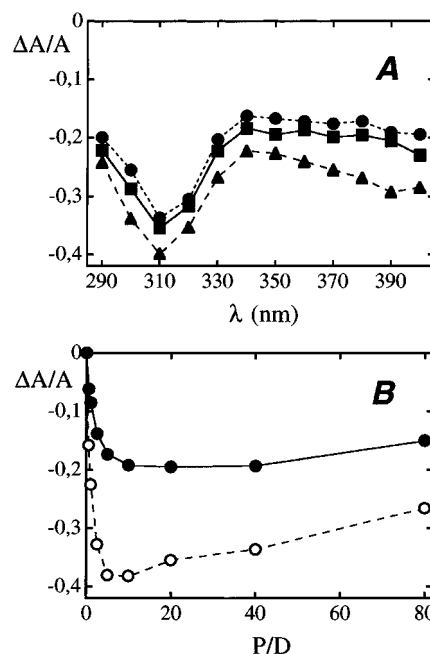


Figure 4. Dependence of the reduced dichroism $\Delta A/A$ on (A) the wavelength and (B) the DNA-phosphate-to-drug ratio. Conditions: (A) (■) calf thymus DNA, (▲) poly(dA-dT)·poly(dA-dT), (●) poly(dG-dC)·poly(dG-dC), P/D = 10, 12.5 kV/cm; (B) (○) 310 nm, (●) 350 nm, 12.5 kV/cm, in 1 mM sodium cacodylate buffer, pH 6.5.

The ELD spectra of the hybrid bound to calf thymus DNA and to the alternating copolymers poly(dA-dT)·poly(dA-dT) and poly(dG-dC)·poly(dG-dC) are shown in Figure 4A. The mode of binding of the drug was analyzed only on the basis of the highest ELD values, obtained when the drug molecules are fully bound to DNA, i.e., for P/D ratios >10 . At lower P/D ratio, the measured ELD values fall significantly due to the appearance of unbound molecules in the solution (Figure 4B). The reduced dichroism is always negative in sign, even in the 350–400 nm region where the salen-Cu unit absorbs the light. The reduced dichroism values do not vary markedly when the drug is bound to calf thymus DNA that contains about 42% A·T base pairs or to the AT and GC polynucleotides; the ellipticine moiety retains much the same orientation whatever the DNA composition. The negative LD measured with the drug–DNA complex at 310 nm (i.e. in the ellipticine absorption band) is equally intense as that measured with the DNA alone at 260 nm ($\Delta A/A = -0.38$), but the LD measured in the salen absorption band (360–400 nm) is only half of that obtained with DNA. This indicates that the ellipticine ring is tilted close to the plane of the DNA bases, consistent with an intercalative mode of binding, whereas the salen substituent does not insert between the base pairs. The orientation of the copper complex can be determined by measuring the angles α and β between the transition moments (of the bases and the dye chromophore, respectively) and the orientation axis of the DNA molecules. With calf thymus DNA, the ELD value in the 350–400 nm band was found to be -0.2 , which corresponds to an orientation of the salen-Cu moiety chromophore inclined at about 65° (β) to the helix axis. The angle is estimated by comparing the reduced dichroism at a given electric field strength for the DNA bases and for the hybrid in their respective absorption bands, assuming a theoretical angle of 90° (α) for the bases with respect to the orientation axis of the particles (9). The angle is 62° if an experimental angle of 72° is taken for

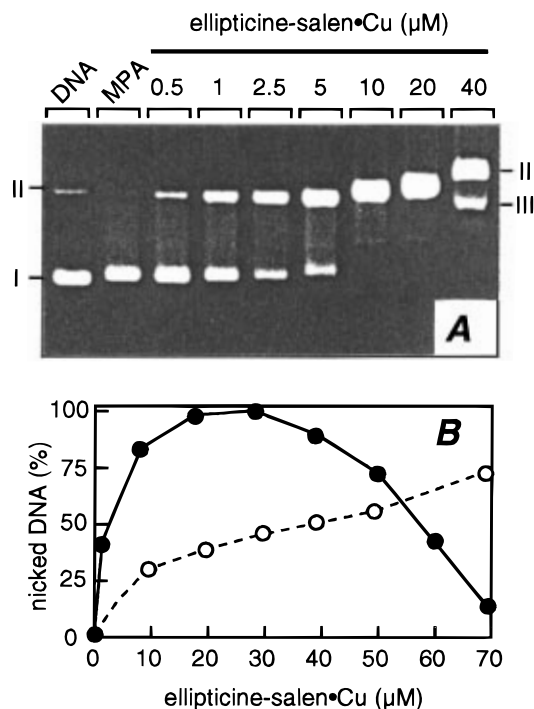


Figure 5. (A) Cleavage of closed circular DNA. Supercoiled DNA (0.7 μg) was incubated at 37 °C for 2 h with the drug at the indicated concentration in the presence of 100 μM MPA. Control lanes refer to the plasmid DNA incubated without drug in the absence (DNA) and presence (MPA) of 2-mercaptopyrionic acid. Forms I, II, and III refer to the supercoiled, nicked, and linear DNA forms, respectively. (B) Comparison of the cleavage efficiency of the conjugate (●) and the salen (○). The plots show the formation of nicked DNA (form II) as a function of the drug concentration. Three gels as shown in (A) were scanned and the results averaged.

the bases (10). Such an orientation is not consistent with a minor groove binding (which usually gives an angle of about 45°). It is more likely that the salen-Cu moiety extends out from the surface of the double helix.³

DNA cleavage was analyzed by monitoring the conversion of supercoiled plasmid DNA (form I) to the nicked circular molecules (form II) and linear DNA (form III). The tests were performed under aerobic conditions in the presence of 2-mercaptopyrionic acid (MPA) as a reducing agent. As shown in Figure 5A, the ellipticine derivative equipped with a salen-Cu^{II} functionality is able to catalyze reductive cleavage of DNA. Incubation of the plasmid for 2 h with 20 μM conjugate suffices to completely convert the form I to the nicked form II, whereas in the same conditions only ~50% of the DNA is cleaved with the salen moiety lacking the ellipticine. The reduced electrophoretic mobility of the nicked DNA reflects the intercalation of ellipticine molecules. The quantitative analysis of the cleavage data reveals that the hybrid compound is considerably more efficient than the salen-Cu complex in producing nicked DNA species (Figure 5B). In other words, the ellipticine moiety

³ The Cu^{II} atom is tetraordinated. The ESR spectrum of the conjugate-Cu complex was obtained from a frozen, aqueous solution (0.1 mM) at 77 K and 9.32 GHz. The magnetic parameters are $A_{||} = 191$ G, $g_{||} = 2.23$, and $g_{\perp} = 2.06$.

⁴ Spin-trapping techniques have shown that the drug can serve as a source of oxygen-based free radicals, with hydroxy radicals OH• probably the ultimate reactive species. In the presence of 5,5-dimethyl-1-pyrroline *N*-oxide (DMPO), solutions of the conjugate-Cu complex containing hydrogen peroxide generate an ESR spectrum characteristic of the DMPO-OH radical adduct ($a_N = a_H = 15.2$ G).

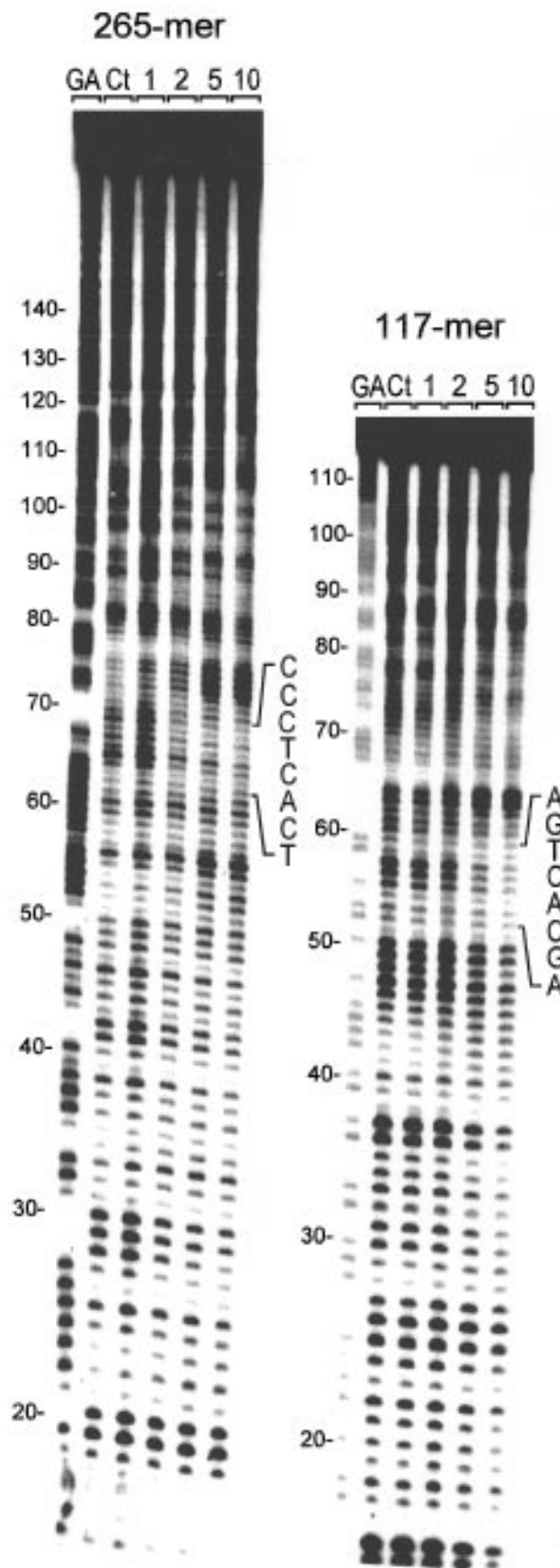


Figure 6. DNase I footprinting of the ellipticine-salen-Cu^{II} conjugate bound to the 265- and 117-mer *EcoRI*-*PvuII* restriction fragments cut out from plasmid pBS. In each case the DNA was 3'-end labeled with [α -³²P]dATP in the presence of AMV reverse transcriptase. The drug concentration (micromolar) is shown at the top of the appropriate gel lanes. The tracks labeled "Ct" contained no drug. The tracks labeled "GA" represent formic acid-piperidine markers specific for purines. Numbers on the left side of the gels refer to the numbering scheme of the fragments. The sequences protected from cleavage are indicated.

contributes significantly to reinforce the single-strand cleavage efficiency of the salen complex.⁴

The capacity of the conjugate to recognize specific sequences in DNA was studied by DNase I footprinting. The gel in Figure 6 shows that the attachment of the salen moiety does not hinder the capacity of the ellipticine chromophore to recognize specific sequences. Two well-resolved footprints encompassing the sequences 5'-CCCTCACT and 5'-AGTCACGA can be detected using micromolar drug concentrations. Complementary DNase I footprinting experiments were carried out with the 160 base pair *tyrT* fragment and, again, binding was shown to occur at various sequences with a preference for GC-rich regions of DNA (not shown). The drug strongly discriminates against runs of adenines or thymines. The sequence selectivity of the conjugate is reminiscent to that of the ellipticine alone (11). The intercalating chromophore imposes its preference for GC-rich sequences.

In conclusion, the experimental results show that the attachment of an intercalating ellipticine chromophore was the correct way to proceed to confer highly efficient cleavage of DNA, the first time this has been achieved with a hybrid intercalator-salen-copper complex conjugate. On the basis of this success, we intend to develop a general strategy for constructing other salen-based molecules as synthetic conjugates that will afford an independent approach to the design of artificial nucleases.

ACKNOWLEDGMENT

This work was supported by grants (to C.B.) from the Association pour la Recherche sur le Cancer and (to C.H. and P.C.) from the Actions de Recherches Concertées contract 95/00-93 and the FNRS, Télévie 7/4526/96. Support by the "convention INSERM-CFB" is acknowledged.

LITERATURE CITED

- (1) (a) Sigman, D. S., Mazumder, A., and Perrin, D. M. (1993) Chemical nucleases. *Chem. Rev.* **93**, 2295–2316. (b) Pratviel, G., Bernadou, J., and Meunier, B. (1995) Carbon-hydrogen bonds of DNA sugar units as targets for chemical nucleases and drugs. *Angew. Chem., Int. Ed. Engl.* **34**, 746–769.
- (2) (a) Muller, J. G., Chen, X., Dadiz, A. C., Rokita, S. E., and Burrows, C. J. (1992) Ligands effects associated with the intrinsic selectivity of DNA oxidation promoted by nickel(II) macrocyclic complexes. *J. Am. Chem. Soc.* **114**, 6407–6411. (b) Woodson, S. A., Muller, J. G., Burrows, C. J., and Rokita, S. E. (1993) A primer extension assay for modification of guanine by Ni(II) complexes. *Nucleic Acids Res.* **21**, 5524–5525. (c) Cheng, C.-C., Rokita, S. E., and Burrows, C. J. (1993) Nickel(III)-promoted DNA cleavage with ambient dioxygen. *Angew. Chem., Int. Ed. Engl.* **32**, 277–278. (d) Muller, J. G., Paikoff, S. J., Rokita, S. E., and Burrows, C. J. (1994) DNA modification promoted by water-soluble nickel(II) salen complexes: a switch to DNA alkylation. *J. Inorg. Biochem.* **54**, 199–206. (e) Burrows, C. J., and Rokita, S. E. (1994) Recognition of guanine structure in nucleic acids by nickel complexes. *Acc. Chem. Res.* **27**, 295–301. (f) Gravert, D. J., and Griffin, J. H. (1993) Specific DNA cleavage mediated by [salenMn(III)]. *J. Org. Chem.* **58**, 820–822. (g) Gravert, D. J., and Griffin, J. H. (1996) Steric and electronic effects, enantiospecificity, and reactive orientation in DNA binding/cleaving by substituted derivatives of [salenMn(III)]⁺. *Inorg. Chem.* **35**, 4837–4847. (h) Bhattacharya, S., and Mandal, S. S. (1995) Ambient oxygen activating water soluble cobalt-salen complex for DNA cleavage. *J. Chem. Soc., Chem. Commun.*, 2489–2490. (i) Sato, K., Chikira, M., Fujii, Y., and Komatsu, A. (1994) Stereospecific binding of chemically modified salen-type Schiff base complexes of copper(II) with DNA. *J. Chem. Soc., Chem. Commun.*, 625–626.
- (3) Routier, S., Bernier, J.-L., Waring, M. J., Colson, P., Houssier, C., and Bailly, C. (1996) Synthesis of a functionalized salen-copper complex and its interaction with DNA. *J. Org. Chem.* **61**, 2326–2331.
- (4) Routier, S., Cotelle, N., Catteau, J.-P., Bernier, J.-L., Waring, M. J., Riou, J.-F., and Bailly, C. (1996) Salen-anthraquinone conjugates. Synthesis, DNA-binding and cleaving properties, effects on topoisomerases and cytotoxicity. *BioOrg. Med. Chem.* **4**, 1185–1196.
- (5) Routier, S., Bernier, J.-L., Catteau, J.-P., and Bailly, C. (1997) Recognition and cleavage of DNA by a distamycin-salen-copper conjugate. *BioOrg. Med. Chem. Lett.* **7**, 1729–1732.
- (6) Rivalle, C., Wendling, F., Tambourin, P., Lhoste, J.-M., Bisagni, E., and Chermann, J.-C. (1983) Antitumor amino-substituted pyrido[3',4':4,5]pyrrolo[2,3-*g*]isoquinolines and pyrido[4,3-*b*]carbazole derivatives: Synthesis and evaluation of compounds resulting from new side chain and heterocycle modifications. *J. Med. Chem.* **26**, 181–185.
- (7) Bourdouxhe, C., Colson, P., Houssier, C., Sun, J.-S., Montenay-Garestier, T., Hélène, C., Rivalle, C., Bisagni, E., Waring, M. J., Hénichart, J.-P., and Bailly, C. (1992) Binding of a distamycin-ellipticine hybrid molecule to DNA and chromatin: spectroscopic, biochemical and molecular modeling investigations. *Biochemistry* **31**, 12385–12396.
- (8) (a) Houssier, C., Hardy, B., and Fredericq, E. (1974) Interaction of ethidium bromide with DNA. Optical and electrooptical study. *Biopolymers* **13**, 1141–1160. (b) Fredericq, E., and Houssier, C. (1972) Study of the interaction of DNA and acridine orange by various optical methods. *Biopolymers* **11**, 2281–2308.
- (9) Houssier, C. (1981) Investigating nucleic acids, nucleoproteins, polynucleotides, and their interactions with small ligands by electrooptical systems. In *Molecular Electro-Optics* (S. Krause, Ed.) pp 363–398, Plenum Publishing, New York.
- (10) Chou, P.-J., and Johnson, W. C., Jr (1993) Base inclinations in natural and synthetic DNAs. *J. Am. Chem. Soc.* **115**, 1205–1214.
- (11) Bailly, C., OhUigin, C., Rivalle, C., Bisagni, E., Hénichart, J. P., and Waring, M. J. (1990) Sequence-selective binding of an ellipticine derivative to DNA. *Nucleic Acids Res.* **18**, 6283–6291.

BC970131Y

ARTICLES

Synthesis and Characterization of High-Molecular Mass Polyethylene Glycol-Conjugated Oligonucleotides

Gian Maria Bonora,^{*,†} Eugenia Ivanova,[‡] Valentina Zarytova,[‡] Barbara Burcovich,[§] and Francesco Maria Veronese[§]

Pharmaco-Chemico-Technology Department, Via Ospedale 72, University of Cagliari, 09124 Cagliari, Italy, Novosibirsk Institute of Bioorganic Chemistry, Novosibirsk, Russia, and Department of Pharmaceutical Sciences, University of Padova, Padova, Italy. Received December 30, 1996[®]

The use of synthetic oligonucleotides as possible drugs for human therapy is usually hampered by their low *in vivo* stability and capacity to achieve high concentrations at their cellular targets. To overcome this, it has been suggested that they be modified chemically. Among the various options, conjugation with short- and long-chain polyethylene glycols (PEGs) has several advantages: PEG is nontoxic and very soluble, reduces immunogenic reactions, and increases the stability of the conjugated molecules. PEG is generally joined to oligonucleotides while bound to the insoluble solid-phase supports, after their synthesis, which does not allow for their being easily scaled up. The use of the liquid-phase approach as an alternative synthetic process, utilizing the PEG polymer both as a soluble, inert synthetic support and a stabilizing agent of the oligonucleotide, is proposed. A new protocol has been set up, characterized by a stable phosphate bond between the support and the oligonucleotide. This method has been tested on a 12mer previously investigated as an antisense agent against HIV. The PEG-conjugated 12mer was efficiently synthesized and purified. It was found that the high-molecular mass PEG chain results in enzymatic stability and does not interfere with the formation of the duplex with its nucleic acid target.

INTRODUCTION

The use of synthetic oligonucleotides as new therapeutic agents is currently of widespread interest (1). These molecules interact with either specific single-stranded RNA messengers, as antisense, (2) or double-stranded genomic DNA, as antigene (3), inhibiting the expression of pathogenic genetic messages. Moreover, these molecules have recently been investigated as new, specific ligands of non-nucleic acid receptors, such as extracellular proteins (4).

The utilization of these molecules as new drugs for human therapy creates new problems related to their low *in vivo* stability and capacity for achieving high concentrations in the biological targets, since they are rapidly degraded by endogenous nucleases and exhibit reduced cellular uptake (5). Their chemical modification, mainly of the sugar-phosphate backbone, is commonly performed (6) to avoid recognition by degradative enzymes and, by increasing their lipophilicity, to enhance cellular penetration. However, these modified oligonucleotides have some disadvantages such as low solubility in a physiological media, toxicity of their metabolites, or inhibition of the degradative process of duplexes brought about by RNase H.

Another solution considers the conjugation of the oligonucleotides with molecules that mask their identity

and confer a stronger hydrophobic character, such as long-chain alcohols (7), steroids (8), cholic acid (9), peptides (10), etc. Recently, the introduction of short- and long-chain polyethylene glycols (PEGs) has been investigated. In fact, it is well known (11) that PEG is a unique molecule that, when covalently bound to a substrate, increases the solubility in organic and aqueous solution, decreases the immunogenic effect, and extends the body lifetime. This nontoxic compound has been used for the preparation of a series of biologically active conjugates (12). In oligonucleotide chemistry, a short PEG chain has been used as a non-nucleosidic linker in triplex-forming molecules (13), synthetic ribozymes (14), loop-forming chains, and circular nucleic acid derivatives (15).

High-molecular mass PEG has recently been introduced at the 3'- and 5'-end of the oligonucleotide chains; the 3'-position has been modified by a PEG-modified solid-phase support (16–18), while the 5'-end reacted with a reactive PEG chain when bound to the solid-phase support (19–22) or after its release (23–25). With these procedures, very often a limited amount of PEG conjugate can be produced, owing to the reduced capacity of the solid-phase processes and its difficult upscaling. Moreover, when a postsynthetic conjugation is performed with high-molecular mass PEGs, the viscosity of their solution hampers the condensation reaction, especially when the oligonucleotides are still bound to an insoluble support.

This problem may be further compounded when large scale production of these conjugated derivatives is needed (26).

A procedure which is based on a new method of oligonucleotide synthesis has recently been proposed to solve these problems (27). During this process, PEG has

* Author to whom correspondence should be addressed. Phone: +39 70 6758570. Fax: +39 70 6758553. E-mail: bonora@chor02.chor.unipd.it.

† University of Cagliari.

‡ Novosibirsk Institute of Bioorganic Chemistry.

§ University of Padova.

® Abstract published in *Advance ACS Abstracts*, July 1, 1997.

been used as a soluble polymeric support for the large scale synthesis of these molecules. In this liquid-phase procedure (called HELP), a PEG unit with a molecular mass between 5000 and 20 000 Da has been employed to produce oligonucleotide chains of up to 20 monomers. To obtain a useful PEG conjugate, that procedure has been modified by introducing a stable bond between the polymer and the growing chain. PEG was then utilized both as a synthetic handle, for the liquid-phase procedure, and as a biological carrier for the final oligonucleotide.

The synthesis of a high-molecular mass PEG-conjugated 12mer is reported here. This sequence was an active antisense against HIV-1 (28). The synthetic protocol, the purification of the final derivative, and the first data on enzymatic stability and binding specificity are described.

EXPERIMENTAL PROCEDURES

Functionalization of Polyethylene Glycol. One gram of monomethoxy polyethylene glycol (MPEG, MW = 9500), corresponding to 0.105 mmol of free OH groups, was coevaporated twice with a few milliliters of anhydrous acetonitrile (AcCN). Dimethoxytrityl (DMT) (2-cyanoethyl)-*N,N*-diisopropyl nucleoside phosphoramidite [0.26 mmol (2.5 \times)] and 1.05 mmol (10 \times) of tetrazole, dissolved in anhydrous AcCN, were added, under argon, to MPEG that had previously been dissolved in the minimum amount of anhydrous AcCN. The mixture was stirred under argon for 5 min and cooled in an ice bath, and the MPEG-nucleoside was precipitated by the slow addition of 5–6 volumes of *tert*-butyl methyl ether (TBME). The product was filtered, washed with ether, recrystallized from ethanol to eliminate any residual amount of reagents or soluble byproducts, and dried.

The phosphite bond between the MPEG and the nucleoside was then oxidized to a phosphate one by dissolving the product in AcCN (1.0 g in 10 mL) and reacting it with 0.6 mL of *tert*-butyl hydroperoxide (TBHP), at 0 °C, under stirring, for 15 min. The product was precipitated with TBME, filtered, washed thoroughly with ether, and dried.

Any unreacted OH groups of the MPEG were capped with a mixture of 2,6-lutidine, *N*-methylimidazole (NMI), and acetic anhydride (0.5 mL each for 1.0 g of MPEG-nucleoside, dissolved in 5 mL of AcCN). The mixture was left under stirring at room temperature for 3 min; the DMT-5'-oligonucleotide-3'-MPEG was precipitated with TBME, filtered, washed with ether, and dried under vacuum over KOH pellets.

Synthesis of MPEG-Conjugated Oligonucleotides. The synthesis of the MPEG-conjugated oligonucleotides was performed according to the phosphoramidite-based procedure previously applied in the liquid-phase synthesis of oligonucleotides (29) as follows.

The fully protected DMT-5'-oligonucleotide-3'-MPEG was dissolved in a concentrated ammonia solution (20 mL for 100 mg of product) and left overnight at 60 °C. The ammonia was eliminated by evaporation with water (two or three times, 20 mL each) and the water solution extracted with ether (three times) and lyophilized. The 5'-DMT protecting group was eliminated by treatment with an acetic acid solution (4:1 v/v; 20 mL for 100 mg) for 30 min at room temperature. The water solution was extracted three times with ether and lyophilized.

The deprotected MPEG-conjugated oligonucleotide was purified by anion-exchange HPLC. The chromatography was performed on a MonoQ HR 5/5 column, eluted with NaCl, the gradient ranging from 0.20 to 0.50 M, at pH

12.00, over 18 min (flow rate of 1.0 mL/min). Detection was by UV absorbance at 260 nm. The product was desalted by a gel-filtration procedure on Sephadex G25-F (2 \times 10 cm), with MilliQ water as the eluent. An alternative desalification procedure was realized by dissolving the product in acetone or methanol (5 mL for 200 mg); after being stirred for 30 min, the solution containing the MPEG conjugate was filtered, or centrifuged, and dried. It was also possible to selectively extract the product from a water solution (5 mL for each gram) with dichloromethane (4 \times 100 mL).

Characterization of MPEG-Conjugated Oligonucleotide. To calculate the reaction yields, the absorption at 498 nm of the DMT group was determined spectrophotometrically (2 mg in 10 mL of a 70% perchloric acid solution in methanol) and the amount of MPEG-bound nucleotide was measured by using the following equation:

$$A_{498} \times \text{milliliters of HClO}_4 \text{ solution} \times \\ 14.3/(\text{milligrams of MPEG-oligonucleotide})$$

A Perkin-Elmer Lambda 5 UV/Vis spectrophotometer was used.

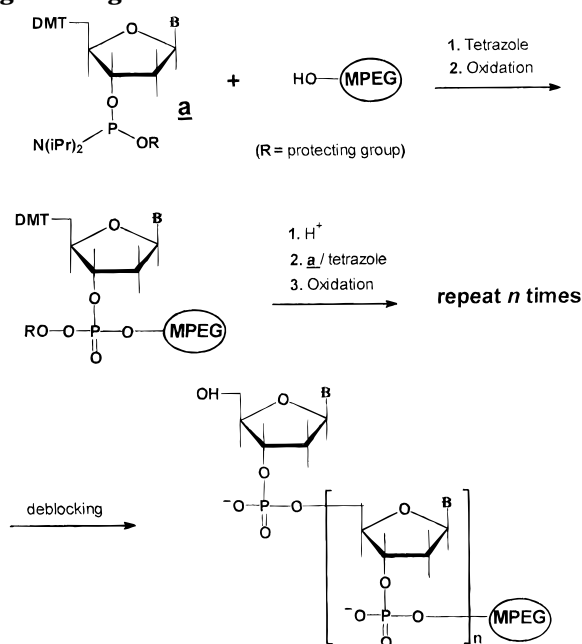
¹H and ³¹P NMR spectra were recorded on a Bruker 400 AM spectrometer, utilizing deuteriochloroform (99.96%) or deuterium oxide (99.9%) as a solvent and TMS as an internal standard for protons and 85% phosphoric acid for phosphorus.

To ascertain the complete removal of reagents, the MPEG conjugates were analyzed by thin-layer chromatography on precoated silica gel sheets 60 F₂₅₄ with the eluant ethyl acetate/acetone/water (5:10:1). The purified compound was analyzed by RP HPLC on a Vydac C₁₈ column (eluant: 0.1 M triethylammonium acetate at pH 7.0; gradient of acetonitrile from 10 to 80% over 60 min) and by IE HPLC on a MonoQ (eluant: gradient of NaCl from 0.05 to 0.5 M at pH 12.00 over 30 min). A WATER 600E apparatus, equipped with a 717 autosampler and a 490E UV/Vis detector, was used.

The starting MPEG, and the final conjugate, were analyzed by GPC on a Biosil Sec-125 column (300 \times 7.8 mm) eluted with 0.1 M Na₂SO₄/0.1 M NaH₂PO₄ at pH 6.8 (flow rate, 0.9 mL/min). A JASCO 880 PU apparatus, equipped with an ERMA Erc-7512 refraction index detector, was utilized.

Thermal Denaturation Studies. The thermal denaturation of oligonucleotide complexes was performed by following the A_{260} variations of solutions containing equimolar amounts of free and MPEG-bound oligonucleotide and complementary sequence. The samples were 1.3 $\times 10^{-5}$ M in 10 mM sodium cacodylate (pH 7.4) containing 0.1 M NaCl and 1 mM EDTA. The temperature inside the cell was increased at a ratio of 0.5 °C/min. More than 600 experimental points for each optical melting curve were collected, with 10 points/(°C step); the curves were fully reversible. The UV detector of a Millichrom chromatograph with a specially designed thermoregulated cell was used (30). The first derivatives of the melting curves were calculated using a linear approximation gradient by 10 experimental points.

Enzymatic Degradation. The enzymatic hydrolysis of the oligonucleotides was performed with a mixture of phosphodiesterase and nucleotidase from snake venom in 0.01 mL of a buffer containing 0.1 optical unit of the compound dissolved in 15 mM MgOAc₂/0.2 mM EDTA/0.1 M Tris-HCl at pH 8.8, and 37 °C. The changes in concentration were followed by HPLC analysis of the samples taken from the mixture on a time scale.

Scheme 1. Liquid-Phase Synthesis of MPEG-Conjugated Oligonucleotides**RESULTS AND DISCUSSION**

Scheme 1 illustrates the liquid-phase method applied for the synthesis of the high-molecular mass MPEG-conjugated oligonucleotides. The OH end groups of the MPEG unit were conjugated with 5'-DMT-protected phosphoramidite nucleosides, using the procedure adopted for the synthesis of the oligonucleotide chains (23). The MPEG-bound product, purified by precipitation from the reaction mixture and filtration, was again left to react with the next nucleotide.

In comparison with the procedures based on insoluble supports, this method had the advantages previously observed in the traditional liquid-phase synthesis of oligonucleotides. Since all the reactions are performed in the solution state, the phase homogeneity may allow for the easy scaling up of the process; moreover, owing to the absence of diffusion problems inside the resin beads, a lower amount of reagent was generally required. It should be recalled that a reduced amount of conjugated product is obtained, when the PEG chain is introduced at the end of the oligonucleotide synthesis on the solid support, owing to the low reactivity of the PEG solutions in these heterogeneous conditions. This drawback, which was further underlined by increasing the PEG molecular mass, was obviously absent in this method which took place under homogeneous conditions. It is also worth noting that the spectral transparency and the great solubility of the PEG moiety, and of its conjugates, allows for the rapid and nondestructive analysis of the various synthetic steps and easy evaluation of the reaction products and its byproducts during the purification processes.

To test the efficacy of this method, the 12mer conjugate with a monofunctional PEG chain, monomethoxy-substituted (MPEG), was synthesized. This oligonucleotide was previously employed to study its antisense activity against HIV (23). A MPEG molecule of a nominal 12 000 Da was used in this study, to obtain a better solubility of the final oligonucleotide chain and verify the effect of the higher molecular mass of the polymer on the biological properties of its conjugate. This polymer used was analyzed by GPC that indicated an average molecular mass of 9500 Da, with low polydispersity.

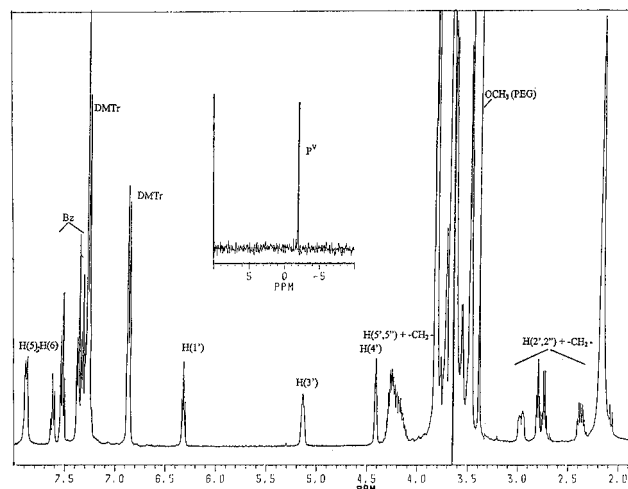


Figure 1. ^1H NMR spectrum of the starting DMT-5'-(*N*-benzoyl)deoxycytidine-3'-MPEG in CDCl_3 . (Inset) Partial ^{31}P NMR spectrum of the same solution (no further signals up to 150 ppm). MPEG methylene signals were suppressed by selective irradiation.

Table 1. Synthetic Cycle (1.0 g of $\text{MPEG}_{12000}\text{-OH}$)

step ^a	reagents	quantity	time (min)
detritylation	TCA solution ^b	20 mL	15
coupling	AcCN	minimum to dissolve	
	0.1 M phosphoramidite	5.0 mL	
	0.5 M tetrazole	4.0 mL	5
capping	capping solution ^b	10.0 mL	5
oxidation	tBHP solution ^b	10.0 mL	15

^a After each step, the sample is precipitated with 5–6 volumes of TBME, at 0 °C; a further recrystallization with 50 mL of ethanol may be required at the end of each cycle. ^b See Experimental Procedures.

The ^1H and ^{31}P NMR spectra of the polymer conjugated to the first nucleotide of the planned oligo chain are reported in Figure 1. Within the limits of instrumental errors, a quantitative reaction of the MPEG was obtained under the reported conditions; the integration values of the nucleotide signals were in a 1:1 ratio with those of the polymeric unit. Moreover, in the ^{31}P NMR spectrum, only the signal from the phosphate bond at -2.2 ppm was visible, which demonstrated the efficacy of the oxidation procedure.

From the UV/vis analysis of the sample, for each gram of MPEG, 95 μmol of nucleotide was measured which corresponded very well with the expected 97 $\mu\text{mol/g}$.

The stability of the phosphate bond between the MPEG and the first nucleoside was evaluated by NMR and TLC analysis of a sample subjected to the same reaction conditions required for the synthesis and the final deblocking of the oligonucleotide chain. The assay indicates that no measurable release of the nucleoside molecule occurred under these conditions.

The MPEG-12mer was obtained following the synthetic protocol reported in Table 1. In all the precipitation steps, TBME was used, instead of diethyl ether (23), because this ether absorbed a lower amount of water, which has an adverse effect during the synthetic process, and also appeared to be more efficient for the complete precipitation of the products.

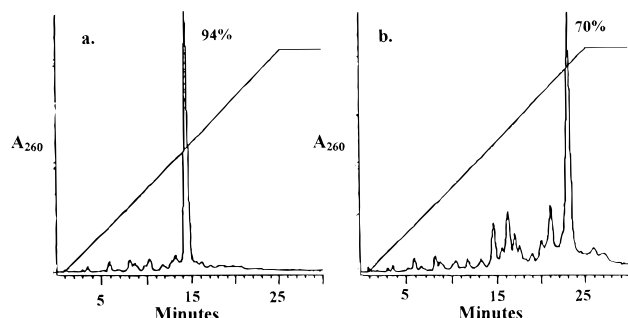
The reaction data of each step of the synthesis of the MPEG-12mer anti HIV are listed in Table 2. A very good coupling yield was observed for each step, as judged from the A_{498} of the derivatives. The overall and the average yields were comparable to those of the solid-

Table 2. Synthetic Data of MPEG-12mer anti HIV (1.0 g of MPEG₁₂₀₀₀-OH)

nucleoside	oligonucleotide bound ($\mu\text{mol/g}$) ^a	step yield (%) ^b
dC	95	98
dG	89	98
dA	85	99
dC	79	98
dG	76	99
dA	72	99
dA	69	99
dC	64	97
dT	60	98
dA	58	99
dC	56	99
dG	54	97

overall yield = 82% average yield = 98.5%
 total amount recovered = 0.9 g (60%) (5815 OD/g after purification)

^a From A_{498} of the DMT group. ^b Calculated on the basis of the increased MW of the conjugate.

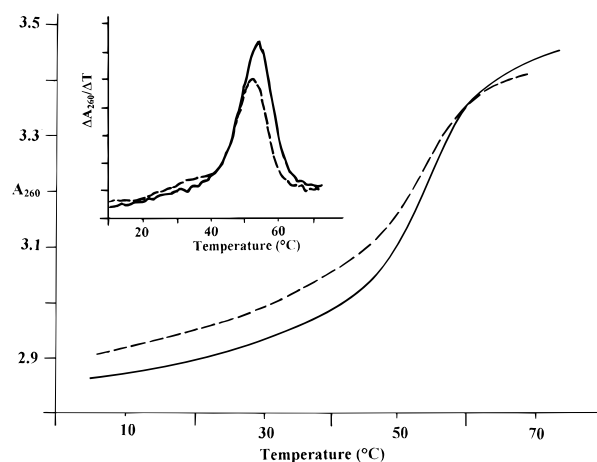
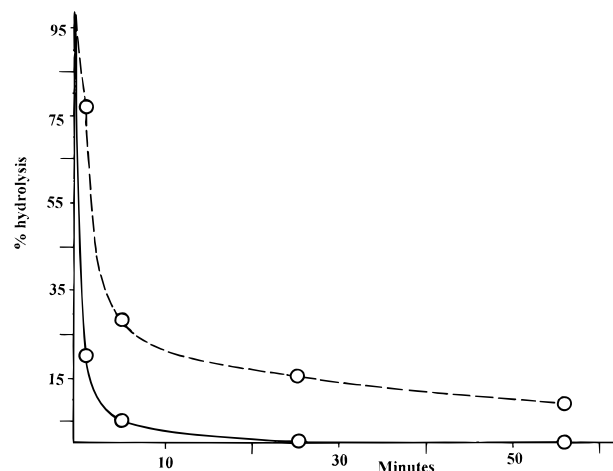
**Figure 2.** IE HPLC of the crude MPEG conjugates: (a) MPEG-6mer-OH and (b) MPEG-12mer-OH. Area values of the main peaks are indicated.

phase synthesis of similar products. We are hopeful that the amount of the final collected oligonucleotide, which in this case was not maximized because of the high number of precipitation steps needed for the purification of the intermediates, could be increased with automation of the process (31). However, it should be recalled that the amount of collectable product was even lower when PEG was introduced with a postsynthetic modification of the oligonucleotide supported on a solid phase, especially if a high-molecular mass polymer is employed.

The purification of the MPEG conjugates was achieved by HPLC initially using a reversed-phase column. Unfortunately, the separation of the final 5'-DMT-protected, fully deblocked, conjugated compounds from shorter sequences was unsuccessful, since the MPEG moiety was similar chromatographically to all the derivatives, and a single peak was always observed, despite the presence of a crude mixture of products. However, the different compounds in the mixtures could be separated by anion-exchange chromatography, since the charge balance of the different oligonucleotide chains was not suppressed by the high-molecular mass MPEG unit. The chromatographic patterns of the crude, fully deprotected 6mer and 12mer are reported in Figure 2; the efficacy of this synthetic procedure was clearly seen.

After purification and desalting, the final compound was further analyzed by GPC. From the elution behavior, the approximate average molecular mass was 13 000 Da, close to the calculated value (13 480 Da).

The final MPEG-12mer was further characterized by thermal denaturation studies. The dissociation of duplexes formed from equimolar concentrations of the conjugated oligonucleotide and the complementary unmodified target was examined. The A_{260} temperature

**Figure 3.** Thermal denaturation profiles of unmodified (unbroken line) and MPEG-conjugated (dashed line) 12mer duplexes. (Inset) First derivatives of the thermal profiles.**Figure 4.** Digestion of unmodified (unbroken line) and MPEG-conjugated 12mers (dashed line). The concentration of the starting oligonucleotides, quantified by HPLC, is plotted versus incubation time.

variations, and their first derivatives, are reported in Figure 3. It has been clearly demonstrated that the introduction of a single, long chain of MPEG at one end of the oligonucleotide has very little, if any, adverse effect on the hybridization properties of the oligonucleotide itself.

The effect of stabilization against the enzymatic degradation in the presence of the MPEG was finally investigated. The disappearance over time of both free and conjugated 12mers, incubated with a mixture of hydrolytic enzymes, is reported in Figure 4. It was possible to observe that, under these conditions, the unprotected oligonucleotide was completely digested in less than 30 min, while during the same period, at least 20–25% of the starting MPEG-12mer was still present, which demonstrated the stabilizing effect of the MPEG when bound to the oligonucleotide. These results are in agreement with those published on oligonucleotide conjugates with PEG chains lower molecular mass (19).

To summarize, the utility of this new, modified liquid-phase method for the preparation of oligonucleotides firmly bound to high-molecular mass PEG chains has been demonstrated. The intrinsic features of this procedure are especially suitable for the large scale production of these derivatives. The first biological data have confirmed that the high-molecular mass MPEG chain could increase the cellular lifetime of its conjugated

molecules without interfering with their capability to interact with the specific target.

The antisense properties of this derivative are now under investigation and will be reported in the near future.

ACKNOWLEDGMENT

The authors thank Dr. Tula Saison-Behmoaras and Prof. Claude Hélène (Museum National d'Histoire Naturelle, Paris) for the stimulating discussions. They are also grateful to Drs. L. Lokhov and N. Komatova, (Novosibirsk Institute of Bioorganic Chemistry, Russia) for the help with the experiments of thermal denaturation and enzymatic degradation. This research was supported by the Progetto Strategico CNR (Italy) ST74 "Oligonucleotidi Antisense" and by grants from MURST (Italy).

LITERATURE CITED

- (1) Cohen, J. S. (1992) Oligonucleotide therapeutics. *Tibtech* 10, 87.
- (2) Gillespie, D. (1992) Perspectives for antisense nucleic acid therapy. *DN&P* 7, 389.
- (3) Thuong, N. T., and Hélène, C. (1993) Sequence-specific recognition and modification of double-helical DNA by oligonucleotides. *Angew. Chem., Int. Ed. Engl.* 32, 666.
- (4) Wyatt, J. R., Vickers, T. A., Roberson, J. L., Buckeit, R. W., Klimkait, T., Deboets, E., Davis, P. W., Rayner, B., Imbach, J. L., and Eckers, D. J. (1994) Combinatorially selected guanosine-quartet structure is a potent inhibitor of human immunodeficiency virus envelope-mediated cell fusion. *Proc. Natl. Acad. Sci. U.S.A.* 91, 1356.
- (5) Heidenreich, O., Kang, S.-H., Xu, X., and Nerenberg, M. (1995) Application of antisense technology to therapeutics. *Mol. Med. Today* 1, 128.
- (6) Sanghvi, Y. S., and Cook, P. D., Eds. (1994) Carbohydrate modifications in antisense research. *ACS Symposium Series* 580, Maple Press, York, PA.
- (7) Shea, R. G., Marsters, J. C., and Bischoffberger, N. (1990) Synthesis, hybridization properties and antiviral activity of lipid-oligodeoxynucleotide conjugates. *Nucleic Acids Res.* 18, 3777.
- (8) Boutorin, A., Guskova, L., Ivanova, E., Kobetz, N., Zarytova, V., Rytte, A., Yurchenko, L., and Vlassov, V. (1989) Synthesis of alkylating oligonucleotide derivatives containing cholesterol or phenazinium residues at their 3'-terminus and their interaction with DNA within mammalian cells. *FEBS Lett.* 254, 129.
- (9) Manoharan, M., Johnson, L. K., Bennett, C. F., Vickers, T. A., Ecker, D. J., Cowser, L. M., Freier, S. M., and Cook, P. D. (1994) Cholic acid oligonucleotide conjugates for antisense application. *Bioorg. Med. Chem. Lett.* 18, 3777.
- (10) Tung, C., Rudolph, M. J., and Stein, S. (1991) Preparation of oligonucleotide-peptide conjugates. *Bioconjugate Chem.* 2, 464.
- (11) Harris, J. M., Ed. (1992) *Poly(ethylene glycol) chemistry. Biotechnical and biomedical applications*, Plenum Press, New York.
- (12) (a) Zalipsky, S. (1995) Functionalized poly(ethylene glycol) for preparation of biologically relevant conjugates. *Bioconjugate Chem.* 6, 150. (b) Zalipsky, S. (1995) Chemistry of polyethylene glycol conjugates with biologically active molecules. *Adv. Drug Delivery Rev.* 16, 157.
- (13) Kessler, D. J., Pettitt, B. M., Cheng, Y.-K., Smith, S. R., Jayaraman, K., Vu, H. M., and Hogan, M. E. (1993) Triple helix formation at distant sites: hybrid oligonucleotides containing a polymeric linker. *Nucleic Acids Res.* 21, 4810.
- (14) Thomson, J. B., Tuschl, T., and Eckstein, F. (1993) Activity of hammerhead ribozymes containing non-nucleotidic linkers. *Nucleic Acids Res.* 21, 5600.
- (15) Rumney, S., IV, and Kool, E. T. (1995) Structural optimization of non-nucleotidic loop replacement for duplex and triplex DNAs. *J. Am. Chem. Soc.* 117, 5635.
- (16) Efimov, V. A., Pashkova, I. N., Kalinkina, A. L., and Chakhmakhcheva, O. G. (1993) Synthesis of conjugates of oligonucleotides with polyethyleneglycol. *Bioorg. Khimi.* 19, 800.
- (17) Bayer, E., Maier, M., Bleicher, K., and Gaus, H. J. (1995) Synthesis of 3' PEG modified oligonucleotides on PS PEG tentacle polymers. *Z. Naturforsch. B* 50, 671.
- (18) De Napoli, L., Di Fabio, G., Messere, A., Varra, M., and Piccialli, G. (1996) New solid-phase approach to obtain 3'-derivatized oligonucleotides. *Gazz. Chim. Ital.* 126, 755.
- (19) Jäschke, A., Fürste, J. P., Nordhoff, E., Hillenkamp, F., Cech, D., and Erdmann, V. A. (1994) Synthesis and properties of oligodeoxyribonucleotide-polyethylene glycol conjugates. *Nucleic Acids Res.* 22, 4810.
- (20) Jäschke, A., Bold, R., Nordhoff, E., Hillenkamp, F., Cech, D., Erdmann, V. A., and Fürste, J. P. (1996) Synthesis and analytical characterization of RNA-polyethylene glycol conjugates. *Nucleosides Nucleotides* 15, 1519.
- (21) Tarasow, T. M., Timmermeier, D., and Zyrniewski, C. (1997) Characterization of oligodeoxyribonucleotides-polyethylene glycol conjugates by EMS. *Bioconjugate Chem.* 8, 89.
- (22) Manoharan, M., Tivel, K. L., Andrade, L. K., Mohan, V., Condon, T. P., Bennett, F. C., and Cook, P. D. (1995) Oligonucleotide conjugates: alteration of the pharmacokinetic properties of antisense agents. *Nucleosides Nucleotides* 14, 969.
- (23) Kawaguchi, T., Asakana, H., Tashiro, Y., Juni, K., and Sueishi, T. (1995) Stability, specific binding capacity, and plasma concentration in mice of an oligodeoxynucleotide modified at 5'-terminal with poly(ethylene glycol). *Biol. Pharm. Bull.* 18, 474.
- (24) Rahman, M. A., Summerton, J., Foster, E., Cunningham, K., Stirchak, E., Weller, D., and Schaup, H. W. (1991) Antibacterial activity and inhibition of protein synthesis in *E. coli* by antisense DNA analogs. *Antisense Res. Dev.* 1, 319.
- (25) Jones, D. S., Hachmann, J. P., Osgood, S. A., Hayaag, M. S., Barstad, P. A., Iverson, G. M., and Coutts, S. M. Conjugates of double-stranded oligonucleotides with poly(ethylene glycol) and keyhole limpet hemocyanin: a model for treating systemic lupus erythematosus. *Bioconjugate Chem.* 5, 390.
- (26) Ravikumar, V. T., Andrade, M., Wyrzykiewicz, T., Scozzari, A., and Cole, D. L. (1995) Large-scale synthesis of oligodeoxyribonucleotide phosphorothioate using controlled-pore glass as support. *Nucleosides Nucleotides* 14, 1219.
- (27) Bonora, G. M. (1995) Polyethylene glycol. A high efficiency liquid phase (HELP) for the large-scale synthesis of oligonucleotides. *Appl. Biochem. Biotechnol.* 54, 3.
- (28) Svinarchuk, F. P., Konevets, D. A., Pliasunova, O. A., Pokrovsky, A. G., and Vlassov, V. V. (1993) Inhibition of HIV proliferation in MT-4 cells by antisense oligonucleotide conjugated to lipophilic groups. *Biochimie* 75, 49.
- (29) Bonora, G. M., Biancotto, G., Maffini, M., and Scremin, C. L. (1993) Large scale, liquid phase synthesis of oligonucleotides by the phosphoramidite approach. *Nucleic Acids Res.* 21, 1213.
- (30) Lokhov, S., Podyminogin, M., Sergeev, D., Silnikov, V., Kutavin, I., Shishkin, G., and Zarytova, V. (1992) Synthesis and high stability of complementary complexes of *N*-(2-hydroxyethyl)phenazinium derivatives of oligonucleotides. *Bioconjugate Chem.* 3, 414.
- (31) Bagno, A., Biciato, S., Dal Bosco, M., Bonora, G. M., and Di Bello, C. (1996) Apparecchiatura e processo per la sintesi automatica di oligomeri in fase liquida. Italian Patent Appl. MI96A001301.

BC970082P

Role of the Central Metal Ion and Ligand Charge in the DNA Binding and Modification by Metallosalen Complexes

Subhrangsu S. Mandal,[†] Umesh Varshney,[‡] and Santanu Bhattacharya^{*,†}

Department of Organic Chemistry and Center for Genetic Engineering, Indian Institute of Science, Bangalore 560012, India. Received November 14, 1996[©]

Several metal complexes of three different functionalized salen derivatives have been synthesized. The salens differ in terms of the electrostatic character and the location of the charges. The interactions of such complexes with DNA were first investigated in detail by UV–vis absorption titrimetry. It appears that the DNA binding by most of these compounds is primarily due to a combination of electrostatic and other modes of interactions. The melting temperatures of DNA in the presence of various metal complexes were higher than that of the pure DNA. The presence of additional charge on the central metal ion core in the complex, however, alters the nature of binding. Bis-cationic salen complexes containing central Ni(II) or Mn(III) were found to induce DNA strand scission, especially in the presence of co-oxidant as revealed by plasmid DNA cleavage assay and also on the basis of the autoradiogram obtained from their respective high-resolution sequencing gels. Modest base selectivity was observed in the DNA cleavage reactions. Comparisons of the linearized and supercoiled forms of DNA in the metal complex-mediated cleavage reactions reveal that the supercoiled forms are more susceptible to DNA scission. Under suitable conditions, the DNA cleavage reactions can be induced either by preformed metal complexes or by *in situ* complexation of the ligand in the presence of the appropriate metal ion. Also revealed was the fact that the analogous complexes containing Cu(II) or Cr(III) did not effect any DNA strand scission under comparable conditions. Salens with pendant negative charges on either side of the precursor salicylaldehyde or ethylenediamine fragments did not bind with DNA. Similarly, metallosalen complexes with net anionic character also failed to induce any DNA modification activities.

INTRODUCTION¹

Design and synthesis of small synthetic systems that recognize specific sites of DNA is an important area of much current research (1). These could be at least in part due to the formation of noncovalently associated complexes by several such molecules with nucleic acids. Many times, such physical complexation may produce important pharmacological effects by interfering with the biological processes in which DNA/RNAs take part. Such investigations also sometimes provide insights for the mechanism of action of naturally occurring antitumor antibiotics (2). Toward this direction, there is a continuing search for new metal complexes that strongly interact with DNA. These studies led to the development of several new reagents. Examples include complexes *e.g.* iron–EDTA (3), copper– or rhodium–1,10-phenanthroline (4, 5), manganese–porphyrin (6), platinum–diamine (7), nickel–cyclam (8), and several photonucleases (9), among others. Examination of the interactions of transition metal complexes with DNA aids in the development of new reagents that are potentially useful in molecular biology (10) and also in the design of putative drugs (11). Utilities of some metal complexes as structural probes (1, 12) for DNA and in drug/protein–DNA footprinting (10, 13) are also known. Sometimes, such studies also

offer useful leads in the elucidation of potential toxicities of various metal complex-based systems (14).

Earlier investigations (16–19) have indicated that, while some metallosalen derivatives bind DNA avidly (15), few others induce effective DNA scission (16–19) or inhibit lymphocyte proliferation (20). Therefore, subtle variation in the structure of the salen unit and variation of the central metal ion influence the effect of the resulting complex on DNA in a widely unrelated fashion. Griffin carefully studied (16) some of these aspects of DNA modification in detail with manganese–salen complexes. Burrows and Rokita synthesized (17) some nickel–salen derivatives which induced DNA cross-linking. More recently, Routier *et al.* examined the interaction of DNA with a functionalized salen–copper(II) complex which induced DNA strand scission in the presence of a reducing agent (18). We also examined the DNA cleavage processes induced by some bis-cationic salen analogues (19). Examination of the above reports makes it clear that much still remains to be understood about the role of salen structure and that of the central metal ion in the DNA binding/modification processes. We thought that a progressive structural variation of the salens with respect to charge on the aryl rings, at the imine portions, and systematic variation of the central metal ion under a given ligand (salen) environment might provide additional insight on the factors involved in the chemistry of binding and DNA modification by such complexes. Herein, we report the synthesis of a number of transition metal complexes based on a few different water-soluble salen derivatives, 1–5. The results of the binding abilities of different metal complexes with native *Escherichia coli* genomic DNA at various salt concentrations and with alkali-denatured DNA and the effects of such binding on DNA melting are included in this report.

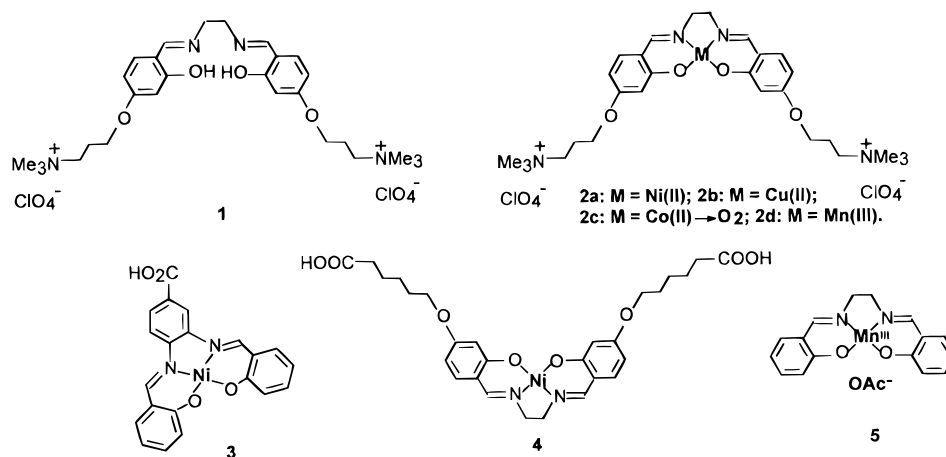
* To whom correspondence should be addressed. Also at Chemical Biology Unit, Jawaharlal Nehru Centre for Advanced Scientific Research, Bangalore 560064, India.

[†] Department of Organic Chemistry.

[‡] Center for Genetic Engineering.

[©] Abstract published in *Advance ACS Abstracts*, August 1, 1997.

¹ **Caution.** Although we did not experience any difficulty while working with these systems, perchlorate salts are potentially explosive!



The DNA cleavage reactions and the nicking patterns produced by different metal complexes are also presented.

EXPERIMENTAL PROCEDURES

General Aspects. Melting points were determined in open capillaries and are uncorrected. Infrared spectra were recorded with a Shimadzu FTIR 8101 infrared spectrophotometer equipped with a DR-8001 workstation. ¹H-NMR spectra were recorded with a Bruker AC-200 (200 MHz) or a Jeol FX-90 (90 MHz) NMR spectrometer using CDCl₃ or the appropriate deuterated solvent. Elemental analyses were performed by the microanalytical division of the Department of Organic Chemistry at the Indian Institute of Science in Bangalore and were run on a Carlo Erba model 1106 elemental analyzer. These are presented as percents. Electronic spectra were recorded on a Shimadzu model 2100 UV-visible spectrophotometer equipped with a TCC-60 temperature controller unit or a Julabo F-10 water-circulating temperature-controlled bath.

Materials. Silica gel (UV₂₅₄) plates (Sigma) were used for TLC. Column chromatography was performed on silica gel (60–120 mesh) from Merck (Schuchardt, Germany). Commercial compounds used in the synthesis and other studies herein were purchased from best known suppliers and used as received; solvents were purified and dried by standard methods. All other materials used for preparing buffers were of the highest quality commercially available. Millipore grade water was used for all the experiments. The enzymes used in this study were obtained from Pharmacia.

Calf thymus DNA (CT DNA) obtained from Sigma Chemical Co. (St. Louis, MO) was purified by phenol-chloroform extraction followed by ethanol precipitation as described previously (21). Solutions of CT DNA in 10 mM Tris-HCl, 1 mM EDTA buffer (pH 7.4) gave a ratio of the UV absorbances at 260 and 280 nm (A_{260}/A_{280}) of >1.9. The DNA concentrations were determined by using an extinction coefficient of 6600 M⁻¹ cm⁻¹ at 260 nm and were expressed in terms of base molarity (22). Melting temperature determinations and the spectroscopic binding studies were performed with CT DNA in 10 mM Tris-HCl, 1 mM EDTA buffer (pH 7.4).

E. coli genomic DNA was isolated and purified as described (23). Briefly, *E. coli* cells (CA 274 strain) were overgrown in LB media, and the cells were subjected to lysozyme treatment, followed by lysis with SDS and proteinase K treatment. The mixture was finally subjected to phenol-chloroform extraction two times, and the DNA was precipitated using 2-propanol and washed with 70% ethanol. Then, the DNA was dissolved in 10

mM Tris-HCl, 1 mM EDTA buffer (pH 7.4) which gave an A_{260}/A_{280} of ~1.9.

The plasmid DNA pTZ19R used herein was grown in *E. coli* cells and isolated in our laboratory as described earlier (19a). The supercoiled plasmid was obtained by CsCl/ethidium bromide density gradient centrifugation.

Synthetic Methods. 4-[[3-(Bromopropyl)oxy]salicylaldehyde (6). A mixture of 138 mg (1 mmol) of 2,4-dihydroxybenzaldehyde and 404 mg (2 mmol) of 1,3-dibromopropane was refluxed in the presence of 140 mg (1.4 mmol) of KHCO₃ in 50 mL of dry acetone for 60 h. At the end of this period, the solvent from the reaction mixture was removed in a rotavapor, 5 mL of water was added to it, and then the solvent was extracted with 3 × 10 mL portions of CHCl₃. The combined chloroform extracts were evaporated to dryness and then purified by column chromatography over silica gel (60–120 mesh) using 2–3% EtOAc in light petroleum (60–80 °C boiling fraction). Upon chromatographic purification, a white crystalline solid was obtained in ca. 60% yield: mp 62–64 °C; ¹H-NMR (200 MHz, CDCl₃) δ 2.3 (2H, m, CH₂CH₂Br), 3.6 (2H, t, CH₂Br), 4.2 (2H, t, CH₂CH₂O), 6.45 (1H, d, ArH₃, J_m = 2.0 Hz), 6.55 (1H, dd, ArH₅, J_m = 2 Hz, J = 9.5 Hz), 7.5 (1H, d, ArH₆, J_0 = 9.5 Hz), 9.7 (1H, s, CHO), 11.5 (1H, s, ArOH); IR (Nujol) (cm⁻¹) 1630 (s), 1510, 1210, 1095. Anal. Calcd for C₁₀H₁₁BrO₃: C, 46.35; H, 4.27. Found: C, 46.42; H, 4.26.

4-[[3-(Trimethylammonio)propyl]oxy]salicylaldehyde Bromide (6a). One hundred milligrams (0.38 mmol) of 6 was dissolved in 20 mL of EtOAc in a screw-top pressure tube. Two milliliters of dry trimethylamine gas was passed into this solution precooled at ~0–5 °C. Then, the screw top of the tube was closed tightly and the tube allowed to stand for 6 h at ambient temperature. At the end of this period, a brownish-white solid was obtained. The solid was collected by filtration and was recrystallized from a mixture of EtOAc/EtOH. Recrystallization afforded a colorless, crystalline, hygroscopic product in practically quantitative yield: mp 152–154 °C; ¹H-NMR (90 MHz, D₂O) δ 2.4 (2H, m, CH₂CH₂CH₂N⁺Me₃), 3.2 (9H, s, N⁺-(CH₃)₃), 3.6 (2H, t, CH₂N⁺Me₃), 4.23 (2H, t, ArOCH₂), 6.52 (1H, d, ArH₃, J_m = 2.0 Hz), 6.68 (1H, dd, ArH₅, J_m = 2 Hz, J = 9.5 Hz), 7.68 (1H, d, ArH₆, J_0 = 9.5 Hz), 9.8 (1H, s, CHO); IR (Nujol) (cm⁻¹) 1630 (s), 3400 (s). Anal. Calcd for C₁₃H₂₀NO₃Br·H₂O: C, 46.44; H, 6.59; N, 4.17. Found: C, 46.41; H, 6.30; N, 4.02.

4-[[3-(Trimethylammonio)propyl]oxy]salicylaldehyde Perchlorate (6b). The above material, 4-[[3-(trimethylammonio)propyl]oxy]salicylaldehyde bromide (6a, 425 mg, 1.3 mmol), was dissolved in 1 mL of water, and the resulting aqueous solution was treated with 1 mL of aqueous NaClO₄ (327 mg, 2.6 mmol). This resulted in

the formation of the corresponding perchlorate salt which precipitated as a white solid. This was filtered and dried in a desiccator, *ca.* 95% yield: mp 140–142 °C; ¹H-NMR (200 MHz, DMSO-*d*₆) δ 2.1 (2H, m, CH₂CH₂CH₂N⁺Me₃), 3.05 (9H, s, N⁺(CH₃)₃), 3.4 (2H, t, CH₂N⁺Me₃), 4.05 (2H, t, ArOCH₂), 6.3 (1H, d, ArH₃), 6.5 (1H, dd, ArH₅), 7.5 (1H, ArH₆, d), 9.5 (1H, s, CHO); IR (Nujol) (cm⁻¹) 1630 (s), 1460 (s), 1375 (s), 1230 (s), 1100 (s), 625 (s). Anal. Calcd for C₁₃H₂₀NO₇Cl: C, 46.23; H, 5.97; N, 4.15. Found: C, 46.21; H, 6.01; N, 4.02.

N,N-Bis[4-[[3-(trimethylammonio)propyl]oxy]salicylidene]ethylenediamine Diperchlorate (1). **6b**, 4-[[3-(trimethylammonio)propyl]oxy]salicylaldehyde perchlorate (250 mg, 0.74 mmol), was dissolved in 10 mL of dry MeOH by careful warming. To this was added 22.2 mg (0.37 mmol) of freshly distilled ethylenediamine, and the resulting mixture was warmed to ~60 °C for 10 min which upon cooling to ambient temperature produced a yellow precipitate. The yellow residue was isolated and washed with cold MeOH and dried (yield *ca.* 80%): mp 258–260 °C; ¹H-NMR (90 MHz, DMSO-*d*₆) δ 2.1 (4H, m, CH₂CH₂CH₂NMe₃), 3.05 (18H, s, N(CH₃)₃), 3.4 (4H, t, CH₂NMe₃), 3.9 (4H, s, =NCH₂CH₂N=), 4.05 (4H, t, ArOCH₂), 6.3–6.45 (4H, m, ArH₃, ArH₅), 7.2 (2H, d, ArH₆), 8.45 (2H, s, ArHC=N); IR (Nujol) (cm⁻¹) 1630 (s), 1610 (s), 1520 (s), 1460 (s), 1210 (s), 1095 (s), 620 (s). Anal. Calcd for C₂₈H₄₄N₄O₁₂Cl₂: C, 48.06; H, 6.34; N, 8.0. Found: C, 47.62; H, 6.33; N, 7.90.

N,N-Bis[4-[[3-(trimethylammonio)propyl]oxy]salicylidene]ethylenediamine–Nickel (II) Bisperchlorate (2a). **1** (55 mg, 0.079 mmol) was suspended in 10 mL of dry MeOH. NiCl₂·6H₂O (15 mg, 0.08 mmol) was added in the form a methanolic solution into this suspension, and the resulting mixture was warmed at 60 °C for 30 min. This gave a deep-red solution which was first allowed to cool to room temperature and then kept in a refrigerator for 48 h. A red-colored, hygroscopic, crystalline precipitate separated out which was collected after filtration, recrystallized from dry MeOH, and dried (yield *ca.* 42%): UV–vis [λ_{\max} (nm), ϵ] 1:1 (CH₃CN/CH₃OH) 348 (25 000), 304 (29 000), 236 (14 000), 211 (20 000); IR (KBr pellet) (cm⁻¹) 600 (m), 730 (m), 920 (m), 1040 (m), 1120 (s), 1200 (s), 1215 (s), 1300 (m), 1420 (m), 1480 (s), 1490 (s), 1530 (s), 1600 (s). Anal. Calcd for C₂₈H₄₂N₄O₁₂Cl₂Ni·2.5H₂O: C, 41.94; H, 5.28; N, 6.99. Found: C, 42.01; H, 5.49; N, 6.99.

N,N-Bis[4-[[3-(trimethylammonio)propyl]oxy]salicylidene]ethylenediamine–Copper(II) Bisperchlorate (2b). The ligand **1** (40 mg, 0.05 mmol) was suspended in 10 mL of dry MeOH, to which a methanolic solution of 16 mg (0.08 mmol) of Cu(OAc)₂·4H₂O was added, and the resulting mixture was warmed for 30 min at 60 °C. The solution slowly turned into a bluish pink color which upon cooling gave a pink crystalline precipitate. The residue was collected by filtration and repeatedly recrystallized from dry MeOH to give a pink hygroscopic solid (yield *ca.* 60%): UV–vis [λ_{\max} (nm), ϵ] (H₂O) 365.5 (10 000), 282.5 (20 000), 249.5 (30 000), 226 (29 000); IR (KBr pellet) (cm⁻¹) 620 (s), 840 (m), 1090 (s), 1110 (s), 1210 (s), 1400 (m), 1540 (m), 1610 (s). Anal. Calcd for C₂₈H₄₂N₄O₁₂CuCl₂·1H₂O: C, 43.10; H, 5.43; N, 7.18. Found: C, 42.89; H, 5.54; N, 7.08. EPR: A_{II} 190.1 G, g_{II} 2.2.

N,N-Bis[4-[[3-(trimethylammonio)propyl]oxy]salicylidene]ethylenediamine–Cobalt(II) Bisperchlorate as a Monomeric Oxygen Adduct (2c). **1** (30 mg, 0.043 mmol) was suspended in 10 mL of dry MeOH. To this was added a methanolic solution of 17.5 mg (0.07 mmol) of Co(OAc)₂·4H₂O, and the resulting mixture was warmed at 60 °C for 30 min. This gave a brownish-red solution which gradually changed into a deep dark brown color

upon standing at ambient temperature in exposure to air. It was kept for 1 week in this manner, from which a dark brown complex was precipitated upon addition of dry ether (yield *ca.* 44%): UV–vis [λ_{\max} (nm), ϵ] (H₂O) 361 (7100), 289 (broad hump), 258 (48 000); FTIR (KBr pellet) (cm⁻¹) 625 (s), 940 (m), 1000 (w), 1090 (s), 1125 (s), 1145 (s), 1200 (m), 1430 (s), 1550 (s), 1600 (s), 1620 (s). Anal. Calcd for C₂₈H₄₂N₄O₁₂CoCl₂O₂·2H₂O: C, 40.97; H, 5.62; N, 6.79. Found: C, 40.94; H, 5.63; N, 6.35 (2d).

N,N-Bis[4-[[3-(trimethylammonio)propyl]oxy]salicylidene]ethylenediamine–Manganese(III) Trisperchlorate (2d). The ligand **1** (66 mg, 0.09 mmol) was suspended in 15 mL of dry MeOH to which was added a methanolic solution of 26.7 mg (0.2 mmol) of Mn(OAc)₃·4H₂O and heated at 60 °C for 30 min. The initial yellowish color of the solution of the Schiff base soon changed into a grayish-black solution from which 70% of the MeOH was removed under vacuum. Upon addition of dry ether to this, a grayish-black solid separates out followed by cooling in a refrigerator. The solid was repeatedly recrystallized from dry MeOH to give a hygroscopic material of 44% yield: UV–vis [λ_{\max} (nm), ϵ] (CH₃CN) 343 (15 400), 303 (21 400), 237 (12 300), 208 (17 400); FTIR (KBr pellet) (cm⁻¹) 630 (s), 850 (w), 1000 (w), 1095 (s), 1110 (s), 1150 (s), 1300 (w), 1400 (w), 1490 (w), 1530 (w), 1600 (s). Anal. Calcd for C₂₈H₄₂N₄O₁₆Cl₃Mn·2.5H₂O: C, 37.49; H, 5.28; N, 6.24. Found: C, 37.32; H, 5.17; N, 6.15.

N,N-Bis(salicylidene)-3,4-diaminobenzoic Acid–Nickel(II) (3). To a solution of 400 mg (3.3 mmol) of salicylaldehyde in 10 mL of MeOH was added with stirring a methanolic solution of 250 mg (1.6 mmol) of freshly recrystallized 3,4-diaminobenzoic acid. From this solution after some time, an orange-colored crystalline solid precipitated out, which was filtered, dried, and then recrystallized from MeOH. This orange Schiff base (100 mg) was dissolved in hot MeOH; to this was added a methanolic solution of 46.7 mg (0.28 mmol) of the NiCl₂, and the resulting mixture was heated at 60 °C for 30 min. This produced a transparent deep red-colored solution which upon standing at ambient temperature gave an orange-red-colored precipitate which was filtered and recrystallized from a mixture of MeOH and CHCl₃ in 80% yield. Anal. Calcd for C₂₁H₁₄N₂O₄Ni·0.5CHCl₃: C, 53.16; H, 3.22; N, 5.76. Found: C, 53.38; H, 3.45; N, 6.05.

[[6-Oxo-6-ethoxyhexyl]oxy]benzaldehyde (7). A mixture of 1.198 g (8 mmol) of 2,4-dihydroxybenzaldehyde and 2 g of ethyl 6-bromohexanoate was refluxed in dry acetone for 2 days in the presence of 800 mg (8 mmol) of anhydrous KHCO₃. Then, the solvent from this reaction mixture was removed, and 5 mL of water was added into the residue. The resulting mixture was extracted with 3 × 30 mL of chloroform. The chloroform extract was evaporated to dryness and then purified by column chromatography over silica gel (60–120 mesh) using 2% EtOAc in light petroleum (60–80 °C boiling fraction). Upon concentration of the eluted fraction, a highly viscous liquid was obtained in *ca.* 50% yield: IR (neat) (cm⁻¹) 3250–3400 (br), 2900 (s), 1715 (s), 1620 (s), 1495 (s), 1200 (s), 1100 (s), 1000 (s); ¹H-NMR (90 MHz, CDCl₃) δ 1.2 (3H, t, CH₂CH₃), 1.5–2.0 (6H, m, OCH₂(CH₂)₃CH₂), 2.4 (2H, t, CH₂COO), 4.05–4.2 (4H, m, ArOCH₂ + COOCH₂CH₃), 6.45 (1H, d, ArH₃, J_m ~ 1.5 Hz), 6.55 (1H, dd, ArH₅, J_m ~ 1.5 Hz, J_o ~ 9.4 Hz), 7.4 (1H, d, ArH₆, J_o ~ 9.4 Hz), 9.8 (1H, s, CHO), 11.5 (1H, s, ArOH).

[[6-Hydroxy-6-oxohexyl]oxy]benzaldehyde (7a). Compound **7** was saponified under refluxing conditions using 2% aqueous NaOH. The resulting reaction mixture was cooled in ice and neutralized by dropwise addition of concentrated HCl under ice-cold conditions. This gave

a white precipitate which was filtered, and the residue was washed with cold water, dried, and then purified by column chromatography over silica gel (60–120 mesh) using 2% MeOH in CHCl_3 . The purified material was recrystallized from EtOAc to afford a solid in 80% yield: mp 124–125 °C; IR (Nujol) (cm^{-1}) 3320 (s), 1710 (s), 1610 (s), 1460 (s), 1370 (s), 1300 (s), 1200 (s), 1050 (s), 860 (s); $^1\text{H-NMR}$ (90 MHz, CDCl_3) δ 1.8 (6H, m, $\text{OCH}_2(\text{CH}_2)_3\text{CH}_2$), 2.2 (2H, t, CH_2COO), 4.0 (2H, t, ArOCH_2), 6.45 (1H, d, ArH_3 , $J_m \sim 1.5$ Hz), 6.6 (1H, dd, ArH_5 , $J_m = 1.5$ Hz, $J_o \sim 9.4$ Hz), 7.3 (1H, d, ArH_6 , $J_o \sim 9.4$ Hz), 9.8 (1H, s, CHO), 11.45 (1H, s, ArOH). Anal. Calcd for $\text{C}_{13}\text{H}_{16}\text{O}_5$, 0.4-EtOAc: C, 62.38; H, 6.83. Found: C, 62.71; H, 6.83.

N,N-Bis[4-[(6-hydroxy-6-oxohexyl)oxy]salicylidene]ethylenediamine–Nickel(II) (4). **7a** (252 mg, 1 mmol) was suspended in 5 mL of dry MeOH. Freshly distilled ethylenediamine (30 mg, 0.5 mmol) was added into this. The resulting yellowing solution was stirred and warmed for 5 min which on prolonged standing at ambient temperature gave a yellow-colored precipitate, **7b**. This was filtered, washed with cold MeOH, and dried (yield of 90%). The Schiff base **7b** (100 mg, 0.18 mmol) was suspended in 5 mL of a mixture of dry MeOH and CHCl_3 . A methanolic solution containing 31 mg (0.18 mmol) of NiCl_2 was added to this, and the mixture was warmed for 30 min at 60 °C. During warming, the yellow suspension got slowly converted to a deep red solution which on cooling and standing at ambient temperature for several hours gave a red-colored crystalline precipitate. It was filtered, and the residue was washed with ice-cold, dry MeOH and then recrystallized from a mixture of MeOH and CHCl_3 to yield a material of ca. 70% yield: UV–vis [λ_{max} (nm), ϵ] [5 mM Tris-HCl buffer (pH 7.4) 376 (7000), 258 (41 000)]; FTIR (KBr pellet) (cm^{-1}) 700 (s), 760 (w), 800 (w), 830 (m), 1110 (s), 1200 (s), 1220 (s), 1540 (s), 1600 (s), 1700 (s). Anal. Calcd for $\text{C}_{28}\text{H}_{34}\text{N}_2\text{O}_8\text{Ni} \cdot 0.75\text{CHCl}_3$: C, 51.17; H, 5.19; N, 4.15. Found: C, 50.84; H, 5.30; N, 4.37.

N,N-Bis(salicylidene)ethylenediamine–Manganese(III) Acetate (5). This was prepared by following a literature procedure (16a). Briefly, 569 mg (2.1 mmol) of *N,N*-bis(salicylidene)ethylenediamine was dissolved in 10 mL of dry MeOH, to which was added a methanolic solution of 442 mg (2.2 mmol) of $\text{Mn}(\text{OAc})_3 \cdot 4\text{H}_2\text{O}$, and the resulting mixture was warmed at 60 °C for 30 min. Then, it was allowed to cool to room temperature. Upon addition of dry ether to this, a gray-black precipitate was obtained. This compound showed all the properties as reported previously (16a) (yield of 70%): IR (cm^{-1}) 1630 (s), 1595 (s), 1560 (s), 1460 (s), 1440 (s), 1385 (s), 1330 (s), 1290 (s), 1200 (m), 1140 (m), 1130 (s), 1080 (m), 1030 (m), 960 (m), 900 (s), 800 (s), 770 (s); UV–vis [λ_{max} (nm), ϵ] (ethanol) 400 (6100), 350 (8000), 310 (16 000), 283 (21 000), 220 (41 000). Anal. Calcd for $\text{C}_{18}\text{H}_{17}\text{N}_2\text{O}_4\text{Mn}$: C, 56.85; H, 4.50; N, 7.37. Found: C, 56.82; H, 4.47; N, 7.11.

Absorption Titration. Absorption titrations were carried out by keeping the concentration of the probe constant while adding a concentrated solution of the *E. coli* genomic DNA in 1 mM Tris-HCl, 0.1 mM EDTA buffer (pH 7.4) in increasing amounts in both the cuvettes until the saturations in hypochromism were observed. The saturation in hypochromism is quantitatively shown by plotting the A_0/A vs [DNA], where A_0 and A are the absorption intensities of the individual metal complexes in the absence and presence of various concentrations of DNA, respectively. The intrinsic binding constants for the different metal complexes with DNA were determined by the half-reciprocal plot method as given in the literature (25). The intrinsic binding constant (K) for a

given complex with DNA was then obtained from a plot of $D/\Delta\epsilon_{\text{ap}}$ vs D according to eq 1, $D/\Delta\epsilon_{\text{ap}} = D/\Delta\epsilon + 1/(\Delta\epsilon K)$ (1) where D is the concentration of DNA in base molarity, $\Delta\epsilon_{\text{ap}} = |\epsilon_a - \epsilon_f|$, and $\Delta\epsilon = |\epsilon_b - \epsilon_f|$, where ϵ_b and ϵ_f are respective extinction coefficients of the complex in the presence and absence of DNA, respectively. The apparent extinction coefficient, ϵ_a , was obtained by calculating $A_{\text{obsd}}/[\text{complex}]$. The data were fitted to eq 1, with a slope equal to $1/\Delta\epsilon$ and a y -intercept equal to $1/(\Delta\epsilon K)$. The intrinsic binding constants (K) were determined from the ratio of the slope to the y -intercept.

Effect of the Addition of Salt on DNA Binding.

To find out the effect of the variation in the ionic strength on the binding abilities of metal complexes with CT DNA, we studied the effects of addition of various salts to a solution containing DNA–**2b** complexes by adding increasing amounts of different salt solutions (30 and 45 mM NaCl or 15 mM MgCl_2) to the **2b**–DNA complex. The effects of such additions were followed by UV–vis absorption spectroscopy (26).

DNA Denaturation and Binding of Metallosalen.

The comparative binding efficiencies of the Ni complex (**2a**) toward double-stranded and alkali-denatured CT DNA were studied by using UV–vis absorption spectroscopy. The denatured CT DNA was obtained by incubating the DNA in 1 M NaOH at room temperature for 10 min. The spectrum of the Ni complex (**2a**) was recorded first; then, 5 μL of alkali-denatured CT DNA was added to this, and the changes in the spectra were then recorded again. The pH of the resulting solution was then slowly decreased by the addition of increasing amounts of HCl until the saturation in binding was reached.

Melting Temperatures. Melting temperatures for DNA in the absence and in the presence of various metal complexes were measured by following the changes in the UV–vis absorption spectra at 260 nm as a function of temperature in a Shimadzu model UV-2100 UV–vis spectrophotometer. The absorption intensities at 260 nm were plotted against individual temperatures in the presence of each metal complex, and the midpoints of the inflection regions in the temperature vs A_{260} curves were taken as the corresponding T_m values (27). The temperatures of the cuvettes were maintained using a Julabo model F-10 water-circulating bath. Each melting temperature determination employed 72 μM (base molarity) CT DNA in 5 mM Tris-HCl buffer (pH 7.4).

DNA Cleavage Experiments. The DNA cleavage or modification reactions induced by different metal complexes in the absence and in the presence of co-oxidants were performed using the supercoiled plasmid pTZ19R (2.9 kbp, Pharmacia) in 20 mM Tris-HCl buffer (pH 7.4). In a typical experiment, the plasmid DNA (0.25 μg /reaction) was incubated in a reaction mixture (10 μL) containing various concentrations of individual metal complexes (either preisolated or prepared *in situ*) in 20 mM Tris-HCl buffer (pH 7.4) at 37 °C. Reactions were initiated by the addition of MMPP (0.5 mM) and were stopped after 5 min by the addition of a terminating agent (5 μL) containing 10 mM β -mercaptoethanol, 20% glycerol, 25 mM EDTA, and 0.05% bromophenol blue/xylene cyanol (1:1). Then, this was kept on ice. The samples were loaded on 1% neutral agarose gel and were subjected to electrophoresis in a horizontal slab gel apparatus using $0.5 \times \text{TBE}$ as the buffer (at 100 V for ~ 1.5 h). After electrophoresis, the gels were stained with a solution of 0.5 $\mu\text{g}/\text{mL}$ ethidium bromide for ~ 60 min and then destained. Bands of DNA were then visualized under UV light (photodyne transilluminator, 312 nm) and photographed (Canon SLR camera with an orange filter) in a darkroom.

Sequencing and Autoradiogram. The sequence or base selectivities in the DNA modification reactions effected by different salen complexes were determined in the following manner. The supercoiled plasmid pTZ19R was linearized with *EcoRI*. After complete digestion of the plasmid with *EcoRI* (confirmed by agarose gel), the DNA was subjected to ethanol precipitation and drying. The DNA prepared in the above manner was used for the different reagent-induced DNA cleavage experiments.

The DNA cleavage reaction conditions for the sequencing experiments were similar to those employed in the agarose gel assays (described above) except that a total reaction volume of 50 μL and 2 μg of plasmid/reaction were used. After incubation for 5 min, 10 μL of the reaction mixture was aliquoted and analyzed by gel electrophoresis on agarose to confirm the reagent-induced DNA cleavage. The residual reaction mixture was first subjected to ethanol precipitation and then dried under vacuum. The dry DNA pellets were then resuspended in water and used as templates for the primer extension reactions. The primer extension reactions were carried out by the adaptation of a literature procedure (28). Briefly, ~ 3 pmol of the ^{32}P -end-labeled primer (300 000 counts, a 19-mer oligonucleotide) and 4 μL of 0.01 M NaOH were added into a solution containing ~ 0.5 μg of the DNA templates. Then, the volume of the resulting reaction mixture was made up to 40 μL which after thorough mixing was kept at 80 $^{\circ}\text{C}$ for 2 min and finally left on ice for an additional 5 min. Into this ice-cold reaction mixture was added 5 μL of the primer extension buffer [0.5 mM Tris-HCl (pH 7.4), 0.1 M MgSO_4 , and 2 mM DTT], and the resulting mixture was again incubated at 45 $^{\circ}\text{C}$ for 3 min. After this, the mixture was kept on ice for a period of 30 min. Then, an aliquot of 5 μL of the dNTP mix (dATP, dTTP, dCTP, and dGTP each at 5 mM) was added to this mixture, and primer extension reactions for each reaction were initiated by the addition of 1 unit of Klenow DNA polymerase at 50 $^{\circ}\text{C}$ for 10 min. Finally, the reactions were quenched by the successive addition of 10 μL of 4 mM ammonium acetate/20 mM EDTA and 180 μL of absolute EtOH. The resulting mixture was then kept at -20 $^{\circ}\text{C}$ for 1 h and pelleted down by centrifugation. The pellets thus obtained were air-dried and resuspended in 8 μL of 80% formamide-denaturing gel loading dye, heated for 2 min at 92 $^{\circ}\text{C}$, then loaded onto a 7% polyacrylamide-bisacrylamide/8 M urea denaturing sequencing gel, and finally electrophoresed at 1500 V until the bromophenol blue touched the foot of the gel (~ 2 h). Then, the gel was autoradiogrammed.

RESULTS AND DISCUSSION

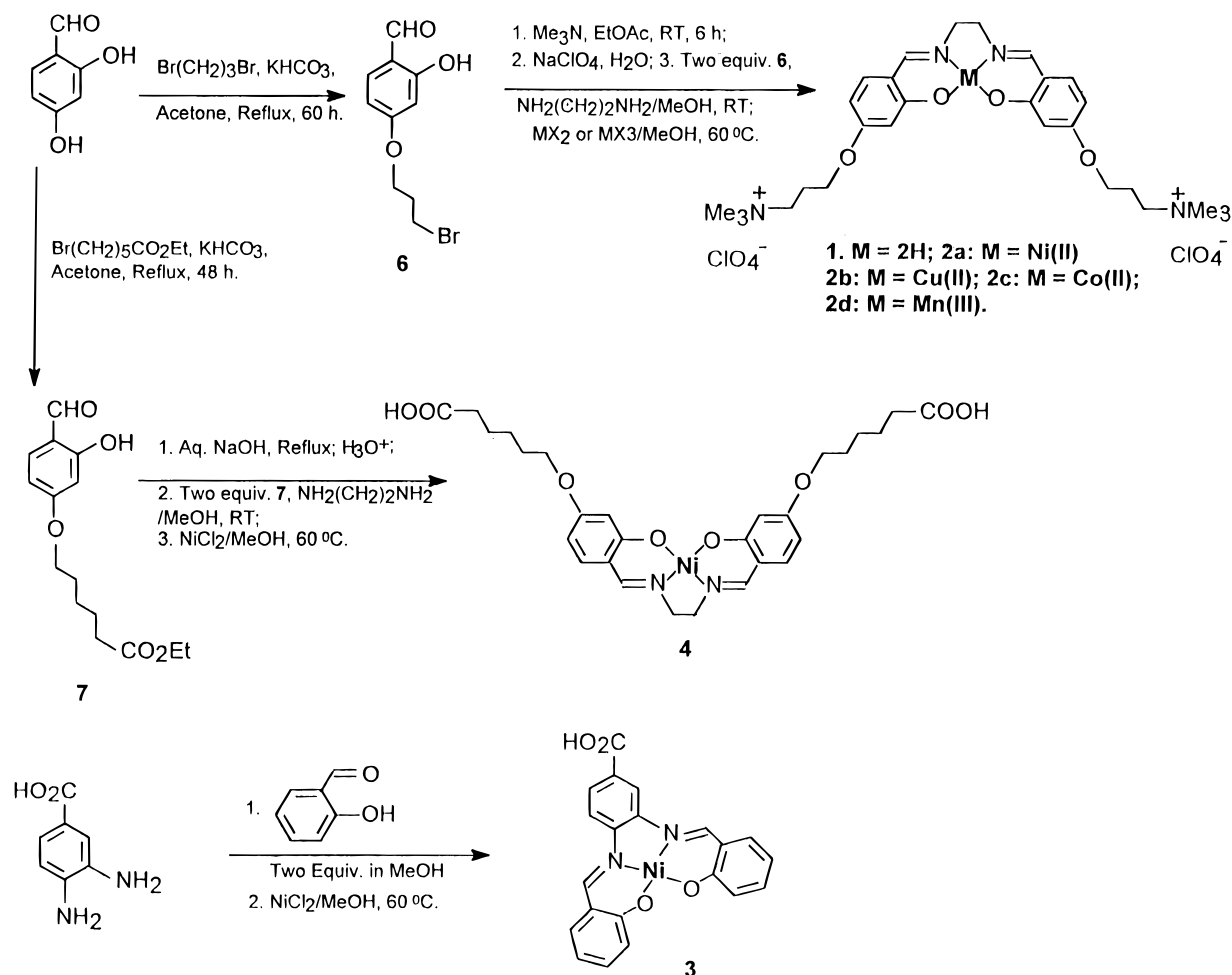
Choice of the Ligand. The tetradentate chelator salen [*N,N*-ethylene bis(salicylideneaminato)] has been widely employed for various purposes in the chemical literature (29) over a long period of time. The utilities of several metal-salen complexes in effecting catalytic, regioselective alkene epoxidation have also been demonstrated (30). Recently, Griffin *et al.* examined in detail the DNA scission activities of an array of Mn(III)-salen derivatives (16). Preferential cleavages of DNA at A-T rich sites by the Mn(III)-salen reagents such as **5** were observed in the presence of the co-oxidant, magnesium monoperoxyphthalate (MMPP). Due to our continuing interest in the studies of metal complex systems that bind DNA and induce DNA scission (19), we sought to examine systematically the interactions that exist between individual transition metal-salen with DNA under comparable conditions. Since salen itself is not soluble in water, we first chose to functionalize the parent salen unit by

covalent appendages with two NMe_3^+ residues (ligand, **1**). This renders the ligand (**1**) and its different metal complexes water-soluble irrespective of the pH of the solution. This also allows these compounds to come closer to the DNA surface due to the favorable electrostatic disposition. It should be mentioned, however, that the idea of the introduction of the cationic residues into salen is not new. Burrows and Rokita (17) developed a bis-cationic Ni(II)-salen derivative which was shown to induce interstrand cross-linking in DNA. Subsequently, Sato *et al.* used a different cationic salen type Cu(II) complex to examine their DNA binding abilities (15). More recently, Bailly and Bernier examined the interactions and the DNA-cleaving properties of the salen-Cu(II) complex containing a pendant alkyl ammonium residue (18). To find the effects of the role of other ligand charges around the metal complexes, two anionic ligands and their corresponding metal complexes (**3** and **4**) have been also synthesized. The syntheses of the ligands and different metal complexes are summarized in Scheme 1.

Synthesis. The synthesis of the ligand **1** began with the functionalization of 4-hydroxybenzaldehyde with 1,3-dibromopropane in the presence of KHCO_3 in dry acetone under refluxing conditions. The product, 4-[(3-bromopropyl)oxy]salicylaldehyde (**6**), thus obtained was quaternized quantitatively upon reaction with Me_3N in EtOAc. The counterion of the quaternary salt was changed to perchlorate by treatment with NaClO_4 , and then the perchlorate salt was converted to the corresponding salen (**1**) in 80% yield upon coupling with ethylenediamine in MeOH. Different metal complexes of this ligand were synthesized on treatment with appropriate metal salts in MeOH. The ligand **3** was prepared by coupling 3,4-diaminobenzoic acid with salicylaldehyde in MeOH, and the corresponding Ni(II) complex was synthesized upon treatment with NiCl_2 in MeOH. For the preparation of salens with pendant negatively charged residues, 4-hydroxysalicylaldehyde was coupled with ethyl 6-bromohexanoate in acetone in the presence of KHCO_3 . This gave **7** in $\sim 50\%$ yield upon chromatographic purification. **7** was then saponified to the corresponding acid (80%) which upon conversion into imine with ethylenediamine gave the bis-anionic salen **7b** in 90% yield. This on complexation with NiCl_2 in a mixture of MeOH/ CHCl_3 afforded the salen **4** in ca. 70% yield. All the final compounds and the intermediates were characterized by UV-vis, FTIR, and ^1H -NMR spectroscopy and by elemental analysis. The details of the synthesis and characterization of each of the new compounds are given in Experimental Procedures.

Absorption Titration. DNA appears to be a convenient target for different metal complex-based reagents (31) as most of the metal complexes contain a variety of potential DNA binding loci. The presence of the nucleobases with ligating abilities and phosphodiester linkages offers scope for direct coordination with a central metal ion in a complex. Furthermore, the coordinatively "unsaturated" sites on the metal ion centers of these complexes may also promote cross-linking at different regions within a long DNA strand or between different strands. In addition to these, other modes of interaction such as ion pairing or hydrogen bonding to minor or major grooves of the DNA and the intercalation of the planar aromatic subunits of some of these complexes into the stacked base pairs may also be possible. The above considerations make it clear that in principle it should be possible to modulate the binding and reactivities of the transition metal complexes with DNA by changing

Scheme 1



the central metal ion, its oxidation state, and the electrostatic character of the ligands of the metal complexes.

In the present study, we investigated the interactions between the newly synthesized salen derivatives (**1**) and its various metal complexes to duplex DNA led to decreases in the absorption intensities with a small amount of red shifts in the UV-vis absorption spectra of the salen species. Figure 1 shows the absorption spectra of the bis-cationic salen analogue **1** and its various metal complexes in the presence and absence of varying concentrations of *E. coli* genomic DNA. Absorption titrations with a given compound were carried out by adding increasing amounts of *E. coli* genomic DNA of a known concentration into a solution [Tris-HCl buffer (pH 7.4)] containing a fixed concentration of the metal complex or the ligand by following changes in the UV-vis spectroscopy after each addition. The addition of DNA was continued until a saturation in the observed spectral changes for a given system was reached. The absorption titration of different metal complexes or the ligand with *E. coli* genomic DNA allowed us to obtain estimates of the binding constants of the individual metal complexes with DNA.

Curve 1 in Figure 1A shows the UV-vis spectrum due to an aqueous solution (pH 7.4 Tris buffer) containing 2.14×10^{-6} M ligand **1** alone in the absence of DNA. Curves 2 and 3 show spectra due to **1** manifested upon addition of increasing amounts of *E. coli* genomic DNA. It is clear that the progressive addition of DNA leads to strong hypochromism in the absorption intensity of **1** finally reaching a saturation at $P/D = 2.3$, where P is

the concentration of the DNA in phosphate molarity and D is the concentration of the compound used in the study (ligand, **1**). The saturation plot obtained by plotting A_0/A against $[\text{DNA}]$ due to this titration is also given (inset of Figure 1A).

Panels B–D of Figure 1 show the results of the UV-visible absorption titration of bis-cationic metal complexes **2a–c**, respectively, in the presence of increasing amounts of *E. coli* genomic DNA. Spectral trace 1 in all of these panels represents the UV-vis absorption spectra of metal complexes **2a–c**, respectively, in pH 7.4 Tris buffer in the absence of any DNA. In each instance, the addition of progressively increasing amounts of DNA resulted in gradual hypochromism in the absorption intensities of the respective metal complexes which finally reached saturation. The insets in panels B–D of Figure 1 show the corresponding saturation plots.

The results of the absorption titration in the presence of progressively increasing amounts of DNA with either tricationic Mn complex **2d** or monocationic Mn complex **5** are shown in panels E and F of Figure 1, respectively. In either of these cases, spectrum 1 (in the absence of DNA) gradually changed to traces 2 and then to 3 upon addition of increasing amounts of DNA. Continuous decreases in the intensities of absorption due to **2d** or **5** were followed by saturation at high concentrations of DNA (insets in panels E and F of Figure 1, respectively).

Isosbestic points are clearly observed in panels A (~290 and ~305 nm), B (~330 nm), C (~290 nm), D (~300 nm), and F (~260 and ~330 nm) of Figure 1 for binding of respective salens with DNA. The presence of the isosbestic points in these titrations suggests that chemical

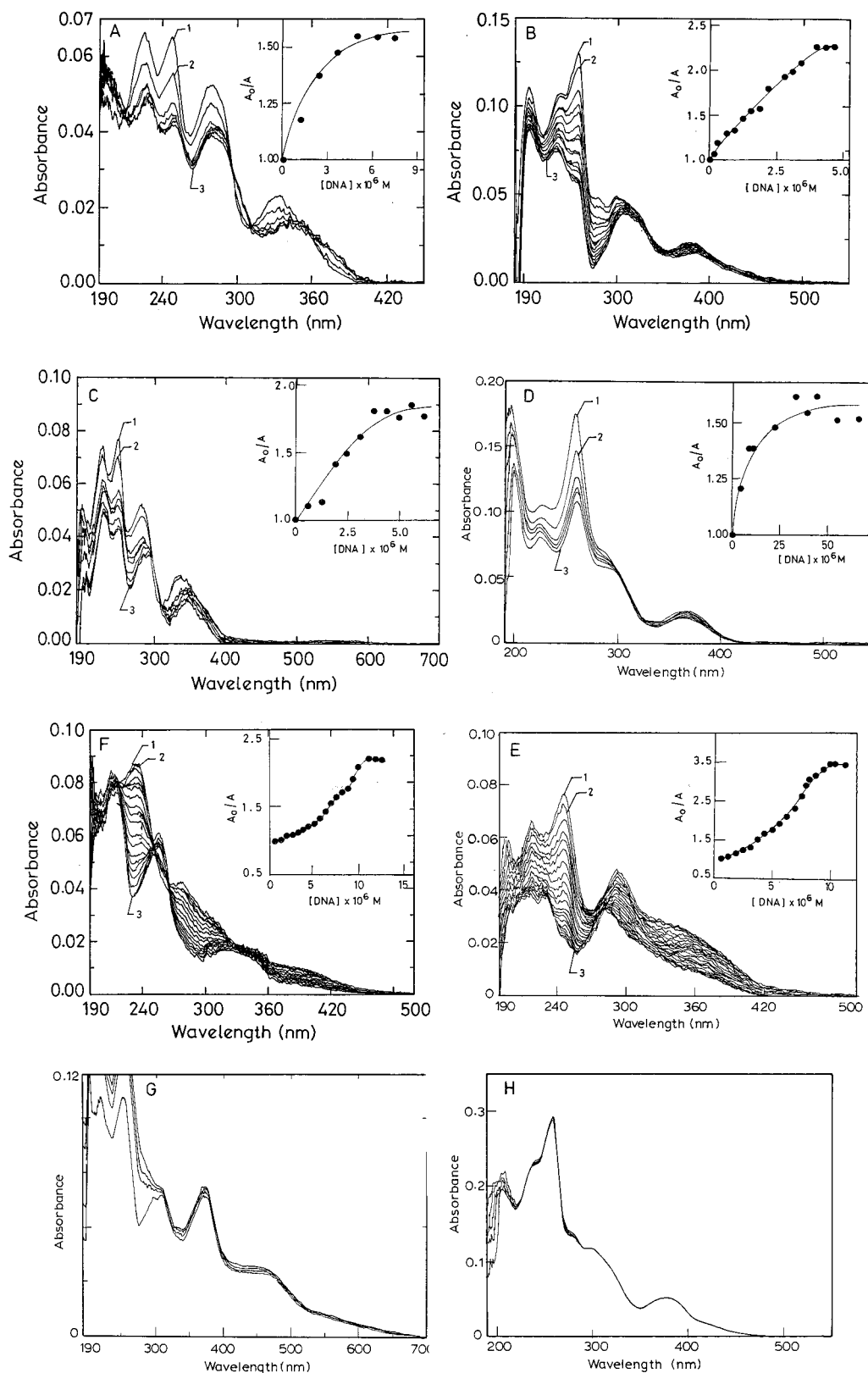


Figure 1. Absorption titration spectra of the ligand and different metal complexes in the presence of *E. coli* DNA. The absorption titrations were carried out by keeping the concentration of the complex constant while adding increasing amounts of *E. coli* genomic DNA until the saturation was reached. In all cases, spectrum 1 represents probe alone in the absence of any DNA; spectra 2 and 3 were obtained upon addition of increasing concentrations of DNA while keeping the probe concentration fixed. (A) **1** vs DNA. $[1] = 2.14 \times 10^{-6} \text{ M}$. (B) **2a** vs DNA. $[2a] = 5.67 \times 10^{-6} \text{ M}$. (C) **2b** vs DNA. $[2b] = 2.6 \times 10^{-6} \text{ M}$. (D) **2c** vs DNA. $[2c] = 3.9 \times 10^{-6} \text{ M}$. (E) **2d** vs DNA. $[2d] = 2.56 \times 10^{-6} \text{ M}$. (F) **5** vs DNA. $[5] = 2.1 \times 10^{-6} \text{ M}$. (G) **3** vs DNA. $[3] = 5.7 \times 10^{-6} \text{ M}$. (H) **4** vs DNA. $[4] = 7.19 \times 10^{-6} \text{ M}$. (Insets) Respective saturation plots. The saturation in absorption intensity hypochromism is indicated by the plot of A_0/A vs $[DNA]$ in phosphate molarity, where A_0 and A are the absorption intensities in the absence and in the presence of varying concentrations of DNA, respectively.

equilibria exist between the bound and the free metal complexes or the ligand with no spectroscopically detect-

able intermediate states in the presence of DNA in each of the above instances. Strong hypochromism and spec-

Table 1. UV–Vis Absorption Spectral Properties of Metallosalens and Metal Free Ligand in the Presence and Absence of *E. coli* Genomic DNA^a

compound	wavelength maxima (nm) ^b		% hypochromism ^c (λ_{\max} , nm)
	free	bound	
1	335, 281, 248	344, 282, 251	30 (335), 20 (281), 33 (248)
2a	381, 259	389, 260	18 (381), 57 (259)
2b	336, 282, 249	345, 292, 250	54 (336), 31 (282), 43 (249)
2c	262, 258	262, 253	25 (262), 34 (258)
2d	293, 245	293, 248	45 (293), 71 (245)
3	450, 372, 300, 250	<i>d</i>	<i>d</i>
4	376, 258	<i>d</i>	<i>d</i>
5	280, 237	280, 237	55 (237)

^a See the text for the details of the experimental conditions.

^b Upon binding with DNA, the λ_{\max} due to the bound complex which was used for the construction of half-reciprocal plots is italicized. ^c *E. coli* genomic DNA was purified by the phenol–chloroform extraction as described in the text. ^d No significant spectral changes were observed.

tral broadening in absorption intensity indicate intense interaction between the electronic states of the complex chromophore with that of DNA bases.

Panels G and H of Figure 1 show the UV–visible absorption titration spectra for the *monoanionic* and the *dianionic* Ni complexes **3** and **4**, respectively, with DNA. Interestingly, in either of these instances, small or no significant spectral changes were observed upon addition of increasing amounts of DNA to solutions containing the above anionic metal complex **3** or **4**.

Experimentally determined parameters from the absorption titration for the different free and DNA-bound metal complexes as well as the metal free ligand are collected in Table 1. The data clearly demonstrate that the electronic spectra of all the cationic metal complexes as well as those of the bis-cationic, water-soluble, metal free ligand are indeed significantly affected upon binding to DNA. This is in marked contrast with the absorption titration involving the anionic metal complexes in the presence of increasing amounts of DNA (panels G and H of Figure 1).

The structural characteristics of compounds **1** and **2a–d** are such that each of them is dicationic in the bivalent oxidation state of the central metal ion. Ligands in such complexes have positively charged residues through a short spacer chain [(CH₂)₃NMe₃⁺]. These pendant NMe₃⁺ residues remain positively charged irrespective of the pH and anionic strength of the media. Thus, the overall positively charged character of the metal complexes provides the basis for electrostatic binding of these compounds with polyanionic DNA.

Under our experimental conditions, the bis-cationic metal complexes, including that of Cu(II), showed strong interaction with DNA as shown by the pronounced hypochromism and red shift. This is in contrast to the observation reported in the DNA binding studies of the Cu(II)–salen analogue by Sato *et al.* It is noteworthy that the ionic strength (50 mM) used by Sato *et al.* was much higher than the one used in the present study. Binding of several other metal chelates with DNA was previously shown to depend on the ionic strength of the media in which the titration experiments were conducted.

Binding Constants of Salen–DNA Association. The association constants of different metal complexes or the ligand with DNA were calculated by employing the method (half-reciprocal plot) using eq 1 as described previously (*cf.* Experimental Procedures). The half-reciprocal plots for different compounds were constructed using the most affected wavelength maxima as deter-

mined from the respective absorption titration experiments. Importantly, the plots of $D/\Delta\epsilon_{\text{ap}}$ vs D resulted in straight lines (Figure 2) for the absorption titration of **1** and **2a–c** with DNA. Individual association constants due to DNA binding with **1** and **2a–c** are given in Table 2. It is important to note that under comparable conditions, however, when the absorption titration data of either **2d** or **5** in the presence of DNA were plotted, the resulting fits did not give linear (straight) half-reciprocal plots. Thus, the saturation plots corresponding to Mn complexes **2d** and **5** (insets of panels E and F of Figure 1, respectively) differed from the other saturation plots given in the insets of panels A–D of Figure 1 with other metal complexes or the ligand **1**. These findings suggest that the binding mode of either of these manganese-based metal complexes (**2d** and **5**) with DNA relative to that of the free ligand or its Co(II), Cu(II), or Ni(II) complex counterparts could be different, although all of the salen complexes showed strong absorption hypochromicities as long as the compounds contained net cationic charge. Similar differences were also apparent while the effects of inclusion of these metal complexes on the DNA melting were examined (see below).

Effect of the Addition of Salt on DNA Binding.

To elucidate the influence of the ionic strength on the DNA binding abilities of the above metal complexes, we then studied the effects of the addition of increasing amounts NaCl and MgCl₂ on the DNA binding of one of the above metal complexes, *e.g.* **2b**. This experiment was performed by progressive addition of several aliquots of concentrated solutions of either NaCl or MgCl₂ into a solution containing fully DNA-bound **2b**. In Figure 3, spectral trace 1 represents the UV–vis absorption spectrum due to the solution containing **2b** alone (2.63 μ M), in the absence of DNA. Spectrum 2 in Figure 3 shows the UV–vis absorption spectra of fully DNA-bound **2b** obtained upon addition of excess CT DNA to the solution containing **2b**. Traces 3 and 4 were obtained upon addition of 30 and 45 mM NaCl to the **2b**–DNA complex. Thus, addition of increasing amounts of NaCl into the **2b**–DNA complex led to an apparent hyperchromism in the absorption intensities of **2b** finally reaching a saturation. While further addition of NaCl did not lead to any spectral changes, addition of a concentrated aqueous solution of MgCl₂ into the above led to further hyperchromism (trace 5, [MgCl₂] = 15 mM).

In a separate experiment, we also examined the effect of the addition of several aliquots of aqueous solutions of MgCl₂ to a solution containing the **2b**–DNA complex (figure not shown). Upon addition of increasing amounts of MgCl₂, the apparent hyperchromism in the absorption intensities of the metal complex was observed, finally reaching a saturation. To obtain the same extent of hyperchromism in absorption intensities of the DNA-bound **2b**, nearly half the concentration of MgCl₂ was required compared to that of NaCl. Notably, the saturation in the hyperchromism in the absorption intensities of the DNA-bound **2b** obtained by the addition of excess MgCl₂ could not be altered by further addition of NaCl.

The hyperchromism observed upon addition of increasing amounts of salt to salen-bound DNA could be explained by considering the enhanced charge neutralization of the negatively charged DNA in the presence of the metal ion of the salt (26). This charge neutralization minimizes the intra and interstrand repulsion between the DNA double helix, promoting the formation of more “compact” DNA structure. Under these circumstances, the average distance between base pairs is decreased. This makes the accommodation of **2b** into the duplex DNA difficult. The dicationic nature of Mg²⁺ ion

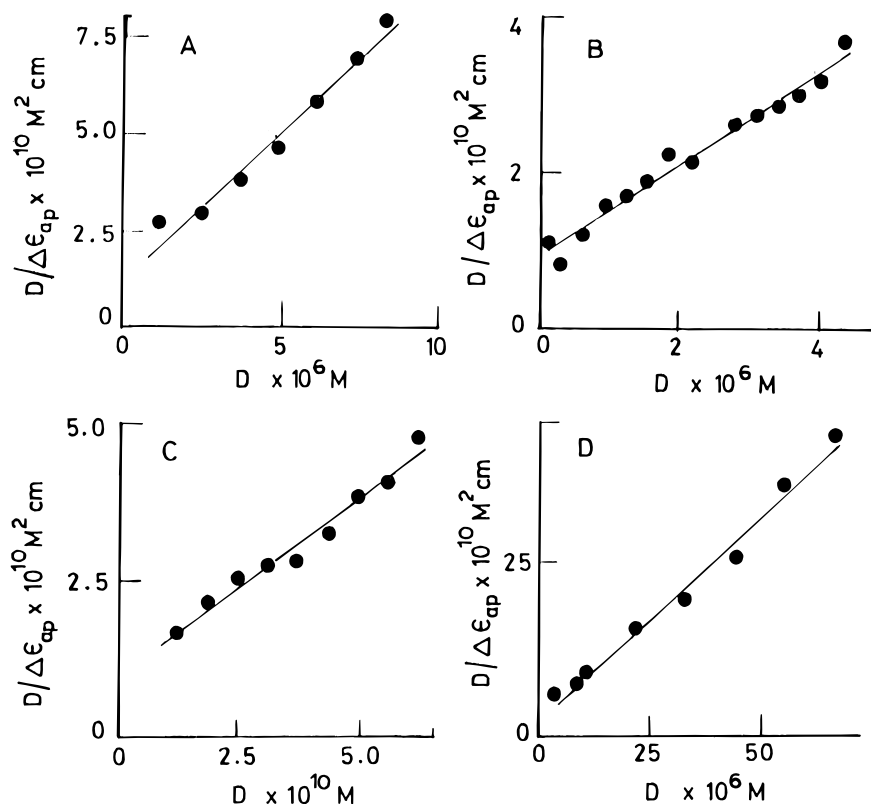


Figure 2. Half-reciprocal plots for binding of different complexes with *E. coli* DNA. The half-reciprocal plots for different complexes were obtained by plotting $D/\Delta\epsilon_{ap}$ vs D according to eq 1 as described in Experimental Procedures. Panels A–D show the half-reciprocal plots for DNA binding due to **1** and **2a–c**, respectively. The binding constants for **1** and **2a–c** were calculated as 3.6×10^5 , 5.2×10^5 , 6.0×10^5 , and $10.0 \times 10^5 \text{ M}^{-1}$, respectively, by taking the corresponding ratio of the slope to y -intercept.

Table 2. Binding Constants and Related Parameters for DNA–Metallosalen Association^a

compound	$10^6[\text{compound}] \text{ (M)}^b$	$10^6[\text{DNA}]^c \text{ (M)}$	$10^{-5}K^d \text{ (M}^{-1}\text{)}$
1	2.1	8.4	3.6
2a	5.7	4.3	5.2
2b	2.6	6.2	6.0
2c	3.9	70.0	10.0
2d	2.6	11.1	<i>e</i>
3	5.7	50	<i>f</i>
4	7.2	180	<i>f</i>
5	2.2	12.4	<i>e</i>

^a For binding constant determination, see the text for details.

^b The concentrations of the compounds were fixed at the given values. ^c Saturating concentration of DNA. ^d K was determined from the ratio of the slope to the y -intercept of each of the half-reciprocal plots as described in Experimental Procedures. We estimate that the values determined for K for the titration experiments are within $\pm 5\%$. ^e Interpolation of the binding titration data did not result in a linear half-reciprocal plot, and hence, binding constants could not be calculated. ^f No significant binding was observed.

affects the charge neutralization of DNA twice as effectively as the monocationic Na^+ ion. This explains why at nearly 50% concentration of MgCl_2 relative to that of NaCl the same extent of hyperchromism in absorption intensities of the **2b**–DNA complex could be attained. Taken together, all of the above observations suggest that intercalation may be important, but all of the above can also be explained on the basis of charge neutralization and may also involve groove binding or phosphate binding.

Binding of the Salen **2a to Denatured DNA.** In the present study, we compared the binding ability of the Ni complex **2a** toward the double-stranded DNA as opposed to that with alkali-denatured DNA. The double-stranded CT DNA was denatured using concentrated, aqueous NaOH . Trace 1 (Figure 4) stands for the

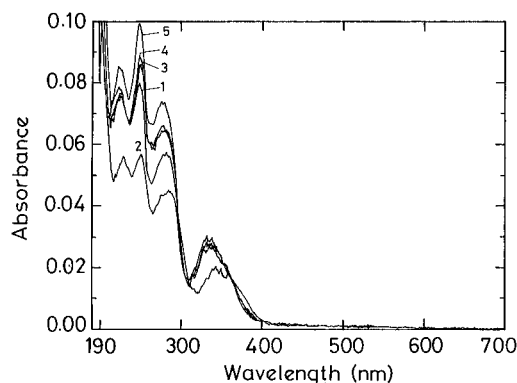


Figure 3. Effect of the addition of salt on DNA binding. This was performed by examining the UV–vis spectra upon addition of progressively increasing amounts of various salts to a **2b**–DNA complex solution: trace 1, **2b** alone, $[\text{2b}] = 2.63 \times 10^{-6} \text{ M}$; and trace 2, with excess CT DNA, $[\text{DNA}] = 5.83 \times 10^{-6} \text{ M}$ in base molarity. Traces 3 and 4 contain the **2b**–DNA complex in the presence of 30 and 45 mM NaCl . Trace 5 contains the **2b**–DNA complex in the presence of 15 mM MgCl_2 .

complex **2a** ($3.35 \mu\text{M}$) alone in the absence of DNA. Spectral trace 2 is obtained after the addition $5.83 \mu\text{M}$ (base molarity) alkali-denatured CT DNA (pH ~ 11) to **2a**. Under these conditions, the absorbance peak at 259 nm was reduced by about $\sim 65\%$ compared to that observed with native double-stranded CT DNA. The decrease in the pH of this solution by progressive addition of small aliquots of aqueous HCl solution led to successive increases in hypochromism reaching a minima ($\sim 55\%$) at around pH 7 (traces 3–8).

The initial, small extent of hypochromism observed in the absorption intensity of the Ni complex **2a** in strongly alkaline media even in the presence of excess DNA suggested a weak binding of the probe **2a** with the

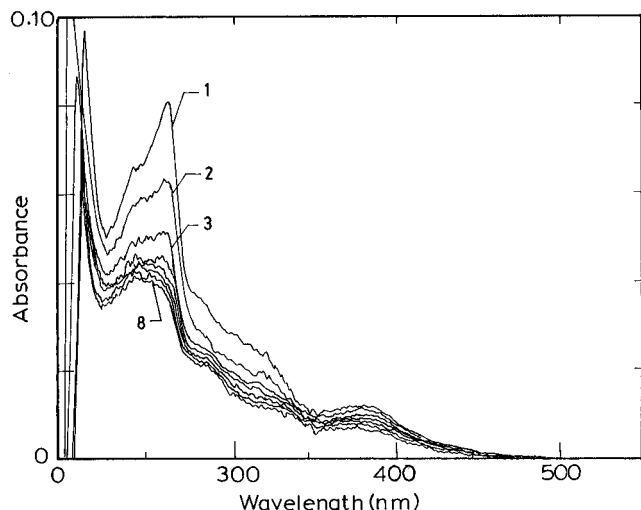


Figure 4. Binding of **2a** to denatured DNA. This was performed by adding an aliquot of alkali-denatured CT DNA into solution of **2a**. An absorption spectrum was recorded, and the same was followed by addition of increasing amounts of aqueous HCl to this mixture to allow progressive slow renaturation. Trace 1 is for **2a** alone in the absence of any DNA; [**2a**] = 3.35×10^{-6} M. Trace 2 shows UV-vis the spectrum of **2a** in the presence of 5.83×10^{-6} M CT DNA ([NaOH] = 5.0×10^{-3} M). Traces 3–7 were obtained by adding successively each time 1.5 μ L of 0.6 M aqueous HCl.

denatured CT DNA. Increasing amounts of HCl addition decrease the pH of the solution by making the conditions more favorable for the renaturation of DNA. Under these circumstances, the formation of more double-stranded DNA duplexes was therefore facilitated. The increase in hypochromism with decreasing pH therefore indicates that there is stronger electronic interaction of the Ni complex with double-stranded DNA upon renaturation. This is in complete agreement with the fact that the absorption hypochromism was maximal at pH ~ 7 where the DNA is present predominantly in the renatured form. A further decrease in pH (below 6.5) also results in the protonation of the DNA bases. Under these circumstances, there is a strong distortion in the DNA structure (32). This was reflected in the reduction in hypochromism with a further decrease in pH (not shown). Taken together, these results clearly demonstrate that the salen **2a** does not physically bind to single-stranded DNA to the extent it does with native duplex DNA.

Effects of Salen Binding on DNA Melting. Additional information concerning the role of DNA binding by different metallosalens was available from the thermal denaturation studies. The melting temperature studies clearly demonstrate that strong interactions between the different cationic metal complexes with CT DNA. The melting profiles of CT DNA in the absence and presence of various metal complexes are shown in Figure 5. Curve 1 in Figure 5 shows the melting profile of 72 μ M CT DNA alone ($T_m \sim 62$ °C) in 5 mM Tris-HCl buffer (pH 7.4). Curves 2–6 show the melting profiles of the CT DNA in the presence of **2a** (1.7×10^{-5} M), **2b** (1.6×10^{-5} M), **2c** (2.1×10^{-5} M), **2d** (2.6×10^{-5} M), and **5** (2.6×10^{-5} M), respectively. These experimentally determined melting temperature data for CT DNA in the absence and presence of different metal complexes are given in Table 3. The binding of either of **2a** or **2b** to DNA led to the enhancement of the melting temperature by ~ 18 and ~ 10 °C, respectively, from that of the DNA alone, and the corresponding melting profiles were also found to be sharp. So the binding of either **2a** or **2b** increased the thermal stability of DNA duplexes as shown by the enhancement in the T_m values of CT DNA in the presence

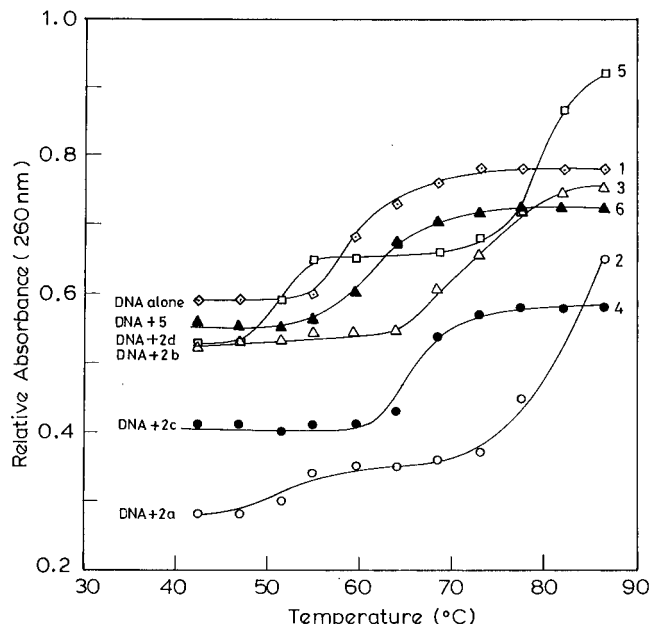


Figure 5. Effect of the inclusion of different metal complexes on the melting of CT DNA. Melting profiles of CT DNA in the presence or absence of different compounds were obtained by plotting the changes in the absorption intensities at 260 nm as a function of temperature. These experiments were carried out with 72 μ M (bM) CT DNA with 5 mM Tris-HCl at pH 7.4: curve 1, CT DNA alone; and curves 2–6, melting profiles of CT DNA in the presence of **2a** (1.74×10^{-5} M), **2b** (1.63×10^{-5} M), **2c** (2.09×10^{-5} M), **2d** (2.59×10^{-5} M), and **5** (2.63×10^{-5} M), respectively.

Table 3. Melting Transitions for Calf Thymus DNA in the Presence of Various Metallosalen Complexes^a

entry	probe	$10^5[\text{probe}]^b$	T_m (°C) ^c
1	<i>d</i>	<i>d</i>	62
2	2a	1.74	80
3	2b	1.63	72.5
4	2c	2.09	67.5
5	2d	2.59	79, 51
6	5	2.63	62

^a The DNA melting was carried out at a DNA concentration of 72 μ M (base molarity). ^b The concentration of the salen used. ^c The melting temperatures were obtained in the presence of salen and are within ± 1 °C. ^d Melting temperature of the DNA alone.

of these compounds. This enhancement in melting temperatures could be due to intercalative binding of the metal complexes with DNA, although other modes of binding are also possible. In the presence of **2d**, a complicated, apparently biphasic melting transition profile with one at ~ 51 °C and another one at ~ 79 °C was observed. This might indicate the differences in the mode with which **2d** interacts with DNA as opposed to **2a**–**c**. The melting profile of DNA in the presence of **5** becomes slightly broadened, although the melting temperature did not change significantly.

In **2a** and **2b**, the pendant positive charges (away from the metal complex core) bring them closer to DNA on electrostatic grounds, leaving the neutral, flat, aromatic region of the complex favorably disposed for further interaction with DNA duplexes. These features in **2a** and **2b** probably contribute to the significant enhancement in DNA melting temperatures. But in the case of Mn(III) complexes **2d**, the complex core bears additional positive charge which probably alters the mode of binding of such complexes with DNA. That is why we see either insignificant changes in T_m upon binding of **5** with DNA or a more complex biphasic DNA melting profile with tricationic **2d**. In the case of Co(II) complex **2c**, the

increase of the DNA melting temperatures was found to be $\sim 5^\circ\text{C}$. It is important to note that, in order to bring a comparable magnitude of absorption hypochromicity, a DNA concentration nearly 1 order of magnitude greater was necessary with this complex relative to that of **2a** and **2b**. The exact reasons for the somewhat modest increases in the DNA melting temperature and the requirement of a higher concentration of DNA during absorption titration are difficult to interpret adequately at this time. However, it could be (i) due to the ability of **2c** to promote DNA scission even in the absence of co-oxidants and (ii) owing to its high oxygen binding capacity (24) the resulting complex may also adopt a nonplanar shape. This deviation from planarity could alter the mode of its interaction with DNA.

DNA Cleavage Studies. The DNA cleavage abilities of different metal complexes in the presence and absence of co-oxidants were investigated with the aid of electrophoresis on agarose gel by noting the conversion of the supercoiled plasmid (form, I, *FI*) to a nicked circle (form, II, *FII*) and then to the completely linear form (form III, *FIII*). As shown in Figure 6A, compounds **2a**, **2d**, and **5** were able to induce oxidative cleavages of DNA. Incubation of the plasmid DNA pTZ19R at 37°C for 5 min with $10\ \mu\text{M}$ **2a**, **2d**, and **5** in the presence of MMPP caused appreciable conversion of form I to the nicked circular form II (lanes 9, 7, and 5, respectively, in Figure 6A). The use of higher concentrations of these reagents ($0.1\ \text{mM}$) and longer incubation ($>15\ \text{min}$) with DNA resulted in double-strand cleavages or even complete degradation (smears) of DNA (figure not shown). Densitometric examination revealed that the DNA nicking efficiencies of tricationic **2d** were a little higher than that of monocationic **5** under comparable conditions. Control experiments verified that any of the above metal complex by itself (in the absence of MMPP) could not affect detectable DNA scission. Significantly, compound **2b** did not show any DNA cleavage activity in the presence or absence of MMPP or any other oxidants, *e.g.* oxone or H_2O_2 (figure not shown). Even with low **2a** concentrations in the presence of MMPP, double-strand scission was appreciable. With the Co(II) complex **2c**, the situation was more complex. It did not appear to show significant DNA nicking when examined on an agarose gel either in the absence or in the presence of MMPP (lanes 10 and 11, respectively). However, more careful examination under a high-resolution sequencing gel confirmed that **2c** also induced considerable DNA modification in the absence of MMPP (see below).

To explore the possibilities of whether a mixture of a given metal ion and the water-soluble ligand **1** could induce DNA cleavage activity, we then went on to examine the DNA cleavage reactions *in situ* by mixing equimolar quantities of **1** with any one of the metal salts, and the reaction products were separated by agarose gel electrophoresis. Figure 6B shows the agarose gel for the DNA cleavage reactions carried out with various mixtures prepared *in situ* by adding individual metal ion to a solution of the ligand **1** in the presence and the absence of co-oxidant MMPP. Lanes 1 and 2 in Figure 6B contain supercoiled plasmid DNA pTZ19R alone and in the presence of $0.5\ \text{mM}$ MMPP, respectively. Lanes 3, 4, 8, 12, and 15 contain $50\ \mu\text{M}$ **1**, manganese(II) acetate, nickel(II) chloride, cobalt(II) acetate, and copper(II) acetate, respectively, in the presence of $0.5\ \text{mM}$ MMPP. Lanes 5, 9, and 16 contain $50\ \mu\text{M}$ mixtures of Mn(II), Ni(II), and Cu(II), respectively, with $50\ \mu\text{M}$ **1** in the absence of MMPP. Lanes 6 and 7 contain DNA treated with 10 and $50\ \mu\text{M}$ *in situ*-prepared Mn(II) complex, respectively, in the presence of MMPP, and lanes 10 and 11 contain 10 and $50\ \mu\text{M}$ *in situ*-prepared Ni(II) complex in the presence of MMPP. Lanes 17 and 18 contained DNA treated with $50\ \mu\text{M}$ of Cu(II) and Cr(III) complex (prepared *in situ*), respectively, in the presence of $0.5\ \text{mM}$ MMPP. Lanes 13 and 14 contain $50\ \mu\text{M}$ *in situ*-prepared Co(II) complex in the absence and presence of $0.5\ \text{mM}$ MMPP, respectively.

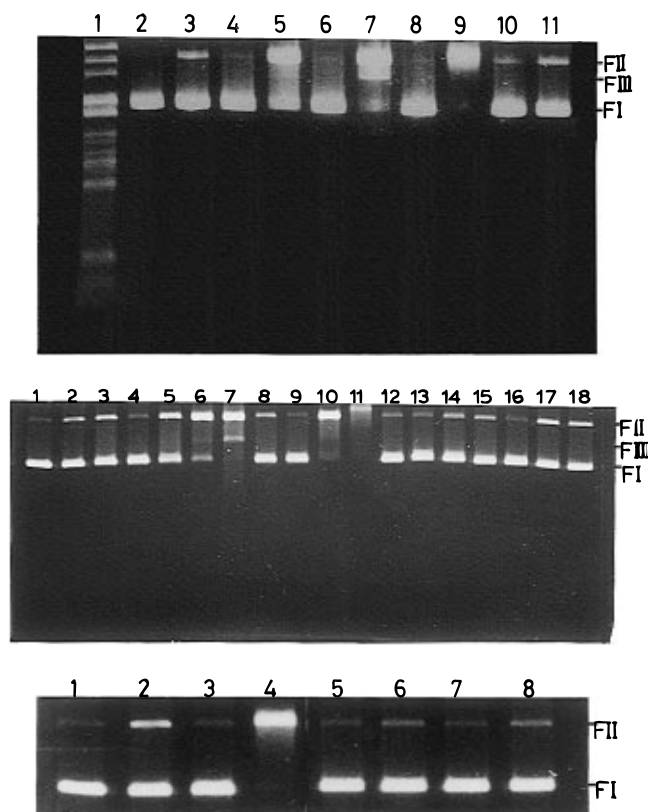


Figure 6. DNA cleavage studies and agarose gel assay. DNA cleavage abilities of the different metal complexes were examined using supercoiled plasmid pTZ19R ($0.25\ \mu\text{g}/\text{reaction}$) in the presence and absence of $0.5\ \text{mM}$ MMPP at 37°C for 5 min in a $10\ \mu\text{L}$ total reaction volume, and the reaction products were analyzed in 1% agarose gel and then stained with ethidium bromide and photographed. (A, top) DNA cleavages by different metal complexes. Lane 1 shows DNA molecular weight markers. Lanes 2 and 3 are supercoiled plasmid pTZ19R alone and in the presence of $0.5\ \text{mM}$ MMPP, respectively. Lanes 4, 6, 8, and 10 contained the same DNA treated with $10\ \mu\text{M}$ **5**, **2d**, **2a**, and **2c**, respectively, in the absence of MMPP. Lanes 5, 7, 9, and 11 contained the same DNA treated with $10\ \mu\text{M}$ **5**, **2d**, **2a**, and **2c**, respectively, in the presence of $0.5\ \text{mM}$ MMPP. (B, middle) DNA cleavages by different metal complexes prepared *in situ*. The different complexes were prepared *in situ* by mixing the water-soluble ligand, **1**, and the respective metal salts in equimolar quantities. Lanes 1 and 2 contain supercoiled plasmid DNA pTZ19R alone and in the presence of $0.5\ \text{mM}$ MMPP, respectively. Lanes 3, 4, 8, 12, and 15 contain $50\ \mu\text{M}$ **1**, manganese(II) acetate, nickel(II) chloride, cobalt(II) acetate, and copper(II) acetate, respectively, in the presence of $0.5\ \text{mM}$ MMPP. Lanes 5, 9, and 16 contain $50\ \mu\text{M}$ mixtures of Mn(II), Ni(II), and Cu(II), respectively, with $50\ \mu\text{M}$ **1** in the absence of MMPP. Lanes 6 and 7 contain DNA treated with 10 and $50\ \mu\text{M}$ *in situ*-prepared Mn(II) complex, respectively, in the presence of MMPP, and lanes 10 and 11 contain 10 and $50\ \mu\text{M}$ *in situ*-prepared Ni(II) complex in the presence of MMPP. Lanes 17 and 18 contained DNA treated with $50\ \mu\text{M}$ Cu(II) and Cr(III) complex (prepared *in situ*), respectively, in the presence of $0.5\ \text{mM}$ MMPP. Lanes 13 and 14 contain $50\ \mu\text{M}$ *in situ*-prepared Co(II) complex in the absence and presence of $0.5\ \text{mM}$ MMPP, respectively. (C, bottom) DNA cleavages by Ni complexes of **2a**, **3**, and **4**. Lanes 1 and 2 contain the DNA alone and in the presence of $0.5\ \text{mM}$ MMPP, respectively. Lanes 3, 5, and 7 contain DNA incubated with $10\ \mu\text{M}$ **2a**, **3**, and **4**, respectively, in the absence of MMPP. Lanes 4, 6, and 8 contain DNA incubated with $10\ \mu\text{M}$ **2a**, **3**, and **4**, respectively, in the presence of $0.5\ \text{mM}$ MMPP.

11 contain DNA in addition to 10 and $50\ \mu\text{M}$ *in situ*-prepared Ni(II) complex in the presence of MMPP. Lanes 17 and 18 contained DNA treated with $50\ \mu\text{M}$ of Cu(II) and Cr(III) complex (prepared *in situ*), respectively, in the presence of $0.5\ \text{mM}$ MMPP. The examination of the electrophoretic profile makes it clear that neither the

metal free ligand nor the ligand free metal ions even in the presence of MMPP could induce any DNA nicking. The DNA nicking was observed only when Mn(II) and Ni(II) were treated with **1** in the presence of MMPP (lanes 6 and 7 and 10 and 11, respectively). In the presence of even micromolar concentrations of either Mn(II)-**1** or Ni(II)-**1** and MMPP, efficient DNA cleavages were observed. However, the combination of **1** with any of the Cu(II) (lane 17), Cr(III) (lane 18), Fe(II), or Zn(II) ions showed no detectable nicking even in the presence of MMPP.

It is evident that in this experiment it is possible to demonstrate that the DNA cleavage activities between the preisolated metal complexes and the metal complexes prepared *in situ* are quite similar. These results further demonstrate that it is indeed possible to modulate the reactivity of DNA cleavage by changing the central metal ion of a complex under the same ligand environment. Moreover, the DNA cleaving ability of different metal complexes could be monitored by using the metal complexes prepared *in situ* without requiring their prior preparation, purification, and characterization.

Role of the Charge on the Metal Complexes. In order to elucidate the role of the charge on the metal complexes toward the DNA cleavage reactions, the DNA modification abilities of monoanionic and dianionic Ni complexes **3** and **4** in the presence and absence of co-oxidant MMPP were examined. The results of these DNA cleavages were compared with that of the bis-cationic Ni complex **2a**. Figure 6C shows the comparative DNA cleavage abilities of **2a**, **3**, and **4**. Lanes 1 and 2 contained the DNA alone and in the presence of 0.5 mM MMPP, respectively. Lanes 3, 5, 7, contained DNA incubated with 10 μ M **2a**, **3**, and **4**, respectively, in the absence of MMPP. Lanes 4, 6, 8 contained DNA incubated with 10 μ M **2a**, **3**, and **4** respectively, in the presence of 0.5 mM MMPP. Thus, while in the presence of MMPP, the cationic Ni complex **2a** cleaves DNA efficiently (lane 4); neither monoanionic **3** nor the dianionic **4** induces and DNA scission under comparable conditions. This inability of **3** and **4** to induce DNA cleavage must be due to their unfavorable electrostatic character which impedes any significant interaction with the DNA. These results emphasize the fact that the presence of cationic charge around the reagent moiety is essential to bringing it close to DNA surfaces. Importantly, the inability of the anionic Ni complexes **3** and **4** to induce DNA modifications further suggest that the active species involved in the DNA cleavage processes described herein with the dicationic Ni complex are not diffusible in nature.

Primer Extension Assay and Autoradiogram. The examination of the DNA cleavage patterns produced by different metal complexes (shown below) has been confined only to those complexes that could apparently produce apparent single- and double-strand breaks in DNA on an agarose gel. The DNA modification patterns produced by the different reagents were examined by performing a primer extension assay. In this experiment, the primer is extended (by Klenow DNA polymerase) to the nick or any other modification in the DNA backbone. The products of this reaction were then analyzed on a high-resolution sequencing gel. Figure 7A shows the chemical modification patterns caused by 20 μ M reagents (**2a**, **2d**, **2c**, and **5**) on the linearized plasmid pTZ19R. Although without appendages to DNA recognition matrices, we did not anticipate any profound selectivities in DNA modification, and we sought to find whether there was any selectivity in DNA modification by various reagents. Toward this goal, we performed the usual

Sanger's sequencing parallel to primer extension reactions (lanes 1–4, G, A, T, and C, respectively.) Lanes 5 and 6 in Figure 7A are untreated DNA and with 0.5 mM co-oxidant MMPP, respectively. Lanes 7, 9, and 11 in Figure 7A contain 20 μ M **5**, **2d**, and **2a**, respectively, without addition of MMPP. Lanes 8, 10, and 12 contain 20 μ M **5**, **2d**, and **2a**, respectively, in the presence of 0.5 mM MMPP. Lanes 13 and 14 showed the DNA modification pattern produced by **2c**, in the absence of MMPP. Thus, these control experiments clearly showed that any of the metal complexes **2a**, **2d**, or **5** did not generate any cleaved products from the plasmid DNA without addition of any co-oxidants (Figure 7A, lanes 11, 9, and 7, respectively). We also found that reagents such as **2d**, **5**, and **2a** cleaved DNA efficiently even at 20 μ M in the presence of 0.5 mM MMPP. The DNA cleavage efficiencies of **2d** and **5** were found to be comparable, while **2a** was found to be somewhat more efficient under comparable conditions. From the analysis of the autoradiogram in base levels, we found that both **2d** and **5** chemically modified in DNA with some selectivity (60–65%) toward the A·T regions of DNA duplexes and the selectivity for both the Mn(III) complexes are almost identical. These observations are consistent with the reports of Griffin in which it was already demonstrated that the related Mn(III)-salen complexes induce A·T selective DNA scission (16). In contrast, Ni(II) complex **2a** preferred to induce nicks in the G·C region (~70%) (19a). Thus, from these results it appears that it is also possible to change the selectivity of DNA modification to some extent by changing the central metal ion in a complex while keeping the ligand environment the same. These intrinsic selectivities, although modest, might indicate prior coordination to preferred base regions of the duplexes by the metal ions of **2a**, **5**, or **2d**. It is noteworthy that the Co complex **2c** alone also induced DNA modifications (without any co-oxidant MMPP) with little G selectivity (lanes 13 and 14, respectively). More significantly, in the presence of MMPP, **2c** did not cleave DNA at all (figure not shown). It is therefore apparent that **2c**-mediated DNA cleavage processes are not related to the DNA nicking events observed with Ni(II) or Mn complexes which required the presence of co-oxidant MMPP.

The autoradiogram in Figure 7B shows the DNA cleavage pattern produced by **2d** and **2a**, respectively, toward supercoiled DNA and linearized DNA to elucidate the dependence of efficiencies and selectivities on secondary structures of nucleic acid. Lanes 6 and 8 in Figure 7B represent linearized and supercoiled plasmid pTZ19R alone, respectively. Lanes 2 and 4 show the supercoiled DNA after treatment with 5 μ M **2d** and **2a**, respectively, in the absence of any MMPP. Lanes 1 and 3 contain supercoiled plasmid after treatment with 5 μ M **2d** and **2a**, respectively, in the presence of 0.5 mM MMPP. Lanes 5 and 7 contain linearized DNA after treatment with 20 mM **2d** and **2a**, respectively, in the presence of 0.5 mM MMPP. Thus, it is quite clear that the efficiency of DNA cleavage produced by either of the reagents **2d** and **2a** was more on supercoiled DNA over its linearized counterpart at higher concentrations of the reagents are necessary for linearized DNA to produce a comparable cleavage pattern.

In order to independently confirm the results obtained from the primer extension reactions, we also carried out parallel control DNA cleavage experiments (not shown) ³²P-end-labeled double-stranded DNA fragments (approximately 200 bp). These results clearly showed that the Mn and Ni complexes could generate cleaved DNA fragments, although in the case of the Ni complex, few additional high-molecular weight bands possibly due to

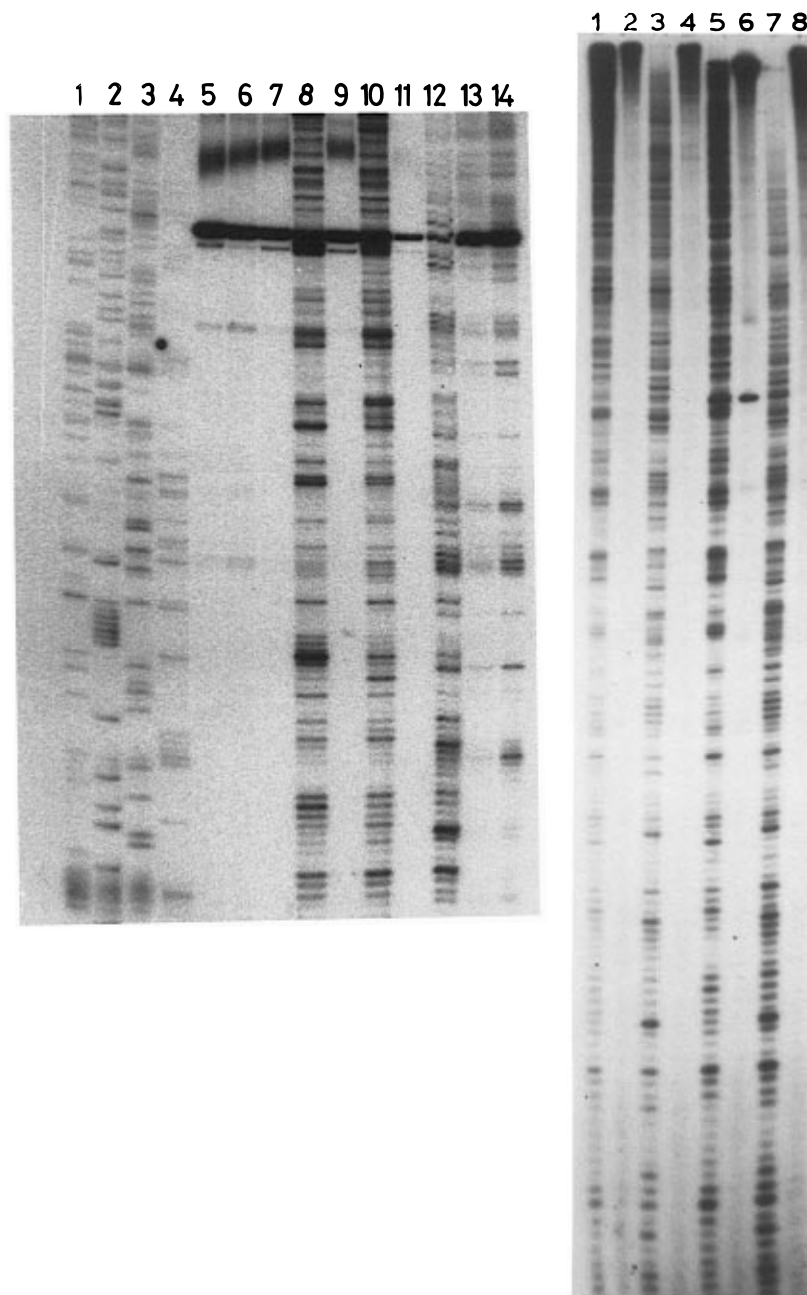


Figure 7. Sequencing and autoradiography. The sequence or the base specificities in DNA modification by different metal complexes in the presence and absence of different metal complexes were determined by performing primer extension. The ^{32}P -end-labeled primer was allowed on the chemically cleaved DNA fragments in the absence of any dideoxy nucleotide, and the primer extension products were analyzed on 8 M urea PAGE and autoradiogrammed. (A, left) DNA cleavage patterns produced by different metal complexes in the absence and presence of cooxidant MMPP. Lanes 1–4 are Sanger's sequencing reactions G, A, T, and C, respectively. Lanes 5 and 6 are untreated DNA and DNA with 0.5 mM MMPP, respectively. Lanes 7, 9, and 11 contain 20 μM **5**, **2d**, and **2a**, respectively, in the presence of 0.5 mM MMPP. Lanes 13 and 14 show the DNA nicking pattern produced by 20 and 100 μM **2c**, respectively, in the absence of MMPP. (B, right) Structural (supercoiled vs linearized) dependence of DNA cleavage efficiencies for **2a** and **2d**. In lanes 6 and 8 are linearized and supercoiled plasmid pTZ19R alone, respectively. Lanes 2 and 4 are supercoiled DNA treated with 5 μM **2d** and **2a**, respectively, in the presence of 0.5 mM MMPP. Lanes 1 and 3 contained supercoiled plasmid treated with 5 μM **2d** and **2a**, respectively, in the presence of 0.5 mM MMPP. Lanes 5 and 7 contained linearized DNA treated with 20 μM **2d** and **2a**, respectively, in the presence of 0.5 mM MMPP.

reagent-induced cross-linking were also seen. The observation of the formation of cross-linked bands is consistent with earlier report of Burrows and Rokita (17b, c).

Possible Mechanism. The active species responsible for the DNA modification by the Ni complexes are probably derived from Ni(III) species. We assume therefore that the scheme proposed by Burrows (17b) persists in the present case also in which a related Ni–salen analogue was used. On this basis, we anticipate the

involvement of an activated Ni(III) species for such profound DNA scission. We also examined the redox behavior of the Ni(II) complex under cyclic voltammetry (not shown). The complexes were found to undergo oxidative polymerization at the electrode surfaces. This finding also suggests a possible ligand–radical coupling involving the phenolic portion of the salen unit, where Ni(II) is oxidized to Ni(III) Goldsby *et al.* reached similar conclusions independently in their studies involving Ni(II)–bis(salicylaldimine) complexes (33). Formation of

ligand–radical should in part be responsible for the DNA cross-linking.

With regard to the chemistry of the Mn complexes, we feel that the DNA cleavages in these instances are affected in the following manner. The combination of the salen–Mn³⁺ and MMPP produces direct DNA nicks through pathways that do not require dioxygen. DNA cleavage releases free, unmodified nucleobases. Such observations are consistent with a plausible mechanism involving deoxyribose CH activation potentiated by an oxidatively activated species such as [salen–Mn(V)O]⁺. The above suggestions are indeed supported in literature from the independent work of Griffin and others (16b, 34).

The mechanistic pathways by which the Co(II)–salen–O₂-mediated DNA modification occurs is currently under investigation. Preliminary studies indicate that a superoxide radical-mediated active species is probably responsible for the observed DNA modification in this instance. In the presence of MMPP, the complex is oxidized to a Co(III) species which does not have ability to activate dioxygen, and hence, this does not possess DNA cleaving ability.

Concluding Remarks. In summary, we have developed several salen-based transition metal complexes which interact with or modify DNA. The binding and DNA modifications by such complexes can be modulated by the charge on the salen unit and more profoundly by the selection of the central metal ion. Only the salens with net cationic electrostatic character bind DNA, and the physical binding of the salen complexes does not occur to denatured (predominantly single-stranded) DNA to the extent that it does with native double-stranded DNA. Thus, probably a combination of the electrostatic and intercalative/groove binding interactions with DNA raise the duplex melting temperatures significantly. The anionic salens neither bind DNA nor induce strand scission irrespective of the central metal ion selected. The supercoiled forms of the plasmid DNA were found to be more susceptible to scission compared to their linearized forms by the cationic salens. Thus, to obtain comparable degrees of DNA cleavage, higher concentrations of the reagents were necessary with the linearized DNA.

The present findings demonstrate that modulation of the reactivities of the salen-based reagents toward DNA is possible and form a basis for further exciting studies. The newly introduced salen derivatives when tethered to suitable nucleic acid structural recognition matrices should be attractive as sequence specific reagents. Elucidations of the exact reaction conditions and mechanistic pathways for such important applications and also for the mapping of DNA tertiary structures are currently underway in our laboratory.

ACKNOWLEDGMENT

We are grateful to the referees for useful comments. S.S.M. thanks CSIR for a senior research fellowship. This work was supported by the funding from DST (INDO-HUNG to S.B.) and by the DBT and DST (to U.V.).

LITERATURE CITED

- (1) (a) Sigman, D. S., Bruice, T. W., Mazumder, A., and Sutton, C. L. (1993) *Acc. Chem. Res.* 26, 98. (b) Barton, J. K., and Pyle, A. M. (1990) *Prog. Inorg. Chem.* 38, 413. (c) Burkoff, A. M., and Tullius, T. D. (1988) *Nature* 331, 455. (d) Riordan, C. G., and Wei, P. J. (1992) *J. Am. Chem. Soc.* 116, 2189.
- (2) (a) Tan, J. D., Hudson, S. E., Brown, S. J., Olmsted, M. M., and Mascharak, P. K. (1992) *J. Am. Chem. Soc.* 114, 3841. (b) Nagai, K., Carter, B. J., Xu, J., and Hecht, S. M. (1991) *J. Am. Chem. Soc.* 113, 5099. (c) Nicolau, K. C., Maligres, P., Shin, J., de Leon, E., and Rideout, D. (1992) *J. Am. Chem. Soc.* 114, 7825.
- (3) Dervan, P. B. (1992) *Nature* 359, 87.
- (4) Sigman, D. S., Mazumder, A., and Perrin, D. M. (1993) *Chem. Rev.* 93, 2295.
- (5) Sardesai, N. Y., Zimmermann, K., and Barton, J. K. (1994) *J. Am. Chem. Soc.* 116, 7502.
- (6) Pratiel, G., Bernadou, J., and Meunier, B. (1995) *Angew. Chem., Int. Ed. Engl.* 34, 746.
- (7) Keck, M.-V., and Lippard, S. J. (1992) *J. Am. Chem. Soc.* 114, 3386.
- (8) Burrows, C. J., and Rokita, S. E. (1994) *Acc. Chem. Res.* 27, 295.
- (9) (a) Breslin, D. T., and Schuster, G. B. (1996) *J. Am. Chem. Soc.* 118, 2311. (b) Breiner, K. M., Daugherty, M. A., Das, T. G., and Thorp, H. H. (1995) *J. Am. Chem. Soc.* 117, 11673. (c) Croke, D. T., Perroult, L., Sari, M. A., Battionti, J. P., Mansuy, D., Helene, C., and Doon, T. L. (1993) *J. Photochem. Photobiol.* 18, 41. (d) Nielsen, P. E. (1990) *J. Mol. Recognit.* 3, 1. (e) Bhattacharya, S., and Mandal, S. S. (1996) *J. Chem. Soc., Chem. Commun.*, 1515.
- (10) (a) Papavassiliou, A. G. (1995) *Biochem. J.* 305, 345. (b) Siltani, A., Long, E. C., Pyle, A. M., and Barton, J. K. (1992) *J. Am. Chem. Soc.* 114, 2303.
- (11) (a) Guajardo, R. J., Hudson, S. E., Brown, S. J., and Mascharak, P. K. (1993) *J. Am. Chem. Soc.* 115, 7971. (b) Stubbe, J., and Kozarich, J. W. (1987) *Chem. Rev.* 87, 1107. (c) Uhlmann, E., and Reyman, A. (1990) *Chem. Rev.* 90, 543.
- (12) Jaeger, J., Santalucia, J., and Tinoco, I. (1993) *Annu. Rev. Biochem.* 62, 255.
- (13) Taylor, S. J., Schultz, P. G., and Dervan, P. B. (1984) *Tetrahedron* 40, 457.
- (14) (a) Kasprzak, K. S. (1991) *Chem. Res. Toxicol.* 4, 604. (b) Tullius, T. D., Ed. (1989) *Metal–DNA Chemistry*, ACS Symposium Series 402, American Chemical Society, Washington, DC. (c) Vahter, M. E. (1988) in *Biological Monitoring of Toxic Metals* (Clarkson, T. W., Friberg, L., Nordberg, G. F., and Sanger, P. R., Eds.) pp 303–321, Plenum, New York. (d) Yamanaka, K., and Okada, S. (1994) *Environ. Health Perspect.* 102 (Suppl. 3), 37.
- (15) Sato, K., Chikira, M., Fujii, Y., and Komatsu, A. (1994) *J. Chem. Soc., Chem. Commun.*, 625.
- (16) (a) Gravert, D. J., and Griffin, J. H. (1993) *J. Org. Chem.* 58, 820. (b) Gravert, D. J., and Griffin, J. H. (1996) *Inorg. Chem.* 35, 4837.
- (17) (a) Woodson, S. A., Muller, J. G., Burrows, C. J., and Rokita, S. E. (1993) *Nucleic Acids Res.* 21, 5524. (b) Muller, J. G., Paikoff, S. J., Rokita, S. E., and Burrows, C. J. (1994) *J. Inorg. Biochem.* 54, 199. (c) Burrows, C. J., and Rokita, S. E. (1994) *Acc. Chem. Res.* 27, 295.
- (18) Routier, S., Bernier, J.-L., Waring, M. J., Colson, P., Houssier, C., and Baily, C. (1996) *J. Org. Chem.* 61, 2326.
- (19) (a) Mandal, S. S., Vinaykumar, N., Varshney, U., and Bhattacharya, S. (1996) *J. Inorg. Biochem.* 63, 265. (b) Bhattacharya, S., and Mandal, S. S. (1997) *Biochem. Biophys. Acta* 1323, 29. (c) Mandal, S. S., Renuka, K., Guru Row, T. N., and Bhattacharya, S. (1996) *J. Chem. Soc., Chem. Commun.* 2725.
- (20) Rajaram, R., Balachandran, U. N., and Ramasami, T. (1994) *Biochem. Biophys. Res. Commun.* 205, 327.
- (21) Muller, W., and Crothers, D. M. (1975) *Eur. J. Biochem.* 54, 267.
- (22) Reichmann, Y., Rice, S. A., Thomas, C. A., and Doty, P. (1954) *J. Am. Chem. Soc.* 76, 3047.
- (23) Maniatis, T., Fritsch, E. F., and Sambrook, S. (1982) *Molecular Cloning*, p 458, Cold Spring Harbor Laboratory Press, Plainview, NY.
- (24) Busetto, C., Cariati, F., Fusi, A., Gullotti, M., Marazzoni, F., Pasini, A., Ugo, R., and Valenti, V. (1973) *J. Chem. Soc.*, 754.
- (25) Pyle, A. M., Rehmann, J. P., Meshoyrer, R., Kumar, C. V., Turro, N. J., and Barton, J. K. (1989) *J. Am. Chem. Soc.* 111, 3051.
- (26) Meehan, T., Gamper, H., and Becker, J. F. (1982) *J. Biol. Chem.* 257, 10479.

- (27) Cory, M., McKee, D. D., Kagan, J., Henry, D. W., and Miller, J. A. (1985) *J. Am. Chem. Soc.* **107**, 2528.
- (28) Sasse-Dwight, S., and Gralla, J. D. (1988) *J. Mol. Biol.* **202**, 107.
- (29) Sheldon, R. A., and Kochi, J. K. (1981) *Metal-Catalyzed Oxidation of Organic Compounds*, Academic, New York.
- (30) (a) Koola, J. D., and Kochi, J. K. (1987) *Inorg. Chem.* **26**, 908. (b) Chen, D., and Martell, A. E. (1987) *Inorg. Chem.* **26**, 1026. (c) Yoon, H., and Burrows, C. J. (1988) *J. Am. Chem. Soc.* **110**, 4087.
- (31) (a) Cheng, C.-C., Goll, J. G., Neyhart, G. A., Welch, T. W., Singh, P., and Thorp, H. H. (1995) *J. Am. Chem. Soc.* **117**, 2970. (b) Groves, J. T., and Kady, I. O. (1993) *Inorg. Chem.* **32**, 3868. (c) Pamatong, F. V., Detmer, C. A., III, and Bocarsly, J. R. (1996) *J. Am. Chem. Soc.* **118**, 5339. (d) Keek, M. V., and Lippard, S. J. (1992) *J. Am. Chem. Soc.* **114**, 3386. (e) Carter, M. T., Rodriguez, M., and Bard, A. J. (1989) *J. Am. Chem. Soc.* **111**, 8901.
- (32) Singleton, S. F., and Dervan, P. B. (1992) *Biochemistry* **31**, 1099.
- (33) Goldsby, K. A., Blaho, J. K., and Hoferkamp, L. A. (1989) *Polyhedron* **8**, 113.
- (34) Srinivasan, K., Michand, P., and Kochi, J. K. (1986) *J. Am. Chem. Soc.* **108**, 2309.

BC970121X

Studies on Base-Boronated Oligonucleotides. 2 (1). Incompatibility of DMT and Cyanoborane Groups during Oligonucleotide Synthesis

Ahmad Hasan,[†] Jeno Tomasz,[‡] and Barbara Ramsay Shaw*

Department of Chemistry, P. M. Gross Chemical Laboratory, Duke University, Durham, North Carolina 27708-0346. Received March 10, 1997*

The cyanoborane ($-\text{BH}_2\text{CN}$) nucleosides and nucleotides are a new class of compounds that mimic natural and synthetic congeners in many ways and exhibit interesting biochemical and biophysical properties. The B–N bond is isoelectronic with the C–N⁺ bond of N⁷-alkylated 2'-nucleosides, as well as the C–C bond of naturally occurring 7-alkyl-7-deazanucleosides. These compounds differ from normal guanosine in that they are incapable of hydrogen bonding at the 7-position. The syntheses of N⁷-cyanoborane 2'-deoxyguanosine, N⁷-(dimethylaminomethylene)-N⁷-cyanoborane 5'-(dimethoxytrityl)-2'-deoxyguanosine (**3**), and N⁷-isobutyryl-N⁷-cyanoborane 5'-(dimethoxytrityl)-2'-deoxyguanosine (**9**) are described. Removal of the dimethoxytrityl (DMT) group from **3** or **9** is accompanied by significant loss of the cyanoborane moiety. Additionally, dimethoxytritylation of a cyanoborated nucleoside leads to partial deboration, thus limiting use of the commercially available 5'-DMT nucleosides as viable precursors in base-boronated oligonucleotide synthesis. The incompatibility of the cyanoborane moiety under DMT removal/addition conditions necessitated the search for an alternative method of protecting the 5'-hydroxyl of the nucleoside. This paper addresses the possible cause of deboration and describes the synthesis of N⁷-cyanoborated nucleosides by a method that avoids transient protection of the sugar hydroxyls.

INTRODUCTION

Boronated nucleic acids are a class of compounds that mimic natural and synthetic congeners in many ways. The base-boronated nucleoside, N⁷-cyanoborane-dG (^{7b}-dG) (**2**), wherein one endocyclic nitrogen is coordinated with the cyanoborane ($-\text{BH}_2\text{CN}$) moiety, resembles the N⁷-methyl-2'-deoxynucleoside and also a naturally occurring 7-deazanucleoside like nucleoside Q found in tRNA (**3**) (see Figure 1). All three compounds preclude hydrogen bonding at position 7 of guanine, and the B–N bond of ^{7b}dG is isoelectronic with the C–N⁺ bond of N⁷-alkylated nucleosides and the C–C bond of 7-alkyl-7-deazanucleosides. Cyanoborated nucleosides exhibit potent antitumor activity in mammalian cell lines, and anti-inflammatory and hypolipidemic activity in mice (**4–6**).

Oligonucleotides having N⁷-cyanoborane 2'-deoxyguanosine units are of particular interest because they are capable of Watson–Crick type base pairing, yet the presence of an N⁷-cyanoborane substituent precludes Hoogsteen-type base pairing as might be found in triplex DNA (**7**). The cyanoborane group also imparts stability toward cleavage of the glycosidic bond; ^{7b}dG is more stable to depurination at acidic pH than is normal dG and is far more stable in both acidic and basic buffers than the corresponding N-alkylated derivatives (**8**). We recently reported that N⁷-cyanoborane 2'-deoxyguanosine triphosphate (5'-^{7b}dGTP) serves as an excellent substrate for DNA polymerases, including the thermostable Vent and Taq polymerases, and is incorporated within an M13mp2 DNA duplex efficiently (**9, 10**). The unique properties exhibited by ^{7b}dG and the resistance of ^{7b}dG

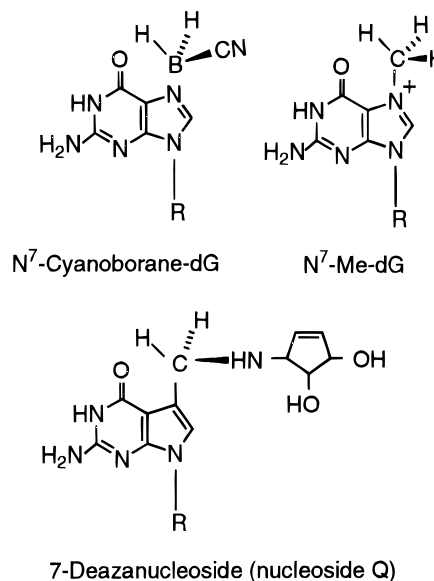


Figure 1. Structure of N⁷-modified nucleosides.

oligos to restriction endonucleases (**10, 11**) have led us to explore chemical methods for the synthesis of monomers and oligomers containing the cyanoborane moiety.

Development of methods for the synthesis of base-boronated oligonucleotides both in solution and on solid support has been one of the main research goals in our laboratory (**2**). Because of their superior stability (**8**), we have focused our attention on oligonucleotides containing cyanoborane modification at the endocyclic nitrogen of the base, especially at N-7 of guanine (**1**). We recently (**1**) reported the synthesis of the nine possible dinucleoside monophosphates containing the ^{7b}dG moiety.

Oligonucleotide synthesis requires protection of functional groups not participating in the condensation reaction. We have attempted the synthesis of boronated oligonucleotides using monomers containing a 4',4'-dimethoxytrityl (DMT) protecting group at the 5'-sugar hydroxyl (**12**) and found that the two groups are incom-

* Author to whom correspondence should be addressed [telephone (919) 660-1551; fax (919) 660-1618; e-mail brs@chem.duke.edu].

[†] Present address: Peninsula Laboratories, 611 Taylor Way, Belmont, CA 94002.

[‡] Present address: Gödöllo, Patota-Kert 6A, x.4, 2100 Hungary.

© Abstract published in *Advance ACS Abstracts*, August 1, 1997.

patible. Substantial loss of the cyanoborane moiety accompanies both the attachment of the DMT group to, and its removal from, the 5'-OH group of ⁷b_dG. A systematic investigation of the possible cause of deboration has been studied, and the results are summarized in the present paper.

EXPERIMENTAL PROCEDURE

Materials and Methods. Compounds **1** (**13**), **4** (**5**), and triphenylphosphine:cyanoborane (**14**) were prepared following the literature procedure. Compound **8** was purchased from Sigma. Bu₄NF (1.1 M in THF) was purchased from Aldrich. Pyridine was distilled from phosphorus pentoxide and stored over 4 Å molecular sieves. THF was freshly distilled from sodium and benzophenone. DMF was distilled from CaH₂ and stored over 4 Å molecular sieves. All other chemicals were of reagent grade.

Thin-layer chromatography (TLC) was run on 0.2 mm Kieselgel 60 F₂₅₄ chromatoplates (Merck). Most of the compounds were visualized under a short-wave UV light. Other compounds were visualized using either I₂ vapors (for **6**) or HCl vapors (for compounds with DMT group) or by heating the chromatograph at 100 °C after the TLC plate was sprayed with 5% sulfuric acid in methanol. Column chromatography was performed on silica gel (60–200 mesh, Baker); the column (i.d. = 2.5 cm) was prepared from a slurry of silica gel (80–85 g) in the first eluent. Fractions of 20–25 mL were collected with a flow rate of ~40 mL/min.

Melting points were recorded on a Mel-Temp capillary melting point apparatus and are uncorrected. NMR spectra of approximately 0.1 M solutions were recorded at ambient temperature on a Varian Associates Model XL-300 spectrometer at 300 MHz (¹H) or on a JEOL FX90Q spectrometer at 28.7 MHz (¹¹B). Chemical shifts are reported in ppm (δ) and are referenced to the internal standard; tetramethylsilane for ¹H or boron trifluoride etherate for ¹¹B. Splitting patterns are expressed as follows: s (singlet), d (doublet), t (triplet), m (multiplet), or br (broad). The presence of exchangeable protons was confirmed by treatment with deuterium oxide (D₂O) followed by reintegration of the NMR spectrum. IR spectra were obtained using a BOMEN MB 100 spectrometer. Fab-MS spectra were recorded on a JEOL JMS 5X102 high-resolution mass spectrometer using 3-nitrobenzyl alcohol as the matrix.

N²-(Dimethylaminomethylene)-5'-O-(dimethoxytrityl)-2'-deoxyguanosine (2). A suspension of **1** (340 mg, 1.0 mmol) (**13**), 4-(dimethylamino)pyridine (8 mg, 0.065 mmol), and DMT-Cl (678 mg, 2.0 mmol) in pyridine (10 mL) was stirred with the exclusion of atmospheric moisture at room temperature (RT). The reaction mixture became homogeneous within 30 min. After 2 h, TLC in CH₂Cl₂/MeOH (90:10 v/v) showed conversion (>95%) of **1** to a much less polar compound. The solution was poured into ice-water (~100 mL) and a yellow oil separated. The mixture was extracted with CH₂Cl₂ (1 × 50, 1 × 25 mL). The combined CH₂Cl₂ extracts were dried over Na₂SO₄, filtered, and evaporated. After evaporation, the oily residue was dissolved in CH₂Cl₂, and the resulting solution was applied onto a silica gel column. The column was eluted with CH₂Cl₂/MeOH (98:2 v/v) (200 mL) followed by a 95:5 mixture of the same solvents (v/v, 2500 mL). Elution was monitored by TLC in CH₂Cl₂/MeOH (95:5 v/v). Fractions containing the product (emerging after about 1000 mL of 95:5 mixture) were pooled and evaporated. After overnight drying at RT and ≤1 mmHg, a pale yellow solid was isolated, which was homogeneous by TLC (*R_f* = 0.11). The isolated yield

of compound **2** was 536 mg (86%): ¹H NMR (CDCl₃) δ 9.35 (s, 1H, NH), 8.53 (s, 1H, CH=N), 7.70 (s, 1H, H-8), 6.78–7.40 (m, 13 H, Ar), 6.39 (t, ³J_{HH} = 6.6 Hz, H-1'), 4.62–4.63 (m, 1H, H-3'), 4.15–4.16 (m, 1H, H-4'), 3.76 (s, 6H, 2 × CH₃O), 3.46 (d, ³J_{HH} = 3.4 Hz, O3'-H), 3.26–3.34 (m, 2H, H-5' + H-5''), 3.02 and 3.07 (2s, 6H, NMe₂), 2.53–2.57 (m, 2H, H-2' + H-2''); Fab-MS calculated for [M + H]⁺ = 625.66, found 625.3.

N²-(Dimethylaminomethylene)-N'-cyanoborane 5'-O-(Dimethoxytrityl)-2'-deoxyguanosine (3). A solution of compound **2** (536 mg, 0.86 mmol) and triphenylphosphine:cyanoborane (970 mg, 3.2 mmol) in THF (16 mL) was heated at reflux with the exclusion of atmospheric moisture for 140 min. TLC in CH₂Cl₂/MeOH (95:5 v/v) showed significant conversion (>50%) of **2** to a less polar compound. After overnight standing at room temperature under anhydrous conditions, the solution was evaporated and the resulting residue was dissolved in CH₂Cl₂ (8–10 mL). The solution was applied onto a silica gel column. The column was eluted with mixtures of CH₂Cl₂/MeOH (98:2 v/v, 200 mL) and (95:5 v/v, 1500 mL). Fractions containing the product were pooled and evaporated to give a solid foam. Yield after overnight drying at RT and 1 mmHg was 299 mg (56%), *R_f* = 0.27: ¹H NMR (CDCl₃) δ 9.99 (s, 1H, NH), 8.58 (s, 1H, H-8), 8.09 (s, 1H, CH=N), 6.82–7.36 (m, 13 H, Ar), 6.26 (t, ³J_{HH} = 6.4 Hz, 1H, H-1'), 4.58 (unres, 1H, H-3'), 4.17–4.18 (m, 1H, H-4'), 3.76 (s, 6H, 2 × CH₃O), 3.56 (d, ³J_{HH} = 4.1 Hz, 1H, O3'-H), 3.23–3.39 (2m, 2H, H-5' + H-5''), 3.07 and 3.17 (2s, 6H, NMe₂), 2.45–2.72 (2m, 4H, BH₂, H-2' + H-2''); Fab-MS calculated for [M + H]⁺ = 664.5, found 664.3.

N²-(Dimethylaminomethylene)-N'-cyanoborane 3',5'-Bis(O-triisopropylsilyl)-2'-deoxyguanosine (5). Compound **4** (6.0 g, 10.4 mmol) was suspended in MeOH (105 mL). *N,N*-Dimethylformamide dimethylacetal (2.77 mL, 20.8 mmol) was added, and the solution was stirred with the exclusion of atmospheric moisture at RT. Crystals started to deposit from the solution after 30 min. Stirring was continued for 1 h, and then the flask was immersed into an ice-water bath for 3 h. The crystals were filtered, washed with ice-cold MeOH (2 × 20 mL), and dried at RT and 1 mmHg overnight to yield 5.3 g (75.7%) of compound **5**, mp 188–190 °C. The product was identical (TLC, ¹H NMR) to that obtained in DMF: Fab-MS calculated for [M + H]⁺ = 674.8, found 674.4.

N²-(Dimethylaminomethylene)-N'-cyanoborane 2'-Deoxyguanosine (6). A solution of 1.1 M Bu₄NF in THF (3.6 mL) was added to a stirred solution of **5** (1.35 g, 2.0 mmol) in THF (10 mL) at RT. Oil separated from the homogeneous solution within 5 min. After 2 h, TLC (CH₂Cl₂/MeOH, 95:5 v/v) indicated complete conversion of compound **5** (*R_f* = 0.44) to a more polar compound **6** (*R_f* = 0.06). The reaction mixture was evaporated, the residual oil was dissolved in a mixture of CH₂Cl₂/MeOH (95:5 v/v, 5 mL), and the solution was percolated through a silica gel column. The column was eluted by a mixture of CH₂Cl₂/MeOH (95:5 v/v). Appropriate fractions containing the product were pooled and evaporated. The residual pale yellow solid was thoroughly washed with THF (altogether 10 mL) until the color disappeared. The white solid was dried at RT and 1 mmHg overnight to yield 558 mg (77%) of compound **6**, homogeneous by TLC: ¹H NMR (DMSO-*d*₆) δ 11.74 (s, 1H, NH), 8.70 (s, 1H, H-8), 8.50 (s, 1H, CH=N), 6.19 (t, ³J_{HH} = 6.4 Hz, 1H, H-1'), 5.24 (d, ³J_{HH} = 3.9 Hz, 1H, O3'-H), 4.97 (t, ³J_{HH} = 5.1 Hz, 1H, O5'-H), 4.26 (unres 1H, H-3'), 3.74–3.75 (m, 1H, H-4'), 3.40–3.52 (m, 2H, H-5' + H-5''), 2.93 and

3.06 (2s, 6H, NMe₂), 2.18–2.56 (2m, 4H, BH₂, H-2' + H-2''); Fab-MS calculated for [M + H]⁺ = 362.17, found 362.17.

Reaction of *N*²-(Dimethylaminomethylene)-*N*⁷-cyanoborane 2'-Deoxyguanosine (6) with DMT-Cl. Two experiments were carried out with ⁷b_dG and DMT-Cl. In the first, compound **6** (362 mg, 1.0 mmol) was treated with DMT-Cl (678 mg, 2.0 mmol) in pyridine (10 mL) and 4-(dimethylamino)pyridine (8 mg, 0.065 mmol). The resulting solution was kept at RT for 2 h. In the other experiment, compound **6** (362 mg, 1.0 mmol) was treated with DMT-Cl (542 mg, 1.6 mmol) in pyridine (6 mL) in the absence of 4-(dimethylamino)pyridine for 65 h at RT. TLC in CH₂Cl₂/MeOH (95:5 v/v) showed that in both cases an identical complex mixture was formed. The most intense product spot had a lower *R_f*-value than **6**.

***N*²-(Dimethylaminomethylene)-*N*⁷-cyanoborane 3',5'-Bis(*O*-triisopropylsilyl)-2'-deoxyguanosine (5) and *N*¹-Methyl-*N*²-(dimethylaminomethylene)-*N*⁷-cyanoborane 3',5'-Bis(triisopropylsilyl)-2'-deoxyguanosine (7).** To a solution of **4** (576 mg, 1.0 mmol) in DMF (5 mL) was added *N,N*-dimethylformamide dimethylacetal (1.0 mL, 7.5 mmol). The pale yellow solution was stirred with the exclusion of atmospheric moisture at RT for 19 h. TLC in CH₂Cl₂/MeOH (97:3 v/v) showed two product spots (**7**, *R_f* = 0.58; and **5**, *R_f* = 0.26) and the pale spot of the starting material (**4**, *R_f* = 0.11). The solution was evaporated to give a thick, yellow oil. After evaporation, the residue was dissolved in a mixture of CH₂Cl₂/MeOH (97:3 v/v, 3 mL), and the solution was applied onto a silica gel column. The column was eluted with a mixture of CH₂Cl₂/MeOH (97:3 v/v). Appropriate fractions were pooled, evaporated, and dried at 40–50 °C and 1 mmHg for 2 h to give 230 mg of **7**, as a thick oil, and 380 mg of **5** as a white solid. Compound **5**: ¹H NMR (CDCl₃) δ 10.39 (s, 1H, NH), 8.57 (s, 1H, H-8), 8.19 (s, 1H, CH=N), 6.35 (dd, ³*J*_{HH} = 5.7 Hz, 1H, H-1'), 4.66–4.68 (m, 1H, H-3'), 4.13 (m, 1H, H-4'), 3.86–3.87 (m, 2H, H-5' + H-5''), 3.18 and 3.20 (2s, 6H, NMe₂), 2.30–2.80 (m, 4H, BH₂, H-2' + H-2''), 1.02–1.08 (m, 42 H, 6 Me₂-CHSi); Fab-MS calculated for [M + H]⁺ = 674.8; found 674.4. Compound **7**: ¹H NMR (CDCl₃) δ 8.54 (s, 1H, H-8), 8.15 (s, 1H, CH=N), 6.34 (dd, ³*J*_{HH} = 5.7 Hz, H-1'), 4.67–4.69 (m, 1H, H-3'), 4.13 (m, 1H, H-4'), 3.86–3.87 (m, 2H, H-5' + H-5''), 3.59 (s, 3H, MeN), 3.16 and 3.21 (2s, 6H, NMe₂), 2.30–2.90 (m, 4H, BH₂, H-2' + H-2''), 1.02–1.08 (m, 42 H, 6 Me₂-CHSi).

***N*²-Isobutyryl-*N*⁷-cyanoborane 5'-*O*-(Dimethoxytrityl)-2'-deoxyguanosine (9).** A mixture of compound **8** (1.04 g, 1.63 mmol) and triphenylphosphine: cyanoborane (1.96 g, 6.5 mmol) in THF (50 mL) was heated at reflux with the exclusion of atmospheric moisture for 1.5 h. The mixture was evaporated, and the residue was taken in CH₂Cl₂ and purified on silica gel column. Elution of the column with 1.0–1.5% MeOH in CH₂Cl₂ gave 452 mg (41%) of pure **9**, followed by unreacted **8** (335 mg, 34%); Fab-MS calculated for [M + H]⁺ = 678.3, found 678.3. The compound was identical with an authentic sample prepared according to the literature (6).

Reaction of *N*²-Isobutyryl-*N*⁷-cyanoborane 5'-*O*-(Dimethoxytrityl)-2'-deoxyguanosine (9) with 2% Benzenesulfonic Acid in CHCl₃/MeOH (7:3 v/v), THF, or Acetonitrile. Stock solutions of benzenesulfonic acid (2%) were prepared in CHCl₃/MeOH (7:3 v/v) (**I**), THF (**II**), or acetonitrile (**III**). Compound **9** (10 mg) was dissolved in **I**, **II**, or **III** (5 mL of each). The solutions were cooled to 0 °C and treated with the stock 2% benzenesulfonic acid solutions (0.5 mL of each in **I**–**III**).

Table 1. Product Distribution of *N*²-Isobutyryl-*N*⁷-cyanoborane 2'-Deoxyguanosine (10) and *N*²-Isobutyryl-2'-deoxyguanosine (11) Formed in the Reaction of *N*²-Isobutyryl-*N*⁷-cyanoborane 5'-DMT-2'-deoxyguanosine (9) with 2% Benzenesulfonic Acid in Various Solvents at 0 °C after 2 min

acid	solvent	products ^a
2% benzenesulfonic acid	MeOH/CHCl ₃ (3:7)	60% 10 , 40% 11
2% benzenesulfonic acid	THF	65% 10 , 45% 11
2% benzenesulfonic acid	ACN	45% 10 , 55% 11

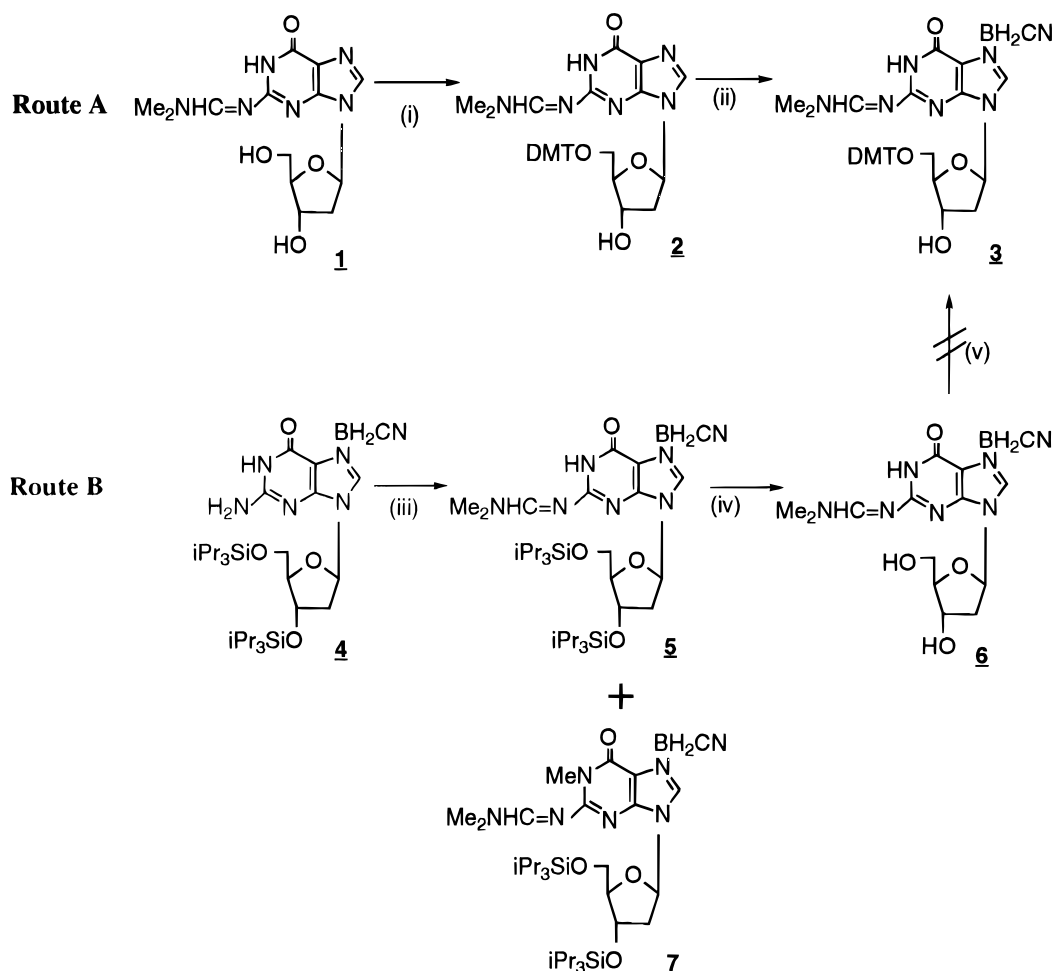
^a The ratio is based on the visualization of TLC spots under UV light. TLC solvent TEA/MeOH/CH₂Cl₂ (2:8:90 v/v/v). dG^{ibu} and dG^{ibu}/BH₂CN were spotted at the same time as the standard for comparison.

After standing for 2 min at 0 °C, the three mixtures were analyzed by TLC in CH₂Cl₂/MeOH/Et₃N (90:8:2 v/v/v). Authentic **10** and **11** were also spotted onto the chromatoplate. Approximate ratios of the products were determined by visual comparison of spot intensities under UV light. Results are summarized in Table 1.

Reaction of *N*²-(Dimethylaminomethylene)-*N*⁷-cyanoborane 5'-*O*-(Dimethoxytrityl)-2'-deoxyguanosine (3) with 0.3 M Dichloroacetic (or Trichloroacetic) Acid in CH₂Cl₂ (13a and 13b). (a) *0.3 M Dichloroacetic Acid.* A solution of 0.3 M dichloroacetic acid in CH₂Cl₂ (2 mL) was added to compound **3** (150 mg). A homogeneous, orange solution was formed immediately. After about 15 s, a precipitate started to deposit from the solution, and the characteristic odor of HCN could be smelled (see eq 1). An aliquot of the mixture was analyzed by TLC, while the bulk of it was applied onto a silica gel column. TLC in CH₂Cl₂/MeOH (9:1 v/v) indicated that a complex mixture including a small amount of **6** was formed. The most intense spot was free of DMT and migrated midway between **3** and **6** on the chromatoplate. The column was eluted by a mixture of CH₂Cl₂/MeOH (95:5 v/v). Three bands emerged by elution with about 1 L of the eluent. The third eluting band, which corresponded to the most intense spot on TLC of the crude mixture, was pooled and evaporated to give 20 mg (18.4%) of **13a**, as an oil, homogeneous by TLC: ¹H NMR (DMSO-*d*₆) δ 11.99 (s, 1H, NH), 9.07 and 9.09 (2s, 1H, H-8), 8.64 (s, 1H, CH=N), 6.598 and 6.602 (2s, 1H, CHCl₂COO), 6.37 (t, ³*J*_{HH} = 6.2 Hz, 1H, H-1'), 5.39 (d, ³*J*_{HH} = 2.6 Hz, 1H, O3'H), 5.12 (d, ³*J*_{HH} = 2.2 Hz, 1H, O5'H), 4.40–4.41 (m, 1H, H-3'), 3.89–3.92 (m, 1H, H-4'), 3.55–3.67 (m, 2H, H-5' + H-5''), 3.06 and 3.20 (2s, 6H, NMe₂), 2.36–2.96 (2m, 3H, BH, H-2' + H-2''); ¹¹B NMR (DMSO-*d*₆) δ -10 to -15 (br); IR (Nujol) ν (cm⁻¹): 2128, 2256 and 2468.

(b) *0.3 M Trichloroacetic Acid.* The reaction was run and the separation was done exactly as described under (a). Observations, including the TLC pattern of the reaction mixture, were quite similar to those obtained for the reaction with dichloroacetic acid. About 15 mg of **13b** was obtained as a TLC homogeneous oil: ¹H NMR (DMSO-*d*₆) δ 12.01 (s, 1H, NH), 9.09 and 9.11 (2s, 1H, H-8), 8.64 (s, 1H, CH=N), 6.38 (t, ³*J*_{HH} = 6.3 Hz, 1H, H-1'), 5.39 (d, ³*J*_{HH} = 4.0 Hz, 1H, O3'H), 5.11 (t, ³*J*_{HH} = 5.1 Hz, 1H, O5'H), 4.40–4.41 (m, 1H, H-3'), 3.89–3.93 (m, 1H, H-4'), 3.41–3.66 (m, 2H, H-5' + H-5''), 3.06 and 3.20 (2s, 6H, NMe₂), 2.36–2.71 (2m, 3H, BH, H-2' + H-2'').

Aliquots of **13b** and **6** (1 mg of each) were dissolved separately in concentrated NH₄OH (0.1 mL for each). The solutions were set aside at RT for 6 h. TLC in CH₂Cl₂/MeOH (8:2 v/v) revealed complete conversion of **13b** to dG and >90% conversion of **6** to ⁷b_dG.

Scheme 1^a

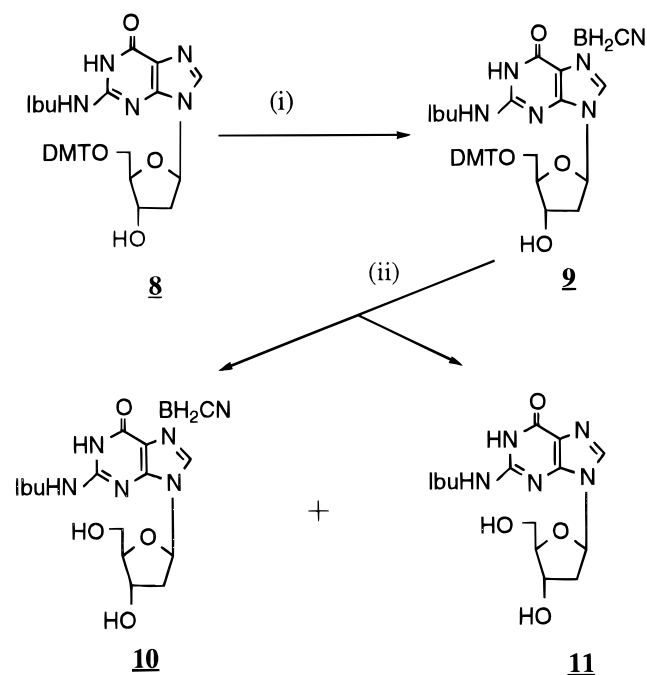
^a (i) DMT-Cl, pyridine, *N,N*-dimethylaminopyridine, RT, 2 h; (ii) $\text{Ph}_3\text{P}:\text{BH}_2\text{CN}$, THF, reflux, 2 h; (iii) $(\text{MeO})_2\text{CHNMe}_2$, MeOH, RT, overnight; (iv) Bu_4NF , THF, RT, 2 h; (v) DMT-Cl, pyridine, *N,N*-dimethylaminopyridine, RT, 2 h, or DMT-Cl, pyridine, RT, 65 h.

RESULTS

We originally intended to use *N*²-(dimethylaminomethylene)-*N*⁷-cyanoborane 5'-*O*-(dimethoxytrityl)-2'-deoxyguanosine (**3**) as a key intermediate for the preparation of oligomers containing ⁷b_dG. Synthesis of **3** was attempted either by cyanoboration of base-protected 5'-DMT-dG (**2**) (Scheme 1, route A) or by dimethoxytritylation of the *N*⁷-boronated 2'-deoxyguanosine derivative (**6**) (Scheme 1, route B). We found that **3** could be obtained only by route A, Scheme 1. Treatment of *N*²-(dimethylaminomethylene)-2'-deoxyguanosine (**1**) (**13**) with DMT-Cl in pyridine (**15**) in the presence of a catalytic amount of *N,N*-dimethylaminopyridine (**16**) gave compound **2**. Compound **2** was converted to **3** by treatment with excess triphenylphosphine:cyanoborane in refluxing THF (**2**). According to route B, treatment of *N*⁷-cyanoborane 3',5'-bis(*O*-triisopropylsilyl)-2'-deoxyguanosine (**4**) (**5**) with *N,N*-dimethylformamide dimethylacetal in MeOH (**17**) gave *N*²-(dimethylaminomethylene)-*N*⁷-cyanoborane 3',5'-bis(*O*-triisopropylsilyl)-2'-deoxyguanosine (**5**). When the reaction was run in DMF (**13**), however, a mixture of **5** and its *N*¹-methyl derivative (**7**) was obtained in an approximate ratio of 3:2. This is consistent with published reports (**17**). Removal of the two silyl groups from **5** to obtain compound **6** was accomplished by Bu_4NF in THF (**18**). Structures of compounds **2**, **3**, and **5–7** were verified by MS and ¹H-NMR spectroscopies (Experimental Procedure). Conversion of **6** to **3**, however, failed. Treatment of **6** with

DMT-Cl in pyridine (**13**, **15**, **16**) gave a complicated mixture of products, including deboronated nucleoside, and not the desired boronated nucleoside **3**.

Treatment of compound **3** under DMT removal/deblock conditions (0.3 M dichloroacetic acid or trichloroacetic acid in CH_2Cl_2 , RT, several minutes) gave the expected product **6** (Scheme 3). Unfortunately, significant decyanoboration also occurred with the concomitant formation of HCN. The major product of the deboronation reaction was sufficiently stable to survive adsorption column chromatography. The NMR and IR spectra of the purified product are consistent with its having a "cyanoborane-acetate" structure (**13a** or **13b**, Scheme 3). The presence of boron in **13a** is confirmed by a broad signal (at -10 to -15 ppm) in its ¹¹B-NMR spectrum. The IR spectrum contains bands at 2468 cm^{-1} (characteristic of B–H stretching) and at 2128 and 2256 cm^{-1} (characteristic of the CN group) (**5**). The ¹H-NMR spectrum of compound **13a** (the CHCl_2COO adduct) has a signal around 6.6 ppm, which we attribute to the dichloromethyl proton. This spectrum also contains overlapping signals between 2.3 and 2.9 ppm, which are due to three protons (B–H, H-2', and H-2''), whereas four protons (B–H₂, H-2', and H-2'') can be found in this region in compound **3**. As a result of the chirality of boron, compound **13a** exists as a pair of diastereoisomers, which display ¹H-NMR resonances at 6.598 and 6.602 ppm for the CHCl_2COO proton and two singlets at 9.07 and 9.09 ppm for H-8. Similarly, compound **13b** has signals at 9.08 and 9.11 ppm for H-8.

Scheme 2^a

^a (i) $\text{Ph}_3\text{P}:\text{BH}_2\text{CN}$, THF, reflux, 1.5 h; (ii) 2% benzenesulfonic acid in $\text{CHCl}_3/\text{MeOH}$ (7:3 v/v) or THF or ACN, 0 °C, 2 min.

The cyanoborane–acetate derivative **13** was quantitatively converted to dG in concentrated NH_4OH at RT within 6 h, with loss of the borane ester. In contrast, the cyanoborane nucleoside **6** was transformed into ^{7b}-dG under identical conditions (no loss of the cyanoborane was detected by TLC).

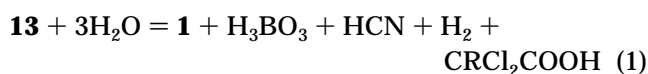
Other reagents for DMT deprotection were also tried. Solutions of 2% benzenesulfonic acid in $\text{CHCl}_3/\text{MeOH}$ (7:3 v/v) or THF or acetonitrile were used instead of 0.3 M dichloroacetic or trichloroacetic acid in CH_2Cl_2 . These reactions were carried out at 0 °C for 2 min, and *N*²-isobutyryl-*N*⁷-cyanoborane 5'-*O*-(dimethoxytrityl)-2'-deoxyguanosine (**9**) was used in place of **3** for these studies. TLC analysis of the reaction mixture revealed the formation of two compounds, *N*²-isobutyryl-*N*⁷-cy-

anoborane 2'-deoxyguanosine (**10**) and *N*²-isobutyryl-2'-deoxyguanosine (**11**) in commensurate quantities. Significant deboronation of the DMT nucleoside derivatives was observed in all three cases (Scheme 2; Table 1).

DISCUSSION

We have found that cyanoborane nucleosides such as **6** react with DMT cations released during DMT deprotection of **3**. This reaction gives products that are analogous to the reaction of amine boranes with halo-carbons to give haloboranes and alkanes and probably proceeds via a similar mechanism (19, 20). The latter reaction is believed to proceed via a transition state involving a reactive carbocation/halide ion pair. The carbocation abstracts hydride anion from the borane moiety, and the halide recombines with the oxidized borane (20). Reaction of the cyanoborane with the DMT cation could be explained by formation of an analogous ion pair intermediate involving a DMT carbonium ion and an acetate **12a** or **12b** (or sulfonate as in Table 1). The DMT cation is liberated from **3** under deblocking conditions and exists as an ion pair with dichloroacetate (**12a**) or trichloroacetate (**12b**) in CH_2Cl_2 solution. The cation probably abstracts a hydride anion from the cyanoborane group, forming dimethoxytritan (**14**), and the coordinatively unsaturated boron intermediate reacts with the dichloroacetate or trichloroacetate to give **13a** or **13b** (Scheme 3). The decomposition of **9** in benzenesulfonic acid solution to give the deboronation product, **11** (Table 1), can be interpreted similarly.

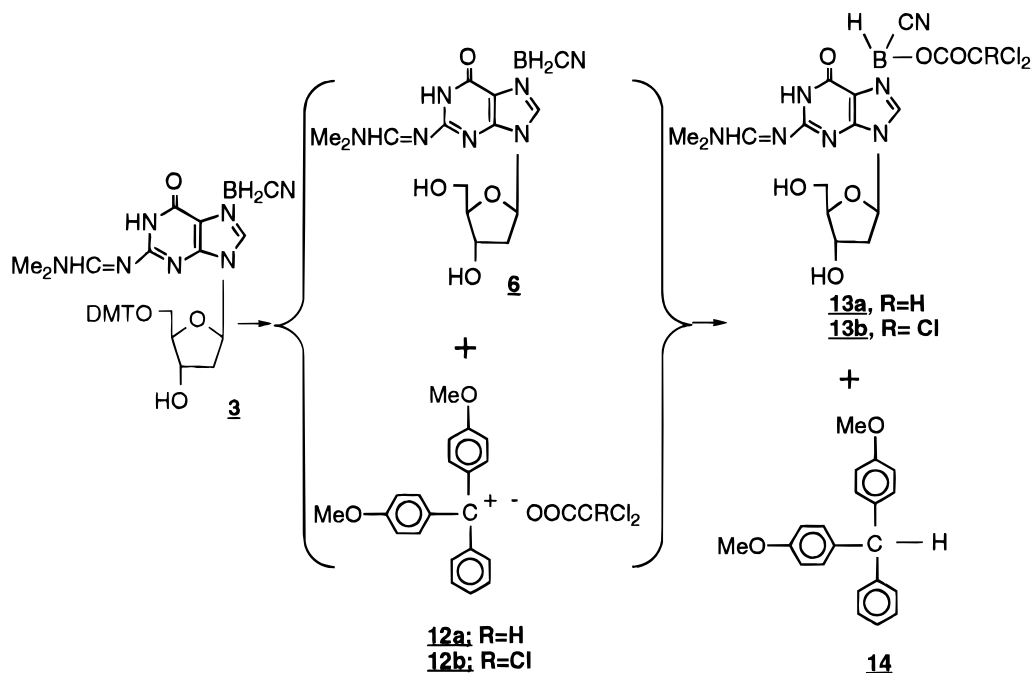
Compounds **13a** and **13b** are sufficiently stable in aprotic solvent to record their NMR spectra, but they decompose in water via intermediates of unknown structure to produce **1**, the deboronation product (eq 1). While



intermediates in the decomposition of **13** might react with more than one equivalent of the DMT cation, we have no evidence to support this theory.

Failure of dimethoxytritylation of **6** probably results from reaction of DMT-Cl with the cyanoborane moiety.

Scheme 3



This reaction leads to unstable products, which ultimately leads to deboronation. The complexity of the mixture, however, makes it impossible to rule out the possibility that additional reactions occur. We conclude that **3** can be synthesized only from **2**, i.e., when dimethoxytritylation precedes cyanoboration.

CONCLUSIONS

Our results clearly indicate the incompatibility of cyanoborane and DMT groups during oligonucleotide synthesis. In the course of investigating the cause of deboronation, we developed an efficient synthesis of the cyanoborated nucleoside **9** starting from *N*²-isobutyryl-5'-*O*-(dimethoxytrityl)-2'-deoxyguanosine (**8**) and triphenylphosphine:cyanoborane. This procedure has an advantage over the prior method (**6**) in that it does not require transient protection of the 3'-OH group (**21**). Since that DMT cation interacts with cyanoborane, it will not be possible to use DMT-derivatized nucleosides for base-boronated oligonucleotide synthesis. To avoid oxidation of cyanoborane by DMT cation, we have synthesized and demonstrated the application of the base-labile 9-fluorenylmethoxycarbonyl (Fmoc) group for transient protection of the 5'-OH function in the solution synthesis of boronated (⁷b_dG) dimer (**1**) and solid phase synthesis of (⁷b_dG)₅dT (**22**).

ACKNOWLEDGMENT

Synthesis of **4** by Tara Richardson (Duke University) and recording of the ¹¹B-NMR and IR spectra by Dr. Anup Sood and of the MS spectra by Dr. George Dubay (Duke University) as well as valuable discussion on several NMR data with Dr. Gy. Dombi (Institute of Pharmaceutical Chemistry, A. Szent-Gyorgyi Medical University, Szeged, Hungary) are gratefully acknowledged. Grant NP-741 (to B.R.S.) from the American Cancer Society is also gratefully acknowledged.

LITERATURE CITED

- (1) For part 1 see: Hasan, A., Li, H., Tomasz, J., and Shaw, B. R. (1996) Base-boronated dinucleotides: synthesis and effect of N⁷-cyanoborane substitution on the base protons. *Nucleic Acids Res.* **24**, 2150–2157.
- (2) Sood, A. H., Spielvogel, B. F., and Shaw, B. R. (1989) Boron-containing nucleic acids: synthesis of cyanoborane adducts of 2'-deoxynucleoside. *J. Am. Chem. Soc.* **111**, 9234–9235.
- (3) Kasai, H., Ohashi, S., Harada, F., Nishimura, S., Oppenheimer, N. J., Crain, P. F., Liehr, J. G., von Minden, D. L., and McCloskey, J. A. (1975) Structure of the modified nucleoside Q isolated from *E. coli* transfer ribonucleic acid. 7-(4,5-*cis*-dihydroxy-1-cyclopenten-3-ylaminomethyl)-7-deazaguanosine. *Biochemistry* **14**, 4197–4208.
- (4) Hall, I. H., Hall, E. S., Chi, L. K., Shaw, B. R., Sood, A., and Spielvogel, B. F. (1992) Antineoplastic activity of boron containing thymidine nucleosides in Tmolt 3 leukemic cells. *Anticancer Res.* **12**, 1091–1098.
- (5) Sood, A., Spielvogel, B. F., Shaw, B. R., Carlton, L. D., Burnham, B. S., and Hall, I. H. (1992) The synthesis and antineoplastic activity of 2'-deoxynucleoside cyanoboranes in murine and human culture cells. *Anticancer Res.* **12**, 335–344.
- (6) Sood, A., Shaw, B. R., Spielvogel, B. F., Hall, E. S., Chi, L. K., and Hall, I. H. (1992) The synthesis and antineoplastic activity of N²-isobutyryl-2'-deoxyguanosine-N⁷-cyanoborane derivatives. *Pharmazie* **47**, 833–838.
- (7) Banks, B. N. (1992) Proton nuclear magnetic resonance studies of boronated nucleosides. Ph.D. Thesis, Duke University.
- (8) Huang, F. (1994) Synthesis and properties of boron-containing nucleic acids. Ph.D. Thesis, Duke University. Huang, F., and Shaw, B. R. (to be published).
- (9) Spielvogel, B. F., Sood, A., Powell, W., Tomasz, J., Porter, K., and Shaw, B. R. (1993) Chemical and enzymatic incorporation of boron into DNA. In *Advances in Neutron Capture Therapy* (A. H. Soloway et al., Eds.) pp 389–393, Plenum Press, New York.
- (10) Porter, K. W., Tomasz, J., Huang, F., Sood, A., and Shaw, B. R. (1995) Cyanoborane-2'-deoxyguanosine 5'-triphosphate is a good substrate for DNA polymerase. *Biochemistry* **34**, 11963–11969.
- (11) Unpublished results.
- (12) Beaucage, S. L., and Iyer, R. D. (1992) Advances in the synthesis of oligonucleotides by the phosphoramidite approach. *Tetrahedron* **48**, 2223–2311.
- (13) Zemlicka, J., and Holy, A. (1967) Preparation of N-dimethylaminomethylene derivatives, a new method of selective substitution of nucleoside amino group. *Collect. Czech. Chem. Commun.* **32**, 3159–3168.
- (14) Das, M. K., and Roy, S. (1985) Convenient and high-yield synthesis of triphenylphosphine-cyanoborane and dihaloboranes. *Synth. React. Inorg. Met.-Org. Chem.* **15**, 53–59.
- (15) Schaller, H., Weiman, G., Lerch, B., and Khorana, H. G. (1963) Studies on polynucleotides. XXIV. The stepwise synthesis of specific deoxyribopolynucleotides (4). Protected derivatives of deoxyribonucleotides and new synthesis of deoxyribonucleosides-3' phosphates. *J. Am. Chem. Soc.* **85**, 3821–3832.
- (16) Chaudhary, S. K., and Hernandez, O. (1979) A simplified procedure for the preparation of triphenylmethylethers. *Tetrahedron Lett.*, 95–98.
- (17) McBride, L. J., Kierzek, R., Beaucage, S. L., and Caruthers, M. H. (1986) Amidine protecting groups for oligonucleotide synthesis. *J. Am. Chem. Soc.* **108**, 2040–2048.
- (18) Corey, E. J., and Venkatesvarlu, A. (1972) Protection of hydroxyl groups as *tert*-butyldimethylsilyl derivatives. *J. Am. Chem. Soc.* **94**, 6190–6191.
- (19) Matsumura, S., and Tokura, N. (1968) Preparation of triethylamine-borane or pyridine-borane in liquid sulfur dioxide and reduction of aralkyl halides with base-borane complex in liquid sulfur dioxide or in nitromethane. *Tetrahedron Lett.*, 4703–4705.
- (20) Ryschkewitsch, G. E., and Miller, V. R. (1973) Polar and free-radical halogenation of amine-boranes with halocarbons. *J. Am. Chem. Soc.* **95**, 2836–2839.
- (21) Studies in our laboratory have proved that transient protection of hydroxyl functionalities during cyanoboration of nucleosides is unnecessary [Tomasz, J., and Shaw, B. R. (manuscript in preparation)].
- (22) Tomasz, J., and Shaw, B. R. Unpublished results.

BC9701205

Biotin Reagents for Antibody Pretargeting. 2. Synthesis and *in Vitro* Evaluation of Biotin Dimers and Trimers for Cross-Linking of Streptavidin

D. Scott Wilbur,* Pradip M. Pathare, Donald K. Hamlin, and S. Ananda Weerawarna

Department of Radiation Oncology, University of Washington, Seattle, Washington 98195. Received April 21, 1997; Revised Manuscript Received July 16, 1997[®]

Polymerization and/or cross-linking of recombinant streptavidin (r-SAv) with biotin derivatives containing two biotin moieties (biotin dimers) or three biotin moieties (biotin trimers) has been investigated as a model for reagents to be used to increase the amount of radioactivity on cancer cells in tumor pretargeting protocols. In the investigation, six biotin dimers and three biotin trimers were synthesized. Most biotin derivatives synthesized had ether containing linker molecules incorporated to improve their aqueous solubility. The synthesized biotin dimers contained linker moieties which provided distances (when fully extended) of 13–49 Å between biotin carboxylate carbon atoms, and the biotin trimers contained linker moieties which provided distances of 31–53 Å between any two biotin carboxylate atoms. All of the biotin derivatives were evaluated for their ability to polymerize r-SAv in solution. When the biotin derivatives were mixed with r-SAv, none of the biotin dimers caused polymerization, but all of the biotin trimers resulted in complete polymerization. Some of the biotin dimers did cross-link r-SAv (to form r-SAv dimers, trimers, etc.), but the percentage of cross-linking was low ($\leq 40\%$). The length of the linker molecule was important in cross-linking of biotin dimers. While linkers which provided distances of 13 and 19 Å between biotin carboxylate carbon atoms did not result in cross-linking, a linker which provided a 17 Å distance resulted in a small ($\leq 10\%$) amount of cross-linking. Also, cross-linking was increased in biotin dimers with linkers which provided distances between biotin carboxylate carbon atoms of ≥ 23 Å. Cross-linking of streptavidin bound in polystyrene wells with biotin dimers and trimers was also examined. In those experiments, an excess of each biotin derivative was incubated at 37 °C for 10–30 min in polystyrene wells containing bound SAv. After the excess biotin derivative was rinsed from the wells, an excess of r-[¹²⁵I]SAv was incubated for another 10–30 min. The amount of r-[¹²⁵I]SAv bound after rinsing the excess from the wells was an indicator of the extent of cross-linking that occurred. The process of alternating additions of reagents was repeated four times to demonstrate that bound radioactivity could be increased with each addition of [¹²⁵I]SAv. The results of cross-linking r-SAv in polystyrene wells paralleled results from cross-linking in solution.

INTRODUCTION

An alternative method to using radiolabeled monoclonal antibodies for cancer diagnosis and therapy, termed "tumor pretargeting", is under investigation by a number of research groups, including our own (1–14). Similar to directly labeled antibodies, pretargeting protocols use monoclonal antibodies as tumor selective binding agents. However, pretargeting protocols involve "two-step" or "three-step" methods to deliver the radioactivity to the cancer cells (3, 14). This multistep approach has an advantage in the fact that the delivery of radioactivity is separated from the pharmacokinetics of the monoclonal antibody (15), making it unnecessary to match the biological half-life of the antibody and the physical half-life of the radionuclide. The antibody pretargeting approach is made possible by the formation of antibody conjugates which bind strongly with another molecule that is used to carry the radionuclide. Because of the very strong binding with biotin (16), antibody conjugates of the proteins avidin (17) and streptavidin (18) have received the most attention in the development of pretargeting methods.

Our interest in the use of biotin/avidin or biotin/streptavidin in pretargeting extends further than the very high binding affinities of these compounds. Avidin (Av)¹ and streptavidin (SAv) are proteins which contain four identical subunits and bind four biotin molecules. The tetravalent biotin binding property of Av and SAv introduces the possibility of increasing the amount of radioactivity localized on cancer cells by increasing the number of (radiolabeled) biotin binding sites available. Indeed, it can be envisioned that an amplification of the number of biotin binding sites can be obtained in a two-step protocol by binding more than one Av or SAv molecule with a poly-biotinylated antibody bound with a cancer cell, or alternatively, an antibody–Av or antibody–SAv conjugate localized at a tumor could potentially bind up to 4 molar equiv of radiolabeled biotin per conjugated Av or SAv (19). In a multistep protocol, an increase in bound radioactivity might be achieved by binding a radiolabeled polybiotin molecule to an antibody–Av or antibody–SAv conjugate on a cancer cell, followed by administration of Av or SAv, and then repeat admin-

* Address correspondence to D. Scott Wilbur, Ph.D., Department of Radiation Oncology, University of Washington, 2121 N. 35th Street, Seattle, WA 98103-9103. Phone: 206-685-3085. Fax: 206-685-9630. E-mail: dswilbur@u.washington.edu.

[®] Abstract published in *Advance ACS Abstracts*, September 1, 1997.

¹ Abbreviations: Av, avidin; BSA, bovine serum albumin; ChT, chloramine-T; cpm, counts per minute; EDC, 1-[3-(dimethylamino)propyl]-3-ethylcarbodiimide hydrochloride; 2 HEDS, 2-hydroxyethyl sulfide; *nca*, no-carrier-added; NCS, *N*-chlorosuccinimide; PBS, phosphate-buffered saline; r-SAv, recombinant streptavidin; rt, room temperature; SAv, streptavidin; TFP, tetrafluorophenyl; TFP-OH, tetrafluorophenol.

istration of the radiolabeled polybiotin molecule (13, 14). The multistep approach appeared to be particularly interesting to us as it introduced the possibility of increasing the quantity of radioactivity on cancer cells in a fractionated dose regime and would, perhaps, allow the use of lower-specific activity radionuclide preparations in therapy.

Although the potential for increasing the amount of radioactivity at the tumor was apparent, it was also apparent that new biotin reagents had to be developed for the cross-linking step as no biotin reagents were available which could be used for this task. Because it was desired that the radiolabeled biotin molecules be excreted via renal clearance, the smallest biotin derivatives possible, biotin dimers and trimers, were of the highest interest. Unfortunately, very little information on the synthesis and properties of compounds containing more than one biotin moiety could be found in the literature. The most relevant studies were those of Green et al. (20), in which it was demonstrated that biotin dimers could be used to polymerize Av. However, the biotin reagents used in their investigation were quite insoluble in water and did not present a means by which radionuclides could be attached. It was apparent that the design of new biotin dimers and trimers for application to human disease would require incorporation of water-solubilizing moieties into the molecules and that the distance between the biotin moieties was very important.

To limit the scope of this investigation, only nonionic compounds containing two or three biotin moieties were synthesized and evaluated for their ability to polymerize recombinant SAV (r-SAV), the protein we have chosen for use in our tumor pretargeting studies (14). The biotin compounds prepared were designed to provide information pertaining to (1) the effect of distances between the biotin moieties on the efficiency of r-SAV polymerization and (2) the use of water-solubilizing linking moieties to improve the water solubility of the new compounds. The biotin compounds prepared in this study did not contain a radiolabeling moiety, as the syntheses of such compounds would be more difficult and the information sought did not require it. In the investigation, six biotin dimers and three biotin trimers were synthesized in which the distances between the biotin moieties ranged from 13 to 54 Å.² Linking moieties which contained two or three ether functionalities were incorporated into most of the molecules to improve their water solubility. Once the molecules were synthesized, the propensity for polymerization of r-SAV by the biotin dimers and trimers was evaluated in solution using size exclusion HPLC and on a SAV-bound surface using commercially available SAV-coated polystyrene wells. Reported here are the results of that investigation.

EXPERIMENTAL PROCEDURES

General. All purchased chemicals were analytical grade or better and were used without further purification. Solvents for HPLC analysis were obtained as HPLC grade and were filtered (0.2 µm) prior to use. Biotin-*d*, 2,2'-(ethylenedioxy)bis(ethylamine) (**2**), 4,7,10-trioxa-1,13-tridecanediamine (**3**), trimelic acid chloride (**9**), 3,5-diaminobenzoic acid (**15**), 2,3,5,6-tetrafluorophenol, 3-aminobutyric acid, chloramine-T, and most other chemicals

were purchased from Aldrich Chemical Co. (Milwaukee, WI). 2,3,5,6-Tetrafluorophenyl trifluoroacetate was prepared as previously described (21). Recombinant streptavidin was obtained as previously described (22). Silica gel chromatography was conducted with 70–230 mesh 60 Å silica gel (Aldrich Chemical Co.). Sephadex G-25 (NAP-10) columns were obtained from Pharmacia Biotech AB (Uppsala, Sweden). Avidin and Reacti-Bind streptavidin-coated polystyrene 96-well plates were obtained from Pierce (Rockford, IL). Melting points were obtained in open capillary tubes on a Mel-Temp II apparatus with a Fluke 51 K/J electronic thermometer and are uncorrected.

Spectral Analyses. ¹H NMR spectra were obtained on a Bruker AC-200 (200 MHz) instrument, and chemical shifts are expressed as parts per million using tetramethylsilane as an internal standard (δ = 0.0 ppm). IR data were obtained on a Perkin-Elmer 1420 infrared spectrophotometer. Mass spectral data (both low- and high-resolution) were obtained on a VG Analytical (Manchester, England) VG-70SEQ mass spectrometer with an associated 11250J Data System. Mass spectral data were obtained by fast atom bombardment (FAB⁺) at 8 keV using a matrix of MeOH/DMIX (thioglycerol/DMSO/TFAA, 90/9/1). Attempts to obtain mass spectral data for compounds **10** and **20** which contain the TFP esters were unsuccessful using several different techniques. The products from reactions involving these compounds had satisfactory HRMS data for identification. ¹H NMR and HPLC were used to assess compound identity and purity (these data are provided in the Supporting Information).

Chromatography. HPLC separations of biotin derivatives were obtained on a Hewlett-Packard quaternary 1050 gradient pumping system with a variable-wavelength UV detector (254 nm) and a Vares ELSD MKIII evaporative light-scattering detector. Analyses of the HPLC data were conducted on Hewlett-Packard HPLC ChemStation software. All reactions were monitored by HPLC. Reverse-phase HPLC was carried out using an Alltech Altima C-18 column (5 µm, 250 mm × 4.6 mm) with a gradient solvent system at a flow rate of 1 mL/min. The gradient mixture was composed of MeOH (solvent A) and 1% aqueous HOAc (solvent B). Starting with 40% MeOH, the initial solvent mixture was held for 2 min, and then the gradient was increased to 100% MeOH over the next 10 min and then held at 100% MeOH for 5 min. Retention times (*t_R*) under these conditions for biotin conjugates were as follows: **1**, 12.9 min; **4**, 7.4 min; **5**, 8.5 min; **6**, 11.6 min; **7**, 7.5 min; **8**, 8.4 min; **10**, 16.6 min; **11**, 2.5 min; **12**, 2.5 min; **13**, 9.2 min; **14**, 10.4 min; **16**, 8.6 min; **17**, 3.8 min; **18**, 9.3 min; **20**, 12.7 min; and **21**, 10.4 min.

HPLC separations of r-SAV and mixtures of r-SAV and biotin derivatives were conducted on a Rainin Dynamax variable-wavelength detector, an isocratic pump, and a Waters Protein Pak Glass 300SW size exclusion column (10 µm, 8.0 × 300 mm; Waters Corp., Milford, MA). The mobile phase consisted of 50 mM potassium phosphate (pH 6.8), 300 mM NaCl, 1 mM EDTA, and 1 mM NaN₃ in deionized water. A flow rate of 0.75 mL/min was used. The retention time of r-SAV under these conditions was 13.7 min. It should be noted that the total peak area for each injection was monitored, and when the area dropped significantly, a 200 µL bolus of 6 N guanidine hydrochloride was injected to clear polymerized SAV from the column. This procedure was particularly important when large excesses of the trimers were being studied.

Estimation of Aqueous Solubility of Biotin Derivatives. The aqueous solubility of biotin compounds was estimated by HPLC. To obtain aqueous concentra-

² Measurements of distances in biotin derivatives were obtained from the computer program ChemDraw3D (Cambridge-Soft Corp., Cambridge, MA) after structural and energy minimization of fully extended, planar conformations of the compounds.

tions, a standard curve for the biotin derivative was first obtained by dissolving a weighed quantity of compound in MeOH, making two dilutions of that solution (to obtain three points), and injecting a 20 μ L volume of the diluted samples to obtain the peak area. Linear regression analysis of the peak areas vs quantity of biotin derivative provided an equation for calculating the concentration in water. The aqueous solubility was measured by adding an excess of biotin derivative to 1 mL of water, mixing occasionally on a vortex mixer while at rt for 10 min, filtering the aqueous solution from the solid present through a 0.45 μ m syringe filter, and injecting 20 μ L of the aqueous solution to obtain the peak area.

Biotin Tetrafluorophenyl Ester (1). This compound was prepared by reaction of biotin with 2,3,5,6-tetrafluorophenyl trifluoroacetate as previously described (14).

3,6-Dioxaoctane-1,8-*N*-dibiotinamide (4). To a solution containing 1.00 g (2.54 mmol) of biotin TFP ester (1) in 150 mL of CH₃CN at 55 °C was added 0.18 g (1.27 mmol) of **2** with stirring. The mixture was cooled to 0 °C, and the precipitate was filtered. Crystallization from CH₃CN gave 0.61 g (1.01 mmol, 40%) of the dibiotin **4** as white crystals: mp 200–203 °C; ¹H NMR (MeOH-*d*₄) δ 4.49 (m, 2H), 4.31 (m, 2H), 3.62 (s, NH, 4H), 3.35 (t, *J* = 5.6 Hz, 4H), 3.35 (m, 4H), 3.31 (m, 4H), 2.93 (dd, *J* = 12.9, 4.9 Hz, 2H), 2.69 (d, *J* = 12.9 Hz, 2H), 2.22 (t, *J* = 7.5 Hz, 4H), 1.63 (m, 8H), 1.44 (m, 4H); IR (KBr, cm⁻¹) 3270, 2920, 2840, 1690, 1640, 1550, 1460, 1320, 1260, 1140; HRMS calcd for C₂₆H₄₅N₆O₆S₂ (M + H)⁺ 601.2842, found 601.2819.

4,7,10-Trioxatridecane-1,13-*N*-dibiotinamide (5). To a solution containing 1.00 g (2.54 mmol) of **1** in 150 mL of CH₃CN at 55 °C was added 0.28 g (1.27 mmol) of **3** with stirring. The mixture was cooled to 0 °C, and the precipitate was filtered. Crystallization from CH₃CN gave 0.65 g (0.96 mmol, 38%) of the dibiotin **5** as white crystals: mp 139–141 °C; ¹H NMR (MeOH-*d*₄) δ 4.48 (m, 2H), 4.30 (m, 2H), 3.64 (m, 4H), 3.62 (m, 4H), 3.54 (t, *J* = 6.2 Hz, 4H), 3.36 (m, 8H), 3.27 (m, 4H), 3.21 (m, 2H), 2.95 (dd, *J* = 12.3, 4.9 Hz, 2H), 2.72 (d, *J* = 12.3 Hz, 2H), 2.21 (t, *J* = 7.2 Hz, 4H), 1.77 (m, 8H), 1.66 (m, 8H), 1.47 (m, 4H); IR (KBr, cm⁻¹) 3270, 2920, 2840, 1690, 1640, 1550, 1460, 1320, 1260, 1140; HRMS calcd for C₃₀H₅₃N₆O₇S₂ (M)⁺ 673.3417, found 673.3397.

3-(Biotinamido)butyrate Tetrafluorophenyl Ester (6). This compound was prepared in three steps as previously described (23). Briefly, reaction of biotin TFP ester with 3-aminobutyric acid and Et₃N in DMF provided the adduct, which was esterified with 2,3,5,6-tetrafluorophenyl trifluoroacetate to provide **6**.

3,6-Dioxaoctane-1,8-*N*-di-(3'-biotinamido)butyrate (7). To a solution containing 0.025 g (0.167 mmol) of **2** in 15 mL of DMF was added Et₃N followed by 0.16 g (0.335 mmol) of **6**. The reaction mixture was stirred at rt for 0.5 h (monitored by HPLC), and the solvent was removed under vacuum. The residue was loaded onto a silica column (2.5 cm \times 35 cm). The column was first eluted with ethyl acetate and then with a mixture of ethyl acetate/methanol. The solvent was removed from eluted fractions containing **7** to give 0.09 g (70%) of colorless solid: mp 186–188 °C; ¹H NMR (MeOH-*d*₄) δ 4.5 (m, 6H), 4.2 (m, 4H), 3.1–3.5 (m, 16H), 2.8 (dd, *J* = 4.6, 12.9 Hz, 2H), 2.6 (d, *J* = 12.6 Hz, 2H), 2.1–2.4 (m, 8H), 1.0–1.5 (m, 20H); IR (KBr, cm⁻¹) 3280, 3060, 2920, 2840, 1695, 1640, 1540, 1260, 1100; HRMS calcd for C₃₄H₅₉N₈O₈S₂ (M + H)⁺ 771.3897, found 771.3894.

4,7,10-Trioxatridecane-1,13-*N*-di-(3'-biotinamido)butyrate (8). To a solution containing 0.1 g (0.45 mmol) of **3** in 15 mL of DMF was added Et₃N followed by 0.43

g (0.9 mmol) of **6**. The reaction mixture was stirred at rt for 0.5 h (monitored by HPLC), and the solvent was removed under vacuum. The product was triturated in 50 mL of CH₃CN and was filtered. The isolated product was dried under vacuum to yield 0.31 g (82%) of **8** as a colorless solid: mp 175–177 °C; ¹H NMR (MeOH-*d*₄) δ 4.4 (m, 2H), 4.2 (m, 4H), 3.4–3.6 (m, 14H), 3.1–3.2 (m, 8H), 2.7–2.9 (m, 3H), 2.6 (d, *J* = 12.6 Hz, 2H), 2.1–2.4 (m, 9H), 1.2–1.6 (m, 18H), 1.0 (d, *J* = 6.6 Hz, 6H); IR (KBr, cm⁻¹) 3280, 3060, 2920, 2840, 1695, 1640, 1540, 1260, 1100; HRMS calcd for C₃₈H₆₇N₈O₉S₂ (M + H)⁺ 843.4472, found 843.4457.

1,3,5-Benzene Tricarboxylic Acid Tris-(2,3,5,6-tetrafluorophenyl) Ester (10). To a solution containing 12.0 g (45.2 mmol) of trimesic acid trichloride (**9**) in 100 mL of CH₂Cl₂ was added 23.26 g (140.1 mmol) of 2,3,5,6-tetrafluorophenol in 150 mL of CH₂Cl₂ and 20 mL (247.2 mmol) of pyridine at 0 °C. The mixture was stirred for 4 h at rt, washed with (2 \times 100 mL) 10% HCl and 3 \times 100 mL of water, dried over anhydrous Na₂SO₄, and evaporated to give 28.0 g (42.8 mmol, 94%) of the triester **15** as a solid. Crystallization from CH₃CN gave a white crystalline solid: mp 156–158 °C; ¹H NMR (CDCl₃) δ 9.31 (s, 3H), 7.10 (m, 3H); IR (KBr, cm⁻¹) 3080, 1760, 1520, 1480, 1270, 1190, 950.

***N*-(8-Amino-3,6-dioxaoctanyl)biotinamide (11).** A 2.80 g (7.13 mmol) quantity of biotin TFP ester (**1**) was dissolved in 300 mL of warm CH₃CN, cooled to rt, and added dropwise over 45 min to a well-stirred solution containing 21.1 g (142 mmol) of diamine **2** in 200 mL of CH₃CN. The reaction mixture was stirred for 4 h, and the solvent was removed under reduced pressure. The resultant oil was triturated in 300 mL of diethyl ether and filtered to give a white solid. The crude product was purified on a silica gel column, eluting with methanol/ethyl acetate (8/2) to give 1.81 g (4.83 mmol) of **11** as a white solid: mp 106–107 °C; ¹H NMR (MeOH-*d*₄) δ 4.50 (m, 1H), 4.31 (m, 1H), 3.62 (m, 4H), 3.52 (m, 4H), 3.36 (m, 2H), 3.2 (m, 1H), 2.92 (dd, *J* = 12.6, 4.9 Hz, 1H), 2.79 (m, 2H), 2.70 (d, *J* = 12.6 Hz, 1H), 2.22 (m, 2H), 1.67 (m, 4H), 1.44 (m, 2H); IR (KBr, cm⁻¹) 3280, 3060, 2920, 2840, 1695, 1640, 1540, 1260, 1100; HRMS calcd for C₁₆H₃₁N₄O₄S (M + H)⁺ 375.2066, found 375.2056.³

***N*-(13-Amino-4,7,10-trioxatridecanyl)biotinamide (12).** This compound was prepared from biotin TFP ester (**1**) and 4,7,10-trioxa-1,13-tridecanediamine (**3**) as previously reported (14).

***N,N,N'*-Tris(8-*N*-biotinamide-3,6-dioxaoctanyl)-benzene-1,3,5-tricarboxamide (13).** To a solution containing 0.15 g (0.21 mmol) of **10** in 5 mL of DMF was added 0.27 g (0.72 mmol) of **11** in 5 mL of DMF at rt. The reaction mixture was stirred at rt for 12 h, and the DMF was removed under vacuum. The solid obtained was purified on silica gel, eluting with methanol/ethyl acetate (7/3). The solvent was removed from eluted fractions containing **13** to give 0.18 g (0.14 mmol, 57%) of a colorless solid: mp 103–105 °C; ¹H NMR (MeOH-*d*₄) δ 8.48 (s, 3H), 4.49 (m, 3H), 4.30 (m, 3H), 3.65 (m, 24H), 3.55 (m, 6H), 3.35 (m, 6H), 3.16 (m, 1H), 2.91 (dd, *J* = 12.8, 4.9 Hz, 3H), 2.69 (d, *J* = 12.9 Hz, 3H), 2.16 (m, 6H), 1.60 (m, 12H), 1.40 (m, 6H); IR (KBr, cm⁻¹) 3280, 3060, 2920, 2840, 1695, 1640, 1540, 1260, 1100; HRMS calcd for C₅₇H₉₁N₁₂O₁₅S₃ (M + H)⁺ 1279.5889, found 1279.5874.

***N,N,N'*-Tris(13-*N*-biotinamide-4,7,10-trioxatridecanyl)benzene-1,3,5-tricarboxamide (14).** Compound **14** was prepared from reaction of 0.31 g (0.70 mmol) of

³ This compound (*N*-biotinyl-1,8-diamino-3,6-dioxaoctane) has been available from Boehringer Mannheim (24).

12 with 0.15 g (0.21 mmol) of **10** according to the procedure used for **13**. After column chromatography, 0.22 g (0.15 mmol, 71%) of **14** was obtained as a colorless solid: mp 106–108 °C; ^1H NMR (MeOH- d_4) δ 8.44 (s, 3H), 4.49 (m, 3H), 4.31 (m, 3H), 3.60 (m, 3H), 3.23 (m, 12H), 2.91 (m, 3H), 2.71 (d, J = 12.7 Hz, 3H), 2.15 (m, 12H), 1.91 (m, 6H), 1.65 (m, 12H), 1.40 (m, 6H); IR (KBr, cm^{-1}) 3280, 3060, 2920, 2840, 1695, 1640, 1540, 1260, 1100; HRMS calcd for $\text{C}_{69}\text{H}_{115}\text{N}_{12}\text{O}_{18}\text{S}_3$ ($M + \text{H}$) $^+$ 1495.7614, found 1495.7638.

***N,N*-Bis(3'-biotinamido)butyryl-3,5-diamidobenzoic acid (16)**. To a solution containing 0.076 g (0.34 mmol) of **15** in 20 mL of DMF was added Et_3N followed by 0.325 g (0.68 mmol) of **6** in 5 mL of DMF. The reaction mixture was stirred at 60 °C for 15 h (monitored by HPLC), and the solvent was removed under vacuum. The solid obtained was purified on silica gel, eluting with methanol/ethyl acetate (8/2). The solvent was removed from eluted fractions containing **16** to give 0.1 g (40%) of a colorless solid: mp 252–254 °C; ^1H NMR (DMSO- d_6) δ 7.9–8.2 (m, 3H), 7.0–7.5 (3s, 1H), 6.6 (d, J = 12 Hz, 3H), 2.8–3.3 (m, 4H), 2.0–2.7 (m, 18H), 1.1–1.9 (m, 19H); IR (KBr, cm^{-1}) 3280, 3060, 2920, 2840, 1695, 1640, 1540, 1260, 1100; HRMS calcd for $\text{C}_{35}\text{H}_{51}\text{N}_8\text{O}_8\text{S}_2$ ($M + \text{H}$) $^+$ 775.3271, found 775.3241.

1-*N*-(13-Amino-4,7,10-trioxatridecanyl)-3'-(biotinamido)butyramide (17). This compound was prepared by reaction of **6** with an excess of the diamine **3** as previously described (23).

***N,N,N'*-Tris(13-*N*-4,7,10-trioxatridecanyl)-3'-[(biotinamido)butyryl]benzene-1,3,5-tricarboxamide (18)**. To a solution containing 0.123 g (0.188 mmol) of **10** in 15 mL of DMF was added Et_3N , followed by 0.3 g (0.565 mmol) of **17**. The reaction mixture was stirred at room temperature for 16 h (monitored by HPLC), and the solvent was removed under vacuum. The residue was loaded onto a silica column (2.5 cm \times 35 cm). The column was first eluted with ethyl acetate and then with a mixture of ethyl acetate/methanol. The solvent was removed from eluted fractions containing **18** to give 0.13 g (40%) of colorless solid: mp 152–154 °C; ^1H NMR (MeOH- d_4) δ 8.4 (s, 3H), 4.5 (m, 3H), 4.1–4.3 (m, 6H), 3.4–3.7 (m, 46H), 3.1–3.3 (m, 16H), 2.9 (dd, J = 4.6, 12.8 Hz, 3H), 2.7 (d, J = 12.6 Hz, 3H), 2.1–2.4 (m, 13H), 1.4–2.0 (m, 33H), 1.0 (d, J = 6.8 Hz, 9H); IR (KBr, cm^{-1}) 3280, 3060, 2920, 2840, 1695, 1640, 1540, 1260, 1100; HRMS calcd for $\text{C}_{81}\text{H}_{136}\text{N}_{15}\text{O}_{21}\text{S}_3$ ($M + \text{H}$) $^+$ 1750.9197, found 1750.9265.

3,6,9-Trioxaundecanedioate Bis-tetrafluorophenyl Ester (20). A 10 g (45 mmol) quantity of 3,6,9-trioxaundecanedioic acid (**19**) was dissolved in 150 mL of anhydrous DMF, and 19 g (115 mmol) of tetrafluorophenol was added, followed by 21 g (108 mmol) of EDC. The reaction mixture was stirred overnight at rt, and the solvent was removed under vacuum. The residue was extracted with 300 mL of ether, and the ether was washed with a saturated NaHCO_3 solution (3 \times 25 mL) and then with water (2 \times 25 mL). The ether solution was dried over anhydrous Na_2SO_4 . Then the ether was removed under vacuum. The resultant product was dried under vacuum at 50–55 °C to yield 15.8 g (76%) of **20** as an oil: ^1H NMR (CDCl_3) δ 3.6–3.8 (m, 8H), 4.46 (s, 4H), 6.9 (m, 2H); IR (neat, cm^{-1}) 1795, 1635, 1520, 1480, 1370, 1270, 1100, 950.

1,11-Bis-*N*-(13-*N*-biotinamide-4,7,10-trioxatridecanyl)-3,6,9-trioxaundecanediamide (21). To a solution of 0.232 g (0.448 mmol) of **20** in 25 mL of DMF was added 0.14 μL of Et_3N , followed by 0.4 g (0.897 mmol) of **12**. The reaction mixture was stirred at rt for 4 h (monitored by HPLC), and the solvent was removed under vacuum.

The residue was loaded onto a silica column (2.5 cm \times 35 cm). The column was first eluted with ethyl acetate and then with a mixture of ethyl acetate/methanol. The solvent was removed from eluted fractions containing **21** to give 0.2 g (42%) of colorless solid: mp 96–98 °C; ^1H NMR (MeOH- d_4) δ 4.8 (s, 4H), 4.5 (m, 2H), 4.3 (m, 2H), 4.0 (s, 4H), 3.4–3.7 (m, 36H), 3.1–3.3 (m, 11H), 2.9 (dd, J = 4.6, 12.8 Hz, 2H), 2.7 (d, J = 12.6 Hz, 2H), 2.2 (t, J = 7 Hz, 4H), 1.3–1.8 (m, 22H); IR (KBr, cm^{-1}) 3280, 3060, 2920, 2840, 1695, 1640, 1540, 1260, 1100; HRMS calcd for $\text{C}_{48}\text{H}_{87}\text{N}_8\text{O}_{15}\text{S}_2$ ($M + \text{H}$) $^+$ 1079.5732, found 1079.5714.

***N*-[13-(*p*-Tri-*n*-butylstannylbenzamido)-4,7,10-trioxatridecanyl]biotinamide (22)**. This compound was synthesized as previously described (23).

***N*-[13-(*p*-Iodobenzamido)-4,7,10-trioxatridecanyl]biotinamide (23a)**. This compound was synthesized as previously described (23).

***N*-[13-(^{125}I -Iodobenzamido)-4,7,10-trioxatridecanyl]biotinamide (23b)**. This compound was prepared as previously described (23). Briefly, to 50 μL of a 1 mg/mL solution of **22** was added 1–5 μL of Na^{125}I in 0.1 N NaOH, followed by 10 μL of a 1 mg/mL solution of NCS in MeOH. After 2 min, 10 μL of a 1 mg/mL aqueous sodium metabisulfite solution was added. The reaction mixture was then drawn into a syringe for purification by HPLC. The purified **23b** was obtained from the HPLC effluent. A small aliquot of **23b** in HPLC effluent was mixed with a weighted amount of **23a** to obtain the specific activity desired.

Radioiodination of Streptavidin. To 25 μL of sodium phosphate buffer (0.5 M, pH 7.4) were added 4 μL (1.19 mCi) of Na^{125}I in 0.1 N NaOH and 167 μL of a 6 mg/mL solution of r-SAv. This was followed by the addition of 19 μL of a 1 mg/mL solution of chloramine-T in water. After 30 s at rt, the reaction was quenched with 1.9 μL of a 10 mg/mL solution of $\text{Na}_2\text{S}_2\text{O}_5$ in water. The entire reaction mixture was placed on a NAP-10 column and eluted with PBS. The fractions containing protein were combined for 1.05 mCi (88%) with a specific activity of 1.07 $\mu\text{Ci}/\mu\text{g}$. A second labeling conducted in the same manner provided 0.45 mCi (79%) ^{125}I -r-SAv with a specific activity of 0.82 $\mu\text{Ci}/\mu\text{g}$. These preparations were used in the binding in coated wells study for experiments 1 and 2, respectively.

Streptavidin Polymerization in Solution. *Procedure A*. A 100 μL aliquot of r-SAv (0.5 mg/mL in PBS) was placed in a microcentrifuge tube. The dimer or trimer was diluted appropriately in 5% DMSO/water. While vortexing, 10 μL of the diluted biotin dimer or trimer was added rapidly. After incubating at rt for 30 min, the entire reaction mixture was injected onto a size exclusion HPLC column and eluted.

Procedure B. This was conducted as was procedure A, except the order of addition was reversed as follows. To a microcentrifuge tube containing 40 μL of PBS was added 10 μL of the appropriately diluted biotin dimer or trimer in 5% DMSO. While vortexing, 100 μL of r-SAv (0.5 mg/mL in PBS) was added slowly.

Streptavidin Cross-Linking Streptavidin-Coated Wells. *Experiment 1*. A Reacti-Bind Streptavidin Coated Polystyrene Strip Plate was washed two times with 100 mM PBS (100 μL /well) prior to use. To lane 1 (12 wells) was added 100 μL of PBS. To lanes 2–7 was added 100 pmol of biotin dimer (**4**, **5**, or **8**) or trimer (**13**, **14**, or **18**) to be tested in 100 μL of PBS. Lane 8 was treated in the same manner with 100 pmol of biotin monomer (**23a**). The plate was then incubated at 37 °C with shaking for 10 min. All the wells were emptied and rinsed with 100 μL of PBS. The PBS was removed, and 25 pmol of ^{125}I -SAv (specific activity of 1 $\mu\text{Ci}/\mu\text{g}$) was added to each well

Table 1. Estimated Distances between Two Biotin Carboxylate Carbon Atoms in the Synthesized Biotin Dimers and Trimers^a

compd no.	distance (Å)	compd no.	distance (Å)
4	13	21	49
16	17	13	31
5	19	14	41
7	23	18	53
8	29		

^a Listed in order of increasing distance.

in 100 μ L of PBS. The plate was incubated at 37 °C with shaking for 10 min. The nonbound [¹²⁵I]SAv was removed, and all wells were washed with 100 μ L of PBS. After removal of the wash PBS, the first three wells of each lane were again filled with 100 μ L of PBS. The remaining wells were filled with 100 μ L of their respective biotin dimer or trimer (as in the first step). The plate was incubated for 10 min at 37 °C, and all wells were rinsed with PBS as before. Another 100 μ L of the [¹²⁵I]-SAv was added to all wells and incubated for 10 min at 37 °C. After removal of the unbound SAv by rinsing of the wells, 100 μ L of PBS was added to the first six wells of each lane. The remaining six wells in each lane were filled with 100 μ L of their respective biotin dimer or trimer and again incubated for 10 min at 37 °C. After removing the liquid in the wells and washing with PBS, 100 μ L of the [¹²⁵I]SAv was again added to each well followed by incubation. The [¹²⁵I]SAv was removed, and the wells were washed with PBS. The first nine wells in each lane were then filled with 100 μ L of PBS, and the remaining three wells in each lane were filled with 100 μ L of their respective biotin dimer or trimer. After incubating and washing, 100 μ L of [¹²⁵I]SAv was again added to each well. After incubating for 10 min at 37 °C, each well was washed with 100 μ L of PBS and all liquid removed. The wells were then separated, and each well was placed in a γ counter and counted. Results of the r-[¹²⁵I]SAv binding data are shown in Figure 5A.

Experiment 2. This experiment was conducted exactly as described in experiment 1, except 100 pmol of biotin dimers (**5**, **8**, **16**, or **21**) and biotin trimers (**13**, **14**, or **18**) was added to wells in lanes 2–8, respectively, and the mixtures were incubated for 30 min at 37 °C. Results of the binding of r-[¹²⁵I]SAv are shown in Figure 5B.

RESULTS

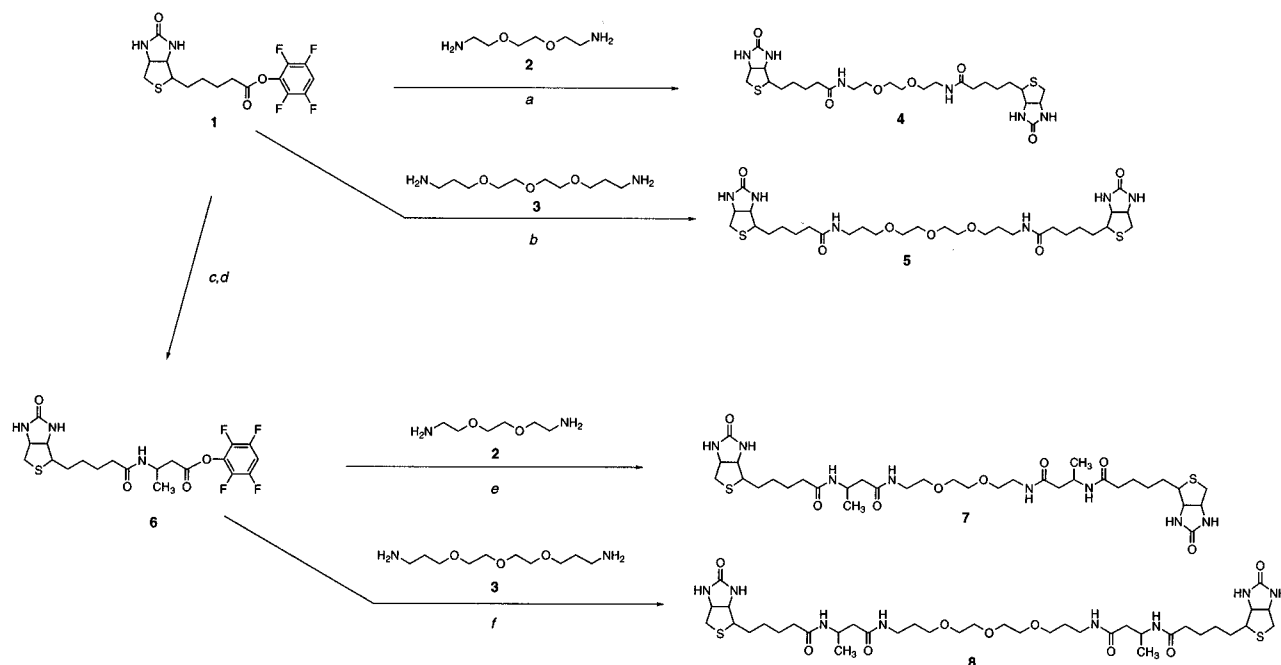
Synthesis of Biotin Derivatives. Six biotin derivatives containing two biotin moieties each (biotin dimers) and three biotin derivatives containing three biotin moieties each (biotin trimers) which have varying distances between biotin carboxylate carbons (Table 1) were synthesized. Biotin dimers **4**, **5**, **7**, and **8** were readily synthesized (Scheme 1) by reaction of 2 molar equiv of biotin TFP ester (**1**) or 3-(biotinamido)butyrate TFP ester (**6**) with 1 molar equiv of the oxadiazines **2** or **3** in DMF. Synthesis of biotin dimer **16** (Scheme 3) was accomplished by reaction of 2 equiv of **6** with 3,5-diaminobenzoic acid (**15**). The coupling of **6** with **15** was conducted under conditions that resulted in a slow reaction, but elevating the reaction temperature to 50 °C resulted in obtaining a reasonable yield of **16**. Synthesis of biotin dimer **21** (Scheme 4) was also readily accomplished by reaction of the cross-linking agent 3,6,9-trioxaundecanedioate bis-tetrafluorophenyl ester (**20**) with *N*-(13-amino-4,7,10-trioxatridecanyl)biotinamide (**12**). Syntheses of biotin trimers **13**, **14** (Scheme 2), and **18** (Scheme 3) were readily accomplished by reaction of 3 molar equiv of *N*-(8-amino-3,6-dioxaoctanyl)biotinamide (**11**), *N*-(13-amino-4,7,10-trioxatridecanyl)biotinamide (**12**), or 1-*N*-(13-

amino-4,7,10-trioxatridecanyl)-3-(biotinamido)-butyramide (**17**) with benzenetricarboxylate tri-TFP ester (**10**) at room temperature in DMF.

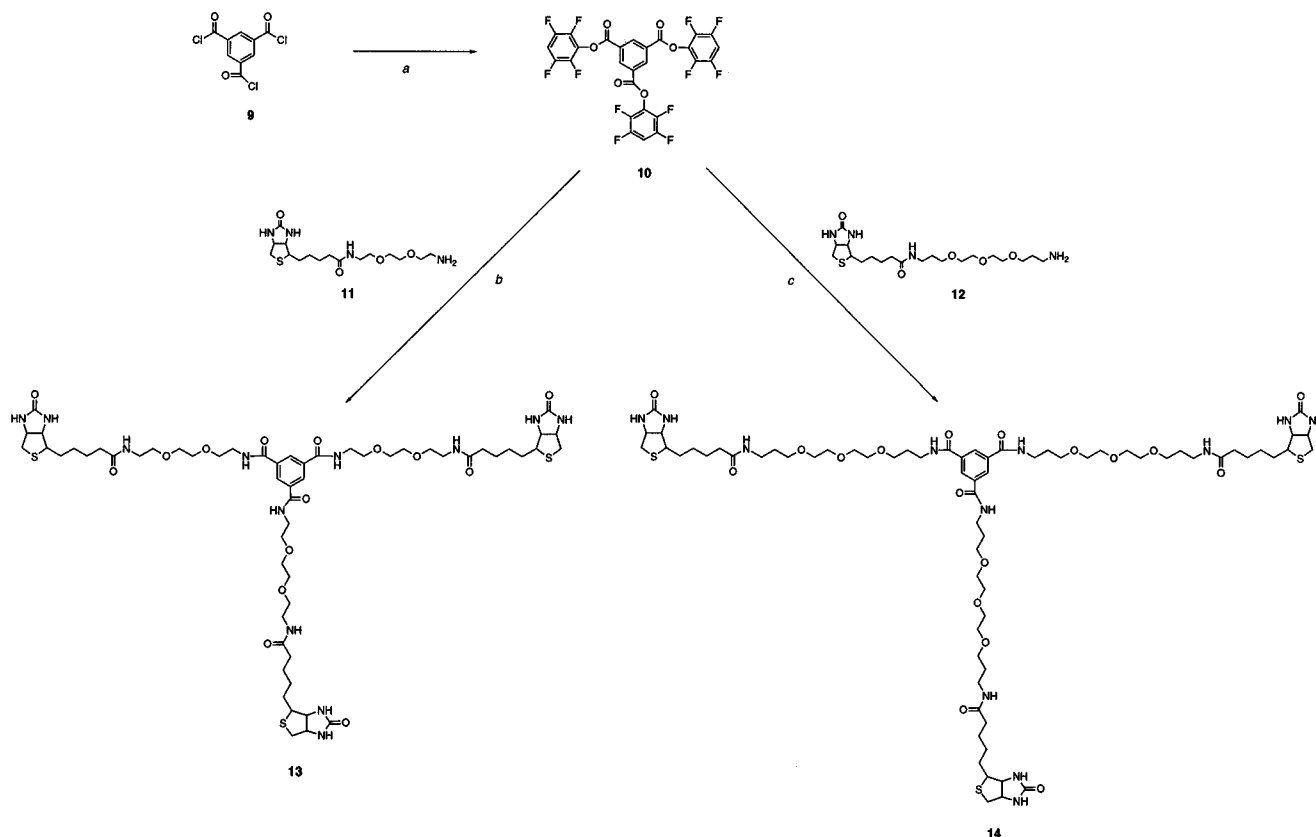
Evaluation of r-SAv Polymerization in Solution. Biotin dimers **4**, **5**, **7**, **8**, **16**, and **21** and biotin trimers **13**, **14**, and **18** were evaluated for their ability to polymerize r-SAv in aqueous solution. To affect polymerization, varying molar quantities of the biotin dimers and trimers were mixed with solutions containing r-SAv in PBS, incubated at rt, and then evaluated by size exclusion HPLC. The chromatograms for mixtures containing 1/1 molar quantities of r-SAv-to-biotin dimer **4**, **5**, **7**, **8**, **16**, or **21** are provided in panels A–F of Figure 1. The chromatograms indicate that only a small percentage of the r-SAv formed what may be r-SAv dimers or trimers, but it is clear that no polymerization occurred.

Contrary to the biotin dimer results, all of the biotin trimers (**13**, **14**, and **18**) dramatically changed the retention time for r-SAv observed by size exclusion chromatography (Figure 2A–C). Indeed, only very high-molecular weight species, eluting at the solvent front, were observed, indicating that complete polymerization had occurred at a 1/1 molar ratio of r-SAv and biotin trimers **13**, **14**, or **18**. Changes in the molar ratio of r-SAv and biotin trimer and in the order of mixing of the components led to very dramatic differences in the product composition as observed for **14** by size exclusion HPLC (Figure 3A–F). Rapid addition of 0.5 molar equiv of the biotin trimer **14** into a solution of r-SAv led to a 1/1 mixture of a high-molecular weight streptavidin polymer and unaltered r-SAv (Figure 3A). Rapid addition of 10 molar equiv of **14** to r-SAv led to a mixture containing approximately 50% polymer, 30% dimer, trimer, tetramer, etc., and 20% r-SAv (Figure 3C). It seems likely that the r-SAv species observed by HPLC (*t_R* = 14 min) was saturated with biotin (i.e. two trimers bound). As one might expect, reversing the additions of reagents by slow addition of 1 equiv of r-SAv to an excess (10 \times) of **14** led to a mixture that had 65% of the (perbiotinylated) r-SAv, and the remaining peaks were higher-molecular weight species, with no polymer observed (Figure 3D). Repeating the foregoing additions with 100 equiv of **14** resulted in a larger shift from polymerization (Figure 3E), with 80% of the (perbiotinylated) r-SAv being observed when the r-SAv was added to the excess **14** (Figure 3F). It was interesting to note that column retention of r-SAv increased slightly as perbiotinylation of r-SAv was achieved (i.e. *t_R* has increased from 13.7 to 14.1 min).

Biotin Cross-Linking of r-SAv with Immobilized SAv. To model cross-linking of SAv on cancer cells, SAv bound to the surface of polystyrene wells was used. Rather than using radiolabeled biotin derivatives, cross-linking was measured by the quantity of [¹²⁵I]SAv retained in the wells after treatment of the bound SAv with biotin derivatives. An initial experiment evaluated triplicate runs having one to four additions of a large excess (100 pmol) of biotin derivatives **4**, **5**, **8**, **13**, **14**, and **18**, alternating with one to four additions of a large excess (25 pmol) of [¹²⁵I]SAv. As controls, triplicate wells were examined in which no biotin was added and in which biotin monomer **23a** was added. In that experiment, the samples were incubated at 37 °C for 10 min after each reagent was added. The picomoles of [¹²⁵I]SAv bound vs additions of biotin derivative and [¹²⁵I]SAv is plotted in Figure 5A. Column 1 of Figure 5A had no biotin added and therefore shows the amount of nonspecific binding occurring. Figure 5A shows that only a very small amount (if any) of cross-linking with [¹²⁵I]SAv was obtained with biotin dimers. Contrary to that, all three biotin trimers provided significant cross-linking under

Scheme 1. Synthesis of Oxadiazine-Linked Biotin Dimers^a

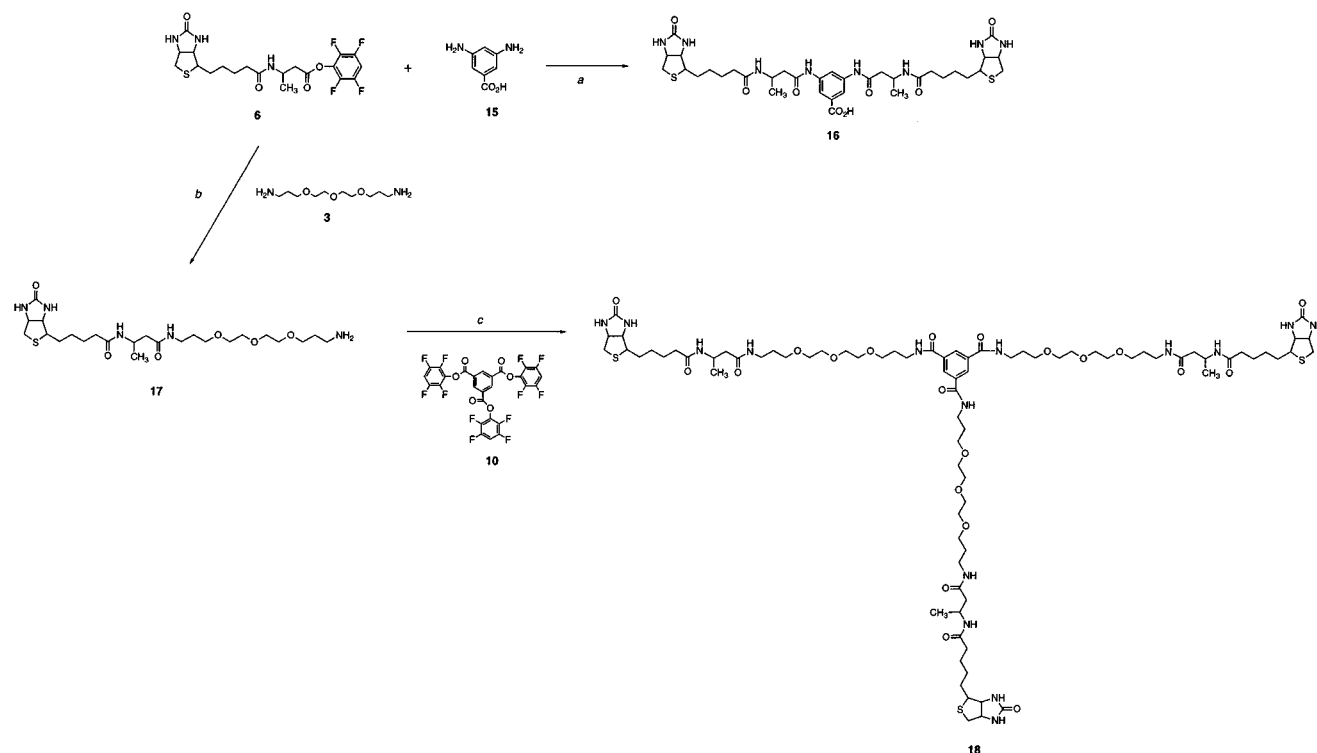
^a (a) **2**, 55 °C, 16–24 h, CH₃CN, 40%; (b) **3**, 55 °C, 16–24 h, CH₃CN, 38%; (c) 3-aminobutyric acid, Et₃N, DMF, 24 h, 98%; (d) Et₃N, TFP-OTFA, 81%; (e) **2**, DMF, rt, 0.5 h, 70%; (f) **3**, DMF, rt, 0.5 h, 82%.

Scheme 2. Synthesis of Oxadiazine-Linked Biotin Trimers^a

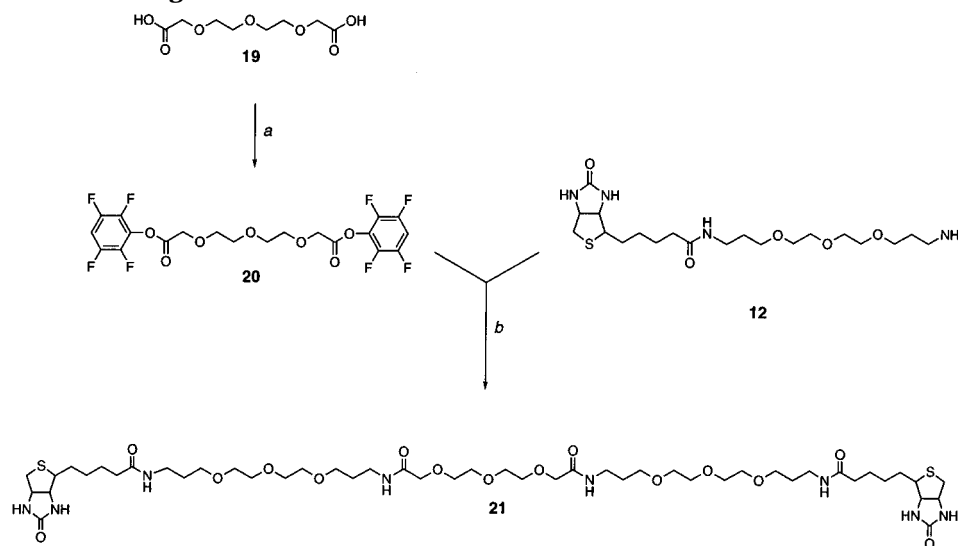
^a (a) **9**, CH₂Cl₂, TFP-OH, pyridine, rt, 4 h, 94%; (b) **11**, DMF, rt, 12 h, 57%; (c) **12**, DMF, rt, 12 h, 71%.

the conditions studied. A second experiment involving [¹²⁵I]SAv binding in SAv-coated wells was conducted with biotin dimers **5**, **8**, **16**, and **21** and biotin trimers **13**, **14**, and **18**. That experiment was conducted to examine cross-linking of dimers **16** and **21**, which had not been evaluated in the first experiment, and to determine if higher quantities of [¹²⁵I]SAv would bind when incubated for 30 min at 37 °C with some of the previously tested

biotin derivatives. The data obtained in that experiment are plotted in Figure 5B. Biotin dimers **16** and **21** did cross-link r-[¹²⁵I]SAv (Figure 5B, first addition), but the amount is quite small and is mostly obscured by a high nonspecific binding of r-[¹²⁵I]SAv brought about by the longer incubation time. More importantly, the picomoles of [¹²⁵I]SAv bound by cross-linking with biotin trimers increased significantly. While optimization of the poly-

Scheme 3. Synthesis of 3-Aminobutyric Acid-Derivatized Biotin Dimer and Trimer^a

^a(a) **15**, DMF, Et₃N, 60 °C, 15 h, 40%; (b) **3**, DMF, Et₃N, rt, 30 min, 90%; (c) **10**, DMF, Et₃N, 40%.

Scheme 4. Synthesis of a Long Oxadiazine Biotin Dimer^a

^a (a) DMF, TFP-OH, EDC, rt, 16–24 h, 76%; (b) **20**, DMF, Et₃N, rt, 4 h, 42%.

styrene well binding assay was not a focus of these studies, it seems likely that the nonspecific binding of [¹²⁵I]SAv could be decreased by including a small amount (i.e. 0.1%) of BSA in the plate washing solution (as is done in antibody-based applications of the Reacti-Bind plates).

The quantities of biotin derivatives and [¹²⁵I]SAv used in the SAV-coated well assay were based on having an excess (i.e. 4×) of the 25 pmol of biotin binding capacity per well that the manufacturer's literature listed. If 25 pmol of biotin could bind, there should be the equivalent of 6.1 pmol of streptavidin in each well. Since binding with a biotin trimer could potentially produce twice the picomoles of bound SAV (assuming two biotins from each trimer bound), then there should be about 12.2 pmol of [¹²⁵I]SAv binding capacity in the wells. In our initial binding experiment (Figure 5A), only about 2.5 pmol of

[¹²⁵I]SAv bound in the first addition, and the quantity per addition decreased with subsequent additions. When the plates were incubated for a longer period of time, the quantity of the first addition doubled to approximately 5.5 pmol of [¹²⁵I]SAv bound, but this was still less than expected. These results were perplexing since a large excess of biotin derivative and [¹²⁵I]SAv had been added in each step. Therefore, some assays were conducted to examine the number of biotin binding sites available per well using a radioiodinated biotin derivative, [¹²⁵I]**23b**. In one assay, 100 pmol of [¹²⁵I]**23b** was added to each of eight SAV coated wells, incubated at 37 °C for 10 min, then rinsed, and counted. The value obtained was 4.16 ± 0.19 pmol of biotin binding/well. Repeat of this assay at 37 °C for 30 min yielded a value of 4.33 ± 0.11 pmol/well, and conducting the assay at rt for 10 min yielded a

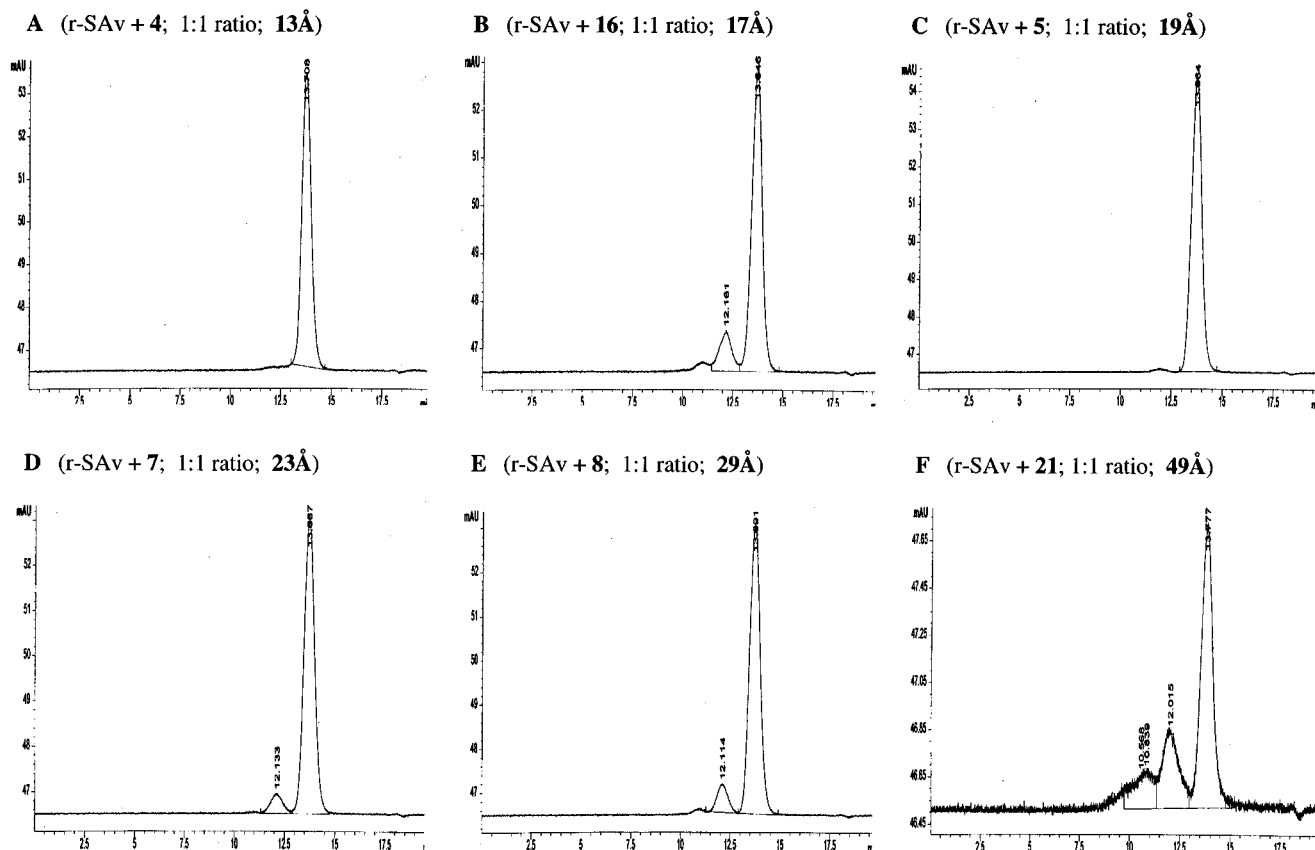


Figure 1. Size exclusion chromatograms of reaction mixtures after mixing r-SAv with biotin dimers **4**, **5**, **7**, **8**, **16**, and **21** at rt for 30 min. The chromatograms are shown in the order (A–F) of the length of the spacer between the biotin carboxylate carbon atoms (distances shown in parentheses). All chromatograms were obtained after addition of 1 molar equiv of the biotin dimer to 50 μ g of r-SAv in 100 μ L of PBS. A chromatogram (not shown) of r-SAv which had not been mixed with a biotin derivative was identical to that seen in panel A. See Chromatography in Experimental Procedures for details of the HPLC equipment and conditions used.

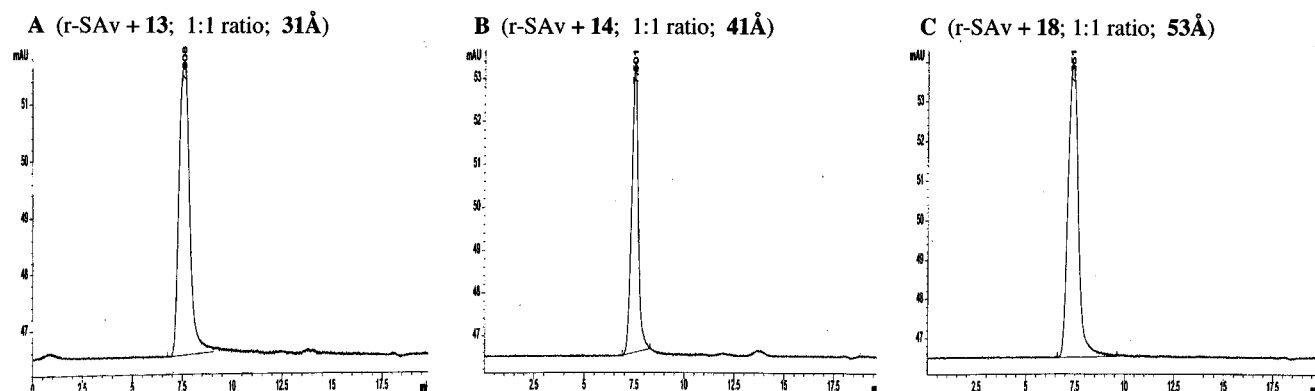


Figure 2. Size exclusion chromatograms of reaction mixtures after mixing r-SAv with biotin trimers **13**, **14**, and **18** at rt for 30 min. The chromatograms are shown in the order (A–C) of the length of the spacer between the biotin carboxylate carbon atoms (distances shown in parentheses). All chromatograms were obtained after addition of 1 molar equiv of the biotin trimer to 50 μ g of r-SAv in 100 μ L of PBS. The retention time (t_R) of monomeric r-SAv under the same HPLC conditions was 13.7 min. See Chromatography in Experimental Procedures for details of the HPLC equipment and conditions used.

value of 4.39 ± 0.16 pmol/well. From this data, a value of 4.2 pmol biotin binding/well was used to assess the results from the cross-linking experiments. Considering that half the amount of biotin trimers can bind as biotin monomers, one might expect 2.1 pmol of r-[125 I]SAv to saturate its binding, which is very close to the amount obtained with an incubation at 37 $^{\circ}$ C for 10 min (Figure 5A). It is difficult to explain the 2 times higher binding observed when the solution is incubated at 37 $^{\circ}$ C for 30 min. However, one explanation might be that an extended incubation period produced higher nonspecific binding of the r-[125 I]SAv and/or biotin derivative and that these residual materials could have resulted in cross-linking in excess of the picomoles of SAV bound. Non-

specific binding of [125 I]SAv is shown in Figure 5B (lane 1, after addition of biotin monomer **23a**). Nonspecific binding of [125 I]**23b** was measured as described above for assessment of picomoles of biotin binding/well, except the biotin binding sites were saturated by incubating the bound SAV with an excess of biotin at rt or at 37 $^{\circ}$ C for 10 or 30 min prior to incubating with [125 I]**23b**. This assay indicated that the amount of nonspecific biotin binding, as assessed with [125 I]**23b**, increased with temperature and time. When the incubation was conducted at rt for 10 min, there was approximately 14% [125 I]**23b** nonspecifically bound; at 37 $^{\circ}$ C for 10 min, 19% [125 I]**23b** was nonspecifically bound, and at 37 $^{\circ}$ C for 30 min, 25% [125 I]**23b** was nonspecifically bound.

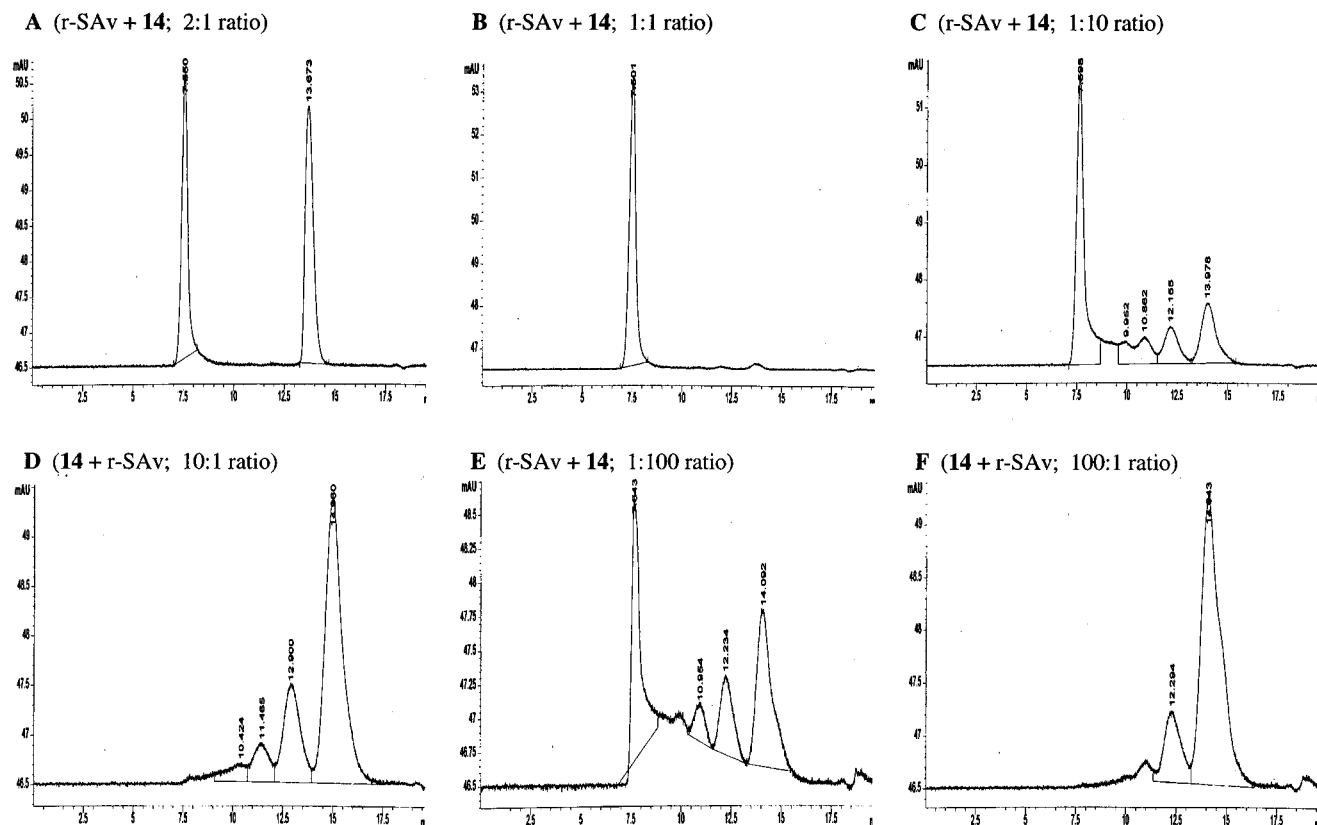


Figure 3. Size exclusion chromatograms of reaction mixtures after mixing r-SAv with varying molar quantities of biotin trimer **14** and reversing the order of addition of reagents. In chromatograms A–C and E, varying quantities of **14** were rapidly added to 50 μg of r-SAv in 100 μL of PBS. In chromatograms D and F, a solution containing 50 μg of r-SAv in 100 μL of PBS was slowly added to a 10 \times or 100 \times molar quantity of **14**. See Chromatography Experimental Procedures for details of the HPLC equipment and conditions used.

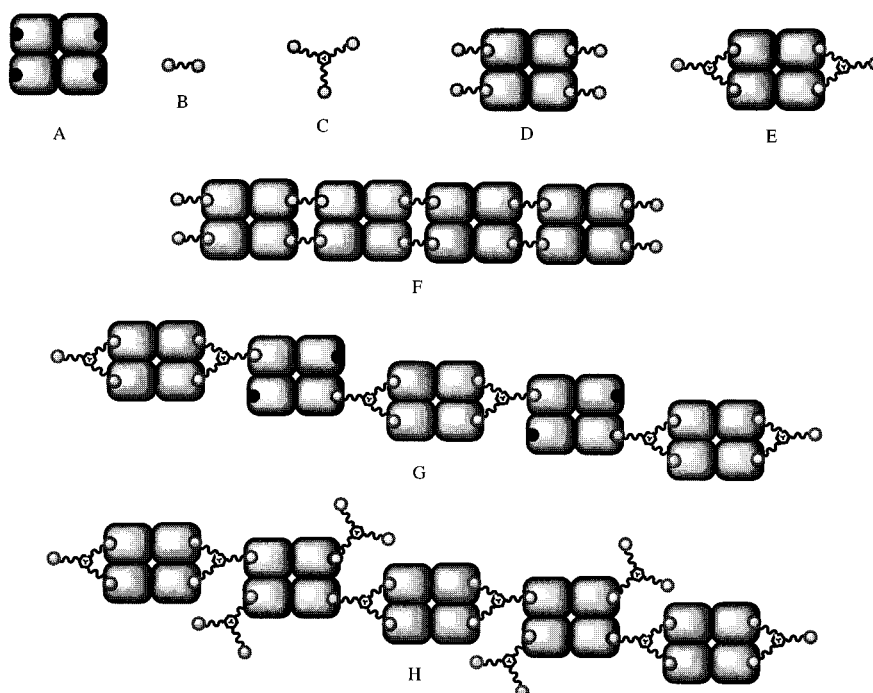


Figure 4. Schematic representations of biotinylated and cross-linked SAv or Av. Schematic A represents Av or SAv with four biotin binding sites (black circles). The representation does not try to show the 222 symmetry of these molecules. Schematic B represents a biotin dimer molecule. Schematic C represents a biotin trimer molecule. Schematic D represents perbiotinylation of Av or SAv with a biotin dimer which is too short to undergo intramolecular binding of the two biotin moieties. Schematic E represents perbiotinylation of Av or SAv with a biotin trimer. Schematic F represents cross-linking or polymerization of Av or SAv with a biotin dimer (having the correct spacing between biotin carboxylate carbons). Schematic G is a representation of cross-linking or polymerization of Av or SAv with 1 molar equiv of a biotin trimer. Schematic H illustrates the potential for branching when an excess of biotin trimer is used for polymerization (it is unclear that this is possible on the basis of molecular modeling).

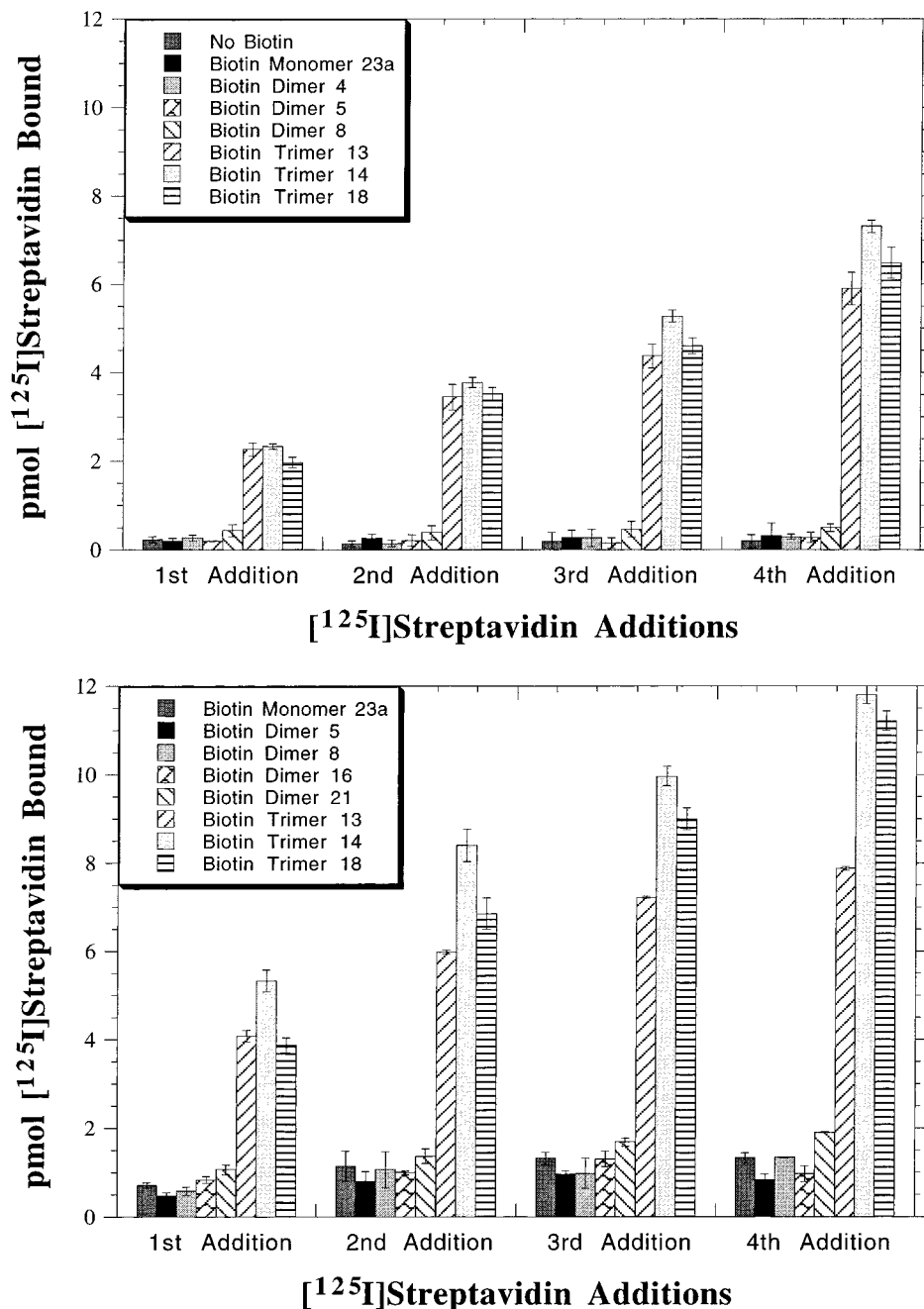


Figure 5. Graph of data obtained for cross-linking of polystyrene-bound SAV and r-[^{125}I]SAV with biotin derivatives at 37 °C for 10 min (top, A) and 30 min (bottom, B). Data were obtained from triplicate runs and are plotted as average \pm standard deviation. The wells had an average ($n = 8$) of 4.2 pmol of biotin binding capacity (as measured by [^{125}I]23b) which equates to 1 pmol of SAV bound. An excess of biotin derivative was added and rinsed with PBS, and then an excess of [^{125}I]SAV was added and rinsed with PBS. This procedure was repeated four times, with the only change being the number of additions of the biotin derivative (i.e. all wells received four additions of [^{125}I]SAV). When one, two, or three additions of biotin derivative were made, 100 μL of PBS was added in the place of the biotin derivative to keep the number of additions and rinses constant. All additions and rinses were made in a volume of 100 μL .

DISCUSSION

The rationale for developing tumor pretargeting methods is based on the fact that directly labeled monoclonal antibodies are limited in their application to cancer therapy due to some inherent problems (15, 25) and that an alternative approach which circumvents some of those problems might have broad application (2). Importantly, the tumor pretargeting approach to cancer therapy has been successfully demonstrated in preclinical studies and is now undergoing clinical evaluation. It should be noted that development of tumor pretargeting methods is more difficult as there are more reagents and more steps involved. However, this increased complexity also offers

the advantage of being able to optimize the reagents and conditions used. Two important factors in the tumor pretargeting approach are the choice of the molecule to be used to carry the radionuclide and the choice of the antibody conjugate that it will bind. We, and other investigators, have chosen to employ the biotin/(strept)-avidin technology (26–28) in tumor pretargeting, as biotin binds streptavidin and avidin with a very high affinity (e.g. 10^{-13} – 10^{-15} M^{-1}), resulting in essentially irreversible binding.

In this investigation, we sought to gain information which would aid in the development of new biotin reagents designed to increase the amount of radionuclide

(attached to a biotin moiety) on cancer cells. We hypothesized that it might be possible to increase the amount of radioactivity bound to cancer cells in antibody pretargeting protocols by utilizing the tetravalent binding nature of r-SAv (or Av). The hypothesis was that a radiolabeled molecule which contained at least two biotin moieties could be administered to bind with antibody-SAv conjugates prelocalized at tumors, leaving some biotin moieties unbound, and subsequent administration of nonlabeled SAv would provide new binding sites for the radiolabeled biotin derivative. Repeat administration of the radiolabeled biotin cross-linking reagent and SAv would again provide more binding sites for radiolabeled biotin, and this process could potentially be repeated many times.⁴ Thus, each administration of radiolabeled biotin dimer or trimer could add radioactivity to the cells pretargeted with antibody. After consideration of the factors involved, it was apparent that investigation of our hypothesis could only be accomplished if the appropriate radiolabeled biotin derivatives were made.

Few investigations involving small molecules containing more than one biotin have been reported.⁵ However, in one particularly relevant investigation, Green et al. described the use of bifunctional biotin derivatives to probe the nature of subunits in Av (20). The bifunctional biotin derivatives evaluated were dimers of biotin or biotinamidobutyric acid produced by reaction of biotin-mixed anhydride with diaminoalkane linkers of various lengths. From their study, it was concluded that (1) the dimensions of Av were $55 \text{ \AA} \times 55 \text{ \AA} \times 41 \text{ \AA}$, (2) the biotin binding site was about 9 \AA below the surface of Av, (3) linkers smaller than 15 \AA did not permit the second biotin molecule to project far enough from the surface of Av to reach a biotin binding site on another Av molecule, (4) linkers of $15\text{--}17.5 \text{ \AA}$ between biotin moieties (carboxylate carbons) resulted in weak binding of the second biotin, and (5) a linker of 18.4 \AA cross-linked Av tightly whereas linkers longer than 20 \AA resulted in intramolecular binding of the second biotin. The linker lengths in biotin dimers reported by Green et al. were used as a guide for designing new biotin dimers.

Although it was apparent from the studies of Green et al. (20) that the biotin dimers had quite a low water solubility, we were not concerned initially about that parameter in the design of new biotin derivatives. However, it became apparent soon after our initial synthetic efforts that biotin dimers which were linked by aliphatic molecules were highly insoluble in many solvents, including water. For example, a biotin dimer synthesized by cross-linking 5-(iodobenzoyl)aminoisophthalate with 1,3-diaminopropane had a water solubility so low that it was barely detectable by HPLC (i.e. $<1 \text{ }\mu\text{g/mL}$). Another biotin dimer, prepared by cross-linking two biotin moieties with 1,12-diaminododecane, had an even lower aqueous solubility. These water solubilities are much lower than biotin's aqueous solubility under the same conditions (e.g. 0.22 mg/mL) (30), presumably due to the fact that the ionization of biotin carboxylate aids in its solubilization. Since the biotin dimers and

trimers were being developed for potential injection into patients, we decided to incorporate water-solubilizing functional groups into their design so that they could be administered in aqueous solutions. Previous studies by our group had shown that ether-containing linkers helped solubilize radiolabeled biotin derivatives (23) and biotinylation reagents (14, 29) for use in aqueous media. Thus, 2,2'-(ethylenedioxy)bis(ethylamine) (2) and 4,7,10-trioxal-1,13-tridecanediamine (3) were used in the design of most biotin derivatives synthesized in the study. The use of the ether-containing linkers greatly improved the aqueous solubility of biotin dimers and trimers over the use of aliphatic linkers. For example, biotin dimer 5, which has a linker length similar to that of the biotin dimer containing diaminododecane (i.e. 19 vs 18 \AA), has an estimated solubility of approximately 9 mg/mL ⁶ at ambient temperature, and biotin trimer 14, which uses the same linker molecule, has a water solubility of approximately 25 mg/mL .⁶

Biotin dimers 4 and 5 were the first water-solubilized biotin derivatives synthesized (Scheme 1) and evaluated for *in vitro* polymerization of r-SAv. On the basis of the previous studies by Green et al. (20), dimer 4, which has a 13 \AA distance between biotin carboxylate carbons, was not expected to polymerize SAv, but dimer 5, which has a 19 \AA linker, was expected to polymerize SAv. However, neither dimer polymerized SAv to any extent (Figure 1A,B). We felt that the length of the linker molecule might be too short; therefore, we prepared dimer 7 in which the distance between carboxylate carbons was 23 \AA . We also prepared biotin dimer 8 to evaluate the effect of an even longer (29 \AA) linker. The biotinamidobutyrate TFP ester (6) was chosen to extend the distance between the biotin carboxylates in 7 and 8 as it had been previously prepared for studies on stability toward biotinidase cleavage (23). Although neither dimer polymerized r-SAv, some cross-linking could be noted as small peaks at higher molecular weight (i.e. 12.1 and 10.6 min).

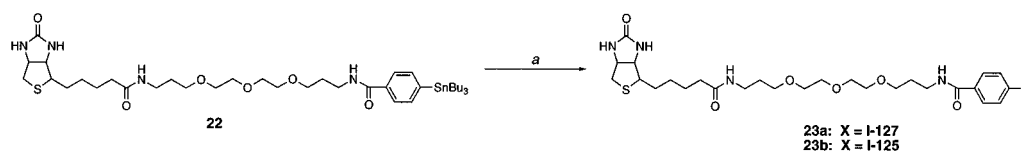
The failure to obtain polymerization of SAv with biotin dimers led to consideration of molecules which contained more than two biotin moieties. Initial consideration was to prepare molecules with four biotin moieties, but it was expected that this would produce linear polymers, limiting the amplification possibilities. However, consideration of molecules with three biotin moieties appeared attractive as one biotin binding site would be left open per cross-linking, and it was thought this might allow branching of the polymeric chain as depicted in Figure 4H. Since it was expected that two of the three biotin moieties in biotin trimers would bind with the same SAv molecule, it seemed that the distance between any two biotins might be >25 but $<55 \text{ \AA}$. Thus, biotin trimers 13 and 14 were synthesized (Scheme 2) and evaluated. Both of these compounds caused immediate polymerization of SAv in solution.

Although biotin trimers 13 and 14 readily polymerized SAv, we still wanted to find a biotin dimer which could polymerize SAv. Our desire to continue to look for biotin dimer was based on the facts that use of biotin trimers resulted in fewer radiolabeled biotin derivatives being bound per SAv molecule as three binding sites would be occupied and in biotin trimers the molecular weights are increased significantly over the dimers, potentially altering the desired renal clearance of biotin molecules to hepatobiliary. This prompted us to evaluate the distances between biotin carboxylates in SAv by molecular

⁴ A schematic representation of this multistep tumor pretargeting approach has been provided in ref 14.

⁵ A biotin dimer used in antibody pretargeting (1), diethylenetriaminepentaacetic acid α,ω -bis(biocytinamide) (DTPA-biotin), is available from Sigma Chemical Co. This biotin dimer has a distance of approximately 32 \AA between the biotin carboxylate carbons when fully extended. It would be expected to undergo intramolecular binding, resulting in both biotin moieties bound to the same SAv molecule (even when the distance between biotin moieties is reduced by metal complex formation).

⁶ The aqueous solubility values must be considered crude estimates as the experiments were not conducted in a rigorous manner.

Scheme 5. Preparation of a Radioiodinated Biotin Monomer^a

^a (a) NCS, NaI, MeOH, 1–5% HOAc.

modeling methods. Molecular modeling of a SAV crystal structure which contains four bound biotin molecules indicated that the biotin carboxylate carbons for biotins on the same face were approximately 20 Å apart and that it is over 60 Å around the molecule to another biotin binding site.⁷ Green et al. (20) reported that the Av molecule appeared to compress 2–3 Å on cross-linking. Although such a compression of Av has not been confirmed, the dynamic nature of the protein is likely to make it possible for the 19.4 Å distance in **5** to be long enough to bind intramolecularly. Therefore, we became interested in synthesizing a biotin dimer which had a distance between biotin carboxylate carbons > 15 but < 19 Å. Synthesis of a biotin dimer with a linker arm between 15 and 19 Å in length could not be readily achieved with an ether-containing linker. However, biotin dimer **16** which contained a carboxylate to aid in water solubilization was obtained by cross-linking **6** with 3,5-diaminobenzoic acid (Scheme 3). In **16**, the biotin carboxylate carbons are approximately 17 Å apart. Examination of a mixture of r-SAv and **16** in solution indicated that a higher percentage of cross-linking⁸ was obtained with it than was obtained with the longer biotin dimer **5**, or the shorter biotin dimer **4**. However, the amount of cross-linking obtained was only about 10%, and no polymerization was noted (Figure 1E). Although there was little optimism for finding a biotin dimer that efficiently cross-linked r-SAv, it had been noted that the increasing length of biotin dimers **7** and **8** had shown a trend toward an increased percentage of cross-linking r-SAv (Figure 1C,D). Therefore, an additional biotin dimer, **21**, which had a much longer linker distance (49 Å) was prepared (Scheme 4) and evaluated. The percentage of r-SAv cross-linked⁸ with **21** was found to be higher (40%), but no polymer was obtained. It seems that it will be difficult, if not impossible, to develop biotin dimers that have a long enough spacer to allow intermolecular binding of the second biotin moiety with another SAV molecule without also being long enough to permit the more facile intramolecular binding of the second biotin with the same SAV molecule. On the basis of the results obtained, we must conclude that biotin dimers will not be useful for rapid, facile polymerization of SAV and, thus, that further studies with biotin dimers for application to *in vivo* tumor targeting are not warranted.

A desire to examine the effect of an increased linker length on cross-linking led to the synthesis of a third

biotin trimer, **18** (Scheme 3). This trimer was prepared to evaluate the effect on r-SAv polymerization with a distance between two biotin moieties of approximately 53 Å. This molecule was of interest as the biotin moieties were separated by a distance that seemed unlikely to result in all three biotin moieties binding with the same r-SAV molecule. Indeed, when a solution with a 1/1 ratio of **18**/r-SAV was mixed, only polymerization was observed (Figure 2C). This result indicates that the third (unbound) biotin moiety is not capable of binding on the opposite face of the same r-SAV molecule as our modeling predicted. However, the extra length did not appear to increase cross-linking of r-[¹²⁵I]SAV with polymer-bound SAV in wells as the percentages bound (Figure 5) were generally less than those observed for the biotin trimer **14**.

Evaluation of the polymerization of SAV in solution was an important step to undertake as it clearly showed the effects of distances between biotin carboxylate carbons, dilution, and varying quantities of biotin compounds on the polymerization process. However, we felt that a better *in vitro* model for the application of the biotin dimers and trimers *in vivo* would be one that would demonstrate an increase in the amount of radioactivity localized to a surface containing bound SAV. The model chosen was SAV-coated polystyrene plates. In that system, the various biotin dimers and trimers (added in excess) could saturate the biotin binding sites, and then [¹²⁵I]SAV could be added to cross-link with available biotin moieties, resulting in a new layer of biotin binding sites. Indeed, SAV-bound wells were a good model as the cross-linking results correlated with the results obtained in solution, and it was easy to detect an increase of the amount of radioactivity bound with each cycle of reagents. The magnitude of increase was less than expected after an incubation for 10 min at 37 °C on the basis of the manufacturer's cited 25 pmol/well biotin binding capacity. However, after a biotin binding capacity of approximately 4.2 pmol/well was measured, the data obtained indicate that at least 1 equiv of r-[¹²⁵I]SAV was added in the first cross-linking step. Although less r-[¹²⁵I]SAV was added in each subsequent addition, the quantity that was added was significant. Assessing the results of the binding to SAV in polystyrene wells was complicated by issues of nonspecific binding of reagents. As our goal was simply to demonstrate that cross-linking can be achieved, optimization of the conditions to decrease the nonspecific binding has not been done. It is clear that increasing the incubation time to 30 min increased the percentage of biotin derivative and r-[¹²⁵I]SAV bound nonspecifically. Further, no difference in biotin binding was noted when the wells were incubated at room temperature or at 37 °C. Therefore, it seems likely that the nonspecific binding could be decreased by conducting the incubations at room temperature. Irrespective of the issues of absolute quantities bound and nonspecific binding, the fact that an increase of radioactivity bound was obtained in each step is very encouraging for continued studies toward *in vivo* application. To our knowledge, this is the first demonstration of a biotin-

⁷ This estimation was made by adding distances between atoms on the surface of the streptavidin molecule from a biotin carboxylate on one face to that of another biotin on the opposite face. Molecular modeling was conducted on a Silicon Graphics, IRIS INDIGO computer running Insight II software (version 2.3.7).

⁸ The percentage of cross-linking refers to the area under peaks eluting between 8 and 12.5 min, presumably the SAV dimer and trimer, relative to the total peak area included in those peaks plus the monomeric SAV peak ($t_R = 13.7$ min) on size exclusion HPLC chromatograms (see Figure 1). The percentage of polymerization found refers to the percentage of very high-molecular weight species eluting with the exclusion volume at 7.6 min.

containing small molecule being able to increase the amount of SAV bound to a surface.

We undertook this study to gain information on the design of biotin derivatives that could be used with r-SAV to increase the amount of radioactivity bound to cancer cells in tumor pretargeting protocols. Although the radioactivity will be delivered to the cancer cells as a radiolabeled biotin derivative, the compounds in this study were not designed with iodine-containing moieties attached as it was felt that those compounds would be more difficult to synthesize, and likely be less water soluble than those investigated. Now that we have gained the information sought, studies are planned to prepare a radiolabeled biotin trimer and evaluate its *in vitro* and *in vivo* cross-linking with r-SAV. As shown in this study, the distance between biotin moieties is very important, but other molecular design features such as inclusion of functional groups to block the amide-cleaving action of serum biotinidase are also critical (23). Additional modifications such as preparing water-solubilized biotin derivatives that contain ionic charged functional groups are planned.

Summary. Six molecules containing two biotin moieties (biotin dimers **4**, **5**, **7**, **8**, **16**, and **21**) and three molecules containing three biotin moieties (biotin trimers **13**, **14**, and **18**) were synthesized and characterized. Investigation of the polymerization or cross-linking of r-SAV in solution and bonding to a solid support was carried out on each biotin derivative prepared. None of the biotin dimers polymerized r-SAV in solution, but some cross-linking to form small adducts (e.g. dimers, trimers, etc.) was noted with biotin dimers having linking moieties of 17 and ≥ 23 Å. Contrary to this, the three biotin trimers synthesized completely polymerized r-SAV in solution when a 1/1 molar ratio of reagents was used. Similar results were obtained in the surface-bound SAV cross-linking experiments as had been observed for polymerization of SAV in solution. On the basis of the results obtained in this study, it seems unlikely that biotin dimers will be found which effectively cross-link SAV, but biotin trimers should be useful for both *in vitro* and *in vivo* applications which require cross-linking of SAV or Av.

ACKNOWLEDGMENT

We thank Dr. Ross Lawrence (Medicinal Chemistry Department, University of Washington) for efforts in obtaining mass spectral data. We thank Dr. Patrick Stayton and Dr. Lisa Klumb for providing r-SAV used in the studies and for their helpful comments on the manuscript. We are grateful for the generous financial support provided by the Department of Energy, Medical Applications and Biophysical Research Division, Office of Health and Environmental Research under Grant DE-FG06-95ER62029.

Supporting Information Available: HPLC chromatograms of compounds **1**, **4–8**, **10–14**, **17**, **18**, **20**, and **21** and ^1H NMR spectra of the new compounds prepared in the research described in this paper (20 pages). Ordering information is given on any current masthead page.

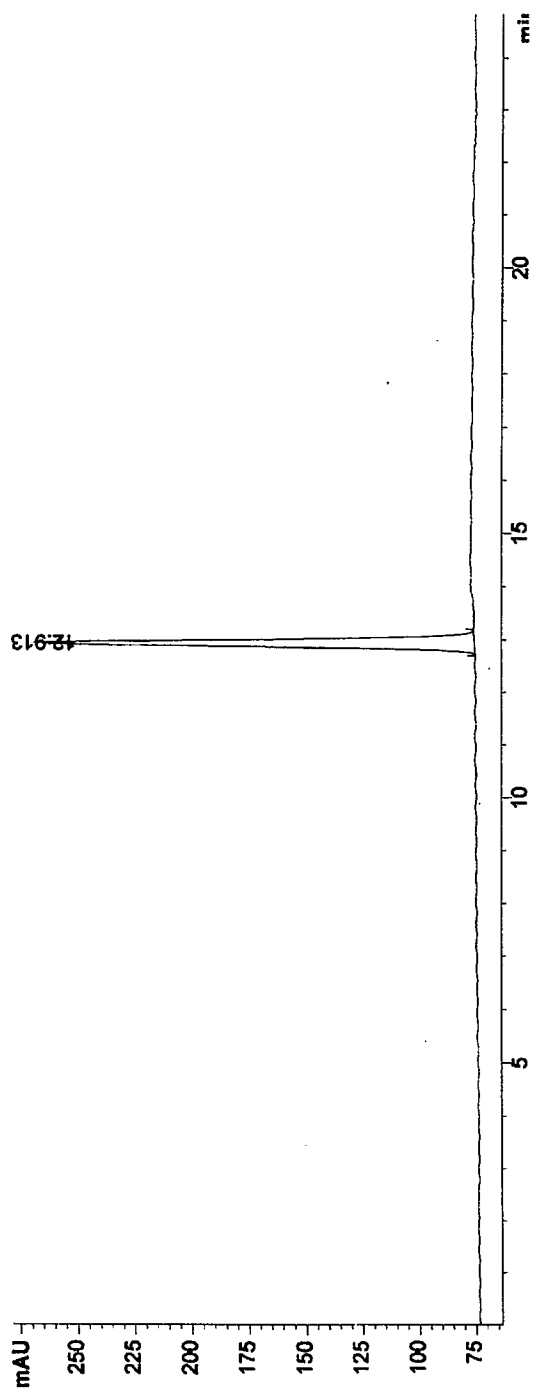
LITERATURE CITED

- (1) Hnatowich, D. J., Virzi, F., and Rusckowski, M. (1987) Investigations of Avidin and Biotin for Imaging Applications. *J. Nucl. Med.* **28**, 1294–1302.
- (2) Goodwin, D. A. (1995) Tumor Pretargeting: Almost the Bottom Line. *J. Nucl. Med.* **36**, 876–879.
- (3) Paganelli, G., Malcovati, M., and Fazio, F. (1991) Monoclonal antibody pretargeting techniques for tumor localization: the avidin-biotin system. *Nucl. Med. Commun.* **12**, 211–234.
- (4) Axworthy, D. B., Fritzberg, A. R., Hylarides, M. D., Mallett, R. W., Theodore, L. J., Gustavson, L. M., Su, F., Beaumier, P. L., and Reno, J. M. (1994) Preclinical Evaluation of an Anti-tumor Monoclonal Antibody/Streptavidin Conjugate For Pretargeted ^{90}Y Radioimmunotherapy in a Mouse Xenograft Model. *J. Immunother.* **16**, 158.
- (5) del Rosario, R. B., and Wahl, R. L. (1993) Biotinylated Iodo-Polylysine for Pretargeted Radiation Delivery. *J. Nucl. Med.* **34**, 1147–1151.
- (6) Jeong, J. M., Kinuya, S., Paik, C. H., Saga, T., Sood, V. K., Carrasquillo, J. A., Neumann, R. D., and Reynolds, J. C. (1994) Application of High Affinity Binding Concept to Radiolabel Avidin with Tc-99m Labeled Biotin and the Effect of pI on Biodistribution. *Nucl. Med. Biol.* **21**, 935–940.
- (7) Oehr, P., Westermann, J., and Biersack, H. J. (1988) Streptavidin and Biotin as Potential Tumor Imaging Agents. *J. Nucl. Med.* **29**, 728–729.
- (8) Pimm, M. V., Fells, H. F., Perkins, A. C., and Baldwin, R. W. (1988) Iodine-131 and indium-111 labelled avidin and streptavidin for pre-targeted immunoscintigraphy with biotinylated anti-tumour monoclonal antibody. *Nucl. Med. Commun.* **9**, 931–941.
- (9) Hashmi, M., and Rosebrough, S. F. (1995) Synthesis, Pharmacokinetics, and Biodistribution of ^{67}Ga Deferoxamineacetyl-Cysteinylbiotin. *Drug Metabol. Dispos.* **23**, 1362–1367.
- (10) Shoup, T. M., Fischman, A. J., Jaywook, S., Babich, J. W., Strauss, H. W., and Elmaleh, D. R. (1994) Synthesis of Fluorine-18-Labeled Biotin Derivatives: Biodistribution and Infection Localization. *J. Nucl. Med.* **35**, 1685–1690.
- (11) Yao, Z., Zhang, M., Kobayashi, H., Sakahara, H., Nakada, H., Yamashina, I., and Konishi, J. (1995) Improved Targeting of Radiolabeled Streptavidin in Tumors Pretargeted with Biotinylated Monoclonal Antibodies through an Avidin Chase. *J. Nucl. Med.* **36**, 837–841.
- (12) Khawli, L. A., Alauddin, M. M., Miller, G. K., and Epstein, A. L. (1993) Improved Immunotargeting of Tumors with Biotinylated Monoclonal Antibodies and Radiolabeled Streptavidin. *Antibody, Immunoconjugates, Radiopharm.* **6**, 13–27.
- (13) Kassis, A. I., Jones, P. L., Matalka, K. Z., and Adelstein, S. J. (1996) Antibody-Dependent Signal Amplification in Tumor Xenografts after Pretreatment with Biotinylated Monoclonal Antibody and Avidin or Streptavidin. *J. Nucl. Med.* **37**, 343–352.
- (14) Wilbur, D. S., Hamlin, D. K., Vessella, R. L., Stray, J. E., Buhler, K. R., Stayton, P. S., Klumb, L. A., Pathare, P. M., and Weerawarna, S. A. (1996) Antibody Fragments in Tumor Pretargeting. Evaluation of Biotinylated Fab' Colocalization with Recombinant Streptavidin and Avidin. *Bioconjugate Chem.* **7**, 689–702.
- (15) Fritzberg, A. R., Beaumier, P. L., Bottino, B. J., and Reno, J. M. (1994) Approaches to improved antibody- and peptide-mediated targeting for imaging and therapy of cancer. *J. Controlled Release* **28**, 167–173.
- (16) Green, N. M. (1963) Avidin. 3. The Nature of the Biotin-Binding Site. *Biochem. J.* **89**, 599–609.
- (17) Green, N. M. (1975) Avidin. *Adv. Protein Chem.* **29**, 85–133.
- (18) Green, N. M. (1990) Avidin and Streptavidin. *Methods Enzymol.* **184**, 51–67.
- (19) Paganelli, G., Riva, P., Deleide, G., Clivio, A., Chiolerio, F., Scassellati, G. A., Malcovati, M., and Siccardi, A. G. (1988) In Vivo Labelling of Biotinylated Monoclonal Antibodies by Radioactive Avidin: A Strategy to Increase Tumor Radiolocalization. *Int. J. Cancer* **2**, 121–125.
- (20) Green, N. M., Konieczny, L., Toms, E. J., and Valentine, R. C. (1971) The Use of Bifunctional Biotinyl Compounds to Determine the Arrangement of Subunits in Avidin. *Biochem. J.* **125**, 781–791.
- (21) Gamper, H. B., Reed, M. W., Cox, T., Viroso, J. S., Adams, A. D., Gall, A. A., Scholler, J. K., and Meyer, R. B. (1993) Facile preparation of nuclease resistant 3' modified oligodeoxynucleotides. *Nucleic Acids Res.* **21**, 145–150.

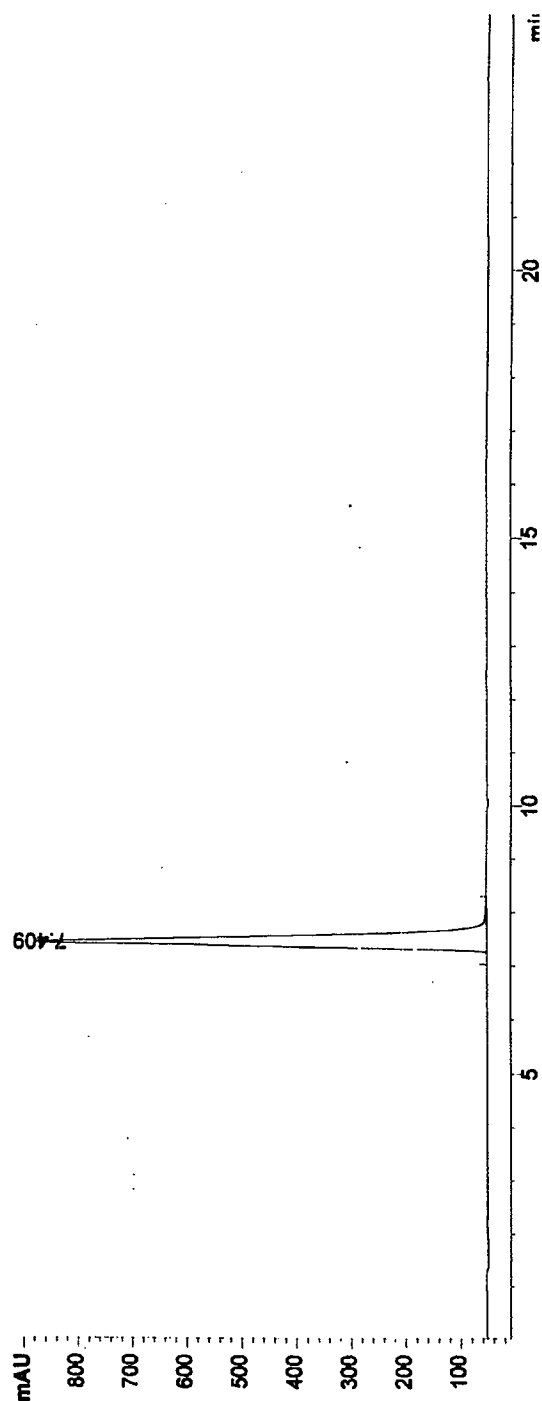
- (22) Chilkoti, A., Tan, P. H., and Stayton P. S. (1995) Site Directed Mutagenesis Studies of the High-Affinity Streptavidin-Biotin Complex: Contributions of Tryptophan Residues 79, 108 and 120. *Proc. Natl. Acad. Sci. U.S.A.* 92, 1754–1758.
- (23) Wilbur, D. S., Hamlin, D. K., Pathare, P. M., and Weerawarna, S. A. (1997) Synthesis, Radioiodination and *In Vitro* Evaluation of Water Soluble, Biotinidase Resistant Biotin Derivatives. *Bioconjugate Chem.* 8, 572–584.
- (24) Dressendorfer, R. A., Heim, J.-M., Gerzer, R., and Strasburger, C. J. (1995) A Non-Isotopic Immunoassay for Guanosine 3',5'-Cyclic Monophosphate Using a Cyclic GMP-Biotin Conjugate as Tracer. *J. Immunoassay* 16, 37–53.
- (25) Buchsbaum, D. J. (1995) Experimental Approaches to Increase Radiolabeled Antibody Localization in Tumors. *Cancer Res.* 55, 5729s–5732s.
- (26) Wilchek, M., and Bayer, E. A. (1990) Introduction to Avidin-Biotin Technology. *Methods Enzymol.* 184, 5–45.
- (27) Diamandis, E. P., and Christopoulos, T. K. (1991) The Biotin-(Strept)Avidin System: Principles and Applications in Biotechnology. *Clin. Chem.* 37, 625–636.
- (28) Wilchek, M., and Bayer, E. A. (1988) The Avidin-Biotin Complex in Bioanalytical Applications. *Anal. Biochem.* 171, 1–32.
- (29) Wilbur, D. S., Hamlin, D. K., Pathare, P. M., Vessella, R. L., Buhler, K. R., Stray, J. E., Stayton, P. S., and Klumb, L. A. (1996) Evaluation of the Effect of Serum Biotin and a Water Soluble, Biotinidase Stabilized, Biotinylation Reagent on the Co-Localization of Fab' and Streptavidin in Tumor Xenografts. *Tumor Targeting* 2, 158.
- (30) Budavari, S., O'Neil, M. J., and Smith, A., Eds. (1989) *The Merck Index*, Merck & Co., Inc., Rahway, NJ.

BC970053E

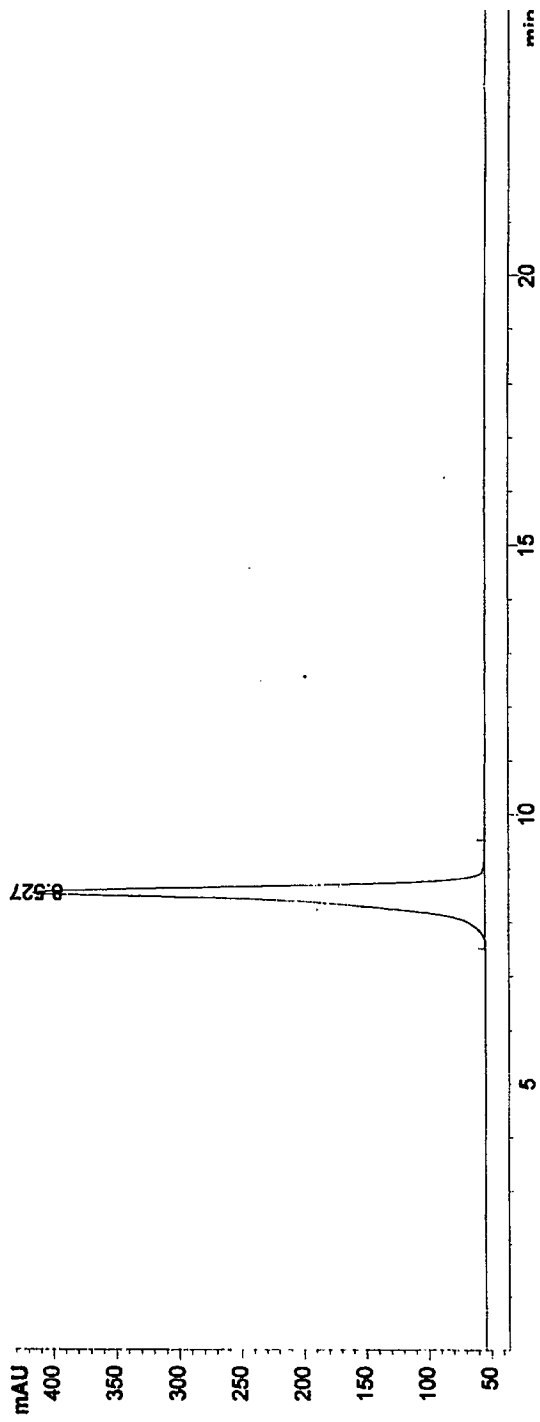
Compound 1



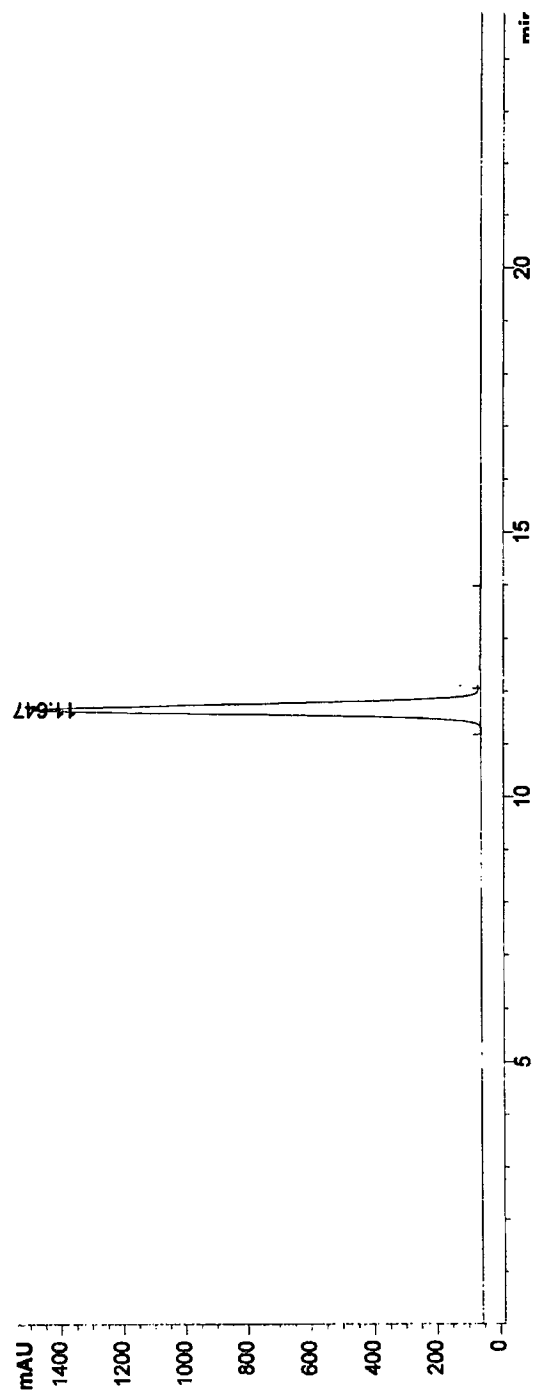
Compound 4



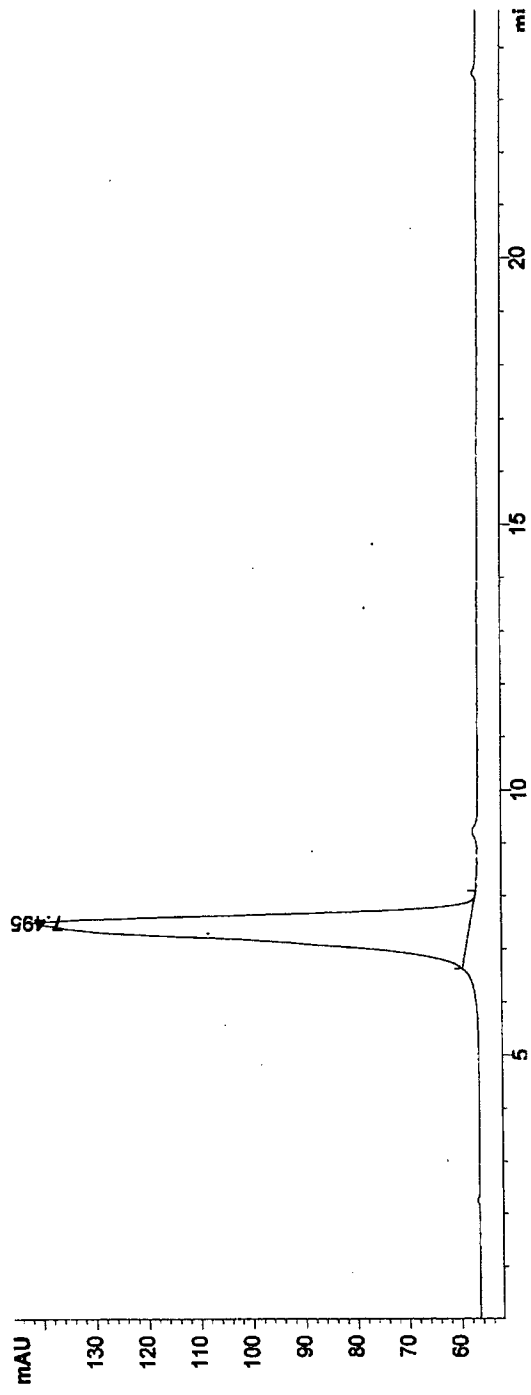
Compound 5



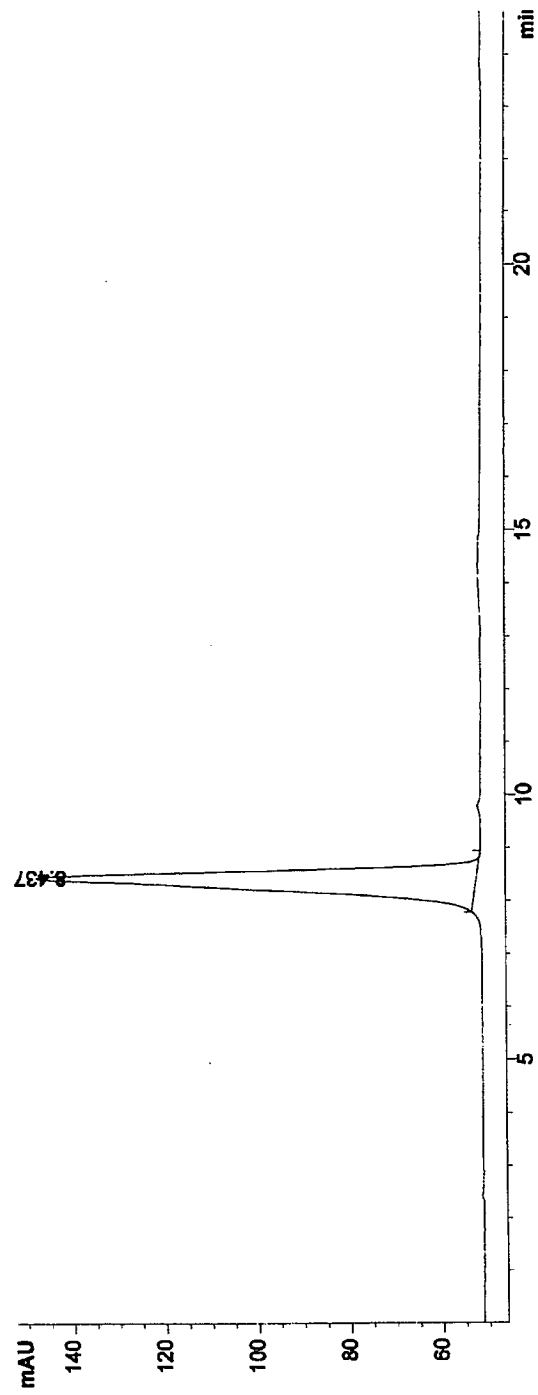
Compound 6



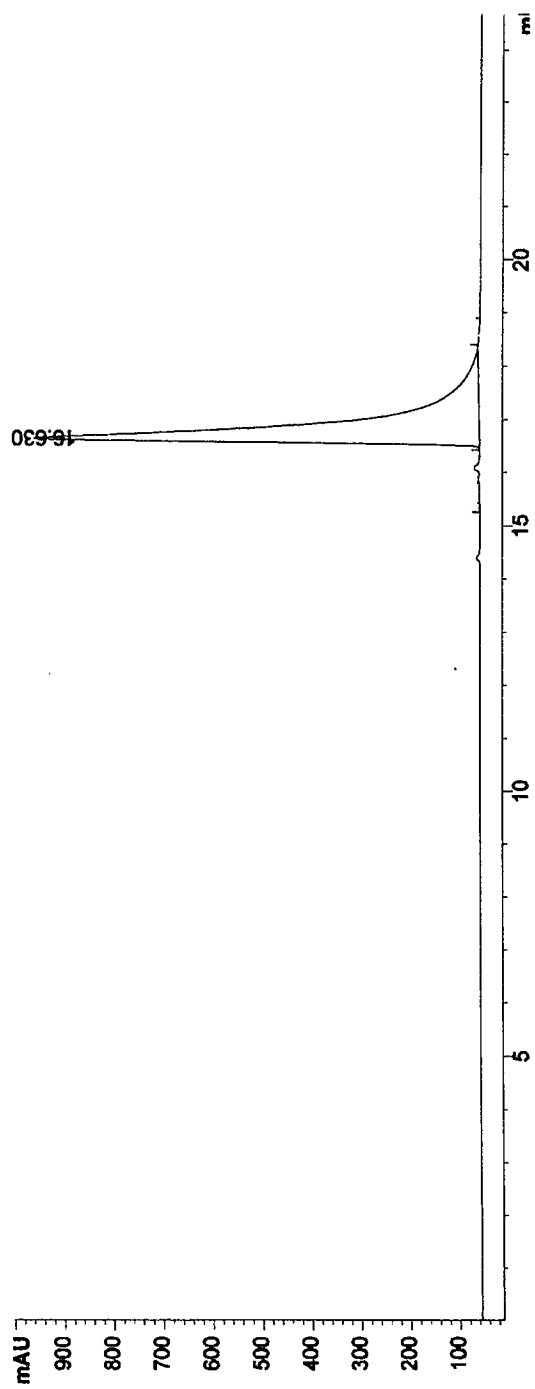
Compound 7



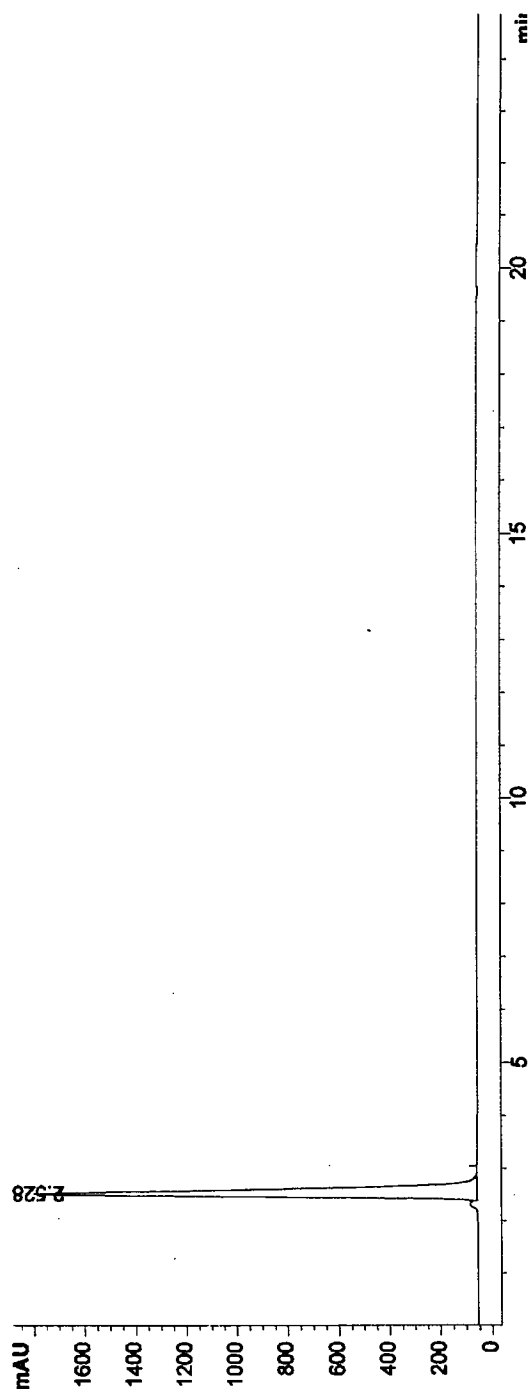
Compound 8



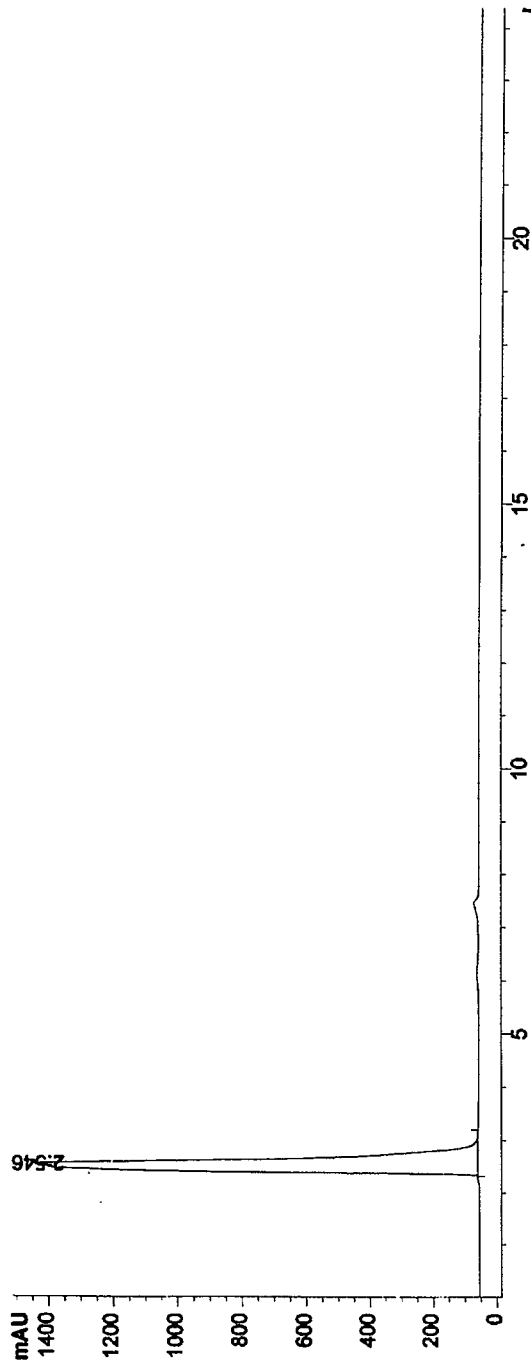
Compound 10



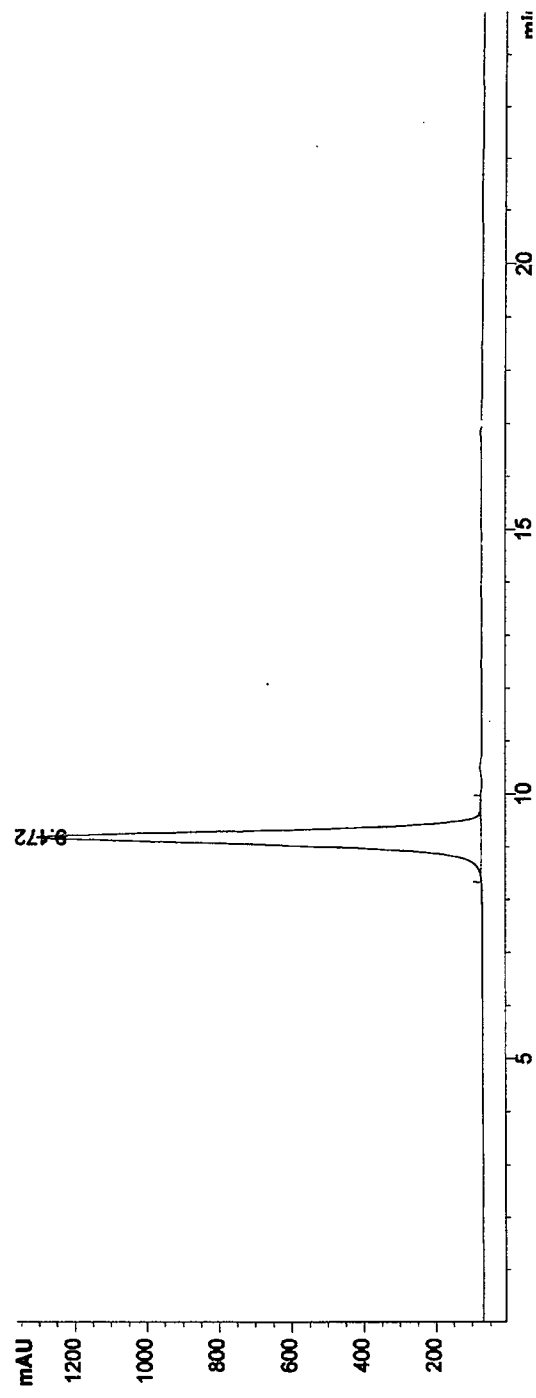
Compound 11



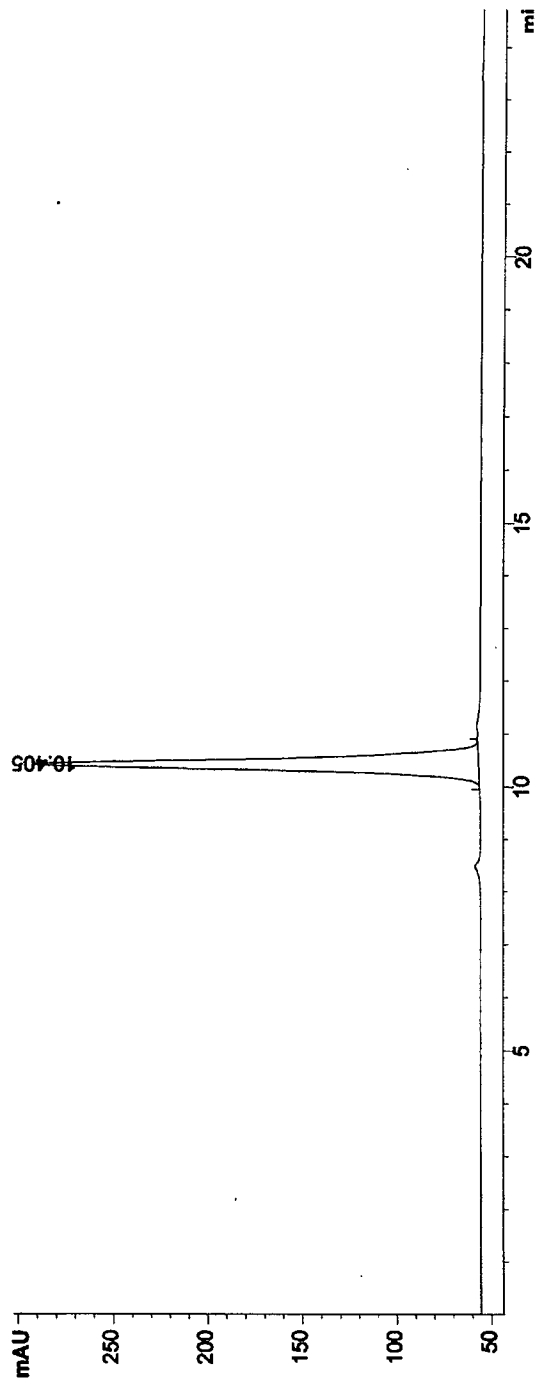
Compound 12



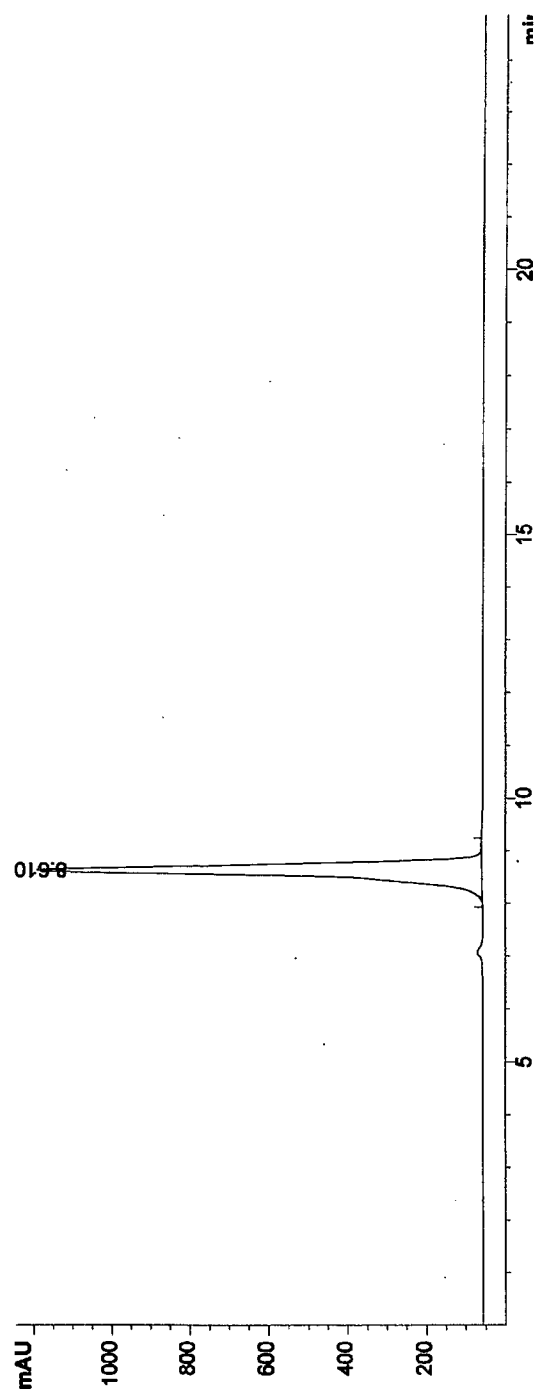
Compound 13



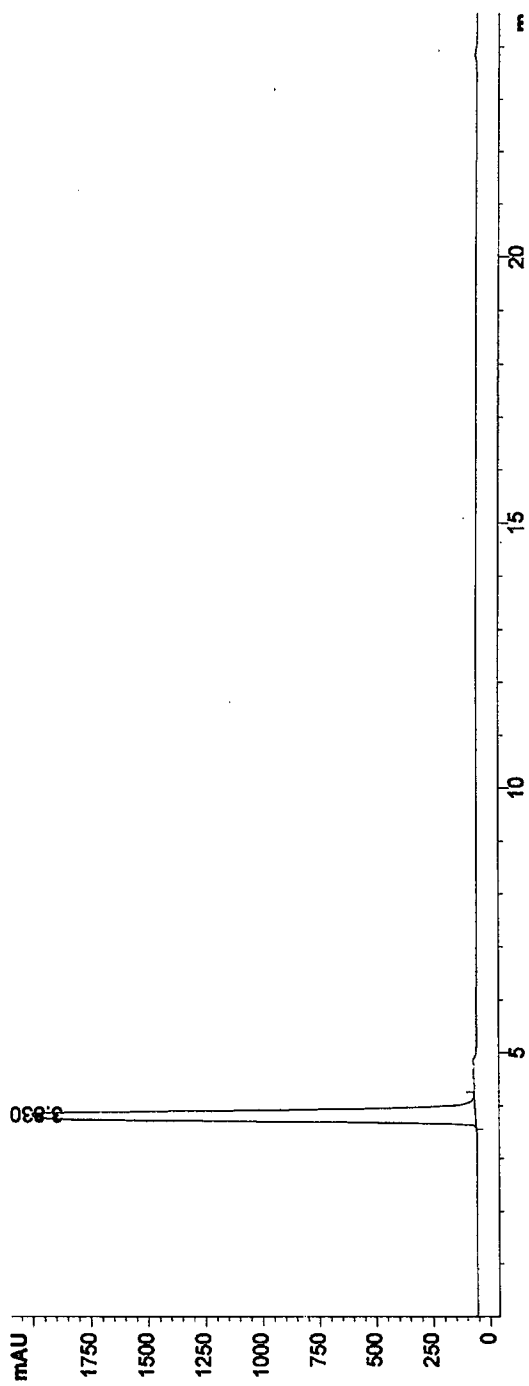
Compound 14



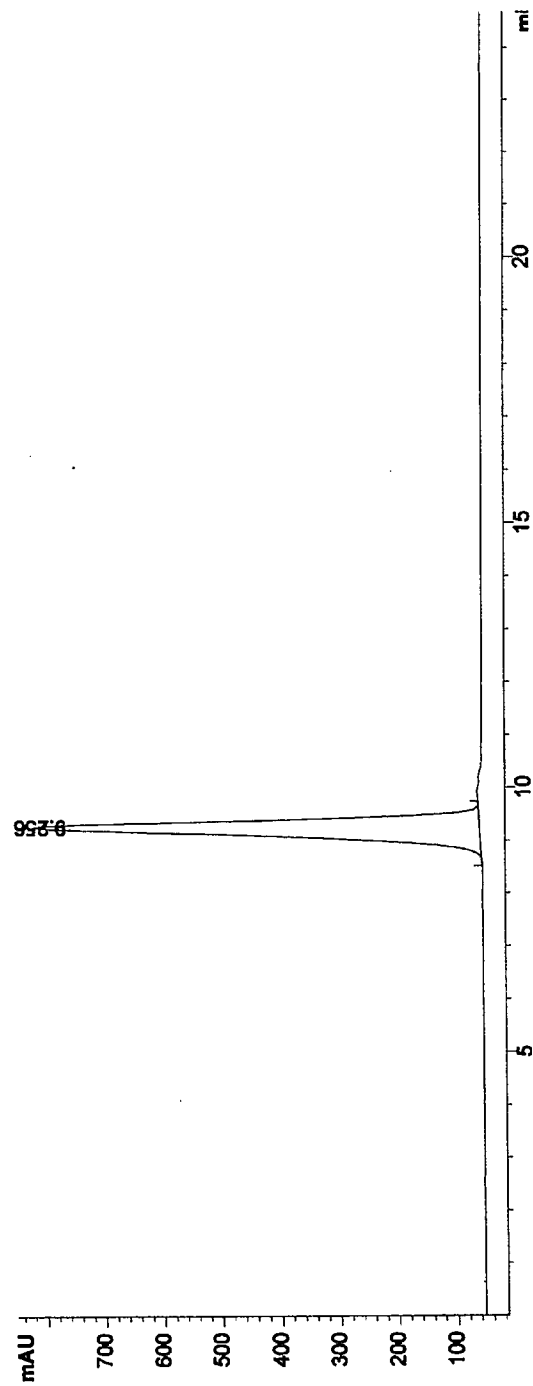
Compound 16



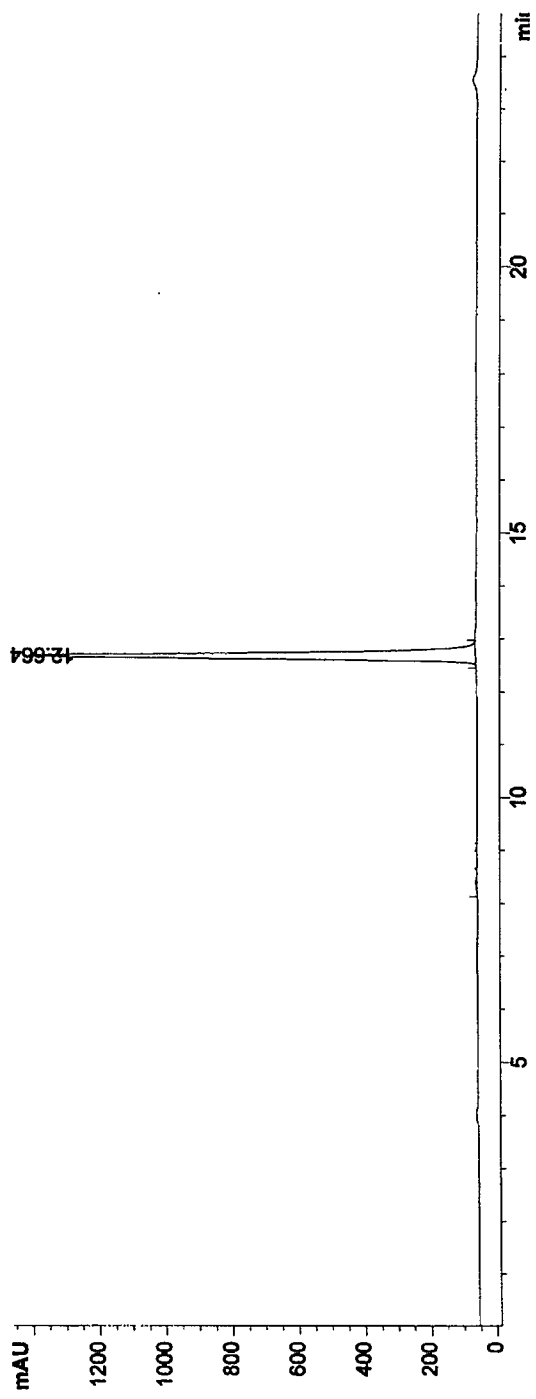
Compound 17



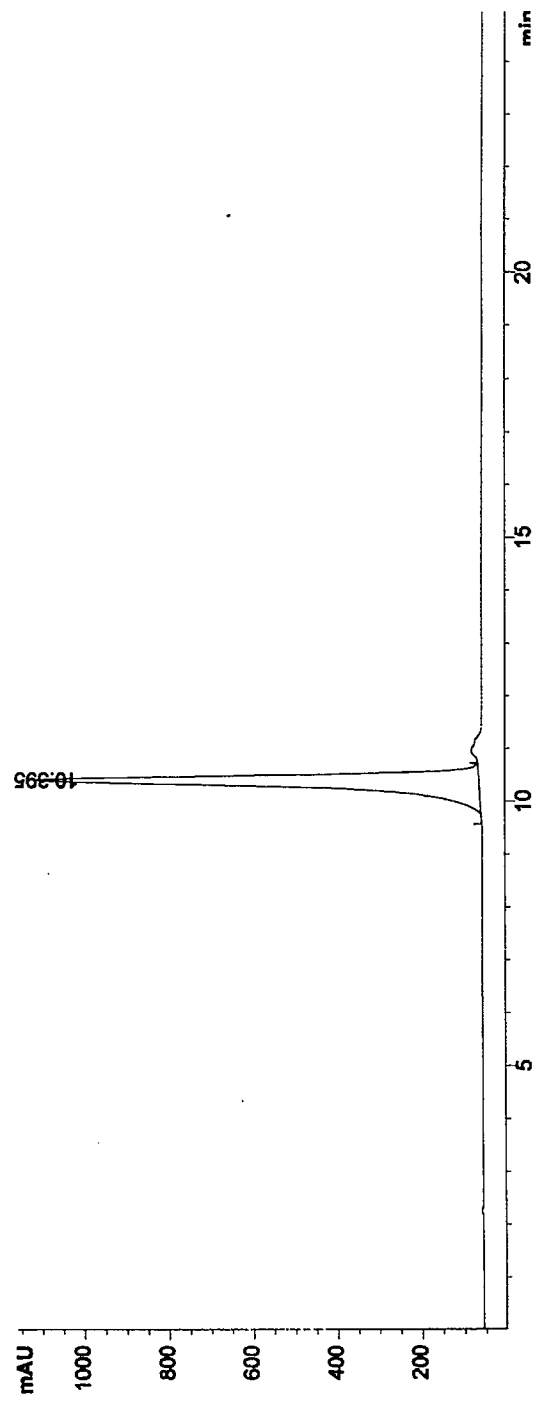
Compound 18

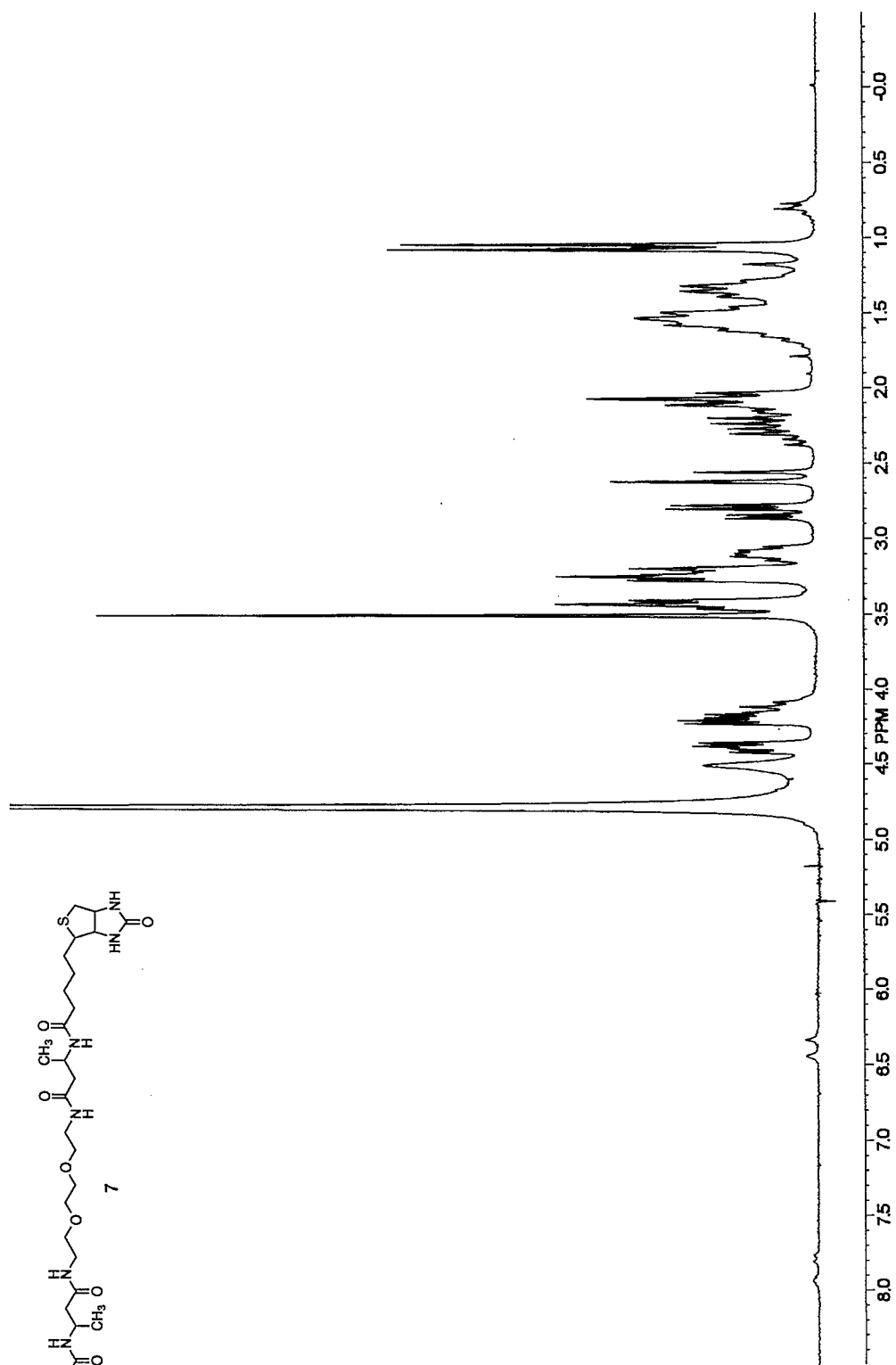
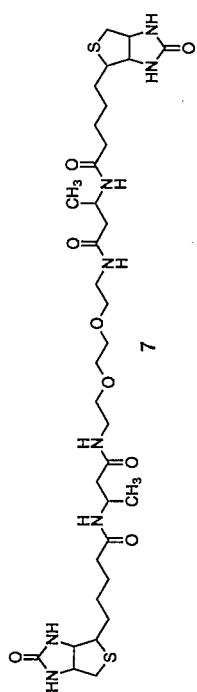


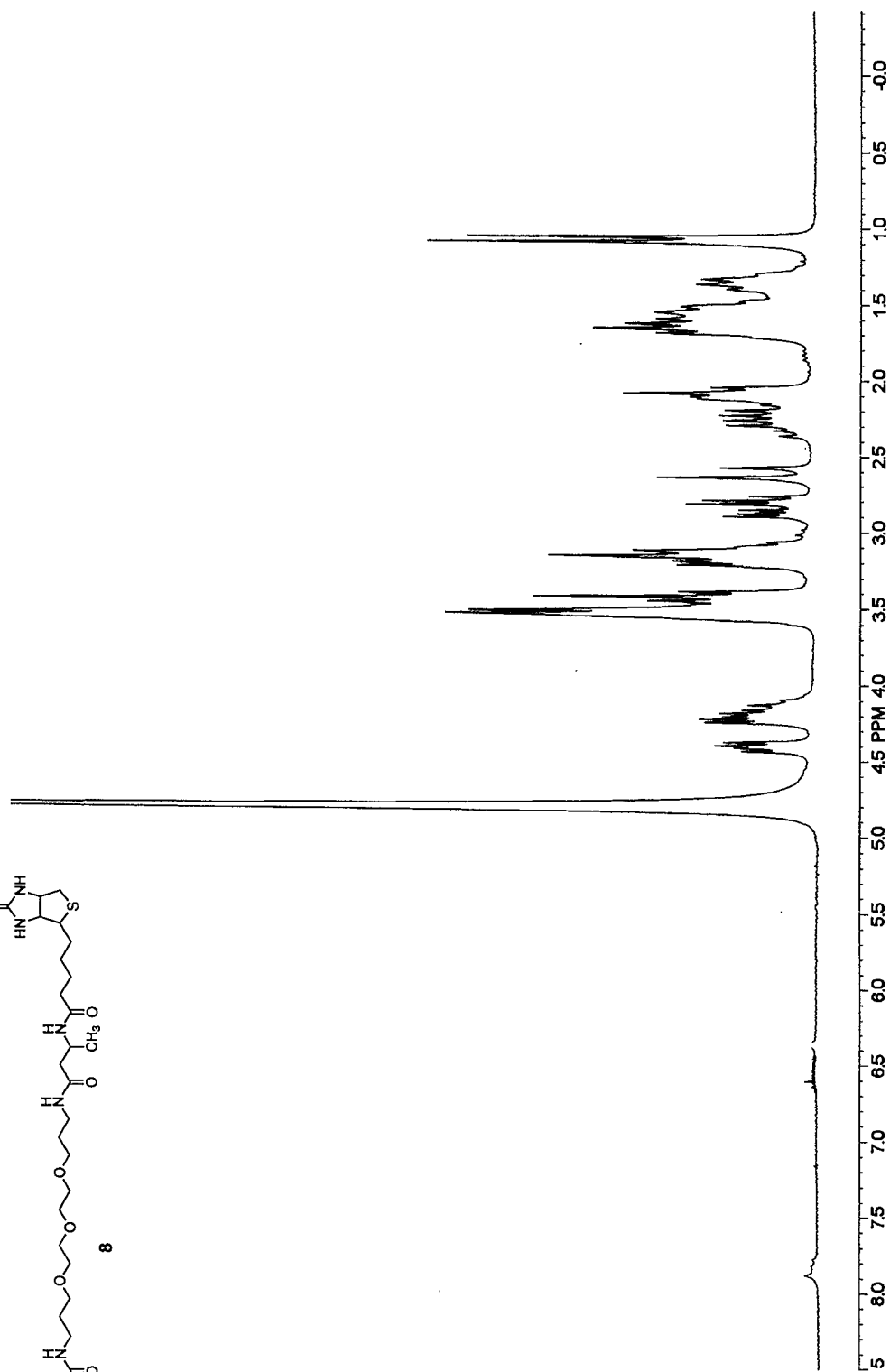
Compound 20

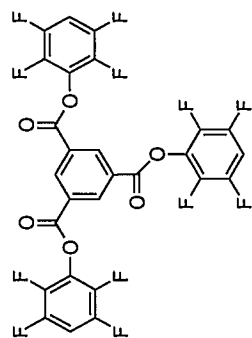


Compound 21

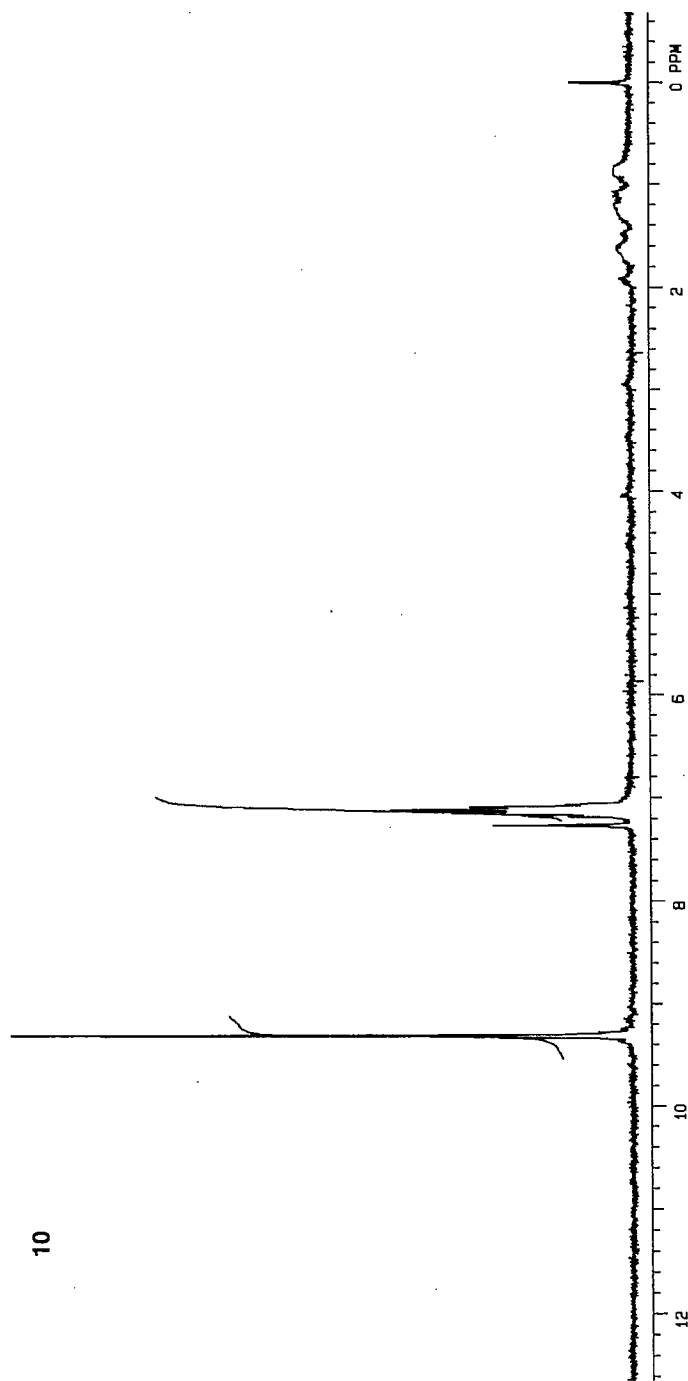


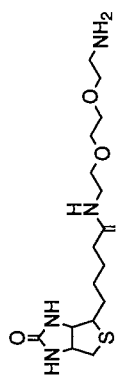




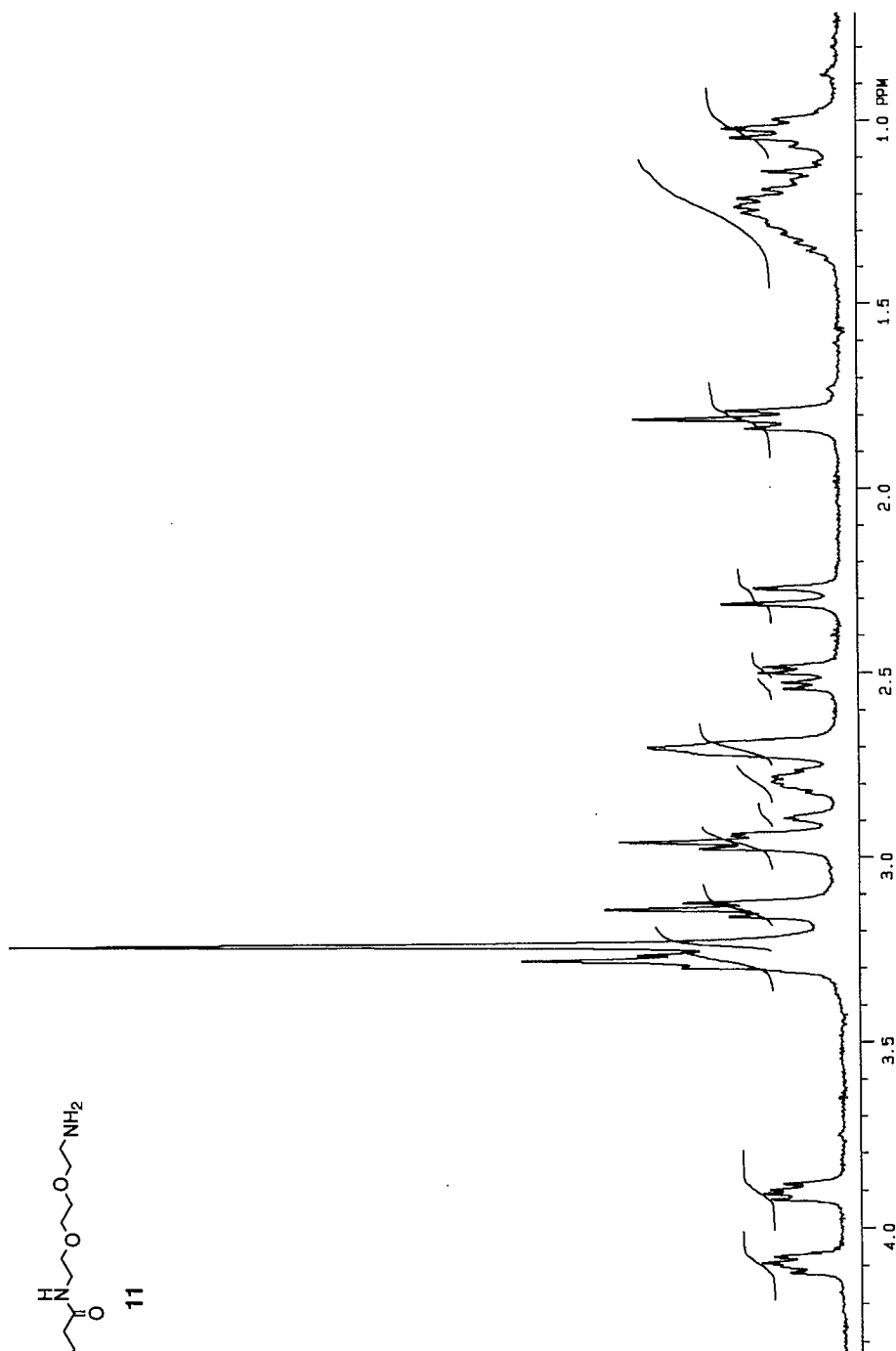


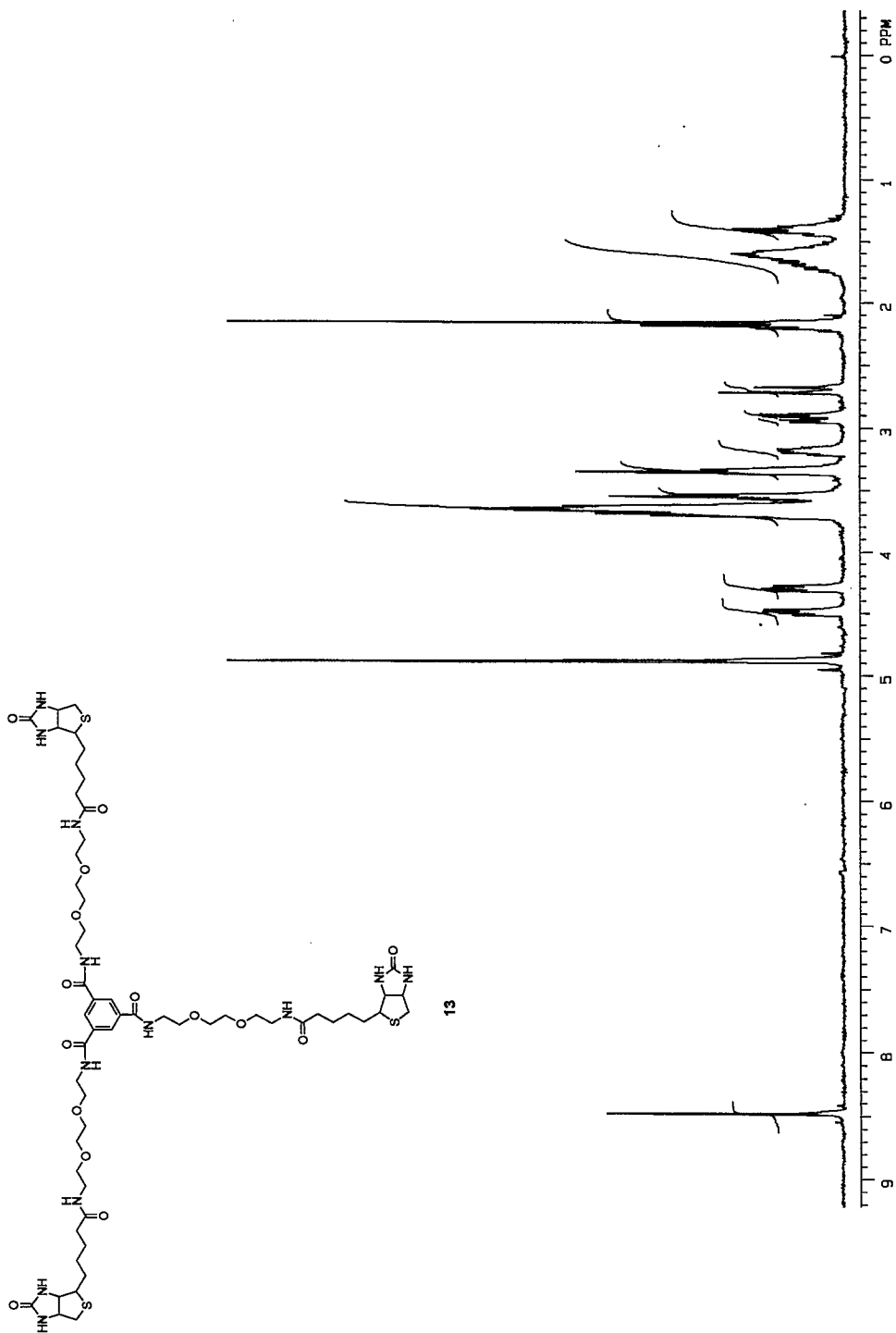
10

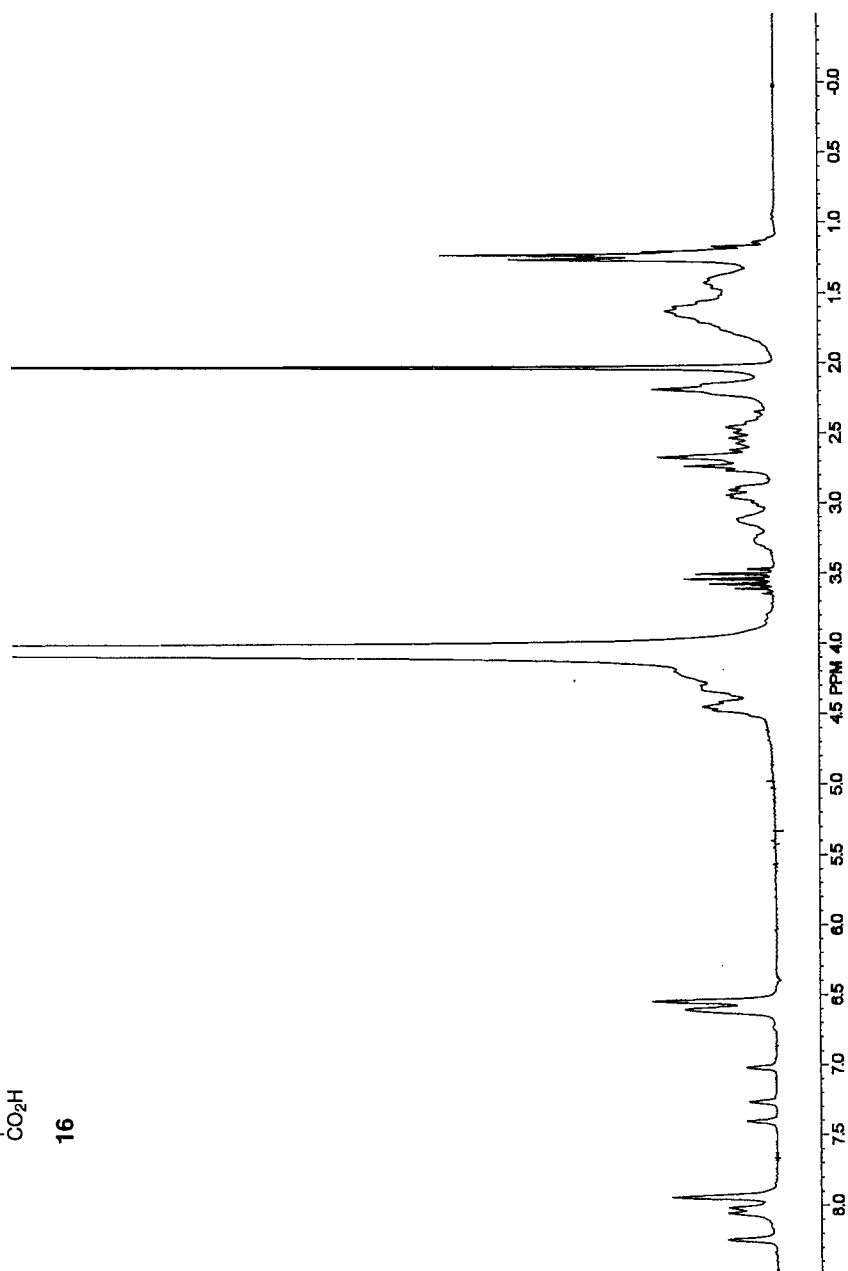
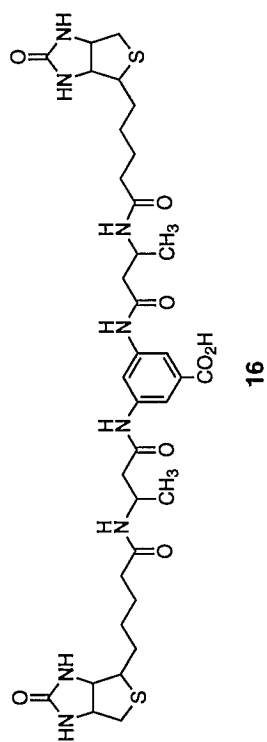


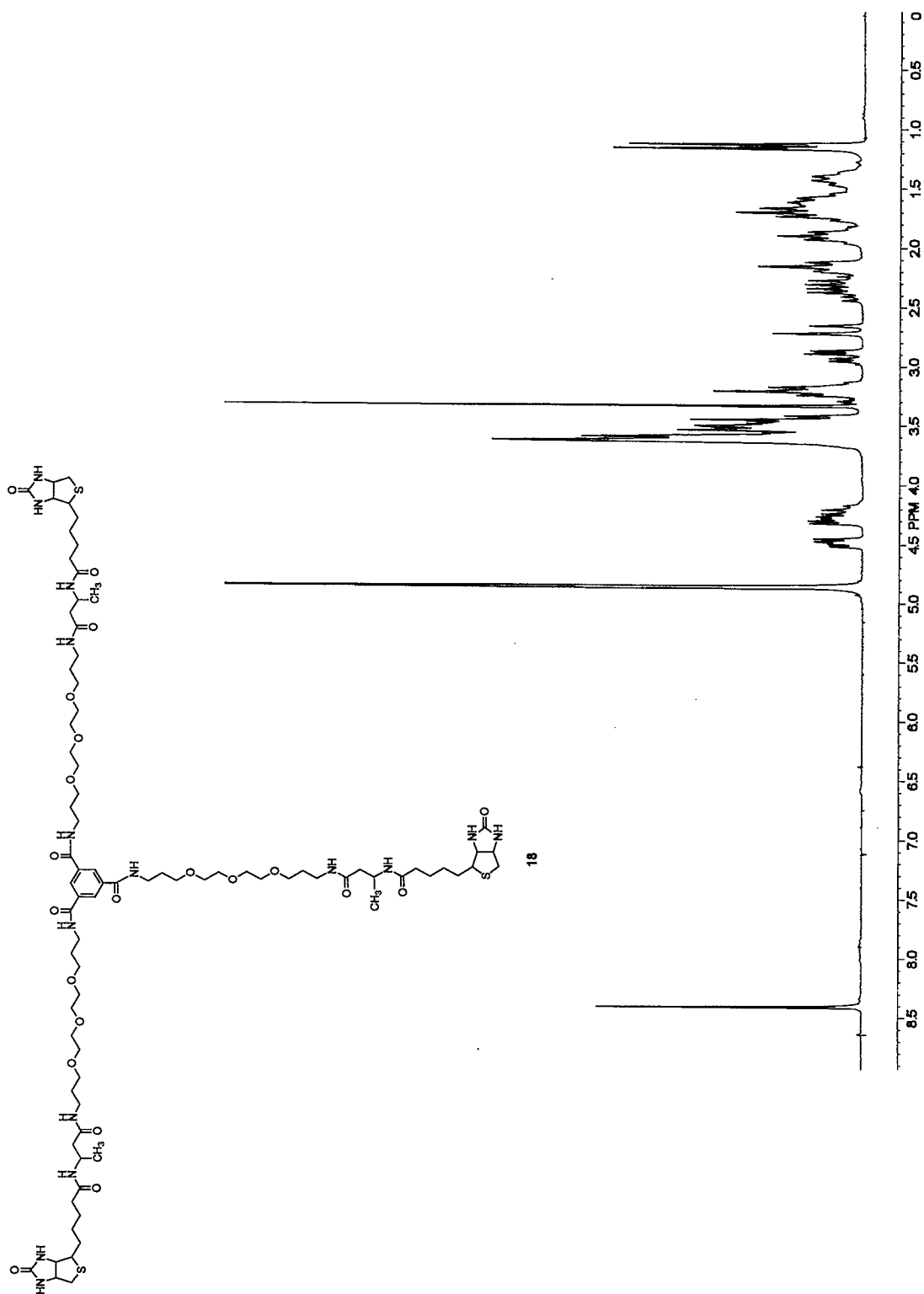


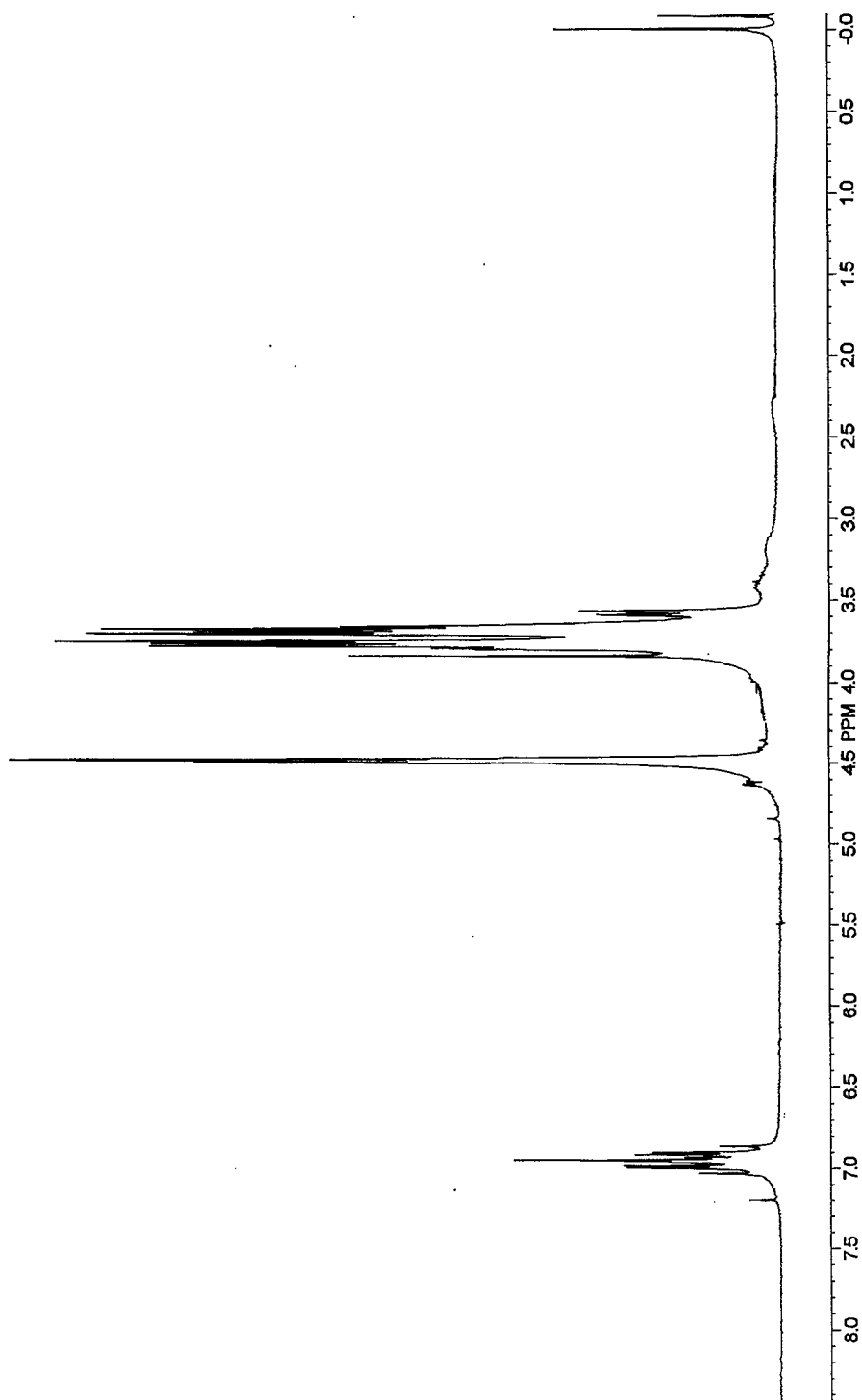
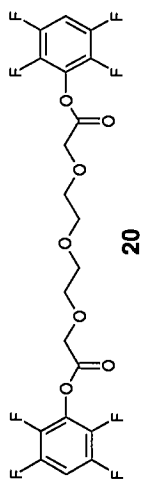
11

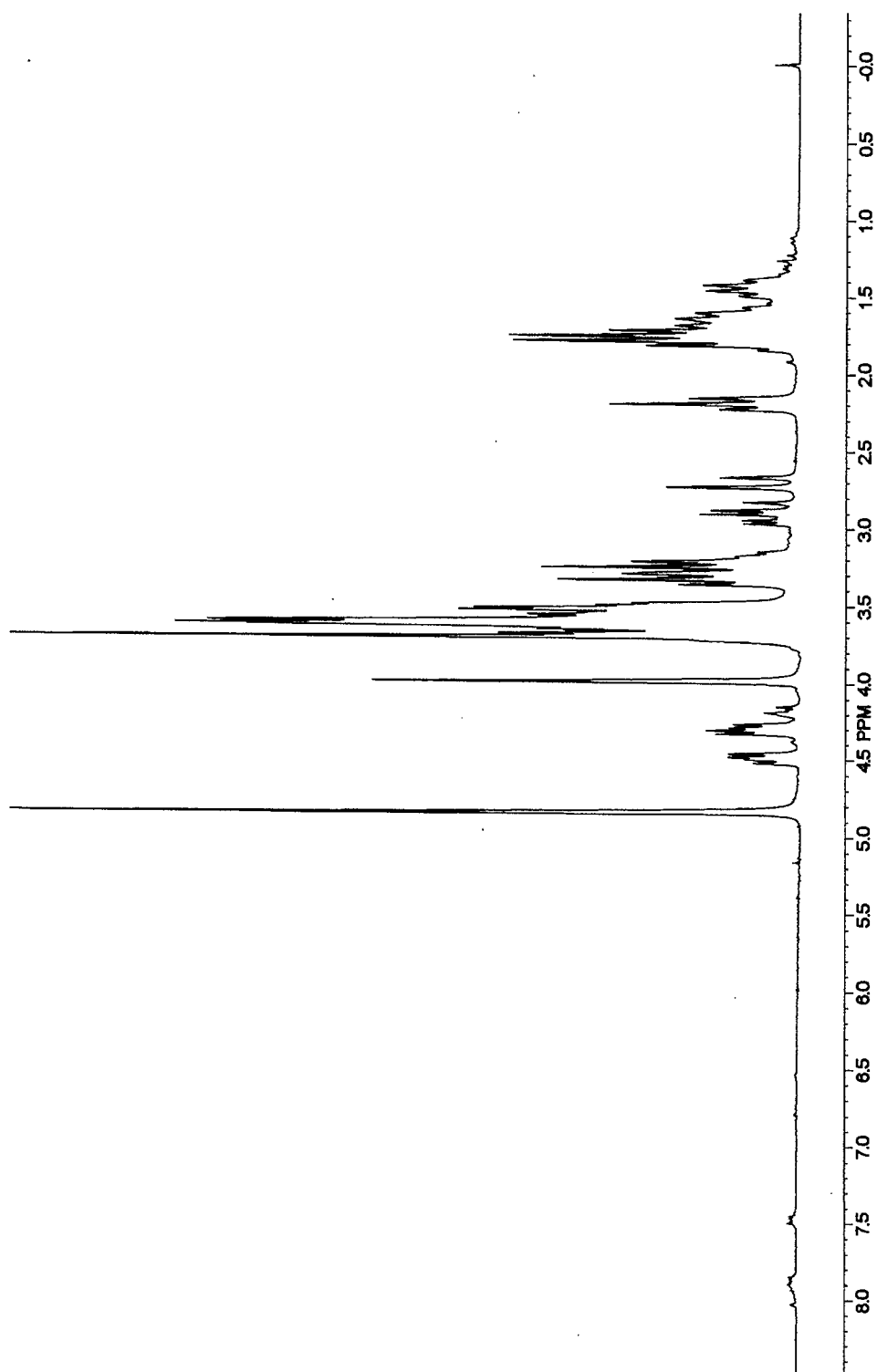
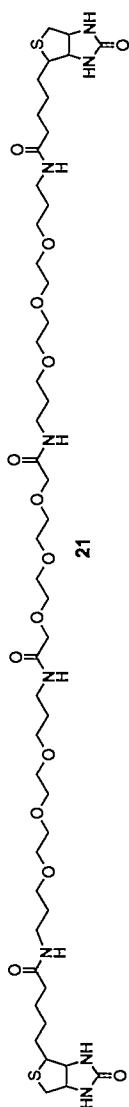












Design of Comb-Type Polyamine Copolymers for a Novel pH-Sensitive DNA Carrier

Shoichiro Asayama,[†] Atsushi Maruyama,^{*,†} Chong-Su Cho,[‡] and Toshihiro Akaike[†]

Department of Biomolecular Engineering, Tokyo Institute of Technology, 4259 Nagatsuta, Midori, Yokohama 226, Japan, and Department of Polymer Engineering, Chonnam National University, 300 Yongbong-dong, Buk-gu Kwangju 500-757, Korea. Received May 21, 1997; Revised Manuscript Received August 4, 1997[®]

The comb-type polycation consisting of a poly[2-(diethylamino)ethyl methacrylate] (PDEAEMA) backbone and poly(L-lysine) (PLL) side chains has been prepared as a novel pH-sensitive DNA carrier. The comb-type copolymer PDEAEMA-*graft*-PLL was prepared by using the macromonomer method, in which a poly(*N*-carbobenzoxymethyl-L-lysine) macromonomer was radically copolymerized with DEAEEMA. The comb-type copolymer exhibited a two-step proton dissociation and a dual ionic character owing to the two cationic segments in the copolymer, as determined by acid–base titration. In addition, the comb-type copolymer caused no significant turbidity even at pH 10, whereas PDEAEMA homopolymer suddenly precipitated out of the aqueous medium above pH 7.5 owing to the deprotonation of amino groups. Furthermore, a ¹H NMR study proved that protonated PLL segments solubilized the comb-type copolymer with a hydrophobic PDEAEMA core at higher pH. Finally, the pH-dependent behavior of the DNA complex with the comb-type copolymer was evaluated. The discontinuous turbidity change of the DNA/PDEAEMA-*graft*-PLL mixture at pH 7.5 suggested that the solubility of the complex varied in response to pH. By circular dichroism measurement, we also found that the comb-type copolymer was capable of varying DNA compaction pH-dependently. In conclusion, we have demonstrated that the comb-type copolymer is capable of sensing a pH signal and outputting the nonlinear change of the physicochemical properties of DNA polyelectrolyte complexes.

INTRODUCTION

Recently, the drug delivery systems using polymeric drug carriers have been studied to effect the efficient delivery of drugs to target sites (1, 2). Among the drug delivery systems, the delivery of genes to target cells as a novel class of clinical application has become one of the topics. For the effective gene delivery by nonviral carriers, the special mechanisms for carrying genes to specific tissues or cells are required. Receptor-mediated gene transfer takes advantage of the ability of receptors on the surface of cells to bind and internalize a ligand (3–8). The components used in the receptor-mediated gene delivery systems include DNAs, receptor-targeting ligands, and linking polycations such as poly(L-lysine) (PLL).¹ The first report of successful DNA transfer and gene expression via receptor-mediated endocytosis was made by Wu and Wu (4), who developed the methods used for the introduction of genes into the liver via the asialoglycoprotein receptor. Many ligands and their models were proposed and investigated as targeting moieties. The polycations conjugated with several ligands, such as transferrin (5), insulin (6), and antibody (7) molecules, have been studied for the efficient internalization of DNA–ligand complexes.

The major shortcomings of these delivery systems are,

however, transient and low levels of transfection activity. These shortcomings are attributed to the barriers existing during the delivery to the final destination, i.e., cytoplasmic space or the nucleus of the target cells. One of the major barriers is the reticuloendothelial system that entraps and scavenges foreign materials in the blood stream. Because most of DNA complexes are the size of a few hundred nanometers, they are liable to be entrapped by the reticuloendothelial system before their arrival at the target tissues or cells (9, 10). Another major barrier of nonviral delivery is the fact that most endocytosed complexes remain entrapped in vesicles and are subsequently degraded by the lysosomal pathway (11).

On the other hand, many viruses have evolved various molecular mechanisms for gaining the efficient entry into cells and escaping lysosomal degradation. For example, some virus particles exhibit the fusogenic activity with endosomal membranes to translocate the viral DNA to cytoplasmic space (12). The mechanics of the direct injection of DNA through the cellular plasma membrane were well documented for the infection of T4 bacteriophages (13). The fact that these viruses display such molecular mechanisms only after the arrival at the target cells is unique. The viruses, therefore, switch on these mechanisms by sensing environmental factors such as pH and/or specific molecules at the target sites.

Such “intelligence” of viral infection pathways has led us to create the nonviral carrier with intelligent functions. The materials internalized via receptor-mediated endocytosis are delivered into acidic endosomal vesicles so that they are subjected to the significant pH change (14). The polymer carriers which are capable of varying their functions in response to pH, therefore, enable us to construct intelligent DNA delivery systems.

In this study, we have prepared a novel comb-type polycation exhibiting a dual ionic property. The comb-type copolymer consists of stronger basic chains of PLL-

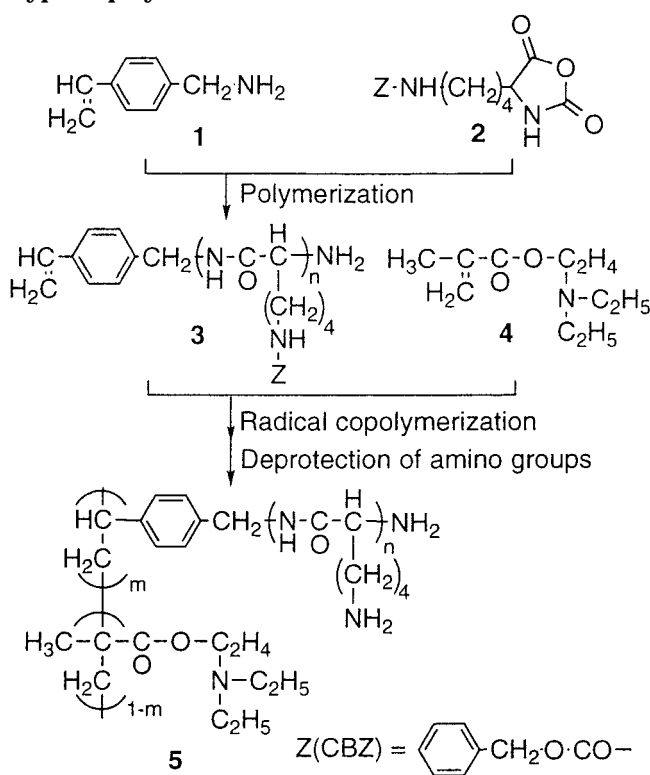
* To whom correspondence should be addressed. Telephone: +81-45-924-5122. Fax: +81-45-924-5815. E-mail: amaruyam@bio.titech.ac.jp.

[†] Tokyo Institute of Technology.

[‡] Chonnam National University.

[®] Abstract published in *Advance ACS Abstracts*, October 1, 1997.

¹ Abbreviations: PLL, poly(L-lysine); PDEAEMA, poly[2-(diethylamino)ethyl methacrylate]; DMF, *N,N*-dimethylformamide; NCA, *N*-carboxyanhydride; CBZ, carbobenzoxy group; V-65, 2,2'-azobis(2,4-dimethylvaleronitrile); GPC, gel permeation chromatography; CD, circular dichroism; *P*_n, number-average degree of polymerization.

Scheme 1. Synthesis of PDEAEMA-graft-PLL Comb-Type Copolymers

grafts and a weaker basic backbone of poly[2-(diethylamino)ethyl methacrylate] (PDEAEMA). The PDEAEMA undergoes the drastic change in protonation degree and solution properties near neutral pH (15, 16). Such a change in the PDEAEMA segment would give pH sensitivity to the DNA complex. It becomes possible to vary complex properties, such as the state of electrical charges and hydrophilic/hydrophobic balance, which are the factors determining the interaction with cellular or endosomal membranes. The higher-order structure of DNA in the complex, which is an influential factor in the transgene expression (17), can be also modified pH-dependently. Furthermore, the pH-sensitive DNA-polycation complexes may allow us to control the release of transgene enhancers, such as fusogenic substances and enzyme inhibitors, in a pH-sensitive manner.

EXPERIMENTAL PROCEDURES

Materials. 2-(Diethylamino)ethyl methacrylate (DEAEMA) was purchased from Wako Pure Chemical Industries, Ltd. (Osaka, Japan) and was distilled under reduced pressure after removing methacrylic acid with a 0.1 M NaOH aqueous solution. Dehydrated *N,N*-dimethylformamide (DMF) was purchased from Kanto Chemical Co., Inc. (Tokyo, Japan), and the calf thymus DNA was from Sigma Chemical Co. (St. Louis, MO). All other chemicals of a special grade were used without further purification.

Synthesis of PDEAEMA-graft-PLL Comb-Type Copolymers. The synthetic route of the comb-type copolymers is shown in Scheme 1. The *N*-carboxyanhydride (NCA) of *N*-carbobenzoyl-L-lysine (2) (18) was dissolved in dehydrated DMF. *p*-Aminomethylstyrene (1) (19) was dissolved in dehydrated DMF and added to the solution of 2. The polymerization reaction was performed with 10 g of CBZ-L-lysine NCA (2) in 100 mL of DMF at a monomer (2)/initiator (1) molar ratio of 20 or 40 (for 72 h at 25 °C). Then, the reaction mixture

was poured into a 10-fold volume of diethyl ether. Precipitate was collected by filtration and washed with diethyl ether, followed by drying *in vacuo*.

The resulting macromonomer (3) and DEAEMA (4) were dissolved in 1 mL of DMF at the total monomer concentration of 300 mg/mL. The radical copolymerization reaction was carried out for 7 h at 47 °C in a sealed glass ampule using 20 mM 2,2'-azobis(2,4-dimethylvaleronitrile) (V-65) as an initiator. After the reaction, the content was poured into a large excess of water, and precipitate was dried *in vacuo*. The crude polymers were dissolved in trifluoroacetic acid, followed by the addition of thioanisole to deprotect CBZ-amino groups. The final concentrations of thioanisole and the polymer were 1.6 and 0.32 mM (based on the CBZ groups), respectively. The deprotection reaction was carried out for 3.5 h at 25 °C. Then, the reaction mixture was poured into a large excess of diethyl ether. Precipitate was redissolved in trifluoroacetic acid and poured again into ether. The precipitate was dried *in vacuo* and dissolved in water, followed by dialysis against distilled water using a Spectra/Por 7 membrane (molecular weight cutoff = 10⁴) to remove unpolymerized macromonomers. After dialysis, the resulting copolymer was obtained by freeze-drying.

Gel Permeation Chromatography (GPC). GPC was carried out using a JASCO 880-PU pumping system (Tokyo, Japan) at a flow rate of 1.0 mL/min at 30 °C with Ultrahydrogel 500 and Ultrahydrogel 250 columns (Japan Waters Ltd., Tokyo, Japan). The aqueous solution containing 0.5 M CH₃COOH and 0.3 M Na₂SO₄ was used as a mobile phase. Three hundred microliters of 1 mg/mL samples was injected into the columns. The detection of the polymers was performed by a refractive index detector (830-RI, JASCO) and a multiangle light scattering detector (Dawn-DSP, Wyatt Technology Co., Santa Barbara, CA).

¹H NMR Spectroscopy. Each polymer (3–5 mg) was dissolved in 700 μL of D₂O (99.95 at. % D; Merck, Darmstadt, Germany), and the pH of the solution was varied by adding a trace amount of a 1 M HCl or 1 M NaOH solution. The pH value was checked with a TOA HM-20E pH meter (Tokyo, Japan) before and after ¹H NMR analysis. ¹H NMR spectra (400 MHz) were obtained by a Varian Unity 400plus spectrometer (Palo Alto, CA), at a probe temperature of 298 K. The chemical shifts are expressed as parts per million using internal water molecules (δ = 4.7 ppm in D₂O) as a reference.

Acid-Base Titration and Turbidity Measurement of PDEAEMA-graft-PLL Solutions. To 1.5 mL of an aqueous solution of the polymer (3.8 mg/mL) was added a 1 M HCl solution (20–30 μL), and the acidic polymer solution (pH 2) was titrated with a 1 M NaOH solution. The titration was carried out by the stepwise addition of 1 M NaOH and stopped at pH 12. The reverse titration was then performed as above, except that 1 M HCl was used. The turbidity of the solution during the titration was measured by monitoring the absorbance at 500 nm with a Beckman DU-640 spectrophotometer (Fullerton, CA).

Circular Dichroism Spectropolarimetry and Turbidity Measurement of the Mixture of DNA and PDEAEMA-graft-PLL. The stock solutions of both DNA (1 mg/mL) and PDEAEMA-graft-PLL (4 mg/mL) in 0.15 M NaCl were mixed together at a final ratio of 1/10 or 10/1 for the lysine unit (PLL-graft) to the nucleotide unit (DNA). The final concentration of DNA was adjusted to 0.1 mg/mL (3 × 10⁻⁴ M based on the nucleotide units). The pH of the mixture was varied from 7 to 8.5 by adding either a 0.1 or 1 M solution of HCl or NaOH.

Table 1. Characteristics of Prepared PDEAEMA-graft-PLL Comb-Type Copolymers^a

sample	mol % of 3 ^b		yield (%)	[lysine]/[DEAEMA] in copolymer
	in feed	in copolymer		
1	1.9	2.5	25	0.46
2	3.7	4.3	24	0.80
3	7.1	8.8	6	1.7
4	1.2	1.5	11	0.44

^a Initiator, 20 mM V-65; reaction temperature, 47 °C; reaction time, 7 h; solvent, DMF. ^b For samples 1–3, P_n (determined by GPC) = 20 and P_n (determined by ¹H NMR) = 18; for sample 4, P_n (GPC) = 30 and P_n (¹H NMR) = 28.

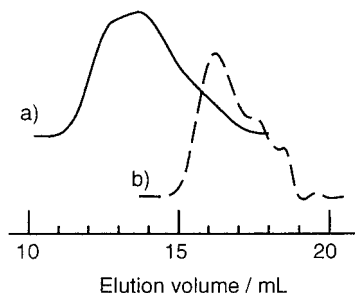


Figure 1. Gel permeation chromatograms of (a) the PDEAEMA-graft-PLL comb-type copolymer (sample 1) and (b) the deprotected CBZ-L-lysine macromonomer: column, Ultrahydrogel 500 + 250; eluent, 0.5 M CH₃COOH + 0.3 M Na₂SO₄; flow rate, 1.0 mL/min; temperature, 30 °C; detection, refractive index.

The circular dichroism (CD) and the turbidity of the mixture were measured at each pH point. The CD was measured with a JASCO J-600 spectropolarimeter in the quartz cell with an optical path length of 1 cm at room temperature. The values of CD in the figure are expressed as molecular ellipticity, calculated for one nucleotide residue in the polynucleotide. The turbidity was measured by monitoring the absorbance at 500 nm. The pH value was also checked after the CD and turbidity measurement.

RESULTS AND DISCUSSION

Synthesis of PDEAEMA-graft-PLL Comb-Type Copolymers. The polymerizations of CBZ-L-lysine NCA (**2**) had progressed homogeneously in the solvent of dehydrated DMF. The vinyl groups were preserved in the resulting polymer (**3**), which was confirmed by ¹H NMR spectroscopy in (CD₃)₂SO (DMSO-*d*₆): δ 5.2 (doublet), 5.8 (doublet), and 6.7 (quartet) ppm. The number-average degree of polymerization (P_n) of the macromonomer (**3**) determined by GPC was almost equal to that determined by ¹H NMR (see footnotes in Table 1) and was proportional to the feed ratio of monomer (**2**) to initiator (**1**). These results confirmed that the resulting macromonomers possessed one polymerizable vinyl end per molecule.

The radical copolymerizations of **3** with DEAEMA (**4**) had progressed homogeneously in DMF. Figure 1 shows the representative GPC profile of the resulting copolymer. The GPC profile indicated that unreacted macromonomers were removed by the purification process, including dialysis. The number-average molecular weight of the each copolymer determined by GPC was about 4.0×10^4 . The ¹H NMR spectra (Figure 2) of the copolymer showed the characteristic signals of both PLL-graft and PDEAEMA backbone: δ 1.3 (methyl protons of the diethylamino group of PDEAEMA), 1.4–1.8 (β -, γ -, and δ -methylene protons of PLL), 3.0 (ϵ -methylene protons of PLL), 3.3 (methylene protons of the diethylamino group

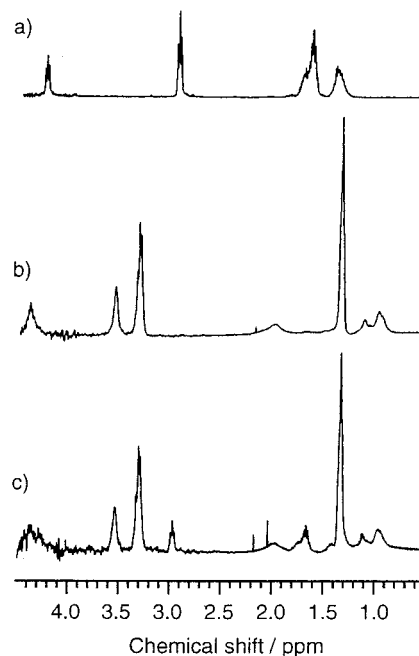


Figure 2. ¹H NMR spectra of (a) PLL, (b) PDEAEMA, and (c) PDEAEMA-graft-PLL in D₂O (pH 2).

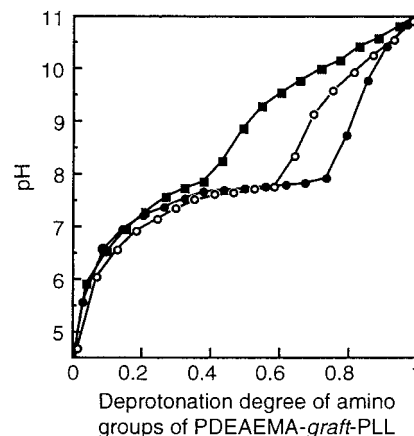


Figure 3. Acid–base titration curves of PDEAEMA-graft-PLL comb-type copolymers: (●) sample 1, (○) sample 2, and (■) sample 3. Acidic polymer solutions were titrated with the stepwise addition of 1 M NaOH. The horizontal axis is normalized as the deprotonation degree based on the total amino groups of the PDEAEMA-graft-PLL comb-type copolymer.

of PDEAEMA), 3.5 (2-methylene protons of PDEAEMA), and 4.3 (α -methine protons of PLL) ppm. No residual CBZ groups were detected in the final polymer samples, indicating the successful deprotection of amino groups. From the signal ratio of ϵ -methylene protons (3.0 ppm) of the PLL-grafts and methylene protons (3.3 ppm) of the PDEAEMA backbone, the content (mole percent) of **3** in the copolymer was determined. As shown in Table 1, the content of **3** in the copolymer was higher than that in feed, which suggested the preferential incorporation of the macromonomers (**3**) in the copolymers under the experimental conditions. Thus, it is possible to obtain the comb-type copolymers with well-controlled graft chains by using the macromonomer method.

pH-Dependent Behavior of PDEAEMA-graft-PLL Comb-Type Copolymers in Water. Figure 3 shows the acid–base titration curves of PDEAEMA-graft-PLL. The comb-type copolymer exhibited two-step proton dissociation. First and second proton dissociation was attributed to that of PDEAEMA (pH 7.5) and PLL (pH 10) segment, respectively. The dissociation profile varied

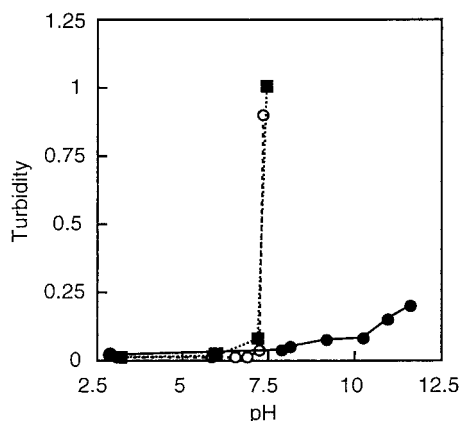


Figure 4. Effect of pH on the solubility of polymers in water: (●) PDEAEMA-*graft*-PLL comb-type copolymer (sample 1, 3.8 mg/mL), (■) PDEAEMA homopolymer (2.7 mg/mL), and (○) homopolymer mixture having the same composition (2.7 mg/mL PDEAEMA and 1.3 mg/mL PLL) as that of the copolymer. The turbidity was measured by monitoring the absorbance at 500 nm of the polymer aqueous solution during the acid–base titration.

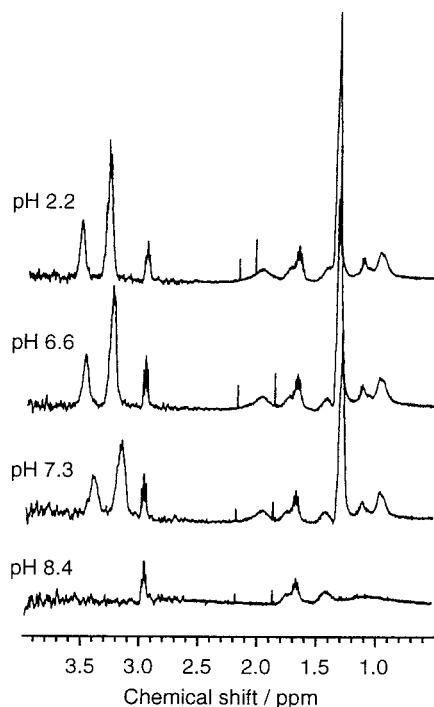


Figure 5. Effect of pH on the ^1H NMR spectra of the PDEAEMA-*graft*-PLL comb-type copolymer in D_2O . The pH was varied by adding a trace amount of 1 M HCl or 1 M NaOH.

according to the composition of the copolymer. Thus, the comb-type copolymer exhibited a dual ionic character owing to the two kinds of cationic segments, i.e., PDEAEMA and PLL, in the copolymer.

It should be noted that the solution behavior of the comb-type copolymer, as shown in Figure 4, was totally different from that of the PDEAEMA homopolymer. The PDEAEMA homopolymer exhibited precipitation above pH 7.5 owing to the deprotonation of the amino groups of the PDEAEMA. The precipitation of PDEAEMA was also seen in the polymer mixture of PDEAEMA and PLL. On the other hand, no significant turbidity was observed for the comb-type copolymer. The solution behavior of the comb-type copolymer was further evaluated by ^1H NMR measurement. As shown in Figure 5, the ^1H NMR signals of the copolymer varied drastically with the change of pH. The deprotonation of diethylamino groups

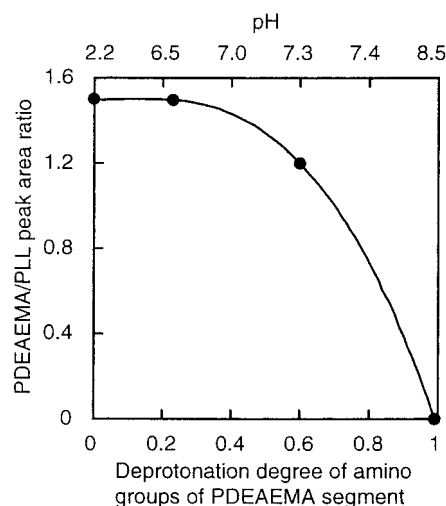


Figure 6. Plot of the ^1H NMR peak area ratio of the PDEAEMA signal at 2.0 ppm to the PLL signal at 3.0 ppm against the deprotonation degree of the PDEAEMA segment. The pH values are also indicated on the top horizontal axis.

was observed by the upfield shifts of the ^1H NMR signals with increasing pH. It is worth noting that the signals of the PDEAEMA segment disappeared at pH 8.4 where the amino groups of the segment were completely deprotonated. The peak area of the signals of the PDEAEMA segment decreased when more than 60% of the amino groups of the segment were deprotonated (Figure 6), whereas no significant change was observed for the PLL segment. As the PDEAEMA homopolymer became insoluble in higher pH, the PDEAEMA segment in the comb-type copolymer probably separated out of water and formed the microprecipitate (microparticle) that caused proton signal shielding (20, 21). The hydrophilic segments of the protonated PLL in the comb-type copolymer would stabilize the microprecipitate of the PDEAEMA segment and protect it from the bulk precipitation, leading to the transparent solution even in higher pH. In this sense, the comb-type copolymer was capable of varying the hydrophilic–hydrophobic balance and higher-order structure, in addition to the total positive charges, in response to the small change of pH of the solution. The pH sensitivity of the comb-type copolymer observed with the turbidity and ^1H NMR measurement was shown to be reversible.

Solubility Change of the Polyelectrolyte Complex between DNA and the PDEAEMA-*graft*-PLL Comb-Type Copolymer in Response to pH. We examined how the pH sensitivity of the PDEAEMA-*graft*-PLL copolymers influenced the properties of their complex with DNA. Figure 7 shows the pH-dependent turbidity change of the DNA solution mixed with an excess amount of the PDEAEMA-*graft*-PLL. Neither the DNA solution nor the PDEAEMA-*graft*-PLL solution exhibited any turbidity. However, the DNA/PDEAEMA-*graft*-PLL mixture exhibited significant turbidity above pH 7.5, and the turbidity decreased discontinuously at pH 7.5. The pH-dependent change of turbidity was almost reversible. Since the PDEAEMA homopolymer became soluble below pH 7.5, the solubility change of the DNA/PDEAEMA-*graft*-PLL complex in response to pH was probably related to the protonation of the PDEAEMA segment in the copolymer. We have already reported that the soluble complexes between DNAs and polycations are available by conjugating water soluble polymer chains such as dextran to polycations (22). In this case, the

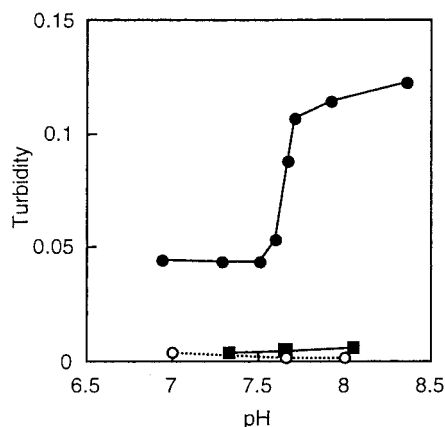


Figure 7. Effect of pH on the solubility of the mixture of DNA and the PDEAEMA-*graft*-PLL comb-type copolymer: (●) mixture of DNA (0.1 mg/mL) and PDEAEMA-*graft*-PLL (sample 1, 1.6 mg/mL) ([amino group]_{PLL-*graft*}/[phosphate group]_{DNA} = 10), (○) DNA alone (0.1 mg/mL), and (■) PDEAEMA-*graft*-PLL alone (1.6 mg/mL) in 0.15 M NaCl. The pH was varied by adding a 1 M solution of HCl or NaOH. The turbidity was measured by monitoring the absorbance of the mixture at 500 nm.

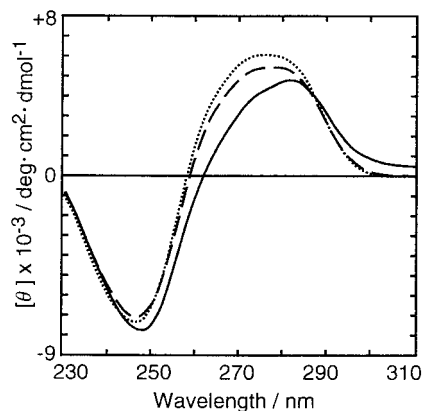


Figure 8. Effect of pH on the CD spectra of DNA in the presence of the PDEAEMA-*graft*-PLL comb-type copolymer: pH 7.7 (solid line), pH 8.2 (dashed line), and DNA alone (dotted line; the spectrum at pH 7.7 and 8.2 overlapped). DNA (0.1 mg/mL) and PDEAEMA-*graft*-PLL (sample 1, 17 μg/mL) were mixed in 0.15 M NaCl ([amino group]_{PLL-*graft*}/[phosphate group]_{DNA} = 0.1). The pH was varied by adding a 0.1 M solution of HCl or NaOH. The molecular ellipticities based on nucleotide units (3×10^{-4} M) are represented.

excess segments of the protonated PDEAEMA should contribute to increasing the solubility of the complex at lower pH.

pH-Dependent Conformational Change of DNA in the Presence of the PDEAEMA-*graft*-PLL Comb-Type Copolymer. To examine further the pH-dependent behavior of the DNA complex with the comb-type copolymer, we studied the structural change of DNA in the presence of the copolymer. Figure 8 shows the CD spectra of DNA in the presence of the comb-type copolymer under the DNA excess condition. We found that the CD spectra of DNA in the presence of the comb-type copolymer varied between pH 7 and 9, whereas those of DNA alone did not vary. The CD spectrum of DNA exhibited the positive peak at around 275 nm and the negative peak at around 246 nm. The ratio of $-[\theta]_{275}/[\theta]_{246}$ is plotted against pH values in Figure 9a to estimate DNA distortion (23, 24). The structure of DNA in the mixture was distorted owing to the complex formation, and the distortion of DNA was enhanced at lower pH. Furthermore, the CD spectrum at lower pH exhibited non-zero values above 300 nm, as shown in Figure 9b. Such "tail" anomalies in the region of the spectrum above

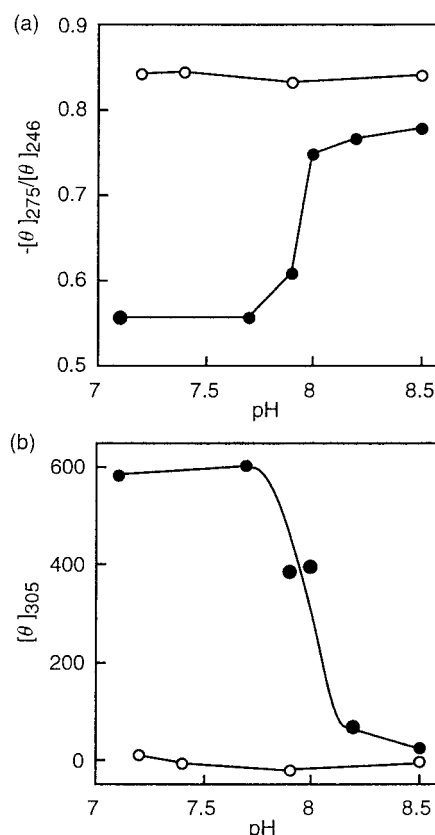


Figure 9. Plot of (a) $-[\theta]_{275}/[\theta]_{246}$ and (b) $[\theta]_{305}$ in the CD spectra against pH: (●) DNA/PDEAEMA-*graft*-PLL mixture and (○) DNA alone.

300 nm (25), where the absorption of the uncondensed DNA goes to zero, are an indication of the formation of large chiral aggregates (26, 27). Taking these results into account, the comb-type copolymer was capable of varying DNA distortion and condensation at a particular pH. The CD spectra varied around pH 8.0, which was a little higher than the proton dissociation pH of the PDEAEMA segment (around pH 7.5). This is reasonable because the dissociation pH of DNA and the PDEAEMA segment should be higher than the proton dissociation pH of PDEAEMA (28). We also confirmed that the pH-dependent conformational change of DNA was reversible.

Conclusion. We have prepared the novel pH-sensitive comb-type copolymer PDEAEMA-*graft*-PLL and evaluated the solution properties of the comb-type copolymer. The comb-type copolymer exhibited unique solution properties in response to pH. The properties were totally different from those of each homopolymer and their mixture. By using the comb-type copolymer as a pH-sensitive polycation, the assembling structure of DNA complexes and the conformation of DNA were drastically varied at a particular pH. The properties of DNA complexes, such as the assembling structure and the compaction of DNA, have been described as factors which influence transfection activity (29, 30); therefore, the comb-type copolymer can be a unique tool for gaining insight into the structure–function relationship in the transfection activity. From a practical point of view, the transition pH value which triggered the response of the DNA complex was a little higher than that desired for sensing acidic endosomal vesicles. It is, however, possible to lower the transition pH value by introducing hydrophobic groups to the PDEAEMA segment (31) or by replacing PDEAEMA with other pH-sensitive polymers. In this study, we have demonstrated that the comb-type copolymer is capable of sensing a pH signal and output-

ting the nonlinear change of the physicochemical properties of DNA polyelectrolyte complexes. The achievement of the pH-induced nonlinear output can be the first step in mimicking the intelligent virus infection pathway with artificial polymer carriers.

LITERATURE CITED

- (1) Ringsdorf, H. (1975) Structure and properties of pharmacologically active polymers. *J. Polym. Sci. Polym. Symp.* 51, 135–153.
- (2) Cartledge, S. A., Duncan, R., Lloyd, J. B., Rejmanová, P., and Kopeček, J. (1987) Soluble, cross-linked *N*-(2-hydroxypropyl)methacrylamide copolymers as potential drug carriers. *J. Controlled Release* 4, 253–264.
- (3) Perales, J. C., Ferkol, T., Molas, M., and Hanson, R. W. (1994) An evaluation of receptor-mediated gene transfer using synthetic DNA-ligand complexes. *Eur. J. Biochem.* 226, 255–266.
- (4) Wu, G. Y., and Wu, C. H. (1987) Receptor-mediated *in vitro* gene transformation by a soluble DNA carrier system. *J. Biol. Chem.* 262, 4429–4432.
- (5) Wagner, E., Cotten, M., Foisner, R., and Birnstiel, M. L. (1991) Transferrin-polycation-DNA complexes: The effect of polycations on the structure of the complex and DNA delivery to cells. *Proc. Natl. Acad. Sci. U.S.A.* 88, 4255–4259.
- (6) Hockett, B., Ariatti, M., and Hawtrey, A. O. (1990) Evidence for targeted gene transfer by receptor-mediated endocytosis: Stable expression following insulin-directed entry of neo into HepG2 cells. *Biochem. Pharmacol.* 40, 253–263.
- (7) Trubetskoy, V. S., Torchilin, V. P., Kennel, S. J., and Huang, L. (1992) Use of N-terminal modified poly(L-lysine)-antibody conjugate as a carrier for targeted gene delivery in mouse lung endothelial cells. *Bioconjugate Chem.* 3, 323–327.
- (8) Wilson, J. M., Grossman, M., Wu, C. H., Chowdhury, N. R., Wu, G. Y., and Chowdhury, J. R. (1992) Hepatocyte-directed gene transfer *in vivo* leads to transient improvement of hypercholesterolemia in low-density lipoprotein receptor-deficient rabbits. *J. Biol. Chem.* 267, 963–967.
- (9) Artursson, P., Edman, P., and Sjöholm, I. (1984) Biodegradable microspheres. I. Duration of action of dextranase entrapped in polyacryl starch microparticles *in vivo*. *J. Pharmacol. Exp. Ther.* 231, 705–712.
- (10) Gabizon, A., and Papahadjopoulos, D. (1988) Liposome formulations with prolonged circulation time in blood and enhanced uptake by tumors. *Proc. Natl. Acad. Sci. U.S.A.* 85, 6949–6953.
- (11) Chowdhury, N. R., Wu, C. H., Wu, G. Y., Yerneni, P. C., Bommineni, V. R., and Chowdhury, J. R. (1993) Fate of DNA targeted to the liver by asialoglycoprotein receptor-mediated endocytosis *in vivo*. *J. Biol. Chem.* 268, 11265–11271.
- (12) Wiley, D. C., and Skehel, J. J. (1987) The structure and function of the hemagglutinin membrane glycoprotein of influenza virus. *Annu. Rev. Biochem.* 56, 365–394.
- (13) Simon, L. D., and Anderson, T. F. (1967) The infection of *Escherichia coli* by T2 and T4 bacteriophages as seen in the electron microscope. *Virology* 32, 279–297.
- (14) Steinman, R. M., Mellman, I. S., Muller, W. A., and Cohn, Z. A. (1983) Endocytosis and the recycling of plasma membrane. *J. Cell Biol.* 96, 1–27.
- (15) Feil, H., Bae, Y. H., Feijen, J., and Kim, S. W. (1992) Mutual influence of pH and temperature on the swelling of ionizable and thermosensitive hydrogels. *Macromolecules* 25, 5528–5530.
- (16) Ishihara, K., Kobayashi, M., Ishimaru, N., and Shinohara, I. (1984) Glucose induced permeation control of insulin through a complex membrane consisting of immobilized glucose oxidase and a poly(amine). *Polym. J.* 16, 625–631.
- (17) Perales, J. C., Ferkol, T., Beegen, H., Ratnoff, O. D., and Hanson, R. W. (1994) Gene transfer *in vivo*: Sustained expression and regulation of genes introduced into the liver by receptor-targeted uptake. *Proc. Natl. Acad. Sci. U.S.A.* 91, 4086–4090.
- (18) Daly, W. H., and Poché, D. (1988) The preparation of N-carboxyanhydrides of α -amino acids using bis(trichloromethyl)carbonate. *Tetrahedron Lett.* 29, 5859–5862.
- (19) Kobayashi, K., Sumitomo, H., and Ina, Y. (1985) Synthesis and functions of polystyrene derivatives having pendent oligosaccharides. *Polym. J.* 17, 567–575.
- (20) Ito, K., Masuda, Y., Shintani, T., Kitano, T., and Yamashita, Y. (1983) Synthesis and interfacial characterization of graft and random copolymers of styrene and 2-hydroxyethyl methacrylate. *Polym. J.* 15, 443–448.
- (21) Crivello, J. V., Conlon, D. A., and Lee, J. L. (1986) Poly(dimethylsiloxane)-vinyl block polymers. I. The synthesis of poly(dimethylsiloxane) macroinitiators containing thermolizable bis(silyl pinacolate) groups in their backbones. *J. Polym. Sci. Polym. Chem. Ed.* 24, 1197–1215.
- (22) Maruyama, A., Katoh, M., Ishihara, T., and Akaike, T. (1997) Comb-type polycations effectively stabilize DNA triplex. *Bioconjugate Chem.* 8, 3–6.
- (23) Li, H. J., Epstein, P., Yu, S. S., and Brand, B. (1974) Investigation of huge negative circular dichroism spectra of some nucleoproteins. *Nucleic Acids Res.* 1, 1371–1383.
- (24) Weiskopf, M., and Li, H. J. (1977) Poly(L-lysine)-DNA interactions in NaCl solutions: B \rightarrow C and B \rightarrow ψ transitions. *Biopolymers* 16, 669–684.
- (25) Reich, Z., Ittah, Y., Weinberger, S., and Minsky, A. (1990) Chiral and structural discrimination in binding of polypeptides with condensed nucleic acid structures. *J. Biol. Chem.* 265, 5590–5594.
- (26) Keller, D., and Bustamante, C. (1986) Theory of the interaction of light with large inhomogeneous molecular aggregates. II. Psi-type circular dichroism. *J. Chem. Phys.* 84, 2972–2989.
- (27) Maestre, M. F., and Reich, C. (1980) Contribution of light scattering to the circular dichroism of deoxyribonucleic acid films, deoxyribonucleic acid-polylysine complexes, and deoxyribonucleic acid particles in ethanolic buffers. *Biochemistry* 19, 5214–5223.
- (28) Abe, K., Ohno, H., and Tsuchida, E. (1977) Phase changes of polyion complex between poly(methacrylic acid) and a polycation carrying charges in the chain backbone. *Makromol. Chem.* 178, 2285–2293.
- (29) Wolfert, M. A., Schacht, E. H., Toncheva, V., Ulbrich, K., Nazarova, O., and Seymour, L. W. (1996) Characterization of vectors for gene therapy formed by self-assembly of DNA with synthetic block copolymers. *Hum. Gene Ther.* 7, 2123–2133.
- (30) Kabanov, A. V., and Kabanov, V. A. (1995) DNA complexes with polycations for the delivery of genetic material into cells. *Bioconjugate Chem.* 6, 7–20.
- (31) Siegel, R. A., and Firestone, B. A. (1988) pH-Dependent equilibrium swelling properties of hydrophobic polyelectrolyte copolymer gels. *Macromolecules* 21, 3254–3259.

BC970097N

***In Vitro* Gene Delivery to Hepatocytes with Galactosylated Polyethylenimine**

Maria-Antonietta Zanta, Otmane Boussif, Abdennaji Adib, and Jean-Paul Behr*

Laboratoire de Chimie Génétique associé au CNRS (URA 1386), Faculté de Pharmacie, Université Louis Pasteur de Strasbourg, BP24, F-67401 Illkirch Cedex, France. Received May 19, 1997[©]

A hepatocyte-directed vector has been developed; it includes several key features thought to favor *in vivo* gene delivery to the liver: electrostatically neutral particles which avoid nonspecific binding to other cells, to the extracellular matrix, and to complement proteins; asialoglycoprotein receptor-mediated endocytosis which may address the complexes to the perinuclear region; and polyethylenimine (PEI)-mediated endosome buffering and swelling as an escape mechanism to the cytoplasm. This system is based on a 5% galactose-bearing polyethylenimine (PEI-gal) polymer which is condensed with plasmid DNA to neutrality. Murine (BNL CL.2) and human (HepG2) hepatocyte-derived cell lines were transfected 10^4 – 10^5 -fold more efficiently than murine fibroblasts (3T3), whether transfection was assessed globally (luciferase expression from the cell extract) or following histochemical staining (β -galactosidase). Under these conditions, over 50% of the hepatocytes were selectively transfected in the presence of 10% serum. Transfection was suppressed by removal of the targeting galactose residues, by their replacement with glucose, or by the addition of excess asialofetuin. Thus, results from comparative and competitive experiments indicate the asialoglycoprotein receptor is involved in transfection of hepatocytes with neutral PEI-gal/DNA complexes.

In vivo gene delivery with nonviral vectors has been demonstrated in many cases and provides the basis for several clinical trials (Nabel, G. J., et al., 1993; Caplen et al., 1994; Nabel, E. G., et al., 1994; Crystal, 1995). However, with some exceptions (Stribling et al., 1992; Logan et al., 1995), efficiency, especially when it comes to the percentage and type of transfected cells, has been rather low (Perales et al., 1994; Thierry et al., 1995; Tsukamoto et al., 1995; McLachlan et al., 1995; Schwartz et al., 1995; Noguezbellin et al., 1996; Stephan et al., 1996; Lee et al., 1996). Most work has been done with cationic lipid/plasmid complexes. Their net ionic charge (i.e. the ratio of cationic vector over anionic phosphate) governs the fate of the resulting particles (Behr et al., 1989; Schwartz et al., 1995; Remy et al., 1995) and leads to a dilemma. Transfection is most efficient only when particles are cationic and thus can be taken up by adherent cells following binding to anionic cell surface proteoglycans (Mislick and Baldeschwieler, 1996; Labat-Moleur et al., 1996); they will however bind to quite similar polyanionic glycans present in the extracellular matrix. Conversely, anionic particles will not be retained, but will not bind efficiently to the cell surface either. The tricky choice of the cationic vector/DNA ratio is further complicated by the fact that around neutrality particles become generally much larger and are unstable (Jaaskelainen et al., 1994); indeed, particle size is an important concern too when considering diffusion within a tissue or escape from the reticuloendothelial system. A way out of this dilemma is development of neutral particles supplemented with a ligand which will prevent complex aggregation and allow cell binding (Remy et al., 1995).

In the pioneering work by Wu and Wu (1987) on hepatocyte targeting with asialoglycoprotein-polylysine/

plasmid complexes, most components for dealing with these problems were empirically present. Calculations with the amounts of cationic vector and DNA they used show that the charge of the complexes was on the anionic side, leading to particles which were stable and diffusible *in vivo*. Efforts in downsizing the particles were undertaken by complex formation in a decreasing salt gradient. Finally, cell binding by the anionic complexes was due to the asialoglycoprotein component. Transgene expression was achieved *in vivo* (Wu et al., 1989, 1991; Wilson et al., 1992; Stankovics et al., 1994; Frese et al., 1994), yet most of the DNA remained for days in intracellular vacuoles (Chowdhury et al., 1993). *In vitro* work showed that these complexes required the lysosomotropic weak base chloroquine to be efficiently released into the cytoplasm (Plank et al., 1992; Midoux et al., 1993; Wadhwa et al., 1995); ip injection of chloroquine prior to gene delivery *in vivo* was even attempted (Merwin et al., 1994).

We recently described a new property for an old compound (Boussif et al., 1995, 1996). Indeed, the versatile cationic polymer polyethylenimine (PEI) was found to be among the most efficient polycationic gene transfer vectors to date. PEI shares endosome buffering capacity with chloroquine, and this "proton sponge" effect provides the basis for endosomal escape for the PEI/DNA complexes. On the other hand, chemical adduction to the ethylenimine network does not seem to interfere with gene delivery (Remy et al., 1997). Therefore, PEI constitutes *per se* an outstanding core for the design of more sophisticated devices. Here, we demonstrate that neutral PEI/DNA complexes bearing galactose residues transfect efficiently and specifically hepatocyte-derived cell lines in the presence of serum and in the absence of any extra membrane-disrupting agent.

EXPERIMENTAL PROCEDURES

Chemicals. Polyethylenimine (25 kDa average M_w), lactose, maltose, and sodium cyanoborohydride were purchased from Aldrich (Saint Quentin-Fallavier, France). Asialofetuin and ethidium bromide were purchased from Sigma Chemical Co. (St. Louis, MO).

* Address correspondence to J.-P. Behr, Chimie Génétique, Faculté de Pharmacie, BP 24, 67401 Illkirch Cedex, France. Telephone: 33 (0)388 676983. Fax: 33 (0)388 678891. E-mail: behr@aspirine.u-strasbg.fr.

[©] Abstract published in *Advance ACS Abstracts*, October 1, 1997.

Glycosylation of Polyethylenimine. PEI (31 mg; 581 μmol of amine functions assuming a mean M_w of 43 Da for the repeating unit) and the disaccharides lactose or maltose (11 mg, 30 μmol , $M_w = 360.3$ Da) were dissolved in 1 mL of sodium borate buffer (200 mM, pH 8.5). After addition of sodium cyanoborohydride (5 equiv/disaccharide), the reaction mixture was incubated for 48 h at 40 °C in a water bath. After cooling to room temperature, the polymeric material was purified by ultrafiltration through an Amicon membrane (cutoff, 30 000 Da, Millipore) and washing with distilled water. Drying of the residue *in vacuo* led to 36 mg of glycosylated polyethylenimine. Carbohydrate quantitation with the resorcinol test led to 5% conjugation. *N/P* calculations for PEI-gal and PEI-glu (see below) were thus based on a mean M_w of 61 Da.

Cell Lines and Cell Culture. NIH 3T3 murine fibroblasts and HepG2 human hepatocarcinoma cell lines were purchased from ATCC (Rockville, MD) and grown in Dulbecco's modified Eagle medium (DMEM). BNL CL.2 murine hepatocytes were kindly provided by E. Wagner (Bender Co., Wien, Austria) and grown in high-glucose DMEM (4.5 g/L). All cell culture media were supplemented with 10% FCS (fetal calf serum, D. Dutcher, Brumath, France), 2 mM L-glutamine (Gibco BRL, Cergy-Pontoise, France), 100 units/mL penicillin (Gibco BRL), and 100 $\mu\text{g/mL}$ streptomycin (Gibco BRL). Cells were maintained at 37 °C in a 5% CO_2 humidified atmosphere. When 80% confluent, they were detached with saline trypsin/EDTA (Gibco, BRL) and grown in new flasks at a 1/10 dilution.

Plasmids. pCMV-luc and pCMV-NLSlacZ, encoding respectively the *Photinus pyralis* luciferase and the bacterial β -galactosidase genes under the control of the cytomegalovirus enhancer/promoter, were kindly provided by M. Scarpa (CRIBI, Padova, Italy). Plasmids were purified from *Escherichia coli* strain XL blue using Qiagen columns (Courtaboeuf, France).

Cell Transfection. Adherent cells were seeded in 24-well plates (Costar, D. Dutcher) the day before transfection so they could reach 60–70% confluence during transfection. All experiments were done in triplicate. Prior to transfection, cells were rinsed and 1 mL of culture medium complemented with 10% FCS was added. Two micrograms of the desired plasmid (from a ca. 1.5 mg/mL solution in 10 mM Tris/1 mM EDTA buffer at pH 7.4) was diluted into 50 μL of 0.15 M NaCl. The desired amount of 25 kDa PEI or glycosylated PEI [from 10 mM stock solutions of PEI, PEI-gal, or PEI-glu in water at pH 7.5; 1 *N/P* equivalent corresponds to the amount of polymer necessary to have one amino group (43 Da mean M_w for PEI and 61 Da for PEI derivatives) per phosphate of nucleic acid (330 Da mean M_w) (Boussif et al., 1996)] was diluted into 50 μL of 0.15 M NaCl, vortexed gently, and spun down.

Fifteen minutes later, the cationic vector was added at once to the plasmid solution [and not the reverse order; see Boussif et al. (1996)], mixed, vortexed, and spun down. The amounts and volumes given above refer to those in a single well and were actually 3-fold larger and distributed in three wells. After ca. 10 min, the resulting mixture was added to the cells and the cell supernatant was uniformly distributed with a gentle horizontal hand rotation. Immediately after, the cell culture dish was centrifuged (Sigma 3K10, Bioblock) for 5 min at 1500 rpm (ca. 280g). The cells were cultured for 24 h and then tested for reporter gene expression.

Luciferase Assay. Luciferase gene expression was measured by luminescence. The culture medium was discarded and cell lysate harvested upon cell incubation

for 30 min at room temperature in Lysis Reagent 1 \times (Promega, Madison, WI). The lysate was vortexed gently and centrifuged for 5 min at 14 000 rpm (ca. 17530g) at 4 °C. Twenty microliters of lysate was diluted into 100 μL of luciferase reaction buffer (Promega), and the luminescence was measured for 10 s (Biolumat LB 9500, Berthold, Wilbach, Germany). The results were expressed as light units per milligram of cell protein (BCA assay, Pierce).

X-Gal Staining. β -Galactosidase gene expression was detected by histochemical cell staining using X-Gal (Euromedex, Souffelweyersheim, France) as described (Boussif et al., 1996).

RESULTS

Synthesis and DNA Binding Properties of the PEI-gal Molecular Conjugate. Several types of ligands have been conjugated to polycations for transferring genes to hepatocytes following endocytosis *via* the asialoglycoprotein receptor: asialoorosomucoid, a natural protein ligand (Wu and Wu, 1987; Cristiano et al., 1993), multiantennary synthetic galactose derivatives (Remy et al., 1995; Plank et al., 1992; Wadhwa et al., 1995; Merwin et al., 1994), and simple galactose groups (Perales et al., 1994; Midoux et al., 1993; Chen et al., 1994; Martinezfong et al., 1994). We opted for the simplest solution as strong binding by individual residues may be unnecessary provided sufficient galactose residues are present on each PEI/DNA particle. The most straightforward way to link galactose to PEI is *via* imine formation of lactose (galactosyl- α 1,4-glucose, see Figure 1) with the amine functions of PEI, followed by *in situ* reduction back to a substituted amine (Martinezfong et al., 1994). This introduces a four-carbon hydrophilic spacer between the polymeric network and the galactose ligand.

The percentage of derivatization is an important factor to consider, too. A rough preliminary screening led to 5% of the total amine functions being a good choice. It should be noted that, in contrast to amide or thiourea linkers, the present sequence of chemical reactions does not decrease the original number of cationic charges borne by the polymer. Furthermore, in contrast to polylysine-based vectors, only a fraction (ca. 25%) of the amine functions of PEI are protonated at physiological pH (Boussif et al., 1995). Complex formation with anionic DNA is expected to increase this fraction, especially at a low PEI/DNA ratio. Some surface charge measurements (zetasizer, Malvern) confirmed this view since complexes were found to be neutral when PEI (nitrogen)/DNA (phosphate) *N/P* = 3. The ratio where DNA binding is complete was assessed by agarose gel electrophoresis of complexes formed between PEI or PEI-gal and plasmid DNA. As shown in Figure 2, all the DNA was retained for an *N/P* ratio of above 2, whether with the native or derivatized polymers. The best conditions for *in vivo* transfection would therefore be around *N/P* = 2–3.

Hepatocyte Transfection in Serum Remains Efficient at Low PEI-gal/DNA Charge Ratios. We recently worked out optimized conditions for transfection with lipopolyamines and PEI which tolerate the presence of serum (Boussif et al., 1996); these conditions have been used here to compare PEI to PEI-gal-mediated transfection for various cation/anion ratios. The pK_a 's of PEI being variable, this ratio was expressed as PEI amine monomer over DNA phosphate (*N/P*). A reasonable assumption is that, above DNA charge neutralization by PEI (*N/P* = 3), excess complexed PEI behaves as free PEI; i.e. every one out of four nitrogen atoms is protonated.

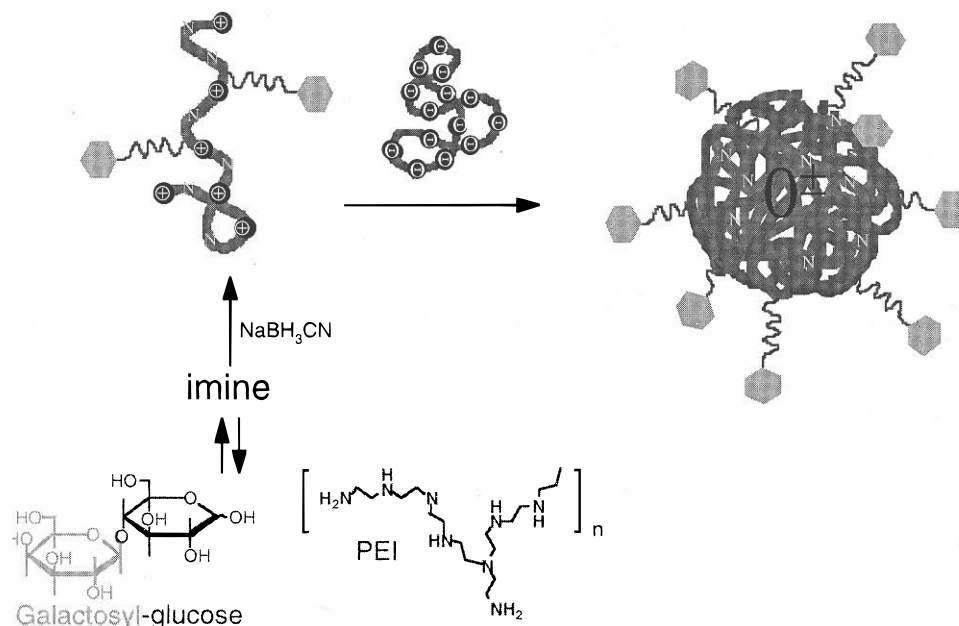


Figure 1. Idealized scheme for the conjugation of galactose to polyethylenimine *via* imine formation with lactose, and subsequent condensation of PEI-gal with plasmid DNA into neutral galactose-bearing complexes (objects are not to scale).

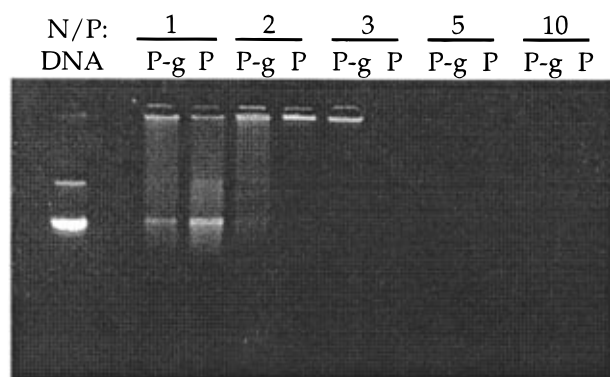


Figure 2. Analysis of complex formation by agarose gel electrophoresis. Above $N/P = 2$ (N/P is the molar ratio of PEI amine functions over DNA phosphates), all the DNA is complexed and remains in the well. pCMV-Luc plasmid DNA (2 μ g) was mixed with increasing amounts of PEI (lanes P) or of PEI-gal (lanes P-g) in a total volume of 100 μ L of 0.15 M NaCl as was performed for the transfection experiments (see Experimental Procedures). After 15 min, 10 μ L of each solution (200 ng/well) was loaded in a well for electrophoretic separation (0.8% agarose in 150 mM Tris-acetate buffer at pH 7; electrophoresis at 65 V for 90 min). DNA was visualized with ethidium bromide.

Adherent 3T3 murine fibroblasts, as expected, were efficiently transfected with cationic PEI/pCMV-Luc complexes ($N/P = 10$ –5, Figure 3a) which bind nonspecifically to anionic cell surface “receptors”. Neutral or anionic complexes ($N/P = 3$ –1) which cannot bind efficiently to the cells displayed poor transfection ability. These results were confirmed histochemically by cell counting after pCMV-NLSLucZ transfection (ca. 80 and $\ll 0.1\%$ transfected cells for $N/P = 10$ and 2, respectively; data not shown). Fibroblasts do not express [$\rho(-)$] the asialoglycoprotein receptor and are not expected to display enhanced PEI-gal-mediated gene delivery. In fact, galactose conjugation seemed even to interfere with the ionic cell binding process, as transfection ($N/P = 10$ and 5) decreased by 1–2 orders of magnitude.

Murine BNL CL.2 hepatocyte (Figure 3b) and human HepG2 hepatoma (Figure 3c) cell lines also were efficiently transfected by cationic PEI/DNA complexes [$>10^9$ LU/(mg of protein)] and showed similar trends toward poor transfection [10^4 – 10^5 LU/(mg of protein)] for

neutral complexes. Here however, galactose-bearing complexes retained high transfection levels down to below neutrality ($N/P = 3$ and 2). Decreasing the vector/plasmid ratio further ($N/P = 1$) led to a sharp efficiency decrease. Indeed, less DNA is complexed (Figure 2), fewer galactose residues are present on the complexes, and DNA may loop out of the anionic complexes and interfere with receptor binding.

Curves shown in panels a–c of Figure 3 are representative of six independent sets of experiments performed with two batches of PEI-gal, pCMV-Luc from several batches, and cells with various passage numbers. Absolute luciferase expression values stayed within 1 order of magnitude for ion-mediated PEI ($N/P = 10$) and galactose receptor-mediated PEI-gal ($N/P = 3$ and 2) transfections. Poor ion-mediated transfection values with neutral PEI/DNA complexes were more scattered (2 orders of magnitude). This had been noticed previously for cationic lipids (Remy et al., 1995) and may be attributed to the fact that neutral complexes are unstable (Jaaskelainen et al., 1994) and that a weak interaction with cells is prone to larger binding variations. Relative values taken from this large set of data however confirmed the conclusions derived above.

Neutral PEI-gal/DNA Complexes Show a 10^4 – 10^5 -Fold Selectivity for Hepatocytes. We compared transfection results obtained on $\rho(+)$ and $\rho(-)$ cells with neutral PEI-gal/DNA complexes in simultaneous experiments to provide an idea of the targeting efficiency in conditions relevant to *in vivo* transfection. A fair comparison should include cells transfectable to similar extents with nontargeted vectors in serum. As shown above, BNL CL.2 [$\rho(+)$], HepG2 [$\rho(+)$], and 3T3 cells [$\rho(-)$] fulfill this condition. With regard to the charge of the PEI-gal/DNA complexes, electrophoresis showed that most of the DNA remained in the well when $N/P = 2$ and that the residual faint smear disappeared when $N/P = 3$ (Figure 2). As discussed in the previous paragraphs, this and surface charge measurements are good evidence for the formation of slightly anionic and neutral complexes at these ratios, respectively.

Transfection of BNL CL.2 and HepG2 hepatocyte cell lines with PEI-gal/pCMV-Luc complexes at $N/P = 3$ and 2 was very efficient [0.6 – 1×10^9 LU/(mg of protein)];

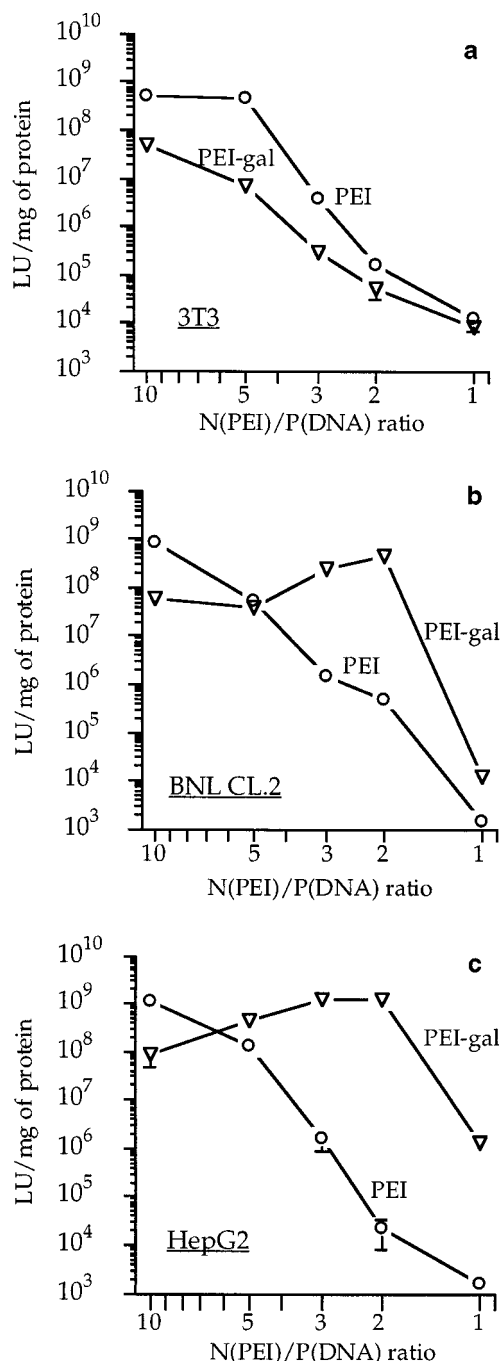


Figure 3. Graph of transfection efficiency vs vector/DNA ratio. 3T3 fibroblast (a), BNL CL.2 (b), and HepG2 (c) hepatocyte cell lines were transfected in the presence of 10% serum with 2 μ g of pCMV-Luc plasmid/well and the desired amount of PEI and PEI-gal as described in Experimental Procedures. Values are the mean \pm SD of three experiments. For most experiments, circles and triangles on the graphs were larger than standard deviations.

transfection of 3T3 fibroblasts was 10⁴–10⁵-fold less efficient (Figure 4). This very large factor was confirmed histochemically following transfection with the pCMV-NLSLacZ reporter gene; BNL CL.2 cells showed >50% blue nuclei (Figure 5), whereas 3T3 cells hardly showed any (0–2 cells/well, i.e. 0–0.002%, not shown).

Transfection of Hepatocytes Is Receptor-Mediated. The external membrane of hepatocytes is rich in receptors that bind and internalize terminal galactose-bearing asialoglycoproteins. Preliminary evidence for the involvement of these receptors in the gene delivery process was inferred from the high level of reporter gene

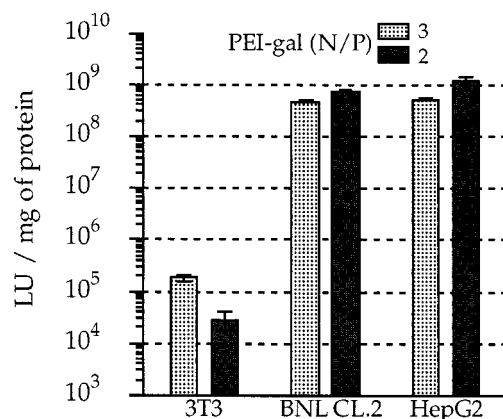


Figure 4. Neutral galactose-bearing complexes deliver genes selectively to hepatocytes. 3T3 fibroblast and hepatocyte (BNL CL.2 and HepG2) cell lines were transfected in a single run with 2 μ g of pCMV-Luc and PEI or PEI-gal (N/P = 2–3) as described in Experimental Procedures. Values are the mean \pm SD of three experiments.

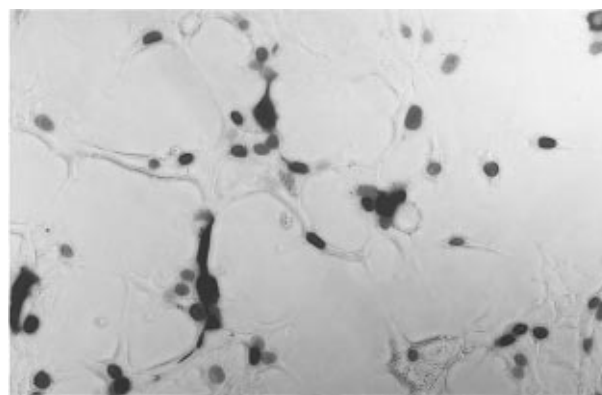


Figure 5. Transfection of BNL CL.2 hepatocytes with neutral PEI-gal/DNA complexes is very efficient. Cells were transfected in 10% serum with PEI-gal and 2 μ g of pCMV-NLSLacZ at N/P = 2. After 24 h, cell permeabilization and histochemical staining with X-gal revealed >50% NLSLacZ-positive cell nuclei. Control experiments at N/P = 2 performed with PEI on BNL CL.2 cells and with PEI-gal or PEI on 3T3 cells showed 0–2 blue nuclei per 10⁵ cells in a well.

expression that was observed with neutral PEI-gal/DNA complexes (see above and compare experiments 1 and 6 with experiment 11 in Figure 6).

Additional evidence came from the following comparisons. Removal of the targeting element (galactose) present on the complexes resulted in complete loss of transfection for ρ (+) cells (Figure 6, experiments 2 and 7 vs 1 and 6); no such change was observed for ρ (–) cells (Figure 6, experiment 12 vs 11). However, a glycosylated vector may have other properties affected besides the targeting phenomenon. We therefore synthesized a 5% glucose-bearing polyethylenimine (PEI-glu) by reacting the disaccharide maltose with PEI under the conditions described for PEI-gal. Transfection of 3T3 cells with PEI-glu was negligible and close to that obtained with PEI-gal (experiments 11 and 13); with hepatocytes, however, transfection became 10000- and 100000-fold less effective (experiments 1 and 6 vs 3 and 8). Finally, asialofetuin (ASF), a natural glycoprotein ligand of the receptor, was added to the cell culture medium during transfection (1 mg/well). This protein was not toxic to the cells, nor did it interfere with receptor-independent transfection (Figure 6, experiments 4 and 9). However, competition between PEI-gal/DNA complexes and ASF (36 molar equiv excess with respect to galactose) decreased transfection to very low levels (Figure 6, experi-

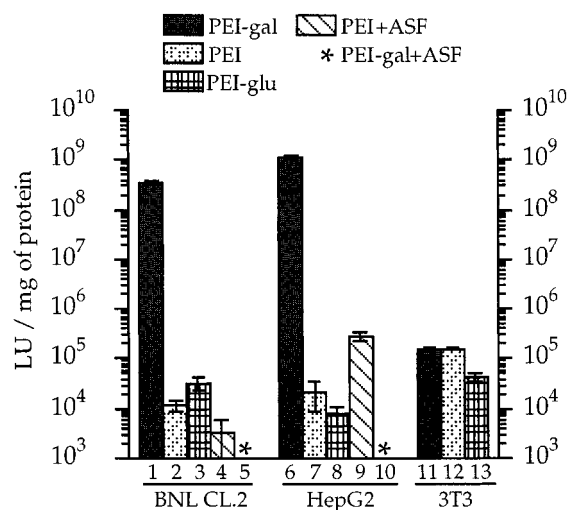


Figure 6. Comparative experiments favoring a receptor-mediated gene delivery process. Cells were transfected with PEI-gal, PEI, or PEI-glu complexed to 2 μ g of pCMV-Luc DNA at $N/P = 2$ in the presence of 10% serum. Luciferase activity was important only for hepatocytes with PEI-gal. Addition of asialofetuin (ASF at 1 mg/well, 36 molar equiv with respect to galactose) 10 min before addition of the complexes abolished transfection in this case also [$*$ is $<10^3$ RLU/(mg of protein)].

ments 5 and 10). Taken together, data from comparative and competitive experiments all point to the involvement of the asialoglycoprotein receptor in hepatocyte transfection with PEI-gal/DNA complexes.

DISCUSSION

Hepatocytes are interesting as target cells for several reasons. The asialoglycoprotein receptor they express is well-characterized and abundant, and its interaction with a ligand leads to endocytosis. Furthermore, the liver is the center organ of several genetic, acquired, and viral diseases amenable to gene therapy (Frese et al., 1994; Ledley, 1993). Successful *in vitro* targeting of hepatocytes has been demonstrated in many cases, with variable (10^4 – 10^5 -fold) selectivities and experimental conditions (Plank et al., 1992; Midoux et al., 1993; Cristiano et al., 1993; Merwin et al., 1994; Chen et al., 1994; Remy et al., 1995; Wadhwa et al., 1995). In our experimental setup, PEI-gal is more selective, with factors in the range of 10^4 – 10^5 -fold. Due to its endosome-buffering property, PEI-gal is also intrinsically more efficient than polylysine-based vectors which require chloroquine (Plank et al., 1992; Midoux et al., 1993; Merwin et al., 1994; Wadhwa et al., 1995), fusogenic oligopeptides (Plank et al., 1992; Midoux et al., 1993), or adenoviral particles (Plank et al., 1992; Cristiano et al., 1993) to be efficiently released in the cell cytoplasm (all these additives would cause either toxicity or immunological problems *in vivo*). Indeed, with neutral complexes and although cells were maintained in 10% serum, over 50% of hepatocytes were transfected, corresponding to 10^9 LU/(mg of protein) with the luciferase reporter gene; these values fell to 0.002% and 5×10^4 LU/(mg of protein) in the absence of the receptor, respectively. Receptor-mediated transfection in our conditions is thus very close to an all-or-nothing process; most of the 10^5 $\rho(+)$ cells in a well [whereas only a few $\rho(-)$ cells] are transfected, leading to the extreme range found above. This interpretation is in agreement with a "quantum" transfection when strongly driven reporter genes are used, as discussed earlier (Boussif et al., 1996).

Other attractive features of this delivery system in relation to targeting of the liver are consequences of its

electroneutrality. The particles should not bind to extracellular matrix anionic proteoglycans, and neutral PEI/DNA complexes have also been shown to have reduced complement activation properties (Plank et al., 1996). Yet on the extreme sides of the fate of a therapeutic plasmid, i.e. complex formation with the vector and nuclear membrane crossing, the most challenging problems remain unsolved. (i) Downsizing of the particles to avoid Kupffer cells and to cross the vascular endothelium fenestration is one problem. Gene transfer *in vivo* with small polylysine-gal/DNA complexes has been reported (Perales et al., 1994); unfortunately, preliminary transmission electron microscopy pictures of PEI-gal/DNA complexes show rather large and polydisperse 100–400 nm particles. (ii) Restricted cytoplasmic diffusion (whether concerning the PEI/plasmid complexes or the free plasmid) and nuclear membrane crossing are the main barriers to gene delivery with cationic vectors (Labat-Moleur et al., 1996; Zabner et al., 1995). Whereas no satisfactory solution for crossing the nuclear membrane has been described so far, hepatocytes may provide a solution to intracellular trafficking. Indeed, in contrast to the forced and "unnatural" endocytosis process of cationic vector/DNA particles (Labat-Moleur et al., 1996), receptor-mediated DNA uptake into hepatocytes with PEI-gal may lead to endosomes which are able to travel along microtubules toward the centrosome, which is located very close to the nucleus (Novikoff et al., 1996).

ACKNOWLEDGMENT

We are grateful to Jean-Serge Remy and Patrick Erbacher for electron microscopy and surface charge measurements. This work was supported by the Association Française de Lutte contre la Mucoviscidose, the Association Française contre les Myopathies, the Association pour la Recherche contre le Cancer, Rhône-Poulenc Rorer (A.A.), and Transgene S.A. (M.-A.Z.).

LITERATURE CITED

- Behr, J., Demeneix, B., Loeffler, J., and Perez-Mutul, J. (1989) Efficient gene transfer into mammalian primary endocrine cells with lipopolyamine-coated DNA. *Proc. Natl. Acad. Sci. U.S.A.* 86, 6982–6986.
- Boussif, O., Lezoualch, F., Zanta, M. A., Mergny, M. D., Scherman, D., Demeneix, B., and Behr, J. P. (1995) A versatile vector for gene and oligonucleotide transfer into cells in culture and in vivo: Polyethylenimine. *Proc. Natl. Acad. Sci. U.S.A.* 92, 7297–7301.
- Boussif, O., Zanta, M. A., and Behr, J. P. (1996) Optimized galenics improve in vitro gene transfer with cationic molecules up to thousand-fold. *Gene Ther.* 3, 1074–1080.
- Caplen, N. J., Gao, X., Hayes, P., Elaszwarapu, R., Fisher, G., Kinrade, E., Chakera, A., Schorr, J., Hughes, B., Dorin, J. R., Porteous, D. J., Alton, E. W. F. W., Geddes, D. M., Coutelle, C., Williamson, R., Huang, L., and Gilchrist, C. (1994) Gene therapy for cystic fibrosis in humans by liposome-mediated DNA transfer: The production of resources and the regulatory process. *Gene Ther.* 1, 139–147.
- Chen, J., Stickles, R. J., and Daichendt, K. A. (1994) Galactosylated Histone-Mediated Gene Transfer and Expression. *Hum. Gene Ther.* 5, 429–435.
- Chowdhury, N. R., Wu, C. H., Wu, G. Y., Yerneni, P. C., Bommineni, V. R., and Chowdhury, J. R. (1993) Fate of DNA Targeted to the Liver by Asialoglycoprotein Receptor-Mediated Endocytosis In vivo—Prolonged Persistence in Cytoplasmic Vesicles After Partial Hepatectomy. *J. Biol. Chem.* 268, 11265–11271.
- Cristiano, R. J., Smith, L. C., and Woo, S. L. C. (1993) Hepatic gene therapy: adenovirus enhancement of receptor-mediated gene delivery and expression in primary hepatocytes. *Proc. Natl. Acad. Sci. U.S.A.* 90, 2122–2126.

- Crystal, R. G. (1995) Transfer of Genes to Humans: Early Lessons and Obstacles to Success. *Science* 270, 404–410.
- Frese, J., Wu, C. H., and Wu, G. Y. (1994) Targeting of genes to the liver with glycoprotein carriers. *Adv. Drug Delivery Rev.* 14, 137–152.
- Jaaskelainen, I., Monkkonen, J., and Urtti, A. (1994) Oligonucleotide-cationic liposome interactions. A physicochemical study. *Biochim. Biophys. Acta* 1195, 115–123.
- Labat-Moleur, F., Steffan, A.-M., Brisson, C., Perron, H., Feugeas, O., Furstenberger, P., Oberling, F., Brambilla, E., and Behr, J.-P. (1996) An electron microscopy study into the mechanism of gene transfer with lipopolyamines. *Gene Ther.* 3, 1010–1017.
- Ledley, F. D. (1993) Hepatic Gene Therapy: Present and Future. *Hepatology* 18, 1263–1273.
- Lee, E. R., Marshall, J., Siegel, C. S., Jiang, C., Yew, N. S., Nichols, M. R., Nietupski, J. B., Ziegler, R. J., Lane, M., Wang, K. X., Wan, N. C., Scheule, R. K., Harris, D. J., Smith, A. E., and Cheng, S. H. (1996) Detailed Analysis of Structures and Formulations of Cationic Lipids for Efficient Gene Transfer to the Lung. *Hum. Gene Ther.* 7, 1701–1717.
- Logan, J. J., Bebok, Z., Walker, L. C., Peng, S. Y., Felgner, P. L., Siegal, G. P., Frizzell, R. A., Dong, J. Y., Howard, M., Matalon, S., Lindsey, J. R., Duvall, M., and Sorscher, E. J. (1995) Cationic lipids for reporter gene and CFTR transfer to rat pulmonary epithelium. *Gene Ther.* 2, 38–49.
- Martinezfong, D., Mullersman, J. E., Purchio, A. F., Armendarizborunda, J., and Martinezhernandez, A. (1994) Nonenzymatic glycosylation of poly-L-lysine: A new tool for targeted gene delivery. *Hepatology* 20, 1602–1608.
- McLachlan, G., Davidson, D. J., Stevenson, B. J., Dickinson, P., Davidsonsmith, H., Dorin, J. R., and Porteous, D. J. (1995) Evaluation in vitro and in vivo of cationic liposome-expression construct complexes for cystic fibrosis gene therapy. *Gene Ther.* 2, 614–622.
- Merwin, J. R., Noell, G. S., Thomas, W. L., Chiou, H. C., DeRome, M. E., McKee, T. D., Spitalny, G. L., and Findeis, M. A. (1994) Targeted Delivery of DNA Using YEE(GalNAcAH)₃, a Synthetic Glycopeptide Ligand for the Asialoglycoprotein Receptor. *Bioconjugate Chem.* 5, 612–620.
- Midoux, P., Mendes, C., Legrand, A., Raimond, J., Mayer, R., Monsigny, M., and Roche, A. C. (1993) Specific Gene Transfer Mediated By Lactosylated Poly-L-Lysine Into Hepatoma Cells. *Nucleic Acids Res.* 21, 871–878.
- Mislick, K. A., and Baldeschwieler, J. D. (1996) Evidence for the role of proteoglycans in cation-mediated gene transfer. *Proc. Natl. Acad. Sci. U.S.A.* 93, 12349–12354.
- Nabel, E. G., Yang, Z. Y., Muller, D., Chang, A. E., Gao, X., Huang, L., Cho, K. J., and Nabel, G. J. (1994) Safety and toxicity of catheter gene delivery to the pulmonary vasculature in a patient with metastatic melanoma. *Hum. Gene Ther.* 5, 1089–1094.
- Nabel, G. J., Nabel, E. G., Yang, Z. Y., Fox, B. A., Plautz, G. E., Gao, X., Huang, L., Shu, S. Y., Gordon, D., and Chang, A. E. (1993) Direct Gene Transfer with DNA-Liposome Complexes in Melanoma—Expression, Biologic Activity, and Lack of Toxicity in Humans. *Proc. Natl. Acad. Sci. U.S.A.* 90, 11307–11311.
- Noguiezhellin, P., Robertlemer, M., Salzmann, J. L., and Klatzmann, D. (1996) Plasmoviruses: Nonviral viral vectors for gene therapy. *Proc. Natl. Acad. Sci. U.S.A.* 93, 4175–4180.
- Novikoff, P. M., Cammer, M., Tao, L., Oda, H., Stockert, R. J., Wolkoff, A. W., and Satir, P. (1996) Three-dimensional organization of rat hepatocyte cytoskeleton: Relation to the asialoglycoprotein endocytosis pathway. *J. Cell Sci.* 109, 21–32.
- Perales, J. C., Ferkol, T., Beegen, H., Ratnoff, O. D., and Hanson, R. W. (1994) Gene Transfer in Vivo—Sustained Expression and Regulation of Genes Introduced into the Liver by Receptor-Targeted Uptake. *Proc. Natl. Acad. Sci. U.S.A.* 91, 4086–4090.
- Plank, C., Zatloukal, K., Cotten, M., Mechtler, K., and Wagner, E. (1992) Gene Transfer into Hepatocytes Using Asialoglycoprotein Receptor Mediated Endocytosis of DNA Complexed with an Artificial Tetra-Antennary Galactose Ligand. *Bioconjugate Chem.* 3, 533–539.
- Plank, C., Mechtler, K., Szoka, F. C., and Wagner, E. (1996) Activation of the Complement System by Synthetic DNA Complexes: A Potential Barrier for Intravenous Gene Delivery. *Hum. Gene Ther.* 7, 1441–1450.
- Remy, J. S., Kichler, A., Mordvinov, V., Schuber, F., and Behr, J. P. (1995) Targeted gene transfer into hepatoma cells with lipopolyamine-condensed DNA particles presenting galactose ligands: A stage toward artificial viruses. *Proc. Natl. Acad. Sci. U.S.A.* 92, 1744–1748.
- Remy, J. S., Abdallah, B., Zanta, M. A., Boussif, O., Behr, J. P., and Demeneix, B. (1997) Gene transfer with lipospermines and polyethylenimines. *Adv. Drug Delivery Rev.* (in press).
- Schwartz, B., Benoist, C., Abdallah, B., Scherman, D., Behr, J. P., and Demeneix, B. A. (1995) Lipospermine-based gene transfer into the newborn mouse brain is optimized by a low lipospermine DNA charge ratio. *Hum. Gene Ther.* 6, 1515–1524.
- Stankovics, J., Crane, A. M., Andrews, E., Wu, C. H., Wu, G. Y., and Ledley, F. D. (1994) Overexpression of human methylmalonyl CoA mutase in mice after in vivo gene transfer with asialoglycoprotein/polylysine/DNA complexes. *Hum. Gene Ther.* 5, 1095–1104.
- Stephan, D. J., Yang, Z.-Y., San, H., Simari, R. D., Wheeler, C. J., Felgner, P. L., Gordon, D., Nabel, G. J., and Nabel, E. G. (1996) A New Cationic Liposome DNA Complex Enhances the Efficiency of Arterial Gene Transfer In Vivo. *Hum. Gene Ther.* 7, 1803–1812.
- Stribling, R., Brunette, E., Liggitt, D., and Gaensler, K. a. D. R. (1992) Aerosol gene delivery in vivo. *Proc. Natl. Acad. Sci. U.S.A.* 89, 11277–11281.
- Thierry, A. R., Lunardiiskandar, Y., Bryant, J. L., Rabinovich, P., Gallo, R. C., and Mahan, L. C. (1995) Systemic gene therapy: Biodistribution and long-term expression of a transgene in mice. *Proc. Natl. Acad. Sci. U.S.A.* 92, 9742–9746.
- Tsukamoto, M., Ochiya, T., Yoshida, S., Sugimura, T., and Terada, M. (1995) Gene transfer and expression in progeny after intravenous DNA injection into pregnant mice. *Nat. Genet.* 9, 243–248.
- Wadhwa, M. S., Knoell, D. L., Young, A. P., and Rice, K. G. (1995) Targeted gene delivery with a low molecular weight glycopeptide carrier. *Bioconjugate Chem.* 6, 283–291.
- Wilson, J. M., Grossman, M., Wu, C. H., Chowdhury, N. R., Wu, G. Y., and Chowdhury, J. R. (1992) Hepatocyte-Directed Gene Transfer In vivo Leads To Transient Improvement Of Hypercholesterolemia In Low Density Lipoprotein Receptor-Deficient Rabbits. *J. Biol. Chem.* 267, 963–967.
- Wu, C. H., Wilson, J. M., and Wu, G. Y. (1989) Targeting Genes—Delivery And Persistent Expression Of A Foreign Gene Driven By Mammalian Regulatory Elements In vivo. *J. Biol. Chem.* 264, 16985–16987.
- Wu, G. Y., and Wu, C. H. (1987) Receptor-mediated in vitro gene transformation by a soluble DNA carrier system. *J. Biol. Chem.* 262, 4429–4432.
- Wu, G. Y., Wilson, J. M., Shalaby, F., Grossman, M., Shafritz, D. A., and Wu, C. H. (1991) Receptor-Mediated Gene Delivery In vivo—Partial Correction Of Genetic Analbuminemia In Nagase Rats. *J. Biol. Chem.* 266, 14338–14342.
- Zabner, J., Fasbender, A. J., Moninger, T., Poellinger, K. A., and Welsh, M. J. (1995) Cellular and molecular barriers to gene transfer by a cationic lipid. *J. Biol. Chem.* 270, 18997–19007.

BC970098F

Neoglycoproteins with the Synthetic Complex Biantennary Nonasaccharide or Its $\alpha 2,3/\alpha 2,6$ -Sialylated Derivatives: Their Preparation, Assessment of Their Ligand Properties for Purified Lectins, for Tumor Cells *in Vitro*, and in Tissue Sections, and Their Biodistribution in Tumor-Bearing Mice

Sabine André,[†] Carlo Unverzagt,[‡] Shuji Kojima,[§] Xin Dong,^{†,||} Christian Fink,[†] Klaus Kayser,[⊥] and Hans-Joachim Gabius^{*,†}

Institut für Physiologische Chemie, Tierärztliche Fakultät, Ludwig-Maximilians-Universität, Veterinärstrasse 13, D-80539 München, Germany, Institut für Organische Chemie und Biochemie, Technische Universität, Lichtenbergstrasse 4, D-85748 Garching, Germany, Department of Biomedical Science-1, Research Institute for Biosciences, Science University of Tokyo, 2669 Yamazaki, Noda-Shi, Chiba 278, Japan, Department of Biochemistry, Glycoconjugate Laboratory, Shanghai Medical University, 138 Yi Xue Yuan Road, Shanghai 200032, People's Republic of China, and Abteilung Pathologie, Thoraxklinik, Amalienstrasse 5, D-69126 Heidelberg, Germany. Received February 19, 1997[®]

Neoglycoproteins were prepared with chemoenzymatically synthesized complex biantennary *N*-glycan derivatives the nonreducing ends of which bear typical sequences found in glycoproteins. A chemically obtained biantennary heptasaccharide–azide was reduced and acylated with a 6-aminohexanoyl spacer. Elongation of the deprotected heptasaccharide using glycosyltransferases yielded a biantennary nonasaccharide with terminal galactose residues and two undecasaccharides terminating with $\alpha 2,6$ - or $\alpha 2,3$ -linked sialic acid. The free amino group of the spacer of these oligosaccharides was converted into an isothiocyanate. Its subsequent coupling to bovine serum albumin gave neoglycoproteins with a yield of 2.4–3.6 glycan chains per carrier molecule. This versatile synthetic pathway allows employment of a wide variety of complex-type glycans, which can be introduced to various test systems *in vitro* and *in vivo* to evaluate potential biomedical applications. Solid-phase assays with biotinylated sugar receptors revealed discriminatory binding properties of the three neoglycoproteins, especially for the mistletoe lectin. This direct assay system is preferable to the measurement of inhibitory capacities with respect to model ligands. Ligand type- and cell type-dependent quantitative differences in the binding properties of the probes were detected by FACScan analyses with a panel of tumor cell lines and by monitoring of staining in tissue sections for small cell and non-small-cell lung cancer and mesotheliomas. Biodistribution of iodinated neoglycoproteins in mice gave a prolonged presence of the sialylated probes in serum. Relative to the nonasaccharide, the uptake, especially of the iodinated neoglycoprotein with $\alpha 2,3$ -sialylated ligand chains, was clearly elevated in mice for kidneys and Ehrlich tumors. On the basis of the documented feasibility of these applications, it is concluded that the further elaboration of glycan chain variants by the described synthetic approach in combination with the given test panel is warranted to evaluate the potential of complex glycan chain-carrying neoglycoproteins for diagnostic and therapeutic purposes.

INTRODUCTION

Due to their enormous structural variability, oligosaccharides are predestined to store and to transmit biological information (1). Physiologically, the recognition of distinct carbohydrate ligands by lectins is involved in various functionally important processes such as cell adhesion or glycoprotein routing (2). This wide-ranging relevance of protein–carbohydrate interactions explains the efforts to construct tailor-made neoglycoconjugates as defined tools to explore medical applications (3, 4). Already experimentally verified possibilities encompass lectin-mediated drug targeting, especially to the C-type asialoglycoprotein receptor of hepatocytes, and lectin visualization in morphological or diagnostic approaches

(5–15). It is reasonable to assume that the extension of the ligand complexity from often used mono- or disaccharides will enhance the selectivity of the synthetic product for respective receptors. Purified glycopeptides obtained from natural glycoproteins are an obvious choice to gain access to the required oligosaccharide part (16, 17). The continuous improvement in the preparative capabilities to produce oligosaccharides by combined chemical and enzymatic synthesis enables us to take an alternative route to neoglycoproteins with complex sugar chains. Having recently described the chemoenzymatic synthesis of the $\alpha 2,6$ -sialylated complex biantennary undecasaccharide attached to asparagine (18), the basis is therefore established to prepare neoglycoproteins with deliberate changes in the terminal part of the sugar antennae to study the ligand properties of the individual variants. Following the experimental description of the formation of the reactive derivatives of the complex biantennary nonasaccharide and the two $\alpha 2,3/\alpha 2,6$ -sialylated undecasaccharides and their conjugation to bovine serum albumin, the structures of the relevant parts being shown in Figure 1, we herein document the

* Author to whom correspondence should be addressed.

[†] Ludwig-Maximilians-Universität.

[‡] Technische Universität.

[§] Science University of Tokyo.

^{||} Shanghai Medical University.

[⊥] Thoraxklinik.

[®] Abstract published in *Advance ACS Abstracts*, October 15, 1997.

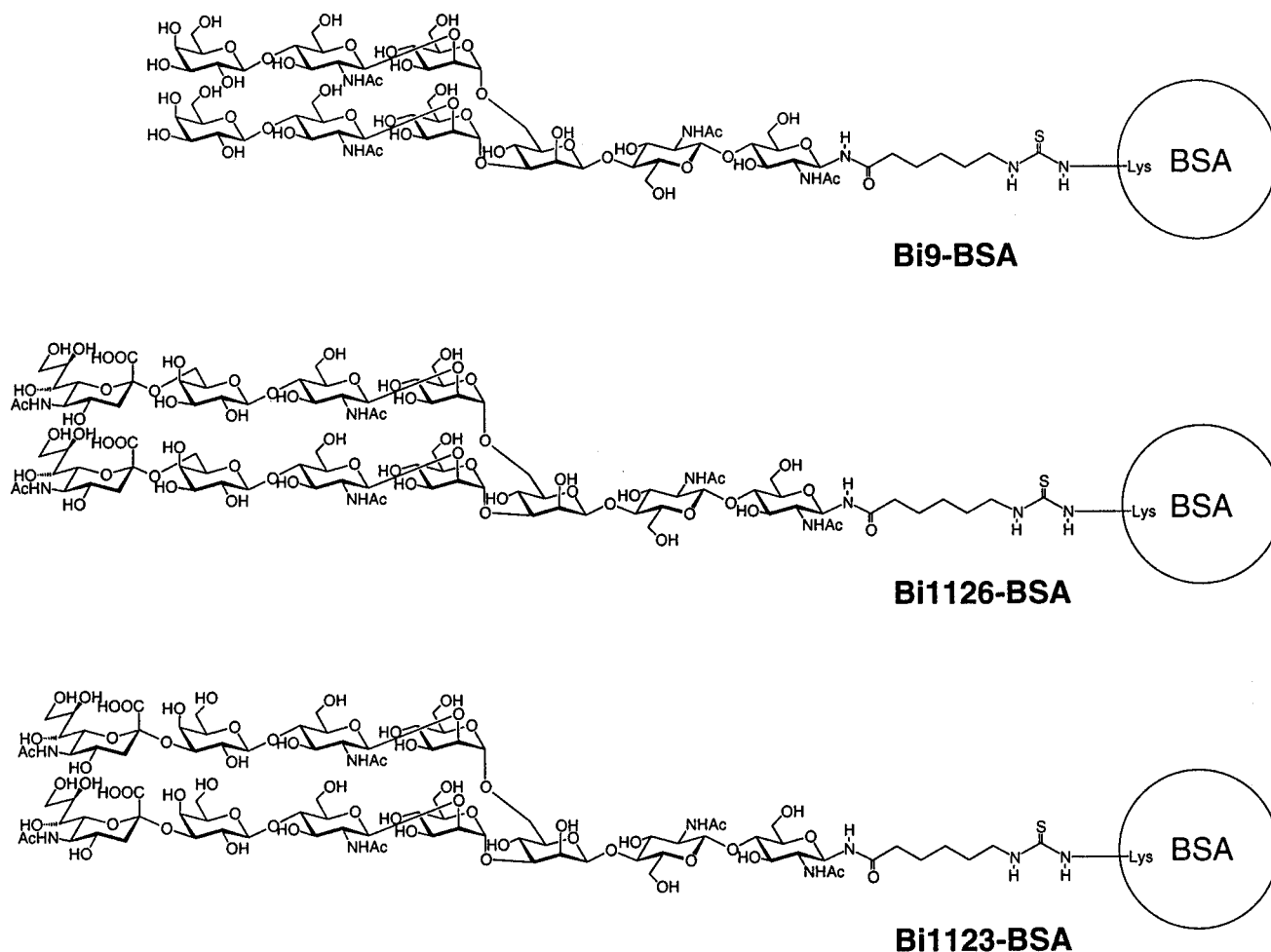


Figure 1. Neoglycoproteins with BSA as carrier for the complex biantennary nonasaccharide **5** (Bi9-BSA) and the two undecasaccharides **6** and **7**, namely the α 2,6-sialylated form (Bi1126-BSA) and the α 2,3-sialylated isomer (Bi1123-BSA). The linker arm and the attachment point to an ϵ -amino group of lysine on the carrier protein are also shown.

comparative analysis of the use of the resulting neoglycoproteins as ligands in solid-phase assays with three different types of purified sugar receptor. To initiate the evaluation of their potential as medical tools, we present the results on binding to purified sugar receptors, to the surface of cells of established tumor lines *in vitro*, and to tumor cells in tissue sections from different types of lung cancer as well as on biodistribution in tumor-bearing mice *in vivo*.

EXPERIMENTAL PROCEDURES

General. NMR spectra were recorded with a Bruker AMX 500 spectrometer. HPLC separations were performed on a Pharmacia LKB gradient system 2249 equipped with a Pharmacia LKB Detector VWM 2141 (Freiburg, Germany). For size exclusion chromatography a Pharmacia Hi Load Superdex 30 column (600 \times 16 mm) was used; RP-HPLC was performed on a Macherey-Nagel Nucleogel RP 100-8 column (300 \times 7.7 mm). Bovine serum albumin (BSA), β 1,4-galactosyltransferase, α 2,6-sialyltransferase, and nucleotide sugars were purchased from Sigma (Munich, Germany), and alkaline phosphatase (calf intestine, molecular biology grade) was purchased from Boehringer Mannheim (Germany). Mass spectra were recorded by Dr. D. Renauer at the Boehringer Mannheim research facility (Tutzing, Germany) on a Voyager Biospectrometry workstation (Vestec/Perseptive) MALDI-TOF mass spectrometer, using 2,5-dihydroxybenzoic acid (DHB) as a matrix. We are grateful to Prof. J. C. Paulson (Cytel Corp., San Diego, CA) for a sample of recombinant α 2,3-sialyltransferase (19).

The structures of the synthetic *N*-glycans were confirmed by the following 2D-NMR experiments: TOCSY, NOESY, HMQC, HMQC-COSY, HMQC-DEPT, and HMQC-TOCSY. NMR spectra were assigned according to the following convention:



The general outline for the derivatization of the synthetic heptasaccharide-azide, prepared previously (20), to the final products with a convenient linker group for attachment to albumin is given in Figure 2.

N'-(6-Benzoyloxycarbonyl-6-aminohexanoylamido)-O-(2-acetamido-2-deoxy- β -D-glucopyranosyl)-(1 \rightarrow 2)-O- α -D-mannopyranosyl-(1 \rightarrow 3)-O-[(2-acetamido-2-deoxy- β -D-glucopyranosyl)-(1 \rightarrow 2)-O- α -D-mannopyranosyl-(1 \rightarrow 6)]-O- β -D-mannopyranosyl-(1 \rightarrow 4)-O-(2-acetamido-3,6-di-O-benzyl-2-deoxy- β -D-glucopyranosyl)-(1 \rightarrow 4)-2-acetamido-2-deoxy- β -D-glucopyranoside, **3 (Bzl₄Bi7AH-Z).** To a 60 mg portion (35.2 μ mol) of **1** dissolved in 2 mL of absolute methanol was added 60 μ L of ethyldiisopropylamine. The flask was filled with an argon atmosphere, and 180 μ L of propane-1,3-dithiol, which efficiently reduces azides to amines (21), was pipetted to the mixture. After 4 h (TLC: 2-propanol/1 M ammonium acetate, 4:1), the reaction mixture was concentrated and

dried under high vacuum for 15 min. Subsequently, the remainder was dissolved in a solution of 80 mg (185 μ mol) of **2**, 40 mg (261 μ mol) of HOBt, and 45 μ L (265 μ mol) of ethyldiisopropylamine in 1.9 mL of *N*-methylpyrrolidone. After complete reaction of the glycosylamine (TLC: 2-propanol/1 M ammonium acetate, 4:1; R_f amine = 0.36; R_f **3** = 0.53), the solvent was removed under high vacuum and the remainder was triturated with 20 mL of water. After centrifugation of the solution, the supernatant was loaded into a plastic syringe and passed through an array of two connected Waters Sep-Pak cartridges followed by 20 mL of water. A first elution with 10 mL of acetonitrile/water 1:4 washed off side products. The product was eluted with 15 mL of acetonitrile/water 3:2, lyophilized, and purified by RP-HPLC (column, Macherey-Nagel Nucleogel RP 100-8, 300 \times 7.7 mm; mobile phase, gradient of 20–45% acetonitrile over 27 min; flow rate, 2 mL/min; detection at 220 and 260 nm). The pooled fractions, containing 38 mg of **3** (56% yield), were lyophilized and analyzed: $[\alpha]^{23}_D = +2.5^\circ$ (0.5, methanol); $C_{92}H_{126}N_6O_{38}$ (1924.02), FAB-MS (thioglycerine) calcd value 1922.8, found 1924 (M + 1), 1946 (M + Na); 1H NMR (500 MHz, DMSO- d_6) δ 8.18 (d, $J_{NH,1} = 9.0$ Hz, 1H, NH-1'), 7.99 (d, $J_{NH,2} = 7.4$ Hz, 1H, NH-2'), 7.90 (d, $J_{NH,2} = 8.8$ Hz, 1H, NH-2'), 7.58, 5.57 (2d, $J_{NH,2} = 8.6$ Hz, 2H, NH-2', NH-2'), 7.37–7.16 (m, 21H, Ar, NH urethane), 5.01–4.94 (m, 9H, H-1', H-1', OH-3', OH-3', OH-4', OH-4', OH-4', CH₂O), 4.75 (d, $J_{OH,4} = 4.9$ Hz, 1H, OH-4'), 4.71 (d, $J_{OH,4} = 4.9$ Hz, 1H, OH-4'), 4.66 (d, $J_{1,2} < 1.0$ Hz, 1H, H-1'), 4.62–4.42 (m, 11H, H-1', H-1', OH-2', OH-6', OH-6', OH-6', CH₂O), 4.36 (d, $J_{1,2} = 8.3$ Hz, 1H, H-1'), 4.32 (d, $J_{gem} = 12.2$ Hz, 1H, CH₂O), 4.23 (d, $J_{1,2} = 8.2$ Hz, 1H, H-1'), 4.19 (t, $J_{OH,6} = 6.6$ Hz, 1H, OH-6'), 3.99–3.94 (m, 2H, H-2', OH-3'), 3.91 (d, $J_{OH,4} = 8.0$ Hz, 1H, OH-3'), 3.88–3.83 (m, 2H, H-2', H-4'), 3.14–3.02 (m, 5H, H-4', H-4', H-5', H-5', H-5'), 2.94 (m, 2H, ϵ CH₂ AH), 2.03 (m, 2H, α CH₂ AH), 1.80, 1.77, 1.73 (3s, 12H, NAc), 1.42 (m, 2H, β CH₂ AH), 1.36 (m, 2H, δ CH₂ AH), 1.18 (m, 2H, γ CH₂ AH); ^{13}C NMR (125 MHz, DMSO- d_6) δ 172.6 C=O amide, 169.8, 169.6, 169.5, 169.3 C=O NAc, 156.1 C=O urethane, 139.3, 138.6, 138.5, 137.3 C-i Ar, 128.4–127.0 C-Ar, 101.6 C-1', 101.2 C-1', 100.3 C-1', 99.9 C-1', 99.8 C-1', 97.6 C-1', 81.6 C-3', C-3', 80.9 C-3', 79.3 C-2', 78.8 C-2', 78.5 C-1', 77.03, 76.97 C-5', C-5', 76.1 C-5', 75.9 C-4', 75.6 C-5', 74.8 C-4', 74.5 C-5', 74.2 C-5', 74.0 C-3', C-3', 73.8 CH₂O, 73.7 C-5', 73.2, 72.3, 71.9 CH₂O, 70.6, 70.4 C-4', C-4', 70.0, 69.9 C-3', C-3', 69.2 C-2', 68.8 C-6', 68.5 C-6', 67.7 C-4', 67.1 C-4', 66.0 C-6', 65.1 CH₂O, 65.0 C-4', 61.6 C-6', 61.2 C-6', 61.1 C-6', 60.9 C-6', 55.7 C-2', C-2', 55.4 C-2', 53.3 C-2', 40.4 C-6 AH, 35.4 C-2 AH, 29.2 C-5 AH, 25.8 C-4 AH, 24.9 C-3 AH, 23.3, 23.0, 22.8 NAc.

N¹-(6-Aminohexanoylamido)-O-(2-acetamido-2-deoxy- β -D-glucopyranosyl)-(1 \rightarrow 2)-O- α -D-mannopyranosyl-(1 \rightarrow 3)-O-[(2-acetamido-2-deoxy- β -D-glucopyranosyl)-(1 \rightarrow 2)-O- α -D-mannopyranosyl-(1 \rightarrow 6)]-O- β -D-mannopyranosyl-(1 \rightarrow 4)-O-(2-acetamido-2-deoxy- β -D-glucopyranosyl)-(1 \rightarrow 4)-2-acetamido-2-deoxy- β -D-glucopyranoside, **4 (Bi7AH).** A 5.5 mg (2.86 μ mol) portion of **3** and 6.6 mg of Pd/C (10%) were suspended in 0.5 mL of methanol and 0.1 mL of acetic acid. The reaction mixture was stirred for 24 h with hydrogen at a pressure of 1 atm (TLC: 2-propanol/1 M ammonium acetate 2:1; R_f = 0.18). The catalyst was removed by centrifugation, and wash steps with methanol/acetic acid 5:1 were repeatedly performed. After concentration of the combined supernatants and washings, the remainder was purified by gel filtration (column, Pharmacia Hi Load Superdex 30, 600 \times 16 mm; mobile phase, 100 mM NH₄HCO₃; flow rate, 750 μ L/min; detection at 220 and 260 nm) and lyophilized. The yield was 3.9 mg

(95.4%), and the analysis provided the following results: $[\alpha]^{23}_D = +0.1^\circ$ (1, H₂O); $C_{56}H_{96}N_6O_{36}$ (1429.39); MALDI-TOF-MS (DHB in H₂O/EtOH = 9 + 1); calcd value 1428.59, found 1452.4 (M + Na); 1H NMR (500 MHz, D₂O) δ 5.17 (d, $J_{1,2} < 1.0$ Hz, 1H, H-1'), 5.11 (d, $J_{1,2} = 9.6$ Hz, 1H, H-1'), 4.97 (d, $J_{1,2} < 1.0$ Hz, 1H, H-1'), 4.83 (d, $J_{1,2} < 1.0$ Hz, 1H, H-1'), 4.67 (d, $J_{1,2} = 7.7$ Hz, 1H, H-1'), 4.61 (2d, $J_{1,2} = 8.4$ Hz, 2H, H-1', H-1'), 4.30 (dd, $J_{2,3} = 2.1$ Hz, 1H, H-2'), 4.24 (dd, $J_{2,3} = 1.7$ Hz, 1H, H-2'), 4.16 (dd, $J_{2,3} = 1.7$ Hz, 1H, H-2'), 2.88 (t, $J_{vic} = 7.5$ Hz, 2H, ϵ CH₂ AH), 2.33 (t, $J_{vic} = 6.9$ Hz, 2H, α CH₂ AH), 2.13, 2.10, 2.05 (3s, 12H, NAc), 1.68–1.60 (m, 4H, β , δ CH₂ AH), 1.39 (m, 2H, γ CH₂ AH); ^{13}C NMR (125 MHz, D₂O, DMSO- d_6 as internal standard) δ 179.0, 176.18, 176.16, 176.06, 176.0 C=O, 102.8 C-1', 102.0 C-1', 101.18, 101.16 C-1', C-1', 101.12 C-1', 98.6 C-1', 82.0 C-3', 81.1 C-4', 80.3 C-4', 79.8 C-1', 78.1 C-2', 77.9 C-2', 77.8 C-5', 77.4 C-5', C-5', 76.0 C-5', 75.9 C-5', 75.1 C-5', 74.9, 74.8 C-3', C-3', 74.4 C-5', 74.2 C-3', 73.5 C-3', 71.7 C-2', 71.5 C-4', C-4', 71.01, 70.97 C-3', C-3', 68.91, 68.87 C-4', C-4', 67.4 C-6', 67.3 C-4', 63.3, 63.2 C-6', C-6', 62.2 C-6', C-6', 61.54 C-6', 61.4 C-6', 56.9 C-2', C-2', 56.5 C-2', 55.4 C-2', 41.0 C-6 AH, 37.1 C-2 AH, 29.0 C-5 AH, 26.6 C-4 AH, 26.1 C-3 AH, 23.9, 23.8, 23.6 NAc.

N¹-(6-Aminohexanoylamido)-O- β -D-galactopyranosyl-(1 \rightarrow 4)-O-2-acetamido-2-deoxy- β -D-glucopyranosyl-(1 \rightarrow 2)-O- α -D-mannopyranosyl-(1 \rightarrow 3)-O- β -D-galactopyranosyl-(1 \rightarrow 4)-(2-acetamido-2-deoxy- β -D-glucopyranosyl)-(1 \rightarrow 2)-O- α -D-mannopyranosyl-(1 \rightarrow 6)]-O- β -D-mannopyranosyl-(1 \rightarrow 4)-O-(2-acetamido-2-deoxy- β -D-glucopyranosyl)-(1 \rightarrow 4)-2-acetamido-2-deoxy- β -D-glucopyranoside, **5 (Bi9AH).** A 4.0 mg portion (2.8 μ mol) of **4** was dissolved in 1400 μ L of a 20 mM sodium cacodylate buffer, pH 7.4. The buffer contained 1.0 mg of BSA, 2.5 μ mol of NaN₃, 1.4 μ mol of MnCl₂, 5.6 mg (8.4 μ mol) of uridine-5'-diphosphogalactose, 6 units of alkaline phosphatase (EC 3.1.3.1) to destroy the inhibitory nucleotide phosphates, as described elsewhere (22), and 120 milliunits of GlcNAc- β 1,4-galactosyltransferase (EC 2.4.1.22). The reaction mixture was incubated at 37 $^\circ$ C, and the pH was maintained at 7.0 by periodic addition of 1 M NaOH. After 24 h (TLC: 2-propanol/1 M ammonium acetate 2:1; R_f = 0.24), the precipitate was removed by centrifugation. The supernatant was concentrated to a volume of 300 μ L, purified by gel filtration (column, Pharmacia Hi Load Superdex 30, 600 \times 16 mm; mobile phase, 100 mM NH₄HCO₃; flow rate, 750 μ L/min; detection at 220 and 260 nm), and lyophilized. The yield was 3.59 mg (73.2%) and analysis provided the following results: $[\alpha]^{23}_D = -1.9^\circ$ (0.5, H₂O); $C_{68}H_{116}N_6O_{46}$ (1753.6770); MALDI-TOF-MS (DHB in H₂O/EtOH = 9 + 1); calcd value 1752.7, found 1776.7 (M + Na); 1H NMR (500 MHz, D₂O, DMSO- d_6 as internal standard) δ 4.92 (d, $J_{1,2} < 1.0$ Hz, 1H, H-1'), 4.86 (d, $J_{1,2} = 9.6$ Hz, 1H, H-1'), 4.73 (d, $J_{1,2} < 1.0$ Hz, 1H, H-1'), 4.57 (d, $J_{1,2} < 1.0$ Hz, 1H, H-1'), 4.42 (d, $J_{1,2} = 7.8$ Hz, 1H, H-1'), 4.38 (2d, $J_{1,2} = 7.8$ Hz, 2H, H-1', H-1'), 4.27, 4.26 (2d, $J_{1,2} = 7.8$ Hz, 2H, H-1', H-1'), 4.05 (m, 1H, H-2'), 3.99 (m, 1H, H-2'), 3.90 (m, 1H, H-2'), 2.68 (t, $J_{vic} = 7.6$ Hz, 2H, ϵ CH₂ AH), 2.08 (t, $J_{vic} = 6.9$ Hz, 2H, α CH₂ AH), 1.88, 1.853, 1.850, 1.80 (4s, 12H, NAc), 1.40 (m, 4H, β , δ CH₂ AH), 1.15 (m, 2H, γ CH₂ AH).

N¹-(6-Aminohexanoylamido)-O-(5-acetamido-3,5-dideoxy- α -D-glycero-D-galacto-2-nonulopyranulosonic acid)-(2 \rightarrow 6)- β -D-galactopyranosyl-(1 \rightarrow 4)-O-(2-acetamido-2-deoxy- β -D-glucopyranosyl)-(1 \rightarrow 2)-O- α -D-mannopyranosyl-(1 \rightarrow 3)-O-[(5-acetamido-3,5-dideoxy- α -D-glycero-D-galacto-2-nonulopyranulosonic acid)-(2 \rightarrow 6)- β -D-galactopyranosyl-(1 \rightarrow 4)-2-acetamido-2-deoxy- β -D-glucopyranosyl)-(1 \rightarrow 2)-O- α -

D-mannopyranosyl-(1→6)-O-β-D-mannopyranosyl-(1→4)-O-(2-acetamido-2-deoxy-β-D-glucopyranosyl)-(1→4)-2-acetamido-2-deoxy-β-D-glucopyranoside, 6 (Bi1126AH). A 4.0 mg portion (2.8 μmol) of **4** was dissolved in 1400 μL of a 20 mM sodium cacodylate buffer, pH 7.4. The buffer contained 1.0 mg of BSA, 2.5 μmol of NaN₃, 1.4 μmol of MnCl₂, 5.6 mg (8.4 μmol) of uridine-5'-diphosphogalactose, 6 units of alkaline phosphatase (EC 3.1.3.1), and 120 milliunits of GlcNAc-β1,4-galactosyltransferase (EC 2.4.1.22). The reaction mixture was incubated at 37 °C, and the pH was maintained at 7.0 by periodic addition of 1 M NaOH. After complete reaction (24 h; TLC: 2-propanol/1 M ammonium acetate 2:1; *R_f* **5** = 0.24), 4.8 mg (6.2 μmol) of cytidine-5'-monophospho-*N*-acetylneuraminic acid and 50 milliunits of β-galactoside-α2,6-sialyltransferase (EC 2.4.99.1) were added. Incubation at 37 °C was continued, and the pH was maintained at 7.0. After 48 h (TLC: 2-propanol/1 M ammonium acetate 1.5:1; *R_f* **5** = 0.32; *R_f* **6** = 0.27), the precipitate was removed by centrifugation. The supernatant was concentrated to a volume of 400 μL, purified by gel filtration (column, Pharmacia Hi Load Superdex 30, 600 × 16 mm; mobile phase, 100 mM NH₄HCO₃; flow rate, 750 μL/min; detection at 220 and 260 nm), and lyophilized. The yield was 3.37 mg (51.5%), and analysis provided the following results: $[\alpha]^{23}_D = -7.1^\circ$ (0.5, H₂O); C₉₀H₁₅₀N₈O₆₂ (2336.19); MALDI-TOF-MS (DHB in H₂O/EtOH = 9 + 1); calcd value 2334.9, found 2359.2 (M + Na); ¹H NMR (500 MHz, D₂O, DMSO-*d*₆ as internal standard) δ 4.93 (d, *J*_{1,2} < 1.0 Hz, 1H, H-1⁴), 4.86 (d, *J*_{1,2} = 9.7 Hz, 1H, H-1¹), 4.76 (d, *J*_{1,2} < 1.0 Hz, 1H, H-1⁴), 4.56 (d, *J*_{1,2} < 1.0 Hz, 1H, H-1³), 4.42 (d, *J*_{1,2} = 7.0 Hz, 1H, H-1²), 4.41 (2d, *J*_{1,2} = 6.9 Hz, 2H, H-1⁵, H-1⁵), 4.249, 4.246 (2d, *J*_{1,2} = 7.7 Hz, 2H, H-1⁶, H-1⁶), 4.06 (m, 1H, H-2³), 4.0 (m, 1H, H-2⁴), 3.92 (m, 1H, H-2⁴), 2.79 (t, *J*_{vic} = 7.6 Hz, 2H, εCH₂ AH), 2.47 (m, 2H, H-3eq^N, H-3eq^N), 2.08 (t, *J*_{vic} = 6.8 Hz, 2H, αCH₂ AH), 1.89, 1.872, 1.869, 1.84, 1.80 (5s, 16H, NAc), 1.52 (dd, *J*_{vic} = *J*_{gem} = 12.1 Hz, 2H, H-3ax^N, H-3ax^N), 1.47 (m, 2H, δCH₂ AH), 1.40 (m, 2H, βCH₂ AH), 1.16 (m, 2H, γCH₂ AH).

N⁶-(6-Aminohexanoylamido)-O-(5-acetamido-3,5-dideoxy-α-D-glycero-D-galacto-2-nonulopyranulosonic acid)-(2→3)-β-D-galactopyranosyl-(1→4)-O-2-acetamido-2-deoxy-β-D-glucopyranosyl)-(1→2)-O-α-D-mannopyranosyl-(1→3)-O-[(5-acetamido-3,5-dideoxy-α-D-glycero-D-galacto-2-nonulopyranulosonic acid)-(2→3)-β-D-galactopyranosyl-(1→4)-(2-acetamido-2-deoxy-β-D-glucopyranosyl)-(1→2)-O-α-D-mannopyranosyl-(1→6)]-O-β-D-mannopyranosyl-(1→4)-O-(2-acetamido-2-deoxy-β-D-glucopyranoside, 7 (Bi1123AH). A 4.0 mg portion (2.8 μmol) of **4** was dissolved in 1400 μL of a 20 mM sodium cacodylate buffer, pH 7.4. The buffer contained 1 mg of BSA, 2.5 μmol of NaN₃, 1.4 μmol of MnCl₂, 5.6 mg (8.4 μmol) of uridine-5'-diphosphogalactose, 6 units of alkaline phosphatase (EC 3.1.3.1), and 120 milliunits of GlcNAc-β1,4-galactosyltransferase (EC 2.4.1.22). The reaction mixture was incubated at 37 °C, and the pH was maintained at 7.0 by periodic addition of 1 M NaOH. After complete reaction (24 h; TLC: 2-propanol/1 M ammonium acetate 2:1; *R_f* **5** = 0.24), 4.8 mg (6.2 μmol) of cytidine-5'-monophospho-*N*-acetylneuraminic acid and 54 milliunits of recombinant β-galactoside-α2,3-sialyltransferase (EC 2.4.99.6) were added. Incubation at 37 °C was continued, and the pH was maintained at 7.0. After 24 h, an additional 4.8 mg (6.2 μmol) of cytidine-5'-monophospho-*N*-acetylneuraminic acid and 54 milliunits of recombinant β-galactoside-α2,3-sialyltransferase (EC 2.4.99.6) were added. Incubation was continued for 24 h (TLC: 2-pro-

panol/1 M ammonium acetate 1.5:1; *R_f* **5** = 0.32, *R_f* **7** = 0.29) followed by removal of the precipitate by centrifugation. The supernatant was concentrated to a volume of 400 μL, purified by gel filtration (column, Pharmacia Hi Load Superdex 30, 600 × 16 mm; mobile phase, 100 mM NH₄HCO₃; flow rate, 750 μL/min; detection at 220 and 260 nm), and lyophilized. The yield was 4.56 mg (69.8%), and analysis provided the following results: $[\alpha]^{23}_D = -3.9^\circ$ (0.5, H₂O); C₉₀H₁₅₀N₈O₆₂ (2336.19); MALDI-TOF-MS (DHB in H₂O/EtOH = 9 + 1); calcd value 2334.9, found 2359.2 (M + Na); ¹H NMR (500 MHz, D₂O, DMSO-*d*₆ as internal standard) δ 4.92 (d, *J*_{1,2} < 1.0 Hz, 1H, H-1⁴), 4.85 (d, *J*_{1,2} = 9.7 Hz, 1H, H-1¹), 4.73 (d, *J*_{1,2} < 1.0 Hz, 1H, H-1⁴), 4.56 (d, *J*_{1,2} < 1.0 Hz, 1H, H-1³), 4.42 (d, *J*_{1,2} = 7.8 Hz, 1H, H-1²), 4.37 (2d, *J*_{1,2} = 6.9 Hz, 2H, H-1⁵, H-1⁵), 4.35, 4.34 (2d, *J*_{1,2} = 7.9 Hz, 2H, H-1⁶, H-1⁶), 4.05 (m, 1H, H-2³), 3.99 (m, 1H, H-2⁴), 3.92 (m, 3H, H-2⁴, H-3⁶, H-3⁶), 2.79 (t, *J*_{vic} = 7.6 Hz, 2H, εCH₂ AH), 2.56 (dd, *J*_{vic} = 4.4 Hz, *J*_{gem} = 12.4 Hz, 2H, H-3eq^N, H-3eq^N), 2.08 (t, *J*_{vic} = 6.9 Hz, 2H, αCH₂ AH), 1.88, 1.851, 1.845, 1.835, 1.80 (5s, 16H, NAc), 1.60 (t, *J*_{vic} = 11.6 Hz, 2H, H-3ax^N, H-3ax^N), 1.47 (m, 2H, δCH₂ AH), 1.41 (m, 2H, βCH₂ AH), 1.16 (m, 2H, γCH₂ AH).

Synthesis of Neoglycoproteins. Coupling of the spaced oligosaccharides was in principle performed by the isothiocyanate reaction protocol, as described (23). In detail, a 0.34 μmol portion of each 6-aminohexanoyl-*N*-glycan (**5–7**) was dissolved in 200 μL of dilute NaHCO₃ (100 mg of Na₂CO₃/10 mL of H₂O) in a 1.5 mL plastic vessel. One microliter (13.1 μmol) of thiophosgene dissolved in 200 μL of dichloromethane was added, and the mixture was vigorously stirred. After the amine was consumed (1.5 h; TLC: 2-propanol/1 M ammonium acetate 2:1; *R_f* value of the nonasaccharide derivative = 0.5; *R_f* value of the α2,3-disialylated derivative = 0.44; *R_f* of the α2,6-disialylated derivative = 0.36), the phases were separated by centrifugation, and the water phase was collected. The organic phase was extracted twice with 100 mL of dilute NaHCO₃. To remove traces of thiophosgene, the combined aqueous phases were extracted twice with dichloromethane. Two milligrams of carbohydrate-free BSA was dissolved in the aqueous solution containing the isothiocyanate derivative. After 6 days at ambient temperature, the neoglycoconjugate was purified by gel filtration (column, Pharmacia Hi Load Superdex 30, 600 × 16 mm; mobile phase, 100 mM NH₄HCO₃; flow rate, 750 μL/min; detection at 220 and 260 nm), and the product-containing solution was lyophilized. To calculate the extent of oligosaccharide incorporation into the protein carrier, a colorimetric assay was employed (24). Gel electrophoretic analysis under denaturing conditions combined with silver staining of the neoglycoproteins was performed, as described (17). In addition to these three neoglycoproteins, lactosylated albumin was produced by the diazonium and phenylisothiocyanate reactions with *p*-aminophenyl β-lactoside (23).

Solid-Phase Assay for Lectin Binding. Thermodynamic binding parameters were determined by immobilization of the neoglycoproteins and asialofetuin, obtained by acidic desialylation of commercial fetuin (Sigma, Munich, Germany), onto the plastic surface of microtiter plate wells and probing of the extent of binding of the labeled carbohydrate-binding proteins, as described (25). The lectins from mistletoe and bovine heart (galactin 1) were purified by affinity chromatography, as described (26). The immunoglobulin G subfraction with preferential affinity for β-galactosides was isolated by sequential affinity chromatographic steps, as described (27). Biotinylation was achieved either with the *N*-

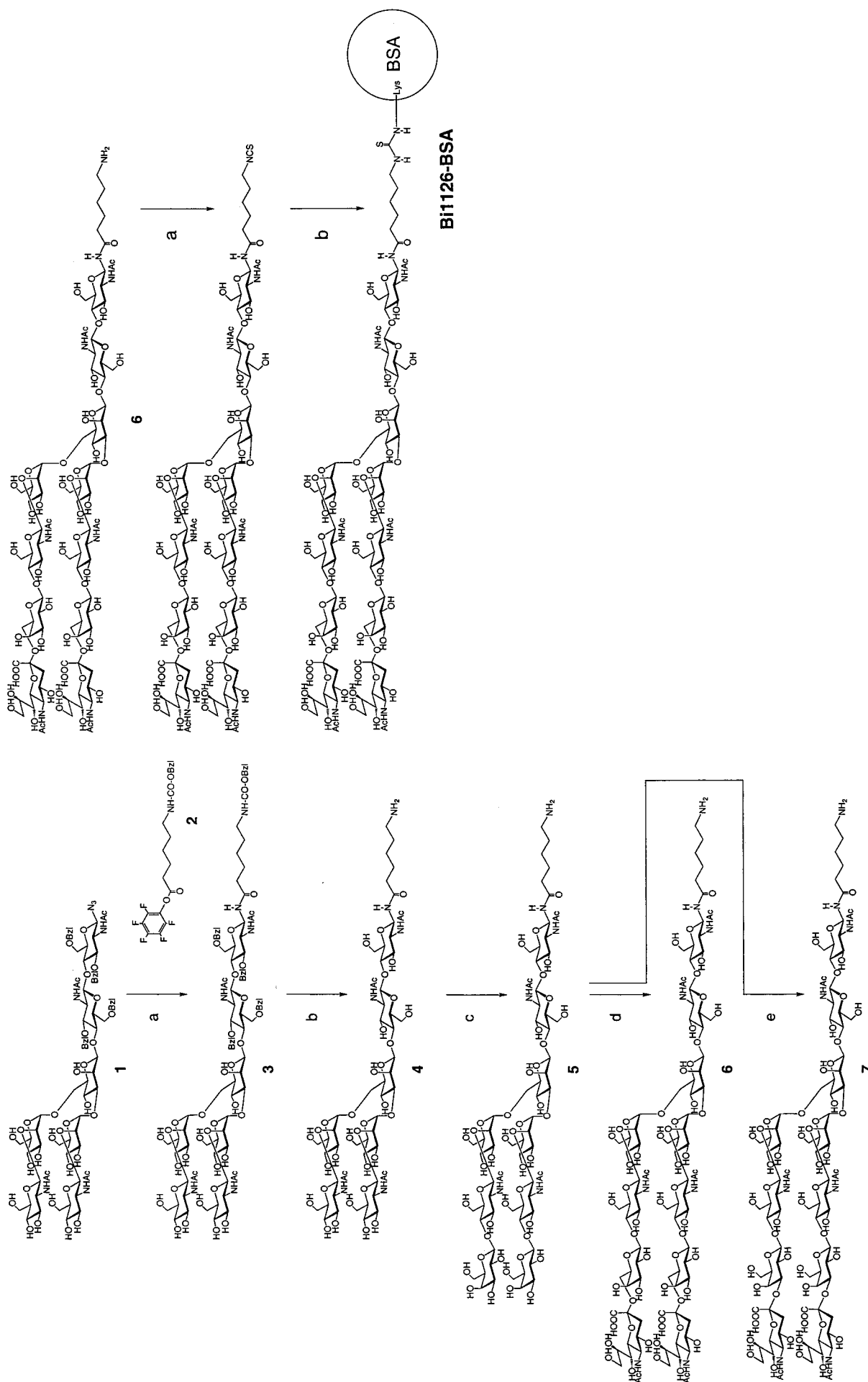


Figure 2. (A, left) Schematic representation of the synthetic pathway to produce spacer-linked galactosylated and sialylated N-glycans: (a) 1, propanedithiol, Et₃N, MeOH; 2, Z-AH-OPfp, 1-hydroxybenzotriazole (1 - 2 = 56%); (b) Pd-H₂, AcOH, MeOH; (c) β 1,4-galactosyltransferase, UDP-Gal, alkaline phosphatase (73%); (d) α 2,6-sialyltransferase, CMP-NeuNAc, alkaline phosphatase (c + e = 70%); AH, 6-aminohexanoic acid; Pfp, pentafluorophenyl (B, right) Activation of the synthetic N-glycans represented by undecasaccharide 6 and coupling to BSA: (a) thiophosgene, CH₂Cl₂-H₂O, NaHCO₃, pH 8.5 (quant.); (b) BSA, H₂O, NaHCO₃, pH 8.5.

hydroxysuccinimide ester derivative in the case of the lectins or with the amidocaproyl hydrazide derivative in the case of the antibody under activity-preserving conditions (27). The experimental series with duplicates were performed at least four times up to the level of saturation for the marker and a fixed amount of substance used for coating, and the data sets were algebraically transformed to obtain the K_D value and the number of bound probe molecules at saturation.

Flow Cytofluorometry. Various tumor cell lines of different histogenetic origin were obtained from the American Type Culture Collection (Rockville, MD). The human pre-B cell line Blin-1 was kindly provided by Dr. B. Woermann (Göttingen, Germany). The tumor cells (myeloid, lymphoid, and epithelial tumor cells) were cultured according to the instructions of the supplier and carefully washed with Dulbecco's phosphate-buffered saline solution containing 0.1% carbohydrate-free BSA to remove any inhibitory serum glycoproteins and to saturate any nonspecific protein-binding sites prior to the incubation with 100 μ g of biotinylated neoglycoproteins/mL for 30 min. The suspension was kept at 4 °C to reduce uptake by endocytosis. Flow cytofluorometric analysis of the thoroughly washed cells using the commercial streptavidin R-phycoerythrin conjugate (Sigma, Munich, Germany) as indicator for quantitative measurement in a FACScan instrument (Becton-Dickinson, Heidelberg, Germany) equipped with the software CON-SORT 30 was performed, as described (28).

Visualization of Neoglycoprotein-Binding Sites in Lung Cancer Tissue Sections. The glycohistochemical procedure for visualizing binding sites for the carbohydrate moiety of biotinylated neoglycoproteins and the control reactions to ascertain the specificity of the protein-carbohydrate interaction has been described in detail elsewhere (29, 30). Lactosylated BSA, asialofetuin, and fetuin after complete sialylation of the three triantennary chains were used as competitive inhibitors for the binding of the nonasaccharide and the α 2,6-sialylated undecasaccharide. Briefly, sections (4–6 μ m thick) of formalin-fixed and paraffin-embedded specimen of disease-free lungs (20 cases), of small cell lung carcinomas (10 cases), of non-small-cell lung carcinomas (adenocarcinomas, epidermoid carcinomas, and large cell carcinomas; 10 cases of each type), and of mesotheliomas (10 cases) were processed by a series of steps including blocking of endogenous peroxidase activity and nonspecific protein-binding sites and subsequent incubation with the biotinylated probe at a concentration of 40 μ g/mL for 60 min at room temperature and with ABC kit reagents as well as the substrates diaminobenzidine/ H_2O_2 for development of the colored, water-insoluble product. A case was considered to be positive when at least clusters of tumor cells were specifically stained.

Organ Distribution of Radioiodinated Neoglycoproteins. Incorporation of ^{125}I into the neoglycoproteins to reach a specific activity of 11.5 MBq/mg of protein was achieved by the chloramine-T method using limiting amounts of reagents (31). The retention of radioactivity in Ehrlich solid tumor-bearing ddY mice (7 weeks old; Nihon Clea Co., Tokyo, Japan) after injection of 28.75 kBq/animal into the tail vein was determined by a γ -counter (Aloka ARC 300, Tokyo, Japan) and expressed as percentage of the injected dose per gram of wet tissue or per milliliter of blood for a group of three to four mice for each type of neoglycoprotein and for each time point, as described (32).

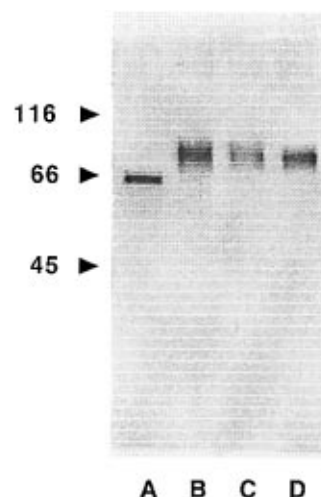


Figure 3. Visualization of the gel electrophoretic mobility under denaturing conditions of sugar-free BSA (A) and the neoglycoproteins with the nonasaccharide (B), the α 2,6-sialylated (C), or the α 2,3-sialylated undecasaccharide (D). Positions of marker proteins for molecular weight designation are indicated by arrowheads.

RESULTS AND DISCUSSION

Preparation of the Neoglycoproteins. Neoglycoproteins carrying defined *N*-glycan ligands were obtained by a combined chemical and enzymatic approach. As a common precursor for the biantennary *N*-glycans the heptasaccharide azide **1** (20) was used. The remaining four benzyl protecting groups could not be removed selectively in the presence of the anomeric azide and facilitated the purification of the protected *N*-glycan **3** by reversed phase chromatography. Reduction to the glycosylamine with propanedithiol and condensation with pentafluorophenylester **2** introduced a suitable spacer. The following hydrogenolytic deprotection of spacer-linked **3** gave the free 6-aminohexanoylated heptasaccharide **4** (Figure 2A). Enzymatic galactosylation of both carbohydrate chains in the heptasaccharide **4** afforded the biantennary nonasaccharide **5**. Sialyltransferases with different specificities allowed rapid derivatization of nonasaccharide **5** to the α 2,6-sialylated undecasaccharide **6** and its α 2,3-linked isomer **7**. High-resolution NMR was used to verify the identity of the synthetic compounds. The NMR data obtained for the final compounds **5–7** were in good agreement with those reported for *N*-glycans isolated from natural sources (33–35). The 6-aminohexanoyl spacer attached to the reducing end of the *N*-glycans can be selectively activated prior to coupling with a carrier protein (Figure 2B). Excess thiophosgene in a biphasic system quantitatively converted the primary amino group to an isothiocyanate that was subsequently reacted with the ϵ -amino function of lysine residues in BSA. The two final steps, which are widely employed for the covalent incorporation of *p*-aminophenyl glycosides into a carrier protein (23), establish a convenient method for attachment of the biantennary sugar chains to BSA.

The yields for the covalent introduction of the bulky nona- and undecasaccharides (10-fold excess during the coupling reaction) were 3.6 biantennary chains for the nonasaccharide, 3.0 chains for the α 2,6-sialylated undecasaccharide, and 2.4 chains for its α 2,3-sialylated derivative. Since the chemical glycosylation will increase the molecular weight of the carrier protein, the results of the colorimetric analysis were corroborated by the measurements of the gel electrophoretic mobilities of the sugar-free carrier protein and the neoglycoproteins (Fig-

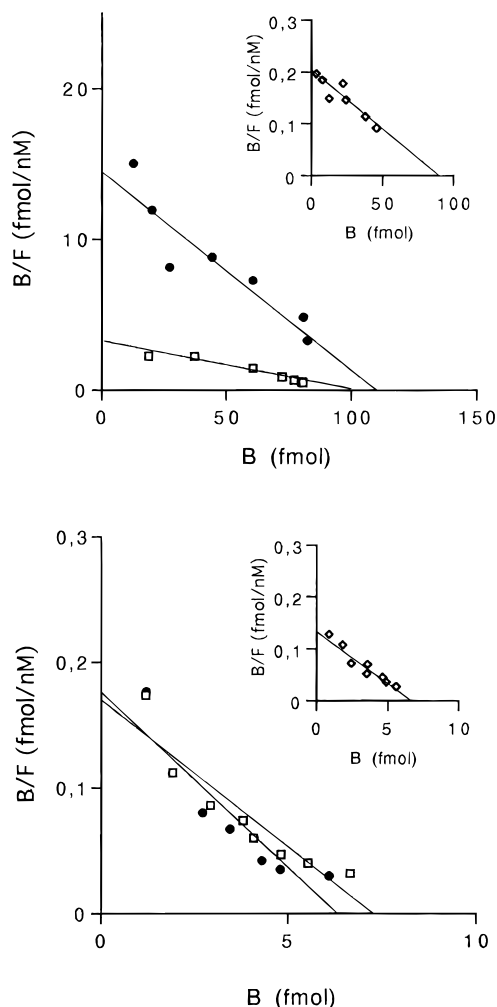


Figure 4. Scatchard plot analysis of the binding of biotinylated galactoside-specific mistletoe lectin (upper part) and immunoglobulin G fraction with enhanced selectivity to β -galactosides from human serum (lower part) to surface-immobilized neoglycoproteins in microtiter plate wells: (\square) nonasaccharide as sugar part, (\bullet) α 2,6-sialylated undecasaccharide as sugar part; (inset) α 2,3-sialylated undecasaccharide as sugar part.

ure 3). It is noteworthy that the presence of the voluminous sugar structures can lead to an anomalous migration behavior. The detection of shifts should therefore only be regarded as semiquantitative evidence. In comparison to other methods for glycan chain conjugation, the degree of modification of albumin by lyso-gangliosides or high mannose-type glycopeptides and a homobifunctional cross-linker yielded a similar extent (17, 36, 37). Since already one sugar chain on a glycoprotein can govern certain aspects of its physiological behavior, as for example seen for plasma clearance (38), these results encourage comparative assays of the three neoglycoprotein preparations to delineate to what extent the structural changes will translate into different properties in the interaction with isolated sugar receptors and binding sites in cells. Having made neoglycoproteins available with the typical termini of complex N-linked chains, it is possible to directly determine the affinity of these oligosaccharide chains for sugar receptors and cell surfaces without having to resort to measuring inhibitory capacities in an indirect system.

Binding to Sugar Receptors and Cells. To evaluate the range in which the sialylation itself and its linkage will affect receptor binding, we selected three phylogenetically unrelated sugar-binding proteins, namely a tetrameric plant agglutinin, dimeric mammalian ga-

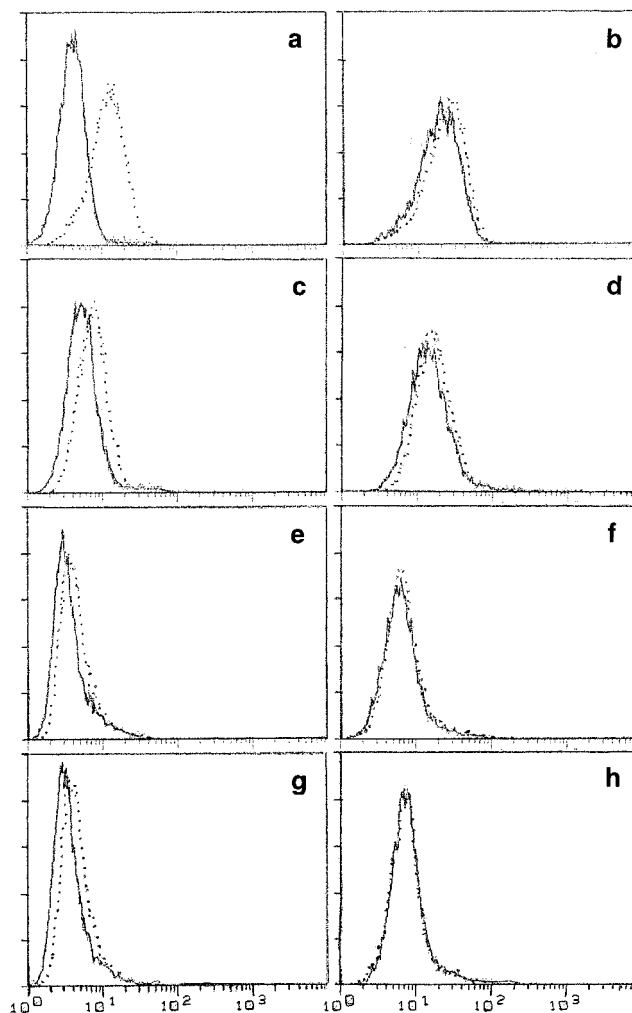


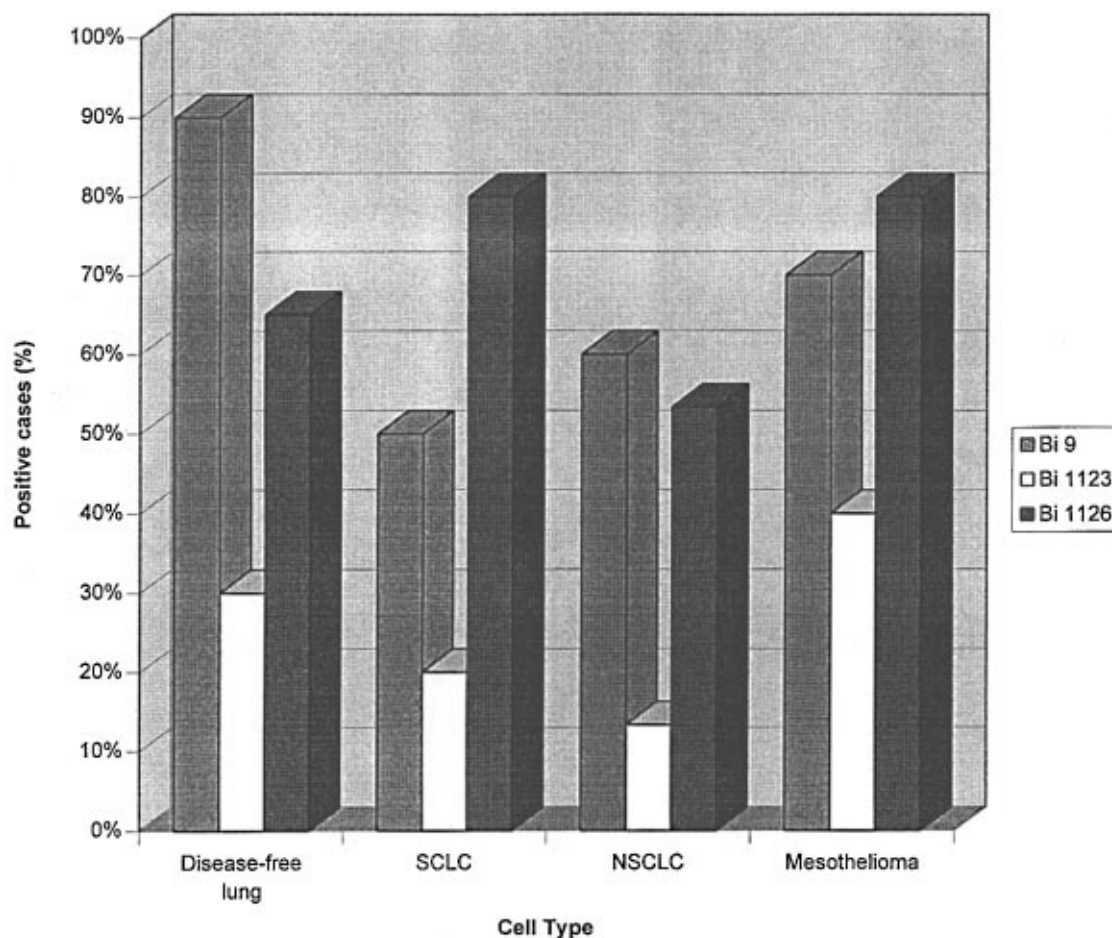
Figure 5. Semilogarithmic representation of the binding of biotinylated BSA (—) and the nonasaccharide-exposing neoglycoprotein ($\cdot \cdot \cdot$), shown in panels a, c, e, and g, as well as of the α 2,3-sialylated (—) and the α 2,6-sialylated ($\cdot \cdot \cdot$) undecasaccharide-exposing neoglycoproteins, shown in panels b, d, f, and h, to cells of the pre-B cell line Blin-1 (a and b), the T-lymphoblastoid line CCRF-CEM (c and d), the colon adenocarcinoma line SW480 (e and f), and the line SW620, established from a lymph node metastasis of the same patient after recurrence of the colon adenocarcinoma (g and h), as monitored in FACSscan analysis employing streptavidin R-phycoerythrin as fluorescent probe.

lectin 1, and a polyclonal immunoglobulin G fraction with enhanced selectivity for β -galactosides from human serum. The neoglycoproteins were presented to the sugar-binding proteins on a plastic surface, and the measurable extent of specific binding was algebraically transformed to Scatchard plots with straight lines. This result raised evidence for the occurrence of a single class of binding sites without exception, as exemplarily shown in Figure 4. It is evident that the site of introduction of the sialic acid can markedly alter the ligand capacity to a receptor, as seen especially for the mistletoe lectin. When saturational levels of lectins or antibody concentrations are reached, the computed maxima of probe molecule binding appeared to reflect the different sizes of the studied proteins, attributing the result to spatial accessibility and orientation of the binding sites (Table 1). Whereas the data for the plant agglutinin are in agreement with inhibition studies, the direct interaction of α 2,6-sialylated sugar chains with galectin 1 was not unequivocally predictable on this basis (39, 40). To determine the differences in these properties between the biantennary chains and either lactose or a glycoprotein with trian-

Table 1. Determination of the Apparent Affinity Constant (K_D) for the Interaction of (Neo)glycoproteins with Sugar Receptors and the Number of Bound Probe Molecules at Saturation for *Viscum album* Agglutinin (VAA), Bovine Galectin 1, and the Human β -Galactoside-Binding Immunoglobulin G Subfraction (IgG) in a Solid-Phase Assay

probe: matrix	VAA		galectin 1		IgG	
	K_D^a	B_{\max}^a	K_D^a	B_{\max}^a	K_D^a	B_{\max}^a
Bi9-BSA (0.5 μ g)	26.7 \pm 11.6	(4.6 \pm 1.9) $\times 10^{10}$	900.1 \pm 176	(42.8 \pm 12.5) $\times 10^{10}$	32.9 \pm 19.6	(0.35 \pm 0.1) $\times 10^{10}$
Bi1123-BSA (0.5 μ g)	938.4 \pm 661	(8.2 \pm 4.4) $\times 10^{10}$	829.5 \pm 501	(42.0 \pm 16.5) $\times 10^{10}$	87.3 \pm 62.7	(0.38 \pm 0.1) $\times 10^{10}$
Bi1126-BSA (0.5 μ g)	8.7 \pm 4.5	(6.1 \pm 1.4) $\times 10^{10}$	1025.5 \pm 619	(48.7 \pm 18.4) $\times 10^{10}$	33.9 \pm 4.6	(0.46 \pm 0.1) $\times 10^{10}$
Lac-BSA (diazot) (3 μ g) ^b	312.4 \pm 190	(4.7 \pm 2.3) $\times 10^{10}$	1127.2 \pm 53.3	(34.6 \pm 17.6) $\times 10^{10}$	139.0 \pm 87.6	(0.70 \pm 0.1) $\times 10^{10}$
Lac-BSA (thio) (0.5 μ g) ^c	13.4 \pm 7.3	(5.1 \pm 0.2) $\times 10^{10}$	516.0 \pm 20.3	(83.3 \pm 6.5) $\times 10^{10}$	7.6 \pm 5.2	(0.65 \pm 0.1) $\times 10^{10}$
ASF (1 μ g) ^d	7.4 \pm 2.6	(4.9 \pm 0.5) $\times 10^{10}$	819.0 \pm 268	(37.5 \pm 10.7) $\times 10^{10}$	69.2 \pm 40.2	(0.43 \pm 0.1) $\times 10^{10}$

^a K_D is given in nM; B_{\max} is expressed as bound probe molecules per well. ^{b,c} BSA was glycosylated either by the diazophenyl derivative (diazot) or by covalent attachment of the *p*-isothiocyanatophenyl derivative (thio) of *p*-aminophenyl β -D-lactopyranoside. ^d Asialofetuin; each value is given as the mean \pm SD from at least four independent experimental series, the quantity of (neo)glycoprotein for coating in μ g/well being given for each type of substance.

**Figure 6.** Quantitative evaluation of the percentage of positive cases for sections of disease-free lungs ($N = 20$), of small cell lung carcinomas ($N = 10$), of non-small-cell lung carcinomas ($N = 30$), and of mesotheliomas ($N = 10$), grouped for the three types of labeled neoglycoprotein, under identical conditions.

tenary sugar chains as ligands, lactosylated neoglycoproteins and asialofetuin were used in the same assay. The different stoichiometric relations in cross-link formation with asialofetuin's three triantennary glycans between the lectins and the antibody fraction had already underscored the importance of spatial factors (41, 42), as similarly noted herein. Ligand clustering by increased conjugation of a lactose derivative or presentation of the triantennary chains of the naturally glycosylated asialofetuin appeared to improve the affinity for the mistletoe lectin (Table 1). This result is in line with an observation previously described with cluster glycosides as inhibitors (43–45). Viewing these data in terms of selectivity, the experiments intimated that purified lectins can exhibit preferences to the chain termini, albeit to an individually variable degree. Further examples of lectins with already documented discriminatory potency to $\alpha 2,3$ - and

$\alpha 2,6$ -sialylated derivatives are given by several I-type lectins (2, 46). Having therefore shown the feasibility to delineate different ligand properties in a defined assay system with purified receptors, the application of the neoglycoproteins could be extended to the monitoring of tumor cell surface binding using established cell lines *in vitro*.

Attachment of the glycan chains obviously conferred ligand properties for cell surfaces to the carrier protein, which depended on the type of oligosaccharide and cell under otherwise identical conditions (Figure 5). Whereas the percentage of positive cells was in the range of 20–30% of the T-lymphoblastoid and colon adenocarcinoma cell populations for the nonasaccharide, the respective values for the two undecasaccharides, which were within the limit of 10%, were between 48 and 74%. Cell batches were deliberately monitored at the same time with the

Table 2. Biodistribution of ^{125}I -Labeled Neoglycoproteins (Percent Injected Dose per Gram of Tissue or Milliliter of Blood) in Ehrlich Solid Tumor-Bearing Mice after 1 h^a

probe: tissue	Bi9-BSA	Bi1123-BSA	Bi1126-BSA
blood	3.07 ± 0.06	25.27 ± 0.98	22.90 ± 0.28
liver	2.42 ± 0.11	3.06 ± 0.20	2.51 ± 0.02
kidneys	3.06 ± 0.07	3.94 ± 0.29	3.36 ± 0.17
spleen	1.19 ± 0.10	2.50 ± 0.12	3.59 ± 0.16
heart	0.82 ± 0.06	3.98 ± 0.11	2.38 ± 0.17
lung	1.27 ± 0.01	2.84 ± 0.15	1.33 ± 0.03
thymus	1.13 ± 0.04	1.54 ± 0.17	2.16 ± 0.06
pancreas	1.20 ± 0.03	1.06 ± 0.04	0.81 ± 0.05
muscle	0.35 ± 0.02	0.06 ± 0.01	0.54 ± 0.04
vertebrae	0.65 ± 0.03	1.50 ± 0.08	1.36 ± 0.12
brain	0.12 ± 0.01	0.04 ± 0.02	0.33 ± 0.02
tumor	1.16 ± 0.09	4.39 ± 0.13	2.79 ± 0.23

^a Each value represents the mean ± SD of three to four animals in each group; the individual dose of the intravenous injection was 28.75 kBq/animal.

probes to avoid occurrence of any shift attributable to the duration of culturing. Qualitatively similar observations were made with other histogenetically different lines, e.g. two prostate and breast carcinoma lines and five leukemia or lymphoma lines (not shown). Having thus shown the occurrence of quantitatively different bindings of the probes to tumor cells *in vitro*, the proven value of neoglycoproteins as tools in tumor diagnosis, discussed elsewhere (11, 14), prompted us to include the determination of the binding properties of the three types of neoglycoprotein to cellular binding sites in a well-defined tumor system, i.e., lung cancer. As shown in Figure 6, specific binding to the sections was nonuniform under identical experimental conditions, the differences being exclusively quantitative. Since discriminatory cell binding was therefore shown *in vitro* and in tissue sections, the next step was to monitor whether the neoglycoproteins may also distribute between different organs with a disparate profile following radioiodination and intravenous injection. To determine the kinetics of organ distribution of the conjugates which were stable in mouse serum for the length of the assay periods, the radioactivity in a panel of organs and in blood was measured for tumor-bearing mice after 1, 6, and 24 h. Relative to the nonasaccharide, the conjugation of the two undecasaccharides prolonged the occurrence of the respective marker proteins in blood, kidneys, and tumor, which showed the relatively largest extent of radioactivity (Tables 2–4). In accordance with previous studies with biantennary glycopeptides (47, 48), no further site of uptake involving a high-affinity receptor could be discerned. However, since modifications of the sugar chains, attainable in our system by chemical and enzymatic methods, indeed shifted the distribution profile of glycopeptides pronouncedly (12, 47, 48), further systematic studies along this route, which are required to clarify the actual extent of carbohydrate-mediated organ retention, appear to be warranted.

In conclusion, complex biantennary nona- and undecasaccharides were prepared by chemical and enzymatic methods as the ligand part of neoglycoproteins. Since the employed approach can readily be extended to introduce glycans with further structural modifications, e.g. tri- to pentaantennary chains with or without core fucosylation, a bisecting *N*-acetylglucosamine residue, and variations at the termini, the results presented in this study of biantennary *N*-glycans have an exemplary character. To demonstrate the practical value of this preparative approach, versatile applications of the synthetic tools are documented in solid-phase assays, for cell

Table 3. Biodistribution of ^{125}I -Labeled Neoglycoproteins (Percent Injected Dose per Gram of Tissue or Milliliter of Blood) in Ehrlich Solid Tumor-Bearing Mice after 6 h^a

probe: tissue	Bi9-BSA	Bi1123-BSA	Bi1126-BSA
blood	0.52 ± 0.06	15.35 ± 1.00	13.95 ± 0.45
liver	0.72 ± 0.02	1.69 ± 0.13	1.81 ± 0.08
kidneys	0.74 ± 0.03	3.31 ± 0.34	2.95 ± 0.08
spleen	0.24 ± 0.02	1.35 ± 0.10	1.07 ± 0.14
heart	0.12 ± 0.00	2.30 ± 0.18	2.35 ± 0.04
lung	0.26 ± 0.04	2.05 ± 0.10	2.09 ± 0.15
thymus	0.18 ± 0.03	1.42 ± 0.13	1.48 ± 0.11
pancreas	0.05 ± 0.01	1.13 ± 0.10	1.06 ± 0.09
muscle	0.05 ± 0.01	0.47 ± 0.03	0.41 ± 0.02
vertebrae	0.12 ± 0.02	0.95 ± 0.06	1.04 ± 0.08
brain	0.02 ± 0.00	0.22 ± 0.02	0.20 ± 0.00
tumor	0.27 ± 0.06	3.33 ± 0.31	3.46 ± 0.25

^a Each value represents the mean ± SD of three to four animals in each group; the individual dose of the intravenous injection was 28.75 kBq/animal.

Table 4. Biodistribution of ^{125}I -Labeled Neoglycoproteins (Percent Injected Dose per Gram of Tissue or Milliliter of Blood) in Ehrlich Solid Tumor-Bearing Mice after 24 h^a

probe: tissue	Bi9-BSA	Bi1123-BSA	Bi1126-BSA
blood	0.17 ± 0.00	5.31 ± 0.41	4.51 ± 0.42
liver	0.33 ± 0.03	0.79 ± 0.05	0.71 ± 0.04
kidneys	0.23 ± 0.03	1.28 ± 0.11	1.01 ± 0.07
spleen	0.11 ± 0.01	0.63 ± 0.04	0.54 ± 0.04
heart	0.07 ± 0.01	0.97 ± 0.09	0.83 ± 0.07
lung	0.10 ± 0.01	0.89 ± 0.05	0.83 ± 0.04
thymus	0.12 ± 0.01	0.80 ± 0.10	0.68 ± 0.05
pancreas	0.07 ± 0.01	0.48 ± 0.05	0.47 ± 0.03
muscle	0.03 ± 0.01	0.30 ± 0.02	0.31 ± 0.02
vertebrae	0.06 ± 0.01	0.42 ± 0.02	0.39 ± 0.02
brain	0.02 ± 0.00	0.09 ± 0.01	0.08 ± 0.01
tumor	0.10 ± 0.01	1.20 ± 0.06	1.05 ± 0.10

^a Each value represents the mean ± SD of three to four animals in each group; the individual dose of the intravenous injection was 28.75 kBq/animal.

binding *in vitro* and in tissue sections, and in biodistribution. Systematic interplay between custom-made synthesis and biological testing is expected to define the position of any member of the array of devisable neoglycoproteins for diagnostic and therapeutic applications.

ACKNOWLEDGMENT

The skilful technical assistance of B. Hofer and the generous financial support of the Deutsche Forschungsgemeinschaft (Grants Ga 349/7-1 and Un 63/2-1) and the Dr.-M.-Scheel-Stiftung für Krebsforschung are gratefully acknowledged.

LITERATURE CITED

- (1) Laine, R. A. (1997) The information-storing potential of the sugar code. In *Glycosciences: Status and Perspectives* (H.-J. Gabius and S. Gabius, Eds.) pp 1–14, Chapman & Hall, Weinheim, Germany.
- (2) Gabius, H.-J. (1997) Animal lectins. *Eur. J. Biochem.* 243, 543–576.
- (3) Lee, Y. C., and Lee, R. T., Eds. (1994) *Neoglycoconjugates. Preparation and Applications*, Academic Press, San Diego, CA.
- (4) Lee, R. T., and Lee, Y. C. (1997) Neoglycoconjugates. In *Glycosciences: Status and Perspectives* (H.-J. Gabius and S. Gabius, Eds.) pp 55–77, Chapman & Hall, Weinheim, Germany.

- (5) Gabius, H.-J. (1988) Tumor lectinology: at the intersection of carbohydrate chemistry, biochemistry, cell biology and oncology. *Angew. Chem., Int. Ed. Engl.* **27**, 1267–1276.
- (6) Monsigny, M., Roche, A. C., Midoux, P., Kieda, C., and Mayer, R. (1988) Endogenous lectins of myeloid and tumor cells: characterization and biological implications. In *Lectins and Glycoconjugates in Oncology* (H.-J. Gabius and G. A. Nagel, Eds.) pp 25–48, Springer-Verlag, Heidelberg, Germany.
- (7) Batra, R. K., Wang-Johanning, F., Wagner, E., Garver, R. L., and Curiel, D. T. (1994) Receptor-mediated gene delivery employing lectin-binding specificity. *Gene Ther.* **1**, 255–260.
- (8) Frese, J., Wu, C. H., and Wu, G. Y. (1994) Targeting of genes to the liver with glycoprotein carriers. *Adv. Drug Deliv. Rev.* **14**, 137–152.
- (9) Bovin, N. V., and Gabius, H.-J. (1995) Polymer-immobilized carbohydrate ligands: versatile chemical tools for biochemistry and medical sciences. *Chem. Soc. Rev.* **24**, 413–421.
- (10) Meijer, D. K. F., and Molema, G. (1995) Targeting of drugs to the liver. *Sem. Liver Dis.* **15**, 202–256.
- (11) Gabius, S., Kayser, K., Bovin, N. V., Yamazaki, N., Kojima, S., Kaltner, H., and Gabius, H.-J. (1996) Endogenous lectins and neoglycoconjugates: a sweet approach to tumor diagnosis and targeted drug delivery. *Eur. J. Pharm. Biopharm.* **42**, 250–261.
- (12) Rice, K. G. (1997) Glycoconjugate-mediated drug targeting. In *Glycosciences: Status and Perspectives* (H.-J. Gabius and S. Gabius, Eds.) pp 471–483, Chapman & Hall, Weinheim, Germany.
- (13) Danguy, A., Camby, I., Salmon, I., and Kiss, R. (1997) Modern glycohistochemistry: a major contribution to morphological investigations. In *Glycosciences: Status and Perspectives* (H.-J. Gabius and S. Gabius, Eds.) pp 547–562, Chapman & Hall, Weinheim, Germany.
- (14) Kannan, S., and Nair, M. K. (1997) Lectins and neoglycoproteins in histopathology. In *Glycosciences: Status and Perspectives* (H.-J. Gabius and S. Gabius, Eds.) pp 563–583, Chapman & Hall, Weinheim, Germany.
- (15) Gabius, H.-J. (1997) Concepts of tumor lectinology. *Cancer Invest.* (in press).
- (16) Rogers, J. C., and Kornfeld, S. (1971) Hepatic uptake of proteins coupled to fetuin glycopeptide. *Biochem. Biophys. Res. Commun.* **45**, 622–629.
- (17) Gabius, H.-J., Brinck, U., Lüsebrink, T., Ciesiolka, T., and Gabius, S. (1991) Glycopeptide-albumin derivative: its preparation and histochemical ligand properties. *Histochem. J.* **23**, 303–311.
- (18) Unverzagt, C. (1996) Chemoenzymatic synthesis of a sialylated undecasaccharide-asparagine. *Angew. Chem., Int. Ed. Engl.* **35**, 2350–2353.
- (19) Wen, D. X., Livingston, B. D., Medzihradsky, K. F., Kelm, S., Burlingame, A. L., and Paulson, J. C. (1992) Primary structure of Gal β 1,3(4)GlcNAc α 2,3-sialyltransferase determined by mass spectrometry sequence analysis. *J. Biol. Chem.* **267**, 21011–21019.
- (20) Unverzagt, C. (1994) Synthesis of a biantennary heptasaccharide by regioselective glycosylations. *Angew. Chem., Int. Ed. Engl.* **33**, 1101–1103.
- (21) Bayley, A., Standring, D. N., and Knowles, J. R. (1978) Propane-1,3-dithiol: a selective reagent for the efficient reduction of alkyl and aryl azides to amines. *Tetrahedron Lett.* **19**, 3633–3634.
- (22) Unverzagt, C., Kunz, H., and Paulson, J. C. (1990) High-efficiency synthesis of sialyloligosaccharides and sialoglycopeptides. *J. Am. Chem. Soc.* **112**, 9308–9309.
- (23) McBroom, C. R., Samanen, C. H., and Goldstein, I. J. (1972) Carbohydrate antigens: coupling of carbohydrates to proteins by diazonium and phenylisothiocyanate reactions. *Methods Enzymol.* **28**, 212–219.
- (24) Monsigny, M., Petit, C., and Roche, A.-C. (1988) Colorimetric determinations of neutral sugars by a resorcinol sulfuric acid micromethod. *Anal. Biochem.* **175**, 525–530.
- (25) Zeng, F.-Y., and Gabius, H.-J. (1993) Determination of carbohydrate-specificity in solid-phase assays. In *Lectins and Glycobiology* (H.-J. Gabius and S. Gabius, Eds.) pp 81–85, Springer-Verlag, Heidelberg, Germany.
- (26) Gabius, H.-J. (1990) Influence of type of linkage and spacer on the interaction of β -galactoside-binding proteins with immobilized affinity ligands. *Anal. Biochem.* **189**, 91–94.
- (27) Dong, X., Amselgruber, W. M., Kaltner, H., Gabius, H.-J., and Sinowatz, F. (1995) Affinity-purified antibodies against α -galactosyl residues from human serum: comparison of their binding in bovine testicular tissue with that of the *Griffonia simplicifolia* lectin and impact of labeling on epitope localization. *Eur. J. Cell Biol.* **68**, 96–101.
- (28) Gabius, H.-J., Engelhardt, R., Hellmann, T., Midoux, P., Monsigny, M., Nagel, G. A., and Vehmeyer, K. (1987) Characterization of membrane lectins in human colon carcinoma cells by flow cytometry, drug targeting and affinity chromatography. *Anticancer Res.* **7**, 109–112.
- (29) Gabius, H.-J., and Bardosi, A. (1991) Neoglycoproteins as tools in glycohistochemistry. *Prog. Histochem. Cytochem.* **22**, 1–66.
- (30) Gabius, H.-J., André, S., Danguy, A., Kayser, K., and Gabius, S. (1994) Detection and quantification of carbohydrate-binding sites on cell surfaces and in tissue sections by neoglycoproteins. *Methods Enzymol.* **242**, 56–65.
- (31) Kojima, S., Shimura, N., Kubodera, A., Takahashi, T., and Oyamada, H. (1991) Radioimmunodetection of human colon cancer in nude mice by a new monoclonal antibody A7 against human colorectal cancer. *Nucl. Med. Biol.* **18**, 847–853.
- (32) Kojima, S., and Gabius, H.-J. (1988) Biodistribution of neoglycoproteins in mice bearing solid Ehrlich tumor. *J. Cancer Res. Clin. Oncol.* **114**, 468–472.
- (33) Joziassse, D. H., Schiphorst, W. E. C. M., van den Eijnden, D. H., van Kuik, J. A., and Vliegthart, J. F. G. (1985) Branch specificity of bovine colostrum CMP-sialic acid: N-acetylglucosaminide α 2 \rightarrow 6-sialyltransferase. Interaction with biantennary oligosaccharides and glycopeptides of N-glycosylproteins. *J. Biol. Chem.* **260**, 714–719.
- (34) Weisshaar, G., Hijama, J., and Renwick, A. C. G. (1991) Site-specific N-glycosylation of human chorionic gonadotropin. Structural analysis of glycopeptides by one- and two-dimensional ^1H NMR spectroscopy. *Glycobiology* **1**, 393–404.
- (35) Tamura, T., Wadhwa, M. S., and Rice, K. G. (1994) Reducing-end modification of N-linked oligosaccharides with tyrosine. *Anal. Biochem.* **216**, 335–344.
- (36) Tiemeyer, M., Yasuda, Y., and Schnaar, R. L. (1989) Ganglioside-specific binding protein on rat brain membranes. *J. Biol. Chem.* **264**, 1671–1681.
- (37) Gabius, S., Kayser, K., Hellmann, K. P., Ciesiolka, T., Trittin, A., and Gabius, H.-J. (1990) Carrier-immobilized derivatized lysoganglioside GM $_1$ is a ligand for specific binding sites in various human tumor cell types and peripheral blood lymphocytes and monocytes. *Biochem. Biophys. Res. Commun.* **169**, 239–244.
- (38) Baenziger, J. U., and Fiete, D. (1980) Galactose- and N-acetylglucosamine-specific endocytosis of glycopeptides by isolated rat hepatocytes. *Cell* **22**, 611–620.
- (39) Abbott, W. M., Hounsell, E. F., and Feizi, T. (1988) Further studies of oligosaccharide recognition by the soluble 13 kDa lectin of bovine heart muscle. *FEBS Lett.* **252**, 283–287.
- (40) Galanina, O. E., Kaltner, H., Khraltsova, L. S., Bovin, N. V., and Gabius, H.-J. (1997) Further refinement of the description of the ligand-binding characteristics for the galactoside-binding mistletoe lectin, a plant agglutinin with immunomodulatory potency. *J. Mol. Recognit.* (in press).
- (41) Mandal, D. K., and Brewer, C. F. (1992) Cross-linking activity of the 14-kDa β -galactoside-specific vertebrate lectin with asialofetuin: comparison with several galactose-specific plant lectins. *Biochemistry* **31**, 8465–8472.
- (42) Gupta, D., Kaltner, H., Dong, X., Gabius, H.-J., and Brewer, C. F. (1996) Comparative cross-linking activities of lactose-specific plant and animal lectins and a natural lactose-binding immunoglobulin G fraction from human serum with asialofetuin. *Glycobiology* **6**, 843–849.
- (43) Lee, R. T., Ichikawa, Y., Allen, H. J., and Lee, Y. C. (1990) Binding characteristics of galactoside-binding lectin (galaptin) from human spleen. *J. Biol. Chem.* **265**, 7864–7871.
- (44) Lee, R. T., Gabius, H.-J., and Lee, Y. C. (1992) Ligand-binding characteristics of the major mistletoe lectin. *J. Biol. Chem.* **267**, 23722–23727.

- (45) Schneller, M., André, S., Cihak, J., Kaltner, H., Merkle, H., Rademaker, G. J., Haverkamp, J., Thomas-Oates, J., Loesch, U., and Gabius, H.-J. (1995) Differential binding of two chicken β -galactoside-specific lectins to homologous lymphocyte subpopulations and evidence for inhibitor activity of the dimeric lectin on stimulated T cells. *Cell. Immunol.* **166**, 35–43.
- (46) Crocker, P. R., Kelm, S., Hartnell, A., Freeman, S., Nath, D., Vinson, M., and Mucklow, S. (1996) Sialoadhesin and related cellular recognition molecules of the immunoglobulin superfamily. *Biochem. Soc. Trans.* **24**, 150–156.
- (47) Chiu, M. H., Tamura, T., Wadhwa, M. S., and Rice, K. G. (1994) *In vivo* targeting function of N-linked oligosaccharides with terminating galactose and N-acetylgalactosamine residues. *J. Biol. Chem.* **269**, 16195–16202.
- (48) Gupta, D., and Surolia, A. (1994) Synthesis of neoglycopeptides and analyses of their biodistribution *in vivo* to identify tissue-specific uptake and novel putative membrane lectins. *Glycoconjugate J.* **11**, 558–571.

BC970164D

Esterase-Triggered Fluorescence of Fluorogenic Oligonucleotides

Alain Laurent,[†] Françoise Debart,^{*,†} Ned Lamb,[‡] and Bernard Rayner[†]

Laboratoire de Chimie Bio-organique, UMR 5625 CNRS-UM II, Case 008, Université Montpellier II, Place Eugène Bataillon, 34095 Montpellier Cedex 5, France, and Unité de Biologie Cellulaire, Centre de Recherche de Biochimie Macromoléculaire, CNRS, 1919 Route de Mende, B.P. 5051, 34033 Montpellier Cedex, France. Received February 21, 1997[©]

In the prooligonucleotide approach, a step of activation by cellular esterases is necessary for the removal of internucleoside phosphate masking groups and subsequent intracellular delivery of active antisense oligonucleotides. The efficacy of this approach implies that prooligonucleotides, once they are taken up by cells, are demasked by esterases during their course to their nucleic acid targets. In this regard, a method for labeling oligomers with esterase-activable fluorogenic tag was designed. The two phenolic functions of carboxyfluorescein were protected by pivaloyl groups, yielding a nonfluorescent lactone which was further activated as a *N*-hydroxysuccinimide ester. Two nuclease-resistant phosphorothioate 18-mer and methylphosphonate 19-mer oligodeoxynucleosides were attached to this biprotected fluorescein derivative via an amino linker at the 5'-end of the oligomers. The two conjugates were assayed for their carboxyesterase substrate ability in different biological media. In the presence of purified esterases or when incubated in serum or cell extracts, both oligonucleotide conjugates became fluorescent. In addition, the phosphorothioate oligoconjugate was microinjected into the cytoplasm of human fibroblasts, and a fast cytoplasmic release of fluorescence was observed with a rapid translocation of the fluorescent oligomer into the nucleus.

INTRODUCTION

The prooligonucleotide concept has been developed by us and others during the past few years (1–5). Prooligonucleotides were designed as a new class of antisense analogs with internucleosidic phosphates masked by enzymolabile protecting groups. Suppression of negative charges and increase of lipophilicity are expected to improve the cellular uptake of these oligonucleotide prodrugs (6–8) and to induce a completely different bioavailability pattern in relation with the route of administration. After intracellular delivery, these uncharged and nuclease-resistant analogs may be converted by cellular esterases to phosphodiester or phosphorothioate oligonucleosides able to elicit RNase H (9). The efficacy of this approach implies that prooligonucleotides, once they are taken up by cells, are demasked by esterases during their course to their nucleic acid targets.

In this regard, the aim of our work was to design a method for labeling oligomers with an esterase-activable fluorogenic tag and to visualize esterase activity within the cell. We report here the synthesis of the 5(6)-carboxyfluorescein derivative protected on the two phenolic functions by pivaloyl groups, yielding the nonfluorescent lactone form. Cleavage of the ester groups by the cellular carboxyesterases would open the lactone to the fluorescent xanthen-3-one derivative. The *N*-hydroxysuccinimide (NHS) ester of the biprotected carboxyfluorescein was then prepared and reacted with the amino linker at the 5'-end of two nuclease-resistant phosphorothioate (ps) 18-mer and methylphosphonate (mp) 19-mer oligonucleosides, yielding the fluorogenic oligonucleotide conjugates **1** and **2**, respectively.

To assess the structure of the fluorogenic conjugates, **1** and **2** were treated with ammonia or pig liver esterase (PLE) and the reaction products were analyzed by HPLC. Furthermore, the fluorescence released upon PLE hydrolysis was measured by fluorescence spectrophotometry. We examined the carboxyesterase substrate ability of the two oligoconjugates **1** and **2** in different biological media including cell culture medium and cell extracts. Finally, we studied the fate of the fluorogenic phosphorothioate oligoconjugate **1** in human fibroblasts after microinjection into the cytoplasm and nucleus.

EXPERIMENTAL PROCEDURES

Materials and Methods. Except as noted, reagents and solvents were commercially obtained and used without further purification. Amine-free *N,N*-dimethylformamide (DMF) (puriss) was purchased from Fluka. Anhydrous methylene chloride (CH₂Cl₂) was distilled from phosphorus pentaoxide. Silica gel TLC was carried out on Kieselgel 60 F₂₅₄ plates (Merck), and compounds were visualized by UV shadowing. Silica gel 60 (Merck 230–400 mesh) was used for flash column chromatography. FAB mass spectra (MS) were recorded on a JEOL DX300 spectrometer operating with a JMA-DA 5000 mass data system in positive ion mode; the ESI mass spectrum was obtained with a Finnigan MAT SSQ 7000 mass spectrometer, and the MALDI-TOF spectrum was recorded on a PerSeptive Biosystems Voyager mass spectrometer. The ¹H-NMR spectra were recorded with a Bruker DRX 400 MHz spectrometer, and chemical shifts were measured relative to CHCl₃ fixed at 7.24 ppm. Reversed-phase HPLC was performed on a Waters 600 E system equipped with a Model 990 photodiode array detector and using a Macherey-Nagel EC Nucleosil 5μ C₁₈ column (150 × 4.6 mm) for analytical purposes and a Waters Delta Pak 15μ C₁₈ 100 Å column (300 × 7.8 mm) for preparative work. The fluorescence spectra were recorded on a Spex-Fluorolog spectrofluorometer Model 1681 (Jobin-Yvon).

* Author to whom correspondence should be addressed [telephone (33) 4 67 14 38 98; fax (33) 4 67 04 20 29; e-mail debart@univ-montp2.fr].

[†] Laboratoire de Chimie Bio-organique.

[‡] Unité de Biologie Cellulaire.

[©] Abstract published in *Advance ACS Abstracts*, October 15, 1997.

3',6'-Bis(*tert*-butyloxy)-3-oxospiro[isobenzofuran-1(3*H*),9'(9*H*)-xanthene]-5(6)-carboxylic Acid (3). To a cooled (ice bath) and stirred solution of 5(6)-carboxy-fluorescein (1 g, 2.6 mmol) in dry pyridine (10 mL) was added dropwise pivaloyl chloride (1.6 g, 1.6 mL, 13.3 mmol). The mixture was stirred at room temperature overnight. The excess of pivaloyl chloride was hydrolyzed with cold water (10 mL), and the volume of the reaction mixture was reduced to 5 mL under reduced pressure. Methylene chloride (10 mL) was then added, and the resulting solution was washed four times with water (50 mL), dried over anhydrous sodium sulfate, and evaporated to dryness under reduced pressure. The residue (1.54 g) was fractionated by flash chromatography on a silica gel (48 g) column (3.5 cm i.d.) using 10% diethyl ether in CH_2Cl_2 (700 mL) and then a stepwise gradient of 1–20% methanol in CH_2Cl_2 as eluants. Fractions containing pure **3** as a mixture of regioisomers (R_f 0.35 for regioisomer **5** and R_f 0.42 for regioisomer **6**, eluant system $\text{CH}_2\text{Cl}_2/\text{CH}_3\text{OH}$ 4:1 v/v) were combined and evaporated to give a colorless foam (766 mg, 1.4 mmol, 53% yield): ^1H NMR (CDCl_3) (regioisomer **6**) δ 1.36 (1s, 18 H, *t*Bu), 6.79 and 7.08 (2m, 6H), 7.85 (s, 1 H, H_I), 8.11 (d, 1 H, H_4 , J_{4-5} = 8 Hz), 8.32 (dd, 1 H, H_5 , J_{5-4} = 8 Hz, J_{5-1} = 1 Hz), 10.57 (br s, 1 H, $-\text{CO}_2\text{H}$); (regioisomer **5**) δ 1.40 (1s, 18 H, *t*Bu), 6.84 and 7.11 (2m, 6H), 7.32 (d, 1H, H_I , J_{1-6} = 8 Hz), 8.43 (d, 1H, H_6 , J_{6-1} = 8 Hz), 8.81 (s, 1H, H_4); MS (+ FAB, glycerol/thioglycerol 50:50, v/v) [$\text{M} + \text{H}$] $^+$ = 545.

1-[3',6'-Bis(*tert*-butyloxy)-3-oxospiro[isobenzofuran-1(3*H*),9'(9*H*)-xanthene]-5(6)-yl]carbonyloxy]-2,5-pyrrolidinedione (4). *N*-[3-(Dimethylamino)propyl]-*N*-ethylcarbodiimide hydrochloride (EDC) (377 mg, 1.96 mmol) and NHS (178 mg, 1.55 mmol) were successively added to a solution of compound **3** (766 mg, 1.4 mmol) in dry CH_2Cl_2 (10 mL). The reaction mixture was stirred at room temperature for 4 h. EDC (54 mg, 0.28 mmol) was then added and stirring was carried on for 3 h. The reaction mixture was evaporated to give a yellowish foam. The residue was dissolved in ethyl acetate (50 mL), and the solution was washed four times with water (100 mL). The organic layer was then dried over anhydrous sodium sulfate and evaporated under reduced pressure. The residue (982 mg) was fractionated on a silica gel (30 g) column (3.5 cm i.d.) using first a gradient of CH_2Cl_2 (10–100%) in cyclohexane and then a gradient of methanol (1–2%) in CH_2Cl_2 as eluants. Pooled fractions containing pure product **4** were evaporated to dryness. The residue was dissolved in dioxane, and the solution was lyophilized to afford a white powder (595 mg, 0.92 mmol, 47% yield): R_f 0.5 (TLC solvent: $\text{CH}_2\text{Cl}_2/\text{CH}_3\text{OH}/\text{CH}_3\text{COOH}$ 97:2:5; 0.5 v/v/v); ^1H NMR (as a mixture of regioisomers **5** and **6** in 2:1 ratio) (CDCl_3) δ 1.36 (br s, 18 H, *t*Bu), 2.95 [m, 4H, $-(\text{CH}_2)_2$], 6.78 and 7.11 (2m, 6H), 7.36 (d, $^{1/3}$ H, H_I of isomer **5**, J_{1-6} = 8 Hz), 7.92 (s, $^{1/3}$ H, H_I of isomer **6**), 8.19 (d, $^{1/3}$ H, H_4 of isomer **6**, J_{4-5} = 8 Hz), 8.40 (dd, $^{1/3}$ H, H_5 of isomer **6**, J_{5-4} = 9 Hz, J_{5-1} = 1.3 Hz), 8.42 (dd, $^{2/3}$ H, H_6 of isomer **5**, J_{6-1} = 8 Hz, J_{6-4} = 1.5 Hz), 8.83 (s, $^{2/3}$ H, H_4 of isomer **5**); MS (+ FAB, glycerol/thioglycerol 50:50, v/v) [$\text{M} + \text{H}$] $^+$ = 642.

Synthesis of 5'-Amino-Linked Oligonucleotides 7 and 8. The phosphorothioate oligonucleoside **5** (sequence 5' AACGTTGAGGGGCATCGT 3') and the methylphosphonate oligo-**6** (sequence 5' TpAACGTTGAGGGGCATCGT 3') were prepared on 1 μmol scale with an Applied Biosystems Model 381A DNA synthesizer. The standard solid-phase β -cyanoethyl phosphoramidite chemistry in combination with Beaucage's reagent (10) was applied to the phosphorothioate oligo-**5** synthesis. The methylphosphonate oligomer **6** was prepared with the ap-

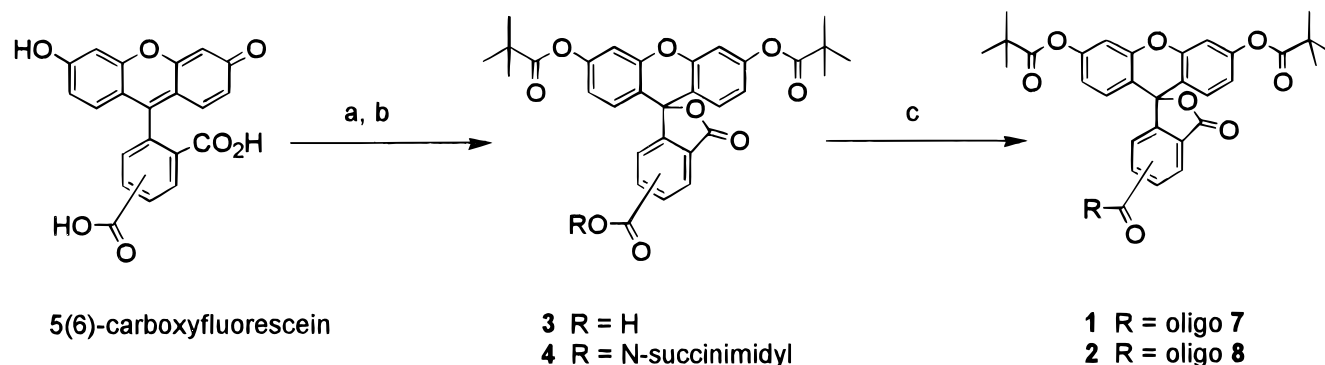
propriately protected nucleoside methylphosphonamidite synthons purchased from Glen Research and according to published procedures (11). Functionalization at the 5'-end of both phosphorothioate (ps) 18-mer and methylphosphonate (mp) 19-mer oligonucleosides **5** and **6** by 1,4 diaminobutane was manually performed on the solid support as previously described (12). After deprotection of **7** by standard ammonia treatment and deprotection of methylphosphonate oligo-**8** according to literature conditions (13), the 5'-amino oligomers **7** and **8** were lyophilized three times and then were reacted with **4** without further purification.

Synthesis and Purification of Fluorogenic Oligonucleotide Conjugates 1 and 2. To a mixture of DMF (105 μL) and 0.1 M $\text{NaHCO}_3/\text{Na}_2\text{CO}_3$ buffer (pH 9) (495 μL) were added successively a solution of 5'-amino-linked oligo-**7** (1.6 mM in water, 100 μL , 28.5 A_{260} units) and a solution of the activated ester **4** (12.5 mM in DMF, 500 μL , 40-fold molar excess). The turbid mixture was stirred vigorously at room temperature for 1.5 h in the dark. The reaction was monitored by HPLC analysis (solvent A = 0.05 M triethylammonium acetate, pH 7; solvent B = 80% acetonitrile in buffer A; linear gradient, from 7% to 63% of B over 20 min and then to 100% of B over 20 min; flow rate = 1 mL min^{-1}). The reaction mixture was loaded onto a Sephadex G-25 column (2 \times 33 cm) equilibrated with 20% ethanol in water, and the crude oligoconjugate **1** was eluted with the same eluant. The oligoconjugate **1** was further purified by preparative reverse-phased HPLC (same eluting conditions as above except 2 mL min^{-1} as flow rate). The pooled fractions were directly desalted through a Sep-Pak C₁₈ (Waters) cartridge following the manufacturer's instructions. The oligoconjugate **1** was eluted with a mixture of acetonitrile and water (50:50, v/v) and then the solvent was evaporated. Yield (measured by UV absorbance at 260 nm) was 25% after purification and desalting with respect to the crude 5'-amino-oligo-**7**: UV spectrum λ_{max} = 256.4 nm; MS (negative ion mode ESI, methanol/water/triethylamine 49:50:1, v/v/v) m/z calcd 6493.4, found 6495.5.

The same procedure as described above was applied for the synthesis and purification of the oligoconjugate **2** except for the following modifications: to a mixture of DMF (170 μL) and 0.1 M $\text{NaHCO}_3/\text{Na}_2\text{CO}_3$ buffer (pH 9) (495 μL) were added successively a solution of 5'-amino-linked oligo-**8** (1.4 mM in water/acetonitrile 50:50, v/v, 100 μL , 25 A_{260} units) and a solution of the activated ester **4** (12.5 mM in DMF, 438 μL , 40-fold molar excess). The turbid mixture was stirred vigorously at room temperature for 0.5 h in the dark. Yield was 23% with respect to the crude 5'-amino-oligo-**8**: UV spectrum λ_{max} = 255 nm; MS (positive ion mode MALDI-TOF, saturated solution of hydroxypicolinic acid in 0.3M diammonium acetate in acetonitrile) m/z calcd 6487.6, found 6485.3.

Esterase Substrate Ability of Fluorogenic Oligoconjugates 1 and 2. *a. HPLC Analysis.* Oligonucleotide conjugate **1** or **2** (18 μM) was incubated at 37 $^\circ\text{C}$ with PLE (80 units mL^{-1}) (Aldrich Chemical Co.) in 25 mM Tris-HCl buffer (pH 7.5). DMSO (6% final concentration in the incubation medium) was added for solubilization of the methylphosphonate derivative **2**. The reaction was monitored by HPLC analysis with the same eluting conditions described above.

b. Fluorescence Spectrophotometry. Oligonucleotide conjugate **1** or **2** (1.1 μM for PLE experiments, otherwise 4.8 μM) was incubated at 37 $^\circ\text{C}$ either in the presence of PLE (8 units mL^{-1}) in 25 mM Tris-HCl buffer (pH 7.5), in RPMI 1640 containing 10% (v/v) heat-deactivated fetal calf serum (FCS; Gibco BRL), or in total CEM-SS cell extracts (14). DMSO (6% final concentration in the

Scheme 1. Synthesis of Fluorogenic Conjugates 1 and 2^a

^a Key: (a) pivaloyl chloride, pyridine; (b) NHS, EDC, anhydrous CH_2Cl_2 ; (c) oligo-7 or oligo-8, $\text{NaHCO}_3/\text{Na}_2\text{CO}_3$ buffer, pH 9, 0.1 M, DMF. Oligo-7, $\text{H}_2\text{N}(\text{CH}_2)_4\text{NHC}(\text{O})(\text{A}_2\text{CGT}_2\text{GAG}_4\text{CATCGT})_3'$. Oligo-8, $\text{H}_2\text{N}(\text{CH}_2)_4\text{NHC}(\text{O})(\text{TpA}_2\text{CGT}_2\text{GAG}_4\text{CATCGT})_3'$. No mark indicates a phosphorothioate linkage, the underscored nucleic bases a methylphosphonate linkage, and the (p) a phosphodiester linkage.

incubation medium) was added for solubilization of the methylphosphonate derivative **2**. The intensity of fluorescence emission (527 nm) was measured as a function of time by fluorescence spectrophotometry upon excitation at 494 nm.

Microinjection and Confocal Fluorescence Microscopy. Human foreskin fibroblasts Hs68 were cultured in CO_2 incubators at 37 °C in Dulbecco's modified Eagle's medium (DMEM) supplemented with 6–10% FCS on 25 mm diameter acid-washed glass coverslips. Cells were microinjected into the cytoplasm and nucleus with a few femtoliters of a solution of 77 μM oligoconjugate **1** in 100 mM HEPES (pH 7.5). Cells were fixed in 3.7% formalin in phosphate-buffered saline (PBS) and were observed with a Leica confocal laser scanning microscope, equipped with a krypton–argon dual-wavelength laser (excitation at 488 nm) (15).

RESULTS AND DISCUSSION

In the present work, we selected the carboxyfluorescein which can exist as a fluorescent xanthen-3-one form or as a nonfluorescent lactone form when the two phenolic functions are esterified. In our approach, we wanted the lactone form to persist all along the conjugate synthesis; for this reason the strategy of coupling the fluorogenic label to the oligomer required the carboxyfluorescein protecting groups to be maintained intact.

Various methods for labeling oligonucleotides with nonradioactive tags have been extensively reported in the literature (16). One of the commonly used approaches is to attach the label at the 5' terminus of the oligomer either by incorporating the suitably protected label phosphoramidite during solid-phase oligonucleotide synthesis or by derivatizing the deprotected oligonucleotide in aqueous medium. In our case, the second procedure of postsynthesis functionalization was more convenient to avoid exposure of the biprotected carboxyfluorescein residue to conditions used during oligonucleotide deprotection (ammonium hydroxide, 55 °C for 5 h). This strategy required the synthesis of a 5'-end-modified oligonucleotide with a primary amino group available for subsequent coupling with the activated ester of the protected carboxyfluorescein **4**.

The NHS ester of the 3',6'-diacetyl-5(6)-carboxyfluorescein is commercially available, but the acetyl groups were not sufficiently stable during the coupling reaction between the oligo derivative and the active ester. We prepared the NHS ester **4** of the more stable 3',6'-dipivaloyl-5(6)-carboxyfluorescein **3**, which has been previously mentioned in the literature (17), but no

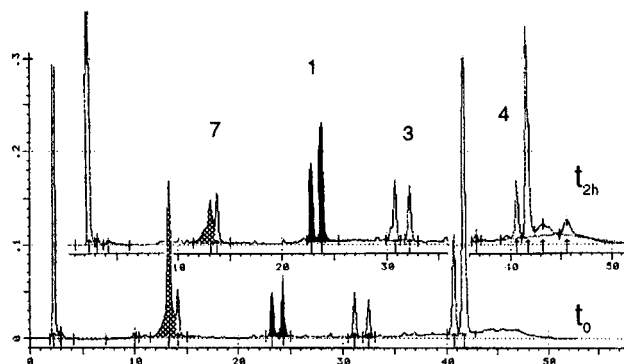


Figure 1. Reversed-phase HPLC chromatogram ($\lambda_{260\text{nm}}$) of the reaction mixture between 5'-aminophosphorothioate oligonucleotide (18-mer) **7** and NHS ester of bis(pivaloyl)carboxyfluorescein **4** at $t = 0$ and 2 h. **1**, fluorogenic phosphorothioate oligoconjugate. **3**, bis(pivaloyl)carboxyfluorescein arising from hydrolysis of **4**.

experimental procedures and data have been reported so far. First, the commercial 5(6)-carboxyfluorescein was reacted with pivaloyl chloride to give the nonfluorescent lactone **3**, which was subsequently reacted with EDC and NHS to yield the NHS ester **4** as described under Experimental Procedures (Scheme 1). In our hands, attempts to synthesize the fluorogenic conjugate with the 5'-amino-linked oligomer prepared with commercially available 5'-amino-modifier C6 (Glen Research) were not satisfactory. Therefore, the functionalization at the 5' end of two nuclease-resistant phosphorothioate **5** and methylphosphonate **6** oligomers was performed manually on solid support after activation of the 5'-hydroxyl group by *N,N*-carbonyldiimidazole (CDI) and then reaction with 1,4-diaminobutane (12). The 5'-amino oligo-7 and -8 obtained were used without purification in the subsequent coupling step with the fluorogenic tag **4**.

The fluorogenic conjugate synthesis was carried out in the dark for 0.5–1.5 h using a 40-fold molar excess of **4** in a 1:1 mixture of DMF and $\text{NaHCO}_3/\text{Na}_2\text{CO}_3$ buffer, pH 9 (18). This coupling reaction was run at pH 9, which was a good compromise to achieve synthesis without loss of pivaloyl groups. The conversion of starting 5'-amino-linked oligonucleotide **7** or **8** into oligoconjugates **1** and **2**, respectively, was monitored by HPLC analysis (Figure 1). Two peaks at $R_T = 23.4$ and 24.2 min corresponding to more lipophilic compounds than the 5'- NH_2 -oligonucleotide **7** ($R_T = 13.3$ min) were tentatively assigned to the isomeric mixture of oligoconjugate **1**. We noticed a similar increase in retention time between the oligoconjugate **2** ($R_T = 25.5$ and 26.3 min) and the starting

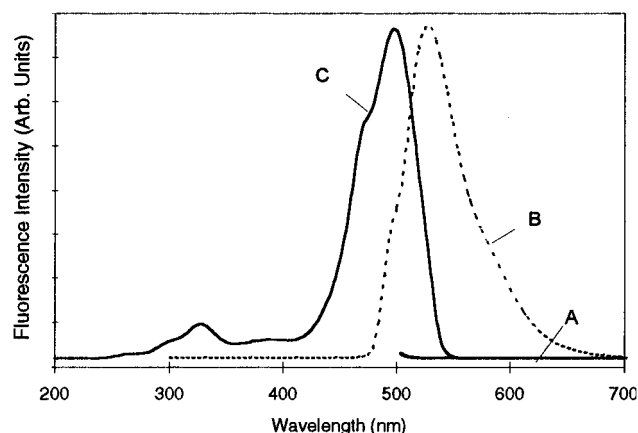


Figure 2. Fluorescence emission spectra upon excitation at 494 nm of the phosphorothioate oligoconjugate **1** before incubation (A) and after 15 h of incubation (B) in cellular extract at 37 °C. (C) represents the fluorescence excitation spectrum of the oligoconjugate **1** after 15 h of incubation in cellular extract.

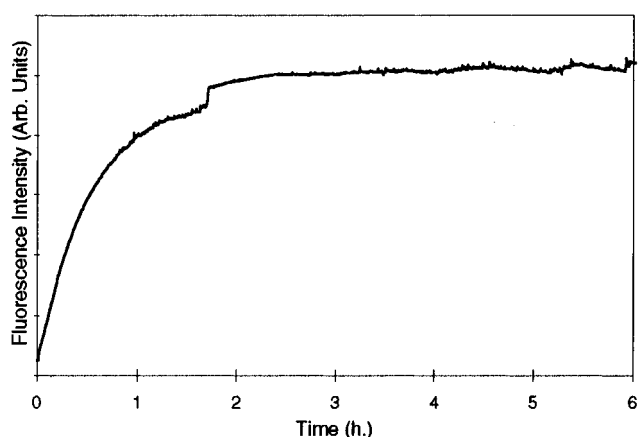


Figure 3. Time course fluorescence at 527 nm (upon excitation at 494 nm) during incubation of **1** at 37 °C with PLE (8 units mL⁻¹). The initial concentration of oligoconjugate **1** was 1 μM in Tris-HCl buffer (25 mM), pH 7.5.

oligonucleotide **8** ($R_T = 15.8$ min). Two extra peaks corresponding to the hydrolysis of succinimidyl ester **4** to carboxylic acid **3** ($R_T = 31$ and 32.5 min) were observed (19). The formation of the oligoconjugates **1** and **2** was monitored at three different wavelengths (245, 260, and 494 nm), and no absorption at 494 nm [characteristic of the unprotected fluorescein derivative (20)] was detected, which indicated that the fluorogenic label was still intact.

Unbound fluorescein derivatives were removed by size exclusion gel chromatography, and oligoconjugates **1** and **2** were further purified by reversed-phase HPLC. These oligonucleotide conjugates were characterized by ESI mass spectrometry for the oligoconjugate phosphorothioate **1** and MALDI-TOF/MS for the methylphosphonate derivative **2**; the molecular weight determined for each compound was found to be in agreement with that calculated.

For further characterization, two samples of oligoconjugate **1** were incubated with either ammonia or PLE. For both chemical and enzymatic hydrolysis, HPLC chromatograms indicated conversion of the starting material into a more polar product. In both cases, products had the same retention time and exhibited an absorption at 494 nm similar to that present in fluorescent conjugates (20). Maximum excitation wavelength was 494 nm, and maximum emission was determined at 514 nm. These experiments were performed with oligoconjugate **2**, and the same data were obtained. These results indicate that fluorogenic oligoconjugates **1** and **2** were deprotected to yield the corresponding fluorescent oligonucleotides.

To determine the carboxyesterase substrate ability of the two oligoconjugates **1** and **2** in biological media, the oligoconjugates **1** and **2** were incubated with PLE or in RPMI 1640 supplemented with 10% heat-deactivated FCS or in total CEM-SS cell extracts, and the fluorescence emission spectra (Figure 2) and the fluorescence curves as a function of time were recorded (Figure 3). All of the curves reach a plateau that corresponds to the deprotected conjugate, and their emission spectra were similar in the three experiments. The fluorescence

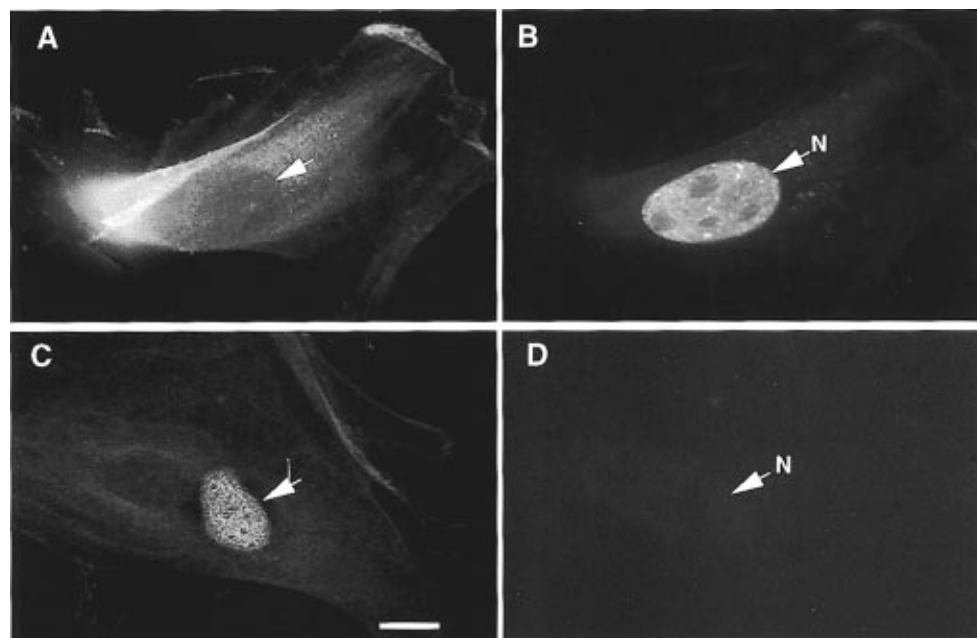


Figure 4. Microinjection of fluorogenic phosphorothioate oligoconjugate **1**. Oligoconjugate **1** was co-injected with an inert rabbit antibody into either the cytoplasm (A and B) or the nucleus (C and D) of human fibroblasts Hs68. Live cells were analyzed 30 min after injection using fluorescence confocal microscopy. Marker antibodies were visualized after staining with Texas-Red conjugated goat anti-rabbit antisera (A and C). Carboxyfluorescein-labeled material is displayed in panels B and D. Scale bar is 5 μm.

intensity increased with a higher rate in cell extracts ($t_{1/2} = 2$ h for **1**, $t_{1/2} = 1$ h for **2**) than in 10% deactivated FCS RPMI 1640 ($t_{1/2} = 6$ h for **1**, $t_{1/2} = 7$ h for **2**), probably because of the higher carboxyesterase content of the former (14). These in vitro experiments confirmed that the oligonucleotide conjugates **1** and **2** are substrates of the esterases.

To investigate the fate of these fluorogenic oligonucleotides within the cell and to visualize the intracellular esterase activity, phosphorothioate oligoconjugate **1** was microinjected into either the cytoplasm or the nucleus of living human fibroblasts. After microinjection into the cytoplasm, confocal fluorescence microscopy revealed primarily a fast emission of fluorescence localized in the cytoplasm (Figure 4). Ten minutes after microinjection, the fluorescence was diffusely distributed in the cytoplasm with some more fluorescent spots attributed to confinement of the fluorescent oligomer to vesicles. This can be explained by an important esterase activity in the vesicles and/or an accumulation of the labeled oligomer in these cytoplasmic organelles. Thirty minutes after microinjection, fluorescence could no longer be observed in the cytoplasm and was essentially located in the cell nucleus. The persistence of fluorescence for > 16 h within the nucleus demonstrated the stability of the linkage between the label and the oligomer in the cells (21, 22). In contrast, when oligonucleotide conjugate **1** was microinjected into the cell nucleus, no detectable fluorescence was observed even after 30 min. This result indicates that esterase activity was predominantly localized in the cytoplasm and that a translocation of fluorescent oligomer occurred from the cytoplasm to the nucleus as already observed with fluorescent oligonucleotides (23). This last result shows that the fluorogenic tag has no effect on the behavior of fluorogenic oligonucleotides as compared to other fluorescent oligomers.

In conclusion, we described the synthesis of fluorogenic oligonucleotides that were obtained by coupling the NHS ester of the bis(pivaloyl)carboxyfluorescein to 5'-amino-phosphorothioate or methylphosphonate oligonucleoside. We provided chromatographic and spectroscopic evidence of the synthesized conjugate identity. We demonstrated that the designed fluorogenic oligonucleotides are substrates of esterases present in serum and in cell extracts. Additionally, we showed that the fluorogenic phosphorothioate conjugate become fluorescent upon esterase-mediated hydrolysis within the cell and that esterase activity was mainly localized in the cytoplasm.

The labeling of prooligonucleotides with this fluorogenic tag is under current investigation as is their cellular uptake in comparison to that of anionic phosphorothioate conjugate **1** and uncharged methylphosphonate conjugate **2**.

ACKNOWLEDGMENT

Financial support for this work was provided through grants from the Association pour la Recherche contre le Cancer and from the Agence Nationale de Recherche sur le Sida. We thank Drs. Frederic Heitz and Anne Fernandez for helpful advice and discussions. We are grateful to Dr. Richard Griffey for MALDI-TOF/MS analysis. The cell extracts were kindly prepared by Dr. A. M. Aubertin.

LITERATURE CITED

- (1) Barber, I., Rayner, B., and Imbach, J. L. (1995) The prooligonucleotide approach I: Esterase-mediated reversibility of dithymidine S-alkyl-phosphorothiolates to dithymidine phosphorothioates. *Bioorg. Med. Chem. Lett.* 5, 563–568.
- (2) Barber, I., Tosquellas, G., Morvan, F., Rayner, B., and Imbach, J. L. (1995) The prooligonucleotide approach II: Synthesis and stability studies of chimeric oligonucleotide models. *Bioorg. Med. Chem. Lett.* 5, 1441–1444.
- (3) Iyer, R. P., Yu, D., and Agrawal, S. (1995) Prodrugs of oligonucleotides: the acyloxalkyl esters of oligodeoxyribonucleoside phosphorothioates. *Bioorg. Chem.* 23, 1–21.
- (4) Tosquellas, G., Barber, I., Morvan, F., Rayner, B., and Imbach, J. L. (1996) The prooligonucleotide approach III: Synthesis and bioreversibility of a chimeric phosphorodithioate prooligonucleotide. *Bioorg. Med. Chem. Lett.* 6, 457–462.
- (5) Tosquellas, G., Morvan, F., Rayner, B., and Imbach, J. L. (1997) The prooligonucleotide approach IV: Synthesis of chimeric prooligonucleotides with 6 enzymolabile masking groups and unexpected desulfurization side reaction. *Bioorg. Med. Chem. Lett.* 7, 263–268.
- (6) Temsamani, J., Kubert, M., Tang, J. Y., Padmapriya, A., and Agrawal, S. (1994) Cellular uptake of oligodeoxynucleotide phosphorothioates and their analogs. *Antisense Res. Dev.* 4, 35–42.
- (7) Spiller, D. G., and Tidd, D. M. (1992) The uptake kinetics of chimeric oligodeoxynucleotide analogues in human leukaemia MOLT-4 cells. *Anti-Cancer Drug Design* 7, 115–129.
- (8) Giles, R. V., Spiller, D. G., and Tidd, D. M. (1993) Chimeric oligodeoxynucleotide analogues enhanced cell uptake of structures which direct ribonuclease-H with high specificity. *Anti-Cancer Drug Design* 8, 33–51.
- (9) Milligan, J. F., Matteucci, M. D., and Martin, J. C. (1993) Current concepts in antisense drug design. *J. Med. Chem.* 36, 1923–1937.
- (10) Iyer, R. P., Phillips, L. R., Egan, W., Regan, J. B., and Beaucage, S. L. (1990) The automated synthesis of sulfur-containing oligodeoxyribonucleotides using 3H-1,2-benzodithiol-3-one 1,1-dioxide as a sulfur-transfer reagent. *J. Org. Chem.* 55, 4693–4699.
- (11) Hogrefe, R. I., Reynolds, M. A., Vaghefi, M. M., Young, K. M., Riley, T. A., Klem, R. E., and Arnold, L. J., Jr. (1993) An improved method for the synthesis and deprotection of methylphosphonate oligonucleotides. *Methods in Molecular Biology: Protocols for Oligonucleotides and Analogs* (S. Agrawal, Ed.) pp 143–164, Humana Press, Totowa, NJ.
- (12) Wachter, L., Jablonski, J.-A., and Ramachandran, K. L. (1986) A simple and efficient procedure for the synthesis of 5'-aminoalkyl oligodeoxynucleotides. *Nucleic Acids Res.* 14, 7985–7994.
- (13) Hogrefe, R. I., Vaghefi, M. M., Reynolds, M. A., Young, K. M., and Arnold Jr., L. J. (1993) Deprotection of methylphosphonate oligonucleotides using a novel one-pot procedure. *Nucleic Acids Res.* 21, 2031–2038.
- (14) Pompon, A., Lefebvre, I., Imbach, J.-L., Kahn, S., and Farquhar, D. (1994) Decomposition pathways of the mono- and bis(pivaloyloxymethyl)esters of azidothymidine 5'-monophosphate in cell extract and in tissue culture medium: an application of the 'on-line ISRP-cleaning' HPLC technique. *Antiviral Chem. Chemother.* 5, 91–98.
- (15) Girard, F., Fernandez, A., and Lamb, N. (1995) Delayed cyclin A and B1 degradation in nontransformed mammalian cells. *J. Cell Sci.* 108, 2599–2608.
- (16) Agrawal, S. (1994) Functionalization of oligonucleotides with amino groups and attachment of amino specific reporter groups. *Methods in Molecular Biology: Protocols for Oligonucleotides Conjugates* (S. Agrawal, Ed.) pp 93–120, Humana Press, Totowa, NJ.
- (17) Theisen, P., McCollum, C., Upadhyaya, K., Jacobson, K., Vu, H., and Andrus, A. (1992) Fluorescent dye phosphoramidite labelling of oligonucleotides. *Tetrahedron Lett.* 33, 5033–5036.
- (18) Acedo, M., Tarrason, G., Piulats, J., Mann, M., Wilm, M., and Eritja, R. (1995) Preparation of oligonucleotide-dexamethasone conjugates. *Bioorg. Med. Chem. Lett.* 5, 1577–1580.
- (19) Fukui, K., Morimoto, M., Segawa, H., Tanaka, K., and Shimidzu, T. (1996) Synthesis and properties of an oligonucleotide modified with an acridine derivative at the artificial abasic site. *Bioconjugate Chem.* 7, 349–355.
- (20) Telser, J., Cruickshank, K. A., Morrison, L. E., and Netzel, T. L. (1989) Synthesis and characterization of DNA oligomers

- and duplexes containing covalently attached molecular labels: comparison of biotin, fluorescein, and pyrene labels by thermodynamic and optical spectroscopic measurements. *J. Am. Chem. Soc.* **111**, 6966–6976.
- (21) Fisher, T. L., Terhorst, T., Cao, X., and Wagner, R. W. (1993) Intracellular disposition and metabolism of fluorescently-labeled unmodified and modified oligonucleotides microinjected into mammalian cells. *Nucleic Acids Res.* **21**, 3857–3865.
- (22) Chin, D. J., Green, G. A., Zon, G., Szoka Jr., F. C., and Straubinger, R. M. (1990) Rapid nuclear accumulation of injected oligodeoxyribonucleotides. *New Biol.* **2**, 1091–1100.
- (23) Leonetti, J.-P., Mehti, N., Degols, G., Gagnor, C., and Lebleu, B. (1991) Intracellular distribution of microinjected antisense oligonucleotides. *Proc. Natl. Acad. Sci. U.S.A.* **88**, 2702–2706.

BC970168I

Incorporation of an Artificial Receptor into a Native Protein: New Strategy for the Design of Semisynthetic Enzymes with Allosteric Properties

Itaru Hamachi,* Tsuyoshi Nagase, Yusuke Tajiri, and Seiji Shinkai

Department of Chemistry and Biochemistry, Graduate School of Engineering, Kyushu University, Fukuoka 812, Japan. Received April 25, 1997*

The sugar-facilitated structure and enzymatic activity change of engineered myoglobins bearing a phenylboronic acid moiety, which were semisynthesized by a cofactor reconstitution method, were studied by the denaturation experiment, spectrophotometric titration of the pK_a shift of the axial H_2O , circular dichroism (CD), and the kinetics of the myoglobin-catalyzed–aniline hydroxylation reaction. Both boronophenylalanine-appended myoglobin [$Mb(m\text{-Bphe})_2$] and phenylboronic acid-appended myoglobin [$Mb(PhBOH)_2$] were stabilized by approximately 2 kcal/mol upon complexation with D-fructose. CD spectral changes and the sugar-induced pK_a shift suggested that the microenvironment of the active site of these myoglobins was re-formed from a partially disturbed state to that comparable to the native state upon D-fructose binding. The correlation of pK_a with k_{cat} (for the aniline hydroxylase activity) and the $\Delta G_D^{H_2O}-k_{cat}$ profile showed that these structural changes of $Mb(m\text{-Bphe})_2$ and $Mb(PhBOH)_2$ were closely related to their sugar-enhanced aniline hydroxylase activity. Thus, the results established that an incorporation of the artificial receptor molecule can be a valid methodology for the design of stimuli-responsive semiartificial enzymes.

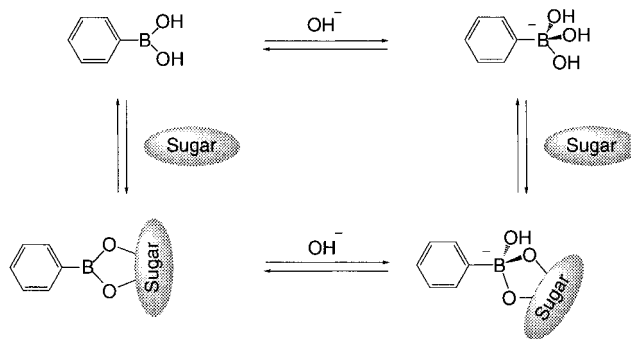
INTRODUCTION

The introduction of unnatural atoms or molecules into naturally occurring enzymes and proteins is one of the most promising approaches for the development of new tailored proteins, which then have potential applications in chemistry and biology (Bell and Hilvert, 1994). Following Kaiser's proposal on chemical mutation (Kaiser and Lawrence, 1984; Kaiser, 1988; Wu and Hilvert, 1989; Petersen and Hilvert, 1995), a more general biosynthetic method that utilizes aminoacylated suppressor t-RNA has been recently advanced by Schultz and co-workers (Cornish et al., 1995). In addition to developing other methodologies for the incorporation of unnatural molecules, the class of unnatural atoms and molecules that can positively act on native enzymes also needs to be expanded. As one example of such an interaction, we preliminarily reported that the sugar-binding ability of phenylboronic acid that has been incorporated into myoglobin can enhance the dioxygen storage capability of the myoglobin molecule (Hamachi et al., 1994a,b). On the basis of the previous findings, the present study demonstrates here that the aniline hydroxylase activity of these engineered myoglobins is facilitated by sugar molecules. The interesting relationship between the structure and the activity change induced by sugars is also discussed in great detail.

RESULTS

Design of Phenylboronic Acid-Appended Myoglobins. Such researchers as Czarnik, Smith, and Shinkai have recently and independently demonstrated that phenylboronic acid is one of the most potentially useful artificial receptors for saccharide molecules (Yoon and Czarnik, 1992; Paugam et al., 1994; James et al.,

1996). A neutral boronic acid (sp^2 configuration of boron) binds a 1,2- or 1,3-diol unit of sugar to form a negatively charged boronate ester (sp^3 configuration) in aqueous solution. Site-specific alteration in the charge and the hydrophilicity can be induced when boronic acid binds with sugar molecules. Thus, phenylboronic acid is expected to be useful for the modulation of structure and/or activity of native proteins.



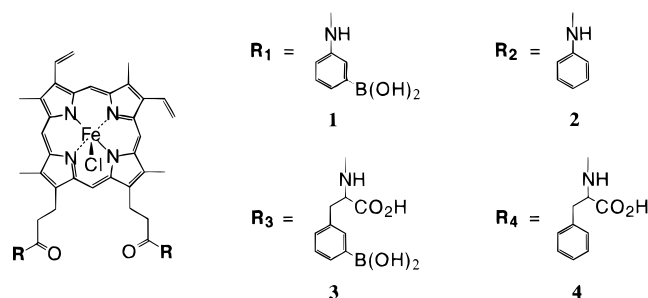
Initially, in this study, heme **1** was synthesized and incorporated into apomyoglobin (apo-Mb) using a conventional cofactor reconstitution method. The resultant $Mb(PhBOH)_2$ displayed a sugar responsive dioxygen storage capability. However, the low yield (30% for the reconstitution) and low stability of $Mb(PhBOH)_2$ and its derivative rendered them unsuitable for detailed analysis.

In an attempt to solve these problems, a more sophisticated design for the phenylboronic acid insertion into myoglobin was used. To retain two carboxylic acid groups, which are usually present in the side chains of the native heme cofactor, an unnatural amino acid, boronophenylalanine, was employed for pendant units. *m*-Boronophenylalanine-appended heme **3** was successfully reconstituted with apo-Mb in an almost quantitative yield [$Mb(m\text{-Bphe})_2$, $\geq 95\%$]. Phenylalanine-appended Mb [$Mb(Phe)_2$, reconstitution of heme **4**, yield $> 90\%$] and

* Author to whom correspondence should be addressed (e-mail itarutcm@mbox.nc.kyushu-u.ac.jp).

© Abstract published in *Advance ACS Abstracts*, November 1, 1997.

aniline-appended Mb [Mb(PhH)₂, reconstitution of heme 2, yield ≈ 50%] were also prepared as control proteins.



After purification using previously reported procedures (Asakura and Yonetani, 1969; Asakura, 1978), the purity of the proteins was assayed using the ratio of Soret absorbance (408 nm) to protein absorbance (280 nm) as a known purity index (Tamura et al., 1973). The ratios were 4.5 for Mb(PhBOH)₂, 4.4 for Mb(PhH)₂, 4.8 for Mb(*m*-BpHe)₂, and 4.7 for Mb(Phe)₂. These are comparable to the value of 4.8 for native myoglobin, indicating that these semisynthetic myoglobins are pure enough to use in the subsequent studies.

Sugar-Facilitated Stabilization of Phenylboronic Acid-Appended Myoglobins. The net stability of the present myoglobins was evaluated by urea-induced denaturation experiments. Increasing the concentration of urea (a denaturant) destroys the three-dimensional structure of myoglobin, resulting in the release of a heme cofactor. This denaturation process can be spectrophotometrically observed by the broadening of the Soret band (Puett, 1973). Figure 1a shows the denaturation curve of Mb(*m*-BpHe)₂ plotting the Soret absorbance changes against urea concentration in the absence and presence of D-fructose. Clearly, Mb(*m*-BpHe)₂ with D-fructose is more resistant to denaturation, relative to that without D-fructose. The conventional linear extrapolation of these denaturation curves gives denaturation free energies ($\Delta G_D^{\text{H}_2\text{O}}$) (Pace, 1986). Table 1 summarizes $\Delta G_D^{\text{H}_2\text{O}}$ values for all of the myoglobin derivatives.

Interestingly, both Mb(*m*-BpHe)₂ and Mb(PhBOH)₂ were stabilized by approximately 2 kcal/mol as a result of D-fructose. On the other hand, the stability of Mb(Phe)₂ (Figure 1b) and Mb(PhH)₂ was not affected by D-fructose. In addition to the sugar-facilitated stabilization of phenylboronic acid-appended myoglobins, there are other important findings related to the design of engineered myoglobins (Table 1): (i) the modification of protoheme at both propionic acid functional groups destabilized the net 3D structure of holo-Mb, (ii) the retention of carboxylic acid groups at heme side chains was effective for the stabilization of reconstituted myoglobins by 2–4 kcal/mol [please compare the $\Delta G_D^{\text{H}_2\text{O}}$ values for Mb(PhH)₂ and Mb(Phe)₂ or for Mb(PhBOH)₂ to Mb(*m*-BpHe)₂].

The intensified heme–apoprotein interactions by fructose were observed for phenylboronic acid-appended myoglobins using circular dichroism (CD) spectroscopy. Figure 2 compares the CD spectra of Mb(PhBOH)₂ in the absence and presence of fructose. A positive peak at 408 nm is due to an induced CD of the heme which is sensitive to the microenvironment of the heme crevice (i.e., myoglobin active site). This peak is clearly intensified by 1.2-fold upon the addition of fructose, whereas two negative (225 and 208 nm) CD peaks and one positive (190 nm) CD peak, which are characteristic of the α -helix structures of myoglobin, scarcely change. Similar CD spectral changes were observed for Mb(*m*-BpHe)₂, but no

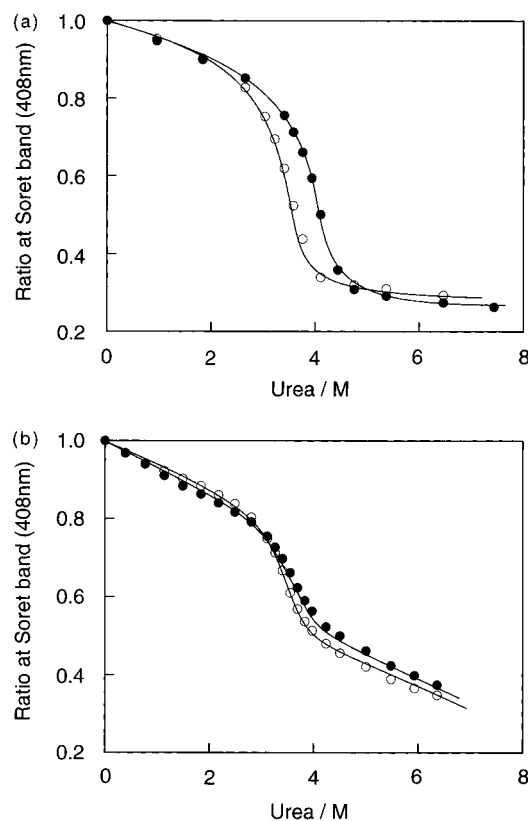


Figure 1. Denaturation curve of the myoglobins derivatives by the addition of urea: (a) Mb(*m*-BpHe)₂ in the absence (○) and the presence (●) of D-fructose (0.1 M); (b) Mb(Phe)₂ in the absence (○) and presence (●) of D-fructose (0.1 M). The slope *m* is a parameter showing the cooperativity factor during the protein denaturation. The values are within 2.2 ± 0.5 , so the cooperativity factors were practically identical in all cases.

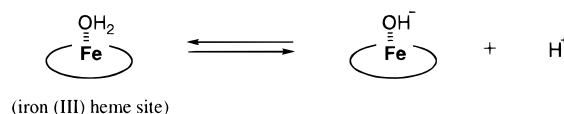
Table 1. Parameters for the Urea Denaturation: Free Energy Changes ($\Delta G_D^{\text{H}_2\text{O}}$) and the Slope (*m*)

	none		D-fructose	
	$\Delta G_D^{\text{H}_2\text{O}}$ (kcal/mol)	<i>m</i> (kcal/mol·M ⁻¹)	$\Delta G_D^{\text{H}_2\text{O}}$ (kcal/mol)	<i>m</i> (kcal/mol·M ⁻¹)
Mb(PhBOH) ₂	6.3	2.3	8.3	2.3
Mb(PhH) ₂	4.5	1.9	4.5	1.8
Mb(<i>m</i> -BpHe) ₂	8.0	2.3	10.1	2.6
Mb(Phe) ₂	8.3	2.4	8.4	2.3
native Mb	14.3	2.7	13.6	2.5

^a $\Delta G_D^{\text{H}_2\text{O}}$ was determined by the following equation: $\Delta G_D = \Delta G_D^{\text{H}_2\text{O}} - m[\text{urea}]$ (Pace, 1986).

fructose-induced changes occurred for Mb(PhH)₂, Mb(Phe)₂, and native Mb by fructose (data not shown). It is clear that the heme–apoprotein interactions are considerably reinforced by the fructose molecules bound to phenylboronic acid sites and not by the fructose dissolved in a solution.

Sugar-Induced pK_a Shift of the Coordinated H₂O. Sugar-induced UV–visible spectral changes in Mb(PhBOH)₂, such as sharpening of the Soret band (408 nm) and intensification of Q-bands (503 and 630 nm) due to aqua-met-Mb with simultaneous lessening of Q-bands (540 and 580 nm) due to hydroxide-met Mb, were evident.



These changes appear to be due to the pK_a shift of a water molecule coordinated to the iron(III) heme center (Brunori

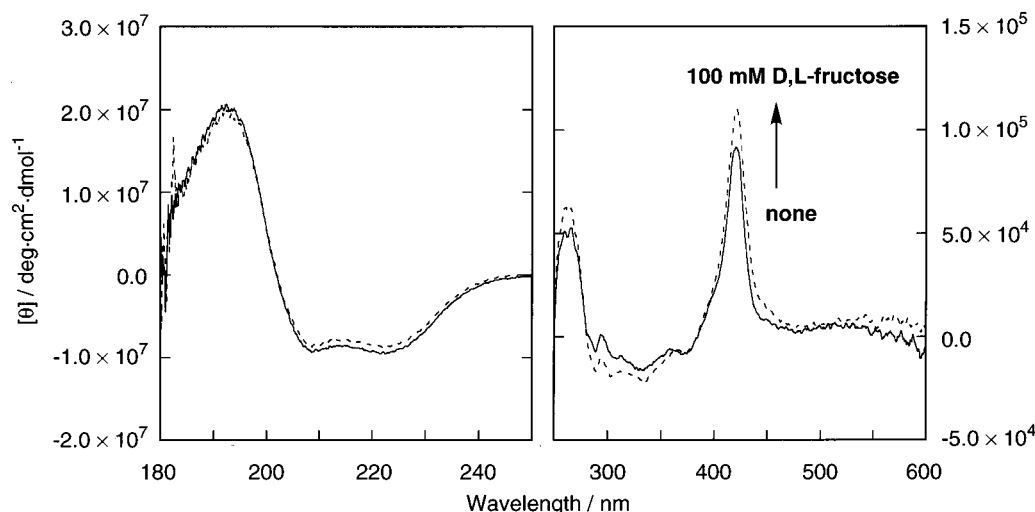


Figure 2. CD spectral changes of the CN-coordinated Mb(PhBOH)₂ in the absence (—) and presence (---) of D,L-fructose (0.1 M). Buffer was Mb(PhBOH)₂ 7 μ M, KCN 10 mM, and 50 mM phosphate (pH 7.5) at 25 °C. The left side (180–250 nm) shows the secondary structure of the protein, and the right side (250–600 nm) shows the induced CD of the heme site. In these experiments, we used low-spin met-Mbs in which a cyanide anion was bound to iron(III) heme because the sugar-induced ligand exchange from hydroxide to H₂O (due to the pK_a shift) can be neglected in this form.

Table 2. pK_a of the Axial H₂O in the Active Center

	none	D-fructose
Mb(PhBOH) ₂	8.0	8.5
Mb(PhH) ₂	8.3	8.3
Mb(<i>m</i> -BpHe) ₂	8.5	9.0
Mb(Phe) ₂	8.1	8.1
native Mb	9.0	9.0

et al., 1968). This suggests that the microenvironment of the active site may be modulated by sugar binding. Table 2 shows the pK_a values of the reconstituted myoglobins in the presence and absence of D-fructose. The modification of the heme propionates clearly appears to cause the acidic pK_a shift seen in all of the myoglobin derivatives. However, the pK_a values for the phenylboronic acid-appended myoglobins were shifted to the basic side by fructose compared to the pK_a value without fructose. In particular, the pK_a of Mb(*m*-BpHe)₂ in the presence of D-fructose became almost identical to that of native myoglobin. This suggests that the microenvironment of the active site of Mb(*m*-BpHe)₂ is re-formed from a partially disturbed state to that comparable to the native state by D-fructose binding. It is highly likely that the bound sugar causes an increase in both the hydrophilicity and the density of negative charge at boronic acid moieties. On the basis of the pK_a values, it is conceivable that D-fructose causes no significant change in the structure of the active site of the myoglobins bearing no sugar-binding sites.

From these sugar-induced spectral changes of Mb(PhBOH)₂, which show a typical saturation behavior with respect to the D-fructose concentration, we can estimate the binding constant of D-fructose to Mb(PhBOH)₂. The Benesi–Hildebrand plot (Benesi and Hildebrand, 1949) gives a good linear relationship against the reciprocal square of the D-fructose concentration, indicating that a 2:1 complex of D-fructose/Mb predominantly formed with an association constant of 8×10^4 M⁻². This value proves that 99% of Mb(PhBOH)₂ binds two molecules of D-fructose in our normal conditions.

Sugar-Enhanced Aniline Hydroxylase Activity of Phenylboronic Acid-Appended Myoglobins. The sugar-induced modulation that was evident not only in the net structure but also at the active site promoted us to investigate whether the enzymatic activity of phenylboronic acid-appended myoglobins can respond to sugar

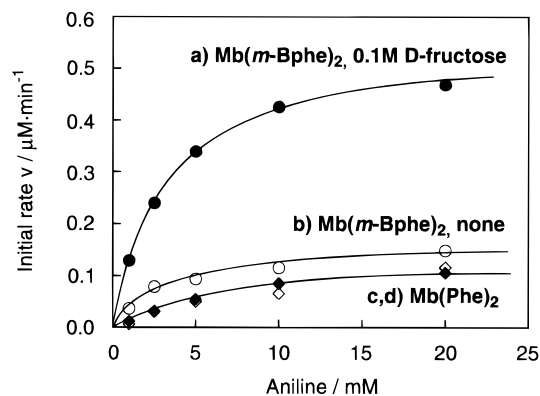


Figure 3. Dependence of the initial rates on aniline concentration in the aniline hydroxylation reaction catalyzed by Mb ([Mb] = 8 μ M): (a) Mb(*m*-BpHe)₂ in the presence of 0.1 M D-fructose; (b) Mb(*m*-BpHe)₂ in the absence of D-fructose; (c) Mb(Phe)₂ in the presence of 0.1 M D-fructose; (d) Mb(Phe)₂ in the absence of D-fructose.

molecules. Therefore, an attempt was made to catalyze the aniline hydroxylation reaction using the myoglobin derivatives according to previously reported methodologies (Mieyal et al., 1976; Kokubo et al., 1987; Hamachi et al., 1995). As shown in Figure 3, the initial rates of generation of *p*-aminophenol were dependent on the aniline concentration and then gradually saturated at >10 mM of aniline. As shown, the initial rates of Mb(*m*-BpHe)₂ were enhanced 3.5-fold by the addition of D-fructose (Figure 3a,b), whereas Mb(Phe)₂ was less reactive and not responsive to D-fructose (Figure 3c,d).

Double-reciprocal plots of the initial reaction rates against aniline concentrations (the Lineweaver–Burk plot) gave good linear relationships and yielded the Michaelis–Menten parameters (k_{cat} and K_m). Table 3 summarizes those parameters for all of the modified myoglobins. The following points in Table 3 should be noted. (i) Most importantly, the net activity (i.e., k_{cat}/K_m) for Mb(PhBOH)₂ and Mb(*m*-BpHe)₂ was facilitated by D-fructose (7.7- and 3.5-fold, respectively), whereas the other myoglobins were unresponsive to D-fructose. (ii) In terms of both the k_{cat} value and the net activity, Mb(*m*-BpHe)₂ in the presence of D-fructose displayed the greatest hydroxylase activity of all the myoglobin derivatives. (iii) Apart from the net activity, the responsiveness

Table 3. Kinetic Parameters of the Aniline Hydroxylase Activity of the Myoglobin Derivatives

	none			D-fructose		
	$k_{\text{cat}} (\times 10^{-2} \text{ min}^{-1})$	$K_{\text{m}} (\text{mM})$	$k_{\text{cat}}/K_{\text{m}} (\text{min}^{-1} \text{ M}^{-1})$	$k_{\text{cat}} (\times 10^{-2} \text{ min}^{-1})$	$K_{\text{m}} (\text{mM})$	$k_{\text{cat}}/K_{\text{m}} (\text{min}^{-1} \text{ M}^{-1})$
Mb(PhBOH) ₂	0.8 ± 0.2	9.4 ± 2.6	0.9 ± 0.3	2.4 ± 0.7	3.5 ± 1.0	6.9 ± 1.9
Mb(PhH) ₂ ^a						
Mb(<i>m</i> -Bphe) ₂	2.1 ± 0.7	3.5 ± 1.1	6.0 ± 2.0	7.0 ± 0.5	3.4 ± 0.4	21 ± 1.0
Mb(Phe) ₂	1.7 ± 0.5	10.8 ± 3.2	1.6 ± 0.5	1.7 ± 0.4	9.9 ± 3.0	1.7 ± 0.4
native Mb	5.6 ± 0.4	8.8 ± 0.9	6.4 ± 0.5	4.8 ± 0.4	4.8 ± 0.6	5.0 ± 0.8

^a The kinetic parameters could not be determined because of its low activity.

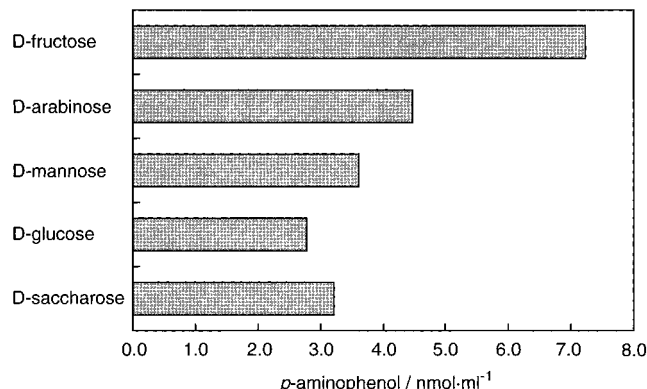
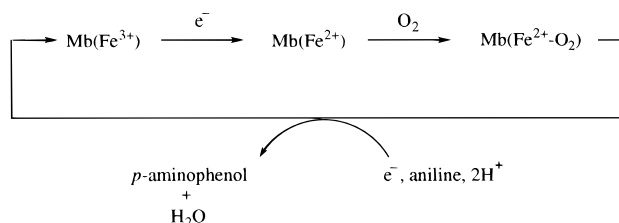


Figure 4. Sugar structure dependence of aniline hydroxylase activity of Mb(*m*-Bphe)₂. The amount of the generated *p*-aminophenol (reaction time = 20 min) was determined according to the phenol–indophenol method (Mieyal et al., 1976; Kokubo et al., 1987; Hamachi et al., 1995). Reaction conditions were described under Experimental Procedures.

[i.e., $(k_{\text{cat}}/K_{\text{m}})_{\text{D-fru}}/(k_{\text{cat}}/K_{\text{m}})_{\text{no D-fru}}$] of Mb(PhBOH)₂ was more efficient than that of Mb(*m*-Bphe)₂. This is mainly ascribed to the fact that the binding affinity ($1/K_{\text{m}}$) was enhanced 3-fold by D-fructose for only Mb(PhBOH)₂, while k_{cat} values were accelerated ~3-fold by D-fructose for both Mb(PhBOH)₂ and Mb(*m*-Bphe)₂.



The aniline hydroxylase activity of Mb(*m*-Bphe)₂ also depended on the sugar's structure (Figure 4). The order of the sugar-facilitated reaction rates (D-fructose > D-arabinose > D-mannose > D-saccharose > D-glucose) corresponds to the binding selectivity of the phenylboronic acid unit to sugar derivatives (Lorand and Edwards, 1959). In addition, the reaction rate shows a saturation curve with respect to the concentration of D-fructose, which corresponded well to the saturation behavior for the preceding D-fructose-induced spectral changes. These results clearly indicate that the sugar molecules bound to phenylboronic acid moieties play an essential role in the enhanced aniline hydroxylase activity.

DISCUSSION

The present results establish that an incorporation of the artificial receptor molecule can be a valid method for the design of stimuli-responsive semiartificial enzymes. Although the Mb-catalyzed aniline hydroxylation reaction is mechanistically complex, the reductively activated O₂ that is bound to the heme oxidizes aniline according to Mieyal's mechanism. The $\text{p}K_{\text{a}}-k_{\text{cat}}$ profile (Figure 5a) shows that the k_{cat} value was promoted along with an

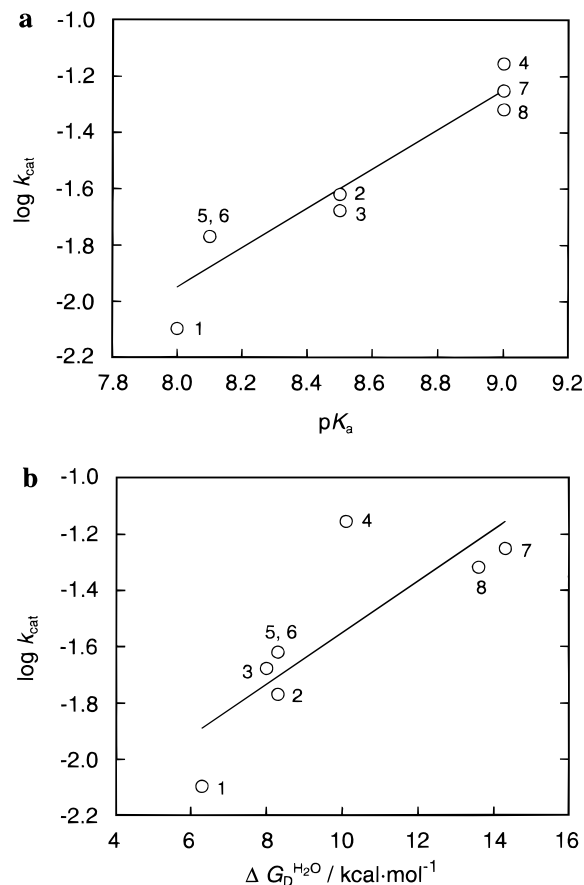


Figure 5. Relationship of the kinetic parameter k_{cat} with (a) $\text{p}K_{\text{a}}$ of the axial H₂O or (b) the Mb structure stability: Mb(PhBOH)₂ (1), Mb(*m*-Bphe)₂ (3), Mb(Phe)₂ (5) and native Mb (7) in the absence of D-fructose, respectively; Mb(PhBOH)₂ (2), Mb(*m*-Bphe)₂ (4), Mb(Phe)₂ (6) and native Mb (8) in the presence of 0.1 M D-fructose, respectively.

increase in the $\text{p}K_{\text{a}}$ of the coordinated water ($\log k_{\text{cat}} = 0.73\text{p}K_{\text{a}} - 7.8$; correlation coefficient = 0.96). The effect of D-fructose on Mb(PhBOH)₂ and Mb(*m*-Bphe)₂ is in this correlation line, implying that the bound D-fructoses induced the considerable $\text{p}K_{\text{a}}$ shift, and as a result, the catalytic efficiency of the myoglobin derivatives was enhanced. In addition, rough correlation (correlation coefficient = 0.82) between $\Delta G_{\text{D}}^{\text{H}_2\text{O}}$ and k_{cat} was observed as shown in Figure 5b. Apparently, the activity increases with protein stability. It is conceivable sugar molecules operate as an active effector on the enzymatic activity, as well as structural stability (see Figure 6).

There are many allosteric enzymes, the activity of which can be regulated by various effectors. Proton and bisphosphoglycerate, for example, are known to lower the dioxygen affinity of hemoglobin (Hb) by factors of 9 and 3, respectively (Imai, 1979; Benesch and Benesch, 1969). The activity of aspartate transcarbamylase is regulated by adenine triphosphate (ATP; 1.5-fold) and cytidine triphosphate (CTP; 0.5-fold) (Kantrowitz et al., 1980). The magnitude of the activity enhancement (3.5–7.7-fold) in

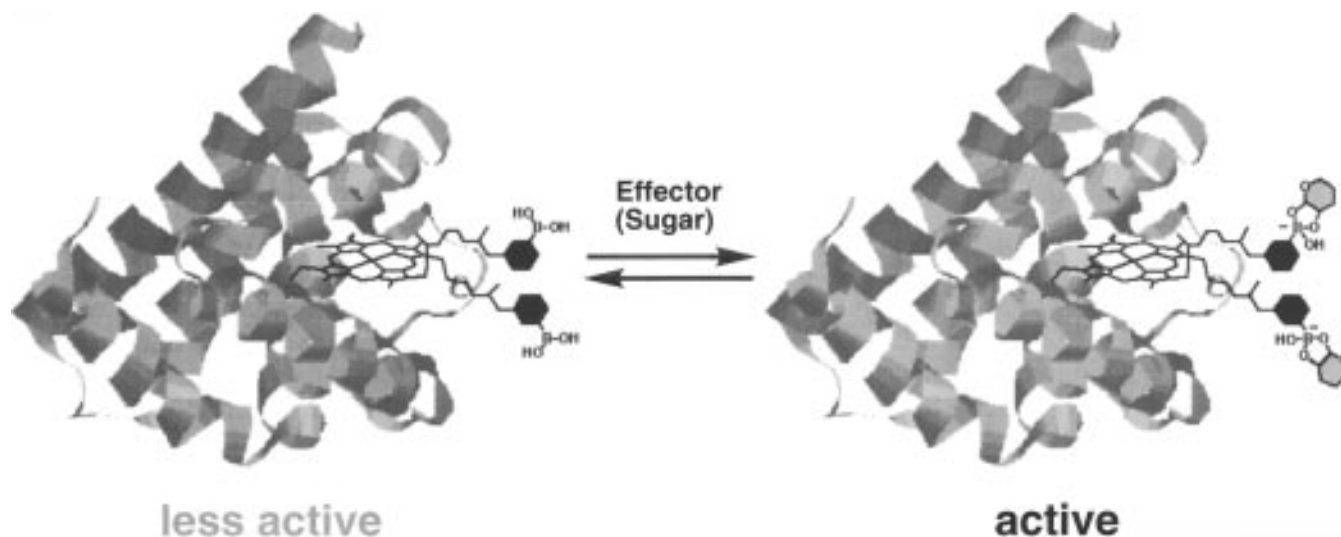


Figure 6. Schematic illustration of our sugar responsive enzymes bearing phenylboronic acid moieties.

our system is not sufficient for practical use as a biosensor, but the activity enhancement is in the same range as that of allosteric native enzymes.

Hemoprotein engineering has been performed primarily by the exchange of axial ligands (to change the electronic state of the heme iron) or the replacement of amino acids located in the active site (to modify its microenvironment) (Egeberg et al., 1990; Raphael and Gray, 1991; Bren and Gray, 1993; Pin et al., 1994; Qin et al., 1994; Adachi et al., 1993; DePillis et al., 1994; Lloyd et al., 1995). In sharp contrast, the present example is unique in its dynamic modulation of activity using the external stimuli that act on a receptor located on the protein surface, not at the active site. This effector-triggered modulation of cofactor–apoenzyme interactions can also be applied to other kinds of cofactor-dependent enzymes.

Although the interaction between boronic acid and sugars is employed as a typical model in this study, we believe that a wide variety of artificial molecular receptors can play a crucial role in the efficient modulation of native enzyme properties (Zuckermann et al., 1988; Corey et al., 1989; Reinhoudt et al., 1989).

EXPERIMENTAL PROCEDURES

Materials. Protoporphyrin IX (PP IX) was purchased from Aldrich. Myoglobin (horse heart) was purchased from Sigma. All chemicals were used without further purification.

General Procedures. Thin-layer chromatography (TLC) was carried out on aluminum sheets coated with silica gel (Merck 5554). Column chromatography was performed on silica 60 (Merck 9385, 230–400 mesh). Melting points were determined on a Micro Melting Point Apparatus Yanaco MP-500D and are uncorrected. UV–visible spectra were recorded on a Shimadzu UV-3000 spectrophotometer. ^1H -NMR spectra were recorded on either a Bruker AC-250P (250MHz) or a JEOL GSX-400 (400 MHz) spectrophotometer. IR spectra were recorded on a Jasco A-100 spectrophotometer. CD spectra were recorded on a Jasco J-720 spectrophotometer.

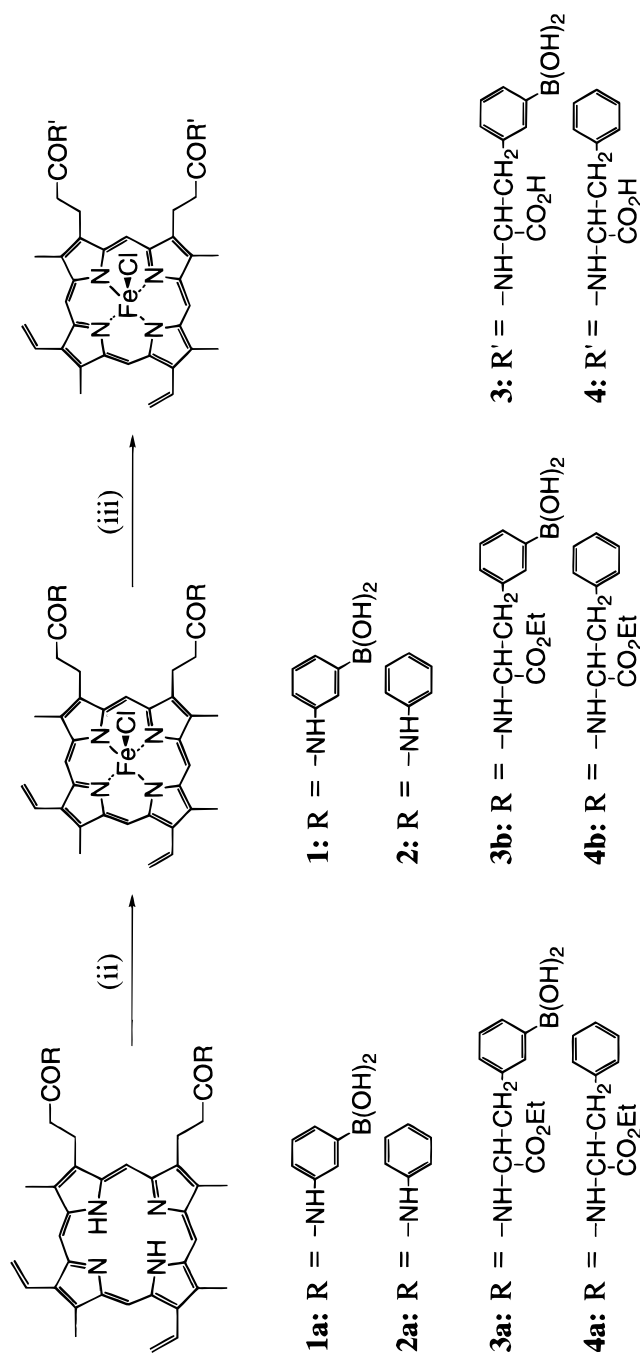
Synthesis. Chemically modified heme derivatives were synthesized according to Scheme 1. *m*-Boronophenylalanine ethyl ester (**5**) was prepared according to the slightly modified procedure of the *para* derivatives reported previously (Snyder et al., 1958).

Synthesis of a *m*-Boronophenylalanine-Appended Porphyrin (3a**).** Under N_2 atmosphere, oxalyl

chloride (0.2 mL) was added dropwise to a suspended dry CH_2Cl_2 solution (12 mL) containing PP IX (100 mg, 0.18 mmol) with ice cooling. After 1 h of stirring at room temperature, the mixture was concentrated and dried in vacuo. The residual dark green solid dissolved in dry CH_2Cl_2 (8 mL) was added dropwise to an anhydrous mixed solvent [pyridine (3 mL)/ CH_2Cl_2 (5 mL)] containing **5**·HCl salt (325 mg, 1.2 mmol). The reaction mixture was stirred at room temperature overnight and then concentrated in vacuo. The residue dissolved in CHCl_3 (100 mL) was washed with acidic water (pH 3) and then with saturated NaHCO_3 aqueous solution. The organic layer was concentrated and applied to column chromatography [silica gel, 3 cm \times 15 cm; solvent, $\text{CHCl}_3/\text{MeOH}$ = 30/1 (v/v)] to yield **6** (58 mg, 33%): mp 210 $^\circ\text{C}$ dec; IR (KBr, cm^{-1}) 3400 (OH), 1735 (ester C=O), 1650 (amide C=O); ^1H NMR (CDCl_3) δ -3.96 (2H, s, NH), 0.68 [6H, m, CH_3 (ester)], 2.69 [4H, m, CH_2 (benzyl)], 3.08 (4H, m, $\text{CH}_2\text{-CO}$), 3.42 [4H, m, CH_2 (ester)], 3.65 (12H, m, CH_3), 4.27 (2H, m, CH), 4.38 (4H, m, CH_2), 6.22, 6.45 (2H each, d each, = CH_2), 6.78, 7.42, 7.53 (4H, 2H, and 2H, respectively; m, t, and s, respectively, ArH), 7.92 (4H, s, OH), 8.53 (4H, m, NH and CH=), 10.24 [4H, m, CH(meso position)]. Anal. Found: C, 65.31; H, 6.01; N, 7.86. Calcd for $\text{C}_{56}\text{H}_{62}\text{N}_6\text{O}_{10}\text{B}_2 \cdot 1.5\text{H}_2\text{O}$: C, 65.44; H, 6.29; N, 8.18.

Synthesis of Iron(III) Complex (3b**).** $\text{FeCl}_2 \cdot 4\text{H}_2\text{O}$ (80 mg, 0.4 mmol) and **3a** (40 mg, 0.04 mmol) were mixed in dry DMF (20 mL) and stirred at 65 $^\circ\text{C}$ for 8 h in the dark. DMF was evaporated off, and the residue was washed with dilute HCl (pH 3, four times). The dark brown solid was purified by reprecipitation ($\text{CHCl}_3/\text{MeOH}/\text{hexane}$) to yield **3b** (35 mg, 85%): mp 250 $^\circ\text{C}$ dec; IR (KBr, cm^{-1}) 3400 (OH), 1735 (ester C=O), 1650 (amide C=O); UV–vis (MeOH, λ_{max}) 502 and 625 nm. Anal. Found: C, 59.79; H, 5.48; N, 7.28. Calcd for $\text{C}_{56}\text{H}_{60}\text{N}_6\text{O}_{10}\text{B}_2\text{FeCl} \cdot 2\text{H}_2\text{O}$: C, 59.73; H, 5.73; N, 7.46.

Synthesis of Heme **3.** A mixed solution [THF (10 mL) and MeOH (4 mL)] containing **3b** (60 mg, 0.06 mmol) and 1 N aqueous NaOH (0.17 mL) was stirred at room temperature overnight. After solvents were evaporated off, the residue was dissolved in 20 mL of H_2O . A black solid was precipitated by acidification (pH 3), and it was further purified by reprecipitation ($\text{CHCl}_3/\text{MeOH}/\text{hexane}$) to afford **3** (20 mg, 35%): mp 250 $^\circ\text{C}$ dec; IR (KBr, cm^{-1}) 3300 (OH), 1710 (carboxylic acid C=O), 1650 (amide C=O). Anal. Found: C, 60.63; H, 5.11; N, 7.98. Calcd for $\text{C}_{52}\text{H}_{52}\text{N}_6\text{O}_{10}\text{B}_2\text{FeCl}$: C, 60.41; H, 5.07; N, 8.13.

Scheme 1^a

^a (i) $(\text{COCl})_2/\text{dry CH}_2\text{Cl}_2$; then R-H, pyridine/dry CH_2Cl_2 ; (ii) $\text{FeCl}_2/\text{dry DMF}$, (iii) OH^-/THF , H_2O .

Other heme derivatives (**1**, **2**, and **4**) were prepared in the same manner. Their analytical data are as follows.

Heme 1. Anal. Found: C, 62.35; H, 5.00; N, 9.34. Calcd for $C_{46}H_{44}N_6O_6B_2FeCl$: C, 62.09; H, 4.98; N, 9.44.

Heme 2. Anal. Found: C, 67.56; H, 5.35; N, 10.06. Calcd for $C_{46}H_{42}N_6O_2FeCl \cdot H_2O$: C, 67.36; H, 5.41; N, 10.25.

Heme 4. IR (KBr, cm^{-1}) 1720 (carboxylic acid C=O), 1640 (amide C=O). Anal. Found: C, 66.12; H, 5.41; N, 8.80. Calcd for $C_{53}H_{52}O_6N_6FeCl$: C, 66.29; H, 5.46; N, 8.75.

Reconstitution of Apo-Mb with Various Heme Derivatives. Chemically modified hemes were incorporated into the heme pocket of apo-Mb according to a slightly modified procedure described previously (Asakura and Yonetani, 1969; Asakura, 1978). Molar extinction coefficients of reconstituted myoglobins were determined by following the conventional pyridine-hemochromogen method (Paul et al., 1953) [ϵ_{409} for Mb(PhBOH)₂ = 147 $mM^{-1} cm^{-1}$, for Mb(PhH)₂ = 138, for Mb(*m*-Bphe)₂ = 197, for Mb(Phe)₂ = 151, and for native Mb = 188]. Myoglobins' concentrations were spectrophotometrically determined using the corresponding values.

Denaturation of Mbs with Urea. Denaturation experiments of the myoglobin derivatives with increasing amounts of urea were conducted according to the reported method (Puett, 1973; Pace, 1986) at [Mb] = 8 μM , 50 mM phosphate buffer (pH 7.5) and 25 °C.

pH Titration of Met-Mbs. Spectrophotometric pH titration experiments were done according to the standard procedure. The pH of the solution was controlled by the addition of an appropriate amount of 1 N aqueous NaOH.

Assay of Aniline Hydroxylation by Mb. Aniline hydroxylase activities were estimated by measuring the amount of produced *p*-aminophenol according to the phenol-indophenol method (Mieyal et al., 1976; Kokubo et al., 1987; Hamachi et al., 1995).

The reaction mixture consisted of a total volume of 1 mL containing appropriate amounts of aniline, 1 mM NADH, 500 μM FMN, 8 μM Mb, and 0 or 0.1 M D-fructose in 50 mM phosphate buffer (pH 7.5). The reaction was initiated by the addition of NADH at 37 °C and terminated by the extraction of the mixture with 1 mL of ethyl ether (three times). The ether layers were combined and evaporated under nitrogen gas at room temperature. The residue dissolved in 1 mL of 0.1 N HCl was mixed with 0.2 mL of 2.5 N Na₂CO₃ and with 5% (w/v) phenol in 2.5 N NaOH. The mixture was then allowed to stand at 37 °C for 30 min. Absorbance of the resultant solution was measured at 630 nm, the absorption maximum of the indophenol derivative (1 nmol of *p*-aminophenol in the standard assay mixture gave a ΔA_{630nm} value of 0.018).

LITERATURE CITED

- Adachi, S., Nagano, S., Ishimori, K., Watanabe, Y., and Morishima, I. (1993) *Biochemistry* 32, 241.
- Asakura, T. (1978) In *Methods in Enzymology* (S. Fleiser and L. Packer, Eds.) Part C, p 446, Academic Press, New York.
- Asakura, T., and Yonetani, T. (1969) *J. Biol. Chem.* 244, 537.
- Bell, I. B., and Hilvert, D. (1994) In *The Lock-and-Key Principles*, (J.-P. Behr, Ed.) P 73, Wiley, New York.
- Benesch, R., and Benesch, R. E. (1969) *Nature* 221, 618.
- Benesi, H., and Hildebrand, J. H. (1949) *J. Am. Chem. Soc.* 71, 2703.
- Bren, K. L., and Gray, H. B. (1993) *J. Am. Chem. Soc.* 115, 10382.
- Brunori, M., Amiconi, G., Antonini, E., Wyman, J., Zito, R., and Rossi Fanelli, A. (1968) *Biochim. Biophys. Acta* 154, 315.
- Corey, D. R., Pei, D., and Schultz, P. G. (1989) *J. Am. Chem. Soc.* 111, 8523.
- Cornish, V. W., Mendel, D., and Schultz, P. G. (1995) *Angew. Chem., Int. Ed. Engl.* 34, 621.
- DePillis, G. D., Decatur, S. M., Barrick, D., and Boxer, S. G. (1994) *J. Am. Chem. Soc.* 116, 6981.
- Egeberg, K. D., Springer, B. A., Martinis, S. A., and Sliger, S. G. (1990) *Biochemistry* 29, 9783.
- Hamachi, I., Tajiri, Y., and Shinkai, S. (1994a) *J. Am. Chem. Soc.* 116, 7437.
- Hamachi, I., Tajiri, Y., Murakami, H., and Shinkai, S. (1994b) *Chem. Lett.*, 575.
- Hamachi, I., Fujita, A., and Kunitake, T. (1995) *Chem. Lett.*, 657.
- Imai, K. (1979) *J. Mol. Biol.* 133, 233.
- James, T. D., Linnane, P., and Shinkai, S. (1996) *J. Chem. Soc., Chem. Commun.*, 281 and references cited therein.
- Kaiser, E. T. (1988) *Angew. Chem., Int. Ed. Engl.* 27, 913 and references cited therein.
- Kaiser, E. T., and Lawrence, D. S. (1984) *Science* 266, 505.
- Kantrowitz, E. R., Pastr-Landis, S. C., and Lipscomb, W. N. (1980) *Trends Biochem. Sci.* 5, 124.
- Kokubo, T., Sassa, S., and Kaiser, E. T. (1987) *J. Am. Chem. Soc.* 109, 606.
- Lloyd, E., Hildebrand, D. P., Tu, K. M., and Mauk, A. G. (1995) *J. Am. Chem. Soc.* 117, 6434.
- Lorand, J. P., and Edwards, J. O. (1959) *J. Org. Chem.* 24, 769.
- Mieyal, J. J., Acherman, R. S., Blumer, J. L., and Freeman, L. S. (1976) *J. Biol. Chem.* 251, 3436.
- Pace, C. N. (1986) *Methods Enzymol.* 131, 206.
- Paugam, M.-F., Valencia, L. S., Boggess, B., and Smith, B. D. (1994) *J. Am. Chem. Soc.* 116, 11203.
- Paul, K. G., Theorell, H., and Åkeson, Å. (1953) *Acta Chem. Scand.* 7, 1284.
- Petersen, E. B., and Hilvert, D. (1995) *Biochemistry* 34, 6616.
- Pin, S., Alpert, B., Cortes, R., Ascone, I., Chiu, M. L., and Silgar, S. G. (1994) *Biochemistry* 33, 11618.
- Puett, D. (1973) *J. Biol. Chem.* 248, 4623.
- Qin, J., La Mar, G. N., Dou, Y., Admiraal, S. J., and Ikeda-Saito, M. (1994) *J. Biol. Chem.* 269, 1083.
- Raphael, R., and Gray, H. B. (1991) *J. Am. Chem. Soc.* 113, 1038.
- Reinhoudt, D. N., Egendebak, A. M., Nigenhuis, W. F., Verboom, W., Kloosterman, M., and Schoemaker, H. E. (1989) *J. Chem. Soc., Chem. Commun.*, 399.
- Snyder, H. R., Reedy, A. J., and Lennarz, W. J. (1958) *J. Am. Chem. Soc.* 80, 835.
- Tamura, M., Asakura, T., and Yonetani, T. (1973) *Biochim. Biophys. Acta* 295, 467.
- Wu, Z.-P., and Hilvert, D. (1989) *J. Am. Chem. Soc.* 111, 4513.
- Yoon, J., and Czarnik, A. W. (1992) *J. Am. Chem. Soc.* 114, 5874.
- Zuckermann, R. N., Corey, D. R., and Schultz, P. G. (1988) *J. Am. Chem. Soc.* 110, 1614.

BC970055Z

Bisintercalation of Homodimeric Thiazole Orange Dyes in DNA: Effect of Modifying the Linker

Dan Stærk, Atef A. Hamed, Erik B. Pedersen, and Jens Peter Jacobsen*

Department of Chemistry, Odense University, Odense M DK-5230 Denmark. Received April 30, 1997[®]

The thiazole orange dye 1,1'-(4,4,8,8-tetramethyl-4,8-diazaundecamethylene)-bis[4-[3-methyl-2,3-dihydro(benzo-1,3-thiazole)-2-methylidene]]quinolinium tetraiodide (TOTO) binds to double-stranded DNA (dsDNA) in a sequence selective bisintercalation. Each chromophore is sandwiched between two base pairs in a (5'-CpT-3'):(5'-ApG-3') site, and the linker spans over two base pairs in the minor groove. The binding of analogs of TOTO in which the linker has been modified is examined. The aim of the study is to utilize the sequence selectivity of the TOTO chromophores to enhance and/or alter the overall selectivity of the binding. One- and two-dimensional ¹H-NMR investigations of complexes between TOTO analogs and various dsDNA oligonucleotides are reported. The following analogs were synthesized and used: 1,1'-(4,4,8,8-tetramethyl-4,8-diazadodecamethylene)-bis[4-[3-methyl-2,3-dihydro(benzo-1,3-thiazole)-2-methylidene]]quinolinium tetraiodide (TOTO10), 1,1'-(5,5,9,9-tetramethyl-5,9-diazatridecamethylene)-bis[4-[3-methyl-2,3-dihydro(benzo-1,3-thiazole)-2-methylidene]]quinolinium tetraiodide (TOTO11), and 1,1'-(6,6,10,10-tetramethyl-6,10-diazapentadecamethylene)-bis[4-[3-methyl-2,3-dihydro(benzo-1,3-thiazole)-2-methylidene]]quinolinium tetraiodide (TOTO13). The results show that with a longer linker the dyes can bisintercalate into two (5'-CpT-3'):(5'-ApG-3') sites separated by one or two base pairs. Bisintercalation in two such "isolated" binding sites yields non-nearest-neighbor bisintercalation in which the linker spans over more than two base pairs. The investigations also showed that an exact length of the linker is not crucial for the site selectivity since TOTO, TOTO10, and TOTO11 are almost equally suitable in binding selectively to the (5'-CTAG-3')₂ sequence. Fluorescence measurements show that TOTO10, TOTO11, and TOTO13 have higher fluorescence quantum yields than TOTO when bound to d(CGCTAGCG)₂. This indicates that the length of the linker in TOTO may not be the optimum one in terms of using the dye as a fluorescence marker.

INTRODUCTION

The search for nonradioactive DNA stains that are stable under gel electrophoretic conditions has led to the synthesis and characterization of a family of homo- and heterodimeric DNA-binding dyes (Benson et al., 1993a,b; Rye et al., 1992). These dyes form highly fluorescent and stable noncovalent complexes with double-stranded DNA (dsDNA¹). Prominent among these are 1,1'-(4,4,8,8-tetramethyl-4,8-diazaundecamethylene)-bis[4-[3-methyl-2,3-dihydro(benzo-1,3-thiazole)-2-methylidene]]quinolinium tetraiodide (TOTO, Scheme 1). The enhancement of the fluorescence quantum yield of TOTO upon complex formation with dsDNA is >1000 (Rye et al., 1992), and *t*_{1/2} for the dissociation of the dsDNA–TOTO complex

under gel electrophoretic conditions is approximately 11 h (Benson et al., 1993). This makes TOTO an excellent choice as a marker with a detection limit of ~4 pg of DNA (Benson et al., 1993a,b).

Recent work in our laboratory has focused on ¹H-NMR studies of the binding mode and sequence selectivity of TOTO with various dsDNA oligonucleotides. We have shown that TOTO binds via bisintercalation preferentially to oligonucleotides containing the (5'-CTAG-3')₂ or the (5'-CCGG-3')₂ sequences (Hansen et al., 1996; Jacobsen et al., 1995). In studies of complex formation in oligonucleotides containing both of these binding sites, we showed that the binding to the (5'-CTAG-3')₂ sequence is favored compared to the (5'-CCGG-3')₂ sequence.

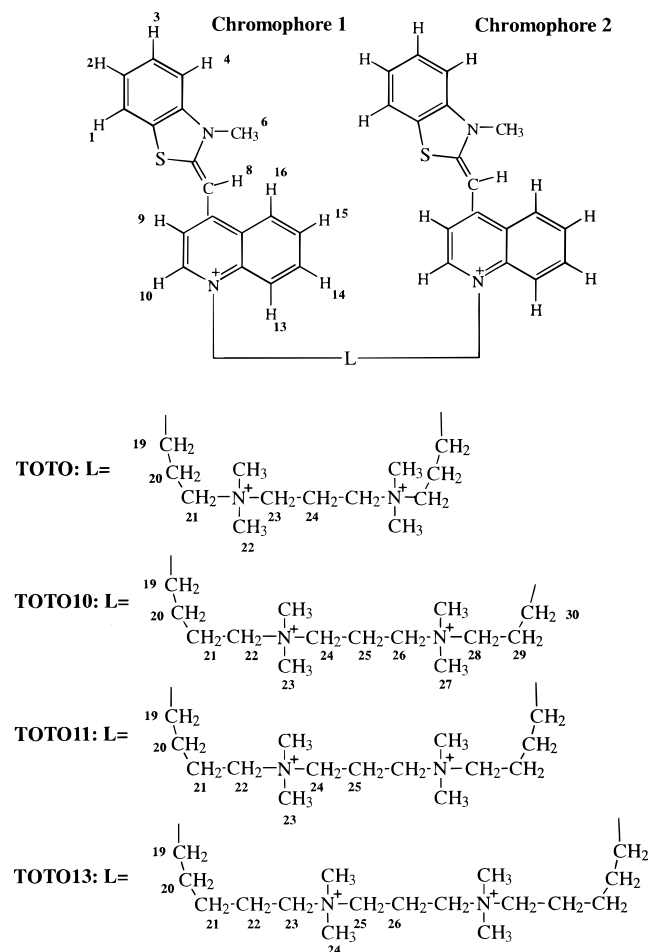
The solution structure of the complex of TOTO bisintercalated in the (5'-CTAG-3')₂ binding site of the d(5'-CGCTAGCG-3')₂ oligonucleotide shows that the sequence selectivity of TOTO is caused by the ability of the TOTO chromophores to adapt to the propeller twist of the nucleobases (Spielmann et al., 1995). This is possible since the benzothiazole ring can twist relative to the quinolinium ring due to the flexible cyanine methine bond between. The benzothiazole is intercalated between two pyrimidine bases and the quinolinium ring between the two purine bases. In contrast to other intercalators, the sequence selectivity of TOTO arises directly from the interaction of the intercalated chromophores with the nucleobases. Although the linker of TOTO adds significantly to the binding strength, it is only a spectator with respect to the sequence selectivity.

With the chromophore responsible for the sequence selectivity, several opportunities for linker modifications are possible to enhance or alter the overall selectivity of TOTO analogs. The bisintercalation of TOTO obeys the nearest-neighbor exclusion principle with the linker

* Author to whom correspondence should be addressed (e-mail jppj@chem.ou.dk).

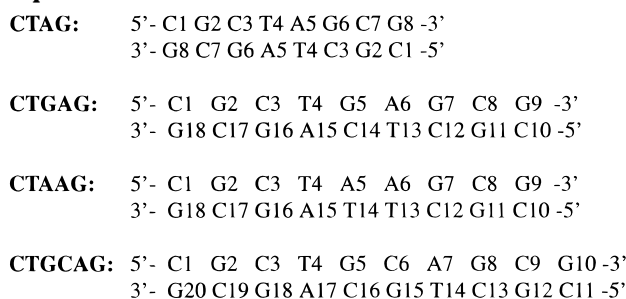
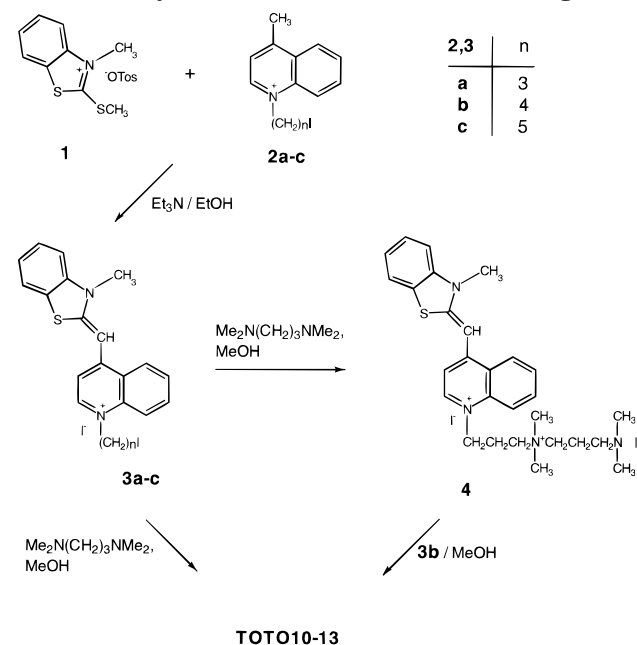
[®] Abstract published in *Advance ACS Abstracts*, October 15, 1997.

¹ Abbreviations: AMBER, assisted model building with energy refinement; DNA, deoxyribonucleic acid; DMSO, dimethyl sulfoxide; dsDNA, double-stranded DNA; DSS, 2,2-dimethyl-2-silapentane-5-sulfonate; EDTA, ethylenediaminetetraacetic acid; HSQC, heteronuclear single quantum coherence; NMR, nuclear magnetic resonance; NOESY, nuclear Overhauser effect spectroscopy; RMD, restrained molecular dynamics; TOCSY, total correlation spectroscopy; TOTO, 1,1'-(4,4,8,8-tetramethyl-4,8-diazaundecamethylene)-bis[4-[3-methyl-2,3-dihydro(benzo-1,3-thiazole)-2-methylidene]]quinolinium tetraiodide; TOTO10, 1,1'-(4,4,8,8-tetramethyl-4,8-diazadodecamethylene)-bis[4-[3-methyl-2,3-dihydro(benzo-1,3-thiazole)-2-methylidene]]quinolinium tetraiodide; TOTO11, 1,1'-(5,5,9,9-tetramethyl-5,9-diazatridecamethylene)-bis[4-[3-methyl-2,3-dihydro(benzo-1,3-thiazole)-2-methylidene]]quinolinium tetraiodide; TOTO13, 1,1'-(6,6,10,10-tetramethyl-6,10-diazapentadecamethylene)-bis[4-[3-methyl-2,3-dihydro(benzo-1,3-thiazole)-2-methylidene]]quinolinium tetraiodide; TPPI, time proportional phase incrementation.

Scheme 1. TOTO Numbering Scheme

spanning over two bases in the minor groove. A priori, there seems to be no structure-based justification that the linker length in TOTO is the optimal one. A slightly longer or shorter linker may enhance the binding strength. Furthermore, a significant longer linker may allow TOTO analogs to bisintercalate in "isolated" (5'-CpT-3'):(5'-ApG-3') sites, i.e. such sites separated by one or two base pairs. Similar considerations on the length of the linker in other bisintercalating agents with completely different chromophores have been reviewed earlier (Wakelin, 1986).

In this paper, we present the results of one- and two-dimensional ^1H -NMR studies of complexes between dsDNA and TOTO analogs with various linker lengths. We have synthesized 1,1'-(4,4,8,8-tetramethyl-4,8-diazadodecamethylene)-bis[4-[3-methyl-2,3-dihydro(benzo-1,3-thiazole)-2-methylidene]quinolinium tetraiodide (TOTO10, Scheme 1), 1,1'-(5,5,9,9-tetramethyl-5,9-diazatridecamethylene)-bis[4-[3-methyl-2,3-dihydro(benzo-1,3-thiazole)-2-methylidene]]quinolinium tetraiodide (TOTO11, Scheme 1), and 1,1'-(6,6,10,10-tetramethyl-6,10-diazapentadecamethylene)-bis[4-[3-methyl-2,3-dihydro(benzo-1,3-thiazole)-2-methylidene]]quinolinium tetraiodide (TOTO13, Scheme 1) and investigated their complexes with various oligonucleotides. These oligonucleotides contain the (5'-CpT-3'):(5'-ApG-3') and the (5'-ApG-3'):(5'-CpT-3') sequences separated by 0, 1, or 2 base pairs (Scheme 2). We found that with a longer linker, TOTO analogs bind into isolated (5'-CpT-3'):(5'-ApG-3') base pairs by bisintercalation. To our knowledge this is the first time that non-nearest-neighbor bisintercalation has been observed.

Scheme 2. Numbering Scheme for the dsDNA Duplexes Used**Scheme 3. Synthetic Path for the TOTO Analogs****SYNTHESIS**

So far, nobody seems to have synthesized TOTO derivatives with extended methylene bridges between the quinolinium ring and the quaternary ammonium nitrogen. In fact, two structures with 4-sulfobutyl are the only examples reported with a chain of more than three carbons attached to the quinolinium nitrogen of the corresponding monomeric cyanine dye (Kagawa and Kawashima, 1989). For the synthesis of the TOTO analogs TOTO10, TOTO11, and TOTO13, we selected the strategy of Brooker et al. (1941, 1942) (Scheme 3) to condense the benzothiazole derivative **1** with the quinolinium compound **2** in the presence of triethylamine in absolute ethanol to give the intermediate cyanine dye **3**, which subsequently was reacted with 0.5 equiv of *N,N,N,N*-tetramethyl-1,3-diaminopropane in refluxing anhydrous methanol according to the procedure of Glazer and o-workers (Benson et al., 1993; Rye et al., 1992) to give the symmetrical derivatives TOTO11 and TOTO13. The starting quinolinium compound **2** was synthesized by treating lepidine with 5 equiv of the appropriate diiodoalkane in refluxing dioxane followed by recrystallization from acetone. The unsymmetrical TOTO10 was synthesized by treatment of **3a** (Brooker et al., 1941, 1942) with *N,N,N,N*-tetramethyl-1,3-diaminopropane in excess followed by reaction with **3b**.

RESULTS

The d(CGCTAGCG)₂ (CTAG) Oligonucleotide. The CTAG + TOTO11 Mixture. The line width observed in

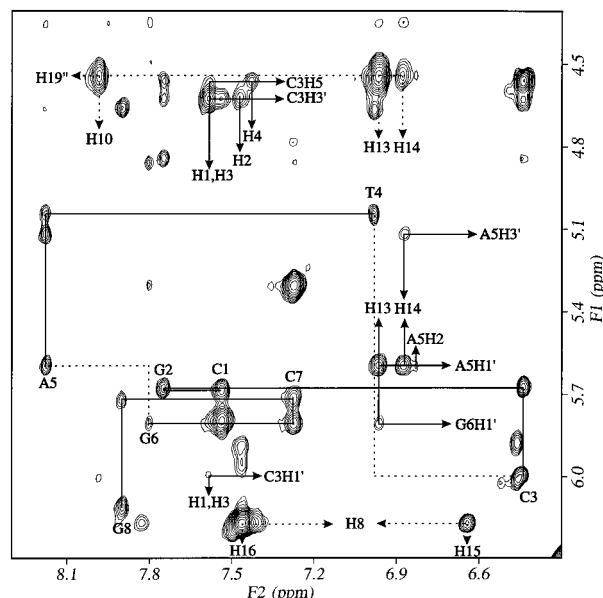


Figure 1. Aromatic to H1' region of a NOESY spectrum (mixing time of 150 ms) of the CTAG–TOTO11 complex at 25 °C. The sequential H1'($n-1$)–H6/H8(n)–H1'(n) connectivity pattern is shown with solid lines. Interruption in the 5'–C3pT4–3' and the 5'–A5pG6–3' binding sites are indicated with broken lines. A few pairs of cross peaks between TOTO11 and the DNA are marked with solid arrows. Intramolecular connectivities between protons from TOTO11 are shown with broken arrows.

the ^1H spectrum of CTAG + TOTO11 is ~ 6 –7 Hz, indicating essentially no dynamic exchange between two or more complexes. Furthermore, only one resonance frequency is observed for the protons on each strand of the dsDNA and for each chromophore. This shows that the CTAG + TOTO11 mixture forms a single complex with dyad symmetry. The CTAG–TOTO11 complex arises from bisintercalation in the 5'–CTAG–3' binding site. The amount of this complex is at least 100 times higher than that of any other complex as seen from inspection of the spectra.

Figure 1 shows the aromatic to H1' part of the NOESY spectrum of the complex. The sequential assignment of the H1'($n-1$)–H6/H8(n)–H1'(n) resonances is shown with solid lines. Interruption due to intercalation in the 5'–C3pT4–3' and the 5'–A5pG6–3' intercalation sites is indicated with broken lines. The large up-field shifts of C3H6 (1.02 ppm), C3H5 (0.85 ppm), T4H1' (0.58 ppm), and T4H6 (0.44 ppm) relative to the free oligonucleotide are caused by the intercalation of the aromatic chromophore. A few cross peaks between the dsDNA and TOTO11 are indicated with unbroken arrows. Combined with the interruption of the connectivity pattern, this establishes binding in the 5'–CTAG–3' site and shows the proximity of the benzothiazole protons H1–H4 and the quinolinium protons H13 and H14 to protons in the 5'–C3pT4–3' and the 5'–A5pG6–3' binding sites, respectively. Intramolecular connectivities between protons from TOTO11 are shown with broken arrows. A characteristic strong cross peak between H8 and H16 on TOTO11 confirms the relative conformation of the benzothiazole and the quinolinium ring as drawn in Scheme 1.

Figure 2 (left) shows the aromatic to H2'/H2'' area of a NOESY spectrum. The aromatic protons yield cross peaks to H2'/H2'' of their own and the previous oligonucleotide except at the 5'–C3pT4–3' and 5'–A5pG6–3' binding sites. Thus, this region is a further strong tool for confirming the bisintercalation in the 5'–C3pT4–3' and 5'–A5pG6–3' sites. H13, H14, and H15 on TOTO11 yield cross peaks to A5 H2'/H2'', while H1 and H3 have cross

peaks to C3 H2'/H2''. The above connectivities show that the benzothiazole is sandwiched between the C3 and T4, while the quinolinium ring is sandwiched between A5 and G6. The methyl group protons of T4 experience an up-field shift of 0.88 ppm and yield cross peaks to H1–H4 of TOTO11. This implies that the methyl group is positioned above the benzothiazole. The relative assignment of H2' and H2'' is based on analysis of the buildup rates of intramolecular aromatic to H2'/H2'' cross peaks (Scheek et al., 1984) (Figure 2, right). The cross peaks with the fastest buildup rate are assigned to H2' and *vice versa*. This analysis was not possible for A5 and G6 due to overlap of the H2'/H2'' pairs.

The ^1H – ^{31}P HSQC spectrum is shown in Figure 3. The ^1H – ^{31}P connectivities (Searle and Lane, 1992) found are in full agreement with the assignment of H3', H4', and H5'/H5'' through NOESY and TOCSY spectra. Normally the dispersion of ^{31}P chemical shift values lies within a range of ~ 0.7 ppm (Roongta et al., 1990). The large dispersion of the ^{31}P chemical shift values of C3, T4, and A5 is due to unwinding of the oligonucleotide upon bisintercalation. A complete assignment of ^1H and ^{31}P chemical shift values of the complex and the free oligonucleotide is given in Table 1.

Intermolecular contacts between the *N*-methyl groups and A5/G6 confirm that the linker crosses the minor groove. The cross peak pattern observed for the CTAG–TOTO11 complex is very similar to that observed for the CTAG–TOTO complex (Spielmann et al., 1995). Restrained molecular dynamics calculations using cross peak intensities in NOESY buildup experiments yielded a structure of the CTAG–TOTO11 complex similar to the structure of the CTAG–TOTO complex (results to be published).

The CTAG + TOTO10 Mixture. Similar to the CTAG + TOTO11 mixture, the mixture of CTAG + TOTO10 forms only one complex. Neither the 1D nor the 2D spectrum shows any sign of more than one compound. The CTAG–TOTO10 complex arises from (5'–CTAG–3')₂ bisintercalation. Only small chemical shift differences are observed between the proton resonances of the two strands, and the observed differences are restricted to the (5'–CTAG–3')₂ binding site. Chemical shift differences of the proton resonances of the two chromophores are also observed and are consistent with the asymmetric bisintercalation. A complete assignment of the chemical shift values of the CTAG–TOTO10 complex compared to those of the free oligonucleotide is given in the Supporting Information (Table 1S).

The CTAG + TOTO13 Mixture. Unlike TOTO11 and TOTO10, the dye TOTO13 forms more than one complex with the CTAG oligonucleotide. The major form (50%) has been identified as the complex with TOTO13 binding in the (5'–CTAG–3')₂ site. In addition to that, two minor forms exist. Severe overlap in the spectra prevents conclusive evidence that would allow identification of the binding sites of TOTO13 in these two minor forms.

The d(CGCTGAGCG):d(CGCTCAGCG) (CTGAG) Oligonucleotide. **The CTGAG + TOTO13 Mixture.** The CTGAG–TOTO13 mixture yields one major form (90%) and one minor form (10%). Dynamic exchange between the major and the minor form yields extensive line broadening and exchange cross peaks. This makes the interpretation of the spectra difficult. The major form is asymmetric and arises from nearest-neighbor bisintercalation in the 5'–CTGAG–3' binding site.

Figure 4 shows the aromatic to H2'/H2'' part of a NOESY spectrum. Interruption in the sequential H2'/H2''($n-1$)–H6/H8(n)–H2'/H2''(n) pattern of the 5'–C3pT4–3', 5'–G5pA6–3', 5'–T13pC14–3', and 5'–A15pG16–3' sequences

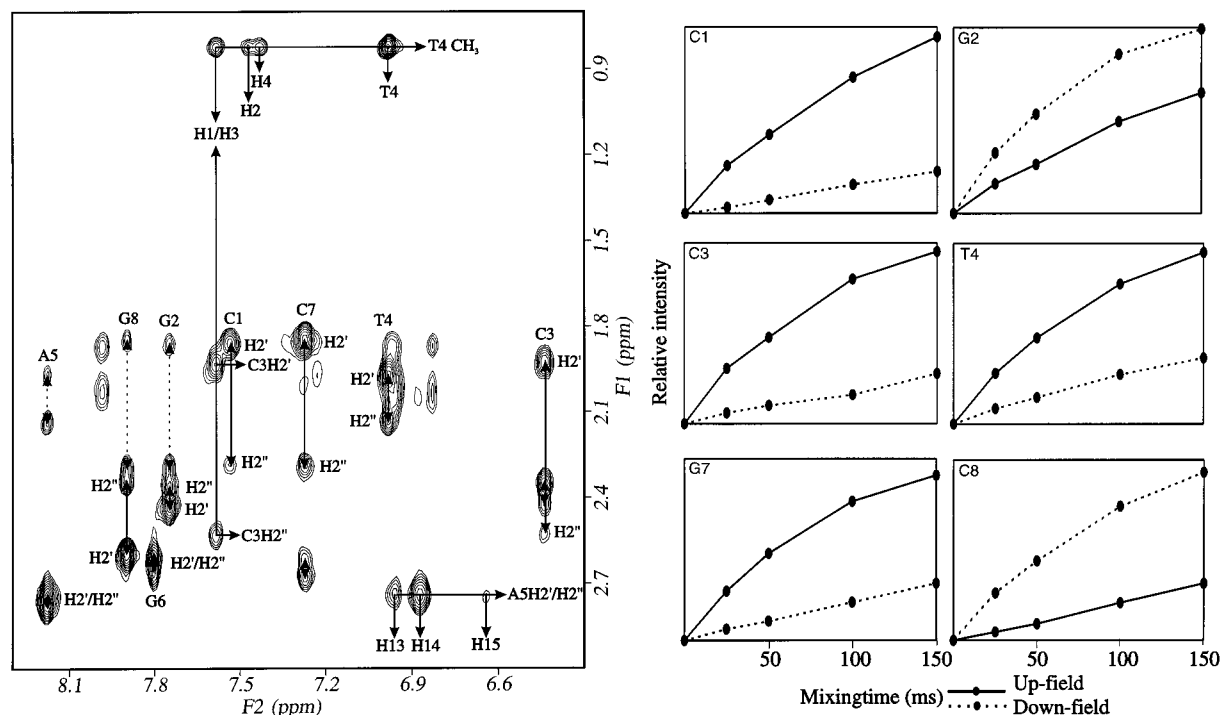


Figure 2. (Left) Aromatic to H2'/H2'' region of a 100 ms NOESY spectrum of the CTAG-TOTO11 complex at 25 °C. Intraresidue connectivities between aromatic protons and H2'/H2'' are shown with solid arrows, and inter-residue connectivities to H2'/H2'' on the previous deoxyribose are shown with broken arrows. A few pair of cross peaks between TOTO11 and the DNA are also marked. (Right) Buildup curves used for the relative assignment of intraresidue connectivities between the aromatic protons and the H2'/H2'' pair.

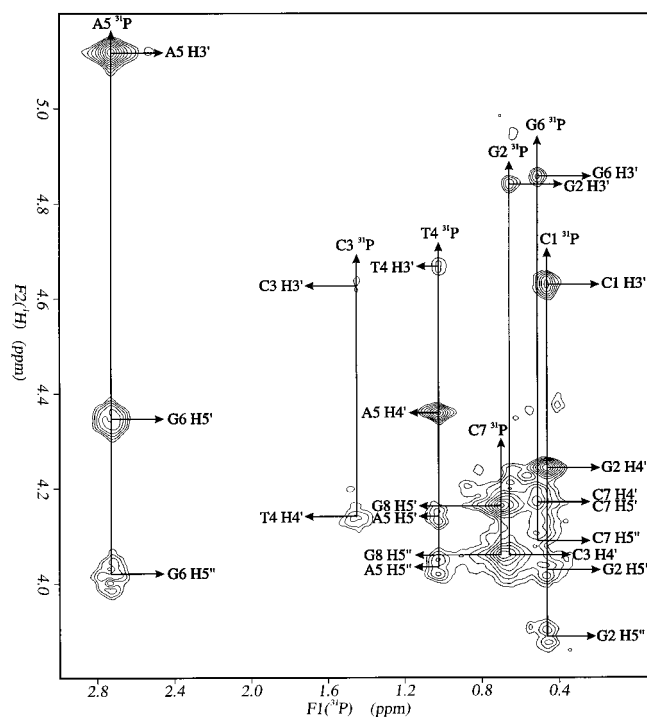


Figure 3. ^1H - ^{31}P HSQC spectrum of the CTAG-TOTO11 complex. The sequential connectivities establish the intrasugar connectivities found through NOESY and TOCSY spectra. ^{31}P chemical shift values are relative to 85% phosphoric acid. The arrows shown indicate the following ^1H - ^{31}P backbone connectivities (Searle and Lane, 1992): intrasidue, $^{31}\text{P}_{(n)} \rightarrow \text{H}3'_{(n)}$; and inter-residue, $^{31}\text{P}_{(n)} \rightarrow \text{H}4'_{(n+1)}$ and $^{31}\text{P}_{(n)} \rightarrow \text{H}5'/\text{H}5''_{(n+1)}$.

is clear evidence of 5'-CTGAG-3' bisintercalation. Cross peaks between A15H2'/H2'' and H13/H14/H15 of one of the chromophores are also consistent with intercalation in the (5'-C3pT4-3'):(5'-A15pG16-3') sequence. Similarly, we observed cross peaks between G5H2'/H2'' and H13/

H14/H15 of the other chromophore consistent with intercalation in the (5'-G5pA6-3'):(5'-T13pC14-3') sequence. A complete assignment of chemical shift values of the major complex and the free oligonucleotide is given in the Supporting Information (Table 2S).

A model of the major form of the CTGAG-TOTO13 complex is shown in Figure 5. The model was obtained from restrained molecular dynamics calculations using 20 intermolecular restraints obtained from cross peak intensities of a NOESY spectrum with a mixing time of 200 ms as described under Experimental Procedures. It is obvious that the linker is positioned in the minor groove crossing from one side of the groove to the other.

A complete assignment of the minor forms is not possible, but exchange cross peaks and exchange-transferred NOEs show that TOTO13 bisintercalates in the 5'-CTGAG-3' binding site. This is demonstrated in the upper part of Figure 4, which is a part of the NOESY spectrum obtained at 25 °C corresponding to the lower part of the figure, which is a part of the NOESY spectrum obtained at 10 °C. Transferred NOEs at 25 °C correlate the resonances of T13 H6 and T13 CH₃ of the major form (6.55 and 0.91 ppm, respectively) with those of the minor form (7.02 and 0.80 ppm, respectively). This is indicated with broken lines. The corresponding transferred NOEs show that H6 and CH₃ of T4_{minor} resonate at 6.54 and 0.92 ppm, respectively.

The CTGAG + TOTO11 Mixture. TOTO11 yields one major form with CTGAG (80%) and one minor form (20%). Both the major and minor forms are asymmetric complexes with nearest-neighbor bisintercalation in the 5'-CTGAG-3' and 5'-CTGAG-3' binding sites, respectively. These complexes are similar to those observed in the mixture of CTGAG + TOTO13. The assignments of the resonances from the major form show many features similar to the spectra of CTGAG + TOTO13 with bisintercalation in the 5'-CTGAG-3' binding site. A complete assignment of chemical shift values of the major

Table 1. ¹H Chemical Shift Values (in Parts per Million) for the CTAG–TOTO11 Complex Compared with Those of the Free Oligonucleotide in Parentheses^a

	C1	G2	C3	T4	A5	G6	C7	G8
H8/H6	7.54 (7.67)	7.75 (8.01)	6.44 (7.46)	6.98 (7.42)	8.18 (8.24)	7.80 (7.71)	7.28 (7.31)	7.90 (7.95)
H5/Me/H2	5.80 (5.95)		4.56 (5.41)	0.83 (1.71)	6.83 (7.40)		5.30 (5.35)	
H1'	5.68 (5.82)	5.67 (5.98)	6.00 (6.00)	5.05 (5.63)	5.60 (6.05)	5.81 (5.73)	5.72 (5.78)	6.10 (6.17)
H2'	1.86 (2.03)	2.43 (2.74)	1.93 (2.08)	1.97 (2.15)	2.75 (2.76)	2.61 (2.52)	1.85 (1.89)	2.59 (2.62)
H2''	2.29 (2.47)	2.35 (2.79)	2.53 (2.53)	2.14 (2.46)	2.75 (2.90)	2.67 (2.62)	2.28 (2.35)	2.34 (2.39)
H3'	4.63 (4.74)	4.84 (5.02)	4.63 (4.78)	4.67 (4.90)	5.12 (5.06)	4.85 (4.97)	4.78 (4.80)	4.67 (4.68)
H4'	4.02 (4.11)	4.25 (4.40)	4.06 (4.27)	4.13 (4.17)	4.36 (4.42)	4.49 (4.38)	4.17 (4.16)	4.16 (4.18)
H5'	3.67 (3.75)	4.02 (4.14)	4.15 (4.27)	(4.11)	4.14 (4.17)	4.02 (4.21)	(4.12)	4.05 (4.08)
H5''	3.67 (3.75)	3.87 (4.04)	4.04 (4.21)	(4.11)	4.04 (4.09)	4.35 (4.21)	(4.21)	4.15 (4.08)
H1/H3		12.77 (13.05)		13.51 (13.79)		12.00 (12.78)		
H4/H6			7.95 (8.30)		7.24 (–)		8.22 (8.36)	
H4/H6			6.59 (6.59)		6.54 (–)		6.43 (6.49)	
TOTO11	TOTO11		TOTO11		TOTO11		TOTO11	
H1	7.59	H10	7.99	H19'	4.04	H23'	3.22	
H2	7.47	H13	6.96	H19''	4.55	H23''	3.26	
H3	7.59	H14	6.88	H20'	2.02	H24'	3.52	
H4	7.43	H15	6.64	H20''	2.02	H24''	3.52	
CH ₃ (6)	3.58	H16	7.46	H21'	1.87	H25'	2.37	
H8	7.17			H21''	1.87	H25''	2.37	
H9	6.46			H22'	3.52			
				H22''	3.52			
phosphate	phosphate		phosphate		phosphate		phosphate	
C1 ³¹ P	0.46	C3 ³¹ P	1.45	A5 ³¹ P	2.73	C7 ³¹ P	0.70	
G2 ³¹ P	0.66	T4 ³¹ P	1.02	G6 ³¹ P	0.52			

^a The values are relative to DSS at 25 °C. ³¹P chemical shift values are relative to 85% phosphoric acid.

form and the free oligonucleotide is given in the Supporting Information (Table 3S).

A similar complete assignment of the minor form is not possible, but transferred NOEs and exchange cross peaks prove that the minor form of CTGAG + TOTO11 arises from bisintercalation in the 5'-CTGAG-3' binding site.

The d(CGCTAAGCG):d(CGCTTAGCG) (CTAAG) Oligonucleotide. The CTAAG + TOTO13 Mixture. The mixture of CTAAG + TOTO13 yields rather broad lines in the spectrum due to exchange between three complexes. The major form (~75%) arises from non-nearest-neighbor bisintercalation in the 5'-CTAAG-3' binding site. This major form constitutes the first complex that has been shown to contain a non-nearest-neighbor bisintercalation of a ligand in dsDNA.

Figure 6 shows the aromatic to H2'/H2'' part of a NOESY spectrum of the CTAAG–TOTO13 complex. Interruption in the sequential H2'/H2''_(n-1)–H6/H8_(n)–H2'/H2''_(n) pattern is observed in the 5'-C3pT4-3', 5'-C12pT13-3', 5'-A6pG7-3', and 5'-A15pG16-3' sequences. More importantly, sequential connectivities for the 5'-T4A5A6-3' and 5'-T13T14A15-3' sequences show that no intercalation takes place in this part of the oligonucleotide, proving that the linker spans over 3 base pairs. Interruption in the sequential H1'_(n-1)–H6/H8_(n)–H1'_(n) pattern confirms the binding site. The aromatic protons on A6 and G7 have cross peaks to H15 and/or H14 on one of the chromophores, while the aromatic protons on A15 and G16 have cross peaks to H15 and H14 on the other chromophore. Furthermore, an up-field shift of ~0.8 ppm of the methyl group protons of T4 and T13 is observed. Such an up-field shift is normally observed in binding sites containing a thymidine (Jacobsen et al., 1995; Hansen et al., 1996). All together, this establishes bisintercalation in the 5'-CTAAG-3' site. A complete assignment of chemical shift values of the major form and the free oligonucleotide is given in the Supporting Information (Table 4S).

A similar complete assignment of the minor forms is not possible, but exchange cross peaks and transferred

NOEs show that the two minor forms arise from nearest-neighbor 5'-CTAAG-3' and 5'-CTAAG-3' bisintercalation, respectively. One aromatic thymidine proton from each of the two minor forms experiences an up-field shift of ~0.5 ppm (not shown). The methyl group protons from these thymidines have an up-field shift of ~0.8 ppm. This large up-field shift is typical when a TOTO chromophore intercalates on the 3' site of a nucleobase. Transferred NOEs from the T4/T13 methyl group protons on the major form to the up-field-shifted thymidine protons on the minor forms are indicated with broken lines in Figure 6. Combined with exchange cross peaks, this makes it possible to assign the binding site of the minor forms.

The CTAAG + TOTO11 Mixture. The mixture of CTAAG + TOTO11 yields complexes similar to those in the CTAAG–TOTO13 mixture, but the ratio between the complexes varies. There is no pronounced major form observed.

The d(CGCTGCAGCG)₂ (CTGCAG) Oligonucleotide. The CTGCAG + TOTO13 Mixture. Dynamic exchange between different forms yields very broad lines in the spectrum of the CTGCAG + TOTO13 mixture. It is not possible to establish the binding sites conclusively. However, it was observed that the thymidine methyl groups in all cases were shifted up-field. A mixture of a symmetric form with intercalation between the 5'-C3pT4-3' and the 5'-A7pG8-3' in the 5'-CTGCAG-3' binding sites and an asymmetric form with intercalation in the 5'-C3pT4-3' and the 5'-C6pA7-3' in the 5'-CTGCAG-3' binding sites is a possible explanation of the features in the spectra. In both cases, this gives a non-nearest-neighbor bisintercalation where the linker spans over more than two base pairs in the minor groove. Complete assignment of the spectra was not possible.

Absorbance and Fluorescence Emission Spectroscopy. Data from absorbance and fluorescence emission measurements of the free dye and the dye–dsDNA complexes are given in Table 2. A red shift of ~35 nm of the absorbance maximum and a blue shift of 38–49 nm of the fluorescence emission maximum are observed upon complex formation. Fluorescence enhancement

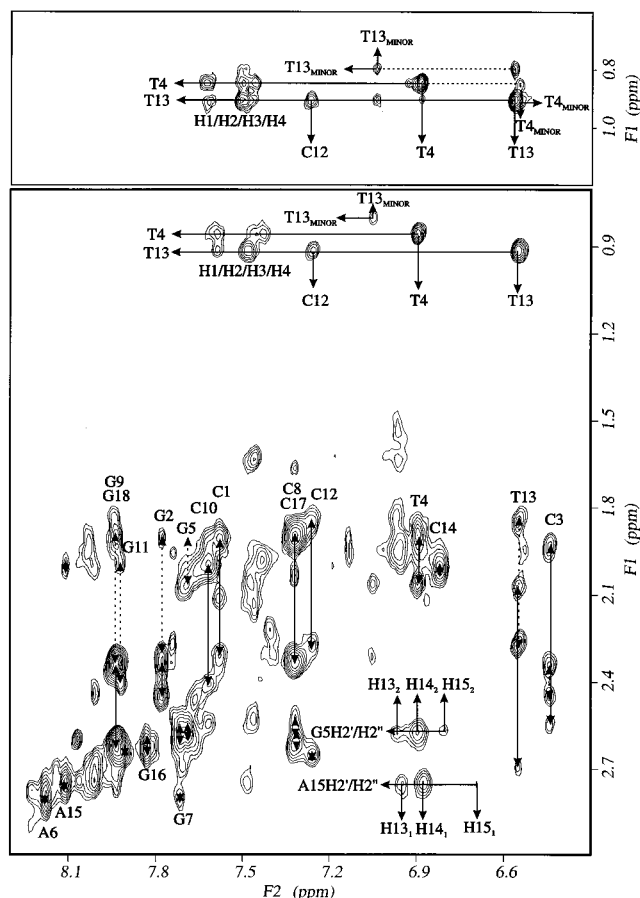


Figure 4. Aromatic to H2'/H2''/methyl area of a NOESY spectra (mixing time of 200 ms) of CTGAG + TOTO13. (Lower part) Spectrum obtained at 10 °C. The H8/H6_(n) → H2'/H2''_(n) connectivities of the major form are shown with unbroken double arrows, while the H8/H6_(n) → H2'/H2''_(n-1) connectivities are indicated with broken double arrows. (Top part) Part of the spectrum acquired at 25 °C. Transferred NOEs used for assignment of the minor form are shown with broken lines.

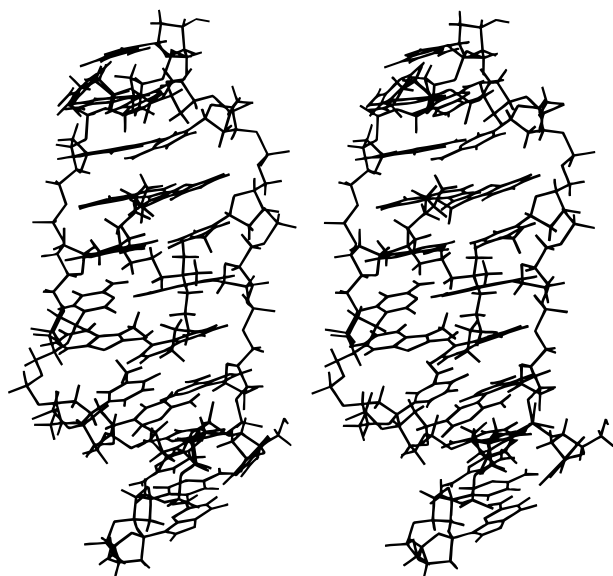


Figure 5. Stereoview of a stickplot of the CTGAG-TOTO13 complex looking into the minor groove. Nearest-neighbor bis-intercalation in the 5'-CTGAG-3' binding site forces the linker between the *N*-methyls to cross the minor groove nearly perpendicularly. Deoxyribose protons have been omitted for clarity.

upon binding to the 5'-CTAG-3' sequence is several thousand for all four dyes, which is much larger than

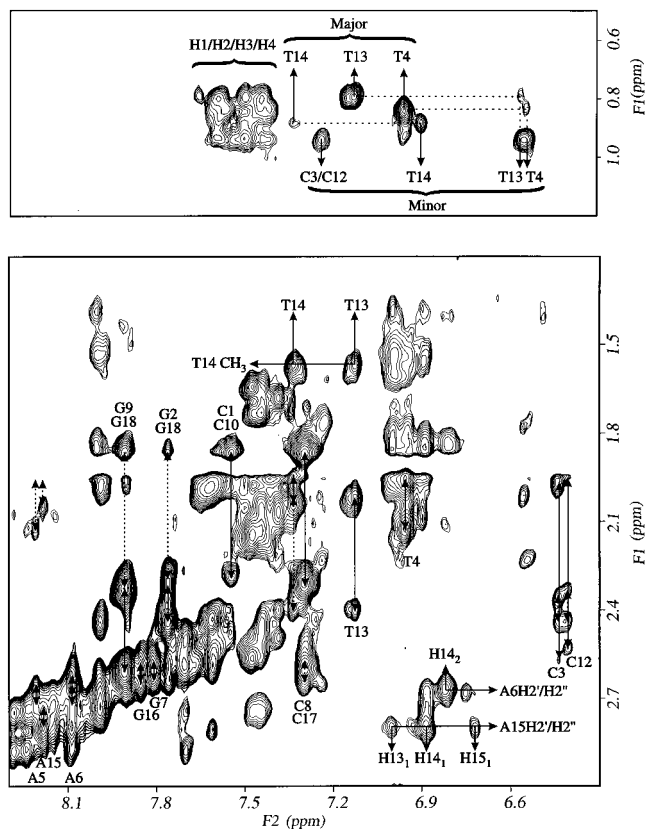


Figure 6. Aromatic to H2'/H2'' part of a NOESY spectrum (mixing time of 200 ms) of the CTAG-TOTO13 complex at 25 °C. (Lower part) The H8/H6_(n) → H2'/H2''_(n) connectivities of the major form are shown with unbroken double arrows, while the H8/H6_(n) → H2'/H2''_(n-1) connectivities are indicated with broken double arrows. (Upper part) Transferred NOEs showing the correlation between the major form and the two minor forms.

the enhancement reported from binding of TOTO to calf thymus DNA (Rye et al., 1992). The uncertainties on the values of the fluorescence enhancement ($F_{\text{bound}}/F_{\text{free}}$) are expected to be very large because the free dye is nearly nonfluorescent and it has not been possible to ensure that the dye was absolutely free of fluorescent impurities. Consequently, we have determined the relative fluorescence intensities at equal normalized absorbance intensities of the dye-dsDNA complexes. The values are given in the last column in Table 2 showing that TOTO10, TOTO11, and TOTO13 have higher fluorescence quantum yields than TOTO.

DISCUSSION

The sequence selectivity and the binding mode of the TOTO analogs to various dsDNA oligonucleotides examined in this work are very similar to those of TOTO. In the CTAG oligonucleotide both TOTO10 and TOTO11 bind exclusively to the 5'-CTAG-3' site. Also, TOTO13 has this sequence as a preferred binding site, but due to the longer linker other binding sites are possible as well. On the basis of the NMR spectra it is somewhat difficult to establish the relative binding strengths of TOTO, TOTO10, and TOTO11 to the CTAG oligonucleotide. However, a comparison of the line width in the NMR spectra indicates that there is no reason to believe that either TOTO10 or TOTO11 binds more weakly or less preferentially to the (5'-CTAG-3')₂ site than TOTO.

The results of the fluorescence spectroscopy experiments using the CTAG oligonucleotide show that the fluorescence quantum yield of TOTO and analogs (Table 2) increases with the length of the linker. Thus, TOTO13

Table 2. Data from Absorbance and Fluorescence Emission Spectra of TOTO Analogs Bound to the CTAG Oligonucleotide

	λ^A (nm)		ϵ (M ⁻¹ cm ⁻¹)		λ^F (nm)		$F_{\text{bound}}/F_{\text{free}}$	rel fluorescence intensity
	free	bound	free	bound	free	bound		
TOTO	479.5	513.5	1.18×10^5	0.81×10^5	565	527	~5000	1
TOTO10	479	512.5	1.16×10^5	0.98×10^5	565	528	~7400	1.2
TOTO11	474	510	0.90×10^5	0.91×10^5	575	526	~2400	1.3
TOTO13	475.5	509.5	1.37×10^5	0.91×10^5	575	527	~6000	1.4

^a A red shift of ~35 nm of the absorbance maximum (λ^A) and a blue shift of 38–49 nm of the fluorescence emission maximum (λ^F) upon complex formation is observed. The fluorescence enhancement upon complex formation, $F_{\text{bound}}/F_{\text{free}}$, is the ratio of the intensities at the fluorescence emission peaks. Measurements were performed in the same buffer with normalized absorbance intensities at the excitation wavelengths. The relative fluorescence emission intensities show that TOTO10, TOTO11, and TOTO13 have higher fluorescence quantum yields than TOTO.

gives the largest enhancement of the fluorescence upon binding to the CTAG oligonucleotide. This effect is not at all correlated to the binding selectivity. One may argue that the most useful fluorescence marker is the one with the lowest selectivity and the highest quantum yield. This would make TOTO13 a better choice as a marker than TOTO.

Both TOTO11 and TOTO13 were observed to give non-nearest-neighbor bisintercalation in oligonucleotides with isolated (5'-CpT-3'):(5'-ApG-3') base pairs. On the basis of the results of TOTO11 and molecular modeling, we refrained from examining the binding of TOTO and TOTO10 to such oligonucleotides since it seems obvious that the length of the linker is too short in these two dyes to accommodate the binding into isolated (5'-CpT-3'):(5'-ApG-3') binding sites.

The CTGAG sequence contains 5'-CpT-3' and 5'-ApG-3' sites separated by one base pair. This is anticipated to lead to non-nearest-neighbor bisintercalation in the 5'-CTGAG-3' binding site of TOTO11 and TOTO13. However, in both cases we observed predominantly nearest-neighbor bisintercalation in the 5'-CTGAG-3' binding site. Earlier results have shown the 5'-CTGA-3' is a good binding site for TOTO, although less favorable than the 5'-CTAG-3' binding site (Jacobsen et al., 1995). The results in the present work demonstrate that this is also the case for TOTO11 and TOTO13. Consequently, it was not possible to observe non-nearest-neighbor bisintercalation in the CTGAG oligonucleotide since the competition from four base pair binding sites is too strong. In the CTAAG oligonucleotide it is more favorable to bisintercalate in a non-nearest-neighbor fashion. The mixture of TOTO13 and CTAAG gives as the major form a complex in which the linker spans over three base pairs. The linker of TOTO11 seems to be slightly too short to really favor the non-nearest-neighbor bisintercalation, although a minor form of that kind was observed in the binding to the CTAAG oligonucleotide.

In case of the CTGCAG oligonucleotide, the linker of TOTO13 was observed to be able to span over four base pairs in the binding to the 5'-CTGCAG-3' site. This is probably initiated by the presence of the 5'-GpC-3' step, which is known to be a very poor TOTO binding sequence (Jacobsen et al., 1995; Spielmann et al., 1995; Hansen et al., 1996).

There seems to be a somewhat rational trend in the ability of TOTO analogs to bind in a non-nearest-neighbor fashion with difficulties in the case of TOTO11, whereas such binding is favored by TOTO13 in some oligonucleotides. However, this behavior probably hides a much more complicated situation than just a simple relation to the length of the linker. The position of the linker in the minor groove is stabilized by electrostatic interactions between the negatively charged phosphate groups on the DNA backbone and the positively charged nitrogen atoms on the linker. It was previously shown

(Spielmann et al., 1995) that the positively charged nitrogens are positioned near the negatively charged phosphate groups between T4 and A5 in the CTAG-TOTO complex with the linker crossing the minor groove. Three CH₂ groups are probably needed to make this crossing. This leaves the first three CH₂ groups of the 4,4,8,8-tetramethyl-4,8-diazaundecamethylene linker with the task of reaching from the intercalating chromophore to the position of the nearest phosphate group. In TOTO11 this can be achieved by the first four CH₂ groups in the 5,5,9,9-tetramethyl-5,9-diazatridecamethylene linker, since it may not be very essential whether there are three or four CH₂ groups in this part of the linker. On the other hand, it may be more crucial for the ability to cross in the minor groove that there are three CH₂ groups between the two positively charged nitrogen atoms in the linker. Preliminary molecular modeling studies have supported these types of considerations on the positions of CH₂ groups in the linker.

In our opinion, the results in this work are best understood if the stability of the complexes is determined not just by the length of the linker but also by the ability of the linker to cross the minor groove so as to place the positively charged nitrogen atoms close to backbone phosphate groups. This makes it understandable that TOTO11 does not bisintercalate in a non-nearest-neighbor fashion, while TOTO13 is able to do so in even the CTGCAG oligonucleotide where the linker has to span over four base pairs. TOTO11 has the optimal length of the linker for nearest-neighbor bisintercalation, while TOTO13 with two extra CH₂ groups in the linker can span much longer in the minor groove.

The non-nearest-neighbor bisintercalation complex of TOTO13 with the CTGCAG was not observed to be kinetically very stable. The linker in the minor groove spans over four base pair, but only two of the four possible phosphate groups can be close to a positively charged nitrogen atom in the linker. This situation is obviously a very dynamic one, giving broad lines in the NMR spectra. The linker may be slightly too short in TOTO13 to span over four base pairs, but more importantly the linker should contain just as many positively charged nitrogen atoms as the number of phosphate groups it meets in the minor groove. A TOTO analog with a 4,4,8,8,12,12,16,16-octamethyl-4,8,12,16-tetraazaundecamethylene linker would probably be optimal for TOTO bisintercalation in the CTGCAG oligonucleotide. Likewise, a 4,4,8,8,12,12-hexamethyl-4,8,12-triazapentadecamethylene linker should be optimal for binding in two isolated 5'-CT-3' sites separated by one base pair.

Recently, Glazer and co-workers (Benson et al., 1995; Zeng et al., 1995) have dealt with the problem of modifying the length of the linker in bisintercalating fluorescent dimeric dyes. In the case of the heterodimeric dyes TOTAB and TOTIN, which are closely related to TOTO, they found that the linker length strongly affected

the emission spectra of the dsDNA-bound dye. In agreement with our work they observed that the energy transfer from donor to acceptor chromophores was optimized in the analog with a linker slightly longer than the 4,4,8,8-tetramethyl-4,8-diazaundecamethylene linker in TOTO.

EXPERIMENTAL PROCEDURES

Synthesis. 1-(4-Iodoalkyl)-4-[3-methyl-2,3-dihydro(benzo-1,3-thiazole)-2-methylidene]quinolinium Iodide (**3**). Equimolar amounts of **1** and **2** were dissolved in absolute ethanol by heating. One equivalent of triethylamine was added, and the mixture was stirred at room temperature for 30 min. The title compound precipitated on addition of ether and was recrystallized from acetone/ether to give a red powder.

3b: yield 75%; mp 216–219 °C; ^1H NMR $[(\text{CD}_3)_2\text{SO}]$ δ 7.00–8.75 (m, 10H, Ar), 6.78 (s, 1H, CH), 4.54 (m, 2H, NCH_2), 3.93 (s, 3H, NCH_3), 3.33 (m, 2H, CH_2I), 1.89 (m, 4H, $2 \times \text{CH}_2$); FAB MS m/z 473 (M^+).

3c: yield 75%; mp 206–209 °C; ^1H NMR $[(\text{CD}_3)_2\text{SO}]$ δ 7.26–8.77 (m, 10H, Ar), 6.85 (s, 1H, CH), 4.58 (m, 2H, NCH_2), 3.99 (s, 3H, NCH_3), 3.29 (m, 2H, CH_2I), 1.83 (m, 4H, $2 \times \text{CH}_2$), 1.46 (m, CH_2); FAB MS m/z 487 (M^+).

1,1'-(4,4,8,8-Tetramethyl-4,8-diazaundecamethylene)-bis[4-[3-methyl-2,3-dihydro(benzo-1,3-thiazole)-2-methylidene]quinolinium Tetraiodide, TOTO10. A suspension of **3a** in anhydrous methanol and 8 equiv of *N,N,N,N*-tetramethyl-1,3-propanediamine were refluxed for 12 h. Evaporation of the solvent and subsequent recrystallization from acetone/ether afforded **4** in 80% yield, mp 230–233 °C. Equivalent amounts of **4** and **3b** in anhydrous methanol were refluxed for 12 h. TOTO10 was precipitated by addition of ether and recrystallized from acetone/ether: yield 85%; mp 238–240 °C; ^1H NMR $[(\text{CD}_3)_2\text{SO}]$ δ 7.26–8.77 (m, 20H, Ar), 6.85 (s, 1H, CH), 6.88 (s, 1H, CH), 4.68 (m, 4H, NCH_2), 4.00 (s, 3H, NCH_3), 3.99 (s, 3H, NCH_3), 3.5–3.9 (m, 8H, $4 \times \text{NCH}_2$), 3.21 (s, 12H, NCH_3), 2.40 (m, 4H, $2 \times \text{CH}_2$), 1.96 (m, 4H, $2 \times \text{CH}_2$); FAB MS m/z 1189 ($\text{M}^+ - 127$). Anal. Calcd for $\text{C}_{50}\text{H}_{60}\text{I}_4\text{N}_6\text{S}_2 \cdot 4\text{H}_2\text{O}$: C, 43.24; H, 4.94; N, 6.05. Found: C, 42.80; H, 4.86; N, 5.70.

1,1'-(5,5,9,9-Tetramethyl-5,9-diazatridecamethylene)-bis[4-[3-methyl-2,3-dihydro(benzo-1,3-thiazole)-2-methylidene]quinolinium Tetraiodide, TOTO11. A suspension of **3b** and 0.5 equiv of *N,N,N,N*-tetramethyl-1,3-propanediamine in anhydrous methanol was heated at reflux for 24 h. Recrystallization from DMF/MeOH afforded the title compound as an orange-red solid: yield 80%; mp 258–261 °C; ^1H NMR $[(\text{CD}_3)_2\text{SO}]$ δ 7.15–8.70 (m, 20H, Ar), 6.76 (s, 2H, CH), 4.68 (m, 4H, NCH_2), 3.94 (s, 6H, NCH_3), 3.61 and 3.49 (2m, 8H, $4 \times \text{NCH}_2$), 3.20 (s, 12H, NCH_3), 2.34 (m, 2H, CH_2), 1.97 (m, 8H, $4 \times \text{CH}_2$); FAB MS m/z 1203 ($\text{M}^+ - 127$). Anal. Calcd for $\text{C}_{51}\text{H}_{62}\text{I}_4\text{N}_6\text{S}_2 \cdot 2\text{H}_2\text{O}$: C, 44.82; H, 4.87; N, 6.15. Found: C, 44.73; H, 4.90; N, 5.78.

1,1'-(6,6,10,10-Tetramethyl-6,10-diazapentadecamethylene)-bis[4-[3-methyl-2,3-dihydro(benzo-1,3-thiazole)-2-methylidene]quinolinium Tetraiodide, TOTO13. The same procedure as for TOTO11 was used: yield 90%; mp 253–255 °C; ^1H NMR $[(\text{CD}_3)_2\text{SO}]$ δ 7.23–8.76 (m, 20H, Ar), 6.82 (s, 2H, CH), 4.62 (m, 4H, NCH_2), 3.98 (s, 6H, NCH_3), 3.40 (m, 8H, $4 \times \text{NCH}_2$), 3.13 (s, 12H, NCH_3), 2.26 (m, 2H, CH_2), 1.91–1.94 (m, 8H, $4 \times \text{CH}_2$), 1.46 (m, 4H, $2 \times \text{CH}_2$); FAB MS m/z 1231 ($\text{M}^+ - 127$). Anal. Calcd for $\text{C}_{53}\text{H}_{66}\text{I}_4\text{N}_6\text{S}_2 \cdot 3\text{H}_2\text{O}$: C, 45.04; H, 5.18; N, 5.95. Found: C, 44.67; H, 5.18; N, 5.69.

Materials. Purified DNA oligonucleotides were purchased from DNA Technology (Aarhus, Denmark) and

used without further purification. The non-self-complementary single-stranded DNA oligomers were added to an equivalent amount of the complementary strand and duplexes formed by annealing from 80 °C over 2 h. In this work four different oligonucleotides have been used (Scheme 2).

Stock solutions of TOTO10, TOTO11, and TOTO13 in DMSO- d_6 were used for complex formation with the dsDNA oligonucleotides according to the procedure described earlier (Jacobsen et al., 1995). A phosphate buffer containing ethylenediaminetetraacetic acid (EDTA), 2,2-dimethyl-2-silapentane-5-sulfonate (DSS), and NaN_3 was added, giving a final concentration in the NMR sample of 10 mM P_i (pD 7.0), 0.025 mM EDTA, 0.1 mM DSS, and 0.01 mM NaN_3 . The complexes were redissolved in 500 μL of 99.96% D_2O (from Cambridge Isotope Laboratories). For experiments in H_2O a mixture of 90% H_2O /10% D_2O (500 μL) was used. The samples were kept under N_2 and remained stable for months.

Absorbance and Fluorescence Emission Spectra. For determination of the absorbance and fluorescence emission spectra of the dye–dsDNA complexes, aqueous solutions of 0.02 mM were used. A phosphate buffer was added, giving a final concentration in a 3 mL sample of 10 mM P_i (pD 7.0), 0.02 mM EDTA, 0.1 mM DSS, and 0.02 mM NaN_3 . After recording of the absorption spectrum, the excitation wavelength for the fluorescence emission was selected to the wavelength of maximum absorbance. A similar aqueous solution of the free dye was prepared and diluted until the absorbance was identical to that of the dye–dsDNA. Once again, the excitation wavelength was selected to the wavelength of the maximum absorbance. The intensities at the fluorescence emission maximum were used to calculate the fluorescence enhancement defined as $F_{\text{bound}}/F_{\text{free}}$. Absorbance spectra were recorded on a Shimadzu UV-160 spectrophotometer, and fluorescence measurements were performed with a Perkin-Elmer MPF-3 fluorescence spectrophotometer. All spectra were recorded at room temperature.

NMR Experiments. The NMR spectra of the free dyes were obtained on a Bruker AC250 NMR spectrometer. All NMR experiments on the DNA–dye complexes were performed at 500 MHz on a Varian Unity 500 NMR spectrometer. NOESY spectra in D_2O were acquired with a mixing time of 200 ms using 1024 complex points in t_2 and a spectral width of 5000 Hz. A total of 512 t_1 experiments with 64 scans each were acquired using the States–Haberkorn–Ruben phase cycle. Furthermore, experiments with mixing times of 25, 50, 100, and 150 ms were acquired for the mixture of CTAG + TOTO11. These experiments were acquired successively without removing the sample from the magnet.

NOESY spectra in H_2O were acquired using 2048 complex points and a spectral width of 10 000 Hz using a NOESY pulse sequence in which the last 90° pulse was replaced by a pulse containing a notch to suppress the water signal (Stein et al., 1995). This ensured suppression of the water signal together with a linear excitation profile over the whole spectral width.

TOCSY experiments in D_2O were acquired with mixing times of 30 and 90 ms using 1024 complex points in t_2 and a spectral width of 5000 Hz. A total of 512 t_1 experiments with 64 scans each were acquired using the TPPI phase cycle.

The ^1H – ^{31}P HSQC experiments were recorded with 1024 complex points and a spectral width of 1000 Hz in both dimensions. A total of 512 t_1 experiments with 288 scans each were acquired using the States–Haberkorn–Ruben phase cycle.

One-dimensional spectra in D₂O were acquired separately. All spectra were recorded at 10 or 25 °C using DSS as reference.

The acquired data were processed using FELIX (version 95.0, Biosym/MSI, San Diego, CA). The TOCSY and NOESY spectra were assigned in the conventional way as described in the literature (Boelens et al., 1985; Feigon et al., 1983; Hare et al., 1983; Scheek et al., 1984, 1983).

Molecular Modeling. The model structure of the CTGAG-TOTO13 complex was made using an isolated spin pair approximation. The assigned cross peaks from a 200 ms NOESY spectrum were integrated and transformed into a restraint file. Twenty structures were calculated using the following restrained molecular dynamics (RMD) protocol: initially 100 and 10 000 cycles of steepest descent and conjugate gradient energy minimization, respectively. This was followed by 28 ps of RMD (steps of 1 fs) with the following temperature profile: 425 K for 4 ps and then cooled to 250 K in 25 K steps of 3 or 4 ps each. Force constants of 50 kJ/mol were used. Finally, the structures were energy minimized using conjugate gradient until the derivative was <0.01. Computational results were obtained using software from Biosym/MSI. Energy minimizations and restrained molecular dynamics were done with the Discover program (ver. 2.9.7), using a modified AMBER force field. Modifications were made to take the thiazole sulfur atoms into account. Graphical displays were obtained by the Insight II molecular modeling system (ver. 95.0).

ACKNOWLEDGMENT

We are thankful to Dr. Paul C. Stein for guidance in setting up the ¹H-³¹P HSQC experiment.

Supporting Information Available: Chemical shift values of CTAG-TOTO10, CTGAG-TOTO13, CTGAG-TOTO11, and CTAAG-TOTO13 (4 pages). Ordering information is given on any current masthead page.

LITERATURE CITED

- Benson, S. C., Singh, P., and Glazer, A. N. (1993a) Heterodimeric DNA-Binding Dyes Designed for Energy Transfer: Synthesis and Spectroscopic Properties. *Nucleic Acids Res.* **21**, 5727-5735.
- Benson, S. C., Mathies, R. A., and Glazer, A. N. (1993b) Heterodimeric DNA-Binding Dyes Designed for Energy Transfer: Stability and Applications of DNA Complexes. *Nucleic Acids Res.* **21**, 5720-5726.
- Benson, S. C., Zheng, Z., and Glazer, A. N. (1995) Fluorescence Energy-Transfer Cyanine Heterodimers with High Affinity for Double-Stranded DNA. I. Synthesis and Spectroscopic Properties. *Anal. Biochem.* **231**, 247-255.
- Boelens, R., Scheek, R. M., Dijkstra, K., and Kaptein, R. (1985) Sequential Assignment of Imino- and Amino-Proton Resonances in ¹H NMR Spectra of Oligonucleotides by Two-Dimensional NMR Spectroscopy. Application to *lac* Operator Fragment. *J. Magn. Reson.* **62**, 378-386.
- Brooker, L. G. S., White, F. L., Keyes, G. H., Smyth, C. P., and Oesper, P. E. (1941) Color and Constitution. II. Absorptions of Some Related Vinylene-homologous Series. *J. Am. Chem. Soc.* **62**, 3192-3203.
- Brooker, L. G. S., Keyes, G. H., and Williams, W. W. (1942) Color and Constitution. V. The Absorption of Unsymmetrical Cyanines. Resonance as a Basis for a Classification of Dyes. *J. Am. Chem. Soc.* **63**, 199-210.
- Feigon, J., Leupin, W., Denny, W. A., and Kearns, D. R. (1983) Two Dimensional Proton Nuclear Magnetic Resonance Investigation of the Synthetic Deoxyribonuclei Acid Decamer d(ATATCGATAT)₂. *Biochemistry* **22**, 5943-5951.
- Hansen, L. F., Jensen, L. K., and Jacobsen, J. P. (1996) Bisintercalation of a Homodimeric Thiazole Orange Dye in DNA in Symmetrical Pyrimidine-Pyrimidine-Purine-Purine Oligonucleotides. *Nucleic Acids Res.* **24**, 859-867.
- Hare, D. R., Wemmer, D. E., Chou, S.-H., Drobny, G., and Reid, B. R. (1983) Assignment of the Non-Exchangeable Proton Resonances of d(C-G-C-G-A-A-T-T-C-G-C-G) using Two-Dimensional Nuclear Magnetic Resonance Methods. *J. Mol. Biol.* **171**, 319-336.
- Jacobsen, J. P., Pedersen, J. B., Hansen, L. F., and Wemmer, D. E. (1995) Site Selective Bis-Intercalation of a Homodimeric Thiazole Orange Dye in DNA Oligonucleotides. *Nucleic Acids Res.* **23**, 753-760.
- Kagawa, N., and Kawashima, Y. (1989) Patent JP 01147451; *Chem. Abstr.* **112**, 108465.
- Roongta, L. G. S., Jones, C. R., and Gorenstein, D. G. (1990) Effect of Distortions in the Deoxyribose Phosphate Backbone Conformation of Duplex Oligodeoxyribonucleotide Dodecamers Containing GT, GG, GA, AC, and GU Base-Pair Mismatches on ³¹P NMR Spectra. *Biochemistry* **29**, 5245-5258.
- Rye, H. S., Yue, S., Wemmer, D. E., Quesada, M. A., Haugland, R. P., Mathies, R. A., and Glazer, A. N. (1992) Stable Fluorescent Complexes of Double-Stranded DNA with Bis-Intercalating Asymmetric Cyanine Dyes: Properties and Applications. *Nucleic Acids Res.* **20**, 2803-2812.
- Scheek, R. M., Russo, N., Boelens, R., and Kaptein, R. (1983) Sequential Resonance Assignments in DNA ¹H NMR Spectra by Two-Dimensional NOE Spectroscopy. *J. Am. Chem. Soc.* **105**, 2914-2916.
- Scheek, R. M., Boelens, R., Russo, N., Van Boom, J. H., and Kaptein, R. (1984) Sequential Resonance Assignments in ¹H NMR Spectra of Oligonucleotides by Two-Dimensional NMR Spectroscopy. *Biochemistry* **23**, 1371-1376.
- Searle, M. S., and Lane, A. N. (1992) ³¹P NMR Investigation of the Backbone Conformation and Dynamics of the Hexamere Duplex d(5'-GCATGC)₂ in its Complex with Nogalamycin. *FEBS* **297**, 292-296.
- Spielmann, H. P., Wemmer, D. E., and Jacobsen, J. P. (1995) Solution Structure of a DNA Complex with the Fluorescent Bis-Intercalator TOTO Determined by NMR Spectroscopy. *Biochemistry* **34**, 8542-8553.
- Stein, P. C., Jacobsen, J. P., and Spielmann, H. P. (1995) Design and Implementation of a Simple Shaped Notch Filter. *J. Magn. Reson. Ser. B* **109**, 93-96.
- Wakelin, L. P. G. (1986) Polyfunctional DNA Intercalating Agents. *Med. Res. Rev.* **6** (3), 275-340.
- Zeng, Z., Benson, S. C., and Glazer, A. N. (1995) Fluorescence Energy-Transfer Cyanine Heterodimers with High Affinity for Double-Stranded DNA. II. Applications to Multiplex Restriction Fragment Sizing. *Anal. Biochem.* **231**, 256-260.

BC970067K

Table 2S. Chemical shift values in ppm for the CTGAG-TOTO13 complex compared with those of the free oligonucleotide in parentheses. The values are relative to DSS at 10°C.

	H1'	H2'	H2''	H3'	H6/H8	H5/H2/Me	H1/H3	H4	H4	H4
C1	5.68(5.80)	1.90(2.00)	2.31(2.44)	4.62(4.73)	7.57(7.64)	5.82(5.91)				
G2	5.69(5.95)	2.34(2.70)	2.44(2.79)	4.85(5.00)	7.77(7.98)		12.81(13.04)	6.68(6.61)	7.98(8.23)	
C3	6.01(6.01)	1.94(2.03)	2.54(2.52)	4.62(4.82)	6.44(7.45)	4.61(5.40)				
T4	5.05(5.66)	2.58(2.01)	2.64(2.36)	4.61(4.85)	6.89(7.28)	0.86(1.65)	13.82(13.87)			
G5	5.19(5.45)	2.58(2.70)	2.65(2.77)	4.60(5.00)	7.68(7.89)		12.30(12.60)			
A6	5.83(6.04)	2.79(2.67)	2.79(2.87)	4.88(5.06)	8.17(8.09)	7.03(7.62)				
G7	5.76(5.72)	2.65(2.44)	2.65(2.60)	4.98(4.95)	7.71(7.63)		12.48(12.79)			
C8	5.73(5.75)	1.89(1.87)	2.33(2.32)	4.81(4.79)	7.32(7.26)	5.34(5.30)		6.49(6.46)	8.25(8.36)	
G9	6.13(6.16)	2.34(2.36)	2.61(2.60)	4.67(4.67)	7.92(7.92)					
C10	5.72(5.80)	2.00(2.00)	2.41(2.44)	4.62(4.73)	7.61(7.64)	5.85(5.91)				
G11	5.88(5.95)	2.66(2.70)	2.66(2.79)	4.81(5.00)	7.92(7.98)		12.95(13.04)			
C12	5.83(5.72)	1.84(2.07)	2.26(2.15)	4.55(4.75)	7.25(7.43)	5.18(5.39)		6.56(6.56)	8.04(8.28)	
T13	6.05(6.05)	2.08(2.15)	2.69(2.51)	4.73(4.88)	6.55(7.43)	0.91(1.63)	14.11(13.87)			
C14	4.30(5.39)	2.02(2.07)	2.02(2.35)	4.65(4.83)	6.82(7.53)	4.61(5.72)		6.84(6.82)	7.88(8.57)	
A15	5.65(5.98)	2.75(2.75)	2.75(2.88)	5.10(5.05)	8.10(8.20)	7.15(7.62)				
G16	5.77(5.72)	2.62(2.49)	2.62(2.60)	4.81(4.95)	7.83(7.68)		12.00(12.86)			
C17	5.73(5.75)	1.89(1.87)	2.33(2.32)	4.81(4.79)	7.32(7.27)	5.34(5.34)		6.49(6.46)	8.25(8.36)	
G18	6.13(6.16)	2.34(2.36)	2.61(2.60)	4.67(4.67)	7.92(7.92)					

TOTO13	Ring1	Ring2	TOTO13	Ring1	Ring2
H13	6.95	6.97	H8	6.22	6.17
H14	6.87	6.89	H9	6.53	6.53
H15	6.70	6.80	H10	8.02	7.94
H16	7.52	7.59	H19'	3.98	3.91
Me	3.60	3.59	H19''	4.45	4.45

Table 3S. Chemical shift values in ppm for the CTGAG-TOTO11 complex compared with those of the free oligonucleotide in parentheses. The values are relative to DSS at 10°C.

	H1'	H2'	H2''	H3'	H6/H8	H5/H2/Me	H1/H3	H4	H4
C1	5.68(5.80)	1.87(2.00)	2.32(2.44)	4.79(4.73)	7.56(7.64)	5.79(5.91)			
G2	5.68(5.95)	2.34(2.70)	2.42(2.79)	4.84(5.00)	7.76(7.98)		12.78(13.04)		
C3	6.02(6.01)	1.95(2.03)	2.50(2.52)	4.63(4.82)	6.49(7.45)	4.60(5.40)		6.73(6.61)	8.00(8.23)
T4	5.27(5.66)	1.95(2.01)	2.10(2.36)	4.74(4.85)	6.95(7.28)	0.77(1.65)	13.75(13.87)		
G5	5.06(5.45)	2.56(2.70)	2.56(2.77)	4.63(5.00)	7.71(7.89)		12.25(12.60)		
A6	5.86(6.04)	2.81(2.67)	2.81(2.87)	4.91(5.06)	8.14(8.09)	7.02(7.62)		6.32(-)	7.22(-)
G7	5.72(5.72)	2.54(2.44)	2.54(2.60)	4.63(4.95)	7.67(7.63)		12.48(12.79)		
C8	5.65(5.75)	1.86(1.87)	2.28(2.32)	4.81(4.79)	7.29(7.26)	5.30(5.30)		6.49(6.46)	8.22(8.36)
G9	6.09(6.16)	2.31(2.36)	2.60(2.60)	4.66(4.67)	7.89(7.92)				
C10	5.75(5.80)	1.86(2.00)	2.31(2.44)	4.79(4.73)	7.58(7.64)	5.80(5.91)			
G11	5.86(5.95)	2.64(2.70)	2.64(2.79)	4.79(5.00)	7.89(7.98)		12.93(13.04)		
C12	5.80(5.72)	1.83(2.07)	2.26(2.15)	4.54(4.75)	7.24(7.43)	5.18(5.39)		6.55(6.56)	8.06(8.28)
T13	6.06(6.05)	2.07(2.15)	2.68(2.51)	4.78(4.88)	6.57(7.43)	0.89(1.63)	14.09(13.87)		
C14	4.46(5.39)	2.04(2.07)	2.04(2.35)	4.67(4.83)	6.86(7.53)	4.60(5.72)		6.87(6.82)	7.75(8.57)
A15	5.68(5.98)	2.76(2.75)	2.76(2.88)	5.10(5.05)	8.14(8.20)	6.94(7.62)		6.37(-)	7.23(-)
G16	5.81(5.72)	2.61(2.49)	2.67(2.60)	4.87(4.95)	7.83(7.68)		12.01(12.86)		
C17	5.65(5.75)	1.86(1.87)	2.28(2.32)	4.81(4.79)	7.29(7.27)	5.30(5.34)		6.52(6.46)	8.25(8.36)
G18	6.09(6.16)	2.31(2.36)	2.60(2.60)	4.66(4.67)	7.89(7.92)				

TOTO11	Ring1	Ring2	TOTO11	Ring1	Ring2
H13	6.94	7.01	H8	6.18	6.14
H14	6.81	6.91	H9	6.49	6.53
H15	6.54	6.70	H10	8.01	7.92
H16	7.44	7.53	H19'	4.04	3.99
Me	3.58	3.58	H19''	4.54	4.54

Table 4S. Chemical shift values in ppm for the CTAAG-TOTO13 complex compared with those of

the free oligonucleotide in parentheses. The values are relative to DSS at 10°C.

	H1'	H2'	H2''	H6/H8	H5/H2/Me	H1/H3	H4	H4
C1	5.65(5.81)	1.87(1.98)	2.29(2.44)	7.55(7.64)	5.79(5.92)		(7.12)	(8.13)
G2	5.68(5.97)	2.36(2.72)	2.44(2.76)	7.76(7.99)		12.77(13.05)		
C3	6.01(5.97)	1.98(2.05)	2.58(2.50)	6.44(7.42)	6.44(5.39)		6.67(6.68)	7.95(8.30)
T4	4.98(5.64)	1.95(2.07)	2.12(2.40)	6.96(7.37)	0.84(1.69)	13.47(13.70)		
A5	5.42(5.86)	2.67(2.72)	2.71(2.87)	8.21(8.25)	(6.89)		(6.37)	(7.74)
A6	5.63(5.94)	2.63(2.62)	2.68(2.80)	8.09(8.06)	(7.43)		(6.06)	(7.57)
G7	5.75(5.71)	2.56(2.43)	2.63(2.61)	7.81(7.59)		12.03(12.82)		
C8	5.71(5.75)	1.87(1.88)	2.31(2.32)	7.29(7.29)	5.33(5.27)		6.47(6.53)	8.19(8.39)
G9	6.11(6.16)	2.34(2.36)	2.61(2.61)	7.91(7.92)			(7.12)	(8.13)
C10	5.65(5.81)	1.87(1.98)	2.29(2.44)	7.55(7.64)	5.79(5.92)			
G11	5.66(5.97)	2.36(2.72)	2.44(2.76)	7.76(7.99)		12.77(13.08)		
C12	5.98(6.04)	1.96(2.15)	2.53(2.58)	6.40(7.46)	6.42(5.39)		6.67(6.70)	7.95(8.23)
T13	4.68(6.04)	2.02(2.15)	2.40(2.58)	7.12(7.46)	0.79(1.65)	13.80(14.16)		
T14	4.95(5.68)	1.94(2.11)	2.03(2.44)	7.33(7.43)	1.57(1.74)	13.31(13.77)		
A15	5.65(6.01)	2.78(2.72)	2.78(2.87)	8.19(8.21)	(7.28)		(6.44)	(7.84)
G16	5.80(5.71)	2.58(2.49)	2.66(2.61)	7.85(7.68)		12.03(12.81)		
C17	5.71(5.75)	1.87(1.88)	2.31(2.32)	7.29(7.26)	5.33(5.32)		6.47(6.56)	8.19(8.39)
G18	6.11(6.16)	2.34(2.36)	2.61(2.61)	7.91(7.92)				

TOTO13	Ring1	Ring2	TOTO13	Ring1	Ring2
H13	7.00	6.97	H8	6.17	6.17
H14	6.88	6.82	H9	6.49	6.45
H15	6.72	6.64	H10	8.00	7.98
H16	7.49	7.46	H19'	3.94	3.97
Me	3.59	3.59	H19''	4.52	4.54

Generation and Characterization of an Anti-CD19 Single-Chain Fv Immunotoxin Composed of C-Terminal Disulfide-Linked dgRTA[†]

Duo Wang,[‡] Quanzhi Li,[‡] Wendy Hudson,[‡] Erica Berven,[‡] Fatih Uckun,[§] and John H. Kersey^{*,‡,||}

University of Minnesota Cancer Center, Biotherapy Institute, and Departments of Laboratory Medicine/Pathology and Pediatrics, University of Minnesota, Minneapolis, Minnesota 55455. Received May 9, 1997[®]

Our laboratory utilized two methods to produce the anti-CD19 immunotoxin containing a single-chain Fv (scFv) FVS191 and a ricin A chain (RTA). The first method produced the recombinant protein FVS191CDRTA from a fusing gene containing sequences encoding FVS191, cathepsin D proteinase digestion site (CD), and RTA. FVS191CDRTA did not show CD19 antigen binding and cytotoxic activity. The second method generated a disulfide-linked FVS191cys–dgRTA from a FVS191cys, the FVS191 with an additional C-terminal cysteine, and a deglycosylated RTA (dgRTA). The formation of FVS191cys–dgRTA is efficient; up to 70% of the proteins participating in the reaction had formed FVS191cys–dgRTA when the molar ratio of FVS191cys to dgRTA was 1:1. A competitive ELISA assay indicated that FVS191cys–dgRTA and the parental monoclonal antibody B43 possessed comparable CD19 binding abilities. The protein synthesis inhibition assay revealed that FVS191cys–dgRTA was toxic to CD19 positive cell lines, but it was less potent than the intact antibody-conjugated B43–dgRTA, which had an $IC_{50} = 2 \times 10^{-11}$ M. ¹²⁵I-labeled FVS191 and ¹²⁵I-labeled B43 were internalized by Nalm-6 cells at 37 °C as demonstrated by internalization studies; this result indicates that cross-linking of CD19 antigen is not required for the endocytosis of CD19 and raises the possibility that the lower cytotoxicity of FVS191cys–dgRTA is not due to the monovalent binding of CD19 by FVS191cys–dgRTA. Our study with anti-CD19 scFv immunotoxin indicates that the formation of a disulfide-linked scFv immunotoxin is an alternative to the recombinant method of producing scFv immunotoxin.

INTRODUCTION

Immunotoxins are cytotoxic molecules designed to eliminate populations of cells that display specific cell surface antigens or markers. An immunotoxin has two functional components: one is the binding domain, which targets the specific marker of a cell; the other is a toxin domain, which kills the target cell. The binding domains of immunotoxins can be a monoclonal antibody (mAb), Fab, F(ab')₂, Fv, or single-chain Fv (scFv). The popular toxic domains of immunotoxins include the ricin A chain (RTA), *Pseudomonas* exotoxin B chain (1–5), or diphtheria toxin A chain (6).

ScFv is a protein fragment composed of immunoglobulin heavy and light chain with a peptide linker connecting the heavy and light chain. A scFv-immunotoxin is a chimeric molecule containing a scFv and a toxin. There are two methods that can be used to generate a scFv immunotoxin. The conventional method is to produce a recombinant fusion protein by genetically linking a scFv gene with a toxin gene. Several scFv immunotoxins have been made using this method, such as B3-(Fv)-PE38KDEL (1, 2), e23(Fv)-PE38KDEL (3), antiTac-(Fv)-PE38 (4), and BR96 sFV-PE40 (5). All of these scFv immunotoxins have been shown to possess antitumor

activity *in vitro* and in animal models bearing human tumor xenografts. The second method of generating a scFv immunotoxin is to build a scFv with C-terminal cysteine and then covalently link the scFv-cys with a toxin through a disulfide bond (7).

The construction of anti-CD19 scFv immunotoxins using the above two methods is described in this paper. CD19, as a pan B-cell antigen, is an ideal target for immunotoxin therapy of B-lineage leukemia and lymphomas (8, 9). Our laboratory has previously constructed an anti-CD19 scFv, FVS191, from a hybridoma producing mAb B43 (10). FVS191cys, a FVS191 containing a C-terminal cysteine, has also been constructed (11). RTA inactivates the 60S ribosomal subunit of eukaryotic ribosomes and has been used for construction of anti-CD19 immunotoxins (12). The RTA gene has been cloned (13); the DNA sequence indicates that RTA has two cysteines. Therefore, RTA can be used to form both recombinant and disulfide-linked immunotoxins.

The recombinant anti-CD19 scFv immunotoxin we produced contained a cathepsin D cleavable peptide (CD) (14); therefore, this protein was named FVS191CDRTA. Deglycosylated ricin A chain (dgRTA) was used to form a disulfide bond with FVS191cys to generate FVS191cys–dgRTA. The characterization of these two proteins is also described in this paper.

MATERIALS AND METHODS

Construction of FVS191CDRTA. FVS191 had been previously cloned in our laboratory (10). To construct the FVS191CDRTA, a DNA fragment containing the sequences encoding cathepsin D proteinase sensitive peptide and RTA was inserted in frame at the 3' end of FVS191 in pFVS191. The nucleotide sequence encoding cathepsin D proteinase sensitive peptide is ACCTGT-TCTTCCTGAACCTGTTCTACCTGA; the RTA gene was

* Address correspondence to this author at Box 86 Mayo, 420 Delaware St. S.E., Minneapolis, MN 55455 [e-mail: kerse001@maroon.tc.umn.edu; telephone (612) 625-4659; fax (612) 624-3069].

[†] This work is supported in part by an Outstanding Investigator Grant Award to J.H.K. (CA 49721) from the National Cancer Institute.

[‡] University of Minnesota Cancer Center.

[§] Biotherapy Institute.

^{||} Departments of Laboratory Medicine/Pathology and Pediatrics.

[®] Abstract published in *Advance ACS Abstracts*, October 15, 1997.

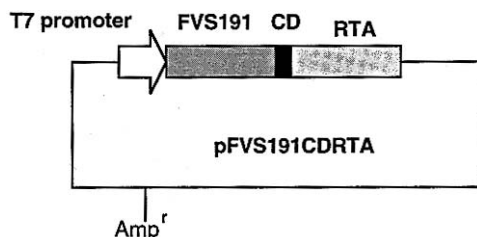


Figure 1. Gene structure of FVS191CDRTA. The fusion gene of FVS191CDRTA is composed of nucleic acids encoding FVS191, cathepsin D sensitive peptide, and RTA. The expression of FVS191CDRTA is under the T7 promoter. The expression vector is derived from pET3b (Novagen).

obtained from a genomic clone of ricin (13). The structure of the expression vector of pFVS191CDRTA is shown in Figure 1.

Production and Purification of FVS191CDRTA. pFVS191CDRTA plasmid DNA was transformed into *Escherichia coli* BL21(DE3) (Novagen, Madison, WI). The transformed bacterial cells were grown in SOB medium (20 g of tryptone, 5 g of yeast extract, 0.5 g of NaCl, 5 g of $\text{MgSO}_4 \cdot 7\text{H}_2\text{O}$, per liter) at 37 °C. When the absorbance of A_{600} of the bacterial culture reached 0.65, production of FVS191CDRTA was induced with 1 mM isopropyl β -D-thiogalactopyranoside (IPTG) for 1.5 h at 37 °C.

FVS191CDRTA was expressed in bacterial cells as inclusion bodies. The method used to isolate FVS191CDRTA inclusion bodies was the same as that described by Wang et al. (11). Briefly, the harvested cell pellets from the above cell culture were suspended in 50 mL of inclusion body separation (IBS) buffer (0.1 M KCl, 0.02 M Tris-HCl, 0.005 M EDTA, 0.1% Nonidet P-40, pH 8.0) by sonication. Lysozyme was added into the cell lysate to a final concentration of 0.2 mg/mL. After incubation at room temperature for 1 h, the cell lysate was frozen at -80 °C. When thawed at room temperature, the cell lysate was sonicated for 10 min and centrifuged at 17000g for 30 min at 4 °C. The pellets were suspended in 50 mL of IBS buffer and added with sodium deoxycholate to a final concentration of 2%. The mixture was stirred at room temperature for 1 h and then centrifuged at 17000g for 30 min at 4 °C. The inclusion bodies were washed with IBS buffer and water.

FVS191CDRTA was refolded according to the method of Buchner (15) with minor modifications. The inclusion bodies of FVS191CDRTA were dissolved in a denaturing buffer [0.1 M Tris, 6 M guanidine hydrochloride, 0.3 M dithioerythritol (DTE), 0.002 M EDTA, pH 8] at room temperature for 2 h. The insoluble materials were removed by centrifugation at 30000g for 30 min. The concentration of solubilized proteins was adjusted to 20 mg/mL with denaturing buffer. Renaturation of FVS191CDRTA was carried out by a rapid 100-fold dilution of the denatured protein into a refolding buffer (0.1 M Tris-HCl, 0.5 M L-arginine, 0.008 M GSSG, 0.002 M EDTA, pH 8) at 10 °C and an incubation at the same temperature for 48 h.

Other refolding methods were also used to refold FVS191CDRTA. Reduced FVS191CDRTA in the above denaturing buffer was dialyzed against phosphate-buffered saline (PBS) buffer containing 0.4 M L-arginine (PBS-arginine buffer) or a buffer composed of 20 mM Tris and 100 mM urea, pH 7.4 (Tris-urea buffer).

After refolding, FVS191CDRTA was dialyzed against PBS to eliminate redox agents and concentrated by ultrafiltration using a YM10 membrane (Amicon, Beverly, MA). The final product of FVS191CDRTA was purified by FPLC using a Superdex 75 (HiLoad 60) column (Pharmacia).

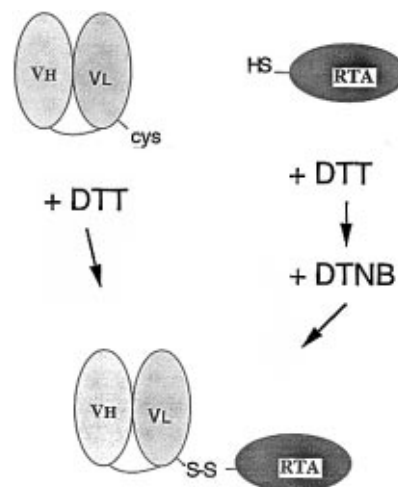


Figure 2. Schematic diagram of the formation of disulfide-linked FVS191cys-dgRTA. DgRTA was reduced with DTT and treated with DTNB prior to conjugation with DTT-treated FVS191cys.

Preparation of FVS191cys-dgRTA. The construction and production of FVS191cys have been described previously (11). The dgRTA was purchased from Inland Laboratory (Austin, TX). Prior to conjugation, dgRTA was buffer exchanged with PBS by dialysis.

A schematic representation of forming disulfide-linked FVS191cys-dgRTA is shown in Figure 2. DgRTA (2 mg/mL) was reduced with 2 mM dithiothreitol (DTT) for 1 h at room temperature and then separated from DTT using a PD10 column (Pharmacia). The DTT-treated dgRTA was immediately reacted with a $1/10$ volume of 25 mM 5,5'-dithiobis(2-nitrobenzoic acid) (DTNB) in phosphate buffer (0.12 M K_2HPO_4 , pH 7.2) at room temperature for 1 h. The DTNB-derivatized dgRTA was then isolated using a PD10 column. At the same time, FVS191cys in PBS buffer was reacted with 2 mM DTT at room temperature for 1 h. After the DTT had been removed by a PD10 column, FVS191cys was reacted with DTNB-derivatized dgRTA at a molar ratio of 1:1 or 1:2. The conjugation was performed at room temperature for 2 h and at 4 °C overnight. The conjugation products were analyzed by a nonreducing SDS-PAGE and kept at 4 °C.

The free sulfhydryl groups of DTT-treated FVS191cys were quantified using DTNB. After DTT-treated FVS191cys had been reacted with 25 mM DTNB in phosphate buffer (0.12 M K_2HPO_4 , pH 7.2) at room temperature for 15 min, the absorbance at 412 nm was measured using a spectrophotometer. The molar concentration of the free sulfhydryl group (C) was calculated according to the equation $C = \text{absorbance}/14150$ (mol/L) (16). The molar concentration of FVS191cys was determined according to the absorbance of FVS191cys at 280 nm.

Preparation of B43-dgRTA. B43 was conjugated to dgRTA by the chemical cross-linker *N*-succinimidyl-3-(2-pyridyldithio)propionate (SPDP, Pierce) using the method of Ghetie et al. (17) with minor modifications. Five milligrams of B43 mAb in 2 mL of conjugation buffer (0.05 M borate acid, 0.3 M NaCl, 0.5% butanol, pH 9.0) was reacted with 30 μL of SPDP (6 mg/mL, in diethylformamide) at room temperature for 30 min. The derivatized B43 was separated from SPDP using a PD10 column (Pharmacia) and dissolved in 2 mL of phosphate buffer (0.1 M sodium phosphate, 0.15 M NaCl, 0.005 M EDTA, pH 6.5). DgRTA in phosphate buffer was incu-

bated with the derivatized B43 at room temperature for 1 h and at 4 °C overnight. The molar ratio of dgRTA to B43 in the reaction was 1:1. After conjugation, free dgRTA was removed by FPLC using a Superdex 75 column (Pharmacia) at a flow rate of 0.5 mL/min. The conjugated B43–dgRTA was separated from free B43 by an open column affinity chromatography. Briefly, Blue Sepharose gel (Supelco Separation Technology, Bellefonte, PA) was packed in a 1 × 20 cm column according to the packing manual of TSK-Gel Toyopearl column. The blue gel column was equilibrated with 50 mL of sodium phosphate buffer (50 mM, pH 7.5) at a flow rate of 2 mL/min. Protein samples were passed through the Blue Sepharose column at a flow rate of 0.3 mL/min. The unconjugated B43 passed through the column; B43–dgRTA, which bound to the column, was eluted with a buffer (0.05 M sodium phosphate, 0.5 M NaCl, pH 7.5) described by Knowles and Thorpe (18).

ELISA Assay. B43 was conjugated to alkaline phosphatase (AP) using a commercial conjugation kit (Pierce, Rockford, IL). The conjugated B43–AP was used directly without further purification. The CD19 antigens used in the ELISA were isolated from CD19 positive Daudi cells using the methods of Siegall et al. (19). The optimal concentrations of CD19 antigen and B43–AP for the ELISA assay were determined by a series of experiments. Before the ELISA assay, the isolated CD19+ membrane proteins (80 µg/mL in H₂O, 50 µL/well) were coated in ELISA plates (Immuron 4, Dynatech Laboratories Inc., Chantilly, VA). These plates were dried in a vacuum desiccator at 4 °C overnight and washed three times with PBS. During the ELISA assay, various amounts of competing proteins (FVS191CDRTA, FVS191cys–dgRTA, or B43 mAb) and a fixed amount of B43–AP were incubated inside the coated plates at room temperature for 1 h. The final dilution of B43–AP in the reaction was 1:2000. The plates were washed four times with PBS before incubation with 100 µL of substrate solution for alkaline phosphatase at 4 °C overnight. The optical density of each reaction well was measured at 405 nm using an ELISA reader.

Cytotoxicity Assay. Blin-1 or Nalm-6 cells were prepared to a final density of 1 × 10⁶ cells/mL in RPMI 1640 medium containing 10% (w/v) fetal bovine serum (FBS), 1% L-glutamine, 1% penicillin/streptomycin, and 20 mM NH₄Cl. One hundred microliters of the cells, along with 50 µL of immunotoxins diluted in the same medium, was plated into wells of the 96-well microtiter plates. The assay was performed in triplicate. After incubation at 37 °C for 48 h in an atmosphere of 5% CO₂, the cells were pulsed with 1 µCi of [³H]leucine (Amersham, Life Science) in 50 µL of the medium for 4 h at 37 °C and frozen at –80 °C. After thawing, the cells were harvested onto GF/F glass microfiber filters (Whatman). Radioactivity was measured using a β scintillation counter (Beckman Instrument). The [³H]leucine incorporation of immunotoxin-treated cells was compared with that of nontreated cells to determine the percent of protein synthesis.

Internalization Assay. FVS191 and B43 mAb were labeled with Na¹²⁵I (New England Nuclear, Boston, MA) using the Iodo-Beads method (Pierce). Nalm-6, in RPMI 1640 medium supplemented with 10% FBS, was used in this assay. Ten micrograms of ¹²⁵I-labeled FVS191 or 10 µg of ¹²⁵I-labeled B43, with specific activity ~5–7 µCi/µg, was incubated with 1 × 10⁸ Nalm-6 cells (5 mL) on ice for 1 h. After incubation, the cells were washed four times with cold, serum-free RPMI 1640 and then suspended in warm RPMI 1640 plus 10% FBS at 0.5 to 1.0 × 10⁸ cells/mL. Aliquots of 5 × 10⁶ cells were transferred to 1 mL sterile test tubes and incubated at 37 °C in a

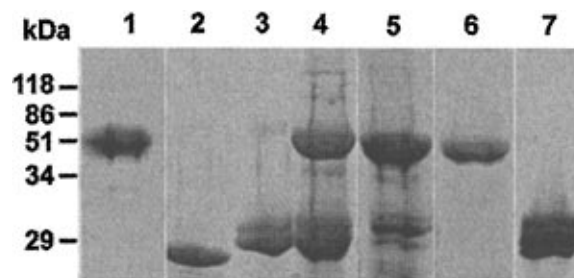


Figure 3. Formation and purification of FVS191CDRTA and FVS191cys–dgRTA. Protein samples were analyzed by a 12% nonreducing SDS–PAGE and visualized by Coomassie blue stain: (lane 1) FVS191CDRTA purified by gel filtration chromatography; (lane 2) FVS191cys used in the chemical conjugation with dgRTA; (lane 3) dgRTA; (lane 4) conjugation products when FVS191cys:dgRTA ratio is 1:2; (lane 5) conjugation products when FVS191cys:dgRTA ratio is 1:1; (lane 6) FVS191cys–dgRTA purified by gel filtration FPLC; (lane 7) DTT-reduced products of FVS191cys–dgRTA. The positions of molecular weight markers are labeled at the left side of the gel.

tissue culture incubator for various time intervals. At each time point, the samples were analyzed for the percents of cell-surface-bound, dissociated, internalized, and degraded FVS191 (or B43), on the basis of a total cell-associated radioactivity at time 0 according to the methods of Press et al. (20). The nonspecific binding of ¹²⁵I-labeled FVS191 or ¹²⁵I-labeled B43 was assessed by incubating the ¹²⁵I-labeled proteins with B43-blocked Nalm-6 cells.

RESULTS

Production of FVS191CDRTA, FVS191cys–dgRTA, and B43–dgRTA. FVS191CDRTA was produced in *E. coli* as inclusion bodies. The optimal amount of FVS191CDRTA was observed when FVS191CDRTA was refolded in buffer containing GSSG. When FVS191CDRTA was refolded in PBS–arginine or Tris–urea buffer, the majority of the protein aggregated; these refolding approaches were not used in future experiments. After the refolding process in GSSG buffer, aggregated FVS191CDRTA was separated; soluble FVS191CDRTA was purified by gel filtration chromatography and examined by SDS–PAGE. The purity of FVS191CDRTA is shown in Figure 3, lane 1.

Figure 3, lane 2, shows the refolded-FVS191cys used to form FVS191cys–dgRTA. Prior to chemical conjugation, the number of DTT-reduced cysteine per FVS191cys was examined. When the concentration of DTT-treated FVS191cys was 3.8×10^{-6} M, the absorbance of DTNB-derivatized FVS191cys was 0.045. According to the formula given under Materials and Methods, the concentration of free sulfhydryl group was 3.1×10^{-6} M; therefore, the ratio of FVS191cys concentration to free sulfhydryl concentration is about 1:1. This result indicated that there was only one cysteine per FVS191cys that had been reduced by DTT.

The formation of FVS191cys–dgRTA was demonstrated by a nonreducing SDS–PAGE. When FVS191cys (Figure 3, lane 2) was reacted with dgRTA (Figure 3, lane 3), a 58 kDa protein (Figure 3, lanes 4 and 5) was formed. When this 58 kDa protein was treated with DTT, it was separated into smaller proteins with the corresponding sizes of FVS191cys and dgRTA (Figure 3, lane 7). This 58 kDa protein is, therefore, the disulfide-linked FVS191cys–dgRTA.

The observed 58 kDa protein (Figure 3, lanes 4 and 5) is not the dimeric dgRTA or the dimeric FVS191cys. The formation of dimeric dgRTA had been prevented by derivatizing dgRTA with DTNB prior to chemical conju-

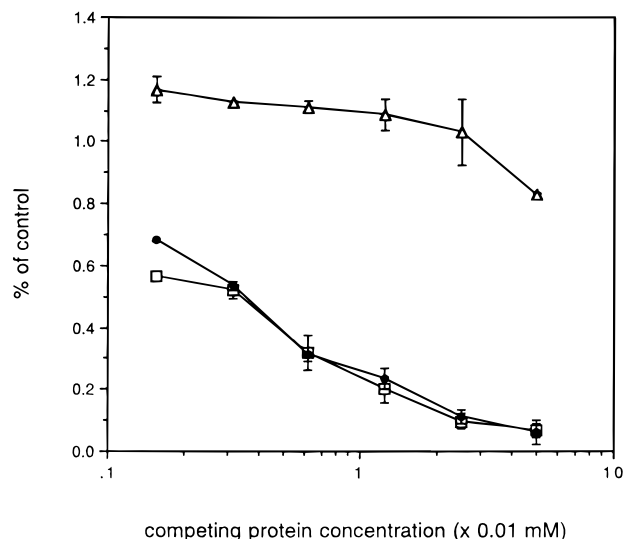


Figure 4. Competitive ELISA to compare the CD19 binding ability of FVS191CDRTA, FVS191cys-dgRTA, and B43. Various amounts of FVS191CDRTA, FVS191cys-dgRTA, and B43 along with a fixed amount of B43-AP were incubated with CD19 antigens. The means of percentage activity of alkaline phosphatase associated with B43-AP were plotted against log molar concentrations of FVS191CDRTA (Δ), FVS191cys-dgRTA (\bullet), and B43 (\square).

gation. Under the conjugation condition, the formation of dimeric FVS191cys was slow (11); it could not compete with the formation of FVS191cys-dgRTA.

The maximum yield of FVS191cys-dgRTA was reached when equal moles of FVS191cys and dgRTA FVS191cys were used in the conjugation. When the mole ratio of FVS191cys to RTA was 1:2, the yield of FVS191cys-dgRTA was ~40% as estimated by a densitometer (Figure 3, lane 4). When that ratio was 1:1, ~70% of proteins formed FVS191cys-dgRTA (Figure 3, lane 5).

FVS191cys-dgRTA was separated from FVS191cys and dgRTA by a gel filtration chromatography. The purity of isolated FVS191cys-dgRTA is demonstrated by Figure 3, lane 6; no FVS191cys or dgRTA was detected.

The formation of covalently linked B43-dgRTA was confirmed by a nonreducing SDS-PAGE (data not shown). After purification by a gel filtration and affinity chromatography, >90% B43-dgRTA was found to have been conjugated with one dgRTA (data not shown).

CD19 Binding of FVS191CDRTA and FVS191cys-dgRTA. The CD19 binding activities of FVS191CDRTA, FVS191cys-dgRTA, and B43 were indicated by the relative activities of B43-AP in ELISA (Figure 4). FVS191cys-dgRTA ($IC_{50} = 1.33 \times 10^{-9}$ M) had a similar CD19 binding ability with B43 ($IC_{50} = 1.3 \times 10^{-9}$ M). FVS191CDRTA did not bind CD19 as indicated by the lack of inhibition of the activity of B43-AP; this result suggested that FVS191CDRTA was not properly refolded.

Cytotoxic Activities of FVS191CDRTA, FVS191cys-dgRTA, and B43-dgRTA. FVS191CDRTA did not show cytotoxic activity to CD19⁺ Blin-1 and Nalm-6 cells as shown by Figure 5. To further evaluate the lack of activity of FVS191CDRTA, a cell-free transcription and translation system of rabbit reticulocyte lysates (Promega) was used. The results showed no evidence of catalytic activity of RTA in the reticulocyte lysates system (data not shown).

However, FVS191cys-dgRTA inhibited protein synthesis of Blin-1 ($IC_{50} = 1.3 \times 10^{-9}$ M) and Nalm-6 cells ($IC_{50} = 1.0 \times 10^{-9}$ M) as shown by Figure 6. With the same cell lines, dgRTA ($IC_{50} > 1 \times 10^{-7}$ M) is 100-fold

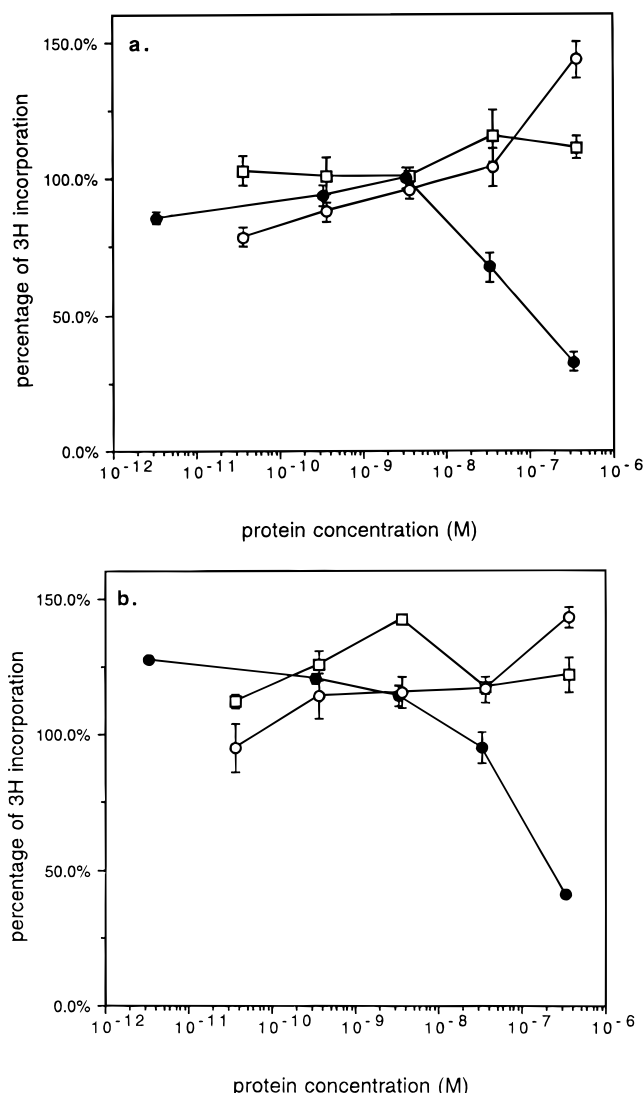


Figure 5. Protein synthesis inhibition assay of FVS191-CDRTA: (a) Blin-1 cells and (b) Nalm-6 cells; FVS191CDRTA (\square), FVS191 (\circ), and dgRTA (\bullet). The percentage of [3 H]leucine incorporation was calculated using the immunotoxin-untreated cells as controls. Data were based on either duplicate or triplicate experiments. The standard deviation is indicated by the vertical bar.

less toxic than FVS191cys-dgRTA. FVS191cys, however, did not show any cytotoxic activity to Blin-1 and Nalm-6.

B43-dgRTA was also potent to Blin-1 ($IC_{50} = 2 \times 10^{-11}$ M) and Nalm-6 ($IC_{50} = 3 \times 10^{-11}$ M) (Figure 7). B43 alone was not cytotoxic to the above two cell lines.

Internalization of FVS191 and B43 by Nalm-6 Cells. Both FVS191 and B43 were internalized by CD19 positive Nalm-6 cells as shown by Figure 8. The internalizations of B43 occurred in the first hour of incubation, and the amount of internalized FVS191 increased from time 0 to the fourth hour of incubation.

DISCUSSION

In this study, we have constructed and compared two different kinds of anti-CD19 scFv immunotoxins: FVS191CDRTA and FVS191cys-dgRTA. The disulfide-linked FVS191cys-dgRTA, but not the FVS191CDRTA, was cytotoxic to CD19 positive cells. The results demonstrating that FVS191CDRTA did not bind to CD19 positive cells and did not inactivate translation in a cell-free transcription and translation system strongly sug-

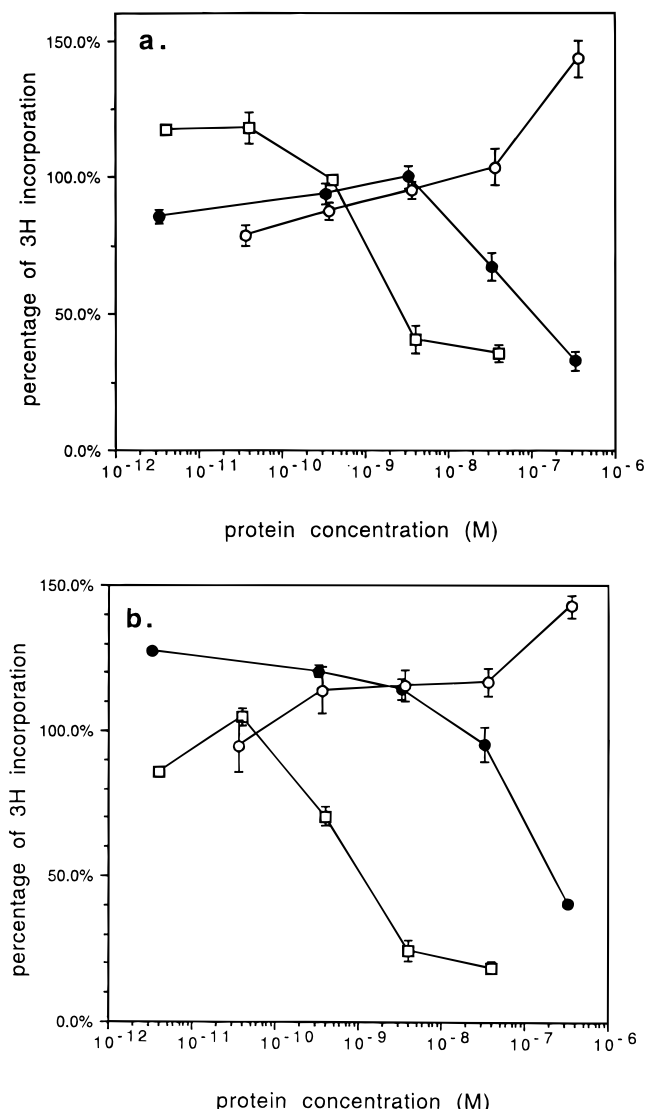


Figure 6. Protein synthesis inhibition assay of FVS191cys-dgRTA: (a) Blin-1 cells and (b) Nalm-6 cells; FVS191cys-dgRTA (□), FVS191 (○), and dgRTA (●). The percentage of [³H]leucine incorporation was calculated using the immunotoxin-untreated cells as standards. Data were based on either duplicate or triplicate experiments. The standard deviation is indicated by the vertical bar.

gest that FVS191CDRTA was not correctly refolded. It is not clear why FVS191CDRTA could not be refolded with the method used in this study; the amino acid sequence, the size, and the chimeric nature of FVS191CDRTA may contribute to the difficulty of refolding.

In comparison to FVS191CDRTA, FVS191cys-dgRTA was produced using the refolded FVS191cys; therefore, the formation of FVS191cys-dgRTA avoids the difficulty of renaturation of the whole immunotoxin. The chemical conjugation provides an alternate method when a recombinant scFv immunotoxin cannot be refolded or when the yield of a recombinant scFv immunotoxin is extremely low.

Our study shows that disulfide-linked scFv immunotoxin can be produced relatively efficiently; ~70% of FVS191cys and dgRTA can form FVS191cys-dgRTA. The yield of refolded FVS191cys from 1 L of cell culture is from 1 to 0.5 mg using the method described in this study. The amount of FVS191cys may limit the large-scale production of FVS191cys-dgRTA. One way to increase the yield of FVS191cys could be to express

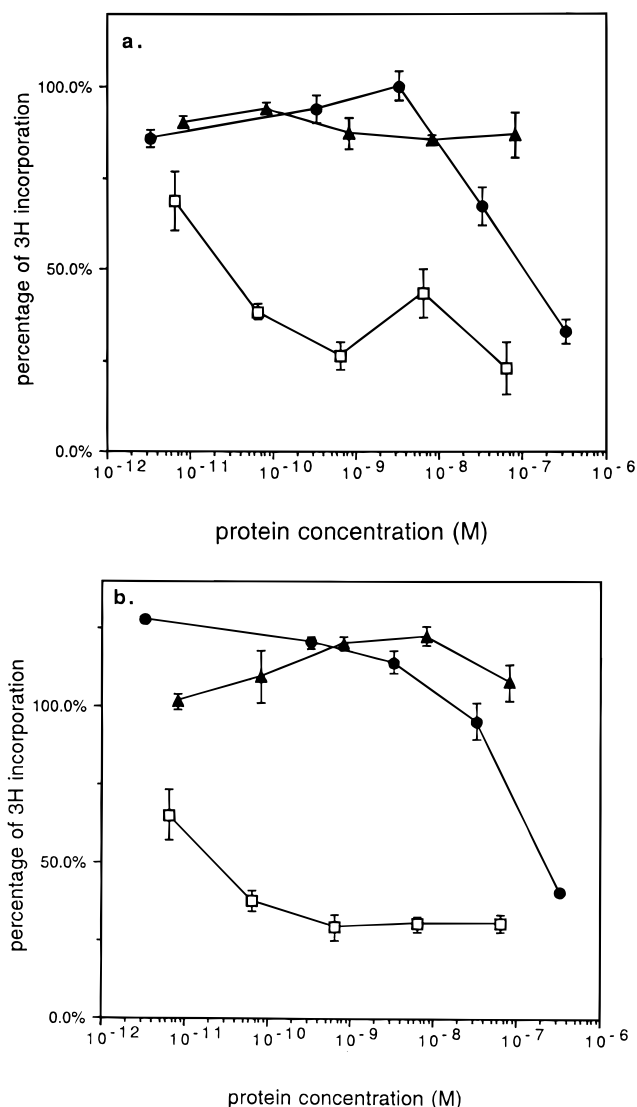


Figure 7. Protein synthesis inhibition assay of B43-dgRTA: (a) Blin-1 cells and (b) Nalm-6 cells; B43-dgRTA (□), B43 (▲), and dgRTA (●). The percentage of [³H]leucine incorporation was calculated using the immunotoxin-untreated cells as controls. Data were based on either duplicate or triplicate experiments. The standard deviation is indicated by the vertical bar.

FVS191cys in the methylotrophic yeast *Pichia pastoris* (21). An anti-CD7 scFvcys fragment, 3A1F, has been reportedly produced (60 mg/L) in *P. pastoris* (22).

The disulfide-linked scFv immunotoxins are homogeneous and smaller in size compared with intact antibody-conjugated immunotoxin. The conjugation of FVS191cys to dgRTA is one to one, unlike the antibody-conjugated molecules which may have more than one dgRTA. FVS191cys-dgRTA is only one-third of the size of B43-dgRTA; thus, it may penetrate tumor tissue better (23–26).

FVS191cys-dgRTA has a lower cytotoxic activity than B43-dgRTA. Several variables can influence the potency of an immunotoxin, such as the affinity of the immunotoxin to the target, the epitope on the target antigen recognized by the immunotoxin, the rate of endocytosis, and intracellular routing of the immunotoxin (27). The ELISA and internalization assay described in this paper were carried out to identify the factors influencing the cytotoxicity of FVS191cys-dgRTA. The ELISA result reveals no differences of CD19-binding ability between FVS191cys-dgRTA and B43 (Figure 4). This indicates that the addition of a disulfide bond to FVS191cys does

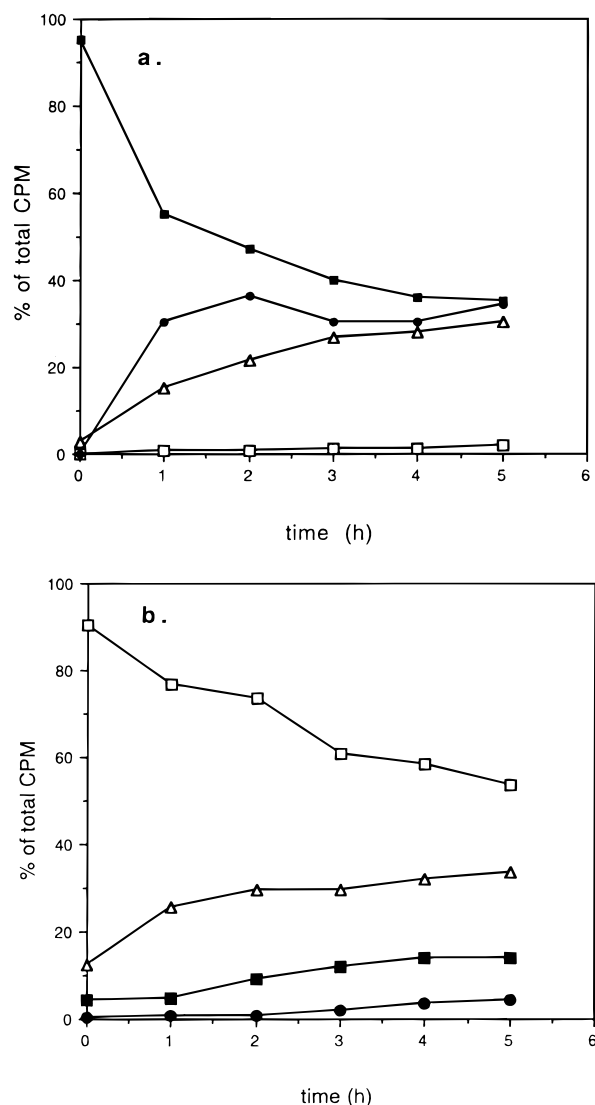


Figure 8. Internalization assay: (a) internalization of ^{125}I -labeled FVS191 by Nalm-6 [the percentage radioactivities associated with cell-surface bound FVS191 (■), internalized FVS191 (△), dissociated FVS191 (●), and degraded FVS191 (□) were calculated on the bases of total CPM at each time point]; (b) internalization of ^{125}I -labeled B43 by Nalm-6 cells [the percentage radioactivities associated with cell-surface bound B43 (■), internalized B43 (△), dissociated B43 (●), and degraded B43 (□) were calculated on the bases of total CPM at each time point and plotted against each time point].

not interfere with its antigen-binding activity. The internalization studies of FVS191 and B43 demonstrated that both FVS191 and B43 were internalized by Nalm-6, although the internalization patterns were slightly different. This result suggests that cross-linking of CD19 is not required for CD19 endocytosis. The extent of internalization of FVS191cys-dgRTA needs further study.

A study of anti-CD22-ricin A immunotoxin conducted by Horssen et al. (28) demonstrates that the cytotoxicity of CD22-ricin A depends on intracellular routing rather than on the number of internalized molecules. Another study conducted by May et al. (27) also reveals that intracellular routing rather than cross-linking or rate of internalization determines the potency of immunotoxins directed against different epitopes of sIgD on murine B cells. These studies suggest that intracellular routing is an important factor in determining the potency of an internalized immunotoxin. It is very likely that the discrepancy in cytotoxic activities between FVS191cys-

dgRTA and B43-dgRTA is due to their differences in intracellular routing.

The efficacy of an immunotoxin *in vivo* is a combination of several effects, such as the stability and the tumor penetration ability of an immunotoxin. Whether FVS191cys-dgRTA will have an efficacy *in vivo* needs to be studied further.

In summary, we compared two different methods to generate scFv immunotoxin and demonstrated that the formation of a disulfide-linked protein is an effective approach to produce anti-CD19 scFv immunotoxin. To our knowledge, FVS191cys-dgRTA is the first anti-CD19 scFv immunotoxin showing cytotoxic activity. However, more work is necessary to develop anti-CD19 scFv immunotoxins with improved cytotoxicity. One possible approach is the development of an immunotoxin made of dimeric scFv. An immunotoxin with dimeric scFv potentially retains the advantages of bivalent binding to antigen and a smaller size in comparison to intact antibody immunotoxin; the reduced size of an immunotoxin should enhance its tumor penetration.

LITERATURE CITED

- Brinkmann, U., Pai, L. H., FitzGerald, D. J., Willingham, M., and Pastan, I. (1991) B3(Fv)-PE38KDEL, a single-chain immunotoxin that causes complete regression of a human carcinoma in mice. *Proc. Natl. Acad. Sci. U.S.A.* **88**, 8616-8620.
- Seetharam, S., Chaudhary, V. K., FitzGerald, D., and Pastan, I. (1991) Increased cytotoxic activity of *Pseudomonas* exotoxin and two chimeric toxins ending in KDEL. *J. Biol. Chem.* **266** (26), 17376-17381.
- Batra, J. K., Kasprzyk, P. G., Bird, R. E., Pastan, I., and King, R. C. (1992) Recombinant anti-erbB2 immunotoxins containing *Pseudomonas* exotoxin. *Proc. Natl. Acad. Sci. U.S.A.* **89** (13), 5867-5871.
- Chaudhary, V. K., Queen, C., Junghans, J. P., Waldmann, T. A., FitzGerald, D. J., and Pastan, I. (1989) A recombinant immunotoxin consisting of two antibody variable domains fused to *Pseudomonas* exotoxin. *Nature (London)* **339**, 394-393.
- Friedman, P. N., McAndrew, S. J., Gawlak, S. L., Chance, D., Trail, P. A., Brown, J. P., and Siegall, C. B. (1993) BR96 sFv-PE40, a potent single-chain immunotoxin that selectively kills carcinoma cells. *Cancer Res.* **53**, 334-339.
- Chaudhary, V. K., Gallo, M. G., FitzGerald, D. J., and Pastan, I. (1990) A recombinant single-chain immunotoxin composed of anti-Tac variable regions and a truncated diphtheria toxin. *Proc. Natl. Acad. Sci. U.S.A.* **87**, 9491-9494.
- Pauza, M. E., Doumbia, S. O., and Pennell, C. A. (1997) Construction and characterization of human CD7-specific single chain Fv-immunotoxins. *J. Immunol.* **158**, 3259-3269.
- Ling, N. R., MacLennan, and Mason, D. T. (1987) B-cell and plasma cell antigens: new and previously defined clusters Leucocyte Typing III. *White Cell Differentiation Antigens* (A. J. McMichael, Ed.) pp 302-335, Oxford University Press, Oxford, U.K.
- Scheuerman, R. H., and Racila, E. (1995) CD19 antigen in leukemia and lymphoma diagnosis and immunotherapy. *Leukemia Lymphoma* **18**, 140-151.
- Becjek, B., Wang, D., Berven, E., Pennell, C. A., Peiper, S. C., Poppema, S., Uckun, F. M., and Kersey, J. H. (1995) Development and characterization of three recombinant single chain antibody fragments (scFv) directed against the CD19 antigen. *Cancer Res.* **55**, 2346-2351.
- Wang, D., Berven, E., Li, Q., Uckun, F., and Kersey, J. H. (1997) Optimization of conditions for formation and analysis of anti-CD19 FVS191 single-chain Fv homodimers (scFv)₂. *Bioconjugate Chem.* **8** (1), 64-70.
- Conry, R. M., Khazaeli, M. B., Saleh, M. N., Ghetie, V., Vitetta, E. S., Liu, T., and LoBuglio, A. F. (1996) Phase I trial of an anti-CD19 deglycosylated ricin A chain immunotoxin

- in non-Hodgkin's lymphoma: Effect of an intensive schedule of administration. *J. Immunother.* 18 (4), 231–241.
- (13) Halling, R. C., Halling, A. C., Murray, E. E., Ladin, B. F., Houston, L. L., and Weaver, R. F. (1985) Genomic cloning and characterization of a ricin gene from *Ricinus communis*. *Nucleic Acid Res.* 13 (22), 8019–8033.
- (14) Lojda, Z., Smidova, J., Barth, A., and Ueberberg, H. (1988) Are Z-Arg-Gly-Phe-Phe-Leu-MNA and Z-Arg-Gly-Phe-Phe-pro-MNA suitable substrates for the demonstration of cathepsin D activity? *Histochemistry* 88, 505–512.
- (15) Buchner, J., Pastan, I., and Brinkman, U. (1992) A method for increasing the yield of properly refolded fusion proteins: single-chain immunotoxins renaturation of bacterial inclusion bodies. *Anal. Biochem.* 205, 263–270.
- (16) Kuwata, K., Uebori, M., Yamada, K., and Yamazaki, Y. (1982) Liquid chromatographic determination of alkylthiols via derivatization with 5,5'-dithiobis(2-nitrobenzoic acid). *Anal. Chem.* 54, 1082–1087.
- (17) Ghetie, M. A., May, R. D., and Till, M. (1988) Evaluation of ricin A chain containing immunotoxins directed against CD19 and CD22 antigens on normal and malignant human B cells as potential reagents for *in vivo* therapy. *Cancer Res.* 48, 2610–2617.
- (18) Knowes, P. P., and Thorpe, P. E. (1987) Purification of immunotoxins containing ricin A chain and abrin A chain using blue sepharose CL-6B. *Anal. Biochem.* 160, 440–443.
- (19) Siegall, C. B., Chace, D., Mixan, B., Garrigues, U., Wan, H., Paul, L., Wolff, E., Hellstrom, I., and Hellstrom, K. E. (1994) *In vitro* and *in vivo* characterization of BR96 scFv-PE40. *J. Immunol.* 152 (2), 2376–2484.
- (20) Press, O. W., Farr, A. G., Borroz, K. I., Anderson, K. A., and Martin, P. J. (1989) Endocytosis and degradation of monoclonal antibodies targeting human B-cell malignancies. *Cancer Res.* 49, 4906–4949.
- (21) Cregg, J. M., Vedvick, T. S., and Raschke, W. C. (1993) Recent advances in the expression of foreign genes in *Pichia pastoris*. *Bio/Technology* 11, 905.
- (22) Eldin, P., Pauza, M. E., Hieda, Y., Lin, G., Murtaugh, M. P., Pentel, P. R., and Pennell, C. A. (1997) High-level secretion of two antibody single chain Fv fragments by *Pichia pastoris*. *J. Immunol. Methods* 201, 67–75.
- (23) Jain, R. K. (1989) Delivery of novel therapeutic agents in tumors: physiological barriers and strategies. *J. Natl. Cancer Inst.* 81, 570–576.
- (24) Fujimori, K., Covell, D. J., Fletcher, J. E., and Weinstein, J. N. (1989) Modeling analysis of the global and microscopic distribution of immunoglobulin G1, F(ab')₂, and Fab in tumors. *Cancer Res.* 49, 5656–5663.
- (25) Sung, C., Youle, R. J., and Dedrick, R. L. (1990) Pharmacokinetic analysis of immunotoxin uptake in solid tumors: role of plasma kinetics, capillary, permeability, and binding. *Cancer Res.* 46, 3960–3978.
- (26) Covell, D. G., Barbet, J., Holton, O. D., Black, C. D., and Parker, R. J. (1986) Pharmacokinetics of monoclonal immunoglobulin G1, F(ab')₂, and Fab in mice. *Cancer Res.* 46, 3969–3978.
- (27) May, R. D., Wheeler, H. T., Finkelman, F. D., Uhr, J. W., and Vitetta, E. S. (1991) Intracellular routing rather than cross-linking or rate of internalization determines the potency of immunotoxins directed against different epitopes of sIgD on murine B cells. *Cell. Immunol.* 135, 490–500.
- (28) Horssen, P. J. V., Van Oosterhout, Y. V., Witte, D. E., and Preijers, F. W. M. B. (1995) Cytotoxic potency of CD22-ricin A depends on internalized molecules. *Scand. J. Immunol.* 41, 563–569.

BC970071W

Libraries of Multifunctional RNA Conjugates for the Selection of New RNA Catalysts

Felix Hausch and Andres Jäschke*

Institut für Biochemie, Freie Universität Berlin, Thielallee 63, 14195 Berlin, Germany. Received June 20, 1997[®]

An *in vitro* selection system was developed for the selection of RNA molecules catalyzing bimolecular reactions between small reactants. The system is based on the direct selection protocol and involves libraries of multifunctional RNA conjugates rather than unmodified RNA transcripts. For the preparation of RNA conjugate libraries, a dinucleotide analog has been designed and synthesized containing a poly(ethylene glycol) linker with an embedded photocleavage site and a terminal attachment site for coupling potential reactants. Reactants are first coupled to the dinucleotide analog by activated ester chemistry and then ligated to the 3'-ends of enzymatically prepared RNA pool molecules, giving libraries of complex conjugates. Species that become attached to biotin on incubation with a biotinylated partner are isolated using streptavidin-derivatized matrices and then subjected to a photocleavage step. Selective cleavage of the linker releases only those RNA species in which reaction has taken place at the linker-coupled reactant, while products with the biotin attached to internal positions of the RNA part remain immobilized. Efficient photocleavage is achieved by laser irradiation at 355 nm, and the released RNAs are intact and amplifiable by reverse transcription. All steps are shown to be compatible with the overall selection procedure, as was shown by performing a model selection cycle. Besides allowing a broader scope of reaction types to be selected for, the strategy relieves the RNA from the requirement to possess substrate properties as well as catalytic activity, and the use of a cleavable linker will suppress the selection of catalysts for side reactions.

INTRODUCTION

Combinatorial RNA¹ libraries have found increasing use for the identification of new ligands and catalysts (Gold et al., 1995; Lorsch and Szostak, 1996). In the most basic versions of *in vitro* selection or SELEX (for Systematic Evolution of Ligands by EXponential enrichment) (Ellington and Szostak, 1990; Tuerk and Gold, 1990), a pool of RNA sequence variants is subjected to a selection (or partitioning) step, and the selected molecules are copied and enzymatically amplified. The ability to iterate the selection amplification cycle ideally allows the isolation of the most active sequences, even when they are exceedingly rare in the initial pool or when they have only a small advantage over competitors. This iterative procedure is possible only because nucleic acids can be copied enzymatically and is not available for organic small-molecule libraries and chemically synthesized peptide or carbohydrate libraries. Due to this property, recursive deconvolution, tagging, or binary coding is unnecessary, and the complexity of libraries used in SELEX experiments is great compared to other classes of compounds.

* Author to whom correspondence should be addressed [telephone (49) 30 838 6023; fax (49) 30 838 6413; e-mail jäschke@chemie.fu-berlin.de].

[®] Abstract published in *Advance ACS Abstracts*, October 15, 1997.

¹ Abbreviations: BSA, bovine serum albumine; cDNA, copy-DNA; CPG, controlled pore glass; DNA, deoxyribonucleic acid; DMF, *N,N*-dimethylformamide; DMSO, dimethyl sulfoxide; DMT, 4,4'-dimethoxytrityl; dNTPs, deoxyribonucleoside 5'-triphosphates; DTT, dithiothreitol; HEPES, *N*-(2-hydroxyethyl)-piperazine-*N'*-(2-ethanesulfonic acid); MALDI-TOF, matrix-assisted laser desorption/ionization time-of-flight (mass spectrometry); NTPs, (ribo)nucleoside 5'-triphosphates; PCR, polymerase chain reaction; PEG, poly(ethylene glycol); RNA, ribonucleic acid; RT-PCR, reverse transcription-polymerase chain reaction; SELEX, Systematic Evolution of Ligands by EXponential enrichment; TBDMS, *tert*-butyldimethylsilyl; Tris, tris(hydroxymethyl)aminomethane.

The most successful strategy for the isolation of RNA molecules with catalytic properties is direct selection. This process requires that the desired reaction be configured so that the catalytic molecules are themselves changed in a way that provides a basis for their enrichment during the selection step (Williams and Bartel, 1996). Selection criterion is ideally the catalysis of a chemical reaction. However, as a catalyst is per definition required to leave the reaction unchanged, catalysis must be coupled with some other principle that leads to a selectable change in the catalyst molecule, and the way this is achieved is self-modification, letting one and the same molecule act as both catalyst and substrate. The principle is illustrated in Figure 1a. A synthetic combinatorial RNA pool (typical complexity 10^{13} – 10^{16} different species) is incubated with a potential reactant that carries an anchor group, which is either a specific functional group (e.g., thiol, thiophosphate, primary aliphatic amine) or an affinity tag (e.g., biotin). Some RNA molecules react and are then covalently linked to that anchor group. These species can be specifically separated from the unreacted excess RNA using suitably derivatized solid supports (e.g., activated thiopropyl agarose or streptavidin agarose). The isolated species are then enzymatically amplified, and the scheme is repeated several times. This strategy has been successfully applied to the identification of RNA catalysts for ligation, alkylation, acylation, transesterification, and phosphorylation reactions (Bartel and Szostak, 1993; Illangasekare et al., 1995; Lorsch and Szostak, 1994; Wilson and Szostak, 1995).

Despite the success of direct selection, however, there are several drawbacks that severely limit its application:

- Since one of the reactants is always the RNA itself, only catalysts for self-modifying reactions of RNA can be identified. If modified monomers were incorporated into RNA pools (Jensen et al., 1995; Wecker et al., 1996), their different chemistry could be exploited, too, but alignment of the substrates has always been controlled by base-

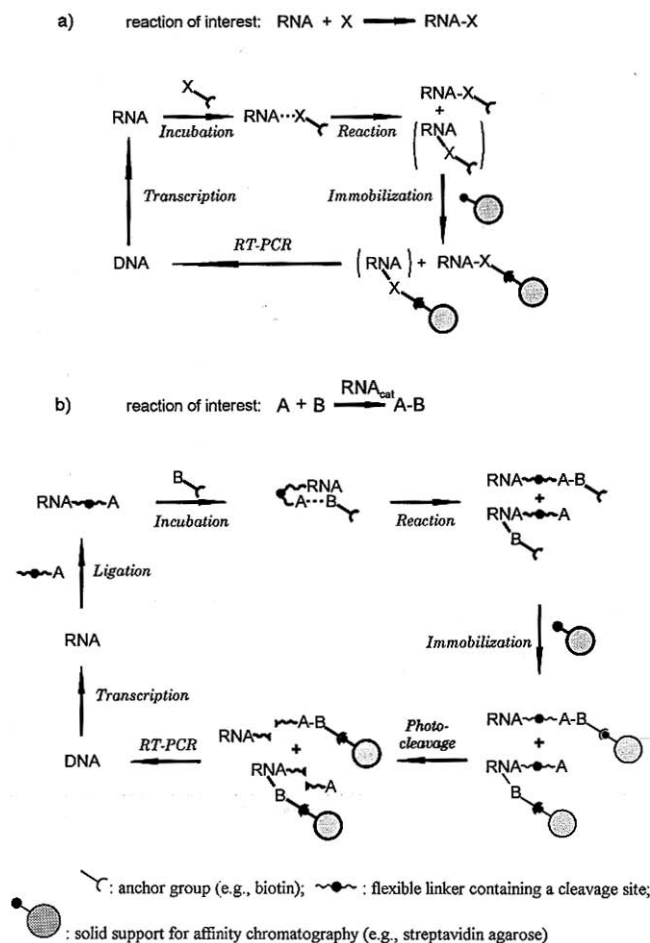


Figure 1. (a) Direct selection of RNA catalysts. The transcribed RNA is incubated with the reaction partner (X) carrying an anchor group (e.g., biotin). The reacted species (including reaction products at internal positions) are separated from the excess of inactive species, e.g., by affinity chromatography. Amplification by RT-PCR yields an enriched DNA pool that is subjected to additional rounds of selection and amplification. (b) Direct selection with linker-coupled reactants. Reactant A attached to a flexible PEG linker is coupled to the RNA transcript by T4 RNA ligase. The RNA conjugates are incubated with reactant B carrying a biotin moiety, which allows subsequent immobilization of the reaction products on streptavidin-agarose. The correct reaction products (reactions at reactant A) can be specifically released by photocleavage of the linker, whereas the products of side reactions with the biotin attached to internal positions of the RNA remain immobilized and are not further amplified.

pairing interactions. Catalysts for reactions between two small reactants, being the basis of biochemistry, prebiotic chemistry, and organic synthesis, could so far not be isolated using direct selection.

- To be selected, the catalytically active RNA molecule must also possess substrate properties. RNA molecules, being excellent catalysts but poor substrates, are eliminated in the selection step.

- Selection criterion is the attachment of the anchor group, while the position of attachment is irrelevant. Therefore, catalysts for side reactions at different positions of the RNA (Illangasekare et al., 1995; Lorsch and Szostak, 1994) or for different chemistries (Wilson and Szostak, 1995) are enriched and finally isolated along with the desired species, as long as these modifications do not interfere with reverse transcription.

Here we describe an approach developed to overcome these limitations involving multifunctional RNA conjugates (Figure 1b). To select for catalysts of a general bimolecular reaction $\text{A} + \text{B} \rightarrow \text{AB}$, the active RNAs have

to acquire a selectable change in a characteristic property as a result of a successful catalysis. This is achieved by coupling one of the reactants (A) to each individual RNA sequence. To allow optimal orientation of the reactant and the RNA, both are tethered by a flexible polymeric linker. By high dilution during the reaction step, self-modification (i.e., reaction of the RNA's "own" reactant) is favored over true intermolecular catalysis. After reaction, the products AB would then be linked to both the anchor group (allowing isolation) and the RNA (allowing amplification). The incorporation of a cleavage site within the linker allows discrimination of side products at the RNA backbone in favor of the desired reaction products at the reactant A.

EXPERIMENTAL PROCEDURES

General. UV-MALDI-TOF mass spectra were obtained on a Bruker Reflex, and IR-MALDI-TOF mass spectra were obtained on a Vision 2000, Model SEQ 1-2-3, Thermo Analysis, Schwartz, Hempstead, U.K. Laser experiments were performed with a Nd-YAG laser, Spektron, SL800 G.

Synthesis of the Dinucleotide Analogs 1a and 1b.

The photocleavable building block **2** was synthesized as described (Ordoukhanian and Taylor, 1996) and incorporated into the dinucleotide analog **1a** by solid phase synthesis on an Applied Biosystems 391 synthesizer using a 1 μmol RNA cycle. 3'-Aminomodifier-C6-CPG support (**3**), DMT-hexaethylene glycol phosphoramidite (**4**), *N*-benzoyl-5'-ODMT-2'-TBDMS-cytidine-3'-O-(2-cyanoethyl)-*N,N*-diisopropylphosphoramidite (**5**), and bis-(cyanoethyl)-*N,N*-diisopropylphosphoramidite (**6**) were from Chemgenes, Waltham, MA (Scheme 2). Cleavage from the solid support and deprotection were performed in a 1 mL mixture of 33% aqueous ammonia and ethanol (3:1) at 55 °C for 24 h and overnight incubation of the lyophilized mixture with 0.4 mL 1 M tetrabutylammonium fluoride in DMF (Aldrich) at room temperature. This solution was diluted with 5 mL of 60 mM NH_4OAc and passed over a 2 mL DEAE-Sephadex A-25 column equilibrated with 0.05 M triethylammonium acetate, pH 7, followed by a 15 mL wash with 0.1 M triethylammonium acetate, pH 7, and elution of the product with 2 M triethylammonium acetate, pH 7. The product fractions were lyophilized and purified by reversed phase chromatography on a HP 1028B liquid chromatograph with a Beckman Ultrasphere C₁₈ column (4.6 \times 250 mm, 80 Å pore) using a 0.1 M triethylammonium acetate gradient, pH 7, containing 0–80% acetonitrile with compound **1a** eluting at ~25% acetonitrile with a total yield of 22%.

Fourteen nanomoles of this compound was biotinylated with 0.7 mg of sulfosuccinimidyl 6-(biotinamido)hexanoate (Sigma) in 100 μL of 0.1 M K_2HPO_4 buffer, pH 8, for 12 h at 25 °C. After quenching with 10 μL of 1 M NH_4OAc , purification by HPLC yielded 5.3 nmol of **1b**.

Transcription. For the preparation of pool RNA, a randomized DNA pool was synthesized as described (Famulok, 1994). Thirty picomoles of this double-stranded DNA template were transcribed in a 100 μL reaction mix containing 80 mM HEPES, pH 7.5, 22 mM MgCl_2 , 1 mM spermidine, 10 mM DTT, 0.12 mg/mL BSA, 4 mM of each ribonucleoside triphosphate (Boehringer Mannheim), 10 μCi [α -³²P]CTP, 100 units of T7 RNA polymerase (Stratagene), and 60 units of RNasin (MBI Fermentas) for 4 h at 37 °C. After DNA digestion with 20 units of DNase I (Boehringer Mannheim) for 30 min at 37 °C, RNA transcripts were purified by electrophoresis on a denaturing 8% polyacrylamide gel, elution, and ethanol precipitation.

For the preparation of 25-mer RNA, a double-stranded DNA template was obtained by hybridization of two oligonucleotides synthesized by standard phosphoramidite chemistry [sequences: 3'-d(AG ATT ATG CTG AGT GAT ATC CTC GAG TCG GAA GTG ACG AGG TGG)-5' and 5'-d(TC TAA TAC GAC TCA CTA TAG GAG CTC AGC CTT CAC TGC)-3']. This template was transcribed under the same conditions as for the RNA pool and purified by electrophoresis on a 15% denaturing polyacrylamide gel.

Ligation. Two hundred picomoles of the 25-mer RNA transcript were incubated with 400 pmol of dinucleotide analog in a 50 μ L reaction volume containing 50 mM HEPES, pH 7.8, 20 mM MgCl₂, 50 μ g/mL BSA, 3.5 mM DTT, 10% DMSO, 0.1 mM ATP, 30 units of RNasin, and 120 units of T4 RNA ligase (MBI Fermentas) at 4 °C for 4 h, and the ligation product was purified as described for the transcript.

For the ligation of the RNA-pool, the RNA molecules were first hybridized with a 3-fold excess of a 20-mer deoxyoligonucleotide [sequence: 3'-d(CCG TGG TGC CAG CCT AGG TG)-5'] complementary to the 3'-end of the pool RNA by heating to 95 °C for 1 min and slowly cooling down to room temperature. Ligation conditions were similar to those for the 25-mer, except for a higher (5-fold) excess of **1a** and a longer ligation time (16 h). Ligated pool RNA was purified on a 8% denaturing polyacrylamide gel.

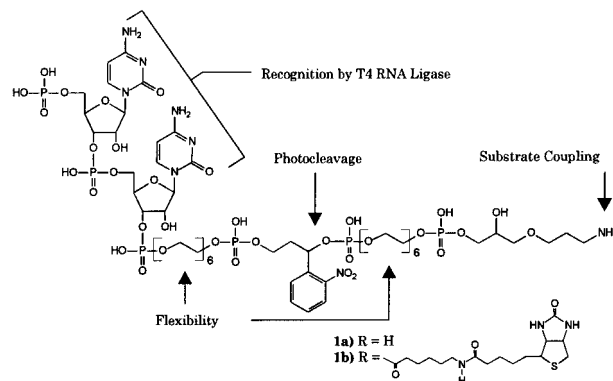
Photolysis. Fifty picomoles of the ligated 25-mer dissolved in 80 μ L of 0.1 M Tris-HCl, pH 7, and 10 mM EDTA was irradiated in a quartz cuvette with a Nd-YAG laser (5 mJ/pulse, 10 ns/pulse, 8 Hz, λ = 355 nm). After 0, 8, 32, and 480 pulses, 10 μ L aliquots were withdrawn and analyzed by electrophoresis on a 15% denaturing polyacrylamide gel.

Immobilization, Photorelease, and RT-PCR. Pool RNA (10 pmol) was immobilized by incubation for 30 min with 20 μ L of streptavidin-agarose on a microcon spin filter prewashed three times with 100 μ L of 3 mg/mL tRNA solution (RNase free, Boehringer Mannheim). Unbound RNA was washed away by subsequent incubation and centrifugation of 200 μ L of tRNA solution (3 mg/mL), 2 \times 200 μ L of 8 M guanidinium hydrochloride, 0.1 M Tris-HCl, pH 7.5, 10 mM EDTA, and 2 \times 200 μ L of tRNA solution (3 μ g/mL). Bound RNA was released by resuspending the agarose in 200 μ L of 3 μ g/mL tRNA solution, irradiation on the filter for 3 min with a Nd-YAG laser (30 mJ/pulse), and washing the agarose three times with 200 μ L of tRNA solution (3 μ g/mL). A 1% aliquot of the obtained RNA was annealed with 200 pmol of primer and subjected to reverse transcription in a 20 μ L reaction mix with 50 mM Tris-HCl, pH 8.3, 75 mM KCl, 3 mM MgCl₂, 10 mM DTT, 0.5 mM dNTPs (MBI Fermentas), and 200 units of Superscript II (Gibco BRL) for 1 h at 37 °C. The reaction mix was then diluted to a 100 μ L volume with the final concentration of 3 μ M of each primer, 20 mM Tris-HCl, pH 8.5, 65 mM KCl, 2 mM MgCl₂, 2 mM DTT, 0.3 mM dNTPs, and 5 units of Taq polymerase (AGS). After 10 cycles of PCR amplification, the resulting DNA was analyzed on a 2% agarose gel and the bands were visualized by ethidium bromide staining.

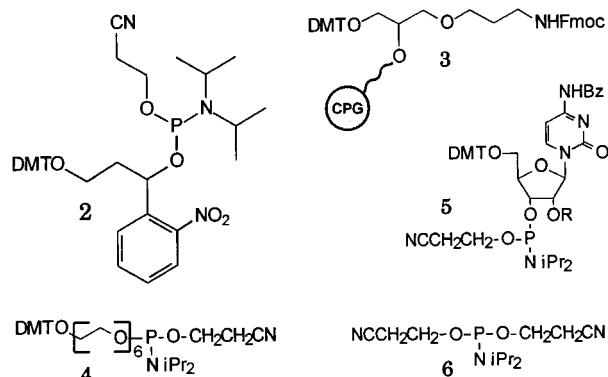
RESULTS

The most essential requirement for the practical realization of the strategy illustrated in Figure 1b was to develop an efficient method to synthesize multifunctional RNA conjugates from RNA transcripts. While numerous strategies exist for the site-specific incorporation of both linkers and non-nucleotide modifiers during chemical synthesis of oligonucleotides (Beaucage and

Scheme 1. Design of Dinucleotide Derivative 1



Scheme 2. Reagents Used in the Synthesis of 1a



Iyer, 1993; Goodchild, 1990), there is currently no method available that would be suitable for direct use in *in vitro* selection schemes. The RNA is enzymatically synthesized in each round of selection, so modification has to occur either during or after enzymatic synthesis. Ideally, linker, cleavage site, and reactant should be combined in one block by chemical synthesis, which then could be introduced in a single step in each selection cycle. As the general method, we chose to use enzymatic ligation of a suitably derivatized substrate with T4 RNA ligase (England and Uhlenbeck, 1978; Igloi, 1996). Poly(ethylene glycol) was chosen as a synthetic linker because of its high flexibility, solubility, and previously described compatibility with oligonucleotide chemistry (Jäschke, 1997; Jäschke et al., 1993, 1996). We decided to use a photochemical cleavage reaction (Ordoukhanian and Taylor, 1996) for its high specificity and for its independence of other chemical parameters (e.g., pH, redox potential, solvent). To combine these features in one molecule, we designed compound **1a** containing the following elements (Scheme 1):

- a 5'-phosphorylated dinucleotide (pCpC) for enzymatic ligation with T4 RNA ligase,
- two hexaethylene glycol units as flexible linkers,
- an *o*-nitrobenzyl derivative as a photolytical cleavage site, and
- a primary aliphatic amino group for coupling of potential reactants by activated ester chemistry.

Compound **1a** was synthesized by automated synthesis introducing the photocleavage site by the use of phosphoramidite **2**, which was prepared as described (Ordoukhanian and Taylor, 1996). Starting with an aminoalkyl-functionalized glass support **3**, hexaethylene glycol phosphoramidite (**4**), compound **2**, hexaethylene glycol phosphoramidite (**4**), and then cytidine phosphoramidite (**5**) (twice) were added sequentially, all employing standard protecting groups (Scheme 2). Finally, chemical phosphorylation was carried out on the synthesizer using

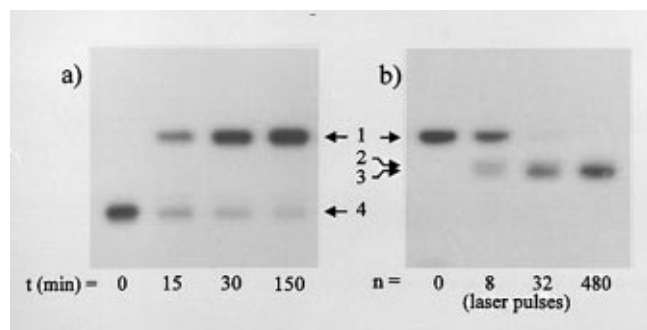


Figure 2. Time course of the ligation of compound **1a** to a 25-mer RNA transcript containing ^{32}P -labeled cytidine residues and photocleavage of the resulting RNA conjugate. (a) Aliquots taken from the T4 RNA ligation mix at indicated times were analyzed on a 15% denaturing polyacrylamide gel and visualized by autoradiography. (b) Purified RNA conjugates obtained by ligation were irradiated in solution at 355 nm with a Nd-YAG laser. Aliquots were taken after exposure to the indicated number of laser pulses and examined by electrophoresis on a 15% polyacrylamide gel. Band index: 1, ligation product; 2, primary photoproduct with attached *o*-nitrosophenylketone; 3, secondary product after β -elimination of vinyl *o*-nitrosophenyl ketone; 4, unmodified 25-mer transcript.

bis(cyanoethyl) *N,N*-diisopropyl phosphoramidite (**6**). After standard deprotection and HPLC purification, compound **1a** was characterized by IR-MALDI mass spectrometry, confirming the correct product composition (calculated $[\text{MH}]^+ m/z$ 1787.2; found $[\text{MH}]^+ m/z$ 1787.3).

To check the desired properties, the dinucleotide analog **1a** was first reacted with an *N*-hydroxysulfosuccinimidyl-activated biotin as a model for the attachment of potential reactants to the primary amino group by activated ester chemistry. Ninety-five percent conversion of the dinucleotide analog was observed by HPLC with the biotinylated product eluting at significantly higher retention times (not shown). The identity of the resulting biotin conjugate **1b** was corroborated by UV-MALDI mass spectrometry (calculated $[\text{M} - \text{H}]^- m/z$ 2125.7; found $[\text{M} - \text{H}]^- m/z$ 2125.5). Due to UV excitation ($\lambda = 377$ nm), additional peaks of the predicted photofragments were detected (calculated m/z 911.9, 1212.8; found m/z 912.2, 1214.2), indicating a photocleavage reaction proceeding in agreement with the accepted mechanism (Pillai, 1980).

The incorporation of the synthetic linker into RNA transcripts—a key step in the modified selection scheme—was studied by ligation with T4 RNA ligase. As rigorous analytics is complicated with randomized pools, first a ^{32}P -labeled RNA 25-mer [sequence: 5'-r(G GAG CUC AGC CUU CAC UGC UCC ACC)-3'] obtained by *in vitro* T7 transcription was incubated with a 2-fold excess of **1a**, and the ligation was followed by electrophoretic analysis of aliquots withdrawn from the reaction mixture at appropriate times. The time course in Figure 2a shows the disappearance of the original 25-mer and the simultaneous formation of the RNA conjugate with up to 95% conversion. No additional bands with lower electrophoretic mobility, indicating circularization or oligomerization products, were detected.

The ligation product was eluted, purified by precipitation, redissolved, and irradiated by an increasing number of Nd-YAG laser pulses ($\lambda = 355$ nm). The rapid and quantitative cleavage of the RNA conjugate after 32 pulses (Figure 2b) correlates with the formation of the photoproducts with higher electrophoretic mobility, which can be resolved into two distinct bands by high-resolution electrophoresis (not shown). The upper band can be assigned to the primary photoproduct, an *o*-nitrosophenyl

ketone, as a result of the photoinduced intramolecular redox reaction, which partially reacts further by β -elimination to release the photoactive moiety leaving a PEG phosphate attached to the 3'-end of the RNA (Ordoukhanian and Taylor, 1996). This secondary product may be assigned to the lower band in Figure 2b. The two photoproducts were unaffected by further irradiation. A 15-fold overexposure did not lead to any additional bands that would indicate photomodification, cross-linking, or dimerization.

To allow the use of the proposed strategy in direct selection, the methods described above have to be compatible with the standard selection scheme without interfering with any other step in the selection cycle. To check the feasibility of the new steps under selection conditions, we performed a selection cycle according to the procedure shown in Figure 1b. Because in the first rounds of a selection project reaction yields are very low and products can often hardly be detected, we substituted the reaction step by artificially creating a situation as it would be after a completely successful reaction. This was achieved by ligating an RNA pool containing two constant sequences for amplification purposes and a randomized domain of 74 nucleotides [sequence: 5'-r(G GAG CUC AGC CUU CAC UGC-N₇₄-GGC ACC ACG GUC GGA UCC AC)-3', complexity of 10^{13} different species (Famulok, 1994)] with biotinylated dinucleotide **1b** leading to species that correspond to the desired reaction products: RNA pool molecules are connected to biotin as an anchor group via a cleavable linker.

Sufficient ligation of the pool required modification of the protocol. A higher excess of the dinucleotide analog and longer incubation times were necessary, and addition of an oligonucleotide complementary to the 3'-end of the pool molecules significantly improved ligation yields, probably by making "buried" 3'-ends accessible to the enzyme. Seventy-five percent yields were obtained in overnight incubation with a 5-fold excess of **1b**. Purified ligation product was incubated with streptavidin-agarose on a spin filter for 30 min. Unbound RNA was washed away under denaturing conditions until no radioactivity could be detected in the filtrate. Eighty percent binding was observed (Figure 3a), while unspecific binding of unmodified RNA transcript was determined to be <2%. The streptavidin-agarose loaded with RNA was resuspended in the same buffer used during the washing procedure and irradiated directly on the spin filter with 480 laser pulses, which brought 90% of the immobilized RNA back into solution. Ten percent of the radioactivity remained stuck to the solid matrix in spite of further irradiation or washing.

To ensure that the photoreleased RNA is intact and functional, it was subjected to amplification by reverse transcription and polymerase chain reaction (RT-PCR, Figure 3b), and an equal amount of unmodified RNA transcript served as a reference. Lanes 3 and 4 in Figure 3b representing the corresponding reaction products demonstrate that even after ligation, immobilization, and photolytical cleavage, appropriate amounts of cDNA with the correct length and purity are obtained.

RNA molecules isolated and released according to this new procedure can thus be amplified and subjected to further rounds of selection as required.

DISCUSSION

Despite the success of direct selection, the range of reactions that can be investigated is severely restricted by the selection for self-modifying RNAs, which limits one reaction partner to be always RNA itself. Even though recent studies successfully extended direct selec-

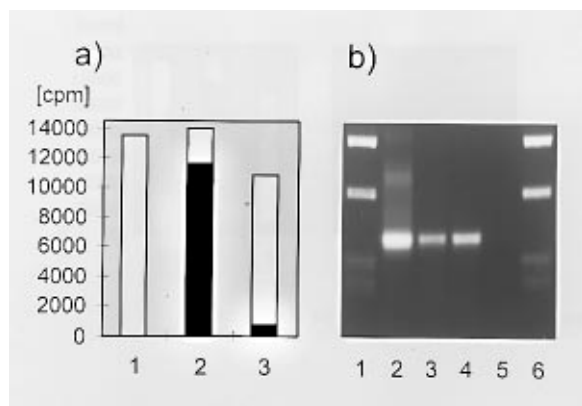


Figure 3. (a) Immobilization of pool RNA-biotin conjugates on streptavidin-agarose and release of the pool RNA by laser irradiation. The amount of RNA at each stage was quantitated by Cerenkov counting; when counting samples in the spin filters, the obtained values were generally ~5% higher than those measured in solution. White: counts in the supernatant. Black: counts immobilized. Bar 1: RNA-biotin conjugates prior to immobilization. Bar 2: after immobilization. Bar 3: after photocleavage of immobilized RNA conjugates. (b) RT-PCR of the photoreleased RNA molecules analyzed by agarose gel electrophoresis: lanes 1 and 6, 100 bp DNA ladders; lane 2, starting DNA pool that was used for transcription; lane 3, RT-PCR product of unmodified RNA transcript (same amount as in lane 4); lane 4, RT-PCR product of the photoreleased RNA molecules; lane 5, RT-PCR without template as a negative control.

tion to reactions on modified nucleotides and cross-linkers (Jensen et al., 1995; Smith et al., 1995; Wecker et al., 1996), catalysis occurs only if these reactants are presented in the context of an oligonucleotide sequence. No example of a directly selected RNA catalyst for reactions between two small, non-oligonucleotide reactants has been described so far. The additional constraint on the selectable structures to have both substrate and catalytic properties reduces the chances of finding a suitable species in sequence space tremendously. From the larger subpopulation of catalytic pool molecules only the tiny fraction with added substrate properties is selectable. This is an intrinsic problem of all strategies to identify catalysts in complex mixtures, as true catalysts are per definition required to leave the reaction unchanged. They can therefore only be selected by coupling catalysis with some other principle that leads to a selectable change in the catalyst molecule, either by combining substrate and catalyst in one molecule and performing a self-modifying reaction (Illangasekare et al., 1995; Lorsch and Szostak, 1994; Wilson and Szostak, 1995) or by using mechanistic inhibitors instead of substrates that form covalent bonds with the catalyst during the reaction (Janda et al., 1997). The complete separation of substrate and catalytic properties by entrapment in liposomes has been proposed recently (Williams and Bartel, 1996), but we have no knowledge of experimental progress in this field.

To gain access to a wider range of reaction types without losing the advantages of direct selection, we designed a selection scheme using oligonucleotide conjugate libraries instead of simple RNA transcripts. Strictly speaking, this is still self-modification (or *cis*-selection). To be selected, the RNA-linker-reactant conjugates—and not the RNA—must possess both substrate and catalyst properties. However, as the substrate properties are provided exclusively by the attached reactant, the RNA part just needs to act as a catalyst. If the RNA acts as a substrate, the respective products are initially selected (i.e., immobilized) but eliminated in the cleavage step, which is in fact a second selection step.

The selection process may still yield byproducts. If the attached reactant contains more than one potential reaction site or if functionalities of the linker are utilized for the attachment of reactant B that are located on the right-hand side of the cleavage site (see **1a**, Scheme 1), then the respective reaction products will be selected, too. However, compared to the situation in standard direct selection where hundreds of potential reactive sites per RNA molecule can give rise to selectable products, the technology described here is a significant improvement of control in the selection step.

The expansion of direct selection from unmodified RNA libraries to libraries of complex RNA conjugates faces strict requirements as only part (i.e., the nucleotide sequence of the RNA part) of the “genetic” information of the conjugate can be transferred through the enzymatic amplification steps. Therefore, the nontransferable parts of information, namely the site of attachment and chemical nature of the linker, must be kept constant to ensure equivalence of the structures in successive generations. For example, random incorporation of nucleoside triphosphates derivatized with a linker-coupled reactant will cause loss of essential information and prevent exponential enrichment of functional species as incompletely represented diversity is created in each round. Due to these requirements, the use of the two termini of RNA transcripts seems the most straightforward approach for site-specific derivatization.

In this work, selective 3'-derivatization has been achieved by the use of the universal linker derivative **1a**, which allows for ligation by T4 RNA ligase, high flexibility by the PEG tether, simple coupling chemistry, and photocleavability. With these functionalities combined in compound **1a** the preparation of the reactant for a selection experiment can be accomplished by standard *N*-hydroxysuccinimide ester chemistry, thereby substantially reducing the synthetic effort. The photolytic cleavage reaction is particularly suited for *in vitro* selection because it offers high stringency as all parameters except irradiation remain constant during the selection.

All steps have been shown to be compatible with the overall selection procedure by performing a model selection cycle. Therefore, the presented selection procedure allows for the first time the design of direct selection experiments with two freely choosable non-oligonucleotide reactants and with the opportunity to control the reaction site. The final proof of the usefulness of this method, however, will be the successful selection of a catalytic RNA species.

The strategy presented here is especially suited to the selection of catalysts for bond formations, but the attachment of an artificial reactant to the RNA pool will also be indispensable in the application of direct selection to bond cleavage or redox reactions. The strategy might therefore serve as a valuable tool for exploring the limits of RNA catalysis.

ACKNOWLEDGMENT

This work was supported by the Deutsche Forschungsgemeinschaft (Grants Ja 794/1-1 and SFB 344, TP B10 to A.J.). We gratefully acknowledge additional support by Prof. V. A. Erdmann, assistance with the laser equipment provided by Dr. S. Ring, and spectrometric measurements performed by Drs. P. Franke, A. Schäfer, E. Nordhoff, and S. Hahner.

LITERATURE CITED

- Bartel, D. P., and Szostak, J. W. (1993) Isolation of new ribozymes from a large pool of random sequences. *Science* **261**, 1411–1418.

- Beaucage, S. L., and Iyer, R. P. (1993) The functionalization of oligonucleotides via phosphoramidite derivatives. *Tetrahedron* 49, 1925–1963.
- Ellington, A. D., and Szostak, J. W. (1990) In vitro selection of RNA molecules that bind specific ligands. *Nature* 346, 818–822.
- England, T. E., and Uhlenbeck, O. C. (1978) 3'-terminal labelling of RNA with T4 RNA ligase. *Nature* 275, 560–561.
- Famulok, M. (1994) Molecular recognition of amino acids by RNA aptamers: An L-citrulline binding RNA motif and its evolution into an L-arginine binder. *J. Am. Chem. Soc.* 116, 1698–1706.
- Gold, L., Polisky, B., Uhlenbeck, O., and Yarus, M. (1995) Diversity of oligonucleotide functions. *Annu. Rev. Biochem.* 64, 763–797.
- Goodchild, J. (1990) Conjugates of oligonucleotides and modified oligonucleotides: a review of their synthesis and properties. *Bioconjugate Chem.* 1, 165–187.
- Igloi, G. (1996) Nonradioactive labeling of RNA. *Anal. Biochem.* 233, 124.
- Illangasekare, M., Sanchez, G., Nickles, T., and Yarus, M. (1995) Aminoacyl-RNA synthesis catalyzed by an RNA. *Science* 267, 643–647.
- Janda, K. D., Lo, L.-C., Lo, C.-H. L., Sim, M.-M., Wang, R., Wong, C.-H., and Lerner, R. A. (1997) Chemical selection for catalysis in combinatorial antibody libraries. *Science* 275, 945–948.
- Jäschke, A. (1997) Oligonucleotide-polyethylene glycol conjugates - synthesis, properties and applications. *Chemistry and Biological Applications of PEG* (J. M. Harris and S. Zalipsky, Eds.) American Chemical Society, Washington, DC (in press).
- Jäschke, A., Fürste, J. P., Cech, D., and Erdmann, V. A. (1993) Automated incorporation of polyethylene glycol into synthetic oligonucleotides. *Tetrahedron Lett.* 34, 301–304.
- Jäschke, A., Bald, R., Nordhoff, E., Hillenkamp, F., Cech, D., Erdmann, V. A., and Fürste, J. P. (1996) Synthesis and analytical characterization of RNA-polyethylene glycol conjugates. *Nucleosides Nucleotides* 15, 1519–1529.
- Jensen, K. B., Atkinson, B. L., Willis, M. C., Koch, T. H., and Gold, L. (1995) Using in vitro selection to direct the covalent attachment of human immunodeficiency virus type 1 Rev protein to high-affinity RNA ligands. *Proc. Natl. Acad. Sci. U.S.A.* 92, 12220–12224.
- Lorsch, J. R., and Szostak, J. W. (1994) In vitro evolution of new ribozymes with polynucleotide kinase activity. *Nature* 371, 31–36.
- Lorsch, J. R., and Szostak, J. W. (1996) Chance and necessity in the selection of nucleic acid catalysts. *Acc. Chem. Res.* 29, 103–110.
- Ordoukhanian, P., and Taylor, J. S. (1996) Design and synthesis of versatile photocleavable DNA building block. Application to phototriggered hybridization. *J. Am. Chem. Soc.* 117, 9570–9571.
- Pillai, V. N. R. (1980) Photoremovable protecting groups in organic synthesis. *Synthesis*, 1–26.
- Smith, D., Kirschenheuter, G. P., Charlton, J., Guidot, D. M., and Repine, J. E. (1995) In vitro selection of RNA-based irreversible inhibitors of human neutrophil elastase. *Chem. Biol.* 2, 741–750.
- Tuerk, C., and Gold, L. (1990) Systematic evolution of ligands by exponential enrichment: RNA ligands to bacteriophage T4 DNA polymerase. *Science* 249, 505–510.
- Wecker, M., Smith, D., and Gold, L. (1996) In vitro selection of a novel catalytic RNA: characterization of a sulfur alkylation reaction and interaction with a small peptide. *RNA* 2, 982–994.
- Williams, K. P., and Bartel, D. P. (1996) In vitro selection of catalytic RNA. *Catalytic RNA* (F. Eckstein and D. M. J. Lilley, Eds.) pp 367–381, Springer, Berlin.
- Wilson, C., and Szostak, J. W. (1995) In vitro evolution of a self-alkylating ribozyme. *Nature* 374, 777–782.

BC9701151

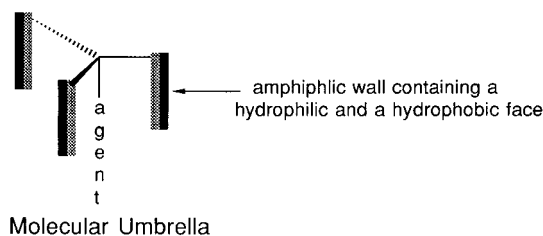
Evidence for Highly Cooperative Binding between Molecular Umbrella–Spermine Conjugates and DNA

Vaclav Janout, Marion Lanier, Gang Deng, and Steven L. Regen*

Department of Chemistry and Zettlemoyer Center for Surface Studies, Lehigh University, Bethlehem, Pennsylvania 18015. Received July 29, 1997*

Double- and tetrawalled molecular umbrella–spermine conjugates (**I** and **II**) have been synthesized, and their binding to calf thymus DNA (CT-DNA), poly[d(AT)], and poly[d(GC)] compared with that of a single-walled analogue (**III**). At moderate salt concentrations (8 mM NaCl), **I** and **II** show significantly greater affinity toward each DNA, relative to **III**; at high salt concentrations (150 mM NaCl), strong binding of **I** and **II** (but not **III**) was maintained toward poly[d(GC)]. Examination of the influence of **I–III** on the melting behavior of poly[d(AT)] has provided strong evidence that the binding of **I** and **II** reflects highly cooperative interactions among DNA-bound conjugates and that the DNA duplex serves as a nucleation site for umbrella aggregation. The implications of these findings for the rational design of novel drug conjugates that operate at the nuclear level, and also novel transfection agents, are briefly discussed.

We have recently introduced a new class of surfactants that can cover an attached agent and shield it from an incompatible environment (1, 2). The design principle upon which these “molecular umbrellas” have been based involves the covalent coupling of two or more rigid “amphiphilic walls” to a central scaffold. Our working hypothesis is that such surfactants will enhance the permeability of pendent polar molecules (e.g., peptides, antisense oligonucleotides, etc.) across lipid bilayers by masking their hydrophilicity. One important issue that we have recently sought to clarify is whether or not an umbrella can adversely affect the binding properties of the attached agent. To probe this question, we synthe-



sized two umbrella–spermine conjugates (**I** and **II**) and examined their DNA binding behavior. Spermine was specifically chosen as a “mock drug” on the basis of its affinity toward DNA and also its strong hydrophilicity (3). For purposes of comparison, the DNA binding properties of a single-walled analogue (**III**) were also investigated. In this paper, we document our discovery that the coupling of a molecular umbrella to spermine results in significantly enhanced DNA binding at physiological salt concentrations. We also present compelling evidence that this binding is highly cooperative in character.

MATERIALS AND METHODS

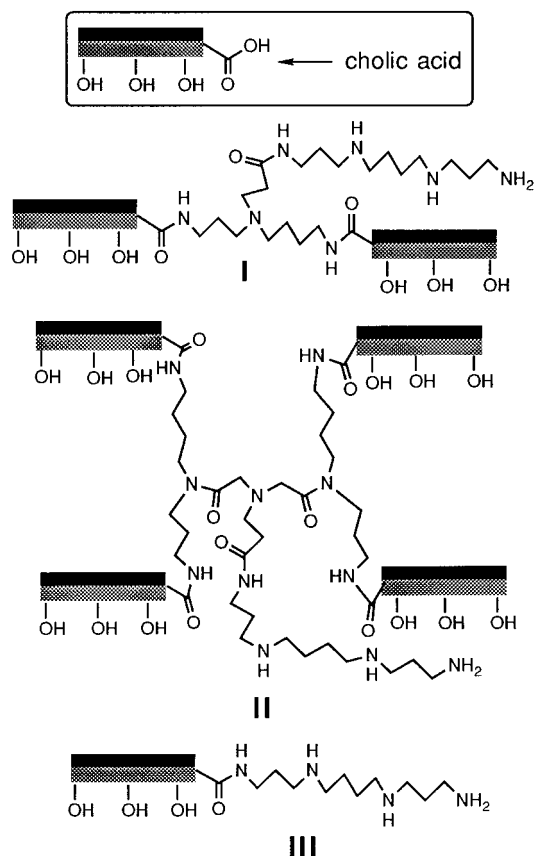
General Methods. Unless stated otherwise, all reagents and chemicals were obtained from commercial sources and used without further purification. *N*-(*O*-Succinimidylcholeate) was prepared using procedures

similar to those previously described (2). EMS silica Gel 60 was used for column chromatography; preparative thin-layer chromatography employed EM Science silica gel 60 F-254. Detection on TLC was made by a combination of sulfuric acid 10% in water, I_2 , and UV (254 and 365 nm). House-deionized water was purified using a Millipore Milli-Q filtering system containing one carbon and two ion-exchange stages. All 1H NMR spectra were recorded on a Bruker 360 MHz instrument; chemical shifts are reported in parts per million and were referenced to residual solvents. High-resolution mass spectra were obtained at the Mass Spectrometry Facility of the University of California, Riverside. Elemental analyses were determined by Midwest Microlab (Indianapolis, IN). Surface tension measurements (23 °C) were made using a tensiometer/micro-balance (NIMA, Model ST9000).

Molecular Umbrella–Spermine Conjugate I. A solution composed of *N*¹,*N*³-spermidinebis[choleic acid amide] (100 mg, 0.11 mmol), ethyl acrylate (0.2 mL, 1.85 mmol), $CHCl_3$ (0.2 mL), and CH_3OH (0.3 mL) was stirred at 40 °C for 16 h. Subsequent concentration under reduced pressure and column chromatography [silica, $CHCl_3/CH_3OH/H_2O$, 103:25:3 (v/v/v)] afforded 85 mg (86%) of conjugated addition product having R_f 0.58 and 1H NMR ($CD_3OD/CDCl_3$, 5:1, v/v) δ 0.67 (s, 6 H), 0.87–2.45 (m, 71 H), 2.45 (m, 4 H), 2.78 (m, 2 H), 3.15 (m, 4 H), 3.33 (m, 2 H), 3.78 (s, 2 H), 3.92 (s, 2 H), 4.11 (q, 2 H). This product was then hydrolyzed by first dissolving it in 2 mL of methanol, followed by addition of 80 mL of 1 M NaOH in methanol. After stirring for 24 h at room temperature, 80 mL of a 1 M HCl solution was added, followed by concentration under reduced pressure. Purification by column chromatography [silica, $CHCl_3/CH_3OH/H_2O$, 103:25:3 (v/v/v)] afforded 79.0 mg of the corresponding acid having R_f 0.52 and 1H NMR (CD_3OD) δ 0.63 (s, 6 H), 0.83–2.15 (m, 68 H), 3.06–3.28 (m, 8 H), 3.32 (m, 2 H), 3.75 (s, 2 H), 3.88 (s, 2 H). Treatment of this acid with *O*-(*N*-succinimidyl)-*N,N,N,N*-tetramethyluronium tetrafluoroborate (TSU) (26.4 mg, 0.086 mmol) and diisopropylethylamine (DIPEA) (11.2 mg, 0.086 mmol) in 0.5 mL of DMF for 4 h at room temperature produced the corresponding activated ester, which was then added, dropwise, to a solution of spermine (44.5 mg, 0.22 mmol) in 0.2 mL of anhydrous DMF. The resulting mixture was stirred for 18 h at room temperature and

* Abstract published in *Advance ACS Abstracts*, October 15, 1997.

then concentrated under reduced pressure. Subsequent dissolution in 1 mL of CH₃OH and precipitation by addition of 10 mL of a saturated aqueous NaHCO₃ solution afforded a colorless solid, which was triturated with water (2 × 10 mL) and purified by column chromatography [silica, CH₃OH/NH₄OH, 3:1 (v/v)] to give 21.0 mg (16%) of **I**, having *R*_f 0.45, mp 151–153 °C, and ¹H NMR (CD₃OD) δ 0.70 (s, 6 H), 0.91–2.25 (m, 74 H), 2.45 (m, 2 H), 2.60–2.72 (m, 12 H), 3.20 (m, 2 H), 3.33 (m, 2 H), 3.78 (d, 2 H), 3.94 (s, 2 H). Anal. Calcd for C₆₈H₁₂₃N₇O₉: C, 69.05; H, 10.48; N, 8.29. Found: C, 68.86; H, 10.51; N, 8.22. HRMS for (C₆₈H₁₂₄N₇O₉)⁺ calcd: 1182.9461. Found: 1182.9413.



Molecular Umbrella–Spermine Conjugate II. To a stirred solution of iminodiacetic acid (0.49 g, 3.68 mmol) in a solution of 9 mL of saturated NaHCO₃/dioxane (4:5, v/v) was added 9-fluorenylmethoxycarbonyl chloride (Fmoc-Cl) (0.95 g, 3.67 mmol) in a few portions at room temperature. After the mixture was stirred in a closed flask for 20 min at room temperature, the solvents were removed under reduced pressure at 40 °C. The resulting oil was then acidified by adding 20 mL of 1 M HCl to give a colorless solid that was dissolved in 20 mL of CHCl₃ and sequentially washed with 1 M HCl (2 × 10 mL) and water (3 × 10 mL). The organic phase was concentrated under reduced pressure, and the colorless solid was recrystallized twice in 30 mL of CH₃OH to give 0.75 g (58%) of the Fmoc-carbamate of iminodiacetic acid having ¹H NMR (CD₃OD/CDCl₃, 5:1, v/v) δ 4.10 (d, 4 H), 4.20 (t, 1 H), 4.34 (d, 2 H), 7.27 (t, 2 H), 7.31 (t, 2 H), 7.58 (d, 2 H), 7.74 (d, 2 H).

To a stirred solution of FmocN(CH₂CO₂H)₂ (19.2 mg, 0.054 mmol) and DIPEA (15.6 mg, 0.12 mmol) in 0.3 mL of anhydrous DMF was added 36.0 mg (0.19 mmol) of TSU. The reaction mixture was stirred at room temperature for 75 min and then diluted with a solution containing 0.2 mL of DMF, 0.1 mL of DIPEA, and 98.5

mg (0.106 mmol) of *N,N*'-spermidinebis[choleic acid amide]. After 24 h of stirring at room temperature, the solvents were removed under reduced pressure, and the residue was dissolved in 1 mL of CH₃OH. Subsequent precipitation by addition into 20 mL of a saturated aqueous solution of NaHCO₃, trituration with water (2 × 10 mL), and purification by preparative thin-layer chromatography [EM Sciences silica, 1 mm, CHCl₃/CH₃OH/H₂O, 65:25:3 (v/v/v)] afforded 0.072 g (69%) of the Fmoc-protected tetrawalled umbrella having *R*_f 0.75 and ¹H NMR (CD₃OD) δ 0.60 (s, 12 H), 0.63–2.19 (m, 132 H), 2.95–3.25 (m, 16 H), 3.35 (m, 4 H), 3.73 (s, 4 H), 3.86 (s, 4 H), 4.00 (br s, 4 H), 4.14 (d, 2 H), 4.35 (t, 1 H), 7.22–7.71 (m, 8 H). Subsequent deprotection was carried out by dissolving 150 mg (0.069 mmol) of the Fmoc-protected tetrawalled umbrella plus 0.10 mL (1.01 mmol) of piperidine in 2 mL of CH₃OH and stirring the solution for 5 h at 40 °C. Removal of solvent under reduced pressure, followed by column chromatography [silica, CHCl₃/CH₃OH/H₂O, 103:27:3 (v/v/v)] afforded 91 mg (67%) of the corresponding amine having *R*_f 0.38 and ¹H NMR (CD₃OD) δ 0.70 (s, 12 H), 0.91–2.30 (m, 132 H), 3.17 (m, 8 H), 3.35 (m, 12 H), 3.54 (br d, 4 H), 3.78 (br s, 4 H), 3.94 (br s, 4 H).

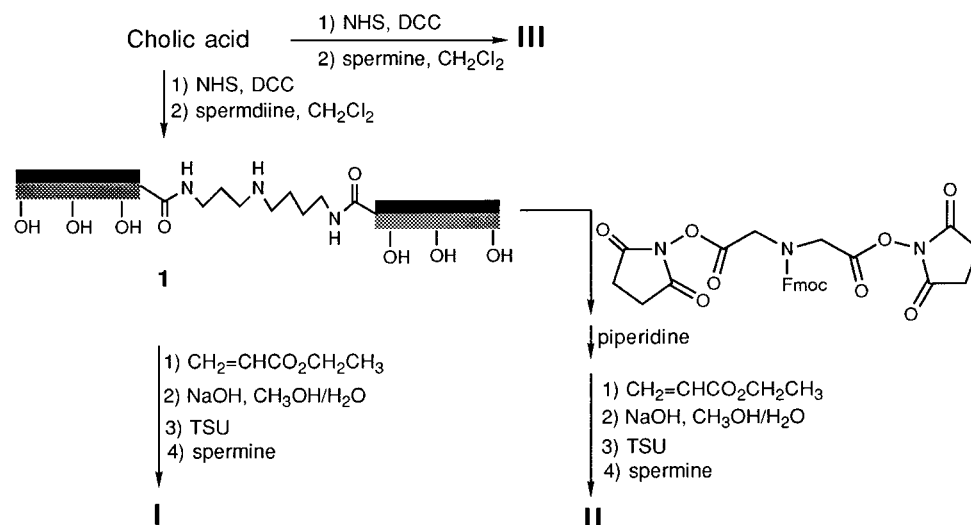
Conjugate addition of 105 mg (0.045 mmol) of the tetrawalled amine to ethyl acrylate (1 mL, 10 mmol) was carried out in 0.5 mL of CH₃OH plus 0.2 mL of CHCl₃ by stirring at 50 °C for 3 days. Removal of solvent under reduced pressure and purification by column chromatography [silica, CHCl₃/CH₃OH/H₂O, 103:25:3 (v/v/v)] afforded 81.8 mg (78%) of the conjugate addition product having *R*_f 0.56 and ¹H NMR (CD₃OD) δ 0.70 (s, 12 H), 0.91–2.25 (m, 137 H), 2.45 (m, 2 H), 2.95 (m, 2 H), 3.15 (m, 8 H), 3.38 (m, 10 H), 3.48 (br d, 4 H), 3.78 (br s, 4 H), 3.94 (br s, 4 H), 4.15 (t, 2 H).

Hydrolysis of the tetrawalled ethyl ester (81.8 mg, 0.0395 mmol) in 2 mL of CH₃OH was carried out by adding 0.05 mL of a solution made from 1 M NaOH/CH₃OH (4:1, v/v) and stirring at room temperature for 1 h, followed by additional stirring for 3 h at 50 °C. After the mixture had cooled to room temperature, 0.05 mL of a 1 M HCl solution was then added and the solvents were removed under reduced pressure to afford 78.0 mg (97%) of the corresponding acid having an *R*_f 0.25 [CHCl₃/CH₃OH/H₂O, 65:25:4 (v/v/v)] and ¹H NMR (CD₃OD) δ 0.70 (s, 12 H), 0.90–2.32 (m, 134 H), 2.52 (t, 2 H), 3.18 (m, 10 H), 3.36 (m, 10 H), 3.70 (m, 4 H), 3.79 (s, 4 H), 3.93 (s, 4 H).

To a stirred solution of the tetrawalled carboxylic acid (100 mg, 0.05 mmol) and DIPEA (8.9 mg, 0.065 mmol) in 0.6 mL of anhydrous DMF was added TSU (19.7 mg, 0.065 mmol). The resulting mixture was stirred at room temperature in a closed flask for 3 h. The solution was then added, dropwise, to a solution of spermine (80 mg, 0.4 mmol) and DIPEA (25 mL). After the reaction mixture had stirred for 24 h at room temperature, the solvents were removed under reduced pressure. Subsequent dissolution in CH₃OH (1 mL), precipitation by addition of a saturated solution of NaHCO₃ (10 mL), trituration with water (3 × 5 mL) and purification by column chromatography [silica, CH₃OH, NH₄OH, 4:1 (v/v)] afforded 58.3 mg (53%) of **II** having *R*_f 0.39, mp 159–161 °C, and ¹H NMR (CD₃OD) δ 0.70 (s, 12 H), 0.91–2.28 (m, 142 H), 2.30–2.90 (m, 12 H), 3.15 (m, 10 H), 3.35 (m, 12 H), 3.55 (br d, 4 H), 3.79 (br s, 4 H), 3.94 (br s, 4 H). Anal. Calcd for C₁₂₇H₂₂₁N₁₁O₁₉·2 H₂O: C, 68.03; H, 9.93; N, 6.87. Found: C, 67.97; H, 9.90; N, 6.84. MS for (C₁₂₇H₂₂₂N₁₁O₁₉)⁺ calcd: 2206. Found: 2207.

***N*'-Spermine Cholic Acid Amide (III).** Cholic acid (0.200 g, 0.5 mmol) was activated by reaction with TSU

Scheme 1



(0.170 g, 0.56 mmol) and 80 μ L (0.5 mmol) of DIPEA in 2 mL of DMF. After the solution had stirred for 5 h at room temperature, a solution that was made from spermine (100 mg, 0.5 mmol) in 8 mL of CHCl_3/THF (1:1, v/v) was added dropwise. The reaction mixture was stirred overnight at room temperature and concentrated under reduced pressure. Subsequent addition of chloroform (10 mL), sequential washing with 3 mL of NaHCO_3 and 3 mL of brine, drying (Na_2SO_4), concentration under reduced pressure, and column chromatography [silica, $\text{CH}_3\text{OH}/\text{NH}_4\text{OH}$ (3:1, v/v)] afforded 34 mg (11%) of a colorless solid having ^1H NMR (CD_3OD) δ 0.70 (s, 3 H), 0.91 (s, 3 H), 1.00–2.30 (m, 35 H), 2.50–3.00 (m, 12 H), 3.12 (m, 2 H), 3.30–3.40 (m, 1 H), 3.78 (br s, 1 H), 3.95 (br s, 1 H). Anal. Calcd for $\text{C}_{34}\text{H}_{64}\text{N}_4\text{O}_4 \cdot 3/4 \text{H}_2\text{O}$: C, 67.34; H, 10.89; N, 9.24. Found: C, 67.11; H, 10.85; N, 9.83. HRMS for $(\text{C}_{34}\text{H}_{65}\text{N}_4\text{O}_4)^+$ calcd: 593.5006. Found: 593.4997.

DNA Binding by Ethidium Displacement. Typically, 3 mL of a 0.01 SHE buffer (8 mM NaCl), 10 mL of an ethidium bromide solution (0.3 mM in 0.01 SHE buffer, 8 mM NaCl), and 10 μ L of a DNA solution (0.3 mM in 0.01 SHE buffer, 8 mM NaCl) were added to a cuvette. The fluorescence intensity at 595 nm was then determined after injection of various volumes of the polyamine conjugate (0.3–1.0 mM, methanolic solution). The excitation wavelength was 547 nm. Analogous experiments that were carried out at “high” salt concentrations used a SHE buffer that was 150 mM in NaCl.

RESULTS AND DISCUSSION

The synthetic approaches that were used to prepare **I–III** are outlined in Scheme 1. In brief, activation of cholic acid with *N*-hydroxysuccinimide (NHS) followed by condensation with spermidine afforded a double-walled precursor, **1**. Subsequent addition of ethyl acrylate, followed by saponification, activation with NHS, and condensation with spermine yielded **I**. The synthesis of **II** followed a similar strategy. Thus, protection of the amino group of iminodiacetic acid with the Fmoc moiety, followed by activation with TSU, coupling with **1**, deprotection, and conjugation with spermine (in a manner similar to that used for the preparation of **I**), afforded the desired tetra-walled umbrella, **II**. Finally, direct coupling of cholic acid to spermine (after activation with NHS) afforded **III**.

To assess the affinity of **I–III** toward DNA, we have used the ethidium displacement technique (4–7). Here, the concentration of each conjugate that is needed to

Table 1. Binding of Molecular Umbrellas to Calf Thymus DNA, Poly[d(AT)], and Poly[d(GC)]

compound	C_{50}^a (μM)			
	CT-DNA	poly[d(AT)]	poly[d(GC)]	poly[d(GC)] ^b
spermine	0.90 (1.0) ^c	2.11 (2.7) ^c	1.15 (1.1) ^c	> 200
spermidine	30.0 (27) ^c			
I	0.40	1.47	0.90	4.45
II	0.32	0.91	0.90	2.20
III	5.52	10.7	10.5	> 200

^a Concentration necessary to displace 50% of DNA-bound ethidium under the following conditions: [DNA-bp] = 1.0 μM , [ethidium] = 1.0 μM , SHE buffer (8 mM NaCl, 2 mM HEPES, 0.05 mM EDTA, pH 7.0); excitation at 547 nm, emission at 595 nm. Values reported are averages of two independent experiments \pm 10%. Methanolic solutions of the polyamine (0–50 μL , 1.0 mM) were injected into 3.0 mL of the DNA-containing buffer at 25 $^\circ\text{C}$. ^b SHE buffer (150 mM NaCl, 2 mM HEPES, 0.05 mM EDTA, pH 7.0); initial fluorescence intensities were \sim 50% of that measured using 8 mM NaCl. ^c Reference 4.

reduce the fluorescence intensity of ethidium by 50% (only DNA-bound ethidium is fluorescent) is taken as a measure of its affinity toward the nucleic acid. Although such “ C_{50} ” values cannot be directly converted into binding constants, since the mode and stoichiometry of binding by ethidium and by the sterol polyamines are uncertain, they do provide a useful qualitative means for probing the effects of polyamine structure on DNA binding. Using experimental conditions similar to those previously described (0.01 SHE buffer: 8 mM NaCl, 2 mM HEPES, 0.05 mM EDTA; ethidium concentration = 1.0 μM ; DNA base pair concentration = 1.0 μM ; pH 7, 25 $^\circ\text{C}$), we obtained C_{50} values for spermine that are in good agreement with those previously reported (4). Since independent studies have estimated a dissociation constant for spermine–DNA complexes in the range of 0.1–1.0 μM under similar conditions, a C_{50} value for spermine of \sim 1 μM reflects very strong DNA binding (7).

A summary of the C_{50} values for **I–III**, spermine, and spermidine, with respect to calf thymus (CT) DNA, is presented in Table 1. Introduction of one amphiphilic wall to the spermine molecule (i.e., **III**) resulted in a significant reduction in DNA binding. The fact that **III** binds more strongly to DNA than spermidine, however, implies that hydrophobic forces and/or hydrogen bonding between the sterol nucleus and DNA contribute to such complexation. That hydrophobic forces are, in fact, of greater importance is indicated by the fact that replacement of the C-7 hydroxyl group of the sterol by a

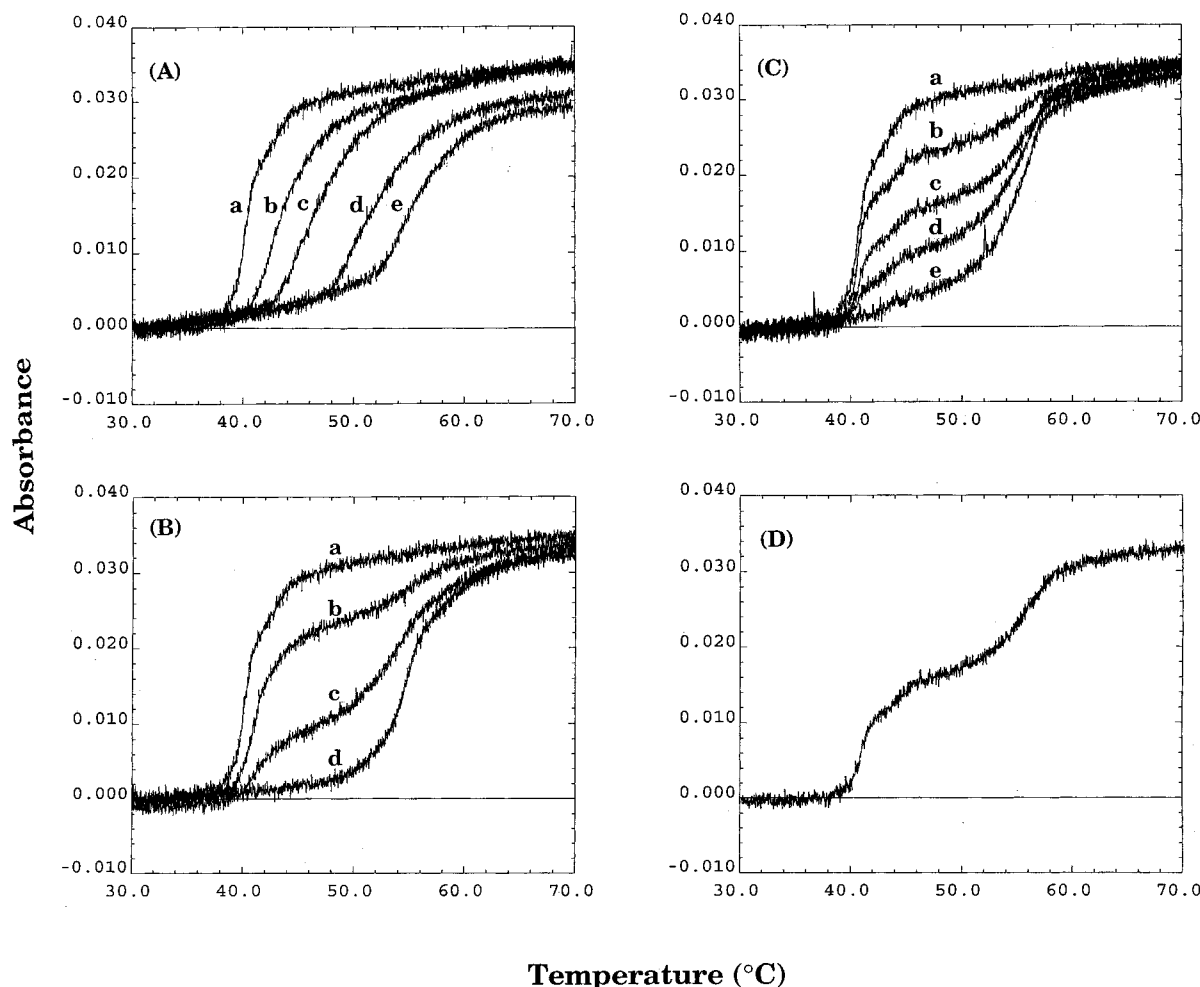


Figure 1. Melting behavior of poly[d(AT)] [0.01 SHE buffer: 8 mM NaCl, 2 mM HEPES, 0.05 mM EDTA; DNA base pair concentration = $6.5 \mu\text{M}$; pH 7.] in the presence of **I**, **II**, and **III**: (A) **III** at (a) 0, (b) 0.065, (c) 0.13, (d) 0.26, and (e) 0.39 μM ; (B) **I** at (a) 0, (b) 0.13, (c) 0.65, and (d) 1.56 μM ; (C) **II** at (a) 0, (b) 0.65, (c) 1.3, (d) 1.95, and (e) 2.6 μM ; (D) **II** at 1.3 μM . In all cases, a heating rate of 2 $^{\circ}\text{C}/\text{min}$ was used; absorbance was determined at 260 nm.

hydrogen atom (i.e., an analogous deoxycholic acid derivative) resulted in considerably stronger binding ($C_{50} = 1.4 \mu\text{M}$, not listed). It is noteworthy, in this regard, that a recent study by Burrows and co-workers has also shown that hydrophobic forces can contribute to the binding of certain amine-containing sterols to DNA (4). When the spermine molecule was attached to the double- and tetrawalled umbrellas, however, significantly greater DNA binding was observed. Similar behavior was found with poly[d(AT)] and poly[d(GC)] (Table 1). In control experiments, inclusion of 2 equiv of cholic acid did not significantly alter the affinity of spermine to poly[d(GC)] or spermidine to CT-DNA (not listed). In addition, the double-walled precursor (**I**) showed negligible binding toward all three types of DNA ($C_{50} > 200$).

Previous studies have shown that the binding of spermine and spermidine to DNA is strongly dependent upon the concentration of Na^+ that is present: the higher the Na^+ concentration, the weaker the polyamine binding (8). This result has been attributed to a competition between the proton-ionized nitrogens of the polyamine and Na^+ , in serving as counterions in the vicinity of the negatively charged DNA. Consistent with these findings, we have observed a dramatic decrease in the binding of spermine to poly[d(GC)] when the Na^+ concentration was increased from 8 to 150 mM (Table 1). Exactly analogous results were observed with **III**. In sharp contrast, the affinity of each of the umbrella conjugates toward DNA was significantly less dependent on salt concentration;

that is, the C_{50} values for **I** and **II** increased by factors of only ca. 5 and 2, respectively. Thus, the difference in DNA binding between spermine and **II** (both having four proton-ionizable nitrogens) at high salt concentrations is quite large, i.e., 2 orders of magnitude.

To obtain further insight into the interactions **I–III** with DNA, we examined their influence on the melting behavior (denaturation) of the duplex poly[d(AT)]. As can be seen in Figure 1, striking differences among these three systems are readily apparent. Thus, addition of **III** leads to a continuous increase in the melting temperature (T_m) in a manner that is very similar to that found with spermine and spermidine (not shown). In the absence of the conjugate, poly[d(AT)] shows a melting temperature of 41 $^{\circ}\text{C}$; with **III**, a maximum T_m of 56 $^{\circ}\text{C}$ is observed (Figure 1). In sharp contrast, incremental addition of the tetrawalled umbrella, **II**, resulted in two distinct melting temperatures, i.e., one that was similar to that of the native DNA and one that corresponded to a stabilized form ($T_m = 56 \text{ }^{\circ}\text{C}$). In this case, incremental addition of the umbrella resulted in a continuous diminution of the former component and an increase in the latter. Qualitatively, the double-walled molecular umbrella, **I**, exhibited behavior that combined those of **II** and **III**. Specifically, the low-temperature transition was gradually shifted to a high-temperature transition, and its overall contribution steadily declined. At high umbrella concentrations, only the high-temperature transition was observed.

Taken together, the effects of **I–III** on the melting behavior of poly[d(AT)] and the enhanced binding of the umbrella conjugates in the presence of a high salt concentration provide compelling evidence for highly cooperative binding and umbrella aggregation along the DNA duplex. Thus, the two distinct melting temperatures that are associated with **II** are a likely consequence of “bare” DNA segments and “stretches” of the duplex that are covered by an aggregated form of the umbrella. As the umbrella concentration is increased, the size and/or number of such aggregates increases. The fact that submicellar concentrations of **II** were used in these melting experiments [critical micelle concentration (cmc) in the identical buffer is 31 μ M; surface tension] further indicates that DNA serves as a nucleation site for aggregation. The continuous increase in temperature of a single transition for **III** also indicates that this conjugate is bound to DNA in a more random fashion. The apparent “mixed” behavior of **I** (cmc = 40 μ M) is a likely consequence of a monomer–aggregate equilibrium that is established on the surface of DNA, where both forms are present in significant amounts. Analogous nucleation phenomena have previously been reported for the binding of cetyltrimethylammonium bromide to DNA (9). Since **III** contains only a single amphiphilic wall, it is not capable of cooperative hydrophobic interactions with neighboring conjugates. With **I** and **II**, however (having two and four amphiphilic walls, respectively), such cooperativity is possible. The high cooperativity that is apparent for the DNA binding of **II** is a likely consequence of the larger number of walls that are present. The relatively modest differences in DNA binding between **I** and **II**, as judged by the ethidium displacement assay, can be readily accounted for if it is assumed that the amphiphilic walls do not play a direct role in the displacement of the dye, e.g., by contacting the DNA. Similar conclusions have recently been drawn for simple bile acid–polyamine conjugates (10). Finally, it should be noted that the cooperativity that we have discovered with these umbrella-based conjugates may also be possible with other small molecules; that is, the presence of amphiphilic walls may not be essential. Our findings do suggest, however, that a prerequisite for such cooperativity is that the ligand contain multiple hydrophobic segments.

In principle, cooperative DNA binding of the type described herein may be exploitable from the standpoint of rational drug design. One can envision, for example, that the attachment of molecular umbrellas to those drugs that act on DNA could result in increased potency due to stronger DNA binding. Moreover, the possibility of enhanced permeation across biological membranes could lead to increased efficacy by improving the drug's accessibility to the cytoplasm and to the nucleus of a cell. In preliminary studies, we have compared the abilities of

I–III to extract CT-DNA from 0.01 SHE buffer into an equal volume of 1-octanol using an umbrella/base pair ratio of 5.0. The percentages of DNA that was extracted were found to be 30, 84, and 3% for **I**, **II**, and **III**, respectively (phosphorus analysis). Although water/octanol partitioning is distinct from water/bilayer partitioning, these results clearly indicate that molecular umbrellas have the ability to transport DNA into a hydrocarbon environment. This capability, together with their ability to maintain strong DNA binding under physiological salt concentrations, is encouraging in terms of their possible use as gene transfer agents. Efforts aimed at exploring the practical potential of umbrella–spermine conjugates are continuing in our laboratories.

ACKNOWLEDGMENT

We are grateful to the National Institutes of Health (PHS Grant GM51814) for support of this research.

LITERATURE CITED

- (1) Janout, V., Lanier, M., and Regen, S. L. (1996) Molecular Umbrellas. *J. Am. Chem. Soc.* 118, 1573–1574.
- (2) Janout, V., Lanier, M., and Regen, S. L. (1997) Design and Synthesis of Molecular Umbrellas. *J. Am. Chem. Soc.* 119, 640–647.
- (3) Schmid, N., and Behr, J.-P. (1991) Location of Spermine and Other Polyamines on DNA As Revealed By Photoaffinity Cleavage With Polyaminobenzenediazonium Salts. *Biochemistry* 30, 4357–4361.
- (4) Hsieh, H. P., Muller, J. G., and Burrows, C. J. (1994) Structural Effects In Novel Steroidal Polyamine-DNA Binding. *J. Am. Chem. Soc.* 116, 12077–12078.
- (5) Cain, B. F., Baguley, B. C., and Denny, W. A. (1978) Potential Antitumor Agents. 28. Deoxyribonucleic Acid Polyintercalating Agents. *J. Med. Chem.* 21, 658–668.
- (6) Stewart, K. D. (1988) The Effect Of Structural Changes In A Polyamine Backbone On Its DNA-Binding Properties. *Biochem. Biophys. Res. Commun.* 152, 1441–1446.
- (7) Morgan, J. E., Blankenship, J. W., and Matthews, H. R. (1986) Association Constants For The Interaction Of Double-Stranded And Single-Stranded DNA With Spermine, Spermidine, Putrescine, Diaminopropane, N¹- and N⁸-Acetylspermidine, and Magnesium: Determination From Analysis Of The Broadening Of Thermal Denaturation Curves. *Arch. Biochem. Biophys.* 246, 225–232.
- (8) Braunlin, W. H., Strick, T. J., and Record, Jr., M. T. (1982) Equilibrium Dialysis Studies Of Polyamine Binding To DNA. *Biopolymers* 21, 1301–1314.
- (9) Mel'nikov, S. M., Sergeyev, V. G., and Yoshikawa, K. (1995) Transition Of Double-Stranded DNA Chains Between Random Coil And Globule States Induced By Cooperative Binding Of Cationic Surfactant. *J. Am. Chem. Soc.* 117, 9951–9956.
- (10) Walker, S., Sofia, M. J., Kakarla, R., Kogan, N. A., Wierichs, L., Longley, C. B., Bruker, K., Axelrod, H. R., Midha, S., Babu, S., and Kahne, D. (1996) Cationic Facial Amphiphiles: A Promising Class Of Transfection Agents. *Proc. Natl. Acad. Sci. U.S.A.* 93, 1585–1590.

BC970142R

New Synthesis and Characterization of (+)-Lysergic Acid Diethylamide (LSD) Derivatives and the Development of a Microparticle-Based Immunoassay for the Detection of LSD and Its Metabolites

Zhuyin Li, K. Goc-Szcutnicka, A. J. McNally,* I. Pilcher, S. Polakowski, S. Vitone, Robert S. Wu, and S. J. Salamone

Drug Monitoring, Diagnostics Research and Product Development, Roche Diagnostic System, Inc., 1080 U.S. Highway 202, Somerville, New Jersey 08876-3771. Received April 24, 1997[®]

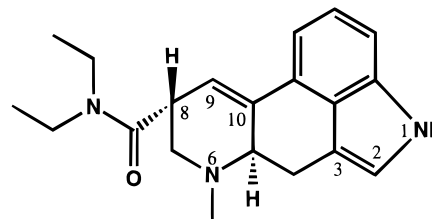
In this paper are reported the synthesis and characterization of three LSD derivatives. On the basis of several analytical characterization studies, the most stable derivative has been selected and a procedure to covalently link the derivative to polystyrene microparticles through a carrier protein has been developed. In addition, two new LSD immunogens have been synthesized and characterized, and from these immunogens antibodies that recognize not only LSD but also several major LSD metabolites have been generated. Using the selected derivative and antibody, a homogeneous microparticle-based immunoassay has been developed for the detection of LSD in human urine with the required sensitivity and specificity for an effective screening assay. The performance of this LSD OnLine assay has been evaluated using the criteria of precision, cross-reactivity, correlation to the Abuscreen LSD RIA and GC/MS/MS, assay specificity, and limit of detection.

INTRODUCTION

(+)-Lysergic acid diethylamide (LSD,¹ Scheme 1) is a highly potent drug that acts on the central nervous system and alters sensory perception, states of consciousness, and thought processes. By causing these altered states, the drug produces severe visual and auditory hallucinations. In addition to these physical effects, the use of LSD has been and continues to be a problem for drug and law enforcement agencies around the world (1–4). Making the problem even more complex is the fact that the detection of LSD in body fluids of users is difficult because the quantities typically ingested are very small (100–250 µg/dose) (4). To date, limited research has been conducted on the chemical properties of LSD. It is, however, known that LSD has an inherent fluorescence, which can be excited at 320 nm and emits at 445 nm. Additionally, under UV light irradiation, LSD can undergo catalytic hydration at the C-9,10 double-bond position. Once hydration occurs, the loss of fluorescence at 445 nm is observed. In alkaline solution, LSD undergoes an epimerization at the C-8 position, resulting in partial formation of iso-LSD. LSD is also unstable under prolonged heat exposure, but the mechanism of the thermal decomposition is not yet fully understood (5, 6).

Under physiological conditions, LSD is rapidly and extensively converted to several known and unknown

Scheme 1. Structure of LSD



metabolic products. At present, several metabolites of LSD in the human body, such as *N*-demethyl-LSD (nor-LSD), 2-oxo-3-hydroxy-LSD, 13-hydroxy-LSD, and 14-hydroxy-LSD, have been tentatively identified; yet only one metabolite (nor-LSD) and the parent compound, both excreted at 1% of the total dose, have been conclusively identified (6–10).

Currently, the measurements of LSD and its metabolites in biological fluids rely on radioimmunoassay methods or HPLC fluorescence methods and very specialized GC/MS/MS methods for confirmation (7–13). These methods produce undesirable radioactive waste or require extensive pretreatment of samples, very specialized equipment, and highly trained personnel. There has been much interest in recent years, because of the reported increased abuse, to develop nonisotopic, highly automated, homogeneous analytical methods to detect or screen for LSD abuse. Due to the lower sensitivities of nonisotopic immunoassays, the instability of LSD under both physiological and nonphysiological conditions, and the lack of information about the majority of the metabolites, the development of nonisotopic immunoassays to date has been a challenge. It is, therefore, extremely important to systematically synthesize LSD derivatives and study the stability of these derivatives for the development of a nonisotopic immunoassay. A conjugate procedure for making a LSD microparticle is also critical for obtaining a highly sensitive LSD assay. In addition, it is very important to generate antibodies that are capable of recognizing not only LSD but also its major metabolites. These antibodies must have low cross-

* Author to whom correspondence should be addressed.

© Abstract published in *Advance ACS Abstracts*, October 15, 1997.

¹ Abbreviations: BTG, bovine thyroglobulin; DMSO, dimethyl sulfoxide; DMF, *N,N*-dimethylformamide; CMC, *N*-cyclohexyl-*N*-(2-morpholinoethyl)carbodiimide methyl-*p*-toluenesulfonate; EDTA, ethylenediaminetetraacetic acid; ELISA, enzyme-linked immunosorbent assay; GC/MS/MS, gas chromatography/tandem mass spectrometry; KPi, potassium phosphate; NHB-H₂O, *N*-hydroxybenzotriazole hydrate; NHS, *N*-hydroxysuccinimide; LSD, (+)-lysergic acid diethylamide; nor-LSD, *N*-demethyl-LSD; NMR, nuclear magnetic resonance; SAMHSA, substance abuse and mental health services administration; TEA, triethylamine; THF, tetrahydrofuran; TLC, thin-layer chromatography; TNBS, trinitrobenzenesulfonic acid.

reactivity to structurally related compounds that are not substances of abuse.

In this paper, we describe the synthesis and characterization of new LSD derivatives used in the development of a microparticle-based OnLine immunoassay. We also describe a new procedure to make a LSD microparticle. Like other OnLine immunoassays, this assay is based on the principle of the kinetic interaction of microparticles in solution (KIMS) (14), in which the drug content in the urine is directly proportional to the inhibition of the microparticle agglutination. Four LSD derivatives were synthesized, two of which (**3** and **7**, Scheme 3) were used to prepare immunogens (**4** and **8**, Scheme 3) for antibody production and three of which (**6**, **7**, and **10**, Schemes 2 and 3) were examined for best stability. From this work the most stable derivative was selected for preparing the conjugate. For the development of this microparticle-based assay, the selected LSD derivative was covalently coupled to a carrier protein, and this conjugate was then covalently linked to microparticles. These newly developed LSD microparticles, together with the properly selected antibodies, were then developed into a competitive displacement immunoassay for LSD with a detection limit of 0.2 ng/mL LSD.

MATERIALS AND METHODS

Reagents. All solvents were obtained from Fisher Scientific (Pittsburgh, PA) unless specified. All flash grade silica gel and silica gel preparative TLC plates were obtained from E. M. Science (Gibbstown, NJ). Protein concentrations were determined by using the Bradford protein assay reagents (15) purchased from Bio-Rad (Hercules, CA), and 2-oxo-3-hydroxy-LSD was purchased from Radian (Austin, TX). LSD, nor-LSD, 1-(3-aminobutyl)-*N,N*-diethyl-*D*-lysergamide, and 1-(3-aminopropyl)-*N,N*-diethyl-*D*-lysergamide (**1a** and **1b**, Scheme 2) (16) and Abuscreen RIA were prepared by Roche Diagnostic Systems (Somerville, NJ). LSD antibodies for the Abuscreen RIA were generated using a LSD analogue derivatized through the indole nitrogen and conjugated to BSA. Carboxylated polystyrene microparticles were obtained from Bangs Laboratories (Carmel, IN). CMC, NHB·H₂O, ovalbumin, and other reagents were obtained from Sigma (St. Louis, MO).

Instrumentation. Fluorescence measurements were carried out by using an LS-5B luminescence spectrometer (Perkin-Elmer, Norwalk, CT). The excitation wavelength was set at 320 nm, and the emission wavelength was measured at 445 nm. Light irradiation was performed using a 20 W desk-top fluorescent light. Proton nuclear magnetic resonance (¹H NMR) spectra were recorded at 400 MHz on an XL-400 NMR spectrometer (Varian, Palo Alto, CA); coupling constants are given in hertz (Hz), and CDCl₃ was used as the solvent. The abbreviations used are as follows: s, singlet; d, doublet; t, triplet; m, multiplet. The OnLine immunoassay was performed using an Olympus AU800 automated analyzer (Olympus, Lake Success, NY).

Synthesis of LSD Labels. *Synthesis of 1-(3-Aminobutyl)-*N,N*-diethyl-*D*-lysergamide and 1-(3-Aminopropyl)-*N,N*-diethyl-*D*-lysergamide (**2a** and **2b**, Scheme 2).* A solution of 900 mg (1.7 mmol) of **1a** in 25 mL of methanol was treated with 0.385 mL (12.3 mmol) of anhydrous hydrazine and stirred at room temperature overnight. The reaction mixture was concentrated at reduced pressure. The residue was treated with 25 mL of a mixture of 9:1 methylene chloride/methanol, and the insoluble solids were filtered off. The filtrate was chromatographed on 200 g of silica gel using 25% methanol

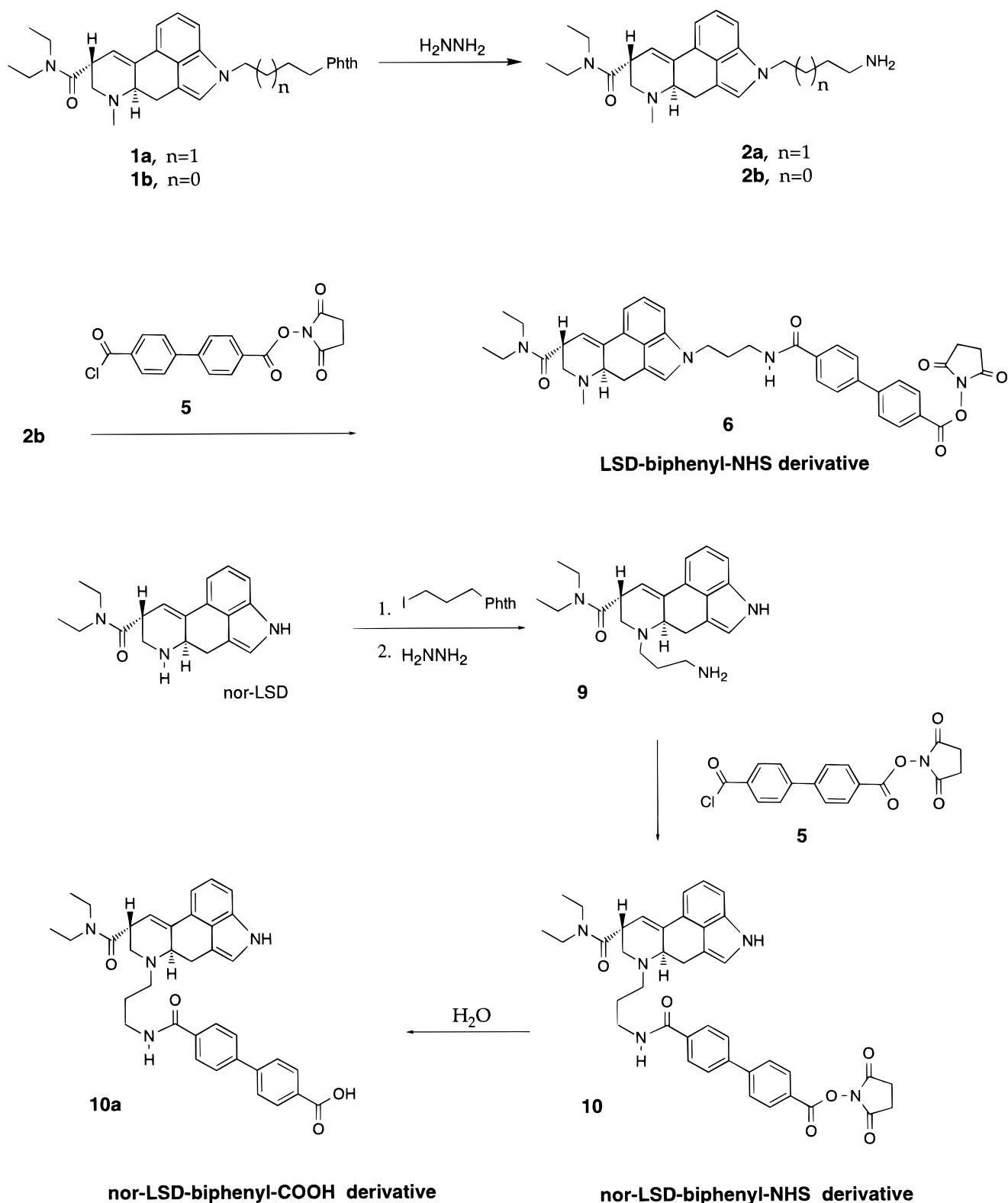
in methylene chloride as an eluent to elute front-running impurities, followed by 2% triethylamine/25% methanol in methylene chloride as an eluent to elute the product to yield 563 mg (83%) of **2a** as a yellow amorphous solid: ¹H NMR (400 MHz, CDCl₃) δ 1.17 (3H, t, *J* = 7.1), 1.24 (3H, t, *J* = 7.1), 1.50–1.60 (2H, m), 1.82–1.92 (2H, m), 2.59 (3H, s), 2.62–2.92 (6H, m), 3.02–3.10 (1H, m), 3.18–3.26 (1H, m), 3.37–3.57 (6H, m), 3.84–3.92 (1H, m), 4.08 (2H, t, *J* = 6.8), 6.33 (1H, s), 6.79 (1H, s), 7.11–7.20 (3H, m); MS, *m/e* 394 (M⁺); HR-EI MS calcd for M⁺ 394.2733, found 394.2731. Likewise, **2b** was obtained using an analogous procedure in 80% yield.

*Synthesis of 1-[[[4-Isothiocyanatophenyl]carbonyl]amino]butyl]-*N,N*-diethyl-*D*-lysergamide (**3**, Scheme 3).* A solution of 370 mg (0.94 mmol) of **2a** in 15 mL of anhydrous THF was cooled to 0 °C and treated with a solution of 190 mg (0.96 mmol) of 4-isothiocyanatobenzoyl chloride (**17**) in 5 mL of anhydrous THF and then stirred at 0 °C for 30 min and then at room temperature overnight; the reaction was driven to completion by adding 0.14 mL (1.0 mmol) of triethylamine and stirred at room temperature for 2 h. The reaction mixture was concentrated at reduced pressure. The residue was dissolved in methylene chloride, washed with H₂O, dried over anhydrous sodium sulfate, and concentrated at reduced pressure. The residue was chromatographed on 200 g of silica gel using 3% methanol in methylene chloride as an eluent to yield 325 mg (62%) of **3** as a tan amorphous solid: ¹H NMR (400 MHz, CDCl₃) δ 1.17 (3H, t, *J* = 7), 1.24 (3H, t, *J* = 7), 1.55–1.65 (2H, m), 1.80–2.05 (4H, m), 2.61 (3H, s), 2.63–2.75 (1H, m), 2.85–2.95 (1H, m), 3.04–3.12 (1H, m), 3.18–3.28 (1H, m), 3.35–3.58 (4H, m), 4.13 (2H, t, *J* = 6.4), 5.97–6.03 (1H, m), 6.35 (1H, s), 6.79 (1H, s), 7.10–7.20 (3H, m), 7.24 and 7.67 (4H, AA' BB'q, *J* = 8.4); MS, *m/e* 555 (M⁺); [α]_D = +47.5° (c 0.91%; CHCl₃).

*Synthesis of 4'-[[2,5-Dioxo-1-pyrrolidinyl]oxy]carbonyl]-[1,1'-biphenyl]-4-carbonyl Chloride (**5**, Scheme 2).* A mixture of 2.0 g (8.2 mmol) of 4,4'-biphenyldicarboxylic acid in 40 mL of anhydrous THF was treated with 5.0 mL (55.0 mmol) of oxalyl chloride followed by 0.02 mL of anhydrous DMF. The reaction was stirred at room temperature for 10 min and then heated to reflux for 90 min. The reaction was then concentrated at reduced pressure to a yellow oil. This was recrystallized from a mixture of THF and ether to yield 1.67 g (73%) of the diacid chloride as yellow needles: ¹H NMR (200 MHz, CDCl₃) δ 7.75 and 8.22 (8H, AA' BB'q, *J* = 8); MS, *m/e* 278 (M⁺).

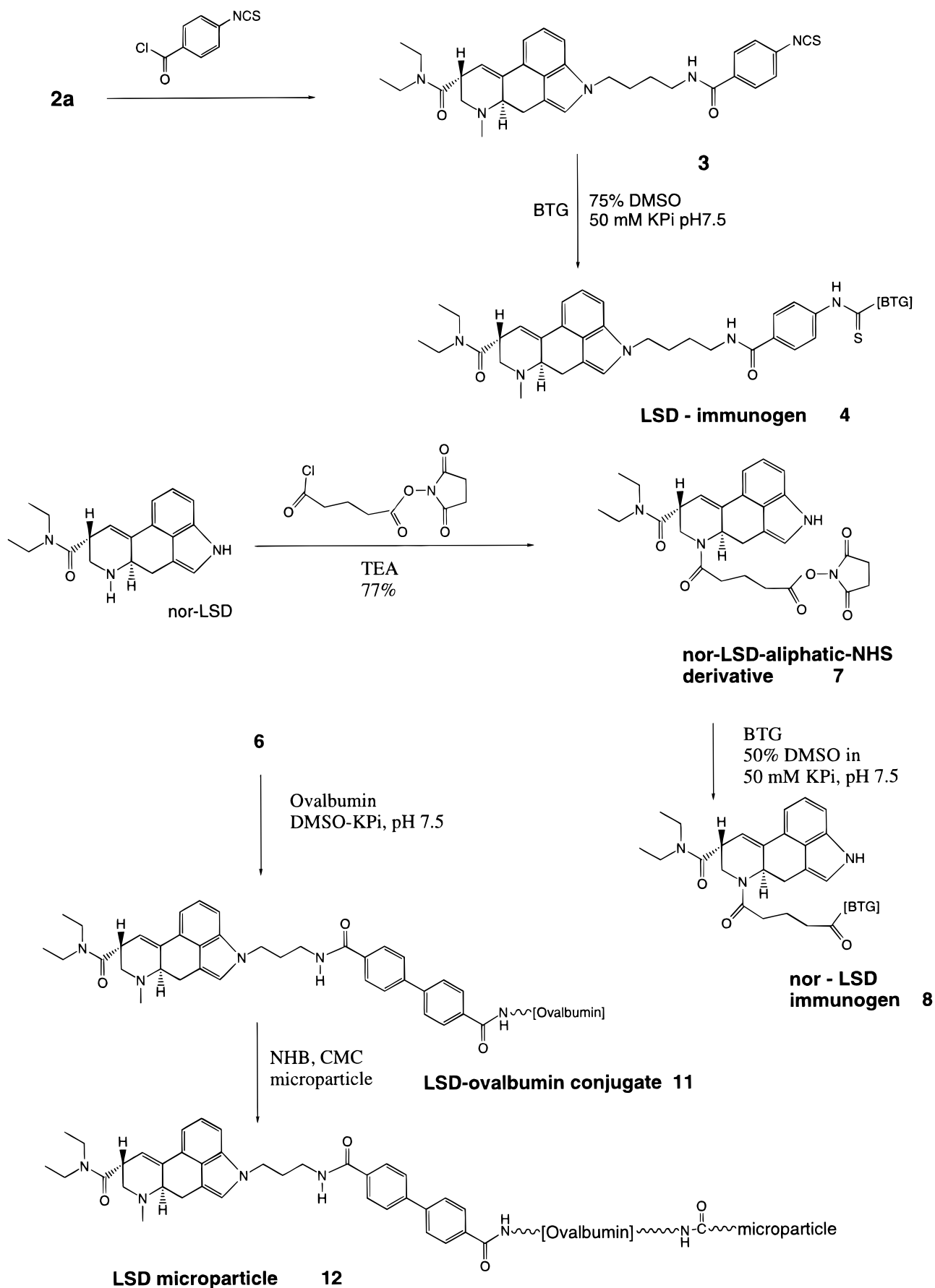
A solution of 1.67 g (6.0 mmol) of 1,1'-biphenyl-4,4'-dicarbonyl chloride in 65 mL of anhydrous THF was treated with 710 mg (6.17 mmol) of *N*-hydroxysuccinimide, followed by 0.835 mL (6.0 mmol) of triethylamine. The reaction was stirred at room temperature for 2 h, after which time it was filtered to remove triethylamine HCl. The filtrate was concentrated at reduced pressure to yield 2.0 g (93%) of **5** as a pale yellow solid: IR (CHCl₃) 1775, 1742 cm⁻¹; ¹H NMR (400 MHz, CDCl₃) δ 2.94 (4H, br s), 7.77 (4H, d, *J* = 8.5), 8.23–8.27 (4H, m); MS, *m/e* 357 (M⁺).

*Synthesis of 1-[3-[[[4'-[[2,5-Dioxo-1-pyrrolidinyl]oxy]carbonyl][1,1'-biphenyl]-4-yl]carbonyl]aminopropyl]-*N,N*-diethyl-*D*-lysergamide (**6**, Scheme 2).* A solution of 850 mg (2.375 mmol) of **5** in 65 mL of anhydrous THF under argon was cooled to 0 °C in an ice bath and then treated with a solution of 900 mg (2.365 mmol) of **2b** in 50 mL of anhydrous THF and 0.6 mL (4.3 mmol) of triethylamine added dropwise over a 20 min period. The reaction mixture was stirred at 0 °C for 1 h and then warmed to room temperature, with stirring, for 1 h. The mixture

Scheme 2. Synthesis of LSD Derivatives

was concentrated at reduced pressure, and the residue was dissolved in 100 mL of methylene chloride. The solution was washed with 100 mL of H_2O , 100 mL of saturated sodium bicarbonate solution, and 100 mL of saturated brine solution, dried over anhydrous sodium sulfate, and concentrated at reduced pressure to a brown residue. This was chromatographed on a short column of 100 g of silica gel using first methylene chloride as an eluent, then 9:1 methylene chloride/ether as an eluent to elute front-running impurities, and then 14:1 methylene chloride/isopropyl alcohol as an eluent to elute the

product to yield 650 mg (39%) of **6** as a cream-colored solid: IR (CHCl_3) 1772, 1743 cm^{-1} ; ^1H NMR (400 MHz, CDCl_3) δ 1.12–1.22 (6H, m), 2.18–2.22 (2H, m), 2.52 (3H, s), 2.60–2.68 (1H, m), 2.72–2.82 (1H, m), 2.93 (4H, s), 3.00–3.10 (2H, m), 3.38–3.58 (7H, m), 3.85–3.92 (1H, m), 4.24–4.32 (2H, m), 5.63–5.71 (1H, m), 6.41 (1H, s), 6.86 (1H, s), 7.20–7.25 (3H, m), 7.36 and 7.57 (4H, AA' BB' q, $J = 8.8$), 7.75 and 8.21 (4H, AA' BB' q, $J = 8.8$); MS, m/e 702 (M^+). An almost equal amount of the dimer was also obtained as a yellow oil: IR (CHCl_3) 3445, 2780, 1653, 1627 cm^{-1} ; ^1H NMR (CDCl_3) δ 1.16 (3H, t, $J = 7.2$),

Scheme 3. Preparation of LSD Protein Conjugates

1.21 (3H, t, $J = 7.1$), 2.15–2.23 (2H, m), 2.51 (3H, s), 2.56–2.64 (1H, m), 2.77 (1H, t, $J = 11$), 2.96–3.03 (1H, m), 3.03–3.09 (1H, m), 3.35–3.47 (5H, m), 3.47–3.55 (2H,

m), 3.80–3.86 (1H, m), 4.20–4.30 (2H, m), 5.90–5.96 (1H, m), 6.85 (1H, s), 7.17–7.25 (3H, m), 7.45 and 7.54 (4H, AA' BB'q, $J = 8.1$); MS, m/e 967 (M^+ H).

Synthesis of 1-[[5-[8 β -9,10-Didehydro-8-[(diethylamino)carbonyl]ergolin-6-yl]-1,5-dioxopentyl]oxy]-2,5-pyrrolidinedione (7, Scheme 3). A solution of 200 mg (0.65 mmol) of nor-LSD in 10 mL of anhydrous THF, under argon, was treated with 161 mg (0.65 mmol) of 5-[(2,5-dioxo-1-pyrrolidinyl)oxy]-5-oxopentanoyl chloride (20, 21), followed by 0.2 mL (1.4 mmol) of anhydrous triethylamine. The reaction mixture was stirred at room temperature for 30 min and then concentrated at reduced pressure. The residue was dissolved in methylene chloride, washed with H₂O and saturated aqueous sodium bicarbonate solution, dried over anhydrous sodium sulfate, and concentrated at reduced pressure to yield 330 mg (98%) of **7** as a yellow amorphous solid: UV (CH₃-OH) λ_{max} 308 (ϵ = 8980); IR (KBr) 3396, 1814–1739, 1634, 1628 cm⁻¹; ¹H NMR (400 MHz, CDCl₃) δ 1.08–1.18 (3H, m), 1.25–1.38 (3H, m), 2.05–2.25 (2H, m), 2.43–3.25 (6H, m), 2.83 (4H, s), 3.28–3.60 (6H, m), [4.26 (d, J = 13.6) (major) and 5.02 (d, J = 13.6) (minor)] (1H, rotamers), [4.73–4.81 (minor) and 5.25–5.33 (major)] (1H, m, rotamers), 6.38 (1H, m), [6.90 (major) and 6.95 (minor)] (1H, s, rotamers), 7.08–7.30 (3H, m), 8.00 (1H, m); MS, m/e 521 (M⁺).

Synthesis of 8 β -6-(3-Aminopropyl)-9,10-didehydro-N,N-diethylergoline-8-carboxamide (9, Scheme 2). Alkylation of nor-LSD with iodopropylphthalimide was carried out according to the procedure of Marzoni and Garbrect (16). The resulting phthalimide derivative (820 mg, 1.65 mmol) in 30 mL of methanol was treated with 0.4 mL (12.7 mmol) of anhydrous hydrazine and stirred at room temperature overnight. The reaction mixture was filtered and concentrated at reduced pressure. The residue was chromatographed on 100 g of silica gel using 2% triethylamine/15% methanol in methylene chloride as an eluent. Fractions containing product were combined and rechromatographed on 150 g of silica gel using 2% triethylamine/15% methanol in chloroform as an eluent to yield 560 mg (93%) of **9** as a yellow amorphous solid: IR (CHCl₃) 3479, 1663, 1624 cm⁻¹; ¹H NMR (400 MHz, CDCl₃) δ 1.17 (3H, t, J = 7), 1.25 (3H, t, J = 7), 1.70–1.80 (1H, m), 1.83–1.93 (1H, m), 1.90 (2H, s), 2.60–2.73 (2H, m), 2.79–2.87 (1H, m), 2.90–2.99 (2H, m), 2.99–3.09 (1H, m), 3.13–3.20 (1H, m), 3.25–3.33 (1H, m), 3.35–3.52 (6H, m), 6.28 (1H, s), 6.88 (1H, s), 7.10–7.17 (2H, m), 7.17–7.23 (1H, m), 8.20 (1H, br s); MS, m/e 366 (M⁺).

Synthesis of 1-[[[4'-[[[3-[8 β -9,10-Didehydro-8-[(diethylamino)carbonyl]ergolin-6-yl]propyl]amino]carbonyl]-1,1'-biphenyl]-4-yl]carbonyl]oxy]-2,5-pyrrolidinedione (10, Scheme 2). A solution of 1.32 g (3.7 mmol) of **5** in 50 mL of anhydrous methylene chloride under argon was cooled to 0 °C and treated with a solution of 535 mg (1.46 mmol) of **9** in 50 mL of anhydrous methylene chloride added dropwise over a 30 min period. After the addition was completed, the reaction mixture was washed with a saturated aqueous sodium bicarbonate solution, dried over anhydrous sodium sulfate, and concentrated under vacuum. The residue was chromatographed on 100 g of silica gel using 5% isopropyl alcohol as an eluent. Fractions containing product were combined and concentrated at reduced pressure to a yellow solid. The solid was redissolved in ether and concentrated five times to remove residual isopropyl alcohol to yield 280 mg (28%) of **10** as a yellow solid: IR (CHCl₃) 3479, 1773, 1743, 1636 cm⁻¹; ¹H NMR (400 MHz, CDCl₃) δ 0.86 (3H, m), 1.11 (3H, t, J = 6.9), 1.82–1.92 (1H, m), 1.93–2.10 (1H, m), 2.70–2.88 (4H, m), 2.93 (4H, s) 3.08–3.20 (2H, m), 3.22–3.38 (4H, m), 3.40–3.60 (4H, m), 3.60–3.70 (1H, m), 3.98–4.08 (1H, m), 6.35 (1H, s), 6.93 (1H, s), 7.15–7.25 (3H, m), 7.61 and 7.95 (4H, AA' BB'q, J = 8), 7.67 and

8.19 (4H, AA' BB'q, J = 8.3), 8.00 (1H, s), 9.05 (1H, br s); MS, m/e 688 (M⁺H); [α]_D = +9° (c 0.355%, CHCl₃).

Preparations of Protein Conjugates. **Synthesis of 1-[[[4'-Isothiocyantophenyl]carbonyl]amino]butyl]-N,N-diethyl-d-lysergamide-BTG (4, Scheme 3).** A solution of 698 mg of BTG in 20 mL of 50 mM KP_i, pH 7.5, was cooled to 0 °C and treated with 58 mL of DMSO, added dropwise, very slowly over a 2 h period. The mixture was treated with a solution of 90 mg (0.16 mmol) of **3** in 2 mL of DMSO, added dropwise very slowly. The reaction mixture was stirred at room temperature for 18 h, poured into a dialysis bag of 50 kDa molecular weight cutoff, and dialyzed 10⁸-fold in 50 mM KP_i, pH 7.5. The resulting conjugate was filtered through a 0.22 μ m sterile filter to yield 116 mL of the LSD-BTG immunogen **4**. The protein concentration was determined to be 5.3 mg/mL. The degree of drug substitution on the BTG protein was determined by the ability of remaining uncoupled lysine residues to react with TNBS (18, 19). Unmodified BTG, at the same concentration as the conjugate, was treated in the same manner with TNBS to provide a control. This procedure produced a yellow complex with an absorbance maximum at 325 nm and was used to calculate the drug substitution expressed as percent modification. The assay showed a 63.8% modification of available lysines on BTG.

Synthesis of 5-[8 β -9,10-Didehydro-8-[(diethylamino)carbonyl]ergolin-6-yl]-1,5-dioxopentyl-BTG (8, Scheme 3). A solution of 700 mg of BTG in 13 mL of 50 mM KP_i, pH 7.5, was cooled to 0 °C and treated with 13 mL of DMSO, added dropwise, very slowly. After the addition was complete, a solution of 84 mg (0.16 mmol) of **7** in 1 mL of DMSO was added dropwise very slowly. The reaction mixture was stirred at room temperature for 18 h, poured into a dialysis bag of 50 kDa molecular weight cutoff, and dialyzed 10⁶-fold in 50 mM KP_i, pH 7.5. The resulting conjugate was filtered through a 0.22 μ m sterile filter to yield the LSD-BTG conjugate **8**. The protein concentration was determined to be 12.1 mg/mL. The TNBS assay showed a 45% modification of available lysines in BTG.

LSD Derivatives Exposed to Fluorescent Light, Oxygen, and Different Solution pH Values. All LSD derivatives (**6**, **7**, and **10**) were placed in quartz cuvettes, and the irradiation experiments were conducted under the following conditions: LSD derivatives were dissolved in DMSO at a concentration of 1 mg/mL and further diluted to 2.6 mM in 10 mM KP_i buffer, pH 7.5, containing 0.09% NaN₃, 5 mM EDTA, and 0.1% Tween 20. The solutions were kept at 2–8 °C in the dark for 3 days to ensure a complete hydrolysis of the NHS ester (e.g. **10a**, Scheme 2). This is indicated by a complete disappearance of the starting material by TLC examination (data not shown). For the stability to light study, samples were exposed to a 20 W desk fluorescent light at room temperature. The distance between the fluorescent light source and the experimental samples was 15 cm. The experimental samples were subjected to irradiation for various times, and then fluorescence from the samples was measured, with λ_{ex} = 320 nm and λ_{em} = 445 nm. Triplicate measurements were performed under each condition. Coefficients of variation were found to be \leq 1.5% for the analytical method. From these data we established that >9% loss in fluorescent intensity represented significant decomposition of the tested compounds. This change of 9% represents three standard deviations from the mean, which is a >99% confidence interval. Corresponding LSD derivatives kept in the dark, at room temperature, were used as controls. These experiments were designed to investigate the effect of indoor light on the stability of the C-9,10 double-bond

position of LSD derivatives and to rank the light stabilities of these derivatives.

For stability to oxygen and solution pH studies, samples were placed in amber glass bottles and saturated with either oxygen or argon. Subsequently, these experimental samples were incubated at 45 °C for 10 days. Samples kept at 2–8 °C in the dark with argon were classified as the control. These experiments were conducted to explore the effect of oxygen, pH, and heat on the stability of the C-9,10 double-bond position of LSD derivatives and to rank the stability of these derivatives under these conditions.

Antibody Generation. Several goats were placed on a modified immunization program, as described by Vaitukaitis (22) using LSD immunogens (**4** or **8**). Briefly, immunogen **4** or **8** was mixed with Freund's adjuvant, and 1 mg of the immunogen containing complete Freund's was injected into multiple sites across the back of each goat. At week two, each goat continued to receive 1 mg of the immunogen containing incomplete Freund's. This injection was repeated twice at 1 week intervals, followed by a monthly injection of 0.5 mg of the immunogen mixed with incomplete Freund's adjuvant for a period of 6 months.

The individual animals were monitored for antibody titer and for cross-reactivity with LSD, nor-LSD, and 2-oxo-3-hydroxy-LSD by an ELISA method. Specifically, a selected derivative was covalently coupled to a carrier protein (ovalbumin). Polystyrene 96 well microtiter plates were coated with 50 μ L of a 1.6 μ g/mL LSD–ovalbumin conjugate in PBS buffer (50 mM KPi , pH 7.2, containing 150 mM NaCl) and allowed to incubate for 2 h at room temperature or overnight at 2–8 °C. The plates were washed with PBS buffer and blocked with 1% BSA in PBS buffer. Fifty microliters of LSD, nor-LSD, or 2-oxo-3-hydroxy-LSD diluted in 1% BSA/PBS buffer at various concentrations or 50 μ L of 1% BSA/PBS buffer without the drug as a control was added into each well. Fifty microliters of the appropriate antiserum in 1% BSA/PBS buffer was then added to each well. The plates were incubated for 1 h at 37 °C and then washed with PBS/Tween 20 buffer. Anti-goat–alkaline phosphatase conjugate and *p*-nitrophenyl phosphate were then used to generate a detection signal. Two criteria were used to select antibodies: (1) affinity of antibodies as estimated by IC_{50} ; (2) inhibition of solid-phase antibody binding by soluble LSD and its major metabolites, namely, nor-LSD and 2-oxo-3-hydroxy-LSD. Once several animals were selected from an immunogen, a pool of antiserum was made and used to develop the immunoassay.

Preparation of LSD–Ovalbumin Conjugate (11, Scheme 3). Seventeen and a half milliliters of ovalbumin solution at 25 mg/mL in 50 mM KPi buffer, pH 7.5, was cooled in an ice bath, and to this was slowly added 10 mL of DMSO. Seven and a half milligrams of selected LSD derivative was then dissolved in 1.5 mL of anhydrous DMSO to make a 5 mg/mL solution. The LSD derivative solution was added dropwise into the ovalbumin solution with stirring, and stirring was continued for 18 h at room temperature. The resulting LSD–ovalbumin conjugate was dialyzed 10^{12} -fold using 30 kDa molecular weight cutoff dialysis bags. The final total protein concentration of LSD–ovalbumin conjugate was determined according to the Bradford protein assay (15).

Characterization of LSD–Ovalbumin Conjugate. To determine the concentration of the noncovalently bound LSD in the LSD–ovalbumin conjugate, the following experiments were conducted: 1.5 mL of 12.5 mg/mL LSD–ovalbumin conjugate in KPi buffer, pH 7.5, was heat stressed at 45 °C in a white nontransparent poly-

ethylene container (HDPE) for 24 h. It was then immediately mixed with 1.5 mL of 40% DMF in 10 mM KPi , pH 7.5. The material was then left at room temperature for 2 h, placed in a ovalbumin precoated Centricon filter (Amicon, Beverly, MA) with a molecular weight cutoff of 30 kDa, and centrifuged at 600*g* for 2 h. The resulting filtrate was then analyzed by fluorescence spectroscopy. Completely hydrolyzed LSD–biphenyl-NHS (**6**) solutions with concentrations ranging from 200 to 3200 ng/mL were used as fluorescence standard, and a linear regression method was used to generate a calibration curve. The concentration of LSD in the filtrate was derived from the standard curve. Filtrate from ovalbumin treated according to the same method as the LSD–ovalbumin conjugate was used as the control for background measurements.

A method was also designed to measure the total number of LSD derivatives per ovalbumin in the LSD–ovalbumin conjugate. The LSD–ovalbumin conjugate was diluted to a concentration of 0.125 mg/mL of total protein, and the fluorescence at 445 nm from the diluted conjugate solution was measured. Ovalbumin treated according to the same method as the LSD–ovalbumin conjugate was used as the control for a blank measurement. Completely hydrolyzed LSD–biphenyl-NHS (**6**) solution concentrations ranging from 200 to 3200 ng/mL were again used as fluorescence standards to generate a calibration curve. Total concentration of LSD molecules per ovalbumin was estimated from the calibration curve.

Preparation of the LSD Microparticle (12, Scheme 3). Ten milliliters of carboxyl-modified microparticle (10% solids) was first washed by centrifugation at 10000*g* with 0.1% Tween 20 in H_2O . To each milliliter of particles was added 20 mL of 0.1% Tween 20 in water, the mixture was centrifuged and decanted, and the particles were subsequently resuspended. This process was repeated five times, and the microparticle concentration was then adjusted to 3% (w/v) with a 0.1% Tween 20 solution. One and two-tenths milliliters of NHB (25 mg/mL, 0.37 mmol), previously dissolved in DMSO, was then added slowly to the 30 mL of microparticle suspension, under rapid stirring conditions, and the suspension was stirred for 10 min at 25 °C. To this suspension was added 1.7 mL of a freshly prepared CMC solution (50 mg/mL, 0.34 mmol), and the mixture was stirred slowly for 3 h at 25 °C. The material was then washed according to the method of centrifugation described above. The washed, activated microparticles (45 mL at 2%) were immediately mixed with LSD–ovalbumin/ovalbumin mixture at different molar ratios (total protein concentration was fixed at 3.1 mg/mL) diluted in 50 mM sodium bicarbonate buffer, pH 8.6, and this mixture was allowed to stir for 15 h at 25 °C. The resulting LSD microparticles were then washed according to the method of centrifugation described above using a wash solution of 10 mM KPi buffer, pH 7.5, containing 0.09% NaN_3 and 0.1% Tween 20. The washed microparticle was then resuspended in this buffer at 1.0% solids (w/v).

Development of the LSD Immunoassay. The LSD immunoassay contains three reagents: (1) the antibody reagent, which was made by placing the titrated antibody in a solution of 50 mM HEPES, pH 6.5, containing 0.1% BSA protein, 0.5% NaCl, and 0.09% NaN_3 ; (2) a reaction buffer containing 50 mM PIPES, pH 7.0, with 2–3% PEG, 2% NaCl, and 0.09% NaN_3 ; and (3) a LSD microparticle reagent, diluted from 1% stock solution to 0.2% solids in a buffer containing 10 mM KPi , pH 7.5, 0.09% NaN_3 , and 0.1% Tween 20. In addition, LSD calibrators at concentrations between 0 and 1 ng/mL in normal urine containing 0.09% NaN_3 were used. The concentration of

these LSD standards were verified by GC/MS/MS method. The antibody concentration was adjusted so that the agglutination of the LSD microparticles was inhibited proportionally to the LSD concentration in the calibrators. The light scattering difference between different calibrators was also maximized in the calibration range (0–1 ng/mL) to obtain maximum sensitivity.

Cross-reactivity to structurally related compounds was conducted as follows: Normal human urine samples were spiked with the structurally related compound of LSD at various concentrations and tested as unknowns in the OnLine assay. The percent cross-reactivity of a structurally related compound was determined using the concentration of the compound that provided displacement equivalent to 0.5 ng/mL (1.5 nM) LSD.

One thousand presumed negative urine specimens were obtained from a large drug abuse screening laboratory. These samples had been previously screened and found to be negative for the SAMHSA five panel (cannabinoids, opiates, cocaine metabolite, amphetamine, and phencyclidine). At the time of analysis, these samples were simultaneously screened for LSD with the Abuscreen RIA and OnLine assay. The Abuscreen RIA has a >99.5% accuracy rate and was used as a reference method in addition to GC/MS/MS method. In addition, LSD positive samples were supplied by Dr. R. Foltz and Dr. D. Kuntz (Northwest Toxicology, Salt Lake City, UT). These samples had been previously screened positive by the Abuscreen RIA and were subsequently confirmed by GC/MS/MS. These samples were received frozen and were stored at -20°C until the day of analysis. For analysis, a qualitative screening assay was performed as follows: a single point calibration standard was used, and its absorbance value was assigned as the cutoff value. A positive result was reported if the sample absorbance value was greater than or equal to the absorbance of the cutoff calibrator.

RESULTS AND DISCUSSION

Synthesis and Stability Studies of the LSD Derivatives. A detailed analytical study of the synthesized LSD derivatives was necessary to determine which derivatives should be used to develop the LSD OnLine assay. The effect of exposure to fluorescent light on the LSD derivatives is shown in Figure 1. The C-9,10 double bond of LSD as previously reported can undergo photocatalytic hydration (5). A potential structure change or instability at this position was indicated by a change in fluorescence intensity when compared to a control. It was demonstrated that the fluorescence intensity of each compound decreased as the exposure time to fluorescent light increased. These results suggested that the order of stability of the LSD derivatives to photon-catalyzed hydration is LSD-biphenyl-COOH (hydrolyzed from **6**) > nor-LSD-biphenyl-COOH (hydrolyzed from **10**) > nor-LSD-aliphatic-COOH (hydrolyzed from **7**). It is hypothesized that the improved stability of **6** may come from the presence of biphenyl group at the N-1 position of the LSD molecule, where the biphenyl moiety can effectively stack on the LSD and exclude water molecules from interaction, thus stabilizing the photolabile C-9,10 center. Such hydrophobic stacking interaction has been documented (23, 24). When the biphenyl modification was at position 6 of the LSD molecule, the biphenyl linker could not effectively stack on the LSD and the protection efficiency was reduced. The aliphatic moiety at position 6 would be predicted to offer little or no protection effect to the LSD molecule, and indeed, this molecule had the least stability under these conditions. The LSD-biphenyl compound (**6**) was chosen for the construction of the

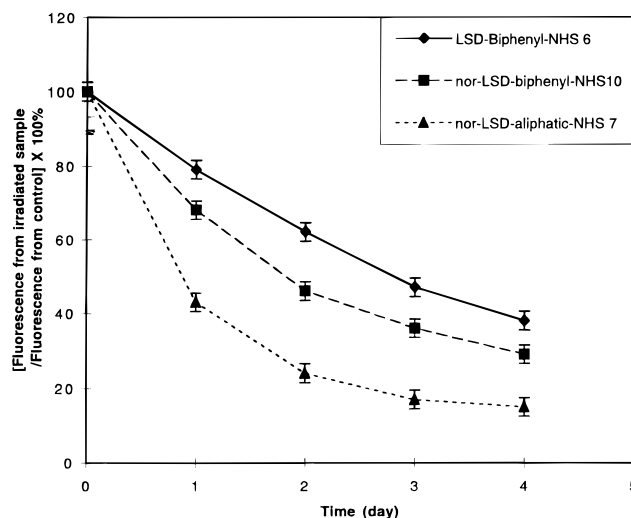


Figure 1. Effect of fluorescent light irradiation on the stability of LSD derivatives. Structural changes of LSD derivatives at the C-9,10 position were indicated by changes in fluorescence intensity. Condition: 2.6 mM LSD derivatives in 10 mM KPi , pH 7.5, buffer containing 5 mM EDTA, 0.09% NaN_3 , and 0.1% Tween 20. All experiments were conducted at 25°C . Corresponding LSD derivatives kept in the dark at 25°C were used as controls. The Y axis represents the fluorescence intensity of irradiated LSD derivatives when compared to their controls. The X axis is exposure time to fluorescent light. Error bar represents ± 2 SD.

conjugate used in the nonisotopic immunoassay. This compound displayed a 50–60% decomposition after having been exposed to the described conditions for 4 days. To ensure good assay stability, this issue was addressed by placing the microparticle reagent containing this derivative in a nontransparent polyethylene container. An accelerated stability study indicated that this container protects the reagent from light to ensure <10% loss at normal room light conditions for 1 year. Further data to emphasize the need not to have decomposition are reflected in cross-reactivity studies of antibodies generated from LSD immunogen (**4**) to completely photodecomposed LSD-biphenyl-COOH (**6**). It was found that the cross-reactivity of this decomposed material was <20% (data not shown), which would cause serious loss in assay sensitivity if the derivative was allowed to decomposed.

Under heating conditions, oxygen may have an effect on the C-9,10 double bond (25). However, it appears from our experiments that oxygen did not affect the stability of the C-9,10 double bond for the LSD derivatives. Since protons can catalyze the hydration of the C-9,10 double bond (5, 25), we explored the effect of pH on the hydration of different LSD derivatives at high temperatures. Solution pH was chosen to be 6.0 or 7.5, because this is the most acceptable pH range for immunochemical reactions. At pH 6.0, in the presence or absence of oxygen, after 10 days at 45°C , compound **10** lost ~20% of its fluorescence intensity, while fluorescence intensity changes for compounds **6** and **7** were negligible. No significant changes in fluorescence intensity were observed for all three compounds when they were kept at pH 7.5 for 10 days at 45°C . The results suggested that the LSD derivatives were more stable in pH 7.5 buffer than in pH 6.0 buffer.

Synthesis of LSD Immunogen and the Generation of LSD Antibodies. Since only 1% of ingested LSD is excreted in urine and the typical ingested dose is very low, it is prudent to generate LSD antibodies that can recognize not only LSD but also LSD metabolites, yet avoid other undesirable ergot alkaloids compounds.

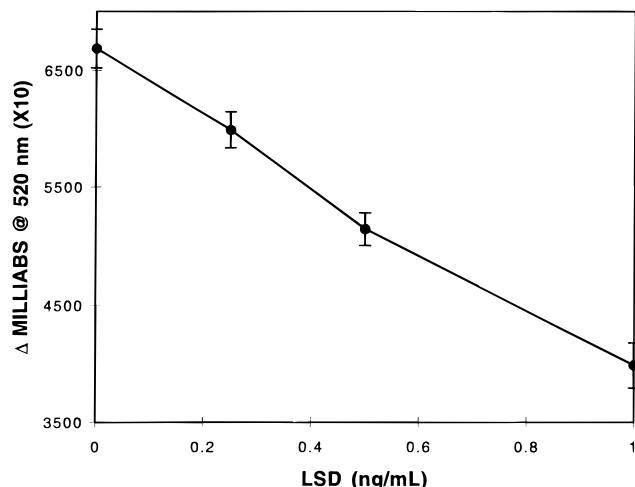


Figure 2. Representative concentration response curve on the Olympus AU800 analyzer of the Abuscreen LSD OnLine assay. Absorbance (ABS) is expressed as the milliabsorbance multiplied by a factor of 10. Error bar represents ± 1 SD.

Table 1. Qualitative Precision of Abuscreen LSD OnLine Assay^a

Within-run	Level 1	Level 2	Level 3	Level 4
LSD (ng/mL)	0.25	0.50	0.75	1.00
Mean ABS* (mA X 10)	6686	5989	5141	3985
SD (mA X 10)	165	154	140	193
CV %	2.5	2.6	2.7	4.9
Day-to-day	Level 1	Level 2	Level 3	Level 4
LSD (ng/mL)	0.25	0.50	0.75	1.00
Mean ABS* (mA X 10)	6587	5860	5156	3977
SD (mA X 10)	198	230	188	194
CV %	3.0	3.9	3.7	4.9

^a The Olympus AU 800 analyzer multiplies the milliabsorbance units by a factor of 10 to report results. Precision was determined to be $<3.0\%$ at 0 ng/mL (blank) urine.

Selectivity of an antibody to a hapten can be directed such that the antibody preferentially recognizes the part of the molecule that is farthest away from the attachment of the hapten to a carrier protein (26). It was assumed that this will allow the antibody to tolerate changes to the hapten near its point of attachment to the carrier protein. Under this hypothesis, we designed two immunogens (**4** and **8**). These immunogens directed antibodies to be less specific regarding changes near the indole ring of LSD (27) or at position 6 of LSD; therefore, cross-reactivity toward 2-oxo-3-hydroxy-LSD, 13-hydroxy-LSD, 14-hydroxy-LSD, and nor-LSD would be predicted to be higher for antibodies generated with immunogen **4**. Antibodies generated from immunogen **8** would be expected to have high cross-reactivity toward 2-oxo-3-hydroxy-LSD and nor-LSD.

LSD-biphenyl-NHS (**6**) was used to construct the LSD-ovalbumin conjugate label for the ELISA method. The binding between the LSD-ovalbumin conjugate label and

Table 2. Cross-Reactivities of Abuscreen OnLine LSD Assay

Compound	Percent Cross-Reactivity	
	by weight concentration	by molar concentration
d-LSD	100	100
2-Bromo- α -ergocryptine	< 0.003	< 0.006
l-LSD (iso-LSD)	2.4	2.4
Lysergic acid N-(methylpropyl) amide	14	14
2-oxo-3-hydroxy-LSD	40	45
Lysergic acid N-(hydroxyethyl) amide	0.03	0.03
d-Lysergic acid	< 0.003	< 0.002
N-desmethyl-LSD (nor-LSD)	36	33
Methylsergide maleate	0.009	0.01
α -Ergocryptine	< 0.003	< 0.004
Ergotamine Tartrate	0.004	0.02
Ergonovine Maleate	0.004	0.005
Serotonin (5-hydroxy-tryptamine)	< 0.003	< 0.001
Tryptophan	< 0.003	< 0.002

the antibodies generated from immunogen **4** can be displaced with LSD (100%), nor-LSD (20%), and 2-oxo-3-hydroxy-LSD (50%). When antibodies generated from immunogen **8** were used, the binding between the LSD-ovalbumin conjugate label and antibodies could be displaced by LSD and had high cross-reactivity to nor-LSD (40%) but had $<20\%$ cross-reactivity to 2-oxo-3-hydroxy-LSD. From the cross-reactivity studies, antibodies raised against immunogen **4** were selected, and, from the derivative stability studies, derivative **6** was chosen for development of a LSD immunoassay.

Preparation and Characterization of LSD-Ovalbumin Conjugate. For a LSD assay, a 1:1 molar ratio between LSD-biphenyl-NHS (**6**) and ovalbumin was used to synthesize the LSD-ovalbumin conjugate stock solution. Since the LSD derivative is a highly hydrophobic compound, it can be trapped in ovalbumin or absorbed on the ovalbumin surface noncovalently. This unbound LSD derivative could be gradually released from the conjugate and could cause poor stability. The unbound LSD derivative could react with titrated antibody and reduce the sensitivity of the LSD assay. Therefore, it was important to develop a reproducible dialysis procedure to remove the unbound LSD from the LSD-ovalbumin conjugate. It was also important to establish a method to measure the noncovalently bound LSD derivatives on the conjugate so that methods could be selected that prevent this from occurring. To accomplish this, the conjugate was denatured at 45°C and then in 20% DMF solvent to release any noncovalently bound LSD derivative. Under these mild denaturing conditions, no protein precipitation was observed. Our results indicated that free LSD derivative accounted for $<0.3\%$ of total LSD derivative loaded on ovalbumin when an extensive dialysis (10^{12} -fold) procedure was used. This procedure was necessary to obtain a stable OnLine LSD assay reagent.

Methods were also developed to quantify the number of the LSD molecules per ovalbumin molecule in the

Table 3.

TOTAL SAMPLE CORRELATION			CHARACTERIZATION OF THE GC/MS/MS VALUES FOR THE LSD POSITIVE CLINICAL SAMPLES																								
<div><div>ABUSCREEN ONLINE</div><div><div>+</div><div>-</div></div><table><tr><td>81</td><td>7</td></tr><tr><td>0</td><td>993</td></tr></table></div>			81	7	0	993	<div>Mean Value for</div> <div><div>LSD:</div><div>0.8 ng/mL</div></div> <div><div>ISO-LSD:</div><div>1.2 ng/mL</div></div> <div>Range</div> <div><div>LSD:</div><div>0.2 -17.5 ng/mL</div></div> <div><div>ISO-LSD:</div><div>0.0 -5.4 ng/mL</div></div> <div>Percentage of Samples in the Following Range:</div> <table><tr><th>Range (ng/mL)</th><th>Sample Number</th><th>Percent</th></tr><tr><td>0.00-0.25</td><td>6</td><td>7.4</td></tr><tr><td>0.26-0.50</td><td>14</td><td>17.3</td></tr><tr><td>0.51-0.75</td><td>20</td><td>24.7</td></tr><tr><td>0.76-1.00</td><td>14</td><td>17.3</td></tr><tr><td>>1.00</td><td>27</td><td>33.3</td></tr></table>			Range (ng/mL)	Sample Number	Percent	0.00-0.25	6	7.4	0.26-0.50	14	17.3	0.51-0.75	20	24.7	0.76-1.00	14	17.3	>1.00	27	33.3
81	7																										
0	993																										
Range (ng/mL)	Sample Number	Percent																									
0.00-0.25	6	7.4																									
0.26-0.50	14	17.3																									
0.51-0.75	20	24.7																									
0.76-1.00	14	17.3																									
>1.00	27	33.3																									
<div><div>ABUSCREEN ONLINE</div><div><div>+</div><div>-</div></div><table><tr><td>81</td><td>0</td></tr><tr><td>0</td><td>0</td></tr></table></div>			81	0	0	0																					
81	0																										
0	0																										

LSD-ovalbumin conjugate stock solution. Since amino groups at the protein surface are used in the coupling, normally, the degree of drug substitution can be determined by the ability of remaining uncoupled amine residues that react with TNBS. However, since the LSD substitution ratio was low (mean < one LSD per ovalbumin), poor results were obtained using the TNBS method. It was found that the number of LSD molecules in the conjugate could be estimated directly using the LSD fluorescence intensity. The fluorescence from ovalbumin at the same concentration as the conjugate was insignificantly small compared to the total intensity. Using completely hydrolyzed LSD-biphenyl-NHS (**6**) as a standard, the conjugates have been shown to contain 0.6–0.8 LSD molecules per ovalbumin molecule. Because coupling of LSD to ovalbumin would change the fluorescence quantum yield from LSD, this method only provided an estimate of the loading of LSD molecules per ovalbumin and was useful for quality control purposes (data not shown).

Synthesis and Characterization of LSD-Microparticle Conjugate. Several different molar ratios of the drug protein conjugate to microparticle were evaluated to determine the optimal ratio that produced the best dose response curve. In the development of a microparticle-based immunoassay, it is important that proper agglutination occurs in the absence of free antigen. To accomplish this, proper amounts of drug protein conjugate must be coupled to each microparticle such that an equivalence point can be reached, allowing the cross-linking of microparticles by antibody. Excess antigen or excess antibody in the system will prevent the formation of the large aggregates produced by cross-linking.

To establish the proper substitution of drug onto microparticle, LSD was first covalently coupled to the ovalbumin protein (stock conjugate) followed by mixing of the LSD-ovalbumin conjugate with ovalbumin at

various molar ratios and coupling the LSD-ovalbumin/ovalbumin mixture to the microparticle. Each coupled microparticle was then titrated against the antibody to determine the performance of each LSD-ovalbumin/ovalbumin molar ratio. The ratio that gave the greatest dose response curve and the lowest nonspecific binding (agglutination rate in the absence of antibody) was selected. This was determined to be a molar ratio of 1:8 (LSD-ovalbumin/ovalbumin).

Development of LSD Assay. Using an endpoint analysis reading at 520 nm, a dose response curve was generated with various concentrations of LSD as shown in Figure 2. The light scattering difference measured by light transmission from 0 ng/mL to the cutoff concentration of LSD (0.5 ng/mL) was > 130 milliabsorbances (mA); the overall difference from 0 to 1.0 ng/mL was > 240 mA. Table 1 shows that the qualitative intra-assay ($n = 20$) and interassay ($n = 100$) precision had CVs of <5%.

Table 2 illustrates the cross-reactivity of the LSD OnLine assay to structurally related compounds of LSD. As expected, this assay had low cross-reactivity to iso-LSD (2.4%, molar concentration); the cross-reactivity to nor-LSD was 25% and to 2-oxo-3-hydroxy-LSD was 32%. The cross-reactivities of other structurally related compounds that are undesirable to detect, such as serotonin, tryptophan, ergotamine, egonovine, and others, were <0.002%. Finally, the limit of detection (LOD) of the assay was determined by performing 20 replicate assays on the 0 ng/mL calibrator. Two standard deviations below the mean yields a LOD of <0.2 ng/mL LSD.

Table 3 shows the correlation of the OnLine LSD screening assay with RIA and GC/MS/MS methods. GC/MS/MS confirmed LSD positive clinical samples were used to study patient correlation. Eighty-one positive samples were tested in the OnLine LSD assay. The distribution of LSD concentration in these samples is also shown in Table 3. Twenty percent of the samples

contained <0.5 ng/mL of LSD according to GC/MS/MS data. Due to the high cross-reactivity to major LSD metabolites, all of these samples were positive by OnLine LSD assay. One thousand presumptive negative samples were also tested; 993 were negative and 7 were positive. All of the presumptive negative samples were found to be negative by RIA. These seven samples that were OnLine positive and RIA negative were found to be GC/MS/MS negative.

CONCLUSION

A homogeneous microparticle-based immunoassay has been developed for the detection of LSD in human urine with the required sensitivity and specificity. Three major issues were considered when this assay was developed: (1) the stability of the LSD derivatives; (2) the stability of LSD microparticles; (3) the cross-reactivity of antibodies. Light, temperature, and solution pH can alter the structure of LSD at the C-9,10 double-bond position. Therefore, it is desirable to prepare and select a derivative that generates a stable LSD microparticle which is able to withstand long-term storage. On the basis of stability studies, we have selected LSD-biphenyl-NHS (**6**) as the best derivative for the development of the LSD OnLine assay. Besides a stable LSD derivative, LSD microparticles free of noncovalently bound LSD are necessary for the OnLine technology to obtain the required assay sensitivity and reagent stability. The conjugation and dialysis procedures reported here have allowed us to minimize unbound LSD in the LSD microparticle reagent and to achieve the targeted sensitivity and stability of the immunoassay. Due to the extent of LSD *in vivo* metabolism and low ingestion dosage, the concentration of parent compound (LSD) in urine is extremely low. To overcome this, we designed and selected an immunogen using a LSD analogue derivatized through the indole nitrogen and conjugated the derivative to BTG. The antibody generated by this immunogen has demonstrated broad reactivity toward LSD and several LSD metabolites. All of these factors were essential in the successful development of the LSD OnLine assay, which demonstrated excellent clinical sensitivity.

ACKNOWLEDGMENT

We thank Dr. D. Kuntz and Dr. R. Foltz for providing the GC/MS/MS data for all of the LSD-positive samples used in this study and Mr. E. Nowaswiat for providing compounds **1a** and **1b**. We also thank Dr. L. Arabshahi, Ms. L. Allison, Dr. K. Savoca, and Dr. K. Schwenzer for their technical help during the development of this assay.

LITERATURE CITED

- (1) Bonner, R. (1992) *Drug Detection Report*, Vol. 1, p 5, Pace Publications, Washington, DC.
- (2) National Institute on Drug Abuse. (April 13, 1993) *Annual National High School Senior Survey*, Rockville, MD.
- (3) National Narcotics Intelligence Consumers Committee (NNICC). (June 1991) *The NNICC Report 1990: The Supply of Illicit Drugs to The United States*, Drug Enforcement Administration, Washington, DC.
- (4) Gold, M. S. (1994) The epidemiology, attitudes, and pharmacology of LSD use in the 1990s. *Psychiatr. Ann.* 24, 124–26.
- (5) Hoffmann, A. (1975) *LSD—A Total Study* (D. Siva Sankar, Ed.) pp 107–140, PHD Publications, Westburg, NY.
- (6) Foltz, R. B., and Foltz, R. L. (1989) Lysergic acid diethylamide (LSD). In *Advances in Analytical Toxicology* (R. C. Baselt, Ed.) Vol. 2, pp 140–158, Year Book Medical Publishers, Chicago, IL.
- (7) Nelson, C. C., and Foltz, R. L. (1992) Chromatographic and mass spectrometric methods for determination of lysergic acid diethylamide (LSD) and metabolites in body fluids. *J. Chromatogr.* 580, 97–109.
- (8) Nelson, C. C., and Foltz, R. L. (1992) Determination of lysergic acid diethylamide (LSD), iso-LSD, and N-deSmethyl-LSD in body fluids by gas chromatography/tandem mass spectrometry. *Anal. Chem.* 64, 1578–85.
- (9) Lim, H. K., Andrenyak, D., Francom, P., and Foltz, R. L. (1988) Quantification of LSD and N-demethyl-LSD in urine by gas chromatography/resonance electron capture ionization mass spectrometry. *Anal. Chem.* 60, 1420.
- (10) Cai, J., and Henion, J. (1996) Elucidation of LSD in vitro metabolism by liquid chromatography and capillary electrophoresis coupled with tandem mass spectrometry. *J. Anal. Toxicol.* 20, 27–37.
- (11) Diagnostic Product Corp. COAT-A-COUNT LSD assay, 1989.
- (12) Roche Diagnostic Systems, Abuscreen RIA LSD package insert, June 1993.
- (13) Peel, H. W., and Boynton, A. L. (1980) Analysis of LSD in urine using radioimmunoassay-excretion and storage effects. *Can. Soc. Forensic Sci. J.* 13, 23–28.
- (14) Looney, C. E. (1984) High-sensitivity light scattering immunoassays. *J. Clin. Immunoassays* 7, 90–95.
- (15) Bradford, M. M. (1983) A rapid and sensitive method for the quantitative determination of microgram quantities of protein utilizing the principal protein-dye binding. *Anal. Biochem.* 72, 245–254.
- (16) Marzoni, G., and Garbrecht, W. L. (1987) N'-Alkylation of dihydro lysergic acid. *Synthesis*, 651–653.
- (17) Ziegler, K., Frimmer, M., Mullner, S., and Fasold, H. (1984) 3-Isothiocyanato-benzamido[³H] cholate, a new affinity label for hepatocellular membrane proteins responsible for the uptake of both bile acids and phalloidin. *Biochim. Biophys. Acta* 773, 11–12.
- (18) Goldfarb, A. R. (1966) A kinetic study of the reactions of amino acids and peptides with trinitrobenzenesulfonic acid. *Biochemistry* 5, 2570–2574.
- (19) Snyder, S. L., and Sobocinski, P. Z. (1975) An improved 2,4,6-trinitrobenzenesulfonic acid method for the determination of amines. *Anal. Biochem.* 64, 284–288.
- (20) Janda, K. D., Schloeder, D., Benkovic, S. J., and Lerner, R. A. (1988) Introduction of an antibody that catalyzes the hydrolysis of an amide bond. *Science* 241, 1188–1191.
- (21) Figli, I., Lerner, R. A., and Janda, K. D. (1991) Enantiofacial protonation by catalytic antibodies. *J. Am. Chem. Soc.* 113, 8528–8529.
- (22) Vaitukaitis, J. (1981) Production of antisera with small doses of immunogen: multiple intradermal injections. *Methods Enzymol.* 73B, 46–52.
- (23) Wiley, R. A., and Rich, D. H. (1993) Peptidomimetics derived from natural products. *Med. Res. Rev.* 13, 327–384.
- (24) Desai, M. C., Vincent, L. A., and Rizzi, J. P. (1994) Importance of parallel vectors and "hydrophobic collapse" of the aligned aromatic rings: discovery of a potent substance P antagonist. *J. Med. Chem.* 37, 4263–4266.
- (25) Morrison, R. T., and Boyd, R. N. (1981) *Organic Chemistry*, 3rd ed., Allyn and Bacon Inc., Boston, MA.
- (26) Erlanger, B. F. (1980) The preparation of antigenic hapten carrier conjugates: a survey. *Methods Enzymol.* 70, 85–104.
- (27) Ratcliffe, W. A., Fletcher, S. M., Moffat, A. C., Ratcliffe, J. G., Harland, W. A. and Levitt, T. E. (1977) Radioimmunoassay of lysergic acid diethylamide (LSD) in serum and urine by using antisera of different specificities. *Clin. Chem.* 23 (2), 169–174.

BC9700594

Probing Biomolecule Recognition with Electron Transfer: Electrochemical Sensors for DNA Hybridization

Mary E. Napier,[†] Carson R. Loomis,[‡] Mark F. Sistare,[†] Jinheung Kim,[†] Allen E. Eckhardt,[‡] and H. Holden Thorp^{*,†}

Department of Chemistry, University of North Carolina, Chapel Hill, North Carolina 27599-3290, and Xanthon, Inc., Park Research Center, Research Triangle Park, North Carolina 27709-2296. Received June 17, 1997[®]

Identifying infectious organisms, quantitating gene expression, and sequencing genomic DNA on chips all rely on the detection of nucleic acid hybridization. Described here is a novel assay for detection of the hybridization of products of the polymerase chain reaction using electron transfer from guanine to a transition-metal complex. The hybridization assay was modeled in solution by monitoring the cyclic voltammetry of $\text{Ru}(\text{bpy})_3^{2+}$ ($\text{bpy} = 2,2'$ -bipyridine) in the presence of a probe strand containing only A, T, and C prior to and after hybridization to a complement that contained seven guanines, which led to high catalytic current due to the oxidation of guanine by $\text{Ru}(\text{bpy})_3^{3+}$. To allow recognition of all four bases in the target sequence, it was shown that inosine 5'-monophosphate was 3 orders of magnitude less reactive than guanosine 5'-monophosphate, suggesting that effective hybridization sensors could be realized by immobilization of probe strands in which inosine was substituted for guanosine; hybridization to guanosine-containing target strands would then provide high catalytic currents. A sensor design was tested in a model system for the detection of a synthetic 21-mer oligonucleotide patterned on the sequence of the ras oncogene, which gave an increase in charge collected of $35 \pm 5 \mu\text{C}$ after hybridization and of only $8 \pm 5 \mu\text{C}$ after exposure to noncomplementary DNA. Independent quantitation of probe and target by radiolabeling showed that the hybridized electrode contained $3.0 \pm 0.3 \text{ ng}$ of target. New sensor electrodes were then prepared for the detection of PCR-amplified genomic DNA from herpes simplex virus type II, genomic DNA from *Clostridium perfringens*, and genomic RNA from human immunodeficiency virus and gave an additional charge of $35\text{--}65 \mu\text{C}$ for hybridization to complementary amplicon and of only $2\text{--}10 \mu\text{C}$ after exposure to noncomplementary DNA.

INTRODUCTION

Electron-transfer reactions of macromolecules are exceptionally well understood at the theoretical level (1, 2), and predictions from these models of the effects of distance and driving force on electron-transfer kinetics have been successfully tested (3, 4). Proper exploitation of this knowledge base should lead to new means for assessing the quantity or quality of the interactions of macromolecules with other biomolecules or small ligands, much in the same way that energy-transfer reactions have been used to study protein–protein complexes (5) and DNA hybridization (6). Energy-transfer approaches, and related photonic methods such as fluorescence polarization (7) and microscopy (8), generally require the attachment of chromophoric labels to one or both of the interacting partners. We report here on an electron-transfer approach to studying DNA hybridization that avoids the attachment of exogenous labels to the target strand by using engineered probes that do not undergo electron-transfer reactions as readily as natural DNA.

Electron-transfer reactions of DNA have been of intense recent interest due to intriguing issues regarding the role of base stacking in the electronic coupling of redox partners (9–13). In particular, one-electron oxidation of the guanine nucleobase in native DNA has been detected by high-resolution gel electrophoresis via the formation of base-labile lesions at guanine following electron transfer (14–16). We showed that this one-

electron oxidation could also be realized by metal complex mediators that were activated electrochemically at potentials accessible in neutral aqueous solution with the appropriate electrode material (17). The guanine–metal electron transfer was detected as a catalytic current enhancement in the cyclic voltammogram of the mediator complex and was observed for complexes with potentials $>1.0\text{--}1.1 \text{ V}$ (all potentials versus Ag/AgCl) (18); later equilibrium titrations confirmed that the thermodynamic potential of guanine oxidation at pH 7 was $E_7 = 1.06 \text{ V}$ (19). The absolute rate constants for electron transfer can be determined from the cyclic voltammetry and offer a sensitive probe of the sequence and structure at the oxidized guanine via existing models for the effects of distance and driving force on the kinetics of electron-transfer reactions (20, 21). In particular, the kinetics of eq 2 have been used to detect single-base mismatches at guanine in solution (20). These observations suggest the engineering of solid-phase sensors by which biomolecular interactions of immobilized DNA are probed using guanine as the redox-active reporter. Because the metal complex is used to carry the electron to the electrode, the nucleic acid can be immobilized in a manner such that direct charge transfer from guanine to the electrode is not required and in which care is taken to preserve the native conformation and recognition properties of the biomolecule. The electrochemical detection of DNA at solid surfaces has been realized previously (22) via oxidation of guanine and adenine (23, 24); however, in these cases electron transfer is efficient only when the DNA is adsorbed onto the electrode surface or incorporated into a carbon paste electrode. In these latter cases,

* Author to whom correspondence should be addressed.

[†] University of North Carolina.

[‡] Xanthon, Inc.

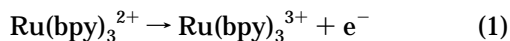
[®] Abstract published in *Advance ACS Abstracts*, October 15, 1997.

the integrity of the biomolecule structure and macromolecular interaction is a concern.

The detection of nucleic acid hybridization at solid surfaces has been used for the identification of infectious organisms in clinical specimens (25, 26), the quantitation of mRNA for gene expression analysis (27), and the sequencing or resequencing of genomic DNA on high-density "chip" arrays (28). Presently, these efforts involve the attachment of a fluorescent label to the target nucleic acid, which is then hybridized with a probe-modified surface and detected after the unhybridized DNA has been washed away from the solid surface. Since detection of photons is required to signal hybridization, analysis of high-density arrays labeled in this manner requires high-resolution fluorescence microscopes. Alternatively, indirect detection of hybridization can be accomplished using sandwich assays when the surface-bound hybrid is subsequently hybridized to an additional signal probe that carries one or more fluorescent labels or enzymes that convert a nonfluorescent substrate to a fluorescent one (25). By attaching multiple enzymes to the signal probes, large signal amplification can be achieved (29); however, the preparation of these multiple enzyme systems is complex. We report here on a system in which the hybridization of *unlabeled*, native DNA can be detected electrochemically at membrane-modified electrodes. Detection of DNA hybridization was realized in model oligonucleotide hybrids, and the practical utility of the sensors was confirmed by detection of the products of polymerase chain reactions (PCR) of genomic material from infectious organisms.

RESULTS

Solution Model. Before the modified electrode sensors were engineered, the hybridization assay was simulated in solution at unmodified indium tin oxide (ITO) electrodes to confirm that the redox chemistry was properly conceived. The mediator chosen was $\text{Ru}(\text{bpy})_3^{2+}$ ($\text{bpy} = 2,2'$ -bipyridine), which exhibits a reversible redox couple at 1.05 V and oxidizes guanine in DNA at high salt by a two-step mechanism (20, 21):



where DNA_{ox} is a DNA molecule in which guanine has been oxidized by one electron. We have shown previously that the rate constant for eq 2 in 50 mM phosphate buffer (pH 7) with 700 mM added NaCl is $1.0 \times 10^4 \text{ M}^{-1} \text{ s}^{-1}$ for double-stranded DNA; at lower ionic strength (50 mM phosphate), the rate constant for eq 2 increases to $1.4 \times 10^5 \text{ M}^{-1} \text{ s}^{-1}$ because of increased binding of the metal complex to DNA and a consequent increase in the local concentration (21). The simulations and kinetic analyses for these scenarios have been described in detail elsewhere (21).

The quasi-reversible cyclic voltammogram of $\text{Ru}(\text{bpy})_3^{2+}$ is shown in Figure 1A. Addition of an oligonucleotide that does not contain guanine produces a small enhancement in the oxidation current (Figure 1B). This oligonucleotide simulates the probe strand in our hybridization assay. Upon hybridization of the oligonucleotide to a longer complement that contains a single guanine in the duplex region and an overhang of three guanines on each end, dramatic catalytic enhancement is observed (Figure 1C). These results suggest a very effective hybridization assay by which, if the probe strand containing no guanines were immobilized to the electrode,

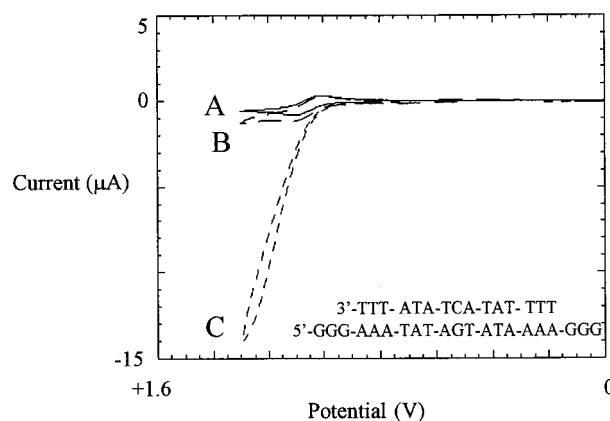


Figure 1. Cyclic voltammograms of $\text{Ru}(\text{bpy})_3^{2+}$ (25 μM) at a scan rate of 25 mV/s in 50 mM sodium phosphate buffer (pH 7) with 0.7 M NaCl: (A) no added oligonucleotide; (B) with 75 μM d(5'-TTTACTATATTT); (C) with the hybrid of the oligonucleotide from (B) with d(5'-GGGAAATATAGTATAAAAAGGG). The secondary structure of the hybrid from (C) is indicated on the figure. Reference electrode: Ag/AgCl. Working electrode: unmodified ITO.

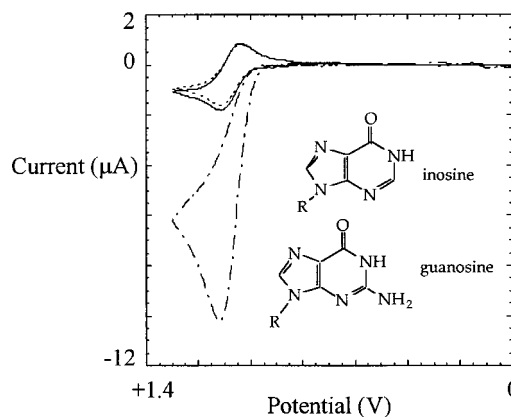


Figure 2. Cyclic voltammograms of (A) $\text{Ru}(\text{bpy})_3^{2+}$ (25 μM) with (B) inosine 5'-monophosphate (0.3 m) and (C) guanosine 5'-monophosphate (0.3 mM). Scan rate: 25 mV/s. Reference electrode: Ag/AgCl. Working electrode: unmodified ITO.

little current enhancement would be observed, but after hybridization to a strand containing multiple guanines, large current enhancements would be produced.

One limitation to the scenario suggested by Figure 1 is that the probe strand could not contain guanine, so a sequence comprised only of A, T, and C was chosen. Such a design would drastically limit the choice of sequences chosen for hybridization. To circumvent this problem, we chose a commercially available guanine derivative that would still recognize cytidine but not donate an electron to $\text{Ru}(\text{bpy})_3^{3+}$. Shown in Figure 2 are the cyclic voltammograms of $\text{Ru}(\text{bpy})_3^{2+}$ in the presence of the mononucleotides guanosine 5'-monophosphate (GMP) and inosine 5'-monophosphate (IMP), in which the guanine base has been substituted by the deaminated hypoxanthine analogue. As expected, a large current enhancement is observed for the guanine mononucleotide, but not for the hypoxanthine mononucleotide, apparently because the exocyclic amine plays a critical electronic role in the guanine oxidation. Digital simulation of the scan rate dependences of the voltammograms shown in Figure 2 gives second-order rate constants for electron transfer to $\text{Ru}(\text{bpy})_3^{3+}$ of $k_{\text{GMP}} = 6.4 \times 10^5 \text{ M}^{-1} \text{ s}^{-1}$ and $k_{\text{IMP}} = 97 \text{ M}^{-1} \text{ s}^{-1}$. Hypoxanthine still recognizes cytidine, so now the engineering of probe strands that recognize all four bases can be envisioned by replacement of guanosine with inosine, and the lower electron-transfer

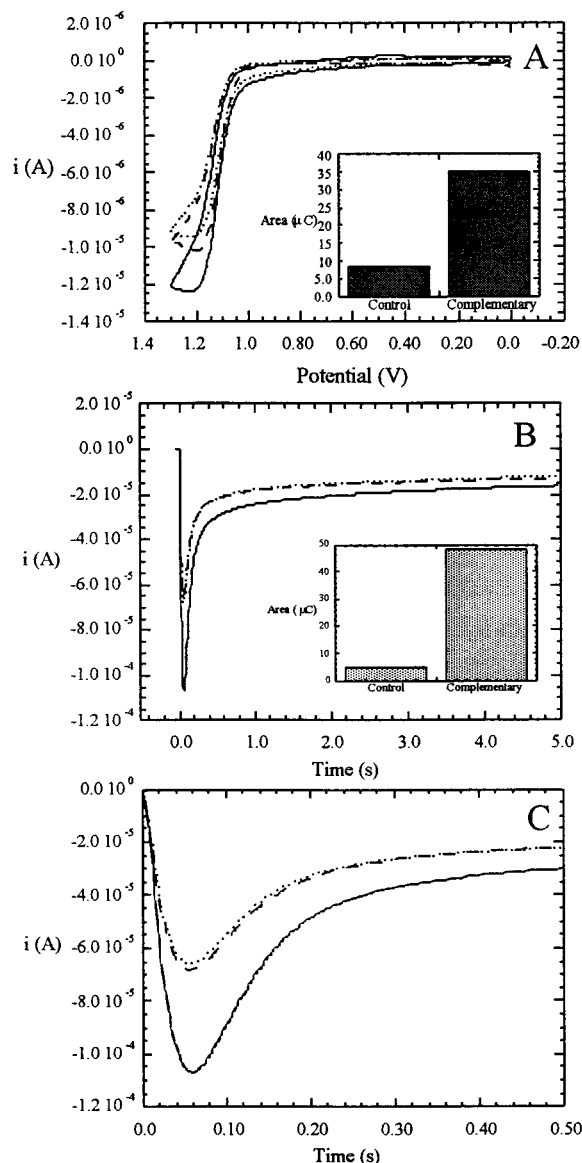


Figure 3. (A) Cyclic voltammograms taken at 25 mV/s of $\text{Ru}(\text{bpy})_3^{2+}$ (100 μM) at the polymer-modified ITO working electrode showing the current (i) measured at the electrode with only the inosine-substituted 21-mer probe attached (dotted) and after exposure to a 200 μL solution of 1 nmol of the complementary (solid) and control (dashed) oligonucleotides. Inset: Integrated charge (in microcoulombs) obtained after subtraction of the current for the unhybridized electrode (dotted) from that after hybridization to the complementary and control oligonucleotides. The charge is $35 \pm 5 \mu\text{C}$ for the hybridization reaction and $8 \pm 5 \mu\text{C}$ for the control. (B) Chronoamperometric traces taken with a potential step from 0 to 1.3 V with $\text{Ru}(\text{bpy})_3^{2+}$ (100 μM) showing current collected at the electrode modified with the 21-mer probe (dotted) and after exposure to the control (dashed) and complementary (solid) oligonucleotides. The dotted and dashed lines appear nearly superimposable on this scale. Inset: Integrated charge in microcoulombs as in (A). (C) Data from (B) replotted on an expanded scale to show the relationship of the complementary (solid), control (dashed), and probe only (dotted) scans.

reactivity of hypoxanthine by nearly 3 orders of magnitude will lead to relatively low currents for the unbound probe. Since hypoxanthine can only form two of the three hydrogen bonds in a Watson–Crick base pair, it may be desirable in the future to use a guanine derivative that is redox-inert but capable of forming all three hydrogen bonds. Accordingly, the reactivity of the nucleotide of 7-deazaguanine was determined as in Figure 2, and the results were very similar to those with IMP ($k = 850 \text{ M}^{-1} \text{ s}^{-1}$). In the study of PCR products discussed below, the

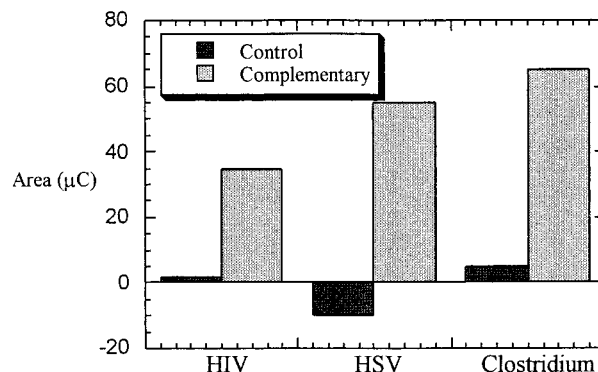


Figure 4. Difference in charge collected in cyclic voltammetry experiments following hybridization of electrode modified with the appropriate probe from Table 1 with the corresponding PCR compared to the current obtained before hybridization. Control reactions involved exposure of the electrode modified with the 21-mer ras probe and the PCR. Data were collected and analyzed as in Figure 3A and gave similar error limits. The negative charge indicated for HSV results from a greater current for the electrode modified with the control probe before hybridization compared to after hybridization.

specificity afforded by inosine substitution was sufficient (Figure 4); however, 7-deazaguanine is clearly an available and attractive alternative.

Sensor Electrodes. As shown by Marchand-Brynaert et al. (30), oxidation of the alcohol chain ends of track-etched microporous poly(ethylene terephthalate) membranes with KMnO_4 results in the formation of carboxylic acid functionalities that can be linked to proteins and amino acids via carbodiimide-catalyzed reaction of amine groups to form amide linkages. We show here that single-stranded DNA probes can also be coupled to the carboxylic acid groups of the polymer membrane via the exocyclic amines of the nucleobases. The DNA attachment was followed by X-ray photoelectron spectroscopy, which showed changes at each step similar to those observed for amino acid functionalization (30) except that peaks due to ionization of phosphorus were apparent following DNA coupling. Similarly, cyclic voltammograms of the membranes exposed to probe with no water-soluble carbodiimide (WSC) resembled the voltammograms of membranes with no exposure to DNA, demonstrating a low degree of nonspecific DNA binding. When attached to ITO electrodes, the covalently attached DNA will be accessible to $\text{Ru}(\text{bpy})_3^{3+}$, which can shuttle electrons from guanine to the electrode surface according to eqs 1 and 2. If inosine-substituted oligonucleotides are used as immobilized probes, then relatively small catalytic currents will be observed. If the immobilized inosine-substituted probes are then hybridized to strands containing guanine, then large catalytic currents are expected due to the shuttling of electrons from the hybridized DNA to the electrode by the $\text{Ru}(\text{bpy})_3^{2+}$ mediator.

The sensor design was first tested using synthetic 21-mer oligonucleotides patterned on the ras oncogene sequence (31) (Table 1). No current above background was observed for the probe-modified electrodes in the absence of $\text{Ru}(\text{bpy})_3^{2+}$ before or after hybridization, indicating that direct electron transfer from the immobilized DNA to the electrode did not occur. However, measurable current due to DNA was always observed in cyclic voltammograms of $\text{Ru}(\text{bpy})_3^{2+}$ at polymer membranes modified with the inosine-substituted 21-mer probe and after hybridization. As shown in Figure 3A, a significant increase in current was observed for the polymer film undergoing hybridization to the complementary 21-mer DNA (solid) when compared to the

Table 1. Oligomer Sequences Used as Probes and Primers

	oligomer sequence
21-mer ras probe	5'-ITACTCTTCTTITCCAICTIT
21-mer complementary	5'-ACAGCTGGACAAGAAGAGTAC
21-mer control	5'-ACATCGAGCTTAAGGTGTCGC
HIV primers	5'-CCGGAATTCTGCAACAACCTGCTG 5'-CCGCTCGAGATGCTGGTCCCA
HIV probe	5'-AAACAAATTCCACAAACTTGC
HSV primers ^a	5'-CGACATCAACCACCTTCGCT 5'-ATGTAGCACGAGGCTGTCTGT
HSV probe ^a	5'-ICCCICACCATCCAACCAACC
<i>C. perfringens</i> primers ^b	5'-TGCTAATGTTACTGCCGTTGATAG 5'-ATAATCCCAATCATCCCAACTATG
<i>C. perfringens</i> probe ^b	5'-CAAAIAATATICAIAITTT

^a Reference 36. ^b Reference 35.

polymer film containing only the inosine-substituted probe (dotted) or after exposure to the 21-mer control sequence (dashed). This current increase suggests that the hybridization event was successful and that electron transfer from the guanines of the hybridized strand to Ru(bpy)₃³⁺ is responsible for the increase in oxidation current. In contrast, very little current increase is observed for the polymer membrane exposed similarly to the 21-mer control DNA. The small increase in current is attributed to a small amount of nonspecific binding of the DNA to the polymer membrane. The inset in Figure 3 shows the charge (in microcoulombs, μC) acquired for the hybridization and control reactions after subtraction of the charge acquired at the probe-modified electrode. Measurement of the charge collected at five entirely different modified electrodes gives an error of $\pm 5 \mu\text{C}$. Exposure of the probe-modified electrodes to 200 μL of 2 mM (in nucleotide) calf thymus DNA produced no current enhancement, demonstrating a significant degree of sequence discrimination.

The 21-mer system was also evaluated by chronoamperometry experiments in which the potential was stepped from a resting potential of 0 V to 1.3 V, where Ru(bpy)₃²⁺ is oxidized. The current was collected for 10 s after stepping the potential; the results for the first 5 s are shown in Figure 3B. As in the cyclic voltammetry experiments, some catalytic current is observed with the probe-modified electrode (dotted) with a much greater increase after hybridization (solid) than after exposure to the control oligonucleotide (dashed). The quantity of charge collected in Figure 3B determined by subtraction of the current at the probe-modified electrode and integration over the entire time period (inset) was similar to that collected in the cyclic voltammetry experiments. The majority of guanine in the film was consumed in both amperometry conducted for 10 s and cyclic voltammetry at a scan rate of 25 mV/s; accordingly, the electrodes could not be re-interrogated after the first scan by either method. While the insets in Figure 3 clearly show that the total charge is significantly greater in both experiments for the hybridization compared to the control, the chronoamperometry data also show significant enhancements in the instantaneous current at early times in the catalytic cycle. The chronoamperometry data are shown on an expanded scale in Figure 3C, where at $t = 0.05$ s there is a 38 μA enhancement in the hybridized case while there is only a 2 μA enhancement for the control.

The quantity of attached and hybridized DNA was independently determined using ³²P-labeled oligonucleotides that were then quantitated by scintillation counting. First, the 21-mer probe was radiolabeled and attached to the film, and the quantity of attached probe was determined. This experiment showed that 8.2 ± 0.8 pmol of probe was attached to the electrode. In a second

series of experiments, the unlabeled 21-mer probe was attached to the electrode and then exposed to radiolabeled 21-mer complement. This experiment showed that 0.43 ± 0.04 pmol of oligonucleotide was hybridized to the film. Thus, the electrodes used in Figure 3 contained 3.0 ± 0.3 ng of hybridized target DNA, and the ratio of hybridized target to total attached probe was $5.2 \pm 0.5\%$.

A number of experiments support the idea that the immobilized DNA resembles its native structure and conformation. The effect of salt concentration in the hybridization buffer is the same as for solution hybridization (32); that is, more efficient and stable hybridization occurred at high salt concentration. Similarly, the effect of salt concentration on the guanine-metal electron transfer was the same as we have observed previously in solution (21): more efficient electron transfer was observed at low salt, at which there is more binding of the metal complex to DNA. The relative reactivities of single-stranded and duplex guanine were similar to that observed in solution (20). We have used the complex Os(bpy)₃²⁺, which is identical in structure to Ru(bpy)₃²⁺ but not sufficiently oxidizing to abstract an electron from guanine (33, 34), to assess whether the films impede diffusion of the mediator. Cyclic voltammograms of Os(bpy)₃²⁺ were identical at the unmodified polymer, probe-modified polymer, and hybridized polymer, demonstrating that the macromolecule does not impede diffusion of the mediator. Finally, the thermal denaturation characteristics for poly(dC)·poly(dG) models were the same in solution and on the polymer film.

The utility of the sensors was demonstrated by showing that the sensitivity and specificity were sufficient for detection of PCR products of biologically significant length in unpurified amplification reactions. Genomic DNA from HSV and *Clostridium perfringens* was amplified using PCR as described elsewhere (35, 36), and the unpurified PCR were hybridized to the polymer films modified with the appropriate probes. Genomic RNA from HIV was amplified by RT-PCR (26) and similarly hybridized. The cyclic voltammograms of the probe-modified and hybridized films were collected along with the appropriate controls. The charge passed during each voltammogram (in microcoulombs) was determined as in Figure 3, inset. The bar graph in Figure 4 shows the differential charge obtained following subtraction of the charge measured at the probe-modified films from that measured at the hybridized films. Controls involved exposing films modified with the 21-mer ras probe to the raw PCR of the HIV, HSV, or *C. perfringens* genomes under the same conditions. An increase in the charge above that for the probe-modified films signals either nonspecific binding in the control case or a successful hybridization event for the complementary case. In all three cases, the complementary hybridization showed a significant increase in charge when compared to the control exposure. The charge increase signifies that the HIV, HSV, and *C. perfringens* amplicons successfully hybridized to the probe attached to the polymer film. In contrast, little or no residual charge was observed for the controls, indicating a minimal amount of nonspecific binding of amplicon or other components of the unpurified PCR to the polymer membrane. The specificity is emphasized by the ability of the electrodes to discriminate large PCR amplicons (247 bp for *C. perfringens*, 561 bp for HSV, and 3.2 kb for HIV) and by the fact that constituents of the PCR, such as genomic DNA or RNA, polymerase, mononucleotides, and primers, do not interfere with the reaction. Finally, controls performed using the HSV probe against the *C. perfringens* PCR and vice

versa were identical with those obtained using the 21-mer control probe.

DISCUSSION

A notable feature of our approach is that the unlabeled target DNA is distinguished from the synthetic probes by a difference in the electron-transfer reactivity. In our assay, instead of distinguishing *duplex* and *single-stranded* DNA [as in ethidium bromide fluorescence (37)], we distinguish *probe* and *target*. The importance of this difference is that our assay is not dependent on bringing double-stranded DNA to the electrode. Thus, our assay is equally well suited for single- or double-stranded DNA as a target. Even more important, single-stranded RNA is an equally suitable target since it contains guanine, which is of particular interest in identifying unamplified genomic RNA from viruses such as HIV or hepatitis C (29), in detecting ribosomal RNA from bacteria (38), or in quantitating cellular mRNA for gene expression analysis (27).

For the studies described here, the probes were attached to the membrane via the endogenous exocyclic amines of the nucleobases, as has also been done for direct attachment to glassy carbon electrodes (22, 39). We have prepared films that behave similarly with synthetic oligonucleotides to which an alkylamine linker was appended. The latter method provides for greater hybridization efficiency and specificity and will be used in the future as required; attachment via the endogenous amines was apparently sufficient for these studies. Further, the data in Figure 3 suggest that the probe strands are present in excess since hypoxanthines are 3 orders of magnitude less reactive than guanines (Figure 2), while the current at the probe-modified electrode prior to hybridization is measurable. Accordingly, the quantitation of the radiolabeled probes shows that there is in fact a 20-fold excess of probe to target at the hybridized electrode. The ability to tune the electron-transfer reactivity of the synthetic probe allows us to maintain the probe strand in excess, which greatly increases the hybridization efficiency, while maintaining requisite sensitivity in terms of the total charge collected (Figure 3, insets) and in chronoamperometric currents (Figure 3C). The ability to vary both the electron-transfer reactivity and loading of the probes allows for tuning of sensitivity and hybridization efficiency in individual assays.

To our knowledge, Figure 4 shows the first use of electrochemical sensors to detect PCR amplicons, although such strategies have been suggested (40). The hybridization reactions were performed with no purification of the reaction mixture following PCR, which indicates that nonspecific binding of other DNA in the reaction mixture did not occur. Further, the results in Figure 2 and elsewhere clearly show that guanosine mononucleotides are particularly reactive, but the results in Figure 4 show that the membranes did not adsorb dGTP, which was present in millimolar concentration in the PCR and would have contributed to the catalytic current in the control reaction if bound to the membrane. As discussed above, the methodology was effective for amplicons varying in length from 247 bp for *C. perfringens* up to 3.2 kb for HIV.

The strategy reported here is distinct from related approaches in which hybridization can be detected without labeling the target nucleic acid. The other electrochemical sensors that operate via voltammetric activation can be divided into two groups. In the first group, the redox chemistry of the nucleobases is monitored by direct electrochemistry (23, 40). This strategy requires that the

DNA is immobilized in a manner that allows electron transfer from the nucleobases directly to the electrode, which is accomplished either by adsorption of the nucleic acid to mercury or by inclusion in carbon paste. In this strategy, maintaining the native structural and recognition properties of the nucleic acid is a concern. The other approach is to monitor the electrochemistry of an exogenous redox indicator that binds more tightly to double-stranded DNA than to single strands (22, 39, 41–43). In this case, higher currents are observed when double-stranded DNA is brought to the electrode. This strategy will be less attractive for single-stranded targets, such as those discussed above, because the only duplex brought to the electrode by the hybridization event will be the small region where the probe is hybridized to the single-stranded target. Other biosensor approaches to hybridization detection are strategies based on surface plasmon resonance (SPR) (44) or the quartz crystal microbalance (QCM) (45), both of which require considerably more expensive instrumentation and immobilization surfaces than the electrochemical apparatus described here with the polymer-modified ITO electrode. The advantages of SPR, QCM, and the double-stranded redox indicator approaches are that engineered (i.e., inosine-substituted) probes are not required and that neither technique consumes the analyzed DNA as occurs with the guanine oxidation described here.

In the future, we envision numerous applications of this approach beyond the detection of PCR amplicons. The attraction of electrochemical biosensors for DNA diagnostics has been discussed elsewhere (41), but, briefly, electrochemical techniques are particularly suited to miniaturization, which brings about a consequent increase in sensitivity due to both the ability to detect small currents and the small volumes analyzed by small electrodes (46, 47). The studies here were conducted using cyclic voltammetry and chronoamperometry; however, modern pulsed methods may offer additional advances in sensitivity and precision (48). The ability of eq 2 to distinguish a single-base mismatch in solution (21) should be conveniently translated to the solid-phase format described here.

EXPERIMENTAL METHODS

Reagents and DNA. The inorganic reagents used in these experiments were of analytical grade or higher. HCl and H₂SO₄ were obtained from Fisher Scientific (Pittsburgh, PA). Water-soluble carbodiimide [WSC, 1-[3-(dimethylamino)propyl]-3-ethylcarbodiimide hydrochloride] and potassium permanganate were obtained from Aldrich (Milwaukee, WI). Na₂HPO₄, NaH₂PO₄, and NaCl were obtained from Maillinkrodt (Phillipsburg, NJ). Water was obtained from a Milli-Q Plus purification system (Millipore, Bedford, MA). Synthetic oligonucleotides (Table 1) were synthesized by the University of North Carolina Department of Pathology and purified using Amicon Micron 3 concentrators with a cutoff of 3000 molecular weight. Genomic DNA from herpes simplex II virus (HSV) and *C. perfringens* bacterial DNA was obtained from Sigma (St. Louis, MO). The RT-PCR of a 3.2 kb fragment from the gp160 gene from HIV was performed using the primers in Table 1 as described elsewhere (26) and was a gift from Trimeris.

Preparation and Activation of the Carboxylated Polymer Membranes. Cyclopore poly(ethylene terephthalate) track-etched membranes with a pore size of 0.4 μ m and a diameter of 25 mm were obtained from Whatman International (Hillsboro, OR). Four circular sample disks, ~8 mm in diameter, were cut from each 25 mm membrane. The carboxylated polymer mem-

branes were prepared following an adaptation of a published procedure (30). The polymer disks were treated with a solution of KMnO_4 in 1.2 N H_2SO_4 (2.5 g/50 mL) for ~18 h at room temperature. The polymer disks were then washed with 6 N HCl (2×30 min, 25 °C) to remove the brown manganese oxide followed by water rinses (3×30 min, 25 °C). The carboxylation of the polymer film was confirmed by XPS analysis with an increase in the O/C ratio from 0.363 to 0.398 following treatment. These results and those obtained at each step in the functionalization compared favorably to those obtained by others in protein immobilization (30). The activation of the surface carboxylate moieties was performed by application of 30 μL of a freshly prepared 10 mM WSC in 20 mM sodium phosphate buffer (pH 7.0) to each side of the polymer disk. After each application, the polymer was allowed to dry. The polymer disks were then rinsed twice with 20 mM sodium phosphate buffer and once with water. The DNA probes were coupled to the activated polymer membranes by application of 0.75 nmol of probe in 10 μL of water to each side of the membrane to give a surface density of ~5 nmol/ cm^2 . The polymer was allowed to dry after each application. The polymer disks were then rinsed twice with 20 mM sodium phosphate buffer and once with water. The polymer disks with the probe attached were now ready for hybridization.

PCR Amplification. All DNA samples were amplified using the PCR method as described elsewhere (35, 36). The reaction tubes contained 80 μL of a solution of ~1 pmol (in nucleotide) sample DNA, 10 mM Tris-HCl (pH 8.4), 50 mM KCl, 200 μM dNTP, and either 2.5 mM MgCl_2 (HIV and HSV) or 3 mM MgCl_2 (*C. perfringens*). The primer sequences (Table 1) were for a 247 bp fragment of the α -toxin gene of *C. perfringens* (35, 49), for a 561 bp amplicon from the *Bgl*II N fragment from HSV (36), or for a 3.2 kb amplicon from the gp160 gene of HIV. The primers were added to a final concentration of 4 μM , and 1–2 units *Taq* polymerase (Perkin-Elmer, Norwalk, CT) was added to the mixture using the hot-start method of preheating the reaction tube to 94 °C for 5 min. The mixtures were subjected to 45 cycles at 94 °C for 1 min, 55 °C for 1 min, and 70 °C for 2 min with an automatic thermal cycler (Perkin-Elmer Model 2400). Each set of amplification reactions contained both positive and negative controls, and each mixture was analyzed by agarose gel electrophoresis to verify that fragments of the appropriate size were produced and that the positive and negative controls behaved appropriately.

Synthetic 21-mer Hybridization. Polymer films to which an inosine-substituted 21-mer probe (Table 1) was coupled were placed into 200 μL of a hybridization buffer of 50 mM sodium phosphate and 800 mM NaCl with 1 nmol of the complementary or control 21-mer DNA. The hybridization buffer and polymer film were heated for 1 h at 50 °C and slowly cooled to room temperature. The polymer membrane was removed from the liquid and washed twice in 20 mM sodium phosphate buffer and once with water prior to electrochemical analysis.

Hybridization of PCR Products. Polymer films modified with the appropriate inosine-substituted probe (Table 1) were placed into the hybridization buffer with a 60 μL fraction of the unpurified HIV, HSV, or *C. perfringens* PCR and heated for 10 min at 95 °C in a total volume of 200 μL . The polymer films were allowed to hybridize in the buffer overnight. As a control, the noncomplementary inosine-substituted ras 21-mer probe was coupled to a polymer membrane and exposed similarly to the PCR. The polymer membrane was removed from the liquid and washed twice in 20 mM sodium

phosphate buffer and once with water prior to electrochemical analysis.

Electrochemical Analysis. Cyclic voltammograms were collected using a PAR 273A potentiostat/galvanostat with a single-compartment voltammetric cell equipped with an ITO working electrode (area 0.32 cm^2), a Pt-wire counter electrode, and an Ag/AgCl reference electrode. In a typical experiment, the polymer membrane was placed on top of the ITO electrode at the base of the voltammetric cell and held in place with an O-ring. Two hundred microliters of 100 μM $\text{Ru}(\text{bpy})_3^{2+}$ in 50 mM sodium phosphate buffer (pH 7.0) was placed into the voltammetric cell and allowed to equilibrate with the polymer film for 20 min. The polymer film covered all of the exposed ITO electrode area so that the $\text{Ru}(\text{bpy})_3^{2+}$ was forced to diffuse through the film to access the working electrode. The porosity of the polymer membrane allowed for adequate diffusion of the $\text{Ru}(\text{bpy})_3^{2+}$. Cyclic voltammograms from 0.0 to 1.3 V were taken at a scan rate of 25 mV/s. A freshly cleaned ITO electrode was used for each experiment, and a background scan of buffer alone was collected and subtracted from subsequent scans. The quantities of charge (in microcoulombs) shown in the bar graphs in Figures 3 and 4 were obtained by integrating the cyclic voltammograms between 900 and 1300 mV and subtracting the charge for the probe-modified films from the charge for the hybridization and control reactions.

Quantitation of Probe and Target by Radiolabeling. The 21-mer probe and complementary target oligonucleotides were 5'- ^{32}P -labeled using T4 polynucleotide kinase and γ - ^{32}P -ATP (6000 Ci/mmol) according to standard procedures (32), and the unreacted ATP was removed by chromatography over a Stratagene NucTrap column. The radiolabeled 21-mer probe (370 cpm/pmol) was attached to the PET membrane by the same strategy described above. The films were washed with buffer and water as in the attachment for electrochemistry, and then the membrane was added to 4 mL of SafetySolve scintillation fluid and counted using a scintillation counter. In a separate experiment, a film to which unlabeled 21-mer probe was attached was hybridized to 44 μM 21-mer complementary target that was ^{32}P -labeled (360 cpm/pmol). The quantity of hybridized target was determined similarly.

ACKNOWLEDGMENT

This research was supported by the David and Lucile Packard Foundation and by Xantho, Inc. We gratefully acknowledge the assistance of Trimeris in the RT-PCR amplification of HIV RNA.

LITERATURE CITED

- (1) Beratan, D. N., Onuchic, J. N., Winkler, J. R., and Gray, H. B. (1992) Electron-Tunneling Pathways in Proteins. *Science* 258, 1740–1741.
- (2) Marcus, R. A., and Sutin, N. (1985) Electron Transfers in Chemistry and Biology. *Biochim. Biophys. Acta* 811, 265.
- (3) Wuttke, D. S., and Gray, H. B. (1993) Protein Engineering as a Tool for Understanding Electron Transfer. *Curr. Opin. Struct. Biol.* 3, 555–563.
- (4) Wuttke, D. S., Bjerrum, M. J., Winkler, J. R., and Gray, H. B. (1992) Electron-Tunneling Pathways in Cytochrome c. *Science* 256, 1007–1009.
- (5) Mitra, R. D., Silva, C. M., and Youvan, D. C. (1996) Fluorescence Resonance Energy Transfer Between Blue-Emitting and Red-Shifted Excitation Derivatives of the Green Fluorescent Protein. *Gene* 173, 13–17.
- (6) Parkhurst, K. M., and Parkhurst, L. J. (1995) Donor–Acceptor Distance Distributions in a Double-Labeled Fluo-

- rescent Oligonucleotide Both as a Single Strand and in Duplexes. *Biochemistry* 34, 293–300.
- (7) Walker, G. T., Nadeau, J. G., Linn, C. P., Devlin, R. F., and Dandliker, W. B. (1996) Strand displacement amplification (SDA) and transient-state fluorescence polarization detection of *Mycobacterium tuberculosis* DNA. *Clin. Chem.* 42, 9–13.
 - (8) Fodor, S. P. A., Rava, R. P., Huang, X. C., Pease, A. C., Holmes, C. P., and Adams, C. L. (1993) Multiplexed Biochemical Assays with Biological Chips. *Nature* 364, 555–556.
 - (9) Arkin, M. R., Stemp, E. D. A., Holmlin, R. E., Barton, J. K., Hörmann, A., Olson, E. J. C., and Barbara, P. F. (1996) Rates of DNA-Mediated Electron-Transfer Between Metallointercalators. *Science* 273, 475–480.
 - (10) Priyadarshy, S., Risser, S. M., and Beratan, D. N. (1996) DNA Is Not a Molecular Wire: Protein-like Electron Transfer Predicted for an Extended π -Electron System. *J. Phys. Chem.* 100, 17678–17682.
 - (11) Olson, E. J. C., Hu, D., Hörmann, A., and Barbara, P. F. (1997) Quantitative Modeling of DNA-Mediated Electron Transfer between Metallointercalators. *J. Phys. Chem. B* 101, 299–303.
 - (12) Melvin, T., Botchway, S., Parker, A. W., and O'Neill, P. (1995) Migration of Photoinduced Oxidative Damage in Models for DNA. *Chem. Commun.*, 653–654.
 - (13) Meade, T. J., and Kayyem, J. F. (1995) Electron Transfer in Synthetic Oligonucleotides Labeled with Ruthenium. *Angew. Chem., Int. Ed. Engl.* 34, 352–354.
 - (14) Hall, D. B., Holmlin, R. E., and Barton, J. K. (1996) Oxidative DNA Damage Through Long-Range Electron Transfer. *Nature* 384, 731–735.
 - (15) Sugiyama, H., and Saito, I. (1996) Theoretical Studies of GG-Specific Photocleavage of DNA via Electron Transfer: Significant Lowering of Ionization Potential and 5'-Localization of HOMO of Stacked GG Bases in B-Form DNA. *J. Am. Chem. Soc.* 118, 7063–7068.
 - (16) Armitage, B., Yu, C., Devadoss, C., and Schuster, G. B. (1994) Cationic Anthraquinone Derivatives as Catalytic DNA Photocleavages: Mechanisms for DNA Damage and Quinone Recycling. *J. Am. Chem. Soc.* 116, 9847–9859.
 - (17) Johnston, D. H., Welch, T. W., and Thorp, H. H. (1996) Electrochemically Activated DNA Oxidation. *Metal Ions Biol. Syst.* 33, 297–324.
 - (18) Johnston, D. H., Cheng, C.-C., Campbell, K. J., and Thorp, H. H. (1994) Transdioxorhenium(V)-Mediated Electrocatalytic Oxidation of DNA at Indium Tin-Oxide Electrodes: Voltammetric Detection of DNA Cleavage in Solution. *Inorg. Chem.* 33, 6388–6390.
 - (19) Steenken, S., and Jovanovic, S. V. (1997) How Easily Oxidizable is DNA? One-Electron Reduction Potentials of Adenosine and Guanosine Radicals in Aqueous Solution. *J. Am. Chem. Soc.* 119, 617–618.
 - (20) Johnston, D. H., Glasgow, K. C., and Thorp, H. H. (1995) Electrochemical Measurement of the Solvent Accessibility of Nucleobases Using Electron-Transfer Between DNA and Metal Complexes. *J. Am. Chem. Soc.* 117, 8933–8938.
 - (21) Johnston, D. H., and Thorp, H. H. (1996) Cyclic Voltammetry Studies of Polynucleotide Binding and Oxidation by Metal Complexes: Homogeneous Electron-Transfer Kinetics. *J. Phys. Chem.* 100, 13837–13843.
 - (22) Millan, K. M., Saraullo, A., and Mikkelsen, S. R. (1994) Voltammetric DNA Biosensor for Cystic Fibrosis Based on a Modified Carbon Paste Electrode. *Anal. Chem.* 66, 2943–2948.
 - (23) Wang, J., Chicharro, M., Rivas, G., Cai, X., Dontha, N., Farias, P. A. M., and Shiraishi, H. (1996) DNA Biosensor for the Detection of Hydrazines. *Anal. Chem.* 68, 2251–2254.
 - (24) Palecek, E., and Fojta, M. (1994) Differential Pulse Voltammetric Determination of RNA at the Picomole Level in the Presence of DNA and Nucleic Acid Components. *Anal. Chem.* 66, 1566–1571.
 - (25) Spargo, C. A., Haaland, P. D., Jurgensen, S. R., Shank, D. D., and Walker, G. T. (1993) Chemiluminescent detection of strand displacement amplified DNA from species comprising the *Mycobacterium tuberculosis* complex. *Mol. Cell. Probes* 7, 395–404.
 - (26) Martin, W. J. (1994) Infectious Diseases. In *The Polymerase Chain Reaction* (K. B. Mullis, F. Ferréand, and R. A. Gibbs, Eds.) pp 406–417, Berkhauser, Boston, MA.
 - (27) Schena, M., Shalon, D., Davis, R. W., and Brown, P. O. (1995) Quantitative Monitoring of Gene Expression Patterns with a Complementary DNA Microarray. *Science* 270, 467–470.
 - (28) Chee, M., Yang, R., Hubbell, E., Berno, A., Huang, X. C., Stern, D., Winkler, J., Lockhart, D. J., Morris, M. S., and Fodor, S. P. A. (1996) Accessing Genetic Information with High-Density DNA Arrays. *Science* 274, 610–613.
 - (29) Holodniy, M., Mole, L., Margolis, D., Moss, J., Dong, H., Boyer, E., Urdea, M., Kolberg, J., and Eastman, S. (1995) Determination of Human Immunodeficiency Virus RNA in Plasma and Cellular Viral DNA Genotypic Zidovudine Resistance and Viral Load during Zidovudine-Didanosine Combination Therapy. *J. Virol.* 69, 3510–3516.
 - (30) Marchand-Brynaert, J., Deldime, M., Dupont, I., Dewez, J.-L., and Schneider, Y.-J. (1995) Surface Functionalization of Poly(ethylene terephthalate) Film and Membrane by Controlled Wet Chemistry: Chemical Characterization of Carboxylated Surfaces. *J. Colloid Interface Sci.* 173, 236–244.
 - (31) Neubaueur, A., Dodge, R. K., George, S. L., Davey, F. R., Silver, R. T., Schiffer, C. A., Mayer, R. J., Ball, E. D., Wurster-Hill, D., Bloomfield, C. D., and Liu, E. T. (1994) Prognostic Importance of Mutations in the ras Proto-Oncogenes in De Novo Acute Myeloid Leukemia. *Blood* 83, 1603–1611.
 - (32) Maniatis, T., Fritsch, E. F., and Sambrook, J. (1989) *Molecular Cloning: A Laboratory Manual*, Cold Spring Harbor Press, Cold Spring Harbor, NY.
 - (33) Welch, T. W., Corbett, A. H., and Thorp, H. H. (1995) Electrochemical Determination of Nucleic Acid Diffusion Coefficients through Noncovalent Association of a Redox-Active Probe. *J. Phys. Chem.* 99, 11757–11763.
 - (34) Welch, T. W., and Thorp, H. H. (1996) Distribution of Metal Complexes Bound to DNA Determined by Normal Pulse Voltammetry. *J. Phys. Chem.* 100, 13829–13836.
 - (35) Daube, G., China, B., Simon, P., Hvala, K., and Mainil, J. (1994) Typing of *Clostridium perfringens* by in vitro amplification of toxin genes. *J. Appl. Bacteriology* 77, 650–655.
 - (36) Lulitanond, V., Chantratita, W., Thammaprasert, K., Nimanahaeminda, K., Matangkasombut, P., and Yoosook, C. (1994) Detection of herpes simplex virus type 2 Bgl II N fragment in paraffin-embedded cervical tissue sections using nested polymerase chain reaction. *Mol. Cell. Probes* 8, 441–447.
 - (37) Waring, M. J. (1965) Complex Formation Between Ethidium Bromide and Nucleic Acids. *J. Mol. Biol.* 13, 269.
 - (38) Scholin, C. A., Villac, M. C., Buck, K. R., Krupp, J. M., Powers, D. A., Fryxell, G. A., and Chavez, F. P. (1994) Ribosomal DNA Sequences Discriminate Among Toxic and Non-Toxic Pseudonitzschia Species. *Nat. Toxins* 2, 152–165.
 - (39) Millan, K. M., and Mikkelsen, S. R. (1993) Sequence-Selective Biosensor for DNA Based on Electroactive Hybridization Indicators. *Anal. Chem.* 65, 2317–2323.
 - (40) (a) Palecek, E. (1996) From Polarography of DNA to Microanalysis with Nucleic Acid-Modified Electrodes. *Electroanalysis* 8, 7–14. (b) Mikkelsen, S. R. (1996) Electrochemical Biosensors for DNA Sequence Determination. *Electroanalysis* 8, 15–19.
 - (41) (a) Wang, J., Cai, X., Rivas, G., Shiraishi, H., Farias, P. A. M., and Dontha, N. (1996) DNA Electrochemical Biosensor for the Detection of Short DNA Sequences Related to the Human Immunodeficiency Virus. *Anal. Chem.* 68, 2629–2634. (b) Wang, J., Palecek, E., Nielsen, P. E., Rivas, G., Cai, X., Shiraishi, H., Dontha, N., Luo, D., and Farias, P. A. M. (1996) Peptide Nucleic Acid Probes for Sequence-Specific DNA Biosensors. *J. Am. Chem. Soc.* 118, 7667–7670.
 - (42) Kelley, S. O., Barton, J. K., Jackson, N. M., and Hill, M. G. (1997) Electrochemistry of Methylene Blue Bound to a DNA-Modified Electrode. *Bioconjugate Chem.* 8, 31–37.
 - (43) Hashimoto, K., Ito, K., and Ishimori, Y. (1994) Sequence-Specific Gene Detection with a Gold Electrode Modified with

- DNA Probes and an Electrochemically Active Dye. *Anal. Chem.* **66**, 3830–3833.
- (44) Peterlinz, K. A., Georgiadis, R. M., Herne, T. M., and Tarlov, M. J. (1997) Observation of Hybridization and Dehybridization of Thiol-Tethered DNA Using Two-Color Surface Plasmon Resonance Spectroscopy. *J. Am. Chem. Soc.* **119**, 3401–3402.
- (45) Okahata, Y., Matsunobu, Y., Ijiro, K., Mukae, M., Murakami, A., and Makino, K. (1992) Hybridization of Nucleic Acids Immobilized on a Quartz Crystal Microbalance. *J. Am. Chem. Soc.* **114**, 8299–8300.
- (46) Fan, F.-R. F., Kwak, J., and Bard, A. J. (1996) Single Molecule Electrochemistry. *J. Am. Chem. Soc.* **118**, 9669–9675.
- (47) Licht, S., Cammarata, V., and Wrighton, M. S. (1989) Time and Spatial Dependence of the Concentration of Less Than 10^5 Microelectrode-Generated Molecules. *Science* **243**, 1176–1178.
- (48) Osteryoung, J. (1993) Voltammetry for the Future. *Acc. Chem. Res.* **26**, 77.
- (49) Titball, R. W., Hunter, S. E. C., Martin, K. L., Morris, B. C., Shuttleworth, A. D., Rubidge, T., Anderson, D. W., and Kelly, D. C. (1989) Molecular Cloning and Nucleotide Sequence of the Alpha-Toxin (Phospholipase C) of *Clostridium perfringens*. *Infect. Immun.* **57**, 367–376.

BC9701149

Development of a Kinetic Model To Describe the Effective Rate of Antibody Oxidation by Periodate

David S. Hage,* Carrie A. C. Wolfe, and Matthew R. Oates

Department of Chemistry, University of Nebraska, Lincoln, Nebraska 68588. Received June 9, 1997[®]

The oxidation of antibody carbohydrate residues by periodate is a common approach used for site-specific antibody modification and immobilization. This study sought to develop a general kinetic model that could be used to describe the effective rate of this oxidation for process control. A detailed analysis of previous data collected for rabbit immunoglobulin G in the presence of excess periodate indicated that the reaction followed a pseudo-first-order mechanism in which two general classes of sites were being oxidized. The first class of sites was oxidized fairly rapidly (i.e., within 15–30 min), while the second class of sites reacted over the course of several hours. From these results, an equation was developed that gave a good fit under a variety of reaction conditions to the production of oxidized sites available for coupling with a hydrazide label. On the basis of this equation, data obtained at several periodate concentrations under the same pH and temperature conditions were used to estimate the apparent rate and equilibrium constants for the oxidation of each class of sites. The values obtained by using this approach could be used not only to predict the effective rate of oxidation at other periodate concentrations but also to provide information on the individual steps involved in the oxidation process.

INTRODUCTION

The oxidation of antibodies by periodate is a popular means for the site-specific modification of antibodies for coupling to solid supports or labeling agents. A number of reviews on the applications of periodate-treated antibodies have appeared previously in the literature (e.g., refs 1 and 2); recent examples of specific applications include those discussed in refs 4–7. During the treatment of antibodies with periodate, diol groups located in the carbohydrate chains of an antibody are cleaved to form aldehyde groups. These aldehydes can then be used as sites for attachment of the antibody to agents that contain free amine or hydrazide residues. The main advantage of this approach is that the carbohydrate residues on antibodies are usually located in regions that are distant from the antigen binding sites. Thus, the use of these residues for antibody modification should result in little or no change in the antibody's final binding activity (1, 2).

Despite the potential usefulness of antibody treatment by periodate, only limited quantitative information is available regarding the actual nature of this reaction. It has been shown that the periodate oxidation of glycoproteins depends on such factors as periodate concentration, reaction time, pH, and temperature (3–6, 8, 9). However, many previous studies with antibodies have examined only some of these parameters in any detail. To overcome this limitation, our group has collected data on the oxidation of rabbit immunoglobulin G (rabbit IgG) under a variety of reaction conditions (10). From this work, a set of empirical guidelines was developed for obtaining various levels of antibody oxidation while also minimizing the loss of antibody activity that occurs as a result of the oxidation process. However, a general model is still

needed that can be used along with this information to predict and follow the periodate treatment of antibodies to obtain a precise means of controlling or adjusting this reaction.

The goal of the present study is to use previous data obtained in work with rabbit IgG to develop a kinetic model and associated equations that can be used to describe the effective degree of antibody oxidation (i.e., the production of aldehyde groups that are available for reaction with a hydrazide- or amine-containing reagent) as a function of time and various reaction conditions that are commonly used during antibody treatment with periodate. This type of model would be potentially useful in allowing for improved control and selection of those conditions that are needed to obtain a given degree of antibody modification for labeling or immobilization. The availability of such a model would also be valuable as a means for studying the mechanisms involved in the periodate oxidation of antibodies or other glycoproteins.

MATERIALS AND METHODS

As discussed previously (10), polyclonal rabbit IgG was selected as the model antibody preparation for this work since it is a common immunological reagent and a number of previous studies on antibody oxidation by periodate have been based, at least in part, on rabbit IgG (5, 8). Furthermore, it was felt that the use of a polyclonal system would help to avoid the variability that has been noted in previous studies examining the effects of periodate oxidation on monoclonal antibodies (3–5, 9). Also, since polyclonal antibody preparations are composed of a large number of distinct antibody lines, this type of system should be fairly representative of the average behavior that would be expected for individual antibody populations when they are treated by a reagent such as periodate.

The polyclonal rabbit IgG was oxidized with periodate as described in ref 10. The effective number of aldehyde groups that were available for coupling was determined by labeling with the hydrazide-containing dye Lucifer yellow CH (LyCH), also as described previously (10).

* Author to whom correspondence should be addressed [telephone (402) 472-2744; fax (402) 472-9402; e-mail dhage@unlinfo.unl.edu].

[®] Abstract published in *Advance ACS Abstracts*, October 15, 1997.

LyCH was obtained from Aldrich (Milwaukee, WI); rabbit IgG and the *p*-periodic acid reagent used to make the periodate solutions (see ref 10 for further details) were from Sigma Chemical Co. (St. Louis, MO). Other chemicals used in this study were of reagent grade quality or better. The degree of antibody labeling by LyCH that was obtained under each set of oxidation conditions was measured by flow injection analysis (FIA), as performed according to procedures given in ref 11.

The simplex optimization method used for analysis of the kinetics of antibody oxidation was performed by a program written in Microsoft QuickBASIC (Redmond, WA). This program was based on a modified version of the procedure given by Noggle (12). For simplex optimization performed with the two-site model, the variance of the fit was calculated by dividing the sum of the squares of the residuals by $N - 4$ degrees of freedom, where N is the total number of points present in the original data set. All simplex optimization studies were carried out by examining the results obtained with at least eight different combinations of estimates for the initial parameters, as selected from points scattered throughout the range of allowable results. All fits were evaluated on the basis of both the residuals or variances that were obtained and a visual comparison of the predicted response versus the experimental data.

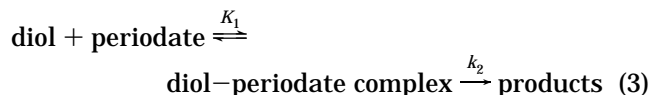
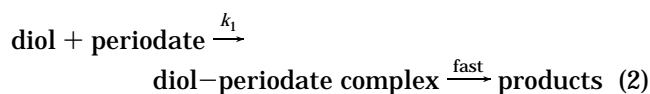
RESULTS AND DISCUSSION

To obtain a model that described the effective rate of antibody oxidation by periodate, an analysis was performed on data previously collected for rabbit IgG in the presence of a known excess of periodate and at various pH values and temperatures (10). The range of test conditions included those typically employed in previous studies involving the periodate oxidation of antibodies (1–9) or other glycoproteins (13–16). In each case, periodate was initially present in at least a 150-fold molar excess versus the amount of antibody in the sample; this resulted in a pattern that consisted of a rapid increase in oxidized sites at short reaction times (i.e., <15–30 min) followed by a much slower increase over longer reaction times (10). The same type of pattern has been noted by others not only in the periodate oxidation of antibodies but also in the treatment of additional glycoproteins by periodate (5, 6, 11, 15–17).

As a first step in developing a kinetic model for antibody oxidation, consideration was given to the various mechanisms that have been proposed for the periodate treatment of other, low molecular weight compounds. For example, studies with various small 1,2-diol compounds have found that periodate oxidation can generally be described by a two-step process:



The first step of this reaction involves the reversible formation of a cyclic intermediate complex between the diol group and 1 equiv of periodate. After this complex is formed, the diol is cleaved at its carbon-carbon bond to form two aldehyde groups (18). There are two extreme cases that can arise from the model in eq 1. In the first case, formation of the diol-periodate complex is the slow step, while in the second case the formation of products from the cyclic complex is rate-limiting. These two situations are represented by the reaction schemes shown in eqs 2 and 3, respectively.



In this series of reactions, k_1 is the forward rate constant for complex formation, k_2 is the rate constant for product formation, and K_1 is the association equilibrium constant for the diol-periodate complex. Both cases in eqs 2 and 3 have been observed in experimental systems (18). For example, simple diols such as ethylene glycol and 2,3-butyleneglycol readily form a cyclic intermediate with periodate but have slow cleavage reactions. On the other hand, highly substituted or hindered diols can have slow formation of the cyclic intermediate, followed by more rapid cleavage of the diol carbon-carbon bond (18).

When a large excess of periodate is present in solution, as was true for rabbit IgG in this study, it is possible to represent either of the cases in eqs 2 or 3 by a pseudo-first-order rate expression. The resulting integrated equations, expressed in terms of the formation of product, are given below (19):

$$B_t = nA_0(1 - e^{-k_{\text{app}}t}) \quad (4)$$

or

$$\ln[1 - (B_t/nA_0)] = -k_{\text{app}}t \quad (5)$$

In eqs 4 and 5, B_t represents the amount of product that is present at time t , A_0 is the initial amount of the reactant, k_{app} is the apparent rate constant for the conversion of A to B, n represents the moles of B that are produced per mole of A that is consumed, and nA_0 is the maximum amount of product (i.e., labeling sites in this study) that can result under the given reaction conditions. Note that the amount of B and A in eqs 4 and 5 can be expressed in terms of either concentrations, moles, or mole ratios (e.g., moles of LyCH per mole of IgG) as long as both A and B are present in the same solution or reaction compartment. Furthermore, the use of the proportionality constant n in these equations is useful in that it allows the reaction rate to be expressed in terms of any product B whose production is proportional with, but not necessarily identical to, the consumption of A (i.e., where A represents diol groups in this case). This makes eqs 4 and 5 valuable in describing antibody oxidation in terms of the effective number of labeling sites that are produced per antibody, since either one or two aldehyde groups can be generated per oxidation event and not all of these aldehydes might be available for labeling due to steric hindrance or other constraints (see discussion at the end of this section).

Although either of the systems in eq 2 or 3 would be expected to fit a pseudo-first-order model in the presence of excess periodate, the actual meaning of k_{app} will differ depending on which situation is present. In the case when complex formation is rate-limiting (eq 2), the value A_0 is equal to the initial amount of diol groups that can take place in the oxidation reaction and the value of k_{app} is given by the equation

$$k_{\text{app}} = k_1[\text{periodate}] \quad (6)$$

where [periodate] is the total concentration of periodate present in solution and k_1 is the forward rate constant for complex formation, as defined previously. In the

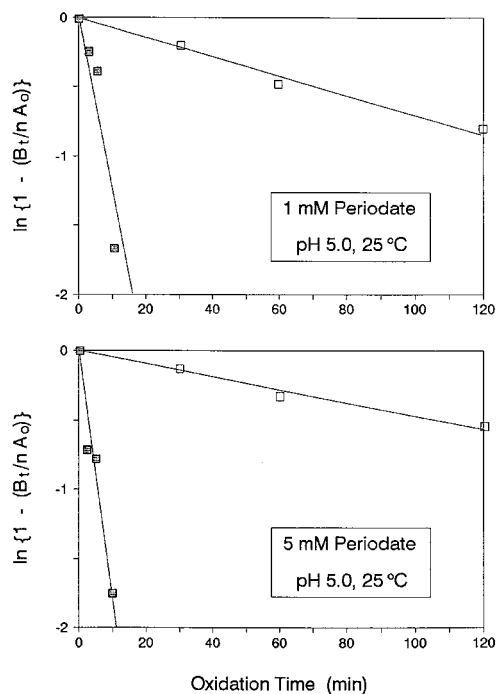


Figure 1. Fit of a first-order rate expression to data for the initial reaction of rabbit IgG with periodate (■) and over longer reaction times after correcting the net response for the contribution predicted by the initial rate analysis (□). This correction assumes the net rate of oxidation can be described by parallel reactions with different reacting sites but similar products (19).

situation when cleavage of the carbon–carbon bond is rate-limiting (eq 3), A_0 is still equal to the total amount of diol groups (both free and complexed) that is present prior to the cleavage reaction; however, k_{app} is now given by the expression

$$k_{app} = k_2 (K_1[\text{periodate}]) / (1 + K_1[\text{periodate}]) \quad (7)$$

The fact that these two cases result in different equations for k_{app} will be used later to help determine which mechanism best describes the oxidation of antibodies by periodate.

Early work in this study examined the fit of a single first-order expression to data obtained for the oxidation of rabbit IgG at pH 5.0 and 25 °C between 0 and 240 min. When this was done, large deviations were noted between the data and the expected response at all of the periodate concentrations that were tested (i.e., 1–100 mM). However, data obtained at short reaction times (0–10 min) did appear to have reasonable agreement with the pseudo-first-order model. This is shown in Figure 1, which illustrates the fit of eq 5 to data obtained at periodate concentrations of 1 and 5 mM. Similar results were obtained when using up to 10 mM periodate. The correlation coefficients for these plots ranged from –0.9459 to –0.9783 for the four to five points in each graph between 0 and 15 min. This indicated that even though data measured over long times did not follow the pseudo-first-order model, the initial rate did seem to fit this type of response. The best-fit values for k_{app} that were obtained from the slopes of these plots were between 0.2 and 0.3 min^{–1} [i.e., (3–5) × 10^{–3} s^{–1}]. The estimated values for nA_0 , as determined by iterative testing, varied from 0.3 to 1.5 mol of LyCH/mol of IgG.

By assuming that the pseudo-first-order fit to the initial data represented a single class of fast-reacting sites, it was possible to use this fit to estimate how many labeling sites were produced by this oxidation process at

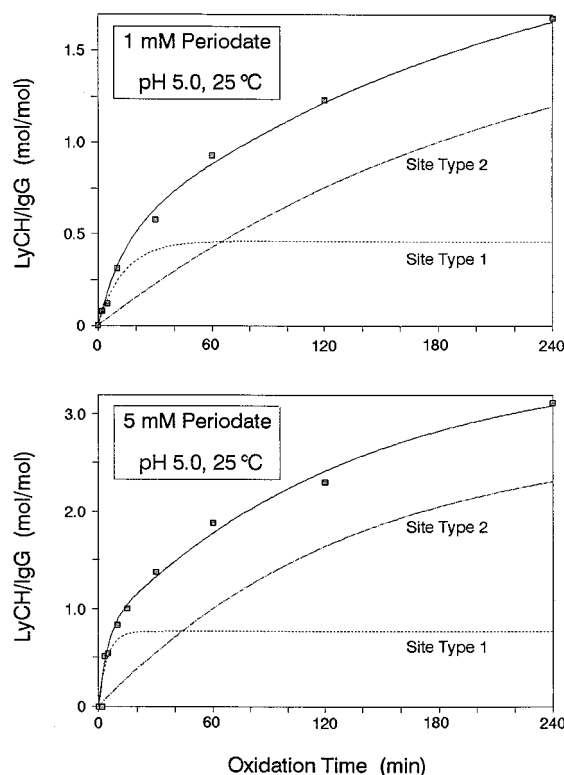


Figure 2. Overall fit of oxidation data for rabbit IgG (■) to a model in which two separate classes of sites for oxidation are present (types 1 and 2). The lines shown in this graph were calculated using eqs 4 and 6, along with the best-fit parameters obtained through simplex optimization.

any given reaction time. These values were then subtracted from the total number of labeling sites that were actually measured. After this was done, the remaining LyCH/IgG levels were replotted according to eq 5, as shown in Figure 1. On the basis of this approach, it was found that the remaining oxidation data again showed good agreement with a pseudo-first-order model. The fits obtained for periodate concentrations of 1–10 mM and reaction times of 0–240 min had correlation coefficients of –0.9641 to –0.9989 over four to five data points. The best-fit values measured for k_{app} were between 0.004 and 0.007 min^{–1} [i.e., (7–12) × 10^{–5} s^{–1}], and the estimated values for nA_0 ranged from 1.7 to 4 mol of LyCH/mol of IgG.

From the results in Figure 1, a model was proposed for the antibody oxidation process in which two distinct classes of sites were present, each following pseudo-first-order kinetics in the presence of excess periodate. On the basis of this model and eq 4, the following equation was developed to describe the overall oxidation process

$$B_t = (nA_0)_1 [1 - e^{-k_{app,1}t}] + (nA_0)_2 [1 - e^{-k_{app,2}t}] \quad (8)$$

where the subscripts “1” and “2” refer to the parameters for the first and second types of sites, respectively.

The fit of eq 8 to each set of oxidation data was tested by using simplex optimization to obtain the best-fit values for $(nA_0)_1$, $(nA_0)_2$, $k_{app,1}$, and $k_{app,2}$. Figure 2 shows the fits that were obtained for data measured in presence of 1–5 mM periodate at 5.0 and 25 °C. In both of the given examples, excellent agreement was seen between the two-site model and the experimental results over the entire range of reaction times that were sampled. The same type of fit was noted when using other periodate concentrations up to 10 mM. The variance of these fits was between 0.003 and 0.005 over 8–10 data points. The

Table 1. Estimated Equilibrium and Rate Constants for the Periodate Oxidation of Rabbit IgG at pH 5.0 and 25 °C^a

oxidation site	nA_0 (mol of LyCH/ mol of IgG)	K_1 (M ⁻¹)	k_2 (s ⁻¹)
site class 1	0.7 (± 0.1)	240 (± 90)	$8 (\pm 3) \times 10^{-3}$
site class 2	1.9 (± 0.7)	600 (± 400)	$3 (\pm 1) \times 10^{-4}$

^a The values in parentheses represent a range of ± 1 SD. The value of nA_0 , or the effective moles of labeling sites that could be generated per mole of IgG, represents the mean result obtained by simplex optimization over five periodate concentrations between 1 and 10 mM and using two separate batches of antibody.

best-fit values for $k_{app,1}$ and $k_{app,2}$ in these plots ranged from 1×10^{-3} to 8×10^{-3} s⁻¹ and from 7×10^{-5} to 40×10^{-5} s⁻¹, respectively, with both of these parameters increasing with periodate concentration. The size of (nA_0)₁ and (nA_0)₂ varied between 0.5–0.8 and 1.2–2.8 mol of LyCH/mol of IgG (see Table 1 for mean values) and showed only random variations as the periodate concentration was changed. Overall, these best-fit parameters gave good agreement with the k_{app} and nA_0 values that were estimated earlier by linear regression analysis, such as performed in Figure 1.

By using the best-fit parameters in Table 1 along with eq 4, it was possible to determine the contribution of each site to the overall extent of oxidation that was measured by the LyCH label. The results are included in Figure 2. The picture that results from this is one in which the first class of sites (type 1) is oxidized within 15–30 min, followed by slower oxidation of the second class of sites (type 2) over a period of at least several hours. This model is consistent with the biphasic behavior that has often been observed for the oxidation of antibodies by periodate (5, 6, 10, 11). In addition, these results agree with past work performed with another glycoprotein, orosomucoid, in which the presence of different classes of sites has been proposed as an explanation for the biphasic nature of the periodate oxidation process (20).

The antibody oxidation process was examined in more detail by studying the concentration dependence of the measured k_{app} values. This was of interest since knowing the expected relationship between k_{app} and periodate concentration would allow the effective rate of antibody oxidation to be estimated at new periodate levels once it has been established for several other periodate concentrations. To study this, plots were made of $1/k_{app}$ versus $1/[periodate]$. According to eqs 6 and 7, one of the following linear relationships should result for this type of plot if the oxidation mechanism is limited exclusively either by the rate of complex or product formation:

$$1/k_{app} = 1/(k_1[periodate]) \quad (9)$$

$$1/k_{app} = 1/(k_2K_1[periodate]) + 1/k_2 \quad (10)$$

For a reaction that is limited by the rate of complex formation, eq 9 shows that a plot of $1/k_{app}$ versus $1/[periodate]$ should result in a linear relationship with a slope of $1/k_1$ and an intercept of zero. For a reaction that is limited by the rate of breaking the diol carbon-carbon bond, eq 10 predicts that a linear response will also result but with a slope that is now given by $1/(k_2K_1)$ and a nonzero intercept that is equal to $1/k_2$.

Figure 3 shows the graph that was generated when a plot of $1/k_{app}$ for site type 1 was made versus $1/[periodate]$. A linear relationship was obtained, as predicted by eqs 9 and 10, with a correlation coefficient of 0.9740 over five points. The best-fit slope for this graph was determined

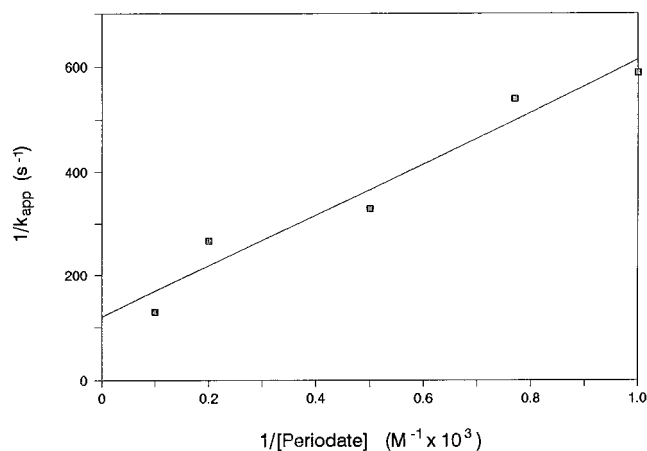


Figure 3. Change in k_{app} with periodate concentration at site type 1 on rabbit IgG. The best-fit parameters are given in the text. The results shown were obtained at pH 5.0 and 25 °C using periodate concentrations of 1, 1.3, 2, 5, and 10 mM.

to be 0.49 ± 0.07 M s (1 SD), and the intercept was 120 ± 40 s. A similar plot was found for site type 2, but with more scatter being present about the best-fit line. In the latter case, a correlation coefficient of 0.7818 was obtained over five points, with a slope of 7 ± 3 M s and an intercept of 3800 ± 1900 s. These linear relationships indicate that such plots should make it easy to estimate k_{app} at new periodate concentrations once this apparent rate constant has been determined at a few surrounding periodate levels.

A further examination of plots such as those in Figure 3 helped to provide some insight into the nature of the antibody-periodate reaction. For example, the data for both classes of sites gave intercepts for plots of $1/k_{app}$ versus $1/[periodate]$ that were significantly different from zero at the 90% confidence level. According to eqs 9 and 10, this supports a model in which periodate and diol groups on the antibody rapidly formed a cyclic complex (as has been shown to form between periodate and low-mass diol compounds—see ref 18), followed by the slow cleavage of this complex to form the aldehyde products. The same mechanism has been used by Nevell (21) to describe the oxidation of cellulose by periodate. By assuming that a cleavage-limited mechanism was indeed present, it was possible to use eq 10 to determine the values of k_2 and K_1 for the two types of sites under the given pH and temperature conditions. The results are summarized in Table 1. For the proposed model, it was found that the two classes of sites had similar, weak equilibrium constants for complex formation, with both K_1 values falling within the range of 200–600 M⁻¹. However, the two classes of sites did differ in the maximum number of available aldehydes that could be generated (nA_0) and in the rate constants for diol group cleavage (k_2). In this case, site type 1 had a smaller value for nA_0 , but the value of k_2 for this type of site was about 25-fold larger than it was for the second class of oxidation sites.

The two-site model that was used in this work to describe antibody oxidation was found to work well not only at pH 5.0 and 25 °C but also at other pH and temperature conditions. Some typical examples are shown in Figure 4. The range of conditions that were examined for antibody oxidation included a pH range of 3–7 (at 10 mM periodate and 25 °C), a temperature range of 4–37 °C (at 10 mM and pH 5.0), and a concentration range of 1–100 mM periodate (at pH 5.0 and 25 °C). In all but two of these cases there was good agreement between the actual data and the two-site model, with total variances that ranged from 0.002 to 0.07 (mean, $0.02 \pm$

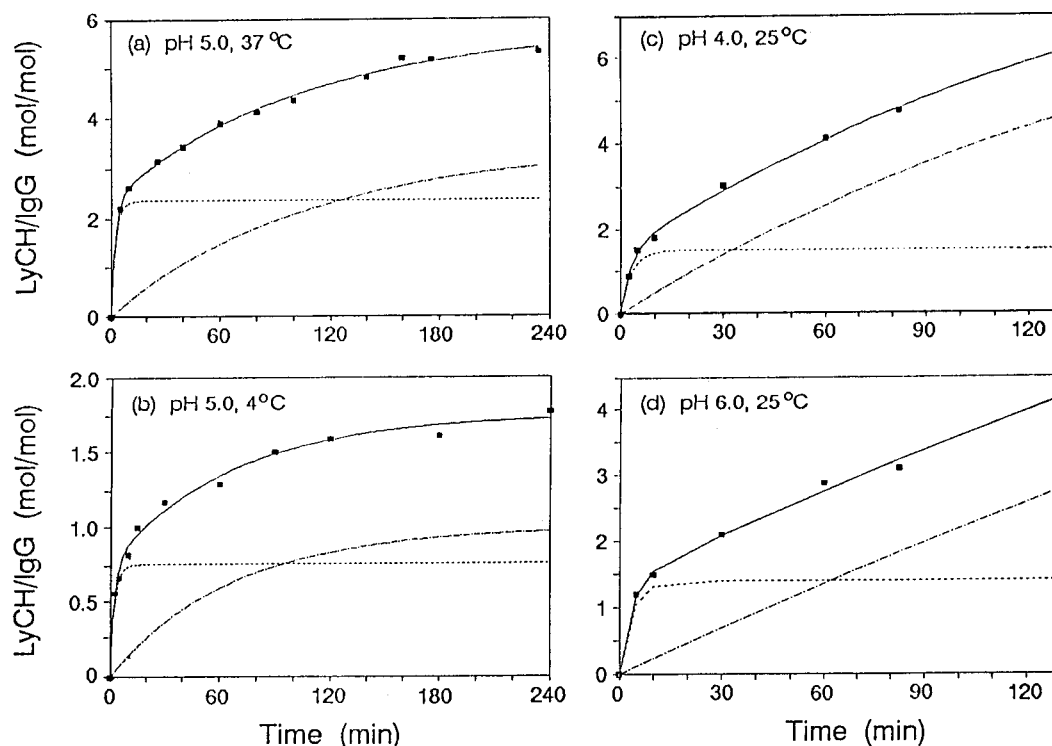


Figure 4. Fit of a two-site model to oxidation data obtained for rabbit IgG (■) under a variety of pH and temperature conditions. The dashed and dotted lines show the estimated contributions due to site types 1 and 2.

Table 2. Actual and Predicted Degrees of Antibody Oxidation by Periodate

oxidation conditions	degree of oxidation (mol of LyCH/mol of IgG) ^a	
	predicted	actual
10 min, pH 7.0, 10 mM periodate, 25 °C	1.0 (± 0.1)	0.9 (± 0.1)
30 min, pH 5.0, 10 mM periodate, 25 °C	2.1 (± 0.1)	2.0 (± 0.1)
60 min, pH 5.0, 10 mM periodate, 25 °C	2.7 (± 0.1)	2.9 (± 0.1)
60 min, pH 4.0, 10 mM periodate, 25 °C	4.1 (± 0.2)	3.6 (± 0.1)

^a The numbers in parentheses represent a range of ± 1 SD.

0.02) over 6–13 points. The only exceptions were those data sets that were measured at 50 and 100 mM periodate. In these two cases, significant deviations were seen from the two-site model at long reaction times (i.e., >1–2 h). This was expected since these same conditions were found to result in the formation of a significant amount of visible precipitate, indicating the possible presence of side reactions due to overoxidation or antibody cross-linking (10).

The accuracy and potential utility of the two-site kinetic model were next tested by using this model to predict the effective rate of periodate oxidation for rabbit IgG. This was done by first using the kinetic fits in Figures 2–4 and related graphs to choose oxidation conditions that would be expected to produce approximately one, two, three, or four active aldehyde groups per IgG. These conditions were next used to oxidize some fresh samples of normal rabbit IgG, with the final extent of oxidation then being measured and compared to the predicted level. The results are summarized in Table 2, with all four test conditions giving good agreement between the actual and predicted degrees of antibody oxidation. Each set of experimental and predicted oxidation levels overlapped within a range of 2 standard deviations, and the absolute differences in these values

varied by only –12.2% to +7.4% (mean, –4.9%). This degree of accuracy was considered to be adequate for most applications since such differences are less than or comparable to the within-day precision of 5% and day-to-day precision of 10–20% expected for the periodate oxidation of rabbit IgG under constant reaction conditions (10).

The carbohydrate structure of a typical antibody (Figure 5) reveals some clues regarding what residues on the antibody carbohydrate regions might be represented by the two types of oxidation sites in the proposed kinetic model. In rabbits and other mammals the oligosaccharides that are attached to IgG are highly heterogeneous in nature (22), with Figure 5 showing the maximum number of sugar units that can be present in a single carbohydrate chain. However, in reality many of the actual carbohydrate chains on rabbit IgG may lack the 1' fucose and/or 4'' *N*-acetylglucosamine residues, or they may contain only a partial extension of the sequences shown in the 4–7 and 4'–7' chains (22).

Although the carbohydrate regions for rabbit IgG are heterogeneous, the aldehydes that can be generated by periodate in these regions could occur through the oxidation of two different types of diol groups: (1) those present as exocyclic diols on sialic acid residues or (2) those within the cyclic structures of other sugars in the carbohydrate chain (13, 15). Of these two types of diols, those present on sialic acids have long been known to have the greatest susceptibility to oxidation by periodate (23). Sialic acids contain diol groups at both the C7–C8 and C8–C9 exocyclic regions. The oxidation of either diol group results in the formation of a free aldehyde in solution and a single aldehyde that is attached to the carbohydrate chain (i.e., $n = 1$ in the term nA_0 , assuming 100% labeling efficiency by LyCH). Studies with other glycoproteins have shown that terminal sialic acids are rapidly oxidized by periodate over a time scale matching that seen for site type 1 in this study (16, 17, 20, 24). In addition, data obtained from previous studies that have examined the extent of rabbit IgG sialylation (25) give

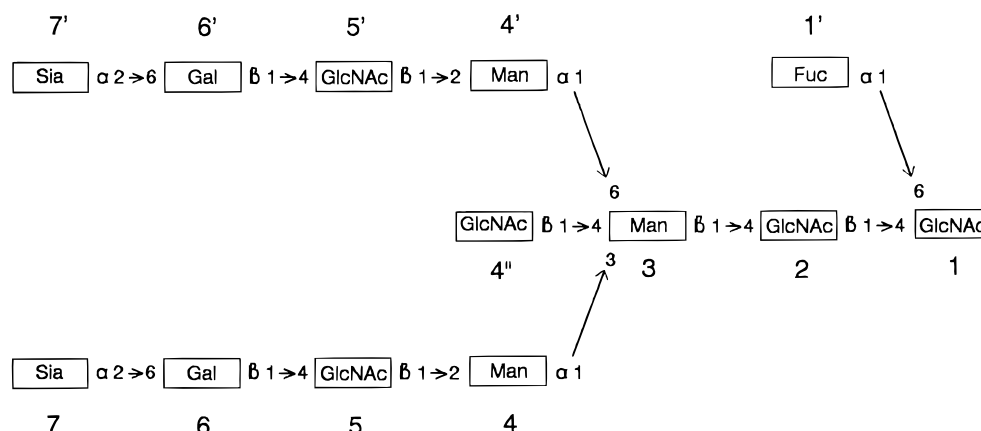


Figure 5. Sequence of the fully extended form of an *N*-linked carbohydrate region on IgG. The abbreviations indicate the locations of sialic acid (Sia), β -D-galactose (Gal), β -D-*N*-acetylglucosamine (GlcNAc), β -D-mannose (Man), and β -L-fucose (Fuc). The numbers below each residue indicate the sugar's position in the chain, based on the scheme of Rademacher et al. (22).

an average number of sialic acids per IgG that shows good agreement with the value of $(nA_0)_1$ in Table 1. On the basis of this information, it was concluded that the first class of oxidation sites (type 1) probably represents the exocyclic diol groups on the sialic acid residues.

The second general type of diol groups (i.e., those suspected to represent cyclic sugar residues) could occur at a variety of locations within the carbohydrate chains. For the fully extended structure shown in Figure 5, diol groups occur within the 1' fucose, 4'' *N*-acetylglucosamine, and two 4/4' mannose residues. Although some of these sugars have more than one pair of adjacent diol groups, a maximum of two aldehydes is produced by the reaction of periodate at any one of these residues. For carbohydrate chains with a partially extended structure, additional pairs of aldehyde groups may be produced by oxidation at a terminal galactose (at the 6- or 6'-positions in the absence of 7 or 7' sialic acids) or a terminal *N*-acetylglucosamine (at the 5- or 5'-positions in the absence of the 6–7 or 6'–7' residues). On the basis of the different combinations of sequences that have been noted in mammalian IgG (22), there is the potential to generate 8–12 aldehydes per carbohydrate chain in the absence of any sialic acid and 6–10 aldehydes per chain when both terminal sialic acids are present (i.e., 4–8 aldehydes from cyclic diols and 2 from sialic acids). Although not all of these sites may be available for labeling due to steric hindrance or other factors, the relatively small nA_0 value noted in Table 1 for site type 2 suggests that only some cyclic diol groups are represented by the second class of sites under normal oxidation conditions. Fucose is one likely source of these groups since studies with other glycoproteins have found this sugar to be readily oxidized by periodate on an hour time scale (16, 17, 20). Terminal galactose residues have also been noted to undergo relatively fast oxidation by periodate, making this sugar another candidate for the type 2 oxidation sites.

Although only a few types of residues might be represented by site type 2 under standard oxidation conditions, more residues might be included in this class of sites when harsher reaction conditions are used. For example, at an oxidation pH <4.5 or at a reaction temperature >25 °C there was an apparent increase in the value of $(nA_0)_2$ that was obtained by simplex optimization. The extent of this increase ranged from a value for $(nA_0)_2$ of 1.9 mol of LyCH/mol of IgG at pH 5.0 and 25 °C to levels of 3.4–8.8 mol of LyCH/mol of IgG at pH 5.0/37 °C and pH 3.0/25 °C, respectively. As discussed earlier, this suggests that other cyclic diols can also fit

within the two-site model but that not all of these are amenable to periodate oxidation unless suitably strong reaction conditions are used. The fact that a relatively good fit is obtained to a two-site model even under this fairly wide range of conditions indicates that if multiple residues are represented by site type 2, then the apparent rate constants for their oxidation must be fairly similar. This is useful since it avoids the need for more complex models to describe the net rate of the oxidation process under these other reaction conditions.

CONCLUSIONS

In summary, this work examined the development of a kinetic model to help describe the effective rate of oxidation of rabbit IgG by periodate to form aldehyde groups for labeling or immobilization. The model that was developed was based on a pseudo-first-order mechanism in which two distinct classes of sites were being oxidized. The first type of site was oxidized fairly rapidly (i.e., within 15–30 min), while the second type of site reacted over the course of several hours. It was proposed that these two classes of sites represented exocyclic and cyclic diol groups, respectively. From the concentration dependence of the apparent rate constants, it was further suggested that this oxidation occurred through a mechanism in which the periodate and carbohydrate residues rapidly form a reversible complex that then undergoes a slower cleavage reaction. On the basis of comparisons that have been made between the carbohydrate regions of mammalian IgG antibodies (22), it is anticipated that the same kinetic model as developed here for rabbit IgG could be applied to other species, including human, sheep, mouse, and bovine IgG.

The model and equations developed in this study are of potential fundamental importance because they provide a basis for examining the kinetic processes that take place during the oxidation of antibodies or other glycoproteins by periodate. This model and these equations are also of interest from an applied viewpoint since they could be used to describe or predict the average number of labeling or immobilization sites that will be generated on oxidized antibodies. As shown in this work, the model developed in this study appears to work under a variety of pH and temperature conditions. It also appears to have the ability to separate the overall oxidation process into the contributions of two distinct classes of sites. This latter ability is of interest since it could allow the oxidation reaction to be tailored to emphasize the treatment of a particular group of carbohydrate residues. This is already done to some extent with glycoproteins through

the use of low temperatures and neutral pH values for the oxidation of sialic acid in the presence of other sugars (14, 25–27). On the basis of the model developed in this work, it should be possible to further refine the conditions that are required for this type of selective oxidation.

ACKNOWLEDGMENT

This work was supported by the National Institutes of Health under Grant GM44931. C.A.W. was supported, in part, by fellowships through the U.S. Department of Education GAANN program and the University of Nebraska Environmental Toxicology and Carcinogenesis graduate program. M.R.O. was supported by a fellowship through the Nebraska Center for Biotechnology.

LITERATURE CITED

- (1) O'Shannessy, D. J., and Quarles, R. H. (1987) Labeling of the oligosaccharide moieties of immunoglobulins. *J. Immunol. Methods* 99, 153.
- (2) O'Shannessy, D. J. (1990) Hydrazido-derivatized supports in affinity chromatography. *J. Chromatogr.* 510, 13.
- (3) Fleminger, G., Solomon, B., Wolf, T., and Hadas, E. (1990) Single step oxidative binding of antibodies to hydrazide-modified Eupergit C. *Appl. Biochem. Biotechnol.* 26, 231.
- (4) Fleminger, G., Hadas, E., Wolf, T., and Solomon, B. (1990) Oriented immobilization of periodate-oxidized monoclonal antibodies on amino and hydrazide derivatives of Eupergit C. *Appl. Biochem. Biotechnol.* 23, 123.
- (5) Abraham, R., Moller, D., Gabel, D., Senter, P., Hellström, I., and Hellström, K. E. (1991) The influence of periodate oxidation on monoclonal antibody avidity and immunoreactivity. *J. Immunol. Methods* 144, 77.
- (6) Morehead, H. W., Talmadge, K. W., O'Shannessy, D. J., and Siebert, C. J. (1991) Optimization of oxidation of glycoproteins: an assay for predicting coupling to hydrazide chromatographic supports. *J. Chromatogr.* 587, 171.
- (7) Ruhn, P. F., Garver, S., and Hage, D. S. (1994) Development of dihydrazide-activated silica supports for high-performance affinity chromatography. *J. Chromatogr. A* 669, 9.
- (8) Hoffman, W. L., and O'Shannessy, D. J. (1988) Site-specific immobilization of antibodies by their oligosaccharide moieties to new hydrazide derivatized solid supports. *J. Immunol. Methods* 112, 113.
- (9) Laguzza, B. C., Nichols, C. L., Briggs, S. L., Cullinan, G. J., Johnson, D. A., Starling, J. J., Baker, A. L., Bumol, T. F., and Corvalan, J. R. F. (1989) New antitumor monoclonal antibody-vinca conjugates LY203725 and related compounds: design, preparation, and representative in vivo activity. *J. Med. Chem.* 32, 548.
- (10) Wolfe, C. A. C., and Hage, D. S. (1995) Studies on the rate and control of antibody oxidation by periodate. *Anal. Biochem.* 231, 123.
- (11) Wolfe, C. A. C., and Hage, D. S. (1994) Automated determination of antibody oxidation using flow injection analysis. *Anal. Biochem.* 219, 26.
- (12) Noggle, J. H. (1992) *QuickBASIC Programming for Scientists and Engineers*, CRC Press, Boca Raton, FL.
- (13) Van Lenten, L., and Ashwell, G. (1971) Studies on the chemical and enzymatic modification of glycoproteins. *J. Biol. Chem.* 246, 1889.
- (14) Lee, K., and Lee, Y. (1994) Transfer of modified sialic acids by *Trypanosoma cruzi* trans-sialidase for attachment of functional groups to oligosaccharide. *Anal. Biochem.* 216, 358.
- (15) Rothfus, J. A., and Smith, E. L. (1963) Glycopeptides. IV. The periodate oxidation of glycopeptides from human γ -globulin. *J. Biol. Chem.* 238, 1402.
- (16) Eylar, E. H., and Jeanloz, R. W. (1962) Periodate oxidation of the α_1 acid glycoprotein of human plasma. *J. Biol. Chem.* 237, 1021.
- (17) Willard, J. J. (1962) Structure of the carbohydrate moiety of orosomucoid. *Nature* 194, 1278.
- (18) Dryhurst, G. (1970) *Periodate Oxidation of Diol and Other Functional Groups: Analytical and Structural Applications*, Pergamon Press, New York.
- (19) Espenson, J. H. (1981) *Chemical Kinetics and Reaction Mechanisms*, Chapters 2 and 3, McGraw-Hill, New York.
- (20) Krotoski, W. A., and Weimer, H. E. (1966) Peptide-associated and antigenic changes accompanying periodic acid oxidation of human plasma orosomucoid. *Arch. Biochem. Biophys.* 115, 337.
- (21) Nevell, T. P. (1957) The mechanism of the oxidation of cellulose by periodate. *J. Textile Inst.* 48, T484.
- (22) Rademacher, T., Homans, S., Parekh, R., and Dwek, R. (1986) Immunoglobulin G as a glycoprotein. *Biochem. Soc. Symp.* 51, 131.
- (23) Ashwell, G., and Morell, A. G. (1974) The role of surface carbohydrates in the hepatic recognition and transport of circulating glycoproteins. *Adv. Enzymol.* 41, 99.
- (24) Popenoe, E. A. (1958) Carbohydrate component of orosomucoid. *Fed. Proc.* 17, 290.
- (25) Massamiri, Y., Durand, G., Richard, A., Féger, and Agneray, J. (1979) Determination of erythrocyte surface sialic acid residues by a new colorimetric method. *Anal. Biochem.* 97, 346.
- (26) Cheresch, D., and Reisfeld, R. (1984) O-Acetylation of disialoganglioside GD₃ by human melanoma cells creates a unique antigenic determinant. *Science* 225, 844.
- (27) Norgard, K., Han, H., Powell, L., Kriegler, M., Varki, A., and Varki, N. (1993) Enhanced interaction of L-selectin with the high endothelial venule ligand via selectively oxidized sialic acids. *Proc. Natl. Acad. Sci. U.S.A.* 90, 1068.

BC9701120

Efficient Chemical Introduction of a Disulfide Cross-Link and Conjugation Site into Human Hemoglobin at β -Lysine-82 Utilizing a Bifunctional Aminoacyl Phosphate

Ronald Kluger* and Xianfeng Li

Lash Miller Laboratories, Department of Chemistry, University of Toronto, Toronto, Ontario, Canada M5S 3H6.
Received September 17, 1997[®]

The creation of a cross-link containing a disulfide into hemoglobin has been accomplished with a site-directed reagent, *N,N*-bis(Cbz-cystinyl)bis(methyl phosphate) (**1**). This is prepared from the reaction of the bis acid chloride of *N*-protected cystine with dimethyl phosphate followed by O-demethylation with methyl iodide in acetone. Reaction with deoxyhemoglobin produces two main products: cross-linked hemoglobin as the bis(cystinyl amide) of the ϵ -amino group of the side chain of Lys-82 of the two β subunits as well as material that has each of the same amino groups modified as the cystinyl amide but not cross-linked. Addition of 2-mercaptoethanol cleaves the disulfide in the material that is not cross-linked while leaving the disulfide intact in the cross-linked species. Dithiothreitol reduces the disulfide in the cross-linked species as well as in the species that is not cross-linked. Spontaneous oxidation in air converts all of the reduced material to the cross-linked bis(cystinyl amide) of hemoglobin. The reagent permits controlled introduction of cystinyl groups at lysyl residues, leading to formation of sulfhydryl groups by reduction and the possibility of re-forming the cross-links or forming conjugates.

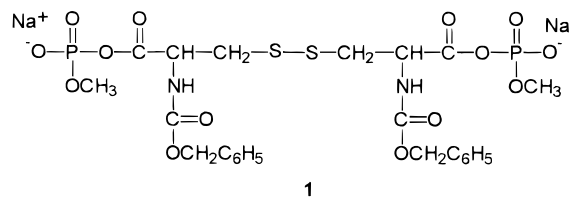
INTRODUCTION

Modified human hemoglobin is a central component of most materials that have been developed as potential blood substitutes (1–5). Cross-linking, either by chemical modification or by genetic engineering, is necessary to stabilize the tetrameric protein. As blood substitutes, cross-linked hemoglobins have to be tolerated in large quantities (6). The functionality introduced by cross-linking or genetic engineering also has the potential for creating sites for bioconjugation. Our laboratory's work on site-directed cross-linking of hemoglobin has established a wide variety of efficient reagents that are anionic electrophiles (3, 7). These materials selectively react with amino groups in the region of hemoglobin that binds the effector 2,3-diphosphoglycerate (DPG) (8, 9). We have also recently reported convenient methods to produce the general class of anionic electrophiles, monoesters of aminoacyl phosphates (10). The reactivity patterns of these molecules suggested that they would be useful for modification of proteins. We now report how modification of the amino acid cystine produces a new site-directed cross-linker, the *N,N*-carbobenzyloxybis(methyl phosphate) of cystine (**1**). This material reacts with hemo-

EXPERIMENTAL PROCEDURES

General Methods. Water was doubly distilled and deionized. All pH measurements were standardized against calibrated buffers using a combination glass electrode. Molecular mechanics was employed to obtain preferred conformations based on several initially estimated structures of bis(*N*-Cbz)cystinylbis(methyl phosphate). The coordinates of deoxyhemoglobin of Fermi and Perutz (11) from the Brookhaven protein database were used for visualization of the structure of the protein. Melting points were obtained in a calibrated oil bath apparatus. Proton NMR spectra were recorded at 200 and 300 MHz with chemical shifts reported relative to TMS or DSS. ¹³C NMR spectra were recorded on the same instruments at 50 and 75 MHz. Carbon chemical shifts were measured relative to chloroform-*d* with TMS at 0. ³¹P NMR spectra were recorded at 120 MHz, and chemical shifts are relative to 85% phosphoric acid in water. Infrared spectra were recorded on a FT-IR spectrometer in KBr pellets. Dr. Alex Young recorded mass spectra by electron-impact (EI) or fast atom bombardment ionization (FAB). The Mass Spectroscopy Laboratory, Department of Medical Genetics, University of Toronto provided electrospray ionization mass spectra. Chemical modification of hemoglobin and analysis followed general procedures as reported for related materials (12,13).

Synthesis of *N,N*-Bis(Cbz-cystinyl) Bis(sodium methyl phosphate) (1**).** *N,N*-Bis(Cbz-cystinyl) dichloride (14, 15) (1.0 g, 1.8 mmol) and sodium dimethyl phosphate (16) (0.54 g, 3.6 mmol; from trimethyl phosphate and 1 equiv of sodium iodide in dry acetone) were suspended in 30 mL of dry tetrahydrofuran at 0 °C under nitrogen and stirred for 1 h. The resulting precipitate of sodium chloride was removed by filtration. Sodium iodide (2.2 g, 14.6 mmol) was added to the filtrate [containing *N*-Cbz-cystinyl bis(dimethyl phosphate), **2**] to replace one methyl group at each phosphate with sodium (17). The mixture was stirred at 5 °C for 48 h. Solvent was removed by rotary evaporation. The result-



1

globin to give cross-linked protein that has amino groups converted to amides joined as a disulfide derivative.

* Author to whom correspondence should be addressed [e-mail rkluger@chem.utoronto.ca; telephone (416) 978-3582].

[®] Abstract published in *Advance ACS Abstracts*, November 1, 1997.

ing solid was crystallized from acetone/ether, producing an off-white powder. This was collected and washed three times with acetonitrile. The powder was dried in vacuum to give 1.0 g (1.35 mmol, 74% yield) of *N*-Cbz-cystinyl bis(sodium methyl phosphate) (**1**) as a white solid, mp > 200 °C: IR (KBr) C=O 1675 cm⁻¹, 1695 cm⁻¹; ¹H NMR (200 MHz, D₂O) δ 7.26 (s, 10H, 2C₆H₅), 4.88 (s, 4H, 2OCH₂Ph), 4.44 (m, 4H, NH and NCH), 3.45 (dd, 6H, J_{P-H} = 11.5 Hz, 2OCH₃), 2.70–3.25 (m, 4H, SCH₂); ¹³C NMR (121 MHz, D₂O) δ 168.3 (d, J_{P-C} = 9.7 Hz, P–O–C=O), 157.29 (C=O), 135.9, 128.4, 128.3, 127.7, 67.1, 53.9 (d, J_{P-C} = 6.4 Hz, OCH₃), 37.8; ³¹P NMR (121 MHz, D₂O) δ –5.4 (q, J_{P-H} = 11.3 Hz); FAB mass (–, glycerol) 717 (38.0, M – Na⁺).

Preparation of Deoxyhemoglobin. A solution of hemoglobin (80 mg/mL in 6 mL of 0.1 M, pH 8, MOPS) in a 50-mL round-bottom flask was immersed in an ice–water mixture. This was connected to a rotating reactor containing tubes for inflow and outflow of gases. Humidified oxygen was then passed through the solution for 1 h with the flask illuminated by a tungsten lamp. The resulting oxyhemoglobin was converted to the deoxy form by passing a stream of humidified nitrogen over the rotating solution for 3 h at 37 °C.

Reaction of **1 with Hemoglobin.** A solution of **1** was added over 15 min to a solution of hemoglobin in buffer (0.5 mM) so that the final concentration of **1** in the mixture was 0.7 mM and that of hemoglobin was 0.25 mM (0.1 M MOPS, pH 8.0). The solution was kept at 37 °C. For reactions with deoxyhemoglobin, the reagent was degassed and was introduced under nitrogen. The reaction was carried out under flowing nitrogen. For reactions with (carbonmonoxy)hemoglobin, the reaction solution was saturated initially with carbon monoxide. After **1** was added to the solution of hemoglobin, the reaction was continued for 2 h. The flask was then disconnected from the rotating reactor, and carbon monoxide was introduced. The solution was passed through a column of Sephadex G-25 equilibrated with 0.1 M, pH 8, MOPS to remove excess reagent. The resulting material (~20 mL) was collected in a vial.

Analysis of the resulting modified hemoglobin was done with a combination of reversed-phase HPLC and ion exchange HPLC following previously reported procedures (12).

Reduction of the Disulfide of Bis(cystinyldeoxyhemoglobin) with 2-Mercaptoethanol. 2-Mercaptoethanol (0.018 g) was dissolved in 1 mL of 0.1 M, pH 8.0, MOPS; 0.1 mL of the solution was added to 1 mL of a solution of the modified hemoglobins from the reaction of deoxyhemoglobin with **1**. The reaction mixture was stirred at 5 °C. Samples were analyzed by reversed-phase HPLC.

Reduction and Oxidation of Modified Hemoglobin with Dithiothreitol. Dithiothreitol (DTT) (0.073 g) was dissolved in 1 mL of 0.1 M, pH 8.0, MOPS; 0.01 mL of the DTT solution was added to 1 mL of the solution of modified hemoglobins from the reaction of deoxyhemoglobin with **1**. The reaction mixture was stirred at 5 °C, and the sample was analyzed by reversed-phase HPLC. After 15 min, the product was passed through a column of Sephadex G-25 equilibrated with 0.1 M, pH 8.0, MOPS to remove excess dithiothreitol. The sample was collected and analyzed again by reversed-phase HPLC.

Product Analysis. Extent of Cross-Linking. A sample of the reaction product (1.0 mL) was passed through a gel filtration column of Sephadex-100 (superfine) that had been equilibrated with 1.0 M magnesium chloride. Under these conditions hemoglobin that is not cross-linked dissociates into αβ dimers. The dimers elute more slowly than do cross-linked tetrameric species. The

extent of cross-linking of globin chains was also determined by polyacrylamide gel electrophoresis in the presence of sodium dodecyl sulfate [SDS–PAGE (18)] on Mini-Protein II Ready Gels (12% polyacrylamide, 0.375 M Tris–HCl, pH 8.8) as reported previously (19). The hemoglobins and globins from HPLC preparations were denatured in 0.065 M Tris–HCl, pH 6.8, 2% SDS, and 10% (v/v) glycerol. Approximately 20 mg of protein was applied to each lane of the gel and processed at 200 V for 1 h. Protein bands on the gel were stained with Coomassie brilliant blue R-250.

Analytical and Preparative Separation of Globin Chains. Modified hemoglobins were separated as intact tetramers by anion exchange HPLC on a SynChropak AX300 column (250 × 4.6 mm) using a mixture of 0.025 M bis-tris and 0.025 M tris with gradients starting from pH 8.5 to pH 6.7. The effluent was monitored at 540 nm. Heme and globin chains were separated by reversed-phase HPLC using 330 Å pore C₄ Vydac columns (250 × 4.6 mm for analytical and 250 × 12 mm for preparative). Developers contained 0.1% trifluoroacetic acid and various gradients of acetonitrile starting at 20% and ending at 60%. The effluent was monitored at 220 nm. Globin chains were recovered from the effluent by lyophilization.

Digestion of Globin Chains. Globin chains were dissolved in 8 M urea to increase susceptibility to hydrolysis and kept at room temperature for 2–4 h. The solution was then diluted to 2 M urea with 80 mM ammonium bicarbonate buffer at pH 8.5. Trypsin (2% of total protein) was added, and the solution was digested for 24 h at room temperature. The hydrolysate was heated in boiling water for 2 min, diluted to 1 M urea with 80 mM ammonium bicarbonate buffer, and further digested with endoproteinase Glu-C (1% of total protein) for another 72 h at room temperature. The hydrolysates were filtered before injection into the HPLC.

Chromatography of Peptides. Peptide fragments were separated by analytical HPLC using reversed-phase C₁₈ columns (3.9 × 300 mm). Developers consisted of 0.1% trifluoroacetic acid in water with gradients of acetonitrile from 0 to 100% over ~2 h. The HPLC effluent was monitored at 214 and 280 nm.

RESULTS

The reaction of *N,N*-bis(Cbz-cystinyl) dichloride with sodium dimethyl phosphate produces *N,N*-bis(CBZ-cystinyl) bis(dimethyl phosphate) (**2**). This is converted by reaction with sodium iodide to **1**. Combination of **1** with deoxyhemoglobin (3:1 reagent/protein) in aqueous buffer produced a set of modified hemoglobins. Under the same conditions, (carbonmonoxy)hemoglobin underwent very little reaction. The resulting proteins from reaction of deoxyhemoglobin and **1** were separated by ion exchange HPLC. Enzymic digestion and mass spectral analysis were used to determine the sites of the modifications resulting from reaction with **1**. The chromatogram of the reaction mixture showed that the solution contained only a small amount of unreacted hemoglobin (aabb) along with two major peaks corresponding to modified tetramers (Figure 1).

Two minor products elute after the major constituents. Further analysis of the components of the modified proteins by reversed-phase HPLC indicates that the two major products have native α chains along with modified β chains (determined by comparison with unmodified protein).

Figure 2 shows the results of HPLC analysis of the reaction mixture under conditions that separate the globin chains. Structural analysis of each component (from digestion, SDS–PAGE, and peptide analysis) in-

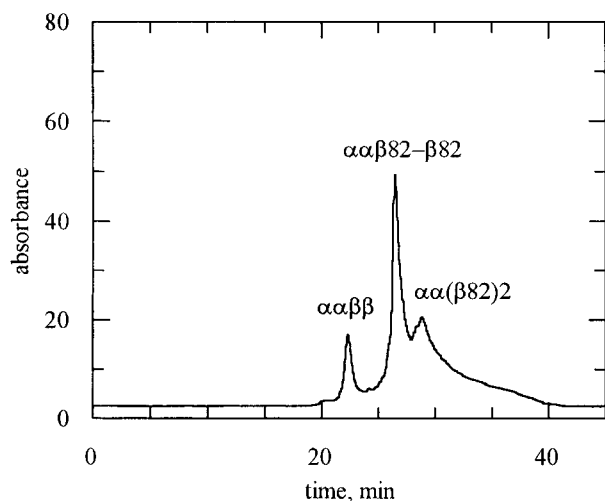


Figure 1. Anion-exchange chromatography (AX-300) of intact tetramers of hemoglobin from the reaction of deoxyhemoglobin with **1**.

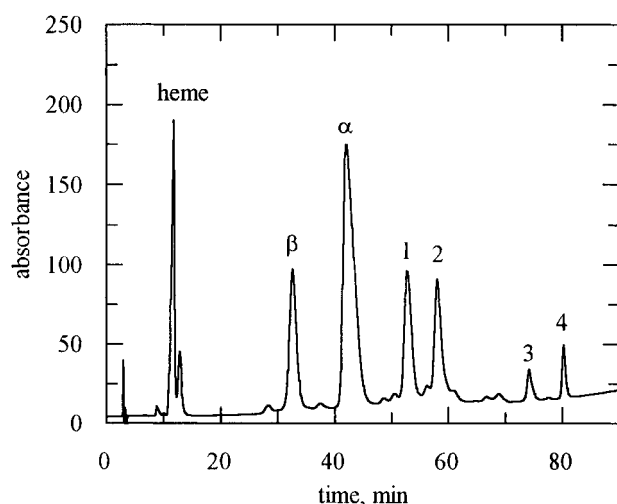


Figure 2. HPLC chromatogram of separated globin chains from the reaction of deoxyhemoglobin with **1**.

indicates that there are two β -modified tetrameric products. Peaks 1 and 2 correspond to modified β subunits. The first peak is material that is modified by reaction with **1** without cross-linking (the cystinyl amide), while the second contains the two subunits cross-linked as the cystinyl bis(amide). Enzymic digestion followed by peptide analysis reveals that in both peaks, modification is at the ϵ -amino group of lysine-82 of the β subunits. Two minor products, peaks 3 and 4, were shown by a similar analysis to be modified α subunits.

Ion-spray mass spectral analysis (20) of material from reversed-phase HPLC gives the molecular weight of the cross-linked β chains as 32 208, consistent with two β chains linked as the N,N -CBZ-cystinyl bis(amide). The peaks from the material that is not cross-linked are consistent with a species in which an amide has formed from reaction of **1** with the lysyl-82 ϵ -amino group, while the second acyl group of the reagent has undergone hydrolysis (Table 1).

Reduction of the Disulfide within N,N -Bis(CBZ-cystinyl) Modified Hemoglobin. The modified hemoglobins were treated with 2-mercaptoethanol. Progress of the cleavage reaction was followed by reversed-phase HPLC. When the modified hemoglobins from the reaction of **1** with deoxyhemoglobin were treated with a 20-fold excess of 2-mercaptoethanol for 1 h, the modified but not cross-linked hemoglobin was reduced to yield two

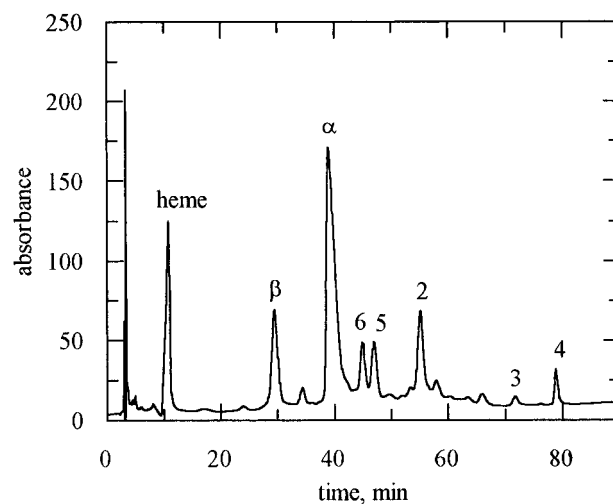


Figure 3. HPLC chromatogram (at early stage of reaction) of separated globin chains from the reaction of hemoglobin that had reacted first with **1** and then with 2-mercaptoethanol.

Table 1. Ion-Spray Mass Spectral Parent Peaks of Modified Globin Chains Obtained from Reaction of Deoxyhemoglobin with **1**

globin chain of hemoglobin	found	expected
unmodified β	15868.80 ± 1.48	15867
modified β -subunit	16359.01 ± 1.50	16357
cross-linked β -subunits	32207.78 ± 1.87	32206
unmodified α -subunits	15127.24 ± 1.55	15126
modified α -subunits	15616.19 ± 1.94	15616

products in approximately 1:1 ratio (Figure 3 shows a chromatogram from analysis early in the course of the reaction). As peak 1 disappears, two new peaks (peaks 5 and 6) appeared with shorter retention times. The structures of these products were established by electrospray ionization mass spectral analysis. Peak 5 is the reduced β chain corresponding to the desired product that results from the cleavage of the disulfide bonds. Peak 6 is the mixed disulfide intermediate (of mercaptoethanol and modified hemoglobin), with a parent mass of $16\ 178 \pm 2$ (calcd 16 180). Thus, the possible products are reduced cross-linked hemoglobin and two hemoglobins with mixed disulfides. However, the reaction of the disulfide of cross-linked hemoglobin with 2-mercaptoethanol proceeded very slowly under the same conditions. Peak 2, corresponding to cross-linked hemoglobin, did not decrease.

The modified protein mixture from the reaction of **1** with deoxyhemoglobin was treated with an excess of 2-mercaptoethanol for a few minutes and analyzed as follows. The C_4 reversed-phase HPLC of the reacted material contains two new peaks (peaks 5 and 6) with smaller retention times than the original peak. Mass spectra reveal that peak 5 is the β chain corresponding to the product that results from the cleavage of the disulfide bonds derived from the protein modified by **1**. The calculated mass of the modified β chain with a cleaved disulfide, a cysteinyl amide, of the β subunit of hemoglobin is 16 105 (found: $16\ 106.7 \pm 1.4$). Peak 6 is the mixed disulfide derived from oxidative coupling of the modified β subunit of cysteinylhemoglobin and 2-mercaptoethanol ($16\ 178 \pm 2$; calcd 16 180). Such a mixed disulfide is consistent with formation of intermediates by this reagent (21, 22).

The reaction of 2-mercaptoethanol with modified (but not cross-linked) hemoglobin is summarized in Scheme 1. The formation of a mixed disulfide intermediate and cleavage occur only with material that is not cross-linked by **1**.

Scheme 1

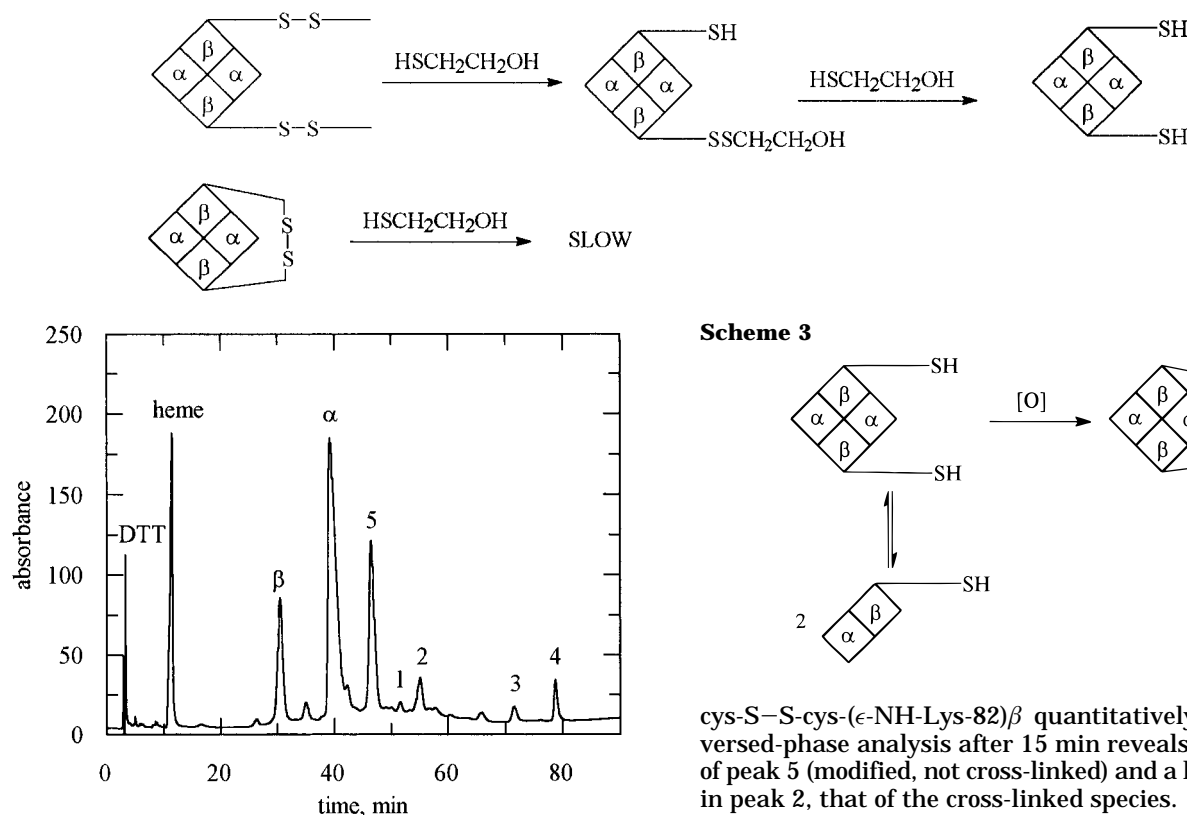
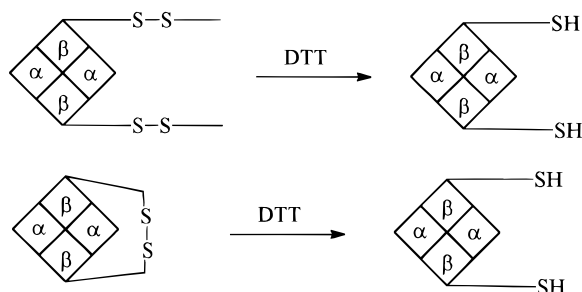


Figure 4. HPLC chromatogram (at early stage of reaction) of separated globin chains from the reaction of hemoglobin that had first reacted with **1** and then with DTT.

Scheme 2

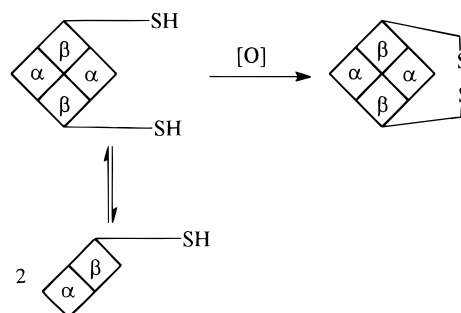


When the solution of modified proteins from the reaction of **1** with deoxyhemoglobin was treated with 4 equiv of the more effective reducing agent DTT (23), all disulfide bonds were cleaved within 15 min. The reversed-phase HPLC showed none of the original peaks derived from the β subunits. There was a single product peak at the position of the cysteinyl derivative of the β subunit. This is the same species generated in the reaction with 2-mercaptoethanol and with the same mass (16 105). The bis(cystinyl amide) [$\alpha\alpha\beta$ -Lys-82-cys-S-S-cys-(Lys-82)- β] is cleaved at the disulfide. Figure 4 shows the reversed-phase HPLC chromatogram of the products from an early stage in the reaction with DTT (showing some remaining unreacted β subunits).

The peaks are numbered as in Figure 3. The bis(sulfide) now appears as peak 5 but, as required, the intermediate from 2-mercaptoethanol (peak 6) is not present. The reaction pattern with DTT is summarized in Scheme 2.

Gel filtration chromatography was used to separate modified protein from excess DTT after reduction. The product in the presence of air and the absence of DTT is rapidly oxidized to produce once again $\alpha\alpha\beta$ -Lys-82(ϵ -NH-

Scheme 3



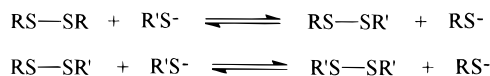
cys-S-S-cys-(ϵ -NH-Lys-82) β quantitatively. HPLC reversed-phase analysis after 15 min reveals the decrease of peak 5 (modified, not cross-linked) and a large increase in peak 2, that of the cross-linked species. Retreatment of the protein solution with DTT once again gives the disulfide-cleaved products exclusively (HPLC analysis). Therefore, the reduction-oxidation procedure is an efficient way to convert material that is not cross-linked into cross-linked material (Scheme 3).

One potential complication with the disulfide-containing cross-linker is the exchange reaction of the disulfides with free sulfhydryl groups within the protein (24). There are six cysteinyl residues per hemoglobin tetramer (three per dimer), with Cys-93 of each of the β chains lying on the surface. HPLC analysis of the globin chains of the cross-linked hemoglobin indicated it was stable at pH 8 for 3 months at 5 °C without degradation. This requires that Cys-93 does not react to cleave the S-S bond of the cross-linked hemoglobin.

DISCUSSION

The reactions of **1** with hemoglobin follow the patterns of other anionic electrophiles. The reagent reacts efficiently only with the deoxy form. Its acylating reaction occurs at residues in the DPG binding site at the ϵ -amino groups of Lys-82 in the β subunits. The reagent does not react with the N-terminal amino groups (Val-1) as do reagents that are bis(methyl phosphate)s derived from simple dicarboxylic acids (25). It is likely that the bulk of the N-protected amino group in **1** produces additional selectivity based on steric effects.

X-ray crystallographic structures of deoxyhemoglobin reveal that the β -Lys-82 ϵ -amino groups are outside the protein at the interface between the DPG-binding site and the surrounding solution (9). By contrast, the α -amino group of the N-terminal β -Val-1 is further within the DPG-binding site. Modeling of the reagent into the structure of deoxyhemoglobin suggests that the reagent binds to the DPG site at the solution interface, limiting reaction to the lysine residues. The steric bulk of two Cbz amino-protecting groups in **1** provides selectivity beyond that found with acyl phosphate monoesters toward amino groups in hemoglobin.

Scheme 4

The reaction of **1** with (carbonmonoxy)hemoglobin gives only a very small amount of product under the conditions that extensively modify the deoxy form. The product that does form is not cross-linked. This result is consistent with the conformational change of hemoglobin in going from the R state to the T state (26). When deoxyhemoglobin binds to ligands such as oxygen and carbon monoxide, the extensive quaternary structural change leads to contraction of the DPG binding site (27, 28). As a consequence, the DPG binding site is not large enough to be accessed by such a bulky reagent.

The disulfides of the two β -chain-modified hemoglobins show different reactivity with β -mercaptoethanol. The reaction mechanism and accessibility of the S-S bonds of modified hemoglobins can explain this difference (21). Reduction of a disulfide by thiol reagents proceeds in two steps. A mixed disulfide of the cleaved disulfide and mercaptoethanol is an intermediate. In the thiol-disulfide exchange process, a large excess of the reagent is required to drive the reaction to completion (Scheme 4).

For the cysteinyl hemoglobin with no cross-links, one end of the reagent is attached to β -Lys-82. The unreacted portion of the large, hydrophilic reagent is probably out of the DPG binding site. Therefore, the disulfide is accessible to 2-mercaptoethanol.

On the other hand, if the β subunits of hemoglobin are cross-linked as the bis(cystinyl) derivative, the S-S bond within the DPG cleft becomes less accessible to the thiol reagent. The DPG binding site protects the disulfide from reduction, and the reaction of that disulfide bond with 2-mercaptoethanol is blocked.

The S-S bond of the cross-linked hemoglobin is cleaved with dithiothreitol, a more effective reducing reagent. When dithiothreitol is used to reduce the S-S bond, the first step is also a thiol-disulfide exchange as with 2-mercaptoethanol. However, once the intermediate is formed, a second molecule of reagent does not participate in the reaction. Instead, an intramolecular reaction can occur, leading to the formation of the stable cyclic disulfide of DTT (23). The intramolecular process has a large entropic advantage in its favor. Since the cross-linked hemoglobin was reduced without the addition of denaturing reagents, the S-S bond is near the outside of the DPG cleft of the cross-linked hemoglobin and is exposed to solvent.

The oxidation of thiols to disulfides by oxygen normally proceeds only in the presence of catalytic quantities of metal ions such as iron and copper (29). The rate of the oxidation of thiols in the same molecule depends on the distance between the thiol groups (29). In the present study, the modified hemoglobin with two free sulfhydryl groups attached at β -Lys-82 is oxidized spontaneously by atmospheric oxygen, quantitatively producing the cross-linked tetramer. It is possible that the iron of the heme facilitates the reaction, especially that which is present as Fe(III) methemoglobin. The result requires that the sulfhydryl groups produced by reduction remain in close spatial proximity to form the disulfide between subunits by oxidation.

CONCLUSIONS

The introduction of specific chemical alterations at defined sites within a protein is complementary to methods based on genetic engineering. The design of **1**

permits site selection based on charge and steric factors. The fact that **1** is an amino acid derivative permits chemical techniques to be used that are extended from the chemistry of peptide formation. A wide variety of side chains, as well as longer peptides for conjugation, can be implemented in combination with the convenient methods we have developed for producing the mixed phosphate-amino acid anhydride.

The use of the disulfide-based reagent in the present study adds further possibilities for applications of cross-linking by converting sites that contain lysyl side chains into those connected as disulfides and also, by reduction, to sites for bioconjugation. For example, after formation, cleavage by reduction permits control experiments to be undertaken as suggested by Uy and Wold (30). If a reagent does not contain a cross-link, modification at both sites by 2 equiv of reagent will permanently prevent formation of a cross-link. However, as we found in this study, cleavage of the disulfide at each site, followed by oxidation, permits spontaneous formation of the cross-link between dimers. This produces a much higher yield of cross-linked materials and suggests an added benefit of the use of such reagents. Finally, these materials should also be useful for studies of protein subunit recombination and for introduction of sites for bioconjugation, as has been reported for genetically engineered variants of hemoglobin that contain additional sulfhydryl side chains.

ACKNOWLEDGMENT

This work was supported by the Protein Engineering Network (PENEC) and by the Natural Sciences and Engineering Research Council of Canada through an operating grant.

LITERATURE CITED

- (1) Chang, T. M. (1997) Recent and future developments in modified hemoglobin and microencapsulated hemoglobin as red blood cell substitutes. *Artif. Cells Blood Substit. Immobil. Biotechnol.* 25, 1-24.
- (2) Walder, J. A., Zaugg, R. H., Walder, R. Y., and Steele (1979) Diaspirins that cross-link β -chains of hemoglobin. *Biochemistry* 18, 4265-4270.
- (3) Kluger, R. (1994) Syntex Award Lecture. Anionic electrophiles, protein modification, and artificial blood. *Can. J. Chem.* 72, 2193-2197.
- (4) Looker, D., Abbott-Brown, D., Cozart, P., Durfee, S., Hoffman S., Mathews, A. J., Miller-Roehrich, J., Shoemaker, S., Trimble, S., Fermi, G., Komiyama, N. H., Nagai, K., and Stetler, G. L. (1992) A human recombinant haemoglobin designed for use as a blood substitute. *Nature* 356, 258-260.
- (5) Kroeger, K. S., and Kundrot, C. E. (1997) Structures of a hemoglobin-based blood substitute: insights into the function of allosteric proteins. *Structure* 5, 227-237.
- (6) Winslow, R. M. (1997) Progress on blood substitutes. *Nat. Med.* 3 (5), 474.
- (7) Kluger, R. (1997) Chemical cross-linking and protein function. In *Protein Function, A Practical Approach* (T. E. Creighton, Ed.) pp 185-214, URL Press, Oxford, U.K.
- (8) Schumacher, M. A., Zhelezanova, E. E., Poundstone, K. S., Kluger, R., Jones, R. T., and Brennan, R. G. (1997) Allosteric intermediates indicate R2 is the liganded hemoglobin end state. *Proc. Natl. Acad. Sci. U.S.A.* 94, 7841-7844.
- (9) Schumacher, M. A., Dixon, M. M., Kluger, R., Jones, R. T., and Brennan, R. G. (1995) Allosteric transition intermediates modelled by cross-linked haemoglobins. *Nature* 375, 84-87.
- (10) Kluger, R., Li X., and Loo, R. W. (1996) 1996 Bader Award Lecture. Aminoacyl ethyl phosphates. Biomimetically activated amino acids. *Can. J. Chem.* 74, 2395-2400.
- (11) Fermi, G., and Perutz, M. F. (1984) The crystal structure of human deoxyhaemoglobin at 1.74 Å resolution. *J. Mol. Biol.* 175, 159-174.

- (12) Jones, R. T. (1994) Structural characterization of modified hemoglobins. *Methods Enzymol.* **231**, 322–343.
- (13) Jones, R. T., Shih, D. T., Fujita, T. S., Song, Y., Xiao, H., Head, C., and Kluger, R. (1996) A doubly cross-linked human hemoglobin. Effects of cross-links between different subunits. *J. Biol. Chem.* **271**, 675–680.
- (14) du Vigneaud, V., and Miller, G. L. (1952) *S*-Benzyl-L-cysteinylglycine. *Biochem. Prepr.* **2**, 74–79.
- (15) Bergmann, M., and Zervas, L. (1932) Über ein allgemeines Verfahren der Peptid-Synthese (On a general method for peptide synthesis). *Chem. Ber.* **65**, 1192–1201.
- (16) Bunton, C. A., Mhala, M. M., Oldham, K. G., and Vernon, C. A. (1960) The reactions of organic phosphates. Part III. The hydrolysis of dimethyl phosphate. *J. Chem. Soc.*, 3293–3301.
- (17) Kluger, R., Grant, A. S., Bearne, S. L., and Trachsel, M. R. (1990) Dicarboxylic acid bis(methyl phosphates): Anionic biomimetic cross-linking reagents. *J. Org. Chem.* **55**, 2864–2868.
- (18) Laemmli, U. K. (1970) Cleavage of structural proteins during the assembly of the head of bacteriophage T-4. *Nature (London)* **227**, 680–685.
- (19) Kluger, R., and Song, Y. (1994) Changing a protein into a generalized acylating reagent. *J. Org. Chem.* **59**, 733–736.
- (20) Fenn, J. B., Mann, M., Meng, C. K., Wong, S. F., and Whitehouse, C. M. (1989) Electrospray ionization for mass spectrometry of large molecules. *Science* **246**, 64–71.
- (21) Means, G. E., and Feeney, R. E. (1971) *Chemical Modification of Proteins*, Holden-Day, San Francisco, CA.
- (22) Fava, A., Iliceto, A., and Camera, E. (1957) Kinetics of thiol-disulfide exchange. *J. Am. Chem. Soc.* **79**, 833–838.
- (23) Zahler, W. L., and Cleland, W. W. (1968) A specific and sensitive assay for disulfides. *J. Biol. Chem.* **243**, 716–719.
- (24) Lomant, A. J., and Fairbanks, G. (1976) Chemical probes of extended biological structures: synthesis and properties of the cleavable protein cross-linking reagent [35S]dithiobis-(succinimidyl propionate). *J. Mol. Biol.* **104**, 243–261.
- (25) Jones, R. T., Head, C. G., Fujita, T. S., Shih, D. T., Wodzinska, J., and Kluger, R. (1993) Modification of human hemoglobin with methyl acyl phosphates derived from dicarboxylic acids. Systematic relationships between cross-linked structure and oxygen-binding properties. *Biochemistry* **32**, 215–223.
- (26) Dickerson, R. E., and Geis, I. (1983) *Hemoglobin: Structure, Function, Evolution, and Pathology*, Benjamin/Cummings Publishing, Menlo Park, CA.
- (27) Perutz, M. (1990) Mechanisms regulating the reactions of human hemoglobin with oxygen and carbon monoxide. *Annu. Rev. Physiol.* **52**, 1–25.
- (28) Perutz, M. (1970) Stereochemistry of cooperative effects in haemoglobin. *Nature* **228**, 726–739.
- (29) Torchinsky, Y. M. (1981) *Sulfur in Proteins*, Pergamon Press, Oxford, U.K.
- (30) Uy, R., and Wold, F. (1977) *Protein Cross-linking*, Plenum, New York.

BC970169A

Preparation and Purification of an End to End Coupled mEGF–Dextran Conjugate

Qinghai Zhao,^{*,†} Ingo Gottschalk,[†] Jörgen Carlsson,[†] Lars-Erik Arvidsson,[‡] Sven Oscarsson,[§] Anders Medin,^{||} Bo Ersson,^{||} and Jan-Christer Janson^{‡,||}

Division of Biomedical Radiation Science, Department of Diagnostic Radiology, Uppsala University, Box 535, S-751 21 Uppsala, Sweden; Pharmacia Biotech AB, S-751 82, Sweden; Department of Chemical Engineering, Mälardalen University, Box 325, S-63105 Eskilstuna, Sweden; and Biochemical Separation Centre, Uppsala Biomedical Centre, Box 577, S-751 23 Uppsala, Sweden. Received February 18, 1997[®]

The amino terminus of mouse epidermal growth factor (mEGF) was coupled directly to the aldehyde end of dextran through a reductive amination procedure. The highest coupling efficiency was ~80% and could be reached after ~24 h of reaction time at pH 8. Gel filtration on Sephadex G-50 Fine removed free mEGF from the conjugate. Preparative polyacrylamide gel electrophoresis was used to separate the conjugate from excess noncharged dextran. The conjugate bound specifically to the EGF receptor on cultured glioma cells as shown in displacement tests with free mEGF. The conjugate was stable in the pH interval 4–9, in 2 M sodium chloride, in 7 M urea, and in human serum and could still bind to the EGF receptor after such treatments. The conjugates are candidates for targeted nuclide therapy.

INTRODUCTION

Dextran has for a long time possessed biomedical interest, primarily as a blood plasma volume expander (DeBelder, 1990; Fassio et al., 1992; Klotz and Kroemer 1987; Moon et al., 1991) but also as a carrier for drug and radionuclide (Andersson et al., 1991; Carlsson et al., 1994; Olsson et al., 1994; Sjöström et al., 1997) delivery. An attractive approach is to couple dextran to a ligand that recognizes a specific receptor on cancer cell membranes. The dextran part is then the potential carrier of the toxic factors such as radionuclides. Targeted therapy with radionuclides for cancer treatment is one main research topic in our laboratory and is therefore discussed in more detail.

Dextran connected to a tumor seeking ligand has potential advantages when used as a radionuclide carrying conjugate for the following reasons:

- There is a reduced risk for biodegradation since dextran has been shown to protect against protein degradation (Andersson et al., 1991; Kato et al., 1990; Marshall, 1978; Srivastava, 1991). The dextran moiety could possibly protect the conjugate from intracellular degradation (Andersson et al., 1991; Blomhoff et al., 1983; Olsson et al., 1994; Sjöström et al., 1997) and also from degradation in the blood circulation (Melton et al., 1987; Yasuda et al., 1990).

- Dextran has potentially high toxicity when loaded with toxic agents but low toxicity due to the EGF and dextran structures since neither dextran (DeBelder, 1990) nor the natural ligand EGF is expected to be toxic. The normal ligand epidermal growth factor (EGF)¹ is known to react only with the EGF receptor and have no known cross-reactivity with other structures (Carpenter,

1987). Thus, EGF is not expected to exert any unwanted blocking of enzymatic reactions or to disturb other cellular processes.

- Control of serum half-life of the conjugate is possible by varying the molecular weight of the dextran. The length of the dextran chains will probably, to a large extent, determine the serum half-life (Emmrich et al., 1977; Klotz and Kroemer, 1987; Lindström et al., 1993).

Furthermore, it is possible that there is a decreased risk for immunogenic reactions against the conjugate in relation to the protein itself. Theoretically, it is possible that the antigenicity could be reduced since the carbohydrate part might "hide" immunogenic sites on the ligand. However, mEGF is a relatively small protein (6 kDa) and such molecules are normally not strongly immunogenic, so this might not be an important factor when EGF–dextran is considered. Dextran is not known to be immunogenic except in those few cases when persons have an immunology-based hypersensitivity to dextran (Klotz and Kroemer, 1987). However, the increased molecular weight of the conjugate in relation to the individual "building blocks" might increase the antigenicity. It is also a risk that new structures appearing in the conjugation point between EGF and dextran might be immunogenic, and this has to be tested in future animal experiments and clinical tests. The situation is complex as shown in other similar cases (Seppala and Makela, 1989), and the question about immunogenic response is important for future therapeutic applications since it might be necessary to give repeated injections of the targeting agent.

These arguments support the ambition to further analyze the basic aspects of dextran–ligand conjugates for targeted radiotherapy. However, each aspect has to be considered with great care since the conjugates will be hybrid molecules consisting of a carbohydrate part, dextran, and a protein, EGF, and such hybrid molecules might attain new unpredicted biological properties.

¹ Abbreviations: CDAP, 1-cyano-4-(dimethylamino)pyridinium tetrafluoroborate; PB, phosphate buffer; PBS, phosphate-buffered saline (at pH 7.2 and 0.15 M PBS); EDTA, ethylenediaminetetraacetic acid; EGF, epidermal growth factor; mEGF, mouse epidermal growth factor; Dex, dextran D14.

* Author to whom correspondence should be addressed (e-mail Qinghai.Zhao@bms.uu.se; telephone +46 18 471 34 33; fax +46 18 471 34 32).

[†] Uppsala University.

[‡] Pharmacia Biotech AB.

[§] Mälardalen University.

^{||} Biochemical Separation Centre.

[®] Abstract published in *Advance ACS Abstracts*, November 1, 1997.

The receptor for EGF is overexpressed in some malignancies such as gliomas, bladder cancers, squamous epithelial carcinomas, and some forms of adenocarcinomas (Bigner et al., 1988; Carpenter, 1987; Filmus et al., 1985; Libermann et al., 1984, 1985; Mendelsohn, 1988; Messing et al., 1992; Ozawa et al., 1989; Sauter et al., 1994; Todderud and Carpenter, 1989) and is a potential target for therapy in those malignancies. The goal with the present study was to design a reasonably well-defined EGF receptor targeting agent, based on the natural ligand EGF conjugated to dextran, for the future delivery of radioactive nuclides of therapeutic interest.

EGF is a 53 amino acid protein with compact structure that binds specifically to the EGF receptor. Human and mouse EGF have 37 of 53 amino acids in common, and the three disulfide bonds are formed in the same relative positions. They have also approximately the same binding efficiency to the human EGF receptor (Carpenter and Cohen, 1976, 1979). We decided to use mouse EGF in the present study since it only has one free amino group, namely the amino terminus (Carpenter and Cohen, 1979). Human EGF has, in addition to the amino terminus, also two lysine residues. Thus, compared to human EGF, mouse EGF might be more suitable for specific amino group coupling to dextran.

Many different protein-dextran conjugates have been developed with various methods. The coupling methods often employed are periodate oxidation of dextran and CNBr or CDAP carbohydrate cyanating procedures (Andersson et al., 1991, 1992; Holmberg et al., 1993, 1994; Löqvist et al., 1993; Olsson et al., 1994; Sjöström et al., 1997). These methods can effectively introduce free amino group containing substances at random positions in the dextran chain. The main disadvantage seems actually to be that the positions on the dextran for linking of the protein are randomly distributed, which gives a heterogeneous mixture of conjugates.

From the view of drug design it would be interesting if the coupling between the tumor seeking ligand and dextran could be limited to one "specific position" in the dextran chain. This could give a more homogeneous conjugate preparation. There seems to be only one such specific position in dextran, and that is the aldehyde group at the end of the dextran chain. Only one such aldehyde group exists per dextran molecule even if some branching exists (Fudui et al., 1982).

The principle mechanisms for selective reductive amination of aldehyde groups have previously been described (Borch et al., 1971; Lane, 1975; Lundblad and Noages, 1984), and some results for coupling of small amino containing molecules to the end aldehyde group have also been described earlier (Yalpani and Brooks, 1985). In the present study we have investigated the possibility of using selective reductive amination of the single aldehyde group of dextran to directly couple to the amino terminus of mEGF.

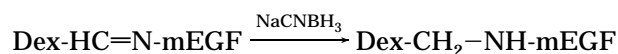
EXPERIMENTAL PROCEDURES

Chemicals. Freeze-dried dextran with a molecular range $14\,000 \pm 500$ was obtained by fractionation of Dextran T10 (Pharmacia Biotech AB, Uppsala, Sweden) by gel filtration on Sephacryl 100 HR (Pharmacia Biotech). This dextran fraction will in the following be called D14. Sodium cyanoborohydride (NaCNBH_3) (article no. 818053) was the product of Merck-Schuchardt, Darmstadt, Germany. Mouse EGF (batch 57.067), tissue culture grade, was purchased from Janssen Biochimica, Belgium. ^{125}I (article no. IMS 30) was from Amersham Laboratories, England.

Equipment. Sephadex G-50 Fine, FPLC System, and PhastSystem are products of Pharmacia Biotech AB. The instrument for preparative electrophoresis, a Mini Prep Cell, was from Bio-Rad Inc., Richmond, CA. A Beckman refractometer was used for continuous registration of the refractive index during chromatography. A Wallac 1480 Wizard gamma counter (Wallac, Finland) was used to count ^{125}I radioactivity. The electronic cell counter was from Coulter Electronics LTD, England.

Radiolabeling. EGF was labeled with ^{125}I according to the chloramine-T method as previously described (Andersson et al., 1991). mEGF (2.5–5 μg) was mixed with 20 μL of pH 7.5, 0.5 M, PB, 10 μL of 0.2% (w/v) chloramine-T, and 10–20 μL of ^{125}I for 1 min. Twenty-five microliters of 0.2% (w/v) sodium bisulfite solution was used to stop the reaction. Excess reagents and free ^{125}I were separated, directly after labeling, from the macromolecules by NAP-5 desalting columns (Pharmacia Biotech AB). Buffer with pH 8.0, 0.05 M, PB was used as washing solution.

Reductive Amination. Dextran D14 (20 mg, 1.43 mmol) was dissolved in 100 μL of iodinated mEGF (1–5 μg , 0.17–0.83 nmol) solution (pH 8.0, 0.05 M PB). NaCNBH_3 (8 mg, 127 mmol) was then added. The reaction was kept going for 24 h (in the range of 0–145 h in the initial tests) at room temperature with continuous stirring. The reductive amination reaction scheme can be written (Dex = dextran D14)



The yield of conjugate production was optimized as a function of the pH of the reaction buffer solution. The reaction conditions were the same as above only that pH values in the range 6.5–8.5 in 0.05 M PB solutions were applied. The uncertainty in each calculated point was estimated from repeated pipettings, variations in the chromatography steps, and Poisson statistics for radioactivity counting. It was then estimated that the error in each measurement was <5%.

Gel Filtration. The reductive amination reaction mixture was applied to a Sephadex G-50 Fine (1 \times 40 cm) column. A Pharmacia HR 10/30 column was used in some cases. The flow rate was 0.2 mL/min, and the fraction volumes were 0.5 mL. Eluents were either 0.09% (w/v) sodium chloride, PBS, or distilled water depending on the application. A refractometer continuously registered the result of the chromatography, and the fractions were then analyzed with the gamma counter.

Analytical Electrophoresis. A PhastSystem for polyacrylamide gel electrophoresis was used to analyze the obtained conjugate solutions. Native 8–15% gradient gels were loaded with 4 μL samples and the samples run at 400 V for half an hour (268 Vh). The gel film was then cut into 30 equally sized pieces for every sample lane. Each piece was transferred to 0.5 mL of PBS and analyzed with the gamma counter.

Preparative Electrophoresis. A discontinuous native-PAGE system for preparative electrophoresis was used to isolate the conjugate from excess amounts of free dextran (dextran without EGF). The system was as follows: 4% stacking gel (7 \times 15 mm) with pH 6.8, 0.125 M, Tris-HCl and 7% resolving gel (7 \times 40 mm) with pH 8.8, 0.375 M, Tris-HCl. Tris-glycine buffer (25 mM Tris, 200 mM glycine) was used as the running and elution buffer. Usually 150–250 μL of sample was mixed with the same volume of sample buffer [pH 6.0, 62.5 mM, Tris-

HCl, 25% (v/v) glycerol, 0.012% (w/v) bromophenol blue]. The electrophoresis was then run at 300 V with constant power and current limits at 1 W and 3 mA for 20 h. The elution buffer was pumped at a rate of 100 μ L/min. The obtained fractions were finally analyzed with the gamma counter.

Dextran Analysis. The dextran concentration in the collected fractions was determined using the phenol method according to Dubois et al. (1956).

Cell Culture. The subclone of the glioma cell line U-343-MG used in this study was originally designated U-343MGaC12:6 and has been characterized in some detail by Westermarck et al. (1982), Nistér et al., (1987), and Werner et al. (1988). Ham's F-10 medium (Kebo, Stockholm, Sweden) supplemented with 10% FCS (Flow, Stockholm, Sweden), L-glutamine (2 mM), and PEST (penicillin 20 IU/mL and streptomycin 20 μ g/mL) (all from Kebo) were used. The culture medium was routinely changed three times per week. Subculture with trypsin was applied normally once a week. The cells in the EGF-binding tests were in all cases not trypsinized for <2 days before the tests since trypsinization might damage the EGF receptors. The number of cells in each of the culture dishes (plastic culture dishes with a diameter of 35 mm, Corning Glass, Corning, NY) used for binding experiments was 5×10^5 .

Displacement Tests. The capacity of normal nonradioactive mEGF to displace the binding of [125 I]mEGF-Dex conjugate was analyzed. Conjugate samples of ~ 5 μ g in 11 mL of F10 medium (complemented with PEST) were prepared. Various concentrations of nonradioactive mEGF in culture medium were used to displace the conjugate binding. The nonradioactive mEGF was given to the cells directly before a constant concentration of radioactive conjugate was added to the culture dishes. In practice, the nonradioactive and radioactive components were given at the same time because the time interval between was only a few seconds. The total medium volume was 2 mL in each dish. The incubations were in all experiments carried out as triplicates. The incubation times were 90 min at 37 °C, which had been found to be suitable for similar types of conjugates in previous studies from our laboratory (Andersson et al., 1991; Olsson et al., 1994; Sjöström et al., 1997).

After incubation, the cultures were washed, 6×1 min, in normal nonradioactive culture medium. The cells were then trypsinized with 500 μ L of trypsin EDTA solution [0.05% trypsin (w/v), 0.02% EDTA (w/v) in buffer] for 15 min at 37 °C. One milliliter of normal culture medium was then added to each dish to obtain a homogeneous suspension of cells. A 0.5 mL fraction of the cell suspension was taken for electronic cell counting. The remaining 1 mL volume was analyzed in the gamma counter using the standard 125 I channel to measure the cell-associated radioactivity.

Stability Tests. The conjugates were exposed to different conditions to test their stabilities. The universal buffers with different pH values and containing different combinations of NaOH, potassium dihydrogen phosphate, boric acid, and diethylbarbituric acid were applied. The choice of these buffers was made since they are often used in biochemical and biological work. NH_4SCN (3 M), urea (7 M), NaCl (1 M) (all three giving high ion strength), or 30% ethylene glycol (hydrophobic) (w/v) was also applied since these are often used for elution in affinity chromatography. We did not apply affinity chromatography in this study, but that might be the case if conjugate specific antibodies are raised in the future. Human serum was also used in the stability tests. The conjugate preparations were collected from gel filtration on the Sephadex

G-50F (1 \times 40 cm) columns, eluted and washed with 0.09% NaCl (w/v). The conjugate fractions were pooled, divided in equally sized fractions, and kept frozen before the tests.

During the stability tests, the [125 I]mEGF-dextran conjugate solutions (in 0.09% NaCl) were mixed with the same volume of universal buffer of different pH or with 6 M NH_4SCN , 14 M urea, 60% ethylene glycol (w/v), or human serum, respectively. The mixtures were incubated at 37 °C for 1 h and then immediately applied to Sephadex G-50 F (1 \times 40 cm) gel filtration. A buffer with pH 7.0 (0.05 M PB) was used to elute and wash the column. The 125 I radioactivity in each fraction was measured with the gamma counter.

Binding to cultured cells was finally analyzed as described above (under Displacement Tests), and 0.5 mg/mL nonradioactive mEGF was in this case added in the culture medium to displace the binding.

RESULTS

After reductive amination, the conjugates were freed from nonreacted EGF by gel filtration on Sephadex G-50 Fine. When a mixture of mEGF-dextran conjugate, mEGF, and dextran D14 was applied to the column, three peaks were obtained (Figure 1a). The first peak contained the mEGF-dex conjugate and free nonreacted dextran. The second peak contained free nonreacted mEGF, and the third peak contained low molecular weight components such as free iodine and salts. It is seen that iodine is released into the low molecular fraction after the conjugation chemistry is carried out. The contents of the first two peaks were confirmed by electrophoresis (see below).

Panels a–c of Figure 1 show that the coupling efficiency increased with time up to about 24 h. Since only mEGF was radiolabeled, only the conjugate could be monitored in the first peak and not the free dextran. Results from several incubation periods are summarized in Figure 1d. The ratio of the conjugate peak radioactivity to the sum of conjugate and nonreacted mEGF peak radioactivities was calculated and defined as the conjugation efficiency. A plateau was reached after ~ 24 h. This reaction time was used in all conjugations. The conjugation efficiency as a function of the pH in the coupling buffer was analyzed the same way. The result is summarized in Figure 2. The maximum efficiency was found to be at around pH 8. This pH was thereafter applied in all conjugations.

A number of conjugation control experiments were then carried out. These are shown in Figure 3. In each panel a reference conjugation chromatogram showing the position of the conjugate and salt peaks is superimposed (dashed lines). Figure 3a shows the result when NaCNBH₃ was omitted from the reaction mixture of dextran and [125 I]mEGF. Only minor amounts of radioactivity could be detected at the position of the conjugate. In another experiment (Figure 3b) the dextran was omitted but NaCNBH₃ was added. Insignificant amounts of radioactivity were found in the conjugation peak, indicating that no aggregation of mEGF molecules takes place due to the presence of NaCNBH₃. A control chromatography of nonconjugate 125 I-labeled mEGF is shown in Figure 3c. Only a very small peak can be seen at the conjugate position.

Figure 4 shows separation of [125 I]mEGF-Dex conjugate and nonreacted [125 I]mEGF by analytical native polyacrylamide gradient gel electrophoresis. The conjugate and mEGF are easily separated. In a separate experiment it was shown that dextran remained at the loading position. This method was used to verify the

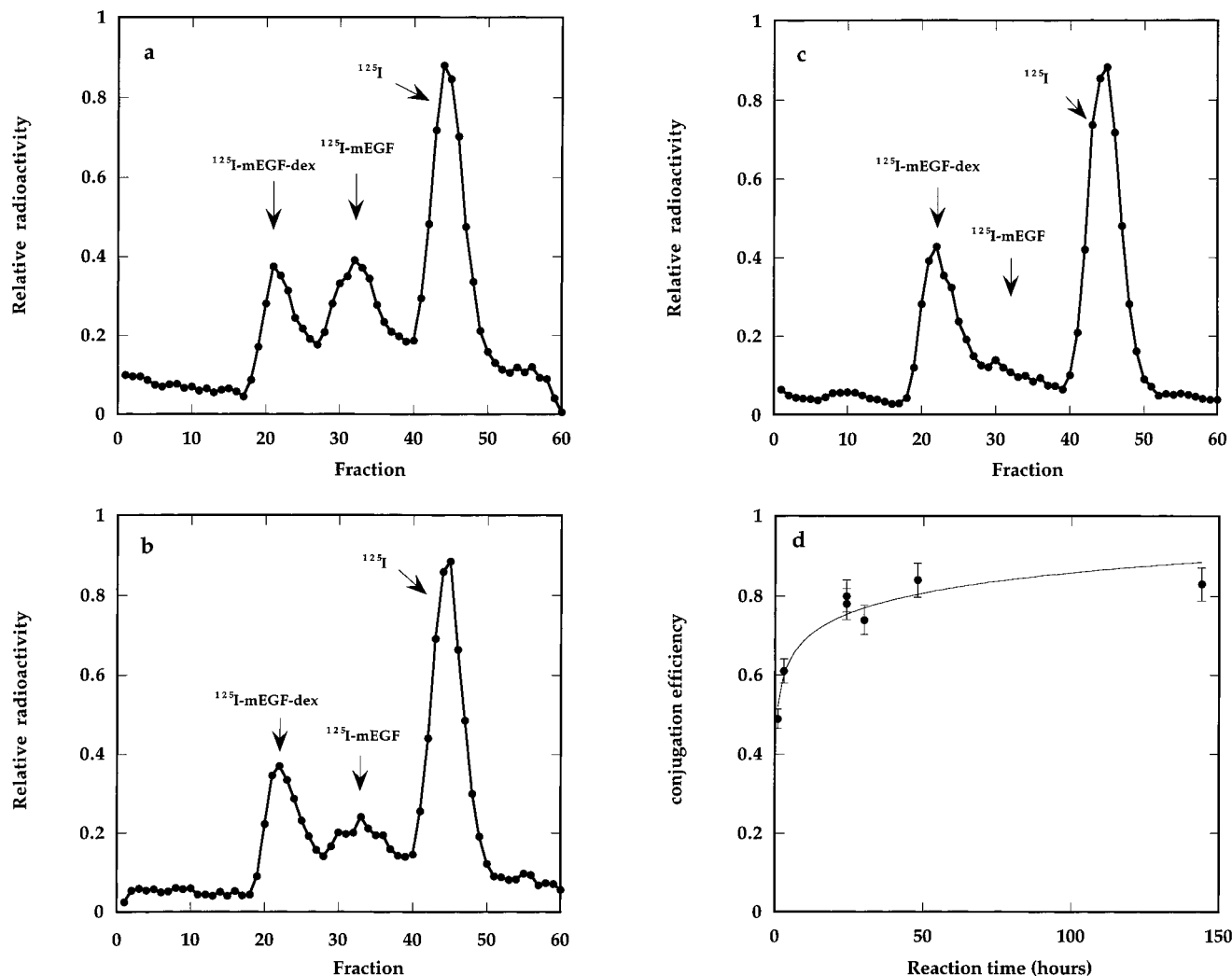


Figure 1. Gel filtration chromatogram after reductive amination of mEGF to dextran. 2.5 μg of [^{125}I]mEGF, 20 mg of dextran D14, and 8 mg of NaCNBH_3 were used in the reaction. The reaction was kept at room temperature (pH 8.0, 0.05 M phosphate buffer). The samples were run on a Sephadex G-50 Fine column (1 \times 40 cm) with a flow rate of 0.2 mL/min. Every fraction of 0.5 mL was measured with the gamma counter (the ^{125}I channel). The results were then normalized to "relative radioactivity" so that the heights of the low molecular weight peaks (marked ^{125}I) were comparable. Panels a, b, and c show chromatograms after 1, 3, and 24 h reaction times, respectively. Panel d shows the coupling efficiency as a function of several applied reaction times. The efficiency is defined as the ratio between the conjugate radioactivity and the sum of conjugate and mEGF radioactivities. The uncertainty in each calculated point was estimated to be not $>5\%$, which is applied as the error bars.

result of the preparative Sephadex G-50 Fine chromatography experiment.

Figure 5 shows the result of a preparative polyacrylamide electrophoresis experiment. The excess amount of noncharged dextran did not move into the 7% polyacrylamide gel but remained at the sample application position (marked B in Figure 5). It could therefore be easily removed from the conjugate solutions. The conjugate migrated more slowly than free mEGF, resulting in an almost baseline separation. Analyses on Sephadex G-50 Fine chromatography and PhastGel electrophoresis confirmed that the first peak was free mEGF and the second was the conjugate.

The result from a cellular displacement test is shown in Figure 6. The EGF-receptor-rich cultured human glioma U-343MG cells were applied. The result shows that the radiolabeled [^{125}I]mEGF-Dex conjugate specifically bound to the EGF receptors on the cell surface without nonspecific interactions since the binding could be completely inhibited by nonradioactive free mEGF.

The stability of the purified [^{125}I]mEGF-Dex conjugate was analyzed by Sephadex G-50 Fine chromatography after exposure to conditions described under Experimental Procedures. The absence of peak broadening and

other changes in the chromatograms (not shown) and lack of radioactivity at the mEGF position support the assumption that the conjugate is stable at pH values of 4–9 and in 3 M NH_4SCN , 7 M urea, 1 M NaCl, 30% ethylene glycol (w/v), or serum. Binding to cultured cells was finally analyzed, and it was shown that such treatments did not inhibit the binding to the EGF receptors. Some variations in binding were seen (Figure 7), but it was only in the case of treatment with pH 9 that the binding decreased significantly in relation to the "positive control" as analyzed with a paired T-test ($p < 0.05$). However, in that case the binding was significantly higher ($p < 0.05$) than in the "negative control" cell sample given 0.5 $\mu\text{g}/\text{mL}$ nonradioactive mEGF to displace the binding. Thus, the conjugate seemed reasonably stable with regard to both the conjugate linkage and the receptor binding.

DISCUSSION

Reductive amination is a nucleophilic addition reaction. The aldehyde group on the reducing end glucose of dextran provides the carbonyl group to the nucleophilic agent, i.e., the N-terminal α -amino group of mEGF. Protonization enhances the reactivity of the carbonyl

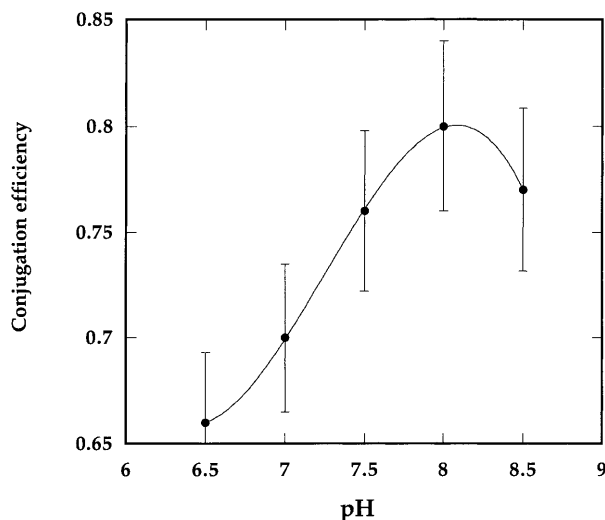


Figure 2. Reductive amination efficiency as a function of the applied pH during conjugation. All reaction times were 24 h (at room temperature). The conjugation solution was run on a Sephadex G-50 Fine (1 × 40 cm) column for gel filtration to separate conjugate and free mEGF. The quotient between the amount of radioactivity in the conjugate peak and the total radioactivity in the conjugate and free mEGF peaks was defined as the conjugation efficiency. The uncertainty in each calculated point was estimated to be not >5%, which is applied as the error bars.

group but reduces the reactivity of the N-terminal amino group of mEGF. Obviously there has to be a compromise, i.e., an optimum pH for the conjugation. The N-terminal α -amino group on a protein or a peptide has a pK value of ~ 8 . This means that most of the terminal amino groups on mEGF should be deprotonated at pH values > 8 . In Figure 2 the reductive amination reaction reached a maximum rate at about pH 8. At this pH the reactivity of the arginine residues in the reaction mixture is significantly reduced since their pK value is 12.

There are two consecutive reaction steps in reductive amination. First, the terminal amino group of mEGF reacts with the aldehyde group on the dextran end and becomes a Schiff base. However, this Schiff base is not stable, especially at acidic pH, so the reaction can reverse to produce free amino and aldehyde groups. Sodium cyanoborohydride (NaCNBH_3) is used to convert the Schiff base into a stable secondary amine.

The amount of the free aldehyde in glucose is, under equilibrium conditions, only $\sim 0.024\%$ in a neutral solution. The situation for the end aldehyde group in dextran is probably the same. On a time scale this means that each end glucose is available in free aldehyde form only on average 0.024% of the reaction time. A consequence of this is that only trace amounts of the Schiff bases would be formed in the reaction if no sodium cyanoborohydride was present. So, when an end glucose opens, exposing a free aldehyde, this group is "captured" by the sodium cyanoborohydride mediated process, giving the stable final product, mEGF-Dex. Thus, it is not surprising that many hours are required to reach a plateau in the conjugation reaction (Figure 1d).

The mEGF-Dex conjugate and the free mEGF have mean molecular masses of 20 and 6 kDa, respectively, and can easily be separated on Sephadex G-50 Fine. However, it was not possible, in this way, to get rid of free dextran since it eluted together with the conjugate. It is essential to remove the free unconjugated dextran since it can in tumor therapeutical applications, after loading with toxic agents, possibly cause unwanted systemic toxic effects to normal tissues. Preparative

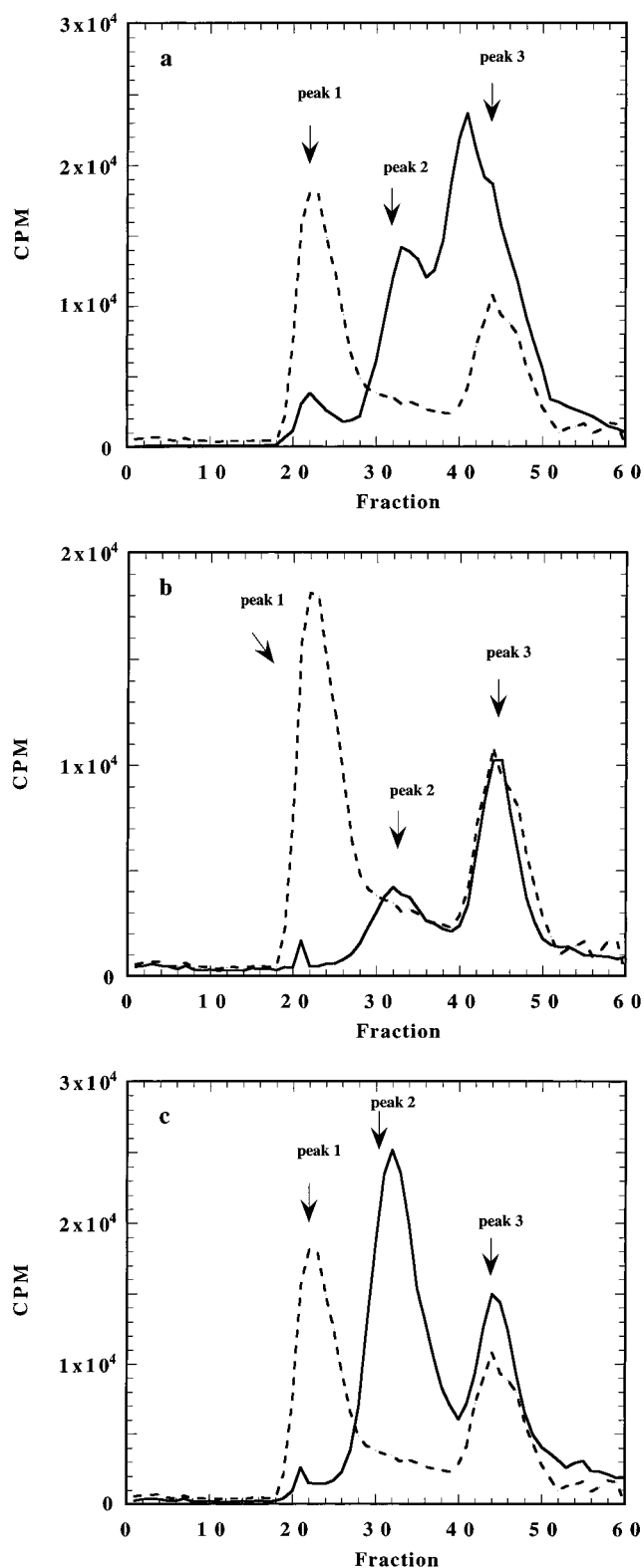


Figure 3. Chromatograms from the control conjugations (solid lines). For comparison, reference conjugate chromatograms are superimposed with dashed lines. The preparations were made with 24 h of reaction time (pH 8.0, 0.05 M phosphate buffer). The gel filtration was run on a Sephadex G-50 Fine (1 × 40 cm) column with 0.2 mL/min flow rate. Every 0.5 mL fraction collected was measured with the gamma counter using the ^{125}I channel giving cpm (counts per minute). Peaks 1, 2, and 3 represent conjugate, free mEGF, and free iodine, respectively. Panel a shows the result when ^{125}I mEGF was incubated with dextran D14 without NaCNBH_3 . Panel b shows the result when ^{125}I mEGF was incubated with NaCNBH_3 without dextran, and panel c shows the result when ^{125}I mEGF was run on the column without prior treatment together with NaCNBH_3 and dextran.

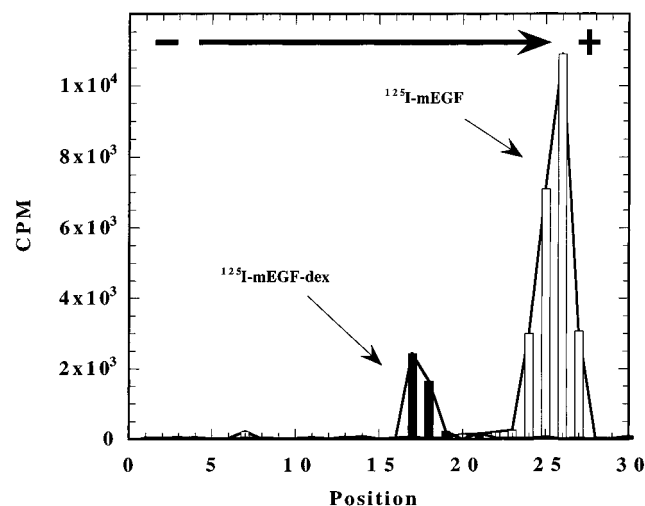


Figure 4. Native gradient polyacrylamide electrophoresis run with the Phast system. Samples of 4 μ L were loaded onto a Phast Gel (8–25% gradient). The electrophoresis was run at 400 V for 30 min with native buffer. Each lane of the gel was then cut into 30 pieces and placed in 0.5 mL of PBS for 30 min. The samples were then measured with the gamma counter using the ^{125}I channel giving cpm. Minus and plus symbols represent the negative and positive electrodes in the electrophoresis, respectively. The arrow shows the migration direction in the electrophoresis. Fraction 5 was the sample loading position.

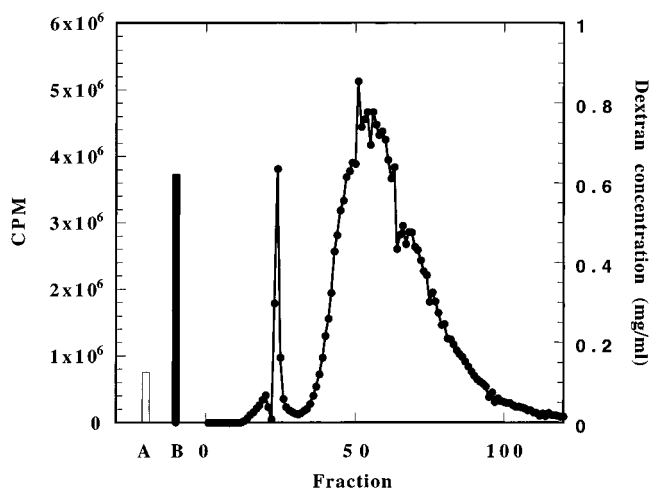


Figure 5. Preparative gel electrophoresis [polyacrylamide gel = 7% T for isolation (4 cm), 4% T for stacking (1.5 cm)]. The electrophoresis was run at 300 V, 3 mA, and 1 W limit using the MiniPrep Cell equipment. A volume of 0.5 mL of conjugate sample (from the Sephadex G-50 Fine separation) was applied. The obtained 1 mL fractions were collected at 0.1 mL/min. The radioactivity was measured in the gamma counter giving cpm, and the obtained data are plotted with solid circles. The symbol A (open bar) shows the remaining radioactivity in the polyacrylamide gel, and the symbol B (solid bar) shows the dextran concentration in a 1 mL buffer solution from the "upper chamber" sample application position (near the negative electrode) after the chromatography run was finished.

polyacrylamide gel electrophoresis was used to purify the conjugate sample from free nonreacted dextran which is noncharged and does not migrate in the electrophoresis gel. Because of the large difference in their molecular weights, mEGF and the mEGF–Dex conjugate could be separated on both analytical and preparative polyacrylamide gel electrophoresis.

The relatively small amount of free [^{125}I]mEGF (~5% of the total radioactivity in Figure 5) most likely was an effect of cross-contamination between the two neighboring peaks in the gel filtration experiment (see for example the peaks in Figure 1a). Thus, preparative electrophore-

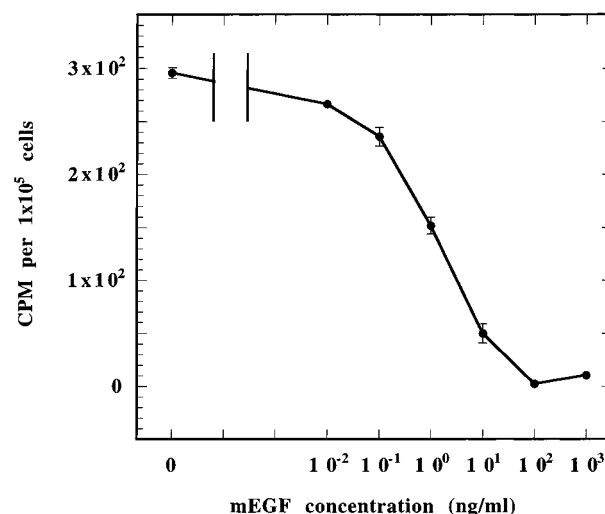


Figure 6. Displacement curve showing the decreasing [^{125}I]mEGF–dextran conjugate binding to U-343MGaCl2:6 cells when increasing amounts of nonradioactive mEGF were added to the incubation medium (each incubation was made at 37 $^{\circ}\text{C}$ for 1.5 h). The [^{125}I]mEGF–dextran samples were taken from Sephadex G-50 Fine separations. Each point corresponds to analysis of three cultures, and mean values and maximum variations were given. The ^{125}I radioactivity was analyzed in the gamma counter giving cpm.

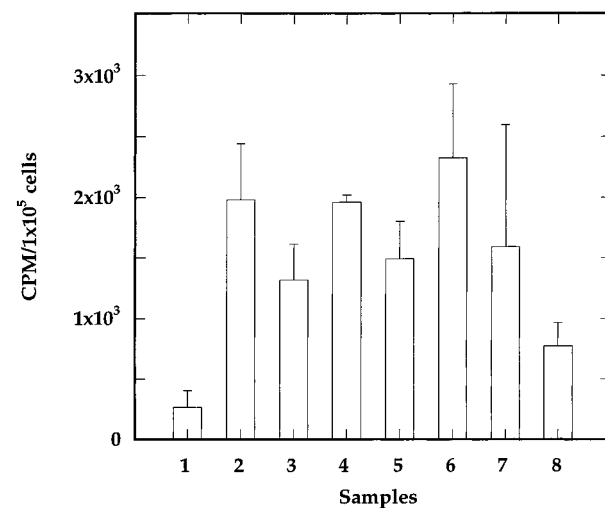


Figure 7. Conjugates were exposed to different buffers to test their stability and their EGF-receptor binding capacity. The receptor binding capacity was tested with U-343MGaCl2:6 cells (1.5 h of incubation with the cells). The histogram shows, from the left, sample 1 [binding of [^{125}I]mEGF–dextran during displacement with 0.5 $\mu\text{g/mL}$ nonradioactive mEGF (negative control)], sample 2 [binding of [^{125}I]mEGF–dextran (positive control)], samples 3–8 [binding of [^{125}I]mEGF–dextran after 1 h of exposure to 3 M NH_4SCN (3), 7 M urea (4), 30% ethylene glycol (5), 1 M NaCl (6), pH 4 (7), and pH 9 (8)]. The ^{125}I radioactivity was analyzed in the gamma counter giving cpm. Mean values and maximal variations from four culture dishes are shown.

sis can efficiently separate the conjugate from excess nonreacted dextran and remove mEGF impurities, resulting in a very pure mEGF–dextran preparation. Possibly the preparative gel electrophoresis method can be optimized to a "one step" purification method giving adequate separation of [^{125}I]mEGF–Dex, [^{125}I]mEGF, and nonreacted dextran.

It is seen in Figure 1 that iodine is released into the low molecular weight fraction after the conjugation chemistry is carried out. The mEGF was purified on a desalting column directly after iodination. However, the iodinated mEGF batches were then stored for different

times (up to 14 days) in relation to the dextranations and therefore free iodine appeared, due to radiolysis, in the final purification step on the Sephadex G-50 Fine column. However, even if the dextranation was made directly after the iodination, some low molecular weight iodine appeared. The reason for this is not clear, but it is not a major problem in future experiments and in the planned clinical tests since the conjugates will be purified directly before injections.

The stability of the conjugate against chemical degradation during exposure to human serum or various pH or ionic strengths and the retained ability to bind to the EGF receptors indicate that the conjugate is suitable for the planned biological experiments and clinical trials. Animal experiments, with transplanted tumors, to analyze the uptake in the tumors as well as in normal tissues are now in progress. Furthermore, we have, together with the oncologists at the university hospital in Uppsala, decided to use the described EGF-dextran for postoperative intracavitary injections (into the cavity left after the operation) in malignant glioma patients to analyze whether tumor cells seem to spread into the surrounding brain tissue. Those tests will be made on patients whose primary operation material proved to contain tumor cells with large amounts of EGF receptors. The EGF-dextran was in the present study labeled with ^{125}I but will be, in the patient studies, labeled with ^{124}I for imaging with PET (and later labeled with ^{131}I if nuclide therapy is requested).

The dextran probably protects the protein ligand against proteolysis, as has been reported in other cases when carbohydrates and proteins have been conjugated (Andersson et al., 1991; Blomhoff et al., 1983; Kato et al., 1990; Marshall, 1980; Melton et al., 1987; Olsson et al., 1994; Sjöström et al., 1997; Srivastava, 1991; Yasuda et al., 1990). In the next phase of this work cytotoxic agents will be coupled to the mEGF-Dex for which optimum conditions have to be developed. A high stability of the conjugate is then essential.

After coupling of toxic agents to the dextran part, the conjugate will be used in targeted treatment of tumors that overexpress the EGF receptor. EGF-based conjugates are known to be internalized (Andersson et al., 1991; Gedda et al., 1996; Olsson et al., 1994), and such conjugates are therefore of special interest when loaded with "short range" radionuclides. Normal cells might also have EGF receptors, but the amount of receptors per cell is dependent on the cell type and whether the cells are up or down regulated, for example, due to normal ligand exposure (Carpenter, 1987). The highest values are in the liver, as has been described in studies on mice and rats (Chabot et al., 1986; Dunn et al., 1986; Murakami et al., 1994; Soley and Hollenberg, 1987). Quantitative data for human liver seem to be lacking in the literature.

The choice of toxic agent, to be coupled to EGF-dextran, is a subject for further research. The optimal choice of the toxic agent might vary from application to application. Radioactive nuclides (such as high-energy beta or alpha emitters), boron-containing compounds, and toxins are all interesting alternatives (Carlsson et al., 1994; Ozawa et al., 1989; Siegfal et al., 1990). It might also be possible to combine EGF-dextran with chelating agents that could chelate radioactive metals of tumor therapeutical interest.

The purpose of this work was to design and develop a well-defined conjugate that binds specifically to the EGF receptor and which can be the starting point for producing toxic tumor targeting agents. An interesting aspect, considering future applications, is that the present

conjugates have a one to one molar ratio of dextran to EGF, enabling the loading of well-defined amounts of toxic agents to each conjugate molecule.

ACKNOWLEDGMENT

WE thank laboratory engineers Veronika Asplund and Ulla Johansson for valuable technical assistance. Financial support was given by the Swedish Cancer Society, the Swedish Medical Research Council, and the Swedish Institute.

LITERATURE CITED

- Andersson, A., Holmberg, A., Carlsson, J., Carlsson, J., Pontén, J., and Westermarck, B. (1991) Binding of epidermal growth factor-dextran conjugates to cultured glioma cells. *Int. J. Cancer* 47, 439–444.
- Andersson, A., Capala, J., and Carlsson, J. (1992) Effects of EGF-dextran-tyrosine-131-I conjugates on clonogenic survival of cultured glioma cells. *J. Neuro-Oncol.* 14, 213–223.
- Bigner, S. H., Burger, P. C., Wong, A. J., Werner, M. H., Hamilton, S. R., Muhlbalier, L. H., Vogelstein, B., and Bigner, D. D. (1988) Gene amplification in malignant human gliomas: clinical and histopathologic aspects. *J. Neuropathol. Exp. Neurol.* 47, 191–205.
- Blomhoff, H. K., Blomhoff, R., and Christensen, T. B. (1983) Enhanced stability of β -galactosidase in parenchymal and nonparenchymal liver cells by conjugation with dextran. *Biochim. Biophys. Acta* 757 (2), 202–208.
- Borch, R. F., Bernstein, M. D., and Dust, H. D. (1971) The cyanohydrinborate anion as a selective reducing agent. *J. Am. Chem. Soc.* 93, 2897–2903.
- Carlsson, J., Gedda, L., Grönvik, C., Hartman, T., Lindström, A., Lindström, P., Lundqvist, H., Löfqvist, A., Malmqvist, J., Olsson, P., Essand, M., Pontén, J., Sjöberg, S., and Westermarck, B. (1994) Strategy for boron neutron capture therapy against tumor cells with overexpression of the epidermal growth factor-receptor. *Int. J. Radiat., Oncol., Biol., Phys.* 30 (1), 105–115.
- Carpenter, G. (1987) Receptors for epidermal growth factor and other polypeptide mitogens. *Annu. Rev. Biochem.* 56, 881–914.
- Carpenter, G., and Cohen, S. (1976) 125-I labeled human growth factor. *J. Cell Biol.* 71, 159–171.
- Carpenter, G., and Cohen, S. (1979) Epidermal growth factor. *Annu. Rev. Biochem.* 48, 193–216.
- Chabot, J. G., Walker, P., and Pelletier, G. (1986) Distribution of epidermal growth factor binding sites in the adult rat liver. *Am. J. Physiol.* 250, G760–G764.
- DeBelder, A. N. (1990) *Dextran*, 2nd ed., Pharmacia Print, Uppsala, Sweden.
- Dubois, M., Gilles, K. A., Hamilton, P. A., Rebers, P. A., and Smith, F. (1956) Colorimetric method for determination of sugars and related substances. *Ann. Biochem.* 28, 350–356.
- Dunn, W. A., Connolly, T. P., and Hubbard, A. L. (1986) Receptor-mediated endocytosis of epidermal growth factor by rat hepatocytes: receptor pathway. *J. Cell Biol.* 102, 24–36.
- Emmrich, P., Baumann, W., and Stechele, U. (1977) Studies on the kinetics and renal excretion of low and high molecular weight dextrans in preterm babies, newborns and young infants. *Eur. J. Pediatr.* 125, 181–190.
- Fassio, E., Terg, R., Landeira, G., Abecasis, R., Salemne, M., Podesta, A., Rodriguez, P., Levi, D., and Kravetz, D. (1992) Paracentesis with dextran 70 vs. paracentesis with albumin in cirrhosis with tense ascites. Results of a randomized study. *J. Hepatol.* 14, 310–316.
- Filmus, J., Pollak, M. N., Cailleau, R., and Buick, R. N. (1985) MDA-468, a human breast cancer cell line with a high number of epidermal growth factor (EGF) receptor, has an amplified EGF receptor gene and is growth inhibited by EGF. *Biochem. Biophys.* 128, 898–905.
- Fudui, K., Moriyama, T., Miyake, Y., Mizutani, K., and Tanaka, O. (1982) Purification and properties of glucosyltransferase responsible for water-insoluble glucan synthesis from *Streptococcus mutans*. *Infect. Immun.* 37 (1), 1–9.

- Gedda, L., Olsson, P., Pontén, J., and Carlsson, J. (1996) Development and in vitro studies of epidermal growth factor-dextran conjugates for boron neutron capture therapy. *Bioconjugate Chem.* 7, 584–591.
- Holmberg, A., and Meurling, L. (1993) Preparation of Sulfhydrylborane-dextran conjugates for boron neutron capture therapy. *Bioconjugate Chem.* 4, 570–573.
- Holmberg, A., Silen, Å., Marquez, M., Bergwall, P., Westlin, J., and Nilsson, S. (1994) An alternative methods of labelling antibodies with ^{99m}Tc . *Antibody, Immunoconjugates, Radiophar.* 7, 149–154.
- Kato, A., Sasaki, Y., Furuta, R., and Kobayashi, K. (1990) Functional protein-polysaccharide conjugate prepared by controlled dry-heating of ovalbumin-dextran mixtures. *Agric. Biol. Chem.* 54 (1), 107–112.
- Klotz, U., and Kroemer, H. (1987) Clinical pharmacokinetic considerations in the use of plasma expanders. *Clin. Pharmacokinet.* 12, 123–135.
- Lane, C. F. (1975) Sodium cyanoborohydride—a highly selective reducing agent for organic functional groups. *Synthesis*, March, 135–145.
- Liebermann, T. A., Razon, N., Bartal, A. D., Yarden, Y., Schlessinger, J., and Scoreq, H. (1984) Expression of epidermal growth factor receptors in human brain tumors. *Cancer Res.* 44, 753–760.
- Liebermann, T. A., Nusbaum, H. R., Razon, N., Kris, R., Lax, I., Soreq, H., Whittle, N., Waterfield, M. D., and Schlessinger, J. (1985) Amplification, enhanced expression and possible rearrangement of EGF receptor gene in primary human brain tumors of glial origin. *Nature (London)* 313, 144–147.
- Lindström, A., Lundqvist, H., and Carlsson, J. (1993) Distribution of ^{125}I after administration of ^{125}I -labeled epidermal growth factor-dextran conjugates in mice. In Annelie Lindström thesis, Targeting to EGF receptors. Preparation of EGF-dextran conjugates and analysis of their metabolism in vitro and in vivo. *Acta Univ. Upsaliensis* 428.
- Lövqvist, A., Lindström, A., and Carlsson, J. (1993) Binding, internalization and excretion of TGF α -dextran associated radioactivity in cultured human glioma cells. *Cancer Biother.* 8, 345–356.
- Lundblad, R. L., and Noages, C. M. (1984) *Chemical Reagents for Protein Modification*, pp 147–162, CRC Press, Boca Raton, FL.
- Marshall, J. J. (1978) Manipulation of the properties of enzymes by covalent attachment of carbohydrate. *Trends Biochem.* 3, 79–83.
- Melton, R. G., Wiblin, C. N., Foster, R. L., and Sherwood, R. F. (1987) Covalent linkage of carboxypeptidase G2 to soluble dextrans. I. Properties of conjugates and effects on plasma persistence in mice. *Biochem. Pharmacol.* 36, 105–112.
- Mendelsohn, J. (1988) Growth factor receptors as targets for antitumor therapy with monoclonal antibodies. *Monoclon. Antibody Ther.* 45, 147–160.
- Messing, E. M., and Rezinkoff, C. A. (1992) Epidermal growth factor and its receptor: markers of—and targets for—chemoprevention of bladder cancer. *J. Cell. Biochem. Suppl.* 161, 56–62.
- Moon, P. F., Snyder, J. R., Haskins, S. C., Perron, P. R., and Kramer, G. C. (1991) Effects of highly concentrated hypertonic saline-dextran volume expander on cardiopulmonary function in anesthetized normovolemic horses. *Am. J. Vet. Res.* 52, 1611–1618.
- Murakami, T., Misaki, M., Masuda, S., Higashi, Y., Fuwa, T., and Yata, N. (1994) Dose-dependent plasma clearance of human epidermal growth factor in rats. *J. Pharm. Sci.* 83, 1400–1403.
- Nistér, M., Wedell, B., Bestsholtz, C., Bywater, M., Pettersson, M., Westermark, B., and Mark, J. (1987) Evidence for progression changes in the human malignant glioma line U-343Ga: analysis of karyotype and expression of genes encoding the subunit chains of platelet-derived growth factor. *Cancer Res.* 47, 4953–4960.
- Olsson, P., Lindström, A., and Carlsson, J. (1994) Internalization and excretion of epidermal growth factor-dextran associated radioactivity in cultured human squamous-carcinoma cells. *Int. J. Cancer* 56, 529–537.
- Ozawa, S., Ueda, M., Ando, N., Abe, O., Minoshima, S., and Shimizu, N. (1989) Selective killing of squamous carcinoma cells by an immunotoxin that recognise the EGF receptor. *Int. J. Cancer* 43, 152–157.
- Sauter, G., Haley, J., Chew, K., Kerschmann, R., Moore, D., Carroll, P., Moch, H., Gudat, F., Mihatsch, M. J., and Waldman, F. (1994) Epidermal-growth-factor-receptor expression is associated with rapid tumour proliferation in bladder cancer. *Int. J. Cancer* 57 (4), 508–514.
- Seppala, I., and Makela, O. (1989) Antigenicity of dextran-protein conjugates in mice. Effect of molecular weight of the carbohydrate and comparison of two modes of coupling. *J. Immunol.* 143 (4), 1259–1264.
- Siegall, C. B., Fitzgerald, D. J., and Pastan, I. (1990) Selective killing of tumor cells using EGF- or TGF- α -pseudomonas exotoxin chimeric molecules. *Semin. Cancer Biol.* 1 (15), 345–350.
- Sjöström, A., Bue, P., Malmström, P. U., Nilsson, S., and Carlsson, J. (1997) Binding, internalisation and degradation of EGF-dextran conjugates in two human bladder cancer cell lines. *Int. J. Cancer* 70, 383–389.
- Soley, M., and Hollenberg, M. D. (1987) Epidermal growth factor (urogastrone)—stimulated gluconeogenesis in isolated mouse hepatocytes. *Arch. Biochem. Biophys.* 255, 136–146.
- Srivastava, R. A. (1991) Effect of glycosylation of bacterial amy-lase on stability and active site conformation. *Indian J. Biochem. Biophys.* 28 (2), 109–113.
- Todderud, G., and Carpenter, G. (1989) Epidermal growth factor: the receptor and its function. *Biofactors* 2, 11–15.
- Werner, M. H., Humphrey, P. A., Bigner, D. D., and Bigner, S. H. (1988) Growth effects of epidermal growth factor (EGF) and monoclonal antibody against the EGF receptor on four glioma cell lines. *Acta Neuropathol.* 77, 196–201.
- Westermark, B., Magnusson, A., and Heldin, C. H. (1982) Effect of epidermal growth factor on membrane motility and cell locomotion in cultures of human clonal glioma cells. *J. Neurosci. Res.* 8, 491–507.
- Yalpani, M., and Brooks, D. E. (1985) Selective chemical modifications of dextran. *J. Polym. Sci.* 23, 1395–1405.
- Yasuda, Y., Fujita, T., Tadakura, Y., Hashida, M., and Sezaki, H. (1990) Biochemical and biopharmaceutical properties of macromolecular conjugates of uricase with dextran and polyethylene glycol. *Chem. Pharm. Bull. Tokyo.* 38 (7), 5053–5056.

BC970173M

Covalent Protein–Oligonucleotide Conjugates for Efficient Delivery of Antisense Molecules

S. B. Rajur, C. M. Roth, J. R. Morgan, and M. L. Yarmush*

Center for Engineering in Medicine and Surgical Services, Massachusetts General Hospital, Shriners Burns Institute, and Harvard Medical School, Boston, Massachusetts 02114. Received February 11, 1997*

Antisense oligonucleotides have been covalently attached to asialoglycoprotein (ASGP) via disulfide bond conjugation chemistry. These conjugates were characterized extensively by an array of chemical, chromatographic, and spectroscopic means. Multiple (approximately six) oligonucleotides can be conjugated to each ASGP molecule. The molecular conjugates were used to deliver antisense oligonucleotides complementary to the mRNA of the interleukin 6 signal transduction protein (gp130) to modulate the acute phase response of hepatoma (HepG2) cells *in vitro*. These conjugates were biologically active, as measured by inhibition of the cytokine-stimulated up-regulation of the acute phase protein haptoglobin. The level of inhibition was comparable to that found with previous technology featuring noncovalent complexes of ASGP–poly(L-lysine) and oligonucleotide. Because of the ability to control the stoichiometry of the conjugate and its unimolecular nature (as opposed to bimolecular for the noncovalent conjugates), this methodology holds great promise for further development and application.

INTRODUCTION

Antisense oligonucleotides have great potential as therapeutic agents. Natural and synthetic analogues of these oligonucleotides have been shown to inhibit gene expression in a variety of *in vitro* and *in vivo* studies. Targets for antisense molecules in clinical and preclinical investigations include cancer, viral diseases, inflammation, and organ transplant rejection (Heidenreich et al., 1995; Agrawal, 1996; Le Doux et al., 1996). Recently, it has been reported that antisense molecules can down-regulate cytokines as well as cytokine receptor expression (Miyajima et al., 1992). For example, cytokines [interleukin 1 α and interleukin 6 (IL-6¹)] and receptors for IL-6, nerve growth factor, and epidermal growth factor have been successfully inhibited by antisense oligonucleotides (Maier et al., 1990; Sariola et al., 1991; Schwab et al., 1991; Keller et al., 1995; Wang et al., 1995; Roth et al., 1997).

Given an efficacious oligonucleotide sequence, the limiting factor in the development of antisense therapeutics becomes delivering the antisense molecule to its target in a particular tissue with satisfactory efficiency, selectivity, and stability. At physiological pH, natural oligonucleotides exist as polyanions and hence do not readily penetrate cell membranes, making it difficult to achieve high intracellular concentrations. Oligonucleotides must therefore be packaged into a vehicle capable of efficient entry into cells. Various methods have been developed to address this problem.

Particularly for liver specific delivery, Wu and Wu (1992) have developed a soluble DNA carrier system that

takes advantage of receptor-mediated endocytosis to achieve internalization. They targeted hepatocytes by complexing oligomeric DNA with asialoglycoprotein–poly(L-lysine) (ASGP–PLL) conjugates. In this system, the negatively charged DNA complexes with positively charged polylysine to form a noncovalent complex, and the asialoglycoprotein, by means of its terminal galactose moieties, augments uptake by binding to a receptor uniquely expressed by hepatocytes, including the transfected cell line HepG2. By utilizing this ASGP–PLL delivery system, we were able to target the mRNA of the IL-6 signal transduction protein (gp130) and modulate the acute phase response of hepatoma (HepG2) cells *in vitro* (Roth et al., 1997). Addition of ASGP–PLL reduced the effective dose of antisense oligonucleotides relative to unconjugated antisense by 10-fold; furthermore, we found that the specificity of action is improved by using lower doses. However, we found that further improvements using the ASGP–PLL conjugates were limited by the physical equilibrium between ASGP–PLL and oligonucleotides and by the toxicity of the ASGP–PLL moiety (Bunnell et al., 1992; C. M. Roth, unpublished data).

In this paper, we describe the covalent conjugation of antisense oligonucleotides to ASGP using the heterobifunctional cross-linker sulfo-succinimidyl 6-[3'-(2-pyridylthio)propionamido]hexanoate (sulfo-LC-SPDP). We describe the synthesis and characterization of these new conjugates as well as their biological activity in an *in vitro* system (Roth et al., 1997). This methodology is generalizable to other antisense sequences and also to other carrier molecules, including alternative ligands for the asialoglycoprotein and ligand/receptor systems for other cell types.

EXPERIMENTAL PROCEDURES

Materials for Oligonucleotide Synthesis and Purification. Unless otherwise stated, all solvents and chemicals were of the highest quality commercially available. Oligonucleotides were synthesized using 2-deoxynucleotide phosphoramidites on a Cyclone Plus DNA synthesizer (Millipore, Bedford, MA) or were obtained from Oligos, Etc. (Wilsonville, OR). The four fully

* Address correspondence to this author at the Center for Engineering in Medicine, Massachusetts General Hospital, Bigelow 1401, Boston, MA 02114 [telephone (617) 726-3474; fax (617) 726-7458].

© Abstract published in *Advance ACS Abstracts*, November 1, 1997.

¹ Abbreviations: IL-6, interleukin 6; ASGP, asialoglycoprotein; PLL, poly(L-lysine); HPLC, high-performance liquid chromatography; SPDP, succinimidyl 6-[3'-(2-pyridylthio)propionamido]hexanoate; 2-PT, 2-pyridinethione; DTT, dithiothreitol; AS, antisense oligonucleotide; ASGP–S–S–AS, asialoglycoprotein–antisense disulfide-containing conjugate.

protected common 2'-deoxynucleoside phosphoramidites containing aryl- or isobutyrylamides and the trityl-protected thiol linker phosphoramidite, 6-(tritylthio)hexanol/2-cyanoethyl *N,N*-diisopropylphosphoramidite, were purchased from Cruachem (Sterling, VA). High-performance liquid chromatography was performed on a system equipped with a dual-wavelength detector. Both purchased and in-house oligonucleotides were isolated on a 9.4 × 250 mm reversed-phase column of ODS-Hypersil at a flow rate of 3.0 mL/min in buffer A: 50 mM TEAA (pH 7.2) with a gradient of acetonitrile (20–80% over 40 min). The purity of the oligonucleotides was evaluated by chromatography on a 250 × 4.6 mm reversed-phase column of ODS-Hypersil at a flow rate of 1 mL/min in buffer B: 20 mM potassium phosphate (pH 5.5) with a gradient of methanol (0–100% over 60 min). Purity of the protein–oligonucleotide conjugates was assessed on a size exclusion column (TSK 3000) at a flow rate of 1 mL/min in buffer C: 0.1 M sodium phosphate/0.1 M sodium sulfate (pH 6.4).

Cell Culture. The human hepatoma cell line HepG2 (ATCC, HB 8065) was maintained in Modified Eagle's Medium, supplemented with 10% fetal bovine serum, penicillin–streptomycin solution (200 units/mL penicillin G activity and 200 µg/mL streptomycin activity), and sodium pyruvate (1 mM) in a humidified atmosphere of 5% CO₂ at 37 °C. The medium was changed every 2 days.

Preparation of *N*-{6-[3'-(2-Pyridyldithio)propionamido]hexanoyl}-ASGP (ASGP–PDP). ASGP was prepared by digesting human α₁-acid glycoprotein with neuraminidase according to the published procedure (Lu et al., 1994). In brief, human α₁-acid glycoprotein was dissolved in PBS, neuraminidase (1 mg/mL in PBS) was added to it, and the mixture was incubated at 37 °C for 1 h. The solution was dialyzed twice against PBS at 4 °C (MW cutoff = 8000).

To 40.56 mg (0.994 mM) of ASGP in 1 mL of PBS (1 ×, pH 7.4) was added 6.42 mg (12.17 mM, 13-fold excess) of sulfo-LC-SPDP (Pierce, Rockford, IL). The mixture was stirred gently for 1 h at ambient temperature. The crude product mixture was then passed through a PD-10 desalting column with PBS elution to remove the byproduct *N*-hydroxysuccinimide and unreacted sulfo-LC-SPDP. The macromolecular fraction was further dialyzed against 1 × PBS (2 × 4 L) through a membrane with 12 000–14 000 MW exclusion limits to remove any remaining *N*-hydroxysuccinimide or sulfo-LC-SPDP. The purity of the conjugates was assessed by running small aliquots through the size exclusion column TSK 3000 with buffer C.

To estimate the number of modified groups, an aliquot of the purified product was treated with DTT to reduce the disulfide bond between the ASGP–PDP moiety and produce 2-pyridine thione **5**, which has a characteristic absorbance with a maximum of 343 nm. One molecule of ASGP–PDP contained about 4 residues of 2-pyridyl disulfide derived from sulfo-LC-SPDP, on the basis of the extinction coefficient of 2-PT (Carlsson et al., 1978).

Synthesis of 5'-Thiol Oligonucleotide. Oligonucleotide **1** was synthesized using standard β-cyanoethyl phosphoramidite chemistry at the 1 µmol scale. A six-carbon (C⁶) thiol linker phosphoramidite (25 mg) was dissolved in 1 mL of acetonitrile and attached to a separate port on the DNA synthesizer. After synthesis of the 15-base sequence, the amidite of the thiol modifier was applied to the reaction column. After completion of the coupling, the column was removed from the synthesizer, washed thoroughly with acetonitrile, oxidized with iodine (0.05 M in THF/pyridine/water 7:1:2) for 30 s using a syringe, and finally washed with acetonitrile and dried

under a stream of argon. The modified sequence was deprotected (concentrated ammonia for 6 h at 50 °C), isolated on a semipreparative column using buffer A, evaporated, and stored at –20 °C in ddH₂O.

Preparation of ASGP–Antisense Conjugates **6 (ASGP–S–S–AS).** The trityl group present on the C⁶ linker of antisense was deprotected according to standard protocols (Figure 1). In summary, the trityl on antisense **1** (216.3 mM, 36.3 OD units) was dissolved in 0.1 M TEAA (360 mL), 1 M silver nitrate (54 mL) was added, and the mixture was vortexed and allowed to react for 30 min. Next, 1 M DTT (84 mL) was added, and the reaction mixture was vortexed and allowed to stand for an additional 20 min. The yellow mixture was microfuged for 5 min and the supernatant collected. The precipitated silver salt was washed twice with 0.1 M TEAA and microfuged, and the supernatants were pooled and stored under argon atmosphere. Excess DTT was then removed by extractions with 2 mL of ethyl acetate (saturated with water and outgassed by bubbling of nitrogen). The resulting oligonucleotide **2** containing a free sulfhydryl group was immediately added to the ASGP–PDP conjugate **3** (36.05 nM, 42.7 mL) in PBS (pH 7.4). The reaction was conducted for 12 h at 20 °C under nitrogen. The disulfide exchange reaction (conjugation) was monitored by an increase in optical absorbance at 343 nm due to 2-PT. The molecular conjugates thus obtained were dialyzed against PBS (4 × 2 L) through a membrane with 12 000–14 000 MW exclusion limits.

The purity of the conjugates was assessed by running analytical aliquots over the size exclusion column (TSK 3000) with buffer C. The amounts of oligonucleotide and protein *c*_{oligo}^{oligo} and *c*_{ASGP–SPDP}^{ASGP–SPDP} in the purified product were determined spectroscopically from the absorbances of the conjugates at 215 and 260 nm, after measuring that of ASGP–SPDP and oligonucleotide individually. That is, the equations

$$A_{215\text{nm}}^{\text{conj}} = \epsilon_{215\text{nm}}^{\text{ASGP–SPDP}} c^{\text{ASGP–SPDP}} + \epsilon_{215\text{nm}}^{\text{oligo}} c^{\text{oligo}} \quad (1)$$

and

$$A_{260\text{nm}}^{\text{conj}} = \epsilon_{260\text{nm}}^{\text{ASGP–SPDP}} c^{\text{ASGP–SPDP}} + \epsilon_{260\text{nm}}^{\text{oligo}} c^{\text{oligo}} \quad (2)$$

(where *A* represents the solvent-corrected absorbance of the indicated compound at the indicated wavelength and ϵ represents the extinction coefficient of the compound) were solved simultaneously for the concentrations of ASGP–SPDP and oligonucleotide.

RESULTS

Synthesis of Compounds. We desired to construct a molecular conjugate of ASGP and antisense oligonucleotides that provides for efficient, tissue-selective cellular uptake and subsequently for release of the oligonucleotide from ASGP for hybridization to its target. For these reasons, we employed SPDP as a heterobifunctional cross-linker that provides a spacer arm that should provide the conjugate sufficient conformational flexibility for the terminal galactose residues to bind to the ASGP receptor and a disulfide linkage that should be reduced in the intracellular endosome (Feener et al., 1990). We employed an antisense oligonucleotide that we have previously found effective in inhibiting the response of HepG2 cells to the cytokine interleukin 6 (IL-6) (Roth et al., 1997).

First, the oligonucleotide was synthesized using standard solid phase synthesis by incorporating the trityl-protected C⁶-thiol linker, 6-(tritylthio)hexanol/2-cyano-

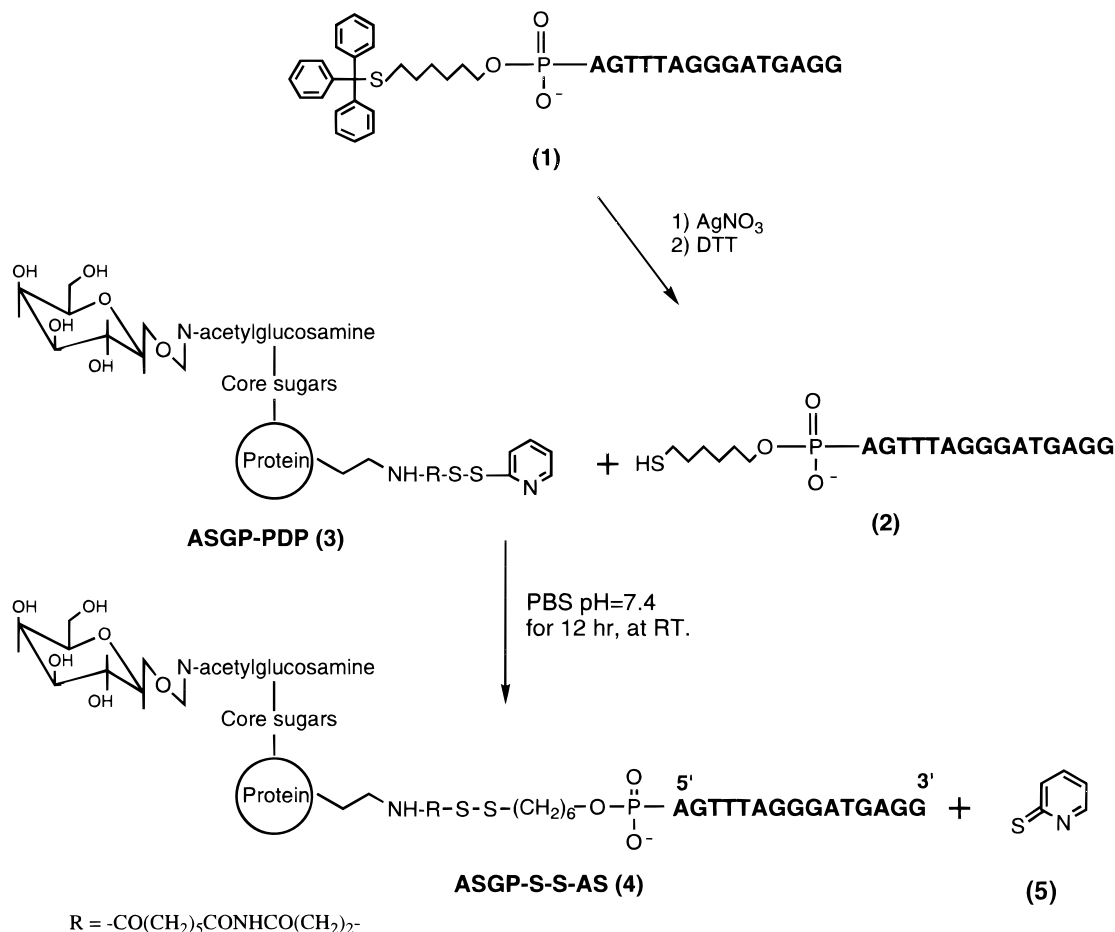


Figure 1. Preparation of ASGP-antisense molecular conjugates (ASGP-S-S-AS). Asialoglycoprotein (α_1 -acid glycoprotein previously treated with neuraminidase) was reacted with sulfosuccinimidyl 6-[3'-(2-pyridyldithio)propionamido]hexanoate (sulfo-LC-SPDP) to produce ASGP-PDP **3**. Antisense oligonucleotide carrying a six-carbon (C⁶) thiol modifier on its 5' end **1** was synthesized by utilizing 6-(tritylthio)hexanol/2-cyanoethyl *N,N*-diisopropylphosphoramidite. The trityl protecting group of the antisense was deprotected with AgNO₃/DTT to form **2**, which was immediately reacted with ASGP-PDP conjugate **3** to obtain the ASGP-S-S-AS molecular conjugate **4**.

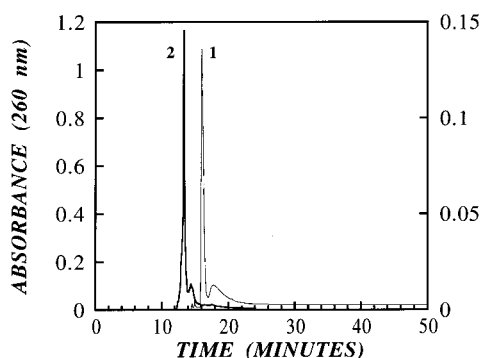


Figure 2. RP-HPLC analysis of the modified antisense oligonucleotide **1** and the deprotected derivative **2**. Analytical aliquots of **1** and **2** were analyzed by using a 250 × 4.6 mm reversed-phase column of ODS-Hypersil at a flow rate of 1 mL/min in buffer B 20 mM potassium phosphate (pH 5.5) with gradient of methanol (0–100% over 60 min).

ethyl *N,N*-diisopropylphosphoramidite, at the 5' end of the sequence. Reversed-phase HPLC analysis of the protected C⁶-thiol-modified oligonucleotide demonstrated an increased retention time due to the presence of the hydrophobic trityl group and the six-carbon aliphatic chain (Figure 2). The trityl group was removed by treatment with silver nitrate, and the product was stored under nitrogen in a solution containing DTT. The deprotection was further confirmed by reversed-phase HPLC. As shown in Figure 2, the trityl-deprotected sequence **2** eluted before its precursor **1**.

The oligonucleotide **2** with a free thiol group was coupled to ASGP bearing pyridyldithiohexanoyl groups introduced by using sulfo-LC-SPDP (Figure 1). The 5'-thiol function reacted with ASGP-PDP **3** bearing dithiopyridinyl groups, leading to conjugates with about six antisense oligonucleotides per ASGP molecule. Conjugation of oligonucleotide to ASGP was monitored by a combination of size exclusion chromatography (SEC) and UV-vis absorption spectroscopy. The purity of the conjugate and the nature of the linkage between ASGP and antisense were evaluated by SEC before and after reduction with DTT. Due to their significant size difference, ASGP and free oligonucleotide are easily distinguished by SEC (Figure 3A,B). This difference was used in the characterization of conjugates. A chromatogram of the crude product mixture before purification showed three peaks at approximately 9.4, 11.6, and 13.8 min (Figure 3C), corresponding to conjugate, free oligonucleotide, and low molecular weight species (probably 2-PT), respectively. After dialysis (12 000–14 000 MW cutoff), only the conjugate ASGP-S-S-AS remained (Figure 3D), eluting with a retention time roughly equal to that of free ASGP. At this point, UV-vis spectroscopy was performed as described below. Upon treatment of the ASGP-S-S-AS with DTT, a new peak eluting at a retention time of 11.6 min, due to free oligonucleotide, was observed (Figure 3E). This clearly shows that the antisense was linked to ASGP by a disulfide bridge sensitive to DTT.

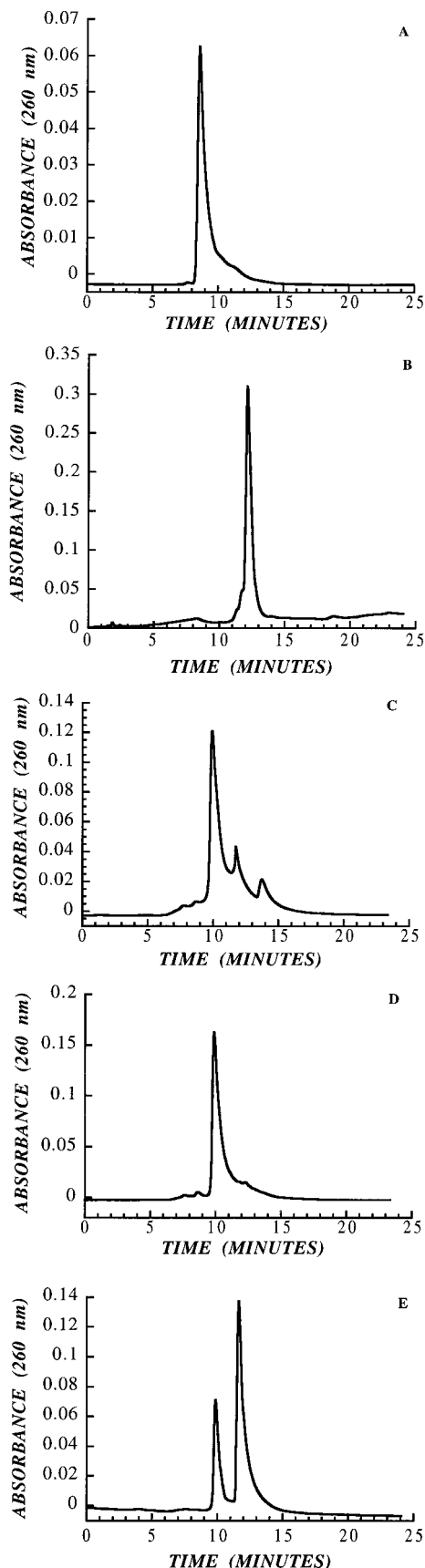


Figure 3. HPLC analysis. Samples were analyzed by size exclusion chromatography on a TSK 3000 column (buffer C): (A) ASGP alone; (B) antisense oligonucleotide (AS130) alone; (C) crude product mixture showing ASGP-S-S-AS **4** (retention time = 9.4 min), unconjugated oligonucleotide (11.6 min), and low molecular weight species (13.7 min); (D) purified conjugate following dialysis of the crude reaction mixture; (E) purified conjugate after 4 h of reduction with DTT.

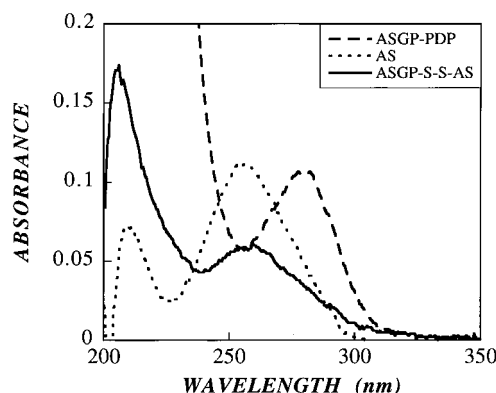


Figure 4. UV-vis spectra of ASGP-PDP (**3**), unconjugated oligonucleotide (AS), and ASGP-S-S-AS (**4**). UV-vis absorption spectra in which the conjugate ASGP-S-S-AS **4** exhibits spectral features of both AS and ASGP-PDP **3**.

Because size exclusion HPLC is not sensitive to chemical composition or to minor differences in molecular weight, we performed absorption spectroscopy to ensure that our purified high molecular weight conjugate indeed contained oligonucleotide. Furthermore, spectroscopy presents a means for quantitation. Figure 4 shows the UV-vis absorption spectra of ASGP-PDP **3**, the 15-mer antisense oligonucleotide (AS130) corresponding to compound **2** (compound **2** itself is not stable in water and could not be tested directly), and purified ASGP-S-S-AS **4**. The conjugate possesses strong absorption at 260 nm due to the presence of oligonucleotide. Furthermore, the presence of protein is indicated by the wavelength shift and increased magnitude of the peak around 210 nm relative to those for oligonucleotide alone. Because of the distinct nature of the spectroscopic transitions for each species, these spectra can be used to quantitate the loading of oligonucleotide per ASGP. The extinction coefficients of ASGP-SPDP and of unconjugated oligonucleotides were determined at 215 and 260 nm. Assuming that the contributions of each molecule to the conjugate add linearly, the absorbances of the purified conjugate at 215 and 260 nm then allow determination of the amount of protein and oligonucleotide contained within them (eqs 1 and 2). We confirmed the amount of protein determined using this method by BCA protein assay. The stoichiometries determined with each method were the same—about six oligonucleotides per ASGP. The batch to batch variation was small; in seven independent batches of conjugates prepared over an 8 month period, the average ratio of oligonucleotide to ASGP was 5.9 ± 1.0 , with a maximum of 7.5 and a minimum of 4.6.

In Vitro Evaluation. We tested the bioactivity of these conjugates using a system that has been the focus of recent investigation in our laboratory (Roth et al., 1997). The synthesized antisense oligonucleotide (AS130) used in our conjugates is complementary to the mRNA encoding gp130, a signal transduction protein central to the response of cells to the inflammatory cytokine, IL-6. Stimulation of HepG2 cells results in the up-regulation of a number of acute phase proteins, including haptoglobin. These acute phase proteins are secreted by hepatocytes into their external environment. We have previously shown that AS130 substantially inhibits the up-regulation of haptoglobin in HepG2 cells (Roth et al., 1997).

To test these new conjugates, HepG2 cells were treated with various concentrations of the ASGP-S-S-AS conjugates (with a stoichiometry of six oligonucleotides per ASGP) for 8 h, after which time the cells were stimulated with IL-6 (5 ng/mL) for 24 h. The medium

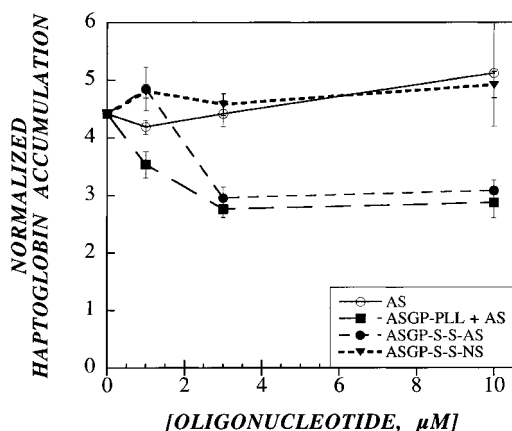


Figure 5. Inhibition of IL-6-mediated acute phase protein production by ASGP-S-S-AS targeted antisense (4). Confluent monolayers of HepG2 cells were incubated with various concentrations of unconjugated antisense oligonucleotide (AS), antisense oligonucleotide with 5 μM ASGP-PLL (ASGP-PLL + AS), covalent antisense conjugate (ASGP-S-S-AS), or covalent nonsense conjugate (ASGP-S-S-NS). After this time, the cells were stimulated with IL-6 for 24 h, after which time the medium was collected and assayed for haptoglobin by ELISA. Results are normalized to control cells that received neither IL-6 nor other treatment.

was harvested, and the haptoglobin secreted over the 24 h time period was quantitated by an ELISA (Roth et al., 1997). The conjugates inhibited the up-regulation of haptoglobin in a dose-dependent manner (Figure 5). Cells receiving no treatment other than IL-6 secreted ~ 5 times as much haptoglobin as basal (unstimulated with IL-6) cells. The cells treated with antisense conjugates—either the complex of ASGP-PLL or the covalent conjugate ASGP-S-S-AS—exhibited less up-regulation of haptoglobin than those that received no oligonucleotide treatment. The sequence of oligonucleotide is important, as conjugates containing a nonsense sequence (same base order as AS130 in scrambled order) demonstrated no inhibition. Furthermore, the presence of a conjugate is required, as equivalent amounts of oligonucleotide to those contained in the conjugates effected no inhibition in the unconjugated form. Therefore, the conjugation to ASGP produced an effective antisense oligonucleotide that inhibits the response to IL-6 in a sequence-specific manner.

DISCUSSION

A number of researchers have recognized the importance of targeted delivery to increase the effectiveness of antisense oligonucleotides. For *in vivo* applications, the delivery of antisense molecules to the target organ is likely to be a critical factor in their effectiveness. A molecular conjugate developed for the delivery of both oligonucleotides and plasmid DNA to hepatocytes is the asialoglycoprotein-poly(L-lysine) (ASGP-PLL) molecule, which provides a ligand (ASGP) for a liver-specific receptor (the asialoglycoprotein receptor) and a positively charged moiety (PLL), which is intended to condense the polyanionic DNA and overcome its electrostatic repulsion from negatively charged cell membranes (Wu and Wu, 1992; Bunnell et al., 1992; Lu et al., 1994). These conjugates have proven biologically effective in several *in vitro* systems and have provided enhanced uptake of oligonucleotides by the liver *in vivo* (Wu and Wu, 1992; Bunnell et al., 1992; Lu et al., 1994; Roth et al., 1997).

Although the ASGP-PLL delivery system has proven effective for *in vitro* studies, it has several drawbacks. For example, polylysine itself has potent toxicity. There-

fore, the quantity of ASGP-PLL that can be used is constrained. Low concentrations of ASGP-PLL were ineffective at condensing DNA and producing biological effect in our assay with IL-6-stimulated HepG2 cells. Moreover, we have found that higher doses of ASGP-PLL ($\sim 25 \mu\text{M}$) cause nonspecific reductions in protein secretion independent of the effects of oligonucleotides (Rajur et al., unpublished data). The ASGP-PLL/oligonucleotide complexes, held together by noncovalent electrostatic interactions, are unstable due to the instability of the electrostatic interaction between the carrier system and the oligonucleotides in ionic media such as blood (Lu et al., 1994). Furthermore, in these ionic conjugates, we have little control over the number of antisense molecules complexed with the carrier system and/or delivered to the target site because it is dictated by a physical equilibrium between the cationic ASGP-PLL and the anionic oligonucleotide. To increase the quantity of complexed oligonucleotide, a much higher quantity of ASGP-PLL is required, as this equilibrium requires ~ 10 – 20 ASGP-PLL molecules per single oligonucleotide (Bunnell et al., 1992; Rajur et al., unpublished data). However, ASGP-PLL that is not complexed with oligonucleotide will compete with the complexed ASGP-PLL for binding sites (Kato et al., 1996). To overcome these difficulties, we have developed a method in which we have eliminated the use of polylysine and covalently conjugated antisense oligonucleotides to asialoglycoprotein by a stable disulfide linkage. The advantage of this method is that the disulfide linkage is stable in the extracellular oxidizing environments typically found *in vitro* and *in vivo* and has the added advantage of undergoing reduction when it reaches the intracellular environment, permitting the release of free antisense within the cytoplasm (Feener et al., 1990).

Approximately six oligonucleotides were conjugated per ASGP molecule using the quantities of reagents described here. This is somewhat greater than the calculated number of PDP groups attached to each ASGP (~ 4). However, the latter estimate is inexact since it is based on low relative absorbance values ($A_{243} \sim 0.02$) and a published extinction coefficient ($8080 \text{ M}^{-1} \text{ cm}^{-1}$; Carlsson et al., 1978) that may depend on the exact buffer conditions. An alternative explanation is that some oligonucleotide binds noncovalently to ASGP. Repeated dialysis against PBS buffer using a 12 000–14 000 MW cutoff membrane did not change the loading ratio of oligonucleotides onto ASGP, so any noncovalent binding was irreversible.

In our experiments, we demonstrated that these conjugates are active *in vitro*, increasing the efficiency of antisense oligonucleotides at inhibiting the acute phase response in a cell culture model. The key advantages of the covalent conjugate relative to ASGP-PLL conjugates are the ability to alter loading via reaction stoichiometry and the inherent stability of the covalent linkage. Furthermore, the amount of ASGP required to target was reduced using the covalent chemistry. Using ASGP-PLL physically complexed to antisense, 5 μM was required to target the 10 μM oligonucleotide sufficiently to produce an effective dose. With the covalent conjugation, $\sim 1.6 \mu\text{M}$ of ASGP was required due to the high loading of oligonucleotide per ASGP (approximately 6:1).

It is noteworthy that neither conjugate was able to provide 100% inhibition, even at higher and repeated doses than those shown here. There are several possible reasons for this behavior, two of which are most plausible. First, the relationship between bound receptors and biological response is nonlinear, and examples are known where only a small fraction of receptors bound results in

maximal biological response (Lodish et al., 1995). Therefore, it is possible that the majority of gp130 (which is a secondary, high-affinity receptor for IL-6, associating with IL-6/gp80 complexes) molecules can be down-regulated before any functional inhibition is observed, and significant levels of haptoglobin up-regulation may be observed even with a small fraction of normal expression of gp130. The second factor is that the oligonucleotides are likely degraded by nucleases during the time course of the experiment, and this may allow sufficient time for the down-regulated gp130 to be newly synthesized, bound, and induce production and secretion of haptoglobin.

A similar approach to ours was developed by Bonfils et al. (1992) for the delivery of oligonucleotides to cells via a mannosylated BSA ligand that binds to membrane lectins. The oligonucleotides were synthesized on a 3'-disulfide derivatized support and conjugated to bovine serum albumin that had been previously 6-phospho-mannosylated (to provide a lectin binding ligand) and derivatized with SPDP. Increased cellular uptake of the conjugates was observed in both macrophages and baby hamster kidney cells as compared to unconjugated oligonucleotide. These conjugates were also found to be stable in culture medium. However, the ability of the conjugated oligonucleotides to act as antisense molecules was not investigated. Our results demonstrate the following: (1) the generalizability of disulfide protein-oligonucleotides to another ligand and cell type and to conjugation via the 5' end of the oligonucleotide; (2) the ability to achieve higher loadings of oligonucleotides (5–6 as compared to 1–2) per protein molecule; and (3) biological activity of oligonucleotide conjugated in this way. These results provide a basis for optimization of oligonucleotide loading for maximum effectiveness and a stable molecule that can be tested *in vivo*.

In summary, we have prepared a molecular conjugate of ASGP and a 15-mer antisense oligonucleotide using disulfide chemistry designed to enhance the delivery of the oligonucleotides to hepatocytes. These conjugates were found to significantly increase the effectiveness of antisense oligonucleotides in an *in vitro* model. This chemistry provides a means to produce stable conjugates with a desired loading of oligonucleotide and to reduce the amount of antisense and carrier required for effective delivery. Further development of these conjugates will involve investigation of their biodistribution, stability, and bioactivity *in vivo*.

ACKNOWLEDGMENT

This work was supported by a grant from the Shriners Hospital for Children (SHCC 8610). C.M.R. was supported by a NIH postdoctoral fellowship (GM-07035).

LITERATURE CITED

- Agrawal, S. (1996) Antisense oligonucleotides: towards clinical trials. *Trends Biotechnol.* 14, 376–387.
- Bonfils, E., Depierreux, C., Midoux, P., Thuong, N. T., Monsigny, M., and Roche, A. C. (1992) Drug targeting: synthesis and endocytosis of oligonucleotide-neoglycoprotein conjugates. *Nucleic Acids Res.* 20, 4621–4629.
- Bunnell, B. A., Askari, F. A., and Wilson, J. M. (1992) Targeted delivery of antisense oligonucleotides by molecular conjugates. *Somatic Cell Mol. Genet.* 18, 559–569.
- Carlsson, J., Drevin, D., and Axen, R. (1978) Protein thiolation and reversible protein-protein conjugation. *N-Succinimidyl 3-(2-pyridyldithio)propionate*—a new heterobifunctional reagent. *Biochem J.* 173, 727–737.
- Feener, E. P., Shen, W. C., and Ryser, H. J.-P. (1990) Cleavage of disulfide bonds in endocytosed macromolecules. A processing not associated with lysosomes or endosomes. *J. Biol. Chem.* 265, 18780–18785.
- Heidenreich, O., Kang, S.-H., Xu, X., and Nerenberg, M. (1995) Application of antisense technology to therapeutics. *Mol. Med. Today* 1, 128–133.
- Kato, Y., Seita, T., Kuwabara, T., and Sugiyama, Y. (1996) Kinetic analysis of receptor-mediated endocytosis (RME) of proteins and peptides: use of RME as a drug delivery system. *J. Controlled Release* 39, 191–200.
- Keller, E. T., and Ershler, W. B. (1995) Effect of IL-6 receptor antisense oligodeoxynucleotide on *in vitro* proliferation of myeloma cells. *J. Immunol.* 154, 4091–4098.
- Le Doux, J. M., Morgan, J. L., and Yarmush, M. L. (1995) Antisense technology. *The Biomedical Engineering Handbook* (J. D. Bronzino, Ed.) pp 1472–1488, CRC Press, Boca Raton, FL.
- Lodish, H., Baltimore, D., Berk, A., Zipursky, S. L., Matsudaira, P., and Darnell, J. (1995) *Molecular Cell Biology*, 3rd ed., p 866, W. H. Freeman and Co., New York.
- Lu, X.-M., Fischman, A. J., Jyawook, S. L., Hendricks, K., Tompkins, R. G., and Yarmush, M. L. (1994) Antisense DNA delivery *in vivo*: liver targeting by receptor-mediated uptake. *J. Nucl. Med.* 35, 269–275.
- Maier, J. A. M., Voulalas, P., Roeder, D., and Maciag, T. (1990) Extension of the life-span of human endothelial cells by an interleukin-1 α antisense oligomer. *Science* 249, 1570–1574.
- Miyajima, A., Kitamura, T., Harada, N., Yokota T., and Arai, K.-I. (1992) Cytokine receptors and signal transduction. *Annu. Rev. Immunol.* 10, 295–331.
- Roth, C. M., Reiken, S. R., Le Doux, J. M., Rajur, S. B., Lu, X.-M., Morgan, J. R., and Yarmush, M. L. (1997) Targeted antisense modulation of inflammatory cytokine receptors. *Biotechnol. Bioeng.* 55, 72–81.
- Sariola, H., Saarma, M., Sainio, K., Arumae, U., Palgi, J., Vaahtokari, A., Thesleff, I., and Karavanov, A. (1991) Dependence of kidney morphogenesis on the expression of nerve growth factor receptor. *Science* 254, 571–573.
- Schwab, G., Siegall, C. B., Aarden, L. A., Necker, L. M., and Nordan, R. P. (1991) Characterization of an interleukin-6-mediated autocrine growth loop in the human multiple myeloma cell line, U266. *Blood* 77, 587–593.
- Wang, S., Lee, R. J., Cauchon, G., Grenstein, D. G., and Low, P. S. (1995) Delivery of antisense oligodeoxynucleotides against the human epidermal growth factor receptor into cultured KB cells with liposomes conjugated to folate via polyethylene glycol. *Proc. Natl. Acad. Sci. U.S.A.* 92, 3318–3322.
- Wu, G. Y., and Wu, C. H. (1992) Specific inhibition of hepatitis B viral gene expression *in vitro* by targeted antisense oligonucleotides. *J. Biol. Chem.* 267, 12436–12439.

BC970172U

TECHNICAL NOTES

Bilayer Distribution of Phosphatidylserine and Phosphatidylethanolamine in Lipid Vesicles

Maria Teresa Roy, Montserrat Gallardo, and Joan Estelrich*

Unitat de Fisicoquímica, Facultat de Farmàcia, Universitat de Barcelona, Avinguda Joan XXIII s/n, 08028 Barcelona (Catalonia), Spain. Received May 28, 1997*

The distribution of phosphatidylethanolamine (PE) and phosphatidylserine (PS) in liposomes was studied as a function of aminophospholipid concentration using fluorescamine as labeling reagent. The method is suitable for such determination since, in the assay conditions, fluorescamine does not penetrate the vesicles nor does it disrupt them. The liposomes were obtained by sonication, extrusion, or mechanical dispersion (MLV). For any kind of vesicle, the percentage of PS in the external monolayer is higher than that obtained for PE in the corresponding vesicles. In extruded PS liposomes, this aminophospholipid is located preferentially in the outer layer, while for PE liposomes the localization depends on the size of vesicle. Sonicated liposomes present an asymmetrical distribution of both aminophospholipids, and the external location of PS or PE always predominates. In contrast, in MLV, aminophospholipids are mainly found in the inner layers of the vesicles, except for liposomes formed by the lowest PS proportion. A remarkable feature of PS liposomes is the reduction of vesicle size, especially in MLV liposomes, in comparison with neutral liposomes.

INTRODUCTION

The molecular architecture of biological membranes is highly asymmetric. Not only is the orientation of membrane proteins asymmetric, but the distribution of phospholipids and fatty acids is also asymmetric (1). The asymmetrical distribution of membrane phospholipids across the lipid bilayer seems to be responsible for cell functions such as coagulation, membrane fusion, and stability (2). In erythrocytes, the best documented system, phosphatidylserine (PS), phosphatidylethanolamine (PE), and probably phosphatidylinositol (PI) are located mainly in the inner monolayer, while phosphatidylcholine (PC) and sphingomyelin (SM) are mostly found in the outermost monolayer (3). This highly asymmetric orientation of lipids is essential to normal homeostasis. Increased exposure of PS on the outer surface of the red blood cell is a signal for sequestration by the reticuloendothelial system. Furthermore, partial loss of PS asymmetry occurs, for instance, in some pathological red blood cells, such as sickle cells. Similarly, tumorigenic cells are bound and lysed by activated monocytes or macrophages, as they express much more PS in their membrane outer leaflet than their nontumorigenic counterparts (4). In platelets, SM and PE are located predominantly in the surface membrane, while PS and PI are in the intracellular membrane (5). Moreover, in platelets, transbilayer asymmetry is rapidly lost upon stimulation by certain platelet antagonists. This phenomenon fulfills an important physiological function in the hemostatic process, since two sequential reactions of the coagulation cascade are dramatically accelerated in the presence of an anionic phospholipid surface (6, 7). PS and PI are

active in thrombin generation but have no role in factor Xa formation. PC and PE do not contribute to thrombin formation but are active in the formation of factor Xa. Although in principle any negatively charged phospholipid is capable of providing a catalytic surface, membranes containing PS exhibit the highest procoagulant activity (8). In view of the weak procoagulant activity of PI and its conversion in the PI cycle upon cell activation, PS is likely to be solely responsible for the formation of procoagulant lipid surfaces in stimulated platelets. It has been known for several decades that platelet activation may result in formation of platelet-derived microparticles with clot-promoting activity. The importance of this material for platelet procoagulant activity has long been underrated. Recently, however, it has become evident that the particles are derived from the cell surface by shedding from the plasma membrane, and shedding of microvesicles appears to be closely associated with surface exposure of PS (7). Electromicroscopy reveals these particles as uni- or paucilamellars. Since this structure is quite similar to liposomes, lipid vesicles could mimic the platelet-derived microparticles or the platelets themselves. Thus, an ability to generate liposomal systems exhibiting asymmetric transbilayer distributions of PS (or PE) may have a number of applications. To this end, we have undertaken the study of the distribution of PE and PS in liposomes obtained by extrusion, sonication, or simple dispersion. These results may help to identify the kinds of liposomes that provide the desired aminophospholipid distribution. This may lead, in turn, to the development of models of biological membrane with a particular PE or PS distribution.

EXPERIMENTAL PROCEDURES

Materials. Soybean PC (Lipoid S-100) was purchased from Lipoid (Ludwigshafen, Germany). PS from bovine spinal cord and PE from egg yolk were obtained from

* Author to whom correspondence should be addressed (telephone + 34-3-4024554; fax + 34-3-4021886; e-mail estelric@farmacia.far.ub.es).

© Abstract published in *Advance ACS Abstracts*, October 15, 1997.

Table 1. Average Size (Expressed as \bar{x} -Average Diameter \pm SD, $n \geq 3$) of the Different Kinds of Liposomes Used

		liposome composition										
type of liposome	pore size (nm)	% PE					% PS					
		5	10	20	30	50	5	10	20	30	50	0
extrusion	400	250 ± 11	247 ± 8	242 ± 10	238 ± 13	210 ± 10	195 ± 27	184 ± 10	174 ± 10	171 ± 10	161 ± 11	255 ± 16
	200	184 ± 6	186 ± 6	170 ± 6	167 ± 3	164 ± 7	137 ± 16	139 ± 2	140 ± 11	140 ± 5	134 ± 12	180 ± 15
	100	111 ± 7	110 ± 8	104 ± 9	109 ± 4	113 ± 1	98 ± 5	95 ± 2	97 ± 8	99 ± 8	106 ± 9	102 ± 5
	50	76 ± 4	78 ± 4	78 ± 6	82 ± 6	84 ± 4	72 ± 3	73 ± 2	72 ± 5	74 ± 5	81 ± 6	84 ± 5
sonication		131 ± 20	127 ± 25	119 ± 19	136 ± 26	117 ± 19	86 ± 8	91 ± 8	76 ± 8	80 ± 7	83 ± 11	121 ± 20
MLV		1350 ± 150	1200 ± 190	1010 ± 210	1160 ± 210	1140 ± 110	560 ± 100	650 ± 160	640 ± 180	650 ± 130	590 ± 190	1350 ± 50

Lipid Products (Nutfield, U.K.). Fluorescamine and Triton X-100 were purchased from Sigma. Organic solvents (methanol, ethanol, chloroform) were obtained from Merck (Darmstadt, Germany) and used without purification. Acetone was of spectroscopic grade (Merck). Saline solution was made with 150 mM NaCl. Borate buffer (pH 8.25) was made at 50 mM concentration and NaCl was added to give an isotonic solution, 310 \pm 10 mOsm/kg.

Preparation of Multilamellar Liposomes (MLV). Phospholipids (PC alone or PC with PS or PE) were dissolved in chloroform in a round-bottom flask and dried in a rotary evaporator under reduced pressure at 50 °C to form a thin film on the flask. The film was hydrated with saline solution to give a lipid concentration of 10 μ mol/mL. Multilamellar liposomes were formed by constant vortexing for 4 min on a vortex mixer and sonication in a bath sonifier for 4 min.

Preparation of Sonicated Liposomes. MLV were sonicated on an ice–water bath with a Branson sonifier (Labsonic U) equipped with a microtip probe and operating at 57 W output for 6 min with three cycles of 2 min and 30 s intervals stand-by in ice bath. The resulting suspension was passed through 0.45 μ m membrane filters to remove the possible titanium particles from the sonifier probe.

Preparation of Extruded Liposomes. MLV were downsized to form oligolamellar vesicles by extrusion at 50 °C in an extruder device (Lipex Biomembranes, Canada) through polycarbonate membrane filters of variable pore size under nitrogen pressures of up to 55 $\times 10^5$ N·m⁻² (9). Liposomes were extruded sequentially through polycarbonate filters (0.8, 0.4, 0.2, 0.1, and 0.05 μ m (Nucleopore, U.S.A.) to obtain liposomes of nominal size of 400, 200, 100, and 50 nm.

Determination of Aminophospholipids. PE and PS were determined spectrofluorometrically using fluorescamine as labeling reagent (10). This reagent was used by Cheung and Forte (11) to label aminophospholipids, but the method is similar to that used by Barenholz et al. (12) to determine PE in liposomes by means of 2,4,6-trinitrobenzenesulfonic acid (TNBS). It was confirmed in advance that fluorescamine had no disruptive effect on liposome structure (data not shown).

Determination of Aminophospholipids in the Outer Vesicle Surface. At room temperature, aliquots (100–200 μ L) of liposomes were diluted with 2.0 mL of borate buffer (pH 8.25). Fluorescamine solution (0.1 mL; 3 mg in 100 mL of acetone) was added, and the vesicle sample was shaken vigorously for 30 s. After 1 min, 2 mL of 1.6% Triton X-100 in borate buffer was added to the sample, followed by mixing. The resulting fluorescence was read within 2 h of reaction by exciting the sample at 381 nm and measuring the emitted radiation at 471 nm.

Determination of Total Aminophospholipids in the Vesicle. Aliquots (100–200 μ L) of liposomes were disrupted with 2.0 mL of 1.6% Triton X-100 in borate buffer (pH 8.25). Fluorescamine solution (0.1 mL) was

added, and the vesicle sample was shaken vigorously for 30 s. After 1 min, 2 mL of borate buffer was added to the sample, followed by mixing. The samples were read as described above.

Photon Correlation Spectroscopy. Vesicle size distribution was determined by photon correlation spectroscopy with an Autosizer II spectrometer (Malvern Instruments, U.K.) at 37 °C. The vesicles obtained by extrusion or sonication, which afforded a unimodal vesicle distribution, were sized by the method of cumulant analysis (13), while the exponential sampling method (14), which does not assume any particular form of distribution, was used to size MLV.

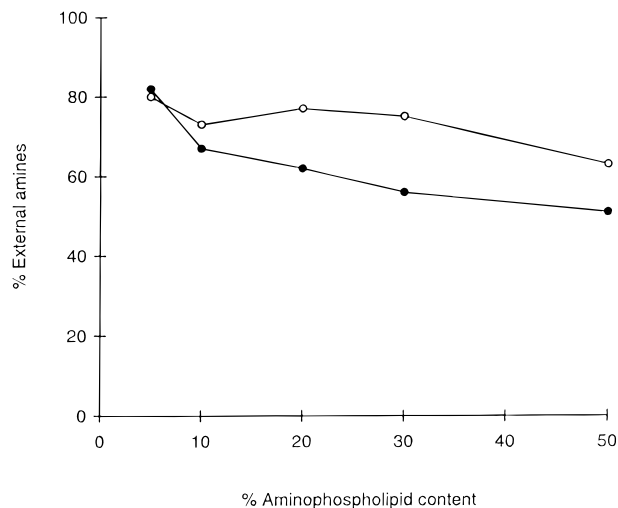
RESULTS

Fluorescamine Assay. The first stage of this investigation was aimed at establishing the validity of the fluorescamine labeling procedures for assaying transmembrane distributions of lipids containing primary amino groups in liposomal systems. We checked the linearity of fluorescence intensity between the range from 0.0125 to 0.300 μ mol of aminophospholipid. On the other hand, we found there was no difference between the results of total and external aminophospholipid when the substance assayed did not present such differences, namely in solutions of bovine serum albumin. In this way, a solution of such protein gave a values of 153 \pm 4 (arbitrary units of fluorescence) ($n = 6$) when it was assayed as external amino groups and 157 \pm 5 ($n = 6$) for total amino groups. A comparison of means showed that at 95.0% confidence interval there were no significant differences between both means ($t = 1.610 < 2.228$). Finally, we checked that at the reagent concentration used, the extent of the labeling was not influenced by the presence of a pH gradient (interior acidic). Liposomes with an acidic interior (achieved with citrate buffer) gave the same result as those obtained in saline solution. Thus, we deduced that, in the experimental conditions of the assay, liposomal membranes were impermeable to fluorescamine and, consequently, we prepared the liposomal samples in saline solution.

Extrusion Liposomes. To assess the distribution of aminophospholipids, three kinds of liposomes were examined. Table 1 shows the \bar{x} -average diameters obtained. On the whole, diameters of PE-containing extruded liposomes were similar to those obtained with neutral liposomes (for example, those formed solely by PC, the sizes of which are displayed in the last column of the table). However, the diameter of vesicles with >20% PE and extruded through 400 and 200 nm membranes was slightly lower than that obtained for PC liposomes extruded through membranes of the same pore size (255 and 180 nm, respectively). In PS-containing liposomes the reduction of vesicle size was even more evident in those vesicles downsized through membranes of 400 and 200 nm. At any PS percentage, the average values were <200 nm for the 400 nm extruded liposomes,

Table 2. Percentage of Aminophospholipid on the External Monolayer of Extruded Liposomes (Values Are the Average \pm SD, $n \geq 3$)

pore size (nm)	liposome composition									
	% PE					% PS				
	5	10	20	30	50	5	10	20	30	50
400	48 \pm 7	43 \pm 5	43 \pm 5	46 \pm 7	44 \pm 1	72 \pm 1	65 \pm 9	60 \pm 5	51 \pm 7	58 \pm 6
200	55 \pm 7	51 \pm 5	51 \pm 5	53 \pm 8	49 \pm 1	77 \pm 6	72 \pm 9	63 \pm 4	62 \pm 5	55 \pm 6
100	69 \pm 7	60 \pm 5	58 \pm 3	60 \pm 6	54 \pm 2	75 \pm 5	72 \pm 6	64 \pm 1	61 \pm 6	56 \pm 7
50	71 \pm 4	65 \pm 4	63 \pm 4	62 \pm 6	56 \pm 3	75 \pm 1	73 \pm 6	68 \pm 3	61 \pm 5	56 \pm 9

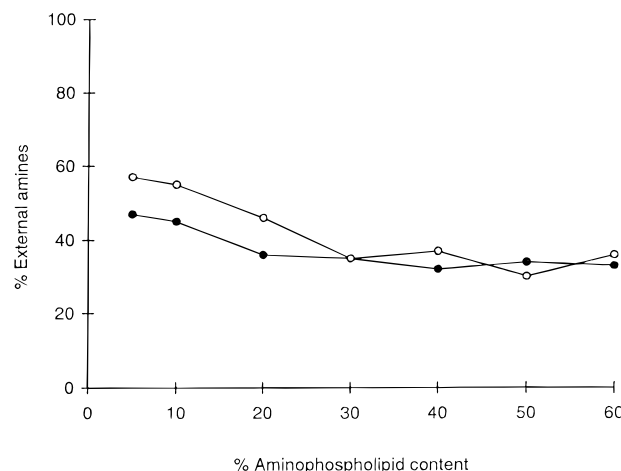
**Figure 1.** Average percentage of external aminophospholipids determined in sonicated liposomes using the fluorescamine assay: (○) PS; (●) PE.

and when vesicles were extruded through a 200 nm membrane, their average diameter never exceeded 140 nm.

The distribution of aminophospholipids between the external and the inner layer (or layers) was determined spectrofluorometrically using fluorescamine as labeling reagent (Table 2). The distribution of PE is defined by two general traits. First, the percentage of aminophospholipids in the external layer increased when the size of vesicles decreased. So, for a given composition, the percentage of external PE in 50 nm liposomes was higher than that obtained in other vesicles. Second, PE tended to distribute on the inside of the vesicle as its proportion increased. As far as PS distribution is concerned, a tendency similar to that described above for the localization of PE in the membrane was found, although for 50% concentration the percentage of external PS barely varies with the reduction of size. The PS content was always >50% irrespective of composition or size. When both distributions were compared, it was observed that below 20% concentration of aminolipid in the membrane, the differences were relatively important, but above such concentration, broadly speaking, the percentages of external amine groups became the same.

Sonicated Liposomes. Diameters of PE liposomes were greater than those of vesicles containing PS (Table 1). Diameters of PS sonicated vesicles were comparable to those of the vesicles extruded by membranes of 50 nm pore size. The aminophospholipid distribution followed the pattern observed in extruded liposomes (Figure 1). At low aminolipid concentrations, both PE and PS showed a tendency to concentrate in the outer surface. This location was reduced in extent when concentration increased. On the other hand, at almost all concentrations, PS was found in a higher extent in the external layer than PE.

Mechanical Dispersion Liposomes. Percentages of

**Figure 2.** Average percentage of external aminophospholipids determined in multilamellar liposomes using the fluorescamine assay: (○) PS; (●) PE.

external aminophospholipids and z-average diameters of multilamellar liposomes are shown in Figure 2 and Table 1, respectively. PE multilamellar liposomes present the classical characteristics of this kind of vesicle: their average diameters were outside the range above the micrometer with relatively important associated polydispersities. PS liposomes, in contrast, showed a lower size—in comparison with neutral liposomes—and the extent of dispersity was lower, too. As in the other types of vesicle, the increment of aminophospholipid percentage favored their localization in the inner layer of the vesicle.

DISCUSSION

Our results show that liposomes containing PS are smaller than PE vesicles or plain PC vesicles. This difference is especially marked in multilamellar liposomes and appears to be independent of PS concentration. This phenomenon has been also noted in other charged vesicles, namely liposomes containing phosphatidic acid, but not to the extent shown in PS liposomes. This fact could be explained by the different structure and morphology of PS dispersions in comparison to those of PC and other neutral or isoelectric phospholipids. In contrast to egg PC, aqueous dispersions of PS exist as a single lamellar liquid crystalline phase up to water content of ~75%. In the absence of salt, pure PS incorporates all of the water between the lipid bilayers, increasing the lamellar repeat distance. The ability of PS bilayers to incorporate large amounts of water is a consequence of the net negative charge of the PS molecule at pH between 5 and 9, giving rise to large repulsive forces between adjacent bilayer sheets. Pure egg PC behaves differently and can incorporate water only up to ~40% water; further addition of water produces a two-phase system, a lamellar liquid crystalline phase in excess water (15). As such liposomes have been formed in saline solution (0.16 M NaCl), the salt must reduce the double-layer repulsion between adjacent bilayers. As

a result of that, water is extruded from the interbilayer space consistent with a decrease of lamellar repeat distance. Hauser (16) proposed that at high water content the multilamellar structures break up, with each lamella sealing off to form closed unilamellar vesicles. The addition of salt would induce aggregation and fusion of the vesicles leading, in equilibrium, to multilamellar structures. The relatively moderate presence of sodium in our liposomal suspension should limit the transformation of multilamellar structures into unilamellar vesicles, and this could explain the intermediate size of PS multilamellar liposomes.

Concerning the aminophospholipid distribution in extruded and sonicated liposomes, there is a predisposition of such lipids to locate in the external monolayer. This is true in general for PS liposomes and characteristic of those PE liposomes extruded through membranes of pore below 200 nm. The preferential localization of PE and PS in the external monolayer is in agreement with the results of Massari et al. (17), who found 67% of external amines in egg PC containing 40% of PS. In contrast, Berden et al. (18) and Barsukov et al. (19) state that in sonicated liposomes, PE or PS had preference for the inside layer of the bilayer. However, the experimental conditions are not equivalent to ours. For instance, these authors did not measure the vesicle size and, although in theory these liposomes might have been unilamellar at the moment of their formation, they could have suffered aggregation and/or fusion during the relatively long time that a measurement by NMR takes.

As it has been already seen in Table 1, the localization of PE shows a clear dependence on actual vesicle size. In PS liposomes the difference of size between the vesicles extruded by the biggest membrane pore and those passed by the lowest are smaller, and this is evidenced by minor and not so clear differences in the PS distribution.

In liposomes obtained by mechanical dispersion the percentage of external aminophospholipid is always <50% and above 20% of amino lipid the amount of external PE or PS barely varies.

As a general rule of aminophospholipid distribution we can affirm that PS and PE tend to locate on the external monolayer, such tendency being influenced by the size of vesicles, or better, by the vesicle curvature. On the basis of theoretical considerations, Israelachvili (21) has predicted an asymmetrical distribution of charged phospholipid molecules between the external and the inner monolayers. This asymmetry in the phospholipid distribution was attributed to the reduced electrostatic repulsion between the negatively charged molecules when these were concentrated more on the outer layers. This analysis agrees quantitatively with the experimental results reported by Michaelson et al. (22) and carried out with vesicles containing phosphatidylglycerol and further predicts that the asymmetric distribution of charged lipid molecules should increase with decreasing radius of curvature and decreasing ionic strength of the suspending medium.

From geometrical relationships, assuming that the bilayer width is 4 nm and that the molecular areas of PC and PS are 70 Å²/mol (22), we can calculate the number of lipid molecules of PS and PC present in a liposome for any PS composition. Thus, liposomes sized to 100 nm may have 44 880 molecules on the external monolayer and 37 986 on the internal. If all lipid molecules were PS, this distribution would involve 54% PS on the external monolayer. We prepared 100 nm extruded liposomes, of which the unique lipid present was PS, and determined the external percentage of PS, using

the fluorescamine method. The value obtained, $54 \pm 2\%$ ($n = 3$), certifies the validity of the method.

We can conclude that the localization of aminophospholipids depends on the amount of charged lipids, as well as the size of the vesicles. In relatively small vesicles (diameter ≤ 200 nm), the natural "site" of such aminophospholipids is the external monolayer. An increase of their concentration reveals that the localization of more molecules is not energetically allowed owing to the repulsive interactions, and the charged lipids must locate in the inner layer. In greater vesicles, the effects of the curvature are not so strong, and the possibility of a symmetrical distribution is open. In MLV liposomes, the higher number of internal bilayers results in a predominance of PS or PE in the inner.

Our results indicate that one can obtain liposomes with a particular PS or PE distribution. The only parameters that may be varied are the size and the aminophospholipid content. Use of liposomes with several bilayer distributions can be a useful tool for the study of the mechanism of coagulation, and, on the other hand, a determined kind of liposomes with a marked coagulant activity could be used as artificial platelets.

LITERATURE CITED

- (1) Op den Kamp, J. A. F. (1979) Lipid asymmetry in membranes. *Annu. Rev. Biochem.* 48, 47–71.
- (2) Zachowski, A. (1993) Phospholipids in animal eukaryotic membranes: transverse asymmetry and movement. *Biochem. J.* 294, 1–14.
- (3) Bretscher, M. S. (1972) Asymmetrical lipid bilayer structure for biological membranes. *Nature New Biol.* 236, 11–12.
- (4) Utsugi, T., Schroit, A. J., Connor, J., Bucana, C., and Fiedler, I. J. (1991) Elevated expression of phosphatidylserine in the outer membrane leaflet of human tumor cells and recognition by activated human blood monocytes. *Cancer Res.* 51, 3062–3066.
- (5) Crawford, N., and Scrutton, M. C. (1987) Biochemistry of the blood platelet. In *Haemostasis and Thrombosis* (T. Bloom and D. P. Thomas, Eds.) pp 47–72, Churchill Livingstone, Edinburgh.
- (6) Bevers, E. M., Tilly, R. H. J., Senden, J. M. G., Comfurius, P., and Zwaal, R. F. A. (1989) Exposure of endogenous phosphatidylserine at the outer surface of stimulated platelets is reversed by restoration of aminophospholipid translocase activity. *Biochemistry* 28, 2382–2387.
- (7) Zwaal, R. F. A., Comfurius, P., and Bevers, E. M. (1992) Platelet coagulant activity and microvesicle formation. Its putative role in hemostasis and thrombosis. *Biochim. Biophys. Acta* 1180, 1–8.
- (8) Rosing, J., Speijer, H., and Zwaal, R. F. A. (1988) Prothrombin activation on phospholipid membranes with positive electrostatic potential. *Biochemistry* 27, 8–11.
- (9) Hope, M. J., Bally, M. B., Webb, G., and Cullis, P. R. (1985) Production of large unilamellar vesicles by a rapid extrusion procedure. Characterization of size distribution trapped volume and ability to maintain a membrane potential. *Biochim. Biophys. Acta* 812, 55–65.
- (10) Udenfriend, S., Stein, S., Böhlen, P., Dairman, W., Leimpruber, W., and Weigle, M. (1972) Fluorescamine: a reagent for assay of amino acids, peptides, proteins, and primary amines in the picomole range. *Science* 178, 871–872.
- (11) Cheung Lee, H., and Forte, J. G. (1979) Asymmetric labeling of amino lipids in liposomes. *Biochim. Biophys. Acta* 554, 375–387.
- (12) Barenholz, Y., Gibbes, D., Litman, B. J., Thompson, T. E., and Carlson, F. D. (1977) A simple method for the preparation of homogeneous phospholipid vesicles. *Biochemistry* 16, 2806–2810.
- (13) Koppel, D. E. (1972) Analysis of macromolecular polydispersity in intensity correlation spectroscopy: the method of cumulants. *J. Chem. Phys.* 57, 4814–4820.

- (14) Ostrowski, N., Sornette, D., Parker, P., and Pike, E. R. (1981). Exponential sampling method for light scattering polydispersity analysis. *Opt. Acta* 28, 1059–1070.
- (15) Atkinson, D., Hauser, H., Shipley, G. G., and Stubbs, J. M. (1974) Structure and morphology of phosphatidylserine dispersions. *Biochim. Biophys. Acta* 339, 10–29.
- (16) Hauser, H. (1984) Some aspects of the phase behaviour of charged lipids. *Biochim. Biophys. Acta* 722, 37–50.
- (17) Massari, S., Pascolini, D., and Gradenigo, G. (1978) Distribution of negative phospholipids in mixed vesicles. *Biochemistry* 17, 4465–4469.
- (18) Berden, J. A., Barker, R. W., and Radda, G. K. (1975) NMR studies on phospholipid bilayers. Some factors affecting lipid distribution. *Biochim. Biophys. Acta* 375, 186–208.
- (19) Barsukov, L. I., Victorov, A. V., Vasilenko, I. A., Evstigne-eva, R. P., and Bergelson, L. D. (1980) Investigation of the inside-outside distribution, intermembrane exchange and transbilayer movement of phospholipids in sonicated vesicles by shift reagent NMR. *Biochim. Biophys. Acta* 598, 153–168.
- (20) Israelachvili, J. N. (1973) Theoretical considerations on the asymmetric distribution of charged phospholipid molecules on the inner and outer layers of curved bilayer membranes. *Biochim. Biophys. Acta* 323, 659–663.
- (21) Michaelson, D. M., Horwitz, A. F., and Klein, M. P. (1973) Transbilayer asymmetry and surface homogeneity of mixed phospholipids in cosonicated vesicles. *Biochemistry* 12, 2637–2645.
- (22) Eisenberg, M., Gresalfi, T., Riccio, T., and McLaughlin, S. (1979) Adsorption of monovalent cations to bilayer membranes containing negative phospholipids. *Biochemistry* 18, 5213–5223.

BC9701050